Q
1
S3
V.80-83
1977-80
SUBJ.
INDEX
A-CRY
N/C
Sci

Physics Abstracts

Volumes 80-83 1977-1980

Cumulative Subject Index

A—Cry

28 July 1983

Inspec
The Institution of Electrical Engineers

© 1981 The Institution of Electrical Engineers

CUMULATIVE SUBJECT INDEX 1977-80

Coverage

The present index provides a subject key to all papers abstracted in *Physics Abstracts* for the years 1977–80. It therefore comprises all relevant entries included in the six monthly subject indexes for the same period.

Subject Headings

In the course of the four years covered by this index the list of subject headings has been revised and new headings have been added. The present index uses the latest (i.e. 1980) version of the list. Entries for articles abstracted in the 1977, 1978 and 1979 volumes have been examined and, where appropriate, re-indexed under the new headings.

Arrangement

The subject headings are arranged in alphabetical order. The entries under each are prepared so that the most significant or 'key' words appear first and thus determine the position and grouping of entries in the alphabetical sequence under each heading.

Where the names of specific inorganic substances are significant under a given heading, the entries relating to them are found as a second alphabetical listing arranged by the chemical formulae of the particular elements or compounds.

Form of entry

The information contained in the subject index may be illustrated by an example.

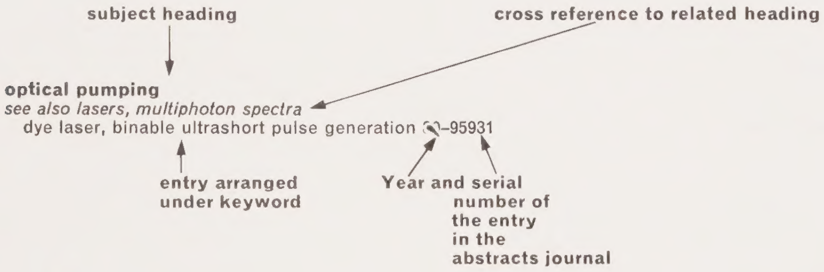
subject heading
cross reference to related heading
optical pumping
see also lasers, multiphoton spectra
dye laser, binable ultrashort pulse generation 80–95931
entry arranged under keyword
Year and serial number of the entry in the abstracts journal

How to use the index

The Subject index provides an alphabetical subject key to the articles included in the abstracts journal. Some general guidance on its use is given below:

1. Look in the index for the name of the specific subject in which you are interested. In most cases this name will be a heading in the index and you will find relevant articles listed under it. The majority of the subject headings fall into the following categories: property, phenomena, substance or named objects, instrument, device, theory, method, process, application, event.
2. Occasionally you will be directed from the subject heading chosen to a different heading under which the relevant or additional articles are listed.
3. If you do not find the subject heading you first chose, try a more general heading.
4. Each entry under the heading relates to an article appearing in the abstracts journal and gives the serial number of that article in the journal preceded by the last two digits of the current year, e.g. 78–12345; i.e. Abstract number 12345 in the abstracts journal for 1978.

   The language of the article, if it is not in English, is also indicated, e.g. optical fibre, three-wave stimulated Raman scattering (French) 0–78902.

   Each entry starts with a Keyword or Keyphrase considered to be most relevant to the heading. On sorting these Keywords, the qualifying prefixes are usually ignored (e.g. n-Ge is sorted under Ge).

   There are three main keyword lists; arabic numerals, alphabetical A–Z, and chemical symbols (organic substances are written and not given as chemical formula). More than one Keyword list may be present under each subject heading.

   For document on, say 'photoemission of silicon' at least two access points 'photoemission' and 'elemental semiconductors' are provided. Under the heading 'photoemission' the Keyword will be 'Si' and under 'elemental semiconductors' the Keyword will also be 'Si'.

   In a case like this, it is advisable and quicker to use the heading 'photoemission' and go straight to the chemical symbol list for 'Si' because there are few entries listed under 'photoemission'.

Printed by Unwin Brothers Limited, The Gresham Press, Old Woking, Surrey

Abbreviations and Acronyms

Abbreviations and acronyms are used in the modifiers in all INSPEC Cumulative Subject Indexes. Individual terms should be readily understood in the context of the subject headings. **Inorganic substances** are usually given by their chemical formulae. Iron and aluminium garnets appear in the formulae lists as MIG and MAG (where M is metal element, e.g. YIG and YAG); $(Pb,La)(Zr,Ti)O_3$ and $Ce_2Mg_3(NO_3)_{12}$ appear as PLZT and CMN respectively. **Organic substances** including **liquid crystals** are not given as formulae but common abbreviations are used.

ABS resin	acrylonitrile-butadiene-styrene
AC	alternating current
ACV	air cushion vehicle
A/D	analogue-to-digital
ADP	administrative data processing
AES	Auger electron spectra(oscopy)
AF	audio frequency
AFC	automatic frequency control
AFL	abstract family of languages
AGC	automatic gain control
AGR	advanced gas-cooled reactor
AM	amplitude modulation
ANS	Astronomical Netherlands Satellite
APACHE	accelerator for physics and chemistry of heavy elements
APR	acoustic paramagnetic resonance
APS	appearance potential spectra(oscopy)
APW	augmented plane wave
ATR	attenuated total reflection
ATS	applications technology satellite
ATWS	anticipated transients without scram
AVC	automatic volume control

BARITT	barrier injection transit time
BBEA	4-butoxybenzal-4′-ethylaniline
BCC	body centred cubic
BCD	binary-code decimal
BFO	beat-frequency oscillator
BWO	backward wave oscillator
BWR	boiling water reactor
BWT	backward wave tube

CAD	computer aided design
CAI	computer assisted instruction
CARS	coherent antiStokes Raman scattering (spectra)
CATV	community antenna TV
CB	citizen band
CBOOA	cyanobenzylidene octyloxyaniline
C-CD	charge-coupled device
CDI	collector diffusion isolation
CDM	code division multiplexing
CDW	charge-density wave
CEM	channel electron multiplier
CEPA	coupled electron pair approximation
CERN	Conseil Européen pour la Recherche Nucléaire
CESR	conduction electron spin resonance
CGTO	contracted Gaussian-type orbital
CHF	coupled Hartree-Fock
CI	configuration interaction
CIEH	charge iterated extended Huckel
CIHY	configuration interaction Hylleras
CNDO	complete neglect of differential overlap
COC	cholesteryl oleyl carbonate
COM	computer output to microform (fiche or film)
COOB	4,4′-cyano-octyloxy-biphenyl
CP	charge, parity
CPA	coherent potential approximation
CPSK	coherent phase shift keying
CPT	charge, parity, time
CRO	cathode ray oscilloscope
CRT	cathode ray tube
CS	coupled states
CSM	continuous slowing down models
CTR	controlled thermonuclear reactor
CVD	chemical vapour deposition
CW	continuous wave

D/A	digital-to-analogue
DBR	distributed Bragg reflector
DC	direct current
DDC	direct digital control
DDL	diode-diode logic
DECENT	distribution of exact classical energy transfer
DESY	Deutsches Electron Synchrotron
DF	Dirac-Fock
DFB	distributed feedback
DH	double heterostructure
DIL	dual-in-line
DITE	divertor in torus experiment
DLTS	deep level transient spectra(oscopy)
DM	delta modulation
DMSO	dimethyl sulphoxide
DMSS	Defence Meteorological Satellite System
DOBAMBC	p-decyloxybenzylidene p′-amino 2-methyl butyl cinnamate
DODS	different orbitals for different spins
DORIS	Dopple-ring-Speicher
DOVETT	double velocity transit time
DP	data processing
DPCM	differential pulse code modulation
DPPH	diphenylpicrylhydrazyl
DPSK	differential phase shift keying
DSC	differential scanning calorimetry
DTA	differential thermal analysis
DV-Xα	discrete variational Xα method

E1,E2	electric dipole, quadrupole
EAS	extensive air shower
EB	exponential Born
EBBA	4-ethoxybenzylidene-4′n-butylaniline
EBR	experimental breeder reactor
EBT	Elmo Bumpy Torus
ECC	emergency core cooling
ECELR	epithermal critical experiment laboratory reactor
ECG	electrocardiography (-gram)
EDA	ethylene diamine
EDP	electronic data processing
EDTA	ethylene diamine tetra-acetic acid
EEBAC	ethyl-4-(4′ethoxy-benzylidene-amino) cinnamate
EEG	electroencephalography (-gram)
EELS	electron energy loss spectra
EFM	extended Flygare method
EHD	electrohydrodynamics
EHF	extremely high frequency
EHP	electron-hole potential method
EHT	extended Huckel theory
EHV	extra high voltage
ELDOR	electron electron double resonance

ELF	extremely low frequency
EM	electromagnetic
EMC	electromagnetic compatibility
EMF	electromotive force
EMG	electromyography(-gram)
ENDOR	electron nuclear double resonance
EOS	earth observatory satellite
EPEN	empirical potential energy function based on interactions of electrons and nuclei
EPMA	electron probe microanalysis
EPR	electron paramagnetic resonance
ERG	electroretinography(-gram)
ERPS	extramolecular relaxation polarisation shift
ERTS	earth resources technology satellite
ESCA	electron spectroscopy for chemical analysis
ESCAR	experimental superconducting accelerating ring
ESFI	epitaxial silicon film on insulator
ESS	electronic switching system
EUV	extreme ultraviolet
EXAFS	extended X-ray absorption fine structure
FBR	fast breeder reactor
FCC	face centred cubic
FDM	frequency division multiplex(ing)
FDNC	frequency dependent negative conductance
FDNR	frequency dependent negative resistance
FEM	field emission microscopy
FET	field effect transistor
FFHR	fusion-fission hybrid reactor
FFT	fast Fourier transform
FFTF	fast flux test facilities
FIM	field ion microscopy
FM	frequency modulation
FPT	finite perturbation theory
FSK	frequency-shift keying
FSGO	floating spherical Gaussian orbitals
FTR	fast test reactor
GAMBIT	gate modulated bipolar transistor
GANIL	grand accelerateur national a ions Lourds
GARP	global atmospheric research programme
GATE	GARP Atlantic tropical experiment
GCFR	gas-cooled fast breeder reactor
GCM	generator coordinate method
GHF-NO-CI	generalised Hartree-Fock/natural orbital/configuration interactions
GIAO	gauge-invariant atomic orbitals
GO	Gaussian orbitals
GOO	generalised Overhauser orbitals
GPM	ground potential model
GSO	general spin orbitals
GTO	Gaussian-type orbitals
GVB	generalised valence bond
HAM	hydrogenic atoms in molecules
HBAB	hexyloxybenzylidene-p' aminobenzonitrile
HBT	N-(p-hexyloxybenzylidene)-p-toluidene
HCDA	hypothetical core disruptive accident
HCP	hexagonal close packed
HEED	high energy electron diffraction
HF	high frequency or Hartree-Fock
HFB	Hartree-Fock-Bogoliubov
HFER	hot fuel examination facility
HFIR	high flux isotope reactor
HFO	Hartree-Fock-Overhauser
HFS	hyperfine structure
HLW	high level waste (radioactive)
HMO	Huckel molecular orbitals
HOAB	heptyloxyazoxybenzene
HOBHA	p-n-heptyloxy-benzylidene-p-n heptylaniline
HOMO	highest occupied molecular orbitals
HORM	hybrid orbital rehybridisation method
HTGR	high temperature gas-cooled reactor
HV	high voltage
HVEM	high voltage electron microscopy
HWR	heavy water reactor
IAEA	International Atomic Energy Authority Agency
IBPBAC	isobutyl 4-(4'-phenylbenzylideneamino) cinnamate
IC	integrated circuit
ICDF	intermediate coupling Dirac-Fock
IDT	interdigital transducer
IEPA	independent electron pair approximation
IF	intermediate frequency
IGFET	insulated gate field effect transistor
IKO	Institute v. Kernph Ouder Amsterdam
I^2L	integrated injection logic
I^3L	isoplanar I^2L
ILS	instrument landing system
IMPATT	impact avalanche transit time
INDO	intermediate neglect of differential overlap
INDOR	internuclear double resonance
ING	intense neutron generator
INO	iterative natural orbital
INTELSAT	international telecommunications satellite consortium
I/O	input/output
IOC-ω	inclusion of the overlap charges in the omega
IR	infrared
IRDO	intermediate retention of differential overlap
ISABELLE	intersecting storage and acceleration
ISR	intersecting storage ring
ISX	impurity study experiment
ITEP	Institute of Theoretical and Experimental Physics
IU	Indiana University
IVO	improved virtual orbitals
JET	Joint European torus
JAERI	Japan Atomic Energy Research Institute
JINR	Joint Institute for Nuclear Research
KEK	Japan National Laboratory for High Energy Physics
KKR	Korringa-Kohn-Rostoker
LAMPF	Los Alamos meson physics facility
LC	inductance-capacitance
LCAO	linear combination of atomic orbitals
LCBO	linear combinations of (semi-localised) band orbitals
LCGO	linear combination of Gaussian orbitals
LCP	large coil program
LCRO	linear combination of Rydberg orbitals
LEC	liquid encapsulated Czochralski
LED	light emitting diode
LEED	low energy electron diffraction
LEP	large electron positron
LET	linear energy transfer
LF	low frequency
LMC	Large Magellanic Cloud
LMFBR	liquid metal fast breeder reactor
LMTO	linear combination of muffin tin orbitals
LOCA	loss of coolant accident
LOCE	loss of coolant experiment
LOFT	loss of flow test facility
LPE	liquid phase epitaxy
LSA	limited space charge accumulation

LSD	local spin density
LSI	large-scale integration
LTE	local thermodynamic equilibrium
LUMO	lowest unoccupied molecular orbitals
LV	low voltage
LWR	light water reactor
MADO	Mulliken approximation for differential overlap
M1,M2	magnetic dipole, quadrupole
MBBA	4-methoxybenzylidene-4′-n-butyl-aniline
MBE	molecular beam epitaxy
MBPT	many body perturbation theory
MCD	magnetic circular dichroism
MCPESCF	multiconfiguration paired excitation SCF
MCZDO	multi-centre zero differential overlap
MEDO	multipole expansion of diatomic overlap
MESFET	metal-semiconductor field effect transistor
MF	medium frequency
MFP	mean free path
MHD	magnetohydrodynamics
MIC	microwave integrated circuit
MIEHM	modified iterative extended Huckel method
MIM	metal-insulator-metal
MIS	metal-insulator-semiconductor or management information system
MIT	Massachusetts Institute of Technology
MMF	magnetomotive force
MNOS	metal-nitride-oxide-semiconductor
MO	molecular orbitals
MOCIC	molecular orbital constraint of interaction coordinates
MODPOT	model potential
MOS	metal-oxide-semiconductor
MOSFET	metal-oxide-semiconductor field effect transistor
MOST	metal-oxide-semiconductor transistor
MRD	multi-reference double excitation
MRINDO	modified Rydberg INDO
MSI	medium scale integration
MSR	molten salt reactor
MSU	Michigan State University
MTBF	mean-time between failures
MTF	modulation transfer function
MTXα	muffin-tin Xα
MUF	maximum usable frequency
MWH	Mulliken-Wolfsberg-Helmholz-semi-empirical method
NAL	National Accelerator Laboratory
NAND	not-and(logic)
NC	numerical control
NCMET	non-closed shell many electron theory
NDDO	neglect of diatomic differential overlap
NDT	nondestructive testing
NEMO	non-empirical molecular orbitals
NEVE	non-empirical valence-electron
NIC	negative impedance convertor
NMR	nuclear magnetic resonance
NNNDO	neglect of non-neighbour differential overlap
NOR	not-or(logic)
NPOST	non-perturbative open-shell theory
NPSO	non-paired spatial orbitals
NQR	nuclear quadrupole resonance
NRC	nuclear regulatory committee
NRM	natural remanent magnetisation
NTO	natural transition orbitals
OAO	orbiting astronomical observatory
OCR	optical character recognition

ODMR	optical detection of magnetic resonance
OER	oxygen enhancement ratio
OGO	orbiting geophysical observatory
OPHF	orbital polarised Hartree-Fock
OPW	orthogonal plane wave
OR	operations research
ORELA	Oak Ridge electron linear accelerator
ORNL	Oak Ridge National Laboratory
OSO	orbiting solar observatory
OTF	optical transfer function
PAA	paraazoxyanisole
PABX	private automatic branch exchange
PAC	perturbed angular correlation
PAHR	post accident heat removal
PAM	pulse amplitude modulation
PAMPUS	photons for atomic and molecular processes and universal studies
PAP	paraazoxyphenetole
PBF	power bursts facility
PBR	pebble bed reactor
PBX	private branch exchange
PC	printed circuit
PCAC	partially conserved axial currents
PCB	printed circuit board
PCGVB	pairwise correlated generalised valence bond
PCILOCC	perturbative configuration interaction using localised orbitals for crystal calculation
PCM	pulse code modulation
PCX	plasma confinement experiment
PDX	poloidal divertor experiment
PEP	positron electron proton
PETRA	positron electron tandem ringbeschleuniger anlage
PF	power factor
PFM	pulse frequency modulation
PHWR	pressurised heavy water reactor
PID(PI,PD)	proportional+integral+differential (derivative)
PLA	phase locked arrays
PLC	programmable logic control
PLL	phase locked loops
PLT	Princeton Large Torus
PM	pulse modulation
PMMA	polmethylmethacrylate
PMDR	phosphorescence microwave double resonance
PNDO	partial neglect of differential overlap
PNO-CI	pair natural orbital configuration interaction
POL	pair orthogonalised Lowdin
POPAE	protons on protons and electrons
POPOP	phenyl-oxazolyl-phenyl-oxazolyl-phenyl
POS	point of sale
PPDP/S	Pariser-Parr-Del Bene-Pople/Segal calculations
PPI	plan position indicator
PPM	pulse position modulation or parts per million
PPP	Pariser-Parr-Pople
PRDDO	partial retention of diatomic differential overlap
PRF	pulse recurrence (repetition) frequency
PROM	programmable read-only-memory or Pockels readout optical modulator
PS	proton synchrotron (CERN)
PSK	phase shift keying
PTFE	polytetrafluoroethylene
PTM	pulse time modulation
PVC	polyvinyl chloride
PWM	pulse width modulation
PWR	pressurised water reactor

QCD	quantum chromodynamics
QDMBPT	quasi-degenerate many-body perturbation theory
QED	quantum electrodynamics
QPSK	quaternary phase shift keying
RAM	random access memory
RBE	relative biological effectiveness
RC	resistance-capacitance
RCNDO	Rydberg CNDO
R & D	research and development
RF	radio frequency
RFI	radio frequency interference
RHEED	reflection high energy electron diffraction
RINDO	Rydberg INDO
RKKY	Rudermann-Kittel Kasuya-Yosida
RLC	resistance-inductance-capacitance
RMS	root-mean-square
ROM	read-only memory
RPA	random phase approximation
RPM	relaxation potential model
SAMO	simulated ab initio molecular orbitals
SAS	small astronomy satellite
SAW	surface acoustic waves
SCF	self consistent field
SCL	space charge limited
SCPT	self consistent perturbation theory
SCR	silicon controlled rectifier
SDM	space division multiplexing
SDO	shielded diatomic orbitals
SEHF	spin extended Hartree-Fock
SEM	scanning electron microscope
SFE	solar flare effect
SGHWR	steam generating heavy water reactor
SHF	superhigh frequency
SHG	second harmonic generation
SIMS	secondary ion mass spectrometer
SIN	Swiss Institute of Nuclear Research
SINDO	scaled INDO
SISAM	spectrometer with interference selective amplitude modulation
SMC	Small Magellanic Cloud
SMS	synchronous meteorological satellite
S/N	signal-to-noise
SOG	strongly orthogonal geminal
SOS	silicon on sapphire
SPA	separated pair approximation
SPC	stored program control
SPEAR	Stanford positron electron asymmetric ring
SPHF	spin polarised Hartree-Fock
SPIN-CIPSI	spin symmetry adapted generalisation of CIPSI
SPS	super proton synchroton (CERN)
SQUID	superconducting quantum interference device
SRMCASE	symmetry-restricted-multiconfiguration annihiliation of single excitations
SSB	single sideband
SSC	sudden storm commencement
SSI	supersonic transport
STD	salinity-temperature-depth or subscriber trunk dialling
STEM	scanning transmission electron microscopy
STO	Slater-type orbitals
STOL	short take-off and landing
STP	Slater-transfer Preuss
SUHFC	spin unrestricted Hartree-Fock with local approximation for correlations
SW	short wave
SWR	standing wave ratio
SXAPS	soft X-ray appearance potential spectrum
TBBA	terephthal-butylaniline
TCNE	tetracyanoethylene
TCNQ	tetracyanoquinodimethane
TCR	temperature coefficient of resistance
TDHF	time dependent Hartree-Fock
TDM	time division multiplex(ing)
TDMA	time division multiple access
TDPAC	time differential perturbed angular correlation
TE	transverse electric
TEA	transversely excited atmospheric
TEM	transverse electromagnetic or transmission electron microscopy
TEXT	Texas Experimental Tokamak
TFTR	Tokamak fusion test reactor
TGFB	triglycine fluoroberyllate
TGS	triglycine sulphate
TGSe	triglycine selenate
TJS	transverse junction stripe
TLD	thermoluminescent dosimeter(-ry)
TM	transverse magnetic
TMMC	tetramethylammonium manganese chloride
TOP	transient overpower accident
TNS	The next step
TRAPATT	trapped plasma avalanche triggered transit
TREAT	transient reactor test facility
TRM	thermoremanent magnetisation
TSC	thermally stimulated currents
TSEE	thermally stimulated exo-electron emission
TTF	tetrathiofulvalinium
TTL	transistor transistor logic
TTT	tetrathiotetracene
TUCA	transient undercooling accident
TV	television
TW	travelling wave
TWT	travelling wave tube
UCHF	uncoupled Hartree-Fock
UHF	ultra high frequency unrestricted Hartree-Fock
UHV	ultra high voltage
UKAEA	United Kingdom Atomic Energy Authority
ULF	ultra low frequency
UMD	unitised microwave devices
UPS	ultraviolet photoelectron spectra
US	ultrasonic
UV	ultraviolet
VB	valence bond
VCR	video cassette recorder
VDM	vector dominance model
VDU	visual display unit
VHF	very high frequency
VLBI	very long base line interferometry
VLF	very low frequency
VLSI	very large scale integration
VOR	VHF omnidirectional range
VPE	vapour phase epitaxy
VRC	visual record computer
VRDDO	variable retention of diatomic differential
VSB	vestigial sideband
VSEPR	valence shell electron pair repulsion
VSWR	voltage standing wave ratio
VTOL	vertical take-off and landing
VTR	voltage transformation ratio or video tape recorder
VUV	vacuum ultraviolet
VVER	water moderated water cooled reactors
WWER	water moderated water cooled reactors
XPS	X-ray photoelectron spectra
ZEBRA	zero energy breeder reactor assembly
ZGS	zero gradient synchrotron
ZPPR	zero power plutonium reactor

Subject Index

1/f noise *see random noise*

A-centres
- alkali halide, activated crystal, absolute quantum yield of stored light sums *(Russian)* 79–56851
- alkali halides, F-centres, ESR in different states of relaxed configuration 80–108067
- alkali halides, microcryst. powders, colour centres, refl. spectra 78–23493
- chars, heat treatment, EPR rel. to temp., A-centers 78–43639
- chars, heat treatment, EPR rel. to temp., spin centres 78–48036
- diamond, natural, impurity complexes, shape and dimens., diffuse X-ray scatt. obs. 78–47398
- diamond, optically active defects, anomalous X-ray scatt. 77–89434
- EPR and spatial extn. of relaxed excited state 79–73812
- α-quartz:Ag, Ag atom paramagnetic centre, $A_{Ag\text{-}Si}$ 78–76308
- tunable IR lasers with F_A(II) and F_B(II) colour centres 78–90420
- Ag halides, fundamental absorption, nature and function of A-centres determ. the extra band at the long wave edge *(Russian)* 80–76060
- CaF_2:Dy^{3+}, fluoresc. spectra, A-centres and B-centres, Stark levels 80–25428
- CaF_2-NaF crysts., F_A centres, 385 and 435 nm absorpt. bands of electron irrad. crysts. 78–2889
- CaO, F_A(Mo) centre, spin coherence zero-field double reson. 78–43689
- CaO, triplet state of F_A centres, ODMR obs. 79–28639
- CaO, undoped and Cl-, F- or Al-doped, X-ray and UV luminesc., electron-hole recombination processes *(Russian)* 78–76528
- CaO:F(Cl)(Al), phosphon, luminesc., electron-hole recombination processes 79–65919
- CaO:Li, thermally quenched, generation of Li^0 centres 80–50382
- CaO:Mo, spin coherence and Stark modulation effect of F_A-Mo centre excited state 77–69733
- CaS, phosphors, hole recombination luminescence *(Russian)* 78–72576
- CsBr:Cu^-, excitation and absorpt. spectra 80–108255
- CsBr(Cl)(I):K(Li)(Na)(Rb), optical absorpt. investig. of F_A-centres 77–44029
- GaP:Cu, deep levels, photoluminesc. and optical cross sections 79–38653
- KBr, ENDOR of F_A(Li) centre meas., 4.2 and 1.8K 77–63320
- KBr:Li(Na), F_A centres, optical detection of ESR 79–99793
- KBr:Tl excitation in fund. absorpt. region, luminesc. and thermolum. 80–50433
- KBr(Cl), F_A(Li)-centre spin-lattice relax. at 4.2K 78–91950
- KCl absorption and emission of F_A(Li) centres under hydrostatic pressure 78–92117
- KCl, additively coloured photochromic crystals, spectral sensitivity *(Russian)* 80–91871
- KCl, and KCl-AgCl, surface positron and positronium states, positron annihilation expts. *(Russian)* 78–39623
- KCl, positron annihilation by positive-ion vacancies, impurities and defect complexes 77–27908
- KCl:Ag(In)(Tl), excitation in fund. absorpt. region, luminesc. and thermolum. 80–50433
- KCl:Cu^- excitation and absorpt. spectra 80–108255
- KCl:Li, X-irrad., F_A centres, thermolum. studies 80–80878
- KCl:Li $(F_2{}^+)_A$ centres, tunable CW laser action 80–87399
- KCl:Li F_A(II) centre laser, pumped by flashlamp-pumped dye laser 80–102737
- KCl:Li^+,Na^+, F_A(II) to F_B(II) centre crystals, CW laser oscill. with extended tuning range 80–32997
- KCl:Li^+ F_A (II) colour-centre laser, mode locking and tunable picosecond IR pulse generation 80–43364
- KCl:Na, absorption from relaxed excited state by F_A and F_B centres 77–44031
- KCl:Na, electron trapping from α_A and F_A-centres, low temp. depend. 80–11444
- KCl:Na, F_A reorientation and $F_A \leftrightarrows F'_A$ conversions, laser induced, kinetic studies 80–10547
- KCl:Na, photodichroic holographic recording, polarisation sensitivity 78–29911
- KCl:Na, photoinduced reorientation of A-centres near room temp. 78–64344
- KCl:Na^+, CW laser action of $(F_2{}^+)_A$-centres, tunable from 1.62 to 1.91 μm 80–32998
- KCl:Na(Li) 78–76016
- KCl:Pb^{2+}, inner-centre luminesc., 8 to 80K *(Russian)* 78–92112
- KCl:Sr, positron annihilation and trapping in A-centres 80–84802
- KCl-Na, F_A, F_B and F_C-centres, wave functions and energy level of bound states 77–8049
- KI:Tl^+ type phosphor, press. effects on triplet relaxed excited states, quadratic Jahn-Teller interaction 78–23510
- KI:Tl, excitation in fund. absorpt. region, luminesc. and thermolum. 80–50433
- NaCl, positron trapping by X-ray produced defects, A-centre form. 77–48273
- NaCl:Ag, excitation in fund. absorpt. region, luminesc. and thermolum. 80–50433
- NaCl:Sr, positron annihilation and trapping in A-centres 80–84802
- RbCl:Li F_A(II) centre laser, pumped by flashlamp-pumped dye laser 80–102737
- RbCl:Li^+,Na^+, F_A(II) to F_B(II) centre crystals, CW laser oscill. with extended tuning range 80–32997
- RbI, luminesc. spectra induced by pulsed Ne^+ and electron beams and X-rays 80–80851
- Si, A-centre formation by vacancy-O_2 recomb., acceptor impurity conc. effect 77–43243
- n-Si, A-centre ionisation energy change due to uniaxial deform. 78–71733

A-centres continued
- Si, amorphous, glow-discharge deposited, ODMR spectrum, deposition temp. and annealing effects 80–50229
- n-Si, complex defect production rate introduced by high energy electron irradiation 77–72635
- n-Si, defect charge states, complex form., gamma-ray effects 80–96564
- n-Si, efficiency of radiation defect generation by electron bombardment, influence of Fermi energy 77–11596
- Si, electron irradiated, O-vacancy pair, EPR of optical absorption 77–16173
- Si, irradiated, nature of 0.97 eV A band luminesc. 77–44049
- Si, lifetime of free vacancies 79–10851
- Si p-n junction, negative annealing of γ-radiation defects 77–43246
- Si, photoionisation cross section 78–39063
- Si, radiation defect clusters, form. kinetics and parameters 77–11545
- Si:Gd, radiation defect form., effect of Gd impurities, elec. and optical meas. 78–71764
- Si:O, A centre, theoretical study 80–75521
- Si:O,C, electron irradiated, indirect vacancy-interstitial recomb., IR absorpt. meas. 77–43209
- Si:Se, impurity states, A- and B-centres, electron, hole thermionic emission rates 80–96813
- n-SiC, thermal defects, ESR study 80–88876
- Sr_2TiO_4:Eu, synthesis, luminesc. of materials 79–11534
- ZnS, Fe^{3+}-Cu^+ complexes and A-centres, g-factor anisotropy *(Russian)* 77–20271
- ZnS:Ga, self-activated emission, A-centre ODMR 79–95685
- ZnS:Pb, blue luminesc., photoexcited EPR spectrum 80–108070
- ZnSe, ODMR expts., A and V^--centres, origin of emission bands 78–80255

A/D conversion *see analogue-digital conversion*

ab initio calculations
- π electron Hamiltonian, ab initio derivation by nonperturbative open shell formalism 78–21846
- A-15 compound, V_3X and Nb_3X, (X=Al, Ga, Si, Ge, Sn), electronic struct., electron-phonon interactions, and low temp. anomalies 79–60701
- AB_2, bent molecule, ab initio force fields, appl. of Simons-Parr-Finlan expansions 79–41218
- absolute rate theory, ab initio calcs., elementary gas phase reaction 80–7757
- acetaldehyde, dichroic effects, computational expts. 80–83424
- acetic acid-formic acid, ‘dimer’, tritium β^--decay causing H^+ transfer, ab initio MO calc. 80–3391
- acetone, ab initio CI valence and Rydberg states, spectral assignments 77–14346
- acetone vapour, mol. assoc., monomer-dimer equilib., thermal cond. meas., MO calcs. 79–52647
- acetylene, and $C_2H_2{}^+$, ionis. pots., photoelectron spectra, ab initio VB calcs. 77–88396
- acetylene, and cation, SCF MOGO calc. of electronic struct. 77–34556
- acetylene, core ionised, core-excited and shake-up states, ab initio MRD-CI methods 80–42950
- acetylene, force consts. of symmetric stretch motions, accurate ab initio calcs. 77–83567
- acetylene, harmonic and anharmonic stretching force consts., ab initio calcs. 78–58587
- acetylene, mol. geometry basis set depend., geometry optimisation ab initio method 79–31382
- acetylene, Verdet consts., ab initio calcs. 77–3390
- acetylene dimer, ab initio HF calc. for 64 conforms. 80–23333
- acrolein, triplet state vertical and adiabatic excitation energies, CI calcs. 78–9083
- adenine, tautomeric forms protonation, ab initio HF Roothaan SCF calcs. 80–78534
- adenine tautomers, relative stabilities, nonempirical MO calcs. 80–21442
- alanine, unionised, ab initio equilib. structs. calcs. 79–68181
- alkali metals, mode Gruneisen parameters, ab initio calc. 77–20091
- alkanes, ab initio calcs. using FSGO, internal rot. 78–82639
- alkanes, linear, elec. struct., evolution of electronic level towards band struct. *(French)* 78–5282
- alkanes, linear, electronic struct., electronic relax. during photoemission *(French)* 78–5283
- alkanes, linear, K-shell ion relax. energy chain length depend. 79–72252
- n-alkanes, methane to n-tridecane, ESCA of core electron relax. and valance bands 77–18978
- alkanes, saturated, ab initio LCAO MO SCF calcs., core ionis., electronic relax. 77–71745
- alkanes, solvent effects, quantum mech., macroscopic electrostatic contribs. 77–30801
- alkyl cadmium, valence and core electron energies, photoelectron spectra, ab initio calc. 78–25613
- alkyl chlorides, proton affinity correl., ab initio SCF calc., MINDO/3, STO and G basis sets 78–33421
- alkyl fluorides, geometries, props. and protonation, ab initio mol. orbital study 79–22588
- alkynoyl cations, struct., charge distrib., ab initio population anal. calcs. 80–58407
- all-trans-polyene, ground state props., ab initio studies 79–47002
- allene, C-C double bond rot. barrier, ab initio open-shell restricted SCF calc. 78–1099
- allene, internal rot. in ground electronic state 77–67975
- allene, transition state for internal rot., HF/STO-3G calcs. with correlation energy corrections 78–25430
- allene, vertical valence ionis. pots., ab initio UB calcs. 79–85917

ab initio calculations continued
- 1H-alloxazine, and derivatives electronic struct., photoelectron spectrosc. and ab initio study 80−106261
- allyl cation and radical, ab initio non-paired spatial orbital wavefunctions 77−26968
- allyl radical, ab initio SCF solns., doublet stability 78−33423
- allyl radical, ionisation potential, ab initio valence bond calcs. 79−31407
- allyl radical, restricted ab initio SCF LCAO solns., doublet stability 77−79539
- amides, geometry from ab initio calcs. 80−23338
- aminoborylpolyynes, intermolecular interaction through triple bonds, internal rot. 80−106370
- aminopolyynes, intermolecular interaction through triple bonds, internal rot. 80−106370
- 18-annulene, geometrical parameters, STO-3G ab initio calc. 80−52867
- aromatic compounds, electrophilic substitution sites, perturbation theory calcs. 77−30800
- atom, KLL Auger spectrum, new developments, line energies, intensities 77−18868
- atom, one-centre integrals of exact effective valence shell Hamiltonian 80−74128
- atom, transition array and energy level distribs. variance, Mo VX-XIV appl. 80−37767
- atom+diatom, ab initio pot. hypersurface anal. fit 79−13785
- atom-atom pot. parameter in azabenzene, dispersion energy calcs. 80−23489
- atomic and molecular processes, developments in ab initio methods 80−63550
- atomic field isotope shift off-diagonal parameter in $(5d+6s)^N$, ab initio evaluation 80−47912
- atomic inner shell electron props., relativistic effects 77−18803
- atomic K-LL Auger spectra in intermediate-coupling scheme with CI, relativistic Dirac Hartree Slater calc. 80−52958
- atomic K-shell Auger rates, level widths and fluoresc. yields, relativistic Dirac Hartree Slater calc. 80−52957
- atomic M-shell radiationless transitions, subshell fluoresc., Coster Kronig yields and X-ray linewidths, relativistic Dirac Hartree Slater calcs. 80−52959
- atoms, singly excited states, oscillator strengths, ab initio calcs. 80−920
- azabenzenes, multipole moments, polarisabilities and long-range interaction coeffs. calcs. 79−89599
- aziridine, ab initio calcs., appl. of convergent SCF procedure 80−47875
- aziridine, anhydrous and hydrated, inversion calc. 78−9272
- cis-azo group, ionisation and excitation energies depend. on bond angle, ab initio MO calc. 79−72236
- azomethane, steric strain relief accompanying isomerisation 79−10230
- B-DNA helix, guanine-cytosine base pair, electrostatic pot. 80−8003
- bases, K^+ affinities ab initio SCF calc. 78−58585
- benzaldehyde, and isomeric phthalaldehydes, dipole moments meas., config., ab initio MO calc. 80−58410
- benzene, ab initio model calc., variational 77−46492
- benzene, ab initio non-paired spatial orbital wavefunction, π-electron correl. energy 77−54509
- benzene, dipole polarisability, finite-field SCF MO calcs. 80−83255
- benzene, electronic struct., mag. susceptibilities, ab initio calcs. 78−74571
- benzene, ground, singlet and triplet states, ab initio VB STO, GTO calcs. 77−75060
- benzene, mol., directional Compton profile, ab initio SCF LCAO MO calc. 78−62857
- benzene, monosubstituted, ring protonation and C_{1s} binding energies, STO-3G calc. 79−29336
- benzene radical anion, ab initio MO calcs., struct. 79−18113
- benzenes, substituted, dihydroxybenzenes, electronic structure, photoelectron spectra and ab initio MO calculations 79−49937
- benzenes, substituted, electronic struct., ab initio calcs., photoelectron spectra 80−58314
- benzenes, substituted, fluoro-derivatives, electronic structure, photoelectron spectra and ab initio MO calculations 79−49937
- benzenes, substituted, methyl-derivatives, electronic structure, photoelectron spectra and ab initio MO calculations 79−49937
- benzenes, substituted electronic structure, photoelectron spectra and ab initio MO calc. 79−49937
- benzyl fluoride, mol. struct., NMR and gas electron diffraction obs., ab initio and mol. mechanics calcs. 80−23574
- beryllocene, gas phase struct., ab initio LCAO SCF calc. 78−41942
- biacetyl, lower excited electronic states, ab initio SCF and CI calcs., absorption band assignment 78−74589
- binary alloys, and intermetallic cpds., struct. and stability, ab initio pseudopot. calcs. 78−34460
- binary complexes, small H-bonded mols. electronic structs., ab initio calcs. 80−74108
- biological molecules, ab initio calcs., small Gaussian basis sets 79−59341
- 2,2′-bipyrimidine, in nematic solvent, conformation, ab initio and PMR determ. 80−47869
- bis(fluoroxy)difluoromethane, ab initio MO calcs. of geometry, torsional barriers 78−90313
- bromomethane, ab initio SCF MO calcs., ionis. pots., dipole moment, config., electronic props. 78−1104
- trans-butadiene, all-valence-electron CI calcs. of electronic spectrum 77−10654
- butadiene, oscillator and rotatory strengths, RPA in ab initio calc. 78−25617
- trans-1,3-butadiene, valence electronic excited states, SCF ab initio GVB and CI calcs. 79−31423
- butadienes, cis- and trans-, ionisation potential, ab initio valence bond calcs. 79−31407
- 1-butanethiol, simulated ab initio MO method calcs. 80−47867
- butatriene, vertical valence ionis. pots., ab initio UB calcs. 79−85917
- trans-2-butene, twisted, oscillator and rotary strengths, ab initio calculations 77−65510
- t-butyl radicals, ab initio geometry calc., ^{13}C hyperfine coupling 77−10580
- carbenes, heterosubstituted, singlet-triplet splitting depend. on heteroatom electronegativity and conform. 80−63553
- carbonyl fluoride, vertical electronic states, ab initio SCF CI calc. 79−49942
- carbonyl halogen substituted cpds., geometric and electronic struct., LCAO-SCF calc. 79−89603
- carbonyl to oxacarbene rearrangement, conformation, ab initio SCF MO calcs. 77−32780

ab initio calculations continued
- carboxylic acid-fluoride system, H---F bond, ab initio MO study 79−76528
- chemical bond transferability, group or loge functions 78−41939
- chemical reaction, force decomposition anal. along reaction coord. 78−27741
- chlorin, ab initio CI calcs. on ground, singlet and excited states, visible spectrum 79−16139
- chloroacetylene, harmonic and anharmonic stretching force consts., ab initio calcs. 78−58587
- p-(N-chlorobenzylidene)-p-chloraniline, cryst., polymorphism, cryst. struct. rel. to mol. conform. 78−75611
- 2-chloroethyl radical, struct., ab initio calcs. 80−83252
- chloromethane+Cl^-, S_N2 reaction, local orbital description, ab initio FSGO method 78−76842
- chloromethyl formate, conformation potential energy surfaces, ab initio calcs. 80−69065
- cluster calculations, unrestricted HF approach, cluster-environment interaction 78−84117
- crystal, ab initio LCAO-HF-contracte GO crystal orbital program 77−55471
- crystal Hartree-Fock theory, ab initio effective potentials 80−103290
- cummulene type infinite chain cryst., energy bands, ab initio Hartree-Fock orbital calc. 78−60066
- cyanamide, ab initio VB wave functions, π-electrons 78−70748
- cyanoacetylene, IR absorpt. bands, integrated intensities, ab initio and LMO calcs. 79−72234
- cyanomethane$^-$, ab initio calcs., electron affinity, stability 77−42239
- cyclic 3- and 4-membered ring cpds., saturated, ab initio struct. anal. 80−58192
- cyclobutadiene, π face bonding with CO, HCN, benzene 79−98180
- cyclobutadiene(-d_1), singlet and triplet ground states, vibr. freqs., MINDO/3 and ab initio SCF calcs. 78−13429
- cyclobutane derivs., nucleophilic substitution, mechanism 77−9057
- cyclopentadienyl radical, pot. surface and vibronic states, ab initio CI calcs. 80−47897
- cyclopentadienyl radical, vibronic valence isomerisation, Jahn-Teller effect, D_{5h} symmetry 79−97986
- cyclopentanone, $n-\pi^*$ transition, vibr. band intensities 80−74116
- cyclopentene, ring puckering, semi-empirical and ab initio calcs. 78−9065
- cyclopropanone, electronic struct., UV photoelectron spectrum 78−33428
- cyclopropyl chloride, ab initio SCF-MO calc., electronic and mol. struct. 78−25425
- cytosine, vertical interaction evaluation methods 79−54772
- diamond, (111) surface states and relax., modelling and using mol. SCF calcs. 78−39186
- diamond, ab initio calcs. of struct. using FSGO method 77−80753
- diamond, electron density, bulk and surface atoms, from ab initio model calcs. 79−4590
- diamond, neutral vacancy, generalised val. bond calc. 77−55493
- diamond, valence band calc. using many-electron theory 80−15434
- diamond clusters and corresponding saturated hydrocarbon ab-initio HF and PCILO calcs. 78−42951
- diatomic isovalent systems, pot. curves, ab initio MRD-CI method 80−83293
- diatomic molecules, book 78−90080
- diatomic molecules, electronic states excitation, atom promotion, ab initio calcs. 78−86772
- diatomic molecules, hydrides, oxides and BeF, spin orbit coupling const., ab initio calcs. 80−63537
- diatomic molecules, linear, substituted fragment series, electronic struct. transferability, mutual at. influence 78−9066
- diatomics, quadratic-quartic force consts. calc. 79−63979
- diazomethane, electronic struct., least energy dissoc. path to CH_2 and N_2 products 78−5131
- dichlorocarbene, electronic spectrum, ab initio CI calcs. 79−85948
- 1,1-dichlorocyclopropane, ab initio SCF-MO calc., electronic and mol. struct. 78−25425
- dicyanoketene, and isomeric forms, heat of form., ab initio STO-3G calcs. 80−58190
- p-difluorobenzene, electronic struct., many-body calc., photoelectron spectrum assignment 77−23421
- difluorobenzenes, X-ray and UV photoelectron spectra, ionis. pots., ab initio GO calcs. 77−61795
- 1,2-difluoroethylenes, ab initio HF comparison of cis and trans energies 77−18786
- diformamide, torsional pot. barriers, ab initio and partition of energy methods 77−88588
- dimethyl ether, internal rot., struct. relax., ab initio SCF calcs. 78−90077
- dimethyl zinc, valence band and Zn 3d levels, electric field gradients 77−88495
- dimethylamine-HCl systems, H-bonded complexes studied by ab initio MO method, dipole moments determ. 80−83253
- p-N,N-dimethylaminobenzonitrile, multiple fluoresc., mechanism 79−45742
- dimethylether, ab initio SCF calcs., force field, IR and Raman intensities 77−79601
- dimethylether, equilib. struct., ab initio SCF calcs. 77−3265
- dipeptide, struct. and bonding, ab initio calcs. 79−53039
- Dirac-Fock theory, multiconfig., relativistic SCF method, appl. to open shell ats. 77−3282
- discontinjous approx. mol. electronic wave functions, ab initio LCAO and VB ZDO appls. 77−50340
- discontinuous approx. mol. electronic wave functions, ab initio LCAO and VB ZDO appls. 77−50340
- dithioformic acid, pot. for rot. about $C(sp^2)$-S bonds, ab initio calc. 80−23572
- dodecahexenes, sudden polarisation effect, ab initio and CI calcs. 80−58160
- dynamical damping in ab initio MO SCF calcs., energy minimisation method 80−18777
- effective core potential method, appl. to Cl_2, F_2, and LiCl 80−32625
- effective core potentials, all-electron calcs. 78−62704
- effective core pots., reduction of all electron to valence electron calcs. 77−14361
- 14-electron isoelectronic series, equilib. geometries and electronic struct. 77−83489
- electronegativity, nonempirical scale, ab initio FSGO wavefunction calcs. 77−26966

ab initio calculations continued
- ethane$^+$, stability and struct., Cl-SCF ab initio calc., Franck Condon anal. 77−54575
- ethane, ab initio MRD-CI calc., 14-25 eV PES region, Rydberg states 78−41962
- ethane, barrier and one electron charge transfer states in strong orthogonal group function theory 78−13421
- ethane cation, relative stability of $^2A_{1g}$, ^2E_g states 80−58140
- ethene, dipole polarisability, finite-field SCF MO calcs. 80−83255
- ethene, general valence force field, ab initio calcs., IR and Raman intensities 77−71746
- ethenediol, σ conjugative interactions role in rot. isomerism 79−31443
- ethenethiol, σ conjugative interactions role in rot. isomerism 79−31443
- ethenol, σ conjugative interactions role in rot. isomerism 79−31443
- ethyl radical, geom. struct., Hartree-Fock calcs. 78−62722
- ethylene, ab initio GO calc. 78−94187
- ethylene, C atom pyramidalisation rel. to bonding, ab initio SCF calcs. 79−93936
- ethylene, C-C double bond rot. barrier, ab initio open-shell restricted SCF calc. 78−1099
- ethylene, core ionised, core-excited and shake-up states, ab initio MRD-CI methods 80−42950
- ethylene, dipole moment derivatives, IR vibr. intensities, STO-3G, 4-31G, calcs. 77−6750
- ethylene, ionisation potential, ab initio valence bond calcs. 79−31407
- ethylene, IR and Raman intensities calc., efficient ab initio computation method 79−45698
- ethylene, lattice dynamics of cryst., ab initio interaction pot. 79−33043
- ethylene, mol. geometry, ab initio calcs., basis set depend. 78−82636
- ethylene, photoelectron spectrum, vibronic coupling effects 79−10090
- ethylene, planar dissociation, electronic rearrangement, states, bonds, ab initio multiconfigurational SCF calcs. 80−27937
- ethylene, pot. energy and dipole moment surfaces, polarisation effect, ab initio CI calcs. 80−106272
- ethylene, quasidegeneracy and effective Hamiltonians, canonical transformation cluster expansion formalism 80−52888
- ethylene, RPA hypervirial relation, ab initio minimal basis calcs. 77−18779
- ethylene, twisted, oscillator and rotary strengths, ab initio calculations 77−65510
- ethylene+cis-N_2H_2, chem. reaction, intermediate geom. calcs. 78−35655
- ethylene+H$\rightleftharpoons$ethyl radical, pot. energy surface, analytic function 79−11779
- ethylene glycol, IR spectra, ab initio calcs., vibr. anal., conformations of isotopic modifications 78−5210
- ethylene molecules, long range forces in multipole expsn., ab initio calcs. 78−9219
- ethylene oxide cation, existence of open isomer, ab initio calcs. 79−22593
- ethylene ozonide, ab initio gradient and MC SCF calc., conformational anal. 80−83290
- ethylene radical cation, electronic states assignments, ab initio SCF CI calcs. 77−10584
- ethylene V state, ab initio study of spatial extension 80−27952
- ethylene-LiF complex, molecular orbital calcs., Li bonding exam. 78−29745
- ethylidene, rearrangement to ethylene, barriers, ab initio MO calcs. 80−104424
- ethynol, ab initio calc., energy levels and geom. struct. of C_2H_2O isomers 78−62716
- ethynol, struct., isomerisation, ab initio SCF MO calcs. 78−41941
- ethynyl radical, emission spectra and pot. energy surface, ab initio MRD CI calc. 79−41099
- excimer lasers, electronic structure, pot. energy curves, radiative transition probabilities, quantum mech. calcs. 79−10284
- ferrocene, metal to ring distance, ab initio MO SCF calcs. 80−47870
- first row atoms, Gaussian basis sets, uniform quality 78−5116
- first row hydride H-bonded complexes *(French)* 80−5479
- first-row atom, uniformly balanced constrained gaussian basis tests 77−65423
- floating orbital geometry optimisation with floating outer-shell basis functions 80−95517
- fluoro sulphuric acid methyl ester, rot. isomerism 78−86964
- 1-fluoro-2-propanol, conformational energies and rot. barrier, ab initio calc. 79−31390
- fluoroacetylene, harmonic and anharmonic stretching force consts., ab initio calcs. 78−58587
- fluorobenzene radical anion, ab initio MO calcs., struct. 79−18113
- fluoroethyl radical, unimol. dissoc., pot. energy characts. and energy partitioning calcs. 80−45488
- fluoroformaldehyde, pot. energy surface characts., substitution effect 80−89505
- fluoromethane, LCAO-Xα-SCF, atoms in mols. theory and appl. 77−57869
- fluoromethanes, ab initio calcs. of K-shell ionisation potentials 77−18784
- fluoromethanes, GVFF from SCF ab initio energies 78−74635
- fluoromethanes, vibr. spectra, force consts. and geom., SCF ab initio calcs. 78−62785
- fluorometh.HF, H-bonded complex, ab initio calcs. *(French)* 80−52866
- fluoromethyl formate, conformation potential energy surfaces, ab initio calcs. 80−69065
- fluoroxyperoxytrifluoromethane, ab initio MO calcs. of geometry, torsional barriers 78−90313
- force constants, appl. of force relaxation method for geometry optimisation 78−66685
- form factors for atoms and ions with $Z \leq 54$ 77−10582
- formaldehyde, $^1A_2$-state, radiative and nonradiative decay calcs., rel. to photochem. decomp. 78−37669
- formaldehyde, $^1A_2$-state, SVL fluoresc.-spectra, absolute radiative lifetime, ab initio CI calcs. 79−63919
- formaldehyde, $^3A''$ state, zero-field splitting param., ab initio CI calcs. 80−99454
- formaldehyde, α-cleavage, feasible forbidden photochem. reaction 77−9092
- formaldehyde, ab initio calcs., appl. of convergent SCF procedure 80−47875
- formaldehyde, and cation, vertical proton affinity in singlet and triplet states 78−90079
- formaldehyde, bond polarity effect on other bonds and lone pairs, LMO calc. 80−9495

ab initio calculations continued
- formaldehyde, electronic struct., dipole moments, mol. polarisability, force fields, ab initio calcs. 80−78531
- formaldehyde, force consts., ab initio CI calcs. *(French)* 78−90093
- formaldehyde, photochem., ab initio calcs. rel. to hydroxycarbene intermediate 79−61880
- formaldehyde, photodissoc., pot. energy surface features 79−79271
- formaldehyde, Rydberg states, excitation energies, oscillator strengths ab initio GVB-CI calcs. 77−54518
- formaldehyde, vibrational band intensities of $^1A_2$-$^1A_1$ transition, ab initio calc. 80−43028
- formaldehyde, X^1A_1, a^3A'' and A^1A'' states, SCF and CI ab initio calcs. 79−36545
- formaldehyde anion radical, hyperfine coupling consts., vibr. depend., ab initio calcs. 80−87150
- formaldehyde-d_0, -d_2, $^1(n\pi^*)$ radiationless transition, ab initio CI calc. 79−767
- formaldehyde-d_0, -d_2, $^1(n\pi^*)$ transition, vibr. struct., ab initio CI calc. 79−766
- formaldehyde-water, heuristic intermol. pot. function, ab initio MO calcs. 78−33566
- formaldehyde.$H_2S(H_2O)$ complexes, ab initio SCF MO calcs., binding energy dispersion contrib. 80−27967
- formamide, ab initio calcs. on ground and excited states 77−83494
- formamide, comparison of theoretical and experimentally determined electron density distrib. 78−82634
- formamide, force consts. and dipole moment derivatives, ab initio MO calcs. 80−95521
- formamide, hydration by H_2O mol., point charge model 77−34569
- formamide, low-lying triplet states, relative energies and conformational preferences 77−3266
- formamide dimer, hydrogen bond, ab initio MO calcs. 78−58588
- formamide dimer, tritium β^--decay causing H^+ transfer, ab initio MO calc. 80−3391
- formamide-glyoxal, charge transfer theory, Mulliken population, ab initio calc., multiconfiguration scheme 80−106392
- formate ion, hydration, ab initio LCMO calcs. 79−59342
- formic acid, and dimer, ab initio MO calcs., ground and excited states 77−83492
- formic acid, conform. hypersurface determ. and analysis 80−1078
- formic acid, dimerisation energy, ab initio calcs., distortion energy effects 79−10022
- formic acid, harmonic force consts., ab initio calcs. and uniqueness problem 79−6834
- formic acid, valence and Rydberg state empirically adjusted ab initio calcs. 77−10609
- formic acid anhydrides, valence force consts., IR spectra, isotope effects 79−93997
- formic acid dimer, hydrogen bond, ab initio MO calcs. 78−58588
- formic acid dimer, tritium β^--decay causing H^+ transfer, ab initio MO calc. 80−3391
- formic acid dimer-t_1, H bonding, β^--decay effects, ab initio calcs. 79−54763
- trans-formic acid geometry, force fields and fundamental vibr. freq., ab initio study 80−87040
- formyl chloride, equilib. geometries and one-electron props., ab initio calcs. 80−47878
- formyl fluoride, equilib. geometries and one-electron props., ab initio calcs. 80−47878
- formyl radical, lower electronic states, ab initio calc. of pot. energy surface, hydrocarbon flame band 79−68287
- formyl-triglycyl amide-H_2O, analytical pot., ab initio calc. 79−48206
- free radical reactions abstraction-addition step, Yamaguchi theory 77−52624
- fully coupled SCF perturbation theory in matrix form, simultaneous perturbations 77−34548
- furan, ionisation pots., transition operator calcs. 77−30771
- Gaussian 70 program, using 128K byte memory minicomputer 79−31375
- Gaussian basis sets, uniform quality 77−34555
- glyoxal, $^3n\pi^*$ states, ab initio STO-3G CI calcs., ΔE_{SCF} transition energies 78−94194
- glyoxal, lowest triplet state, excitation energies, electron correl. effects 78−5147
- glyoxal-alkali (alkaline earth metal) complex, ab initio MOSCF calc., chelate effect 79−31386
- graphite, band theory, Fermi surface constructed, ab initio energy band calc. 77−11841
- graphite, electronic struct. exact exchange HF calcs. 80−65438
- ground state atoms, Van der Waals coeffs., polarisabilities and oscill. strengths calcs. 79−93913
- guanidinium ion, rot. barriers, ab initio calcs. 78−41923
- guanine, tautomeric forms protonation, ab initio HF Roothaan SCF calcs. 80−78534
- guanine tautomers, relative stabilities, nonempirical MO calcs. 80−21442
- 2-haloethanols, torsional interaction, IR spectra, ab initio calcs., 2-dimens. model 80−74160
- halogen atom, 1s hole states, ionisation, ab initio SCF calcs. 78−17568
- halogen diatomic molecule, 1s hole states, ionisation, ab initio SCF calcs. 78−17568
- heterobenzenes, electronic struct., π electron mag. susceptibility anisotropy 79−59353
- all-trans-1,3,5-hexatriene, excited electronic states calcs., spectra assignments 79−22606
- trans-1,3,5-hexatriene, low-lying $\pi\pi^*$ excited states, ab initio STO method 77−3284
- trans,trans-1,3,5-hexatriene, valence electronic excited states, SCF ab initio GVB and CI calcs. 79−31423
- hybridisation for arbitrary orbital 77−57852
- hydrides, first row, $AH_2(H_3)(H_4)$, and positive ions, chemical equilibria, correl., ab initio calc. 78−35714
- hydrides, first row, localised MOs, size-energy relation, at initio LMO GO calcs. 77−50351
- hydrides, second row, ab initio calcs. using FSGO basis, mol. parameters correlation 78−901
- hydrides, ten electron, localised orbitals, moment analysis 78−41945
- hydrocarbon radicals, ab initio calc. of spin densities 79−93938
- hydrocarbons, average elec. polarisabilities and mag. susceptibilities, ab initio valence electron calcs. 80−87033
- hydrocarbons, bond functions, for ab initio calcs. 80−5469

ab initio calculations continued
hydrocarbons, double-zeta quality ab initio mol. fragment calcs. with pseudopots. 79—85879
hydrocarbons, small, electron momentum distribs. in π orbitals from (e,2e) expts. 80—14239
β-hydroxy acrolein, lower excited states, electronic struct. and H-bonding, ab initio SCF and CI calcs., photochemical mechanism 80—83278
β-hydroxyacrolein, intramol. H bonds, orbital and transition energies, ab initio SCF and SCF CI calcs. 77—14345
5-hydroxyindole, near ab initio and pseudopotential calcs. 77—71749
hydroxymethylene radical cation stability, CH_2O^{+} isomers, ab initio MO study 80—42965
2- and 4- hydroxypyridine tautomers, ab initio SCF LCAO MO calcs. 79—81154
hydroxytryptamines, near ab initio and pseudopotential calcs. 77—71749
ice, cubic, LCMO calc. of energy bands 77—51656
imidazole, quadrupole coupling consts. interpretation, ab initio field gradient calcs. 80—58282
imidazolium cation, near ab initio and pseudopotential calcs. 77—71749
inert gas, atomic photoionisation, Dirac-Fock calcs., branching ratios and angular distrib. in p shells 80—63601
inert gas dimer ions, electronic struct., chem. binding 79—31376
inert gas fluorides, covalent and ionic states, ab initio CI calcs. 78—78634
inert gas oxides, low-lying electronic states, ab initio CI calcs. 77—57888
interconversion pot. energy surfaces, geometries, electronic structs. 78—35660
intermolecular energies calculation from delocalised pictures, artifacts and elimination 80—18899
intermolecular energy, CI ab initio calc., correction for basis superposition error 79—85904
intermolecular forces, ab initio calcs. applicability and accuracy 80—18898
intrinsic reaction coordinate ab initio SCF calc. method 77—48626
ion+atom, intermediate energy, electron capture cross-section calcs. 78—42206
ion-atom collision, electron capture, at. expansion method 79—45833
ion-molecule equilibria in solvolysis, secondary β ^2H isotope effects, hyperconjugation 80—50874
ionic iron group compounds, nuclear quadrupole interactions, role of antishielding effects 78—47748
ionisation potential, vertical, inner and valence shells, ab initio SCF MO CI perturbation calc. method 78—74800
10H-isoalloxazine, and derivatives electronic struct., photoelectron spectrosc. and ab initio study 80—106261
isoelectronic sequence, X-ray spectra 80—87071
isomerism, directional effects of σ conjugation 78—37769
isopropyl radical, pot. energy surfaces, ab initio UHF calcs. 80—106258
ketene, ab initio calc., energy levels and geom. struct. of C_2H_2O isomers 78—62716
ketocarbene-ketene rearrangement, reaction path, ab initio calc. 78—20008
ketone, H abstraction, feasible forbidden photochem. reaction 77—9092
KLL Auger transition energies, relativistic multiconfig. calcs. 77—18873
Koopmans atomic valence electron ionisation energy, 1/Z expansion method, reorganisation corrections 78—78623
β-lactam antibiotics, ab initio SCF-MO-LCAO calcs., amidic bond breaking, methoxy substitution effect 80—78533
large molecule, ab initio calcs. using mol. fragments, floating spherical Gaussian basis sets characts. 77—42233
large molecules, mol. fragment basis, generalisation, for ab initio calcs. 80—91438
LCAO-Xα-SCF, atoms in mols., theory and appl. 77—57869
linear mols., π orbital electron energy contrib. to reaction heat 80—76539
linear rigid rotors, scattering calcs., ab initio intermol. pots. fitting 77—83680
linear triatomic hydrides, ab initio SCF CI electric dipole moments 79—31410
liquid alloys, binary, entropies, ab initio calcs. 77—47599
liquid metals and alloys, struct. and thermodynamic props., ab initio calcs. 77—84621
lithium acetylene, SCF MOGO calc. of electronic struct. 77—34556
local electronic structure in molecules, Hartree-Fock theory 77—79541
localised Wannier functions, numerical calc. from ab-initio Hartree-Fock wave functions 79—60671
magnesium chlorin, ab initio CI calcs. on ground, singlet and excited states, visible spectrum 79—16139
magnesium porphine, ab initio CI calcs., electronic absorpt. spectra 78—78639
mass spectrometry, energetics of theory, review 78—319
maximum overlap mol. orbitals versus ab initio HF-SCF-MO calc. dipole energy 78—9070
MC-SCF theory, modified one-electron Hamiltonian, iteration convergence 79—6871
metallic glasses, stability, microscopic calcs. 79—32914
metalloenzymes, model for biological active sites, ab initio calcs. 80—104551
methane, ab initio calcs., appl. of convergent SCF procedure 80—47875
methane, and -t_1, β-decay, ab initio SCF MO calcs. 77—71842
methane, and isotopic forms, anharmonic force field, equilib. struct. 79—76365
methane, bonding, electron pairs, size and shape parameters, Gaussian basis set MO calcs. 80—27935
methane, coord. bond calcs. 80—58129
methane, excited states, photochem., ab initio calcs. 77—14371
methane, force consts., ab initio CI calcs. *(French)* 78—90093
methane, mol. nuclear spin-spin coupling, ab initio SCF perturbation theory 78—33525
methane, multipole moments and polarisabilities 79—85910
methane, orbital relax. energy for single and double ionis. from valence shells 80—106253
methane $+H_2O$, pairwise interaction pot. function, ab initio SCF MO calc. 79—22786
methane cation, photodissoc., ab initio RHF and MRD CI calcs. 80—95695
methane derivatives, stabilisation of planar tetracoordinate C, substituent effects, RHF/STO-3G calcs. 77—6671
methanediol, bond length distortions and torsion pots., ab initio calcs. 79—6836
methanethiol, force consts., anharmonic vibr. 78—21898

ab initio calculations continued
methanol, ab initio calcs. of K-shell ionisation potentials 77—18784
methanol, coord. bond calcs. 80—58129
methanol, equilib. struct., general valence force field, ab initio calcs. 77—3265
methanol, force consts., anharmonic vibr. 78—21898
methanol dimer, intermol. function from ab initio calcs. 80—32629
methyl cation, force consts., ab initio calcs. with differentiated estimation of integrals 77—67974
methyl chloride, ab initio SCF-MO calc., electronic and mol. struct. 78—25425
methyl chloride, force consts., anharmonic vibr. 78—21899
methyl cyanides and isocyanides, isomerisation, ab initio (STO-3G) geometry optimised calc. 78—46265
methyl fluoride, coord. bond calcs. 80—58129
methyl fluoride, force consts., anharmonic vibr. 78—21899
methyl fluoroformate, isomer conformation, CNDO and ab initio STO calcs. 80—58151
methyl glyoxal, $^3n\pi^*$ states, ab initio STO-3G CI calcs., ΔE_{SCF} transition energies 78—94194
methyl halides, mol. force field at SCF ab initio levels, quantum-mechanical calc., LCAO-MO method 80—106319
methyl ion, electrostatic force theory appl. to mol. geometry ab initio verification 79—98002
N-methyl m-fluoroaniline, conformational anal., microwave spectra obs. 80—58247
s-methyl nitrite, methyl group rot. barriers in cis and trans forms, ab initio calcs. 80—74111
methyl radical, ab initio projected unrestricted Hartree-Fock calcs. 78—58582
methyl radical, hyperfine coupling consts., vibr. depend., ab initio calcs. 80—87150
methyl radical and anion, electron affinity determ., ab initio SCF and CI calcs. 78—5149
methyl vinyl sulphide, syn-gauche equilib., force field and ab initio calcs., microwave and Raman spectra 80—23573
N-methylacetamide, vertical excitation energies, ab initio SCF CI calcs. 79—45647
methylamine, affinities for $H^+(Li^+)(K^+)(CH_3{}^+)$, ab initio SCF calculations 80—102443
methylamine, coord. bond. calcs. 80—58129
methylamine, force consts., anharmonic vibr. 78—21898
methylamine-HCl systems, H-bonded complexes studied by ab initio MO method, dipole moments determ. 80—83253
methylamine-t_1-NH_3, β^- decay effect on H-bond, ab initio LCAO SCF MO calc. 78—76894
methylene, $^1B_1$-$^1A_1$ separation, ab initio 80—106251
methylene, electron affinity, $^1A_1$-$^3B_1$ T_0-value, ab initio MRD-CI method calcs. 78—50478
methylene, force consts., ab initio calcs. with differentiated estimation of integrals 77—67974
methylene, photoelectron spectra, singlet and triplet state calcs. 78—42127
methylene, singlet-triplet excitation energy, relativistic correction 80—69059
methylene, singlet-triplet separation, ab initio calcs. 78—74582
methylene, singlet-triplet separation, configuration interaction study 78—13438
methylene, singlet-triplet splitting, ab initio calc. 78—5128
methylene, vibronic anal., ab initio CI pot. curves calcs. 78—50479
methylene$+H_2\rightarrow$methane, ab initio CI calc. on SCF level, insertion reaction min. energy path 80—7774
methylene anion, electron affinity, $^1A_1$-$^3B_1$ T_0-value, ab initio MRD-CI method calcs. 78—50478
methylene anion, vibronic anal., ab initio CI pot. curves calcs. 78—50479
methylene ion, pot. energy surfaces of excited states, ab initio GTO SCF CI calcs. 78—58602
methylene manganese, electronic struct., equilib. geometry, ab initio SCF calcs. 77—71747
methylene peroxide, struct., energy levels, ab. initio UHF and MRUHF NO CI calcs. 80—83287
methylenimine, $n\rightarrow\pi^*$ transition, ab initio SCF MO CI calc. 78—58584
o-methylhydroxylamine, ionisation energies, He I photoelectron spectra, orbital calcs. 77—88497
molecular, geometry optimisation in ab initio SCF calcs., appl. of Hellmann-Feynman force 79—49927
molecular ab initio CI pot. curves, mol. wavefunctions and vibr. freqs. comparison of methods 80—27956
molecular cubic anharmonicity constants, normal coord. ab initio calcs. 79—36595
molecular deuteron quadrupole coupling freqs. calc. 78—29801
molecular electron scatt., ab initio theory including polarisation 78—50640
molecular electron scattering, theory and calc. techniques 80—63841
molecular electron scattering cross-sections, ab initio calcs., incl. polarisation 78—5341
molecular energy gradient, ab initio HF program 79—89606
molecular fragment calculations with pseudopots. 79—93905
molecular geometry optimisation in mols. with second row atoms 77—42232
molecular inner-shell photoabsorpt., shape resonances, extended X-ray absorpt. fine struct. 77—18979
molecular ionisation potential, quark influence, ab initio SCF calcs., appl. to H_2O and SO_2 79—10058
molecular multipole magnetisability, mag. shielding, multiple SCF perturbation theory 77—34549
molecular quadratic potential functions, calc. MO constraint of interaction coordinates 78—74631
molecular single/multiphoton dissoc., ab initio theory 78—17735
molecular spin-spin coupling consts., mol. vibr. contrib., calc. methods comparison 80—23402
molecular static polarisability, ab initio SCF wave functions 80—74106
molecular systems, saddle points and min. energy paths, constrained simplex optimisation procedure 80—42943
molecular vibrational wave functions, semiclassical Gaussian basis set method 80—9583
molecule, 1st row, geometry optimisation, using bond function augmented basis sets 78—905
molecule, polar, anion, ab initio ground state pot. energy surfaces, electron affinity 79—49958

ab initio calculations continued
- molecule, polar, anion ab initio ground state pot. energy surfaces calc. 80—47923
- molecule with second-row atoms, bond functions in SCF calcs. 77—14349
- molecules, atomic potentials, transferable, new general methodology 79—45624
- molecules, bond contributions to electronic energies, ab initio STO 3G calcs. 77—6669
- molecules, electron distrib., ab initio anal. 80—47866
- molecules, energy partitioning scheme for ab initio SCF calc. interpretation 79—93918
- molecules, ground state props., coupled cluster and MBPT methods appl. 80—47881
- molecules, ionis. pot., SAMO-ZDO method 78—41947
- molecules of rows 1-3, equilib. geometries, orbital energies, ab initio rel. to pseudopot. calcs. 78—82613
- monofluoromethane, force consts. and IR intensities, ab initio SCF finite difference method 78—86783
- monofluoromethane, X-ray photoelectron spectral linewidth of F core, ab initio HF calc. 78—62841
- monothioformate anion, protonation site, ab initio SCF calc. 79—47894
- monothioformic acid, pot. for rot. about C(sp^2)-S bonds, ab initio calc. 80—23572
- multi-config. SCF super-CI calc., density matrix formulation 80—78547
- naphthalene, dipole polarisability, finite-field SCF MO calcs. 80—83255
- naphthalene, LCAO SCF MO CI calcs., integral approx. scheme using semiorthogonalised orbitals 79—6873
- p-nitroaniline, cryst., electronic excited states, config. interaction calcs., UV spectrum 78—10913
- nitromethane, ab initio SCF MO calcs. of geom. and bond energies 79—31381
- nitromethane, torsional barriers, electronic spectrum 79—59424
- nitromethyl anion, ab initio SCF ab initio MO calcs. of geom. and bond energies 79—31381
- nitrosomethane, ground state and nonvertical n-π^* excitation energy calcs. 80—18804
- non-linear transport theory, field depend. of carrier screening 80—29415
- nucleation and molecular clustering about ions, energetics and structure 79—41260
- nucleic acid bases, Zn^{2+} binding, ab initio SCF (pseudopot.) calcs. 80—12052
- one-electron eigenenergies for class of atomic model pots., exact calcs. 77—23399
- one-electron props. variation with changes in mol. geometry, electronic and nuclear components partitioning 77—83491
- open-shell SCF calcs. with model pot. method 77—57875
- organic compound, substituent π-conjugative effects, ab initio calcs. 79—45633
- organic mols., IR intensities anal., hybrid orbital rehybridisation model, mol. charge distrib. 78—74630
- organolithium cpds., ab initio SCF-MO calcs. of C-Li bond character 77—410
- oscillator strength sum rule, hydrodynamic analogy to quantum mechanics 79—26873
- oxalic acid, theoretical deformation density, ab initio Hartree-Fock calcs. 79—32982
- oxirane cation, struct. rearrangement following vertical ionisation, ab initio CI calc. 80—58191
- oxiranylidene, struct., isomerisation, ab initio SCF MO calcs. 78—41941
- oxirene, ab initio calc., energy levels and geom. struct. of C_2H_2O isomers 78—62716
- oxoniomethylene cation, rearrangement to hydroxymethyl cation, barriers, ab initio MO calcs. 80—104424
- ozone, ${}^1A_1$ ground state, dipole moment function, ab initio SCF and CI calcs. 80—32628
- papain models, active site α-helix and ion pair stability 80—74265
- partial at. charges calc. from ab initio mol. electrostatic pots., appls. 78—70739
- peptide architectural units, ab initio SCF MO calcs. 78—96004
- peptide linkages, H bonding effects, review 77—10783
- periodic systems electronic struct., LCAO SCF ab initio HF calcs. method 80—65419
- perturbational MO analysis of ab initio SCF-MO wave functions 77—57867
- perturbational molecular orbital analysis, hybrid lone pairs problem 79—89608
- phenol-phenyl complex, electrostatic mol. pot. contour maps, MODPOT and VRDDO calcs. 80—102463
- phenyl cation, singlet, triplet state mol. geometries, energies, ab initio UHF STO calcs. 77—6672
- phosphate-H_2O-Na^+ system, interactions 77—30773
- photochemical reaction, avoided crossings in excited states potential energy surfaces 78—76881
- photochemistry, sudden polarisation effect 79—34328
- photoionisation cross-section, molecules, orthogonalised-plane-wave approx. 79—41202
- photosynthetically relevant mols., electronic structural props. 80—16902
- PMDA, ab initio SCF MO wavefunctions for ground and excited states 79—10028
- point charge model approach to intermol. interaction coeffs. 80—18897
- point charge model approach to mol. elec. polarisability 80—18797
- polar molecules, electron affinities, ab initio calcs., dipole moments 79—89623
- polarization Green's function with multiconfiguration self-consistent-field reference states 80—37724
- polyacetylene:$ASF_5(AsF_6)(SbF_6)(PF_6)$, metallic, band theory 80—49570
- polyacetylene type infinite chain cryst., energy bands, ab initio Hartree-Fock orbital calc. 78—60066
- polyatomic closed-shell systems, ab initio Hartree-Fock instabilities 78—78628
- polyatomic molecules, bond functions, for ab initio calcs. 80—5469
- polyatomic molecules, IR absorpt. bands, integrated intensities, ab initio and LMO calcs. 79—72234
- polycytosine, ab initio energy band struct. 77—70415
- polydiacetylene backbone sequence, electronic structs., unrestricted HF approach 78—63975
- polydiacetylenes, band struct., ab initio cryst. orbital method, and transport props. calc. 78—26811
- all-trans polyene, ab initio studies 80—43222
- polyene, different orbitals for different spins 79—69392

ab initio calculations continued
- polyene, energy bands, ab initio Hartree-Fock cryst. orbital calcs. 77—89717
- polyenes, photoiosomerisation, triplet pot. energy surfaces and normal mode anal. 80—108700
- polyethylene, band structure, linear combination of localised orbitals calc. 77—62808
- polyethylene, conform. stability, 1-electron levels, long-range effects calcs. 80—28123
- polyethylene, one-, three-dimensional, energy band struct., ab initio calcs. 79—95330
- polyglycine, band struct., ab initio SCF LCAO calcs. 79—22874
- polyglycine chain, electronic struct. and transport props., ab initio Hartree-Fock crystal orbital calc. 79—42448
- polymer, FSGO model, X-ray diffr. struct. factor calcs. 77—46660
- polymeric chains and Mott insulators, similarities w.r.t. electronic correl., AMO method *(French)* 80—24775
- polymers with defects, energy bands, ab initio SCF crystal orbital calcs. 78—30884
- polymethineimine, all-trans, ab initio cryst. orbital calcs. 79—77530
- polyyne, linear infinite chain, ground-state props., ab initio studies 79—95306
- polyynes, intermolecular interaction through triple bonds, internal rot. 80—106370
- porphine, ab initio CI calcs., electronic absorpt. spectra 78—78639
- position space LCAO wave function, momentum space variation approx., many centre integrals 80—27926
- potential energy surfaces of chemical reactions, review 80—35505
- prop-1, 2-dienyl radical, ab initio SCF HF MO calc., electronic struct. and one electron props. 77—42231
- propane, vertical electronic spectrum, ab initio MRD-CI calcs. 78—70810
- propene, force constants, SCF ab initio calcs. 77—34780
- n-propyl radical, and propane, struct., ab initio calc. 79—98006
- protein, electron-transport type, H-bonding, ab initio MO 80—51039
- protein, structure and bonding, quantum theory, ab initio calcs. 80—61509
- protein architectural units, ab initio SCF MO calcs. 78—96004
- pseudo pot. model Hamiltonian, spin-orbit splitting, intercombination and relativistic orbital reorganisation 78—25424
- pseudopotential for FSGO calcs., appl. to Li compounds 77—75043
- pyrazine, excited and N_{1s} ionised states, ab initio calcs. broken orbital symm. 80—27931
- pyrazine, lowest triplet state, phosphoresc., intersystem crossing 78—5269
- pyridine, π-electronic structs., ab initio VB calcs. 78—70749
- pyridines, monosubst., H_2O complexes, n-π^* transitions, H bonding, MO theory 80—95550
- pyrrole, excited state electronic struct., ab initio SCF and CI calcs. 78—78644
- pyrrole, ground state, (π-π^*) state, ab initio SCF CI calcs. 78—33438
- pyrrole-acetonitrile, H-bonded complex, ab initio MO calcs. 80—102440
- rare earth ternary borides, coexistence of magnetism and superconductivity 79—73630
- rare earth ternary borides, RRh_4B_4, supercond., re-entrant magnetism, energy band calcs. 78—52140
- relativistic effects in ab initio effective core pot. studies, appl. to $HgCl_2$, AuCl, and PtH 79—93933
- relativistic effects in oscillator strength calculations, ab initio methods 80—9519
- Ruedenberg relation, in ab initio calcs. of at. and mol. SCF energies 79—89596
- satellite struct. of electron spectra, CI and vibronic coupling, dynamical calc. 80—53044
- saturated hydrocarbon polymers, conform. stability, 1-electron levels, long-range effects calcs. 80—28123
- SCF calculations, molecular, optimal damping factor, dynamical damping 79—54762
- second-row hydrides, nucl. spin-spin coupling consts., ab initio calcs. 80—95647
- self-consistent electron pair theory, methods and appls. 77—10579
- semiconductor, dynamical effective charges, pseudopotential calc. 78—30881
- 1,3-sigmatropic rearrangements, ab initio calcs., basis set and electron correl. effects 80—104428
- silaethylene, singlet-triplet energy separations 77—57866
- silaethylene, triplet carbenoid isomers, thermodynamic stability 78—90076
- silanes, ab initio calcs. using FSGO, internal rot. 78—82639
- silyl radical, conform., hyperfine struct., nonempirical calcs., vibr., effects 79—97998
- simulated ab initio MO method, appl. to second row elements in mols. 80—47867
- simulated ab initio molecular orbital method, resolvent technique 79—41094
- small, medium and large systems, ab initio and approx. rigorous calcs. 78—62714
- $(Sn)_x$ chain, energy band struct., Hartree-Fock and CDW solns. 79—23885
- solid electrolyte, mobility paths for MI_4^{-3} clusters, ab initio electronic struct. calcs. 80—70458
- spin and charge density theoretical determ., review 77—75045
- spirohydrocarbons, strained, bond angles, interatomic distances, semiempirical and ab initio calcs. 80—95533
- superexchange interactions, models, prospects for ab initio calcs. 77—69281
- supermolecule calcs. with additive procedure, intermolecular interactions and binding energy 80—52880
- surface flow of dilute gas in model pores, free mol. flow calc. in adsorbent force field 80—6100
- surface states, three-dimens. cryst. ab initio SCF LCAO calc., impurity clustering 78—56201
- surfaces and interfaces, quantum chemical calc. methods 80—49849
- TCNE-benzene, charge transfer theory, Mulliken population, ab initio calc., multiconfiguration scheme 80—106392
- teaching instruction using ab initio computer program 77—78937
- tetracyanoquinodiamine, LCAO-Xα-SCF atoms in mols., theory and appl. 77—57869
- tetrafluoromethane, X-ray photoelectron spectral linewidth of F core, ab initio HF calc. 78—62841
- 3,3,4,4-tetramethyldiazetine, photoelectron spectra, ring size effects on azo group ionis. pots. 77—61793

ab initio calculations continued
tetrathiofulvalene, LCAO-Xα-SCF atoms in mols., theory and appl. 77–57869
thermal dissociation vibrational relaxation at high temps. 79–74367
thieno(3,2-b)thiophene, electronic and vibr. spectra, vapour phase and cryst. 77–34654
thiocarbonates, mol. struct., S-substitution effect *(French)* 80–23335
thiocarbonyl halogen substituted cpds., geometric and electronic struct., LCAO-SCF calc. 79–89603
thioformaldehyde, electronic struct., dipole moments, mol. polarisability, force fields, ab initio calcs. 80–78531
thioformyl ion, theoretical study 78–37553
thionitrates, mol. struct., S-substitution effect *(French)* 80–23335
thiophene, single cryst., UV spectrum, ab initio CI calcs. 79–19898
thiourea, ground and first excited triplet state configs., ab initio SCF calcs. 79–89597
thiourea, struct., hydration, ab initio SCF calcs. 80–58142
third-row hydrides, core d-electrons, FSGO struct. optimisation method 77–50382
thirene, ab initio SCF calc., thermodynamic stability 78–25420
three atom ab initio energy surface calc. 78–82663
three-electron bonds, strengths, ab initio LCAO MO CI calcs. 80–87046
toluene, mol. struct., ab initio calcs. 80–106262
transition metal atoms, neutral and ion val. states, electron correlation, ab initio effective val. Hamiltonian calc. 80–99449
transition metal atoms interactions with PF$_3$ and CO ligands, MO calcs., boundary props. of adsorption systems 79–85896
transition metal complexes, counterintuitive orbital mixing in semiempirical, ab initio MO calcs. 78–90078
transition metal hydrides, homoleptic, electronic structure, ab initio calcs. 79–89601
transition metal nitrides, liquid interactions, ab initio LCAO MO SCF calcs. 79–18256
transition metal nitrosyls, ab initio HF calcs. 78–90082
transition metal surface atom interaction with ethylene and acetylene MO calc. 80–6623
transition metal trifluorides, mol. and electronic structs., ab initio restricted Hartree-Fock calcs. 79–63900
transition metals, supercond. transition temp., ab initio calc. 80–25036
transition state determination and characterisation ab initio calcs. 77–28975
triatomic dihydride molecules, Walsh's rules and small bond angle states 80–106255
triatomic molecules, linear, substituted fragment series, electronic struct. transferability, mutual at. influence 78–9066
triatomic molecules, vibr. energies, wavefunctions, ab initio calc. 78–17652
trichlorofluoromethane, dissoc. electron attachment, pot. curves calcs. 79–98231
trichlorofluoromethane anion, dissoc. electron attachment, pot. curves calcs. 79–98231
trifluoroacetic acid, ab initio MO calcs. of geometry, torsional barriers 78–90313
trifluoromethyl cyanides and isocyanides, isomerisation, ab initio (STO-3G) geometry optimised calc. 78–46265
trimethylene diradicals, geometry optimisation ab initio SCF CI calcs., energy gradient 79–85903
trioxolane, methyl substituted, stability, pseudorotation, electronic effects in final ozonide 79–45654
trioxolanes, methyl substituted, stability, pseudorotation, electronic effects in primary ozonide 79–49961
trioxolanes, pseudorotation surface, mol. struct. and conform. 79–45653
tryptamine, near ab initio and pseudopotential calcs. 77–71749
TTF-TCNQ, Landau free energy function, CDW-libron interaction, sp. ht. near phase transitions 80–19963
unimolecular decay, nonadiabatic interactions, transition probability as function of Massey parameter 80–35503
unitary group irreducible representation subduction coeffs. 80–37723
unsaturated hydrocarbons, dipole polarisabilities, STO-4G calcs. 80–83255
valence-shell MO calc. with pseudopot. 78–907
van der Waals forces between mols. 78–62868
vibrational excitation calcs. by sudden approx., pot. energy surface choice 77–27158
vinyl alcohol, struct. from ab initio calcs. 78–29857
vinyl fluoride, geometries, props. and protonation, ab initio mol. orbital study 79–22588
vinyl isocyanate, and vinylcyano ether, geometry and conform., ab initio minimal STO-3G MO calcs. 80–23337
vinylcyano ether, and vinyl isocyanate, geometry and conform., ab initio minimal STO-3G MO calcs. 80–23337
n-vinylformamide, torsional pot. barriers, ab initio and partition of energy methods 77–88588
VSEPR model and Pauli exclusion principle, mol. geom. determ. and validity 79–31380
water, proton affinity, many-body Rayleigh-Schrodinger perturbation theory 78–92497
water+glycine(serine) zwitterions, interaction pots., ab initio SCF LCAO calcs. 78–48747
water dimers, stability, CNDO/2 and STO-3G calcs. 79–760
water-imidazole, H bond interrupted chain, cooperative effects, STO-3G ab initio calcs. 80–63535
X$_3$YO molecules, ab initio MO calcs., geometry, electronic struct. 78–41940
Z=114, Dirac-Fock one-centre calcs., tetravlent hydride prediction 77–34551
Z=11 to 103, theoretical, L-shell Coster-Kronig energies 77–83524
Ziegler-Natta type catalysis, reaction pathway, ab initio SCF-LCAO-MO calcs. 78–56891
Ag, 4d-subshell absorpt. spectra, ab initio Hartree-Fock calcs. 79–18139
Ag, electronic and mag. structure calcs. of mag. impurities 80–80213
Al II, $^3F^0$ Rydberg series, energy levels, multiconfigurational HF procedure 80–47882
Al-Ga(Sn), ab initio calcs. of partial enthalpy and result for enthalpy of mixing 79–43197
Al-H$_2$O, mol. complex, electronic struct. calcs. 78–66465
Al$_2$(Al$_2^-$)(Al$_2^+$) configurations, ab initio study, LCAO, STO, MO-SCF and CI calcs., binding energy *(French)* 80–91447
Al$_2$Cl$_6$, ab initio LCAO SCF minimal basis set calc., struct. 79–49943
Al$_2$F$_6$, ab initio LCAO SCF minimal basis set calc., struct. 79–49943

ab initio calculations continued
AlH$^+$ radical cation, EPR matrix isolation obs., hyperfine components calcs. 80–14158
AlH$_3$, AlH$_3^-$, ground electronic states and geometries, ab initio calcs. 77–57863
Al$_c$Mg$_{1-c}$ liquid alloys, vols. and entropies of mixing, calc. 80–75363
AlOH$\rightarrow$HAlO system, intramol. rearrangement, ab initio calc. of pot. surfaces and min. energy paths, geom. parameters 80–32623
Ar, aqueous soln., dil., energy and struct., pair pot. energy function, Monte Carlo calc. 80–54107
Ar, KLL and KLM Auger electron spectra, obs. and relativistic multiconfigurational Dirac-Fock calc. 78–50524
Ar, solid, n=1 surface excitons and LO-TO splittings of bulk excitons 79–73445
Ar, solid-liq. transition and mech. props., modified cell theory 79–23703
Ar, total state energies, L-, M-electron processes, ab initio CI investig. 77–18801
Ar+H$^+$, subshell electron capture cross sections 79–89771
Ar+HHe$^+$, ab initio pot. energy data, SCF-LCAO calcs. 80–63530
Ar$_2$ $^1\Sigma_u^+$ excimer state, photoionis. cross section 78–70882
Ar$_2$, accurate ab initio calc. of intermol. energy 80–18899
Ar$_2$, excited state pot. curves, ab initio CI calc. 78–78643
Ar$_2$ van der Waals dimer, intermol. pot., SCF CI ab initio calcs. 80–106274
Ar$_2^+$, bound-free absorpt. cross section for Π and Σ states 78–5140
Ar$_2^+$, electronic struct., pot. energy curves, spectroscopic consts. 79–18114
ArF, laser emission, ab initio config. interaction calcs. on electronic states 78–63083
ArF$_2$, ab initio diatomics in mols. pot. surface, spin-orbit coupling 79–3519
Ar$_2$F, electronic states, ab initio POL CI calcs. 78–66474
ArHCl, ab initio FGO calc. 78–50467
ArHF, van der Waals complex, ab initio RHF calc., struct. 79–76339
ArHO, van der Waals complex, ab initio RHF calc., struct. 79–76339
ArKr$^+$, absorpt. spectra, ab initio calc. of potential energy curves 78–74568
ArO, lasing, low-lying electronic states, ab initio config. interaction calcs. 78–63084
Au, ab initio effective core pot., Dirac-Hartree-Fock and Hartree-Fock calcs. 78–33426
Au, ground and excited states, pot. energy curves, relativistic effects calcs. 79–31416
Au$_2$, ground state, ab initio effective core pots., relativistic effects calcs. 79–31377
Au$_2^+$, ab initio SCF calcs. using relativistic effective core pot. 80–95524
AuH, AuCl, relativistic effective core potentials 78–86767
BF$_3^-$, geometric struct. of ground state, ab initio calc. 78–5130
BH, ab initio spin-projected EHF method pot. curve calcs. 79–10054
BH, electron density, basis set, electron correl. effects 78–74581
BH$^+$, spin-extended Hartree-Fock ab initio calculations for small radicals 78–70746
BH$_2$, Walsh's rules and small bond angle states 80–106255
BH$_2^+$, BH$_3$, force consts., ab initio calcs. with differentiated estimation of integrals 77–67974
B$_2$H$_5^+$, FSGO ab initio calc. of geometry, CNDO/2 calc. 78–41943
B$_2$H$_6$, quadratic valence force field, rel. to ethene 79–3382
B$_2$H$_n$, struct., ab initio SCF calcs. *(French)* 79–22598
B$_3$H$_n$, struct., ab initio SCF calcs. *(French)* 79–22598
(BHNH)$_n$, band structure, ab initio calcs. 79–23895
(BH$_2$NH$_2$)$_n$, band structure, ab initio calcs. 79–23895
B(I) hydrides, ab initio calcs., proton and hydride affinities 79–10029
BN, cubic, ab initio SCF calcs., band struct., ground state props. 78–51891
BN, electronic struct., exact exchange HF calcs. 80–65438
B$_3$N$_3$H$_6$, electronic struct., mag. susceptibilities, ab initio calcs. 78–74571
B$_2$O$_3$, bipyramidal struct., stability, ab initio SCF-MO calcs. 80–99446
BOH$\rightarrow$HBO system, heterovalent isomerism, ab initio calc. of pot. surfaces and min. energy paths, geom. parameters 80–32622
(B(OH)$_3$)$_2$, hydrogen bond, ab initio MO calcs. 78–58588
Ba I, low-lying, even-parity levels, ab initio relativistic SCF MCDF calcs. 78–37568
Ba II, 5p excitation, relativistic anal., multiconfig. Dirac-Fock calcs. 80–69240
Ba II, ab initio calc. of isotope shifts 78–37555
Ba, quantum defect param., ab initio calcs. 80–78525
Be cluster, multibody expansions, convergence 80–23594
Be complexes, binding and orbital energies, biological systems ab initio calc. 80–102442
Be compounds, electronic structure, configs., energy, bonding, of small mols. and complexes 78–13420
Be I, B I, C I, N I and O I isoelectronic series, tables of oscillator strengths of transitions 80–37779
Be I, energy level calcs. using model pot. and cores approxs. 77–14353
Be I, energy level calcs. term systems, convergence to Be II 2s limit 77–14354
Be, polarisability and London coeff., ab initio variation perturbation calc. 79–13635
Be$_n^-$ (n=2,3,4), electronic struct., ab initio calcs. 78–17560
BeF, A $^2\Pi$ state config., ab initio MO calcs. 80–95532
BeF, spin orbit coupling const., ab initio calcs. 80–63537
BeH, BeD, linewidth, indirect predissoc., anomalous isotope effect, ab initio calc. 77–58101
BeH radical, hyperfine splitting const., electronic energy, UHF-type, CCI calcs. 80–52909
BeH, spin-extended Hartree-Fock ab initio calculations for small radicals 78–70746
BeH$_2$, force consts., ab initio calcs. with differentiated estimation of integrals 77–67974
BeH$_2$, pot. energy curve, minimal basis ab initio VB calcs. 78–50477
(BeH$_2$)$_x$, polymer, ab initio calcs., cryst. orbital method 79–37659
BeO$_2$, and anion, dimerisation energy and binding of electron, ab initio calc. 79–45628
BeO$_2^-$, electron binding, ab initio calc. 79–45628
BeO(BeO), electron affinity and dipole moment, ab initio calc. 78–41938
(Be(OH)(NH$_3$)$_2$)$^+$ model for biological active sites, ab initio calcs., comparison with Zn complex 80–104551

ab initio calculations continued

- $Be_2(^1\Sigma_g{}^+)$, binding energy, ab initio pot. curves, interacting correlated fragments method 80−63557
- $Be(2^3P)$+methane, reaction, ab initio MO calcs. 79−8431
- Bi, parity-nonconserving optical rotation 79−63968
- $Br^{25+}+Br^{25+}$. correlation diagrams, inner-shell vacancy prod., characteristic X-rays 77−83503
- BrCl, photoelectron spectrum, assignments 78−5284
- BrF, He(I) photoelectron spectra, interpretation 79−13766
- $Br^-(H_2O)_n$, hydration energies, orientation, ab initio-LCAO SCF MO calcs. 80−27944
- BrN_3, VPS obs., comparison with ab initio and semi-empirical calcs. 80−53043
- BrNCO, VPS obs., comparison with ab initio and semi-empirical calcs. 80−53043
- C allotropes, diamond, graphite, gas-solid interface, electronic struct. HFR calc. 80−54745
- C, effective valence shell Hamiltonian, ab initio calcs. 78−82611
- C III, IV, V Auger lines obs., beam-foil excitation, ab initio calcs. 77−54601
- C, one-centre integrals of semiempirical theories of valence, ab initio calcs. 80−102441
- C^-, effective valence shell Hamiltonian, ab initio calcs. 78−82611
- C^{n+}, (n=1,2,3) effective valence shell Hamiltonian, ab initio calcs. 78−82611
- C-C bonds, single, double, triple, electron density distrib., X-ray diffr. data accuracy rel. to ab initio calcs. 79−89805
- C-H bond, acidity in organic mols. and anions, SCF MO calcs. 77−83497
- C-H-X H bonded systems, ab initio MO calcs. 79−6835
- C_2, bond order values, ab initio calcs. and basis set depend. 80−32605
- C_2, $X^1\Sigma^+{}_g$, $6^3\Sigma^-{}_g$ states, perturbations, ab initio CI calcs. 77−83490
- C_3, electron spectrum, ab initio MRD CI calcs. 78−90089
- C_3, ground and excited states, vibr., pot. curves, CI calcs. 77−83509
- C_3, ground state pot. surfaces, analytical functions 80−83304
- C_3, Renner effect, vibronic levels and wavefunctions, ab initio variational method 80−14127
- CD, Λ-type doubling in excited rot. levels 77−57979
- CF_3, $CF_3{}^-$, and $CF_3{}^+$, optimised struct. and bonding, ab initio SCF MO calc. 80−23334
- CF_3O^-, bonding, ab initio calcs. 77−50350
- CH, Λ-type doubling in excited rot. levels 77−57979
- CH, one-centre integrals of semiempirical theories of valence, ab initio calcs. 80−102441
- CH^+, $a^3\Pi$-$b^3\Sigma^-$ transition moment, ab initio calcs. 80−87047
- CH^+, excited states, pot. curves and transition moments determ. by ab initio CI methods 80−106286
- CH^+ indirect nucl. spin-spin coupling const., Hartree-Fock and polarisation propag. calcs. 78−9170
- CH_2 and $CH_2{}^+$, valence states, ab initio calcs. 79−6859
- $CH_2{}^+$, Walsh's rules and small bond angle states 80−106255
- $CH_3\cdot$+ethylene, transition state, ab initio calc. 78−48640
- $C_2H_2+OH^-\rightleftharpoons C_2H^-+H_2O$, equilib. consts., ab initio SCF and CEPA calcs. 78−3361
- $C_2H_3{}^++HF$, interaction, struct. and stability, ab initio calcs. 80−58347
- $C_2H_7{}^+$, ab initio SCF, CI, CEPA-PNO struct. and energy calcs. 78−94197
- CH_3CO', low lying states, struct., energetics, ab initio STO calcs. 77−61682
- CH_3NN', low-lying states, struct., energetics, ab initio STO calcs. 77−61682
- $C_2H_5O^+$ and $C_2H_5S^+$, stability, proton affinity, ab initio SCF, CEPA PNO, MINDO/3 and MNDO calcs. 79−59357
- CH_2SiH_2, ab initio GO calc. 78−94187
- $(CH_3)_2X$ molecules, perturbational MO anal., methyl rot. barriers, fragmentation mode 77−88386
- C_3Li_4, structure calculations 78−5364
- CN^-, electron density distrib., theoretical and expt. determ. 77−61683
- CN^-, spectrosc. consts. for ground and excited states, ab initio, CI calcs. 80−78551
- CN^+, ab initio full CI calcs. 78−50480
- CN^+, ground state, identity, ab initio CI calcs. 80−5468
- CN^+, lowest $^1\Sigma^+$ and $^3\Pi$ states, ab initio CI pot. curves calcs. 79−85905
- C_2N_2, and $C_2N_2{}^+$, electronic struct. UV and PE spectra 80−23304
- C_2N_2, satellite struct. of electron spectra, CI and vibronic coupling, dynamical calc. 80−53044
- $(CN^-;e^+)$ complex, ab initio LCAO SCF calc., positron affinity and excitation energy 79−49945
- $CN^-.e^+$, positron energy levels, rel. to Rydberg levels of Na, NO 79−86089
- CO, ab initio calcs. of the derivative of the static polarisability 79−3597
- CO, core ionis., electric field depend. 78−13424
- CO, core ionisation single orbital relax. energy, LCAO-SCF basis set depend. 79−89604
- CO, indirect nucl. spin-spin coupling const., Hartree-Fock and polarisation propag. calcs. 78−9170
- CO, low energy electron scatt., ab initio study, frame-transform. theory 77−83732
- CO, nonempirical PRDDO scheme and calcs. 80−37739
- CO, polarisability derivatives, bond length depend., SCF and CI calcs. 80−58162
- CO, X-ray K-absorpt. spectra, vibr. fine struct., ab initio restricted HF calc. 78−86883
- CO^+, ab initio pot. energy curves, full valence CI with minimal STO 79−72361
- $CO+H_2$, pot. energy surface anisotropy in nonreactive region, ab initio calcs. 78−29832
- $CO+H_2$, thermal energy collision, ab initio pot. energy surface 79−45788
- $CO+Li^+$, pot. energy surface, equilib. distance, SCF calcs., correl. effects 77−3430
- CO_2, $1\pi_g{}^3\,2\pi_\mu{}^1$ config., ab initio eqn. of motion excitation energies 77−50376
- CO_2, ab initio SCF calcs., force consts., vibrs., pot. energy surface 78−5209
- CO_2, anomalous energy minima surfaces 78−86791
- CO_2, collision-induced Raman spectrum, theoretical studies 80−63646
- CO_2, dimer struct. CNDO/2 and ab initio calcs. 77−71753
- $CO_2\ H^+$, geom. struct., ab initio mol. orbital study 78−62939
- CO_2, ionised states, core and valence, ab initio HF calcs. 77−79597

ab initio calculations continued

- CO_2, localised mol. orbitals, ab initio PRDDO SCF calc., isoelectronic struct. 78−25441
- CO_2, low energy electron (positron) collisions, ab initio adiabatic polarisation pots. 80−14240
- CO_2, mol. quadrupole moments, mag. shielding and spin-rot. tensors 79−22609
- CO_2, nonempirical PRDDO scheme and calcs. 80−37739
- CO_2, polarisabilities, quadrupole and dipole moments, nucl. geom. effects 79−63899
- CO_2, spin polarised photoelectrons, synchrotron excited 80−43101
- CO_2, static polarisabilities, ab initio SCF HF calcs., internucl. separation depend. 78−9073
- CO_2, stretch-stretch interaction force const., electron correlation influence, ab initio CI study 80−58161
- CO_2+H_2, rot. transfer, ab initio intermol. pot. energy surface 80−58354
- $CO_2+H_2(D_2)$, ab initio LCAO-MO-SCF intermolecular pot. energy surface, V→T transfer 77−50489
- CO_2+He, rot. inelastic collision, ab initio SCF, electron gas and pot. energy surfaces 80−83468
- CO_2+Ne, intermol. pot. in repulsive short-range region, ab initio 80−69204
- $CO_3{}^{2-}$, localised mol. orbitals, ab initio PRDDO SCF calc., isoelectronic struct. 78−25441
- $CO(CN)_6{}^{3-}$, electronic struct., LCAO SCF MO calcs. 79−18112
- CS, perturbation parameters between valence states 77−26975
- $C^-(^4S^0)$, attachment energies, ab initio calc. 77−30768
- CS_2, mol. quadrupole moments, mag. shielding and spin-rot. tensors 79−22609
- Ca, quantum defect param., ab initio calcs. 80−78525
- $Ca_2{}^+$, pot. energies in Ca^+ and Rydberg Ca** collisions with Ca 79−27055
- $CaF_2{:}Np^{3+}(U^{3+})$, cryst. field splittings, ab initio MO calcs. 77−20520
- CaH, low lying electronic states, ab initio SCF-CI calcs. 80−52893
- Cd, effective core potentials calcs. rel. to bond lengths and energies 78−66464
- Cd, field gradients, temp. depend., electronic and lattice contribs., ab initio study 79−42501
- Cd, nuclear quadrupole antishielding effects, ab initio theory 78−34814
- Cd, nuclear quadrupole interaction theory using first-principles pseudopotential 79−73482
- CdS, cubic, ab initio band struct. calcs. within local density functional formalism 78−87910
- Ce II, isotope shift and screening, pseudo-relativistic HF calc. 78−90096
- Cl^-, pair polarisability, ab initio SCF MO energies 78−70741
- Cl-containing systems, core Auger and core electron binding energy shifts, ab initio LCAO SCF MO UHF calcs. 77−30777
- Cl_2, ground and ionised states, Koopman's theorem and Mo relax. in ab initio calcs. 78−1035
- Cl_2, inner shell excited states, X-ray absorpt. spectra, HF calcs. 80−78536
- $(Cl_2)_2$, binding, dispersion energy predominance 78−25421
- $(Cl_2)_2$, config., ab initio calc. 79−41098
- $Cl_3{}^-$ energy surface, comparison of CNDO and ab initio results 77−23445
- ClF_4 radical, geom., ab initio MO calcs. 79−89610
- $ClF(ClF_2{}^-)(ClF_3)$, ground and ionised states, Koopman's theorem and Mo relax. in ab initio calcs. 78−1035
- $ClF(ClF_2{}^-)(ClF_3)$, localised MO ab initio calc., Gaussian orbital ab initio calc. 80−14083
- $ClHCl^-$, deuteron quadrupole coupling const., nuclear mag. shielding, geometry depend. 78−58586
- ClN_3, VPS obs., comparison with ab initio and semi-empirical calcs. 80−53043
- ClNCO, VPS obs., comparison with ab initio and semi-empirical calcs. 80−53043
- ClNSO, ground state geometry, ab initio calcs. 80−106259
- $ClO_n{}^+$, ClO_n and $ClO_n{}^-$ (n=1 to 3), ab initio calcs., localised MO and nature of Cl-O bond 80−69070
- Cl_2O, ab initio vertical ionis. pot., corrections to Koopmans' theorem 78−25749
- $ClO(X^2\Pi_i)$, radical, He(I) photoelectron spectrum, ΔSCF calcs. 79−72359
- $Cl.+XHC{=}CH_2$, free radical reaction theory, ab initio calc. 77−52624
- Co (0001), photoemission, exchange-split energy-band dispersions 80−35059
- Co, Auger spectrum, ab initio MO LCAO SCF CI calc. many electron contribs. 80−87169
- Co-porphine, ab initio LCAO SCF MO calcs. 79−6860
- $CoCl_4{}^{2-}$, electronic energy levels calc. by conventional and Xα Hartree-Fock methods 78−66470
- CoO, ab initio SCF and CI calcs. on d-d transitions, $CoO_6{}^{10-}$ cluster d-electron localisation 77−35897
- CoO, ionisation, electron density relax. effects. ab initio calcs. 78−50466
- CoO, valence photoelectron spectrum, relative intensities, limited CI calcs. 79−63918
- $CoO_6{}^{10-}$, ionisation, electron density relax. effects. ab initio calcs. 78−50466
- Cr, band struct., X-ray emission bands, self-consistent calc. 77−28104
- Cr II-VI, struct. and transition probabilities, ab initio calc. using Thomas-Fermi central pot. 79−3360
- $CrOCl_3$, electronic structure and valence ionisation energies, obs. by ab initio and SW-Xα methods 80−69073
- Cs, discrete level raising into far continuum, oscillator strength to shape reson. transfer 78−78624
- Cs, photoionis. of 6s electron, spin-orbit interaction, ab initio calc. 79−81191
- $CsH^-CsH^+(CsH)$, ab initio ground-state pot. energy curves, electron affinities 78−41946
- $CsNpF_6$, cryst. field splittings for Np^{5+}, ab initio MO calcs. 77−20520
- Cu (001) monolayer, electronic struct., self-consistent LCAO calc. 79−4606
- Cu (100) film, chemisorbed N_2, electronic struct. 77−59315
- Cu, elec. field gradient due to interstitial positive muon 78−31142
- Cu, electronic and mag. structure calcs. of mag. impurities 80−80213
- Cu film, surface electronic struct., determ. by ab initio calc. 77−43679
- Cu/Ni coherent modulated structures, electronic struct. and magnetism 80−103620
- CuCO, linear, ab initio RHF-MO calcs., rel. to adsorption 79−26883
- CuCl, bonding, ab initio pseudopot. calcs. 79−6857

ab initio calculations continued

CuCl, electronic struct., ab initio HF SCF MO calcs. of $CuCl_4^{3-}$ cluster 78−95262
CuCl, electronic struct. by LCAO and LMTO methods, direct gap semiconductor 80−59868
$CuCl_4^-$, ESCA satellite intensity, ab initio SCF calcs. 80−74103
$CuCl_4^{2-}$, charge distrib. and ligand field splitting calc. 77−62879
$CuCl_4^{2-}$, electronic energy levels calc. by conventional and Xα Hartree-Fock methods 78−66470
$CuCl_2(Cl_4^{2-})(Cl_6^{4-})$, electronic struct. studies by SCF, MSXα and INDO method 80−74119
$CuF_2(F_6^{4-})$, electronic struct. studies by SCF, MSXα and INDO methods 80−74119
CuO, ab initio HF-MC-SCF with GTO basis set, dissoc. energy and bond length 80−47890
$CuSO_4.5H_2O$, EXAFS, rel. between Debye-Waller factor and thermal parameters meas. by neutron diffr. 80−84803
$D+H_2$ reaction, transition state theory calculations, kinetic isotope effect explanation 80−66784
D_2, c, I and i states, pot. energy curves and vibr. levels, Born-Oppenheimer approx. 78−931
D_2^+, dissociative recombination cross sections 79−59568
D_3 Rydberg states, spectroscopic B_0 consts. 80−74109
D_3^+, ab initio vibr. intervals and vibr. freq. refinement 80−47968
D_3^+, rot.-vibr. spectrum, ab initio calcs. 80−95595
D_3^+, vibr. spectra, ab initio calcs. 77−83562
DCN, electronic spectra, vibr. struct., ab initio calc. 78−9166
D_2O, cubic anharmonicity constants, normal coord. ab initio calcs. 79−36595
DOD, vibr. intensities, ab initio and empirical calcs. 80−78592
DOD, vibr. intensities, ab initio and empirical calcs., band strengths 80−78593
$ErRh_4B_4$, supercond., electronic struct. and reentrant magnetism 78−10340
Eu, exchange integral, spiral spin configuration, ab initio calcs. 79−47275
$EuMo_6S_8$, Chevrel phase, RE mag. isolation and supercond. 80−44470
F $(^2P_{1/2})+H_2$, quenching, classical path calcs. 79−22800
F, ab initio effective valence shell Hamiltonian for neutral and ionic valence states 80−74117
F, isoelectronic sequence, X-ray spectra 80−87071
F^- hydration, ab initio MO calcs., fractional charge model 77−34547
$F+H_2 \rightarrow HF+H$ energy profile, minimal basis ab initio VB calcs. 78−50477
F^- + fluoromethane, S_N2 reaction, ab initio LCAO SCF calcs. 77−81402
F + ethylene, transition state, ab initio calc. 78−48640
F_2, electron impact excitation, dissoc. of lowest electronic state 80−63839
F_2, ground and ionised states, Koopman's theorem and Mo relax. in ab initio calcs. 78−1035
F_2, valence electronic states, $^1\Pi_u \leftarrow X^1\Sigma_g^+$ absorption spectrum 79−63920
FBO, electronic struct. calcs. 77−30772
FCN, CNF, isomer pairs, mol. orbitals calcs., using PLA and LEDO integral approx. methods 78−13418
F_2CS, pot. surfaces, X^1A_1, a^3A_2 and $a^3A_2(b_1)$ states, ab initio SCF calcs. 78−86795
$FClO^+$, radical cation, struct. and electronic props., ab initio RHF SCF MO calc. 80−52883
FH, indirect nucl. spin-spin coupling const., Hartree-Fock and polarisation propag. calcs. 78−9170
$FH-OH_2$(dimethyl ether), H-bonded complexes, cubic force consts. calcs. 80−47868
FH_2^+, reactive processes, ab initio MCSCF-CI and diatomics in mols. calc. 78−56881
FH_3^+, stability, ab initio calcs. 77−30775
$FHCl^-$, deuteron quadrupole coupling const., nuclear mag. shielding, geometry depend. 78−58586
FHF radical, struct. and stability, ab initio SCF and CI calcs. 77−71887
FHF^-, deuteron quadrupole coupling const., nuclear mag. shielding, geometry depend. 78−58586
FHF^-, H bonds, vibr. dynamics calcs. 80−23397
FNNF, mol. struct., cis effect 80−91434
FNO, four electron three centre bonding units, ab initio valence bond calcs. four electron three centre bonding units, ab initio valence bond calcs. 80−27949
FNO, ground and lowest excited states, SCF ab initio calcs. 78−37544
F_2O, geometry, electron spectrum, vert. ionis. pot. ab initio calc. 80−58187
FOCl, ab initio vertical ionis. pot., corrections to Koopmans' theorem 78−25749
$(F^-;e^+)$ complex, ab initio LCAO SCF calc., positron affinity and excitation energy 79−49945
$F^-.e^+$, positron energy levels, rel. to Rydberg levels of Na, NO 79−86089
Fe (111), photoemission, exchange-split energy-band dispersions 80−35059
Fe complex, $[Fe(CN)_6]^{3-}$, electronic struct., optical transitions, XPS, Mossbauer isomer shift, valence ionisation pot., SCF-MSX calc. 79−6864
Fe, electronic structure of nontransition element impurity atoms 77−73023
Fe, ferromagnetic, hyperfine fields; SCF calcs. 77−8061
Fe III-VI, struct. and transition probabilities, ab initio calc. using Thomas-Fermi central pot. 79−3360
Fe^{2+} and Fe^{3+} hydrate clusters, aq. electron exchange reaction, ab initio RHF MO calc. of inner shell reorganisations, vibr. freq. 80−102564
$Fe(CN)_6$, Mossbauer isomer shift const., ab initio SCF calcs. 78−43751
FeF, electronic states, ab initio calcs., UV spectrum elucidation 78−74570
FeF_6, Mossbauer isomer shift const., ab initio SCF calcs. 78−43751
Fe_xO, wustite, width of d-level final-state struct. obs. in XPS 78−19633
GaAs (110), chemisorption of O and Al, ab initio theory 80−75612
GaAs (110), reconstruction and oxidation initial stages, ab initio calc. 80−49473
GaKr, low-lying electronic states, PE curves, transition moments, emission coeffs. 79−6894
$GdMo_6S_8$, Chevrel phase, RE mag. isolation and supercond. 80−44470
Ge_2, multiplet struct. and charge distrib. 79−26881
GeH_2, struct. determ., restricted HF calcs. 80−87030

ab initio calculations continued

GeH_3^-, electronic struct., electron affinity, inversion barrier, ab initio SCF Gaussian basis calc. 80−63552
GeO, mol., VUV photoelectron spectra, $X^2\Sigma^+$ state 79−72358
H atom, relativistic quantum mech. as weak-field limit of nonlinear theory 79−6878
H atom finite chains, HF solns. stability and symmetry breaking, independent particle model calcs. 80−87035
H, chemisorbed on Be(0001) surface, mol. orbital cluster theory 79−15002
H, electron scattering, optical pot. methods 80−102569
H halides, ab initio SCF calc. of dipole polarisabilities 79−89600
H, He atmosphere, hyperfine press. shift, MCSCF-variational procedure 77−6735
H-bonded systems, cyclic and bifurcated, ab initio MO calcs. 79−41100
$H+Br_2 \rightarrow HBr+Br$, pot. energy surface, ab initio generalised valence bond calc. 78−73026
$H+C^{2+}(C^{3+})(N^{2+})$, radiative charge transfer, rate coeffs., pot. energy curves 77−88554
$H+D_2$ reaction, transition state theory calculations, kinetic isotope effect explanation 80−66784
H + HCl, barriers for abstraction and exchange reactions 77−48629
H^- + methane → methane + H^-, nucleophilic substitution, ab initio pot. energy classical trajectory anal. 78−68886
$H^+ + CO\ (^1\Sigma)$, ground state pot. energy surface, ab initio SCF calc., protonated equilib. geometry 80−83301
$H^+ + H_2$, inelastic collisions at 3.7 eV, close cou-ing calcs. 77−34734
$H^+ + H_2$, rot. and vibr. excitation, energy loss obs. 80−63773
$H^+ + H_2$, vibr. excitation, ab initio CI pot. energy surface calcs. 80−74228
$H^+ + H_2$, vibr.-rot excitation, ab initio CI pot. energy surface calcs. 80−74229
H_2, D_2, photoionisation, body-frame Hund's case b description 78−94295
H_2, electron elastic low energy scatt., ab initio pseudostates calc. 78−9247
H_2, electron impact excitation, $\nu \leq 4$ vibr. levels, theory 80−18940
H_2, electron impact low energy rot. and vibr.-rot. excitation cross sections, static exchange approx. 79−89799
H_2, electron repulsion matrix elements, asymptotic form, adiabatic representation 80−87038
H_2, electron scatt., vibr. and vibr.-rot. excitation 79−22853
H_2, electronic states, adiabatic energy corrections, CI ab initio calc. 77−83502
H_2 H_2, intermol. energy, CI ab initio calc. 79−85904
H_2, HD, c, I and i states, pot. energy curves and vibr. levels, Born-Oppenheimer approx. 78−931
H_2 metastable state, spin-rot. coupling, ab initio calcs. 77−18804
H_2 molecule dimer, ab initio SCF intermolecular interaction energy calcs. 80−78537
H_2, octapole magnetisability, multiple SCF perturbation calc. with STO basis set 77−34550
H_2, repulsive intermol. pot. 80−32794
H_2, triplet state, molecular polarisability calcs. 80−63860
H_2, Verdet consts., ab initio calcs. 77−3390
H_2^+, dissociative recombination cross sections 79−59568
H_2^+, nonadiabatic vibrational energies, ab initio calcs. 78−90142
H_2-H_2 intermol. pair pot., ab initio SCF-CI surface 80−91457
H_2-He, nucl. shielding, ab initio coupled HF calc. 79−89690
H_2+Ar, vibr. energy transfer rate, ab initio calcs. 78−82821
H_2+H_2, interaction polarisability comparison with the He diatom, ab initio SCF calcs. 80−27943
H_2+H^+, low energy rot. excitation, ab initio differential inelastic cross section calcs. 77−88542
$(H_2)_2$, ab initio calcs., perturbation dispersion energy versus CI treatment 77−26976
H_3, CI calc. of three dimens. pot. energy surface 78−56882
H_3, Rydberg states, spectroscopic B_0 consts. 80−74109
H_3, three atom ab initio energy surface calc. 78−82663
H_3^+, ab initio calcs. of vibr. spectrum 77−6753
H_3^+, ab initio vibr. intervals and vibr. freq. refinement 80−47968
H_3^+ rot.-vibr. spectrum, ab initio calcs. 80−95595
$H_3^+ + H_2 \rightarrow H_5^+ \rightarrow H_2 + H_3^+$, ab initio GO pot. surface, C_{2V} symmetry 77−25252
H_4 excimer, electronic and geom. struct., ab initio CI calc. 79−76348
H_4, ground and excited states, SCF MO CI calcs. 77−6693
H_4, pot. energy surfaces, valence bond calcs. 80−74129
H_4^+, ground and excited state pot. energy surfaces and geom. struct., SCF and CI calcs. 78−78769
H_n^+ (n=3,5,7,9,11), stability, struct., ab initio MO calcs. 78−74810
$(H\text{-}He)^-$, ab initio calcs. 80−63799
HBr^{n+}, highly charged, repulsion energies, nucl. internal conversion, ab initio calcs. 79−76341
HC_2 radical, electron affinity, ab initio SCF and CI calcs. 78−50468
HCC^+, equilib. struct., rot. const. 79−98003
HCCN, a cyanocarbene, geom. struct., electron correl. effects 80−1077
HCCN, free radical, matrix isolation spectra and ab initio calcs. 78−46329
HCN and HNC, analytic functions from pot. energy surfaces 78−62743
HCN, CNH, isomer pairs, mol. orbitals calcs., using PLA and LEDO integral approx. methods 78−13418
HCN, dipole moment derivative, sign anomaly, CGTO ab initio calc. 78−74795
HCN, electronic spectra, vibr. struct., ab initio calc. 78−9166
HCN, ground state pot. surfaces, analytical functions 80−83304
HCN, HNC, electronic reorganisation, with core ionisation 78−94196
HCN, IR and Raman vibr. intensity changes due to Li^+ interaction 79−45712
HCN, SCF ab initio ground state pot. energy surface, geometry, rel. to HCN^- 78−78646
HCN, vibr. energies, wavefunctions, ab initio calc. 78−17652
HCN^-, ab initio calcs., electron affinity, stability 77−42239
HCN^-, SCF ab initio ground state pot. energy surface, geometry, rel. to HCN 78−78646
HCN^+, A and B $^2\Sigma^+$ states, pot. surfaces, ab initio SCF calcs. 80−27959
HCN^+, photoelectron spectra of third electronic state, ab initio calc. of pot. energy surface 78−70871
HCN-CO complex, charge transfer theory, Mulliken population, ab initio calc., multiconfiguration scheme 80−106392

ab initio calculations continued

$H_2CN^+H_2 \rightarrow HCN^+H+H_2$, ab initio GO SCF pot. energy surface, saddle point, reaction path 77−50379

HCNO, isomers, geometry, spectra, rot. and force consts., ab initio calcs. 77−34574

HCO and HNO, pot. energy functions for ground state surfaces 79−89620

HCO_2^+, geom. struct., ab initio mol. orbital study 78−62939

H_2CO^+ ion, unimolecular decay paths of electronically excited species 79−3359

HCO′, low lying states, struct., energetics, ab initio STO calcs. 77−61682

HCS^+-CSH^+, struct. and stability, ab initio SCF calcs., CNDO calcs. 80−32608

HCS^+-CSH^+ system, pot. surface for H abstraction, internuclear bending for ground and excited states 78−29744

H_3CS^+, struct. ab initio (4-31G) SCF calc. 79−68201

HCl, bond dependence of dipole polarisabilities 78−74573

HCl, infinite chain, ab-initio electronic band struct., MUNICH-CHAIN program 77−8017

HCl, K-emission and -absorpt. spectra, vibr. struct., ab initio calcs. 77−79629

HCl, mol. cryst., angles of H-bonded mols., ab initio calcs. 78−6037

HCl, solid, ferroelec., comparative calcs. 77−8529

HCl^-, resonance states, CI calcs., pot. energy curves 78−29755

HCl^+, effective Hamiltonian, ab initio calc. 79−45632

$HCl^+(DCl^+)$, spin-rot. consts., Van Vleck approx., ab initio calcs. 77−34610

HD, elec. dipole vibr.-rot. spectrum, line strengths, ab initio calcs. 78−25514

HD, indirect nucl. spin-spin coupling const., Hartree-Fock and polarisation propag. calcs. 78−9170

HD, nuclear spin coupling const. calc., using ab initio LCAO MO SCF method 78−25558

HD^+, dissociative recombination cross sections 79−59568

HD^+, nonadiabatic vibrational energies, ab initio calcs. 78−90142

HD_2^+, vibr. spectra, ab initio calcs. 77−83562

H_2D^+, vibr. spectra, ab initio calcs. 77−83562

HDO, line strengths and intensities, ab initio calcs. 79−72300

HF, ab initio HF-STO perturbation Auger transition rate calc. 79−72368

HF, Auger spectra, correl. effects, energies and wavefunctions, ab initio CI calc. 80−14125

HF, Auger transition energy calcs. 77−34704

HF, bond dependence of dipole polarisabilities 78−74573

HF chain, ab initio cryst. orbital calcs., basis set depend. 78−34746

HF dimer, stabilisation energies, harmonic free constants, intermolecular vibration, SCF and CEPA PNO calcs. 79−98177

HF, force consts., ab initio CI calcs. *(French)* 78−90093

HF, geometries, props. and protonation, ab initio mol. orbital study 79−22588

HF, K-emission and -absorpt. spectra, vibr. struct., ab initio calcs. 77−79629

HF, mag. shielding and susceptibility, ab initio finite perturbation calcs. using GIAOs 77−6670

HF, nucl. spin-spin coupling consts., finite perturbation and sum-over-states calcs. 79−85893

HF, nuclear spin-spin coupling, ab initio SCF perturbation theory 78−33525

HF oligomers, Gibbs free energies, gas. equilib., ab initio calc. 79−20456

HF, orbital relax. energy for single and double ionis. from valence shells 80−106253

HF, pot. energy curve, minimal basis ab initio VB calcs. 78−50477

HF, solid, ferroelec., comparative calcs. 77−8529

HF^- and $(HF)_2^-$, ab initio calcs., electron affinity, stability 77−42239

HF^+, ab initio valence band calcs. 79−6869

HF-cyclic ethers H-bonded complexes, calorimetry, IR spectra and MO calcs. 79−52738

HF+formyl fluoride, multiple site reactivity, ab initio GO supermol. calc. 78−11498

$HF+H^-$, reaction, ab initio pot. energy surface calcs. 79−39127

HF+HF, ab initio pot. surface, ang. depend. fit calcs. 77−19006

$(HF)_2$, energy decomp. anal. of H-bonding, ab initio SCF MO calcs. 77−57868

$(HF)_2$, intermol. pot. function, ab initio 6-31G calc. 79−18254

HF_2^-, four electron three centre bonding units, ab initio valence bond calcs. 80−27949

$(HF)_n$, $n=1\text{-}\infty$, ab initio hydrogen bond and electronic parameters, phonons 77−14342

H_2F_2 and H_3F_3 clusters, molecular structures, ab initio calcs. 80−83532

$HF^+(DF^+)$, spin-rot. consts., Van Vleck approx., ab initio calcs. 77−34610

HFF radical, struct. and stability, ab initio SCF and CI calcs. 77−71887

HN_3, ground $^1A'$ state, SCF and CI calcs., conform., geom., vibr. freqs. and dissoc. 80−18806

H_3N-BH_3, cryst., electronic struct., ab initio, MO calcs., fractional charge model 77−34547

H_3N-HF, energy decomp. anal. of H-bonding, ab initio SCF MO calcs. 77−57868

$HNC \rightarrow HCN$, transition state determination and characterisation ab initio calcs. 77−28975

HNCO, barrier to linearity, ab initio SCF and CI calcs. 79−3363

HNF_2 and DNF_2, photoelectron spectra, vibr. struct. obs, ionisation pot. determ., ab initio calcs. of ionic geometry 80−83418

HNF_2, force consts., geometry, ab initio Hartree-Fock calcs. 77−57864

H_2NF, force consts., geometry, ab initio Hartree-Fock calcs. 77−57864

HNN′, low-lying states, struct., energetics, ab initio STO calcs. 77−61682

HNO, four electron three centre bonding units, ab initio valence bond calcs. 80−27949

HNO, ground and lowest excited states, SCF ab initio calcs. 78−37544

HNO, HON, electronic reorganisation, with core ionisation 78−94196

HNO, isomerism, low lying electronic states, ab initio MRD-CI calcs. 80−83291

HNO, vibr. freqs. from anharmonic ab initio/empirical PE functions 79−76406

HNO^+, ab initio pot. surface, and isomerisation barrier of lowest states 79−22622

ab initio calculations continued

HNO^+, ab initio SCF and CI comparison of struct. and spectra, rel. to NOH^+ 77−26972

HNO^+, vertical spectra, heat of form., ab initio MRD-CI calcs. 79−49934

HNO_2, isomers, protonation mechanism, electrostatic pot. prediction limits 78−11506

H_3NO^-, ab initio calcs., electron affinity, stability 77−42239

HNOO, singlet and triplet diradicals, unrestricted 79−97975

HNSi, struct. and microwave freqs. calcs., rel. to interstellar emission lines 78−36648

HO-H...OHX, $X=H$, CH_3, NH_2, OH, F, H-bonds, electron donor substituted, mol. orbital calc. 78−13422

HO_2 and HOCl, struct., vibr. freqs., IR intensities, ab initio calcs. 79−98007

HO_2^+, ab initio calc. of three lowest states 78−62711

H_2O, 1s shake-up spectrum, ab initio equiv. cores, improved virtual orbital and CI calcs. 77−46597

H_2O, ab initio SCF CI calcs., ground state energy, config. and force consts. 77−18782

H_2O affinity for $Li^+(Na^+)(K^+)$, ab initio SCF calcs. 80−58125

H_2O, and D_2O, Feshbach-reson. and dissoc. electron attachment 79−41246

H_2O, bonding electron pairs, size and shape parameters, Gaussian basis set MO calcs. 80−27935

H_2O, core 1s and 1b, photoelectron bands, vibr. excitations, ab initio calcs. 80−63543

H_2O, cubic anharmonicity constants, normal coord. ab initio calcs. 79−36595

H_2O dimer, intermolecular pot. functions from ab initio calcs. 80−5473

(H_2O), electron affinity, ab initio SCF calcs. 79−76343

H_2O, electron density, basis set, electron correl. effects 78−74581

H_2O, equilib. struct., ab initio SCF calcs., general valence force field 77−3265

H_2O, force consts., ab initio calcs. with differentiated estimation of integrals 77−67974

H_2O force consts., ab initio CI calcs. *(French)* 78−90093

H_2O, free energy of liq. water, ab initio Monte Carlo calc. 78−83975

H_2O, line strengths and intensities, ab initio calcs. 79−72300

H_2O, mol., Compton profile, directional, polarisation functions 79−36706

H_2O, nucl. spin-spin coupling consts., finite perturbation and sum-over-states calcs. 79−85893

H_2O, nuclear spin-spin coupling, ab initio SCF perturbation theory 78−33525

H_2O, open-shell SCF calcs. with model pot. method 77−57875

H_2O, orbital relax. energy for single and double ionis. from valence shells 80−106253

H_2O, perfect pairing valence bond model, ab initio SCF calcs. 77−6689

H_2O, rot.-vibr. Schrodinger eqn. soln., bond lengths and angles, force consts. 79−41151

H_2O, VSEPR model and Pauli exclusion principle 79−31380

H_2O, vibr. freqs. from anharmonic ab initio/empirical PE functions 79−76406

H_2O , ab initio calcs., electron affinity, stability 77−42239

H_2O^+, ab initio SCF study of low lying electronic states, monopositive ions 79−49946

H_2O-H_2S supersystem, ab initio LCAO MO SCF calcs. of H bonding 79−89607

H_2O-lysozyme, interaction, intermol. pot. calcs. 77−75250

H_2O+Li^+, ab initio GTO calc. of vibr. intensity changes of spectroscopic parameters 78−58583

$(H_2O)_2$, energy decomp. anal. of H-bonding, ab initio MO calcs. 77−57868

H_2O_2, geometry, internal rot. barriers, electron correl. calcs. 78−70751

H_2O_2, hindered rot. pot., strongly orthogonal geminal calcs. 77−71751

H_2O_2, hindered rot. pot. recreation, electron pair wavefunction transferability 77−71752

$(H_2O)_n$, $n=2$ to 8, correlation energies, ab initio and SCF calcs. semiempirically corrected 80−43223

H_3O radical, stability, ab initio UHF-CI calcs. 78−5137

H_3O^+, ab initio CI calcs. of excited states 77−30796

HOCl, ab initio MRD CI calc., electronic spectrum, dissoc., heat of reaction, formation 78−21857

HOCl, ab initio vertical ionis. pot., corrections to Koopmans' theorem 78−25749

HOCl, photodissoc., ab intio SCF CI calcs. 78−50604

HOCl, vibr. freqs. from anharmonic ab initio/empirical PE functions 79−76406

HOD, vibr. intensities, ab initio and empirical calcs. 80−78592

HOD, vibr. intensities, ab initio and empirical calcs., band strengths 80−78593

HOF, vibr. freqs. from anharmonic ab initio/empirical PE functions 79−76406

$H_3O^+(H_2O)_n$, H^+ motion energetics, ab initio calcs. 78−25413

HOT, vibr. intensities, ab initio and empirical calcs. 80−78592

HOT, vibr. intensities, ab initio and empirical calcs., band strengths 80−78593

$H_2O.H_2O$ and $H_2O.Ne$, excited, first order interaction energy, ab initio calc. 80−32598

$HO_2.H_2O(NH_3)$ complex form., ab initio calcs., min. energy configs. 77−14340

H_2O...HF complex, force field, vibr. freqs., equilib. geometry bond energy, ab initio calc. 77−65450

HPN-HNP, isomerisation energies, ab initio MRD-CI calcs. 80−106271

HPO, mol. struct. and props., ab initio, calc., Gaussian lobe orbital 78−62713

HS_2, ground and first excited states, geometry, ab initio SCF calcs. 78−50657

HS_2 radical, ab initio calcs. of geometry and spectra 77−34552

HS_2, rotamers, electronic and geometrical structs., ab initio floating GO basis calcs. 78−74572

HS_n^-, $n=1\text{-}4$, electronic struct., ab initio Hartree-Fock-Slater calcs. 80−74107

HS_n^{2-}, $n=1\text{-}4$, electronic struct., ab initio Hartree-Fock-Slater calcs. 80−74107

H_2S, electron density, basis set, electron correl. effects 78−74581

H_2S, electronic struct., ab initio CI SCF calc., spectra assignments 77−10586

H_2S, gas-phase, states in valence photoelectron spectrum 78−94284

H_2S, ground and excited states, SCF and CI calcs. 77−414

- **ab initio calculations** continued
  - H_2S, KLL Auger spectra of S, ab initio LCAO SCF calcs. 77—65515
  - H_2S, KLL Auger spectrum, obs. and ab initio SCF CI calc. 78—50654
  - H_2S, mol. polarisability and derivatives, ab initio SCF CI calc. 79 59597
  - H_2S_n, $n=1$-4, electronic struct., ab initio Hartree-Fock-Slater calcs. 80—74107
  - HSO, ground and first excited states, geometry, ab initio SCF calcs. 78—50657
  - HSO radical, ground and excited first states, ab initio SCF and CI calcs. 77—30776
  - HSO-HOS, isomerisation energies, ab initio MRD-CI calcs. 80—106271
  - H_2SO hypothetical molecule, nonempirical STO calc. of chem. bonds 80—23307
  - HSiC-HCSi, isomerisation energies, ab initio MRD-CI calcs. 80—106271
  - HSiN and HNSi, analytic functions from pot. energy surfaces 78—62743
  - HSiN, struct. and microwave freqs. calcs., rel. to interstellar emission lines 78—36648
  - HSiN-HNSi isomers, MRD-CI calcs. of struct. and stability 78—82635
  - H_2SiO, electronic struct., dipole moments, mol. polarisability, force fields, ab initio calcs. 80—78531
  - H_2*, energy and occupation curves, wave functions, natural spin orbital anal. 77—83493
  - H.HF, H-bonded complex, ab initio calcs. *(French)* 80—52866
  - He, electron scattering, optical pot. methods 80—102569
  - He, quantum-mechanical calculations 77—14350
  - He-LiH, rot. inelastic collisions, ab initio pot. energy surface calcs. 80—87208
  - $He+(H^+)(D^+)$, mobility and diffusion, runaway effect 80—33727
  - $He+ArH^+$, ab initio pot. energy data, SCF-LCAO calcs. 80—63530
  - $He+H_2$, collision-induced dipole, ab initio VB calc. 78—94202
  - $He+H_2$, pot. energy surface, ab initio calcs., van der Waals const. determ. 80—106372
  - $He+H_2$, Van der Waals pot., ab inito SCF model 78—74728
  - $He+H_2^+(H^+)$, interaction pots., comparison with values from ion mobility data 77—14518
  - $He+H^+$, differential scatt., 1-12 eV, high resolution beam meas. 80—58348
  - $He+H^+(D^+)$, runaway mobility obs. 80—38517
  - $He+He^+$, 2 and 3 keV, one and two electron excitations in He, quantal treatment 78—37730
  - He+He(Li), intermol. forces, ab initio VB calc. using nonorthogonal basis set 80—23490
  - He+LiH, rot. inelastic collisions, dynamics 80—87209
  - He+LiH, rot. inelastic collisions, state-to-state cross sections determ. 80—87210
  - $He^+ + He$, He_2^+ mol. collision complex, pot. energy curve spectrum 77—19008
  - He_2, ${}^1\Sigma_g{}^+$ states, pot. curves, ab initio multiconfig. SCF calcs. 77—46632
  - He_2, polarisability and collrision induced Raman spectra 80—48005
  - HeH^+, spectroscopic characts. in ground and first excited triplet states, Dunham pot. approach 77—42234
  - HeH_2, collision induced dipole IR spectra, ab initio SCF LCAO calc. 79—89737
  - $HeHe_2^+$, doublet, ab initio pot. energy surface calcs. for ground and lower excited state 79—63898
  - $(HeLi)^{2+}$, ab initio PE curves, coupling matrix elements, for $He^{2+}+Li$ 79—22822
  - $HeNO_2$, molecular geometry and stability 78—90075
  - $HeNe^+$, collisional form., excitation, pot. energy curves calcs. 77—6697
  - $He_2{}^+ X^2\Sigma_u{}^+$ state, ab initio CI calc., pot. energy curve, vibr. and rot. levels 77—3263
  - Hf III, multiconfig. Dirac-Fock theory, relativistic SCF method 77—3282
  - Hg, effective core potentials calcs. rel. to bond lengths and energies 78—66464
  - HgBr, ab initio CI calcs., spectroscopic parameters 79—72245
  - HgCl, ab initio CI calcs., spectroscopic parameters 79—72245
  - HgH, $HgCl_2$, relativistic effective core potentials 78—86767
  - $H_n{}^+$($n=7$, 9, 11, 13), geometry optimisation, ab initio SCF calcs 80—53180
  - $HoRh_4B_4$, electronic struct. and reentrant magnetism 78—10340
  - $I^{25+}+Te^{24+}$, $I^{43+}+Au^{69+}$, $I^{25+}+Au^{51+}$, correlation diagrams, inner-shell vacancy prod., characteristic X-rays 77—83503
  - I_2, HFS and mag. parameters of B state, ab initio calc. 79—45865
  - IF, He(I) photoelectron spectra, interpretation 79—13766
  - INCO, VPS obs., comparison with ab initio and semi-empirical calcs. 80—53043
  - In, Fermi surface dimensions, ab initio KKRZ calc. 77—89686
  - KC_8, intercalated graphite, electronic and cryst. struct. 80—44472
  - KCl, Compton profile anisotropies, charge and momentum distrib., LCAO-SCF-MO calc. 79—3500
  - K_2Cs, Laves phase, chemical bonding, electronic charge density distrib. pseudopotential calcs. 79—77549
  - K_7Cs_6, μ-phase variant, chemical bonding, electronic charge density distrib. pseudopotential calcs. 79—77549
  - KF, ab initio SCF MO energy, dipole moment and polarisability 80—1085
  - KN_3, ab initio calcs. of elec. props. of $N_4{}^-$ 79—95363
  - Kr, solid, $n=1$ surface excitons and LO-TO splittings of bulk excitons 79—73445
  - $Kr_2{}^+$, electronic struct., pot. energy curves, spectroscopic consts. 79—18114
  - $Kr_2Cl(F)$, ab initio diatomics in mols. pot. surface, spin-orbit coupling 79—3519
  - KrF, electronic states, ab initio CI calcs., spin-orbit coupling, pot. curves, dissoc. energy, dipole moments 77—38619
  - KrF, electronic states, ab initio POL CI calcs. 78—66474
  - KrF, fluoresc. spectrum, theoretical modelling using electronic potential curves 78—63086
  - KrF, laser emission, ab initio config. interaction calcs. on electronic states 78—63083
  - KrO, lasing, low-lying electronic states, ab initio config. interaction calcs. 78—63084
  - Li (100), O adsorption, cluster models, ab initio HF LCAO theory 78—71978
  - Li, adsorption of methyl groups, complex form., STO calcs. 77—9124
  - Li chain, disordered system, ab initio cryst. orbital calcs. 77—47715
  - Li cluster, chemisorption of H, ab initio HF calcs. 77—76670
- **ab initio calculations** continued
  - Li clusters, dissociative chemisorption of H_2, ab initio SCF-MO calcs. 79—77918
  - Li complexes $((C_2H_2X_2)_2Li)^n$ where $X=S$, O, binding and orbital energies, biological systems ab initio calc. 80—102442
  - Li compounds, electronic structure, configs., energy, bonding, of small mols. and complexes 78—13420
  - Li, Gaussian basis sets, uniform quality 78—5116
  - Li H^-, mol. orbital calcs., diffuse functions for basis sets, electron affinity 78—25436
  - Li linear chain, ab initio calcs., cryst. orbital method 79—37659
  - Li^+, ab initio SCF binding energies, with $-NCO$, $-CO$, $-COO-$, O, N, and $-CN$ 77—50352
  - Li^+ hydration, ab initio MO calcs., fractional charge model 77—34547
  - Li^+, pair polarisability, ab initio SCF MO energies 78—70741
  - Li-H_2O(ethylene) 78—66465
  - Li-like ions, fine struct. in $1s2p^2\ {}^4P$ and $1s2s2p\ {}^4P^0$ states 78—66471
  - Li^+-H_2O complex, charge transfer theory, Mulliken population, ab initio calc., multiconfiguration scheme 80—106392
  - Li^+-ligand complexes, NMR appl. ${}^7Li$ chemical shifts, expt. and ab initio studies 80—63670
  - $Li+H_2$, rot. and vibr. transitions, close-coupling calcs. 77—58136
  - $Li+H_2O \rightleftharpoons LiOH+H$, equilib. consts., ab initio SCF and CEPA calcs. 78—3361
  - $Li^+ + CO$, differential cross-sections, ab initio CI vibrotor pot. energy surface calcs. 78—46421
  - $Li^+ + CO$, rot. excitation, ab initio CI pot. energy surface, classical mech. and coupled states calcs. 78—25665
  - Li^+ + ether(thioether)(amide), pair pots., ab initio LCAO SCF MO calcs. 80—58184
  - $Li^+ + He$ collisions, K-shell vacancy sharing, ab initio LCAO-SCF, CI calcs. 77—19054
  - Li_2, ${}^3\Sigma_g{}^+$-${}^3\Sigma_u{}^+$ excimer emission, ab initio calcs. 80—91608
  - Li_2 SCF polarisability, polarisation potentials 79—89602
  - $Li_2{}^-$, electronic struct., ab initio calcs. 77—34553
  - $Li_2{}^+$, $X^2\Sigma_g{}^+$, ${}^2\Sigma_u{}^+$, $A^2\Pi_u$ and ${}^2\Pi_g$ states, electronic struct. vibr. spectra, ab initio calcs. 79—36507
  - Li_{2n}, ($n=1$, 2, 3), stable cluster configs., ionisation pots., binding energies, vibr. freqs., al initio SCF and CEPA calcs. 80—14265
  - Li_3, BO hypersurface and vibronic states, coupled electron pair approx. 78—94203
  - Li_3, potential energy surface and config., RHF CI calc. 77—34562
  - Li_4, plane configs., ab initio SCF calc., rel. to condensation *(French)* 77—4062
  - $LiAlF_4$, struct. pot. energy surface, Li^+ migration, ab initio LCAO SCF calcs. 80—23305
  - $LiAlH_4$, $LiBH_4$, ab initio calc. of geom. struct., charge distrib., bonding and pot. energy surfaces 80—18796
  - $LiBF_4$, nonrigid mol. struct. and stability, ab initio calcs. 80—83259
  - $LiBH_4$, non-rigid complex molecule, ab initio calcs. of pot. energy surface and geometric struct. 77—6678
  - $LiBH_4$, pot. surface and geometry, ab initio calcs. 78—86771
  - $LiBH_4$, struct., pot. surface, ab initio calcs. 79—41092
  - $LiBeF_3$, pot. energy surface, struct., stability and internuclear distances, ab initio calc. 80—58147
  - $LiBeH_3$, ab initio calc. of pot. surfaces and geometry 79—10024
  - $LiBeH_3$, pot. surface, struct., ab initio calcs. 77—88385
  - LiCa, laser chemiluminesc. 80—93759
  - LiCl, Compton profile anisotropies, charge and momentum distrib., LCAO-SCF-MO calc. 79—3500
  - Li_2Cl^+, mass spectra, struct., stability, expt. and theory 77—554
  - Li_2Cl^+, triplet polarisability, ab initio MO calc. 79—98244
  - $Li_nCl^{(n-1)+}$, energy cluster expansion convergence 80—91715
  - LiF, ab initio SCF MO energy, dipole moment and polarisability 80—1085
  - LiF, cohesion energy, compressibility and density, ab initio calc. 77—72648
  - LiF, F centre study by mol. SCF calcs. 80—44530
  - LiF^-, ground and excited states, ab initio calcs. single config. and multiconfig. SCF calcs. 80—52873
  - LiF-NH_2 adduct, mol. consts., ab initio SCF LCAO MO calcs. *(French)* 78—13423
  - Li_2F^+, mass spectra, struct., stability, expt. and theory 77—554
  - Li_2F_2, struct., force fields and normal mode freqs., ab initio calcs. 80—83260
  - $LiF(LiF^-)$, electron affinity and dipole moment, ab initio calc. 78—41938
  - LiH, adsorption of He, ab initio calc. 78—38952
  - LiH, crystalline, surface struct., quantum mechanical ab initio calc. 77—1281
  - LiH, insulator-metal transition press. calc. 78—34769
  - LiH, laser irradiated, single/multiphoton dissociation, ab initio theory 78—17735
  - LiH, LiH^-, pot. energy curves, electron affinity, spectroscopic consts. 78—5129
  - LiH, $LiHe^+$ and $LiHe_2{}^+$ systems, ab initio SCF LCAO calcs. of stability and spectroscopic consts. 77—71748
  - LiH, linear chain, ab initio calcs., cryst. orbital method 79—37659
  - LiH, positron affinity, ab initio LCAO MO SCF calc. 78—82870
  - LiH, SCF ab initio calcs. with noninteger Slater orbitals 77—26969
  - LiH^+, spin-extended Hartree-Fock ab initio calculations for small radicals 78—70746
  - LiH-NH_3(ethylene)(acetylene), struct. and props., SCF ab initio calcs. 80—106250
  - LiH+He, rot. inelastic collisions, rigid shell models 80—99545
  - $(LiH)_3$ complex, SCF interaction energy nonadditivity 80—91437
  - $LiH^-(LiH)$, ab initio ground-state pot. energy curves, electron affinities 78—41946
  - $Li(H_2O)^+$, config. ab initio GAUSSIAN 70 calcs. 79—49939
  - LiNO, four electron three centre bonding units, ab initio valence bond calcs. 80—27949
  - $LiNO_3$, mol. struct. ab initio calcs. 79—26884
  - $Li^+NO_3{}^-$ ion pairs and hydrated ion pairs, MO calcs., matrix isolation data 78—46267
  - Li_2O , electronic struct. and config., ab initio SCF study 79—85898
  - Li_2O_2, ab initio geometry, vibr. freqs., ionis. pots., and force consts. 77 65421
  - $LiOH^-$, electronic struct. and config., ab initio SCF study 79—85898
  - LiON, four electron three centre bonding units, ab initio valence bond calcs. 80—27949
  - Mg cluster, multibody expansions, convergence 80—23594

ab initio calculations continued
Mg I, $^3F^0$ Rydberg series, energy levels, multiconfigurational HF procedure 80–47882
Mg I, extensions to the doubly excited spectra in the vacuum uv 79–6901
Mg, polarisability and London coeff., ab initio variation perturbation calc. 79–13635
Mg_2, Mg_2^+, electronic struct., pot. energy curves, multiconfig. SCF calcs. 78–5124
MgH, and MgD, $B'^2\Sigma^+$-$X^2\Sigma^+$ band system, ab initio CI calcs. 79–93970
MgH, X and $B'\ ^2\Sigma^+$ and A $^2\Pi$ ab initio CI calc. 79–31415
MgO(MgO^-), electron affinity and dipole moment, ab initio calc. 78–41938
$Mg^{2+}.nH_2O+PO_4H_2^-$, binding mechanisms, SCF ab initio calcs. 79–22586
Mn III-VI, struct. and transition probabilities, ab initio calc. using Thomas-Fermi central pot. 79–3360
Mn-C_2H_2 and Mn-C_2H_4, π-bonded, pot. energy curves, SCF calc. 78–5136
$MnCl_4^{2-}$, electronic energy levels calc. by conventional and $X\alpha$ Hartree-Fock methods 78–66470
MnO, SCF CI calcs., ground and first excited states, bonding mechanism 77–14347
Mo, band struct., X-ray emission bands, self-consistent calc. 77–28104
N, ab initio effective valence shell Hamiltonian for neutral and ionic valence states 80–74117
$N+H_2^+$, triplet state ab inito CI pot. energy surfaces 78–74729
N^++H_2, triplet state ab inito CI pot. energy surfaces 78–74729
N_2, ab initio calcs. of the derivative of the static polarisability 79–3597
N_2, ab initio MO-LCAO-SCF and Gordon-Kim intermolecular pot. for seven different orientations 80–95522
N_2, bond order values, ab initio calcs. and basis set depend. 80–32605
N_2, core photoelectron line shape, localisation role 79–59512
N_2, core-ionised, core-valence excited and shake-up states, all electron MRD CI calc. 78–21858
N_2, electron elastic low energy scatt., ab initio pseudostates calc. 78–9247
N_2, electron impact, reson. vibr. excitation, ab initio R matrix calc. 80–32842
N_2, electron scattering, 13.6 eV, coupled channel treatment calcs. 79–64106
N_2, electron-mol. adiabatic polarisation pots. and ab initio SCF polarisabilities 80–9499
N_2, low energy electron (positron) collisions, ab initio adiabatic polarisation pots. 80–14240
N_2, MRD CI calc., lowest dissoc. limits 78–21859
N_2, multiple moments, polarisabilities and anisotropic long range interaction coeffs. 80–43206
N_2, photoelectron spectra, valence region strong shake-up bands, Koopman's theorem breakdown 79–72354
N_2, polarisabilities, quadrupole and dipole moments, nucl. geom. effects 79–63899
N_2, Raman intensities calcs., ab initio method 80–52993
N_2, Raman intensity, ab initio calc. 80–1028
N_2, static polarisabilities, ab initio SCF HF calcs., internucl. separation depend. 78–9073
N_2, X-ray K-absorpt. spectra, vibr. fine struct., ab initio restricted HF calc. 78–86883
N_2^{n+}, Coulomb explosion following heavy ion impact, ab initio SCF calc. 79–18277
$(N_2)_2$, Van der Waals molecule, struct. and internal rot. barriers determ., interaction pot. from ab initio calcs. 80–91626
N_3^-, low-lying excited states 79–31425
N_3^-, theoret. electron density distrib. cf. expt. density distribs. of NaN_3 and KN_3 77–46489
$NCNO\rightleftharpoons NC+NO$, ground state pot. energy surface, ab initio calcs. 77–90593
NCO^+, partial pot. energy surfaces, ab initio SCF CI calcs. 78–37554
NCl_3, ab initio LCAO SCF calc. for ground state, inversion barrier 78–25426
NF_3, NF_3^-, and NF_3^+, optimised struct. and bonding, ab initio SCF MO calc. 80–23334
NH^+, pot. curves, ab initio CI calcs., equilib. distances 78–17579
NH_2, ab initio calcs., appl. of convergent SCF procedure 80–47875
NH_2, pot. energy curves of X^2B_1, A^2A_1, $^2B_2$ valence-shell and $\pi_u{}^23s$-type Rydberg states calc. by CI 80–74138
NH_2 radical, (NH_2^+), ab initio SCF study of low lying electronic states 79–49946
NH_2, X^2B_1, A^2A_1 and B^2B_2 states, ab initio SCF CI calcs. 78–29746
NH_2^+, low lying states, ab initio MRD-CI pot. surface calcs. 79–89611
NH_2^+, quintet states, pot. energy surfaces, ab initio SCF MO calc. 78–25419
NH_2^+, triplet state ab inito CI pot. energy surfaces 78–74729
$NH_2^-+H_2\rightleftharpoons NH_3+H^-$, chem. equilib., ab initio calcs. 79–34282
NH_3, ab initio SCF calcs., force consts., vibrs., pot. energy surface 78–5209
NH_3, affinities for $H^+(Li^+)(K^+)(CH_3^+)$, ab initio SCF calculations 80–102443
NH_3, affinity for $Li^+(Na^+)(K^+)$, ab initio SCF calcs. 80–58125
NH_3, bonding electron pairs, size and shape parameters, Gaussian basis set MO calcs. 80–27935
NH_3, first triplet state, photodissoc. and Rydbergisation investig. 80–53067
NH_3, geometry changes during inversion, ab initio calcs. 78–5154
NH_3, IR absorption band integrated intensities, ab initio and LMO studies 80–23458
NH_3, lone pair contributions to the IR intensities 80–63630
NH_3, lowest triplet state geometry, SCF and CEPA-PNO calc. 80–914
NH_3, mol. nuclear spin-spin coupling, ab initio SCF perturbation theory 78–33525
NH_3, NH_3^+ ion, electrostatic force theory appl. to mol. geometry ab initio verification 79–98002
NH_3, orbital relax. energy for single and double ionis. from valence shells 80–106253
NH_3, photodissoc., ab initio SCF and CI calcs. 78–21984
NH_3, vibr. excitation in soft X-ray emission and core ESCA spectra 80–69163
NH_3^+, two-mode Jahn-Teller effect calcs. 80–83297
NH_3-CO_2 complex, matrix isolation IR spectrum, struct., ab initio SCF calcs. 78–5209

ab initio calculations continued
NH_3-lithium halide complex, ab initio calcs., Li bond rel. to H bond 77–14343
NH_3+2H_2, triplet n3S Rydberg state, ab initio UHF CI SCF calc. 80–53095
NH_3+SO_3, donor-acceptor adduct form., ab initio calcs. 78–82612
$NH_4^++LiH(H^-)$, substitution and abstraction reactions, ab initio calcs. 77–48624
NH_5^+, stability, ab initio calcs. 77–23419
N_2H_2, model rearrangement system, electron correlation and basis set effects 80–3317
N_2H_2, $N_2H_2^+$, ab initio calcs., electronic struct., geometries relative energies 77–46487
N_2H_2+ethylene reaction, H transfer, ab initio SCF GO calcs. 77–44469
NH_2CO', low-lying states, struct., energetics, ab initio STO calcs. 77–61682
NH(D) radical, and isotopic species, laser mag. reson., hyperfine parameters 77–10694
NH_xF_{3-x}, geometry changes during inversion, ab initio calcs. 78–5154
$N_2H_2(N_2D_2)$, ground and first excited state small vibr. coupling, ab initio CI calc. 78–62791
NH(NF)(NCl), effective spin-spin parameter and singlet-triplet transition intensities, ab initio calc. 78–9067
NH_2OH, ionisation energies, He I photoelectron spectra, orbital calcs. 77–88497
NH_2T, β-decay, ab initio SCF MO calcs. 77–71842
NH_2TNH_3, β^- decay effect on H-bond, ab initio LCAO SCF MO calc. 78–76894
$NH_2(X^2B_1)$ radical, and ND_2, ionisation pot., vibr. anal., ab initio calcs. and vacuum UPS obs. 80–53047
$NH_2.HF$, H-bonded complex, ab initio calcs. *(French)* 80–52866
NO, core photoelectron line shape, localisation role 79–59512
NO_2, electronic states, pot. energy surface calcs. 77–6673
NO_2, ground state pot. surface, ab initio LCAO MO SCF calcs. 80–102461
NO_2, lowest quartet state theoretical excitation energy 79–68221
NO_2, optimisation of diffuse Gaussian exponents 79–3364
NO_2, peroxy isomer, stability, ab initio SCF calcs., bond strength 77–14605
NO_2, vertical electronic spectrum, SCF and CI calcs. 77–30878
NO_2, vertical electronic spectra, ab initio calcs. 78–66538
NO_2^-, ab initio VB wave functions, π-electrons 78–70748
NO_2^-, optimisation of diffuse Gaussian exponents 79–3364
NO_2^-, solvated, in H_2O, ethanol, cyanomethane, and DMF lowest n-π^* transition 79–85960
NO_2^-, vertical electronic spectra, ab initio calcs. 78–66538
NO_2^+, gas phase equilib. geometry, force consts., vibr. freq., dipole moment function MCSCF/CI calcs. 80–78520
NO_2^+, vertical electronic spectra, ab initio calcs. 78–66538
$(NO_2)_2$, struct. and force fields of isomers, ab initio calcs. 77–18783
N_2O, spin polarised photoelectrons, synchrotron excited 80–43101
N_2O^+, ground state potential energy surfaces 77–27175
N_2O^+, pot. energy hypersurface characts. calc. in $O^++N_2\rightarrow N+NO^+$ react. 78–60996
NOF and ONF, ab initio calcs. of geometry and electronic struct. 79–76342
NOH isomerism, low lying electronic states, ab initio MRD-CI calcs. 80–83291
NOH^+, ab initio pot. surface, and isomerisation barrier of lowest states 79–22622
NOH^+, ab initio SCF and CI comparison of struct. and spectra with HNO^+ 77–26972
NOH^+, vertical spectra, heat of form., ab initio MRD-CI calcs. 79–49934
$N_2O(X^1\Sigma^+)\rightarrow N_2(^1\Sigma_g{}^+)+O(^1S)$, photodissoc., exact collinear calcs. 77–30937
$N^{2+}(^2P^0)+H$, charge transfer, ab initio CI pot. curves and coupling-matrix elements 80–37878
$N^{3+}(^1S)+H$, charge transfer, ab initio CI pot. curves and coupling-matrix elements 80–37878
$N(^4S)+N^+(^3P)=N^+(^3P)+N(^4S)$, gerade-ungerade splitting of N_2^+ pots., cross sections 77–30987
^{14}N quadrupole coupling consts., ab initio calcs. 80–58283
$^{14}NH^+(^{15}NH^+)(^{14}ND^+)$, ab initio CI calc. Λ type doubling in $X^2\Pi$ states 78–82714
Na $A^1\Sigma_u{}^+\rightarrow X^1\Sigma_g{}^+$ system, transition moments and radiative lifetimes calcs. 77–34697
Na, electron ionis., ejected electrons ang. distrib. 77–50541
Na I, isoelectronic sequence, X-ray spectra 80–87071
Na^+, interaction with purine and pyrimidine bases of nucleic acids 77–64005
Na+Ne, Na(3p) excitation 80–1056
$Na+Xe+\hbar w$, collisions in presence of nonresonant lasers 80–99567
Na^++ether(thioether)(amide) interaction, pair pots., ab initio SCF LCAO MO calc. 79–36721
Na_2, $^3\Sigma_g{}^+$-$^3\Sigma_u{}^+$ excimer emission, ab initio calcs. 80–91608
Na_3, electronic struct., pot. energy surface, ab initio CI study 78–70996
$NaAlH_4$, $NaBH_4$, ab initio calc. of geom. struct., charge distrib., bonding and pot. energy surfaces 80–18796
NaAr, $X^2\Sigma$, $A^2\Pi$ and $B^2\Sigma$ state, ab initio CI calcs. 78–9085
$NaBH_4$, struct., pot. surface, ab initio calcs. 79–41092
NaCl, Compton profile anisotropies, charge and momentum distrib., LCAO-SCF-MO calc. 79–3500
$NaCl^-$, mol. orbital calcs., diffuse functions for basis sets, electron affinity 78–25436
Na_2Cl^+, mass spectra, struct., stability, expt. and theory 77–554
NaF, ab-initio calc. of cohesion energy, compressibility and density 78–71782
Na_2F^+, mass spectra, struct., stability, expt. and theory 77–554
NaF(NaF), electron affinity and dipole moment, ab initio calc. 78–41938
NaH^-, mol. orbital calcs., diffuse functions for basis sets, electron affinity 78–25436
NaH^-(NaH), ab initio ground-state pot. energy curves, electron affinities 78–41946
NaK, ab initio and pseudopot. energy curves 78–90068
NaSCN, and similar salts, Na atomic charge determ. by numerical integration 80–28944
Na(1s), X-ray photoelectron spectrum, binding energy, at. compared with metal 78–70800

ab initio calculations continued
- $Na^+.nH_2O+PO_4H_2$, binding mechanisms, SCF ab initio calcs. 79–22586
- Nb, band struct., X-ray emission bands, self-consistent calc. 77–28104
- NbC, phonon anomaly rel. to Fermi surface 77–11853
- Ne, atomic interaction energy, basis set effects in SCF calcs. 77–83678
- Ne, atomic struct. calc., symmetry adapted pair functions, Rayleigh Schrodinger HF variational perturbation theory 80–42944
- Ne, Auger spectra, correl. effects, energies and wavefunctions, ab initio CI calc. 80–14125
- Ne, autoionising resons. near 575 Å, ab initio relativistic RPA calc. 80–32681
- Ne, solid, lattice relax. model of $n=1$ exciton emission 79–47492
- Ne, solid, $n=1$ surface excitons and LO-TO splittings of bulk excitons 79–73445
- $Ne+H_2$, Van der Waals pot., ab inito SCF model 78–74728
- $Ne+H^-(D^-)$, electron detachment, dynamical phenomenon 80–106305
- Ne_2, solid, a priori calc. of $n=1$ valence exciton 78–10364
- Ne_2, van der Waals mols., interatomic energy, SCF supermol. ab initio calcs. 77–42370
- Ne_2^+, electronic struct., pot. energy curves, spectroscopic consts. 79–18114
- $Ne_2^+ +He$, pot. energy surface, reaction cross sections, ab initio calcs. 80–11881
- Ne_2F, ab initio diatomics in mols. pot. surface, spin-orbit coupling 79–3519
- Ne_2F, energy surfaces, application of molecular electronic struct. theory 78–25452
- NeH_2^+, ab initio potential surfaces, frozen orbital approximation calcs. 78–41927
- Ne_nH clusters, ab initio LCAO MO SCF calc., struct. and energy 78–66704
- Ne_nH^+ clusters, ab initio LCAO MO SCF calc., struct. and energy 78–66704
- $NeHe_2^+$, extended valence bond diatomic calcs., applications to method of diatomics-in-molecules 79–45635
- Ni (001), chemisorption of CO and C_2H_2, final state mol. relax. 77–62752
- Ni, (001) surface, local density of states, asphericity of pot. and charge transfer, ab initio self-consistent calcs. 79–15064
- Ni (100), chemisorption of O(S), geometry of overlayers 78–2373
- Ni (100) and (111) surface, chemisorption of CO, tight-binding theory 77–20395
- Ni (111), photoemission, exchange-split energy-band dispersions 80–35059
- Ni, adsorbed CO, core level spectrum, satellite struct., ab initio HF-LCAO calc. 80–40233
- Ni, electronic structure of nontransition element impurity atoms 77–73023
- Ni, FCC, H-Ni_n self-consistent electronic screening charge density 79–33255
- Ni, ferromagnetic, electronic struct. and hyperfine field of nonmag. impurities, calc. 80–70658
- Ni III-VI, struct. and transition probabilities, ab initio calc. using Thomas-Fermi central pot. 79–3360
- Ni, $M_{II,III}$ spectrum, ab initio calculation 80–83276
- Ni surface, (001), H_2 dissociative adsorption, calc. 80–101036
- Ni+Ni, exchange interactions and exchange integrals 80–37849
- Ni+Ni interaction, ab initio HF and CI calcs. 79–59535
- NiCO, linear, ab initio RHF-MO calcs., rel. to adsorption 79–26883
- NiCO, liquid interactions, ab initio LCAO MO SCF calcs. 79–18256
- $NiCl_4^{2-}$, charge distrib. and ligand field splitting calc. 77–62879
- NiCu molecule, electronic states determ. by ab initio HF and CI methods 80–69087
- NiF_2+CO, Ar matrix isolated, ab initio MO calcs. 78–92458
- NiNaK, mol., intersection of pot. energy surfaces, ab initio calcs. 79–36557
- $Ni(Ni)_2$-ethylene cluster complex 78–82641
- NiO, ab initio SCF and CI calcs. on d-d transitions, NIO_6^{10-} d-electron delocalisation 77–35896
- NiO, H chemisorption, cluster model, bonding 78–38939
- Ni(001) surface states, surface magnetisation, electron spin polarisation 80–88612
- O, ab initio effective valence shell Hamiltonian for neutral and ionic valence states 80–74117
- O I, isoelectronic sequence, X-ray spectra 80–87071
- O^{n+}, $n=1$ to 4, gas and foil-excited, 2-18 MeV, projectile Auger spectra 79–59414
- $O+H_2$, classical trajectory calcs., ab initio surface, singlet state, rate consts. 80–66786
- $O+H_2$, pot. energy surfaces and reaction rates, ab initio calcs. 80–63531
- $O+H_2$, trajectory calcs., fitted ab initio pot. energy surface 79–74358
- O_2, $^3\Pi_g$ diabatic Rydberg states, ab initio CI calcs. 80–95554
- O_2, core photoelectron line shape, localisation role 79–59512
- O_2, effective spin-spin parameter, ab initio calc. 78–9067
- O_2, excited state geometries and energies, ab initio pot. energy surfaces 78–5151
- O_2, ground state, ab initio pot. curve calcs. 77–83510
- O_2, RH-GTO-MCSCF calc., 1s photoelectron spectra, multiplet intensity ratio 78–5134
- O_2, Rydberg states, $^3\Sigma_g$, $^3\Sigma_u^1$, $^3\Pi_g$, $^1\Pi_g$, $^1\Sigma_g^+$ symm., ab initio CI study 80–99460
- O_2, valence states, ab initio config. interaction calcs. 78–25448
- O_2^-, ab initio pot. curves of $X^2\Pi_g$, $A^2\Pi_u$, $a^4\Sigma_u^-$, $^2\Sigma_u^-$ states 78–66483
- O_2^+, $^4\Pi$ states, spin-spin coupling consts., ab initio calc. 79–97981
- O_2^+, ab initio CI STO calc. 78–74585
- O_3, ab initio projected unrestricted Hartree-Fock calcs. 78–58582
- O_3, ab initio UHF and UHF-natural orbital CI studies 80–102452
- O_3, ab initio VB wave functions, π-electrons 78–70748
- O_3, approximate spin extended HF calcs., singlet and triplet states 78–78621
- O_3, conformation, ab initio HFS method calc. 79–36526
- O_3, cyclic, stability, ab initio GVB-POL-CI calcs. 78–915
- O_3 depletion, ClO influence 77–75052
- O_3, line and band strengths in IR spectra, variational calcs. 80–87112
- O_4 molecule, SCF-CI calcs. 80–78517
- OCS, mol. quadrupole moments, mag. shielding and spin-rot. tensors 79–22609
- OCS photolytic laser, for fusion reasearch 78–59002

ab initio calculations continued
- OCl_2^+, radical cation, struct. and electronic props., ab initio RHF SCF MO calc. 80–52883
- OF_2, photoelectron spectra, ionisation energies, ab initio many-body Green's function calc. 79–89709
- OH, spin-extended Hartree-Fock ab initio calculations for small radicals 78–70746
- OH-HF, H-bonded complex, ab initio calcs. *(French)* 80–52866
- $OH+H_2 \rightarrow H_2O+H$, rate constant, ab initio calc. 80–45478
- $OH+H_2 \rightarrow H_2O+H$, reaction product vibr. distribs, quasiclassical trajectory, calcs. 80–85162
- $OH^- +CO_2 \rightarrow HCO_3^-$ react., MO-LCAO-SCF calcs., energy barrier 78–76846
- OH_4^+, stability, ab initio calcs. 77–30775
- OH_n, ab initio LCAO SCF calcs. of ionisation pot., electron, proton, H and hydride affinities 77–88387
- O_3H^+, isomeric structs. ab initio MO calcs. 80–83270
- OH(OD), spin-rot. consts., Van Vleck approx., ab initio calcs. 77–34610
- OHT, β-decay, ab initio SCF MO calcs. 77–71842
- ONCN, IR spectra isotope shifts and ab initio calc. for harmonic force field 79–13715
- ONCl, vibr. freq., anharmonic ab initio/empirical pot. energy functions 80–99457
- ONF, geom. and electronic struct., ab initio calcs. 79–76342
- $O^-(^2P^0)$, attachment energies, ab initio calc. 77–30768
- $O^+(^4S)+N_2(X^1\Sigma_g^+) \rightarrow NO^+(X^1\Sigma^+)+N(^4S)$, MCSCF potential energy surface for collinear $^4\Sigma$ pathway 80–63540
- P, ab initio effective valence shell Hamiltonian for neutral and ionic valence states 80–74117
- PH_2 radial, pot. energy curves. config., ab initio SCF-MO calcs. 77–50419
- P_2H_4, conformation, ab initio, HF, PNO-CI and CEPA calcs. 77–46495
- PH_xF_{3-x}, geometry changes during inversion, ab initio calcs. 78–5154
- PH(PF), effective spin-spin parameter and singlet-triplet transition intensities, ab initio calc. 78–9067
- $PH_2(PH_2^+)(PH_2^-)$, electronic structure, ab initio LCAO MO SCF calcs. 79–10027
- PN, valence state interactions, ab initio and semiempirical estimates 78–74567
- $PN(X^1\Sigma^+)$, VUV photoelectron spectrum 78–1024
- $P_2(X^1\Sigma_g^+)$, He I photoelectron spectrum, ab initio and semiempirical calcs. 77–34691
- Pb, ab initio band struct. calcs. 80–75502
- Pb+Pb quasimolecules ab initio calc. of K X-ray spectra 78–21941
- PbS(PbSe), ab initio SCF calcs. using relativistic effective core pot. 80–95524
- $Pd(CO)_4$, ab initio LCAO MO SCF results invalidate pseudopot. calc. 77–6675
- Pt, ground state configs., ab initio HF calcs. 80–42987
- $Re_2Cl_8^{2-}$, $Re_2Cl_8^{3-}$, ab initio calcs. of metal-metal bond 78–82633
- S, ab initio effective valence shell Hamiltonian for neutral and ionic valence states 80–74117
- S_2, effective spin-spin parameter, ab initio calc. 78–9067
- S_3, conformation, ab initio HFS method calc. 79–36526
- S_3, open and ring isomers, electronic struct., ab initio SCF calcs. 77–57862
- S_4^{2+} and S_4^{2-}, structure investigation by ab initio calcs. 80–69066
- SCN^-, electron density distrib., theoretical and expt. determ. 77–61683
- $(SCN)_2$, prep., UV photoelectron spectrum and structure 80–28059
- SF_2, ab initio LCAO MO SCF calcs., elec. struct., mol. props. 77–14344
- SF_2, generalised VB calcs. of electronic struct. 77–57881
- SF_2, photoelectron spectra, ionisation energies, ab initio many-body Green's function calc. 79–89709
- SF_4, generalised VB calcs. of electronic struct. 77–57881
- SF_6, ab initio electronic struct., and photoelectron spectral assignment 79–54764
- SF_6 and SF_6^+, excited states investig. 77–57882
- SF_6, generalised VB calcs. of electronic struct. 77–57881
- SF_6, KLL Auger spectrum, obs. and ab initio SCF CI calc. 78–50654
- SF_6, KLL spectra of S, ab initio LCAO SCF calcs. 77–65515
- SH, ionis. pot. of $(X^2\Pi_i)$ radical, ab initio ΔSCF calc. with electron correl. 79–98153
- SH_3^+, struct., ab initio HF calcs. 79–31371
- SN, electronic states, ab initio, SCF, and CI calcs. 77–75053
- SN, struct., vibr. spectra, ab initio calcs. 78–66475
- SN^+, struct., vibr. spectra, ab initio calcs. 78–66475
- $(SN)_x$, 1-D chain, ab initio treatment, HF LCAO calc. 77–1349
- $(SN)_x$, different orbitals for different spins 79–69392
- $(SN)_x$, electronic props., ab initio LCAO HF orbital calc. 77–51635
- $(SN)_x$, quantum chem. calcs. of electronic struct. 78–6257
- S_2N_2, $(SN)_x$, $(x=2$ or 3), minimal STO-3G basis HF ab initio LCAO SCF MOC, geometry 78–903
- S_2N_2, electronic states, ab initio, SCF, and CI calcs. 77–75053
- S_2N_2, semiempirical electronic struct. calcs., applicability testing, and for $(SN)_x$ 77–6681
- S_2N_2, struct., vibr. spectra, ab initio calcs. 78–66475
- SO_2, analytical pot. functions, several surface minima 78–5158
- SO_2, effective spin-spin parameter and singlet-triplet transition intensities, ab initio calc. 78–9067
- SO_2, ground state, ab initio and MOD POT calcs. 78–66466
- SO_2, KLL Auger spectra of S, ab initio LCAO SCF calcs. 77–65515
- SO_2, KLL Auger spectrum, obs. and ab initio SCF CI calc. 78–50654
- SO_2, SF_2, SO_2F_2, bond function parameter transferability 77–30770
- SOH, ground and first excited states, geometry, ab initio SCF calcs. 78–50657
- SOH radical, ab initio SCF and CI calcs., electronic states and transitions 77–46488
- ^{35}S compounds, beta decay, transition probabilities, ab initio calcs. 77–61387
- SbH_3, inversion barrier, ab initio SCF calcs. 78–78615
- Si (111), chemisorption of H, localised model, ab initio HF-LCAO calc. 80–6930
- Si (111), surface relax., mol. SCF calcs. 78–91522
- Si (111) surface reconstruction, milk-stool model, quantum chem. ab initio calc. 80–49477
- Si, ab initio effective pots. 77–69222
- Si, ab initio effective valence shell Hamiltonian for neutral and ionic valence states 80–74117
- Si, ab initio self consistent calcs., charge density and band struct., Wannier function scheme 79–69409

ab initio calculations continued

- Si III, $^3F^0$ Rydberg series, energy levels, multiconfigurational HF procedure 80—47882
- Si, neutral vacancy, generalised val. bond calc. 77—55493
- Si_2, multiplet struct. and charge distrib. 79—26881
- SiF_3, low-lying electronic states, ab initio HF calcs. 77—54512
- SiH_3 radical, hyperfine coupling consts., vibr. depend., ab initio calcs. 80—87150
- SiH_4, ab initio Hartree-Fock SCF-LCAO-MO method 78—94195
- SiH_4, SiH_3F, SiH_2F_2, CH_3SiH_3, core Auger shifts, ab initio LCAO MO SCF calcs. 78—904
- SiH_4^+, struct, stability, ab initio calcs. 79—13632
- Si_2H_4 ground state struct., ab initio SCF calcs., singlet silylsilylene 80—27945
- Si_2H_4, Si-Si double bond, ab initio GO calc. 78—94187
- Si_2H_6, barrier to internal rotation 78—66680
- Si_2H_6, bond lengths, photoelectron spectrum, mol. orbitals calcs. 78—5132
- SiH_2F_2, ab initio Hartree-Fock SCF-LCAO-MO method 78—94195
- SiH_3F, ab initio Hartree-Fock SCF-LCAO-MO method 78—94195
- SiH_3NCO, geometric struct., ab initio MO calc. 79—13834
- Si_2H_6O, geom. and electronic struct., ab initio MO calc. 79—97972
- SiH_3X (X=H, F, NH_2, OH), coord. bond calcs. 80—58129
- SiO $^3\Pi$ valence states, struct. and perturbations 79—59369
- SiO^+, vac. UV photoelectron spectra, ab initio mol. orbital and $X\alpha$ calcs., $(X^1\Sigma^+)$ state 78—46395
- SiO_2, mol., ab initio SCF calcs., ground state stability, struct., vibr. freqs. 78—86781
- $(Si_2O_7)^{6-}$ bitetrahedra, in silicates, total energy surface, ab initio calc. 78—23056
- SnH_2, struct. determ., restricted HF calcs. 80—87030
- $SnMo_6S_8$, Chevrel phase, RE mag. isolation and supercond. 80—44470
- $SnMo_6Se_8$, Chevrel phase, RE mag. isolation and supercond. 80—44470
- Sr, quantum defect param., ab initio calcs. 80—78525
- TCNQ, ab initio SCF LCAO band struct. calc. 80—70608
- TOT, vibr. intensities, ab initio and empirical calcs. 80—78592
- TOT, vibr. intensities, ab initio and empirical calcs., band strengths 80—78593
- TTF, ab initio SCF LCAO band struct. calc. 80—70608
- TaC, phonon anomaly rel. to Fermi surface 77—11853
- $ThO_2:Np^{4+}$, cryst. field splittings, ab initio MO calcs. 77—20520
- Ti complex, bis cyclopentadienyl $Ti:N_2$, liquid interactions, ab initio LCAO MO SCF calcs. 79—18256
- Ti, neutral and ion val. states, electron correlation, ab initio effective val. Hamiltonian calc. 80—99449
- TiF_2, TiF_4, X-ray emission, core level chem. shift calcs. 80—53010
- TiH_4, X-ray emission, core level chem. shift calcs. 80—53010
- TiH_3F, X-ray emission, core level chem. shift calcs. 80—53010
- $TiS_2(Se_2)$, core states, energy bands, and valence densities of states 79—95322
- $TiSe_2$ (IT), structurally induced semimetal-to-semicond. transition, ab initio LCAO calc. 78—51896
- TlCl, ground-state props., Wannier functions, and electronic struct., ab initio self-consistent calc. 80—80178
- TlCl, self-consistent electronic struct. and ground state props. 80—15451
- TlH, ab initio SCF calcs. using relativistic effective core pot. 80—95524
- U, ab initio effective core pots., relativistic corrections 78—50483
- U^{n+} (n=0 to 6), electronic struct., multiconfig. Dirac-Fock calcs. 79—45646
- UF_5, electronic struct. and geometry, ab initio calcs. using relativistic ECP 80—32606
- UF_6, UF_6^+, and UF_6^-, electronic struct., ab initio calcs. using relativistic core pots. 79—97987
- V, band struct., X-ray emission bands, self consistent calc. 77—28104
- VO, $^4\Pi$ states, spin-spin coupling consts., ab initio calc. 79—97981
- W (001), surface phase transition, electronic contribs., surface susceptibility, ab initio self-consistent thin-film energy band calc. 80—29255
- W, single cryst., coated with ferromagnetic layer, Fermi vel. using band calcs. 79—11307
- WO_6^{6-}, in lattice electronic struct., luminesc. ab initio calcs. 78—6337
- X_3YOH molecules, ab initio MO calcs., geometry, electronic struct. 78—41940
- Xe, ab initio effective core pot., Dirac-Hartree-Fock and Hartree-Fock calcs. 78—33426
- Xe, solid, n=1 surface excitons and LO-TO splittings of bulk excitons 79—73445
- Xe subshell photoionisation, multichannel k-matrix calc., spin orbit interactions 80—63600
- Xe^++Ag, quasimolecular L and Ag L X-ray excitation thresholds, electron correl., calc. and expt. 78—78793
- Xe_2, dispersion damping functions and interaction energy calcs. 80—78673
- Xe_2^+, electronic struct., pot. energy curves, spectroscopic consts. 79—18114
- XeF, laser emission, ab initio config. interaction calcs. on electronic states 78—63083
- XeF_5^+, pseudopot. SCF MO studies, steric aspects of struct. and force fields, Jahn-Teller effect 80—99444
- XeF_6, pseudopot. SCF MO studies, steric aspects of struct. and force fields, Jahn-Teller effect 80—99444
- XeF(Cl)(Br)(I), covalent and ionic states, spectroscopic props., ab initio CI calc. 78—90092
- XeO, lasing, low-lying electronic states, ab initio config. interaction calcs. 78—63084
- Xe_2*, Xe_2^+, Xe_2, pot. energy curves, relativistic ab initio effective core pots. 78—86800
- YRh_4B_4, supercond., electronic struct. and reentrant magnetism 78—10340
- Zn, field gradients, temp. depend., electronic and lattice contribs., ab initio study 79—42501
- Zn, nuclear quadrupole antishielding effects, ab initio theory 78—34814
- Zn, nuclear quadrupole interaction theory of ground state of ^{67}Zn nucleus 79—73481
- Zn_2, ab initio SCF LCAO MO calcs., contracted basis set effects 77—83495
- Zn_2, electronic states, CI calcs., rel. to Hg_2 77—10601
- $ZnCl_2$, pseudopot. calcs. of mol. electronic props. 77—30779
- $(Zn(OH)(NH_3)_2)^+$, model for biological active sites, ab initio calcs., comparison with Be complex 80—104551
- $ZrS_2(Se_2)$, core states, energy bands, and valence densities of states 79—95322

abacs *see nomograms*

aberrations

aberrations in optics and particle optics only

see also lenses; optical instrument testing; particle optics

- aberrated pupils, apodisation, anal. 79—98298
- achromatic imaging, of distant objects, with plane, concave holographic gratings 78—94372
- achromatized wedge scanner design 77—88948
- acousto-optic frequency shifter, beam quality, heterodyne interferometry meas. 78—79127
- adaptive optics, atmospheric compensation, book contrib. 79—31972
- adaptive optics, book 79—31921
- adaptive optics, coeffs. adaptive estimation 77—88659
- adaptive optics coefficient estimation 77—19179
- adaptive optics in astronomy, rubber mirrors to compensate for atm. aberrations, book contrib. 79—35150
- adaptive optics in high energy laser systems, book contrib. 79—31971
- adaptive optics technology overview, book contrib. 79—32030
- ametropia determination with laser refractor 78—35907
- anastigmatic electron deflection system between beam-shaping lens and probe target 79—27155
- annular aperture, light distrib. from diffr., aberration correction using mirror lenses *(German)* 80—69325
- annular aperture lenses for scanning optical microscopy, spherical aberration 77—65054
- annular pupil system, use of orthogonal polynomials, appl. to Fraunhofer diffr. 78—50714
- aplanatic waxicon insensitive to tilt errors, for high power laser beam transport 80—74460
- apochromat planar lens 133 mm f/6.3, astigmatism and longit. chromatic aberration meas. *(German)* 79—75636
- apochromatic pancratic objective component chromatic aberration formulae 79—76795
- apochromats from four types of glass, components for broad spectral region 79—32026
- apodisation for minimising intensity diffr. pattern second moment in systems with aberrations 79—81358
- apodising filters, numerical exam., second moment of the point spread function 80—106611
- apodized optical systems with third-order spherical aberrations, MTF 80—9823
- aspheric surface primary characts., analysis using Delano diagram *(German)* 78—90381
- aspherical deformations, rotationally symmetrical, representative model *(German)* 78—90375
- aspherical surface testing, interferometer optical system modification 79—7236
- aspherical wavefront testing by shearing interferometer 77—31144
- astigmatic coherent processor analysis 78—78927
- astigmatic Gaussian beams in travelling-wave resonators 77—723
- astigmatism, pupil shape effects 79—98307
- astigmatism due to surface cylindricity, vectorial representation *(Russian)* 78—87121
- astigmatism effects in electron microscope meas. of domain wall widths 79—19753
- astigmatism of central and peripheral cornea, asymm. meas. by photokeratoscopy 78—64981
- astronomical telescopes, high resolution field correctors for better observing sites 80—4257
- astronomical three mirror anastigmatic telescope design 77—87265
- asymmetric electrostatic lens for field-emission microprobe applications 79—75656
- automatic correction of optical systems by accurate ray tracing *(Spanish)* 80—53401
- axial hologram lens with remote entrance pupil, cancellation of aberration 80—32933
- axial holographic lenses, monochromatic aberrations 79—98321
- axicon and related optical component diagnostic techniques 80—14417
- axisymmetric electrostatic post-deflection lenses third-order distortion 80—32898
- bicylinder mirror aberrations, effects on multipassage mag. mass spectrometer props. *(French)* 79—75651
- bifocal lens designs, marginal aberrations 78—48927
- binoculars, high magnification, optical characts. and aberration graphs 77—7170
- bipotential lens, with axial pot. function $\Phi(\mu)=V\exp(K_0\arccos\mu)$ 77—23606
- birefringence elements in optical systems, generalisation of pupil function 78—55310
- Bragg diffraction imaging, aspect ratio restoration by holographic lenses 79—46122
- Bragg-diffraction imaging 79—64463
- Cassegrain telescope, corrector lens system using wide field doublet *(Japanese)* 77—91427
- Cassegrain telescope, wide-field, design and performance 77—2338
- catadioptric lenses, two-component, small zonal spherical aberration *(German)* 79—50366
- catadioptric objective, development *(German)* 80—102796
- cathode lens having a quasispherical field 80—95782
- cathode lens model, third-order chromatic aberrations 79—81352
- cathode lenses, with combined elec. and mag. fields, third order aberration theory 79—41317
- caustic point displacement due to generalised bending, third-order approx. 80—83656
- caustic surface calcs. in geom. optics, analytical illum. monitoring 77—3643
- charged particle beam focusing, using aberrational quadrupole lens system 79—26180
- charged-particle beam, current density distrib. calcs. 77—27238
- chromatic, CF chromatic aberration-free projection system, optical microscopes appl. 78—89534
- chromatic aberration, effect of yellow ocular filter, fish eye 80—8046
- chromatic aberration first-order theory, secondary spectrum correction with common glasses 78—90382
- chromatic aberrations of real rays, role of each lens in optical system 80—102655
- chromatic and spherical aberrations of single glass lenses, holographic correction 79—86226
- chromatic-aberration-free microscope optics 80—86395

aberrations continued
- chromatically corrected objective lens, of electron microscope, test *(German)* 79—892
- chromatism transverse, effect on transfer characts. of optical systems 79—908
- coherent fast IR wavefront aberration sensor interference problems 80—74499
- coherent information processing by a pair of lenses in spherical wave illumination 80—95816
- coherent optical adaptive Modal Wavefront Control System 77—19295
- collimator, single element gradient index design 78—9426
- colour distribution in polychromatic line spread function, aberration influence 77—7014
- colour image evaluation from tristimulus values transfer functions measurements 80—87333
- colour image form., optical transfer functions for tristimulus values 78—33685
- coma, optimally balanced, influence on refractive images of annular object *(Czech)* 78—50710
- coma corrector for parabolic reflector telescope off-axis guiding 80—82196
- coma-free two-mirror systems, astronomical appls. *(Russian)* 77—64641
- combined focusing and deflection systems, electron trajectory aberration formulae 78—45756
- compensation for inclined beam aberrations in lens-hologram system *(Russian)* 77—19381
- computation accuracy of aberational diffr. images 80—87328
- computer algebra, unconventional electron lens calcs. 77—67542
- concave diffr. grating, astigmatism compensation, comparative characts. 79—32067
- concave grating efficiency meas. at grazing incidence 78—33825
- concave grating mirror stable resonator, astigmatism in field distrib. of reson. modes *(Chinese)* 79—50324
- concave spherical gratings with compensated astigmatism in Rowland mountings 78—30081
- concave stigmatic grating mech. prod. on spherical surface 80—38109
- condenser objective, single field, advantages and limitation for min.-exposure 80—87292
- condenser synthesis, astigmatism-free, using spherical mirrors 78—50887
- confocal scanning microscope, image form. 80—68249
- confocal unstable resonator beam props., astigmatism due to Brewster angle windows 78—46670
- conical porthole, deep-water, deformation effect on optical characteristics 79—76859
- conical SELFOC fibres, third order aberration coeffs., gradient-index lens design 77—27357
- contact lenses, soft, apparatus for longit. spherical aberration meas. 79—79684
- contemporary optics, book 79—81353
- continuous system without symm., Lagrangian aberration theory 77—34815
- correction, expt. criteria for use of deconvolution methods 78—18492
- correction using inverse convolution 80—23629
- cosmic X-ray spectroscopy, transmission grating behind grazing incidence telescope 77—64654
- crossed lenses, electron optical characts., trajectory anal., aberrations from axial pot. profile 80—63909
- crossed lenses, theoretical and expt. study of electron-optical lenses 80—95780
- curved crystal spectrometer, geometrical aberrations analytical and numerical study 78—78002
- curved Fresnel surface, primary aberration contribs. 79—13913
- curved graded index medium, aberration analysis 80—14295
- curved graded-index fibres as image relays, aberrations 79—55219
- curved zone plates and Fresnel lenses, third-order aberrations 77—72043
- cylindrical electrostatic mirror analyser, image line aberrational expansion, nonplanar trajectories 79—41327
- data processing using volume holograms in far field zone 78—17867
- decentered concave mirror in three-mirror concentric objective, for astigmatism correction 78—46749
- Defelction distortion in scanning electron-beam systems 78—74835
- deflection effect of light reflected from moving mirror in ether theory 80—91749
- deflection systems combined with mag. lenses, optical props. 80—31938
- depth imaging of pupil *(German)* 77—58270
- design techniques, for desk and pocket calculators 78—71181
- differential ball screw actuator driven deformable mirror design and performance 80—33137
- diffracted wave field aberrations 78--94376
- diffraction and aberration effects, wave optical calc. 80—83549
- diffraction grating, a spherical, elimination of aberrations 80—33181
- diffraction grating, geometric optical theory 80—32904
- diffraction grating geometrical aberration theory 79—55068
- diffraction images of bar and edge objects, influence of optimum balanced coma 78—74850
- diffraction pattern obs. with computer-generated holograms 80—102681
- diffraction patterns for optical systems with pupils of non-uniform transmittance 80—87470
- diffraction patterns of off-axis gaussian beams in optical system with astigmatism and coma 78—55309
- diffraction theory of image form., aberration function 80—9822
- diffuse system design, optimum conditions, appl. to optical system 78—50886
- diffuser, weak, speckle pattern, spherical aberration effect 80—87476
- discharges, selfluminous, schlieren system for time and space resolved photography 80—87471
- distortion elimination by eigenfunction method 79—7087
- double focusing mass spectrometer, second order, aberrations, stigmatism 78—21256
- double Gauss basic lenses, design *(German)* 80—53398
- doublet, single-radius, paraxial properties and errors correction *(Czech)* 79—76791
- dye laser resonator, CW, astigmatism compensation using lenses 78—29978
- Ebert parabolised monochromator, coma compensation 79—81526
- einzel lens, depend. of aberration consts. on magnification 77—75404
- elastooptical constants and refractive index, thermo-optical method for meas. 80—7327
- electric-magnetic focusing deflection system, relativistic aberrations formulae 78—13653

aberrations continued
- electron beam, axis with curvature and torsion, inner and outer problems soln. 77—592
- electron beam deflection error assessment, expt. technique 80—78757
- electron beam deflective aberration free system using moving objective lens 77—61908
- electron beam scanning systems, aberration elimination 80—78756
- electron beams, aberration averaging, image and deflection component design 78—74830
- electron beams, shaped practical focus-deflection system 79—76572
- electron lens, magnetic, min. spherical aberration 80—87287
- electron lens, rotationally symmetric, with curved charged transparent foils, third order spherical and axial chromatic aberrations *(German)* 77—10827
- electron lens, spherically corrected, apochromatic *(German)* 77—22620
- electron lens, system for correction of spherical aberration 80—5676
- electron lens, unipotential, focal and aberration props. calc. 77—68162
- electron lens aberration coeffs., computer calc. using CAMAL 77—38798
- electron lens doublet, crossed, six electrode, stigmatic operation 79—13888
- electron lens spherical aberration correction by holography 79—85203
- electron lenses, wave aberration from superposition diffractograms 77—71411
- electron lenses between TEM specimen and an electron spectrometer for energy-loss spectral resolution optimisation 80—101886
- electron lenses consisting of two double cylinders, design, spherical aberration calcs. 80—23613
- electron lenses with electron-transparent foils, geometric and chromatic aberrations 77—10828
- electron micrograph computer image processing, error sensitivity as resolution limit 79—71570
- electron microscope, 3-dimens. imaging, curved axis electron optics *(German)* 79—13889
- electron microscope, chromatic aberration effects on lattice images of defects 80—107210
- electron microscope, chromatic field aberration compensation *(German)* 77—10149
- electron microscope, high resolution, EM 400, chromatic aberration effects compensation and thick specimen imaging 77—41738
- electron microscope, HV, objective lens aberrations *(Japanese)* 80—52364
- electron microscope, mag. energy filter, for error-free image, second order approx. *(German)* 77—191
- electron microscope energy filter, correction of second order aberrations *(German)* 77—22624
- electron microscope image interpretation, instrumental, environmental conditions *(Polish)* 79—30623
- electron microscope image reconstruction problems 79—75661
- electron microscope objective lens focus and spherical aberration meas. 77—54024
- electron microscope spiral distortion correction double-lens system 80—68327
- electron microscope spiral scanning attachment for corrections of spherical aberration effects 79—2889
- electron microscope transfer functions determ. from wave aberration function 77—87883
- electron microscopes, electron source size in field-emission gun 79—71575
- electron microscopes, imaging characts., third order aberration theory exam. *(German)* 78—32926
- electron microscopy, aberration correction 80—86531
- electron microscopy, dark field image of weak phase objects *(German)* 77—10150
- electron microscopy, field emission transmission, sub-angstrom resolution 80—82851
- electron microscopy, focused image production through visible-optics correction of defocusing and spherical aberration 79—6231
- electron microscopy, HV, accurate stigmating using optical diffr. pattern of micrograph 78—49941
- electron microscopy, image correction methods, exptl. anal. 79—12889
- electron optical systems, reduction by optimisation techniques 80—87290
- electron optics, algorithm computation using Chebyshev polynomials 79—27156
- electron optics, paraxial eqn. asymptotic solns., singular perturbation theory, chromatic aberrations of cathode electron optics 79—41320
- electron optics, spherical aberration, for teaching 78—54135
- electron optics, wave aberration, sign conventions 77—589
- electron optics achromator using three elec.-mag. quadrupoles *(German)* 77—61166
- electron optics optimisation using dynamic programming 77—61907
- electron optics system, multielement with third-order aberration 79—41321
- electron probe, compensation, dynamical focusing with stigmator 80—87291
- electron probe forming systems, optimisation with respect to aberrations and vertical beam landing 80—68291
- electron spectrometer, electrostatic prism type 79—40647
- electron-optics, two-lens projection systems, reduction of third-order distortion 80—48134
- electrostatic 77—50601
- electrostatic analyser, electrode geometry tolerance calcs. 77—23611
- electrostatic double cylinder lenses, spherical aberration coeffs. and focal props. 79—86124
- electrostatic energy filter, telescopic, with cylindrical mirror analysers 80—87296
- electrostatic immersion lens with minimum spherical aberration, dynamic programming search 78—25789
- electrostatic lenses, unipotential aberration in accelerating mode *(French)* 78—46504
- electrostatic lenses for control of ion or electron beams 80—32897
- electrostatic mirror, axisymmetric, two-electrode paraxial props., aberrations 78—71025
- electrostatic mirror, two-electrode, transaxial, aberrations, gap depend. 77—27242
- electrostatic mirror, two-electrode, transaxial, cardinal elements, aberrations 77—27241
- electrostatic one-foil lenses, round, electron optical properties, charges induced on foil 80—53203
- electrostatic prism, dihedral, for spectrometer aberration coeff. 79—26178

aberrations continued
electrostatic round lenses, asymptotic aberration coeffs., systematic transformations 78—74828
electrostatic telescope system, 3 electrode with mirror, spherical aberration elimination 77—50606
electrostatic transaxial lens, curved charged particle beam focusing, image coords. and aberrations 78—46503
elliptical square-law medium, astigmatic Gaussian beams 78—94427
energy analyzer, two-stage with cylindrical mirrors, aberration reduction 79—40640
equivalent concentric systems *(Russian)* 77—64659
extended circular target, diffr. images in presence of coma 77—58250
extrameridional aberrations of spherical surface at large angles of incidence 77—50623
eye, astigmatism induced by pterygium 78—40139
eye, chromatic stereopsis, opposition of photometric and dioptric factors *(Italian)* 78—56986
eye, chromoretinoscopy and its instrumentation 80—94201
eye, fish, chromatic aberration and effect on refr. state 78—64985
eye, high-order aberrations, subjective meas. 77—1994
eye, human, pupil diameter and depth-of-field as meas. by laser speckle 78—15826
eye, hypermetropia rel. to chromatic aberration in small animals 78—40140
eye, in strabismic amblyopia, optical aberrations rel. to visual loss 78—48788
eye, longit. chromatic aberration meas. by chromoretinoscopy 78—56967
eye, subjective meas. of monochromatic aberrations 78—35837
eye chromatic aberration, effects on accommodation response 78—69042
Fabry-Perot etalon, optical thickness error compensation 78—49889
factor analysis methods for designing complicated optical systems 80—28303
far-field diffraction, partial coherence, primary astigmatism 79—22899
field emission gun, electron optical characteristics *(German)* 79—893
field emission gun SEM column electron-optical performance obs. and model 80—68328
first surface simplified aspherising procedure *(Russian)* 78—63013
flat-field spectrograph design, holographic grating appl. 80—68264
foil lens characts. for spherical aberration correction of strongly excited magnetic lens 79—71567
Foucault, phase edge and wire optical test 80—96046
four-colour thin apochromat design 79—27364
four-component system design for optical data processing 78—42282
four-element lens systems of Cooke-triplet family design considerations 80—57404
Fourier optics described by operator algebra 80—48163
Fresnel diffraction effects on high-resolution images, spherical aberration effect 79—27153
Fresnel lens, colour-corrected linear convex, for solar concentration 80—45640
Fresnel zone plates, image form. with short wavelength radiation 77—58437
fundamental chromatism coefficients 78—1317
Gaussian beam, free-space propagation, wave eqn. solns. 78—87008
Gaussian beam astigmatism, meas. by Ronchi grating interferometer 79—3635
Gaussian beams, off-axis, aberrated Fraunhofer diffr. patterns 78—66753
generalised ray tracing, caustic surfaces, bending and merit function for optical design 80—102612
geodesic lens, axially symmetric, geometrical theory 80—33238
geodesic lenses, aberration-corrected rounded edge, profile calcs. 80—10048
geodesic lenses, spherical aberration correction and fabrication tolerances 79—27435
glass active elements of pulse-periodic lasers, thermal lenses 79—89914
glass sampling, of simplex variants and of multiplets *(German)* 78—90484
Golay-type static multi-slit spectrometer 78—295
graded index fibre profile determ., interferometric method 80—14481
graded index media, fifth order aberrations 77—27258
graded-index medium, non-parabolic, meas. of aberrations by Ronchi interferometer 79—36843
graded-index optical waveguide characteristics meas. 79—14108
gradient index optical imaging systems, topical meeting, Rochester, USA (May 1979) 80—12851
gradient index optical lenses, use, design, fabrication and refr. meas. 78—13780
gradient index SELFOC lens, aberration improvement 80—14425
gradient index spherical lens design for selfcoupled optical pickup system 80—14427
grating detectability, aberration effect evaluation in visual instruments 79—55073
grating mounting with large aberrations, aberration balancing 78—66906
gratings, concave, mounted in Seya-Namioka monochromator, polarisation characts. 79—18526
grazing incidence optics, total transverse aberration function 78—45765
grazing incidence spectrometer, astigmatism correction method 77—82659
grazing incidence system, primary aberrations 77—88644
grille spectrometer efficiency, effect of aberrations 78—70195
Hadamard spectrometer, curved slits used to increase throughput 80—95149
half-symmetric image geometry 78—66773
hexapole spherical aberration corrector 79—76571
higher order chromatic aberrations, pupil coordinates *(Chinese)* 80—69335
hologram lens, axial, on spherical substrate with remote pupil, aberrations 80—95849
hologram lens, compensating method for spherical aberrations 77—23634
hologram lens system, astigmatism and coma reduction 80—53238
hologram lenses, spherical aberration compensation for short- wave shift in reconstructing radn. 77—19206
hologram optical elements anamorphotic props. with astigmatism 79—98319
hologram scanner, interferometric zone plate, for point-of-sale systems, aberration corrections 79—81383
holograms, Fresnel copies, aberration props. 80—99676
holographic aberration compensation of optical system, computer modelling 77—50640
holographic binary information image reconstruction, aberrations, shrinkage effects 78—78967

aberrations continued
holographic concave grating design 80—1153
holographic diffraction grating on toroidal substrate, astigmatism 80—58482
holographic diffraction gratings, astigmatism compensation 80—48428
holographic display of diffraction patterns, third and fifth order aberrations 80—9829
holographic elements, axisymmetrical, third order aberrations 80—69341
holographic elements as lenses, third-order aberrations, design parameters 78—9425
holographic flat field lens with no first order astigmatism 77—10995
holographic grating, imaging props. 78—5563
holographic grating scanner with aberration corrections 77—61924
holographic gratings formed on aspheric substrates for aberration correction 78—63187
holographic image deformation, optical modification at reconstruction 80—83567
holographic image magnification, new methodology 80—95851
holographic image motions due to reconstruction light source movements, deform. analysis applic. 77—10866
holographic imaging, geometrical analysis 80—43291
holographic interference pattern parameters adjustment, aberrations effect 78—17875
holographic interferometer instrument errors for narrow reference beam 77—640
holographic interferometry method, Francon's, meas. of MTF, wavefront aberration 79—3647
holographic lens element, astigmatism free 77—46784
holographic lens system, method for wave aberrations calc. 80—28175
holographic memory, lens aberrations effect on storage capacity 77—19202
holographic memory, parameter optimisation allowing for aberration 79—55085
holographic microscopy, aberrations, due to wavelength shift, elimination technique 78—74861
holographic optical element design and construction 78—55315
holographic optical elements, third-order aberration theory and generalised aplanatic condition 80—74314
holographic optical elements for incoherent polychromatic imaging 80—69349
holographic particle sizing high-resolution system 79—81392
holographic plane grating, stigmatic mounting 78—25817
holographic plane gratings, self-focusing, aberrations 77—58450
holographic reflective lenses for compact optical data processor 77—34829
holographic scan aberration correction 77—83828
holographic scanner, for CO_2 laser materials processing, aberration analysis 79—18367
holographic screens production with third order spheric aberration compensation *(Russian)* 78—90404
holographic visor helmet-mounted display, optical design 79—86149
holography, aberration coefficient estimation 80—63949
holography advantages for physical structure meas. and recording 80—95843
Hunt aberration generator 78—59119
hyperchromatic lens, expressions for first order chromatic aberrations 80—91879
illumination, relative, easy calc. 80—63920
illumination distribution calc. in image plane 77—31125
image contrast loss in presence of chromatic magnification difference, numerical estimate 80—95823
image formalism, diffraction at straight edge, partially coherent illum., aberrations *(Chinese)* 80—43267
image formation with coherent and partially coherent light 77—88658
image optimisation by apodisation filters in optical systems with residual aberrations 80—53223
image quality criterion, second moment of diffraction point spread function 80—9818
image reconstruction, computerized, fragment size choice 80—78785
image-forming reflection system testing by grazing-incidence Linnik interferometry 79—76891
imaging in the presence of random wave aberrations 79—76607
imaging system, incoherent, diffr. images asymptotic behavior 80—1139
incoherent annulus object diffraction images in presence of primary astigmatism 79—22904
infinitely-thin-component optical system design principle 79—76794
integrated acousto-optical spectral analyser waveguide geodesic lens correction 79—50241
interferogram aberration evaluation program 80—13130
interferogram fringe pattern reduction, automated system 80—47097
interferometric testing method with computer-generated holograms, aberration balancing 78—46845
interferometry, multiwavelength testing using modified Twyman-Green interferometer 78—59169
ion microscope aberrations and image form., study by magnetic anal. of beam from HF source 78—55293
ion optical props., aberration, crossed toroidal elec., mag. fields as mass spectrometer *(Chinese)* 80—82843
IR coating nonuniformity effect on precision optical systems, compensation by auxiliary laser 80—78926
IR scanning radiometer data interpretation 79—30541
IR wavefront aberration sensor for high-energy laser system, interference problems 79—98422
isoplanatism in optical systems, image form. 80—1144
Lagrangian coefficients calc. of systems without symmetries, recond. and third order local coeffs. 77—10845
large-aperture interferometer with low-resolution holographic corrector plate 80—74315
laser, astigmatism and coma appl. to thermal blooming reduction, expt. demonstration 79—98449
laser, double-current-confinement channelled-substrate struct., near-field and beam-waist position 80—106553
laser adaptive optical control with closed-loop estimation and predictive filtering 77—19298
laser beam, highly aberrated, propag. in nonquadratic plasma waveguide 77—84441
laser beam, intensity mapping aberrations 78—66855
laser beam, phase compensated, propag. through atm. turbulence 78—83012
laser beam expander design corrected for Petzval curvature 80—74461
laser beam printer scanning system with f-θ lens 80—78942

aberrations continued

- laser beam steerer-expander device, two-mirror afocal telescope design 78—46700
- laser beam thermal lensing in SiO_2 plate 78—63148
- laser heated IR windows, interferometric meas. 77—46748
- laser resonator, compensation of coma and astigmatism 77—34898
- laser self-focusing suppression through low-pass spatial filtering and relay imaging 78—74938
- laser speckle in presence of spherical aberrations in imaging geometry 79 81373
- laser system, high energy, optical distortion, active control 78—83019
- laser system, high energy, optical distortion sources 78—83018
- laser system, high energy, thermally induced optical distortion 80—38051
- lattice image formation, many-beam theory, TEM 80—38879
- lens, cemented doublet, 3rd order aberrations calc. 77—88889
- lens, double Gaussian objective, design *(German)* 80—64134
- lens, gradient-index rod, aberrations in multimode optical fibre devices 80—69487
- lens, gradient-index rod, appl. in optical fibre communication systems 80—69488
- lens, gradient-index rod, evaluation by imaging 80—69485
- lens, gradient-index spherical, design for optical pickup systems 80—69483
- lens, multi-element, defective surfaces, tilt meas. 78—66886
- lens, photographic gradient singlet, design techniques based on total aberrations 80—69479
- lens, radial gradient-index, with zero Petzval aberration, third-order aberrations 80—69484
- lens, residual wave aberration due to schlieren, diminished image quality *(German)* 77—14788
- lens, three-component objective, lateral aberration graphs, design 77—54771
- lens, three-electrode , crossed, electron focusing, spherical aberration 78—33659
- lens, three-element, optimisation by damped minimum method *(German)* 77—23726
- lens aberration weighted coeffs., belastung (strain) indicator of optical system correctability 77—46783
- lens aberrations, influence on signal in space filtering scheme *(Russian)* 78—37815
- lens aberrations determination by speckle interferometry *(French)* 79—72653
- lens aspherical effect on image defects *(German)* 78—9332
- lens design, analytic merit function based on Buchdahl's aberration coeffs. 77—755
- lens design, least squares fitting of Zernike's polynomials to wave aberration function 80—83660
- lens design parameters, 35 mm format enlarging lenses, survey 80—13168
- lens design program 79—86233
- lens design with simultaneous image spot, optical path difference, diffraction MTF and Seidel abberation minimisation 80—74459
- lens model of high-energy atm. laser propag. 78—69454
- lens objectives, visible and UV, for microscopes and microspectrophotometers 79—75591
- lens optimisation using Walsh functions, FEE-based criterion 78—79097
- lens system, distortion by means of numerical transformation *(German)* 80—64132
- lens system design with extended depth of focus, Version 14 optimisation program 78—90489
- lens wavefront aberration, interferometric examination techniques 80—69498
- lens waveguides, influence on beam capacity 77—54785
- lens-hologram optical system, monochromatic aberrations 79—3760
- lenses, crossed, electron optical image position, ang. magnification aberration 78—50691
- lenses calc., thin, modified relations using Caddington variables *(Czech)* 78—50885
- lensless matched filter, operating principle, third order holographic aberration 77—7013
- Lick, Kitt Peak and Hale reflectors, scales and distortion coeffs. for prime-focus correctors 77—22071
- linear coma, optimum balanced, influence on disc spread functions 78—37814
- longitudinal, calc. by stereo-self-collimation method *(Russian)* 80—91878
- low-aberration focusing fibre, optimum diffusion exchange and heat treatment 78—1378
- Luneberg apodization problem 80—87302
- magnetic analyser, sector type, with fringing field, geometric image aberration *(Japanese)* 78—8465
- magnetic condenser-objective lens, for high resolution microscope, optical characts. 78—25788
- magnetic deflection systs., aberration correction 78—66740
- magnetic einzel lens, satisfying anastigmatic and achromatic conditions 80—87288
- magnetic energy filter, without second-order aberrations 80—86524
- magnetic field distribs. with min. spherical aberration, dynamic programming 78—9313
- magnetic filter 1 MV, second order image abberations 77—61165
- magnetic imaging filter, electron optical experiments 80—87295
- magnetic lens, by foil lens, appl. to STEM 80—87294
- magnetic lens aberration formulae 80—95781
- magnetic lens and deflection system, electron optic props. and aberrations *(Chinese)* 77—58244
- magnetic lens spherical aberration correction with foil lens 77—67537
- magnetic lens third-order field geometrical aberration of single slot lenses forming electron probe 79—3619
- magnetic lenses, single-pole, for field emission electron gun systems 79—31784
- magnetic prism, design, for TEM energy filter 80—86523
- magnetic spectrometer, corrected second-order aberrations 80—87013
- magnetic spectrometer design with corrected second-order aberrations, theory 78—89604
- magnetic spectrometers, approx. and ideal design, appl. to STEM 78—8475
- Marechal evaluation of Strehl definition, Dini expansion of wave aberration function 78—71043
- mask linewidth meas. effects of optical microscope operating parameters 77—37977

aberrations continued

- mass spectrometer uncoupled, sector charged particle analyser, image props. 78—70218
- matrix treatment of primary aberrations, for optical system design 77—50622
- maximum Strehl intensity ratio intensity ratio image plane determ., remarks *(German)* 78—71038
- mechanically ruled and holographic concave diffr. grating parameter relationships 80—87543
- meniscus Fresnel lenses, primary aberrations 77—27328
- meniscus-concave mirror systems, misaligning effects *(Russian)* 77—53426
- merit function, diffr. based, for automatic lens design *(Chinese)* 80—5809
- metallic film apodising and attenuating filters, phase shifts and aberrations 78—90514
- metallic thin film apodising and attenuating filters, phase shifts and aberrations 80—87552
- micro-optic directional coupler, aberration losses 80—48395
- micro-optics quality testing 79—27368
- microprobe instrument, spherical aberration correction, using zone plates 79—45899
- microwave holographic imaging through aberrating media with phase-modulated ref. beam 78—42303
- minicomputer optical design and analysis program 79—14075
- mirror, electrostatic, transaxial, for large-incidence ang. ion beams 78—37798
- mirror, electrostatic, two-electrode transaxial, for large incidence ang. electron beam 78—37797
- mirror system, meridional aberration summation, spherical surfaces with arbitrary decentring angles 77—71931
- models of optical systems 80—9821
- modular optical design, control of fifth-order aberrations 79—55199
- moments of images aberrated by turbulences undersampling errors in meas. 80—1137
- monochromatic aberrations, third order, correction of four lens objective 78—87123
- monochromatic aberrations in systems without symm., general and accidental identities 77—616
- monochromator, glancing incidence, with corrections for astigmatism and spectral-line curvature 80—43466
- monochromator, Seya-Namioka type, vertical astigmatism correction *(Japanese)* 79—76841
- monochromator, telescopic, in CTEM, with cylindrical mirror analysers 80—87296
- monochromator mounting with ruled diffr. grating at 45° off-plane 80—87479
- monochromator using concave holographic grating and plane mirror, imaging props. 80—99856
- monochromators with off-axis mirrors, distortion and split-image curvature 78—59141
- moving objective lens and Fraunhofer condition for predeflection 79—41316
- mutual coherence function in radio astronomy 79—75115
- nonaligned systems, off-centre aberrations 79—10263
- null Ronchi grating from spot diagrams 78—5548
- objective, 3-mirror design, optical scheme 78—55431
- objective, concentric, longitudinal spherical aberrations calc. method *(Russian)* 78—71184
- objective design with reduced secondary spectrum 77—7172
- objective for holographic recording devices 79—32028
- objective lens, with compensated axial chromatic aberration, for electron microscope 80—87293
- objective time-varying lateral aberration meas. 79—76797
- objective using a planoidal mirror 80—28297
- oculars of optical sights, for target and hunting guns 77—58419
- off axis systems, limit of validity of plate diagram 78—29903
- off-axis gaussian beam, third order spherical aberration, diffr. pattern 77—14665
- off-axis gaussian beam focusing props. optical system primary spherical aberration depend. 79—76735
- open stable cavity with axial symmetry, aberration corrections 80—43372
- ophthalmic lens distortion display 78—7338
- ophthalmic lenses, longit. spherical aberration and its effect on visual acuity 80—99816
- optical collimating system alignment by shearing plate 78—79126
- optical components testing for thermal imaging systems 78—33911
- optical design education program, desktop computer appl. 79—84922
- optical image quality number rel. to wave aberration polynomial coeffs., best image plane position determ. *(Spanish)* 77—68180
- optical receiver system, narrow-field, spherical aberration effect on radiation power losses 80—28299
- optical relay, system design, secondary colour reduction 78—83067
- optical storage focus error detection, skew beam and Foucault knife-edge techniques 80—102649
- optical system, automatic correction routine 80—58464
- optical system aspherical area shape predeterm. method *(German)* 80—28294
- optical system planning and design *(Italian)* 80—69490
- optical system testing, interferogram analysis, point spread function and OTF determ. 79—76616
- optical system tolerancing, encircled energy performance prediction 80—78935
- optical system with magnification chromatism, MTF 79—31818
- optical system with symmetry plane fourth order aberrations *(Russian)* 77—58417
- optical systems, entropy and neguentropy *(French)* 80—102608
- optical systems, refractive index nonlinearity influence *(Russian)* 78—58921
- optical video discs, read-out system diffraction theory, focus error aberration influences 79—50338
- optical wavefront distortion compensation in real time 77—17219
- optical wavefunctions, inversion of integral equation for system distorted by aberrations 79—98304
- optical waveguide, intrinsic, in medium with saturated nonlinearity, theory 80—14405
- optimal reference sphere determ. 79—89859
- optimum apodizers, performance, primary coma effects 79—98557
- OTF, numerical calc. from lens design data *(Korean)* 80—19085
- pancratic objectives, aberration stabilisation during focusing 80—102799

aberrations continued

- parabolic gradient index lens, SELFOC, chromatic aberration in imaging system 80—14422
- parametric image convertor with freq. rise, phase aberrations *(Russian)* 78—9455
- parametric image upconversion, thickness aberrations investigation rel. to multi-transverse mode pump 78—13765
- partially coherent imagery with spherical aberrations *(German)* 79—59641
- particle optics, telescope electrostatic system with removable spherical aberrations 77—6989
- particle optics, telescope electrostatic system with removable spherical aberrations 77—6990
- periscope, secondary colour correction 77—7169
- phase aberration correction via stimulated Brillouin scatt. 78—37944
- photogrammetry, distortion calibration, lateral chromatic aberration effects, operational data reduction 79—35881
- photogrammetry of Earth, atmos. refr. compensation 80—56339
- photographic gradient singlet, total aberrations 80—13177
- photographic lenses for low cost high production, design example 79—85193
- photographic multilens system image field curvature and residual spherical aberration mutual correction *(Russian)* 77—87857
- photographic objective axial ray bundles achromatisation and Staeble-Ligotsky isoplanasie condition *(Russian)* 78—65988
- photographic Wood lens, third order aberrations 77—26413
- planar optical elements, dispersion props. 79—3811
- plane grating monochromators, fourth-order aberrations 77—62056
- plane parallel lenses, prep., theory 79—3761
- plastic gradient index lens fabrication and image evaluation 80—14426
- point-source image energy centre of gravity, location accuracy, aberrations effect 79—27192
- precision objectives, high resolution, image-forming quality *(German)* 78—87120
- precision optical element testing by phase meas. interferometry 80—74520
- primary coma, influences on partially coherent imagery 79—76609
- principles, w.r.t. electronics engineer appl. 77—83818
- prism, cone-shaped, combined elec./mag. fields, relativistic particle optics 78—50690
- prism, wedge-shaped, combined elec./mag. fields, relativistic particle optics 78—50689
- prism binoculars, wide-angle eight-fold magnification 77—10997
- projection system, wavelength and coherence effects 80—64136
- proximate ray tracing and wave aberration coeffs. 77—597
- pyrometric system, precision, residual aberration effect calc. 79—71456
- pyrometric system image quality in temp. meas. of nonisothermal objects 78—41312
- quadratic structure functions describing random tilted phase fields 80—95799
- radial refractive index gradient optical element, off-axis aberrations 80—14423
- radiation pyrometer temp. meas., effect on metrological characts. 78—77920
- radioastronomy, aperture synthesis meas. processing, tangent-plane aberration, new transform 79—8847
- rapid system, correction method *(Russian)* 79—98300
- ray tracing, generalised, caustic surfaces 79—23043
- real time interferogram simulation by analogue device, aberration generation, CRT display 79—54181
- reflecting telescope design, appl. of plate diagram 79—94321
- reflector phased array aberration effects, optical modelling *(Russian)* 78—16290
- refractive index gradient tolerance in optical elements 78—71179
- refractive null corrector design for testing aspheric surfaces 77—19377
- rhomb laser beam sampler, two-grating, inherent aberration correction, inverse filter description 80—37954
- Ronchi test, practical formulae and experimental verification 80—43490
- Ronchi test formulae, theory 80—23817
- rotational symmetric aspheric in compensated interferometers, computer-generated-holography testing 80—33128
- round lens aberration correction 80—78758
- satellite acquired image geometric distortion correction 79—74588
- scalar diffraction theory, exact solns. 80—78778
- scanning optical microscope, spherical aberration effect on imaging props. 79—58783
- scanning rate restrictions in monochromators 80—48430
- Scherzer's formula and the correction of spiral distortion in the electron microscope 77—71407
- Scherzer theorem and ideal lenses 77—67547
- schlieren instrument, amplitude transfer charact., Monte Carlo method 80—28336
- schlieren photography, aberration and diffr. effects on resolution 77—34040
- Schmidt achromatic corrector plates for near IR, spherical aberration elimination 78—28515
- Schmidt achromatic correctors, off-axis aberration 78—45223
- Schmidt telescopes, achromatic condition *(Japanese)* 78—89062
- secondary colour aberration limited system performance estimation 79—23041
- secondary spectrum correction with normal glass 77—62032
- Seidel aberrations, in TV zoom lenses, modular construction method 78—311
- Selfoc conically graded medium, aberration anal. 80—1142
- Selfoc lens, aberration improvement by glass composition and ion exchange process parameter choice 80—69486
- Selfoc lens as imaging system, chromatic aberration 80—69480
- SEM objective lens, spherical and chromatic aberration coeffs., meas. method 78—21286
- sextupole corrector limitations 80—102604
- sextupole system for spherical aberration correction 80—43246
- shearing interferogram evaluation improvement *(German)* 80—27339
- simple lens shape effect on image curvature 79—50368
- single lens, longitudinal-chromatic and spherical aberrations, ray-tracing method estimation 78—1311
- single-polepiece magnetic lens axial field distrib. 80—69317
- single-polepiece objective and projector lenses for electron microscope 80—68326
- slow scan SEC vidicon system coupled to telescope 77—25945
- space charge ion optics, influence of chromatic aberrations 78—55294

aberrations continued

- Space Telescope pointing control fine guidance subsystem design 80—82201
- speckle interference fringes, lens aberration effects 80—105700
- speckle interferometry, lens aberration effects, optical system pupil complex amplitude changes *(French)* 79—50237
- speckle photography, effect of lens aberrations 78—32866
- spectacle lenses, astigmatic, technological construction *(Russian)* 80—99817
- spectacle lenses, hard resin, comparative study of bitoric effect 80—91877
- spectral line aberration in concave grating spectrometer, deconvolution appl. *(Japanese)* 79—26141
- spectrograph, with transparent holographic grating 80—57395
- spectrophotometer, UV-visible, high throughput, optical and optomechanical design 80—95155
- spherical, eye, contrib. of cornea and lens 79—100597
- spherical, new optical solns. for close focusing 79—97453
- spherical aberration, single crossed electrostatic lens 77—54662
- spherical aberration measurement of photographic lenses, using solid-state image sensor 80—23812
- spherical concave gratings, off-plane stigmatic imaging 77—38808
- spherical mirror folded cavities, astigmatism elimination and regulation *(Chinese)* 78—90431
- spherical mirrors for IR imaging, astigmatism 78—33804
- spherical surface, large incidence angle 77—617
- spherical surfaces, extrameridional aberrations anal., with large decentring angles 77—68181
- spherochromatism correction system for high-speed spectrographs *(Russian)* 77—61129
- spheroidal geodesic lenses for integrated optical processing, design 77—27385
- STEM, defocus and astigmatism, automatic correction method 80—68298
- STEM, post specimen optics, corrected spectrometer 77—38062
- STEM optical system, practical considerations, review 78—21301
- stigmatic grazing incidence spectrometer, using toroidal mirror as focusing element 79—71539
- stigmats using two curved Fresnel surfaces 80—38084
- Strehl intensity applicability as image quality criterion *(German)* 80—28166
- superachromatic triplets, design method 80—64133
- superachromatization, glass combination selection 78—1315
- surface errors rel. to optical performance, effect of mid- and high-spatial freqs. 79—59789
- telephoto apochromat lenses, design 80—31924
- telescope, AZT-24, design formulas for construction elements 79—35133
- telescope system, IR Galilean, attachment for information scanning device, aberrations 78—46751
- telescope with severe aberration, MTF for speckle interferometry 78—12103
- telescope with two magnifications, residual aberration 77—14790
- telescope-spectrometer combination, optical props. 80—87455
- TEM, electronic prod. of hollow cone illum. 77—54026
- TEM, spiral distortion correction 78—32942
- TEM, viewing arrangement improvements 78—32941
- TEM, wave aberration sign 77—22623
- TEM micrograph image restoration, of weak-phase object using computer *(Japanese)* 79—71571
- TEM multilens imaging system design for minimum distortion at low magnifications 79—12897
- testing optical systems, speckle shearing interferometer *(French)* 77—65616
- thermal imaging system resolution and S/N ratio, optical aberration effect 79—81552
- thin three lens cemented components, performance calc. 77—75652
- third order for negative system astigmatism and coma anal. *(Russian)* 78—30039
- third order formulae for optical systems with Fresnel surfaces *(Russian)* 78—63014
- third order in optical system with one symmetry plane, analytic expression obtention *(Russian)* 77—34832
- three lens cemented objectives, spherical aberration correction 77—88894
- three-actuator deformable water-cooled mirror 80—33134
- three-lens cemented component calcs., reduced secondary spectrum 80 102800
- toroidal holographic gratings, design and performance *(Japanese)* 79—27412
- transfer function of optical systems with small residual aberrations, schlieren effects *(German)* 80—32923
- transmission grating, facet-type, aberrations for cosmic X-ray and XUV spectroscopy 78—85851
- triple monochromator a spectrometer in Raman scatt. *(French)* 80—96007
- triplets of 2-electrode astigmatic tubular lenses, spherical aberration 79—50203
- truncated sinusoidal test and exptl. MTF meas. 78—25806
- turbulent medium, optical resolution with adaptive phase compensation 77—46692
- two-coordinate acousto-optical prismatic deflector geometry *(Russian)* 77—58428
- two-electrode tubular lens, astigmatic, spherical aberrations 77—34804
- two-electrode tubular lens, astigmatic, spherical aberrations, object position effects 77—34805
- two-mirror telescopes, image quality estimation and utilisation in cosmic astronomy *(Russian)* 79—96911
- uncentred surface system, field aberrations of object meridional points 78—82923
- unstable optical resonators with tilted spherical mirrors, design eqns. 78—74930
- UV holographic microinterferometer and probe beam design for plasma probing 80—59270
- varifocal compensated lens for flow cells irrad. 79—27357
- virtual image display using Fresnel lenses 80—1295
- visual instrument astigmatism, accommodation compensation 79—34563
- visual optical systems, aberration tolerances 77—73529
- wave, transverse and longit. values, aberration approx. optical systems *(Russian)* 80—28167
- wave aberrations caused by misalignments of aspherics, and their elimination 80—33127
- wavefront aberration difference function, variance 77—3543

aberrations continued
wavefront aberration polynomial, calc. 80—102614
wavefront analyser using max. likelihood algorithm, phase aberration meas. 77—46694
wavefront compensation error due to finite corrector-element size 77—46693
wavefront distortion sensing for adaptive optics system control 77—19293
wavefront interpretation with Zernike polynomials 80—78776
wavefront plot, aberrations, point spread function, three dimens. *(German)* 78—46521
waxicons for high-power chemical lasers, interferogram analysis 80—14418
wedge scanner, achromatisation 77—7205
wedge scanner, design 77—39058
Wollaston prism as convergent light beam splitter 79—14092
X-ray transmission gratings, aberrations, testing, astronomical appl. 79—25508
Zernike circle polynomials, appl. in optics 77—67182
Zernike polynomial generalisation, optimum balanced wavefront aberrations for annular apertures 80—95805
Zernike-Tatian polynomials for interferogram reduction 80—37077
zero Petzval curvature radial gradient index lens, third-order aberrations 80—14424
zonal spherical aberrations in optical systems, correction, use of aplanatic lens 79—27360
zone plate, profiled, chromatic props. calc. 80—28328
zoom lenses, aberrations analysis using Delano and aperture diagrams *(German)* 77—88888
zoom null lens design for optical component and system testing 80—23811
zoom projection lens, optical level system, paraxial characts. 80—53399
C graphitic, high resolution electron microscopy imaging, phase contrast transfer functions in electron optical aberrations 79—77463
CO_2 laser Antares fusion system optical diffraction computation 80—74424
Ge, polycrystalline thermal-imaging lens, optical requirements 80—69495
Li cylindrical lens for high energy particle focusing, aberrations 77—14649
PbO glass, thermal focusing of elliptically shaped optical beams, astigmatism effect 79—18489
SF_6, multiwavelength phase conjugation using multiline CO_2 TEA laser 80—91847
SF_6, phase conjugation at 10.6 μm by resonantly enhanced degenerate four-wave mixing 79—64271

abrasion
see also hardness; wear
abrasive and impact abrasive wear testing equipment for materials at elevated temps. 78—7136
abrasive particle shape control and quantitative eval. apparatus 78—4586
active abrasive conc. determ. by static method based on etch figure stars count 80—74544
alumina on stainless steels and Inconel, gasless ion plated films 77—40476
asbestos-reinforced friction materials, wear and thermal processes 80—40559
body rotating in viscous abrasive medium, wear *(Russian)* 79—79114
boride coatings, under elec. heating conditions, hydroabrasion wear resist. on Armco Fe and steel 80—55543
boronised coating on steel, sliding and abrasive wear, corrosion resist. 78—11428
brass, abrasive wear, critical grit size effect *(Japanese)* 80—11783
brass, magnetoabrasive machining, optimum conditions 80—30172
brittle abrasive material, rating capability for elastic deformation 78—56680
ceramic glaze, abrasion resistance 79—38984
composite materials, water lubrication, wear studies 80—60984
cutting tools, diffusive wear, mag. field effect 80—60985
dentin, human, effects of irradiation on wear resistance, microhardness and acid solubility 79—96634
diamond, polycrystalline tool, wear in rock removal processes 78—64724
diamond-abrasive polishing, of breakdown and exhaustion of lubricating and cooling liquids 79—96196
dimethacrylate resins dental composite, abrasion and wear props. 79—96710
ductile metals, velocity depend. of erosion by solid particles, at low incidence angles 78—87311
elastohydrodynamic film thickness, meas. of artificially produced dents and grooves 80—36975
electroplated diamond-composite abrasion-resistant coatings 79—61737
erosivity and mechanoluminescence *(German)* 80—25873
exoelectron emission for tribomechanical surface treatment *(German)* 77—4870
Fe, cast, high Cr, hardfacing of roll, wear resistance and thermal durability 80—7686
flexural fatigue and surface abrasion 78—15504
float glass, commercially produced, thermally toughened and untoughened, surface damage resistances on air and tin side 79—61612
friction machine, residual stresses meas., appl. to wear resist., surface wear 78—60906
gas-abrasive wear tests, methods and apparatus, neutral gas flow 77—25209
glass, material removal mechanism by free abrasive grinding 77—52510
glass, surface damage by abrasive contact, effect on strength 80—85066
glazed surface, abrasion resistance testing *(German)* 77—32728
glazes with improved abrasion resistance *(German)* 80—11798
granular composition changes due to wear in abrasives *(Russian)* 79—79115
granular materials, abrasive, failure and strength characts. in US field, test unit 80—85112
graphite, sliding against C, dusting wear regime 80—97595
grinding efficiency increase, using abrasive tool with filler *(Russian)* 80—7687
grinding resist. materials, review 80—108586
hard coating on metal surfaces, abrasive wear resist. meas. 79—20327
hardfacing alloys in impact abrasive loading, wear resistance, temp. effects 79—87737
Hayes alloy no.716, Fe-Cr-Ni-Co-W-Mo-Si-C-B (26, 22, 12, 3.5, 3, 1.2, 1.1, 0.4 wt.%), hardfacing alloy 80—100802
Haynes Stellite 6B, Al_2O_3 particle erosion of surface, SEM obs. 78—88545

abrasion continued
Haynes Stellite 6B, particle erosion damage, TEM obs. 78—88546
high speed rubbing, thermomechanical interactions 80—83769
high-speed friction, intensity calc. 80—103416
impact, abrasion, wear, review *(German)* 78—88536
inorganic nonmetallic building material with rough surface, abrasion test using pneumatic apparatus for thickness meas. *(German)* 79—52553
instrumentation engineering, laser beam appls. in drilling, welding, cutting, definite abrasion and surface treatment *(German)* 80—108608
Kevlar-29, flexural fatigue and surface abrasion 78—15504
Large optical component grinding and polishing condition selection 79—81579
low-alloy steel, abrasive wear resistance, effect of C content, annealing quenching 77—56115
martensitic steel, abrasive wear resistance, effect of tempering strain martensite 77—56116
metal, abrasive wear resistance rel. to physicomechanical props. 79—91804
metal, coated abrasive belt grinding, relation between wear of grain cutting edge and material removal 80—16507
metal, impact abrasive wear, anal. 79—43443
metal, kinetic friction re-examination using modified pin and disc machine 80—55547
metal erosion by solid particles, high-speed photography 78—39919
metal surfaces, abrasion mechanism rel. to groove sizes, shapes 79—20216
metal surfaces, abrasive wear theory based on shear effects 80—89363
metal wear energy balance under abrasive and boundary friction, expt. 78—85006
metal-insulator pairs, sliding behaviour 80—66671
metal-metal metal-polymer sliding, wear mechanisms, review 79—70174
metals, abrasive finishing with refractory carbide micropowders, surface struct. 80—11842
metals, abrasive wear and impact and arc erosion, exam. of comparative tendencies of metal loss 79—15811
metals, abrasive wear testing under conditions of rolling friction 79—15894
metals, effects of microstruct. on wear resistance 78—92367
metals and alloys, abrasion wear testing 77—40493
minerals, impact abrasion by windblown dust or snow 77—70647
monocrystal surface layer damage depend. on abrasive working parameters *(Russian)* 80—76368
non-magnetic material wear in presence of magnetic field 80—60982
optical glass surfacing, using loose abrasives, impregnated diamonds and electro-plated diamonds 78—50956
optical material radiation strength, dissipative characteristic 79—27344
optical surface shaping, contact problems 80—74540
oxide thickness in shutdown fission reactor meas., abrading system appl. 79—63720
particles, abrasive, mech. strength determ. 79—87781
phenolic resin, linen impregnated, abrasion, SEM obs. 78—64742
photographic migration images, liquid developed, fixing and abrasion resistance 80—4792
physicochemical processes during frictional contact leading to H_2 generation *(Russian)* 77—52496
plastic accurate convex hyperbola prod. using pantograph and rotating abrasive drum 79—98513
platilon UO1, use in artificial blood pumps, fatigue resist. and mech. props. 79—84026
PMMA, abrasion, SEM obs. 78—64742
PMMA, abrasion resistance, use in dentistry 79—83434
PMMA, quartz- and glass-particle reinforced, abrasive wear 80—97594
polyethylene: (Dy_2O_3), mech. props. and transfer to steel surfaces 80—16496
polyethylene, ultra-high mol. wt., wear mechanisms in total joint replacement 77—52929
polyethylene, ultrahigh mol. wt., wear props. 79—84001
polyethylene prostheses, radiation crosslinking improvement of shock- and abrasion-resistance 77—60307
polyethylene-Fe, wear resistance on steel counterbody, exam. 78—68826
polymer impregnated gypsum cast, mech. props. 79—100107
polymer surfaces, abrasion mechanism rel. to groove sizes, shapes 79—20216
polymer-polymer and metal-polymer sliding wear mechanisms, review 79—70174
polymeric thin coating, mechanochem. degradation, substrate effects 79—79134
polymers, abrasive wear resistance rel. to physicomechanical props. 79—91804
polymers, cryst., hard-elastic fibres, morphology mech. props., mechanisms, review 77—32612
powder, ultra fine, surface roughness effect on formation by rotating friction mill *(Japanese)* 78—95709
powders, ultra fine prod. by rotating friction mill, mechanism in initial wear region *(Japanese)* 80—25589
profile meas. system, on-line computer controlled 77—52603
PTFE, abrasion, SEM obs. 78—64742
PTFE, wear, sliding speed, contact press. and rubbing surface temp. 80—76372
PVC, filled with SiC particles, abrasion resistance *(Japanese)* 78—7055
quartz dental composites, acrylic acid grafted on particles by gamma-radiation 80—66840
refractory abrasion test machine for use at high temp. 79—52505
refractory metal, disturbed layer depth on abrasive lapping with TiC, NbC, WC micropowders 77—44391
refractory metal carbides, abrasive props. of micropowders for lapping 77—63821
refractory transition metal, abrasive polishing mechanism 77—12745
Relite-base alloy compositions wear caused by sliding abrasive material stream 78—95813
rocks, pebble abrasion studies 80—4004
rocks hardness and abrasiveness determ., suggested methods 78—96313
rubber, rel. to growth of cracks, theory and expt. 79—38988
sandpaper, standardised, for Taber abraser, influence of relative humidity an abrasive quality *(Japanese)* 79—8369
secondary nucleation, influence of crystal brittleness and degree of supersaturation using in growth *(Italian)* 78—23836
sedimentary material in Atlantic Ocean, shore abrasion 79—2217
slab, surface displacements for high speed rubs 80—83767
sliding contact, friction, wear, temp. anal. 80—93659

abrasion continued

- sliding wear test apparatus, design and statistical evaluation, polymeric restoratives evaluation 80—21237
- solid lubrications dynamics, obs. using Micro Contact Imager 78—85002
- solid target, abrasion and evaporation by focused CO_2 TEA laser radiation *(German)* 77—40305
- stainless steel rod adaptor, failure anal. in Fast Burst Reactor 77—54307
- steel, abrasive wear resistance, effects of microstruct. 78—92367
- steel, alloy, electroslag remelting effect, an impact-abrasive wear resistance 80—55541
- steel, alloy, friction with cast Fe, boundary and oil-abrasive, adsorption effect 80—55546
- steel, alloy, types CT40, CT40X, CT45, texture form. 80—25721
- steel, austenitic, fracture toughness effects on friction force in abrasive wear *(German)* 77—4860
- steel, austenitic, high Mn, abrasive wear resistance *(Korean)* 77—25162
- steel, austenitic, precipitation hardenable, friction and wear under abrasive conditions *(German)* 77—59951
- steel, C, wear resistant, review of abrasive adhesive and rolling wear *(Korean)* 79—24624
- steel, Cr-C (18, 0.9 wt.%), cavitation, abrasion resistance, effect of unstable austenitic struct. *(Russian)* 77—16695
- steel, Cr-Ni-Nb, LKh16N4B, high temp. frictional characts. 80—21118
- steel, high C, resist. to crack propag. and abrasive wear, role of retained austenite 79—83330
- steel, high speed tool, diffusion wear model 79—29230
- steel, inclusion chemistry control for machinability enhancement 80—85067
- steel, medium C, 45, deposition of composite, wear resistant Ni-B-Cr coating 78—11420
- steel, Mn, wear resistant, review of abrasive adhesive and rolling wear *(Korean)* 79—24624
- steel, scoring and scuffing on lubricated sliding surfaces, Mossbauer study 80—7690
- steel, stainless, austenitic, CC Ni-Al, γ-phase, fracture mechanical aspects of abrasive friction, wear, chip formation 78—72865
- steel, stainless, epoxide butt joints, effect of abraded and Ar ion bombarded surfaces on ultimate tensile strength 80—16638
- steel, tool, abrasive wear rate rel. to fracture toughness and microstructure *(German)* 79—29232
- steel, tool, maraging, based on N12M10, exam. of hardening, crack resistance and wear *(Russian)* 79—34047
- steel, type Kh12M, rel. between structural inhomogeneity and wear resist. *(Russian)* 80—66672
- steel, using Al_2O_3 or Fe_2O_3 suspension, mag. and dielec. emulsion prep. 78—27826
- steel, wear due to paper and printer ribbon exam. 79—15812
- steel, wear of single abrasive grains, using pin on disc wear test *(Japanese)* 78—44230
- steel, wear resistance, determ. using MI-1M machine 80—25943
- steel, wear resistance during abrasive wear, comp. and struct. effects 80—35337
- steel, wear resistance of low temp. nitriding treatment 80 - 89357
- steel 40 kH, wear resistance in oil abrasive environment, various grinding methods *(Russian)* 77—70184
- steel Kh12, impact abrasive wear improvement by TiC coating 77—70187
- steels, N-implanted, surface hardness and abrasive wear resist. 80—50746
- strain gauge protection, sealants suitability determ. 78—4610
- superficial plastic deformations by particles *(French)* 80—40540
- surfaces, wear, lubricant additive effects, AES appl. 77—44445
- test device, for rapid wear resist. determ. using converted lathe 79—87780
- testing, automatic device for discrete batching small amounts of abrasive suspension 79—87782
- topography of abraded surfaces rel. to contact area and abrasion mechanism 80—58986
- transition metal borides, abrasive props. 77—63808
- transition metal carbides, X-ray investig. of abrasive action 77—52497
- transparent materials, defective surface layer formation during abrasion, laser-induced breakdown *(Russian)* 78—53007
- tribological system and wear factors, worn vol. load and sliding distance calc. 80—21122
- vacuum metallised surfaces, protection by clear coatings 80—35392
- wear mechanism, grit size effect 80—16501
- wear mechanism review 78—72891
- wear of soft surface against rough hard surface, model 79—33034
- wear resistance, hardfacing, review 78—72937
- wear resistance, surface treatments, selection procedure, review 78—72892
- white cast Fe, abrasive wear 80—108587
- Al anodised layer, exam. of factors affecting abrasion resistance 79—34207
- Al FCC single crystal, crystal rotation accompanying scratch deform. *(Japanese)* 79—15733
- Al, polycrystalline, abrasion, deform., fatigue, study by exoelectron microscope *(Japanese)* 78—74108
- Al, SiC paper, low speed abrasion, strain rate effects 79—20208
- Al-Al_2 eutectic, abrasive fragmentation *(Czech)* 78—64715
- Al-Al_2Cu, eutectic composite, abrasive fragmentation *(Czech)* 80—30110
- Al-Al_3Ni, eutectic composite, abrasive fragmentation *(Czech)* 80—30110
- Al-steel mixture, wear resistant, produced by compaction by discrete shock waves 80—84882
- Al_2O_3, abrasive, wear in simulated hot grinding 78—56784
- Al_2O_3 rod, damaged, mech. strength, surface defects effect, appl. as insulators *(German)* 80—76330
- Au-Fe-Ni layer coating, Fe and Ni conc. meas. by X-ray diffr. *(German, English)* 80—34330
- β-B, abrasive props. 77—63808
- B coating on steel 45, effect of abrasive particle size on wear 78—44225
- B-based paste, abrasive props. 80—21114
- B-Cu(Al) coating on steel 45, effect of abrasive particle size on wear 78—44225
- C fibre, flexural fatigue and surface abrasion 78—15504
- C steel, abrasive wear resistance, effect of C content, annealing, quenching 77—56115
- Co, superalloy, attritious wear in grinding 77—32696
- Cr-C facing alloys, effect of B on phase composition and facings props. during abrasive wear 80—21117

abrasion continued

- Cu, FCC single crystal, crystal rotation accompanying scratch deform *(Japanese)* 79—15733
- Cu, SiC paper, low speed abrasion, strain rate effects 79—20208
- Cu, thermally stimulated exo-electron emission 80—11547
- Cu-Ag solder composite, plastic deform. below worn surfaces 77—36670
- Cu-Sn-P (5, 1-5 wt.%), effect of P on friction and wear characts. 80—16494
- Cu-Zn, thermally stimulated exo-electron emission 80—11547
- Fe alloy granule reinforced Cu M2 wear resistance in rubbing with lubrication 80—16490
- Fe, cast, abrasive wear rel. to lamellar or spheroidal graphite content *(German)* 78—85000
- Fe, cast, grey, abrasive wear rate rel. to fracture toughness and microstructure *(German)* 79—29232
- Fe, cast, grey, martensitic, lamellar, internal notch effect on abrasive wear *(German)* 79—29231
- Fe, cast, surface temperature effect on dry sliding wear 80—60983
- Fe, cast, white Cr alloyed, wear resistance, effect on abrasive hardness 78—64722
- Fe, degree of charging of surfaces polished by TiC and synthetic diamond micropowders 78—60880
- Fe, ductile, with different secondary struct., abrasive wear *(German)* 80—25871
- Fe, SiC paper, low speed abrasion, strain rate effects 79—20208
- Fe-based materials, wear resistance, surface hardening processes, review 78—72894
- Fe-C alloys abrasion resist. materials, review 80—108586
- Fe-C-Cr-Mo(Ni)(V), white cast, effect of abrasion on carbide microstructure *(German)* 78—88540
- Fe-Cr-Mo, white cast, optimising fracture toughness and abrasion resist. 80—85042
- Fe-Cr-Mo alloy castings, thick-section, factors affecting 80 ·108374
- Fe-Mn-C (11.5, 0.2 to 1.6 wt.%), water quenched, effect of C on phase composition, abrasion, plasticity *(Russian)* 78—35445
- Fe-TiC pseudofused composite magnetoabrasive powders, props. 80—100926
- GaAs(-GaP) single cryst., defect distrib. near abraded surface 80—92533
- GaP single cryst., defect distrib. near abraded surface 80—92533
- $Gd_3Ga_5O_{12}$, garnet substrate, surface polishing, damage, abrasion, brittle fracture model *(German)* 77—73357
- $Gd_3Ga_5O_{12}$, garnet substrate surfaces, working damage, electron microscope investig. 77—77605
- Hf-B, abrasive props. 80—16489
- MgO single cryst., impact wear characts. 80—76374
- Mo alloy sphere, three-body abrasive wear with small size diamond abrasives 80—76373
- Mo_2B_5, monocryst., grain size, abrasive and strength props. 80—11787
- NaCl single crystal, stained by abrasion, struct. defects *(Russian)* 79—74262
- Na_2O-B_2O_3-SiO_2 glass fibre, plastic coating influence on strength 80—58697
- Na_2O-CaO glass, abrasion-resistant, high strength 80—76369
- Ni, deformed by filing, fine struct. obs. *(Russian)* 77—21309
- Ni sputtered coating microstructure on mechanically activated cathode *(Russian)* 79—91586
- Ni-Cr (20 wt.%), high temp. frictional characts. 80—21118
- Ni-Cr-B-Si, hard faced with WC, exam. of abrasion and wear props. 79—34202
- Ni-Cr-Mo-C hardfacing alloy, hardness and abrasive wear resistance 79—79117
- Ni-SiC(WC), dispersion hardened coating, chemically deposited using electroless baths, exam. of protection props. 79—34208
- Ni-Zn ferrites, hot-pressed, key props. 78—15348
- Si, anodic oxidation for abrading thin layers from wafers *(German)* 77—25176
- Si, mechanically treated surface, chem. state *(Russian)* 80—11805
- Si, near (111), fracture by painted indenter, SEM study 80—71734
- Si, near (111) slices, scratches made by diamond stylus 77—12726
- Si, reactivity with organic nitrogen compound, rel. to polishing *(Russian)* 79—70192
- SiC, abrasive, wear in simulated hot grinding 78—56784
- SiC, abrasive paper, variables affecting degradation 79—43444
- SiC, attritious wear in grinding 77—32696
- SiC, chem. stability, mech. and thermal props. rel. to appls. 80—21103
- SiC, single cryst., friction and wear behaviour in sliding contact with various metals 80—21112
- β-SiC/Si abrasive resistant material, prep. and props. 80—20878
- SiO_2, fused material removal mechanism by free abrasive grinding 77 52510
- SiO_2 reinforced decorative laminates, abrasion resistance, abrasive paper deterioration 77—16696
- Ta_2O_5, reactive DC sputtering deposited films with magnetron-plasmatron, mechanical elec., optical props. 80—25566
- Ti alloys, grinding, effect on surface struct. 80—25878
- Ti, degree of charging of surfaces polished by TiC and synthetic diamond micropowders 78—60880
- Ti, oxide layer form. in acid soln., electrochem. and optical props. 78—48560
- Ti-Al-C(N) system cpds., abrasive power, glass grinding 77—63820
- Ti-Al-Cr-Mo, type VTZ-1, machinability, using different abrasive materials *(Russian)* 80—97593
- Ti-Al-Mo, type VT14, machinability, using different abrasive materials *(Russian)* 80—97593
- Ti-B, abrasive props. 80—16489
- Ti-Cr, sintered, friction and wear, structural factors 78—60843
- Ti-Cr-TiC, sintered, friction and wear, structural factors 78—60843
- Ti-TiC system, sintered, friction and wear, structural factors 78—60843
- TiC, pseudofused powder, abrasive props. 77—77589
- TiC-B, struct. and mech. props. 80—55461
- TiC-TiB_2 alloys, composition effect on surface layer rupture at various temps. 80—25879
- TiN decorative coating, ion plating on steel and Stellite, and abrasion resist. 78—11441
- TiO_2, reactive DC sputtering deposited films with magnetron-plasmatron, mechanical elec., optical props. 80—25566
- W_2B_5, monocryst., grain size, abrasive and strength props. 80—11787
- WC-Co cemented composites, abrasion by quartz 80—16495
- WC-Co hard alloys, hot-pressed, wear resist. under abrasive friction, heat treatment effect 80—66555
- Zn, thermally stimulated exo-electron emission 80—11547

abrasion continued
Zr-B, abrasive props. 80—16489
ZrC based cermets, strength and gas-abrasive wear resistance 77—25163

abrasive wear *see abrasion*

absolute gravity *see gravity*

absolute pressure measurement *see pressure measurement*

absolute temperature *see temperature*

absorbers (surge) *see surge protection*

absorption
for absorption of substances see sorption
see also acoustic wave absorption; electromagnetic wave absorption
gas flow, recirculating, in packed columns, mass transfer and mixing, cell model 80—69913
LiBr absorption, solar air conditioning system, low and high temp. cycles 80—81425

absorption spectra *see spectra*

absorption wavemeters *see wavemeters*

abundance ratio *see element relative abundance; isotope relative abundance*

a.c. generators
see also asynchronous generators; synchronous generators
cryo, He cooling system selection and efficiency *(French)* 77—26305
cryo, magnet field transient change calc. *(French)* 77—26303
fusion reactor, ohmic heating energy storage for power reactor, costing 78—58495
superconducting, 2 GW, cryogenic aspects *(French)* 77—26304
superconducting, 50 MVA thermal design of cryogenic rotor 79—58710
superconducting, simulation of rotating liq. He transfer union 77—84116
wind turbine driven, 5 kW, with automatic load matching device, field testing 79—70418
X-ray tube single- and three-phase generator performance comparison *(Japanese)* 79—92354

a.c. machines
see also a.c. generators; a.c. motors; asynchronous machines; synchronous machines
superconducting, rotor refrigerant circuit operating as zero mechanical work thermal pump, liquid He rotating cryostat 79—58717

a.c. motors
see also induction motors
optical diamond turning air-bearing spindle and eddy-current motor 80—5851
two-phase servo master-slave manipulators, triac output control system 79—9213

a.c. network analysers *see network analysers*

acceleration
see also acceleration control; acceleration measurement; accelerometers
α-particles, heating and acceleration 79—12376
auroral electrons acceleration mechanisms 80—77210
ball, radius of gyration determ., using air track, undergrad. demonstration 78—49606
cardiac function modification by synchronised oscill. accel. 80—56089
charged body free fall motion in gravit. field, field energies and equivalence principles 78—49740
charged particles in solar flares, accel. in presence of micro-turbulence 77—53528
cloud and rain drops, accel. to terminal vel. 77—78334
cosmic rays accel. in shock fronts 78—24415
cosmic rays acceleration by moving magnetic mirrors, efficiency 79—44310
cosmic rays in interplanetary space accel. to relativistic energies 79—21111
crystal resonators with increased immunity to acceleration fields in any shock/vibration environment 80—91953
electron acceleration to mildly relativistic energies by strong plasma turbulence 77—31437
electrons acceleration by weak MHD turbulence, energy spectrum, radiosources appl. 79—88582
explosion-induced accel. of cylindrical metal liners, form stability anal. 78—83425
explosive propulsion of bodies in plane and cylindrical symm. 77—58544
extended bodies, accel. and weight in relativity theory 77—33746
eye level acceleration forces experienced with rotation on the horizontal bar 80—45937
flow, separated, supersonic, caused by throttling in round duct 78—63446
flow downstream of gas injection, wall temp., heat transfer, accel. effect 79 1251
galactic cosmic rays, accel. mechanism and transport, model 79—35077
human $+G_z$ tolerance, objective ultrasonic determ. method 78—3619
human acceleration response, heat and acute dehydration effects 80—30907
humans exposed to centrifugation, optoelectronic ear oximeter calibration 78—92734
impact accelerations, short, features for reproduction 79—32351
impact experiments, appl. of rectangular-bore gas gun 77—41588
interplanetary energetic particles accel. by transit time damping 77—2311
interplanetary energetic particles accel. mechanisms 77—2312
ion collective acceleration, by intense relativistic electron beam, localised pinch model 78—87460
jerk: the time rate of change of acceleration 79—5928
laminar boundary layer, acceleration on partially moving surface *(Russian)* 77—51032
monkey/hunter problem and possible solutions 79—75306
particle acceleration in solar flares by cyclotron damping of cascading turbulence 79—44433
particle reflection by MHD shock waves, energy spectrum and pitch angle distrib. 79—35126
Phobos secular acceleration, value and origin 78—89100
plasma sheet, adiabatic accel. of ions induced by convection 78—88997
primary cosmic rays origin, intergalactic suprathermal grains, accel. mechanisms 79—25412
pulmonary blood flow, spatial distribution in dogs in increased force environments 78—92664
quasar absorption line clouds, radiative accel. 78—57683
relativistic energy and momentum triangles, modified versions applicable to accelerated motions 79—88803
relativistic negative acceleration components 78—86058
ridig body rotation in 3D space from body fixed linear acceleration meas 80—68040

acceleration continued
road vehicle stopping distance, weight transfer effect, for teaching 79—25800
solar flare, particle acceleration in turbulent current sheet 79—35232
solar flare particles pulsed accel., plasma turbulence, ion-acoustic and Langmuir waves 78—96450
solar wind, deposition of momentum and energy by MHD waves 77—37493
solar wind He ions superheating and superacceleration 80—12631
solar wind heating and acceleration, implications of coronal fast waves evanescence 78—89147
spherical shell accelerating in fluid medium, generation of waves 78—13843
statistical particle acceleration models for Cassiopeia A supernova remnant 78—57606
steady plane isochoric flows, acceleration and pressures 78—81845
stochastic acceleration of particle in random pot., renormalised canonical perturbation theory 77—27233
superconducting dipole magnet models of combined type 79—31301
supermassive black holes, accel. by emission of asymmetric radiation 77—45481
supernova explosions, relativistic electrons accel. 78—28710
teaching acceleration and velocity, racetrack game 80—31458
teaching of accelerated motion, by 'racetrack' game 78—62022
water drops accel. to terminal vel., drag coeff. 78—61506

acceleration control
see also acceleration measurement
nuclear power station earthquake simulator 78—5681
spacecraft relative motion around orbiting station, guidance method 78—16263
vestibular research, rotating room acceleration and damping 79—84048

acceleration measurement
see also acceleration control
acceleration due to gravity, absolute determ. *(Chinese)* 79—71426
accelerometer, VM20, features, appls. *(German)* 77—41576
accelerometer/velocimeter, range of 10^5 g to 10^{10} g and time resolution of few nanoseconds 77—45826
accelerometers, performance characteristics and selection, review 79—177
bioradiotelemetry with 9-channel accelerometer for head crash impact accel. meas. 77—86655
bone in vivo properties determ., effect of soft tissue on wave propag. and vibr. tests 78—3660
constant angular acceleration unit, USSR standard, metrological characts. 79—30430
discreteness periods, selection 79—30433
doubly integrating vibration accelerometer random input anal. *(Russian)* 78—77873
education, homodyne microwave Doppler velocimetry, accel. meas. 77—78920
electrocapillary acceleration meters, electrolyte composition selection 80—73331
electrocapillary acceleration meters with electrolyte in gel form 80—73330
falling objects accel. due to gravity, Doppler effect, student microwave expt. 80—105472
flux gradient accelerometer, working model tests 77—26274
gas gravimeter use for variable linear acceleration meas. 78—77875
gravitational, appl. of desk calculator 80—73336
gravitational acceleration meas. using falling ball, teaching 78—28896
gravity, inertial navigation, covariance analysis of periodic traversing 80—95087
hand-arm energy dissipation in using vibratory tools and accel. levels 78—96116
holographic double exposure method for quadratic motion analysis 77—61927
homodyne microwave Doppler velocimetry, accel. meas. 77—78920
human motion three-dimensional monitoring by optoelectronic means, calibration 77—86658
iliac crest, acceleration transmission to sensor *(German)* 77—21542
impact motion acceleration transducer system, piezoelectric, with mechanical waveguide, anal. of processes 79—30436
laser ballistic gravimeter, meas. of absolute acceleration due to gravity 80—12569
linear, 10^{-3} to 2×10^2 m/sec^2, Soviet primary standard for measurement unit 77—79070
linear, steady/LF alternating equipment and standards for metrological support 78—45601
low-reactive meas. of motion, trnasducer effects on body under investigation *(German)* 80—105621
motion parameter measurement by comparison with motion of standard 79—30434
piezoelectric acceleration sensors, lower limiting frequency and indication threshold *(German)* 80—95093
piezoelectric accelerometers, effect of strain sensitivity on accel. meas. of flexural vibrations 80—58991
plastic plate velocity measurement, as continuum, by streak camera technique 78—37095
platforms, rotational and turning, kinematics 79—30220
projectile, using stroboscopic picture, teaching demonstration 78—36779
sensor device for recording vibrations of tall structures 80—95084
sensor for heart implantation *(German)* 79—57802
solid body motion parameters, determination reliability improvement using redundancy methods 79—30431
telemetric human movement correction using computer and electrostimulating device 77—86656
transducer design and characteristics *(Hungarian)* 78—29097
tuned equipment-structure systems, response spectra design methods 79—3952
Weibull distrib. function for analysis of data obtained by accelerated tests *(Spanish)* 79—54113

accelerators (particle) *see particle accelerators*

accelerometers
see also acceleration measurement
atmospheric thermal balance meas. by radiation pressure on satellite microaccelerometer 79—2380
biodynamic subminiature piezoresistive accelerometer performance evaluation 78—20340
bioradiotelemetry, 9-channel, for head crash impact accel. meas. 77—86655
blind person's rocking motion sensor and recorder 77—52921

accelerometers continued
BM transducer characts. and appl. to mouse behavioural stages classification 80—56309
Cactus, on Castor satellite, Earth's radiative balance meas. *(French)* 78—81530
Cactus accelerometer, for Earth radiation budget meas. *(French)* 79—84482
Cactus accelerometer, in-orbit performance on D5B satellite 78—61698
Cactus accelerometer for meas. below 10^{-9}g, payload for Castor satellite *(French)* 79—75505
Cactus accelerometer on Castor satellite, flight results synthesis for accels. below 10^{-9}g 80—77251
CACTUS high sensitivity accelerometer, in-orbit electrification of proof mass *(French)* 77—64589
calibration, industrial noise meas. appl. *(German)* 77—80039
chronobiological movement transducer *(Spanish)* 80—89902
doubly integrating vibration accelerometer random input anal. *(Russian)* 78—77873
Earth radiation budget, accelerometer direct meas. *(French)* 80—46287
electro-mechanical sensors, mechanical compensation methods influence on error characts. *(German)* 78—16786
electrocapillary acceleration meters, electrolyte composition selection 80—73331
electrocapillary acceleration meters with electrolyte in gel form 80—73330
element with gas dynamic suspension, subharmonic oscillation anal. *(Russian)* 79—88948
EM accelerometer with adjustable rigidity and damping, static/dynamic accel. detect. *(German)* 80—105625
finger tremor amplitude and freq. artefact reduced routine meas., portable equipment *(German)* 78—85407
floated pendulum accelerometers, performance measurements 80—31718
flux gradient accelerometer, working model tests 77—26274
FM telemeter for human limb movement characterisation 77—86680
gait analysis automated accelerometry system 77—90934
gravimetric calibration 79—71444
gyro type for inertial navigation vibrating sensitive element reliability improvement *(Russian)* 77—57302
human motion analysis, assessment of derivative determining technique 77—90838
impact, Impul's-3 calibration apparatus 80—8964
implantable, for cardiac performance telemetering 77—86670
induction generator type, transient characts. and Law-Novotny expression development *(Japanese)* 79—88921
linear, with centrifuge, methods of eliminating systematic errors in calibration 79—71399
microwave noncontacting accelerometer for gravitational wave antenna, supercond. cavity 77—30076
microwave parametric accelerometers, prototype Nb gravitational radiation antenna 79—44841
ocean wave spectral density meas. with analogue filtering 77—41230
oesophageal accelerometer evaluation for cardiac function noninvasive meas. 79—92458
pendulum, vibration errors *(Russian)* 78—77874
pendulum accelerometer, student expt. 79—58506
performance characteristics and selection, review 79—177
piezoceramic accelerometers, construction and appls. 79—50686
piezoceramic accelerometers and associated instrumentation for vibration meas. 80—10073
piezoceramic cardiovascular acceleration transducer 79—39536
piezoelectric, effect of strain sensitivity on accel. meas. of flexural vibrations 80—58991
piezoelectric, magnetic fastening using new magnetic material $SmCo_5$ 79—77035
piezoelectric accelerometers *(German)* 80—22334
piezoelectric ceramic sensors appl. 79—6100
piezoelectric impact, effect of damping on dynamic error 79—30435
piezoelectric type, range of 10^5 g to 10^{10} g and time resolution of few nanoseconds 77—45826
piezoresistive accelerometers, appl. in meas. of hand and arm vibr. transmission characts. 77—64075
polished metal sphere and microaccelerometer, for absolute meas. of Earth's radiation balance *(French)* 79—29900
reading error compensation, algorithm *(Russian)* 77—26282
rotational angular acceleration and velocity meas. by miniature linear accelerometers 78—12679
seafloor instrumentation systems development, multifunctional, USA project 79—53584
seismic sensors, mechanical, frequency charact., influencing factors *(Japanese)* 78—85722
shock pendulum for calibrating and testing accelerometers *(German)* 80—31719
signature verification, data recovery 80—101791
single process integral parameter meas. method 77—5792
strain sensitivity test device 80—52173
superconducting, using Nb-on-sapphire RF resonator 79—49210
superconducting accelerometers, gravitational wave detection, and general gravit. expts. 78—45555
superconducting gravity gradiometers 79—29868
systematic-error correction in accelerometer testing on standard vibratory testers 79—71423
testing using apparatus for exact production of accelerations less than g, errors 79—71424
time-average hologram fringe pattern interpretation 77—38838
triaxial acoustic current meter for small-scale ocean turbulence resolution 77—41232
triaxial vector accelerometry for quantifying tremor and ataxia 78—28116
VM20, features appls. *(German)* 77—41576
wind-driven wave parameters determ. at automated buoy stations 79—21064
Si accelerometer, batch fabricated 80—73328
Si piezoresistive accelerometer power transfer factor *(German)* 80—37017

accidents
see also electric shocks; explosions; safety
accident handling in Federal Republic of Germany 78—53530
accidents during work, mapping of reasons using error beams by function sensed computations of admission probabilities *(German)* 80—68027

accidents continued
AGR system for nuclear process heat, primary circuit component materials 78—13233
aircraft accidents related to weather 79—84463
aircraft crashes in thunderstorm downbursts, analysis 78—53693
alternative containment designs, value/impact comparison, containment failure and safety aspects 79—13464
atmospheric diffusion of pollutants after hypothetical accidents at nuclear plants *(German)* 77—64421
behaviour of previously failed fuel rods under power ramp and film boiling operation 79—49745
blowdown process, bubble growth by expansion and dissolution in variable pressure field 78—15723
breeder reactors, SNR300, cooling system failure, effects *(German)* 78—695
BWR loss-of-coolant accident, peak-clad temp. probability distribs. 77—74952
BWR passive containment system, LOCA safety features 79—13466
Candu reactor moderator effectiveness as LOCA heat sink 79—81021
car accidents, correl. of field injuries and GM Hybrid III dummy responses 80—108939
CEGB nuclear power station emergency arrangements 78—55050
CEGB nuclear power station emergency monitoring procedures 78—55053
charcoal spill, release of absorbed radioactive fission gases Kr and Xe 77—50262
concrete slab perforation by missiles, nuclear plant appl. 77—38352
concrete slab perforation by missiles, nuclear plant appl. 77—38353
concrete slab perforation by missiles, nuclear plant appl. 77—38354
condensed vapour following core disruptive accident, particle-size distribs. using first-generation model 78—13295
conference on nuclear power and fuel cycle, Salzburg, Austria, (May 77) 79—26503
containment blowdown following LOCA, press. and temp. transients and COPDA results 78—13303
core disassembly calculations, vapour press. eqn. of state, VENUS-II code studies 78—8908
Creys Malville station, Super Phenix project safety *(French)* 79—30948
Creys-Malville station, safety arrangements *(French)* 79—30946
criticality accidents, dosimetry using activations of blood and hair 80—89857
criticality accidents at facilities processing fissile material, characts., detect. and action procedures *(French)* 78—55054
dissociating N_2O_4 power plants, safety and accident response *(Russian)* 79—31066
Dutch reactor safety studies, Rasmussen report eval. *(Dutch)* 79—81016
earthquakes connected with human engineering activity, tectonic and tectonophysical conditions for occurrence 77—81802
ECCS top spray, restrictive effect of ascending steam on falling water 79—49704
European in-pile investigations of fast breeder reactor safety *(French)* 79—26653
fast breeder reactor accidental releases, influence of physico-chemical form on consequences 79—74574
fast breeder reactor floor response spectra direct calc. 77—38327
fast reactor, time series analysis and forecasting for ANL TREAT expts. 78—13289
fast reactor boiling detection by noise analysis 79—13449
fast reactor disassembly, fuel vapour expansion work energy calcs., effect of eqn. of state uncertainties 78—8940
fast reactor whole core accidents, fission products role 78—54854
FBR accidental releases, implications of dose-mortality relationships 80—46064
FBR LOF accident, first visual in-pile fuel disruption experiments 79—49747
FBR notional accidental releases, effect of duration on consequences 80—94296
fission reactor, industrial accident involving radiation exposure in Washington State, worldwide impact 77—3122
fission reactor, PWR, with loss of coolant, computer-aided calc. *(Slovak)* 78—29594
fission reactor LOCA, transient flow boiling anal. method 79—26549
flash floods, American National Weather Service (NWS) warning and disaster preparedness program 79—25289
fuel element damage at Three Mile Island Nuclear Power Station, thermodynamic aspects *(German)* 79—93739
fuel failure behaviour of unirradiated fuel rods under reactivity initiated accident conditions *(Japanese)* 79—30955
fuel-pin failure threshold, effect of pellet density and axial restraint 78—17367
fusion reactor LOCA, performance of shield and magnet 77—67880
fusion reactor LOCA accidents in Li cooled fusion blankets 78—777
fusion reactors, air detritiation operation, computer model and scale expt. 78—66413
fusion-fission hybrid blanket designs, accidental criticality 78—778
fusion-fission hybrid power reactor, blanket cooling under LOCA conditions 78—775
gamma radiation dosimetry, Al_2O_3 TLD 78—57076
gas-cooled fast breeder reactor depressurisation transients without scram, anal. 77—14246
GCFR, effect of accidental steam entry on reactor parameters 78—33277
GCFR, fission gas release and molten fuel motion for slow overpower transient 78—17369
GCFR, thermal radiation effects on subassembly wall failure 78—8938
GCFR core support structural assembly, seismic response via modal synthesis 78—89942
German nuclear power stations, assessment of accident risks 80—18517
Harrisburg reactor accident in 1979, lessons to be learned *(German)* 80—91233
HCDA, radiological consequences, attenuation due to radiative cooling 78—13296
HCDA due to transient overpower, model for prediction of press. in core and upper plenum 78—8926
HCDA in FFTF, dynamic anal. of hydraulic press. wave propag. in plastically deforming pipe 78—8876
HCDA in LMFBR, UO_2 mech. response to transient heating 77—14237
heat transfer from round-bottom pool with internal heat generation, expt., LMFBR appl. 79—13470
high-level waste solidification plant, contribs. to risk evaluation 78—17356

accidents continued
- HTGR, consequence anal. of hypothetical accidents, core heatup and afterheat removal 78—58381
- HTGR, control rod ejection accident, comparison of one- and two-dimens. models 78—13279
- HTGR, fuel failure anal. following LOCA, post-accident temp. response 78—13276
- HTGR, maximum pot. hazard of ultimate accident sequence initiated by PCRV leak 78—13278
- HTGR, unlimited core heatup, fission product release, hypothetical accident anal. 79—6754
- HTGR containment, layering and combustion following depressurization accident 78—13277
- HTGR fission product release following LOCA 79—13457
- HTGR hypothetical accidents, consequences following breach of primary circuit and safeguard failure *(German)* 78—58390
- HTGR PCRV depressurisation accident, anal. of gas circulation using HAZARD code 79—54561
- HTR, expt. JAERI, safety anal. of fission product behaviour and hypothetical accident *(Japanese)* 78—66330
- HTR pebble bed heat transport, particularly radiation, in hypothetical accidents *(German)* 79—49791
- HWR, explosive rupture of power channel pressure tube 78—70605
- hypothetical meltdown accident, large-scale steel melt/concrete interactions test 78—17387
- ICEPEL code comparisons for flexible pipe elbow loop 79—49772
- ignition and extinguishment in simulated LMFBR accident conditions 78—8932
- in-core molten fuel pool expt., heat flux and struct. ablation 79—13407
- in-pile post accident heat removal facility, feasibility study 79—49774
- industrial explosions and fires, sparks from charged stack plumes 77—5315
- industrial radiography, accidental over-exposure to ^{192}Ir source 77—56472
- industrial radiography radiation exposures, causes, safety training program 80—17141
- investigation, advance prep. 78—57083
- ionising radiation, conclusions from unusual events in German Democratic Republic 78—53520
- ionising radiation exposure, dose estimation using TSC in human nail 78—73253
- laboratory instrumentation, causes of accidents and prevention 79—80594
- laser fusion power stations, potential accidents 78—776
- liquefied natural gas spills on land and water, dispersion hazard 77—45141
- liquid cooled fast reactor HCDA, fluid filled vessel response to internal explosions 79—49771
- LMFBR, accident conditions, theoretical anal. of Na fire using SPOOL-FIRE code 77—14248
- LMFBR, accident progression for loss-of-heat-sink with scram 79—81022
- LMFBR, accidental Na release as peroxide aerosol, effect on tomato and lettuce *(French)* 78—8997
- LMFBR, acoustic anal. of TREAT safety test R8 78—13290
- LMFBR, bubble worth calcs. using probability table method 78—13306
- LMFBR, cladding meltdown phase for loss-of-heat-sink event during shutdown 78—8923
- LMFBR, Clinch River, assessment of containment response to hypothetical core melt-through accident 78—8928
- LMFBR, Clinch River, consequences of boiling in radial blanket due to hypothetical major pipe leak 78—8922
- LMFBR, Clinch River, humidity effect on burning rate of Na droplets, Fick's eqn. anal. 78—13297
- LMFBR, Clinch River, LOCA in one heat transport loop without reactor trip 78—8924
- LMFBR, Clinch River Plant, pipe rupture simulation using DEMO code 78—8927
- LMFBR, Clinch River Plant, sensitivity for radiological consequences to var. in aerosol parameters 78—13294
- LMFBR, containment, safety anal., conf., San Francisco (Aug. 1977) 77—71664
- LMFBR, containment building response to HCDA, risk assessment, computer anal. 77—71678
- LMFBR, containment codes appl., response predictions in HCDA conditions 77—71670
- LMFBR, core meltdown event, transient containment response, inherent retention capability 77—71677
- LMFBR, dynamic response of reactor vessel to HCDA 77—71674
- LMFBR, flow instabilities of molten core debris pool following accidents 78—8931
- LMFBR, fluid-to-struct. heat transfer effects on structural damage pot. 79—81023
- LMFBR, fuel motion pot. due to volatilisation of metallic fission product inclusions 79—49746
- LMFBR, HCDA, accident energetics assessment 77—71667
- LMFBR, HCDA, core debris behaviour, interaction with concrete 77—71676
- LMFBR, HCDA anal., effects on reactor struct., radiological consequences 77—71666
- LMFBR, heat and mass transfer behind heated reactor cell liner following hot Na spill 78—17388
- LMFBR, hypothetical LOCA, fission gas role in transition phase development 78—8935
- LMFBR, inherent safety features 80—106145
- LMFBR, large, systematic method for constructing low Na void heterogeneous cores 78—13220
- LMFBR, LOFT for loss-of-piping-integrity transient, expt. data and COBRA-3M comparison 78—17370
- LMFBR, molten cladding film relocation following HCDA, large wave dynamics 78—17365
- LMFBR, molten fuel pins, Sandia's safety research program, United States 77—10484
- LMFBR, multichannel cladding relocation model for loss-of-flow accident 78—17366
- LMFBR, natural convective cooling of fuel debris bed following HCDA 78—8929
- LMFBR, nucl. performance of reactor designed to preclude energetic HCDAs 78—13307
- LMFBR, parametric safety analyses for reduced energetics in PLBR-sized core 78—13298
- LMFBR, prompt critical excursion, disassembly energy release for mech. damage evaluation 77—71668

accidents continued
- LMFBR, SNR-300, HCDA anal. by failure incoherence modelling, HOPE computer code 77—88237
- LMFBR, SNR-300, HCDA expt. simulation, theory reliability test 77 71675
- LMFBR, struct. response to HCDA, appl. of coupled Euler Lagrange computer program 77—71671
- LMFBR, thermal radiation effects on subassembly wall failure 78—8938
- LMFBR, unified model for fission gas release and Na boiling in reactor coolant channel 78—8921
- LMFBR accident material compatibility studies for PAHR in-core molten pool expt. 78—8933
- LMFBR accidents, licensing decisions and safety research 79—26651
- LMFBR core disruptive accident anal., heat transfer effects 77—74949
- LMFBR debris bed simulation expt., in-reactor expt. 79—13404
- LMFBR fuel assembly, edge blockage in 19-pin Na-cooled bundles 78—13292
- LMFBR HCDA, fuel condensate solidification onto steel struct. in above-core region 78—17364
- LMFBR HCDA, heat transfer from pool of molten UO_2 to concrete slab 78—8930
- LMFBR HCDA, hydrodynamic/neutronic coupled code FX2-POOL 77 -23219
- LMFBR HCDA, molten fuel freezing in shield plug 78—8941
- LMFBR HCDA, pipe rupture following earthquake, accident course 78—8925
- LMFBR HCDA, simulation of fuel-speed pool during transition to transition phase 78—8937
- LMFBR HCDA, study of natural convection in porous media with heat generation 77—51114
- LMFBR HCDA, vapour bubble-liquid slug heat transfer, Taylor instability mechanism 78—8939
- LMFBR HCDA, wave propagation ICECO code predictions in rigid 2-dimens. vessel 79—49770
- LMFBR HCDA analysis, effect of condensation on dispersion of closed boiling UO_2 78—8936
- LMFBR head closures, dynamic struct. response to HCDA 78—70617
- LMFBR LOF accident, analysis of in-pile fuel disruption experiments 79—49748
- LMFBR maximum critical accident, assessment using theory of aerosols coagulation 77—3121
- LMFBR prompt burst calcs., FX2-TWOPOOL code for hydrodynamics, thermodynamics and neutronics 79—49767
- LMFBR safety against propagation of local subassembly failures, CDA conditions 77—18673
- LMFBR safety analysis, computer code for determ. of aerosol attenuation in leakage paths 78—13293
- LMFBR safety and fuel cycle, accident anal. 79—26650
- LMFBR simulated meltdown configs., reactivity worths 79—81036
- LMFBR vessel structural response to HCDA, model tests *(Japanese)* 77—67829
- LMFBRs evaluation of local accidents out-and in-pile expts. 79—26652
- LOCA, condensing heat transfer coeff. based on mass condensation 78—13304
- LOCA, fuel element behaviour during high-temp. transients, ELOCA code 79—81043
- LOCA, quench phenomena correlation for bottom flooding 79—54520
- LOCA anal. in Federal Republic of Germany, computer models 79—26642
- LOCA capability code for utility appl. 78—21690
- LOCA in LWR, props. of core melts, viscosity thermal cond., specific heat 77—14247
- LOCA mathematical models for PWR safety analysis *(Russian)* 79—30963
- LOFT L2-4 test and FLOOD4 code, PWR reflood behaviour anal. *(Japanese)* 79—97824
- Lucens reactor accident, alarm and surveillance 78—50283
- LWR, accidents, effects and damages 80—22961
- LWR, commercial, evaluation of human errors and operator reliability 78—17373
- LWR, fission gas release high-burnup fuel during transient heating 78—13283
- LWR, fuel rod microstruct. changes associated with post-DNB operation during power-cooling-mismatch 78—21688
- LWR, LOCA conditions, fuel rod behaviour, code system SSYST-Mod 1 calcs. 77—88248
- LWR, LOCA separated air-water two-phase flow, mathematical anal. *(Japanese)* 79—36334
- LWR, pipe system failure characts., effects on plant availability and capacity 78—17375
- LWR, post-LOCA γ-ray energy redistrib. and effects 78—13280
- LWR, power cooling mismatch accident, molten fuel radial motion and cladding melting 80—13638
- LWR, thermal interaction of molten core materials with water 78—17383
- LWR 1300 MWe system, design of containment to withstand core melt 78—66335
- LWR accidents, containment venting and filtration approaches 79—13465
- LWR blow down accident, French studies, assessment codes *(French)* 79—26641
- LWR core barrel model, circular cylindrical shell, dynamic response to nonaxisymm. loading 77—88247
- LWR core melt, steam explosion parametric study *(German)* 77—6527
- LWR core meltdown, activity release and aerosol characts. 78—82469
- LWR fuel elements, behaviour under accident conditions 79—26545
- LWR fuel failure under reactivity initiated accident conditions, NSRR experiments *(Japanese)* 79—36340
- LWR fuel reprocessing and mixed oxide fuel fabrication plant safety 79—26710
- LWR hydrogen formation during core melt accident 78—50267
- LWR hypothetical core meltdown, vapour explosion potentials at high interface temp. 79—13476
- LWR LOCA analysis, TRAC-1D code for Standard Problem 2 78—13288
- LWR post-accident aerosol removal, steam condensation expt. 79—13456
- LWR power plants, radioactivity release in LOCA uncertainties 79—26639
- LWR pressure boundary failure and LOCA studies 79—26640
- LWR ruptured fuel rods in LOCA, fission product release, computer modelling 79—49780

accidents continued
- LWR safety research in the Federal Republic of Germany 79−26638
- LWR with superheated steam isolation valve, blowdown expts. 79−625
- LWRs, accident prevention study 78−66356
- LWRs at Harrisburg and Mulheim-Karlich, safety systems comparison *(German)* 80−22966
- mixed-oxide fuel fabrication plant, large commercial, accident radiological risk assessment 78−17401
- mobile He cooling loop system for post-accident heat removal expts. 79−13403
- molten core debris contact with Na, particulate debris bed formation expt. 79−13405
- molten fuel-coolant interaction studies, simulated reactor accident, windscale shock tube rig 78−58363
- MSBR, locked rotor accident anal., point reactor model 79−54521
- National Arrangements for Incidents involving Radioactivity, NAIR 78−65136
- neutron dosimetry methods for accidental exposures, Czechoslovak intercomparison 78−57075
- non-nuclear energy systems, accidents and unscheduled events 79−52861
- NORHAV—a Nordic reactor safety evaluation project 79−26619
- nuclear, emergency planning and preparedness 80−57887
- nuclear, HCDA, REXCO code, comparison with flexible vessel expts. 78−70618
- nuclear, Three Mile Island anal. 80−18457
- nuclear accident dosimetry, blood-Na meas. 80−57979
- nuclear accident dosimetry intercomparisons at US Health Phys. Research Reactor (1965-1978) 80−32520
- nuclear accident dosimetry system, Czechoslovakia 80−57978
- nuclear accident dosimetry system for criticality accidents 77−88288
- nuclear accident dosimetry systems, Czechoslovak-Hungarian comparison 79−45437
- nuclear accident features affecting emergency measures 78−55055
- nuclear accident phenomena, human elements *(French)* 78−57084
- nuclear accidents, review 79−618
- nuclear accidents, review 79−3207
- nuclear accidents, use of mobile remote-handling equipment *(French)* 78−53525
- nuclear accidents in power stations of Electricite de France, protection organisation *(French)* 78−55049
- nuclear contamination, radionuclide inhalation reduction using indoor shelter 77−34478
- nuclear emergency conditions, monitoring and handling 78−57082
- Nuclear Energy Research Centre, Mol, Belgium, emergency plan organisation in event of major accident *(French)* 78−53527
- nuclear energy system, fuzzy set theoretic approach to systems analysis 78−17352
- nuclear fuel, irradiated, highly radioactive, safe transportation 77−74956
- nuclear fuel cycle, risk estimation, evaluation, and management 78−17350
- nuclear fuel cycle plants, accident anal., special completeness proof for licensing 80−817
- nuclear fuel transportation in Canada, emergency planning 78−50411
- nuclear industry safety criteria 77−65302
- nuclear installation safety assessment criteria in UK 79−26615
- nuclear installations safety, report on 1977 IAEA conference *(Dutch)* 77−83047
- nuclear plant building walls, differential press. during tornadoes, computer program 77−38349
- nuclear plant column section seismic design subjected to three components of earthquake 77−38355
- nuclear plant equipment response to aircraft impact 78−50416
- nuclear plant risks assessment 78−50281
- nuclear plants, protection against chemical explosion induced shock waves 77−38351
- nuclear power, human factors, safety system problems and risk assessment 80−22968
- nuclear power plant, aircraft impact, simplified derivation of reaction-time history 78−89958
- nuclear power plant, failure probability of battery system following loss of AC power 78−17376
- nuclear power plant, fast alarm system to optimise protection of public 78−55048
- nuclear power plant, fire hazard 78−50269
- nuclear power plant, Three Mile Island, breakdown *(Hungarian)* 80−18454
- nuclear power plant, Three Mile Island accident, commission report 80−32372
- nuclear power plant, TMI-2, breakdown consequences *(Hungarian)* 80−18455
- nuclear power plant blast effects due to gas cloud explosions 77−38350
- nuclear power plant emergencies, prevention of excessive irrad. of staff and population *(Russian)* 78−50286
- nuclear power plant safety, West German policy *(German)* 80−57865
- nuclear power plants risks assessment, German Risk Study *(German)* 80−57866
- nuclear power reactor accidental release, isopleth method for population reaction 79−13533
- nuclear power reactor emergency medical assistance programmes 78−53532
- nuclear power station, coolant unsteady flow, with discharge from high-pressure vessel *(Russian)* 79−89448
- nuclear power station, due to loss of coolant, multiple-element model and computer solution 78−66358
- nuclear power station, hot water leakage from first loop, 22.8 MPa initial pressure, flow characts. 78−66357
- nuclear power station, Three Mile Island, accident, malfunction development, prevention *(Hungarian)* 80−68846
- nuclear power station at Harrisburg (TMI-2) fuel element defects quantitative calc. *(German)* 80−23105
- nuclear power station leak, ^{133}Xe from Three Mile Island 80−89696
- nuclear power stations, HTGR risk assessment, operator actions, event and fault tree anal. 80−63330
- nuclear power stations, in New England, seismic risk anal. 77−86785
- nuclear power stations, prevention, 1300 MW nuclear reactor steam isolating valve blowdown tests *(German)* 80−22967
- nuclear power stations *(Portuguese)* 80−68844
- nuclear power stations in Italy, district emergency exercises 78−55052
- nuclear reactor, assessment by reliability technique 77−30653
- nuclear reactor, human errors in high stress situations, data and assessment 78−17374

accidents continued
- nuclear reactor, impulse-initiated gas release triggering vapour explosion 78−17384
- nuclear reactor, LOCA, strain in Zircaloy clad of fuel pins 78−699
- nuclear reactor, LOCA causing core meltdown, vapour explosion caused by water entrapment with melt 78−17382
- nuclear reactor, post-accident heat transfer, Leidenfrost temperature for spherical fuel particles 78−17371
- nuclear reactor, radioactive releases and waste disposal, CEGB Research Division report 78−46145
- nuclear reactor, struct. shielding against gamma-ray sources, dose reduction factors 78−13251
- nuclear reactor, thermal decomp. of concrete in hypothetical fuel meltdown accident 78−17386
- nuclear reactor accident, dosimetry calcs., comparison with expt. data 79−36422
- nuclear reactor accident, human exposure to radiation, biological consequences 78−7407
- nuclear reactor accident dispersion model, direction depend. probability limits consistent with NRC practice 78−17372
- nuclear reactor accident risk calcs., models and data 80−47613
- nuclear reactor accidents, meas. of crit. environmental exposure by I radioisotopes 78−57081
- nuclear reactor concrete shield, interaction with molten core material, heat flux determ. 78−17385
- nuclear reactor LOCA reflood phase, hydrodynamics, moving control vol. method 78−704
- nuclear reactors, LOFT, contribution to safety 80−106139
- nuclear reactors, molten fuel-coolant interaction modelling, INTER and CEFRA *(Czech)* 78−66352
- nuclear reactors, radioiodine air sampling system, separation into gaseous and particulate fractions 80−57962
- nuclear reactors, radiological emergency monitoring and instrumentation, Federal guidance 80−57961
- nuclear reactors, UK standards and procedures 79−81032
- nuclear safety exercises carried out in French industrial facilities *(French)* 78−55051
- nuclear spent fuel overheating in pool drainage accident, protection 79−85639
- nuclear spent fuel shipping systems, full scale tests in extremely severe accident environments 79−26582
- nuclear wastes, risk evaluation model, on-site meteorological data 80−36155
- oxide crust thermal stress effect in LMFBR accident 79−13471
- PBF, cladding temperature, deform., and failure threshold 78−13281
- PBF blowdown tests, thermal hydraulic and mechancial deformation 79−81024
- plutonium, biologically important physicochemical props. and methods of human contamination *(French)* 80−98004
- post-LOCA containment atmospheres, physical state 79−76087
- power plant effluents, gaseous, AEOLUS code for dispersion during normal, sea-breeze, and accident conditions 78−11993
- power reactor, seismic trip system, risk assessment 78−17377
- prompt burst energetics experiments, UC series, fuel cladding coolant systems 79−49768
- prompt burst excursion experiments, fuel pin modelling 79−49769
- PWR, determ. of typical accidents and consequences, rel. to emergency planning *(French)* 78−50285
- PWR, LOCA performance test of upper heat injection system 79−81028
- PWR, LOCA test, effect of LOFT pressurizer on RELAP4/MOD5 modelling 78−13286
- PWR, meltdown accident risk-analysis 79−45375
- PWR, peak cladding temp. sensitivity to LOCA reflood parameters 78−86639
- PWR, Three Mile Island, Pennsylvania, USA LOCA 79−89398
- PWR accident prevention, extra instrumentation for Ringhals 2 station, Sweden 80−63369
- PWR coolant system under seismic and LOCA loads, dynamic anal. 77−6512
- PWR ice condenser plant, dominant accident sequences 79−85646
- PWR LOCA, drift flux appl. to transient two-phase level swell 79−81027
- PWR LOCA, effect of cold-leg injection of low press. coolant, ROSA-II study *(Japanese)* 78−17334
- PWR LOCA, ROSA-II severe hot leg break for core cooling during blowdown *(Japanese)* 79−9769
- PWR LOFT project, design and results *(Dutch)* 80−42735
- PWR main circulation pipe breakdown, mathematical model for primary circuit processes *(Russian)* 77−38368
- PWR power plant, assessment of underground siting as engineered safety factor 78−13316
- PWR reactor, steam generator accidents, rel. to impurity enrichment in boiling on surface coated with porous struct. 78−2365
- PWR reactor with reactivity perturbations, accident anal., methodical approach *(Czech)* 79−22402
- PWR reflood simulation of FLECHT-SET system using RELAP4/MOD6 78−13285
- radiation accident casualties, organisation and planning of medical aid *(French)* 78−53528
- radiation accident casualty, organisational forms of medical care in German Democratic Republic 78−53529
- radiation accident caused by ^{192}Ir radiography source 78−53514
- radiation accident handling, conf., Vienna, Austria (Feb.-Mar., 1977) 78−53518
- radiation accident management, participation of nucl. medicine technologists 77−56486
- radiation accidents, effects on public, casualty management 78−53519
- radiation accidents, follow-up study programme for irrad. persons 78−53522
- radiation risks in nuclear industry, comparison to other jobs 80−18680
- radioactive, high-level vitrified waste, risk anal. of repository in geologic salt formation 78−17362
- radioactive, low- and intermediate-level waste, risk anal. of road transport in Netherlands 78−17359
- radioactive glove box accident, surgical treatment of wound contaminated by ^{239}Pu and Am *(French)* 78−53521
- radioactive high-level waste management systems in Germany, risk analysis 78−17354
- radioactive material transport, statistical anal. of low-radiation packages 77−88286

accidents continued
radioactive materials, IAEA transport information collection system, influence on improved safety measures 80—63413
radioactive waste, risk analysis for management system, safe design 78—17351
radioactive waste management system 78—17353
radioactivity incidents, national arrangements, review 80—102355
radioactivity release to environment, late effects on population 78—15861
radiological accidents, operational organisation *(French)* 78—53531
Radiological Emergency Response Planning and Preparedness Training Programmes, USA 78—57079
radiological emergency response training programme 78—57080
radiological major accidents, USA planning guides 78—53526
radionuclide users in Israel, surveillance and accident prevention 78—57077
Rasmussen report on reactor safety, retrospective and prospective view 79—26632
reactor accident consequences, estimated, effect of appl. of surface depletion model 80—30622
reactor accidents and the environment 79—30940
reactor containment leakage from Na fire anal., response surface method, SPOOL-FIRE code 79—18004
reactor containment liner seismic reliability under statistical uncertainty, cracking 78—89948
reactor incident duct plugging by aerosol deposits, simple model 79—49782
reactor large-bundle LOCA expts., fuel rod ballooning probabilistic analysis 79—13462
reactor molten clad relocation during unprotected undercooling transient 77—38348
reactor radioactive products transport, model, air concentration in working rooms *(Russian)* 77—42110
Reactor Safety Study (Wash-1400) and implications for radiological emergency response planning 78—50284
reactor single core subassembly model, coupling of struct. and coolant response 78—8934
risk assessment in absence of complete data, freq.-consequence model 77—83062
risk evaluation of high level waste solidification plant 78—50273
road accidents in Ahmedabad city (1972-5), possible effects of geomagnetic fluctuations 78—15958
SAREF test fuel motion reactivity feedback, experimentally based limits 79—49775
semiscale isothermal blowdown, appl. of self-initialized RELAP4 momentum eqn. 78—13287
Seveso, environmental contamination assessment, effectiveness of treatments 80—3558
SGHWR safety design and evaluation 79—26636
simulated meltdown experiment, modified diffusion coeffs. for neutron streaming 78—33278
Soviet nuclear disaster, 1957-8, radioactive waste origin 80—45823
spent fuel casks under extreme accident conditions, behaviour prediction 77—71663
spent reactor fuel, risk analysis of alternatives from reactor pool until final disposal 78—17355
spent-fuel rail cask system, high-speed impact and fire test 79—59206
steam generator, modular, liquid Na heated, pressure and temp. loading in breakdown situation *(Czech)* 78—50264
Swiss emergency organisation for nucl. and chem. accidents 78—57078
Swiss Federal Institute for Reactor Research emergency organisation 78—55047
thermal explosions, fragmentation requirements for detonation 78—71368
thermal power reaction, 3-dimens. transient anal., finite difference and spacetime synthesis methods 79—17989
Three Mile Island, Unit 2 accident, noble gas releases 80—47616
Three Mile Island, accident account and status of nuclear security *(French)* 79—81033
Three Mile Island, Japan Safety Commission preliminary report *(Japanese)* 80—22972
Three Mile Island, lessons learned in maintenance and reliability 80—57929
three mile island, LWR *(Korean)* 80—32355
Three Mile Island accident conclusions and recommendations *(German)* 80—47588
Three Mile Island incident, Atmospheric Release Advisory Capability, response and support 80—57889
Three Mile Island incident, operator/instrumentation interactions 80—57890
Three Mile Island incident, Pennsylvania's emergency preparedness and response 80—57888
Three Mile Island malfunction, monitoring, radiation exposure 80—57960
Three Mile Island nuclear power station, viewpoint of member of Commission of Enquiry 80—83190
Three Mile Island reactor accident, radiological consequences 80—27771
THTR 300 MW(e) prototype reactor, safety anal. under extreme accident conditions 79—31087
traffic accidents correl. with rainfall, St. Louis area 79—16604
transient fission gas release effects on carbide fuel failure dynamics 79—49762
transient process dynamics in reactor with dissociating coolant *(Russian)* 77—42050
transportation of nuclear waste material, risk analysis 78—17357
TREAT TOP experiments, applicability to post failure dynamics 79—49765
tREAT TOP test H6—preliminary results for transient overpower 79—49763
tREAT transient overpower experiment R12 79—49764
UMFBR molten core debris and core containment material interactions 79—13469
US reactor safety principle evolution, accidents and safety systems 79—26613
vitrified high-level radioactive waste, rail transportation, fault tree anal. and accidental release 78—17358
vitrified high-level waste, calcs. of radioactivity release due to leaching in final disposal 78—17360
VVER-440 reactors, emergency operating conditions following main circulation pipe failure, computer aided anal. 79—9823
WWER reactor safety problems, LOCA prevention *(Russian)* 79—26629

accidents continued
X-ray fluoroscopy, acute radiation injury caused by faulty use during cardiac procedures 77—9272
Zircaloy clad fuel rod burst behaviour in simulated PWR LOCA 79—36337
^{241}Am source ingestion, case report 78—28088
^{60}Co 20 Ci source, site radiography incident 78—53523
^{60}Co 3000 Ci source accidental fall and retrieval in teletherapy room 78—53524
^{60}Co hot cell accidental exposure 77—9261
^{60}Co teletherapy unit, mech. fault affecting source position 77—73562
^{203}Hg-methyl mercury chloride retention in man after inhalation 77—9277
I radioisotopes, high efficiency mixed species air sampling, readout and dose assessment system 78—57074
^{125}I accidental inhalation, bioassay and thyroid monitoring results 78—24151
^{115m}In specific activity determination, for nuclear accident dosimetry 79—3248
NH_3, liquid anhydrous, spill onto water, air pollution 77—73846
N_2O_4 gas cooled fast reactor power stations, nuclear and chemical safety *(Russian)* 79—26655
Na pool fuel vapour and aerosol transport in HCDA 79—13455
Pu accidental release at Thule, Greenland, environmental behaviour 77—56656
$^{106}RuO_4$ in lung, in vivo meas. and dosimetry 78—53515
UF_6 centrifuge cascade, power supply loss accidents anal. 79—13502
UO_2 fission vapourised fuel, aerosol close in sampling, accident safety 79—49779
UO_2 heat-generating, molten, interaction with MgO brick 79—13468
UO_2 molten, interactions with steel and graphite 79—49700

accommodation coefficient *see sorption*

accounts data processing
nuclear inventory and management system program for fuel accounting 78—13245

accumulation layers
Gunn diode, anode domain disappearance dynamics, computer simulation calcs. 80—6859
heterostructure solar cells, polycryst., grain boundary effects 78—52063
III-V compounds, electron transport in quantised inversion and accumulation layers 79—60935
inhomogeneous media, surface plasmon dispersion 77—28229
ionic solids, surface phonon-plasmon coupling (surface plasmarons) 80—54497
MOS structures, quasi-2-dimens. system, review 79—33352
p-n heterojunctions, forward-biased, charge accumulation 80—107902
semiconductor, quasi-two-dimens., polar-optical phonon scatt. 78—72237
semiconductor coatings, space charge effects on triboelec. charge exchange 80—54763
semiconductor surface space charge layers, subband struct., perturbation theory 80—84497
semiconductor surfaces, electron-electron interaction and electronic props. of space-charge layers 78—60210
semiconductor-piezoelectric structs., surface pot. influence on acoustoelec. interaction 78—10516
semiconductors, with deplation or accumulation layers, surface plasmon dispersion 77—1464
X-band oscillators, voltage distrib. using SEM 78—38152
p-CdTe-Langmuir film interface, prep., characters. and MIS struct. 80—92998
n-GaAs MIS structs., native oxide, effect on interface props. and removal by sputter etching 79—11228
GaAs MOS structure, props. of surface carriers 77—20453
n-GaAs-anodic oxide MIS devices, inversion and accumulation layer form. at elevated temps. 79—60934
GaAs-insulator interface, elec. props. 78—95370
p-GaSb, accumulation zone effect on photocond. *(French)* 77—24582
GaSb, localised carrier interaction with LO phonons, Raman interference lineshapes 80—93338
n-Ge, low-energy Ar^+ ion bombard. effect on electron scatt. 77—66205
$Hg_{1-x}Cd_xTe$-oxide interfaces, MIS capacitance characts. 80—49926
InAs, heteroepitaxial, far IR refl. and transmission meas., surface and interface effects 80—16044
InAs surface accumulation layers, magneto-transconductance study 80—49948
InAs surface layers, oscillatory transport coeffs. 78—64136
InAs, two dimensional accumulation layer, Anderson localisation 80—107871
InSb (110), cleaved, gap states, field effect meas. 80—84501
InSb based MIS structs., charge accumulation in insulator layers 80—6993
n-InSb, in MIS struct., sub-mm cyclotron reson. obs. 77—39912
InSb, localised carrier interaction with LO phonons, Raman interference lineshapes 80—93338
p-InSb·MIS struct., field effect studies 80—80386
n-InSb, surface accumulation layer, sub mm electron cyclotron reson. 78—6576
$Pb_{1-x}Sn_xTe$ epitaxial films, adsorption-induced accumulation layer form. on surface 80—60117
n-PbTe, accumulation layer, quantised surface states 80—20279
PbTe, surface space charge layers, magnetorefl. study 78—52475
PbTe, surface space charge layers, magnetorefl. study 78—64349
PbTe surfaces, tunnelling spectroscopy in MOS and Schottky barrier junctions 80—49945
Si (100), surface space charge layer, inter-subband optical transitions 77—15931
Si (100) surface accumulation layer, subband struct. and inter-subband absorpt. in strong mag. field 78—39177
Si (100) surface electrons, effective mass and collision time 78—34909
Si (100) surface electrons, effective mass and collision time 78—64081
Si, (100) surface space-charge layer, intersubband cyclotron combined resonances 79—69571
Si, accumulation layer, intersubband-cyclotron combined resonance, theory 80—20278
Si MOSFET structs., photocond. meas. rel. to intersubband transitions 78—64127
n-Si, surface cond. anisotropy in accumulation layers 78—10536
Si, surface space charge layer, electron subbands, mag. field effect 77—20393

accumulation layers continued
  Si, temp. depend. of inter-subband transitions, many-body effects 79−60899
  Si, thermally oxidised surfaces, electron mobility in inversion and accumulation layers, MOS devices 80−103753
  n-Si-SiO_2 interface, hot carrier surface thermo EMF depend. on surface band bending 80−44734
  ZnO, accumulation layers, correlated behaviour of Hall mobility and work function 78−60185
  ZnO, adsorption of H, space charge accumulation layers effect on secondary ion yields, H conc. meas. 79−83087
  ZnO crystals, adsorbed dye laser, charge transfer, field effect and spectrally sensitised photocond. meas. 80−49815
  ZnO, ESR and NMR studies of adsorbed H_2 *(Japanese)* 80−50186
  ZnO electrolytic contact quantisation effects, self consistent quantum calcs. 79−60920
  ZnO, field-effect mobility in accumulation layers on polar surfaces 79−73509
  ZnO single csytals quantised accumulation layers, Hall mobility of electrons 79−60909
  ZnO surface, quantised accumulation layer magnetoresistance, spin scattering model 79−69529
  ZnO, surface phenomena, interpretation by compensation model 78−95323
  ZnO, surface phonon-plasmon coupling (surface plasmarons) 80−54497
accumulators *see secondary cells*
acidity *see pH*
acids, organic *see organic compounds*
acoustic analysis
  acoustic resonance in vaneless radial diffusers with swirling flows 79−18882
  aneurysm detection using one-bit correl. 80−17175
  annular and circular fan duct noise, radial and circumferential mode meas. 79−68529
  atmospheric infrasound waves recording method and computer anal. *(Russian)* 78−65407
  auditory analysis of sound, review 80−104593
  automatic speaker verification by cepstral analysis 80−91998
  cylinder, rotating, line-source radiation scatt., distant field calc. 77−50795
  dolphins, importance of isolation and anal. of emotional signals *(Russian)* 79−43934
  finite element, automobile exhaust system design appl. 78−51003
  gas turbine annular vortex shedding acoustic resonance analysis *(Japanese)* 80−14526
  infrasound signals, dynamic spectral anal. by FFT *(Chinese)* 78−1453
  lagged signal power spectrum in cross correl. 78−9502
  layer potentials for two dimensional mechanical vibrations *(French)* 78−59337
  LMFBR, acoustic anal. of TREAT safety test R8 78−13290
  LMFBR, acoustic anal. on Na boiling expt. in FFM Bundle 3B, Test 4 78−13291
  modal anal. of vibrating structures using transient excitation 77−62220
  modal analysis techniques, computer based, review 79−18651
  normal mode sound field in shallow water, positive sound vel. gradient, random fluctuation surface *(Chinese)* 77−34982
  off-axis beam pattern analysis using replica pulse representation 77−54821
  optimum resolution of signals with varying freq. 78−13862
  phonothyreogram and phonocardiogram frequency spectrum analysis by minicomputer, ECG reference time signal 79−83966
  piping systems, gas, time domain identification of standing wave parameters 79−18558
  plane two-dimensional motion in acoustic medium caused by kinematic excitation, Laplace transform study *(Russian)* 80−43503
  power cepstrum for echo detect. in multi-peaked wavelets 77−14855
  power flow between linearly coupled oscillators, statistical energy anal. 77−84022
  pulsed emission evaluation, freq. anal. appl. 78−18126
  random response of identical, one-dimensional coupled subsystems 80−102915
  rectangular cavity with rigid incomplete partition, acoustic modes 77−84031
  reverberation chamber LF sound power injection analysis and response averaging 78−42496
  ring source, fluctuating, with const. vel., power and freq. spectrum emitted 77−50796
  room acoustics analyser using public telephone line and computer 77−35004
  rotating machine flaw detection, acoustic signature analysis and time-domain techniques 79−50525
  ship propeller induced underwater acoustic disturbance obs. 79−68463
  signal rate of change distribution, gramophone player 80−79083
  soft tissue characterisation by US backscatter analysis 77−21586
  source location on spherical or plane surface 78−92421
  spectral information display in colour ultrasonogram 77−21584
  synthesis of sound by continuous spectral transformation *(French)* 80−79100
  Thermo-Acoustic Sensing Technique for noninvasive tissue analysis 77−64117
  time selector for acoustic spectrosc. 80−87660
  time-delay spectrometry, practical appl. in field 80−79082
  tissue US signal analysis methods 79−57737
  transfer function estimation, effect of reverberation, digital signal processing appl. 79−18616
  US spectrometry, physical basis *(German)* 79−7265
  US spectroscopy, impulse response eval. of US echoes *(German)* 78−26012
  US tone-burst spectroscopy, influence of phase cancellation and pulse shape artifacts 80−81276
  vibration of viscoelastic orthotropic layered cylinderical shell in acoustic medium, numerical anal. 77−54828
  Al alloy D16, supersaturated solid soln., decomp. process, electron microscope obs. and acoustic anal. *(Russian)* 79−15650
  AlMgSi, adhesive jointing, acoustic anal. *(German)* 78−7168
acoustic applications
  see also ultrasonic applications
  acoustic emission, structural calibration technique for quantitative appl. 78−9509
  aerofoil stall measurements, with acoustic flow control 80−23991
acoustic applications continued
  aerosol particles, sonic agglomeration 77−29411
  aerosols, single particle dia. and aerodynamic relaxation time from motion in acoustic field 77−80205
  aerospace acoustic emission instrumentation and applications 77−33322
  anemometer for boundary layer eddy correl. 80−56637
  atmosphere acoustic and radio acoustic exploration, effects of sound nonlinear absorpt. *(Russian)* 80−94567
  atmosphere acoustic sounding technique, appls. to siting studies 78−81467
  atmosphere remote sensing, performance of echosonde antenna 78−1474
  atmosphere sounding, appl. to boundary layer obs. from top of steep mountain 80−98409
  atmospheric sounder, design, wind velocity meas. appl., review 79−53528
  beacon guidance system for walking blind aid 80−81676
  beam forming with vibrator arrays, seismic field tests near Tulsa and Handy 78−61338
  bone fracture healing, sonic diagnosis 77−21580
  book, general aspects 78−30146
  bubble counting, review 77−42673
  buried pipe detection in sand using impulsive sound *(Japanese)* 77−88996
  cased wells logging, effect of excited wave freq. on results *(Russian)* 78−40707
  coagulation of aggregates of submicron particles in airborne dust 77−35011
  coastal breezes, dispersive, monostatic acoustic sounding system *(French)* 78−7683
  convection, instability, crit. slowing, config. inversion acoustic obs. 78−34133
  cryogenic liquids, technique for producing uniformly charged drops 77−49733
  crystallisation of supercooled liquid in sound field, steady-state dynamics 80−15223
  current meter for small-scale ocean turbulence resolution 77−41232
  diagnosis using nonlinear effects, asymptotic feasibility anal., props. of layer on halfspace object 78−63248
  Doppler sounder for wind profile meas. in boundary layer 78−65413
  dry hot rock hydraulic fracture characterisation acoustic instrumentation 77−33221
  elastic moduli meas., acoustic resonance method, temp. depend. 78−18264
  extrusion, benefit of vibrations 78−51135
  fast reactor safety, TREAT test R12, acoustic data anal. 79−93778
  fission reactor flow-induced control element movement, expt. investigation using noise analysis 80−788
  fracture toughness testing using acoustic emission monitoring 80−100918
  free gas concentration in liquids, rapid anal. by acoustic method 78−91041
  gas analyser design and performance 78−11603
  gas-liquid mixtures, flowing, gas conc. meas., acoustic method 78−59448
  granular media, density measurement, plane strain conditions, acoustic method *(Polish)* 80−62635
  high data rate acoustic telemetry system design 80−43573
  hot-wire acoustic method for convection meas. in gases and liqs. 78−45617
  imaging, visualization and characterization, conf., Houston, TX, USA (Dec. 1979) 80−106672
  imaging aid for the blind 80−104810
  impact sound stressing, appl. to lifetime control in Si 77−85238
  jet, free, aeroacoustic characterisation *(French)* 79−41727
  layered media, asymptotic analysis of nonlinear effects in acoustic diagnostics 77−84090
  leak detect. in LMFBR steam generator 78−29589
  leak detection in pressure vessels during hydraulic tests *(French)* 80−789
  level measurement for material arranged in arbitrary fashion in tank, errors 80−17921
  levitation, acoustic, liq., solid props. meas. appl. 80−43565
  levitation system, parametric study 80−74692
  LMFBR, acoustic anal. from Na boiling tests using THORS bundle 6A 79−31033
  LMFBR, acoustic resonances as means of blockage detection 79−93752
  LMFBR, effects on noncondensable gas bubbles on propag. of boiling acoustic noise 77−46364
  LMFBR boiling acoustic detection sensitivity, PFR commissioning expts. 79−13452
  LMFBR HCDA, appl. of acoustic agglomerators for suppression of Na-fire aerosols 79−54525
  LMFBR hypothetical accident, use of sonic agglomerators for aerosol particle suppression 79−36370
  LMFBR Na vapour bubble collapse detection 79−13451
  LMFBR steam generator leak, meas. of sound produced during steam injection into Na 79−93782
  LMFBR surveillance technique development 79−13448
  LWR primary coolant leakage detection using acoustic monitoring system 80−700
  materials testing methods, review 79−43504
  metal cutting, separation process tool tip, fracture detection, acoustic emission method *(Japanese)* 80−1388
  metals, thermal props. at high temps. meas., acoustic method 79−14222
  methane gas plumes, in atmosphere, tracking via acoustic sounder 80−55968
  microscopy, recent developments *(Japanese)* 78−79177
  microscopy, scanning acoustic, Gray scale 78−94494
  microscopy using scanning laser beam as remote sensing microphone 77−81382
  modal anal. of vibrating structures using transient excitation 77−62220
  monitoring of industrial chem. waste at deep water dump site 79−34466
  N-substituted amides, liquid, acoustic spectroscopy method for H-bond studies 79−96303
  NDT, failure prevention, test methods and equipment *(German, English)* 79−52560
  NDT using acoustic emission methods 80−28375
  neutrino detection, high-energy, using acoustic pulse from hadron shower *(Russian)* 77−38580
  noise measurements for plant surveillance and anomaly detection in nuclear power stations 79−97853
  nonlinear scanning and signal processing; bulk and surface wave interaction theory 77−50797
  nuclear power plant diagnostic system using noise anal. 78−50279

acoustic applications continued

- nuclear power station acoustic monitoring equipment 79—76076
- nuclear reactor core meltdown, acoustic meas. of penetration of molten metallic pool into concrete 80—13544
- ocean bed carbonate sediments, acoustic stratigraphy 80—21709
- ocean current parameters meas. from drifting ship 77—49189
- ocean density profile remote sensing by acoustic pulses, numerical algorithm 77—70893
- ocean tomography, for large scale monitoring 80—4119
- oceanographic free-fall instruments, position determ. using acoustic navigation system 77—29490
- oceanography, acoustics for sediment suspensions and shallow thermoclines 77—9523
- oceanography, remote acoustic monitoring of natural suspensates and slope/shelf water intrusions 79—2241
- particle agglomeration due to hydrodynamic collisions between monodisperse aerosols 80—26191
- particle agglomeration of aerosols under standing-wave condition 80—30627
- particle beam recording using acoustic detector 77—30727
- physical acoustics, review *(Polish)* 79—55258
- pipe gas flow, fluid-wall mass transfer, sonic oscills. enhancement 77—910
- pipeline flow measurement 80—43808
- plasma coatings, elastic properties, acoustic meas. *(Russian)* 80—97519
- polymers, defect elementary movement orientation from acoustic expts. 79—94927
- pulsed, inhomogeneous gas heating, acoustic wave temp. determ. 77—55175
- radiative absorption at surface, investig. of induced SAW rel. dispersion 77—51585
- reactor diagnosis by acoustic meas. methods, magnetostrictive and piezoelec. high-temp.-resistant sensors 80—32411
- reactor fuel pin rupture detection system, using meas. of time differential of acoustic emissions 80—102282
- reference equivalent, phonetic test to subjective meas. *(Polish)* 79—98572
- reflection acoustic microscopy, contrast 78—55533
- research over past 50 years, review 80—96151
- resonance-tracking circuit for acoustic levitation expts. 78—46874
- respiratory rate monitor using microphone pickup 79—79617
- river bedload transport measurement, calibration of acoustic device 80—56620
- rock structure analysis method *(Russian)* 80—85760
- sodar application in aviation 80—31132
- sonar mapping of lake bottom sapropel and sea shelf sediments *(Russian)* 77—9562
- Space Shuttle external insulation, acoustic emission inspection 78—16276
- specific heat of coatings, using transient acoustic Doppler effect 79—81706
- stress determ., improvement of accuracy 78—15631
- submarine sediments, automatic recognition by sonoprobe survey, acoustic reflection pattern model *(Japanese)* 80—85776
- tensile testing, acoustic emission signals interpretation 77—9030
- thermosonimetric investigation, of crystn. in metallic glasses 80—75180
- tube inspection, new device characteristics 77—68343
- ultrarelativistic charged particles traversing stable liquids, acoustic emission, particle detection possibility 77—61653
- underwater acoustic communications, swept carrier method for multipath interference suppression 79—3835
- underwater construction teams tracking, appl. of portable acoustic system 79—3874
- underwater surveys by submersibles, acoustic navigation system 79—5683
- US testing, time-domain deconvolution technique for signal identification 79—20306
- vacuum system protection for synchrotron radiation storage ring, acoustic delay line efficiency 79—88965
- velocimetry, corrected ray theory 79—41774
- vibration and shock testing of industrially produced substances, acoustic emission analysis *(German)* 80—3279
- viscosimeter technique for shear viscosity meas. 77—958
- volume gauge, infrasonic gas-dynamic, with pressure pulsations stabilisation 77—5806
- weightless liquid systems, acoustic manipulation in space 77—49716
- H_2 uniform solid spheres, prod. via acoustic excitation 77—74409
- Na boiling in LMFBR, acoustic detection using pulsed system 79—97839
- Na test loop boiling, acoustic detection expts. 79—13487

acoustic arrays

- 32 kW Doppler sonar for ocean internal wave meas. 80—46296
- acoustic beacon-aided navigation in the deep ocean 79—32166
- acoustic range for the measurement of the noise signature of aircraft during flyby operations 79—23134
- acoustic telescope appls. in architectural acoustics 80—5873
- acoustic-emission source location using 'face-centered' transducer arrays 79—24708
- acoustics, speech and signal processing, IEEE international conf., Washington, DC, USA, 1979 Apr. 79—55275
- acousto-optic deflector, anal. and design of flat transducer array 79—18527
- adaptive array processing, time and frequency domains 79—59874
- adaptive beam forming processor formulation 80—91967
- adaptive beamformer, adaptive or null-steering arrays 79—18621
- adaptive beamforming algorithm for resolving directions of sources in correlated field incident on array 80—64297
- adaptive cross-sensor beam forming with planar arrays 78—18121
- adpative antenna arrays, underwater, review 79—64467
- aliased arrays, processing, errors concerning calc. of max. likelihood estimator 79—41523
- ambient-sea-noise directionality measurement and processing 78—16025
- ANGUS, acoustically navigated geological undersea surveyor 80—4120
- annular array design and logarithmic processing for ultrasonic imaging 79—34615
- annular array search units, potential appl. in conventional US testing systems 80—35446
- atmospheric echo sounder, design from loudspeaker elements 78—87226
- axial field of parametric acoustic radiator 80—33290
- background noise spatial coherence, influence on high resolution passive methods 79—64387
- beam forming with vibrator arrays, seismic field tests near Tulsa and Handy 78—61338

acoustic arrays continued

- beamforming a towed line array of unknown shape 78—63230
- bearing estimation for source endfire to array 79—50515
- bias in bearing estimation resulting from source motion 78—29084
- bidimensional array design for B- and C-scan US imaging system 79—47877
- billboard array, high resolution cross-sensor beamforming 79—41520
- bispectral synthesizer for random signal with preassigned power spectrum 79—50513
- broadband constant directivity transducer, array shading function 79—14188
- broadband echo ranging system for measuring the frequency characteristics of fish schools 79—64390
- broadband parametric array with Gaussian primary directivity patterns 80—96066
- broadside vertical array in shallow water, comments on array gain 80—19138
- broadside vertical array in shallow water, reply to comments on array gain 80—19139
- broadside vertical line array gain in shallow water 79—41497
- calibration using standing wave tube as absolute sound power source 79—81674
- circular transducer array for ultrasonic inspection of plates and sheets 79—29293
- clustered sensor array, turbulent boundary layer induced noise suppression 80—96121
- coherence estimates for signals propagated through acoustic channels with multiple paths 79—50479
- compact planar array nearest-neighbour mutual interaction estimation 79—46160
- computer interface of ultrasonic flowmeters 78—38426
- computer-controlled acoustic beam steering and focusing with variable frequency array transducers 80—38191
- conformal array beam patterns and directivity indices, comments 79—41524
- conformal array beam patterns and directivity indices 78—55523
- crossarray beamforming with a parametric receiving array and a line array 80—79078
- curved face parametric projector design 78—51032
- CW coherence meas. at low freq. for long underwater paths 80—106654
- cylindrical array synthesis 78—38123
- cylindrical arrays with directivity patterns uniformly approximating a predetermined function, synthesis 78—38123
- cylindrical hydrophone array, analysis of acoustic fill time effects 80—19163
- digital beamforming 78—50989
- digital image focusing in the near field of a ralpled acoustic perture 77—60232
- digital phase shift beamformer, design and implementation 79—1034
- directional response control by modification of diffracted field 78—66973
- directional response of arrays with side baffles, geometrical diffr. theory 79—23115
- directivity patterns of plane-aperture arrays calcs. from meas. of radiated-field spectrum 80—38145
- dynamically focused array imaging systems, induced Doppler distortions 79—46117
- dynamically focused US diagnostic phased array 78—61232
- echo sounder array, for atm. surface layer vorticity meas. 78—7810
- edge-bonded surface-acoustic-wave transducer array 80—1395
- eigenvector decomposition of correlation matrices 80—96118
- electrically steered line array of piezoelectric vibrators 80—35486
- electroacoustic sound sources for non-directional sound radiation *(German)* 79—3876
- electromechanical coupling coeff. depend. on width to thickness ratio for plank shaped piezoelectric transducers 80—33383
- electronic high speed sector scan ultrasonic tomography improved in directivity by using signal processing technique 77—44729
- electronic sector scanning ultrasonotomography and its applications to cardiac diagnosis 77—66829
- element failure and random errors effect on sidelobe level for linear array 80—106670
- environmental influences on acoustic array design and performance in shallow water 80—83721
- etched arrays for medical imaging 79—25057
- farfield angular radiation pattern generated from arrayed piezoelectric transducers 80—33401
- fluctuations of the angle of arrival at a line array by a plane wave propagating in the ocean 80—43515
- four probe array for NDT 80—35499
- Fourier series method for detect. and localisation of acoustic signals in noise background 79—3861
- full-aperture beam forming delay line for wave direction-finding 80—48527
- gain for signals and noise having amplitude and phase fluctuations 80—43548
- gain limitations of passive vertical line array in shallow water 80—96117
- Gaussian acoustic signal detection using array processors, performance eval. 80—83696
- HF piezoceramic array, acoustical decoupling characts. of onionskin paper backing material 79—81675
- high resolution cross sensor beamforming for uniform line array 78—50988
- high-efficiency narrowband transducers and arrays, development 80—58880
- high-gain, nonstationary and nonuniform oceanic background 80—64263
- high-speed stress detection and imaging, 100-element acoustic phased array 79—47876
- highly directional acoustic beams, penetration into sediments 80—14511
- holographic piezoelectric integrated array, system anal. 80—79067
- hydrophone array response calc. errors due to two dimensional beam pattern assumption 78—66972
- hydrophones, linear array, robust formulation of optimum cross-spectral beamformer 79—68495
- hydrophones, optimum turbulent boundary layer induced noise suppression with suboptimum realizations 80—19161
- IC transducer array using electronically-addressed bulk acoustic wave Fourier transform device 80—74637
- image reconstruction, effect of spatial sampling 78—51021
- imaging of a two dimensional target by means of hologram matrix-an ultrasound experiment 79—23145
- imaging using impulsive sound 79—10431

acoustic arrays continued

- impedance image reconstruction, reflection and transmission techniques 79—53202
- in-line reflective array compressor 80—74626
- infinite periodic array of vibrating strips in plane acoustically compliant baffle 77—68305
- irregular, amplitude shading coeffs., steering, beam pattern generation 78—83178
- large time-bandwidth acousto-optic signal processors 79—46118
- line and planar, effects of random shading, phasing errors and element failures on beampatterns 79—64468
- line array, analytic expansion technique for ambient noise directionality determ. 79—90088
- line arrays, expt. data rel. to design 77—84099
- linear, waveguide attenuator using Helmholtz resonators, design calc. for zeroth normal mode 80—87602
- linear array real time US scanners, add-on modification for three dimens. displays 78—61229
- linear scanning with zone plate comparison with cylindrical focalisation 80—79091
- linear sonar array processor finite impulse response digital filter design 80—43549
- magnetostrictive transducer at air-water surface, effect of spherical scatterer on radiation reactance 80—48531
- marine seismic refl. data acquisition using extended arrays 78—77340
- mathematical model of sound amplifying systems in halls *(French)* 79—37090
- maximum entropy array processing 79—90087
- maximum entropy array processing for estimating bearing and strength of source 79—90087
- maximum entropy spectral estimation of frequency and arrival angle 80—96129
- maximum likelihood estimation of the position of a radiating source in a waveguide 79—90085
- maximum-likelihood estimation of source parameters from time-sampled outputs of a linear array 77—75751
- microphones, cross-correlation analysis for noise source location in industry 79—18601
- monolithic ultrasound array 79—3877
- monopole receiver and radiator arrays, continuous, active sound suppression 79—94386
- Moored Acoustic Buoy System suspended Kevlar array technology 80—43572
- motion limitations of an acoustic holographic system utilizing a scanned linear array 78—5616
- moving fibre optic hydrophone based on intensity modulation 80—43455
- multielement, characterisation by acousto-optic diffraction 80—99911
- multielement array underwater acoustic instrumentation 80—43571
- multielement sonar receiving array operating in reverberant environment 79—1020
- mutual interaction of nearest neighbours in compact planar array 78—50979
- mutual radiation impedances between pistons 79—1016
- near-field transient acoustic beamforming with short pulse arrays 79—57738
- noise correlation functions for arbitrary receiver orientation and steering direction in vertically anisotropic, azimuthally isotropic noise fields 80—58864
- noise immunity in presence of weak external disturbances 79—64386
- noisy acoustic signal sources, optimal meas. of coords. by group of acoustic arrays 80—87659
- nonlinear acoustics 8th symposium, conf., Paris, France, July 1978 80—33277
- nonlinear and thermal acoustic sources 79—23122
- nonlinear generation of LF component in atmosphere for intense modulated acoustic wave *(Russian)* 79—98522
- nonlinear parametric sound reception in freq. range 10 to 20000 cps, expt. research 80—33391
- nonlinear sound generation by hadron showers 80—36465
- ocean receivers for acoustic signals from moving radiating sources, computer-aided analysis 79—59859
- optimal array processing for case of strong localized interference using appl. of adaptive beamforming 79—41521
- optimal array processing for case of strong localized interference, comments on rapid approximation 79—90084
- optimum detection of signals in non-gaussian noise 78—38149
- optimum range and bearing estimation with randomly perturbed arrays 80—96119
- opto-acoustic transducers for potentially sensitive ultrasonic imaging 78—5625
- parametric, beam pattern and propag. curve for air *(Japanese)* 80—83693
- parametric, beam penetration into marine sediments 80—33324
- parametric, characterisation of materials at oblique angles 80—96164
- parametric, effect of finite aperture 80—106648
- parametric, nonlinear interaction of finite-amplitude sound waves 80—53529
- parametric, nonlinear interaction of two collinear, spherically spreading bearing 80—48484
- parametric, suppression of finite-amplitude primary wave attenuation, use of bubbles 80—74563
- parametric acoustic array max. conversion efficiency anal. 78—71242
- parametric acoustic array theory 78—38119
- parametric acoustic arrays, theory 80—33289
- parametric acoustic receiving array, experimental, band elimination processor 79—90086
- parametric acoustic receiving array vibration sensitivity anal. 78—66971
- parametric acoustic source model 77—46836
- parametric array, selected mode excitation in shallow-water sound propagation 78—59182
- parametric arrays in air with applications to atmospheric sounding 80—33390
- parametric arrays with intermediate directivity in water, expt. study 80—74569
- parametric echoscanner for medical diagnosis 80—36041
- parametric excitation of ultrasonic beams in a dissipative medium 79—18570
- parametric radiator, influence of dispersive medium on characts. 78 94470
- parametric receiving array response to transducer vibration 80—74570
- parametric receiving array with large aperture, expt. 79—64469

acoustic arrays continued

- parametric receiving arrays, modulation characts. 80—33393
- parametric sonar performance calculator 80—33392
- parametric transmitting arrays, symmetric and asymmetric, weak interaction model for axial difference-freq. field 79—81599
- partially random sonobuoy array directivity index analysis 80—43518
- partitioned signal detection by discrete cross-spectrum analysis 80—91966
- passive ranging errors due to receiving hydrophone position uncertainty 79—41522
- passive ranging of acoustic source 78—71241
- passive source location with array meas. 79—64410
- passive tracking acoustic array evaluation, nonlinear filtering lower bound algorithms 80—96088
- penetration into a sand sediment of difference-frequency sound generated by a parametric array 78—63227
- performance sensitivity of array detectors to a priori spatial knowledge 78—55524
- periodic dot arrays, selective reflection of SAW 80—74624
- phase arrays, multi-mode operation using noise signals 80—96157
- phase decorrelation effects on array beam scanning 79—3860
- phase-shift beamformer, narrowband, suitable for IC implementation 80—58865
- phased, infinite periodic, investigation of acoustic field 80—58836
- phased array beam steering, phase error grating lobes 79—48313
- phased array US imaging, computerised anal. 79—70598
- phased array US imaging, real-time digital scan conversion and multidimensional processing 79—48363
- phased array US imaging delay line bandwidth reduction 79—50552
- phased array US imaging with multiscan processing 79—57736
- phased arrays, defect classification and direct reconstruction *(German)* 80—35448
- phased-array US scanners, coarse phase quantisation effects 79—57739
- pulsed thermoacoustic array, near field 79—95083
- radiation patterns of acoustical arrays with quantized time delays 80—74566
- random and partially random, statistical props. of beampatterns 80—64301
- range estimation using acoustic sensor subarray parallax, passive 79—72759
- real-time and frequency-domain processor simulation 79—81643
- real-time B-scn echography, appl. in obstetrics and gynaecology 80—41140
- rectangular transducer elements for ultrasonic arrays 77—80046
- reflection of finite-amplitude waves in a parametric array 77—84036
- reflective arrays, coupled mode vector anal. and flowchart 79—7241
- reflective dot array for high-performance signal processing, development 80—74623
- rejection of sonar interference of finite bandwidth by amplitude shading of transducer arrays 78—38151
- robust sequential detection of weak signals in undefined noise 80—58861
- SAW resonator filters, synthesis using various coupling mechanisms 78—33967
- scattering from oceanic microstructure detection with a large aperture array 79—98530
- scattering of sound by sound, relation to the parametric receiving array 78—90563
- shading function design for array transducers in electronic scan US tomography *(Japanese)* 77—84100
- shading of acoustic and antenna arrays, ability of Lagrange multiplier method to control side lobes 79—98553
- shading of acoustic and antenna arrays, criteria used in Lagrange multiplier technique for obtaining coeffs. 79—98552
- shape meas. using active/passive acoustic techniques 80—23824
- signal processing, comments on errors 80—19164
- signal processing methods for imaging using sonar transducers 78—18122
- slotted acoustic waveguides, propag. characts. *(Japanese)* 78—46859
- slotted transducer arrays with matched backings for underwater imaging 80—38214
- small-aperture directional hydrophones 79—3828
- sonar, passive range estimation 80—53583
- sonar beamforming by CCD scan conversion for SAW chirp-Z transform 80—43552
- sonar Doppler phased array antennas, coherent imaging and holographical processing, metaxial theory 79—72521
- sonar systems, digital beam forming 80—91950
- sound source reconstructions using a microphone array, holographic technique 80—96132
- space-time signal processing, optimal versus conventional detectors 79—27467
- sparse array technique, min. output variance, S/N ratio 78—83177
- spatial aliasing of broadband signals, frequency wavenumber analysis 79—1031
- spherical, reconstruction of three dimens. US reflectivity images 80—38203
- statistical array-synthesis problem, general soln. 80—87646
- statistical measures of beam output noise due to shipping 79—3836
- statistical moments of the excitation distribution function in the array-synthesis problem 79—27460
- steered planar nearfield transducer calibration array 78—59214
- steered surface acoustic arrays, optimal excitation 79—18564
- steered vertical line arrays, response to anisotropic noise 79—90103
- strip-shaped acoustic radiators, near and farfield 79—50475
- synthetic focus digital acoustic imaging for nondestructive evaluation 79—52611
- technique for measuring the sound of a moving tire 78—33969
- telescope for transportation noise meas. 79—94426
- thickness-extensional trapped energy mode transducer array, increased bandwidths and mode shapes 80—74633
- Three Array Processor beamforming system 80—43550
- tissue parametric stimulation by inductive transducer and US phased array 79—92320
- towed arrays, hydroacoustic sources of locally generated sound, hose material 80—23822
- towed arrays, hydrodynamics 80—23823
- towed hydrophone array detection system 79—2401
- towed sonar array, modelling of steady state and transverse dynamic motion 78—30112
- towed-line array, iterative technique for ambient-noise horizontal-directionality est. 78—55525
- transducer array for acoustical holography *(Japanese)* 77—80029

acoustic arrays continued
  transient-free pulsed acoustic sinusoids generated with phased-array speakers 77−54847
  transmit/receive 2D ceramic piezoelectric arrays, construction and performance, medical, NDT appls. 78−87223
  two-dimensional monolithic mosaic transducer array 79−46156
  undersea acoustic holographic transducer array development 78−59209
  undersea platform location by acoustic signature processing 80−43519
  underwater, acoustic line array operation in water layer 80−5866
  underwater, optimization technique 79−64405
  underwater acoustic source location and motion estimation, joint reduction of bias and variance 80−96087
  underwater C-mode US imaging by electronically scanned coaxial circular spherical receiving array 78−59222
  underwater calibration of individual elements, LF technique 77−79997
  underwater focused nonuniformly spaced arrays, 2-dimensional, minimax optimization 79−59897
  underwater imaging system using multi-frequency ultrasonic holography 79 98556
  underwater propagation in shallow water expts. for long range communication systems 80−33323
  underwater sound, measurement of freq. dependence of normal modes in shallow water 79−7262
  US beam scanning by SAW transducer arrays 79−55266
  US imaging, correction for refraction and attenuation 80−30817
  US imaging sonar 79−3831
  US imaging using direct imaging and phased arrays 79−64460
  US imaging using electronic scanning for NDT 79−66230
  US imaging with an acoustic lens 77−46868
  US medical diagnostic imaging, digital scan convertors 79−66581
  US multiple freq. array for improved diagnostic imaging 79−14170
  US phased array diagnostic instrument with microcomputer *(Japanese)* 79−88146
  US real time imaging with hand-held linear array scanner, clinical experience 79−62317
  US real time imaging with hand-held linear array scanner, technical description 79−62316
  US receiving array having power response 80−74653
  US receiving array with strip type piezotransducers 78−42511
  US scanners, phased-array, angular response of piezoelectric elements 79 64471
  US transducer, broadband directional reception 80−96126
  US transducers, electric coupling effects in acoustic imaging 80−43587
  US video system for underwater imaging 78−94471
  vertual line array, deep-water signal transmission and background noise 79−86283
  vorticity meas. in surface layer using echo sounder arrays 78−7810
  wideband annular US imaging array response 79−55306
  wideband array synthesis 78−38120
  wideband Fresnel focusing array response, echography appls. 80−74640
  Si array/$LiNbO_3$ gap-coupled imaging devices 79−46057
  ZnO integrated optical transducer arrays 79−50444

acoustic delay lines
  see also ultrasonic delay lines
  chalcogenide glasses, photoelastic props. 78−55420
  dispersion characts. of tubular waveguides *(Russian)* 79−3866
  microwave delay line, freq. charact. 77−842
  oscillator, band I, 10 GHz, with noise compressed by acoustic delay line *(French)* 78−16818
  quartz, doubly-rotated-cut, SAW and SBAW 80−74584
  quartz, Y cut crystal second harmonic generation in SAW *(French)* 80−34285
  recirculating pulse generator, meas. of acoustic surface wave velocity changes 78−5619
  SAW, for GHz SAW oscillators, fabrication and performance 79−14185
  SAW, towards an ideal photon correlator 80−68252
  SAW delay line, variable, using magnetostrictive metallic glass film overlays 78−63240
  SAW delay line fabrication by direct optical projection 79−81667
  surface acoustic wave delay line, tunable, using layered piezoelectric-liquid-piezoelectric structure 79−94431
  surface wave delay line, temp. dependence of surface wave diffraction on α-quartz 77−15674
  synchrotron radiation storage ring beam lines, delay line efficiency 79−88965
  $LiNbO_3$, ion implanted, acoustic model of SAW delay lines *(French)* 78−55540
  $LiNbO_3$-gap coupled Schottky diode memory correlator, grating coupled optical imaging 80−64143
  $LiTaO_3$-SiO_3, temp. compensated SAW device fabrication 79−76923

acoustic detectors *see acoustic transducers*

acoustic devices
  see also acoustic delay lines; acoustic generators; acoustic microscopes; acoustic microwave devices; acoustic parametric devices; acoustic radiators; acoustic receivers; acoustic resonators; acoustic transducers; bells; surface acoustic wave devices; ultrasonic devices
  active vibration-suppression systems, automation 78−18098
  active vibration-suppression techniques for mechanical systems with many degrees of freedom 78−18101
  agglomerator for control of particulate emission 80−33413
  amplifier, activity integrator, lab. studies of wood boring insect larvae appl. 79−16357
  amplitude-frequency charact., temp. instability effect of matching layer 78−59220
  artificial acoustic anisotropy of a controlled piezoelectric element 77−50848
  atmospheric sounder, design, wind velocity meas. appl., review 79−53528
  audiometer, history of development rel. to psychological and physiological acoustics 77−45664
  conical acoustic lens, fabrication and test results 78−51019
  conical acoustic lens, opto-acoustic feasibility design 78−51020
  coupler for reciprocity calibration of microphones 77−75754
  cylindrical interferometer, theoretical criterion for end face alignment 77−14861
  electronic signal processing devices, photoelastic materials, nonlinear elastic interactions *(French)* 79−41525
  elliptic lenses, history 80−96158
  filter components for ANSI standard psychoacoustic testing 78−83198
  filtering schemes for signals propagating through random multipath medium 80−58862

acoustic devices continued
  focusing device, with interdigital transducer 78−9520
  focusing radiators and acoustics lenses, field structure 77−50792
  geophysical prospecting, nuclear and acoustic logger for cased well and open hole studies 77−87098
  imaging applications of US and acoustic methods *(Dutch)* 78−27719
  Lamb wave focusing device 80−79093
  lenses, two-layer, focal plane field 77−35005
  levitation devices for processing materials, limitations 80−74694
  LMFBR HCDA, appl. of acoustic agglomerators for suppression of Na-fire aerosols 79−54525
  loudness meter for temporally variable sounds 78−3508
  magnetoelastic waves in YIG rod, inhomogeneously magnetised, propag. characts. 78−15006
  multichamber sound reflector, design parameters 78−94500
  nonlinear orifice impedance correlation curves 77−23837
  orifice under turbulent boundary layer 77−23838
  photographic flash unit triggered by acoustic shock wave, cct. details 80−101862
  planar grating of compliant cylindrical shells, use as shielding for sonar receiver 77−31157
  quartz sand, pilot tests of acoustic device for dressing 78−7271
  research over past 50 years, review 80−96151
  solid-state device conference, Tokyo, Japan (Sept. 1976) 77−76901
  sound source location system for jet engines 77−14864
  Spacelab passive atmospheric sounders 77−82113
  surface skimming bulk wave transducers, specific appls. 79−81678
  thermometers with W resonators 79−32153
  weak speech amplification device with suppression of respiration noise 80−30929

acoustic dispersion
  see also ultrasonic dispersion
  acoustic spectroscopy, H bonds investigation, N-butyl acetamide association in solns. 80−5891
  air-water fogs, audible sound propag. 78−1473
  anisotropic cylindrical crystal, strain wave propag., theory 77−11062
  anisotropic rods of rectangular cross-section 78−1463
  collinear h.f. sound beams, nonlinear interaction in weakly dispersive media 77−807
  crystals, sound wave conservation laws 78−5597
  ear-defenders, active noise reduction system, aircrew flying helmets appl. 79−18602
  Fermi surface local flattening effect of acoustic wave absorpt. and dispersion *(Russian)* 79−51471
  fluids, corrections to linear hydrodynamics eqns., low-freq. sound dispersion *(Russian)* 79−3990
  gyrotropic tensor, in crysts., activity rel. to cryst. class 80−107378
  heat transfer in acoustic wave 78−5599
  n-heptane-nitrobenzene, critical fluid, ratio of sound dispersion to attenuation 79−55826
  jet noise, amplification by higher-mode acoustic tone 78−9664
  liquid-gas system near critical point, sound attenuation and dispersion, renormalisation group calcs. 79−42149
  liquids acoustic relaxation mechanism, using coherent optoacoustic spectroscopy scheme 80−5890
  metals, sound absorption and dispersion temp. depend. associated with Fermi surface plateaus *(Russian)* 80−65166
  multimode waveguide with uneven walls, sound attenuation 78−83147
  nematic-smectic A phase transition, sound attenuation and dispersion 79−82286
  noise attenuation over an absorbing terrain, theoretical models comparison, aircraft noise appl. 79−18572
  orthogonal fibre reinforced viscoelastic composites 78−42558
  piezoelectric crystals, surface modes, acoustic wave propagation 80−20026
  plane sound waves in air, dispersion rel. to finite-amplitude saturation 78−1465
  plasma, acoustic wave interaction, diagnostics appl. 78−83541
  polymers, highly oriented, elastic wave dispersion relations 78−51618
  polyurethane foam plate, response to acoustic noise impulse *(French)* 79−1033
  pulse, dispersion and damping in medium with high thermal cond. 77−27409
  quasi-Lorentz gas, Temkin-Dobbins formula 78−55502
  rarefied gas, acoustic dispersion, hydrodynamic soln. 77−68630
  Rayleigh waves, surface tension dispersion effects 80−14513
  relaxation phenomenon influence on propgation, relativistic theory *(French)* 77−37754
  SAW, in anisotropic media, anal. of roots of dispersion eqns. 79−14997
  SAW velocity dispersion induced by laser radiation absorpt. 77−51585
  smectic and nematic liquid crystals, acoustic props. near transition, hydrodynamic theory 79−77731
  solid, phase and group vels. determ. for dispersive waves 78−81848
  sound absorption coefficient measurement in reverberation chambers 79−18653
  surface layer structure estimation from Rayleigh wave dispersion, sparse data case 79−14995
  transmission paths in dispersive systems, determ. of importance 77−72106
  trimethylamine-water critical fluid, ratio of sound dispersion to attenuation 79−55826
  US materials testing, three layered medium, dispersion relation for interference waves 78−72980
  waveguides, discretely-layered, Holmholtz eqns., radiation conditions for boundary value problems 79−14134
  waveguides, Doppler effect under conditions of sound dispersion 79−86277
  wide cylindrical tubes with wall-mounted resonators, sound attenuation 77−11063
  wideband wavefront reconstruction in two-dimensional dispersive space 77 31191
  Al, nonlinear sound wave interactions, sound attenuation in weak superconducting state *(Russian)* 80−75310
  Ga, nonlinear sound wave interactions, sound attenuation in weak superconducting state *(Russian)* 80−75310
  ^{3}He critical fluid, ratio of sound dispersion to attenuation 79−55826
  ^{4}He, liq., pressurized, attenuation and dispersion of first sound near superfluid transition 78−14524
  Ni crystals in strong mag. field, EM excitation and vel. dispersion of sound *(Russian)* 80−39837

acoustic dispersion continued
- Si guided-wave acousto-optical devices 80—102864
- Xe, critical fluid, ratio of sound dispersion to attenuation 79—55826
- Xe, sound propag. near critical pt. 79—82285

acoustic echoes *see echo*

acoustic emission
- *see also ultrasonic materials testing*
- 23rd International Aerospace Instrumentation Symposium tutorial, Las Vegas (1977) 78—12074
- acoustic emission, amplitude distrib. anal. 80—66713
- Admiralty Metal, transgranular stress corrosion crack propag. 80—89402
- aerodynamically generated sound, mathematical formalisation of Lighthill's theory 77—62245
- aerospace acoustic emission instrumentation and applications 77—33322
- air conditioning and ventilation systems, sound emission prediction 77—7252
- Al alloy AK4-1, acoustic investigation of ageing 79—34083
- algorithm for computing the coordinates of an acoustic-emission source 79—94432
- amplitude distrib., information content 80—108666
- amplitude estimation model 79—68476
- amplitude response variations effect on nonlinear props. 78—48605
- appliance acoustic emission determ. facility development 77—58507
- applications *(Japanese)* 80—93726
- asbestos cement, resistance to crack growth 79—29185
- automatic acoustic emission analysis system with programmed control *(Russian)* 78—46866
- automatic digital equipment for recording acoustic emission signals 80—102948
- aviation and astronautics, conference, Tel Aviv (1977) 78—81517
- B fibre reinforced Al, real-time NDT during fatigue loading 77—86264
- Bauschinger AE peak detection of back stress component in flow stress *(Japanese)* 78—6977
- blown flap, upper surface, sound generation in vicinity of trailing edge 77—75902
- boiling, nucleate type, boiling acoustic emission and bubble dynamics 77—46893
- boiling water in annular channel *(Russian)* 77—54302
- bone, human, acoustic emission in restressing 80—3704
- bone acoustic emission diagnosis, soft tissue effects 79—48362
- bone mammalian, testing 80—76783
- bone tissue, human, subjected to longit. extension 77—25495
- boride coatings on steel effect of Cu impurities in reaction mixture on brittleness, acoustic emission meas. 80—16581
- bovine femur crack detection 79—48312
- α-brass, acoustic emission signals in plastic deform., amplitude distrib. *(Japanese)* 78—6978
- α-brass, Bauschinger AE peak detection of back stress component in flow stress *(Japanese)* 78—6977
- brass, burst acoustic emission during Bauschinger effect 77—48475
- $\beta'+\gamma$- brass, two-phase, acoustic emission from β' plastic flow and γ cracking 80—16452
- brief crack propagation event 79—64397
- brittle material, surface energy determ. from AE, automatic system 79—91899
- brittle material, wear, acoustic emission obs., effect of ion aggregates in Rebinder-Westwood environment 78—48536
- brittle materials, book contrib. 78—11484
- brittle tensile fracture of cylindrical and flat specimens 77—62211
- brontides, natural atmospheric explosive noise 80—12523
- BWR power plant availability improvement by acoustic emission monitoring 79—9809
- calcite, sound emission on dislocation annihilation *(Russian)* 80—54246
- calibration of acoustic emission systems using He gas jet 77—835
- cartilage generated noise, computer-aided acoustical correl. 78—40391
- CBOOA, acoustic emission at liq. cryst. transitions prod. by thermo-optically excited defects 79—95137
- ceramic and glass ceramic, AE meas. under maintained load *(German)* 79—43315
- ceramics, thermal shock resistance meas. by AE *(German)* 79—70233
- charged particle beams in liqs., elastic wave excitation, microscopic bubble acoustic emission 80—43516
- circular plate, noise reduction by polyurethane foam covering 77—62102
- combustion zones, nonlinear acoustic phenomena 80—38156
- composite grip design for extraneous noise elimination during AE testing 79—15915
- composite materials, crack growth, conc. criterion 80—65146
- concrete, acoustic emission at prior loading meas. method 78—27703
- continuous self-inspection of acoustic emission instruments 79—96275
- COOB, acoustic emission at liq. cryst. transitions prod. by thermo-optically excited defects 79—95137
- Corson alloys, AE during tensile deform. *(Japanese)* 79—61654
- crack and fracture behaviour, simultaneous acoustic emission and SEM techniques *(German)* 79—96240
- crack growth and coordinate determ. by acoustic emission 79—5119
- crack growth measurement, instrum., expt. 77—73421
- crack propagation, acoustic emission transients meas., appl. to low alloy steel 79—8407
- CrMoV, surface coating to prevent oxidation during high temp. AE 80—16539
- crystal lattice, beam instability and collective disturbance *(Russian)* 77—8676
- cutting Al alloy on lathe, acoustic emission rel. to tool sharpness 77—42675
- data acquisition system for processing and recording of signals, on-line 80—57266
- defect coordinate determ. by calibration of AE method 80—35473
- defect coordinate determ. in struct. with arbitrary surface, AE method 79—66239
- defect coordinates in anisotropic shells, plates, determination using acoustic emission 78—80707
- defect development, temporal and spatial variation of elastic constant 80—85127
- defect dimension determination by acoustic emission 80—104381
- detection, calibrated capacitance transducer 78—71256
- detection system sensitivity, direct comparison method 78—56848
- detection technique, industrial NDT appl. *(Japanese)* 78—27721
- digital memory, storage and source isolation 78—27712
- dislocation pile-up formation, by Frank-Read source, emission of sound 79—37705

acoustic emission continued
- dual-gate depletion-mode FET/piezoelectric film transducer 79—50563
- ductile materials, acoustic emission and fracture 77—56059
- earthquake precursory acoustic emission, sound source direction formula *(Chinese)* 80—89961
- earthquake sounds generated by body wave ground motion 77—9351
- efficiency eval. of AE systems 79—39079
- elastic plate, acoustic emission and transient waves 79—41506
- elastic porous media, acoustic phenomena 78—25997
- elastic stress monitoring 78—53176
- electroacoustic, analytic and diagnostic equipment 78—63249
- electron beam welds, NDT by AE to detect lack of fusion *(German)* 77—56193
- energy measurement and significance in acoustic emission testing 78—31594
- engineering diagnostic appl. *(Russian)* 77—44439
- engines, exhaust manifold design and cylinder firing order effect on short term spectrum 77—14845
- ethanol, aq. subcooled soln., acoustic phenomena during nucleate boiling 78—10181
- failure prediction on basis of acoustic emission 80—104382
- fatigue crack growth, AE monitoring 78—27706
- fatigue crack growth in aircraft wing test, AE detection 78—60925
- fatigue crack propagation monitoring 79—86313
- fatigue damage detection, book contrib. 79—100326
- fatigue damage monitoring of 80—97673
- fatigue detection and rating by acoustic emission, review 80—104380
- fatigue life prediction, acoustic emission signals distrib. anal. 80—25852
- fatigue monitoring, new technique 77—28938
- fatigue testing, use of standard equipment and background noise effects elimination, expt. 77—73423
- fibre reinforced composite, fibre/matrix adhesion, AF testing *(Japanese)* 77—70254
- fibre reinforced composite failure analysis 78—80691
- fibre reinforced composite laminate, fracture mode determ. by AE 79—57187
- fibre reinforced composites, AE monitoring review 79—11735
- fibre reinforced composites, strain rate effect on AE 78—44193
- fibreglass rings, ultimate load determ. by AE method 78—48604
- finite elastic cylinder longitudinal collinear impact acoustodynamics 77—75743
- flexurally vibrating beam-reinforced plate, compensation of radiation 77—68302
- for aircraft wing fatigue crack tests 77—16769
- fracture, ductile, acoustic emission interpretation 80—35300
- fracture monitoring with simultaneous recording of acoustic emission signals 80—55599
- fracture toughness testing, inspection technique 78—68860
- gas flow in duct, self-excited oscillations 78—55670
- glass, acoustic emission obs. during heating through glass temp. 80—84253
- glass, Gaussian size distrib. of rigid particles, AE anal. 78—62181
- glass, wear, acoustic emission obs., effect of ion aggregates in Rebinder-Westwood environment 78—48536
- glass fibre reinforced plastic, acoustic emission 80—104294
- glass reinforced laminates, damage accumulation during tensile loading 79—83262
- glass reinforced plastic, acoustic emission investigation of deformation and fracture 77—16756
- glass sphere mixture, polydisperse system, AE anal. 78—62180
- granite microfracture, source process rel. to earthquake prediction 80—104919
- granodiorite, fracture under uniaxial compression, mech. and AE meas. *(Japanese)* 78—56748
- graphite fibre reinforced epoxy, impact damaged, acoustic emission 79—91875
- graphite fibre reinforced epoxy laminate, containing interlaminar paper inclusions, AE monitoring 79—34229
- graphite fibre reinforced polyimide acoustic emission spectral anal. 79—47850
- graphite materials, mech. characts. under stress using acoustic emission analysis *(German)* 79—15881
- graphite reinforced epoxy laminates, imminent fracture detection using acoustic emission 79—20302
- graphite/epoxy laminates, T300/5208, effect of curing stresses on first ply failure 79—43329
- Green's function for plate acoustic emission 77—50798
- high alumina cement pastes, accelerated conversion 77—36726
- hydraulic component fatigue crack acoustic emission inspection 77—40513
- impact and solid body accel. sound energy 77—62099
- impact excitation of vibrations in the acoustic spectral inspection method 79—70273
- impact of elastic sphere on thin plate, radiation of transient sound 80—38168
- industrial appl. 78—68850
- infrasonic signals from thunder 79—70846
- inorganic materials, acoustic emission meas of H_2 embrittlement 80—11742
- instrument for crack detection by AE 79—52582
- intensity, calc. using fracture kinetic concept and phenomenological model 78—85110
- intensity calc. using kinetic concept of disruption 79—50499
- internal friction measurement of metals using sound emission during vibration 77—77715
- ionosphere sound generation, theory 80—41604
- Langmuir soliton formation with ion-acoustic densiton emission 78—75328
- laser beam incident on plane interface, thermal acoustooptical effect 77—11639
- leak detection, attenuation of elastic waves in pipelines 78—27711
- leak detection in pressure vessels during hydraulic tests *(French)* 80—789
- linear convertor, for acoustic emission signals 78—9512
- linear vortex over plane with projecting edge, sound radiation 77—811
- liquid crystals, defect dynamics study 78—91232
- liquid half-space bounded by solid layer optical generation of sound 80—38158
- LMFBR, acoustic anal. of TREAT safety test R8 78—13290
- LMFBR, acoustic anal. on Na boiling expt. in FFM Bundle 3B, Test 4 78—13291

acoustic emission continued
locally distributed boundary of a half-space, axisymm. emission 78—42485
locator, receiving channels, selection of number 80—108676
materials testing appl., plastic strain and growing cracks identification 80—81252
materials testing methods, review 79—43504
measurement transducers, comparison of piezoelec. and optical sensors 79—14192
metal, polycryst., electron or proton irrad., coherent acoustic emission *(Russian)* 77—81355
metal cutting, separation process tool tip, fracture detection, acoustic emission method *(Japanese)* 80—1388
metallic bars, acoustic emissions during flexion *(French)* 80—48625
metals, mechanical props., testing and modelling 80—25811
metals, rel. to NDT *(French)* 77—56207
methanol, excitation of acoustic radiation by pulsed proton beam *(Russian)* 77—80580
microwave irradiated materials, anal. 78—24095
monitoring, weld flaws detection appl. 80—11866
monitoring activities in deep-level coal seams, bed rocks instability obs. *(Japanese)* 80—10071
monitoring difficulties overcome by optical detectors 78—60968
monitoring of multipass submerged arc welding 77—73394
multilayered piezoelectric transducers, amplitude-freq. characts, anal., to determine acoustic emission receiver configuration 78—42507
NDT, principles of acoustic emission and measuring techniques 80—28375
NDT, transducer parameter and interpretation 77—40508
NDT appls., review 78—11489
NDT of aircraft struct. 78—53177
near surface region of solid, H_2 effect on deform. and fracture, Rebinder-Westwood effect 79—39001
nematic liquid crystal, acoustic emission, depend. temp. 79—55654
noise intensity during cracking 77—846
non destructive testing technique, improvement in noise immunity 80—21213
nondestructive testing appl. 80—11854
nondestructive testing cast iron, Cu alloy, and Al alloy 77—25221
nondestructive testing method, twinning characts. in In 77—4873
nuclear power plant availability improvement by acoustic emission surveillance 79—3213
nuclear power plant piping, weld inspection, by in-process acoustic-emission monitoring 77—14823
nuclear reactor components, NDT using acoustic emission *(Spanish)* 80—57871
nuclear reactor components inspection *(German)* 79—45373
nuclear reactor pressure vessels, US pulses propag. by means of acoustic emission *(German)* 80—3274
nuclear reactor system, subcooled nucleate pool boiling, intensity and power spectral density of acoustic emission 78—17282
optical detection using Michelson interferometer and laser 77—90510
optical interfereometer and auxiliary direct viewing system 79—79217
optimisation using acoustic emission transducers 80—48539
oxide coating, thermal sprayed, AE study of porosity 80—25927
oxide films on $MoSi_2$, cracking under heat cycling, acoustic emission determ. *(Russian)* 80—30067
oxide thermal-sprayed coating on steel, acoustic emission 80—21247
particle size analysis, irregular shape particles, from acoustic emissions 79—61825
particle size distrib. charact. by AE 78—62179
piezoelectric receivers, amplitude-freq. response determ. for acoustic emission 80—87699
piezoelectric transducers, single acoustic signal distortion 80—87637
pipe with turbulent air-flow, acceleration response and acoustic power spectral meas. 77—19484
plastically deformed crystal, bubble formation mechanism in liq. He *(Russian)* 78—85066
point sources on road, analysis of noise emission *(Japanese)* 77—23804
polymeric liquid, viscoelastic, gas bubble pulsations and assoc. dissipation effects 80—59079
porcelain enamel layers on steel, H_2 induced fracture of layers 78—76752
postweld eval., by AE 79—96252
powder, particle size and size distrib. determ. from acoustic emissions 77—53861
pressure vessel inspection, during water-pressure testing, NDT 77—1901
pressure vessels, AE during fatigue crack expansion 80—108675
pressure vessels, C-fibre reinforced plastics, detection, immersion technique 77—1902
pressure vessels, elastoplastic fracture modelling 80—35303
pressure vessels, thin-walled, containing surface flaws, fracture mechanics and acoustic emission exam. of failure 78—84981
pressure vessels and steel pipes structures anal. under creep conditions 77—25237
pressure vessels hydrotest, acoustic emission monitoring 77—46206
pulse shape, relaxation and acceleration pulses 80—64250
pulse signature anal., optimal design and eval. criteria 77—48596
pulsed emission evaluation, freq. anal. appl. 78—18126
PWR acoustic monitoring instrumentation 78—17309
PWR acoustic monitoring instrumentation 79—89488
Pyrex glass, near-surface H embrittlement, effect on deform. and fracture props. 79—29180
quadrupole near fluid interface, sound refl. and radiation 78—9475
quantitative application, structural calibration technique 78—9509
quartz, Dauphine twinning, stress-induced, acoustic emissions 80—6414
quartz, thermally excited state relax., acoustic and EM pulse obs. *(Russian)* 77—40293
quartz ferrobielastic twinning, electrical and acoustic emissions 79—56731
random signal parameters, computer calc. 77—44454
rectilinear dislocation annihilation, acoustic emission, exact soln. 80—44209
refractories, fatigue behavior, effect of texture and crack kinetics, AE anal. *(German)* 80—21061
refractory, fracture under thermal shock, AE study 80—25865
remote sensing technology developments and appl. *(Japanese)* 79—8701
rock fracture, assoc. microacoustic signals anal. 78—32070
rock mechanics, appl. of AE *(Japanese)* 78—56845
rock mechanics appl., rel. to earthquake prediction *(Chinese)* 78—24279

acoustic emission continued
rocks, acoustic emission and creep at high confining press. and differential stress 77—73716
rocks, failure processes and AE under compression *(Japanese)* 78—56749
rocks, microfracture *(Japanese)* 78—7020
rocks, wide-band optical-mechanical system for high temp. and press. emissions meas. 78—1525
sandstone, fracture toughness and acoustic emission characts. *(Japanese)* 79—34810
SEM, combined deformation/heating stage, acoustic emission role meas. 80—101892
service life of equipment in creep, AE appl. to technical diagnostics 79—96271
ship hull, acoustic radiation from point excited rib-reinforced plate 77—80003
signal recovery technique appl. to AE anal. of martensitic transformation 78—60965
signal sorting by computerised pattern recognition 77—40516
signals, unit for recording and reproduction 80—79039
simulation by SiC grain brittle fracture and elastic sphere impact, freq. anal. 78—55504
small components production testing, review 80—16632
snow, acoustic emission response 79—87801
solids, acoustic wave emission, absorpt. and propag. in THz range 80—65164
sonic pulses generated during boiling of underheated liquid, time and spectral characteristics 80—107373
sound production in moving stream, Lighthill's acoustic analogy, jet noise 78—79313
source identification using signal anal. 77—44415
source localisation, application of correlation techniques 78—87220
source location, using face centred transducer array 79—24708
source location on spherical or plane surface 78—92421
source mechanism identification by energy spectrum anal. 77—19489
Space Shuttle external insulation, acoustic emission inspection 78—16276
spectra, laboratory comparisons 80—108658
spectral anal. 79—43496
spherical material parts, defect coordinates, location via acoustic emission method 78—35626
spherical shell accelerating in fluid medium, generation of waves 78—13843
spherical void expansion into isotropic elastic medium 80—102914
spot welding process, acoustic emission signals, anal. *(German)* 78—44296
stacking fault energy rel. to total elastic power 78—14365
statistical investigation of acoustic-emission pulse distrib. 80—87638
steel, 45, acoustic-emission signals, rel. to struct. 79—52297
steel, acoustic emission anal., during fatigue crack growth 77—56090
steel, acoustic emission associated with phase conversions 79—70275
steel, acoustic emission in deformation, at various strain rates and sign change 78—44188
steel, acoustic emission sources and dislocation patterns 80—61040
steel, acoustic-emission analysis of fracture-toughness tests 80—55596
steel, austenitic, types A533B and A508, acoustic emission and deformation processes during tensile tests 79—74212
steel, austenitic stainless, acoustic emission during cyclic deformation *(Japanese)* 79—43314
steel, austenitic stainless, acoustic emission during tensile tests, H_2 assisted fracture 79—100257
steel, austenitic stainless type 304L, temp. depend. of acoustic emission accompanying plastic deform. 79—74217
steel, carbide cracking as source of acoustic emission 78—19872
steel, ferritic, magnetomechanical acoustic emission for residual stress NDT 80—71149
steel, high strength, alloy, initiation of cracks at delayed fracture, AE study 78—72868
steel, high strength low alloy, acoustic emission meas. from crack opening displacements 80—7732
steel, high strength low-alloy, AE appl. to nondestructive testing 79—83419
steel, high-strength castings, AE study of intercrystalline crack form. 80—104403
steel, HSLA and Low C, weldment, AE monitoring 79—87800
steel, low, effect of pressurisation on acoustic emission characts. during tensile testing 78—92304
steel, low alloy, acoustic emission during ductile fracture, isothermal tempering effect 79—83241
steel, low alloy, isothermal tempering effect on acoustic emission during ductile fracture 80—85047
steel, low C, structural, AE rel. to crack tip plasticity *(Japanese)* 79—66150
steel, low-alloy, study of deformation and fracture processes by acoustic emission transient anal., SEM and optical microscopy study 79—43311
steel, mild, 1019 AISI, acoustic emission generated during deform. 80—60921
steel, mild, acoustic emission during magnetisation, stress effects 79—82854
steel, mild, subject to three point bending and tensile load, acoustic emission 80—3154
steel, nitride coated, brittleness eval. by AE *(Chinese)* 78—11453
steel, nuclear reactor pressure vessel materials, AE assessment 79—83422
steel, plastic zone growth, quantitative evaluation of acoustic emission, book contrib. 79—100328
steel, press. vessel, acoustic emission and ductile crack growth 78—11320
steel, pressure vessel, acoustic emission during loading by pulsating internal press. *(German)* 78—19973
steel, rail, AE use for mech. tests 80—35467
steel, Si-Mn-Ni-Cr-Mo, acoustic emission during stress corrosion cracking appl. to materials testing 78—53042
steel, stainless, austenitic type 304, martensite transform, acoustic emission identification, opt. microscopy obs. 80—81062
steel, stainless, Cr-Mn (21, 14 wt.%), grain boundary precipitation and fracture *(Japanese)* 79—100149
steel, stainless, SUS 304, acoustic emission signals in plastic deform., amplitude distrib. *(Japanese)* 78—6978
steel, stainless SUS 304, Bauschinger AE peak detection of back stress component in flow stress *(Japanese)* 78—6977
steel, stainless type SUS 304, diffusion welded joints, sound emission during tensile testing *(German)* 80—61062
steel, strength, acoustic monitoring 80—35479

acoustic emission continued
steel, structural, elastic limit determ. by acoustic emission 80−66716
steel, welded specimen AE testing by external static loading of cold cracking susceptibility 78−40013
steel HF-1, acoustic emission during extension, frequency content variation 77−81301
steel laminate, acoustic emission rel. to fracture at 77K *(Russian)* 80−93633
steel parts, martensite form., hardening cracks, acoustic emission investig. possibility 79−29177
steel pressure vessel, notched, acoustic emission meas. during pressurisation 78−21638
steels, eutectoid 79−15889
stoneware sewer pipes, resonant frequency and acoustic emission meas. *(German)* 77−9010
stress wave emission, appl. to anal. of crack propag. in metals 77−63837
structural fatigue crack acoustic emission monitoring 77−32755
structure radiation of simple emitters, radiated sound power *(French)* 77−19471
supersonic heat source, sound radiation 78−1688
supersonic jet, underexpanded, impinging on barrier, sound field 78−9495
supersonic jet noise spectrum, discrete component 78−9493
surfactant, aq. subcooled soln., acoustic phenomena during nucleate boiling 78−10181
system for monitoring components and struct. in severe fatigue noise environment 77−63869
technological strength and nondestructive methods of testing during heat treatment 78−85090
temperature dependence 78−53136
temperature investigation 78−44336
test apparatus 80−61041
thermoelastic generation of 20 MHz wave, pulsed excitation of constrained surface 77−35007
threshold discriminator, automatic *(French)* 80−23851
timber drying process 80−102940
time-domain deconvolution technique for signal identification 79−20306
transducer calibration *(Czech)* 80−106697
transducer calibration temperature sensitivity checking technique 78−18144
transducer construction principles evaluated 78−59239
transducer for inspecting weld quality 79−94444
transient recorders for acoustic emission studies 80−83717
turbine spiral acoustic emission during pressure testing 80−28391
turbulent boundary layer over inhomogeneous boundary 77−68297
tyre/road noise mechanism study 77−19485
ultrarelativistic charged particles traversing stable liquids, acoustic emission, particle detection possibility 77−61653
ultrasonics symposium, Annapolis (1976) 77−19469
US cavitation emission from insonated plant tissues 78−59185
US crack detection, emission pulses amplitude and crack size correlation 77−90568
US materials testing, beam shaping effects and optimisation *(German)* 80−85122
vibrating body acoustic field calc. via Schenck numerical method *(French)* 80−69589
weld inspection, AE analysis *(German)* 77−36698
weld joint, fatigue crack progress, acoustic emission frequency determ. *(German)* 78−19971
weld monitoring, in-process, with acoustic emission 80−16620
welded structure reliability estimation, appls. 80−93702
welding, crack formation monitoring equipment and acoustic emission method 80−89451
Al, AE under plastic deform., appl. of spectral anal. energetic anal. of moving US source *(French)* 77−77543
Al, acoustic emission from moving dislocations during tensile tests 77−19964
Al, acoustic emission signals in plastic deform., amplitude distrib. *(Japanese)* 78−6978
Al, acoustic emission under plastic deform., spectral anal., dislocation mean free path 78−84934
Al alloy, 2124-T851, rel. to fracture toughness 78−7109
Al alloy, acoustic emission power, strain rate depend. 77−4808
Al alloy, acoustic stress wave emission during plastic deform., dislocation motion explanation 77−36697
Al alloy, fracture toughness testing, acoustic emission, inspection technique 78−68860
Al alloy, galvanic corrosion monitored by acoustic emission 77−90499
Al alloy 7039, AE spectra, laboratory comparisons 80−108658
Al alloy 7075, acoustic emission sources during plastic deform. 78−27573
Al alloy 7075-T6, acoustic emission response 79−87801
Al alloy D16T, acoustic emission temp. depend. 78−53136
Al alloy D16T, acoustic-emission signals, rel. to struct. 79−52297
Al alloy electrode, corroding, acoustic emission 80−60997
Al alloys, superplastic, tensile deform. behaviour *(Japanese)* 78−27558
Al, and Al alloys 6061 and 2024, burst acoustic emission during Bauschinger effect 77−48475
Al anodic films, acoustic and electron-emission during deform. 80−80143
Al, Bauschinger AE peak detection of back stress component in flow stress *(Japanese)* 78−6977
Al, plastic deform. of poly- and single-crystals, AE study 79−24579
Al, polycrystalline, acoustic emission energy release, grain size and flow stress depend. 80−11722
Al-Cu (4 wt.%), AE during deform., effect of ageing at 170°C 78−64597
Al-Cu-Mg, acoustic emission during tensile testing 80−7632
Al-Mg, acoustic emission during tensile testing 80−7632
Al-Mg solid soln., AE during plastic deform. 78−64592
Al-Mg(Si), acoustic emission signals in plastic deform., amplitude distrib. *(Japanese)* 78−6978
Al-Ni, thermoelastic phase transform., acoustic emission 80−3039
Al-Zn-Mg, acoustic emission meas. during tensile testing, reproducibility of results 80−50782
Al_2O_3, crack detection caused by thermal shock, AE technique *(Japanese)* 80−21248
Al_2O_3, dielec. breakdown mechanism determ. acoustic signature anal. techniques 80−11337
Al_2O_3, fracture toughness testing by AE *(German)* 79−70234

acoustic emission continued
Al_2O_3, polycrystalline, fracture toughness and acoustic emission rel. to microstructure, temp. depend. 80−11745
Al_2O_3, unflawed polycryst., tensile failure, SEM and acoustic emission expts. 78−27598
β-Al_2O_3-Na_2O, AE during breakdown under Na^+ transport 78−67860
B fibre reinforced epoxy resin, real-time NDT during fatigue loading 77−86264
Be, welded acoustic emission 78−39976
BeO, dielec. breakdown mechanism determ. acoustic signature anal. techniques 80−11337
C fibre and glass fibre hybrid reinforced plastics, review of physical properties 80−55496
C fibre reinforced plastic aircraft structural appl., non destructive testing 78−35599
C fibre reinforced plastic, fatigue failure mechanism identification, AE detection using piezoelectric strain gauge 79−96239
C fibre reinforced plastic, deform. and failure using AE method *(Russian)* 80−40630
C materials, mech. characts. under stress using acoustic emission analysis *(German)* 79−15881
Cd, grain size effect on acoustic emission generated during plastic deformation 78−80609
Cr-Ni-Mn, type 4340, acoustic emission interpretation of ductile fracture processes 80−35300
Cu, acoustic emission signals in plastic deform., amplitude distrib. *(Japanese)* 78−6978
Cu, acoustic emission under action of single elec. pulse discharge *(Russian)* 77−59071
Cu, Bauschinger AE peak detection of back stress component in flow stress *(Japanese)* 78−6977
Cu, grain size effect on acoustic emission generated during plastic deformation 78−80609
Cu, single crystals, amplitude and freq. response to 1-dimens., transient stress waves 78−14399
Cu-Al (12 wt.%), acoustic emission related to props. 79−34032
Cu-Al (7.9 wt.%), burst acoustic emission during Bauschinger effect 77−48475
Cu-NbTi, composite conductor, acoustic emission 80−97032
β-CuZn, acoustic emission rel. to stress induced martensitic transformation 80−81061
α-Fe, acoustic emission signals in plastic deform., amplitude distrib. *(Japanese)* 78−6978
Fe, magnetomechanical acoustic emission for residual stress NDT 80−71149
Fe, porous, volume strained, correlation between strength and acoustic props. 77−16770
Fe, pure, tensile deform., sources of acoustic emission 78−19814
Fe static loading over wide deform. and temp. range, acoustic emission, plastic flow, fracture 77−90424
Fe, static loading over wide deform. and temp. range, acoustic emission, fracture, plastic flow 77−90425
Fe-Ni (29.58 wt.%), acoustic absorpt. and emission associated with martensitic transform. 79−34035
Fe-Ni-C, martensitic transform., new investigation method *(French)* 79−91881
Fe-Ni-C (32.7, 0.01 wt.%), athermal marrtensitic transition investigation by acoustic emission *(Russian)* 79−91645
Fe-Ni-Mn, martensite, aged, grain boundary embrittlement 79−96144
Fe-Si (3 at.%), acoustic emission response 79−87801
Fe-Si (3 wt.%), strain aged polycrystalline samples, AE study of deform. 77−63696
$Fe_{40}Ni_{40}P_{14}B_6$, metallic glass, acoustic emission generated during viscous flow 78−39853
$Fe_{40}Ni_{40}P_{14}B_6$, Metglas 2826, acoustic emission during viscous flow 78−42915
GAP:N LED, acoustic emission study of defects 79−86799
GaAs, during deformation, acoustic emission rel. to cracks, dislocations 80−35441
GaP:N LED, acoustic emission, NDT of dislocation motion 78−91759
H_2O, acoustic rad. from ionising particles 78−71793
He gas jet noise source, absolute calibr. for acoustic emission appls. 78−59228
He gas jet use in AE anal. 78−80701
In, emission characts. of twinning, nondestructive testing evaluation 77−4873
$LaNi_4Fe$, H_2 absorpt. cracking, acoustic emission characts. *(Japanese)* 80−66631
Mg, burst acoustic emission during Bauschinger effect 77−48475
MgO and MgO-dolomite, crack detection caused by thermal shock, AE technique *(Japanese)* 80−21248
Mo single crystal, crystallographic feature of brittle fracture, AE study 79−43415
Na boiling acoustic emission burst detection in parasitic noise 79−3214
NaCl, work hardening, acoustic emission 79−100167
NaCl-KCl mixture, electrical, electromag., and acoustic props. *(Russian)* 78−30759
NaCl(I), acoustic radiation generated by ionising particles 78−87726
Na_2O-CaO-SiO_2, origins of acoustic emission in fracture 78−72889
Nb-H system, temp.-stimulated acoustic emission, hydride precip. 80−3044
Nb-Ti wires, microplastic behaviour, acoustic emission, appl. to training effect in supercond. magnets 77−26356
NbTi, dynamic stress effects, supercond. magnet training problems 78−49870
NbTi, superconductor, acoustic emission during flux jump 80−39724
NbTi-Cu, composite superconductor, acoustic emission 80−84546
Ni, acoustic emission during magnetisation, stress effects 79−82854
Ni base superalloy, fatigue crack opening load variation with meas. location 80−16425
Ni-Cr-Ti-Al/Au-Ni brazed joint, high temp., AE under elev. temp. and loading *(German)* 78−31597
RbI, single crysts., mosaic struct. changes, press. induced 77−51507
α-SiC, uniaxial compressive damage at low homologous temps., AE and SEM obs. 79−91736
Sn, acoustic emission generated during rapid heating of single crysts. 77−63659
steel, C, magnetomechanical acoustic emission for residual stress NDT 80−71149
Ta, acoustic emission induced by hydride formation 80−76257

acoustic emission continued
ThO_2, sintered, fracture props. studied by Hertzian indentation technique 80—50703
Ti, grain size effect on acoustic emission generated during plastic deformation 78—80609
Ti-Al-V (6, 4 wt.%), high temp. cyclic oxidation, AE monitoring 79—83413
Ti-Ni, thermoelastic phase transform., acoustic emission 80—3039
W, acoustic emission under action of single elec. pulse discharge *(Russian)* 77—59071
Zn, single cryst., in metal melt, plastic deform. and fracture obs. by acoustic emission *(Russian)* 78—56737
Zn, single crystal, acoustic emission during twinning 78—11468
Zn-Al (0.4 wt.%), grain size effect on acoustic emission generated during plastic deformation 78—80609
Zr alloys, acoustic emission during tensile testing 77—90433
Zr during deformation, expt. 77—73425

acoustic equipment
see also acoustic arrays; acoustic wave interferometers; ultrasonic equipment
acoustic reflex threshold temporal integration, instrumental effects 77—77910
active band-pass filter for infralow freqs. 80—53578
active sound-suppression system, single-mode waveguide, bandwidth meas. 80—87605
amplitude and statistical distrib. analysers, basic characts., applications, selection criteria 79—1027
anemometer based on turbulent pressure fluctuations 78—16179
atmosphere acoustic sounder, appl. to methane gas plumes tracking 80—55968
atmospheric sounder, balloonborne, design and construction 78—57353
atmospheric sounder, phase sensitive, phase shift correl. with temp. profile 78—49170
audible warning devices, effectiveness on emergency vehicles 78—87200
audio noise dosimeters, comparison of available equipment, ANSI standards, use in mines 79—1026
audiometer, screening, and real-time computer techniques 78—81009
circuit for acoustic detect. of natural stream bedload transport oscillations 77—45168
digital audio systems, future prospects *(Japanese)* 80—83725
digital sound spectrograph for speech signal anal. 78—63251
directive acoustic spectrum analyser using moving microphones 78—66992
emitter medium receiver type system, phase charact. calc. 80—33409
equivalent continuous noise levels, instrument design, electronic 77—65654
filters, arbitrary profile, circular cross section, finite element simulation 77—11059
Fresnel zone and diffraction fields anal. near boresight of acoustic radar antennas 80—64318
Fresnel zone plate, for focusing of sound waves *(German)* 80—5888
GenRad 2512 portable digital spectrum analyser, simplicity of operation due to interactive display, technical specifications 80—64326
Geological Undersea Surveyor, Acoustically-Navigated, for Mid-Atlantic Ridge appl. 80—4120
HF radio acoustic sounder, atm. wind and temp. remote meas. 78—32235
high frequency atmospheric acoustic sounders 79—84489
history of acoustical measurements and instrumentation, historical review 77—45666
holography and radiation source detection *(Japanese)* 78—18128
impedance head, for mechanical admittance meas. on violin sound post 77—23833
instrumentation for dynamic meas. in sound and vibration 77—72124
integrating real-time noise analyser for portable field operation 79—1037
integrating sound level meters, response to impulsive sounds 79—50547
kit of instruments for statistical research 78—87215
laser-pistonphone for microphone calibration 77—58519
layered matching systems, synthesis technique 78—18141
level meas. in nuclear waste liquor tanks using acoustic pulse-reflection meter 80—86265
levitation and manipulation method for controlling liquid samples in microgravity expts. 80—74666
lining design, finite length tuning concept expt. verification 77—31170
measuring apparatus, for acoustic impedance of brass instruments 78—1518
measuring instrums. over past years, review 80—96152
microscope, acoustic zone plate variable-illuminating-angle system 80—106684
microwave-acoustic Doppler radar system, wind and wind shear meas. at Dulles Airport 78—32233
miniature sound level meter, development 77—31166
mirror, for sound source location in wind tunnel 78—30372
moored acoustic buoy system (MABS) 77—49187
muffler, low-pass filter, for small two-cycle engines 79—18585
muffler chambers, flow-reversing, anal., testing and design 77—11085
navigation systems for submersibles, appl. to precise underwater surveys 79—5683
noise meas. systems and equipment 78—83189
nuclear power station acoustic monitoring equipment 79—76076
phonocardiograph modulator design trends 78—24171
portable acoustic tracking system, for underwater construction teams tracking 79—3874
portable digital spectrum analyser by GenRad, Model 2512 78—57933
radar systems, appl. of microcomputers 80—106685
radio-acoustic sounder for tropospheric temp. meas. 78—53728
reference sound sources, characts. and calibration 78—9515
reflectors, for receiver sound control in auditoria 77—68328
seafloor earthquake meas. system, acoustic telemetry 79—5689
sonar, directional accuracy of small ring arrays 77—31181
sonoprobe survey, automatic recognition of submarine sediments *(Japanese)* 79—39985
sound analyser, undergraduate lab. expts. 80—82600
sound insulation meas. for light struct. *(Chinese)* 79—10427
sound level meter and microphones for intensity meas. 78—83194
sound level meters, comparative listing 79—50546
sound level meters, modern standards and features 78—83191
sound-level meters, instrum., meas., and environmental limitations 79—1039
sounder for lower atm. remote probing 77—17243

acoustic equipment continued
source location techniques, comparison of acoustic telescope and polar correlation 79—37098
spectral analysers, amplitude accuracy limitations 79—1042
spectral analyzers, survey of currently available models 79—1040
tactual sound localizer for deaf *(Japanese)* 77—86707
transponder navigation 79—59896
undersea acoustic transponders, locations optimal estimation 79—5684
underwater communications system for small submersible, design 79—5666
vibration generation techniques using induction motors 77—42790

acoustic field
3-D objects, calc. by integral eqn. methods 80—74558
accelerated sphere in arbitrary fluid medium 78—50966
acoustic diffuser characteristics for amateur user, concert hall appl. *(Italian)* 80—91961
aerodynamically generated sound, mathematical formalisation of Lighthill's theory 77—62245
aerofoils, laminar wakes and noise pattern 79—37341
aerosols, highly dispersed, with elec., acoustic fields, collision rates 79—47986
allowance for temporal variablity of random inhomogeneities of a medium in connection with the local method 79—32144
ambient noise horizontal directionality meas. with linear arrays 77—7270
angle probes, influence of membrane dimensions on sound field 79—23168
anisotropic cylindrical crystal, strain wave propag., theory 77—11062
arbitrarily electroded piezoelec. plate acoustic spatial response determ. 80—99910
Ariane launch vehicle, model firing tests, acoustic field, heat flux, press. distrib. 78—4062
Atlantic bottlenose dolphin, echolocation signal propag. 78—88721
autonomous active systems for sound field suppression in single mode waveguides 77—50831
axisymmetric spherical radiator with mixed boundary conditions, press. field calcs. 77—46827
axisymmetric surfaces, analytic method for sound field prediction 79—50480
axisymmetric transducers, with various boundary conditions, single integral computer method for Green's function 80—87591
axisymmetric transmission system with sound absorbing wall, finite element anal. 77—88974
baffled piston transducer, analytical model for nearfield 80—96168
baffled piston wideband acoustic near- and far-field transients 79—46154
barrier or pillar, many-sided, diffracted acoustic field *(Japanese)* 79—18559
beam reinforced plate, acoustic radiation 79—18580
boundary layer of viscous heat cond. medium, acoustic streaming 79—86544
cardiac acoustic model for computer-aided surface acceleration mapping 78—35791
circular array of acoustically rigid elliptical-cylindrical scatterers, plane wave diffr. 77—31151
circular cylindrical grating with open gaps, infinite 79—90051
circular ducts, multimodal far-field acoustic radiation pattern using mode cutoff ratio 79—32107
circular piston, effect of mean flow on radiation 79—50486
circular piston, influence of acoustically compliant baffle on sound radiation 78—5598
circular piston, nearfield shading effect calc. by ring-function method 77—34974
closed homogeneous lenses, field struct. in focal region 77—68289
coherent optics methods appl. to acoustic field investigations 80—106691
compact planar array nearest-neighbour mutual interaction estimation 79—46160
compensation, in active noise-suppression problem, influence of random errors 77—14852
concave radiator in infinite baffle *(Japanese)* 79—18560
concert hall design, lateral and ensemble reflection requirements 80—91964
concert halls, subjective preference tests for acoustic fields simulated by aid of computer 80—23838
confined beam in viscous medium, sound field near boundary 78—18092
correction of near-field acoustic meas. using arbitrary meas. transducers 78—66996
cross-spectral density meas. in partially reverberant fields 78—30140
crystals, conservation laws in media with freq. disperion 78—5597
cuboidal spaces, computer-aided geometrical field analysis of directional props. 80—19157
CW line spectra, determination of struct. using integration time and acoustic multipaths 79—59860
cylinder, rotating, line-source radiation scatt., distant field calc. 77—50795
cylindrical array synthesis 78—38123
cylindrical radiator, method of estimation 79—64371
cylindrical radiator with mixed boundary conditions 79—18563
diffracted field, layer potential representations 78—30108
diffracted field formed by rigid scatterers in field of harmonic point sound source, compensation 78—18112
diffuse, pressure transformation to external ear, body and head 79—68523
diffuse sound field around objects in a reverberant room *(Japanese)* 79—1030
diffuse vibration field propag. in structs. with periodic inhomogeneities 80—86093
directivity of loudspeaker and subjective hearing event *(German)* 78—79174
directivity of sound sources on noise field *(Japanese)* 77—84075
disc radiator calc. using Kirchhoff surface integral, simplification 79—86275
disc with or without baffle *(French)* 79—98541
discrete approximation of spherical Huygens surface 78—38114
duct acoustic pressure distrib., Galerkin isoparametric finite element analysis 80—27144
ducted noise source, numerical spatial marching techniques for prediction of press. distribs. 79—46098
ducts, mode-matching analyses of coupled fields, boundary conditions 79—32108
echo sounder transducer field plotter 78—59238
edgetone sound, prediction of amplitude 80—74568

acoustic field continued
- effective acoustic centre, redefinition 77—84028
- effective sound field eval. with distance law for sound press. *(German)* 77—32742
- elastic shells, reciprocity theorem 79—32129
- enclosure, 2-dimens., stationary sound field, continuous obs. *(Japanese)* 79—32143
- end-fire line arrays, nearfield beam patterns 77—46857
- energy optimisation using secondary sources *(French)* 80—53518
- equivalent elec. ccts. based on finite-element approach 79—7238
- equivalent elec. circuit using finite element method *(Japanese)* 77—50790
- Exhibition Hall of Yamaha Sportland TSUMAGOI, auditorium sound field control 78—13858
- factorization by means of 2 concentric spherical sensing surfaces 80—64247
- far field amplitudes of diffraction and radiation problems, general relation 77—34973
- far field sound wave generation in liquids by laser pulse 78—83882
- far-field ambiguity of monopole, possibility for active control 77—14828
- fibrous absorber, near-fibre acoust. field for regular fibre arrangements *(German)* 77—801
- finite element simulation of acoustic filters with sound absorbing wall *(Japanese)* 77—84032
- finite-amplitude sound wave field resonator nonlinear losses 78—1469
- flow, transversely sheared, unsteady motion scatt. and distortion 79—59997
- fluid acoustic wave scatt. by temp. and vel. inhomogeneities 79—50491
- focusing radiators and acoustics lenses, field structure 77—50792
- focusing transducers, study of parametric radiation *(French)* 79—41486
- formation by superposition with phase shift *(Russian)* 78—18087
- Fourier analysis to calculate fields around bodies of complex form *(Russian)* 78—46486
- Fredholm integral equation, 1st kind for acoustic diffraction calc. *(Russian)* 80—58834
- free field rooms for industrial applications 80—48518
- gas-liquid mixture, acoustic disturbance propag. 78—9473
- geological materials, acoustic fluidisation prod. by strong transient wave field, theory and appls. 80—85653
- harmonics of the difference freq. in saturation limited parametric sources 78—30110
- highland bagpipe, radiation pattern in open air 77—75752
- horn loudspeaker, anal. of acoustic radiation by finite element method 80—96171
- hydrophone LF calibration, field nonuniformity effect avoidance 78—42486
- impulsively accelerated bodies, approx. method for sound field eval. 77—50825
- Indian Ocean, fluctuation spectrum of US field scattered by inhomogeneities 79—88367
- infinite elliptical cylindrical radiators array with mixed boundary conditions, sound field 78—1538
- infinite planar baffles problem in acoustic radiation and its expt. verification 79—98520
- infinite plate reinforced by finite beam set and driven by point force, sound radiation anal. 78—1496
- infinite plate wave properties, influence of reinforcing beam 77—50821
- integral soln. of 3-D radiation problems 77—68293
- intersection of pipe with plenum, acoustic inertial end correction 80—64246
- irregular waveguide, average acoustic field attenuation 78—1459
- Isom's thickness noise formula, extension to near field 80—53520
- jet, of gas, axisymmetric, free, steady-state, sound emitted, review *(French)* 78—67244
- jet, turbulent, quasi-periodic structure 79—81935
- jet mixing noise, hot and cold, scaling laws based on geometric acoustic model 79—37306
- jet noise source distrib., from far-field cross-correlations 77—84039
- Lagrangian and Eulerian representations of linear acoustic fields *(French)* 79—41477
- Lamb wave optical detect. in fused SiO_2 80—106690
- laser beam incident on plane interface, thermal acoustooptical effect 77—11639
- lenses, two-layer, focal plane field 77—35005
- linear array, far-field directivity patterns, electrical analogue simulation 77—804
- liquid, laser excited acoustic field, effect of surface perturbation 77—15499
- liquid excited by spherical acoustic radiator, bubble dynamics 77—68679
- liquid half-space, sound generation by FM modulated laser beam 78—38781
- liquid layer floating on liquid half-space, acoustic field generated by laser beam 78—51615
- liquid surface scanned by laser beam, acoustic field of moving optoacoustic antenna 79—90108
- machine panels, insertion loss, meas. and evaluation 78—87193
- mapping, nematic liquid crystal array appls. 79—91402
- membrane, infinite, acoustic radiation due to fluid loading discontinuity 78—90579
- microsphere probe for pressure field meas. up to 10 MHz 80—96159
- modal radiation impedances for semi-infinite unflanged circular ducts including flow effects 79—72738
- mode representation of the noise field in a wedge 79—86299
- motor vehicle noise propagation, prediction technique 77—75744
- moving body, thickness noise formula for acoustic far-field 79—81630
- moving media, randomly inhomogeneous, probabilistic characteristics of noise fields 79—64383
- moving source in superfluid, sound pressure and temp. fields 79—90054
- moving sources, intensity of acoustic field 79—32106
- multielement acoustic array characterisation by acousto-optic diffraction 80—99911
- multimode waveguide, active sound fields suppression system 78—18113
- multimode waveguide with periodic boundaries, acoustic field of volume-velocity sources 78—94463
- music fields, effects of early multiple reflections on subjective preference judgements 79—41517
- narrow sound bundle reflected from irregular surface, amplitude and phase var. 77—46825
- narrow-strip transducer, radiation pattern theory 80—96165
- near field of flat acoustic radiators, anal. 77—31148

acoustic field continued
- near sound press. field during plane wave scatt. at circular cylinder *(Russian)* 77 75731
- nearfield axial levels of exponentially shaded end-fire arrays 77—39127
- noise barriers, Z-lines method appl. to anal. of far field diffr. 77—50822
- noise correlation functions for arbitrary receiver orientation and steering direction in vertically anisotropic, azimuthally isotropic noise fields 80—58864
- noise environments, use of coherence and phase data between two receivers 78—59194
- noise field, anal. of structural-vibr. related noise contrib. 77—84077
- noise field, evaluation of integral in spatial-correl. theory 77—88981
- noise fields, factorisation and active suppression, nonsteady problem 77—27426
- nonlinear interaction of fields with plates under harmonic excitations 79—23246
- nonlinear oscillating gas bubble in compressible liquid, translational motion in an inhomogeneous sound field *(German)* 80—53495
- nonmagnetic metal, calc. of acoustic field prod. by EM US transducer 77—11101
- nonrectangular reverberation chamber design and construction 78—83196
- normal mode sound field in shallow water, positive sound vel. gradient, random fluctuation surface *(Chinese)* 77—34982
- ocean, tidally varying sound speed and currents rel. to deep ocean total field 77—79995
- off-axis beam pattern analysis using replica pulse representation 77—54821
- open ended cylindrical pipe or cone and rod or slab 77—84021
- optical registration system for pulsed sound fields 79—90102
- optical-acoustic probing of heterogeneous condensed media 80—38211
- opto-acoustic antenna, floating, acoustic field statistical characts., surface waviness depend. *(Russian)* 78—1536
- oscillating body of revolution, sound field anal. 78—90583
- oscillating circular plate, axial field, meas. and anal. 77—7235
- paper membrane sound generation by impulsive tension 78—90581
- parametric acoustic arrays formed by diverging sound beams 77—27418
- parametric acoustic source, numerical method for nearfield calc. 78—63221
- parametric acoustic sources, model for difference-freq. radiation 77—46836
- parametric acoustic transmitting arrays, symmetric and asymmetric weak interaction model for axial difference-freq. field 79—81599
- parametric source aperture factors 77—841
- Pekeris operator, resolvent in dispersive media *(French)* 79—41488
- penetration into a sand sediment of difference-frequency sound generated by a parametric array 78—63227
- phased array beam steering, phase error grating lobes 79—48313
- phased arrays, infinite periodic 80—58836
- phonocardiographic microphones, air cavity characteristics, effect of vibrations, room noise 77—81611
- piezoelectric hydrophones US output assessment 79—23176
- piezoelectric polymer transducers, effect of acoustic radiation on equivalent circuit 79—94380
- piezoelectric radiators, field homogeneity enhancement 77—68358
- piezoelectric transducer wedge-shaped, ang. displacement of sound beam 77—35009
- piezoelectric transducers, single acoustic signal distortion 80—87637
- plate reinforced with projecting beam, long-wave diffr. field 78—9469
- plate with line impedance discontinuities, acoustic transmission and scatt. 78—90553
- plates joined at right angles with fluid contact, diffraction problem 78—18224
- point source in rectangular space bounded by thin elastic walls, acoustic field 80—96050
- point source radiation near cylindrical jet in motion 77—31169
- point source radiation through composite medium 77—31150
- pressure field alongside manikin's head, rel. to in situ hearing aid tests 77—90805
- pulsating sphere in rectangular waveguide, field suppression 77—68287
- pulsed US fields, integrated acousto-optical effect 77—31193
- quadraphonic sound field analysis method and appl. *(Japanese)* 77 75730
- radial spatial coherence from near ocean surface source 78—30117
- radiating sources, conditional sampling technique appl. 77—68322
- radiation field computation for sound channels using coherence theory 78—79152
- radiation fields, interpretation in terms of sub-beams 77—50788
- radiation press. on an absorbing sphere 78—79154
- radiator directivity pattern calc. from near-field sound meas. 78—83149
- Raman Nath parameter calc. for entire field of baffled planar transducer 80—74689
- rays reflection from curvilinear boundary in medium, field amplitude calc. 77—33874
- realtime echographic imaging system, acoustic field study *(Italian)* 79—96636
- reconstruction of acoustic wave fields, weighting factors, seismic appl. 78—28330
- rectangular reverberant room, sound press. correl. coeffs. 78—18115
- rectangular reverberant room, sound pressure correl. coeff. *(Japanese)* 78—38146
- rectangular room, instantaneous excitation of one-dim. sound waves *(German)* 78—87201
- reflectivity field reconstruction from line integrals over circular paths 80—58863
- resonantly vibrating surface, nearfield determ. of complex radiation efficiency and intensity distrib. 79—55262
- reverberant room, rectangular, correlation coeffs. of sound pressure 79—76914
- reverberant sound field spatial cross-correlation 79—68496
- reverberation chamber, space variance for rectangular modes 77—75746
- reverberation room sound pressure level spatial averaging by microphone array and traverse 77—58515
- rigid prolate spheroid, short wavelength diffracted surface pressures 77—84018
- rigid sphere vibrating parallel to plane wall, near field 80—102910
- room impression index, definition on basin of subjective examination *(German)* 78—87202
- rooms, field anal. by finite element method *(Japanese)* 79—27465
- sawtooth sound waves, diffr. and radiation 77—808
- scattered field, of circular array of acoustically compliant elliptical cylindrical scatterers 77—14831

acoustic field continued
- secondary flow beside cylinder in complex sound field 79—14376
- semiinfinite plate, immersed in a fluid, flexural modes 77—50819
- shadow-optical colour imaging technique for sound field pressure distrib. meas. 79—64464
- shallow water, transition ranges, bottom-reflection loss *(Chinese)* 77—58500
- shear wave scatt. by flat-bottomed hole in Al, intensity distribution mapping 77—19503
- short pulse US transducers, field phenomena 79—23170
- solid layer, field of elementary source of elastic strain waves 79—18561
- sound and vibration fields coupling in compensation of radiation from plate at subcritical freqs. 78—18110
- sound and vibration fields suppression, synthesis of systems 78—9494
- sound generation and transmission in flow ducts with axial temperature gradients 78—90551
- sound pressure levels behind large storage tanks, reflection effects 77—50826
- source extraction in random field 79—50514
- sparse line array, cross-sensor beam forming 77—39126
- spatial cross-correl. of acoustic pressures in steady and decaying reverberant sound fields 77—7232
- spatial varaition of decaying fields, commnets on investigations 79—90073
- spherical, acoustic radiation pressure on rigid sphere 80—64251
- spherical and ellipsoidal Huygens surfaces, discrete approx. for suppression of sound fields 80—87594
- spherical radiator in presence of spherical impedance scatterers 78—38111
- spherical source near scattering sphere, radiation characts. 77—7228
- spherical sources of finite size, acoustic radiation load coupling 77—79982
- spherical wave diffraction by absorbing plane farfield vel. pot. 77—46830
- spherical wave reflection at fluid plane interface with porous medium 78—42484
- spheroidal body at interface, sound scattering 79—94387
- standing wave acoustic field, stable arrays of reson. bubbles 77—79988
- standing wave field, meas. of radiation press. on sphere 77—79989
- stochastic boundary-value problems, solns. using digital simulation of space-random fields 79—41510
- strip-shaped baffled flat sources, near and farfield calcs. 79—50475
- submerged cylindrical target, comparison of schlieren and holographic techniques 78—38157
- submerged elastic shell, acoustic radiation 78—90572
- subsonic jet, acoustic far field, azimuthal struct. *(French)* 79—14150
- superdirective spherical radiator, max. directivity conditions 77—84019
- supersonic jet, underexpanded, impinging on barrier, sound field 78—9495
- supersonic optoacoustic antenna, acoustic field 78—1540
- target recognition using theory based on Bojarski's identity *(French)* 79—41479
- thin cylindrical shell, point-driven, with rigid massive septa, sound radiation 77—803
- three dimensional acoustic radiation, problems, boundary integral solns. 79—3818
- three dimensional objects, stable soln. for integral eqn. formulation 80—106647
- three-dimensional flow in highly-loaded axial turbomachine, vorticity effects 78—26130
- time transformation of acoustic eqn., flow effects on sound field, wind tunnel noise meas. appl. 78—87198
- Tollmien-Schlichting waves, sound field 78—18090
- transducer, US sound field diffr. losses, numerical calc. *(German)* 77—3705
- transient, microphone method for energy meas. 80—102942
- transparent-solid US transducer field visualisation 79—55285
- turbulent shear layer, sound and aircraft noise, spectral broadening 79—37076
- turbulent shear layer, sound transmission 79—37075
- two-dimensional, anal. by integral eqn. upon the periphery *(Japanese)* 79—81591
- underwater, CW source motion effects on total acoustic field, isospeed channel appl. 77—7242
- underwater sound, bottom-reflected field defocusing in inhomogeneous antichannel 78—1484
- underwater sound, press. and intensity fields from spherical compliant-tube Luneburg lens 77—46842
- underwater sound, simulation of reverberation from surface of sea *(French)* 77—14836
- underwater sound, use of linear system theory in acoustic radiation and scatt. anal. 77—75729
- underwater sound, wide-angle field in ocean with range-depend. vel. profiles 77—79993
- underwater sound field, fluctuations using parabolic vel. profile 77—31159
- uniaxial waveguide, sound field calc. from combination normal mode-ray technique 77—50800
- US, experimental study of integrated optical effect using light diffraction technique 80—23848
- US, in liq., kinetics of number of cavitation bubbles 77—15085
- US, visualisation using microphone matrix *(German)* 79—32151
- US concentrators, spheriform and cylindriform 77—50816
- US field calibration from acousto-optic data using Fourier techniques 77—84054
- US fields, Gaussian-Laguerre description for circular piston 80—64239
- US fields investigation, appl. of holographic interferometry 78—1519
- US fields of different freqs. in liquids, cavitation effects under simultaneous action 79—94396
- US fields radiated into liquid by normal modes of plate driven by pulsed beam 78—50995
- US focusing transducers, field pattern criteria 79—14196
- US pressure and interference fields *(German)* 80—89436
- US tissue characterisation by backscattered field space-time processing 79—48305
- US transducer field, appl. to standard probe transducers 77—840
- US visualisation in air *(French)* 78—87212
- US visualization using small Al flakes *(Japanese)* 78—33973
- velocity monopole source, power radiated under reverberant and freefield conditions 79—46107
- vibrating bodies, calculation of sound fields *(Japanese)* 80—48493

acoustic field continued
- vibrating bodies in homentropic potential flow at low Mach number 80—23826
- vibrating porous material surface sound radiation *(Japanese)* 79—68474
- vibrating rigid body, calc. via Schenck numerical method *(French)* 80—69589
- vibrating sphere near rigid or compliant wall, near field and impedance 78—94476
- visualisation by optical holography 78—59216
- wall shear layer of infinite duct, acoustic field generated by single line source 78—1455
- wave characteristics rel. to EM waves *(Japanese)* 78—46858
- wave incident on moving plane 78—63218
- waveguides, excitation of sound pressure field by spherical pulse 78—50971
- waveguides, sound pressure field variation as function of refractive index 78—94464
- wedge with curved faces, field near edge 80—87592
- $LiIO_3$ single crystal, surface acoustic wave parameter meas., coherent optics method 80—106691

acoustic generators
- *see also earphones; loudspeakers; photoacoustic effect*
- acoustic pressure generation by laser beams 79—18575
- axial dynamic, model of theoretical acoustic system 79—14181
- biomedical noise generator for masking click stimuli 80—108980
- circular piston, effect of mean flow on radiation 79—50486
- coherent THz acoustic wave launching by far IR photon-phonon conversion 77—39135
- convergent ultrasounds generation in air, via sources using flexurally vibrating circular diaphragms 77—50845
- digital generation, of acoustic excitation impulses 78—90618
- digital reverberation and echo apparatus *(German)* 79—50554
- disc-rod US tool, gain enhancement technique 77—35010
- Doppler thermooptical source of US waves 80—58852
- duct with axial temp. gradient, sound transmission and generation 77—62084
- edgetone, fluid mechanics 78—13835
- electroacoustic and aerodynamic calibrated sound sources compared 78—55543
- EM generation of US guided waves in ferromag. metal polycrysts., model 78—22236
- ferroelectric cylinders, radially polarised, electroacoustic sensitivity calc. by normal-mode methods 77—62131
- gait trainer for hemiplegic patients with lower limb sensory loss 78—48940
- gas-jet, HF high-intensity 79—64376
- gas-jet sound generator, Hartmann type, influence of jet temp. on characts. 78—51025
- heat engine, travelling wave, based on pistonless Stirling engine 80—19127
- Helmholtz resonator as high-power deep-submergence LF source 80—74576
- horn excited by Hartmann-Sprenger tube, aeroacoustical phenomena 80—91948
- hydrodynamic siren, influence of rotor-stator spacing on hydroacoustic characts. 78—18135
- hydrodynamic sound generation mechanism 79—32172
- impulse source, continuous spectrum, appl. to polyurethane foam acoustic response meas. *(French)* 79—1033
- infrasound and pressure waveform generator, compact, for small cavity appls., animal research 80—104830
- laser beam generation of sound in solid 77—11639
- laser thermooptical sound source in liquid, anal. of wave zone 80—87631
- linear pulse selector for US investigs. 78—5623
- liquid waveguide, sound generation by absorpt. of modulated laser radiation 78—1539
- mechanical waveguide using circular cylindrical rod for HF intense US production *(Japanese)* 78—33983
- metal, EM generated ultrasound, position dependent amplitude 79—37763
- motor car horn diaphragms, free vibr. anal. 80—74687
- moving point sources, intensity of acoustic fields *(German)* 80—102879
- multi-blade fan as reference sound source, influence of reflecting plane *(Japanese)* 80—19189
- music research programmable tone generator presenting melodic and harmonic patterns 77—56381
- noise, pseudo-random for sound absorption and buildings, insulation testing *(Spanish)* 78—13861
- nonlinear and thermal, due to thermoviscous heating of fluid by modulated sound wave 79—23122
- optoacoustic sound focusing device using YAG laser 80—87692
- optoacoustic sound-focusing device based on laser beam absorption in thin liquid film 79—90107
- oscillating circular plate, axial field, meas. and anal. 77—7235
- parametric acoustic sources, model 77—46836
- parametric array, finite amplitude waves refl. 77—84036
- parametric sound generators, theory 77—50849
- parametric sources, interaction of nonlinearity-limited spherical beams 80—43508
- particle agglomerator for particulate emission control, use under standing-wave condition 80—30627
- particle agglomerator for particulate emission control 80—26191
- piezoceramic transducers for generation of acoustic pulses having prescribed shape 80—87691
- piezoelectric ceramic buzzers for high sound levels 80—92005
- PMOS programmable sound generator, microprocessor-compatible, electronic music appls. *(German)* 80—79092
- pulsed electron flux, acoustic waves generation, for nondestructive inspection 80—5905
- radial US vibration generation by circular plate 79—18663
- randomly fluctuating sources on 2 coaxial rings, direct and inverse problems 80—33270
- resonance frequencies in T-tube 79—14136
- SAW generation using CW laser, NDT appl. 80—87683
- sound generation by long laser pulses incident on liquid surface 80—5900
- sphere impacting on thin square plate, acoustic generation mechanism 80—74591
- spherical sources of finite size, acoustic coupling 77—79982
- stepped pressure concentrator, anal. of reson. freq., gain, and press. distribs. under reson. and nonreson. conditions 78—90619

acoustic generators continued
structure radiation of simple emitters, radiated sound power *(French)* 77—19471
tapered piezoelectric bar transducer with transverse polarisation of piezoceramic, acoustic props. 78—1537
thermoelastic expansion flexible acoustic probe 80—16618
thermooptical sound generation problems, method of transfer functions 79—64478
thyristor impulse generator 79—10441
transducer-receiver configuration, flexible, activated by laser 80—83724
underwater parametric acoustic source beamwidth control 78—75011
underwater parametric source, specialized drive waveforms 78—33985
underwater projector, improvement of fidelity using technique involving modern control theory 79—98549
underwater sound, operating freq. choice for miniature transmitters in fresh waters 77—54826
US pulse excitation method for solids 78—5624
US shear waves, EM detection and generation in supercond. Sn 77—19468
US tomography using laser-generated acoustic fan beam 79—83862
virtual sources, non-contributive 80—38151
vortex, separation of acoustic energy and spent-air jets 80—102953
vortex sound generators 78—50975
whistler nozzle, formula for acoustic resonance freqs. 79—72741
wideband general-purpose US generator for biological object handling 79—48381

acoustic holography
acousto-optics, conf., San Diego, Calif., USA (Aug 1976) 77—58463
aperture synthesis with frequency sweeping 79—23146
apodized holograms numerical reconstruction 77—31187
applications and theory review, background and current status 78—74866
b-scan Fourier transform holography 79—83421
biomedical applications, state of art and future 80—67175
bispectral holography, theory 77—84086
coherent optical defectoscopy, signal processing, materials testing appl. *(German)* 78—7110
computer reconstruction of acoustic sources from holographic detect. 78—38153
crack detection of rotor forgings by US holography 77—66730
FM pulse sound holographic imaging 79—55270
Fourier holograms, long-wavelength, recording and reconstructing schemes 78—87029
Fourier transform, lensless, expt. and digital simulation results *(Japanese)* 78—30133
GaAs holographic grating transduction from bulk to surface acoustic waves 77—31199
graphite composite aircraft structures, flaw detection by US methods 78—44288
Green's theorem, potential theory, angular spectrum *(French)* 78—18127
hologram matrix image reproduction expt. 79—55271
hologram matrix sonar 79—41526
hologram matrix US imaging method 79—46120
image enhancement by electronic differentiation 77—19204
imaging, super-resolution, using sequential estimation of hologram 79—68499
imaging applications of US and acoustic methods *(Dutch)* 78—27719
imaging technique without wavelength resolution limit 80—99898
lens theory and construction 78—55536
liquid surface imaging 78—53175
liquid surface method, optical processing of acoustic information *(French)* 77—68339
liquid surface system, effect of minitank membrane on minitank transfer function 79—81645
long-wave imaging with super-resolution by wavelength diversity 80—102675
long-wave small-amplitude holograms, recording and reconstruction 79—18627
long-wavelength hologram focusing parameters, estimation method using focused pattern 80—14304
longwave holography, double circular scan format generation 80—43555
M-sequence combination of spatial and temporal modulation 80—38183
materials testing, defects reconstruction by signal locus curves *(German)* 78—92435
mechanical scanned hologram method and optical reconstruction *(Korean)* 80—28385
medical and biological applications 79—8528
medical diagnosis appls. 77—81545
methods, concepts, and appls. 79—64411
motion limitations, using an electronic reference 77—58512
moving acoustic source image reconstruction by temporal reference holography 78—79171
multifrequency holographic imaging system, investigation 79—81644
multifrequency synthetic detecting holography, geophysics appls. *(Chinese)* 77—64444
NDT appl., techniques 79—86300
near-surface defects, US detection and analysis *(German)* 80—93728
numerical image reconstruct., applicability conditions for Fourier transform *(Japanese)* 78—59208
numerical restitution, finite aperture and sampling effects *(French)* 79—72760
passive holographic sonar, new system using polyspectral anal. 77—39124
passive imaging systems, effective utilisation of spectral spread 78—71250
phase samples, improved image quality *(French)* 80—79088
piezoelectric integrated acoustic array, system anal. 80—79067
and radiation source detection *(Japanese)* 78—18128
raster choice 78—74867
real-time acoustic imaging using light modulator comprising LiTaO$_3$ crystal 80—5879
reconstructions from hologram, digital and optical 80—23842
resonance echo holograms, acoustooptic conversion of wave fronts 77—62112
review, status of research 77—58511
sapce-frequency equivalence recombination with holography 80—48522
SAW memory, monolithic, with long storage time 77—80026
SAW memory, using semicond. laser 77—80024
scanned, motion effects on image quality 78—71249
scanned linear array, motion limitations 78—5616
seismic data processing applications 80—46268

acoustic holography continued
seismic imaging by holography, techniques and appls. 79—66831
Sonoscan, real time microprocessor based imaging system 80—38184
sound source location on complex vibrating structures 77—7264
sound source reconstructions using a microphone array 80—96132
speckle size 78—13864
steel, stainless, LWR appl., US and AE testing of welds 79—36330
submerged cylindrical target, comparison of schlieren and holographic techniques 78—38157
summary of acoustical holography development work *(German)* 80—53567
survey of techniques and developments 80—23841
threefold seismic or acoustic holographic interferograms for improved reconstructed-image definition and contrast 80—23844
transducer array for acoustic holography *(Japanese)* 77—80029
transient acoustic radiation source imaging 78—1516
two-dimensional target imaging using hologram matrix, ultrasound experiment 79—23145
two-dimensional target imaging using multifreq. hologram matrix, 1 MHz ultrasound expts. 80—64305
undersea acoustic holographic transducer array development 78—59209
underwater, systems characts. and appls. 78—33945
underwater acoustic hologram correction for nonuniform relative motion 79—46119
underwater acoustic holographic image reconstruction for moving objects 78—75019
underwater acoustic holographic viewing experimental system 79—46121
underwater imaging system using multifreq. US holography 79—98556
underwater synthetic aperture imaging using acoustical holography 79—3863
US, holograms, recording via suspension method 77—14857
US hologram numerical reconstruction in NDT *(German)* 80—97667
US holographic visualisation *(Slovak)* 79—41527
US holography, electronic reference generation of spherical wave by microcomputer 79—81646
US holography for defect size meas. at inservice inspections of nuclear components 79—45372
US holography with crossed linear transducers using spatial reference 77—84088
US holography with electronic reference wave incidence variation 77—84087
US imaging and holography, devices, medical uses *(French)* 77—827
US imaging techniques for medical diagnosis *(French)* 80—26304
US indications, use of acoustic holography in tandem arrangement for interpretation *(German)* 77—16763
US testing, flaw image form. *(German)* 77—56196
US transducer vibration amplitude distrib. meas. by holographic technique *(Japanese)* 77—88999
US transducer vibration amplitude distribution meas. 77—42678
US two-dimensional imaging by means of multifrequency hologram matrix 80—19165
US-field display device with transducer and LED linear arrays, appl. to US holography 80—23843
weld flaw study using ultrasonic holography *(Dutch)* 78—68855
wideband signals, ang. resolution, image intensity 78—83182
wideband wavefront reconstruction in two-dimensional dispersive space 77 31191
B$_{12}$GeO$_{20}$, cryst. powder, phonon electroacoustic echo signal storage 78—68055
CdS, photocond. cryst. characterisation of electron-trap responsible for acoustic holographic echoes *(French)* 79—19544
H$_2$O, cavitation nuclei conc., holographic and hydrodynamic obs. 78—83440
LiNbO$_3$ SAW devices, SAW and bulk wave propag., freq. shift holography *(Japanese)* 79—59895
LiNbO$_3$, SAW excitation and propagation patterns, frequency translated holographic obs. 77—80690

acoustic imaging
see also acoustic holography
2-D acoustic Fourier transform of optical images 80—74308
abdominal abscesses detection, role of ^{67}Ga-scintigraphy, ultrasonography and computerised tomography 80—17096
abdominal diagnosis, combined, complementary appl. of echoscopy, echotomography and echography 80—21507
abdominal ultrasonography, clinical appl. 80—30826
acoustic seeing aid for blind *(Polish)* 80—8215
aid for the blind 80—104810
air gap diode acoustic imaging and scanning 79—50524
analogue fast Fresnel transform methods 79—46116
anthropomorphic torso section phantom for US imaging 80—45987
arc array with automatic sector scan echo signals presentation system *(Italian)* 79—96637
arrays, direct imaging and phased, US imaging appls. 79—64460
attenuation reconstruction from back-scatt. US 80—30821
B-scan imaging with automated water-delay system 80—98041
B-scan viewing using backward wave propagation 80—33352
Benthic Untethered Multipurpose Platform for underwater acoustic TV 80—46319
bidimensional array design for B- and C-scan US imaging system 79—47877
biliary ductal system, status demonstating ability of ultrasonography and computerised tomography 79—92310
biliary tree gas appearance in US B-scan 78—80930
biomedical ultrasonics, signal processing aspects 78—7418
biomedical US B-scanning, computer simulation 80—81675
bispectral passive imaging system for machine-system diagnosis 78—63239
blood velocity analysis during pulsed Doppler US imaging of carotid artery disease 77—29189
body organ volume determination by US scanning 80—17034
Bragg diffraction imaging, aspect ratio restoration by holographic lenses 79—46122
Bragg diffraction imaging, influence of US absorpt. in water of Bragg cell 77—31188
Bragg diffraction imaging for medical use 78—53462
Bragg diffraction imaging systems, speckle size 78—13864
Bragg diffraction scanner for ultrasonic tissue characterisation in vivo 77—77949
Bragg imaging in the reflection mode and designs for improved optics 80—17040

acoustic imaging continued
Bragg-diffraction imaging 79−64463
Bragg-diffraction imaging system with partially coherent light illumination 79−14175
brain US imaging through skull 80−51185
brass/water interface leaky Rayleigh wave reflectivity loss meas. 78−59187
breast echography, possibilities, results and indications *(French)* 78−7408
breast tissue characterisation in vivo by US TOF computed tomography 80−51186
broadband focusing through converging lens, linear systems approach 79−3817
broadband US tomography 80−26311
cardiac parameter extraction from 2-dimens. US images 77−25533
carotid arteries, high definition imaging using standard commercial US 'B' scanner 79−88142
carotid artery imager, CW Doppler US and spectrum analyser 79−57731
carotid bifurcation scanner, differential velocity display with colour coding 77−21588
carotid bifurcation tomographic scanner, US Doppler colour coded vel. display 77−25529
cellular mechanical and chemical analysis, recommendations of workshop on future of biomedical instrum. 80−81776
coal seam acoustic imaging 79−53585
coaxial circular spherical array for US imaging 78−9513
coherent optics methods appl. to acoustic field investigations 80−106691
composite material delamination visualisation, US pulsed schlieren method 79−70289
computed tomography of breast, progress 80−51196
computerised tomographic reconstruction, breast scans 80−41216
conical acoustic lens, fabrication and test results 78−51019
conical acoustic lens, opto-acoustic feasibility design 78−51020
contact B-scanners, calibration method 79−23161
cylindrical transducer scatter scanner for medical ultrasonographic imaging 80−96154
data collection aperture, based on long-wavelength imaging system 80−99905
diagnostic US, prospects and limitations 80−98040
diagnostic US role of computer 80−8111
diffraction tomography, experimental results 80−76818
discrete-time Doppler frequency meter for blood flow imaging 79−57704
display system using computer generated integral photograph, appl. to US images 78−87021
Doppler US system, for internal organs imaging 79−5332
dynamically focused array imaging systems, induced Doppler distortions 79−46117
dynamically focused electronic sector scanner based on CCDs 80−98042
dynamically focused US diagnostic phased array 78−61232
echo and reconstruction imaging via adaptive ray tracing 79−83867
echo-shadow method of visualizing foreign bodies 80−3742
echo-tomographic imaging with SAW processing, ultrafast 80−74639
echocardigram, automatic anal. and VTR recording 80−8112
echocardiogram computer-assisted interactive interpretation 78−80938
echocardiographic, graphic representation of 2-dimens. structs. in motion 79−70597
echocardiography, clinical appls. of new techniques 80−36050
echocardiography, two-dimens., wall motion and thickening quantification by computer-aided contouring 78−80937
echocardiography, US, picture processing of 2-dimens. data 77−77958
echographic diagnosis of lesions of the abdominal aorta and lymph nodes 80−17033
echographic phased array for medical diagnostics, dynamically focused insonification 80−89813
echography, in vivo A-scan dynamic autocorrel. anal. 80−51192
echography, real time, contrib. to diagnosis and management of palpable breast lumps 80−17027
echomammography: indications and limitations in tumours with or without calcification *(French)* 80−36039
echopyelographic visualisation of pacemaker induced contractility in calyceal structs. of human kidney 78−48850
echotomograph, ultrafast, using optical processing of US signals 80−51180
electronic ccts., book 80−99899
electronic devices, nondestructive testing by acoustic microscopy 79−37094
electronically-addressed bulk acoustic wave Fourier transform device 80−74637
etched arrays for medical imaging 79−25057
fault detection by scanning acoustic microscopy 77−80040
film for US imaging 79−88143
fluid velocity vector and temp. fields reconstruction, three-dimens., from acoustic transmission meas. 78−51261
focusing device with IDT on thin piezoelectric plate 80−1398
focusing device with interdigital transducer, image prod. 78−9520
foetal growth estimation from US image meas. 80−101239
gall-bladder kinetics, real-time US study method 79−100682
gallstones, acoustic shadow formation 80−98047
gastric motility measurement, non-invasive US pulse-echo scanning method 77−64101
generalized image synthesis from projections 80−67579
grating acoustic scanner characteristics measured by an optical probe 80−74662
grating acoustic scanner for material defects 79−47878
grating acoustic scanner for underwater imaging and NDT 79−57198
gray tone display processor for CRT, US materials testing appl. 78−44284
grey-scale US images, local diagnoses and artefacts identification *(German)* 77−86571
heart diagnosis, electronic sector-scanning cross-sectional echocardiograph, model SSH-10A 79−57732
heart wall motion quantification using computerised US technique 78−40279
hepatic metastases detect. by grey-scale US scanning 78−73179
high-resolution blood flow imaging system using binary phase coded pseudonoise sequences 79−57703
high-speed stress detection and imaging, 100-element acoustic phased array 79−47876
holograms of acoustic field, moire processing 78−55539
improvement using statistical estimation theory 79−46115

acoustic imaging continued
impulsive sound method *(Japanese)* 78−33971
impulsive sound method 79−10431
information processing application in US imaging systems *(Japanese)* 77−65655
instant photographic technique 78−58079
interdigital transducer for acoustic imaging 77−80020
isochrone convergence imaging of pulse echoes 77−68338
jet noise meas., source location, appl. to acoustic mirror, telescope and polar correl. techniques 78−83169
Lamb wave optical detect. in fused SiO_2 80−106690
laser scanned acoustical imaging systems, demodulation scheme 79−59826
layer-by-layer endography of multiply scattering objects 79−48303
left ventricular dimensions and dynamics during coronary occlusion determ. by B-scan US in dog model 78−48849
lens, solid acoustic, pulse and freq. response anal. *(Russian)* 78−46873
light optical imaging, of focused US field *(German)* 80−3275
$LiNbO_3$ wedge waveguide apodised interdigital transducer evaluation 77−27451
linear array acousto-optical modulator devices 77−39072
linear scanning with zone plate comparison with cylindrical focalisation 80−79091
liquid crystal cell, mixed nematic-cholesteric, US field visualisation 78−1524
liquid-solid interface, acousto-optic diffr. with crit. angle incident light 78−37801
liver diagnosis, estimating acoustic attenuation coeff. slope from reflected US signals 80−5876
mammographic US image correlation with histopathologic sections 80−101240
materials for acoustic lenses suitable for acoustic imaging 79−72771
medical, shadowing due to calculi and gas collections, differentiation 80−98048
medical, transmission media for ultrasonography 80−98050
medical B-scan US, technical factors influencing the imaging of small anechoic cysts 80−98049
medical imaging, ceramic and PVF_2 transducers compared 79−57734
medical imaging techniques, developments, review 80−26324
medical ultrasonics, USA National Science Foundation incentive programme 77−66831
medical ultrasonics conference, Munich (May 1975) 77−32945
medical US, spread energy method, use of time gain control 80−108988
medical US echoscopic meas., random error sources *(Croatian)* 78−44569
medical US imaging, improvement of sensitivity or reduction of dose 80−74641
medical US imaging, overview of principles and instrumentation 79−66579
medical US imaging, use of fibre optic recorder 77−5057
medical US imaging light intensity perception charact., stochastic noise influence 80−98053
medical US imaging technology status 78−24174
medical US phantoms, water-based gels 80−81671
medical US systems, spread energy method, theory 80−14533
microprocessor-controlled digital compound scan system 79−57735
microscopy conference, Reston, VA., USA (Apr. 1977) 78−45683
microscopy in high-pressure gases 80−43561
microscopy of excised tissue 80−17041
microscopy review, historical development 78−46877
microscopy using scanning laser beam as remote sensing microphone 77−81382
monolithic acoustic retina resolution improvement 79−55305
monolithic cascade CCD ultrasonic lens applications 78−22231
multiplicative and additive processing comparison 80−64303
muscle mechanics obs. by acoustic microscopy 78−48952
narrow-strip transducer, radiation pattern theory 80−96165
NDT application, electronic scanning 79−66230
NDT using acoustic imaging devices 77−81381
nematic liquid crystal acoustic image detector, resolution expt. 78−46871
nematic liquid crystal retinas for direct 2D acoustic images *(French)* 80−69617
nematic liquid crystals, appl. as image detectors 79−41537
nonperiodic wave diffr. anal. *(French)* 80−48486
objects buried in seafloor sediment using focused US transducer 80−79036
ocean, New England shelf-slope water mass interfaces, imaging 78−3784
ophthalmic US B-scanner 80−30804
optical registration system for pulsed sound fields 79−90102
optical scanning, photo integration technique *(French)* 79−32147
optically-controlled acoustic transducers, piezoelect. and electrostrictive 80−74638
optimum apodizers, performance, primary coma effects 79−98557
opto-acoustic transducers, improved equivalent cct. 80−74658
opto-acoustic transducers for sensitive US imaging 78−5625
optoacoustic transducer characteristics for US imaging 79−50560
orbital tissue visualisation by A-scan echography 77−77953
pancreatic disease, study by multiple imaging modalities 80−17094
pancreatic lesion visualisation and documentation by diagnostic US 78−11708
pancreatic US, systematic approach to scanning technique 79−74731
PCB, nematic liq. cryst., US imaging, convertor, acousto-optical effect 78−59218
phantom for imaging biological fluids by US and computerised tomography scanning 80−104692
phase contrast imaging with electronic scanning 77−31190
phase imaging in reflection with acoustic microscope 78−30136
phase samples, improved image quality *(French)* 80−79088
phased array beam steering, phase error grating lobes 79−48313
phased array US imaging, real-time digital scan conversion and multi-dimensional processing 79−48363
phased array US imaging delay line bandwidth reduction 79−50552
phased array US imaging with multiscan processing 79−57736
piezoelectric elements of array, tall, narrow, vibration mode 80−74690
PMMA Doppler scatt. optical determ. of US radiation patterns 79−76930
prostate tumour diagnosis by pattern recognition in US sectional pictures 79−83866
prostate US sectional pictures, pattern recognition for tumour diagnosis 80−51194

acoustic imaging continued
prostatic carcinoma treatment planning, US imaging rel. to computerized tomography 80—3786
pulse echo US, intensity meas. errors assess. when using miniature hydrophones 80—3743
radiotherapy treatment planning, appl. of US imaging *(German)* 78—53463
radiotherapy treatment planning and follow-up of superficial tumours, US B-scan appl. 78—11721
random signal analyses 78—42499
raylography, acoustic medium characterisation and imaging, non-biological model expt. 77—25528
raylography, freq. domain deconvolution technique for pulse echo ultrasonography 77—25527
real-time real-space US scanning principle 79—70594
real-time US imaging, dynamically variable electronic delays 79—46142
real-time US imaging with shear, Rayleigh, and Lamb waves 77—32759
reconstruction in parallel processing analog electronic systems, secondary images 79—81638
reconstructive tomography and applications to ultrasonics 79—66578
reflection acoustic microscopy, acoustic material signatures 79—46139
reflective acoustic microscope, signal processing, image enhancement 78—75022
reflective strip swept-frequency imaging 77—31192
renal imaging with radionuclides, US and computerised tomography 80—17095
renal pelvic dilatation in children after fluid intake demonstration by US scanning 77—77951
review, status of research 77—58511
rotating M-sequence phase disc and correl. anal. 79—3870
SAW transducer array for surface defect imaging in metals 80—74660
scanning acoustic microscope, contrast and image performance 79—55280
scanning acoustic microscope, image enhancement using analogue filters 78—18131
scanning acoustic microscope, nonlinear imaging of edge 78—38158
scanning acoustic microscope, phase imaging 77—7268
scanning electron microscopy, US imaging technique 80—95192
scanning laser acoustic microscope, biomedical research and materials science appls. 78—46878
scanning microscope, characteristic material signatures 78—63259
scanning microscope, image resolution 78—26011
scanning microscopes with partially coherent source and detector 78—58923
scanning microscopy, Gray scale 78—94494
scanning of optical images using acoustoelectric memory correlator struct. 80—74632
schlieren method sensitivity for LF US wave visualisation 78—55501
schlieren quantitative visualization, using closed circuit TV system 78—46867
schlieren stroboscopic apparatus, defect visualisation 79—87811
sea ice, sidescan sonar imagery, Arctic Ocean 79—25339
sector-scan imaging devices 79—86311
seismic data, source receiver coincident profiles 79—92615
seismic imaging of faults in multi-moded coal seams 80—85778
serial tomogram 3D imaging, processing system 79—83859
shadow-optical colour imaging technique for sound field pressure distrib. meas. 79—64464
signal analysis applied to medical imaging 80—17038
signal processing, review 79—64403
signal processing in ultrasonics, conf., London, England, Jan. 1980 80—33351
slotted transducer arrays with matched backings for underwater imaging 80—38214
small-area ultrasonotomogram magnification and smoothing 77—86572
soft tissue characterisation by US backscatter analysis 77—21586
Sokolov image convertor tubes 77—19494
solid material joints, visualisation using transmission-type scanning acoustic microscope 77—90511
sonar echo imaging, using elasto-optic material and laser interferometer 77—58501
sonar imaging with synthetic aperture technique 78—33943
Sono Diagnost R multi-element scanner, use for upper abdomen US diagnostics 80—17028
SonoChromascope, US B-scan image acquisition, display and recording 80—30818
sonoscan, new US imaging technique 79—83403
spatial sampling effect on image reconstruction 78—51021
spectra-colour ultrasonography, instantaneous power spectra, theoretical anal. 80—51190
steel, acoustoelastic stress field imaging technique, stress field contour plots 79—77033
super-resolution, using sequential estimation of hologram 79—68499
super-resolution imaging system using waves with a limited frequency bandwidth 79—41519
super-resolution passive imaging system using algebraic reconstruction 80—79081
survey of techniques and developments 80—23841
synthetic aperture sonar system prototype 77—46867
synthetic focus digital acoustic imaging for nondestructive evaluation 79—52611
Talbot-Schlieren interferometric method to see US waves 77—10099
thermographic-photographic technique for US intensity pattern characterisation 80—106689
thick specimen visualisation with reflection acoustic microscope, acoustic field distribution 79—76922
three dimensional display using fly's eye lens 79—81668
three dimensional US reflectivity imaging, reconstruction with spherical transducer arrays 80—38203
three-dimensional display improvement 78—59225
three-phase interdigital transducer for acoustic imaging in fluids 79—72774
time of flight tomography, reconstruction of US vel. distribs. in soft tissue 77—48850
tissue characterisation by acoustic microscopy 77—64123
tissue characteristion, static and moving, high spatial resolution US meas techniques 80—51187
tissue quantitative characterisation by US, review 80—81670
tissue refractive index and attenuation distrib. reconstruction from time-of-flight and amplitude profile 77—64113

acoustic imaging continued
tissue refractive index spatial distrib. meas. by US computer assisted tomography 78—69161
tissue US attenuation and velocity meas. by direct and phase-contrast imaging 77—64114
tissue US parameters, quantitative cross-sectional imaging 79—53277
transmission microscope optimisation 78—51022
transmit/receive 2D ceramic piezoelectric arrays, construction and performance, medical, NDT appls. 78—87223
transparent-solid US transducer field visualisation 79—55285
two-dimensional photoacoustic image processing with longitudinal waves 79—50244
two-dimensional target imaging using hologram matrix, ultrasound experiment 79—23145
ultrasonic imaging systems, including Sokoloff tube 79—98575
ultrasonic symposium, Phoenix, AZ, USA (Oct. 1977) 79—46096
ultrasonics symposium, Annapolis (1976) 77—19469
ultrasonographic diagnosis of pancreatic diseases 78—7416
ultrasonography rel. to computerised tomography in upper abdomen and retroperitoneum exam. 80—21506
ultrasonotomography with electronic sector scanning, cardiac diagnosis appl., features 77—66829
ultrasound image coding, mammograms appl. 77—81544
underground remains detection, acoustic meas. with computer data processing 79—76921
underwater, real-time signal processing techniques 79—90089
underwater, systems characts. and appls. 78—33945
underwater, techniques and characts. 79—64462
underwater C-mode US imaging by electronically scanned coaxial circular spherical receiving array 78—59222
underwater imaging using US image convertor tube 77—19499
underwater US image convertor optimal working frequency estimation *(Russian)* 78—30111
underwater US video system *(German)* 78—94471
unipolar acoustic pulses, quantitative schlieren visualization 78—38125
US, as aid to cancer radiation therapy treatment planning 77—12982
US, backscatter enhancement from collagen microspheres, dog liver, erythrocyte suspension 80—94281
US, computerized, digital data acquisition system 79—39454
US, electric coupling effects in transducer array 80—43587
US, for weld inspection 77—86254
US, intraoesophageal, heart dynamics 80—94303
US, piezoelec. face plate response anal. 79—14169
US, piezoelectric transducers design 78—9525
US, single-channel reduced-bandwidth SAW-based processor 80—74636
US, speckle reduction in ultrasound B-mode scans 78—22233
US, super-resolution, by combined spectral and aperture synthesis 77—84055
US 2-dimensional scanning of excised brain, normal anatomy 77—77950
US 3D imaging and vol. from series of arbitrary sector scans 80—8109
US A-scan pulse-echo scanner performance, transfer functions, biomedical appl. 79—25055
US abdominal scanners survey, clinician's viewpoint 79—66582
US annular array with dynamic focusing 77—32947
US applications, conference, Brighton (1977) 78—59223
US attenuation reconstructive tomography 80—30822
US B-mode images of human tissue, real-time speckle reduction 80—74634
US B-scan, pancreas scans of cystic fibrosis sufferers, amplitude anal. 80—94302
US B-scan, theory of image formation, technique for restoration 80—94300
US B-scan recording on video tape-recorder 78—77095
US backscattering from human tissue, model 77—40715
US backscattering from human tissue, rel. to imaging 77—86576
US biomedical micro-array technology for improved image quality *(German)* 80—98052
US blood flow imaging model eqns. and implications 79—48308
US camera for patient diagnosis *(French)* 77—37028
US carotid arteriography, real-time system 78—24108
US computed tomography, cancer detect. appl. 80—30820
US computerised tomography, var. of acoustic speed with temp. in excised human tissues 80—51150
US computerised tomography scanner evaluation 79—48301
US contrast agents, aqueous solns. for biomedical appls. 80—41157
US data, moving heart surfaces extraction 80—8114
US delay technique using phased array imaging system 80—30810
US diagnosis, 2-dimens. colour display of spectral information 77—21584
US diagnosis, basic principles 80—17037
US diagnosis, human abdominal tissue phantom 80—51152
US diagnosis, newer clinical imaging appls. 80—30825
US diagnosis, tissue simulators 80—51153
US diagnosis, transmission tomography by reconstruction compared with pulse-echo imaging, tissue-equiv. test objects 80—51154
US diagnosis review 79—92307
US diagnostic techniques, basic principles *(Dutch)* 80—3744
US digital image focusing in near field of sampled acoustic aperture 77—60232
US display system, using colour TV, tissue disease diagnosis appl. 79—29576
US dynamic imaging, high resolution 80—17042
US echoaortocardiography, Kymo-two-dimensional, aortic root diagnosis appl. 78—24110
US echocardiographic system, two-and three-dimensional, computerised, atrial septal defect detection appl. 78—20237
US echography appl. to artificial heart performance studies 78—44728
US echography for medical diagnosis *(French)* 80—26305
US echotomography for intrahepatic vessel and duct structure diagnosis 77—90868
US field focusing upon transmission using annular transducer 78—44574
US grey scale display on storage oscilloscope system 78—3569
US grey scale scanner dynamic range testing 78—69169
US grey scale sonoarterographic imaging 77—25532
US high-resolution 3-dimens. real-time imaging system 77—86575
US image processing, appl. to film recorded images 77—25531
US image reconstruction using acoustoelectronic lens device 78—18137
US image sequences, logical neighbour operations appl. 80—8113
US images corrected for refr. and attenuation, comparison of high resolution methods 80—30817
US imaging, clinical information, comparison of two types in detect. of focal intrahepatic lesions 77—64100

acoustic imaging continued
US imaging, single-transducer technology, state of art review 77—843
US imaging and holography, devices, medical uses *(French)* 77—827
US imaging by acousto-optic interaction in Raman-Nath diffr. regime 79—55260
US imaging cell for direct visualisation of defects in solids 79—20324
US imaging equipment, quality control problems 78—69171
US imaging modalities for medical appls. 80—81669
US imaging of neoplasms 80—17032
US imaging over view, appls. and future trends 80—48536
US imaging sonar, design and construction 79—3831
US imaging system, digitally controlled electronically scanned and focused 80—74659
US imaging system, high resolution for defect detect. 78—53169
US imaging system using moving random phase mask and third order correlation function anal. 78—63244
US imaging system using random phase mask and stationary-point receiver 77—80035
US imaging systems, high-resolution, real-time 78—69160
US imaging techniques for medical diagnosis *(French)* 80—26304
US imaging using Bragg diffraction *(French)* 79—81664
US imaging with convergent acoustic lens 77—46868
US impedance image reconstruction, reflection and transmission techniques 79—53202
US impediography, quantitative characterisation of lesions in vivo 80—17039
US in medical diagnostics, for teaching 78—49620
US lateral and range resolution improvement by optical computer 79—53203
US liver sector scans, echoes across diaphragm 78—69165
US medical diagnostic imaging, digital scan convertors 79—66581
US medical diagnostic imaging systems, methods and terminology 79—66580
US multiple freq. array for improved diagnostic imaging 79—14170
US multiple section tomogram simultaneous display equipment 78—61227
US ophthalmological diagnostics and therapy *(Croatian)* 78—44570
US ophthalmological signal acquisition and image enhancement 78—57045
US phased array sector scanning, medical diagnosis, review 80—36038
US pseudosources, non-surgically implanted in tissue, appl. 78—3572
US pulse echo digital processing 77—32948
US pulse-echo scanning, echo struct. 77—52857
US real time imaging with hand-held linear array scanner, clinical experience 79—62317
US real time imaging with hand-held linear array scanner, technical description 79—62316
US real time scanner, performance meas. 77—29191
US real-time B-scan machine attachment for three-dimensional display 78—61229
US real-time echographic imaging system, acoustic field study *(Italian)* 79—96636
US real-time image computerised anal. 79—70598
US real-time two-dimensional ECG images, direct conversion 77—60233
US renal diagnosis, clinical results 78—28027
US scanning diagnosis systems, design fundamentals 80—26308
US scanning microscope, high resolution 78—1529
US signals, physiological measurements and numerical analysis 77—86577
US spectral tissue identification by colour-coded B-scan display 77—64112
US synthetic aperture imaging resolution 77—25530
US techniques *(Japanese)* 80—19190
US time-of-flight tomography, computerised, breast pathology appl. 78—24107
US tissue analysis, comprehensive system 80—51189
US tissue characterization in vivo, broadband integrated backscatter 80—74635
US tomography, refr. index and attenuation images rel. to breast tissue types 80—17036
US tomography for umbilical cord complications diagnosis 77—90867
US tomography in cardiology 80—30824
US tomography techniques survey 80—30823
US tomography using laser-generated acoustic fan beam 79—83862
US transducer 2-D array technology, state of art review 77—844
US transducer characterisation using cholesteric liquid crystals 78—42512
US transducers for imaging, modelling *(French)* 80—26302
US transmission image reconstruction, inverse scatt. and tomography 78—61231
US transmission tomography 80—94301
US transmission tomography by reconstruction, imaging soft tissue through bone 77—70512
US vascular imaging, Doppler method, improvement 78—24106
US vibration visualization in piezoelectric ceramics using IR telethermography 78—33966
US visualisation, using milling yellow colloidal water soln. flow birefr. props. 80—53585
US visualization and characterization, conf., vol.8, Key Biscayne, FL, USA (May-June 1978) 80—83720
US wavefront visualisation using holographic interferometry 80—48526
ventricular circumferential segmental shortening, from US sector scanning images in ischaemic dogs 79—70599
visualization and characterization, conf., Houston, TX, USA (Dec. 1979) 80—106672
wavefront reconstruction acoustic imaging using two dimensional arrays 80—74661
wedged piezoelectric transducer with improved signal-to-scattered-noise ratio 79—3880
wideband annular US imaging array response 79—55306
wideband Fresnel focusing array response, echography appls. 80—74640
zero-order Raman-Nath method for acoustic beam longitudinal character visualisation 78—71252
Al, acoustoelastic stress field imaging technique, stress field contour plots 79—77033
InSb/$LiNbO_3$ gap-coupled convolver operation at 77K 79—50242
$LiIO_3$ single crystal, surface acoustic wave parameter meas., coherent optics method 80—106691

acoustic impedance
see also acoustic wave velocity
absorbers, dimensioning of facings for acoustically effective structural elements *(German)* 80—74600
artificial mastoid type 4930 *(German)* 78—27970
audiometric impedance meas. instrumentation 77—78005
axisymmetric spherical radiator with mixed boundary conditions radiation impedance 77—46827
baffled circular piston, radiation impedance deduced from transient state 77—79980
boundaries of finite impedance, errors in literature on nearby sound propag. 79—98525
brain, normal and abnormal, attenuation, vel. and impedance 80—45955
brass instruments, acoustic impedance meas. apparatus 78—1518
breast cancer connective tissue content correl. with US attenuation 80—45997
bubble activity in acoustically excited spherical flask, obs. 78—42488
circumferential slit in circular cylinder, radiation impedance 80—19120
compact planar array nearest-neighbour mutual interaction estimation 79—46160
cylindrical duct with impedance walls, attenuation calc. 78—83146
cylindrical shell in rigid baffle, model efficiencies of sound radiation and additional mass coeffs. 78—38129
dissipative mufflers with locally reactive lining, modelling 78—13849
dog lungs, input impedance from Fourier anal. of response to transient pulse pressure excit. 79—5309
duct acoustics, integral equation methods for nonuniform duct with variable impedance 77—58498
ear, acoustic reflex, factors influencing acoustic-immittance characts. 80—56062
ear, hearing loss prediction from acoustic reflex thresholds 78—3511
ear, interactions among tympanometric variables 78—27964
ear, meas. of temporal characts. and filter response of electroacoustic impedance instruments 78—3512
ear, tympanometric asymmetry 78—27963
ear, tympanometry in normal neonates 80—3651
ear simulators, constants meas., for earphone calibration 78—27960
eardrum, human, impedance from external ear transform. characts. meas. 77—86508
elastic cylinder, radially driven, input impedance on lateral surfaces 77—14830
electret US transducer performances and prospects 78—59244
electrostrictive US transducer electroacoustic efficiency and load matching 79—68541
engine exhaust system, acoustic characts. in presence of mean flow 77—837
fibre masses, closed front, amplitude depend. damping 78—83144
fibrous absorber, wave impedance for elementary cells model, numerical results *(German)* 77—802
filled polymer materials, simple approx. method, US velocity meas. 80—64314
floors impact testing, impedance problems *(German)* 77—825
fluid machinery manifold impedance meas. 78—42501
grass covered ground, impedance models 77—79992
ground surface, point impedance rel. to atmospheric sound propag. 77—50805
hearing, acoustic-reflex growth and loudness 80—35916
hearing, freq. acoustic reflex, multiple probe meas. 80—56065
hearing, impedance and tone screening of schoolchildren 80—108985
hearing, impedance changes elicited by tactile and electrocutaneous stimulation 80—56066
Highland bagpipe, acoustics of the chanter and reed 78—94491
horns, quasi-standing waves 80—79071
influence of grazing flow, cylindrical wall cavity 80—69784
inhomogeneous elastic slab impedance soln. 79—44745
irregular cavity acoustic impedance, finite element analysis 78—42483
Kundt's tube, determination of wall impedance by means of FM transmitter signal *(German)* 80—102878
$LiNb0_3$ wedge waveguide apodised interdigital transducer evaluation 77—27451
line transfer and line drive admittance approx., free wavenumbers, fluid-loaded panels 80—64432
lining design, finite length tuning concept expt. verification 77—31170
low-loss wide-band US transducer design for noninvasive medical appls. 79—44021
lung, distributed response of complex branching duct networks 78—57027
magnetostrictive transducer at air-water surface, effect of spherical scatterer on radiation reactance 80—48531
marine sediments, in situ acoustic impedance meas. method 78—9519
mastoid, human, model of mech. system imitating acoustic props. 78—80886
measurement, impulse method, normal impedance at oblique incidence 80—53582
measurement, pulse-tube and direct point meas. methods 80—96164
measurement technique for a black box, fixed position press. meas. 78—1523
measurement technique for a black box at low freqs. using shorter impedance tube 78—1522
measurement technique using sine sweep excitation and known vol. vel. method 79—3869
measurement using const. vol. vel. sources 80—74651
measurement using sine excitation and known volume velocity technique, comments 79—98570
medical imaging, ceramic and PVF_2 transducers compared 79—57734
modal radiation impedances for semi-infinite unflanged circular ducts including flow effects 79—72738
mutual radiation impedances between pistons 79—1016
neonatal acoustic reflex, static and dynamic impedance obs. 80—104597
nondestructive eval. using unipolar transducers 80—76471
nonlinear orifice impedance correlation curves 77—23837
ocean bottom input impedance meas., particle vel. hydrophone appls. 78—94475
orifice in infinite thin plate, linear acoustic resistance, theory *(Chinese)* 78—90546
orifice under turbulent boundary layer 77—23838
p-n-pentyl p′-cyanobiphenyl, anisotropic viscosity, US meas. 77—31581
perforated facings with porous backing material as sound absorbers 77—62115
perforated plate, nonlinear acoustic resistance *(Chinese)* 79—23119

acoustic impedance continued
- piezoceramic tubes with capped or shielded ends, diffr. consts. and radiation impedances 78—1534
- piezoelectric transducer with inhomogeneous acoustic load, equivalent circuit 79—32174
- piezoelectric transducers, thickness mode, front face mech. impedance effects 77—31197
- pistons in a plane wall, calculation of mutual impedance 80—19119
- plate reinforced with projecting beam, impedance treatment of long-wave diffr. 78—9469
- plate terminated by liquid, transfer constant and input impedance ang. depend. 77—11103
- plate with line impedance discontinuities, acoustic transmission and scatt. 78—90553
- porcine skin, acoustic impedance variations at burn-nonburn interfaces 79—2114
- porous layers, impedance meas. rel. to damping in reson. absorbers *(German)* 77—14825
- pulsating gas flow, aeroacoustic charact. eval. method 79—46141
- pulse echo waveform rel. to acoustic characteristics of continuous medium 80—67145
- quadrupole near fluid interface, sound refl. and radiation 78—9475
- radiation impedance of pistons operating in homogeneous layer 80—87596
- rectangular panel in infinite baffle, acoustic impedance 79—94399
- rectangular piston radiation impedance 78—33937
- resonator, effect of initial impedance on vibr. combustion *(Russian)* 77—9082
- reverberation time, absorption and impedance, theoretical model used for calcs. of a room 78—90601
- rigid sphere vibrating parallel to plane wall 80—102910
- screen, evaluation, numerical method 78—13831
- seabed acoustic impedance, normal incidence seismic profiles 77—81822
- shear-wave transducers for laboratory sediments 78—51033
- single-transducer coupler for diagnostic pulsed Doppler or pulse-echo US instrumentation 78—61236
- specific acoustic impedance of organic liquids, interdependence on surface tension *(Polish)* 80—39223
- speech, vocal tract losses, influence on damping of reson. freqs. 78—85325
- stiffening ring, longitudinal-mode and flexural-mode impedances 78—83320
- stratified media, acoustic impedography *(French)* 79—3816
- stratified media, elastic waves at normal incidence, inverse problem 80—33509
- stratified media with specific impedance profiles, investigation method *(French)* 79—41490
- surface impedance, meas. technique for oblique incidence angles at 10-160 kHz 77—54848
- surface wave device, diffr. and guiding via impedance inhomogeneities 78—13828
- surface waves on complex impedance ground 78—55491
- thick walled tube with hot flow, standing-wave tube technique 77—75753
- thin annular diaphragm of electromechanical transducers, acoustic impedance calc. *(Czech)* 77—3708
- tissue characterisation by US frequency-dependent attenuation and scatt. 77—66832
- tissue structures characterisation, method of obtaining an impedance profile 80—67171
- transducer arrays, numerical calc. method for acoustic interaction *(Japanese)* 78—9521
- trombones, objective and subjective assessment of quality 80—23847
- tube, meas. combustion process admittances 80—64320
- tympanic membrane acoustic admittance in aging ear 79—100630
- unbaffled cylindrical pipe outlet, impedance for plane wave incident at outlet 79—55256
- underwater sound, impedance calculations for refracting layer 79—90065
- unflanged duct exit, high temp. effects on radiation impedance 77—84069
- US diagnosis principles and tissue characteristic impedances 79—83861
- US impedance image reconstruction, reflection and transmission techniques 79—53202
- US impedance profiling, analytical and physical model 77—64121
- US impediography, deconvolution and processing procedures and corrections 77—64122
- US impediography, quantitative characterisation of lesions in vivo 80—17039
- US tool, radial mode, with statically loaded inner surface, acoustic input impedance 78—183
- US transducer damping by multilayer front face 79—55301
- US velocity meas., fixed-path interferometer, phase error elimination 78—83197
- vibrating sphere near rigid or compliant wall, near field and impedance 78—94476
- violin sound post, mechanical admittance meas. rel. to post action 77—23833
- waveguides at cutoff freqs. 78—59215
- He, bulk, Kapitza conductance, acoustical mismatch 77—76637
- ^{3}He, liq., transverse acoustic impedance, Landau theory 78—51778
- ^{3}He, normal, acoustic impedance, variational theory 79—42334
- ^{3}He, superfluid, acoustic shear impedance meas. 77—11759
- Si rubber, room temp. vulcanized, compounded with various powders 79—81614
- W-PVC composites, fabrication rel. to performance 80—76218

acoustic insulating materials *see noise abatement*

acoustic intensity
- *see also acoustic noise; loudness*
- acoustically coupled rooms, reverberation time extension, directional microphone appl. *(German)* 79—41518
- average sound intensity in shallow water with negative vel. gradient *(Chinese)* 78—1477
- binaural summation of the loudness of pure tones 78—92638
- brainstem evoked response, relationship of latency and amplitude with sound intensity 79—20551
- Brillouin scattering in reflection and transmission modes, rel. to intense acoustic flux, relation linearity test 80—45098
- city streets and tunnels, expressions for stationary sound pressure level 80—19159
- clouds and fog, sound attenuation obs. 77—34981
- dilatometric method for US intensity meas. 79—3865

acoustic intensity continued
- discrimination of intensity as function of freq. and sensation level 77—36944
- fibre masses, closed front, influence on acoustic damping 78—83144
- hearing perception, preceding stimulus effect on identification 80—51120
- high fidelity sound, perception of sound and music 80—42014
- machine, meas. technique of acoustic power with an intensity meter 78—83188
- moving point sources, intensity of acoustic fields *(German)* 80—102879
- moving source in semi-space with stratified medium 80—87617
- moving sources, intensity of acoustic field 79—32106
- noise distribution prediction in underground enclosures, from free-field meas. 77—7253
- noise intensity discrimination, bandwidth and masker presentation effects 77—9209
- ocean acoustic propag., long range, statistical anal. of signal intensity 78—90569
- radiators moving with supersonic vel., interaction 77—815
- randomly inhomogeneous medium with reflecting boundary, wave intensity fluctuations 80—42075
- rectangular rooms, prediction of intensity using geometrical acoustics 80—23837
- resolution and relation to loudness matching 80—108908
- resonantly vibrating surface, nearfield determ. of complex radiation efficiency and intensity distrib. 79—55262
- rock music sound levels and spectra rel. to hearing damage 79—68517
- sonometry, sound audibility, serial noise from machines and equipment *(French)* 77—21537
- sound channel intensity distrib. using coherence theory 78—79152
- steady source in built-up area, sound level decay with distance 77—72109
- underwater amplitude fluctuations due to temp. microstructure 80—19140
- US intensity, primary determ. method using elastic sphere radiometer 77—68342
- velocity monopole source, power radiated under reverberant and freefield conditions 79—46107
- CdS, thermal equilib. phonon populations, acoustic intensity meas. by Brillouin scatt. intensity obs. 80—45098
- GaAs, thermal equilib. phonon populations, acoustic intensity meas. by Brillouin scatt. intensity obs. 80—45098

acoustic intensity measurement
- absorption, classroom experiment 80—42016
- air-handling ducts and plants, direct sound intensity measurement method *(German)* 80—102944
- American National Standard S1.21-1972 qualification procedures 77—62120
- amplitude changes in harmonic signals, psychoacoustic investigations of discernibility *(Polish)* 80—38193
- appliance acoustic emission determ. facility development 77—58507
- audiometer, automatic digital, for mass hearing examinations 80—33379
- barriers used in foundry industry, investigation of sound transmission paths 80—48515
- Bayerischer Rundfunk carnival, comparison with audience comments *(German)* 78—13860
- biomedical pulse echo US, intensity meas. errors assess. when using miniature hydrophones 80—3743
- Bruel and Kjaer acoustic level recorder type 2306, interfacing to a digital computer for a graphical output 80—53572
- club noise control by electronic power reduction 78—51004
- cochlear excitation, electric circuit model and overpressure meas. in guinea pigs *(French)* 78—85316
- cross-spectral 2 microphone method, Fourier analysis technique 79—18649
- cross-spectral density meas. in partially reverberant fields 78—30140
- cross-spectral method of measuring acoustic intensity without error caused by instrument phase mismatch 79—14176
- digital registration and rational evaluation of measured data of acoustic emission *(German)* 80—19178
- dual-beam sonar system for individual fish target strength meas. 77—3704
- ducts with mean flow, microphones cross correlation method 79—86282
- ear protectors, use of sound levels for assessing adequacy 80—104771
- ear-borne sound level dosimeter 77—11099
- environmental effects on microphones and Type II sound level meters 77—62127
- equivalent continuous noise levels, instrument design, electronic 77—65654
- error propagation analysis of four sound-power measurement techniques 80—48529
- fibre optic acoustic sensors with increased sensitivity due to composite structures 80—5834
- field sound level calibrators for sound measuring instruments 80—19197
- flames and inaccessible places, microphone probe design for scound meas. 77—62114
- frequency averaging method for investigation of scattered field from rough surfaces 80—38169
- hearing protectors, meas. of real-ear attenuation, SABS 572 1973 80—53581
- household vacuum cleaners, effect of reduction in measurement locations below measurement standards 79—18647
- hypernasal speech, oral/nasal intensity ratio meas. 79—83804
- impact sound loudness meas. *(Japanese)* 79—98546
- instrumentation for sound power determinations 80—19196
- integrating sound level meters, response to impulsive sounds 79—50547
- light column display of sound pressure levels 79—41536
- loudness meter for temporally variable sounds 78—3508
- loudness of narrowband noise pulses 80—38194
- loudspeaker efficiency *(Spanish)* 79—3871
- loudspeakers efficiency determ. method 78—51028
- low frequency, reverberation process 79—46110
- low frequency, sound power meas. 79—41514
- machine, meas. technique of acoustic power with an intensity meter 78—83188
- machine panels, insertion loss, meas. and evaluation 78—87193
- machinery noise source analysis using surface intensity measurements 80—43543
- mechanical input power meas. method for wall structures 80—19176
- meter for acoustic power of small machine in a room 78—33975

acoustic intensity measurement continued
microphone signals, cross-spectral density for acoustic intensity meas. 78—9514
microphones for sound-level meas. 78—83190
multi-blade fan as reference sound source, influence of reflecting plane *(Japanese)* 80—19189
multielement acoustic array characterisation by acousto-optic diffraction 80—99911
noise abatement exercises, instrument using amplifiers and probes *(German)* 80—1389
noise meas. systems and equipment 78—83189
nondirectional sound sources in layer of fresh-water reservoir 80—58845
optical fibre power dividers, acoustic sensitivity 80—5835
piston source, circular, meas. of fundamental and second harmonic pressures in acoustic field 79—46101
pitch and influence of intensity, binaural diplacusis 79—34571
power, US, power meas. via acousto-optic method 77—832
precision acoustic meter *(French)* 78—71254
procedure for measuring sound intensity near vibrating surface 80—53580
reactive acoustic field, complex wattmeter meas. 79—41535
real time system for acoustic measurement and analysis and its applications *(Japanese)* 79—68522
resonator, cylindrical disc-type, acoustic performance 79—18657
reverberation chamber LF sound power injection analysis and response averaging 78—42496
reverberation chambers, using standing-wave tube 79—81674
reverberation room ANS qualification error sources and effects 77—58514
reverberation room ANS qualification for discrete frequency sound power level meas. 77—62122
reverberation room ANS qualification with microphone traverse and LF absorption 77—62123
reverberation room qualification with computer-controlled instrumentation system 77—58516
reverberation room sound pressure level spatial averaging by microphone array and traverse 77—58515
room acoustics correction, using Shure analyser *(German)* 80—58873
schlieren optical filtering for light diffracted from US beam 80—87672
semianechoic chamber sound power meas. by traversing microphone 77—62116
shear wave scatt. by flat-bottomed hole in Al, intensity distribution mapping 77—19503
sound level meter meas. accuracy 78—59211
sound level meter with octave band filters and two microphones 78—83194
sound level meters, comparative listing 79—50546
sound level meters, freq. response and directional characts. in presence of operator 79—23159
sound level meters, modern standards and features 78—83191
sound level meters, use and abuse 80—19198
sound power from machines and loudspeakers using type 4205 power source 80—1392
sound pressure within ear, monitoring for noise exposure meas. 77—52799
sound-level meter, innovative high school teaching project 80—4495
source strength reciprocity meas. in arbitrary surrounding 77—54850
structure-borne sound, procedure for meas. sensitivity of building structures to stationary excitation *(German)* 80—64287
structure-borne sound and its transmission, measuring procedure 79—50509
tissue characterisation by US backscattering 79—70595
tones, AM, dependence of fluctuation strength on sound parameters *(German)* 79—34569
traffic noise, meas. by L_{eq} and L_{α} *(Japanese)* 79—1024
transient sound fields, microphone method for energy meas. 80—102942
two microphones method 77—68346
underwater sound pressure unit, 0.01 to 1 Hz, USSR state standard 78—38160
US beam power meas. calorimeter bridge for 1 to 15 MHz 77—27446
vibrating cylinder, surface intensity measurements for determination of machine noise 80—43577
$LiNbO_3$, electrostatic probe for absolute measurement of SAW amplitude 79—50543

acoustic magnetic resonance
see also acoustic nuclear magnetic resonance; acoustic paramagnetic resonance
double acoustic magnetic resonance in crystals, review 77—32291
molecular fragmentary composition, determ. by IR, EPR and US mag. reson. spectra *(Russian)* 78—13624
semimetAl, acoustic cyclotron reson., sound interaction with cyclotron waves *(Russian)* 77—35959
W, Doppler-shifted cyclotron reson. along nonprincipal cryst. directions *(Russian)* 79—4725

acoustic measurements *see acoustic variables measurement*

acoustic microscopes
acoustical imaging, US visualization and characterization, conf., vol.8, Key Biscayne, FL, USA (May-June 1978) 80—83720
basic principles and applications 78—18133
ceramic components nondestructive testing, comparison with SEM and optical microscopy results 80—58875
characteristic material signature studies 78—63259
conference, Reston, USA (Apr. 1977) 78—45683
dark field acoustic microscopy 80—96149
developments, review *(Japanese)* 78—79177
diagnosis, microscopy of excised tissue 80—17041
Gray scale for scanning acoustic microscopy 78—94494
high resolution US microscope 78—1529
high resolution using mechanical scanning, review 79—98571
using high-pressure gases 80—43561
history, principles and appls. *(Russian)* 77—75763
history and review 78—46877
IC nondestructive evaluation by improved reflective scanning acoustic microscope 79—50551
image enhancement using analogue filters 78—18131
imaging, visualization and characterization, conf., Houston, TX, USA (Dec. 1979) 80—106672
introduction to microscopy by light, electrons, X-rays and ultrasound 79—49283

acoustic microscopes continued
LSI surface analytical techniques applied to electronic components [Si LSI chip inspection] 80—81392
materials characterization appls. 79—74335
microwave frequency, determ. of mech. props. of materials 80—48535
modulation transfer function modulation transfer function 79—64454
muscle mechanics study appls. 78—48952
NDT of electronic devices 79—37094
nondestructive material testing appls. 80—48537
optical wavelengths, resolution 78—71251
optical wavelengths 78—71251
phase imaging in reflection 78—30136
photoacoustic, principle and appl. to semiconductor industry 80—14525
photoacoustic, solid surface and subsurface struct. obs 78—68481
photoacoustic, thermal wave microscopy, physical processes 80—74652
photoacoustic, with resolution of several microns 79—64456
photoacoustic microscope, plastic deform. detect. in polycrystalline metal 80—35435
photoacoustic microscope using Q-switched Nd:YAG laser 79—18637
photoacoustic thermal-wave microscopy, high resolution studies 80—74647
piezoelectric transducer based, principle and appl. 80—1387
planar acoustic microscope lens using Rayleigh to compressional conversion 80—87668
principles and appls. 78—18133
recent developments *(Japanese)* 78—79177
reflection, contrast as function of elec. props. of surface under study 78—55533
reflection, ray interpretation of material signature 80—1386
reflection acoustic microscope appl. to study of polymer materials 80—28922
reflection acoustic microscopy, acoustic material signatures 79—46139
reflection microscope, acoustic signatures, physical model 80—48532
reflection-type contrast 78—55533
reflective, signal processing 78—75022
reflective, signal processing image enhancement 78—75022
reflector geometry for acoustic microscopy and NDT 79—47874
rock section imagery 79—12292
SAW dispersion and film thickness meas. using reflection acoustic microscope 80—10769
SAW dispersion and film thickness measurement, Au film appl. 80—53575
scanning, acoustic contrast of structs. buried inside object 80—74664
scanning, fault detection appls. 77—80040
scanning, for IC diagnostics 78—6086
scanning, for IC diagnostics 78—13877
scanning, image formation with partially coherent source and detector 78—58923
scanning, image resolution 78—26011
scanning, in refl. mode, angular-spectrum approach to contrast 79—10437
scanning, nondestructive testing appl. 80—16612
scanning, nonlinear imaging of an edge 78—38158
scanning, nonlinear imaging of edge 78—38158
scanning, phase imaging 77—7268
scanning, Quate and Lemons instrument, operation and appls. 77—84095
scanning, with ZnO film concave transducers 80—74663
scanning acoustic microscope, contrast and image performance 79—55280
scanning acoustic microscope, image enhancement using analogue filters 78—18131
scanning acoustic microscope examination of Si IC 78—13877
scanning acoustic microscope for IC defect testing 80—38190
scanning acoustic microscopy for study of interfaces in solid-state devices 80—99907
scanning image resolution 78—26011
scanning laser, material science and biomedical appls. 77—81382
scanning laser, principles and appls. 78—46878
scanning laser acoustic microscope, principles and analytical capabilities 79—18655
scanning laser acoustic microscope 79—7263
scanning laser acoustic microscope appl. to US vel. meas. of mammalian collagen threads 79—43972
scanning laser acoustic microscope applications *(German)* 80—3271
scanning laser acoustic microscopy, techniques and appls. 79—55279
scanning microscope, characteristic material signatures 78—63259
scanning microscopes, resolution criteria rel. to radiation detection technique 80—33388
scanning microscopy, Gray scale 78—94494
subcellular detail resolution 80—56313
subsurface structure detection by scanning photoacoustic microscopy 80—6323
surface interior planes acoustic microscopy 80—5886
techniques and applications *(Dutch)* 78—27719
techniques and appls. (1979) 79—64461
thick specimen visualisation and joint characterisation by scanning acoustic microscope 79—47875
thick specimen visualisation with reflection acoustic microscope, acoustic field distribution 79—76922
transmission, optimisation 78—51022
transmission, phase measurement using AM carrier 80—74665
transmission microscope optimisation 78—51022
transmission scanning, single lens 80—87669
transmission-scanning, visualization of solid material joints 77—90511
US high resolution microscope 78—1529
US imaging, resolution comparable to light micrographs 80—23852
zone plate variable-illuminating-angle system 80—106684
SiO_2 sputtered film performance as acoustic antireflection coating at sapphire-H_2O interface 80—106686

acoustic microwave devices
see also acoustic transducers; surface acoustic wave devices
1.2 GHz temperature stable SAW oscillator 78—59226
2.148 GHz SAW oscillator 80—74680
400 MHz to 2.3 GHz acousto-optic deflectors 79—50416
acousto-optical, 0.2 to 18 GHz, using ZnO piezoelectric transducers 77—58465
bulk ware resonators and filters with fundamental mode >100 MHz 77—42671
composite bulk acoustic resonator properties and applications 77—27434
delay line, freq. charact. 77—842

acoustic microwave devices continued
- interdigital transducer and 1.1 GHz SAW oscillator, photolithographic contact printing *(Japanese)* 78–33981
- interdigital transducers for SAW devices at GHz freqs. form. by electron beam lithography 80–4702
- Josephson junction appl. to hypersonic generation and detection *(Polish)* 77–14870
- laser modulation, acousto-optical 78–1282
- photoacoustic detection system for investigation of ferromag. resonance in films 80–80613
- piezoelectric film transducer of $\lambda/4$ operation, microwave ultrasound in liquid generation, effective attenuation analysis *(Japanese)* 78–30145
- SAW oscillator, status and designs review 78–55542
- scanning acoustic microscope examination of Si IC 78–13877
- surface-skimming bulk wave controlled quartz crystal oscillator 78–59250
- GaAs n-n^+ epitaxial structure for CW electroacoustic amplifier 78–59235
- SiC delay line at 9.43 GHz, acoustic props. study 80–65169

acoustic mode of crystals *see lattice dynamics*

acoustic noise
- absorption, impulse method of meas. normal impedance at oblique incidence 80–53582
- absorption, panel system design 80–87649
- absorptive barrier noise control, theory *(Japanese)* 77–3700
- acoustical enclosure, airtight, methods for predicting the insertion loss 79–18607
- acoustically excited jet, discrete noise spectrum, vortex pairing 80–74847
- acoustooptic modulator intensity servo, optical isolation and amplitude noise reduction 79–98472
- additive masking effects of noise bands of different levels 78–57021
- aeroacoustic measuring techniques in or outside turbulent flows 80–53534
- aeroacoustics, book contrib. 77–50807
- aeroacoustics of advanced turbopropellers, noise prediction 80–69598
- aerodynamic, scatt. by hard and soft surfaces 77–68326
- aerodynamic, various theoretical approaches *(French)* 78–34116
- aerodynamic noise, acoustic interference effects and role of Helmholtz number 79–94392
- aerodynamic noise, theoretical modelling 79–37077
- aerodynamic noise from wave-turbulence interaction 80–14679
- aerodynamic noise generated by high speed electric train 79–18591
- aerodynamic sound generation by unsteady subsonic flows around rigid bodies 80–69798
- aerodynamic sound problem in relaxing medium, appl. of Green's functions 78–22363
- aerodynamically generated, refl. at solid boundary, boundary layer turbulence *(French)* 80–43694
- aerodynamically generated noise, especially jet noise *(French)* 78–14002
- aerodynamically generated sound, extension to relaxing media 78–90567
- aerofoils, laminar wakes and noise pattern 79–37341
- agricultural tractor operator noise, investigations on cab 80–43529
- air, outflow from porous materials and noise reduction theory of porous diffuser *(Chinese)* 79–50785
- air bubbles, production, pulsation and damping, in dil. polymer solns. 80–69879
- air conditioning and ventilation systems, sound emission prediction 77–7252
- air conditioning plants, sound attenuators, attenuation characts. 78–30123
- air conditioning system, subjective responses and meas. 78–83168
- air traffic, general control measures, case study of Torrance Municipal Airport (California) 80–83702
- air-conditioning systems, acoustical characts. of certain flow-spoiling devices 77–50832
- airbase noise contours prediction 79–1025
- airborne noise, personal calculator program for A-weighted sound pressure level and noise ratings 80–23828
- airborne noise level criteria for buildings 80–10075
- airconditioning and ventilating systems, sound emission prediction 78–30122
- aircraft, anomalous attenuation, meteorological and ground effects 79–14138
- aircraft, appl. of theory of acoustic radiation from moving sources 80–53526
- aircraft, diffraction of high speed jet at subsonic flight 77–50806
- aircraft, effect on sleep of babies 77–77928
- aircraft, effects of background traffic noise and signal duration on subject assessment 79–86288
- aircraft, engine over wing config. 77–58505
- aircraft, fuselage, light, interior noise, laboratory studies 78–90596
- aircraft, general aviation, ground noise level changes derived from cockpit noise levels 78–9488
- aircraft, general aviation types, interior noise, acoustic field studies 78–90595
- aircraft, noise, basic aeroacoustic research, industrial appl. 80–69596
- aircraft, noise and vibration ride comfort criteria 79–41512
- aircraft, noise shielding 77–54840
- aircraft, residents sleep interference near airport 77–54843
- aircraft, Siements airport noise monitoring systems 80–99895
- aircraft, sound generated near trailing edge of upper surface blown flap 77–75902
- aircraft, the Netherlands, legal and economic factors 80–72112
- aircraft, trade off between noise and number 77–80009
- aircraft, variation of community response with time of day 79–34462
- aircraft engine, high-temperature high response fluctuating pressure meas. probe 78–13855
- aircraft flyover noise, modelled by acoustic scatt. by moving prolate spheroid 78–94458
- aircraft fuselage, sound transmission under flight conditions 77–7255
- aircraft interiors, turbulent boundary layer noise 77–11087
- aircraft jet noise reduction test facility 77–11096
- aircraft noise, effects on mental health 79–5316
- aircraft noise, responses of Chinese firemen 77–39157
- aircraft noise and premature birth 79–5324
- aircraft noise at Japanese bases, forecast contours *(Japanese)* 77–88982
- aircraft noise effects and reduction, Canadian environmental policy 78–33950

acoustic noise continued
- aircraft noise exposure forecast contours, retrieved using algorithm *(Japanese)* 80–19153
- aircraft noise generation, appls. of diffraction theory 80–53532
- aircraft noise index, psychological assessment 78–55507
- aircraft noise meas., cause of structural vibrations 78–87187
- aircraft noise propag., review 80–64258
- airfoil trailing edge noise, near-wake struct. and unsteady pressures at trailing edge 80–69794
- airfoil trailing edge noise, pressure field at trailing edge: effect on radiated noise 80–69795
- airport noise, effect of flight path dispersion 77–14848
- AM noise, rate and modulation thresholds detect. by mass 78–85320
- AM wide-band noise, perception of nonspectral pitch 77–9205
- ambient noise directionality determination, analytic expansion technique 79–90088
- anaesthesia during tooth hard tissue operations, BN-1 apparatus 78–85350
- analysis, Cranfield Institute of Technology, SPAG minicomputer system 80–96162
- analysis of noise emissions from point sources on road *(Japanese)* 77–23804
- angle synchronous contact sensing for noise investigations, anal. of gear wheels machining errors appl. *(German)* 79–68477
- annoyance, performance, and mental health related to noise 80–96104
- annoyance due to different sources, activity interference patterns 80–48504
- apartment blocks, noise transmission through wood joist floors, sound insulation methods 80–38178
- arbitrarily shaped body, integral approach to acoustics prediction 77–84040
- arbitrary random noise and vibration waves, statistical consideration of peak distribution 80–23836
- Ariane launch vehicle, acoustic environment *(French)* 79–81620
- array processor for noise and interference suppression 77–23815
- array processors for noise and interference suppression and signal-to-noise resolution enhancement, error corrections 78–30132
- atmospheric propagation, review 77–84065
- attenuation over an absorbing terrain, theoretical models comparison, aircraft noise appl. 79–18572
- audibility and effective loudness of sirens and speech in automobiles 77 16935
- audiometric testing, A-weighted equivalents of permissible ambient noise 78–69107
- auditory evoked response with homophasic and antiphasic signal and noise, masking level difference quantification 80–41045
- auditory fatigue influence on masked pure tone thresholds 77–9207
- auditory impairment danger from inpulse noise, CHABA and the Federal Republic of Germany comparison 80–45920
- auditory localisation, behavioural compensation limits in earmuff listening conditions 77–36947
- auditory masking effects on lip movements during speech 78–65061
- auditory perception nonlinear model with autocorrel. feedback 80–81615
- auditory system, pitch of amplitude-modulated low-pass noise and predictions by temporal and spectral theories 80 -67095
- auditory threshold assessment in extended HF range, with impedance measurements 80–61592
- automobile exhaust systems, measurement of acoustic parameters 80–53591
- automobiles, interior noise levels running in city streets 79–23127
- automobiles, noise annoyance from power drive train 79–90077
- axial flow fans, aeroacoustic mechanism for rotor-vortex interactions 79–3849
- axial-flow fan, quadrant duct bend effect on noise emission *(German)* 77–27539
- axisymmetric turbulent boundary-layer flow, noise generation 77–47001
- background noise levels in United Kingdom, prediction model 77–14843
- barrier attenuation in presence of ground, line integral theory 80–33300
- beam output noise due to shipping, statistical meas. 79–3836
- bearings, rolling, varying compliance vibrations 78–90582
- bias assessment in surveys of symptoms attributed to noise 79–3852
- binaural interaction theory based on auditory nerve data, tone detect. in noise 77–36950
- biological effects, autonomic system activities 80–83700
- biological effects, autonomic system activity and performance on a psychomotor task in noise 80 -89790
- biological effects other than hearing, review of animal expts. 79–5314
- biomedical noise generator for masking click stimuli 80–108980
- bispectral passive imaging system for machine-system diagnosis 78–63239
- blade force and sound generation for annular cascade in distorted flows 77–58504
- blast propagation, statistics of amplitude and spectrum 78–63224
- boom induced window response and damage 79–81604
- boundary layer noise generation, role of surface shear stress fluctuation 80–23994
- British passenger trains, noise meas. and prediction 80–14516
- broadband noise impulses, subjective duration and temporal masking patterns 77–36943
- building barriers for traffic noise protection 77–68324
- buildings, damping prediction by power flow methods of structure borne sound 78–33952
- buildings, service sysems noise, review 77–34997
- built-up urban environments, propag. of sound generated by point source 80–58841
- burning vortex ring, turbulent, acoustic emission 78–94676
- calculation of noise transmission between dwellings, partitions and flanking structures 80–43545
- car and motorcycle speed and cross-country races, noise inconvenience to local residents 77–84064
- cavitation noise, subharmonic component 77–14851
- cavitation zone of marine propellor, noise emission 77–14853
- centrifugal fan noise reduction by acoustically lined casing 78–1494
- centrifugal fans, geometrical parameter influence on sound power level 79–37084
- channel flow, convective vel. to wall press. fluctuations, numerical simulation 78–94829
- chemical industrial plants, ambient noise meas. *(German)* 77–68327
- circular flow ducts, broadband noise atten. spectra, measured and predicted 78–63237
- circular plate, noise reduction by polyurethane foam covering 77–62102

acoustic noise continued
circular saw blades, aerodynamic noise generation 79—24929
circular saws, aerodynamic noise source, point dipole model 79—50503
circumferential slit in circular cylinder, radiation impedance 80—19120
closed building, sound pressure level forecasting program *(French)* 78—13856
cloth curtains, effect to noise field *(Japanese)* 80—1379
clustered sensor array, turbulent boundary layer induced noise suppression 80—96121
coaxial jet, aeroacoustic characts., sound power spectral density 77—62285
coaxial jet noise and isothermal jets 79—86423
cocktail parties, acoustical aspects 77—80008
cold heading equipment noise and control 80—43538
cold subsonic coaxial jets, emitted noise *(French)* 79—37308
collinear interaction of noise with finite amplitude tone 78—55490
combustion generated noise, spectrum using Fourier transform techniques 78—1500
combustion generated noise from turbulent diffusion gaseous flames 78—38135
combustion noise, flow induced, suppression using appl. of DC elec. field 80—38176
combustion noise, sources in open turbulent pre-mixed flames 77—51127
combustion-driven oscillations in small tube 79—52664
community annoyance, effect of emergency vehicle audible warning devices 78—87200
community noise, scaling of loudness, noisiness and annoyance 77—11086
community noise surveys, stratification to improve design efficiency 79—81623
community sound level prediction, convolution method 77—11084
compressible axisymmetric jet sound radiation by instability waves 80—69792
compressible fluid flow in pipes and valves, acoustic noise calcs. *(French)* 77—19477
control by thick barrier, excess attenuation of noise band 77—62103
control equipment noise reduction, steam power, chemical, petrochemical industries appl. 78—51002
control valve cavitation and aerodynamic noise level estimation 77—84076
control valve noise prediction 79—72754
convected turbulence, vortex shedding influence on noise generation 77—3830
core noise and jet noise separation, mean square pressures 80—69779
correlation coeffs. in annoyance studies comments 77—75737
correlation technique appls. to noise and vibration anal. 79—81617
crustal structure estimation from acoustic reflection meas., Cramer-Rao bound 77—5369
cumulative noise measure for general annoyance prediction of traffic and aircraft noise 77—80010
cutting Al alloy on lathe, acoustic emission rel. to tool sharpness 77—42675
cylinders, aerodynamic noise vs. drag relationships 79—32550
deep-water background noise, estimate of envelope spectra 79—86283
defensive activation toward noise 79—5318
dental drill with noise, vibr. radiointerference reduction 78—85450
dental instrument noise studies, canine evoked response audiometry system 77—29226
depth-mode cavity resonance in turbulent flow 79—1017
detector, Hunt transit, performance estimates 79—68494
Deutsche Bundesbahn, noise caused by trains with and without sound protection screen 77—68316
Deutsche Bundesbahn exptl. line, vibration and structure borne noise 77—68320
dieing machine, 300 ton, acoustic and vibratory characts. 80—43541
diesel electric locomotives, SD40-2 noise under various operating conditions 80—102924
diesel engine, freq. content of surface vib. rel. to noise reduction 77—80011
diesel engine noise generation, diagnosis and control 80—58857
diesel engine powered installations, noise reduction programme 80—96106
diesel engine radiating surface identification by partial coherence technique 78—42490
diesel engines, high-speed, influence of piston slap and crankshaft torsional vibration on engine struct. noise 80—53555
diesel engines, open chamber, knock-induced cavity resonances 79—81624
diesel engines, piston slap, assessment of contribution to overall noise and vibration 80—79055
diffraction around wedge, appl. to factory design 78—42494
diffraction by absorbing semi-infinite plane in moving fluid 77—50830
diffraction by screen above locally reacting, infinitely large plane 78—79158
digital recording of levels using programmable calculator 79—23130
directivity of radiation from acoustic monopoles and dipoles, appls. to noise control 80—53515
directivity of sound radiated from large aperture in building 80—38148
directivity of sound sources on noise field *(Japanese)* 77—84075
disc brakes, location of squeaking noise, using laser holography *(German)* 78—37834
discrete frequency sound generation by fluid flows 80—69812
distant shipping noise statistics, Edgeworth series 78—55496
Dounreay Fast Reactor surveillance, noise analysis development 79—3215
duct, cylindrical, with acoustically absorbing internal surface 78—38142
duct, supersonic flow downstream oscillations from abrupt cross section increase, nozzles 80—74976
duct noise radiation, aircraft turbojet and turbofan engines 80—23834
ducted source, numerical spatial marching techniques for prediction of press. distribs. 79—46098
duration effect on annoyance *(Japanese)* 77—50828
duration effect on annoyance 79—14151
duration subjective impression rel. to ambient noise 78—44554
ear protectors, relation of attenuation to noise spectra 80—96100
ear reflex threshold shift in chinchillas following a prolonged exposure to noise 79—100631
ear-borne sound level dosimeter 77—11099
earplugs, real-ear noise attenuation and effectiveness 78—87199
EBR-II, obs. of amplitude modulated 12 Hz effect in upper plenum acoustic expt. 78—33241
eddy generated noise *(French)* 80—19363

acoustic noise continued
effect of noise and vibration on human beings, summary of symposium, Southampton Univ. (Dec. 1978) 80—35958
effect on performance of a psychomotor task, sorting during 90 dB(A) of pink noise 80—64283
electric arc 78—9890
in electric arcs *(French)* 80—28865
electric transmission lines, overhead, use of acoustic menu in assessing human response to corona noise 80—19149
electric utilities, impact of noise control regulations 78—33958
electrical equipment, noise generation mechanisms and characts., selecting quiet equipment and correcting noisy devices 80—64286
emission meas. for regulation 77—62108
engine intake noise, high freq., ray-theory approach 80—69595
environmental, evaluation *(Japanese)* 77—68308
environmental, health effects of noise exposure, review 79—5313
environmental, relationship to air pollution levels 80—69594
environmental, tendencies in subjective assessment 80—72111
environmental, urban, computer aided evaluation and control *(Japanese)* 79—88033
environmental aspects, low-noise olefines plants design 80—3561
environmental noise, conclusions and recommendations of conf. Gothenburg 1977 79—5325
environmental noise, exposed population size determ. 79—3851
environmental noise, medical effects, Conf., Gothenburg, Sweden, 1977 79—5311
environmental noise, review of biological effects on humans 79—5315
environmental noise annoyance evaluation *(Japanese)* 78—18106
environmental noise exposure, medical effects, review of basic considerations 79—5312
environmental noise protection of fibre optic hydrophone 79—98471
environmental noise rating and standardisation 77—58508
environmental noise seasonal variations 77—84062
environmental noise system, statistical anal. of mutual relation between two-component noises 80—102917
excess noise from supersonic underexpanded jets in flight 80—69815
excited jets, aerodynamic characterisation of broadband noise amplification 79—32491
exhaust noise and its control for construction equipment 80—43531
exposure and reaction to noise of inhabitants of Sendai *(Japanese)* 80—19151
exposure meas. of varying levels by noise records 79—23141
external sound level prediction, statistical eval. of accuracy 80—23829
factor of safety, calc. method and appl. to air and noise pollution 80—94140
factory noise effects on performance of psychomotor tasks 80—38177
fan drives on construction equipment 80—43530
fanjet engines, discrete freq. noise reduction modelling 80—106652
fans, blowers, dynamic compressors, noise emission, acoustic test methods *(French)* 77—19478
fans, loudness rating programme 79—24930
fans, low tip speed, axial flow, noise mechanism separation and design considerations 77—14849
fans, low tip speed, axial flow, vortex shedding noise 77—80014
fans noise generation, various types comparison 78—63238
fast breeder reactor, liquid metal, noise in upper plenum 79—81622
filtered N-wave sonic booms, subjective loudness and annoyance 79—50505
flame, laminar premixed gaseous, amplification of propagating acoustic signal 79—29357
flexible cylinder, structural-acoustic response of mech. excitation, finite element anal. 79—3839
flexible membrane, acoustic wave scatt. near reson., panel deflection and vel. pot. field 77—42657
flight effect of Michalke and Michel vis-a-vis Lighthill's model 80—59018
flow acoustic interaction near a plane heat conducting compliant boundary 80—69809
flow noise in ducts, excitation of side-branch cavity 77—11182
flow noise level determination in ducts 79—86421
flow noise past rod, wind tunnel expts. 78—50978
flow over rectangular cavities, induced tones and press. oscills. meas. 79—32493
flow-generated, acoustic power and head losses of silencers *(Japanese)* 79—23309
flow-generated noise through pipe walls, transmission at acoustic pipe coincidence 80—53767
fluctuating, effects of standard deviation and fluctuation freq. of sound level on annoyance *(Japanese)* 79—18583
fluctuating noise, effective sound level prediction *(Japanese)* 79—27462
fluctuating noise annoyance meas. using magnitude estimation method *(Japanese)* 79—27461
fluid inhomogeneities as sources of noise 77—11181
fluids, acoustic wave propag., damping, flows in pipes *(French)* 77—19467
free gas jets, acoustic field emission *(French)* 78—42595
free round cold subsonic jet, noise from axisymmetric shear flow, numerical results 79—77206
free round cold subsonic jet, noise from axisymmetric shear flow, analytical results 79—77207
free shear layer tone phenomenon, probe interface 78—71324
free turbulent shear flow, acoustic pressure fluctuations due to large scale coherent structs. 80—14677
frequency response testing in noisy environment, time domain averaging 77—14856
fresh water, absorpt. rel. to operating freq. choice for miniature transmitters 77—54826
fuselage-shaped body, interaction with aerodynamic noise 80—53533
gas flow in duct, self-excited oscillations 78—55670
gas stream in axisymmetric channels, acoustic disturbance propagation, gas-turbine noise appl. *(Russian)* 79—32131
gas turbine combustion, perturbations produced by unsteady combustion and heat addition 80—53764
gas turbine combustors, noise source mechanisms, expt. determ. 80—69597
gas turbine exhausts, core noise 78—13850
Gaussian intensive noise spectrum evolution, plane wave in lossless fluids 80—69581
gear noise, real-time bispectral anal. appl. to contactless diagnosis 77—84066
generation by laminar flames in tubes 79—86422

acoustic noise continued
  generation by steady airflow down corrugated duct 80—106660
  gliders, aerodynamic noise 78—38307
  gradient hydrophone flow noise 77—75758
  ground-borne, building vibration control, use of natural rubber mounts 80—87643
  growth function for human response to large-amplitude impulse noise 79—16222
  halls, effect of background noise on insonification, mathematical model *(French)* 78—13857
  hearing, effects of noise and signal intensity, on dichotic chords pitch mixture 78—3501
  hearing, human, specific and nonspecific noise effects *(French)* 77—21538
  hearing, temporal gaps detect. as meas. of auditory sensation decay 77—36953
  hearing ability, effect of noise *(Chinese)* 79—62267
  hearing damage, temporary and permanent threshold shifts *(German)* 77—77902
  hearing distribution in population with ageing and exposed to noise 77—48815
  hearing hazard, occupational, obs. on heavy industry workers 77—81512
  hearing loss, noise-induced vasoconstriction rel. to pattern A personality 80—35917
  hearing loss due to noise and sodium salicylate combined effects, obs. 77—52798
  hearing loss estimation tables for long-term noise exposure 78—15848
  hearing protector attenuation of random noise, testing 77—46866
  hearing reflex threshold for noise stimuli 80—108916
  hearing temporary threshold shift from noise exposure in squirrel monkey 78—88715
  hearing threshold levels of N.Carolina industrial employees, race and sex variations 80—97939
  hearing threshold shifts following 3 days noise exposure in chinchilla 78—88712
  heat diffusion as source of aerodynamic sound 77—7382
  helicopter rotor noise, Mach number scaling law correction 79—72753
  helicopter rotor noise, simplified Mach number scaling law 78—83167
  helicopter rotors, sound radiation props. for free field and near absorptive plane surface 80—102885
  high speed trains, aerodynamic noise study 80—48512
  high speed trains, noise annoyance 77—68313
  high speed trains, role of aerodynamic noise in wayside levels 78—13851
  high-temperature supersonic jet, noise spectrum 79—94691
  higher order mode effects in circular ducts and expansion chambers 80—96058
  highway traffic noise prediction, state of the art review 77—65651
  homogeneous turbulence, uniform distortion, generation of pressure fluctuations 77—27519
  Hong Kong, reverberation time in high-rise areas 78—59197
  hospital noise level measurement 80—51025
  hot jet, crossed beam technique for characterisation of noise sources *(French)* 77—35284
  household vacuum cleaners, effect of reduction in measurement locations below measurement standards 79—18647
  HTGR, acoustic environment determ. 79—89352
  hydroacoustics, role of surface shear stress fluctuations 80—69808
  hydrofoil cavitation noise and inception, boundary layer development 77—55057
  hyperbaric chamber, noise levels and hearing damage to divers 77—62107
  immunological effects of auditory stress 79—5323
  impact noise, review and bibliography 79—3848
  impact noise in buildings, meas. equipment *(Japanese)* 77—88986
  impact noise level criteria for buildings 80—10075
  impact noise prediction, acceleration noise 79—72752
  impact of sphere with slab, transient sound radiation 79—23128
  impact sound insulation, new rating system 77—11082
  impulse and impact, review of current knowledge 80—79056
  impulse noise assessment, evaluation of C-weighted L_{dn} 77—84068
  impulse noise exposure, simulated work-week, hearing loss 79—74687
  impulsive discharge noise, balloon burst and engine exhaust systems, acoustic pulse parameters determ. 78—90588
  impulsive noise reduction on gramophone records 80—87689
  impulsive sounds, large amplitude, human response to house vibr. caused by sonic booms or air blasts 78—90589
  impulsively accelerated bodies, approx. method for sound field eval. 77—50825
  incoherent jet noise line source, for scale modelling *(Japanese)* 80—33337
  incompressible viscous fluid, turbulently generated sound, pressure probability struct. 80—33581
  indoor noise environments due to outdoor noise sources 79—76911
  induced vibration, fatigue cracks in aircraft skin panels, prediction of edge crack growth 80—69737
  induced vibration in buildings, propag. model 80—74602
  industrial, effect of occupational exposure upon hearing 79—83801
  industrial, monitoring workers' hearing 80—81621
  industrial impact/impulsive noise source study 78—1493
  industrial noise, biological effects other than on hearing 79—5320
  industrial noise, effect on blood pressure in humans 79—5321
  industrial noise, fatigue and recovery of human acoustic stapedius muscle reflex 79 -53159
  industrial noise control, costs and legal requirements 78—33957
  industrial noise exposure, practical hearing conservation programme 80—12161
  industrial noise legal situation 80—12042
  industrial noise onset effects on physiological and psychological functions 80—91959
  industrial noise regulation, acoustic press. level limits *(French)* 77—19480
  industrial process burners, suppression methods 80—74597
  industrial process control valve systems, noise analysis 78—79163
  industry, choice of engineering or administrative controls or personal protection 78—33956
  infrasonic noise at Mid Atlantic Ridge near 37°N 77—25691
  infrasonic sea noise, meas. and experimental problems 78—11902
  infrasound, exptl. study of levels in transportation 78—88726
  infrasound, problems on environmental pollution *(Japanese)* 80—35805
  infrasound effects on task performance 77—56421
  inside passenger vehicles, acceptable noise levels 77—19474

acoustic noise continued
  insulation, domestic roofing, expt. facilities of meas. laboratory, test details 80—79058
  insulation, multiple layer walls, prediction of output probability distribution of noise level 80—69593
  insulation, window-glasses, most effective window configurations 80—87655
  intensity discrimination, bandwidth and masker presentation effects 77—9209
  intensity discrimination of band-noise signals as function of duration and bandwidth 78—27959
  intermittent truck noise effects on deep sleep 79—5310
  intermodulation product pair, masking and growth 78—20185
  Isom's thickness noise formula, extension to near field 80—53520
  jet, acoustic noise due to turbulence, directivity and Mach no. depend. 79—72921
  jet, aerodynamically generated noise *(French)* 77—75951
  jet, annular, discrete freq. noise generation props. and flow pattern 77—51092
  jet, cold, subsonic, acoustically active turbulent structs., conditional sampling anal. *(French)* 79—18881
  jet, edgetone oscillation analysis *(Japanese)* 79—10599
  jet, flow noise anal. 78—1654
  jet, large scale structure 78—34174
  jet, large-scale turbulent struct., noise prod. 79—7394
  jet, noise modelling by geometrical acoustics, outside silence cone 78—34177
  jet, noise radiated from convecting quadrupoles, flight effects 79—32601
  jet, nonisothermal, acoustic energy 77—7431
  jet, of gas, axisymmetric, free, steady-state, sound emitted, review *(French)* 78—67244
  jet, sound power output, turbulent jet into gas with different sp. ht. 78—94789
  jet, subsonic hot free, coherent structures in mixing zone, acoustic effects 79—4052
  jet, subsonic sound propagation due to a source near the duct exit 78—83446
  jet, supersonic, cold, coaxial, acoustic, flow characts. 80—1656
  jet, supersonic, noise, Reynolds number depend. 78—14053
  jet, turbulent, noise, coherent struct. 77—89176
  jet, turbulent source coherence effect on noise 79—32599
  jet aeroplane noise, effects on facial expression, EEG and manual responses, human subjects 80—98006
  jet aircraft, relation between static and in-flight directivities 79—86289
  jet engine exhaust noise, orderly struct. as a source 78—94786
  jet engine exhaust noise, source coherence 78—94787
  jet exhaust noise, large-scale struct. importance 78—94792
  jet exhaust noise, prediction of in-flight levels 78—87178
  jet exhaust noise, role of shear-layer instability waves 77—47054
  jet exhaust noise, shear layer instability effect 78—94791
  jet flow, noise directivity, peak spectra freq., and Strouhal no. *(Japanese)* 78—9489
  jet flow field during screech 77—15086
  jet flow noise mechanisms and principal notions 78—1653
  jet flow noise with fluid dilatation as source fluctuation, causality correlation analysis 79—72742
  jet flow turbulence generated, edge dissipation 80—103020
  jet flows, correlation techniques to detect azimuthally coherent structures 80—53765
  jet mixing noise, hot and cold, scaling laws based on geometric acoustics model 79—37306
  jet mixing noise generation, eval. of Lighthill analogy using LV turbulence, source location and spectral noise data 80—69803
  jet noise, amplification by higher-mode acoustic tone 78—9664
  jet noise, appl. of cepstral techniques to ground refl. effects in acoustic spectra 77—31165
  jet noise, characts. of shock assoc. noise 77—54831
  jet noise, characts. of turbulent mixing noise 77—54830
  jet noise, cross-spectral densities, extension of Ribner's theory 80—69804
  jet noise, current research 79—32602
  jet noise, external boundary-layer flow effect in flight 77—75901
  jet noise, geometric acoustic model inside the cone of silence 78—34117
  jet noise, geometric acoustics model, computer prediction program 78—34118
  jet noise, shear term role 77—72114
  jet noise and large scale instability waves, effect of upstream tones 80—69790
  jet noise in flight, prediction, importance of jet temp. 80—69814
  jet noise in flight prediction from static tests 80—61490
  jet noise prediction, nonlinear Lilley equation 80—69805
  jet noise source distrib., from far-field cross-correlations 77—84039
  jet noise source modification due to forward flight 78—63466
  jet noise suppressors, lab. comparison 78—59193
  jet nozzle, meas. of plane-wave noise radiation 77—58758
  jet propulsion aircraft noise, two-point correlation model 78—42493
  jet turbulence, interaction with pure tone sound 78—94790
  jets, cold, direct measurements of correlation between axial in-jet vel. fluctuations and far-field noise 79—81629
  jets, effect of spatial source coherence 78—38138
  jets, elliptical, stability and noise 78—38377
  jets, hypersonic, high temp., noise rel. to gas parameters *(Russian)* 79—32132
  jets, two parallel flow, noise reduction, exptl. investig. 79—41723
  jets, two-point correlations, comments and reply 79—32492
  laboratory air blowers 78—61975
  laminar wake behind airfoil, noise generation 77—42842
  legal remedies for noise and vibration problems 80—10084
  LF environmental noise annoyance, expt. study 77—36941
  LF industrial noise problem 80—33339
  LF masking patterns 77—36955
  LF noise, effect on people, review 78—92673
  LF tone-burst stimuli, determ. of freq. following response, humans and cats 79—83796
  LF transmission through walls of rectangular ducts, effects of external lagging 80—53544
  lifting boundary in low Mach number flow, sound scatt. anal. 77—42648
  linear predictive coded speech digitisers, background noise spectral subtraction 80—96140
  liquid fuel flames in open air, noise from jet and flames *(French)* 77—19476
  LMFBR, acoustic anal. of TREAT safety test R8 78—13290

acoustic noise continued
  - LMFBR, acoustic anal. on Na boiling expt. in FFM Bundle 3B, Test 4 78—13291
  - LMFBR, acoustic resonances as means of blockage detection 79—93752
  - local spectrum of underwater ambient noise field 79—37078
  - loudness discomfort level and acoustic reflex threshold for speech stimuli 80—76762
  - loudness discomfort level and acoustic reflex threshold for normal and sensorineural hearing-impaired subjects 80—76763
  - loudness perception, for short-duration tones in masking noise 78—65047
  - low frequency noise breakout from air conditioning ducts, abatement 80—74594
  - low frequency sound radiation due to the interaction of unsteady flows with a jet pipe 80—69787
  - low level sound, estimation of subjective annoyance using sound character as an objective physical attribute 80—35902
  - low Mach number aerodynamic noise theory 80—69796
  - low Mach number duct flows, combustion noise generation by chemical inhomogeneities 80—92237
  - low pressure axial flow fans, effects of rot. freq., blade thickness and profile 78—59195
  - low Reynolds number supersonic air jets, noise generation by instabilities 80—23831
  - low-frequency noise waves, parametric excitation in nonlinear medium 78—9472
  - machine, meas. technique of acoustic power with an intensity meter 78—83188
  - machine noise, octave sound-power level calc. 78—1503
  - machinery, control by vibration control 77—34999
  - machines employing circular saw blades 80—43533
  - machines influence assessment, outside condensing power plant, with four 200 MW blocks *(Czech)* 79—57548
  - marine structures, noise exposure and control 77—84079
  - masking level differences for temporal masking 77—64050
  - maximum acceptable noise levels in quiet rooms *(German)* 77—68307
  - maximum likelihood detection and estimation for harmonic sets 80—96116
  - mechanical structures, noise and vibration conf. Repino, Leningrad, 1977 Oct. 79—18579
  - mechanism of the development of noise in hydro-systems as the result of fluctuations in delivery flow *(German)* 79—7256
  - minimized sonic boom waveforms, subjective loudness 79—16221
  - minimum acoustical requirements for school buildings 80—79059
  - mining industry, characterization of noise environment, control methods 80—53556
  - mode representation of the noise field in a wedge 79—86299
  - monaural and binaural signal detect., role of dynamic cues 77—36952
  - monitoring and instrumentation 79—12301
  - motor vehicle noise propagation, prediction technique 77—75744
  - motor vehicle racing and shooting noise 78—55510
  - moving media, randomly inhomogeneous, probabilistic characteristics of noise fields 79—64383
  - moving point source above finite impedance reflecting plane 78—59179
  - muffler chambers, flow-reversing, anal., testing and design 77—11085
  - multiple input systems, effect of input cross spectra on freq. response estimation 79—55261
  - multiple input/scalar output problem, source identification 80—96105
  - multivariate joint probability expression of general random processes, finite expansion terms 80—69592
  - municipal noise control program development 79—74577
  - Murphy's laws appl. in noise control engineering 77—65650
  - N-wave sonic booms, subjective loudness tests 79—16220
  - New York City, environmental noise codes 78—59202
  - noise, aerodynamically generated, fluid flow eqns. *(French)* 80—74848
  - noise cancelling microphone with piezoelectric plastic diaphragm, coupled oscillator theory 80—43581
  - noise generation by transonic open rotors 80—69599
  - noise measurement, engineering aspects, techniques of noise evaluation 77—39178
  - noise reduction between two rooms connected by ventilation duct, anal. 80—10074
  - noise-induced sleep disturbances and their effects on health 79—5317
  - nonlinear noisy medium, sound absorpt. 77—35000
  - nonlinear waves attenuation, interaction with noise 77—50801
  - notched-noise masker, appl. to auditory filter shape determ. 77—90806
  - nozzle, subsonic flow, entropy noise, model 79—60046
  - nozzles, acoustic disturbance from gas nonuniformities 78—34179
  - nuclear power stations, environmental acoustic protection *(French)* 80—19155
  - nuclear reactor system, subcooled nucleate pool boiling, intensity and power spectral density of acoustic emission 78—17282
  - occupational exposure, audiometric and audiologic services 77—64056
  - occupational exposure, otolaryngologist's role in hearing conservation 77—64055
  - occupational exposure, permanent threshold shift, from an A-weighted Leq of 89 dB 78—92644
  - occupational noise standard, 29 CFR 1910.95, problems in enforcement 80—43528
  - ocean, ambient sea noise directionality meas. and processing techniques 78—16025
  - ocean, statistical anal. of ambient noise 77—79996
  - ocean acoustic background noise, detection of sinusoids 80—33347
  - ocean ambient noise levels, freq-freq. correls. 77—64302
  - office work interruption and psychological effects 78—42492
  - oil burner, industrial, reduction of infrasound generation 79—76909
  - open plan offices, comparison of NIC′ and ΔdBA rating schemes for speech privacy 79—3854
  - open plan offices, effect of V-form ceilings 77—50835
  - open wind tunnel jet flow, convection and refraction of acoustic waves *(French)* 77—24007
  - open-plan offices, role of acoustic screening 80—87650
  - opencast coalmining, principal noise sources 80—81505
  - optimum signal detect. in non-Gaussian noise 78—38149
  - outdoor process plant design, atm. noise attenuation calc. 79—70497
  - outdoor propagation of finite-amplitude noise 80—33338
  - overhead HV lines, noise, publications review *(Czech)* 80—23827
  - paper membrane sound generation by impulsive tension 78—90581
  - party wall and floor transmitted noise nuisance survey 78—42491
  - perforated facings with porous backing material as sound absorbers 77—62115

acoustic noise continued
  - petro-chemical industrial plants, piping networks, noise abatement 80—28381
  - physiological acoustics and health 80—96103
  - piezoelectric semiconductor, nonlinear acoustic noise amplification theory, phonon distrib. function basis 78—47837
  - pipe walls, randomly vibrating, broadband sound-power radiation efficiency estimation 77—62104
  - pipe with fluid flow, sound wave reflection at end *(Japanese)* 79—68457
  - pipe with turbulent air-flow, acceleration response and acoustic power spectral meas. 77—19484
  - pitch of noise signals, evidence for central spectrum 77—36942
  - PL/1 computer program for calculating subjective noise characts. 78—59192
  - plane noise barriers, integration of far field diffr. by surface mapping 77—54829
  - plates with irregular shock response, sound power level and noise reduction parameters *(German)* 79—81616
  - pneumatic control valves, noise characts. 80—53562
  - pneumatic silencers for exhaust valves and parts ejectors 77—84080
  - point source radiation near cylindrical jet in motion 77—31169
  - point source radiation through composite medium 77—31150
  - Poisson transduction of noise stimuli, results of computer simulation 77—86512
  - power law transformation giving short term integrators producing time-intensity trades for noise bursts 78—40190
  - power press, relationship between force waveform and sound radiation 80—74596
  - power transformer prediction and control 79—18648
  - power transformers, recent reduction techniques, Fuji product appl. 77-72113
  - predicting annoyance from detectability of low-level sounds 80—19148
  - propagation along finite impedance boundary, aircraft ground noise appl. 78—9487
  - propagation around thin half-plane numerical calc. 78—9486
  - propagation in open air, obstruction effects, propag. around finite plane on ground *(Japanese)* 77—39160
  - propagation in open air, obstructions effects, sound diffr. by 1/4 infinite plane *(Japanese)* 77—39159
  - propagation models, railway lines 80—48500
  - propagation over hard ground for distances under 200 ft, exp. study, community noise appl. 79—18600
  - property line noise control limits, statistical representation 77—54842
  - protection of occupationally exposed workers 79—92392
  - pseudo-Gaussian noise signals, for hydrophone calibration 77—84045
  - pseudorandom noise excitation of auditory evoked pots., spectral anal. 79—83795
  - psychoacoustics, effect of noise on signal detect. 78—3514
  - pulsation noise damping from small air bubbles in water 80—64253
  - punch press, mean square pressure of transient oscillator 80—23830
  - quarry blasting, sound propag. expts. 79—24928
  - radiated noise level calc. of mechanical impact using tapping machine *(French)* 80—87639
  - radiation, from axisymmetrically driven three-layer struct. 78—1507
  - radiation efficiencies, beams in flexural vibration 80—53541
  - radiation properties of a turbulent jet excited by a sinusoidal acoustic disturbance 80—69789
  - rail noise annoyance in residential areas 77—68311
  - rail traffic, wave reflections from slotted tunnel portals 78—18108
  - rail traffic conf., Derby, England, 1976, March 77—68309
  - rail traffic noise, survey *(German)* 77—821
  - rail traffic noise duration relations *(German)* 77—27423
  - rail traffic noise sources 77—68310
  - rail vehicle internal noise, sources and mechanisms 77—68318
  - railway, effect on sleeping subjects 80—48509
  - railway, environmental controls for new housing sites 80—48505
  - railway, environmental impact in Britain 80—48508
  - railway, wheel/rail noise research 80—48496
  - railway coaches, static and moving tests 80—48498
  - railway floating track slab resolution for noise and vibration reduction 77—68321
  - railway ground noise, underground systems 80—48490
  - railway ground vibrations, propagation and wayside effects 80—48489
  - railway noise, effects on nearby residents, survey 78—18114
  - railway noise and estimation, for newly established line in Japan *(Japanese)* 79—10428
  - railway noise levels in residential areas 77—68317
  - railway noise prediction and control from bridges and elevated structures 77—68319
  - railway noise propagation 77—68315
  - railway passenger coaches, structure-borne noise suppression *(German)* 80—91957
  - railway traffic, Dutch study 80—48511
  - railway tunnels, structure-borne sound levels and spectra 80—48499
  - railway wayside noise, high-speed trains 80—48497
  - railways, conf. Oct. 1978, Lyon, France 80—48495
  - random noise and vibratory system, multivariate state probability expression using unified statistical treatment *(Japanese)* 79—18584
  - rectangular cavity, two-dimens., acoustic modes, damping 77—31149
  - rectangular jets, heated high vel., noisc characts. 79—94604
  - rectangular opening, directivity and distance decay characts. 78—42495
  - rectangular reverberant room, correl. coeffs. of narrow band noise 78—18115
  - reduction by barriers on finite impedance ground 80—33301
  - reduction by multiple acoustic screens, influence of physical factors *(French)* 78—13844
  - reflex adaptation to combined steady-state and repeated pulse stimuli 78—44555
  - regulations in small cities, inexpensive community assessments 77—54841
  - relationship between sound power level and sound pressure level, laboratory and domestic environments, use of noise data 80—74599
  - research index, for UK (1975/1976) 77—7257
  - resonators, concentric tube, with unpartitioned cavities, anal. 78—90587
  - resource letter on environmental noise control 78—61949
  - rigid shell, oscillatory flow through perforated surface, sound generation 79—18950
  - ring source, fluctuating, with const. vel., power and freq. spectrum emitted 77—50796
  - ringing noise arising from free vibration, impact noise prediction 80 28377
  - ripple noise, models of pitch and pitch strength 79—90075

acoustic noise continued

- rising speed, effect on annoyance *(Japanese)* 77—68323
- rivers, acoustic noise from breaking ice 78—53671
- road noise, effects of tyre tread and road surface 77—14850
- road traffic, a socioeconomic approach to subjective responses 80—67022
- road traffic, close proximity vehicle noise survey method 80—102926
- road traffic, close to light motor vehicles 80—83701
- road traffic, community reactions from social survey in Manchester 77—84073
- road traffic, control of noise level of moving vehicles 80—99894
- road traffic, correct building placement, noise emitted by single source in open space 80—87647
- road traffic, effect of skewness and standard deviation on sampling errors 80—35803
- road traffic, effect of structure-borne tunnel vibrations on buildings 80—48492
- road traffic, equally spaced line sources model *(Japanese)* 78—33954
- road traffic, exponentially distrib. vehicles model *(Japanese)* 77—88983
- road traffic, highway noise barrier perceived benefit 80—102920
- road traffic, highway noise barriers, optimum weight with respect to effectiveness and cost 80—67021
- road traffic, human response in residential areas 80—55962
- road traffic, improvements to the equally-spaced vehicles model, grouping effect *(Japanese)* 80—55963
- road traffic, kerbside study of vehicles 80—79050
- road traffic, meas. accuracy using digital instrums. 80—79075
- road traffic, meas. radiating height of cars and lorries, effectiveness of sound barriers 80—64325
- road traffic, noise generated by single vehicles in freely flowing traffic 78—38139
- road traffic, noise propag., scale model anal. 78—59196
- road traffic, noise propag. in streets, multiple-reflection diffuse-scatt. model 78—87190
- road traffic, noise with interrupted flow 77—62106
- road traffic, prediction of time pattern of fluctuating sound levels *(Japanese)* 80—55965
- road traffic, prediction problem for various types of vehicles and multilanes *(Japanese)* 77—3699
- road traffic, relationships between multidimens. correlation props. of intensity and higher order information, Stratonovich's stochastic theory for random points system 80—87645
- road traffic, statistical theory based on component response waves composition 77—84070
- road traffic, statistical treatment in arbitrary sound propag. environment *(Japanese)* 78—59199
- road traffic, subjective annoyance, lab. expt. on students 80—102921
- road traffic, test procedures *(Japanese)* 78—38141
- road traffic, traffic passing through road intersections controlled by roundabouts, model 80—64280
- road traffic, traffic-induced building vibration 80—96098
- road traffic, use of sloped barriers for noise abatement 80—102925
- road traffic acoustic behaviour near traffic lights, computer simulation 78—90597
- road traffic Monte Carlo simulation methods, effect of vehicle spacing on results 80—72110
- road traffic noise, community response prediction 77—80012
- road traffic noise, individual diffs. in sensitivity from public surveys 78—33953
- road traffic noise, new theoretical model *(Japanese)* 80—35804
- road traffic noise and sleep disturbance 77—42659
- road traffic noise attenuation by masonry subdivision perimeter fence 79—74578
- road traffic noise control, systematic trial and eval. diagrams *(Japanese)* 79—23132
- road traffic noise in Hong Kong 78—30125
- road traffic noise levels on high rise building balconies 79—50504
- road traffic noise levels prediction 77—14842
- road traffic noise monitoring, errors between sampled data and continuous data 79—81618
- road traffic noise nuisance in residential areas, individual responses 77—31167
- road traffic noise poly-freq. spectral anal. based on filtered Poisson process model 79—52998
- road traffic noise prediction *(Japanese)* 78—13853
- road traffic noise studies based on traffic flow models 79—52999
- road traffic total noise exposure and time average statistics *(Japanese)* 79—70499
- road vehicle vibration analysis, digital modal analysis system 80—38173
- road vehicles, noise at roundabouts 78—90594
- road-traffic noise rating using continuous judgement by category *(Japanese)* 78—83170
- rock music sound levels and spectra rel. to hearing damage 79—68517
- rolling-contact noise generation in wire stranding machines, use of elastomers 80—43534
- rotary lawn mower noise control methods 77—34995
- rotary scrap chopper noise 80—53549
- rotor blades, radiation characts. of acoustic sources in circular motion 77—23803
- rotor blades in low-pressure axial flow fan, chord length and camber effects on noise 77—42661
- round free jet, aerodynamic noise, propagation of wavelike disturbances 80—69806
- scattering by density gradients 78—13836
- schoolchildrens' mental performance levels, aircraft noise effects 79—70495
- self-induced sound generation by flow over perforated duct liners 77—54990
- service evaluation tests on locomotives, AMTRAK Northeast corridor 80—48506
- service system noise faults survey at Liverpool University 77—7251
- shear layer instability noise produced by various jet nozzle configurations 80—69791
- shear turbulence, acoustic field, convective amplification, jet noise appl. 77—23943
- shielding, mathematical theory 77—54839
- ship noise, source level model for propeller blade rate radiation 80—43513
- shooting-range noise annoyance threshold variation 79—70498
- signal detection and localization, Fourier series method appl. to signal in noise background, comments 80—106671

acoustic noise continued

- signal processing, sparse array technique, min. output variance, S/N ratio 78—83177
- site selected variables effect on human responses to traffic noise 80—61491
- site selected variables effect on human responses to traffic noise 80—61492
- sleep, disturbance by noise 78—92645
- small air jet and quiet valve noise obs. 78—83165
- social surveys, on noise annoyance 78—87189
- sonar interference rejection by amplitude shading of transducer arrays 78—38151
- sonar target transfer function estimation in presence of noise and clutter 77—62110
- sonic boom of supersonic transport aircraft, effects on ecological environment 80—106661
- sonic booms, pressures inside room with open window 80—69602
- sonic booms, simulated, and inner-ear bleeding of chinchillas 79—16247
- sonic pulses generated during boiling of underheated liquid, time and spectral characteristics 80—107373
- sonometry, sound audibility, serial noise from machines and equipment *(French)* 77—21537
- sound generation and propagation in flows, inhomogeneous convected wave equation 80—69813
- sound generation and simulated emission by vortex flows 80—69797
- sound generation by flow-acoustic coupling 80—69793
- sound generation by head-on collision of two vortex rings 80—69801
- sound generation in a flow near a compliant wall 80—53766
- sound generation in flows, conf. Göttingen, Germany (Aug. 1979) 80—67937
- sound insulation, domestic roofing systems 80—96109
- sound isolation tests of residential buildings, correlation with subjective privacy opinions, standard sound source requirements 80—64323
- sound levels, use for assessing adequacy of hearing protectors 80—104771
- sound pressure levels behind large storage tanks, reflection effects 77—50826
- sound production in moving stream, Lighthill's acoustic analogy, jet noise 78—79313
- sound radiation from a simulated jet flow, calc. of vortex configuration and sound field 80—69786
- sound recording and reproduction quality eval. in motion picture studio recording room *(Russian)* 78—55518
- sound scattering in an urban street 78—51000
- sound sinks in flows, low freq. sound absorpt. of jets 80—69788
- sound source location techniques 80—69802
- sound spectra radiated by gas jets, influence of closely located solid surfaces 80—69800
- source position determ. by conditional sampling technique 77—19497
- Space Shuttle, environmental effects during launch and reentry 78—85681
- spatial correlation theory for noise field, evaluation of integral 77—88981
- speaker verification algorithm for noisy utterances 80—91992
- speech adaptive noise cancellation by short-time Fourier transform 80—91976
- speech comprehension ability of hard-of-hearing, calc. model *(Dutch)* 78—73165
- speech extraction from noise by adaptive digital filtering *(Japanese)* 78—13863
- speech intelligibility, noise effects in cases of presbyacusis 80—96139
- speech intelligibility, temporal interruptions with and without intervening noise 77—32911
- speech intelligibility and S/N ratio in high noise *(Japanese)* 77—73533
- speech intelligibility improvement in the presence of noise to combat hearing impairment 77—11091
- speech noise suppression filter for narrowband vocoder 80—91977
- speech wideband noise reduction by spectral weighting 80—96146
- spherical shell, constrained fluid-loaded, vibrations and noise associated with response to turbulent boundary layer excitation 79—90239
- splitter plate acoustics, zones of silence in sound wave-jet flow interaction 79—3819
- sports areas, reverberation and noise levels 78—9497
- sports-related noise or trauma, effects on hearing 77—64057
- standard noise impression change for field evaluation *(Japanese)* 77—72116
- standardisation, activities of ISO *(Japanese)* 80—19154
- statistical anal. of nonstationary random noise *(Japanese)* 77—84074
- statistical estimation of percentage of overexposed noise-impacted workers 78—92671
- statistical prediction of vibr. distrib. and random noise in higher level region *(Japanese)* 79—1023
- statistical treatment of random noise in digital form *(Japanese)* 77—23805
- steam hammer, scale model and on-line computer investigation 79—23137
- steam hammer noise, noise prediction using a small scale model 78—90598
- steam turbines, 200 MW, with accessories, noise reduction research and development 80—91958
- stochastic signal locally optimum detect. in non-Gaussian noise 78—38148
- STOL aircraft engine-wing system jet flap impact noise meas. 80—96101
- Strouhal number influence on flight effects on jet noise radiated from convecting quadrupoles 80—69781
- structural dynamics, modal anal. 78—39993
- structural freq. response testing, impulse technique 78—39992
- structural noise and vibration problem solution by statistical methods 79—23126
- structural-acoustic combined systems, modal synthesis for LF forced/free props. 77—88980
- structural-vibr. related noise, anal. technique 77—84077
- structure radiation of simple emitters, radiated sound power *(French)* 77—19471
- structure-borne noise of concrete floors 77—42665
- structure-borne sound, transmission of free waves across rib on panel 77—39248
- structures under impact loading, finite element modelling as tool for noise analysis and control 80—43535
- subjective analysis of acoustic noise *(German)* 79—46109
- subjective experiments (e.g. aircraft noise anal.), use of changeover designs 77—82380

acoustic noise continued
subsonic free-jet, directional characts. 80—23820
subsonic jet, acoustic far field, azimuthal struct. *(French)* 79—14150
subsonic jet, noise study by method of causality *(French)* 77—7428
subsonic jet in simulated motion, sound radiation 80—74846
subsonic jet issuing from semi-infinite cylindrical pipe, sound interaction 78—22395
subsonic jet noise, peak Strouhal freq. as function of Reynolds number 79—77196
subsonic jet noise, prediction method for flight effects 78—1502
subsonic MHD channel, acoustic props., calc. for longitudinal oscills. 77—35405
subsonic nozzle flow, response to acoustic and entropy disturbances 77—75958
subway trains, retrofit noise control of rapid transit cars 80—48502
supersonic, jet flow from nozzle, coords. of acoustic cross-section 78—5778
supersonic air flow through high press. gas valves into atm., noise and flow pattern obs. 80—59067
supersonic flow, cumulative nonlinear distortion of acoustic wave 78—22367
supersonic jet, acoustic perturbations *(Russian)* 77—58751
supersonic jet, acoustic reflections effect on discrete component of noise spectrum 79—68775
supersonic jet, imperfectly expanded, model describing sound generation 79—4053
supersonic jet, Mach wave emission 78—26172
supersonic jet, underexpanded, impinging on barrier, sound field 78—9495
supersonic jet flow over obstacle, discrete tones generation 78—1708
supersonic jet noise spectrum, discrete component 78—9493
supersonic jet noise suppression by coaxial cold/heated jet flows 78—63468
supersonic jets, acoustic radiation using double-pulse holographic interferometry 80—14678
supersonic quiet wind tunnel development 78—38437
supersonic round jet, flow characts. of large scale wave-like struct. 77—89178
suppression in speech using spectral subtraction 79—46124
surface effect vehicles, design problems 80—74598
surface generated noise in stratified ocean, spatial correlation 80—87620
surface noise from turbulent hot jet, temperature effects 80—69782
tapered unconstrained beams, vibration damping 78—51106
tempo sensation of burst signals *(Japanese)* 77—77913
temporal recognition masking or interference 77—25464
temporary threshold shift from transportation noise 79—90074
temporary threshold shift produced by varying noise exposures 77—64042
temporary threshold shifts in humans exposed to octave bands of noise 79—74688
test of speech intelligibility in noise 77—64048
thickness noise formula for acoustic far-field for body in arbitrary motion 79—81630
thin cylindrical shell, effect of cavity resonances on sound transmission 79—3850
thin elastic plate, acoustic wave scatt. near reson., panel deflection and vel. pot. field 77—42657
threshold shift and cochlear pathology in the Mongolian gerbil 78—65035
threshold shift in chinchilla from daily exposure to noise 77—36954
time delay bias errors in estimating frequency response and coherence functions 79—18614
time sampling, uncertainty in sound level eval. 77—42658
time transformation of acoustic eqn., flow effects on sound field, wind tunnel noise meas. appl. 78—87198
tone/noise combination effect on speech intelligibility rel. to aircraft noise 77—50824
towed-line array, iterative technique for ambient-noise horizontal-directionality est. 78—55525
tractor cab noise affect on the hearing perception of drivers 79—83791
traffic, acoustical correlates of aversiveness 79—41511
traffic, reverberant meas. rel. to noise level prediction 78—75013
traffic, road vehicle tyre/road noise mechanism study 77—19485
traffic, sampling errors with gamma headway distributions 77—84072
traffic noise, annoyance testing *(German)* 77—19473
traffic noise, attenuation around buildings 78—1498
traffic noise, meas. by L_{eq} and L_{α} *(Japanese)* 79—1024
traffic noise, model investigation on acoustical performance of courtyard houses 80—10077
traffic noise, responses of Chinese firemen 77—39157
traffic noise above ideal reverberant city, aerial meas. 77—50827
traffic noise annoyance, lab. study 77—80013
traffic noise in a high-rise city 78—94482
traffic noise reduction by closed balcony shielding on buildings 78—33951
traffic noise screening effect by buildings *(German)* 80—10076
traffic noise spectra, simulation model 77—46865
traffic noise survey, Turin, Italy 77—84063
traffic noise transmission, model *(Hungarian)* 79—86291
traffic noise vertical distrib. in Hong Kong 77—19475
traffic system noise propagation characts. estimation trial 79—53000
trailing edge noise, semi-infinite rigid plate, theoretical review 79—37307
trailing-edge turbulent flow noise, incident surface pressure field effect 78—90865
train induced ground vibration, propagation pathway prediction 80—48491
train noise, prediction of equivalent mean energy level from relatively short parts of railway lines 80—38172
trains, annoyance in residential areas from noise and vibration 80—48503
trains, attenuation by tree belts, pilot study 80—48501
trains, high speed train noise impact in AMTRAK's Northeast corridor 80—48507
trains passage, noise investigation *(German)* 77—822
tramway noise in city traffic 77—68312
transducer flow noise, rejection using coherence function method 77—84067
transformer noise reduction by acoustic compensation 78—38134
transformer substation, effect on urban environment 77—3701
transmission lines, high-voltage, coronal discharge noise depend. on instantaneous rainfall rate 80—98471
transonic tip speed propeller noise, quadrupole sources 79—55263

acoustic noise continued
transonic wind tunnel, noise level effect on model characts. *(French)* 78—71411
transportation, ride quality criteria 79—90076
transportation noise, LF, effects on human performance tests 77—19483
transportation systems, importance in France 80—48510
tube bank, in-line, acoustic reson. generation mech. 78—46958
turbojet, internal 80—87644
turbojet engine noise interaction of entropy fluctuations with turbine blade rows 77—80149
turbomachinery, multiple blade rows, semi-actuator disc model for sound transmission calc. 78—38137
turbomachinery, semi-actuator disk model, single blade row 78—13852
turbomachinery for central power stations, review of vibration and noise 80—23835
turbulence, heat transfer in gas *(Russian)* 78—46962
turbulence generated, acoustic radiation from bodies in unsteady flows 80—69799
turbulence generated noise, coherent struct. model 78—94675
turbulence generated noise on both sides of double layer jet 77—47056
turbulence generated sound, mean flow calcs. of large eddy struct. and flow-acoustic interaction 80—69785
turbulence-generated, air flow in pipes with various fittings 80—74849
turbulence-generated noise in pipe flow, book contrib. 78—59385
turbulent boundary layer over inhomogeneous boundary, sound emission 77—68297
turbulent flame, acoustic noise *(Russian)* 79—32708
turbulent flow noise generation, role of tornado-like vortices 80—69811
turbulent jet, acoustic emission from coherent structures *(French)* 77—65775
turbulent jet, acoustic power distrib. 78—67238
turbulent jet, noise spectrum calc. 78—67236
turbulent jet, sound radiation due to nonlinear interaction of instability waves 79—50720
turbulent jet, sound transmission expts. 79—32600
turbulent jet, trailing edge noise mechanism 79—41720
turbulent jet flow, aeroacoustic interaction, review 80—87765
turbulent jet mixing noise, aircraft, in-flight simulation expt. 78—1501
turbulent jet mixing rates with self-excited acoustic oscills. 78—47008
turbulent jet noise, press. depend. for choked and subsonic jets *(Chinese)* 78—67235
turbulent noise from low-pressure axial flow fans, model 77—42660
turbulent shear flow, large-scale coherent structure 78—94671
turbulent shear layer, sound and aircraft noise, spectral broadening 79—37076
turbulent shear layer, sound transmission 79—37075
tyre noise, meas. and anal. technique 78—33969
underground enclosures, noise distrib. prediction from free-field meas. 77—7253
underwater, determ. of spatial coherence using model *(French)* 79—41487
underwater, radiated noise due to boundary-layer transition 80—33319
underwater, sound and infrasound prod. by nonlinearly interacting ocean waves 77—11069
underwater, VLF attenuation from deep-water ambient noise field meas. 77—11070
underwater ambient noise levels meas., Cochin backwaters 79—25256
underwater noise spectra produced by fishing boats affecting albacore catch, comment 80—58844
underwater sound, attenuation of surface-generated noise received deep 78—9481
underwater sound, cancellation of turbulent boundary-layer press. fluctuations 77—88978
underwater sound, effect on directional accuracy of small ring arrays 77—31181
underwater sound, noise rel. to signal hearing estimation via FFT and Prony algorithms 77—46855
underwater sound, theoretical model of ambient noise in low-loss, shallow water channel 80—64265
unflanged duct exit, high temp. effects on radiation impedance 77—84069
unified noise index, formulation 77—50823
uniform noise invironment tests, protection of impaired hearing 79—81658
unsteady aerofoil theory, small perturbation expns. 78—14037
urban, relative importance of different sources 78—51001
urban noise, effect on cardiovascular function in rhesus monkey 79—5322
urban noise, field study, noise sources, effects on humans 79—5319
urban noise, math. model for noise level prediction 78—90599
urban noise level variation and attenuation with height 80—10078
urban sound level decay with distance 77—72109
urban traffic, sound pressure prediction 77—84071
urban traffic noise, contrib. of heavy vehicles 78—38136
US transmission line of probe for hot metal inspection, spurious signals 80—66754
USA, 1977 state noise restrictions 78—59203
USA, environmental noise control programs 78—59201
USA National Measurement System 78—38102
USA urban noise survey, community response 78—90586
USSR basic state standard of noise control 79—23142
vaneless diffuser, sound propag. and transmission 80—19121
vehicle noise attenuation over short grass 80—19146
vehicular queue, statistical anal. 77—80015
Viennese Subway stations, noise control problems 77—68314
vocal output and preferred listening level rel. to ambient noise 79—68500
vortex noise emission in flow past vibrating rigid bodies 79—23310
vortex noise from rotating blades 78—38143
vortex pairing in jet noise generation 80—69807
vortex shedding noise of aerofoils in smooth flow 77—80147
vortex sound at low Mach number, appl. to various flow fields 78—46978
vorticity waves in swirling duct flows, sound generation 77—62261
wake, supersonic, of transverse circ. cylinder, laminar to turbulent transition, external noise effect 78—38367
wake cutting aerofoil *(French)* 77—917
wall jet flow, compliant walls, influences of flow convection and refraction on sound radiation 80—74595
wall-pressure spectrum in turbulent boundary layer, rel. to noise generation by boundary layer-surface interactions 80—69810
water boiling in annuli under forced convection, boiling noise 79—1062

acoustic noise continued
- water drop impact noise *(German)* 77—75736
- water flow through orifice, polymer additives effect on cavitation and noise 79—98768
- waveguide with monopole radiators and dipole receivers, active noise suppression 80—102928
- white-spectra stimuli, place clues rel. to direct use of time information in hearing 77—90803
- wind and ground plane attenuation effects on sound propag. near ground 80—10080
- wind tunnel, sound source location using acoustic mirror 78—30372
- wing in forward motion, trailing edge acoustic source radiation 80—69780
- word discrimination scores, effect of marking by noise 80—41047
- work places, industrial installations, noise levels, limits *(French)* 77—19479
- CdS, intensity fluctuations of nonlinearly amplified phonons, Brillouin scatt. meas. 77—90163
- CdS, photoconducting, surface acoustic noise amplification by carrier drift 78—72208
- Fe-Cr-Al, attenuation and vel. of acoustic shock waves, amplitude depend. 78—63810
- He gas jet noise source, absolute calibr. 78—59228
- Na boiling acoustic emission burst detection in parasitic noise 79—3214
- Te, acoustoelectric current flow, acoustic refraction effect 79—19637
- ZnO, intensity fluctuations of nonlinearly amplified phonons, Brillouin scatt. meas. 77—90163

acoustic noise measurement
- 500 MW power station, methods *(German)* 78—55517
- acoustic barrier performance, scale model studies of effects of wind 77—23806
- air conditioning, noise measurement by concave reflector, new method 77—68344
- air conditioning system, subjective responses and meas. 78—83168
- air tools, portable, noise evaluation standards 80—23855
- air-handling ducts and plants, direct sound intensity measurement method *(German)* 80—102944
- aircraft, general aviation, ground noise level changes derived from cockpit noise levels 78—9488
- aircraft, meas. of noise signature using remotely-operated multiple array acoustic range 79—23134
- aircraft and missiles, effect of intense noise on equipment 79—3853
- aircraft and road traffic, noise indexes rel. to responses of firemen 77—39157
- aircraft engine exhaust noise, flight effects, use of Bertin Aerotrain 78—13847
- aircraft noise, effect of small vars. in height of microphone above ground surface 77—23813
- aircraft noise exposure prediction, method, problems 78—9491
- aircraft noise monitoring concepts of instrumentation 80—33397
- aircraft noise monitoring systems, requirements 80—23849
- aircraft voice communications, expt. study 79—81662
- airfoils at high Reynolds numbers, investigation using adjacent plane jets 80—28372
- airports, noise exposure, problems of definition of metrics 79—90079
- ambient noise horizontal directionality meas. with linear arrays 77—7270
- amplitude and statistical distrib. analysers, basic characts., applications, selection criteria 79—1027
- analysis, measurement and remedies *(French)* 79—81621
- analysis techniques *(Japanese)* 78—18105
- angle synchronous contact sensing for noise investigations, anal. of gear wheels machining errors appl. *(German)* 79—68477
- annoyance functions and scaling performance for LF noise 80—38196
- annular and circular fan duct noise, radial and circumferential mode meas. 79—68529
- appliance sound power meas., acoustic test facility 77—58507
- artificial head system, transmission errors causes and improvements *(German)* 80—106700
- atmospheric probing, appls. of external noise spectrum model 80—58858
- audio noise dosimeters, comparison of available equipment, ANSI standards, use in mines 79—1026
- automobiles, acoustic noise measuring techniques in automobile development *(German)* 78—79178
- axial flow fan sound power, acoustic loading effects 77—68348
- axial flow fans, noise and aerodynamic characts. 80—43536
- axial flow fans with nonuniformly distrib. stator rows, interaction tones reduction 77—14847
- bat detection instruments 80—69609
- blast noise measurement, recording system 77—88984
- buses, noise levels in New York City and Albany metropolitan areas 80—76684
- cavitation tunnel hydroacoustic transfer function, meas. and anal. *(Croatian)* 80—92002
- cement works, fundamental principles *(Hungarian)* 79—86290
- circuit-breakers, impulse sound levels of high voltage devices, DIN standard *(German)* 79—94401
- city area noise propag. using scale models and field measurements *(Japanese)* 80—19152
- city noise mapping, grid method with Rohde and Schwarz integrating sound level meter ELDO 4 80—48533
- coherence and phase data between two receivers, use in eval. of noise environments 78—59194
- community, industrial noise control conf., Inter-Noise 78, San Francisco, USA, 1978, May 79—18594
- community noise surveys, stratification to improve design efficiency 79—81623
- computer and business equipment, standardization of noise emission measurements 80—53589
- control valves, measurement from pipe vibration *(French)* 77—39158
- corona discharge from water drops, on HV overhead power lines, expt. 80—33851
- correlation measurement method for rotating sources of noise 80—64279
- data accumulation equipment *(Japanese)* 78—42503
- data anal. using digital techniques 78—83193
- data logging system requirements for noise monitoring 77—68351
- diesel engine, freq. response and multiple coherence function of noise generation system 77—7254
- digital instruments, Bruel & Kjaer products review 78—94493
- digital voltmeter for noise and vibration meas. 78—55538
- domestic noise control and measurement *(Spanish)* 80—1380

acoustic noise measurement continued
- dosimeters and noise exposure ratings 77—31173
- duct noise active attenuation meas. 78—90592
- electric machines, meas. errors *(Hungarian)* 80—96102
- electrical apparatus, signal processing techniques appl. 77—75765
- electroacoustic, analytic and diagnostic equipment 78—63249
- emission detection system sensitivity, direct comparison method 78—56848
- energy mean level and decibel mean level relations for arbitrary sound level distribs. 80—14530
- engineering aspects, techniques of noise evaluation 77—39178
- engines, exhaust manifold design and cylinder firing order effect on short term spectrum 77—14845
- environmental, evaluation *(Japanese)* 77—68308
- environmental noise measurements, undergraduate research project 78—12472
- environmental noise monitoring installation 80—33396
- environmental random noise distrib., prediction using generalized time-discrete Fokker-Planck eqn. 80—102918
- equivalent continuous noise level meter requirements 78—83195
- equivalent continuous noise levels, instrument design, electronic 77—65654
- equivalent continuous noise levels, Leq meters 77—68353
- excess attenuation of noise propag. over ground *(Japanese)* 80—19128
- exhaust system, procedures for evaluation of acoustical performance 79—18645
- exposure measurement, monitoring of sound press. within ear 77—52799
- exposure monitoring for an individual for one month 78—30124
- fans, blowers, dynamic compressors, acoustic test methods, noise emission *(French)* 77—19478
- fission reactor flow-induced control element movement, expt. investigation using noise analysis 80—788
- fluctuating noise, meas. and anal. system *(French)* 80—64316
- fluid power equipment, noise analysis and control, PDP 11/40 minicomputer dynamic analysis system, graphical presentation of results 80—64327
- Fourier analyser signal processing system 77—68335
- frequency spectra interpretation guide 78—22235
- gas turbine wideband combustion noise obs. *(Japanese)* 80—11890
- generalised system and equipment 78—83189
- ground-to-ground, by synchronized integration technique *(Japanese)* 80—19188
- hearing protectors, effectiveness meas. 79—14180
- heavy trucks, indoor simulation of SAE recommended practice J366b 80—53588
- helicopter; rotary wing; wind tunnel 77—19501
- helicopter impulsive acoustic noise signature recording in flight 78—9477
- helicopter noise rating, development of proposed impulse correction 80—96107
- helicopters, experimental investigations of flight conditions and noise 80—19193
- high speed trains, aerodynamic noise study 80—48512
- high speed unequally spaced fan rotor, method 80—96163
- holographic detection of acoustic sources, computer reconstruction 78—38153
- housing, classes of acoustical comfort, measurement and control methods 79—23143
- hydraulic pumps, methods 79—79433
- hydraulic pumps, standard methods for airborne noise meas. 79—50548
- icebreakers, noise accompanying breakup of ice by hull 79—94402
- impact noise testing on floors, comparison of methods 79—46111
- impact sound loudness meas. *(Japanese)* 79—98546
- impulsive and continuous noise, combined dose meas. 80—102929
- impulsive noise, accuracy of measurement, health hazard appl. 79—18652
- indoor large machinery, sound power meas. by two-surface method 77—39152
- induction motors, 3-phase, laminated cores, sound level theory, meas., and results *(Polish)* 80—92004
- industrial acoustic pattern recognition *(German)* 77—80038
- industrial compressor sound level meas. *(German)* 80—14520
- industrial machinery, acoustic environment improvement for in situ meas. 77—39155
- industrial machinery, sound power determ., environmental corrections 77—39153
- industrial machinery, surface acoustical intensity method for in situ meas. 77—39156
- industrial machines, determ. of sound performance for multi-position machines *(German)* 80—43523
- industrial noise, health problems and meas. *(Hungarian)* 77—27424
- industrial noise, random sampling techniques for in-plant use 79—27464
- industrial noise control, health hazard, legal implications 78—33955
- industrial noise dose for setting hearing loss risk limits 78—1504
- industrial noise level meter calibration procedures 77—62125
- industrial sound meas., transducer function, basic theory *(German)* 77—80037
- industrial time-varying noise, methods *(Polish)* 77—54851
- infants in incubators, measurement of noise exposure and possibilities of hearing damage 80—53545
- infrasonic ambient noise, nonacoustic noise interference 80—19135
- infrasonic flow noise, meas. by H-58 omnidirectional hydrophone 77—47119
- infrasonic sea noise measurement, experimental problems 78—11902
- instrumentation, evaluation method, calibration *(German)* 77—80039
- integrating real-time noise analyser for portable field operation 79—1037
- integrating sound level meter ELDO 4 77—75761
- integrating soundlevel meter ELDO 2, industrial appl. 78—42505
- internal combustion engines, models for predicting piston impact noise 80—53553
- jet engine noise meas., flowing duct sound separation probe 78—13878
- jet engine noise source location, polar correl. technique 77—62105
- jet flight simulator, shear layer refraction and facility-to-flight corrections 78—13845
- jet noise, flight effects, use of Bertin Aerotrain 78—13848
- jet noise, source location, appl. of acoustic mirror, telescope and polar correl. techniques 78—83169
- jet noise diagnostics, spurious sound generated by hot-wire turbulence interaction 80—33304
- jet noise sources, meas. using shallow surface-wave simulator 77—80146
- jet position transducer, experimental investigation of noise characts. 79—37103

acoustic noise measurement continued

- job shop environment, analysis for noise regulations 80—45840
- L_a evaluation level, estimation using sequential and non-sequential type algorithms *(Japanese)* 79—37099
- laboratory for vibration and acoustic measurements, organization 79—76925
- large chamber for road vehicles and large machines, instrum. room and services room *(German)* 77—72121
- LF noise annoyance using dB(A) as predictor 80—38195
- LMFBR diagnosis, electrochemical and physical methods 79—97787
- LMFBR Na-cooled 7-rod bundle acoustic and temp. noise obs. 79—13391
- locomotive, stationary, in-cab noise level measurements 79—14155
- loudness determ. methods *(French)* 77—34996
- machine, meas. technique of acoustic power with an intensity meter 78—83188
- machine noise, conf., St. Louis, USA (Nov. 1974) 77—39151
- machine noise, determination from surface intensity measurements on vibrating cylinder 80—43577
- machine noise transmission, device for meas. and comparison with computation 80—28380
- machine tools noise meas. techniques 77—31172
- machinery acoustic noise meas. standards and reference sources *(French)* 78—83185
- machinery noise measurement and control, conf., W.Lafayette, IN, USA (Apr/May 1979) 80—43526
- machinery noise source analysis using surface intensity measurements 80—43543
- machines influence assessment, outside condensing power plant, with four 200 MW blocks *(Czech)* 79—57548
- magnitude estimation technique for impulsive and steady machine noise 80—53590
- mean energy density, noise level determ. 78—51018
- mean level determination methods 80—28390
- meter for acoustic power of small machine in a room 78—33975
- methods and instrum. *(German)* 77—42670
- microphone selection and use for engine and aircraft noise meas. 79—90104
- microphone windscreens, acoustic sensitivity 78—38133
- microphones for sound-level meas. 78—83190
- microprocessor based noise analysers 79—18654
- mine ventilation fan, spectral anal. *(Russian)* 80—53584
- miniature sound level meter, development 77—31166
- model rotors, LF broadband noise 79—90057
- motorway free-flow traffic noise obs. 78—90591
- moving noise sources, far-field pressure measurement 80—53547
- noise and number index, definitions of parameters 80—61489
- noise exposure of inhabitants of Sendai and their reaction *(Japanese)* 80—19151
- noise level meas. using optical fibre interometric hydrophone 80—87673
- noise source location, use of microphone coupler, BOTSEAR 80—43576
- non-Gaussian noise, detection of signals using optimum processing structures 79—7260
- nuclear power plant diagnostic system using noise anal. 78—50279
- nuclear power stations, noise meas. for plant surveillance 79—97853
- ocean, radiated noise meas. from data buoys and cycloidal propellers 78—33960
- ocean, spatial, noise spectrum meas. in ocean for small observation baseline 80—102902
- oceanic wind speed and stress estimation from ambient noise meas. 79—74963
- offices, open-plan, noise barrier performance 79—76927
- optical fibre interometric hydrophone appl. 80—87673
- outdoor noise monitoring microphone installation and calibration *(Japanese)* 78—42504
- outdoor noise of coal-fired power plants 80—76683
- personal noise dosimeter response to impulsive noise, measurement errors 79—18646
- pile driving devices 80—23832
- pipe with turbulent air-flow, acceleration response and acoustic power spectral meas. 77—19484
- plasterboard sound reduction indices and meas. 78—87196
- Poznan district post and telecommunication premises, reduction problems *(Polish)* 79—37088
- prediction method for traffic noise in urban Sydney 77—34994
- pressure transformation from diffuse sound field to external ear, body and head 79—68523
- pressure vessels, acoustic equipment for leak detection during hydraulic tests *(French)* 80—789
- punch press load-radiation characts. 77—68350
- quarry blast waves, simulated, subjective loudness 79—72751
- quarrying, use of electronic transient recorders for meas. explosion noise and vibration 80—67023
- R20 computer centre, noise level meas. *(Hungarian)* 79—41513
- radiating sources, conditional sampling technique appl. 77—68322
- railway noise and estimation, for newly established line in Japan *(Japanese)* 79—10428
- railway trains, acoustic telescope applications 79—94426
- railways, meas. on noise protection screens *(German)* 80—102916
- rain and wind in trees effect on sound levels 79—76926
- real-time frequency analysers for acoustic noise control 78—83192
- real-time room-acoustic analyzer using tone burst signal from loudspeaker *(Japanese)* 80—10087
- regulations and methods for noise measurement *(German)* 80—69610
- reverberation room ANS qualification error sources and effects 77—58514
- reverberation room ANS qualification for discrete frequency sound power level meas. 77—62122
- reverberation room ANS qualification for wideband and discrete frequency source meas. 77—58518
- reverberation room ANS qualification with microphone traverse and LF absorption 77—62123
- reverberation room qualification with computer-controlled instrumentation system 77—58516
- review of noise measurement 80—33381
- road traffic noise, analysis of sequence of sound level readings *(Japanese)* 80—35806
- road traffic noise, comment on survey method 79—37083
- road traffic noise, influence of averaging time 80—28393
- road traffic noise, simulated, measurement of annoyance 80—28379

acoustic noise measurement continued

- road traffic noise, traffic control effect on noise evaluation index 80—51024
- road traffic noise data, appl. of multivariate joint probability function of state variables with quantized levels 80—36836
- road traffic noise prediction calc. on straight road in suburbs *(Japanese)* 80—19147
- Rome road traffic noise, 24-hour obs. and statistical analysis *(Italian)* 80—87651
- rotating noise sources, correl. meas. method, math. model construction *(Croatian)* 77—39150
- rotating sources of noise, correl. method *(Croatian)* 78—46869
- school teachers' subjective response to aircraft noise 79—70496
- sea noise, LF ambient levels in S.Fiji Basin 79—72744
- signature anal. for noise source identification 77—68336
- signature analysis systems with Fourier analyzer 78—87195
- sound absorption coefficient, reverberation chamber appl. 79—18653
- sound attenuation, air-to-ground propag., effects of temp., humidity gradients 79—1019
- sound insulation meas. for light struct. *(Chinese)* 79—10427
- sound level meter display attachment, small no. of samples metering 80—79076
- sound level meter output measurement, use of digital voltmeter 80—79077
- sound level meters, digital hold for maximum value 79—76928
- sound level meters, modern standards and features 78—83191
- sound power estimation in free field above refl. plane 77—39154
- sound reduction in small elec. appliances, investigation using time average holography *(German)* 79—37086
- sound transmission loss 77—19486
- sound-level meter design and future developments 80—43560
- sound-level meters, instrum., meas., and environmental limitations 79—1039
- sounding, ambient noise elimination method *(Japanese)* 78—1506
- soundlevel meter ELMOT improvements, motor vehicle noise measurement appl. 78—42506
- soundlevel meters, Rohde and Schwarz, official approval, W.Germany 78—46872
- Space Shuttle, prediction of acoustic environment in payload bay 80—102919
- spectral analysers, high speed, vessel noise freq. anal., comparative advantages *(Croatian)* 79—55278
- standardisation, activities of ISO *(Japanese)* 80—19154
- standardisation and subjective aspects hearing damage prevention appl. *(German)* 78—9496
- standardised methods, effects on ear prevention *(Spanish)* 78—15857
- standards 77—35001
- structure-borne sound levels, effects of walls and floors in multistorey buildings *(German)* 78—94483
- supersonic transport planes, generation of local ground noise 80—38174
- supertanker radiated noise spectra in deep ocean, origin 78—33959
- surface transportation vehicles, sound meas. standards 80—14531
- tape recorders, portable, FM- and direct-recording types comparison 79—1028
- temporal sampling strategies for noise monitoring, development 79—98542
- test acoustic chambers 78—87218
- test facility modification for ANS qualification 77—62121
- textile machine noise charact. meas. under production condition 78—5611
- tone sound power, reverberant room appl. 77—19502
- traffic, microsampling technique 79—55264
- traffic in housing estate, model *(Hungarian)* 79—86291
- traffic noise, effect on speech communication and annoyance, anechoic chamber meas. 79—18590
- traffic noise at signalized intersection, influence of traffice structure *(Japanese)* 79—37082
- traffic noise measurement method and results *(Spanish)* 78—59219
- traffic noise measurements in Antwerp and Brussels and their relation with annoyance 80—33332
- transducer measurements, flow noise rejection using coherence function method 77—84067
- TREAT reactor, acoustic monitoring of IRT-10 test 78—8944
- turbine-generator sound level meas. using directional microphones 79—68520
- turbojet noise suppression investigations using hydrodynamic press. meas. and cross-correlation techniques 78—79157
- underwater noise from fishing-boats, freqs. affecting albacore catch 79—90063
- underwater sound, background ambient noise estimation from spectral anal. of time series 77—84046
- underwater sound, measurement of acoustic noise effects on behaviour of marine organisms 80—106657
- units and traceability *(Japanese)* 78—18104
- unsteady noise from letter-handling machines, automatic classification of noise levels 80—79085
- urban areas, method for predicting equivalent noise levels 80—19177
- urban built-up areas, external reverberation times 77—14846
- USSR acoustic noise metrological improvement 78—42502
- vehicle noise, stationary test method 77—34998
- vehicle noise, using correlation techniques, expt. 77—68349
- vehicle sound emission meas. 79—76910
- velocity, procedure *(German)* 79—93106
- VLF wind-generated noise produced by turbulent pressure fluctuations in atmosphere near ocean surface 80—19137
- wall and floor noise insulation field tests 78—1511
- wind noise, expts. on human beings 78—92648
- work environment evaluation with reference to noise 80—23833
- worker exposure, types of measurement and accuracy 80—23854

acoustic nuclear magnetic resonance

- absorption and dispersion 77—36143
- amplifier-generator for nuclear acoustic resonance spectrometer 80—27324
- antiferromagnet, acoustic nuclear resonance, self-induced transparency *(Russian)* 79—91304
- antiferromagnets, EM and acoustic response echoes of nuclear spin system *(Russian)* 79—69747
- autodyne detector using FETs 79—17457
- corundum, hexadecapole transitions, acoustically induced, of ^{27}Al nuclei *(Russian)* 80—50205

acoustic nuclear magnetic resonance continued
- III-V semiconductors, electric field gradient-elastic tensor components, acoustic NMR obs. 80—25229
- incoherent phonons, nuclear acoustic resonance 80—7180
- liquids, spin lattice relaxation, sound coherence 80—97128
- magnetically ordered media, self-induced transparency in nucl. acoustic reson. 79—69733
- metal, cubic, dipole-nuclear acoustic resonance, electron band struct. influence 79—19787
- metal, electron mediated nucl. spin-phonon interaction 77—1604
- metals, nucl. acoustic reson., quantum theoretical treatment 79—42846
- multiple-scan direct and lock-in detection schemes, metal single cryst. appls. 80—66050
- spin quantisation, in field of strong acoustic wave 78—19344
- spin system kinetics for spin quantisation by strong acoustic field 78—15052
- transmission oscillator US spectrometer with new calibration technique 77—67486
- Al, acoustic NMR saturation studies 79—73835
- Al, anomalous nucl. acoustic reson. signals 77—20732
- Al, nuclear acoustic resonance, influence of longitudinal and transverse magnetoresistivity 79—24222
- Al-Zn (0.14 at.%), signal amplitude and phase, temp. depend. 79—8058
- Al_2O_3, corundum, acoustic enhancement of NMR lines 80—29632
- $Al_2O_3{:}Cr^{3+}$, corundum and ruby, ^{27}Al quadrupole, transitions, acoustic and elec. saturation 77—90071
- Co, acoustic nucl. spin echo obs. at 4.2K *(Russian)* 78—6599
- CsI, acoustic NMR, role of incoherent phonons *(Russian)* 78—80230
- CsI crystal, incoherent phonons, nuclear acoustic resonance 80—7180
- CsI, nuclear spin echo for ^{127}I, magnetoacoustic excitation *(Russian)* 77—4578
- CuBr(Cl)(I), electric field gradient-elastic tensor components, acoustic NMR obs. 80—25229
- Ga, liq., nucl. acoustic reson. Knight shift, rel. to spin-lattice relax. 78—19351
- Ge, electric field gradient-elastic tensor components, acoustic NMR obs. 80—25229
- InSb, acoustic NMR, role of incoherent phonons *(Russian)* 78—80230
- n-InSb, EM wave resonant absorpt. 78—2757
- $KMnF_3$, acoustic nucl. spin echo *(Russian)* 77—48088
- LiF:Co(Mg), defect mechanism of nucl. quadrupole spin-phonon coupling 77—8445
- Mo electric field gradient tensor, electronic contrib., nucl. acoustic reson. determ. 78—48059
- NaCl, pure and doped, nucl. acoustic reson. 79—69746
- $NbH_{0.026}$, nucl. acoustic reson. of interstitial H 79—51867
- Pd, nucl. acoustic reson from 4-200K 80—25247
- PrF_3, van Vleck paramagnetic, nuclear acoustic resonance of ^{141}Pr using US *(Russian)* 79—78539
- $RbMnF_3$, acoustic nucl. spin echo *(Russian)* 77—48088
- Sn, white, nuclear acoustic reson., Knight shift 80—71204
- Ta, Knight shift and hyperfine fields, core polarisation contrib., nucl. acoustic reson. determ. 79—51868
- Ta, with mobile H impurities, anomalous nuclear acoustic reson. line shape 77—20730
- ^{181}Ta nuclear acoustic reson. line shapes, quadrupole exchange contrib. 79—61242
- $TmVO_4$ type crystals with cooperative Jahn-Teller effect *(Russian)* 77—28460
- $TmVO_4$-type crystals, dipole nuclear spin-phonon coupling and US absorpt., theory 77—24753
- ^{51}V, nucl. acoustic reson. absorpt. and dispersion via coupling to mag. dipole moment 77—48065
- W, acoustic NMR line shape, effect of demagnetisation 79—95654

acoustic paramagnetic resonance
- acoustic solid effect due to US stimulated transitions between NQR levels 77—12249
- borosilicate glass US attenuation saturation by microwaves, low-temp. obs. 77—36114
- cubic crystals, pseudo-tetragonal APR spectra 80—88861
- degenerate semiconductor, conduction electron acoustic spin resonance, oscillations of absorbed power 80—108075
- dielectric crystal, Jahn-Teller effect, study of paramagnetic ions 80—84634
- impurity centres exchange interaction caused by elementary excitations in solids, temp. depends. 80—25193
- liquid, APR line form. induced by anisotropic spin-lattice interactions *(Russian)* 78—52338
- liquid, effect of APR on sound refl. at solid-paramag. liq. interface 78—35025
- liquids, spin lattice relaxation, sound coherence 80—97128
- molecular cryst., phonon scatt. times below 10K, optically-detected APR 78—88228
- semiconducting film with paramag. admixture under EPR conditions *(Russian)* 77—63266
- semimetal, degenerate, conduction electron acoustic spin resonance, oscillations of absorbed power 80—108075
- spectrometer using Bragg diffraction of laser light 80—27326
- spin-system saturation in paramagnet, rel. to reson. rot. of acoustic polarisation plane 77—32245
- 1,2,4,5-tetrachlorobenzene, multiple-quantum spin-phonon interactions, acoustically-induced phosphoresc. obs. 77—40150
- transverse hypersonic waves at 9.4 GHz appl. to APR and attenuation meas. 78—33970
- vibronically coupled systems, cluster model 79—19540
- Al_2O_3, $3d^4$ ion study by cross-relaxation 79—99755
- $CaO{:}Cr^{2+}$, APR spectra 79—87313
- $CaO{:}Cr^{2+}$ Jahn-Teller system, APR spectrum, zero strain site energy level diagram 79—99756
- $CaO{:}V^{3+}$ orbital triplet, intermediate Jahn-Teller effect, APR 80—34758
- $KMgF_3{:}Cr^{2+}$, dynamic Jahn-Teller effect 77—66416
- $KMgF_3{:}Fe^{2+}$, anomalous acoustic relax. absorpt. and APR 80—88864
- $LiNbO_3$, photorefractive sensitivity, dependence on impurity Fe^{2+}/Fe^{3+} ratio, EPR and APR data 79—73893
- $LiNbO_3$:Fe, optical damage, Fe ion conc., EPR and optical spectra evaluation 79—42933
- $MgO{:}Cr^{2+}$, APR spectra 79—87313
- $MgO{:}Cr^{2+}$, APR under applied stress 80- 88865
- $MgO{:}Cr^{2+}$, dynamic Jahn-Teller effect, APR obs. 77—20693

acoustic paramagnetic resonance continued
- $MgO{:}Fe^{2+}$, microwave acoustic relaxation losses 78—43635
- $ThO_2{:}U^{4+}$, paramag. acoustic reson. absorpt. in cubic field 77—20680

acoustic parametric amplifiers
- degenerate parametric amplification, theory 77—27414
- piezoelectric semiconductor, US parametric amplification effects, contributions to nonlinear material coefficients 80—34144
- GaAs n-n$^+$ epitaxial structure for CW microwave electroacoustic amplifier 78—59235

acoustic parametric devices
- *see also acoustic parametric amplifiers; acoustic parametric oscillators*
- arrays, beam pattern and propag. curve for air *(Japanese)* 80—83693
- arrays, historical background and theory 78—5621
- arrays, max. conversion efficiency anal. 78—71242
- arrays, model for difference-freq. radiation 77—46836
- arrays with intermediate directivity in water, expt. study 80—74569
- curved face parametric projector for marine sediment penetration 78—51032
- cylindrical waveguide, sound generation theory 77—50849
- dispersive acoustic systems, nonlinear and parametric phenomena 78—55489
- high data rate acoustic telemetry system design 80—43573
- low-frequency parametric radiator, experimental study 77—39128
- nearfield calc. for parametric acoustic source 78—63221
- radiating parametric antennas, review 80—102898
- receiving array response to transducer vibration 80—74570
- receiving arrays, modulation characts., 80—33393
- rectangular aperture sources, source level and beam pattern prediction 78—63219
- saturated receiver, analysis 80—33386
- selected mode excitation in shallow-water sound propagation 78—59182
- sonar performance calculator 80—33392
- US radiator, influence of dispersive medium on characts. 78—94470

acoustic parametric oscillators
- azimuthal angle of T-D mode induced scatt. from parametric ion-acoustic wave 78—75322
- source for underwater acoustic communications 77—7247
- transient parametric acoustic sources 80—10060

acoustic radiators
- *see also acoustic generators; Doppler effect*
- aircraft engines, duct noise radiation in turbojet and turbofan engines 80—23834
- antenna, based on existing microwave dish-antenna, for acoustic remote sensing 79—72770
- arbitrary elastic structure in infinite inviscid fluid, acoustic radiation and scatt. 79—7318
- arbitrary shape, directivity pattern calc., near-field press. meas. on surface of finite circular cylinder 80—87677
- axisymmetric spherical radiator with mixed boundary conditions, press. field calcs. 77—46827
- axisymmetry parametric, weak interaction model 79—90053
- baffled circular piston, radiation impedance deduced from transient state 77—79980
- baffled piston wideband acoustic near- and far-field transients 79—46154
- baffled thin rectangular plates, radiation efficiencies 77—27405
- beam reinforced plate, acoustic radiation 79—18580
- ceramic transducer, for transient acoustic pulses generation in water 78—1483
- circular duct with hyperbolic horn, sound radiation modes 80—96096
- circular piston, influence of acoustically compliant baffle on sound radiation 78—5598
- circular piston, nearfield shading effect calc. by ring-function method 77—34974
- circular plate, edge-clamped, sound radiation study using optical holography 77—836
- compensating sources in active suppression systems, effectiveness of placement criteria 78—18099
- complex mechanical structures, sound radiation determ. using reciprocity principle 79—23124
- composite plates, thick fluid-loaded, structural response function 79—94381
- concave radiator in infinite baffle, acoustic field *(Japanese)* 79—18560
- concentric piston radiator, influence of thickness of finite rigid baffle on directivity 79—64373
- controlling sources, for active noise suppression in waveguide 78—5613
- cylinder, rotating, line-source radiation scatt., distant field calc. 77—50795
- cylindrical, method of estimation of acoustic field 79—64371
- cylindrical radiator with mixed boundary conditions, acoustic field 79—18563
- cylindrical shell, coupled vibrations giving high intensity US radiators 78—59236
- cylindrical shell driven by line force, sound radiation 78—94480
- cylindrical steel shells in water, thick-walled *(German)* 80—102899
- cylindrical tubes, high-intensity US radiators *(Japanese)* 80—33404
- delay and Doppler parameters, max. likelihood estimation 78—9503
- diesel engine radiating surface identification by partial coherence technique 78—42490
- directivity pattern calc. from near-field sound meas. 78—83149
- disc, radiation coupling to plane and back or to disc, exact soln. 77—46828
- disc radiator calc., using Kirchhoff surface integral, simplification 79—86275
- disc with or without baffle, acoustic field study *(French)* 79—98541
- echosonde antenna, effects of phase-front distribs. on radiation patterns 77—39123
- echosonde antennas, echo carrier freqs. and antenna dimensions rel. to performance 78—1474
- elastic shell, appl. FEM to coupled structural-acoustic radiation system 80—83691
- elastically supported circular plate, sound radiation 79—41507
- electroacoustic sound sources for non-directional sound radiation *(German)* 79—3876
- engine exhaust system, acoustic characts. in presence of mean flow 77—837
- estimation of source motion from time delay and time compression measurements 80—58860
- ferroelectric cylindrical shells, appl. of one-dimensional finite elements to normal mode anal. 77—31163

acoustic radiators continued

- finite element simulation of acoustic transmission system with radiation 79—3862
- flame acoustic radiation rel. to flame loudspeakers 78—59227
- fluid-loaded plate, real roots of eqn. defining free wavenumber 79—94398
- focusing radiators and acoustics lenses, field structure 77—50792
- free-jet, turbulent, experimental investigation of acoustic radiation 79—46102
- gas-jet generators, design characts. 80—87695
- hard-walled ducts, formulae for sound radiation 78—13830
- harmonic point source, compensation of diffracted field formed by rigid scatterers 78—18112
- horn and silencer design, FEM anal. of acoustic transmission/radiation systems 80—87589
- horn design for focused SAW radiation into waveguide 78—1542
- ill-posed diffraction problem and quasisolution 80—87593
- impact of sphere with slab, transient sound radiation 79—23128
- infinite elliptical cylindrical radiators array with mixed boundary conditions, sound field 78—1538
- infinite periodic array of vibr. strips in plane acoustically compliant baffle 77—68305
- infinite periodic slotted array, sound radiation 77—11105
- infinite planar baffles problem in acoustic radiation and its expt. verification 79—98520
- infinite plate driven by moving load, sound radiation 79—64396
- infinite plate reinforced by finite beam set and driven by point force, sound radiation anal. 78—1496
- infinite thin plate driven by longitudinal force 78—50998
- interdigital transducer, use as transmitter in acoustic focusing device 78—9520
- low-frequency parametric radiator, experimental study 77—39128
- membrane, infinite, acoustic radiation due to fluid loading discontinuity 78—90579
- monopole arrays, continuous, active sound suppression 79—94386
- moving sources, radiation props. in free field and near absorptive plane surface, helicopter blade noise 80—102885
- nearfield axial levels of exponentially shaded end-fire arrays 77—39127
- off-axis beam pattern analysis using replica pulse representation 77—54821
- open ended cylindrical pipe or cone and rod or slab 77—84021
- organ flue pipes, sound prod. 77—7265
- organ pipes and edge tones, jet drive mechanisms 77—831
- oscillating spheroids, acoustomechanical characts. 77—34991
- parametric, liquid containing gas bubbles 80—87615
- parametric acoustic radiators, high-power, operating characts. 78—94469
- parametric acoustic sources of rectangular aperture, source level and beam pattern prediction 78—63219
- parametric antennas, review 80—102898
- parametric source aperture factors 77—841
- parametric sources, interaction of nonlinearity-limited spherical beams 80—43508
- parametric US radiator, saturation-limited operation 78—94467
- periodic line-supported plate, approx. theory for sound radiation 79—37080
- piezoceramic cylindrical transducer, increase of bandwidth via two transition layers 77—14871
- piezoceramic plates, tunable HF high-power radiator 79—18664
- piezoceramic tubes with capped or shielded ends, sensitivity above omnidirectional freq. range 78—1534
- piezoelectric, field homogeneity enhancement 77—68358
- piezoelectric polymer transducer, effect of acoustic radiation on equivalent circuit 79—94380
- piezoelectric radiator of longitudinal acoustic waves with an inhomogeneous elec. field 80—87693
- piezoelectric transducer, wedge-shaped ang. displacement of sound beam 77—35009
- pinger modification to transmit water temp. data 79—39895
- pipe walls, randomly vibrating, broadband sound-power radiation efficiency estimation 77—62104
- piston, in waveguide with elastic plates in walls, radiation efficiency 77—50850
- piston, operating in homogeneous layer, radiation impedance 80—87596
- piston radiator, extensions to theory 79—50478
- piston radiator, second harmonic generation 79—32123
- plane, near field anal. 77—31148
- plane sound sources, radiation pattern *(German)* 77—42639
- plane waveguide with one perforated wall, calc. of radiation characts. 80—102886
- plate, loss factor, influence of fluid flow vel. *(German)* 77—820
- plate radiation compensation at subcritical freqs., coupling of sound and vibr. fields 78—18110
- plate with water loading, US radiation due to Lamb waves *(Japanese)* 77—3690
- point source between thin elastic plates, fluid immersed, roots of dispersion relations 80—87601
- point-driven elastic plate, influence of shear, rotary inertia and longitudinal vibrs. on acoustic emission 80—5871
- power output, calc. by integrating energy flux over distant control surface 80—87587
- pulsating sphere in rectangular waveguide, field suppression 77—68287
- pulsed electron flux, acoustic waves generation, for nondestructive inspection 80—5905
- pulsed radiolysis acoustic wave generation in liquids 79—8446
- radiation impedance of infinite elliptical cyclinder in system of like radiators 80—102911
- randomly fluctuating sources on 2 coaxial rings, direct and inverse problems 80—33270
- rectangular panel in infinite baffle, acoustic impedance 79—94399
- rectangular plate complex mode vibration and sound radiation 78—83163
- rib-reinforced plate, point excited, acoustic radiation 77—80003
- ring source, fluctuating, with const. vel., power and freq. spectrum emitted 77—50796
- rotor blades, radiation characts. of acoustic sources in circular motion 77—23803
- scalar wave source in compliant baffle, impulse response function 79—50481
- short column vibrator, apparent elasticity analysis and applications 78—59242
- sonar synthetic-aperture systems, characts. and comparison with nonsynthetic-aperture systems 77—62092

acoustic radiators continued

- sound fields from vibrating bodies, calculation *(Japanese)* 80—48493
- spherical and ellipsoidal Huygens surfaces, discrete approx. for suppression of sound fields 80—87594
- spherical source near scattering sphere, radiation characts. 77—7228
- spherical sources of finite size, acoustic coupling 77—79982
- strip radiator, power output considerations 80—69577
- strip-shaped baffled flat sources, near and farfield calcs. 79—50475
- superdirective spherical radiator, max. directivity conditions 77—84019
- supersonic motion with variable accel., interaction of acoustic multipoles 77—815
- surface, rheological behaviour of liquid 79—94573
- thermal sources, sound generation 77—34977
- thin beam-reinforced plates and shells, wideband sound radiation 79—18581
- thin cylindrical shell, point-driven, with rigid massive septa, sound radiation 77—803
- three dimensional acoustic radiation, problems, boundary integral solns. 79—3818
- three-layer structure, axisymmetrically driven, acoustic radiation 78—1507
- underwater data communication US standing-wave radiator 79—46104
- underwater horns, directivity 78—18138
- unflanged duct exit, high temp. effects on radiation impedance 77—84069
- US exponential solid horn, finite element analysis 78—94496
- velocity monopole source, power radiated under reverberant and freefield conditions 79—46107
- vibrating circular plate, freq. depend. of acoustic radiation *(Japanese)* 79—90070
- vibrating porous material surface sound radiation *(Japanese)* 79—68474
- Al plate excited by free turbulent jet, generation of vibrs. and atmospheric sound *(German)* 80—102908

acoustic reactance *see acoustic impedance*

acoustic receivers

see also microphones

- adaptive cross-sensor beam forming with planar arrays 78—18121
- array, 1.5 MHz 8-element 77—838
- coaxial circular spherical array for US imaging 78—9513
- controlling receivers, for active noise suppression in waveguide 78—5613
- electroacoustic transducers, experimental scheme for dynamic behaviour anal. 78—9518
- interdigital transducer, use as receiver in acoustic focusing device 78—9520
- medical ultrasonics, piezoelectric materials study 80—76819
- monopole arrays, continuous, active sound suppression 79—94386
- ocean acoustic background noise, detection of sinusoids 80—33347
- ocean mooring monitoring, acoustic phase tracking technique 78—30138
- optical fibre acoustic sensor 77—72119
- optimization of acoustic receiver noise performance 77—84097
- parametric acoustic receiving array vibration sensitivity anal. 78—66971
- piezoelectric, sensitivity determ. by impedance method 77—11104
- saturated parametric receiver, analysis 80—33386
- sonar, digital phase shift beamformer, design and implementation 79—1034
- sparse line array, cross-sensor beam forming 77—39126
- symmetric line array, source passive location, variance bounds 78—9480
- transducer-receiver configuration, flexible, activated by laser 80—83724
- underwater acoustic signals receiver, freq. shift arrival time determ. 79—3875
- underwater acoustic wave direction-finding by full-aperture beam forming delay line 80—48527
- underwater US image convertor optimal working frequency estimation *(Russian)* 78—30111
- US phase-insensitive receiver theory and CdS acoustoelectric convertor 79—47871
- vector acoustic receivers, calibration method *(Russian)* 77—46876

acoustic resistance *see acoustic impedance*

acoustic resonators

- 220 MHz acoustic bulk wave resonator and filter realisation 78—59245
- 300 MHz oscillators using SAW resonators and delay lines 78—59255
- ageing mechanisms 79—46161
- application in gas phase conc. meas. in flowing gas-liq. mixture 78—59448
- bar-shaped resonators excited electromechanically in flexural vibration, equiv. electric circuit 77—42677
- blood clotting characterisation by US digital fixed path interferometer 78—44670
- cavity, scalar Green's function, numerical calcs. using integral eqn. *(French)* 79—32110
- cavity normal modes and normal freqs., Green's function numerical study *(French)* 79—32111
- cell discrimination by US Gaussian resonator and lens 77—21587
- closed cavity, cylindrical, excitation of nonlinear acoustic resonances by unsteady heat input 79—41483
- combustion driven oscillators, plane wave theory anal. 80—102951
- complex cavities, reson. props. of violin-shaped and guitar-shaped cavities 77—50838
- composite bulk acoustic resonator properties and applications 77—27434
- concentric tube, with unpartitioned cavities, anal. 78—90587
- coupled SAW grating resonator filter synthesis 77—23821
- cylindrical, disc-type, acoustic performance 79—18657
- cylindrical piezoelec. transducer, influence on spectrum of natural freqs. 80—87694
- cylindrical wide tube with wall-mounted axisymm. resonators, sound attenuation 78—1460
- definition of quality factor, errors in Q from width of an input impedance peak 80—69572
- distributed, model for a two dimens. resonator 80—64275
- eccentric spherical cavity, calc. of acoustic resonant frequencies 78—90548
- elastic spherical shells, fluid-filled, isolation of resonant component in acoustic scattering 79—46106
- electromagnetic cavity resonator, excitation and detection of acoustic waves 80—33399
- electromechanical devices using thin Si diaphragms 78—13879
- externally coupled resonator-filter (ECRF), loss minimizing 79—41542
- filters with open end, finite element prediction of transmission characts. 80—33349
- finite-amplitude sound wave field resonator nonlinear losses 78—1469

acoustic resonators continued
flexural piezoelectric bimorph vibrator, spurious response suppression *(Japanese)* 78—59233
flexural-mode mechanical filter resonances 77—27435
flow-tone effects, forced oscillations of separated shear layer 80—64256
gas analyser design and performance 78—11603
gas turbine annular vortex shedding acoustic resonance analysis *(Japanese)* 80—14526
gravitational wave detection, low temp. antenna designs 77—17900
grooved reflective array SAW compressor and resonator performance 77—23820
hall reverberation time modification appls. *(Dutch)* 78—22227
heat exchanger tube bank duct acoustic resonances 78—90550
helical, technique for broadband tuning, MHz to GHz range 78—94502
Helmholtz resonance cells for dye laser excited optoacoustic spectroscopy 80—9048
Helmholtz resonance effect in photoacoustic cells 79—75602
Helmholtz resonator, considered as limit case of reson. tube, theoretical and expt. study *(French)* 80—53496
horizontal-shear surface wave grating resonators 78—59249
impacting oscills. simulation of resonator with vibrating wall *(Japanese)* 78—9483
influence of depth on acoustical props. 80—58838
jet driven Helmholtz oscillator, optimum parameters and operation 80—53600
multimode SAW resonators, optimum design 77—23823
NMR detector, autodyne, using FETs 79—17457
nomograms-aided calc., for pneumatic-acoustic automation appl. 77—11098
non-rectangular reverberation chambers, resonance freq. and eigenfunctions, calculation by finite element analysis 80—64324
nonlinear oscillation theory 78—50974
one-port SAW resonators using long IDTs and their application to narrow band filters 79—76934
open and closed end pipes, for teachers 78—81774
open tube, nonlinear oscillations 78—18091
photoacoustic cell design, reson. enhancement, background signals 78—4700
photoacoustic cell resonances from standard ultrahigh vacuum components 79—12862
piezoelectric plates with rectangular electrodes, two-dimensional energy trapping 77—27458
pipes, open ended, end corrects. determ. for fundamental reson. freq., material effects *(Korean)* 77—27443
portable monolithic IC sonar unit *(French)* 78—13868
pressure sensing SAW resonator 77—23850
PVF$_2$ film composite resonator for concave focusing US transducer 79—46155
quartz, electron irradiated, optical and anelastic absorptions and resonator freq. 78—64385
quartz plates, acoustic reson. vibr., Berg-Barrett X-ray diffr. method 80—40063
quartz rotated Y-cut crystal with two different electrodes 77—84098
quartz SAW resonator deep etching 78—59248
quartz SAW resonator tuning by shorted reflector opening 78—59246
rare earth-Fe rod, US resonance with large eddy currents 80—54933
rectangular cavity, two-dimens., acoustic modes, damping 77—31149
rectangular cavity in viscous gas flow, numerical anal. of acoustic resonance 79—64378
resonant oscills. in tube with jet inlet 78—59440
SAW, distributed-feedback, design, computer model and construction *(Flemish)* 80—5899
SAW, radiation losses formed by interdigital type reflectors 80—69603
SAW, VHF and UHF, Q-factors reflective array design, calc. method *(Dutch)* 77—34988
SAW, with interdigital transducers anal. rel. to electrode loading effect 78—9517
SAW delay line and resonator oscillators for phase locking 78—59254
SAW filter for radio receiver 79—7271
SAW grating cascades, bulk scatt. loss 77—46869
SAW grating resonators, modes 78—42498
SAW grating resonators, reflection-dependent coupling 77—23822
SAW interdigital transducer, inverse phase, suppression of direct transmission in resonator filters *(Chinese)* 78—79181
SAW quartz, two-port design 77—23819
SAW resonator cavities with unidirectional transducers 77—23849
SAW resonator coupling and multimode filter design 77—23824
SAW resonator filters, improved temp. stability using multiple coupling paths 80—19175
SAW resonator filters using tapered gratings 78—87224
SAW resonator filters with enhanced out-of-band rejection 80—19179
SAW resonator Q rel. to fabrication tolerances 77—27452
SAW resonator reflector and transducer characteristic effects 77—39168
SAW resonators, comparison of metal strip and waffle iron arrays 78—51030
SAW resonators, using long IDTs, coupled mode anal. 79—76933
SAW resonators on quartz, loss reduction and cavity maximizing 79—41543
SAW resonators using withdrawal weighted reflectors 80—19180
SAW two-port, terminal characts., S-matrix approach 77—23848
SAW two-port resonator using long interdigital transducers *(Japanese)* 78—33982
SAW X-ray topographical representation 79—47870
second-harmonic generation in resonator of multilayered interference filter type 80—58840
shallow bulk acoustic wave generation by interdigital transducers 79—51411
side-branch pipe resonators, flow-induced tones 80—64243
single side branch Helmholtz resonator in circular duct, air flow effects 77—79986
spherical, for temp. and thermophysical prop. meas. in dilute gases 80—53573
spherical cavities in viscoelastic materials, fluid-filled, determination of shear absorption 79—7239
steam means, Gentilly-I generating station, acoustic phenomena 78—89944
stepped pressure concentrator, anal. of reson. freq., gain, and press. distribs. under reson. and nonreson. conditions 78—90619
surface wave resonators, characts. from Fabry-Perot cavity anal. 77—39131

acoustic resonators continued
teaching demonstration using eddy currents from Fisher burner 78—28902
tetrahedral, exact soln. of natural mode problems 80—64248
trapped-energy ceramic resonator with improved response characts. *(Japanese)* 78—9522
tunable variable bandwidth/frequency SAW resonator 78—59247
US cell, new design for millilitre liquid samples 78—87213
US confocal resonators, for vel. meas. in freq. range 20 to 1000 kHz 77—14867
US spectrum, RF field in multidomain struct. 78—68056
variational soln. using field-source reaction concept 79—55302
vibrational combustion parameters rel. to resonator impedance *(Russian)* 77—9082
violin cavity, reson. modified by He or CO$_2$, for teachers 79—35484
viscosimeter technique for shear viscosity meas. 77—958
voltage-controlled SAW resonator oscillators 77—27450
CO$_2$ pulse-periodic laser, gas stream gasdynamic perturbations, acoustic waves 79—94208
LiNbO$_3$ hypersonic wave absorption, attenuation temp. depend. 78—18710
$Sr_xPb_{1-x}(Zr_{0.545}Ti_{0.455})O_3$, piezoelec. resonator, preparation and props. *(Rumanian)* 80—28402
ZnO, film, SAW resonators 78—83199

acoustic streaming
air, sound wave propag. *(French)* 79—59858
boundary layer of viscous heat cond. medium, acoustic streaming 79—86544
drop evaporation rate in forced convective flow with transverse sound fields 78—51224
droplet-laden gas, acoustic streaming rel. to high-intensity sound attenuation 77—62082
dynamic characts. in field of acoustic dipole 78—50973
Eckart flow in conducting liq. or gas, acoustoelectric current prod. 79—27707
fluids, enhancement of absorption coeff. of acoustic waves due to acoustic streaming 78—9471
gas bubbles, influence of microstreaming on growth due to rectified diffusion 78—51232
ideal incompressible liquid, streaming generated by oscillations of a sphere 77—31412
intravascular thrombus induction in vivo using localised hydrodynamic shear stresses 80—97997
liquid oscillations, steady streaming over infinite plate 80—19125
MBBA nematic liquid crystals excited by 20 MHz US surface waves 80—76003
melts of transparent organic substance simulating metals 80—5861
multidimensional, numerical anal. 77—962
nematic liquid cryst., acousto-optic effect, acoustic streaming 80—88964
nematic liquid cryst., response to acoustic field, streaming component and instability 80—80747
nematic liquid crystal acoustic image detector, resolution expt. 78—46871
nematic liquid crystals, acoustically induced birefringence 78—38126
nonsteady quasi-one-dimensional acoustic streaming in unbounded volumes with hydrodynamic nonlinearity 80—87611
pipe flow with high viscosity, acoustical streaming and thermal effects 77—15122
plant tissue acoustic microstreaming induced by Doppler foetal heart detector 79—62292
review, nature and modern developments 79—37079
solid spheres in oscill. fluids, mass transfer review 77—42902
US absorpt. in liquid containing gas bubbles 80—5863
US perturbation obs. at cellular level 78—61214
viscous fluid, self-defocusing of sound beam 77—14833
Hg, acoustic streaming meas. 79—64380

acoustic superradiance
acoustors, superadiationless phase transition, theory and expt. detect. *(Russian)* 78—71805
crystals with paraelectric impurities, superradiative transitions, acoustic and EM excitation 78—66872
octupole and hexadecapole dynamics in solid state physics, algebraic struct. 77—88682
phonon avalanche, and propagation effects 79—69195
phonon-type superradiative phase transition *(Russian)* 77—27961
quantum theory, one-dimensional solid 78—10128
ruby, spin level population inversion, coherent phonon amplification and generation *(Russian)* 77—24364
KCl:Li$^+$, coherent excitation by EM and acoustic waves, induction and echo signal study 78—67773
KCl:OH$^-$ type dipole-phonon system, superradiative phase transition *(Russian)* 78—71806

acoustic surface wave devices *see surface acoustic wave devices*

acoustic surface waves *see surface acoustic waves*

acoustic transducers
see also acoustoelectric transducers; ultrasonic transducers
acoustical imaging, US visualization and characterization, conf., vol.8, Key Biscayne, FL, USA (May-June 1978) 80—83720
acousto-optic deflector, anal. and design of flat transducer array 79—18527
acousto-optic sensor development 80—14542
acousto-optic transduction used in optical hydrophones 80—14541
amplitude and phase statistical dispersion 77—68357
apodized ID transducers in wedges, radiation conductance 78—38164
array directional response anal., model 78—66973
arrays, numerical calc. method for acoustic interaction *(Japanese)* 78—9521
backscattering formula 80—96064
baffled piston transducer, analytical model for nearfield 80—96168
boundary layer acoustic monitor for hypersonic turbulence transition determ. 78—34237
broadband constant beamwidth, theoretical new approach 78—90616
broadband piezoelectric transducer design 78—51029
broadband probe, for studies of acoustic surfaces waves 78—23904
bulk acoustic wave devices employing interdigital transducers 77—23841
bulk acousto-optic interactions in thin film waveguides, for GHz modulators 78—42471
bulk-wave, field distributions for surface-skimming 79—64472
calibration *(Czech)* 80—106697

acoustic transducers continued
- capacitance transducer, calibrated, for detection of acoustic emission 78—71256
- capacitive, appl. to sound vel. measurements in TTF-TCNQ 79—72775
- ceramic, for transient acoustic pulses generation in water 78—1483
- circular, piston, maximum sound pressure available when displacement limited 79—81676
- combustion driven oscillators, plane wave theory anal. 80—102951
- condenser electret transducer design principle 78—59231
- curved face parametric projector for marine sediment penetration 78—51032
- detector for beta and gamma radiation *(German)* 79—63876
- edge-bonded surface-acoustic-wave transducer array 80—1395
- efficiency measurement using self-reciprocity techniques 80—58881
- electroacoustic transducer on 90° ferroelec. domain struct. theory 80—43585
- electrodynamic drivers, monotone performance optimisation using tubular couplers 77—7279
- electromechanical, constructed from MOS movable-gate-field-effect struct. 79—1043
- element factor for periodic transducers, analytical results 80—43493
- EM-acoustic transducer as elastic-wave ellipsometer for meas. of material property variations 79—46143
- emission detection system sensitivity, direct comparison method 78—56848
- emission transducer calibration temperature sensitivity checking technique 78—18144
- emission transducer construction principles evaluated 78—59239
- equivalent cct. parameters calc. for radially polarised piezoceramic sphere 80—14538
- fibre optic acoustic sensors with composite structure, analysis 80—19087
- fibre optic acoustical detector probe 80—91916
- flextensional, in LF wide-band high-power sound source 79—3883
- flextensional transducer design trends 80—43588
- flow noise, rejection using coherence function method 77—84067
- flowmeters, multiple and single path, sources of error, accuracy, appls. 79—94749
- focusing, study of parametric radiation *(French)* 79—41486
- grating and meander-line transducers for magnetoelastic surface-wave excitation, comparison 79—50557
- HF piezoceramic array, acoustical decoupling characts. of onionskin paper backing material 79—81675
- imaging, visualization and characterization, conf., Houston, TX, USA (Dec. 1979) 80—106672
- impedance transducer, for in situ meas. of marine sediments 78—9519
- impulse response modelling of SAW transducers 79—81665
- industrial sound meas., transducer function, basic theory *(German)* 77—80037
- interdigital transducer, in acoustic focusing device 78—9520
- interdigital transducer for acoustic imaging 77—80020
- interdigital transducer for Lamb wave devices for AM, influence of electrical termination 79—41549
- interdigital transducer in layered anisotropic semiconducting struct., elec. input admittance matching 78—22238
- interdigital transducers, bulk wave generation near SAW reson. in $LiNbO_3$ 80—33402
- interferometric acoustic sensor, single optical fibre 78—38161
- intermetallic compound, $TbFe_2$ elastic modulus magnetic field dependence 80—87698
- J-9 underwater sound projector, freq. response in typical experimental tank 79—50556
- jet position transducer, experimental investigation of noise characts. 79—37103
- laminated first-order transducers, acoustomechanical characts. 80—14537
- laser-activated transducer-receiver, flexible configuration 80—83724
- level transducers resistor type, coupled with AC supply amplifier systems, theoretical and experimental behaviour *(Italian)* 80—79051
- line hydrophone array, low-freq. technique for underwater calibration of individual elements 77—79997
- LMFBR steam generator, acoustic detection of small leak Na-water reaction 78—29589
- magnetostrictive sonar transducer, hollow spherical scatterer effects on radiation resistance at air-water surface 77—39125
- magnetostrictive underwater sound transducers, use of rare earth alloys 80—19204
- medical US, linear-filter model for signal transmission process 80—17026
- mutual interaction of nearest neighbours in compact planar array 78—50979
- narrow-strip transducer, radiation pattern theory 80—96165
- noise and vibration meas. methods *(German)* 77—42670
- nonlinear effects in vicinity of HF transducer 80—38152
- ocean current sensors, performance assessment 79—25345
- optical fibre bending loss modulation sensor, multimode 79—50564
- parametric acoustic arrays, historical background and theory 78—5621
- parametric antenna radiation, approx. soln. *(French)* 77—42680
- piezoactive complex vibratory systems, matrices of parameters for six-pole equivalent circuits 77—68304
- piezoceramic cell, fluid-filled, response to pressure generated by axial laser pulse 79—72746
- piezoceramic tubes with capped or shielded ends, sensitivity above omnidirectional freq. range 78—1534
- piezoelectric transducer, composite, of low freq. acoustic flaw detector, natural freq. calc. 80—89450
- plane discrete, array with interacting elements, statistical parameters 77—34993
- plate terminated by liquid, transfer constant and input impedance ang. depend. 77—11103
- pneumatic-acoustic automation appl., nomograms-aided resonator calc. 77—11098
- pneumoacoustic, amplitude meas. for linear dimens. control 79—17387
- polyvinylidene fluoride transducers, underwater acoustic meas. 79—14184
- pulse echo method for acoustic vel. meas., transducer effect 77—42676
- quadrature 3 phase unidirectional transducer 79—81672
- rare earth iron magnetostrictive underwater sound transducer 78—13881
- reciprocity calibration in unconventional acoustic geometries 78—83200
- SAW, frequency band broadening of phase shifters 78—55532
- SAW, withdrawal weighting combined with series sections weighting 79—81666
- SAW bandpass filter design, approx. parameter anal. *(Russian)* 80—23858
- SAW broad-band filters, tap weight enhancement 78—22239

acoustic transducers continued
- SAW filters, fundamentals of design, interdigital transducer circuit model, book contrib. 79—50520
- SAW generation in crysts. with high dielec. const. 78—83203
- SAW interdigital transducer, inverse phase, suppression of direct transmission in resonator filters *(Chinese)* 78—79181
- sonar, towed type, portable, for ocean acoustic meas., features 78—69550
- sonar transducer arrays, amplitude shading for interference rejection 77—62094
- sonar transducer arrays, image prod., signal processing methods comparison 78—18122
- standing-wave tube, use as an absolute sound power source in reverberation chambers 79—81674
- steel, acoustoelastic stress field imaging technique, stress field contour plots 79—77033
- surface barrier volume wave transducer 80—33403
- surface wave, very narrow aperture, acoustic diffr. effects 78—22240
- testing, using high-power DUMILOAD device 77—3707
- three-phase interdigital transducer for acoustic imaging in fluids 79—72774
- torsional vibrators, design by computer optimisation *(Japanese)* 80—33405
- transformations in acoustical transduction based on optical principles 80—53594
- turbulent boundary layers, freq.-wave-vector spectrum determ. using acoustic transducer 78—38430
- underwater cylindrical piezoceramic transducer, increase of bandwidth via two transition layers 77—14871
- underwater transducers, bandwidth extension by FM signal correl. methods 77—62086
- underwater transducers, gain characts. meas. by FM signal modulated by smoothed random telegraph signal 78—18130
- underwater transducers, nearfield measurement system for computing farfield radiation characts. 80—10101
- underwater transducers materials, suitability of polyvinylidene fluoride 78—1531
- unidirectional, group type, tuning method 79—68535
- unidirectional focusing device with group of three electrodes 80—10104
- US impulse thickness gauges, comparison of three element and single element transducers 78—72988
- vibration pickup on soil surfaces, horizontal resonant freqs. 80—10102
- Al, acoustoelastic stress field imaging technique, stress field contour plots 79—77033
- Cu-NbTi, composite conductor, acoustic emission 80—97032
- R-Fe octagonal transducer 80—74684
- Ga and alloy high-temp. couplants 79—14195
- $KTaO_3$, light-sensitive surface-barrier generation of acoustic vol. waves 78—63252
- $LiNbO_3$ SAW devices, SAW and bulk wave propag., freq. shift holography *(Japanese)* 79—59895
- $LiNbO_3$ X-cut plate shear transducer, direction of displacement 78—51031
- $Pb(Zr,Ti)O_3$ ceramic, interconnected porous, props. 80—43579
- Si-PVF_2 integrated acoustic transducer arrays 80—74683

acoustic variables control
- *see also noise abatement*
- domestic noise control and measurement *(Spanish)* 80—1380
- petro-chemical industrial plants, piping networks, noise abatement 80—28381

acoustic variables measurement
- *see also acoustic intensity measurement; acoustic noise measurement; acoustic wave velocity measurement; Q-factor measurement; ultrasonic measurement*
- absorption coeff. in situ meas. by correlation technique 77—27444
- absorption in rooms 77—39161
- acoustic characteristics of flow through duct systems, transfer function technique 79—18650
- acoustic coupling between rooms, meas. system using decrease in sound level method *(French)* 80—69611
- acoustic emission rate, combined deformation/heating stage, for SEM 80—101892
- acoustic emissions, meas. at high temp. and press. by wide-band optical-mechanical system 78—1525
- acoustic reflex adaptation in humans 79—2082
- acoustics, time delay estimation in presence of source or receiver motion 77—88977
- active-impedance termination method using travelling-wave equipment, error estimation 79—94429
- aeroacoustic measuring techniques in or outside turbulent flows 80—53534
- amplitude calc. method for reflection from rigid spherical body *(Japanese)* 77—50791
- amplitude variations in compact cassette tape recorders, measuring set with oscilloscope display *(German)* 79—32156
- architectural acoustics measurements by impulsive excitation *(Japanese)* 80—64292
- attenuation of hearing protectors, meas. by real-ear threshold-shift method, standardised tests 78—1508
- audiometric impedance meas. instrumentation 77—78005
- auditory system, pitch of amplitude-modulated low-pass noise and predictions by temporal and spectral theories 80—67095
- automatic reverberation time meas. 79—68518
- automobile development appl. *(German)* 78—87219
- automobile exhaust systems, measurement of acoustic parameters 80—53591
- brass instruments, acoustic impedance meas. apparatus 78—1518
- broadcasting studio, 'Deutsche Welle' building construction and meas. *(German)* 80—106668
- building acoustics, history of meas. in America (1920-1940) 77—45663
- chamber reverberation time, holographic meas. 79—68519
- combustion process admittance measurement, acoustic impedance tube technique 80—64320
- concert halls acoustics, spatial impression, lateral refls., musical level *(German)* 78—79164
- concert-hall acoustics, multidimensional description of subjective judgement *(German)* 77—72117
- conductor, acoustic band investig. by obs. of weak sound signal absorpt. *(Russian)* 77—75733
- correction of near-field acoustic meas. using arbitrary meas. transducers 78—66996

acoustic variables measurement continued
- correlation coeffs. of sound pressure in rectangular reverberant room 79–76914
- coupling device for transfer characteristics measurement, earphones, hearing aids appl. *(German)* 77–75756
- cultural centre reconstruction, acoustic tasks and measurements *(Hungarian)* 80–106666
- direction location of infrasound waves, meas. on jet planes *(German)* 80–92000
- directive spectral analysing system using moving microphone *(Japanese)* 80–33348
- directivity of loudspeaker and subjective hearing event *(German)* 78–79174
- directivity pattern, near-field press. meas. on surface of finite circular cylinder, arbitrarily-shaped acoustic radiators 80–87677
- ear static acoustic-immittance measurements 80–76758
- earphones, reference equivalent threshold sound pressure levels, audiometric zero 79–3872
- elastic vibrations parameters evaluation *(Russian)* 80–38181
- electret condenser microphones, design for meas. purposes 80–79086
- enclosure, 2-dimens., stationary sound field, continuous obs. *(Japanese)* 79–32143
- evaluation instrumentation, Bruel-Kjaer Co. *(Russian)* 80–1390
- exhaust of IC engine, acoustic characts. meas. 77–837
- floors, structure-borne sound meas., problems of impact testing *(German)* 77–825
- fluid machinery manifold impedance meas. 78–42501
- Gentilly-1 steam mains, hydrodynamic oscills., acoustic anal. 79–97771
- geophysical structure estimation from acoustic reflection meas. 78–7818
- Gulyaev-Bleustein and Rayleigh wave reflection , rel. to signal processing appl. 77–80028
- HF SAW phase/amplitude meas. using phase sensitive laser probe 79–14171
- history of acoustical measurements and instrumentation, historical review 77–45666
- holograms of acoustic field, moire processing 78–55539
- HP3582A spectrum analyser using digital signal processing 80–43567
- hydrophone quartz transducer stability analysis 77–11102
- impedance, sine sweep excitation and known vol. vel. method 79–3869
- impedance meas. instrument, for ear characteristics meas. *(Hungarian)* 78–36012
- impedance meter, middle ear, deafness diagnosis appl. 77–25460
- impedance of a black box, fixed position press. meas. 78–1523
- impedance of a black box at low freqs. using shorter impedance tube 78–1522
- impedance of marine sediments, in situ meas. method 78–9519
- impulse noise assessment, evaluation of C-weighted L_{dn} 77–84068
- impulse response meas. of acoustic transmission system, digiral computer processing *(German)* 80–91999
- impulse response of acoustically absorbent materials *(French)* 79–1033
- infrasound, investigations into measurement and analysis, development of measuring system *(German)* 79–50541
- interior acoustics CAD *(Polish)* 78–59205
- Karl-Marx-Stadt, great hall, small hall, sound absorption of furnishings *(German)* 77–58509
- lake surface reverberation, statistical props. 79–1020
- laser interferometer, acoustic vibration meas. 78–71253
- laser velocimeter, directional non-contact meas. of press. level, spectral components and noise 77–834
- lateral, phantom sources generated by two loudspeakers, localisation 77–54849
- LF coherent underwater transmission range meas. system, portable 77–88976
- LMFBR, acoustic surveillance of anomalous events 78–37397
- LMFBR, boiling stability tests on THORS Na loop 78–37396
- LMFBR core simulation, Na loop safety facility, P2 expt., LOCA, acoustic meas. 78–33264
- loudspeaker, frequency response measurment in echo chamber *(German)* 77–75762
- loudspeaker driver parameters, time domain measurement implemented with digital computer 79–59901
- loudspeaker measurement, by application of digital techniques 77–68345
- loudspeaker signal displacement meas., optical method 78–51023
- loudspeaker testing limitations *(German)* 79–37105
- M-sequence modulated acoustic signal propagation meas. *(Japanese)* 78–18132
- manual and Bekesy thresholds, noise-exposed subjects, test-retest reliability 80–81622
- motion picture theatres, acoustic response measurements and standards 77–19496
- muffler characts., acoustic impulse technique 78–59217
- multidelay system coherence function meas. 79–68530
- multidimensional audio, meas. and hearing sound quality 79–64458
- multiplier unit for acoustic and electronic wattmeters 77–79118
- musical sounds, digital meter for tonal error meas. *(German)* 77–830
- nearfield array for use in acoustic backscattering cross section meas. 77–14862
- noise generation by control equipment, steam power, chemical, petrochemical industries appl. 78–51002
- noise source investigation, anechoic, reverberation rooms, industrial acoustic problems appl. 77–75742
- nonlinearity coefficient in benzene and toluene, interferometric meas. *(French)* 77–1175
- optical determ. of low US powers of circular piston transducers 80–64319
- n-paraffins, generalised eqn. of state from acoustical meas. 78–51642
- pitch, detection probability of continuous signal parameter change evoking blurred change 80–41055
- pitch, new contour display in connection with sound spectra *(German)* 77–833
- pitch, poststimulatory pitch shifts for pure tones 80–97934
- pitch and intensity changes, dynamic approach to perception 80–33378
- pitch estimation algorithm for speech and music 79–14173
- pitch extraction method based on peak detection and AMDF *(Korean)* 80–102935
- pitch of noise signals, evidence for central spectrum 77–36942
- pitch of vibrato tones 80–35911
- polarisation of acoustic waves in quartz rod, electrodynamic meas. method *(Russian)* 77–75764
- power, use of semiconductor strain gauges, US medical probes 80–87679

acoustic variables measurement continued
- power of plane sound waves, method and apparatus *(Polish)* 80–79087
- power response of loudspeakers using monitor 80–87674
- pseudo-continuous-wave monitor for measuring acoustic props. of substances 79–68525
- pulsating gas flow, aeroacoustic charact. eval. method 79–46141
- pulsed acoustic sinusoids generated with phased-array speakers, transient free 77–54847
- radiation fields, complex values of pressures on two concentric spheres 80–96161
- Rayleigh disc in aligned nematic liquid crystal for acoustic field detect. 77–11094
- re-entry vehicle acoustic/vibration environment expt. 78–20620
- re-entry vehicle flight tests, boundary layer acoustic meas. 78–16275
- reference equivalent, phonetic test to subjective meas. *(Polish)* 79–98572
- reference sound sources, characts. and calibration 78–9515
- reflection coefficient in liquid layer, error of interference methods 77–14865
- reflection from obstructions in pipes with flow, meas. method 78–63246
- reflex meas., esitmate of freq. selectivity of human auditory system 79–83797
- regenerative sound system investigation using time-delay spectrometry 78–51006
- reproduced sound in rooms, standards of measurement, computational procedure 77–54844
- reverberation house construction, acoustic power meas. appl. *(German)* 78–51024
- reverberation room sound absorpt. meas. precision assessment 78–59210
- reverberation time meas. using digital freq. analyser 77–80033
- reverberation time meter *(Japanese)* 79–37100
- RF vibr. crystals, inverse problem of Mossbauer spectroscopy 79–37081
- room acoustics analyser using public telephone line and computer 77–35004
- room resonance measurement techniques *(German)* 80–53586
- SAW diffraction effects from very narrow surface transducers 78–22240
- shallow water horizontal spatial coherence meas. 78–5605
- shear waves polarisation meas., optical method 77–35006
- short-range propagation, coherency recovery by pilot signal *(Japanese)* 80–53499
- signal form distortion, in absorptive medium *(Russian)* 78–46856
- signal mean frequency meas. *(Russian)* 78–81441
- signal rate of change distribution, gramophone player 80–79083
- small-chamber method applied to investigations of sound-absorbing systems at high sound pressure levels 78–94497
- solutions in alcohols, ultrasonic vel. and density meas. used to calc. compressibility, intermol. free length and salvation no. 80–96150
- sonometry, sound audibility, serial noise from machines and equipment *(French)* 77–21537
- sound absorption of rooms, using reference sound source 77–62109
- sound attenuation by barriers, estimation via calculating charts *(Japanese)* 78–30126
- sound detection, fibre-optic technique 78–13871
- sound level, decibel unit, definition and eqns. *(Italian)* 79–9201
- sound pressure in insert earphone couplers and real ears 78–65152
- sound source location in wind tunnel, using acoustic mirror 78–30372
- source location techniques, comparison of acoustic telescope and polar correlation 79–37098
- speech synthesis from vocal tract area function acoustical measurements 79–64446
- standing sound waves, particle vel. detect. via hot wire anemometer 77–62124
- stereophony, artificial head, tone meas. *(German)* 80–106702
- surface acoustic impedance, meas. technique for oblique incidence angles of 10-160 kHz 77–54848
- system matrix parameter determ., transient test principles 79–68527
- system matrix parameter determ., transient test results 79–68528
- target identification through parameter estimation and imagery by interferometric methods *(French)* 79–41539
- time-delay spectrometry, practical appl. in field 80–79082
- transfer characteristics, acoustic systems with long reverberation, narrowband digital signal processing *(Japanese)* 80–64304
- transient recorders for acoustic emission studies 80–83717
- two microphone random excitation technique to determ. acoustic props. in a tube 77–62118
- tyre noise, meas. and anal. technique 78–33969
- underwater acoustic measurements, appl. of FM signal modulated by smoothed random telegraph signal 78–18130
- underwater explosions, scaling law for shock waves 77–14838
- underwater sound, ambient sea noise directionality meas. and processing techniques 78–16025
- underwater sound, array shape measurement using active/passive acoustic techniques 80–23824
- underwater sound arrival angle estimation by multiple cross-correlation meas. 78–66978
- US energy density meas. in liquids *(Polish)* 78–5617
- US transducer directivity, semi-automatic meas. 77–84102
- US transducer power output meas. using modulated radiation pressure 78–59230
- US transducer vibration amplitude distrib. meas. by holographic technique *(Japanese)* 77–88999
- USA National Measurement System 78–38102
- violin sound post, mechanical admittance meas. rel. to post action 77–23833
- vocal pitch extraction and visual display using computer 77–52807
- voice frequency meas. using fast freq. meter *(German)* 78–3518

acoustic velocity *see acoustic wave velocity*

acoustic wave absorption
- *see also noise abatement; ultrasonic absorption*
- absorption coeff. in situ meas. by correlation technique 77–27444
- acoustic liner, interaction with incident sound 79–81857
- active, broad-band, duct carrying uniformly flowing fluid 80–74556
- active, Huygens principle, free space, waveguide with uniform flow examples, mathematical treatment *(French)* 77–42644
- active absorption via first order eqns. of acoustics, use of distribs. *(French)* 79–90045
- active sound absorpt. for high atten. at low freqs. 77–84023
- active sound attenuation, secondary sources *(French)* 79–90044
- admittance figure approach to processing acoustic interferometry meas. 79–50539

acoustic wave absorption continued
- air, absorption in 10-100 kHz range, NPL report 77—7239
- air-to-ground propag., effects of temp., humidity gradients 79—1019
- air-water fogs, audible sound propag. 78—1473
- air-water two phase medium, acoustic velocity and attenuation meas. 77—58513
- airborne sound, damping by laminated building components *(German)* 80—102877
- aircraft noise, excess attenuation of high freq. 78—33939
- anisotropic sound energy flow effects in reverberation room plane absorber meas. precision 78—55482
- antiferromagnet, low temp., absorption of sound 79—69711
- antiferromagnet, sound damping by phonon-magnon interaction, high Neel temp. *(Russian)* 78—43626
- antiphase signal for sound attenuation in ducts, expt. 77—31168
- architectural acoustics, sound transmission between absorbing parallel planes 80—33344
- architectural acoustics 80—64288
- atmosphere, nonlinear absorpt. of sound in problems of acoustic and radio acoustic exploration *(Russian)* 80—94567
- atmosphere, sound attenuation through interaction with internal gravity waves *(Russian)* 77—3693
- atmospheric, 10 to 10^5 Hz 80—53531
- atmospheric absorpt. of wave train producing freq. shift 80—64255
- attenuation, and propag. speed, of elastic waves in materials under uniaxial static compression, installation for determ. 80—21233
- attenuation by absorptive barriers *(Japanese)* 78—59198
- attenuation coeffs. of acoustic normal modes in shallow water 77—86932
- attenuation in lined ducts, theory for splitter type silencers 77—23801
- axisymmetric transmission system with sound absorbing wall, finite element anal. 77—88974
- backscattering, cross section for an absorbent sphere 80—64236
- baffle, composite compliant, response to mech. and acoustical vibrs. 79—10421
- baffles, effectiveness against flexural wave noise 79—90069
- baffles in closed spaces, dependence of effectiveness on nature of closed space, economic and annoyance factors 80—67019
- bands of noise, influence of atmospheric absorption on propag. 79—98524
- barriers, sound attenuation estimation via calculating charts *(Japanese)* 78—30126
- beamlike dynamic vibration absorbers, anal. 80—53539
- Berea sandstone, effects of pore fluids on bulk and shear attenuation 80—51386
- binary mixture, high-frequency sound absorpt. near crit. separation point 78—83881
- Boltzmann-Enskog equation, nonlinear, acoustical approx. for elastic sphere system 78—41252
- borosilicate glass, EM wave effects on acoustic absorpt. at low temp. 77—47866
- during brittle-plastic transition, theory 79—27595
- bubbly liquid, acoustical cross sections rel. to bubble-size spectra determs. 78—9735
- building insulation meas. dependence on type of loudspeaker *(German)* 78—75021
- building materials, noise abatement appl. 77—23808
- cellulose solutions, acoustic relax. mechanisms *(Russian)* 79—90733
- ceramics containing volatiles, mechanisms for attenuation 80—74560
- circular ducts, effect of expansion chamber 78—55485
- circular flow ducts, broadband noise atten. spectra, measured and predicted 78—63237
- circular lined ducts, nonlinear attenuation 79—23118
- clouds and fog, sound attenuation obs. 77—34981
- cocktail parties, importance of ceiling and wall sound absorpt. 77—80008
- coefficient, locally reacting patch of arbitrary shape 80—79049
- combustion duct, attenuation by fuel droplets and soot particles 80—74549
- complex elasticity of crystals, small variations meas. by acousto-optical method 79—3867
- compressional wave attenuation in deep ocean sediments 80—79033
- concert hall, musical instruments directivity rel. to efficiency of acoust. refl. or absorpt. *(German)* 77—829
- conductor, acoustic band investig. by obs. of weak sound signal absorpt. *(Russian)* 77—75733
- conductors, quantum acoustic bleaching, acoustic zones 80—70324
- confined beam in viscous medium, sound field and energy losses near beam boundary 78—18092
- constrained viscoelastic damping composites, FEM analysis 80—83743
- corrugated surface, effective absorption coeff. 79—32119
- cosmic ray detection, acoustic radiation by charged atomic particles in liquids, theoretical anal. 79—89526
- coupling of finite element acoustic absorption models 80—53497
- covered panels, sound insulation characteristics of panels having porous material coverings *(Japanese)* 80—33334
- critical binary mixtures, sound propag., mode coupling theory, validity breakdown 80—65159
- crystals with Jahn-Teller centres, sound absorpt. 79—37765
- cylindrical duct with impedance walls, attenuation calc. 78—83146
- cylindrical wide tube with wall-mounted axisymm. resonators, sound attenuation 78—1460
- damping, fluid induced, in refrigeration machinery manifolds 78—83164
- decay rate of sound in a reverberation chamber versus humidity and temperature 79—50473
- deep ocean LF attenuation data review 80—33318
- defect structure near phase transition pt., effect on solid props. *(Russian)* 79—37838
- degenerate semiconductor, nonparabolic, acoustic wave absorption/amplification coefficient 78—64069
- dielectric solids, acoustic wave propagation, phonon relax. time 80—44263
- dilute magnetic alloys, electron sound absorpt., disordered mag. impurities, spin glasses *(Russian)* 80—80503
- dimensioning of facings for acoustically effective structural elements *(German)* 80—74600
- discontinuous waves in nonlinear media, form. and attenuation 78—5601
- dissipative mufflers with locally reactive lining, modelling 78—13849
- domestic roofing sound insulation, expt. facilities of meas. laboratory, test details 80—79058
- double layer grating of hollow elastic bars, plane wave diffr. 79—86278
- double walls, influence of cavity-volume damping on air layers stiffness *(German)* 77—80016

acoustic wave absorption continued
- double walls, sound transmission loss and cavity absorbent materials *(Japanese)* 78—79167
- duct, air conditioning, active sound absorpt. 78—90555
- ducts, attenuation of lined plenum chambers, meas. and theory 79—81625
- ear protection systems, attenuation produced at each normal freq., Noise Reduction Rating calc. *(Spanish)* 80—109041
- elastic floor coverings, effect of thickness and hardness on impact sound insulation props. *(Japanese)* 80—79053
- electron sound absorpt. coeff. Fermi surface local geometry changes *(Russian)* 80—15437
- elliptical pipes, acoustic insulation *(German)* 80—28376
- enclosure, thermoviscous dissipation at walls, normal mode theory 78—83171
- equivalent absorpt. area of room in steady-state condition and reverberation *(German)* 80—102931
- expansion chamber mufflers, optimisation of silencing characteristics and positioning *(Japanese)* 80—33333
- experiment in classroom 80—42016
- explosion waves, atmospheric attenuation 77—31155
- felt sound absorption rel. to airflow resistance, obs. 77—58506
- Fermi surface local flattening effect of acoustic wave absorpt. and dispersion *(Russian)* 79—51471
- ferrodielectric, sound absorption due to interaction with magnons *(Russian)* 77—69663
- ferrodielectric, sound wave damping, due to phonon-magnon interactions 77—36107
- ferroelectric, acoustic props., at second-order phase transition, effect of polarisation fluctuations 77—85664
- ferromagnets and antiferromagnets, EM and acoustic energy attenuation in many-domain magnets 80—7140
- fibrous absorber, model theory for regular fibre arrangements *(German)* 77—801
- fibrous absorber, theory for elementary cells model, and numerical results *(German)* 77—802
- fibrous materials, comparison between expt. and theoretical sound absorpt. props. 80—28378
- finite sound absorbing panels, edge phenomena 77—27425
- flass, phonon avalanches, exptl. conditions for obs. 78—71822
- flexural wave transmission across line inhomogeneity on plate in liquid 80—38159
- floor coverings, impact noise reduction expts. *(Japanese)* 80—33331
- floor sound insulation, analysis using L_C and L_A *(Japanese)* 80—79054
- fluids, enhancement of absorption coeff. of acoustic waves due to acoustic streaming 78—9471
- fluids, one and two dimensional, hydrodynamics, viscosity, heat conductivity, kinetics *(Russian)* 80—79972
- foliage as low-pass filter, expts. with model forests in anechoic chamber 80—33303
- Franz-type wave, rel. and attenuation, generation on outside of solid cylinders in water *(French)* 80—28370
- fresh water, absorpt. rel. to operating freq. choice for miniature transmitters 77—54826
- Fresnel integrals for calculating sound reduction of absorbing screens 80—53494
- furnishings, Karl-Marx-Stadt, great hall, small hall, reverberation *(German)* 77—58509
- gas mixture, modified rough sphere model, rel. to sound absorpt. 78—93597
- gas-bearing sediments, eqns. based on model of resonating gas bubbles 80—87630
- gas-bearing sediments, eqns. based on model of resonating gas bubbles 80—87670
- gas-vapour droplets, nonuniform mixture, acoustic wave attenuation 78—83154
- gases, liquids and solids, relationship with props., research during past 50 years, review 80—96089
- geographic variation contour chart for Atlantic, Indian and Pacific Oceans 80—36303
- geophysical acoustic logging, signals limited spectrum rel. to time interval and damping determ. accuracy *(Russian)* 79—39971
- glass isolating panes, influence of gas filling on sound isolation *(German)* 77—80017
- graphite, giant quantum attenuation of sound waves 80—54741
- hearing protector attenuation of random noise, testing 77—46866
- heavily doped compensated piezoelectric semiconductor, sound absorpt. coeff. calc. *(Russian)* 79—15194
- n-heptane-nitrobenzene, critical fluid, ratio of sound dispersion to attenuation 79—55826
- high-intensity sound, attenuation in droplet-laden gas 77—62082
- high-Q materials, measurement of HF losses using Fabry-Perot acoustic interferometer 80—5887
- Huygens principle appl. to active sound absorbers, approx. *(French)* 77—42640
- impulse method of measuring acoustic normal impedance at oblique incidence 80—53582
- in-duct acoustic props. meas., transfer function method, expt. 80—106688
- in-duct acoustic props. meas., transfer function method, theory 80—106644
- inhomogeneous absorbing solid, self-focusing of intense hypersonic and US beams 77—84038
- insulating material losses and performance factors *(Spanich)* 78—55516
- interferometer nonlinear transducer motion 79—50540
- intermediate state superconductor, kinetic props. of corrugated and thread struct., sound attenuation *(Russian)* 80—54843
- irregular cavity acoustic impedance, finite element analysis 78—42483
- irregular waveguide, average acoustic field attenuation 78—1459
- Ising type model, elastically coupled, effects of dipolar forces on crit. sound attenuation in uniaxial systems 80—50158
- lagging configurations for noise reduction, insertion loss 77—84078
- Landau damping in regular wave interaction with noise 80—33284
- landscaped office, effect of screens on sound attenuation 78—94486
- laser light diffraction, appl. to meas. of acoustic and acousto-optic props. of crystals *(Polish)* 78—76425
- layered media, strong nonlinear and dissipative effects 78—1472
- LF acoustic reduction of rectangular panel 79—32142
- LF sound waves propag. in Arctic channel with irregular ice boundary 77—11079
- lined curved ducts, rectangular cross-sect. 78—1454
- lined plenum chambers in ducts, attenuation 79—37071

acoustic wave absorption continued
- liquid, US-induced birefringence, Brillouin scatt. linewidth, sound absorption coeff. 78—27180
- liquid with gas bubbles, acoustic wave self-transparency effect *(Russian)* 80—14509
- liquid with gas bubbles, acoustic wave unresonance absorpt. *(Russian)* 78—14404
- liquid-gas system near critical point, sound attenuation and dispersion, renormalisation group calcs. 79—42149
- liquids containing gas bubbles, effect of polymer additives 78—38779
- liquids near critical points, cubic term in complex bulk viscosity eqn. 79—95082
- low-freq. absorption in seawater, borate-complex relaxation 80—36304
- lower thermosphere, acoustic wave dissipation rel. to atmosphere heating 77—53266
- magnetic systems, one-dimensional, sound attenuation at finite temps. 77—63247
- marine sediments, water-saturated, infinite amplitude absorpt. rel. to finite-amplitude wave propag. 78—1476
- metal, BCC, tensor of deform. of cryst. lattices by impurity atoms *(Russian)* 77—7711
- metal, Fermi surface local geometry effects on phonon spectrum, acoustic props. *(Russian)* 77—55333
- metal, longwave sound, absorpt. coeff., in phase transition of $2^{1}/_{2}$ kind *(Russian)* 78—39008
- metal, low-freq. longit. sound attenuation, viscous and induction mechanisms 77—8152
- metal, phonon spectra, singularities caused by local geometry of Fermi surface 78—91401
- metal, Pippard sound-attenuation oscillating angular depend. *(Russian)* 80—103613
- metal, SAW absorption with and without external mag. field *(Russian)* 77—31936
- metal, sound absorpt. coefficient at phase transition of order $2^{1}/_{2}$, effect of geometry of const. energy surfaces 77—39769
- metal surface, resonant absorpt. of sound *(Russian)* 78—95216
- metal with several carrier groups in strong mag. field *(Russian)* 77—47868
- metals, Fermi surface geometry, effect on sound absorpt. and vel. 79—7775
- metals, HF sound propagation, nonlinear effects, review 80—88279
- metals, sound absorption and dispersion temp. depend. associated with Fermi surface plateaus *(Russian)* 80—65166
- metals and semimetals, two-phonon sound absorption in quantising mag. field 79—28382
- model sealing laws for sound absorptive boundaries 77—75727
- monopole receiver and radiator arrays, continuous, active sound suppression 79—94386
- multilayer sound absorbing panels, edge phenomena *(Japanese)* 77—42641
- multitone decay variance in reverberation room 80—87653
- N-wave propagating in circular tube, nonlinear attenuation and wall effects 78—50972
- narrow gap semiconductor, sound absorpt. in strong EM field 77—55590
- nematic liquid crystals, sound attenuation, near clear point, microscopic derivation 78—34605
- nematic-smectic A phase transition, sound attenuation and dispersion 79—82286
- noise control, sound absorptive systems review 78—30127
- noise control barrier attenuation, estimation procedures 80—33340
- noise control panels, system design 80—87649
- noise propag. along finite impedance boundary, aircraft ground noise appl. 78—9487
- nonlinear noisy medium, sound absorpt. 77—35000
- nonlinear waves attenuation, interaction with noise 77—50801
- nonuniform duct, with variable impedance, integral equation methods in duct acoustics 77—58498
- nozzle flow, low Mach no. sound attenuation 79—50721
- oblique incidence sound absorpt. characts. of materials using cross-correlation methods *(Japanese)* 78—83172
- ocean, l.f. attenuation and seawater bulk viscosity, Be and B influence 77—3696
- ocean, pH depend. of low-freq. sound absorpt. 77—49072
- ocean floor, refl. and attenuation obs. at 4 kHz 77—2140
- ocean microbubbles, in situ acoustic meas. 77—37207
- ocean sediments, experimental studies of attenuation 80—10067
- ocean sediments, math. model 77—91104
- oceanic layered finestructure in Arctic, acoustic variability, 10 to 60 kHz 79—90060
- one-dimensional system, cond. and longitudinal sound attenuation above Peierls transition point 77—28168
- open-cell polyurethane foam, induced mass of an equilateral triangular cylinder moving in an incompressible irrotational fluid 80—64237
- optimised multisectioned acoustic liners 80—19145
- outdoor process plant design, atm. noise attenuation calc. 79—70497
- Pacific Ocean, geographic variation of LF sound absorption 79—44189
- S.Pacific Ocean, transmission loss regions on acoustic cross-section, (Project Kiwi One) 80—36330
- partition airborne-sound transmission loss, effect of sound-absorptive facings 78—79166
- perforated facings on porous backings, calculation of specific normal impedance 80—64281
- perforated facings with porous backing material as sound absorbers 77—62115
- personal computer program for air absorpt. 80—96065
- phase transitions, caused by inhomogeneity of transition parameter *(Russian)* 79—23698
- piezoelectric semiconductor, weakly inhomogeneous theory of sound absorption 80—15574
- pine trees, swept freq. meas. 79—50494
- polymers, amorphous, acoustic loss factor rel. to struct. 77—51446
- polystyrene solution, in toluene and cyclohexane, acoustic absorption and dynamic compressibility 77—55321
- polyurethane foam plate, response to acoustic noise impulse *(French)* 79—1033
- polyvinylidene fluoride film, acoustic loss factor and piezoelectric coupling coeff. 77—81058
- porous and permeable material characteristics *(Spanish)* 78—14405
- porous elastic solid containing compressible viscous fluid *(French)* 80—38149

acoustic wave absorption continued
- porous material, absorption mechanism of sound pulse, Fourier transform anal. 80—38170
- porous material, estimation of reverberant sound absorpt. coeff. *(Japanese)* 78—83145
- porous materials, absorption coeff. in different media *(Japanese)* 77—84033
- porous materials, flexible, sound absorption 79—32115
- porous materials vibrations, radiations anal. 80—87640
- porous plates in fluids, sound absorpt. props. near rigid walls 80—87730
- propagation models for absorbent materials 80—53524
- quartz, lattice attenuation of longitudinal sound 79—86847
- quartz, vacancy attenuation of elastic waves at high temp. 79—86846
- radiation press. on an absorbing sphere 78—79154
- reactive acoustic attenuator, effects of flow on performance 79—55257
- rectangular multielement acoustically lined ducts, sound attenuation 77—84030
- rectangular parallel layers, sound attenuation, effect of boundaries *(German)* 78—18082
- rectangular rooms, reverberation time dependence on wall diffusion and room shape *(German)* 80—102932
- resonance absorbers, effects of additional damping *(German)* 77—14825
- reverberant sound absorpt. coeff. of plane porous material, theory *(Japanese)* 78—79168
- reverberation room ANS qualification error sources and effects 77—58514
- reverberation room ANS qualification with microphone traverse and LF absorption 77—62123
- reverberation room modifications for ANS qualification 77—58517
- reverberation room sound absorpt. meas. precision assessment 78—59210
- reverberation time, absorption and impedance, theoretical model used for calcs. of a room 78—90601
- rigid porous absorbing materials, finite element model 79—32114
- road traffic noise, highway noise barriers, optimum weight with respect to effectiveness and cost 80—67021
- rock elastic wave absorption meas. and recording instrument *(Russian)* 79—29891
- room acoustic absorption meas. using reference sound source 77—62109
- rooms sound absorpt. meas. 77—39161
- rubber compounds, measurement using automatic progressive wave apparatus 79—91866
- sand, water-saturated, broadband meas. of acoustic attenuation 80—83719
- SAW and anomalous sound absorpt. for fluid-fluid interface 80—74562
- SAW electronic absorption, temp. depend. 77—55585
- schoolroom acoustic insulation check allowing for boundary absorption *(Hungarian)* 80—106664
- screens, role in open-plan offices 80—87650
- sea water, chemical relaxation involving Mg and carbonic acid 79—68466
- sea water, sound absorpt. 78—1481
- sea-floor sub-bottom absorption profiles, acoustical effects 79—41500
- seawater, attenuation due to chem. relax.-absorpt. 79—34851
- seawater, chemical relaxation studies using resonator method 80—96073
- semiconductor, acoustoelectric phenomena in variable elec. field *(Russian)* 79—51637
- semiconductor, sound absorption at very low temps. 79—95089
- semiconductor films, narrow-joined, sound propagation, in strong EM wave field *(Russian)* 80—39483
- semiconductors, HF sound propagation, nonlinear effects, review 80—88279
- semiconductors, semimetals, electron heating by phonons, acoustic absorpt. and acoustoelectric current quantum oscills. *(Russian)* 79—19639
- SF-14 flint glass, acoustic vel., absorpt. coeff. and photoelastic consts. rel. to acoustooptical parameters 79—56762
- shallow water sound propag. overlying consolidated bottom 77—816
- ships, structure borne sound attenuation 78—33947
- shock pulses in Al rods, amplitude-dependent attenuation 78—55503
- simple fluids, order-parameter fluctuations near crit. point, Ornstein-Zernike theory 78—34416
- single and double walls, simplified L_α evaluation method, statistical evaluation of noise control mechanisms *(Japanese)* 80—33336
- single monopole noise source in air duct, very low freq. noise abatement, diesel engine exhaust 80—64282
- single-layer wall with porous layer, acoustic reduction 79—27466
- sludge, cohesive, dynamic props. *(Japanese)* 80—45580
- small-chamber method applied to investigations of sound-absorbing systems at high sound pressure levels 78—94497
- solutions with critical point of unmixing, acoustic relax. *(Russian)* 79—95085
- solvents, acoustic relax. mechanisms *(Russian)* 79—90733
- sound absorption materials, effects of outdoor exposure 77—88985
- sound attenuation by multiple barriers 80—43524
- sound attenuation in magnetic field at the $2^{1}/_{2}$-order phase transition *(Russian)* 80—100487
- sound insulation meas. for light struct. *(Chinese)* 79—10427
- sound panels, estimation of transmission loss by statistical energy analysis 80—64278
- sound propagation conf., France (May 76) *(French)* 77—42638
- sound sinks in flows, low freq. sound absorpt. of jets 80—69788
- sound-absorbing wedge, reflection characts., glass wool props. *(Japanese)* 80—64322
- space absorber composed of porous materials, reverberant sound absorption coeff. 78—55519
- sphere, sound refl. 78—18084
- spherical wave, diffr. by absorbing plane 77—46830
- stratosphere and ionosphere, LF waves relax. absorpt. *(Russian)* 78—65356
- structure borne sound in ducts by impedances attached to side *(German)* 80—102876
- superconducting alloy, sound absorpt. and longit. collective oscills. *(Russian)* 77—32122
- superconductor, bulk, absorption of SAW in presence of supercurrent 79—28443
- superconductor longitudinal acoustic wave absorpt., nonlinear effects, hysteresis *(Russian)* 79—19691
- superconductors, dirty layer, fluctuation sound attenuation, depend. on critical temp. *(Russian)* 80—34553
- superconductors, thread-like structure, sound attenuation in intermediate state *(Russian)* 77—32118

acoustic wave absorption continued
superconductors with mag. impurities, theory of longitudinal sound attenuation *(Russian)* 79—11268
surface ducts, attenuation 78—63231
tangential momentum accommodation coeff. meas. by acoustic vel. and absorpt. obs. for He, He on W 80—66867
thermally conducting medium, dispersion and damping of acoustic pulse 77—27409
traffic noise, attenuation around buildings 78—1498
transmission loss prediction for building elements 79—32139
trimethylamine-water critical fluid, ratio of sound dispersion to attenuation 79—55826
tubes, sound distrib. control by auxiliary driving sources, air conditioning duct appls. 79—14133
turbulence, acoustic energy conversion to turbulent kinetic energy 78—63420
two-phase medium, sound wave absorpt. and dispersion 78—94466
underwater, in viscoelastic medium containing short cylindrical cavities 77—84049
underwater absorption of sound by sound 78—59180
underwater sound, acoustic absorpt. by $MgCO_3^0$ ion-pair relaxation 79—74914
underwater sound, attenuation of surface-generated noise received deep 78—9481
underwater sound, CW propag. loss meas. rel. to background ambient noise levels estimation 77—84046
underwater sound, high-freq. scatt. from cylindrical shells coated with viscoelastic absorbing layers 78—1478
underwater sound, influence of range-depencent environments on low-freq. volume attenuation meas. 77—46845
underwater sound, pH depend. of low-freq. absorpt. in ocean 77—84052
underwater sound in shallow water with rough boundaries, attenuation of coherent component 77—62091
urethane foams for noise abatement, physical and acoustical props. 79—18592
vehicle noise attenuation over short grass 80—19146
vibrating porous plate in fluid *(Japanese)* 79—81590
vibration-absorbing coatings, constrained, optimality 77—823
vibration-absorbing coatings, detachable, investigation of energy losses 79—90078
vibrational energy propag. in absorbing structs. 78—9596
viscous attenuation in suspensions and high-porosity marine sediments 80—74577
wall, finite element simulation of acoustic filters *(Japanese)* 77—84032
wall absorption coeff. derivation, complex impedance, for normally and obliquely incident waves *(French)* 77—54823
wall and floor noise insulation field tests 78—1511
wall covered with sound-absorbing cubes, absorpt. coeff. *(German)* 77—84081
wall systems, design for desired STC ratings 79—18608
water, supercooled liq., high freq. sound vel. and absorpt., thermodynamic singularity, 228K 77—76489
waterfilled US testing tanks, appl. of filled rubber material system to echo absorpt. 80—96059
waveguide, fluid-filled, with transverse resistivity, mode-selective sound attenuation 78—1452
wide barriers, acoustical scale model study of sound attenuation 78—1499
wind and ground plane attenuation effects on sound propag. near ground 80—10080
window-glasses, most effective window configurations 80—87655
wood joist floors, sound insulation 80—38178
Al alloy, strain response to acoustic excitation, statistical props., comparison with C fibre reinforced plastic 79—43502
Al, fluxural oscillations in longitudinal mag. field, sound attenuation, magnetoelasticity *(Russian)* 80—54844
α-$AlPO_4$, berlinite, temperature-compensated surface and pseudo-surface acoustic wave props. 77—51584
Bi, giant quantum attenuation of sound due to electronic phase transitions 79—60718
Bi, magnetoacoustic attenuation peak at low temp. 79—91105
Bi, magnetoacoustic attenuation, tilt effect 79—91106
Bi-Sb alloys, magnetoacoustic attenuation, tilt effect 79—91106
$Bi_{12}GeO_{20}$, acoustic vel., absorpt. coeff. and photoelastic consts. rel. to acoustooptical parameters 79—56762
$Bi_{12}SiO_{20}$, acoustic vel., absorpt. coeff. and photoelastic consts. rel. to acoustooptical parameters 79—56762
C fibre reinforced plastic, strain response to acoustic excitation, statistical props., comparison with Al alloy 79—43502
CdS, acoustic wave attenuation, phonon viscosity and dislocation drag 80—70319
CdS, heavily doped compensated piezoelectric semiconductor, sound absorpt. coeff. calc. *(Russian)* 79—15194
CdS, SAW absorpt., effect of transverse electron drift 77—76879
CdS-ZnTe, acoustoelectric domain injection across interface, propag. loss, elastic consts. 77—51778
CdS(Se), piezoelec. semicond., sound absorption 80—60051
CdSe, heavily doped compensated piezoelectric semiconductor, sound absorpt. coeff. calc. *(Russian)* 79—15194
Fe-Cr-Al, attenuation and vel. of acoustic shock waves, amplitude depend. 78—63810
GaAs, phonon viscosity tensor 78—34570
GaP, elastic moduli and attenuation of elastic waves 77—51429
GaSb, acoustic wave attenuation, phonon viscosity and dislocation drag 80—70319
Ge, phonon viscosity tensor 78—34570
Ge:Sb, acoustic attenuation, uniaxial stress effects 78—59863
HD+He, relax. and kinetic cross-sections, DWBA calcs. 79—41782
H_2O, acoustic relaxation in critical region *(Russian)* 80—92609
^{3}He critical fluid, ratio of sound dispersion to attenuation 79—55826
^{4}He, liq., pressurized, attenuation and dispersion of first sound near superfluid transition 78—14524
^{4}He, solid, phase transition 80—15333
InSb, phonon viscosity tensor 78—34570
$KCl{:}OH^-$, paraelec. system, acoustic susceptibility in strong phonon-coupling approx. 78—71801
KH_2PO_4, longit. sound attenuation, strain depend. pseudo spin coupling mechanism 77—85666
$LiNbO_3$, LF sound attenuation, internal friction 78—63804
$LiNbO_3$-CdSe layer structure, SAW absorpt., elec. field effects 80—65355

acoustic wave absorption continued
$MgAl_2O_4$, influence of nonstoichometry on acoustic wave attenuation 79—65146
Mn-Cu alloy, high-damping, acoustic shock pulse attenuation and vel., stress amplitude and temp. depend. 77—15503
N_2, moist, relaxation freq., sound tube meas. 78—1058
NH_4, halides, sound attenuation near lambda point 77—66002
$NH_4Br(Cl)$, anomalous sound attenuation above lambda point 78—51617
Nb, clean supercond., fluctuations and sound attenuation near $T_{c2}(B)$ 77—15996
Ni crystals in strong mag. field, EM excitation and vel. dispersion of sound *(Russian)* 80—39837
Ni film, mag. field depend. surface acoustic wave attenuation meas. 77—20674
Ni-SiO composite film, acoustic damping capacity and struct. *(Russian)* 77—59070
O_2, gas, intermol. pot. for spectra, acoustic absorpt., rot. relax., etc. 79—68224
O_2-CO_2 mixture, temp. difference of molecular vibr. relaxation freq. from 300 to 675K 80—74238
O_2-H_2 mixture, temp. dependence of molecular vibr. relaxation freq. from 300 to 675K 80—74238
O_2-He mixture, temp. dependence of molecular vibr. relaxation freq. from 300 to 675K 80—74238
Pb, fluxural oscillations in longitudinal mag. field, sound attenuation, magnetoelasticity *(Russian)* 80—54844
Se, amorphous, acoustic behaviour in terms of model involving stochastic reson. 79—23681
Si, phonon viscosity tensor 78—34570
SiO_2, silica, amporphous, acoustic absorpt. in range 1 to 20K and 15 to 65 MHz 77—24357
α-Sn, gapless semicond., sound propag., RPA calc. 77—31721
Sn, sound absorption giant resonance, produced by coherent mag. breakthrough *(Russian)* 80—6700
Sn, sound attenuation and velocity depend. on mag. field *(Russian)* 80—29446
Sn, thin film, supercond., acoustic wave absorpt., quasiparticle distrib. 78—10603
TiO_2, acoustic vel., absorpt. coeff. and photoelastic consts. rel. to acoustooptical parameters 79—56762
V, fluxural oscillations in longitudinal mag. field, sound attenuation, magnetoelasticity *(Russian)* 80—54844
Xe, critical fluid, ratio of sound dispersion to attenuation 79—55826
Xe, sound propag. near critical pt. 79—82285
$Zn_xCd_{1-x}Te$, resonant Brillouin scattering *(Japanese)* 79—15474

acoustic wave amplification
see also acoustoelectric effects
Bleustein-Gulyaev wave amplification in tetragonal and hexagonal crystals 77—7959
degenerate parametric amplification, theory 77—27414
degenerate semiconductor, amplification of sound by temp. gradient 77—20366
degenerate semiconductor, nonparabolic, acoustic wave absorption/amplification coefficient 78—64069
dielectric/piezoelectric layered waveguide, surface acoustic wave amplification *(Russian)* 78—23138
disc-rod US tool, gain enhancement technique 77—35010
flame, laminar premixed gaseous, amplification of propagating acoustic signal 79—29357
halls, sound amplifying systems, model *(French)* 79—37090
non-linear ultrasound absorption in an electromagnetic wave field under quantum size effect conditions 78—87745
nonuniform flow, sound amplification 78—83158
piezoelectric semiconductor, amplification and vel. change of acoustic waves due to external temp. gradient 78—84260
piezoelectric semiconductor, inhomogeneous, amplification of acoustic wave 79—69561
piezoelectric semiconductor, plasmon enhanced sound amplification in mag. field 77—39900
piezoelectric shear SAW amplification in periodic structures on solids 79—90055
piezoelectric-semiconductor corrugated boundary, reflected acoustic wave amplification *(Russian)* 78—30819
piezoelectric-semiconductor interface, periodically irregular, electron absorp. and acoustic wave amplification 79—42361
piezosemiconductor film, surface-mode acoustic wave amplification 79—46907
SAW amplifier, saturation power 77—39133
SAW slow shear waves in periodic structures, electronic damping and amplification 80—19124
semiconducting film with paramag. admixture under EPR conditions *(Russian)* 77—63266
semiconductor, acoustoelectric phenomena in variable elec. field *(Russian)* 79—51637
semiconductor, monopolar, anisotropic, US amplification at intermediate freq. *(Russian)* 77—35965
semiconductor, validity criteria of phenomenological theory of electron obs. and amp. of sound 78—91733
semiconductor film, piezoelec., quantum acoustoelec. interaction, thickness depend. *(Russian)* 79—47126
shock wave amplification in nonequilibrium system of liq. and solvent gas bubbles 79—18936
size-quantised films under ESR conditions 80—70322
Stoneley wave amplification at interface between piezoelectric semicond. and dielectric crystal 79—19441
Stoneley wave amplification between two piezoelecs. separated by thin semicond. film 79—14998
TGS, ferroelec. single crystal, low freq. nonlinear effects 80—84490
thermal fluctuations during amplification of magnetoacoustic surface waves 78—88158
thermopiezosemiconductor critical drift velocity for US amplification 78—60169
thermopiezosemiconductors 78—76114
weak acoustic signal enhancement using parametric mode interaction 79—94391
Al, nonlinear sound wave interactions, sound attenuation in weak superconducting state *(Russian)* 80—75310
CdS crystal, SAW amplification, bulk and acoustic noise 80—39637
Ga, nonlinear sound wave interactions, sound attenuation in weak superconducting state *(Russian)* 80—75310

acoustic wave amplification continued
GaAs n-n$^+$ epitaxial structure for CW microwave electroacoustic amplifier 78−59235
$LiNbO_3$-liquid-CdS-liquid-$LiNbO_3$ structure, acoustic wave propag. and amplification 77−42654
$LiNbO_3$-SiO_x-InSb-SiO_x monolithic acoustoelectronic amplifier with pulsed power supply 79−56269
Te, acoustoelectric current flow, acoustic refraction effect 79−19637
Tl_3TaS_4, piezoelec. semicond., acoustic wave generation, amplification material appl. *(Russian)* 78−72464

acoustic wave attenuation *see acoustic dispersion; acoustic wave absorption; acoustic wave scattering; acoustic wave transmission; ultrasonic absorption*

acoustic wave diffraction
see also ultrasonic diffraction
absorbant wall panels, modal analysis *(French)* 80−79060
absorbing semi-infinite plane in moving fluid 77−50830
acousto-optic modulator efficiency optimisation, sound diffraction profile model and expt. 80−106615
aeroacoustics and aircraft noise generation, appls. of diffraction theory 80−53532
aircraft, diffraction of high speed jet at subsonic flight 77−50806
airfoil trailing edge, incident acoustic wave diffr., flow depend. 78−26143
arrays with side baffles, directional response using geometrical diffr. theory 79−23115
axisymmetric transducers, with various boundary conditions, single integral computer method for Green's function 80−87591
baffles, symmetrical planar, sound diffraction *(Czech)* 78−90558
barrier, absorptive, noise attenuation calc. *(Japanese)* 77−3700
barrier attenuation in presence of ground, line integral theory 80−33300
barrier or pillar, many-sided, diffracted acoustic field *(Japanese)* 79−18559
barriers on finite impedance ground for noise reduction 80−33301
characteristic wave numbers for simple source formulations of acoustic radiation and diffraction problems 78−38109
circular array of acoustically rigid elliptical-cylindrical scatterers, plane wave diffr. 77−31151
circular cylinders encased in partial annular layers 80−58837
composite, layered, Love wave diffr. by stress-free crack in plane interface 80−33501
confined beams, nonlinear effects and diffr. 78−1470
continuous noncircular cylinder, echo signal calc. using Kirchhof integral *(Russian)* 79−68453
cracks, diff. of elastic waves 78−79161
curved surface, wave propag. 78−37793
cylindrical pulse diffr. by metallic half plane, boundary value problem, direct transform technique 80−69573
cylindrical shell, fluid filled, plane acoustic press. pulse diffr. 78−90559
diaphragm in circular waveguide, scattering matrices 80−87598
diffraction waves on arbitrary surface, Gaussian functional integral method 79−76902
discontinuity line in boundary surface curvature, acoustic wave diffraction *(Russian)* 79−37072
double layer grating of hollow elastic bars, plane wave diffr. 79−86278
double-layer waveguides, normal mode diffraction 78−94462
elastodynamic diffraction, by periodic rough surface (stress-free boundary) 78−13826
elliptic cylinder, acoustic press. wave diffraction and radiation *(Russian)* 79−32113
far field amplitudes of diffraction and radiation problems, general relation 77−34973
farfield scatt. from prolate spheroid, meas. and anal. 78−94459
finite element analysis of elastodynamic fields near running cracks 78−34066
finite sound absorbing panels, edge phenomena 77−27425
finite-amplitude sound beams in nonlinear medium 78−1471
Fredholm integral equation, 1st kind for acoustic diffraction calc. *(Russian)* 80−58834
generalized Fourier transform diffraction theory for parabolically anisotropic media 78−38107
grating consisting of fluid-filled hollow elastic bars 80−38143
half-plane with discontinuous boundary conditions 77−72108
heterogeneous media, perturbation method, mathematical treatment *(French)* 77−42645
HF, non-linear effects in tubes 80−87614
homogeneous ellipsoid, scalar problem of LF diffr. *(Russian)* 77−68286
ill-posed diffraction problem and quasisolution 80−87593
impedance cylinders of large wave dimensions 80−64249
inhomogeneous media, derivation of generalised parabolic equation and evolution of Gaussian beams 79−64377
inhomogeneous periodic surface, diffr. ang. and freq. depend. 78−1458
Lamb waves by finite crack in elastic layer 80−64244
layer potential representations of diffracted field 78−30108
layered media, strong nonlinear and dissipative effects 78−1472
long-wave diffraction by plate reinforced with projecting beam 78−9469
model of nonreflecting anisotropic medium 80−5856
multiple screens, diffr. theory rel. to noise reduction *(French)* 78−13844
noise barrier model, diffraction by acoustically penetrable or electromagneticlally dielectric half plane 78−5595
noise barriers, Z-lines method appl. to anal. of far field diffr. 77−50822
noise diffraction around wedge, appl. to factory design 78−42494
noise propagation around thin half-plane, numerical calc. 78−9486
noise propagation in open air, obstruction effects, propag. around finite plane on ground *(Japanese)* 77−39160
noise propagation in open air, obstructions effects, sound diffr. by 1/4 infinite plane *(Japanese)* 77−39159
noise reduction by absorptive barrier 77−84061
nonlinear effects, acoustic focusing systems 79−32126
ocean, diffr., refl. and interf. during near grazing and near normal ocean surface backscatt. 78−90570
optical theorem, plate-fluid system 80−87595
parabolic reflector 80−58835
pencil conical beam diffraction on acoustically soft sphere *(Ukrainian)* 78−90547
perforated screen, sound diffraction, vortex shedding influence 80−69849
piezoceramic tubes with capped or shielded ends, diffr. consts. and radiation impedances 78−1534
plane, grating of acoustically compliant circular cylinders partially coated with perfectly compliant material 80−87604

acoustic wave diffraction continued
plane grating formed by hollow elastic bars, partial domains technique 77−14829
plane noise barriers, integration of far field diffr. by surface mapping 77−54829
plane pulse diffraction by thin arbitrarily shaped obstacles 80−96053
plane scalar wave by locally reacting, planar, finite scattering surface 80−48481
plane wave, by semicircular infinite soft strip 77−84025
plane wave, by two staggered parallel soft or rigid strips 79−1015
plane wave, diffraction by strip of finite thickness 77−27410
plane wave diffr. by semicircular infinite strip, comment 78−83134
plane wave diffraction by two parallel half-planes 80−5858
plane wave diffraction by wedge with finite impedance 78−38106
prolate spheroidal radial function of third kind, asymptotic formula 80−42077
α-quartz, temp. dependence of surface wave diffraction 77−15674
rectangular aperture in soft plane screen 80−96055
rectangular wide barriers for sound reduction, approx. formula for calculation 80−38175
rigid cylinder, nonstationary diffraction of spherical and cylindrical waves *(Russian)* 78−13832
rigid elliptical cylinder, echo signal determ. using Kirchhoff integral *(Russian)* 78−13833
rigid planar screens, diffr. of arbitrarily oriented directional sources 78−83137
rigid prolate spheroid, short wavelength diffracted surface pressures 77−84018
rigid scatterers in field of harmonic point sound source, compensation of diffraction field 78−18112
rigid sphere, nonstationary diffraction of spherical and cylindrical waves *(Russian)* 78−13832
SAW diffraction in quartz 80−38160
SAW filter design with diffraction compensation 80−74672
sawtooth sound waves, diffr. and radiation 77−808
screen above locally reacting, infinitely large plane 78−79158
seismic signal processing using inverse diffraction technique 80−74608
semiconductor, diffraction transverse acoustoelectric effect 77−35967
shadow-optical colour imaging technique for sound field pressure distrib. meas. 79−64464
shear normal mode diffraction by surface crack in elastic plate 79−94549
shock wave, weak plane, at wedge, reflection and diffr. 77−72111
shock wave diffraction, nonlinear problem soln. *(Russian)* 78−75171
simultaneous Wiener Hopf eqns., Fredholm integral type soln. wave diffraction appl. 80−57100
slitted screen, thick, diffraction induced on plane wave 79−68455
sound pulse diffraction by circular cylinder 78−30107
sound reduction by barriers *(Japanese)* 79−68479
spherical, ground models 80−74555
spherical diffraction by wedge of arbitrary angle, comparison of theoretical solns., expt. verification *(Japanese)* 80−53498
spherical wave, diffr. by absorbing plane 77−46830
statistically stationary traffic noise shielding by simple obstacles 78−90590
sub-beams interpretation of radiation fields, diffr.-induced sub-beam spread 77−50788
surface ducts, attenuation 78−63231
surface wave transducer, very narrow aperture acoustic diffr. effects 78−22240
surface waves, diffr. and guidance 78−13828
target identification, transfer functions and impulse responses *(French)* 79−41480
target recognition, 2 theoretical techniques using geometrical optics and physical optics theories *(French)* 80−53509
thin foil wing, subsonic speed, closed solution 79−64368
thin phase grating diffr. eqn. solns. 78−54198
thin screen, study of shielding efficiency *(French)* 78−87188
thnadners, shaped noise barriers for control of diffracted sound 79−50502
three-dimensional elastodynamics, geometrical theory of diffr. 77−46829
traffic noise, diffr. and attenuation around buildings 78−1498
transducer array directional response anal., model 78−66973
two-dimens. waves, diffraction by cylindrical cavity in half-space 79−23110
underwater sound, computations of strength and diffraction parameters for real and canonical oceans 80−33320
variable density cylinder, plane wave diffr. 78−50977
vibrations of hollow elastic cylinder in partial annular layer of finite thickness 80−14506
vorticity at sharp edge, sound diffraction by perforated screen, low Mach number grazing flow 80−53805
waveguide field approx. to soln. of Helmholtz eqns. *(Russian)* 77−57171
wedge near thin elastic plate 77−68290
wedge with curved faces 80−87592
wide barriers, acoustical scale model study of sound attenuation 78−1499
wide trapezoid barrier, plane acoustic wave diffraction 77−34976
KH_2PO_4 electro-optic modulator crysts., piezoelec. induced acoustic transients 80−70316

acoustic wave diffusion *see acoustic wave scattering*

acoustic wave effects
see also acoustic magnetic resonance; acousto-optical effects; acoustoelectric effects; biological effects of acoustic radiation; sonoluminescence; ultrasonic effects
acoustic vibration of a liquid filled distorted circular cylindrical shell 79−3840
aerosol particles, ellipsoidal, relative velocity in acoustic field 80−58854
aerosol systems, acoustic field effects 80−89529
aerosols, highly dispersed, with elec., acoustic fields, collision rates 79−47986
Bjerknes forces in viscous medium and acoustic coagulation of aerosols 77−68680
bubble, spherical gas, nonlinear response to multi-freq. acoustic excitation 80−38480
bubble in liquid subject to tension pulse, model 79−55406
bubbles, forced oscillation damped by acoustic radiation 80−33664
bubbles and drops driven by modulated acoustic radiation stresses, shape oscillation and static deformation 80−33274

acoustic wave effects continued
cavitation, fluid-solid boundary, US cleaning and cavitation erosion 80—65158
cavitation gas bubble in compressible liquid, influence of inhomogeneous sound field on motion 80—6131
critical sound pressure level in mass transfer processes, analytic expressions 78—90633
cylinder, forced convective heat transfer, sound wave effects 80—43699
cylinder in near-critical flow, influence of acoustic surface vibrs. on drag 78—5729
displacement of infinite elastic plate submerged in ideal liquid, examination of displacement field 80—74557
drop evaporation rate in forced convective flow with transverse sound fields 78—51224
drops driven by modulated acoustic radiation pressure, quadrupole resonance, experimental props. 80—33275
duct flow, compressible laminar flow, superimposed sound field effect 77—75933
gas bubble kinematics under strong acoustic wave press. in liq. *(Russian)* 79—94708
gas bubbles, influence of microstreaming on growth due to rectified diffusion 78—51232
geological materials failure, role of acoustic fluidisation 80—85653
glass vessel shattering by sound waves, chamber for expt. 80—17752
heat transfer in turbulent flow 78—59394
hydrocarbon drops levitated in water, acoustically forced shape oscill. 79—47987
induced vibration, fatigue cracks in aircraft skin panels, prediction of edge crack growth 80—69737
influence of grazing flow on the acoustic impedance of a cylindrical wall cavity 80—69784
interaction of acoustic waves and microwave radiation fields: depletion and mixing effects 79—90056
interaction of induced sound with flow past a square leading edged plate in a duct 80—69783
ionic crystals, structurally modulated, elasticity and its limits, yielding and melting 80—49295
jet noise, amplification by higher-mode acoustic tone 78—9664
jets, free, turbulent, acoustic effect, dual nature 78—18325
laminar boundary layer, acoustic field effect for compressible liquid *(Russian)* 77—68617
laminar pipe gas flow, fluid-wall mass transfer, sonic oscills. enhancement 77—910
levitation, acoustic, liq., solid props. meas. appl. 80—43565
levitation of liquid drops, calc. of nonspherical distortion 80—74693
linear acoustic loading in straight pipes 80—96060
liquid crystals acoustic storage effect 78—94992
liquid dispersion, suspended impurities effects on wave excitation in sound field 80—81372
liquid surface, ripples, generation by parametric subharmonic reson. with sound waves 77—46849
mass transfer from cylinders to air stream 79—32127
mutual radiation impedances between pistons 79—1016
nonpolar liquids, cavitation threshold under ionising acoustic radiation 79—37074
plasma jet mixing, with surrounding gas, effect of sound radiation 79—82053
polymer, stress-relaxation apparatus, stress and vibration relaxation in sound frequency range 77—1905
polyurethane foam plate, response to acoustic noise impulse *(French)* 79—1033
pulsating gas bubbles in acoustic field, thresholds for surface waves 80—33665
pump wave, high intensity, appl. to degenerate parametric amplification of sound 77—27414
radiation pressure on sphere in standing wave field, meas. 77—79989
rotation effects on flow past flat plate due to standing sound field 80—24028
sieving of fine powders by sonic oscillating air column *(Japanese)* 78—95712
solar atmosphere, gravity waves generation by HF acoustic waves, Cherenkov radiation *(Russian)* 77—17265
solar chromosphere, temperature distribution, acoustic wave heating 77—53508
solar chromosphere models, short period acoustic heating theory appl. *(Italian)* 78—85926
solid body first-order torques and spinning velocities in intense sound field 77—23798
spacecraft structure, acoustic excitation analysed by Statistical Energy Method 77—58502
sphere suspended in fluid, vel. in sound wave 77—23800
steam, film condensation in tube, heat transfer, vibr. effect 78—51044
supersonic boundary layer, external acoustic perturbations *(Russian)* 78—34152
turbulent boundary layer, compressible, extended mixing length appls. 78—94655
two-dimensional shear layer, instability wave excitation by sound 79—32541
underwater sound, generation of surface waves *(Russian)* 77—46841
unstable laminar boundary layer, response to acoustic excitation 79—98681
vortices, acoustic destabilisation 79—32533
wake, artificial control of laminar-turbulent transition 78—34139
water jets, two-dimensional, effects of applied sound *(Japanese)* 78—79353
As-S glasses, acousto-induced structural changes, optical props. 80—49122
Ca, acoustic effect in crystallisation and melting *(Russian)* 79—51238
H_2O, contact angle measurement, effect of acoustic energy 78—95207
^{4}He solid-liquid interface mobility under 1 MHz sound wave *(French)* 80—100373

acoustic wave interference
see also acoustic wave interferometers; acoustic wave interferometry
aircraft noise measurement, interference of direct and ground-refl. waves, height depend. 77—23813
atmospheric turbulence effects on interference of sound waves above finite impedance boundary 79—41493
birdsong, consequences of interference patterns 80—102881
combination tones, student demonstration 79—58507

acoustic wave interference continued
correlation of the phase and amplitude fluctuations between direct and ground-reflected sound 80—96067
ear, airborne sound destructive interference applicability for personal sound protection *(German)* 77—66817
frequency band broadening of phase shifters of SAW 78—55532
laboratory acoustic interference expts., refl. effects 77—22353
multifrequency Bragg acousto-optic deflector, laser beam AM suppression 80—53426
multipath interference nulls in long-range, low-frequency acoustic propagation by normal modes 80—33315
ocean, diffr., refl. and interf. during near grazing and near normal ocean surface backscatt. 78—90570
optimal array processing for case of strong localized interference using appl. of adaptive beamforming 79—41521
plane noise barriers, integration of far field diffr. by surface mapping 77—54829
reflection microscope, acoustic signatures, physical model 80—48532
SAW, velocity, attenuation and reflection meas., interf. acoustical method 79—18638
SAW filter triple transit suppression by mech. and regeneration reflection cancellation 77—23829
seismic data colour TV display system 79—74995
sound pulses interfering in continuous stratified medium, reciprocal action *(German)* 77—68285
superposition paradox, explanation, teaching approach 80—41999
underwater sound in shallow sea, influence of bottom on interference struct. of acoustic field 80—102900
US materials testing, three layered medium, dispersion relation for interference waves 78—72980
US pressure and interference fields *(German)* 80—89436

acoustic wave interferometers
see also acoustic wave interferometry
acoustic interferometer, cylindrical, theoretical criterion for end face alignment 77—14861
blood clotting characterisation by US digital fixed path interferometer 78—44670
complex apparatus for viscous and elastic prop. meas. at high press. of liquids 78—9734
correlation interferometers rel. to binaural perception and resolving power of bats *(French)* 78—80883
cylindrical interferometer, theoretical criterion for end face alignment 77—14861
echosonde interferometer for atmospheric research 78—57347
exact fractions interferometer algorithm and circuitry 77—39182
Fabry-Perot, for measuring HF acoustic losses in materials with high Q-factor 80—5887
Fabry-Perot interferometer using α-quartz as acoustic mode converter 79—23152
shock-loaded solids, wave profile measurement 79—94564
sound speed measurement in liquids, moderate accuracy interferometer 77—50844
UHF US interferometer, for liquids 78—22234
US, high press. elastic moduli meas. 77—4140
US manometers for low and medium vacua 77—67455
US pulse-phase interferometer, appl. of $LiIO_3$ cryst. as wide-band transducer 77—14868

acoustic wave interferometry
see also acoustic wave interferometers
admittance figure approach to processing acoustic interferometry meas. 79—50539
Fabry-Perot interferometer for determ. of acoustic parameters of fused quartz 79—41532
gas constant meas. in Ar by acoustic interferometry 77—7492
nonlinear transducer motion 79—50540
reflection coefficient meas. in liquid layer, error of interference methods 77—14865
target identification through parameter estimation and imagery by interferometric methods *(French)* 79—41539
threefold seismic or acoustic holographic interferograms for improved reconstructed-image definition and contrast 80—23844
US attenuation or velocity meas. 80—58874
US field in fluids, pseudo-stationary fields 79—81610
US holograms, recording via suspension method 77—14857
US velocity meas., fixed-path interferometer, phase error elimination 78—83197
SF_6 gas acoustic dispersion obs. by double-crystal US interferometry *(Japanese)* 79—4100
UF_6 gas acoustic dispersion obs. by double-crystal US interferometry *(Japanese)* 79—4100
WF_6 gas acoustic dispersion obs. by double-crystal US interferometry *(Japanese)* 79—4100

acoustic wave propagation
see also acoustic dispersion; atmospheric acoustics; Doppler effect; liquid helium sound propagation; seismic waves; shock waves; surface acoustic waves; ultrasonic propagation; underwater sound
2D finite amplitude acoustic waves radiating from flat plate in arbitrary periodic vibrations 80—33283
above absorbing surfaces, model study, anechoic chamber exp. results 79—18568
absorbant fluid, Fourier propag. theory for linear and nonlinear acoustics *(French)* 80—33288
absorbent materials, models for propag. 80—53524
absorbing boundary conditions for wave equation 78—59320
accelerated sphere in arbitrary fluid medium 78—50966
acoustic interactions in media with weak periodic inhomogeneities 79—32124
acoustic sources, nonlinear and thermal, due to thermoviscous heating of fluid by modulated sound wave 79—23122
aeroacoustic source distribution, integral representation, general theory 79—50492
aeroacoustic source distribution, two dimensional model flows 79—50493
aeroacoustics, appl. of linear wave theory conservation eqns. 78—9476
AGARD special course 80—53522
air, vibrations of cavity-backed panel anal. *(French)* 80—38164
air, weak nonlinear waves, struct. and propag., effect of vibr. relaxation 79—64683
air-gun arrays for marine prospecting, pressure pulse theory 77—39177
aircraft noise propag., review 80—64258

acoustic wave propagation continued
airway geometry determ. by anal. of acoustic pulse response meas. 78—28026
amplitude density of finite amplitude wave, effect of nonlinear propag. distortion 79—68462
anisotropic layered medium, plane wave transmission 78—83150
anisotropic rods of rectangular cross-section 78—1463
aperiodic transition layers and waveguides 80—43498
arbitrary continuously stratified environments, propagated, reflected and transmitted acoustic waves 78—13829
architectural acoustics, field and model expts. on solid-borne sound *(Japanese)* 80—64290
array processing using freq.-wavenumber approach 78—66974
asymmetric double exponential waveform, weak-shock soln. for nonlinear propag. 80—10061
asymptotic solution for sound propag. above impedance boundary 80—87582
atmosphere, attenuation of explosion waves 77—31155
atmosphere, MHD wave propag. in presence of rot. and variable mag. field 79—40024
atmosphere, parabolic approx. 79—3824
atmosphere, vertical propag. of powerful sound beam *(Russian)* 77—64375
atmosphere and oceans, wave disturbances 78—32209
attenuation, and propag. speed, of elastic waves in materials under uniaxial static compression, installation for determ. 80—21233
axisymmetric acoustic wave radiation by locally perturbed impedance boundary of half-space *(Ukrainian)* 79—50474
axisymmetric channels of slowly varying cross section, 3-dimens. acoustic disturbance propag. 79—90266
barriers, tree-lined earth, effects on sound propag. 79—18588
beam displacement, cycle distances, and attenuations for rays and normal modes 80—74580
beam-type disordered periodic systems. flexural wave motion 79—50636
bearing estimation, when source is endfire to array 79—50515
Benard convective instability, anomalies in sound propag. 77—34975
bent thin-walled waveguides, attenuation and pre-bend build-up 80—69576
bilayered media, stress wave propag. 79—90047
Blasius boundary layer, sound and Tollmien-Schlichting waves 79—10578
Bleustein-Gulyaev waveguides with gratings, anal. Bleustein-Gulyaev waveguides with gratings, anal. 80—1391
blood, deoxygenated sickle cell blood and haemoglobin S soln. 78—3453
bone, wave propag. in piezoelectric two-layered cylindrical shell with hexagonal symmetry 78—55487
boundaries of finite impedance, errors in literature on nearby sound propag. 79—98525
bulk-to-surface mode conversion by periodic corrugations at boundary of solid 79—64392
Burgers eqn., finite-amplitude propagation through gas droplet mixture 80—33282
caustics and spreading of adjacent acoustic rays 80—64241
CDW, quasi two dimens., phason and sound wave coupling 80—92839
channels constituted by moving and motionless targets, simulated varying, active identification *(French)* 79—41478
characteristic wave numbers for simple source formulations of acoustic radiation and diffraction problems 78—38109
charged particle hydrodynamic acoustic radiation in water *(Russian)* 77—54459
chromosphere, radiatively damped acoustic waves, hydrodynamic code 77—13300
circular ducts, effect of expansion chamber 78—55485
circular pipes, mode-selective energy transfer to pipe wall vibration 80—87586
circular piston, effect of mean flow on radiation 79—50486
circular tubes of arbitrary radius, sound propag. theory 77—27408
classical Lamb problem, time-harmonic soln. for elastic head waves 78—63215
closed tube, nonlinear resonant acoustic oscillators, finite rate theory 80—92171
closed-cycle high-energy pulsed lasers, investigation and management of waves 80—38153
coarse grained eqns. of propagation in two-phase random media 79—86280
coaxial circular cylinders of two elastic phase materials, pulse propagation 79—72747
colloidal crystals, ordered suspensions of charged latex spheres, acoustic shear waves 80—6466
combustion chamber, acoustic mode excitation by vortex shedding 80—19150
composite, fibre-reinforced, layered, harmonic elastic waves, dispersion 78—63223
composite thin-plates, equivalent microwave network analysis 79—3820
compressible inviscid linearly-sheared parallel flow, characterisation of acoustic disturbances 80—69848
compression waves scatt. from fluid filled spherical cavities in solids, modal resonance determ. 79—94529
conference, Marseille, France, 1978, May *(French)* 79—41484
confined beam in viscous medium, sound field characts. near beam boundary 78—18092
confined beams, nonlinear effects and diffr. 78—1470
confined sound beams, scale invariance and asymptotic solns. of Zabolotskaya-Khokhlov eqn. 77—11065
conical, excitation of an elastic half-space by a buried line source 80—64245
conservation laws for sound waves in media with frequency dispersion 78—5597
continuously coupled distributed coupling transducers, elec. and acoustic waves 77—50847
convergent sound beam in nonlinezr medium 78—1468
Cooper coupling, increase due to strong longitudinal sound 80—49990
correlation coeff. meas. for signals with stationary additive noise 78—94489
correlation of the phase and amplitude fluctuations between direct and ground-reflected sound 80—96067
corrugated surface, horizontal shear surface wave propagation 77—7957
cosmic ray detection, acoustic radiation by charged atomic particles in liquids, theoretical anal. 79—89526
critical binary mixtures, sound propag., mode coupling theory, validity breakdown 80—65159
critical freq. of flat plates in dense fluids *(German)* 80—38165

acoustic wave propagation continued
crystal classification by acoustic props. 78—79547
crystal lattice, beam instability and collective disturbance *(Russian)* 77—8676
crystal with spatial dispersion, circular dichroism 78—26632
cubic crystal, acoustic waves, Christoffel elastic eqns., and elastic consts. 79—51205
cubic crystals, elastic surface wave propagation 78—2357
curved ducts with central partition 78—55486
CW line spectra, determination of struct. using integration time and acoustic multipaths 79—59860
cylindrical acoustic waveguide containing moving viscous fluid, modal pattern anal. 79—32105
cylindrical duct with impedance walls, attenuation calc. 78—83146
cylindrical shells with finite regions of structural discontinuity, wave propag. 78—13841
cylindrical surfaces with nonuniform vel. distribs., radiated power and radiation loading 78—50969
cylindrical tubes containing slightly rarefied gas 79—23114
deep-water vertically directional beams, estimates of envelope spectra 79—86283
detonations, sound ranging in atmosphere, anal. problems 79—94393
dielectrics, phys. models of 1/f noise 77—71272
diffuse vibration field propag. in structs. with periodic inhomogeneities 80—86093
diffusivity of nonlinear wave propagation in pipes 80—33286
directivity of radiation from acoustic monopoles and dipoles, appls. to noise control 80—53515
directivity of sound radiated from large aperture in building 80—38148
directivity pattern calc. from near-field sound meas. 78—83149
discontinuities in linear, nonlinear acoustics *(French)* 78—46857
discontinuous or layer media, unidimensional propag. of transient signals 80—87265
dispersive fluid-filled tubes, asymptotic analysis 80—43500
dispersive systems, determ. of transmission path importance 77—72106
Doppler effect in special relativity for teaching 78—24609
duct, cylindrical, with acoustically absorbing internal surface 78—38142
duct, with axial sound speed variation, exact soln. 79—81588
duct of variable area, effect of flow on quasi-one-dimensional wave prop. 77—84037
duct propag., eigenvalue computation, integration scheme 77—46839
duct with liquid layer lying over half-space (Pekeris branch cut) 79—68464
duct with varying cross section and viscous mean flow, acoustic wave propag. 80—96267
ducted propag., asymptotic theory based on local evanescent wave fields 78—55484
ducts, acoustic characts. of bends 80—74554
ducts, finite element simulation 78—38115
ducts, mode-matching analyses of coupled fields, boundary conditions 79—32108
ducts, modified Galerkin method 79—10423
ducts, nearly annular, acoustic propagation 78—83141
ducts, nonhomogeneous, acoustic energy flux 79—7243
ducts, sound production and propagation 79—41473
ducts, sound propagation in parallel sheared flows, mode estimation 80—79026
ducts, theoretical aspects of wave eqn. and other props. *(French)* 80—53516
ducts containing sheared flows, analysis using geometric acoustics 80—33269
ducts with flow, damping, section discontinuity effects *(French)* 77—6576
elastic bars, phase boundary propagation, dynamic elastic bar theory, sound wave interactions 80—69706
elastic nonhomogeneous media, one dimensional response to acoustic sources 78—18083
elastic porous media, acoustic phenomena 78—25997
electron gas, nonlinear theory of sound wave propag. *(Russian)* 79—76904
elliptical waveguides, comparison of rigid and soft walled *(Japanese)* 77—42642
emission of sound by ionised inhomogeneity in nonuniform flow 78—30365
energy eqns. for acoustic fields in stationary and moving fluids 80—53525
energy-absorbent media, wave theory generalisation *(Russian)* 78—77725
explosion shock wave propagation in hollow circular cylinder *(Japanese)* 80—10175
explosive signals in shallow water, computer simulation 78—79160
explosive wave profile transformation, time constant derivation 80—48485
exterior problems of acoustics, integral eqns. soln. 79—27455
ferroelectric, acoustic activity near ferroelectric transition 77—90114
ferroelectric, acoustic props., at second-order phase transition, effect of polarisation fluctuations 77—85664
ferromagnet magnetisation, influence of high intensity longitudinal sound waves 80—103875
ferromagnetic conductor, cylindrical, acoustic wave propag., EM field behaviour 80—88857
fibrous networks in viscous media, acoustic theory of wave motion 78—59177
field suppression beyond narrow slit in rigid baffle, long wave approx. 80—102890
finite amplitude sound beam propag. in dissipative medium, nonlinear eqn. 79—32122
finite amplitude two-dimensional waves in rectangular duct induced by arbitrary periodic excitation 79—72739
finite beams, general expressions 78—38105
finite element simulation of acoustic transmission system with radiation 79—3862
finite-amplitude sound wave distortion cancellation *(Japanese)* 77—14832
finite-amplitude sound waves in inhomogeneous medium with caustics 77—68295
finite-amplitude wave, propag. through water-saturated marine sediments 78—1476
finite-amplitude wave propag. in media of various degrees of nonlinearity 80—53528

acoustic wave propagation continued
finite-length fluid cylinder, surface wave interpretation of eigenfrequencies 80—58831
fission reactor core control and monitoring *(Russian)* 80—5292
flames, vibrating, in tubes, dynamical props. 77—31388
flexural wave transmission across line inhomogeneity on plate in liquid, radiation of sound 80—38159
flow-duct acoustics, adjointness props. for differential systems with eigenvalue-depend. boundary conditions 77—50787
fluctuating media, propag. in oceans and atmosphere 77—53073
fluid consisting of two interacting components, analysis *(French)* 78—5844
fluid velocity vector and temp. fields, reconstruction, three-dimens., with aid of computer 78—51261
fluid-filled borehole, aysmptotic methods for first compressional head wave arrival 79—50482
fluids, acoustic wave propag., damping, flows in pipes *(French)* 77—19467
fluids, finite-amplitude effects 77—50794
fluids, HF short-wavelength fluctuations 77—50793
foliage effects on transmission through vegetation, expts. with model forests in anechoic chamber 80—33303
forward-scatter approx. 77—46832
free-jet, turbulent, experimental investigation of acoustic radiation 79—46102
freewave propagation through combinations of periodic and disordered systems 80—43494
frequency shift of wave train due to atmospheric absorpt. 80—64255
frequency-separated waves, fluctuations during reflection in randomly inhomogeneous medium 79—90049
fully developed turbulent pipe flow, low Mach number wall turbulence—sound interaction 80—6148
Galaxy, hot interstellar matter effect of sound wave propagation in hot gas 80—109511
gas, dissociating, sonic wave propagation, formation of shock waves 80—64672
gas, real, viscous, heat-cond., acoustic nonequilib. phenomena 78—47086
gas filled tubes, thermoviscous regions for principle and higher modes 80—96057
gas mixtures, disparate mass, double sound propag., theory 80—33724
gas phase reaction systems, sound interaction 77—84024
gas stream in axisymmetric channels, acoustic disturbance propagation, gas-turbine noise appl. *(Russian)* 79—32131
gas with porous medium obstacle, scalar Helmholtz eqn. 80—74552
gas-liquid mixture, acoustic disturbance propag. 78—9473
gas-liquid mixture, arbitrary amplitude acoustic wave propag. 78—38122
gas-liquid mixture, self-action mechanisms 78—38118
gasdynamics, nonequilib., sonic discontinuities growth and decay 78—34209
Gaussian beams, nonlinear propag. 80—87609
generalised wave theory applied to low frequency and deep water sound propagation *(French)* 80—53505
generalized beam pattern assoc. with approx. solns. of source extraction integral eqn. 78—51009
glass, insulating, thermal, acoustic props., low temp. anomaly microscopic model 80—28921
granular solid, one-dimens., small amplitude wave behaviour 78—59339
ground, spherical wave diffraction model 80—74555
ground-to-ground noise propag., measurement by synchronized integration technique *(Japanese)* 80—19188
guided, rigorous asymptotic theory of evanescent waves 80—64238
guided acoustic waves in the ocean, review 79—39753
guided mode propagation, parabolic approx. 80—43506
half-space with sinusoidal boundary 80—19116
halogens, crystallised, acoustic wave velocity calc. from phonon curves *(French)* 77—1180
hard sphere system, surface tension, compressibility, bulk modulus press. coeffs. and Rao's acoustical parameter 80—80027
harmonics, generation by longitudinal elastic waves 77—79991
harmonics of the difference freq. in saturation limited parametric sources 78—30110
HF, non-linear effects in tubes 80—87614
high thermal conductivity mecia, model equations for the nonlinear acoustics 78—90565
higher order mode effects in circular ducts and expansion chambers 80—96058
horn loudspeaker, anal. of acoustic radiation by finite element method 80—96171
hybrid ray-mode formulation of ducted propagation 79—50477
hydrophone array response calc. errors due to two dimensional beam pattern assumption 78—66972
in-duct acoustic props. meas., transfer function method, expt. 80—106688
in-duct acoustic props. meas., transfer function method, theory 80—106644
incompressible flow with density as function of time *(French)* 80—53517
industrial sound meas., transducer function, basic theory *(German)* 77—80037
infinite plate with losses, flexural vibrs. in fluid 78—83319
infrasonic signals from thunder 79—70846
infrasound waves, in the Earth's atmosphere *(Russian)* 78—32143
inhomogeneous anisotropic media, 3-dimensionally, geometrical acoustics 79—64372
inhomogeneous anisotropic media, ray approx. 78—83153
inhomogeneous granular solid, one dimens. accel. waves, speed, amplitude 78—87288
inhomogeneous media, diffraction of sound waves, derivation of generalised parablic equation and evolution of Gaussian beams 79—64377
inhomogeneous medium, Poincare-Lighthill-Kuo method 78—83133
inhomogeneous medium with slightly varying sound vel., confined beam propag. 78—1467
intense sinusoidal pressure waves in air, finite amplitude distortion 80—33273
intensity distrib. in sound channels, coherence theory 78—79152
internally excited three-layer cylindrical shells, acoustic reduction 80—5874
inverse scattering problem 78—38103
ionised gas in applied mag. field, acoustic instabilities 78—9719
ionising particle beam interactions with liquids, acoustic effect, laser beam simulations 80—23262

acoustic wave propagation continued
ionospheric plasma, weakly ionised quasihydrodynamics approx. *(Russian)* 77—82079
isothermal shock waves in nonhomogeneous medium 77—55017
isothermal shock waves in perfect gas, density increase 77—55016
isotropic materials, rod shaped, elastic moduli and Poisson ratio determ. method 80—55606
isotropic viscous weakly compressible medium, eqn. limits problem *(French)* 80—8808
jet, free, aeroacoustic characterisation *(French)* 79—41727
jets, wave propag. on acoustically perturbed jet 79—81592
Lagrangian and Eulerian representations of linear acoustic fields *(French)* 79—41477
Lagrangian-mean flow, exact theory of nonlinear waves 79—37331
laminated composite, horizontal shear surface waves 77—80687
laminated composite, nonlinear transient pulse propag., interface reflection effect 78—63222
Landau damping in regular wave interaction with noise 80—33284
layered acoustic waveguide, group delay time, temp. coeff. var. 78—83152
layered metal structure, acoustic size effect, sound attenuation anisotropy *(Russian)* 79—46752
layered systems, direction control 80—103557
LF multipath fluctuations in the ocean, statistical anal. 78—90571
LF transmission through walls of rectangular ducts, effects of external lagging 80—53544
linear, perfect fluid at rest with piecewise indefinitely differentiable characteristics appl. *(French)* 78—55488
lined ducts with flow, finite element formulation of eigenvalue problem 80—23819
liquid, nonviscous, laser-induced acoustic waves 78—63808
liquid, simple, perturbation theory for sound prop. vel. *(Russian)* 77—15500
liquid crystals, acoustical activity 78—83880
liquid with gas bubbles, acoustic wave self-transparency effect *(Russian)* 80—14509
liquid with nonlinear friction-velocity relationship, asymmetry phenomenon *(Russian)* 78—22913
liquid-saturated open cell foam in circular tube 79—41470
liquid-vapour mixture, acoustic wave propag. 78—90972
liquids, relation between sound vel. and mean vel. of thermal motion of molecules 79—14885
liquids acoustic relaxation mechanism, using coherent optoacoustic spectroscopy scheme 80—5890
locally distributed boundary of a half-space, axisymm. emission 78—42485
long-range tracking, Doppler effects 78—30116
longitudinal waves, theory, radiation press. problems appl. 78—25998
Love wave interaction in thin film with periodic surface corrugation 79—14130
lungs, sound wave propag. in acoustic ducts 77—12981
M-sequence modulated acoustic signal propagation meas. *(Japanese)* 78—18132
magneto-acoustic waves, generation and radn. in compressible fluid 77—68699
magnetoelastic media, nonlinear effects 77—27413
Mandel'shtam and sound propagation in microscopically inhomogeneous media 80—101704
marine sediments, penetration as function of physico-mech. characts. *(French)* 80—33324
mathematical techniques for soln. of problems 80—53514
measurement of short-range propagation, coherency recovery by pilot signal *(Japanese)* 80—53499
melts of transparent organic substance simulating metals, acoustic streaming 80—5861
mesosphere, acoustic-gravity waves propagation 78—44912
metal, nonlinear interaction of strong and weak sound waves 78—59865
metals, HF sound propagation, nonlinear effects, review 80—88279
metals, higher sound harmonic generation in momentum nonlinearity regime *(Russian)* 78—38783
metals, sound pulse spike like transport near acoustic cyclotron resonance *(Russian)* 80—100617
MHD medium, acoustic pulse propag., disperison *(Russian)* 78—5809
micropolar thermoelastic solids, entropy inequality and accel. waves 78—47538
minerals, acoustic non-linearity parameters 78—20392
modal theory, broad-band active sound absorption in a duct carrying uniformly flowing fluid 80—74556
mode theory of propag. in bilinear medium, WKB approx. 77—7229
moving fluids, transport eqns. and acoustic motion 80—53523
moving sources in flow, appl. to aircraft noise 80—53526
moving thermal source, acoustic perturbations in medium 80—87597
multi-blade fan as reference sound source, influence of reflecting plane *(Japanese)* 80—19189
multimodal far-field acoustic radiation pattern using mode cutoff ratio 79—32107
multimode waveguide, active sound fields suppression system 78—18113
multimode waveguide with uneven walls, sound attenuation 78—83147
multipath channels, comments on coherence estimates 80—58832
multipath signal, individual pulse resolution, signal processing techniques 78—83176
multipath signals, narrowband, with and without FM or phase modulation, first-order statistics 79—98550
multiple paths, coherence estimates 79—50479
N-shaped sound pulse propag. behaviour *(Japanese)* 77—84034
near-sonic duct flows, linear acoustic theory 77—75728
nematic liquid crystal, order parameter fluctuations and anomalous sound propag. just above clearing point, critical dynamics 80—15224
nematic liquid crystal near transition to isotropic liquid 79—19320
noise propag. along finite impedance boundary, aircraft ground noise appl. 78—9487
noise propagation around thin half-plane, numerical calc. 78—9486
nonhomogeneous elastic rods, similarity soln. of wave propagation 78—59323
nonisothermal atmosphere, rel. to solar five minute oscills. 80—31276
nonlinear, induced by vibr. cylinder, 2-dimens. case 79—23120
nonlinear, induced by vibr. cylinder, 3-dimens. case 79—23121
nonlinear adiabatic waves in self-gravitating gas, astrophys. appl. 78—28512
nonlinear diatomic chain, initial-velocity disturbance 77—1186

acoustic wave propagation continued
nonlinear elastic medium, mutual focusing of sound waves *(Russian)* 78—26001
nonlinear interaction of two collinear, spherically spreading sound beams, appl. to parametric acoustic arrays 80—48484
nonlinear media, statistical characts. of random quasimonochromatic waves 78—38116
nonlinear media containing chaotic inhomogeneities, equation closure for average field 79—81601
nonlinear one-dimensional waves in near-sonic flows 79—41701
nonlinear propag. of sound beams with uniform amplitude distrib. 80—102896
nonlinear propag. of waves induced by infinite vibrating cylinder 80—33279
nonlinear propagation of axisymmetric beam in nondispersive medium 77—34979
nonlinear propagation of finite amplitude sound wave through circular pipe, simulation 78—13834
nonlinear wave propagation, analytic solns. for accel. waves, non-equilib. effects 78—94890
nonlinear wave propagation, spectral and pseudospectral methods, turbulent sound wave appl. 77—5672
nonlocal diffusion theory of wave propagation in highly viscous liquids 80—102897
nonstationary, propagation in ideal liq. layer 79—68458
nonuniform ducts, wave-envelope technique 78—9464
normal mode amplitudes in random ocean, statistical theory 78—50981
ocean, internal waves, acoustic refractive index modulation, parabolic moment eqns. 80—83698
ocean, long range acoustic propag., statistical anal. of signal intensity 78—90569
ocean, long-range, transfer function for motional source 79—14140
ocean, sound propagation in an ocean shelf zone of arbitrary profile 78—90576
ocean, two-point coherence function models with inhomogeneous background and anisotropy 80—81922
ocean bottom roughness effects on LF propag. 79—41501
ocean ducts, range dependent, acoustic flux formulae 80—96075
ocean sound channel with range depend. parabolic sound speed profile, normal modes 78—33941
ocean surface ducts with rough boundaries 78—55493
oceanic finestructure effects on acoustic transmission, numerical simulation 80—43511
oceanic guided waves, acoustic flux methods 80—96077
oceans, three dimensional sound ray paths in basins, troughs and near seamounts using ray invariants 78—30113
octylcyanobiphenyl, second sound propag. and smectic response function, forced Rayleigh scatt. obs. 79—86693
one-component gas, relativistic Burnett eqns. and sound propag. 77—15150
open waveguides, phase vel. bounds 77—58497
outdoor propagation of finite-amplitude noise 80—33338
outdoor sound, ground and building scattered sound fields, black body radiation analogue 80—69579
outdoor sound propagation over hard ground for distances under 200 ft, exp. study, community noise appl. 79—18600
P-wave seismograms from continuously varying transition zones, acoustic media 78—20361
parabolic approx., correction based on second range derivative 79—14146
parabolic waveguide, statistical theory of propag. 80—102887
parabolic-coherence function model 79—23111
parallel jets exhausting from ducts 80—64257
parametric acoustic array, similarity theory and dimensional anal. 78—38119
Pekeris operator, resolvent in dispersive media *(French)* 79—41488
phonon drag by acoustic waves in solids 77—27947
physical and technical acoustics, conf., Parnu, USSR (Apr. 1976) 78—1451
piecewise uniform ducts, momentum and energy theorems 80—74550
piezoelectric boundary waves propagating along SiO_2 and $LiTaO_3$ interface, characts. 79—14149
piezoelectric cryst., excitation and energy flux of acoustic harmonic 79—15404
piezoelectric crystal, acoustic activity 78—26631
piezoelectric crystal, acoustic activity and other effects due to spatial dispersion 78—2808
piezoelectric crystal, energy flow and group vel. of sound waves 77—39633
piezoelectric crystal, three-field electroacoustic parametric interactions 79—1740
piezoelectric crystals, acoustic waves, group vel. characts. 80—92613
piezoelectric crystals, surface modes, acoustic wave propagation 80—20026
piezoelectric hexagonal crystal, acousto-EM modes *(Spanish)* 77—4602
piezoelectric rods, hexagonal crystal symmetry, wave propagation 78—56429
piezoelectric semiconductor, longit. phonon-plasmon interaction, density gradient inhomogeneity 79—56156
pipe, arbitrary temp. and flow profiles effect in sound speed 78—9467
piston source, circular, meas. of fundamental and second harmonic pressures in acoustic field 79—46101
plane harmonic waves, infinite isotropic medium having embedded doubly periodic array of cylindrical fibres 80—87607
plane sound sources, radiation pattern *(German)* 77—42639
plane wave fluctuations of arrival angle at line array 80—43515
plane wave normal and oblique interaction with plane shock, wavenumber jump conditions 78—1466
plane-layered medium, strong sound wave propag. 77—34980
plasma, ion acoustic soliton, Boussinesq eqn. description 79—46449
plasma ion-acoustic waves excitation by piezoelectric surface acoustic wave 80—10381
plastic flow, discontinuous, acoustic wave spectrum resulting from interaction with unstable thermal mode 77—27937
plate excitation, difference of structure-borne-sound levels in point excitation and large area excitation *(German)* 80—53538
plate in turbulent pressure-fluctuation field, vibrations and sound radiation 78—38130
plates, rectangular elastically supported, vibration and sound radiation 77—72112
point source in certain built-up urban environments 80—58841

acoustic wave propagation continued
point source in one-dimensional, randomly inhomogeneous medium, with specularly reflecting walls 80—105514
polarisation effects in crystal acoustics, linear and nonlinear 80—5855
polarisation field for body waves in anisotropic elastic media, topological nature 80—49309
polyacrylamide gel, audiofrequency very slow propagating mode 79—74429
polymers, highly oriented, elastic wave dispersion relations 78—51618
porous elastic solid containing compressible viscous fluid *(French)* 80—38149
porous media, fluid-filled, propag. and decay 79—7248
potential field induced by an acoustic wave incident upon a moving plane 79—37342
pre-seismic sound *(Chinese)* 79—34760
pressure wave, two dimens. cylindrical, excited by moving load, propag. in acoustic medium 77—68300
product of matrices, random transfer in harmonic longitudinal acoustic wave *(French)* 78—5596
proton beam effects in fluid media, acoustic signal prod. 78—38162
pulse-modulated intense wave in atm., low freq. component nonlinear generation *(Russian)* 79—98522
pulsed radiolysis acoustic wave generation in liquids 79—8446
pulsed signal models, representation by ordered sequence of uniform information elements magnitudes *(Russian)* 80—38180
quartz, acoustoelectric methods 80—84359
quartz, fused, elastic wave excitation by charged particle beam 77—89474
quasilinear hyperbolic systems, propag. of weak discontinuities when charact. shock occurs 78—79153
radiating gases, sonic wave propagation 77—47114
radiation by plane structures with diffuse flexural-wave field 80—102912
radiation from a submerged elastic shell subjected to a time harmonic internal press., calc. 78—90572
radiative acoustics eqn., effect of non-transverse magnetic field 77—87252
random, methods of analysis 80—53527
random media, propag. in frozen oceans 77—50814
random media, theory and appl. of wave propag. and scatt., review 77—75376
randomly perturbed one dimens. wave eqn., multiple-scales space-time anal. 78—8247
in rarefied gas, linearised BGK model calcs. 79—64369
rarefied gas, solns. of linearised modeled Boltzmann equation 80—53912
Rayleigh and Langevin radiation press. magnitude calc., longit. wave propag. theory appl. 78—25999
Rayleigh wave, propag., isotropic elastic material with homog. strain 78—94460
rectangular duct, propag. in shear flow with temp. gradient, investigation using finite-element analysis 79—94379
rectangular ducts with sinusoidal undulations 80—74551
rectangular parallel layers, sound propag. effect of boundaries *(German)* 78—18082
rectangular piston radiation impedance 78—33937
relativistic theory of influence of relaxation phenomenon on sound propag. *(French)* 77—37754
relaxing gas, nonlinear waves propag., weak influence of relax. 77—55100
resolvent of Pekeris operator with Neumann condition 78—38110
resonance interaction of sound waves with plane parallel flow 77—814
ribbed cylindrical shell immersed in liquid, dispersion curves and coeffs. of distribution function 80—87736
rigid 3-dimens. waveguides, anal. of propag. using eigenfunction expansion of Helmholtz eqn. 80—83690
rigid planar sharp bends and bifurcation ducts 80—87585
rods, elastic, linear, nonhomogeneous, propag. and decay of shock and accel. waves 78—83278
rotational flows, as example of flow-acoustics 77—75903
sand, water-saturated, broadband meas. 80—83719
sapphire rod, numerical description of torsional vibrs. 77—51435
sapphire rod, wave propag. 77—51434
SAW propagation study based on coherent light diffraction *(Russian)* 79—14172
sediment shear wave effects on ocean bottom refl. loss, ray path anal. 80—96084
sediments, penetration of highly directional acoustic beams 80—14511
self-detection of finite amplitude sound waves with large Reynolds numbers 78—5600
self-excitation of subharmonics in rectangular ducts 77—46838
self-induced sound generation by flow over perforated duct liners 77—54990
semiconductor, acoustic studies progress *(Japanese)* 80—49310
semiconductor films, narrow-joined, sound propagation, in strong EM wave field *(Russian)* 80—39483
semiconductors, HF sound propagation, nonlinear effects, review 80—88279
semimetals, higher sound harmonic generation in momentum nonlinearity regime *(Russian)* 78—38783
shallow ocean water, Naval Research 79—25258
shallow sea, infrasonic field structure determ. with machine expt. 80—14512
shallow-water propagation, investigation using reduced scale model *(French)* 79—3825
shallow-water sound propagation 79—5493
shear layer with linear velocity profile, closed-form solns. for sound propag. 80—6074
shear waves, rotary activity under helicon-phonon interaction 80—2412
shear waves in an infinitely extended medium perforated with a row of cylindrical ducts 79—32116
signal form distortion, in absorptive medium *(Russian)* 78—46856
signal processing, sparse array technique, min. output variance, S/N ratio 78—83177
silencing systems, acoustic charact. anal., 4-terminal matrices of tube system *(Japanese)* 80—10082
silencing systems, acoustic charact. anal., attenuation const. of plane wave in tube *(Japanese)* 80—10081
slotted acoustic waveguide propagation expts. *(Japanese)* 78—46859
slow waveguide, in water, Helmholtz eqn. soln. 78—30114
solar atmosphere, acoustic waves interaction with mag. flux tubes 80—85911

acoustic wave propagation continued
solar atmosphere, acoustic waves propag. and chromosphere temp. rise 79—16911
solar atmosphere, efficiency of one-dimens. hydrodynamic codes 78—57520
solar atmosphere, heating of chromosphere and corona by sound waves 79—21246
solar atmosphere, radiative damping of acoustic waves 77—53496
solar atmosphere, shock wave development from acoustic waves, theoretical temp. min. 77—53497
solar atmosphere, spectral line profiles, acoustic wave effects 80—46517
solar atmosphere and solar wind, momentum and energy transport by waves 78—4162
solar atmosphere upper layers, convective noise waves dissipation in mag. struct. 78—65600
solid, low temp., first and second sounds interaction *(Russian)* 79—86841
solid superconductors, Ginzburg-Landau and linear elasticity eqns. 78—95395
solids, acoustical props. 77—51448
solids, how the structure of a medium is seen by an acoustic wave 80—65163
sonar range prediction, inherent errors 78—66977
sonic boom propag. in thermosphere 80—33305
sonic discontinuities propagation through thermally conducting and dissociating gases 78—30311
sound beam, self defocusing in presence of acoustic streaming 77—14833
sound propagation along an impedance surface, numerical calcs. 80—87590
space-time processing of acoustic signals in waveguides 80—5878
space-time structure of acoustical field anal. by means of optical Fourier transform *(French)* 80—87583
spark-gap, electrodes, acoustic phenomena in erosion 80—64796
spatial coherence of acoustic signals in randomly inhomogeneous waveguides 77—58521
spectral analysis of wave perturbations in D-layer and F-layer 80—21873
spherical wave interaction with elastic spherical shell, comments and reply 77—50789
splitter plate acoustics, zones of silence in sound wave-jet flow interaction 79—3819
standing wave analysis for duct with temp. gradients 77—62085
stellar winds, radiative amplification of sound waves in OB stars 79—96999
stochastic waves, temporal moments, mutual coherence function 78—20979
structure-borne sound, procedure for meas. sensitivity of building structures to stationary excitation *(German)* 80—64287
sub-beams interpretation, appl. to radiation fields 77—50788
submerged structures, doubly asymptotic approximations for transient motions 79—14132
subsonic nozzle flow, propag. of acoustic and entropy disturbances 77—75958
Sun, acoustic mode overstability in polytropic atmosphere 78—49413
superfluid, Poisson's formulas for wave propagation 78—38891
surface waves on anisotropic substrates, transverse amplitude dependence 79—7242
surface waves on complex impedance ground 78—55491
survey of investigations, historical, propag. in ideal and non-ideal media *(French)* 80—53513
temperature behaviour, piezoelectric coupling in quartz, $LiNbO_3$, $LiTaO_3$, Tl_3VS_4, acoustic surface wave propag. *(French)* 78—35093
temperature gradient effects, thin shear layer expansion 77—14826
TGS crystal, generation of second acoustic harmonics 78—18711
thermal self-action of sound waves, theory 77—3692
thermally conducting and radiating gases 78—42679
thermally conducting medium, propag. of acoustic pulse 77—27409
thermoacoustic waves in cylindrical porous tube, Rijke tube limit *(French)* 80—74553
thermooptically excited acoustic pulses propag. 80—102891
thermosphere, wave-induced diffusion effects on acoustic-gravity waves 78—61637
thick specimen visualisation with reflection acoustic microscope, acoustic field distribution 79—76922
thin plate, longitudinal- and flexural-mode attenuation by periodic surface corrugations 79—90048
in thin-walled nonuniform elastic tubes containing incompressible inviscid fluid 77—79981
transformation operators and wave propagation in a spherically stratified medium 79—18569
transonic flow, excitation of nonlinear plane waves by volume sources 80—38154
transverse acoustic wave at solid-solid interface 79—32118
triangular pulses with discontinuous edges, interaction with shock waves 77—50802
tubes and flexible hoses carrying moving liquid excited in transverse vibrations, nonconservative boundary-value conditions 79—63056
turbulent dipole, sound generation, model 77—68296
turbulent jets using organ pipe flue 80—91946
turbulent media, scatt. and interaction of sound with sound *(Russian)* 79—18571
two dimensional acoustically lined duct, sound radiation from open end 78—33936
two-dimensional solids and hexatic liq. crysts., nonlinear hydrodynamic props., theory 80—100169
typhoons, detection and appl. of associated acoustic waves *(Chinese)* 79—34996
unbaffled cylindrical pipe outlet, impedance for plane wave incident at outlet 79—55256
unbounded elastic plate influence on point source radiation 78—1456
underground gas-filled pipes, accompanying surface displacements 80—83692
underwater, acoustic line array operation in water layer 80—5866
underwater, intensity fluctuations spectrum in internal wave freq. range 80—64268
underwater, multipath, impact of ocean acoustic transfer function on coherence of propagations 79—59861
underwater, temp. variation of acoustical props. of laboratory sediments 80—96069
underwater, Virtual modes and mode amplitudes near cutoff 79—81607
underwater acoustic fluctuations, aspects of apex approximation 79—41498

acoustic wave propagation continued
underwater acoustic surface duct propagation model based on radiation transport eqn. 80—46196
underwater duct problems, variational anal. techniques 78—90574
underwater parametric acoustic source beamwidth control 78—75011
underwater propagation in deep channels, analysis *(French)* 79—72745
underwater propagation in shallow water expts. for long range communication systems 80—33323
underwater propagation prediction measuring system at sea, WPA prototype 78—69552
underwater sound, passive localisation of moving source 79—3826
underwater sound, pseudoresonances and virtual modes 79—14144
underwater sound propagation in presence of randomly perturbed parabolic profile 78—94477
underwater US pulse propag. and reflection by small targets 78—50986
undostatic interactions, in travelling elastic wave 77—46834
unified wave propagation theory, tenuous random medium 78—4491
urban and forest areas, prediction of noise appl. *(German)* 80—38142
urban environment, sound attenuation at street intersection 78—13846
vaneless diffuser, sound propag. and transmission 80—19121
vapour-droplet mixtures, small perturbation propagation 78—95111
vapour-liquid mixture, propagation of acoustic disturbances, model 80—103058
vibrational energy propag. in absorbing structs. 78—9596
vibrationally excited gas, in elec. discharge, sound propag. 78—18370
viscoelastic rod with temp.-depend. props., propag. theory 77—54822
viscous heat-conducting gas, wave propag., Poisson type integrals calcs. 78—38445
wall jet flow, compliant walls, influences of flow convection and refraction on sound radiation 80—74595
water, acoustic cavitation threshold and tensile strength, theory 79—42131
water, laser-induced acoustic waves 78—25996
wave amplitude variance in random medium with nonuniform background 78—38104
wave propagation and underwater acoustics, book 78—90577
wave-front method for dynamics of high damping bar 77—23895
wave-guides, slowly-varying, acoustic and liquid wave propag. 78—4490
wave-theory peaks in range-averaged channels of uniform sound velocity 80—96076
waveguide, fluid-filled, with transverse resistivity, mode-selective soond transmission 78—1452
waveguide, limited frequency sound suppression 78—83148
waveguide, rough boundary, spatial and temporal correl. functions for stochastic part of sound field 78—90560
waveguides, discretely-layered, damping of normal and surface waves, depend. of vel. on losses 79—14135
waveguides, group vel. direct calc. from dispersion curve 77—27407
waveguides, irregular, with compliant or rigid walls, approximate wave eqns. solns. 79—90050
waveguides, nonuniform structural, long-wavelength asymptotic solns. for axisymmetric compressional waves 79—50485
waveguides with moving medium, energy transport 77—46837
weak shock waves in chemically reacting gas *(Russian)* 78—42681
wideband array synthesis method 78—38120
wind speed distribution, effect on sound propag. outdoors *(Japanese)* 79—1018
Young sound wave propagation in thin electrically loaded piezoelectric waveguide 78—38112
Zabolotskaya-Khokhlov eqn., exact solns. determ. via symmetries 77—805
Al, acoustic non-linearity parameter in cubic crysts. 77—51444
Al alloy rod, wave profiles generated by short shock pulse 78—6125
CdS, electro-acoustically active, AC impedance meas. 80—103726
CdS, semicond., coexistence of surface and bulk acoustic waves in acoustoelec. domains 80—44404
Cu, acoustic non-linearity parameter in cubic crysts. 77—51444
$CuCl_2$, aqueous soln., nonlinear conversion of acoustic pulses with thermooptic excitation 80—14510
He, superfluid, detection of second-sound shock waves using fast-response superconducting thin-film probe 79—63237
He-Ne mixtures, disparate mass, double sound propag., theory 80—33724
^{3}He-He II dilute solution, fourth sound velocity 80—70498
^{4}He superfluid films, geometry induced third sound splitting 80—96712
InSb, magnetoacoustic wave excitation by acoustic wave propagation 80—88597
KCl, acoustic non-linearity parameter in cubic crysts. 77—51444
KH_2PO_4, electro-optic modulators, transient acoustic waves 79—59809
KH_2PO_4 electro-optic modulator crysts., piezoelec. induced acoustic transients 80—70316
$LiNbO_3$, anisotropy and phase velocities of prop. of elastic waves 79—1478
$LiNbO_3$, opposed interaction of acoustic waves 77—24360
$LiNbO_3$ SAW devices, SAW and bulk wave propag., freq. shift holography *(Japanese)* 79—59895
$LiTaO_3$-SiO_3, temp. compensated SAW device fabrication 79—76923
Mn-Cu alloy, acoustic shock pulse characts., stress amplitude and temp. depend. 79—19323
$Mn_{0.53}Zn_{0.35}Fe_{2.12}O_4$, and Ti substituted, acoustic losses 79—24207
NH_3 halides, acoustic anomalies above critical temps., volume magnetostriction type terms 80—2123
NaCl, acoustic non-linearity parameter in cubic crysts. 77—51444
RbCl(Br)(I), acoustic non-linearity parameter in cubic crysts. 77—51444
Xe, liq., acoustic nonlinearity parameters *(German)* 79—77685

acoustic wave reflection
see also echo; reverberation; ultrasonic reflection
2-dimensional reflecting medium over circular domain, exact soln. of reconstruction 80—64299
absorbing sphere, sound refl. 78—18084
aircraft noise measurement, interference of direct and ground-refl. waves, height depend. 77—23813
amplitude calc. method for reflection from rigid spherical body *(Japanese)* 77—50791
anisotropic solids interface, acoustic wave refl., transmission and mode conversion 79—76903
arbitrary continuously stratified environments, propagated, reflected and transmitted acoustic waves 78—13829
architectural acoustics 80—64288

acoustic wave reflection continued
atmosphere, Concorde sonic booms as probe of temp.-wind parameters 77−91323
atmospheric phenomena, analytical solns. of wave eqn. 80−53530
auditoriums, effect of direct reflections 80−33345
backscattering from very rough water surfaces 79−41499
bivariate beamshaping in elliptic case, numerical method for reflector surface design 77−27225
boundary between piezoelec. ceramic and water 80−87588
boundary layer effects on weak shock wave and sound wave refl. at shallow incidence 78−22373
cochlea, one-dimensional model illustrating resonance 80−61581
composite plates, thick fluid-loaded, structural response function 79−94381
composites of wood, steel and rubber, underwater acoustic reflection 79−94394
concert hall, musical instruments directivity rel. to efficiency of acoust. refl. or absorpt. *(German)* 77−829
concert hall design, lateral and ensemble reflection requirements 80−91964
concert hall design for orchestral balance in seats behind stage 80−91963
concert hall problem, coherence length and diffuse reflection formulation 80−91962
contact interface, total reflection of SH waves in presence of slip and friction 79−98519
corrugated surface, Rayleigh and Waterman theories 80−96063
crustal structure estimation from acoustic reflection meas., Cramer-Rao bound 77−5369
curvilinear boundary in medium, calc. of field amplitude in refl. of rays 77−33874
cylindrical cavity in absorptive medium, elastic wave reflection 78−55582
cylindrical shell, evaluation procedure for refl.-reduction coating 78−9468
cylindrical shells with finite regions of structural discontinuity, refl. and transmission efficiencies 78−13841
diffuse sound reflection by max. length sequences 77−7230
discrete layered media, structure estimation accuracy 79−23108
ducts, acoustic characts. of bends 80−74554
elastic cylinders and spheres immersed in fluids 78−30106
elastodynamic diffraction, by periodic rough surface (stress-free boundary) 78−13826
enclosure, thermoviscous dissipation at walls, normal mode theory 78−83171
finite amplitude wave refl. in parametric array 77−84036
fish, target strength at any aspect 78−30115
flowduct area discontinuity, experimental investigation of acoustic pressure reflection coeff. 80−33302
fluid-solid boundary, cavitation effects, bubble collapse, US cleaning and cavitation erosion 80−65158
forward reflection from rough sea surface statistical anal. 78−50983
frequency-separated waves, fluctuations during reflection in randomly inhomogeneous medium 79−90049
Fresnel zone plate, for focusing of sound waves *(German)* 80−5888
gas-bearing sediments 80−87630
geometric properties for refl. fields from general surface, finite difference method 77−84026
geophysical structure estimation from acoustic reflection meas. 78−7818
ground reflection, nonlocal boundary conditions 79−18573
ground reflection effects on measured acoustic spectra, appl. of cepstral techniques 77−31165
guide step analysis 78−1487
Gulyaev-Bleustein and Rayleigh wave reflection from rectangular and curves ends of cryst. 77−80028
harmonic acoustic waves, refraction to tunnelling transition 79−46099
high-resolution ocean subbottom survey data analysis model 80−46211
impedance cylinders, calc. of differential cross sections 79−41474
in-duct acoustic props. meas., transfer function method, expt. 80−106688
in-duct acoustic props. meas., transfer function method, theory 80−106644
inhomogeneous layers, optimal distrib. of density and dilation modulus 80−19117
interacting finite amplitude waves, reflection and distortion, initial boundary value problem 80−53699
interface between elastic waveguides, variational method for modal solns. 77−84027
interface of two highly stressed elastic half-spaces 78−63213
isothermal shock wave, from rigid wall 77−55035
laboratory acoustic interference expts., refl. effects 77−22353
Laval nozzle, reflection of acoustic waves from subcritical inner parts 77−27574
layered elastic absorptive cylinders, matrix theory 77−46826
layered medium, sound refl. coeff. freq. and ang. response 77−11078
LF sound waves propag. in Arctic channel with irregular ice boundary 77−11079
liquid layer, error of interference methods for relf. coeff. meas. 77−14865
liquid surface, influence of condensation or evaporation 79−46097
liquid-solid interface, plane sound wave reflection and refraction in mag. field 80−38150
living room loudspeaker performance problems *(German)* 79−90081
lossy liquid-lossless isotropic solid interface, reflection coeff. 79−72733
loudspeaker cabinet reflection effects 79−64451
magnetoelastic ribbon position sensor 79−80603
model of nonreflecting anisotropic medium 80−5856
moving and rotating barriers, math. anal. 78−93539
moving material interface, freq. modulation and wave number conservation 77−7231
multichamber sound reflector, design parameters 78−94500
multilayered media, layer-indexed acoustic reflection model 80−43517
multiple refl. from rough surface, correl. characts. 77−68288
N-wave reflection at open end of circular pipe, nonlinear reflection meas. 80−79027
narrow beam sound waves, rigid cylindrical tube 80−69578
noise, aerodynamically generated, refl. at solid boundary, boundary layer turbulence *(French)* 80−43694
noise suppression, multiple relf. rel. to sound fields compensation 77−14852
nonlinear effects in vicinity of HF transducer 80−38152
obstacle in one-dimens. medium with random inhomogeneities 80−58839

acoustic wave reflection continued
obstacle in waveguide, acoustic wave transmission and reflection 80−102893
obstructions in pipes with flow, meas. method 78−63246
ocean, diffr., refl. and interf. during near grazing and near normal ocean surface backscatt. 78−90570
ocean, Stoneley wave effects on plane wave reflection coeffs., bottom reflection characts. 78−87180
ocean bottom, ray theory model of acoustic interaction 79−98532
ocean bottom, space scales of reflected signal fluctuations 79−90066
ocean bottom, technique for meas. plane-wave refl. coeff. 80−96081
ocean bottom and surface, correlation measurement of reflection coeff. 80−58848
ocean bottom interaction, plane wave reflection loss model based on numerical integration 79−10425
ocean bottom layering influence on reflected FM signal characts. 78−50991
ocean bottom plane-wave reflection loss model including sediment rigidity 80−33311
ocean bottom reflected signals, isotopicity of correlation characts. 79−86284
ocean bottom reflection data processing by digital deconvolution 77−33223
ocean bottom reflections, nonparametric estimation of plane wave refl. coeff. 79−7252
ocean bottom-reflected pseudonoise signals, correlation with transmistted signal 80−58846
ocean floor, refl. and attenuation obs. at 4 kHz 77−2140
ocean sediments, math. model 77−91104
ocean surface, acoustic sidebands obs. in CW tones at long ranges 77−7244
oceanography, acoustic reflection profile display using dot matrix plotter with minicomputer 77−9548
outdoor environment, refl. simulation for assisted reverberation effect 78−13825
outdoor sound, ground and building scattered sound fields, black body radiation analogue 80−69579
paramagnetic liquid, effect of APR on sound refl. at solid-liq. interface 78−35025
Pekeris model, reflection loss and mode attenuation 79−98534
phased arrays use in very shallow water 78−1482
piezoelectric crystal, acoustoelectrical waves, double refl. and birefr. 80−11047
piezoelectric-semiconductor corrugated boundary, reflected acoustic wave amplification *(Russian)* 78−30819
piezoelectrics, elastic wave leakage across gap 78−6204
pipe with fluid flow, sound wave reflection at end *(Japanese)* 79−68457
pipes, open ended, end corrects. determ. for fundamental reson. freq., material effects *(Korean)* 77−27443
plane compressional wave reflection on free surface, reflection coeffs. 77−31152
plane hyperdetonation shock wave reflection from rigid wall 78−75167
plane reflector in scatt. medium, sound refl. calc. 77−810
plane wave reflection, existence of Stoneley waves as loss mechanism 79−50498
plane wave reflection from a plate immersed in and floating on a liquid 78−83132
plane waves from flat boundary in micropolar half space, graphical method 77−11060
point source radiation near cylindrical jet in motion 77−31169
point source radiation through composite medium 77−31150
pseudo-steady single-Mach reflection, reconsideration of shock polar soln. 80−99893
pulse-echo technique for determ. of parameters of liquid-filled shells 78−1462
quadrupole near fluid interface, sound refl. and radiation 78−9475
quartz wedge, reflection, transmission and conversion of normally incident SAW 80−2257
randomly inhomogeneous medium with reflecting boundary, wave intensity fluctuations 80−42075
Rayleigh waves from periodic corrugations of surface in oblique incidence 80−58850
raypath reflection model for layered media with source and receiver in different layers 80−83704
reactive acoustic attenuator for air conditioning 78−38140
reciprocity principle in duct acoustics 80−74545
reconstruction of reflectivity field from line integrals over circular paths 80−58863
reflective acoustic linear performance, length effect 77−14827
resonance interaction of sound waves with plane parallel flow 77−814
resonance theory of acoustic reflection and transmission through a fluid layer 79−41471
resonance theory of acoustic waves interacting with an elastic plate 80−33268
road traffic, noise propag. in streets, multiple-reflection diffuse-scatt. model 78−87190
rolled sheet, artificial surface cracks, reflection of normal shear waves 80−89448
rough sea surface reflected signal and sea wave spectrum 78−94474
rough surface sound reflection, surface wave effects *(Russian)* 80−1377
SAW from row of dots for SAW devices 79−90052
SAW reflection and bulk wave loss characts. of groove reflector grating 77−39129
SAW reflection and bulk-wave conversion at single shallow groove 77−51586
SAW reflection by strips, grooves and arrays of strips and grooves 78−63214
SAW reflection from finite system of periodic perturbations 80−10059
SAW reflection from thin-strip overlays, first-order coeff. 80−1376
SAW reflector, metallic strip grating expts. for Al metallisation thickness on quartz and $LiNbO_3$ 78−13875
sea irregular surface, amplitude and phase var. of refl. narrow sound bundle 77−46825
sedimentary ocean, reflection from sea bottom with linearly increasing sound speed 80−33312
seismic reflection profiles of marine sediments, staitistical anal. 79−2385
shear body wave, reflection in case of conical reflection 79−95090
shock pulse reflection at solid-solid interface 77−19466
shock wave, weak plane, at wedge, reflection and diffr. 77−72111
shock wave reflection from concave surface, numerical simulation 79−18913

acoustic wave reflection continued
- shock wave-acoustic wave interactions in elastic solids 79—98521
- silicate glasses, phonon echoes at low temp., coherent acoustic echo generation 79—65163
- slotted tunnel portals 78—18108
- solid-liquid interface, surface wave reflection from periodic irregularities 79—18562
- sound attenuation by wide barriers, effects of ground refl. 78—1499
- sound pressure levels behind large storage tanks, reflection effects 77—50826
- spark-gap, electrodes, acoustic phenomena in erosion 80—64796
- spatial impression of concert halls, lateral refls., musical level *(German)* 78—79164
- spherical enclosure, uniformly absorbing, effect of surface roughness on reverberation time 79—14160
- spherical sound wave reflection from rigid sphere 78—66969
- spherical wave from reactive impedance boundary, Cagniard's method modification 77—11064
- spherical wave reflection at fluid plane interface with porous medium 78—42484
- spherical waves, reflection from locally reacting plane surface, numerical calcs. 80—87590
- square plate, refl. meas. by FM signal modulated by smoothed random telegraph signal 78—18130
- star atmosphere, acoustic wave refl. in transition region 80—36607
- statistical theory for sound radiation and reflection from duct 79—81585
- statistically stationary traffic noise shielding by simple obstacles 78—90590
- target recognition, 2 theoretical techniques using geometrical optics and physical optics theories *(French)* 80—53509
- thermosphere, lower, investigation by reflected natural infrasound obs. 79—21089
- thick specimen visualisation with reflection acoustic microscope, acoustic field distribution 79—76922
- torsional waves in semi-infinite cylindrical rod connected to elastic half space 80—96095
- transverse waves in absorbing solid, refl. coeff. 78—9470
- underwater, refl. and lateral waves for Sommerfeld model 77—11074
- underwater, sound, nonlinear reflection of short impulsive waves at water surface 80—33298
- underwater detonation wave, reflection from water surface 80—87628
- underwater pulse reflected from water surface, spectrum 80—87627
- underwater shadow zones in horizontal plane 79—41494
- underwater sound, Al cylindrical shells immersed in water 79—7251
- underwater sound, amplitude fluctuation spectra of tone-burst signals refl. from ocean surface 77—3695
- underwater sound, backscattering, from thin air-filled spherical shells 78—13838
- underwater sound, bottom refl. coeff. rel. to negative bottom loss and critical-angle shift 77—46853
- underwater sound, ocean bottom loss and mode attenuation per cycle 79—90061
- underwater sound, plane-wave reflection coeff. for inhomogeneous plane waves 79—90059
- underwater sound, refl. from absorbing and nonabsorbing cylinders 78—1479
- underwater sound, reflection from a variable-index half space 78—94472
- underwater sound, scattering by sea surface 80—106656
- underwater sound refl. from bottom with sound vel. and density gradients 80—102901
- underwater US pulse propag. and reflection by small targets 78—50986
- viscoelastic plates, model resonance analysis of transmission and reflection loss 79—72734
- water, free surface, metastable effects associated with press. pulse refl. 80—6463
- waveguide reflectors, effectiveness study 80—87599
- Al rods, waveform variation of reflected acoustic shock pulse due to work hardening 77—21167
- CdS, acoustoelectric interaction at wave reflection points 78—2528
- CdS-ZnTe, acoustoelectric domain injection across interface, propag. loss, elastic consts. 77—51778
- KH_2PO_4 electro-optic modulator crysts., piezoelec. induced acoustic transients 80—70316
- $KTaO_3$, light-sensitive surface-barrier generation of acoustic vol. waves 78—63252
- $LiNbO_3$ interfaces, SAW reflection, light scatt. meas. 80—34286
- $LiNbO_3$, surface acoustic wave device, obs. of bulk waves by freq. shifted holography 77—19505
- $LiNbO_3$, Y-Z, Rayleight-wave reflection from groove 79—51408
- SiO_2 sputtered film performance as acoustic antireflection coating at sapphire-H_2O interface 80—106686

acoustic wave refraction
- *see also acoustic dispersion; ultrasonic refraction*
- aircraft wake vortices, tracking system based on acoustic refr. scatt. 77—46840
- atmosphere, echo sounding, refr. effects, multilayer model appl. 77—84041
- atmosphere, infrasound refr. by upper atmosphere winds 77—33229
- atmospheric phenomena, analytical solns. of wave eqn. 80—53530
- atmospheric refractive turbulence effect on Radar-Acoustic Sounding Systems, range limitations 77—41195
- atmospheric sound, propag. over layer with large refr. index 77—50805
- Fresnel zone plate, for focusing of sound waves *(German)* 80—5888
- Helmholtz eqn., test of Born and Rytov approx. using Epstein problem 78—63212
- inhomogeneous absorbing layer, refractive index distrib. 78—38117
- lens, solid acoustic, pulse and freq. response anal. *(Russian)* 78—46873
- liquid-solid interface, plane sound wave reflection and refraction in mag. field 80—38150
- nonuniform wind, error in Rayleigh's theory 79—72743
- ocean, sound speed profile, modification to improve accuracy of parabolic eqn. technique 78—1480
- open wind tunnel jet flow, convection and refraction of acoustic waves *(French)* 77—24007
- piezoelectric crystal, acoustoelectrical waves, double refl. and birefr. 80—11047
- shallow water propagation under downward refr. conditions 77—34983
- shear layer refraction theories, comparison, parameters for open jet wind tunnel shear layer correction 78—90556
- sound beam, self defocusing in presence of acoustic streaming 77—14833

acoustic wave refraction continued
- underwater sound, focusing by spherical compliant-tube Luneburg lens, theory 77—46842
- underwater sound, refr. rel. to objects depths determ. method 77—34986
- underwater sound in refractive channels, bottom loss effects in diffusion loss 78—9482
- underwater sound in upward-refr. ocean, sideband struct. prod. by refr. at rough surface 77—46847
- Te, acoustoelectric current flow, acoustic refraction effect 79—19637

acoustic wave scattering
- *see also ultrasonic scattering*
- aerodynamic noise scatt. by hard and soft surfaces 77—68326
- aircraft wake vortices, tracking system based on acoustic refr. scatt. 77—46840
- anisotropic random medium, numerical calc. 79—81587
- arbitrary elastic structure in infinite inviscid fluid, acoustic radiation and scatt. 79—7318
- atmosphere, scattering from locally homogeneous turbulence 78—87177
- atmosphere, sound attenuation through interaction with internal gravity waves *(Russian)* 77—3693
- backscattering, cross section for an absorbent sphere 80—64236
- backscattering from a plate with a thickness discontinuity 80—96056
- backscattering from elastic cylinders of finite length underwater 77—50811
- backscattering from very rough water surfaces 79—41499
- backscattering of sound by disturbed sea surface 77—11077
- biological sound scatterers in water, acoustic size measurement 80—38199
- bulk-to-surface mode conversion by periodic corrugations at boundary of solid 79—64392
- buried inhomogeneities, general 3-D formalism 78—94461
- capped sphere partially insonified at circular spot, monostatic and bistatic cross sections 77—62081
- chemically reacting systems, sound wave attenuation, thermodynamic interpretation 80—43505
- circular array of acoustically compliant elliptical cylindrical scatterers, scattered field 77—14831
- circular cylinder, acoustically compliant, scattering of confined sound beam 79—94385
- city streets and tunnels, expressions for stationary sound pressure level 80—19159
- coated hollow cylinder in water, sonar cross section 77—46844
- coherent scattering from randomly rough surfaces *(French)* 80—53503
- combustion duct, dispersion by fuel droplets and soot particles 80—74549
- compression waves scatt. from fluid filled spherical cavities in solids, modal resonance determ. 79—94529
- convex shell, sound wave scatt. pattern, high freq. asymptotics 80—96051
- cross section prediction from spectrum model of temperature fluctuations 79—81603
- cylinder, direct and inverse scatt. problems, Dirichlet boundary conditions 80—95774
- cylinder, inverse scattering problem, determ. of shape from far field data 80—83543
- cylinder, rotating, line-source radiation scatt., distant field calc. 77—50795
- cylinders and spheres with complex impedance, approximate methods 79—41472
- cylindrical shells, resonance scatt. 78—83138
- density gradients 78—13836
- diffusion in reverberation chambers 77—50842
- directional spectral spreading in randomly inhomogeneous media 80—19133
- disturbed water surface, acoustic amplitude variations *(Russian)* 77—11058
- Doppler effects, for randomly moving scatterers and platforms 77—62093
- echoes scattered by random fluctuating surface, statistical model *(French)* 77—11066
- echosonde signals, excess attenuation 80—83694
- Eckart's formulation, surface correlation effect on average scattered pressure 80—96070
- elastic and viscoelastic obstacles immersed in fluid, acoustic wave scatt. 80—69583
- elastic cylinder submerged in water, scattered form function determ. 78—30105
- elastic cylinders, HF scattering 79—90046
- elastic cylinders and spheres immersed in fluids 78—30106
- elastic shells, fluid-coupled spherical, transient response to incident pressure pulse 79—68454
- elastic spherical shells, fluid-filled, isolation of resonant component 79—46106
- elastic wave scatt. by randomly distributed and oriented scatterers 79—50483
- ellipsoid differing from surrounding medium in compressibility only, LF scatt. 79—18566
- ellipsoids, acoustically soft, LF scattering of plane wave *(Russian)* 78—46855
- elliptical cylinders, scatt. matrix for elastic waves 78—59324
- ethyl alcohol, angular distrib. of scatt. press. to carrier press. ratio 77—27942
- excess attenuation of noise propag. over ground *(Japanese)* 80—19128
- exterior Neumann problem for reduced wave eqn. in spherically symm. medium, constructive methods of soln. 77—50799
- farfield scatt. from prolate spheroid, meas. and anal. 78—94459
- ferromagnet, acoustic wave scatt. and reemission by moving domain walls 77—24713
- fibrous absorber, model theory for regular fibre arrangements *(German)* 77—801
- field of spherical radiator in presence of spherical impedance scatterers 78—38111
- finite beams, general expressions 78—38105
- finite elastic cylinder in water 80—96062
- finite elastic struct. immersed in acoustic medium, finite element anal. of vibr. 79—7254
- fish, target strength at any aspect 78—30115
- fish backscattering cross section, swimbladder effect in gadoid and mackerel 80—89787
- flaws, reciprocity theory appl. 78—72941
- flexible membrane, acoustic wave scatt. near reson., panel deflection and vel. pot. field 77—42657

acoustic wave scattering continued
  - fluid, by temp. and vel. inhomogeneities, parabolic approx., numerical soln. 79−50491
  - fluid-loaded cylindrical shell, resonant component isolation in acoustic scatt. 80−5864
  - forward and specular scattering from randomly rough surfaces, Fresnel phase approximation appl. *(French)* 80−53504
  - forward scatt. approx. by circular cylinder 78−32689
  - forward-scatter approx. 77−46832
  - fuselage-shaped body, interaction with aerodynamic noise 80−53533
  - gas bubbles, effect of backscattered acoustic wave on bubble oscillation 79−1021
  - gas bubbles in liquid, multipole resonances in sound scattering 79−81606
  - giant monopole resonances in the scattering of waves from gas-filled spherical cavities and bubbles 79−50476
  - impedance cylinders, calc. of differential cross sections of geometrical reflections 79−41474
  - impedance cylinders of large wave dimensions 80−64249
  - impulse response meas. in sound scattering from sphere in air *(French)* 80−87581
  - inhomogeneity of medium, determination by means of sound signals 80−87610
  - inhomogeneous medium, spherically stratified, direct and inverse scatt. problems 78−71239
  - integral formulation for randomly rough surfaces *(French)* 80−53193
  - inverse scalar wave scatt., statistical estimation *(Russian)* 78−54200
  - inverse scattering problem 78−38103
  - irregular solid waveguides with defects, variational method for soln. of diffraction problems 80−5857
  - irregular waveguide, average acoustic field attenuation 78−1459
  - jet engine sound scatt. by aircraft fuselage, coordinate stretching 79−23123
  - layered elastic absorptive cylinders, matrix theory 77−46826
  - layered elastic and viscoelastic obstacles in water 80−96061
  - LF backscattering by wind-generated air bubbles undersea with large-scale roughness 79−86285
  - LF expansions using Waterman's T-matrix method 79−94382
  - LF sound waves propag. in Arctic channel with irregular ice boundary 77−11079
  - lifting boundary in low Mach number flow, sound scatt. anal. 77−42648
  - long wavelength acoustic radiation; radiation pattern of penetrable body, theory 80−14508
  - long-wave diffraction by plate reinforced with projecting beam 78−9469
  - low frequency field calc., iterative method 78−29876
  - low roughness rigid surface, scattering of boundary wave generated by grazing incidence at slightly rough rigid surface 80−10064
  - low roughness surfaces, scattering of spherical pulses 80−10065
  - magnetostrictive sonar transducer, hollow spherical scatterer effects on radiation resistance at air-water surface 77−39125
  - marine organisms, acoustic target strengths 79−46103
  - matrix method of optimal truncation, scalar wave illustration 80−62479
  - matrix theory of elastic wave scatt., conservation law 78−63217
  - membranes and plates, with line constants, acoustic scattering 78−90554
  - metal, Raman scatt. of sound in quantising mag. field 78−60171
  - methyl alcohol, angular distrib. of scatt. press. to carrier press. ratio 77−27942
  - mode conversion rates, due to scatt. from ocean bottom roughness 78−63228
  - molten salt, hydrodynamic correlation functions 77−31577
  - multi-obstacle, sample source formulation with accuracy checks 80−19118
  - multilayered elastic body embedded in infinite material, acoustic wave scatt. theory 80−69584
  - multimode waveguide with uneven walls, sound attenuation 78−83147
  - multiple scatt. between a rigid steel cylinder and plane, underwater 77−23793
  - multiple scatt. of waves from lattice, theory 78−16697
  - multiple scattering in randomly inhomogeneous medium, allowance for Doppler effect 78−1461
  - multiple scattering of elastic waves by bounded obstacles 80−43496
  - music reproduction in small rooms, theory *(Spanish)* 78−38155
  - n-propyl alcohol, angular distrib. of scatt. press. to carrier press. ratio 77−27942
  - nematic liquid crystals, sound attenuation, near clear point, microscopic derivation 78−34605
  - noise control barrier attenuation, scattering by trees 80−33340
  - noise propagation in open air, obstruction effects, propag. around finite plane on ground *(Japanese)* 77−39160
  - nonlinear interaction between two fully collimated plane-wave beams, secondary radiation *(Chinese)* 77−34978
  - nonlinear scattering of sound by sound 79−10424
  - nonspecular backscattering from finite plates 79−72736
  - ocean, diffr., refl. and interf. during near grazing and near normal ocean surface backscatt. 78−90570
  - ocean, scattering of sound by internal waves 79−14141
  - ocean, two-point coherence function models with inhomogeneous background and anisotropy 80−81922
  - ocean bottom roughness effects on LF propag. 79−41501
  - ocean bottom-reflected pseudonoise signals, correlation with transmistted signal 80−58846
  - ocean floor, mode conversion in shallow water 77−84050
  - ocean floor, refl. and attenuation obs. at 4 kHz 77−2140
  - ocean surface, acoustic sidebands obs. in CW tones at long ranges 77−7244
  - ocean surface characteristics affecting acoustic scatt. 80−46194
  - ocean surface probing for measurement of directional-frequency spectrum 80−79032
  - ocean-surface directional-frequency spectra, inverse scattering problem 80−79031
  - one-dimensional vel. inversion, numerical results 80−64240
  - optical theorem for scatt. of strain waves by inhomogeneities of plane boundary of solid 80−102888
  - oscillating spheroids, acoustomechanical characts. 77−34991
  - N Pacific Ocean, regional depend. of low-freq. attenuation 77−62090
  - pair-correlated scatterers, random distribs., acoustic bulk parameters 79−23112
  - physical optics farfield inverse scatt., mathematical inversion technique for nondestructive eval. 80−69580
  - physical optics farfield inverse scatt. in the time domain 77−23789
  - piecewise uniform ducts, momentum and energy theorems 80−74550
  - piezoelectric wave, transient scattering from crack 80−43499

acoustic wave scattering continued
  - planar gratings of compliant cylindrical shells, plane wave scatt. 77−31157
  - plane harmonic elastic P and S wave scatt. by spherical inclusions and cavities 78−89353
  - plane surfaces, scattering integrals approximations, acoustic waves appl. *(French)* 80−53501
  - plane wave at circular cylinder, struct. of near sound press. field *(Russian)* 77−75731
  - plane wave scattering by Schroeder diffusor, mode-matching approach 80−43501
  - plane waves, reciprocity relations for scatt. by finite obstacle 77−49602
  - plate with line impedance discontinuities, acoustic transmission and scatt. 78−90553
  - point sources scatt. by moving prolate spheroid, aircraft noise appl. 78−94458
  - potential scattering, inverse problem formal solns. 77−2555
  - prolate spheroids, EM vs acoustic backscattering 78−46854
  - quadratic sound channel, first order scatt. resulting for temp. fluctuations 78−83136
  - random, methods of analysis 80−53527
  - random inhomogeneous isotropic medium, determination of correlation function 80−19122
  - random media, theory and appl. of wave propag. and scatt., review 77−75376
  - Rayleigh scattering from N acoustical scatterers, second-order, approximate formula 79−81589
  - Rayleigh surface waves, propag. along corrugated solid boundary 80−87600
  - Rayleigh wave scattering from topographical irregularities at oblique incidence 78−38927
  - Rayleigh waves from periodic corrugations of surface in oblique incidence 80−58850
  - rectangular room of various proportions, calc. of scattered sound field 80−53564
  - resonances in sound scattering from water droplets in air 80−33306
  - resonant acoustic scattering by swimbladder-bearing fish 78−87183
  - resonant scatt. from spherical cavities in elastic and viscoelastic media 78−79150
  - resonant scattering of elastic waves from spherical solid inclusions 80−74547
  - resonating fields inside elastic scattering objects 80−106645
  - reverberation room ANS qualification error sources and effects 77−58514
  - reverberation room modifications for ANS qualification 77−58517
  - ribbon-shaped scatterer, appl. of transition matrix 80−10058
  - rigid body with thin liquid coating 78−50968
  - rigid scatterers in field of harmonic point sound source, compensation of diffraction field 78−18112
  - road traffic, noise propag. in streets, multiple-reflection diffuse-scatt. model 78−87190
  - room-acoustic directional diffusivity model *(Hungarian)* 80−106665
  - rough interface between two fluids, coherent acoustic scatter 80−96074
  - rough surface backscatter anal. for surface with 2 types of roughness at small grazing angles 80−14505
  - rough surface scattered field, freq. averaging method for determination of average intensity 80−38169
  - rows of cylindrical obstacles in shallow water 78−87182
  - SAW grating cascades, bulk scatt. loss 77−46869
  - SAW reflective-array-compression filters, nonsynchronous scatt. loss 78−71246
  - SAW scatt. by post spacers 79−27456
  - scattering by sea surface, props. *(French)* 80−53502
  - scattering matrix for spheroids 79−68456
  - scattering of sound by sound, relation to the parametric receiving array 78−90563
  - sea surface, locally irradiated, correl. functions of amplitude fluctuations *(Russian)* 79−29777
  - sea surface backscatter under shadowing conditions 78−94473
  - sea surface inhomogeneities, sound scatt. phase function shape in shadowing conditions *(Russian)* 80−94530
  - sea surface scattering at rough boundary, interaction models 79−7247
  - sea surface scattering channel and undersea communications, modelling 79−1022
  - semiconductor, sound absorption at very low temps. 79−95089
  - semimetal, Raman scatt. of sound in quantising mag. field 78−60171
  - SH waves, multiple scatt. by arbitrary cross section cylinders 78−63216
  - shear layer, thin and thick, linearised theory with causality 77−42643
  - shear-wave scattering from spherical fluid obstacles in solids, resonance theory 80−43497
  - silicone rubber cylinders and spheres 78−79149
  - smooth elastic obstacle, adaptation of transition matrix method 80−87584
  - solid, low temp., first and second sounds interaction *(Russian)* 79−86841
  - solid waveguide with periodic boundary corrugations, multiple sound scatt. 79−94384
  - sound field calculation, three dimens. objects, integral equation methods 80−74558
  - source above rough absorbent plant 80−64289
  - spectral domain formulation 80−10057
  - spherical cavities in viscoelastic materials, fluid-filled, determination of shear absorption 79−7239
  - spherical source near scattering sphere, radiation characts. 77−7228
  - spherical targets, dynamics of acoustic resonance scattering appl. to gas bubbles in fluids 80−10068
  - spherically stratified medium, construction of solns. 78−90557
  - spherically stratified medium, soln. 79−64370
  - spherically stratified medium and bounded obstacle, integral equation 79−32120
  - spheroidal bodies near fluid-solid interface 78−18088
  - spheroidal body at interface 79−94387
  - stationary waves, scattering by elastic obstacle immersed in fluid 80−43495
  - statistical model for backscattering from a randomly fluctuating surface 79−27459
  - statistically rough surface, wave scatt., book 80−73116
  - stratified media, acoustic impedography *(French)* 79−3816
  - stratified media with specific impedance profiles, investigation method *(French)* 79−41490

acoustic wave scattering continued
submerged elastic bodies, resonance excitation by sound scatt., linear approx. theory 78—55495
submerged plate with finite number of reinforcing ribs 80—74586
submerged plate with one reinforcing rib 80—74585
superfluid, acoustic turbulence, first and second sound kinetic eqn. soln. *(Russian)* 78—43193
surface cracks, SAW excitation, length and depth resonances 79—8403
surface roughness and frequency dependence of backscattered field *(French)* 80—53506
surface scatt. from moving rough surface 79—7246
surface wave formation and resonance relation *(French)* 80—8809
surface wave scatt. from elastic cylinders, Regge poles 78—50967
surface waves, by edges of thin surface layers at oblique incidence 78—18085
target recognition using theory based on Bojarski's identity *(French)* 79—41479
thin elastic cylindrical shell submerged in water, backscatter calc. from Kirchhoff approx. 78—30104
thin elastic plate, acoustic wave scatt. near reson., panel deflection and vel. pot. field 77—42657
thin plate, effect of line-discontinuity admittance on sound scattered by plate vibration 78—55494
thin plate, longitudinal- and flexural-mode attenuation by periodic surface corrugations 79—90048
thin stiffened Al plate, underwater acoustic backscattering and echo struct. characts. 78—55492
time-frequency-space generalised coherence and scatt. functions 78—5603
time-varying shallow water channel weighting function meas. 78—5606
transducer, backscattering formula 80—96064
transformation operators and wave propagation in a spherically stratified medium 79—18569
transient scatt. by arbitrary axisymm. surfaces 78—79151
turbulent jet, power spectrum of scattered signal 79—94695
turbulent media, scatt. and interaction of sound with sound *(Russian)* 79—18571
underwater, diffusion loss in stratified sound channel 77—11072
underwater, multiple bounce channels, scatt. function 78—83162
underwater, VLF attenuation from deep-water ambient noise field meas. 77—11070
underwater, volume scatt. strength obs. at 2 kHz in NE Atlantic 77—11073
underwater acoustic scatterers, classification, experimental appls. involving fish 79—41502
underwater acoustic surface duct propagation model based on radiation transport eqn. 80—46196
underwater Fermat paths, phase and amplitude 78—79159
underwater forward scatt. and freq. depend. on medium 79—50496
underwater scattering by marine organisms, review 80—64269
underwater scattering channels, signal correl. function after several reflections 77—7246
underwater sound, acoustic estimation of oceanic scatt. layer comp. 77—86909
underwater sound, amplitude fluctuation spectra of tone-burst signals refl. from ocean surface 77—3695
underwater sound, backscattering, from thin air-filled spherical shells 78—13838
underwater sound, backscattering spectra of preserved zooplankton 77—79994
underwater sound, connection between small-waveheight solns. of ocean surface scatt. problem 78—13839
underwater sound, cylindrically symm. formulation for spatial coherence loss 77—34985
underwater sound, forward surface freq. spreading, physical models 79—14145
underwater sound, high-freq. scatt. from cylindrical shells coated with viscoelastic absorbing layers 78—1478
underwater sound, ocean bottom backscattering strengths at low grazing angles 79—14143
underwater sound, scattering by sea surface 80—106656
underwater sound, use of linear system theory in acoustic radiation and scatt. anal. 77—75729
underwater sound diffusion loss in refractive sound channels, bottom loss effects 78—9482
underwater sound in shallow water with rough boundaries, attenuation of coherent component 77—62091
underwater sound scattered by rough surface of upward-refr. ocean, sideband struct. 77—46847
underwater sound scattering from fluid sphere, appls. to marine organisms 77—46846
urban built-up areas, external reverberation times 77—14846
virtual sources, non-contributive 80—38151
vol. reverberation from scatt. layers and biological meas. 78—81194
waveguide, rough boundary, spatial and temporal correl. functions for stochastic part of sound field 78—90560
waveguide inhomogeneities single-scatter theory 77—7245
wide-band plane wave scattering and transmission by fluid loaded plates 80—106646
wideband acoustic characterisation method for fish schools and long-range propag. channels 80—43551
KH_2PO_4 electro-optic modulator crysts., piezoelec. induced acoustic transients 80—70316
$LiNbO_3$, Y-Z, SAW scatt. from groove 78—60019

acoustic wave transmission
see also ultrasonic transmission
air layers in double walls, influence of cavity-volume damping on stiffness *(German)* 77—80016
air-water two phase medium, acoustic velocity and attenuation meas. 77—58513
airborne sound coupling into earth, freq. dependence 80—74567
aircraft fuselage, sound transmission under flight conditions 77—7255
anisotropic solids interface, acoustic wave refl., transmission and mode conversion 79—76903
arbitrary continuously stratified environments, propagated, reflected and transmitted acoustic waves 78—13829
architectural acoustics, sound transmission between absorbing parallel planes 80—33344
architectural acoustics 80—64288
atmosphere, sound attenuation by turbulence 77—7238

acoustic wave transmission continued
axisymmetric transmission system with sound absorbing wall, finite element anal. 77—88974
band-limited power flow into enclosures 78—9485
boundary between piezoelec. ceramic and water 80—87588
building elements, use of thin plates for improving transmission loss 80—102930
building materials, noise abatement appl. 77—23808
building structures, power flow methods for sound transmission assessment 77—31177
CBOOA, isotropic, nematic, smectic-A phases, Brillouin scatt. 80—11421
circular ducts, method of weighted residuals with trigonometric basis functions 78—59174
circular plate, insulation characts. for single sound pulse 78—18086
circular plate, sound pulse transmission characts. 78—59170
circular plate, transmission of sound pulse 77—79985
concrete plate junctions 80—87652
cylindrical shells with finite regions of structural discontinuity, refl. and transmission efficiencies 78—13841
deep ocean, anal. of acoustical effects of receiver-source motion at intermediate ranges 80—96082
diffracted and penetrating, acoustic pathways through barriers 80—102880
diffraction grating formed by hollow elastic bars, sound transmission coeff. 77—14829
displacement of infinite elastic plate submerged in ideal liquid, examination of displacement field 80—74557
dissipative mufflers with locally reactive lining, modelling 78—13849
duct, nonuniform, finite element method for acoustic transmission 78—83140
duct acoustics, integral equation methods for nonuniform duct with variable impedance 77—58498
duct with axial temp. gradient, sound transmission and generation 77—62084
ducts, circular, with compressible mean flows 80—74900
ducts with uniform flow, acoustic energy transmission 79—72737
elastic plates, vibration and sound transmission due to a spherical sound wave *(Japanese)* 80—33330
ferroelectric with orientational transition, coupled elastic, EM and polarisation oscill. spectrum 79—8103
filters, arbitrary profile, circular cross section, finite element simulation 77—11059
finite-amplitude sound waves in inhomogeneous medium with caustics 77—68295
floors, problems of impact testing *(German)* 77—825
free waves on panel, transmission across rib 77—39248
free-field loudspeaker system, system function, design of compensating cct., state-space methods *(Japanese)* 80—53566
gas with porous medium obstacle, scalar Helmholtz eqn. 80—74552
gas-bearing sediments 80—87630
glass isolating panes, influence of gas filling on sound isolation *(German)* 77—80017
glass panels, transmission loss and vibr. in nonreverberative conditions 77—7258
guided sound transmission through double partition, exact soln. 77—7233
harmonic acoustic waves, refraction to tunnelling transition 79—46099
heavily-damped cylindrical fuselage 78—83166
homomorphic deconvolution, reverberant and distortional channels 78—90606
horn and silencer design, FEM anal. of acoustic transmission/radiation systems 80—87589
impulse response meas. of acoustic transmission system, digiral computer processing *(German)* 80—91999
inhomogeneity of medium, determination by means of sound signals 80—87610
insulator, transparent, laser breakdown, acoustic characts. 80—50269
interdigital transducers, quasiacoustic wave propagation, field theory anal. 78—66998
interface between elastic waveguides, variational method for modal solns. 77—84027
interface three-phonon processes, Kapitza conductance and pulse expt. applications 80—2261
lagging configurations, acoustic transmission rel. to effective noise reduction 77—84078
laminated plate, reinforced by beams of different mech. impedances 78—90584
landscaped office, effect of screens on sound attenuation 78—94486
layered anisotropic media, construction of input wave impedances by direct tensor method 79—94136
layered media, strong nonlinear and dissipative effects 78—1472
layered metal structure, acoustic size effect, sound attenuation anisotropy *(Russian)* 79—46752
LF acoustic reduction of rectangular panel 79—32142
LF sound pressure at various Reynolds numbers 80—87613
lined plenum chambers in ducts, attenuation 79—37071
lung sound transmission meas. 78—28149
maisonettes, flanking transmission of sound, effect of woodwool shuttering in party floors 78—94487
mechanical input power meas. method for wall structures 80—19176
metallic film, coherent hypersound point excitation in millimetre microwave region *(Russian)* 78—2204
microballoon reinforced plastics, acoustic and mech. props. rel. to hydrophone applic. *(Japanese)* 77—7793
mode-selective sound transmission in fluid-filled waveguide with transverse resistivity 78—1452
moving material interface, freq. modulation and wave number conservation 77—7231
muffler chambers, flow-reversing, anal., testing and design 77—11085
N-fold walls, unified theory for sound shielding charact. determ. *(Japanese)* 79—90082
nematic liquid crystals, sound attenuation, near clear point, microscopic derivation 78—34605
noise control, sound barrier systems review 78—30127
noise transmission through stiffened panels 80—102922
obstacle in waveguide, acoustic wave transmission and reflection 80—102893
ocean eddy effects on sound transmission 78—11905
oceanic, calc. of strength and diffraction parameters 80—74572
oceanic layered finestructure in Arctic, acoustic variability, 10 to 60 kHz 79—90060
open plan spaces, technique for sound pulse transmission anal. 79—23151

acoustic wave transmission continued

- partition and glass windows, influence of vibration damping on acoustic transmission *(French)* 77—31176
- periodically framed parallel plates, sound transmission 77—50833
- piezoelectrics, elastic wave leakage across gap 78—6204
- pipe walls, presence of flow, use of reverberation chambers 80—102883
- plate, orthotropic multilayered, acoustic transmission loss 78—83143
- plate, orthotropic multilayered, vibr. modes, acoustic transmission 78—83142
- plate pair, interconnected at discrete set of points 77—806
- plate terminated by liquid, transfer constant and input impedance ang. depend. 77—11103
- plate with line impedance discontinuities, acoustic transmission and scatt. 78—90553
- plywood panels, effect of orthotropy on sound transmission 79—41515
- point source radiation near cylindrical jet in motion 77—31169
- point source radiation through composite medium 77—31150
- pulmonary dysfunction detection using sound transmission 77—37031
- pure tone transmission, detect. in medium with time-varying time delay, functional analysis 79—86296
- quartz rod, electrodynamic method of acoustic wave polarisation meas. *(Russian)* 77—75764
- quartz wedge, reflection, transmission and conversion of normally incident SAW 80—2257
- radiating gas, nonlinear attenuation of plane pulses, shock wave formation *(Russian)* 77—35259
- radiation efficiency estimation through walls 79—81634
- reactive acoustic attenuator, effects of flow on performance 79—55257
- reciprocal transmission in midocean environment, current monitoring appl. 78—11907
- reciprocity principle in duct acoustics 80—74545
- rectangular duct, LF transmission through walls 79—81598
- rectangular ducts, LF acoustic transmission 79—37070
- reflective acoustic linear performance, length effect 77—14827
- resonance theory of acoustic reflection and transmission through a fluid layer 79—41471
- resonant interaction of sound with electrons, sound transmission *(Russian)* 79—7774
- reverberant sound, transmission through orthotropic viscoelastic multilayered plates 80—102884
- scalar wave transmission, through small apertures, appl. of isoperimetric inequalities 79—32109
- shock wave-acoustic wave interactions in elastic solids 79—98521
- single-layer wall with porous layer, acoustic reduction 79—27466
- solar atmosphere, acoustic wave energy transmission across mag. flux sheath 78—20802
- sound generation and transmission in flow ducts with axial temperature gradients 78—90551
- sound transmission from air into rough ocean, expt. 77—11071
- structure-borne power flow, beams and pipes, cross spectral density methods 80—106742
- subsonic nozzle flow, response to acoustic and entropy disturbances, transmitted acoustic waves soln. 77—75958
- thin cylindrical shell, effect of cavity resonances on sound transmission 79—3850
- thin elastic plate, reinforced at discrete set of points 77—806
- thin panel backed by rectangular cavity 80—28382
- transmission loss of apertures, reverberent room method 78—1510
- turbomachinery, multiple blade rows, semi-actuator disc model for sound transmission calc. 78—38137
- turbomachinery, semi-actuator disk model, single blade row 78—13852
- turbulent shear layer, sound transmission 79—37075
- underwater explosive sources, model evaluation and data interpretation 77—11068
- underwater sound, acoustic cross-section of S.Pacific Ocean, (Project Kiwi One) 80—36330
- underwater sound, influence of range-depencent environments on low-freq. volume attenuation meas. 77—46845
- underwater sound, point source transmission of broadband sound through sinusoidal ocean surface 79—14142
- unsealed window sound insulation rel. to frame construction 79—68485
- vaneless diffuser, sound propag. and transmission 80—19121
- viscoelastic plates, model resonance analysis of transmission and reflection loss 79—72734
- wide-band plane wave scattering and transmission by fluid loaded plates 80—106646
- wood joist floor-ceiling systems, sound-insulating efficiency upgrading 78—1515
- wood joist floors, noise transmission, insulation methods 80—38178
- CO_2 pulsed laser system, acoustic suppression 80—74378
- CdS-ZnTe, acoustoelectric domain injection across interface, propag. loss, elastic consts. 77—51778
- TeO_2, acoustic beam electronic steering 79—98569

acoustic wave velocity

see also acoustic dispersion; liquid helium sound propagation; shock waves; ultrasonic velocity

- ABA poly(styrene-b-butadiene) copolymer, physical props., casting solvent effects 77—55935
- acetic acid, meas. at freqs. of 5 to 20 kHz in small-volume cells 78—9516
- acoustic wave interaction, diagnostics appl. 78—83541
- adsorbed monolayer, substrate-induced strain and orientational ordering 79—82460
- alcohols, dil. aqueous solns., isentropic compressibility behaviour from sound vel. meas., dissolution mechanism 80—30269
- amorphous dielectrics, universal relaxation time at low temp. 80—55026
- amorphous insulators acoustic props. at low temps., ultrasonic attenuation, dielec. props. *(French)* 77—72658
- anhydrite, shock compressed, vel. of sound meas. 78—10123
- aqueous salt solns., as function of conc., temp., and press. 78—79668
- aromatic compound-carbon tetrachloride, liq. mixture, sound vel. theories 78—2199
- atmosphere, Concorde sonic booms as probe of temp.-wind parameters 77—91323
- beamforming when the sound velocity is not precisely known 80—96123
- Boltzmann-Enskog equation, nonlinear, acoustical approx. for elastic sphere system 78—41252
- Bose gas, imperfect, quasiparticle sound velocity, temp. depend. 78—51761
- Bose liquid, dense hard sphere, vel. of sound 79—69308

acoustic wave velocity continued

- boson system, struct. factor and sound vel. 78—34668
- CBOOA, isotropic, nematic, smectic-A phases, Brillouin scatt. 80—11421
- o-chlorophenol-acetone (ethyl methyl ketone), thermodynamic and transport props. 80—92686
- clathrate hydrates, longitudinal acoustic vel. 80—88275
- coesite, elasticity meas. by Brillouin scatt. 77—44978
- collisionless regime, amplitude dependent sound velocity *(Russian)* 78—52037
- colloidal crystals, ordered suspensions of charged latex spheres, acoustic shear waves 80—6466
- compressible classical Heisenberg chain, phonon dynamics and sound velocity 80—96604
- compressible liquid flow with heat transfer 79—14131
- computer model for generating World ocean sound velocity profile 80—87624
- contained spherically symmetric fluid, sound speed from natural freq. spectra 78—61344
- crystalline films, dispersion law and struct. transition, Fermi line geometry, acoustic spectrum, resist. min. *(Russian)* 79—7764
- cubic crystal, acoustic waves, Christoffel elastic eqns., and elastic consts. 79—51205
- cylindrical steel shells in water, thick-walled, distrib. of normal surface vel. *(German)* 80—102899
- dichlorodifloromethane, liq. Refrigerant 12, meas. at 26.7°C 77—89497
- p-dioxane-water mixtures, adiabatic compressibilities and sound vels., temp. depend. 79—28044
- diphenyl-diphenyl ether mixture, Dowtherm vapour, speed of sound meas. 79—18989
- dolomite, shock compressed, vel. of sound meas. 78—10123
- doped displacive ferroelectrics, sound vel. change 80—45013
- elastic body, general stress-velocity expressions in acoustoelasticity 79—81722
- electron beam pulse generated waves, in Cu, Al, ionic crysts. *(Russian)* 77—76463
- electron gas, sound velocity variation under de Haas-van Alphen conditions 79—60681
- ethane, fluid, saturated, compressed, sound velocity meas., compressibility, sp. ht. determ. 77—76488
- fermion one-dimensional many-body system, SCF approx. 77—62699
- ferroelectric piezomaterials, pyrochlore struct. high sound-propagation velocity 78—43791
- ferroelectric with orientational transition, coupled elastic, EM and polarisation oscill. spectrum 79—8103
- filled polymers, dynamic shear modulus and acoustic velocity, filler content depend. 80—60900
- finite amplitude sound wave in circular pipe. vel. rel. to nonlinear propag. simulation 78—13834
- fluids composed of hard convex particles, rel. to vel. depend. on molecular size and shape 77—43282
- Franz-type wave, rel. and attenuation, generation on outside of solid cylinders in water *(French)* 80—28370
- fused quartz, determ. of acoustic and acousto-optical parameters using acoustic interferometry 79—41532
- gas, ideal, thermomech. effect, adiabatic velocity of HF sound 77—47137
- gas mixtures, chem. reactive, sound speed calc. *(Russian)* 77—35261
- gas-bearing sediments, eqns. based on model of resonating gas bubbles 80—87630
- gas-bearing water-saturated sediment, sound vel. as function of bubble distrib. 79—39703
- gases, liquids and solids, relationship with props., research during past 50 years, review 80—96089
- glass, acoustic phonons lifetime at low temps. 78—26650
- glycerine, meas. at freqs. of 5 to 20 kHz in small-volume cells 78—9516
- heat exchanger tube bank duct acoustic resonances 78—90550
- n-heptane, self-excited thermoacoustic oscills. in heat transfer 78—79186
- hollow cylindrical rod compressed by axial pressure 80—19276
- homogeneous isotropic material, high press. eqn. of state and sound vels. to fourth order elastic consts. 79—37806
- homogeneous viscoelastic mixtures, speed of sound 80—33272
- human skull, acoustic losses and vel. meas., rel. to diagnostic imaging 78—69159
- inert gas crystal, acoustic velocity, theory 79—55831
- inhomogeneous granular solid, one dimens. accel. waves, speed, amplitude 78—87288
- inhomogeneous media model for acoustic vel. calc. in tissues 79—43945
- intensity meas. in duct with mean flow 79—86282
- intermediate valence metals, renormalisation of collective excitations, acoustic wave vel. near electronic transition 79—82539
- isotropic elastic materials, propag. vels. as functions of stress or strain 79—72740
- Kaprolon, compressibility, elec. cond., sound vel. behind shock front 78—95105
- liquid, calc. method 78—67834
- liquid, Gruneisen parameter rel. to Rao's acoustical parameter 80—92581
- liquid, principle of corresponding states, dynamic props. 77—89358
- liquid, simple, perturbation theory for sound prop. vel. *(Russian)* 77—15500
- liquid, thermophysical properties rel. to compressibility 78—83964
- liquid metal, acoustic wave velocity calc. within limits of hard sphere model *(Russian)* 78—43072
- liquid-gas mixtures, sound speed in water-air and water-steam 77—84029
- liquids, relation with mean vel. of thermal motion of molecules 79—14885
- liquids containing gas bubbles, effect of polymer additives 78—38779
- long range propag. in oceans, signal speed variations 78—50984
- lubricant, glass transition, light scattering study 79—29228
- magnetic materials, elastic props., review 80—7142
- mantle rocks, thermally activated point defects interpretation of low vel. zone 78—88806
- marine sediments, sound velocity gradients 79—68465
- marine sediments and rocks, sound vel.-density relations 78—50982
- metal, cyclotron reson. and geometric oscills. of sound velocity 77—20230
- metal, electron-phonon drag and interaction of first and second sound 77—66009
- metal, Fermi surface local geometry effects on phonon spectrum, acoustic props. *(Russian)* 77—55333
- metal, light scatt. from surface acoustic phonons 78—76484

acoustic wave velocity continued

- metal, phonon spectra, singularities caused by local geometry of Fermi surface 78—91401
- metal, theory of electronic transport of sound packets in parallel mag. field *(Russian)* 78—84261
- metals, Fermi surface geometry, effect on sound absorpt. and vel. 79—7775
- metals, sound pulse spike like transport near acoustic cyclotron resonance *(Russian)* 80—100617
- methyl alcohol, meas. at freqs. of 5 to 20 kHz in small-volume cells 78—9516
- mixed metal chloride acousto-optical props. *(Russian)* 78—60419
- mobile dislocation density determ. from sound velocity 79—19258
- nonideal gaseous mixtures, prediction of acoustic vels. 78—67306
- nuclear matter, compression and speed of sound 80—27584
- ocean cyclonic eddies, effects of sound-speed variations on short-range transmission 80—33316
- ocean sediments, math. model 77—91104
- ocean velocity profile, horizontal range, and travel time series expansions 78—5604
- one-dimensional vel. inversion, numerical results 80—64240
- N.Pacific mesoscale phenomena, oceanographic model and acoustic survey comparison 80—46195
- N.Pacific Ocean, west, depth, var. of temp., salinity and sound vel. meridional gradients 80—51429
- paraffin, shock compressed, vel. of sound meas. 78—10123
- n-paraffins, generalised eqn. of state from acoustical meas. 78—51642
- paramagnet, velocity of sound, temp. depend. modification due to spin-phonon interaction, phonon relax. 78—19303
- piezoelectric crystal, acoustic transverse wave polarisation and energy flow in external static fields 80—19123
- piezoelectric semiconductor, amplification and vel. change of acoustic waves due to external temp. gradient 78—84260
- piezoelectric semiconductor, weakly inhomogeneous theory of sound absorption 80—15574
- pipe, arbitrary temp. and flow profiles effect in sound speed 78—9467
- plexiglas, shock compressed, vel. of sound meas. 78—10123
- polarised ferroelectric ceramic, acoustic vel. anisotropy 79—55835
- polydimethylsiloxanes, rubbery and liq., hypersonic sound vel., Brillouin spectra meas. 80—75308
- polydisperse, vapour-liquid mixtures, acoustic velocity, damping decrement 80—66881
- polyether ester-PVC blends, annealed, dynamic mechanical and sonic velocity behaviour 80—25740
- polyethylene, shock compressed, vel. of sound meas. 78—10123
- polymer additive effects on sound propag. in water containing bubbles 77—50810
- polymers, aliphatic and aromatic, mean mol. orientation factors, from IR spectra and acoustic method 80—70142
- polymers, amorphous, transverse waves vel. rel. to struct. 77—51446
- polymethylpentene, LF acoustic relaxation 78—38784
- polystyrene-polyvinyl methyl ether blends, dynamic mech. and sonic vel. behaviour 79—34090
- polyvinylidene fluoride, US transducers, dielec. and acoustic losses 80—48541
- polyvinylidene fluoride-PMMA blends, dynamic mech. props. and sonic velocity, cryst. phase transitions 78—26454
- porous solid, generalised p-α model, eqn. of state, sound vel. 80—65154
- potential energy effects in liquids 79—81595
- protein, globular, compressibility in water at 25°C 80—40951
- PTFE, shock compressed, vel. of sound meas. 78—10123
- pure material, in two-phase solid-liq. melt regime, eqns. 77—55342
- quartz, He$^+$ ion implanted, SAW velocity, influence of annealing 79—14996
- quartz glass, Ti-doped, acoustic props., thermal stability 77—24356
- quartz plates, acoustic reson. vibr., Berg-Barrett X-ray diffr. method 80—40063
- quartzite, shock compressed, vel. of sound meas. 78—10123
- Raman-Nath theory, mol. struct., liq. mixture, temp. depend. lab. teaching 77—33796
- rare earth orthochromites, mag. interactions and weak ferromagnetism 78—52220
- sandstone elastic wave velocity, function of moisture content 80—56459
- sea salts, relative sound vels. at 25°C 77—84042
- seawater at high pressure, sound speed meas. 78—13837
- seawater sound speed eqns. for varying salinity and temp. 78—81193
- sediment cores from W.North Atlantic, laboratory and in situ compressional-wave vel. meas. 79—57866
- sedimentary rocks, anisotropy due to overburden press. 80—56455
- semiconductor, opaque, light scatt. from surface acoustic phonons 78—76484
- SF-14 flint glass, acoustic vel.. absorpt. coeff. and photoelastic consts. rel. to acoustooptical parameters 79—56762
- shock waves, generation by pulse chamber ignited by HV ignition spark 77—24039
- shock-compressed porous solids *(Russian)* 78—71788
- shock-compressed uniform solid, lateral discharge ang. semiempirical formula *(Russian)* 78—55910
- silicate minerals, phonon cond. and mean sound vel., linear relationships 77—21761
- simple fluids, semiempirical calcs. using perturbation theory 80—28892
- solids, evaluation of finite strain eqns. of state using lattice models 80—96620
- steam mixture of bubble struct., sound velocity, damping decrement 79—55444
- stress determ., improvement of accuracy 78—15631
- superconductor, temp. depend., nonlinear effects *(Russian)* 77—4468
- surface acoustoelectric waves, electrostriction-induced, at interface between media 77—16255
- tangential momentum accommodation coeff. meas. by acoustic vel. and absorpt. obs. for He, He on W 80—66867
- TGS, SAW phase velocity in b-plane 77—85043
- thermodynamic speed of sound, equation of state, virial form 77—27406
- thermosphere, lower, sound rel. from natural infrasound ten years obs. 79—21089
- triethylamine/alcohol mixtures, theoretical evaluation of sound vels. and AB interactions 78—18706
- triethylamine/phenol mixtures, theoretical evaluation of sound vels. and AB interactions 78—18706
- two-phase flow, nonequilib. subsonic/supersonic, acoustic vel. obs. 78—42642

acoustic wave velocity continued

- underwater, observed sound speed profile, appl. to Gaussian quadrature ranges 77—46851
- underwater, sound-speed field perturbation and phase modulation by internal waves 77—46852
- underwater ray theory for sound speed profiles with two dim. variation 78—50987
- underwater sound, approximate ray angle diagram from vel. profile 77—46843
- underwater sound, effects of currents and tidally varying sound speed on deep ocean propag. 77—79995
- underwater sound, wide-angle field in ocean with range-depend. vel. profiles 77—79993
- underwater sound field, fluctuations using parabolic vel. profile 77—31159
- underwater sound speed profile, modification to improve accuracy of parabolic eqn. technique 78—1480
- underwater velocity inversion in a stratified medium with separated source and receiver 80—96071
- viscous liquid, acoustic and thermal props., phenomenological models 79—82393
- water, eqn. of state determ. from sound speed eqn., spl. vol. and compressibility 77—47538
- water, LF sound velocity and related thermodynamic props. 79—73255
- water, subcooled, choked expansion and the isentropic homogeneous equilib. model for 2-phase flow 78—91034
- water, supercooled liq., high freq. sound vel. and absorpt., thermodynamic singularity, 228K 77—76489
- Wilson's sound speed meas. reevaluation for pure water 77—23794
- AgI, B1 phase, high press. elastic props., thermally activated rel. anomaly 80—44261
- AgI, sound vels. near phase transitions with negative dP/dT 78—83885
- Al and its alloys, dynamic determ. of Gruneisen coeff. 77—24418
- Al, mobile dislocation density determ. from sound velocity 79—19258
- α-$\mathrm{AlPO_4}$, berlinite, temperature-compensated surface and pseudo-surface acoustic wave props. 77—51584
- Ar gas constant determ. from speed of sound meas. 78—9746
- Ar, liquid, velocity of second meas. and thermodynamic stability *(Russian)* 79—4374
- Ar-He, liq. soln., perturbation theory *(Russian)* 77—47512
- $\mathrm{Ba_2Si_2TiO_8}$, fresnoite, SAW props., expt. and calc. 78—43229
- $\mathrm{Ba_2Si_2TiO_8}$, fresnoite single cryst. SAW characts. 79—37913
- $\mathrm{Bi_{12}GeO_{20}}$, acoustic vel., absorpt. coeff. and photoelastic consts. rel. to acoustooptical parameters 79—56762
- $\mathrm{Bi_{12}SiO_{20}}$, acoustic vel., absorpt. coeff. and photoelastic consts. rel. to acoustooptical parameters 79—56762
- Ce, renormalisation of collective excitations, acoustic wave vel. near electronic transition 79—82539
- $\mathrm{CeAl_2}$ sound vel. in high mag. fields 79—78500
- $\mathrm{CeSn_3}$, mode softening and elastic consts., acoustic vel. meas. 80—88242
- Co-P, amorphous, sound propagation 77—62586
- $\mathrm{Cs_2NaBiCl_6}$, optical, photoelastic, acoustooptic props. 80—55064
- Cu, zero to first sound transition, inelastic-neutron scatt. data 77—31738
- $\mathrm{D_2}$, solid, melting curve, meas. of P, V, T and longitudinal sound velocity 79—37814
- $\mathrm{D_2O}$, heat capacity, compressibility and speed of sound 79—82284
- $\mathrm{D_2O}$, sound speed rel. to normal water as a function of temp. and press. 78—2201
- Fe-Cr-Al, attenuation and vel. of acoustic shock waves, amplitude depend. 78—63810
- $\mathrm{FeCl_2}$, metamagnetic, sound propag. near tricritical point 78—48024
- $\mathrm{(Fe_{1-x}Mn_x)_3Si}$, mag. phase diagram determ. 77—24697
- Ge, molten, temp. depend., MP to 1400K 77—15498
- n-$\mathrm{H_2}$, equation of state from PVT and sound vel. meas., 75-307K, 2-20 kbar 77—62609
- p-$\mathrm{H_2}$, FCC, equation of state and lattice dynamics, temp. depend. 77—76521
- p-$\mathrm{H_2}$, liq., equil. bulk props., perturbation theory approach and quantum effects *(Russian)* 77—89551
- p-$\mathrm{H_2}$, solid, elastic consts., Brillouin scatt. obs. 79—8149
- $\mathrm{H_2}$, solid, melting curve, meas. of P, V, T and longitudinal sound velocity 79—37814
- He, dense gas, transport eqns., shear viscosity and acoustic vel., quasiparticle kinetic eqn. calcs. 80—53906
- He, liq. and vapour phases, thermodynamic and thermophysical props. calc. using HEPROP computer program 80—6529
- ^{4}He, gas, second virial coeff., acoustic determ., 1.28-2.13K 80—69965
- $\mathrm{Hg_2X_2}$, X=Cl, Br, I, acoustic props., cryst. lattice bonds 78—30700
- KF-PbO-$\mathrm{SiO_2}$ glass shear wave velocity and its temp. depend. *(Japanese)* 78—30702
- $\mathrm{K_2O}$-PbO-$\mathrm{PbF_2}$-$\mathrm{SiO_2}$ glass shear wave velocity and its temp. depend. *(Japanese)* 78—30702
- $\mathrm{K_2ReCl_6}$, elastic constants, softening of acoustic modes, obs. by Brillouin scattering 80—71440
- $\mathrm{K_2SnCl_6}$, elastic constants, softening of acoustic modes, obs. by Brillouin scattering 80—71440
- $\mathrm{LiNbO_3}$, anisotropy and phase velocities of prop. of elastic waves 79—1478
- $\mathrm{LiNbO_3}$, diffusion of Co, Ni, Zn and Cu and its effect on acoustic velocity 77—84847
- $\mathrm{LiNbO_3}$, photocond. induced by $\mathrm{N_2}$ laser, piezoelec. reson., acoustic wave rel. determ. *(Japanese)* 78—2521
- $\mathrm{LiNbO_3}$, photoinduced grating contrib. to acoustic wave vel. 77—77154
- $\mathrm{LiNbO_3}$:Ti, in-diffused waveguide, acousto-optical meas. of optical field profiles 79—23054
- $\mathrm{Li_2O.2SiO_2}$, ceramic, prep. of oriented microstructure by unidirectional solidification of melts 80—71614
- Mn-Cu alloy, high-damping, acoustic shock pulse attenuation and vel., stress amplitude and temp. depend. 77—15503
- MnO, multidomain single cryst. and monodomain cryst., crit. and elastic behaviour, T_N to 300K 77—66407
- $\mathrm{N_2}$-He mixture, speed of sound, temp. depend. at high press. 77—84388
- $\mathrm{NH_4H_2PO_4}$, Z-cut, SAW props. 80—84358
- $\mathrm{(NH_4)_2SiF_6}$, elastic constants, softening of acoustic modes, obs. by Brillouin scattering 80—71440
- $\mathrm{(NH_4)_2SnCl_6}$, elastic constants, softening of acoustic modes, obs. by Brillouin scattering 80—71440
- $\mathrm{N_2O_4}$ liquid *(Russian)* 79—59863
- $\mathrm{N_2O_4}$, sound dispersion and velocity mol. dissoc. effects *(Russian)* 80—1730

acoustic wave velocity continued
(Na,Li)NbO_3 ceramic, optimum prep. conditions and characterisation 78—3079
NaCl, high press. eqn. of state and sound vels. to fourth order elastic consts., 270 kbar 79—37806
NaCl, polycrystalline, acoustic vels. at 300K from 2.5 to 270 kbar 77—27945
NaCl, shock compressed, vel. of sound meas. 78—10123
Ne-H_2 mixture, liquid vapour phase equilib., sound vel., compressibility, thermodynamic perturbation theory obs. *(Russian)* 80—39306
Ni crystals in strong mag. field, EM excitation and vel. dispersion of sound *(Russian)* 80—39837
Ni-P, metallic glass, acoustic wave vel. log. temp. depend. *(French)* 77—72659
Pb, thermodynamic characterisation at high temp. 80—103494
$Pb_2KNb_2O_5$, SAW props., rel. to device appl. 78—71923
PbO-containing binary systems, acoustooptic props. from comp. and density 80—76000
$PbTi_xZr_{1-x}O_3$, piezoelectric ceramic, sound velocity temp. coefficients 77—12315
$PrCu_2$, Jahn-Teller transition, susceptibility, elec. resist., thermal expansion and acoustic meas. 77—20276
α-Pu, longit. and shear sound vels., press. to 50 kbar, elastic moduli 77—20015
Se, trigonal, normal mode calcs. 80—84259
Si amorphous film, acoustic study using Rayleigh waves 80—75312
Si film, hydrogenated amorphous, Brillouin scatt. 78—72538
Si, liq., sound vel. meas. 79—77684
Si rubber, room temp. vulcanized, compounded with various powders 79—81614
SiO_x amorphous films, acoustic study using Rayleigh waves 80—75312
SiO_x, thin film on YZ-$LiNbO_3$, SAW props. 80—84356
$SmCrO_3$, spin reorientation phase transition, second order nature 77—80950
α-Sn, gapless semicond., sound propag., RPA calc. 77—31721
Sn, sound attenuation and velocity depend. on mag. field *(Russian)* 80—29446
$SrCl_2$, elastic constants and acoustic wave velocity, temp. variation 78—6118
Te-Se liquid mixtures, sound vel. meas., adiabatic compressibility determ. 80—65161
TiO_2, acoustic vel., absorpt. coeff. and photoelastic consts. rel. to acoustooptical parameters 79—56762
TmSe, first obs. of negative elastic const. 80—103409
V_3Si, neutron irrad., sound velocity, magnetic susceptibility and upper critical field 78—88074
$Y_3Fe_{5-x}Ga_xO_{12}$, inhomogeneous stress effect on ferromagnetic resonance, elastic consts. from sound vel. meas. 79—24219
YIG, sound vel., temp. depend., phonon scatt. processes 80—96598
ZnO-PbF_2-SiO_2 glass, shear wave velocity and its temp. depend. *(Japanese)* 78—30702
ZnO-SiO_2-Si layered structure, SAW props., anal. 77—62729

acoustic wave velocity measurement
see also ultrasonic velocity measurement
acoustic flowmeter, for open channels, accuracy 79—68876
acoustic pipe entrance, experimental study of vel. field *(French)* 80—33395
acoustic surface wave velocity measurement, pulse technique 78—5618
admittance figure approach to processing acoustic interferometry meas. 79—50539
air-water two phase medium, acoustic velocity and attenuation meas. 77—58513
amorphous polymers, meas. of LF shear-wave vel. to determine influence of space network of linkages 80—19194
Bermuda Eleuthera Acoustic Range environmental meas. buoy 77—41229
calcareous ooze and chalk, Ontong Java Plateau, W Pacific, sound vel., sonobuoy data 78—40542
clapping method 80—82620
compact bone sample, distrib. of sonic plesio-velocity 79—96611
complex elasticity of crystals, small variations meas. by acousto-optical method 79—3867
computer-controlled system for measuring two-dimensional acoustic velocity fields 80—35462
continuous recording of shock waves, appl. to sound speed meas. 78—5708
dichlorodifluoromethane, liq. Refrigerant 12, meas. at 26.7°C 77—89497
digital electronic instrument, comments on errors 80—14528
Earth crust, synthetic sonic logs as process for stratigraphic interpretation 79—88483
education, speed of sound meas. expt 79—71181
Fresnel zone and diffraction fields anal. near boresight of acoustic radar antennas 80—64318
gas constant meas. in Ar by acoustic interferometry 77—7492
gas-bearing sediments 80—87670
gases, dilute, temp. and thermophysical prep. meas., using acoustic resonators 80—53573
geophysical acoustic logging, signals limited spectrum rel. to time interval and damping determ. accuracy *(Russian)* 79—39971
interferometer nonlinear transducer motion 79—50540
liquid metal column, acoustic velocity meas. across diameter 80—14527
liquids, meas. at freqs. of 5 to 20 kHz in small-volume cells 78—9516
liquids, moderate-accuracy interferometer for sound speed meas. 77—50844
marine sediments containing gas hydrates, thermal cond. and acoustic wave vel. meas. 79—79819
musical acoustics wave motion experiment, phase vel. meas. using spring 80—8762
near-borehole elastic wave linear velocimeter *(Russian)* 77—60492
ocean density profile remote sensing pulses, numerical algorithm 78—20429
phase velocity meas. using CW feedback technique 78—83187
pulse echo method for acoustic vel. meas., transducer effect 77—42676
resonance tube principle *(Japanese)* 77—42672
rocks sound velocity determination, suggested methods 78—81433
rubber compounds, using automatic progressive wave apparatus 79—91866
sand, water-saturated, broadband meas. 80—83719
SAW velocity measurement, high accuracy method 80—38189
seawater, microprocessor-based instrument 80—67440

acoustic wave velocity measurement continued
shock-loaded solids, wave profile measurement 79—94564
solid, phase and group vels. determ. for dispersive waves 78—81848
sonar system, transfer function model 77—7275
sonobuoy position meas., sound speed adaptive estimation 79—72773
standing-wave systems, resonant, errors in wave velocity meas. 79—10436
steel, stainless, Cr-Ni-Mn, N strengthened, low-temp. elastic props. determined from sound velocity measurements 79—70109
surface wave, recirculating pulse generator 78—5619
thiophene, hypersonic wave propag. vel. in 2.7 GHz range, existence of vibrational relaxation 80—33377
underwater acoustic measurement, FM signal correl. methods 77—62086
wide rivers, acoustic flow meas. 79—72975
H_2, rot. energy, specific heat, temp. depend. determ., demonstration 78—12465
Li, seeded flames, excitation, laser radiation absorpt., sound vel., optoacoustic effects obs. 80—43345
Na seeded flames, excitation, laser radiation absorpt., sound vel., optoacoustic effects obs. 80—43345

acoustic waveguides
3-layer, wave numbers and phase difference between components of sound field 80—38144
active noise suppression 78—5613
active noise suppression in waveguide with monopole radiators and dipole receivers 80—102928
anisotropic elastic waveguide normal-mode anal., appl. to Rayleigh-Love wave mode converter 79—23113
autonomous active systems for sound field suppression in single mode waveguides 77—50831
average field attenuation in irregular waveguide 78—1459
bent thin-walled, acoustic wave propag., attenuation and pre-bend build-up 80—69576
Bleustein-Gulyaev waveguides with gratings, anal. Bleustein-Gulyaev waveguides with gratings, anal. 80—1391
circular, acoustic diffraction by diaphragm, scattering matrices 80—87598
circular pipe, simulation of finite amplitude sound wave nonlinear propag. 78—13834
cylindrical, containing moving viscous fluid, modal pattern anal. 79—32105
diffraction field, approx. to soln. df Helmholtz eqns. *(Russian)* 77—57171
discretely layered, damping of normal and surface waves, depend. of vel. on losses 79—14135
discretely-layered, Holmholtz eqns., radiation conditions for boundary value problems 79—14134
dispersive acoustic systems, nonlinear and parametric phenomena 78—55489
Doppler effect under conditions of sound dispersion 79—86277
double-layer waveguides, normal mode diffraction 78—94462
duct acoustic pressure distrib., Galerkin isoparametric finite element analysis 80—27144
with elastic plates in walls, sound radiation from piston 77—50850
elastic strip with fluctuating parameters, flexural wave characts. 79—23116
elastic surface waves guided by edge of semiinfinite slit 78—1457
elastic waveguide slow torsional wave sensors 79—46748
elliptical cross-section, numerical anal. by mode-matching method 79—23109
elliptical waveguides, comparison of rigid and soft walled *(Japanese)* 77—42642
energy transport in waveguides with moving medium 77—46837
evanescent waves for guided propag., rigorous asymptotic theory 80—64238
excitation of sound pressure field in ideal waveguide by spherical pulse 78—50971
finite-length fluid cylinder, surface wave interpretation of eigenfrequencies 80—58831
fission reactor core control and monitoring *(Russian)* 80—5292
flowduct area discontinuity, experimental investigation of acoustic pressure reflection coeff. 80—33302
fluid-filled thin cylindrical elastic shell, normal modes with point force excitation 79—94550
grating waveguide modes 78—59172
Helmholtz and parabolic equations for sound propag., relation between solns. 77—84048
horn design for focused SAW radiation into waveguide 78—1542
hybrid ray-mode formulation of ducted propagation 79—50477
impedance of acoustic and structural waveguides at their cutoff frequencies 78—59215
irregular, with compliant or rigid walls, approximate wave eqns. solns. 79—90050
irregular solid waveguides with defects, variational method for soln. of diffraction problems 80—5857
isotropic elastic waveguides, numerical anal. by mode-matching method 78—9465
isotropic elastic waveguides, rectangular rods, mode-natching method 78—9466
layered acoustic waveguide, group delay time, temp. coeff. var. 78—83152
limited frequency sound suppression 78—83148
linear array of Helmholtz resonators, design calc. for zeroth normal mode 80—87602
maximum likelihood estimation of position of radiating source 79—90085
mechanical waveguide using circular cylindrical rod for HF intense US production *(Japanese)* 78—33983
mode-selective transmission in fluid-filled waveguide with transverse resistivity 78—1452
multimode waveguide, active sound fields suppression system 78—18113
multimode waveguide with periodic boundaries, acoustic field of volume-velocity sources 78—94463
multimode waveguide with uneven walls, sound attenuation 78—83147
nondispersive propag. of elastic strain waves in rectangular cross section solid waveguide 79—18565
nonlinear interaction of elastic waves with reson. *(Russian)* 78—6206
nonuniform structural, long-wavelength asymptotic solns. for axisymmetric compressional waves 79—50485
obstacle in waveguide, acoustic wave transmission and reflection 80—102893

acoustic waveguides continued
- oceanic waveguide, normal mode theory of acoustic Doppler effects 79—50497
- overlay ridge waveguide SAW mode analysis 79—46100
- overlay SAW waveguides, analytical method for characts. determ. 79—94383
- parabolic, statistical theory of propag. 80—102887
- periodic, wave propagation 79—84969
- phase vels. in open waveguides 77—58497
- piezoactive, anisotropic, dispersion relations for normal waves 77—88975
- planar, acoustooptic interaction 79—23150
- planar, bounds on soln. of Helmholtz equation 80—14507
- plane waveguide, acoustical-gravity waves interaction and self-action *(Russian)* 78—36221
- plane waveguide with one perforated wall, calc. of radiation characts. 80—102886
- point acoustic source between thin elastic plates, fluid immersed, roots of dispersion relations 80—87601
- propagation in aperiodic transition layers and waveguides 80—43498
- quartz, film acoustic surface waveguides, electrically controllable polarisation conversion and its appl. 79—76924
- reflectors, effectiveness study 80—87599
- rigid 3-dimens. waveguides, anal. of propag. using eigenfunction expansion of Helmholtz eqn. 80—83690
- rods and clad rods, elastic waves anal., tutorial review 78—94608
- rough boundary, spatial and temporal correl. functions for stochastic part of sound field 78—90560
- rough walled, acoustic propagation in material of fluctuating refr. index 78—90549
- SAW guide step analysis 78—1487
- SAW metallic gratings, equivalent circuit of step discontinuity, rel. to SAW devices 80—33389
- SAW special total reflection on anisotropic crystals 79—56054
- SAW waveguides, types and props., book contrib. 79—50488
- shear SAW in periodic structures on solids 79—90055
- side-branch pipe resonators, flow-induced tones 80—64243
- single-mode, active sound field suppression 78—38113
- single-mode, bandwidth of active sound suppression system 80—87605
- single-mode transmission and backscatter measurements in laboratory waveguide 80—64259
- slotted acoustic waveguide propagation expts. *(Japanese)* 78—46859
- slow waveguide, in water, Helmholtz eqn. soln. 78—30114
- solid waveguide with periodic boundary corrugations, multiple sound scatt. 79—94384
- sound pressure field variation as function of refractive index 78—94464
- space-time structure of acoustical field anal. by means of optical Fourier transform *(French)* 80—87583
- stochastic instability of rays in inhomogeneous media 79—64379
- straight pipes, linear acoustic loading 80—96060
- strip surface waveguide, diffr. and guidance anal. 78—13828
- surface acoustic waveguides, microwave network anal., flat overlay guides 77—27411
- surface acoustic waveguides, microwave network anal., rectangular ridge guides 77—23790
- travelling wave lens for high-speed optical scanners 79—36991
- unbaffled cylindrical pipe outlet, impedance for plane wave incident at outlet 79—55256
- uniaxial, sound field calc. from combination normal mode-ray technique 77—50800
- US transmission line of probe for hot metal inspection, spurious signals 80—66754
- wedge, mode representation of noise field 79—86299
- wire with weak surface corrugation, mode coupling of guided elastic waves 80—33271
- Young sound wave propagation in thin electrically loaded piezoelectric waveguide 78—38112
- B fibre reinforced W double coaxial composition rod, waveguide, normal mode US propag. 79—100317
- LiNbO$_3$, diffusion of Ti, surface acoustic waveguide formation 77—79998
- LiNbO$_3$, Y-cut, SAW $\Delta V/V$ waveguides in arbitrary propag. directions 79—81602
- LiNbO$_3$:He$^+$, ion implanted SAW guides, air-gap Si convolver data 78—42500

acoustic waves
- *see also acoustic emission; magnetoacoustic effects; shock waves; surface acoustic waves; ultrasonic waves*
- acoustic field in stratified media of variable viscosity, Green's functions 80—4545
- acoustogravity wave generation in Earth's atmosphere 79—66776
- boiling, nucleation centres interaction, obs. technique 78—14065
- α Bootis atmosphere, acoustic flux rel. to temp. minima and Wilson-Bappu effect 79—62825
- Burgers equation, sawtooth soln. decay 80—31529
- characteristics rel. to EM waves *(Japanese)* 78—46858
- chromospheres of late type stars acoustic wave heating and temp. minima heights 78—20818
- composite compliant baffle anal., comments 80—48482
- crystal nonlinear electroacoustics, dynamical eqns. and constitutive relations 79—56734
- crystals, optical method for meas. of shear waves polarisation 77—35006
- CW far-infrared laser scattering from a laboratory plasma ion acoustic wave 80—106974
- detection of high-energy particles in water 79—59307
- dielectric crystals, externally deformed, phonon transport eqn. 77—27956
- direction location of infrasound waves, meas. on jet planes *(German)* 80—92000
- discontinuous waves in nonlinear media, characts. 78—5601
- Doppler research in the nineteenth century 80—86070
- Earth atmosphere, acoustical-gravity waves interaction and self-action in plane waveguide *(Russian)* 78—36221
- elastic transitions of second order, dynamical renormalisation group method 79—40512
- elastic-acoustic system, response to press. source in acoustic medium 77—75833
- electroacoustic wave variational expression derivation 78—1488
- EPR spin system saturation characts., acoustic wave excitation *(Russian)* 80—66013
- gas dynamics with relaxation effects, acoustic waves, nonequilibrium atmosphere effects, review 78—79390

acoustic waves continued
- gas flow into duct, self-excited oscillations 80—33647
- generation by strip propellers, non-uniform liq. stream 80—96094
- gravity waves, quasi-simple wave solns. 77—75930
- gravity-acoustic waves, self-localisation, non-linear effect in non-uniform atmosphere 79—8761
- Green's function for plate acoustic emission 77—50798
- harmonic wave reflection, effect of thermoelastic scatt. 80—14613
- hot plasma, white noise excitation, sum of ion acoustic waves 78—42736
- infrasonic pulses detect. from thunderclouds 77—29362
- infrasound, atmospheric, detect. by homing pigeons 77—29156
- infrasound, investigations into measurement and analysis, development of measuring system *(German)* 79—50541
- infrasound generated by Concorde used to monitor stratospheric winds 80—51492
- inhomogeneous, visual characts., optical holographic interferometry 80—102943
- inverse source problem of scalar waves, acoustic and EM examples 77—30015
- ionospheric acoustic-gravity waves, Doppler sounding, rel. to storm detection and prediction 79—2326
- Lamb and SH wave propag. in layer with initial stresses 77—35076
- late-type stars, acoustic energy generation rel. to chromospheres 78—7986
- line, unusual parametric effects 80—5854
- linear waves in radiating scatt. grey medium, effect of transverse mag. field 77—56911
- magnetic bubble lattice propagation control by standing acoustic waves 79—82841
- material properties associated with dynamic deformation of matter, acoustics and the props. of materials 80—64234
- negative-energy waves, investigation of normal modes 80—102889
- nonlinear acoustics of pipes and ducts in gas, breakdown of acoustic approx. 79—3823
- nonlinear elastic interactions between acoustic bulk and surface waves 77—50797
- nonlinear hyperbolic waves, comparison of three perturbation methods 77—7236
- nonlinear resonance effects in closed shock tubes with varying cross section 77—50803
- nonlinear sonic wave, excitation by quasi-monochromatic Alfven pumping 80—106649
- open pipe exits, flow during acoustic resonance, vortices and boundary layers 80—92224
- open tubes, resonant oscillations of gas 77—68628
- poly(vinylidene fluoride) piezoelectric film, Lamb and shear wave propagation *(French)* 80—44256
- production in polar medium, by radiation, possible detection method appl. 80—63493
- proton beams in fluid media, acoustic signature 79—59317
- pulse propag. in nonlinear media, linear approx. 79—94390
- quartz substrate, surface and bulk acoustic waves excited by interdigital transducers, optical diffr. study *(Chinese)* 78—50965
- radiated, vibrating strip, power output considerations 80—69577
- Rubens flame tube demonstration of standing sound waves 80—8760
- scheelites, external lattice vibr. modes and elastic wave vels., dispersion relations 79—33050
- shock wave-acoustic wave interactions in elastic solids 79—32370
- solar atmosphere, acoustical-gravity waves interaction and self-action in plane waveguide *(Russian)* 78—36221
- solar atmosphere, penetrative instabilities theory in presence of thermal dissipation 80—109406
- solar atmosphere, sound generation by Alfven waves with random phases 78—7979
- solar chromosphere, acoustic shock waves dissipation and H$^-$ radiation 78—96454
- solar non-isothermal atmosphere, linear hydrodynamical eqns. coupling with radiative transfer 78—20794
- solar photosphere, effect on spectral line profiles for Na I and O I 80—17558
- solar transition zone and corona, wave refl. and wave disorder 79—12453
- sound pulse generation, by thermal sources 77—34977
- spectral theory for acoustic wave eqns., generalised Neumann boundary conditions 78—59173
- sphere impacting on thin square plate, acoustic generation mechanism 80—74591
- standing waves, in gas liq. medium 78—9474
- stellar atmospheres, short period acoustic wave mechanism for chromospheric heating *(German)* 80—109421
- stellar chromospheres of late type stars, acoustic wave heating and temp. minima heights 78—20818
- stellar penetrative atmosphere, convective, gravity and acoustic instabilities 79—84783
- stratified compressible flow, inhomogeneous acoustic-gravity wave eqn. 77—80174
- subharmonic nonlinear acoustic resonances in open tubes 77—72404
- subsonic flow past flat bodies with blunt tail sections, vortex shedding associated waves 77—68616
- supersonic flow, separated, self-excitation of acoustic oscillations 77—7411
- terrestrial atmosphere acoustic-gravity waves, generation mechanisms *(Russian)* 78—85621
- thermoacoustic vibration generation, in heated channel laminar flow 78—14029
- thermoacoustic vibrations of subcritical press., vibrs. onset mechanism 77—47026
- time transformation of acoustic eqn., flow effects on sound field, wind tunnel noise meas. appl. 78—87198
- transient acoustic emission signals, stochastic model 79—72749
- transonic gas flow, optical excitation of intense acoustic waves 80—74564
- triangular pulses with discontinuous edges, interaction with shock waves 77—50802
- tunnel effect for linearised quantum eqns. of elasticity 77—26188
- turbulent liquid pipe flow, thermoacoustic oscills. 78—9635
- turbulent shear layer, instability waves, radiation of sound 80—79341
- variational expressions systematic derivation 78—93536
- visualisation of progressive acoustic wavefronts using Koster prism 80—5701
- water heated by laser pulses 77—50812
- He, thermoacoustic oscillations in nonuniformly heated tubes 80—33441

acoustic waves continued
- ^{4}He superfluid, acoustic vibration field density of states in piecewise const. parameter media 80—6483
- $LiNbO_3$, bulk wave generation near SAW reson. by interdigital transducer 80—33402
- Y-Z $LiNbO_3$, radiation patterns of bulk acoustic modes from finite interdigital transducer 80—43491
- TeO_2, elastic wave parametric instability kinetics in dielectrics *(Russian)* 80—45035

acoustical laboratories
- *see also anechoic chambers; reverberation chambers*
- ambient noise indices, control instruments and systems *(French)* 79—76913
- appliance acoustic emission determ. facility development 77—58507
- audio equipment technical laboratory, Toshiba Audio Center 79—55284
- noise exposure effect on human body investigation *(Japanese)* 77—40709
- nonrectangular reverberation chamber design and construction 78—83196
- research laboratory design for the Rensselaer Polytechnic Institute 77—80036
- reverberant room, calibration by reverberation decay method 77—19502
- test facility modification for ANS qualification 77—62121

acoustics
- *see also acoustic applications; acoustic devices; acoustic equipment; acoustic noise; anechoic chambers; architectural acoustics; atmospheric acoustics; audio acoustics; hearing; musical acoustics; photoacoustic effect; sound reproduction; ultrasonics; underwater sound; vibrations*
- Acoustical Soc. Amer., 98th meeting, Salt Lake City, Utah, USA (Nov. 1979) 80—14501
- Acoustical Soc. Amer. 96th meeting, Hawaii, 1978 Nov. 78—90545
- Acoustical Soc. Amer. 97th meeting, Cambridge, MA, USA, 1979 Jun. 79—64367
- Acoustical Soc. America, plenary sessions celebrating 50th anniversary, Cambridge, MA, USA (Jun. 1979) 80—94914
- Acoustical Soc. of America in historical perspective 80—96047
- acoustics, speech and signal processing, conf., Tulsa, USA, 1978, April 78—63242
- acoustics, time delay estimation in presence of source or receiver motion 77—88977
- bibliography, references to contemporary papers 77—79979
- closed space, sound levels decrease *(French)* 80—14503
- cocktail parties, acoustical aspects 77—80008
- conference, physics in industry, Dublin, Ireland (9-13 March 1976) 77—60887
- conference, San Diego, California (Nov. 1976) 77—7227
- conference, University Park, Pa. (June 1977) 77—50784
- conference on acoustics, speech and signal processing, Denver, CO, USA (Apr. 1980) 80—83689
- contemporary acoustics, brief review *(Chinese)* 79—37069
- contemporary papers references, 1980 80—96049
- course, sound and light in the arts 77—22340
- cross-spectral anal., statistical parameters of estimators 78—83180
- cutting-out techniques *(French)* 79—41476
- effective acoustic centre, redefinition 77—84028
- flow acoustics, characteristic phenomena 77—75903
- future accomplishments, summary of conjectures based on plenary sessions of ASA 50th anniversary 80—96048
- historical account of Wallace C. Sabine's notebooks 77—49545
- history, from Echo to 18th century *(German)* 79—76915
- history, golden age of 19th century 78—12526
- history, Kircher's 'Phonurgia nova' *(German)* 78—81788
- history of American acoustics, conference, Washington, DC (Apr 1976) 77—45660
- history of American acoustics, introductory comments 77—45661
- illustrated technical talks, planning and preparation guidelines 77—9832
- International Standards organisation for acoustics *(Japanese)* 80—14502
- jet turbulence, interaction with pure tone sound 78—94790
- John Tyndall's demonstrations on sound (1854-82) 77—22362
- magnetoelastic media, nonlinear acoustic effects 77—36109
- Mossbauer absorpt. spectrum oscillation with acoustic modulation 79—87345
- nonlinear acoustics of pipes and ducts in gas, breakdown of acoustic approx. 79—3823
- numerical evaluation of singular integrals in interface separation, new quadrature formulae 80—74559
- physical acoustics, history and future, review 77—49548
- physical acoustics, International School of Physics, Course 63 (Varenna, Italy, 1974 Aug. 5-17) 77—50785
- physical and technical acoustics, conf., Parnu, USSR (Apr. 1976) 78—1451
- physical and technical acoustics, conference, Zvenigorodskii, USSR (Sep. 1977) 78—18081
- physical and technical acoustics and ultrasonics, conf., USSR (Apr. 75) 77—800
- principles and appls. *(German)* 77—3689
- quantum, liquids, spin lattice relaxation, sound coherence 80—97128
- references to contemporary papers 79—86274
- references to contemporary papers on acoustics 79—41468
- research in Australia *(Japanese)* 80—10056
- resonance, open and closed end pipes, for teachers 78—81774
- review, acoustics in perspective *(Chinese)* 79—37068
- source extraction problem, general formulation 77—84043
- Soviet acoustics, progress in ninth five-year plan (1971-1975) 77—14824
- stability of difference schemes for multidimensional equations of acoustics 80—105512
- structural information theory of sound 77—14822
- system identification, from multiple input/output data, comment and reply 78—83179
- teaching, sixth form physics course 79—62973
- undergraduate teaching, 'demonstration cart' 79—35481
- units, change to SI problems *(German)* 77—27403
- variable systems subjected to arbitrary source functions and boundary conditions 77—7234
- wave packets, propag. and spreading theory 77—13521

acousto-optical devices
- *see also acousto-optical effects*
- 2-D image processing applications 80—53231
- 400 MHz to 2.3 GHz acousto-optic deflectors 79—50416
- acoustic emission monitoring difficulties overcome by optical detectors 78—60968

acousto-optical devices continued
- acousto-optic deflector, holographic distortion correction *(Russian)* 77—75690
- active optical devices, seminar, San Diego, CA, USA (August 1979) 80—101664
- adaptive Fourier transformation by acousto-optic convolver 79—55079
- anisotropic acoustooptic deflector, using otically active uniaxial crysts. 78—66928
- astronomical radio spectrograph for spectral integration 78—69694
- beam quality, of acousto-optic frequency shifters 78—79127
- binary input hologram recording with single acoust-optical modulator *(Russian)* 77—58287
- Bragg deflection of guided optical wave by surface acoustic waves in $LiNbO_3$ Ti-diffused waveguides 79—14118
- Bragg deflector, wide-band guided wave, using tilted-finger chirp transducer 80—14440
- Bragg deflector, wideband, guided wave, technology and applic. 77—58471
- Bragg deflector, wideband guided-wave, using tilted-finger chirp transducer 80—74510
- Bragg diffraction imaging, aspect ratio restoration by holographic lenses 79—46122
- broadband acousto-optical deflector, design and performance characts. *(Chinese)* 80—10011
- broadband chirp transducers for integrated optics spectrum analyzers 80—74514
- broadband matching of piezo-transducers for acousto-optical devices *(Russian)* 80—64329
- bulk acousto-optic interactions in thin film waveguides, for GHz modulators 78—42471
- bulk acousto-optic interactions in thin film waveguides, gigahertz modulators 79—32091
- chalcogenide glasses, optimum glasses for acoustic delay lines and deflectors 78—55420
- chalcopyrite crystal acousto-optical props. 79—46054
- colinear thin film acousto-optical scanner 77—79944
- conference, San Deigo, Calif., USA (Aug 1976) 77—58463
- correlator with two-dimensional reference transparency, testing 80—106485
- correlators, real-time and memory devices using acousto-optic processing 78—46533
- correlators, review 77—58473
- correlators, spatial or time integrating, review 78—9341
- deflection cell, scanning of image-carrying light beams 80—14459
- deflector, 200 MHz bandwidth, using stepped array transducer 77—58467
- deflector, (x,y), with 32×32 positions resolution 79—72683
- deflector, bandwidth increase method 80—99861
- deflector, planar optoacoustic, expt. 78—74995
- deflector, resolution criteria 80—43265
- deflector for 1-D hologram, page-composer technique 79—81397
- deflector for laser beams, design and appl. *(Czech)* 78—5573
- deflector for TV and oscillograph displays 77—39099
- deflector of luminous radiation parametric excitation of sound *(Russian)* 78—33850
- detector integration acouto-optic signal processing 79—72519
- direct modulation of light by sound 79—72715
- Doppler signal simulator for optical heterodyne receiver parameter meas. 79—80684
- Fabry-Perot acoustic interferometer for measuring HF acoustic losses in materials with high Q-factor 80—5887
- Fabry-Perot cavity acoustooptic modulator for internal laser modulator *(Japanese)* 77—88814
- fibre interferometer for reflective surface motion meas. 80—13127
- fibre loss, dispersion and polarisation meas. by acousto-optical tunable filter 80—102855
- fibre optic acoustic sensor, modulation processes 80—58771
- fibre optic acoustic sensor, single coiled monomode fibre 80—102826
- fibre optic acoustic sensors with increased sensitivity due to composite structures 80—5834
- fibre optic hydrophone, using single-mode and multimode fibres, sensitivity 78—13882
- fibre optic interferometric sensor for acoustic detect., thermally induced optical phase effects 80—74479
- fibre-optic acousto-optical modulator 79—98499
- fibre-optic microphones and hydrophones compared with conventional devices 79—72717
- film deflector, efficiency for Gaussian beam 78—13791
- film waveguide, SAW signal convolution 77—27428
- FM wide-band system using optical techniques 79—64308
- Fourier transform., real-time, via acousto-optics 79—46112
- frequency shifter for CO_2 laser velocimeter 80—100042
- gap-coupled Schottky diode array/$LiNbO_3$ imager for scanning of optical images 80—74632
- gas analyser with acoustooptic detector and semiconducting generator based on Gunn diode *(Russian)* 80—101141
- guided acoustic travelling wave lens for high-speed optical scanners 79—36991
- guided beam deflector design, fabrication, and applications 77—19433
- guided wave acoustooptic Bragg diffr., optical pulse compression, light beam scanning 78—38053
- guided wave acoustooptics, fundamental principles and wideband appls. 79—37038
- guided-wave, with appls. to wideband communications and signal processing, progress review 80—58801
- guided-wave acousto-optic interaction on Si substrate 79—37050
- heterodyning image processor, OTF 80—5833
- HF acousto-optic mode conversion and deflection 77—54776
- HF crystal acousto-optic deflectors, 0.5-1.5 GHz 78—5576
- holocinematography, high speed, acousto-optic beam deflection for spatial freq. multiplexing 78—74860
- holographic binary data recording with multichannel acousto-optical modulator *(Russian)* 79—94178
- holographic data recording phase-random mask production by multichannel acousto-optical modulator *(Russian)* 79—94179
- hydrophone, coupled waveguide, using intensity modulation 80—14431
- hydrophone, fibre-optic, description and advantages 80—58770
- hydrophone, moving fibre optic, based on intensity-modulation mech. 80—43455
- hydrophone, optical, using acousto-optic transduction 80—14541

acousto-optical devices continued
image and hologram convertor based on acousto-optical effect in liquid cryst. 80—76002
image Fourier transform correlator using US light modulator *(Russian)* 77—58264
image processing using space-to-temporal freq. conversion 80—87340
imaging, analogue fast Fresnel transform methods 79—46116
incoherent image two-dimensional Fourier transform by optoacoustic transducer 79—50243
information processing using surface acoustooptic interaction, side entry config. 78—42461
integrated acousto-optical spectral analyser waveguide geodesic lens correction 79—50241
integrated optic Bragg spectrum analyser design 80—33237
integrated optic spectrum analyser, design of Bragg cell 80—74515
integrated optical detector array, waveguide, and modulator, based on Si technology 77—11049
integrated optical RF spectral analyser acousto-optical readout scheme 79—50446
integrated optics A/D convertor based on bulk acousto-optic interaction 80—69552
interferometer signal processing by acoustooptic correlation devices, radio astronomy applications 80—8543
interferometric acoustic sensor, single optical fibre 78—38161
IR scanning by SAW modulation 79—80687
isolator for stabilisation of optically pumped submm. lasers 79—31918
large time-bandwidth acousto-optic signal processors 79—46118
laser alphanumeric character generator for line printer and COM 80—33067
laser beam deflector guided wave acoustooptic Bragg diffraction *(German)* 77—19417
laser beam deflector quality factor N/τ, comparison of holographic and acousto-optical deflectors *(French)* 78—55318
laser beam intensity modulator *(Slovenian)* 80—43429
laser beam modulation appl., comparison with electro-optical devices 80—43380
laser beam modulation using US acousto-optic modulator 79—3730
laser beam phase detector, HF chem. laser beam phase fluctuation meas. 80—48317
laser beam scanning by acousto-optic deflector array 80—10017
laser detection using tunable acoustooptic filters 78—29159
laser Doppler anemometry, acousto optic cell performance, investigation *(Portuguese)* 77—89217
laser Doppler velocimeter with variable frequency shift for combustion flow meas. *(Japanese)* 78—67294
laser interferometer, acoustic vibration meas. 78—71253
laser modulator, freq. and intensity control system for CW lasers 77—88804
laser modulators, for microwave frequencies 78—1282
laser pulse generation and modulation devices 78—25899
laser scanned acoustical imaging systems, demodulation scheme 79—59826
laser scanner, using acoustic travelling wave technology 77—58470
laser scanner high resolution deflector 78—46827
laser spectrometer, high resolution, appl. to H_2O vapour spectrum 80—86450
laser velocimetry using acousto-optical modulators 80—33715
lensless convolver using SAW device with polarisation discrimination detect. 78—79170
light modulator, waveguide, using Raman-Nath diffr. of vol. acoustic wave 80—48437
light modulator for laser image recording on cinefilm *(Russian)* 79—89027
linear array acousto-optical modulator devices 77—39072
liquid crystal cell, mixed nematic-cholesteric, US field visualisation 78—1524
loss modulation for mode locking of Nd:YAG laser, optical pulse generator 79—64260
matched filtering with multichannel US modulators *(Russian)* 77—58426
memory correlator, long duration, using acousto-photorefractive effect 78—79124
memory correlator based on photoinduced surface storage of SAW patterns in $LiNbO_3$ 80—74309
memory correlator using acousto-photorefractive effect 78—71248
microwave, 0.2 to 18 GHz, using ZnO piezoelectric transducers 77—58465
modulation of pumping laser, for CW dye laser mode-locking 79—18456
modulator, appl. to laser Doppler anemometers 78—83082
modulator, for intracavity laser intensity modulation, 0.01 Hz to 1.2 GHz 79—41400
modulator, for single sideband Doppler-free double reson. Stark spectroscopy 79—44935
modulator, improved contrast using spatial filtering 78—9448
modulator, intracavity, 212.8 nm pulse burst generation of Nd:YAG laser 78—74934
modulator, laser beam transverse mode and polarisation effects on perform. 77—58469
modulator, liq. and solid, freq. characts. and coupling composition 77—62069
modulator, metrological certification of photodetection devices 80—23727
modulator, mode-locking CW Nd:YAG laser, optical spectra obs. by interferometer 79—7134
modulator, phase modulation technique to determine freq. response of piezoelectric transducers 80—38023
modulator, reduction of thermal distortion of diffracted light 80—5837
modulator, standing wave, thermal detuning effects 78—71197
modulator, temporal response, geom. optics model in low scatt. efficiency limit 77—34935
modulator, wide bandwidth, design procedure 78—5569
modulator and driver for CW dye laser 77—61984
modulator efficiency optimisation, sound diffraction profile model and expt. 80—106615
modulator for CO_2 laser rangefinder using heterodyne detect. 80—102825
modulator for gas laser radiation, using acoustic surface waves 78—25901
modulator for laser beam position sensor 78—46705
modulator for mode-locked CW Nd:YAG laser 80—87419
modulator for mode-locked phosphate glass oscillator *(Japanese)* 79—13999

acousto-optical devices continued
modulator for optical heterodyne interferometer 77—5896
modulator for ruby laser, by US surface waves on resonator mirror 77—50699
modulator in high scattering efficiency regime, temporal response, algorithm 79—50377
modulator intensity servo, optical isolation and amplitude noise reduction 79—98472
modulator temporal response, physical optics model in low scatt. efficiency limit 78—66897
modulator using acoustic Fabry-Perot resonator, for gas laser mode locked operation 79—45976
modulator using coupled plane waveguides 80—69527
modulator-deflector for light beam 79—55224
modulators, applications and device technology 77—58468
modulators, computer controlled laser interferometer 80—56294
modulators, for laser freq. changes 78—74932
modulators, nonreciprocal transmission phenomena 78—33898
modulators, shutters and deflectors, areas of appl. 79—94359
modulators, switches and deflectors, physical principles and Czechoslovak developments *(Czech)* 80—19090
modulators and wide-band deflectors, dense and ultradense flint glasses appl. *(Russian)* 80—2721
modulators for laser beams 77—19355
monochromatic light source with electronically variable wavelength 80—102791
movie camera, laser based, operation and applications 80—57405
multibeam acousto-optic modulator efficiency stabilisation 80—43439
multichannel acousto-optical modulator control system *(Russian)* 79—72525
multichannel acoustooptic modulator for real-time recording and optical processing 79—10399
multichannel signal processing using acoustooptic techniques 80—19160
multifrequency Bragg acousto-optic deflector, laser beam AM suppression 80—53426
multimode fibre coupler-type acoustic sensor, optical intensity modulation 80—102945
multiplexer for fibre-optical systems 77—27370
multiplexer/demultiplexer terminals, appl. to laser communication system, expt. results 78—25959
nematic layer as active element for acoustic information transform. 77—20824
nematic liquid cryst., isotropic phase, pulse acoustic-optic modulator 80—95993
nematic liquid crystal acoustic image detector, resolution expt. 78—46871
nematic liquid crystal acoustooptical image convertor 78—18062
noncollinear UV acousto-optical tunable filter 80—102832
optical computing, conference, London (1978) 79—72511
optical fibre acoustic sensor 77—72119
optical fibre power dividers, acoustic sensitivity 80—5835
optical fibres as microphonic instrumentation transducers 77—17970
optical fibres for acoustic detection, sensitivity measurement 79—50542
optical probe for meas. local elastic props. in transparent media 79—14174
optical processing systems, seminar, Huntsville, USA (May 1979) 80—46732
optical signal and image processing, conference, San Diego (1977) 78—74853
optical video disc, acoustooptic travelling wave transcription signal recording 79—36986
optical waveguide, metal diffused, TE-TM mode conversion 78—42411
opto-acoustic transducer, for biomed. diagnostic imaging, equiv. cct. and simulation 77—60283
opto-acoustic transducer structs., recent investigations 80—74688
optoacoustic cell with improved performance for NO detect. 77—66987
optoacoustic sound-focusing device based on laser beam absorption in thin liquid film 79—90107
parallel channel wideband receiver 80—48447
particle motion detection in transparent liquids, Fourier transform acoustooptical system performance 80—87680
PCB, nematic liq. cryst., US imaging, convertor, acousto-optical effect 78—59218
photochromic film waveguide, acousto-optical props., integrated optics appl. 80—33207
photorecorder, 1 GHz bandwidth 77—57365
planar, SAW loss meas. using light beam diffraction 78—74996
planar acoustic waveguide, acoustooptic interaction 79—23150
planar deflector, with colinear propagation of optical and surface acoustic waves *(Russian)* 77—62053
planar guided-wave Bragg modulators, integrated optic communication appls. 80—38131
Pockels readout optical modulator, acoustooptic snapshot, optical, signal spectrum analyser 78—90494
polarisation interferometry 78—32864
polarisation modulator, 200 to 2400 nm transmission band *(Russian)* 80—14472
processor, light diffr. by acoustic wave 79—76586
processors for wideband electronic signals 78—79137
programmable acousto-optic tunable filter 80—74511
programmable filter characteristics and applications in optical computing 79—72716
pulsed acousto-optical modulator RF driver for laser mode locking 78—90438
Q-switch, ultrasonic, for Nd:glass laser 80—64034
Q-switches for Nd:YAG lasers 79—7166
radio astronomy spectrometer for processing of MM-wave signals 80—4253
radioastronomy, RATAN-600 radiotelescope, acousto-optic spectrograph 80—46398
radiospectrometer, high resolution, for mm wave astronomy 78—4109
Raman-Nath standing-wave mode-locking switch, modulation index 80—78980
raster-scanned laser display using TeO_2 acousto-optical deflector 77—10930
Rayleigh interferometer, two-freq., acoustooptical transform. of spatial and time freqs. 79—75579
real time two crystal correlator 78—42497
real- and near-real-time signal processing 80—10024
real-time Fourier spectrum analysis applic. 77—58285

acousto-optical devices continued
- real-time optical Fourier spectrum analysis using acousto-optic diffr. 78−5430
- real-time radar and sonar signal processing 79−72515
- RF spectral analyser, integrated optics structure employing acousto-optic effect 77−27389
- RF target simulator 80−102843
- SAW, applications 77−59198
- SAW acousto-optic modulators for integrated optics 79−90032
- SAW acousto-optical light diffraction grating, gas laser tuning *(Russian)* 78−33759
- SAW acousto-optical total internal reflection modulator 77−19435
- SAW Broadband modified chirp transducers for integrated optics spectrum analyser 80−58802
- SAW delay line acousto-optic signal processing devices 79−94328
- SAW delay line signal processors using acousto-optic interactions, real time system 80−28384
- SAW device for optical image processing 78−71051
- SAW electrostrictive mixing in optical waveguides 77−27390
- SAW integrated optics spectrum analyser, development progress 80−58803
- SAW time integrating correlator 80−64295
- scanner design, resolution 77−39045
- scanning laser acoustic microscope 79−7263
- Scophony light valve, comparison with flying spot scanner 80−33147
- semiconductor acoustic DFB laser, high speed repetitive Q-switching 78−83007
- sensor development 80−14542
- side band spatial elimination associated with acoustooptical pulse-picking 79−59732
- side-entry surface acousto-optic interaction signal processor 80−48174
- signal processing, time-integrating, acousto-cptic 80−102641
- signal processing activities of United States Army 80−48172
- signal processing system architectures and applications 80−102652
- signal processor, multichannel 78−66990
- signal processors based on light polarization discrimination techniques 80−74310
- signal processors using multichannel SAW correlation and convolution 80−74611
- snapshot Pockels Readout Optical Modulator 77−19193
- solar radio spectrograph 78−73631
- spectral analyser at RATAN-600 radio telescope, first test *(Russian)* 80−51668
- spectrograph, for radioastronomy *(Russian)* 79−25506
- spectrum analyser for radar signal processing 78−78942
- spectrum analysers, RF, using TeO_2 crystals *(Russian)* 77−7263
- spectrum analysers for radioastronomy, expt. *(Russian)* 77−29652
- spectrum analysis, wideband high-resolution, hybrid technique 79−76597
- spectrum analyzer, time- and space-integrating 80−9983
- standing wave US Bragg cell, appl. to laser communication system, theory 78−25958
- standing wave US Bragg cell, appl. to laser communication system, expt. results 78−25959
- state of the art and potential, review 77−58464
- surface acousto-optic lens, Fourier and Mellin transform props. 78−78926
- surface wave modulator and correlator, for optical link 78−38040
- surface-wave acousto-optic signal processors 80−102640
- TE$\rightleftharpoons$TM mode convertor utilizing doubly confined optical and acoustic waveguide struct. 78−83087
- thin film, theory and experimental results 77−58472
- time integrating acousto-optic signal processors 80−48176
- time-integrating acousto-optical correlator design and performance 80−106618
- transducer array, anal. and design for light diffr. 79−18527
- transducer bandwidth, layer thickness determ. *(Chinese)* 80−53593
- trichromatic acousto-optical laser-beam deflector for TV scanning *(Czech)* 79−98502
- tunable acoustooptic narrow band optical filters, appl. computer-controlled spectroscopy 77−75705
- tunable filter, for optical coherent detect. 77−88932
- tunable filter, guided-wave, using collinear TE-TM mode conversion 80−102852
- tunable filter, theory and practice 77−58466
- tunable filter based on collinear acousto-optic interaction in Zno thin film opt. waveguides 80−74509
- tunable filter for staring IR sensor, performance 80−36407
- tunable filter spectrometer development 80−101848
- tunable filters, review 78−5570
- tunable switched directional couplers of two thin film waveguides using SAW 78−75003
- tunable TE-TM mode convertor on diffused waveguide 80−53477
- TV picture production, modulated laser beam 79−55237
- two dimensional image scanning of movies using surface acousto-optic interaction 79−94352
- two-coordinate acousto-optical prismatic deflector geometry *(Russian)* 77−58428
- two-dimensional acoustic processor 79−72514
- ultrasonic symposium, Phoenix, AZ, USA (Oct. 1977) 79−46096
- ultrasonics symposium, Cherry Hill (1978) 79−50472
- US lateral and range resolution improvement by optical computer 79−53203
- US light modulators, multichannel optical processing and spectral anal. of radio signals 77−23763
- US modulator in interferometer arm, for photodetector amplitude-freq. charact. meas. 77−10112
- US transducer, liq. cryst. cell for US visualisation *(German)* 78−79179
- US transducers, integrated acousto-optical effect prod. by pulsed sound fields 77−31193
- US-optical correlator for spatial freq. meas. 80−95995
- variable-ratio laser beam splitter 79−81538
- waveguide components, planar, critical assessment and development trends *(Czech)* 80−23777
- wideband acousto-optic radiometry 78−77983
- wideband integrated optic signal processors, review 79−89864
- wideband programmable filter 80−102842
- wideband thin film modulators and switches, for optical communication 78−63206
- As_2S_3, film waveguide, acoustooptic deflection and modulation of light by stationary phase grating struct. 80−5841
- As_2S_5, thin film optical waveguide 78−83051

acousto-optical devices continued
- CO laser driven spectrophone, humidity trace detection in H_2 and air 79−20477
- CdS-$LiNbO_3$ monolithic two-dimensional Fourier transformer 79−72516
- CdTe acousto-optic and electro-optic waveguide modulators 77−42624
- GaAs, optically pumped laser with acoustic distributed feedback 78−82977
- GaP pulse modulator 78−46814
- Ge acousto-optical deflector performance at 10.6 μm 80−102835
- He-Ne laser device, for US devices power meas. 77−832
- α-$LiIO_3$, piezoelec. mat. for acoustooptic cells, piezoelectric transducers 78−95575
- $LiNbO_3$, acoustically tuned optical filter, electrostatic field effect 77−58443
- $LiNbO_3$, acousto-optic interaction with surface waves, for image scanning 77−3673
- $LiNbO_3$ acousto-optic convolver with large time-bandwidth product 77−27432
- $LiNbO_3$ acousto-optical SAW interaction multicolour image scanner 77−58483
- $LiNbO_3$ acousto-optic memory correlator 77−88992
- $LiNbO_3$, acousto-optic interaction, phase grating production 79−41454
- $LiNbO_3$, acoustophotorefractive effect, appl. at acousto-optic memory correlator 78−15145
- $LiNbO_3$ acoustophotorefractive memory correlator enhancement 79−55080
- $LiNbO_3$ crystal acousto-optical tunable filter 77−19434
- $LiNbO_3$ crystal acousto-optic tunable filter 79−55245
- $LiNbO_3$, diffused waveguide for acoustooptical signal processing 79−90029
- $LiNbO_3$, high freq. plane acousto-optical light modulators *(Russian)* 78−79106
- $LiNbO_3$ planar HF acousto-optic modulator construction and expts. 79−76863
- $LiNbO_3$ TE-TEM light mode convertor using acousto-optic interaction, expt. 78−46794
- $LiNbO_3$ TE-TM mode convertor, using collinear acoustooptic interaction 77−19407
- $LiNbO_3$ waveguide, thin-film optical filtering using acoustooptic interaction 79−81572
- $LiNbO_3$, wedge shape cryst. optical modulation, diffr. by natural freq. US standing waves 77−75685
- $LiNbO_3$:Ti, Y-cut thin film waveguide, acousto-optical deflector, electro-optical modulator *(Russian)* 77−39115
- $LiNbO_3$:Ti thin film acousto-optic deflector 77−75698
- $LiNbO_3$-gap coupled Schottky diode memory correlator, grating coupled optical imaging 80−64143
- $LiNbO_3$-Ge, modulator for CO_2 lasers 78−42365
- $LiNbO_3$-Ge acousto-optic modulator for 10.6 μm CO_2 laser 80−99776
- $LiNbO_3$-Ge acoustooptic modulator *(Japanese)* 80−69542
- $LiNbO_3$-pn-diode airgap convolver struct. optical scanner using single SAW pulse 80−64144
- $PbMoO_4$ acousto-optical modulator for wideband laser recording system 79−89942
- $PbMoO_4$, polychromatic acousto-optical deflector *(Russian)* 77−58429
- Si array/$LiNbO_3$ gap-coupled imaging devices 79−46057
- Si diode storage correlator optical imaging and memory characteristics 77−23772
- Si guided-wave acousto-optical devices 80−102864
- Ta_2O_5 optical waveguide, colinear interaction between acoustic and optical waves in planar waveguide, radiation into substrate 80−53452
- Te acousto-optic modulator, props., for IR laser beam control *(Russian)* 77−72073
- TeO_2 acousto-optic laser deflector scanning 80−14486
- TeO_2 acousto-optic laser beam deflector using shear wave propag. slightly off (110) crystal axis *(Japanese)* 80−102818
- TeO_2 acousto-optical tunable filter with microcomputer control 80−102833
- TeO_2 broad bandwidth devices bonded with Sn 78−50910
- TeO_2 crystal multichannel acousto-optic modulator 77−39100
- TeO_2 monocrystal acousto-optical deflector design and testing *(Russian)* 79−98460
- TeO_2 noncollinear IR tunable acousto-optical filter 79−23086
- TeO_2, paratellurite deflectors, bandwidth, scanning linearity *(Chinese)* 78−90501
- TeO_2 rapid optical spectrum analyser *(Japanese)* 77−27360
- TeO_2 shear wave acousto-optical device with polarisation filtering 80−106619
- TeO_2 time-integrating acousto-optical correlator for chirp spectrum analyses 80−106474
- TeO_2 volume-acoustic-wave generator acousto-optical device, appl. in laser Doppler velocimeter 79−90030
- Tl_3AsSe noncollinear acousto-optic tunable filter, operation at 10 μm 79−41434
- Tl_3AsSe_3 10.6 μm tunable acousto-optic filters 79−55248
- ZnO integrated optical transducer arrays 79−50444
- ZnO piezoelec. film, fabrication and appl. *(Japanese)* 78−23616
- ZnO thin films, surface acousto-optic interaction, diffr. 77−3685

acousto-optical effects
- *see also acousto-optical devices*
- 2-D acoustic Fourier transform of optical images 80−74308
- acoustic emission optical interfereometer and auxiliary direct viewing system 79−79217
- acoustic shear waves polarisation meas. 77−35006
- acoustic system, rapid variation in focal length 79−81641
- anisotropic diffraction by acoustic waves, induced anisotropy 77−50614
- anisotropic diffraction by bulk acoustic waves 77−23784
- anisotropic graded index waveguide, acoustooptic interaction efficiency freq. depend. 80−23776
- anthracene, mol. crystal, meas. of US attenuation coeff. by optoacoustical methods *(French)* 80−70317
- apatite type crysts., acousto-optical props. 80−100644
- bonded interface defect testing by differential interferometric Stoneley wave meas. 80−76444
- Bragg light scattering at elastic waves, acoustic activity in crysts. *(Russian)* 77−62587
- Bragg-diffraction imaging 79−64463
- Brillouin scattering by Stoneley waves, elasto-optic and surface ripple mechanisms 80−71435
- chalcogenides, prod. and acoustooptic props. *(Russian)* 78−63158

acousto-optical effects continued
- chalcohalide glasses of Ge-As-S-I system, acousto-optical parameters 77—36199
- coherent optics methods appl. to acoustic field investigations 80—106691
- colinear interaction between acoustic and optical waves in planar waveguide, radiation into substrate 80—53452
- collimated laser beam interactions with SAW-induced bulk particle motion 79—76742
- complex elasticity of crystals, small variations meas. by acousto-optical method 79—3867
- cooling liquid, absorption of flashlamp radiation with phase transition in medium 80—5868
- crystal, phenomenological theory of optical and acoustic prop. interactions 77—4621
- cyclobutanone, absorpt. of pulsed IR radiation and decomp., joulemeter and opto-acoustic obs. 80—58328
- cylindrical light beam diffr. on wideband US signal 78—50698
- DFB film laser tuning using acoustic wave 77—58359
- dielectric permeability sound wave induced nonlinear modulation *(Russian)* 80—16008
- dielectric waveguides, optoacoustic interaction, Raman-Nath type diffr. 78—87153
- diffraction by standing and travelling sound waves, anal. 77—600
- diffraction by US wave, spectral line calcs. and limitations of approximate solns. *(Russian)* 77—3532
- diffraction of divergent beam by intense waves 77—83808
- diffraction of laser light, nonlinear liquids, ultrasound propagation 80—64270
- diffraction of light by sound in solids, review 79—18577
- diffraction of light on ultrasound, phase geometry variation analysis 80—106441
- diffraction spectrum of light transmitted by superimposed US wave and diffuser 79—89848
- diffused waveguide, acoustooptic interaction efficiency of TE modes, freq. depend. 80—53455
- diffused waveguide, generalised parameters describing acoustooptic interaction 80—91924
- double phase-matching function 79—41332
- ferroelectric bodies, deformable, coupled acousto-optic modes 80—96093
- ferroelectric crysts., meas. using optical heterodyning and Raman diffr. by US waves 79—18640
- ferroelectric mats., conf., Novosibirsk, USSR (Sep. 1976) 78—76393
- Fraunhofer diffraction pattern by ultrasonic phase grating with laser point source 77—79747
- frequency shift of EM waves by indirect parametric interaction with acoustic radiation 77—38983
- fused quartz, determ. of acoustic and acousto-optical parameters using acoustic interferometry 79—41532
- gas analysis, laser optical-acoustic spectroscopic method 79—66383
- Gaussian light beam, diffr. by plane acoustic waves at oblique incidence 80—69326
- Gaussian light beam diffr. by acoustic waves 79—64173
- glass, flint, dense and ultradense, meas. and appl. *(Russian)* 80—2721
- glass, magneto-optical properties of US light diffr. 78—76437
- glass 7059, film acousto-optical props. for integrated optical Bragg cell 79—55251
- guided optical beam scatt. by surface acoustic waves 79—98508
- guided wave Bragg diffr., phased SAW array in LiNbO$_3$ 77—58439
- gyrotropic crystals, acoustic, light diffr. by US 79—56765
- gyrotropic media, diffr. of light by acoustic waves 78—72485
- high laser light intensity diffraction by sound 78—2822
- hologram, 3-dimens., optical charact., acoustic field effects 77—10877
- holograms of acoustic field, moire processing 78—55539
- impurity relaxation in nonresonance field, phonon amplification *(Russian)* 80—100310
- integrated, numerical procedure 80—91944
- integrated optics, mode interaction phenomena, exact anal., and its appl. to acousto-optics 78—42465
- intense laser beam diffraction by long US wave in liquid column 78—60421
- interaction efficiency calc. 80—103940
- isotropic media, strong acousto-optic interaction, multiple plane wave scattering 79—76580
- Lamb wave optical detect. in fused SiO$_2$ 80—106690
- Lamb wave propag. on isotropic plates, second harmonic acousto-optic interaction 80—34886
- laser beam modulation by Fresnel acousto-optic conversion 77—27371
- laser beam spatial coherence control by progressive US wave 80—78885
- laser intracavity acousto-optical modulation 77—19356
- laser light diffraction, appl. to meas. of acoustic and acousto-optic props. of crystals *(Polish)* 78—76425
- laser output power stabilisation appl. *(Polish)* 79—13994
- laser radiation intensity distrib. meas. using Bragg diffraction of light 80—64092
- laser speckle reduction by US modulation 79—3638
- laser speckle reduction in image plane by US modulation of spatial coherence 80—106459
- light coherence reduction by amplitude-modulated US wave 79—3624
- light diffraction, adjacent US beams 80—87629
- light diffraction, elastic surface wave parallel to light beam, expt. investigation 78—82904
- light diffraction by acoustic wave in acousto-optical processor 79—76586
- light diffraction by acoustic waves, anisotropic medium 77—90127
- light diffraction by acoustic waves, appl. to testing of thin film piezoelectric transducers 77—23840
- light diffraction by amplitude modulated US wave 80—1127
- light diffraction by two adjacent parallel US waves, soln. of boundary value problems 78—90358
- light diffraction by US beam in homogeneous isotropic dielectric plate, anal. 78—82905
- light diffraction by US waves, in optically active crystals 77—43965
- light diffraction efficiency for acousto-optic interactions over wide wavelength interval 80—45036
- light modulation assoc. with periodic deform. with liquid crystal layer 78—52471
- light passage, through US beam in homogeneous isotropic dielec. 77—599
- light temporal modulation, in thick-screen diffr. by ultrasound beam plus amplitude grating 77—50755
- light temporal modulation by two antiparallel sound beams, thick-screen treatment 77—68256

acousto-optical effects continued
- light wave diffr. by complex spectral composition US 80—95939
- light-induced grating, possible energy transfer control by acoustic vibrs. 80—28267
- linear anisotropic crystals, acousto-optic interactions, general theory 79—99850
- liquid, photoelastic, EM wave-excited, radiation from uniformly moving charge 79—13882
- liquid, US vel. determ. using optical diffr. by short acoustic pulses, for teaching 79—62963
- liquid, US-induced birefringence, Brillouin scatt. linewidth, sound absorption coeff. 78—27180
- liquid containing gas bubbles, thermal generation of sound 78—50994
- liquid crystal film, imaging of US in air 80—38166
- liquid crystals, instabilities generated by US field, review 78—91235
- liquid crysts., effect due to anisotropic attenuation, new developments and appls. 80—76002
- liquid US diffraction of light, Fresnel approx. 80—48135
- liquid-solid interface, acousto-optic diffr. with crit. angle incident light 78—37801
- liquids, US induced birefringence, temp. depend. study by optical farfield method 78—16826
- MBBA, light scatt. by disclinations, spatial coherence props. 77—8544
- MBBA, nematic liq. cryst., ultrasound produced rolls, spatial coherence props. of scatt. light 78—75534
- MBBA nematic liquid crystals excited by 20 MHz US surface waves, acousto-hydrodynamic effects 80—76003
- MBBA-EBBA mixture, nematic layers with homogeneous orientation, acousto-optical props. 77—20824
- metal, isotropic, Brillouin scatt. 78—80367
- methane(-^{13}C), absorpt. spectra. optoacoustic laser meas. 78—37635
- methylammonium aluminium sulphate, third order elastic consts. from stress shifted reson. freqs. 78—55905
- milling yellow colloidal water soln. flow birefr. props. for US visualisation 80—53585
- mixed metal chloride acousto-optical props. *(Russian)* 78—60419
- molecular crystals, triply-excited impurity centres, effect of acoustic wave on phosphorescence 78—27115
- molecular parameter calc. from acoustically induced optical diffusion data 77—48144
- Mossbauer radiation spectrum passed through vibr. resonant medium 80—40022
- multielement acoustic array characterisation by acousto-optic diffraction 80—99911
- multifrequency acousto-optic diffraction in optically birefringent media 80—74300
- multifrequency acoustooptic diffraction, coupled mode formulation 77—6996
- multiple plane-wave scatt., explicit formalism 80—99621
- naphthalene, mol. crystal, meas. of US attenuation coeff. by optoacoustical methods *(French)* 80—70317
- NDT by acousto-optical imaging, resolution 78—53165
- nematic liquid cryst., acousto-optic effect, acoustic streaming 80—88964
- nematic liquid cryst., response to acoustic field, streaming component and instability 80—80747
- nematic liquid crystal, birefringence obs., model 77—55767
- nematic liquid crystal, US induced birefringence and opacity 77—28544
- nematic liquid crystals, acoustically induced birefringence 78—38126
- nematic liquid crystals, homeotropically oriented, spectral studies of acoustooptical interaction 80—88965
- nematic oriented film, birefringent stripe pattern generation by ultrasonic waves 77—76301
- nonlinear acoustics 8th symposium, conf., Paris, France, July 1978 80—33277
- nonlinear acoustoelectro-luminescence excited by SAW 80—45143
- nonreciprocal effect, during light passage through US beam 80—106443
- optical coherence modulation by two ultrasonic waves 80—1120
- optical coherence modulation by US waves, partial coherence depend. on US parameters 80—58453
- optical fibres, acoustic modulation of light propagation 80—33209
- optical fibres, phase modulation of coherent light using HF sound 78—87142
- optical fibres, single-mode, Brillouin spectrum 79—46032
- optical fibres, single-mode, normal acoustic modes and Brillouin scatt. 79—76760
- optical materials, elasto-optic coefficient determ. under static loading, by acousto-optic and Brillouin scatt. techniques 79—4787
- optical waveguide, interaction between optical and acoustic surface waves, expt. 77—19428
- optical waveguide, light diffraction by oppositely propagating SAWs 79—41453
- parallel optical flat SAW meas. by reflective interferometry 79—76931
- parametric effects anal., in optics 80—102619
- partial coherence control, of light wave modulated by progressive US wave 79—76581
- pentacene, in p-terphenyl, electronic excitation transport, acousto-optical effects 78—72079
- p-n-pentyl-p′-cyanobiphenyl, nematic phase, mapping of acoustical fields 79—91402
- photochromic film waveguide, acousto-optical props., integrated optics appl. 80—33207
- photoelastic film, fluctuations of acoustic waves and light scattering *(Russian)* 77—28543
- photoelasticity, nonlinear, in impure crystals, theory 80—108179
- piezoceramic cell, fluid-filled, response to pressure generated by axial laser pulse 79—72746
- piezoelectric crystals, acousto-optic props. exam., light scatt. by thermal acoustic phonons 78—48144
- piezoelectric crystals, surface modes, acoustic wave propagation 80—20026
- piezoelectric semiconductors, photoelasticity and acousto-optic diffr. 80—29715
- PMMA Doppler scatt. optical determ. of US radiation patterns 79—76930
- polarised light in materials research, birefr., electro-, magneto-, elasto- and acousto-optics 77—48143
- probing of heterogeneous condensed media 80—38211
- pulsed sound fields, integrated acousto-optical effect in US transducers 77—31193
- quartz, fused, light scatt. by SAW on refl. and transmission 79—24288

acousto-optical effects continued

- Raman-Nath acousto-optical interaction, geometrical interpretation of image form. *(French)* 77−34836
- Raman-Nath parameter for entire sound field, calc. for baffled planar transducer 80−74689
- resonance echo holograms, acoustooptic conversion of wave fronts 77−62112
- rhodamine 6G solns., acousto-optical distortions induced by pump lamp radn. 79−73898
- ruby, optical detect. of 10^{12} Hz acoustic phonons 77−36272
- SAW, light scattering on internal refl. 78−64345
- SAW field pattern visualisation in multistrip structures 78−9511
- SAW holographic visualisation, improved S/N ratio *(French)* 78−75023
- SAW standing waves, heterodyne optical probing of partial standing waves 78−13870
- semiconductor, absorption of EM and sound waves in strong coupling case, effect of acoustic superlattice 78−26630
- semiconductor, sound-induced anomalous transmission of light below plasma edge 78−68475
- semiconductor film, size-quantised, EM wave absorpt. coeff. in coherent hypersonic wave field 80−29819
- semiconductor junction lasers, resonant acousto-optic interaction in degenerate semicond. 80−19036
- SF-14 flint glass, acoustic vel., absorpt. coeff. and photoelastic consts. rel. to acoustooptical parameters 79−56762
- solids, high speed anal. of light spectrum *(French)* 80−95156
- sound generation, by optical radiation heating 77−34977
- sound generation in liquid half-space with inhomogeneous surface layer 79−91403
- stimulated acoustooptical effects due to nonlinear photoelasticity 80−103941
- strong field interaction, Gaussian beams 80−95790
- surface acoustic wave diffr. of light beam propag. parallel to surface 78−66752
- surface acousto-optic interaction on nonpiezoelectric substrates 79−46090
- surface polariton interaction with periodic surface struct. 77−47879
- tellurites, acousto-optical criterion estimation 79−82945
- temporal modulation of light beam, diffraction by real stationary US field in liquid 80−83551
- TGS, photoelastic const. behaviour new ferroelectric transition 78−19441
- TGSe, cryst., US vel., crit anomaly and electromech. effects 79−55832
- thermal nonlinearity effects of thermooptical sound generation 80−38146
- thermooptical sound generation problems, method of transfer functions 79−64478
- thin film elastic constants and SAW velocity and attenuation meas. 79−56101
- thiourea, room temp. photoelastic consts., Brillouin scatt. obs. *(French)* 78−15182
- time-resolved, opto-acoustic spectroscopy, nonradiative yields and rate consts. 78−58052
- triphenylphosphite, acoustically induced birefringence 80−93274
- ultrasound modulated laser light, resolution of illuminated double-slit object 80−37959
- uniaxial ferroelectric, US vel. and absorpt. anisotropy and crit. anomalies, acousto-opt. obs. 78−95574
- US fields, experimental study of integrated optical effect using light diffraction technique 80−23848
- US imaging by acousto-optic interaction in Raman-Nath diffr. regime 79−55260
- US modulation of γ-radiation 79−24249
- US vel. in acoustooptically active solids, laser beam probing of standing wave 78−33965
- US wave 3D meas. in transparent solids, Doppler-shifted light scatt. technique 78−90613
- US wave anisotropic Bragg diffraction of light *(Russian)* 77−10833
- vibration-induced modulation in bent optical fibre waveguide 78−1405
- visualisation of progressive acoustic wavefronts using Koster prism 80−5701
- wavefront correction in real time for atm. distortion, Bragg diffr. by acoustic wave 77−42500
- ZnO film acousto-optical props. for integrated optical Bragg cell 79−55251
- AgCl, single cryst., optical, acoustic and acousto-optical props. *(Czech)* 78−76417
- Al, Brillouin spectra, light scatt. cross section for surface ripples 80−71434
- α-Al_2O_3, trigonal crystal, optical heterodyne detection using collinear acousto-optic interaction 78−66927
- As-Ge-Se and As-Ge-Se-Sb glasses acousto-optic props. 77−27327
- As_2S_3, amorphous, acoustic flux, optical transmission *(Japanese)* 79−82946
- As_2S_3, amorphous, acousto-induced struct. change, Brillouin scatt. meas. 79−27928
- As_2S_3, amorphous, US attenuation obs. 79−46756
- Au sols, acoustically induced birefringence 80−93274
- BCl_3, visible fluoresc., IR laser induced, acousto-optical effects *(Chinese)* 79−78733
- Bi-Sb-O-I glasses, acousto-optic props. 77−31121
- $Bi_{12}GeO_{20}$, acoustic vel., absorpt. coeff. and photoelastic consts. rel. to acoustooptical parameters 79−56762
- $Bi_{12}GeO_{20}$, finite amplitude SAW distorted rippling profiles, optical probing obs. 80−34287
- $Bi_{12}SiO_{20}$, acoustic vel., absorpt. coeff. and photoelastic consts. rel. to acoustooptical parameters 79−56762
- $CaWO_4$ collinear diffr. by oppositely directed acoustic beams 80−16007
- CdS, charge in energy gap caused by acoustic domains 77−20822
- CdS, coherent interaction of externally generated 35 GHz of sound with light 77−43964
- CdS, epitaxial film, conductivity control by S vacancy form., light modulation appls. 77−4455
- CdS, equivalent gap alteration by light scatt. by acoustic domains 77−85687
- CdS, influence of Lamb US waves on exciton spectra *(Russian)* 80−7374
- CdS, light scatt. by Bleustein-Gulyaev waves on refl. and transmission 79−24288
- CdS, optical modulation caused by acoustic domains 77−85689
- CdS/$LiNbO_3$ system SAW convolution signal photoenhancement obs. 77−27431

acousto-optical effects continued

- $CsAl(SO_4)_2.12H_2O$, third order elastic consts. from stress shifted reson. freqs. 78−55905
- $CsCuCl_3$, phys. props. 77−62511
- CsH_2AsO_4 and $Cs(H_xD_{1-x})_2AsO_4$, acoustooptical and photoelastic props. 78−27181
- $Cs_2NaBiCl_6$, optical, photoelastic, acoustooptic props. 80−55064
- $CsPbCl_3$, refr. index and birefr., struct. transition effects 77−90126
- $CsSrCl_3$, refr. index and birefr., struct. transition effects 77−90126
- CuBr, photoelastic tensor, acousto-optical meas. 77−12359
- CuCl, photoelastic tensor, acousto-optical meas. 77−12359
- CuI, photoelastic tensor, acousto-optical meas. 77−12359
- GaAs, Brillouin spectra, light scatt. cross section for surface ripples 80−71434
- GaI, Brillouin spectra, light scatt. cross section for surface ripples 80−71434
- $Gd_2(MoO_4)_3$, photoelastic tensor components 77−48146
- Ge, electron-hole drops, inflammation radiation under action of ultrasound *(Russian)* 79−7788
- Ge, photoelastic consts. determ. 78−68474
- Ge-Pb-Bi-O glass, photoelasticity, glass transition limits 79−33670
- ^{4}He, superfluid, tensile strength and visible US cavitation 77−7920
- Hg-As-S modulating glasses, optical parameters and struct. *(Russian)* 78−63159
- Hg-As-S-I system, glasses, optical and acousto-optical props. 78−83053
- InSb, submillimeter radiation diffr. by electron-density waves 80−7328
- $KAl(SO_4)_2.12H_2O$, third order elastic consts. from stress shifted reson. freqs. 78−55905
- KD_2PO_4, cryst. high-freq. modulation in Pockels cell, acoustic phenomena 78−1336
- $K(H_{1-x}D_x)_2PO_4$ polarised impurity cluster effects in light scatt. expts. 80−29716
- KH_2PO_4 and $K(H_xD_{1-x})_2PO_4$, acoustooptical and photoelastic props. 78−27181
- KH_2PO_4, cryst. high-freq. modulation in Pockels cell, acoustic phenomena 78−1336
- KH_2PO_4, photoelastic const. behaviour new ferroelectric transition 78−19441
- Li, seeded flames, excitation, laser radiation absorpt., sound vel., opto-acoustic effects obs. 80−43345
- $LiBi(MoO_4)_2$, acoustooptic characteristics 79−8118
- $LiIO_3$ and quartz, piezoelectric transducers, acoustic field distrib., Bragg diffr. method, quartz crystals 80−97231
- $LiIO_3$ single crystal, surface acoustic wave parameter meas., coherent optics method 80−106691
- $LiNbO_3$, acousto-photorefractive effect 77−88878
- $LiNbO_3$, acoustophotorefractive effect, appl. at acousto-optic memory correlator 78−15145
- $LiNbO_3$, acoustophotorefractive effect, phenomenological theory 79−78649
- $LiNbO_3$, and $LiTaO_3$, finite amplitude SAW distorted rippling profiles, optical probing obs. 80−34287
- $LiNbO_3$, collinear light diffr. by transverse acoustic waves 77−52040
- $LiNbO_3$, cryst., US vibrating laser beam diffr. *(Russian)* 78−31172
- $LiNbO_3$, diffusion waveguide, acousto-optic mode conversion at surface wave freqs. *(Russian)* 78−1348
- $LiNbO_3$, film lightguide, pulse signal convolution in acoustooptic interaction *(Russian)* 78−1345
- $LiNbO_3$ film on Al_2O_3, optical guided wave mode conversion by Love waves 79−46055
- $LiNbO_3$ laser beam/SAW mode conversion 79−46056
- $LiNbO_3$, leaky SAW and guided light Bragg interaction, theoretical anal. 78−72484
- $LiNbO_3$, light induced ultrasonic wave velocity change, refractive index 80−97236
- $LiNbO_3$, light scatt. by Rayleigh waves on refl. and transmission 79−24288
- $LiNbO_3$, optical waveguide, anisotropic planar, acoustooptic interaction 77−68273
- $LiNbO_3$, optical waveguide, diffr. of modes by standing elastic surface waves *(Russian)* 78−1343
- $LiNbO_3$ optical waveguide surface, acoustooptical interaction for TE modes, metallisation effect 80−69541
- $LiNbO_3$, partial waves of SAW, direct meas. by light scatt. 78−66994
- $LiNbO_3$, phase and amplitude relations between fundamental and second harmonic SAW 77−69157
- $LiNbO_3$, photoinduced surface storage of SAW patterns 80−74309
- $LiNbO_3$ pure and Fe doped, IR induced acousto-photorefractive memory effect 80−80746
- $LiNbO_3$, SAW, suppression of harmonic generation, light diffr. determ. 80−84355
- $LiNbO_3$, trigonal crystal, optical heterodyne detection using collinear acousto-optic interaction 78−66927
- $LiNbO_3$, unguided light deflection via SAW 77−8543
- $LiNbO_3$, Y-Z cut, surface to bulk mode wave conversion, at interfaces ang. spectrum meas. 78−47652
- $LiNbO_3$, y-z, x-z and $41^{1}/_{2}$-x cuts, SAW SHG, laser probing 77−31153
- $LiNbO_3$, y-z crystal, line shape of light scattered by SAW upon total internal refl. 79−24287
- $LiNbO_3$, y-z cut, light scatt. from SAW 78−6652
- $LiNbO_3$:Ti, in-diffused waveguide, acousto-optical meas. of optical field profiles 79−23054
- $NH_4Al(SO_4)_2.12H_2O$, third order elastic consts. from stress shifted reson. freqs. 78−55905
- $NH_4H_2PO_4$, acoustooptical and photoelastic props. 78−27181
- Na seeded flames, excitation, laser radiation absorpt., sound vel., opto-acoustic effects obs. 80−43345
- $NaBi(MoO_4)_2$, photoelastic props., acousto-optical figure of merit meas. 78−60420
- NaCl:Mn^{2+}, elastic wave damping, 300-1800 MHz, acousto-optical obs. 79−69198
- Nd:glass laser with US modulated emission 80−48309
- Nd:YAG acousto-optically mode-locked CW laser performance and stability criteria 77−38934
- Ni, Brillouin spectra, light scatt. cross section for surface ripples 80−71434
- $Pb_{1-x}Ba_xMoO_4$, refr. index. and photoelastic consts. 77−63393
- $PbCl_2$ crystals, acousto-optical props. and photoelasticity 80−40085
- $Pb_5(GeO_4)(PO_4)_2$, crysts., acousto-optical props. 80−100644
- $Pb_5(GeO_4)(VO_4)_2$, crysts., acousto-optical props. 80−100644
- $PbMoO_4$, acousto-optic interaction at high optical intensities 79−42942

acousto-optical effects continued
$PbMoO_4$, diffr. modulator, two separate opposing US waves 77—3676
$PbMoO_4$, SAW props. 78—63920
PbO-containing binary systems, acoustooptic props. from comp. and density 80—76000
$Pb_3(P_{1-x}V_xO_4)_2$, ferroelastic, acoustooptic props. of single crysts. and solid solns. 79—69809
$Pb_5(SiO_4)(VO_4)_2$, crysts., acousto-optical props. 80—100644
$PbTeO_2$, acousto-optic interaction at high optical intensities 79—42942
RbH_2AsO_4, acoustooptical and photoelastic props. 78—27181
RbH_2PO_4, acoustooptical and photoelastic props. 78—27181
Se, amorphous, acousto-optic props., 10.6 μm 77—43966
Si_3N_4 film acousto-optical props. for integrated optical Bragg cell 79—55251
SiO_2, finite amplitude SAW distorted rippling profiles, optical probing obs. 80—34287
SiO_2, fused, photoelastic coeffs., freq. depend. 77—4619
SiO_2, phase an amplitude relations between fundamental and second harmonic SAW 77—69157
α-SiO_2, trigonal crystal, optical heterodyne detection using collinear acousto-optic interaction 78—66927
Ta_2O_5 film acousto-optical props. for integrated optical Bragg cell 79—55251
Te, acousto-optic props. at 10.6 μm 79—91401
Te, acousto-optical props. at wavelength of 10.6 μm 80—76001
Te acousto-optically phase-matched noncollinear optical SHG obs. 79—50353
Te, acoustoelec. domain induced transparency at 11 μm 78—27182
Te, acoustoelectric domain induced transparency near 11 micron 77—85727
TeO_2, cryst., acousto optical RF spectrum analyser, double diffr. *(Russian)* 77—7263
TeO_2 crystal, parametric excitation in an acoustic interferometer 79—64381
TeO_2, light diffr. by slow acoustic waves 80—29717
TeO_2, single crystals, acousto-optic props., optical information processing *(Russian)* 77—55768
TiO_2, acoustic vel., absorpt. coeff. and photoelastic consts. rel. to acoustooptical parameters 79—56762
TlBr-TlI KRS-5 single crystals, acousto-optical characts. 78—71165
TlCl-TlBr single cryst., acousto-optic characts. 77—52039
TlCl-TlBr solid solution, photoelastic constants obs. *(Russian)* 78—39526
$TlMnCl_3$, refr. index and birefr., struct. transition effects 77—90126
ZnO, photoelastic consts., absolute sign determ. by Biegelsen method 79—1749
ZnO thin film opt. waveguide, collinear acousto-optic interaction and appl. to tunable opt. filter 80—74509
ZnO thin films, surface acousto-optic interaction, diffr. 77—3685
ZnSe, dielec. const. strain depend., spectral behaviour by acousto-optic method 77—48147
ZnSe, resonant Brillouin scatt. by injected acoustic waves 77—12394

acoustoelasticity *see elasticity*

acoustoelectric devices
see also acoustoelectric transducers
bulk acoustic wave devices employing interdigital transducers 77—23841
controllable electroacoustic phase shifter 79—81640
driven equilibrium Fourier transform sensor operating at 100 MHz 80—74612
Exhibition Hall of Yamaha Sportland TSUMAGOI, auditorium electroacoustic technology 78—13858
Hungarian developments, BEAG activities 78—46860
impedance meas. instrum., temporal response determ., hearing study appl. 78—3512
integrating correlators; four-wave interactions 79—98547
measuring equipment for noise anal. and machine diagnosis 78—63249
memory correlator using GaAs Schottky diodes 78—66989
memory correlators, fabrication, experimentation and anal. 79—32179
monolithic layered piezoelectric-semicond. structures, acoustoelectric coupling 77—32050
optical image in slow surface states in Ge read out by SAW 77—79942
piezoelectric transducers, energy method for impedance calculation 77—72126
SAW, wideband signal processing 77—27442
SAW convolver in monolithic MIS struct., basic characts. 77—23791
SAW devices based on interaction of SAW with electrons in semicond. 77—80025
SAW image scanner applications 79—45912
Schottky diode/$LiNbO_3$ acoustoelectric integrating correlator 77—88990
signal storage device, DIAM, appl. to adaptive correl. *(French)* 77—7272
transmission scanning acoustic microscope, single lens 80—87669
two-layer systems with an air gap, interaction of Rayleigh waves with electrons 77—39901
ultrasonics symposium, Cherry Hill (1978) 79—50472
$LiNbO_3$ acoustoelectric memory correlator struct. for scanning of optical images 80—74632
$LiNbO_3$-gap coupled Schottky diode memory correlator, grating coupled optical imaging 80—64143
$LiNbO_3$-InSb amplifier production, role of protective films 78—95220
$LiNbO_3$-pn-diode airgap convolver struct. optical scanner using single SAW pulse 80—64144
Si array/$LiNbO_3$ gap-coupled imaging devices 79—46057
ZnO/Si SAW devices 80—80332

acoustoelectric effects
acoustic surface wave broadband generation on GaAs by conversion from acoustoelectrically amplified bulk waves 77—54852
acoustic system, rapid variation in focal length 79—81641
acoustic wave interaction with microwave radiation field 80—6913
acoustic wave resonant transmission across piezoelectric gap 78—87855
anisotropic semiconductor, absolute instability for locked packet of sound waves *(Russian)* 77—35969
anisotropic semiconductor, US amplification, kinetic theory, chain fraction method *(Russian)* 78—68054
anisotropic semiconductor, with traps, kinetic theory of acousto-electrical effect in nonhydrodynamic collision region *(Russian)* 79—24019
auditoria speech amplification space and electro-acoustics study *(Dutch)* 77—68330
backward waves and acoustic scanning, nonlinear interaction of vol. and surface waves 80—79040

acoustoelectric effects continued
bipolar conductivity investigs. using ohmic and acoustoelec. currents in Hall effect 77—32027
borosilicate glass, EM wave effects on acoustic absorpt. at low temp. 77—47866
Brillouin scattering in reflection and transmission modes, rel. to intense acoustic flux, relation linearity test 80—45098
Brillouin surface ripple scattering by solids, for acoustoelec. amplified bulk acoustic waves 78—39559
ceramic cylinders, LF voltage-press. sensitivity 78—2805
charged-particle stream, wave interaction, nonlinear effect 80—80310
cubic crystal/cubic crystal interface, transverse surface acoustoelec. wave propag., due to electrostriction 77—66082
degenerate nonparabolic semiconductor, acoustoelec. absorpt. theory 77—85269
degenerate semiconductor, amplification of sound by temp. gradient 77—20366
degenerate semiconductor, nonparabolic, acoustic wave absorption/amplification coefficient 78—64069
dielectric crystals, nonlinear electroacoustic, fundamentals and appl. 80—34489
dielectrics, electric, optical and acoustic interactions from Lagrangian representation, book 80—2715
disordered semiconductor, DC hopping cond., photon- and US-induced, microscopic theory 77—76872
domain injection, semiconductors *(Japanese)* 80—91945
Eckart flow in conducting liq. or gas, acoustoelectric current prod. 79—27707
elastic nonlinearities in dielec., piezoelec., and pyroelec. crysts. 78—79155
electroacoustic wave variational expression derivation 78—1488
electroluminesc. excitation by SAW, nonlinear effects 80—16104
electron drag by coherent Lamb phonons in quantising magnetic field 80—80330
electrostrictive solid, acoustic to EM wave conversion 78—91734
EM radiation in amplified sounds, theory 77—80812
ferroelectric bodies, deformable, coupled electroacoustic eqns. 80—96092
ferroelectric material, r.f. echo 78—95549
ferrolectric cylinders, radially polarised, electroacoustic sensitivity calc. by normal-mode methods 77—62131
ferromagnet, continuous EM-acoustic conversion, normal skin effect case, expt. *(Russian)* 77—59304
frequency anal., optimized octave, half-octave and third octave bandpass filters *(German)* 79—64470
n-GaAs, semidegenerate, acoustoelec. gain and lattice attenuation, X-ray Brillouin scatt. and elec. meas. 79—15193
n-Ge US attenuation due to donors and acceptors 77—28223
heavily doped compensated piezoelectric semiconductor, sound absorpt. coeff. calc. *(Russian)* 79—15194
information storage in piezoelectric semiconducting single crystals 78—15101
inhomogeneous semiconductor, acoustoelectric interaction, elec. cond. 79—95453
insulator, modulation oscills. of travelling EM wave 80—24962
insulators, dynamics of electroacoustic waves 79—28381
interdigital transducers, quasiacoustic wave propagation, field theory anal. 78—66998
laminar piezodielectric-dimensionally quantised semiconductor film struct., acoustoelectronic effects 80—75607
α-$LiIO_3$ powders, temp. depend. of electro-acoustic echo 80—66115
liquid crystal, US attenuation, elec. field effects 77—15304
longitudinal carrier waves in solids, coupled mode anal. *(Korean)* 78—43403
many valley semiconductor, US propag., nonlinear effects 77—59305
many-valley semicond. anisotropic acoustoelectric effect, thermo-EMF anisotropy fluctuation depend. on ultrasound freq. 79—69562
metal, acoustic breakdown, electron energy spectrum *(Russian)* 78—18948
metal, acoustoelectric effects, anisotropy *(Russian)* 78—91732
metal, EM generation of ultrasound in static mag. field 78—14768
metal, EM sound generation in cyclotron reson. regime *(Russian)* 77—69381
metal, EM to acoustic energy conversion, temp. depend. 77—51780
metal, Fermi surface local geometry ultrasonic absorpt. ang. depend., Pippard oscill. spectrum *(Russian)* 79—19507
metal, longwave sound, absorpt. coeff., in phase transition of $2^1/_2$ kind *(Russian)* 78—39008
metal, low-freq. sound attenuation, viscous and induction mechanisms 77—8152
metal, nonlinear EM absorption of short-wave sound *(Russian)* 78—43446
metal, strong and weak sound waves propag., nonlinear effects *(Russian)* 78—60168
metal, surface acoustoelectric H-waves, theory 77—69159
metal, US generation by EM radiation, surface scatt. effects 80—24973
metallic thin films, attenuation and phase vel. of SAW interacting with charge carriers 79—46136
metals, acoustic attenuation in collision regime, variational principle 79—82648
metals, acoustoelectric current for conductivity electron arbitrary dispersion law *(Russian)* 80—49829
metals, anomalous sound propag. by cond. electrons 80—11048
metals, EM generation of ultrasound, theory 80—103727
metals and alloys, EM acoustic reson. for elastic moduli meas. 80—15573
MIM diode, US effect on tunnel current for normal and supercond. metals 77—16006
narrow gap semiconductor, sound absorpt. in strong EM field 77—55590
non-linear ultrasound absorption in an electromagnetic wave field under quantum size effect conditions 78—87745
noncollinear interaction with RF elec. field 79—69566
nondegenerate semiconductor with ionised impurity scatt., acoustic wave amplification 77—11965
nonlinear piezoelectric crystal, acoustic wave direct transformation to microwaves 78—10521
p-n junction, US wave effect on effective current relaxation time in base 77—4434
parametric excitation of acoustic waves in presence of electron currents *(Russian)* 80—80328
parametric generated high efficiency oscillations in acoustoelectric oscillators 78—10518

acoustoelectric effects continued
- parametric interaction of EM and acoustic waves in solids, theory 78—60166
- phonon echo in crystals 77—1641
- phonon echoes *(French)* 77—51461
- phonon echoes and amplification of ultrasonic waves in a microwave electric field 79—19635
- piezo-semiconductor plates, effect of diffusion of charge carriers *(Russian)* 80—65633
- piezoceramic, electroelastic plane wave propag. *(Russian)* 77—55752
- piezoelectic crystals, hexagonal, acoustoelectric wave excitation 77—76880
- piezoelectric, coupled surface, electroacoustic waves 78—2355
- piezoelectric ceramic, excitation of acoustoelectric oscills. by ionising radiation 78—56191
- piezoelectric crystal, acoustoelectrical waves, double refl. and birefr. 80—11047
- piezoelectric crystal, electro-acoustic effects on phase vels. of acoustic and EM waves *(French)* 79—15401
- piezoelectric crystal, parametric interaction of 550 MHz elastic wave with 1100 MHz elec. pump field 77—11966
- piezoelectric crystal, three-field electroacoustic parametric interactions 79—1740
- piezoelectric hexagonal crystal, acousto-EM modes *(Spanish)* 77—4602
- piezoelectric material, phonon electroacoustic echo under acoustic reson. conditions *(Russian)* 77—48131
- piezoelectric material, r.f. echo 78—95549
- piezoelectric powder, electroacoustic echo 77—8517
- piezoelectric powder, electroacoustic echo form. by FM mechanism 78—19421
- piezoelectric powder, freely-falling, electroacoustic echo 79—91104
- piezoelectric powder, mech. of long-time phase memory 79—42899
- piezoelectric powders, dynamic electroacoustic echo and recording *(Russian)* 79—87397
- piezoelectric semiconductor, acoustic wave combinatorial scatt. by electrons *(Russian)* 77—11963
- piezoelectric semiconductor, acoustic wave synchronisation 77—11964
- piezoelectric semiconductor, acoustic waves parametric excitation 79—47128
- piezoelectric semiconductor, acoustohelicon waves, parametric excitation 79—38135
- piezoelectric semiconductor, amplification and vel. change of acoustic waves due to external temp. gradient 78—84260
- piezoelectric semiconductor, dissipative, amplification of spin waves 79—24000
- piezoelectric semiconductor, effect of strong doping on sound attenuation 80—2120
- piezoelectric semiconductor, frequency mixing of acoustic waves in oscillatory and DC elec. fields, theory 77—35966
- piezoelectric semiconductor, influence of thermal quenching of photocond. on US amplification. 77—4410
- piezoelectric semiconductor, inhomogeneous, amplification of acoustic wave 79—69561
- piezoelectric semiconductor, n-type, heavily doped, laser beam modulational instability 79—99570
- piezoelectric semiconductor, nonlinear acoustic noise amplification theory, phonon distrib. function basis 78—47837
- piezoelectric semiconductor, nonlinear interaction of quasicollinear acoustic waves 77—59306
- piezoelectric semiconductor, plasmon enhanced sound amplification in mag. field 77—39900
- piezoelectric semiconductor, resonant microwave absorption by electrons in strong piezoacoustic wave 77—85270
- piezoelectric semiconductor, second acoustic harmonic generation of acoustoelectronic waves 77—43669
- piezoelectric semiconductor, shock waves and acoustoelec. domains 77—32049
- piezoelectric semiconductor, stationary acoustic wave nonlinear theory 77—76878
- piezoelectric semiconductor, surface electroacoustic wave, excitation by drifting cond. electrons 77—66083
- piezoelectric semiconductor, transversely magnetised, parametric instability of acoustic waves 79—65521
- piezoelectric semiconductor, ultrasound amplification, hard regime 77—89810
- piezoelectric semiconductor, US absorption 80—44670
- piezoelectric semiconductor, weakly inhomogeneous theory of sound absorption 80—15574
- piezoelectric semiconductor film, quantum acoustoelectric interaction 79—15197
- piezoelectric semiconductor film, Rayleigh wave amplification, quantum theory approach 77—69158
- piezoelectric semiconductor film, surface mode phonon amplification theory 78—34691
- piezoelectric semiconductor SAW convolver, convolution voltage enhancement due to carrier transverse drift 80—1381
- piezoelectric semiconductors, acoustic phonon conduction electron interaction, Brillouin scatt. theory 77—40255
- piezoelectric semiconductors, acoustoelectric interactions on cylindrical surfaces 80—6914
- piezoelectric semiconductors, acoustoelectric surface phonon-conduction electron interaction 79—42360
- piezoelectric semiconductors, growth of wave discontinuities 80—34488
- piezoelectric semiconductors, nonlinear noise amplification 78—60167
- piezoelectric semiconductors, surface phonon acoustoelectric interaction, elastic anisotropy effects 80—6610
- piezoelectric semiconductors, US ionisation of shallow impurities 77—43538
- piezoelectric shear SAW amplification in periodic structures on solids 79—90055
- piezoelectric-semiconductor, layer struct. transverse acoustoelectric effect 79—69565
- piezoelectric-semiconductor struct., nonlinear acoustoelectric effects for large amplitude SAW 80—92942
- piezoelectrics, electroacoustic echo at doubled freq. 78—15100
- piezoelectrics, tensor description of electroacoustic echo effect 78—19103
- piezosemiconductors, second harmonics of acoustoelectric current 80—80329
- plasma, electrosound waves in strong HF field *(Russian)* 77—31466
- powders, phonon electroacoustic echoes, storage mechanisms 80—75606

acoustoelectric effects continued
- quartz, film acoustic surface waveguides, electrically controllable polarisation conversion and its appl. 79—76924
- quartz, SAW propagation, acoustoelectric methods 80—84359
- Rayleigh sound absorpt. in normal and supercond. metals *(Russian)* 78—43233
- SAW electronic absorption, temp. depend. 77—55585
- SAW slow shear waves in periodic structures, electronic damping and amplification 80—19124
- semiconductor, absorpt. and amplification of sound at intermediate freq. *(Russian)* 77—55586
- semiconductor, absorpt. and amplification of US at moderate freq. 78—19102
- semiconductor, acoustoelectric phenomena in variable elec. field *(Russian)* 79—51637
- semiconductor, acoustoelectronic phenomena in alternating elec. field, theory 79—11187
- semiconductor, acoustomagnetoelectric effects in inelastic scatt. of electrons by optical phonons 77—4372
- semiconductor, anisotropic acoustoelectric effect at medium US freq. and anisotropy compensation effect 77—55588
- semiconductor, diffraction transverse acoustoelectric effect 77—35967
- semiconductor, electron absorption and amplification of HF ultrasound, kinetic theory 77—32051
- semiconductor, electron-hole droplet, US absorption 77—89814
- semiconductor, electronic absorption and amplification of acoustic waves 78—39166
- semiconductor, EM generation of ultrasound 79—51639
- semiconductor, extrinsic, parametric reson. of acoustic and optical phonons at low temps. 78—10519
- semiconductor, impurity acoustoconduction, nonlinear theory 77—15914
- semiconductor, monopolar, anisotropic, US amplification at intermediate freq. *(Russian)* 77—35965
- semiconductor, n-type, lightly doped, hopping acoustoconductivity mechanism 80—65635
- semiconductor, narrow cond. bands, hypersound amplification in quantising elec. field 77—89811
- semiconductor, nondegenerate, interaction between electrons and strong piezoelec. wave *(Russian)* 77—90106
- semiconductor, parametric reson. of acoustic and optical phonons at low temp. 77—51779
- semiconductor, parametric resonance of acoustic and opt. phonons 77—15915
- semiconductor, photostimulated impurity absorpt. of US 77—62962
- semiconductor, planar acoustomagnetoelec. effect, theory 80—60052
- semiconductor, thermoelectric amplification of sound 80—2427
- semiconductor, ultrasound absorption, intermediate frequency, nonlinear effects 79—28380
- semiconductor, unipolar, acoustophotoelectric effect theory 77—55577
- semiconductor, US absorption of moderate freq., electron distrib. function perturbation 77—55587
- semiconductor, validity criteria of phenomenological theory of electron obs. and amp. of sound 78—91733
- semiconductor film, piezoelec., quantum acoustoelec. interaction, thickness depend. *(Russian)* 79—47126
- semiconductor film, US propagation in quantised elec. field *(Russian)* 80—60050
- semiconductor in mag. and US wave fields, electronic density of states *(Russian)* 78—72056
- semiconductor structure, inhomogeneous, transverse acoustoelectric effect 80—39638
- semiconductor surface characterisation using SAW 80—11069
- semiconductor with energy-dependent relax. time, acoustoelectric absorpt. 79—56268
- semiconductor with negative differential conductivity, amplification of SAW by transverse current 79—7741
- semiconductor-piezoelectric structures, surface pot. influence 78—10516
- semiconductors, acoustoelectric current at moderate US freq. 80—29444
- semiconductors, current instabilities, theory and expts. *(Hungarian)* 77—39857
- semiconductors, degenerate, acoustodielectric effect, permittivity modulation by acoustic wave in resonance conditions 80—92944
- semiconductors, electron absorption and amplification of sound at intermediate freqs. 80—54740
- semiconductors, electron absorption of ultrasound in strong elec. field, oscills. 79—69563
- semiconductors, narrow band gap, superlattices, acoustic wave absorpt. and amplification 80—29445
- semiconductors, nonlinear electroacoustic echo 80—92943
- semiconductors, semimetals, electron heating by phonons, acoustic absorpt. and acoustoelectric current quantum oscills. *(Russian)* 79—19639
- semiconductors nonlinear acoustoelectric effects 77—69382
- semimetal, acoustic plasma wave excitation 78—10520
- semimetal, US propag., nonlinear effects 77—59305
- shear SAW in high permittivity three-layer system *(Russian)* 80—80048
- SHG in elec. field 77—11962
- p-Si US attenuation due to donors and acceptors 77—28223
- slow shift SAW in attenuating piezo-electric and piezosemicond. surface structs. 78—79872
- solids, transverse SAW in microwave field 80—92945
- sound velocity, amplitude dependent, in collisionless regime *(Russian)* 78—52037
- Stoneley wave amplification between two piezoelecs. separated by thin semicond. film 79—14998
- superconducting loop, bimetallic, acoustically generated mag. flux 77—16010
- superconductors, difference between acoustoelec. and thermoelec. effects 79—38246
- superconductors, thermoelectric and acoustoelectric effects, influence of mutual drag of excitations and phonons 80—44761
- superlattice, hypersound amplification by a quantizing electric field 80—6915
- surface acoustic and electrostatic wave excitation by electron beam 77—24473
- surface acoustoelectric waves, electrostriction-induced, at interface between media 77—16255
- surface-wave devices, gap-coupled, transverse modes 79—46138
- TGS, acoustic emission, threshold electric field 79—60874
- TGS, ferroelec. single crystal, low freq. nonlinear effects 80—84490
- thermopiezosemiconductor critical drift velocity for US amplification 78—60169

acoustoelectric effects continued
thermopiezosemiconductors, amplification of longitudinal acoustic waves 78−76114
three pulse echo detection and electroacoustic recording *(Russian)* 79−47129
TsTS polarized ceramic film, Lamb waves near. crit. freq. study *(Russian)* 78−52039
ultrasonic pulsed measuring instrums., signal shape anal. 80−87678
wave excitation in piezoelec. crystals by narrow metallic electrodes 79−69777
wave mechanism of external fields effect on crystallisation 80−19733
Wigner crystal, long-wavelength excitations in strong mag. fields 79−82533
$Ag_3SbS_3(AsS_3)$, electroacoustic echo, ultrasonic wave attenuation *(Russian)* 80−88280
Ag_3SbS_3. piezoelec. semicond., residual cond., ultrasound photoabsorpt. *(Russian)* 78−72465
Al rod, US amplitude distrib. generated by direct EM method 78−2526
Al-ZnO-SiO_2-Si monolithic MIS struct., charge-transfer device using SAW 79−11229
α-$AlPO_4$, berlinite, temperature-compensated surface and pseudo-surface acoustic wave props. 77−51584
n-AlSb, acoustoelectric effect due to piezoelectrically active wave 80−80331
As_2S_3, glass, US attenuation, enhanced after elec. field removal 79−65145
Au film, ultrathin evaporated, acoustoelectric meas. of electron mobility and diffusion 80−65707
$B_{12}GeO_{20}$, cryst. powder, phonon electroacoustic echo signal storage 78−68055
$BaTiO_3$, acoustic wave interaction with microwave radiation field 80−6913
$BaTiO_3$, isotropic dielectric, US vel. and longit. elec. field *(Russian)* 78−38785
Bi, acoustic plasmon excitation 77−89793
Bi, stationary I-U curve, falling portion under phonon generation conditions 79−15195
CdS, acoustic noise amplification along c_6 axis, Brillouin scatt. obs. 78−19101
CdS, acoustic-wave-induced increase in cond. 77−59307
CdS, acousto-voltaic effect, asymmetric electron ejection from trap levels *(Russian)* 80−65634
CdS, acoustoelec. interaction, influence of surface pot. 77−1455
CdS, acoustoelectric current fluctuations 79−24020
CdS, acoustoelectric fluctuations 79−7866
CdS, acoustoelectric interaction at wave reflection points 78−2528
CdS, acoustoelectric mobility measurement for X-ray excited carriers 77−15916
CdS, acoustoelectronic current SHG 80−6916
CdS, carrier density nonlinearity of interacting acoustic fluxes 77−51781
CdS crystal, SAW amplification, bulk and acoustic noise 80−39637
CdS, drift mobility in presence of trapping-recomb. centres 78−19054
CdS, efficiency of acousto-electrical effects, meas. by bridge method *(Russian)* 77−76881
CdS, electro-acoustically active, AC impedance meas. 80−103726
CdS, epitaxial film, conductivity control by S vacancy form., light modulation appls. 77−4455
CdS, even acoustoelec. current due to Lamb waves, freq. depend. 80−20256
CdS film, second harmonic generation by transverse acoustic wave 77−51782
CdS, heavily doped compensated piezoelectric semiconductor, sound absorpt. coeff. calc. *(Russian)* 79−15194
CdS, high intensity US amplification *(Russian)* 77−28222
CdS, intensity fluctuations of nonlinearly amplified phonons, Brillouin scatt. meas. 77−90163
CdS, Lamb US wave induced luminesc., green edge radiation *(Russian)* 79−91509
CdS large- and small-signal lattice attenuation, Brillouin scatt. obs. 79−47130
CdS, lattice attenuation meas. by US injection method 78−76480
CdS, lattice attenuation meas. by acoustic domains 80−49827
CdS, nonlinear electronic absorption of US waves 79−15196
CdS, obs. of acoustically induced space charge gratings 77−7203
CdS, photocond., acoustoelec. fluctuations 79−24022
CdS, photocond. cryst. characterisation of electron-trap responsible for acoustic holographic echoes *(French)* 79−19544
CdS, photocond. meas. using surface wave acoustoelec. current 77−8131
CdS, photoconducting, surface acoustic noise amplification by carrier drift 78−72208
CdS, photoconductive, convolution voltage enhancement due to carrier transverse drift in SAW convolver 80−1381
CdS, photoconductive, obs. of high intensity sound self-defocusing 80−24972
CdS, photoconductive, transverse electric current effect on SAW propagation 79−47127
CdS, piezoelec. polycryst. film layer struct., acoustic harmonic generation 77−89812
CdS, piezoelectric semiconductor, frequency mixing of acoustic waves in oscillatory and DC elec. fields 77−35966
CdS, piezoelectric semicond., acoustoelectric current of Lamb waves *(Russian)* 77−89815
CdS plate, amplification of elastic waves by transversely drifting injected carriers 79−7868
CdS plates, noise amplification as function of drift field intensity, conductivity and freq. *(Russian)* 79−73556
CdS, SAW meas. of surface elec. props. 77−20387
CdS, SAW superheterodyne amplification 77−55589
CdS, semicond., coexistence of surface and bulk acoustic waves in acoustoelec. domains 80−44404
CdS, semicond. piezoelec. crysts., US investigation of acoustoelectric characts. 77−1456
CdS single cryst., melt growth, improvement of elec. characts. 79−38734
CdS, single crysts., rel. to US luminesc. 80−76092
CdS surface, transverse acoustoelec. voltage inversion 77−47885
CdS, surface acoustoelec. current due to Rayleigh wave, ambient medium effects and surface state changes 77−69383
CdS surface spectroscopy using acoustic surface waves, spectral response 77−69402
CdS, thermal equilib. phonon populations, acoustic intensity meas. by Brillouin scatt. intensity obs. 80−45098

acoustoelectric effects continued
CdS, time investig. of parametric interactions of thick oscillators 77−47867
CdS, transverse acoustoelec. effect, for SAW optical image scanning 77−11001
CdS, transverse acoustoelec. effect rel. to SAW intensity 78−26917
CdS, US dispersion of high intensity waves, nonlinear electron absorpt. *(Russian)* 78−26916
CdS:Cu, US absorpt. in heavily doped piezoelec. semicond. 79−11189
CdS-$LiNbO_3$ separated medium convolver, illumination effects 77−72766
CdS-$LiNbO_3$ structure, acoustoelectric interaction of surface waves with inhomogeneously distributed free carriers 77−43668
CdS-$NiCl_2$ interface, elec. props. using SAW techniques 79−56302
CdS-ZnTe, acoustoelectric domain injection across interface, propag. loss, elastic consts. 77−51778
n-CdS(Se), bipolar photocond. and acoustoelectric current 79−19636
CdS(Se), piezoelec. semicond., sound absorption 80−60051
CdSe, effect of heat treatment in Se vapour, photocond. acoustoelec. effect and surface morphology 78−39152
CdSe, heavily doped compensated piezoelectric semiconductor, sound absorpt. coeff. calc. *(Russian)* 79−15194
CdSe-$LiNbO_3$, semicond.-piezoelec. layer struct., acoustic-wave-induced increase in cond. 77−59307
$CdSe_xTe_{1-x}$ crystal, acoustoelec. oscillations affected by surface treatment *(Russian)* 78−10517
p-CdTe, bipolar photocond. and acoustoelectric current 79−19636
CdTe, bipolar photoconductivity exam. 78−6410
$CuPbSbS_3$, piezoelectric semiconductor, electron-phonon interaction, temp. depend. 77−51464
n-GaAs epitaxial film, surface mode phonon amplification, numerical analysis 78−34691
n-GaAs, IR luminesc. emitted by travelling acoustoelec. domains 78−27329
n-GaAs, IR luminescence from acoustoelectric domains 77−55822
n-GaAs, IR luminescence of acoustoelectric domains 78−31258
n-GaAs, impact ionisation initiated by acoustoelectric effect 78−52038
GaAs n-n^+ epitaxial structure for CW microwave electroacoustic amplifier 78−59235
n-GaAs, piezoelec. semicond., nonlinear interaction of acoustic waves with microwave elec. fields 79−42593
GaAs, piezoelectric, absorpt. edge broadening by acoustoelec. amplified phonons 77−16302
n-GaAs, piezoelectric semiconductor, influence of acoustic phonon disturbances on conductivity 78−91697
GaAs, SAW meas. of surface elec. props. 77−20387
GaAs, surface characterisation using SAW 80−11069
GaAs, thermal equilib. phonon populations, acoustic intensity meas. by Brillouin scatt. intensity obs. 80−45098
GaAs:Cr (Cr-Te), and undoped, transverse-acoustoelec.-voltage spectroscopy 79−99586
GaAs:Cr excess electron lifetime determ. by US method *(Czech)* 77−20336
n-GaP, acoustoelectric effect due to piezoelectrically active wave 80−80331
GaP, surface characterisation using SAW 80−11069
GaP, transverse acoustoelec. voltage spectroscopy 80−49828
Ge, photoacoustic effect, free flexural vibrs. damping 77−89813
InAs, transverse acoustoelec. voltage spectroscopy 80−49828
InAs/$LiNbO_3$ structure, SAW generated transverse acoustoelectric voltage, image scanning and signal processing appl. 80−49826
n-InSb, acoustoelectric amplification, temp. depend., 77 to 135K 79−51638
InSb, acoustoelectric effect at 77K 78−72209
n-InSb, acoustoelectric gain coeff., nonlinear elec. field depend. 78−76115
n-InSb, acoustoelectric instability, effect of nonparabolic band struct. 79−60875
n-InSb, acoustoelectronic interaction, effect of alternating electric field 79−11188
n-InSb, acoustomagnetoelec. effect, 20-120K, sign reversal obs., and Hall mobility 77−24592
n-InSb, degenerate, acoustomagnetoelec. effect obs. 78−72207
n-InSb, ferroelec. semicond., transverse acousto-elec. effect *(Russian)* 78−30958
n-InSb, helicons, parametric decay 80−34472
n-InSb, noise, round trip acousto-electronic amplification, anodic piezoelectric transducer *(Russian)* 78−23139
n-InSb piezoelectric semiconductors, carrier temp. effect on transverse phonon-helicon interaction 77−15886
n-InSb, reversal of sign of acoustoconductivity effect 78−2527
n-InSb, threshold field dependence on sample length, 77K 78−76116
n-InSb, transversely magnetised, parametric instability of acoustic waves 79−65521
n-InSb, US absorption in alternating elec. field *(Russian)* 78−30959
n-InSb, Wigner cryst., long-wavelength excitations in strong mag. fields 79−82533
InSb-NiSb system, anisotropic, acoustomagnetoelec. effect, theory 79−24021
KCl:Li^+, phonon generation by EM excitation, mechanism 80−2129
$LiIO_3$, transverse gap elastic waves, expt. 80−59576
$LiNbO_3$, crysts., elec. field influence on hypersonic wave propag. 80−44668
$LiNbO_3$, electroacoustic echo excitation with aid of surface waves 77−14834
$LiNbO_3$, electroacoustic correlation memory effect 78−88001
$LiNbO_3$, electroacoustic coeffs. 79−69564
$LiNbO_3$, film, Lamb waves near. crit. freq. study *(Russian)* 78−52039
$LiNbO_3$, piezoelec., SAW interaction with secondary electrons 80−80708
$LiNbO_3$-CdS, layered structure, acoustoelectric surface current kinetics 78−43232
$LiNbO_3$-CdS, layered struct., transverse acoustoelectric effect 79−69567
$LiNbO_3$-CdS, layered structure, transverse acousto-electric current 80−44669
$LiNbO_3$-CdS layer structure, temp. depend. of acoustoelectric current 79−7867
$LiNbO_3$-CdSe structure, electroacoustic effects and signal convolution 80−10098
$LiNbO_3$-InSb struct., electroacoustic interaction temp. depend. 79−69336
$LiNbO_3$-Si, acoustoelectronic memory, effect of band-bending 80−70771

acoustoelectric effects continued
$LiNbO_3$-Si(CdTe) structure, acoustoelectronic interaction between SAW and transverse drift current 77—69424
$LiNbO_3$-Si(Ge) layer struct., acoustoelectronic phenomena 77—55556
$LiTaO_3$, crysts., elec. field influence on hypersonic wave propag. 80—44668
$LiTaO_3$, electroacoustic coeffs. 79—69564
$MgSO_4$, aq. soln., electrolytic conduct. affected by US waves 79—23997
$Pb_5Ge_3O_{11}$, acoustic emission, threshold electric field 79—60874
$Pb_3MgNb_2O_9$ diffuse phase transition, Brillouin scatt. and acoustic phonons 78—76401
$Pb_{0.975}Sn_{0.025}Se$, film, acoustic wave modulation of electron current 78—64067
Se, trigonal, acoustoelectric current saturation 80—60053
Se_xTe_{1-x}, acoustoelectric current saturation 80—60053
Si, photoacoustic effect, free flexural vibrs. damping 77—89813
Si, SAW meas. of surface elec. props. 77—20387
Si, surface characterisation using SAW 80—11069
Si, surface props. using SAW attenuation in adjacent $LiNbO_3$ 79—87131
Si wafer, surface exam. of ion-implantation using SAW convolver 77—72897
n-Si-SiO_2-ZnO-Al, SAW convolver in monolithic MIS struct. 77—23791
SiC, absorption of US waves 78—72210
SiC, sound absorption 78—88000
SiO_x-GaAs, vacuum evaporated system, acoustoelec. signal, interface props. 80—75646
Sn, electron drag by sound waves obs. *(Russian)* 77—35968
Sn, u.s. surface generation, below 20K 78—2353
Te, acoustoelec. domain induced transparency at 11 μm 78—27182
Te, acoustoelectric current flow, acoustic refraction effect 79—19637
Te, acoustoelectric domain induced transparency near 11 micron 77—85727
Te, acoustoelectric instability of current, mag. field influence 79—73547
Te, carrier density nonlinearity of interacting acoustic fluxes 77—51781
Tl_3TaS_4, piezoelec. semicond., acoustic wave generation, amplification material appl. *(Russian)* 78—72464
V, US waves interaction with cond. electrons, double-pulse comparison spectrometer appl. 78—1526
ZnO film, longit. elastic wave attenuation, 9.4 GHz 78—18888
ZnO, intensity fluctuations of nonlinearly amplified phonons, Brillouin scatt. meas. 77—90163
ZnO monolithic SAW device, separation of storage effects 79—18611
ZnS, prebreakdown electrolum., domain form. and negative resist. effects 80—84788

acoustoelectric transducers
see also earphones; headphones; hydrophones; loudspeakers; microphones
bulk wave generation in $LiNbO_3$ surface wave device by interdigital transducer, hologram 77—19505
capacitive tap weighted SAW transducers 77—80041
continuously coupled distributed coupling transducers, elec. and acoustic waves 77—50847
dielectric acoustoelectric transducer, freq. characts. 78—38167
dynamic behaviour analysis, experimental scheme 78—9518
electret transducer equations by Lagrange's equation 78—83202
electret-slot-effect-transducer, two-port eqns. *(German)* 78—75024
electromechanical devices using thin Si diaphragms 78—13879
EM periodic SAW transducers 78—13880
energy balance problem *(German)* 78—26014
ferroelectric cylinders, radially polarised, electroacoustic sensitivity calc. by normal-mode methods 77—62131
ferrofluids, appl. as acoustic transducer material 80—58877
flat conductor, EM SAW transducers, fields 77—23842
grating-array acoustic-surface-wave transducers and reflectors 80—58884
history in America (up to 1940) 77—45665
hydroacoustic transducers of fixed operating freq., elec. imped. matching *(Croatian)* 79—55287
interdigital transducers, equiv. cct. parameters from surface waves dispersion relations 77—39187
interdigital transducers, generation and detection of surface and bulk acoustic waves 77—39186
interdigital transducers, scatt. parameters 77—39188
layered matching systems, synthesis technique 78—18141
matching systems calc. 79—94445
multicomponent ring transducers, mechanical loss resistance calc. technique 78—38166
multilayer, with active layers electrically connected in parallel, transfer functions and resistance 80—5902
multilayer electroacoustic transducer containing active layers 79—64482
noise measurement, engineering aspects, techniques of noise evaluation 77—39178
phase insensitive, operation and optimisation procedures, comparison with piezoelectric transducer 78—90617
piezoelectric double-diffused MOS transducer 77—80043
piezoelectric polyvinylidenefluoride films for diaphragm material 80—10100
piezoelectric properties of synthetic polymer films, transducers appl. *(Italian)* 79—98577
polyvinylidene fluoride film for high freq. US transducers, acoustic wave reson. meas. 77—81058
polyvinylidene fluoride foil appls. *(German)* 78—22243
pulse detector, appl. of current amplification by vibrating membrane of piezoresistive semicond. 78—75025
quartz transducer, multimodality influence on US vel. and attenuation meas. 77—11100
radiating magnetostrictive transducers, impedance determ. 79—32173
rotation sensor using EM-SAW transduction 77—31194
SAW, microfabrication technique for Al electrode 77—80042
SAW IDTs, long, and resonators, coupled-mode analysis *(Japanese)* 79—27477
spaced interdigital transducers, SAW probing 77—80045
stretched circular membrane, vibrational props. *(Japanese)* 77—42655
tapered piezoelectric bar transducer with transverse polarisation of piezoceramic, acoustic props. 78—1537
thin annular diaphragm of electromechanical transducers, acoustic impedance calc. *(Czech)* 77—3708
transmission matrices 78—51027
two-dimensional, amplitude-frequency characts. 77—46878
US phase-insensitive receiver theory and CdS acoustoelectric convertor 79—47871

acoustoelectric transducers continued
US tone-burst spectroscopy, influence of phase cancellation and pulse shape artifacts 80—81276
wide-band projecting transducer 77—84096
$LiNbO_3$ acoustic conversion, piezoelect. surface wave behaviour at discontinuities 77—31198
SbSI materials, piezoelectric props. rel. to use as electroacoustic transducers 78—52445

acoustooptics *see acousto-optical effects*

actinide alloys
see also actinide compounds; plutonium alloys; uranium alloys
conduction electron polarisation, model density of states 79—37949
conference, Baden-Baden, Germany (Sept. 1975) 77—19807
conference on rare earths and actinides, Durham, England (July 1977) 78—84115
cubic intermetallic cpds., var. from localised to itinerant magnetism 77—20534
electronic energy band structure, 5f electrons role 77—28107
electronic structure, conf., Grenoble, France (30 Aug-1 Sept. 1978) 80—6685
electronic structure, conf. Wroclaw, Poland (Sept. 1976) 77—85124
Fermi surface meas. 80—6698
fission reactor fuel, irradiation effects 78—86606
fuel alloys, recycle technology 79—59245
intermetallic compounds, containing d-transition metal, hydrogenated, magnetism 80—34609
liquid alloys of actinides and lanthanides, thermodynamic props. 77—55366
localised crystal field states in metallic actinide cpds., neutron inelastic scatt. obs. 78—14697
localised versus itinerant character of 5f electron states 77—28138
magnetic ordering in intermetallics, review 77—20598
magnetic properties, review 78—84383
magnetic properties, review 79—4649
magnetism of actinide metallic systems 80—7076
metastable phases production by splat cooling 77—21134
non-stoichiometric intermetallic cpds., elec. resist. temp. depend. 79—1597
resistivity temperature dependence due to localised spin fluctuations 77—8083
silicides, atomic volume deviations and supercond. T_c 80—75203
spin fluctuations effect, model approach 77—28404
thermoelectric power of nearly magnetic systems 78—84197
transition metal actinides nearly mag., low-temp. magnetoresist. 78—39091
transition metal alloy disordered host, actinide impurity localised magnetism 77—51883
transition metal alloys, binary system constitution diagram interrelations *(Russian)* 80—7535
transition metal-actinide dilute alloy, disordered occurrence of localised magnetism, CPA calc. 77—63096
valence fluctuation model, physical prop. response 80—6791
AmB_2 (B=Al, Co, Fe, Rh, Ru), crystal structure, mag. props. of Laves phases 77—27851
$AmFe_2$, high temp. mag. props., 300 to 1100K 79—51757
$AmFe_2$, magnetisation, neutron diffr. and Mossbauer expts. 77—63137
$AmPt_5$, preparation and cryst. struct. *(French)* 78—42959
Bi-Th system, heats of form. 80—89517
Ce-Th, mag. suscept. and sp. ht. 79—78411
$Ce_{0.736}Th_{0.264}$, induced mag. form factor 79—78307
$Ce_{0.74}Th_{0.26}$, induced magnetic form factor, polarised neutron studies 80—25078
$Ce_{0.74}Th_{0.26}$, mixed valence alloy, spin dynamics 78—10708
$Ce_{0.8}Th_{0.2}$, inelastic neutron scatt. meas. 79—47066
$Ce_{1-x}Th_x$, mixed valence systems, spin dynamics and mag. ordering 78—68162
Dy-Th, single cryst., mag. susceptibility, transitions, anisotropy 80—54873
Fe-Th, amorphous, charge transfer and mag. props., ^{57}Fe Mossbauer spectra 79—19719
Gd-Th, Curie temp. and saturated mag. moment, nonmag. solute effects 78—39301
$Gd_xTh_{1-x}Ru_z$, coexistence of supercond. and spin glass mag. freezing 77—28283
$La_{0.80}Th_{0.20}Ce$, re-entrant supercond. matrix-impurity system additive pair breaking 77—69460
$(La_{1-x}Th_x)_{1-n}Ce_n$, supercond. mag. alloy, effect of interconfigurational fluctuations 78—19175
Ni-Th (1 at.%), surface comp., temp. and O_2 exposure effects, AES study 80—80914
Np intermetallics, NpM_2Si_2, (M=Cr, Mn, Fe, Co, Ni, Cu), Mossbauer and magnetization expts. 78—31138
$NpAl_4$ clusters, band struct., variational Xα calc. 79—4508
$NpAl_4$, clusters, X_α calculations *(Japanese)* 79—82519
$NpCo_2Si_2$ and $NpFe_2Si_2$, itinerant magnetism obs. 77—28406
$NpCo_2Si_2$, mag. props., high press. studies with ^{237}Np(60)-resonance 80—39924
$NpCo_2Si_2$, mag. struct., neutron diffr. determ. 80—93084
$NpCu_2Si_2$, mag. struct., neutron diffr. determ. 80—93084
$NpFe_2$, high temp. mag. props., 300 to 1100K 79—51757
$NpFe_2$, lattice distortions in ferromag. phase, X-ray obs. 80—15774
$NpFe_2$, magnetisation, neutron diffr. and Mossbauer expts. 77—63137
$NpFe_2$, Mossbauer diffr., combination type maxima, hyperfine interactions on nuclei 80—25263
Np_6Fe, existence and cryst. chemistry 77—51349
$NpFe_{2-x}Co_xSi_2$, mag. and hyperfine props. 79—51887
$NpFe_{2-x}Co_xSi_2$, mag. and hyperfine props. 80—7247
$NpIr_2$, itinerant antiferromagnetism 79—61154
NpM_2Ge_2 (M=Cr, Fe, Co, Ni, Cu), Mossbauer and magnetisation meas. 77—1555
$NpNi_2$, lattice distortions in ferromag. phase, X-ray obs. 80—15774
$NpOs_2$, band magnetism due to f-electrons, T_c 77—73039
$NpOs_2$, itinerant ferromagnet, sp. ht., 3-25K 77—63212
$NpPd_{3-x}Rh_x$, Mossbauer spectra, hyperfine interactions and mag. ordering 77—20783
$NpRe_2$, mag. susceptibility 78—68182
$NpRu_2$, spin fluctuation cpd., sp. ht., 3-25K 77—63212
$NpSn_3$, band magnetism due to f-electrons, T_N 77—73039
$NpSn_3$, itinerant f-electron antiferromag. obs. 77—8315

- **actinide alloys** continued
  - $(Np_{1-x}U_x)Fe$, Mossbauer spectra, magnetism and hyperfine interactions 80—20529
  - Pd-Th, thermodynamic stability 79—55903
  - $Pd_xTh_{1-x}Pu$, magnetism of actinide impurity 77—51883
  - Pt-actinide diatomic mol., calc. dissoc. energy 78—78832
  - RhTh, mol. vapour above Th-U-Rh-graphite, dissoc. energy, mass spectra 78—78832
  - Tb-Th, mag. ordering temps., susceptibility meas. 80—25136
  - $Tb_{0.20}Dy_{0.22}Ho_{0.58}Fe_{1.95}$, grain-oriented, permeability, magnetomechanical coupling and magnetostriction 79—78491
  - Th-Bi-H, hydride form. and supercond. 77—36007
  - Th-Ce-H, hydride form. and supercond. 77—36007
  - Th-Cr, supercond., press. meas. to 20 kbar 80—88667
  - Th-Cu, amorphous, thermal stability, crystn., DSC and elec. resist. study 80—107060
  - Th-Dy, dil., supercond. Th, paramag. relax. of Dy moments, Mossbauer study 80—39957
  - Th-Dy, dil., type I superconductor, paramag. Dy moment relax., Mossbauer spectra study 80—65755
  - Th-Fe (20 to 70 at.%), amorphous alloy, electrical resistivity and thermal stability 80—33901
  - Th-Gd(Tb)(Dy)(Ho)(Er)(Tm)(Lu) (1 at.%), Heisenberg exchange, residual resist. meas. 80—75558
  - Th-La-H, hydride form. and supercond. 77—36007
  - Th-Mn alloy, mag. props. and effect of H_2 absorpt. 78—19250
  - Th-Mo(Re), high temp. phase diagram, thermodynamic props. of refractory metal solutes in liquid Th 77—25022
  - Th-Os(Ir) system, phase diagram and thermodynamic props. *(German)* 79—47958
  - Th-Pu (20 wt.%) metal fuels, compatibility with cladding alloys for FBR appls. 80—102242
  - Th-Pu-U-Zr (20, 4, 8 wt.%) metal fuels, compatibility with cladding alloys for FBR appls. 80—102242
  - Th-U, Kondo alloys, spin and phonon resistivity independ. 78—47777
  - Th-U (20 wt.%) metal fuels, compatibility with cladding alloys for FBR appls. 80—102242
  - Th-U alloy fast reactor fuel element, design basis considerations 79—54503
  - Th-U alloy fuel behaviour in organic-cooled reactor 78—86605
  - Th-U metal alloys, LMFBR appl. 77—83040
  - Th-U metallic fuel, irradiation performance 78—86608
  - Th-U Na-bonded metal fuel, transient heating test 78—86607
  - Th-U-Pu metal alloys, LMFBR appl. 77—83040
  - Th-U-Pu-C-O-N, kernel migration for HTGR fuel 77—38335
  - Th-Y, absolute thermoelec. power values 77—20303
  - Th-Y-Ce, supercond., magnetisation of Ce impurities, sp. ht. meas. 78—47904
  - Th-Y-H, hydride form. and supercond. 77—36007
  - Th-Zr, BCC phase, supercond. props. 79—87178
  - Th-Zr, supercond. transition temp. depend. on constitution 78—88056
  - Th-Zr-H, hydride form. and supercond. 77—36007
  - $ThAl_4$ clusters, X_α calculations *(Japanese)* 79—82519
  - $ThBe_{13}$, lattice spacings and susceptibilities 80—65778
  - $ThC_{0.063}$ single crystal, elastic consts., 4.2-300K 77—90386
  - $ThCo_5$ itinerant electron metamagnetism, polarised neutron study 80—39742
  - $ThCo_5$, lattice consts., magnetisation, and anisotropy fields 79—78364
  - $ThCo_5$, mag. transition due to Co moment change, metamagnetism of 3d-band 77—63184
  - Th_7Co_3, effect of absorbed H_2 on mag. behaviour 80—60184
  - $ThCo_{5-x}Al_x$, homogeneity regions, X-ray powder diffr. study 79—77554
  - $Th_7Co_3(Fe_3)$, spin-pairing state investig. via Josephson current between weakly-coupled superconductors 77—47942
  - $ThFe_3$, H_2 absorption effect on mag. props. and struct. 77—40045
  - $ThFe_5$, mag. props., ferrimag. moment arrangement 79—33475
  - $Th_{1-x}Fe_x$ amorphous alloys, mag. props. and Mossbauer spectra 79—91326
  - Th_7Fe_3, H induced change from supercond. to mag. ordered state 79—28525
  - Th_7Fe_3, Mossbauer spectra, mag. props. 80—15852
  - $ThFe_{5-x}Al_x$, homogeneity regions, X-ray powder diffr. study 79—77554
  - $ThFe_2Ge_2$, magnetisation, 4.2-273K 77—8310
  - $ThMg_2$, cubic Laves compound, sp. ht. rel. to supercond. 79—82356
  - $ThMn_{12}$ type structure, role of elongated rhombic dodecahedron in alloy structures 79—32946
  - $ThMn_2$, Th_6Mn_{23}, H_2 absorption effect on mag. props. 77—89931
  - $ThMn_{5-x}Al_x$, homogeneity regions, X-ray powder diffr. study 79—77554
  - $Th_6Mn_{23}H_x$, H induced mag. ordering obs. 77—85423
  - $ThNi_5$, methanation catalyst, AES and characteristic energy loss spectra 78—56915
  - Th_7Ni_3, effect of absorbed H_2 on mag. behaviour 80—60184
  - ThPt, valence bands, XPS spectra 80—50520
  - $ThRe_2$, mag. susceptibility 78—68182
  - $ThRu_2$, type II supercond., ESR of Nd^{3+} meas. 79—28444
  - $ThRu_2:Nd^{3+}$, supercond. state, ESR investigation 79—78514
  - $Th_{65}Sc_{35}Ce$, supercond., magnetisation of Ce impurities, sp. ht. meas. 78—47904
  - $ThSn_3$, inelastic neutron scatt. 80—11165
  - Th(U)-Re, high temp. phase diagram, thermodynamic props. of refractory metal solutes in liquid Th 77—25022
  - $Th_{1-x}Y_xCo_{5-y}Fe_y$, lattice consts., magnetisation, and anisotropy fields 79—78364
  - $U_{1-x}Th_xAl_2$, ferromag. spin fluctuation system, sp. ht. and elec. props. 77—20604
  - $U_{1-x}Th_xAl_2$, mag. susceptibility, low temp. depend. 80—11173
  - W-Th, atomic structure of grain boundaries 79—33003
  - W-Th, mean square strain, use of approx. methods for Fourier series coeffs. for X-ray diffr. lines *(French)* 77—31549
  - $Y_{1-x}Th_xFe_3$, saturation magnetisation, fields up to 120 kOe, comp. depend. 77—8283

- **actinide compounds**
  - *see also compounds of individual actinides, e.g. uranium compounds*
  - *see also actinide alloys*
  - actinide (V) dioxocations, coordinating props. 77—27869
  - actinyl complexes, hyperfine interactions 80—10928
  - alkali metal actinide complex halides, thermochem. and struct. props. 80—7847
  - band structure and bonding calcs. 80—10871
- **actinide compounds** continued
  - binding and transition energies, expt. and theoret. comparison, review 78—50497
  - BOA valence bonding with f-character 80—6790
  - bond lengths in oxygen and halogen compounds of d and f elements 79—37653
  - borides, mag. props., book contrib. 78—47978
  - carbides, lattice defects and rel. to phys. props., review 77—27874
  - conduction electron polarisation, model density of states 79—37949
  - conference, Baden-Baden, Germany (Sept. 1975) 77—19807
  - crystal and magnetic props. *(French)* 77—27857
  - dioxides, cryst. growth by chem. transport 80—16166
  - dioxides, electronic struct. and ionicity 80—10872
  - dioxides, low temp. lattice parameters, Neel pt. behaviour 77—27867
  - double orthovanadates and orthoarsenates, struct. evolution due to cationic and anionic substitutions 77—19938
  - electronic configurations correlation 80—6385
  - electronic structure, conf., Grenoble, France (30 Aug-1 Sept. 1978) 80—6685
  - electronic structure, conf. Wroclaw, Poland (Sept. 1976) 77—85124
  - ESCA spectra, intense shake-up satellites, model 78—50589
  - f-electron systems with fluctuating valence, phase transitions 80—6789
  - ferromagnetic, with mag. axial symmetry, temp. depend. of magnetisation 77—40044
  - ferromagnetic properties, book contrib. 80—75727
  - halides and oxides, stability study, energy difference between trivalent and tetravalent metal states 78—79553
  - hexahalometallate (IV) complexes, A_2MX_6, A=alkali metal or ammonium, M=lanthanide or actinide, X=F or Cl, lattice energies and thermochem. 79—60307
  - hydrides , Mossbauer studies, book contrib. 79—82906
  - ligand fields calcs., strong and intermediate fields, tensor algebra 80—42922
  - ligand ordering parameters, nephelauxetic and spectrochem. series 77—76777
  - magnetic and structural props., review 77—63132
  - magnetic ordering and struct. transforms. 77—20596
  - magnetic properties, review 78—84383
  - magnetic properties, review 79—4649
  - metallic systems, magnetism 80—7076
  - monopnictides, anomalous mag. props., planar coupling theory 80—60245
  - neutron scatt. studies 80—75716
  - oxalates, separation from high level radioactive waste by precipitation 79—49720
  - oxide/rare earth oxide system, high temp. vaporization, valence effects 79—99309
  - oxides, chem. bonding, mol. cluster theory 80—10526
  - oxides, electronic props., review 77—28115
  - oxides, preparation of metals and refractory cpds. 80—16229
  - oxides, uniformly dense aerosols prod. by gas phase neutralisation of acidic droplets 80—26427
  - oxinides, thermodynamic props. and high temp. chem. behaviour, comparison with lanthanide oxides 79—100127
  - pnictides, single cryst. and film growth by CVD 80—16165
  - radioactive target preparation and characterisation 80—18734
  - radioactive waste, transmutation in PWR thermal reactors 80—18491
  - reduction in molten halides 77—29088
  - silicides, atomic volume deviations and supercond. T_c 80—75203
  - specific heat meas., review 80—6524
  - spectroscopic techniques for electronic props. meas. 80—11427
  - structure, mag. and related props., review 80—6389
  - thermal reactor fuel cycles, actinide wastes toxicity limitations *(German)* 80—99220
  - transuranic chalcogenides and pnictides, prep. and cryst. chem. 80—16255
  - valence transitions and intermediate valence states 79—42496
  - X-ray diffractometer for work with actinide metals and compounds at low temps. 80—316

- **actinide metal compounds** *see actinide compounds*

- **actinide metals** *see actinides*

- **actinides**
  - *see also individual actinides, e.g. uranium*
  - adsorption by Mn and Fe oxides in soils and sediments 79—66422
  - adsorption on silica gel, for urinary gross α activity determ. 79—88155
  - aqueous ions, chemical thermodynamics, book 77—60108
  - atomic volumes calc. 80—15042
  - atoms, non-relativistic Hartree-Fock X-ray scattering factors 78—37602
  - atoms and ions, electronic struct. *(Japanese)* 79—6856
  - band structure and bonding calcs. 80—10871
  - band structure Fermi surface, magnetisation density 78—84140
  - band theory approach 80—15440
  - binding and transition energies, expt. and theoret. comparison, review 78—50497
  - burn-up characteristics, feasibility study for nuclear incineration 79—85706
  - burnup, alternative waste management techniques 79—59210
  - chemical separation from PUREX raffinates using organic solvents 78—66676
  - chemical thermodynamics, book 77—60107
  - conference, actinide nuclear transmutation, Ispra, Italy (April 1977) 79—85698
  - conference, Baden-Baden, Germany (Sept. 1975) 77—19807
  - conference on rare earths and actinides, Durham, England (July 1977) 78—84115
  - Coulomb ten U and 5f electron excitation energies calc. 77—11867
  - electronic energy band structure, 5f electrons role 77—28107
  - electronic excitation energies calcs. 80—54592
  - electronic structure, conf., Grenoble, France (30 Aug-1 Sept. 1978) 80—6685
  - electronic structure, conf. Wroclaw, Poland (Sept. 1976) 77—85124
  - electronic structure, Hubbard's alloy approx. 79—73665
  - electronic structure, role of 5f electrons, Dirac-Slater wave function structure 77—28108
  - electronic structure and props., review 77—62813
  - elimination by fissioning in generic actinide burner reactor 79—93756
  - environmental, pot. carcinogenic effects 80—30780
  - EPR, expt. techniques, electronic and nuclear props. 78—52337
  - fast reactor recycle as waste management alternative, performance calcs. 78—13269
  - Fermi surface meas. 80—6698

actinides continued
  ferromagnetic properties, book contrib. 80—75727
  health effects of man-made actinides rel. to natural radionuclides 80—61647
  heavy element decay data, reactor related calcs., current status 79—97772
  incineration and transmutation in thermal and fast reactors 79—85707
  incineration strategies, UK 79—85704
  industrial dusts, lung clearance studies at NRPB 78—65137
  inertial confinement fusion pellet centre burnup of fission reactor actinide waste 79—31181
  ions, AnO_2^{2+}, in CO_3^{2-} media, Raman scatt. 79—13718
  ions, EPR in solids, review of 1973 literature 77—69675
  ions, tetrapositive, nucl. hexadecapole antishielding factors 79—26909
  ions in crystals, corrections to cryst. field Hamiltonian 79—33268
  ions in solids, EPR 80—51968
  K X-ray energies, natural widths and intensities 80—37768
  lattice vibrations role in transport props. determ. 77—28158
  ligand field theory 77—59269
  localised versus itinerant character of 5f electron states 77—28138
  long lived, disposal, irrad. expts, production assessment nuclear data 79—85712
  magnetic and structural props., review 77—63132
  magnetic properties, review 78—84383
  magnetic properties, review 79—4649
  magnetoresistance, low temp. calc. 77—59278
  metals and semimetallics, electronic structure *(Japanese)* 79—37941
  monazites, nuclear waste, synthesis, ideal actinide hosts for geologic disposal 79—22406
  Mossbauer isomer shifts, book contrib. 79—87362
  nearly ferromagnetic, coupled d- and F-band model 77—63211
  nuclear incineration feasibility study 79—85705
  nuclear materials, actinide determ. review of procedures at Rockwell Hanford Operations 79—81050
  oxidation potential 80—5495
  partitioning in LWR fuel reprocessing, conceptual methods 79—85810
  passive neutron activation for environmental transuranic and moisture assay 80—21431
  Periodic Table subclassification 77—26109
  preparation and refining 78—84705
  production in different HTR fuel cycle concepts 79—85753
  production in nuclear reactors, reduction in Th-U fuel cycle *(German)* 80—9386
  radioactive waste, biological hazards, consequences for LMFBR fuel recycling 80—86960
  radioactive waste, decay heat estimation, summation calcs. and Standard eqns. 80—63317
  radioactive waste, geological disposal, chemical factors controlling environmental actinide sorption 80—13713
  radioactive waste processing, consequences of separation of long-lived α-emitters *(Czech)* 80—5251
  radioactive waste storage, interaction of actinides and humic acid 80—13715
  radioactive waste storage, mineral-contributed anion effects on the retention of trivalent actinides in the environment 80—13717
  reactor fuel reprocessing wastes, removal of actinides by solubilisation and solvent extraction 79—36384
  reactor waste recycling strategies, burn-up and transmutation studies 79—85700
  recycling, nuclear data uncertainties 79—85711
  recycling and recovery in fission reactor wastes 79—85699
  recycling in power reactor fuel cycle *(French)* 79—85714
  research developments since 1950 78—84116
  self-consistent relativistic muffin-tin calc., atomic vol. and bulk modulus Ac-Am 78—72065
  sensitivity studies and nuclear data requirements 79—85710
  separation from high activity liquid waste, OXAL process *(French)* 79—85813
  separation from high level radioactive fuel reprocessing waste 79—85809
  separation in highly active nuclear waste solns. *(French)* 79—85812
  separation in nuclear fuel and wastes, hazard assessment 79—85806
  short lived, neutron cross sections for transmutation, Van de Graaff accel. study 79—85713
  Slater-Koster interpolation scheme 80—6708
  solutions, differential alpha radiography using solid state track detectors 80—71932
  solvent extraction by trilaurylammonium nitrate carboxylic acid mixtures 79—22444
  specific heat, Debye temp. 80—15258
  spin fluctuation theory, for mag. and elec. props., appl. to actinides 78—91869
  stellar spectra and actinide astronomy 77—78769
  structural properties rel. to F electrons 78—83951
  susceptibility meas. using micro-mag. susceptometer 80—13112
  synthesis from oxides and single cryst. growth 80—16229
  target prep. for synthesis of transactinide elements 80—23206
  target preparation by focused ion beam sputtering 80—23219
  thermodynamic properties 78—35716
  thermoelectric power of nearly magnetic systems 78—84197
  trans Cm isotope build-up in thermal reactors 79—85709
  transmutation, nuclear fuel cycle impact studies 79—85752
  transmutation, research activity status, Japan 79—85807
  transmutation, Swedish studies 79—85703
  transmutation and chemical separation from radioactive waste 79—85808
  transmutation in nuclear power reactors, neutron physical feasibility 79—85701
  transmutation of by-product actinides to reduce high-level radwaste storage times 80—95384
  transmutation-partitioning, technological impacts on nuclear fuel cycle 79—85751
  transmutations in radioactive waste management scheme 79—26611
  transplutonium element symposium, Baden-Baden, Germany (September 1975) 77—28974
  transport properties and sp. ht., role of optical and acoustic phonons 77—15821
  transPu elements, chem., phase anal., X-ray powder diffr. techniques 77—70388
  transuranic element elimination during fission reactor fuel reprocessing *(French)* 77—26857
  transuranic element separation from radioactive waste and fuel reprocessing *(French)* 79—85811

actinides continued
  transuranic elements, in situ. conc. determ. using passive neutron monitoring 79—87933
  transuranic elements in radioactive wastes, long term hazards, removal requirements *(French)* 77—26848
  transuranic neutron flux meas. in radwaste using leached hull monitor 79—85606
  transuranium processing plant, chem. process engng. 77—54338
  transuranium processing plant, remote processing practices, equipment changing and modification facilities 77—54339
  valence fluctuation model, physical prop. response 80—6791
  valence transitions and intermediate valence states 79—42496
  waste incineration, UK and European investigations 79—85702
  X-ray 3d spectra, 4f and 5f states 78—84681
  X-ray diffractometer for work with actinide metals and compounds at low temps. 80—316
  XPS, many-electron effects, comparison with rare earths 80—7466

actinium
  see also nuclei with ......
  soil, U and Ac series nuclides radioactive disequilibrium 80—4014

actinium compounds
  actinium (III) axalate decahydrate, lattice consts. 78—2102
  dihydirdes, structs. and stabilities 80—107146
  AcH, $^1\Sigma$ state, Dirac-Fock one-centre calcs. 80—23301

actinometers *see radiometers*

actinometry *see radiometry*

activation analysis *see chemical analysis by nuclear reactions and scattering*

active antennas
  gravitation radiation detection, active resonant antennas, sensitivity and noise 79—30346

active circuits *see active networks*

active filters
  analogue CCD and SAW filters 77—39172
  band-pass filter for infralow freqs. 80—53578
  biomedical signal conditioning CCD transversal filter 77—52901
  Butterworth filter model of basilar membrane displacement 77—29159
  charge transfer transversal filters, applications in nuclear detectors 77—54466
  education, psychoacoustical expts. with all pass networks 79—25787
  Gaussian filter for nuclear pulse amplifiers, direct synthesis, freq. domain anal. 77—3239
  HEPI accelerator, active filter of annular electromagnet 78—33338
  high-gain, narrow-band, amplifier using active filters for ionosphere measurement 77—56760
  L-shaped, transistorised, stabilisation large current precision measuring ccts. appl. 77—53940
  laser Doppler microscope period meas. signal analyser *(Japanese)* 79—88998
  programmable, characts., hearing equipment appl. *(Swedish)* 78—36055
  PS booster at CERN, longit. active damping system electronics, tracking band pass filters 77—83297
  recursive, determination of pulse density of output terminal 79—72769
  spectroscopy, noise reduction by low pass filter for DC signal, appl. chlorophyll-a fluoresc. 80—87249
  time variant filter performance in 1/f noise, Si(Li) detector-opto feedback FET system 77—57830
  tunable notch filter for solvent elimination from PMR spectra 80—22405

active networks
  see also active filters; gyrators; impedance convertors
  attenuator, for medical US pulse-echo systems 77—40835
  biomembrane electronic cct. model utilising time variant negative res. 78—88696
  nuclear spectroscopy systems, active zero-pole cancellation feedback loop 79—9972
  thermocouple dynamic error correction cct. 78—77909

active nitrogen *see nitrogen*

active oxygen *see oxygen*

actuators
  see also electric actuators
  arm prosthesis, gas-press. actuated fingertip mechanism *(Japanese)* 77—66872
  arm prosthesis, hydraulically actuated, performance criterion 77—48951
  attitude and orbit control systems, conference, Noordwijk (1977) 78—65480
  helenoid actuators applied to deformable mirrors 80—74454
  mechanical actuator, stepper motor, appl. to control of scientific apparatus 78—62683
  multiactuator deformable mirror evaluations 80—14416
  multiactuator mirrors, wavefront error compensation capabilities 79—59797
  nuclear steam system, globe main steam isolation valve unbalanced forces and novel actuator design 78—50288
  optimum configuration in mirror deform. for phase compensation of thermally bloomed laser beam 80—8423
  sectional mirror, optoelectronic control system 78—20645
  solar collectors, design and data rate requirements of computer-based sun following system 79—83573
  surface configuration control by conc. loads applic., mirrors case 79—94317

adaptive control
  see also adaptive optics; adaptive systems; model reference adaptive control systems
  biological control mechanisms for complex motor systems 80—81573
  biological system modelling appl. 77—40628
  cloud chamber adaptive closed-loop expansion control system 79—93889
  digital computer applications to process control, conference, The Hague (1977) 78—49808
  dimensional gauging using scanning laser beam 78—57898
  distributed parameter system control, conference, Coventry (1977) 79—3897
  EEG phasic event detection by microprocessor 78—57091
  eye continuous movement monitoring, proportional-integral adaptive system *(German)* 79—16320
  eye tracking as sequential input adaptive process 79—88074
  image bandwidth compression, scene analysis algorithms and rule-based controller 80—95819
  lungs long-term forced ventilation control excitation 77—60296
  nuclear reactor systems, appl. of stable adaptive schemes 80—13635
  nuclear reactor systems, nonlinear loosely coupled core reactor 80—672

adaptive control continued
- nuclear reactor systems, stable adaptive control systems appl. 79—9765
- orthoses for lower extremities, study 78—48932
- parameter identification and adaptive control, applic. to nuclear reactor systems 80—22970
- polymers, molecular weight distribution 80—58434
- prosthesis control system, complete hand/arm 80—109059
- prosthetic arm decentralised control hierarchical approach 77—40924
- PWR power plant self-tuning control and simulation 79—9827
- saccadic eye movement controller considerations 78—27949
- satellite communications wideband polarisation separation network 77—78394
- scanning background-limited IR sensor with adaptive threshold signal processing logic, performance 80—37082
- semicircular canal afferent response system identification 78—27927
- spacecraft, nonstationary, coordinate-parametric control via multidimensional asymptotically stable adaptive systems 80—101522
- spacecraft final descent vel. control in Mars atmosphere, autonomous navigation algorithm 77—29620
- stochastic object, suboptimal adaptive control 79—30371
- stretch reflex system in human forearm, adaptive control characts. 79—83758
- temperature control system synthesis for superheated steam *(Polish)* 79—75518
- US transducer, realisation algorithm *(Russian)* 77—54853
- wind energy conversion system control, on-line, performance in turbulent wind environment 79—48069

adaptive optics
- *see also optical phase conjugation*
- aberration coefficient estimation 77—19179
- active mirror characterisation by heterodyne interferometry 79—59799
- active mirror testing by stroboscopic interferometry 79—58782
- active optical systems, real-time control over optical wave fronts 78—71187
- adaptive holographic matched spatial filter for pattern recognition 77—7011
- alignment accuracy of Helios CO_2 laser 80—33071
- alignment system for Helios CO_2 fusion laser 80—33070
- amplitude phase distortions correction of wave propag. in turbulent atm., efficiency 79—27178
- astronomical image processing digital techniques 78—81555
- astronomy, rubber mirrors to compensate for atm. aberrations, book contrib. 79—35150
- atmospheric compensation, radial Ronchi grating lateral shear interferometer, book contrib. 79—31972
- atmospheric optical propagation through strong turbulence, adaptive techniques appl. 79—66802
- bandwidth specification for phase corrector and servo control 77—46799
- bimorph piezoelectric flexible mirror constructed from glass plates and $Pb(Zr,Ti)O_3$ ceramic 79—59787
- book 79—31921
- circular membrane reflector made by surface bending due to electrostatic tension 80—91876
- closed loop adaptive, target effects 77—88934
- closed-loop simple system for real-time optical phase meas. 79—63302
- coherent optical adaptive Modal Wavefront Control System 77—19295
- coherent optical adaptive techniques and compensated imaging systems, survey 78—42296
- components, seminar, Washington (1978) 79—59792
- components, seminar, Washington USA (Apr. 1979) 80—31421
- continuous deformable mirror multidither coherent optical adaptive system operation 77—19296
- continuous deformable mirror multidither coherent optical adaptive system characteristics 77—19297
- deformable metal mirror characterisation techniques 79—59798
- deformable mirror adaptive optical system 77—46796
- deformable mirror design and resonance damping 79—59794
- deformable mirror design for wavefront correction in CO_2 laser fusion system 80—74427
- deformable mirror for wavefront error correction in Gemini CO_2 laser fusion system 80—74426
- deformable mirror system using polyvinylidene fluoride piezoelec. film 80—74455
- deformable mirrors for wavefront error correction, piezoelectric material requirements 80—78928
- deformable mirrors with bimorph actuators 80—33135
- deformable-mirror system, computer-aided, using differential angle control 79—27356
- diamond turned metal optics, book contrib. 79—32104
- differential ball screw actuator driven deformable mirror design and performance 80—33137
- discrete actuator deformable mirror 80—33133
- dispersion correctors for compensated imaging, atm. dispersion minimisation 77—46695
- dither systems for space telescopes 77—49301
- dynamic-focusing mirror system, umbrella-type 79—36971
- elastomer storage device evaluation for optical signal processing 80—48444
- film photopot detector characteristics for adaptive optical systems 79—59741
- focusing of light in inhomogeneous nonlinear medium, interf. criteria 80—99633
- Fourier transformation by acousto-optic convolver 79—55079
- glint tracking by adaptive optical techniques 77—19458
- helenoid actuators applied to deformable mirrors 80—74454
- heterodyne receiver arrays in turbulent atm., joint signal current probability distrib. 79—81368
- heterodyne receivers for atmospheric optical communications 80—58663
- image chopping techniques, fast meas. of irradiance distrib. parameters 79—36839
- image phase conjugate laser adaptive control, isoplanatic effect simulation 77—19294
- image quality enhancement *(Russian)* 80—28163
- images aberrated by turbulence, undersampling errors in moments meas. 80—1137
- integrated imaging irradiance sensor for phase conjugate adaptive optics 80—33138
- interferometer, radial grating lateral shear heterodyne, for real-time wavefront meas. 80—77843
- intracavity tip/tilt adaptive control system 79—59728

adaptive optics continued
- IR multidither deformable-mirror COAT system expts. 80—1289
- IR phase conjugation adaptive array 77—46790
- isoplanatic degradation of tilt correction and short-term imaging systems 80—53219
- Large Space Telescope mirror figure control, adaptive optical techniques 77—22076
- laser adaptive optical control with closed-loop estimation and predictive filtering 77—19298
- laser adaptive resonator expt. config. 78—55386
- laser and electro-optical systems, conf., San Diego, CA, USA (Feb. 1980) 80—62392
- laser beam, phase compensated, propag. through atm. turbulence 78—83012
- laser beam control process, closed loop considerations 77—88660
- laser beams, high energy, adaptive phase and amplitude control, book contrib. 79—31971
- laser beams 77—88833
- laser engineering and appls., conf., Washington, USA (May-June 1979) 80—1216
- laser resonator, intracavity deformable mirror adaptive optical system 78—87078
- laser resonator, intracavity phase variations 77—88793
- laser resonator active control techniques 78—71122
- laser resonator adaptive techniques, multidither COAT system 78—42360
- laser resonator adaptive techniques for CO_2 laser, phase error correction 79—59729
- laser system, high energy, optical distortion, active control 78—83019
- laser wavefront analyser for diagnosing high-energy lasers 79—59740
- laser wavefront analyzer for diagnosing high-energy lasers 79—59738
- least-squares wave front errors of minimum norm 80—48137
- membrane mirror performance as adaptive optical element 77—46782
- membrane mirrors for image compensation system, performance and manufacture 77—42587
- microdensitometer precision focus control 79—58769
- mirror positioner, tip/tilt, high performance 79—59795
- modal wave-front estimation from phase derivative meas. 79—89856
- modal wavefront compensative system performance, finite bandwidth effect 79—81361
- monolithic deformable mirror/heat exchanger unit evaluation 80—33139
- multiactuator deformable mirror evaluations 80—14416
- multiactuator mirrors, wavefront error compensation capabilities 79—59797
- multidither adaptive optical system, 69-channel hybrid controller 80—33136
- multidither adaptive optical systems with zonal control of deformable mirrors 77—46795
- multidither adaptive optics, estimation and control 77—50757
- multidither adaptive optics system, speckle interactive effects 77—46797
- multidither adaptive optics system operation 80—33141
- multidither coherent optical adaptive techniques 77—46793
- multidither hillclimbing adaptive optical system, secondary intensity maxima correction 80—106593
- multidithered segmented COAT mirror, surface wave control 78—46752
- N-loop ensemble reference phase control system, stability 77—46794
- nonlinear, adaptive spatial filter for image classification *(Russian)* 78—42292
- nonlinear adaptive system, characteristic purposes 80—28273
- nonlinear holographic gratings for high energy laser beam sampling 80—14476
- nonlinear optical phase conjugation for laser systems 78—79072
- nonlinear optical phase conjugation for pulsed laser systems 78—59092
- optometer, refractive error correction optical system with continuously variable spherocylindrical power 79—62385
- overview of technology, book contrib. 79—32030
- passive return-wave 77—88933
- pattern recognition, hybrid parallel optical and serial digital processing systems 80—99657
- performance with extended dynamic targets 77—46798
- phase aberration correction via stimulated Brillouin scatt. 78—37944
- phase adaptation by nonlinear techniques, optical propag. distortion compensation, book contrib. 79—31973
- phase compensation, optical resolution through turbulent medium 77—46692
- phase compensation for multiple pulse thermal blooming 77—50732
- phase conjugate adaptive optical systems, convergence 77—46688
- phase conjugate adaptive optics using perimeter phase meas. 77—46791
- phase conjugate optics and real-time holography 78—83034
- phase conjugate reflection, pulsed 10.6 μm, via intracavity degenerate four-wave mixing 78—87097
- phase determination of amplitude modulated complex wavefront 78—55305
- phase estimates from slope-type wave-front sensors 78—66770
- phase expansion coefficients spatial correlation, propag. through atm. turbulence 79—80021
- phase values reconstruction from phase differences, matrix formulation 79—59642
- phased array expt. with independent laser sources, compensation for atm. effects 78—42367
- phased arrays driven by independent laser oscillators 80—33005
- piezoelectric bimorph plate, adaptive optical element analysis 79—50389
- reading machine, multifont adaptable automatic, for blind people 80—104814
- real time atmospheric compensation, active optical imaging 77—49307
- real-time optical processing using the liquid crystal light valve 80—63936
- resonator, annular, adaptive mirror effects on performance 80—58596
- sectional mirror, optoelectronic control system 78—20645
- sharpness criterion, rel. to redundant spacing interferometry 78—5427
- single mode fibre polarisation stabilisation 80—58724
- speckle cancellation techniques, computer simulation 80—48161
- speckle effects 77—19410
- stellar image real-time atm. compensation by active wavefront control 78—45242
- surface configuration control by conc. loads applic., mirrors case 79—94317
- surface configuration control of nonuniformly heated shells, actuators effectiveness 79—94318
- systems analysis using two-dimensional FFT algorithm 80—78986
- technology, historical review and prospects 79—59793
- technology status and prospects 80—33132
- thermal blooming, theoretical aspects of compensation 78—32226

adaptive optics continued
- thermal blooming cell design for adaptive optics evaluation 80—33096
- thermal blooming cell design for use in evaluating adaptive optics 80—102780
- thermal blooming compensation, equivalent thin lens model 78—87108
- thermal blooming compensation with multidither COAT system 78—33789
- thermal blooming reduction vice phase correction, experimental demonstration 79—98449
- thermal defocusing of light beams, phase conjugation compensation method 80—64123
- thermal self-action problems and their compensation 80—106579
- thermal-blooming compensation, using closed-loop adaptive single parameter system 78—94407
- three-actuator deformable water-cooled mirror 80—33134
- tracking turbulence induced tilt errors with shared and adjacent apertures 77—46792
- two-wavelength optical phase control system 80—33140
- wave front mutual coherence function corrected by zonal adaptive optics 79—72490
- wavefront analyser using max. likelihood algorithm, phase aberration meas. 77—46694
- wavefront compensation error due to finite corrector-element size 77—46693
- wavefront correction using photon echo 78—9417
- wavefront distortion estimate, least-square fitting to phase difference meas. 77—46689
- wavefront distortion sensing for adaptive optics system control 77—19293
- wavefront meas. control, and conjugation, adaptive optical system aspects 79—59796
- wavefront sensing by phase retrieval 80—106478
- wavefront sensing systems compared 79—58766
- wavefront sensing using white light sources 80—1146
- wideband adaptive optics for imaging, real time atm. compensation 77—45320
- HF chemical laser, phase control for coherent optical recomb. 79—72580
- HF chemical laser phase control servo system 80—33063
- KCl:LiCl photodichroic crystals as adaptive spatial filters 79—72713
- KF:LiF photodichroic crystals as adaptive spatial filters 79—72713
- $Pb(Zn,Ti)O_3$ piezoelectric electrically deformable diffraction grating 80—78963

adaptive systems
- *see also adaptive control; adaptive optics; cognitive systems; learning systems; model reference adaptive control systems; pattern recognition; self-adjusting systems*
- adaptive neuronlike layer net as a control learning system 79—74631
- analogue neural net dynamics, qualitative analysis *(Russian)* 78—27920
- atmosphere echo sounding, Doppler shift extraction hy adaptive linear-prediction filtering 77—64453
- beam forming processor formulation 80—91967
- carotid artery pressure, noise-resistant trigger cct. 77—48889
- chemical dynamics applics. 77—32768
- deconvolution, processing technique for time-varying seismic data 77—91287
- delay element for seismic noise cancellation 79—74994
- eye tracking as sequential input adaptive process 79—88074
- industrial robot, orientation angle calc. method *(Russian)* 80—42192
- learning in networks with minimal disruption 79—74628
- living self-organising systems analysis, bionic aspects *(Russian)* 77—52732
- lungs, artificially ventilated, mechanical properties monitoring, parameter estimation 77—21642
- multi-dimensional asymptotically stable adaptive systems, appl. to nonstationary spacecraft coordinate-parametric control 80—101522
- N-loop ensemble reference phase control system, stability 77—46794
- natural terrain scenes, segmentation-based boundary-modelling processor 80—99661
- nonstatistical parameter estimation adaptive algorithms 80—91995
- nuclear reactor systems, appl. of stable adaptive schemes 80—13635
- passive sonar system adaptive processor 78—5622
- pulmonary parameter identification adaptive analogue tracker 77—48911
- ripple noise pitch detection by human, adaptive model 78—73166
- saccadic ocular dysmetria simulation using sampled-data model 77—56373
- seismic signals deconvolution, adaptive filter structs. 80—98451
- side scan sonar data, adaptive sample set construction 80—43554
- sonobuoy position meas., sound speed adaptive estimation 79—72773
- speaker verification algorithm for noisy utterances 80—91992
- speech adaptive noise cancellation by short-time Fourier transform 80—91976
- time-varying images, object displacement estimation adaptive algorithm 80—99668
- underwater sound passive detection 78—5607
- visual acuity meas. computer-aided system *(German)* 79—2144
- voice amplification, adaptive method for feedback suppression *(German)* 80—106676

adders
- digital level detector, using BCD adders 79—75528
- electroluminescent, short-lived memory and time param. *(Russian)* 77—52768
- image processing, digital, parallel logic device and half-adder circuit 80—10027
- $LiNbO_3$/CdS integrated optical half adder circuit 79—76877

adding machines *see calculating apparatus*

adherence *see adhesion*

adhesion
- ABS polymers, deposited in internal magnet magnetron sputtering system, adhesion of Cu films 79—83121
- ABS-2 plastic, etching rate rel. to electroless Cu adhesion *(Russian)* 78—35542
- acrylate adhesive coating on glass substrate, mech. props. determ. using transfer functions of US oscillations *(Russian)* 79—87644
- acrylic bone cement containing second phase dispersions, strength 77—81663
- acrylic bone cement viscosity characterisation 79—79690
- acrylic bone cement-stainless steel interface, shear strength 77—86706
- acrylic cements for fixation of orthopaedic implants 79—84000
- acrylic copolymer adhesives, performance of polar and non-polar, relevance of glass transition temp. 79—39119
- adhesive, pressure sensitive, radiation curing, literature review 77—86283

adhesion continued
- adhesive bond testing, US trapped modes in layered media 77—32761
- adhesively bonded metallic panels, 2-ply, finite element and integral eqns. anal. of fatigue crack growth 78—92347
- aerosol cluster, mol., sticking probability to solid surface 77—12833
- alloy, selective stripe, electrodeposition and hot flow techniques, metallurgical characteristics 80—50567
- alumina, effects of intense proton beams 79—63261
- alumina-acrylic composite bone cement 79—79689
- alumino-chromo-phosphate adhesive, chem. interaction with α-Fe substrate, Mossbauer obs. 80—40596
- aluminophosphate adhesive, chem. interaction with α-Fe substrate, Mossbauer obs. 80—40596
- anaerobic adhesive bonding sealing and retaining properties 78—48610
- anodic, and free anodic film on Al substrate, deform.-strength props. *(Russian)* 77—69203
- apparatus, for adherence, wear resist. and thermal shock meas. of thin films 78—72943
- Araldite, high vacuum sealant at liq. N_2 temp. 80—57319
- axially loaded butt joints, stress strain behaviour 79—74209
- axisymmetric butt joints, stress anal. in torsion and tension, response of adhesives 78—63397
- bimetallic adhesive force at small separation 77—35823
- bimetallic interface energies 78—2545
- biomembranes, bivalent cations effect 78—64946
- blood platelet adhesion obs. in flow chamber 79—79589
- bond strength, and stressed state during breaking *(Russian)* 80—76478
- bond strength classifier algorithm 79—91906
- bond strength prediction, Fisher linear discriminant function 79—61808
- bond US inspection, aspects of model anal. and pattern recognition 78—31611
- bonded Al-CFRP single lap joint strength 79—29328
- bonded interface defect testing by differential interferometric Stoneley wave meas. 80—76444
- bonded joint, new test method for prediction of environmental resistance 78—7102
- bonded joints, adhesive nonlinearities, optimal length, performance 79—1103
- bonded lap joints, elastic stresses theory 78—55563
- bonded plate or membrane strips, exam. of adhesive fracture 78—59342
- bonded surface durability, wedge test 78—31591
- bonded tubular lap joint, stress anal. 78—18253
- bone cements, mech. props. effects of antibiotics, strain rate, temp. and age 77—60298
- bone-cement interface bond enhancement technique 78—31980
- boride RF sputtered wear-resistant coatings, XPS study of adherence 79—34191
- brittle rod, optimum specimen shape for compression tests, gluing technique effects 80—50797
- cadmium arachidate monolayer transfer from air-water interface to solid, contact angles 77—55424
- carbide RF sputtered wear-resistant coatings, XPS study of adherence 79—34191
- cement based on $Ca(OH)_2$ and polymethylphenylsiloxane, high-temperature high-strength props. 77—36439
- cement mortar-epoxy resin mortar, durability of jointing of successive pours with epoxy resin adhesive *(Japanese)* 77—8793
- cement mortar-K cement mortar, durability of jointing of successive pours with epoxy resin adhesive *(Japanese)* 77—8793
- cemented carbides, physical and chem. nature 80—76265
- ceramic/metal layer adhesion mechanism for metallization of electronic ceramics, elec. props. *(German)* 80—76381
- ceramics using synthetic adhesives made in Poland, resistance tests *(Polish)* 80—35365
- coatings, adhesion strength, meas. using microindentation method 80—40640
- colloidal particles, interaction force, calc. of electronic component 79—11829
- composite glass shells, bonded joint efficiency during external hydrostatic pressure cyclic loading 79—57079
- composite material/metal sheet bonded, finite element anal. of patched cracks 80—10192
- composites, adhesion between two crystals, theory 80—104417
- concrete, joints glued with reaction resinous mortar, photoelastic exam. *(German)* 78—76825
- concrete, strength, shrinkage strain and deterioration down to −160°C *(Japanese)* 80—100886
- contact interaction between spherical surfaces under press. in various media *(Russian)* 77—7958
- contact of deformable bodies, influence of adhesive forces 77—70281
- contacting bodies under conditions of adhesional interaction, Hertz problem *(Russian)* 79—81820
- corrosion protective coatings, organic, performance evaluation of adhesion and permeability 78—64764
- crystalline particles at sphere-plane contact, nondiffusional deform. under capillary forces 78—15329
- α-cyanoacrylate adhesive in first monolayer on bulk Al surface, IR spectra, H-bond form., stretching vibr. 80—87119
- cyclic stress testing of adhesive bonds 79—15820
- debond dynamics for elastic strip, Timoshenko beam props. and steady motion 78—55604
- Debonding of circular second phase particles 78—5688
- dentistry, adhesion 79—20715
- deposit-substrate systems, adhesion testing 80—50814
- diamond surface soldered to metal film, contact strength determ. device 78—60910
- dielectric coating adhesion improvement of diamond turned mirrors, ion polishing surface prep. 79—23102
- dielectric coatings on Be substrate based mirrors 77—62034
- diffusion bonding, in Ar atmosphere, investigation *(Japanese)* 78—11491
- diffusion effects on adhesion energy of two crystals 78—2380
- disperse materials, fine layers, autohesive strength, meas. installation 80—40644
- double cantilever beam, adhesive fracture specimen, crack tip stress field anal. 78—55602
- double cantilever beam adhesive joint, cohesive fract., stress anal 77—65721
- double lapped composite joints, efficiency in bending, of steel/B reinforced Al or epoxy adherends 78—68870

adhesion continued

- double-lap adhesive bonded joints, approx. solns. by means of asymptotic expansions *(French)* 79—90191
- E-glass textile filaments, wetting characts. 80—80030
- elastic adhesion problems, rel. to linear fracture mechanics *(French)* 80—14617
- elastic particles and solid surface, electrostatic rel. to mol. component 77—42787
- elastic solids, tangential force effect on adhesive contact 77—62216
- elastic sphere, deformation and sticking to a rigid plane, mol. force effect 80 106720
- elastomers, surface roughness, friction and adhesion 80—66674
- electric discharge sintering, metal powder+punch electrode reactions 78—11148
- electrodeposit, on metallic substrate, peel test for determ. adhesion 80—50815
- electron beam curing, beam voltage effects on mech. props. and chem. struct. 77—70201
- electropolymerisation, on electrodes, book contribs. 80—50854
- EM tensile adhesion test method 80—50804
- epoxide resin, self-toughening mechanism on Al substrate 79—70293
- epoxide resin cured with aliphatic dicarboxylic acids, fatigue behaviour *(Japanese)* 79—79092
- epoxy adhesive layers, interlaminar stress distrib. in nonlinear range 79—39117
- epoxy Al bonded, adhesive joints under complex loading, development of failure criterion 78—92344
- epoxy based structural adhesives, time-temp. cure behaviour, torsional braid anal. 80—55621
- epoxy laminate, surface prep. to promote electroless Cu bonding 77—21300
- epoxy polymer, glass microsphere-filled, glass transition temp. *(Russian)* 79—24489
- epoxy resin, curing accelerator effect on props. and ingredients *(Japanese)* 78—27726
- epoxy resin, glass bead-filled, elastic moduli, interfacial slippage effect anal. 78—76688
- epoxy resin adhesives, capillary flow and bond strength 80—71883
- epoxy resin bond layer, prep. methods, ultimate thickness 80—71884
- epoxy resin EhDT-10, temp.-time rel. of strength 80—25798
- epoxy resin-Al alloy 5086, scarf joint test specimen, mixed mode adhesive fracture, bond angle effect 78—68768
- epoxy resins, adhesion to metals fracture mech. study 77—4888
- epoxy system, inelastic electron tunnelling spectroscopy appl. 79—15952
- epoxy type adhesives, solidification temp. conditions rel. to strength *(Russian)* 79—56972
- epoxy-metal joints, environmental fracture and effects of shrinkage stresses 80—16635
- epoxy-metal powder mixtures, cryo-tip refrigerator appl., heat transport 78—37013
- epoxy-resin join with Teflon-glass fabric double layer material, adhesion strength determ. method 77—77681
- ethylene-methyl acrylate, random copolymer, review 80—108330
- exoelectron emission for tribomechanical surface treatment *(German)* 77—4870
- fatigue resistant adhesive 77—4834
- femoral stem size and design effects on cement extrusion pressure, hip replacement 79—79692
- fibre reinforced composite, fibre/matrix adhesion, AF testing *(Japanese)* 77—70254
- fibre reinforced composites, metal clad, debonding risk 80—3132
- fibre reinforced polyester composite, interface strength *(Japanese)* 78—15646
- film, adhesion stability and peeling off from substrate 77—24501
- film, adhesive failure, rel. to interfacial structure 80—50820
- film, diamond indentation and draw tester for meas. of ultra-adherence 78—72944
- film, evaporated, adhesion meas. methods 80—50822
- film adhesion testing, simple real-time holographic interferometry method 78—92411
- film adhesion testing, use of fracture mechanics concepts 80—50802
- film-substrate bond strength, meas. by laser spallation 80—50821
- filmed structures, hardness and adhesion meas., scratch technique 80—50805
- flame-sprayed coatings, adhesion testing 80—50812
- fluoropolymer adhesive joints, fracture and surface anal. by SEM and ESCA 77—55434
- fluoropolymers, ion-beam textured, adhesive bonding 79—87752
- fracture mechanics of blister test specimen, effect of adhesive layer elasticity 77—16778
- fracture toughness meas., CDCB specimens 77—4874
- galvanic coatings, adhesion after strain hardening, test device 80—71837
- glass, surfaces joined by optical contact, spectral absorpt. of water layer 78—46852
- glass ball rolling on adhesive viscoelastic material, contact area 79—52394
- glass bonded Pt-Au thick film conductor, adherence fracture energy, Al_2O_3 substrate effects 77—56075
- glass fibre reinforced epoxy/Al alloy bonded joint, mean strength, moisture effects 79—20106
- glass fibre reinforced polyester, epoxy-polyamide, single lap joint, tension-shear strength *(Japanese)* 78—11494
- glass fibre reinforced polyester, single lap joint, tension-shear strength *(Japanese)* 78—11494
- glass fibre reinforced polyester resin, interfacial bond strength, effect of surface treatment 77—21303
- glass fibres-resin interface studies 80—93531
- glass-enamel coatings, effect of firing method on adhesion 79—24647
- glass/polymer/glass plate in temp. field, failure 80—43674
- glue joints, axisymmetric with optimal shearing stress distrib. within glue layer *(Polish)* 79—66256
- graphite, fibre reinforced Sn-Pb investment castings, tensile strength 77—48487
- graphite, of melted Al, Ga and In, 300 to 1200K *(Russian)* 77—15663
- graphite reinforced epoxy steel scarf joint, adhesively bonded, exam. of failure 78—92350
- graphite-epoxy composite, hydrothermal ageing 77—21189
- high temp. bonding, piezoelectric transducers, adhesive tests 80—43586
- ice single crystal, friction of steel ball load, velocity and temp. depend. *(Japanese)* 78—88537
- improvement by gas-plasma contaminant removal 79—39112

adhesion continued

- indentation with perfect adhesion, wave propag. anal. 77—23919
- inelastic electron tunnelling spectroscopy studies 78—92440
- interface crack tip, adhesion loss model 80—38335
- interface forces and interactions, roughness and ductility depend. 77—24476
- interfacial energy-contact angle relation 79—91904
- ion plating, evaporation sources, gaseous media, and transport modes 80—80984
- ion polishing for diamond-turned mirror dielectric coating adhesion 80—1370
- ionic crystals, adhesion energy, calc. for NaCl type crysts. 77—43437
- joint, cohesive bond strength prediction 79—83436
- joint failure, adhesive/electronically conducting substrate, exam. of electrochemical aspects 78—60979
- joint strength, effect of change in surface morphology of adherend 77—36672
- joint strength testing under normal rupture and shear stresses 79—52500
- joint under combined stress, expt. study of strength 79—74339
- joints, adhesive, effect of structural parameters on stressed state 79—41630
- joints, calc. of internal stresses under temp. variation *(Russian)* 77—70273
- joints, testing using US probe 79—57182
- lambda tight cement, for low temp. techniques 79—35752
- laminates, fracture, effect of adhesive layers 78—90791
- larch arabogalactan solns. as optical cement 77—75723
- laser CVD, film physical props. and applications 80—93493
- layer, double torsion method of crack propag. study 79—83412
- leucocyte adhesion studied quantitatively by multiple internal reflectance-IR spectroscopy 77—56562
- light and electron emission in breaking of adhesive bonds under high vacuum 80—55190
- liquid, to solid surface, contact angle rel. to dielectric constant 80—10741
- liquid-liquid interfaces in isolation, and in interaction, review 77—47651
- locus of failure, bond failure in adhesive joints, experimental methods 80—50801
- locus of failure, implications for adhesion meas. 80—50818
- lubricated contacts, adhesive wear 80—16491
- measurement, of preformed film to solid 80—50819
- measurement, of thin films, thick films and coatings 80—50817
- measurement techniques, of thin films, thick films and bulk coatings, conf. Philadelphia, USA (Nov. 1976) 80—46729
- metal, wear characts., mechanisms 77—32697
- metal adhesion experiment for Spacelab 78—88621
- metal adhesion to ionic surface 78—18914
- metal adhesive bond quality meas., digital US signal analysis 79—47863
- metal base+hard electrolytic Fe, adhesion strengths, quantitative determ. method 77—77680
- metal coatings, obtained by vacuum evaporation and sputtering, mech. props. rel. to prep. conditions 77—59239
- metal cutting, direct SEM obs. of adhesion and frictional sliding 80—104412
- metal elements, adhesively bonded, cracked or with discontinuities, analysis procedures 78—90793
- metal film on polymer base, US test device 79—91865
- metal hot sprayed deposit adhesion quality factors 79—83365
- metal panels, adhesively bonded, cracked, fracture anal., crack tip stress intensity factors 78—90792
- metal particles produced by gas evaporation, form., growth and interaction 80—16220
- metal surface, AES anal. in adhesion, friction and wear 78—53179
- metal surfaces, adhesion theory, electron distribution tail effective length *(Russian)* 79—99430
- metal to ceramic joint, problems of characterizing the adherence 79—43552
- metal to polymer, temp.-depend. determ., rapid method 77—51610
- metal-metal interface, effect on adhesion and friction 77—24488
- metal-polymer, ply-separation resist. polymer polarity effect *(Russian)* 80—61064
- metal-polymer joint, meas. of temp. dependence of joint strength 80—50824
- metal-polymer splices, adhesive bond destruction and strength w.r.t. electrochem. interaction 79—20339
- metal-to-metal bonds, stress analysis in hostile environments 79—20338
- metal/ceramic system, adhesive energy, meas. techniques 80—50803
- metallic adhesion 79—73463
- metallic films, vapour deposited on polymer, ageing, adhesion, elec. cond., electrochem. pot. *(Russian)* 79—33362
- metallic interfaces, local and nonlocal contribs. to adhesive energies 77—85085
- metallic interfaces, self-consistent electronic densities and adhesive energies 78—72005
- metallic layers/non-metallic substrates, micro-contacting problems *(German)* 80—55624
- metallic sliding contact, resistance at single point, friction force *(Japanese)* 78—11343
- metallurgically bonded plates, structural integrity determ. by high energy impulse 79—39111
- metals, adhesion theory for two surfaces 80—20270
- metals, fundamental nature 79—52616
- metals, ion-beam textured, adhesive bonding 79—87752
- metals, surface pretreatment effect on joint bond strength by cyanoacrylate adhesive Kanokonlit-E *(German)* 79—57202
- metals, theory of adhesion *(Russian)* 77—44455
- metals, with lattice of different types, theory of adhesion, incl. dislocations *(Russian)* 78—7165
- mica, surface free energy dispersive component, adhesion to water and n-alkanes 77—55435
- mica, surface free energy nondispersive component, adhesion to polar liq. 77—55436
- microsphere removal by SAW displacement field 79—45884
- mirror, diamond-turned, adherent dielec. coating 78—33810
- modelling possibilities of the mass transfer processes 79—74338
- multicomponent thin film formation on K8 glass 79—72726
- multilayer interference film, mass production by roll coating *(Japanese)* 79—81577
- Mylar film/adhesive/Al foil laminate, mech. interactions 80—81112
- NDT characterisation of metallic substrate surfaces prior to adhesive bonding 78—53166

adhesion continued
- Nylon 12, short-time adhesion, rel. to diffusion properties *(Japanese)* 79—70294
- optical, struct. and mechanical properties 79—76772
- optical cements, commercial, trials and meas. *(French)* 79—50452
- optical coating adhesion characterisation pull-off tests 79—14128
- organic films, plasma polymerised, adhesion and cohesion on metal substrates 78—3259
- organo tin polymers, glow discharge formed, interface composition and adhesion 79—82467
- orthodontic adhesive joints, adherend topography effects 77—52916
- orthodontic direct bonding systems, stress anal. 77—56513
- oxide, vacuum deposited layer adhesion to glow-discharge treated-surfaces *(Russian)* 77—44372
- particle adhesion upon impaction 79—52784
- particles, effect of elastic contact deformation 77—29048
- particulates, glass, removal mech. from solid surface 79—50676
- passivation films, on Sn plate, lacquer adhesion, ESCA exam. of constitution and effects 80—40776
- peel mechanics with constraints 79—23285
- peeling mechanics of elastic strip from rigid substrate, large bending 77—80122
- PET fibres, adhesivity improvement by plasma surface treatment 79—15823
- photosensitive materials which change their adhesion to a substrate due to the action of light *(Russian)* 79—97464
- physical chemistry of surfaces, book 77—25310
- physical mechanisms of adhesion of solids, review *(French)* 78—6231
- physical modelling, US attenuation effects 78—7141
- piezoceramic benders, circular, bond stresses 78—21124
- plasma coating, fused, strength of adhesion to base by gas flame soldering 78—23894
- plasma spraying, coatings and composite materials 78—3247
- platelet adhesion to solid surfaces, effects of plasma proteins and substrate wettability 78—35814
- PMMA femoral cement compactor for total hip replacement 79—79688
- polyacrylonitrile, plasma deposited, adhesion to plastics 80—50745
- polyamide-Cu(Ni) oxalate, oxalate decomposition kinetics, in polymeric medium, thermogravimetry and DTA 78—52749
- polybutadiene, adhesive, uncured linear flexible-chain polymers of narrow molecular mass distrib., fracture in triaxial stress 79—43550
- polycaprolactam, crystallisation effect on adhesion to Al 77—66742
- polyester-polyurethane interpenetrating polymeric network glues, props. 80—16640
- polyethylene, adhesion to Cu, substrate topography effect 79—74340
- polyethylene, high density, adhesion strength to St. 3 steel 78—23920
- polyethylene, melting against Al, XPS obs. 77—32700
- polyethylene, oxidised, energy of adhesion with polar and nonpolar liquids 77—55427
- polyethylene, self-adhesion, surface polarity effect, meas. by Ca^{2+} adsorpt. 79—11759
- polyethylene, theory of adhesion to alkali halide crystals, allowance for boundary dislocations 77—70280
- polyethylene coatings, vac. deposited on Al and Cu 79—61793
- polyethylene films, adhesive props. improvement by corona discharge appl. *(French)* 78—92438
- polyethylene terephthalate monofilaments, friction and adhesion 79—52386
- polyethylene-steel adhesive bond strength, rel. to ultrathin layer of polymer remaining on metal 77—70279
- polyethylene/Cu(Zn) adhesion, role of surface topography 80—35500
- polyethyleneterephthalate, film, props. of adhesive layer adsorbed on surface 79—56067
- polyethyleneterephthalate film, influence of crystallisation on adhesive and cohesive props. 79—56100
- polyhedral particles, adhesion forces in liq. medium 79—70380
- polyisobutylene-glass adhesion bond, macroscopic contact form. 79—39113
- polymer, adhesion phenomena and influence of various factors, work of adhesion *(Polish)* 80—3292
- polymer, particle-filled, elastic moduli, interfacial slippage effect anal. 78—76688
- polymer adhesion ability enhancement by block copolymer incorporation *(Russian)* 80—61065
- polymer adsorption/adhesion, smooth surface, mech. stress effects *(Russian)* 78—50672
- polymer coated graphite fibres, adhesion to epoxy matrix 79—15644
- polymer film, adhesion, structure-time analogy 79—70292
- polymer film, in adhesive joint contact layer, intermol. interaction with substrate and filler *(German)* 79—8421
- polymer film, plasma-deposited, adhesion to plastics 80—50745
- polymer films, to metals and non-metals, principles and meas. methods *(Czech)* 78—80709
- polymer laminate films, thin composite, adhesive strength determ. 79—57178
- polymer matrix composites, component interaction mass spectrometry investigation *(Russian)* 80—35511
- polymer systems for adhesive applications, radiation curing, lap shear strength props. 80—66842
- polymer to solid substrate 77—70278
- polymer-metal adhesive bonds, shear resist., polymer crystn. effect 80—89462
- polymeric adhesive layer, interlaminar stresses, direct determ. 77—86237
- polymeric composite, interphase, physico-chemical problems 80—16262
- polymeric materials, high-energy electron emission, in breaking adhesive contact 79—65981
- polymers, adhesional strength, review *(Russian)* 79—52619
- polypropylene, neutron irradiation effect on weldability and adhesion *(Japanese)* 79—60405
- polypropylene coating, glow-discharge-polymerised, adhesion and hydrophilicity 79—15829
- polysilicane gel on glass plate, elastic deformation in adhesion of solids 78—60010
- polysiloxane-metal oxide interfaces, bonding mechanism, surface anal. by XPS and static SIMS 78—15643
- polystyrene-polyethylene block copolymer, deformation ratios, Poisson ratio and adhesion, dilatometric obs. 80—60937
- polyurethane, adherence on glass 78—83336
- polyurethane adhesive, interface reactions with Al surface after surface treatments 77—81384
- polyurethane adhesives, modified, struct. *(German)* 79—100333

adhesion continued
- polyurethane cement, viscosity and shear strength, components influence *(German)* 80—93729
- polyvinyl alcohol-Cu interface, XPS study 79—83093
- polyvinylbutyral, high density, adhesion strength to St. 3 steel 78—23920
- powder metal sprayed coatings, bond strength, influence of surface preparation 78—11150
- propag. of cracks, effect of humidity 77—86133
- PTFE-Al, adhesion joints, effect of Cu and CuO 78—53183
- PTFE/graphite bond in H_3PO_4 environment, electrochemical exam. of joint failure 78—60979
- PVC, filler effect on adhesion to Cu 80—45476
- refractory metal powder adhesion forces on metallic substrates, electrostatic eval. method 77—52564
- reinforced composite pull-out forces, effect of matrix stresses 77—21334
- rigid rodlike molecules adsorption onto planar surface, dispersion interactions, statistical mech. anal. 80—29265
- rubber, friction coefficient, role of adhesion *(French)* 77—52495
- rubber, peeling initiation and propag. 78—76824
- rubber adhesion and friction, surface charge contribution 77—80826
- rubber to metal bonding, XPS appl. 78—15648
- rubber-brass interface, adhesion failure, XPS study 80—40671
- rubber-metal interface, adhesion mechanism, XPS study 80—65382
- rubbery polymer film, on glass surface, interfacial dislocations spontaneously created by peeling 78—73011
- SEM specimen mounting epoxies, aerosols, and adhesive tapes 79—71580
- short-range interactions mediated by a solvent with surface adhesion 78—71973
- silicide RF sputtered wear-resistant coatings, XPS study of adherence 79—34191
- silicone rubber, on Perspex, surface topography effects 78—15644
- soda-lime glass, chemically modified, water contact angle, adhesional wetting 77—55426
- solar cells design, with improved glass, adhesives and heat dissipation 80—76636
- soldered thick-film conductor, adhesion meas. technique 80—50811
- solid particle, in liq. medium, hydrodynamic method of adhesive forces meas. 79—68826
- solid surfaces in contact, adhesive force 79—15026
- solid-fluid interface, wetting and adhesion, thermodynamic aspects 80—89525
- solids, stickiness 80—88438
- solids in vacuum, contact adhesion, single asperity experiments 77—11149
- solids in vacuum, deform. and interfacial energy 78—22306
- sputtered refractory carbides, adhesion to metal substrates, improved 80—76481
- steel, adhesive wear, heat treated load effect 78—11344
- steel, austenitic stainless, friction in vac. at elevated temps. 80—55542
- steel, bonded with epoxy resin, effect of adhesive bond thickness on mech. resist. *(French)* 77—63882
- steel, Cr plated, laser treatment 80—21191
- steel, double-layer, adhesion strength determ. method 77—63857
- steel, galvanised, with paint coating, adhesion failure, XPS study 80—40671
- steel, joints glued with reaction resinous mortar, photoelastic exam. *(German)* 78—76825
- steel, low-C, bond form. between powder layer and dense basis during hot pressing 79—24669
- steel, machining, adhesion mechanism of built-up edge and layer on rake face of cutting tool 79—47784
- steel, mild and stainless, fretting wear, role of adhesion and delamination 78—35533
- steel, stainless, epoxide butt joints, effect of abraded and Ar ion bombarded surfaces on ultimate tensile strength 80—16638
- steel, stainless, liquid phase bonding with Ni-P plating *(Japanese)* 78—7082
- steel, stainless, on Al_2O_3, adhesive energy, meas. techniques 80—50803
- steel, stainless, surface prep. for adhesive bonding 77—52546
- steel, stainless, surface preparation for adhesive bonding, surface characteris. techniques 77—56132
- steel sheets, overlapped, glued with nonuniform epoxy resin layer, strength tests *(German)* 78—15647
- steel substrate, coating applied by explosive energy, adhesive strength 77—70235
- steel-aluminium plates, exam. of adhesion strength by impulse loading 78—84943
- steel/SiO_2-Al_2O_3 glaze, adhesive behaviour of metallic cation glaze exchanged on acid site struct. *(Japanese)* 79—66216
- steels, stainless, surface characterisation rel. to adhesive bonding chem. etching, SEM, AES, XPS and electron probe microanal. 80—88416
- stiffened panels, stringers bonded to cracked orthotropic sheet, stress intensity factors 79—50647
- Stoneley wave study of adhesively bonded interface 80—49530
- strain gauges, performance in pressurised water at 50°C, reactor pressure vessels testing 79—35713
- strength determ. apparatus for gunite coating on refractory masonry, breakaway tests 78—35618
- strength measurement of electroplates, device 78—56843
- strengthening of adhesive joints by dislocations 77—89659
- stress corrosion testing of adhesive bonds 80—16514
- structural bonded joints, fatigue crack growth of adhesive bond line cracks 78—92346
- styrene-diene block copolymers, pressure sensitive adhesives, morphology and viscoelastic behaviour 77—52419
- sublayer, influence on stability and photographic characteristics of AgBr evaporated layers *(Bulgarian)* 80—42281
- superconducting magnet, effect of adhesion between turns 78—89507
- surface, topography rel. to adhesion props. 79—96280
- surface anal. techniques appl. 80—65381
- surface and interfacial aspects, review 80—108690
- surface chemistry studies, anal. appls. 80—88440
- surface contacts, tribological props. 79—19469
- surface energy, theory and appls., symposium, New York, USA (Apr. 1976) 77—55422
- surface science in metallurgy, review 79—42388
- tensile bond strength, effect of aspect ratio, for butt joint of internal fracture 80—50823
- test specimens, mechanical charact. and optimum geometry of joints 80—16639
- testing, coating to substrate, specimen prep. device 79—43518

adhesion continued
thermal resistance of high viscosity adhesive layer 77—1269
thermally sprayed coating adhesive strength testing method 79—83432
thermally sprayed nonfused coating, adhesive bond strength NDT 79—83433
thermosetting acrylic adhesives, electron beam curing 80—16634
thermostatic glass-float adhesiometer 79—43519
thick film, to ceramic, destructive and nondestructive meas. 80—50809
thick film conductor, adhesion meas. 80—50808
thick film terminations on chip components, adhesion meas. methods 80—50810
thick specimen visualisation and joint characterisation by scanning acoustic microscope 79—47875
thin film adhesion meas., semiautomatic installation 79—96245
thin film growth, surface self-diffusion coeff., adhesion energy of evap. material 78—84080
thin films, adhesion determination, electron and laser beam appls. 80—71833
thin films, meas. device 80—66720
tooth, artificial-denture base joint, adhesion, fracture mech. 79—16350
transducer bonding material investigations, US delay lines *(Japanese)* 80—79097
tubular lap joint, nonlinear stress-strain anal. 80—16637
urea-formaldehyde resin/wood materials, book 80—73114
US bond evaluation, anal. of problem 80—71847
US ellipsometer design and performance 79—57196
US spectroscopic NDT 78—76805
US wave interaction with adhesive bonds, modelling concepts 77—21335
vesicles, large, anal. of adhesion to surfaces, expt. procedure 80—109063
vinyl ester adhesive/Al lap shear specimens, electron beam curing 79—20337
viscoelastic bodies, adhesion and fracture mechanics, review 78—83336
viscoelastic solid, kinetics *(French)* 77—89065
viscoplastic medium, asymmetric breakdown of thin layer between two sand surfaces 79—94503
viscoplastic medium, formation of contact with solid surface under pressure 79—69320
wedge adhesive joint, nonuniform stress distrib. under combined normal and shear stresses 79—18837
weldbonded joint deform., finite element simulation 78—35636
wet particulate systems, pendular band strength between unequal-sized spherical particles 80—104418
wetting angle determ. method for adhesive and material to be joined *(German)* 77—62709
work of adhesion, technique for eval. 78—19969
Ag electroplated lead frames, surface struct. rel. to bonding behaviour, IC prod. *(German)* 79—11010
Ag, evaporated film, density, adhesion, intrinsic stress, substrate temp. effects 77—15709
Ag film, adhesion changes on 10 MeV electron irrad. *(Russian)* 77—43460
Ag, film, chem. deposited, agglomeration, SEM and TEM obs. 80—59828
Ag film, evaporated, adhesion meas. 80—50822
Ag film, on amorphous C and Si substrates, dispersion force contrib. to adhesion *(French)* 80—59842
Ag films deposited from hot hollow-cathode source, ion pre-cleaning energy 77—8754
Ag, fine particles, adhesion and sintering, TEM exam. 78—44053
Ag, granular thin films, adhesion measurement 80—50807
Ag-Au thin films, interdiffusion, pore formation, stress effects, adhesive effects *(Russian)* 79—82502
Al, adhesively bonded and weld bonded aircraft struct. subjected to acoustic excitation, determ. of sonic fatigue life 78—92351
Al alloy, 2024-T3, adherend surface, chem. comp., effects of chem. and thermal treatments 78—39939
Al alloy, adhesive-bonded-laminated, fatigue props. 80—50695
Al alloy, surface preparation for adhesive bonding, surface characteris. techniques 77—56132
Al alloys, contamination, automated nondestructive inspection 80—16629
Al alloys, epoxy bonded sheet, fatigue crack initiation, propagation 79—15776
Al and Al alloy anodised oxide films, for adhesive bonding appls., AES and SEM study 80—66689
Al epoxy bonded joint, determ. and appl. of COD 80—30078
Al film, evaporated, adhesion meas. 80—50822
Al film, on amorphous C and Si substrates, dispersion force contrib. to adhesion *(French)* 80—59842
Al film+vitreous silica substrate, reaction 77—86380
Al, joints glued with reaction resinous mortar, photoelastic exam. *(German)* 78—76825
Al plasma sprayed coating adhesion to mild steel, substrate pretreatment effect 79—83391
Al, prepared for adhesive bonding, oxide morphologies 79—70203
Al, surface energy and adhesion props. 80—10774
Al, thin film on fused quartz, threshold adhesion failure, meas. by stylus method 80—50806
Al, thin foil, adhesion and friction, rel. to observed dislocation density 78—64706
Al/Sn, composite, kinetics of adsorption softening of solid interface *(Russian)* 79—61619
Al/Sn interface, effect of plastic deformation on structure and adhesion strength of interface *(Russian)* 79—28218
Al-Al adhesive bond system, US determ. of bond strength due to surface prep. variations 77—21336
Al-Cu-Mg-Mn (4.5, 1.5, 0.6, wt.%), alloy 2024-T81, plates, adhesively bonded, exam. of fatigue crack growth 78—92349
Al-epoxy adhesive joints, cohesive-interfacial mixed-mode fracture 79—39110
Al-epoxy adhesive systems, opening and edge-sliding fracture toughness 78—95805
Al-graphite adhesion and contact angle, effects of metal additives *(Japanese)* 78—60008
Al-Ni with multiple layer plasma coating, exam. of cohesion strength *(Russian)* 80—7714
Al-polymer joint, meas. of temp. dependence of joint strength 80—50824
Al-steel mixture, wear resistant, produced by compaction by discrete shock waves 80—84882
Al-Zn-Mg-Cu-Cr, (5.6, 2.5, 1.6, 0.3 wt.%), laminates, 8 and 22 layers, adhesively bonded exam. of fatigue crack propag. 78—92345

adhesion continued
Al-Zn-Mg-Cu-Cr, (5.6, 2.5, 1.6, 0.3 wt.%), alloy 7075, plates, adhesively bonded, exam. of fatigue crack growths 78—92348
AlMgSi, adhesive jointing, acoustic anal. *(German)* 78—7168
Al_2O_3 and Al_2O_3-Y_2O_3, plasma spraying, microstruct., porosity and adhesion 77—32710
Al_2O_3 detonation deposited coatings, porosity and adhesion, processing parameters effects 79—70227
β-Al_2O_3, field assisted bonding to metals 80—45474
α-Al_2O_3, growth and adhesion on Pt-Al alloys 77—8994
α-Al_2O_3 protective scale, influence of Pt 77—16749
Al_2O_3/Nb laminates, metal to ceramic joints, adherence props. 80—45386
Al_2O_3/Nb/Al_2O_3 joint, solid state bonded, exam. of bond fracture strength 78—76826
Au film, on amorphous C and Si substrates, dispersion force contrib. to adhesion *(French)* 80—59842
Au film on oxide or glass with interposed fluoride film 78—19667
Au, fine particles, adhesion and sintering, TEM exam. 78—44053
Au fine particles, adhesion, role of twinning and surface energy, TEM obs. 78—72009
Au, immersion plating on Al, adhesion and contact resist. 79—39033
Au on oxidised Si with metal adhesion layer, ageing props. 77—11820
Au to Al_2O_3 solid state reaction bond, effect of ambient atmosphere 78—67914
B coatings on graphite, fusion reactor appl. 80—23147
B(C) fibre reinforced matrix, matrix-fibre interaction depend. on metallic dopants *(Russian)* 80—76479
B_4C coating, erosion rates under H^+ ion bombard., fusion reactor appls. 80—39179
Be coating, erosion rates under H^+ ion bombard., fusion reactor appls. 80—39179
Bi, liq., in fused alkali chloride binary mixtures, electrocapillary phenomena 77—40553
C, diamond-like, produced by RF glow discharge of hydrocarbon gases, props. and coating rates 80—21146
C fibre, friction, expt. and adhesion theory 77—1877
C fibre-reinforced plastic joints, fatigue life, stress distrib. analysis 80—55497
C film, diamond-like, ion deposited, hardness and mech. stability 80—2314
Co, particle formation by evap., electron microscopy obs. of interaction processes 80—104053
Cr film, trivalent, cathodic deposition, as bonding interface between Cu and polyethylene 80—76201
Cr pyrolytic coating, effect of support metal mech. props. on formation *(Russian)* 80—7713
Cr-SiO cermet thin films, thickness effect on density, resist., adhesion and annealing coeff. 77—69432
Cr_2O_3, RF sputtered coating for wear appls., on Inconel X-750 foil, prep. and props. 80—40605
Cu film, adhesion changes on 10 MeV electron irrad. *(Russian)* 77—43460
Cu film, evaporated, adhesion meas. 80—50822
Cu film, on amorphous C and Si substrates, dispersion force contrib. to adhesion *(French)* 80—59842
Cu, flux adhesion, and spreading coefficient 80—15379
Cu, metallic adhesion, use of fracture mechanics and contact resistance meas. 77—70271
Cu, on thermally oxidised Si, EM tensile adhesion test method 80—50804
Cu to Au, surface treatments and surface impurities 77—15701
Cu to polyethylene, reactions of CuO with Cu or polymer 79—39118
Cu/Cu single crystal, explosion clad bonding, TEM obs. 77—62763
Cu-Al_2O_3 composite coating, electrodeposited, exam. of particle-cathode adhesion during formation 79—33954
Cu-Ni(Ag)(Al), diffusion bonding 77—62687
Cu-to-glass adhesion 77—44386
Fe, Armco, friction in vac. at elevated temps. 80—55542
Fe, bonding of Al, growth of intermediate phases, effect of O and N impurities 78—27680
Fe laminates, superplastic bonding 80—25981
Fe, metallic adhesion, use of fracture mechanics and contact resistance meas. 77—70271
Fe, particle formation by evap., electron microscopy obs. of interaction processes 80—104053
Fe surfaces, effect of adsorbed atoms, AES study 80—39456
Fe-Al, diffusion bonding 77—62687
Fe-C (graphite), adhesion and wettability of graphite *(Russian)* 80—20008
Fe-Ni, exam. of mech. adhesion, with vitreous coating 79—20336
Fe-Ni-Cr-Al-Y, oxidation mechanism, Y addition effect on kinetics and oxide adherence 80—97623
GaO_xN_y films and multilayer systems, passivation of GaAs 80—11809
Ge films, adhesion to substrates, effect of Ar^+ ion irrad. 79—11047
MgO-Al_2O_3-SiO_2 glass/polysulphone adhesive failure, ISS and SIMS obs. 80—55626
Mo, siliconised, adhesive interaction with Nb and unprotected Mo 77—48569
MoS_2 film, adhesion to oxidised metal surfaces, XPS meas. 78—22972
$MoSi_2$ on Mo, coating by local heating 77—81335
NI dendrites on Al, CVD, selective solar photothermal absorber 78—52683
Na_2O; SiO_2, use as US transducer bond 79—83437
Nb film sputtered onto Cu substrate, microstruct. and supercond. props. 77—85370
Ni coatings on Al alloy substrates, adhesion strength, meas. using microindentation method 80—40640
Ni films, adhesion on graphite 80—80141
Ni, particle formation by evap., electron microscopy obs. of interaction processes 80—104053
Ni/ThO_2, adhesive energy, meas. techniques 80—50803
Ni-Al_2O_3, composite coating, electrodeposited, exam. of particle-cathode adhesion during formation 79—33954
Ni-Cr/ThO_2, adhesive energy, meas. techniques 80—50803
Ni-Cr-Co, Mo, Ti, Y and R alloying additions influence on oxidation *(Russian)* 80—40587
Ni-SiC coating adhesion to Al alloy, metal interdiffusion *(Russian)* 80—66697
Ni-W surfaces in contact, deform. and adhesion at very low loads 80—39457

adhesion continued
$NiCr_2O_4$, plasma-sprayed coatings, props. 77−59999
PLZT/TFPD thermal/flash protective lens assembly, polarised delamination investigation 80−78929
Pb, electrolytic refining, adhesion of anode slime on anode surface 78−44047
Pb film, deposition using low-energy ion beam, Rutherford backscatt. and TEM anal. 77−59699
Pb film, deposition using low-energy ion beam, Rutherford backscatt. and TEM anal. 77−70003
Pd membrane, sorption of H_2, adhesion and penetration probabilities, extreme values 80−101040
Pd-C (graphite), adhesion and wettability of graphite *(Russian)* 80−20008
Pd+MgO, reaction and bonding below MP of starting materials, obs. in TEM 77−21419
Pd+SiO_2, reaction and bonding, below MP of starting materials, obs. in TEM 77−21419
Pt-Au, thick film, adherence meas. and evaluation 80−50813
Pt-Au glass-bonded printed thick-film conductor, adherence fracture energy 77−9037
Pt-C (graphite), adhesion and wettability of graphite *(Russian)* 80−20008
Rh-C (graphite), adhesion and wettability of graphite *(Russian)* 80−20008
$SbS_xSe_{1-x}I$ layer elec. and ferroelec. props., mech. stress effects *(Russian)* 80−50279
Se film on brass, ESCA interface study 78−43269
Se-Ni-Mylar multilayered struct., interfacial bonding effect on adhesion, ESCA obs. 79−95274
Si surface, wetting by Pb, Sn, Ge in H_2+HCl 78−43210
Si, surface doped with metal impurities, water adhesion energy *(Russian)* 77−89620
Si, thermosprayed, bonding to glass ceramic 78−23848
Si_3N_4/Zr joint, solid state bonded, exam. of bond fracture strength 78−76826
Si_3N_4/Zr laminates, metal to ceramic joints, adherence props. 80−45386
SnO_2 coating, scratch resistance and suitability for glass artificial heart valves *(German)* 79−12028
Ta film sputtered onto Cu substrate, microstruct. and supercond. props. 77−85370
Ta_2O_5, anodic oxide film, adhesion, ductility and fracture, spectrophotometric thickness meas. and SEM obs. 79−99460
Ti, adhesional reactions with refractory metals 79−29280
Ti alloy, fretting wear, role of adhesion and delamination 78−35533
Ti ion planted coating on steel 77−70217
Ti metal-metal interface, adhesion energy, surface treatment and ion implantation effects 80−107660
Ti, of melted Al, Ga and In, 300 to 1200K *(Russian)* 77−15663
Ti-Cu, evaporated adhesion after electroplating 79−82475
TiB_2 coating, erosion rates under H^+ ion bombard., fusion reactor appls. 80−39179
TiC abrasion-resistant coatings, glow discharge assisted CVD 79−83392
TiC coating, erosion rates under H^+ ion bombard., fusion reactor appls. 80−39179
TiC coatings, RF sputtered, on 440-C steel, adherence, friction, and wear props. 79−47823
TiC reactively sputtered coatings on Ti-Al-V (6,4 wt.%), adherence, XPES and wear study 80−25565
TiC, TiVC, on steel, sputter deposited, adhesive quality 77−12531
TiC, vapour deposited coatings, elec. resist., mag. susceptibility and adhesion meas. 77−44395
TiC(N) overlay coating on stainless steel, Ti or Al, effect on physicomechanical and wear props. 80−40603
TiN, CVD growth in US field, effect on adherence and hardness 77−59696
VBe_{12} coating, erosion rates under H^+ ion bombard., fusion reactor appls. 80−39179
W fibre reinforced epoxy resin, strength of metal-polymer adhesive contact, time-temp. depend. 78−68753
W, plasma coating, thick, struct. and mech. props. 77−28716
WC, sputter deposited coatings, elec. resist., mag. susceptibility and adhesion meas. 77−44395
WC_x formation during pyrolysis of WCl_6 and toluene, coating props. 77−36682
WSi_2 on W, coating by local heating 77−81335
Zn coatings on steel, adhesion strength determination by centrifugal method 77−56149

adiabatic compression, plasma *see plasma heating*

adiabatic demagnetisation *see magnetic cooling*

adion *see adsorption*

administrative data processing
see also distributive data processing; educational administrative data processing; financial data processing; management information systems; manufacturing data processing; medical administrative data processing; word processing
BWR power plant, computerised core component accounting system shortens shuffling time 80−699
fissile material inventory and criticality control system, on-line, INMACS 79−89486
nuclear fuel accountability and control, use of novel data collection and processing techniques 79−85749

admittance, electric *see electric admittance*

admittance, electric, measurement *see electric admittance measurement*

ADP *see administrative data processing*

ADP (ammonium dihydrogen phosphate) *see ammonium compounds*

adsorbed layers
see also monolayers
acetic acid, on Cu (100), interaction with formic acid, EELS study 80−76120
acetonitrile, adsorbed on ZnO, IR spectrum species identification *(French)* 79−82967
acetonitrile, on MgO, IR and TPD study 80−70528
acetylene, adsorbed on type 13X zeolites, inelastic neutron scatt. 78−14584
acetylene, and deuterated derivative, adsorbed on Ag exchanged zeolite, inelastic neutron scatt. 78−6229
acetylene, chemisorbed on metal surfaces, geometric and electronic struct., UPS obs. and HF LCAO calc. 79−86988

adsorbed layers continued
acetylene, chemisorbed on Ni (111), ind. vibrs., high resolution electron energy-loss meas. 79−90877
acetylene, chemisorbed on W(100), geometry distortion 77−30919
acetylene, on transition metal, surface at.-mol. interaction, MO calc. 80−6623
acetylene, on W (111), vibr. states, EELS 77−66090
acetylene adsorbed on Fe containing segregated C, hydrogenation, C-1s XPS spectra obs. 80−84366
acetylene on Pt (111), nature of adsorption state, surface vibrs. meas. 77−76657
acetylene overlayers on Pt (111), surface, surface struct. and bonding, LEED analysis 77−85067
acoustic phonons, obs. method using Brillouin scatt. in adsorbed monolayers 80−59804
adatom, valence shell energy level shift *(French)* 78−67900
adatom binding site, UV photoemission intensity modulation, angle-resolved 79−47589
adatom elastic interactions due to substrate anisotropy and cluster size 78−43253
adatom geometry and chemisorption energy on simple metal 77−66093
adatom indirect interaction energy, separation distance depend. 79−42386
adatom indirect interaction on Si, Ge surfaces, theory 80−44696
adatom interaction with solid substrate, effect of mechanical stress on chem. pot. 80−10784
adatom laser stimulated migration and multiphoton excitation, relax. and reaction enhancement 79−39200
adatom monolayer, on model transition metal surface, densities of states, chemisorption effects 78−26769
adatom on transition metal surface, vibr. model using pair interactions 80−15357
adatom valence-level position variation on metal surface 80−88611
adatom-surface interaction potential, vibr. spectrum 80−103581
adsorbed film monolayer melting, dual symm. systems, periodic struct. *(Russian)* 80−107405
adsorbed layers, Maxwell Wagner and Debye processes, differentiation using temp. depend. of dielec. loss 79−28195
adsorbed monolayer parameter determ. by full current spectroscopy method *(Russian)* 80−70539
adsorbent effects on props., empirical relns. 78−6217
AES, chem. state effects, for water and simple organic cpds. 78−72687
AES, chemical-state effects 78−92566
Ag, on AgCl cryst., luminesc. fatigue 80−66281
albumin, adsorption on SiO_2 80−10777
algumin, on polystyrene, contact angle meas. 80−61508
alkali halide, on GaAs (110), adsorpt.-desorpt. processes and phase transitions 78−2361
alkali halides, on Ag photocathode, effect on work function 79−78824
alkali metal, on W (011) or Mo (011), disordering, LEED obs. *(Russian)* 77−89655
alkali metal chemisorbed layers, changes in work function due to charge transfer 78−18900
alkali metals, on metal substrates, electronic struct. 79−87139
alklylammonium ions, adsorpt. potential determ., at soln.-solid interface 79−56068
amino acid monolayers and ordered films on Cu, surface struct. LEED 78−38968
amino acid overlayers, on Ag, XPS and SIMS study 79−86986
amino acid overlayers, static SIMS exam. 79−83074
amino radical adsorbed on zeolite, extra coupling with ^{23}Na 77−7963
amorphous and ordered films on metal surface, electron state of adsorbed atoms *(Russian)* 79−51425
angle resolved photoemission, multiple scatt. approach 78−72693
anisotropic long range elastic interaction between adatoms 79−33185
anthracene, chemisorbed on Al_2O_3, radiative and nonradiative processes 79−36686
aromatic ring ompounds adsorbed on Al-AlO_x-Pb and Mg-MgO-Pb, inelastic electron tunnelling 79−59521
atom, on metal surface, appl. of Hellmann-Feynman theorem 79−95262
atom-surface 3-9 interaction, bound state vibr. spectrum 78−14615
atoms, electronic struct. and UPS, appl. to O on Ni 78−15281
atoms, surface band splitting, theory, with appl. to He/graphite 80−60058
atoms and molecules, photoelectron spectra, review 78−27372
atoms on metal surfaces diffusion parameters, binding energy and dipole moment 79−51422
atoms on metallic surface, SCF approx. of atomic ordering 77−7976
Auger electron spectroscopy 77−85851
autoionisation bands due to one-centre resonances in adsorbed layers, theory 80−59790
bacteria, attachment to solid surface, influence of substratum critical surface tension 79−79493
benzene, adsorbed at metal surface, obs. of vibrational modes 80−6649
benzene, adsorbed on porous vycor glass, adsorpt. spectrum 80−9615
benzene, adsorbed on silica, laser Raman spectra 77−3367
benzene, chemisorbed on Pd (100), angle-resolved photoemission symm. anal., polarisation depend. and lateral interactions 79−91568
benzene, chemisorption on (111) surface of Pt, LEED and Auger spectroscopy obs. 78−30823
benzene, deuterated and chemisorbed on glass, vibr. bands, Raman scatt. study 80−84737
benzene, on Al_2O_3, Raman spectroscopy study 80−65358
benzene, on graphite, diffusive motion on basal planes, neutron scatt. study 79−42385
benzene, on Pt(111), electronic energy losses 79−46931
benzene, Raman spectra using pulsed laser and gated detection 77−74529
benzene adsorbed on graphite, melting and orientation, NMR study 80−100403
benzene adsorbed on Pt(111) and Ni(111) surfaces, vibr. loss spectra 79−23838
benzene adsorbent mesopores, capillary evaporation and struct. 80−107614
benzene on graphitized C black, adsorbed layer mobility 78−6216
benzenes, on Cr, IR multiple refl. spectra recording via cuvette attached to spectrophotometer 78−298
bitransitions in molecule reorientation processes in adsorbed layers *(Russian)* 79−99416
bond geometry, determ. using photoemission 78−71951
bonding determ. by desorption methods 77−62746

adsorbed layers continued
Born-Green-Yvon eqn., two-dimensional, with anisotropic interac. 78—79882
Bose liquid, ground-state energy calc. 77—20157
bubble with adsorbed film, migration in Hele-Shaw cell, rel. to materials processing in space 79—28912
butadiene iron tricarbonyl, adsorbed on graphite, diffusion and melting, Mossbauer meas. 79—61270
butane, on graphite, struct. and dynamics, empirical interatomic pots. 79—99417
butane, on graphite, struct. and dynamics, neutron scatt. study 78—87870
butane on graphite, intramol. and surface vibr. modes, inelastic neutron scatt. obs. 77—72780
1-butene, on δ-Al_2O_3, isomerisation, IR study 80—76554
1-butene adsorption on delta alumina, microgravimetric-IR study 80—75432
butyl alcohol, pumping down curve, P(t), rel. to adsorption isotherm *(Japanese)* 80—52249
t-butyl cyanide, adsorbed on silica, laser Raman spectra 77—3367
capillary condensation theory, adsorbates liq. or gaseous props. 80—80028
carbon tetrachloride, adsorbed on silica, laser Raman spectrum 77—3367
carbonaceous surface contamination growth on ion bombard. 77—90229
β-casein, adsorpt. isotherm, at air-water and air-oil interfaces 79—79461
β-casein, adsorption kinetics, surface denaturation 79—79460
β-casein, molecular structure of adsorbed film 79—79462
catalytic reaction, high temp. IR obs. 78—88655
ceramic, compaction during pressing, green strength, effect of adsorbed layers *(German)* 78—6880
chain, structure, Monte-Carlo simulation *(Russian)* 77—19122
chemisorbed atoms, atomic and extra-atomic relax. and IR catastrophe in core spectra 77—48304
chemisorbed layers, electron beam damage, tunnelling spectra obs. 77—76672
chemisorbed on metal surface, optics by reflectance of p-polarised light 79—78706
chemisorbed phases, phase transitions 80—107656
chloroethylene, adsorbed on silica, laser Raman spectra 77—3367
chloroform, adsorbed on silica, laser Raman spectrum 77—3367
chlorophyll, electrochem. behaviour 78—31778
chlorophyll-a on aerosil, absorpt. spectra 78—53327
cholesterol, adsorbed monolayer on aerosil, IR spectra 78—15753
chondroitin-4-sulphate biopolymer, adsorption on adsorbed collagen 79—79459
clustering, bulk vapour pressure behaviour 79—4473
collagen biopolymer, on solid surfaces 79—79459
colloid particles with adsorbed polyelectrolyte, electrophoresis 79—47991
colloid stabilisation by polymers, excluded volume effects 77—60129
commensurate-incommensurate phase transitions on restricted substrate area 80—49513
commensurate-incommensurate transition and domain walls 80—107654
commensurate-incommensurate transitions, substrate defects effect 80—75437
condensed adsorption layers, effect on electrode reaction rates 80—93769
contamination layers, XPS meas. 78—31301
core level photoemission from adsorption layers, book contrib. 78—95673
core level spectra, correlation effects 78—68605
core level spectra of adsorbates, exactly soluble limits of model 78—80459
core level spectroscopy of adsorbed atoms, soluble relax. model 79—8226
core level spectroscopy of adsorbed atoms and molecules, surface relax. energies, theory 77—89830
core photoelectron spectra, shake up and relaxation effects 79—47595
core photoelectron spectra, shape 79—47596
core-level spectra spectral function calculation, time depend. approach 79—43096
correlation effects, s-d hybridization in substrate 80—107886
crystal growth from soln., thermodynamic formalism for adsorbed layers 77—76336
cyanide, on Ag, at electrolyte interface, enhanced Raman effect 79—28767
cyanogen adsorbed in Pt (100), UPS 77—36351
cyanopyridine, isomeric forms, adsorbed of Ag electrodes, Raman scatt., orientational specificity 79—69822
cyclohexane, adsorbed on silica, laser Raman spectra 77—3367
cyclohexane, thin crysts. and monolayers on Ag(111) surface, LEED 79—11014
cyclohexane on graphitized C black, adsorbed layer mobility 78—6216
deep level spectroscopy, many body effects 80—39441
density of states, impurity atom effects 80—92958
designed monolayers assemblies 79—37915
diatomic adsorbed on electrode, reson. Raman scatt. 79—51421
dibenztetrathiafulvalene, absorbed on Au, Al, ionisation and polarisation energies of mol., UPS meas. 78—79886
diffusion and capture of adatoms by clusters in film deposition 78—2385
diffusion and density fluctuations on solid surfaces 80—39452
diffusion on single cryst. surface 78—38969
diffusion on single crystal surfaces, influence of lateral interactions 78—38953
dimethyl ether, condensed multilayers, electron bombard. effects, AES line-shape anal., XPS, and desorption meas. 80—7450
1,1-diphenylethylene, adsorbed on porous Vycor glass, reson. Raman spectrum, surface species identification 78—42066
directional photoemission, book contrib. 78—95674
dislocation geometry 79—23604
disordered overlayers, diffuse LEED intensities, multiple scatt., theory 79—4476
disordering due to supercond. transition in metal substrate 80—50022
dye, adsorbed on ZnO electrode, sensitisation mechanism, from reson. Raman spectrum 78—42066
dye laser, on ZnO cryst., charge transfer 80—49815
dye molecules adsorbed on Ag, Au and Cu films, absorpt. and luminesc. study 80—103981
dye pair, chromophorically degenerate, adsorbed on AgBr, supersensitised photoconductance 79—61887
dynamics, neutron scatt. obs., book contrib. 77—89505
elastic interaction between adatoms near distortive phase transition 80—80080
elastic interaction of two adsorbed atoms 77—72791

adsorbed layers continued
elastic interactions between surface adatoms and between surface clusters 78—10283
electric double layer in electrochem. systems, dense part, model, adsorbed mols. 77—25282
electrochemical phase formation 80—55309
electrode, anisotropy of optical props. 80—60534
electrode-electrolyte interface, solid film props., review of expt. techniques 77—77780
electrolytic double layer, light absorpt., electrochromic changes 78—84551
electron binding energies reference level problem in photoelectron spectra of solids and adsorbates 78—63936
electron bombardment induced luminesc. and bremsstrahlung of adsorbed mols. on Ta (111) *(Russian)* 78—31290
electron density oscills. around adatom 79—87138
electron spectroscopies of adsorbed atoms, relax. shifts, satellites and sum rules 80—11539
electron spectroscopy of solid surface, quantitative, electron inelastic mean free path 79—92041
electron spectroscopy of surfaces, review 78—92169
electron state of adatoms at high coverages 79—28400
electron-impact vibr. excitation, specular selection rule 80—80051
electron-stimulated desorption ion imaging of adsorbate distrib. 80—103572
electronic state of adatom, depend. on conc. 78—72001
electronic states, adsorbate induced rel. to photoemission, book contrib. 78—95326
electronic states of adatom, correlation effects, self-consistent T-matrix calc. 80—44691
electronic transforms, near boundary separating mag. and nonmag. states 80—92961
ellipsometry applied to surface films and film growth 78—39619
enhanced Raman scattering by adsorbates on metals, including nonlocal metal response, nonradiative modes excitation 80—88994
epoxy films, in polished metal mirrors, refl.-absorpt. IR spectrosc. and ellipsometry obs. 79—78765
epoxy system, on Al_2O_3 inelastic electron tunnelling spectra 79—15952
ethane, on graphite, struct. and dynamics, empirical interatomic pots. 79—99417
ethanol, dissoc. adsorption on porous glass, IR obs. 79—23830
ethoxysilanes, on BK 7 glass, IR spectra *(German)* 78—30834
ethylene, adsorbed on Na zeolite, uniaxial rot., translational dynamics 78—91538
ethylene, chemisorbed on metal surfaces, geometric and electronic struct., UPS obs. and HF LCAO calc. 79—86988
ethylene, chemisorbed on W(100), geometry distortion 77—30919
ethylene, on Pt(111), electronic energy losses 79—46931
ethylene, on transition metal, surface at.-mol. interaction, MO calc. 80—6623
ethylene adsorbed on Ag, photon-induced field ionisation mass spectroscopy 80—6639
ethylene adsorbed on Ag exchanged zeolite, inelastic neutron scatt. 78—6229
ethylene-^{14}C, on Ni sheet, determ. by autoradiography method 77—63989
EXAFS for adsorbate-substrate characterisation 77—43430
face centred rectangular lattice gas model, ground state struct. 78—38936
fatty alcohol, oil-water interface adsorption, high-press. effect on phase transition 79—99395
fibrinogen, on polystyrene, contact angle meas. 80—61508
field emission from metallic substrate, effect of adsorption 78—35259
field emission through semiconductor and dielectric layers on metal 77—12501
film, on BCC cryst., modelling of order-disorder transition, Monte-Carlo method 78—60033
film, surface backscatt. phonon pulse time delay, heat-sensitive detector obs. 78—22927
fixed molecule high energy photoelectron ang. distribs. 78—39667
flavanthrene molecules, stationary stochastic adparticle flip-flop as a precursor to surface diffusion 80—15371
fluctuation in adsorbed phases 78—14573
formaldehyde, adsorbed on W(100) single cryst., XPS obs. of decomp. 77—4927
formic acid, on Cu (100) interaction with acetic acid, EELS study 80—76120
formic acid, on Ni surface, decomp., dipole interactions effects 80—61143
furan, adsorbed on NaCl, evidence of new condensed phase, IR spectra *(French)* 80—16028
gas, localised adsorption on patchwise heterogeneous surfaces, effect of local correl. between adsorbed mols. *(German)* 80—44432
gas, on solid adsorbents, thermodynamics *(Rumanian)* 80—10786
gas atom scattering by adsorbed layer, hard sphere theory *(Russian)* 79—38704
gas-solid processes, generalised Langevin theory, continuum elastic treatment of surface lattice dynamics 80—6612
gases on solid surfaces, mobile and localized adsorption, theory 80—65379
on graphite, time to formation of adsorbed molecular monolayers at contact spots during friction 77—43425
gravimetric measurement of sorption isotherms, errors 78—67905
ground state structure of adsorbates on square lattice net, 3rd neighbour interactions 78—26765
groups of sites used in statistical calculations, Bethe's method *(French)* 77—70334
growth kinetics under high adatom conc., surface diffusion parameters 77—28088
halogens, on Ni, effect on surface self-diffusion *(French)* 80—24723
heterogeneous systems, self-diffusion, NMR pulsed field gradient *(German)* 78—60341
1-hexene-water(-D_2O), field-induced surface reactions, field ionis. mass spectra obs. 78—95949
hydrocarbon molecules, strongly adsorbed, contamination rate reduction 79—1550
hydrocarbons, adsorbed on Ru(001), characterisation by electron-stimulated desorpt. 78—71958
hydrocarbons, short-chain, on small particles, appl. of neutron scatt. to struct. and dynamics study 79—4481

adsorbed layers continued

- hydrocarbons, substituted, monolayers on Pt (100) surface, AES quantitative anal., calibration 78−31724
- hydrocarbons chemisorbed on SiO_2-supported Ni, chem. composition *(German)* 79−92002
- ice, monolayer ledges on basal surfaces 77−35809
- incommensurate two-dimensional crystal, ground state, spectrum, phase diagram 79−19458
- indirect long-range oscillatory interaction between adsorbed atoms 78−71997
- inelastic electron tunnelling intensity, depend. on adsorbate conc. 79−68284
- inelastic scattering of slow electrons from adsorbed molecules 80−50485
- inert gas, LEED exam. 77−47306
- inert gas, Percus Yevick theory for gas to condensed phase transition 77−7968
- inert gas absorbate-substrate system, surface phonons, superstructures 77−15676
- inert gas atom adsorbed on graphite surface, excitation spectrum 78−71943
- inert gas atoms on alkali halide crystal, variation of adsorption heat 77−85049
- inert gas monolayers on graphite, nonregistered-registered phase transition 79−77894
- inert gases, on graphite, cleavage face, 2-dimens. condensation, crit. temps. 80−20032
- inert gases, on graphite solidified layer struct. and density *(French)* 78−18893
- insoluble monolayer, ionised, of surfactant, thermodynamic eqn. of state 79−8450
- instability of an adatom lattice, and fluctuations of the field emission current 79−15024
- interface total reflection and surface wave obs. 80−108292
- ion scattering from solid surface *(Japanese)* 80−50501
- IR ellipsometric spectroscopy 80−39434
- IR photoacoustic spectra in 4000 to 2000 cm^{-1} region using broadband source 79−26149
- IR photoacoustic spectroscopy of solids and surface species 80−90909
- IR spectroscopy, 200-800°C, vessel design 77−41704
- IR spectroscopy, reflection-absorption, of adsorbed layer systems, review, book contrib. 80−84747
- Ising model for monolayers of coadsorbed atoms, phase transitions 80−19909
- island films, diffusive mass transfer, review 80−20054
- isobutyl alcohol adsorpt. on Al_2O_3, gravimetry, IR investigs. 79−1546
- isoquinoline, adsorbed on Ag, surface enhanced Raman spectrum 80−100400
- isothermal desorption spectroscopy for 2-dimens. condensed phase obs. 77−69181
- Kapitza resistance, heat transfer rel. to adsorbed monolayer *(Russian)* 78−51758
- laser intracavity adsorption spectra of surface-active substances and aerosols *(Russian)* 79−57343
- laser stimulation of surface reactions by excitation of adsorbed molecules 77−56242
- lattice dynamics of disordered surfaces 79−60616
- lattice fluid model, real-space renormalisation group method 80−17882
- lecithin, adsorbed monolayer on aerosil, IR spectra 78−15753
- LEED beams, adlayer induced, near order-disorder transitions, Monte Carlo study 79−82438
- LEED examination of interaction of adsorbed atoms 78−95237
- LEED from disordered overlayer, model calc. 78−84074
- LEED studies of defect surface structs., review 77−80685
- LEP, electron positron storage ring, vac. chamber, glow discharge surface cleaning 80−58010
- Light emitted from molecules adsorbed on a metal surface 78−18907
- light metal atoms, raising of superconductor critical temp. *(Russian)* 78−84337
- light scattering by adsorbed molecule, classical theory 79−51944
- light scattering by adsorbed mols. located near solid surface 79−18247
- light scattering of adsorbed mol. near solid surface 79−56069
- long-range order in two dimensions 79−65307
- lysozyme, adsorpt. isotherm, at air-water and air-oil interfaces 79−79461
- lysozyme, adsorption kinetics, surface denaturation 79−79460
- lysozyme, molecular structure of adsorbed film 79−79462
- macromolecular, conform. and thermodynamics at liq./solid interface 77−11782
- macromolecules, energy of interaction between two spherical particles 78−53271
- medical polymers, chem. problems, conf., Prague, Czechoslovakia (Aug. 1977) 80−56996
- metal, modification of surfaces, effect on electrocatalysis, review 80−61110
- metal, on single crystal planes, kinetic investig. of structural changes and desorption, Au (111)/Bi^{3+} appl. 80−54500
- metal, positive secondary ion and sputtered atom energy distrib., surface contamination effect 77−32485
- metal adatom pair, on metal surface, effective interaction, from FIM expts. 78−22953
- metal on III-V semiconductor surfaces, adatom interactions, photoemission obs. 79−33898
- metal substrate, thin film form., appl. of AES and ESCA *(French)* 80−50903
- metal surface, adsorbed mole. low energy electron scatt., appl. to Ni-CO 79−56896
- metal surface, adsorbed molecules, inelastic scatt. of slow electrons 78−9916
- metal surface, influence of submonolayer films on props., calc. *(Russian)* 80−2273
- metal surface, single crystal with hexagonal symmetry, ordering of adatoms *(Russia)* 77−89653
- metal surface, with adsorbed at., XPS intrinsic plasmon satellites, dispersion and lifetime effects 79−56151
- metal-InP contacts, intermediate adsorbed layer effect on electronic props. 80−39674
- metal-solution interface with adsorbed molecules, enhanced light scatt. 79−82989
- metallic thin film, vacuum deposition, early stage obs. using microbalance technique and electron microscopy *(Japanese)* 80−54554
- metallic thin films, low adsorption coverage, microscopic calc. of elec. cond. 79−15236

adsorbed layers continued

- metals, oxide coated, environment-sensitive mechanical behaviour 77−32722
- methane, on graphite, orientational phases, Monte Carlo calc. 80−2263
- methane, on graphite, struct. and dynamics, neutron diffr. and inelastic scatt. 78−87869
- methane, submonolayer on graphite, two-dimens. fluid 79−37920
- methane adsorbed on γ-Al_2O_3, γ-radiolysis 80−3375
- methane adsorbed on graphite basal plane, first order melting transition, triple point 80−2269
- methane adsorbed submonolayer on graphite, structural transitions between epitaxially ordered phases 80−96740
- methane-d_4, adsorbed on graphon, neutron scatt. study 79−60640
- methane-d_4 monolayer films on graphite, neutron diffr. studies of phases 80−96739
- methanol, condensed multilayers, electron bombard. effects, AES lineshape anal., XPS, and desorption meas. 80−7450
- methanol, on graphite, proton mag. relax. times obs. 77−51590
- methanol on Ag (110) catalyst, oxidation 78−88556
- methyl alcohol, on silica, low temp. thermally stimulated depolarisation spectra fine struct. 79−78611
- methylpyridine adsorbed on Ag, surface enhanced Raman spectra 80−83376
- microscopic electronic theory 77−85112
- microsurfaces, obs. using thermal desorption spectroscopy combined with TEM and transmission electron diffr. 79−90888
- migrating adatom capture by point capture centres, for 2-dimens. substrate lattices 78−43236
- migration of adsorbed atoms on disordered surfaces, theory 80−54516
- mobile monolayer adsorption, critical props. of Bergmann's model *(German)* 78−84073
- mobile physically adsorbed layer, dynamics 79−95271
- mobility of adatom on metal surface, density functional approximation calc. 80−103577
- molecular chains, config. props. effect on surface coverage 79−42371
- molecular clusters adsorbed on conductor surfaces *(Russian)* 80−80078
- molecular complex, adsorbed on metal, charge transfer model of Raman intensity enhancement 79−13720
- molecular vibrations, inelastic scatt. of electrons, model for mols. on metal surface 78−34718
- molecule, angle-resolved and variable impact energy electron vibr. excitation spectroscopy 80−76119
- molecule, in electrochem. systems, Raman scattering 80−60563
- molecule above metal surface, damping of mechanism for excited state 78−92160
- molecule adsorbed on solid, NMR, paramag. relax. times *(Russian)* 77−39737
- molecule vibrational energy on metals, heterogeneous relax. 79−42362
- molecules, chemisorbed on metal surface, spectrosc., electron gas effects 80−54504
- molecules, EELS selection rule 80−49495
- molecules, on metal surface, hole recoil, vibrational shake-up and photoelectron lineshapes 80−55265
- molecules, on metallic surface, reson. Raman scatt. 79−45729
- molecules, Raman and fluoresc. enhancement by surface roughness 80−102511
- molecules adsorbed on electrode surfaces, Raman scatt. theory 79−13724
- molecules adsorbed on metals, low energy electron inelastic scatt. exam. 79−46526
- molecules on metal surface, vibr. excitation due to electron impact 79−46912
- molecules on size-quantising film, pulsed inversion 79−90889
- monocarboxylic acids, chemisorbed on Al_2O_3, tunnelling spectroscopy 78−91545
- monolayer of patches covered by mobile and localised adsorbed mols. 78−72004
- monolayer on graphite, neutron scatt. studies 80−107655
- monolayers, intrinsic defects, deep potential relief surface *(Russian)* 79−99415
- monolayers, Lennard-Jones system, melting in external field 80−65362
- monolayers, neutron scatt. meas. 79−65306
- monolayers, nonregistered, lateral compression effects calc. 80−6641
- monolayers, order, disorder transitions, classification and characterisation, review 80−52149
- monolayers, oriented phase transitions *(Russian)* 78−75936
- monolayers, oriented second order phase transitions *(Russian)* 79−65315
- Monte Carlo studies, surface physics appl., book contrib. 79−82426
- multicomponent gas and liquid mixtures, adsorption heterogeneous solid surfaces *(German)* 80−44430
- multicritical phenomena at surfaces 77−32208
- multilayer adsorbed films, mol. theory 80−80058
- multiple layer adsorption, on foreign substrate, surface roughness and surface free energy variation 77−24497
- multiple overlayers, effect on ellipsometric parameters 77−32457
- naphthalene, chemisorbed on Al_2O_3, radiative and nonradiative processes 79−36686
- neopentane-d_{12}, adsorbed on TiO_2, neutron scatt. study 79−60640
- neutral atoms, on metal surfaces, excitation spectrum 79−23832
- neutral molecules adsorbed on dielec. surface, excitation spectrum 78−71943
- neutron diffraction and inelastic scatt. from adsorbed mols. 78−87869
- Ni, adsorption residual C removal by electron beam irrad. and heat treatment *(Chinese)* 80−88421
- nitrilotri (methylenephosphonic acid), adsorption on $BaSO_4$ crystals, effect on crystal growth 78−88417
- p-nitroaniline, adsorbed layer, core ionisation, negative shake-up energy 79−56913
- NMR, effect of migration between physical and chem. absorpt. sites 77−21422
- nonequilibrium frontal ion adsorption dynamics in a long bed when the double layer is taken into account 79−69349
- nonpolar molecules, adsorbed on metal surface, depolarisation interaction 78−51820
- nonuniform charge distribution, phase transitions, Hartree-Fock calcs. 80−54525
- octane-water interface, water photo-oxidation in presence of adsorbed porphyrins 78−64933
- one-dimensional incommensurate structures at finite temperatures 80−103567

adsorbed layers continued
- one-dimensional model crysts., surface density of states, rel. to adsorbed molecule 80—107889
- order-disorder transition, effect on work function 80—59791
- order-disorder transition, Ising model, LEED superlattice beam intensity distrib. 80—65371
- order-disorder transition classification, realisation of four-state Potts model 77—51605
- ordered adlayers, density of surface states, Green's function calc. method 77—85291
- ordered adlayers, electronic struct. 79—38142
- ordered overlayers, chemisorption energy, multiadatom effects 78—14581
- ordered overlayers, on FCC metal surface, electronic struct. calcs. 79—60906
- organic compound, two-dimensional condensation with adsorbed mol. reorient. 78—61051
- organic molecules, Si-SiO_2 interface as electrode for electrical and ellipsometric meas. 80—15366
- organic solvent, on Si surface *(Russian)* 78—91537
- organic surfactant molecules reorientation on electrode surface, electrochem. kinetics 80—45522
- oriented molecules, inelastic low energy electron scatt. 78—72653
- oriented overgrowths, pairwise interaction approach 77—62759
- oscillatory indirect interaction between adsorbed atoms, non-asymptotic behaviour in tight-binding models 78—72000
- phase transformations, approx. law of corresponding states 77—59209
- phase transition, λ, elementary approx. statistical-mech. treatment 80—6627
- phase transitions, in systems with competing interactions 78—14963
- phase transitions, review 80—44433
- phase transitions in adsorbed films on transition refractory metals 77—51606
- phenanthrene, chemisorbed on Al_2O_3, radiative and nonradiative processes 79—36686
- phenol, adsorbed layer, inelastic electron tunnelling spectral lineshapes below 100 mK 78—31000
- phosphor adsorbates, luminesc. quenching, activator location effects 77—52172
- phosphor-silica gel substrate, oxygen quenching anomaly of afterglow 77—77275
- phosphorescence experiments using adsorbed dyes 77—26114
- photoelectron angular distrib. from cryst. field split adatom levels 77—63533
- photoelectron core level spectra calc. 77—85896
- photoelectron diffr. aximuthal patterns, struct. sensitivity 80—107644
- photoelectron line shapes, vibr. excitation and hole delocalisation effects 79—95905
- photoelectron spectra, collective effects, relax. and localisation of hole levels 80—52950
- photoelectron spectra, line shapes and relaxation effects 79—69956
- photoelectron spectra, review 79—52072
- photoelectron spectroscopy, adsorption geometry and surface crystallography *(French)* 80—50519
- photoemission, adsorbate induced, book contrib. 78—95668
- photoemission, ang.-resolved, independent atomic centre approx. 78—84701
- photoemission, angle-resolved, from adsorbates, book contrib. 78—95669
- photoemission from adsorbed molecules, atomic dipole theory 78—84695
- photoemission from clean and adsorbate covered single cryst., appl. of simple selection rules 79—33896
- photoexcitation theory rel. to angle-resolved UPS and surface EXAFS 80—39426
- phthalocyanine monolayers and vapour-grown films, surface struct., LEED 77—35830
- physisorbed atoms on metallic surfaces, atomic size effect on polarisability 78—43242
- physisorbed layer on elastic substrate, commensurate-incommensurate phase transition 79—56074
- pinacyanol dye, adsorbed on CdS substrate, aggregation effect on mol. electronic states 80—37757
- pinacyanol sensitizer adsorbed on CdS, spectral sensitization at low surface density 79—47973
- plasmon mediated interaction between physically adsorbed atoms in presence of metallic surface 78—71991
- polar solvent molecule interactions in the adsorbed state 80—21299
- polarisation energy from opt. data 77—72792
- polyacetylene, polymerisation and Raman spectra on zeolite and alumina surfaces 79—13721
- polyimide, adsorption modification of surface of macroporous SiO_2 80—6624
- polymer, conformation, excluded vol. effects 78—2372
- polymer, on particles in suspension, thickness meas. by mag. birefringence 80—42191
- polymer chain in restricted environment, Monte Carlo simulation 77—46663
- polymer chains, surface restricted self avoiding walks span, mol. weight depend. 80—65360
- polymer film, in adhesive joint contact layer, intermol. interaction with substrate and filler *(German)* 79—8421
- polymer flexible lattice chain in limited vol., behaviour *(Russian)* 78—70992
- polymers, adsorbed, excluded vol. effects, Monte Carlo investigation 79—95259
- polymers, adsorbed molecules, configurational behaviour, computerised dynamic display 79—874
- polymers, hydrodynamic thickness, Navier-Stokes eqn. calcs. 77—65726
- porous solid with below-freezing pt. adsorbate, isothermal adsorption and dimensional changes obs. 78—75925
- porous texture, determ., anal. of adsorption isotherms 79—77897
- on powder minerals, influence on mech. props. 77—25084
- propane, on graphite, struct. and dynamics, empirical interatomic pots. 79—99417
- propiolic acid, in thin film tunnel junctions, hydrogenation and deuteration, IETS obs. 80—45547
- protein adsorbed layers on field-emitter tips, removal by UV radiation 80—104836
- proteins at interfaces, fluoresc. spectroscopy study 80—12315
- pseudopotential of adparticle on substrate near second-order phase transition 80—80065
- PVA adsorbed on polystyrene latex particles, flocculation and stabilisation, concentration effects 80—45569

adsorbed layers continued
- pyrazine, on Ni (111), UV spectroscopic ellipsometry obs. 79—86997
- pyridine, adsorbed on Ag, 210-243 cm^{-1} mode in surface enhanced Raman scatt. 80—89003
- pyridine, adsorbed on Ag electrodes, ang. resolved Raman spectra 80—16017
- pyridine, on Ag, Ramam intensity enhancement by surface plasmons 80—7334
- pyridine, on Ag (100), (111) and polycryst. electrode surfaces intense Raman spectra 78—72492
- pyridine, on Ag electrode with graphic C overlayer, Raman spectra obs. 80—103954
- pyridine, on Ag surface, enhanced Raman scatt., ultrahigh vac. study 80—88993
- pyridine, on Ag surface, Raman active librational modes 80—65359
- pyridine, on Au substrate with Ag monolayer, giant Raman effect 80—63637
- pyridine, on Cu(Au) electrode, angle-resolved Raman spectroscopy 80—52991
- pyridine adsorbed on Ag, reson. Raman scatt. 80—25380
- pyridine adsorbed on Cu (110) surface, photoemission selection rules 80—100751
- pyridine adsorbed onto roughened Ag electrode, Raman band intensity 78—48160
- pyridine-d_5, physisorbed thin film on Ag surface, enhanced Raman scatt. study 80—20620
- Raman scattering, molecules absorbed on bumpy metal surface 79—15448
- Raman scattering by adsorbed molecules on metal surface, intensity enhancement, theory 80—54518
- Raman scattering from molecules adsorbed on metal surfaces, enhancement, theory 79—99882
- Raman scattering from molecules adsorbed on metal surfaces 80—65374
- Raman scattering from oriented molecules, angle resolved, group theory 79—47425
- Raman spectra of adsorbed molecules, theory 79—37922
- rare gas (111) adsorbate-substrate systems, thermal expansion and stability, soft phonons 79—69352
- rare gas adsorbates on simple metals, optical excitation, configurational switching, charge transfer 80—107643
- rare gas monolayers, order-disorder phase transforms., CDW and mass density waves 80—39281
- rhodamine 6G and rhodamine B adsorbed on AlH_3, luminesc. spectra during AlH_3 photolysis 80—55171
- rhodamine 6Zh, on stilbene mol. cryst., role of excitonic and radiative mechs. of energy transport 80—108276
- rhodamine B, on Ag electrode, anisotropy of optical props. 80—60534
- rhodamine B adsorbed on anthracene, electron-hole pair in external elec. field 79—73558
- rhodamine B adsorbed on NaCl, photoelectric meas. and contact charging 79—19643
- rhodamine B dye, on PbO powder layers, charge storage and photocond. 78—64056
- rigid rodlike molecules adsorption onto planar surface, dispersion interactions, statistical mech. anal. 80—29265
- rose bengal, adsorbed on ZnO electrode, reson. Raman spectra 78—76446
- rotating disk, in liquid surface with adsorbed film, torque 78—32685
- salts, field ion emission, field desorption and ionic cond. 77—16473
- SC Cr, on W (011) or Mo (011), disordering, LEED obs. *(Russian)* 77—89655
- semiconductor, positive secondary ion and sputtered atom energy distrib., contamination effect 77—32485
- semiconductor interface and overlayer electronic struct., review 80—49841
- semiconductor sensitised photolysis and latent image structure 79—24768
- on semiconductor surface, H recomb., nonequilib. charge carrier generation *(Russian)* 79—91126
- semiconductor/adsorbate system, local density of states calcs. *(German)* 80—60062
- serum albumen, bovine, adsorption kinetics, surface denaturation 79—79460
- serum albumin, bovine, adsorpt. isotherm, at air-water and air-oil interfaces 79—79461
- serum albumin, bovine, molecular structure of adsorbed film 79—79462
- shapes of islands of chemisorbed atoms as probe of long-range interadatom interactions 79—65320
- solid surface, mol. dynamic processes interaction with laser radiation 80—71943
- solution film adsorbed on cryst. surface, NMR investig. 77—8426
- solvents adsorbed on insulating substrate, ionic conduction 79—33180
- specific heat of adsorbed gases, cryostat design 79—58695
- spreading pressure, direct meas. 77—15692
- spreading pressure 78—38971
- spreading pressure of adsorbed film 79—73408
- sputtering by low energy ions 77—62758
- stainless steel surface, low energy ion scatt. of adsorbed layers *(Japanese)* 77—1774
- STEM use for two-dimensional molecular assemblies construction 78—24201
- stepped substrate-adsorbed layer interaction, selective effect on epitaxy 78—14616
- sticking of adsorbates, electron-hole mech., soluble model 80—49512
- stilbene:rhodamine-6Zh, luminesc. of adsorbed mols., excitonic energy transfer to surface 78—31255
- structural and electron alterations, electron-phonon interaction effects *(Russian)* 78—87880
- structural and electronic reconstructions in adsorbed layer on metal surface 78—84280
- submonolayer films on metallic surface, struct. and props. review 78—38972
- substrate-adparticle system, phonon instabilities 79—90861
- superelastic electron scattering *(French)* 78—56039
- surface atomic and electronic struct. studied with synchrotron radiation 80—80945
- surface defects and thermodynamics of chemisorbed layers 80—80068
- surface diffusion calcs. 80—107633
- surface diffusion of adatoms and clusters, mol. dynamics simulation 79—99411
- surface diffusion of adsorbed species 80—80070
- surface diffusion on solids, model 78—6214

adsorbed layers continued
surface diffusion on transition metals, pair potential calcs. 80—39446
surface electron states, effects of isolated adatoms 77—85294
surface electronic props., effect of isolated adsorbed atoms 79—60905
surface electronic struct. and UV photoemission 77—62975
surface enhanced Raman scatt. on rough metal surfaces 80—93307
surface enhanced Raman scattering surface plasmon model 80—108211
surface enhanced Raman spectra, image dipole description, critical review 80—87125
surface EXAFS study of adsorbate Auger electron intensity on single cryst. surfaces 78—66562
surface film phase transitions, conf., Erice, Sicily, Italy (Jun. 1979) 80—105429
surface films, thermodynamics of Volta effect 77—51604
surface phonons and superstructures 77—62731
surface plasmon effects on satellites in XPS 79—61493
surface plasmon enhanced light absorption by adsorbed molecules 80—40176
surface properties variational calcs., binding energy, Lang model 80—29279
surface reactions, dipole interactions effects 80—61143
surface structure and dynamics, neutron scatt. studies, review 79—60639
surface structure of solids and adsorbates by LEED 78—94953
surface tension and spreading press. for mobile and registered layers 78—38960
surfactant adsorption on metal surface, effect on electrochem. reaction kinetics 80—40703
tetrafluoromethane adsorbed on graphite, adsorption isotherms, crit. temps. *(French)* 80—34312
tetramethylethylene, adsorbed on silica, laser Raman spectra 77—3367
tetramethyltin, on graphite, nature of 2 D diffusion 80—84372
thermal desorption and conversion kinetics, AES study 78—71959
thermodynamic relations of Pippard's type for dielectric and magnetic properties of adsorbed layers near a λ-transition 78—79881
thermodynamic theory of clustering and percolation transitions 77—47697
transition metal, 5d, dipole moments of single adatoms on W (110) 77—47674
transition metal, on transition metal surface, interaction between adatom and substitutional impurity atom 79—56076
transition metal adatoms, on transition metal, tight-binding theory of interactions 77—1304
triangular Ising model, phase diagram 78—10631
tribenzylmethylammonium sulphate, condensed adsorbed layer, effect on electrode reaction rate 80—93769
trimethyl tin chloride adsorbed on grafoil, Mossbauer study 80—80643
triphenyl tin chloride adsorbed on grafoil, Mossbauer study 80—80643
trypaflavine, on silica gel, luminesc. quenching, activator location effects 77—52172
two dimensional incommensurate crystal theory, thermodynamics *(Russian)* 80—49524
two-dimensional order-disorder phenomena, Monte Carlo simulation 78—67904
two-dimensional phase transitions, review 80—39419
two-dimensional system, monolayers, permeation and evaporation resistance, attractive forces effects 78—67892
UPS, angle-resolved, initial state symmetries from polarisation effects 80—40227
valence photoemission from adsorbates, book contrib. 78—95672
Van der Waals film adsorbed on graphite, two-dimensional phase transitions 80—107653
van der Waals interaction between molecules, spatial dispersion effects 77—79672
vibration of adsorbed molecules, effect on electron capture by deep centers 80—29458
vibrational frequencies of chemisorbed molecule rel. to interaction with surface 80—54519
vibrational modes, surface atom freq. spectrum, mean correl. displacements *(French)* 78—2206
vibrational normal modes obs. by neutron scatt. 79—19443
vibrations, large-angle inelastic electron scatt., theory 80—75427
water, adsorbed in monolayer hydrate of halloysite, NMR obs. of mol. motion 78—95226
water, adsorbed multilayers on quartz, surface forces 80—6597
water, adsorption on SiO_2, neutron scatt. study 79—60643
water, chemisorbed on Pt (111), EELS spectra, vibr. freqs. 80—80920
water, condensed multilayers, electron bombard. effects, AES line-shape anal., XPS, and desorption meas. 80—7450
water, detection of OH groups for adsorption centres in plant tissues, dielectric relaxation *(Japanese)* 80—7999
water, effect on epitaxy of polycyclic aromatic quinone on alkali halides 79—28239
water, on Al_2O_3, Raman spectroscopy study 80—65358
water, on cellulose, NMR relaxation times 79—78552
water, on NaCl surface, absorpt. and thickness meas. 80—16001
water, on porous glass, proton spin-lattice relax. meas. by pulse NMR 78—84053
water, on Pt(100), bonding, electron energy loss spectra 80—34311
water, on silica, low temp. thermally stimulated depolarisation spectra fine struct. 79—78611
water, on $ZnSO_4.7H_2O$, meas. of water physically adsorbed rel. to water of crystallisation *(Japanese)* 80—6622
water, polymolecular adsorbed layer on quartz surface, IR absorption spectra 80—9595
water adsorbed on AnSe ATR plate, absorpt. coeff. meas. of NaF coating 80—35000
water adsorbed on CaF_2, internal reflection spectroscopy 79—15549
water adsorbed on cellulose, mech. relaxation at low temps. 77—43277
water adsorbed on IR optical material, evaporation rel. to surface breakdown 80—35020
water molecules, interaction with surface hydroxyls, IR spectra 78—43244
water on IR optical elements, effect on laser breakdown threshold 77—79886
water-liquid system, solid-adsorbed, dispersion medium density changes 77—9137
wetting film and capillary layer, transition layer 79—23807
work function, local, surface with adsorbed atom islands 80—7462
XPS, core ionisation, negative shake-up energy 80—100749
XPS, line shapes and multiple lines 78—84702
XPS, many-body effects 80—55266

adsorbed layers continued
XPS, plasmon effects on core level spectra 78—60547
XPS, plasmon versus shake-up satellites 78—48286
XPS, solid-state and adsorbate shifts, equivalent cores calc. 79—28888
$^{15}N_2$ monolayer, on Grafoil, reson. photon scatt. 80—34832
Ag monolayer on (111)Si surface, Schottky barrier, interface electronic nature and epitaxy 79—77934
Ag, on AgCl cryst., luminesc. fatigue 80—66281
Ag, on Si (111), electronic and cryst. struct., Schottky barrier form. obs. 78—84091
Ag-electrolyte interface, enhanced Raman scatt. of adsorbed molecules, background continuum obs. 79—73926
AgBr emulsion grains, adsorbed dyes, light-induced ESR spectra 80—88862
Al, on Si (111), theoretical study 78—95366
Al-adsorbed monolayer-Al junction, elec. cond. mech. 78—95386
Ar adsorbed on graphite, nonregistered-registered phase transition 80—39414
Ar, determ. of porous texture of solids 79—77897
Ar film, phase transition phenomena 77—62741
Ar, monolayer adsorbed on graphite, lattice dynamics 78—75946
Ar monolayer adsorbed on graphite basal planes, heat capacity 80—6636
Ar, on Ag, Auger spectrum film thickness depend. 77—8691
Ar, on Al, differential refl. spectroscopy, local field effect 80—80811
Ar on $CdCl_2$ cleavage face, two-dimens. condensation of second adlayer 79—99413
Ar, on graphite, adsorption of first layer, 55 to 62K 79—28197
Ar, on graphite, multilayer adsorbed films, mol. theory 80—80058
Ar, on metal, polarisation due to short range interaction with substrate 80—39428
Ar, two-dimensional structs., modified cell theory 80—20033
Ar-N_2 liquid soln., selective adsorption on graphite, struct. study, mol. dynamics calc. 80—59806
^{36}Ar, on MnI_2 and PbI_2 cleavage faces, layer-like charact., neutron diffr. obs. 79—86994
As, model for autodoping mech. in Si epitaxial growth 80—7505
Au, adsorbed on W (100), electron field emission revealing unmasked surface reson. 79—15595
Au, on AgBr dispersion in gelatin, transient absorpt. spectra, latent image form. and decay 80—66837
Au, on Pt, adatom surface diffusion energies, Lennard-Jones pair pot. calcs. 79—77923
Au, on Si (111), 2-dimens. condensed phase obs. by isothermal desorption spectroscopy 77—69181
Au, on W field emitter, (110) and (211) planes, effect on work function 77—12503
Au overlayers on GaSb surfaces, adatom interactions, photoemission obs. 79—33898
Au, surface comp. anal., by ion-forwarded electron spectra 77—31850
Au, surface diffusion on W, spreading behaviour 79—99421
Au+Ag adsorbed layers on Si, dispersed struct. formation 78—22952
Ba adsorbed layer on Mo (011), surface diffusion *(Russian)* 80—6658
Ba, on 4d or 5d metal, work function, O_2 coadsorpt. effects, thermionic emission obs. 78—11064
Ba, on Ir (111), thermionic emission obs. 77—85881
Ba, on W, Auger and work function meas., impregnated W cathode model 79—43073
Ba-O system, on W, Auger and work function meas., impregnated W cathode model 79—43073
BaO, multilayer and monolayer, on W substrate, AES and work function meas. 77—24921
BaO, on Si photofield cathode, work function and emission props. *(Russian)* 78—68608
Be adsorbed layers on W(110) and (100), work function and loss spectra meas. 80—6638
Bi, evaporated on W, work function obs. by field emission method 78—6834
Bi^{3+} monolayers on Ag(111), two-dimens. phase formation, desorption obs. 77—15680
Bi_2S_3, evaporated on W, work function obs. by field emission method 78—6834
Br, on Au(100), EELS Obs. 80—50483
Br on Pt(111), $M_{2,3}M_{4,5}V$ and $M_{4,5}VV$ Auger spectra 79—69926
Br, on Si single cryst., X-ray standing waves obs. at cryst. surface 80—96417
Br_2, adsorbed layer on zeolites, Raman spectra, aromatic bromination catalysis 80—3408
Br_2 adsorbed on Grafoil, EXAFS investig. 77—51602
Br_2, chemisorbed on zeolites, Raman spectra 80—93301
Br_2 chemisorption on V, layer struct., Na adsorption effects 80—101039
Br_2, on Au electrode, anisotropy of optical props. 80—60534
Br_2 on graphite, EXAFS 77—43430
Br_2-graphite systems, adsorbed and intercalated, EXAFS 78—72638
C 1s contaminant buildup on conductors (insulators) in X-ray ESCA 78—95981
C adsorbed on Ni, coadsorption of Pb or Sn, AES study 80—54521
C adsorbed on Ni (100), LEED struct. anal., substrate distortion 80—6637
C, dissolution into (110) face of Ni, 600-913K 80—49504
C electrode breakdown voltage dependence on adsorbed gases 78—75465
C layers on W, Auger signal intensity in differential and energy distrib. mode spectra 79—78799
C, on Fe(100), adsorbate coverage determ. by LEED, AES and XPS 80—103566
C on Ir and Pt substrates, effects on NaCl mol. beam condensation 77—66593
C, on Mo (110), oxidation, electron diffr., contact pot. difference, and AES obs. *(Russian)* 79—52430
C, on Ni surface, location of adsorbed atoms, surface channelling meas. 80—84373
C, on Pt, determ. of monolayer coverage by AES 79—46916
C, on Pt, stability and struct. of high Miller index forces in vacuum and with adsorbed C and O 77—76651
C, on W FEM tips, adsorbed layer conc. using nucl. microanal. *(French)* 80—29860
C^+, on metal surface, removal by Ar^+ impact, 20-30 keV, in plasma 77—76103
CC LaB_6, adsorption on Ta, work function 80—20039
CD_4, on PbI_2 cleavage faces, layer-like charact., neutron diffr. obs. 79—86994
CN^-, on Ag, bonding exam. by electrorefl. 77—80700

adsorbed layers continued
CN$^-$, on Ag surface, Raman active librational modes 80—65359
CO adlayers, on Cu(100) and Cu(111), struct., LEED pattern reinterpretation 79—28209
CO, adsorbed, lateral interactions on vibr. spectrum 79—46954
CO, adsorbed c(2×2) layer on Ni, Cu(001), struct. 80—88428
CO, adsorbed layer, electron impact, electron impulsive ionisation spectroscopy obs. 80—60720
CO adsorbed on Ag, Au films, enhanced Raman scatt. mechanism in ultrahigh vacuum 80—107645
CO adsorbed on clean metal surfaces, sputtering effects, combined analytical techniques 80—35047
CO, adsorbed on Cu film, optical constants 79—78645
CO adsorbed on graphite, fluid-registered solid transition 80—59796
CO, adsorbed on jellium, surface plasmon relax. energies 80—70537
CO, adsorbed on metal surface, collective vibr. modes, dipole interactions 78—50533
CO adsorbed on Ni, energy depend. of vibr. excitation, electron energy loss spectra 79—28201
CO adsorbed on Ni, valence band photoemission, SCF MO CNDO calc. 80—100754
CO adsorbed on Ni (100), UPS study 79—76473
CO, adsorbed on Ni and Cu(100) surfaces, LEED study of c(2×2) struct. 79—86983
CO, adsorbed on Ni(Pt), intermediate UPS/XPS synchrotron radiation study 78—52633
CO adsorbed on Pd surface, Penning ionisation by metastable He beam, theory 80—60735
CO, adsorbed on Pt, adsorbate induced electron losses 79—46959
CO, adsorbed on Pt (111), oxidation process, reflection-absorpt. IR study 78—76468
CO, adsorbed on Rh/Al_2O_3 catalyst, interaction with NO, IR study 79—70369
CO adsorbed on stepped Ni surface, vibrs. from electron energy loss spectra 79—73406
CO adsorbed on transition metal zeolite, ^{13}C NMR study 79—52751
CO adsorbed on W, electron-stimulated ion desorption 80—59797
CO adsorbed on W, electron-stimulated desorption, photoemission, relax. energy 80—100401
CO adsorbed on W(100), electron and photon-stimulated desorption 79—99414
CO, adsorption sites on Pt (111), surface vibr. modes, electron energy loss meas. 77—43422
CO adsorption state on W, FEM obs. *(Japanese)* 77—62738
CO, an alkaline earth oxide, reflectance spectra 79—28781
CO and NO, coadsorbed on Ru(001), adsite symmetry by electron energy loss 79—99412
CO, c(2×2) on Ni (001), surface geometry determ. by deep-core-level XPS 80—40224
CO, c(2×2) on Ni (100), photoemission orientation determ. 79—19974
CO, c(2×2) on Ni(001), struct. by LEED, self-consistent scatt. pot. 80—70536
CO, catalytic oxidation on ferrites, IR spectrosc. investig. 80—89524
CO, chemisorbed, CNDO calcs. of mol. struct. *(German)* 79—96368
CO, chemisorbed layer on Au(Pt), mag. phase transition obs. *(Russian)* 77—77083
CO, chemisorbed monolayer on Pt or Au, mag. phase transition, thermomagnetic study *(Russian)* 80—34319
CO, chemisorbed on Al_2O_3-supported Rh-Cu catalysts, IR spectra *(French)* 80—60559
CO, chemisorbed on alumina-supported transition metals, inelastic electron tunnelling spectra 77—31871
CO chemisorbed on Fe, low energy vibr. modes studied by tunnelling spectroscopy 80—78590
CO, chemisorbed on Ni (100) struct., dynamical LEED expts. 78—34710
CO, chemisorbed on Ni (111), bond energies 80—100398
CO, chemisorbed on Ni(100)p(2×2)O surface and Ni(100)c(2×2)O surface, struct. and vibrs. 78—2375
CO, chemisorbed on Ni(111), vibr. spectra from electron energy loss spectra *(French)* 78—22951
CO, chemisorbed on Ni{001} surface, LEED study of mol. orientation in c(2×2) struct. 79—86982
CO chemisorbed on Pt, IR refl.-absorpt. spectra, absorbate island struct. 80—84385
CO, chemisorbed on Rh (111), dissociation probability, isotopic exchange and AES meas. 80—40743
CO chemisorption on Pd, Ag, PdAg, SIMS, XPS study 80—84382
CO, coadsorbed with O and Rh, desorption spectra, Langmuir-Hinshelwood reaction anal. 79—47965
CO, condensed film, UPS linewidths 78—31294
CO, determ. of porous texture of solids 79—77897
CO molecular adsorbed on Mo (110) surface, electronic states, photoemission spectra 80—65363
CO, on Ag films, Raman scatt. study 79—78672
CO, on $BaTiO_{3-x}$, Auger spectroscopy of surface layers 79—42343
CO, on Cu (100), vibr. excitations and struct., EELS and LEED study 80—39437
CO, on Cu (100), vibr. excitation cross-sections 80—75441
CO, on Cu surface, cluster calc. using SCF-Xα-scatt. wave method 77—62742
CO, on metals, ion impact desorption, adsorption energy depend. 80—39442
CO, on metals, valence photoemission book contrib. 78—95672
CO, on Mo (100), surface kinetics, photoemission study method 80—80941
CO, on Ni, core level spectrum, satellite struct., ab initio HF-LCAO calc. 80—40233
CO, on Ni, high press., low temp. Raman spectra 78—6219
CO, on Ni, laser-induced desorption expts. 79—1548
CO, on Ni (001), angle-resolved polarisation-dependent photoemission, adsorbate orientation 77—4716
CO, on Ni (100), adsorbate vibr. EELS, large-ang. defl. 80—44405
CO, on Ni (100), EELS and concomitant surface anal. 80—7453
CO, on Ni (100), freq. and amplitude of localised vibrs., cluster calc. 80—6616
CO, on Ni (100), surface struct., LEED meas. 80—6647
CO on Ni (100) electron energy-loss spectra 79—47570
CO, on Ni (110), dissociation 77—31875
CO, on Ni (110), molecular desorption anal. 77—31874

adsorbed layers continued
CO, on Ni (111), isothermal desorption, UPS study, time-resolved approach 80—39440
CO, on Ni (111) surface, angle-resolved photoemission meas. 77—16463
CO, on Ni (111) surface, Raman spectra 79—28769
CO, on Ni and Pd, obs. using thermal desorpt. spectroscopy combined with TEM and transmission electron diffr. 79—90888
CO, on Ni(001), orbital energy spectrum 78—2369
CO, on Ni(100) surface, angle resolved UV photoemission 78—56570
CO, on Pd, photoelectron spectra, 40-180 eV, adsorbate sensitivity enhancement 78—80453
CO, on Pd (100), geometrical struct., LEED and high-resolution EELS study 80—20037
CO, on Pd (100), lateral interactions, effect on work function, UPS, and IR spectra 79—77904
CO on Pd (111) surface, metastable He impact, electron emission, energy and ang. distrib. 80—60744
CO, on Pd (210), inclined bonding config., electron stimulated desorption and LEED obs. 80—39430
CO, on Pd/Al_2O_3, IR study 80—108193
CO, on Pd(100), band formation, calcs. and photoemission expts. 79—95463
CO, on Pt (100), electron energy loss, mol. levels 77—15688
CO, on Pt surface, IR spectrum obs. in presence of free CO 78—74654
CO on Ru, adsorbed particle interactions, lattice gas quasi-chem. approx. 80—49529
CO, on Ru (001) surface, electron induced desorption 77—59215
CO, on Si (111), ion scatt. obs. 80—59810
CO, on supported Pt catalysts, temp. programmed desorption 79—46915
CO, on transition metal surface, electronic struct., localised orbital pseudopot. method 80—39653
CO, on W, FEM expt., pseudoclean pattern *(Japanese)* 78—34701
CO, on W, He metastable atom bombard., secondary electron emission 79—47581
CO, on W (110), LEED meas. 77—59213
CO, on W (210), surface struct., LEED obs. 79—82449
CO, on W(210) surface, surface struct. rel. to adsorbed N_2 79—15009
CO, oriented molecule, photoelectron ang. distrib., energy depend. 80—76152
CO, oriented molecules, vibrationally inelastic electron scatt. 78—67907
CO, oxidation on Ir films, IR absorpt. spectroscopy 80—71398
CO, Photoelectron angular distrib. of C and O K-shell ionisation 78—52628
CO, reaction with H_2 on Ni(001), extended muffin-tin orbital theory 80—76557
$CO+O_2$, chemisorbed on Ru(001), surface reaction, electron energy loss spectra 79—46924
CO_2, determ. of porous texture of solids 79—77897
CO_2 film, on KBr, density fluctuations 79—42391
CO_2, on Al_2O_3, Raman spectroscopy study 80—65358
CO_2, on $Fe(OH)_3$ 79—66344
CO_2, on Ru (001), characteristic slow electron energy loss meas. 79—47562
Cl, adsorption-desorption props. and surface struct. chem. on Cu (111) and Ag (111) 77—89648
Cl, chemisorbed layer on Si (111), SCF LCAO calcs. of Si band struct. 78—88010
Cl, chemisorbed on Ni(100), LEED and angle-resolved AES obs. 79—95258
Cl, on Ag(111), props., struct., AES study 78—72024
Cl overlayer on Cu (100), adatom bonding effects, photoemission study 80—104044
Cl$^-$ ions, labelled, adsorbed on Ag surface, diffusion 80—39413
Co, on Pt, electron wave interference 79—33332
Co, on W surface, interaction of He metastable atoms with surface 79—91558
Cs adsorbed on Cu (111) surface, oxidation effect on UPS 79—78826
Cs and Cs-O, on GaP (100) surface, thermal desorption props. *(Japanese)* 80—15368
Cs and Cs-O covered Ag, surface plasma waves, ATR study 80—39451
Cs atoms and ions on W (001) face, thermal desorption kinetics 79—28210
Cs monolayer on Cu(111), dilution of electron gas by O adsorption, plasmon energy losses 79—47036
Cs, on Cu (111), electronic surface band energy 80—2443
Cs, on Cu (111), XPS exam. of Cu surface state and Cs valence electrons 79—19647
Cs on graphite, dissolution, lamellar cpd. form. *(French)* 80—100399
Cs, on metal surface, effects on photon and secondary ion emission during sputtering 80—35038
Cs, on Mo (100), negative ion form. by sputtering, work function depend. 78—39645
Cs, on Ni (100) surface, electron binding energies of core levels 78—18896
Cs, on Pt (100), surface struct., LEED anal. 77—89654
Cs$^+$, adsorpt. potential determ., at soln.-solid interface 79—56068
Cu, adsorbed on W (100), electron field emission revealing unmasked surface reson. 79—15595
Cu, on polystyrene, unusual core level spectra, XPS obs., surface electronic struct. 79—24415
Cu on Pt electrode, optical props., electronic struct. 77—69855
D, on graphite (0001), vibr. spectrum, at. beam scatt. obs. 80—92779
D_2, on W (111), vibr. states, EELS 77—66090
D_2, solid, porosity of solid gas layers, appl. to cryosorption pump *(Japanese)* 80—20031
D_2O adsorbed on Pt surface, exchange react. with H_2, ^{18}O 77—80695
Fe, on W (100) surface, field emission microscopy study 79—15015
$FeCl_2$, adsorbed monolayers, gamma-ray reson. 77—8478
Fe_2O_3 amorphous layer on graphite, Mossbauer spectra, superparamag. props. 80—60474
Ga, (3×3) superstructure on W(011) and Mo(011), FIM obs. 79—99425
Ga on W and Mo (001), struct., FIM obs. 80—103576
GaAs, positron annihilation rel. to surface treatment *(Russian)* 77—44081
GaP:Cs-O simultaneous adsorption, oxidation interface chemical struct. 80—103584
H adsorbed on Nb, distrib., electron-stimulated desorption ion imaging 80—103572
H atom recombination at Ge surface, elec. cond. and chemomag. effect *(Russian)* 79—91125

adsorbed layers continued
H atoms, chemisorbed on cluster, indirect interactions, Grimley-Pisani model and tight-binding calc. 80—65370
H atoms, on W (001), collision of gas phase H atom, dynamics 77—10726
H, chemisorbed atom, surface charge fluctuations effect on spectral density 80—65368
H, chemisorbed on metal substrate, vibr., freq. shifts due to adatom interactions 80—39407
H chemisorbed on metal surface, electron correl., friction coeff. 78—60026
H, chemisorbed on Ni, order-disorder transitions on (111) surface, LEED observation 78—47668
H, chemisorbed on Ni (111), order-disorder transition, cluster-variation method 80—15372
H, chemisorbed on transition metals, effect of surface spin fluctuations 80—75613
H, chemisorption geometry on Ni (111), LEED, thermal desorption, and work function meas. 80—39433
H, in contact with He surface, Bose condensation, adsorption isotherms and stabilty 80—107638
H on Be, secondary ion emission, coverage dependence 80—35043
H, on graphite (0001), vibr. spectrum, at. beam scatt. obs. 80—92779
H, on jellium surfaces, charge density oscills. and adatom-adatom interaction 79—42389
H, on Mo (001) surface, band structure self-consistent calc. 80—15585
H, on Mo(001), self-consistent electron struct. 80—44693
H on Ni (110), adatom configuration, He diffr. study 80—103569
H, on Pt (111), vibr. modes, EELS study 80—15377
H on Pt (111) surface, backscattering, channelling spectra, H adsorption, surface relaxation 80—71552
H, on Si (100) surface, LEED and AES meas. 78—60016
H, on Si {100}(1×1) surface, LEED study 78—67910
H, on stepped Pt surface adsorption sites study by EELS 80—49521
H, on W, surface cond. and intrinsic surface states, surface refl. spectra 80—15378
H on W (001), atomic nature of β-states, electron energy loss spectra 77—76664
H, on W (100), struct. determ. by surface vibr. modes anal., EELS obs. 80—39435
H, on W (100) and Ni (111), angle-resolved and variable impact energy electron vibr. excitation spectroscopy 80—76119
H, on W (100) face, fluctuation, thermal impurity depinning and commensurate-incommensurate transition of CDWs 79—42611
H, on W (100) surface, induced lattice reconstruction, surface vibr. obs. 79—19445
H, on W surface, Cl_2 scatt. 80—20743
H, proposed struct. on Ni(111) 79—60628
H_2 adsorbed layers on Ta and Pt, energy loss spectra *(French)* 79—83069
H_2, adsorbed on Ni, inelastic neutron scatt. 78—18898
H_2 adsorbed on Pd black, vibr. spectrum assignments, inelastic neutron scatt. obs. 78—71942
H_2 adsorbed submonolayer, ortho-para separation coeff., mol. alignment and rot. levels 77—7971
H_2, adsorption on graphite, dynamics, neutron scatt. study 79—60641
H_2 adsorption on Rh-TiO_2 catalyst., surface states, NMR spectrosc. investig. 80—103891
H_2, chemisorbed on Pt black, incoherent inelastic neutron scatt. study 79—60642
H_2 chemisorbed on W, vibr. states, electron energy loss spectra 77—31877
H_2 chemisorbed on W, vibr. spectra characts., adsorption sites 80—70535
H_2, J=1, orientational props. on Grafoil surface, mean field theory 80—15361
H_2, on Al_2O_3, diffusive motion, neutron scatt. study 79—42394
H_2 on CoO, MnO magnetic surfaces, ortho$\rightleftharpoons$para conversion 79—47969
H_2, on Cu, adsorbate induced photoemission, book contrib. 78—95668
H_2, on Ni (111), LEED intensity spectra, 173K 79—28192
H_2, on Ni (111) surface, Raman spectra 79—28769
H_2, on Ni laser-induced desorption expts. 79—1548
H_2, on Ru(110), UPS and work function meas. 79—99424
H_2, on Si and Ge surface, cluster model approach for electronic struct. 78—56205
H_2, on W (001), LCAO calc. of band struct. 77—8168
H_2 on W (011) face, bidimensional lattice *(Russian)* 79—7744
H_2, on W (111), vibr. states, EELS 77—66090
H_2, on W surface, energy spectra for electron stimulated desorption of H^+ calc. 78—79892
H_2, on ZnO, effect on ESR and NMR *(Japanese)* 80—50186
H_2, oriented molecules, vibrationally inelastic electron scatt. 78—67907
H_2, ortho-para conversion, magneto-catalytic reaction, quantum formulation 80—108750
H_2 overlayer on Ni(111), geometry, order and disorder 79—65311
H_2, solid, porosity of solid gas layers, appl. to cryosorption pump *(Japanese)* 80—20031
H_2O, adsorbed, surface-induced NMR line splittings and augmented relax. rates 78—64288
H_2O adsorbed layer on powdered quartz, thermal effects on DTA 79—100161
H_2O adsorbed layers on NH_4Cl, NH_4I powders, adsorpt. isotherms, heats of adsorpt. 79—1545
H_2O, adsorbed on kaolinite clays, dielec. props. 78—76381
H_2O molecule in pores of zeolites, intermed. state of enhanced mobility 78—60027
H_2O, ordered monolayer adsorbed on KCl (100), secondary ion mass spectra 77—76660
H_2O vapour, chemisorbed on Hg, Ag, Pb, Ga, Fe, Pt, effect on surface props. 78—60187
H_2O+CO_2, photoassisted reaction on $SrTiO_3$ (111) face, methane form. 78—76878
H_2S absorpt. on zeolites with varied Si/Al ratios 78—60029
H_2S, on Ni(100), (111), ang. distrib. of Auger electron emission *(Japanese)* 78—43963
H_2S, on Ru(110), evidence for SH species, UPS and work function meas. 79—99424
^{3}H, on Ni sheet, determ. by autoradiography method 77—63989
H(1×1), on W (100), H ν, vibrational mode, IR study 80—60582
He film, adsorbed, NMR measurements 80—107605
He film, density profile 78—10252
He film, from two to three dimens.,, review 78—47633

adsorbed layers continued
He film, multilayer adsorbed, in restricted geometries, book contrib. 79—99391
He film, ordered, finite size effect, crit. parameters and three-state Potts model 77—31836
He films, physisorbed low-density submonolayer thermodynamics, potential scatt. theory calcs. 79—95243
He monolayer, sp. ht., low-density phase modification produced by substrate changes 77—76642
He, on graphite, band struct. effects in heat capacity 80—59788
He on graphite, band struct. and thermodynamic props. 80—80349
He, on graphite surface, anisotropic He-C pair interaction 80—96738
He on W surface, accommodation coeffs. calcs. 80—66866
He, solid, porosity of solid gas layers, appl. to cryosorption pump *(Japanese)* 80—20031
He-Xe layer interaction on carbon black 77—59172
^{3}He, absence of BCC nucleation on Grafoil substrate, 30-320 mK 79—19422
^{3}He, adsorbed film on Grafoil, NMR, intermediate and near-monolayer coverages 79—46878
^{3}He adsorbed layers, antiferromag. indirect exchange 79—99389
^{3}He, adsorbed monolayers, dipolar anisotropy effects in spin relax 77—7940
^{3}He, adsorbed monolayers, nuclear magnetic relaxation for two dimensional systems 80—103534
^{3}He adsorbed on Grafoil, nuclear spin relax. and atomic motion 79—51369
^{3}He, adsorbed on Grafoil surface, ground state, thermodynamic anal. 79—19421
^{3}He, adsorbed on graphite, NMR relax, times 79—51374
^{3}He adsorbed on superfluid ^{4}He surface, ripplons and heat conduction meas. 80—49459
^{3}He film, submonolayer and multilayer, adsorbed on Grafoil, pulsed NMR study 80—49456
^{3}He films adsorbed on Grafoil, NMR relax. times 79—28171
^{3}He, liq., reinforcement of low temp. surface ferromag. instability due to ^{3}He-wall attraction 79—51373
^{3}He, on Grafoil, interlayer exchange 77—72736
^{3}He, on graphite, mag. props., 2-D gas behaviour 78—47631
^{3}He, on graphite, NMR relax. times below 4.2K 78—38898
^{3}He, on graphite, nucl. mag. susceptibility below 4.2K 77—20155
^{3}He on graphite 78—87842
^{3}He, on graphite and other substrates, NMR studies 79—65286
^{3}He, on MgO, nucl. mag. relax. props. 80—49457
^{3}He, on solid Ar, desorption heat capacity 80—10735
^{3}He, on solid Ne, desorption heat capacity 79—4452
^{3}He, on solid Ne, desorption heat capacity 79—51383
^{3}He, specific heat second layer adsorbed on Grafoil 78—87843
^{3}He-^{4}He, on graphite, nucl. mag. susceptibility below 4.2K 77—20155
^{3}He-^{4}He mixture, adsorbed film, systematic exptl. study 80—107603
^{3}He-^{4}He mixtures, superfluid film, on Vycor substrate, superfluid mass and transition temp. 79—51385
^{4}He film, adsorbed, few atomic layers, excitations, two-dimensional roton. 80—39381
^{4}He film growth on graphite, MgO, and Mylar substrates, vap. press. meas. 80—70499
^{4}He films, on graphite substrate, layering and thermal cond., heat capacity and vapour press. meas. 79—51386
^{4}He films adsorbed on graphite, transition temp., entropies, internal energies and heats of desorption, vapour press. meas. 80—2238
^{4}He monolayer, multicritical behaviour from triangular lattice gas model 77—74328
^{4}He, on disordered substrate, heat capacity meas. 0.08-1.3K 80—2239
^{4}He, on Ne-plated graphite, single particle and liquid state props. 77—72738
^{4}He on Nuclepore filter, specific heat *(Japanese)* 78—79852
^{4}He, on solid Ne, desorption heat capacity 80—10736
^{4}He, on Vycor glass, superfluid transition 77—72737
^{4}He, second layer film on graphite, liquefaction 78—47632
^{4}He superfluid film, adsorbed in Vycor substrate, superfluid mass and transition temp. 79—51385
^{4}He superfluid film, adsorbed on Al_2O_3 powder, surface tension sound 80—24691
Hg adsorbed on W, thermal desorption kinetics, theory 80—59792
I adsorbed on Ag(111), photoelectron diffr. aximuthal patterns, struct. sensitivity 80—107644
I chemisorbed on Au, AES and LEED study 80—100405
I, on Ag (111), geometry and bond length, surface EXAFS 78—71952
I^- ions, labelled, adsorbed on Ag surface, diffusion 80—39413
I_2,I_3^-, adsorbed layers, on unroughened Pt electrode, Raman spectra 78—31689
I_2, adsorbed on Ag(111), Cu(111), and Cu(110), surface EXAFS study 80—40186
I_2, chemisorbed on zeolites, Raman spectra 80—93301
In, chemisorption of O_2, XPS and static SIM spectral study 80—80055
In film, $\sqrt{3}$ and $\sqrt{31}$ submonolayer superstructures on Si (111) isothermal desorption, RHEED meas. 79—86992
InSb, irrad. real and clean surfaces, work function 78—95336
Ir, on Pt, adatom surface diffusion energies, Lennard-Jones pair pot. calcs. 79—77923
K adsorbed on W, field emission flicker noise power 80—59795
K, on Fe(100), adsorbate coverage determ. by LEED, AES and XPS 80—103566
K, on Ni (100), plasmon losses in electron energy loss spectra 79—61480
k, on Re (10$\bar{1}$0) surface, electron-adsorption props. 79—33192
K, on W, stimulated ionisation by Na, Cs beams, energy depend. 78—31292
K, on W (112) planes, flicker noise field emission obs. 78—26774
K, on W(112) planes, temp. depend. of noise spectral density functions 78—2992
Kr absorption on graphite, monolayer regime phase diagram 80—49507
Kr, adsorbed monolayer, expt. vs. 2-dimens. Lennard-Jones fluid eqns. of state predictions 79—69223
Kr adsorbed on graphite, commensurate-incommensurate transitions, low temp. theory 80—103582
Kr adsorbed on graphite, nonregistered-registered phase transition 80—39414
Kr, adsorption meas. on SiC coated UO_2, small surface area determ. 80—44429
Kr layer on graphite, heat capacity 79—60621
Kr monolayer on graphite, disregistry transition 78—30825

adsorbed layers continued

- Kr, monolayers adsorbed on (0001) graphite, continuous phase transitions 78—34698
- Kr, on graphite, commensurate to incommensurate transition 80—80079
- Kr, on graphite, finite size effect and temp. depend., multicritical phase diagrams 79—42372
- Kr on graphite, neutron diffr. obs. 77—72789
- Kr, on graphite, Potts lattice gas, renormalisation-group treatment 78—67908
- Kr, on graphite, X-ray diffr. from 2-D solid 78—75498
- Kr, on metal, polarisation due to short range interaction with substrate 80—39428
- Kr, submonolayer, adsorbed on graphite, melting, X-ray scatt. obs. 78—95234
- La, on 4d or 5d metal, work function, O_2 coadsorpt. effects, thermionic emission obs. 78—11064
- La, on W (011) or Mo (011), disordering, LEED obs. *(Russian)* 77—89655
- La, on W (112), strongly anisotropic interaction *(Russian)* 77—11798
- MgO, adsorbed layers of S containing small paramag. ions, g-tensors, spin densities 78—46270
- Mo, surface sensitive structure in angular resolved photoemission *(French)* 77—40326
- N (1×1), on Ti (0001), underlayer geometry, electronic struct. calcs. and UPS meas. 80—54751
- N, on Cu (100), electronic props., UPS, XPS and Auger spectra 77—66088
- N, on Cu (110), temp. depend. evolution, Auger line shape 78—2376
- N, on W (001) clean surface, long-range inhibition by N of displacive phase 80—2266
- N_2 adsorbed on Ni (001) surface, p(2×2) struct., LEED and AES study 80—54515
- N_2 adsorbed on W, effect of SIMS sputtering induced recomb. anal. 80—55243
- N_2 adsorbed on W(100), vibr. spectra, bonding struct., LEED study 80—84387
- N_2 adsorbent mesopores, capillary evaporation and struct. 80—107614
- N_2, condensed film, UPS linewidths 78—31294
- N_2, dense monolayer on graphite cleavage face, phase transition 78—56034
- N_2, determ. of porous texture of solids 79—77897
- N_2, monolayer adsorbed on graphite, lattice dynamics 78—75946
- N_2 monolayer on graphite, sp. ht. and u.p., size and steric effects 77—85073
- N_2, NO, N_2O, dry air, chemisorbed on transition metals at high pressures, XPS 77—20990
- N_2 on Ag (111), electronic props., XPS and UPS 78—10279
- N_2, on graphite, Mossbauer obs. 80—18060
- N_2 on Ni, valence band photoemission, SCF MO CNDO calc. 80—100754
- N_2, on W (210), surface struct., LEED obs. 79—82449
- N_2, on W(210) surface, surface struct., rel. to adsorbed CO 79—15009
- N_2, on W{411} and W{320}, sticking probability and coverage determ. 80—54528
- N_2, oriented molecules, vibrationally inelastic electron scatt. 78—67907
- ND_3, adsorbed on graphon, neutron scatt. study 79—60640
- NH_3, adsorbed on $CaCl_2$ and $CaBr_2$, IR and far IR spectra 77—24478
- NH_3, adsorbed on silica gel, neutron scatt. investig., mol. vibrs., rots. 77—51608
- NH_3, on amorphous silica, Raman scatt. obs. 80—11948
- NH_3, on graphite, struct. and dynamics, neutron diffr. and inelastic scatt. 78—87869
- NH_3, on Ir (111), mol. adsorbate structs. from angular-resolved photoemission 80—76141
- NH_3, on Si (111) surface, electron energy loss spectroscopy 78—2374
- NO, adsorbed layer, electron impact, electron impulsive ionisation spectroscopy obs. 80—60720
- NO, adsorbed on Cu, species identification, struct., dissoc. chemisorption, desorption, UV photoelectron spectroscopy 78—52635
- NO, adsorbed on Rh/Al_2O_3 catalyst, interaction with CO, IR study 79—70369
- NO, first adsorbed layer on graphite, BN, and lamellar halides, critical and triple point temps. 78—91548
- NO, on cleavage face of lamellar halides, polymorphic phase changes 77—31900
- NO, on Si (111) surface, electron energy loss spectroscopy 78—2374
- NO_2 on Cu, ultrahigh vacuum ESR studies 80—97729
- Na adsorbed on Ni, photoemission, directional memory effects 80—100753
- Na adsorbed on Ni(100), photoelectron diffr. aximuthal patterns, struct. sensitivity 80—107644
- Na, adsorbed on W(110) plane, ordering, theoretical anal. 78—18892
- Na adsorption on V, effect on Br_2 chemisorption 80—101039
- Na c(2×2) overlayer on Ni (001), surface struct. effects via photoexcited core electron diffr. 79—74063
- Na c(2×2) overlayer on Ni (001), core level excitation effects, synchrotron radiation UPS study 80—40234
- Na, on Al, adatom valence-level position variation 80—88611
- Na, on Cu (111), UPS study of surface electronic struct. 80—80350
- Na, on Ni (100), plasmon losses in electron energy loss spectra 79—61480
- Na, on Ni substrate, hybridisation between s and p resons., jellium model 80—6932
- Na, on Ni(001), core-level photoelectron diffraction 78—95659
- Na, on Ni(001), photoelectron diffr. effects in core-level photoemission 80—76144
- Na, on Pt(III), electronic struct. 78—19117
- Na, on W (100), binding props. calc. 80—49522
- Na-Br coadsorption on Ag (111), NaBr island formation 78—38944
- NaF coating defects and impurities affecting damage threshold and absorptance 79—14065
- Nb-Nb_xO_y-Pb Josephson tunnel junction form. and ageing, adsorbed gas effect *(Russian)* 78—14899
- Ne, on exfoliated graphite, vapour press. meas., 15-30K 79—69350
- Ne, on metal, polarisation due to short range interaction with substrate 80—39428
- Ne, solid, porosity of solid gas layers, appl. to cryosorption pump *(Japanese)* 80—20031
- Ni (001), adsorbed S, crystallography by LEED, appl. of iso-intensity map method 79—19128

adsorbed layers continued

- Ni, electrocrystallisation, reaction mechanism, appl. of impedance meas. *(French)* 80—103597
- Ni, on W, effect on surface self-diffusion FEM characts. *(French)* 77—1296
- Ni, on W (111), surface site geometry and diffusion characts. of Ni atoms 78—71953
- Ni, quasiatomic excitation, causing energy loss peak, UPS 78—72691
- Ni(001) surface N adsorption due to ion beam irrad., surface struct. LEED study *(Chinese)* 80—84364
- No, on graphite, melting and polymorphism 78—84063
- O (2×2) overlayer on Ir (111) surface, LEED study 80—2264
- O adsorbed on Al (111) surface, surface struct., LEED and SEXAFS data 80—92782
- O adsorbed on CdS, EPR of O radicals, temp. depend. 80—80612
- O adsorbed on clean metal solid surfaces, sputtering effects, combined analytical techniques 80—35047
- O adsorption on Cu (001) surface, effect on surface barrier, LEED study 80—84378
- O, c(2×2) on Cu (001), surface geometry determ. by deep-core-level XPS 80—40224
- O c(2×2) overlayer on Ni (100), angle-resolved photoemission study 79—33903
- O, chemisorbed on Al (100), photoemission ang. depend., MO cluster model calc. 78—76576
- O, chemisorbed on W (110), order-disorder transform., theory compared with LEED data 79—7748
- O chemisorption on Cu(100) surface, angle-resolved UPS study 80—84384
- O, chemisorption on W (110), Monte Carlo modelling of phase changes 78—71969
- O, coadsorbed with CO on Rh, desorption spectra, Langmuir-Hinshelwood reaction anal. 79—47965
- O, on Al, ang. depend. of plasmon loss features in XPS 78—43987
- O, on Al (100), overlayer electronic struct. 77—85058
- O on Be, secondary ion emission, coverage dependence 80—35043
- O, on Cu (001), Ar^+ bombarded, particle ejection, ang. depend. 80—50489
- O, on Cu (100), ejection by ion bombardment of atomic and mol. species 79—42373
- O, on Cu (100), electronic props., UPS, XPS and Auger spectra 77—66088
- O, on Cu (100), ion bombard., ejected atom energy distrib., classical trajectory calc. 79—100011
- O on Cu vicinal surfaces, LEED study 80—103575
- O, on Fe(100), adsorbate coverage determ. by LEED, AES and XPS 80—103566
- O, on metals, ion impact desorption, adsorption energy depend. 80—39442
- O, on Ni, electronic struct. and UPS 78—15281
- O, on Ni, photoemission intensities from core states 78—95654
- O, on Ni, sputtering 77—36335
- O on Ni, sputtering by low energy ions 77—62758
- O, on Ni (001), electronic struct., KKR calc. 78—56200
- O, on Ni (100), effects on secondary election spectra 80—50480
- O on Ni (100), electron energy-loss spectra 79—47570
- O, on Ni (100), overlayer electronic struct. 79—47144
- O, on Ni (100), rapid LEED intensity meas. 80—44420
- O, on Ni (111), adlayer phases and binding sites 80—80069
- O, on Ni (111), order-disorder transition 79—82447
- O on Ni {100}, crystallographic effects in low energy ion scatt., local ion-atom neutralisation 80—84377
- O, on Ni surface, interaction of He metastable atoms with surface 79—91558
- O, on Ni surface, location of adsorbed atoms, surface channelling meas. 80—84373
- O, on polycryst. W, W(100), and V, electron stimulated desorption of O^+ ions 79—99428
- O, on Pt (111), chemisorbed and oxide states, low energy ion scatt. obs. 80—65372
- O, on Si (111), ion scatt. obs. 80—59810
- O, on stepped W (100) surface, electron stimulated desorption ion ang. distribs. 80—20035
- O, on UHV cleaved Si (111), electronic transitions 78—39183
- O, on W, order-disorder transition, theory 78—38811
- O, on W (110), island size determ., response function and substrate struct., LEED meas. 79—42414
- O, on W (110), three-adatom non-pairwise interaction, Monte Carlo simulations 79—82466
- O, on W(100) and (110), electron stimulated desorption 79—33181
- O ordered overlayer on Al (111), angle-resolved photoemission, band struct. 80—40229
- O single layer on Au, ferromag. props., thermomag. effect *(Russian)* 78—64256
- O_2, adsorbed layer on graphite film, mag. susceptibility 78—43241
- O_2 adsorbed on Cu (110) surface reaction with CO, ellipsometry, AES, LEED study 80—6635
- O_2, adsorbed on PbSe, XPS (UPS) obs., lattice diffusion and sticking coeff. 78—52637
- O_2 adsorbed on Pd (111) surface, UPS and thermal desorpt. characts. 80—54754
- O_2 adsorption on Ni(110) surface, LEED and ion scatt. study 80—84386
- O_2 adsorption on Pt (111) surface, UPS, EELS and thermal desorption study 80—100409
- O_2 and WO_2 adsorption on W (110) 80—34317
- O_2 chemisorbed on Hg, Ag, Pb, Ga, Fe, Pt, effect on surface props. 78—60187
- O_2, chemisorbed on Si (111), bonding geometry, electron yield EXAFS meas. 80—50461
- O_2, determ. of porous texture of solids 79—77897
- O_2 layer on W, $Ar^+(Ar^{+,m})(Ar^{2+})$ impact, electron emission obs. 80—60740
- O_2, on Ag, EPR of O_2^-, rate of angular reorientation 78—72413
- O_2 on Ag (111), electronic props., XPS and UPS 78—10279
- O_2 on Cu, ion-bombarded, ejected particle ang. distrib. 78—95643
- O_2, on Cu (100) single crystal surface, oxidation 80—11846
- O_2 on Cu (100) surface, LEED study 80—100408
- O_2, on Fe surface, effect on chem. reaction kinetics 80—55572
- O_2, on GaAs(Pt), surface electronic struct. (surface chem.) using synchrotron radiation 78—53254
- O_2, on graphite, heat capacity meas. 80—49511

adsorbed layers continued
O_2, on graphite, mag. phase transition, theory 78–38811
O_2, on graphite phase diagram, mag. ordering, neutron scatt. obs. 79–73401
O_2, on Mo surface, low-energy ion scatt. study 79–1807
O_2, on Ni (001), angle-resolved UPS 77–40333
O_2, on Ni (111) surface, Raman spectra 79–28769
O_2, on Pt, stability and struct. of high Miller index forces in vacuum and with adsorbed C and O 77–76651
O_2, on Ru (001), characteristic slow electron energy loss meas. 79–47562
O_2 on Si, EPR, comparison with free mol. 77–69176
O_2, on Si (111) surface, electron energy loss spectroscopy 78–2374
O_2, on SiO_2 supported W, EPR evidence for surface mobility of O_2^- 78–84046
O_2, on SnO_2, EPR meas. *(Japanese)* 78–10750
O_2 on Ta, effect on kinetics of H_2 absorption, 77-700K 79–95169
O_2, on Ta, electron stimulated desorption, bound states 77–85082
O_2, on Vycor and Grafoil substrates, mag. susceptibility as probe of restricted geometry 79–51436
O_2, two-dimensional, on graphite, props. calc. 80–103568
O_2^-, on GaAs surface, EPR spectrum HFS 77–40118
O_2^- species adsorbed on Ce-X zeolites, identification by ESR 77–27096
O_2-CO coadsorbed complexes evolving from Ag surface, mass analysed thermal desorption spectra 77–60121
O_2+CO, chemisorbed on Ru(001) surface reaction, electron energy loss spectra 79–46924
O_3, field ionisation at Ir surface 78–35273
OH adsorbed on Ni, energy depend. of vibr. excitation, electron energy loss spectra 79–28201
OH, on Pt(111), identification by electronic struct. and vibrs. 80–49509
P adsorbed on Ni, coadsorption of Pb or Sn, AES study 80–54521
P, chemisorbed on Ni(100), LEED and angle-resolved AES obs. 79–95258
P, on Ni (100), effects on secondary electron spectra 80–50480
Pb adsorption on P or C contaminated Ni, AES study 80–54521
Pb, adsorption on W(100), W(110) substrates, pairwise interaction model using Morse pot. 80–6657
Pb electrode, combined electroreflectance and double layer effects 77–85692
Pb monolayer, double layer with Sn, growth on Al (111), struct. 80–70567
Pb, monomolecular film on Ag electrode, anisotropy of optical props. 80–60534
Pb on Cu, Auger electron spectroscopy 77–85851
Pb on Cu vicinal surfaces, LEED study 80–103575
Pb, on Ni (100), effects on secondary electron spectra 80–50480
Pb, on W (100) surface, field emission microscopy study 79–15015
Pb, underpotential adsorption, cathodic deposition, on Ag(111) and (100) *(German)* 80–108363
Pd, on Si surface, effect on electronic props. *(Russian)* 79–91124
Pd on W (110), long range interatomic interactions with coadsorbed Re, W 80–59789
Pd on W (110) surface, growth, struct., stability, desorption 80–59794
Pd, on W FEM tips, adsorbed layer conc. using nucl. microanal. *(French)* 80–29860
Pd, surface diffusion on W, spreading behaviour 79–99421
Pd, surface diffusion on W, anisotropy effects due to substrate struct. 79–99422
Pt, on Pt, adatom surface diffusion energies, Lennard-Jones pair pot. calcs. 79–77923
Rb, chemisorbed on Ag (111), struct., and reactivity towards NO 79–28207
Rb, on Ni (100), plasmon losses in electron energy loss spectra 79–61480
Re on W (110), long range interatomic interactions with coadsorbed Pd 80–59789
Re_2, on W (211) surface, dissoc., thermodynamics 78–87861
Rn, adsorption on surface of elastically deformed body 80–10775
S, $(\sqrt{2}\times\sqrt{2})R45°$, on Pd(100), adsorbate induced surface reson. obs. in photoemission 80–7470
S on Ag (111), electronic props., XPS and UPS 78–10279
S, on AgBr dispersion in gelatin, transient absorpt. spectra, latent image form. and decay 80–66837
S, on Cu (100), electronic props., UPS, XPS and Auger spectra 77–66088
S on Cu vicinal surfaces, LEED study 80–103575
S on Cu∼(111), selective effect of substrate steps rel. to adsorbed layer interaction 78–14616
S, on Fe, effects on surface reaction kinetics and surface self-diffusion 78–7234
S, on Fe(100), adsorbate coverage determ. by LEED, AES and XPS 80–103566
S, on Mo (001), effect on CO adsorption 79–86981
S on Ni, photoelectron diffr. data 80–29851
S, on Ni, sputtering 77–36335
S on Ni (100), effect on photoelectron spectra *(French)* 77–36360
S on Ni (100), surface, effects of S-coverage *(French)* 77–36360
S, on Ni (110), layer struct. from anal. of LEED pattern 79–73407
S, on Ni surface, interaction of He metastable atoms with surface 79–91558
S on Ni surface, oxidation studied by AES 79–83505
S, on Ni(100), (111), ang. distrib. of Auger electron emission *(Japanese)* 78–43963
S, on polycrystalline Ni surface, H_2^+ ion induced desorption 78–84069
S, on Ru(110), evidence for SH species, UPS and work function meas. 79–99424
S, role in dissolution and passivation of Ni and Ni-S alloys 79–66340
SF_6, on Ru (001), XPS exam. 77–55866
SF_6, physical adsorption on Ru (001), XPS expts. 77–69178
SO_2 on gas-covered Pt surface, thermal accommodation coeff. 80–10346
Sc, on 4d or 5d metal, work function, O_2 coadsorpt. effects, thermionic emission obs. 78–11064
Se c(2×2) overlayer, on Ni (001) surface, angular resolved UPS 78–76584
Se, c(2×2) overlayer, on Ni (001), angle resolved UPS, resonancelike peaks 79–87562
Se on Ni, photoelectron diffr. data 80–29851
Se, on Ni, photoemission intensities from core states 78–95654
Se, on Ni (001), photoelectron diffr. obs. 80–40223
Se, on Ni (100), electronic orbitals, angle-integrated UPS 78–72224

adsorbed layers continued
Se, on Ni(001), resonancelike peaks in angle-resolved UPS 79–69955
Se on Ni(100), normal photoelectron diffr. of Se 3d level 79–11501
Si, adsorption site on Ni, photoelectron intensity modulation 79–47589
Si, chemisorbed on Ni(100), LEED and angle-resolved AES obs. 79–95258
Si, ordered monatomic film on W(100) face, dynamic props. 77–89634
Si, positron annihilation rel. to surface treatment *(Russian)* 77–44081
SiO_2 on BeO, effect on TSEE 80–76159
Sn adsorption on P or C contaminated Ni, AES study 80–54521
Sn, monolayer, double layer with Pb on Al (111), layer growth, struct. 80–70567
Sn, on Ni (100), effects on secondary electron spectra 80–50480
Sn on W and Mo (001), struct., FIM obs. 80–103576
Sr submonolayers adsorbed on Mo crystal, LEED and contact pot. study 80–2271
^{182}Ta-containing Ta sheet, radioactive electron emission spectrum (exoelectrons), surface elec. field and Auger effects 78–72705
Te, on Ni, photoemission intensities from core states 78–95654
Te, on Ni (001), photoelectron diffr. obs. 80–40223
Te, on Ni(001), core-level photoelectron diffraction 78–95659
Te, on Ni(001), photoelectron diffr. effects in core-level photoemission 80–76144
Te overlayer, c(2×2), on Ni surface, 4d levels, angle resolved photoemission cross section, atomic and solid-state effects 80–29853
TiO_2 in non-aqueous liquids, effects of mol. architecture of long chain fatty acids on dispersion props. 80–40751
Tl, underpotential adsorption, cathodic deposition, on Ag(111) and (100) *(German)* 80–108363
$^{205}Tl^+$ adsorbed on hydrated silica, NMR relax. chem. shift 78–72427
W adatoms, on Ir(110), surface diffusion by atomic exchange mech. 80–49508
W, adsorbate covered, field emission energy distrib., overlayer geometry effects 77–8730
W, adsorbed Sm, conc. depend. of lifetime and heat of adsorption of Sm atoms 79–69364
W, diatomic cluster migration on W {100} plane, elementary displacement steps 80–88436
W film, adsorbed Th layer, work function, temp. depend. 77–28701
W on W (110), long range interatomic interactions with coadsorbed Pd 80–59789
W on W(001), struct., FIM obs. 80–103576
Xe, adsorbed monolayer, THEED intensity meas. 78–84075
Xe adsorbed monolayer, two-dimens. Lennard-Jones system, melting 79–28071
Xe adsorbed on Ag, lateral compression effects calc. 80–6641
Xe adsorbed on Ag(111), structural and thermodynamic studies 80–6640
Xe adsorbed on Cu, NaCl, stepped and disordered surfaces, two-dimens. phase transformations 80–103580
Xe adsorbed on graphite (0001) surface, monolayer liquid and solid struct. 80–65400
Xe adsorbed on Pd (110), anomalous 5p photoemission, electron binding energies 80–100750
Xe, incommensurate overlayer on Ag (111), dynamical calc. of LEED 78–30828
Xe, monolayer on Ag(111) surface, lateral struct. and Xe-Xe interactions 77–1311
Xe, on Au and Ti, electronically excited atoms coupling to cond. states 77–89642
Xe, on graphite, finite size effect and temp. depend., multicritical phase diagrams 79–42372
Xe, on graphite (0001), 2-dimens. condensed phase obs. by isothermal desorption spectroscopy 77–69181
Xe, on Ni (100) and Fe (100), UPS 79–33897
Xe, on $NiCl_2$, phase transition identified as 2D polymorphic transform. 78–56040
Xe, on Pd (100), angular-resolved photoemission 79–43102
Xe, on Pd (100), lateral interactions, effect on work function, UPS, and IR spectra 79–77904
Xe, on Pd (110), anomalous 5p photoemission 80–7471
Xe, on Pd-Pt, Ir, and Ru, 5p photoemission, local surface struct. influence 80–2920
Xe, on W, UPS, $P_{3/2}$ level splitting mechanism 77–31880
Xe, physisorbed layer, UPS spectra, lateral interaction 78–92174
Xe, physisorbed monolayer on graphite, dynamical and thermal props. 80–34292
Y, on 4d or 5d metal, work function, O_2 coadsorpt. effects, thermionic emission obs. 78–11064
Zn, electrocrystallisation, reaction mechanism, appl. of impedance meas. *(French)* 80–103597
Zr, adsorbed on W(Ta)(Re), low-temp. mobility, surface struct. 77–20197

adsorption
see also heat of adsorption
A-type zeolites, of hydroxymethyl radicals, electron spin echo obs. 78–21947
accommodation and adsorption of gases on solid surfaces at low temps. 80–49518
acetate ions adsorbed on Ag particles in aqueous soln. Raman spectra 80–69148
actinides, adsorption by Mn and Fe oxides in soils and sediments 79–66422
adenine, adsorption on Ag halide grains *(German)* 79–39175
adsorbed layers, general principles of construction of structural models 80–84351
adsorbed on Ni, electronic surface reson. of Ni(001)c(2×2)S, LEED obs. 79–24051
adsorption on Pt electrode surface, struct. and comp. exam. by LEED and AES 79–70342
aerosols, atmospheric, gaseous nitrates adsorption by particles in urban and rural area 80–94123
aerosols, flowing, attachment of ^{220}Rn decay products using aerosol centrifuge 80–61167
albumin, human serum, adsorption studies, feasibility of radiolabelling 78–85359
aliphatic acids, thermodynamics of adsorption at air/aqueous soln. interface 80–10752
aliphatic alcohol, thermodynamics of adsorption at air/aqueous soln. interface 80–10752

adsorption continued
alkali halide, band struct. of selectively adsorbed atoms 79—28399
alkali halide, screw dislocations in puncture rosettes, motion-starting-stresses, surface-active media effects *(Russian)* 78—10051
alkali halide (100) surface, adsorbed monomers and dimers, pot. surfaces, diffusion dissoc. 77—66769
alkali halide (100) surface, potential energy of isolated Au atom above surface 77—89650
alkali halide adsorbate motions and reactions at surface defects, mol. beams 77—59205
alkali halide surfaces, adsorbate binding energies and struct. at surface defects 77—59206
alkali halides, atomic interaction pot. on (100) face *(German)* 80—15380
alkali halides, heterogeneous adsorption, photoelec. work function changes 77—69175
alkali halides, of gas, stress depend. of chem. pot. 78—91541
alkali halides, of inert gas atoms, pot. energy calcs. 78—67902
alkali halides of CO_2, field induced vibr. splitting, IR spectra 78—46334
alkaline earth oxides, of CO, reflectance spectra obs. 79—28781
alkaline earth oxides, of O_2 , electron transfer, EPR obs. 78—76296
n-alkane, long-chain even, adsorpt. energies of n-alkane mols., rel. to cryst. growth kinetics 78—42933
n-alkanes, adsorption into bimolecular lipid layers 80—88435
allophane adsorber, removal of atmospheric gaseous hydrocarbons *(Japanese)* 77—78412
alloys, of O, Auger spectra 78—14600
alumina, of electron acceptors, adsorption isotherm, ESR and electronic spectra 77—48681
γ-alumina surface, adsorbed benzene high-temp. IR spectra *(German)* 79—28757
anthracene, radical cation, EPR, acidic surface anisotropic rot. diffusion 78—27095
artificial liver support, protein-bound metabolite adsorbent equilibrium props. 79—20709
artificial liver support, protein-bound substance removal kinetics 79—20710
atom migration, on solid surface, dynamical theory 77—1293
atom pair recombination, on solid surface, dynamics pot. calcs. 78—7197
atom surface scatt., reflection and sticking coeffs., short range forces, low energy limit 80—40208
atom-surface bound states, surface averaged pot. energy function 77—11789
atom-surface scattering, selective adsorption phenomena, elastic theory 79—100012
atomic beam and mol. beam scatt. from cryst. surfaces in quantum regime, review 78—35244
atomic collision processes rel. to vacuum system, review 80—54290
atomic interaction dipoles, perturbation theory 80—78680
atomic scattering, reson., from solid surfaces, atomic band struct. effects 77—85871
Auger matrix element, multicentre, ang. depend. calc. for solids and adsorbate systems 78—92151
batch adsorption for pore diffusion with film resistance and an irreversible isotherm 78—84047
bentonite, adsorption of chloramine T 79—92001
benzene-chlorobenzene, benzene-toluene, perfect binary liquid mixtures on silica gel, adsorption thermodynamics 80—44428
benzene-toluene, perfect binary liquid mixtures on silica gel, adsorption thermodynamics 80—44428
binary crystal, growth mechanism, dissoc. adsorption effect 78—26465
binary liquid mixtures adsorption onto solid surface, effect of surface heterogeneity 80—44411
binary mixtures flowing through activated C, adsorpt. interference 80—107635
biological homopolymer, theory of 1D adsorpt. on to 80—51034
biopolymer, charge carriers origin and mobility, adsorbed water effects 79—92461
biporous media, influence of double layer on dynamics of ion adsorption 79—11827
black foam films stability, review 80—104463
block copolymers, chromatographic separation on porous adsorbents *(Russian)* 79—66392
block copolymers, selective adsorpt., surface tension meas. *(Japanese)* 79—69323
blood proteinpolymer interfacial behaviour, influence of hydrophilic-hydrophobic type of microphase separated struct. *(Japanese)* 80—12051
bombardment induced light emission, chem. effect 77—28672
bonding and surface structure, review 77—4252
borosilicate glass, porous, surface area change with acid treatment, adsorption of N_2 and H_2O *(Japanese)* 78—44244
bovine serum, meas. at interfaces by drop volume technique 78—60009
brass, of Hg, effect on mech. props *(Russian)* 79—29267
breakthrough curves for adsorption-desorption, modelling using statistical moments 79—37916
Brownian particles, reversible adsorption and reversible coagulation, kinetic eqns. 79—16045
Brunauer-Emmett-Teller surface areas, automatic low-cost determ. 77—55441
caffeine in aq. electrolyte, adsorpt. isotherm and solute activities from spreading pressure-surface charge data 78—14576
calorimetry, adsorption, for studying surface phenomena 79—40574
capillary, effect of surface condition on crystallisation of aq. solns. 79—56037
capillary condensation and absorption processes 79—28175
capillary condensation and adsorption, adsorptive pot. boundary layer approx. 78—2366
capillary condensation and adsorption, Gibbs free energy, unitary approach 77—76643
capillary phenomena in cylindrical pores, appl. to pore size anal. 80—15340
carbon black, of He isotopes, effects of preadsorbed Xe 77—59172
carbons, active, micropore filling and adsorption of simple gases, Dubinin theory 77—47661
catalysis reaction studies on single cryst. surface in XHV system limitations 77—9126
catalyst, polycryst., of O, Auger spectra 78—14600
catalyst, polycryst., oxidation, Auger spectra 78—14600
cationic dyes, adsorbed ionisation energy, local environment effects 79—34337

adsorption continued
cellular resting pot., eqns. according to surface adsorption theory 80—35861
cellulose, mol. motions, role of water, temp. and morphology 77—89386
cellulose film, moisture effect on phys. and mech. props. 80—40450
ceramic, specific surface area meas. by gas adsorption 78—11144
chabazite, of Ar-N_2 mixture, test of eqns. for gas mixture adsorption on heterogeneous surface 78—60030
chain molecules with polar head, scaling description 78—3378
charcoal, of Se in environmental water, preconc., neutron activation anal. appl. 77—44551
charcoal, of V, from sea and surface waters, neutron activation anal. appl. 77—44549
charcoal, wood, of N_2, methanol, cyclohexane 79—28973
charcoal filter, adsorpt. of radioactive I, safety evaluation *(Japanese)* 78—33267
charcoal filters, NDT of residual adsorption capacity 80—89523
charged system, two-dimens. comparison with neutral particle adsorption 80—80077
chemoepitaxy and chemoendotaxy on metals 77—11827
chemostress coefficient, adatom-solid substrate interaction 78—91540
chemostress effect in ionic crysts. and metals 79—28193
chlorobenzene-bromobenzene, perfect binary liquid mixtures on silica gel, adsorption thermodynamics 80—44428
chromatographic determ. of isotherms by step and pulse method, apparatus and data processing 78—6215
chrysotile, of organic micropollutants, XPS and gas solid elution chromatography exam. 78—80790
classical quadrupoles on triangular net, orientational ordering calcs. 80—2262
CO_2 condensed layers, cryosorption pumping characts. for He, thermal spike effects 79—80635
coexisting mobile and localized adsorption 79—19455
coherent potential approximation 79—33193
colloid stability theory, direct operational determ. of disjoining pressure 80—40752
colloidal capillary-porous body, mass transfer parameters, adsorpt., osmotic moisture 78—11563
colloidal plates, parallel, polymer adsorption, excluded volume effects, polymer-solvent interactions 80—45568
colloids, rel. to thermodynamic stabilisation 80—81369
colloids, solvation force between particles, Monte Carlo calc. 80—21328
competitive adsorption from binary liquid mixtures, adhesive hard sphere model 80—2265
competitive equilibrium adsorpt. model 79—42367
computer simulation 79—65308
conference on solid-vacuum interface, Amsterdam, Netherlands (June 78) 79—42342
conference on surface science, York, England (March 1977) 78—14540
contact sorption moisture exchange in vacuum, mass exchange kinetics *(Russian)* 79—19468
copper phthalocyanine film, electroconductivity, effect of adsorption 77—85356
copper phthalocyanine film, electron acceptor surface states due to O_2 adsorption 80—88586
cosmic dust grains of Ar, rel. to interstellar Ar depletion and grain temps. 80—51848
covered surface, adsorption dynamics, model 77—51594
crocidolite, of organic micropollutants, XPS and gas solid elution chromatography exam. 78—80790
crosslinked elastomer, of Rn 80—10775
cryogenic molecular adsorption refrigeration systems, design theory and performance 79—58722
crystal growth, stochastic models, diffusion and relax. kinetics 79—37642
crystal surface discrete dipole layer effect on surface barrier shape 79—95468
crystal-electrolyte interface, pot. drop effects on surface at. electronic levels 78—19123
crystal-solution interface, localised adsorpt. in one layer 79—46582
curved surface physisorption, small spherical particles or pores 77—7964
cycling zone adsorption, travelling wave, continuous flow equilib. staged model 78—64874
α-cyclodextrin surface, adsorbed gases effects on positron annihilation 79—65952
cylindrical channel walls, adsorption from fluid in Poiseuille flow 78—84048
density functional theory, computer simulation 80—24735
density profile, improved calc. 77—31876
diamond, of gases and metals 77—72758
diamond lattice, of polymer chain, span calc., self-avoiding walk model 77—15679
diatomic molecular gas, vibr. excited, on surface, accommodation coeff. *(Russian)* 78—38973
dielectric adsorbent, energy of interaction with monolayer 77—4259
diffusion-controlled reactions on a two-dimensional lattice 80—71940
digital timer for electroadsorption studies 77—90670
N,N-dimethyl aniline, adsorpt. on Ag colloids, surface enhanced Raman spectra obs. 80—97251
dipolar hard spheres, adsorpt. onto smooth hard wall in elec. field, density profile 79—67221
Disjoining pressure of thin layers of binary solutions 78—15716
disperse system adsorption on hydrated solid phase surface exchange cations effect 78—64893
dissociative adsorption, quantum chem. theory, diatom-solid potentials 78—73087
distribution function of adsorption energy in relation to the overall adsorption isotherm 79—1542
Duralumin, adsorpt. of Hg, effect on mech. strength, creep, fatigue, embrittlement *(Russian)* 79—29267
dust, of SO_2, in atmosphere 78—96287
dynamical and geometrical effects on the physisorption of atoms 80—70531
E-glass fabric, post heat-treatment temp. on moisture adsorption and elec. cond. 79—70178
electrical double layer, ion adsorpt. and discrete charge effects, self-consistent calcs. 80—76516
electrocatalysis, surfaces modified by metal adatoms, review 80—61110
electrocatalysts, of CO, reversible poisoning, air pollution appl. 77—37363
electrochemical electrode-ion adsorption parameters, zero charge pot. conc. depend. 80—40706

adsorption continued
electrochemical reaction kinetics, in presence of surface-active substances, eqn. selection 79—34322
electrochemical system, diffusion layer theory, exptl. test 78—35701
electrochemical system, impurity ion adsorpt. process on reactant transfer processes 80—45519
electrode, enhanced Raman scatt. from adsorbed molecule 79—95767
electrode, metal, effect of solvent interaction on elec. double layer struct., adsorpt. 78—61023
electrode adsorption effects in Cs-Ba grid-controlled switching element 80—19626
electrode-solution interface, AC polarographic data anal., computer program 80—3400
electrode-solution interfaces, role of water 78—40058
electrodes, adsorption isotherm equation, thermodynamic form 79—69369
electrolyte flocculation of stabilised potassium 79—43638
electrolytes, strong, specific adsorption, electrical double layer, interface excess activity coeff. 80—49523
electron beam induced adsorption, enhanced adsorpt. due to ion beam 77—11778
electron energy loss spectroscopy, book contrib. 77—63509
electron microscope contamination by surface diffusion of adsorbed hydrocarbon mols., theory 80—99013
electronic state of adsorbate on single crystal, anal. using angle-resolved photoelectron spectroscopy 80—11541
ellipsometry work at Gakashuin University from 1955, review 80—9019
epoxy polymer, glass microsphere-filled, glass transition temp. *(Russian)* 79—24489
epoxy resin, mobility of sorbed water, low resolution PMR method 80—11276
equilibrium, anomalies near crit. points of substrate 78—79895
equilibrium constant calc. for generalised surface-layer model 77—20199
equilibrium surfaces, adsorption energy 77—31896
EXAFS for adsorbate-substrate characterisation 77—43430
exponential adsorption isotherm, modified form 78—87864
factor VIII, native and modified, surface adsorption and mol. interactions, ellipsometric obs. 80—104555
ferricytochrome c, rate of interaction with negatively charged lecithin liposomes 77—16914
fibrinogen, native and modified, surface adsorption and mol. interactions, ellipsometric obs. 80—104555
field adsorption, correction to short-range binding energy, isolated dipole pair approx. 79—100027
field adsorption, monopole-dipole interaction 79—19979
field emission current fluctuation, power spectral density *(Japanese)* 78—88407
field emission microscopy appls. 79—65982
field emitter, adsorpt. effects on emission, theory 78—2996
film, thermodynamic theory of clustering and percolation transitions 77—47697
film, vapour deposited, growth morphology, effect of absorbed gas 78—11370
film boiling, effect of adsorption characts. on minimum temp. 80—79114
film growth kinetics under high adatom conc., surface diffusion parameters 77—28088
FIM, gas supply function, expt. determ. from adsorption rate 80—100402
finite harmonic oscillator chain with surface impurity, dynamics 80—59776
fission product and actinide adsorption on silica gel, for urinary gross α activity determ. 79—88155
fission reactor fuel reprocessing, adsorptive removal of rare gases 79—31094
fluid with strong interparticle repulsions, adsorpt. isotherms, Percus-Yevick theory 78—10276
fly ash particles, water accretion, refract. index and accreted layer thickness 80—58462
flyash from coal combustion, S and Cl adsorpt., cloud nuclei form. 77—21887
force between adsorbing walls separated by Lennard-Jones liq., Monte Carlo calc. 80—15363
formaldehyde, on Ru(110), UPS study, 80K 78—73080
formate ions adsorbed on Ag particles in aqueous soln. Raman spectra 80—69148
fracture processes, adsorption-sensitive, control and appl. 77—52468
free energy change, direct eval. from single adsorption isotherm 77—35807
Freundlich and Dubinin-Radushkevich isotherms, model 77—20194
gas, installation for studying static characts. of porous and nonporous materials 80—81361
gas, surface areas calc. using programmable calculator 78—15706
gas adsorption data analysis, pore size and size distribution determ., review 78—63939
gas atmosphere quantitative analysis adsorption chamber 80—85234
gas atom scattering by adsorbed layer, hard sphere theory *(Russian)* 79—38704
gas chromotography, modified geophitised C black adsorbent 79—96358
gas diffusion eqn., recoil/sticking probabilities at wall 77—51149
gas-liquid interface of rising bubbles, adsorption rate determ. *(Japanese)* 80—6595
gas-solid, spectrophotometric obs. using IR vacuum cell 79—80703
gas-solid interface, EPR centres induced by microwave gas plasma 78—80215
gas-solid interface, surface stress and tension 79—60627
gas-solid processes, generalised Langevin theory, solid models convergence 80—49489
gas-solid surface sticking probabilities, internal mode depend. 78—6213
gas-surface interaction theory 79—87002
generalised surface-layer model calculations, refinements 78—3348
Gibbs adsorption equation, phenomenological interface theory 79—23834
glass, adsorption of Au, AES study, electron bombardment effects 80—65380
glass, BK 7, of ethoxysilanes, IR spectra *(German)* 78—30834
glass, in detergent solns., protein adsorption 78—44401
glass, of Rn 80—10775
glass, surface cond., effect of impurity adsorption *(German)* 78—30971
glasses, porous, of water, thermoosmotic flow, filtration investig. 78—53248
grain boundaries decohesion energy, solute adsorption influence 80—65009

adsorption continued
grain boundary cohesion, resulting from solute segregation, pair bonding theory 80—88166
grain boundary segregation theory in terms of surface adsorption analogues 78—15407
graphite, adsorbed methanol, proton mag. relax. times obs. 77—51590
graphite, adsorbed water vapour, CH_4 release from graphite, desorption study 79—51420
graphite, adsorption and migration of O_2, CNDO/2 calcs. 79—28205
graphite, adsorption of CH_4, Kr, Xe, substrate deform. meas. 80—54520
graphite, adsorption of CO, fluid-registered solid transition 80—59796
graphite, adsorption of cyclohexane *(Italian)* 77—55439
graphite, adsorption of Xe and Kr, first layer study 79—73397
graphite, Ar monolayer, adsorpt. isotherms LEED geometry and intenstiy meas. 79—65316
graphite, exfoliated, of benzene, −70 to −5°C *(French)* 79—33177
graphite, exfoliated, of cyclohexane, −25 to −70°C *(French)* 79—33178
graphite, He scattering, bound state reson. and inelastic effects 79—28876
graphite, interaction with Cs, study of surface diffusion, computer simulation 78—30837
graphite, N adsorption, surface homogeneity changes on gasification 79—51396
graphite, of Ar, Lennard-Jones 9:3 adsorptive system, Percus-Yevick and hypernetted chain theories 80—20030
graphite, of Ar, orientational ordering of incommensurate monolayers, LEED obs. 78—95233
graphite, of Br_2, EXAFS 77—43430
graphite, of first layer of Ar, 55-62K 79—28197
graphite, of H_2, 63 to 90K *(French)* 77—11791
graphite, of H, effect of non-orthogonality between localised orbitals of adsorbed atom 77—43435
graphite, of He, surface band splitting, theory 80—60058
graphite, of inert gas, phase transitions using Landau model 79—69243
graphite, of inert gas microcluster, temp. depend., mol. dynamics study 80—80056
graphite, of inert gases, solidified layer struct. and density *(French)* 78—18893
graphite, of methane, mobility of 2-dimens. hypercrit. fluid, neutron scatt. obs. 77—20193
graphite, of methane, NMR pulsed field gradient method, diffusion coeff. meas. 80—15362
graphite, of methane, phase transitions and orientational order, mol. field theory 79—95257
graphite, of methane in first monolayer domain, thermodynamic props. *(French)* 80—29275
graphite, of N_2, Ar, monolayer two-dimensional phase change, calorimetric investig. 77—47669
graphite, of $N_2(H_2)$, orientational ordering, theory 80—2262
graphite, of neopentane, NMR pulsed field gradient method, diffusion coeff. meas. 80—15362
graphite, of neopentane, quasi two-dimens. fluid, NMR 80—102525
graphite, of NH_3, NMR pulsed field gradient method, diffusion coeff. meas. 80—15362
graphite, of O_2, graphical determ. of entropy of adsorpt. *(French)* 77—11790
graphite, of O_2, mag. phase transition, theory 78—38811
graphite, of O_2, partially localised, partially mobile monolayer films, adsorption isotherms 80—107646
graphite, of o-H_2 (p-D_2), NMR, orientational behaviour, weak crystal field 78—75935
graphite, of trimethyl tin chloride, mol. orientation, recoilless gamma reson. 77—76663
graphite, sliding against C, dusting wear regime 80—97595
graphite, Xe-plated, of Ar, virial coeffs. and interatomic pots. 77—9125
graphite (0001), ^{4}He selective adsorption, level crossings 80—71556
graphite (0001), inelasticity in He scatt. 80—76127
graphite (0001), of Xe, kinetics using AES 77—72782
graphite (0001), scattering and selective adsorption of H_2 (D_2) 80—71553
graphite basal plane surface, selective adsorption of ^{3}He and ^{4}He 80—6650
graphite fibre, Type-A, surface comp. and energetics 77—70024
graphite selective adsorption from Ar-N_2 liquid soln., mol. dynamics calc. 80—59806
graphite surface, adsorbed Cs, dissolution, lamellar cpd. form. *(French)* 80—100399
graphite surface, asymptotic interaction with He, H, and H_2 79—99429
graphite surface interaction with He atom 80—34316
graphite-Br system, intercalation threshold, ellipsometric investigation 78—26760
graphite/inert gas adsorption, modified Buckingham pot., virial coeff. anal. 79—65312
graphitised C black, of inert gases, gas-solid virial coeffs. 78—75928
graphitised C black, of inert gases, Henry constant, rel. to intermol. interaction pot., review 78—22948
graphitised C black, of methane, rot. tunnelling, neutron scatt. obs. 79—15000
graphitised carbon black, of Ar, (methane), surface excess isotherms, gravimetric determ. 78—51816
graphitized C black, continuous phase transitions of adsorbed Kr monolayers 78—34698
graphitized C black, virial coeff. theory of Kr adsorption 78—34697
graphon, of Ar, high press. and temp., gas density profile theory 78—67903
haemoperfusion through fixed-bed adsorber 78—31976
halide, of O_2, bidimensional condensation *(French)* 78—75941
halloysite, $Al_2O_3(SiO_2)_3(H_2O)_2$, NMR study of adsorbed water, molecular motions 78—95226
hard sphere gas interacting with hard wall, density profile, virial expansion 78—63928
hard sphere mixture on to plane surface, Percus-Yevick approx. 77—31878
hard sphere/hard wall interaction, local density, adsorption theory *(German)* 79—77925
hard spheres near hard wall, comparison of adsorption theories 78—38934
hard-sphere fluid, monolayer adsorption profile, adsorption isotherm 79—33182
heat of adsorption determ., expt. methods 79—42370

adsorption continued
Henry's constant, pre-exponential factor *(German)* 78—22961
Henry constant, rel. to intermol. interaction pot., review 78—22948
heterogeneous micropore systems, filling, generalisation of Dubinin-Radushkevich eqn. 77—47664
heterogeneous nucleation systems, crit. conditions characterising formation 78—56023
heterogeneous reactions, bimolecular, following Langmuir-Hinshelwood mechanism, rates 79—84907
heterogeneous solid surface, adsorption from multicomponent gas and liq. mixtures *(German)* 80—44430
heterogeneous solid surface reflection, in scope of adsorption thermodynamic quantities, on basis of Langmuir model *(German)* 78—30831
heterogeneous solid surfaces, of gases, calc. using model of associated adsorbate 78—34699
heterogeneous surface, adsorpt. energy distrib., surface topography effects 77—89649
heterogeneous surface, gas mixture adsorpt. equilib. at const. total press. 77—55442
heterogeneous surface, gas mixture adsorption, expt. data analysis 78—60030
heterogeneous surface, isosteric heats of components in mixed gas adsorpt. 77—55445
heterogeneous surface, localised and nonlocalised adsorpt. theory 78—14572
heterogeneous surface, of gas mixtures, energy distrib. 77—85079
heterogeneous surface, topography effects on adsorpt. energy, asymptotically correct condensation approx. 79—7753
heterogeneous surface adsorption, energy distrib. function, virial anal. 77—28080
heterogeneous surfaces, multilayer BET adsorpt. of atoms, thermodynamic functions *(German)* 79—95267
heterogeneous surfaces, of atoms, monomol. adsorpt. thermodynamic functions *(German)* 79—90891
heterogeneous surfaces, of multicomponent liq. mixtures 79—56073
high-current multirod cathode, influence of absorption effects on characts. 80—20756
homogeneous solid surface, monomolecular adsorption of single gases, model 79—4477
homogeneous solid surfaces of binary gas mixtures, theory 79—42387
homogeneous surface, adsorpt. of single gases statistical thermodynamics 78—79877
homogeneous surface, competitive adsorption of binary gas mixtures *(German)* 79—33195
homogeneous surfaces, statistical mech. of collisions which lower desorption rate *(German)* 78—84072
homopolymer chain adsorpt. on uniform surface 78—53316
homopolymer chain adsorption on homogeneous surface, theoretical model 77—70403
human red cell membranes, surface adsorpt. of dextrans 78—15799
hydrocarbons, formation on metal surfaces in fusion reactors 80—21322
hydrodynamic interfacial instability, mechanical, chem. and elec. constraints, review 80—34278
hydrogen embrittlement, adsorpt. model. and equilibrium crack growth meas. 80—108574
hyrocarbons, on activated C, rel. between adsorption and polarizabilities 80—76558
ice, I_h, water monomer on basal plane, static interaction model 78—18891
ice, of CO_2, H_2S, propane, gas hydrate form. investigs. 79—39191
II-VI semiconductors, of H_2, O_2 and N_2, effect on thermoemission of positive ions *(Russian)* 77—28676
III-V semiconductor-oxide interface states, photoemission obs. of energy levels induced by adsorpt. 80—93000
immiscible incompressible fluids, interfacial convective instability, diffusional exchanges, adsorption-desorption processes 80—70504
immunology, Ni plated slides, effect of metallic shield on cosmic radiation effects 80—56317
Inconel 600, fusion reactor vac. vessel, air, N, adsorpt., thermal desorpt., heat treatment effects 78—54880
inelastic electron tunnelling spectroscopy, rel. to vibration energy levels of adsorbed mol. or atom 79—4479
inert gas atoms, physisorbed, dipole moments of atoms 79—33175
inert gas ion milling processes, etch-rate ratio of oxides to nonoxides, increase using halocarbon gases 80—93663
inert gas solid, in inert gases, sp. ht. of adsorbates calc. 77—1302
inert gas solid layer, of H_2, sorption capacity meas. 79—90865
integral equation, new method of solution 77—28076
interface atomic structure, interface roughness, calc. *(Russian)* 80—103587
interfacial cohesion, adsorption-induced losses 80—65010
interfacial tension var. with supersaturation, one-layer adsorpt. model 80—103563
intermolecular surface forces in plane densely packed hexagonal model 80—59785
interstellar amorphous ice grains, H_2 form. and importance for planetary atmospheres 80—26933
interstellar grains surface activity, adsorbed mol. ions rel. to diffuse spectral bands 77—26040
inverse power law potentials about polygonal prisms and in polygonal cavities 78—95232
inverse power law potentials in rectangular configurations 79—28213
ionic, quantitative approach 80—49522
ionic crystal, anisotropy of adsorption for mol. SCF MO LCAO calcs. 77—89643
ionic crystal, gas-solid interaction potential, adsorption sites and surface migration 80—24738
ionic crystal, phys. adsorption of nonpolar gases, localised and mobile phases, hopping adsorbates 80—24739
ionic crystal, space charge polarisation involving electrode reaction with surface adsorption 77—12019
ionic crystal surface, electrostatic interaction energies 79—23831
IR frequency shifts, coverage dependence 79—19464
iron phthalocyanine film, electroconductivity, effect of adsorption 77—85356
island film growth, cluster size distrib. 80—107665
isolated discharge electroerosion craters, interelectrode surfactant effect *(Russian)* 79—83462
isostere equation, comparison with that based on John's isotherm eqn. 79—42368

adsorption continued
isotherm, exponential possibility of adsorbent heterogeneity determ. 77—7969
isotherm, statistical mechanics, summation of virial expansion for eqn. of state 79—15007
isotherm and solute activities from spreading pressure-surface charge data 78—14576
isotherm equation based on vacancy solution theory 80—65356
isotherm extrapolation, John's method, linearity range implication 80—34293
isotherm for study of interfacial and biological phenomena 77—59207
isotherm shape, mol. theory 79—90867
isotherms, Adamson and Ling's analysis 77—31906
isotherms, Adamson and Ling's analysis 77—31907
isotherms for heterogeneous substrates, improved CAEDMON program 79—77895
jellium, of H, simple model 77—69171
jellium surface, interaction with H_2 80—29259
Jovanovic isotherm, theoretical validity 79—73400
kaolinite, of H_2O, volume expansion lattice deform. 80—45555
kinetic analysis of Langmuir and Jovanovic models 79—33191
kinetic eqn. under electron bombard. conditions *(Russian)* 79—77893
kinetics analysis using Ritchie's equation 79—90871
kinetics of gas adsorpt. on solid, alternative to Elovich eqn. 78—14579
Kisliuk model for adsorption and desorption kinetics 79—73409
β-lactoglobin, meas. at interfaces by drop volume technique 78—60009
Lennard-Jones 9:3 adsorptive system, Percus-Yevick and hypernetted chain theories 80—20030
lipid bilayer, of cytochrome c 78—69001
lipid bilayer membranes, spectrophotometric and elec. correls. of cyanine-dye adsorpt. 80—85358
liquid, of polymer 77—20166
liquid alloy, surface tension and surface adsorpt. determ. *(French)* 79—69325
liquid film, falling, O_2 adsorpt. with zero order react. in entrance region 80—64652
liquid mixture, adsorption on solid, equilib., thermodynamics correlations 78—84045
liquid-liquid interfaces in isolation, and in interaction, review 77—47651
liquids capillary rise, contact angle and film jumps 77—66076
local densities of states near a crystal surface with disordered overlayer 79—15201
localised, on homogeneous solid surface, Berezin-Kiselev model 80—10780
localized monolayer adsorpt. of gas-mixtures on heterogeneous surfaces, stat. thermodyn. 78—2371
low energy ion backscattering, struct. anal. 78—15271
low energy ion scattering analysis of surface and thin film composition *(French)* 77—59663
low-density gas, motion and absorption in porous medium, stochastic calcs. 77—7449
lunar soil 15081,2, adsorpt. of methanol and water, microcrystallinity determ. 77—87292
lysozyme absorpt. meas. at interfaces by drop volume technique 78—60009
macromolecular adsorption, onto inorganic substrate, surface struct. 79—69342
macromolecule, on charged surface, weak electrostatic attraction 77—19118
magnetic surfaces, ortho to para H_2 conversion 79—34362
mean sojourn time of molecules on surfaces, meas. in practical vacuum system *(Japanese)* 80—57315
mean spherical model for interacting particle adsorpt. 77—4260
measurement using pulse gas chromatography of adsorption rate consts. in packed bed 79—48002
membranes, linear laminated media, permeation, sorpt. 79—1966
metal, adsorbate vibrational excitation by inelastic electron scatt. 77—43428
metal, Friedel oscillations around adatom 78—30967
metal, light reflection, adatom characts. depend. 78—10918
metal, of gas, general rule 77—85078
metal, of H_2, interaction between gas atoms on approach to surface 78—14609
metal, of $H_2(O_2)(CO)$(benzene), exptl. aspects of angle-resolved photoemission 78—15294
metal, of H_2 and N_2, permeation through metal barrier, adsorpt. processes 78—63879
metal, of He, HF calc. of repulsive pot. contrib. 77—43434
metal, of He, interaction energy, quantum mech. density functional formalism calc., comp. with expt. 78—67911
metal, of inert gas, interaction energy, quantum mech. density functional formalism calc. 78—67911
metal, of molecule monolayer, IR spectra exam. by surface EM wave spectroscopy 78—71967
metal, perfectly imaging, physical adsorption of atomic H, variational cals. 79—33188
metal, with low adsorption activity, diffusion coeff. of H, steady-state flow method 80—10795
metal, with substitutional disorder, density of states, Green's function theory 78—23145
metal, work function changes due to absorpt. 77—7972
metal, XPS satellite spectra of adsorbed atoms 77—20993
metal ammine complexes, metal extraction by adsorption, using low rank coals 79—11530
metal film, evaporated, of gases, rel. to surface area 78—79909
metal films, evaporated, with BCl_3, HCl, interaction, adsorpt. 78—75945
metal ion adsorption, nucleation effects *(German)* 78—68635
metal ion electroreduction, ion-induced adsorpt. 80—21297
metal of O_2, effect on sputtering-induced photon and ion emission 77—28674
metal oxide, of molecules, UPS studies, review 80—84374
metal oxide surfaces, of electron acceptors, strength and distrib. of electron donor sites 78—84055
metal substrate, adsorption systems, relationship between work function and degree of adsorption coverage 79—83092
metal surface, adatom pair interaction asymptotics, degenerate electron gas permittivity 80—29281
metal surface, adsorbed molecule giant Raman scatt. mechanisms 79—51960
metal surface, adsorbed molecule vibration excitation low energy electron scatt. 78—18910

adsorption continued
- metal surface, alkali adsorption, finite barrier model, bounded electron gas static semiclassical response 78—72221
- metal surface, atomic and mol. beam scatt., review 80—40203
- metal surface, electron density depend. on modulation, adsorption, diffusion 80—54526
- metal surface, interaction with neutron mol. 77—80701
- metal surface, kinetics of adsorpt., desorpt. and migration, review 79—46921
- metal surface, reactivity, review of electron spectra 77—62748
- metal surface, reson. interaction with neutral mol. 77—80702
- metal surface, review 79—37912
- metal surface, review *(Russian)* 79—46963
- metal surface, sticking probability, correl. with adsorbate-induced electron struct. 80—39425
- metal surface, vibr. motion of adsorbed molecules, inelastic scatt. of electrons, model 78—34718
- metal surface, work function change on simultaneous adsorption of atoms of two different elements 78—60184
- metal surface electronic barrier, elec. field effect in presence of adsorbate, Thomas-Fermi model 80—49864
- metal surface $H_2 \rightleftharpoons H+H$ reaction rel. to catalysis, friction coeff. calc. 77—77807
- metal surface region, electrostatic energy and screened charge interaction for different Fermi surface shape 80—70631
- metal surface struct. and initial stages of reactivity, review 78—68837
- metal surfaces, adsorbate spectra, vac. UV differential reflectivity obs. 79—28783
- metal surfaces, of H, adsorption mechanisms 79—69368
- metal surfaces, of inert gases, density functional approach 77—85061
- metal surfaces, radioactive contamination 80—68771
- metal surfaces self-diffusion of single atoms and diffusion of adatoms, activation energies calc. 80—24732
- metal tip profile change meas. for evaporation rate determ. 77—24403
- metal-adsorbate system, appl. of cluster model theory, book contrib. 80—24991
- metal-electrolyte interfaces, optical reflectance specta, interpretation 80—93263
- metal-H system, hydride formation in high press. range 80—65235
- metal-sapphire interface, effect on shear strength of adsorbed species 80—49485
- metallic films, adsorption studies using modulated surface plasmon reson. 79—82439
- metallic membrane interface, mass transfer 80—81366
- metallic substrate, metal atom adsorption, enthalpy calc. 80—100406
- metallic surface, coupling to fluctuating atomic dipole, screening of point charge by surface plasmons 77—59217
- metallic surface, of inert gas atoms, collective effects in physical adsorption 79—19456
- metallic surfaces, adsorption of inorganic and organic molecules, mechanism and effects, exam. *(German)* 78—51828
- metallic surfaces, thin film appls. 78—75943
- metallic thin film, electrical resistance, effect of gas adsorption review *(Rumanian)* 79—82691
- metals, adsorption potential in hydrodynamical model 80—100396
- metals, of atoms, Green's function formalism for studying electronic struct., local density of states calc. 80—107884
- metals, of gases, review *(Japanese)* 79—46930
- methane as fuel, solid state storage device study using physisorption data *(German)* 79—96414
- methyl iodide removal by Ag impregnated Al and zeolite 78—53719
- mica, of aq. poly(ethylene oxide) soln., force meas. between mica surfaces 79—23833
- mica, of propylene from isomerisation of cyclopropane 79—74376
- microcrystallites, LCAO-MO calcs, in HMO approx., influence of lattice distortion adsorption, absorpt. of gases *(German)* 78—30584
- microporous solid, electrical double layer on surface 80—11955
- microscopic approach onset of multilayer adsorption 77—47650
- minerals, inorganic, of aqueous heavy metals, expts. 78—49006
- Mischmetal-Ni alloy, H_2 adsorption and desorption *(Japanese)* 77—47668
- mixed gas adsorption, homogeneous solid surface, adsorbate-adsorbate assoc. model 80—96742
- mixed gas adsorption, on heterogeneous solid surface, kinetics 78—95231
- mixed gas adsorption, review of theories 78—75942
- mixed gas adsorption on solids, Bragg-Williams approximation 79—19465
- mixed sterically-stabilised dispersions, equilib. aspects of heteroflocculation 80—45570
- modulated molecular beam mass spectrometry, anal., appl. to nonlinear systems 78—56944
- molecular adsorption, effective reson. Raman spectra 80—97730
- molecular adsorption, ratios between rates of thermal dissociation, desorption and diffusion 79—95265
- molecular dumbbells with distinguisable ends, 1-D neighbour pair degeneracies 78—34735
- molecular sieves, adsorpt. of atmospheric gases, comparison of 13X and 4A at low temp., press. *(German)* 80—88423
- molecular sieves, bi-porous, sorption kinetics, expt. and theory comparison for batch systems 79—87873
- molecular sieves, bi-porous sorption kinetics, math. models for systems with rectangular equil. isotherm 79—87872
- molecules adsorbed on rough surfaces, Rayleigh, Mie and Raman scatt. 80—83378
- monolayer adsorption from multicomponent gas mixtures, lateral interactions and surface heterogeneity effects on kinetics 79—90890
- monolayer films, partially localised, partially mobile, adsorption isotherms, temp. depend., theory 80—107646
- monolayer formation on solid surface as friction protection 78—47663
- monolayer localised and mobile adsorption from gaseous phase onto solid surfaces, unified description of kinetics 80—10797
- monolayer mobile adsorption, 2-D hard disc model, perturbational method 78—38932
- monolayer model for gas adsorption on random topology of heterogeneities 79—23827
- monolayer-covered surface, surfactant adsorpt., Gibbs eqn. calcs. 80—59781
- Monte Carlo calcs., grand canonical ensemble, long-range corrections 78—30826
- montmorillonite, of N_2, H_2O, cyclohexane vapours, specific surface area 79—29406

adsorption continued
- multicentred adsorbed particles, configurational entropy and blocking coeff. 77—60118
- multicomponent surface phase, comp. determ. from gas adsorption data 80—88417
- multilayer adsorption isotherms, step formation, lattice model investig. 78—14575
- multilayer adsorption of gases on solid surfaces, heterogeneity effects 79—28212
- multiple layer, lattice gas model 78—38956
- multisite adsorption, mean field theory and Monte Carlo simulation 79—60630
- N_2O refrigerator, thermodynamics and thermoelectric condenser design 80—108809
- naphthalene, adsorbed on silica gel surface, biphasic photochemistry, time-resolved spectra 80—30252
- nearly free electron metal surface, at. chemisorption 78—14588
- neutron scattering from adsorbed mols., surfaces and intercalates, review, book contrib. 80—84394
- nickel phthalocyanine film, electron acceptor surface states due to O_2 adsorption 80—88586
- 9-nitroanthracene, semiconductive props., gas adsorpt. effect 79—65471
- nitrobenzene, adsorbed radicals, oxide surface chem., ESR 77—21417
- noble metal film, of O_2, modulated surface-plasmon reson. in situ meas. 77—77311
- nonequilibrium distributions on lattice, operator formalism 79—4468
- nonequilibrium parametric pump, steady state predictions 77—49736
- nonisothermal one-component sorption in adsorbent particle, interparticle heat transfer 80—70523
- nonisothermal sorption within adsorbent particle, heat and mass balance 79—19452
- nonlinear adsorption isotherms, breakthrough curve *(German)* 79—86978
- nonlinear diffusion-reaction problem, dissipative structs., stability anal. 79—1938
- nonplanar geometry, physical adsorption 78—79887
- nonpolar molecules, adsorption into lipid bilayer membranes 80—61517
- oil-water interface, electroadsorption and electrocapillarity 80—44393
- one-dimensional lattice model, thermodynamic functions calc., matrix method 79—37917
- optical examination and monitoring of surfaces, review 79—67375
- optical filter, moisture penetration patterns 77—767
- optical glass, surface layer structure after grinding and polishing, Kr sorption meas. 77—31122
- optically oriented atoms, surface thermal relax. adsorption thermodynamics 77—24480
- organic compound, two-dimensional condensation with adsorbed mol. reorient. 78—61051
- organophilic montmorillonites, of methanol-benzene mixtures, effect of surface modification 78—84056
- oxide surfaces, adsorbate spectra, vac. UV differential reflectivity obs. 79—28783
- partial localisation model *(French)* 80—70526
- particle absorption rates at high cell concs., Monte Carlo simulation 80—94141
- patchwise heterogeneous surface, applic. of extended model of associated adsorbate 78—14617
- patchwise heterogeneous surface, localised adsorption of gases, effect of local correl. between adsorbed mols. *(German)* 80—44432
- patchwise heterogeneous surface, thermodynamics of localised and nonlocalised adsorpt. 77—1299
- pendular ring condensation on spherical adsorbent, surface tension curvature depend. 79—46926
- Percus-Yevick and hypernetted chain theories, second and third virial coeffs. for hard-sphere gas 78—60031
- perylene, anthracene, radical cation, EPR, acidic surface anisotropic rot. diffusion 78—27095
- 1-phenylpyrazolidin-3-one adsorption on metal electrodes, obs. 79—100391
- phosphatidylcholine hydration, adsorpt.-desorpt. isotherm and PMR 78—15781
- photoemitter, adsorpt. effects on emission, theory 78—2996
- phthalocyanine films, metal-free, adsorbed o-chloranil effect on surface photovoltage 80—34485
- physical adsorption, high press. and temp., gas density profile theory 78—67903
- physical adsorption, vacuum microbalance studies 80—76551
- physics of transitions, introduction 78—26660
- planar surface, rigid rodlike mol. adsorption, long range dispersion interactions, statistical mech. anal. 80—29265
- plane surface, of macromols., computer rel. to real expts. *(Russian)* 79—56077
- plant tissue, of water, detection of OH groups for adsorption centres, dielectric relaxation *(Japanese)* 80—7999
- plasma etching, mech., review 79—83348
- plasma protein interaction with polyion complex studied by circular dichroism and UV spectroscopy *(Japanese)* 80—12316
- plasmon satellites and relax. shifts in adsorption spectroscopy of adsorbed atoms 77—59204
- polar molecules, spontaneous surface polarisation during adsorption 79—42381
- polarographic maximum suppression by substituted vinyl quinolones 79—57325
- poly(vinyl pyrrolidone), silicone grafted, for contact lenses, surface props. and stability of thin tear film 80—17194
- poly (N^{α},N^{ϵ}-terephthaloyl-L-lysine) membrane for artificial red blood cells, interaction with serum proteins *(Japanese)* 80—12061
- polybutadiene, adsorption behaviour, surface tension exam. *(Japanese)* 78—31690
- polyethylene, self-adhesion, surface polarity effect, meas. by Ca^{2+} adsorpt. 79—11759
- polyethylene terephthalate film, surface modification by corona discharge, adsorption and wettability 77—86212
- polyethyleneterephthalate, film, props. of adhesive layer adsorbed on surface 79—56067
- polymer, scaling theory 77—35811
- polymer adsorption at interface, self-avoiding random walk anal. 77—1085
- polymer adsorption into surface pores, computer simulation, phase transition *(Russian)* 78—51824
- polymer adsorption on small spheres, scaling approach 78—3377

adsorption continued
polymer adsorption/adhesion, smooth surface, mech. stress effects *(Russian)* 78—50672
polymer attached to surface, dynamics, bead and spring model 78—75931
polymer carbons, water vapour adsorption, porosity, and surface chem. 79—52753
polymer charcoal, adsorpt. isotherms of organic vapours 80—96731
polymer config. on interaction with interface 78—47659
polymer cryovacuum adsorbent, high efficiency, N_2 adsorption 79—63249
polymer films, electret state and adsorption during injection 79—69770
polymer flexible lattice chain in limited vol., behaviour *(Russian)* 78—70992
polymer random flight chain, surface adsorbed, end-to-end mean value 78—22060
polymeric composite, interphase, physico-chemical problems 80—16262
polymeric molecules adsorption, statistical mechanics appln. 80—84365
polymers, adsorbed molecules, configurational behaviour, computerised dynamic display 79—874
polymers, adsorption transition, excluded vol. effects, Monte Carlo and enumeration calcs. 78—67906
polymers, of gases, sorption, permeation investigs., review 78—67868
polymers, of molecules, Green matrix local impurity SCF calcs. 80—92778
polymers, of plasma proteins, Fourier transform IR spectrometry 80—16899
polymers in mixed solvents, preferential adsorpt. coeff. rel. to mol. dimens. 80—103237
polymolecular adsorption on heterogeneous surfaces, statistical thermodynamical eqns. *(German)* 78—30830
polyox dilute aqueous solns., flow resistance mechanisms in porous media 79—41747
polystyrene, γ-Fe_2O_3 powder filled, mag. films, packing and particle orientation *(Japanese)* 80—104115
polystyrene, of albumin and fibrinogen, contact angle meas. 80—61508
polystyrene, porous gel, solute elution behaviour in high performance liq. chromatography 78—92524
polystyrene latex particles, of poly(vinyl alcohol), influence of temp. 78—85206
polyvinyl acetate, γ-Fe_2O_3 powder filled, mag. films, packing and particle orientation *(Japanese)* 80—104115
polyvinyl acetate film, charge retention, adsorbed water vapour effects, TSC obs. 77—32321
polyvinyl butyral, γ-Fe_2O_3 powder filled, mag. films, packing and particle orientation *(Japanese)* 80—104115
pore size measurement, comparison of methods 80—62622
porous, media, of radioactive gas, diffusion, adsorpt. *(Russian)* 77—27591
porous glass, of ethanol, IR obs. 79—23830
porous solids, pore struct. anal. using adsorpt. data, appl. to active C 77—32763
powder surface area determ., simple continuous flow apparatus 77—16777
precursor intermediates in adsorption, desorption and reaction 80—108731
probe, vibrating capacitor type, for surface and adsorption studies 78—10274
protein adsorption and immunological reactions at liq./solid interface, ellipsometry obs. 77—52948
protein adsorption at liq.-solid interface, ellipsometric estimation of film thickness 78—44740
proteins, of non-paramag. compounds, spin probe investigation 78—65153
proteins, on polymer surfaces, structural changes 80—89712
pyrene adsorbed on silica gel surface, biphasic photochemistry, time-resolved spectra 80—30252
Pyrex glass capillary tubes, effect of adsorbed water vapour on liq. water flow 80—92759
pyridine, adsorpt. on Pt/Al_2O_3, electron accepting sites 80—71947
Quantum theory of adsorption of isolated adatoms 78—22957
quartz, of water, appl. of Hill-de Boer eqn. 79—15008
quartz, surface cond. adsorbed gas effects 77—85297
quartz surface, of chlorosilanes and n-alkanes 79—4466
quinone adsorption on electron-donor and electron-acceptor centres of oxiphenol radical *(Russian)* 79—39138
radioactive waste, geologic storage, effect of adsorption of Tc and I radioisotopes by minerals 80—83203
radioactive waste, sorption of actinides in igneous rocks 80—95367
radiotracer method investig. appls. 80—70525
rare earth, of $H_2(D_2)$, adsorpt. and absorpt. 77—4257
rare earth metal film, O_2 and H_2 contamination effect on elec. resist. 77—80856
rare earth metal films, of water, XPS obs. of oxidation 77—31888
Rebinder effect in breakdown of dielectrics 77—44328
reconstructed surfaces, effect of adsorbed atoms or mols. 78—95214
refractory materials, emission and adsorption props., rel. to electronic struct., review 77—76899
regenerated cellulose-activated charcoal membrane adsorpt. characts. for haemoperfusion *(Japanese)* 80—12298
relaxation energies in XPS, calc. for adsorbate 78—15283
rigid rod adsorption, on solid surface, lattice model 77—85051
rocks of Xe and Kr, rel. to Mars regolith adsorption and atmosphere rare gases concs. 78—49358
rough surfaces, adsorpt., capillary condensation 79—1544
rubber latex, natural, mechanical and chemical stability enhancement, by potassium fatty-acid soaps 79—96034
selective, correlation of intensity features with at.-surface pot. Fourier components 79—15013
semi-infinite crystal with surface impurity, electronic states 79—24046
semiconductor, interface form., initial steps, surface states and thermodynamics 80—49503
semiconductor, nonpolar, empty surface states and surface order effects on sorption 77—85281
semiconductor, photoemission meas. of surface and bulk states 80—25527
semiconductor, with defects adsorbed mols. and metal overlayers, electronic structure 79—95466
semiconductor gas detector, for gas chromatograph, electroadsorption phenomena *(Russian)* 78—7307
semiconductor surface, review 79—37912
semiconductors, adsorption, boundary layer and electron theories *(German)* 78—95236
Si, complexing mechanism, effect of ion etch rate 79—70197

adsorption continued
SI units, in adsorption expts., replacement of Langmuirs and exposure proposed 78—62175
silica, of water:Cu(II), EPR spectrum, freezing props. of water 77—4555
silica, of water, stepwise multilayer adsorpt., 130-150°C 78—14574
silica (metallised) gels, thermal cond., 10-200K, cryogenic appls. 78—79828
silica gel, adsorption from soln. of benzene-cyclohexane mixture, surface heterogeneity 79—23826
silica gel, Mn^{2+} adsorption rel. to H_2O adsorpt., EPR study 79—5180
silica gel, of H_2O, pore struct., effect of washing 79—52786
silica gel, surface cond., effect of impurity adsorption *(German)* 78—30971
silica gel, toroidal amorphous microporous, low-temp. adsorption of N_2 79—57305
silica gel for low temp. regenerator of cryogenic refrigerator 77—17994
silica gels, surface treatment, adsorption properties *(Japanese)* 78—95855
silicate glass, hydration in steam atmosphere 80—85211
SIMS, appl. to surface anal., review 80—40204
SIMS, solid surface investig. applications *(Rumanian)* 80—49510
soil-water system interfacial reactions and heavy metal adsorption 78—3832
solid electrolyte-metal interface adsorption layer capacitance calc. *(Russian)* 80—59697
solid gas, porosity, appl. to cryosorption pump *(Japanese)* 80—20031
solid particle interaction, adsorpt. effects 78—11569
solid surface studies, recent progress *(Japanese)* 80—15347
solid surfaces, photoemission from adsorbed atom valence orbital and surface plasmon emission, model Hamiltonian calcs. 80—50525
solid surfaces, surface heterogeneity in physical adsorption 79—23829
solid surfaces, surface processes, and solid/gas interactions 80—73125
solid-electron interactions, conf., Southampton, England (Apr. 1976) 77—44570
solid/gas interfaces, in situ Fourier transform IR spectroscopy 80—37100
solid/liquid adsorption equilib., kinetic studies using isotopic mol. exchange method 80—88427
solid/liquid interface interactions, IR spectroscopy obs., review 80—40733
solids, amorphous and crystalline, condensing from gas phase, nucleation, growth and transform. 80—24745
solids, of gas mixtures, review 79—28211
solute transport in soils, two-site adsorption-desorption model evaluation 77—41101
solutes in aqueous fissures in porous rocks, effects of adsorption on transport 80—94553
solution, different-sized mols., orientation effects, surface region, lattice model 79—1540
solution adsorption, from liq. chromatography 78—84054
specific adsorption of ions, differential capacity meas. in binary electrolyte solns. 80—26025
spherical particles adsorption, statistical mechanics appln. 80—84365
Spheron 6, surface group obs. using gaseous reagents, surface acidity evolution during heat treatments *(French)* 77—66767
static AES technique, appls. 78—84685
statistical mechanics, cluster expansion of adsorption isotherm, grand partition function 77—69162
statistical mechanics, virial expansion, eqn. of state and isotherms *(German)* 78—95235
statistical mechanics, virial expns. in 3D model 79—77891
statistical mechanics of adsorption processes 79—40460
statistical mechanics of short chain mols. at interface 77—43426
steel, alloy, friction with cast Fe, boundary and oil-abrasive, adsorption effect 80—55546
steel, high-strength, lowering, influence of H_2, H_2S, HCl and CH_4 gases *(Russian)* 79—52440
steel, of H_2, correl. with H_2 embrittlement 77—36645
steel, quenched surface layer hardness rel. to adsorption contact fatigue *(Ukrainian)* 80—40478
steel, room temp. O_2 adsorption in ultra-high vacuum system 77—20188
steel, segregation and adsorption of S, influence on carburisation and nitrogenation 80—66701
steel, stainless, exoelectron emission, effect of gas press. and sample temp. during slow electron excitation 79—61505
steel, stainless, of O ions 79—1547
steel, stainless, oxidised, of Cs 78—84061
steel, stainless, type 304, surface treatment effect on protium uptake, AES anal. 77—59984
steel cutting and grinding, surface adsorption effects 78—39938
steel fatigue in surface active media, adsorption facilitation mech. 80—55586
steels, strength reduction by adsorpt., stress corrosion *(Russian)* 79—29265
STEM, at. resolution, adsorpt. and diffusion of heavy atoms on light element substrates 77—24484
sticking coefficient at low temp. for atoms on solid surface 78—22955
sticking coefficients of atoms on solid surfaces at low temperatures 79—95263
substrate-split localised adsorbate levels, spin polarisation effects in photoemission 79—19971
superconductor, raising of critical temp. *(Russian)* 78—84337
surface, adsorbed atoms thermal desorption, one dimens. microscopic model, weak binding case 80—96729
surface, coverage of foreign atoms as function of adsorption, sputtering and diffusion rates 79—69354
surface, solid, of microdrop, stability, dynamics 78—51790
surface, use of vacuum ultramicrobalance 79—71465
surface adsorbed molecules, internal optic modes, mol. dipole model 80—100395
surface band theory and surface transport props. 77—43680
surface chemical bond, book 80—22147
surface coating, adsorpt. of Cs ions on constituent materials 78—23843
surface crystallography and bonding, book contrib. 80—24724
surface dipole layers, forces between plates 80—70793
surface EXAFS study of adsorbate Auger electron intensity on single cryst. surfaces 78—66562
surface interaction with adsorbed molecules, desorption 77—31874
surface interaction with adsorbed molecules, dissociation 77—31875
surface properties of materials, Conf., Missouri, USA (August 1977) 78—87867

adsorption continued
surface properties variational calcs., binding energy, Lang model 80—29279
surface science in metallurgy, review 79—42388
surface states in (111) covalent faces, effect of alkali adsorbates 79—42601
surfaces, of ideal polymers, conformational props. 77—3501
surfactant adsorpt., electrokinetic investig., appls. to AgI, latex particles 80—3363
symmetrical adsorption thermodynamics, case of noninert adsorbent 80—80059
temperature behaviour of adsorption system of particles, generalised Frumkin isotherm 79—90886
ternary systems, high temp. adsorption 79—77914
terylene film, electret state prod. using electrochem. injection, adsorbed states, frozen field 79—91344
tetracene, radical cation, EPR, acidic surface anisotropic rot. diffusion 78—27095
theory, concept of adphase 79—37919
thermodynamic theory 80—93794
thermodynamics data, Henry constants, small surface coverage, n-m-potential for adsorbent-adsorbate energy *(German)* 78—30833
thermodynamics of adsorpt. excess quantities, comprehensive treatment 78—10281
Thermodynamics of adsorption and Gibbsian distance parameters in two and three-phase systems 78—10282
thermodynamics of gas adsorpt. 79—73396
thioindigo, adsorbed on Al_2O_3, photoisomerisation 80—89503
toluene-bromobenzene, perfect binary liquid mixtures on silica gel, adsorption thermodynamics 80—44428
toluene-chlorobenzene, benzene-toluene, perfect binary liquid mixtures on silica gel, adsorption thermodynamics 80—44428
transition and free-electron like metals, of alkali metals, valence electronic struct., wave-function matching calcs. 78—72235
transition metal, of CO, AES obs. 77—35818
transition metal, of rare-earth atom, effects of changes in valence state 79—69367
transition metal, tight-binding theory of interactions between transition metal adatoms 77—1304
transition metal atoms interactions with PF_3 and CO ligands, MO calcs., boundary props. of adsorption systems 79—85896
transition metal carbide, behaviour in Cs or K plasma 77—20979
transition metal carbides, of Cs(K), adsorpt. energy, thermionic emission 77—7978
transition metal carbonyl complexes, UV and X-ray photoelectron spectra, effect of adsorbed CO 79—4897
transition metal oxides, UPS, LEED and AES studies of mol. adsorption 79—4480
transition metal surface electronic struct., influence of size and roughness 78—14785
transition metal surfaces, independent electron theory of atomic interactions 79—60903
transition metal surfaces, polycrystalline, of inert gases, tangential momentum accommodation coeffs. meas. 79—95270
two-dimensional lattice gas, improvement of quasi-chemical approx. for localised adsorption 79—69356
two-dimensional mobile phase, virial expansion, Unit Compressibility Law 77—72790
two-dimensional triangular octopolar array, orientational order and phase transitions 79—95257
two-particle correlation function for fluid-solid surface interaction 78—79880
ultrahigh vacuum adsorption, Haul-Gottwald empirical isotherm origin 78—21149
ultrahigh vacuum chamber for Raman studies of gases adsorbed on metals 78—81991
unified description from Henry range to liq. layer form. *(German)* 78—22962
uracil in aq. electrolyte, adsorpt. isotherm and solute activities from spreading pressure-surface charge data 78—14576
vacancy solution theory of adsorption from gas mixtures 80—65357
vacuum measurements, standard devices 79—71464
vacuum pump, pumping speed and condensation coeffs. determ. 78—21156
van der Waals interaction between molecules, spatial dispersion effects 77—35817
Van der Waals model, adsorption of gas on solid substrate 80—29271
vapour adsorption and outgassing by solder sealing glass, ultramicrogravimetric meas. using ultrahigh vac. system 79—80580
vibration excitation of adsorbed mol. due to plastic deform. accompanying fracture 77—15488
vibrational modes of absorbed atoms 77—69172
virial expansions for hard spheres on structureless wall 78—10277
virial series, Lennard-Jones 12-6 and 9-3 and square well potentials 80—45558
virial theory, critical discussion 80—54506
volatile chlorides, adsorption isotherms meas. using radionuclides and chromatography 78—76902
volcanic rocks, of nucleoside phosphates, rel. to origin of life 77—91273
Vycor glass, of ^4He from ^3He-^4He mixtures 78—84023
Vycor porous glass, of carbonium ions, reson. Raman spectra 78—84571
water, autoadsorption and surface entropy in 20-50° temp. range 77—28065
water, press. effects on surface tension, adsorpt. of hydrocarbon gases and CO_2, 0-50°C 78—56024
water, supercooled, role of adsorption in mech. of heterogeneous crystallisation 79—95125
water at interfaces, mol. struct. and dynamics 77—31873
water vapour adsorption isotherm, improved measurement method *(Japanese)* 78—6220
and wetting, unified theory using Percus-Yevick eqn. for hard spheres with surface adhesion 77—31879
wetting fluids, evaporating menisci, capillarity and multilayer adsorption 80—29248
zeolite (Itaya), of H^+, NH_4^+, Cd^{2+}, Cu^{2+} *(Japanese)* 78—95951
zeolite surface, of Cu^{2+}, Cr^{3+}, Co^{2+} ions, EPR, optical spectroscopy investig. *(German)* 79—95266
zeolites, A-type, crystn. from Na-K silicaalumo gels, and characts. 79—52780
zeolites, type 13X, acetylene adsorption, inelastic neutron scatt. 78—14584

adsorption continued
γ-Al_2O_3, physisorption and reaction of $Mo(CO)_6$, IR spectra obs. 80—80064
Ag (100), underpotential adsorption of Tl and Pb, mean field theory and Monte Carlo simulation 79—60630
Ag (110), adsorption, O_2-induced, and reaction of H_2, water, CO, and CO_2 80—55714
Ag (110), of S, equilib. segregation isotherm, selvedge model 79—90883
Ag (110) surface, adsorption of mol. O_2 species 80—103578
Ag (110) surface, of Na and Na+O_2, LEED, thermal desorption and AES meas. 77—31883
Ag (111), adsorpt.-desorpt. props. and surface struct. chem. of Cl 77—89648
Ag (111), adsorption of acetic and propanoic acids, LEED obs. 80—80073
Ag (111), of I_2, surface EXAFS exam. 79—82446
Ag (111), ordered and damaged surfaces, O_2 adsorption, O_2+CO interaction 78—14583
Ag (111), Xe monolayer adsorption, LEED obs. 77—1307
Ag (111) surface, ethylene adsorption, XPS and UPS investigation 80—103573
Ag, adsorpt. of acetonitrile, surface enhanced Raman spectra obs. 80—97251
Ag, adsorpt. of benzene (deuterobenzene), surface enhanced Raman spectra obs. 80—97251
Ag, adsorpt. of pyridine, surface enhanced Raman spectra obs. 80—97251
Ag, adsorption and surface reaction of formic acid 80—40741
Ag coating on refractory metals, energy struct. determ. at two monolayer thickness 80—100392
Ag electrode, enhanced inelastic light scatt. caused by adatoms 80—89013
Ag electrode, of metal ions, kinetics, surface struct. 78—79873
Ag film, discontinuous, of alkali halide mols., effect on elec. cond. 80—2487
Ag film, ellipsometric response to CO adsorption 80—103571
Ag film, vac. deposited, internal stress and its depend. on gas adsorption 80—6683
Ag halides, of water, mol. studies of ice-forming capabilities 77—31872
Ag, I_2 adsorption site on Ag(111), X-ray anal. 78—84679
Ag islands, on Al_2O_3 substrate, adsorption of ethanol, inelastic electron tunnelling spectra and TEM obs. 79—90884
Ag, of 1,2-dichloromethane, surface-plasmon modulated reson. 79—83045
Ag, of Ar curved surface physisorption, small spherical particles or pores 77—7964
Ag, of aromatic hydrocarbons, heat of adsorption, coating and fine struct. *(German)* 79—23844
Ag, of Cl, AgCl epitaxial layer form., RHEED 78—14642
Ag, of Cl monolayer, enhanced Raman intensity 79—95766
Ag, of Cl_2, on low index surfaces, energetics and structures 79—82440
Ag, of ethylene and propylene, enhanced Raman spectra obs. 80—95607
Ag, of Hg, work function changes 77—7966
Ag, of monomolecular films of Pb, anisotropy of optical props. 80—60534
Ag, of O, surface species identification by XPS, high press. 79—28191
Ag, of O_2^-, catalytic oxidation mechanism 78—61046
Ag, of organic dye, excited mol. decay near metal surface, energy transfer to plasmon surface polaritons 80—50440
Ag, of pyridine, giant Raman scatt. 79—95768
Ag, of pyridine, on (110) surface, UPS, AES and flash desorption meas. 80—92776
Ag, of rhodamine B, anisotropy of optical props. 80—60534
Ag, of S, adsorpt. effects on electrodeposition 79—20001
Ag, single crystal, adsorption of metal ions on (111) and (100) surfaces *(German)* 78—68636
Ag surface, of inert gases, physisorption energies 78—71944
Ag, surface roughness induced electronic Raman scatt. 80—50347
Ag-Au, nucleation and growth on substrates, adsorption energy 79—77956
Ag-Sn system intermetallic formation rate, H_2 adsorption effect 79—90819
AgBr emulsion, latent image speck size, characteristic curve anal. 79—34338
AgBr, of cyanine, pH depend. 78—62254
AgBr, of thiolic antifoggants, chem. struct., adsorpt., ESCA investig. 78—32907
AgBr single crystals, adsorption and orientation of cyanine dyes 79—20431
AgBr surface, vibr. freq. of adsorbed Ag atom, LCAO-MO calc. *(Russian)* 79—2866
$Ag(CN)_2$, adsorption on activated charcoal 79—82455
$Ag(CN)_2$, adsorption on activated charcoal, kinetics and thermodynamics 79—82456
AgCl, surface crystallisation, due to colloid adsorption 80—54544
AgI aerosol, ice forming activity, UV irrad. effect 80—71950
AgI, of water, CNDO calc. 77—4254
AgI surface, of water, effective pair pot. model 80—100394
Ag_2O film, prep. and effect of O_2, Ar and H_2 gases *(French)* 78—14637
Ag(111), adsorption of Xe, structural and thermodynamic studies 80—6640
Ag(111), of Xe, monolayer, lateral struct. and Xe-Xe interactions 77—1311
Ag(111) surface, of I, cluster calc. with Xα scattered wave method 77—31894
Al (100), of Pb and Sn, prep. and props. of monolayers 79—15018
Al (100), with adsorbed O, Xα-scatt. wave cluster approach 80—49851
Al (111), adsorption of O_2, possible ordered struct. 80—44412
Al (111), angle-resolved UPS obs. of 2-dimens. band structs. of S, Se and Te 80—60059
Al (111), of O, band dispersion and symmetry, photoelectron spectrosc. obs. 79—61490
Al (111), of O_2 at 30K, UPS obs. 79—60635
Al, adsorption and decomp. of methanol, UPS, XPS and thermal desorption obs. 79—82441
Al, alkali metal adion-surface interaction energy, density formalism calcs. 78—68069
Al, anodised, of ^{90}Sr, prep. of radiation sources 79—36454
Al, anodised, of ^{90}Sr and ^{90}Y, oxide layer thickness, Al purity, temp. depend. studies 79—82458
Al, anodised, of ^{90}Y, prep. of radiation sources 79—36454

adsorption continued

- Al, film, adsorption of O_2 and N_2 77—24486
- Al film, nucleation and growth on C layers, adsorption energy and surface diffusion 79—99451
- Al, of alkanes, thermal accommodation coeffs., translational and internal gas-solid energy exchange 78—92506
- Al, of hydrazine derivatives, inhibiting dissoln. in HCl soln. 80—50759
- Al, of NH_3, KVV Auger spectra, deconvoluted spectra 80—50508
- Al, of O_2, AES, XPS, and LEED obs. 79—46938
- Al, of O_2, H_2O, gases, effect on exoelectron emission from rubbing surfaces 79—1816
- Al, of O_2, intrinsic and extrinsic plasmon coupling, XPS of adsorbed atoms core states 78—10278
- Al, of O_2, relation between energy-band and cluster model 78—52048
- Al, of O_2 and CO, interatomic Auger transition spectroscopy 80—11521
- Al, of small molecules, photoelectron spectra, surface plasmon spectroscopy 79—47148
- Al, propane adsorption SIMS and EID obs. 77—69167
- Al surface, hydrasine and NH_3 adsorption and decomp., XPS obs. 80—92783
- Al, tunnel junction, barrier layer structure, mol. adsorption mechanisms *(Russian)* 79—31634
- Al/Sn, composite, kinetics of adsorption softening of solid interface *(Russian)* 79—61619
- Al-Al oxide-Pd tunnel junctions, exposed to H_2, inelastic electron tunnelling spectra 80—20327
- Al-Al_2O_3-Au device, adsorption of Cl_2, effect on current-voltage characts., press. depend. 80—65704
- Al-Al_2O_3-Au(Al), capacitance, water sorption effects 77—43738
- Al-Cu, liq. alloys, surface tension meas. *(French)* 78—18875
- Al-Cu (4 wt.%), fatigue crack propag. role of adsorption in H_2S, Hg and moist air *(French)* 78—15580
- Al+NO_3^-, reactions between metal and aq. nitrate solns., XPS 77—12825
- Al_2O_3, adsorption and orientation of sulphonic acids, tunnelling spectroscopy obs. 78—34707
- Al_2O_3, adsorption of H_2O, energetics, effects of adsorption temperature on surface processes 78—60028
- Al_2O_3, adsorption of HCl and water vapour 79—73398
- Al_2O_3, alumina, adsorpt. of saturated hydrocarbons, gas-solid chromatography based on compensation effect 80—26053
- Al_2O_3 film pore size distribution meas., adsorpt.-desorpt. vs. TEM methods 77—74357
- γ-Al_2O_3, heat treated, of SO_2 79—56070
- Al_2O_3, inelastic electron tunnelling spectroscopy of adsorbates, MgO comparison 80—88686
- γ-Al_2O_3 interface with electrolyte solns, adsorption of ions, surface conductance, ion mobility and surface pot. 80—75622
- Al_2O_3, mass spectroscopic investig. of chem. reactions between adsorbed species 77—40600
- Al_2O_3, of 2-butanol, PMR spectra 79—19457
- Al_2O_3, of benzoic acid, benzoate ion binding energy 79—60629
- Al_2O_3, of Cs, Sr, Eu, Co, and Cd 80—99240
- Al_2O_3, of ethanol, acetic acid and acetaldehyde, inelastic electron tunnelling spectra, surface vibr. struct. determ. 80—35572
- Al_2O_3, of $Fe(CN)_6$, tunnelling spectra, isotope shifts 80—29262
- α-Al_2O_3, of $H(H_2)$, microweighing and X-ray obs. *(German)* 78—51825
- Al_2O_3, of isobutyl alcohol, gravimetry, IR investigs. 79—1546
- γ-Al_2O_3, of methane, γ-radiolysis, reaction kinetics 78—95940
- Al_2O_3, of NH_3, KVV Auger spectra, deconvoluted spectra 80—50508
- Al_2O_3, of pyridine, rel. to surface acidity meas. 80—35611
- Al_2O_3, of TCNQ anion radical salts, EPR and electronic spectra 77—72776
- Al_2O_3, pure and SiO_2 coated, surface props., catalytic activity 79—79287
- Al_2O_3, Raman spectroscopy study of adsorbed molecules 80—65358
- Al_2O_3 surface adsorption effects during inelastic electron tunnelling spectroscopy *(French)* 79—822
- Al_2O_3-B_2O_3 system, phase comp. and sorption props., Al salts chem. nature influence 79—51426
- β-Al_2O_3-Na_2O, of Na, surface electronic struct. calcs. 80—75431
- Ar, adsorption on graphitised C black, eqns. of state predictions vs. expt. 79—69223
- As-Se, glassy, surface phenomena, gas adsorption effects on elec. props. 79—42621
- As_2Se_3, glassy, with adsorbed $H_2O(NH_3)(NO_2)(O_2)(CO_2)(CO)$, surface cond., photocond. 78—80038
- As(111), of As_4, thermal accommodation coeffs. determ., vibr. surface method 77—1319
- Au, (320) and (311) surfaces, of Pb, LEED and AES obs. 79—86998
- Au, adatom beam scatt. expts. on NaCl and KBr (100) surfaces 79—77924
- Au electrode, of metal ions, kinetics, surface struct. 78—79873
- Au electrodes, of Br^-, specular reflect. investig. 78—61047
- Au electroplate on Cu, water vap. adsorption 77—69168
- Au film, adatom surface diffusion at low temps., elec. resist. study *(French)* 80—65376
- Au film, electrical resistivity, influence of metallic adsorption *(French)* 79—19677
- Au film, evap., temp. change and gas adsorpt. effect on opt. consts., ellipsometric obs. *(German)* 80—89081
- Au film, multiple attenuated total reflection spectroscopy, initial growth process 79—19490
- Au film, vac, deposited, internal stress and its depend. on gas adsorption 80—6683
- Au film, work function changes upon water contamination 80—44705
- Au film electrode, electrochem. adsorpt. of O_2, elec. resist. obs. *(French)* 79—29372
- Au of Br_2, anisotropy of optical props. 80—60534
- Au, of CO, high resolution UPS 78—39666
- Au, of iodide ion, depend. on electrode crystallographic orientation 79—15020
- Au, of O_2, Auger spectra 78—87879
- Au, of Pb, formation of $AuPb_2$ epitaxial layer, LEED, AES study of Au/$AuPb_2$ interface 78—71988
- Au, of water or Hg, work function changes 77—7966
- Au, of Xe, electronically excited atoms coupling to cond. states 77—89642
- Au, of Xe and CO on (100), LEED, AES, EELS, surface pot. 77—15691
- $Au(CN)_2$, adsorption on activated charcoal, kinetics 79—82457

adsorption continued

- Au(III) and polycrystalline surfaces, O_2 adsorption, LEED, AES and energy loss spectra 80—34310
- BN, of Ar, thermodynamic values calc. from pot. parameters *(German)* 79—95268
- BN, of methane in first monolayer domain, thermodynamic props. *(French)* 80—29275
- BN_3, adsorpt. of Ar, Kr and Xe 79—73395
- BN_3, adsorption of Xe and Kr, first layer study 79—73397
- Ba monoatomic film on W (110), characteristic electron energy loss 80—100720
- BaO, surface states, reflectance spectra, impurity effects 77—20873
- $BaTiO_3$, of O_2, mechanism calc. 78—63927
- $BaTiO_3$, of $O_2(H_2)$, effect on work function and spontaneous polarisation *(Russian)* 78—6211
- $BaTiO_3$ polymorph, hexagonal, low temp. and surface CO_3 adsorption and desorption 80—80713
- Be, clean and O covered, secondary-ion emission energy depend. 80—50502
- BeO ceramics, thermally stimulated exoelectron max., effect of H_2 adsorption 79—43109
- BeO ceramics, thermostimulated exoemission and adsorption centres 78—27386
- BeO, exoelectron emission from hydrated and dehydrated surfaces 80—11545
- Bi adsorption, and condensation on W 79—73394
- Bi film, adatom surface diffusion at low temps., elec. resist. study *(French)* 80—65376
- Bi film, on Si(111) substrate, MBE deposition kinetics 80—10817
- Bi, of organic cpds. 80—20038
- $Bi_xSb_{2-x}Te_3$, 2-dimens. cryst. interface props. of Bi overlayer UPS obs. 78—34881
- $Bi_2(Ti_{1-x}S_x)_3$, thin crysts., adsorpt. effects on elec. cond. 78—19034
- C, activated, adsorption in countercurrent flow 80—70524
- C, activated, adsorption rate constants prediction for various vapours 80—40735
- C, activated, equil. adsorption coeffs. of Kr and Xe at low partial press. 77—52673
- C activated, of 0.98 mol.% Ar, vol. adsorption capacity 78—75933
- C, activated, of I_2, pore struct. 77—31870
- C, activated, of O_2, H_2S, catalyst for H_2S oxidation, electrochem. model *(German)* 78—35717
- C, activated, surface oxidised, of organic vapour, paramag. props. 77—32238
- C, activated, vol. adsorption capacity for selected trace contaminants 78—56031
- C, activated, vol. adsorption capacity, 25°C, org. trace gases 79—16036
- C, activated and impregnated, adsorption and desorption isotherms of phosgene and chloroform 77—70333
- C, activated and impregnated, adsorption of HCN and H_2O vapour mixtures 80—39412
- C amorphous film, atomic imaging using the dark-field annular detector in the STEM 80—6331
- C black, graphitised, adsorpt. of gases 79—42366
- C black, graphitized, of benzene and cyclohexane, exptl. determ. of models 78—6216
- C fibres, of organic liqs., surface characts. investig. using flow calorimetry 78—48694
- C fibres, PAN-based of N_2, surface characts. 78—35536
- C, from methanol-benzene solutions 78—14568
- C, glass tip, field emission current instability due to dislodgement of adsorbed mol. 80—11544
- C membranes, graphitised in situ, adsorpt. meas. using steady state flows and time lags 79—33183
- C, micropore analysis 78—14570
- C, micropore volumes from isotherm eqn. 78—14569
- C, microporosity, determ. from isotherm eqns. 79—51419
- C, microporous, gas adsorption 78—22956
- C molecular sieve prep. by pore blocking 78—15324
- C, of Ag and U, scanning-transmission electron microscope obs. 77—51597
- C, of Br from CCl_4 soln. 78—10273
- C, of gas, rate depend. on granule size and gas flow velocity 78—56033
- C polymeric chains, reduced from poly(tetrafluoroethylene), N adsorption 80—89488
- C, porous, of Kr, Henry's constant, pre-exponential factor *(German)* 78—22961
- CO, on Pt or Pd surface, oxidation kinetics 79—61903
- CO+N_2O catalytic reaction on Sc_2O_3 and MgO, kinetic obs. 79—29389
- CO_2, adsorption and capillary condensation on clays rel. to Mars volatile storage and atmospheric history 80—72833
- CO_2, solid, of Ar, density functional theory, computer simulation 80—24735
- CaF_2, adsorption mechanism in selective etching 77—7727
- CaF_2, crysts., adsorption processes in selective etching 80—39098
- CaF_2 surface, of water, IR internal reflection spectra 79—77920
- $CaHPO_4$, powder and granules with starch mucilage binder, compressed, low temp. N adsorption obs. of surface area 80—80998
- CaO, of O_2, O_2^- ion form. 80—61155
- CaO with adsorbed metal, photoexcited ions and electron emission *(Russian)* 77—40324
- CaO:Mn phosphor, surface radical recomb. and cathodoluminesc. *(Russian)* 78—6787
- Cd sorption and accumulation in sediment of Tama River 79—74924
- $CdCl_2$ cleavage face, Ar adsorpt., two-dimens. condensation of second adlayer 79—99413
- $Cd_xHg_{1-x}Te$, vacancy mech. of resorption of Hg droplets 80—39070
- CdO thin film conductivity, H_2O and CO adsorption effects 79—56340
- $Cd(OH)_2$, adsorption props. of surface, gas-chromatographic investigation 79—66343
- CdS, O and CO adsorption effects on surface pot. *(Russian)* 77—47686
- CdS, of N_2, CO, and O_2, total current spectrum interpretation 77—85857
- CdS powder, surface O_2 adsorption, ESR studies 79—65738
- CdS, surface energy levels, O(C) adsorpt., AES study *(Japanese)* 78—88008
- CdS:Li film, of O_2, effect on photocond. 78—34854
- CdTe, clean and oxidised surfaces, O_2 sticking coeff., ionicity effects, XPS expts. 77—85887
- Ce^{3+}, oxidation kinetics in X zeolite on O_2 adsorpt. 78—3373
- $CeCo_5$, adsorption and desorption charact. of H_2 *(Japanese)* 77—47667

adsorption continued

- $CeNi_4Al$, mag. susceptibility, H adsorption-desorption cycle effects 80–107990
- CeO_2 in O_2 atmos., adsorption and elec. cond. props. 79–23836
- Co (0001), adsorption of O_2 and CO, XPS and UPS study 79–74050
- Co, adsorption by Mn and Fe oxides in soils and sediments 79–66422
- Co, adsorption-desorption kinetics of CO, surface carbide form. effects 80–103574
- Co film, evaporated, of H_2, surface pot. meas. 77–31890
- Co film, texture and adsorption of CO *(German)* 77–24485
- Co film, work function changes upon water contamination 80–44705
- Co, of O_2, CO and CO_2, XPS and UPS *(French)* 77–36362
- Co, pure surfaces, adsorpt. of water and decomp. *(German)* 80–26054
- Co^{2+} ion removal in high temp. water using TiO_2 79–89376
- $Co(OH)_2$, adsorption props. of surface, gas-chromatographic investigation 79–66343
- ^{60}Co removal from waste water, adsorption on activated charcoal with oxine 78–58365
- Cr (100), of O_2, and initial oxidation at room temp. 80–20034
- Cr (111) face, of O_2, LEED and RHEED meas. *(French)* 78–39955
- Cr, of O_2, effect on ion bombard. induced photon and secondary ion emission 77–90231
- Cr, photon emission due to Ar^+ ion bombard., adsorbed and recoil-implanted O effect 80–80872
- Cr, secondary negative ion emission, effect of adsorbed O_2 *(Russian)* 79–28881
- Cr_2O_3 dissociation in presence of C in Ar, CO and vac. atm., Cr_3C_2 form. *(Russian)* 80–35570
- Cr_2O_3 polycrystalline powder, crystallite sizes and surface areas 77–66086
- $Cr(OH)_3$, adsorption props. of surface, gas-chromatographic investigation 79–66343
- $Cr_2O_3.SH_2O$, heat-treated, narrow particle size distrib., surface props. 78–85210
- $CrVO_4$, adsorption of methanol, IR spectra *(Russian)* 79–51435
- Cr(111), of O, photoemission exam. 79–19976
- Cs ion source, SF_6 adsorpt., thermionic emission 80–71557
- Cs monolayer on Cu(111), of O, dilution of electron gas, plasmon energy losses 79–47036
- Cs, oxidation, adsorbate-induced structs., UPS obs. 79–47828
- Cs, trace quantities in NaCl soln., seawater, adsorption behaviour on paper *(Russian)* 77–73766
- CsBr, of methanol, IR spectrometric obs. *(French)* 78–46343
- CsCl, of methanol, IR spectrometric obs. *(French)* 78–46343
- CsI, of Ar-O_2 mixture, test of eqns. for gas mixture adsorption on heterogeneous surface 78–60030
- CsI, of methanol, IR spectrometric obs. *(French)* 78–46343
- Cu (100), coadsorption of O_2 and Cs, effect of O_2 on Cs work function 79–15014
- Cu (100), diatomic mol. scatt., energy transfer and dissociative adsorption 79–46961
- Cu (100), of CO, UV and X-ray photoelectron spectra, LEED 78–56037
- Cu (100), of Pb and Bi, coadsorption, LEED and AES study 79–15017
- Cu (100), with adsorbed CO, $X\alpha$-scatt. wave cluster approach 80–49851
- Cu (100) of H_2, dissociation, classical trajectory calcs. 77–1947
- Cu, (100) surface, Auger emission ang. depend., overlayer effects 78–39637
- Cu (100) surface, of O_2, CO and water, EELS study 80–2260
- Cu (110), ion-induced adsorption of O_2 80–54510
- Cu $(\bar{1}10)$, low energy Ne^+ ion scatt. meas. 79–51431
- Cu (110), O adsorption, low-energy ion bombardment investigation 80–34302
- Cu (110), of CO, electron energy loss vibr. spectra and LEED obs. 79–77902
- Cu (110), of pyridine, angle-resolved photoemission, selection rules 80–40231
- Cu (110) surface, interactions with O_2, N_2O, ellipsometry, AES, LEED study 80–6635
- Cu (111), adsorpt.-desorpt. props. and surface struct. chem. of Cl 77–89648
- Cu (111), hydroxylation and dehydroxylation, XPS obs. 80–7850
- Cu (111), of CO, rel. to surface prep. 78–6223
- Cu (111), of O_2 from 23°C to 400°C, AES, LEED and ellipsometric meas. 79–65317
- Cu (111) and (110), of I_2, surface EXAFS exam. 79–82446
- Cu (111) surface band energy shift upon adsorption of Cs and O, angle-resolved UPS study 80–40228
- Cu (111)/Cs, adsorption-induced changes of photoemission spectra and surface electronic struct. 80–55260
- Cu (210) surface, of O_2, LEED and AES meas. 78–71998
- Cu, adsorbed mol. monolayers, UV-visible spectra 78–72619
- Cu, adsorption and surface reaction of formic acid 80–40741
- Cu adsorption of O_2, N_2O on (100) surface, reaction with CO 80–103583
- Cu, electrolytic coating, brighness and adsorption of surface-active additives 80–100963
- Cu, electrolytic deposition, adsorption of substances used as brighteners 79–66220
- Cu film, of CO, effect on resist., negative p-values 77–85083
- Cu film, pure and CO covered, work functions 79–91570
- Cu film, work function changes upon water contamination 80–44705
- Cu films, adsorption of O, study of gravimetric uptake and work function 79–33179
- Cu, influence of cryst. orientation on work function, with and without adsorbed S *(French)* 78–76134
- Cu, membrane, permeation of H_2, adsorpt. on entry side 79–99371
- Cu of Ag, pairwise interaction approach to adsorption of oriented overgrowths 77–62759
- Cu, of CO, angle-resolved UPS and adsorbate induced struct. 78–71983
- Cu, of CO, high resolution UPS 78–39666
- Cu, of CO, on (110), LEED, surface pot., IR spectra 77–66092
- Cu, of CO, polycryst. surface, SIMS 78–14585
- Cu, of CO and Xe, (311), electron energy loss spectra 77–63507
- Cu, of Cs, on (111) surface, photoelectron spectra, angle averaging 79–83100
- Cu, of H, potential energy curves, pairwise additive model calcs. 78–73087
- Cu, of H and H_2, HMO studies 77–15682
- Cu, of H_2O and Br_2, on (100) face, Helmholtz layer model system 80–92777

adsorption continued

- Cu, of N, LEED, data averaging, objective approach 77–15668
- Cu, of NO, NH_3 and N_2H_4, photoelectron spectra 78–6830
- Cu, of NO, species identification, struct., dissoc. chemisorption, desorption, UV photoelectron spectroscopy 78–52635
- Cu, of O, on (001) face, core-level XPS, azimuthal anisotropy 79–19969
- Cu, of O, on (001) surface, deep core level XPS anisotropy 78–72690
- Cu, of O_2, H_2O, gases, effect on exoelectron emission from rubbing surfaces 79–1816
- Cu, of Pb, on stepped and low index surfaces, LEED, AES and desorption anal. 79–46942
- Cu, of S, Cl, adsorpt. effects on electrodeposition 79–20001
- Cu, of Xe, stay time meas. 78–56044
- Cu polycrystals, oxidation, secondary ion energy spectra 80–71788
- Cu, secondary negative ion emission, effect of adsorbed O_2 *(Russian)* 79–28881
- Cu surface, (001), O_2 adsorption effect on surface barrier, LEED study 80–84378
- Cu surface, (110), methanol adsorption, XPS, UPS and thermal desorpt. study 80–84388
- Cu surface, of Sr^{2+}, ^{90}Sr tracer expt., immersion time conc. and temp. depends. 78–87863
- Cu surface (100), adsorption of O_2, LEED study 80–100408
- Cu surfaces, O_2 adsorbed, exam. of structure by LEED, O_2 pressure-temp. diagram *(Japanese)* 78–79884
- Cu vicinal surfaces, LEED study, S, O and Pb adsorption effects 80–103575
- Cu-Ni, of H_2+CO, interaction in (110) single cryst. surface, TDS and UPS obs. 80–80052
- Cu-Ni (110), of CO and H_2, UPS, thermal desorption, AES,and LEED study 80–80087
- Cu-Sn system intermetallic formation rate, H_2 adsorption effect 79–90819
- CuCO, linear, ab initio RHF-MO calcs., rel. to adsorption 79–26883
- Cu_5FeS_4, bornite, O_2 adsorpt. effect on surface struct. by AES 77–15669
- CuO powder, surface area determ. by adsorpt. of stearic acid and pyridine 80–107636
- CuO-Cr_2O_3 based oxide, catalyst, adsorption of fluorobenzene, binding energy of F 1s electrons *(French)* 79–69346
- Cu(100), adsorption and incorporation of O_2 78–56042
- Cu(100), of Xe monolayers, thermodynamics and kinetics, LEED and AES obs. 79–99423
- Cu(110), adsorption of O_2 and its reaction with CO 80–15373
- Cu(111), of Cs, struct. and electronic props. 78–23147
- $DyFe_3$, of H, effect on mag. props. 77–63129
- Er, film, evap., CO effect on work function 78–39188
- $ErFe_2$ surface, effect of H and O adsorption, spin polarised photoemission study 80–29854
- $ErFe_3$, H_2 sorption, mag. and struct. props. of hydrides 80–34831
- Fe (001), of CO, random occupation of adsorption sites, LEED exam. 78–63930
- Fe (001) surface, initial reaction with water vap. 77–69173
- Fe (100), of Br_2, AES, LEED, work function, and thermal desorption study 80–15375
- Fe (100), of carbon tetrachloride, AES, LEED, work function, and thermal desorption study 80–15376
- Fe (100), of Cl_2, AES, LEED, work function, and thermal desorption meas. 79–82465
- Fe (100), of I_2, AES, LEED, thermal desorption, and work function study 80–15374
- Fe (100), of tetrabromomethane, AES, LEED, work function, and thermal desorption meas. 80–39422
- Fe (11O), coadsorption of K and 0_2, XPS, UPS, AES, and LEED study 80–80084
- Fe (110), adsorption and decomposition of ammonia 79–69345
- Fe (110), K promoted, of CO, UPS, XPS, AES, and flash desorption obs. 79–82463
- Fe (110), of C, N, O, S, CO, NO, and C_2H_2, UPS and LEED/Auger meas. 77–72773
- Fe (110), of K, LEED, AES, UPS and XPS meas. 79–77919
- Fe (110), of Xe, UPS obs. 79–33897
- Fe (110) surface, adsorption and decomposition of NH_3, identification of surface species using SIMS 79–90862
- Fe, adsorption and surface reaction of formic acid 80–40741
- Fe and Fe-C(1.54 wt.%) alloy, electrocapillary curves in liq. sodium tetraborate 79–91968
- Fe, Armco, D penetration, mass spectrometric obs. 78–47606
- Fe, evaporated, adsorbed acetylacetone, XPS study 80–76133
- Fe film, work function changes upon water contamination 80–44705
- Fe, H_2 embrittlement and H_2 adsorption 80–89401
- Fe liquid, C saturated, decarburization by CO_2, effect of S 79–11726
- Fe, molecular adsorption and dissociative chemisorption of N_2, XPS obs. 79–99427
- Fe, of acetic acid and ethylenediamine, XPS study 80–76132
- Fe, of alkanes, thermal accommodation coeffs., translational and internal gas-solid energy exchange 78–92506
- Fe, of CO, polycryst. surface, SIMS 78–14585
- Fe, of CO, resistance changes, work function change and thermal desorption meas. 79–19450
- Fe, of CO and H, effect of preadsorption of one on adsorption of other 79–19451
- Fe, of ethoxysilanes, XPS 77–89639
- Fe, of N_2, temp. controller for filament heating appl. *(Japanese)* 77–51603
- Fe, of N_2 and NH_3, 80-290K, XPS and UPS obs. 77–31901
- Fe, of NO, low press. anal., XPS, UPS 77–7970
- Fe, of O_2, H_2O, gases, effect on exoelectron emission from rubbing surfaces 79–1816
- Fe, of O_2, oxidation 80–108730
- Fe, of O_2, oxide formation, XPS/UPS obs. 77–85074
- Fe, polycrystalline, H_2 adsorpt. and embrittlement, work function changes 80–96741
- Fe, segregation and adsorption of S, influence on carburisation and nitrogenation 80–66701
- Fe surface, purposeful modification by gas adsorption, charact. by photoemission 78–71955
- Fe surfaces, adhesion, effect of adsorbed atoms, AES study 80–39456
- Fe surfaces, adsorption, segregation and reactions of non-metal atoms, LEED and AES obs. 80–59783
- Fe-As melts, surface tension, density, adsorption *(Russian)* 80–92757

adsorption continued
Fe-CR alloys, ion-etched, surface comp., effect of adsorbed CO, AES obs. 79−46896
Fe-Ni-Cr-C, ferritic, of P, segregation to free surface, 723 to 823K 78−48411
α-Fe_2O_3, surface struct., adsorptive interactions rel. to rusting process, IR spectra 79−34363
Fe_2O_3:Mn, surface props. 79−65302
Fe_3O_4, effect of Al ion on formation and structure *(Japanese)* 77−59727
Fe_xO_y, of H_2O, oxidation and reduction effects on adsorption 78−43237
FeOCl-pyridine intercalate, mechanism, nucleation and diffusion 80−49420
$Fe(OH)_3$, of CO_2 79−66344
$Fe(OH)_3$, of CO_2 rel. to prep. method 79−39192
α-FeOOH, surface struct., adsorptive interactions rel. to rusting process, IR spectra 79−34363
FeS_2, adsorption mechanism in selective etching 77−7727
Fe(100), of CO and H_2, C, O, S and K adlayer effects 80−71573
Fe(110), of K, UPS and XPS meas. 80−95675
Fe(110) surface covered with C, O, N, S, CO adsorption, photoemission spectroscopy study 80−54527
Fe(111), of hydrazine, UPS and XPS 79−46956
α-Fe(111), of water, adsorption under the influence of 2.5 keV electrons 79−28199
GaAs, (100) surfaces, reconstructed, ang. resolved photoemission from surface states, adsorption and annealing effects 80−16143
GaAs (110), adsorption of Cs 77−72794
GaAs (110), adsorption of O_2, H_2, H_2O and H_2S, surface photovolt. spectroscopy 80−49499
GaAs (110), atomic struct. of clean and As covered surfaces, LEED study 80−49476
GaAs (110), coadsorption of Cs and O_2, initial oxidation, soft XPS obs. 80−10793
GaAs (110), low O_2 exposure effects on electronic surface props. 79−47146
GaAs (110), of alkali halides, adsorpt.-desorpt. processes and phase transitions in adsorbed layers 78−2361
GaAs (110), of In, N, P, and As, UPS and EELS study, tight-binding calcs. 80−49496
GaAs (110), of O_2, oxide form., XPS/UPS study 80−49497
GaAs (110) face, of one Cs atom, mol. orbital study *(French)* 78−38958
n-GaAs (110) surface, Cs adsorption, work function meas., adsorption site model 79−23839
GaAs (110) surfaces, ordered and disordered, O_2 adsorption, XPS meas. 80−49498
GaAs (111), Ga-As-H-Cl CVD system, adsorption of Cl, GaCl, As, As_4, Ga, AsGaCl, 973 to 1223K, equilib. adsorption layers 79−23858
GaAs (111) epitaxial film, adsorption of Cs, Cs+O ellipsometric study 80−29282
GaAs, adsorbed O, (110), surface electronic struct., synchrotron irradiated photoemission 78−43453
GaAs, adsorption enhancement by electron beam excitation of gas mols. 78−43238
GaAs, ambient-enhanced photoluminesc. props., mol. adsorption and gas-flow effect 79−99925
GaAs, clean and oxidised surfaces, O_2 sticking coeff., ionicity effects, XPS expts. 77−85887
p-GaAs, field electron emission current-voltage characts., effect of Au and O adsorption 80−45219
GaAs, of Cs, on epitaxially grown (001), (111) and $(\bar{1}\bar{1}\bar{1})$ surfaces 78−38924
GaAs, of Cs(Rb)(Na), LEED, AES, EELS study 78−68068
GaAs, of O_2, adsorption states and Ga depletion, UPS, AES, and thermal desorption meas. 79−46952
GaAs, of O_2, elec. props. *(French)* 78−34690
GaAs, of O_2, influence of cleavage defects on interaction 80−66684
GaAs, of O_2, surface chemistry and electronic struct., photoemission meas. using synchrotron radiation 77−20985
GaAs, of O_2, work function and photovoltage meas. 77−1446
GaAs, of Sb_2, surface state exam. by energy loss spectra 77−15935
GaAs, of Zn, thermal desorpt., at. beam adsorpt., AES, SEM, RHEED 78−14591
GaAs, oxide film influence on adsorption and electrophys. props. 79−42369
GaAs surface, O_2 sorption and excitonic effects, photoemission expts. 77−85055
GaAs:Cs, oxidation process, UPS obs. 80−50511
GaAs-O_2 system, electron beam induced adsorption, ion beam effects 77−11778
GaAs(P), adsorption and field-desorption of O_2 and Au, FEM studies 80−34304
GaAs(110) surface, adsorption of water and methanol, UPS study 80−6632
GaAs$(\bar{1}\bar{1}\bar{1})$As surface, 3 states, comp., struct., surface states and O_2 sticking coeffs. 77−66080
GaP (001), of Cs, photoemission meas. 78−87874
GaP (100), prep. of negative electron affinity surface by Cs adsorption 80−10768
GaP, (100) surface, thermal desorption props. of Cs and Cs-O adsorbed layers *(Japanese)* 80−15368
GaP, adsorption and desorption of Cs, LEED, AES, and photoemission meas. 80−70532
p-GaP electrodes with metal adatoms, surface states form. due to impregnated H 80−54778
p-GaP, field electron emission current-voltage characts., effect of Au and O adsorption 80−45219
GaP, O_2 adsorpt. monitoring by Auger spectroscopy, electron beam effects 77−72777
GaP, O_2 adsorpt. monitoring by Auger spectroscopy, electron beam effects 78−6218
GaSb, adsorption and desorption of Cs, LEED, AES, and photoemission meas. 80−70532
GaSb, of O_2, surface chemistry and electronic struct., photoemission meas. using synchrotron radiation 77−20985
Gd-Fe(Co) amorphous films, O_2 adsorption, effect on perpendicular anisotropy 80−34713
$GdCo_2$, of H_2, effect on mag. props. 77−20185
$GdFe_3$, of H, effect on mag. props. 77−63129
Ge (111), of Cd, combined RHEED-mol. beam obs. 77−4255

adsorption continued
Ge (111), of K and Cs, effect on surface elec. props. 79−90880
Ge (111), of oxygen, electron-beam enhanced reaction, AES meas. 77−4256
Ge (111), of polar molecules, surface recomb. centre neutralization 79−38147
Ge (111) Cd adsorption, struct. and surface coverage, RHEED-mol. beam obs. 77−4265
Ge (111) clean surface, of O_2, and electron work function 80−59779
Ge (111) of Cd, struct. and surface coverage, RHEED-mol. beam obs. 77−4265
Ge (111) of K and O_2, rel. to work function, K thermodesorpt. spectra 78−79874
p-Ge (111) surface, Cs adsorption work function meas., adsorption site model 79−23839
Ge, (111) surface, of O_2, photoemission yield spectroscopy of electronic surface states, sticking coeff. 79−91122
Ge, adsorption-desorption kinetics of H_2, O_2 and other gases, catalysis 77−47684
Ge electrode, of halide ions, effect on cathodic characts. 79−57238
Ge film, elec. resist., long term stability rel. to ambient atmosphere changes 78−2597
Ge films, of H_2O vapour, IR spectra 80−6628
Ge heteroepitaxial film, ethanol pulsed adsorption effect on elec. cond. 80−93014
Ge, of Ar, Kr and Xe on (111) plane, adsorpt. pot. 78−26768
Ge, of Au, effect on I-V characteristics, field emission study 78−67925
Ge, of metal atoms, effect on surface electron props. 77−55597
Ge, of N_2 and CO, adsorption potentials and trapped electrons role 79−90872
Ge, of O, enhancement by elec. field of polarity facilitating field-ion emission 79−65325
Ge, of O_2, degree of freedom of rot. and translational motion of O particles 79−23842
Ge, of water, neutralization of surface recomb. and fast capture centre 79−33184
Ge photocathodes, Au absorbed photofield emission current spectral investigation 80−29856
Ge surface, Ar atoms scatt., energy accommodation coeffs. 77−90230
Ge:Na (111) surface, of O_2, adsorpt. rate, work function, surface cond. changes investig. 78−79875
GeO_2, highly dispersed, produced by plasmochemical method, adsorption props. *(Russian)* 77−70275
H adsorption and desorption, self-consistent model calc. 79−46943
H storage by use of cryoadsorbents 80−45783
H-mordenite, of benzene *(German)* 79−90892
H_2 embrittlement adsorption or decohesion, mechanism 80−97643
H_2, permeation through metal barrier, adsorpt. processes 78−63879
H_2, recombination on interstellar grains, translational and rot. energy 79−17045
H_2, solid, H atom adsorpt. time and energy, hyperfine freq. meas. 79−50155
H_2 storage using cryoadsorbents, 65 to 150K, comparative evaluation 79−74548
$H_2+D_2 \rightarrow 2HD$ on stepped Pt surface, selective adsorption effect 78−20066
HF adsorption, by smelter-grade aluminas, during Al smelting 80−80075
^{4}He, adsorpt. and sp.ht. in 0.2 μm Nuclepore filters 77−35773
^{4}He, liq., surface, interaction with atomic H, Euler Lagrange eqn. 79−77850
^{4}He, superfluid film third sound meas. as capillary condensation probe in probe material 80−20005
Hg electrode, of n-butanol, diffusion layer theory, exptl. test 78−35701
Hg, of water vapour, critical anal. of expt. data *(Spanish)* 79−82435
Hg/aqueous solution interface, elec. double layer in presence of adsorbed ions 79−83469
Hg/electrolyte contacts, adsorption model for double layer capacitance 80−44706
Hg/electrolyte interface, of ethylammonium bromide from H_2O, D_2O solns., solvent props. 79−83459
Hg/$Na_2B_4O_7.10H_2O$ contacts, double-layer capacitance, temp. depend. 80−44707
Hg-gas interface, electrocapillary effects, CH_2Cl_2 adsorption in CF_4 77−32798
Hg-KI solution interface, specific adsorption of I ions, electrical double layer, interface excess activity coeff. 80−49523
HgTe, vacancy mech. of resorption of Hg droplets 80−39070
$HoFe_3$, of H, effect on mag. props. 77−63129
I_2, adsorbed on silica, reson. Raman spectrum 78−42066
IO_3^- adsorption by hematite, appl. to radioactive waste storage 80−22992
In, of O_2, CO, CO_2, and water, AES study 79−82451
In-Sn liquid alloy, of 2-butanol vapour, effect on surface tension and surface comp. 79−14981
InP (110), low coverage adsorption, SIMS study 80−49500
InP, ambient-enhanced photoluminesc. props., mol. adsorption and gas-flow effect 79−99925
InP, cleaved surface, metal contact props. and influence of intermediate adsorbed layers 80−49905
InP, of O_2, surface chemistry and electronic struct., photoemission meas. using synchrotron radiation 77−20985
InP surface, of Cl, electron spectroscopic obs. 78−56036
InSb (110), clean, O_2 adsorption, AES, LEED, RHEED and field effect meas. 80−49501
InSb (110) surface, LEED and surface conductivity during gas adsorption 77−62760
InSb, of Cs(Rb)(Na), LEED, AES, EELS study 78−68068
InSb(111) surface, of O_2, LEED and surface cond. meas. 78−15559
Ir (100), of Xe, local surface struct., UPS study 80−39429
Ir (110), O adsorbed, surface struct. anal. using hybridisation model 80−44423
Ir (110), of CO, O_2, H_2, N_2, ethylene and benzene 78−38961
Ir (110), of CO, reaction with O_2, transient study 80−30284
Ir (110), of O_2, LEED obs. 79−77880
Ir (111), of benzene and pyridine, electronic transitions sensitivity to molecule-surface orientation, energy loss spectra 80−45184
Ir (111) surface, of O_2, kinetics of CO oxidation reaction, appl. of XPS 77−31886
Ir, adsorbed gases, field desorption from field ion tips 80−59793

adsorption continued
- Ir, adsorption and condensation of Sm, thermal desorption mass spectra and thermionic emission meas. 79—69362
- Ir, clean and adsorbate covered surfaces, field emission energy distrib. spectra 80—25535
- Ir, field depend. of spectral line energy of He-H_2 adsorbate 79—78853
- Ir, of CO on evaporated film, IR refl.-absorpt. spectroscopy 80—34925
- Ir, of H_2, influence of surface steps and clusters, field emission investig. 77—28698
- Ir, of H_2 and O_2, surface reaction, thermal desorption and FEM obs. 79—52774
- Ir, of N_2, field emission exam. of effect of steps on surface potential 78—30829
- Ir, of N_2 and Xe, weak adsorption, field emission meas. 77—24479
- Ir, of O_2, H_2, effect on Ir work function 77—66094
- Ir, of O_2, work function changes by continuous meas. method 79—33328
- Ir-C, of Sm, adsorption and initial stages of condensation 79—69366
- $Ir_4(CO)_{12}$ EELS and AES rel. to CO adsorption on Ir 80—35021
- Ir(110), of O, structure of c(2×2)O overlayer 79—19463
- Ir(110)-(1×2) reconstructed, of S, AES study 79—42384
- K, oxidation, adsorbate-induced structs., UPS obs. 79—47828
- KBr, of Ar and Kr, potential energies calc. 78—71993
- KCl (001), water covered cold surface, H atom diffr. 77—66565
- KCl, LEED-AES study of oriented adsorption of TCNE 77—62737
- KCl, of H_2O, on (100), ordered monolayer, SIMS 77—76660
- KCl with adsorbed metal, photoexcited ions and electron emission *(Russian)* 77—40324
- KCl:Tl, of H_2, O_2 and N_2, effect on thermoemission of positive ions *(Russian)* 77—28676
- $KNbO_3$ catalysts, ferroelectric, for reactions involving CO and NO , and adsorption of NO 80—30282
- Kbr surface, residence times of Au atoms, time-of-flight meas. 80—10788
- Kr-plated graphite, of ^4He monolayer, possible Ising transition 80—34298
- LaB_6 (100), of O_2, UPS and LEED study 80—49519
- LaB_6, of O_2, measurement using retarding potential method in axial magnetic field 79—80719
- $LaNi_5$, adsorption and desorption charact. of H_2 *(Japanese)* 77—47667
- $LaNi_5$, Pauli paramagnet, adsorption of H, proton and ^{139}La NMR 79—78535
- $LaNi_{4.6}In_{0.4}$, H_2 absorption props., desorpt. pressure calc., and decomp. pressures 79—24827
- $LaNi_{4.6}Sn_{0.4}$, H_2 absorption props., desorpt. pressure calc., and decomp. pressures 79—24827
- Li, of methyl groups, complex form., STO calcs. 77—9124
- Li, of O, (100) surface, cluster models, ab initio HF LCAO theory 78—71978
- LiF, ^4He scatt., selective adsorption induced intensity maxima 78—72667
- LiF (001), elastic and inelastic scatt. of He and Ne, selective adsorption 77—66564
- LiF (001), He adsorpt., theory of selective adsorpt., azimuthal and polar dependent intensities 79—60624
- LiF (001), multiple Debye-Waller effects at selective adsorption in atom-surface scattering 80—76126
- LiF (001), of H_2, molecular orbital calc. 78—87878
- LiF, He at. scatt., bound state reson. data anal. 78—39644
- LiF, of ^4He, band struct. effects 79—73402
- LiF, of He, bound state reson. calc. in atom-solid scatt. 77—1779
- LiF, selective adsorption of ^3He and ^4He, atomic beam scatt. meas., binding energies 78—63935
- LiF, thermally stimulated exoemission, radiation defects and adsorpt. centres 78—11087
- LiF, thermostimulated exoemission, adsorbed layer effects 78—11085
- LiF type surface, He scatt., selective adsorption intensities, attractive corrugated wall model 79—28874
- LiF(001), ethanol-covered, atomic H scatt. 77—31905
- LiH, of H_2, on (100 surface), FSGO calcs. *(German)* 79—33196
- LiH, of He, ab initio calc. 78—38952
- Mg, of O_2, at 100 and 300K, XPS, UPS and X-ray AES meas. 78—18901
- Mg, polycryst., of O_2 at 100 and 300K, XPS, UPS, XAES 78—18906
- Mg vermiculite, adsorbed water mol. orientation, elec. pot. calc. 78—26763
- MgBr, of NO, triple pt. of first monolayer on cleavage face 78—6227
- $MgCaH_{3.72}$, synthesis and struct. *(Japanese)* 78—84751
- $MgCr_2O_4$-TiO_2, porous ceramics, humidity-sensitive electrical conduction 80—107782
- MgO, adsorption mechanism in selective etching 77—7727
- MgO, coadsorpt. of CO_2 and O_2, UV irrad., ESR of radicals 78—6572
- MgO, crysts., adsorption processes in selective etching 80—39098
- MgO, dissolution mechanism in acids 80—39296
- MgO, inelastic electron tunnelling spectroscopy of adsorbates, Al_2O_3 comparison 80—88686
- MgO, of acetonitrile, IR and TPD study 80—70528
- MgO, of CO, IR spectra 80—2751
- MgO, of CO, vibration excitation on fracture 77—15488
- MgO, of CO,(N_2),(NO),(O_2), 77 to 150K, mol. motion anal. 78—84051
- MgO, of Cs and Li, AES, LEED, work function, and secondary electron emission meas. 80—44407
- MgO, of H_2O vapour, at high temps., IR spectra 77—47687
- MgO, of H(H_2), microweighing and X-ray obs. *(German)* 78—51825
- MgO, of NO, adsorbate dimer form., heat of dissoc., EPR obs. 78—82755
- MgO, of O_2, $(O_2^-)_s$ form., thermal activation, reducing gas effects, EPR 77—9119
- MgO powder, surface area determ. by adsorpt. of stearic acid and pyridine 80—107636
- MgO single cryst., γ-irrad. in presence of O_2, H_2 and H_2O adsorbates, thermostimulated surface cond. 80—34499
- MgO:Mo, of propylene, oxidation reactions, surface structs., IR absorpt. spectra obs. 80—66868
- MgO-CoO, of O_2, EPR, volumetric investig. 80—10782
- MnO, hydrated, adsorpt. of Cs and Sr radioisotopes 78—3822
- MnO_2 coated Al_2O_3 and SiO_2 supports, N adsorption obs. of dispersion modes 80—81363
- MnO_2 porous powders, Al_2O_3 and SiO_2 coated, changes in surface free energy for N adsorption 80—84363
- MnO_2:Li(Mo)(V), of Zn^{2+} ions, kinetics, ^{65}Zn γ-ray scintillation investig. 80—70529

adsorption continued
- ^{54}Mn radionuclide adsorption characts. in waste water on oxine-impregnated activated charcoal 79—89394
- Mo (011) face, of Sr and La, influence of substrate electronic struct. on props. 78—60032
- Mo (100), adsorption sites of CO, electron stimulated desorption and LEED meas. 80—49516
- Mo (100), condensation of Cu and Ag, early stage comparison with W(100) 80—80072
- Mo (100), emission and work function, K adsorption effects 78—11060
- Mo (100), of CO_2 and trimethylamine, adsorbed O effect, LEED and AES obs. 80—39443
- Mo (100), of O_2, AES, LEED, work function, and desorption meas. 80—6654
- Mo (100), of W, effect on surface reson. 79—65983
- Mo (110), of Cs and O_2, common adsorption, work function and thermal stability by contact pot. method 80—44427
- Mo, (110) and (111) faces, joint adsorption of Cs and O, and emission props. 78—2364
- Mo (111) planes, of NH_3, preferential nitriding, FEM study 80—66877
- Mo, (112) face, Sr submonolayer adsorption 80—2271
- Mo (112) surface, of LI film, LEED and contact pot. method 80—10794
- Mo, adsorption of CO, O_2, metastable He de-excitation spectroscopy and UPS study 80—34314
- Mo, chromizing, formation of ordered solid soln. *(Russian)* 78—11402
- Mo, coadsorption of CO_2 and O_2, AES and SIMS obs. 79—46928
- Mo, field depend. of spectral line energy of He-H_2 adsorbate 79—78853
- Mo field emitter, of Se, field emission meas. 77—31889
- Mo field emitter, of Te, on single cryst. faces 78—34714
- Mo, ion bombard., ion and photon yields, CO adsorption effect 80—89098
- Mo, of CO, dissociation, comparison with carburised (100) surface 77—15689
- Mo, of Hg, work function change 77—7966
- Mo, of K, work function depend. on surface coverage 77—11788
- Mo, of N_2, surface coverage 78—60036
- Mo, of NH_3, and catalytic decomposition, field emission study 78—14596
- Mo, of O_2, low energy SIMS and electron induced desorpt. exam. 77—76667
- Mo, of O_2 and C_s, simultaneous adsorption struct., emission props., thermal stability 80—66878
- Mo, of Te, field emitter 77—69177
- Mo, refl. of metastable He atoms, O_2 adsorption effects 79—11493
- Mo surface, clean and gas covered, He* impact, deexcitation, pot. energy transfer mechanism 80—60743
- MoF_6 reduction by H, chemical kinetics eqn., adsorbed component interactions *(Russian)* 80—35569
- MoO_3, highly dispersed, produced by plasmochemical method, adsorption props. *(Russian)* 77—70275
- MoO_3, of water 79—77898
- Mo_2O_3-Al_2O_3, reduced catalyst, of O_2, O^- form. 78—85197
- MoS_2, of Cs and O_2, LEED, Auger and work function meas. 78—71994
- Mo(100), of Co, LEED, AES, study 78—87873
- Mo(100), of H_2, photoemission rel. to surface resonances and surface reconstruction 80—44417
- Mo(110) and (100) surface, surface reson. states and adsorption of 4d atoms 78—71982
- Mo(112), of Sr, interaction of adatoms 79—7754
- N_2, permeation through metal barrier, adsorpt. processes 78—63879
- N_2, thermomagnetic effect, Knudsen gas between Au surfaces, low temp. 78—30405
- NH_4Cl, powder, of H_2O vapour, isotherms, heat of adsorpt. 79—1545
- NH_4I, powder, of H_2O vapour, isotherms, heat of adsorpt. 79—1545
- NO, on W, dissociative, FEM obs. 77—4258
- Na loop in fission reactor, of I_2, Xe production, degassing investig. 77—34410
- Na montmorillonite, of water, adsorption meas. at −5°C 78—65540
- Na zeolite and Sc substituted zeolite, selective adsorption 79—90887
- NaBr, of Ar and Kr, potential energies calc. 78—71993
- NaBr, water preadsorbed, of organic vapours *(Japanese)* 78—18897
- NaCl (100), of Xe, AES and LEED meas. 77—11792
- NaCl, dislocation movement, effects of adsorpt. of octadecylamine *(Russian)* 77—51372
- NaCl, of Ar, gas-solid virial anal. 77—55444
- NaCl, of Ar and Kr, energy distrib. using numerical algorithm HILDA 77—55443
- NaCl, of CO, electrostatic interaction energy 78—74592
- NaCl, of CO, N_2 and H_2, electrostatic interaction energies 79—23831
- NaCl, of CO_2, gas-solid interaction potential, adsorption sites and surface migration 80—24738
- NaCl, of methane, adsorpt. pot., localised and mobile phases, hopping adsorbates 80—24739
- NaCl, of N_2, electrostatic information energy 78—74592
- NaCl surface, residence times of Au atoms, time-of-flight meas. 80—10788
- $NaCl_4$ on Pt and Ir surfaces, adsorption kinetics 80—84393
- NaF, He atomic beam refl., selective adsorpt. transitions, band-struct. effects 77—11781
- NaF, of ^4He, effect on intensity of diffr. atomic beam 77—12480
- NaF, selective adsorption of ^3He and ^4He, atomic beam scatt. meas., binding energies 78—63935
- Nb (110), of O_2, variation in work function, retarding field and thermionic emission meas. *(French)* 79—78823
- Nb, adsorbed O_2, effect on polarised Balmer radiation from scatt. H^{2+} 80—99569
- Nb, evaporated film, of CS_2 and H_2S, 195 to 473K 79—33197
- Nb film, of SO_2, adsorpt., corrosion 78—79897
- Nb, interaction with O_2, AES and low-energy SIMS meas. 79—47832
- Nb, of H, sticking coeff. calc. 80—59803
- Nb, of O_2, continuous meas. of surface pot. variations using mirror electron microscope 77—47680
- Nb, of O_2, electron-stimulated desorption study 79—11017
- Nb, of O_2 and N_2, on (100) planes, LEED-AES obs. 77—69186
- Nb, surface, coverage of O atom as function of adsorption, sputtering and diffusion rates 79—69354
- Nb_2O_5, hydrated gel, prep. conditions on pore struct., adsorpt. meas. 78—3068
- $NbSe_2$, of Cs and O_2, 200-300K 78—26767
- $NbSe_2$(2H)-hydrazine, intercalation cmpd., kinetic studies by transmittance meas. at 1600 nm 78—71981

adsorption continued
Ni 78−7099
Ni (001), of N_2, c(2×2) struct. form 80−80083
Ni (001) and (001)c(2×2)S adsorbed, electronic surface resonances by LEED 79−24051
Ni (001) surface, electronic struct. of ordered S overlayers 80−84835
Ni (100), adsorption of C, LEED struct. anal., substrate distortion 80−6637
Ni (100), clean and chalcogen-covered, electron ejection by metastable He atom impact 79−8217
Ni (100), dissociative chemisorption and mol. adsorption of NO 80−65373
Ni (100), of C, substrate reconstruction, LEED constant momentum transfer averaging study 80−39445
Ni (100), of chalcogen, orbital identification in INS and UPS spectra 77−43427
Ni (100), of chalcogen, structure, force consts., binding energies and photoemission, importance of final state multiplet splitting 78−71966
Ni (100), of O2, and reduction of surface oxide by H_2 80−108741
Ni (100), of water $(O_2)(H_2)$(CO), combined XPS/LEED/SIMS exam. 79−83075
Ni (100), of Xe, UPS obs. 79−33897
Ni (100) of O_2, surface phonons 78−2359
Ni (100) surface, coadsorption of Sn on Pb, P or O contaminated surface, AES study 80−88437
Ni (100) surface, of H_2S and S, ang. distrib. of S Auger emission 77−32475
Ni, (100) surface, secondary electron spectra, adsorbed elements effects 80−50480
Ni (100)-p(2×2)C surface, of H_2, CO and CO_2 and decomp. of formic acid 79−91995
Ni, (110), (100) and (111) surfaces, coadsorption of CO and H_2S, surface coverage meas. by SIMS 79−90876
Ni (110), clean and S covered, atomic struct., medium energy ion scatt. 79−61483
Ni (110), interaction with O_2, electron energy loss spectra and AES obs. 79−47826
Ni (110), of CO and CO_2, electron bombard. effects, AES and electron stimulated ion desorption obs. 79−51430
Ni (110), of H, substrate reconstruction, LEED constant momentum transfer averaging study 80−39445
Ni (110), of O_2, obs. by electron microscopy, AES and LEED *(French)* 77−62732
Ni (110), S and O adsorbed, surface struct. anal. using hybridisation model 80−44423
Ni (110), struct. anal. during O_2 adsorption, low energy ion scatt. meas. 79−82424
Ni (110), surface relax., O_2 coverage effects, medium energy ion scatt. obs. 79−28181
Ni, (110) surface, methane interaction kinetics, AES-LEED-ellipsometry 77−62756
Ni (110) surface, of fermic acid, modulated mol. beam scatt. anal. 79−89032
Ni (111), adsorption and decomp. of hydrocarbons, high resolution EELS study 80−40739
Ni (111), adsorption sites of CO using IR reflection-absorption spectroscopy 79−69355
Ni (111), coadsorption of CO and hydrocarbons, $C\equiv O$ bond weakening 79−90863
Ni (111), dehydrogenated adsorption of ethylene, thermal desorption and AES study 80−29274
Ni (111), of acetylene, identification of CH species by electron energy loss spectra 79−15022
Ni (111), of acetylene and ethylene, surface structs., LEED and AES obs. 79−60636
Ni (111), of CO, H_2 and O_2, Raman spectra 79−28769
Ni (111), of CO, LEED, AES, thermal desorption, work function, and IR system meas. 79−77903
Ni (111), of CO and O LEED and low-energy ion scatt. investigation 79−65324
Ni (111), of chalcogens, angle-resolved photoemission 80−40230
Ni (111), of ethylene and acetylene, vibr. spectra from electron energy loss *(French)* 78−34696
Ni (111), of H_2, LEED intensity spectra, 173K 79−28192
Ni (111), with submonolayer of O, H or C_2H_2, surface phonons obs. by EELS 80−39403
Ni (111) and (110), laser-induced charge transfer to adsorbed CO, photoemission expts. 80−59798
Ni (111) face, of CO, CO stretching vibr., high resolution electron loss spectroscopy 78−14605
Ni (111) of ethylene at room temp., surface complex vibr. from electron energy loss spectroscopy 79−73404
Ni (111) surface, of Cl 77−85069
Ni {100}, of O, low energy ion scatt. study 80−39420
Ni, adsorption of CO on (001) surface, XPS for adsorbate geometry 79−65314
Ni, atmospheric corrosion, moisture adsorption and indoor corrosion rates 80−71799
Ni catalyst, Al_2O_3 supported, of CO in H_2-He, effect of H_2S on IR spectrum 78−71945
Ni catalyst, H_2+CO, adsorption, co-adsorption, reaction, neutron inelastic spectroscopy method 79−99408
Ni, clean and gas-adsorbed surfaces, ang. distribs. of Auger electrons 78−39636
Ni, evaporated, adsorbed acetylacetone, XPS study 80−76133
Ni film, evaporated, galvanomag. props., oscill. due to CO adsorption 77−1496
Ni film, interaction with O_2, AES, EELS, work function, and gravimetric meas. 80−75433
Ni film, of CO, effect on resist., negative p-values 77−85083
Ni film, of water, change in work function *(German)* 79−42365
Ni film, vacuum deposited, ethylene adsorption and reactivity with adsorbed H, surface pot. meas. 79−86995
Ni film, work function changes upon water contamination 80−44705
Ni films, of ethylene, adsorpt. and decomposition, coverage depend. meas. 80−96743
Ni, ion bombard., ion and photon yields, CO adsorption effect 80−89098
Ni metal cluster, of CO, mol. orbital calc. 78−18895
Ni, of acetic acid and ethylenediamine, XPS study 80−76132
Ni, of acetylene, on stepped surface, dehydrogenation 79−52752

adsorption continued
Ni, of benzene, ang. distrib. of electrons photoemitted from benzene mols. 77−69968
Ni, of benzene, on (100) and (111) faces, LEED and high resoln. electron energy loss spectra 78−6224
Ni, of CO, adsorbed mol. bond config. and orientation, ang. resolved photoemission 77−44506
Ni, of CO, binding and energy level shifts, NiCO and Ni_2CO electronic struct. 78−34882
Ni, of CO, coverage, backscatt. coeff. from ^{14}C radiation 78−30824
Ni, of CO, effect on galvanomagnetic and magnetic props. 78−43490
Ni, of CO, electron field emission, energy distrib. 79−8231
Ni, of CO, high press., low temp. Raman spectra 78−6219
Ni, of CO, mol. orientation, ion scatt. 78−71949
Ni, of CO, on (001), orbital energy spectrum 78−2369
Ni, of CO, on (100), bonding struct., vibr. excitations 77−15687
Ni, of CO, polycryst. surface, SIMS 78−14585
Ni, of CO on stepped surface, adsorpt.-desorpt. behaviour, LEED, AES, thermal flash desorpt. study 78−71984
Ni, of H, extended Huckel theory 78−10286
Ni, of H, isotherms 77−11776
Ni, of H, on (110) surface, structural investig. by He diffraction 79−86984
Ni, of H and H_2, HMO studies 77−15682
Ni, of H_2, activation mechanism, extended Huckel calc. *(French)* 79−42379
Ni, of H_2, demagnetisation of surface due to absorption 77−80990
Ni, of H_2, effect on electron spin polarisation 78−14933
Ni, of H_2, initial sticking coeff. for polycryst. O_2 and S covered surface 78−63937
Ni, of N_2, photoemission and electronic struct., cluster calcs. 80−97403
Ni, of NO, ground and core hole states, config. depend. HF LCAO SCF calc., relax. and binding energy 80−29453
Ni, of O_2, H_2O, gases, effect on exoelectron emission from rubbing surfaces 79−1816
Ni, of O_2, oxidation 80−108730
Ni, of S, diffusion, multiple binding sites, photoelectron spectra, LEED struct. 77−66569
Ni, of S(Se), surface bonding mechanism for ang. resolved photoemission 79−69360
Ni, of Xe, Kr and CO_2, stay time meas. 78−56044
Ni, photon emission due to Ar^+ ion bombard., adsorbed and recoil-implanted O effect 80−80872
Ni, secondary negative ion emission, effect of adsorbed O_2 *(Russian)* 79−28881
Ni small clusters, of Na, local densities of states 80−88466
Ni surface, (110), O_2 adsorption, LEED and ion scatt. study 80−84386
Ni surface, adsorpt. and decomp. of formic acid, obs. using combined SIMS-FDS-AES system 78−40076
Ni, surface, coadsorption of Pb or Sn with P or C, AES study 80−54521
Ni surface, coverage and desorption of CO flash desorption spectrum 80−49493
Ni, surface, single-atom self-diffusion FIM study, hydrogen adsorption effects 80−103548
Ni surfaces, of at., mol. H_2, semi-empirical CNDO MO calcs. *(German)* 79−95465
Ni surfaces, of S, directional UV photoemission 78−15295
Ni, ultrathin film, field effect meas., influence of CO adsorption 80−11108
Ni, with Te overlayer, surface sensitivity of MeV He ion scatt. 79−56904
Ni/SiO_2, of CO, scavenging effect of H_2, in situ Fourier transform IR spectra obs. 80−39410
Ni-Al, Raney nickel catalyst, surface texture studied by N_2 adsorption and ESCA *(French)* 79−69348
Ni-Cu (30 at.%), H(D) penetration, reversed kinetic isotope effects 77−43387
Ni-Fe, of O_2, oxidation 80−108730
Ni-Sn system intermetallic formation rate, H_2 adsorption effect 79−90819
NiCO, linear, ab initio RHF-MO calcs., rel. to adsorption 79−26883
NiCr film, gas adsorption during electron beam deposition *(Polish)* 79−20492
NiO, (100) surface interaction with SO_2, electron diffr. and Auger spectrosc. obs. *(French)* 80−97728
NiO, of CO+N_2O, catalysed reaction in Neel transition region 78−53258
NiO, prepared by thermal decomp. of $Ni(OH)_2$, microporosity and irreversible water vapour adsorption 80−80060
$Ni(OH)_2$, adsorption props. of surface, gas-chromatographic investigation 79−66343
Ni(100), of chalcogens 80−6648
Ni(100), with adsorbed K^+, He^+ impact, Auger deexcitation spectrosc. 79−100010
Ni(110), of ethylene and decomp. 77−85071
Ni(111), coadsorption of CO and H_2, surface carbide influence, vibr. electron energy loss obs. 79−52772
Ni(111), of acetylene, benzene form., vibr. spectra 78−95952
Ni(111), of acetylene, chemisorbed O_2 effects, CH formation 78−18902
Ni(111), of CO, absolute coverage determ., AES and LEED 77−76661
Ni(111) surface, of CO, CO_2, carburisation, AES meas., electron beam-induced effects 77−48588
Ni(111) surface, of H_2, at low temps., LEED meas. 78−56045
Os, of O_2 and H_2 in H_2SO_4 soln. 79−61873
P transport through sandy soils, nonlinear reversible adsorption-desorption model 77−66940
PO_4^{3-} adsorption equilibria in lake sediments 79−66354
Pb halides, of water, mol. studies of ice-forming capabilities 77−31872
PbS (100) surface, adsorption of O_2, effect on electronic struct., UPS study 80−54756
PbS, adsorption mechanism in selective etching 77−7727
PbS, hot-pressed compact, elec. behaviour, adsorbed atmos. gas effects 77−66601
$Pb_{1-x}Sn_xTe$ epitaxial films, adsorption-induced accumulation layer form. on surface 80−60117
PbTe (111), of O_2, UPS and XPS exam. 78−71962
PbTe (111) epitaxial films, localised electron irrad. effects on elec. props. and O_2 sorption 80−49472
Pd (100), with CO adlayer, band formation, calcs. and photoemission expts. 79−95463

adsorption continued
Pd (110) surface, adsorption of S, characterised by LEED *(French)* 80—88422
Pd (111), electronic states calc. and adsorbate-induced photoemission struct. interpretation 78—60179
Pd (111), of NO, LEED, UPS, and thermal desorpt. expts. 77—69179
Pd (111), of O_2 and NO, LEED, photoelectron spectra and thermal desorpt. expts. 77—69180
Pd (111), scattering, adsorption, and absorpt. of H_2 and D_2, mol. beam study 80—29277
Pd black, of H_2, adsorpt. props. rel. to PtO irrad. 77—11796
Pd cluster, adsorption/desorption of CO, AES and thermal desorption meas. 80—75436
Pd film, of H_2 or O_2, reciprocal titration of gases, film surface area determ. 77—1318
Pd film, vacuum deposited, ethylene adsorption and reactivity with adsorbed H, surface pot. meas. 79—86995
Pd film, work function changes due to adsorbed H_2, surface and interface dipoles 80—96972
Pd, influence of adsorbed H on positron lifetime spectra 80—25480
Pd layer, adsorption and absorption of H_2, kinetic analysis of models 77—47679
Pd, of benzene, ang. distrib. of electrons photo-emitted from benzene mols. 77—69968
Pd, of CO, on (111) surface, catalytic oxidation, mol. beam investig. 78—88656
Pd, of CO, polycryst. surface, SIMS 78—14585
Pd, of CO, UPS of CO on Pd clusters, binding energy, d-electron emission particle size depend. 79—4888
Pd, of H_2, piezoelectric quartz microbalance meas. 79—60626
Pd, of NH_3, NH_x and N, decomposition of NH_3 and hydrogenation of N, AES 77—1315
Pd ribbon, of H_2, thermal desorption and work function meas. 80—70538
Pd, surface, coverage and desorption of CO flash desorption spectrum 80—49493
Pd wire, of H_2, heat of adsorpt., sticking probabilities 78—43240
Pd/Al_2O_3, of CO, IR study 80—108193
Pd-Ag, influence of adsorbed H on positron lifetime spectra 80—25480
Pd-Cu, influence of adsorbed H on positron lifetime spectra 80—25480
Pd-TiO_2 Schottky barrier, work function depend. on adsorbed species 80—54782
Pd-ZnO Schottky-barrier diode, H_2 sensitivity 80—11085
PdAg wire, of H_2, heat of adsorpt., sticking probabilities 78—43240
PdAu wires, of H_2 78—43239
Pd(001), of CO, LEED, electron energy loss spectra study, surface struct. effect on weak chemisorpt. bonding 78—71987
Pd(100) surface, of O, obs. of O^- and O^+ during electron bombardment 79—95883
Pd(110) surface, adsorption of Xe, AES, UPS, LEED, work function, flash desorption 80—6633
Pd(111), of CO and O_2, mutual interactions, transient product formation 78—87871
Pt (100), (110), and (111), form. of Cu monolayer, optical and electrochem. studies 79—99419
Pt (100), CO or C_2N_2 adsorpt. induced backscatt. enhancement 77—90227
Pt (100), cyanogen adsorbed layers, electron energy loss spectrum 78—14592
Pt (100), of acetylene or ethylene, intermolecular forces and kinetics of adsorption 78—75930
Pt (100), of H_2S, intermolecular forces and kinetics of adsorption 78—75930
Pt (100), of NO, 40-400°C, LEED, AES, XPS and UPS obs. 77—35820
Pt (100), of S 78—14606
Pt (100) (5×20) and (1×1) surfaces, stability and reactivity, adsorption of H 80—75434
Pt (110), of acetylene, LEED, AES and desorption meas. 77—62749
Pt (110), surface structs. during S adsorption, LEED pattern interpretation model 77—69184
Pt (111), adsorption of acetic and propanoic acids, LEED obs. 80—80073
Pt (111), clean and oxidised, binding states and sticking coeffs. of CO and H_2 77—72787
Pt (111), coadsorption of CO and hydrocarbons, $C\equiv O$ bond weakening 79—90863
Pt (111), interaction with water, thermal desorption, UPS, and XPS study 80—80088
Pt (111), O_2, CO and C_2H_2 adsorption and cooxidation, AES *(German)* 78—14619
Pt (111), of CO, XPS, UPS, TDS and dynamic meas. of work function 79—65322
Pt (111), of CO, XPS, UPS, thermal desorption, and work function meas. 79—77905
Pt (111), of Co, electron energy loss spectroscopy and IR reflection spectroscopy 77—85729
Pt (111), of H_2, obs. by dynamic meas. of work function 79—77915
Pt (111), of H_2 and O_2, and their interaction kinetics 77—55461
Pt (111), of NO, EELS, thermal desorption, LEED, and AES study 80—80086
Pt (111), surface reaction with acetylene ethylene, and H_2, EELS 78—71947
Pt (111) and (100) superlattices formed by dissociative adsorption of HI, LEED, AES, and thermal desorption studies 80—55715
Pt (111) and Pt(S)-12(111)×(111) surfaces, of 0, thermal desorption, AES, XPS, and LEED study 80—70534
Pt (111) surface, stepped, of O_2, CO, C_2N_2 and ethylene 78—71992
Pt, adsorption and catalytic reactions of H_2, CO, and O_2 80—81362
Pt, adsorption and decomp. of ethylene, 90 to 500K 79—46933
Pt, adsorption and desorption of O_2 on (110) surface, thermal desorpt., LEED/AES obs. 77—72788
Pt adsorption of CO, O_3 NH_3, surface composition, AES and temp. programmed desorption meas. 80—34313
Pt, adsorption of water, H_2 and reaction between H_2 and adsorbed O 80—49514
Pt black, of H_2, adsorpt. props. rel. to PtO irrad. 77—11796
Pt, electrochemical adsorpt. of H_2, adsorpt. states, tensiodynamic meas. 77—20196
Pt electrode, compact layer struct., absorpt. EHT calcs. 77—16828
Pt electrode, of H, dynamic impedance meas. 79—74393
Pt electrodes, of Au, in aq. HCl 78—56914

adsorption continued
Pt film, discontinuous, of alkali halide mols., effect on elec. cond. 80—2487
Pt film, vacuum deposited, ethylene adsorption and reactivity with adsorbed H, surface pot. meas. 79—86995
Pt film, work function changes upon water contamination 80—44705
Pt, low index surface, adsorption of O_2 reduction intermediates at steps 79—70343
Pt, of activated N_2 on single cryst. faces 77—85070
Pt, of Ar, thermal accommodation coeffs., 300 to 1350K 80—30272
Pt, of CO, adsorption site investigation by IR reflection spectra 78—14565
Pt, of CO, binding states, desorption and adsorption kinetics 77—85065
Pt, of CO, electron energy loss spectral study of surface vibrs. 77—69160
Pt, of CO, IR reflection absorpt. spectra, 1875 cm^{-1} band 79—65852
Pt, of CO, low temp. vibr. mode, site occupation, electron energy loss spectra 80—29263
Pt, of CO, mol. internal optic modes, mol. dipole model 80—100395
Pt, of CO, O_2, H_2, thermal desorpt. spectra 78—14607
Pt, of CO, O_2, H_2, UV photoemission spectra 78—14608
Pt, of CO, on (111), photoemission, 40-150 eV 77—16465
Pt, of CO and D_2, absolute coverage meas. using nucl. microanal. 80—54511
Pt, of CO(C_2N_2)(Benzene)(ethylene), Auger spectra 79—52077
Pt, of CO(NO), on SiO_2-supported surface, IR spectrosc. obs. 80—92780
Pt, of Cs field-emission microscopy 78—51822
Pt, of cyclopropane, NMR and PMR obs. 77—51591
Pt, of ethylene and acetylene, on (111) surface, LEED intensity obs. 77—51592
Pt, of H, (111) surface, role of at. steps. 77—15690
Pt, of H, electrode surface exam. by LEED and AES 77—47665
Pt, of H, face specificity, field emission probe-hole microscope obs. 77—11783
Pt, of H_2, electrolyte environment and crystallite size effects 78—27774
Pt, of H_2, recording contact pot. changes using precise diode method 79—88982
Pt, of H_2 and CO on (110) clean and oxidised surfaces 77—28078
Pt, of $H_2(D_2)$ on (111) or (332) surface, H_2+D_2 exchange reaction, mol. beam obs. 79—66269
Pt, of N_2, thermal desorption meas., α and β-status 77—15696
Pt, of N_2 and Xe, weak adsorption, field emission meas. 77—24479
Pt, of O, Auger spectra 78—14600
Pt, of O, preanodised or passivated, DTA 77—16733
Pt, of O_2, AES, LEED and thermal desorption spectroscopy exam. 78—79891
Pt, of O_2, isotopic exchange and thermal desorption *(French)* 78—43249
Pt, of O_2, on (110) surface, Ar^+ bombardment effects on reactivity 80—89099
Pt, of O_2, surface struct. effects on rate, data assessment 78—43251
Pt, of O_2, surface struct. depend., LEED, AES, and electron energy loss spectra 79—46934
Pt, oxide layers on electrode surface anisotropy of optical props. 80—60534
Pt particles supported on SiO_2 gel, reaction between adsorbed H_2 and O_2, low press. 77—52668
Pt, polycrystalline, coadsorption of CO and H_2 77—59220
Pt, stepped surface, adsorpt. and decomp. of NO and NH_3, LEED, AES, and thermal desorption expts. 78—38943
Pt, stepped surface, of H_2 and D_2, reaction probability, reactant ang. of incidence effects 77—47670
Pt, surface, (111), O_2 interactions, UPS, EELS and thermal desorption study 80—100409
Pt surface, CO oscillatory oxidation, theory 80—85215
Pt surface, CO oscillatory oxidation, theory 80—85216
Pt surface, coverage and desorption of CO flash desorption spectrum 80—49493
Pt surface, of water, D_2O+H, $D_2{}^{16}O+{}^{18}O$ exchange reacts. 77—80695
Pt surface, oscill. oxidation of CO 77—4926
Pt surfaces, of H, field emission study 77—24477
Pt, surfaces (111) and 6(111)×(111), CO adsorption, EELS and thermal desorption spectroscopy 78—91547
Pt/MgO catalyst, of H_2, 300-873K *(French)* 78—38967
Pt-electrolyte interface laser speckle movements related to electrode pot., H_2 adsorb. 78—40052
Pt-graphite catalyst, of H, ESR obs. 79—24818
Pt-Pd, of CO(NO), on SiO_2-supported surface, IR spectrosc. obs. 80—92780
Pt(S)-[9(111)×(111)] face, of O_2, flash desorption, LEED and AES obs. 77—69182
Pt(100), of ethylene 78—18905
Pt(111), of Br, irreversible order-disorder transition 79—69361
Pt(111), of K, UPS and XPS meas. 80—95675
Pt(111), of NO, anal. of adsorption processes and surface reactions, vibration spectroscopy 78—87868
RE, of K, work function changes, FEM obs. 77—72772
Ra A (^{218}Po) adsorption to monodispersed aerosol 80—32535
Rb, oxidation, adsorbate-induced structs., UPS obs. 79—47828
Re $(10\bar{1}0)$ of k, electron-adsorption props. 79—33192
Re, adsorption, oxidation, and hydrogenation of CO, XPS, UPS, and thermal desorption study 80—71571
Re, catalytic activity during adsorption of HD 79—69358
Re, coadsorption of ethylene and O_2, thermal desorption study *(French)* 78—85194
Re, dissociative and mol. adsorption of H_2O and NO *(French)* 79—69344
Re, field depend. of spectral line energy of He-H_2 adsorbate 79—78853
Re filament, of CO and H_2, temp. controller for filament heating appl. *(Japanese)* 77—51603
Re, interaction with F_2 and fluorides at low temp. and high press. 78—39700
Re, interactions between adsorbed HD or D_2 and CO 79—86987
Re, of Au, on low index planes, FEM 78—14597
Re, of CO, effects of surface steps on CO β state *(French)* 78—43250
Re, of CO, on basal (0001) and stepped $|14(0001)\times(10\bar{1}1)|$ planes 78—14594
Re, of H, within wide temp. range 80—10778
Re, of Hg, work function change 77—7966
Re, of O_2, effect of struct. defects, steps and kinks 80—29269
Re, oxide formation and surface rearrangement, field ion microscope obs. 77—28936

adsorption continued
Re, polycryst., of C, CO, H_2 and C_2H_4, work function changes *(French)* 77−28075
Re, polycryst. and (0001) single cryst., ethylene and acetylene adsorption 78−38947
Re tip, condensation remoulding, field emission microscopy 78−2995
Re, with adsorbed O_2, Na ionisation, field reversal and surface ionisation expts. 77−90232
Re(0001), of O_2, CO, NO, and H_2O, XPS, UPS and temp. programmed desorption 80−71574
Rh (110), S adsorbed, surface struct. anal. using hybridisation model 80−44423
Rh (110), S-adsorbed, LEED crystallographic determ. of struct. 80−44422
Rh (111), catalytic reaction between adsorbed O_2 and H_2, LEED obs. 79−52773
Rh (111), co-adsorption of H_2 and CO segregation of co-adsorbed species 80−65361
Rh (111), coadsorption of O_2 and H_2 below 140K 80−29276
Rh (111), interaction with O_2, thermal desorption spectra, AES and LEED obs. 79−51428
Rh (111), of CO, thermal desorption mass spectrometry and LEED meas. 79−77917
Rh (111), of O_2, AES, LEED, and thermal desorption mass spectra meas. 79−77900
Rh, coadsorption of CO and H_2, thermal desorption mass spectroscopy meas. 79−46948
Rh dispersed on Al_2O_3, of CO, ^{13}C NMR obs. of adsorbed states 80−96733
Rh, of $C^{16}O$ and $C^{18}O$, inelastic electron tunnelling spectra obs. 79−65331
Rh, of CO, inelastic electron tunnelling spectra obs. 79−46962
Rh, of CO, on (110) face 78−6225
Rh, of CO and H_2, on (111) surface, 2-dimens. phase separation 80−107634
Rh, of CO+H_2 mixtures, reflection-absorption IR and thermal desorpt. obs. 78−6226
Rh, of H_2, mass spectra 78−38970
Rh supported catalyst particles, of CO, inelastic electron tunnelling spectra 79−3509
Rh(100), of H_2S, (2×2) surface struct., LEED anal. 79−99426
Ru (0001) surface, adsorption and desorption of NH_3, effects of electron beam 78−38955
Ru (0001) surface, of H_2, N_2 and NH_3, AES, LEED and thermal flash desorption meas. 78−38954
Ru (001), coadsorption of O_2 and CO, uptake and flash desorption meas. 80−39450
Ru (001), of CO, IR spectra, LEED, and thermal desorption meas. 80−70533
Ru (001), of CO, temp. depend. ordering processes 80−80773
Ru (001), of H_2S and S, LEED, UPS, AES, and thermal desorption meas. 79−99420
Ru (001), of NO, inelastic electron scatt. dissoc. energies adsorbed state depend. 78−95956
Ru (001), of NO, KPS, UPS, and X-ray AES meas. 80−6655
Ru (001), physically adsorbed SF_6, XPS expts. 77−69178
Ru ($10\bar{1}0$) of NO and CO, dissoc. 77−72783
Ru ($10\bar{1}0$), decomp. of formic acid, depend. on adsorption temp. 79−79245
Ru ($10\bar{1}0$), dissociative adsorpt. of NO, LEED and AES expts. 77−90642
Ru (110), of H_2S, H_2, and S, UPS and work function change meas. 79−78834
Ru ($11\bar{2}0$), of O_2, H_2, and CO, ellipsometry-LEED study 80−103570
Ru, clean and S covered, adsorption and desorption kinetics of CO 80−6643
Ru, clean and S covered, adsorption and desorption kinetics of H_2 80−6644
Ru electrodes, adsorption and surface reactions, cyclic voltammetry and X-ray emission spectrometry 78−61018
Ru field emitter, of H_2, field-induced redistrib. processes 79−78854
Ru, of CO on (001) surface, IR spectra and LEED 79−37914
Ru, of NO, on (001) surface, EELS obs. 80−20741
Ru, physisorbed SF_6, XPS interpretation 77−89830
Ru(110), of H_2S, H_2, and S, UPS and work function meas. 79−99424
S adsorption in coal, content meas., using X-ray radiometric analysis 80−26077
SF_6 purification in const. temp. adsorption process, appl. to electrostatic accelerators 78−29672
SI, of O_2, early stages, AES, LEED, and XPS obs. 79−46937
SO_2 adsorption on mixed metal films 79−87003
SbSI, adsorption polarisation and depolarisation currents 77−43942
SbSI, of methanol $(O_2)(H_2)$, polarisation switching processes, effect of surface electron states 77−90115
SbSI, of $O_2(H_2)$, effect on work function and spontaneous polarisation *(Russian)* 78−6211
Sc (0001), H adsorption, geometric vs. electronic factor in surface electronic structure 80−70788
Sc, crystal surface, N and O adsorption, refl. electron energy loss spectra obs. 80−20742
Se, amorphous film, inverse/combined photoadsorption and photodeposition, light-temp. interference 79−46977
Si (100), H adsorption, MeV ion scatt. study 80−80071
Si (100), oxides formed in Cs-O adsorbed films, ionisation loss spectra, Auger spectra 79−69365
Si, (100) surface, Auger emission ang. depend., overlayer effects 78−39637
Si (111), adsorpt. of O and stimulated oxidation by electron bombardment, AES 78−14599
Si (111), adsorption of Cl, H, Si, SiCl, $SiCl_2$, equilib. adsorption layers 79−23858
Si (111), growth and etching vectors, adsorption and step reconstruction 79−23548
Si (111), O and CO sorption, ion scatt. obs. 80−59810
Si (111), of C_2H_2, low-energy electron loss spectroscopy obs. 77−1303
Si (111), of Cl, electronic energy states, cluster-type calcs. 79−47149
Si (111), of Cs, LEED, work function and thermal desorpt. 78−14590
Si (111), of $H_2S(H_20)(0_2)$, electron energy loss spectra exam. 77−39736
Si, (111) 7×7 surface, of Al, electron energy loss spectroscopy and LEED 77−43432

adsorption continued
Si (111) surface, O_2 adsorption, atomic steps and residual gas effects 80−54517
Si (111) surfaces, cleaved, electronic structure following Al adsorption 80−75610
Si (111)7×7, dangling-bond surface states and O_2 adsorption, reflectometric study 79−99600
Si, adsorption-desorption kinetics of H_2, O_2 and other gases, catalysis 77−47684
Si, CVD from SiH_4-HCl-H_2 system, rate-determining reactions and surface species 80−84405
Si, cleaved surface, metal contact props. and influence of intermediate adsorbed layers 80−49905
Si, crystallisation in Si-H-Cl system, adsorpt. layer comp. 77−15697
Si, epitaxial layer, growth mechanism from ion-molecular beams 80−2299
Si, etching using XeF_2 vapour, adsorption/desorption process 79−43449
Si gas-sensitive microtransducer, cond. variation with pulsed ethanol adsorption *(Russian)* 80−50915
Si, of Cs, (100)2×1 surface, LEED 77−62747
Si, of gases, electron energy loss spectral study of surface vibrs. 77−69160
Si, of H_2S, on (111) 7×7 surface, LEED and AES 78−38966
Si, of metal atoms, effect on surface electron props. 77−55597
Si, of O, Auger spectra 78−14600
Si, of O, chem. shift of Si 2p core level in SiO_x, relax. contrib. 79−47141
Si, of O_2, light sensitive electron loss meas. on surface 79−24396
Si, of O_2, UPS, new adsorption state 78−34702
Si, of water (O_2), surface charging during illumination, effect of various surface treatments 79−51651
Si, oxidation comparison with O_2 adsorption, SIMS 78−15273
Si, photon emission due to Ar^+ ion bombard., adsorbed and recoil-implanted O effect 80−80872
Si, planar and O_2 etched (111) surface, CO adsorption, AES, SEM, ESD, flash desorption mass spectra 78−63934
Si, pure and with adsorbed Al(Au), thermal expansion and at. vibr. singularities 77−89635
Si, surface, (111) 2×1, cleaved, O_2 adsorption, low-energy electron loss spectra 79−15840
Si surface interacting with adsorbed gases, paramag. props., EPR study 80−34772
Si surface structure, Si (111)7×7, Si (111)$\sqrt{19}\times\sqrt{19}$ Ni, Si (111)5×1 Au, RHEED 77−62452
Si surfaces, amorphous, hydrogenated, and monocryst., AES and LEED, comparative study *(French)* 80−44398
Si wafer, chemically etched, surface roughness by gas adsorption techniques 80−15398
Si:H, amorphous, plasma deposited, cond. adsorbate and insulating layer effects 80−49749
Si:H film, amorphous, elec. cond., effect of adsorbed gases and illumination 78−88048
Si/SiO_2, adsorbed methanol, light scatt. from clusters 79−33721
Si-SiO_2 microsensor, surface conductivity effect of aliphatic alcohol molecule adsorption *(Russian)* 78−34887
SiO_2 (silicalite), hydrophobic crystalline mol. sieve, organic mols. preferential adsorpt. 78−30598
SiO_2, adsorption of H_2O, surface treatment and methylation effects 78−84058
SiO_2, CVD film, hydration props., ellipsometry meas. 78−22986
SiO_2 film, ion bombarded, attenuated total refl. method obs. of H capture 79−95863
SiO_2 film, on Si wafer, surface roughness by gas adsorption techniques 80−15398
SiO_2 films, of H_2O, sintering effects investig. 79−66031
SiO_2 gel, adsorption curves of O_2, EPR *(Russian)* 79−52776
SiO_2 gel, irrad., adsorpt. of NH_3, neutron scatt. 79−33194
SiO_2 gel, macroporous, modification of surface by adsorption of thin layer of polymer 80−6624
SiO_2 gel, meso-porous, of N_2, pore size distrib. calc. 77−4941
SiO_2, gel, motion of NO_2 radicals adsorbed on surface, ESR spectrum averaging-out 77−60119
SiO_2 glass, porous, of inorganic cations, in distilled water medium 79−24814
SiO_2, highly dispersed, produced by plasmochemical method, adsorption props. *(Russian)* 77−70275
SiO_2, of albumin 80−10777
SiO_2, of cetyl pyridinium bromide, adsorpt. pH depend., mechanism 79−20466
SiO_2, of H_2O, O_2, H_2, He, adsorpt. rel. to EPR relax. time *(German)* 79−95645
α-SiO_2, of $H(H_2)$, microweighing and X-ray obs. *(German)* 78−51825
SiO_2 of water and methyl alcohol, thermally stimulated depolarisation currents 79−78611
SiO_2, P-doped amorphous, porous and hydrophilic, water adsorpt. and IR spectra obs. 80−80061
SiO_2 surface, adsorpt. pot. and electrophysical props. *(Russian)* 79−91123
SiO_2 surface, Ar plasma-treated, O_2 adsorption reactivity, EPR obs. 79−51418
SiO_2 surface, of Cu^{2+}, Cr^{3+}, Co^{2+} ions, EPR, optical spectroscopy investig. *(German)* 79−95266
SiO_2 surface defects, influence of adsorbed O_2 EPR spectra 80−7163
SiO_2, vitreous, He solubility, 100 to 1350 atm., 5 to 80°C 79−4414
SiO_2:Al gel, gamma rad. effects, depend. of H_2 adsorption and colour centre form. on Al content 79−69156
SiO_2:Co(II), of H_2O, coord. lifetime, surface effect, NMR obs. 80−34299
SiO_2-liquid heptane interface, adsorption of organic liqs., IR spectra obs. 79−57295
SiO_2-Na_2CO_3, sodium Erevanit-25, sintering, struct. 79−43284
SiO_2-Si stratified system surface charges, adsorption and desorption effects *(Russian)* 80−49942
SiO_2-ZrO_2 adsorbents, coprecipitated, porous struct. rel. to form. conditions 78−53263
Si(100), (1×1)H struct., averaged LEED 77−62720
Si(100) surface, of H, effect on struct., LEED meas. 78−14602
Si(111), ion-bombard., O_2 adsorption, SIMS study 80−70522
Si(111), of Ag, cohesive energy and 2-dimens. phase diagram, AES exam. 78−43246

adsorption continued
- Si(111), of HBr(Cl), AES, electron energy loss spectra and electron impact desorption exam. 78−43243
- Si(111), partial monolayers of H, UV photoemission, disordering effect 77−1308
- Si(111), water vap. and O_2 interactions, EELS 78−14571
- $SmCo_5$, adsorption and desorption charact. of H_2 *(Japanese)* 77−47667
- Sn, O_2 precursor adsorption, chemisorption activation energy 78−71950
- SnO_2, of H_2O, isotherms 78−56038
- SnO_2, of $O_2(CO)(H_2O$ vapours), effect on cond. 78−76067
- SnO_2, of water, adsorption anomaly rel. to pretreatment 79−28194
- SnO_2, of water, anomaly, effects of cryst. growth of solid 80−10779
- SnO_2, sintered, of Ar, meas. and calcs. 77−69164
- SnO_2 thin film gas sensor, prep. 80−39691
- SnO_2:ThO_2, exposed to CO gas, self-oscill. phenomenon 78−68032
- SrO, surface states, refl. spectra, impurity effects 77−20873
- $SrSO_4$, surface crystn., on $BaSO_4$, isotope exchange and electron microscopy study 80−34332
- $SrTiO_3$, (111) face, photoassisted reaction of adsorbed H_2O+CO_2, producing methane 78−76878
- $SrTiO_3$, of O_2, electron energy-loss spectra obs. 80−89521
- Ta (112), oxidised, emission and work function, K adsorption effects 78−11060
- Ta auto-cathodes, effect of O_2 on emission and surface diffusion *(Russian)* 79−77892
- Ta, caesiation, AES at very low energies 77−69946
- Ta, evaporated film, of CS_2 and H_2S, 195 to 473K 79−33197
- Ta film, of SO_2, adsorpt., corrosion 78−79897
- Ta film, vacuum-deposited, gas adsorpt. effects on photoelec. props. 78−15298
- Ta, interaction with F_2 and fluorides at low temp. and high press. 78−39700
- Ta, of $CO(CO_2)$, FEM and flash filament method exam. 78−43245
- Ta, of Cs, direct meas. of adsorpt. isobars 78−43235
- Ta, of H_2, mass spectra and field-emission obs. 77−76673
- Ta, of K, work function depend. on surface coverage 77−11788
- Ta, of LaB_6, work function 80−20039
- Ta, of O_2, FEM obs. of work function changes 78−26771
- Ta, oxidation comparison with O_2 adsorption, SIMS 78−15273
- Ta, simultaneous interactions with Cl_2 and O_2 under low press. and high temp. 80−71938
- TaS_2 (2H), of $NH_3(N_2H_4)$(pyridine) (O_2) gases, intercalation, X-ray diffr. investig. 77−12828
- Ta(100), of Au, model 77−1321
- Te film, atm. comp. influence on elec. surface props. 78−26980
- Te film, H_2, during Te electrodeposition on Sn in Sn/Te/electrolyte system 77−63923
- $Te_{50-x}Se_{50}Sn_x$, thin films, elec. cond. and thermoelectric power meas. *(French)* 80−80335
- Th, of O_2, XPS study 80−7473
- Ti (0001), H adsorption, geometric vs. electronic factor in surface electronic structure 80−70788
- Ti evaporated film, adsorption and replacement of methane, CO and NO *(Japanese)* 78−22949
- Ti, evaporated film, of CS_2 and H_2S, 195 to 473K 79−33197
- Ti, film, evap., CO effect on work function 78−39188
- Ti film, of SO_2, adsorpt., corrosion 78−79897
- Ti, of O, on polycryst. film at room temp., UPS and XPS 77−89645
- Ti, of O_2, CO and CO_2, SIMS expts. using 500 eV primary Ar^+ ions 77−72785
- Ti, of O_2, XPS exam. *(French)* 78−23858
- Ti, of Xe, electronically excited atoms coupling to cond. states 77−89642
- Ti, oxide layer growth by dry oxidation at 25°C, ESCA obs. *(French)* 80−45434
- Ti, photon emission due to Ar^+ ion bombard., adsorbed and recoil-implanted O effect 80−80872
- TiH_x film, kinetics of H_2 interaction 80−6620
- TiO_2 (rutile), (001) and (110) faces, UPS and LEED obs. 80−45206
- TiO_2, clean and hydrated, surface sites, XPS 80−35052
- TiO_2, OH^- adsorption on defect site, electronic struct. 79−47150
- TiO_2, of neopentane, NMR pulsed field gradient method, diffusion coeff. meas. 80−15362
- TiO_2, of water, IR spectra 78−14577
- TiO_2, rutile, of acetic acid-d_4, IR obs. 78−30827
- TiO_2, rutile, of O_2 and CO, effect on oscills. in elec. resist. 79−91068
- TiO_2, rutile, pure and SiO_2-coated, adsorption of N_2 and Ar, 77.4K, microcalorimetry obs. 80−80062
- TiO_2 surface, of O_2, heat cleaned, O_2^- radical form., EPR 77−35806
- TiO_2 suspension, adsorption-desorption of IO_3^- 80−93804
- TiO_2, X-irrad., adsorpt. of O_2, EPR meas. 78−80211
- TlCl, of water vapour, 273, 283 and 293K 78−56035
- TlI, of water vapour, 273, 283 and 293K 78−56035
- TlTe, melt, elec. cond., surface tension, microhardness, influence of impurities 80−88551
- Tl_2Te_3 melt, impurities effect on surface tension polytherm and adsorption obs. 77−7947
- ^{205}Tl, NMR studies *(Rumanian)* 79−82888
- Tn decay products, ats. and ions, adsorption probability on submicron particles 79−39803
- U (VI) extraction from sea water, by adsorption on gel particles containing $Ti(OH)_4$ *(Japanese)* 77−54347
- U binding, by brown coal, from seawater, IR spectroscopic obs. 78−82855
- U extraction from seawater, tests of adsorbents 78−36198
- U extraction from seawater using composite absorbents 80−24730
- U, of water and O_2, XPS study 80−7473
- UO_2 pellets, retention and release of water 79−67923
- U(VI), extraction from sea water using polyacrylamide gel containing metal hydroxides 78−54861
- V (100), sorption investig. using total current spectroscopy of slow electrons 77−8694
- V, extended fine struct. above L-shell appearance pot. thresholds, CO adsorption effects 78−92148
- V, oxidised in air during laser irradiation, switching effect *(Russian)* 80−24977
- V surface interaction with O_2, H_2, H_2+O_2 and H_2O, SIMS, EID 77−62753
- V_2O_5, interaction with adsorbed propene, IR emission spectra obs. 79−90881

adsorption continued
- W (001), disordered CO and O_2 overlayer effect on electron spin polarisation in LEED 79−60632
- W (001), of N_2, effect on LEED electron spin polarisation and intensity profiles 80−65377
- W (001), ordered CO overlayer effect on electron spin polarisation in LEED 79−60633
- W (001), surface reconstruction and reordering by H adsorption, MeV ion scatt. 79−23835
- W (001) adsorbate system, directional photoemission of polarised electrons 77−36374
- W (001) surface, of CO, electron energy loss spectra 78−71999
- W, (001) surface, reconstruction and reordering by H adsorption, MeV ion scatt. studies 79−82443
- W (001) surface with adsorbed Cs, core-level photoemission anisotropy 78−11076
- W (001) surface with adsorbed S, struct. and effect on CO adsorption 79−86981
- W (011), of Ag, LEED, AES, and work function meas. 79−86990
- W (011) face, of Sr and La, influence of substrate electronic struct. on props. 78−60032
- W (100), coadsorption of CO and H_2, CO/H surface complex obs. 79−4478
- W (100), coadsorption of H and CO, photoemission and thermal desorpt. investig. 77−28079
- W (100), coadsorption of Zr and O_2 at high temp. 80−6653
- W (100), condensation of Cu and Ag, early stage comparison with Mi(100) 80−80072
- W (100), Cs and O_2 coadsorbed, high photoemission efficiency 77−55862
- W (100), H adsorbate low energy electron vibrational excitation 80−84375
- W (100), O covered, ion scatt. spectroscopy 77−73205
- W (100), of Au, Cu, Ta, Nb, Mo, and Ir, effect on surface reson. 79−65983
- W (100), of CO, thermal desorption and work function meas. 80−29273
- W (100), of Cl_2, LEED and AES study 79−90878
- W (100), of ethylene at 80K and decomposition to acetylene, AES obs. 79−66353
- W (100), of La, depend. of work function, heat of adsorpt. on surface coverage, contact potential study 78−67912
- W (100), of O_2, AES, desorption, LEED and work function obs. 77−1317
- W (100), of Zr, AES, LEED, thermal desorption, and work function meas. 80−39444
- W (100), physisorption of Xe, Lennard-Jones model, mol. dynamics study 80−34308
- W (100), total hemispherical emissivity meas., sensitivity to O_2 adsorption 80−79964
- W (100), with ordered C overlayer, of O_2 and CO, UPS meas. 79−77907
- W (100) and (110) surfaces, of H_2, CO, O_2 and I_2, chemical effects in N_7 VV Auger spectra 77−32474
- W (100) with adsorbed Au and Cu layers, electron field emission revealing unmasked surface reson. 79−15595
- W (110), (112), of Cs and O_2, common adsorption, work function and thermal stability by contact pot. method 80−44427
- W (110), coadsorption of Ba and Cs, work function of surface under equilibrium conditions 79−15025
- W (110), codeposition of Cs and O, Cs_2O form. 80−44425
- W (110), dipole moments of single 5d metal adatoms field emission meas. 77−47674
- W (110), mobility of adsorbed O, 300 to 800K, field emission current meas. 79−33187
- W (110), of alkali atoms, trapping probabilities and desorption kinetics 77−62754
- W (110), of Be, film growth and struct. 80−75477
- W (110), of N_2, thermal desorpt. and work function meas. 77−1294
- W (110), of O, adatom interaction energies, Monte Carlo calc. 78−71948
- W (110), of O_2, LEED, AES, and thermal desorption meas. 78−38957
- W (110), oxygenated and oxidised, Cs absorption 80−44424
- W (110) and (100), adsorption of Xe and coadsorption with O, work function and thermal desorption meas. 80−39448
- W (110) and (100) planes, sticking coeffs. of CO, O_2, and Xe 79−82464
- W (110) and (111) surfaces, KCl adsorption-desorption behaviour 80−75442
- W (110) mobility and two-dimens. compressibility of adsorbed Xe, field emission current fluctuation method 80−80089
- W (110) plane, of CO, electron impact desorption, thermal desorption and work function meas. 77−85064
- W (110) stepped surface, of O, electron stimulated desorption, atomic steps and defects influence 80−80091
- W (110) surface, of H, band struct. and adsorbate geometry, surface-reflectance-spectroscopy 80−44416
- W (111), 0_2 and CO adsorption, angle resolved electron stimulated desorption, LEED and AES 80−6645
- W (111), (211), and (311), of W single atoms, surface site geometry determ. by FIM 80−39447
- W (111), field adsorption of He, array model 80−59800
- W (111), of O_2, AES, LEED and electron stimulated desorption obs. 79−46935
- W (112), of La, coating growth and struct. obs. *(Russian)* 78−14618
- W (112) face, of La monolayer, LEED and contact pot. difference meas. *(Russian)* 77−1316
- W (211) planes, of Mo, direct obs. of atomic processes by field ion microscopy 77−59219
- W {100}, coadsorption of N_2 with O_2 or C, AES obs. 77−35821
- W, adsorbed gases, field desorption from field ion tips 80−59793
- W, adsorpt. surface migration and thermal desorpt. of LaB_6, field emission microscopy 79−56075
- W, adsorption and condensation of Fe, meas. by thermal desorption in time-of-flight mass spectra 79−15023
- W, adsorption and early stages of condensation of Ag and Au on single cryst. surface 78−6212
- W, adsorption of Ga, In and Sn, field emission, FIM 77−16470
- W, adsorption of La, specific characts. *(Russian)* 79−1543
- W, adsorption of Pb on W(100), W(110) substrates, pairwise interaction model using Morse pot. 80−6657

adsorption continued
- W, alkali metal adion-surface interaction energy, density formalism calcs. 78–68069
- W, catalytic activity during adsorption of HD 79–69358
- W, coadsorpt. of Ni and K, average work function change 79–28190
- W, coadsorption of La and B, field emission and field ion microscopy 80–104049
- W, coadsorption of Th and H, FEM exam. 79–90869
- W evaporated film, adsorption and replacement of methane, CO and NO *(Japanese)* 78–22949
- W faces, of Ba and Cu atoms, work function changes during simultaneous adsorption 80–65378
- W, field depend. of spectral line energy of He-H_2 adsorbate 79–78853
- W field emitter, of Cu, field emission energy distribs. 77–59677
- W field emitter, of Se, field emission meas. 77–31889
- W field emitter, of Te, on single cryst. faces 78–34714
- W field emitter, surface migration and overgrowth of LaB_6 77–85902
- W filament, of CO, temp. controller for filament heating appl. *(Japanese)* 77–51603
- W foils, of Sm, kinetics meas. by flux modulation method 79–69363
- W, gas-surface interaction in atom-probe FIM 77–40336
- W, interaction with F_2 and fluorides at low temp. and high press. 78–39700
- W, ion induced secondary electron emission, probe for adsorbed O 80–55251
- W, K atom beam impact, mean residence time of K^+ and ionisation efficiency 77–73208
- W, LEED and electron microscopic investigs., review *(Hungarian)* 77–47654
- W, low-index planes, of Pb, probe-hole field emission microscopy obs. 77–47677
- W, methane dissoc. by adsorption-desorption process 78–92511
- W, of Ag, adsorption and desorption kinetics, mass spectra obs. *(German)* 79–46951
- W, of Ag, on (001), (011) and (111), work function changes 77–62757
- W, of Ag, substrate temp. effect on relation between work function and coverage, FEM obs. 80–2272
- W, of alkali metal vaps., thermal accommodation 80–24729
- W, of Au, field emission microscopy exam. of work function, correlation with LEED and RHEED meas. 78–35276
- W, of Ba and Ti, work function meas. 80–100411
- W, of Be, crystallites growth, FEM obs. 78–26799
- W, of Be, work function changes and scatt. electron energy losses 79–46947
- W, of benzene, isothermal ramped field desorption technique 79–82450
- W, of CO, adsorbate characterisation by UPS, XPS and X-ray AES 77–15683
- W, of CO, adsorption state at 300 to 80K *(Japanese)* 77–85057
- W, of CO, electron energy loss spectral study of surface vibrs. 77–69160
- W, of CO, FEM expt., pseudoclean pattern *(Japanese)* 78–34701
- W, of CO, FEM obs. of adsorption state *(Japanese)* 77–62738
- W, of CO, mol. orientation, ion scatt. 78–71949
- W, of CO, polycryst. surface, SIMS 78–14585
- W, of CO on (100), surface vibrs., EELS 77–62745
- W, of $CO(H_2)(O_2)$, surface reflectance spectroscopy on low index planes 78–71965
- W, of C(O), Auger signal comparison using differential and integral Auger spectra 78–76561
- W, of Cs(Te), work function, field emission meas. surface film effects 78–19645
- W, of Cu, Ag and Pb, pairwise interaction approach to adsorpt. of oriented overgrowths 77–62759
- W, of Cu, FIM and FEm obs. of nucleation, epitaxial growth and interface form. 78–26800
- W, of Cu, probe hole field emission spectra 78–14612
- W, of Cu and Pd, adsorpt. energies 79–51464
- W, of Dy, Ho, Er, field emission electron study 80–100393
- W, of Fe, work function and field emission obs. *(Japanese)* 78–91536
- W, of Ga, In and Sn, rel. to field emitter tip stability 77–12500
- W, of Gd, in field ion microscope *(Russian)* 77–47662
- W, of H, PMR meas. of adsorption state, surface migration 78–10275
- W, of H on (100), electron stimulated desorption, structural model 77–66091
- W, of H_2, D_2 and C_2H_2 on (111), EELS 77–66090
- W, of H_2, FEM study of binding states *(Japanese)* 78–2370
- W, of H_2 and CO, field emission current instability, freq. spectrum 77–32509
- W, of H_2 in presence of adsorbed H 77–51594
- W, of $H_2(N_2)(NH_3)$, thermal desorption and pulsed time of flight mass spectra anal. 80–30285
- W, of K, field emission flicker noise, coverage depend. 78–35262
- W, of La and B, field emission meas. 78–47662
- W, of La and O layers, work function changes *(Russian)* 77–35816
- W, of methane, on (100) and (111), work function meas. 78–38963
- W, of N_2, CO, and O_2, total current spectrum interpretation 77–85857
- W, of NO and NO_2, FEM obs. 80–84390
- W, of Ni, effect on surface self-diffusion FEM characts. *(French)* 77–1296
- W, of O, order-disorder transition, theory 78–38811
- W, of O_2, (110), electron impact and thermal desorption at high temp. 78–30821
- W, of O_2, electron stimulated desorpt. study, 300K, kinetics, order-disorder transition 78–71985
- W, of O_2, N_2 and Co, on (100) planes LEED-AES obs. 77–69186
- W, of O_2 and H_2, on (100), effect on NVV Auger spectra, comp. to band struct. calcs. 78–72643
- W, of Te, field emitter 77–69177
- W, or methanol, decomposition obs. 77–31887
- W, potential of He atom above field adsorbed He or Ne atoms 78–35267
- W, powder, gas adsorption and desorption *(Russian)* 80–75429
- W ribbon, with adsorbed CO, CO_2, or methane electron beam induced C deposition, AES obs. 77–89651
- W stepped surface, adsorption and desorption of O, LEED, AES and work function obs. 77–47675
- W surface, (100) adsorbed N_2, vibr. spectra, bonding struct., LEED study 80–84387
- W surface, polycryst., N_2 adsorption states 80–100404
- W surface, static skin effect and transverse electron focusing, effect of adsorbed layers *(Russian)* 79–91036

adsorption continued
- W, surface adsorption processes following electron excitation, cathodeluminescence studies 80–100390
- W, surface diffusion of adsorbed O, secondary electron emission study 80–76117
- W tip, condensation remoulding, field emission microscopy 78–2995
- W, trapping and desorption of alkali atoms on clean and O_2 covered (110) surface 77–11786
- W, with adsorbed Pd, field emission obs. of adsorpt., diffusion and self-diffusion 78–38945
- W:La, B coadsorption and work function, FEM and FIM obs. 79–52087
- W-Re (3%) alloy, W adatom-substitutional Re atom interaction, FIM obs. 77–89626
- W-ZrC (25 wt.%), eutectic alloy, thermionic emission and adsorption props. 79–69951
- WC, microcrystalline, mol. dynamics, motion of H_2O and H_2 mols. adsorbed on surface, catalytic activity 78–71941
- WO_n, of O_2 (propene), adsorption, struct., rel. to catalysis 78–51826
- W_2O_{5-x} film, of water, excess current noise 78–6421
- W(100), chemical effects in electron loss spectrum 77–4705
- W(100), I adsorption at room temp., LEED and AES study 80–84389
- W(100), of H, nondipole electron impact vibr. excitations obs. 78–63922
- W(100), of O_2, H_2, N_2, CO, NO and water, adsorbate densities determ. 77–1320
- W(100) surface resonance, effect of Cu adsorption 77–59201
- W(110), adsorption of CO, mobility of CO 79–46955
- W(110), of Cs and O_2, surface anal. 77–89656
- W(110), of Na, ordering, theoretical anal. 78–18892
- W(110), of Xe, 77 to 90K, LEED study 79–42382
- W(110), substrate strain induced interaction of adatoms 80–96744
- W(110) vicinals, adsorption of N_2, step sites as dissoc. centres 80–6642
- W(111), of Ni, surface site geometry, diffusion charact. 78–75944
- W{100}, of N_2, surface disorder effects on work function change 77–20192
- W{100} surface, co-adsorption of Cu and O_2, AES, thermal desorption, LEED and work function meas. 78–38950
- W{411} and W{320}, sticking probability and coverage determ. of N_2 80–54528
- Xe substrate, thin Ar films, phase transitions 79–42244
- Xe-plated graphite, of Ne, virial coeffs. 78–18904
- Zn (0001), of Te, UPS investigation 79–91563
- Zn-Bi liquid alloy, surface tension and surface adsorpt. determ. *(French)* 79–69325
- $Zn_xHg_{1-x}Te$, vacancy mech. of resorption of Hg droplets 80–39070
- ZnO $10\bar{1}0$ surface, reaction of O_2, AES, LEED, EPR, desorpt., surface cond. and work function expts. 78–95950
- ZnO $(000\bar{1})$, of alkali metal, anomalous behaviour of Na 78–79883
- ZnO $(000\bar{1})$ and $(10\bar{1}0)$ surfaces, clean and contaminated, reactivity to Cl_2 79–61904
- ZnO, (0001) surface, of O, AES and refl. electron energy loss spectra 79–46927
- ZnO, adsorbing p- and n-type dyes, surfaces pot., UV light illum. effect 80–75624
- ZnO, dye adsorption, contact pot. difference 80–27365
- ZnO film, of O_2, logarithmic law 79–42392
- ZnO, nonpolar surface, adsorption and desorption of CO and CO_2 79–65321
- ZnO, of Ba, effect on low energy cathodolum. 78–60522
- ZnO, of Br_2 and I_2, γ-irrad. induced centres 80–54513
- ZnO, of ethylene, adsorption rate spectra, freq. response method 78–51817
- ZnO, of H, field emission meas. work function determ. 77–21009
- ZnO, of H, space charge accumulation layers effect on secondary ion yields, H conc. meas. 79–83087
- ZnO, of H and O, ellipsometric spectroscopy of nonpolar $(1\bar{1}00)$ surface 79–33651
- ZnO, of H_2O vapour, annealing and grinding effects 78–68656
- ZnO, of isopropyl alcohol, (acetone), decomp., IR and kinetic obs. 80–59780
- ZnO, of merocyanine dye, spectral sensitisation of photocond. 77–47854
- ZnO, of N_2, 76.8 to 87.3K, expt. isotherms 77–31869
- ZnO, of O_2 and CO, electron energy loss spectra meas. 78–14601
- ZnO, of rhodamine B, on (0001) face of single cryst. electrode 78–31645
- ZnO polar surfaces, H and O_2 exposed, ion irrad., and heat treated, cond., EELS study 80–71525
- ZnO powder, adsorption of O_2, H_2, light effects *(Japanese)* 78–95230
- ZnO powder, CO_2 desorption during electron irrad. and interaction with atomic H 77–89638
- ZnO, powder, of methanol, electron spectrosc. obs. 79–52076
- ZnO powder, with adsorbed methanol, appl. of XPS method for surface anal. 78–40104
- ZnO powder layers, of Rose Bengal dye, effect on surface potential and photovoltage obs. *(Japanese)* 79–24003
- ZnO, with adsorbed metal, photoexcited ions and electron emission *(Russian)* 77–40324
- ZnO-NiO:Li_2O n-p heterojunction, contact resist., effects of water vapour 80–34506
- ZnS, surface, work function and luminesc. phenomena, effect of H,H_2O and O_2 adsorpt. 78–10538
- $ZnSO_4.7H_2O$, meas. of water physically adsorbed rel. to water of crystallisation *(Japanese)* 80–6622
- ZnS(Se)(Te), clean and oxidised surfaces, O_2 sticking coeff., ionicity effects, XPS expts. 77–85887
- ZnSe(100) surface, of O_2, anomalous oxidation props. 78–15558
- ZnTe clean and adsorbed O_2 (110) surfaces, UV photoemission spectra *(Japanese)* 80–93456
- ZnTe, of CO_2, H_2, CO_2-H_2, manometric and mass-spectroscopic investig. 77–35808
- Zr, adsorption and absorpt. of CO, NO, N_2, O_2, and D_2, dissoc. and diffusion 80–80085
- Zr base alloy, fatigue crack propag., role of adsorption in H_2S, Hg and moist air *(French)* 78–15580
- Zr, photon emission due to Ar^+ ion bombard., adsorbed and recoil-implanted O effect 80–80872
- Zr-Al intermetallic compounds in SAES ST101 getter, surface anal. during stimulated pumping 79–67945
- $Zr(BH_4)_4$ catalytic reactions on Al_2O_3, inelastic electron tunnelling spectra 80–75425
- ZrC and ZrC-Re alloys, adsorption of H 79–19467

- **adsorption** continued
  - ZrC, work function, effect of H_2 adsorpt., thermionic emission expts. 78—2970
  - ZrC(—Re), of H_2, effect on thermionic emission 78—48269
  - $Zr(HPO_4)_2$, of pyridine, IR spectra, acidity 78—92377
  - ZrS_2Cs_x, adsorpt. of H_2, mol. sieving effect *(French)* 79—65305
- **advertising**
  - commercial large-scale laser displays using path-controlled galvanometers 77—17963
- **aerials** *see antennas*
- **aerodromes** *see airports*
- **aerodynamics**
  - *see also hypersonic flow; jets; shock waves; supersonic flow; transonic flow; turbulence; wind tunnels*
  - ablating body, solution for stable shape *(Russian)* 78—75162
  - ablating body shape, numerical soln. method *(Russian)* 78—75134
  - ablation of melting bodies, effect of temp.-depend. heat capacity 79—37431
  - acceleration wave propagation, modification in theorem of Bailey and Chen 79—12621
  - acoustic dipole model for aerodynamic noise prediction, effect of motion 77—80148
  - acoustic disturbance propagation in gas stream, gas turbine noise appl. *(Russian)* 79—32131
  - acoustic mirror, for sound source location in wind tunnel 78—30372
  - adaptive-wall wind tunnel, iterative anal. of subsonic flow 78—22364
  - aeroacoustic source distribution, integral representation, general theory 79—50492
  - aeroacoustics, book contrib. 77—50807
  - aeroacoustics, theoretical modelling 79—37077
  - aerobionic systems in flapping-wing flight *(Russian)* 77—64066
  - aerodynamic theory, gas turbulence, Deutsch law 80—53758
  - aeroelastic stability of wide span surface structs., wind vels., flutter, binary divergence 78—26083
  - aeroelasticity in separation streamline flow 80—5979
  - aeroelasticity of unsteady aerodynamics, force calc. methods *(French)* 78—75095
  - aerofoil, dynamic forces acting, subsonic instabilities *(French)* 78—67213
  - aerofoil, in transonic cascade, choking flutter 77—75885
  - aerofoil, incompressible potential flow, second order approx. theory 80—69860
  - aerofoil, oscillating, viscous incompressible flow, finite element anal. 80—38427
  - aerofoil, thin, near-inviscid supercritical flow, numerical soln. 78—14038
  - aerofoil, thin, windward surface shock layer, hypersonic flow 78—34158
  - aerofoil, two-dimens., in incompressible flow, unsteady motion 78—67171
  - aerofoil, wake effects in finite amplitude nonsteady motion 77—23963
  - aerofoil at high angle of incidence in longitudinal oscillations 79—72969
  - aerofoil cascade with sinusoidal vibration, induced velocity in wake *(Japanese)* 77—15031
  - aerofoil flutter, vibration and stability of a bar in a stream of gas *(Russian)* 79—32548
  - aerofoil stall in wind tunnel, meas. stall props. with acoustic flow control 80—23991
  - aerofoil with jet flap, incompressible flow past 78—59414
  - aerofoils, laminar wakes and noise pattern 79—37341
  - aeronautical technique utilising laser and microwave beams *(Russian)* 77—3838
  - aft-body drag reduction, combined boat-tailing and base blowing at M=3 77—23988
  - aft-loaded airfoil, boundary layer displacement effect and wake near trailing edge 78—22366
  - aggregates, solid, aerosols, dynamic shape factors meas. appls. 80—61165
  - air, outflow from porous materials and noise reduction theory of porous diffuser *(Chinese)* 79—50785
  - air diffuse discharge, gasdynamic effects 78—81294
  - air pollution, contaminant movement, Galerkin finite element method 80—74902
  - air wall-jet immersed in uniform flow, aerodynamic forces on circular cylinder 77—62287
  - air-conditioning systems, acoustical characts. of certain flow-spoiling devices 77—50832
  - airborne plume dispersion, 2-D computer hydrodynamic simulations 80—45837
  - aircraft, subsonic, longitudinal, lateral and crossed aerodynamic derivatives computation 79—81915
  - aircraft design technology, fluid dynamics computer program assessment data base 80—1637
  - aircraft dynamics, unsteady airloads prediction, aeroelastic anal. 78—71346
  - aircraft jet noise reduction test facility 77—11096
  - aircraft vortex wakes, neutral atmospheric effects on dissipation 79—32528
  - aircraft wing weight optimisation with static aeroelasticity constraints *(Russian)* 79—23240
  - airfoil, circulation control via rotating cylinder 77—7401
  - airfoil, oscillating, exact soln. by integral eqn. 77—84270
  - airfoil, thin, pulsating, HF subsonic flow 79—59998
  - airfoil flow, unseparated, potential distrib. and circulation, non-mapped complex variable method 80—83811
  - airfoil in supersonic and hypersonic flow, wedge problem 79—41705
  - airfoil interference in two-dimens. steady flow 78—71356
  - airfoil noise measurement for high Reynolds numbers, investigation using adjacent plane jets 80—28372
  - airfoil optimisation, transonic flow finite element anal., book contrib. 80—1633
  - airfoil singular integral eqns., generalised Theodorsen soln. 78—1682
  - airfoil trailing edge, incident acoustic wave diffr., flow depend. 78—26143
  - airfoil with oscillating jet flap, press. distrib. meas. 77—23976
  - airfoils, lifting, design procedure in transonic flow by integral method *(German)* 77—35163
  - airfoils near stall, numerical soln. in optimised boundary fitted curvilinear coordinates 79—77156
  - airfoils placed near ground or in tunnels, flow with separation *(German)* 79—37345
  - annular aerofoil theory, experimental verification *(Russian)* 79—14420
  - arc (electric) in transverse aerodynamic and mag. fields, approx. model 80—24285
- **aerodynamics** continued
  - architectural, wakes of surface-mounted cubes 79—12183
  - asymmetric flow past wings, nonlinear-discrete vortex method 78—71351
  - asymmetric stress tensor in gas dynamics 77—58738
  - asymmetrically swept wings, flutter 77—23972
  - atmosphere, dissipative effects, convective instability *(French)* 80—77058
  - atmospheric turbulence, aircraft response, math. modelling 78—81274
  - atomic analysis, aerosol aerodynamics effects 78—48709
  - atomisation units for powder metallurgy, gasdynamic and acoustic props. 80—66451
  - attitude motion of Skylab for revisit mission, digital computer simulation 79—16794
  - automobiles, air and rolling resistance effects 77—11
  - aviation and astronautics, conf., Tel Aviv and Haifa, Israel, May 1976 77—31319
  - axial turbine blades, spatial streamline flow calcs. using pot. flux of incompressible liq. 80—59000
  - axisymmetric bodies, aerodynamic coeffs. in supersonic flow *(Russian)* 78—34153
  - axisymmetric cylinder aerodynamic drag, base cavities effects 80—14723
  - axisymmetric nonstationary flow around an obstacle in a cylindrical tube 79—77169
  - axisymmetric rigid body in air, stability of unperturbed motion *(Russian)* 78—86146
  - base pressure correlation technique, turbulent supersonic flow, conical bodies 77—89146
  - beam, pretwisted, slender, coupled torsional and longitudinal vibr. 79—18770
  - Bernoulli forces on an elliptical cylinder by a nonuniform flow, aerodynamic lift 80—1619
  - bird flight, wake behind finch 80—81629
  - blade force and sound generation for annular cascade in distorted flows 77—58504
  - blades, three-dimens. annular array, aerodynamic forces with nonsteady flow 80—99991
  - blades, vibr. due to rotating stall, aerodynamic force meas. 80—92172
  - blower tunnels with wide-angle diffusers, aerodynamic design 78—1771
  - blown flap, upper surface, sound generation in vicinity of trailing edge 77—75902
  - bluff structures, aerodynamic mechanism of torsional flutter 80—53689
  - bodies disposed from aircraft, dynamic flight characteristics *(Polish)* 78—18311
  - bodies with arbitrary cross section, aerodynamic coeffs. 79—68741
  - body of revolution, slender, nonlinear normal forces, Reynolds no. influence *(German)* 78—51191
  - body oscillating in supersonic stream, entropy and total energy 79—86456
  - body shape for minimal radiative heat inflow, spacecraft atmospheric entry *(Russian)* 78—77457
  - boundary layer, laminar, subsonic, strong slot injection, triple deck theory 80—74831
  - boundary layer shear stress distribution calc. 79—98701
  - bow wave distance for infinitely long plate in ultrasonic flow *(German)* 79—81920
  - breakdown of continuous multidimensional gasdynamic flow from weak discontinuity theory 77—51075
  - bridges, buffeting due to wind action 79—14321
  - bridges, flutter due to wind action 79—14320
  - buoyant plumes behaviour on release at ground level, lab. wind tunnel obs. 80—30624
  - cambered airfoil in generalised sinusoidal flow perturbations, lift, moment and press. distrib. 79—37343
  - cambered blade, unsteady aerodynamic force due to nonuniform amplitude gusts 80—19418
  - cascade, with large-deflection oscills., unsteady aerofoil theory, numerical soln. *(Japanese)* 78—67211
  - cascade airfoil aerodynamic design, exact method based on conformal transformation *(Italian)* 79—41599
  - cascade flow, transonic anal., by conformal mapping and relax. techniques 77—75934
  - cascades, supersonic and transonic compressor, unstarted choked regime calc. *(Chinese)* 80—43730
  - cascades, unsteady flow, sinusoidal gusts having different phase for each blade 78—14034
  - cavities, suppression of aerodynamically induced pressure oscillations 79—98523
  - cavity flow, broadband noise generation, vortex model 77—75900
  - centrifugal and unsteady aerodynamic force field 79—1127
  - channel flow, unsteady, of compressible gas with shock waves, appl. to gasdynamic laser 77—72327
  - channel height effect on nearcritical flow past circular cylinder 80—14818
  - channels with rough surfaces, heat exchange intensification *(Russian)* 80—53779
  - cold gas, noninteracting particles, nonlinear periodic motion *(Russian)* 80—14868
  - complex aerofoils, compressible flows, isoparametric Hermite cubic element 80—1617
  - compound lifting surfaces at high supersonic flight speeds 77—19622
  - compressed gas, nonsteady transonic flow, modified Khokhlov method study 80—79347
  - compressible flow around an aerofoil or a cascade, up to shockfree transonic range 78—22365
  - compressible flow around lifting profiles near permeable walls *(French)* 77—68614
  - cone with arbitrary surface deviations in supersonic gas flow, aerodynamic characts. 77—19620
  - conference on unsteady flow, Ottawa, Canada, (Sept. 1977) 78—71347
  - conformal representation of arbitrary multiconnected airfoil sections 78—30308
  - conical gas flows, two-dimens. unsteady problems 77—51085
  - conservative scheme for eqns. of gas dynamics *(Russian)* 79—50755
  - constrained and unconstrained flow about pitching foil 78—26137
  - converging bi-conical pipe, 3-dimensional internal blocking *(French)* 79—50751
  - convex body aerodynamics in rarefied mol. flow, kinetic theory 78—59424
  - corner, right dihedral interaction between turbulent boundary layer 79—86414
  - corner and junction flow, complete aircraft aerodynamics, lecture 78—22325

aerodynamics continued
cylinder in cross flow, skin friction and vortex shedding freqs. 78—94758
cylinders, aerodynamic noise vs. drag relationships 79—32550
cylinders placed in turbulent plane mixing layer, time-averaged aerodynamic forces 80—28524
Darrieus rotor, aerodynamic analyses comparison 80—61264
delta wing, oscillating, with attached shock wave, flowfield theory 77—84276
delta wing equations, high freq. solns. 79—46337
design, wind tunnel tests and numerical methods compared 77—27635
detached flow around wing in ideal fluid, vortex sheet break-up 77—11200
difference eqns., gasdynamic, convergence of Newton's iterative soln. *(Russian)* 77—39304
difference schemes for aerodynamics 77—35160
diffuser, conical, tangential boundary layer blowing, flow struct. and efficiency 77—47033
discontinuous solns. of differential eqns. using generalized differentiation 78—33940
discrete vortices method and multidimensional singular integral eqns. theory 80—19421
dissociating gas, relativistic flows, growth and decay of weak waves, shock wave formation 80—69949
disturbance fields of unsteady singularities in uniform motion 78—71355
drag, supersonic wave, of planar singularity distribs. 78—83430
drag minimisation anal. 77—72319
drag minimised bodies, given length and base, Newtonian theory calcs. 77—84267
drag on heated spheres and cylinders, effective Reynolds no. 77—89090
drag reduction spike, fluctuating pressure wind-tunnel meas. 78—30310
Drive and Ascent Satellite, aerodynamic characts. rel. to lower ionosphere research programme 80—77252
duct, plane, with sudden expansion, aerodynamics 79—94722
dust entrainment in shock-induced turbulent air flow, dust entrainment 80—43763
electroacoustic and aerodynamic calibrated sound sources compared 78—55543
electrostatic precipitators, gas flow distribution effects 80—53804
elliptic cylinder unsteady aerodynamics and vortex induced oscillations, test results 78—94746
excited jets, aerodynamic characterisation of broadband noise amplification 79—32491
exhaust jet, swirling, noise and flow characts. obs. 77—75950
expanding body entry into planetary atmos. 77—37584
finite element formulation for subsonic and transonic flow 80—28526
finite-particle scheme for three-dimens. gas dynamics 78—67218
flame, atm. press., ion sampling aerodynamic disturbance by sampling system 77—60142
flame, counterflow diffusion, struct. in elec. field, interferometric obs. 80—16685
flapping wing propulsive efficiency for plane parallel flow (bionics) *(Russian)* 77—32919
flat plate boundary layer flow model and spherical particle drag expt. 79—18871
flat plate skin friction meas. by splitter plate method 80—38385
flight effect of Michalke and Michel vis-a-vis Lighthill's model 80—59018
flow in pipelines, self-similar solns. to eqns. *(Russian)* 79—10584
flow past airfoils with oscill. jet flaps, quasisteady theory 78—63467
flow past circular cascade of arbitrary profiles 77—39303
flow resistance in channels from acceleration of gas injected through walls *(Russian)* 77—80217
flow separation, incipient, viscous interaction, laminar and turbulent boundary layers, similitude props. 77—72325
flow study using holographic interferometry *(French)* 78—5833
flows with heat addition, review 77—916
flutter eqn., continuation and direct soln. 78—34047
Galerkin finite element-finite difference soln. of laminar boundary layer flows 78—42586
gas dynamic flow fields with discontinuities, computational method checking test 80—36864
gas dynamic variational problems, nonlinear programming methods *(Russian)* 77—51074
gas dynamics, self-adapted algorithms 80—38432
gas dynamics eqn. boundary conditions in Chapman-Enskog Boltzmann eqn. soln. 80—96284
gas flow, one-dimens., non-steady, invariant transformation of eqns. 77—39270
gas flow in duct, self-excited oscillations 78—55670
gas flow in non-uniform pipe, gas-line model, acoustic wave anal. 80—14726
gas flow into duct, self-excited oscillations 80—33647
gas flows, selfgravitating, thermodynamic processes and radiation, numerical method 80—14848
gas flows in gravitational field *(Russian)* 78—67212
gas in pipelines, stationary subsonic flow *(Russian)* 79—98743
gas motion near symmetry centre for energy release on the periphery, shocks 80—33626
gas of variable density, channel flow, discontinuity evolution 77—58734
gas-particle mixture flows, aerodynamic problems, French contribs. 77—42909
gas-particle mixture flows, fundamentals and applics., review 77—42913
gas-particle mixture flows, German R&D 77—42910
gas-particle mixture flows, report of European developments 77—42908
gas-particle mixture flows, research at Von Karman Inst., Belgium 77—42912
gas-particle mixture flows, UK research survey 77—42911
gas-solid interactions, rel. to reduction of aerodynamic friction and aerothermal heating 79—95896
gasdynamic equations, multiatomic gases with different elastic and inelastic rates 79—81993
Gifting propeller operation characts. by computer aided numerical anal. 80—6068
gliders, aerodynamic noise 78—38307
Goethert's rule with improved boundary condition 78—26138
ground effect wings, minimum induced drag 77—7367
H-shaped section cylinder in laminar and turbulent flows, aerodynamic charact. 80—106813
Hausdorff representation of positive polynomials and convex approx., aerodynamic shapes simulation 80—38430
heat diffusion as source of aerodynamic sound 77—7382

aerodynamics continued
heat transfer for tube banks in transverse streamline air flow with high Reynolds numbers *(Russian)* 79—94619
heat transfer in turbulent boundary layers on porous plate, gas cooling film 79—98714
heating of bodies with deep cavity 79—86454
heating test, use of melting liq. crysts. 79—77299
helical gas flow, restrictions on instabilities 79—98745
helicopter blade, lifting line concept appl. to blade computation *(French)* 79—77163
helicopter multibladed rotor flutter, effect of phase angle 77—7333
helicopter rotor, nonlinear mathematical simulation of unsteady flow past rotor 79—86442
high angle of attack aerodynamics (conf. Sandefjord, Norway (Oct. 1978)) 79—77159
high speed photography, in aeroballistic range, track facilities of von Karman gas dynamics facility 78—37094
high-gradient magnetic separation in region of high aerodynamic loading 79—86108
higher order panel method for general analysis and design appl. in subsonic flow 77—55022
hot-wire probes in low speed flow 79—82010
hovering, ground effect, fluid flow model 79—94643
hydraulic drag on banks of profiled twisted tubes in cross-flow of gas *(Russian)* 79—7381
hydroplaning of a rotating cylinder on water 78—63522
hydroplaning plate, lift, drag 78—63523
hypersonic aerodynamics, limiting shock layer *(Russian)* 78—30316
hypersonic blunt-slender cones, artificially induced boundary layer transition 80—28496
hypersonic body shape optimisation, principal approx. methods 78—5765
hypersonic bow shock interaction with ice crystal, aerodynamic shattering criterion 77—27558
hypersonic flow, around slender blunt body 77—35164
hypersonic flow, conical wing-body combination, thin shock layer theory appl. 79—46339
hypersonic flow, ice crystal-shock layer interaction 78—30317
hypersonic flow, separation behind aerofoil 77—42864
hypersonic flow, slender vehicle dynamics, viscous interaction or support interference 78—71363
hypersonic flow around blunt bodies, surface friction, physiochemical processes in shock layer 78—46997
hypersonic flow on slender wing *(Russian)* 79—10588
hypersonic flow past power-law bodies 77—42863
hypersonic flow with attached shock waves over plane delta wings 77—27556
hypersonic flow with axisymmetric body, optimal control solution, with aid of computer 78—4474
hypersonic slender-body theory, parallel-source correspondence 78—26151
hypersonic source flow field, aerodynamical anal. of body in hypersonic source flow field *(Chinese)* 80—59066
hypersonic three-dimensional shapes, optimal surfaces and total drag coeffs. 80—59068
hypersonic turbulent boundary layer, surface cooling, multiple slot injection 78—9653
hypersonic unsteady airfoil aerodynamics, viscous and elastic perturbation effects 78—26150
improved free-vortex, subsonic aerodynamic window 80—23663
inclined turbulent jet exhausting from flat plate into turbulent subsonic crosswind 77—42885
incompressible flows, 2-D, potential flow past aerodynamic body, subsurface panel method 80—74901
incompressible laminar boundary layer, three-dimensional, hyperbolicity of integral equations of momentum 77—27505
incompressible lifting surface anal. with wake roll-up 77—42859
industrial aerodynamics, conference, Aachen 80—17712
initial-boundary value problems 77—65750
internal gas flow anal. by large particles method *(Russian)* 78—79355
inviscid fluid conservation law eqns., coeff. matrices for implicit finite difference soln. 78—42580
inviscid gas, expansion into near vacuum, contact front-primary shock regime, particle path formulation 80—59070
inviscid hyperbolic flow, computational algorithms tests 80—27140
inviscid ideal gas flow, direct simulation methods 80—48733
ionospheric rocket-borne mass spectrometer, Monte Carlo prediction of +ve ion collection 80—8459
isothermal gas, straight compression wave due to pressure pulse driven flat piston 80—69873
isotope separation by gaseous diffusion, aerodynamic effects 78—59469
jet, aerodynamically generated noise *(French)* 77—75951
jet, subsonic hot free, coherent structures in mixing zone, acoustic effects 79—4052
jet entering fluidised bed, aerodynamics and mass transfer 80—14809
jet noise, external boundary-layer flow effect in flight 77—75901
jet noise source distrib., from far-field cross-correlations 77—84039
jets, free, turbulent, acoustic effect, dual nature 78—18325
Joukowski airfoil, unsteady viscous flow, bound-vorticity distrib., numerical anal. 78—51169
Jovian atmospheric probe, mass loss, shape change, real-gas aerodynamic effects 78—4055
knuckleballs, aerodynamics and spin 77—22344
Korteweg de Vries eqn., soliton soln., Hugoniot conditions for gas dynamics 80—42069
laminar boundary layer, finite amplitude high frequency oscillations 80—6024
laminar boundary layer on curvilinear thermally conducting surface, optimum suction *(Russian)* 77—54968
laminar bubble separation, stalling, lecture 78—22325
laminar wing flow, tip vortex stability 77—19611
laser, chemical, pressure recovery, 1D flow model, comparison with DF laser results 77—71979
laser Raman diagnostics using coherent antiStokes scattering *(French)* 77—35280
laser velocimeter appl. *(Spanish)* 80—53902
laser velocimetry principles and appls. *(French)* 78—63518
levitation technique for containerless high temp. studies on liquids and solids 77—29046
lift correction to transonic equivalence rule 77—62273
lifting boundary in low Mach number flow, sound scatt. anal. 77—42648
lifting surface, varying thickness shear layer, soln. using kernel function 77—89137

aerodynamics continued
lifting surface in unsteady motion in inviscid fluid 78—14036
lifting wing calcs., spanwise integrations, computational economy improvement 78—71344
lifting-line theory, alternative treatment as perturbation problem 79—27663
liquid sheet sprayed by air stream, aerodynamic stability 80—1528
low perigee aerodynamic heating during orbital flight of Atmospheric Explorer 77—45290
low speed wind tunnel contractions, optimum design 79—77157
low vel. airflow calibration and research facility 80—1718
luffing in 2-dimens. sails, analytical theory 79—32549
lung, dispersion of inhaled particles in humans, model 78—11689
Mach number expansion, of Navier-Stokes equations, Lighthill's theory to non-adiabatic cases 78—83372
magnetoaerodynamic forces on oscill. circular cylindrical shell, simple harmonic motion 79—1257
mass transfer and mixing in packed columns, recirculating gas fraction, cell model 80—69913
metallic tethers in ionospheric plasma, electrodynamics and aerodynamics 78—69652
MHD convection, free, near plane and axisymmetric bodies 79—94728
model rotors, investigation of generated LF broadband noise 79—90057
multiconnected airfoil systems, inverse problem, book contrib. 80—1515
multidimensional gasdynamics, Riemann invariants concept generalisation 79—68735
around multiplane, steady, plane and inviscid flow 77—23980
multivelocity multitemperature mixture of gases, gasdynamic eqns. 79—77052
Navier-Stokes eqns., bluff body aerodynamics, numerical simulation methods 78—75115
Navier-Stokes eqns. for viscous and potential flow about arbitrary 2-D bodies 77—65730
Navier-Stokes stationary 2-D eqns. in parabolic form, optimal control *(French)* 77—72321
noise, aerodynamically generated, fluid flow eqns. *(French)* 80—74848
noise, scatt. by hard and soft surfaces 77—68326
noise, various theoretical approaches *(French)* 78—34116
noise generated aerodynamically *(French)* 79—77090
noise generation by wake cutting aerofoil *(French)* 77—917
non-oscillatory circular lifting re-entries 79—37340
non-stationary I-D problems, computational methods *(Russian)* 77—19618
nonequilibrium flow past thin profile 77—84344
noninertial deformable rot. coordinate system, unsteady gasdynamic flow eqns. 80—43726
nonlifting airfoil, response to streamwise gusts 77—65753
nonlinear formulation for low-frequency transonic flow 78—94761
nonslender body, minimal drag determ. 77—39306
nonstationarity near cylinder in air cross-flow *(Russian)* 79—7382
nonstationary unidimensional entropic gas flow, dynamic functions, reduced vels. *(Russian)* 77—51073
nonuniform parallel stream, slender wing theory, flow and lift 80—74830
nozzle flows with boundary layer, CO_2-N_2-He, gain coefficients 80—14312
nozzles with turbulent high temp. gas flow, heat transfer 80—24068
nuclear power plants, aerodynamic and thermodynamic effects on environment *(German)* 80—61469
numerical investigation by net-characteristic method 80—19420
numerical solution of a class of integral equations arising in two-dimensional aerodynamics 78—62086
ogive cylinder, mag. suspended, subsonic flow, reverse Magnus flow, turbulent boundary layer 78—51153
ogive cylinder at high angle of attack in transonic flow, experimental investigation of support interference 80—10260
open tubes, resonant oscillations of gas 77—68628
operating theatre, air flow patterns 80—94439
operating theatre, air flow patterns 80—94440
optimum re-entry configuration via the method of steepest decent 79—37339
oscillating airfoil surfaces in supersonic flowfield, time-variant aerodynamics 79—77167
oscillating airfoils with controls in ventilated wind tunnels, aerodynamic interference, subsonic flow 80—74905
oscillating flow over aerofoil, vel. field, surface press. 78—75164
oscillating wings, three-dimensional nonlinear unsteady potential flow calcs. 79—41689
oscillatory subsonic piecewise continuous kernel function method 78—5763
Oseen flow, unsteady, around flat-plate airfoil 78—5723
over-wing-blowing configurations, characts. determ. 78—5774
panel structural optimisation under supersonic flutter conditions *(Italian)* 79—41600
parachute influence on motion of axially symmetric air dropped object *(Polish)* 79—14243
parachute opening flowfield computation, using He bubble technique, high-speed photography and computer graphics appl. 78—30374
parallel circular cylinders, finite height 80—103013
parallel jets systems, aerodynamics calc. *(Bulgarian)* 80—28543
particle streams in crossflow, aerodynamic interaction at Reynolds numbers around 10^4 79—81946
perfect gas, vortex sheet, separation from smooth body at large Reynolds number *(French)* 80—74908
piston, magnetic field effect, self-similar magnetogasdynamic problem with radiative heat transfer 80—64578
plane gas flow, restrictions on instabilities 79—98745
plane jet curvature in bounded cross flow with stagnant zone 79—46355
plane nonstationary self-similar gas flow with energy liberation in shock waves 79—77182
plate, elastic, under aerodynamic tension, flutter, bending stiffness effect 78—30208
plate with vertical cylindrical projection, aerodynamic coeffs., approx. method 80—48746
pollutant transport eqn., 3-D, numerical algorithm 80—106811
pollution distrib., test results and numerical solution *(German)* 79—8686
polyatomic chemically reacting gases, hydrodynamic eqns. 79—32711
potential field induced by an acoustic wave incident upon a moving plane 79—37342
potential flow around multiconnected airfoil sections 78—30309
potential flow over wing with free vortex 78—63444

aerodynamics continued
potential flow round a body, induced forces and moments *(Russian)* 77—31318
potential flow with directional variation of source mass flow singularity 77—35109
potential unbounded flows, finite element method 79—88813
Prandtl-Meyer function soln., hybrid computer method 77—11164
pressure pulsations at cylinder at Mach 0.5-0.9, step effect 79—86453
pressures on a slender body at high angle of attack in a very low turbulence level air stream 79—77164
projectile motion, air resistance, speed depend. 77—75932
propeller wake, stalling conditions, 3-dimens. flow field obs. 78—46972
random choice method for gas dynamics problems soln. 77—55106
rarefied gas expanding in vacuum, asymptotic props., jet for flow field *(Russian)* 77—55041
ray method for solving gas dynamics equations *(Russian)* 79—27659
re-entry, streaming, of vel. and temp., in oscill. boundary layers 78—83358
real gas effects in cryogenic wind tunnels 78—94760
rectangular cylinders in heaving mode, aeroelastic instability 79—3954
rectangular prisms, galloping in smooth and in turbulent flow 77—75840
relaxing gas, nonlinear waves propag., weak influence of relax. 77—55100
rigid shell, oscillatory flow through perforated surface, sound generation 79—18950
roll of slender wings at incidence in separated flow 77—3840
rolling missile, apsidal limits 79—3909
Savonius rotor, aerodynamic performance testing in wind tunnel 80—61266
segmented-conic body, flow structure close to lateral surface and formation of breakaway zones 77—58727
separated air flow, surface orientation effects 79—98709
separated flow around flat plate, influence of vortex diffusion 77—19613
separated flow types over slotted wings 80—38458
shape optimisation for bodies in supersonic flow 80—38438
shear flow, inviscid parallel, aerodynamic effects 78—1680
shear layer with linear velocity profile, closed-form solns. for sound propag. 80—6074
shock layer blunt body problem, aerodynamic heating, effect of chemical reactions of injected gas *(Japanese)* 79—94739
shock tube flows, unsteady non-equilibrium, discretisation of boundary layer terms 80—14742
shock tube mass flow measurement using thermocouple-anemometer 79—77300
shock wave front propagation, numerical solution of hyperbolic initial-boundary value problem *(German)* 80—6095
shock wave localisation, by shock-capturing results of computation of gas dynamics problems 80—83815
shock wave reflection, regular to Mach transition, Monte Carlo simulation 77—75936
shock wave visualisation, by elec. discharge radiation 77—72371
shocks, magneto-radiative, axisymmetric, equatorial propagation 80—79349
short-fetch wind waves, aerodynamic lift and drag from Lagrangian wind and current vectors 80—72553
Shuttle/Spacelab platform in near Earth ionospheric plasma, aerodynamics 80—8517
simple bodies in two-phase flow, aerodynamic drag 80—96294
single particle drag coeff. in still air 80—33620
slender bodies and wings, vortex asymmetries 78—9644
slender bodies of revolution, subsonic normal force, centre of pressure, boundary layer method 80—48735
slender lifting body with permeable surface, curvilinear motion 77—58713
slim profile relaxation drag minimisation in near solidified subsonic flow *(German)* 79—81916
slots, circumferential gas streams in running channels *(Russian)* 80—74980
smooth profile in perfect incompressible fluid in irrotational motion, periodic solns. to eqns. of motion *(French)* 79—41703
solar magnetic flux tubes, aerodynamic lift on thin cylinder in convective flows 79—101126
solar magnetic flux tubes physics, aerodynamic lift 79—101125
sonic boom, nonlinear propag., including asymm. effects, numerical soln. program 77—72326
sonic nozzles, expt. study using gas flow dimensionless characts. 79—81945
sound diffraction by perforated screen, low Mach number grazing flow 80—53805
sound generation, mathematical formalisation of Lighthill's theory 77—62245
sound generation, uniform mean flow near infinite compliant wall 80—53766
sound problem in relaxing medium appl. of Green's functions 78—22363
sound wave transmission through nonuniform circular ducts 80—74900
space probe or meteorite reentry, mass loss and shape change with radiative heating 80—31198
space transport system, aeromanoeuvering orbit transfer vehicles 78—4060
spacecraft, optimal aerodynamic attitude control 80—77250
spheroids, harmonically oscillating, unsteady airload prediction, analytical soln. 78—51184
spinning cone, spin rate effect on side force 78—71349
spinning shells, Magnus characts., empirical calc. method 78—26072
spray pyrolysis, aerodynamics of nozzles 79—68782
sprays, drop trajectories, aerodynamic drag effects, computing methods 77—72347
square prisms, interaction in two flow fields 78—9632
stable flow past a wing, appl. of method of discrete vortices 80—74889
static aeroelastic characts. of guided launch vehicle, effect of misalignments 79—14313
stationary supersonic flow of compressible fluid, distrib. eqns. *(French)* 77—62278
stochastic properties of complex nonlinear oscillation regimes 80—8919
straight wing in circular cross section in wind tunnel, induced drag 77—15055
structural response to turbulent forcing field, decomposition calc. method 77—72282
subcritical flows past lifting profile *(French)* 77—72322
subsonic aerodynamics, finite element approach 79—55399
subsonic aerodynamics, finite element method appl. 77—47038

- **aerodynamics** continued
  - subsonic aerodynamics, sixth order direct solver for Poisson and Helmholtz eqns. 79—77160
  - subsonic aircraft, aerodynamic forces for aeroelastic anal., doublet-lattice method *(Italian)* 79—41598
  - subsonic and slightly supercritical aerodynamic flow, rapid finite-difference computation 77—23979
  - subsonic and supersonic aerodynamics, SOUSSA computer code 78—71352
  - subsonic bluff body wakes, measurement of fluctuating pressures 80—10249
  - subsonic flow, diverging, stability aspects, time-dependent method 80—74906
  - subsonic flow around delta wing, vortex breakdown pt. stabilisation 77—39305
  - subsonic flow past an oscillating cascade with finite mean flow deflection 80—74907
  - subsonic flow past pulsating airfoil 78—71348
  - subsonic flowfield, three dimensional geometrics, correction for viscous effects 79—98744
  - subsonic gas flow over convex corner, density jump *(Russian)* 77—65755
  - subsonic gasdynamic flow, stability anal. for gas in varying cross-section channel *(Russian)* 78—46992
  - subsonic gasdynamic flow stability 79—86451
  - subsonic high-angle-of-attack flow 78—38358
  - subsonic laminar viscous gas flow in flat channels and in shadow regions *(Russian)* 79—50749
  - subsonic rotational and transonic mixed flows, numerical simulation using fast super-dashpot time-dependent technique 80—83813
  - subsonic wind tunnels with slight perforation 79—68738
  - supercavitation flow past thin lifting surfaces *(Russian)* 78—34171
  - supercritical jet flapped airfoil, relax. soln. for transonic flow 77—23984
  - supercritical profile with oscill. control surface in subsonic flow *(French)* 78—71357
  - supersonic, leeside flowfields of planar delta wings, Reynolds number 79—60003
  - supersonic air flow through high press. gas valves into atm., noise and flow pattern obs. 80—59067
  - supersonic airfoil design by numerical optimisation 79—98750
  - supersonic cascade with strong in-passage shocks, unsteady flow 78—14041
  - supersonic cascades, aerodynamic anal., response predictions 78—34160
  - supersonic cascades, aerodynamic anal., unsteady press. field 78—34159
  - supersonic cone flow at high angle of attack, numerical simulation, laminar and turbulent flow 79—77178
  - supersonic flow, Lorentz-like coord. transform. 79—37348
  - supersonic flow around a wing, analogue modelling 80—28530
  - supersonic flow around flattened bodies and sharp tip wings 79—46341
  - supersonic flow around wings with attached shock wave on leading edge, num. soln. 77—51080
  - supersonic flow field meas. of slender cone at high angle of attack 79—77177
  - supersonic flow generation for circular cascade of aerofoils, design of annular nozzle *(French)* 77—7433
  - supersonic flow over hemisphere-cylinder at incidence up to 19° 78—59419
  - supersonic flow over sharp-edged wings 79—10587
  - supersonic flow past laser beam 78—38366
  - supersonic flow past solids of revolution, small perturbation theory 79—68742
  - supersonic flow past thin sharp bodies with intensive blow *(Russian)* 77—31329
  - supersonic flutter of heated circular cylindrical shells with temperature-dependent material properties 78—71289
  - supersonic gas axisymmetric flow past pointed body of revolution *(Russian)* 77—55034
  - supersonic gas jet, penetration into the ground *(Russian)* 80—28544
  - supersonic gas stream, stationary, conical flow about plane wedge and circular cone 80—74912
  - supersonic lifting surface, finite element anal. and collocation method 78—1687
  - supersonic local zone near wing profile of infinite span, flow calcs. 79—32565
  - supersonic potential flow, panel flutter, finite element calc. 78—26152
  - supersonic separated turbulent boundary layer, laser velocimetry meas. 77—35274
  - supersonic theory by potential gradient method 77—42862
  - supersonic wings with subsonic leading edges, minimum drag *(German)* 77—15058
  - supersonic-transonic flow, thin airfoil in stratified atmosphere 78—5764
  - supersonic/hypersonic flow past an oscillating flat plate at high angles of attack 79—14424
  - surface structural tests, systems approach to analysis design 77—16760
  - swirled gas flame aerodynamics, empirical results 77—58804
  - symmetric gas flows, D props. of a system of eqns. 80—4535
  - symmetrical flow past double wedge at subsonic Mach nos. 78—51182
  - tandem cylinders in motion, mathematical model for aerodynamic forces, aeroelastic appls. 77—62270
  - temperature gradient meter for gas flow study 79—86539
  - terrestrial atmosphere, low-density gaseous body motion, rel. to Tunguska catastrophe 79—84554
  - test chimney stack construction, two-phase flow model *(French)* 77—37392
  - thick wing, two-dimens. aerofoil, boundary conditions 77—62274
  - thin airfoil theory, for subsonic flow, soln. of Possio integral equation 77—23978
  - thin airfoil theory, HF, for subsonic flow 77—23977
  - thin assemblies, aerodynamic tests via two-component Si strain-gauge device 78—3263
  - three-dimensional gasdynamic flows, variational principle in Euler description, vortex conservation 80—48731
  - Timoshenko bar, aerodynamic stability, time- and space-harmonic balance *(German)* 80—83812
  - trailing edge vortices behind rectangular wing, expt. study *(German)* 77—72305
  - transonic, integral eqn. formulation for lifting profiles and wings 78—38363
  - transonic aerodynamic flows, fast semidirect computing method 77—3842
  - transonic aerodynamics, finite element method, book contrib. 79—32556
- **aerodynamics** continued
  - transonic aerodynamics, variational formulation and finite element anal., book contrib. 79—32555
  - transonic airfoil problem, variational principles 78—42626
  - transonic axisymmetric pot. flow around inlets, Cartesian mesh soln. 77—72323
  - transonic cascades, numerical design 79—10585
  - transonic flow, two- and three-dimens., perturbation soln. method 79—1208
  - transonic flow, unsteady, implicit shock-fitting computational scheme 78—94763
  - transonic flow, unsteady, turbulence modelling, compression waves developing into shock wave 80—74909
  - transonic flow, unsteady inviscid, local linearisation soln. for pitching bodies of revolution, $M_\infty=1$, stability anal. 77—31322
  - transonic flow around airfoil, finite-difference calc., computer code 78—26147
  - transonic flow around bodies of rotation *(Russian)* 78—87357
  - transonic flow on axially symmetric torus 80—28527
  - transonic flow over body of revolution, perturbation theory and numerical body 79—60000
  - transonic flow past wedge, drag and sonic line shape 78—26148
  - transonic flow simulation by tracking and blowing *(German)* 80—6081
  - transonic indicial method, shock motion effect 78—94769
  - transonic profile flow at incidence with shock 79—4031
  - transonic profile flow with shock, supercritical flow 77—15056
  - transonic viscous flow around 3D wings 79—37346
  - transonic wind tunnel, noise level effect on model characts. *(French)* 78—71411
  - tube, cylindrical, sudden expansion, turbulent flow meas. by laser Doppler velocimeter 80—75003
  - tube drag in different rows of banks in transverse streamline air flow *(Russian)* 79—94583
  - tubes with ball seatings, basic groups, appl. in flowmeters *(Russian)* 78—67287
  - turbine cascade flow, surface-oriented coords. in num. simulation 77—55018
  - turbine cascades, rotating annular, test facility of DFVLR, measurement and evaluation 80—14866
  - turbomachine airfoil cascades, variational and dual extremum principles for aerodynamic problems *(Chinese)* 80—43729
  - turbomachine cascade wing profile oscills., aerodynamic damping, ang. of attack influence 79—37344
  - turbomachine combustor, analysis and modelling of flow *(French)* 79—46401
  - turbomachinery ring chamber, oscillatory behaviour of confined ring vortex 80—6075
  - turbulence generated noise on both sides of double layer jet 77—47056
  - turbulent air flow in infinite medium spatial speed distrib. *(Rumanian)* 80—53826
  - turbulent flow around plate with elastic surface *(Russian)* 77—54982
  - turbulent flow of incompressible liquid in planar channel, axial curvature effects 80—87762
  - turbulent flow past circular cylinder, free-stream turbulence effect obs. *(Japanese)* 80—10229
  - turbulent separating boundary layer, subsonic, integral prediction method 80—1623
  - turbulent transonic flow about lifting aerofoil 79—4032
  - turbulent wake, behind slender propeller-driven bodies 78—38335
  - two-airfoil systems, with aerodynamic interference, flutter anal. 78—51181
  - two-element airfoil, conformal mapping, including multiply connected regions 77—23981
  - ultracentrifuge, thermally-controlled, for isotopic separation, gasdynamic features 77—54362
  - unidimensional gas flow prod. by piston in nonmonotonic motion *(Russian)* 77—42871
  - unsteady, modelling, for arbitrary motions 78—14033
  - unsteady aerodynamic modelling for arbitrary motions 80—19433
  - unsteady aerodynamics of lifting surfaces using computer, book contrib. 77—51076
  - unsteady aerofoil theory, small perturbation expns. 78—14037
  - unsteady airfoil, Kutta condition *(Japanese)* 80—92155
  - unsteady airloads on oscill. wings and bodies 78—71354
  - unsteady airloads on wing-store configs. in subsonic flow 78—71358
  - unsteady airstream, two-dimens. viscous flow past aerofoil, numerical predictions 78—75166
  - unsteady boundary layers, separated and attached, review 78—71313
  - unsteady boundary layers with reversal and separation 78—75163
  - unsteady gas dynamics, least squares finite element approach 78—26134
  - unsteady gas flow from piston in channel with moving walls *(Russian)* 79—77162
  - unsteady hypersonic gas-dynamic eqns., approx. solns. *(Russian)* 77—35165
  - unsteady laminar separation and stall from aerodynamic surfaces 80—59090
  - unsteady lifting-line theory for wing 77—11215
  - unsteady MHD forces on oscillating shell, transient soln. 79—64775
  - unsteady separated flow, aerodynamic characts., vorticity field 80—38457
  - unsteady subsonic and supersonic inviscid flow 78—71350
  - unsteady subsonic and supersonic pot. aerodynamics for complex config. aircraft 77—72320
  - unsteady thin aerofoil theory, lift and moment calc. 79—4029
  - unsteady transonic flow about oscillating airfoil, perturbation soln. 77—23985
  - unsteady two-dimensional flow over oscillating airfoil, Dowell's method 77—31321
  - unsteady viscous flow around aerofoil, numerical soln. procedures 78—75165
  - upwind second-order difference schemes for aerodynamic flow 77—23975
  - Venera 9 and 10, aerodynamics and dynamics during motion in Venus atmosphere 77—91399
  - vertical manoeuvers of aircraft 77—82385
  - vibrating airfoil in transonic flow *(Russian)* 77—39308
  - Viking entry vehicle, aerodynamic behaviour, ground test and flight results 79—16821
  - viscous compressible flow at high Reynolds number, global approach and coupling approach 80—48742
  - viscous gas eqn., movable net difference scheme *(Russian)* 79—50838
  - viscous gas equations, numerical solution, difference schemes, moving grids 80—48730

aerodynamics continued
viscous transonic cascade flows around airfoil, coord. system for numerical calcs. 78—42627
viscous-inviscid flow interaction method, using blowing and suction flows 79—1154
vortex flow aerodynamics, review of developments rel. to design 79—77140
vortex lift predictions for cambered wings 77—31311
vortex shedding noise of aerofoils in smooth flow 77—80147
vortex-induced side force on slender bodies 79—14408
wake-induced flutter of cylinder in wake of another 77—80167
wakes, unsteady, airfoils and cascades, rel. to predictions 77—72300
water vapour-N_2, nonstationary rarefaction wave, nonequilib. condensation obs. 77—75937
weak shock wave stability in gas-dynamic context *(Russian)* 80—6093
wind energy conversion, wind driven turbines, review 80—7909
wind energy generator system, tornado-type, latent heat from moist air, effect on vortex 80—30365
wind tunnel test program for determining effect of spin on boundary-layer transition at Mach numbers 5 and 8 on 9-deg. cone configurations 80—14864
wind turbine blade, non-linear dynamic response 79—81771
wind turbines, machine performance and rotor aerodynamics 80—74904
wind velocity gust factors, analytical expression and wind tunnel simulation 80—31107
windmill design and testing 79—43717
wing, 3-dimens. boundary layer calc. method 80—1622
wing, leading edge transition 78—38361
wing, rectangular, with tip clearance in channel, aerodynamic characts. 78—59415
wing, swept, 3-dimens. turbulent boundary layer, numerical anal. 80—1621
wing, swept-back, boundary layer laminar/turbulent stability 78—38284
wing, three-dimensional, hypersonic flow around 77—19621
wing, trailing line vortices, axial flow 79—32534
wing, unsteady lift and pitching moment at Mach no. 0.38-1.28 78—34151
wing aerodynamic characts., modelling ground plane effect 79—32553
wing aerodynamic characts. at hypersonic speed, slip effect 79—81917
wing in forward motion, trailing edge acoustic source radiation 80—69780
wing in motion near rigid wall, asymptotic theory *(Russian)* 78—38359
wing moving near solid wall, asymptotic theory 79—68737
wing moving with subsonic vel., shock wave effect 79—64684
wing of finite span, free vortices 79—64685
wing section theory of Kutta and Zhukovski, book contrib. 80—1514
wing tip-shed vortex, decay, injected air jet modification 78—63434
wing-body interference at hypersonic speeds *(Japanese)* 78—30315
wings, delta, for supersonic aircraft, lift with leading-edge vortices, at low speeds 79—14422
wings, lift and pitching moment meas. in oscill. gusts 78—71353
wings, low aspect ratio, computation of nonlinear characts. 79—41690
wings near ground, nonlinear unsteady one dimensional theory 80—79344
yawed slender wings, Abel integral eqns. for wake strength 79—32552
yawed wedge, local heat transfer 78—18295
$2NO_2 \rightleftarrows N_2O_4$, condensation, heat transfer and aerodynamics *(Russian)* 80—19932

aeronomy *see meteorology; terrestrial atmosphere; upper atmosphere*

aerosols
see also foams
absorption coeff. of airborne particles rel. to measurable bulk props. 77—45154
absorption of solar, diffuse and reflected visible radiation *(Russian)* 78—96291
acid sulphate in atmosphere aerosol, detection from S/N ratio 80—61494
acoustic field effects 80—89529
acoustic particle agglomeration due to hydrodynamic collision between monodisperse aerosols 80—26191
acoustic particle agglomeration of aerosols under standing-wave condition 80—30627
actinide industrial dusts, lung clearance studies at NRPB 78—65137
actual light scattering coefficient as meas. in haze and fog 79—80013
aerodynamic particle size calibration of optical particle counters 77—5879
aerosol monitoring and control, using size distrib. 79—57534
aerosol particles diffusion and gravitational settling in tube 78—90976
aerosol precipitation from laminar gas stream, free convection effect 78—83459
aerosol size distribution retrieval, simulated aureole data inversion in presence of multiple scatt. 79—74957
aerosols of marine air, submicron size distrib. and CCN supersaturation 80—77041
aggregates, solid, aerosols, dynamic shape factors meas. appls. 80—61165
air, aerosol-induced breakdown, two-dimensional modelling 79—90368
air particulate element conc. over USA 80—76679
air particulate matter collected on filter, X-ray fluoresc. anal., filter absorpt. corrections 77—60166
air particulates, automatic time sequence filter sampler for proton induced X-ray emission anal. 77—60171
air pollutants, particle acid content determ. method 77—37448
air pollutants three-dimens. distrib. in Los Angeles basin 78—61542
air pollution, detection and meas. of 10^{-4} to 10^{-1} μm particles *(French)* 80—7985
air pollution, from combustion, particle size distrib., health hazards 78—81394
air pollution meas. using laser radar data processing system 79—57559
air pollution sources and sinks, stochastic models for SO_4^{2-} particles and windblown dust 79—100930
air-borne particles, meas. of nasal tract filter efficiency 77—56492
airborne aerosol mass conc. meas. by Nd:glass laser/parabolic mirror lidar 77—21937
airborne dust pollution monitor 80—55971
airborne fibre sampling method for pollution detection using separated deposition 77—82031
airborne lidar aerosol measurements during the ASSESS II mission 78—73489
airborne particles, leaching solns., Gran's plot, acid-base titration 79—79432
airborne particulate sampler, wind tunnel testing, using monodisperse particles 77—82053

aerosols continued
airborne particulates sources, identification and relative importance estimation 80—72105
airborne sampling system for plume monitoring 79—21027
airborne sea salt sedimentation meas., effects on vegetation 78—3847
Aitken counter, portable photo-recording, for small atm. aerosols detect. 78—57355
Aitken nuclei meas., Black Hills, S.Dakota, green area filtration effect 78—3928
Aitken particles and cloud condensation nuclei in smelter plume 80—40937
Aitken range size distrib. meas. in N.Atlantic 80—98404
n-alkane pollutants, N.Atlantic gas and particle concs. in troposphere 80—7969
alpha recoil aerosol penetration of HEPA filters 77—66867
ambient aerosols, particulate S chemical state determ. by PIXE anal. 79—5225
ammonium sulphate vapour pressures, nucleation of new particles in atmosphere 79—81708
amosite fibres, collection efficiency of nuclepore filters 78—81341
analysis by proton induced X-ray emission anal., spectral anal., computer program 77—60167
Ankara atmosphere, trace elements and size distribs. determ. by thermal neutron activation anal. 78—81377
Antarctic, particle anal., comp. 80—77091
Antarctica, radioactive pollution of near-surface air *(Russian)* 77—29393
aqueous, crystallising, gas capture, role of gas adsorpt. in ice surface 79—39191
aqueous, optical thickness change due to CO_2 laser pulses 77—75591
aqueous, thermal clearing by laser radiation *(Russian)* 78—28312
aqueous aerosol cloud containing medium, light beam propag., thermal self-interaction 80—91750
aqueous polydisperse aerosol, bleaching by high intensity beam 77—58394
Arctic aerosol and snow compositional differences 79—88377
artificial mist, laser radiation propag., intensity fluctuations *(Russian)* 78—37806
asbestos aerosol electron microscopy and analysis *(French)* 77—37461
asymmetric deposition motion in circ. tube, anal. by Laplace transform methods *(Chinese)* 79—37379
N Atlantic marine aerosol, chemical relationships 77—53136
atmospere, particulate NO_3 size distrib. and chem. comp., Nagoya area, Japan 78—11980
atmosphere, above Black Sea, spectral transmission and sky brightness *(Russian)* 80—94603
atmosphere, absorpt. of visible light, spectrophone meas. 78—4000
atmosphere, acid sulphate aerosols existence and NH_3 gas conc. 77—81998
atmosphere, aerosol angular scatt., in situ photometric obs. 77—9492
atmosphere, aerosol anomalies preceding earthquakes 79—16407
atmosphere, aerosol characterization for particulate S, health effects 79—20984
atmosphere, aerosol comp. rel. to K/Na ratios in dew drops 77—91190
atmosphere, aerosol concs. prediction in plumes subject to dry deposition 78—28307
atmosphere, aerosol content determ. from photometric obs. of stars 78—92976
atmosphere, aerosol contrib. to stellar extinction oscills. caused by atmospheric disturbances 80—56606
atmosphere, aerosol effect on remote sensing aerospace information 80—4101
atmosphere, aerosol effects on light transmission, Smithsonian Astrophysical Observatory meas. 80—17374
atmosphere, aerosol effects on polarisation of scatt. light from point source *(Russian)* 80—4106
atmosphere, aerosol flow, transit-time lidar velocimeter detect. 77—13127
atmosphere, aerosol models rel. to optical propag. 79—100947
atmosphere, aerosol optical attenuation statistics, spring and autumn 79—84484
atmosphere, aerosol particle conc. variation with relative humidity *(Russian)* 78—32146
atmosphere, aerosol particles induced error in satellite retrieved temp. profiles 80—98449
atmosphere, aerosol properties rel. to solar aureole, photogrammetry 78—57315
atmosphere, aerosol scattering indicatrices under clear sky conditions in 0.55 to 2.4 μ spectral region *(Russian)* 80—94600
atmosphere, aerosol species optical consts. rel. to radiation balance determ. 77—17163
atmosphere, aerosol-induced heating effects on convective boundary layer 78—69409
atmosphere, aircraft studies during GATE radiation subprogram 78—81408
atmosphere, Aitken particles, dynamics *(German)* 79—53413
atmosphere, Al particles from space rocket launching 80—81503
atmosphere, ambient sulphate aerosols laser-Raman monitoring 78—69532
atmosphere, ambient sulphate particles size discrimination and chemical comp. by diffusion sampling 78—69528
atmosphere, anal. of water-soluble S compounds 78—96282
atmosphere, Antarctic aerosol origins and props. 80—90197
atmosphere, Antarctica, seasonal and frontal vars. on aerosol conc. 79—70855
atmosphere, Arctic haze bands, probable Asian desert origin 77—78349
atmosphere, atoms and ions attachment rate, nuclei conc. and humidity effects 79—62555
atmosphere, aureole around UV source at finite distance 78—77320
atmosphere, aureole phase function interp., logarithmic derivative method *(Russian)* 77—45148
atmosphere, automatic mass conc. meas. techniques 77—64459
atmosphere, Barrow, Alaska, cloud condensation nuclei 77—29386
atmosphere, characts. over India, role in warm rain process 79—92573
atmosphere, charge of aluminosilicate pollutant particles, depend. on thermal history 80—97840
atmosphere, chem. comp. of particles with diameters >1 μm over Tasmania 77—87014
atmosphere, chemical characterisation, progress and problems 78—68969
atmosphere, climatology of aerosols in Europe, Project OPAQUE 79—66784
atmosphere, cloud 80—56571

aerosols continued
atmosphere, composition, PIXE anal. 79—53004
atmosphere, composition meas. for Florida by time series anal. 80—89688
atmosphere, conc. meas. by lidar 78—85693
atmosphere, conc. statistics for N. tropical Atlantic region 78—32188
atmosphere, condensation nuclei and weather on Mount Kenya 80—82012
atmosphere, condensation nuclei conc. meas. on aircraft flight 79—58010
atmosphere, condensation nuclei conc. records, 1965-77, SW.Germany *(German)* 79—84422
atmosphere, condensation nuclei vertical profiles 79—79956
atmosphere, conductivity meas. in lower stratosphere over Poona, aerosol effects 77—70750
atmosphere, content from ERTS (LANDSAT) obs., comment 78—28282
atmosphere, counting efficiency of condensation nuclei counters 78—36293
atmosphere, detection by solar occultation technique, horizon radiance inversion 77—9539
atmosphere, diffuse atmospheric scatt. corrections to solar radiometry 79—80015
atmosphere, direct formation by reaction of NH_3 and SO_2 77—29377
atmosphere, direct observations of aerosols attached to falling snow crystals 80—17362
atmosphere, downward particulate transport to aerosol layers 77—78348
atmosphere, dust aerosols, activation analysis experience at Karlsruhe Nuclear Research Center 78—3941
atmosphere, dust grains mean radius rel. to transparency meas. on Maidanak mountain *(Russian)* 80—72627
atmosphere, effect on contrast reduction in remote sensing of Earth surface 80—101431
atmosphere, effects on diffuse and direct solar radiation at Earth's surface 77—37406
atmosphere, effects on total O_3 estimation from UV radiance meas. 79—8662
atmosphere, effects on turbidity 77—78420
atmosphere, elemental analysis for SO_2 contamination source determination *(French)* 77—41159
atmosphere, elemental conc. meas., Quillayute, Washington, (USA) 78—36270
atmosphere, EM wave scatt., spectral-zonal functions *(Russian)* 80—21824
atmosphere, erroneous elemental mass-size functions from high vol. impactor 79—20997
atmosphere, expt. meas. of inhomogeneities 78—77304
atmosphere, extinction at 500 nm in urban and rural air at Milwaukee, USA 79—100946
atmosphere, extinction coeff. from outgoing solar radiation meas. in O_2 0.76 μm band *(Russian)* 79—8690
atmosphere, extinction effects on Dobson meas. of total O_3 79—84431
atmosphere, Fe conc. and sources determ. by Mossbauer technique 79—79442
atmosphere, fine aerosol particles and light absorpt. in 8-12 μm transparency window *(Russian)* 78—16159
atmosphere, five year record of fall-out in Liege industrial region 78—81375
atmosphere, formaldehyde conc. and contrib. to rainwater 78—57243
atmosphere, from Jungfraujoch, Switzerland, chem. comp. 77—45056
atmosphere, gas-particle conversion meas. for coal fired power station plumes 80—81502
atmosphere, gaseous and particulate nitrates conc. meas. 77—45137
atmosphere, gaseous nitrates adsorption by particles in urban and rural area 80—94123
atmosphere, granulometric spectrum, in slightly polluted marine atm. 78—44893
atmosphere, growth kinetics during SO_2 oxidation 78—96255
atmosphere, H_2SO_4 constituent reaction with O,N,OH 80—90168
atmosphere, H_2SO_4 particulate form. in coastal area 80—90113
atmosphere, haze and fog vertical struct., effects on visible and IR extinction 79—58086
atmosphere, haze microstruct. and refr. index from scatt. light polarisation characts. *(Russian)* 79—29852
atmosphere, hexagonal ice crystals as cause of 46° halo and its arcs 80—82065
atmosphere, Hg, As and Br quantitative analysis 79—12179
atmosphere, homogeneous two-layer particles, relative humidity and light scatt. *(Russian)* 77—82007
atmosphere, humidity effects on gravit. settling and Brownian diffusion 78—32203
atmosphere, ice forming nuclei in N. Caucasus 77—78364
atmosphere, ice nuclei, no detectable effects from coal-fired power plant plume 77—21888
atmosphere, ice splinter production during riming 78—85662
atmosphere, impaction on nuclepore filter, collection efficiency 79—20475
atmosphere, incoherent optical propag. effects 78—92987
atmosphere, individual microparticles identification via micro-Raman spectrometer 78—68970
atmosphere, individual particle scatt. and single-burst digital correl. for wind remote meas. 79—100980
atmosphere, individual submicron sulphate particles detect. technique 78—69527
atmosphere, influence on shortwave radiative transfer, pyranometer meas. errors 79—21050
atmosphere, influence on thermal effects of stratosphere O_3 depletion at 85°N latit. 78—81279
atmosphere, information exchange concerning suspended particulates pollution in European Community 80—7979
atmosphere, inhomogeneities struct. and dynamics in ground layer, light scatt. 77—81955
atmosphere, instrumental anal. of light element comp. 78—69516
atmosphere, interactions with NO_x and O_3 78—81342
atmosphere, investigation in Complex Atmospheric Energetics Experiment (CAENEX) 78—3904
atmosphere, IR extinction rel. to aerosols mass conc. 79—84473
atmosphere, IR transparency window, 10-13 μm, H_2O and aerosol effects in winter and summer *(Russian)* 80—105048
atmosphere, Israel, pollution sources detection by X-ray fluoresc. 79—52975
atmosphere, K-rich aerosol emission by tropical forest *(French)* 79—100551

aerosols continued
atmosphere, large aerosol particles in convective storm environment 80—41512
atmosphere, large condensation nuclei meas. using laser photoelec. spectrometer *(Russian)* 78—65408
atmosphere, large particle scatt. coeffs. approximation for total O_3 determ. 80—82091
atmosphere, large particles ingestion by cloud, ice nucleation by freezing 77—37308
atmosphere, lidar meas. problems in hazy visibility conditions 77—9572
atmosphere, lidar obs., containerisation of heavy system for environmental protection control 78—36336
atmosphere, light absorpt. in UV *(Russian)* 78—16160
atmosphere, light beam coherence through optically dense turbid layer 78—55300
atmosphere, light scatt., generalisation of Rayleigh-Gans-Rocard approach 77—7006
atmosphere, light scatt. altitude depend., soln. by Monte Carlo methods *(Russian)* 77—60465
atmosphere, light scatt. coeff. of marine boundary layer 80—82052
atmosphere, light scattering problem, integral formulation 78—63010
atmosphere, limitation on electrical measures 78—69431
atmosphere, low-level aerosols as cause of anomalous gray shades in DMSP visible imagery 80—77111
atmosphere, marine, trace elements in size separated aerosols 79—20989
atmosphere, maritime, SO_4^{2-} sources over N.Atlantic Ocean 79—20904
atmosphere, maritime aerosol near Europe, albedo and 632.8 nm absorpt. 80—90136
atmosphere, mass conc. meas. by Nd:glass lidar, ASSESS II Spacelab mission simulation *(German)* 78—69649
atmosphere, mass loadings evaluation from multispectral extinction data 79—12221
atmosphere, mean bulk densities of dry samples 78—32204
atmosphere, meas. at Algarve coast, Portugal 79—58062
atmosphere, meas. by DFVLR mobile lidar system 77—53248
atmosphere, measurement problems 79—66839
atmosphere, meteorological transport of particulate material to South Polar Plateau 80—51481
atmosphere, microphysical parameters from complex optical meas. *(Russian)* 77—13123
atmosphere, Mie optical cross-sections calcs., sensitivity to size distribs. sampling errors 77—2243
atmosphere, minor and trace elements emissions and particle size distribs. at coal-fired power plants 79—92108
atmosphere, moist, equilib. sizes and size spectra of aerosols *(Russian)* 79—12194
atmosphere, mol. and aerosol scatt. rel. to effects of diffuse radiation on O_3 photodissoc. 80—109210
atmosphere, motion due to inertia, Brownian diffusion, phoretic and elec. forces 79—53460
atmosphere, MTF and PSF calcs. rel. to space-meteorological photography, multiple scatt. effect 79—66792
atmosphere, multielement characterisation 77—41152
atmosphere, multiwavelength contrast telephotometry, aerosol extinction and visibility determ. 79—66842
atmosphere, natural organic aerosols of terrestrial origin 80—36381
atmosphere, near IR absorpt. due to soot particles *(Russian)* 80—82055
atmosphere, N.England particle sizes in 0.25-5.0 μm range 77—70812
atmosphere, new particle formation in presence of existing aerosol 80—81962
atmosphere, nonautomotive components of Pb detect. in St. Louis region 79—12260
atmosphere, obs. at Barrow, Alaska, effect of wind direction 80—85704
atmosphere, obs. of Denver Brown Cloud 80—81961
atmosphere, particle collisions with cloud drops and raindrops, elec. fields and charges effects 77—25748
atmosphere, particle size, opt. and geom. determs. *(German)* 77—91259
atmosphere, particle size distrib. statistical characts. rel. to light attenuation coeffs. *(Russian)* 78—53702
atmosphere, particle sources over Australia 79—20907
atmosphere, particles and trace gases meas. in St. Louis area 79—16600
atmosphere, particles characterisation by Raman spectroscopy 77—49188
atmosphere, particles chem. diameter meas. with scintillation analyser *(French)* 79—88036
atmosphere, particles scavenging by falling water drop, lab. expt. 79—5572
atmosphere, particulate nitrate and HNO_3 in air of equatorial Pacific 80—85702
atmosphere, particulate S compounds phys. props. 78—96285
atmosphere, Pb aerosol concs. in Teheran 79—21011
atmosphere, peak short term dustfall meas. from dust generating industry 78—81386
atmosphere, physical characts. 78—69430
atmosphere, planetary radiation balance, climatological consequences 78—36242
atmosphere, pollution monitoring above urban site by Lidar meas. *(French)* 77—25780
atmosphere, precipitation scavenging rates of background aerosol 78—85648
atmosphere, produced by α-particles, evolution of <0.02 micron particles *(French)* 79—43640
atmosphere, propagation calcs., use of average complex refr. index 78—57314
atmosphere, props. rel. to visible and near IR light attenuation up to 30 km *(Russian)* 78—61558
atmosphere, Pt metals analysis by neutron activation 78—3989
atmosphere, pyrheliometric ratioing for apparent atm. transmission determ. 79—96809
atmosphere, quartz dust, in situ absorption meas. using reson. CW laser spectrophone 77—73860
atmosphere, radiation attenuation in absorpt. bands of moistened particles *(Russian)* 78—65384
atmosphere, radiation model of polluted boundary layer 77—49168
atmosphere, radiation modulation of aerosol state by moving clouds *(Russian)* 78—88916
atmosphere, radioactive, filter testing, Winfrith, double automatic Pollak counter 78—33301
atmosphere, Raman/aerosol signal ratio obs. for visibility meas. 79—100953
atmosphere, relative aerosol content determ. from ERTS obs. 77—37303

aerosols continued
atmosphere, remote sensing of particle size distribs., analytical inversions 78—73508
atmosphere, remote sensing of particle size distribs., analytical inversions 78—73509
atmosphere, remote sensing using laser radar techniques 79—66841
atmosphere, Rn content determ. in uranium mine *(French)* 78—32195
atmosphere, role in attenuation of 10.6 μm radiation *(Russian)* 78—45000
atmosphere, S aerosols characts. in Florida, PIXE anal. 79—21030
atmosphere, S level meas. using continuous flame photometric detect. system 80—81508
atmosphere, Saharan dust affecting radiative transfer rates, model 80—90149
atmosphere, sampling and anal. system for particulate S monitoring 79—21029
atmosphere, sampling by in situ and standard methods 79—66840
atmosphere, scatt. aerosol effects on optical mass of real atmosphere *(Russian)* 77—2239
atmosphere, scatt. coeff. as function of visibility and wavelength, empirical formula 79—34944
atmosphere, scatt. meas. of irregular particles versus Mie theory 78—58918
atmosphere, scattering matrix for pairs of absorbing dielectric spheres *(Russian)* 78—32147
atmosphere, scavenging by clouds and raindrops, elec. charge effect 79—53459
atmosphere, scavenging of aerosol particles by cloud drops and small rain drops, elec. field effect 80—82001
atmosphere, shortwave spectral characts. over desert, calc. from CAENEX-70 data 79—100956
atmosphere, single-stage and multiple-stage particulate scrubbing, comparison 77—37356
atmosphere, size and comp. at Mauna Loa Obs., Hawaii 77—78333
atmosphere, size distrib. and turbidity meas. over St. Louis, Project METROMEX 79—16670
atmosphere, size distrib. meas. with particle Doppler shift spectrometer 78—69515
atmosphere, size distrib. of water-soluble and insoluble particles 78—36218
atmosphere, size distribution in Nagoya area 78—3931
atmosphere, size spectra from inversion of optical scatt. and spectral extinction 79—62578
atmosphere, size-fractionated aerosol comp. in Charleston, W.Virginia 80—89687
atmosphere, sky brightness fluctuations in daytime *(French)* 80—81959
atmosphere, small ions attachment rate to aerosol particles 79—39817
atmosphere, SO_4^{2-} conc., sampling and anal. techniques 78—28304
atmosphere, SO_4^{2-} long-distance transport rel. to visibility, London, England 79—21015
atmosphere, soil derived, extinction between 0.55 and 10.6 μm 77—91264
atmosphere, solar occultation technique using Skylab coronagraph 77—9540
atmosphere, solar radiation absorpt., cloud and aerosol effects on heating rate 78—57319
atmosphere, solar radiation absorpt. 77—37407
atmosphere, solar radiation absorpt. by aerosol, spectrophone meas. 79—80027
atmosphere, sources identification in St. Louis area using factor anal. 79—12200
atmosphere, South Pole aerosol characterization using Raman microprobe 80—26580
atmosphere, spectral meas. of direct and scatt. solar radiation 78—3949
atmosphere, S.Pole, chem. comp. determ. by instrumental neutron activation analysis 78—3988
atmosphere, S.Pole aerosol props., 1978 obs. 80—41484
atmosphere, St. Louis in airborne pollutant meas. 78—3937
atmosphere, steady-state coagulation eqns. and particle size spectrum model *(Russian)* 77—41115
atmosphere, steel mill plume, ice nuclei and aerosol obs. 80—89693
atmosphere, stratified aerosol layers meas. by searchlight probing technique 78—92892
atmosphere, structure function of conc. fluctuations 78—92980
atmosphere, sulphate and nitrate assay via ion chromatography anal. 78—68974
atmosphere, sunlight scattering, Rayleigh and Mie theory 80—56605
atmosphere, surface layer, visible and IR attenuation statistical characts. *(Russian)* 80—4104
atmosphere, surface layer aerosols variability, spectral transmittance method *(Russian)* 78—69448
atmosphere, thermodynamic props. and aerosol patterns in St. Louis downwind plume 79—16603
atmosphere, thunderstorm ice nucleation study, Colorado, USA 80—90135
atmosphere, total organic aerosol conc. estimate 77—37289
atmosphere, trace element concs. over Lake Michigan 80—81968
atmosphere, trace elements concs. in UK aerosol, 1975 survey results 77—25759
atmosphere, turbidity meas. across Los Angeles Basin 78—92982
atmosphere, turbidity meas. via polarisation of UV light of daytime sky 78—20517
atmosphere, ultragiant urban particles conc. meas., St. Louis, Missouri, USA 77—49159
atmosphere, urban, aerosols distrib. rel. to mixing depths numerical simulation 80—105024
atmosphere, urban, radiative effects of elevated aerosol pollutant layers on temp. struct. in urban atmosphere, radiative effects of elevated pollutant layers 80—97841
atmosphere, urban, soot determ., by optical absorption technique 80—108824
atmosphere, urban aerosol comp. and mass, particle size depend., rel. to visibility level 77—91258
atmosphere, urban and rural, aerosols influence on warming 79—16671
atmosphere, urban visibility degradation, multivariate statistical anal. 79—62579
atmosphere, UV communication based on scattering effect 79—3736
atmosphere, vertical optical struct. determ. from angular depend. of IR radiation *(Russian)* 78—32223
atmosphere, visibility, turbidity and light scatt. obs. 80—105047
atmosphere, visibility meas. using long-path laser transmissometer 78—85751

aerosols continued
atmosphere, visibility reduction, linear system theory of visual acuity appl. 78—11997
atmosphere, visibility reduction by sulphates in photochemical smog 77—21904
atmosphere, visual range and relative humidity relationship from aerosol meas. 77—56728
atmosphere, water uptake and equilib. sizes at high relative humidities 78—61516
atmosphere, X-ray fluoresc. anal., book 77—41217
atmosphere, X-ray fluoresc. anal., filter attenuation corrections 78—35740
atmosphere, X-ray fluorescence anal. *(Spanish)* 77—87045
atmosphere, X-ray quantitative anal. of high vol. filter samples 79—70501
atmosphere aerosol, mass concentration from Lidar-solar radiometer expt. 80—90171
atmosphere aerosol, study of chemical components in Kashmir region 80—94594
atmosphere aerosol attenuation, influence on atmospheric and oceanic temp. determ. by remote sounding *(Russian)* 78—81430
atmosphere aerosol boundary layer effects on brightness oscillations of daytime sky 78—81406
atmosphere aerosol concentration global distrib., 162-238 millibar altitude 80—56591
atmosphere aerosol particle counter and size analysers with automatic correction 80—41574
atmosphere aerosols, meas. of trace metals in Antarctic snows, (1914 to 1974) 79—34867
atmosphere aerosols from municipal wastewater plants, monitoring 79—80050
atmosphere albedo change induced by aerosol 80—56604
atmosphere boundary layer, fog and haze, visibility and particle size distrib. 80—109195
atmosphere composition, Nigeria during dry dusty season 80—81960
atmosphere dust, eval. using nuclear methods *(French)* 80—7993
atmosphere dust, meas. via personal CIP type sampler 78—81469
atmosphere dust loading, 1923-54, pyrheliometric and circumsolar sky radiation obs. 80—46240
atmosphere H_2SO_4, extinction, absorpt., backscattering and mass content relations 80—101403
atmosphere ice nuclei, bacterial sources 77—5292
atmosphere ice nuclei, terrestrial and marine biogenic sources 77—5291
atmosphere ice platelets, IR radiation attenuation 80—66141
atmosphere obs. revealing volcanic activity of Mauna Loa, Hawaii 80—76950
atmosphere observations at Kingston, Jamaica, using lidar system 78—36284
atmosphere of South American continent, S and trace elements concs. in aerosols 78—57245
atmosphere of Sudan Gezira, chem. composition and pH 80—51518
atmosphere off W.African coast, Na, Cl and Br composition 80—77053
atmosphere optics, scatt. by particles and mols., book 77—5323
atmosphere particulate matter, role in anthracene photooxidation 80—61487
atmosphere particulate pollution, climatological effects 78—85678
atmosphere particulates, Mn desorption rel. to Mn distrib. in Pacific Ocean 80—56494
atmosphere particulates measurement, anal. and calibration techniques 78—69531
atmosphere pollution dust dynamics, study via ^{222}Rn descendants radioactivity meas. *(Rumanian)* 80—12524
atmosphere salinity used to determine ocean salinity flux 80—104986
atmosphere snow and ice particles, influence on elec. field above Arctic Ocean *(Russian)* 79—48537
atmosphere soil-derived dust, Christiansen effect in IR spectra, Rayleigh limit 80—105046
atmosphere submicron aerosols, losses in aluminised Mylar bags 79—58114
atmosphere sulphate aerosol, meso-scale transport obs. in rurual East Midlands, England 80—94124
atmosphere sulphate aerosols, diurnal var. at rural sites in E.United States 80—30621
atmosphere turbidity monitored by satellite, obs. of reflected sunlight 80—51471
atmospheres, reflective dust blanket rel. to Earth albedo sudden change and ice age onset 79—44241
atmospheric, laser beam propag., UV, visible and IR regions *(Russian)* 78—28313
atmospheric, microscopic samples molecular analysis, using Raman microprobe 80—57391
atmospheric, neutron activation anal. system appl. 77—81442
atmospheric, particle conc., meteorological factors effect 80—4060
atmospheric, particle size distribs. evolution via Brownian coagulation, num. simulation 80—41513
atmospheric, simultaneous Al, Si determ. by neutron activation anal. 80—72116
atmospheric, solar radiation absorpt., visual photometric meas. technique 80—85750
atmospheric, sulphate and nitrate level calcs. 80—26056
atmospheric, use of lidars, laser rangefinders 80—51580
atmospheric aerosol, absolute element concs., PIXE and AAS, comparison 78—85237
atmospheric aerosol, turbidity characts. determ. from spectral actinometric obs. 78—92986
atmospheric aerosol constituents, absorpt. coeff. rel. to imaginary refr. index 79—74956
atmospheric aerosol extinction measurements, multiple scatt. corrections 80—98445
atmospheric aerosol particles, optical props. 78—11995
atmospheric aerosol size distribution determ., optical attenuation meas. *(Chinese)* 80—72570
atmospheric aerosol studies using solar aureole radiometer 77—53240
atmospheric background aerosol, elemental conc. and particle size distribs., PIXE anal. 77—49139
Atmospheric Cloud Physics Laboratory on Space Shuttle, image dissector for size and position of statically suspended particles 80—26616
Atmospheric Cloud Physics Laboratory simulation, vorticity transport eqn. solns. 80—94690
atmospheric degradation of electrooptical system performance 79—34940
atmospheric environmental research, appl. of lasers *(German)* 80—97849

aerosols continued
atmospheric extinction and absorpt., effects of particulate complex refr. index and size distribs. 79—29849
atmospheric from naturally occurring aerosols, rel. to particle size statistics, 3.8 μ meas. 78—49136
atmospheric IR aerosol extinction, 3 to 5 and 8 to 15 μm spectral regions, relative humidity effects 79—62581
atmospheric light scatt. meas. extension into UV using integrating nephelometer 79—74955
atmospheric measurements with calibrated two- and three-freq. lidars 78—36334
atmospheric models, contrast attenuation factors calc., for remote sensing 80—4135
atmospheric nonspherical aerosol particle characterisation with electrooptical nephelometry 80—77106
atmospheric optical transmission modelling and prediction schemes 79—53519
atmospheric particles, S assessment along urban freeway, proton induced X-ray emission anal. 77—60172
atmospheric particulates, chemical characterisation via light scatt. method 78—69533
atmospheric pollutant propagation anal., appl. of indicator activation method 79—88039
atmospheric remote sensing by aerosol lidar backscatter *(Dutch)* 80—4110
atmospheric scattering from marine aerosols, ELOS optical communications system 79—29862
atmospheric transverse velocity single-beam meas. 78—53747
atmospheric turbidity caused by air pollutants, assessment 79—100941
atmospheric ultrafine particles and ions, form. from trace gases 77—25742
atmospheric vertical distribution, meas. by Skylab photographic coronagraph 77—60568
atmospheric water vapour and aerosol optical depth determ. by remote sensing 78—65389
atomic analysis, aerosol aerodynamics effects 78—48709
atomisation of liquid by impinging jets, expt. and theory 78—87373
atomisation of petrol in internal combustion engine 78—27829
atomisation of solns., US method, aerosol dispersion, sensitivity, reproducibility *(Russian)* 77—1964
atomizing jets, ultra-high speed filming 79—68777
attachment coeffs. of ^{212}Pb atoms and ions on monodisperse aerosols 79—66367
attenuation effect on O$_3$ determ. with Dobson spectrophotometer 77—45186
background aerosol characts. from daytime sky meas. *(Russian)* 78—36276
background aerosol comp. on Chacaltaya Mtn., Bolivia 77—91188
backscattered fraction in two-stream approxs. 77—45150
bacterial aerosol, deposition and round-nose wedge in interception region 77—81520
balance equations, homogeneous and nonhomogeneous, similarity solns. 77—9130
beam broadening in randomly inhomogeneous cloudy aerosol medium *(Russian)* 78—58911
benzo(a)pyrene, distrib. with respect to particle size in submicron atm. aerosols 79—74563
benzo(a)pyrene and C black combined aerosol form., rel. to air pollution and health hazards 78—80796
binary gas mixture, drop thermophoresis 80—93806
binary homogeneous nucleation theory, limiting behaviour 78—92517
biomedical influence, conf., Dusseldorf, Germany (Oct. 1979) 80—94915
bipolar ionic atmosphere, equilib. charge distrib. on aerosols 79—70830
Bjerknes forces in viscous medium and acoustic coagulation of aerosols 77—68680
bleached zone, probe radiation propag., intensity and phase fluctuations 80—67411
breakdown, electrical, due to pulsed, RF, and static fields 77—76242
brick dust in air, aerosol, photophoresis in optical radiation field 77—12836
Brownian, thermo- and diffusiophoretic forces effect on aerosol capture 77—16869
Brownian coagulation 77—9133
Brownian coagulation and diffusive deposition of monodisperse particles 78—23967
Brownian coagulation in rarefied gases 77—36794
Brownian coagulation in transition regime 77—86383
Brownian coagulation in transition regime 78—11571
Brownian diffusion to face of Nucleopore filter 79—88025
brush fires, influence on W.African atmospheric aerosols *(French)* 79—34883
California stratus, ^{34}S/^{32}S ratios rel. to aerosol and cloud drop origin 77—29407
capture on horizontal rotating disc, collection efficiency of particles calc. *(French)* 77—63960
carbonaceous aerosols mass monitoring with spectrophone 79—92112
cascade particle analyser for aerosol size distrib. and mass conc. 79—71583
catalytic oxidation of SO$_2$, expt. under atm. conditions 79—1941
centrifuge, calibration at unmatched relative humidities between stream and aerosol air 79—41775
charge deposition on charged particles of arbitrary shape 78—3386
charge distribution, meas. via variable freq. electrostatic mobility analyser 78—77945
charged, particle deposition in conducting tube 79—98792
charged dielectric particle, electrostatic with charged conducting drop, atmospheric appls. 77—25749
charged spray, evaporation in elec. field *(French)* 77—29054
charging by α-ionizing radiation in electric field 78—11566
charging migration and EHD transport 78—88660
chemical components of particles in lower troposphere above central Europe 77—29354
chemical composition measurement, use of laser induced mass spectrosc. instrument 80—97848
chimney plumes, partial penetration of inversion layer, model 80—7974
city plume aerosol size distrib. and turbidity meas. 77—37408
classification pulse amplitude analyser 78—61587
clean air aerosol, chem. components depend. on air mass and meteorology *(German)* 79—53412
climate contemporary changes due to solar const. aerosols and radiative transfer *(Russian)* 77—41140

aerosols continued
climate model, zonally averaged, aerosols affecting temperature 80—77102
climatic effects *(French)* 79—84360
cloud condensation nuclei, meas. using horizontal thermal gradient spectrometer 80—77158
cloud condensation nuclei, microstruct. meas. in Kenya high-frequency hail area 79—53484
cloud condensation nuclei flux, continental surface meas. 79—53443
cloud condensation nuclei in urban environment, effects on cloud microphysical model 80—82004
cloud condensation nuclei on USA Atlantic seaboard 77—5310
cloud drop growth by condensation, air parcel model 78—7729
cloud droplet spectra, effect of nuclei spectra 77—64364
cloud droplets, interception collection efficiencies 78—3381
cloud particles, effects of nearest neighbour interactions on evaporation rate 77—2209
clouds, ice nucleation by aerosol particles 80—61864
coagulation, initial size distrib. effect 80—104469
coagulation, kinetics 79—39209
coagulation, simplified model 77—56254
coagulation and condensation, dynamic behaviour 77—25312
coagulation and diffusion in turbulent jet 79—23355
coagulation of aerosols, appl. to LMFBR max. critical accident assessment 77—3121
coagulation of aerosols with broad initial size distributions 78—15717
coagulation rate measurement, of high Knudsen number aerosol 80—71954
coagulation theory, new aspects *(Russian)* 79—8453
coal-dust aerosol, radiation-absorbing coeff., effect of spectral comp. of radiation and particle size 77—23859
coastal aerosol sampling instruments, Californian workshop 78—7681
coastal meas. by 1.06 μm Mie lidar scatt. 80—98403
collection efficiency by water drops in subsaturated air 78—28273
collection efficiency of micro-perforated plates 79—64760
collection efficiency of nuclepore filters with asbestos fibres 78—57351
collision rates in highly dispersed aerosols with elec., acoustic fields 79—47986
combination coeffs. of small positive ions with submicron particles 78—27830
combustion products, Raman scatt., fluoresc. interference 78—15728
complex permittivity meas. at microwave, two coupler method 78—21167
concentration measurement using beta gauge *(French)* 79—53012
condensation fume, nature and origin of particles 79—39221
condensation nuclei, balloonborne meas. using condensation nuclei counter 77—64460
condensation nuclei, counter with inherent size resolution capability 78—81470
condensation nuclei conc. over Mediterranean Sea 77—45057
condensation nuclei counters, calibration and intercomparison 79—83684
condensation nuclei counters, efficiency improvement for particle detection 80—7983
condensation nuclei counters at South Pole, calibration 80—98470
condensation nucleus counters, comparisons, comments 77—56758
condensing turbulent annular-mist flow, wall and interfacial shear stress 78—94812
conducting particles in non-conducting gas, hydromagnetic thermal convection instability 79—53709
continuum source particle beam properties, comput. modelling 80—26062
corona ion generator for removing dust and aerosol particles in rooms *(Finnish)* 77—66883
coronene, distrib. with respect to particle size in submicron atm. aerosols 79—74563
correl. with N.Hemisphere average temps. during Little Ice Age 80—82050
corundum particle aerosol, nonlinear propag. of laser radiation 79—23033
counter, photoelectric, calibration by sedimentation method 80—99031
creeping motion of aerosol aggregate composed of two touching spheres 77—47077
cyclone, reverse flow, efficiency anal., using monodisperse methylene blue-uranine 78—34142
cylindrical particles, diffusophoretic force in binary gas mixture 78—68936
cylindrical particles, overall drift angle in sedimentation 79—50777
cylindrical particles, thermophoresis under creep conditions 78—68935
cylindrical surface, aerosol particle capture, thermophoresis forces 80—103060
decay in human lung during breath holding 79—66480
deposition, diffusion model description *(German)* 78—59446
deposition in entrance of parallel-plate channel, gravity effect 80—83834
deposition in human lung, computational model 77—44579
deposition of particles in model airways 80—72192
deposition of polydisperse aerosol in human respiratory tract, models 78—24085
deposition on plate in turbulent flow 78—87380
detector, in cryogenic systems 78—81986
dibutylphthalate, supersaturated vapour, aerosol form. by mixing of flows 79—39212
dielectric and absorbing nonspherical particles, scatt. and polarisation props. 77—34823
differential scatt. coeff. to mass conc. ratio, spectronephelometer, cascade impactor obs. 80—72628
diffuse radiation, models with aerosols and common absorbing gases, data sets 79—44235
diffusion, polydispersivity, unipolar charging, charging mobility analysis 78—61059
diffusion, polydispersivity unipolar charging, particle dielectric constant and ion mobility effects 78—61058
diffusion and sedimentation in horiz. cylinder 78—3385
diffusion and sedimentation in Poiseuille tube flow 78—59463
diffusion sampling method for ambient aerosol size discrimination with chemical comp. determ. 77—37349
diffusophoresis along curved surface 78—83432
diffusophoresis of nonspherical aerosol particles in a free molecular flow 80—43765
dioctyl phthalate, polydisperse, spectronephelometer studies 79—21797
dioctylphthalate, monodisperse aerosol, automatic method of determ. Stokes size of particles 79—93096
direct visible spectra and aerosol optical depths at urban and rural locations during summer 1975 at Milwaukee, meas. 79—29857

aerosols continued
  - discharge in heterogeneous medium 80—38858
  - discharger, electrostatic, for helicopters *(French)* 80—28863
  - discrete coagulation eqn., approx. analytical soln. 80—55722
  - dispersed composition analysis, small-size optical instrument design 77—17257
  - dispersion aerosols for transport of deuteron and ^{84}Kr induced reaction products 77—34502
  - dispersion analysis by Kvant optoelectronic classifier 78—12739
  - dispersion analysis of aerosols, optoelectronic instrument adjustment 77—74476
  - dispersity analysis, automatic photoelec. analyser for size range 0.3-40 μm 80—57251
  - Dobson total O_3 meas., aerosol effect 80—12463
  - drop, submicron size, evap. in continuum and non-continuum regimes 79—43639
  - drop size prod. by plain-jet airblast atomizer 78—3375
  - droplet aerosol optical bleaching, influence of free convection 80—9924
  - droplet motion in optical radiation field for small Knudsen number values 78—35730
  - droplet size and conc., simple transmittance meas. 77—9511
  - droplet-laden gas, attenuation of high-intensity sound 77—62082
  - dry deposition, filtration model rel. to trace metal deposition from atmosphere 78—73441
  - dust particles in atmosphere, effects and size distribution *(Dutch)* 79—52974
  - dust sampling system collection effeciency rel. to particle density and size 77—37456
  - dust storm in Israel, dust property obs. 80—90162
  - dust storms, aerosol and momentum mixing, fast-response meas. 78—65364
  - dye solution aerosols as laser active media 80—95887
  - dynamics in low atmosphere, correlation lidar meas., method error 79—68785
  - electret filters for high efficiency air cleaning 80—56569
  - electric arc, plasma stream form., aerosol particles effect 78—51390
  - electrical analyzer, performance under nonideal conditions 79—66372
  - electrical plume detection, theory and meas. 80—7984
  - electrification of β-active aerosol particles in external elec. field, influence of stopping power of gaseous medium 79—20473
  - electro-aerosols, precipitation in the airways, effect of electrostatic scatter 80—108929
  - electro-optical sensors use, prediction of atmospheric effects 79—53522
  - electrodiffusion precipitation of charged particles onto cylindrical channel walls 79—14463
  - electrolyte aqueous soln. drops, ion emission due to laser heating 78—59063
  - electrostatic collection of aerosol particles on sphere at intermediate Reynolds numbers 77—36799
  - electrostatic collection of particles on sphere 79—47994
  - electrostatic image force charged particle deposition in rectangular and cylindrical channels with laminar flow 78—83491
  - electrostatic metallic spray theory 77—25317
  - electrostatic precipitation, Reynolds no. range 10-100 77—86388
  - electrostatic spraying of liquids, role of Joule heating 77—32837
  - electrostatically charged, particle deposition in hollow cast of human larynx-tracheobronchial tree 79—43953
  - elemental abundances of S, K and P in aerosols from S.American rain forests 79—100910
  - elemental composition in particle size fractions, human respiratory uptake 77—48726
  - elemental composition of atmospheric aerosols and ice nuclei 78—3882
  - ellipsoidal aerosol particles in binar binary gas mixture, diffusophoresis under hydrodynamic conditions 80—66888
  - ellipsoidal particles in acoustic field, relative velocity 80—58854
  - EM radiation scattering by soft particles, Mie series appl. 79—36824
  - EM scattering by cluster of spheres, soln. using Debye potentials 79—31800
  - emission spectroscopy, use of plasma jet and aerosol desolvation system 77—86425
  - environmental aerosol sampler, particle size depend. of collection efficiency 78—12002
  - equation of motion for small aerosol in a continuum 78—3895
  - equilibrium surface area rel. to vol. prod. rate 78—61066
  - eruption clouds in Guatemala, atmospheric studies 80—41505
  - ethylene, obtained from gas cylinder, particle size distrib. 80—55723
  - evolution downwind of St. Louis, visibility reduction 79—53514
  - extinction in 0.2-40 μm wavelength range, meteorological effects 80—17371
  - fast breeder reactor accidental releases, influence of physico-chemical form on consequences 79—74574
  - fibrous media, dendritic deposition of aerosol particles, inertial impaction and interception 80—74945
  - filtered air, particle production expts. using UV radiation 78—24336
  - filtration efficiency of granular bed, triboelec. effects 80—38487
  - fine particle charging by unipolar ions, review and expt. 78—88658
  - fine particles clustering, experiment 80—26937
  - flash holography investigation of atmospheric aerosols 78—16217
  - Floc density, porosity and void ratio in colloidal systems and aerosols 78—3383
  - flow, disperse drop composition meas. 78—55682
  - flowing, attachment of ^{220}Rn decay products using aerosol centrifuge 80—61167
  - flowing aerosol, particle size distrib. *(German)* 78—20076
  - flows in finite tubes in random orientation, sedimentation 79—50778
  - fluid jet impinging upon void aerosol impactors 78—63472
  - fluorides, particulate, stack sampling by trapping on dry holders *(French)* 80—7986
  - fly ash nucleation props. in coal-fired power-plant plume 79—5607
  - flyash from coal combustion, S and Cl adsorpt., cloud nuclei form. 77—21887
  - fog, thermal emissivity 80—95795
  - fogs, optical probing, homogeneous particle model 79—66790
  - formation, growth, general dynamic eqn., H_2SO_4/H_2O aerosol simulation appl. 79—47990
  - formation, vapour condensation of various humidities, size spectra model *(Russian)* 80—12483
  - formation in reacting gases, relation of surface area to gas-to-particle conversion rate 78—48696
  - gamma emitting aerosol lung clearance studies, adjustable response detector 77—56451

aerosols continued
  - gas jet recoil transport system, aerosol formation using pure gas as carrier 79—97921
  - gas-jet transport system, aerosol size-depend. props. 77—79493
  - gas-jet transport system, optical investigation 77—14289
  - gasdynamic laser, two-phase mol. vibr. relax. in gas-aerosol system 79—45807
  - generators used in 3-D laser Doppler velocimeter 80—10331
  - global surface irradiance, effect of aerosol props. and surface reflectivity 80—76611
  - granulometric distrib. rel. to atmospheric pollution influences 77—37341
  - graphitic C, optically absorbing component of urban aerosol particles, photoacoustic meas. 79—96493
  - gravity settling in horizontal rectangular tube with diffusion 77—84310
  - greenhouse effects of some atmospheric constitutents 79—70882
  - ground level meas. of N.Greenland summer tropospheric aerosol 78—85645
  - growth by condensation, general dynamic eqn., exact solns. 79—39218
  - growth in urban plume, obs. 77—37390
  - hailstone nuclei formation, role of giant aerosols *(Russian)* 80—56530
  - haze stratification, rel. to slant meteorological visibility 79—100954
  - health hazards, biohazard safety cabinet design testing 79—16362
  - heat transfer in pipe flow 78—9684
  - heavy metals pollution of mountain watershed, impact of ski basin 79—20903
  - heterogeneous condensation, in cylindrical channel and on aerosol particles 79—57298
  - heteromolecular nucleation and condensation, multi-dimens. theory 78—92518
  - high-vol. samples, X-ray diffraction compound analysis 77—49176
  - holographic method of small particle analysis 79—13924
  - holographic reconstruction configuration, automatic assessment 77—7031
  - Homer City power plant plume, aerosols and ice nuclei meas. 79—74570
  - hot, β-active, charging in variable electric field 77—11280
  - hot, β-active charging in turbulent flow 77—19642
  - hot β active emission electrification in varying force fields 80—7868
  - human respiratory airways, diffusional deposition of airborne particles in curved tract 77—81519
  - humid atmosphere, water droplet vaporis. model with natural convection 78—33999
  - humidity effect in flow resistance of loaded fibrous filters 77—29451
  - hydrocarbon vapour, spontaneous condensation in submerged turbulent jet 79—64721
  - hydroscopic particle humidification process, electrooptic scatt. meas. 80—77107
  - hygroscopic particle size, air humidity depend., applic. to lung dynamics 77—90841
  - ice nucleation mechanisms of submicron aerosol particles 79—20947
  - impactor design 77—29448
  - impactor performance, effect of boundary layers 77—60133
  - inhalation apparatus, technique of continuous and intermittent working 78—36038
  - inhalation exposure system, microprocessor-controlled for repeated exposure of animals to aerosols 79—70726
  - inhaled aerosol transport into blood and retention, rel. to alveolar microenvironment 77—25630
  - injection methods of solids and liquids into HF plasma, anal. appls. 79—39257
  - intense light propag. in gaseous medium with solid microfilling, theoretical analysis *(Russian)* 78—25797
  - interaction with surfaces past which they flow 77—80198
  - ionisation path formation in gases by laser beam with retractable focus 79—18992
  - ionised gas, charged aerosol particles effect on thermal and elec. conds. 80—28593
  - IR attenuation by atm. H_2O, lab. study of role of mol. and aerosol contribs. *(Russian)* 79—34945
  - IR extinction by aerosols with Junge size distrib. 80—51537
  - IR laser propag. 79—53521
  - IR radiation scattering, atmos. heating and cooling rates 80—72630
  - IR spectra of soil-derived atmospheric dusts, Christiansen effect 80—26608
  - IR spectrometry, theory and appl. to spectroscopic effects of atmospheric constituents 80—101428
  - IR wavelengths extinction by aerosols in coastal fog 78—81400
  - isokinetic sampler for particle flux determ. 77—91279
  - jet, turbulent, normalised radial conc. profiles meas. using laser-Doppler anemometer 77—84311
  - JROE II LIDAR, atmospheric measuring instruments *(Italian)* 78—3957
  - Jupiter, upper atmosphere aerosol content from Ganymede eclipse obs. 77—41349
  - Jupiter atmosphere, aerosol absorpt. latit. vars. from 0.6 to 1.1 μ spectrophotometry 80—46468
  - Jupiter atmosphere, atmospheric aerosol props. from near IR polarisation studies 78—85899
  - Jupiter atmosphere, NH_3 haze rel. to high resolution obs. between 30 and 50 μm 80—46462
  - Jupiter stratosphere, acetylene photopolymers aerosol 80—31244
  - kinematic coagulation calcs. in variable-speed gas stream 80—19491
  - Knollenberg light scattering counters, response characts. 79—66369
  - Labadie Power Plant plume, lidar obs. of particulate density distrib. and behavior 80—55956
  - Lake Michigan dry deposition loading by airborne particulate matter 77—29410
  - laminar flow in cylindrical tube, conc. distrib. of free and attached Rn and Tn decay products 79—29412
  - laminar flow through inclined circ. tubes, gravitational deposition of particles 77—89192
  - laminar tube flow, gravitational deposition of growing aerosol particles 80—59099
  - large aerosol particle thermophoresis theory, comparison of two methods 80—26060
  - large particle, diffusional phoresis theory 79—55408
  - large particles, collection by high capacity preseparator 80—16884
  - large particles, photophoresis in optical radiation field 77—12836
  - large particles volatile, diffusion-phoretic motion 77—56259
  - large spherical particles, absorpt. efficiencies, approximation scheme 79—31798
  - laser aerosol deflector for energy parameters meas. 78—25916

aerosols continued
laser applications in particulate analysis, multiple ratio single particle counter 78−35732
laser beam clearance of water aerosol, change in transmittance at 0.63 and 1.06 μm 78−37933
laser beam deflector, operation at high radiation intensities 80−9922
laser beam hygroscopic aerosol interaction 77−79888
laser beam transmission, coagulation-sedimentation effects 80−36393
laser beam-exploded aerosol, light focusing and defocusing 80−8426
laser intracavity adsorption spectra of surface-active substances and aerosols *(Russian)* 79−57343
laser pulse interaction with aerosol particles 77−7097
laser radiation intensity fluctuation in fine-droplet water aerosol at 630 nm 80−4109
latex, doublet particles, response of Knollenberg light scatt. counters 80−37152
latex, laser spectrometer for submicronic aerosols, photoelec. determ. of conc. acid dispersity 79−54244
layer depth remote meas. by microwave-modulated laser *(Russian)* 78−57338
lidar antenna aerosol vol. optical field scatt., laser atmospheric sounding 77−88641
lidar equation for inhomogeneous atm., double-scatt. approx. 79−29855
lidar meas., error analysis and simulation 80−26617
lidar obs. at 0.7 and 10.6 μm wavelength 78−69459
lidar observations, flight tests of continuous long-distance system *(German)* 78−36338
lidar observations, planned operation of multidisciplinary airborne lidar 78−36335
light scattering, obs. of polarisation and intensity 80−51541
light single scattering rel. to photographic solar aureole meas. 77−5448
light source in photoelec. aerosol counters *(Russian)* 79−100969
light wave fluctuations in turbulent atmosphere 80−48157
lipid composition of marine aerosols, sea surface microlayer and subsurface water 80−17297
liquid and solid, size distrib. meas. by Doppler shift spectroscopy 78−33674
liquid atomisation, using US piezoelectric resonators *(German)* 79−66359
liquid in centrifugal atomizer, air vortex radius 77−80201
liquid particles, aerosol and hydrosol, separation by size in thermal fields 80−101044
liquid-drop aerosol, laser beam distortion in illumination channels *(Russian)* 77−14727
liquid-droplet smokes and fogs, IR extinction spectra 77−78416
liquid-gas interface, heat and mass transfer 78−30338
LMFBR, accidental Na release as peroxide aerosol, effect on tomato and lettuce *(French)* 78−8997
LMFBR, Clinch River Plant, sensitivity for radiological consequences to var. in aerosol parameters 78−13294
LMFBR, filtration of Na fire aerosols 79−30998
LMFBR aerosols, size dependent density, gravitational collision efficiency 79−93789
LMFBR containments, post-accident conds., gravitational agglomeration of aerosols 79−36369
LMFBR containments, severe post-accident conds., approx. in aerosol behaviour models for source-term calcs. 79−31064
LMFBR HCDA, appl. of acoustic agglomerators for suppression of Na-fire aerosols 79−54525
LMFBR hypothetical accident, use of sonic agglomerators for aerosol particle suppression 79−36370
LMFBR mixed-oxide fuel aggregates, dynamic shape factors 79−67853
LMFBR postulated accident, aerosol behaviour within containment, Na$_2$O agglomerate props. 79−36368
LMFBR safety analysis, computer code for determ. of aerosol attenuation in leakage paths 78−13293
lower atmosphere, acoustic and optical dynamics study *(Italian)* 77−91327
lung, deposition of inhaled particles, airway generations of normal subjects 80−67125
lung airways aerosol deposition, two-component theory 79−34582
lung airways aerosol impaction model 77−90840
lung burdens of low-energy photon-emitters, interlaboratory comparison of meas. techniques 79−20671
lung scintiphotography with dry aerosol, generation and delivery system 78−24126
LWR core meltdown, activity release and aerosol characts. 78−82469
LWR post-accident aerosol removal, steam condensation expt. 79−13456
magnetite powder, detection of steel structural heterogeneities, using mag. aerosol method 78−44314
mammalian lung airways, aerosol deposition in anatomical models, theoretical evaluation 80−81627
marine, meas. using laser scattering spectrometer system 78−36316
marine, organic and inorganic Cl gas concs. and particulate Cl size distrib. 78−32187
marine aerosol, Bermuda, alkali and alkaline earth chemistry 77−70727
marine aerosol alkali and alkaline earth metal chemistry 77−70726
marine aerosols influx into atmosphere, influence of coastal-zone physicogeographic conditions 79−29818
marine atmosphere, extreme E. Pacific Ocean Aitken nuclei concs. 77−37305
marine atmosphere, lightly polluted, condensation nuclei conc. correl. smokes 78−81376
marine atmosphere, mineral and sea salt aerosol concs. 79−58039
marine atmosphere particulate matter, organic C conc. and particle size distrib. 78−32139
marine atmosphere particulate Na and Cl vertical distrib. 77−37304
maritime, over-the-horizon optical propag. effects 80−41547
maritime air, aerosol distribs., IR scatt. coeffs. 77−45050
maritime coastal haze, optical properties *(Russian)* 79−25327
Mars atmosphere, aerosol characts. from isophotes 77−29699
Mars atmosphere, condensates rel. to phase function meas., July to November (1976) 78−20677
Mars atmosphere, O$_3$ layer and two aerosol layers detect. by Mars 5 spacecraft UV obs. 78−49357
Mars atmosphere, two-component aerosol rel. to opacity during July-November (1976) 78−20676
mass distribution, meas. using centrifuge with quartz oscills. *(German)* 79−92004
mass extinction coefficients estimated for nonabsorbing spherical aerosol particles in the geometric scattering regime 80−87310

aerosols continued
medical nebulizer produced, droplet size distrib., evaporation effect 78−24084
membrane filter mounts and quick-change device for aerosols and liq. suspensions 77−53873
mesosphere, aerosol layer contrib. to polar albedo 77−60467
mesosphere, turbidity from twilight obs. 77−5318
meteoritic aerosols, twilight optical charact. modification during Perseid meteor shower *(French)* 80−46255
microscopic particles, heating by laser beams 78−50838
middle atmosphere aerosol, remote sensing techniques 80−109269
midlake region, aerosol mass conc. and scattering coeff. 80−61839
mixed salt aerosols, phase transform. and droplet growth in moist atmosphere 79−52783
mixed-salt particle suspension in moist air, phase transform. and growth 77−12832
molecular aerosol cluster, sticking probability to solid surface 77−12833
molecules embedded in small particles, Raman and fluoresc. scatt., coherent results 79−41338
molecules embedded in small particles, Raman and fluoresc. scatt., incoherent results 79−41337
monitoring system for alpha-in-air, real-time 80−23155
monodisperse, 0.01 μm steady-state charged fraction meas., ion-particle attachment coeff. ratio 77−60136
monodisperse, 0.1-0.4 μm, size meas. by polarisation ratio of 90° scatt. light 80−40754
monodisperse, mass concentration, laser monitoring 80−98878
monodisperse, quantitative analysis using IR differential absorpt. analysis 79−24931
monodisperse, uniform electrical charging 77−56256
monodisperse aerosol particles, 0.627 μm scatt. from spheroidal 2 μm cladosporium and cubical 4 μm NaCl 80−9804
monodisperse particles dry deposition on simulated grass surfaces 78−81396
movement in lake-land breeze circulation, pollution study 80−31101
moving droplet, bleaching kinetics by CO$_2$ laser radiation 78−13743
multi-droplet system in vapour flow, time-evolution, mathematical formulation 79−41733
multicomponent, coagulation eqn., with/without particle growth 78−35727
multiple light scatt., inverse problems 79−98289
multiple light scattering, theory for dispersive media with spherical particles *(Russian)* 80−94599
nasal deposition during inhalation, theoretical study 79−34581
natural ice-forming nuclei surfaces, elemental comp. 78−3881
Neptune atmosphere, aerosol particles rel. to UV albedo 80−82295
neutron activation analysis for 14 volatile heavy metals as constituents of aerosol particles 80−16891
nitrate conc., SO$_2$ photochem. effects 77−49103
nitrate detection in aerosol particles using nitron 79−12280
noctilucent cloud aerosol particles, temp. profiles *(Russian)* 78−16093
noctilucent cloud particles, sunlight scattering rel. to characts. 78−11945
noctilucent clouds, circularly polarised light detect. rel. to ice crysts. growth 79−48568
Nolan-Pollak condensation nucl. counter, droplet growth rate, supersaturation 77−60480
nonlinear optics degenerate four-wave mixing medium 80−43390
nonspherical particles, orderly motion 80−7867
nonspherical particles size distrib. from scatt. meas., Mie theory 78−58909
nonvolatile aerosol particles capture by growing or evaporating drops 77−36797
nonvolatile particles, capture by large evaporating or condensing drops 78−3388
nozzle-inlet design, for aerosol beam instruments 80−6183
nuclear accidents, behaviour of airborne aerosols 80−746
nuclear fission aerosol products, bioindication using needles of common pine tree 79−100550
nuclear reactor post accident aerosols, gravitational collision efficiency 80−32375
Nuclepore filters, anomalous filtration of solid particles 79−12283
nuclepore filters, clogging, cap form. model 79−20468
oceanic, ^{55}Fe and stable Fe forms and availability 79−12241
one-dimensional unsteady gas flow *(Russian)* 77−35223
optical backscatter by aerosols of high relative humidity 77−34825
optical coherence, atm. effects 80−82064
optical component protection in dusty environments, electrostatic techniques 80−58657
optical depth of Saharan dust, NOAA 3 VHRR reflected radiance meas. 78−65390
optical device for examination of mixed phase aerosols 80−86404
optical extinction coefficients, practical upper limits 79−72486
optical extinction in 0.5-14 μ wavelength range 78−57318
optical extinction meas. in polydispersion, forward scatt. corrections 79−7075
optical extinction measurements, forwardscattering corrections in aerosol media, monodispersions 78−94367
optical particle counters, field comparison 79−12279
optical particle counters behaviour, comparative assessment 79−57550
optical particle sizing counter for in situ meas. 79−75489
optical particle sizing counter for in situ meas. 79−75490
optical properties of cigarette smoke aerosols 79−7073
optical thickness at marine boundary layer, rel. to satellite meas. 80−17326
organic compounds in aerosol samples 78−73463
organic constituents, effect on fog and clouds 78−73465
organic liquid surface, charged drop formation from bubble bursting 77−14634
organic material in atmospheric aerosols 78−73464
organic pollutants, particle size distribs. in urban, rural and seashore aerosols 80−55958
Pacific marine aerosol, continental component identification by combined neutron activation and SEM with X-ray anal. 78−3990
particle, nonequilib. bipolar charging 78−3382
particle 79−50776
particle analysis for sulfate, nitrate, elemental comp., Los Angeles 80−7971
particle capture by drops, thermodiffusionphoresis and Brownian motion effects *(Russian)* 79−39791
particle charging in continuum regime 78−90349
particle charging using beta sources, elect. and mag. fields 79−36429

aerosols continued
particle coagulation by Brownian motion 79—96375
particle concentration over Chicago, comparison of method 80—7981
particle content study in atmosphere, clear atm. and at cloud edges *(Russian)* 80—21794
particle deposition from laminar flow 79—47988
particle deposition in channel due to diffusion and electric charge 78—90978
particle deposition in fibrous media with dendritic pattern 77—60124
particle deposition in flow through model filters 78—1740
particle deposition in human respiratory tract, sampling apparatus 79—96719
particle deposition in human respiratory tract model 78—24086
particle deposition in sampling lines, expts. 78—81472
particle diffusivity in turbulent pipe flow 78—1731
particle dimensions, equipment for transmitting dispersed compositions and measuring characts. 79—70384
particle distributions, inertial sizing using laser velocimeter method 80—53901
particle fallout rate under nonisothermal conditions 78—7238
particle growth and size distrib., humidity effects, effects on visibility 77—25321
particle inertial impactors, calculation of optimum geometries 80—24115
particle mass and charge determ. by one electron differentials 79—66368
particle motion, stochastic nature, analytical approach 77—86385
particle neutralisation to Boltzmann's equilib. by corona discharge 78—61064
particle optical constants and disperse aerosol comp., phase scattering function *(Russian)* 80—61898
particle response to impulse at small Knudsen no. 78—90977
particle separation efficiencies of wire grids 78—87381
particle separation property of impactor stage with nonstationary flow *(German)* 78—18335
particle settling and diffusion from stationary gas in tube or duct 77—52678
particle settling in flow in parallel plate channel, diffusion effect 79—66371
particle size classifier with parallel plate electrostatic device 80—95070
particle size depend. of condensation nuclei counter 79—20476
particle size determination by light scattering, unknown refractive index 78—95957
particle size distrib., dynamic behaviour, coagulation, condensation, nucleation and removal 78—35726
particle size distrib., effect of concentration of dispersed liquid 77—60128
particle size distrib., theoretical and meas. over Milwaukee 80—7970
particle size distribution, information provision of brightness and polarisation phase functions *(Russian)* 78—44998
particle size distribution, Rocky Mountain air in winter 79—100887
particle size distribution errors of ratio-type single-particle counters 77—21898
particle size distribution meas. using electronic cascade impaction 80—72652
particle size distributions, laser Doppler velocimeter meas. 77—35273
particle size meas. by microcomputer-modified elec. analyser 80—40756
particle size meas. by optical methods, review 80—40746
particle size meas. by scintillation counting, inhalation technique development *(Slovak)* 79—74750
particle size measurement, optical particle counter calibration by Doppler shift spectrometry 80—68173
particle size measuring device, using spectral transparency and small angle scatt. methods 80—95069
particle size spectrometer, microcomputer-modified 79—39329
particle sizing, AC/DC quotient method 77—37462
particle sizing by laser beam Mie scatt., computer program 77—37457
particle sizing by laser Doppler dynamic relaxation time meas. 77—21897
particle sizing by optical scattering counters 77—21896
particle time-of-flight spectrometry 77—37451
particle-droplet inertial collisions 79—47989
particle-size classification by opposing jets, secondary effects 79—70383
particle-small ion combination coeffs., size depend. 77—25320
particles, collecting, handling and mounting for SEM characterisation 79—21867
particles, dendritic deposition of metal fibres 80—40755
particles from oil-fired burners, size distrib. characterisation using Beta distrib. 78—81384
particles in flow type chamber, coagulation, deposition 80—69908
particles sizing, influence of chemical struct. 78—81471
particulate collection, low loading conditions, filter inefficiencies 77—70721
particulate detection by metal-coated Nuclepore filters 77—37463
pattern recognition using laser radar *(Japanese)* 80—51028
penetration through high efficiency filters 79—27690
percolation clusters in nucleation theory 79—52785
photochemical aerosol formation, primary pollutants effects *(Japanese)* 78—57305
photochemical aerosols in Titan atmosphere, identification 80—31249
photochemical and condensational var. of submicron aerosol particles *(Russian)* 78—40611
photochemical production of submicron particles of very narrow size distrib. 79—29491
photochemical smog, gas-to-particle conversion, organic aerosol growth rates 77—73826
photoelectric analyser, theoretical anal. of optical detector 79—67455
photoelectric analyser pickup, optical method of forming counting vel. 79—93270
photoelectric counter, use of laser light sources *(Russian)* 79—100969
photophoresis, low Knudsen number spherical particles 77—63965
photophoretic motion, particles $\ll$ light wavelength, gas collisional effect 77—90646
photophoretic motion of nonvolatile particles, thermal diffusion effect 78—79364
physical-chemical transformation processes, thermal-optical anal. *(Russian)* 80—12482
pipe, turbulent aerosol flows at high wall temps., heat transfer 80—74862
PIXE anal. of urban aerosols on heavy loaded membrane filters 77—49138
planetary atmosphere, polarisation state, aerosol and Rayleigh scatt. 77—49171

aerosols continued
planetary atmospheres, aerosol effect on radiative transfer 80—109383
planetary atmospheres, aerosol volumetric scatt. coeff. determ. from absorption bands obs. 78—24480
plasma, cond. determ. 79—55464
plasma, highly-dispersed aerosol, nonisothermal, thermionic electron density function determ. 78—91066
plasma, nonequilib. aerosol, electrophys. props. 80—38543
plasma production by CO_2 laser beam, brightening channel 80—6272
plume models, application of rainfall statistics 79—84355
plume opacity related to particle mass concentration and size distribution 79—74566
pneumatic nebuliser efficiency enhancement through appl. of elec. field 78—95966
pollen and spores, long distance transport in troposphere 78—73466
pollutant mass density function multimodality 77—70807
polluted atmosphere, new particle form. in presence of aerosol 79—24926
pollution, St. Louis urban plume, form. and transport of secondary air pollutants 77—5316
pollution in Beijing, China, effect of weather conditions *(Chinese)* 80—108825
polycyclic aromatic hydrocarbons in long-range transported air pollutants 77—78410
polydisperse, growth in adiabatic condensation nuclei counter, finite expansion time 79—79306
polydisperse aerosol number and mass conc. meas. by elect. aerosol anal. 80—108753
polydispersions, Rayleigh-Gans approx. appl. to light scatt. 79—44249
polystyrene, monodisperse, attachment of ^{220}Rn and ^{222}Rn delay products 80—41256
polystyrene latex particles, particle sizing by forward lobe scatt. intensity ratio 78—71031
polystyrene latex sphere beams, secondary electron emission 77—24914
polystyrene monodisperse ^{51}Cr tagged aerosol prod. using aerosol centrifuge 78—92519
power plant plume, induced snowfall prod. 78—81284
precipitation of aerosol particles on a fixed evaporating droplet 80—7869
precipitation of aerosol particles on an evaporating droplet in a turbulent gas flow 80—7870
proton activation analysis of environmental and ecological pollution determ. 78—3994
proton scattering anal. of atmospheric particulate matter 77—25778
pulmonary regional electroaerosol deposition model 79—83842
pulse shaper for optoelectronic aerosol classifier 79—16049
pulsed laser-induced shattering of water drops 80—50471
pyrotechnically produced, use as atmospheric tracers 77—41236
radiative transfer through turbid atmosphere, single-scatt. solution 79—16663
radioactive, atmospheric contamination inside buildings, absorbed dose estimation *(Spanish)* 78—8998
radioactive, attenuation of airborne debris following LMFBR HCDA 80—13650
radioactive aerosol, human inhalation administration technique, deposition/clearance expts. 77—60312
radioactive aerosol charging, transient mean particle charge 78—23973
radioactive aerosol surveillance system evaluation 80—57984
radioactive aerosols, atmos. conc. monitoring, radionuclide anal. 80—21427
radioactive fallout in atmospheric dust, results to end of (1978) 79—79997
radioaerosol delivery, US nebuliser system 77—2050
radioelement transfer in marine aerosols *(French)* 78—24338
Raman-line splitting, surface waves of liquid drop in EM field 77—69826
Rayleigh scatt. props., nephelometer meas. 79—29865
reacting gases, aerosol formation, theory 80—55725
reacting gases, aerosol formation, theory 80—55726
reactor incident duct plugging by aerosol deposits, simple model 79—49782
receiving optical antenna, sensitivity to scatt. aerosol particle, laser location of atm. aerosols 77—70847
respirable aerosol mass conc. meas., using piezoelec. microbalance 78—69518
respirable aerosol sampler using two Nuclepore filters 77—91278
respirable fraction definitions, matching air sampler penetration curves 77—90827
roadway aerosol filter samples, proton-induced X-ray emission analysis 77—41233
rocket effluent, effect on ice nucleation 79—88446
Royco aerosol particle counter 225, data processing system and modified system props. 80—37005
Saharan aerosols, complex refractive index between 300 and 700 nm 77—81970
Saharan dust radiative characts. at solar wavelengths 77—81969
Saharan dust transport and deposition over Italy and S.Europe 80—41504
salt nuclei, size rel. to critical supersaturation 78—44940
salt spray, patterns of airborne salt across forested barrier island 80—8381
sampling thin-walled tube aspiration coeff. 77—37460
Saturn atmosphere, atmospheric aerosol props. from near IR polarisation studies 78—85899
Saturn atmosphere upper layers, aerosol particles props. *(Russian)* 78—40867
scattered radiation, effect on O_3 photodissociation 79—2371
scattering albedo determination using sky brightness measurements in UV *(Russian)* 80—21822
scattering and extinction coeff. simultaneous meas. in portable multipass cell 79—62588
scattering function determ. with telephotometer 80—105055
scavenging, in-cloud, rel. to aerosol particle size, mechanisms 78—16108
scavenging of spherical particles by charged thin ice plates, efficiency 78—44934
sea salt aerosol, atmospheric temp. sensors contamination 80—82095
sea spray and coastal aerosol effects on transmission 79—39861
sea spray comp. and aerosol generation, detergent effect on oil slicks 77—29325
sedimentation, natural, visual, photographic and laser sonde obs. *(Russian)* 78—32216
sedimentation, spontaneous, of sub-micron fractions, in confined space, expts. *(Russian)* 79—5182

aerosols continued
sedimentation in closed finite tubes in random orientation 79—24841
SEM autoradiography for location and study of microscopic β-active particles 77—57425
SEM specimen mounting epoxies, aerosols, and adhesive tapes 79—71580
separation, chainlike form. of particle deposits 77—77813
settling under convective stirring conditions, quiescent boundary layer thickness 79—66364
simulated, Be content by proton scatt. anal. 79—5217
simultaneous diffusion and sedimentation in rectang. tube 77—11266
single droplet, size and mass meas. using electrodynamic balance 80—89535
single particle aerodynamic relaxation time analyser 77—80205
single particles, transient analysis with multi-electrode flame ionization detector 80—23246
size and charge distrib., appl. of four-parameter distrib. model 78—85213
size determ. by holographic disdrometry 79—7104
size distrib. approx. determ. method 77—45188
size distrib. characterisation, modified beta density function 78—69432
size distrib. determ. from mobility distrib. of charged fraction 78—61065
size distribs. from inversion of spectral optical depth meas. 79—80020
size distribution, chemical composition, and optical properties of urban and desert aerosols in Israel 80—41503
size distribution, electrical analyser performance under nonideal condition 77—36798
size distribution, fractionator for large-scale sampling 77—9140
size distribution, meas. by combined light scatt. and centrifugation 77—10083
size distribution by inverting spectral turbidity data 80—95796
size distribution by means of laser-induced fluoresc. 77—40576
size distribution meas. by impactors, data inversion via nonlinear programming 77—2258
size distribution meas. with cascade impaction instrument using quartz crystal microbalance sensing elements 78—65904
size evaluation, response function optimisation of light scatt. instruments 79—50214
size spectrum determ. in turbulent medium using coherent Doppler meas. 79—96841
sizing using slotted virtual impactor 78—57350
sky intensity information content, polarisation meas. at right angles to solar direction 78—81401
smog episode, Los Angeles, pollutant transport in daytime sea breeze regime 79—5605
smoke aerosol microstruct. and refr. index, optical determ., inversion method 80—36399
smoke aerosols, optical absorption to extinction ratio, photoacoustic determ. 80—58459
smoke/dust cloud temporal analysis algorithm 80—98484
smokes, atmospheric, gravitational seidmentation, velocity *(Russian)* 78—85619
smokes, atmospheric, optical probing, homogeneous particle model appl. *(Russian)* 78—77328
soil-derived atmospheric dusts, particle absorption contributions to mass extinction coefficients 80—61896
solar radiative heating, in presence of aerosols 79—16665
solid aerosol collection in spouted bed, electric field effect 78—91019
solid particle concentration profiles in turbulent jet, laser Doppler anemometer meas. and theoret. calcs. 79—27686
solid particles, diffusive evaporation, laser spectrochemical analysis 79—92040
solid phase motion, large Reynolds no., carrying agent drag 78—79363
sonic agglomeration of c black aerosol particles 77—29411
soot conglomerate destruction dynamics in pulsed laser radiation field 80—58617
South America, PIXE system for air pollution meas. 77—49157
South Pole, particulate trace elements, conc. and size distrib. 79—79937
spark discharge generator for laser Doppler measurements in turbulent flames 80—59139
spectral attenuation of sunlight at Mauna Loa 80—41494
spectral photometry using compact spectrometer 79—2396
spectrometer using two-pulse Fraunhofer holography, fibrous particle motion anal. 80—58476
spectronephelometer, automatic scanning integrating, visible and IR spectra 77—79165
spherical particle phoresis in multicomponent gas mixtures 78—22446
spherical particles, collision with water drops, impaction and electrical effects 78—28272
St. Augustine volcano eruptions, airborne meas. and obs. 77—49053
St. Louis aerosol, variation of elemental composition with particle size 77—49137
stearic acid, laser spectrometer for submicronic aerosols, photoelec. determ. of conc. acid dispersity 79—54244
Stokes drag forces for small particles, kinetic corrections to aerosol gravitational collisional efficiency 80—95386
Stokes size of particles, automatic method 79—93096
stratiform clouds particles, meas. of local mean radii and concs. *(Russian)* 77—53158
stratosphere, aerosol and gaseous constituents from spacecraft solar extinction data, inversion retrieval 79—74961
stratosphere, aerosol conc. at Mildura, Australia following 1974 Fuego eruption in Guatemala 77—5276
stratosphere, aerosol conc. using iterative method from twilight polarization meas. 78—20464
stratosphere, aerosol layer, climatic effects, review 78—81331
stratosphere, aerosol layer visible and IR optical props. influence on global climate 77—2240
stratosphere, aerosol particle size distrib. meas. 80—51578
stratosphere, aerosols latit. vars. 79—58040
stratosphere, airborne lidar meas. during winter (1973) 77—33159
stratosphere, Aitken nuclei meas. with aircraft-borne instrument 77—64399
stratosphere, Aitken particles, nature and sources 77—87050
stratosphere, balloon obs. of particle layer injected by aircraft at 23 km 78—81283
stratosphere, change in nature of aerosol at 34°S 78—28286
stratosphere, detection, ground based techniques, laser usage 80—17390
stratosphere, dust meas., (1970-1977) 78—73445
stratosphere, electrical parameters and aerosols, meas. *(Japanese)* 80—31087

aerosols continued
stratosphere, environment monitoring system, benefit assessment 78—73507
stratosphere, fluorocarbon hazard to O_3 layer, assessment 79—79963
stratosphere, from Agung volcano eruption, solar radiation absorpt. estimation 77—87072
stratosphere, global content vars. rel. to fluctuations of solar radiation and temp. in troposphere 78—81327
stratosphere, global time vars. of aerosol burden and source considerations 77—25739
stratosphere, interaction of Cl and Cl_2 with H_2SO_4 and water, surface reactions at low temps. 79—79288
stratosphere, laser radar meas. *(Japanese)* 80—21810
stratosphere, long term vars. after Fuego volcano eruption, lidar obs. 79—16597
stratosphere, lower, aerosol microstruct. sounding with multifreq. lidar 80—56645
stratosphere, lower, simultaneous balloon meas. of elec. cond. and aerosols 77—73813
stratosphere, meas., southern hemisphere, time vars., rel. to 1974-75 volcanic eruptions 79—48551
stratosphere, microphysical processes affecting aerosol particles 78—7709
stratosphere, microstruct. from sounding by multifrequency lidar *(Russian)* 77—64374
stratosphere, Mount Agung eruption as test of glogal climatic perturbation 78—69440
stratosphere, multi-ion complexes, implications for aerosols and trace gases 80—61872
stratosphere, $NOHSO_4$ and $NOHS_2O_7$ identification in aerosols, rel. to N oxides pollutants removal 79—39795
stratosphere, O_3 and aerosol monitoring using orbiting photodetectors 77—78445
stratosphere, O_3 and Aitken nuclei conc. correl. over Americas 77—49141
stratosphere, optical props. and size distrib. effects on heating rates 79—12222
stratosphere, optical thickness meas. at Adelaide (35°S) 79—44248
stratosphere, particles physical state and nature of undissolved granules 78—28275
stratosphere, post-Fuego aerosol layer, lidar meas., radiative and thermal implications 77—56679
stratosphere, post-volcanic aerosol decay, lidar meas. 79—53444
stratosphere, remote anal. by differential scatter lidar system 78—69524
stratosphere, S hemisphere meas. by impactor and in situ single-particle detect. 78—73437
stratosphere, satellite monitoring systems, SAM II and SAGE 80—82082
stratosphere, steady-state aerosol model 79—53445
stratosphere, two-colour lidar meas. 77—25752
stratosphere aerosol, determ. of characteristic parameters *(French)* 80—8387
stratosphere aerosol, modification by supersonic transport and space shuttle operations, climatic implications 80—98408
stratosphere aerosol content var., rel. to atm. transparency and direct solar radiation 80—82035
stratosphere aerosol event, 1974-1975, balloon obs. of time development 77—45084
stratosphere aerosol layer, Earth zonal radiation balance perturbation 80—56602
stratosphere aerosol layer, simulated lidar return from one-dimensional model 79—44247
stratosphere aerosol meas. by solar occultation method 77—45090
stratosphere aerosol size distrib., lidar obs. at 0.6943 μm and 1.06 μm 77—41120
stratosphere and troposphere, obs. of condensation nuclei on circumpolar airliner flight 80—51475
stratosphere and troposphere SO_4^{2-} aerosol layer, form. and evolution model 80—21801
stratosphere lidar obs. at Menlo Park, California 77—21865
stratosphere particles, collection and analysis techniques 80—17306
stratosphere particles, detect. of ^4He rel. to extraterrestrial origin 77—56878
stratosphere particles, optical props., instrumentation and techniques for meas. 80—17389
stratosphere pollution, albedo and radiative equilib. temp. changes 77—45092
stratosphere sulphate aerosol, kinetics of growth by condensation in homogeneous medium *(Russian)* 80—94566
stratosphere sulphate aerosol layer, processes, models, obs. and simulations 80—109212
stratosphere sulphate aerosols, contrib. of OCS emissions rel. to climate 80—41524
stratospheric, causing errors in Umkehr vertical O_3 profile 79—70849
stratus clouds, shortwave radiative effects of unactivated aerosol particles 77—64382
submicrometre particle detector and size analyzer 79—75672
submicron aerosols, collection efficiencies of spheres, rel. to washout in atm. 78—81395
submicron particles, controlled generation *(Italian)* 77—48688
sulphate aerosol, estimated dry deposition vels. over E United States and surrounding regions 80—56507
sulphate and nitrate mixing ratios obs. near tropopause 80—61835
sulphate concentration, Southwestern Desert of US, X-ray emission anal. 80—8378
sulphate particle formation by heteromol. nucleation and condensation in cavities 80—26183
sulphates in atmospheric particulates, analysis 79—83685
sulphates in photochemical smog, atm. visibility reduction 77—21904
sunphotometer aperture effects on atmospheric turbidity meas. 79—84483
supercooled fog, −20°C, influence of aersol particle size on AgI ice-forming activity 79—53465
surface aerosols in Cape Verde Is., physical and chemical props. 78—85640
suspensions of charged particles, laminar tube flow, entrance deposition 80—59100
temperature and energy exchange in Earth's atmosphere 77—45082
thermal analysis for in situ detection of aerosol pollutants 77—37364
thermal collection of aerosol particles on larger liq. droplets 77—3867
thermal diffusophoresis of droplets of a liquid solution in a binary gas mixture 80—43766
thermal force, on aerosol particle 78—1724

aerosols continued

- thermal slip of binary gas mixture along spherical aerosol particle surface 78−34168
- thermophoreses velocity and coeff. of thermal slip of gases 77−7416
- thermophoresis, development of theory 79−55407
- thermophoretic deposition, from laminar-flow gas streams 77−58766
- thin flat, EM wave scatt. and absorpt. 80−91723
- Titan, optical props. and vertical distrib. of aerosols in atmosphere 80−46471
- Titan atmospheric aerosol distribution, constraint 79−96964
- trace constituents in Indian west coast SW monsoon aerosols 80−81967
- transuranic, online high sensitivity measurement system 77−65334
- transuranium oxides, uniformly dense aerosols prod. by gas phase neutralisation of acidic droplets 80−26427
- tropical atmosphere, influence of stratospheric aerosols on solar and longwave radiative fluxes 77−25743
- tropical N.Atlantic Ocean, aerosols water-soluble K, Ca and Mg contents 80−72598
- troposphere, aerosol mass conc. deduction from 1.06 μm lidar meas. 79−25323
- troposphere, aerosol monitoring using Spacelab lidar system 77−21876
- troposphere, effect on atmospheric IR cooling rates 78−88886
- troposphere, from dust storms, SW United States 79−20932
- troposphere, lower, seasonal vars. in aerosol vertical profiles *(Russian)* 78−16092
- troposphere, particle size distrib. skewness and mode radius relationships 77−45121
- troposphere, particles physico-chemical property models 78−92898
- troposphere, SO_4^{2-} aerosols chem. props. 78−96254
- troposphere, trace gases in summer, background levels in Greenland 80−72609
- troposphere aerosols having soil-derived component, commonalities in measured size distribs. 77−60454
- troposphere light scattering, particle shape influence 80−90220
- troposphere over equatorial N.Atlantic Ocean, dust conc. rel. to Sahelian drought 77−78356
- troposphere particulate matter, N_2O decomposition 79−16014
- troposphere sulphate aerosol burden, linear eight-box model for global S cycle 80−56506
- tropospheric, effect on surface and surface-atmosphere radiation budgets 80−17375
- tropospheric fallout fluxes of Pb, Cd, Cu, Zn, Ag in Antarctica and Greenland 79−58007
- turbulent coagulation in pipe flow 79−37385
- turbulent migration phenomenon 80−53836
- turbulent pipe flow, depend. of particle deposition velocity on particle inertia 77−35219
- two-layer spherical liquid particle with solid core, thermophoresis 79−39211
- ultradisperse condensational, formation by plasma-jet powder evaporation *(Russian)* 80−55721
- ultrafine particle size meas., diffusion battery anal. 79−92010
- ultrafine particles in gas, information on size, surface props. from photoelectron emission 78−68598
- ultrasonically produced aerosol droplet size rel. to liquid viscosity 79−47998
- unipolar diffusion charging in continuum regime 77−25319
- Uranus atmosphere, aerosol particles rel. to UV albedo 80−82295
- Uranus clouds, particle comp. 80−31253
- urban, Boston area, multivariate anal. for element sources identification 77−37357
- urban, characterisation and hazard assessment 77−41157
- urban aerosol, size-fractionated, C, N and O determ. by particle elastic scatt. anal. 78−81466
- urban aerosols, optically absorbing component identification as graphitic C 79−34939
- urban aerosols at St. Louis, pollutant source strength-rainfall relationships investigation 80−77059
- urban aerosols in Nagoya area, Si and Al concs. for atmospheric soil particles characterisation 80−26581
- urban air, total suspended matter estimation, comparison of three methods 77−37416
- urban atmosphere, thin layer brown haze form. 77−56685
- urban climate, model of aerosol effect 77−66978
- urban plume particulates collected on Anderson 8-stage impactor stages, chemical anal. 78−69433
- urban pollutant, size distrib. 78−3925
- urban troposphere, photochemistry, kinetic study 77−45058
- urban-suburban air pollutant transport, chemical and physical transformations 77−37399
- vaccine atomiser for liquid aerosol immunisation 77−81638
- vagal blockade effects on lung mechs. in normal man 80−8081
- Venus, atmospheric aerosol distrib. changes, 1972-75 period 77−64681
- Venus, cloud microstructure, optical props., H_2SO_4 atmosphere-aerosol study 80−72808
- Venus atmosphere, aerosol model 80−101545
- Venus atmosphere, B-layer and C-layer aerosols rel. to UV cloud model, polarimetric evidence 80−82250
- Venus atmosphere, cloud particles, Venera 9 and 10 nephelometric meas. 77−78695
- Venus atmosphere, H_2SO_4 aerosols characts. from isophotes, spacecraft obs. 78−81575
- Venus atmosphere, IR extinction meas. from Pioneer Venus IR radiometer expt. 79−48719
- Venus clouds, aerosol size distrib., coagulation sedimentation and turbulent mixing effects 77−71041
- Venus clouds, H_2SO_4 aerosol medium IR optical props. and spectrum 78−65526
- Venus clouds, particle size distrib. meas. 79−48717
- Venus stratosphere, aerosol layer discovery by Pioneer orbiter cloud photopolarimeter 79−48713
- virtual impactor aerosol separators, analytical study 80−42874
- virtual impactor for particle classif. and generation of test aerosols with narrow size distribs. 80−30626
- visibility in turbid media with coloured illumination 79−72489
- visibility var. over SW.United States, historical databases of pollution effects 80−21424
- visibility-reducing aerosols in Los Angeles air basin 78−16157
- volatile binary solutions, ion-induced nucleation 79−47992
- volatile particles, large-size, theory of photophoretic motion 77−9132
- volcanic, rel. to tropospheric mean temp. 77−33168

aerosols continued

- volcanic activity dust veil index, apparent periodicity 79−92514
- volcanic ash particles, influence of shape on atmospheric settling vel. 79−84364
- volcanic dust veils causing Earth surface temp. drops 80−85726
- volcanic eruption cloud dispersion in stratosphere, lidar and numerical models for Vulgan Fuego and Augustine 77−56682
- volcanic Fuego eruption, aerosol density, temp. and particle content determ. 80−90050
- volcanoes, airborne particles emissions meas. 79−2203
- vortex jet streams, impingement zone, particle motion soln. and expt. 77−65773
- wake of cylinder, local particulate vel. 77−11238
- water, propagation of intense radiation at 10.6 μm 80−5692
- water, pulsed laser radiation action pulsed laser radiation action 80−14378
- water aerosol, evaporation during transport through atmosphere *(Russian)* 79−88408
- water droplet aerosol interaction with EM radiation, temp. field and refractive index distrib. model 78−3899
- water droplet clouds, rate of evaporation, stability 79−52782
- water droplets suspended in turbulent flow, evaporation rate rel. to $Ca(CO_3H)_2$ soln. drops 79−90771
- Wilson Cloud form. by low altitude nuclear explosions, water aerosol and droplets characts. 78−53704
- X-ray absorption spectra for chem. characterisation of atmospheric aerosols 80−61501
- X-ray absorption spectra for chem. characterisation of atmospheric aerosols 80−72121
- X-ray fluoresc. anal. 78−85269
- X-ray fluoresc. anal. of loaded filters, X-ray scatt. appl. in absorpt. corrects. calcs. 78−7311
- α-emitting aerosols, on-line monitor 78−46236
- β-active, emission electrification in external field 78−83497
- β-active aerosol particles, stationary charge distribution 79−92581
- ^{99m}Tc labelled aerosol particles rel. to ^{81m}Kr ventilation imaging for lung function assess. 79−100716
- AgCl, solid monodisperse aerosols, in He jet system, for unstable nuclide transportation 79−22507
- AgI aerosol, studies of ice-forming activity, verification of theory 80−101406
- AgI aerosol particle size, struct. rel. to ice forming activity 80−61164
- AgI aerosol particles, influence of cryst. struct. on their ice-forming activity 79−16048
- AgI aerosols, particle size influence on cryst. struct. 80−2000
- AgI, ice forming activity, UV irrad. effect 80−71950
- AgI, ice nucleation at different supercooled fog temps. *(Russian)* 77−27983
- AgI, preliminary tests of cumulus cloud seeding technique 78−57352
- AgI surface, adsorption of water, effective pair pot. model 80−100394
- ^{7}Be aerosols content increase over Pacific Ocean during strong jet stream 77−78373
- ^{7}Be bearing aerosols mean residence time in troposphere 77−87018
- Br from vehicle exhausts, model for dispersion 77−37367
- C aerosol visibility vs. particle size distrib. 78−88911
- C particulate, airborne, photacoustic and absorption spectrum using tunable dye laser 80−4102
- C sphere aerosol, black smoke opacity, calc. variation with particle size and refr. index 79−72488
- CO_2 aerosol/hypersonic air stream interaction, gasdynamic CO_2 laser energy characts. 80−48211
- CO_2 laser action on wateraerosol, efficiency, optical thickness, water content 77−66774
- CS_2, aerosol form. by laser, kinetics study and photoreaction products chem. nature study 80−21324
- Ca-DTPA, effect of inhaled aerosol on long-term $Pu(NO_3)_4$ effects 77−66861
- $CaCO_3$ aerosols, coagulation rate meas. 79−96374
- Cd, metallic precipitates, crystallography dendritic origin of hexagonal prisms 79−66366
- Cd, Pb, Mn in particle size fractionated aerosols, flameless atomic absorpt. determs. 78−69434
- $^{144}CeO_2$, effects of repeated inhalation exposure, mouse obs. 80−104676
- $^{144}CeO_2$, inhalation exposed mice, toxicity, dosimetry and ^{144}Ce retention 80−89874
- ^{60}Co long-lived γ-emitting aerosols, max. allowable emission rate from nuclear power station 80−32532
- Cu, meas. in aerosol particles produced by ocean 79−58050
- CuS aerosol prepared by burning pyrotechnic mixture, crystallisation activity 78−96279
- Fe aerosol powders, oxidised, nucl. gamma reson. study *(Russian)* 79−1725
- Fe aerosoled fine particles, Mossbauer spectra 80−7223
- Fe, aerosoled ultrafine particles oxidation 80−21183
- Fe aerosols in atmosphere, source determ. by gamma-ray spectroscopy 77−41235
- Ga, liq. particles-$He(N_2)(CO_2)$(air), nonequilib. Laval nozzle flow calib., numerical soln. 77−75967
- HNO_3-water, homogeneous nucleation, relative humidity depend. 78−71846
- H_2O-droplet, CO_2 laser beam clearing process, transmission function ratios 78−88919
- H_2O-H_2SO_4 system, nucleation, aerosol form. 77−70327
- H_2O-H_2SO_4-ion aerosol particles, ultrafine, stratospheric form., ion-induced nucleation 80−72608
- H_2O-organic aerosol-n-heptane reverse-type micellar soln., neutron small-angle scatt. *(French)* 80−26059
- HSO_3^-, aerosols form. from SO_2 oxidation by O_3 in cloud droplets 78−44894
- H_2SO_4 aerosol, filter sampling of air, possible artifacts 80−82079
- H_2SO_4, aerosol, form. by flash photolysis of SO_2-gas mixtures 79−66307
- H_2SO_4 aerosol growth, kinetic model 77−37340
- H_2SO_4, aerosol particles props. in subsiding air over Japan 79−20986
- H_2SO_4 aerosol particle size measured by impaction method 80−31134
- H_2SO_4, aerosols form., expt. and theory 78−96256
- H_2SO_4, air pollution, new detector, aerosol mobility chromatograph 78−96297
- H_2SO_4 in atmosphere, heterogeneous reactions and role as tropospheric sinks 80−72612
- H_2SO_4 meas. in aerosol samples during METROMEX 79−100548
- H_2SO_4 secondary aerosol form. in urban atmosphere 77−33137

aerosols continued
H_2SO_4, secondary particles form. and growth, kinetic aerosol model 79−29492
H_2SO_4-H_2O, aerosol form., nucleation calcs. 78−31709
H_2SO_4-H_2O, vapour mixture, temp. depend. of nucleation, aerosol form. 77−86350
H_2SO_4-H_2O aerosols nucleation rate in presence of ionisation source 80−104464
H_2SO_4-H_2O droplets in atmosphere, equilib. size and comp., quick estimation method 79−66767
H_2SO_4-H_2O solution aerosol particles nucleation in stratosphere 77−56678
H_2SO_4-water, homogeneous nucleation, relative humidity depend. 78−71846
^{115}In aerosol generation technique for atm. tracer obs. 80−26190
KBr pellet spectroscopy, H_2SO_4 effect 79−88034
KCl, solid monodisperse aerosols, in He jet system, for unstable nuclide transportation 79−22507
^{85}Kr aerosol discharge devices, fabrication and use 79−1969
La_2O_3, aerosol, controlled production technique 78−76929
$Mg+O_2 \rightleftharpoons MgO+O$, shock-tube study of evap. and oxidation kinetics 80−16651
MnZn ferrite particles, mag. filtration from air streams 77−4945
$(NH_4)_2SO_4$, aqueous solns. and cryst., optical consts. meas. rel. to atm. aerosol props. 77−52034
$(NH_4)_2SO_4$, atm. particles conc. and size distrib., rural conditions 79−74564
$(NH_4)_2SO_4$, production under elevated temp. inversion in Cleveland Country, model 78−81397
NO_2+SO_2 aerosol, form. kinetics, irrad. by 488 nm light 78−40067
$^{15}N/^{14}N$ ratios in gaseous NH_3, NO_2 and NO_3^- in aerosols and precip. 78−44896
Na, aerosol effects on ionisation detector characts. 79−49243
Na aerosols and fires, expts., LMFBR safety anal. data 77−71650
Na burning, aerosol release, temp., O conc. depend., LMFBR safety anal. 77−83049
Na, form. and sedimentation, physico-chemical and semiempirical relations, review *(Czech)* 79−30956
Na pool fuel vapour and aerosol transport in HCDA 79−13455
Na-fire aerosol filtration in nuclear reactors 80−68853
NaCl, aqueous, fixation and microscopic sizing 80−16734
NaCl as natural sea salt nuclei and laboratory controlled recrystallization 78−24337
NaCl, monodisperse aerosol, preparation and growth 77−86389
NaCl monodisperse aerosols, appl. in cloud droplet nucleation expts. 80−82003
NaCl particle generation 79−16606
NaCl, single cubic particles, suspended in laser beam, optical size determ. 78−33673
NaCl, solid monodisperse aerosols, in He jet system, for unstable nuclide transportation 79−22507
NaCl soln., no particle fragmentation during evaporation 77−91189
NaCl-gas reactions, atmospheric, in situ TEM studies 80−104544
Na_2O aerosol gravitational fallout rate, validation of computer code for fast reactor accident anal. 80−18535
Na_2O aerosols, aerodynamic props. 80−23011
Na_2O, behaviour in closed chamber under thermal convection flow in LMFBR accident 77−57723
^{95}Nb inhalation in beagle dogs, deposition and retention, dosimetry 78−35959
P containing particles, deposition velocity over southern Lake Huron 79−83666
P, red, atmospheric aerosol, absorption to extinction coeff. ratio meas. 80−90217
Pb compounds identification in urban aerosols, rel. to health hazard 78−44991
Pb dry deposition onto snow surface 77−37288
^{210}Pb, atmospheric fluxes determ. from soil profiles 79−2346
^{210}Pb from nucl. explosions in environment 78−21774
PtI_4, X-ray fluoresc. anal., particle size correction method 78−48705
Pu compounds, release from contaminated burning Na, LMFBR safety evaluation 77−23224
Pu containing, charge distribution from mixed-oxide reactor fuel fabrication lab. 79−5181
Pu fumes, aerodynamic and dissolution behaviour of laser-ignited droplets 79−13438
Pu isotopes, maximum permissible inhalation values 79−70640
$Pu(NO_3)_4$, long-term effects of inhalation, influence of inhaled Ca-DTPA 77−66861
PuO_2 aerosol, acute inhalation, predictive model of early mortality 80−36028
$^{238,239}PuO_2$ inhalation toxicology in Syrian golden hamsters 77−86552
$^{238}PuO_2$ particle inhalation, pulmonary tissue local dose computation 79−92385
$^{239}PuO_2$, in vivo solubility in rat lung 78−28093
$^{239}PuO_2$ inhalation, rat pulmonary connective tissue modification by internal α-irrad. 79−92302
PuO_2-UO_2-Na aerosol, from LMFBR HCDA conditions, characterisation 78−94104
^{239}Pu and ^{233}U droplets burning in air, aerosol generation investig. rel. to inhalation hazards 79−67959
^{239}Pu, characterisation inside safety enclosures of mixed fuel fabrication facility 79−13501
$^{239}PuO_2$, inhalation exposure of miniature swine 79−11976
$^{239}PuO_2$ inhaled by rhesus monkeys, cytogenetic and other biological effects 80−108968
Ra A (^{218}Po) adsorption to monodispersed aerosol 80−32535
Rn daughters in atmospheric air, efficiency of HV-70 filters for sampling 80−108827
Rn, vertical diffusion coeffs., wash-out and deposition effects 77−68726
Rn-Th monitor for earthquake prediction research 78−73532
S aerosol, of S. American troposphere 80−67401
S, and trace metal content of nonurban and marine aerosols, PIXE anal. 77−49136
S compounds, techniques for chem. comp. determ. 78−95976
S containing aerosols, continuous meas. and speciation by flame photometry 78−95974
S containing aerosols, continuous in situ meas. by flame photometry and thermal analysis 78−96296
S containing aerosols, physical characts. 78−96284

aerosols continued
S, determ. in submicrometric aerosols, SO_2-denuder appl. for continuous meas. 79−8699
S dry deposition onto snow surface 77−37288
S, in atmosphere, meas. via compact X-ray fluoresc. analyser 78−68971
S pollutants in atm., conf., Dubrovnik, Yugoslavia (Sep. 1977) 78−96281
S pollutants in atm., conf., Dubrovnik, Yugoslavia (Sept. 1977) 79−20965
S, SO_4^{2-} and related species, sampling and anal. of atm. aerosols 78−96283
S, total conc. meas. using pulsed electrostatic precipitator and flame photometer 78−95975
SO_2 and sulphates, residence times under non-steady-state conditions 80−77092
SO_2, heterogeneous conversion to SO_4^{2-}, rel. to urban air pollution 78−80789
SO_2 mass spectrometric obs. in stratosphere 77−33200
SO_2 oxidation in aqueous aerosols rel. to conversion to sulphates in dispersing plumes 77−70806
SO_2 oxidation over atmospheric aerosol, absorption over V_2O_5 and C 77−70811
SO_2, oxidation via OH radical, rel. to atm. fate of HSO_x radicals 79−62559
SO_2 photo-oxidation products, smallest particle size detectable by condensation nucleus counters 78−24364
SO_2, photooxidation, aerosol evolution, rel. to air pollution 78−81392
SO_2 to sulphate conversion processes in atmosphere 77−37389
SO_2-alkane-H_2O gaseous mixture, photoinduced nucleation and quantum yields 79−96348
$SO_2+H_2O+O_2(N_2)(Ar)$, condensation nuclei form., ion polarity and age depend. 79−39220
SO_4 aerosol, geographical extent in Midwestern and Southern USA 77−49145
SO_4^{2-} aerosol form., CO effect, smog chamber expt. 79−74925
SO_4^{2-} aerosol form. and growth in stratosphere 79−5604
SO_4^{2-} aerosol layer in stratosphere, formation and evolution model 80−17327
SO_4^{2-}, air pollution, large-scale spatial and temporal distrib. 79−20981
SO_4^{2-}, airborne particles, size meas. and chem. comp. by diffusion sampling 78−45007
SO_4^{2-}, atm. hazes and long-range pollution transport, satellite detect. 79−20975
SO_4^{2-} containing aerosols, dynamics, review 78−96286
SO_4^{2-}, individual submicron size particles detect. method 78−95973
SO_4^{2-}, particle size depend. on relative humidity 79−20906
SO_4^{2-}, quantitative determ. in aerosol particles 79−20474
$^{35}SO_2$ interaction with atmospheric particulates 77−41137
SiO_2, electron spectroscopic chemical analysis and X-ray $K_{\alpha 1}$ line spectra *(Russian)* 77−66775
SnO_2 aerosols, Lamb-Mossbauer factor *(French)* 80−81375
$^{99m}TcO_4^-$, diffusible aerosol inhalation for imaging pulmonary ischaemic lesions 77−37047
Tn decay products, ats. and ions, adsorption probability on submicron particles 79−39803
U, radiation exposure assoc. with surface U mining 77−64140
U, specific α radioactivity meas. rel. to size using aerosol centrifuge 79−76255
UO_2, condensed vapour following core disruptive accident, particle-size distribs. using first-generation model 78−13295
UO_2 fission vapourised fuel, aerosol close in sampling, accident safety 79−49779
U_3O_8, ^{235}U enriched, characterisation using solid state track recorders 78−17538
Zn, condensation in heat-pulse cloud chamber, prismatic and spherical particle form. 77−9135
Zn, metallic precipitates, crystallography dendritic origin of hexagonal prisms 79−66366
^{95}Zr from Chinese atmospheric thermonuclear explosions, appl. to stratospheric transport parametrisation 79−2342

aerospace
see also aerospace computing; aerospace control; aerospace instrumentation; aerospace propulsion; aerospace simulation; aerospace test facilities; aircraft; ground support systems; space research; space vehicles; terrestrial atmosphere
acceleration effects in women after 15 days bed rest, fluid and electrolyte shifts 77−48881
aeronautical meteorology, progress and challenges 78−53692
astronaut visual working capabilities, rel. to external conditions logical approach *(Russian)* 77−5088
aviation and astronautics, conf., Tel Aviv and Haifa, Israel, May 1976 77−31319
computerised planning in ESA 80−4223
economics, forward-looking financial planning in ESA 80−4221
economics, investment planning in ESA 80−4222
European Space Research and Technology Centre (ESTEC) 78−69651
kinematic tools, vectorial mechanics and variational method 79−30218
O'Neill space colonies, prospects for realisation 77−87230
patrol balloon, long duration flight *(Japanese)* 79−80218
plasma coating technology appls. 78−44026
radiation protection for space colonies 77−86651
space colonisation, preliminary cost benefit anal. 77−87231
space colonisation, two new propulsion systems 77−87232
space rescue involving human vacuum exposure, possibilities 77−44762
space technology and scientific satellites, conf., Rome, Italy (Mar. 1977) 77−82107
spacecraft launch planning using Markov theory on meteorological data 77−45091
Spacelab and Space Transportation System, management and programme 77−45280
systems and electronics, IEEE conference, Washington D.C., USA 26-29 Sept (1976) 77−5420

aerospace applications of computing *see aerospace computing*

aerospace computer control
see also aerospace computing
coverseal particle detection using X-ray 78−21313
flexible CAMAC based data system for Space Shuttle scientific instruments 79−45603
Ionosphere sounding satellite control, automated system 77−60572

aerospace computer control continued
- Ionospheric Sounding Satellite, automated control system *(Japanese)* 77–78607
- Ionospheric Sounding Satellite, command system *(Japanese)* 77–78609
- Ionospheric Sounding Satellite, summary of control centre *(Japanese)* 77–78606
- Ionospheric Sounding Satellite, telemetry receiving system *(Japanese)* 77–78610
- Ionospheric Sounding Satellite control, tracking system *(Japanese)* 77–78608
- IR Astronomical Satellite (IRAS), on board computer, design 79–80191
- IR Astronomical Satellite (IRAS), on board computer software 79–80192
- remote programming, real time computers, space flight on-board expts. *(German)* 78–53791
- SEASAT-A satellite radar altimeter design 77–5415
- SIRIO satellite dynamics and control in geostationary orbit *(Italian)* 77–82108
- star tracker, microprocessor controlled CCD, STELLAR design 78–53792
- type U CAMAC controller for the Spacelab multi-crate, multi-processor system 79–45604
- UK-6 satellite, computer command system 79–25440
- unmanned (or manned) vehicles, automatic rendezvous with space station 80–77249
- Viking lander remote diagnostic techniques 78–57426
- Viking Orbiter uplink command generation and validation simulation 77–22040
- wind tunnel system, for architectural and industrial testing, Oxford University 78–22443
- X-ray astronomy balloon, microprocessor-controlled payload 79–62716

aerospace computing
- *see also aerospace computer control*
- 23rd International Aerospace Instrumentation Symposium tutorial, Las Vegas (1977) 78–12074
- ablation, multidimens., embedding in inverse heat cond. problem, finite difference method 78–94508
- aerodynamics of axisymmetric body, in Newtonian hypersonic flow, optimal control initial states conversion 78–4474
- aerospace instrumentation, conference, Las Vegas, Nev., USA, (May 1977) 78–12075
- aerospace systems and electronics, IEEE conference, Washington D.C., USA, 26-29 Sept (1976) 77–5420
- aircraft noise exposure forecast contours, retrieved using algorithm *(Japanese)* 80–19153
- artificial satellite attitude determ. system, Taiyo (1975-014A) *(Japanese)* 77–17319
- artificial satellite nonconvex solar battery panel mounting, optimal ang. determ. 79–39291
- Astronomical Netherlands Satellite, orbit prediction 79–21139
- axisymmetric transonic flow around slender bodies, hybrid computation 77–42861
- conformal representation of arbitrary multiconnected airfoil sections 78–30308
- cyclic thermoplasticity finite element analysis by subvolumes 77–42749
- data management systems, remotely sensed space data 79–92600
- design, unsteady boundary layers with reversal and separation 78–75163
- duct of arbitrary cross section, parabolic procedure for three-dimens. compressible viscous flow prediction 79–94716
- dynamic discharge arc driver, computer-aided circuit simulation 77–24219
- flow, unsteady two-dimensional subsonic, transonic and supersonic flow calcs. 77–55021
- fuselage min. weight design subjected to pure torsion 78–1582
- gas turbine annular vortex shedding acoustic resonance analysis *(Japanese)* 80–14526
- interplanetary missions, trajectory analysis computing, ESTEC program 79–21129
- Ionospheric Sounding Satellite control, data recording and anal. system *(Japanese)* 77–78611
- Jupiter orbiter propulsion anal. 78–45189
- Kalman filter algorithms, use of Givens transformation techniques, for orbit determ. 78–4473
- laminar trailing edge stall, triple-deck eqns. num. soln. 77–55020
- large deflection anal. of tail-wheel struct. of light aircraft 78–83272
- laser transit anemometer system, for measurements in supersonic flow 80–10332
- lifting wing calcs., spanwise integrations, computational economy improvement 78–71344
- microprocessor, SBP9900, radiation test 77–75002
- Navier-Stokes equations solution method for viscous effects in transonic flow 77–55023
- nuclear reactor, rocket propulsion, optimisation problem, calculus of variation 80–27694
- orbit transfer of rocket between elliptic orbits, globally optimal solns. 78–8236
- orbital transfer using two fixed-magnitude impulses 78–81518
- parachute opening flowfield computation, using He bubble technique, high-speed photography and computer graphics appl. 78–30374
- periodic satellite coverage pattern generation computer graphic system 77–37496
- planetary boundary layer equations soln. using sensitivity analysis 77–54957
- plasma sheaths of satellite and spherical probe, static and dynamic behaviour, simulation 77–25907
- reinforced organic composite, graphite, or C-C, ablation, mathematical modelling 79–41564
- rocket propellants, thermodynamic evolution, extension of Huff's method 78–75054
- Salyut-6 spacelab, data acquisition and logging system incl. speech 80–61979
- satellite location by tone-code trilateration 77–9653
- satellite navigation, Chebyshev approximations for compression of Ephemerides 80–61993
- shear modulus of superplastically formed sandwich cores 79–32286
- shells of revolution under axisymmetric and asymmetric loadings, linear elastic dynamic analysis program using finite element analysis *(Japanese)* 80–106719
- shock wave reflection, regular to Mach transition, Monte Carlo simulation 77–75936

aerospace computing continued
- solar power satellite concept, electronic systems 79–92065
- sonic boom, nonlinear propag., including asymm. effects, numerical soln. program 77–72326
- space shuttle reentry, unsteady nonequilib. chemically reactive flow, parallel computation 78–47065
- Spacelab data processing system, 125 MS computer *(French)* 77–78594
- streaming, of vel. and temp., in oscill. boundary layers 78–83358
- subsonic and supersonic aerodynamics, SOUSSA computer code 78–71352
- subsonic flow higher order panel method for general analysis and design appl. 77–55022
- supersonic flow about elliptic cones with large semiaxis ratio, num. soln. method 77–58729
- supersonic flow around blunt bodies with combined cross sections, num. comput. 77–58728
- supersonic wave drag of planar singularity distributions 78–83430
- test meas. symposium, San Diego (1976) 77–41284
- thin shell mixed method formulation, large displacement and dynamic analysis 77–35032
- transonic axisymmetric pot. flow around inlets, Cartesian mesh soln. 77–72323
- transonic flow, bow shocks comput. method 77–55027
- transonic flow, far-field boundary conditions solution 77–55024
- transonic flow, steady three-dimensional, finite vol. soln. of Euler eqns. 77–55028
- transonic flow, three-dimens., flow analysis using STAR-100 computer 79–94644
- transonic flow numerical calculation methods and problems 77–58723
- transonic flow over two-element airfoil systems, num. comput. of inviscid irrot. flow eqns. 77–55026
- transonic flow problems 77–58725
- transonic nozzle flow, rotational, relaxation solution 78–30312
- unsteady aerodynamics of lifting surfaces using computer, book contrib. 77–51076
- unsteady aerodynamics research, data acquisition using minicomputer 80–10337
- viscous flow over flat plate, comput. method developments 77–54970
- wind tunnel testing, conference, Rhode-St-Genese (1976) 77–27634
- wind tunnel transonic test section wall interference minimisation *(French)* 77–27550

aerospace control
- *see also air traffic control; attitude control*
- aeromanoeuvering orbit transfer vehicles, for space transport system 78–4060
- aeroplane, deformable control systems, numerical anal. of lateral dynamic stability 78–51057
- aircraft power plants noise control, mixer nozzle appl. 77–42662
- artificial satellites, conf., Rome, Italy (Mar. 1978) 78–96384
- astrodynamics conf. (Provincetown, MA, USA, June 1979) 80–82583
- astronaut transfer in weightlessness, biomechanical model 78–96106
- astronomy satellite SAS-3 general description 77–2324
- aviation and astronautics, conference, Tel Aviv (1977) 78–81517
- avionic multiterminal data link, fibre-optic interconnection system 78–46805
- coordinate-parametric control of nonstationary spacecraft, multidimensional asymptotically stable adaptive systems appl. 80–101522
- cruise engines optimal thrust in interorbit flights, analytical determ. 78–4069
- Drive and Ascent Satellite, orbit control for lower ionosphere research 80–77252
- dynamics problems, gradient method for optimal control 78–69638
- flight path, navigation strategy for Mariner Jupiter/Saturn 1977 mission 77–5411
- Geos 1 and 2 satellites, keV plasma expt., real-time ground-based computer control 80–41695
- gravitational physics experiments in space 80–8896
- gravity gradiometers for improved orbit estimation 80–8523
- International Space Hall of Fame Dedication Conference, Alamogordo, New Mexico (Oct. 1976) 77–56814
- interstellar travel, optimum transfer in uniform motion 78–20614
- Lambert's problem, recursive formulation for enhanced computation time 77–89016
- Mars descent trajectories using parachute-rocket system for soft landing 78–69640
- Mars descent vehicle, aerodynamic braking arc control algorithm 79–84629
- Mars entry vehicle, lifting spacecraft control and ballistics 78–16264
- Mars orbit emplacement using atmospheric braking, control algorithm 78–69639
- Mars probe, optimal atmospheric entry trajectories with two-dimensional control 77–91400
- oblate planet orbiter, optimal low-thrust takeoff from orbit 77–60580
- optimisation algorithm for spacecraft flight trajectory between Earth and Moon 80–72754
- optimum low-thrust multiple rendezvous between inclined orbits 78–4086
- orbit transfer, three burn, optimal, nonlinear programming trajectory simulation 77–84133
- orbital transfer, optimal, low-thrust, limited power, elliptical orbits 78–4087
- Pioneer 11 post-Jupiter trajectory midcourse manoeuvre sequence for Saturn targeting options 78–7857
- proportional counters, thin-window, rocket-borne, gas press. control system 78–17512
- SAS-3, power and thermal subsystems 77–2325
- SAS-3 delayed command system 77–2327
- SAS-3 X-ray astronomical satellite, programmable format telemetry system 77–2328
- satellite, gravitational stabilization system, optimum parameters 77–41280
- satellite, optimal trajectory-meas. program and meas. error effects 77–53409
- satellite eccentricity oscills., compensation with stabilizer 78–69643
- satellite flexibility experiment design, control/flexible structure interaction 77–70970
- satellite rendezvous trajectories determ., autonomous system 77–53392
- shuttle reentry trajectory optimisation, perturbation method appl. 77–67021

- **aerospace control** continued
  - soft landing guidance algorithms based on terminal control principles 78—73602
  - Solar Maximum Mission satellite, hard X-ray imaging spectrometer control 79—80194
  - sounding rocket attitude estimation using star sensor data 79—25435
  - Space Shuttle orbiter, remote manipulator system 79—21150
  - space vehicle motion in vicinity of collinear libration point, statistical estimates in control problem 78—4067
  - spacecraft, rotation control by mass ejection 77—41278
  - spacecraft charging, neutralisation via electron emitter *(Japanese)* 80—94673
  - spacecraft detumbling, using movable telescoping appendages 77—54868
  - spacecraft final descent vel. control in Mars atmosphere, autonomous navigation algorithm 77—29620
  - spacecraft four-impulse planetary landing and return under time constraints 79—62711
  - spacecraft minimum time Earth-Mars orbit transfer, conjugate gradient method 77—87244
  - spacecraft optimal accel. with electroreactive engine with bound on thrust vector 77—53393
  - spacecraft relative motion around orbiting station, guidance method 78—16263
  - spacecraft trajectory optimal correction, pulse count constraint, combinatorial method 77—64598
  - spacecraft trajectory optimisation using closed soln. of constant thrust-accel. motion 77—25926
  - spaceship, fission-engined series-staged, overall payload-optimal control 77—2320
  - starship, single-stage constant-power, optimal exhaust vel. programming 78—20613
  - three-impulse min.-time orbital transfer generation, numerical method 78—73607
  - transonic flow, unsteady force and moment alleviation by control devices in airfoil 78—71362
  - two-terminal trajectories, global anal., geometric and kinematic family struct. 78—4085
  - vehicles in close near-circular orbits, optimal multimomentum transfers 77—41290
  - Venera 9 and 10, flight control 77—78598
- **aerospace engines**
  - 23rd International Aerospace Instrumentation Symposium tutorial, Las Vegas (1977) 78—12074
  - aircraft, atmospheric pollution, reduction measures *(French)* 77—81994
  - aircraft engine inlet guide vanes, acoustic fatigue due to intake flow distortions 80—53542
  - aviation and astronautics, conference, Tel Aviv (1977) 78—81517
  - gas turbine annular vortex shedding acoustic resonance analysis *(Japanese)* 80—14526
  - gas turbine wideband combustion noise obs. *(Japanese)* 80—11890
  - GEOS, apogee motor, technical features 78—4071
  - jet engine, air-breathing 79—7172
  - jet engine noise meas., flowing duct sound separation probe 78—13878
  - jet engine noise source location, polar correl. technique 77—62105
  - jet exhaust noise, prediction of in-flight levels 78—87178
  - laser-air reaction motor, using laser breakdown of air, expt. model *(Russian)* 77—7106
  - noise, high response fluctuating pressure meas. probe 78—13855
  - noise reduction modelling, discrete freq. noise 80—106652
  - nuclear rocket engine, gaseous-fuelled, reactivity effects 77—54354
  - rocket engine plume radiation, measurements in space simulation chamber 79—97437
  - supersonic jet noise spectrum, discrete component 78—9493
  - turbo-jets, fan noise reduction by single- and double-wall barriers 80—87648
  - turbojet, internal noise generation 80—87644
  - turbojet and turbofan, duct noise radiation through a jet flow 80—23834
  - Viking Mars lander, hydrazine terminal descent engine, thermal design 77—87234
  - Ni alloy protection against hydrogen embrittlement, by Cu electroplating 80—76416
- **aerospace ground equipment** *see ground support equipment*
- **aerospace instrumentation**
  - *see also aircraft instrumentation; Langmuir probes*
  - 23rd International Aerospace Instrumentation Symposium tutorial, Las Vegas (1977) 78—12074
  - airborne system, for vertical air vel. meas. 80—77159
  - amplitude stabilised scanning generator for probing system for plasma research 77—56807
  - artificial satellite gamma telescope, Kosmos-461 79—97480
  - AUOS-MAGIK satellite, instruments and measurements *(German)* 79—88562
  - conference, Las Vegas, Nev., USA, (May 1977) 78—12075
  - conference, nuclear and space radiation effects, San Diego, Calif., USA (July 1976) 77—20376
  - cosmic-ray fluxes, expt. determ. 78—85778
  - cryogenic instrumentation for spacecraft 79—54138
  - cryogenic systems for spacecraft 80—86319
  - design and development for space environment 78—4077
  - dewar, liq. He, for space expts., long-term cooling feasibility 77—33323
  - electron emitter, appl. to spacecraft charge neutralisation *(Japanese)* 80—94673
  - electronic systems, explanation of basic principles for layman 79—29972
  - electronic units development, on-board, used in rockets and satellites *(Spanish)* 77—91401
  - electrostatic discharge monitoring, on Meteosat spacecraft 80—17463
  - engine noise, high response fluctuating pressure meas. probe 78—13855
  - fibre optic connector system characteristics, aerospace user's viewpoint 78—46804
  - gravity gradiometers for improved orbit estimation 80—8523
  - Hadamard transform X-ray telescope, characts. *(Japanese)* 80—94714
  - HF generator for supplying quadrupole mass spectrometer *(Rumanian)* 77—29628
  - holographic head-up display 79—50266
  - IEEE conf., scintillation and semiconductor counters and nucl. power systems 77—54389
  - induced background radiation, gamma and X-ray meas. 78—85821
  - International Space Hall of Fame Dedication Conference, Alamogordo, New Mexico (Oct. 1976) 77—56814
  - IR Astronomical Satellite (IRAS), on board computer, design 79—80191
- **aerospace instrumentation** continued
  - IRAS telescope, maintaining temp. at 2K using superfluid He dewar 79—54143
  - Kuiper Airborne Observatory, far IR photometer 79—66926
  - Landsat multispectral scanner, calibration of thermal band 79—97438
  - laser gyro progress 78—46704
  - laser ranging systems, NASA applications 78—81527
  - liquid-trap heat pipe thermal diode for cooling components 80—27292
  - Lyman α camera, for high resolution solar Lyman α filtergrams 80—82323
  - magnetometer, ring-core type, for space vehicles, geomag. fluctuations high-sensitivity obs. *(Japanese)* 80—94671
  - Meteosat imaging payload, functional aspects 78—36424
  - Meteosat in-orbit calibration, appl. to lunar thermal props. obs. 80—17511
  - Meteosat spacecraft, elec./mech. configurations 78—36423
  - microprocessor, SBP9900, radiation test 77—75002
  - modular system, standardised, for space scientific instruments 77—71005
  - Multipurpose Utility Pointing and Stabilisation System *(Italian)* 77—82114
  - NASA Lear Jet, liquid He cooled grating spectrometer for far IR astron. obs. 79—66925
  - operation in adverse environments, conference, London (1976) 78—189
  - particle telescopes, anisotropies meas. by multiple telescope system 77—82103
  - radiation coloration and bleaching of Schott optical glasses temp., time depend. 77—19981
  - radioactivity induced in scintillator materials 78—85822
  - rocket geomagnetic aspect horizontal component sensor *(Japanese)* 78—24421
  - SAS-3, power and thermal subsystems 77—2325
  - SAS-3 X-ray astronomical satellite, programmable format telemetry system 77—2328
  - satellite borne microwave sensors, remote sensing of Earth physical parameters 79—80060
  - satellite image plane scanner for earth observations 79—97436
  - satellite thermal imager for Defense Meteorological Satellite Program 79—97435
  - satellite-gyrostat reorientation, optimal attitude control 80—61980
  - scatterometer for investigating underlying surfaces, optimization of characts. 80—67436
  - scientific instrument development problems and solns. 77—82111
  - SEASAT-A satellite project, for oceanographic research 79—84496
  - SEASAT-A satellite radar altimeter design 77—5415
  - Shuttle/Spacelab mission, instrumentation requirements and provisions 77—70972
  - Shuttle/Spacelab missions, low power CAMAC and NIM modular system for spaceflight use 77—70973
  - Skylab colour TV as primary data recording system 77—60569
  - solar instruments for Solar Maximum Year review 80—90404
  - solar stratospheric station, automatic, construction, selection of variant *(Russian)* 79—96913
  - solid cryogens usage in space research *(French)* 77—134
  - space optics, conference Huntsville, Alabama (1979 May 22 to 24) 80—62385
  - space optics, imaging X-ray optics workshop, Huntsville, Alabama (1979 May 22 to 24) 80—62384
  - space probe, automatic setting of range of amplifying path 77—67019
  - Space Shuttle Orbiter wideband PCM tape recorder 77—64614
  - Space Shuttle project avionics 80—17465
  - space suit cooling, automatic control of human thermal comfort 80—109046
  - Space Telescope pointing control fine guidance subsystem design 80—82201
  - spacecraft instrumentation radioisotope thermoelectric generator 78—85824
  - spacecraft IR detector, cooling down to 85K using solid cryogen cryostat 79—54122
  - spacecraft systems, evaluation of acceptance testing 79—16797
  - Spacelab Picpab expt., phenomena induced by charged particle beams obs. 80—17443
  - Spacelab scanning IR telescope, refrigeration using 79—54141
  - star tracker, microprocessor controlled CCD, STELLAR design 78—53792
  - Sun position sensors using fibre optic selector 77—49262
  - telescope, double roll-out solar array appl. 79—52939
  - telescope, low-cost, pointing control system 77—5430
  - telescope mirrors, surface configuration control by conc. loads appl. 79—94317
  - test meas. symposium, San Diego (1976) 77—41284
  - Voyager Sun sensor, CdS detector, radiation effect test, simulator 79—23644
  - CdTe detector, Cl doped, for reentry vehicle appl., development electronics 77—45288
  - ^{4}He, superfluid, properties in zero gravity, appl. as cryogen on spacecraft 77—31822
- **aerospace propulsion**
  - *see also aerospace engines*
  - air-scooping nuclear-electric propulsion for advanced orbital transportation missions 78—45188
  - attitude and orbit control systems, conference, Noordwijk (1977) 78—65480
  - cruise engines optimal thrust in interorbit flights, analytical determ. 78—4069
  - Drive and Ascent Satellite, on-board propulsion subsystem rel. to lower ionosphere research programme 80—77252
  - Earth resources rocket, enriched air propulsion system 77—2259
  - electrostatic/EM ion collection techniques, interstellar appls. 77—70974
  - EM slingshot system for space propulsion 78—77462
  - flows with heat addition, aerospace appls. 77—916
  - future space travel and astronauts, technical problems *(Italian)* 79—80244
  - GEOS, auxiliary system, technical features 78—4071
  - impulsive plasma accelerators, tests under cosmic conditions 77—53399
  - interstellar ramjets infeasibility 78—81520
  - interstellar rocket, laser powered, mass ratio and instantaneous efficiency 79—21134
  - ion beam injection into magnetosphere, from solar power satellite engine 80—82149
  - ion-propelled space tug optimisation 78—53798

aerospace propulsion continued
- jet engine, air-breathing 79—7172
- large payloads, launching into Earth orbit by intense relativistic electron beams 79—21135
- laser-powered interstellar ramjet 77—70975
- low-thrust propulsion, rel. to optimal takeoff from orbit about oblate planet 77—60580
- MHD, by laser radiation absorption 77—3998
- MPD arcjet, effect of strong mag. field on physical processes 77—89324
- near-wake phenomena, with and without external compression, axial and radial air injection effects 80—10273
- nuclear, NASA's thermionic technology program, 1978 status, objectives and plans 79—48159
- nuclear, out-of-core thermionic power conversion system 79—48160
- nuclear, UF$_6$ gas fueled reactor development, NASA-sponsored program 79—49829
- nuclear gas-phase rocket motor, MHD rot. of conducting fluid in crossed field *(Russian)* 78—47059
- nuclear reactor, rocket propulsion, optimisation problem, calculus of variation 80—27694
- nuclear rocket engine, gaseous-fuelled, reactivity effects 77—54354
- rocket exhaust plumes, short-duration, rapid-scan instrumentation for spectrally and spatially resolved radiance measurements 80—13164
- rocket nuclear reactors, laminar flow, temp.-viscosity induced instabililities in gaseous heated channel 77—18689
- rockets, early stages in theory of propulsion and dynamics 78—16
- satellite flexibility experiment design, control/flexible structure interaction 77—70970
- series-staged fission powered starship, direct propulsion 78—61706
- solar electric propulsion stage applications 78—4059
- solid rocket fuel, new law for crack propagation 80—53712
- space colonisation, two new propulsion systems 77—87232
- Space Shuttle external tank for main propulsion system 77—73922
- staged thermonuclear microexplosions prospects 77—91405
- starship, flight optimisation via time plus energy minimisation criterion rel. to powerplant 79—44330
- student experiment, rocket propulsion project 77—9839
- thermionic conversion appl., USSR activity and 1978 status, comparison with USA status 79—48158
- turbine cascades, rotating annular, test facility of DFVLR, measurement and evaluation 80—14866
- U plasmas, fissioning, for space vehicle power, propulsion, terrestrial appls. 77—3145

aerospace simulation
- *see also aerospace test facilities*
- active noise reduction system for ear defenders 78—92748
- aerofoil stall props. with acoustic flow control 80—23991
- aircraft engine exhaust noise, flight effects, use of Bertin Aerotrain 78—13847
- Ariane launch vehicle, model firing tests, acoustic field, heat flux, press. distrib. 78—4062
- ASSESS II Spacelab mission simulation results *(German)* 78—69649
- attitude motion of Skylab for revisit mission, digital computer simulation 79—16794
- AURORA machine studies of air chem., cond. and boundary layer 78—32144
- complex structure fatigue life prediction using critical location concept 78—59348
- dynamic discharge arc driver, computer-aided circuit simulation 77—24219
- Earth resource satellite attitude meas. and control requirements 78—65482
- facilities, conf., Shrivenham, England, (Sept. 1977) 77—80251
- flight simulator viewing lens, triplet design 80—74457
- glass particles impacting on metal barriers, piercing, stony meteorite simulation 78—89043
- holographic Pancake Window reflective system 80—1165
- human motion and force sensory mechanism model 80—8094
- hypersonic shock tunnel, development for aerospace simulation 79—41777
- ionosphere, simulation of satellite flight using synthesised plasmas *(French)* 78—16269
- ionospheric flight conditions simulation 79—16796
- jet flight simulator, shear layer refraction and facility-to-flight corrections for noise meas. 78—13845
- jet noise, flight effects, use of Bertin Aerotrain 78—13848
- laboratory investigations 79—58217
- large-aperture holographic visual simulator 80—102679
- long arc simulated lightning attachment testing using 150 kW Tesla coil 80—70074
- micrometeoroid impact, laboratory simulation 78—57510
- modal test methods and applications 78—79252
- moving atmosphere simulation by rotating phase plate 80—79021
- multiple radiation effects facility for testing materials exposed to space environment 79—48644
- optical beacon/tracker system simulation, turbulent atmospheric propag. 79—53525
- orbit transfer, three burn, optimal, nonlinear programming trajectory simulation 77—84133
- payload model, modal confidence factor in vibration testing 79—27607
- planetary atmosphere probes, flight characts., scale model expts. 78—7854
- planetary spacecraft, Jovian environment simulation, materials hardening and mass shielding 80—36472
- plasma chamber, elec. field meas. with double probes, atm. appl. 79—64909
- plasma diffusion in space simulation beam-plasma discharge 79—60108
- plasma sheaths of satellite and spherical probe, static and dynamic behaviour, simulation 77—25907
- RF target simulator using acousto-optical device 80—102843
- rocket engine plume radiation, measurements in space simulation chamber 79—97437
- satellite geomagnetic substorm charging simulation 79—96886
- satellite plasma sheaths, streaming instabilities, elec. equilib., one-dimens. particle simulation 77—22036
- satellites integration and test phase optimisation *(French)* 80—17464
- Skylab simulator visual displays and training for joint obs. programmes 77—60566
- Skynet, system-generated EM pulse testing with exploding-wire photon 79—25433

aerospace simulation continued
- Space Shuttle lightning current distrib., circuit modelling and exptl. verification 78—49293
- Space Shuttle Orbiter, flow angle and mass flow rate meas. in unknown flowfield 79—77306
- space shuttle reentry, unsteady nonequilib. chemically reactive flow, parallel computation 78—47065
- spacecraft, meteoroid impacts effect on attitude motion, analytical model 78—73608
- spacecraft trace contaminant concentration, toxokinetic/toxodynamic model 79—83952
- star simulator design 78—85814
- starry sky simulator, optical system and cell unit 77—60575
- step-stare spaceborne optical system image motion compensation 80—90322
- step-stare spaceborne optical system smear compensation by focal plane manipulation 80—82172
- subsonic jet noise, prediction method for flight effects 78—1502
- transonic flow, wind tunnel wall and viscous effects, numerical simulation 77—27552
- turbulence model development expts. with numerical simulations 77—27551
- turbulent jet mixing noise, in-flight simulation expt. 78—1501
- variable area flowmeter calibration, gas flow modelling 78—14115
- visual simulation and image realism, seminar, San Diego, USA (Aug. 1978) 80—3639
- wind tunnel particle and droplet field holography 79—76642
- wind tunnel transonic test section wall interference minimisation *(French)* 77—27550
- wind tunnel water droplet size distrib. interferometer 79—80673

aerospace test facilities
- *see also wind tunnels*
- acoustic emission instrumentation and applications 77—33322
- acoustic environmental testing 79—3853
- aerodynamic heat transfer meas. using transient techniques 77—80258
- aerothermodynamic test techniques at AEDC von Karman gas dynamics facility 80—14863
- aircraft jet noise reduction test facility 77—845
- airframe material defectometry, quantitative test specifications *(German)* 80—89427
- attitude and orbit control systems, conference, Noordwijk (1977) 78—65480
- balloon-borne slow-scan TV camera performance test *(Japanese)* 80—12635
- cardiopulmonary stress test data acquisition and control systems 79—79673
- environmental testing, climatic, features of McKinley laboratory 79—16798
- fatigue-critical structure, optimal periodic proof test based on cost-effective and reliability criteria 77—63838
- hypersonic re-entry vehicle heat transfer meas. in separated laminar base flow 78—61708
- instrumentation symposium, San Diego (1976) 77—41284
- IR measurement facility, low-background large-aperture, design 79—21125
- IR measurement facility, low-background large-aperture, performance 79—21126
- jet noise reduction test facility 77—11096
- laser Doppler velocimeter for high speed combustion flow meas. 77—80255
- laser testing methods, holographic interferometry 77—7039
- microphone selection and use for engine and aircraft noise meas. 79—90104
- modal test methods and applications 78—79252
- multiple radiation effects facility 79—48644
- NASA Long Duration Exposure Facility, for space testing and qualification of optical instrums. 79—5725
- noise technology laboratory facilities, Boeing Commercial Airplane Co. 79—18603
- non-metallic materials, flaw detection by tomodensitometry *(French)* 79—20295
- nosetip ablation holography in 10 MW plasma arc facility 78—20621
- nosetip recession meas. using implanted radioactive sources, error analysis 78—16272
- satellite geomagnetic substorm charging simulation 79—96886
- satellites integration and test phase optimisation *(French)* 80—17464
- solar array sample accelerated thermal cycling facility 79—96458
- solid propellant stress transducer evaluation 80—81245
- space qualification of optical instruments, using long duration exposure facility 78—85826
- Space Shuttle external insulation, acoustic emission inspection 78—16276
- variable area flowmeter calibration, gas flow modelling 79—90353
- Viking Lander environmental test programme 77—56810
- Viking lander remote diagnostic techniques 78—57426
- Voyager Sun sensor, CdS detector, radiation effect test, simulator 79—23644

a.f. amplifiers *see audio-frequency amplifiers*

AFC *see automatic frequency control*

afterglows
- $1s_5$ level density meas. by fluorescence, effect of dye laser intensity 78—67474
- adsorbate phosphor-silica gel substrate, oxygen quenching anomaly of afterglow 77—77275
- air, afterglow plasma, interaction with glass, Cu, steel walls, calorimetric method obs. 78—14177
- air, high-current electron beam interaction causing press. reduction 80—28867
- air, press. effects on spectral features excitation 78—38563
- 3,4-amino-N-methylphthalimide, intermolecular orientational relax. 'upwards', fluorescence spectra displacement *(Russian)* 79—78748
- Balmer Hβ line profiles, mag. field effects on afterglow plasma 80—1849
- carbazole, crystalline, room temp. afterglow 78—27314
- decaying plasma, nonequilib. props. during afterglow modulation by acoustic waves 80—103144
- dense plasma afterglow, theory 78—9882
- density decay in diffusion-controlled atomic-gas plasma 79—7442
- diagnostics, instantaneous triple-probe method for direct display of plasma parameters in low density continuum plasma 80—84000
- diffusion cooling, electron energy balance 78—5852
- drift waves, short-circuit effects 77—35431

afterglows continued

- electron energy distrib., radial variation 78–71570
- electron energy distrib. function, expt. determ. by electronic instrum. 79–32840
- electron energy distrib. meas., Langmuir probe characteristics 77–80350
- electron energy distribution function, probe meas. in Ar afterglow 79–60195
- electron energy distribution function in afterglow discharge 79–10725
- electron temp. relax. in afterglow plasma 78–51280
- electron-ion recombination coefficient in afterglow, continuity equation, numerical solution 80–28598
- flowing afterglow plasma ion source, appls. 80–87955
- fluorescence de-excitation function recording, one-quantum method, error anal. *(Russian)* 77–65925
- free plasma column, afterglow on switching off UHF power *(Russian)* 77–15265
- functions, multistop method investig., dead time registration effects *(Russian)* 79–10719
- glass, colour centre form. by UV irrad., afterglow, thermolum. and EPR obs. 78–10047
- higher diffusion modes, in early afterglow 78–1802
- hollow cathode stationary afterglow apparatus, for at. props. studies 78–63619
- inert gas, excimer form., VUV emission obs. at low press. 80–38755
- inert gas afterglow, anisotropic props. 79–1362
- inert gas afterglow plasmas, cyclotron emission and electron thermalisation 77–84545
- inert gas discharge, electron-atom bremsstrahlung, time decay 78–63620
- inert gas recombination afterglow, spectral line shapes 80–940
- inert gases, metastable atom diffusion, state decay, VUV obs. from discharge afterglow 80–44061
- ion composition of plasma of pulsed discharge in He, H_2^+ current time evolution 80–54046
- ionic recombination in flowing afterglow, at. and mol. ions 79–1361
- kinetic reactions, pulsed afterglow technique obs. in Ar-II plasma 80–48854
- lower hybrid waves, propag. in toroidal plasma 80–83927
- magnetically confined afterglow/at. beam, technique for α ion+atom cross section determ. 77–34750
- magnetised plasma, in dielectric chamber with thermionic emitter, enhanced diffusion 79–64901
- marine green alga, Ulva fenestrata, afterglow in the ms and ds intervals of attenuation 80–104636
- metal vapour laser, afterglow electron energy balance 79–76678
- molecular photodissociation, recomb. afterglow, quenching var., activator penetration to region inaccessible to quencher 80–64813
- multistop method of afterglow functions investig., dead time influence on meas. accuracy 80–1874
- $N_2^*+NO(H_2O)$, vibr. excited quenching temp. depend., flowing afterglow 77–54595
- nonisothermal plasma electron ensemble, nonstationary behaviour, kinetic description 80–59171
- Penning collision processes, review *(Japanese)* 79–64092
- phosphor, stationary recombinatorial luminesc. without thermal transitions, model 79–8193
- phosphors, containing O, excitation spectra of recombination 78–10952
- pulsed DC discharge afterglow, electron conc. and temp., double-probe technique 78–63632
- pulsed discharge, formation of He_2 in afterglow 77–15259
- radiation escape kinetics, radiation captured by plane optically thick layer 80–95593
- RF discharge plasmas, mag. field effects, probe and microwave meas. 77–7594
- shock-radiative recombination rate in afterglow of He plasma 79–4205
- simulation of plasma afterglow by computer code GLOWCODE 77–39480
- spectral line profile of low-press. afterglow plasma in mag. field 80–6285
- water, vapour RF discharge, low press., afterglow, spherical plasmoid, optical diagnostics 78–38568
- Z-discharge plasma, low-temp., time evolution, diagnostics 79–37548
- Ar, 1s states deactivation by N_2 and SF_6, pulsed afterglow, kinetic absorption obs. 77–50398
- Ar, afterflow stability boundaries, plasma oscillation modes in mag. field 78–38486
- Ar, afterglow, pulsed discharge, acoustic oscills. in emitted radiation 77–89309
- Ar decaying pulsed discharge plasma, acoustic waves density modulation 80–103143
- Ar, electron-atom bremsstrahlung continuum, afterglow decay *(German)* 78–83626
- Ar, line radiation of plasma in early afterglow 80–38745
- Ar, low press. discharge afterglow, dissoc. recombination, microwave diagnostics 78–9876
- Ar, metastable $^3P_2$ deactivation in afterflow, plasma characts. 78–55769
- Ar, metastable state production, microwave and DC discharges in flowing afterglows 78–46463
- Ar, spectra and microphotograms, dissociative recombinations 78–26365
- Ar, stationary afterglow obs. of singly charged atomic ions, three-body rate coeffs. 80–38757
- Ar-Ti hollow cathode afterglow, energy transfer mechanisms and excited metallic ion prod. 80–43857
- $Ar+Ar(^3P_2)(^3P_0)$, flowing afterglow metastable decay rates, diffusion, two- and three-body rate consts. 78–73027
- $Ar+Kr(^3P_2)$, flowing afterglow metastable decay rates, diffusion, two- and three-body rate consts. 78–73027
- Ar+methane, CH chemiluminesc. in flowing afterglow 78–64839
- $Ar+N_2$, N_2 molecule, formation of $C^3\Pi_u$ and $B^3\Pi_g$ in early afterglow 79–34305
- $Ar+N_2$, pulsed microwave discharge, early afterglow and radiative transitions, Penning ionisation 78–9874
- $Ar+Xe(^3P_2)$, flowing afterglow metastable decay rates, diffusion, two- and three-body rate consts. 78–73027
- $Ar^{*+}+Kr$, flowing afterglow, energy transfer reaction and quenching rates 80–23529
- $Ar^*(3p^54p)_i+Ar(^1S_0)$, collisional population transfer rate coeffs., 300K 79–10177
- BaS:Cu, thermoluminesc. and decay 78–80426
- Br_2, thermal electron dissoc. attachment rate consts., meas., in flowing afterglow 77–10773
- C afterglow laser, recombination-pumped 77–50657

afterglows continued

- CO, $a^3\pi$ state, IR radiative decay of vib. levels 77–30870
- CO-He-O_2, species concentrations in glow discharge and afterglow, mass spectra, laser conditions 78–14241
- CO_2, press. effects on spectral features excitation 78–38563
- CO_2:He:N, glow discharge instability 80–6313
- CO_2-He, species concentrations in glow discharge and afterglow, mass spectra, laser conditions 78–14241
- CS+He, Penning ionisation, $CS^+(B^2\Sigma^+\rightarrow A^2\Pi_i)$ fluoresc., flowing afterglow 80–14197
- CaF_2, doped, colour centre form. by UV irrad., afterglow, thermolum. and EPR obs. 78–10047
- CaS, phosphor, tunnel luminescence *(Russian)* 78–72577
- $CaWO_4$, phosphors, energy storage, afterglow decay and thermolum. meas. 77–12422
- Cl_2, thermal electron dissoc. attachment rate consts., meas., in flowing afterglow 77–10773
- Cs-He afterglow, spectral emission from excited Cs ions, 380-750 nm 79–82116
- CsI:Tl single crystal gamma-optical converting screens, factors influencing relative afterglow intensity 79–8173
- Cu/CuCl double pulse laser, dissoc. pulse, afterglow, and laser pulse model 80–91775
- Cu-vapour-He laser discharge, metastable decay rates 79–86164
- F_2, thermal electron dissoc. attachment rate consts., meas., in flowing afterglow 77–10773
- $Ge(^3P_0)+N_2O$, reaction rate const. meas., in flowing afterglow 77–77731
- H^- affinity radiation, theoretical study of negative absorption 80–38001
- H_2, electron energy-loss spectra in afterglow, ground state vibr. conc. 77–31012
- H_2 molecular lines, in H_β region, in low press. afterglow discharge 79–60199
- H_3^++XCN, flowing afterglow, rate const. meas. 77–40533
- $H_3O^+(D_3O^+)$ plasma, dissociative ion electron recombination, rate coeffs. 80–63747
- $H_3O^+(H_2O)_n$, ion clustering, diffusion, flowing afterglow obs. 77–12799
- $H_3S^++HCN\rightleftharpoons H_2CN^++H_2S$, equilib., rate coeffs. and proton affinity, flowing afterglow 78–56885
- He, afterglow, intermediate press., plasma discharge parameter time depend. calc. 79–19102
- He afterglow, Rydberg states collisional radiative transfer, He^+ electronic recombination 77–62401
- He, afterglow of low-press. glow discharge, recombination processes 78–26366
- He, afterglow of pulsed discharge, elec. and optical meas. 78–26329
- He afterglow plasma, $He(2^3S_1)+e\rightarrow He(1^1S_0)+e+KE$, rate const., electron energy distrib. 78–71571
- He, afterglow plasma, interaction with glass, Cu, steel walls, calorimetric method obs. 78–14177
- He, afterglow produced by microwave surfaguide, spectroscopic diagnostic, electron and He_2 rot. temp. 80–44042
- He, cryogenic, recombination plasma decay *(Russian)* 79–4104
- He discharge, high-pressure, rapid formation of He_2 $a^3\Sigma_u^+$ and $b^3\pi_g$ molecules 79–37571
- He, electron energy distrib. and collisions during decay, peculiarities 78–63621
- He, excited state formation from He_2^+ in afterglow, theory 79–22802
- He, flowing afterglow, N_2, CO, CO_2, N_2O collisionally excited neutral and ionic emission 77–51248
- He I 4^3D, ^3F-2^3P line struct., in low-press. linear discharge 79–14523
- He, low-press. weakly ionised magnetoplasma, acoustic wave generation 80–44059
- He, plasma, afterglow and inertial expansion, numerical soln. of relax. kinetics 77–27769
- He plasma, stepwise excitation, electron energy distrib. and density at metastable states 77–84413
- He plasma in electron beam-excited discharge, atm. press., relax. obs. and model 79–37569
- He pulsed arc, Thomson scatt. diagnostics 80–24297
- He pulsed discharge, collisional electronic and rot. relax. of mol. He_2 77–61784
- He pulsed discharge, He_2 mol. formation in early afterglow, time-resolved spectra 78–63585
- He^+, He_2^+ and metastable He and He_2 densities in afterglow, mass spectroscopy 77–24221
- He-Cd, Cd^+ excited state prod. by Penning and charge exchange reactions 77–15252
- He-Cd mixture, Penning ionis. and nonreson. charge exchange in afterglow 79–72414
- He-H plasma, H_3^+ ion density decay, mass spectral obs. 77–3987
- He-Hg afterglow plasma, time resolved double probe study 78–18444
- He-Hg pulsed discharge afterflow, metastable He+Hg inelastic collision 78–50627
- He-Ne, afterglow of low-press. glow discharge, recombination processes 78–26366
- He-O microwave discharge afterglow, O_2 metastable emission bands obs. 79–64015
- $He+CS_2$, metastable atoms, energy transfer processes 80–83466
- He+He, (2^3S) and (2^1S) metastable states, direct and assoc. ionisation rate consts. in afterglow, electron energy spectra 79–13812
- He+Ne, afterglow, metastable state energy transfer, spectra 80–43167
- He+OCS, emission spectra in He afterglow 80–87139
- He+water (cyanomethane), afterglow, excitation and quenching reactions, optical pumping 78–35690
- He_2 high press. afterglows, reviews 80–64823
- $He(2^3S)$, bi- and ter-mol. deexcitation reaction rate coeffs. meas. in afterglow 79–36748
- $He(2^3S)$, quenching rates meas., in pure afterglow 77–75206
- $He(2^3S)+H_2O(H_2S)$, energy transfer processes, reaction products, UV and visible obs. in flowing afterglow 78–85138
- $He(2^3S)+Ne(Ar)(N_2)(CO)(CO_2)(CH_4)$, high press. afterglow, bi- and termolecular de-excitation rates 77–27168
- $He(2^3S_1)+Na(K)(Rb)(Cs)$, Penning ionis. in stationary afterglow 78–42184
- $He(3^3S)$ decay rates in high-press. afterglow 79–41898
- Hg+He, afterglow, $Hg^+(7^2P_{1/2}, 7^2P_{3/2})$, excitation processes, rate consts. *(Russian)* 78–29848
- $Hg_2(Hg_3)$, violet emission, formation and decay kinetics, luminesc. time resolved spectra 79–76464

afterglows continued
$Hg(6^3P_0)+Hg(6^3P_2)$, line excitation and population decay in afterglow 80−74242
$KCl:Eu^{2+}$ crystals, photostimulated afterglow investigation at room temp. 80−108259
Kr afterglow plasma, electron energy distrib. funtion 80−38748
Kr, afterglow spectra of pulsed discharge, levels populated by dissociative recombination 78−83640
Kr, Kr-N_2, metastable Kr atoms, spectra, collisions 77−427
Kr microwave afterglow, Kr_2^+ dissoc. recombination coeff., electron temp. depend. 78−30501
Kr, stationary afterglow obs. of singly charged atomic ions, three-body rate coeffs. 80−38757
Kr-N_2 plasma, afterglow ion prod. and loss processes 77−11401
$Kr^+ + 2Kr \rightarrow Kr_2^+ + Kr$, reaction rate const. in afterglow period 77−9044
$Kr^*(Kr^+)+NF_3$, rate consts., electron attachment coeffs., flowing afterglow 78−13578
Mg ($^3P_1$) metastable atom afterglow quenching rate consts. with various mols. 77−6720
$Mg(^3P)+K(Ca)$, energy transfer and excimer form. in flowing afterglow 77−60049
N, ($2p^3\ ^2P^0$) state, form. and depletion in N afterglow 79−49951
N afterglow laser, recombination-pumped 77−50657
N afterglow plasma, diffusion and recombination, microwave cavity expts. 79−90479
N, glow discharge instability 80−6313
$N+N \rightarrow N_2$, recombinational afterglow spectra, 10-300K 78−44355
N_2 afterglow, chem. reactions rel. to plasma props, appl. to toluene polymerisation 80−3346
N_2, afterglow, short-lived, electron and ion density enhancement obs. 78−63625
N_2, afterglow plasma, interaction with glass, Cu, steel walls, calorimetric method obs. 78−14177
N_2, B^3pi_g state vibr. levels, obs. in Lewis-Rayleigh afterglow 77−6797
N_2, catalysis and quenching by SF_6 78−51376
N_2 discharge plasma, radial distrib. profile of atom conc., Lewis-Rayleigh afterglow radiation 77−89312
N_2, glow discharge, ionis. mechanism 78−13613
N_2, Lewis-Rayleigh afterglow, spectrum 77−61757
N_2, Lewis-Rayleigh afterglow spectrum 79−64938
N_2, light intensity radial distrib. current and press. depend. *(German)* 77−11434
N_2, mol. excitation, in glow discharge and afterglow 78−63623
N_2, pink afterglow, ionisation and ion conversion mechanisms 78−63624
N_2, Rayleigh-Lewis and pink afterglows, mechanisms 78−63622
N_2-H_2 mixture, glow discharge, ionisation and excitation obs. 78−67505
$N_2+Ar(Xe)$, $\Lambda^3\Sigma_u^+$ state energy pooling in flowing afterglow, Herman IR system 80−83503
$N_2+N_2^+$, first negative bands, excitation cross-section calcs. 77−68100
$N_2^+(B^2\Sigma_u^+)$, $N_2(C^3\Pi_u)$ and $N_2(C'^3\Pi_u)$ molecules, emissions obs. in yellow N_2 afterglow 80−63649
NH_4^+, in afterglow, electron recomb. coeffs. mass spectrometric meas. 77−6927
NH_4^+, mutual neutralisation, with simple and clustered positive (negative) ions 78−44372
$NH_4^+.(NH_3)_n$, in afterglow, electron recomb. coeffs. mass spectrometric meas. 77−6927
N_2O-He, species concentrations in glow discharge and afterglow, mass spectra, laser conditions 78−14241
$N_2O+He(He^+)$, in afterglow, $N_2^+(N_2O^+)$ optical emission obs. 79−68251
N(^{4}S) recombination rate in Lewis-Rayleigh afterglow 79−58968
Na-Ne-Ar, low-pressure discharge, AC operated, time-resolved afterglow 77−43099
$Nd_xLa_{1-x}P_5O_{14}$, laser properties 79−22957
Ne, 1s atom prod. by recombination, press. depend. 78−59716
Ne, 2p levels prod. by dissoc. recomb. in afterglow, recomb. coeffs., level population 80−43855
Ne, $2p_1$ level relax. and populations of $1s_2$ and $1s_4$ in afterglow 78−9111
Ne, $2p^53s^3P_2$ to ground state, electron collisions of the second kind, rate consts. 79−27090
Ne afterglow, recombination processes, microwave quenching 79−14624
Ne afterglow plasma, electron energy distrib. function 78−63587
Ne, collisional transfer coeffs. between 2p levels, in afterglow, laser excitation obs. 80−43856
Ne, diffusion, collisions, decay freqs., fluoresc. obs., calcs. 78−59715
Ne, early afterglow, electron temp. at few torr press. *(French)* 77−4013
Ne, electron-atom bremsstrahlung continuum, afterglow decay *(German)* 78−83626
Ne, excited atoms reactions in pure afterglow, plasmas using resonance absorpt. spectrometry 80−33835
Ne, low press. discharge afterglow, dissoc. recombination, microwave diagnostics 78−9876
Ne, low-press., atom densities of first excited state 80−38750
Ne, negative afterglow, pulse excited, at. spectral lines, microwave quenching 78−63591
Ne, temporal decay, electron distrib. function and macroscopic parameters relax. 78−18374
Ne, Townsend discharge afterglow, decay rate of metastable ats. 80−44011
Ne-He and Ne negative afterglows, microwave quenching and recombination processes, Ne spectral emission 77−80307
Ne-He DC glow discharge electron density decay, microwave cavity obs. 78−91167
$Ne+CS_2$, metastable atoms, energy transfer processes 80−83466
$Ne^+ + Zn$, charge exchange and Penning ionisation in pulsed discharge afterglow 79−7007
$Ne_2^+ + e$, in recombination afterglow, line intensity decay complex struct. 79−7503
O/NO afterglow, absolute N_3 conc. determ. in NaN_3 thermal decomp. 79−100351
O_2-He afterglow, $O_2(C^1\Sigma_u^-, C^3\Delta_u, A^3\Sigma_u^+)$ generation from at. recomb. fluoresc. obs. 79−31576
$OH^- + O$, $OH^- + CO$, reaction rates, mechanism, flow discharge chemilum. obs. 77−52610
$SF_5^- + SF_3^+$, ion recombination, flowing afterglow, cross section meas. 77−44473
$SF_6^- + SF_5^+$, ion recombination, flowing afterglow, cross section meas. 77−44473
α-SiC, afterglow stimulated by IR radiation *(Russian)* 80−89066

afterglows continued
Sn hollow cathode laser, emission obs. from Sn II, I transitions 80−106509
Xe, afterglow, $6s_{12}$ metastable atom density decay rate 78−63612
Xe afterglow, $6s'(^1/_2)_0$, $6s'(^1/_2)_1$ at. states, collisional relax., population decay 78−63617
Xe, afterglow, metastable atom deactivation, electron collision effects 77−23441
Xe, line transition probabilities, in afterglow plasma, light absorpt. obs. 77−30807
Xe, pulsed discharge, visible line afterglow emission obs., excimer form. 80−38754
Xe, radiation imprisonment of $1s_4$ resonance line 79−82115
Xe, radiative and collisional deexcitation of reson. states, absorpt. and emission obs. 80−38742
Xe-N_2, afterglow, $6s_{12}$ metastable atom density decay rate 78−63612
Xe_2^+, dissoc. recomb. in afterglow, rate coeff., excited state prod. 77−46647
Zn afterglow diffusion coeff. for metastable Zn atoms 77−23542
$Zn_4O(BO_2)_6$:Tb, phosphoresc. study *(Spanish)* 80−16105

AGC *see automatic gain control*

age (Earth) *see geochronology*

age determination, radioactive *see radioactive dating*

age hardening *see precipitation hardening*

ageing
see also precipitation hardening; strain ageing
acrylonitrile-styrene copolymer melts, rheological behaviour *(German)* 77−51012
adhesives, thermosetting acrylic, electron beam curing 80−16634
age temperature shifting rel. to phenomenological theory of annealing and precipitation hardening 78−15428
Al alloy, type AK4-1T1, effect of high temp. ageing, on endurance of thin walled joints 78−80570
Al alloy AK4-1, acoustic investigation of ageing 79−34083
alloy, ageing-type, single cryst. deform. and hardening 78−23716
alloy, overaged and dispersion hardened, dislocation bowing computed from Orowan relations 77−19949
alloy, role of anisotropy in elec. resist. of Guinier-Preston zones 77−36515
alloy, struct. transform. during ageing, book contrib. 78−11199
alloy, with correlated system of second phase particles, X-ray and electron scatt. *(Russian)* 77−59738
alloys, disordered, residual resistivity due to clustering, ageing effects 80−65521
alloys, radiation effects on ageing and precipitation, review 80−29956
Alnico 5, two-phase separation during ageing, Mossbauer study 80−7533
anisotropic viscoelastic ageing materials, linear irreversible thermodynamics and phenomenological consts. 77−14922
austenite solid soln., decomposition, effect of struct. of initial state *(Russian)* 77−48442
austenitic stainless steel, 18 Cr-11 Ni, directly aged, nucleation of $M_{23}C_6$ carbides *(Polish)* 78−52806
austenitic steel, ageing after deform. in pre-martensitic state, internal friction meas. *(Russian)* 77−77477
austenitic steel, hardened by thermomechanical treatment with ageing, influence of stabilisation on mech. props. *(Russian)* 77−52356
austenitic steel, mechanical properties, effect of high temp. thermomechanical treatment and post-deform. ageing *(Russian)* 78−39809
brass, high-speed strain effect on struct. and props. *(Russian)* 77−59855
brass, martensitic transform., short range order effect 79−61586
α-brass, quenched, secondary defect form. during ageing, TEM obs. 78−88482
β-brass, spinodally decomposed, morphology and characts. 80−60863
Brightray S, lattice contraction during ageing 80−3030
bronze, sintered, mech. props. 77−28839
butadiene-styrene latexes, ageing *(Polish)* 79−70098
cable insulation for nuclear power station, deterioration testing *(Japanese)* 80−27743
capacitor, ceramic, $BaTiO_2:La_2O_3$ and $BaTiO_3:La_2O_3.3TiO_2$, permittivity ageing obs. *(Korean)* 80−25325
cathodoluminophor, nature of ageing 78−10994
cellulose fibre, gamma-irrad., and storage effects on props. *(Russian)* 80−61121
cellulose-PAN copolymer, luminesc., ageing effect 78−64401
ceramic/metal layer adhesion mechanism for metallization of electronic ceramics, elec. props. *(German)* 80−76381
class 1E electronic equipment qualification, ageing evaluation using Arrhenius techniques 79−45361
composite insulating materials, fatigue behaviour, influence of superposition of elec., mech. and environmental stresses 80−97590
creep modelling incorporating initial strain and ageing 80−58939
creep theory, thermodynamic pots. *(Russian)* 78−63318
creep theory for ageing bodies, with growing slit 78−63329
creep theory problems for ageing bodies with growing slits and cavities 80−69678
Cu-Co, dil., rotational hysteresis of Co fine particles 78−23301
CW stripe lasers, thermal-impedance ageing characteristics 80−64018
diamond-metal strip, strength props. 79−61678
dielectric materials, anal. using equiv. circuits *(Bulgarian)* 77−66467
Duralumin, effect of alloy purity and ageing on fracture mechanism, and resultant toughness 79−5049
E-glass fibre strength, effect of forming and ageing atmos. 78−92283
electrochemically formed layers, kinetic and structural consequences 80−61109
Elinvar, Cr addition effect on modulus of elasticity and thermoelastic coeff. 77−90387
enamel slips, control of rheological props. 79−29136
endurance limit, ageing effect *(Japanese)* 79−20077
epoxy resin insulation, adapted models selection problems for electric ageing *(German)* 80−89365
ester-imide varnishes, electroinsulating, thermal resist. *(Polish)* 78−84014
fission reactor system reliability prediction, appl. of Bayes eqn. 77−67797
fluoroplastics, heavy charged particle detectors 79−26821
Geiger counter, self-quenching, anode surface changes with ageing 80−58025
gelatin film, deuterated, IR absorpt. spectra, heat treatment and ageing *(Russian)* 78−39621

ageing continued
glass, ageing use, photothermal processing, sorptive and luminescence props. *(Polish)* 78—11250
glass fibre reinforced Al alloy, formed by hot extrusion, heat-treatment 77—24988
glass fibre reinforced cement, review of reinforcing theory, ageing, stress/strain relations 78—44165
glass fibre reinforced plastic greenhouse sheets, ageing behaviour, natural and artificial weathering *(German)* 80—81226
glass fibre reinforced plastic laminates, strength and deformability, artificial ageing effect 80—60893
glass fibre reinforced plastics, ageing by boiling in water, effect on physicomech. props. 80—60892
glass fibres, types E and A, surface composition, effect of ageing, reduction, exam. using X-ray photoelectron spectroscopy 79—20223
glass optical fibres, UV-cured, epoxy-acrylate coated, environmental effect on long-term strength 78—5582
glass reinforced polyamide 6, fatigue strength after heat treatment, ageing and coating of Al-containing lacquer *(Polish)* 80—89347
graphite fibre filled polyimide composite prepreg laminates, room-temp. ageing effect 80—81093
graphite-epoxy composite, hydrothermal ageing 77—21189
graphite-epoxy resin, hydrothermal ageing 77—52367
Hastelloy, C-276, H transport rel. to ageing treatment 80—75384
Hastelloy, H_2 embrittlement in H_2S environments, impurity segregation effects 80—71724
Hastelloy N, Si additions, comp. of eta carbide after ageing 78—52816
hereditary solid, optimum form for system with reinforcing elements *(Russian)* 79—81727
high alumina cement concrete, quality, thermal anal. investig. 79—15912
high molecular weight polyethylene for HV cables, characterisation using size exclusion chromatography 80—66897
high-temp. behaviour of inelastic metals 77—4830
Incoloy 800, and 800H, proposed specification changes 79—43298
Incoloy 800, mechanical props., heat treatment and appl., conf., Petten, Netherlands (March 1978) 79—43296
Incoloy 800, review of structural charact., heat treatment and comp. effects 79—43297
Incoloy 800, use up to 550°C, creep ductility 79—43369
Incoloy 800H, high temp. low cycle fatigue, ageing and cold working effect 79—43277
Incoloy 800H, high temp.-low cycle fatigue, ageing and cold working effect on initial stress/strain curve 79—47720
Incoloy 903, microstruct. and effect of H_2 charging 77—86143
Inconel 600, effects of ageing and misorientation on intergranular corrosion *(Japanese)* 79—79158
Inconel 617, microstruct., mech. props., thermal ageing effect 77—36557
Inconel alloy 718, exam. of struct., properties and continuum synthesis of ductile fracture 78—76736
Inconel X750, positron annihilation study of ageing and creep 80—29824
insulation corona discharge, ageing process, expt. 77—43095
iron, pure, tensile deformation behaviour under high pressure *(Japanese)* 80—16381
island films, coalescence kinetics, ageing rate, Kahlweit approx. *(Russian)* 80—59838
Langmuir multilayer assembly film structure, stability on ageing 77—39740
loaded column, creep and ageing optimisation problems stress-strain state *(Russian)* 79—46226
lubricating oil, ageing parameter determ. by IR spectroscopy *(German)* 80—27360
martensite ageing, influence of neutron irradiation *(Czech)* 78—84859
metal carbide, magnetron-sputtered, solar selective absorbing surfaces 79—92079
metal layered contacts, low temp. diffusion *(German)* 80—6538
metal strips, welded, aged, reduction of deformations *(Russian)* 80—97508
metallic films, vapour deposited on polymer, ageing, adhesion, elec. cond., electrochem. pot. *(Russian)* 79—33362
metallic glasses, atomic clustering exam. using positron annihilation methods 77—84655
metals, quenched, vacancy cluster form. process 80—92706
Metglas 2826 ribbon, voids formation during crystallisation 80—108428
MOS structs. formed on stain films on Si wafers, electrophysical props. *(Russian)* 78—52095
multilayer winding around hollow cylinder, creep and ageing optimisation problems stress-strain state *(Russian)* 79—46226
new particle phase spatial distribution, computer calcs. *(Russian)* 79—83202
Ni-Cr-Mo-Ti-Al, quenching and ageing effects on props. of type 36NkhTYuM8 79—52275
Nimonic, ageing, role of quenched-in vacancies 77—52363
Nimonic 105, overaged, creep and fatigue crack growth 77—86138
Nimonic 80A, lattice contraction during ageing 80—3030
Nimonic 80A, order hardening, comparison between revised theory and expt. 80—93565
Nimonic type, elastic interphase strains on ageing effects on extinction *(Russian)* 77—66646
Nomex, fibre, mech. props., environmental effects, incl. sunlight and ionising rad. effs. 77—36560
nonlinear creep theory of an ageing body, principle of correspondence *(Russian)* 80—33469
nonuniform hereditory-ageing media, creep theory 77—35059
nonuniformly ageing materials, equations of state in nonlinear creep theory 77—75824
Nylon 6, pressurized heat treatment effect on fatigue props. 79—87669
nylon-6,6, creep meas. at const. temp., humidity 78—95883
optical fibre, rupture stress rel. to ageing *(German)* 78—38009
optical fibre, UV cured epoxy acrylate coated, zero stress ageing effect on strength 80—58753
optical fibre splice, using arc fusion method, protection and reliability 80—69565
optical fibre stress-optical degradation obs. 78—1402
optical fibres, GeO_2-$B_2O_3SiO_2$, ageing effects of moisture on fatigue and tensile strength 80—66539
optical fibres, plastic-coated fused silica, ageing and static fatigue 79—46067
optical fibres, surface compressive strength, increase after ageing under load 79—46065
optical fibres, UV curable epoxy acrylate coated, long-term mech. behaviour 78—95802

ageing continued
optical waveguide performance before and after storage 79—27392
Ostwald ripening and its application to precipitates and colloids in ionic crystals and glasses [Review] 78—80548
Ozhennite, yield point, effect of ageing stress 77—21223
parallel plates, one-dimens. diffusion-controlled growth 80—55410
PBI fibre, mech. props., environmental effects, incl. sunlight and ionising rad. effs. 77—36560
PET film, metallized reflecting surface, ageing under natural conditions, destructive factors identification 79—83340
phenolic resin filled and unfilled, mech. relaxation behaviour, effects of temp. and time *(German)* 78—6963
photographic materials, non-Ag 79—24780
photometers, drift errors evaluation method *(German)* 77—10087
plasma etched SAW resonator ageing effects 77—39148
plastics, materials testing, application-oriented test standardisation *(French)* 78—85061
PMMA, ageing characts., sub-atm. pressure partial discharge obs. 80—1867
PMMA, viscoelastic props. in plastic zone, cooling rate effect 80—40418
polycaprolactam film, subjected to 9 kV elec. discharge, X-ray obs. *(Russian)* 79—23536
polycarbonate, viscoelastic props. in plastic zone, cooling rate effect 80—40418
polycarbonate film, fission track etching characts., UV and ageing effects 79—76296
polydimethyl siloxane-b-styrene-b-dimethyl siloxane block copolymer, morphology, mech. props. 80—64930
polyester foil, static polarisation depend. on heat ageing 78—60688
polyester varnishes, electroinsulating, thermal resist. *(Polish)* 78—84014
polyethylene, ageing in extreme cold climate *(Russian)* 77—59897
polyethylene, cross linking by energy rich radiation, mech. and elec. props. *(German)* 78—20035
polyethylene, effect of Se on electrical and mechanical strength, after mechanical and electrical ageing *(Russian)* 79—52396
polyethylene, ionising radiation effects crosslinking with accelerated electrons, ageing, SCC *(Polish)* 79—52701
polyethylene, partial discharges degradation effects, expt. 77—7617
polyethylene, prediction by isothermal differential scanning calorimetry 78—11485
polyethylene resin coated paper formulation for photography 80—4794
polyethylene stabilized with home-made antioxidants, thermal resistance *(Polish)* 79—52328
polyethylene terephthalate, glass-rubber transition determ., small-angle X-ray scatt., ageing 78—95145
polyimides, effect of orientational stretching on thermal aging 80—11721
polymer, accelerated ageing data processing using linear regression analysis 78—39815
polymer, ageing and stabilisation, struct.-kinetic aspects *(Russian)* 79—52660
polymer, glassy, ageing, scanning calorimeter meas., theoretical prediction 79—10810
polymer ageing through exposure to light, device *(French)* 80—30126
polymer glasses, aged, enthalpic state determ. by scanning calorimetry 80—6528
polymer glasses, enthalpy relax., scanning calorimetry technique 80—90851
polymeric dielectric materials exposed to partial discharges, degradation product anal. 79—4765
polymers, atmospheric resistance, distrib. function determ. and anal. *(German)* 80—81225
polymers, stress-enhanced chemiluminesc. 80—40628
polyphenylene oxide, with and without impact resisting polystyrene, photo-oxidative ageing, Cu and Fe trace effects *(German)* 79—100191
polyphenylene oxides, high temp. ageing effect on struct. and props. *(Japanese)* 77—70078
polypropylene, thermal stabilizer content effect on props., processing and ageing *(Polish)* 79—70099
polystyrene fibre, ageing effects on elongation to fracture *(German)* 78—76750
polyurethane foam solar concentrator, thermal and thermohydrolytic ageing 78—92281
polyvinyl dispersion, ageing *(Polish)* 79—70098
polyvinylidene fluoride, ageing effects on thermally stimulated currents 77—1634
polyvinylidene fluoride film, biaxially oriented, charact. for transducer appl. 80—88931
precipitates, Ostwald ripening, general kinetics 78—27808
precipitates, reaction-controlled Ostwald ripening, in steady state, general kinetics 78—35715
PVC, antiplasticisation rel. to ageing and nonlinear viscoelasticity 78—52929
PVC, rigid, physical ageing effect on elec. props. 78—10836
PVC surfaces, natural and stabilised, composition, ageing, oxidation and weathering, ESCA obs. *(French)* 80—61139
PWR pressure components reliability and residual life evaluation and precipitation 79—20191
radiation, of halophosphate phosphors, recombination processes effect *(Russian)* 80—7424
radiation concentrators with silazane protective coatings, UV exposure, tests 78—79092
Rene 95, as hot isostatically pressed (HIP) and HIP+forged, low cycle fatigue 80—25854
resins, thermoplastic, glass-fibre-reinforced, performance at elevated temperatures obs. 79—95067
rubber, C-black loaded SBR, elec. cond., effect of milling and thermal-oxidative ageing 77—55529
rubber, effect of Se on electrical and mechanical strength, after mechanical and electrical ageing *(Russian)* 79—52396
rubber, natural, with furnace soot or acetylene black, natural ageing and dielectric props. *(German)* 78—19795
rubber, natural and accelerated, comparison 79—24625
rubber, nitrite, heat ageing, light scatt. method study *(Russian)* 80—40407
rubber, rupture life calc. 77—59933
rubber mixtures, synthetic, natural ageing effects on dielec. props. 77—24778
rubber-brass interface, adhesion failure, XPS study 80—40671
rubber-channel black mixtures, natural ageing effects on dielec. props. 77—24777

ageing continued
- safety-system instruments for nuclear plants, impact of IEEE Std. (323-1974) 80–52753
- sapphire :Ti^{4+}, deformation history effects on precipitation hardening 79–83209
- SAW deeply-etched resonators, long-term aging improvement 79–55290
- SAW oscillator frequency stability developments 78–59253
- secondary cells with C-air electrodes in alkaline electrolytes, ageing mechanism study 80–101087
- semiconducting electrodes, defect doped, ageing effects 79–69592
- semiconductor, apparent ageing, caused by defect migration, dark and photocond. 79–11169
- semiconductor homojunction lasers, gradual degradation process expt. *(Polish)* 77–68213
- semiconductor junction lasers in optical fibre links *(German)* 79–32042
- silica optical fibres, ageing polymer-coated fused specimens in pH solns., tensile strength and dynamic fatigue 79–46063
- silica reflectors, ageing under flash lamp light pulses *(Russian)* 77–54737
- silk, spider, tensile, fracture strength, elongation and ageing effects 80–41072
- single crysts., fatigued age-hardenable, dislocation structure *(German)* 80–54247
- soda glass, ageing effect of HF discharge on conductivity and dielec. const. 78–39138
- solar collector DC reactively sputtered metal carbide and silicide selective surface props. 79–62029
- spark switches, high repetition rate, with Al and brass electrodes, surface ageing 80–106997
- sputtered in Ar-N_2 atm., elec. and struct. props. 80–15636
- sputtered metal silicide solar selective absorbing surfaces 78–52671
- sputtered particles-substrate, temp. overaging *(Russian)* 80–40385
- stainless steel, 36NKhTYu, highly deformed, discontinuous γ'-phase precipitates cell boundaries, formation during ageing 79–87641
- stainless steel, types 304 and 308, fatigue crack growth at elevated temps. 77–46288
- stainless steel aged by discontinuous precipitation mechanism ultrafine grain and mech. props. *(Russian)* 77–70053
- steel, 10Kh11N20T3R, brittle fracture susceptibility rel. to grain size *(Russian)* 77–59901
- steel, 18% Ni maraging, fatigue strength, effect of ageing treatment 78–23805
- steel, 30KhG and 30KhN, carbide formation, Mo alloying effects *(Russian)* 78–48402
- steel, 36NKhTYu, ageing to produce ultrafine grains, discontinuous precipitation *(Russian)* 77–81277
- steel, 37Kh12N8G8MFT, precipitation hardening, hardness meas. and electron microscope exam. *(Russian)* 79–38843
- steel, 4340, quenched, tempered, and austempered, effect of plastic strain followed by ageing on elastic limit 78–31446
- steel, $\alpha \rightarrow \gamma$ transformation during rapid heating of N18K9M5T and N25 77–59788
- steel, alloy, ageing characts., precipitation and coarsening of VC, TiC, and V-Ti-C in ferrite 78–84874
- steel, alloy, cluster formation susceptibility in 40 KhN, influence of isothermal working in H_2 *(Russian)* 78–56643
- steel, alloy, hardened, electrochem. characts. and stress corrosion cracking, ageing and cold treatment effects 80–108639
- steel, alloy, maraging, 250-grade, ductility and toughness of hot isostatically pressed powder 78–52925
- steel, alloy, type 36NKhTYu, plastic deformation, effect of surface condition on initial stage 78–84929
- steel, alloy 36NKhTYu, deformation resistance, grain size effect *(Russian)* 78–11271
- steel, alloy maraging, type Kh13N8D2TM, conditions for formation of stable austenite 78–84868
- steel, austenite, abnormal decomposition kinetics and mechanism *(Russian)* 80–55344
- steel, austenite, carbide strain hardened, strength and plasticity, effect of Mn content *(Russian)* 80–97500
- steel, austenitic, 800H, effect of hardening processes on initial stress-strain curve 78–84846
- steel, austenitic, aged, stress induced martensitic transform., mech. props. *(Russian)* 79–87632
- steel, austenitic, ageing and plastic deform. effect on struct. and mech. props. of N15Kh5G3T3 *(Russian)* 80–71691
- steel, austenitic, alloyed with N, decomposition of solid solution 78–23712
- steel, austenitic, cold worked 10Kh11N23T3MR, structural transformations, aging effect, electron microscope obs. 80–40402
- steel, austenitic, Cr-Mn, Kh4G18F, microstruct. and mech. props. during tensile deform. *(Russian)* 79–20114
- steel, austenitic, Cr-Ni-Mo, Mo effect on lattice parameters and chem. comp. of σ-phase and $M_{23}C_6$ carbides 77–70072
- steel, austenitic, Kh12N20T3R, ageing, submicroscopic struct. role in dispersion hardening *(Russian)* 78–64549
- steel, austenitic, martensitic transform., alternating elastic stressing effects 77–86029
- steel, austenitic, mechanical strength, effect of mech. and heat treatment 77–12659
- steel, austenitic, Mn-Al-V-F2, EM characts. after nitriding, aging, austenitizing, NDT of nitrided layer depth 79–11750
- steel, austenitic, Nb modified, HSLA, interaction between recrystallisation and precipitation during high temp. determ. 79–100187
- steel, austenitic, Ni-Ti, alloy N35T5, ageing, magnetisation and Curie temp. depend. on plastic deform., Mossbauer studies *(Russian)* 79–69669
- steel, austenitic and duplex 308 stainless, mech. of intergranular corrosion and pitting corrosion 79–91846
- steel, austenitic cladding, stability of fuel element for gas-cooled fast reactors *(Russian)* 77–83042
- steel, austenitic Cr-Mn, $M_{23}C_6$ carbide precipitates comp., heat and thermomech. treatment influence *(Russian)* 80–40361
- steel, austenitic Fe-Mn-V-C, ageing characts., discontinuous precip. nature 80–84940
- steel, austenitic Mn-Ni, alloying element influence on struct. and mechanical props. *(Russian)* 80–35256
- steel, austenitic stainless, aged and deformed, growth and dissolution of NbC particles 78–39782
- steel, austenitic stainless, biphase, ferritic, ageing and thermomech. treatment effects on struct. and props. 80–35226

ageing continued
- steel, austenitic stainless, Cr-Ni-Mo-Mn, Mo, Mn and ageing effects 78–35413
- steel, austenitic stainless, creep props., effect of high temp. ageing, SEM 80–97516
- steel, austenitic stainless, matrix precipitation of Cr_2N, due to P addition, TEM exam. 79–4973
- steel, austenitic stainless, MC precipitate comp., APFIM study 80–104161
- steel, austenitic stainless, Ni-alloyed, Cr_2N precipitation, interface struct. and morphology 80–11644
- steel, austenitic stainless, precipitation of $M_{23}C_6$ carbide by ageing *(French)* 79–52216
- steel, austenitic stainless, type FV 548, effect of ageing on void swelling on cold worked samples 79–37744
- steel, austenitic stainless, types 304, 316, tensile props., effect of exposure to Li and LiH 80–35219
- steel, C, hardened, cold-drawn or shot-peened, residual stresses rel. to temp. *(French)* 77–77494
- steel, C, yield point determ. rel. to grain size, deform., ageing and temp., dislocation theory *(Serbian)* 79–34120
- steel, C type U10A, X-ray diffr. investig. of carbide residues after deform. and tempering *(Russian)* 77–81275
- steel, Co-Cr-Mo type HY-180M, mech. props. and SCC, overageing effect 80–108634
- steel, Co-W-Mo-V-Ti-C (25.3, 12.8, 6.2, 0.5, 0.5, 0.05 wt.%), martensitically aged, structural transformation, and strengthening mech. *(Russian)* 79–15676
- steel, Cr, ferritic, N_2 effect on 475°C embrittlement 79–83313
- steel, Cr, H-dislocation interaction 79–8307
- steel, Cr-Mn(Ni), Mn and Ni additions, effect on corrosion resistance and hardness 80–104342
- steel, Cr-Mn-W(Mo), W and Mo addition effect on carbide form. in type 30 KhG *(Russian)* 79–87638
- steel, Cr-Mo (2.25, 1.0 wt.%), temper embrittlement, effect of P, Sn, comp. and carbide precip. 80–85036
- steel, Cr-Mo (2.25, 1.0 wt.%), temper embrittlement, effect of Mn, Si, comp. and carbide precip. 80–85037
- steel, Cr-Mo (2.25, 1.0 wt.%), thermally aged and Na decarburised, stress-rupture props. 80–21102
- steel, Cr-Mo (2.25, 1 wt.%), temper embrittlement trace elements, Mo, intercritical heat treatment effects 77–36634
- steel, Cr-Mo (2.25, 1 wt.%) annealing, high strain rate tensile props. 77–25117
- steel, Cr-Mo-V, brittle failure, heat treatment and influence of cold plastic deform. 78–72858
- steel, Cr-Mo-V (0.5, 0.5, 0.25 wt.%), creep crack growth in notched bend test, microstruct. effect 77–21261
- steel, Cr-Ni (32.8 wt.%), tensile props. and fracture of two phase Fe alloy austenite and ferrite *(Japanese)* 79–8344
- steel, Cr-Ni-Mo-V-Nb (12,8,1,1.5,0.4 wt.%) Ce addition effects on strength and hardness *(Russian)* 78–15454
- steel, Cr-Ni-W(Mo), W and Mo addition effect on carbide form., X-ray obs. *(Russian)* 79–87639
- steel, crack propagation stress wave obs. of brittle fracture *(German)* 77–56110
- steel, deformation ageing of 40Kh, effect on impact resistance and tensile strength *(Russian)* 78–31427
- steel, deformed, Kh18N10T, ageing under gradually increasing load 77–90383
- steel, ELA, coercive force, differential meas., room temp. ageing study 77–71351
- steel, ferritic, strengthened by VC interphase precipitation, cleavage 79–74171
- steel, ferritic, with interstitial N, continuous precipitation and clustering 80–7585
- steel, ferritic stainless, embrittlement 80–85041
- steel, high-strength low alloy, Nb(CN) precipitation and coarsening during hot compression 80–97514
- steel, high-strength maraging, N18K9M5T, improvement in mech. props. under applied stress influence during ageing 80–20985
- steel, high-strength maraging, N18K9M5T, nitriding effect on fracture resist. 80–21092
- steel, low C, crack propagation energy rel. to temp., time factors 79–29179
- steel, low C, Mb-Nb, reheated, quenched, tempered, microstruct. 77–36550
- steel, low C, Mn-Nb, quenched and tempered, microstruct. and props. 77–36549
- steel, low C, weldable, precipitation hardening rel. to low cycle fatigue *(Czech)* 79–15686
- steel, low C Cr-Ni, temper embrittlement by antimony, Ti addition effects 77–32683
- steel, low pearlite, Nb microalloyed, ageing at 600°C, mech. props. *(German)* 77–36542
- steel, low-C, gas nitrocarburised, aged, fatigue behaviour 80–40514
- steel, maraging, 18% Ni content, exam. of age hardening-grain size relationships 78–84833
- steel, maraging, 18 Ni, welded joints ageing props. obs. *(Japanese)* 80–40401
- steel, maraging, 18 wt.% Ni, solution heated and aged, surrface damage during machining, unlubricated 78–15599
- steel, maraging, 18 wt.% Ni, tensile props., effect of aged struct. and austenite grain size 77–48511
- steel, maraging, 18Ni300, ageing, electron diffr. and microscope obs. *(Polish)* 79–34070
- steel, maraging, ageing kinetics and struct. of N12K7M5TYu, effect of high temp. deform. of austenite *(Russian)* 80–84960
- steel, maraging, ageing study by internal friction meas. 77–12660
- steel, maraging, Co-Ni-Mo (20,15,5 wt.%), environmentally assisted fracture 77–52547
- steel, maraging, crack resistance, effect of external stress during ageing *(Russian)* 77–59902
- steel, maraging, effect of deformation on props. 80–21032
- steel, maraging, heating of thin samples with brief ageing, N6G4M, ON18K9M5T 78–52866
- steel, maraging, influence of microstructure, strain rate and temp., on tensile props. 80–11733
- steel, maraging, intermetallic phases precip. study by electron microscopy *(Polish)* 80–89217

ageing continued
- steel, maraging, investigation with lower Ni and Co contents *(Chinese)* 78−84812
- steel, maraging, Ni (18 wt.%), grain boundary precipitation, scanning Auger electron obs. 78−3132
- steel, maraging, Ni (18 wt.%), with aged struct. at low temp., delayed failure crack and fracture toughness 78−7047
- steel, maraging, Ni-Co-Mo, ageing and evolution peak at 470°C, calorimetric anal. *(Japanese)* 79−100156
- steel, maraging, Ni-Co-Mo (18,10,5 wt.%) precipitation *(Japanese)* 78−15402
- steel, maraging, plastic deform. effects on ageing kinetics *(Russian)* 77−77508
- steel, maraging, solubility of Fe-Mo-Co (10, 0 to 20 wt.%) Laves phase, depend. on Co *(Russian)* 79−100145
- steel, maraging, steady state unidirectionally solidified, austenite reversion and determ. 77−25118
- steel, maraging 18%Ni, calorimetric anal. of ageing *(Japanese)* 80−89264
- steel, maraging alloy, intermetallic compound solubility, thermodyanmic calcs. *(Russian)* 80−40363
- steel, maraging low-Ni, isothermal martensitic transformations *(Russian)* 78−88465
- steel, maraging N18K9M5T, crack propag. resistance under stress corrosion 77−70224
- steel, maraging Ni-Co-Mo, precipitation, elec. resist. meas. *(Japanese)* 78−11228
- steel, maraging type with 18% Ni, ageing treatment effect on fatigue crack propag. 80−16411
- steel, martensitic, age hardening with Cu, Nb additions, exam. of hardness 80−7681
- steel, martensitic, ageing, effect of H_2 on stresses in process of $\gamma\to\alpha$ transformation *(Russian)* 80−76252
- steel, martensitic, ageing, thermal recovery 77−56011
- steel, martensitic, ageing of 05kh3N2MD2, hardness depend. on tempering temp. *(Russian)* 79−24544
- steel, martensitic, Cr-Ni-Co-Mo-Ti, Kh12N8K5M3TYu, ageing of C free martensite *(Russian)* 79−1884
- steel, martensitic, delayed fractures suppression, by neutron irradiation *(Czech)* 78−67743
- steel, martensitic, medium alloy, quenched state, deform. hardened, ageing effects *(Russian)* 77−21179
- steel, martensitic, submicrostructure alterations in ageing and plastic deform. *(Ukrainian)* 79−79032
- steel, martensitic stainless, type 05Kh13N4m, strength and embrittlement, early stages of martensite decomp. effect 80−35227
- steel, martensitic-ageing, etching technique, for revealing struct. inhomogeneities 80−61035
- steel, microalloyed, alloy carbide precipitation during isothermal ageing 80−3077
- steel, mild, etching method for revealing plastic deformation 78−72825
- steel, mild, N_2 on oxidation resistance 79−61786
- steel, mild, tensile deformation, behaviour under high pressure *(Japanese)* 80−16381
- steel, mild, yield strength and fracture toughness, microstruct. effect, heat treatment 78−27615
- steel, Mn-Ni-Al, nonmagnetic, carbide-intermetallic strengthening 79−83208
- steel, Mo, energy structure X-ray anal. using TEM 80−84036
- steel, multicomponent duplex stainless, high temp. precipitation of α' 80−20939
- steel, N27Yu2T2B, elec. and thermal cond., 4.2 to 200K, Wiedemann-Franz law *(Russian)* 79−78076
- steel, Ni, maraging, H_2 diffusion, diffusivity and solubility *(Japanese)* 79−42311
- steel, Ni (19 and 24 wt.%), austenite thermal stabilisation at sub-zero temps. 77−52324
- steel, Ni (21 wt.%), ageing, nitrided case struct. investigation 80−35416
- steel, Ni-(Cr)-Ti, thermomechanical and heat treatment effects on retained austenite *(Russian)* 77−66661
- steel, Ni-Cr, (4,1, wt.%), isothermal embrittlement, AES exam. of grain boundary segregation 78−60814
- steel, Ni-Cr, P induced temper embrittlement, Mo effect 77−86148
- steel, Ni-Cr, SCC, grain boundary impurity effect 80−30150
- steel, Ni-Cr, temper embrittled, electron microscope and X-ray microstruct. obs. 79−38870
- steel, Ni-Cr, temper embrittlement, intermediate tempering treatments 80−60944
- steel, Ni-Cr, temper embrittlement by Sn 77−86149
- steel, Ni-Cr temper embrittlement by P 77−40448
- steel, Ni-Cr-Ti, thin bands, cold working, props. and struct. of 36NKhTYu 79−78994
- steel, Ni-Mn-Al-V, nonmagnetic, ageing, dispersion hardening, microstruct., phase comp., mech. props. *(Russian)* 79−34046
- steel, Ni-Ti, high-alloy, precipitation hardening, fatigue strength 79−79103
- steel, Ni-Ti-Al, 36NTYu, heavily deformed, subgrain struct. due to discontinuous precipitation of γ' phase *(Russian)* 79−52218
- steel, pearlitic, heat-resist., secondary phase precipitation, deform., and fracture during creep *(Russian)* 80−50669
- steel, phase separation, effect of plastic deform. and heat treatment *(Polish)* 78−92295
- steel, plain C, quench ageing avoidance, critical cooling rate *(German)* 79−52244
- steel, quench ageing, effect, of Mn content on C and N precipitation and mech. props. *(German)* 78−31409
- steel, rotor, Ni-Cr-Mo-V, reversible temper embrittlement 77−36656
- steel, sheet, 5-7 mm thick, method for assessing susceptibility to ageing 77−63850
- steel, spring alloy, microstruct. and props. at low temps. 77−44286
- steel, stainless, 316, 304, LMFBR primary piping materials, mech. props., review 77−25151
- steel, stainless, 316, neutron irradiation embrittlement, pre-irradiation treatment and composition modification 80−3171
- steel, stainless, 36NkhTYu, heavily deformed, subgrain struct. due to discontinuous precipitation of γ' phase *(Russian)* 79−52218
- steel, stainless, aged 304, twin boundary cavitation during creep 77−86099
- steel, stainless, austenitic, Cr-Ni-Mn-Si-Mo-C alloy, 13Khi8N10G3S2M2, elastic moduli exam. after thermomechanical treatment *(Russian)* 79−24558

ageing continued
- steel, stainless, austenitic, H_2 induced transformation obs. *(Japanese)* 80−11640
- steel, stainless, austenitic, precipitation hardening and N_2 effects obs. *(Rumanian)* 77−55973
- steel, stainless, C-Cr-Ni-Mn-V , non mag., aged, struct. and mech. props. *(Russian)* 78−56666
- steel, stainless, Cr-Mn (21, 14 wt.%), grain boundary precipitation and fracture *(Japanese)* 79−100149
- steel, stainless, Cr-Ni, maraging, effect of Mo, Co additions on hardening 78−84835
- steel, stainless, Cr-Ni-Co (13, 4.5, 0 to 13.8 wt.%), Co effect on martensite ageing *(Russian)* 77−66660
- steel, stainless, fatigue, influence of ageing and plastic deformation *(Russian)* 79−15857
- steel, stainless, fatigue crack morphology of type 304 cycled at const. stress amplitude at elev. temps. 78−64671
- steel, stainless, ferritic, electron microscope obs. of precipitation hardening *(French)* 79−34049
- steel, stainless, ferritic, subjected to 475°C embrittlement, exam. of fracture toughness 78−84982
- steel, stainless, ferritic and duplex, Mossbauer effect study of 475°C embrittlement 78−52933
- steel, stainless, high-strength 0Kh11N10M2T, phase transform. 77−70046
- steel, stainless, maraging, Cr-Co, effect of ageing on microstruct., TEM and neutron diffraction exam. 78−84867
- steel, stainless, maraging, high strength, exam. of ageing embrittlement *(Japanese)* 78−84972
- steel, stainless, maraging, high strength, notch toughness, effect of ageing *(Japanese)* 78−11311
- steel, stainless, maraging high strength, embrittlement on low temp. ageing *(Japanese)* 79−100155
- steel, stainless, martensitic, ageing, strength/structural charact. relationship 77−90426
- steel, stainless, martensitic, crack resistance of type VNS-2, heat treatment effects 79−100196
- steel, stainless, radiation-thermal treatment, N_2O_4 coolant action, intergranular corrosion *(Russian)* 78−58357
- steel, stainless, sensitization, C content and ferrite morphology effect 80−89400
- steel, stainless, solution treated FV 548, irradiated with 22 MeV C^{2+} and 46.5 MeV Ni^{6+} ions void swelling 78−22771
- steel, stainless, stress relieved, microstruct. transformations resulting from ageing 80−71644
- steel, stainless, surface treatment, X-ray photoelectron spectrosc. study 80−50764
- steel, stainless, SUS 321, thermal ageing effect on high temp. low cycle fatigue life *(Japanese)* 80−29988
- steel, stainless, two phase, variation of tensile and impact strength with heat treatment 79−34085
- steel, stainless, type 07Kh16N6, heat treatment 79−66158
- steel, stainless, type 304, solution-annealed and thermally aged, correl. of high- and low-cycle fatigue data 78−15532
- steel, stainless, type 316, cold worked, precipitation response to neutron irrad. 80−34073
- steel, stainless, type 316, influence of preirrad. thermal-mechanical treatment on phase stability and swelling 79−55792
- steel, stainless, type 316, microstruct. changes in creep ductility, SEM, TEM, optical microscopy and X-ray diffr. study 79−38927
- steel, stainless 12kh18N9T, wire, mechanical and heat treatment effect on static and cyclical strength *(Russian)* 78−35410
- steel, stainless 304 sol. of annealed and thermally-aged, high-cycle fatigue behaviour 80−100923
- steel, stainless AISI 316, fatigue crack growth, effect of grain size on threshold stress intensity 78−44216
- steel, stainless precipitate phasee in type 321 after ageing 17 years at 600°C 78−27525
- steel, stainless type 316, neutron irradiated, or themally aged diamond-cubic η phase formation, TEM study 79−99249
- steel, steam pipes, 12Cr1MoV, selection of allowable stresses based on minimum possible strength data 80−104237
- steel, strengthened by surface plastic deform., tempering effect on physicomech. props. *(Russian)* 78−35409
- steel, structural, Bauschinger effect *(French)* 78−23787
- steel, thin sheets, C and N contents determ. by internal friction *(German)* 78−27715
- steel, tool, maraging, based on N12M10, exam. of hardening, crack resistance and wear *(Russian)* 79−34047
- steel, type IN-787, for use in Arctic, low temp. effects on mech. props. 80−76310
- steel, type Kh13N9D2MT martensitic aged, struct. and mech. props. *(Russian)* 80−93600
- steel, type N18K9M5T, maraging, rate of movement change of fatigue cracks as result of ageing *(Russian)* 79−70149
- steel, ultrahigh strength, monotonic and cyclic stress strain curves 80−35268
- steel, unalloyed, brittle fracture, effect of prestrain and ageing *(German)* 78−19857
- steel, VN precipitation after heat treatment 79−29067
- steel, W, high C, amorphous, rapidly quenched from melt, mech. and thermal props. 79−38874
- steel, work-hardenable, N26T low magnetic phase, fatigue strength effect of surface treatment 77−48546
- steel 03Kh12N10MT, mech. props. at low temps. 77−16615
- steel AF1410, wear against stainless steel, repetitive impact, microstruct. effect 79−74263
- steel low C, fatigue strength of notched specimen, low-temp. quenching and quench ageing effects 79−100173
- steel strips, elec., grain-oriented, effect on stress-relief annealing treatments on permeability and ageing 78−23832
- steel strips, elec., grain-oriented, effects of ageing on mag. AC permeability 78−23833
- steel turbine casings, residual life determ. 80−93585
- steel VNS-2, damping capacity, magnetomechanical, phase transform. effects 78−31445
- steels, austenitic, microdefect accumulation during creep, effects of heat treatment, hardening 79−24550
- steels, low-C, aged after quenching, rel. between micro-cracks and coaxing effect *(Japanese)* 80−81159

ageing continued
steels, nitrided age-hardened, for blanking punches, chipping resist. props. *(Japanese)* 80—89340
stretched wires as standards of straightness *(German)* 80—36976
styrene alpha methylstyrene copolymer, microcrack development under atmospheric ageing 77—86210
TGS:Cr^{3+}, polarisation reversal and ageing mechanisms, EPR meas. 79—8044
TGS, deuterated, dielectric props., ageing 77—16257
TGS, spontaneous polarisation and coercive field from 30 to 1000 Hz 77—66464
TGSe, deuterated, dielectric props., ageing 77—16257
thermistor stability, ageing in constant temp. baths 79—21745
Ticonal with magnetic texture, struct. damages during ageing 77—16626
Tishomingo Fe meteorite, microstructural study rel. to ageing 79—16898
transition metal amorphous alloys with metalloid elements, embrittlement/crystn. relationship *(Japanese)* 79—96134
1,3,5-trithiane, single cryst., thermal treatment or ageing, photocond. meas. 77—11959
tube, thin walled plastic, subject to ageing, cyclic loading *(Russian)* 79—68600
Udimet 500, microstructural instability in industrial gas turbine engine vane 77—28833
Udimet 520, γ' phase composition variation with ageing 77—8866
viscoelastic contact, aging 80—64486
Zircaloy-2, yield pts. obtained by ageing at two stresses 80—81091
Ag film, Ge coated, electrical resistance and ageing *(Russian)* 80—103759
Ag film, on mica, microstruct. changes 78—72013
Ag, vacuum condensate, effect of Ge coatings on ageing kinetics *(Russian)* 77—59340
Ag-Pd-Cu, contact-spring props., fatigue and spring limit *(Japanese)* 79—29117
AgBr:Sr, stress induced anomalies in internal friction, logarithmic decrement 79—66095
AgI hydrosols, kinetics and mechanics of colloid systems formation 80—101045
(Al,Ga)As DH lasers, temp. accelerated ageing and degradation characts. 78—22130
(Al,Ga)As double-heterostructure lasers degraded, deep-level changes during accelerated ageing at high temps. 80—74356
Al alloy, AK4-1, dispersion-hardening, US effects on ductility and thermal resist. *(Russian)* 77—32582
Al alloy, precipitation hardening, creep deform. effect 77—16601
Al alloy 01205, mech. props. at cryogenic temps. 79—29206
Al alloy 2024, relief of residual quenching stresses *(Korean)* 79—70091
Al alloy 2024-T3, work hardening in surface layers and bulk during fatigue 78—48428
Al alloy 2036, thermomechanical treatment on struct. and props. 79—29109
Al alloy 6061, high-purity, precipitation hardening, prior strain and ageing effect 77—66651
Al alloy 6061, thermomechanically treated elev. temp. mech. props. 79—8310
Al alloy 7001, ageing effect on hardness and tensile props. rel. to delay time till quenching 78—92286
Al alloy 7075, fracture props., effect of thermomechanical treatment 78—60793
Al alloy 7075, influence of overageing at 175°C on fatigue crack growth rate *(French)* 77—56010
Al alloy 7075, precipitation hardening, toughness and microstruct. *(Japanese)* 78—15509
Al alloy AL22, influence of ultrasonics application on creep during multistage ageing *(Russian)* 79—91708
Al alloy AZ5G, age hardening heat treatment effect on mech. props. microstruct. *(French)* 77—52370
Al alloy D16, supersaturated solid soln., decomp. process, electron microscope obs. and acoustic anal. *(Russian)* 79—15650
Al alloys, dil., quenched, foreign element effects on dislocation loop form. 80—54239
Al alloys, fracture, grain size effect 78—60781
Al, alloys, thermomechanical working effect on mech. props. *(Russian)* 77—21181
Al alloys aged, local plastic strain distrib. by selected areas channelling patterns 77—44349
Al contact of p-type Si surface-barrier diode, ageing 77—32077
Al film, nucleation-grown, RF sputtered, Mayadas-Shatzkes cond. 77—1498
Al, high purity 6061, thermomechanical treatment 77—44277
Al, sputtered film, thermal ageing, thickness dependent effects 78—6462
Al/Ge(Si) thin film couples, accel. ageing 80—44726
Al-Ag, discontinuous decomposition *(Polish)* 78—52808
Al-Ag, struct. of two-layer film 79—23851
Al-Ag, type-II superconductor, torque oscillations in mag. field *(Russian)* 80—103800
Al-Ag (1.03 at.%) alloy elec. resist. meas. above room temp., Ag atom configuration correlation 78—35534
Al-Ag (4 wt.%), scattering of conduction electrons, effect of size and internal struct. of GP zones *(Japanese)* 77—21149
Al-Ag (up to 40 at.%), exam. of anelastic phenomena and structural state 78—76693
Al-Ag alloy, ageing exam. by X-ray electron spectroscopy and electron diffr. exam. *(Russian)* 78—60685
Al-Ag alloy, second ageing stage, diffuse electron and X-ray scatt. *(Russian)* 78—68711
Al-Ag(10 at.%), supercond., flux pinning, torque meas., decomp. effect 77—1525
Al-Al$_2$Cu, aligned eutectic, precipitation, TEM and microhardness meas. 78—27529
Al-Al$_2$O$_3$-metal capacitor, capacitance and power factor rel. to voltage and temp. changes 80—54802
Al-Au (0.2 wt.%), precipitation mechanism and creep behaviour 80—3058
Al-Cu, effect of alloy purity and ageing on fracture mechanism, and resultant toughness 79—5049
Al-Cu (1.7 at.%), EXAFS study of precipitation 79—100151
Al-Cu (3 wt.%), stress aged, GP zone struct. by X-ray diffuse scatt. meas. *(Japanese)* 80—71653
Al-Cu (3 wt.%) single cryst., stress aging, oriented precipitation *(Japanese)* 80—71652

ageing continued
Al-Cu (3.71 wt.%), stress oriented precipitation of Guinier-Preston zones and θ' 78—52809
Al-Cu (4 wt.%), AE during deform., effect of ageing at 170°C 78—64597
Al-Cu (4 wt.%), aged to contain Guinier Preston zones, crystallographic fatigue crack growth 78—60832
Al-Cu (4 wt.%), naturally aged, early stages of G.P. zone form. 77—90355
Al-Cu (4 wt.%), precipitation sequence of metastable phases, NMR meas. 78—23713
Al-Cu (4 wt.%), reversion charact. *(Japanese)* 77—21150
Al-Cu (4 wt.%), single crystal, anisotropy in plane strain compression 77—36599
Al-Cu (4 wt.%), supersaturated and aged conditions, high strain deform. 80—60907
Al-Cu (4 wt.%), TEM obs. of intergranular corrosion 79—91835
Al-Cu (4 wt.%), θ' phase coalescence 79—56985
Al-Cu (4 wt.%), with θ' precipitates, relation between elastic limit and hardness *(French)* 79—5018
Al-Cu (4 wt.%) alloy, precipitation hardened, single crystal, directional plastic behaviour, exam. 78—39788
Al-Cu (4 wt.%) alloy, reversion characts. *(Japanese)* 79—56989
Al-Cu (4 wt.%) alloy, reversion process of Guinier-Preston zones, ^{63}Cu NMR obs. 80—60871
Al-Cu (4.6 wt.%), cold work and ageing influence on ductility and fracture behaviour *(Japanese)* 80—89295
Al-Cu (5 wt.%), ageing, extinction effects *(Russian)* 77—81283
Al-Cu (5 wt.%) alloy, ageing during relax. of elastic stresses, X-ray diffr. expts. *(Russian)* 77—59821
Al-Cu alloys, condensed films, metastable states 79—15046
Al-Cu full coherent precipitation hardened alloy, high temp. cyclic deform. 80—25711
Al-Cu-Mg, dil. alloys, ageing response *(Korean)* 77—28832
Al-Cu-Mg, type 2036, deformation at ageing temp., effect on struct. and props. 80—7605
Al-Cu-Mg (1.3, 1.3 at.%) alloy, natural ageing, meas. of quenching vacancy dislocation loops 79—15704
Al-Cu-Mg (2.0, 1.1 wt.%), Ostwald ripening of S' precipitates *(Korean)* 79—38831
Al-Cu-Mg (2.6, 0.4 wt.%), Fe, Si, Mn and Ti addition effects on age-precipitation *(Japanese)* 80—20937
Al-Cu-Mg alloy, struct. of Guinier-Preston zones *(Russian)* 79—1870
Al-Cu-Mg type 2036, thermomech. treatment, flow stress anal., effect in mech. props. 80—93584
Al-Cu-Mg-Ag casting alloy, precipitation hardening in artificially aged condition 79—1874
Al-Cu-Mg-Mn-Fe-Si, alloy D16, effect of mechanisothermal treatment on mech. props. 78—56674
Al-Cu-Mg-Mn(-Zn-Cr), low temp. deformed, ageing and mech. props. 79—1881
Al-Cu-Mg-Si-Fe-Mn-Ti, Si, Fe, Mn and Ti effect on precipitation in solid soln. *(Korean)* 79—66064
Al-Cu-Mg-Si-Mn (2.5, 0.7, 0.7, 0.5 wt.%), alloy AK6, US inspection of heat treatment quality 78—76681
Al-Cu-Mg(:Fe,Si) alloys, double-ageing, resist., hardness meas. 77—28822
Al-Cu-Mn-Mg-Fe-Si (4.48, 0.66, 1.55, 0.43, o.23 wt.%), alloy D16, relationship between intercrystallite corrosion depth, and elec. cond. 79—20220
Al-Cu-Si-Mg (4, 0.8, 0.8 wt.%) alloy, GPB zone formation during room temp. ageing 77—44263
Al-Cu-Sn, ageing process, effect of Sn atoms, ^{119}Sn Mossbauer spectra obs. 80—7598
Al-Cu-Sn (3.4, 0.28 wt.%), Mossbauer anal. of Sn behaviour during ageing 78—31431
Al-Cu-Zn alloy, ageing, X-ray and electron diffr. meas. *(Russian)* 78—39806
Al-CuAl$_2$, directionally solidified eutectic, structural changes during strength tests *(Russian)* 80—7543
Al-Cu(Ag), tensile ductility, effect of ageing and impact velocity *(Japanese)* 78—15465
Al-Cu(Mg), age-hardenable, US cavitation erosion mechanisms, effects of comp. and heat treatment 78—53002
Al-Cu(Mg), low freq. internal friction during plastic deform. *(Chinese)* 80—103420
Al-Cu(Zn, Ag, Mg$_2$Si), intermediate precipitates, stability, X-ray, elec. resist. and hardness study 80—3063
Al-Fe, dil., Mossbauer spectra of implanted ^{57}Fe, ageing behaviour 80—7233
Al-Fe-Si commercial alloy, elevated temp. low cycle fatigue behaviour under rotating bending 79—47766
Al-GaAs interface, thermal ageing of Al film, optical microscopy and SEM obs. 77—20203
Al-Ge (2 wt.%), quenched and aged, deform. slip line obs. 78—51544
Al-Ge alloy, effect of high press. on phase equilibrium *(Russian)* 79—1844
Al-Li, ageing mechanism, metastable δ' phase and stable δ phase precip. *(Russian)* 77—8858
Al-Li, alloy, ageing, δ'-phase precip., effect of quenching conditions *(Russian)* 78—19761
Al-Li (2.8 wt.%), ageing in US field, precip. hardening *(Russian)* 80—29968
Al-Li (6.72 at.%), δ' coherent solvus determ. on ageing at 20 to 200°C, X-ray scatt. 77—25056
Al-Li alloy, annealing of vacancies and ageing, resist. and TEM obs. 77—21172
Al-Li alloy, thermal anal. of precipitation 78—15417
Al-Li solid soln., decomposition exam. by secondary ion ion emission *(Russian)* 78—68696
Al-Li system, δ' coherent miscibility gap determ. by small-angle X-ray scatt. 77—77483
Al-Li-Mn (2.8, 0.3 wt.%), recrystallised sheet, fracture behaviour, SEM and TEM study 80—97566
Al-Mg, ageing process, effects of Ag additions and pressure *(Russian)* 80—45321
Al-Mg, Si alloy, void form. under different precip. conditions, after Al ion irrad. 80—59529
Al-Mg, single crystal, ultrasonic meas. of elastic consts. during isothermal ageing 78—11263

ageing continued
- Al-Mg (5.7 wt.%) alloy, pre-precipitation, elec. resist. investig. 77—32601
- Al-Mg alloy, AL24M, decomp. kinetics and ageing mechanism *(Russian)* 80—45269
- Al-Mg alloys, initial decomposition exam. by X-ray diffr. *(Russian)* 77—77482
- Al-Mg$_2$Si, ageing sequence study by electron microdiffr. 80—81068
- Al-Mg$_2$Si(1.42 wt.%), aged, dislocation structs. caused by plastic deformation 80—25786
- Al-Mg-Ag, age effect on age hardening *(Japanese)* 78—52831
- Al-Mg-Be, solid soln. decomposition, metallographic study 77—16577
- Al-Mg-Li alloy, metastable S′-phase, struct. *(Russian)* 80—103291
- Al-Mg-Si, Guinier-Preston zones, inception and effect on ageing *(Hungarian)* 79—11627
- Al-Mg-Si, precipitation of cube-shaped phases, electron diffr. study using TEM *(Japanese)* 79—43251
- Al-Mg-Si, thermomechanically treated, age-hardening 78—11236
- Al-Mg-Si, type 6010, microstruct. characts. influence on formability, heat treatment 80—81090
- Al-Mg-Si solid solution under stress, solute atom clustering during ageing 78—31430
- Al-Pt (2 wt.%), rapidly solidified alloy, metastable phase formation and decomposition 79—52194
- Al-Si, internal friction and Si precipitate nucleation 78—60690
- Al-Si, neutron small angle scatt. study 79—43255
- Al-Si (1.2 and 0.6 wt.%), single crystal, dispersion hardened with SiC, Bauschinger effect and work hardening 79—43360
- Al-Si (9 wt.%), precipitation hardening during isothermal ageing 80—29969
- Al-Si-Cn-Mg, alloy AL32, ageing of castings produced by pressure die castings 78—56650
- Al-Si-Cu-Zr, ageing kinetics *(Russian)* 80—76274
- Al-Si(Cu)(Zn-Mg-Cu), extraction and phase anal. 79—15673
- Al-Zn, ageing alloy, zonal decomposition stage, new effects in X-ray diffr. anal. *(Russian)* 79—4982
- Al-Zn, dil. alloy, ageing and reversion, annealing curves, X-ray obs. 78—88485
- Al-Zn, discontinuous decomposition *(Polish)* 78—52808
- Al-Zn, G.P. zone form., temp. limit 80—16317
- Al-Zn, resistivity anomalies in Guinier Preston zones *(French)* 78—6937
- Al-Zn 6.8 at.%, Guinier-Preston zones *(French)* 79—87640
- Al-Zn (10 wt.%), ageing at low temp., solute conc. fluctuation effects *(Japanese)* 79—4969
- Al-Zn (10 wt.%), ageing at low temp., effects of fluctuation of solute conc. 80—76287
- Al-Zn (10 wt.%), ageing at low temp., effects of fluctuation of solute conc. 80—76288
- Al-Zn (10 wt.%), ageing behaviour, calorimetric study 80—45328
- Al-Zn (10 wt.%), solute conc. fluctuation effects on ageing at low temp. 79—57023
- Al-Zn (15 at.%), structural changes during post ageing between 125°C to 215°C 80—40399
- Al-Zn (15 at.%), supersaturated alloy, growth and decomposition kinetics 80—29965
- Al-Zn (15 wt.%), calorimetric ageing study 80—45330
- Al-Zn (18 at.%), position of coherency spinodal curve 78—23660
- Al-Zn (2 and 4 wt.%), ageing and elec. cond. reversion *(Japanese)* 79—4983
- Al-Zn (30 wt.%), metastable phases, transformation kinetics, quenching rate effects meas. 77—55960
- Al-Zn (30 wt.%), precipitation sequences and transformation kinetics, X-ray diffr. and TEM obs. 77—55959
- Al-Zn (38 at.%), TEM study of precipitation processes or different microstructures during ageing 80—93561
- Al-Zn (3.9 wt.%), single crysts., fatigued age-hardenable, dislocation structure *(German)* 80—54247
- Al-Zn (40 wt.%), mechanical properties after thermal cycling 78—3150
- Al-Zn (60 or 71 wt.%), natural ageing *(Russian)* 78—48367
- Al-Zn (6.5 at.%), fatigue props., effect of ageing and thermomech. treatment 78—27620
- Al-Zn (6.8 at.%), decomposition, electron microscope study *(French)* 77—40422
- Al-Zn (6.8 at.%), neutron small angle scatt., interparticle interference 77—77514
- Al-Zn (6.8 at.%) alloy, elec. resist. temp. depend. rel. to ageing processes 77—77486
- Al-Zn (6.8 wt.%), effects of ageing temps. on microhardness and resistivity *(Japanese)* 78—35408
- Al-Zn (8-25 wt.%), solid solns., residual resist. during clustering 80—97483
- Al-Zn alloy, resist. and X-ray small angle scatt. during GP zone form., theory *(French)* 79—29070
- Al-Zn alloys, room temp. decomp. of metastable phases precipitated at 200°C 78—84814
- Al-Zn changes in inner-electron binding energies during ageing, electronic spectra study 77—28816
- Al-Zn-Fe-Si, Fe and Si effects on precip., TEM and X-ray diffr. obs., ageing at 90°C 77—48439
- Al-Zn-Mg, decomp. kinetics and ageing mechanism *(Russian)* 80—45269
- Al-Zn-Mg, duplex ageing effect on tensile props. 79—91721
- Al-Zn-Mg, effect of microstruct. and corrosive environments on stress corrosion cracking *(Japanese)* 79—79159
- Al-Zn-Mg, plastic deform. influence on structural transform. and mechanical props. *(Russian)* 80—7623
- Al-Zn-Mg, polygonized struct. in extrusions, thermal stability and mech. props. 80—50659
- Al-Zn-Mg, precipitation of η' phase, heat treatment, electron microscope obs. 78—68699
- Al-Zn-Mg, solid soln. decomp., 20 to 200°C 79—38830
- Al-Zn-Mg, TEM and calorimetric study 80—76290
- Al-Zn-Mg, zone composition change during ageing 79—29110
- Al-Zn-Mg (3.6, 1.95 wt.%), ageing and plastic deform., effect on structure, electron microsc. and X-ray diffr. study *(Russian)* 80—81108
- Al-Zn-Mg (4.5, 2.5 wt.%), fatigue crack propag. 77—86171
- Al-Zn-Mg (4.5 at.%, 2 or 3 at.%), decomposition behaviour during continuous cooling, XSAS and TEM examination 80—16264
- Al-Zn-Mg (4.5 at.%, 2 to 3 at.%), decomp. behaviour during continuous heating 80—29922

ageing continued
- Al-Zn-Mg (4.8, 1.1 wt.%), second phase dissolution, calorimetry study 79—100193
- Al-Zn-Mg (5,1 wt.%), decomp. process, TEM study 80—71660
- Al-Zn-Mg (5,2 wt.%), TEM of early stages of precipitation 77—40423
- Al-Zn-Mg (5.9, 2.9 wt.%), ageing effects on microstruct. 80—16306
- Al-Zn-Mg (6,1.5%), influence of ageing and cold work on tensile and fracture props. *(Japanese)* 78—52842
- Al-Zn-Mg (6.0, 2.5 wt.%), aged, grain, size depend. of fracture toughness 78—48495
- Al-Zn-Mg alloy, Ag addition and pre-precipitation treatment, influence on GP zone growth 80—71658
- Al-Zn-Mg alloy, effect of heat treatment and ageing on elec. resist. of η' precipitates 77—48441
- Al-Zn-Mg alloy, thermomechanically treated, precip. behaviour 78—84856
- Al-Zn-Mg alloy 7075, effect of thermal and mechanical pretreatments, on Guinier-Preston zone 78—39817
- Al-Zn-Mg alloy V95, two-stage ageing kinetics, mech. props. effects 79—83238
- Al-Zn-Mg alloys, decomposition kinetics, resistivity meas., extended jump model 78—84766
- Al-Zn-Mg alloys, H$_2$ bubbles in embrittlement 78—19868
- Al-Zn-Mg alloys, role of dispersed transition metal intermetallic compounds 79—96088
- Al-Zn-Mg and Al alloy 7050, age hardenable, microstruct., effect of monotonic and cyclic straining 77—36633
- Al-Zn-Mg granules and bands rolled from them, heat treatment 80—100862
- Al-Zn-Mg-Cu, optimum treatment combination for thermochemical processing 77—44278
- Al-Zn-Mg-Cu alloy 7075, SCC from T6 to overaged T7X 77—90487
- Al-Zn-Mg-Cu-Cr-Zr, high strength Cr and Zr addition effects 77—59820
- Al-Zn-Mg-Li alloys, effect of Li on thermal props. 79—24515
- Al-Zn-Mg-Ti, Ti effect on microstructure during ageing 78—64568
- Al-Zn-Mg(Mg-Ti), TEM exam. of early stage ageing behaviour, exam. of precip. kinetics 78—56645
- Al-Zn-Mg(3.2, 2.2 wt.%), deform. strengthened by Guinier Preston zones 77—52343
- Al-Zn(10 at.%), supersaturated solid soln., structural charact. of decomposition 77—70027
- Al-Zr (0.22 wt.%), hardness and struct. changes during prolonged ageing at 350, 400 450°C *(Japanese)* 79—52281
- (Al-Mg-Si)-Al$_2$O$_3$, SAP type, ageing 79—96055
- AlCuMgPb, microstruct. and flow stress during deform. at 573K 77—81307
- AlGaAs DH laser, self-pulsations due to proton bombarded region self-annealing during ageing 80—99728
- (AlGa)As DH laser degradation due to facet oxidation 78—42336
- AlGaAs DH short wavelength lasers, internal stress and degradation 79—68393
- (AlGa)As laser, CW, accelerated ageing effect on optical props. 77—38898
- (AlGa)As oxide-defined strip lasers, self-sustained oscillations, ageing effects 80—32991
- AlGaAs-GaAs double heterostructure laser lifetime, point defect generation model calcs. 80—32992
- AlGaAs-GaAs remote junction heterostructure laser, recomb. enhanced annealing effect 79—98355
- Al$_x$Ga$_{1-x}$As DH laser, accelerated ageing and uniform mode of degradation 77—83874
- Al$_x$Ga$_{1-x}$As DH stripe-geometry lasers, degraded, capacitance spectroscopy 77—14715
- Al$_x$Ga$_{1-x}$As heterojunction laser diode, accelerated step-temperature ageing 78—46599
- Al$_2$O$_3$ hot pressed, high density, effect of grain size on grinding 78—39723
- Al$_2$O$_3$ humidity sensor, ageing improvement *(Japanese)* 80—100863
- AlZn alloys, ageing zone stage duration depend. on quenching temp. *(Russian)* 77—55993
- AlZn, disordered, residual resistivity due to clustering, ageing effects 80—65521
- AlZnMg alloy, precipitation hardened, strength 78—39786
- As$_2$Se$_3$, amorphous, electrophotographic props., photodecomp. effect 78—49918
- As$_2$Se$_3$, in evaporated layer systems, electric field forming and ageing processes 77—12021
- Au film, void growth in early stages of ageing and electromigration 78—38991
- Au films on Si substrate, solid-solid reactions 78—95369
- Au on oxidised Si with metal adhesion layer, ageing props. 77—11820
- Au, pure metal and Au-Sn dil. alloy, vacancy clusters, quenching and ageing 78—76671
- Au thin films, material transport instabilities accompanying ageing *(German)* 80—7601
- Au/Pb thin film couple, room temp. interdiffusion study 79—28154
- β-Au-Cu-Zn, martensitic transformation temps. ageing and quenching effect 79—47687
- Au-Fe ion implanted alloy, Mossbauer conversion electron scatt. 80—88898
- Au-Ge thin film couples, activation energy for interdiffusion, accelerated ageing studies 79—82671
- Au-Pb-In solder joints, layer growth, ageing 77—32764
- BaTiO$_3$, exam. of anomalous pyroelectric effect above Curie point 79—33613
- Be bronze, struct. and props. after ageing under load 78—84932
- Be, fracture and strength properties, dynamic ageing effects 80—81202
- Be-bronze BrB2, struct. and phase transform. during mechano-thermal treatment *(Russian)* 80—11667
- Be-Cu alloy, props., precipitation hardening effects and appl. *(Italian)* 79—83207
- Bi film, granular, enhancement of laser machining and ageing characts., using Mg$_{0.25}$In$_{0.75}$ sensitising layer 77—62020
- Bi-Sb interface, film, thermoelectricity, ageing differential efficiency *(German)* 78—60146
- Bi$_2$O$_3$, thermally-grown capacitor-film, dielec. props. 80—2480
- Bi$_2$O$_3$ vacuum deposited films, dielec. props., 90 to 298K, freq. range 0.1 to 10 kHz, ageing effect 80—55036
- C fibre reinforced plastic laminates, axial and short beam shear fatigue 78—15492

ageing continued
CC Al-Zn-Mg (4.5,1(2)(3) at.%), decomposition during ageing, preageing and cooling rate influence 80−20938
CU-Zr-(Cr), powder metallurgical alloys, thermomech. treatment effect on props. 80−50660
CdS:Cd(In), Cu- or defect-compensated, optical ageing rel. to storage cond. 78−84247
CdS-Cu_xS solar cell, ageing due to thermally produced changes in Cu_xS film 77−8181
CeO_2 coating of laser optical components, electron microscope obs. 80−43342
Co-Cr-C alloys, $M_{23}C_6$ precip. mechanism 78−44130
Co-Cu-Fe-Ce, mag. characteristics of sintered permanent magnets 78−60312
Co-Cu-Fe-Sm magnet, microstruct. exam. after ageing, TEM meas. 77−48555
Co-Fe-Nb alloy, mag. precipitation-hardening and Bloch wall pinning 78−80173
Co-Fe-Nb semihard mag. alloy, mag. precip. hardening 77−8960
Co-Fe-Ti (12,6 wt.%), semihard permanent magnet, magnetic precipitation hardening 78−52830
Co-Fe-Ti alloy, precipitation hardened, rel. between struct. and mag. props. 78−95470
Co-Ni-Cr-C, carbide precipitation 79−29065
Co-Ni-Cr-Mo (35, 20, 10 wt.%), MP35N, TEM study of phase transformations 80−81054
Co-Ni-Cr-Nb, effect of Fe addition on precipitation behaviour 80−29962
Co-Ni-Cr-Nb (40, 18, 1.8 wt.%), precipitation behaviour of NbC, effect of ageing temp. on morphology 80−89227
Co-Si-B, embrittlement by crystallisation *(Japanese)* 78−48513
Co-Ti (9 at.%), decomp. kinetics, elec. resist., hardness, and saturation magnetisation during ageing *(Russian)* 80−50587
Co-Ti alloys, martensitic transformation depend. on ageing, cryst. struct. 79−91649
Co-Ti-Fe (3, 1 to 2 wt.%), spinodal decomposition 80−100839
$(Co_{0.83}Cu_{0.17})_6Ce$, cryst. struct. and mag. props., decomp. during ageing *(Russian)* 79−37661
Co_4CuCe, cryst. struct., mag. characts., ageing and decomposition *(Russian)* 79−4272
$Co_{75}Si_{15}B_{10}$, amorphous, crystallisation study *(Japanese)* 78−9959
Co_5Sm sintered magnet, effect of surface conditions on mag. props. 79−28556
Cr steel, austenite, abnormal decomposition kinetics and mechanism *(Russian)* 80−55344
Cr/Au layered films, microstruct. and interdiffusion during ageing, 423 to 573K 79−46965
Cr-Co-Fe, for telephone receiver mag. use 80−45318
Cr-Co-Fe permanent magnet anisotropic alloys, plastic deform., ageing, particle alignment temp. 80−35254
Cr_2O_3-Al_2O_3, solid soln., effect of Cr on point of zero charge 78−61021
CsI:Na, crystal, kinetics of decay of surface solid soln. 79−23810
Cu, cold rolling, mechanical props., ageing, annealing, recrystallisation, plastic strain *(Russian)* 80−35202
Cu, cyclic strain hardening under deform. at various temps. 79−43273
Cu, discontinuous film, ageing effect on elec. cond. 79−24084
Cu film, ageing effect of thermoelectric power 78−2584
Cu, polished mirror, optical props. ageing 77−79912
Cu wire leads with Sn60Pb coating, effect on props. *(Polish)* 80−35231
Cu-Al, α_2 phase form. process 77−48464
Cu-Al-Co, precipitate-free zones near grain boundaries, growth kinetics, TEM obs. 80−40368
Cu-Al-Ni (14.3, 4 wt.%), ω-phase form. during quenching and ageing *(Russian)* 80−25686
Cu-Al-Ni Marmen alloys, rapid solidification and ageing 80−76245
Cu-Al-Ti, formation of modulated structure rel. to barrier nucleation of new phase *(Russian)* 77−32580
Cu-Au film, aged, strength failure due to Kirkendall porosity 79−77969
Cu-Be, SCC in NH_3 80−104326
Cu-Be (2 at.%), plastic deform. and dislocation substruct. 80−76307
Cu-Be (2 wt.%), alloying addition effects on grain boundary reaction *(Japanese)* 80−49236
Cu-Be (2 wt.%), plastic deformation influence on ageing, granular microhardness *(Russian)* 80−55474
Cu-Be (2.1 wt.%), discontinuous precipitation *(Japanese)* 78−19766
Cu-Be alloys, ageing kinetics, ultrasonic effects *(Russian)* 79−78997
Cu-Be alloys, relationship between discontinuous precipitation and continuous precipitation 79−100144
Cu-Be-Co, cuboid (Co, Cu, Ni, Fe)Be inclusions, metallography, ageing effects 80−11645
Cu-Be-Co (1.8, 0.2 wt.%), TEM obs. of precipitates, ageing charact. *(Korean)* 77−66648
Cu-Be-Ni (1.9, 0.32 wt.%) solution treated alloy, age induced vol. changes in structural transformations *(Russian)* 79−100179
Cu-Be-Ni-Ti-Mg (2, 0.3, 0.2, 0.02 to 0.4 wt.%), multiple step ageing *(Russian)* 78−19786
Cu-Be-Ni-Ti-Mg bronze, alloying element influence on minimum thermo EMF, cold working *(Russian)* 80−34426
Cu-Co (2 wt.%), single crysts., fatigued age-hardenable, dislocation structure *(German)* 80−54247
Cu-Co alloy, ageing and reversion phenomena 79−91718
Cu-Co-Fe, dil. alloy, low temp. resistivity maxima, deform. and ageing effects *(Russian)* 79−87091
Cu-Cr, isothermal decomp. diagrams 79−38791
Cu-Cr, precipitation hardened, wear 78−3234
Cu-Fe, dil., diffusion and ageing processes, Mossbauer study 80−7245
Cu-Fe, dilute, low temp. heat capacity in mag. field, superparamagnetism 80−39804
Cu-Fe, growth kinetics and interfacial energy of coherent γ-Fe particles *(Japanese)* 78−19765
Cu-Fe, implanted, Mossbauer study, rel. to annealing temp. 78−31135
Cu-Fe, Mossbauer studies of ageing and precip. 79−38415
Cu-Fe, precipitation processes during aging, TEM, resistivity, hardness study *(Japanese)* 80−35221
Cu-Fe (2.46 wt.%), reversion phenomena and cold-working effect *(Japanese)* 80−35204
Cu-Fe system, ageing and reversion phenomena study 80−89274
Cu-Mn (38 to 58 wt.%), age hardened, exam. of precipitation and strengthing 78−72782
Cu-Mn alloy, effect of ageing on mag. props. 77−28366
Cu-Mn mictomagnet, effect of ageing on mag. moment 77−43841

ageing continued
Cu-Nb (0,4 at.%), splat quenched, aged, superconductivity *(Japanese)* 77−63018
Cu-Nb-Sn dil. alloys containing Nb_3Sn precipitates, superconductivity 78−43507
Cu-Ni-Al, ageing charact., optical TEM, X-ray, hardness obs. 79−29079
Cu-Ni-Al, grain boundary reaction under isothermal ageing at 623 to 973K *(Japanese)* 79−70090
Cu-Ni-Al, review 80−7564
Cu-Ni-Be (30, 0.5 wt.%), grain boundary reaction after ageing and quenching, obs. *(Japanese)* 79−70089
Cu-Ni-Be-(Al) (30,0.5,(0.2-2) wt.%), Al addition effect on grain boundary reaction *(Japanese)* 80−54254
Cu-Ni-Cr (28, 2.8 wt.%), spinodal alloy, microstruct. and tensile props. 78−39858
Cu-Ni-Fe, spinodal alloy, heat treatments for improved mech. props. 79−5024
Cu-Ni-Fe alloy, quenched and aged, deformed, low-temp. elec. resist. meas. *(Russian)* 77−52514
Cu-Ni-Nb (30,1 wt.%), precipitation 77−86035
Cu-Ni-Nb-Al, correlation of γ' and γ'' precipitates phase stability 80−25704
Cu-Ni-Nb-Al, formation of γ' and γ'' precipitates 78−76655
Cu-Ni-Sn (15, 8 wt.%), prior deform. effect on spinodal age hardening 80−108465
Cu-Ni-Sn (15, 9 wt.%), age hardening accompanying phase transition 78−64551
Cu-Ni-Sn (4-15, 4-8 wt.%), strip strengthened by spinodal decomp., stress relax. in bending 80−7616
Cu-Ni-Sn spinodal substitute for Be-Cu alloy 80−35217
Cu-Ni-Zn-Mn fine grained precipitation-hardenable alloy, high strength and ductility 80−100805
Cu-Si(Ge), dissoc. dislocations pinning by Suzuki effect *(French)* 79−100223
Cu-Sn (25 wt.%), struct. changes with ageing *(Russian)* 77−40421
Cu-Sn-Mg, precipitation, effect of thermomechanical treatment *(Japanese)* 79−4970
Cu-Sn-Ni alloys, mech. props. after thermomech. treatment 79−79009
Cu-Sn(-Al), quenched and aged, struct. of phases *(Russian)* 80−49184
Cu-Ti, ageing effect on internal friction and elastic props. *(Russian)* 77−28842
Cu-Ti, deform. effect on precipitation and recrystallisation, electron microscope study 77−70115
Cu-Ti, lattice parameter change during ageing *(Japanese)* 78−35411
Cu-Ti, Zr effects on cellular precipitation 77−16587
Cu-Ti (Zr), strength improvement by thermomechanical treatment *(Japanese)* 78−48426
Cu-Ti (3.5 wt.%), aged by US strain, struct. and props. *(Russian)* 80−21003
Cu-Ti (4 wt.%), aged, stress corrosion cracking in Cu-NH_3 solutions, effect of pH, Cu and NHz conc. 78−88562
Cu-Ti (4 wt.%), ageing, X-ray study 77−56012
Cu-Ti (4 wt.%), combined recrystallization and precipitation 79−29072
Cu-Ti (5 wt.%), effect of cold work on ageing behaviour, TEM study *(Japanese)* 79−78991
Cu-Ti alloys (0.5 to 4.0 wt%) ageing charact. determ. 79−20089
Cu-V-Ga dil. alloys with V_3Ga particles, supercond. props. and microstruct. 78−39278
β_1-Cu-Zn mixed crystal, metastable structural Umklapp process, isothermal phase transform. *(German)* 78−22798
Cu-Zn-Al, martensitic transform., short range order effect 79−61586
Cu-Zn-Al, memory alloy wire and ribbon reversible martensitic transformation, ageing effect, review 80−7564
Cu-Zn-Al (26, 4 wt.%), martensitic transform. temp. variation after low temp. ageing 79−15666
Cu_3Au-Co, single crystal, overaging mechanism 79−20081
Cu_3Au-Co, underaged, ordered and disordered single crystal, hardening mechanisms 78−3134
CuNiCr, IN838, heat treatment effect on fatigue and corrosion fatigue behaviour 80−20982
$Cu_{46}Zr_{54}$, devitrification effect on mech. props. 80−30082
$Cu_{56}Zr_{44}$ metallic glass, devitrification and its effect on mech. props. 80−33893
Fe, cast, increase in yield strength, after phase transformations 78−44125
Fe, cast, interdendritic dispersed graphite, dissolution kinetics on heating, excess time *(Russian)* 77−52360
Fe, high-purity, low-temp. mag. relax. after thermal ageing and demagnetisation 77−85502
α-Fe, influence of C and ZrH_2 on static and cyclic creep behaviour 78−39856
α-Fe, nitrided, aging at room temp. 80−71679
Fe particles in Hg, ferromag. liquid, mag. props., ageing effects 77−12154
α-Fe, quench ageing of N_2, effect of soln. heating and quenching temps. *(German)* 77−55991
Fe, quenched-in hydrogen, yield stress decrease of prestrained specimens 80−16454
α-Fe, strengthening kinetics due to deformation ageing, impurity atom sources *(Russian)* 80−55435
Fe, varying purity, internal friction, H-dislocation interactions 77−52377
α-Fe-Al, migration of C, mag. permeability disaccommodation meas. 77−36100
Fe-Al (15 at.%), short range order form. kinetics *(Russian)* 78−3146
Fe-Al-C, low C, precip. of carbides and cementite after quenching and ageing 78−52814
Fe-Al-C alloys, C migration and mag. aftereffect, mag. permeab. disaccommodation and long-range order meas. 79−8020
Fe-Al(Ti), O containing, mag. aftereffect and disaccommodation meas., time depend., activation energy, and ageing props. 80−88836
Fe-Al(24.3 at.%)-C alloy, magnetic permeability disaccommodation, 260-400K 80−93144
Fe-Be, formation of quasi-periodic distrib. of precipitates during ageing *(Russian)* 78−56642
Fe-Be (16.5 or 19.5 at.%), four-phase model of struct. in initial ageing stages *(Russian)* 78−48430
Fe-C, ageing late stages, diffusional coalescence of precip. along dislocation lines *(Russian)* 77−25060
Fe-C, martensite, struct., Mossbauer meas. 80−40000
Fe-Co-Cr, Cr effect on struct. of ordering 78−35407

ageing continued
Fe-Co-Ni-Si-B amorphous alloy, magnetostriction and permeability, effect of annealing 79—1701
Fe-Co-Si(B), amorphous ferromagnet, mag. after effect on soft mag. props. 80—84626
Fe-Co-V, ordered and disordered, dynamic ageing *(French)* 80—16355
Fe-Co-V (2 wt.%), gamma phase 77—36514
Fe-Co-V(2%) alloy, correl. of resistivity with microstructure 78—72896
Fe-Co-W-C steel, M_6C carbide behaviour during ht. treatment *(Russian)* 77—66658
Fe-Cr (25wt.%), continuously cooled, embrittlement 77—36636
Fe-Cr-Co, ductile magnet alloys, mech. props. 80—85001
Fe-Cr-Co, mag. alloys, Mossbauer spectra 78—19386
Fe-Cr-Co, magnetic domain walls, Lorentz microscopy 80—103854
Fe-Cr-Co (28, 10.5 wt.%) ductile magnet alloy, humidity-induced H_2 embrittlement 80—89406
Fe-Cr-Co (31 wt.%, 23 wt.%), microstruct. and mag. props., ageing and thermomag. treatment effects 78—76769
Fe-Cr-Co alloys, (5-9 wt.% Co), obtained by slow cooling under mag. field, permanent magnet props. 80—75797
Fe-Cr-Co-Mo, microstruct., hardness, mag. props., influence of isothermal tempering and heat treatment 79—79129
Fe-Cr-Co-V alloy, microstruct. and mag. props. 78—68221
Fe-Cr-Co-V-(Ti) hard magnets, V and V-Ti effects on mag. and mech. props. 79—91810
Fe-Cr-Ni-Nb-C, austenitic, splat quenching 78—72798
Fe-Cr-Ni-Ti-Al, superalloy, Ti, Ni, Al, H_2 variations effect on mech. props. 78—3188
Fe-Cr(55 wt.%), phase decomp. early stages and clustering *(Japanese)* 80—55403
Fe-Cu, modulated microstruct., continuous cooling effect, hardness and electron microscope obs. 79—87665
Fe-Cu (2 wt.%), furnace cooled, ageing and steam oxidation 78—23744
Fe-Cu(2, 4 and 6 wt.%), sintered, precipitation hardening 77—66653
Fe-Mn, struct. and props., effect of Nb, C and Si alloying *(Russian)* 77—90360
Fe-Mn-Al-C, hardening during ageing, 450-750°C *(Russian)* 78—3135
Fe-Mn-C, anomalous changes in austenite and martensite lattice parameters 80—50636
Fe-Mn-Nb-V, high Mn, dispersion strengthening 77—16602
Fe-Mn-Ni, fracture toughness, thermomechanical treatment effects 78—60794
Fe-Mn-Ni base maraging alloys, age hardening 79—74170
Fe-Mn-Ti alloys, austenitic, precipitation strengthened 80—25714
Fe-Mn-V-C austenitic steel, discontinuous precipitation, morphological changes 80—3078
Fe-Mo (13-20 at.%) binary alloys, spinodal decomp. on ageing, TEM and X-ray diffr. study 80—97503
Fe-Mo (15.5 and 19.5 at.%), modulated struct., heat treatment effects, TEM obs. 79—100192
Fe-Mo (3at.%), internally nitrided, precipitate, morphology and chemistry 78—44128
Fe-Mo alloys, spinodal decomp. and modulated struct. form. on ageing *(Japanese)* 79—100184
Fe-Mo-Au, orienting of precipitating Au particles by external elastic stress 77—73279
Fe-Mo(V), nitrided by const. activity ageing, X-ray studies 77—32720
Fe-N, precipitated $Fe_{16}N_2$ nitride distrib. during isothermal ageing 77—21143
α-Fe-N, supersaturated solid solns., N atom precip. kinetics, resist. meas. 80—60864
Fe-N (0.022 wt.%), quenched, N precipitation during isothermal ageing 77—28820
Fe-N single crystals, solid soln. stress assisted nucleation of α'' precipitates 78—52810
Fe-N(C), solid soln., metastable and stable, interstitial atom config. 77—36512
Fe-Nb creep resistant alloy, precipitate free zones elimination 80—16312
Fe-Ni (31 at.%), austenitic, ageing, absence of at. order 77—11502
Fe-Ni martensitic alloys, age hardening 79—47736
Fe-Ni-Al, struct. of aged austenite *(Russian)* 77—52357
Fe-Ni-Al (30, 4wt.%), ageing, peculiarities of struct. state *(Russian)* 79—57008
Fe-Ni-Al-Ti alloy, N27Yu2T2, aged austenite, diffuse electron scatt. distrib. during martensitic deform. *(Russian)* 78—60669
Fe-Ni-Al-(Cu) (12, 0.5, 0.5 to 3 wt.%), Cu addition strengthening at 77K, mech. props. 80—60875
Fe-Ni-C, martensitic, mech. charact., effect of ageing and tempering *(Slovak)* 78—19791
Fe-Ni-C, martensitic, modulation of local C atom cumulation during ageing *(Slovak)* 78—19790
Fe-Ni-C, model alloy, intercrystalline brittleness caused by segregation and precipitation in austenite *(Slovak)* 79—70073
Fe-Ni-C, N31, martensitic point lowering by microplastic deform. and room temp. ageing *(Russian)* 77—25049
Fe-Ni-C (31.24, 0.21 wt.%) effect of deformation and ageing after deformation, on martensitic transformation temp. 78—76650
Fe-Ni-Co-Ti, martensite cryst. lattice tetragonality, $\gamma\rightleftharpoons\alpha$ transform. *(Russian)* 79—61587
Fe-Ni-Co-W(Mo) (18.65, 8.99, 4.87 wt.%), ageing characts., 380-530°C 80—60876
Fe-Ni-Cr, austenitic, creep strength and ductility, effect of γ' precipitation 77—36597
Fe-Ni-Cr alloy 800, minor alloying element effect on creep, ageing microstruct. 78—27572
Fe-Ni-Cr-Si alloy 800, Si effect on creep and age hardening 77—48444
Fe-Ni-Mn, martensite, aged, grain boundary embrittlement 79—96144
Fe-Ni-Mn martensitic alloy, precipitation 77—12630
Fe-Ni-Mo (16.4, 8.1 wt.%), effect of substituting Mo by W during ageing 80—29991
Fe-Ni-Si-Mn-Cr(Co-Mo), effect of prolonged aging on mag. props. 80—16513
Fe-Ni-Ta (-Co), alloys, Co effect on martensite ageing at 300-600°C *(Russian)* 80—20972
Fe-Ni-Ti, martensite, tetragonality, X-ray obs. 77—63665
Fe-Ni-Ti, shape recovery depend. on hardening *(Russian)* 79—83259
Fe-Ni-Ti, undeformed metastable alloy, cellular decomposition of austenite during ageing *(Russian)* 79—100178
Fe-Ni-Ti (27.4, 2 to 3 wt.%), aged, stress induced martensitic transform., mech. props. *(Russian)* 79—87632

ageing continued
Fe-Ni-Ti (30, 6 wt.%), austenitic, discontinuous coarsening of lamellar cellular precipitates, morphology 79—78967
Fe-Ni-Ti (30, 6 wt.%), austenitic, discontinuous coarsening of lamellar cellular precipitates, growth kinetics 79—78968
Fe-Ni-Ti (31.2, 5.3 wt.%), γ-phase ageing effect on martensitic transform. *(Russian)* 77—28814
Fe-Ni-Ti alloy, ageing mechanism, neutron diffr. expts. *(Russian)* 78—48403
Fe-Ni-Ti martensitic alloy, γ' particle effect on crystallisation struct. *(Russian)* 78—44129
Fe-Ni-Ti-C (31, 4, 0-18 wt.%), coherent precipitates in austenite, effect on martensite substruct. 77—52327
Fe-Ni-V, effect of low temp. ageing on props. during high temp. ageing *(Russian)* 78—39811
Fe-Ni-V, nitrided austenitic alloys, modulated substitutional interstitial solute atom clustering 79—74160
Fe-Ni-V alloy, ageing of martensite *(Russian)* 78—39808
Fe-Ni-V-(CO) alloy, lattice parameter variation during ageing *(Russian)* 78—39812
Fe-Ni-(Cu) (12, 0.5 to 3 wt.%), Cu addition strengthening at 77K, mech. props. 80—60875
Fe-P-C, embrittlement by crystallisation *(Japanese)* 78—48513
Fe-Pt (24 at.%), colour metallographic technique, for studying microstructural reproducibility, in martensitic transformations 78—72954
Fe-Si-B, embrittlement by crystallisation *(Japanese)* 78—48513
Fe-Ta alloy, mech. drawn and aged, exam. of electrical resistivity, hardness, microstruct., and mag. props. *(Japanese)* 78—48545
Fe-Ti-C, rapidly quenched by splat-cooling 80—84923
Fe-W-Cr-Mo-Co with austenitic phase, magnetic and mech. props., cold working and ageing effects *(Japanese)* 78—60678
$(Fe_{1-x}Co_x)_y$PBAl metallic glasses, influence of composition and ageing on Curie temps. 77—85445
FeN alloy, coercive force, effect of $Fe_{16}N_2$, anisotropic model 77—85501
$Fe_{32}Ni_{36}Cr_{14}P_{12}B_6$ metallic glass, effect of pre-ageing on glass transition temp. 80—100326
$Fe_{40}Ni_{40}P_{14}B_6$ glass, struct. relax., ferromag. reson. and X-ray scatt. 79—90566
$Fe_{40}Ni_{40}P_{14}B_6$ metallic glass, ferromag. reson., spin waves, thermal ageing and long-range order effects 80—25214
$(Fe_{0.5}Ni_{0.5})_{75}P_{16}B_6Al_3$ glass, struct. relax. as origin of Curie temp. ageing 78—84418
Fe_2O_3-Al_2O_3, solid solns., effect on Fe on point of zero charge 78—61021
$Fe_{75}P_{16}B_6Al_3$, aged metallic glass, Mossbauer effect 79—91318
$Fe_{78}Si_{10}B_{12}$, amorphous alloy crystallisation study *(Japanese)* 78—9959
Fo-Fe-Nb, cold-worked and aged, mag. props. and microstruct. 80—34690
GaAlAs/GaAs kink-free narrow-stripe proton-isolated injection DH lasers 80—58534
GaAlAs-GaAs DH laser diodes, long-life diodes for optical fibre communication 80—48246
$Ga_{1-x}Al_xAs$ DH laser, accelerated ageing test 79—76688
$Ga_{1-x}Al_xAs$ DH laser diode, long-lived, high-power, facet coated 80—58564
$Ga_{1-x}Al_xAs$ double heterostruct. lasers, aging characts. 79—72569
$Ga_{1-x}Al_xAs$ laser, buried heterostruct., stable operation during accelerated ageing at 70°C 79—7125
GaAs, photo-field cathode, ageing and surface state effects *(Russian)* 77—28703
GaAs-AlGaAs transverse junction stripe laser, single mode behaviour after 12000 hr ageing test 78—66831
GaP, surface layers produced by chemical treatment, comp. and struct. 79—96173
GaP:ZnO, LED, degradation, temp. and current depend. 79—87144
Ge, photo-field cathode, ageing and surface state effects *(Russian)* 77—28703
He-Cd segmental tube laser ageing *(Bulgarian)* 79—18441
Hf-Nb (30 to 50 at.%) exam. of beta phase decomposition processes 78—76674
$Hf_{0.65}Nb_{0.35}$, superconducting alloy, transition temp. and flux line pinning 77—43772
HfO_2, monoclinic, microcracking, elasticity, internal friction, thermal expansion meas. 79—29195
$(Hf_xZr_{1-x})_{80}Nb_{20}$, precip. of high vol. fraction of ω-phase particles 79—8304
InGaAs-InGaP vapour-grown ternary heterojunction laser struct., reliability 79—98385
InGaAsP/InP injection lasers for long wavelength (1.1 to 1.6 μm) optical communication 80—58582
InGaAsP-InP, double heterostructure laser lifetime, point defect generation model calcs. 80—32992
InGaAsP-InP buried heterostructure lasers emitting at 1.3 μm, accelerated ageing characts. 80—95898
InGaAsP-InP DH lasers, degradation by In solder 79—98402
InGaAsP-InP DH LED, high temp. aged, dark-spot defects, TEM obs. 80—66300
InGaAsP-InP vapour-grown quaternary heterojunction laser struct., reliability 79—98385
$In_{1-x}Ga_xAs_yP_{1-y}$-InP DH laser, 10000 h continuous CW operation, dark-line and dark-spot defects 79—98384
KCl:Pb, impurity distrib., light scatt. and microhardness study, heat treatment 80—96562
KCl:Pb^{2+} crystals, precipitation, density changes, nucleation mode, lattice relaxation, heat treatment 79—66066
LiF, refractive index, effect of ageing, wavelength range 460-1000 nm 80—84707
LiF:Co, flow stress changes during precipitation 80—92594
LiF:Mg^{2+}, TLD-100, solution treatment temp. and ageing effects 77—56480
LiF:OH, neutron irrad., interstitial H-centres, ESR obs. 80—93175
$LiNbO_3$:Fe spatial holograms, use of thermal fixing *(Russian)* 80—74311
LiO_2-$2SiO_2$, glass, devitrification with ageing 78—79536
LuOOH, $Lu(OH)_3$, growth from gel on ageing, X-ray diffr. patterns 80—24386
Mg alloy, quenched-in defect behaviour, effect on flow stress 79—61625
Mg-Al (9 wt.%), ageing via cellular reaction, microanal., cell boundary vel. meas. 78—11230
Mg-Al-Zn (9wt.%Al), sand cast, preferred orientation and mechanical props. *(Japanese)* 80—20979

ageing continued

- Mg-Ce, workability, aging characts. and tensile strength 80−55416
- Mg-Ga (6 wt.%), precipitation, lattice const., ageing effects *(Chinese)* 79−43279
- Mg-La, workability, aging characts. and tensile strength 80−55416
- Mg-Li-Al (31, 1 at.%), heat treated, precipitation 80−40364
- Mg-Tb, (up to 45 wt.%), phase diagram, and mech. preps. 80−16277
- Mg-Y-Nd-Zn-Zr (2,2,0.3, 0.7 wt.%), heat treatment effect on casting dimensional stability, alloy mech. props. 78−44146
- Mg-Zn alloy, aged, one dimensional transition phase β'_2, crystallographic obs. *(Chinese)* 80−60865
- MgCd wire, elongation during disorder-order transform. *(Russian)* 80−104148
- MgF_2-Na_3AlF_6 thin film deposits, quenched ageing by chopping 80−97364
- MgF_2-PbF_2, multidielectric stacks as interf. filters, ageing characts. *(French)* 77−34939
- Mn-Cu, alloying behaviour and high damping capacity 80−35160
- Mn-Cu alloys, mechanical damping at 40 kHz 78−23755
- Mn-Cu structural alloys, physicomechanical props. 77−12652
- MnCu, neutron scatt. near crit. comp., effects of stress and ageing 79−19722
- $Mn_{17.5}Cu_{82.5}$, mictomag. 800 hours at 373K, alternating mag. susceptibility meas. on fast quenched wire 78−3157
- MnO-CoO-O_2, semicond. solid solns., ageing effects on elec. cond. 78−23085
- Mo alloy, long-term ageing effects on ductility and microstruct. 77−44348
- Mo, blistering and surface roughening, room temp. ageing effects Ar^+ ion bombardment 78−34550
- Mo, high purity single crystal doped with C, low temp. mech. props. 77−77544
- Mo-Zr-C (0.063, 0.06 wt.%) alloys, ageing, effect of cold deform. by hydrostatic extrusion 79−57001
- Mo-Zr-C (0.63, 0.06 wt.%), quenched and deformed, structural changes during heating to ageing temp. *(Russian)* 79−1879
- Na_2O-SiO_2, glass, devitrification with ageing 78−79536
- Na_2O-SiO_2:Au+CeO_2, Au particle nucleation 80−81066
- Nb alloy SVMTs, high-temp. ageing, struct. and morphology of hardening phases *(Russian)* 80−40390
- Nb alloys, long-term ageing effects on ductility and microstructure 77−44348
- Nb, blister form. on single crystal under Ne^+ ion bombardment 78−71772
- Nb, cold-worked, Snoek-Koster relaxation transient period, comparison with Schoeck's theory 79−34086
- Nb, deformed, temp. effects on ageing, interstitial conc. depend. *(French)* 77−21182
- Nb superconducting films, penetration depth measured with Nb-NbO_x-PbIn Josephson junctions 79−42691
- Nb-H, behaviour of H in Nb, relation to mech. props. 78−80572
- Nb-Nb_3Al superconductor, fabrication by quench-age method 77−40403
- Nb-Nb_xO_y-Pb Josephson tunnel junction form. and ageing, adsorbed gas effect *(Russian)* 78−14899
- Nb-Nb-Al-(Cr), γ/γ'-δ type eutectic, fatigue, effect of composition and microstruct. 78−48520
- Nb-Ti (60 at.%), aged, TEM exam. of precipitation process *(Japanese)* 78−48409
- Nb-Ti superconducting alloy, critical current density, heat treatment effects *(Japanese)* 78−14909
- Nb-Ti-Zr, superconducting, ageing effect on critical current density *(Japanese)* 79−61747
- Nb-Ti-Zr, superconducting, critical current density and microstruct. correlation *(Japanese)* 79−61748
- Nb-W-Mo-Zr (5, 2.1, 0.92 wt.%), creep resist., high temp. ageing in vacuum 80−71716
- Nb-W-Mo-Zr-C, strength and ductility, prolonged high-temp. soaking effect 80−55483
- Nb-Zr-C alloy, creep in vacuum, prolonged high-temp. ageing effects *(Russian)* 78−56692
- Nb-Zr-C alloy, effect of ageing on high temp. strength *(Ukrainian)* 79−52249
- Nb-Zr-C alloy, long term strength rel. to carbide precipitate geometry *(Ukrainian)* 78−92266
- Nb-Zr-C alloy, struct. changes during stressed and unstressed ageing at 900, 1100°C *(Russian)* 79−29064
- Nb-Zr-C welding solid solutions, ageing kinetics, influence of inclusion elements *(Russian)* 80−100853
- $Ni_{75}Si_8B_{17}$, amorphous alloy, crystallisation study *(Japanese)* 78−9959
- Ni alloy 718, intermetallic second phase obs. using electrolytic extraction and SEM 79−34074
- Ni alloy EI617, creep, effect of preliminary heat treatment on struct. and props. 77−21195
- Ni alloy Mar M200, directionally solidified Hf additions, effect of vol.% γ' on creep rupture 78−27526
- Ni base alloy IN 738 LC, overaged, creep and fatigue crack growth 77−86138
- Ni base superalloy IN-738, γ' precipitate coarsening during ageing and creep 79−52271
- Ni, cathodically H charged, isothermal ageing 79−15703
- Ni, deformed, struct. form. during annealing, Ni_3Al type ordered phase precipitation *(Russian)* 80−45325
- Ni-Al, order hardening, comparison between revised theory and expt. 80−93565
- Ni-Al (12.8 at.%), irradiation enhanced coarsening 79−66060
- Ni-Al (14 at.%), two stage ageing effect on spatial distrib. of γ'-phase particles *(Russian)* 78−39805
- Ni-Al-Cr, strain hardening, participation of various slip systems *(Russian)* 79−24536
- Ni-Al-Cr(Ti), ageing kinetics and γ'-phase particles spatial distrib. under applied load *(Russian)* 77−32598
- Ni-Al-Mo (12.7, 21.6 wt.%), directionally solidified eutectic composite, precipitation 80−108454
- Ni-Al-Ti cast superalloy, eutectic transform. on ageing *(Chinese)* 79−100110
- Ni-base alloy, age hardened, stress corrosion cracking resistance, plastic deform. and microstruct. relation 77−63829
- Ni-base superalloy, conventional and powder metallurgical, σ-phase precipitation 80−11646
- Ni-Be alloys, struct. and phase stability in neutron bombardment field *(Russian)* 77−76467

ageing continued

- Ni-C (1.8 at.%), precipitation of graphite and NiC TEM obs. 77−52334
- Ni-Co-Al alloys, continuous precip., SEM, TEM, X-ray diffr. study 80−89220
- Ni-Co-Cr-Mb-W-Ta, Cr, Mb, W, Ta effects on σ phase occurrence 77−36507
- Ni-Cr, deformed, struct. form. during annealing, Ni_3Al type ordered phase precipitation *(Russian)* 80−45325
- Ni-Cr-Al-Ti alloy, KhN78TYu, heavily deformed, subgrain struct. due to discontinuous precipitation of γ' phase *(Russian)* 79−52218
- Ni-Cr-Fe-Mo-Co (21.41, 19.28, 8.64, 2.16 wt.%), Hastelloy alloy X, exam. of thermal stability 78−84865
- Ni-Cr-Mo-Fe-Mn, Kh12M23, intermetallic phases exam. *(Russian)* 78−39740
- Ni-Cr-Mo-W-Al-Ti, heat-resist., phase comp. 80−76250
- Ni-Cr-Ta alloy, precipitation hardening, 650 to 800°C 77−59798
- Ni-Cr-Ti (19.51, 4.2 wt.%), quench-ageing and fracture *(German)* 77−70088
- Ni-Cr-Ti-Al alloys, precipitation of γ' phase during single and combined ageing treatment *(Russian)* 77−52328
- Ni-Cr-Ti-Al-Fe-Co (19.65, 2.40, 1.37, 0.78, 0.52 wt.%), strength of γ' hardened alloy, ageing exam. 78−88501
- Ni-Cr-Ti-Al-Mo-Nb-Fe (13-16, 2.35-2.75, 1.3-1.7, 2.8-3.2, 1.8-2.2, 2.0 wt%), heat resistant props, mech props. struct., stepwise ageing effects *(Russian)* 78−76666
- Ni-Cr-W(Mo)(Ti)(Al), long range ordering of matrix of complex heat resistant alloys *(Russian)* 77−77509
- Ni-Cu-Si, Si effect on structural changes during ageing, TEM and X-ray obs. 78−15438
- Ni-Cu-Si (38,5 at.%), changes in modulated struct. during ageing early stages *(Japanese)* 79−100183
- Ni-Fe solid soln., precip. hardened, paramag.-ferromag. transition on ageing 78−52255
- Ni-Fe-Cr superalloy 718, heat treatment effect on room temp. and elevated temp. fracture toughness response 80−100922
- Ni-Fe-Nb-Al (11.2, 8.09, 79.66 wt.%), modulated struct. growth process rel. to ageing *(Chinese)* 80−66541
- Ni-maraging weld metal, increasing fracture toughness by heat treatment 78−72871
- Ni-Ni_4Mo, strengthening by ordered precipitates 77−86041
- Ni-P, amorphous electrodeposited alloys, phase-separation *(Japanese)* 80−54140
- Ni-Si-B, embrittlement by crystallisation *(Japanese)* 78−48513
- Ni-Ti (10 wt.%), X-ray study of ageing of plate and powder 77−1847
- Ni-Ti (8 and 10 wt.%) alloy, aged, precipitation behaviour at 550 to 950°C, X-ray and electron microscopy exam. 78−39785
- Ni-Ti (9.6 wt.%), mag. study on phase decomposition *(Japanese)* 80−15758
- α-Ni-Zn, continuous precipitation kinetics *(Russian)* 78−76652
- Ni-Zn, physical-chemical metallurgy *(German)* 80−108390
- NiAl martensite, Ni-rich, precip. of Ni_3Al, mechanism 77−86033
- NiCr thin film resistor, 'clean vacuum' deposition equipment suitability obs. *(Polish)* 79−15611
- Ni_3Fe, short range order determ. after heat treatments 79−96044
- $(Ni_{1-x}Fe_x)_{1-y}S$, anomalous thermal hysteresis in metal-semicond. transition 80−39640
- Ni_4Mo, stoichiometric and quenched, short range order and order-disorder transform. 79−78955
- NiO:Mn, microhardness, plasticity, ageing effects 79−43291
- PLZT ceramic, ageing, dielec. props. 80−88940
- PLZT, effect of ageing on temp. depend. of permittivity, for ferroelectric and antiferroelectric compositions 78−48121
- PLZT, reduced, exam. of ageing phenomena, using dielectric hysteresis *(German)* 79−33647
- PLZT transparent ceramics, electro-optical anisotropy due to hot pressing 77−12720
- Pb-Ag (0.068 wt.%), Ag precipitation kinetics and activation energy 80−66517
- Pb-As (~0.01 wt.%), enhanced precip. phenomena, invest. of mechanism by elec. resist. meas. 80−104162
- Pb-Ca-Sn, effect of Sn additions on precipitation behaviour, of Pb-Ca alloys *(German)* 78−52821
- Pb-Cd (1.5 wt.%) discontinuous precipitation, metallographic study *(Japanese)* 77−48440
- Pb-Sb (1 wt.%), highly averaged, fracture behaviour 79−8366
- Pb-Sb battery grids, ageing behaviour obs., effects of casting and cooling 79−100517
- Pb-Sb-As (1.1-1.8, ~0.01 wt.%), enhanced precip. phenomena, invest. of mechanism by elec. resist. meas. 80−104162
- PbIn superconducting films, penetration depth measured with Nb-NbO_x-PbIn Josephson junctions 79−42691
- $PbNb_2O_6$, O defects and elec. props. anomalies 79−42898
- $Pb_xSn_{1-x}I_2$, thin films, photosensitivity, ageing and annealing effects *(Russian)* 78−6804
- $Pb(Zr,Ti)O_2$ ceramic, surface barrier electroreflectance, hysteresis, ageing 80−80752
- $Pb(Zr,Ti)O_3$ ceramic, permittivity and resonant frequency ageing, space charge field effects 77−85657
- $Pb(Zr,Ti)O_3$ ceramics, space charge field meas. by ferroelec. domain switching current, piezoelec. reson. freq. ageing characts. 80−7296
- $Pb(Zr,Ti)O_3$ ceramics, DC field sintering preparation, piezoelectric props., ageing behaviour 80−81211
- $Pb(Zr,Ti)O_3$:Fe(Nb) ceramic, elec. and electromechanical props., depend. on dopants 80−81212
- Pd film, VPE growth on Au(111), interface struct. 79−95297
- Pd-Ag-Cu (35,25 at.%), determ. of ageing transformations by resist. meas., metallography, TEM and X-ray diffr. 79−4967
- Pd-H, dil. α-phase, influence of deform. on low-temp. sp. ht. 77−31783
- Pd-H, nature of the 50K anomaly, residual resist. 79−7818
- Pd-Ni-Si amorphous alloys, crystn. process during isothermal ageing 80−89275
- $PdH_{0.73}$, 50K transition, γ-ray and neutron diffr. study 79−14932
- $Pd_{100-x-y}Si_xFe_y$, amorphous, ^{57}Fe Mossbauer spectra, X-ray diffr., ageing behaviour 79−28651
- Pt-Co, magnetically hard, struct. and morphology, electron microscope study 79−82171
- Se, amorphous, struct. relax. effects, obs. by mech. props. *(French)* 79−51201
- Se, amorphous films, evaporated, ageing and crystn., DTA 80−65413
- Se amorphous layers, dielectric relax. in glass transition range, ageing 79−82923

ageing continued
Se electrophotographic films, ageing effects on structure and properties 77–47699
Se film, noncryst., ageing and crystn. obs., tentative struct. model 80–2295
Se, vitreous, elastic coeffs. about glass transition temp. US study *(French)* 80–19865
Si ion-controlled diodes, acid-base exposure effects, Si-SiO_2 interface state density 80–96984
Si, photo-field cathode, ageing and surface state effects *(Russian)* 77–28703
Si, Schottky diode ageing, influence of metal electrode O diffusion coeffs. 79–99620
Si, stacking fault form. model during oxidation and ageing, defect clustering 77–24322
Si-Au Schottky diodes, role of O in formation mechanics 79–42639
p-Si-$In_{2-x}Sn_xO_{3-y}$ solar cells, thermal degradation mechanisms 80–55841
Si-SiO_2 interface, thermally grown, surface pot. inhomogeneities after stress ageing 80–92993
Si_3N_4 thin film, reactively sputtered, struct. and elec. props. 80–88656
SiO_2-Si interfaces, surface state form. during bias-temp. stress aging 79–78193
SiO_2-ZrO_2 adsorbents, coprecipitated, porous struct. rel. to form. conditions 78–53263
Sm-Co, decomp. kinetics when aged, X-ray mag. props. and metallography study *(Russian)* 78–56644
$SmCo_5$ permanent magnet, liq. phase sintered, hysteresis loops, ageing, temp. depend. *(Chinese)* 77–51921
$SmCo_5$, permanent magnet stability, during long-term ageing *(Chinese)* 80–55428
$Sm_{1-w}MM_w(Co_{1-x-y}Cu_xFe)_z$, (MM-mischmetal), mag. meas. and metallographic exam. 77–56119
Sn coating on Cu wire, growth of diffusion layer due to ageing effect *(Polish)* 80–34227
Sn-Ni, electrodeposited, thermal stability 77–52319
Sn-Ni metastable alloy, surface film comp., time depend., XPS 78–60870
Sn-Pb surfaces ageing, detrimental effect in PC fabrication 80–108625
SnO_2, sputtered film, thermal ageing, thickness dependent effects 78–6462
SnPb 38, superplasticity, effect of ageing *(Czechoslovakian)* 77–32644
$Sr_{0.75}Ba_{0.25}Nb_2O_6$, ceramic ageing dielec. props. 80–88940
steel, 36NKhTYu, aged, rate of discontinuous precipitation of γ'-phase, short high-temp. treatments *(Russian)* 78–11226
steel, austenitic stainless, 18 Cr-11 Ni, effect of boron on nucleation of $M_{23}C_6$ carbides *(Polish)* 78–84808
steel, Cr-Ni, ferrite precip. *(Japanese)* 80–35187
Ta-Al-N thin film resistors with improved elec. props. 80–100544
Ta-N (0.6 to 6.5 at.%), supersaturated solid soln., precipitation 79–96028
Ta-N (4 at.%), TEM obs. of ordering 79–96021
Ta-O solid soln., interstitial ordering and precipitation at 100 to 270°C, exam. 78–52813
Ta-O supersaturated solid solution, precipitation processes, hardness change meas. 80–25712
Ta-W-Hf, embrittlement, effect of composition 77–21247
$Te_{80}Ge_{15}Pb_5$, DSC sensitivity to controlled ageing in glass transition region 80–71673
ThO_2:Y_2O_3, electrochem. cell, complex impedance, temp. and freq. depends. 77–1458
Ti alloy, hardening heat treatment, alloying element effects development trends 78–95759
Ti alloy, VT16, decomposition of metastable β-phase *(Russian)* 78–68710
Ti alloy, VT23, ht. treatment effects on fracture *(Russian)* 78–80623
Ti alloy VT16, strengthening heat treatment in vacuum 79–79013
Ti alloy VT22, hardening during thermomechanical treatment, precipitate particle internal struct. *(Russian)* 79–91657
$\alpha+\beta$Ti alloy VT3-1, drop forgings, grain orientation and props., combined mech. working, hardening and high-temp. heat treatment influence *(Russian)* 80–20973
$\alpha+\beta$ Ti alloys, fracture, influence of phase comp. in VT16 and VT9, quenching effects *(Russian)* 78–56665
β IIITi alloys solution treated and aged, estimation of precipitate volume fraction using Young's modulus 78–39781
Ti, commercial purity, stress relaxation expt. 77–48472
α-Ti, hydride precipitation, resistometric investigation, isothermal ageing effects *(Japanese)* 77–81265
Ti, passive oxide layer form. in H_2SO_4, ageing with and without photoexcitation *(French)* 80–45432
Ti, yield pts. obtained by ageing at two stresses 80–81091
Ti/Cu/(Au) thin films thermocompression bonds degradation by thermal ageing 80–66546
Ti-Al (27.3 wt.%), arc melted, microstruct. 79–61577
Ti-Al film, struct. and elec. props. 80–7002
Ti-Al-Cr-Mo-Fe(V)(Zr), effect of structure and heat treatment on tensile strength, ductility, fatigue limit and notch sensitivity 78–56711
Ti-Al-Cr-Mo-U, alloy VT22, phase composition and fatigue strength 78–3219
Ti-Al-Cr-Mo-V, alloy VT22M, exam. of ageing and phase transitions *(Russian)* 79–11641
Ti-Al-Mo-Cr alloy weldment containing orthorhombic martensite, auto-tempering behaviour and alpha precip. strengthening 80–84976
Ti-Al-Mo-V (8, 1, 1 wt. %), stress corrosion cracking and slow strain rate H_2 embrittlement 78–48569
Ti-Al-Sn (5, 2.5 wt.%), annealing of near-basal hydrides 80–20989
Ti-Al-V, alloy 685, fatigue life, creep and dynamic strain ageing effect, 25 to 400°C *(French)* 80–45384
Ti-Al-V (6, 4 wt.%), cavitation induced erosion, under mill annealed, soln. treated and aged, and beta annealed conditions 79–8371
Ti-Al-V (6,4 wt.%), cyclic stress-strain response 77–21170
Ti-Al-V-Cr-Mo-Zr (3,8,6,4,4 wt.%), beta-C, microstruct. effect on mech. props. 78–27577
Ti-Al-V-Cr-Zr-Mo (3, 8, 6, 4, wt.%), phase transforms. 79–100113
Ti-Al-V-Sn(Mo-Fe), heavy section extrusion, fabrication and mech. props. 78–6985
α-Ti-Al-Zr (6.16, 5.23 wt.%), alloy IMI 685, electron microscope observations of strain induced hydrides 78–72828
αTi-Al-(Zr), embrittlement due to ageing 78–56673

ageing continued
Ti-Cr, phase transformation, appl. of Philips STEM400 system 80–25689
Ti-Cr (15 at.%), aged omega phase, electron microscope exam. 78–72783
Ti-Cr(Mo), alpha precipitation kinetics 78–68697
Ti-Cu-Al(Zr)(Sn)(Nb)(Mo), heat treatable alloys, effect of alloying on strength, tensile props. 78–56671
β-Ti-Fe, (7.1 wt.%) exam. of ω phase formation, by X-ray diffr. and Mossbauer spectroscopy 78–52800
α-Ti-Fe(0.22 wt.%), ω phase form. during ageing 77–52355
β-Ti-Mo, alloy, struct. changes during deformation and ageing *(Russian)* 78–39791
Ti-Mo, martensitic alloy, decomposition by nucleation and growth and spinodal mechanisms 79–61590
$\beta-$Ti-Mo, thermal instability, hardness and tensile deform. *(Japanese)* 80–71703
β-Ti-Mo-Cr-Al (8, 4.5, 2.5 wt.%), metastable, tensile ductility, α-phase morphology and distrib. effect 77–86098
Ti-Mo-Fe (3, 0.13 at.%), metastable phases, Mossbauer study 80–7243
Ti-Mo-Fe-Cr-Al, alloy VT3-1, influence of constitution on fracture toughness *(Russian)* 77–77559
Ti-Mo-V-Fe-Al (8,8,2,3, wt.%), exam. of stress controlled fatigue response 79–61734
β-Ti-Mo-V-Fe-Al (8,8,2,3 wt.%), metastable, high cycle fatigue crack initation, grain size effect 77–86145
β-Ti-Mo-V-Fe-Al (8,8,2,3 wt.%), metastable alloy, microstruct. and mech. props. ageing time and temp. effect 78–64569
Ti-Mo-Zr-Sn (11.5, 6, 4.5 wt.%), β III, mech. props. rel. to heat treatment 80–84961
Ti-Mo-Zr-Sn (11.5, 6.0, 4.5 wt.%) alloy, struct. as affected by processing history 80–84972
Ti-Mo-Zr-Sn-Fe-C-Si alloy, β-III, cold deform. and annealing, effect on struct. and mech. props. *(Russian)* 79–24533
β-Ti-Mo-Zr-Sn(11.5, 6, 4.5 wt.%), metastable phase III, microstruct. and age hardening response 80–84945
Ti-Mo-Zr(-Al) (15, 5 (3) wt.%), quenched and aged metastable β-phase, crystallography, morphology and decomposition 80–76262
Ti-Nb, cold strained, exam. of ω and α phases, precipitated during ageing *(Russian)* 79–11620
Ti-Nb alloys, Fe, Mo, V, Ta alloying additions on microstruct. after combined treatment *(Russian)* 77–59826
Ti-Nb-V(25 wt.%, 15 wt.%), precipitation of β and ω phases during ageing at 350°C 77–8838
Ti-Nb-Zr-Fe-Mo-V, cold worked, struct. and phase transform. during ageing 78–3153
Ti-V (19 at.%), aged ω-phase precipitation, incomplete proximity effect 78–60252
Ti-V (27 and 30 wt.%), fatigue crack propag., in single and poly. crystals 79–5048
Ti-V-Mo-Cr system, β-phase stability 80–55353
Ti-V-Si, Si effects on precipitation and strengthening 77–55970
Ti-V-Si (30, 1 at%), quenched and aged, hardness, tensile behaviour and phase transform. 79–11646
βTi-V-Si (40, 1 at.%), Si effect of precipitation and age hardening 77–63676
α-Ti-Zr-W, effect of W impurity on mech. preps. 80–16392
α-β TiAl-Sn-Zr-Mo (6,2,4,6 wt.%), age hardening 79–61604
TiC, ageing and ordering phenomena *(Russian)* 78–39807
TiC, TiVC, on steel, sputter deposited, adhesive quality 77–12531
$TiH_{1.8}$, tritiated, NMR of ^3He formed by β-decay, radiation damage, ageing 77–24751
TiN_x, cryst. and internal structs., electron diffr. and microscopy 77–27861
TiO_2, rutile ceramic, in strong electric field *(Polish)* 78–52869
TiO_2, rutile ceramics, capacitors, anomalous cond. 78–14836
TiO_2, rutile ceramics capacitor, elec. cond. meas. 78–14836
$Ti_xZr_{1-x70}Nb_{30}$, ω phase precipitation 79–34042
U-Mo-Nb-Zr-Ti (0.75, 0.75, 0.75, 0.5 wt.%), heat treatment effect on microstruct. and mech. props. 78–23729
U-Mo(2 wt.%), mech. props., effect of ageing 77–8914
U-Nb (14 at.%), martensitic and polymorphic transformations 80–60861
U-Nb-Zr (7.5, 2.5 wt.%), elastically bent, ageing induced shape instability 77–16622
U-Nb-Zr (7.5, 2.5 wt.%), texture development role in shape memory effect 79–87661
U-Ti (0.75 wt.%), quench rate sensitivity, effect on microstruct., mech. props., ageing 77–70077
U-Ti(0.75 wt.%), mech. props., effect of ageing 77–8914
V, plasticity and strength change in temp. range 20 to 1000°C impurity effects 80–35235
V-N system, phase formation *(Russian)* 78–39739
VC_xN_y, superstructure induced by ageing, neutron diffr. obs. *(Russian)* 80–49195
V_3Ga, supercond. A15 phase, prep. by controlled precip. 80–81000
W, diffusion barrier between Ni-Cr-Al coatings and Ni eutectic alloys in gas turbines 79–24673
W, hot emitter, surface struct. change during baking above 2000K 79–65971
W, with impurities, grain boundaries, effect on high temp. plasticity *(Russian)* 79–79057
Y, polycrystn., plastic deform. at different deform. speeds, dislocation glide *(Russian)* 80–93598
Zn film, RF sputtered, ageing processes 78–84322
Zn film, RF sputtered, thickness dependence variations in electrical resistance 79–42674
Zn, sputtered film, thermal ageing, thickness dependent effects 78–6462
Zn-Al-Cu-Mg (22, 0.5, 0.01 wt.%), superplastic alloy, strengthening mechanism *(Japanese)* 77–55975
Zn-Al(22 wt.%), alloy sheet, superplastic, cold-rolling effects on mech. props. and microstructure *(Japanese)* 80–71671
Zn-Cd liquid/Fe-Ni-Al mag. powder, effective viscosity of composites *(Russian)* 80–54424
ZnO, black, possible use as spectrally selective coating for low temp. solar collectors 79–994
ZnS, electrolum. phosphors, surface phenomena occurring during ageing *(Russian)* 79–33842
ZnS, electroluminophor, ageing rate, voltage effects *(Russian)* 78–84662
ZnS electroluminophors, ageing effects *(Russian)* 78–15231
ZnS, photocell, transient photoelec. phenomena 79–82687

ageing continued
ZnS:(Cu, Cl), electroluminesc., voltage effect on ageing rate 79—95848
ZnS:Cu, halogen, electroluminescent cells, visible light and DC voltage effects on ageing 77—69914
ZnS:Cu,Er,Cl film, ageing and forming, DC electroluminesc., impact excitation 79—47522
ZnSe electroluminescent diode, ageing effects 77—8660
Zr, yield pts. obtained by ageing at two stresses 80—81091
Zr-Al (4.6 wt.%), microstruct. effect on mech. props. 79—20080
Zr-Cu (1.6 wt.%), near eutectoid, active eutectoid decomposition ageing and quenching effects 80—2993
Zr-Nb (2.5 wt.%), quenched-and-aged, neutron irradiated, 573 to 923K, damage struct. 79—99247
Zr-Nb alloy, isothermal decomposition at elevated temp. 78—27470
Zr-Nb-V-Al (Fe) alloys, decomp. of β solid soln., metastable and equilib. phases 79—11632
Zr-Sn-Mo (6, 1 wt.%), creep and creep rupture 78—23778
Zr-Ta (5 wt.%) martensite, β_1 precipitation, thermodynamics 79—74164
ZrO_2, crystallisation from $Zr(OH)_4$, effect of water vapour, heat treatment and grain size *(Japanese)* 79—19170
ZrO_2, MgO partially stabilized, microstruct. development during ageing 79—91710
ZrO_2, partially stabilised ceramics, strengthening, post-sintering heat treatment 80—97518

ageing characteristics *see ageing*

agriculture
see also farming
60 Hz electric field effect on plant growth and development 77—81534
acreage estimates using LANDSAT data, interactive software systems 77—78504
aerial data processing, automatic, for agricultural resources inventory and survey expt. 77—78505
afforestation effects on streamflow of large Soviet rivers 78—7675
agrometeorological data, information flow organization and processing automation 77—78430
agrometeorological survey, management of resources *(Italian)* 77—81989
air pollution by N_2O from fertiliser, causing atmos. warming 80—94579
ancient Mesopotamia, barley harvest dates rel. to temp. 79—5597
animal wastes, pollutant transport in runoff water, review 80—97831
anisotropic reflection properties of vegetated surfaces 77—82010
astronomy of Hopi Indians, agricultural and theological aspects 78—36472
bioclimatic coefficients and water consumption coeff., change with respect to climatic zones *(Russian)* 77—53169
biogeochemical cycles, role of atmosphere 79—79427
black locust biomass, surface mine reclamation 80—7894
cadastral maps and new technical developments *(German)* 77—70589
California, agricultural water demand information, remote sensing 79—2315
canopy interception, measure of loss from hydrologic budget 78—11928
chlorinated pesticides, in soils of Everglades National Park and adjacent agricultural areas 79—92098
chronobiology in plants 80—56328
citrus orchards, diseased, automatic interpretation of IR aerial colour photographs 77—56749
climatic change effects on food production, statistical models limitations 78—57303
conference, basic sciences and agriculture, New Delhi, India (Oct. '75) 80—51939
cover type separability in visible and IR remote sensing 77—29473
crop and soil bidirectional reflectance factor calibration, remote sensing field research 80—86382
crop canopy index values for various canopy densities 79—53420
crop damage by hail, effect of wind and shelter by trees 77—45097
crop damage by hail, wind effects and hailcube meas. 77—17173
crop discrimination, radiowave backscatter from vegetation, water cloud model 78—57274
crop drying and weather stabilisation, large orbiting mirrors to reflect sunlight 80—45632
crop identification and area estimation by computer aided LANDSAT data anal. 77—78503
crop response to hail suppression seeding, Nelspruit project, South Africa 78—57257
crop rows, effect on thermal radiation from terrestrial surface 78—16016
crop types remotely sensed by radar, side-looking method 80—46280
crops, Landsat data, pattern recognition, temporal trend analysis 78—65440
cultivated and natural vegetation mapping 77—56781
deep well irrigation power system, solar photovoltaic concentrator system appl. 79—92082
dew duration forecasting, Pendleton, Oregon, using simple weather obs. 79—70857
digital crop identification, high-altitude versus Landsat imagery 79—25357
drought effects on agriculture in United Kingdom, 1975-76 period 78—57298
drought in England and Wales, 1975-6, effect on agriculture 78—88890
drought in upper Midwest, USA, 1931 to 1969 period 79—70880
dust storms, Great Plains, USA, lessons 79—29486
effective rainfall analysis at Parbhani, India, rel. to irrigation planning 79—96794
effects of microwave energy on Acacia longifolia 79—53190
energy budget over grasslands, eddy correl. sampling technique 77—78446
EPR applications 80—56298
European agriculture rel. to climatic change 78—85679
evapotranspiration est. from thermal scanner meas. of crop temp. 77—5324
Everglades Agricultural Area, USA, soil temp. obs. in winter nighttime 80—56559
expansion in late 19th century rel. to CO_2 levels in atmosphere 78—53717
fertilizer rel. to N_2O atmospheric life cycle and O_3 reductions 78—16140
field burning practice, downwind particulate pollution 80—97836
flood inundation of agricultural land, LANDSAT digital image anal. 80—61913
Forest Service, US Dept. of Agriculture, digital terrain model appls. 79—84086

agriculture continued
genetic and physiological process control by magnetic methods *(Russian)* 79—2088
geomorphology, land exploitation organisation Svencionys upland structure and development *(Russian)* 78—20423
geothermal hot water for controlled horticulture 80—108783
German solar flat plate air collector development 79—62075
grass canopy spectral reflectance, 500-1000 nm, asymptotic value 77—64442
grass canopy spectral reflectance, soil spectra contributions 77—87126
greenhouse solar distillation and cultivation materials 79—74496
groundwater contamination, Holt County, Nebraska, USA 80—12033
growing season length as climatic indicator, fluctuations 80—61887
growing season variations in China in historical past, from written records *(Chinese)* 80—109246
Gujarat, India, short period rainfall characts. rel. to crop planning 79—96791
hail suppression, crop protection, involvement of society 79—8677
hail volume model extrapolation from surface meas. 77—21871
hail-prevention operations, cost effectiveness estimation methods anal. 78—93013
hailstorm damage to vegetation, LANDSAT remote sensing epxt. *(Italian)* 77—81986
hailstripes, aerial photographs of crop damage patterns 78—3848
Haryana State, India, cumulative periods of rainfall statistical distrib. rel. to crop planning 79—96792
Haryana State, India, rainfall patterns rel. to crop planning 79—100902
heat recovery from nuclear plants for agriculture and pisciculture 78—37464
historic climate correl. with wheat prices and wages 78—81346
horizontal-axis wind-turbine system for pumping duties in Third World agriculture, design 80—61259
identification of rice-growing land from teledetection data *(French)* 79—96775
India, effects of drought 77—56707
industrial complex environmental impact, Whatcom County, Washinton, USA 79—57532
International Solar Energy Congress, New Delhi (1978) 79—57357
IR aerial photography for agriculture, potato blight detection 80—13174
Iraq, frost phenomena and damage 77—73795
Irish solar energy developments 79—57378
irrigation, connection between soil and groundwater 80—26554
irrigation, influence on radiation balance of Earth surface and components 79—29863
irrigation, kinematic model 79—5529
irrigation and groundwater salinity, river basin salt balance management 77—78276
irrigation detection in the Loire-Britanny river basin *(French)* 79—96774
irrigation in Karnataka State, in India, wind power and potential appls. 80—108782
irrigation plants using solar or wind power, comparison w.r.t. cost, maintenance and reliability 79—70425
Israel, water shortage and supply, long-run policy for agriculture 78—61454
Kuwaiti solar energy research, development and demonstration programme 79—57371
land biota changes rel. to C cycle and atm. CO_2 77—70785
land-use mapping, evaluation of LANDSAT image data 80—101443
land-use mapping by machine processing of LANDSAT-1 data 77—78467
LANDSAT agricultural monitoring program to monitor corn in Iowa 77—78495
LANDSAT agriculture landuse survey, Texas 77—82050
LANDSAT data for determining unharvested winter wheat acreage 77—78508
LANDSAT digital data for classifying vegetative cover 77—78543
LANDSAT digital data for detect. of moisture stress by Green Index Number method 80—17423
LANDSAT digital data for forest vegetation and land classification, in Minnesota 77—78528
Landsat views of Earth, book 78—7643
laser applications *(Chinese)* 77—68216
loamy sand, Flanders hilly region, quantitative rill and gully erosion study 77—81936
maize canopy, eddy momentum fluxes 77—91203
Malawi solar energy utilisation prospects 79—57379
micrometeorology aspects, field crops and glass houses *(Dutch)* 77—64389
microwave probe for subsurface soil moisture profiling 78—65939
moisture meas. methods, review *(Polish)* 79—2776
New Zealand, temp. record, historical data and agricultural implications of climatic var. 80—61886
nitrogenous fertilisers and soil as atmospheric N_2O source 78—61419
NMR, pulsed, appls. 80—56297
optical radiation influences on plants and animals, appls. *(Japanese)* 78—44556
perennial grasses potential yield and yield shortfall due to water deficit, agroclimatic estimate 78—61450
phosphate fertilizers, leaching from agricultural soils to groundwater 79—20901
phosphate fertilizers, occupational dose from natural radionuclides 79—100751
photosynthesis bioenergetics 80—61521
photovoltaic powered irrigation and grain drying expt., 25 kW, US development 79—70442
physics in agriculture, various applications 80—31481
plant and soil monitoring, from tethered balloon, multispectral radiometry 78—3958
plant canopies reflectance meas. using spectroradiometer 80—56658
plant Pb uptake near roads in Eqypt 79—12255
poly chlorinated biphenyls, in soils of Everglades National Park and adjacent agricultural areas 79—92098
power station waste heat utilisation for fish farming and agriculture *(German)* 80—101080
prairie region of Canada, hailstorm damage problem 80—109204
products, development possibilities of energy resources *(German)* 80—21355
radiation and isotopes appl., development trends 78—55041
radioisotope applications in agriculture, hydrology, medicine industry etc., booklet 78—35947

agriculture continued
remote sensing, agricultural cover types separability in spectral channels and wavelength regions 80—98468
remote sensing, environmental potential survey in Japan 78—57374
remote sensing, max. likelihood estimation of signature transformation algorithm 77—78497
remote sensing, use of photographic imagery and pattern classification techniques 77—64454
remote sensing applications 80—56329
remote sensing data, harvest prediction, man computer optimal system *(Italian)* 77—82059
remote sensing of natural resources using satellite and aircraft scanner data for Finland 79—100988
reservoir management for irrigation, chance-constrained linear programming 79—2317
Saskatchewan, 1971 growing season, CO_2 concs. over native grassland 77—45120
satellite remote sensing appls. 77—25788
sediment graph model based on instantaneous unit sediment graph 79—53394
shelled, dielectric loss and moisture meas. using microwave technique 77—77142
soil, moist, emissivity in microwave range, temp. effect 79—29797
soil and plant improvement by ferromagnetic additives *(Russian)* 77—66882
soil erosion processes meas. in German area of Moselle river valley 77—81937
soil moisture deficit estimation from meteorological factors 79—20890
soil moisture IR thermography remote sensing through agricultural crop 80—109147
soil moisture meas. by remote microwave radiometry 79—48526
soil moisture vars. under bare conditions rel. to rainfall at Pune and Delhi, India 79—96777
soil organic C rel. to CO_2 cycle and atm. CO_2 conc. 79—58063
soil warming, simultaneous heat and mass transfer governing eqns., waste heat utilisation 78—94562
soil warming, waste heat from nuclear power station 78—37463
soilborne pathogenic fungus population reduction by 2.45 GHz irradiation 80—3719
solar desalination appl., greenhouse installation in Grenoble *(French)* 80—55806
solar drying of crops, using no-glass flat plate collectors, analytical model 79—70465
solar energy, photosynthetic conversion in agricultural systems, incremental model 79—70457
solar energy utilisation, crop starting tunnels for vegetable growing season increase, test results 79—70438
solar energy utilisation, India's 1978 development trends 79—74509
solar heating, Czechoslovak projects *(Czech)* 79—70430
solar heating equipment appl., use of heat tube 79—57412
solar power utilisation in developing countries, conf. report, Varese, Italy (March 1979) 80—40834
solar pumping engine, irrigation, 7.5 W, with liquid piston, design and analysis 79—74537
solar pumps development, irrigation, 1978 status review 79—74506
solar pumps development in India, using biomass as auxiliary heat source 79—70461
solar technology and methods for appl. of solar energy to European agriculture 80—76616
space-borne remote sensing *(Italian)* 80—109333
spring runoff from arable land and saline soils *(Russian)* 77—21811
St. Louis area, land use and cover correl. with meteorological anomalies 79—12201
stratified acreage estimates in Illinois crop-acreage expt. using LANDSAT data 77—78501
subsurface drainage and irrigation, expt. evaluation of theoretical solns. 78-61465
surface runoff, New Zealand, P transport, effect of fertiliser and grazing cattle 77—53094
terrain classification using colour imagery, algorithms 77—78466
tobacco shreds, effect of glycerol and sucrose additions on props. *(Japanese)* 78—85113
Uttar Pradesh, influence of droughts on ground water supplies in Himalayan region 77—56708
UV radiation meas. in agricultural production, instrument *(Russian)* 78—65969
vegetation and crop development mapping, table look-up procedure 77—78531
vegetation canopy modelling for signature correction/anal. 77—78515
vegetation changes with maturity, solar elevation effects on sequential LANDSAT imagery 77—45159
vegetational surface, gaseous pollutant transfer 77—2233
water budget and potential reserves of East Africa source region of Nile 79—100880
water potential evaporation from crops surfaces, eqn. adaptable to remote sensing use 77—64334
weather and crop spraying, N.Nigeria 77—81983
weather modification, economic context 79—20936
weather modification, insurance perspective 79—20937
weather modification economics, review, future anal. 79—20927
weather service, New Jersey, user survey 80—4065
weighing apparatus for hydraulic lysimeter in the Western Australian cereal belt 79—12276
wheat, plant canopy light absorption model 78—88913
wheat acreage estimation, LANDSAT-based, two phase sampling 77—78502
wheat canopy reflectance, Suits' spectral model appls. 78—7811
wheat field 2,4-D herbicide concs., pollution aspects 77—17213
wind furnace systems, advanced, for residential and agricultural heating and power supply 79—48070
wind turbine appl. in tropical countries, bird scarer for orchards and grain fields 79—70423
windmill for use in irrigation, with horizontal axis sail 80—21368
winter wheat acreage estimation in Kansas, cloud cover effect on LANDSAT data 77—78509
winter wheat yield on Great Plains, Landsat data and soil moisture evaluation 78—65351
world predicament and climatic change, need for interdisciplinary research 78—57300
^{14}C, liquid scintillation counting efficiency, volume and quenching effects 79—76270

agriculture continued
N fertilised soil, N_2O evolution rates 79—16656
N fertilisers, perturbation of stratospheric O_3, independent variables anal. 78—73505
N fertilizer and stratospheric ozone 79—21007
NH_3, in troposphere, effect of nitrate fertilisers 80—85701
NH_4^+ fertilisers and soil N_2O emission, effects of acetylene and water content 79—83672
NO_3^--N export from drainage basins, Toronto, Ontario 79—66729
N_2O in soil, losses dissolved in drainage water 79—43797
P loading of lake from non-point agricultural sources, uncertainty analysis 78—81262

air
see also terrestrial atmosphere
acetylene-air flame, energy transfer from laser excited Na, Li, optoacoustic pulses 78—25490
acetylene-air flame, Li(Na)(K)(Mg)(Ca) damping consts., Lorentz collisions, mag. field effect 80—66805
acoustic and US absorption in 10-100 kHz range, NPL report 77—7239
action potentials in single axons, effects of hyperbaric air and hydrostatic press. 80—56007
adsorption of atmospheric gases on mol. sieves 13X and 4A at low press. and temps. *(German)* 80—88423
aerosol composition, Nigeria during dry dusty season 80—81960
aerosol particle size distrib., Rocky Mountain air in winter 79—100887
afterglow, press. effects on spectral features excitation 78—38563
afterglow plasma, interaction with glass, Cu, steel walls, calorimetric method obs. 78—14177
air positive corona discharge between coaxial cylinders, critical density estimation 78—67595
air-acetylene flame, atom form., theory 78—7208
air-acetylene flame, multichannel apparatus detect. limits using atomic absorpt. spectra 80—76586
air-CO_2(He), probe for conc. meas. 79—4098
air-dielectric interface, EM wave reflection and transmission in terms of polarisation, education 80—105458
air-H_2 (methane) mixtures, ignition energy by capacitive discharge *(French)* 80—10446
air-H_2 flame, temp. profile, two-line at. fluoresc. method meas. 77—71328
air-H_2O, two phase upflow across horizontal tube bundles, void fraction and flow pattern 80—92201
air-moving arc interface, optical anal. at atm. press. 79—90482
air-propane flame, chem. anal. of reaction zone by Raman spectra 78—64837
air-SF_6 mixture, breakdown voltage and discharge extension of long gaps 77—84550
air-steam mixtures, heat transfer to moving droplets 78—90997
air-water choked flow in short pipes 77—84314
air-water separated critical flow *(Japanese)* 78—42650
air-water two-phase flow in vertical pipe, heat transfer *(Japanese)* 77—24011
analysis by X-ray spectroscopy 77—52689
arc, wall-stabilised, step and sinusoidal current change response 80—103209
arc discharge high-temp. transport obs. 78—71577
arc temp. meas. by N_2^+ integrated emission coeffs. 80—59314
arcs, very high current gas blast local voltage and cross-sectional areas correlation 80—38779
atmospheric, pure rot. CARS obs. 80—99511
atmospheric tritiated water vapour, condensation-evaporation model 77—29326
blast wave, variable energy, shock trajectories, flow field densities 77—68620
blast waves, cylindrically converging, in normal atm. conditions 80—92180
blunt flat plates, air flow, 2-D, thermal boundary layer characteristics, nose shape effects 80—92121
boundary layer airflow under stable conditions, aircraft obs. 77—37295
breakdown, submillimetric laser induced 78—67446
breakdown and corona characts. under AC voltage for rod to plane air gaps *(Japanese)* 79—84416
breakdown formative time lag rel. to gap geometry, pressure, and overvoltage 79—18994
breakdown in crossed elec. and mag. fields, modified Paschen's law 80—24121
breakdown in superimposed DC and HF electric fields 78—67571
breakdown initiated by particle in laser beam 77—58875
breakdown pot. reduction by pulsed lamp 79—94767
breakdown potential, pulse lamp irrad. effects *(Russian)* 78—83518
breakdown potential 6.2 MHz elec. field, perpendicular mag. field, 350 G, 500 G, 0.5-8 torr 77—35422
breakdown threshold meas. using pulsed HF(DF) laser 77—11423
breakdown voltages, from normal to cryogenic temps. 78—59692
bubble, oscillating, in water, appl. of subharmonic threshold to damping meas. 77—31374
bubble, rising behaviour in superposed liquid layers 77—62294
bubbles, in water, thermal effects and damping mechanisms in forced radial oscills. 77—31375
buoyancy demonstration 80—67988
BWR, air clearing in H_2O-type press. suppression systems, scaling laws 79—54563
BWR, air clearing in H_2O-type press. suppression systems, scaling laws 79—54564
S.California coastal air, Rn series disequilib. 78—49087
cascade ionisation by strong microwave field at low press. *(Russian)* 79—98854
chemisorbed on transition metals at high pressures, XPS 77—20990
circulation and precipitation formation in rolled stratocumulus *(French)* 77—9473
coal fired power station affecting downwind air quality, Montana, USA 80—108821
collection and analysis techniques, troposphere and stratosphere 80—26566
composite discharge plasma, rate of heating of dry air as function of voltage and density *(Russian)* 79—37513
compressed, liq. water solubility 78—34631
compressed, uniform field gap spark breakdown 77—11410
compression, pneumatic-freq. method for volume determ. of complex shape bodies *(Polish)* 79—49199

air continued
- conduction current, effect of cross mag. field 79—18990
- convection, free, from horizontal cylinder to air (water) (Si oils), correlation eqns., viscous dissipation 78—5632
- corona, alternating, with superimposed DC field, at threshold voltage 80—1860
- corona current, negative, depend. on O_3 density, 46.87 kPa 80—1852
- corona discharge, electron density meas. by microwave resonant cavity method 77—68881
- corona discharge, low-velocity heat transfer to flat plate 79—77112
- corona discharge, thermal energy positive ion extraction through Al and Au films 80—38801
- corona discharge ion density and mobility obs. 78—67594
- corona discharges in atmospheric air under AC voltage, observation *(Japanese)* 79—84417
- corona negative discharge, low energy humid air ions, etching effect on Al foil 80—40593
- cyclohexane-NO_2-air mixtures, photochem. particulate form. 78—11529
- DC corona Trichel pulse development at atm. pressure, obs. 78—67588
- density direct determination in balance through artifacts characterised in evacuated weighing chamber 79—88916
- density equation and mass unit transfer 79—88918
- diffuse discharge, gasdynamic effects 78—81294
- diffusion of fluoromethanes 77—15154
- diffusion rate in Au thin layers 80—100359
- discharge, DC, plasma microwave propag. const. determ. by slab technique 80—53992
- discharge, DC point-to-plane, temp. patterns, Michelson interferometry 80—54061
- discharge, electrode free, appl. to plasma deposition of films *(Russian)* 80—16197
- discharge, grazing, incomplete gas temp. and electron density diagnostics 79—55600
- discharge, HF, bipolar, reduced press., elec. macroparameter diagnostics 80—1854
- discharge, high-current, nanosecond, explosive cathode processes and contraction 80—10449
- discharge, HV diffuse, gas stream temp. inlfuence 79—32842
- discharge, impulse breakdown processes at low press. 80—44021
- discharge, low-press., between polymer dielecs., characts. 80—10448
- discharge, pulsed, high-current, channel temp. profile 77—27768
- discharge, sputtered cathode metal atoms, time-resolved light emission 78—71601
- discharge, turbulent flow stabilisation effect *(Russian)* 79—99010
- discharge, wall stabilised arc, current step changes, conductance transient effects 78—87547
- dissociated, hypersonic flow over blunt axisymmetric body, nonsteady heat exchange 79—37319
- dissociating, non-equilibrium laminar boundary-layer 77—952
- dissociation by field-accelerated electrons, macroscopic props., rel. to pure O_2 80—61118
- dry, electron lateral diffusion to mobility ratio 80—6203
- dry and moist, primary ionisation coeffs., secondary ionisation coeffs. for water surface 78—65376
- education, gas pressure gauge for student expt., mol. weight determ. by law of atm. 79—25795
- EHF clear air refractivity calc. procedure 78—57266
- EHF propag. in clear air, modelling 79—58075
- electric breakdown, leader development and mechanism under impulse voltage *(Japanese)* 77—80390
- electric breakdown, positive point-plane gap, critical press. prediction, v_c/press. characts. 78—87583
- electric breakdown between coaxial cylinders in crossed elec. and mag. fields 78—5963
- electric breakdown by long laser spark 79—64822
- electric breakdown by pulsed laser radii 80—1731
- electric breakdown under sustained appl. field, influence of floating particles *(German)* 79—94830
- electric breakdown voltage, 300-2100K *(Russian)* 78—51370
- electric breakdown voltage hysteresis, electrode coating effects 78—87553
- electron backscattering coeffs., 100 eV to 5 keV 80—9750
- electron beam, relativistic, interaction with air 80—48904
- electron radial diff. coeff. to mobility ratio 77—19666
- electron-photon cascade curves 79—44322
- electrons, field-accelerated, in dry air and pure O_2, macroscopic props. comparison *(French)* 80—59161
- electrostatic forces effect on thermodynamic props. and equilibrium composition 78—55710
- EM cascades caused by electrons and photons, 10-100 GeV, longit. development 79—21120
- enriched air propulsion system, Earth resources rocket 77—2259
- enthalpy meas. by LiCl humidity sensors 80—90858
- entrainment at solid/liquid/gas interface 77—1276
- entrainment coeff. of convective air in hail-producing clouds *(French)* 77—53151
- flashlamp in air, optical inhomogeneity due to light absorpt. heating of air 79—64299
- flow, annular, air-water, interfacial drag and wall layer height 77—39324
- flow, glow discharge, voltage, current oscills. 79—55585
- flow, laser velocimetry in untreated air shock, Teflon seeding technique 77—84348
- flow and heat transfer around in-line tube banks with pyramidal roughness 78—18152
- flow in vertical tube, laminar and turbulent heat transfer 78—71332
- flow of turbulent air boundary layer with slot-injected He, vel. and density profiles meas. 77—42808
- flows in triple point shock configurations, anal. thermodynamics *(Russian)* 79—32569
- fluid dynamic equations, acoustic energy conservation, vibrational relaxation effects 78—90566
- formaldehyde, in marine air and rainwater, wet season obs. 80—85703
- formaldehyde composition of air over N.Germany coast, obs. 80—26584
- gap corona pulse delay obs. and HV insulation design 79—19117
- gap discharge zone probabilistic features 78—67582
- gas, heated, elec. breakdown parameters 80—103202
- gas breakdown, cross-field, in coaxial cylinder geometry 79—82029
- gas breakdown by pulses from a CO_2 laser 80—6206
- glacier structure and flow rel. to elongated air bubbles in ice *(Japanese)* 78—88861
- glow discharge, flowing, negative ion density increase with press. 80—28821

air continued
- glow discharge in turbulent flow 20 to 200 m/s *(Russian)* 77—65921
- glow discharge plasma, electron energy balance 77—43092
- glow plasma, X-band heterodyne generation by microwave mixing 77—35391
- grazing discharge at air/glass interface, X-ray emission 80—33846
- heat transfer efficiency from rough plate 80—48704
- heat transfer in laminar natural convection in cubical cavity 80—24022
- heated, optical breakdown, mol. ion reactions influence 80—96341
- heated air, ascending bubbles, interaction with ambient cold air 79—84362
- heating by flashlamp radiation, ballistic and calorimetric meas. *(Russian)* 78—5843
- HF corona discharge ignition characteristics 78—67589
- HF discharge, unipolar determ. of gas and rotational temperature *(German)* 77—1033
- high current discharge temp. and density 77—62427
- high temp. elec. breakdown characts., theory and obs. 78—87581
- high-current discharge, current-carrying zone investig., induction method *(Russian)* 78—26355
- high-current discharge cond. zone, HF mag. field probe 78—71589
- high-current pulse discharge, near-electrode process dynamics 78—71602
- humidified by boiling water, ion content, sensitive cell meas. 80—53913
- humidity meas., microwave refractometer using Fabry-Perot interferometer 77—18073
- humidity measurement above 100°C 78—226
- hygroscopic particle size, air humidity depend., applic. to lung dynamics 77—90841
- hyperbaric air, modification of synaptic facilitation and bursting patterns in Aplysia californica 80—56008
- hypersonic flow, in shock tunnel, mass spectrometric analysis 77—31328
- hypersonic wake, electron recomb. coeff. temp. depend. meas. 79—27834
- ion concentration, pollution aspects *(French)* 78—16125
- ion mobility of ions created under atm. press. 77—969
- ionisation coefficient of air stressed at high voltage, meas. using photomultiplier 78—1786
- ionisation path formation by laser beam with retractable focus 79—18992
- ionized, as wind tunnel tracer 78—22435
- ions, biological impact 77—1972
- irradiated, N_2^+ 1st negative band reson. absorpt. calcs. 77—30850
- isobutane-air, in packed bed, heat and mass transfer, axial mass dispersion 78—75200
- jet, turbulent, evaporation of water drops 77—55077
- jets, axisymmetric, turbulence mixing of gases with different densities 77—58749
- laser breakdown, very long spark prod. *(Russian)* 77—1031
- laser breakdown near solid, thermal stress cracking effects reducing threshold 79—69924
- laser breakdown near solid targets, by pulsed CO_2 laser radiation *(Russian)* 78—26362
- laser breakdown of air initiated from dust particle, laser beam shutter 79—68412
- laser exploded, emission processes affecting development of explosion 79—7417
- laser induced gas breakdown threshold at 1.06 micron 80—28594
- laser-evaporated microplasma radial glow and temp. distrib. 78—67387
- laser-induced breakdown over long distances 80—33795
- laser-initiated ionisation channels, form., characts. 77—89345
- laser-produced spark ionisation channel effect on long discharge 78—67468
- leader breakdown process, positive/negative, problems 77—11427
- LF coherent antiStokes Raman spectroscopy 79—13727
- light flash excited by γ-ray source, electric field effect 79—14514
- liquefaction, from Cailletet and Pictet to microkelvin 79—40
- liquefaction systems, optimum operating conditions 77—61075
- liquid, transport of neutron and secondary γ-rays from 14 MeV source 78—50234
- long air gap minimum breakdown voltage and time estimation 78—67575
- long rod-to-plane air gap voltage/time characteristic for switching impulses 78—67576
- low threshold breakdown, near target, by pulsed laser radiation *(Russian)* 78—22594
- methanol-water-air mixing, in perforated disc type stirring cascade, power dissipation, mechanism and correlation 79—1238
- microwave breakdown field calc., resonator and rectangular waveguide expt. 79—41789
- microwave gas breakdown, ionisation pot., qualitative theory 80—43837
- moist air, ion content and IR absorption 80—41493
- molecular diffusion in water, experimental determ. of coeff. 77—28029
- multichannel spark form. 80—87976
- natural convective oscillatory flow from heated wire on axis of horizontal cylinder 77—72295
- negative ions evolution, computer simulation *(French)* 77—21869
- negative point-plane corona, electrical characts. 78—71567
- negative pulseless corona to spark breakdown transition condition 80—54062
- neutron-stimulated luminescence 78—86567
- non-self-sustained discharge plasma ionisation instability obs. 78—71609
- non-self-sustaining discharge, ionisation instabilities *(Russian)* 78—26268
- nonlinear susceptibility and self-focusing *(Russian)* 79—86224
- O_2 electron attachment coeff. meas., O_2 partial press. depend., in dry air *(German)* 79—13821
- optical breakdown, initation by absorbing water droplets 80—10352
- optical breakdown, interferometric investigation 80—100064
- optical breakdown threshold reduction near dielectric surface 77—51211
- optical detonation threshold, press. depend., rel. to Ar 79—23438
- outflow from porous materials and noise reduction theory of porous diffuser *(Chinese)* 79—50785
- parallel discharge growth during impulse breakdown, mechanism *(German)* 78—63607
- particulate element conc. over USA 80—76679
- particulate nitrate in marine air of equatorial Pacific 80—85702
- particulates in Montana air, element composition, background study 80—77034
- photochemical pollution, weekend-weekday differences 78—3921
- plasma, breakdown, effect on absorpt. coeff. of metal target irradiated by CO_2 laser 79—52052
- plasma, CO_2-TEA laser breakdown, average temp. depend. on physicochemical target props. 77—19738

- **air** continued
  - plasma, dense, nondegenerate, electron transport, thermal cond. *(Russian)* 79–98865
  - plasma, gas-discharge, meas. of electron energy loss distrib. 77–35418
  - plasma, laser-produced, decay time *(Russian)* 79–98941
  - plasma, optical absorpt. coeff. at 1000 atm, 13000K, N_2^- photodissoc. 80–64691
  - plasma, optical emission, localised oscill. mode obs. 80–83903
  - plasma, prod. by CO_2 laser interaction with plane target *(French)* 78–9806
  - plasma, radiowave interaction, electron velocity, collision cross-section depend. 80–103155
  - plasma, shock heated, nonequilib. submillimetre emission *(Russian)* 78–1869
  - plasma, shock wave-induced, transverse mag. field interaction simulation 78–38463
  - plasma, slow burning gasdynamics, due to Nd laser beam *(Russian)* 80–108715
  - plasma, surface treatment of polyester fabric, effect on surface struct., props. 78–95831
  - plasma, TEA CO_2 laser-produced, using solid targets, induced shock waves 80–64729
  - plasma source, pulsed high-intensity elec. discharge between parallel plates 80–1857
  - point-to-plane gap corona and breakdown in supersonic airstream 78–67573
  - point-to-plane negative corona discharge in axial airstream 78–67585
  - positive column of high-voltage diffuse discharge, nonstationary processes 80–64802
  - positive corona discharge time lag obs. 79–27849
  - positive point corona current continuous component 78–67586
  - positive point-to-plane corona, continuous and pulse components 79–19119
  - predischarge current meas. in compressed air 78–87555
  - pressure, as function of internal energy and density, algorithm *(Russian)* 77–58829
  - propane-air flame-generated turbulence, approach stream turbulence effects 79–64793
  - propane-air mixture, turbulent combustion, model 79–64792
  - propane-air mixture, turbulent combustion zone, initial temp. fluctuations influence on reaction evolution *(French)* 79–15998
  - propane-O_2-air flame, temp. meas. by laser Raman spectroscopy 77–5833
  - pulsed corona discharge channel fast heating process 78–67560
  - radiant heat transfer coefficient for blunt body in hypersonic flow, similarity law 80–33705
  - radiative cooling behind strong shock waves 78–91030
  - radioactive fallout in air and rain over United Kingdom 77–73847
  - Rayleigh scatt. props., nephelometer meas. 79–29865
  - Rayleigh scattering 79–1342
  - refractive index meas. with improved Rayleigh interferometer *(Chinese)* 77–57383
  - relative humidity control, error comparison for various sensors, accuracy 77–10034
  - relativistic electron beam on air, He and H_2, charge neutralisation press. depend. *(Russian)* 77–19668
  - RF breakdown in longit. mag. field, diffusion theory validity 77–39491
  - rod-to-plane air gap breakdown under negative impulse voltage 78–67563
  - rod-to-plane air gap impulse-voltage delayed streamer and leader formation 78–67570
  - rod-to-plane air gap impulse-voltage primary and secondary streamer obs. 78–67569
  - rotating partially filled cylinder, horizontal, steady flow soln. 77–84260
  - self focusing of laser beam as a whole 77–88875
  - separation, energetic, influence of vortex-tube configurations and length 77–7400
  - shock activation of supersonic nozzle with overexpansion, jet form. 78–18330
  - shock photoionisation, radiation from shock heated gas 79–7438
  - shock wave radiation, low inertia pyroprobe meas. *(Russian)* 77–31333
  - sound absorption, HF meas. 78–1475
  - sound generator, vortex, separation of acoustic energy and spent-air jets 80–102953
  - space charge limited current in N_2 and air, high pressure effect 79–32735
  - space charges in rod-to-plane gap, impulse voltage meas. *(Japanese)* 80–87970
  - space-time distribution of refractive index of air in Mongolia 78–81335
  - spark discharge, numerical simulation 77–89340
  - spectrochemical analysis, nonlinear least squares method for IR spectra 78–15738
  - stable flow over complex region, linear model 79–53466
  - steam-air mixture, condensation, transport and thermodynamic props. *(Japanese)* 78–34251
  - strongly reflected shock wave trajectories, vel. parameters *(Russian)* 77–23993
  - subsaturated air, aerosol particle collection efficiency by water drops 78–28273
  - superdetonation waves, propag. towards laser beam, vel. meas. *(Russian)* 77 -35159
  - supersonic radiation waves, excitation by CO_2 laser 79–90433
  - temperature measurement, using rot. Raman spectra 78–62200
  - thermal activity coeff. meas., periodic-heating method 80–42218
  - thermal conductivity, 400-1200K 78–75249
  - thermal conductivity computation in 400 to 1600K range 78–5841
  - thermal transpiration, theory and expt. comparison, molecular and transition flow 79–32579
  - Trichel corona, negative ion form. 77–35425
  - turbidity of Barcelona's air, anal. of 1971-7 obs. *(Spanish)* 80–36375
  - turbulence, free-stream, control by means of honeycombs 77–35122
  - turbulence effects heat transfer from cylinders in crossflow at critical Reynolds no. 79–98707
  - turbulent boundary layer analysis for air and combustion products *(Russian)* 78–5732
  - turbulent flow in circular pipe, temp., velocity profiles, heat transfer, flow resist. 79–55370
  - turbulent flow in heated channel, effect of gravitational field 80–64533
  - ultrapure, molar density at 298.15K for mass transfer buoyancy corrections 79–88917
  - undervoltage breakdown between parallel plates 79–60099
- **air** continued
  - unionized, enhanced light emission from positive corona 79–37568
  - US assisted radiant heat transfer into water and air 79–46169
  - UV irradiation of filtered air, particle production expts. 78–24336
  - viscosity rel. to ionis., skin friction of wetted oscill. disc 78–34252
  - volcanic contamination indicating volcanic activity of Mauna Loa, Hawaii 80–76950
  - W values and backscatt. coeffs. for slow electrons in air, dosimetry appls. 80–19551
  - wake, hypersonic, ionised, free electron attachment coeff. meas. 79–27835
  - water-air interface, overall heat transfer coeffs., humidity and density profiles, turbulent pulsations *(Russian)* 78–22349
  - water-air plug-train system, press. wave propag. characts. 80–59058
  - water-air spray, dispersion characts, orifice shape depend. 78–34182
  - water/air surface tension, effect of air diffusion and interface struct. 77–4246
  - weak nonlinear waves, struct. and propag., effect of vibr. relaxation 79–64683
  - weakly-ionised, secondary electron distrib., produced by electron source distrib. 80–6211
  - wire/plane electrode air discharges in strong nonuniform field *(Rumanian)* 79–68964
  - Yaounde, Cameroon, particulates in urban and rural air *(French)* 80–61478
  - Al-air, seawater activated secondary cell 80–26128
  - Ar-air, transformer plasmatron, LF discharge, electrical and energy props. 80–103200
  - Ar-air arc, stabilised, spectroscopic methods of temp. meas. *(Russian)* 80–38854
  - CO-air streams, selective oxidation of H_2 before CO electrochem. anal. 77–63978
  - $CO+H_2$ combustion in air, gasdynamic laser operating on combustion products, construction, amplification coeff. *(Russian)* 77–7075
  - CO_2-air, heat transfer from cylindrical anemometer probe 77–84256
  - CO_2-air, open cycle laser, generated power depend. on pulse repetition freq. *(Russian)* 77–19231
  - CO_2-air mixtures, mol. rot. temp. determ., absorpt. spectra calcs. 77–30851
  - $CO_2+O_2(N_2)$(air), bending mode vibr. deactivation rate, 1500-350K, shock tube meas. 77–38714
  - H-air, laminar diffusion flames, chem. nonequilib. effects model 78–48654
  - HCN compact CW laser, output increased by He, Ar, air and O_2 buffer gases 79–10293
  - HNO_3 in marine air of equatorial Pacific 80–85702
  - He-air, thermal cond. meas., conc. depend., 315K, 330K *(Russian)* 78–71421
  - I partition equilibrium between air and NaOH aq, effect of CO_2 conc. 78–78474
  - NH_3 content Southern Ocean air 80–61871
  - NO_2 composition of air over N.Germany coast, obs. 80–26584
  - O_3 composition of air over N.Germany coast, obs. 80–26584
  - O_3 conc. affected by hydrocarbon emission from car factory 80–76674
  - O_3, conc. at ground-level, Oslo, Norway, summer 1977 obs. 80–81965
  - $OH(A^2\Sigma^+)$ quenching rates and fluoresc. efficiency in air, rel. to atmosphere 80–14199
  - SF_6-air mixture impulse discharge characteristics of 30 cm gaps 78–67572
- **air bases** *see airports*
- **air blast circuit breakers**
  - arc characts., depend. on electrode position 79–23470
  - core electron temperature at current zero, 3 kA, spectral meas. 78–87526
  - electrical gradient during high current phase, plasma probe methods 78–87527
  - energy clogging, current and voltage meas. at different press. 78–87531
  - local electrical properties, near current zero, optimisation 78–87516
  - post-zero current and power loss meas. 79–19106
  - very high current arcs, elec. conductance of arc gap 78–87524
- **air bubbles** *see bubbles*
- **air clutches** *see clutches*
- **air compressors** *see compressors*
- **air conditioning**
  - *see also ventilation*
  - air assisted thermoelec. air conditioner humidifier (SATEACH) 80–108802
  - air based solar heating systems, phase charge energy storage, optimum physical properties 79–43742
  - antifreezing circuit design, Boolean algebra appl. *(German)* 77–64914
  - astronomical observations, building design effect on photographic zenith tube obs. 80–85856
  - Brazilian development of low-cost houses, evaporative and night sky cooling system design and testing 79–62132
  - broadcasting studio, 'Deutsche Welle' building construction and meas. *(German)* 80–106668
  - building solar-climate control systems, control options evaluation by simulation 80–40844
  - BWR, heating, ventilation and air conditioning systems *(Japanese)* 80–91212
  - cool storage as a means for residential air conditioning electrical load management 80–30590
  - cooling and dehumidifying coil, heat, mass and momentum transfer 79–192
  - diesel-driven chiller system, with multi-tank thermal storage system, computer simulation 79–48187
  - ducts, active sound absorpt. 78–90555
  - dust control, measurement methods *(Hungarian)* 80–35810
  - education, air conditioners, second law efficiency, energy efficiency ratio and performance coeff. 78–36742
  - energy saving control system, using heat storage tank *(Japanese)* 80–72087
  - fan systems and energy 80–6145
  - for energy savings 80–52211
  - heat exchanger, indirect, thermodynamic calc. *(German)* 77–23862
  - house energy conservation measures obs. and evaluation, using minicomputer, Philips expt. house (West German project) 79–61951
  - intersecting plane turbulent air jets, appl. 79–86476
  - laboratories, automatic temp. control and meas. *(Japanese)* 78–86245

air conditioning continued
- laboratory temperature control, modified window air conditioner 80—68192
- low frequency noise breakout from air conditioning ducts, abatement 80—74594
- noise, subjective responses and meas. 78—83168
- noise abatement for induction motors in air/air heat-exchangers for ventilation *(Hungarian)* 80—102923
- noise control by auxiliary driving sources, air conditioning duct appls. 79—14133
- noise measurement by concave reflector, new method 77—68344
- noise suppression 77—11083
- PWR nuclear power station, heating, ventilating and air conditioning systems *(Japanese)* 80—91213
- reactive acoustic attenuator 78—38140
- rectangular ducts, LF acoustic transmission 79—37070
- solar, based on LiBr absorption devices, computer-aided performance predictions 79—62134
- solar, CAD w.r.t. maximum solar heat gain 79—57466
- solar, evacuated tubular solar collectors and LiBr absorption system integration 79—62135
- solar, heating and air conditioning 80—61290
- solar, intermittent cycle, NH_3/H_2O absorption system, expt. evaluation in Florida 79—62133
- solar, natural environmental control of houses in Northern India 79—62151
- solar, of financial building (1100 m^2) 79—57465
- solar, of mobile home, performance in Kuwait environment obs. 79—62130
- solar, retrofitting of existing residence, combined heat and electricity generation, expt. results and economic assessment 79—61952
- solar, stochastic simulation expts. 79—57415
- solar, using evacuated tabular collectors, digital simulation and design, comparison with actual performance 79—61949
- solar absorption cooling systems, small scale, feasibility study 79—74502
- solar absorption refrigeration 80—76651
- solar air conditioning, LiBr absorption 80—81425
- solar air conditioning with solid absorbents, earth and underground water cooling 80—72018
- solar augmented and assisted 80—7918
- solar chemical heat pump/storage system for air conditioning 80—55886
- solar cooling, heating and hot water supply for hospital, evacuated glass tube solar collector system appl. 80—26155
- solar cooling with air collectors by desiccant/r bed method 80—30412
- solar desiccant dehumidifier development 80—30411
- solar energy, research, applications, water heating, space heating, air conditioning and hothouse heating *(French)* 79—100487
- solar energy transition and materials problems 80—26115
- solar evaporation and refrigeration units, assurance of specified energy parameter values, statistical analysis 80—93848
- solar flate plate evacuated collector design 79—62099
- solar heat pump plant for space heating in winter, air conditioning in summer 80—76615
- solar heating and cooling system for domestic use *(Japanese)* 80—108787
- solar integrated collector-heat storage systems for natural air conditioning 80—51002
- solar powered, NH_3/H_2O absorption unit design and performance 79—62129
- solar powered Rankine cycle system, 18-ton, analysis and design 79—52897
- solar Rankine cycle air conditioner *(Japanese)* 80—72076
- solar regenerator buoyancy effects, study 79—68709
- solar selective surface absorption and IR emissivity calorimetry 79—62098
- solar system, liquid desiccant, with flywheel storage system 79—52909
- solar thermal energy storage using methanol based heat pumps 80—30587
- solar total energy system, for US Army base buildings, conceptual design and large-scale expt. 79—52899
- solar total energy system, preliminary design for large building supply 79—52898
- sound attenuators, attenuation characts. 78—30123
- sound attenuators, ideal characts. 77—54836
- sound emission prediction 77—7252
- sound emission prediction 78—30122
- space heating, solar air heaters, aerodynamic drag investigation 80—40899
- storage of thermal energy, annual cycle, ice storage and three-coil heat pump 80—55917
- surgery cell with laminar air flow *(German)* 79—16335
- technical meteorology, technical and commercial appls. *(German)* 80—46231
- underground railway tunnel microclimate, calc. method *(Russian)* 79—68548

air permeability *see permeability*

air pollution
- *see also air pollution detection and control; smoke*
- 2,4-D herbicide, long-distance transport and damaging levels in Washington vineyards 77—17213
- 12th International Colloquium, Paris (1976) 77—37377
- 1977 Clean Air Act amendments and industrial expansion 79—79426
- acid content vars. of rainwater during single precip. event 79—57990
- acid precipitation, soil Al leaching response effects on high-elevation watersheds in NE.United States 80—12442
- acid precipitation and forest ecosystem, symposium (Columbus, Ohio, 1975, May 12-15) 77—37322
- acid precipitation at Ithaca, New York, origin of air masses 79—16655
- acid precipitation effects, Norwegian SNSF-project on forest and fish 77—37411
- acid precipitation in central Texas, chemical comp. 77—37329
- acid precipitation in N.E. United States 77—37328
- acid precipitation in Norway 77—37371
- acid precipitation meas., interpretation and review 77—37323
- acid precipitation meas. in Norway 77—37324
- acid precipitation rel. to S and N oxide emissions over Canada 77—37338
- acid rain, neutralization in Hubbard Brook ecosystem 79—74922
- acid rain and cation leaching in Douglas fir ecosystem 77—78392
- acid rain and interactions with dust 77—37326

air pollution continued
- acid rain rel. to S compounds long range transport, chem. aspects 78—81391
- admixtures, atmospheric diffusion in calm conditions 80—40935
- Adrigole, Ireland, halocarbon concs. 1970-75 period 77—70809
- advection equation soln., using second-order moments with and without width correction 78—85655
- advection-diffusion model for pollutant dispersion near roadways 79—21003
- advection-radiation fog near Lake Michigan, visibility meas. 77—81996
- aerosol, ambient sulphate particles size discrimination and chemical comp. by diffusion sampling 78—69528
- aerosol, individual microparticles identification via micro-Raman spectrometer 78—68970
- aerosol, particle size, opt. and geom. determs. *(German)* 77—91259
- aerosol, photochem. prod. of submicron particles of very narrow size distrib. 79—29491
- aerosol conc. statistics for N. tropical Atlantic region 78—32188
- aerosol effects on atmospheric transmission, Smithsonian Astrophysical Observatory pyrheliometric meas. 80—17374
- aerosol elemental composition in particle size fractions, human respiratory uptake 77—48726
- aerosol extinction at 500 nm in urban and rural air at Milwaukee, USA 79—100946
- aerosol granulometric distrib. rel. to atmospheric pollution influences 77—37341
- aerosol growth in urban plume, obs. 77—37390
- aerosol meas. at Algarve coast, Portugal 79—58062
- aerosol movement in lake-land breeze circulation, pollution study 80—31101
- aerosol optical extinction coefficients, practical upper limits 79—72486
- aerosol particle analysis for sulfate, nitrate, elemental comp., Los Angeles 80—7971
- aerosol particle size distrib., theoretical and meas. over Milwaukee 80—7970
- aerosol particle time-of-flight spectrometry 77—37451
- aerosol particles influence on warming of urban and rural atm. 79—16671
- aerosol pollution, urban, physical demonstration of cloud modification 80—56571
- aerosol sources and sinks, stochastic models for SO_4^{2-} particles and wind-blown dust 79—100930
- aerosols, anal. of water-soluble S compounds 78—96282
- aerosols, effect on rate of new particle form. 79—24926
- aerosols, electrostatic interaction of charged dielectric particle with charged water drop 77—25749
- aerosols, from Jungfraujoch, Switzerland, chem. comp. 77—45056
- aerosols, granulometric spectrum, in slightly polluted marine atm. 78—44893
- aerosols, influence on thermal effects of stratosphere, O_3 depletion at 85°N latit. 78—81279
- aerosols, IR extinction rel. to mass conc. 79—84473
- aerosols, mass density function multimodality 77—70807
- aerosols, particle collisions with cloud drops and raindrops, elec. fields and charges effects 77—25748
- aerosols, size distrib. characterisation, modified beta density function 78—69432
- aerosols, SO_4, NH_4, NO_3 particulates size distribution in Nagoya area 78—3931
- aerosols, trace element conc. over Lake Michigan 80—81968
- aerosols from coal-fired power plant plume, no detectable ice nuclei 77—21888
- NW.Africa, snowfield acidity (1977-79) 80—98370
- aircraft effects, Canadian environmental policy 78—33950
- aircraft emission during high altitude cruise operation, study 77—29427
- Airways Surface Obs. data for pollution potential prediction model 77—29423
- Aitken nuclei meas., Black Hills, S.Dakota, green area filtration effect 78—3928
- aldehydes, formation by photochemical reactions *(Japanese)* 78—88648
- aldehydes in air, gas chromatography 79—12284
- n-alkane pollutants, N.Atlantic gas and particle concs. in troposphere 80—7969
- alkyl Pb and Se compounds, detect. via gas chromatograph-microwave plasma detector 78—68975
- alkylbenzene concentration study in New South Wales 77—70817
- aluminosilicate particles, charge state depend. on thermal history 80—97840
- ambient air pollutants, statistical models with reference to Los Angeles Catalyst Study (LACS) data 80—30620
- ambient air quality maintenance data system applied to coal-fired electric generating stations 80—3560
- AMS symposium (Reno, Nevada, 15-18 January 1979) 79—66745
- Ankara atmosphere aerosol, trace elements and size distribs. determ. by thermal neutron activation anal. 78—81377
- annual average concentration around single source, rapid estimation technique 78—81382
- Antarctica, radioactive pollution of near-surface air *(Russian)* 77—29393
- anthropogenic gases, climatic alteration 77—53179
- Arctic aerosol and snow compositional differences 79—88377
- artificial radionuclides, depositional history in Ross Ice Shelf, Antarctica 79—88027
- asbestos, rel. to use of quarried serpentine rock 77—91261
- asbestos particulate concs. in Thetford Mines area of Quebec 77—37394
- atmosphere, Al particles from space rocket launching 80—81503
- atmospheric analysis, using laser, from orbiting satellite 77—9571
- atmospheric chemistry, recent advances 79—12204
- atmospheric circulation and pollution analysis using hydrodynamic models *(Italian)* 79—100892
- atmospheric coolants operation from cooling towers *(French)* 79—66427
- atmospheric diffusion model for short distances and complex topography 77—37386
- atmospheric diffusion transport models, variational imbedding soln. 77—37381
- atmospheric dispersion, completely Lagrangian random-walk model 78—81380
- atmospheric dispersion calcs. for nuclear plants, EFFAIR code 79—18007
- atmospheric dispersion models for calc. of pollutant conc. levels 79—100552

air pollution continued

atmospheric pollution 1978, conference, Paris, France, (April 1978) 78—81373

atmospheric radioactivity, dose calcs., incurred from deposited activity and cloud activity 80—3551

atmospheric radioactivity inside buildings, absorbed dose estimation *(Spanish)* 78—8998

automobile exhaust pollutants diffusion 79—52985

Beijing, China, weather conditions effect on pollution *(Chinese)* 80 108825

Belgium, meteorological episodes increasing air pollution 78—81374

Belgium, SO_2 and smoke daily concs. from 1968, Jan. to 1973, Mar. *(Flemish, French)* 77—82003

Belgium 1973-4 SO_2 and smoke pollution *(French, Flemish)* 77—41147

benzo(a)pyrene and C black combined aerosol form., rel. to air pollution and health hazards 78—80796

bi-Gaussian atmos. diffusion model, influence of turbulence typing scheme for environmental anal. of nuclear power 80—3554

bifurcated cooling tower plume, math. model of drift deposition 79—58002

biogeochemical cycles, role of atmosphere 79—79427

biomass burning, C flux between biosphere and atmos. 80—97838

biosphere, radioactive contamination, influencing factors, 1962-76, Hungary *(Hungarian)* 78—92711

Bombay Airport, urbanisation and industrial development effects on air temp. 77—53167

Bombay heavy metal particulates due to road traffic 80—97837

Boston, air quality during fuel shortage 77—64424

boundary layer, pollutant field from multiple sources *(Russian)* 78—69443

boundary layer, radiation model 77—49168

boundary layer model, two-dimens., appl. to Nanticoke region, Lake Erie north shore 79—66750

boundary layer thermal stability diurnal and seasonal var. at Poona, rel. to pollution 77—53130

box models for air quality simulation 79—70474

breakdown voltage of air, effect of sand particle pollution 78—81363

British Isles, aircraft sampling of halocarbons 77—73832

Budapest, SO_2-sulphate relationships 77—70810

buildings, indoor airborne radioactivity calcs. 80—63305

Bulgaria, radionuclide composition and activity over Bulgaria in 1976 79—88018

buoyant axisymmetric plume in atmospheric inversions, entrainment characts. 77—82004

buoyant plume in stably stratified boundary layer, max. ground conc. 80—72573

buoyant plume rise in atm. inversions 77—41114

buoyant plumes behaviour on release at ground level, lab. wind tunnel obs. 80—30624

bus lane network for pollution reduction simulation 79—52991

BWR airborne ^{131}I releases during operation 80—23033

Calgary, air quality affected by Chinooks, acoustic sounding expt. 80—16876

California stratus, $^{34}S/^{32}S$ ratios rel. to aerosol and cloud drop origin 77—29407

Canada, prairie cities increased sunshine due to natural gas use as fuel 77—17211

Canadian urban air quality, 1971-1975 period 79—70479

carbon tetrafluoride, atmospheric content, sources and residence time 80—61879

Charleston, W.Virginia, size-fractionated aerosol composition 80—89687

chemical analysis, gaseous, aerosol and particulate methods, review 80—7876

chemical composition of Norwegian snowpack, rel. to air pollution 79—20871

chemical reactions, second-order, in turbulent fluid, model, formulation and validation 79—20349

chemical reactions, second-order, in turbulent fluid, model, appl. to atm. plumes 79—20350

chemistry of polluted air reactions at 55°N 80—98382

Chicago Area Program, mesoscale meteorology 78—77294

Chiltern, Oxon. (1951-1977), dose rate, air ionisation, radioactive fallout 79—6775

chimney height for optimal air pollution reduction 80—26588

chimney plumes, partial penetration of inversion layer, model 80—7974

chimney stacks, prediction transport, dispersion air pollutants, computer program appl. 77—73836

chinook weather effects 78—61534

chlorinated hydrocarbons in ambient air, washout effect and diurnal var. 78—28305

chloro-hydrocarbons, interaction between atmospheric pollutants *(French)* 80—7976

chlorocarbon industry impact on atmospheric O_3 layer 78—40648

chlorofluorocarbon residence times in stratosphere, two-dimens. model 80—45834

chlorofluorocarbons, photodecomposition under simulated tropospheric conditions *(German)* 79—53408

chlorofluorocarbons 11 and 12, observability of possible atmospheric removal processes 77—25773

chlorofluorocarbons and ozone depletion in the lower atmosphere 79—53498

chlorofluorocarbons in stratosphere, O_3 layer depletion calc. using two-dimensional model 80—109221

chlorofluoromethane, computer based policy analysis to reduce human health impacts 80—89698

chlorofluoromethane induced IR cooling, effect on general circulation model 80—90122

chlorofluoromethane induced O_3 depletion, atmos. chem. theory 80—51477

chlorofluoromethane photolysis in stratosphere, effect on O_3 conc. 80—109197

chlorofluoromethanes, atm. O_3 depletion, two-dimens. time-depend. model 78—24341

chlorofluoromethanes, $CHFCl_2$ and CHF_2Cl, diffusion and chem. reaction 77—70804

chlorofluoromethanes, contradiction of stratospheric O_3 depletion prediction 78—49099

chlorofluoromethanes CCl_2F_2 and CCl_3F in Wuppertal-Dusseldorf region, ground level meas. 78—73478

chlorofluoromethanes effect on atm. surface temp. 79—70832

air pollution continued

chlorofluoromethanes effect on O_3 layer rel. to stratosphere natural structure 79—84436

chlorofluoromethanes in stratosphere, vertical distrib. 78—73476

chlorofluoromethanes in upper troposphere and lower stratosphere, vertical distrib. 78—73477

chronology of events (up to 1970) 80—7975

climate, human influence, conference, Manlo Park, California (1979 February 21 to 22) 80—62381

climate and climatic change, numerical simulation 79—16643

climate change, anthropogenic effects, review 78—28293

climate effects *(French)* 79—84360

climate variability, effects of volcanoes, pollution and CO_2 78—28292

climatic effects, review 78—28291

cloud, motion of a large dusty buoyant thermal with a vortex ring 79—48561

cloud condensation nuclei from paper mill, calc. effects on rainfall 78—11970

cloud condensation nuclei from paper mill, measured effects on clouds 78—7721

cloud condensation nuclei from paper mill effluents, induced fog *(French)* 78—96270

cloud condensation nuclei on USA Atlantic seaboard 77—5310

cloud dose data file fast correction for changes in dispersion parameters 78—80969

clouds, shortwave albedo, pollution effects 78—7755

by CO_2, report summary *(German)* 78—44993

CO, air pollution rel. to HO tropospheric concs. in N and S hemispheres 78—32140

coal conversion technologies, health and environmental effects 80—81493

coal fired power station affecting downwind air quality, Montana, USA 80—108821

coal fired power station plumes, gas-particle conversion meas. 80—81502

coal smoke, diurnal variation, harmonic anal. *(Rumanian)* 79—21009

coal smoke particles, atmospheric natural radioactivity *(Rumanian)* 78—53723

coal-fired power plants, effects on cloud and precip. processes 79—20933

coal-fired power plants, minor and trace elements emissions and particle size distribs. 79—92108

coal-fired power station, heavy metal fallout to nearby pond 80—76667

coal-fired power station, particulate nitrates in plume 80—81498

coal-fired power station pollution, physics 79—44659

coastal breezes, dispersive, monostatic acoustic sounding system *(French)* 78—7683

collective dose commitments from the release of radioactive nuclides to the atmosphere 80—3556

combustion aerosols, particle size distrib., health hazards 78—81394

combustion engine exhaust pollution in Netherlands *(Dutch)* 80—101138

comparison study between city and desert by neutron activation analysis 77—41155

concentration, statistical parameters determ. from truncated data set 77—37414

concentration calcs., algebraic element (Scator) appls. 77—91277

concentration pattern determ. in one wind direction *(Dutch)* 77—70821

concentration pattern determ. over long period *(Dutch)* 77—70822

condensation nuclei conc. over Mediterranean Sea 77—45057

condensation nuclei conc. records, 1965-77, SW.Germany *(German)* 79—84422

conference, proceedings of 14th international colloquium, Paris (May 1980) 80—98760

conference, Rochester, NY, USA (May 1979), polluted rain 80—82585

conservation of species equation with chemical terms, soln., numerical methods 78—36265

contemporary climate changes, natural and anthropogenic factors 79—34938

continuous point sources, conc. Gaussian distrib. calc. *(Dutch)* 78—61546

continuous point sources, effects prediction *(Dutch)* 78—61545

continuous point sources, German calc. models *(Dutch)* 78—61548

continuous point sources Gaussian distrib. anal. *(Dutch)* 78—61611

convection, moist plume from a cooling tower *(French)* 79—84400

convective boundary layer, max. ground level conc. 80—41474

cooling pond heat transfer, numerical model study and water vapour plume production 80—8380

cooling tower, plumes, stationary model *(German)* 80—4082

cooling tower buoyant plume simulation using Lagrangian convection model *(French)* 79—88450

cooling tower drift deposition, modelling and monitoring 79—20992

cooling tower effluents at conceptial power parks, potential weather modification 78—11951

cooling tower plume effects on total solar radiation 79—12177

cooling tower plume rise and visible plume length, prediction and obs. 77—45053

cooling tower plume vortices, time-lapse photography 79—20950

cooling tower plumes, interaction with atm., numerical model simulation *(French)* 80—94126

cooling tower plumes, Lagrangian conveection model, representation of isolated thermals *(French)* 79—88449

cooling tower plumes, max. rise formula appl. 77—45142

cooling tower plumes, natural draught snowfall obs. 77—2215

cooling tower plumes and drift, mathematical models 80—45836

cooling tower plumes from energy centres, predicted climatology 78—61541

cooling tower plumes obs. and models 79—20991

cooling tower plumes simulation, model calibration at Meppen power station *(German)* 80—94130

cooling tower salt drift, potential biological impacts 79—88022

cooling towers, effects, review *(German)* 77—73800

cooling towers affecting rainfall, statistical study 80—109202

cooling towers effects and their reduction *(Czech)* 80—51021

Copenhagen area urban aerosols on heavy loaded membrane filters, PIXE anal. 77—49138

damage to material objects, economic evaluation 80—76692

dark smoke, Greater London area, vehicular and domestic emissions relative importance 78—36269

data analysis using combined interactive graphic presentation and clustering technique 79—83656

data uncertainty rel. to environmental decisions 80—104535

Denver Brown Cloud, obs. of C particles in aerosol 80—81961

Denver Brown Cloud, spectral absorption of solar radiation 78—16158

air pollution continued
- deposition velocities determination, limitations 78—44903
- deposition velocities over water 79—8683
- dewatered pipeline coal dust pollution model 77—37401
- dichlorodifluoromethane, UV absorpt. cross sections temp. depend., stratospheric appls. 77—64423
- dichlorodifluoromethane, UV photodissoc. cross-section, 223 and 296K 79—52729
- dichlorofluoromethane pollution, conc. obs. in background troposphere air 80—97843
- diffusion, pseudospectral soln. 78—32172
- diffusion, steady state 3-D model, numerical anal. *(Japanese)* 79—79984
- diffusion, steady state model, effect of terrain 79—92582
- diffusion eqn. for line sources, analytical steady soln. 79—12244
- diffusion from ground-level source in turbulent boundary layer, Lagrangian statistical anal. 80—12517
- diffusion from point sources, orthogonal collocation 79—12249
- diffusion of pollutants after hypothetical accidents at nuclear plants *(German)* 77—64421
- diffusion parameters estimation, use of routine meteorological data 78—85649
- diffusion plume model, estimation of model parameters *(Japanese)* 79—79983
- diffusion problems soln., pseudo-spectral and orthogonal collocation method 79—12170
- diffusion transport, variational imbedding calc. method 77—73785
- diffusion-deposition-resuspension problem, formulation and soln. 77—2229
- difluorodichloromethane, spectral data evaluation for atm. sensing 79—62582
- dimethyl sulphide, biologically prod., contrib. to global S cycle 77—70786
- dimethyl-N-nitrosamine, assessment is urban air 78—81378
- dispersal, three-dimens. particle-in-cell method, comparison to regional tracer studies 78—92967
- dispersal from point source into boundary layer, Ekman-type model 80—105039
- dispersal in tropical region, use of stability and freq. wind roses 80—97846
- dispersal of pollutants over complex terrain, steam plant in Tennessee valley 80—97833
- dispersing plume, crosswind geometry, second-order reaction 80—61480
- dispersion, model for continuous shoreline fumigation 79—100914
- dispersion, modelling by smeared conc. approximation 78—81381
- dispersion, modelling using cubic splines and chapeau functions 79—83662
- dispersion, overlay technique, topography problem, long term conc. 78—81389
- dispersion, transformation and deposition using Green's function method 79—83663
- dispersion during calm wind situations, analytical modelling 78—81385
- dispersion from area sources in convective turbulence, model 78—28303
- dispersion from elevated point source in convective planetary boundary layer 79—12245
- dispersion from elevated source in convective boundary layer 80—85312
- dispersion from elevated source in convective planetary boundary layer 79—12246
- dispersion from ground-level source, appl. of mixed-layer similarity scaling 80—105021
- dispersion from tall stack, into shore line environment 80—97832
- dispersion from tall stacks, correl. spectroscopy appl. 78—3932
- dispersion in flow over shoreline of large water body, model 79—100913
- dispersion in horizontally-homogeneous boundary layer 78—36263
- dispersion in stratified planetary boundary layer, numerical simulations 79—12251
- dispersion in turbulent shear flow, theory 79—88393
- dispersion model (gaussian), incorporating temporal vertical stability variations 80—104526
- dispersion models incorporating fast reversible chem. reactions 77—73784
- dispersion near highways, gas tracer release study 80—7972
- dispersion near roadways, simple line-source model 79—5600
- dispersion of chemically reacting plume 79—34453
- dispersion of gases, aerodynamic aspects, test results and numerical solution *(German)* 79—8686
- dispersion of gases into atmosphere from volatile liq. evaporation, diffusion model *(Dutch)* 79—79425
- dispersion of instantaneous pollutant release, eddy diffusion model 77—87067
- dispersion of pollutants, Gaussian moment-conservation diffusion model 80—85317
- dispersion over highways, wind and temp. study of turbulence 80—12038
- dispersion parameters, tracer expts. and theory 80—76680
- diurnal variations of O_3 and other pollutants in urban area 79—74568
- dosage population product in Venice, modelling and forecast 79—57546
- Drax coal fired power station, CEC remote sensing campaign results 80—76681
- drift droplets deposition estimation from natural draught cooling tower 79—16647
- dry deposition from point source, pseudospectral simulation 79—2362
- dry deposition in initial phase, related to long distance transport of pollutants 79—83667
- dust, aggregates of submicron particles, acoustic coagulation 77—35011
- dust, long-lived beta-activity, freq. distrib. anal. 77—73835
- dust generating industry, peak short term dustfall meas. and effect on residential development 78—81386
- dust loading of atmos., 1923-54, pyrheliometric and circumsolar sky radiation obs. 80—46240
- dust particles in atmosphere, effects and size distribution *(Dutch)* 79—52974
- dust transport in Maricopa County, Arizona 79—70824
- dustfall from isolated cement works, implications for residential development 77—37403
- EBR-II building complex, wake and dispersion models rel. to released material 77—91186
- effective chimney heights estimation based on rawinsonde obs. 78—85684
- electrical climate relationship 77—73837
- elemental conc. and particle size distribs. in background aerosol 77—49139
- elemental concentration meas., Quillayute, Washington, (USA) 78—36270
- emission, transmission and immission, fundamentals *(Dutch)* 77—70820

air pollution continued
- emission inventory for Greater London 79—5608
- emissions from alternative electricity generation fuel cycles, health hazards evaluation 78—11791
- emissions over urban area sources, atmospheric transport 79—12184
- energy and air pollution consequences of traffic systems management 79—52990
- energy consumption effects on climate 79—29848
- energy use and climatic changes 79—29846
- N.England, aerosol particle sizes in 0.25-5.0 μm range 77—70812
- N.W. England, coastal site, ambient air quality determ. 80—89690
- NW.England, pollution at rural site, transport of tropospheric photochemical ozone 80—61481
- NE.England and Midlands, plumes visible on 78—45035
- environmental assessment for air pollution abatement, diffusion model evaluation 79—57547
- environmental effects from nuclear energy, effects of small radiation doses 79—2312
- environmental pollution by nuclear fission products 78—85607
- environmental pollution regional distribution, pattern model for prediction 79—57501
- environmental radiation dose assessment of a growing nuclear industry 80—3553
- environmental radioactive releases from nuclear installations, computer simulation of effects 80—3550
- environmental radioactivity meas. in the EEC, 1977, for air, deposition, water and milk 79—62162
- ethylene, high resolution spectroscopy with diode laser heterodyne system 77—91300
- Europe, long range transport 77—37371
- exhaust pollution, data reliability 80—3559
- factor of safety, calc. method and appl. to air and noise pollution 80—94140
- fallout observation, Chinese A-tests 80—27820
- fallout of highly radioactive particles originating from the Chinese nuclear explosions *(Japanese)* 79—63813
- fast breeder reactor accidental releases, influence of physico-chemical form on consequences 79—74574
- field burning practice in farming, downwind particle obs. 80—97836
- fission products and ^{222}Rn in N.Atlantic air 80—77074
- flames, convective mass transfer, appl. to air pollutants distrib. *(German)* 79—52662
- Flin Flon, Manitoba, fallout in vicinity of base metal smelter 80—55959
- Florida, aerosol composition meas. by time series anal. 80—89688
- fluorocarbon mixing and photolysis, eddy diffusion, tropospheric lifetime 79—62551
- fluorocarbon-11, estimated future atmos. concs. for various tropospheric removal rates 77—21892
- fluorocarbon-O_3 theory, one-dimens. modelling of atm. 79—70831
- fluorocarbons, destruction of stratospheric O_3 77—9459
- fluorocarbons, global distrib. 79—53407
- fluorocarbons, lifetime determ. methods 79—20920
- fluorocarbons, world production and release, 1975, rel. to stratospheric O_3 78—3919
- fluorocarbons conc. meas., model validation 77—45138
- fluoromethanes, tropospheric lifetime against reactions with OH 77—64366
- fluorotrichloromethane, spectral data evaluation for atm. sensing 79—62582
- fluorotrichloromethane in N.American troposphere and stratosphere 79—79430
- fly ash, from coal power plants, radioactivity 79—62161
- fly ash nucleation props. in coal-fired power-plant plume 79—5607
- fly ash particles, effect of chem. variability on cell exposure 79—16172
- fly ash particles, surface oxidation of SO_2 under low relative humidity conditions 79—62160
- fly ash particles, water accretion, refract. index and accreted layer thickness 80—58462
- flyash from coal combustion, S and Cl adsorpt., cloud nuclei form. 77—21887
- flying dust lead content determ. using atomic absorption method *(Hungarian)* 77—21893
- forced plume characteristics 78—18286
- formaldehyde, concs. in rain water and on atmospheric aerosol 78—57243
- formaldehyde, in troposphere and stratosphere, meas. by high resolution IR absorpt. spectroscopy 79—84371
- formaldehyde, photodecomposition in tropospheric clean air *(German)* 79—53405
- formaldehyde+Br, reactions, rate consts. by EPR 80—93736
- formaldehyde+F reactions, rate consts. by EPR 80—93736
- formaldehyde in air, photodecomposition, CO and H_2 quantum yields 79—66311
- Freon 21, evidence for presence in atmosphere 79—62565
- Freon-12, absorpt. coeffs. for CO_2 laser radiation, press. and temp. depend. 78—55170
- frequency distribution of pollutant concs. 77—37352
- fumigation, lab. simulation 77—78390
- furnaces, heat transfer and pollution *(French)* 79—16001
- gaeous and particulate pollutants transport, interconversion and removal, model, urban plume appl. 78—44984
- gamma-rays from extended sources, energy distrib. calc., rel. to remote spectroscopy 78—61586
- gas absorption coefficients at CO_2 laser wavelengths, remote sensing appl. 78—40647
- gas phase chemical reactions in atmosphere, evaluated kinetic and photochemical data 80—101671
- gas-particle plumes from finite-size combustion sources, dynamics 78—30341
- gaseous and particulate F compounds accumulation by forage vegetation and limed filter paper samplers 77—78407
- gaseous pollutant transfer to vegetational surface 77—2233
- gaseous pollutants mesoscale transport, math. modelling 78—44986
- gaseous reactor wastes, dispersal forecasting *(French)* 78—8995
- Gaussian diffusion-deposition model for elevated point sources 77—49156
- Gaussian plume dispersion over rough terrain 79—12250
- Gaussian plume model, parameters for ground-level and elevated sources from diffusion eqn. 80—82010
- Gaussian plume model evaluation at Dickerson power plant 78—24358
- Gaussian plume model parameters determ. from diffusion-convection eqn. integration 78—81399

air pollution continued
- Gaussian puff model simplification for real-time minicomputer use 77—81997
- geothermal energy, environmental problems, air and water pollution, subsidence, induced seismicity, blowouts, noise, review 80—55797
- N. Germany, plume concs., statistical analysis *(German)* 77—91260
- global pollution and climatic change, review 77—13120
- Gran's plot, acid-base titration 79—79432
- greenhouse effects of some atmospheric constitutents 79—70882
- Greenland, NH_4^+, SO_4^{2-}, Cl^-, Ca and Na in snow and ice, natural and anthropogenic origins 79—70815
- ground level air spectra at 9, 92 and 993 m path lengths 77—73823
- ground level concentration calc. for different sampling periods and chimney locations 77—37378
- ground level trajectory of diffusing cloud, wind vector turning effect 79—12232
- halocarbon conc. meas. in southern hemisphere 79—5602
- halocarbon depletion of O_3 layer, climate effects 80—98436
- halocarbon lifetimes and conc. distrib. using two-dimens. tropospheric model 79—12180
- halocarbons, decomp. by natural tropospheric ions 77—21889
- halocarbons, global budget analysis 79—34881
- halocarbons, hydrocarbons and SF_6, global distrib., sources and sinks, rel. to 0_3 depletion 80—4088
- halocarbons, meas. in W. Europe 78—36272
- halocarbons, SF_6 and N_2O concs., rel. to tropospheric OH conc. 77—45069
- halocarbons in stratosphere, chemical studies using Concorde aircraft, air sampling equipment 79—80058
- halomethanes, electron impact dissoc., tropospheric lifetimes *(German)* 79—50141
- halomethanes, electron scavenging props., rel. to ozonosphere 79—50143
- halomethanes in troposphere and stratosphere, O_3 depletion 80—16866
- heat releases from elec. power generating plants, effects 80—40942
- heated stack effluents in disturbed flows, wind tunnel modelling 79—92564
- heavy metal levels related to wind direction, Belgian North Sea coast 79—83665
- hemispheric mean surface temp., nonequilib. model, pollution effects 77—49150
- high oxidant days in Melbourne, atmospheric characts. 79—70484
- highway traffic, heavy metals contamination of roadside soils and plants in Alexandria district, Egypt 78—81171
- hill affecting turbulent diffusion from point source in stratified flow 80—56505
- historical survey and research projects *(Dutch)* 79—83674
- Homer City power plant plume, aerosols and ice nuclei meas. 79—74570
- humid plume interaction with stratocumulus cloud *(French)* 79—16605
- central Hungary, precipitation amounts, steelworks effects 79—20943
- hydrocarbon+N oxide mixtures in air, photochemistry 79—53427
- hydrocarbon emission from car factory affecting O_2 level, Wisconsin, USA 80—76674
- hydrocarbon mixtures, photochemical reactivities 78—61533
- hydrocarbons, assoc. with airborne particles, dispersion and transport 79—20990
- hydrocarbons, emission sources in 1974, Los Angeles-Palm Springs area 77—78408
- hydrocarbons emissions inventory in United Kingdom 79—62158
- hydrometeorology, pollutants atmospheric transport to water systems 78—96240
- hydrometeors, pH detailed struct. 79—92111
- industrial area, neutron activation analysis and evaluation of results 77—41156
- industrial area, pollutant concs., deposition vs. transport effects 79—12243
- industrial area pollution, occurrence affected by wind direction 80—89691
- industrial chimney stack plumes, large elec. fields 78—44987
- industrial cumulus, numerical simulation, comparison with obs. 79—12202
- industrial odorous pollution rel. to perceived sensory discomfort 77—37391
- industrial site, local weather effects on air pollution, field studies 77—53165
- industrial stack plumes, elec. fields 77—5315
- industrial-residential mixed area, air quality numerical model *(Chinese)* 80—3546
- insecticide, DDT and DDE in New York rain following Pacific N.W. spraying 77—29425
- integrated energy systems, environment impacts 78—73506
- inversion descent in mountain valleys, air pollution implications 79—62550
- ion comp. and episodic var. rel. to arctic snowfield contamination 77—91159
- ion concentration, pollution aspects *(French)* 78—16125
- ionic composition of rain during sixteen convective showers 79—58003
- ions, large and positive, hourly variation of source intensity, Ovieda *(Spanish)* 80—51449
- Istanbul overall air pollution obs. 77—37398
- Japan, measurement of elec. cond. and small ion mobility, pollution aspects 78—92931
- Japan, O_3 and temp. distrib. rel. to pollutant profiles *(Japanese)* 77—70768
- Labadie Power Plant plume, lidar obs. of particulate density distrib. and behavior 80—55956
- Lake Michigan, sulphate deposition in stable atmos. conditions 80—81494
- Lake Michigan dry deposition loading by airborne particulate matter 77—29410
- laser absorption techniques 77—9570
- lasers in air pollution detection, review 77—9569
- lead alkyls concentration obs. 80—85313
- lidar measurement problems in hazy visibility conditions 77—9572
- Liege industrial region, five year record of atmospheric fall-out 78—81375
- light pollution and possible measures 78—49139
- liquefied natural gas spills on land and water, dispersion hazard 77—45141
- liquid-droplet smokes and fogs, IR extinction spectra 77—78416
- literature review, 1974-6 period 77—78405

air pollution continued
- Livermore Regional Air Quality model, appl. in San Francisco Bay area 78—92966
- Livermore Regional Air Quality model, concept and development 78—92965
- local meteorological situations, statistics and pollution potentials *(Spanish)* 79—29813
- London, pollutant levels, 1500-1900 period 78—44982
- London, summer 1976 photochemical pollution 79—16648
- London, urban plume, early obs. 78—88907
- long range pollutant transport, Lagrange model 80—61851
- long-distance transportation model incorporating washout and dry deposition components 77—2228
- long-range transport, meteorological aspects 79—20969
- long-range transport, OECD study assessment 79—20967
- long-range transport modeling review 80—108823
- long-range transport modelling, OECD study 79—20970
- long-range travel of airborne material with dry deposition 77—49101
- Los Angeles, oxidant and precursor trends 79—16649
- Los Angeles, particulate sulphate and air quality, annual data multivariate analysis 80—61483
- Los Angeles Reactive Pollutant Progam (LARPP), anal. of processes affecting oxidant and precursors 80—61479
- Manchester, air pollution episode 79—84464
- marine atmosphere, lightly polluted, dark smokes and acid pollution study 78—81376
- mass consistent atmospheric flux model (MASCON) for complex terrain regions 78—92964
- mass consistent model for wind fields over complex terrain 78—92906
- mass diffusion from point source in turbulent shear layer 78—92968
- material damage functions 80—76693
- mercaptans+$O(^3P)$, reaction rate consts., O_2 effect 79—52630
- Merseyside, England, assessment difficulties for area values and trends 80—104538
- mesoscale air quality model appl. to long range pollution problems 78—81388
- mesoscale dispersion expts., trajectory-diffusion modelling 80—61837
- mesoscale models, use in studying pollution *(French)* 79—84411
- mesoscale transport and air quality in remote location 80—40938
- metal-containing particles, release into atm. from vegetation 77—41135
- metals, airborne, in industrial districts, conc. rels., dust anal. 80—72107
- metals, Pb, Cd, Cu, Zn, Ag, in deposited snow, atmospheric pollution, effect of human activity compared to volcanoes *(French)* 80—67018
- metals in Walker Branch Watershed, atmospheric input and origin 77—86956
- meteorology of air pollution conf., New Orleans, USA (March 1980) 80—90603
- meteorology of long-range transport 79—20966
- methane, conc. over ocean, var. with latit. 78—81372
- methane, troposphere vertical profile, eastern USA in winter 80—77035
- methane content of atmospheric surface layer and vertical air column, synchronised meas. *(Russian)* 79—88407
- methane flux from wetlands areas rel. to mean air temp. 77—78382
- methanethiol+OH radical, reaction rate const., 299-426K 77—40525
- methanol (dimethyl ether)+Cl, absolute rate consts., 200-500K, stratospheric chem. appl. 79—66271
- methyl chloroform, atmospheric residence times rel. to HO tropospheric concs. 78—32140
- methyl chloroform, impact on stratospheric O_3 78—53722
- methylamine+OH radical, reaction rate const. 299-426K 77—40525
- microclimatic and mesoclimatic stability indices, statistical relation, rel. to pollutants diffusion *(Spanish)* 78—44964
- microwave absorpt. coeffs. of atmospheric pollutants and constituents 77—64378
- midwest USA, ^{85}Kr concs. 77—73834
- mineral dusts, electron microscope anal., environmental monitoring 77—81877
- mineral dusts and asbestos fibres, health hazards 77—86732
- mineral dusts in environment, health hazards 77—87068
- minor species meteorological control of lower stratosphere 79—12171
- mixing during pollution incident, acoustic and temp. meas. 79—12234
- modelling, data gathering and processing 79—52984
- modelling of effects in forests 77—37370
- monodisperse particles dry deposition on simulated grass surfaces 78—81396
- monomethylamine, dilute mixtures, decomposition, shock tube studies, IR emission obs. 79—96301
- Monte Carlo anal. 77—78415
- motorways, Pb from motor exhausts 79—12248
- multiple source Gaussian air quality model, validation 78—16146
- multivariate air pollution models, computationally economical identification technique 79—57545
- natural cycle of gases *(German)* 79—53404
- natural sky radiance and smoke stack radiance spectral characts. meas. and modelling, 3.8-5.5 μm region 79—66797
- Netherlands, SO_2 conc., source areas, dispersion model 80—61482
- neutron activation anal. of air dust, environmental data evaluation problems 80—21425
- New Jersey, formaldehyde, statistical anal. 77—73833
- New York, particulate sulphate and air quality, annual data multivariate analysis 80—61483
- New York City, air pollution, aerometric station representation 77—49154
- New York City, air pollution, validity of single station representation 77—49153
- New York City air, caffeine occurrence 77—91191
- New York State, possible anthropogenic causes of local climate trends in four cities 80—105044
- New Zealand, suspended particles in Dunedin and Milton, 1975 meas. 77—53182
- nitrate in suspended particulates, rel. to weather, S.Ontario, Canada 80—76678
- nitrates, gaseous, concentrations, investigations in urban and rural area 80—94123
- nitrates over Ontario, weather pattern rel. to suspended particle composition 80—17365
- non Boussinesq forced plumes 77—81995
- nonBoussinesq forced plumes 79—57997
- northern hemisphere, temp. trend to year 2000, prediction 79—16646
- S.Norway, heavy metals and chlorinated hydrocarbons 79—12239
- nuclear accidents, behaviour of airborne aerosols 80—746

air pollution continued
nuclear and thermal power engineering sources, comparison *(Russian)* 79—70494
nuclear energy and the environment 77—50304
nuclear industry, radiation doses, health risks from various power sources 80—57899
nuclear installations, environmental surveillance programme, Spanish experience 77—65336
nuclear plant airborne effluent variable-trajectory puff advection model modifications 78—94149
nuclear power and environmental pollution, British Royal Commission Report evaluation 77—71705
nuclear power stations, radioactive emissions, heat emissions, other environmental effects 79—22491
nuclear reactor accident, effects of wind shift and cross-plume concentration models on calculated accident consequences 80—3555
nuclear reactor accident dispersion model, direction depend. probability limits consistent with NRC practice 78—17372
nuclear reactor accident risk calcs., models and data 80—47613
nuclear reactors, Three Mile Island malfunction, monitoring, radiation exposure 80—57960
nucleation model, for nonuniform vapour, cluster diffusion effects 77—4206
ocean data and information services, appl. to air pollution problems 78—69463
oil fired power station SO$_x$ critical conc. calc. *(Dutch)* 78—61547
oil refinery plume chemical composition, obs. in Los Angeles, USA 80—104524
oil slick burning in Arctic, adverse atm. effects during clearing of spills 80—16875
open field burning emissions and plume concs., depend. on meteorology, field conditions and ignition technique 78—36266
organ-specific radiological impact of airborne effluents from model PWR and FBR reprocessing plants 80—3825
organic compounds+OH, reaction rate consts., photochem. air pollution 78—7171
organic compounds photooxidation, rates, reactivity and mechanism for reaction with OH radicals 80—72104
organic constituents of particulate matter, total conc. estimate 77—37289
organic micropollutants, adsorpt. on chrysotile and crocidolite, rel. to carcinogenic props. 78—80790
organic micropollutants in precipitation in Norway 78—36262
organic pollutants, particle size distribs. in urban, rural and seashore aerosols 80—55958
organic pollutants in airborne particulate matter and gas phase 79—12238
organochlorine removal processes from atmosphere 80—51472
organochlorine residues in rainwater 78—73495
organolead compounds adsorbed on atmospheric particulates in urban air 77—73831
origin and residence times of pollutants, determ. via ^{14}C content 78—69445
oxidant air quality statistical prediction model for land use and transportation planning 77—87064
ozonosphere, chemical-kinetic criteria of effect of substances of natural and anthropogenic origin *(Russian)* 78—53699
ozonosphere, CIX pollution, effects on temp. struct. and O$_3$ distrib. 78—57246
particle acid content determ. method 77—37448
particle deposition, sensitivity to depositional velocity 80—55954
particle flux determ. using isokinetic sampler 77—91279
particle sources over Australia 79—20907
particles from oil-fired burners, size distrib. characterisation using Beta distrib. 78—81384
particles in urban air, mol. nature, high-resolution mass spectrometry 78—24360
particulate, contrib. to visibility 77—73852
particulate, planetary radiation balance, climatological consequences 78—36242
particulate air pollution meas. 79—70502
particulate concentrations in Eastern Australia and Papua New Guinea (1971 to 1976) 78—28257
particulate content in Yaounde, Cameroon, rel. to Intertropical Front 79—12240
particulate deposition, eddy correl. meas. 78—3930
particulate element conc. over USA 80—76679
particulate matter emitted by Mount Etna volcano, heavy metal chem. 78—61491
particulate pollution, climatological effects 78—85678
particulate pollution in Delhi due to Indraprastha power plant 79—21000
particulate thermal coagulation and downstream transport from urban area source, math. model 78—44985
particulates, chemical characterisation via light scatt. method 78—69533
particulates and gaseous pollutants measurement, anal. and calibration techniques 78—69531
passive contaminant vertical dispersion in surfac layer 79—62547
pathways of atmospheric pollutants, conf., England (Nov. 1977) 79—70488
pattern identification, large-spatial, of air pollution by combined model of source-receptor matrix and revised GMDH 79—57543
pattern recognition applic. to prediction 77—37404
Pb concentration variation at two stations in Perth, 1974-76 period 80—94127
peroxyacetyl nitrate, absorpt. by grass, soil and water surfaces 77—45139
peroxynitric acid form. in photochem. smog in urban atm. 77—63885
perturbed atmosphere thermal struct. and relaxation rates, photochemical radiative convective model 80—8408
pesticide, DDT translocation by resuspension over Pacific N.W. forests 77—29422
pesticides and heavy metals in Bavarian snow 80—61488
photochemical aerosol formation, primary pollutants effects *(Japanese)* 78—57305
photochemical air pollution formation simulation 80—81504
photochemical air pollution potential form. in United Kingdom, numerical estimation method. form in United Kingdom 80—76682
photochemical and condensational var. of submicron aerosol particles *(Russian)* 78—40611
photochemical haze over Greater London 78—36281
photochemical levels and particulates, predictive techniques for new city 77—70818
photochemical numerical model 80—40943

air pollution continued
photochemical oxidant transport, mesoscale lake breeze and synoptic-scale aspects 77—2232
photochemical pollutants day of weak vars. in St. Louis, USA 79—20988
photochemical pollutants from N oxides 78—36271
photochemical smog, effect of latit. on form. pot. 77—2227
photochemical smog, fresh emissions, admixing effects 79—12237
photochemical smog, gas-to-particle conversion, organic aerosol growth rates 77—73826
photochemical smog, rate parameters and computer simulation 78—48677
photochemical smog, transferred contaminant air pollution model *(Japanese)* 78—32217
photochemical smog enhancement by N,N′-diethylhydroxylamine in polluted ambient air 77—91262
photochemical smog formation, solar spectral distrib. 79—52983
phytotoxic admixtures, standardisation and meas. of max. permissible concs. 79—8685
Pittsburgh, SO$_2$ in steady winds, air quality management 77—49155
planetary boundary layer, air pollution statistical anal. rel. to meteorological conditions 77—37379
planetary boundary layer effects, numerical model 77—41143
plume diffusion over hilly terrain, validity of Gaussian model 80—3552
plume dispersion, 2-D computer hydrodynamics simulations 80—45837
plume dispersion from ground level sources in simulated atmospheric boundary layers 79—12231
plume dispersion model (gaussian), compared to obs. of NO$_x$ from HNO$_3$ works 80—104525
plume dispersion modelling for inversion breakup at power plant 78—3933
plume dispersion near large buildings, simulation in wind tunnel, flow field 77—70724
plume dispersion near large buildings, simulation in wind tunnel, concentration field 77—70725
plume from steel mill, ice nuclei and aerosol obs. 80—89693
plume model simulation with curved trajectory on data of diffusion expt. 79—52986
plume nonturbulent dispersion in complex terrain 77—45054
plume opacity related to particle mass concentration and size distribution 79—74566
plume rise, jet discharge into flaming ambient fluid, model 80—7973
plume rise at large distances from multiple-source region 78—85683
plume rise from multiple sources: A new model 79—34451
plume rise model for multiple sources appl. to power plant cooling towers 80—40939
plume spread in calm environment, for negative buoyancy case 80—55952
plume stability relationships 80—17304
plume structure and trajectories, lidar meas. 79—58016
plume trajectories, comparison of observations and model predictions 77—87062
plumes from power stations, ionisation effects 78—88909
plumes in inversion conditions, cross-sectional asymmetry, pollution 80—30619
plumes subject to dry deposition, concs. prediction 78—28307
point source, peak/mean concs., long term statistics 79—34457
point source plumes, optimal diffusivity 78—85667
point source pollution dispersion, meas. and modelling of conc. 80—81973
pollutant gas analysis, linear regression math. model defining conc. relationships 80—61486
pollutant trapping by local circulation, obs. 77—37397
pollutants long distant transport, analytical diffusion model 80—94125
pollutants vertical diffusion, study using airborne gas-chromatography and numerical modelling 78—69435
pollution level, stat. prediction by Kalman filtering method 79—57535
polycyclic aromatic hydrocarbons, in particles from coke oven, size distrib., health hazards 78—36268
polycyclic aromatic hydrocarbons in long-range transported aerosols 77—78410
polynuclear aromatic hydrocarbons, atom. distrib. 78—3934
polynuclear aromatic hydrocarbons and particulate conc. in urban air 80—76675
population exposure doses from USSR power plants, evaluation, prediction, regulation *(Russian)* 79—26776
positive ion concentration, in urban centre, meas. method *(Spanish)* 80—4059
power plant chimney plume, dispersion and chemical reactions 79—12178
power plant emissions over Lake Michigan, O$_3$ formation 79—74575
power plant plume, induced snowfall prod. 78—81284
power plant plumes, visual impact, model 79—16664
power stations, radiological impact from model coal-fired power plants and from nuclear systems 80—3557
practical air pollution model at signalised intersections in Tokyo metropolitan area 79—52987
precipitation, trace element analysis by neutron activation analysis 77—41154
prediction, based on observed data 79—57538
prediction model of air pollution adapted to pattern of daily fluctuation 79—57539
prediction via third order shaping filter modelling 79—57536
proper functions of two-dimens. field, matrix method and integral eqn. method 79—21002
pseudospectral dispersion model, inter grid sources representation 79—12259
pseudospectral model for pollutant dispersion 77—56727
puff pollutant dispersion model with wind shear and dynamic plume rise 79—57996
quality modelling, digital terrain data appl 79—84440
quality standards derivation on basis of risk considerations 79—79429
radiation exposure due to exhaust air of nuclear fuel reprocessing plant *(German)* 80—57940
radiation hazards from emissions of thermal and nuclear power stations, comparative study 79—34460
radiative effect, latitudinally depend. radiation calcs. with clouds 79—34942
radiative effects of elevated pollutant layers 78—65382
radiative transfer in polluted atmosphere, conference, San Diego, California (1979 August 29 to 30) 80—62376
radiative transfer in polluted urban planetary boundary layer 78—7708

air pollution continued
radioactive ^{133}Xe in plume from Three Mile Island nucl. reactor 80—89696
radioactive cloud, external gamma dose model 79—85828
radioactive contamination by Cosmos 954, obs. of lichens 80—55960
radioactive discharges, use of census data in assessing collective doses 79—59271
radioactive dust captured by wind from Earth's surface, radioactive fallout *(Russian)* 80—16869
radioactive effluent discharges, European Community, 1972-76, radiological aspects 79—41019
radioactive effluent gases from nuclear power industry, ambient contamination *(Spanish)* 78—61540
radioactive fallout at South Pole, 1954-1978 T content of snow 80—16867
radioactive fallout in air and rain, results to end of (1978) 79—79997
radioactive fallout in air and rain over United Kingdom 77—73847
radioactive fallout on Milan 1976-7, influence of Chinese nuclear expts. *(Italian)* 78—58501
radioactive fission products, washout by rain *(Spanish)* 79—92399
radioactive inert gas release by nuclear reactors in West Europe 77—50305
radioactive particulates in gaseous effluents at nuclear fuel reprocessing facility 79—9848
radioactive plume in atmosphere, depletion calc., and exposure from deposited activity 79—66561
radioactive pollution, atmospheric, concentration time integral *(German)* 80—26378
radioactive pollution evolution, influence of jet stream *(Spanish)* 79—100549
radioactive pollution from nuclear power stations, accident anal. 79—63782
radioactive release from nuclear facility, dose calcs. using on-site meteorological data 77—40798
radioactive releases, estimation of inhalation doses using gross monitors 79—13532
radioactive waste, risk anal. of high-level waste management systems in Germany 78—50272
radioactivity dispersion, population dose calc. 78—85381
radioisotope environmental dispersion models, evaluation of uncertainties 80—46074
radioisotopes, resuspended, possible importance of short-term exposure 80—85501
radionuclide and chemical pollutants, pulmonary effects *(French)* 80—8102
radionuclide release assessment, importance of vars. in deposition vel. 78—80979
radionuclide releases to atmosphere, dose reduction factors from indoor residence 80—56219
radionuclides, doses while travelling under well-established plumes 77—54369
radionuclides decomposition in glaciers 80—40934
radionuclides from nuclear facilities, diffusion calcs. *(German)* 80—61484
radionuclides in N.European air due to Chinese nucl. explosions 80—108826
rainfall frequency values, air pollution effects 78—7697
rainfall statistics, application of aerosol plume model 79—84355
rainfall vars. around thermal power station 78—3846
rainwater chemical composition 30 km downwind from industrial complex 77—37395
reactive pollution dispersion 78—16085
reactor accident consequences, estimated, effect of appl. of surface depletion model 80—30622
reactor airborne plume deposition estimation model evaluation 78—94148
reactor near-stack dose calc., diffusion model applicability 78—94147
reactor waste air plumes, diffusion in atmosphere 77—53183
regional air quality, estimation using GMDH 79—57544
regional scale numerical models 77—25770
removal mechanisms and processes *(Dutch)* 77—70824
respirable aerosol sampler using two Nuclepore filters 77—91278
Rijnmond, Netherlands, SO_2 concs., comparison with Gaussian plume model obs. 80—85314
road traffic, relationship to noise pollution levels 80—69594
rocket effluent, effect on ice nucleation 79—88446
rocket exhaust, $Al+SO_2$, high temp. fast flow reactor obs. of kinetics 80—30226
Rome, obs. of urban heat island during summer season 80—85717
roof-level plume interaction with downwind building 79—12233
Rustavi, USSR, coordinated radiation and meteorology study, CENEX-72 77—78413
Saint John, New Brunswick, air quality and precipitation meas. 77—37369
saline drift deposition meas. from natural draught cooling towers 77—73825
salt deposition model for natural draught cooling tower, sensitivity anal. 79—83655
salt emission and deposition from nucl. cooling tower 80—40941
sampling pump, personal, for hospital operating staff 79—12019
San Francisco air basin, biogenic emission related to high ozone levels 79—83676
sea breeze rel. to pollution over gulf region 78—11977
sea spray comp. and aerosol generation, detergent effect on oil slicks 77—29325
seasonal extinction due to aerosol at Kottamia Observatory site 80—46253
semirural area, three-year study of pollution episodes 79—5603
Seveso, environmental contamination assessment, effectiveness of treatments 80—3558
short-lived radionuclides of unknown origin in Sweden (1976) 78—32219
simple box model revisited 79—34456
skyshine dose due to gamma-rays from nucl. power plant *(Japanese)* 79—29917
small ion conc., influence of smoke, SO_2 and wind speed 78—3896
smelter plume, Aitken particles and cloud condensation nuclei 80—40937
smog episode, Los Angeles, pollutant transport in daytime sea breeze regime 79—5605
smoke and SO_2 long-term mean conc. in England and Wales country areas 77—37360
smoke cloud plumes from forest fires in Canada, satellite obs. 78—24367
smoke concentrations, frequency of fog in Midlands, England 79—84458

air pollution continued
smoke dispersion modelling, meteorological methods appls. *(German)* 80—51496
smoke plume data and vertical diffusion parameters meas. *(Russian)* 78—36227
smoke plumes, meas. of effective stack height with lidar *(German)* 77—9490
smoke plumes in surface layer, cross section diffusion *(Russian)* 80—104532
smoke plumes SO_2 conversion *(Dutch)* 77—70825
smoke plumes visual effects, computer simulation 79—66429
smoke pollution index system for rapid source-strength determ. 77—29450
snow strong acidity on Mt. Blanc rel. to air pollution 78—81259
soil particles mass concentration rel. to visibility 77—73849
solar radiation influence obs., three examples 77—37314
soot in urban atm., determ. by optical absorption technique 80—108824
source height dependence of lateral and vertical dispersion characts. 79—70823
Space Shuttle, environmental effects during launch and reentry 78—85681
spatial conc. estimation, new proposal for those which absorb optical energy 79—57533
spatial correlation analysis of air pollution data in an urban area 79—12236
spatial distrib., objective interpolation formulae 78—65412
SSTs, nitrogen fertiliser and stratospheric ozone 79—21007
St. Augustine volcano eruptions, airborne meas. and obs. 77—49053
St. Louis, Missouri, pollutant source strength-rainfall relationships investigation 80—77059
St. Louis, Missouri, USA, incident solar radiation, urban-neural differences 80—109247
St. Louis aerosol, variation of elemental composition with particle size 77—49137
St. Louis area airborne pollutant meas. 78—3937
St. Louis urban plume, O_3 and aerosols, form. and transport of secondary pollutants 77—5316
statistical analysis of data rel. to meteorological conditions 77—70816
statistical distrib. over urban area 77—37400
statistical prediction by mixed order multi-variable AR scheme in Japan 79—57537
statistics, in France, 1974 *(French)* 77—25777
steady state two-dimens. transport over area source, nonequilib. theory, pollutant dispersion 79—79924
steam boiler convective heating surface fouling with ash, NO_x formation dependence 79—83678
steam-gas power stations, pollution reduction by multi-stage high-sulphur residual fuel oil combustion 77—9487
steel industry, effects on rainfall within 200 km 77—56714
stratified boundary layer, tensor diffusivity of inert trace constituent 77—56675
stratosphere, aerosol content vars. rel. to fluctuations of solar radiation and temp. in troposphere 78—81327
stratosphere, Aitken particles, nature and sources 77—87050
stratosphere, chemistry of ozone depletion 77—91256
stratosphere, chlorofluorocarbon effects, O_3 photochemistry 77—41160
stratosphere, CO_2 and chlorofluoromethanes simultaneous effects on O_3 79—74940
stratosphere, effects of pollution on sulphate aerosol layer on global climate 80—109212
stratosphere, Fuego volcano eruption, O_3 and Aitken nuclei meas. 77—49141
stratosphere, gas composition, comparison of one-, two- and three-dimens. models 79—70870
stratosphere, influences on and effects of changes in O_3 *(French)* 77—5271
stratosphere, NH_3 injection detected from change in nature of aerosol 78—28286
stratosphere, numerical model of effect of N oxides on O_3 77—53269
stratosphere, O_3 reduction by natural NO_x and man-made pollution, model 77—60461
stratosphere, O_3 reduction due to pollution, system-theoretic model 77—73848
stratosphere, review of Climatic Impact Assessment Programme (CIAP) 78—16153
stratosphere, trace gas concs. during 1976 in N.Hemisphere 80—67016
stratosphere aerosol, modification by supersonic transport and space shuttle operations, climatic implications 80—98408
stratosphere and troposphere, H_2, CO, N_2O, methane, chlorofluoromethanes, vertical profiles meas. 79—84384
stratosphere chlorofluorocarbons, NO photolysis rel. to effects on O_3 layer 77—29399
stratosphere chlorofluorocarbons, possible O_3 depletions and Earth surface UV radiation changes 80—94577
stratosphere Cl, prospects of HOCl as inert Cl reservoir 79—12207
stratosphere O_3 reduction estimates, effects of water vapour changes 78—73444
stratosphere particle layer injected by aircraft at 23 km, balloon obs. 78—81283
stratospheric aerosols, albedo and radiative equilib. temp. changes 77—45092
stratospheric effects from aviation 79—16657
street air pollution meas. and opinion survey 77—37383
submicron aerosols, collection efficiencies of spheres, rel. to washout in atm. 78—81395
subway, New Jersey, IR anal. of sulphates, nitrates, bromates, SiO_2, acrolein, $(NH_4)_2SeO_4$ pollutants 78—36273
sulphate, dry deposition on snow surface 77—2231
sulphate aerosols, diurnal var. at rural sites in E.United States 80—30621
sulphate conc. in N.W. United States, 'STATE' program of the EPA 80—76673
sulphate concs. in New YOrk State, summertime trajectory analysis 79—34882
sulphate particle formation by heteromol. nucleation and condensation in cavities 80—26183
sulphate washout from stack plumes 77—37327
sulphates in Canada, long-range transport 79—16561
sulphates in photochemical smog, atm. visibility reduction 77—21904
surface boundary conditions arising from particulate plume dispersion 79—79944

air pollution continued
- surface boundary layer, deposition-resuspension process effect, simulation 80—16860
- surface contamination, air conc. and horizontal fluxes estimation 79—5599
- surface depletion model for Gaussian plume deposition 77—49152
- surface layer, turbulent moment calculations for application to air pollution transport 79—84354
- suspended matter, Valencia, hourly measurements *(Spanish)* 80—30618
- synoptic weather maps and typical local conditions *(Spanish)* 78—88891
- Teheran atmosphere, Pb conc. 79—21011
- telephone exchange contact reliability, effect of H_2S and organic vapours *(Polish)* 79—74573
- terrestrial thermal balance, influence of human activity *(French)* 79—74553
- test chimney stack construction, two-phase flow model *(French)* 77—37392
- tetra-alkyl Pb compounds in urban air 78—16149
- tetraalkyllead, natural source 79—2367
- tetrachloromethane, UV photodissoc., mechanism and quantum yield 79—52723
- tetrafluoromethane, v_3 vibr.-rot. band identification in balloon-borne IR solar spectra 79—100894
- theoretical methods, basic concepts 79—83669
- thermal pollution, large-scale, regional climatic effects simulation with NCAR general circulation model 79—53478
- thermal pollution from fuel and energy consumption, effects on weather and climate 78—61539
- thermal power station environment, airborne elec. and microphys. obs. 77—37354
- time model of lowest atmospheric layers pollution in towns and industrial complex areas *(Ukrainian)* 77—53180
- tolerance levels and norms, threshold values establishment *(Dutch)* 78—49129
- Toronto, city light pollution and night sky spectra 79—16668
- toxic effects, exposure-effect diagram *(Dutch)* 78—49130
- toxic gas dispersion, DENZ computer program 80—45842
- trace chemicals in atmosphere, ozone depletion *(German)* 79—96492
- trace constituents during May 1976 over continental United States 78—16084
- trace constituents transfer past air-sea interface 79—62544
- trace element concentrations in Valencia region under typical meteorological conditions *(Spanish)* 78—44992
- trace elements, environmental health hazard aspects *(Czech)* 78—7756
- trace elements in United Kingdom atmosphere, 1975 survey results 77—25759
- trace gases and pollutants, data compilation on mag. tape 78—44995
- trace gases vertical conc. from solar radiation absorpt. spectra *(Russian)* 78—69442
- trace metal aerosol, dry deposition meas. and filtration model 78—73441
- trace metals, natural and anthropogenic emissions, global inventory 79—66428
- trace metals and sulphates, record in Greenland Ice Sheet core 78—7667
- traffic control and surveillance system for anti-pollution programme *(Japanese)* 77—56726
- transfer across cavity region behind two-dimens. fence 79—70476
- transfer into water bodies, model 77—33118
- transfer model possibilities and criticisms 77—37382
- transport, air quality models development for limited wind fetch 80—104533
- transport, contaminant movement, Galerkin finite element method 80—74902
- transport, short- and medium-range material balance 77—37373
- transport across North Sea and English Channel 78—24357
- transport and deposition from point source, analytical model 77—70805
- transport and diffusion, puff-on-cell model 78—85682
- transport and diffusion in near wake regions of surface-mounted cubes 79—12183
- transport and structure in laser troposphere 80—85319
- transport and turbulent dispersion over rugged mountainous terrain 79—84349
- transport between troposphere and stratosphere 80—105034
- transport eqn., 3-D, numerical algorithm 80—106811
- transport in atmospheric turbulent boundary layer, finite-element numerical modelling 80—77061
- transport in planetary boundary layer, stack and inversion height effects, model 80—16865
- transport in Upper Silesian Industrial District, deposition and washout 78—92960
- transport near buildings, wind tunnel expts. 78—11984
- transuranic nuclides depositional history in S.Greenland firn layers 77—86953
- trichlorofluoromethane, transport processes indicator in urban atmosphere 78—36264
- trichlorofluoromethane, tropospheric lifetime 78—3920
- trichlorofluoromethane, UV absorpt. cross sections temp. depend. stratospheric 77—64423
- trichlorofluoromethane, UV photodissoc. cross-section, 223 and 296K 79—52729
- trichlorofluoromethane reaction rate with atmospheric-like ions 77—70723
- tropopause, sulphate and nitrate mixing ratios obs. 80—61835
- troposphere, composition, natural and effects of pollution 78—28262
- troposphere, interhemispheric gradients of CF_2Cl_2, $CFCl_3$, CCl_4 and N_2O 78—81289
- troposphere, methane and ethane conc. meas. in nonurban area 78—32184
- troposphere, N_2O continuous meas. 78—81318
- troposphere, NO_2 vertical column abundance, optical absorpt. meas. 78—85632
- troposphere, OH and peroxy radicals in polluted air 79—62560
- troposphere, reduced S, H_2S role 78—49123
- troposphere, Sahara dust cont. over N.Atlantic from air cond. meas. 78—92897
- troposphere, trace gases and free radicals, two-dimens. model 78—32214
- troposphere aerosol, trace gases in summer, background levels in Greenland 80—72609
- turbidity caused by air pollutants, assessment 79—100941
- turbidity meas. across Los Angeles Basin 78—92982
- turbidity of Barcelona's air, anal. of 1971-7 obs. *(Spanish)* 80—36375

air pollution continued
- turbidity rel. to atmospheric contamination, helicopter soundings *(Spanish)* 77—9499
- turbulent atmosphere, pollution release, exposure freq. distrib. from multiple cloud sources 78—57255
- turbulent atmospheric transport, Monte Carlo simulation and comparison with exptl. data 79—53479
- turbulent diffusion, gradient transfer theorem generalisation 80—12036
- turbulent diffusion, gradient transfer theorem generalisation, plume dispersion spectral diffusivity model 80—12037
- turbulent diffusion, of particles in air, analytical numerical method 78—32257
- turbulent diffusion, Sutton's formula criticised *(French)* 79—44223
- turbulent diffusion from sources near obstacles with separated wakes, eddy diffusivity model 79—81865
- turbulent diffusion from sources near obstacles with separated wakes, conc. meas. near cylinder 79—81866
- turbulent diffusion in boundary layer with Rossby number similarity 78—92896
- turbulent diffusion in cloudless summer atmosphere, radar study 77—91228
- turbulent diffusion in Ekman boundary layer 77—73783
- turbulent diffusion model, K-theory 80—89697
- turbulent diffusion of pollutants in atm. boundary layer 77—41113
- turbulent mass transfer in boundary layer, plume dispersion *(French)* 80—61850
- N.E.United States, acid precipitation, pH and acidity 77—53184
- W. United States, acidic precipitation, pH value obs. 80—89695
- NE.United States, photochemical air pollution 79—83677
- E.United States, pollution distrib. in moving high pressure system 79—83664
- SW.United States, visibility var., historical database 80—21424
- upper atmosphere, comparison of satellite self-contamination expts. and scatt. return flux calcs. 78—40722
- urban, area-source model 77—37358
- urban, HOlzworth model for meteorological potential, correction 78 -11983
- urban, multiple-source plume models, general math. struct. 77—87061
- urban, spectral meas. of direct and scatt. solar radiation 78—3949
- urban aerosol, effects on cloud microphysical model 80—82004
- urban aerosols, Boston area, multivariate anal. for element sources identification 77—37357
- urban aerosols, characterisation and hazard assessment 77 -41157
- urban aerosols, size distrib. 78—3925
- urban air quality index, proposals and computations 78—16155
- urban and industrial pollution, Houston, Texas, hydrocarbon meas. 77—78406
- urban area, photochemical pollutants, atmospheric parameters effect 77—17212
- urban areas, solar energy flux predictions 80—30394
- urban aserosol comp. and mass, particle size depend., rel. to visibility level 77 - 91258
- urban atmosphere, prediction of long-term mean and mean square pollutant concs. 77—2226
- urban atmosphere, radiative effects of elevated pollutant layers on temp. struct. and pollutant dispersion 80—97841
- urban atmospheres, modelling of temp. and pollutant conc. distribs. 77—45143
- urban atmospheric chemistry and statistics for contamination resistance improvement 77—45127
- urban centres, traffic CO emissions 77—21895
- urban heat island in subtropical environment rel. to city size 77—33170
- urban photochemical product concs., effects of entrained species 79—92566
- urban photochemistry, O group anal. and O_3 prod., theory 78—48626
- urban planetary boundary layer, effects on thermal struct. and dispersion 78—11986
- urban plume particulates collected on Anderson 8-stage impactor stages, chemical anal. 78—69433
- urban pollutants inorganic nonmetallic species, precipitation scavenging by convective storm systems 80—12039
- urban pollutants scavenging by thunderstorm rainfall, numerical expt. 79—12261
- urban suspended matter continuous sampling over large grain size spectrum 78—3924
- urban temp. field dynamics in Calgary area 77—17168
- urban ultragiant aerosol particles conc. meas., St. Louis, Missouri, USA 77—49159
- urban-rural complex, air pollution effects, two-dimens. numerical simulation 78—81369
- urban-rural solar radiation and atm. turbidity, meas. in Los Angeles basin 79—80024
- urban-suburban air pollutant transport, chemical and physical transformations 77—37399
- urbanisation and pollutant effects on thermal struct. in various climatic regimes 78—61500
- vehicle emission rate depend. on road speed, mass balance techniques 80—97839
- vehicle generated air pollutants, correl. study 79—21012
- vehicular Pb concs. rel. to airborne particulate Br levels 77—91254
- Venetian region, air pollution episodes real-time forecasting, advection-diffusion model 80—77096
- Venetian region, real-time forecasting of air pollution episodes via Kalman predictor 80—82046
- Venice, SO_2 pollution levels, meteorological factors 77—91253
- Venice area SO_2 concentration, real time prediction 80—55953
- Venice region, real-time forecast, advection-diffusion model 80—72102
- Venice region, real-time forecast, Kalman predictor 80—72103
- vertical diffusion from ground-level source, Lagrangian similarity modelling 80—51480
- vertical diffusion from sources near ground 79—62548
- vertical dispersion in neutral surface layer, Markov Chain simulations 79—88399
- viscous incompressible flow problems, two-dimens., Navier-Stokes eqns. soln. and contaminant effects 77—58638
- visibility reduction due to pollution at Bombay Airport during monsoon season 78—32225
- visibility rel. to surface wind at Gutersloh, Germany, smoke pollution effects 79—29853
- visibility-reducing aerosols in Los Angeles air basin 78—16157

air pollution continued

- Vizcaya, Spain, B, Mg, Cr, Mn, Fe, Co, Ni, Pb, Ga, Ge and Si conc. in atm. and rainwater *(Spanish)* 78−57264
- Vizcaya, Spain, Na, Mg, Cr, Al, Ti, Cu, Ag, Zn, Co and Ni content in sedimentable powders *(Spanish)* 78−57265
- volatile fission product atmospheric release from nuclear reactors and fuel reprocessing plants 79−34461
- volcano eruption cloud particles, St. Augustine, Alaska 78−57186
- Washington, D.C., chemical element balances and pollution sources 79−12174
- waste heat release from nuclear power plant, convective cloud model appl. 79−34452
- water vapour effect, damp air and plumes *(Dutch)* 77−70823
- wet and dry removal of particles and gases 77−73845
- wet plume rise from cooling towers in strong winds 77−33182
- wind speed averaging in pollutants conc. equation 78−57307
- workplace carcinogens, respirator selection, US standards review 77−79076
- Yaounde, Cameroon, particulates in urban and rural air *(French)* 80−61478
- β-active aerosol particles, stationary charge distribution 79−92581
- Ag cloud seeding of Florida cumuli, rainwater conc. obs. 80−56563
- ^{41}Ar dose distributions due to atm. release from HWR, including wind effects 77−14271
- Br compounds in stratosphere, O_3 depletion due to chem. reactions 80−98391
- Br from vehicle exhausts, model for dispersion 77−37367
- Br/Pb ratios in atmospheric particulate matter over Perth, W.Australia, 1971-6 var. 79−34455
- C sphere aerosol, black smoke opacity, calc. variation with particle size and refr. index 79−72488
- CH_3O_2+NO, rate const., flash photolysis and kinetic spectroscopy 79−70305
- CO abundance, geographical, seasonal and secular vars. *(Russian)* 78−53700
- CO, air quality criteria using a COHb model 80−16864
- CO, anthropogenic emissions, implications for atm. CO-OH-CH_4 cycle 77−49160
- CO, comments on appl. of one-dimensional mixing models 77−45086
- CO, conc. in Sheffield, var. 80−16863
- CO dispersal in city streets, wind tunnel modelling 78−3927
- CO, dispersion at ground level rel. to nocturnal inversion 79−92563
- CO from vehicle emission in urban area cold engine startups 80−104527
- CO generated from road traffic, rel. to traffic parameters 80−81500
- CO near highways, line source dispersion models, comparison 79−12247
- CO, troposphere vertical profile, eastern USA in winter 80−77035
- CO_2 and climate, model of geographically nonuniform effects 80−90143
- CO_2 and global warming, effect on regional climate 80−77099
- CO_2, anthropogenic, possible influence on atmospheric temp. 80−51486
- CO_2, atm. conc., logistic source function calcs. 78−24368
- CO_2, atmos. var. at Mauna Loa Obs., Hawaii during 1964-71 period 77−37365
- CO_2, atmos. var. at S.Pole in 1957-71 period 77−37366
- CO_2, atmospheric response to deep-sea injections of fossil-fuel CO_2 80−31090
- CO_2, biosphere as source and/or sink 79−88030
- CO_2, climatic effects of increasing content 79−88029
- CO_2, climatological significance of doubling of atmospheric conc. 80−101426
- CO_2 conc., effects of different future energy strategies, rel. to global climate 79−83640
- CO_2, conc. vars., cycles and trends 79−84381
- CO_2 content of atmosphere, role of C storage by forests and oceans 78−53718
- CO_2, decrease during 1963-69 period 79−84380
- CO_2 diurnal and seasonal vars. in air over Tehran 77−37396
- CO_2, form. from fossil fuel combustion in atm., effect on climate 79−2359
- CO_2 from fossil fuel burning and global C budget 80−77080
- CO_2, future atm. level prediction using atm. and ocean models 78−61549
- CO_2, global problem of increasing levels 79−88032
- CO_2, impact on snow and water surfaces cooling 79−92569
- CO_2 in atmosphere, $^{13}C/^{12}C$ vars. in last 22 yrs. 80−104530
- CO_2 in atmosphere, climate-C budget model 80−98381
- CO_2 in atmosphere, significance of deforestation 79−74572
- CO_2 in urban atmosphere, dependencies and trends 80−16870
- CO_2, increasing concs. effect on heating rates 80−17376
- CO_2, industrial pollution affecting ^{13}C tree ring dating method 80−51586
- CO_2 input from burning wood 78−81368
- CO_2 levels rel. to global C cycle, modelling perturbations 80−31114
- CO_2, ozone, and water vapour, atmospheric content variation meas. *(Dutch)* 79−70838
- CO_2 pollution, climate sensitivity study with global climate mathematical model 80−31117
- CO_2 problem, increase from fossil fuel combustion 79−16623
- CO_2, uncertainties associated with effect on global climate 79−88028
- CO_2, wood vs. fossil fuel as source 77−53162
- $COCl_2$ (phosgene) in ambient air of California 77−13119
- COS and CS_2 conc. meas. 77−73830
- ^{14}C and ^{3}H, continuous monitoring, sensitive method *(German)* 77−372
- ^{14}C produced in advanced FBR fuels, potential radiation doses 77−40799
- ^{14}C released to atmosphere, dynamic model for estimating radiation dose to world population 80−89852
- ^{14}C released to atmosphere as CO_2, population dosimetry 78−35958
- Cd, Pb, Mn in particle size fractionated aerosols, flameless atomic absorpt. determs. 78−69434
- Cl effects on O_3 layer, zonally averaged two-dimens. model 79−84435
- Cl particulate distrib. in Houston-Galveston area 79−12252
- Cl^- ion concentrations in river, spring waters in Okinawa Honto, origin *(Japanese)* 79−39324
- $Cl+O_3 \rightarrow ClO+O_2$, rate consts. meas. 77−60059
- $ClO+NO_2 \rightarrow ClNO_3$, reaction rate consts., stratospheric appl. 77−78306
- $ClO+NO_2 \rightarrow ClONO_2$, fall-off curves, N inclusion effects 77−63910
- $ClO+O(NO) \rightarrow Cl+O_2(NO_2)$ rate consts. meas. 77−60059
- ^{60}Co, inhaled, long-term clearance 79−79663
- Fe aerosols in atmosphere, source determ. by gamma-ray spectroscopy 77−41235
- α-Fe_2O_3, analysis of car exhaust by Mossbauer spectroscopy 78−92963

air pollution continued

- ^{55}Fe and stable Fe forms and availability in oceanic aerosols 79−12241
- H fuel, health benefits derived from a planned hydrogen community 80−55947
- H^+ in E United States precip., concs. behaviour 78−92962
- H_2 fuelled aircraft, kinetic model anal. of pollution 80−40816
- HCl production mechanism, in cloud, chemical model with trace gases 77−37325
- HF meas. in upper stratosphere 77−45070
- HNO_2, obs. of lower atmos. pollution in W.Europe 80−72106
- HNO_3 in rural air, meas. 79−79422
- HNO_3 vapour and particulate NO_3^-, global tropospheric meas. 78−88904
- HNO_3-water, homogeneous nucleation, relative humidity depend. 78−71846
- $HO_2+NO \rightarrow OH+NO_2$, kinetics temp. depend. 80−3313
- H_2O_2 in rural air, meas. 79−79422
- HONO (nitrous acid), obs. in urban atmosphere by differential optical absorpt. 80−76677
- H_2S, distant source sensing by statistical treatment of air quality data 77−70808
- H_2S in troposphere, photochem. production reactions 80−90112
- H_2SO_4 aerosol growth, kinetic model 77−37340
- H_2SO_4, aerosols form., expt. and theory 78−96256
- H_2SO_4 formation in urban atmosphere, flame photometric obs. *(French)* 77−41136
- H_2SO_4 secondary aerosol form. in urban atmosphere 77−33137
- H_2SO_4, secondary particles form. and growth, kinetic aerosol model 79−29492
- H_2SO_4-water, homogeneous nucleation, relative humidity depend. 78−71846
- HT single release in a room, radiation dose 78−74513
- ^{3}H, environmental surveillance, sensitivity to natural fluctuation of tritiated water vapour in troposphere 77−88287
- ^{3}H, environmental transport from atm. release of mol. ^{3}H 78−11987
- ^{3}H, in working area of nuclear power stations 77−71699
- Hg emissions from geothermal power plants 77−73838
- Hg emissions from wastes stored near Cl manufacturing plant 77−66938
- Hg fallout in Hawaii 78−61551
- I deposition velocity rel. to environmental transport of radioiodine from air to milk 77−66866
- ^{131}I concentrations in air, milk and antelope thyroids in southeastern Idaho 80−89871
- $^{131}I_2$, $CH_3{}^{131}I$, radioactive, airborne, diffusion coeffs. 79−2142
- K-rich aerosol emission by tropical forest *(French)* 79−100551
- Kr activity meas. using ^{85}Kr 77−78454
- ^{85}Kr conc. 80−93756
- ^{85}Kr concentration in atmosphere over USSR (1971-1975) 78−37453
- N oxides, release by burning of fossil fuels, rel. to acidity of rain and snow 80−26590
- NH_3 fluxes into free atmosphere over W.Germany evaluation 80−94132
- NH_3, gas complex analysis method, resonance absorption with pulsed laser light *(Japanese)* 80−36421
- NH_3 gas conc. and acid sulphate aerosols existence 77−81998
- NH_3, in troposphere, effect of nitrate fertilisers 80−85701
- NH_3, resulting from accidental spills of liquid anhydrous NH_3 onto water 77−73846
- NH_4^+, NO_3^-, in rain water collected at Julich, Germany, N isotope comp. 78−57284
- $(NH_4)_2SO_4$ aerosol production under elevated temp. inversion in Cleveland Country, model 78−81397
- NO, absorpt. characts. of γ-0 band 79−39845
- NO, gas complex analysis method, resonance absorption with pulsed laser light *(Japanese)* 80−36421
- NO, NO_2, deposition onto soil and cement surfaces, lab. meas. 79−70477
- NO, NO_2, O_3 conc. meas. at ground level at unpolluted maritime site 78−3951
- NO, troposphere content, 0-7 km altitude over clean and polluted areas 80−51478
- NO_2, absolute integrated intensity for 3.44 μm band 77−3418
- NO_2, determ. from solar and lunar spectra in visible region obs. from ground *(French)* 79−53511
- NO_2, emission inventory for Canada 80−97835
- NO_2, from supersonic transports, latitude-dependent stratospheric O_3 depletion 77−45051
- NO_2 meas. in ambient air, Dutch-German programme 77−29443
- NO_3, detect. in polluted troposphere by differential optical absorpt. 80−77036
- NO_3 in troposphere, obs. of content in mountain air 80−72582
- NO_3 particles size distrib. and chem. comp., Nagoya, area, Japan 78−11980
- NO_3^- in E United States precip., concs. behaviour 78−92962
- NO_x atmospheric chemistry, significance of HO_2NO_2 78−11971
- NO_x, conc. in Sheffield, var. 80−16863
- NO_x emission, from thermal energy plants, review of preventive measures *(Croatian)* 78−3935
- NO_x emissions of high-altitude aircraft, effects on O_3 conc. 78−32176
- NO_x from SST and subsonic aircraft emission, potential O_3 column increase 78−11979
- NO_x removal rate in urban atmosphere 80−56524
- NO_x, urban pollution in Genoa, Italy 78−11981
- N_2O, atmospheric fluxes from N_2O supersaturated surface waters 78−57223
- N_2O cycle, sources and sinks 79−70871
- N_2O emission from soils, effects of acetylene and soil water content 79−83672
- N_2O from fertiliser, causing atmos. warming 80−94579
- N_2O from fertilisers and O_3 content of stratosphere, latitudinal effects 80−36370
- N_2O, global atmos. composition and residence time 80−51519
- N_2O, potential of soil as natural sink 77−21772
- N_2O, prod. by coal and fuel oil combustion 77−21890
- N_2O, rates of evolution from N fertilised soil 79−16656
- N_2O, sources, sinks and vars. meas. 78−85631
- N_2O sources and sinks, O_3 reduction due to industrial fixed N fertilizers 77−78383
- N_2O, sources and sinks, review 77−37374
- N_2O, three-dimens. distrib. and variability, numerical simulation three-dimens. distrib. and variability, numerical simulation 79−58006
- N_2O, tropospheric lifetime against reactions with OH 77−64366

air pollution continued
- $NO(NO_2)+O_3$ reactions in power plant plumes 78—3923
- $^{15}N/^{14}N$ ratios in gaseous NH_3, NO_2 and NO_3^- in aerosols and precip. 78—44896
- O_3, absorpt. by grass, soil and water surfaces 77—45139
- O_3 affecting ground-level oxidant concs. at Santa Rosa 78—16112
- O_3 depletion, uncertainty in calcs. from stratospheric photochemistry model 79—16567
- O_3 depletion chemistry 79—70872
- O_3, depletion resulting from nitrogen oxides pollution *(Russian)* 78—16154
- O_3 determ. with Dobson spectrophotometer, aerosol effects 77—45186
- O_3 effects on lung function, appl. of short-lived positron emitting tracer 77—25552
- O_3 elevated levels from natural sources 79—62552
- O_3 formation dynamics in cities 80—31112
- O_3, global distribution, effects of pollutants, book contrib. 77—29429
- O_3, ground level conc., rel. to regional transport of pollutants 78—44990
- O_3 in troposphere, evidence for significant in situ photochemical source 80—72619
- O_3 in urban air at night, Jerusalem and Tel-Aviv 80—89689
- O_3 layer, fluorocarbon hazard assessment 79—79963
- O_3 layer depletion 80—104534
- O_3 layer depletion by supersonic flight, rel. effects of latitude and altitude 77—64360
- O_3 levels from plant damage in British Isles 79—21008
- O_3 long-range transport across mid-W. and E. United States 78—16147
- O_3, sources and transport in NE. United States 79—92110
- O_3 sources in NE.USA, air pollution assessment 80—41482
- O_3, stratospheric, perturbation by N fertilisers, independent variables anal. 78—73505
- O_3, stratospheric, spectroscopy with CO_2 waveguide laser 77—13117
- O_3 surface concentration forecasts for polluted areas, Model Output Statistics appl. 80—12035
- O_3 transport in St. Louis area 79—16650
- O_3, tropospheric, long-range transport 78—61514
- O_3, tropospheric, photochemical prod. and influence on climate 80—36365
- O_3+cis-2-butene+formaldehyde→propylene ozonide, gas phase reaction mechanism 77—33132
- OCS, anthropogenic emissions rel. to contrib. to stratospheric aerosols and climate 80—41524
- OH+dimethyl sulphide, flash photolysis reson. fluoresc. rate consts. determ., pollution aspects 78—95913
- OH+halocarbons rate consts., appl. to tropospheric degradation 79—52622
- OH+OCS(CS_2), flash photolysis reson. fluoresc. rate consts. determ., global S cycle 78—95914
- P, atmosphere contrib. to aquatic system 79—100545
- P containing particles, deposition velocity over southern Lake Huron 79—83666
- Pb, atmospheric long range transport to Denmark 80—94131
- Pb baseline in troposphere, anthropogenic sources effects 78—7757
- Pb concs. rel. to 1000 mb geostrophic back trajectories at Quillayute, Washington 77—29421
- Pb, contamination, rel. to traffic density *(German)* 79—70470
- Pb, dispersion from motor exhausts 79—70491
- Pb, dry deposition on snow surface 77—2231
- Pb dry deposition onto snow surface 77—37288
- Pb, effects on children, Steinbuch's Lernmatrix appl. 77—44878
- Pb, from petrol engine exhaust, deposition on plant and soil surfaces 77—87063
- Pb in subalpine pond sediments, anthropogenic source var. 80—85315
- Pb near roads in Egypt 79—12255
- Pb, V, Cd, Zn, Cu, conc. in snow of Mt. Blanc rel. to air pollution 78—81258
- Pu, air concs. near Rocky Flats, $^{239+240}Pu$ 78—16150
- Pu isotopes in Antarctic snow layers, deposition and accumulation 79—70820
- Pu toxicity hazards, cancer fatalities 77—66864
- $^{239}PuO_2$, cancer risk, max. permissible conc. in air 79—25108
- Ra A (^{218}Po) adsorption to monodispersed aerosol 80—32535
- ^{222}Ra short lived daughter disequilibrium in a mixed maritime and continental atmosphere 80—108822
- ^{226}Ra background levels in lower troposphere from coal burning 77—37361
- Rn 80—7977
- Rn air concs. in certain houses 79—79662
- Rn, atmospheric, accumulation in calcite caves 80—104531
- Rn concentration in Norwegian dwellings 79—70485
- Rn, concentration of ^{222}Rn, ^{220}Rn and decay products in room air, exhalation, ventilation and deposition effects 78—73261
- Rn daughter concentrations in different atmospheres 80—85316
- Rn daughters, dose conversion factors 79—70641
- Rn decay products, concs. in mine air 77—9280
- Rn decay products, influence of elec. charge and humidity on diffusion coeff. 80—6192
- Rn dose calculations for inhalation of ^{222}Rn, ^{220}Rn and daughters 77—64133
- Rn, evolution in neutral atmospheres *(Spanish)* 80—4058
- Rn exposure and human disease, impact of energy conservation in residential buildings 80—56225
- ^{220}Rn and ^{222}Rn, decay products, diffusion coeffs. in air and Ar 79—90366
- ^{220}Rn decay products attachment to flowing aerosols using centrifuge 80—61167
- ^{222}Rn, conc. in free air *(Hungarian)* 80—94128
- ^{222}Rn concentration in tunnel air, atmospheric press. and precipitation effects *(Japanese)* 80—97845
- ^{222}Rn decay products, conc. in basement lab., working levels 77—40797
- ^{222}Rn, diffusion and exhalation meas. from U mill tailings pile 79—92109
- ^{222}Rn in biologically produced gas from reactor cooling pond 78—80976
- ^{222}Rn, release to atm. due to UK coal combustion, annual rate of release determ. 80—17143
- S aerosols, in atm., phys. props. 78—96285
- S airborne transport over N.Atlantic 78—20507
- S and N, acid precipitation in the Pittsburgh, Pennsylvania area 80—94129
- S and trace elements in aerosols from South American continent, conc. relationships 78—57245

air pollution continued
- S, and trace metal content of nonurban and marine aerosols, PIXE anal. 77—49136
- S balance and washout by precip. in industrial atm. *(Russian)* 79—100898
- S budget of eastern N.America, anthropogenic and natural contribs. 80—97834
- S budget over Europe, residence times 79—70475
- S compounds, meso-scale transport obs. in rurual East Midlands, England 80—94124
- S compounds, natural and man-made emissions in Europe 79—20968
- S compounds conc. in remote continental and oceanic areas 79—20983
- S compounds homogeneous oxidation in atmosphere 78—96258
- S compounds long term deposition calc. for Europe 79—20971
- S compounds long term region patterns in Europe 79—20973
- S compounds transform. and removal, time-dependent diffusion model 79—20972
- S compounds wet removal from atmosphere 79—2363
- S containing aerosols, physical characts. 78—96284
- S dry deposition onto snow surface 77—37288
- S, estimated dry deposition vels. over E United States and surrounding regions 80—56507
- S, in deposited snow, effect of human activity compared to volcanoes *(French)* 80—67018
- S isotopic comp. in atm. precip. around Sudbury, Ontario 78—81361
- S, linear eight-box model for tropospheric global cycle 80—56506
- S, natural and anthropogenic emissions in Central Europe, calc. from atm. meas. 77—73827
- S, over NE. United States, statistical trajectory model 77—73828
- S oxide pollutants, SURE/MAP3S obs. comparison with regional model predictions 80—81501
- S pollutant removal from atmosphere by rain, modeling method 80—85318
- S pollutants, long-range transmission, simulation, two-dimens. pseudospectral dispersion model 78—57306
- S pollutants dispersion over western Europe 79—70490
- S pollutants in atm., conf., Dubrovnik, Yugoslavia (Sep. 1977) 78—96281
- S pollutants in atm., conf., Dubrovnik, Yugoslavia (Sept. 1977) 79—20965
- S, release by burning of fossil fuels, rel. to acidity of rain and snow 80—26590
- S wet fallout scale, geographical var. in S. Sweden 79—16653
- SO and SO_2 deposition and transformation rates during transport over Atlantic Ocean, comment 77—66975
- SO_2, adsorption and oxidation on atmospheric particles 78—96287
- SO_2, aerosol-catalysed oxidation, expt. under atm. conditions 79—1941
- SO_2 air pollution, decomposed model design for assessment of utility measure 79—66426
- SO_2 and SO_4^{2-}, dry and wet removal from atmosphere 79—2361
- SO_2 and SO_4^{2-} conc. relationship in urban and industrial air 79—2360
- SO_2 and smoke, ground level concs. in urban areas of UK rel. to meteorology 79—12253
- SO_2 and sulphates in rain, urban and rural Norfolk, England 80—55955
- SO_2 at ground level, air pollutant dispersal, Forth Valley, Scotland 80—81497
- SO_2, atmospheric removal rate meas. using ^{38}S tracer *(German)* 79—53411
- SO_2, atmospheric transport and conversion to sulphates 79—16654
- SO_2 conc., urban built-up area, Japan 79—21006
- SO_2 conc. and wind in Venice, Italy, spectral anal. 77—73824
- SO_2 conc. decrease near Rotterdam rel. to meteorological parameters during 1961-74 winters 77—37359
- SO_2 conc. determ. using HBr laser *(Russian)* 78—69484
- SO_2 conc. in Milan urban atmosphere in winter *(Italian)* 78—53721
- SO_2, conc. rel. to sulphate dry deposition on snow 77—2231
- SO_2 concentration distributions in Paris region (1962-72) *(French)* 77—37402
- SO_2 concentration in Norwegian air rel. to sulphates in precipitation 77—37385
- SO_2 concentrations, maximum, and averaging time, in industrialised area of Bilbao (Spain) 80—51020
- SO_2 concentrations of Venice air, time series anal. 79—57540
- SO_2 daily meas., PVC sample line interference, comment 77—70815
- SO_2 density prediction for Tokyo, adaptive transformation network method 79—5609
- SO_2 deposition to pine forest, radioactive tracer method 78—20508
- SO_2 deposition velocities to snow, N.Canada 79—70478
- SO_2 diffusion-coupled oxidation 78—65371
- SO_2, dispersion and wet deposition from power plant plume 80—16861
- SO_2, distrib. in Venice using air quality simulation model 79—88394
- SO_2, dry deposition on forests and grasslands 79—16652
- SO_2 dry deposition to land and water surfaces 77—49158
- SO_2 effect on precipitation and soil S content and acidity in Alberta 77—73843
- SO_2, emission inventory for Canada 80—97835
- SO_2 emissions in Mediterranean region, remote meas. 79—20987
- SO_2 from sour gas plants in Alberta 77—37372
- SO_2, gas complex analysis method, resonance absorption with pulsed laser light *(Japanese)* 80—36421
- SO_2, Helsinki study of district heating effect 79—21010
- SO_2, heterogeneous conversion to SO_4^{2-}, rel. to urban air pollution 78—80789
- SO_2, high conc. duration in urban atm. 78—11982
- SO_2, homogeneous oxidation mechanism in troposphere 78—96257
- SO_2, in India, containment and use in agriculture 78—28309
- SO_2 in Sheffield industrial area, precipitation scavenging 77—29424
- SO_2 in St. Louis, numerical simulation of parametric effects 79—12235
- SO_2 levels in Sarnia area, Ontario, modelling 77—37368
- SO_2 long-distance transport, numerical model 79—44238
- SO_2 low core, equilibria between air and water 78—16137
- SO_2 max. conc. rel. to av. time and av. conc. in urban area 79—34454
- SO_2 meas. in ambient air, Dutch-German programme 77—29443
- SO_2 measurements for stability classification schemes, stack plume dispersion, Maryland 80—16862
- SO_2, mesoscale air quality model appl. 78—81388
- SO_2, mesoscale transport over English Midlands 78—44983
- SO_2, movement in atmosphere *(Dutch)* 80—97844
- SO_2, NH_3 and CO_2 reversible washout and acid rain prod. 79—83657
- SO_2, NO_2, meas. in ambient air, International Comparison Programme 77—87066

air pollution continued
- SO_2, NO_2, solar UV radiation effect on photochem. reactions 77–21894
- SO_2, norm determ., technical meas. aspects *(Dutch)* 78–49131
- SO_2 over E. United States, regional residence time 79–16651
- SO_2, oxidation, precursor effects, rel. to air pollution 79–1960
- SO_2, oxidation by O_2 and O_3 in aq. soln., kinetics, rel. to atm. rate processes 79–20905
- SO_2 oxidation in clouds and rain, O_2, O_3 and H_2O_2 role 79–84351
- SO_2 oxidation in coal-fired power plant plumes 77–87065
- SO_2, oxidation in moist atm., aerosol growth kinetics 78–96255
- SO_2 oxidation in smelter plume 78–3922
- SO_2 oxidation in stored rainwater samples, rel. to Mn content 79–84352
- SO_2 oxidation over atmospheric aerosol, absorption over V_2O_5 and C 77–70811
- SO_2 oxidation to SO_4 in urban atmosphere 80–81964
- SO_2 oxidation to sulphates in dispersing plumes 77–70806
- SO_2 oxidation to sulphate in troposphere, model predictions 80–81963
- SO_2, oxidation via OH radical, rel. to atm. fate of HSO_x radicals 79–62559
- SO_2 photochem. effects on nitrate conc. in aerosols 77–49103
- SO_2, photochem. oxidation 79–70873
- SO_2, photooxidation, aerosol evolution, rel. to air pollution 78–81392
- SO_2 plume detect. 400 km from source 78–24361
- SO_2 pollutant dosages in urban areas 80–81499
- SO_2 pollution in Montreal, Canada, anal. of meteorol. and source factors 80–104537
- SO_2, pollution zones definition and assessment 78–81383
- SO_2 regional transport, three-dimensional grid model 77–37375
- SO_2, removal from atm. by dew 78–81370
- SO_2, reversible washout by rain, improved model 79–2364
- SO_2, SO_4 and Aitken nuclei airborne meas. over Denmark, long-range transport 78–3950
- SO_2, SO_4^{2-}, budgets and turn-over times 79–20980
- SO_2, SO_4^{2-}, transport over Mediterranean 78–81390
- SO_2 source determination by meteorology and elemental aerosol analysis *(French)* 77–41159
- SO_2, stochastic modelling and dosage area product forecast 79–5601
- SO_2 to SO_4 transformation rate from atm. conc. data, aircraft meas. 77–73829
- SO_2 to sulphate conversion processes in atmosphere 77–37389
- SO_2 transfer resistance of European soils, laboratory meas. 77–37384
- SO_2, transform. and scavenging processes, plume transport model 79–20976
- SO_2, transmission on local, regional and continental scale 79–20974
- SO_2, turbulent diffusion above and within forest 77–45055
- SO_2, vertical distrib., influence of clouds and rain, one-dimens. model 79–20982
- SO_2 washout and rain composition, model 78–28253
- SO_2, washout coeff., data from ground level monitoring network 79–74926
- SO_2-lime plaster interaction *(German)* 77–86378
- SO_3 emissions remote meas. from Asama Volcano, Japan *(Japanese)* 79–70772
- SO_4 aerosol, geographical extent in Midwestern and Southern USA 77–49145
- SO_4 dispersion, wind, temp. and conc. fields 78–3929
- SO_4^{2-} aerosol form., CO effect, smog chamber expt. 79–74925
- SO_4^{2-} aerosol form. and growth in stratosphere 79–5604
- SO_4^{2-} aerosol particles size depend. on relative humidity 79–20906
- SO_4^{2-} aerosols long-distance transport rel. to visibility, London, England 79–21015
- SO_4^{2-} conc. in precip. 79–100915
- SO_4^{2-}, conc. in rainwater, obs. by European Atmospheric Chemistry Network 79–2365
- SO_4^{2-} containing aerosols, dynamics, review 78–96286
- SO_4^{2-} in E United States precip., concs. behaviour 78–92962
- SO_4^{2-}, NO_3^-, NH_4^+, contrib. to acidity of rain 79–2327
- SO_4^{2-}, natural sources in tropical humid area *(French)* 78–81371
- SO_4^{2-} production in rain and raindrops in polluted atm. 79–88388
- SO_4^{2-} production rel. to cloud water acidity 79–5546
- SO_4^{2-}, tropospheric aerosols chem. props. 78–96254
- ^{35}S content of coolant gas in Windscale AGR, gas chromatographic and radiochemical anal. 78–73125
- $^{35}SO_2$ interaction with atmospheric particulates 77–41137
- T release from nuclear power stations 80–23032
- THO, prediction of flux from air to plant leaves 80–26381
- ^{99m}Tc, atmospheric release, dose evaluation 79–25119
- ^{132}Te in lower troposphere, airborne levels and lifetime 79–12242
- Tn decay products, ats. and ions, adsorption probability on submicron particles 79–39803
- U, in situ mining, Wyoming State regulations and environmental monitoring 79–88510
- UO_2 inhaled particle distrib. and clearance on first bifurcation and trachea of rats 78–73267
- V in particulate matter, statistical control of results 77–41153
- V, meas. by neutron activation analysis 77–41239
- V, transport from urban to remote marine areas 77–37355
- ^AXe, A=133,135, interference with low-energy meas. systems 80–89872

air pollution detection and control
- absorption spectrum Fourier transform for air pollutant meas. 80–81514
- acid precipitation, development of regulatory programs in USA 77–73842
- acid sulphate in atmosphere aerosol, detection from S/N ratio 80–61494
- acidity, man-made, determ. using Gran's titration method 79–5606
- acoustic agglomerator for control of particulate emission 80–33413
- acoustic particle agglomeration due to hydrodynamic collision between monodisperse aerosols 80–26191
- acoustic particle agglomeration of aerosols under standing-wave condition 80–30627
- adaptive diagnostic model for air quality management 79–20996
- advection eqn. numerical analysis 77–13118
- aerosol, monodisperse, quantitative analysis using IR differential absorpt. analysis 79–24931
- aerosol, particles chem. diameter meas. with scintillation analyser *(French)* 79–88036
- aerosol, Pt metals analysis by neutron activation 78–3989
- aerosol, S.Pole, chem. comp. determ. by instrumental neutron activation analysis 78–3988
- aerosol automatic mass conc. meas. techniques 77–64459
- aerosol characterization for particulate S, health effects 79–20984

air pollution detection and control continued
- aerosol classification pulse amplitude analyser 78–61587
- aerosol collection efficiency of nuclepore filters with asbestos fibres 78–57351
- aerosol concentration deduction from 1.06 μm lidar meas. 79–25323
- aerosol detection, condensation nuclei counters, efficiency improvement 80–7983
- aerosol detection using solar aureole radiometer 77–53240
- aerosol fibre, airborne fibre, sampling method for pollution detection using separated deposition 77–82031
- aerosol fractionator for large-scale sampling, impacting jet system 77–9140
- aerosol loaded filters, X-ray fluoresc. anal., absorpt. corrects. calcs. 78–7311
- aerosol loaded filters, X-ray fluoresc. anal., filter absorpt. correction 77–60166
- aerosol mass conc. meas. by Nd:glass lidar, ASSESS II Spacelab mission simulation *(German)* 78–69649
- aerosol measurement, particle deposition in sampling lines 78–81472
- aerosol measurements with calibrated two- and three-freq. lidars 78–36334
- aerosol mobility chromatograph, new detector for H_2SO_4 air pollution 78–96297
- aerosol monitoring and control, using size distrib. 79–57534
- aerosol multielement characterisation 77–41152
- aerosol particle concentration over Chicago, comparison of methods 80–7981
- aerosol particle size distribution errors of ratio-type single-particle counters 77–21898
- aerosol particle size spectrometer, microcomputer-modified 79–39329
- aerosol particle sizing by laser Doppler dynamic relaxation time meas. 77–21897
- aerosol particle sizing by optical scattering counters 77–21896
- aerosol particles, S assessment along urban freeway, proton induced X-ray emission anal. 77–60172
- aerosol particles and trace gases meas. in St. Louis area 79–16600
- aerosol particles characterisation by Raman spectroscopy 77–49188
- aerosol pattern recognition using laser radar *(Japanese)* 80–51028
- aerosol S compounds, techniques for chem. comp. determ. 78–95976
- aerosol S content, continuous flame photometric detection system 80–81508
- aerosol samples, Israel, pollution sources detection by X-ray fluoresc. 79–52975
- aerosol samples, simulated, Be content by proton scatt. anal. 79–5217
- aerosol sampling, chemical heterogeneity revealed by atomic absorption and X-ray photoelectron spectroscopy 80–55970
- aerosol sampling and anal. system for particulate S monitoring 79–21029
- aerosol sampling by in situ and standard methods 79–66840
- aerosol sampling thin-walled tube aspiration coeff. 77–37460
- aerosol sizing using slotted virtual impactor 78–57350
- aerosol sources identification in St. Louis area using factor anal. 79–12200
- aerosols, Aitken range size distrib. meas. in N.Atlantic 80–98404
- aerosols, atmospheric, neutron activation anal. system appl. 77–81442
- aerosols, automatic time sequence filter sampler for proton induced X-ray emission anal. 77–60171
- aerosols, chemical characterisation, progress and problems 78–68969
- aerosols, composition, PIXE anal. 79–53004
- aerosols, detection and meas. of 10^{-4} to 10^{-1} μm particles *(French)* 80–7985
- aerosols, elemental conc. meas., Quillayute, Washington, (USA) 78–36270
- aerosols, erroneous elemental mass-size functions from high vol. impactor 79–20997
- aerosols, from dust storms, SW United States 79–20932
- aerosols, instrumental anal. of light element comp. 78–69516
- aerosols, limitation on electrical measures 78–69431
- aerosols, meas. by horizontal thermal gradient cloud condensation nucleus spectrometer 80–77158
- aerosols, remote anal. by differential scatter lidar system 78–69524
- aerosols, size distrib. meas. with particle Doppler shift spectrometer 78–69515
- aerosols, sulphate and nitrate assay via ion chromatography anal. 78–68974
- aerosols, X-ray fluoresc. anal., filter attenuation corrections 78–35740
- aerosols, X-ray quantitative anal. of high vol. filter samples 79–70501
- aerosols impaction on nuclepore filter, collection efficiency 79–20475
- air quality evaluation, daily profiles method *(French)* 78–92969
- air-monitoring instruments, review 78–61590
- airborne air quality meas. system design and operation 77–78414
- airborne mineralogical dusts, metallic elements determ. by energy dispersive X-ray fluorescence anal. 80–76569
- airborne particles, quantitative meas. by laser beam *(Japanese)* 77–29426
- airborne particulates, in industrial Greek city, X-ray fluoresc. 78–27857
- aircraft engine emission surveillance 79–74562
- aircraft engine pollutant emission, reduction measures *(French)* 77–81994
- aircraft/groundstation air monitoring minicomputer data processing system 77–64439
- airport environs, air pollution, remote monitoring by laser systems 80–17368
- airport fencing for air pollution reduction, wind-tunnel expt. *(Japanese)* 80–12034
- alkali emission and fixation during pressurised fluidised bed combustion of coal 80–30352
- alpha recoil aerosol penetration of HEPA filters 77–66867
- ambient air analysis, area survey and sampling mobile laboratory 80–104528
- ambient air monitoring, microprocessor appls. 79–48201
- ambient air monitoring system in Melbourne 77–70819
- amosite fibres, collection efficiency of nuclepore filters 78–81341
- analysis and control instrumentation and organisation *(French)* 78–20549
- analyzer, automatic, calibration system, zero and span standardization 79–16107
- areal air pollution source shaping and location for downwind community protection 77–37380
- aromatic hydrocarbons, in airborne particulates, gas chromatography/mass spectrometric, NMR analyses 77–13116

air pollution detection and control continued
artificial radioactivity migration in environment, survey of models 79—96487
asbestos, X-ray diffr. anal., calibration standards 78—69517
asbestos aerosol electron microscopy and analysis *(French)* 77—37461
assessment of operating rules *(Dutch)* 78—53720
atmosphere dust, eval. using nuclear methods *(French)* 80—7993
atmosphere pollution dust dynamics, study via ^{222}Rn descendants radioactivity meas. *(Rumanian)* 80—12524
atmospheric dispersion models, comparison between critical sector and overall-site techniques 80—16873
atmospheric NO$_2$ total content meas. by absorption spectroscopy *(Japanese)* 80—12469
atmospheric pollutant propagation anal., appl. of indicator activation method 79—88039
Atmospheric Release Advisory Capability, 1977 update 78—49127
atmospheric trace gas IR monitor, airborne, nondispersive 79—8719
atomizing high-energy scrubber design, test of math. model 78—24359
Australian atmospheric contamination after 1974 French Pacific tests, cyclotron anal. by proton activation 79—57311
automated environmental monitoring system for pollution studies 80—81513
automated measuring systems, sampling, anal. and results 77—21885
automated monitoring of atmospheric pollution *(German)* 80—4069
automatic analysis of pollution, spectroscopic methods *(Spanish)* 80—81516
automatic measuring networks in W. Germany 77—37388
automatic monitoring network, statistical approach to online control 77—41164
automatic sequential precipitation sampler, chem. anal., rel. to acid rain problem 79—83681
automobile ejections control model 77—21900
automobile exhaust emission meas. and testing procedures, error statistics, survey *(German)* 77—73839
automobile exhaust particulate emissions, containing H$_2$SO$_4$, X-ray fluoresc. anal. technique 77—60173
automobile exhaust pollutants, neutron activation analysis, distrib. of Pb particulate 78—3943
automotive exhaust gas catalysts, radiometric determ. of Pt and Pd attrition 78—31740
background pollution characteristics 79—57531
baghouse maintenace, opacity monitoring technique 79—34459
balloon-borne stratospheric grab-sampling system for air pollution meas. 77—29504
baseline air monitoring, Australian initiative 79—96490
benzo(a)pyrene, distrib. with respect to particle size in submicron atm. aerosols 79—74563
beta counting for fallout analysis 79—92106
beta gauge for measurement of aerosol concentration *(French)* 79—53012
beta-active microscopic particles, location and study by SEM autoradiography 77—57425
biological surveillance of pollutants using plants 80—76689
blast furnace cast house emission control 80—30623
brief infrequent random releases, atm. dilution estimation 79—83652
BWR power plant stack effluent inert gas nuclide monitor 79—3255
carbonaceous aerosols mass monitoring with spectrophone 79—92112
cascade impaction instrument using quartz crystal microbalance sensing elements, particle size distrib. meas. 78—65904
cascade impactor meas. of size distrib. of organic pollutants in particulate matter 79—57553
cement kiln dust emission control by electrostatic precipitator, meas. 79—52989
centralised supervision system, in Fos-Etang de Berre region 78—81410
charcoal tube sampling technique, meas. accuracy 78—69508
chemical analysis of atmospheric dust *(Dutch)* 79—16713
chemical factory, air monitoring anal. and instrum. technology *(German)* 77—21886
chemical industry problems and solutions 77—9488
chemical laboratory, airborne contaminants monitoring, USA regulations 80—12869
chimney discharges, dust level determination, equipment charact. *(French)* 78—3948
chimney plume particulate and gaseous pollutant conc. and mass flow, IR radiometry 77—37393
chimney stack sampling, traverse point location for HP calculator program 80—94139
Chinese nuclear explosion, Jan. 1976, anal. of fission products 77—26884
chlorinated hydrocarbon, dry aerial deposition rate, meas. techniques 80—81506
chlorobenzenes determination by gas chromatography with photoionis. detection 80—35809
chloromethyl methyl ether, on-column reaction GC determ. in ambient air 78—20093
chrysler's electronic lean burn system 80—16868
chrysotile asbestos, photoacoustic spectrum using CW HF laser 80—7980
chrysotile asbestos determ. in rainwater 78—44895
cigarette smoke, diode laser meas. of methane, ethane and H$_2$O vapour concs. 80—97847
city plume aerosol size distrib. and turbidity meas. 77—37408
classification of pollutants and pathways in atmosphere 79—70489
climatic change, long-term, prod. by fossil fuel usage, proposed space obs. 79—29844
CO dose meter for working places exposed to extreme peaks of CO contamination 78—81096
coal, combustion, radiological aspects 80—61485
coal fired power stations, EPA regulations and radiological dose commitment 79—52980
coal-fired power plants, inertial cascade impactor appl. 79—12278
coastal nuclear power stations, gaseous release dilution meas. 79—52981
coherent anti-Stokes Raman scattering, for quantitative gas anal. 78—68968
collective dose commitment for estimate of radioactive pollution, concept and calcs. *(German)* 78—74504
combustion, flame propagation through stratified charge combustion channel, model 79—64795
combustion gases, radiation treatment to remove SO$_2$ and NO$_x$ 77—70322
compressed air, pollution level meas. *(Polish)* 79—88040
computerised monitoring system, program system *(Japanese)* 78—81414

air pollution detection and control continued
computerised tomography for two dimens. remote pollution monitoring 79—39330
conc. meas. at Baring Head, New Zealand 79—100931
concentration fields determination, comparison of interpolation methods for sparse data 80—51575
condensation nuclei counters, calibration and intercomparison 79—83684
condensation nuclei counters, counting efficiency 78—36293
condensation nuclei counters at South Pole, calibration 80—98470
condensation nucleus counters, smallest particle size detectable, appl. to SO$_2$ photo-oxidation products 78—24364
conference on nuclear power systems, Washington, USA (1978) 79—41045
contaminant diffusion in freely convective boundary layer, meas. by acoustic sounding 79—34966
continuous monitoring instrumentation, selection, maintenance 78—77316
continuous monitoring of airborne particulates in an industrial plant 80—51029
control philosophy in UK 79—70493
cooling tower drift eliminators, design study for collection efficiency 78—7760
cooling tower plume models, importance of meas. *(German)* 77—66985
cooling tower plumes, lidar meas. *(German)* 77—25781
corona ion generator for removing dust and aerosol particles in rooms *(Finnish)* 77—66883
coronene, distrib. with respect to particle size in submicron atm. aerosols 79—74563
correlation spectrometry meas. of air pollution, 2nd CEC remote sensing campaign, report 78—88908
correlation spectroscopy appl. to dispersion from tall stacks 78—3932
corrosion test site selection *(French)* 80—16893
Curie point pyrolysis system for hydrocarbon anal. 77—77854
data interpretation via pollution roses, appl. to data from meas. systems near refineries 78—81379
dense particulate system, particle size meas. device based on scatt. light 78—45006
density distrib., flow pattern in Tanabe area, Japan, numerical anal. *(Japanese)* 78—96289
Denver air quality, effects of meteorological and climatological factors 79—84350
deposition research using rain gauges *(Dutch)* 78—81367
detector sampling by minicomputer and multicomponent chemical unit *(French)* 77—37452
determination by Stark modulated microwave spectroscopy 78—57337
dichlorodifluoromethane, spectral parameters for atm. sensing 79—84481
diesel engines effects *(Croatian)* 80—55961
differential absorption lidar systems for atm. gases remote meas. 78—69525
differential absorption lidars, reference range 80—89700
differential lidar detection, alternate-pulse wavelength switching of dye laser 78—25890
differential-absorption lidar technique for remote meas. of atm. gases 78—61603
diffusion battery, screen type, theory 80—95208
diffusion model for use with directional samplers 79—62549
diffusion sampling method for ambient aerosol size discrimination with chemical comp. determ. 77—37349
directional dust gauges, collection efficiency 77—37415
dispersion, wind speed remote meas. using video equipment *(French)* 80—7990
dispersion and transport within coastal regions, tracer study of power plant emissions 79—62545
dispersion and transport within coastal regions, tracer study of industrial emissions 79—62546
dispersion correlation spectroscopy, mask optimisation procedures 77—73857
dispersion from large area sources, finite element technique 80—16874
dispersion model validation for Keihin area, Japan 79—57528
dispersion studies, long-term, temporal sampling requirements 79—39325
drop size distribution airborne meas. for drops >60 μm diameter 78—45008
dust, airborne, respirable fraction, performance characts. of samplers matched to them 78—53438
dust, polarisation and interference microscopy appls. 78—61544
dust aerosols, activation analysis experience at Karlsruhe Nuclear Research Center 78—3941
dust analysis using LMA 10 laser microspectral analyser 78—24385
dust content of gas meas. by laser *(French)* 77—64486
dust control equipment available in GDR *(German)* 79—74571
dust control using chemical retardants 78—3945
dust cyclone operation, anal. 78—57362
dust filter type AFA, X-ray analysis 77—41142
dust gauges, directional, analytic expression for collection efficiency 79—21062
dust in flue gas., radiometric monitoring method *(German)* 77—29452
dust measurement 79—39331
dust meter, EIP-9M, with optical and inductive-charge transducers 79—17595
dust particle deposition in human respiratory tract, sampling apparatus 79—96719
dust pollution monitor 80—55971
dust sampler, CIP type, for personal use 78—81469
dust samples, neutron activation anal. using high-rate loss-free gamma spectroscopy system 78—61129
dust sampling system collection effeciency rel. to particle density and size 77—37456
Dutch airborne equipment charact. *(Dutch)* 78—20534
Dutch national air pollution monitoring system, local and reference point 78—69465
dye laser, high energy pulsed, for atm. sounding 79—39868
education, undergraduate project using sulphation plates 77—49527
effluent gases due to radioactive waste heat treatment, purification, techniques *(French)* 77—23230
electret fibre appl., non-woven, high efficiency 80—76691
electret filters for high efficiency air cleaning 80—56569
electrical aerosol plume detection theory and meas. 80—7984
electrical conductivity meas. rel. to pollution determ. 77—91233
electrochemical methods of determining gas traces 80—16753
electrochemical methods use *(German)* 80—26187
electrochemical technique using porous electrode sensors 77—17261
electron beam particulate analysis of air samples 80—40785

air pollution detection and control continued
electron capture detectors operating in tandem, theory 80−61493
electronic detector for conducting particles and fibrils 79−62164
electrostatic precipitation technology development, stack gas ionisation by electron beams 78−57346
electrostatic precipitators, cold-side, at coal-fired power plants, effects on aerosol emissions 79−92108
elemental analysis at sub parts per trillion concs., via SONRES 78−81465
emission measurement design with respect to urban sanitation *(German)* 80−104536
emissions from nonferrous plants, neutron-activation anal. 80−21343
emissions from refinery 80−35800
emmission meas. network, Baden-Wurtemberg *(German)* 79−52977
ENEL's air quality monitoring, thermoelectric plant installation, VHF transmission of data *(Italian)* 77−82064
energy related pollutants study in NE.United States, MAP3S program 79−20978
energy resources development, European Community Italian Centre activities *(Italian)* 80−785
environmental aerosol sampler, particle size depend. of collection efficiency 78−12002
environmental chemistry, anal. techniques, conf., Barcelona, Spain, (Nov. 1978) 80−88038
environmental data acquisition systems, SMART-I and CLEVER COUNTER 79−48196
environmental diagnostics using laser beams 80−35802
environmental dispatch simulation and emission dispersion modelling 78−32221
environmental impact assessment, meteorology 78−49124
environmental measurement, conf., Gaithersburg, Maryland, USA (Sept. 76) 78−69504
environmental measurement and control *(Japanese)* 80−26184
environmental monitoring, the role of electronic system in India 77−41146
environmental monitoring instruments 80−45825
environmental monitoring systems, current status in India 77−41144
environmental monitoring systems, health hazards in India 77−41145
environmental particulates, anal., X-ray techniques 77−56322
environmental protection *(Japanese)* 78−16152
environmental radioactivity prior to the Kori nuclear power plant operation 79−6773
environmental samples, X-ray fluoresc. anal., particle size correction method 78−48705
epidemiology, causality, and public policy 79−97177
ERDA nuclear plants, radiation levels in environmental vicinity 78−9002
ethane, in air, IR spectra, optical-acoustic investig. *(Russian)* 78−74663
ethylene, air pollution monitoring, computer controlled CO_2 laser absorpt. system 80−89699
ethylene, in air, IR spectra, optical-acoustic investig. *(Russian)* 78−74663
ethylene dibromide in urban air 79−70481
ethylene in exhaust gas, optoacoustic detect. using line-selectable CO_2 laser 78−56947
ethylene in gas mixtures, optoacoustic detect. in urban areas and fruit storage chambers 79−87886
ethylene remote meas. using CO_2 differential absorpt. lidar 78−49122
ethylperoxy radical$+NO_2$, reaction rate const. meas. 80−21262
Europe, air pollution monitoring organisation 77−37412
European Community, information exchange concerning pollution by S compounds and suspended particulates 80−7979
evaporative cooling tower drift eliminators, comparative performance evaluation 78−11985
exhaust gas radiation treatment, NO oxidation and NO_2 reduction 78−80765
exhaust gas radiation treatment, SO_2 oxidation in moist O_2-N_2 mixture 78−80766
factor of safety, calc. method and appl. to air and noise pollution 80−94140
fall out measurement techniques and apparatus *(Dutch)* 77−25774
fallout nuclides determ., 19th Chinese test 78−82520
fertilizers, nitrogenous and phosphate, pollution problems from manufacture 79−34450
filter material selection for airborne radioactive ^{131}I and methyl iodide sampling 79−83673
filter media suitable for air pollutant analysis (HNO_3, nitrates and acidity) 80−104541
filtration efficiences of selected filter types 79−57551
fine particulate emissions control electrostatic precipitation efficiency improvement 77−45140
fine particulate emissions from coal-fired power plant, size distrib. 77−45135
fission product release, inclusion in AVR fuel cycle strategy program *(German)* 79−74576
fission reactor accident health effects, incorporation of plume trajectories in CRAC code 80−47617
fission reactor pollutant dispersion computation 80−47621
flue gases, extractive stack sampling system for cont. emission monitoring 79−96494
flue systems, computer anal. of soot particles *(French)* 79−83675
fluidized bed combustion of plastic waste with coal, removal of HCl 80−30347
fluoride concentration meas. methods *(Dutch)* 77−82002
fluorides, gaseous and solid, meas. in atmosphere *(Dutch)* 80−3567
fluorocarbon, detect. using computer simulated IR solar spectra 77−53217
fluorocarbon measurements, interlaboratory comparison 79−70483
fluorosensor systems using N_2 and KrF lasers 80−21428
fog density monitoring in pollution chamber 78−45059
forest fire sources, microwave radiation spectra 80−52314
fossil fuel flames, pollutant monitoring 77−41149
Fourier interference spectrometric detection of atmospheric pollutants 80−35813
Fourier IR air monitor, description and appls. 79−16106
Fourier transform IR absorpt. spectroscopy, airborne, for atm. comp. meas. 78−61604
Fourier transform IR spectroscopy appl., conf., Columbia, USA (June 1977) 78−58067
Fourier transform IR system, km pathlength, for trace pollutants detect. and meas. 79−5624
Fourier transform spectroscopy appl., far IR 78−58069

air pollution detection and control continued
Fourier transform spectroscopy meas. 78−61564
French local networks, examples and software *(French)* 77−37459
fusion reactor air detritiation operations, computer modelling and bench-scale testing 79−85784
gamma exposure rate, real time simulation by puff model 80−47618
gas analyser, portable, 1920 to 1978 development 78−61124
gas analyser with acoustooptic detector and semiconducting generator based on Gunn diode *(Russian)* 80−101141
gas analyzers, testing instrums. 79−8715
gas chromatographic method for low benzene concs., determ. *(German)* 80−21429
gas chromatography-mass spectrometry anal. *(Japanese)* 79−79424
gas complex analysis method, resonance absorption with pulsed laser light *(Japanese)* 80−36421
gas conc. cells for S oxides and S-bearing pollutants sensing 77−70842
gas cyclone fitted deswirler, efficiency 79−12254
gas detection by dye laser and Fourier transform method 79−57558
gas mixtures, kinetic studies rel. to gas lasers and pollutant detect. 79−48013
gas monitoring system performance tests and specifications 79−16659
gas monitors for in situ source emission, field experience 79−16660
gas trace anal. by laser-induced Schlieren technique 80−9929
gas trace monitor, control of toxic gases 80−61499
gaseous air pollutants, sample collection and spiking *(Dutch)* 80−3568
gaseous air pollution control *(Dutch)* 80−3548
gaseous criteria pollutant methodology and standards for USA Clean Air Act 80−94133
gaseous effluent standards comparison for nuclear and fossil fuel power prod. facilities 80−32536
gaseous hydrocarbons, removal with allophane adsorbers *(Japanese)* 77−78412
gaseous impurities, atm. press. ionisation mass spectrometric anal. technique 77−56263
gaseous impurities continuous automatic meas. *(Dutch)* 77−82000
gaseous impurities meas., sampling and calibration methods *(Dutch)* 79−83687
gaseous pollutant monitoring by mm-wave microwave rot. spectroscopy 79−48197
gaseous release monitoring and γ spectrometric analysis *(French)* 79−3259
gases, remote meas. using discretely tunable IR gas laser 77−49199
gaseus pollutants, analytical control, review 80−101140
German laws, standards, guidelines and limiting values *(Dutch)* 78−57312
glass industry, review 78−3936
global collective dose commitments, long lived radionuclide release 79−26780
global sulphur cycle study, reaction rate determination, atmospheric modelling appl. 78−92902
graphitic C, optically absorbing component of urban aerosol particles, photoacoustic meas. 79−96493
grid filters, collection efficiency, effect of Stokes and Reynolds numbers 78−61592
ground level SO_2 concentration automatic meas. grid in Holland *(Dutch)* 77−82001
halocarbons, gas chromatography detect. 78−85739
halocarbons in atmosphere, global monitoring stations 79−57555
halofluorocarbons, background levels in situ quantification 78−69530
halogen air pollution gauge, apparatus based on secondary emission of Pt 80−85320
halogenated compounds, meas. in air over Europe 77−37351
heat-electric power station for Cologne *(German)* 79−20999
heavy metals, Belgian network meas. of atmospheric concs. 77−70833
heavy metals in particulate matter, comparison of analysis techniques 77−41151
high acidity measurement, comparative tests near industrial installations in Fos-Etang de Berre region 78−81464
high-S coal, continuous sorbent regeneration in pressurized fluid bed combustion 80−30351
high-volume preparation of air to standard quality for zeroing analyzers 80−90829
holocamera for particulate studies 79−22919
holographic droplet image analysis by TV camera and table calculator via IEC-Bus 78−36337
Hong Kong, air particulates, nondestructive multielement determ. by neutron activation analysis 80−12040
hot fuel examination facility, air sampling system 79−13541
hot particle physical props. determ. 79−3251
housing estate heat supply methods comparison, computer based investigation *(Hungarian)* 79−2366
HV-70 filters, efficiency for sampling short-lived Rn daughters 80−108827
hydrocarbon concentrations, measuring methods *(Dutch)* 78−36300
hydrocarbons, aromatic and aliphatic, gas chromatographic determ. in airborne matter 79−79434
hydrocarbons, volatile, detection and meas. in atm. review 77−64492
hydrofluorocarbon monitoring using telluric absorption line *(German)* 78−49133
impurity concentration meas., instrument calibration *(Dutch)* 77−66983
impurity concentration meas. methods survey *(Dutch)* 77−70826
impurity concentration meas. sampling errors, statistical anal. *(Dutch)* 77−70828
incinerator smog reduction by US vibration induced water mist 77−32845
incoherent optical heterodyne detection 79−16679
indoor-outdoor relationshiops for airborne particulate matter of outdoor origin 79−83654
industrial atmosphere submicroscopic asbestos fibre evaluation 79−74585
industrial atmospheres, pollutant analysis, pollution prevention *(French)* 80−89692
industrial atmospheric pollutant remote analysis by Raman lidar 80−12047
industrial chimney design for satisfactory emission *(Dutch)* 78−81364
industrial complex environmental impact, Whatcom County, Washinton, USA 79−57532
industrial flare flames, smoke detection and control by electric fields 78−81360
industrial gaseous effluent contaminant removal 77−25771
industrial source emission meas. needs 77−41165
instrumentation, evidence of electronic malpractice 77−37453

air pollution detection and control continued
interferential detector of atmospheric pollutants 80—108830
intermittent gaseous release from nuclear plant, probability distrib. of atm. dispersion factor 78—11994
intracavity laser Raman spectrometer, appls. 78—65973
ion chromatographic anal. of air pollution samples, appls. 80—30625
ion detecting and measuring system with wide dynamic range 79—2870
ionisation large area gridded chamber, low level α-spectrom. appl. 78—49128
ionisation type smoke detector, model for response 78—88933
IR gas analyser, non-dispersive, for industrial processes and environment protection *(Hungarian)* 80—55735
IR heterodyne detection technique, line profiles for CO_2, C_2H_4, NH_3 77—42359
IR laser heterodyne spectroscopy for trace gases remote detect. 78—61606
IR laser technique for SO_2 conc. determ. *(Russian)* 78—69484
IR parametric oscillator source for remote air pollution monitoring 77—21936
IR spectrometer INFRAMEK-E operational principles *(Hungarian)* 78—54474
IRAN-1,2, plants, calc. of radioactive releases 79—18056
iron and steel industry technology 77—21891
Kawasaki City air pollution monitoring and telemetry system 77—37464
kraft mill effluents control in Finland 79—52988
Kyoto University reactor, airborne radioactivity from primary coolant 80—22959
laboratory vehicle for air-pollution measurements with computer-controlled data acquisition and navigation system *(German)* 79—39327
LANDSAT 1 MSS imagery, plumes visible over NE.England and Midlands 78—45035
large fuel reprocessing plant, anticipated chem. emissions 78—5004
laser absorpt. method based on use of two freqs. 79—21004
laser absorption spectrometer, long path length, effect of scintillation and multiwavelength coherence 78—40653
laser absorption spectroscopy for point monitoring of gases ambient concs. using tunable lasers 78—61607
laser absorption system, computer-controlled, monitoring of ethylene and vinyl chloride 78—49182
laser apparatus for remote sensing of air pollutants 77—37458
laser application to atmospheric environmental research *(German)* 80—97849
laser emission and emission meas. of gaseous pollutants *(German)* 78—40665
laser gas analysers, freq. modulation appls. 80—85246
laser high sensitivity point monitoring of atm. gases 78—73523
laser incoherent heterodyne detection 77—87130
laser monitoring, book 77—25799
laser monitoring techniques for trace gases 78—69521
laser photoelectric spectrometer for large condensation nuclei meas. *(Russian)* 78—65408
laser PROBE technique, density profile meas. of specific constituent 78—28320
laser radar data processing system 79—57559
laser radar system, mobile computerised, stack plume obs. 80—56644
laser spectroscopic detection 80—17366
laser spectroscopic techniques 79—57557
laser spectroscopy, conf., San Diego, USA (Aug. 1978) 80—13153
laser systems appl. to atm. monitoring 78—69520
laser two-photon ionisation spectroscopy, real time monitoring of atmospheric pollutants 80—7996
laser velocimetry of distance smoke plume 78—28345
laser velocimetry techniques using CO_2 laser 78—61623
laser-Raman microprobe anal. of suspended particulates 80—76687
laserbeam, detection appl., signal processor charact. *(Japanese)* 77—78449
leaf cuticular features as indicators of environmental pollution 77—73840
Leningrad, air pollution forecasts *(Russian)* 77—53181
level prediction by nonphysical models based on Kalman filtering 77—29428
lichen indicator appl. in PIXE and NRA environmental studies 80—61744
lidar, airborne continuous long-distance system, flight tests *(German)* 78—36338
lidar, differential absorpt., from Space Shuttle, for atm. trace constituents meas. 78—45179
lidar, multidisciplinary airborne, planned operation 78—36335
LIDAR data, simulated, air pollution model parameter estimation 78—28302
lidar mobile systems, for atmospheric gaseous pollutants meas. 80—35814
lidar observation of plume dispersion in northern Alberta 79—83679
lidar observations of atmosphere at Kingston, Jamaica 78—36284
lidar observations of Labadie Power Plant plume, particulate density and behaviour obs. 80—55956
LIDAR observations of plume diffusion at Rancho Seco Generating Station 78—11991
lidar return signal geometrical compression, atm. remote sensing appl. 78—57329
lidar system, heavy, for environmental protection control, containerisation 78—36336
lidar system, two-freq. downward looking, for atm. monitoring 78—69523
lidar system using tunable dye lasers for pollution monitoring 80—3562
lidar systems for atmospheric pollution monitoring 78—53765
LIDAR teledetection and measurement of minority atmospheric constituents for pollution control *(French)* 80—7992
literature review, 1974-6 period 77—78405
London, smoke control rel. to Global Solar Radiation Index vars. at Kew 77—17217
long path monitoring of ambient gases, CO_2 versus semiconductor diode lasers 79—16682
Los Angeles basin, pollutants three-dimens. distrib. 78—61542
luminescence, automatic meas. of SO_2 and oxides of nitrogen, optical technique *(Dutch)* 80—3565
LWR plant, plume exposure monitoring system 80—42875
LWR stowaway fuel cycle effluent projections 78—94110
magnetic particle fallout recorded in recent ombrotrophic peat sections 78—61519
magnified dark-field image holographic recording 77—19214
mapping, provisional, of pollution effects indicators 78—81387
marine atmosphere, trace elements in size separated aerosols 79—20989

air pollution detection and control continued
maximum concentration, statistical anal. by autocorrelation and non-stationarity 80—16885
measurement by incoherent optical heterodyne detection 79—48203
measurement errors and sampling methods *(Dutch)* 77—70827
measuring apparatus and systems, problems connected with development *(Rumanian)* 80—72117
membrane filters in air anal., review 79—79316
Merseyside, England, assessment difficulties for area values and trends 80—104538
mesoscale pollution transport, quantitative evaluation 79—70825
metals determ. in air particulates, graphite furnace atomic absorption spectrometry app. 80—94134
meteorological information system for response to nuclear power station accidental release of radioactivity 80—16888
meteorological satellites development, new trends 79—29964
meteorology, rel. to 1976 USA Clean Air Act amendments 78—11989
methane, global anthropogenic emission into atm. *(Russian)* 79—100547
methane, in air, IR spectra, optical-acoustic investig. *(Russian)* 78—74663
methane concentration in surface air layer from IR absorpt. meas. *(Russian)* 77—29366
methane gas interferometer for coal mine safety 78—44423
methane gas plumes, tracking via atmospheric acoustic sounder 80—55968
methane remote meas. by continuously tunable IR lidar 79—21025
methanol trace detection using phase fluctuation optical heterodyne spectroscopy 80—68266
method review, esp. long path optical meas. *(Italian)* 77—91329
methyl iodide removal by Ag impregnated Al and zeolite 78—53719
4,4′-methylenebis(2-chloroaniline), air sampling and anal. method 79—79420
methylhydrazine, electrochem. oxidation on Au, appl. to gas monitoring 79—39248
MHD process, coal-fired, NO_x control 79—52947
microconcentrations of gases determ., metrological certification of meas. methods 80—55972
middle atmosphere, minor constituents, chemistry and transport, conf., Seattle, USA (Aug. 1977) 79—84428
mobile laboratory for ultratrace amounts of atmospheric contaminants 79—83670
modified Andersen impactor and All Weather Sampler Inlet, wind tunnel tests 78—3926
monitoring, computer automation of CO_2 laser long-path absorption system 78—92971
monitoring, electrical techniques, solid laser appls. *(Italian)* 77—82069
monitoring, instrumentation and methods 80—72118
monitoring, on site automatic analysers, review *(French)* 78—81451
monitoring and instrumentation 79—12301
monitoring at source and in environment, equipment and law enforcement 77—91263
monitoring by pulsed dye laser 79—48204
monitoring network, nontelemetric, in Hungary *(Hungarian)* 77—64422
monitoring networks, automatic systems 78—93009
monitoring of pollution above urban site by Lidar meas. *(French)* 77—25780
monitoring philosophy 79—70492
monitoring system, minicomputer-based 77—66984
monitoring system design by spatial sample stratification 79—83680
monitoring systems for radioiodine and inert gases, evaluation 80—95480
MOSFET, Pd gate, to monitor H_2, H_2S and NH_3 78—44645
motor vehicle air pollution analysis, automated X-ray fluorescence technique *(French)* 77—41234
multicomponent, multipoint infrared ambient air monitor, microcomputer-controlled 80—40945
multielement analysis of environmental sampelsdby samples by X-ray fluoresc. spectrometry 78—69513
multigas analyser for automobile exhaust 77—49198
multiple gaseous air pollutants, point monitoring method by tunable laser *(Japanese)* 80—81515
multispectral obs. of pollutants, near UV imaging system 77—70892
multiway sorption filters, development and use for radioactive iodine removal from air 78—61543
municipal wastewater plants, air pollutants monitoring 79—80050
national environmental monitoring system 78—77329
national network of stations, conc. variations, statistical methods *(Dutch)* 79—88042
natural site monitoring, expt. philosophy, equipment performance *(Italian)* 77—82065
network experiments, design criteria, for regional-scale pollutant transport and transform. 79—20993
neutron activation anal., meas. in semi-arid zone 78—36317
neutron activation analysis 77—25772
neutron activation analysis for 14 volatile heavy metals as constituents of aerosol particles 80—16891
neutron activation analysis in trace element detect. and meas. 77—41158
neutron activation analysis using 14 MeV neutrons, Al, Si, Fe and Pb conc. meas. 77—91257
NIMBUS-7, global atmosphere pollution monitor 79—21149
nitrate, artifact, formation on filter media, interference effects 79—83668
nitrate determ. using HNO_3 collection on NaCl impregnated filters 80—81509
nitrates, gaseous and particulate, conc. meas. 77—45137
nitrosamine, air sampling sorbents testing 80—77026
N-nitrosodimethylamine, trapping for GC/MS analysis 78—20094
noise considerations in millimeter-wave spectrometers, air pollution detection appl. 80—57367
Nolan-Pollak condensation nucl. counter, droplet growth rate, supersaturation 77—60480
non-methane hydrocarbons, monitoring via photoionisation 78—73549
nondestructive neutron activation analysis of environmental samples using low-energy photon spectrometry 78—3995
nonimaging airborne geophysical and miscellaneous systems 77—56777
nuclear fission aerosol products, bioindication using needles of common pine tree 79—100550
nuclear installations, radioactivity release, air monitoring, emergency procedures 78—70610
nuclear pollutant release assessment, JEREMIAH computational system environmental transport and dose calcs. 78—94150
nuclear power plant radioactive emission meas. and control *(German)* 77—79484

air pollution detection and control continued
nuclear power plant vent-air monitoring by nuclide-specific detection system 79—3249
nuclear power station accidental activity release, effect of meteorological parameters 80—17142
nuclear power station radioactive emissions meas. and control, survey 79—85818
nuclear power station stack effluents, radiation monitoring 78—46179
nuclear power stations, atmospheric pollution, nature and extent of unplanned releases, review 79—57530
nuclear reactors, radioiodine air sampling system, separation into gaseous and particulate fractions 80—57962
nuclepore filters, clogging, cap form. model 79—20468
objective air monitoring site selection for large point sources 78—36267
objective sensor placement for sampling regional turbidity 79—5626
odorous organic compounds, evaluation of catalysts for vapour phase oxidation 79—70482
odour analyser, automatic, for atmospheric sulphide anal. *(Japanese)* 80—50924
odour detection, instrumental techniques *(Dutch)* 79—16658
odour intensity measurement techniques *(Dutch)* 77—25775
olfactometer, environmental odour emission analysis, hospital appl. *(German)* 78—7754
online, two level prediction method 77—21952
Ontario air pollution incidents and wind variability 79—70822
Ontario Hydro nuclear power plant stack effluent monitoring 79—3254
opacity monitoring 79—100557
optical fibre network system for air-pollution monitoring over wide area by optical absorption method 80—10002
optical methods, laser beam based apparatus *(Czech)* 79—21001
optical methods appl., resonant fluorecence, Raman scattering and LIDAR *(Czech)* 78—81359
optical methods of pollution detection *(Czech)* 78—69444
optical particle counters behaviour, comparative assessment 79—57550
optimal timings and number of observations determ., w.r.t. cost 79—88026
organic component analysis using capillary GC/MS/computer technique 78—80799
organic compound extraction from airborne particulate matter 77—33181
organic compounds, evaluation of Cd_3O_4 catalysts for oxidation 77—37353
organic effluent toxicity from nuclear fuel reprocessing, rel. to carcinogenecity 78—5005
organic gases and vapours meas. in air *(Dutch)* 80—3566
organic micropollutants in precipitation in Norway 78—36262
organic pollutants, determ. via gas chromatography after cryogenic sampling 78—81468
oxidant control strategy, short term, statistical testing 79—20995
ozone analysers, for industrial plant monitoring and control *(Japanese)* 78—57308
Pacific marine aerosol, continental component identification by combined neutron activation and SEM with X-ray anal. 78—3990
Paris regional air pollution monitoring network optimisation *(French)* 77—37387
Paris street, atmospheric pollution survey network 78—81463
particle analysis, SIMS appl. 79—43695
particle collection efficiencies by single droplets, calc., inertial impaction, Brownian diffusion and electrostatics 79—57525
particle size depend. of condensation nuclei counter 79—20476
particle size detection efficiency of condensation nucleus counter 80—55967
particle sizing, 0.05 to 5.0 μm, using laser instrument 78—61624
particle-induced X-ray emission anal., 2 MeV protons 80—45833
particles, matching sampler penetration curves to definitions of respirable fraction 77—90827
particles, surface composition, AES, X-ray photoelectron spectroscopy appl. 79—43694
particles, surface toxic elements, ion microprobe and Auger electron spectrometric anal. 78—7753
particles in urban air, mol. nature, high-resolution mass spectrometry 78—24360
particulate air contamination in Puerto Rico, student project 79—58504
particulate C and SO_4^{2-} species identification by Raman spectroscopy 79—5625
particulate chem. composition, use of laser induced mass spectrosc. instrument 80—97848
particulate control for coal-fired boilers 80—35801
particulate detection by metal-coated Nuclepore filters 77—37463
particulate detector, ionisation type, space charge effects 77—41587
particulate emission monitor calibration in gas-solid suspension 77—37454
particulate material, trace elements analysis by nucl. activation techniques 78—3991
particulate material in stack effluent of coal-fired power plant, comp. and size distrib. 77—45136
particulate matter, conc. on membrane ultrafilters, neutron activation anal. 79—52841
particulate matter, multitechnique examination 77—41150
particulate matter, suspended, X-ray fluoresc. anal., semicond. detector X-ray spectrometer construction, calibration 77—56321
particulate matter anal., X-ray fluoresc. spectrometer standardisation, reference sample 77—60176
particulate matter catch from EPA and ASME-ASTM sampling trains 78—73547
particulate matter collected on filters, chamber for weight determ. 79—57552
particulate matter concentration, moving filter technique, PIXE analysis, two hour resolution 79—92107
particulate sample X-ray fluoresc. anal., multichannel spectrometer, computerised 77—60170
particulate sampler, size selective, modification and operation 78—36294
particulate sampler, wind tunnel testing, using monodisperse particles 77—82053
particulate size distrib. and refr. index, new lidar-radiometer method 80—77153
particulate volume conc. determ. by atmospheric Mie scatt. method *(Korean)* 80—45835
particulates collected on filters, X-ray fluoresc. anal., least-squares method appl. 77—60168
particulates collected on filters, X-ray fluoresc. anal., self-absorpt. effects, digital simulation 77—60165

air pollution detection and control continued
particulates sources, identification and relative importance estimation 80—72105
pathways of atmospheric pollutants, conf., England (Nov. 1977) 79—70488
pattern recognition appls. 79—70480
peak-mean concs. from point source, long term statistics 77—70813
personal sampling devices for atmospheric contamination monitoring *(French)* 80—57986
PESA advances in air pollution sampling 80—51023
pesticides, chlorinated, gas chromatographic anal. using electron capture detector *(Japanese)* 80—55764
phosgene, spectrophone meas. at selected CO, CO_2 laser wavelengths 78—57310
photoacoustic detector characts. at CO_2 laser freqs. 79—100554
photoacoustic effect and appls., review 79—41786
photochemical oxidants occurrence at high latits. 79—74567
photochemical smog, control meas. using diethylhydroxylamine additive to atmos. 79—52982
photochemical smog, minicomputer based prediction system for reducing acute damage 79—57541
photochemical smog dynamics and control strategies *(Japanese)* 78—32220
photocolorimetry *(Russian)* 77—40610
photosmog inhibitors, O atom reaction rate constants 79—12185
piezoelectric microbalance, for respirable aerosol mass conc. meas. 78—69518
PIXE anal. of urban aerosols on heavy loaded membrane filters 77—49138
PIXE analysis of atmospheric gases, cryogenic conc. technique 79—53005
PIXE applications, conf. 77—48715
PIXE data handling, statistical techniques 77—52715
PIXIE, advances in air pollution sampling 80—51023
plume chemistry studies at Alberta power plant 79—74565
plume control from cooling towers, new designs 78—7758
plume dispersion from cooling towers, EPRI research program 78—7759
plume monitoring, airborne sampling system 79—21027
plume transport and diffusion studies using fluoresc. lidar 80—101139
point source pollution dispersion, meas. and modelling of conc. 80—81973
pollutant gases, monitoring from space using passive microwave techniques 80—76690
pollutant ground-level concentration, field meas. of benefits of increased stack height 80—76676
pollutant plumes, remote sensing from Landsat 78—40689
pollution transport, monitoring via Atmosat balloon for tropospheric research 78—7775
polycyclic aromatic hydrocarbons, long-range transport 79—83653
polyurethane, foam, for organic material sampling in ambient air 78—20080
population exposure to air pollution, satellite-aided evaluation 79—92116
portable LIDAR for antipollution problems *(German)* 79—74583
power plant effects on environment, protection measures *(German)* 80—26574
power plant plume, submicron particle size distribs. determ. 79—57526
power plant stack emission vel. and SO_2 conc., IR TV appl. 77—49197
power plant stack emissions, trace element analysis techniques 78—3938
power stations, stack emission monitoring systems, for air pollution detection and control 79—100558
precipitation acidity measurement, error anal. applied to indirect methods 80—72108
prediction of pollutant concentration for air pollution control 79—52992
preseparator for large particle collection 80—16884
programs for meas. *(Dutch)* 80—3549
protection of air quality, role of tall stack 78—24362
proton activation analysis for determ. of F_2 pollution from brick kiln 78—20504
proton activation analysis of environmental and ecological pollution determ. 78—3994
proton scattering anal. of atmospheric particulate matter 77—25778
pulp mill stack plume meas., LANDSAT satellite multispectral scanner subsystem data appl. 78—88905
pulsed electrostatic precipitator and flame photometer for total S aerosol conc. meas. 78—95975
quadrupole mass spectrometry applics., book contrib. 77—25622
quality criteria, biological response modelling 79—79431
quality monitoring, international approach 79—83661
quantitative analytical spectroscopy using scanning tunable dye laser 78—81362
quantitatively analysing spectroscopy by continuously scanned tunable dye laser 77—78486
α-quartz, collected on PVC membrane filters, X-ray diffr. determ. 77—70392
radiation exposure near nuclear power plants, remote monitoring system 79—18055
radioactive, tritium activity meas., in exhaust gases from nuclear power stations *(German)* 77—25322
radioactive aerosol dispersiveness in main ventilation system 78—70650
radioactive aerosol surveillance system evaluation 80—57984
radioactive aerosols, atmos. conc. monitoring, radionuclide anal. 80—21427
radioactive aerosols, filter testing, Winfrith, double automatic Pollak counter 78—33301
radioactive contaminant unplanned release meas. and countermeasures 78—89994
radioactive discharges from nuclear plants monitoring, state of art *(German)* 77—42174
radioactive effluent release reduction, Japanese LWRs 79—31078
radioactive fallout in air and rain, results to end of 1977 78—82535
radioactive fallout water deactivation using sorption props. of clinoptilolite, vermiculite, bentonite 79—43995
radioactive gas monitoring by silicone oil absorbent scintillation counter 80—12044
radioactive gaseous effluents, AEOLUS code for dispersion during normal, sea-breeze, and accident conditions 78—11993
radioactive gaseous effluents, relase trends from US PWR reactors 1977 80—95481
radioactive material release to atmosphere, calc. of consequences with TIRION-4 code 79—29494
radioactive particle meas. at HFEF/N 80—18687

air pollution detection and control continued
- radioactive surface contamination, resuspension models 80—16872
- radioactive tracer appls. to ventilation and air pollution studies, review 78—28306
- radioactivity meas. appl. *(Hungarian)* 77—36840
- radioactivity meas. at Nuclear Research Institute, using scintillation probe and GM-tube *(Czech)* 78—88906
- radioactivity standards for environmental monitoring, prep. 78—80816
- radioiodine volatilisation problem, soln. using plexiglas iodination box 77—56484
- radiometer, airborne dual-channel IR heterodyne, for atm. meas. 78—57369
- radiometry methods (Soc. Photo-Optical Instrum. Engrs., Proc. vol.91, San Diego, 26-27 Aug. 1976) 77—70880
- radionuclide airborne release assessment, determ. of atm. stability categories 78—73504
- radionuclide concentration determ. in ground level air 79—24927
- radionuclide inhalation reduction using indoor shelter after nuclear accident 77—34478
- radionuclides, chronic releases to atmosphere, resuspension models 80—16871
- radionuclides in pine needles, washing effect as meas. of fallout 79—43799
- radiosonde system, 403 MHz, for boundary layer study 78—85723
- rainwater, trace elements determ. by neutron activation analysis 78—3944
- Raman lidar for quantitative pollutant meas. from stationary source 78—36291
- Raman microprobe appl., microscopic samples molecular analysis, particle characts. determ. 80—57391
- Raman scattering analytical techniques using tunable lasers 78—61134
- reactor containment air contamination, sampling and measurement techniques *(French)* 78—89997
- real-time meas. transformation and statistical processing 78—24365
- real-time urban power dispatch with ambient air quality constraints 79—57542
- reference meas. methods and systems, workshop proc. (Bilthoven, Netherlands, 1977 December 12-16) 79—79444
- relative Raman scatt. cross-sections of pollutant gases and vapours 80—100061
- remote detection, appl. of $LiNbO_3$ tunable parametric oscillator 78—59089
- remote meas. expts., estimation of surface temp. 79—70854
- remote meas. of HCl, CH_4 and N_2O, using chem. laser lidar system 77—21910
- remote meas. of tropospheric pollution from aircraft 77—49195
- remote meas. using laser techniques *(Italian)* 79—70889
- remote meas. using mobile Fourier transform interferometer 80—12043
- remote measurement of gases using discretely tunable IR lasers 77—87118
- remote measurement using tunable lasers 77—60499
- remote monitoring using discretely-tunable IR gas lasers and heterodyne detect. techniques 78—61605
- remote monitoring with YAG:Nd laser pumped $LiNbO_3$ parametric oscillator 77—46767
- remote probing, generalised method for environmental surveillance 78—57363
- remote sensing, active and passive systems 77—70889
- remote sensing, rot. Raman spectroscopy using Fabry-Perot interferometer, background rejection method 77—71384
- remote sensing, via computer assisted correl. spectrometer 78—4002
- remote sensing by correl. spectroscopy, instrumental response characts. 79—5623
- remote sensing from space 78—61621
- remote sensing of pollutant gases, at CO_2 laser wavelengths 78—40647
- remote sensing of pollutants by satellite, correl. spectroscopy techniques 77—64456
- remote single ended monitoring system, 1.4. to 4 μm range 78—3974
- research animals, monitoring of airborne tritium evolution 79—39526
- residual carbonaceous material, in urban airborne particulates, Raman microprobe obs. 78—69441
- resonant optoacoustic cells for trace gas analysis 79—11840
- respirable airborne crystalline silica, determ. polymorphs, silicosis 80—45832
- retrospective analysis of air samples in UK for 1957 to 1974 period 78—3942
- roadway aerosol filter samples, proton-induced X-ray emission analysis 77—41233
- rocket exhaust effluents from space shuttle model, meas. using electrets 79—53548
- rocket fuels, CO_2 laser absorption spectra and photoacoustic detection 80—104540
- rotating disc, particle migration in turbulent boundary layer 78—22333
- rotational Raman spectroscopy of gases using interferometry 77—73494
- RWE environment protection organisation outline and functions *(German)* 80—101552
- S aerosols characts. in Florida, PIXE anal. 79—21030
- sampling filters, charged particle induced X-ray fluorescence anal. *(French)* 78—27852
- sampling of particulate nitrate with glass fibre filters, errors 78—16169
- sampling system, radio-controlled, for diffusion expts. 79—79440
- sampling system at HFEF/N 79—45441
- satellite techniques, equipment Conf. on Earth resources electronics Rome, Italy (Mar.77) *(Italian)* 77—82056
- satellite-aided evaluation of population exposure in USA 80—40936
- scalp hair as monitor of population exposure to environmental pollutants, nucl. activation analysis 78—3940
- Schottky barrier chemical sensor, Pd-Si, for H_2 detect. 78—44646
- scrubber, US device for air/water mixing 77—33180
- selective modulation radiometer for gaseous pollutant remote sensing *(French)* 78—20550
- selective quantitative measurement of pollutants, appl. of CO and CO_2 lasers 78—69526
- semiconductor sensors, reducing gas defect. *(German)* 80—55974
- sequential precipitation sampler, design and operation 77—70844
- single-stage and multiple-stage particulate scrubbing, efficiency and power comparison 77—37356
- sinter plant emissions control equipment 77—66982
- smell meas., status *(Japanese)* 78—92661
- smoke, natural sedimentation, photographic, visual and laser sonde obs. *(Russian)* 78—32216

air pollution detection and control continued
- smoke and dust clouds, lidar observation at 0.7 μm, 10.6 μm 78—49181
- smoke density meter, maximum sensitivity determination, flue gas optical density spectral analysis appl. 78—69500
- smoke detector design and smoke props. 79—63331
- smoke gas purification automated process control system *(Russian)* 77—52712
- smoke plume dispersion meas. at large distances from source 79—20998
- smoke plumes, application of lidar 80—51026
- smokes, atmospheric, optical probing, homogeneous particle model appl. *(Russian)* 78—77328
- smokestack emission, meas. via. DFVLR mobile lidar system 77—53248
- snow as an accumulator of air pollutants 77—73841
- SO_2 max. surface conc. from moderate-sized power plant rel. to power plant load 79—83659
- sodar acoustic echo sounder for use in air pollution meteorology, low level stability and wind velocity monitors 80—108828
- solid radwaste combustion, development of wire cloth filter for flue gas scrubbing 79—71919
- sonic agglomeration of c black aerosol particles 77—29411
- soot particle conc. meas. by near IR extinction coeff. *(Russian)* 80—82055
- source inventory for Tehran, methodology and approach 79—52996
- South America, PIXE system for air pollution meas. 77—49157
- South Pole aerosol characterization using Raman microprobe 80—26580
- spacecraft trace contaminant concentration, toxokinetic/toxodynamic model 79—83952
- Spacelab atmospheric trace contaminant meas. and identification 79—70387
- spatial concentration estimation method using IR absorption 77—73865
- spectral absorption patterns, detect. and estimation, anal. methods 77—87059
- spectral absorption patterns, detect. and estimation, system appls. and design 77—87060
- spectral image analysis device, Chromotron 80—83683
- spectral interference correlation method 79—8727
- spectrometer, laser absorpt., for high sensitivity pollution detect. 78—57373
- spectrometer, PbSe diode laser, for air pollution monitoring and mineral prospecting 77—82044
- spectrophone measurement of absorpt. coeffs. at CO_2 laser wavelengths 80—26193
- spectrophone measurement of IR laser absorpt. by atm. dust 77—9513
- spectrophone measurement of visible light absorpt. by aerosols 78—4000
- spectroscopic method, monitoring with pulsed lasers, numerical filter design *(Japanese)* 79—43801
- stack close to building, necessary height determ. by wind tunnel study 77—2225
- stack dust monitor based on particle counting and sizing 79—83683
- stack effleunt monitor in-place testing 79—3257
- stack gas monitor, β scintillation detector+Ge(Li) detector system, environmental γ dose *(Japanese)* 79—3246
- stack gas monitoring system for warning and control in Chiba Prefecture 79—57561
- stack monitoring of long-lived α-emitters, review of meas. techniques 79—48195
- stack plume downwash prediction formula, comment 79—12256
- stack plume obs. by laser radar *(Japanese)* 78—11990
- stack release radioactivity monitoring with digital processing 79—3253
- standard apparatus, metrological warranty of gas-analysis instrums. 79—21005
- standardisation of methods and facilities 79—8684
- standards, administrative aspects *(Dutch)* 78—57311
- stochastic modelling and dosage area product forecast 79—5601
- stratosphere, methane meas. and predictions 79—84432
- stratosphere, $NOHSO_4$ and $NOHS_2O_7$ identification in aerosols, rel. to N oxides pollutants removal 79—39795
- stratosphere, trace constituents, in situ meas. 79—8676
- stratosphere, trace gases detection *(German)* 79—53003
- stratosphere minor constituents, concs., chemiluminescence in situ instrums. and techniques 80—16886
- stratospheric gas monitoring, two-photon spectroscopy, Doppler-free technique 77—9514
- stratospheric O_3 and aerosols, economic anal. of environment monitoring system 78—73507
- stratospheric O_3 density meas. using lidar, feasibility 77—60493
- subway air pollutants, (sulphates, nitrates, bromates, SiO_2, acrolein $(NH_4)_2SeO_4$) IR anal. 78—36273
- sulfur dioxide concentration automatic digital recording system 77—25776
- sulphate aerosol, individual submicron particles detect. technique 78—69527
- Sulphate Regional Experiment (SURE) in NE.United States 79—20977
- sulphates in atmospheric particulates, analysis 79—83685
- survey aircraft for sample collection and anal. *(Dutch)* 78—81366
- survey vehicle for air pollution monitoring *(Dutch)* 78—81365
- suspended particulates, field sampling techniques 79—12258
- tackishade sampling to measure airborne radioactivity *(Hungarian)* 80—94136
- tele-detection apparatus using combination light scatt. spectra *(Russian)* 77—49193
- teledetection of atmospheric pollutants by differential absorption of a CO_2 laser at two frequencies *(French)* 80—7991
- teledetection of gaseous atmos. pollutants, data acquisition and anal., pollution mapping *(French)* 80—7989
- teledetection of gaseous atmospheric pollutants *(French)* 80—7988
- test gas atmospheres, calibration standards, generated by gas phase titration 78—69507
- testing instrums., standardisation and determ. of dynamic errors 79—8714
- thermal analysis for in situ detection of aerosol pollutants 77—37364
- thin dust layers, particle size effects automatic correction, computer appls. in spectrometry 79—83539
- thin film sulphate test for submicron particles 77—70814
- Thre Mile Island, Unit 2 accident, noble gas releases 80—47616
- tin inorganic compounds, separation and determ. in environmental samples 79—79416
- town air basin pollution levels prediction by empirical statistical regression anal. *(Ukrainian)* 79—34887
- toxic gas detection, appl. of MOS devices 78—76908

air pollution detection and control continued
  toxic gas microconcentration determ. by automatic belt photometer *(Russian)* 78−28347
  toxic gas monitor based on laser photoacoustic spectrometer *(German)* 80−12046
  trace amounts of toxic substances, meas. techniques and standards 80−26188
  trace analysis, selection of calibration gas standards 77−91255
  trace element analysis of radiological effluents from coal-burning power plants 80−21426
  trace elements, meas. accuracy using neutron activation anal. 78−69509
  trace elements levels in Glasgow 79−88024
  trace gas monitoring system, with tunable diode laser, improvements 80−16882
  trace metals, global cycles, anthropogenic impact 80−3547
  trace-gas remote analysis, optoacoustic radiometry limitations 80−108759
  transmission holography limitations in particle analysis 77−19213
  transparency meas., computer prediction *(Italian)* 77−91333
  transuranic aerosols, online high sensitivity measurement system 77−65334
  transuranic elements in air at nuclear reprocessing plant, monitoring system 80−63409
  trapped atmospheric contaminants, IR anal., solvent extraction technique 77−73479
  troposphere, ^{3}H in water vapour, rel. to reactor release detect. 78−11988
  troposphere, photochemical and physical transformations, obs. by tunable lasers 77−60460
  troposphere, photochemical mechanisms, computational methods 78−49084
  troposphere, pollutants from industry, domestic coal burning and vehicles *(German)* 79−52973
  tunable diode laser instruments, appl. advanced meas. and anal. 77−75600
  tunable semiconductor diode laser system for long-path monitoring 78−69522
  tunable-diode-laser IR spectroscopy applics. 80−40798
  turbulent atmospheric transport, Monte Carlo simulation, radioactive pollution appl. 78−61550
  turbulent dispersion concentration valves, system for wind tunnel meas. 79−5191
  two-wavelength double-pulse tunable dye laser for differential absorption lidar 77−21939
  urban aerosol, size-fractionated, C, N and O determ. by particle elastic scatt. anal. 78−81466
  urban aerosols, optically absorbing component identification as graphitic C 79−34939
  urban air, total suspended matter estimation, comparison of three methods 77−37416
  urban suspended matter continuous sampling over large grain size spectrum 78−3924
  USA air quality protection measures 77−60463
  USSR environmental pollution obs. and monitoring system 80−85322
  USSR Hydrometeorological Service, automation of data collection and processing 79−34994
  UV diffuse-direct ratios meas. with compact double monochromator 78−49144
  UV double-beam photometer, for atm. O_3 calibration 78−69505
  variable selectivity photoionisation analyser, hydrocarbon vapour detection 80−81511
  vehicle emission control, nitrogen oxides reduction on industrial furnace 79−52995
  vehicle exhaust emissions, meas. and testing procedures survey and criticism *(German)* 77−56299
  Venetian region, industrial emissions real-time control using Kalman predictor 80−82046
  Venice, air pollution survey and stonework deterioration 79−62159
  Venice, Italy, air pollution indicated by isotopic anal. of rainwater and stonework 79−79992
  venturi scrubbers, optimum design 78−16148
  venturi-jet scrubber, gas absorpt. with chem. reaction, performance study 78−81393
  vinyl chloride, air pollution monitoring, computer controlled CO_2 laser absorpt. system 80−89699
  virtual impactor aerosol separators, analytical study 80−42874
  virtual impactor for particle classif. and generation of test aerosols with narrow size distribs. 80−30626
  visibility at ground level, two meas. methods 80−82078
  volatile fission products from nuclear fuel cycle and power stations, pollution effects *(Russian)* 79−31152
  volatile organic compounds determ. in city air, gas chromatography techniques 78−12003
  water vapour isotopes, spectrophone meas. at selected CO, CO_2 laser wavelengths 78−57310
  weather changes and air pollution, meteorological meas., brief survey *(French)* 80−17359
  West German LWR power plant stack monitoring, legal and technical aspects 78−89988
  West German nuclear plant airborne radioactive effluent monitoring 78−89990
  West German nuclear power plant airborne radioactive release control 79−13549
  wet cooling system for power plants, atm. impact of plumes and fogging 78−7761
  wind tunnel testing of flue gas dispersion 79−12282
  working level survey meter 3R-WL, meas. of α-particles from ^{218}Po and ^{214}Po 78−25330
  X-ray absorption spectra for chem. characterisation of atmospheric aerosols 80−61501
  X-ray absorption spectra for chem. characterisation of atmospheric aerosols 80−72121
  X-ray fluorescence anal. of air particulates, S content meas. 79−20491
  X-ray fluorescence analysis, radioisotope-induced, applic. to Zn and Pb determ. 77−17214
  X-ray fluorescence spectroscopy, proton induced elemental trace anal. 77−36831
  X-ray photoelectron spectroscopy *(French)* 77−36837
  X-ray spectroscopic method 77−52689
  Zagreb, pollution reduction measures, 1974-76 results *(Croatian)* 77−37362
  Zephyr radar system for meteorological measurements 80−90228

air pollution detection and control continued
  Ag, neutron activation analysis 77−17215
  Al electrolysis units, air washing tests *(French)* 79−29493
  Al, simultaneous determ. with Si in atmospheric aerosols by neutron activation anal. 80−72116
  ^{41}Ar release from TRIGA reactor, comparison of γ-ray detectors 78−57309
  As, tropospheric, conc. determ. over marine and continental regions 79−70486
  As, tropospheric, enrichment, sources and flux 79−70487
  C in suspended particulates, meas. technique 80−76686
  C particulate, airborne, photacoustic and absorption spectrum using tunable dye laser 80−4102
  CO absorption meas. using long-path laser, system improvements 80−3563
  CO, condensation nuclei and O_3, meas. on aircraft flight 79−58010
  CO, determ. by portable IR tester 80−89569
  CO, determ. in air by reversible poisoning of electrocatalysts 77−37363
  CO pollution and its control in Japan 79−52994
  CO, remote sensing using freq. doubled CO_2 laser radiation 80−67025
  CO, sensitive optoacoustic detection by reson. absorpt. 78−44981
  CO-air streams, selective oxidation of H_2 before CO electrochem. anal. 77−63978
  CO_2, atmospheric environmental control technology 80−104529
  CO_2, gas chromatographic meas. using electron capture detect. 79−57549
  CO_2 IR laser velocimetry, processing techniques and applications 80−87831
  CO_2 tunable dual-line laser for atmospheric spectroscopy and pollution monitoring 78−3977
  CO_2-laser long-path absorption system, computerised, error anal. 79−25340
  ^{14}C activity and distrib. in gaseous effluents from PWRs 79−85829
  ^{14}C production and discharge in BWRs 79−52979
  $^{14}CO_2$ meas. in Karlsruhe Reprocessing Plant exhaust air 79−3231
  $ClONO_2$ collection using impregnated filters, simulation 79−12257
  ^{60}Co, gamma radioactive source, buildup factor determination for meas. in air *(Rumanian)* 78−49132
  ^{137}Co, gamma radioactive source, buildup factor determination for meas. in air *(Rumanian)* 78−49132
  ^{137}Cs, time variation of low concentrations in rain water 79−43994
  F determ. in atm. samples by $^{19}F(p,\alpha)^{16}O$ react. using low energy accelerator 78−85239
  F, stack sampling apparatus for the collection of gaseous and particulate pollutants *(French)* 80−7986
  Fe, characterisation in environmental samples by Mossbauer technique 79−66433
  Fe conc. and sources determ. by Mossbauer technique 79−79442
  Ge(Li) system for low level radioactive gas monitoring 78−9038
  HC-NO_x photochemical smog, smog chamber simulation model *(Japanese)* 77−29087
  HCl, absorption coeffs. for DF laser radiation, pollution detection appl. 77−27059
  HCl automatic control in air by electrochem. methods 79−96491
  HCl detector for environmental monitoring 78−24366
  HCl, determ. in ambient air at ppbv level 79−74579
  HCl gas in ambient air, detection using coated piezoelec. quartz cryst. 78−92532
  HF, CW chemical laser for remote pollution monitoring and process control, HF conc. in Al plant 79−48200
  H_2H_4, electrochem. oxidation on Au, appl. to gas monitoring 79−39248
  HNO_2, obs. by UV differential optical absorpt. 80−72106
  HNO_3, atmospheric monitoring, chemiluminesc. method 79−16062
  HNO_3, particulate nitrate and acidity measurement in ambient air filter media 80−104541
  HNO_3 vapour line parameters meas. by CO laser transmittance 79−26976
  H_2S in air, preconc., determ. by flame photometric detection 78−92535
  H_2S, new anal. method for remote areas 79−21028
  H_2SO_4 aerosol, filter sampling of air, possible artifacts 80−82079
  H_2SO_4, aerosol particles props. in subsiding air over Japan 79−20986
  H_2SO_4 and particulate strong acidity measurement techniques, evaluation 80−104542
  H_2SO_4 and SO_4^{2-}, determ. in Netherlands, 1971-76 period 79−21031
  H_2SO_4 and SO_4^{2-}, meas. in particulate matter from coal and oil combustion 79−74569
  H_2SO_4, dissociation and absorpt. consts., ultrahigh resolution obs. of 8.2, 11.3 μm bands 78−70825
  H_2SO_4 meas. in aerosol samples during METROMEX 79−100548
  H_2SO_4 mist monitor, semicontinuous 80−61495
  H_2SO_4, vapour, foreign gas broadening diode laser spectroscopy in IR 78−36261
  H_2SO_4-H_2O droplets in atmosphere, equilib. size and comp., quick estimation method 79−66767
  HT-HTO in air meas. system 80−21433
  ^{3}H, conc. in atmospheric precip., rivers, and seas, USSR 79−74560
  ^{3}H contamination monitoring using centralized control *(French)* 80−63407
  ^{3}H control strategies in PWRs, cost effectiveness 77−38360
  He tracers for detection of gaseous atmos. pollutant emissions *(French)* 80−7987
  Hg determ. in troposphere *(German)* 79−53406
  Hg dispersion, expt. meas. 79−92565
  Hg vapour conc. meter, construction and performance 79−2759
  I, A=123 to 135, derived air concs. annual limits 78−31909
  I radioisotopes, high efficiency mixed species air sampling, readout and dose assessment system 78−57074
  I trapping in ventilation system, user guide to codes ITRAP-A(B)(S)(L) 79−93843
  ^{125}I airborne vapour detection 80−51027
  ^{125}I thyroid dose calc., air and water conc. limits 79−88195
  ^{131}I, airborne conc. at Swierk nuclear research centre 1975-1977 80−7978
  ^{131}I, airborne conc. in nuclear medicine lab. 79−34674
  ^{131}I airborne release from PWR, determ. of sources 80−17138
  ^{131}I, comparison of calculated and meas. values 77−34477
  ^{131}I, concs. during thyroid therapies 79−25122
  ^{131}I filters, design against weathering 80−32524
  ^{131}I, gamma radioactive source, buildup factor determination for meas. in air *(Rumanian)* 78−49132
  In trace amounts, extraction and neutron activation determ. 80−12045

air pollution detection and control continued
^{115}In aerosol generation technique for atm. tracer obs. 80−26190
KBr pellet spectroscopy, H_2SO_4 effect 79−88034
^{85}Kr, radioactive pollution in atmos., Warsaw 1975 to 1977, meas. methods 79−34458
^{85}Kr, seasonal and annual concs. at 30-150 km from point source 79−20994
^{85}Kr waste encapsulation, in amorphous alloy 80−47589
NH_3, conc. determ. on long path from CO_2 laser radiation reson. absorpt. 79−29904
NH_3, gas conc. meas. using ring oven technique 80−81507
NH_3 microdetermination by ring oven technique 77−45164
NH_3 monitoring using Stark microwave cavity resonator 80−61500
NH_3, photoacoustic spectroscopy at 9 μm, 10 μm $^{12}C^{16}O_2$ laser wavelengths 79−21014
NH_3 remote atmospheric sensing by multiphoton sequential photodissociative excitation 79−48199
$(NH_4)_2SO_4$, atm. particles conc. and size distrib., rural conditions 79−74564
NO, absorpt. characts. of γ-O band, rel. to atm. meas. 78−57316
NO, automatic meas., luminescence appls. *(Dutch)* 79−88041
NO, collection method and conc. determ. *(French)* 77−81999
NO, combustion gas sampling system and valves for sampling during engine expansion process 78−24380
NO decomp. in industrial exhaust gases by electron beam irradiation 79−29490
NO isotopes, spectrophone meas. at selected CO, CO_2 laser wavelengths 78−57310
NO measurements in CH_4-O_2-N_2 flame by laser fluorescence 80−61178
NO, optical detection in air, gamma band fluoresc. *(German)* 77−60494
NO photometric process analyser using resonance absorption method 80−57360
NO, reson. absorpt. meas. with CO laser, spectroscopic data for pollution monitoring 77−37350
NO, self-N_2- and O_2-broadened linewidths 5.4 micron band, quadrupole moment 77−30930
$NO/NO_2/O_3$ monitors, intercalibration 78−69529
NO_2 and SO_2 pollution near industrial area, meas. and remote sensing equipment *(French)* 79−74928
NO_2, atmospheric concentration determ. dye laser differential lidar system 78−32250
NO_2 decomposition by electron beam irradiation treatment of exhaust gases 79−79423
NO_2 fluorescence monitor with flashlamp pumping atm. tests 77−64443
NO_2, gas chromatographic meas. using electron capture detect. 79−57549
NO_2, laser and flash lamp fluoresc. monitors, comparison 80−17367
NO_2 monitoring in stack gas, chemiluminescence appl. 79−57560
NO_2, optoacoustic detect. using pulsed dye laser 78−27835
NO_2, remote sensing of air pollution using optical multichannel analyser 79−79439
NO_2 spatial distribution, detectivity estimation of DAS lidar 78−92991
$NO_3{}^-$, particulate, lab. and field studies of major sampling interferences 79−92105
NO_x, atmospheric monitoring, chemiluminesc. method 79−16062
NO_x chemiluminescent analysis using diffusion interface module 78−40095
NO_x emissions from coal-fired MHD power plants, simplified correlations for prediction 80−97842
NO_x emissions from domestic kerosene-fired and gas-fired appliances 79−88023
NO_x emissions from European cars, control 79−48198
NO_x in flue gases, determination various methods, comparative evaluation 79−53014
NO_x in flue gases, measuring instruments, calibration and checking 79−53015
NO_x reduction on Fe-based catalysts containing V 79−12285
NO_x removal by absorption reaction, using MARTZCLEAN reagents based on $NAClO_3$ and K_2CO_3 *(Japanese)* 80−61147
NO_x removing reagents, based on $NaClO_2$ and K_2CO_3 (MARTZCLEAN) *(Japanese)* 79−52976
N_2O emission from soils during nitrification of fertiliser 78−57313
^{24}Na, gamma radioactive source, buildup factor determination for meas. in air *(Rumanian)* 78−49132
Nd:glass laser/parabolic mirror lidar for airborne aerosol mass conc. meas. 77−21937
O_3 and other gases diurnal conc. cycle and destruction at ground 79−79972
O_3, atmospheric profile, airborne dual-channel IR heterodyne radiometer meas. 78−57369
O_3 calibration methods, accuracy 78−69506
O_3 depletion, supersonic gas sampling error 77−33193
O_3 eddy correlation flux meas. by fast respnse sensor 78−45009
O_3 formation and control strategy options for Sydney, precursor distrib. 80−16859
O_3, monitoring apparatus, chemiluminescence reaction with ethylene 78−96310
O_3 monitors calibration, modification of KI method for improved stoichiometry 79−88037
O_3, photochemical, nocturnal depletion at rural site 79−57527
O_3, photochemical generation, sources, air sampling programme 79−66430
O_3, reference methods, international comparative programme 79−88038
O_3, total content meas. using Dobson spectrophotometer 80−72643
O_3 variations in Auckland, comparison between city and urban regions 80−17350
P compounds, pollutants, concentration measurements with flame photometric apparatus 80−16883
Pb compounds identification in urban aerosols, rel. to health hazard 78−44991
Pb micro fall-out, furnace atomic absorption spectrometry appl. 78−49125
Pb, nonautomotive components detect. in St. Louis region 79−12260
Pb ore dust, pollution analyser using Harwell 6000 series electronics 79−5649
Pb salts, inorganic 80−77081
PbSe detector appl. design and performance 78−24378
$Pb_{1-x}Sn_xSe$ diode laser absorption spectrometer, pollution detection equipment 78−40672
^{210}Pb, radiochem. determ. in U ores, air dusts 77−56266

air pollution detection and control continued
^{210}Pb, time variation of low concentrations in rain water 79−43994
^{210}Pb tropospheric residence time 78−85396
^{210}Po determ. in air, radiochem. separation and α-counting method 78−73113
Pu fallout detection using fission tracks prod. with neutron irrad. spectra 80−95479
Pu laboratory stack monitoring, computerised system 79−3256
Ra, annual rate of release to atmosphere as result of coal combustion in UK 80−93787
Ra daughters in air, meas. by gamma spectrometry 80−30628
^{220,222}Rn daughters, 2-count filter method for meas. in air 80−63480
Rn and Tn air concentrations in dwelling rooms *(Hungarian)* 77−78409
Rn, at active U mines and mills, emission and control 80−41264
Rn barrier to reduce indoor airborne Rn progeny 78−73262
Rn continuous monitor response to transient Rn concs. 80−32519
Rn daughter airborne conc. meas. in atmosphere 80−37636
Rn daughter concentrations in air of dwellings in Great Britain 78−77118
Rn daughter products, ionisation large area gridded chamber appl. 78−49128
Rn daughter products, reduction by plateout on air mixing fan 79−57529
Rn daughter sampling, relative filter efficiencies 77−56725
Rn daughters in air, conc. meas. by α-spectrom. 78−32218
Rn flux from U mill tailings, attenuation by consolidation 79−66563
Rn, short lived daughters, detection method *(Chinese)* 80−42889
^{222}Rn flux through multilayered covers cover U mill tailings 80−95487
Rn/Tn daughter air conc. meas. by filter method, general formula 78−70711
^{222}Rn concentration meas. by plastic detectors to determ. environmental α-emitters from natural sources 80−91292
^{222}Rn daughter conc., meas. sensitivity computer optimisation 78−49126
^{222}Rn daughter prods. meas. using diffusion sampler 80−81510
^{222}Rn daughters, meas. of low conc. in air 78−28308
^{222}Rn determination in air and water, sampling and meas. methods 77−9278
^{222}Rn low conc. meas. in air, α-scintillation method 78−92970
^{222}Rn, passive environmental monitor based on exoelectron dosimeter 78−82523
^{222}Rn short lived decay products in air, collection efficiency of Whatman GF/A filter 78−20526
Ru, determ. in automobile exhaust-emission, by chem. ionisation mass spectrometry 78−61079
S, compact X-ray fluoresc. analyser 78−68971
S compounds, isotopic tracing of pollution *(Italian)* 77−53078
S compounds, large scale study in Canada 79−20979
S compounds, large-scale spatial and temporal distrib. 79−20981
S compounds, pollutants, concentration measurements with flame photometric apparatus 80−16883
S, concentration and valence state in pollution samples, X-ray fluoresc. anal. 79−48027
S containing aerosols, continuous meas. and speciation by flame photometry 78−95974
S containing aerosols, continuous in situ meas. by flame photometry and thermal analysis 78−96296
S, determ. in submicrometric aerosols, SO_2-denuder appl. for continuous meas. 79−8699
S, $SO_4{}^{2-}$ and related species, sampling and anal. of atm. aerosols 78−96283
SF_6 and tracer gases, electron capture detection method 77−25785
SF_6, trace detection using phase fluctuation optical heterodyne spectroscopy 80−68266
SF_6 tracer technique for near-stack reactor effluent dispersion studies 78−11992
SO_2, 4 μm $\nu_1+\nu_3$ band, Doppler-limited and atmospheric spectra 77−27064
SO_2, absorption spectrum, meas. using frequency doubled pulsed dye laser 80−87144
SO_2, absorption spectrum, meas. using frequency doubled CW dye laser 80−87145
SO_2 air pollution levels modelling and forecasting, statistical approach 78−81398
SO_2 and H_2SO_4 emissions from chem. plant, precision estimates 79−83682
SO_2 and nitrogen oxide automatic monitors, laboratory and field calibration *(French)* 77−37455
SO_2, atmospheric, fluoresc. monitoring using NO γ-bands 78−73121
SO_2, atmospheric, sampling and anal. with PbO_2 plate, Huey plate 79−62163
SO_2, atmospheric concentration determ., dye laser differential lidar system 78−32250
SO_2, atmospheric concentrations, meas. using laser absorption spectrometer 79−96497
SO_2 automatic control in air by electrochem. methods 79−96491
SO_2, automatic meas., luminescence appls. *(Dutch)* 79−88041
SO_2, city concs., box model and acoustic sounder anal. 80−7982
SO_2 collection efficiency with 0.5 N KOH-impregnated filters 78−16168
SO_2 collection from low-vel. jets, efficiency 79−16683
SO_2, conc. determ. for coal-burning power plant stack, Fourier spectrometry appl. 77−49196
SO_2, continuous-running, direct-reading recorder 78−53743
SO_2 conversion to $SO_4{}^{2-}$, meas. during manned balloon flight 79−83658
SO_2 daily volumetric meas., PVC tubing acid release effects 77−29449
SO_2 detect. in stratosphere, analytical technique 77−5314
SO_2 detection, appl. of dye laser differential absorpt. lidar 77−88784
SO_2 detection using thermal radiation at 53.53 GHz rot. reson. 77−78411
SO_2, downwind conc. from Four Corners Generating Station 80−47620
SO_2, dry deposition, field meas. with stirred chamber 79−88021
SO_2, emission control alternatives for coal fired power stations 79−52978
SO_2 emission control and dispersion contrib. to ambient standards achievement 79−83660
SO_2 emission reduction, from steam generators burning pulverised brown coal *(German)* 78−53724
SO_2 emissions in Mediterranean region, remote meas. 79−20987
SO_2 gas pollution of Osaka city, optimal discharge control 79−52993
SO_2, high vol. sampling for isotopic studies 79−70500
SO_2 in gas mixtures, determ. using X-ray absorpt. detector with gas chromatography 77−29069

air pollution detection and control continued
SO_2, in O_2-variable gases, potentiometric determ. using solid state detector 78—20505
SO_2 in power station plumes, differential lidar meas. 79—57556
SO_2, interferential Fourier correl. of spectrum *(French)* 79—21059
SO_2, long path meas. with correl. spectrometer 78—44988
SO_2, long-path automatic monitoring using diode laser system 79—29892
SO_2, long-term monitoring method using permeation sampling, development 80—26189
SO_2, low conc. meas. using diode laser correlation spectrometer 77—91301
SO_2 mass spectrometric obs. in stratosphere 77—33200
SO_2 molecules in air, remote sensing methods assessment *(Japanese)* 78—96288
SO_2, new anal. method for remote areas 79—21028
SO_2 optical depth meas., mask correlation spectrophotometry 77—82066
SO_2, optoacoustic detect. in air-pollution control below parts per billion level 78—41355
SO_2 plume in atmosphere, remote sensing mask correl. spectrosc. method 80—55966
SO_2 pollution electricity generation, policy options for control 80—51022
SO_2, potentiometric determ. using solid state detector 78—16151
SO_2 remote meas. at 4 μm with continuously tunable source 78—77365
SO_2 remote meas. by continuously tunable IR lidar 79—21025
SO_2, remote sensing, $^{12}C^{18}O_2$ laser line absorption cross-sections 79—16661
SO_2 remote sensing by correl. spectrometry and differential lidar 78—96298
SO_2 removal from waste gases, citrate process demonstration at 60 MW power plant 79—100553
SO_2 rural background pollution meas. network 77—37465
SO_2, SO_4^{2-}, vertical distrib. in lower troposphere 79—79428
SO_2 small automatic monitoring network, practical experiences 78—81462
SO_2, stationary source, quantitative meas. using Raman lidar 78—36291
SO_4^{2-} aerosol hazes and long-range pollution transport, satellite detect. 79—20975
SO_4^{2-} aerosols, ambient, laser-Raman monitoring 78—69532
SO_4^{2-}, airborne particles, size meas. and chem. comp. by diffusion sampling 78—45007
SO_4^{2-} in aerosol particles, sampling and anal. techniques 78—28304
SO_4^{2-}, individual submicron size particles detect. method 78—95973
SO_4^{2-}, quantitative determ. in aerosol particles 79—20474
SO_4^{2-}, spatial and temporal distrib. in United States 79—20985
SO_x removal by absorption reaction, using MARTZCLEAN reagents based on $NAClO_3$ and K_2CO_3 *(Japanese)* 80—61147
Si, simultaneous determ. with Al in atmospheric aerosols by neutron activation anal. 80—72116
$SiO_2+Al_2O_3$ particulate emission from calcining of clay, removal using electrostatic precipitator 79—24925
SnO_2 gas sensor, fast-detecting, prep. 80—61497
^{90}Sr, time variation of low concentrations in rain water 79—43994
^{90}Sr tropospheric residence time 78—85396
T forms released from nucl. prod. complex, detection and meas. 77—54372
T in air, scintillation detection using liquid adsorbent 79—76291
T, in PWR, sources, releases, monitoring, management and environmental impact 80—18690
T monitoring methodology using SiO_2 desiccant, appl. to research reactor facility 80—21434
T, role in radiation safety in nucl. fuel cycle *(Russian)* 80—56227
T species, sources and reactions 80—21432
Tn daughter products, ionisation large area gridded chamber appl. 78—49128
U mill tailings, meas. of surface Rn flux, effect of moisture content 78—5056
U mill tailings pile, health effect estimations 77—40800
U, specific α radioactivity meas. rel. to size using aerosol centrifuge 79—76255
U_3O_8, ^{235}U enriched aerosol, characterisation by solid state track recorders 78—17538
^{133}Xe, simple method of air monitoring 79—83949
^{133}Xe waste storage and retrieval, clinical use 77—86649
Zn ore dust, pollution analyser using Harwell 6000 series electronics 79—5649

air pumps *see compressors*

air terminals *see airports*

air traffic
meteorological support to low-level flights, charts with plotted meteorological parameters 79—66772
monthly international airline passenger data, Box-Jenkins modelling appl. 77—87633
noise, general control measures, case study of Torrance Municipal Airport (California) 80—83702
noise at Japanese bases, forecast contours *(Japanese)* 77—88982
nuclear fuel transport by air, feasibility and economics 78—94154
solar power station hazards, photometric photography of dazzling heliostat mirrors *(French)* 80—61295
supersonic transport, model predictions of latitude-dependent stratospheric O_3 depletion 77—45051

air-traffic control
see also aircraft
airport wind reports, optimum averaging time for along-runway and across-runway components 77—17177
Glissada laser landing system 79—31920
meteorological conditions forecasting procedures, development and improvement 78—92950
meteorological radar system appls., economical aspects 79—62543
radar system developments 80—26651
satellites appl., European Space Agency activities *(German)* 80—8516
tracking system, based on acoustic refr. scatt. by wake vortices 77—46840
weather surveillance near airports using Doppler radar 80—46272
wind shear detection radar, for airport use 80—51565

aircraft
see also aerospace control; aerospace instrumentation; air-traffic control; helicopters
accidents in thunderstorm downbursts, analysis 78—53693
accidents related to weather 79—84463

aircraft continued
acoustically excited panels, growth rate of bending induced edge cracks 78—5697
aeroacoustics of advanced turbopropellers, noise prediction 80—69598
aeroautoelasticity, active control and suppression of flutter in aircraft *(Russian)* 78—67079
aerodynamic flow, vortex-induced side force on slender bodies 79—14408
aeroelastic analysis, unsteady airloads prediction 78—71346
air pollution sample collection and anal. equipment *(Dutch)* 78—81366
airbase noise contours prediction 79—1025
aircraft noise meas., cause of structural vibrations 78—87187
aircraft wing weight optimisation with static aeroelasticity constraints *(Russian)* 79—23240
airframe material defectometry, quantitative test specifications *(German)* 80—89427
airline meteorology, early days 77—49544
airport noise, effect of flight path dispersion 77—14848
ambient and cabin air O_3 conc. simultaneous determ. 80—90198
angular vibration of aircraft structs., prediction 77—39253
angular vibration power spectral density prediction model 78—83323
avionic multiterminal data link, fibre-optic interconnection system 78—46805
ballistic descent, stabilisation transient processes 77—53395
building sound insulation against aircraft noise, German federal regulation 79—90083
Concorde, use in stratosphere chemical studies 79—80058
Concorde sonic booms as probe of atm. temp.-wind parameters 77—91323
conducting tubes in polarized plane wave fields, surface currents and charges 78—42256
crack detection, in engineering elements using bleeding system 79—66226
cumulative noise measure for general annoyance prediction of traffic and aircraft noise 77—80010
electric airplane, high-altitude, remotely powered, for environmental appls. 80—17470
EM fields, hazards to aircraft 79—88456
in EM pulse from nuclear explosion, induced currents and charges 78—42258
in EM pulse from nuclear explosion, surface currents and charges 78—42257
emissions effect on ozone in natural atm., numerical model 80—40943
engine exhaust noise, flight effects, use of Bertin Aerotrain 78—13847
fatigue crack growth prediction, aircraft structures, under flight-by-flight loading 79—50651
fibre reinforced composite aircraft materials, design allowables 80—81204
flight effect of Michalke and Michel vis-a-vis Lighthill's model 80—59018
flyover noise, modelled by acoustic scatt. by moving prolate spheroid 78—94458
gliders, aerodynamic noise 78—38307
graphite fibre filled phthalocyanine composites, cure cycle investigation 80—81030
ground noise levels of general aviation aircraft, changes derived from cockpit noise levels 78—9488
infrasound, effect on people, exptl. study of levels 78—88726
IR emission meas. using versatile sensitive radiometer 77—70887
IR segmented composite window design 80—106621
IR window material using GaAs, development 77—72038
jet exhaust noise, prediction of in-flight levels 78—87178
jet flight simulator, shear layer refraction and facility-to-flight corrections for noise meas. 78—13845
jet noise, flight effects, use of Bertin Aerotrain 78—13848
jet noise, relation between static and in-flight directivities 79—86289
jet noise in flight prediction from static tests 80—61490
jet noise reduction test facility 77—11096
jet propulsion aircraft noise, two-point correlation model 78—42493
lightning transient anal. for aircraft, flux induced voltage transients on low-loss transmission lines 79—36814
lightning triggered by aircraft in Japanese winter thunderstorms 77—5309
Lockheed WC-130 aircraft for aerial weather reconnaissance 79—66816
metal fatigue crack detection using nondestructive evaluation (NDE) methods 80—71826
Meteorological Research Flight work during GATE 77—2248
military avionics interconnection fibre-optic data bus 78—46806
minimum noise landing trajectories model *(Spanish)* 80—53546
motion in atm. turbulence, math. modelling 78—81274
Munich Aircraft Noise Survey, appl. of unified noise index 77—50823
navigational almanacs for small computers, calculators 79—62726
noise, annoyance and activity interference patterns 80—48504
noise, appl. of theory of acoustic radiation from moving sources 80—53526
noise, basic aeroacoustic research, industrial appl. 80—69596
noise, effect on sleep of babies 77—77928
noise, engine over wing config. 77—58505
noise, excess attenuation at high freq. 78—33939
noise, generation near trailing edge of upper surface blown flap 77—75902
noise, insulation of buildings 78—55508
noise, interior, general aviation types of aircraft, acoustic field studies 78—90595
noise, interior, light aircraft fuselage laboratory studies 78—90596
noise, responses of Chinese firemen 77—39157
noise, Siemens airport noise monitoring systems 80—99895
noise, spectral broadening by turbulent shear layer 79—37076
noise, subjective anal. expts., use of changeover designs 77—82380
noise, trade off with number of events 77—80009
noise, transmission through turbulent shear layers 79—37075
noise, UK noise and number index, definitions of parameters 80—61489
noise, variation of community response with time of day 79—34462
noise and other pollution effects, Canadian environmental policy 78—33950
noise and vibration, ride quality criteria 79—90076
noise and vibration ride comfort criteria 79—41512
noise assessment, effects of background traffic noise and signal duration 79—86288
noise attenuation over an absorbing terrain, theoretical models comparison 79—18572
noise exposure forecast contours, retrieved using algorithm *(Japanese)* 80—19153

aircraft continued
noise exposure prediction method, problems 78—9491
noise generation, appls. of diffraction theory 80—53532
noise generation by transonic open rotors 80—69599
noise identification system by correlation technique 79—23131
noise in flight, prediction, importance of jet temp. 80—69814
noise index, psychological assessment 78—55507
noise monitoring, concepts of instrumentation 80—33397
noise monitoring systems, requirements 80—23849
noise near airport, sleep interference of residents 77—54843
noise pollution, numerical representation, control methods 79—3846
noise propag., review 80—64258
noise propagation, meteorological and ground effects 79—14138
noise reduction measures 78—1505
noise scattering by density gradients 78—13836
noise shielding 77—54840
noise signature, meas. using remotely-operated multiple array acoustic range 79—23134
noise technology laboratory facilities, Boeing Commercial Airplane Co. 79—18603
nonconservative system resonance, modal analysis 78—42557
optical fibre communication, A-7 ALOFT economic analysis, EM interf. and pulse tests 78—42448
passenger entertainment, dual language Super 8 mm sound system 80—4785
prism-scanning panoramic camera for reconnaissance aircraft 77—79181
psychophysiological techniques applied to aircraft design and other operational problems 80—26384
radial-bolt-hole cracks in mechanically fastened aircraft structs., measurement of size using Doppler shift 80—55597
radiation exposure meas. in aircraft from transported radioactive goods 79—22488
radio oceanography using aircraft, inherent problems 77—25792
radiometry and spectroscopy of stratosphere from aircraft 77—70890
radiooceanography appl., inherent problems 77—17241
rudder-bars force meas. *(French)* 78—49825
skin, lightning damage simulation 78—87575
solar thermal aerostat research station (STARS) 80—17471
sound diffraction of high speed jet at subsonic flight 77—50806
sound radiation from convecting monopole and dipole sources in jet flow, forward vel. effects 79—94603
sound transmission into heavily-damped cylindrical fuselage 78—83166
sound transmission under flight conditions 77—7255
STOL aircraft and helicopters, interior noise control 80—14519
STOL aircraft engine-wing system jet flap impact noise meas. 80—96101
stratosphere pollution, review of Climatic Impact Assessment Programme (CIAP) 78—16153
stratospheric aircraft, aerosol particle exhaust layer obs. at 23 km 78—81283
stratospheric effects from aviation 79—16657
subsonic jet noise, prediction method for flight effects 78—1502
supersonic, sonic booms, pressure inside rooms and effect on plaster/wood walls 80—69602
supersonic transport planes, generation and reduction of local ground noise 80—38174
supersonic transports operations, stratospheric aerosol modification and climate implications 80—98408
tail-wheel struct. of light aircraft, large deflection anal. 78—83272
takeoff procedures, effectiveness for noise abatement 80—16880
thunderstorm-induced low-level wind variation effects 77—91217
tracking system, based on acoustic refr. scatt. by wake vortices 77—46840
turbojet noise, subsonic nozzle response to acoustic and entropy disturbances 77—75958
turbulent boundary layer noise 77—11087
turbulent jet mixing noise, in-flight simulation expt. 78—1501
US inspection system for composites 80—81274
vibration isolation for high-performance cameras 77—74543
voice communication, operational noise environment, expt. study 79—81662
waverider, appl. of flows with heat addition 77—916
wing fatigue crack testing using acoustic emission source technique 77—16769
Al aircraft alloy, fatigue resistance improvement by laser shock 80—93654
H_2 fuelled aircraft, kinetic model anal. of pollution 80—40816
ZnS(Se) multispectral window materials, production processes 77—73237

aircraft communication
flying helmets, active noise reduction system 79—18602
ocean surface meteorological buoy and aircraft VHF link 80—46298
optical fibre, cost models for A-7 aircraft ALOFT project 78—59131
optical fibre multiterminal data system for aircraft, based on time division multiplexing 78—46811
optical fibre technology for military aeronautic appl. *(French)* 78—46813

aircraft instrumentation
airborne, reconnaissance, data collection, conf., Washington, DC, USA, March 1978 79—32078
airborne clock synchronisation by minimum variance methods 77—37853
aviation, meteorology, forecasting systems, TECAM '79 conf. 80—94569
benchless laser structural model, control system 79—81464
benchless laser with autoalignment for airborne electro-optical systems 79—76723
colour radar displays for weather detection and groundmapping 79—92608
EM environment meas. near thunderstorm cells 78—49180
microwave radiometer stepped-frequency, 4.5 to 7.2 GHz, remote sensing appl. 79—80062
MTF anal. for post-flight image eval. 79—31827
multispectral aerial imagery capabilities for military geographic information acquisition 77—82054
piezoelectric transducer, appl. to aviation industry 77—12314
quasi-optical radiometer receiver design 78—8447
radar displays for weather detection and groundmapping 79—92608
radar system, forward looking IR, effect of ZnS CVD windows 78—46816
radiometers, millimeter-wave, multi-channel, dual frequency, high altitude obs. of atmospheric water vapour 79—80061
ring laser gyro, military appl. 78—42370
scanner, multispectral, optical system design 80—74458

aircraft instrumentation continued
structural fatigue crack acoustic emission monitoring 77—32755
tactical reconnaissance system, real-time, KA-102A EO LOROP camera 79—30599
X-ray tube with variable focus, use in NDT 79—80734
Cu/H_2O axially-grooved heat pipes, fabrication and performance testing for space vehicle appls. 80—37028

airfields *see airports*

airglow
see also atmospheric spectra; aurora; nightglow; sky brightness; twilight
artificial polar aurora region, external airglow meas. 78—16227
cryogenic spectrometry in 1-2.5 μm range 77—70886
dayglow spectrum, far UV N and N_2 emissions 78—28361
diurnal variation and seasonal depend. rel. to solar semidiurnal tidal wind 77—21965
electron precipitation causing 630 nm emission enhancement, high-altitude auroral zone 80—85803
electrons ejected from rocket exciting optical emission 80—51592
enhancement during ionospheric modification by intense radiowaves 77—60531
equatorial north-south aligned airglow depletions and F-layer irregularities 78—45074
EUV, AEROS and TAIYO satellite results 80—46340
EUV and visual obs. from Spacelab 77—22201
EUV dayglow, obs. by He gas absorpt. cell 79—12326
EUV dayglow, spectra, atomic and ionic emissions, 530-1240 Å 79—70904
F-region, $N(^2D)$ chemistry from airglow and atm. comp. meas. 78—16241
F-region airglow, anal. of consistency of ground-based obs. with 80—98496
Fabry-Perot spectrometer for airglow studies, with large aperture and high resolution 80—67424
far UV radiation background at high galactic latits., D2B-Aura satellite obs. 79—17143
Feyerverk experiment, airglow induced by electron injection 77—13160
general study of upper atm. *(Chinese)* 79—75039
gravity wave induced Brunt-Vaisala oscillations 79—53603
ground-based observatories intercalibration with AE-C satellite 77—41210
ionosphere, airglow emission vars. due to solar EUV flux changes, calcs. 79—44293
ionosphere, equatorial, airglow data rel. to irregularity patch form., motion and decay 80—67456
ionosphere, predawn, conjugate photoelectrons, rocket obs. 79—29931
ionosphere heating by radio waves, effects on airglow emissions 78—77403
IR airglow and O radiative association 80—12582
IR emissions in auroral regions, origin 77—33247
magnetosphere dayside cleft region, photometric obs. at 6300 Å 80—41586
mesopause, energy characts. of internal gravity waves obs. by OH emission *(Russian)* 79—12324
O I, 6300 Å airglow enhancements by high powered HF radiowaves *(Portuguese)* 80—41592
optical baffling system, high rejection, for airglow separation from background 78—7802
optical phenomena, review including airglow and aurora 77—70831
photometric systems, comparison at observatories in Arecibo and Stara Zagora 79—48575
Photozavr modulation photometer for artificial aurorae/airglow 79—21076
polar airglow, mag. ordering obs. 78—57378
polar atmosphere, penetration by monoenergetic and unidirectional proton beams 77—29528
predawn 630 nm airglow and conjugate photoelectrons, direct meas. 78—49196
radiometry methods (Soc. Photo-Optical Instrum. Engrs., Proc. vol.91, San Diego, 26-27 Aug. 1976) 77—70880
semi-annual variations, of airglow emissions intensities 78—28360
space sciences, conf., Trivandrum, India (Jan. 1977) 78—69586
spectrometer, Fabry-Perot instrument for daytime use 80—77156
temperature measured by obs. of emission lines, using new interferometer aperture 80—82075
twilight, photographic obs. from Skylab 77—60505
twilight, Raman scattering spectrum 79—92596
twilight spectrum, new diffuse emission bands obs. 80—72662
UV airglow, rocket obs. at 1530 Å 77—33704
UV dayglow, mesosphere and thermosphere H distrib. from Lyman α and β obs. 80—109290
UV spectrum, effect on zodiacal light spectroscopy at 20° elongation 78—20728
visible events 80—12584
visible spectrum, detection and study 77—70903
visual obs. from space 79—96850
VUV global observations made by satellite, 110-290 nm region 80—90272
wave component identification, multiple-point method 78—73526
weak airglow emissions, meas. with programmable scanning spectrometer 80—8469
0 I, 63 μm emission as cooling mechanism in thermosphere and ionosphere 79—16732
CO_2 4.3 μm emission, excitation mechanism involving OH and N_2 79—16731
H, geocoronal Lyman β and Balmer α emissions meas. during Apollo 16 mission 77—37476
H Lyman α, meas. rel. to local perturbations of H density distrib. near exobase 78—24400
He I 584 Å dayglow emission and exospheric He seasonal-latitudinal var. 79—75007
He I 584 Å dayglow obs. by rocket-borne reson. absorpt. cell 77—64503
He I 584 Å line meas., contrib. of O II 537 and 581 Å lines 77—41253
Mg II 29800 Å airglow obs., ionospheric equatorial Mg^+ ion distrib. 80—26673
Mg II equatorial airglow altitude distrib. 79—2418
N, far UV dayglow emissions 80—90271
N I 5200 Å rel. to temp.-depend. model of odd N species in thermosphere 78—16226
N, NO, airglow rel. to concs. diurnal variability 77—78549

airglow continued
N_2 3371 Å dayglow emission, excitation by photoelectron impact 77—33236
N_2 dayglow intensity from photoelectron impact 80—46331
N_2 dissociation by electron impact and EUV photoabsorpt., rel. to aurora and airglow 78—58847
N_2, far UV dayglow emissions 80—90271
N_2, fluoresc. efficiencies of electrons, 4900-10500 Å wavelength range 77—61870
N_2, solar activity effect on (0,0) second positive band 77—70902
$N_2^+(A^2\Pi_u)$ Meinel band deactivation cross sections 78—66635
NO 5.3 μm emission, effect of thermosphere N_2 anharmonic mols. vibr. relaxation 79—12322
NO abundance meas. in equatorial upper atm. 77—78547
NO airglow, 2150 Å (1,0) γ-band intensity meas. with polarising NO photometer 78—45076
NO, density profile from airglow obs., 72-120 km altitude 80—105094
NO γ-bands rel. to temp.-depend. model of odd N species in thermosphere 78—16226
NO, high-latit. airglow obs. in lower thermosphere 77—37467
Na I D lines dayglow diurnal var. obs. at Poona 78—69558
Na I emission from Jupiter Region C, attributed to terrestrial airglow 77—64696
O, 557.7 nm spectral emission mechanism at 100 km altitude 80—61933
O atom corona, of fast atoms during solar max., airglow obs. 80—101469
O emission rel. to shortwave radio absorpt. in winter 80—77184
O, green line intensity rel. to O atom density *(Chinese)* 80—90269
O I 1304 Å, nadir intensity/column prod. rate ratio rel. to airglow studies 77—45213
O I 5577 Å, altitude profiles rel. to $O(^1S)$ prod. in lower thermosphere 77—33235
O I 5577 Å, Na I D lines and OH band emissions, diurnal var. and seasonal depend. 77—21965
O I 5577 Å and 6300 Å line widths meas., laboratory discharge lamp source appl. 80—4148
O I 5577 Å line depend. on E_s-layer 77—67006
O I 5577 Å wave var. and meteor zone wind speed 79—62637
O I 557.7 nm forbidden line emission structure 79—35027
O I 5588 Å green line airglow emission rel. to HF wintertime absorption in D-region 79—58148
O I 630 nm profile, daytime thermospheric temps., wind vels. and emission intensities 79—58144
O I 6300 Å, Fabry-Perot interferometer meas. rel. to global model of exospheric temp. 77—53265
O I 6300 Å airglow, relationship to ionospheric F-region parameters 78—36354
O I 6300 Å airglow rel. to O atoms creation and destruction 79—8735
O I 6300 Å airglow spectrum, appl. to exosphere global temps. determ. 77—33234
O I 6300 Å airglow structures within intertropical arc, movements 78—36352
O I 6300 Å emission in twilight airglow, thermospheric temperature depend. 77—45215
O I 6300 Å forbidden line high resolution obs. 77—41252
O I 6300 Å line, ground meas. for exospheric temp. determ. 77—67003
O I 7990 Å branching ratio, lab. study, rel. to airglow and auroral emissions 79—775
O I airglow, $3s'\ ^3D^0$ and $3d\ ^3D^0$ levels excitation and radiative decay 79—80064
O I green line airglow, obs. during Winter Anomaly Campaign (1957/76) 78—45075
O II 537 and 581 Å lines contrib. in He I 584 Å dayglow meas. 77—41253
O II 7319-7330 Å dayglow, meas. and theory 77—37475
O II 7320-7330 Å emissions meas. at twilight 78—88962
O, spectral line shape in upper atm. following dissociative excitation 80—105097
O-H atmospheric model rel. to OH emission problem 77—60503
O_2 1.27 μm airglow, middle latit. meas. rel. to mesospheric O_3 concs. 80—72606
O_2 1.27 μm airglow emission, zenith angle dependence 77—45216
O_2, (0-1) spectral emission band in upper atmos. 80—61933
O_2 emission from atom recomb. 79—31576
O_2, fluoresc. efficiencies of electrons, 4900-10500 Å wavelength range 77—61870
O_2, OH, NO_2, NO emissions, Spacelab obs. 77—21967
$O(^1D)$ formed by $N(^2D)+O_2$ reaction in thermosphere, 6300 Å dayglow implications 80—90270
$O_2(^1\Delta_g)$ airglow, emission height profile meas. during winter anomaly event 78—45077
OH airglow layer (90 km), atmosphere warming during 1976-77 winter *(Russian)* 79—88518
OH airglow nature 77—64505
OH and O I emission intensities, lunar tidal effects 77—60506
OH emission, 5-1 band rot. temps. rel. to waves in emission layer and F_2-layer 78—45065
OH emission, nature of internal gravity waves obs. 77—41246
OH emission, obs. rel. to mesosphere internal gravity waves propag. range *(Russian)* 79—16575
OH emission, spectrometric thermometry rel. to internal gravity waves in upper atmosphere *(Russian)* 78—16224
OH emission, waves and winds, 80-100 km altitude 78—93025
OH Meinel bands, in airglow, rot. temp., radiative lifetime 78—61643
OH Meinel bands intensity distrib., OH* quenching mechanisms 78—65447
OH near IR emissions, Spacelab image intensifying TV obs. 77—21966
OH, submicron bands correl. studies during Spacelab simulation 79—25381
OH, vibrationally excited states, time and altitude vars. 80—41589
OI 5577 Å line, ground obs. 77—70900
$O^+(^2P)$ airglow, meas. rel. to ionisation freq. vars. during solar cycle 21 80—77195
$O^+(^2P)$ ionisation freq. determ. using satellite airglow and neutral comp. data 77—5384
$O^+(^2P)$ twilight airglow, thermospheric comp. changes estimation 79—62635
$O(^1S)$ airglow, lab. prod. rate coeff. meas. 79—53604
$O_2(^1\Sigma)$ airglow, gravity waves interaction theory 79—29918
O_2(0-1) 8645 Å atmospheric band, ground obs. 77—70900
T 80—41588

airmail *see postal services*

airports
25 kW Fresnel lens/photovoltaic concentrator application experiment at Dallas—Fort Worth Airport 80—89647
acoustic-microwave Doppler radar system, wind and wind shear meas. at Dulles Airport 78—32233
aeronautical meteorology, progress and challenges 78—53692
airbase noise contours prediction 79—1025
aircraft noise, the Netherlands, legal and economic factors 80—72112
airline meteorology, early days 77—49544
Airways Surface Obs. data for pollution potential prediction model 77—29423
Baghdogra, India, thunder occurrence over airport 78—20499
control tower cab, optical design 80—58661
environs, air pollution, remote monitoring by laser systems 80—17368
fencing for air pollution reduction, wind-tunnel expt. *(Japanese)* 80—12034
fog, warm, modern thermo-kinetic dispersal system for commercial airports 80—51576
general aviation airport, practical noise abatement 77—65653
helicopter environmental noise impact obs. and evaluation 80—104539
meteorology, aviation weather, automation in prediction procedures 78—49080
noise at Japanese bases, forecast contours *(Japanese)* 77—88982
noise control agency and Noise Bureau Factor proposals 77—23802
pressure jump detector array, gust front detect. at Dulles Airport 78—32234
schoolchildrens' mental performance levels, aircraft noise effects 79—70495
United States, recorded and predicted wind speeds 79—88457
Vandenberg Air Force Base and effects of Space Shuttle 77—64608
weather events, recurrence probabilities of weather events 80—51491
weather forecasting, operational use of panoramic lightning recorder 77—78482
weather service, future trends 78—53694
weather surveillance near airports using Doppler radar 80—46272
weather-related aircraft accidents, analysis 78—53693
wind reports, optimum averaging time for along-runway and across-runway components 77—17177
wind shear detection radar, for airport use 80—51565

alarm systems
artificial kidney, wearable, monitoring instrumentation 77—64154
audible, liquid level detection, thermistor appl. 79—12764
audible training aid for visually impaired infants, motion activated 80—36193
Caorso nuclear power station airborne and liquid radioactive release monitoring systems 79—13553
computerised monitoring of vinyl-chloride monomer for job safety 79—21727
digital level detector, using BCD adders 79—75528
Doppler, ultrasonic piezoelectric transducers with IC aux. ccts. appl. *(Italian)* 78—42508
electric field variation during low solar activity *(Japanese)* 79—40032
electronic thermometer with adjustable alarm setting *(French)* 79—63209
eneuresis alarm system, programmable op. amp., CMOS logic, Min. of Health Perf. Spec. 79—39600
gamma radiation, portable, with audible/visual warnings 78—8390
heart-beat monitoring circuit with missed beat alarm 77—56500
industrial IR detector markets and device limitations 80—86432
ink-writing recorder, warning device indicating stoppage of paper 77—5111
IR, intrusion, passive, thermopiles appl. 80—47104
IR forest fire alarm system 80—86429
IR systems and equipment design and applications *(German)* 80—52316
Large Azimuthal Telescope program control system 79—16829
leg-load alarm system for partial-weight-bearing walking exercise *(Japanese)* 79—29658
line isolation monitor with adjustable alarm level for hospital elec. systems 77—56496
line sensor used to monitor a distant transducer 79—6145
LMFBR steam generators, safety alarm system, water leakage detection *(Czech)* 78—33268
mechanical respirator, ventilation failure detector cct. *(Spanish)* 77—52913
motion picture rerecording, warning system devices and electronic digital counter utilisation *(Russian)* 80—95177
mulitary appls., portable US warning tape, perimeter warning device for combat troops 80—19200
multicomponent, multipoint infrared ambient air monitor, microcomputer-controlled 80—40945
nuclear facilities entry control system design 79—85688
nuclear power plant, fast alarm system to optimise protection of public 78—55048
nuclear reactors, computer modules appl. *(German)* 79—49788
partial weight-bearing walk, limb load alarm system 79—29661
perimeter security system using ^{137}Cs γ-ray beams 77—18713
radio emergency warning system, earthquake prediction appl. *(Japanese)* 78—85497
remote control audio system, using Doppler shift 79—64477
stack gas monitoring system for warning and control in Chiba Prefecture 79—57561
stack release radioactivity monitoring with digital processing 79—3253
Swiss Federal Institute for Reactor Research emergency organisation 78—55047
technology, IR applications 80—86431
urban hydrology, US National Weather Service programme 77—37267
US switch appl., two-board design 78—46870
ventricular fibrillation alerting device 77—78024

albedo
absorbing-scattering semitransparent planar layer, flat temp. waves 78—90683
aerosol scattering albedo determination using sky brightness measurements in UV *(Russian)* 80—21822
NW.America albedo increase following Pleistocene explosive eruptions, climatic effects 80—61789
anthropogenic effects 78—28238
asteroid 1976 AA, diameter and albedo, radiometric obs. 77—82145
asteroids, diameters and albedos 77—56870

albedo continued

- asteroids, radiometric diameters and geometric albedos from 10 and 20 μ photometry 77—53456
- asteroids, radiometric method for remote determ. 77—82148
- asteroids, review of sizes and albedos 77—60708
- asteroids, rotation rates, pole positions and shapes 80—17531
- asteroids, surface albedo and colour contracts 80—36547
- asteroids 1978 CA and DA, UBV photometry, rotation periods, albedos and diameters 78—36489
- atmosphere, finite plane-parallel, forward and backward scatt. effect on spherical albedo 79—92592
- atmosphere, heat budget and albedo determ. using balloon-borne pyranometers 79—58135
- atmosphere, inhomogeneous, with anisotropic light scatt. and small true absorpt., albedo 79—62742
- atmospheric shortwave and longwave radiative flux, mid-ocean obs. 80—12547
- aurora and nightglow satellite obs., contamination due to scatt. by clouds and snow 78—77385
- auroral albedo profile over snow-covered ground, rocket obs. 78—77384
- biosphere-albedo feedback and climate modeling 79—53508
- Callisto, IR emission spectra 80—82264
- clay soil/sand mixtures, reflectance 80—56475
- climate model, zero-dimens., with ice-albedo and greenhouse feedback, catastrophes and resilience 79—80007
- climatic changes due to intensive solar energy production, albedo modification 78—85680
- climatic model experiments, simulated changes, solar energy conversion effects 78—81354
- climatic models of Budyko-type, nonlinear albedo-temp. coupling effects 77—45129
- clouds, horizontally inhomogeneous, albedo and refl. radiance 77—78417
- clouds, shortwave albedo, pollution effects 78—7755
- cloudy atmosphere, radiative transfer model, solar radiation and cloud struct. 79—21016
- Comet West (1975n), scatt. phase function of cometary dust, 0.5 to 18 μ 77—29731
- concrete, effect of azimuthal angle on fast neutron albedos 78—8866
- concrete, meas. of albedo number using ^{60}Co, ^{137}Cs sources 79—26768
- concrete, neutron number and dose albedo 79—93681
- continents, albedo during ice age rel. to tropical climate 78—16144
- cosmic ray albedo determ. from meas. in stratosphere 79—80134
- cosmic ray flux, altitude depend., polar orbiting satellite obs. 80—46353
- cosmic ray flux in atm., primary and splash albedo components, polar orbiting satellite meas. 79—25415
- decelerating neutrons absorption in multizonal absorbing rod, rod effectiveness *(Russian)* 80—556
- Deimos, normal albedo and photometric function from Viking orbiter images 80—72838
- Deimos, spectral evidence for carbonaceous chondrite surface comp. 80—41754
- desert formation mechanisms 77—70707
- desert region, surface albedo and vertical vel. relations 78—11953
- desert region, variable surface albedo effects on atm. circulation 77—49123
- deserts, positive feedback from high albedo 77—21863
- Duluth-Superior Harbour, ice albedo distrib. rel. to growth rate 79—2299
- Earth, albedo contrast and glaciation due to continental drift 79—74950
- Earth, Albedo correl. with upper atmosphere Na abundance 77—87140
- Earth, albedo rel. to effects of diffuse radiation on atmospheric O_3 photodissoc. 80—109210
- Earth, atmosphere aerosol induced albedo change 80—56604
- Earth, global albedo, contrib. from troposphere nonspherical aerosol 80—90220
- Earth, ice-cap albedo feedback rel. to energy-balance climate models stability theorem 80—56594
- Earth, IR radiation budget, diurnal variation obs. 80—51538
- Earth, latitudinal depend. rel. to radiation press. perturbations of near-Earth satellite 78—24444
- Earth, Mars and asteroids, palaeoglaciation due to solar radiation reduction *(French)* 79—34857
- Earth, monitoring technique from LANDSAT data 77—78516
- Earth, reflected solar radiation, for satellite solar battery power increase 77—33318
- Earth, zonal and global albedoes depend. on reflectivity regional vars. 80—17377
- Earth's surface, radiance of natural formations 79—62515
- Earth albedo, anthropogenic changes and effects on climate 80—81893
- Earth albedo contribution to satellite solar array perf. 78—40798
- Earth albedo model in spherical harmonics 80—41445
- Earth albedo sudden change, climatic effects 79—44241
- Earth atmosphere, middle UV, obs. by TAIYO satellite *(Japanese)* 79—44281
- Earth climate affected by land surface albedo changes 80—98434
- Earth ground albedo to visible light using diffuse light radiometer 80—51465
- earth radiation budget: simulation of fluxes and accelerometric measurements *(French)* 79—84482
- Earth radiation budget, Nimbus 6 meas., first 18 months 80—12493
- Earth surface, albedo change effects on drought in semi-arid regions 78—32128
- Earth surface, albedo rel. to aerosol scatt. indicatrices determ. in 0.55 to 2.4 μm region *(Russian)* 80—94600
- Earth surface, albedo rel. to Monte Carlo simulation of twilight obs. *(Russian)* 77—33186
- Earth surface, effects in satellite auroral photometry 77—56737
- Earth surface, new model, D5B satellite meas. interpretation 79—21020
- Earth surface, remote sensing, contrast reduction due to haze 80—101431
- Earth surface albedo, atmospheric transfer function influence on aircraft and satellite meas. *(Russian)* 77—60464
- Earth surface albedo, reduction monitoring by LANDSAT 78—32104
- Earth surface albedo, satellite meas. over NW.Africa 79—2368
- Earth surface reflectivities in arid regions from LANDSAT MSS data 77—53189
- Earth surface UV reflectance, meas. from airborne platform 80—98453
- Earth-atmosphere albedo change due to stratospheric aerosol pollution 77—45092
- Earth-atmosphere sensitivity, albedo sensitivity to stratospheric aerosols rel. to zonal radiation balance 80—56602

albedo continued

- emittance, directional, of semi-infinite scattering medium with refr. index >1 79—94471
- 433 Eros, IR albedo and thermal props. from radiometric and refl. light obs. 80—31231
- ESRO IV satellite solar array influence 78—40797
- fast neutron albedo for Fe, concrete and Fe-covered concrete radiation shields 79—76151
- forest and grassland, radiation balance comparative study 77—17196
- Galilean satellites, radar obs. during 1976, results 78—61788
- global surface model, land use basis 80—12394
- ground, determination by remote sensing, theory 79—88438
- Hyperion, radius and albedo from 20 μ obs. 79—40136
- Iapetus, near IR reflectivity of dark and light faces 80—26800
- Iapetus, normal reflectance from lunar occultation obs. 78—85897
- ice age beginning, instantaneous glacierisation, albedo rate change and feedback effects 80—105006
- ice caps, albedo feedback effects on global climate, 2-D energy balance model 80—67407
- ice-albedo feedback effects on energy-balance climate models 78—7749
- interstellar dust, single-scatt. albedo rel. to diffuse galactic light models 78—8118
- interstellar dust, UV albedo from scattered UV radiation obs. around λ Orionis 80—56918
- interstellar dust, UV albedos from galactic UV background meas. 77—13504
- interstellar dust grains in Barnard Loop Nebula, far UV imagery rel. to albedo 77—29911
- interstellar dust in HD 200775/NGC 7023 complex, far UV albedo and phase function 80—51832
- interstellar grains in Orion Nebula, UV albedo from far UV imagery 78—4326
- interstellar UV grain albedos rel. to C I 79—92818
- Io, albedo distrib. on surface 79—53761
- Io, albedo stability and colour markings, historical meas. 79—96951
- Io, spectrum, S-containing mixtures and surface albedo 79—40127
- Io, surface albedo rel. to laboratory samples 78—53865
- Io, UV albedo curve and evidence for SO_2 80—36561
- Io spectral albedo, implications of Na and K doped NH_3 frosts reflectance spectra 78—84561
- Jupiter, Lyman α albedo, Copernicus UV obs. 80—94747
- Jupiter, Lyman alpha albedo calc. from hydrocarbon and H I photochemistry 80—105194
- Jupiter, near IR spectral albedo 80—31242
- Jupiter, UV albedo for Rayleigh scattered radiation, multichannel spectrometer obs. 77—25974
- Jupiter cloud zones, IR obs. rel. to scatt. props. 77—29712
- Lake Kainji, W.Africa, water columns movement, LANDSAT data 79—25284
- local energy exchange dynamics and climatic boundary conditions, solar energy conversion effects, preliminary examination 78—81355
- lunar, soils, mineral comp. determ. from spectral behaviour of albedo 79—21207
- lunar charged particle albedo, Luna 22 data 80—56729
- lunar normal albedo, digital file from photographic data 77—78684
- lunar soil, relationship between surface chemistry and albedo, Auger electron spectroscopy 77—60677
- lunar surface chemical composition from albedo and colour index 77—87296
- lunar surface reflective props. 77—33366
- Lyman α albedo of Jupiter rel. to solar activity 80—98601
- major planets, effects of Raman scatt. in atmospheres 78—28571
- Mars, atm. optical props. during 1971 dust storm 77—13274
- Mars, bolometric albedo vars. rel. to radio brightness longit. depend. 80—21937
- Mars, IR photometric function and bolometric albedo 77—29698
- Mars, longit. var. of radiometric albedo, thermal inertia and 2.8 cm brightness temp. 80—105191
- Mars, opposition effect, Viking Orbiter 1 obs. of Chryse-Acidalia region 79—44397
- Mars, soil density map rel. to surface albedo, topography and geology 80—109388
- Mars, surface struct. from optical and IR refl. spectrum and thermal props. 77—29690
- Mars, thermal and albedo mapping during Viking primary mission 78—20683
- Mars, UV geometric albedo during dust storm, TD1A and OAO-2 satellites obs. 77—91459
- Mars, variable surface albedo features study during Viking primary mission 78—20678
- Mars atmosphere, optical props. during 1971 dust storm *(Russian)* 78—93138
- Mars surface, global colour vars, obs. 78—65527
- Mercury, regolith containing Fe^{2+}, refl. spectra, 0.65-2.5 μm 80—56736
- Mercury albedo features, IAU nomenclature 78—53848
- Mercury albedo features, longits. and nomenclature 78—53849
- Mercury and Moon, EUV albedos 77—33378
- mesosphere, aerosol layer contrib. to polar albedo 77—60467
- meteoroid albedo and size distrib. in 0.3-4.8 AU range 78—36539
- meteoroids from Periodic Comet d'Arrest, particle size distrib. and albedo 78—53876
- Milne problem and spherical albedo, law of darkening, forward and backward scatt. effects 78—77483
- Moon, effect of transient lunar events, possible mechanisms 80—82238
- Moon, far UV albedo meas. by Apollo 17 77—37513
- Moon, geometric albedo and full Moon magnitude 77—33374
- Moon, Heiligenschein and albedo differences at zero phase angle 79—21205
- Moon, soil and rock chem. comp. effects, solar wind darkening mechanism 78—28552
- Moon, true normal albedo, photometric function and three-dimensional scatt. indicatrix 80—101538
- natural illuminance of Earth's surface 77—70794
- Neptune, UV albedo meas. 80—82295
- neutron, level meas. method 80—106097
- neutron dosimeter, description and calibration data 77—65389
- neutron flux, exponentially damped, exptl. determ. of albedo on vacuum-liq. H_2 boundary 78—4977
- neutron reflection from concrete, differential characts. of current number albedo 77—71633
- neutron scatt. energy-dependent albedo calc. 79—9659

albedo continued
neutron streaming through ducts in shields, Albedo-Monte-Carlo method usefulness 79—89345
neutron transport theory, F_N method, appl. and numerical results 79—30878
ocean chlorophyll content airborne meas. under cloudy sky, Gulf of Guinea appl. 79—25359
ocean surface absorption of short-wave radiation and albedo *(Russian)* 77—60415
ocean-atmosphere system, sea foam effect 77—81899
ocean-atmosphere system, spectral struct. of refl. solar radiation field *(Russian)* 77—33086
Pageos 1 balloon satellite, orbital effects of direct solar and Earth albedo radiation pressure 79—88566
Periodic Comet Tempel 2, optical spectrophotometry at 3 AU distance, albedo, nucleus radius 80—26814
Phobos, composition, evidence for carbonaceous chondrite surface from spectral anal. 78—49365
Phobos, evidence for carbonaceous chondritic composition from multicolour obs. with Viking lander cameras 78—49366
Phobos, normal albedo and photometric function from Viking orbiter images 80—72838
planetary albedo and long-term climatic change numerical modelling 78—77315
planetary atmosphere, single-scatt. albedo determ. for Rayleigh-scatt. atmosphere with true absorpt. 80—94704
planetary solids near opposition, laboratory study of limb-darkening 78—36477
planets, solar activity effects 79—75177
Pluto, light variation, surface albedo distrib. 77—82160
Pluto, methane frost, IR photometry obs. 77—22136
power reactor nodal anal., albedo conditions 79—80989
radiative source function, isotropically scatt. medium, refr. index effect 77—83805
radiative transfer, inverse soln. by F_N and Monte Carlo methods 80—109352
radiative transfer albedo problem in inhomogeneous isotropically scatt. atmospheres 80—36398
radiative transfer eqn. exact soln. for semiinfinite plane-parallel isotropic scatt. atm. 79—12396
random media, active remote sensing, depolarisation effects 80—82090
Rayleigh atmosphere single-scatt. albedo, determ. from polarisation meas. 79—35117
reactor cavity radiation streaming, albedo Monte Carlo methods 79—89363
reactor radiation streaming anal. using spherical harmonics expansion of albedo data 79—89367
Rhea, normal reflectance from lunar occultation obs. 78—85897
Sahel region, Africa, surface albedo vars. investigation during recent drought (1967 to 1974) 80—76981
satellite auroral photometry, spectral albedo corrections 77—49208
Saturn, far UV albedo from rocket obs. of spectrum 78—53867
Saturn, limb darkening and brightness temp., 1.30 cm interferometry obs. 80—82279
Saturn, near IR spectral albedo 80—31242
Saturn B-ring, optical reflectance polarimetry interpretation 80—31248
Saturn ring particles, albedo and size rel. to A-ring azimuthal brightness var. 78—32391
Saturn ring particles, single-scatt. albedo from 3.71 cm wavelength interferometric obs. 79—96962
Saturn rings, model constraints from radar obs. of polarisation and albedo 80—82277
singly scattered gamma radiation, albedo 79—40783
slab reactor with finite reflectors, criticality 79—26475
snow albedo following dustfall, satellite remote sensing 80—17385
snow- and ice-covered regions, multiple reflections between clouds and surface 77—45131
soil, water content estimation via total solar reflectance and spectral band ratioing 77—60479
solar proton albedo neutron flux north-south asymm. meas. 79—75061
solar radiation reflected from Earth, brightness field, atm. transmission function calc. *(Russian)* 80—4105
spectral bidirection refl. props. meas., at 0.52 μm, for savannah, bog, pasture, and coniferous forest vegetation 78—40649
spheroidal particles, randomly oriented, light scatt. 80—58461
sunlit Earth, Ar fluorescent X-rays from atmosphere during solar flares 77—13142
terrestrial atmosphere and climate long-term stability rel. to clouds 79—74951
terrestrial natural surfaces, reflected solar irradiance indicatrices and albedo effects 79—62514
Titan, albedo wavelength depend. rel. to atmosphere photochemical aerosols 80—31249
Titan, normal reflectance from lunar occultation obs. 78—85897
Triton, diameter and reflectance, spectral and radiometric obs. 80—17546
Trojan asteroids, albedo and reflection spectra rel. to comp. 80—56751
Trojan asteroids, radii and albedo 77—33399
Uranus, albedo and spectral features from IR obs. 80—82299
Uranus, methane band geometric albedo and limb brightening 79—84742
Uranus, UV albedo meas. 80—82295
Uranus ring particles, albedo from optical search 77—67067
Uranus rings, geometric albedo upper limit 78—36510
Uranus rings, low albedo rel. to ice sputtering by radiation belt protons 78—89116
vegetation reflectivity, effect on atmospheric radiance and polarisation 78—40650
Venus, albedo vars. rel. to atmospheric dynamics, winds, circulation and turbulence 77—78706
Venus, global thermal emission and radiometric albedo *(Russian)* 78—4132
Venus clouds, H_2SO_4 aerosol medium IR single scatt. albedo 78—65526
Venus surface, Venera-8 optical meas. interpretation 79—8864
Venus surface panoramas, photometric analysis of Venera 9 and 10 obs. 77—78686
water, neutron number and dose albedo 79—93681
γ-ray albedo from surface of reflecting barrier 78—1154
Al, meas. of albedo number using ^{60}Co, ^{137}Cs sources 79—26768
Fe, neutron number and dose albedo 79—93681

alclad *see aluminium alloys*

Alfven waves *see magnetohydrodynamic waves; solid-state plasma*

algebra
see also Boolean algebra; linear algebra; matrix algebra
*-algebra, decomposition of families of unbounded operators 77—10159
affine Lie algebra $A_1^{(1)}$, explicit construction 78—89626
algebra generated by Hodge's star and external differential 79—92926
array algebra techniques in multilinear least squares problems 78—36296
associative Hamiltonian algebras 78—69975
automatic dimensional analysis using symbolic maths. 77—57173
Banach, Hilbert boundary problems, associated abstract singular integral eqn. *(Russian)* 77—22370
C*, conference, Varenna, Italy (July-August 1973) 77—17753
C*, derived algebras 77—17763
C*, in quantum statistical mechanics 77—17910
C*, tensor products 77—17764
C* algebra, completely positive maps 78—49716
C* simple algebras, generated by isometries 78—20936
C*-algebra, amenability of cross products 78—20937
C*-algebra, complete positivity and asymptotic abelianness 77—60892
C*-algebras and Jordan algebras, spectral theory 77—9893
C*-dynamical systems, small perturbations 79—80458
CAMAL language for algebra, appl. to electron optics 77—38798
canonical anticommutation relation algebra, implementation of automorphisms and derivations 77—22369
canonical Schwartz spaces and generalized operators 79—30284
CAR representations generated by CCR representations, non-Fock extension 77—45672
Clifford algebra and Maxwell eqns., vector formulation 77—67302
clustering prop. for arbitrary primary state 77—30097
cohomology of action differential forms 77—33832
colloquium, lattice theory, Szeged, Hungary (Aug 1974) 77—60890
complete sets of observables on the sphere in four-dimensional Euclidean space 78—70015
completely positive mappings on algebras of unbounded observables 77—45674
computer, unconventional electron lens calcs. 77—67542
conference on Lie admissible formulations, Cambridge, USA, (Aug. '79) 80—36765
conformal superalgebra, new representations 77—61199
connected partially ordered set of events in time measurement 80—77640
deformation theory and quantisation, sympletic struct. 78—45493
deformation theory and quantisation 78—45494
differential equations, symm. *(Russian)* 77—74193
differential operators, elliptic-hyperbolic, factorisations and fundamental solns. 77—67187
division rings with evolution 78—89296
dual covariance algebras, duality 77—17748
education, exterior algebra and exterior differential forms for electromagnetic problems 80—57037
education, logarithms! and estimation 78—36748
electron propagator theory for mol. electron binding energies and photoionis. intensities 80—47848
energy spectrum of extremal invariant states 78—24
enveloping, recent results and complete proofs, book 77—17752
enveloping algebras in representation theory 77—17865
equations, appl. to symm. of non-differential eqns. of phys. *(Russian)* 77—78952
ergodic theory in von Neumann algebras 80—9104
Euler's number, relationship to natural logarithms 80—27105
exceptional Lie algebras, quartic trace identity 79—58897
external EM interaction with relativistic fields, finite algebra 77—2722
fermion system thermodynamics, appl. of class of dissipative evolutions 80—46960
filtered K-algebra, p-form continuity 77—22368
finite closed systems, relaxation, algebraic approach 77—29985
finite electron no. system, approx. Green's-functions algebraic formulations 80—47849
Fourier optics described by operator algebra 80—48163
free scalar charge field, local nets of algebra of observables 80—99039
Galileian formulation of spin, explicit realisations 80—62505
generalised Poisson bracket and associated natural one-form 77—37719
generalized deformations of nonassociative algebras. Definition and some simple examples 80—36887
generalized Grassmann algebras with applications to Fermi systems 80—57174
graded Lie algebra, Killing form 77—29984
Grassmann variables, possible interpretation of theories 77—79001
Hilbert spaces, Gleason measures on infinite tensor product 77—26200
Hilbert spaces, nested, spectral props. in class of operators and group representations 78—4459
K-flows quasi-free reversible, generalised 78—54297
Kubo-Martin-Schwinger boundary condition in Neumann algebras 79—75443
lattice system equilib. states, semi-quantum, AF algebra 78—45576
Lie algebras, finite and infinite, physics and deformation theory 77—33831
linear gauge theory algebraic struct., spontaneously broken symmetry, quantisation, massive gauge field 79—2906
many electron correl. problem, unitary group approach via spin algebra graphical methods 80—47902
mathematical approximations in physical systes, rules and useful appl. *(Hungarian)* 79—25783
modular operator, local observables, in von Neumann algebras, duality in QFT, CPT invariance 78—81793
molecule, skeleton-ligand interactions, algebraic invariant investig. 80—52853
near-rings theory and applics., book 77—37720
net cohomology over Minkowski space 78—93561
Neumann, asymptotic ratio set, temp. states, statistical mechanics 78—12640
Neumann algebra, automorphisms of quantum logics 77—30049
nilpotent Lie algebra, dimension of ideals *(French)* 77—67184
nonassociative algebra, bibliography 80—36793
nonassociative algebra history, Lie, Jordan and power associative algebras 80—37170
nonassociativity in particle physics and Caley-Graves' octonions 80—37171
noncommutative algebra, two point function calcs. 78—57734

algebra continued
- normal states and unitary equivalence of von Neumann algebras 77–17754
- normal varieties of algebras, Ω-algebras *(Russian)* 80–68019
- octonionic Hilbert spaces, Poincare group, SU(3) for coloured quark scheme 77–2791
- octonions in quantum mechanics 80–27479
- operator, theory of derivations 77–17762
- operator algebra and quantum statistical mechanics, book 80–41965
- operator algebras and Banach spaces, perturbation of flow 78–49630
- para-Grassmann algebras and para-Fermi systems 79–44783
- para-Grassmann algebras with applications to para-Fermi systems 80–57175
- perturbation theories, algebraic aspects 80–31539
- perturbation theory, so(4,2) algebraic soln. of H ground state in strong mag. field 80–47845
- physics, algebras, manifolds and fibre bundles 79–44709
- Poincare $IO_{3,1}$, centraliser subalgebras 79–6294
- Poincare $IO_{3,1}$, coordinate transforms. and centraliser subalgebra, algebra Casimirs 79–6295
- Poisson Lie algebra deformations, quantum mechan. 77–74261
- positive cone, Radon-Nikodym theorems, relative Hamiltonian, appl. of Tomita Takesaki theory 77–17758
- pseudo-Lie algebra, finite dimens. representations 77–60898
- pseudo-quartenion and pseudo-octonian Lie-admissible algebras 79–2948
- quantum communication channels 78–28998
- quantum field theory, local algebra type 77–45932
- quantum theory, *-algebra, state space transition probability 77–5699
- quantum theory, dilations of irreversible evolutions 78–65794
- quasifree completely positive semi-group generator for nonequilibrium statistical mechanics 79–25963
- scalar extensions in universal algebra *(French)* 79–53956
- Scator appls. to air pollution conc. calcs. 77–91277
- semisimple Lie algebra, completely integrable classical system 77–74215
- semisimple Lie algebras highest weights 77–60888
- spectral subspaces of 1-parameter groups of automorphisms 77–17761
- spinors, visual geometry and algebraic props. 80–31625
- statistical physical axioms and GL-spaces 78–29042
- structural loop Lie operators, definition of vector l-fields *(Russian)* 77–74186
- structure theory of factors, asymptotically Abelian C*-algebras 77–17759
- subalgebra of similitude algebra and invariants 77–29983
- superalgebra generalisation, 3-colour extension of OSP (4,1) de Sitter and SU(2,2;1) Wess-Zumino superalgebras 79–330
- superconformal 77–65134
- supergravity models, superalgebra stability *(Russian)* 80–52109
- superpositioned exponential processes, resolution and parameter evaluation *(German)* 78–89294
- tensor product composition of algebras in Bose and Fermi canonical formalism 77–71177
- test function algebra positive elements, symmetrisation 77–37715
- thin shells, algebraic constraints for weak C^1 continuity 78–4458
- Tomita-Takesaki theory, classification of type III factors 77–17756
- Tomita-Takesaki theory for von Neumann algebras with separating and cyclic vector 77–17755
- two centre problem, linear algebra of integrals *(Russian)* 78–89368
- U(12) failure in quantum chromodynamics 77–67576
- unbounded operators in statistical mechanics, *-algebras for quantum mechanics formulation 79–6046
- von Neumann, faithful normal states 77–17760
- von Neumann algebra, conditional expectations 78–45459
- von Neumann algebras, complete normal dissipations 78–89358
- von Neumann algebras, conditional expectation and commutativity 78–36789
- von Neumann algebras, unbounded derivations 77–26125
- von Neumann of type III, structure, crossed products 77–17757
- Wigner's theorem generalisation, struct. of projection-valued states 78–36868

algorithm theory
- *see also computational complexity; programming theory*
- annular plate, algorithm for numerical soln. of critical buckling 78–83275
- chemical reactions, tree construction by algorithm, using tabular pot. functions 77–70286
- education, implications of algorithm theory for instructional design 78–81735
- fast least-squares algorithms, on-line data fitting, for physics teaching 77–33787
- image formation, super-resolution derivation by analytical continuation methods 78–29915
- Kalamboukis tests of Davidson algorithm, comments, nuclear structure 80–86822
- open-shell SCF secular eqn., iterative algorithm soln. 80–52868
- power series, class of algorithms for obtaining rational approximants 78–54169
- three-body system, computation method for eigenvalues and eigenvectors 78–24681
- water network anal. using node recording algorithms and admittance matrix 78–85613

algorithms (computer listings) *see subroutines*

aliphatic compounds *see organic compounds*

alkali metal alloys
- *see also caesium alloys; lithium alloys; potassium alloys; rubidium alloys; sodium alloys*
- alkali metal liq. binary systems, thermodynamic props. at high temps. 80–15262
- alkali metal-Au alloys, elec. props. 78–84187
- alkali metal-H, liq. and solid, mol. orbital approach, solvation energies 77–4201
- binary intermetallic compounds, OPW calc. of struct., bonding and stability 77–43169
- charge transfer and percolation 79–95372
- diatoms, pot. curves, selected valence electron SCF MO calc. 79–10053
- dilute alloys, lattice relax., energy of mixing 77–84936
- dilute binary alloys, equilib. at. vol. and compressibility 80–70295
- dilute binary solutions, heat of formation 78–75840
- liquid semiconductors, struct. and electronic props. 78–2403

alkali metal alloys continued
- nontransition element/alkali metal systems, direct calorimetric exam. 78–84775
- specimen preparation for thermal analysis up to 1500°C 77–28948

alkali metal compounds
- *see also alkali metal alloys; alkali metal halides; caesium compounds; francium compounds; lithium compounds; potassium compounds; rubidium compounds; sodium compounds*
- afghanite, stacking variation, TEM study 79–99219
- alkali + inert gas molecule, far wing line broadening, quasistatic theory 79–22762
- alkali borate glass networks, π-electron distrib. SCF INDO LCAO-MO calc., O basicity 78–79924
- alkali bromides, soln. in propylene carbonate, dissociation, radius and no. of ion solvation *(French)* 79–70319
- alkali disulphide species, $M^+S_2^-$, laser photoluminescence spectra in solid Ar at 12K 79–5148
- alkali graphite intercalation compound, evidence for alkalilike cond. bands 80–45201
- alkali hydrides, bulk props. prediction from molecular behaviour 78–51468
- alkali metal actinide complex halides, thermochem. and struct. props. 80–7847
- alkali metal cation-electron pair in ethers, optical spectra, coordination effects 77–66788
- alkali metal glass, elec. cond. meas. method 79–66250
- alkali metals in graphite, organic molecule effects, aromatic hydrocarbons *(French)* 78–27433
- alkali metapenodates, chem. shift, NMR obs. 80–48015
- alkali-aggregate reaction particle size effect on expansion *(Japanese)* 78–31374
- alkali-alkaline earth ceramic solid solutions, with tetragonal tungsten bronze struct., low freq. optical modes 78–76477
- alkali-alkaline earth silicate glasses, IR refl. spectra *(Japanese)* 78–52505
- alkali-alkaline-earth silicate glasses, IR reflection spectra *(Japanese)* 78–19491
- alkali-anthracene ion-pairs and triple-ions in solution, far IR spectra 79–78663
- alkaline trihydrogen selenites, ferroelec. phase transitions, Raman spectra 77–8525
- alkanoates, solid-state transitions, diffractometric and conductometric meas. 79–60507
- alum salts, cubic, Debye temp., elastic consts. averaging 80–54332
- aluminophosphate glasses, ionic cond. mechanism 80–15299
- antimonide photocathodes, prep. and props. 78–84693
- antimonides, photocathodes, emission and work functions 79–78836
- azides, diamag. susceptibility, rel. to cryst. struct. 79–24127
- bifluoride, struct. parameters determ. from NMR spectra anl. of two-spin system 77–89353
- binary selenites, formed by reaction of alkali metal and Ga selenites, comp. and props. 77–24941
- bisulphites, and disulphites, solid and soln., and isotopic forms, Raman spectra assignments 79–42968
- borate and silicate glasses, γ-irrad., paramag. SO_3^- radicals 79–42838
- borate binary glass, energy storage behaviour studied by thermoluminesc. 80–50432
- borate glass:S, blue and green coloration, absorpt. spectra 79–87470
- borate glass, mech. and dielec. relaxs. and interpet. 78–27159
- borate glasses, phase separation 79–41965
- borate glasses, Raman study at high temps. 80–93306
- borate glasses, single and mixed, viscosities 80–92701
- borates, vitreous and cryst., vibr. spectra and struct. comparison 78–23470
- borosilicate glasses, phase separation obs. using SEM-EDX technique 80–76224
- bromides, photofragment spectra, 266 nm, bond energies and excited state symmetries 80–53072
- carbonates, fused, electrochemical oxidation of H_2 and CO, fuel cell anode appl. 80–72040
- chalcogenides, crystal binding, analysis in Born model of cohesion 78–38652
- chalcogenides, electronic polarizabilities and ion sizes 80–59432
- chalcogenides, van der Waals pots. determ. 78–83767
- chloride-$AlCl_3$, molten mixture, vap. pres. meas. 78–87779
- complex uranyl phosphites, synthesis and comp. 80–35516
- cryptand complex, with anion or solvated electron, optical absorpt. spectra 78–52526
- cyanide, aq., chem. dissolution of Au anode, electron stoichiometry 80–40697
- cyanide, lattice energy calc. from hydration enthalpy 77–35506
- cyanides, He I photoelectron spectra 79–64046
- cyanides, lattice energies calcs. 77–47375
- cyanides, mol. excitons, X-ray excited emission spectra obs. 80–66287
- deuterides, cohesive energy, lattice energy eqn. 77–35501
- difluorides, MHF_2, ^1H and ^{19}F NMR 78–2753
- dithioferrates (III), electronic struct. and hyperfine interactions, $X\alpha$ calcs. 80–100448
- double salts, $MM'BX_4$ (M=alkali; M'=alkali or NH_4^+; $BX_4=SO_4$, BeF_4, etc.), theory of phase transitions 79–99837
- feldspars, structure energies 80–6387
- ferrocyanides, $A_2BFe(CN)_6$, A=alkali metal, B=alkaline earth metal, structural aspects 78–14326
- fluo-perovskites, weakly discontinuous phase transition, linear birefringence obs. 80–11362
- fluoantimonates, dielectric props. and structural phase transitions *(German)* 80–25274
- fluorides, thermodynamics and kinetics of O incorporation 77–84778
- fluorite crysts., modified electronic charge density 77–62502
- fluoroaluminates, dissoc. enthalpies, mass spectrometric determ., heat of form. 80–97720
- fluoroborates, ^{19}F chem. shift, multiple pulse zero crossing NMR obs. 79–9230
- franzinite, stacking variation, TEM study 79–99219
- germanate crystals and glasses, struct. and stability, IR spectra meas. 80–64911
- germanate glass, Ge co-ord. number change *(Japanese)* 77–58958
- germanate glasses, He permeability, diffusivity and solubility 79–51308
- glass, alkali-alkaline earth nitrates, Raman spectra, vibr. perturbations effect 79–8132

alkali metal compounds continued
glass, ion motion and mixed alkali effect analysis 78—30793
glass, rapidly quenched, alkali ion cond. 80—107559
glass, single- and mixed-alkali, high field cond. and ionic jump processes 78—38873
glasses:Cu^{2+}, near IR electronic spectra, effect of alkali contents 78—27267
glasses, alkali-silicate, chem. stability, cations coordination, leaching vacancy mechanism 80—35526
glasses, alkali-silicate, chem. stability depend. on cation O_2 structs. 80—35527
glasses, ionic motion, ^{7}Li NMR obs. 78—27107
glyoxal-alkali (alkaline earth metal) complex, ab initio MOSCF calc., chelate effect 79—31386
graphite intercalation compounds, alkali and halogen, electronic props., conductivity and optical reflect. *(German)* 80—49837
graphite intercalation compounds, neutron scattering study 78—30597
graphite intercalation compounds *(French)* 78—27431
graphite intercalation cpds., selection rules and restricted valence band self-convolution for KVV Auger transition 80—29832
graphite-alkali metal intercalation cpds., electronic props. 80—45202
graphite-alkali metal intercalation cpds., IR, active lattice mode obs. 80—45072
graphite-alkali metal-benzene ternary intercalation compounds thermal and X-ray anal. *(French)* 78—27434
halides, bond order correl. with dissoc. energy 80—32596
hexachloroniobate and hexachlorotantalate compounds, thermodynamic props. from VP meas. 79—34345
hexachlorotellurate, $A_2(TeCl_6)$, (A=Cs, Rb, K), IR and Raman spectra, lattice and internal modes, phase transition 78—6659
hexahalometallate (IV) complexes, A_2MX_6, A=alkali metal or ammonium, M=lanthanide or actinide, X=F or Cl, lattice energies and thermochem. 79—60307
hydrate layered chalcogenide, anisotropic mobility of water, NMR, for $A_x{}^+(H_2O)_y[TaS_2]^{x-}$, (A=Na, K, Cs) 79—65744
hydride arc, laser initiated, H^- production 80—32550
hydride molecules, pot. energy function, rot. const., vibr. const., and binding energy 80—99532
hydrides, bond forces, parameterless calc. 78—47275
hydrides, cohesive energy, lattice energy eqn. 77—35501
hydrides, ionic-covalent config. mixing, pot. curves 77—34576
hydrides, lattice props. from interacton pot. energy function 80—100199
hydrides, repulsion interaction 78—26488
hydrides, thermodynamic props. calc. using ionic pots. 78—10155
hydrides, VB calcs., equilib. internuclear separation, dissoc. energies 77—71756
hydrides, Woodcock pot. calcs. 80—43136
hydroxides, clusters in gas phase, high press. mass spectrometry, atmospherical implications 80—58436
hydroxides, dissoc. energies and bond lengths, ion props. depend. 78—86801
hyperoxides, ionic π-electron systems, magnetogyration 80—93155
indates and thioindates, prep., props. and struct. 80—35517
inert gas-alkali metal excimer molecule, possibility of existence 79—76354
inert gas-alkali metal mol., gaseous transient, D-line emission obs. 77—38688
intercalated graphite, C XVV Auger lineshape anal. 80—104019
intercalates, alkali metal and alkali metal hydroxide with TaS_2, lattice parameters, supercond. transition temps. 80—25029
intercalation and substitution-intercalation cpds. in dichalcogenide hosts, factors affecting ion mobility 80—59707
intercalation compounds, prep. methods and cryst. struct. 79—99156
intercalation compounds *(French)* 78—27442
intercalation compounds with graphite, evidence for alkali-like conduction band, UPS study 80—45208
intercalation compounds with graphite, large anisotropy and stage depend. 80—44795
intercalation compounds with TaS_2, X-ray anal. and supercond. transition temp. 78—31007
intercalation compounds with $TiS_2(Se_2)$, $VS_2(Se_2)$ and $CrS_2(Se_s)$, phys. props. 80—44179
iodates, chem. shift, NMR obs. 80—48015
iodates, lattice dynamics of $IO_4{}^-$ mol. vibr. 79—42157
iodides, photofragment spectra, bond energies and excited state symmetries 80—5589
ionic conductors with sheet structures, ion mobility and influences 80—107522
isoalkanoates, thermal behaviour, differential scanning calorimetry 78—34600
$M^IM^{IV}IO_6$, vibr. spectra (M^I=Na,K,Rb,Cs,NH_4; M^{IV}=Ge,Sn,Pb) 77—42325
metaborates, dissoc. energies and bond lengths, ion props. depend. 78—86801
metaborates, vapour over heated solid, XPS, obs. 80—87171
metaniobates, electron spectra of polycrystals, 0.06 to 25 μm 77—20868
metaphosphate glass, dielec. relax. at medium temp. 79—24257
metaphosphate glass phosphors, M_2O-R_2O_3-P_2O_5 (R=Y or rare earth), fluoresc. props., activator conc. effect 80—89058
metaphosphate glasses, low frequency Raman scattering and glass transitions 79—95745
metaphosphate glasses, M_2O-R_2O_3-P_2O_5 (R=Y or rare earth), glass transition temps. and coeffs. of linear thermal expansion 80—88343
metaphosphate glasses, $n(M_2O.P_2O_5).(1-x)Y_2O_3.xTb_2O_3.3P_2O_5$, M=Li, Na, K, excitation and emission spectra 80—40150
metaphosphate glasses exam. of temp. dependence of thermooptical const. 78—88286
metaphosphate glasses exam. of thermooptical and photoelastic props. 78—88287
metatantalates, electron spectra of polycrystals, 0.06 to 25 μm 77—20868
mixed alkali glasses, IR reflection spectra *(Japanese)* 78—19491
mixed halides, A_nCY_6, spectra by cryst. field theory 79—4820
molten carbonates, eval. as latent heat thermal energy storage materials 80—30586
molten salt mixtures, binary, excess thermodynamic props. and US vel. *(French)* 77—27943
molten salts physical props. data compilation rel. to energy storage 79—92090
molybdates, nonstoichiometric, IR spectra rel. to vacancy struct. *(French)* 78—43867

alkali metal compounds continued
molybdates $M^IM^{III}(MoO_4)_2$, M^{III}=Al,Sc,Fe,In, struct. transitions phenomenological approach 78—51674
monoxides, bond distance, dissoc. energy and vibr. freq., electron gas model 77—30846
multialkali photocathodes, secondary emission characts. 78—84687
nitrate, lattice energies and related thermodynamic props. 77—51344
nitrates, lattice energy, standard heat of formation, electron affinity 78—91295
nitrates, melting presssure curves up to 5 kbar 77—15547
nitrates, molten, isothermal compressibility obtained from adiabatic thermal press. coefficients 79—95065
nitrates, molten, pVT data, internal energies, eqn. of state 78—43098
nitrates, molten, pVT data, thermal press. coeffs., compressibilities 78—43097
nitrates, molten, Rb^+ and Cs^+ ion tracer diffusion coeffs. meas. 80—70437
nitrates, molten, thermodynamic study *(French)* 77—31781
nitrates, Raman and Brillouin scatt., temp. influence and freq. of $NO_3{}^-$ ion *(French)* 79—69833
nitrates, Raman spectra, interionic interactions effect on bond lengths, dissoc. energies and vibr. 79—36653
nitrates calc. of heat of fusion using quantum mechanical relations 80—6491
nitrites, molten, combination scatt. spectra, freq. shifts, jumps at melting, line widths *(Russian)* 77—40241
nitrocomplexes, planar dynamic Jahn-Teller effects 77—15804
nitroprussides, Mossbauer spectra, dehydration effects 79—24237
NMR spectra of alkali metal nuclei, shielding and quadrupole coupling consts. 78—84487
optical surface, target containing alkali metals and alkaline earths, chemical sensitisation after ion bombardment 80—3227
oxide glass, composition dependence of activated processes, mixed alkali effect 79—77525
oxide-Al_2O_3-SiO_2 glass, EPR 78—91930
oxides, effect on refr. index of optical glasses *(Russian)* 78—22182
oxides, M_2O^+, $M_2O_2{}^+$, M_3O^+, $M_3O_2{}^+$, heats of formation 80—16715
oxides, O two electron affinity from cohesive energies 78—25736
oxides in binary system with WO_3, phase relations 79—8290
oxides in vitreous silica, effects on viscosity 78—64580
perchlorates, elec. transport during struct. transforms. 78—59971
perrhenates, UV photoelectron spectra 78—50575
phosphate glass, mech. and dielec. relaxs. and interpet. 78—27159
phosphates, $Sn(MPO_4)_2.H_2O$, (M=Li, Na, K) struct. and vibr. spectra 80—39030
polyaluminates, synthesis, solar furnace appl. 78—84746
polyether-alkali metal salt adducts, cond. investigation rel. to use as solid electrolytes 80—59708
polyphosphates, vitreous, mol. weight distrib. determ. by gel-chromatography 79—50173
polyphosphates, vitreous IR spectra 80—16043
rare earth double orthophosphates with alkali metals, conc. depend. of luminesc. props. 80—100673
rare earth double orthophosphates with alkali metals, spectroscopic obs., struct. and chem. nature 80—100674
salt solution, Ar saturated, sonoluminesc. as acoustic cavitation probe 79—60437
silicate:Nd_2O_3 glasses, coloured, dichroism *(Polish)* 79—99919
silicate glass, CuO doped, ESR spectra of Cu^+, quadrupole effects 78—64265
silicate glass, internal friction, influence of red/ox ratio of multivalent ions 78—31447
silicate glass, isothermal mech. loss spectrum, appl. of Rheovibron 80—88260
silicate glass, suitability of small angle neutron scatt. for struct. determ. 78—22663
silicate glasses, high temp. relax. mechanisms 80—70134
silicate glasses, secondary relax. transitions 80—88261
silicate glasses, struct. and thermal props. 80—84075
silicate glasses in aqueous solutions, leaching kinetics rel. to surface pot. 80—11803
suboxides, structure and bonding, book contrib. 80—972
suboxides, thermal and struct. anal., elec. and optical props., photoelectron spectra 79—47587
sulphates, $SO_4{}^{2-}$ optical and spectroscopic props., cryst. environment effect 77—40224
TCNQ salt, alkali transition metal, elec. cond. and phase transition 78—43370
TCNQ salts, charge transfer enhanced IR absorpt. spectra 77—28558
TCNQ salts with alkali metals, intensities of IR absorpt., electronic transfer magnitude 78—6691
ternary chlorides, $ABCl_3$ type, optical props. 78—35111
ternary molten salt phase diagrams, computation 79—100118
ternary sulphides, $A_xMo_3S_4$, and hydration products, cryst. struct. 78—42989
ternary sulphides, A_xMoS_2, and hydration products, cryst. struct. 78—42989
tetrachloroaluminates, vapor characterisation by photoelectron spectrosc. 80—81388
tetracyanoplatinate (FHF), one-dimens. conductors, IR spectra 77—77184
tetrafluoroaluminates, matrix isolated IR spectra 80—985
tetrafluoroaluminates, vapor characterisation by photoelectron spectrosc. 80—81388
tetrafluoroborates, intramol. force fields and mean vibr. amplitudes 80—2743
titanates, $(A_2Ti_6O_{13})_n.A'Ti_4O_9$, (A=Na, K, Rb)(A′=Ba, Pb, Sr), intergrowth in tunnel structures 80—28995
trihalogeno-plumbates, $M[PbX_3]$, cryst. growth struct. and spectra *(German)* 79—90632
triple-ion species of alkali metals, ESR spectral hyperfine multiplets, linewidth effects 77—83624
tungstates, $M^IM^{III}(WO_4)_2$, M^{III}=Sc,In, struct. transitions, phenomenological approach 78—51674
tungsten bronzes, cluster model 78—10351
tungsten bronzes, dynamic fluctuations between local struct. states in supercond. TI phase 78—26981
tungsten bronzes, enhanced supercond. T_c, possible explanation 78—14850
tungsten bronzes, inhomogeneous, numerical simulations of Hall effect 77—43551

alkali metal compounds continued

- tungsten bronzes, struct. and supercond. 79—82703
- tungsten bronzes, superconductivity at press. up to 20 kbar 79—38226
- uranates, struct., phys. and chem. props., preparation methods, review *(Japanese)* 79—14764
- uranyl acetates, cubic crysts., optical spectra fine struct. 77—1693
- uranyl nitrates, IR spectra, force constants, bond orders 77—30873
- uranyl propionates, cubic crysts., optical spectra fine struct. 77—1693
- AMO_2, M=transition metal, stability rel. to coordination *(French)* 77—19933
- (Ag-M)Br, (M=Na, K, Rb, Cs) molten mixtures, molar vols. and molar conductivities *(French)* 79—77788
- $AlM_xH_{1-x}(SeO_3)_2.nH_2O$, M=alkali metal, hydrothermal crystallization, thermal decomp. 77—90265
- Al_2O_3-SiO_2-X_2O (X=alkali metal) glass, acid resist. 80—21140
- C fibre layered compounds with alkali metals, prep. 80—20809
- $CsMHoF_6$, (M=Na, K, Rb), mag. behaviour *(German)* 80—65774
- Eu double metaphosphates with alkali metals or H, luminesc. props. 80—100675
- α-F_2O_3:alkali metal hydroxides, reduction, Mossbauer spectra 80—16672
- Ga_2O_3-SiO_2-X_2O (X=alkali metal) glass, acid resist. 80—21140
- hydrate layered chalcogenide, anisotropic mobility of water, NMR, for $A_x{}^+(H_2O)_y[NbS_2]^{x-}$, (A=Na, K, Cs) hydrate layered chalcogenide, anisotropic mobility of water, NMR 79—65744
- $Li_2B_2O_5$ glass, phase separation 79—41965
- $MLnO_2$, Ln=Y or Gd, synthesis and physicochem. props. 77—48216
- $M^+{}_3M^{3+}(VO_4)_2$, $M^+{}_2M^{4+}(VO_4)_2$, M^{3+}=Sc, La, B, Al, Ga, In, M^{4+}=Ti, Zr, Sn, phosphors 77—48217
- M_2O-MnO-B_2O_3 glasses, M=Li, Na, K, glass-forming region and physicochem. props. 78—63678
- $M_2O(MF_y)$-BeO-P_2O_5 glasses, M=alkali metal, alkaline earth, Cd or Zn, glass-formation 78—67656
- MoS_2 intercalation compounds, reaction with alkali and alkali earth metals, band struct., superconductivity 78—26541
- SiO_2-Al_2O_3-RO-R_2O type glass additions, sintering of porcelain bodies 80—45265
- V_2O_5 bronzes, single cryst., elec. cond., 300 to 900K 77—20369
- WO_3-P_2O_5 alkali glasses, electrochromic, electron-ion processes 80—25341
- YCl_3-MCl melt, M=Cs, K, Li, Raman spectra 77—59567

alkali metal halides

see also compounds of individual alkali metals, e.g. sodium compounds

- absorption spectra, freq. and temp. depend. of vibr. bands 80—2787
- activated, physical phenomena and optical data processing appl. *(Russian)* 80—80819
- activated crystal, absolute quantum yield of stored light sums *(Russian)* 79—56851
- activator centres, excited state transitions, bleaching dynamics 79—4527
- activity and brittle fracture, effect of lattice of point defects 79—15785
- adhesion to polyethylene, theory, allowance for boundary dislocations 77—70280
- adsorbed on GaAs (110), adsorpt.-desorpt. processes and phase transitions 78—2361
- adsorption, of inert gas adatoms, pot. energy calcs. 78—67902
- adsorption heat of inert gas atoms, variation 77—85049
- adsorption of CO_2, field induced vibr. splitting, IR spectra 78—46334
- adsorption on discontinuous Ag and Pt films, effect on elec. cond. 80—2487
- aggregation process of divalent metal impurities, order of reaction, fractional time conc. depend. 80—107308
- air enthalpy meas. by LiCl humidity sensors 80—90858
- aliovalent impurities, periodic distrib., self consistent approach 79—69149
- alkali halide: $Ge^{2+}(Sn^{2+})(Pb^{2+})$, T-centres, absorpt. spectra, energy level diagram 77—73157
- alkali halide: monovalent cation, recomb. luminesc. $(V_K+e)_A$-type emission 77—28615
- alkali halide: O^{2-}, photoluminesc. spectra, phonon using struct. *(Russian)* 78—2912
- alkali halide: $Tl^+(In^+)(Sn^{2+})(Pb^{2+})(Cu^-)$, charge transfer absorpt. band 79—73977
- alkali halide:alkaline-earth cations, defect structs. examined by methods based on Mott-Littleton techniques 80—59487
- alkali halide:CN^-, Kerr effect and birefringence from paraelectric CN^- defects 78—43838
- alkali halide:Cr^+, Szigeti charge and correl. with hyperfine coupling const. 80—96831
- alkali halide:$CrO_4{}^{2-}(MoO_4{}^{2-})(MnO_4{}^-)(ReO_4{}^-)$, frozen solns., absorption spectra, 4.2-300K 79—87467
- alkali halide:$Cu^+(Ag^+)$, luminesc. spectra and lifetime, high-press. effects 78—35194
- alkali halide:Eu^{2+} , spin Hamiltonian, cryst. field consts. calcs. 79—51537
- alkali halide:$H^-(D^-)$, local modes and colour centre absorpt. bands, analogy 80—60632
- alkali halide:Hg, EPR and optical props. 78—91933
- alkali halide:Me^{2+}, nearest-neighbour theory of dipole polarisation and depolarisation, cation vacancies 77—16243
- alkali halide:Mn^{2+}, spin-Hamiltonian parameters anal., superposition model applicability 79—28592
- alkali halide:NCS, force field calc. 79—51224
- alkali halide:Tl^+-like ions, triplet state lifetime, hyperfine interaction 80—2844
- alkali halide, molecular processes of condensation and evaporation 79—69237
- alkali halides: cation with s^2 ground-state configuration, absorption bands assignment 80—97310
- alkali halides: $SCN^-(CNO^-)$, absorption bands temp. depend. *(Russian)* 77—77260
- alkali halides:Ga^+, Jahn-Teller effect, EPR study 78—43690
- alkali halides, bond forces, parameterless calc. 78—47275
- alkali halides, F-centre trapping of conduction electrons, photocond. study 78—56179
- alkali metal halides, F-centre luminesc. rel. to cryst. chemical parameters 80—29780
- Anderson-Gruneisen parameter evaluation 80—24617
- aqueous area solutions, conc., viscosity meas. 79—23759
- aqueous solutions, extrinsic $O_2{}^-$ ions, spectral props. *(Russian)* 78—6766
- aqueous solutions, hypersonic sound vel. and absorpt. meas. 78—30699

alkali metal halides continued

- aqueous solutions, IR absorpt. ν_1 (CN) band parameter temp., conc. study *(Russian)* 80—80801
- avalanche impact ionisation, in optical breakdown 79—42895
- band centre shift of SH^- and SD^- impurities 77—16346
- base for graft polymerisation of polystyrene *(German)* 79—100365
- binary mixtures, molten, excess enthalpies, calc. 80—3397
- binding energies of vacancy pairs 78—51533
- binding energy, atomisation energy 78—18576
- birefringence, annealing effects, photoelasticity 78—72483
- boiling, melting points rel. to mol. wt. 79—46785
- Born repulsive parameters and dielectric behaviour 77—72579
- Born-Mayer repulsive parameters, overlap parameters, free ion electronic charge densities 79—98179
- bound polarons, vibronic theory, appl. to F-centre excited states 78—84150
- brittle fracture of single crysts. and active struct. of cleavage surfaces 79—28039
- bromide, molten, struct. by X-ray diffr. 77—4033
- bromide-VBr_2 systems, cryst. struct., DTA investig. *(German)* 78—72766
- bulk modulus, temp. variation 80—92588
- cathodoluminescence of ionic crystals containing self-localising excitons 78—6785
- cation and anion vacancy motion in NaCl and CsCl type structs., comparison of migration entropy 77—62519
- cation impurity-cation vacancy complex, equilib. conc. calc. 80—19834
- cation motion energy parameters, dielectric relax. meas. 78—30784
- CESR of dendritic metal phase precip. 77—24744
- charged dislocations for case of saturated region 79—46657
- chemostress effect in ionic crysts. and metals 79—28193
- chloride:Mn^{2+}, spin Hamiltonian parameters, binding energies for cation vacancy complexes 80—96461
- chloride, molten, interdiffusion of Ag^+ *(Japanese)* 79—60530
- chloride aqueous solutions, ^{35}Cl relax. rates of chloride ions 77—88471
- chloride crystal, F centre energy level shift and splitting in O^- field 80—70640
- chloride-$MgCl_2$ system, solid and molten states, struct. props., Raman spectra 80—76011
- chlorides: $F^-(Br^-)(I^-)$, anion impurities substitution, energies of soln., association and migration 78—83831
- chlorides, aq. soln., ion-solvent and solvent-solvent interactions, X-ray obs. 80—44107
- chlorides, aqueous solns., high precision viscosity meas. 80—10695
- chlorides, I^- or Br^- doped, optical investigation of atomic hydrogen centres 78—88351
- chlorides, interionic pots. 77—47372
- chlorides, Mn doped, luminesc. spectra and decay *(German)* 77—48234
- chlorides, modified electronic charge density 78—79554
- chlorides, molten, Ag^+ impurity diffusion 80—59685
- chlorides, molten, metal transport reactions in isothermal system *(German)* 77—63568
- chlorides, molten, metal transport reactions in isothermal system *(German)* 77—63569
- chlorides, molten mixtures with UCl_4, physicochemical props. 78—38915
- chlorides, photofragment spectra, bond energies and excited state symmetries 80—87190
- chlorides, thermal diffusion in H_2O, D_2O, potentiometric calcs. 78—18807
- chlorides, thin film, crystal-vacuum (100) surfaces, mol. dynamics computer simulation 80—34288
- cleavage in ultrahigh vacuum apparatus, surface charge meas. 78—12708
- cluster ions and mol. ions in salt field desorption 80—40238
- cohesive energies, effect of three body interactions 77—76516
- cohesive properties, analysis using density functional formalism 79—90592
- colour centre lasers, tunable CW IR, using $F_A(II)$, $F_B(II)$, M and $F_2{}^+$ centres 77—88725
- colour centres, binding energy of F_{e+}', M_{e+}' and R_{c+}' centres, positron trapping 79—69460
- colour centres, positively charged long-lived excited states and spontaneous tunnel transitions 79—82552
- colour centres, thermal annealing, monomolecular and bimolecular sequence of kinetics 78—47373
- coloured crystal, possibility of Auger effect as result of positron capture 78—14381
- coloured crystals, light amplification at activator centres 80—2795
- compressibility, force const. and IR absorpt. freq. 77—27955
- Compton profiles, anisotropies 80—20730
- crystal, optical emission following pulsed 10.6 μ irrad. 79—28847
- crystal, pot. parameters, Hellman function calcs. 80—2181
- crystal anharmonic effects, modified Gruneisen relation 79—99290
- crystal binding, electronic delocalisation *(French)* 77—24286
- crystal binding energy, long and short range forces 80—75200
- crystal binding energy formula, halogen, H, D electron affinity 77—35501
- crystal containing molecular centres, IR absorpt. spectra, 77-630K 79—99863
- crystal deformation, F-spectrum electric and strain fields 79—56256
- crystal electronic polarisability, ion size and dielectric const., hydrostatic press. effects 78—26487
- crystal growth, physical vapour transport method for low dislocation density crysts. 78—43992
- crystal properties, cohesive energy, bulk modulus and press. depend., interionic force model 80—15035
- crystal structural stability and repulsion 79—65028
- crystals, doped, optical absorption and MCD spectra, Gaussian quadrature calc. 80—7367
- crystals, force consts., IR absorpt. freq., logarithmic pot. function calcs. 78—2832
- crystals and melts, far IR emission 77—51527
- Czochralski growth, dynamical aspects, use of optical diameter controller 78—31332
- damage by UV laser radiation 80—76110
- DC breakdown strength at room temp., calc. 79—24260
- Debye temperature, elastic consts. averaging 80—54332
- defect centres, chalcogen^{2-} vacancy centres, absorpt. and fluoresc. spectra 78—48204
- defect energy, shell-model calc., crystal-independent interionic potential parameters 79—28141
- defect formation, kinetics 78—67713

alkali metal halides continued
- defect formation, model of excitonic mech. 78−91337
- defect formation, model of excitonic mechanism 78−38696
- defect formation volume, temp. and press. depend. 78−26563
- defect production in cation sublattice, mechanisms 80−96510
- defect recombination, V_k-A^0 pairs, diffusion-controlled, incorporating Coulomb interaction and annihilation 78−23044
- deformation dipole model, rel. to dielectric props. 78−72454
- deformation spectroscopy, dislocation interactions with electron and hole centres 78−10983
- deformed single crystals, dislocation struct. formation *(Russian)* 77−7733
- diamagnetic susceptibility, interatomic charge transfer effect 78−50660
- diatom+inert gas, inelastic scatt., short-lived complex form. 79−13796
- dibenzo-18-crown-6 complex, ESCA, binding energy 78−50584
- dielectric const., press. depend. from Szigeti relations 79−19828
- dielectric const. temp. depend. 78−43770
- dielectric constant, Clausius-Mossotti and Mott-Littleton theories 79−82910
- dielectric constant, electronic, evaluation of second order strain derivatives 78−2792
- dielectric constant, high freq., press. derivative model calcs., electronic polarisation 80−7255
- dielectric constant and polarisability strain derivatives 77−90088
- dielectric constants, electronic and static, strain derivative theory 79−95701
- dielectric constants, first and second order strain derivatives 78−47719
- dielectric constants, vol. depend., and effective charge parameter, under hydrostatic press. 78−14689
- dielectric properties under hydrostatic press. 79−38436
- diffusion of H and H_2, activation energy calcs. 77−51546
- diffusion of monovalent ions 78−30790
- dipolar point defects, studied by ITC 80−6405
- dipolar relaxation induced by AC field in divalent metal doped crystals 79−19833
- dipole pseudo-spin glasses, collective excitations 80−59617
- dipolons, graphical method for binding energy determ. 78−59805
- dislocation dynamics studied by nucl. spin relax. meas. 80−108091
- dislocation internal friction, orientation depend. 78−48439
- dislocation mechanism of electrification during cleavage 77−24353
- dislocation motion, nucl. spin relax. study *(Dutch)* 79−78556
- distortion of ionic cryst. by vacancies 77−89429
- divalent impurity diffusion, penetration plot deformation 80−24666
- doped, AC field induced impurity-vacancy dipole relax. 79−11385
- doped, F-centre accumulation efficiency temp. depend. 77−76394
- doped, thermal expansion at low temps., rel. to glasses 80−96672
- doped angle crystals, latent hardening 78−51607
- doped single crystals, plastic anisotropy 78−26575
- dynamics of nonrelaxed and self-trapped holes *(Russian)* 80−80607
- effective ionic charge and interionic separation, correl. 77−19896
- elastic constants, eval. of 3rd order and press. depend. of 2nd order elastic consts. of ionic crysts. 79−77668
- elastic constants, many-body effects and press. derivative 77−35621
- elastic constants, temp. depend., pseudopot. calc. 80−65120
- elastic consts., anomalous temp. depend., phonon-lattice interaction 80−107354
- elastic dielectrics, Gruneisen parameter, effective ionic charge volume derivative 80−84273
- elastic moduli determ. 78−91373
- elasto-optic coefficients, signs 78−64346
- electric-dipole ordering of tunnelling impurity centres 80−2215
- electrification by plastic deform., mechanism 78−26935
- electron beam excited, luminesc. and cond. of nonideal degenerate electron-hole plasma 78−10488
- electron elastic reflection and secondary emission, 1 to 30 eV obs. 78−11037
- electron emission, photo- and thermostimulated, ultrahigh vacuum conditions *(Russian)* 80−66383
- electron impact, elastic scatt., model, static and static exchange calcs. 78−94321
- electron irradiated, depth distrib. profiles of colour centres 79−27977
- electron momentum distrib. and Compton profiles 79−13631
- electron spin transfer in alkali chlorides and alkali bromides doped with divalent vanadium 78−87949
- electron sputtered atoms, energy distrib., time of flight method 78−48263
- electron sputtering process, mechanism 77−55857
- electron stimulated dissociation 80−34301
- electron trapping by alkali ion impurities 78−47809
- electron-ion emission due to ionisation of surface atoms 77−16474
- electron-phonon interactions, review 78−63991
- electronic dielectric const. strain derivative, photoelasticity 77−4620
- electronic strain polarisability constants 80−29677
- electronic structure calculation, CNDO semi-empirical methods *(Russian)* 80−10909
- emission band of F-centre 80−76071
- emission spectra of O_2^- and NO_2^- centres at high hydrostatic press. 78−10943
- ENDOR dynamics of F-centres, cross relax. effect 77−40151
- epitaxial growth, role of lattice fitting 78−34728
- equation of state Gruneisen formulation 78−30733
- equations of state under high press. 78−55935
- exchange charge polarisation, dielectric const., Dick and Overhauser model 78−55832
- exchange charge shell model analysis of strain derivatives of static polarisability, effective charge parameter 78−91296
- excited complexes, instrument for quenching studies 79−17511
- excitonic mechanism of defect form. 77−47737
- extended-ion approximation and pressure shifts in F-band energies 80−49223
- F_A(II)-centre emission process, molecular model 77−28616
- F_A-centre optical absorption, lattice statics theory 79−43004
- F^--centres, thermal and photolytic decay processes 78−95053
- F centre luminescence polarisation, stress induced, temp. dependence 79−56857
- F-centre, cluster-Bethe lattice treatment 78−63762
- F-centre, impurity pseudopotential screening 79−15121
- F-centre, laser, continuously tunable near IR *(German)* 80−1207
- F-centre, relaxed excited state, vibronic theory of Stark effects 77−85691
- F-centre, stabilisation process in first colouring stage 79−19246

alkali metal halides continued
- F-centre, vibronic scheme of relaxed excited state 79−90989
- F-centre absorption and ground state in halides with NaCl struct. 77−62524
- F-centre absorption energy calc. 79−78715
- F-centre accumulation, radiation induced, temp. depend. 80−59460
- F-centre coupling to lattice modes 79−77596
- F-centre decay, temp. effects, Arrhenius depend., rel. to NH_3 radiolysis 77−48662
- F-centre lasers, tunable IR emission 78−59030
- F-centre photoionisation, semicontinuum model 79−99509
- F-centre spin-lattice relax., theory and MCD meas., phonon-modulated HFS 77−43883
- F-centres, binding energies of positron to F and F′ colour centres 78−87667
- F-centres, cation vacancy model, rot. mechanism 77−76393
- F-centres, dynamic equilib. with F_2-centres at room temp. 79−51103
- F-centres, emission and relaxed excited state for NaCl structured halides 79−42060
- F-centres, EPR in relaxed excited state, detection via saturated optical pumping 78−6606
- F-centres, ESR in different states of relaxed configuration 80−108067
- F-centres, first order Raman scatt. *(French)* 78−2828
- F-centres, formation time 80−15477
- F-centres, influence of purity of crystals on stability of F-centres and interstitials 78−91336
- F-centres, optical pumping, spin-orbit and hyperfine coupling 77−16360
- F-centres, saddle-point configuration, molecular model parameter 80−107234
- F-centres, vibronic problem in higher excited states 78−10931
- F-colouring, role of impurities 80−64995
- far IR reststrahlen spectra, γ-induced changes 77−40244
- FCC, PO_4^{3-}-Al^{3+}(Sb^{3+}) anion-cation impurity mol. complex, IR absorpt. obs. *(Russian)* 77−16317
- FCC→SC pressure phase transition 80−44315
- film, low energy electron scatt. 78−26928
- fluorides, ^{19}F chem. shift, multiple pulse zero crossing NMR obs. 79−9230
- fluorides, dil. aq. solns., conductance at 25°C 77−69105
- fluorides, ESR study of interstitial atomic H centres 79−56609
- fluorides, thermoluminescent glow-peak shapes 77−28639
- fluorides mol. Compton profiles, parallel-perpendicular anisotropies 79−94038
- fracture, exciton mechanism of complex active centre formation 79−33033
- fracture, intense electron-beam pulse, initiated, Monte Carlo modelling 77−69038
- free energies of solid phase, Debye-Huckel theory 80−15263
- freezing point depression in binary liq. mixtures 77−43312
- Frenkel defect generation in cation sublattice, shock recomb. mechanism *(Russian)* 77−31656
- Frenkel defect pairs formation mechanism *(Russian)* 80−10542
- g-tensor analysis of S^- and Se^- centres, ESR 80−84650
- gamma irradiated, positron annihilation 79−23643
- geometries, force consts., charge distribs., FSGO model pot. calcs. 77−88379
- growth shape stability, dendrite and prominences appearance *(Hungarian)* 80−7489
- Gruneisen parameter, vol. depend. anal. 80−2135
- Gruneisen parameter and dielectric props. 77−31747
- halide dioxide radical form., H_2O_2 decomposition of halide-coated surface, EPR obs. 80−7851
- heat and entropy of evaporation, Trouton's rule generalisation 79−77735
- heat of formation for high-conc. substitutional defects, model 78−10048
- heat pipe apparatus for coloration of laser-quality alkali halide crystals 78−74917
- heterogeneous adsorption, photoelec. work function changes 77−69175
- heteronuclear XY^- defects, spin Hamiltonian parameters anal. 80−88509
- high field transients, three-level model 79−91055
- high pressure phase transformations, transformed fraction and reaction rate meas. 78−51667
- high-field transients, three-level model 77−59289
- high-pressure submillimetric-wave spectra 79−33694
- hole capture kinetics, influence of autolocalised and zone holes *(Russian)* 80−54714
- hole localisation at two halogenide ions, polaron theory *(Russian)* 77−69268
- hole self-localization and capture, temp. depend. 80−92526
- hologram, high-efficiency recording by selective colloidal centre destruction 80−63955
- implantation of ^{57}Fe, conversion electron Mossbauer spectroscopy technique 80−40012
- impurities, monovalent, and impurity pairs, lattice distortions 77−68984
- impurity, diatomic, molecular, rot. barrier height and librational modes 77−11491
- impurity aggregation kinetics for divalent impurity dipoles 78−79630
- impurity-vacancy complexes, association and orientation energies 78−51578
- impurity-vacancy dipole interaction with relaxed and nonrelaxed holes *(Russian)* 78−75661
- impurity-vacancy dipoles, activation energy 79−33013
- inhomogeneous transport at low temp. 77−43382
- interaction potential, Gruneisen parameter, compressibility 78−14304
- interatomic forces, Born model anal. on US data 78−55833
- interionic potentials, based on elastic consts. and equilib. eqns. 77−47374
- interionic potentials, completely cryst. independent specification of Born-Mayer potentials 78−55828
- interionic potentials, cryst. independent shell parameters and fitted Born-Mayer pots. 78−55827
- interionic repulsive force, and compressibility of ions 77−11500
- interionic repulsive short-range interaction pot., lattice energy calc. 80−96466
- interstitial motion during radiation damage and sputtering processes 80−54230
- intrinsic point defects, generalised Mott-Littleton approach 77−51698
- iodide, molten, struct. by X-ray diffr. 77−4033
- iodides, free exciton reson. luminesc. lines 77−77272
- iodides in acetone, press. effects on Walden products, ion-solvent interactions 80−3398
- ion hydration numbers in aq. solns., mol. dynamics calcs. 77−62464

alkali metal halides continued
ion irradiated, using 1 MeV He$^+$, Pooley excitation mechanism 80—2093
ion migration, barrier heights, shell model calcs. 77—35742
ion sizes and short range repulsive interactions 79—37652
ionic compressibilities and radii 80—24397
ionic conductivity plots, curvature as consequence of anharmonicity 77—76597
ionic crystal:transition metal, excitation and trapping at impurity sites 79—33776
ionic crystals, impulse compression temps. 80—100307
ionicity trends in diamagnetism and its temp. depend. 79—19717
IR absorpt. in molecules, clusters and microcrystals 78—80363
IR absorption spectrum, lattice vibrs., freq. and temp. depend. 79—65864
IR laser window material extrinsic absorption 79—14049
IR materials, high transparency, state of the art 77—27326
IR spectra, freq. and temp. depend. of charact. lattice vibrs. 79—65861
IR transparent materials and components 77—19374
irradiated, annealing 78—92494
irradiated, chemiluminesc. process during dissolution *(Russian)* 78—92133
irradiated, colloidal centre growth, model 77—19946
irradiated, first-stage F-centre prod. 80—107231
irradiated, formation of Z centre 80—103326
irradiated, recombination of radiation defects *(Russian)* 80—39151
irradiated at room temperature, stored energy 80—79839
irradiation stability obs. using X-ray emission meas. *(Russian)* 80—66326
irradiation-induced defects 80—107316
island metal films, effect of ionisation of condensing flux and transverse electric field on nucleation 80—107675
isomorphous salts in aq. solns., viscosity 78—95173
isothermal compressibility calc., 0-1000K 77—7784
Jahn-Teller induced B absorption band of Tl$^+$-type centres 77—12410
laser, CW single mode colour centre, freq. behaviour and linewidth 77—88728
laser damage morphology simulation 80—35015
laser induced breakdown, 10.6 μm, reproducibility 77—62023
laser induced breakdown of halide crysts., avalanche ionisation theory *(Russian)* 77—44095
laser induced damage *(Russian)* 79—43070
laser volume damage anisotropy 77—89469
laser-induced damage, CaF$_2$:Er^{3+} laser radiation at 2.76 μm 79—91539
laser-induced damage, role of avalanche multiplication and multiphoton absorption 80—48316
lasing action of F_2^+-centres, 0.9-2 μm 78—29957
lattice dynamic and static props., appl. to KCl 77—7798
lattice dynamics, long wavelength optical mode freq. and Anderson-Gruneisen parameter 80—65182
lattice dynamics calc., extended three body force shell model 78—47491
lattice dynamics using breathing shell model 80—88285
lattice energies, empirical calcs. 77—58967
lattice energy, binding, indeterminancy principle theory 78—59777
lattice energy, from modified Kapustinskii-Yatsimirskii eqn. 78—34461
lattice props. from interorbital-distance-related-repulsion approach 78—22809
lattice relaxation around tetragonal and rhombic defects 79—95110
lattice vibrations, effect of NO$_2^-$ impurity molecule, theory 77—35654
lifetime of carriers and excitons before self trapping 77—85236
linear dichroism spectra, stress-induced, reorientation of O$_2^-$ and NO$_2^-$ impurity ions *(Russian)* 80—45127
liquid, crit. consts., dense gas formulation 79—23700
local and reson. modes due to hydide ions, U-centres and additive cation impurities 79—77710
local vibration modes excitation by ions, moving dislocation steps *(Russian)* 77—31696
localised mode due to U-centre 77—20036
luminescence, colour centres and radiation-tunnel transition 79—4846
luminescence, high press. expts. on In-, Cu$^+$-, and Ag$^+$-doped specimens 79—43017
luminescence, ion-induced, effect of CN radical impurity 77—16402
luminescence, polarized type A, from Sn centres, model for excited states 78—10945
luminescence and stored light sum for fundamental absorpt. region excitation 78—6738
luminescence by ion impact, −160 to 200°C 77—8654
luminescence excited by vacuum UV lasers 78—10941
luminescence of Tl$^+$-like centres, Ga$^+$-centre polaris. effect 79—33806
luminescence polarisation and low-temp. photoinduced orientation change in O$_2$ and S$_2$ mol. centres 78—6735
luminescence quenching of F-centres 80—50417
luminescence spectra of aq. solns. with O^{2-} anion impurities *(Russian)* 77—69876
luminescence spectra of O$_2^-$, S$_2^-$ and NO$_2^-$ mol. ions, peculiarities of electron-phonon interaction 77—52174
lyoluminescence mechanism, gamma and additively coloured crysts. dissolving in pure water 80—100693
M-centre, lifetime data for excited state 78—35193
M-centres, computer-generated polarisation holography 78—46538
mass transport, contrib. of vacancy defects 79—46831
matter transport rel. to point defect parameters 80—107488
melt, estimation of struct. models by comparing vol. parameters 77—89368
melting, appl. of microscopic theory 78—79748
melting, dislocation theory, cooperative effects 78—59934
melting, mechanical instability 77—89524
melting, molecular dynamics study 80—15220
melting and boiling points vs. Coulomb pot., parabolic behaviour 80—70375
melting mechanism, vol. and enthalpy changes 79—55866
melting temperature, influence of press. 77—84896
melting temperatures, press. depend. 79—77726
microcryst. powders, colour centres, refl. spectra 78—23493
microhardness and atomic vibr. freq. relation 80—75297
migration enthalpy and entropy for cation vacancy motion 77—35750
migration enthapy of cation vacancy, correl. with MP 77—76606
mixed, impurity centre local vibrs., comp. depend. of spectral parameters 80—79898
mixed, U-centre localised modes 80—100319
mixed crystals, volume thermal coeff. of expansion, calc. 80—96671
mode Gruneisen parameters, ab initio calc. 77—20091

alkali metal halides continued
molecular centre symm. groups, roto-vibronic spectra *(Russian)* 80—88283
molecular clusters, equilib. geom., form. energy and vib. spectrum 78—55269
molecular dissociation energy, by photofragmentation spectroscopic method 79—76527
molecular ion cluster emission in SIMS, parity rule applics. *(French)* 80—63882
molecular orbital theory, relativistic, in Dirac Slater model *(Japanese)* 78—66480
molecular quadrupole coupling, vibr. and rot. effects, Morse oscill. calcs. 77—6805
molecule, electronic polarisability, ionic radii and repulsive pot. parameters, mol. consts. 80—87242
molecule, hyperpolarizability and dissociation energy 79—72439
molecule, improved interaction pot., spectroscopic consts. calc. 79—86024
molecule, interaction pot. 79—36720
molecule, zero point Compton profile anisotropies and bond polarities, correl. 80—78659
molecules, binding energy, relativistic effects 77—14370
molecules, force const. and vibr. amplitudes calc. using electron gas model 80—87245
molecules, interaction potential 78—58612
molecules, zero point Compton profile anisotropy rel. to nucl. charge 79—64054
molten, crit. consts. calc., dense gas formulation 80—44100
molten, eqn. of state in restricted primitive model 77—7644
molten, ionic radii and X-ray diffr. patterns 78—59732
molten, mode coupling theory of charge fluctuation spectrum 80—92451
molten, statistical mechanics 80—19683
molten, struct. determ. by X-ray scatt. 78—87609
molten, surface tension, compressibility, viscosity, self-diffusion, calcs. 77—7946
molten salt mixtures, enthalpy of mixing, theory, Monte Carlo calcs. 77—72691
molten salts, struct. by X-ray diffr. 77—4033
morphology of growth and evaporation surface 78—79544
mosaic structure determ., rapid X-ray method 79—37584
Mott-Littleton dielectric theory 78—80274
multiphonon absorption, quasiselection rules 77—24844
multiphonon recombination processes 79—38643
nonradiative Auger effect, oppositely charged defect centres, autoionisation-tunnel relax. of electron excitation 78—72112
nuclear spin-lattice relaxation, impurities effect 78—19362
octupole polarizability modifications of Clausius-Mossotti relation 80—49179
off-centre displacement of univalent impurity ions 79—23632
optic mode Gruneisen parameters 78—43088
optic mode Gruneisen parameters and strain derivatives, Born-Mayer and Sziegti model 78—55929
optical breakdown, 1.06 to 0.172 μm 78—35089
optical breakdown, damage threshold calcs. 79—95708
optical breakdown, multiphoton carrier generation theory 79—19953
optical breakdown, role of colloidal particles 80—50270
optical components, cryst. growth from melt 78—50955
optical components, finished, forging 77—46824
optical components, for high power lasers *(Rumanian)* 79—18462
optoelectronic properties 80—25330
Ostwald ripening and its application to precipitates and colloids in ionic crystals and glasses [Review] 78—80548
overlap repulsion, pot. energy function for Bohr-like atoms 77—15344
pelleting technique for solid sampling in IR spectroscopy 78—87171
phenomenological potentials 79—37654
phonon dispersion relations, using extensions of shell model 79—77702
phonon spectra moments 77—4163
phosphor:Eu^{2+}, explosive loading method form., spectra, luminesc. characts. *(Russian)* 78—35212
phosphor, Ag-doped, luminesc. rel. to formation of complex compounds *(Russian)* 80—11454
phosphors, Pb^{2+}(Sn^{2+}) doped, luminesc. props., press. effects to 140 kbar 77—40278
phosphors, Tl$^+$ depend, uniaxial stress effects 78—48202
phosphors, Tl doped, press. effect on emission spectra at low temps. 77—85771
photodichroic, as optical processing elements 78—83056
photodichroic crystals use for coherent opt. data processing 77—68248
photoelastic constants, effect of many body forces 78—47464
photoelastic consts., short range polarisability effect 80—80748
photoelastic effect anal. 77—12358
photoelasticity, exchange charge polarisation effect 77—81046
photoelectric yield spectra, 10 to 40 eV photon energy 79—28887
photoelectron spectra of ionic mols. using mol. beam technique 78—50576
photoemission, energies and lineshapes 80—89119
photoemission on mech. stimulation, mechanism *(German)* 77—85819
photon induced sputtering 80—35013
piezo-optical properties, temperature dependence 78—92050
piezooptical coeffs. temp. depend., macroscopic and microscopic parameter contrib. 77—4622
plastic deformation, effect of solid film coatings *(Russian)* 77—25167
plastic deformation, original stage, exposed to US waves, dislocation multiplication 78—47383
Poisson ratio and Gruneisen parameter, vol. depend. anal. 80—96614
polarisability analysis using Narayan-Ramaseshan repulsive pot. 77—76353
polarisation energy for core states 80—10903
polarity, nucl. charge depend., empirical formula 79—26870
polarization, photoinduced, rel. to exchange between vacancy and impurity 80—59914
polarization dichroism in the optical spectra of Jahn-Teller excitons 79—69435
polycrystalline, use as IR optical waveguide fibres 80—58750
polymorphic phase transition 77—80618
polymorphic transformations, sudden, theoretical considerations 78—51666
positron annihilation, Doppler broadening meas. 78—26806
positron annihilation, expt. techniques, positron states, book contrib. 80—2894
positron annihilation and capture at M- and R-centres *(Russian)* 77—85829

alkali metal halides continued
positron lifetime and Doppler broadening spectra in crysts. 79—8208
positron localisation at negatively charged centres 77—8055
pulsed laser induced damage at DF laser wavelengths 77—46751
radiation damage, mechanisms, review 80—107315
radiation damage products, impurities and colour centres, review *(German)* 78—10086
radiation hardening mechanism, dislocation-interstitial elastic interaction 79—23636
radiolysis, growth of colloidal metal inclusions 78—92493
rare earth ion doped, optical props., review 79—15492
refractive index calculation 80—88949
relative stabilities of NaCl, CsCl and cubic ZnS structures 80—19745
repulsive hardness parameters, crystal-independent 80—64947
repulsive softness parameter anal. 80—107102
resonance Raman scattering, electron-phonon interaction for F centres 78—68519
rocksalt-type, quadratic electrostrictive effects 77—24796
Schottky defect correl. of form. enthalpy and melting point 78—43015
screw dislocations in puncture rosettes, motion-starting-stresses, surface-active media effects *(Russian)* 78—10051
second-neighbour interaction potential 78—91298
secondary electron emission statistics, photomultiplier appl. 79—47564
secondary emission, under bombard. by multiply charged Ar^+-Ar^{5+} and Kr^+-Kr^{5+} ions 78—11046
selectively adsorbed atoms, band struct. 79—28399
self trapped exciton, optical detection of spin relax. processes 78—60358
self-trapped holes, ESR *(Japanese)* 79—73811
short range interactions, static polarisabilities 78—71702
single crystals, high purity, prod. purification characts. *(Hungarian)* 77—52229
slow muon flux spectra, model requiring const. negative muon Coulomb capture ratios 79—65133
softness parameter, additivity rule 80—1959
solid soln. hardening, dislocation motion and interaction with solute ions, stress effects 79—32994
solid soln. spectroscopy, investigs. by F. Klement *(Russian)* 80—8767
solid solns., lattice parameter and heat of form. 80—79739
solid solutions, Stokes losses for crystalline vibrs. in impurity O_2^- anions luminesc. spectra *(Ukrainian)* 79—43012
solubility press. coeffs. and solvent isotope effect 80—96649
solution, H_2O and D_2O, O isotope fractionation, and soln. struct. 78—22629
solution phonon wings in luminescence spectra *(Ukrainian)* 79—52001
solutions, aq., interionic forces and thermodynamics *(German)* 79—52688
solutions, homogeneous nucleation glass form., press. depend. 78—51649
solutions, in methanol, halide ion solvation, IR obs. 79—22703
solutions, ionic hydration, review 78—92501
solutions, tetrahedral hydration of ions, Raman obs. 78—55804
solutions, US determ. of hydration numbers 78—20027
solutions in DMSO, modelling of interactions 79—77469
specific heat anomaly, Ising model, Monte Carlo calcs. 78—47989
spectral characteristics of Ga^+, In^+ or Tl^+ impurities, cryst. field effect 77—24880
spin lattice relax. and g-shift 80—15799
sputtering, thermal effects, review 80—35033
sputtering and cluster formation, mass spectra and SIMS 79—19959
sputtering of molecules, low-energy electron bombardment 80—35026
stability and melting 78—71839
static dielectric behaviour, vol. depend., many-body interactions effects 78—2786
static polarisability, vol. depend. 78—52428
strain defects, low temperature props., heuristic model 79—82245
strain polarisability parameter, evaluation 77—35617
structures in compressible ions theory 80—33971
substrate, epitaxial crystn. of isotactic polypropylene 78—26787
substrate, epitaxy of polycyclic aromatic quinone, effect of adsorbed water 79—28239
substrate, gas adsorption, stress depend. of chem. pot. 78—91541
substrates, calc. binding of deposited Au atoms 79—33208
substrates, for epitaxial crystallisation of S_2N_2, $(SN)_x$ 77—24496
substrates for condensation of Au, film struct., stability and growth *(French)* 78—38989
supersonic seeded molecular beam, vibr. relax. 78—17761
surface, (100), NaCl struct., differential ionic relax., shell model 77—69151
surface, atomic interaction pot. on (100) face *(German)* 80—15380
surface, Au clusters, size depend. of valence bands, XPS study 80—65647
surface, diffr. intensities in He scatt., topographic curves 78—15274
surface (100), adsorbed monomers and dimers, pot. surfaces, diffusion dissoc. 77—66769
surface (100), potential energy of isolated Au atom above surface 77—89650
surface energies, surface tensions and surface struct. 79—60610
surface impurity distribution, Fick's 2nd law calc. 77—47673
surface light emission, 10.6 μm laser pulse irradiation *(Russian)* 78—27352
surface migration of small crystallites, Monte Carlo calc. with continuous time 78—26783
surface step structure 77—31853
surfaces, adsorbate binding energies and struct. at surface defects 77—59206
surfaces, adsorbate motions and reactions at surface defects, mol. beams 77—59205
surfaces, step struct. 78—79866
surfaces, step structures 78—79865
Suzuki phase, continuum model for periodic incorporation of aliovalent impurities 79—33012
Szigeti effective charge, temp. depend. 78—38653
Szigeti effective charge parameter, strain derivative, lattice dynamics and dielectricity 79—7571
thermal expansion, rapid increase near melting point 77—51521
thermally stimulated depolarisation of NCO^- centres 80—80678
thermo-optical props., 120-580K *(Russian)* 79—91414
thermoluminescence and X-ray induced luminescence 79—28830
thermoreflectivity spectrum, 5 to 9 eV, band struct. and spin-orbit splitting of Γ-exciton 77—81123
thin films, crystal-vacuum (110) interfaces, mol. dynamics computer simulation 80—34289

alkali metal halides continued
thin films, high-field electron injection, ionic cond., photocond. 80—75665
thin films, photoacoustic determ. of optical absorptance of highly transparent solids 79—40632
third order elastic constants, NaCl struct. 77—35620
three body interaction effects on cohesive props. 78—83770
three-body interactions, effect on electronic polarisabilities and photoelastic behaviour 79—47382
transition metal halide-alkali halide binary melt, spectra by cryst. field theory 79—4820
transparent, with inclusions, laser-induced stresses 79—28012
transport phenomena, appl. to solid state devices 78—55976
transverse optic mode Gruneisen parameter 80—39244
transverse-optic modes and anharmonic self-energies, temp. and press. depend. 77—11649
triboluminescence spectra 80—66312
trimer formation due to dimer-dipole aggregation 77—62561
two-photon absorpt. 80—50292
two-photon absorpt. coeffs., 355 and 266 nm 78—83037
U_2 centres, cluster-Bethe lattice calc. for electronic density of states 79—4531
U-centre, electronic struct., self-consistent model 79—65406
U-centre electronic struct., cluster-Bethe-lattice calc. 80—107737
U-centre pairs, localised modes 77—7813
UV high-power laser material, refractive props. and optical constants 80—106555
UV laser window material absorption obs. 79—14012
UV photodissoc., metal-atom resonance-line lasers 80—58529
UV photoelectron spectra at high temp., interpretation 78—17718
UV transparent materials, 355 and 266 nm absolute two-photon absorption coeff. obs. 79—18493
V_c^--centres, vacancy induced splitting of excited states, Sn^{2+} structure 78—51931
V_K and $(XY)^-$ centres, hyperfine struct. using valence band wave functions 77—11873
V_k-centre, electrostatic energy 79—27978
V_k-centres, thermal motion theory *(Russian)* 77—47451
V_k-centres, vibr. modes, calc. 80—84269
vacancy comaplex formation and binding energies in zeroth approx. 80—24441
vacancy energy of movement, zeroth order calc. 77—89571
vacancy entropy of formation due to anharmonic effects 77—62521
vacuum UV absorption spectra, exciton splitting rel. to exchange interaction 78—23494
van der Waals dipole-quadrupole interactions, estimation 77—80441
van der Waals interaction energy eval. 78—71705
van der Waals pots. determ. 78—83767
vibration modes due to single ion impurities 79—51225
vibrational amplitudes of atoms near melting points, Lindemann's melting law 77—89522
vibrational modes due to three impurity cluster 78—75773
vibronic spectra of O_2^- and NO_2^- ions in alkali halides, press. effects 78—52532
whisker crystal, X-irrad., elec. breakdown, temp. and F-centre conc. depend. *(Russian)* 77—8504
X-ray induced colour centre and halogen aggregate form. 80—96565
X-ray induced strain effects rel. to time of irrad. 78—6120
XPS, trapped electrons at F-centres and anion defects, photoionis. cross sections 77—90249
Z_1-centres, peculiarities of thermolum. 80—103999
B+CsF(RbF)(KF)(NaF), gas phase chemiluminescence reaction 77—29013
CN^- doped, internal modes reson. hybridization 79—42194
$CdCl_2$-NaCl, KCl molten salt mixtures, US velocity and adiabatic compressibility obs. 78—75730
Cu^+-doped, absorpt., emission and lifetime data, temp. depend. 77—4671
Eu^{2+} cation vacancy complexes, binding energies 80—96513
Eu^{2+}-doped, spin-Hamiltonian parameters, superposition model calcs. 80—96830
F_2^-, mag. reson. absorpt. spectrum 77—73079
K halide solids, lattice dynamics, three body force shell model studies 79—55841
KCl far IR complex permittivity meas. by dispersive Fourier transform spectroscopy, 7 to 300K 80—15940
KI:NO_2^-, first-order Raman scatt. meas. 77—52085
Mn^{2+} doped, powder EPR *(Spanish)* 77—48036
$MnCl_2$-alkali metal chloride melts, Raman spectra of $MnCl_4^{2-}$ ion 79—24310
NH_2^- dipole centre paraelectric alignment, UV electroabsorpt. and Kerr effect 77—12413
NH_4^+ ions in alkali halide lattice, inelastic neutron scatt. 78—14407
NH_4^+ lattice impurity, hindered rot. energy levels calc. 80—10514
NaCl-type crystals, ionic polarisabilities, pseudopot. calc. 80—88913
NaCl-type structure, MgO epitaxy, RHEED meas. 78—67920
O_2^- impurity luminescence in alkali halide frozen solns. 79—87488
$PbCl_2$-MCl, (M=Li, Na, K, RB, Cs), molten systems, thermoelec. power 77—62658
RbCl:NO_2^-, first-order Raman scatt. meas. 77—52085
ReO_4^- doped, saturable absorber at 10.6 μm 80—53384
S_2^--doped, laser-excited spectra and reorientation of S_2^- 77—28563
Tl^+ doped, magneto-optical rot. dispersion anomaly near absorpt. bands 77—63400
UI_6-alkali metal halide system, prep. 80—50568
VO^{2+}-doped, elec. cond. and IR absorpt. obs. 77—8607

alkali metals
see also caesium; francium; lithium; potassium; rubidium; sodium
adsorption, on free-electron like and transition metals, valence electronic struct., wave-function matching calcs. 78—72235
adsorption, on metal surface, finite barrier model, bounded electron gas static semiclassical response 78—72221
adsorption on Ni, depend. of electron state of adatom on conc. 78—72001
alkali atom+alkyl oxide cross-sections, hard-sphere model 78—7176
alkali atom+inert gas atom, $^2P_{1/2}$ state depolaris., mag. field effect 78—33590
alkali atom+methane derivative, collisional ionisation, nitromethane, perfluoromethyl bromide (iodide) electron affinities 78—66639
(alkali atom)$^+$+(halogen atom)$^-$, recombination 78—7192
alkali ion+alkali atom, differential scatt. meas. 78—62903

alkali metals continued
- alkali metal:H(0), impurity investigation using residual resist. and optical absorpt. meas. 79−95816
- alkali metal:halogen, charge transfer excitations 79−95815
- alkali metal:inert gas, optical absorpt. by impurity, cluster Bethe lattice calc. 77−8612
- alkali metal, model potential calculation of binding energy and compressibility 78−91632
- alkali metal+Hg, scatt. cross-sections, pseudopot. calcs. 78−9225
- alkali metal atom+inert gas atom, hyperfine transition spectral line shift, quantum corrections 78−82655
- alkali metal-ammonia solns., spin site exchange mechanism for electron relax. times 78−27077
- alkali metal-H, liq. and solid, mol. orbital approach, solvation energies 77−4201
- alkali metal-molten salt mixtures, thermal EMF calcs., Rice and Pitzer models 78−20057
- alkali metal-NH_3 solution, Hall effect and cond. at metal-nonmetal transition 78−2530
- alkali trimers, LEPS pot. energy surfaces, equilib. geometries, vibr. force consts. 79−22624
- alkali-inert gas system, mol. band profiles of induced dipole transitions 78−42135
- alkali-rare gas atom systems, electronic collisionally induced transition dipole moments 79−98195
- ammonia-metal solutions containing cryptands, metal anion and trapped electrons form. by evap. 79−100340
- anions, formation 78−5159
- anions, photodetachment cross-sections and multipole polarisabilities, extended asymptotic model 78−42028
- anomalous positive thermopower 79−65449
- arc discharge, high current, anode near-electrode layer, spot formation and sheath breakdown 80−38835
- Ashcroft pseudopotential, unified study of props. 80−39239
- atom, autoionising levels excitation by electron impact 77−19085
- atom, Bloch theory appl. to optical pumping and mag. reson. 79−59403
- atom, dynamic polarisability, dispersion forces, at. levels light shifts, model pot. 77−31017
- atom, dynamic polarisability, variational calcs. with mode pot. *(Russian)* 78−902
- atom, dynamic polarisability dispersion eqn., dispersion interaction of atoms 79−26902
- atom, effective ionisation cross section determ. for H, Li, Na, Cu, Ag, Au and Fr, classical theory *(Russian)* 77−30998
- atom, electron impact excitation of autoionis. states 79−54971
- atom, excited hyperfine and Stark parameters, meas. and calc. 78−86814
- atom, excited states, radial matrix elements and radiative lifetimes 79−59375
- atom, excited states energy levels ordering 77−67968
- atom, fine-struct. of excited nd and nf states, at. core effect 78−58606
- atom, flame emission apparatus for teaching 77−29976
- atom, ground state coherence, transversal relaxation rates, Zeeman shifts 77−6888
- atom, heavy, polarised, circ. dichroism of ang. distrib. of photoelectrons 80−37789
- atom, high ang. momentum Rydberg states, quantum defect core polaris. depend. 77−18808
- atom, hyperfine shift and interatomic pots. in inert buffer gas 80−5491
- atom, hyperfine struct., review of exptl. methods 77−31019
- atom, in inert-gas solid, at level struct. calc. pseudopot. method 80−9532
- atom, laser three-photon absorpt., ionisation cross-sections *(French)* 78−5182
- atom, modulated optical absorption transients weights 77−6887
- atom, near-resonant two-photon ionis., non-Coulomb phase shifts of photoelectron partial waves 80−106302
- atom, outer-shell photoelectron ang. distrib. 80−37797
- atom, perturbed by rare gases, dipole moments of S-P transitions 80−27979
- atom, photoabsorption by scaled Thomas-Fermi method 77−46549
- atom, polarisability calc. using Laplace method *(Russian)* 79−89803
- atom, polarised, spin-deposited photoelectrons from two-photon ionisation 79−63971
- atom, positron and electron low energy scatt., JWKB approx. 77−14579
- atom, positron elastic scatt. cross-sections, vel. distrib. functions 78−42218
- atom, quantum beats in photoionis. by fine struct. levels coherent superposition 79−6922
- atom, quasiadiabatic polarisation pot. for elastic electron-atom scatt. 77−6929
- atom, radioisotopes, hyperfine spectroscopy, nucl. props. 80−57677
- atom, Rydberg state Stark struct. 80−37754
- atom, S-state, +H(inert gas), long-range interaction theory 77−50490
- atom, screened potential model, for at. energy levels and oscill. strengths 79−36516
- atom, spin polarisation of photoelectrons, one-quantum photoeffect 80−37790
- atom, Stark and photoabsorption spectrum, density of oscillator strengths, atom c.f. semiconductor spectra 80−83318
- atom, Stark effect for hyperfine structure sublevels and splitting of $n^2S_{1/2}$ states *(Russian)* 79−3401
- atom, Sternheimer shielding functions calcs. 79−76352
- atom, transition oscillator strengths in discontinuous and continuous spectra, review 80−52937
- atom, two-photon ionis. using elliptically polarised light 79−98052
- atom, two-photon ionis. via reson. intermediate state 78−42023
- atom, two-photon ionis. with two light beams, photoelectron polaris. 80−43011
- atom, two-photon ionisation, polarisation effects 78−1039
- atom, two-photon ionisation with two light beams, polarisation effects 79−81190
- atom, two-photon S-S transitions, press. broadening and shift by rare gases 79−6916
- atom, two-photon transitions to Rydberg levels, dye laser reference wavelengths 78−94221
- atom, valence electron ground states, nonlocal Hellmann model potentials 78−50476
- atom+atom, laser-induced ionis. collisions 78−5333
- atom+atom nonresonant collisions (with rare gas), intramultiplet relax. 77−6902
- atom+H^{+}, charge exchange, eikonal approx. 80−32830

alkali metals continued
- atom+H^{+}, valence and core electron capture cross-section 79−94081
- atom+$H^{+}(C^{+})(O^{+})(S^{+})$, charge exchange, negative ion formation 79−50128
- atom+H, interaction potentials 80−63736
- atom+H(inert gas), long-range interaction, S-state alkali atom 79−76480
- atom+halogen mol., ion pair form., trajectory model 77−16800
- atom+halogen molecule, electron contact, model system *(Dutch)* 79−50111
- atom+He(2^3S), Penning ionisation by slow collisions 77−50512
- atom+HX, (X=F,Cl,Br,I), reaction, semiempirical pot. surfaces calcs. 79−74362
- atom+inert gas, adiabatic pots. 79−81254
- atom+inert gas, collisional broadening and shifts, semiempirical pots. calcs. 77−10727
- atom+inert gas, collisional shifts and broadening of Voigt contour 80−27983
- atom+inert gas, line profiles, width, shift and asymmetry, square well pot. approx. 80−52936
- atom+inert gas, three-body interaction, secondary satellites of alkali line 77−83683
- atom+ion coupling energy, internuclear separation depend. 77−14523
- atom+Mg^{+}, effective charge exchange cross section, 20 to 1000 eV 77−42398
- atom+N_2, thermal ionis. rate coeff. 77−30982
- atom+N_2 collision, temp. depend. of vibr. relax. time 77−34725
- atom(dimer)+MF_6, (M=Mo,W,U), ionis. reactions, electron affinities 77−81398
- atom (highly excited)+atom (ground state), collisional quenching cross sections 80−43146
- atom (ion)+inert gas, collision studies of quasi-one-electron systems 80−63750
- atom dimer polarisation transfer, atom-molecule-exchange reaction 78−13574
- atom in solid matrix, bistable state, optical trapping between levels 79−81187
- atomic and molecular collisions in intense light beams, quantum aspects *(Russian)* 79−6903
- atomic beam source, three-stage oven design 77−42443
- atomic collisions, dimer intramultiplet mixing 80−1059
- atomic collisions, photon absorpt. cross-section and quasimol. transitions *(Russian)* 77−75285
- atomic electron scatt., polarised orbitals method modification 79−22835
- atomic multiphoton inoisation probability, Green's function model pot. 78−25498
- atomic multipole polarisability, extended Coulomb approx. 78−33451
- atomic properties, pseudopotential calc. depend. *(Russian)* 78−38997
- atomic resonance levels relax., hyperfine struct. effect 77−38725
- atomic two-photon ionis. by unpolarised light, depolaris. effects 79−59409
- atomic vapour, optically pumped, longit. relax. in hyperfine states 77−57908
- atoms, charge exchange, exciplex or excimer form. in plasma 80−75026
- atoms, electron impact excitation, integrated cross-section calc. 78−62921
- atoms, excitation transfer in slow collisions between identical particles *(Russian)* 78−78799
- atoms, excited state, laser photoionisation theory, hyperfine coupling effect 80−102493
- atoms, ground state correl., photoelectron spectra, multiconfig. Hartree-Fock calcs. 77−50471
- atoms, highly excited Rydberg states, fine struct. 80−58402
- atoms, mag. reson. spectrum, rapid spin exchange effects 78−25460
- atoms, oscillator strengths, nonlocal Simons pot. anal. 80−32795
- atoms, outer p shells multiplet and satellite struct., photoelectron spectra 80−87039
- atoms, resonance interaction, resonance lines self-broadening, adiabatic pot. curves 77−83676
- atoms, Rydberg state emission oscill. strength minima 80−32662
- atoms, Rydberg states, Stark ionisation 80−52933
- atoms, spin-polarised, near-reson. two-photon ionis., light polarisation effects 80−106308
- atoms, static polarisability, lower bounds, oscill. strength calcs. 77−75074
- atoms, Van der Waals energies calcs., variation-perturbation method 77−510
- atoms, van der Waals energy of interaction with aggregated Au film 77−11829
- atoms, vapour states, laser spectroscopy and applic., review 80−68260
- atoms, Zeeman coherences relaxation in ground state by spin-exchange and sudden collisions 77−50402
- atoms+H^{+}, charge exchange, eikonal approx. calcs. 80−78703
- atoms+molecules reactions, electronically excited atoms and alkali metal atoms analogy 80−76490
- atoms and anions, electron affinity, model pot. CI and SCF calcs. 77−38609
- BCC, lattice dynamics, modified Bhatia model 77−51455
- binding energy, non-parametric calc. *(Russian)* 77−27844
- binding energy calc. *(Chinese)* 80−911
- borate glass, Li^{+} motion, ^{7}Li NMR spectra, nucl. relax. 80−34804
- bulk modulus and eqns. of state under press. 80−88293
- bulk properties, computer simulation 78−30729
- cation pairs, lumiensc. with dichromate anion 80−83409
- Cauchy relations, violation for elastic moduli 79−69179
- chemisorbed layers, changes in work function due to charge transfer 78−18900
- chemisorbed on metal substrates, electronic struct. 79−87139
- chemisorption on metallic surface, using density functional formalism 77−7975
- chemisorption on Re surface, bond, valence energy level broadening *(French)* 79−33176
- classical one-component plasma, melting parameter 78−47092
- clusters in gas phase, high press. mass spectrometry, atmospherical implications 80−58436
- cohesive energy, calc. based on interatomic approach 80−43209
- cohesive energy, dielectric function calcs. 78−2060
- cohesive energy, teaching 80−90630
- colliding atoms, optical excitation to state of quasibound motion *(Russian)* 78−58784
- colloidal plasma theory, electron droplet collision temp. 77−3914

alkali metals continued
- compressibility, contrib. of John Bardeen 80—57057
- compressibility and binding energy, Shaw's optimised model pot. 78—26620
- condensed phase, free energy, Debye-Huckel theory calcs. 80—79958
- contact term, use of local spin density functional method 80—58158
- crystalline and alkaline, eqns. of state, zero compression isotherms *(Russian)* 80—103446
- dendritic phase precip. in alkali halide, CESR 77—24744
- dense plasma ionisation and cohesion, critical density and press., approx. formulas 80—59253
- dense vapour, anomalously large elec. cond., positive complex ions form. 80—19547
- density of states effective masses, liq. and solid phases, model pseudopot. calc. 77—76738
- dialkalis, VB calcs., equilib. internuclear separation, dissoc. energies 77—71756
- diatomic isovalent sequence, free-mol. electronic transition intensity consts., systematics 78—42137
- diatomic molecular ions, core-core interaction pots. 79—18251
- diatomic molecule, ground state, opt. prod. and orientation, review *(Russian)* 79—27046
- diatomic system, three states nonadiabatic coupling calcs. 77—57896
- diatoms, pot. curves, selected valence electron SCF MO calc. 79—10053
- diffusion in $LiNbO_3$ single crysts. 77—84989
- dimer+halogen mol. (IBr)(ICl) thermal chemi-ionisation reactions, products, energies 77—63903
- dimer-He anisotropic interaction pot., influence on transport cross sections 80—9677
- dimers, ${}^1\Sigma_g{}^+$ ground state, density functional theory 78—37573
- dimers, photodecomp. 79—27049
- double frequency microwave reson. in hyperfine struct. of ground state *(Russian)* 77—51993
- effective ion-ion potential, compressibility and force consts. 80—70158
- elastic and thermal props. by pseudopotential method 80—19899
- elastic constants, temp. depend. 78—51603
- elastic moduli, chem. trends, pseudopot. method 80—107355
- elastic moduli, third order, calc. *(Russian)* 77—51427
- elasticity moduli, third order, temp. depend. *(Russian)* 78—63798
- electrical and thermal cond. in weak mag. fields 80—65535
- electrical resistivity, phonon-limited, low temp., validity of empirical expressions 79—23945
- electrical resistivity, temp. depend. 78—64022
- electron relaxation time energy depend., electron-phonon resist. 79—60805
- electron-electron scattering in terms of dielectric and vertex functions 79—95351
- electron-phonon drag effects in elec. cond. and thermoelec. power 77—15824
- electronic magnetic susceptibilities calc. 78—52204
- equation of state, partial press. contrib. 80—107401
- equation of state and vol. depend. of thermodynamic props., pseudopot. theory 78—18738
- equations of state and density meas. installation 77—43307
- Fermi surface topological changes due to uniaxial stresses 80—92810
- film, granular, multipole oscillations in small hemispherical particles 79—78774
- film, inert gas impurities, optical excitation spectra obs. 77—24876
- film, inert gas impurities, optical spectra, rel. to inert gas solids 77—24878
- film, inert gas impurities, sharp pair spectra and excited states 77—24877
- film, inert gas impurities, X-ray edge and recoil problems in optical excitation spectra 77—24879
- flash lamp, absolute spectral distrib. and radiant output 78—66510
- ground state alkali molecules, mag. shielding and spin-rot. interaction 80—87186
- Gruneisen parameter, temp. variation 80—107396
- Gruneisen parameter and temp. depend. of elastic consts. 80—39317
- Gruneisen parameters, calc. using non-central force model 77—1242
- Gruneisen parameters, influence of press. on lattice anharmonicity and temp. depend. 80—79905
- heat of desorption from refractory material surfaces 80—75430
- high pressure effect on supercond. and high temp. resist. 77—47917
- HMPA:alkali metal, density of states in band gap, EPR and optical correlations 79—61201
- homologous ions series, Stark broadening trends 80—105157
- homonuclear dimers, quasi-static wing profiles of self-broadening reson. lines 80—48042
- hyperfine interactions of excited states, Brueckner and natural orbitals 77—3283
- impurity in hydrocarbon fuels combustion prod. plasma, elec. cond. 79—55466
- inert gas-alkali metal, inhomogeneous mixture, nonequilib. processes under conditions of T-layer form. 78—91079
- interatomic potential, pseudopotential method 79—68294
- intercalates with graphite, basal plane elec. resist. 80—44685
- intercalation compounds, ionicity, struct., size, intercalation amount, ion mobility anal. 80—39041
- intercalation compounds with graphite, interlayer screening and mag. susceptibility 80—44794
- intercalation with graphite and Hg 80—44183
- internal energy, heat of mixing, entropy, dielectric function 80—88340
- ion, thermionic emission from zeolites 79—4887
- ion, with filled shell, dipole polarisability 80—9501
- ion+atom, charge exchange cross sections 79—26871
- ion+atom, differential scatt. cross sections 77—28999
- ion+atom collision, symmetric charge exchange, below 1 keV, cross sections calcs. 77—532
- ion+inert gas, interaction pots., gaseous ion mobilities 77—54584
- ions, electron impact ionisation, binary encounter model 80—23557
- ions, in aq. solns., limiting equiv. cond. rel. to water viscosity 77—1252
- ions, interdiffusion with H^+ ions in glass surface, extended Boksay-Doremus theory 80—34254
- ions, pair formation with oixphenol radicals *(Russian)* 79—39138
- isoelectronic series, transition probabilities, oscill. strengths, lifetimes, branching ratios 78—33470
- lasers, reson. line, based on alkali halide photodissoc. 79—72560
- lattice anharmonicity 79—19341
- lattice dynamics, a priori pseudopot. calc., comparison of statistical and Lindgren cond.-core exchange approxs. 77—72662

alkali metals continued
- lattice dynamics, dispersion curves using second-order perturbation theory 80—79893
- lattice excitation dispersion relations 80—100314
- lattice sp. ht. and thermal vibrs. 78—30768
- lattice vibrations, homology 80—44267
- lattice vibrations and Gruneisen parameter 78—59917
- law of corresponding states, pseudopotential theory 77—59095
- law of corresponding states 77—15535
- liquid, calc. of enthalpy of soln. of nonmetals and elec. resist. 77—55225
- liquid, collective excitations and short-range order 78—63665
- liquid, effective interionic interaction, many particle effects *(Russian)* 77—39530
- liquid, elec. resist., exchange and correlation effects 77—1403
- liquid, electrical resistivity and thermoelec. power, Harrison's method 79—78066
- liquid, Fermi energy, density of states, electronic props., exchange and correl. effects 80—96774
- liquid, internal energy, chem. pot., critical consts. 78—34422
- liquid, law of corresponding states, microscopic basis 77—47539
- liquid, mag. susceptibility rel. to theories of electronic struct. 77—1536
- liquid, nonlocal harmonic model potential, appl. to elec. props. 80—6802
- liquid, O_2 pot. and O_2 distrib. coeffs. between alkali and struct. metals 80—65231
- liquid, reactions with refractory metals and oxides, relevance to reactor technology 80—85173
- liquid, resist. and struct. factor, temp. depend. 77—62466
- liquid, salt solns., phase equilib., and chem. 78—73040
- liquid, self-diffusion coeffs. calcs. 78—2274
- liquid, soln., chemistry as elucidated from elec. resist. studies 77—52636
- liquid, solubility and solns. of nonmetals 77—51505
- liquid, thermoelectric power, optimised model pot. calcs. 80—29391
- liquid alkali metal-solid metal interfaces, chemistry and physics 77—51576
- liquid metals, US absorption due to electrons and phonons 79—28046
- liquid structure, from 1st-principles pseudopot. calc. 79—41941
- local Heine-Abarenkov-type model pot. 79—87031
- low temp. plasma ionisation by fast electron beam, effective cross section calc. 79—14572
- $M+XF_6$, X=S,Se,Te,Mo,W,Re,Ir,Pt, collisional ionisation 78—55226
- magnetic property volume depend., Knight shifts, electron spin response 80—88729
- Matthiesen rule deviations rel. to CDW 80—29385
- metals, cohesive properties, energy density functional-pseudopotential method 79—73462
- metastable magnetic crystal, aligned electronic spins, mag. props. 77—77035
- methyl iodide+alkali metal reaction cross section energy depend. 77—28991
- migration and accumulation in Si-SiO_2, interface struct. 80—107574
- migration in SiO_2 film of alkali ions, elec. meas. 80—39359
- model pseudopot., energy-independ. for second-order elastic consts. and phonon spectra 77—62890
- molecules, laser radiation absorpt., at. excitation processes 80—32785
- muon Knight shift 79—56656
- negative ions, autodetaching sub ${}^2P_{1/2}$ threshold states 79—22611
- neutron activation analysis at 14 MeV for determ. of O_2 conc. 78—11602
- optical spectra, agreement with theory *(French)* 78—72558
- optimized model potential, thermoelec. power in liq., phonon freqs. 78—2467
- paramagnetic gas in radiation field, magnetisation 78—78667
- phonon dispersion, axially symmetric model 80—34152
- phonon dispersion, binding energy, compressibility, elastic consts., electron screening and Ashcroft pot. calcs. 80—65174
- phonon dispersion, phenomenological model 79—60445
- phonon dispersion and electron gas pressure, theory 78—2208
- phonon dispersion curve crossing in $(\zeta 00)$ direction 78—38795
- phonon frequencies, depend. on atomic mass 79—14901
- phonon spectra, rel. to ion-ion pot. 77—80591
- phonon-limited electrical resistivity 78—6346
- phonon-phonon scattering relax. times, rel. to elec. resist. 77—39813
- phosphate glass, Li^+ motion, ${}^7Li$ NMR spectra, nucl. relax. 80—34804
- plasma, in hollow cathode arc, low-press. current limiting 80—6304
- plasma resonance, line shape 77—39765
- plasmon line width variation due to interband transitions 78—47822
- positive ion Rydberg states, pseudopotentials, local exchange approx. calcs. 77—14337
- positive muon spin rotation frequency, Knight shift meas. 79—38421
- pressure influence on absolute zero isotherms, polymorphic transform., phonon spectra *(Russian)* 80—49363
- pseudopotential calcs. of binding energy, compressibility and resistivity 79—65025
- quasimolecule, exchange interactions of atoms with valence s electrons 77—83677
- rare-gas impurity in metal host, absorpt. edge, extra-orbital relax. model 79—4825
- RKKY oscillations in surface spin density 77—20512
- scattering at high-energies intermol. potential determ. 77—46609
- secondary cells, nonaqueous electrochem. behaviour of alkali and alkaline earth metals 80—35665
- seeded plasma, calc. of thermal nonequilib. near-electrode region 77—55186
- silicate glass, Li^+ motion, ${}^7Li$ NMR spectra, nucl. relax. 80—34804
- solid, atomic properties, pseudopot. calcs. 77—89512
- solutions, cation-electron interactions 78—73037
- sorption on W (110), trapping probabilities and desorption kinetics 77—62754
- Stark profiles, of reson. lines, model microfield method appl. 79—26931
- submonolayer on metal substrate, geom. struct. rel. to electronic props. 77—85080
- supercritical, density of states, effect of nonorthogonality 77—59243
- surface props., Rayleigh-Ritz variational calcs. 79—69570
- susceptibility, paramag. and electronic 78—52205
- thermal accommodation on W 80—24729
- thermal expansion, elastic constants, phonon freq. anisotropy *(Russian)* 79—1516
- thermal expansion and Gruneisen parameters 78—38857
- thermal plasma data on collisional transition probabilities from 1000 to 8000K 77—72406

alkali metals continued
thermal properties and Gruneisen parameters, employing model pot. 78−71815
thermal resist. and Lorenz number due to conduction electron-phonon scatt. 80−29377
thermodynamics, anharmonic effects *(Russian)* 78−43145
thermopower and elec. cond., relationship at low temps. *(Russian)* 80−92882
trace diffusion of nuclear reaction products in polycryst. Ta 78−22896
trapped positron, effect of vacancy migration on annihilation 77−48271
trimers, London pot. energy surfaces 79−6893
trimers, semiempirical pot. energy surfaces calcs. 78−25649
trimers, spin population, config. determ. 80−42937
vacancy formation energy calcs., electron density functional method 80−19801
vapour, excited by electron impact, ejected-electron spectra from autoionising levels 80−37893
vapour, fifth harmonic generation by laser beam 78−33774
vapour, induced optical anisotropy in laser radiation field *(Russian)* 80−38525
vapour, IR image upconversion using two-photon resonant optical four-wave mixing 80−58632
vapour, nonresonant excitation of fluoresc. *(Russian)* 77−10633
vapour, optical breakdown threshold, bremsstrahlung theory *(Russian)* 77−79694
vapour, population inversion possibility in I using alkali metals 79−94221
vapour, reson. radiation, diffuse and selective reflection 77−50611
vapour, seventh and ninth order nonlinear susceptibility meas. 79−55186
vapour, two-photon reson. four-wave mixing process, phase matching 77−14772
vapour arc discharge, source for pumping YAG:Nd^{3+} laser 80−78924
vapour condensation from gas flow (He,Ar,N_2), heat and mass transfer 78−75192
vapour discharge, low-press., energy balance eqns. 80−87969
vapour O-O transition resonance line obs. *(Russian)* 78−57999
vapour systems, nonreson. third harmonic generation of I laser radiation 79−3746
wire, low temp. elec. resist., size and temp. depend. 77−76958
X-ray fluorescence, near absorpt. threshold *(Russian)* 77−4704
CaF_2:alkali metal cation, thermal depolarisation study 80−108147
CaF_2:Li(Na)(K)(Rb), dielec. relax., activation energy, rel. to vacancy pair reorientation 80−88917
$D+M \rightarrow D^- + M^+$ (M=alkali metal atom), ion-pair form. 78−58779
GaAs, surface segregation of implanted alkali metals, photoemitter prep. and characts. *(French)* 78−60544
H-alkali metal vapour plasma, charge exchange role in optical props. 80−59284
$H^- + M^+$ (M=alkali metal atom), ion-ion recombination 78−58779
He-alkali metal quantum magnetometer 80−17965
He^++alkali metal, charge exchange, He metastable beam form., composition 79−89775
He^++alkali metal atom, ionisation cross sections, binary encounter approx. with HF electron vel. distrib. 78−55225
He^++Na(K)(Cs), 5-100 keV, electron capture form. of fast metastable He 78−74760
$M+H_2$, exchange reactions and rot. transfer effects on transfer coeffs. 77−66749
NH_3-alkali metal solutions, metal-nonmetal transition Hall mobility, electrodeless meas. 78−56194
S_2Cl_2+alkali metal, matrix reaction, S_2Cl absorpt. spectrum 79−5149
S_2Cl_2+alkali metal, matrix reaction, examination by laser excitation 79−5148
Si:alkali metal, Si amorphous film, heavy doping by alkali ion implantation 80−2045
UF_6+e^-(K)(Na)(Cs), positive and negative ion formation, electron affinity, bond dissoc. energy 77−75314
ZnTe: group I element, absorption saturation *(Russian)* 78−35183

alkaline earth alloys
see also barium alloys; beryllium alloys; calcium alloys; magnesium alloys; strontium alloys
Ca-Zn liquid alloys, thermodynamics 79−52173
Ga-Mg(Al), metallic glasses, stability, microscopic calcs. 79−32914
Mg-Ca(Sr)(Ba), liquid, thermodynamic charact. *(German)* 77−59757

alkaline earth compounds
see also barium compounds; beryllium compounds; calcium compounds; magnesium compounds; radium compounds; strontium compounds
alkali-alkaline earth ceramic solid solutions, with tetragonal tungsten bronze struct., low freq. optical modes 78−76477
alkali-alkaline earth silicate glasses, IR refl. spectra *(Japanese)* 78−52505
alkali-alkaline-earth silicate glasses, IR reflection spectra *(Japanese)* 78−19491
alkaline earth precious metal hexahydroxides, prep. and characterisation 79−90610
alkaline-earth-Os ternary oxide system, solid state prep. and reactions, cryst. struct., mag. and elec. props. 79−24739
aluminophosphate glass, electron irrad., EM pulses during thermoexcitation 79−42107
carbonate, thermal decomp. in vac., dielec. method appl. 77−16802
chalcides with NaCl-type structure, third-order elastic consts. 80−70292
chalcogenides, anal. of electronic polarisabilities of ions 78−30579
chalcogenides, atomis. energy, electron affinity, mean amplitude of vibr. *(German)* 79−51045
chalcogenides, cryst. polarisabilities and ion sizes, calcs. 77−68941
chalcogenides, cryst. radii of ions 77−15340
chalcogenides, crystal binding, analysis in Born model of cohesion 78−38652
chalcogenides, crystal parameters calcs. using repulsive interaction pot. 79−37795
chalcogenides, electronic polarisabilities and ionic radii of metal and chalcogenide ions in cryst. state 80−100198
chalcogenides, electronic polarizability of ions, effect of crystal potential 78−26490
chalcogenides, interionic repulsive short-range interaction pot., lattice energy calc. 80−96466
chalcogenides, ion sizes and short range repulsive interactions 79−37652
chalcogenides, lattice energy, from modified Kapustinskii-Yatsimirskii eqn. 78−34461
chalcogenides, Madelung potential, ionic radii 78−2061

alkaline earth compounds continued
chalcogenides, static dielec. const. 78−84513
chalcogenides, van der Waals pots. determ. 78−83767
chlorides, photoelectron spectra, geometry 78−29816
citrate electrolyte, Ni electrodeposition, cathodic process rate *(Russian)* 79−8440
diatomic alkaline earth halides, multiplet splitting, extended Huckel approach 80−74127
feldspars, homogeneous and heterogeneous polymorphic transformations 79−15659
ferricyanide hydrates, $M_3[Fe(CN)_6]_2.12H_2O$, Mossbauer spectra 79−99805
fluoride:Gd^{3+}(Eu^{2+}), model of ligand hyperfine interaction 80−6792
fluoride, CeF_3(UF_4) doped, solid electrolytes, in galvanic cells 80−3501
fluoride, doped with trivalent rare earths, migration entropy for bound fluorine motion 80−71303
fluoride based solid solns., ion transport 80−107545
fluorides:rare $earth^{2+}$, photionis. thresholds 79−78132
fluorides, crack propag., cryst. props. effects 78−75720
fluorides, cryst. growth in reactive atmosphere 80−80962
fluorides, crystal growth using CF_4 and C_2F_4 as reactive atmos. processing agents 77−8747
fluorides, elasto-optic coefficients, signs 78−64346
fluorides, electronic and static dielec. consts., strain derivative theory 79−95701
fluorides, EPR of triplet state of self-trapped excitons 78−43684
fluorides, F-centre annealing and intrinsic luminesc. 79−65937
fluorides, F-centre luminesc. rel. to cryst. chemical parameters 80−29780
fluorides, high transparency IR material 77−27326
fluorides, ion transport, mechanisms and energetics using interatomic pot. 77−55382
fluorides, luminesc. excited by vacuum UV lasers 78−10941
fluorides, orbital binding energy and ionicity relations, XPS meas. 80−97399
fluorides, pulsed laser induced damage at DF laser wavelengths 77−46751
fluorides, radiation damage and photochromism in doped and undoped crysts. 79−51148
fluorides, thermoluminescent glow-peak shapes 77−28639
fluorides, UV window and coating materials, two-photon absorpt. coeffs. 79−59734
fluorite type crystal, effects of anharmonicity and disorder on Raman scatt. at high temp. 78−80349
fluorite-type crystals, universal valence bands 77−35864
glass, alkali-alkaline earth nitrates, Raman spectra, vibr. perturbations effect 79−8132
glyoxal-alkali (alkaline earth metal) complex, ab initio MOSCF calc., chelate effect 79−31386
Group IIA hydrides and halides, ionic bonds 80−18789
halide, dipolar point defects, studied by ITC 80−6405
halide crystals, thermal transport of charged point defects 80−15293
halides, aq. solns., activity and osmotic coeffs. 78−53242
halides, electron spectroscopy of crystals, book 80−36786
halides, electronic polarizabilities and ion sizes 80−59432
halides, rare earth ion doped, optical props., review 79−15492
halides, refractive index, wavelength and temp. derivatives 80−88948
halides, solid soln. spectroscopy, investigs. by F. Klement *(Russian)* 80−8767
halides, thermodynamic and structural props., computer simulation 78−75849
halides, transport phenomena, appl. to solid state devices 78−55976
halides, van der Waals pots. determ. 78−83767
hexaboride single crystals, microhardness meas. 80−21087
hexaborides, electron fractography 77−8906
hydrides, MH^+, MH_2, M=Be, Mg, Ca, Sr, Ba, Ra, relativistic (nonrelativistic) HF one-centre expansion calcs. 80−52908
hydroxide layered materials, prep. and growth, book contrib. 78−19649
hydroxyapatites, elec. cond., charge carrier identification 78−67855
iodides, photoelectron spectra, geometry 78−29816
ionic crystal containing self-localising excitons, cathodolum. 78−6785
metal oxides, new catalysts for CO-H_2O induced liquefaction of coal 80−30335
metaphosphate glass phosphors, MO-R_2O_3-P_2O_5 (R=Y or rare earth), fluoresc. props., activator conc. effect 80−89058
metaphosphate glasses, MO-R_2O_3-P_2O_5 (R=Y or rare earth), glass transition temps. and coeffs. of linear thermal expansion 80−88343
metaphosphate glasses exam. of temp. dependence of thermooptical const. 78−88286
metaphosphate glasses exam. of thermooptical and photoelastic props. 78−88287
mixed fluoride crystals, nucl. radiation effects 80−80831
mixed hydrogenated fluorides, local mode absorpt. 77−81130
mixed oxides, with U, EPR spectra 78−27090
molten carbonates, eval. as latent heat thermal energy storage materials 80−30586
molybdates, luminesc. centres, EPR meas. *(Russian)* 77−28442
molybdates, U activated, scheelite struct. luminesc. props. vibr. modes and quenching temp. 80−60651
niobate based ceramics, synthesis, struct., elec. cond., mag. props. *(Czech)* 80−45259
nitrites, molten, combination scatt. spectra, freq. shifts, jumps at melting, line widths *(Russian)* 77−40241
optical surface, target containing alkali metals and alkaline earths, chemical sensitisation after ion bombardment 80−3227
orthosilicates, gamma-irrad., ESR spectra 79−51853
orthovanadates:rare earth ions, spectroscopic props. 77−16363
oxide:Cu phosphors, electroluminesc. 77−32440
oxide, irrad. stability obs. using X-ray emission meas. *(Russian)* 80−66326
oxide based compounds, thermodynamic study using CaF_2 electrolyte 78−53241
oxide based phosphors, photon multiplication and secondary electron-hole pairs generation *(Russian)* 80−66262
oxide-silicate glasses, elastic props. and struct. 77−24273
oxides, adsorption of CO, reflectance spectra obs. 79−28781
oxides, analysis of press. derivatives of second order elastic consts. 77−35618
oxides, crystalline second-neighbours contrib. to repulsive energy 79−51044

alkaline earth compounds continued
- oxides, electron thermoemission and tunnelling emission *(Russian)* 77-44113
- oxides, electron transfer between adsorbed O_2^- ions, EPR obs. 78-76296
- oxides, emission props. in CO_2 stream 80-100742
- oxides, eval. of 3rd order and press. depend. of 2nd order elastic consts. of ionic crysts. 79-77668
- oxides, F-centre luminesc. rel. to cryst. chemical parameters 80-29780
- oxides, luminesc. excited by vacuum UV lasers 78-10941
- oxides, Mollwo-Ivey relation between peak-colour absorption energy and average O ion spacing 77-90179
- oxides, O two electron affinity from cohesive energies 78-25736
- oxides, occurrence in sunspots and cool stars 78-85933
- oxides, photoelastic consts. 78-71781
- oxides, point defect props., band struct., lattice simulation calc. 80-19797
- oxides, surface emission active centres 80-100741
- oxides, third order elastic constants 77-35620
- oxides in binary system with WO_3, phase relations 79-8290
- perovskite oxides, point defects, elec. cond., and electron energy spectra 80-70706
- phosphate glasses, $45RO.5Al_2O_3.50P_2O_5$, (R=alkali earths), electron beam irrad., exam. of charge accumulation and light-sum kinetics 79-4336
- phosphates, H prod. by thermochemical water-splitting cycles based on Ce and alkaline earth phosphates 80-55945
- phosphites, $M^{II}PO_3H.xH_2O$, cryst. struct. *(French)* 80-24413
- photoluminescent spectra of surface states 79-47505
- silicate:Nd_2O_3 glasses, coloured, dichroism *(Polish)* 79-99919
- silicates, Cr^{2+} solid solubility 77-76564
- sulphates, crystallisation kinetics 79-43119
- supersaturated solutions, precipitation induction errors, a method for determ. 79-5175
- ternary molten salt phase diagrams, computation 79-100118
- tetraborates, doped, radiothermoluminesc. detectors, dosimetric characts. 77-61665
- transition metal ternary and quaternary oxides, ATO_3, $ATi_{1-x}T_xO_3$, and $AZr_{1-x}T_xO_3$, prep., mag. props. and struct. 79-15277
- tungstates, luminesc. centres, EPR meas. *(Russian)* 77-28442
- tungstates, U-doped, perovskite struct., luminesc. quenching, QMSCC calcs. 80-71470
- uranates, struct., phys. and chem. props., preparation methods, review *(Japanese)* 79-14764
- zirconate, perovskite type, X-ray K-absorpt. edge, chem. shift 79-91529
- Al_2O_3-SiO_2-MO-Fe_2O_3 glass, M=Ca, Mg, Ba, Sr, UV and EPR absorpt. spectra 80-89018
- BaB_2O_4-RF_2, R=Mg, Ca, Sr, Ba, glass form., struct. and props. 80-84077
- $Ba(PO_3)_2$-alkaline earth fluoride glasses, pseudobinary, elec. cond. and dielec. losses 77-7890
- $M_2O(MF_y)$-BeO-P_2O_5 glasses, M=alkali metal, alkaline earth, Cd or Zn, glass-formation 78-67656
- Mo-alkali earth oxides, multiple phase system calc. of phase equilibria using thermodynamic analysis *(Russian)* 79-56964
- MoO_3-MO system, M=alkaline earth metal, eutectic coordinates on phase diag. 77-44227
- MoS_2 intercalation compounds, reaction with alkali and alkali earth metals, band struct., superconductivity 78-26541
- Na_3AlF_6-LiF-CaF_2-AlF_3-Al_2O_3, electrolyte, exam. of phase equilibria, review 79-11590
- PbO-MoO_3-MO and PbO-WO_3-MO systems, M=Ca, Ba, Mg, Sr, perovskite type cpds. detection 80-108404
- SiO_2-Al_2O_3-RO-R_2O type glass additions, sintering of porcelain bodies 80-45265
- W-alkali earth oxides, multiple phase systems, calc. of phase equilibria, using thermodynamic analysis *(Russian)* 79-56964
- ZnB_2O_4-RF_2, R=Mg, Ca, Sr, Ba, glass form., struct. and props. 80-84077

alkaline earth metals
- *see also barium; beryllium; calcium; magnesium; radium; strontium*
- alkali halide:alkaline-earth cations, defect structs. examined by methods based on Mott-Littleton techniques 80-59487
- alkaline earth flame chemistry, photometric meas. of $H_2+O_2+N_2$ flames with/without Ca, Sr, Ba additions 79-8439
- atom, correl. lines, Rydberg excitation and ionisation pots. 77-6705
- atom, electron impact double electron excitation and autoionisation calcs. 77-68121
- atom, flame emission apparatus for teaching 77-29976
- atom, multiphoton ionis. spectroscopy of even- and odd-parity states 78-86973
- atom, multiphoton ionisation spectroscopy 78-82703
- atom, photoabsorption by scaled Thomas-Fermi method 77-46549
- atom, quasiadiabatic polarisation pot. for elastic electron-atom scatt. 77-6929
- atom+D, D^- ion production, multiple charge-transfer collisions 79-89776
- atom+inert gas ion, double ionisation, cross section and defect energy *(Russian)* 77-83703
- atomic multiphoton spectra, high Rydberg states 77-68022
- atomic multipole polarisability, extended Coulomb approx. 78-33451
- atoms, doubly excited, autoionising states and interference profiles 80-52949
- atoms, high Rydberg states, multichannel quantum defect theory 79-72250
- atoms, static polarisability, lower bounds, oscill. strength calcs. 77-75074
- atoms and ions, regularities within Stark widths of reson. lines 78-78662
- binding energy calc. *(Chinese)* 80-911
- bound diatomic molecules, covalent bonding concept in undergrad. chem. courses 80-22177
- determination, mechanism of buffer action of La and Sr *(Russian)* 79-29441
- homologous ions series, Stark broadening trends 80-105157
- ion, impurity in liq. ^4He, struct. 77-39714
- ion, valence electron ground states, nonlocal Hellmann-model potentials 78-50476
- liquids, pseudo-Gruneisen parameter, temp. depend. 77-7873
- muon Knight shift 79-56656

alkaline earth metals continued
- positive muon spin rotation frequency, Knight shift meas. 79-38421
- secondary cells, nonaqueous electrochem. behaviour of alkali and alkaline earth metals 80-35665
- separation and identification by circular thin layer chromatography 79-66385
- surface plasmons, excitation 79-28310
- surface props., Rayleigh-Ritz variational calcs. 79-69570
- trace diffusion of nuclear reaction products in polycryst. Ta 78-22896
- vapour, excited by electron impact, ejected-electron spectra from autoionising levels 80-37893
- vapour, soft X-ray gain 77-23655
- X-ray emission spectra, atomic interaction effects *(Russian)* 79-69905
- N_2O-CO flame, alkaline earth catalyzed chain reaction chemiluminesc. 77-40548

alkalinity *see pH*

allotropism *see polymorphism*

alloy steel
- 1Kh18N9T, physico-mech. props. after boring in metallic melts *(Russian)* 78-56736
- 2S96D, fatigue crack propag. theory 78-5692
- 12Kh18N9T, high intensity US absorpt. 79-86845
- 12Kh18N9T-TiB_2, eutectic alloy, high temp. props. 78-84931
- 30KhGSNA, strength under combined compound stresses and corrosive environment *(Russian)* 78-56803
- 35KFN10, X-ray diffr. investig. after thermomech. treatment *(Russian)* 77-48457
- 40Kh, surface working effects on crack resist. *(Russian)* 78-56734
- 40Kh, thermally strengthened, influence of loading rate and sea water on K_{1c} value *(Russian)* 78-56799
- 40KhNMA, fretting-corrosion in vacuum-chromized Ti alloy VT3-1 couple *(Russian)* 78-56804
- A533 B, fatigue crack propagation, grain size and temp. effects 78-56727
- A533B1, neutron irrad., flow growth characts. by acoustic monitoring 80-100918
- A533B, fatigue crack growth of irradiated pressure vessel steels in simulated, reactor-grade water environment 80-97582
- A-533 B, J_{1c}-testing, statistical eval. of different techniques 78-56828
- abrasive machining of types CT45, CT50 and CT40X, textures formed 80-25721
- acoustic emission, amplitude distrib. anal. 80-66713
- ageing characts., precipitation and coarsening of VC, TiC, and V-Ti-C in ferrite 78-84874
- ageing to produce ultrafine grains, discontinuous precipitation, in 36NKhTYu *(Russian)* 77-81277
- Al-killed, sheets, effect of strain path changes on formability 79-43347
- alternating bending, fracture surface appearance of Ck 45 *(German)* 78-52995
- API 5LX-X60, pipe fatigue strength under cyclic internal pressure, inner surface defects 79-38980
- austenised at low and high temps. toughness evaluation of AISI 4340 77-16621
- austenite grain growth, role of V, Nb, N alloying additions 77-44255
- austenite grain size, determ. 79-74332
- austenite transformation in hot rolled strips 80-55407
- austenite/ferrite interface, struct. and diffr. effects, TEM exam. 80-16308
- austenitic, ageing and plastic deform. effect on struct. and mech. props. of N15Kh5G3T3 *(Russian)* 80-71691
- austenitic, grain size, tempering effect on brittle fracture susceptibility 80-55534
- austenitic, heavily doped, linear expansion meas. 80-103501
- austenitic, Mn and Mn-Cr, thermal expansion *(German)* 77-59127
- austenitic, Mn-Ni-Cr, Mn effects on cracking *(German)* 77-59889
- austenitic, Ni free, TEM exam. of corrosion 78-85029
- austenitic transform., temp.-conc. range of form. 79-100135
- austenitic-martensitic, phase comp., struct. and mech. props. 80-29974
- bainite, ε-carbide precip. *(Russian)* 77-66647
- bainitic, morphological characteristics 78-68682
- bainitic and martensitic transform., isothermal studies 77-36497
- bainitic transformation, suppression in steels *(Russian)* 80-76247
- ball bearing, fatigue damage, influence of dispersed phases in martensitic matrix 80-108549
- bearing, induction hardened, rolling contact strength *(Japanese)* 80-93568
- bearing, tricresyl phosphate treated, Auger anal. of type AISI 52100 79-52413
- bearing type En 31, surface-ground, residual stress and fatigue property comparison 80-60975
- bending fatigue resistance, size effect and prediction 79-43411
- bimetal faced with austenitic ferritic stainless steel, fracture toughness *(Russian)* 78-35482
- bimetal with austenitic stainless steel, H permeability 80-107572
- boiler plate, comp. effects on SCC resist. *(Russian)* 78-11400
- boride coatings, spectroscopic thickness determ. 80-85099
- boriding in powdered mixture with high activity 80-30164
- brass clad plate/roll bonded Ni clad, fatigue crack growth behaviour 80-40484
- brittleness, elastic props., abrasive wear stability of type Kh12M steel *(Russian)* 80-66672
- carbide formation, Mo alloying effects, in 30KhG and 30KhN *(Russian)* 78-48402
- carbide lattice, kinetics of its destruction in NC6 *(Polish)* 78-92280
- carbide phase determ. by annealing in moist H_2 *(German)* 79-39231
- carbide transitions during post-strain ageing and tempering *(Russian)* 78-95741
- carbonitride comp. and solubility calcs. *(Russian)* 77-70052
- carbonitrided 25khGT, 25KhGM, exam. of hardenability and phase composition 78-44272
- carburisation, internal oxidation of excess carbides *(Russian)* 80-25903
- carburised, kinetic parameter determ. *(Rumanian)* 79-29259
- carburised, transform. of residual austenite, mag. field effects *(Russian)* 80-29952
- carburized case parameters, effect on props. of 20Kh3MVFA and 12Kh2N4A 78-52989
- case hardened, MnCr, shot peening effect on bending fatigue strength *(German)* 78-56777
- case hardened and structural steel fracture obs. by SEM *(German)* 77-60032

alloy steel continued
case hardened gas carbonitrided, holographic interferometry study of plastic flow *(German)* 77−77723
case hardening and carbonitriding treatment, comparative effects on operation props. *(French)* 77−59991
case-carburized, low alloy, rolling contact fatigue 78−35518
case-hardened, 12KhN3A, friction austenite, electron diffr. obs. *(Russian)* 77−21286
case-hardened cast, contact endurance rel. to austenizing *(Russian)* 78−56805
cast, fatigue from notches 77−16678
cast, fatigue strength probability characts. determ. 77−70173
cast, heat-resist., subcrit. crack growth 80−97581
cast, high speed, solidification, $(Fe,Mo)_6C$ form., struct. 79−24514
cast, low alloy, fracture toughness 77−4835
cast, optimal alloying, carburising effect 80−50771
casting properties, correlation anal. *(Bulgarian)* 79−83192
cementite decomposition during plastic deform., alloying element effects 78−84768
cementite phase dispersion change during tempering *(Russian)* 80−93577
chemicothermal treatment, diffusional basis 80−104343
cladded with monolayer austenitic stainless steel, heavy section, residual stresses *(German)* 78−35420
cluster formation susceptibility in 40 KhN, influence of isothermal working in H_2 *(Russian)* 78−56643
coarsening at high temp. of small carbide particles dispersed in ferrite 77−52335
cold formability *(French)* 78−60681
cold rolled, low alloy, rimming steel, radiation capacity *(Russian)* 78−14486
cold rolled, transformer type, decarburising annealing, Mossbauer cryst. struct. anal. *(Russian)* 80−11294
cold worked, original struct. effect on softening during heating 80−60882
cold-formed, low pearlite, Nb alloyed, Nb effects, precipitation, recrystallisation *(German)* 77−8832
complex alloy steel, X-ray diffr. determ. for struct. changes during quenching and tempering 77−56004
complex carbide V-Nb-C layer form. in fused borax bath *(Japanese)* 77−56150
composite mode cracks, K_I-K_{II}, brittle fracture study *(Chinese)* 80−55494
composite with 30.% TiC, sintered, wear resist. 80−100815
compression, high strain rate, 4130 steel 79−34099
concentration of B, solubility depend. on introduction of rare earth metals *(Russian)* 80−65226
constructional, fatigue cracking in corrosive media 78−85081
constructional and tool steels, heat treatment effects on elec., mag. and mech. props. expt. 77−77719
constructional material, K_{1c} determ. from mech. props. and struct. parameters *(Russian)* 77−60010
constructional materials, brittle failure resistance, calc. characts., expt. methods 77−77662
corrosion, alternating current effect 80−30141
corrosion fatigue, effect of NaCl and shot peening, in AISI 6150 79−8391
corrosion fatigue crack growth in NaCl soln., waveform effect in SNCM2 80−21163
corrosion fatigue strength determ. *(Japanese)* 80−25910
corrosion in artificial seawater, alloying element effect *(Chinese)* 80−21150
corrosion in artificial seawater, alloying element effect *(Chinese)* 80−21151
corrosion resistance, alloying effects 77−70225
corrosion resistance in liquid metals *(Czech)* 77−50245
corrosion stability to double iodate-iodide salt melt in H prod. *(Russian)* 80−55593
corrosion-impact-cyclic strength of boring bars, effective hardening treatment 78−53034
Cr-Mn, unstable austenite, martensitic transform., effect of alloying, heat treatment, and deform. 78−19751
Cr-Mo (2.25,1 wt.%), exposed to H_2-H_2O-H_2S environment, fatigue crack growth 80−40623
Cr-Mo (2.25, 1 wt.%), small changes effect in impurity elements, creep life 80−25790
Cr-Mo (2.25, 1 wt.%), temper embrittlement, trace elements, Mo, intercritical heat treatment effects 77−36634
Cr-Mo-V, cyclic deformation under out-of-phase loads 80−40428
Cr-Mo-V steel turbine rotor, fatigue tests 78−39912
Cr-Ni-(Mn), mech. props. at low temp. 77−70118
crack arrest toughness determination 78−72867
crack profile meas. and correlation with mech. props. *(German)* 80−21108
crack propag. anal. in delayed fracture under repeated load, internal friction model 79−79064
crack propagation, acoustic emission transients meas. 79−8407
crack propagation vel. in delayed failure under cyclic load, temp. and freq. depend. in JIS SNCM8 79−43381
crack resistance, yield strength, ductile-brittle transition temp., optimum tempering of 24Kh2NMFA 77−63787
crack tip stress and strain fields and fracture behaviour 78−22304
creep limit and long-term strength, parametric eval. method, for X8CrNiNb1613 80−100996
creep tests on 12Kh1MF, structural changes 77−63746
CrMoV, quantitative stereological anal. and creep-resistance *(Czech)* 80−30030
CrMoV, surface coating to prevent oxidation during high temp. AE 80−16539
Croloy Cr-Mo, stress corrosion cracking in high temp. caustic soln. 77−59964
Croloy steel for LMFBR steam generator, meas. of T permeation 80−68775
crystallographic texture perfection in sheet with S,Mn inhibitors *(Russian)* 79−91709
cyclic strength after strain hardening and tempering, precip. hardened 40FT 78−52988
cylindrical notched specimen, four-point bending, crack resist. tests 80−53735
cylindrical tubes or shells, mild steel, quasi-static piercing 80−45351

alloy steel continued
damping behaviour and fatigue strength correlation, in type Ck22 and St52-3 *(German)* 80−39211
deep drawing sheet, annealing effect on coercive force *(German)* 80−29573
deep drawing sheets, influence of strain- and stress-rátios on preferred orientation change 79−91690
deformability at 600 to 950°C 77−70117
deformation, rapid dynamic, at −196°C 80−104220
deformation and fracture props. in type 12KhN4MDA steel, on extension and twisting *(Russian)* 80−55504
deformation broaching, of type 38kHMYuA and 38KhNMYuA bushings 80−108473
deformation resistance, grain size effect *(Russian)* 78−11271
deformation study, positron lifetime and hardness correlation, in type 4340 79−87649
deformed N32 sheet, $\alpha\rightarrow\gamma$ transform., struct., texture conc. var. depend. on plastic deform. *(Russian)* 79−66050
delayed retardation phenomena of fatigue crack growth, exam. 78−56745
denitriding annealing, effect on mech. props. of 08kp 79−52461
density and thermal expansion in liq. and solid states 80−96668
determination of minor impurities and alloying constituents, appl. of inductively coupled plasma spectrometry 80−90903
die, mech. props. high temp. thermomech. treatment 79−20086
die, thermal fatigue resistance, high temp. thermomech. treatment effect 80−50715
die steels for cold plastic working, powder metallurgy, characts. 78−68649
die types 4Kh5MFS and 5Kh2MNF, nitriding in vibrofluidised bed 80−35410
diffusion modelling of carburization 79−24657
discontinuous precipitation of γ'-phase of alloy 36 NKhTYu, influence of short high-temp. treatments *(Russian)* 78−11226
dislocation structure changes, susceptibility to damage in type 12Kh1MF steel after thermomechanical working *(Russian)* 80−66545
double ligament tensile test in deformation processing 77−32753
ductile-brittle transition temp., variation with grain size 78−27640
ductility, hydrostatic press. effects 78−80615
duplex ferritic/martensitic, design for improved mech. props., heat treatment, TEM obs. 77−63697
effect of Co on 18Kh2N4MA, struct. and mech. props. 78−44147
elastic and fatigue charact. 77−21267
electrical, mag. hysteresis representation in numerical modelling of mag. fields 80−88813
electrical and thermal cond. of N27Yu2T2B, 4.2 to 200K, Wiedemann-Franz law *(Russian)* 79−78076
electrode, erosion resist., influence of C and carbide-forming elements *(Russian)* 78−11389
electroslag remelting effect, an impact-abrasive wear resistance 80−55541
electrotechnical, losses on mag. aftereffect *(Russian)* 77−66388
electrotechnical steel, hysteresis curves, plotting *(Russian)* 78−76269
embrittled N18K8M3TYu, toughness enhancement by double quenching 77−59922
embrittlement during tempering *(Russian)* 77−90436
emission spectrochemical analysis of Nb, effect of Mn, interference for Nb II 3194.977 Å 77−21457
emissivity, integrated normal with low heat conductivity coeffs. of type Kh23N18 80−103504
eutectic carbide, composition change due to heating, exam. 80−16353
eutectoid, partitioning of Si during pearlite growth, electron microscopy study 79−83201
eutectoid pearlitic, exam. of microstructures dominating ductility *(Japanese)* 78−84917
failure characts. of steel 15G2AFDps, effect of loading freq. and temp., SEM exam. of failure surface 78−84995
fast reactor steels and alloys, neutron damage development, irradiation conditions, chemical composition 80−34082
fatigue, under const. and variable amplitude loading, air environment effect on type D6AC 80−35386
fatigue crack closure over stress ratio range, stress intensity threshold, in HT80 78−80619
fatigue crack development at low temps., type 10GN2MFA 79−57110
fatigue crack growth, in presence of welding residual stresses *(Russian)* 80−71739
fatigue crack growth, near threshold, prior austenite grain size effect 78−39903
fatigue crack growth from a surface flaw 78−68803
fatigue crack growth in steel, A533 grade B, class 1, in PWR coolant 77−77584
fatigue crack growth under random load, mean stress and amplitude distrib. 77−73319
fatigue crack initiation and propag. at notch tip, HY140 steel 78−80647
fatigue crack initiation and propag. at notch tip, HY180 steel 78−80647
fatigue crack propag. work coeff., of type HT60 80−16422
fatigue crack propagation in high strength alloy containing retained austenite 80−16432
fatigue crack propagation rate in types 15KP, ST3, 15G and 10G251 with different yield strengths 78−52987
fatigue cracking under polymodal stress *(French)* 79−91787
fatigue life diagrams plotting, of type 30 KhGSNA 79−70246
fatigue limit during bending, inelastic strain effects 77−44355
fatigue resistance when strengthened by nitrides and welded joints, grades 14G2AFD and 15G2AFDps 78−95790
fatigue strength, of notched specimens with regard for cyclic plastic strains of type 1Kh2M 79−43414
fatigue strength and fracture, diamond grinding effect 80−55532
fatigue strength estimation, separation method suitability *(German)* 78−27644
fatigue strength improvement, by subcritical quenching 78−44153
fatigue strength rel. to absolute dimensions and stress conc. 79−43410
fatigue testing of spherical sample, subjected to forced bending *(Croatian)* 77−36712
fatigue to brittle fracture transition at low temp., stress raiser effect 77−12696
ferrite, transform. kinetics, grain size, alloying element effect, carbide precip. 80−93560
ferrite-carbide struct., cold plastic deform. 77−90408
ferrite-pearlite, ductile fracture, pearlite colony morphology and hydrostatic press. effect *(Japanese)* 78−15510

alloy steel continued
ferrite/martensite dual phase, compositional anal., TEM 80—85253
ferritic, As effect on grain size 77—70062
ferritic, Cr-Mo, corrosion behaviour in reducing environment of coal fired MHD generator 80—104322
ferritic, Cr-Mo (2.25, 1 wt.%), annealed, time depend. strain controlled fatigue, nuclear steam generator appl. 77—8915
ferritic, Cr-Mo (2.25, 1 wt.%), C and Nb influence on structural transformations *(French)* 80—84925
ferritic, Cr-Mo-V (0.5, 0.5, 0.25 wt.%), creep and fracture, microstructural instability effects 77—63734
ferritic, damping, logarithmic decrement meas. by torsion pendulum *(German)* 79—74195
ferritic, screening studies for evaluation for nucl. process heat system 78—13236
ferritic, strengthened by VC interphase precipitation, cleavage 79—74171
ferritic, surface hardening by gas nitriding, process improvements 80—97499
ferritic, void swelling during irradiation, suppression mechanisms 80—6441
ferritic, void swelling response after fast reactor irradiation 80—6437
ferritic alloy DT02, oxidation behaviour in CO_2 or Ar with H_2O and H_2, 823-123K 80—3249
ferritic Cr-Mo type, microanalysis of precipitates using TEM 80—108688
ferritic-pearlitic, low C, low alloy, low temp. effects on fatigue strength 79—5057
Ferrotic C, fatigue crack propag. theory 78—5692
fine 42NKhTYuA alloy wire, hysteresis loop and differential permeab. after US and conventional drawing 79—15818
fission reactor steels for use in PWRs, props. and development 77—38336
forgings, cylindrical, nonsteady temp. fields during cooling, calc. 80—16346
forgings, H precipitation kinetics, diffusion to voids, effect on shattercrack formation 80—16344
formation of special carbides, theory *(Russian)* 77—21153
fracture and fracture energy, subject to static, impact and repeated impact bending 77—63799
fracture and high temp. props. of 4340, 533K to 1255K 78—60821
fracture in creep at temp. near 0.5 MP, type 12Kh1MF *(Russian)* 77—32675
fracture mech. specimen, effect of fatigue precracking condition *(German)* 77—21240
fracture mechanics, K_{Ic} values determ. in elastic-plastic material behaviour range 80—45376
fracture mechanics parameters, influence of specimen thickness on types RSt 37-2, st52-3, StE70 and 30CrNiMo8 *(German)* 80—66614
fracture obs., shell-shaped fracture 77—25153
fracture of 10G2S1, subjected to low-temp. fatigue 80—89350
fracture resist. assessment from stable crack length *(Russian)* 79—15765
fracture strength investigation under various types of loading 78—7042
fracture toughness, cyclic and static, low temp. effect in 08kp and 03Kh13AG19 steels *(Russian)* 79—52344
fracture toughness, directional, and sulphide modification 78—27618
fracture toughness, of medium and low-alloy steel with ferriticpearlitic struct. 79—15787
fracture toughness, pressure vessel appl. *(Czech)* 79—79094
fracture toughness, single specimen determ. for J_{Ic} 80—100989
fracture toughness, type 4340, effect of partially dissociated N_2 78—80642
fracture toughness and dynamic strength, surface active agent effects *(Russian)* 78—56812
fracture toughness and strength, effect of heat treatment on microstruct. in 300M 78—15436
fracture toughness depend. on Cl_2 environment, type 4340 79—100295
fracture toughness props. for nuclear bolting appl. 78—35514
free cutting steel with MnS inclusions tensile flow and fracture 78—11290
fretting corrosion, exam. of secondary structures 79—100292
friction, redistribution of alloying elements in active layer of type 1Kh17N2 *(Russian)* 77—81326
friction surface and lubricant nature, effect on adsorption and temp. stability of lubricant layers 78—15544
friction with cast Fe, boundary and oil-abrasive adsorption effect 80—55546
fully killed, nonmetallic inclusions, microprobe and metallographic exam. 80—30196
grain boundary anal.,, H_2 embrittlement effects, scanning AES 79—43256
grain boundary proeutectoid ferrite formation, direct obs. method 80—3074
grain oriented, 3 wt.% Si, high permeability obs. 77—1881
grain size effect on mech. props. 78—44207
graphite dissolution, segregation and diffusion *(Russian)* 78—11201
graphitised elastic modulus and internal friction, temp. depend. 80—35242
grinding wheel loading meas. using neutron-activated workpieces 79—5070
Hadfield, cast and crystallised, deform. resist. of grain boundaries *(Russian)* 77—21216
hard, high speed and tool, linear elastic fracture mech. appl. 78—48518
hard layer prod. by electrospark alloying with TiC-Ni-Mo alloys 77—59998
hard-alloy/U8 C alloy steel weld, local internal stress region boundaries 77—59846
hardenability, role of B and P segregation 80—97486
hardened, electrochem. characts. and stress corrosion cracking, ageing and cold treatment effects 80—108639
hardened and tempered parts, nondestructive magnetic inspection 78—95889
hardened and tempered parts, nondestructive magnetic inspection 79—1929
heat resistant, 12Kh1MF and 15Kh1M1F, damage accumulation during prolonged high-temp. creep 79—57026
heat resistant, type 15Kh1M1F, study of long term cyclic strength under soft asymmetric and rigid loading 79—57076
heat resistant, type Kh8CrNiNb1613, approach to numerical soln. of problem of predicting long-term strength by summary diagrams 79—56988

alloy steel continued
heat resistant 15Kh1M1FL, cast, crack development at various stages of fracture, prolonged load 77—63802
heat resisting, type 15Kh1M1F, exam. of structural stability and props. *(Russian)* 79—29104
heat treated, alloying element distrib. effects, mech. props. 78—84876
heat treated, stresses and cracks form. *(Czech)* 80—20977
heat treated low alloy 12GN2MFAYu testing temp. influence on fatigue strength *(Russian)* 80—40501
heat treatment, mag. quality control method of 30KhN2MFA and 40Kh 80—108662
heat treatment, mech. props., wear, fracture toughness for cutting tool 78—19864
heat-resistant, 12Kh1MF, yield point rel. to dislocation density and cryst. lattice spacing *(Russian)* 77—44291
heat-treated, crack resist. in seawater 80—104347
high alloy, strain induced martensite and austenite influence on crack formation *(Russian)* 80—21007
high alloy ledeburitic, wear and corrosion resistant coating by chemical vapour deposition 78—92403
high C, amorphous, produced by rapid quenching from melt, hardness and strength 78—59764
high C, high alloy, $M_{23}C_6$ type carbides, effect of alloying elements on defect struct. and hardness 80—16481
high Cr, substrate, TiB_2 coating prep. by CVD and interaction with substrate 79—24680
high Mn, austenite grain size, effect of rolling and V, Ti and Zr additions *(Korean)* 77—12632
high Mn, heat resistant, alloying additions, effect on mech. props. *(Korean)* 77—12631
high Mn, mech. props., strain induced martensitic transform., effect of austenite predeformation 77—16649
high Mn alloy G22, phase transform. during plastic deform. 77—16576
high speed, AISI M2 and M7, fracture toughness 77—86141
high speed, anode potential determ. of tempering quality 78—53139
high speed, atomised powder, defects in parts produced by hot isotactic pressing 78—60612
high speed, cast R6M5, carbide transform. during high temp. treatment 77—90375
high speed, cutting tools, carbide heterogeneity change during hot extrusion 80—16390
high speed, fixed time integration-emission spectral anal. and employment of high freq. induction melting-centrifugal casting samples *(Japanese)* 80—89567
high speed, hardened, for drills, mech. and cutting props. 79—43407
high speed, irradiated, absolute tool wear determ. by γ-γ coincidence counting of radiotracers 77—73352
high speed, M2, fracture behaviour and fracture toughness 79—24609
high speed, microstruct. effect of splat cooling 79—61624
high speed, plasticity depend. on plastic strain gradient *(Russian)* 79—57048
high speed, powder, cold isostatic compaction effect on thermophysical props. 78—52717
high speed, R12, R18, R6M5, R9K5, R14F4, annealing effect on props. 77—90373
high speed, R18 and R6M5, rolled and annealed carbide phase investigation 77—90374
high speed, rapid stepless cyclic method annealing 80—16352
high speed, sintered, and wrought, type T6 strength and toughness 80—30102
high speed, steel R18, hot deformation and recrystn. 80—16391
high speed, TiC-coated, machining of steel 4340, tool life 78—11435
high speed, tool, cyanided, wear charact. 78—48542
high speed, type R6M5K5, secondary and red hardness of marquenching 80—16350
high speed, W-Mo-Cr-V, production by powder metallurgy 77—12574
high speed, wear resistance of white layer formed by vacuum oil quenching *(Japanese)* 78—11336
high speed, wear resistant coating of Ti(N,C,O), CVD 78—92406
high speed, working curve, sample production for spectrochemical anal. from Fe dilution method *(Japanese)* 78—53050
high speed M2, charact. of solidification struct. within dendritic core 78—27504
high speed R6M5, secondary inheritance investigation by austenite recrystallisation 77—90367
high speed R6M5K5, excess carbide size and distrib. effect on grain size 77—90356
high speed R8F8K7M6, cast, forged, sintered, struct. and props. 77—77516
high speed S6-5-2 Si content effect on solidification *(German)* 78—11213
high speed steel powder, S and O reduction in a H_2 gas stream 80—61015
high speed tool, diffusion wear model 79—29230
high speed tool, laser surface melting 79—24654
high speed tool, rapidly quenched, exam. of solidification struct. 78—39758
high speed tool, roughness and wear characteristic of spark-eroded surfaces 79—52390
high speed tool, sliding contact in magnetic field, model for cross diffusion 79—79121
high speed type M-50 and 18-4-1, fracture and fatigue 80—16457
high strength, alloy initiation of cracks at delayed fracture, AE study 78—72868
high strength, Cr, Cr-Mo, Ni-Cr, and Ni-Cr-Mo, diffusion of H_2, effect of quenching and tempering 77—90384
high strength, environmental effects on initiation and propag. of fatigue cracks 77—86216
high strength, HSLA metallurgy in Europe, review 77—48614
high strength, increasing resistance to cracking, use of overheating before quenching *(Russian)* 77—25135
high strength, low alloy, critical stress for delamination fracture 79—1907
high strength, low alloy, low cycle fatigue, composition, thickness effects 79—57100
high strength, low alloy, mech. behaviour, deform. rapidity influence *(French)* 79—57056
high strength, low alloy, mech. props. 78—60739
high strength, low alloy, plate, impaired ductility in sheared edges 78—60727

alloy steel continued
high strength, low alloy, rare earth treated, ductile fracture mech. 78—64658
high strength, low alloy, response to cyclic plastic deform. 78—7035
high strength, low alloy, splitting of tensile and impact specimens 77—63777
high strength, produced by extrusion of Ni-coated steel powder, enhanced fracture resist. 80—81169
high strength, residual stresses during low cycle fatigue 79—29201
high strength, treatment effect on ductility and strength 80—60880
high strength, type 90 Mn V8, stress corrosion crack velocities in NaCl soln. 80—21161
high strength, type SAE 4340, depend. of fracture toughness on crack velocity 79—47772
high strength, use of metallic melts as lubricant-coolant, in drilling *(Russian)* 79—57201
high strength AISI 4130, H_2 assisted cracking 78—48522
high strength HP 9-4-20, retained austenite influence on fatigue crack propag. 80—21106
high strength low alloy, acoustic emission meas. from crack opening displacements 80—7732
high strength low alloy, high strain fatigue behaviour 77—86180
high strength sheets, finite element anal. of crack propag. expts. 80—40498
high strength steels HT80, HY130, quenching and tempering effect on H_2 diffusion *(Japanese)* 78—64565
high strength structural mats., microstruct. influences on fatigue and fracture resist. 78—56728
high temperature thermomechanical treatment, Cr effects on props. 77—12651
high V-W-Mo, high speed, phase composition and struct. of atomized powders 77—90323
high-alloy, creep, expt. investigation above 900 degrees C 80—81134
high-alloy, phases *(Chinese)* 78—95728
high-alloy bearing, LTMT effects on ht. resist. and contact fatigue resist. 77—44354
high-alloy die steel, electrothermal treatment 80—29996
high-alloy die steel, heat resistance and crushing strength, low-temp. thermomech. treatment effects 77—52372
high-C, amorphous, mech. props. and thermal stability 80—76361
high-speed, atomised powders and sintered blanks, particle size effects 77—44188
high-speed, cast, mech. props. at high temps. 79—20135
high-speed, low-temp. mag. cycling effect on ferromag. struct. 80—100928
high-speed, N effects on struct. and props. 77—59799
high-speed, portable salt bath for rapid anal., high frequency current heating 77—70256
high-speed, quenched and tempered notch toughness, ultimate and yield strength in tension and compression 78—95782
high-speed, struct. changes investigation by hot hardness and quench dilatometry *(French)* 80—76249
high-speed tool, Nb addition effect on hardening 79—34048
high-speed tool, properties, powder metallurgy prep. method *(Czech)* 80—60800
high-speed tools, cemented carbide ion plating, cost and cutting performance 80—30174
high-strength, Cr (1 to 15 wt.%) effect on crack initiation stress *(Russian)* 77—16725
high-strength, endurance in air and NaCl soln., loading freq. effects *(Russian)* 78—56810
high-strength, fatigue, interaction effects between trace impurities and environment 80—66651
high-strength low alloy, H_2 attack, 350-510°C 80—97636
high-strength low-alloy, stress corrosion cracking in NaCl solution *(Japanese)* 78—92401
high-strength maraging, N18K9M5T, improvement in mech. props. under applied stress influence during ageing 80—20985
high-strength maraging, N18K9M5T, nitriding effect on fracture resist. 80—21092
high-temp. combined ht. treatment and mech. working, C content effects *(Russian)* 78—52854
homogenisation of sulphide inclusions 77—32605
hot rolled, low C, low alloy, bainitic alloying addition effects on microstruct. and props. 77—36546
hot rolled Al killed sheet, strain ageing control 79—61628
hot rolled M1 tool type, microparticle distributions and mech. response 77—44279
HSLA, grain size and substruct. control by alloying and thermomech. treatment, review 80—3082
HSLA, HAZ microcrack study in multilayer welding *(Chinese)* 79—100172
HSLA, V effect on mech. props. *(Korean)* 80—29987
HSLA, weldment, AE monitoring 79—87800
HSLA steel, AE appl. to nondestructive testing 79—83419
HSLA type 4340, hydrogen diffusivity and solubility, correl. with embrittlement and SCC phenomena 79—83323
Hugoniot parameters to 320 GPa, dynamic yield strengths and phase transition press. 80—75331
HY-130 steel, shallow spherical cap buckling under uniform external press. 77—23902
hydrogen embrittlement and H_2S cracking resist., effect of alloying elements and struct. 79—38953
hydrogenation and embrittlement under neutron irrad. in contact with water *(Russian)* 77—52529
impact and tensile props., Si effects 79—24614
instrumental anal., use of HF induction melting and centrifugal casting *(Japanese)* 77—56280
interaction with Nd^{3+}-glass laser light 78—92147
intergranular segregation of Cr, Mn, Sn in as-quenched state, AES *(Japanese)* 78—19764
ion nitrided and ion-softnitrided, comparison of compound layers in SACM1 and SCM3 *(Japanese)* 79—8386
ion-softnitriding effects on metallurgical props. of nitrided layer in Cr-Mo and Cr-Mo-Al alloy *(Japanese)* 79—5079
killed ingot, freezing process liq. core movement *(Russian)* 80—20921
ledeburite, fracture during hot plastic deformation exam. 78—56755
lightly alloyed, S effect on failure following controlled rolling *(Russian)* 79—57086
liquid, interface with $MnO-SiO_2-ZrO_2$ molten slag systems, wetting angles, surface tension *(Czech)* 79—19432

alloy steel continued
localised corrosion resistance of M50 bearing steel, improvement by ion implantation 80—16602
low, dual phase, high strength, exam. of energy absorption by structual collapse 80—7640
low, exam. of microstructure, in type PZhK-1000 soldered joint by metallography 79—52257
low, Ni-Cr, tempered martensite embrittlement 80—7669
low alloy, 10KhSND, 16G2AF, welded joint low-cycle fatigue during crack form. and propag. during biaxial bending 79—11704
low alloy, 18KhMVTCh, corrosion cracking resistance in sulphide environments *(Russian)* 78—31571
low alloy, 45, depth length relationship of fatigue crack developing in circular specimens during bending 79—11705
low alloy, A533B, fatigue crack prop. 78—35517
low alloy, acoustic emission during ductile fracture, isothermal tempering effect 79—83241
low alloy, alloying constituents, XES determ. 78—73126
low alloy, at. absorpt. anal. using electrically dispersed sample 79—74459
low alloy, atmospheric corrosion in marine environments 80—30142
low alloy, B, quenchability and microstructure *(French)* 79—47727
low alloy, brittle fracture, quenched and tempered 80—11677
low alloy, C, corrosion fatigue crack growth, waveform effect *(Japanese)* 79—29274
low alloy, C-Ni-Cr-Mo (0.36 wt.%), impact toughness rel. to microstruct. *(Korean)* 77—21188
low alloy, cleavage fracture, fine scale precipitation dispersion effect, TEM obs. 78—60788
low alloy, cold resistance, effect of nitrides, carbonitrides, carbides, Cu precipitates 77—16594
low alloy, crack branching in delayed fracture 79—79067
low alloy, crack form. during stress relief in heated zones *(German)* 79—74242
low alloy, creep crack growth, microstruct., fatigue effects 80—7672
low alloy, creep damage and the remaining life concept 80—59574
low alloy, effect of grain size, and amount of pearlite on fracture resistance 79—100255
low alloy, exam. of fatigue crack, growth, and Paris Law parameter relationship 78—92343
low alloy, fatigue crack growth rate in high temp., high purity oxygenated water 80—40622
low alloy, fatigue crack nucleation under high cycle fatigue and uniaxial loading 79—79060
low alloy, fatigue crack propag. in deaerated distilled water 77—25177
low alloy, fatigue fractographs *(Japanese)* 78—92335
low alloy, Fe-Cr-C, austenitizing temp. effect on microstruct. and mech. props. 80—16341
low alloy, ferritic-pearlitic, carbonitride hardening 80—104174
low alloy, fibrous component zones size, depend. in fracture on impact test temp. and notch radius 80—21076
low alloy, H_2S embrittlement, susceptibility, alloying effect 79—91797
low alloy, high strength, correlation between fracture toughness, tensile props., fracture morphology 78—60789
low alloy, high strength, ductile failure criteria for blunting crack 78—64657
low alloy, high strength, hot compression dynamic precip. and coarsening of Nb(CN) 80—97514
low alloy, impurity and strength effect on H_2 induced cracking 78—27625
low alloy, influence of accelerated weathering on corrosion 80—55565
low alloy, isothermal tempering effect on acoustic emission during ductile fracture 80—85047
low alloy, macrosegregation 80—11647
low alloy, martensite twinning, direct anal. 80—2040
low alloy, Mn-P, temper brittleness, rare earth mischmetal effect *(Chinese)* 80—104249
low alloy, naval, stretch zone width meas., COD for ductile crack initiation 78—68813
low alloy, Nb effect on cold resist. 79—38954
low alloy, particle coarsening reactions, effect of cold deform. 80—71664
low alloy, pearlite block, exam. of crystallographic features, formation processes *(Japanese)* 78—84799
low alloy, precracked, crack growth and propag., repeating load effect in delayed failure 78—19861
low alloy, press. vessel, fracture toughness in post yield regime 77—16671
low alloy, pressure vessel and piping, factors affecting notch toughness 79—61730
low alloy, quenched, tempered martensite embrittlement, role of retained austenite and cementite 79—74251
low alloy, quenched and tempered, formation of stony fracture during forging 79—79059
low alloy, relationship between stationary creep rate and time to rupture *(Czech)* 79—70165
low alloy, rolled, nondestructive impact strength testing by coercive force meas. 79—52601
low alloy, S and Mn influence on high temp. strength and ductility after solidification from melt *(German)* 80—81106
low alloy, serrated flow and thermomechanical treatment *(Korean)* 80—30026
low alloy, SMCM 8, tempered, fractographic study of stress corrosion cracking *(Japanese)* 79—66214
low alloy, SNCM 8, quenched, tempered, prior austenite grain size effect on stress corrosion cracks *(Japanese)* 79—66215
low alloy, strength, Cr and N effects 80—104277
low alloy, study of deformation and fracture processes by acoustic emission transient anal., SEM and optical microscopy study 79—43311
low alloy, temper embrittlement and ternary equilib. segregation 80—60958
low alloy, tempered martensite embrittlement and crack initiation *(Japanese)* 79—66149
low alloy, test for determining reheat cracking susceptibility of heat affected zones *(French)* 80—16633
low alloy, thermally fatigued, fracture toughness 78—72872
low alloy, toughness, effect of packet size and lath width 77—16677
low alloy, type 10KhN1M, heat-treated, struct. and resist. to thermal embrittlement 79—15788
low alloy, type 12Kh1Mf, effect of thermal cycling on life under creep conds. 79—57075
low alloy, type 15G2AFDps, describing cyclic-creep processes with parametric eqn. 79—57074

alloy steel continued
low alloy, type 3sp, effect of temp. at end of rolling on mech. props., and coercive force 78–72799
low alloy, type 4340, quenched and tempered, effect of plastic strain followed by ageing, on torsion fatigue resistance 78–92360
low alloy, type A533B-1, fracture toughness meas. using small specimen strength ratio 79–70143
low alloy, type A553B, fracture toughness meas. using elect. potential method *(Japanese)* 80–93722
low alloy, type AISI 4340, martensitic transformation, TEM study 80–3043
low alloy, type SNCM 8, rotor disc, exam. of fracture, using a J integral approach 78–92352
low alloy, welded joints, cracking during heat treatment 80–7724
low alloy, X-ray fluorescence anal., matrix corrections, minicomputer program 80–3458
low alloy 10KhSND, thermal embrittlement when held for long periods at 340 to 450°C 77–70178
low alloy 30khGSNA, quenched grain refinement influence on impact strength *(Russian)* 80–20974
low alloy and mild, stress corrosion cracking in CO-CO_2-H_2O 77–21308
low alloy ferritic, sub-micron cavity nucleation, SEM obs. 78–95753
low alloy low C, types 45, 10GN2MFA, 15G2AFDps, fracture toughness characts. under cyclic loading 79–11703
low alloy medium C, sliding interfaces, division of heat and surface temp. rel. to oxidative wear 78–64712
low alloy Mn-Sb(2, 0.12 wt.%), reversibility of temper embrittlement, studied by XPS and AES 77–32667
low alloy press. vessel steel, fracture toughness determ. from invalid compact tension specimens 77–4848
low alloy sheet materials, 30KhGSA, regression anal. of critical stages of fracture process 79–15786
low alloy structural, pre-treatments to enhance graphitisation, dilatometric and optical microscopy study *(Japanese)* 79–78992
low alloy type 14Kh2GMR, high strength, welded joint, impact toughness, welding thermal cycle and tempering effects 80–3157
low alloy weldment cracking causes creep resisting 78–56760
low alloyed (Mo,Cr,B), structural and mech. props., report *(French)* 80–25691
low alloys, exam. of stress corrosion cracking in H_2S environments by const. strain rate method 79–29260
low alloys, high strength, stress corrosion cracking in saturated $Ca(OH)_2$ solns., due to Cl^- and SO_4^{2-} additions 78–88567
low alloys, Ni, exam. of stress corrosion cracking in S environment 79–20256
low and medium C content, relaxation phenomena in volume changes during tempering *(Russian)* 79–100176
low C, 15Kh2MFA and 15Kh2NMFA, neutron irrad. embrittlement, effect of P, Sb and Sn impurities 80–85055
low C, 18KhNMFA, quenched and tempered, fracture resist., nonmartensitic transformation products effect 79–96054
low C, cold-rolled, good and bad paintability, AES, SEM and X-ray diffr. characterisation of surfaces 79–42344
low C, Cr-Ni (25, 25 wt.%), σ phase form., prestrain effects *(Japanese)* 78–92260
low C, effects of pre-treatment on graphitisation behaviour *(Japanese)* 78–84860
low C, high C, bainite transform., heat treatment effects *(Czech)* 77–63661
low C, increased damping capacity, mathematical planning method *(Russian)* 80–45332
low C, low alloy, electron beam heat treatment of thin bands 78–3156
low C, low alloy, ferritic-pearlitic, high temp. mech. treatment, cooling effect 80–104193
low C, low alloy, Mossbauer study of retain austenite 78–48434
low C, Mb-Nb, reheated, quenched, tempered, microstruct. 77–36550
low C, Mn, recrystallisation and grain growth in hot rolling 79–47714
low C, Mn, strain hardening parameters, electron microscope obs. 77–63690
low C, Mn, surface segregation of Mn during annealing 77–36555
low C, Mn effect on recrystallisation and texture *(French)* 80–3110
low C, Mn surface segregation during annealing, kinetic studies 78–27528
low C, Mn-Nb, quenched and tempered, microstruct. and props. 77–36549
low C, Nb-V microalloyed, Nb, V effect on impact and toughness props. 78–15515
low C, rapidly solidified laser surface alloyed, electron microprobe obs. 79–70201
low C, structural transform. during deform. and annealing *(Russian)* 79–91707
low C, with Mo and B, proeutectoid γ to ferrite transform. *(French)* 77–73270
low C Cr-Ni, temper embrittlement by antimony, Ti addition effects 77–32683
low C Mn-V, VC effects on strength and brittleness 77–70055
low pearlite, low alloy, low temp. strength props., heat treatment 77–12658
low pearlite, Nb microalloyed, ageing at 600°C, mech. props. *(German)* 77–36542
low pearlite, Ti addition effect on transform. behaviour *(German)* 77–90343
low S, overheating 77–21185
low strength, strain induced fracture 79–43382
low-alloy, 35khN2VL, cold resistance determination, quick method 80–100997
low-alloy, BCC lattice, texture form. by drawing and pulling through non-powered rolls *(Russian)* 77–25100
low-alloy, bearing, mech. props., carbide behaviour effect *(Korean)* 80–93615
low-alloy, blunt-notched, fracture mechanism and failure assessment 80–16450
low-alloy, case carburised, retained austenite effect on contact fatigue strength 80–30096
low-alloy, creep, expt. investigation above 900 degrees C 80–81134
low-alloy, electron fractographic analysis of fatigue fractures 79–38965
low-alloy, etchant for revealing austenite grain boundaries 80–85098
low-alloy, fracture toughness and brittle fracture, S and rare earth additions effect 79–87720
low-alloy, fracture toughness characts., loading rate effect 80–100897

alloy steel continued
low-alloy, hardened deoxidised, delayed failure, influence of internal adsorpt. of impurities 80–60974
low-alloy, high strength, deforms. during cold crack developments in welded joints 80–81142
low-alloy, plastic deform. mechanisms under dynamic loading 80–100883
low-alloy, props. with nitride and Cu hardening at low temps. *(Russian)* 80–40372
low-alloy, residual elements, effect on props. 80–66643
low-alloy, transform. of austenite, cooling rate effect 79–38821
low-alloy, V effect on mech. props. 80–35312
low-alloy cast steel, high-strength, fracture toughness 77–56109
low-alloy pipe, low-cycle fatigue in H_2-evolving media, S content and sulphide inclusion effects *(Russian)* 78–11398
low-alloy pipe, resist. to fracture, S content and sulphide inclusions effect 79–96128
low-alloy samples with fatigue crack, work of crack propag. and fracture toughness 79–38959
low-alloy Si-Mn, uphill diffusion of C, at brazed joint with pig Fe 78–44280
low-alloy steel, abrasive wear resistance, effect of C content, annealing quenching 77–56115
low-alloy steel, bending, effect of strain rate on dynamic stress factors 77–56046
low-alloy steel, effect of B on radiation embrittlement 78–691
low-alloy structural 16G2 and 16GFR, struct. and props. after quenching and tempering 80–76280
low-alloyed, C-content influence on high temp. strength and ductility after solidification from melt *(German)* 80–81105
low-C, Al-stabilised, texturing during annealing *(Russian)* 78–19777
low-Mn low-C, susceptibility to brittle fracture 80–76340
loy allow, elastoplastic strain evaluation in crack weakened cross sections by fracture mechanics 80–45380
machining, 12L14, effect of Pb and Te on hot-shortness mechanism 80–104190
machining of steel 4340, by TiC-coated high speed steel tool 78–11435
magnetisation direction in interaction domains in demagnetised type YuNDK24 *(Russian)* 79–99720
marageing, austenite formation, stability, transformation to martensite *(Russian)* 79–91646
marageing 300 grade, serrated flow in austenitic state 80–30041
maraging, 0Kh6N8M7S, effect of Cr, Ni and Mo on hardness 80–21093
maraging, 18% Ni, effect of solution and ageing treatments, on microstruct., tensile props., fracture toughness 78–80648
maraging, 18% Ni, fatigue strength, effect of soln. treatment and inclusions 78–23805
maraging, 18 Ni, welded joints ageing props. obs. *(Japanese)* 80–40401
maraging, 18 wt.% Ni, solution heated and aged, surface damage during machining, unlubricated 78–15599
maraging, 18 wt.% Ni, tensile props., effect of aged struct. and austenite grain size 77–48511
maraging, 18 wt.% of Ni, annealed, surface damage during machining, lubricated conditions 77–59948
maraging, 18Ni300, ageing, electron diffr. and microscope obs. *(Polish)* 79–34070
maraging, 250-grade, ductility and toughness of hot isostatically pressed powder 78–52925
maraging, 300 grade, low temp. elastic props. 78–27555
maraging, $\alpha \to \gamma$ transform. rate *(Russian)* 77–8821
maraging, α to γ transform. and austenite stabilisation *(Russian)* 79–52212
maraging, (18 wt.% Ni), solution annealed, exam. of cryogenic tensile, fatigue, and fracture props. 78–92311
maraging, and HY-80, deform., hydrostatic pressure effect 77–36596
maraging, Co-Ni-Mo (20,15,5 wt.%), environmentally assisted fracture 77–52547
maraging, Cr-Co, effect of ageing on microstruct., TEM and neutron diffraction exam. 78–84867
maraging, Cr-Ni-Ti, effect of Ti addition on hardness and energy scatt. 79–15687
maraging, crack resistance, effect of external stress during ageing *(Russian)* 77–59902
maraging, DI52, low cycle fatigue in gaseous H_2 *(Russian)* 78–35478
maraging, effect of deformation on props. 80–21032
maraging, effect of thermal cycling (γ to and from α) on props. 80–20986
maraging, electron fractographic analysis of fatigue fractures 79–38965
maraging, fatigue crack growth, during impact tests, exam. of kinetics 78–88525
maraging, Fe-Cr-Co-Mo, phase transforms. during high temp. austenitisation and solid soln. decomp. *(Russian)* 80–66524
maraging, fracture toughness data, comparison with equivalent energy and energy per unit area data 78–52965
maraging, fracture toughness of thin sections 78–27616
maraging, grain refinement due to cyclic heat treatment 78–52971
maraging, hardening mechanism of quenched samples, tempering *(Czech)* 79–78989
maraging, Hart's model in hydrogen embrittlement 79–24621
maraging, heating of thin samples with brief ageing, N6G4M, ON18K9M5T 78–52866
maraging, high strength, gaseous H_2 embrittlement 77–86147
maraging, hot work die use, mech. props., heat resistance 77–70081
maraging, inert gas atomised, hot isostatic pressing temp. effect 79–24460
maraging, influence of microstructure, strain rate and temp., on tensile props. 80–11733
maraging, intermetallic phases precip. study by electron microscopy *(Polish)* 80–89217
maraging, investigation with lower Ni and Co contents *(Chinese)* 78–84812
maraging, N12K7M5TYu, fracture influence of high-temp. thermomechanical treatment on characts. *(Russian)* 78–27591
maraging, Ni, H_2 assisted crack growth 77–73346
maraging, Ni, stress corrosion cracking 78–35563
maraging, Ni (18 wt.%), fatigue crack initiation and propag. in earlier stage *(Japanese)* 77–8937
maraging, Ni (18 wt.%), with aged struct. at low temp., delayed failure crack and fracture toughness 78–7047

alloy steel continued
maraging, Ni-Co-Mo, ageing and evolution peak at 470°C, calorimetric anal. *(Japanese)* 79—100156
maraging, Ni-Co-Mo, precipitation, elec. resist. meas. *(Japanese)* 78—11228
maraging, Ni-Co-Mo (18,10,5 wt.%) precipitation *(Japanese)* 78—15402
maraging, Ni-Co-Mo (18, 8, 5 wt.%), fatigue strength charact. *(German)* 77—21241
maraging, notch strength 77—56056
maraging, plastic deform. effects on ageing kinetics *(Russian)* 77—77508
maraging, precipitation hardening, strength and struct. *(German)* 79—47701
maraging, prior austenite grain size effect on tensile ductility and fracture toughness 79—100226
maraging, SCC, subcritical flow growth, comparison of aircraft alloys in NaCl soln. 78—53028
maraging, Se microalloying, machinability improvement 80—21116
maraging, solubility, of Fe-Mo-Co (10, 0 to 20 wt.%) Laves phase, depend. on Co *(Russian)* 79—100145
maraging, steady state unidirectionally solidified, austenite reversion and deform. 77—25118
maraging, thermally embrittled, TiC precipitation 77—25055
maraging, thin sheet, fracture toughness testing *(German)* 77—66728
maraging, type 200, effect of freq. on cyclic crack growth, in salt water environment 78—64680
maraging, type Kh13N8D2TM, conditions for formation of stable austenite 78—84868
maraging, type N18K9M5T, rate of movement change of fatigue cracks as result of ageing *(Russian)* 79—70149
maraging *(Russian)* 79—78962
maraging 18%Ni, calorimetric anal. of ageing *(Japanese)* 80—89264
maraging 18 wt.% Ni, annealed, surface drainage during machining, unlubricated conditions 77—59947
maraging 250-grade, fatigue crack growth model, notch analysis of fracture approach 78—52984
maraging 350, produced by powder metallurgy, mech. props. 78—15334
maraging alloy, intermetallic compound solubility, thermodyanmic calcs. *(Russian)* 80—40363
maraging low-Ni, phase transformations *(Russian)* 78—88465
maraging N18K9M5T, crack propag. resistance under stress corrosion 77—70224
maraging Ni (18 wt.%), grain boundary precipitation, scanning Auger electron obs. 78—3132
maraging Ni-Co-Mo, strengthening by repeated strain ageing *(Japanese)* 79—100157
maraging steel, ageing study by internal friction meas. 77—12660
maraging type with 18% Ni, ageing treatment effect on fatigue crack propag. 80—16411
martensite structural singularities during tempering, electron diffr. study *(Russian)* 79—100177
martensitic, alloying element effect on coarsening behaviour of cementite particles in ferrite 80—66518
martensitic, fatigue crack form. associated with cyclic slip deform. along prior austenite grain boundaries 78—60831
martensitic, heavily doped, linear expansion meas. 80—103501
martensitic, Ni-Cr-Mo, fatigue crack initiation and propag. in water 77—9000
martensitic point, influence of cooling rate on position *(Russian)* 79—70063
martensitic transform. effect on stress development during quenching in type 60 NCD 11 *(French)* 79—91712
martensitic transform. microkinetics, in type N24M5 78—56637
martensitic transformation, ferrite and alloy carbide interrelation 80—3040
martensitic transforms. during deform. of types N28, N29, N30 and N31 78—56639
mechanical properties, morphology, transform. kinetics and composition interrelations 77—86146
mechanical properties after warm extrusion 77—12668
mechanical props. at low temps. 77—16615
mechanical props. meas. by acoustic methods, chem. composition influence 80—104384
medium C, B addition effect on mech. props., fine structure 80—11752
medium C, fatigue failure, alloying influence *(Russian)* 80—21081
medium C, microalloying with V and Ti, effect on hardness and structure 80—11750
medium C H2KhMFA, quenched and tempered, fracture resist., nonmartensitic transformation products effect 79—96054
medium strength, SEM obs. of fracture surfaces, cleavage fracture model 77—36649
metastable alloys, singularities of $\alpha \to \gamma$ transform. and hardening *(Russian)* 79—52210
micro-alloying, effect on improving properties, in R6M6 78—6939
micro-duplex structure, neutron diffr. anal. of texture and its development 79—91692
microalloyed, alloy carbide precipitation during isothermal ageing 80—3077
microalloyed, fine grained, mech. props., effect of hot dip galvanising *(German)* 77—36679
microalloyed, recrystallisation, precipitation effect 79—47695
microalloyed, types V1599, V1600, V1286, NbCN precipitation in undeformed austenite 80—89230
microalloyed review of development 79—47699
microsegregation in forging, electron microprobes testing *(Croatian)* 77—36516
microstruct. and fracture of steel 52100, exam. as function of austenitising in temp. range 800 to 1100°C 78—76673
microstructure characteristics, statistical processes *(German, English)* 78—95884
microstructure of cup and cone fracture surface, effect of size of disperse phase particles *(Russian)* 78—68762
mild, decomp. of CCl_4 and corrosive action 80—45420
mild, low cycle fatigue crack propag. at a notch under pulsating load 80—40492
mild, signature response, for friction and wear 80—40541
mild, yield point phenomena in fission reactors, effect of neutron irrad. and N_2 conc. 80—45365
mild Cr welding, 550°-850°C heating effects on structure and toughness 79—24540

alloy steel continued
multielement determ. by computer-controlled X-ray spectrometry 77—56318
natural gas environment effects on strength *(Russian)* 78—11401
NBS standard alloy steels, Co content, X-ray fluoresc. anal. 78—31734
nitride phase hardening, precipitation and solution kinetics after heat treatment 78—95756
nitrided age-hardened, for blanking punches, chipping resist. props. *(Japanese)* 80—89340
nitriding, effect on struct. and internal stresses 80—30162
nondestructive mag. quality control method in heat treatment of 30KhN2MFA and 40Kh 80—108662
nonmagnetic 40KhNM, corrosion resistance, melting procedure effects 77—70226
nonmartensitic decomposition of austenite, fracture strength of high tempered products *(Russian)* 78—11304
notched beam, fatigue crack emanates from notch root, fracture strength 78—72866
nuclear pressure vessel, SA533B-1 and SA302B, fracture toughness prediction using crit. fracture stress and strain models 80—25855
nuclear reactor pressure vessel steels, optimum chem. comp. rel. to props. 80—93517
oriented Si steel, magnetisation hysteresis loops prediction 78—64221
oxidation of Cr-Mn alloy, sub-cinder layer role as protective coating *(Russian)* 80—93686
oxidation of structural steels in gas-cooled reactors 80—45447
oxidation reaction of Si and Mn during CO_2-O_2 arc welding 77—60116
oxidation resistance, N effect 80—66706
oxidation resistance at elevated temps., effect of various alloying additions 77—56134
pearlitic, Cr-Mo, Cr-Mo-V, and Mo-V, heat resist., Mo content rel. to mech. props. 79—20134
pearlitic, creep-induced micropore healing kinetics of 12MKh and 15Kh1M1F, TEM obs. *(Russian)* 80—71690
pearlitic, heat-resist., secondary phase precipitation, deform., and fracture during creep *(Russian)* 80—50669
peritectic transformations, influence on initial struct., solidification, grain boundaries *(Russian)* 80—66621
pipe, large diameter, load carrying ability, failure charact. 79—5055
plastic deformation, type 36NKhTYu, effect of surface condition on initial stage 78—84929
plastic deformation depend. on grain size in type 08KP low C steel *(Russian)* 80—66580
plastic deformation of 15KhM1 and 20KhM1 with thermal cycling 80—89310
plasticity and resist. to deform. of MhN77TYuR, deform. parameters effect 77—63750
plate, rolling direction determ. with notched bend test specimen *(German)* 77—60003
plate, thickness and rolling ratio influence on inclusion behaviour 80—16340
plates, comparison of dynamic tear and Charpy V notch impact props. 78—92357
pore formation in creep, precip. hardening, 1Kh12V2MF 77—63747
positron lifetime and X-ray particle size meas. during high cycle fatigue of AISI 4340 79—5053
potentiostatic control limitations in stress corrosion crack growth meas., in NaOH soln. 78—53031
potentiostatic development of structures 78—95887
powder forged, fatigue, surface treatment effect 80—85048
powder metallurgical steels, using Mn-Cr(V)-Mo-C master alloys, development 80—50576
powder metallurgy hot forging for differential pinion gear 78—15337
precipitation behaviour under high temp. conditions, photoemission electron microscope obs. 80—108456
precipitation effect on microstruct. and mech. props. *(French)* 80—25708
preparation for instrumented anal., HF induction melting and centrifugal casting 78—48607
pressing die X45 CrNiWMoVCo 9.9, test results *(German)* 80—50785
pressure effect on reverse martensitic transform. and mech. props. for N30 and N29T *(Russian)* 79—38824
pressure tank plates, heat-treatment effects and mech. props. *(German)* 80—40409
pressure tank plates, yield point influence on brittle fracture, tensile strength *(German)* 80—40539
pressure vessel, A508 C1 2 steel, microcrack formation during stress-relief annealing of a weldment 78—80629
pressure vessel, irradiated type A533B-1, reference fracture toughness curves 80—100921
pressure vessel, with defects, failure anal. 77—44361
punch, for blanking tools, method of wear resist. determ. 80—55600
PWR primary circuit constituent materials, design features verification *(French)* 79—17976
quality, effect of methodic factors on quality of S replicas 79—24691
quench ageing, effect of Mn content on C and N precipitation and mech. props. *(German)* 78—31409
quenched, high strength, shot blast hardening effect on repeated impact bending 79—1914
quenched, types 37KhGSTF and 44KhGSTF, X-ray diffr. testing of heat treatment 78—56834
quenched 40Kh2N5SM and 18KhNVA, nature of delayed fracture 77—90456
quenched and tempered, fatigue crack propag., effect of mean stress 77—59914
quenched carbonitrided, multicycle fatigue failure 80—104283
radiation embrittlement, heat treatment effects 78—19893
rail, fracture tough, exam. of wear in rollers, subject to creep 79—15808
rapid anal., use of central laboratory computer *(German)* 77—48703
rare earth addition effects and behaviour, review *(Chinese)* 79—43257
rare earth additions review 78—72786
recrystallisation after hot deformation 77—44268
rectangular beam, stress-strain anal. of cyclic plastic bending and torsion 78—90734
reheating quenched steel to improve plasticity and notch toughness 77—63701
residual stress distrib. effect on fatigue crack growth 79—57111
resistance functions, of alloy 30KhGSA in tension and torsion 80—16397
restricted durability, subject to pure bending with rotation 77—90431
reversible temper brittleness kinetics *(French)* 78—35498
reversible temper embrittlement, book contrib. 78—11334

alloy steel continued
Rheocast, struct. and props. 77–28804
Rheocast high performance alloy, solid-liquid phase charact. 77–28803
rolled 15 MND 6, nuclear reactor cell material, determination of non-cracking threshold *(French)* 79–52367
roller-bearing, high-temp. wear resistant coating treatment *(German)* 79–24629
rolling wear study of misaligned cylindrical contacts 80–108590
rolls for cold-rolling mills, surface hardening, contact fatigue strength 79–24664
RPV type, toughness values compilation, temp.-range validity 77–48611
rust analysis by Mossbauer spectroscopy 79–43487
secondary hardened, microstruct. rel. to mech. props. 80–25851
secondary recrystallisation props. of multilayered types St2kp and 10Kh18N10T steel *(Russian)* 80–66533
segregation embrittlement 80–60958
semi-high speed, martensite degradation due to fatigue *(French)* 79–91615
sheet, crack-propag. resist. in heat-affected zone in presence of H, rolling direction and preliminary plastic tensile strain effects 80–60971
sheet deformation, criteria for determ. of deformation limit G *(German)* 80–21000
sheet material with laminar coating, damping capacity improvement 79–66098
Si-Mn-Cr-C (1.1, 0.9, 1.0, 0.29 wt.%) 30KhGSA, heat treatment effect on strength and toughness 78–15437
silver, elastic limit, bending strength, and ductility rel. to tempering temp. after quenching 78–95764
sintered, Cr-Mo, CaF addition effects on struct. heterogeneity 78–60611
sintered, high speed, with Ti(C,N) additions 78–11160
sintered, low alloy, isothermal transformations, porosity effects 80–3032
sintered, maraging, N14K7M5T, mech. props., effect of Ti additions 77–25081
sintered, Ni-Cr-Mo additions, struct., props., thermomechanical treatment effects 77–12657
sintered Cu, hardenability *(Japanese)* 77–48527
sintered type M2 high speed, heat treatment response and cutting props. 78–15336
sintering, reaction kinetics of Fe and graphite powders 77–55907
soft magnetic steels, coercivity meas. 77–41659
softening of heat affected zone under postweld tempering 77–21196
softening process in deformed type 15GYuT, metallographs *(Russian)* 78–52840
solubility of W and Mo in Ti(C,N)$_x$ 80–16276
spheroidised pearlitic, superplasticity of USA *(Russian)* 78–19826
splat cooling of Fe-Mo-C alloy, microstruct. changes 78–84855
spring, fatigue life testing, universal machine 78–11479
spring alloys, microplastic deform. and endurance limit 80–81197
spring leaf retainer with variable ductility, processing error, cold working error *(German, English)* 79–70267
static and fatigue strength, tension and compression test results 78–95810
statistical fatigue props. of heat treated JIS steel S 45 C and SK 5 SCM 3 and SNCM 8 78–44222
steel, 30N9K4, effects of Mo, V, and N on grain growth, tempering, hardenability, strength and toughness 78–44202
steel, 35NiCr18, bainite transformation, study with aid of hot stage microscope 80–76253
steel, alloy structural, anomalous grain growth 80–20984
steel, alloy type 25KhN3MFA, tempering of bainitic structure 80–20983
steel, Co, shrinkage kinetics of sintering and dependence on carbon content 79–100087
steel, Cr (17 wt.%), influence of Mo on intergranular corrosion *(French)* 80–21182
steel, Cr-Mn eutectoid, pearlite growth kinetics and partitioning 80–29963
steel, Cr-Mo-V, high-temp. cumulative damage for stage I crack growth 78–19883
steel, CrMoV, creep-resistant, quantitative struct. parameter *(Czech)* 80–35266
steel, ferritic and austenitic, microstruct. study by means of replicas taken from components at 100°C 80–81256
steel, high Ni, orientational variations of martensite transform. during deform of metastable austenite 78–84805
steel, HSLA, V and N effect on recovery and recrystn. during and after hot working 80–84973
steel, low alloy, rel. between over-heating embrittlement and behaviour of S, Auger spectroscopy anal. *(Japanese)* 79–79088
steel, low strength, strain induced fracture 79–43382
steel, low-alloy sheet, welded hydraulic turbine volute chamber, strength and toughness 78–68820
steel, medium C, Mn, type 42Mn2 cylinders, flake immunisation by hot working *(Chinese)* 80–66540
steel, Mn-Si, for springs, metallographic study, present phases rel. to mech. props. *(French)* 80–21090
steel, Ni-Co-Mo-Ti, maraging, electron diffr. obs. of second phase *(Chinese)* 80–11655
steel, Ni-Cu, shrinkage kinetics of sintering and dependence on carbon content 79–100087
steel, structural, crack growth under cyclic load, stress intensity factor 79–87709
steel 30L, critical size of nometallic inclusions in fracture 79–83322
steel St3, kinetics of form. and struct. of thermodiffusional protective coatings 77–56158
steels, heat-treated, nature of high sensitivity to stress raisers 80–21051
strain ageing effect on strength and toughness, susceptibility to strain hardening, in type 15Kh2NMFA 79–57028
strain energy anomalies, plastic strain mechanisms *(Russian)* 79–52300
strength, static, dynamic, interrelation 79–15725
strength parameters and crack growth energy correl., notched alloy steel specimens 77–73334
strength-toughness relationship 77–70137
strengthening by strain tempering, deform. effects 78–15424
stress concentration, effect on endurance of type 16GNMA under repeated static loading 79–43412
stress corrosion crack, electrode pot. distrib. 77–90506
stress corrosion cracking in deionised water, temp. effects. on 300M 78–53029
stress corrosion cracking of 65G, simulated field trials of inhibitor KXO in H_2S cracking *(Russian)* 78–31573

alloy steel continued
stress intensity factor of bearing steel GCr15, S effect *(Chinese)* 77–73300
structural, addition of solid SiO, effect on ductile fracture 80–16465
structural, bending moments and tensile creep, relaxation bending test device 79–70245
structural, BS 4360-50C, stress ratio and freq. effect on fatigue crack growth 80–21068
structural, CK10, temp. and freq. depend. of stress-strain behaviour under cyclic loading *(German)* 79–38888
structural, crack growth under cyclic load, stress intensity factor 79–87709
structural, CrN-modified, tempering and quenching effects on struct. and props. 77–59835
structural, ductile and brittle fracture resist. in stable crack growth stage 79–52369
structural, effect of rare earth metals on cold temper brittleness 79–29202
structural, exam. of mech. props. when under impulsive loading *(Czech)* 79–91742
structural, heat treated, impurities effect on embrittlement susceptibility and temper brittleness 79–38955
structural, high-strength, stress-strain curves, shape effects *(German)* 80–45343
structural, lithoidal fracture surfaces *(Russian)* 77–8905
structural, macroscopic and microscopic features of fracture 80–81179
structural, microalloyed, precipitation hardening, strength and struct. *(German)* 79–47701
structural, St37-2, crack tip displacement and flow curves *(German)* 79–47747
structural, St37-2, large plastic deform., fracture behaviour, COD concept validity *(German)* 79–47764
structural, type 30KhGSA, effect of thermomech. treatment on strength, fracture toughness and fatigue props. 80–11676
structural, wide plate tensile testing eval. *(German)* 80–100969
structural and phase changes of type ST.5 steel after high temp. heating *(Russian)* 80–55439
structural changes during thermocyclic working of type Kh16N11M3 steel, dislocation struct. *(Russian)* 80–54243
structural components, flaw assessment based on cleavage fracture hypothesis 78–60804
structural heterogeneity of 70 ton ingots γ to α transform. in dendritic sections 77–70047
structural low-alloy, radiation hardening, rel. to embrittlement *(Russian)* 77–21243
structural sheet, high-cycle fatigue crack growth under in-plane biaxial loads 80–40495
structural steel, electron fractographic patterns of fatigue fracture under cyclic loading 77–56094
structural steel, type St3S, hardness, random functions 80–76329
structural transformations during heat treatment, and wear resistance of steel U20Kh6T2D 78–88484
structure and properties after nitriding in molten salts, steel 08kp with Al diffusion coating 80–35418
structure steels 4Kh4VMFSSh and 45Kh3V3MFSSh, grain size, hot deform. and austenitising effects 80–76286
sulphide corrosion cracking resistance, test procedure and eval. 77–63842
sulphide cracking resistance, strengthening method influence, 40Kh steel 80–55577
sulphide inclusion behaviour during mechanical treatment of AISI 4340 78–3151
surface burnishing effect on low cycle corrosion fatigue *(Russian)* 77–16730
surface hardening by 2 kW CW CO_2 laser, En8 steel 79–83396
surface plastic deform., effect of heating conditions, types 45, 40 Kh 78–53033
surface quality improvement, thermomech. treatment 80–61020
temper brittleness of complex alloy structural steels 78–44209
temper brittleness of type 30Kh2N2SMK5 79–96129
temper embrittlement, comp. influence 80–66658
temper embrittlement, review 79–20154
temper embrittlement and embrittling intergranular segregates, Mo effects *(French)* 79–91788
temper embrittlement control progress 78–72797
temperature profile, IR obs. during pull tests 77–44427
temperature-time dependence of long-time structural strength, type 15kh1M1F 79–100232
tempered martensite embrittlement, and retained austenite, exam. 78–56754
tempered martensite embrittlement mechanisms 79–8351
tempering of steel R6M5 after quenching with rapid heating 77–56002
tensile test, regulated, strength and deform. characteristic values, consistency *(German)* 80–93712
tensile testing of 20Kh and 38Kh2N2Va steels, deform. rate effect 79–70115
tensile tests, −196 to +20°C 79–61692
tension test, computer simulation of deform. to fracture 79–11667
tension-compression tests, cyclic, macroscopic changes of length, of type Ck45 *(German)* 80–40424
testing cracked specimens for impact bending, expt. planning method appl. 80–71831
thermal and electro-physical props. of various heat resisting stampings *(Russian)* 78–51698
thermodynamic aspects of gas-metal heat treating reactions 79–24547
thermodynamic prediction of Ae_3 temp., additions of Mn, Si, Ni, Cr, Mo, Cu 78–64524
Ti (0.1 to 0.55 wt.%), strengthening by carbide precipitation 77–25062
tool, abrasive wear rate rel. to fracture toughness and microstructure *(German)* 79–29232
tool, and high speed steel samples, high frequency induction melting and centrifugal casting method for prep. in instrumental anal. *(Japanese)* 79–43232
tool, blanking punch, chipping behaviour *(Japanese)* 79–100250
tool, chipping resistance testing method for blanking punches *(Japanese)* 79–100308
tool, cold hydrostatic extrusion rel. to struct., props. 79–20068
tool, cutting blades, heat treatment in fluidised bed, hardening 79–20087
tool, fatigue crack propagation, acoustic monitoring 79–86313

alloy steel continued
tool, fully annealed, cantilever beams, nonlinear damping for nonsinusoidal strain 79—47762
tool, hardened, crack propag. under cyclic load *(German)* 79—24596
tool, high heat resist., density and extension coeff. *(Russian)* 79—51282
tool, high speed, wear, effect of magnetisation on tool life 80—89361
tool, high speed multispeed tool life tests with radioactive tools 78—44338
tool, high-strength, mech. props. in compression, tempering temp. effect 79—83240
tool, improvement of props. by ion implantation 80—16601
tool, low alloy, methods of revealing austenitic grain 80—25949
tool, M2, laser surface melted, heat treatment effects on struct. 79—70086
tool, maraging, based on N12M10, exam. of hardening, crack resistance and wear *(Russian)* 79—34047
tool, martensite plate size, austenitization 79—24549
tool, martensitic hardened, reagent for revealing austenitic grain size 80—21207
tool, martensitic plate arrangement following austenisation 77—40420
tool, material related model for thermal fatigue in hot work appl. 79—91791
tool, quenching procedure effect on distortion, tool life 80—50657
tool, TiC coated by CVD, wear resistance 79—34196
tool, type Kh12M structural inhomogeneity rel. to wear resist. *(Russian)* 80—66672
tool, type KhVG, carburising and quenching, effect on fracture toughness 80—29997
tool, type M2, laser melting and heat treatment, microstruct. charact. 79—100188
tool, type U10A and R6M5, phase comp. and phys. props. after hydrostatic extrusion 79—96053
tool steel, retained austenite estimation during tempering, DTA *(German)* 77—28831
tool type M2, surface hardening and microstruct. refinement by laser melting, electron beam melting, heat treatment *(Korean)* 79—70093
toughness evaluation of AISI 4340, austenitized at high and low temps. 77—86155
transformations from austenite 77—25045
transformer, formation of perfect cubic texture in thin sheets *(Russian)* 78—80557
transformer, textural barriers to grain growth after cold rolling and annealing *(Russian)* 78—39796
transformer steel magnetic loss variation due to nonuniform normal press. *(Russian)* 79—91250
TRIP, warm extrusion, process control and tensile props. 80—16338
TRIP steels, fatigue strength 80—108552
type 08Kh15N5D2T, martensitic, high temp. embrittlement *(Russian)* 79—70153
type 25GS, increasing fatigue resistance by surface plastic deformation 78—88530
type 37KhN3MF, austenite grain growth depend. on structural inheritance *(Russian)* 79—61582
type AISI 4340, quenched and tempered, U-notched bend specimens, effect of H_2 on fracture 79—61716
type HF-1, microstruct. effects on fracture toughness, ductility, strength 79—74255
ultrahigh strength, Si addition and retain austenite effect on SCC, quenched and tempered 78—48567
ultrahigh-strength, near threshold fatigue crack propag., microstructure effects 77—86168
uphill diffusion during homogenization 77—90381
US attenuation, heat treatment effects 78—44315
vitreous enamel coating effect on mech. props. of surface layers 80—35424
warm extrusion effects on struct. and mech. props. 77—44311
wear particles, spheroid form. by cavitation erosion 79—52382
wear resistance, change through hardened layer 79—96153
wear resistance, mech. props. and struct. effects 80—35338
wear resistant diffusion coatings of B-Cr(Si) on type U8 78—56823
weld, deformation criteria of low cycle failure 78—39875
weld metal, contrib. to mechanism of Nb(C,N) precip. *(Slovenian)* 78—84816
weldments, heat-affected zone struct. 79—24552
welds, distrib. of Cr, Ni, Mn, Si, Ti, laser emission microanal. method 78—61110
Whittemore gauge length meas., reliability 77—36669
work hardening effect on martensitic transform. cond. *(French)* 80—16329
X-ray fluoresc. anal., interelement correction, models, computer program 77—56315
yield point, temp. depend. anomaly for steel OKh18N10T, subjected to low temp. thermal cycling *(Russian)* 78—48489
Al alloying addition effect on resistance to hydrogen embrittlement 77—59925
Al killed, density changes, void growth in biaxial stress fields, plastic deformation 80—71692
Al killed, rolled sheet, plastic anisotropy theory based on yield function of fourth order 78—31458
Al killed BOP, degreased and annealed, surface exam. *(German)* 77—52686
Al, quenched, tempered, orientation of precipitated Fe_xC particles, X-ray obs. *(Russian)* 79—29063
Al semikilled, $(Fe_xMn_{1-x})O.Al_2O_3$ inclusions, deoxidation, thermodynamic conditions 80—60830
Al steel, austenite, martensite cryst. struct. changes on γ irrad. 79—90699
Al steel, κ'-martensite struct. and $\kappa' \rightarrow \alpha_m$ transform., X-ray diffr. *(Russian)* 77—59786
Al, steel, relax. twins in martensite, electron diffr. and electron microscopy *(Russian)* 78—47391
Al treated steel for sulphide corrosion resistance 77—63826
Al-C, austenitic, microstruct., Mossbauer obs. *(Russian)* 80—29655
Al-C, redistribution of C during tempering *(Russian)* 77—90371
Al-Cr, $FeO.(Al_xCr_{1-x})_2O_3$ inclusions, thermodynamics 80—60831
Al-Cr-Mo, nitride hardened roller, surface fatigue failure under pure rolling and sliding rolling contacts 79—79183
Al-Cr-Mo, nitride hardened rollers, surface fatigue resistance under pure rolling and sliding-rolling contacts 79—79184
Al-killed, deep drawing, texture control as affected by processing variables 79—91689

alloy steel continued
Al-killed, fatigue life for program loading of multiple repeated two step stresses *(Japanese)* 80—66632
Al-stabilised steel, texture formation in continuous annealing, effect of coiling temp. of hot strip 79—91688
Al-steel, cementite isolation, Mossbauer anal. 80—93225
Al-Ti-Nb-(Mo), low-alloy, toughness improvement through Ti additions 80—66525
Al-Ti-V-(Mo), low-alloy, toughness improvement through Ti additions 80—66525
Al-Ti-(Mo), low-alloy, toughness improvement through Ti additions 80—66525
Al-V-(Mo), low-alloy, toughness improvement through Ti additions 80—66525
B, depth distrib. meas. using time of flight method and $^{11}B(p,n)^{11}C$ reaction 80—71986
B distrib. in reactor fuel cladding after Na exposure and high-temp. 77—57719
B segregation assessment 77—63627
B-Si, Cu addition effect on mag. props. 80—89366
BN extraction, and identification, IR anal. 80—85254
C and low-alloy steel inherent austenitic grain size determ., exam. of methods used 78—85071
C-Cr (0.6, 13 wt.%), friction during working stresses and rheological charact. at high temps. *(Russian)* 77—66702
C-Cr of surface residual stress by heat treatment 80—97501
C-Cr-Mo-V, high speed, exam. of fracture toughness and critical flow anal. 78—72848
C-Cr-Mo(Cr-W)(Mo-W)(Cr-Mo-W), high C amorphous crystallisation behaviour *(Japanese)* 79—94911
C-Cr(Mo)(W), high-C, amorphous, crystn. behaviour *(Japanese)* 79—94911
C-Mn, accelerated H_2 charging in aq. H_2SO_4 at 0.2% yield stress 80—30144
C-Mn, anisothermic oxidation 79—66195
C-Mn, corrosion cracking, role of microstresses and crystal lattice stresses *(Russian)* 77—25190
C-Mn, corrosion in acidic soln., metallurgical factor effects 79—70206
C-Mn, elevated temp. embrittlement under impact loading 77—44366
C-Mn, environmentally assisted fatigue crack propag., stress waveform and hold-time effects 79—79175
C-Mn, fatigue crack growth retardation following load reduction 79—70141
C-Mn, stress corrosion cracking in PO_4 solns. over range of potentials and PHs 79—39021
C-Mn, threshold stress intensity range in fatigue 80—30058
C-Mn, types SA-516-70, SA-105-B, fracture energy criterion determ. by static and dynamic testing 80—40651
C-Mn-Cr-Mo (0.4, 0.8, 1.1, 0.25 wt.%) C, Ni, Mo, Cr addition effects on toughness of bainite 78—11327
C-Mn-Nb, Nb microalloying, weldable, structural, recrystallization and precipitation induced by high temp. deform. *(French)* 79—61632
C-Mn-Nb, structural, for seamless line pipe tube, brittle fracture resistance *(Czech)* 77—70161
C-Mn-P, P effect on mech. props. 77—63745
C-Mn-Si, dual phase stress-strain curves, deformation behaviour 79—52324
C-Mn-V-Al-N, fine grained steel, relationship between ferrite and austenite grain size 80—3001
C-Mn-V-Cb-N, high strength low alloy, controlled-rolled 80—100803
C-Mn-(Cr), structural changes during stress cycling after heat treatment and cold rolling *(Russian)* 78—19787
C-Mn(-Nb), weldable, high temp. thermomechanical treatment 79—15709
C-Mo-P, intergranular fracture and grain boundary segregation, P, H, Mo effects *(Japanese)* 79—15775
C-Ni-Cr (0.6, 1, 1 wt.%), grain boundary segregation of S, N, P, As, Sb and Bi *(Japanese)* 78—15405
CC Cr-Mo-V, heat resisting, creep, probabilistic physical granulation *(Czech)* 79—70125
CC Cr-Mo-V (1,1,.25 wt.%), Mo_2C-V_4C_3 precipitation, creep rupture test *(Japanese)* 79—70070
Ce-Nb, addition effects on hot plasticity *(Russian)* 77—66680
Co (2 wt.%), effect of Co on pearlite growth 77—90359
Co-Cr-Mo, type HY 180, correl. between advanced NDT evaluation methods and fracture mech. parameters 80—97675
Co-Cr-Mo HY 180M, SCC in NaCl, temp. effect 80—108633
Co-Cr-Mo type HY-180M, mech. props. and SCC, overageing effect 80—108634
Co-Cr-Ni-Mo-Mn (39.65, 20.25, 15.33, 7.08, 1.9 wt.%) carbide formation during tempering after plastic deformation 80—16330
Co-Ni-Cr-Mo AF 1410 wear against stainless steel, repetitive impact, microstruct. effect 79—74263
Co-Si-Cr-Mo(2,2,1,0.3 wt.%), eutectoid, alloying additions effect on pearlite interlamellar spacing *(German)* 80—40327
Co-W-Mo-Cr-V, high-speed tool, splat quenching, props. and struct. 80—76294
Co-W-Mo-V-Ti-C (25.3, 12.8, 6.2, 0.5, 0.5, 0.05 wt.%), martensitically aged, structural transformation, and strengthening mech. *(Russian)* 79—15676
Cr, 5KhGSVF, tempering resistance, mech. props., Cu addition effect 79—79012
Cr (0.5 wt.%), austenite-pearlite transformation 80—97480
Cr (1 to 5 wt.%), effect on transform. of Cr content and all round press. of 25 kbar *(German)* 78—11219
Cr (10 wt.%), precip. free ferrite form., STEM 80—84941
Cr (12-18 wt.%), transformation behaviour *(German)* 80—40349
Cr (13 wt.%), fatigue, effect of toughness *(Japanese)* 78—7025
Cr (13 wt.%), sintered, organometallic complex addition effects on mech. props. 80—25595
Cr (13 wt.%), tempered, quenched, fatigue resistance in corrosive medium *(French)* 78—23870
Cr (13 wt.%), wear of Al bronze on steel in presence of aviation fuel 80—11781
Cr (17 wt.%), ferritic, influence of Mo on intergranular corrosion 80—30139
Cr (17 wt.%), stainless, hot-rolled texture, effect on cold-rolled and annealed textures 80—55425
Cr (1.7 and 2.5 wt.%), segregation of S and P to prior austenite grain boundary, stress effect *(Japanese)* 77—55962

alloy steel continued
Cr (2%), austenite decomp., phase diagrams and struct. form. kinetics 80−76223
Cr (3 wt.%), $\gamma \rightarrow \alpha$ transformation singularities in intermediate transformation temp. interval *(Russian)* 79−91644
Cr (3.51, 3.74, 3.56 wt.%), bainite transform. of deformed austenite 77−32574
Cr (4 wt.%), Cr_7C_3 precipitate growth during tempering, effect of Cr diffusion *(Russian)* 79−52219
Cr (40 wt.%), Sn and P segregation effects on impact toughness *(Chinese)* 77−73313
Cr (9 wt.%), oxidation in CO_2, early stages study by AES 78−7080
Cr (9 wt.%), SiO_2 vapour deposited coating, exam. of corrosion protective props. 78−88563
Cr, and Cr-Mo-Ni austenite decomposition, deform. effects, ferrite reaction 79−1842
Cr and Cr-Ni-Mo, refining effect on low cycle fatigue strength, resistance to hydrogen embrittlement 78−44208
Cr, austenitic boundary layers, form. by short laser pulse reaction 78−88555
Cr bearing, carbide phase precipitation during tempering, Mossbauer, X-ray diffr. studies *(Russian)* 79−87636
Cr, brittleness onset during high-temp. tempering *(Russian)* 77−81276
Cr, carbide form. depend. on Mn, Cr, V additions, cementite stabilisation, microstruct. *(Russian)* 80−55399
Cr, carburising kinetics, in endothermal atm. 80−76410
Cr, carburising with high-activity carburiser 80−76412
Cr, cast, fracture toughness and fatigue crack propagation, structural components of hydro-turbines, in water and air 78−68822
Cr, coated with TiC, prep. and props. 80−76414
Cr, cold roll, frictional heating surface damage 80−76289
Cr, corrosion fatigue testing 79−70247
Cr, corrosion resist., tempering after air-hardening in rolling heat *(German)* 80−45324
Cr, cyclic creep in complex stress system, 20-400°C 79−91764
Cr, cyclic re-austenitizing 80−35222
Cr, EM excitation and recording of US 80−34748
Cr, exam. of surface layer after electrochemical treatment, effect on mech. props. *(Russian)* 80−7727
Cr, feasibility of electrochem. corrosion protection 79−70220
Cr, ferritic, corrosion morphology, electrochem. pot. and Mo additions effect *(French)* 80−45439
Cr, ferritic, N_2 effect on 475°C embrittlement 79−83313
Cr, ferritic, oxide scale etching 79−70204
Cr, H-dislocation interaction 79−8307
Cr, high C, Cr effect on superplasticity 79−15729
Cr, high C, in situ transform. of cementite to M_7C_3 and internal defects of M_7C_3 by tempering 78−31412
Cr high C, ingot macrostruct., effect of diffusion annealing, solidification condition *(Chinese)* 78−15429
Cr, high strength, hot dip galvanized delayed fracture *(Japanese)* 78−15512
Cr, high-C hardened rolls, parameters for short tempering times 79−38865
Cr, hypereutectic, ShKh15, exam. of thermal props., 298 to 1173K *(Russian)* 79−28334
Cr, hypereutectic, structural, critical rates of impact, kinetics of failure 80−35325
Cr ion implanted, corrosion behaviour 80−11840
Cr, long-time exposure to N_2O_4, effect on mech. props. *(Russian)* 78−48573
Cr, lower bainite transform., significance of carbide precip. 80−97476
Cr maraging steel, internal friction, 120 to 700K *(Polish)* 79−96075
Cr modified, heat resist. rel. to thermomech. treatment 79−20084
Cr, nonoriented, mag. props., texture 77−1880
Cr, phase transform., effect of high temp. plastic deform. *(Slovak)* 78−19837
Cr, pitting corrosion, temp. depend. *(Czech)* 79−39039
Cr, previous deformation influence on strength, ductility, in biaxial tension, low temps. 79−90718
Cr, quenched and tempered struct. effect on H diffusion coeff. and solubility *(Japanese)* 78−52857
Cr, softening during tempering, austenitising effect 79−96052
Cr steel, austenite, abnormal decomposition kinetics and mechanism *(Russian)* 80−55344
Cr steel, $\alpha \rightarrow \gamma$ transformation, studied by internal friction meas. *(French)* 77−25043
Cr, steel, tempering, initial stages of carbide form., electron diffr. *(Russian)* 78−19760
Cr, surface damage during friction, struct. effect 80−35339
Cr, thermodynamic anal. of facing process using other metals 78−60878
Cr turbine casings, residual life determ. 80−93585
Cr, type 403, high C, low C, backscatter Mossbauer spectroscopy 80−40001
Cr, type Kh, (GOST 5950-51), in biaxial tension, effect of charact. of preloading on low-temp. ductility and strength 79−15749
Cr, V additions effect on brittleness near 475°C *(Russian)* 78−19890
Cr with metastable austenite, wear resist., temp. effect 80−76370
Cr-Al, sulphidation behaviour, 750°C, preoxidation effect *(French)* 78−15566
Cr-C, (2.14, 1.08 at.%) tempered, resistance to small plastic deformation, strain relaxation *(Russian)* 78−56698
Cr-C, carbide coating by CVD, interlayer form. 80−11574
Cr-C, segregation of P, C, and Cr to γ-boundary and carbide/γ-interface *(Japanese)* 79−61593
Cr-C (1, 1 wt.%), hot ductility and S segregation 80−66594
Cr-C (12, 0.2 wt.%) growth of grain boundary ferrite allotriomorphs, photoemission electron microscope exam. 78−88468
Cr-C (13, 0.15 wt.%), bainitic, transform. *(German)* 78−11218
Cr-C (3.74, 0.86 wt.%), stress assisted bainitic transform. *(Czechoslovakian)* 77−32573
Cr-C-Mn (Ni), struct. prop. rel., design of struct. steels for high strength and toughness 80−97491
Cr-Cu-Mn-C, HT 80, effect of grain size, on sensitivity to reheat cracking *(German)* 78−72856
Cr-Cu-Mo, ductile fracture, microvoid effects *(Japanese)* 80−108542
Cr-Mi-Mn type 4340, hydrogen bearing environment effect on K_{Iscc} 80−104325
Cr-Mn, annealing effect on mech. props. for cryogenic appl. *(Russian)* 78−19788

alloy steel continued
Cr-Mn, austenitic $M_{23}C_6$ carbide precipitates comp., heat and thermomech. treatment influence *(Russian)* 80−40361
Cr-Mn, carbide transform. *(Russian)* 79−33997
Cr-Mn, exam. of phase composition and carbide form. *(Russian)* 79−20057
Cr-Mn, laws governing discontinuous yield under tensile strain in liquid He 77−63760
Cr-Mn, low-cycle fatigue at 20 and −196°C 80−81196
Cr-Mn, metastable constitution diagram and phase transforms. *(Russian)* 80−50590
Cr-Mn, non-metallic inclusions anal. with increased N content *(Bulgarian)* 79−82259
Cr-Mn, powder forged, fracture processes and fracture toughness 78−72870
Cr-Mn, strain hardening, 4.2 to 293K 80−81076
Cr-Mn, with increased N content, X-ray spectral microanalysis *(Bulgarian)* 78−53304
Cr-Mn (13, 19 wt.%), for liquefied natural gas appl., material and weld props. 79−61735
Cr-Mn (13, 19 wt.%), for liquefied natural gas appls., material and weld props. 79−61736
Cr-Mn type, martensite struct. after quenching and HTMT, X-ray diffr. obs. 80−84975
Cr-Mn-Si, type 10KhSND, resist. to low-cycle deformation of low temps. 79−87696
Cr-Mn-Si steel, heat-treatment quality, higher harmonics of EMF obs. 78−60941
Cr-Mn-Si-Ni, 30CrMnSiNi2A, fracture toughness parameter K_{ISCC} 80−21099
Cr-Mn-W(Mo), W and Mo addition effect on carbide form. in type 30 KhG *(Russian)* 79−87638
Cr-Mn(Ni), Mn and Ni additions, effect on corrosion resistance and hardness 80−104342
Cr-Mo, (9, 1 wt.%) appl. of electron energy loss spectrometry to precipitate morphology 78−48414
Cr-Mo, alloy SCM3, hydrogen embrittlement, delayed fracture, exam. *(Japanese)* 78−64620
Cr-Mo, annealed, creep and rupture, heat treatment effects 79−24548
Cr-Mo, annealed, interaction solid soln. hardening, precipitation effects on creep 79−4974
Cr-Mo, annealed, microstructural effects on creep-rupture behaviour 79−57120
Cr-Mo, cast and forged, differenc in mech. props. 77−48465
Cr-Mo, crack decoration in oxides by electrodeposited metals *(German, English)* 79−70266
Cr-Mo, creep resistant, creep, effect of carbide precipitation *(German)* 77−52398
Cr-Mo, effect of Mo on high-temp. props. 80−85005
Cr-Mo, ferritic, grain boundary segregation, X-ray microanal. by STEM 80−66740
Cr-Mo, grain size effect on ductile brittle transition 79−24615
Cr-Mo, H embrittlement in H_2S environment, Mo effect 80−76415
Cr-Mo, hardened, fatigue life, effect of programmed load history *(Japanese)* 79−20160
Cr-Mo, heat fatigue, effect of technical factors 79−79058
Cr-Mo, heat treated steels of equal tensile strength, varying toughness *(German)* 80−25727
Cr-Mo, high tension, delayed fracture, fundamental study *(Japanese)* 77−48531
Cr-Mo, high-temp. props. and constitutive equations 79−34146
Cr-Mo, impact fatigue crack growth at low temps. *(Japanese)* 80−104266
Cr-Mo, low alloy, effect of stress intensity rate and stress ratio on corrosion fatigue crack growth enhancement 79−39022
Cr-Mo, low alloy, stress corrosion cracking and corrosion fatigue 79−47806
Cr-Mo, low-alloy, material selection for nuclear LMFBR steam generator 78−54834
Cr-Mo, martensite to ferrite transform. by fatigue deform. *(French)* 79−66056
Cr-Mo, materials specifications for AGR steam generators 80−42772
Cr-Mo, notched specimens, statistical eval. of fatigue life and fatigue limit and life distrib. *(Japanese)* 79−61702
Cr-Mo, notched specimens, fatigue strength distrib. *(Japanese)* 80−66633
Cr-Mo, oxidised, mechanism of crack decoration of oxides by electrodeposition 80−97560
Cr-Mo, pitting and crevice corrosion, exam. *(Japanese)* 78−64769
Cr-Mo, press. vessel material, yield surface behaviour, investigation techniques 79−61658
Cr-Mo, pressure vessel material, hydrogen embrittlement evaluation *(Czech)* 79−38950
Cr-Mo, quenched, carbide reactions during tempering 80−89229
Cr-Mo, quenched and tempered struct. effect on H diffusion coeff. and solubility *(Japanese)* 78−52857
Cr-Mo, secondary relaxation, correspondence of steady state creep *(Japanese)* 79−83250
Cr-Mo, structural carbonitrided at low temps., rotating bending fatigue strength *(Japanese)* 77−48534
Cr-Mo, tempered, cementite precipitation along twin boundaries 80−45309
Cr-Mo, type EN19 80−25717
Cr-Mo, V effects on recrystallisation *(Russian)* 77−66654
Cr-Mo, vacuum deposited Al film 79−70231
Cr-Mo, X-ray elasticity constants at high specimen temp. *(German)* 80−35239
Cr-Mo (1, 0.5 wt.%), heat treated creep failure, role of stress state 79−5047
Cr-Mo (1.25, 0.5 wt.%), creep, fracture, Ti and Ti+B effects 77−36603
Cr-Mo (1.25, 0.5 wt.%), creep and rupture, temp. and stress effects 77−86096
Cr-Mo (20, 1 wt.%), creep rupture tests, at 500°C loading times up to 300000 hours *(German)* 80−25828
Cr-Mo (2.25, 1 wt.%), annealing, high strain rate tensile props. 77−25117
Cr-Mo (2.25, 1 wt.%), annealed, heat treatment effect on tensile props. 78−11243
Cr-Mo (2.25, 1 wt.%), annealed, tertiary creep behaviour 79−43326
Cr-Mo (2.25, 1 wt.%), corrosion in molten NaOH, rel. to reactor boiler wastage 77−90497

alloy steel continued

- Cr-Mo (2.25, 1 wt.%), corrosion behaviour in simulated HTGR He environment 79−54495
- Cr-Mo (2.25, 1 wt.%), creep-fatigue testing from thermal transient effects in CRBRP reactor 78−21660
- Cr-Mo (2.25, 1 wt.%), creep and high temp. low-cycle fatigue tests 80−85061
- Cr-Mo (2.25, 1 wt.%), damage accumulation and microstruct. changes during creep 80−3129
- Cr-Mo (2.25, 1 wt.%), decarburization carbide effects in high temp. Na *(Japanese)* 78−15403
- Cr-Mo (2.25, 1 wt.%), in high temp. Na, heat treatment and metallurgical struct. effects 77−16619
- Cr-Mo (2.25, 1 wt.%), interrelationship between creep deform. and creep rupture 79−61664
- Cr-Mo (2.25, 1 wt.%), oxidation effect on hold time fatigue behaviour 80−30161
- Cr-Mo (2.25, 1 wt.%), quenched and tempered, diffusion and solubility of H_2 *(Japanese)* 79−65255
- Cr-Mo (2.25, 1 wt.%), relationship between minimum creep rate and time to fracture 78−56759
- Cr-Mo (2.25, 1 wt.%), SCC and temper brittleness, P grain boundary segregation effect 80−55571
- Cr-Mo (2.25, 1 wt.%), strain hardening shakedown load during bending 80−20958
- Cr-Mo (2.25, 1 wt.%), thermal fatigue cracking caused by repeated quenching from high temps. 77−52469
- Cr-Mo (2.25, 1 wt.%), weld metal, high temp. crack growth, effect of tempering, prestrain and grain refinement 78−27622
- Cr-Mo (2.25, 1 wt.%) effect of heat treatment on tensile props. 78−23745
- Cr-Mo (2.25, 1 wt.%) pipe, high temp. fatigue and creep strength 80−85060
- Cr-Mo (2.25, 1 wt.%) steel, T permeation rate at 400 to 500°C, rel. to LMFBR conditions 78−17319
- Cr-Mo (2.25, 1.0 wt.%), fracture-mechanisms, tensile specimens 80−85039
- Cr-Mo (2.25, 1.0 wt.%), Mn and Si effect on temper embrittlement, comp. and carbide precip. effects 80−85037
- Cr-Mo (2.25, 1.0 wt.%), P and Sn effect on temper embrittlement, comp. and carbide precip. effects 80−85036
- Cr-Mo (2.25, 1.0 wt.%), time of flight atom probe, quantitative microanal. metallurgical appl. 80−86498
- Cr-Mo (2.25, 1.0 wt.%) alloy steel, thermally aged and Na decarburised, stress-rupture props. 80−21102
- Cr-Mo (2.25, 1.00 wt.%), bainitic, strain rate effects on elevated temp. tensile behaviour 78−35461
- Cr-Mo (2.8, 1.6 wt.%), atom probe anal. of bainitic phase boundaries 80−71990
- Cr-Mo (3 wt.%), temper embrittlement 77−36647
- Cr-Mo (9, 1 wt.%), microstructural instability during creep, heat treatment effects 78−48472
- Cr-Mo (9,1 wt.%), austenitized in $\gamma+\delta$ phase field, secondary hardening and tempering 78−11247
- Cr-Mo low alloy ferritic steel, meas. of alloy and impurity elemental distrib. using STEM 80−35601
- Cr-Mo low C steel forgings, material capabilities 77−42105
- Cr-Mo low-alloy, additive remedy for temper brittleness 80−66659
- Cr-Mo pressure vessel steel, improvement through electroslag remelting 77−42104
- Cr-Mo SMC3, statistical fatigue props. eval., heat-to-heat variations 78−7048
- Cr-Mo steel types JIS SCMV 2, SCMV 3 and SCMV 4, high-temp. high-cycle fatigue props., press. vessel appls. *(Japanese)* 80−93650
- Cr-Mo type, tube, long-time stressed condition *(German)* 77−59888
- Cr-Mo weld metal, reheat cracking, residual elements and microstruct. influence 80−66553
- Cr-Mo weld metal, trace element embrittlement suppression by creep strength effects 80−66656
- Cr-Mo:P (2.25, 1 wt.%), stress relief cracking, effect of P segregation 80−89324
- Cr-Mo-Mn-Si-W (3, 1.95, 1.55, 1.45, 0.95 wt.%), struct. and props. 80−104175
- Cr-Mo-Ni-Nb, Nb effect on mech. props. *(German)* 80−30012
- Cr-Mo-Ni-V, dynamic stress intensity factor meas., possibilities and limits *(German)* 80−93719
- Cr-Mo-Ni-WV (6, 4, 3, 2 wt.%), tempering and secondary hardening, TEM obs. *(Chinese)* 80−104245
- Cr-Mo-Ti, oxidised, sunlight absorber, struct. and thermal efficiency 77−125
- Cr-Mo-V, 1% Cr, chem. comp. and struct. effect on deform. props. *(German)* 79−1888
- Cr-Mo-V, biaxial cyclic deformation behaviour 80−16431
- Cr-Mo-V, biaxial cyclic deformation behaviour 80−21057
- Cr-Mo-V, cast, creep resistant, rare earth addition effect on deoxidation, nonmetallic inclusions and mech. props. *(German)* 79−66067
- Cr-Mo-V, cast, strain intensity approach of high temperature fatigue crack growth and failure 79−20175
- Cr-Mo-V, combined Cr-Mn addition effects on hardenability 78−7046
- Cr-Mo-V, creep, effect of microstruct., heat treatment, transform. temp. 78−11248
- Cr-Mo-V, creep crack growth temp. depend., 525 to 600°C 78−64634
- Cr-Mo-V, creep deform. under const. and cyclic temp. 79−38914
- Cr-Mo-V, creep fatigue interactions obs. 78−44214
- Cr-Mo-V, creep fatigue interaction 78−60841
- Cr-Mo-V, creep fracture microstruct. effects 78−64668
- Cr-Mo-V, creep/fatigue interaction 78−64632
- Cr-Mo-V, cyclic oxidation and crack growth during high strain fatigue 78−31586
- Cr-Mo-V, environmental crack growth during isothermal high strain fatigue and temp. cycling 79−5082
- Cr-Mo-V, excessive temp. effect on creep behaviour, structure and hardness *(German)* 80−30054
- Cr-Mo-V, fatigue, failure probability based on residual strength 78−68797
- Cr-Mo-V, fatigue crack growth rate and threshold under oxidising conditions 79−20272
- Cr-Mo-V, heat treated, mech. props. *(German)* 80−25724
- Cr-Mo-V, high temp. low cycle biaxial fatigue 80−30063
- Cr-Mo-V, high temp. steam pipe weld, defect distrib. and growth 80−25979

alloy steel continued

- Cr-Mo-V, initiation and growth of cracks in biaxial fatigue 80−30064
- Cr-Mo-V, isothermal decomp. of austenite and carbide precip. 79−38832
- Cr-Mo-V, low alloy, creep fatigue interaction 78−64673
- Cr-Mo-V, low alloy, V effect on creep *(Czech)* 77−86088
- Cr-Mo-V, low cycle fatigue crack propag. at a notch under pulsating load 80−40492
- Cr-Mo-V, Low-cycle fatigue under out-of-phase loading conditions 78−7051
- Cr-Mo-V, medium strength, correlation between crack initiation, propag. and microstruct. 78−60787
- Cr-Mo-V, normalised and tempered, size and geometry effect on creep cracking behaviour 78−64630
- Cr-Mo-V, notch geometry influence on creep rupture props. *(German)* 80−30055
- Cr-Mo-V, power station component, fracture toughness and fatigue characts. 79−20192
- Cr-Mo-V, press. vessel, fracture, effect of tempering 78−60799
- Cr-Mo-V, rupture ductility rel. to cavitation, density and SEM obs. 79−34142
- Cr-Mo-V, rupture strength and thermal fatigue, charact. investigation 78−72857
- Cr-Mo-V, steamline bends, restorative heat treatment effects 78−68716
- Cr-Mo-V, strength and ductility in creep, purity influence 80−66598
- Cr-Mo-V, stress relief cracking mechanism 78−64669
- Cr-Mo-V, stress rupture, notch influence, temp. depend. *(German)* 80−60945
- Cr-Mo-V, stress rupture strength at high temps. *(German)* 80−40474
- Cr-Mo-V (0.5, 0.5, 0.25 wt.%), creep crack growth in notched bend test, microstruct. effect 77−21261
- Cr-Mo-V (0.5, 0.5, 0.25 wt.%), creep crack growth at 565°C 77−73323
- Cr-Mo-V (0.5, 0.5, 0.25 wt.%), bainitic and martensitic, tempered, creep crack growth 77−86136
- Cr-Mo-V (0.5, 0.5, 0.25 wt.%), heat treated, microstructure effect on threshold region fatigue 78−56757
- Cr-Mo-V (0.5, 0.5, 0.25 wt.%), comparison of methods of correlating creep crack growth 78−60826
- Cr-Mo-V (0.5, 0.5, 0.25 wt.%), creep crack growth, temp. effect 78−64667
- Cr-Mo-V (0.5, 0.5, 0.25 wt.%), steel, low alloy, creep behaviour at engineering stresses 79−74218
- Cr-Mo-V (0.5, 0.5, 0.25 wt.%), microstruct. effects on fatigue at intermediate and high crack growth rates 79−74247
- Cr-Mo-V (1, 0.5, 0.25 wt.%), long-time stress relaxation props. 77−12666
- Cr-Mo-V (1, 0.5, 0.25 wt.%), stress relax. data anal. using total strain-time parametric method *(Japanese)* 80−104198
- Cr-Mo-V (1, 1.25, 0.25 wt.%), creep crack growth *(Japanese)* 79−43399
- Cr-Mo-V (1 wt.%) oxidation assisted crack growth during high cycle fatigue at 550°C 77−16742
- Cr-Mo-V (1.35, 1.0, 0.25 wt.%) exam. of mech props, comparison with mathematical model predictions *(Czech)* 79−91740
- Cr-Mo-V (2.65-2.86, 0.68-0.7, 0.3-0.35 wt.%) hydrogen embrittlement resist. evaluation *(Czech)* 80−35308
- Cr-Mo-V crack growth during strain fatigue at 825K 78−39890
- Cr-Mo-V creep crack growth, relation between engineering and metallurgical factors 78−11321
- Cr-Mo-V low-alloy, high-temp. ductility and crack growth, impurities effect 80−66652
- Cr-Mo-V low-alloy, mech. props. and stress relief cracking, effects of impurities and deoxidation practice 80−66599
- Cr-Mo-V low-alloy, prior austenite grain boundary embrittlement by B 80−66657
- Cr-Mo-V low-alloy, stress relief cracking, impurity and alloy content effects 80−66654
- Cr-Mo-V low-alloy with high residual element content, cavitation control 80−66663
- Cr-Mo-V pipe, high temp. main steam pipe, residual stresses in butt welds. 80−21059
- Cr-Mo-V press. vessel, crack growth under creep 78−60827
- Cr-Mo-V pressure vessel, microstruct. parameters and yielding rel. to plastic deform. 80−89318
- Cr-Mo-V steel, creep rupture tests on notched cylindrical specimens at 600°C 77−32670
- Cr-Mo-V type X 41 CrMoV 5 1, austenized, carbide detection by etching *(German, English)* 79−91884
- Cr-Mo-V-Nb, supercooled austenite isothermal decomp., struct., strength and fracture characts. 80−60966
- Cr-Mo-V-Nb-B, creep rupture strength *(Japanese)* 79−83301
- Cr-Mo-V-P, quenched, temper brittleness in relation to V and P concs. 78−52986
- Cr-Mo-V-W, crack-growth and thermal-mech. fatigue 80−21072
- Cr-Mo-V-(W), for bolts, stress relaxation data 78−60699
- Cr-Mo-W, splat quenched, formation of metastable austenite 80−84974
- Cr-Mo-W-V, long term creep rupture props., turbine blade *(Japanese)* 77−59909
- Cr-Mo-W-V, long time stress relaxation props. *(Japanese)* 77−59841
- Cr-Mo-W-V-Ti-B, transformation mechanism and fine structure of (M-A) phase, TEM study *(Chinese)* 80−66500
- Cr-Mo-(Ni-V), temper embrittlement by P and Sn, effect of rare earth additives 79−61721
- Cr-Mo-(Ni), fracture resistance, H_2S in H_2 effect *(French)* 80−16461
- Cr-Mo-(V), microstruct. effect on high-temp. props. *(Czech)* 80−89300
- Cr-Mo-(V) austenitic, creep resist., high-temp. props. residuals effect 80−66600
- Cr-Mo(-Al), NH_3 gas addition to N_2-H_2(-C_3H_8) gas mixture and its effect on nitrided layer *(Japanese)* 80−35403
- Cr-Mo(-V), ductility and heat resistant prop. prediction rel. to fine struct. and solid soln. state 79−15751
- Cr-Mu-W, carbide form., W effect 80−76259
- Cr-Ni, austenitic, nonmetallic inclusions modification using rare earth metals *(Russian)* 80−40369
- Cr-Ni, bainitic habit plane determ. 79−1927
- Cr-Ni, carbide transform. *(Russian)* 79−33997
- Cr-Ni, case hardened rollers, surface fatigue failure under pure rolling and sliding rolling contacts 79−52472
- Cr-Ni, cladding material, deform., failure, rigid loading scheme 79−91765
- Cr-Ni, detonation spraying of WC-Co with automatic powder feed 80−25558

alloy steel continued
- Cr-Ni, effect of tempering under load on mech. props. 80−16354
- Cr-Ni, ferrite precip. *(Japanese)* 80−35187
- Cr-Ni, hydrogen effect on strength, ductile and fracture characts. 79−38960
- Cr-Ni, Kh23N18, self lubricating composite, frictional props., Ag-Cu-Zn-Cd lubricant 78−11340
- Cr-Ni, laws governing discontinuous yield under tensile strain in liquid He 77−63760
- Cr-Ni, long-time exposure to N_2O_4, effect on mech. props. *(Russian)* 78−48573
- Cr-Ni, maraging, effect of Mo, Co additions on hardening 78−84835
- Cr-Ni, microstruct. effect on temper brittleness *(Korean)* 79−70092
- Cr-Ni, pendant drop melt extracted, struct. and props. 80−76242
- Cr-Ni, rock-like fracture *(Chinese)* 78−31497
- Cr-Ni, rolled and sintered, to produce capillary structured filter material, exam. of mech. props. and production 80−16235
- Cr-Ni, SUS 304, thermal fatigue props. 80−21071
- Cr-Ni, soaking at forging temp., effect on struct. and mech. props. *(Czech)* 78−64628
- Cr-Ni, strain hardening, 4.2 to 293K 80−81076
- Cr-Ni, surface tension and limit wetting angle in contact with CaO-SiO_2-Al_2O_3-Na_2O-CaF_2 melts *(Czech)* 79−37908
- Cr-Ni, tensile strength and cooling curve, regression anal. 79−57070
- Cr-Ni, type 4340, high-strength, new inhibitors for crack arrestment in corrosion fatigue 80−100941
- Cr-Ni, type EP810VD and EP842, effect of stress conc. on fatigue strength at elevated temps. 79−57115
- Cr-Ni (1.47, 1.48 wt.%), lath martensite microstruct. and props., cold rolling effect 80−55422
- Cr-Ni (2.25, 1 wt.%), role of Mo in P-induced temper embrittlement 80−35316
- Cr-Ni (32,8), two phase austenite-ferrite alloy, fatigue behaviour *(Japanese)* 79−79091
- Cr-Ni steel, strengthening by elastic deform. at −196°C 77−55987
- Cr-Ni-Al, intergranular crack investigation, by etching *(Chinese)* 79−43457
- Cr-Ni-C (3, 1, 0.6 wt.%), grain boundary sulphide precip. and hot ductility *(Japanese)* 80−71654
- Cr-Ni-Cu (14, 5, 2 wt.%), phase transform. and props., preliminary heat treatment effect 79−79011
- Cr-Ni-Mn, type 4340, acoustic emission interpretation of ductile fracture processes 80−35300
- Cr-Ni-Mn, type 4340, decarburisation by gaseous atomic hydrogen 80−30160
- Cr-Ni-Mn, type 4340, H_2 embrittlement, stress state, thickness and delayed failure in bending 80−71746
- Cr-Ni-Mn, type 4340, modified double cantilever beam model for K_{Ic} determ. *(Chinese)* 80−54306
- Cr-Ni-Mn, type AISI 4340, correl. between advanced NDT evaluation methods and fracture mech. parameters 80−97675
- Cr-Ni-Mo, 'light spots', fractographic anal. 79−29204
- Cr-Ni-Mo, 'spots' *(Chinese)* 80−104248
- Cr-Ni-Mo, combined B and rare earth metal additions effect on microstruct. impact strength and hardness 79−38963
- Cr-Ni-Mo, dynamic and static softening behaviour at hot forming temp. *(German)* 80−25728
- Cr-Ni-Mo, handbook data for type 34KhN1M 79−78960
- Cr-Ni-Mo, resist. to corrosion and corrosion-fatigue in seawater 80−104346
- Cr-Ni-Mo, resistometric study of austenitization and carbide dissolution, preliminary anealing *(Czech)* 77−59829
- Cr-Ni-Mo 40KhN2MA, magnetostriction used in inspection after heat treatment 80−108673
- Cr-Ni-Mo steel, low-cycle fatigue in sea water, mechanism *(Russian)* 77−59970
- Cr-Ni-Mo-Mn, wetting of TiC, expt. planning investigation 80−60822
- Cr-Ni-Mo-V, austenite form. during heating, influence of recrystn. during tempering *(Russian)* 80−104188
- Cr-Ni-Mo-V, ductile fracture during tensile loading 80−45381
- Cr-Ni-Mo-V, magnetic induction, struct. dependence *(Czech)* 80−50141
- Cr-Ni-Mo-V, Mossbauer austenitometry and mag. props. 80−40003
- Cr-Ni-Mo-V, plate, type HY130, exam. of elastic-plastic R curve 79−29157
- Cr-Ni-Mo-V-Nb (12,8,1,1.5,0.4 wt.%), Ce addition effects on strength and hardness *(Russian)* 78−15454
- Cr-Ni-Mo-W-Nb, for bolts, stress relaxation data 78−60699
- Cr-Ni-Nb, containing controlled particle dispersions, creep strength 77−52425
- Cr-Ni-Si (18.15, 17.64, 2.4 wt.%), rare-earth additions effect on impact fracture *(Chinese)* 80−66617
- Cr-Ni-Ti, austenitic stainless, creep deform. effects on intergranular TiC dispersion stability 78−84912
- Cr-Ni-Ti (18, 8, 0.7 wt.%), creep rupture tests, at 500°C loading times up to 300000 hours *(German)* 80−25828
- Cr-Ni-Ti-B, grain size effect on mech. and struct. props. *(French)* 80−45361
- Cr-Ni-W(Mo), W and Mo addition effect on carbide form., X-ray obs. *(Russian)* 79−87639
- Cr-Ni-(Mo), cast, intercritical heat treatment *(Czech)* 80−89268
- Cr-plated, H_2 distrib., laser-mass spectrometer investig. 78−61113
- Cr-Si, oxidation resist. in high pressure CO_2, Si effect 80−66704
- Cr-Si-Mn-ΔV-Ti-Nb-Mo, effect of Vi, Ti, Mo, Nb additions on substructure, mech. props. *(Russian)* 79−34108
- Cr-Si-Mn-Ni-Mo-C, resist. to deform. and fracture, C effect 80−71757
- Cr-steel, influence of ultrasound on tempering processes *(Russian)* 78−52827
- Cr-steel 80−16303
- Cr-V, fatigue strength and fatigue failure at complicated states of stress 77−56057
- Cr-V, hardened sping, surface finish effect on fatigue strength *(Japanese)* 79−61708
- Cr-V (1.5, 0.5 wt.%), cavitation, effect of temp. and C content 78−64638
- Cr-V (1.5, 0.5 wt.%), ferritic, effect of temp. and microstruct. on creep damage 79−5023
- Cr-W, quenched, carbide reactions during tempering 80−89229
- Cr-W-Mo-Co, high-speed, from atomised powders, mech. and cutting props. 80−66556
- Cr-W-V-Mo (3.9 to 4.5, 1.5 to 2, 0.9 to 1.2, 3.9 to 4.4 wt.%), heat resistant, type 8Kh4M4V2F1-Sh, mech. props. 80−16464

alloy steel continued
- CrMo and CrMoV, creep resistant, ductile-brittle transition temp., precipitation effects *(German)* 78−19856
- CrMo, cast, fatigue tests under varying stress amplitude and varying temp., cumulative damage *(Japanese)* 78−27605
- CrMo(M)V, creep rupture tests, at 500°C loading times up to 300000 hours *(German)* 80−25828
- CrMoV (1 wt.%), creep crack propag. rates, prediction using C* parameter 77−90449
- CrMoV (1 wt.%), high temp. creep and fracture 77−36598
- CrMoV, carbide phases precipitation *(Czech)* 80−29961
- CrMoV, compact tension specimen, thickness effect 78−68764
- CrMoV, creep and creep strength under alternate tension/compression *(Czech)* 77−63728
- CrMoV, creep resistant, cast, creep rupture and creep *(German)* 77−70098
- CrMoV, creep resistant, quantitative struct. parameter use in props. prediction *(Czech)* 80−108481
- CrMoV, failure in post yield regime using single edge notched tension specimens 78−68765
- CrMoV, low alloy, coarsening rate and activation energy of M_4C_3 and M_7C_3 carbides *(Czech)* 80−108480
- CrMoV, low alloy, creep resistant, temp. and stress depend. of time to rupture *(Czech)* 77−70160
- CrMoV, low alloy, dispersed phase of VC, hardening mechanism *(Czech)* 78−60676
- CrMoV, low alloy, quantitative stereological anal. of carbide phase, comparison of methods *(German, English)* 79−91886
- CrMoV, low alloy, quantitative stereological anal. of carbide phase, struct. stability during creep *(German, English)* 79−96262
- CrNi, etchability of austenite *(German, English)* 80−11860
- CrNiMo, cantilever beam method to investigate J_{Ic} and J_{Iscc} *(Chinese)* 78−15488
- CrNiMoV, weld metal, hot cracking resistance during electroslag welding, effects of Cr 79−87732
- Cu, fission reactor vessels, neutron embrittled, exam. of technique for in situ thermal annealing 79−29114
- Cu, precipitation hardening, strength and struct. *(German)* 79−47701
- Cu, precipitation hardening, struct. and fracture *(German)* 79−61696
- Cu-Mn-Zn, Zn addition effects in powder forgings produced by liquid solid alloying 78−11157
- Cu-Ni-Mo (2, 2, 0.25 wt.%), sintering, kinetic characts. 80−60805
- Cu-steel composites for intense pulsed mag. field generation 80−42245
- Cu-Zn, brass clad, fatigue crack growth behaviour 80−40484
- Fe-Al-C steel, singularities of struct., electron microscope and electron diffr. analysis *(Russian)* 77−77476
- Fe-C-Cu (0.21, 0.2 wt.%), neutron-irradiated, resolution of C atoms, internal friction meas. 78−31442
- Fe-C-Mo, dynamics of transform. interface, ferrite-austenite interface 78−52795
- Fe-C-Mo, dynamics of transform. interface, at intermediate temps. 78−52796
- Fe-C-Si alloy, lattice parameters of cementite after quenching 78−11198
- Fe-C-Si-S, liquid, desulphurisation with CaO, exam. of reaction mechanisms 78−80742
- Fe-C-Zn (0.45 wt.% C, 1.56 wt.% Zn), pearlite transformation during continuous cooling 78−80538
- Fe-Co-Cr-Mo, maraging, age hardening, Mossbauer study 80−40002
- Fe-Co-Cr-W-Ni-C, alloy KKhVN, transforms. during annealing and nature of hardening *(Russian)* 78−56653
- Fe-Co-W-C steel, M_6C carbide behaviour during ht. treatment *(Russian)* 77−66658
- Fe-Cr-C, steel carbide formation during chromising, exam. in terms of ternary phase diagrams 78−56818
- Fe-Cr-C (10,0.2 wt.%) isothermally transformed, carbide distrib., microstruct. development 80−3076
- Fe-Cr-C alloys, equilibrium partition coeffs. for ferrite/liquid, austenite/liquid 78−39744
- Fe-Cr-C system, isothermal sections, 873 to 1373K, computer plotting 78−6894
- Fe-Cr-Mn-C, high temp. oxidation, X-ray and weight gain meas. *(Russian)* 78−15571
- Fe-Cr-Mo-C, X-ray investigation after friction and oxidation 78−52997
- Fe-Cr-Mo-Si-V, various steels, short rod stress intensity factor tests up to 700K, exam. 78−60815
- Fe-Cr-Ni-Mo-Al, (13, 8, 2, 1, wt.%), H_2 effects on fracture, exam. 78−60809
- Fe-Mn (32.5 and 38.3 wt.%), steel sheet, exam. of form limit diagrams and damage 78−48461
- Fe-Mn (8 wt.%), improvement of cryogenic mech. props. through thermal/mech. treatments 79−79098
- Fe-Mn-C, cast iron and steel, Mn effects on struct. 78−23696
- Fe-Mn-C (11.5, 0.2 to 1.6 wt.%), water quenched, effect of C on phase composition, abrasion, plasticity *(Russian)* 78−35445
- Fe-Mn-C austenitic steel, deform. twinning and mech. props. 77−59868
- Fe-Mn-C system, isothermal sections, 873 to 1373K, computer plotting 78−6893
- Fe-Mn-Cr-C (20, 4, 0.5 wt.%), hyperquenched and predeformed, mech. props. *(French)* 78−23786
- Fe-Mn-Si-C, minimum of elec. resist. near LNT *(Russian)* 77−66707
- Fe-Mn-Ti (12, 0.2 wt.%), improvement of cryogenic mech. props. through thermal/mech. treatments 79−79098
- Fe-Mn-V-C austenitic, ageing characts., discontinuous precip. nature 80−84940
- Fe-Mn-(Cr)-C, intermediate phase form. during martensite form. 77−12626
- Fe-Mo-C low-alloy, photoelectron microscopy of diffusional transformations 77−44242
- Fe-Mo-C system, isothermal sections, 973 to 1273K, thermodynamic analysis 78−6895
- Fe-Ni, effect of metallurgy on stress corrosion cracking, and hydrogen embrittlement 78−60885
- Fe-Ni-C, ausformed, ductility of martensite *(Japanese)* 77−48490
- Fe-Ni-C, FCC, effect of two gamma states on C activity 78−6897
- Fe-Ni-C, lenticular martensitic alloy, fractured at liquid N_2 temps., crack propag. mode *(Japanese)* 77−48524
- Fe-Ni-C, single cryst., singularities of distrib. of Ni and C *(Russian)* 77−77467
- Fe-Ni-C (19 to 30, 0.04 to 0.8 wt.%) alloys, transformation of martensite in austenite, optical and electron microscopic exam. *(Russian)* 78−35382

alloy steel continued
- Fe-Ni-C (31, 0.1 wt.%), kinetics of deform. induced martensite, shock loading and grain refinement effects 78—15395
- Fe-Ni-C (31, 0.1 wt.%), metastable austenite, fractography 77—59919
- Fe-Ni-C (9, 0.1 wt.%), effect of intercritical tempering on impact energy, exam. of mech. props. 78—52861
- Fe-Ni-C austenite, metastable, influence of prior deform. on yield stress 78—15461
- Fe-Ni-Cr steel, mag. susceptibility and magnetoresistance, temp. depend. *(Ukrainian)* 77—73004
- Fe-Ni-Cr-C, ferritic, P segregation to free surface, 723 to 823K, AES 78—48411
- Fe-Ni-Cr-C, martensitic transform. effect of austenite prestrain above M_d temp. 78—15398
- Fe-Ni-Cr-Mo, exam. of tapered tensile specimen, for stress corrosion threshold stress testing 78—53055
- Fe-Ni-Cr-Mo-V-C, H_2S stress corrosion cracking, effects of overload, exam. 78—60886
- Fe-Ni-Cr-Mo-V-C, HY130, effect of H_2 and impurities on brittle fracture, review 78—60765
- Fe-Ni-Cr-Sb-C effect of Ni, Sb, on temper embrittlement 78—60813
- Fe-Ni-Mn-Si-Cr-Ni-Mo, effect of metallurgy on stress corrosion cracking, and hydrogen embrittlement 78—60885
- Fe-Ni-Mn-steel 48, struct. defects effect on interdiffusion 80—15314
- Fe-Ni-Mo-C, Mossbauer investig. of secondary hardening, carbide form. *(Russian)* 77—44260
- Fe-Si, high permeability, processing effect on recrystn. and deform. 77—12716
- Fe-Si (3 wt.%), AlN-inhibited, Se effect on primary grain recrystallisation 77—12715
- Fe-Si (3 wt.%), Bauschinger effect, computerised evaluation method 80—93625
- Fe-Si (3 wt.%), cold rolled, effect of primary recrystallisation texture, on behaviour of secondary recrystallisation 78—39802
- Fe-Si (3 wt.%), grain oriented, MnS-AlN-inhibited, precipitate morphology 77—12648
- Fe-Si (3 wt.%), hot rolled sheet steel, ductile-brittle transition temp. *(Chinese)* 78—31498
- Fe-Si (3 wt.%), secondary recrystn., struct. inhibition, permeability improvement 77—12713
- Fe-Si (3 wt.%), transformer steel, grain-oriented, magneto-optical domain obs., magnetisation mechanism 77—12364
- Fe-Si (3 wt.%) high-permeability grain-oriented steel, quenching effect on primary recrystn. texture development 80—84956
- Fe-Si (3 wt.%) steel, oriented, stress depend. mag. props., coating effects 80—34729
- Fe-Si-C, liquid alloy, activity of Si and C *(Russian)* 78—11203
- Fe-Si-C melt, Si and C activity *(Russian)* 77—55364
- Fe-Si(6.5 wt.%) steel, core mat. development *(Korean)* 78—60852
- Fe-Ti-Si-Ni-P-C-S, H_2 segregation kinetics *(Russian)* 78—18832
- Fe-V-C (1, 0.2 wt.%), austenite formation 80—84927
- Fe-V-W-Mo-Cr-C, exam. of carbide transformation 80—16299
- $Fe_{70}Cr_{30}$, disordered, X-ray spectra study of electronic struct. 77—77324
- G-Mo type, welded joints, thermal fatigue testing 78—3278
- GCFR fuel pin claddings, oxidation behaviour in He environment 80—16594
- H_2 embrittlement, stress state and delayed failure of types AISI 4340 and A-106 80—45400
- Mg effect on precipitation of C and or N, and mech. props., during strain ageing *(German)* 78—35387
- Mn (0.9 wt.%), hydrogen embrittlement resist. evaluation *(Czech)* 80—35308
- Mn (1 to 10 wt.%), Mossbauer, X-ray and electron microscope studies of martensite 78—56621
- Mn (13.5 wt.%), hardening mechanism during friction 79—96152
- Mn (16 to 20 wt.%) metallographic analysis method 80—50791
- Mn (1.10 to 1.55 wt.%), reactor vessel material, assessment of weld heat affected zone mech. props. 79—29217
- Mn (high), austenitic, creep rupture, p addition and two-step soln. heat treatment effects *(Korean)* 80—93646
- Mn, acicular ferrite high-strength low-alloy, low temp. mech. props., pipe-line appl. 80—55472
- Mn and Mn-Ti, cryogenic mech. props. and intergranular brittleness *(Korean)* 79—70164
- Mn, as rolled bainitic, tensile, impact and machinability props., transport appl. 78—88503
- Mn, cyclic creep in complex stress system, 20-400°C 79—91764
- Mn determ. by AES and APS 79—48001
- Mn, diffusion of C, Si, V, W, electron probe microanalysis *(Czech)* 77—59149
- Mn, effect of Mn on corrosion *(Czechoslovakian)* 77—28933
- Mn form. of twinned struct. *(Russian)* 78—64542
- Mn, H_2 emibrittlement mechanism *(Korean)* 78—68774
- Mn, mandrels, wear resist., surface layer chem. comp. influence *(Russian)* 79—52444
- Mn, Mn influence on martensitic transform in presence of strain *(Russian)* 80—20934
- Mn, plastic deformation, shape recovery during γ to and from ε, ε' transformations *(Russian)* 79—83196
- Mn, sintered, production, effect of initial Fe powder struct. on mech. props. 80—104095
- Mn, softening during tempering, austenitising effect 79—96052
- Mn, solutioning of castings in salt baths 78—23871
- Mn steel, tempering, initial stages of carbide form., electron diffr. *(Russian)* 78—19760
- Mn steel with varying Mn content, diffusion of ^{48}V and ^{59}Fe *(Czechoslovakian)* 77—35743
- Mn, surface crack exam. by eddy current technique 77—9007
- Mn, tempered cementite crystals, carbide phase segregation, X-ray study *(Russian)* 78—35391
- Mn, type 35SGM, magnetic, electrical, and mech. props. after tempering and hardening 79—66086
- Mn, ummachined samples, impact figure testing 78—56838
- Mn, wear resistant, review of abrasive adhesive and rolling wear *(Korean)* 79—24624
- Mn-Al-C, hardening during ageing, 450-750°C *(Russian)* 78—3135
- Mn-B-V, low alloy, transform. singularities *(Russian)* 80—104116
- Mn-C, formation of filamentary V(C,N) precipitates during diffusional $\gamma\rightarrow\alpha$ transform *(Russian)* 79—1865
- Mn-C (1, 0.1 wt.%) strip, hot rolled, P effect on mech. props. 78—27532

alloy steel continued
- Mn-C steel, X-ray K-absorption spectra of $(Fe_xMn_{1-x})_3C$ *(Russian)* 78—6813
- Mn-C-O, phase equilibrium, Mn effects at liquidus temp. *(Russian)* 77—66625
- Mn-Cr, blank hardened, shot peening effect on bending fatigue strength *(German)* 78—35402
- Mn-Cr, normalised, shot peening effect on bending fatigue strength *(German)* 78—35401
- Mn-Cr, nuclear reactor pressure vessel, effect of Mn and C content on irrad. response 79—20196
- Mn-Cr, tempered, case hardened, shot peening effect on bending fatigue strength *(German)* 79—24645
- Mn-Cr-B (1.46, 1.03, 0.003 wt.%), lath martensite microstruct. and props., cold rolling effect 80—55422
- Mn-Cr-Cu, effect of Cr and Cu on ductility when deformed 78—44175
- Mn-Cr-V, crack propag. resist. at hardness indentation, and fracture toughness *(German)* 79—29220
- Mn-Cr-V, structural changes during solution annealing *(Czech)* 78—84864
- Mn-Cr-V, tool, quenched and tempered, fracture toughness *(German)* 80—25726
- Mn-Mo, castings, mech. props., Cu and Sn trace elements effect 80—66596
- Mn-Mo-Nb, high strength, ductile, acicular ferrite struct. 77—21191
- Mn-Mo-Nb-C, transform. charact. and struct. during continuous cooling 79—29057
- Mn-Mo-Ni, embrittling effects of residual elements 80—66655
- Mn-Mo-Ni (A533 B), ductile-brittle transition, material fracture temp. depend., Gauss distrib. function 80—97574
- Mn-Mo-Ni-Cr, bainitic, microstruct. and mech. props. *(French)* 80—16362
- Mn-Mo(3, 0.4 wt.%), specimen fracturing device for ion microprobe analyser, appl. to grain boundary segregation 77—21341
- Mn-Nb-Al-C, crack progag. and hot ductility during straightening concast strand 80—66646
- Mn-Ni-C system, pressure effect on melting diagram *(Russian)* 77—55943
- Mn-Ni-Cr diffusion of Fe, Mn, Si, V and W *(Czech)* 77—59148
- Mn-Ni-Cr-Mo, high tensile strength, control-rolled, transformation textures 79—83225
- Mn-Ni-Mo, PWR pressure vessel, irrad. induced embrittlement, chemical composition effect *(French)* 79—20195
- Mn-Ni-Mo (0.68, 2.02, 0.48 wt.%), hydrogen embrittlement resist. evaluation *(Czech)* 80—35308
- Mn-Ni-Mo low alloy steels for nuclear appl., toughness and heat treatment 80—5239
- Mn-Si, 16GS sheet mag. method of NDT of mech. props. 80—21211
- Mn-Si, 17G2S, VN and NbV dispersion hardening effect on mech. props. 78—3137
- Mn-Si, fatigue, level of prior cyclic stresses effect 80—89348
- Mn-Si, St 52-3, cleavage fracture toughness, temperature and notch sharpness influence *(German)* 80—35291
- Mn-Si, St 52-3, fracture toughness determ. from yield strength and cleavage fracture strength *(German)* 80—35292
- Mn-Si, thin sheet impact strength study *(Czech)* 80—59571
- Mn-Si-Cr-Mo, dual phase, as-rolled, continuous cooling transformation diagram to optimize composition 80—100829
- Mn-Sn(-Nb), extra low C, shear transformation struct. *(German)* 80—60873
- Mn-steel, cryst. geometry in formation of ε'-, ε-, $\aleph'$- and α-martensitic phases *(Russian)* 78—76648
- Mn-steel, influence of ultrasound on tempering processes *(Russian)* 78—52827
- Mn-Ti, structural, brittle fracture resistance, Ti addition effect *(Czech)* 80—45392
- Mn-Ti-B-rare earth, distrib. of B *(Chinese)* 78—84811
- Mn-V, nitrided age-hardened, for blanking punches, chipping resist. props. *(Japanese)* 80—89340
- Mn-V, pressure vessel material, hydrogen embrittlement evaluation *(Czech)* 79—38950
- Mn-V (0.04 to 0.06 wt.%), strain ageing characts. rel. to mech. props. 80—84969
- Mn-V-Mo high-strength heat-treatable sintered 80—50575
- MnMoNi, pressure vessel, stress relief cracking 79—43404
- MnMoNiCr, pressure vessel, stress relief cracking 79—43404
- MnS inclusions in free-cutting steel, X-ray, light and scanning electron microscopy 77—77685
- Mo, energy selective X-ray anal. using TEM 80—84036
- Mo, quantitative anal. of carbides formed during tempering 78—64571
- Mo, X-ray elastic consts. as function of plastic strain *(German)* 78—31436
- Mo, X-ray elasticity constants at high specimen temp. *(German)* 80—35239
- Mo-Cr, X-ray elastic consts. as function of plastic strain *(German)* 78—31436
- Mo-Cr (3 wt.%), CrC formation in isochronal tempering, electron microscope study 80—7584
- Mo-Cr-Ni-Mn alloy with TiC, optimum comp. and manufacture conditions, Mn effect 80—84896
- Mo-high purity steel, tempering behaviour 80—7600
- Mo-Nb, sheet, fracture toughness evaluation *(Slovak)* 79—38948
- Mo-Nb (2.5, 0.035 wt.%) Mo content effect on sulphide stress cracking resistance 80—21157
- Mo-V, creep rupture strength, rel. to microstruct. *(German)* 78—35467
- Mo-V, creep rupture strength, heat treatment effects *(German)* 78—72834
- Mo-W, high speed, best quenching heat treatment 78—84852
- Mu-Cr-Mo, high-strength heat-treatable sintered 80—50575
- N-Cr-Mn, influence of nitride phase on corrosion behaviour *(Bulgarian)* 79—61798
- NO_x to NO_2 conversion in metallic materials, expts. *(German)* 80—55716
- Nb,(V), (Al), hot rolling, laboratory simulation, recrystn. of austenite 80—97512
- Nb, controlled-rolled into ferrite temp. range, soln. temp. and rolling effects 80—11678
- Nb, deform., recrystn. and precip. interaction 80—97515
- Nb, HSLA, low temp. fatigue props. 80—40490
- Nb, high and medium C, austenite grain growth 78—11249

alloy steel continued
Nb, microalloyed, hot rolled, Nb(CN) precip. and austenite recrystn. 80−97513
Nb microalloyed dual phase, etching technique 80−71809
Nb-Mn, Molytor 53, Bauschinger effect, computerised evaluation method 80−93625
Nb-Mo, HSLA, low temp. fatigue props. 80−40490
Nb-Mo, Mo effect on sulphide stress cracking resistance 80−16552
Nb-stabilised, orientation depend. of cell size and recrystallisation texture development 79−91682
Nb-V, cold rolled, HSLA, prod. by precipitation hardening, annealing 78−88471
Nb-Va microalloyed, mech. props. *(French)* 80−35252
NbCN precipitation in HSLA steel, exam. by electrical resistivity meas. 78−84822
Ni, 11.6%, quenched cylinder residual stresses, boring/turning and X-ray diffr. obs. *(German)* 80−93586
Ni, 9 wt.%, welded joints on LNG carriers mech. props. and fracture toughness 80−85017
Ni (1 to 9 wt.%), Mossbauer, X-ray and electron microscope studies of martensite 78−56621
Ni (17 wt.%), martensitic deform. temp., cryst. struct. effect *(Russian)* 80−66576
Ni (19 and 24 wt.%), austenite thermal stabilisation at sub-zero temps. 77−52324
Ni (19 wt.%) thermal stabilisation of austenite 78−15397
Ni (21 wt.%), ageing, nitrided case struct. investigation 80−35416
Ni (23 wt.%), crack propag. in the presence of H_2 *(French)* 78−15517
Ni (3.5 wt.%), heavy rotor forgings, temper embrittlement, metallurgical investigations *(German)* 80−16471
Ni (5 and 9 wt.%), for liquefied natural gas appl., material and weld props. 79−61735
Ni (5 and 9 wt.%), for liquefied natural gas appls., material and weld props. 79−61736
Ni (5 wt.%), corrosion fatigue 78−27683
Ni (5.5 wt.%), fatigue fracture toughness, crack propag., at low temp. 78−68823
Ni (9 wt.%), effect of repeated tempering on notch strength *(Japanese)* 79−43280
Ni (9 wt.%), static and dynamic fracture toughness 77−36664
Ni (9 wt.%), tempered, mech. stability of retained austenite 79−24521
Ni (wt.%), mech. props., effect of alloying 77−48462
Ni, antifriction material, sintered, determination of elastic moduli 79−96070
Ni, cross girder connections, fatigue strength, design stress 78−64700
Ni, cryogenic fracture toughness enhancement through grain refinement 77−36651
Ni, high-strength, impact fatigue strength, heat treatment conditions effect 80−76285
Ni ion implanted, corrosion behaviour 80−11840
Ni, low alloy, low strength, stress corrosion cracking in sulphide environment 79−47812
Ni, maraging, H_2 diffusion, diffusivity and solubility *(Japanese)* 79−42311
Ni, martensitic transformation induced by pulsed mag. field in type 52X2H23 79−15667
Ni, medium C, impact fatigue strength 79−79104
Ni, microstruct., plastic zone size and crack propag. 78−60790
Ni, recrystallisation mech. during laser treatment 80−50658
Ni, sintered, physical and mech. props. rel. to homogeneity 79−38762
Ni, sintered, relation between microstruct., microchemistry and mech. props. 78−64504
Ni steel, neutron irrad. effects on tensile props., microstructure effects 77−69005
Ni, struct. change of hot-worked austenite during post-deform. holding 80−35228
Ni-(Cr)-Ti, thermomechanical and heat treatment effects on retained austenite *(Russian)* 77−66661
Ni-Al, γ-phase, fracture mechanical aspects of abrasive friction, wear, chip formation 78−72865
Ni-B, B effect on temperability and microstructure 79−15710
Ni-Co-C (9,4,0.2 wt.%), enthalpy, sp. ht. to 2000K 79−10960
Ni-Co-Cr, high-strength medium C, Cr effect on props. 80−76339
Ni-Co-Mo, dynamic stress intensity factor meas., possibilities and limits *(German)* 80−93719
Ni-Co-Mo, fatigue crack growth, during impact tests exam. of kinetics 78−88525
Ni-Co-Mo (17.55, 8.02, 4.92 wt.%) maraging, lath martensite microstruct. and props., cold rolling effect 80−55422
Ni-Co-Mo-Ti, hot formed, recrystallization and grain boundary precipitation effect on mech. props. *(German)* 79−66073
Ni-Co-Mo-Ti microfractographical features, embrittlement and grain size influence on fracture behaviour *(German)* 80−30053
Ni-Cr, 36NKh, thermal expansion under stress at −253°C 78−22871
Ni-Cr, (4,1, wt.%), isothermal embrittlement, AES exam. of grain boundary segregation 78−60814
Ni-Cr, anodic dissoln. in NaCl solns. at high current densities *(Russian)* 80−76396
Ni-Cr, case hardened rollers, macroscopic and microscopic changes in surface layer due to rolling contact 77−77518
Ni-Cr, case-hardened roller, rolling contact fatigue life, effect of changing rolling direction 77−77519
Ni-Cr, cast, tempering embrittlement due to impurities, Auger spectroscopy exam 80−11683
Ni-Cr, corrosion on N_2O_4 flow 520-890K and 8-9 MPa *(Russian)* 80−3256
Ni-Cr, cyclic re-austenitizing 80−35222
Ni-Cr, enthalpy of martensitic transform. 77−63670
Ni-Cr, exam. of caustic stress corrosion cracking, comparison with type 304 stainless steel 79−29261
Ni-Cr, oxide layer form., SIMS obs. 79−52464
Ni-Cr, P doped, tempered martensite embrittlement 80−30089
Ni-Cr, P induced temper embrittlement, Mo effect 77−86148
Ni-Cr, SCC, grain boundary impurity effect 80−30150
Ni-Cr, Sb doped, solute segregation and brittle fracture 80−85033
Ni-Cr, Sb doped, temper embrittlement susceptibility intercritical heat treatment effect 78−64570
Ni-Cr, solute segregation and intergranular brittle fracture 80−108568
Ni-Cr, surface hardened, rolling contact fatigue failure 80−16608
Ni-Cr, temper embrittled, electron microscope and X-ray microstruct. obs. 79−38870

alloy steel continued
Ni-Cr, temper embrittlement by Sb, Ni, Cr effects 77−36628
Ni-Cr, temper embrittlement by P 77−40448
Ni-Cr, temper embrittlement by Sn 77−86149
Ni-Cr, temper embrittlement, intermediate tempering treatments 80−60944
Ni-Cr, type AC/HT-2, grain diameters, US attenuation 80−89429
Ni-Cr (35, 18 wt.%), bainitic, invariant plane strain theory, determ. of habit planes and orientation relationships 80−55388
Ni-Cr low alloy, effect of Mo on tempered martensite embrittlement 80−3187
Ni-Cr steel, case-hardened surface durability in rolling contact fatigue testing 77−63684
Ni-Cr-Fe base, radiation enhanced precip. and dissolution of precipitates, point defect kinetics and dislocation obs. 80−108467
Ni-Cr-Mn, type 4340, exam. of intergranular brittle fracture, by impact tests, Auger spectroscopy 78−52978
Ni-Cr-Mo, 106 *(German)* 80−35215
Ni-Cr-Mo, alloy SNCM8, mech. strength under combined alternating strength 78−64690
Ni-Cr-Mo, alloys SNCM8, SAE 4161, heat treated, residual stress at fatigue fracture surface *(Japanese)* 78−64622
Ni-Cr-Mo, bar, subject to combined static and repeated bending and torsion fatigue strength criterion 80−40496
Ni-Cr-Mo, cleavage fracture toughness, temperature and notch sharpness influence *(German)* 80−35291
Ni-Cr-Mo, crack growth in different media, test frequency effect *(German)* 79−66194
Ni-Cr-Mo, cyclic creep under increasing stress condition, constitutive eqn. 80−93593
Ni-Cr-Mo, ductile fracture, microvoid effects *(Japanese)* 80−108542
Ni-Cr-Mo, electroslag refined, fracture toughness and fatigue behaviour 80−81171
Ni-Cr-Mo, fracture toughness determ. from yield strength and cleavage fracture strength *(German)* 80−35292
Ni-Cr-Mo, increase of crack initiation time in delayed fracture by fatigue accumulation *(Japanese)* 78−11312
Ni-Cr-Mo, Ni effect on fracture toughness, heat treatment effect *(Korean)* 79−91781
Ni-Cr-Mo, quenched and tempered, nothced bar tensile tests *(German)* 80−35247
Ni-Cr-Mo, SAE 4340, influence of air temp. and water vapour content on fatigue behaviour 79−43463
Ni-Cr-Mo, SNCM8 exam. of delayed fracture using fracture mechanics *(Japanese)* 78−52961
Ni-Cr-Mo, TRIP steel, exam. of transformation behaviour 78−76718
Ni-Cr-Mo, type 4340, equivalence of K_{Ic} and J_{Ic} fracture toughness meas. for range of yield stress 79−38934
Ni-Cr-Mo, weld, stress corrosion cracking, metallurgical effects 79−43468
Ni-Cr-Mo (11, 5, 3 wt.%), maraging, corrosion cracking in chloride and alkaline solutions 80−55576
Ni-Cr-Mo (2.5 wt.%), elevated temp. fatigue, effect of zero load rest period 77−8943
Ni-Cr-Mo and Ni-Cr, impact strength, effect of modified ausforming *(Japanese)* 79−11692
Ni-Cr-Mo SNCM8, delayed fracture, specimen thickness and threshold stress intensity effect *(Japanese)* 80−104268
Ni-Cr-Mo steel, corrosion and cavitation-erosion resist. *(Russian)* 78−11395
Ni-Cr-Mo-U, ferritic, B segregation and high temp. embrittlement 78−7040
Ni-Cr-Mo-V, corrosion fatigue crack growth in NaOH soln., cathodic pot. effect 80−89403
Ni-Cr-Mo-V, exam. of temper embrittlement susceptibility 78−76737
Ni-Cr-Mo-V, fatigue crack growth rate, specimen thickness and stress relief effect 77−40445
Ni-Cr-Mo-V, fatigue crack growth, effect of aq. and H_2 environment 79−79173
Ni-Cr-Mo-V, for rotor appl., elastic-plastic fracture mechanics, finite element method appl. 80−1489
Ni-Cr-Mo-V, hydrogen bearing environment effect on K_{Iscc} 80−104325
Ni-Cr-Mo-V, reversible temper embrittlement 77−36656
Ni-Cr-Mo-V, stress corrosion cracking 77−52542
Ni-Cr-Mo-V, temper embrittled, crack initiation strength *(Japanese)* 77−52474
Ni-Cr-Mo-V, turbine rotor shaft, fracture toughness, validity criterion for K_{IC} 78−72861
Ni-Cr-Mo-V, type HY130, temper embrittlement due to Si intergranular segregation, effect on H_2 induced cracking 78−76735
Ni-Cr-Mo-V low-alloy, additive remedy for temper brittleness 80−66659
Ni-Cr-Mo-V steel disc, rolling contact fatigue and residual stress on contact surface 77−32671
Ni-Cr-Mo-V turbine disc steel in NaOH soln., corrosion fatigue crack growth rate, applied pot. effect 80−60998
Ni-Cr-P (0.06 wt.%), influence of intercritical heat treatment on temper embrittlement susceptibility 78−52863
Ni-Cr-S-P-Mn-Si, residual stress meas. by X-ray diffr. 80−71688
Ni-Cr-Ti, thin bands, cold working, props. and struct. of 36NKhTYu 79−78994
Ni-Cr-Ti-P, Ti and P solubility effect on free surface segregation 79−11628
Ni-Cr-(Mo), quenched and tempered struct. effect on H diffusion coeff. and solubility *(Japanese)* 78−52857
Ni-Cu-Mo-C, powdered, influence of cooling rate after sintering on preps. 79−95969
Ni-G rollers, case hardened, surface durability in pure rolling and sliding-rolling contacts 79−61739
Ni-maraging weld metal, increasing fracture toughness by heat treatment 78−72871
Ni-Mn, directional martensitic transform. expt. 79−11613
Ni-Mn (16, 2 wt.%), 40 N16G2, single crystal, stabilisation and destabilization mechanisms *(Russian)* 78−23732
Ni-Mn-Al-V, nonmagnetic, ageing, dispersion hardening, microstruct., phase comp., mech. props. *(Russian)* 79−34046
Ni-Mo, powder forged, as-forged props., effect of process variables 77−59715
Ni-Mo, powder forged, fracture processes and fracture toughness 78−72870
Ni-Mo, sintered, martensitic transformation due to cold working, metallographic study 78−44127

alloy steel continued
- Ni-Mo-C (2.0, 0.2, 0.4 wt.%) sintered, struct. transforms. and mech. props. after quenching 80—66557
- Ni-Mo-C (5, 0.5, 0.5 wt.%), sintered effects of powder and sintering variables on props. 80—104093
- Ni-Mo-Cr, critical value of J-integral determ. *(German)* 80—25827
- Ni-Mo-Cr, elastic plastic material, critical stress intensity factor determ., fracture mech. method *(German)* 79—11694
- Ni-Mo-Cr, embrittling effects of residual elements 80—66655
- Ni-Mo-V, fatigue crack growth, H_2 gas environment effect *(Japanese)* 80—104340
- Ni-Mo-V fracture toughness data, comparison with equivalent energy and energy per unit area data 78—52965
- Ni-P (8 wt.%), protective coating for wear and corrosion resistance of steel 77—21329
- Ni-S-(Mn), ferrite to austenite transform. effect on sulphide precipitation 77—86025
- Ni-Si 300M type, acoustic-emission analysis of fracture-toughness tests 80—55596
- Ni-Si-Nb (1.5,0.02,0.03 wt.%), fatigue crack growth under bending *(French)* 80—21089
- Ni-Sn, temper embrittled, interaction detect. by Mossbauer spectroscopy 77—86176
- Ni-steel U8 system, struct. defects effect on interdiffusion 80—15314
- Ni-Ti, precipitation hardening, fatigue strength 79—79103
- Ni-Ti-Al, 36NTYu, heavily deformed, subgrain struct. due to discontinuous precipitation of γ' phase *(Russian)* 79—52218
- Ni-Ti-Al, martensitic, coherent γ'-phase particles and influence on $\alpha \rightarrow \gamma$ transformation *(Russian)* 79—29056
- NiCr, random load fatigue crack propag. 78—64692
- NiCrMo, medium, C, overheated, fractographic study *(Chinese)* 80—66616
- NiCrMoV, stress corrosion cracking, cold work effects 78—11383
- NiMoCr waterquenched steel, for BWR press. vessel, fast neutron fluence evaluation, irrad. behaviour *(German)* 77—34369
- Ni(3 wt.%), hydrogen embrittlement, standard qualification tests 79—74259
- Ni(9 wt.%), isothermal bainitic transform., thermomechanical effects on mech. props. *(German)* 80—40383
- P content, 110G13L, effect on elastic moduli and internal friction 78—23753
- Pb inclusions in free-cutting steel, X-ray, light and scanning electron microscopy 77—77685
- Se addition effects, form. of existance in various chem. comp. *(Russian)* 79—56986
- Si (3 wt.%), corrugated texture perfection, mag. anal. 80—88745
- Si (3 wt.%), cube-on-edge oriented, high permeability, mill processing and mag. props. 77—86045
- Si (3 wt.%), grain oriented, core losses *(Japanese)* 78—60303
- Si (3 wt.%), grain oriented, lowest core loss 78—91887
- Si (3 wt.%), high permeability, grain oriented 78—91886
- Si (3 wt.%), hot rolled, effect of initial texture on secondary recrystallisation *(Czech)* 79—91711
- Si (3 wt.%), loss prediction, from distorted waveforms 78—76273
- Si (3 wt.%), prediction of magnetisation hysteresis loops for distorted waveforms 79—47303
- Si (3 wt.%), struct. and preferred orientation, annealing parameters influence *(Czech)* 80—89248
- Si (3 wt.%), textured, secondary recrystn., precip. annealing effect *(Japanese)* 80—71662
- Si (6.5 wt.%), fibre and sheet, Mn, Ni and Al additions influence research on mech. and magnetic props. *(Slovak)* 79—5064
- Si (low), martensite struct. and mech. props. *(Korean)* 80—93614
- Si, bainite transform. 79—100134
- Si, braking rapid cracks by pulse of current 77—16683
- Si, coated grain oriented sheet, grain detection by Hall probe 78—11470
- Si, commercial, O_2 diffusion coeff. determ. *(Slovak)* 79—39040
- Si, commercial, ordering after heat treatment, Mossbauer meas. 80—7556
- Si determination by 14 MeV neutron activation-high resolution γ-ray spectroscopy 77—1967
- Si dual-phase, mech. props and microstruct. anal. 80—40444
- Si, electron irrad. in HVEM, void swelling, Si role 80—54285
- Si, grain-oriented, high permeability, dissoln. and precip. of AlN and MnS 80—89223
- Si, high permeability grain-oriented, AlN precip. study 79—83337
- Si, highly-oriented, domain and grain obs. methods, using ferromagnetic colloid technique 80—11856
- Si killed steel, effect of Al addition to Zn on phase composition and morphology of products of Fe-Zn reaction *(Polish)* 78—85021
- Si, lower bainite morphology *(Czech)* 79—78959
- Si, metallography of bainitic transform., carbide precipitation 78—27527
- Si, non-magnetic, minimum electroresistivity, −268 to 0°C *(Russian)* 79—91021
- Si, nonoriented elec. sheet, solute oxidation effect on mag. props. 79—83335
- Si, permeability change due to stress variation after demagnetization in Rayleigh region 80—88854
- Si steel sheet, single sheet tester for 20 Hz to 20 kHz range *(Japanese)* 77—70251
- Si, steel sheet static mag. props., elastic tensile stress effect 78—47999
- Si, textured, alloying addition inhibition effects on grain orientation and growth *(Japanese)* 79—43270
- Si, transformer steel, supplementary domain struct. of misoriented grains *(German)* 78—14979
- Si, upper bainite morphology *(Czech)* 78—64537
- Si, with coating, grain-oriented, domain pattern measurements *(Japanese)* 79—38353
- Si-Al, non-oriented elec., internal oxidation and nitridation effects on mag. props. 79—83336
- Si-Cr-Mo-W-V (2,4,1,3,2 wt.%), heat treatment and props. 80—16349
- Si-Mn, 27SG, heat treated sheets, underwater explosive forming *(Polish)* 79—34052
- Si-Mn, ferrite-pearlite structs., fatigue crack propagation *(Russian)* 79—34126
- Si-Mn, hypereutectoid, type HF-1, brittle fracture, fragmentation due to blast loading 80—50699
- Si-Mn, melt, surface tension *(Russian)* 78—43212
- Si-Mn, non-magnetic, minimum electroresistivity, −268 to 0°C *(Russian)* 79—91021

alloy steel continued
- Si-Mn-C (1.6-2.0, 0.4-0.6, 1.1-1.4 wt.%), cast graphitised, heat treatment effects on mech. props. and wear resist. 79—96050
- Si-Mn-Ni-Cr-Mo, acoustic emission during stress corrosion cracking appl. to materials testing 78—53042
- Si-Mn(Mn-Cr), heat treated, exam. of microfractographic aspects of fatigue cracks *(Japanese)* 78—52959
- Si-Ni gas turbine, blade material, corrosion fatigue testing 79—70247
- Si-P-C, low C, varying Si content, cold rolled annealing 80—3090
- SiO_x inclusion formation on introduction of solid SiO into molten steel *(Russian)* 78—80530
- Sn (1.5 wt.%), specimen fracturing device, appl. for ion microprobe analyser, appl. to grain boundary segregation 77—21341
- Ti, hot-rolled, inhomogeneity of mech. props. *(Chinese)* 80—55455
- Ti inclusion nucleation, effect on crack formation *(Czech)* 79—91782
- Ti microalloyed, structural precipitation hardening, struct. and fracture *(German)* 79—61696
- Ti-C, threshold fatigue behaviour, effect of grain size and yield strength 79—91790
- Ti-microalloyed, deep drawing, texture control as affected by processing variables 79—91689
- Ti-V, Ti and V effects on precipitation, hardness and annealing *(German)* 77—55968
- TiC-Kh6V3M steel alloy, reaction during sintering and heat treatment 78—60617
- TiC-steel alloy, struct. form. during sintering, strength, rel. to heat treatments 77—59717
- TiC-steel alloys, structure formation during sintering 77—59732
- TiC-steel compact prod. by sintering in vacuum and in Ar or H_2 atmos. 77—63616
- TiC-steel composite, effect of method of Cr additions on props. 78—15341
- V and V-N, high strength, mech. props. and strain ageing, processing variables effects 77—59819
- V, carbide eutectic presence, solidification and struct. 80—50624
- V containing dual-phase, yielding and strain ageing, early stages 80—25794
- V, high C content, faceted Mn sulphide formation on crystn., thermomech. treatment effect on dendritic struct. *(Russian)* 80—50621
- V high-strength low-alloy for low temp. use, tensile and yield strength 79—70118
- V interface, diffusion above 500°C *(German)* 79—28156
- V, precip. and transform. kinetics, effect of N 80—97485
- V, steel tempering, initial stages of carbide form., electron diffr. *(Russian)* 78—19760
- V strengthened dual phase, deform. and fracture props. 78—48467
- V-C, as-quenched, struct. of lath martensite and occurrence of retained austenite 79—96033
- V-Nb, sheet, fracture toughness evaluation *(Slovak)* 79—38948
- V-Nb, supercooled austenite isothermal decomp., struct., strength and fracture characts. 80—60966
- V-Nb, V, Nb effects on strength and formability of cold rolled sheets 77—55979
- VN precipitation after heat treatment 79—29067
- W (12%), eutectic carbides struct. and comp. during heating 80—76283
- W content, rapid anal., scattered radiation recording using γ-absorpt. method 77—73489
- W fibre reinforced Ni-Cr steel, TiN coated fibre, protective props. *(Russian)* 79—66201
- W, high C, amorphous, rapidly quenched from melt, mech. and thermal props. 79—38874
- W, microstruct. and hardness, splat quenching effect 80—76293
- W, quantitative anal. of carbides formed during tempering 78—64571
- W, R18, self lubricating composite, frictional props., Ag-Cu-Zn-Cd lubricant 78—11340
- W, recrystallisation mech. during laser treatment 80—50658
- W-Co-Mo-Cr-V-C (8.5, 8.1, 4.5, 3.5, 2.2, 1.02 wt.%), phase composition, struct. and props. 80—104163
- W-Cr (3 wt.%), CrC formation in isochronal tempering, electron microscope study 80—7584
- W-Cr-V, high-speed tool, splat quenching, props. and struct. 80—76294
- W-high purity steel, tempering behaviour 80—7600
- W-Mo, high speed, hot deform. and heat treatment effect on props. 77—90372
- W-Mo, tool, heat treatment effect on props. 80—50656
- W-Mo, tool, hydrostatic extrusion and tempering, wear resistance effect 80—50728
- W-Mo, types R6M5 and R6M5K5, decarburising layer evaluation 80—21164
- W-Mo-Co, high-speed tool, struct. and props., cooling rate effect at primary crystn. temp. 80—76241
- W-Mo-Co-Cr-V, production from atomized powder 80—20837
- W-Mo-Cr-V, blanks welded to steel 45, optimal high temp. tempering 80—16351
- W-Mo-Cr-V tool steel, laser surface melted, struct., heat treatment effect 80—76424
- W-Mo-V-Cr(6,5,2,4 wt.%), 56-5-2, microstruct. produced by melting and powder metallurgy *(German, English)* 77—63591
- W-Mo-V-TiC, powder, TiC effect on milling, pressing and sintering 78—60607
- W(-Mo), sintered high-speed, naphthalenelike grain form., quenching effect on fracture toughness 80—30103
- WC surface hardened, serviceability by Ni, Cu-Ni and V alloying additions 77—21290

alloying additions
- A-15 diffusion layers, influence of additions of growth and supercond. props. *(German)* 80—11130
- Al alloys, influence of solid soln. elements and precipitation as correlation of formability parameters with texture 79—91696
- alloy, binary, crystallisation under parabolic stability *(Russian)* 79—70054
- alloy, heat-resistant, alloying and heat treatment effects on struct. and strength 78—95758
- alloys, temper embrittlement, impurities and alloying elements role, review 80—66649
- Alnico 5 alloy, S and Ti additions effect rel. to non-metallic inclusions, coercive force and grindability 80—89375
- Alnico alloys, effect of Ce addition on mag. props. 78—2699
- brass leaded, effect of Al, Sn, Fe on solidification, differential thermal analysis exam. *(Russian)* 79—29041

- **alloying additions** continued
  - bronze, sintered, Zr addition effects on struct., hardness, wear resistance *(Russian)* 77—70019
  - bronze matrix, Be alloying addition effects on supercond. props. of Nb_3Sn monofilament wires 79—87222
  - chemically stabilised, sensitisation and corrosion resist., heat treatment depend., precipitation steel, stainless, Cr-Ni 79—38827
  - Cunial MNA13-3, Mn addition effect on props. 80—21035
  - diffusion into liq. Fe *(Russian)* 78—79791
  - Elinvar, Cr addition effect on modulus of elasticity and thermoelastic coeff. 77—90387
  - ferrite, transform. kinetics, grain size, alloying element effect, carbide precip. 80—93560
  - fibre reinforced composite, alloying effect on interphase interaction, thermodynamic calc. *(Russian)* 79—74134
  - hardened, martensite struct. characts., Cu and Al additions effect *(Russian)* 78—19709
  - Incoloy, evaluation for use in nuclear process heat appl. 78—13234
  - Incoloy 800, and 800H, proposed specification changes 79—43298
  - Inconel, type 600, Li corrosion inhibitions by Al additions 80—108646
  - liquid alloy, O_2 activity coeff. 77—4925
  - Magnico alloy, with Si, Nb, Ti effect of Ub on mag. props. and grindability 77—63811
  - metal film, vacuum deposited, grain struct., influence of impurities and alloying elements *(Russian)* 78—56048
  - metal interaction with gases and C, conf., Stuttgart, Germany (Sept 1977) *(Russian)* 79—57134
  - metals and alloys, trace element detection by atom probe microanalysis 80—66910
  - mischmetal-$Ni_{5-x}Al_x$ ternary alloys, Al addition effects on structural and H_2 absorpt. props. 79—52761
  - Nichrome based dispersion hardened material, Ti, Y, Zr addition effects on crystallisation *(Russian)* 79—74143
  - oxidation resistance, high-temp., improvement by alloying additions 80—66702
  - Permalloy, corrosion resist. and mag. props., effect of Cr addition 77—86219
  - Permalloy-Rh, film, influence of Rh on corrosion resist. and mag. props. 80—3235
  - refractory compound fibre reinforced cpd. materials, diffusional reaction, effect of alloying calc. 80—20851
  - restorational carbonisation in one and two phase states *(Russian)* 80—65225
  - Silumin, AlSi10Mn, struct. and mech. props., Na modification effects 77—63786
  - solidification enhancement using Bi and Te *(Italian)* 80—7540
  - steel, 12Kh18N9T-TiB_2, eutectic alloy, high temp. props. 78—84931
  - steel, 18Kh2N4MA, Co effect on struct., and mech. props. 78—44147
  - steel, 30KhG and 30KhN, carbide formation, Mo alloying effects *(Russian)* 78—48402
  - steel, 30N9K4, effects of Mo, V, and N on grain growth, tempering, hardenability, strength and toughness 78—44202
  - steel, Al alloying addition effect on resistance to hydrogen embrittlement 77—59925
  - steel, Al-Ti-(Mo), Al-Ti-V-(Mo), Al-Ti-Nb-(Mo) and Al-V-(Mo) low-alloy, toughness improvement through Ti additions 80—66525
  - steel, alloy, 55Kh20G9AN4, corrosion resistance, alloying effects 77—70225
  - steel, alloy, mechanical properties, morphology, transform. kinetics and composition interrelations 77—86146
  - steel, alloy, Mn-Cr-Cu, exam. of ductility when deformed, alloying addition effects 78—44175
  - steel, alloy, temper embrittlement, comp. influence 80—66658
  - steel, aluminising, thermodynamic anal. of phase transforms. 80—76413
  - steel, austenitic, corrosion-resistant, strengthening by alloying with N_2 78—95757
  - steel, austenitic, Cr-Ni, nonmetallic inclusions modification using rare earth metals *(Russian)* 80—40369
  - steel, austenitic, Cr-Ni (18, 15 wt.%), oxidation resist., metallic alloying additions effect 79—52419
  - steel, austenitic, Cr-Ni (20, 25 wt.%), containing B and Ti additions, splat quenching, X-ray and TEM study 79—74186
  - steel, austenitic, Cr-Ni-Mn (21, 4, 9 wt.%), heat resistant, grain boundary reaction, effect of alloying elements *(Japanese)* 77—52331
  - steel, austenitic, Cr-Ni-Mo, Mo effect on lattice parameters and chem. comp. of σ-phase and $M_{23}C_6$ carbides 77—70072
  - steel, austenitic, grain growth in 16G2S. 16G2SF, AND 09G2SF, As effect 77—70060
  - steel, austenitic, high-speed, austenite grain growth, W addition effects 79—20085
  - steel, austenitic, high-temp. crack resist., B and Mo influence *(Russian)* 80—16435
  - steel, austenitic, intercrystn. corrosion and mech. props., inflence of Cr, N and Nb *(German)* 80—50747
  - steel, austenitic, Kh17N13M3T, activation characts. of rupture, 630-730°C, Sb and Nb microalloying effects *(Russian)* 79—5033
  - steel, austenitic, Mn-Ni-Cr, Mn effects on cracking *(German)* 77—59889
  - steel, austenitic, Ni-Cr high alloy, N_2, P and Ni effect on stress corrosion cracking and stacking fault energy *(Czech)* 78—60875
  - steel, austenitic, nitrided, creep, effect of N_2 and Ti and prior deform. 78—23789
  - steel, austenitic, phase composition of Kh14N16 with Zr, Ti, Nb and N additions after quenching and tempering 77—90378
  - steel, austenitic Mn-Ni ageing , alloying element influence on struct. and mechanical props. *(Russian)* 80—35256
  - steel, austenitic stainless, 08Kh18N10T, hot-worked precipitation kinetics and struct. of dispersed phases, Ti effect 80—29964
  - steel, austenitic stainless, B effect on corrosion resistance 78—35569
  - steel, austenitic stainless, Cr-Ni-Mo-Mn, Mo, Mn and ageing effects 78—35413
  - steel, austenitic stainless, hot plasticity, Y additions effect 79—83270
  - steel, austenitic stainless, in boiling $MgCl_2$ solns., alloying elements effect on stress corrosion cracking and K_{ISCC} *(Japanese)* 80—93692
  - steel, austenitic stainless, metastable, Si effects, unlubricated adhesive wear, oxidation resistance, solid soln. hardening 77—59949
  - steel, austenitic stainless, Mo effect on mech. behaviour in inert medium and hot Cl^- medium *(French)* 79—43482
  - steel, austenitic stainless, Mo-bearing, ellipsometric meas. of passive films, optical constants *(Japanese)* 78—85041
  - steel, austenitic stainless, N-alloyed 80—108490

- **alloying additions** continued
  - steel, austenitic stainless, stacking fault energy, effect of N 80—107279
  - steel, austenitic stainless Ni-Cr, heat resist. and comp. of non-metallic inclusions, effect of La, Nd, Pr and Ce 80—76315
  - steel, austenitic stainless stacking fault energy, effect of C, exam. 78—80553
  - steel, austenitic type EI-69, carbide transformations on precipitation of C from austenite *(Russian)* 80—97487
  - steel, B-Si, grain-oriented, high induction, Cu impurity effects 80—89366
  - steel, bearing GCr15, stress intensity factor, S effect *(Chinese)* 77—73300
  - steel, C, alloying addition effect on austenite-cementite boundary *(Czech)* 77—85991
  - steel, C, diffusion of H_2, SCC via martensite form. cooling rate changes on Mn and Ni addition *(Russian)* 78—56813
  - steel, C, Mossbauer effect exam. of effect of alloying elements 78—2781
  - steel, C and HSLA, grain size and substruct. control by alloying and thermomech. treatment, review 80—3082
  - steel, C-Mn-Cr-Mo (0.4, 0.8, 1.1, 0.25 wt.%) C, Ni, Mo, Cr addition effects on toughness of bainite 78—11327
  - steel, C-Mo-P, intergranular fracture and grain boundary segregation, P, H, Mo effects *(Japanese)* 79—15775
  - steel, carbide form. depend. on Mn, Cr, V additions, cementite stabilisation, microstruct. *(Russian)* 80—55399
  - steel, carburised, alloying effect on props., mathematical-statistical determ. 78—19794
  - steel, Ce, Nb, addition effects on hot plasticity *(Russian)* 77—66680
  - steel, cementite decomposition during plastic deform., alloying element effects 78—84768
  - steel, Co (2 wt.%), effect of Co on pearlite growth 77—90359
  - steel, Co-Si-Cr-Mo, eutectoid, alloying additions effect on pearlite interlamellar spacing *(German)* 80—40327
  - steel, cold worked, alloying additions effect on 200°C internal friction peak *(Russian)* 77—8867
  - steel, cold-formed, low pearlite, Nb alloyed, Nb effects, precipitation, recrystallisation *(German)* 77—8832
  - steel, cold-worked, alloying elements effect on cementite decomp. during plastic deform., Mossbauer study 79—82900
  - steel, comp. and processing effects on microstruct. and props. rel. to low temp. applic. 77—52365
  - steel, continuously cast slab, liquid-solid interface obs. by Pb additions to mould 77—21128
  - steel, Cr, 5KhGSVF and 0Kh16Mk, tempering resistance, mech. props., Cu addition effect 79—79012
  - steel, Cr, ferritic, corrosion morphology, electrochem. pot. and Mo additions effect *(French)* 80—45439
  - steel, Cr (17 wt.%), influence of Mo on intergranular corrosion *(French)* 80—21182
  - steel, Cr-Mn, unstable austenite, martensitic transform., effect of alloying, heat treatment, and deform. 78—19751
  - steel, Cr-Mn(Ni), Mn and Ni additions, effect on corrosion resistance and hardness 80—104342
  - steel, Cr-Mn-W(Mo), W and Mo addition effect on carbide form. in type 30 KhG *(Russian)* 79—87638
  - steel, Cr-Mo, effect of Mo on high-temp. props. 80—85005
  - steel, Cr-Mo, H embrittlement in H_2S environment, Mo effect 80—76415
  - steel, Cr-Mo, Mn and Si effect on temper embrittlement, comp. and carbide precip. effects 80—85037
  - steel, Cr-Mo (1.25, 0.5 wt.%), creep, fracture, Ti and Ti+B effects 77—36603
  - steel, Cr-Mo (2.25, 1.0 wt.%), temper embrittlement, effect of P, Sn, comp. and carbide precip. 80—85036
  - steel, Cr-Mo (2.25, 1 wt.%), small changes effect in impurity elements, creep life 80—25790
  - steel, Cr-Mo (2.25, 1 wt.%), temper embrittlement trace elements, Mo, intercritical heat treatment effects 77—36634
  - steel, Cr-Mo and Cr-Ni-Mo, V effects on recrystallisation *(Russian)* 77—66654
  - steel, Cr-Mo and Ni-Cr-Mo-V low-alloy, additive remedy for temper brittleness 80—66659
  - steel, Cr-Mo-(Ni-V), temper embrittlement by P and Sn, effect of rare earth additives 79—61721
  - steel, Cr-Mo-(V) austenitic, creep resist., high-temp. props. residuals effect 80—66600
  - steel, Cr-Mo-Ni-Nb, Nb effect on mech. props. *(German)* 80—30012
  - steel, Cr-Mo-V, cast, creep resistant, rare earth addition effect on deoxidation, nonmetallic inclusions and mech. props. *(German)* 79—66067
  - steel, Cr-Mo-V, combined Cr-Mn addition effects on hardenability 78—7046
  - steel, Cr-Mo-V, low alloy, V effect on creep *(Czech)* 77—86088
  - steel, Cr-Mu-W, carbide form., W effect 80—76259
  - steel, Cr-Ni (14, 5 wt.%), 00Kh14N5M, tempering resist., mech. props., Cu addition effect 79—79012
  - steel, Cr-Ni (16,14 wt.%), Si effect on texture, grain growth after rolling or recrystallisation *(French)* 77—55986
  - steel, Cr-Ni (2.25, 1 wt.%), role of Mo in P-induced temper embrittlement 80—35316
  - steel, Cr-Ni-Mo, combined B and rare earth metal additions effect on microstruct. impact strength and hardness 79—38963
  - steel, Cr-Ni-Mo-V-Nb (12,8,1,1.5,0.4 wt.%) Ce addition effects on strength and hardness *(Russian)* 78—15454
  - steel, Cr-Ni-Sr (18.15, 17.64, 2.4 wt.%), rare-earth additions effect on impact fracture *(Chinese)* 80—66617
  - steel, Cr-Si, oxidation resist. in high pressure CO_2, Si effect 80—66704
  - steel, Cr-Si-Mn-ΔV-Ti-Nb-Mo, effect of V, Ti, Mo, Nb additions on substructure, mech. props. *(Russian)* 79—34108
  - steel, creep-resistant pipe steel, influence of chemical comp. on formability *(German)* 78—84900
  - steel, CrNiMoV, weld metal, hot cracking resistance during electroslag welding, effects of Cr 79—87732
  - steel, effect of ε-Cu precipitates on H discharging phenomena *(Japanese)* 80—7583
  - steel, emission spectrometric determ. of Al *(Japanese)* 80—16750
  - steel, fatigue life, structural parameters and chem. comp. effects, rel. to test parameters 77—59928
  - steel, ferritic, Cr-Mo (2.25, 1 wt.%), C and Nb influence on structural transformations *(French)* 80—84925
  - steel, ferritic, creep resist., high-temp. props. residuals effect 80—66600
  - steel, ferritic, Mo addition effect on corrosion resistance, X-ray photoelectron study 79—74285

alloying additions continued
- steel, ferritic (17 wt.% Cr), influence of Mo on intergranular corrosion 80—30139
- steel, ferritic stainless, Cr-Mo, Mo effect on pitting pot., AES anal. 78—95852
- steel, high C, high alloy, $M_{23}C_6$ type carbides, effect of alloying elements on defect struct. and hardness 80—16481
- steel, high Cr, V additions effect on brittleness near 475°C *(Russian)* 78—19890
- steel, high Mn, austenite grain size, effect of rolling and V, Ti and Zr additions *(Korean)* 77—12632
- steel, high Mn, heat resistant, alloying additions, effect on mech. props. *(Korean)* 77—12631
- steel, high Mn austenitic, creep rupture, p addition and two-step soln. heat treatment effects *(Korean)* 80—93646
- steel, high purity plain C, eutectoid, alloying additions effect on pearlite interlamellar spacing *(German)* 80—40327
- steel, high speed S6-5-2 Si content effect on solidification *(German)* 78—11213
- steel, high strength, Nb(C, N) precipitation in austenite, effect on mech. props. *(Japanese)* 77—21186
- steel, high-speed cutting, struct. and props. Co addition effects *(Russian)* 77—21177
- steel, high-speed tool, Nb addition effect on hardening 79—34048
- steel, high-speed tool, VC additions, properties, powder metallurgy prep. method *(Czech)* 80—60800
- steel, hot rolled, low C, low alloy, bainitic alloying addition effects on microstruct. and props. 77—36546
- steel, HSLA, V and N effect on recovery and recrystn. during and after hot working 80—84973
- steel, HSLA, V effect on mech. props. *(Korean)* 80—29987
- steel, hypoeutectoid, alloying effect of graphitisation *(Japanese)* 79—52270
- steel, impact and tensile props., Si effects 79—24614
- steel, influence of rare earth additions on low-temp. fracture toughness *(Russian)* 79—52346
- steel, lightly alloyed, S effect on failure following controlled rolling *(Russian)* 79—57086
- steel, liquid bath, shooting methods for projecting buoyant alloy additions, expt. and mathematical eval. 77—21047
- steel, low alloy, 15Kh2MFA and 15Kh2NMFA, neutron irrad. embrittlement, effect of P, Sb and Sn impurities 80—85055
- steel, low alloy, corrosion in artificial seawater, alloying element effect *(Chinese)* 80—21150
- steel, low alloy, corrosion in artificial seawater, alloying element effect *(Chinese)* 80—21151
- steel, low alloy, ferritic, As effect on grain size 77—70062
- steel, low alloy, H_2S embrittlement, susceptibility, alloying effect 79—91797
- steel, low alloy, reactor pressure vessel, effect of Mn and C content on irrad. response 79—20196
- steel, low alloy, S and Mn influence on high temp. strength and ductility after solidification from melt *(German)* 80—81106
- steel, low alloy, strength, Cr and N effects 80—104277
- steel, low C, Al-killed, effect of V on mag. props. 79—83339
- steel, low C, cold rolled sheet, Cu effect on recrystallization texture *(Chinese)* 79—74173
- steel, low C, containing P, Mg effect on annealing texture, mech. props. and plastic anisotropy 78—27536
- steel, low C, impact and tensile props., effect of Si 77—36526
- steel, low C, Mn effect on recrystallisation and texture *(French)* 80—3110
- steel, low C, Nb-V microalloyed, Nb, V effect on impact and toughness props. 78—15515
- steel, low C, Si effect on gas nitriding, surface hardness *(Japanese)* 77—48582
- steel, low C, type AISI 1010, effect of Se, Te additions on fatigue props. 78—92359
- steel, low C Cr-Ni, temper embrittlement by antimony, Ti addition effects 77—32683
- steel, low C hot rolled sheet, drawability improvement by Al addition *(Ukrainian)* 79—78996
- steel, low C Mn-V, VC effects on strength and brittleness 77—70055
- steel, low pearlite, Ti addition effect on transform. behaviour *(German)* 77—90343
- steel, low-alloy, austenite grain growth, role of V, Nb, N alloying additions 77—44255
- steel, low-alloy, fracture toughness and brittle fracture, S and rare earth additions effect 79—87720
- steel, low-alloy, transform. of austenite, cooling rate effect 79—38821
- steel, low-alloy, V effect on mech. props. 80—35312
- steel, low-alloyed, C-content influence on high temp. strength and ductility after solidification from melt *(German)* 80—81105
- steel, low-C and low-alloy types, Nb effect on cold resist. 79—38954
- steel, low-C contaning Ti, sheets, recrystn. texture effects on plastic strain ratio and deep-drawing *(Chinese)* 80—66527
- steel, low-C martensitic, Ni addition influence on toughness and ductile-brittle transition 80—30099
- steel, machining, 12L14, effect of Pb and Te on hot-shortness mechanism 80—104190
- steel, maraging, 0Kh6N8M7S, effect of Cr, Ni and Mo on hardness 80—21093
- steel, maraging, Cr-Ni-Ti, effect of Ti addition on hardness and energy scatt. 79—15687
- steel, maraging, hardening mechanism of quenched samples, tempering *(Czech)* 79—78989
- steel, maraging, Se microalloying, machinability improvement 80—21116
- steel, maraging, solubility of Fe-Mo-Co (10, 0 to 20 wt.%) Laves phase, depend. on Co *(Russian)* 79—100145
- steel, maraging, structural recrystallisation, alloying element effects 77—70080
- steel, maraging alloy, intermetallic compound solubility, thermodyanmic calcs. *(Russian)* 80—40363
- steel, martensitic, age hardening with Cu, Nb additions, exam. of hardness 80—7681
- steel, martensitic, alloying element effect on coarsening behaviour of cementite particles in ferrite 80—66518
- steel, martensitic, Cr-Ni, grain refining and phase transforms. effect on plasticity *(Russian)* 78—39837
- steel, martensitic, tempered, C and low alloy, hardness, effect of alloying additions 78—27629

alloying additions continued
- steel, medium C, fatigue failure, alloying influence *(Russian)* 80—21081
- steel, medium C, microalloying with V and Ti, effect on hardness and structure 80—11750
- steel, medium C 80—11752
- steel, medium Cr, B effects on struct. and toughness 77—21265
- steel, Mg effect on precipitation of C and or N, and mech. props., during strain ageing *(German)* 78—35387
- steel, microalloy V-Nb, V, Nb effects on strength and formability of cold rolled sheets 77—55979
- steel, microalloyed, review of development 79—47699
- steel, microalloyed with Ce, La, Nd, effect on crystal structure and thermal fatigue and resistance *(Russian)* 79—34136
- steel, mild, cold rolled, texture and plastic anisotropy rel. to alloying and precipitation *(French)* 80—108475
- steel, mild, N_2 on oxidation resistance 79—61786
- steel, Mn-C (1, 0.1 wt.%) strip, hot rolled, P effect on mech. props. 78—27532
- steel, Mn-C-O, phase equilibrium, Mn effects at liquidus temp. *(Russian)* 77—66625
- steel, Mn-Cr-Mo, Mn-V-Mo, high-strength heat-treatable sintered 80—50575
- steel, Mn-Ni-Cr-Mo, high tensile strength, alloying addition and rolling conditions effect on transformation texture 79—83225
- steel, Mn-Te, structural, brittle fracture resistance, Ti addition effect *(Czech)* 80—45392
- steel, Mo-Nb (2.5, 0.035 wt.%) Mo content effect on sulphide stress cracking resistance 80—21157
- steel, Nb,(V), (Al), hot rolling, laboratory simulatory recrystn. of austenite 80—97512
- steel, Nb-Mo, Mo effect on sulphide stress cracking resistance 80—16552
- steel, Ni (9 wt.%), mech. props., effect of alloying 77—48462
- steel, Ni-Co-Cr, high-strength medium C, Cr effect on props. 80—76339
- steel, Ni-Cr, P doped, tempered martensite embrittlement 80—30089
- steel, Ni-Cr, P induced temper embrittlement, Mo effect 77—86148
- steel, Ni-Cr, temper embrittlement by Sn 77—86149
- steel, Ni-Cr low alloy, effect of Mo on tempered martensite embrittlement 80—3187
- steel, normalised, C-Mn-P, P effect on mech. props. 77—63745
- steel, pearlitic, Cr-Mo, Cr-Mo-V and Mo-V, heat resist., Mo content rel. to mech. props. 79—20134
- steel, pearlitic atom probe microanal., computer controlled 77—66781
- steel, plate, alloying, normalising, controlled rolling 77—48459
- steel, quench ageing effect of Mn content on C and N precipitation and mech. props. *(German)* 78—31409
- steel, R6M6, Nb, Zr, Ti micro-alloying effects on properties 78—6939
- steel, rail, toughness, effect of Sn, SEM exam. 80—97569
- steel, rare earth addition effects and behaviour, review *(Chinese)* 79—43257
- steel, rare earth additions, effect on physicomechanical props. 77—12639
- steel, rare earth additions review 78—72786
- steel, rare earth metal additions effects on mech. props. 78—52829
- steel, Se addition effects, form. of existance in various chem. comp. *(Russian)* 79—56986
- steel, Si, textured, alloying addition inhibition effects on grain orientation and growth *(Japanese)* 79—43270
- steel, Si (6.5 wt.%) Mn, Ni and Al additions influence obs., on mech. and magnetic props. *(Slovak)* 79—5064
- steel, sintered, Cr-Mo, CaF addition effects on struct. heterogeneity 78—60611
- steel, sintered, high speed, with Ti(C,N) additions 78—11160
- steel, sintered, maraging, N14K7M5T, mech. props., effect of Ti additions 77—25081
- steel, solubility of W and Mo in $Ti(C,N)_x$ 80—16276
- steel, stainless, 10Kh18N9TL, S, Se, Te and Bi additions effect on mech. props. 79—83312
- steel, stainless, corrosion prevention by rare earth metal addition 79—20289
- steel, stainless, Cr, Mo effects on passivation AES and electrochemical anal. 79—74292
- steel, stainless, Cr-Ni, maraging, effect of Mo, Co additions on hardening 78—84835
- steel, stainless, Cr-Ni-Co (13, 4.5, 0 to 13.8 wt.%), Co effect on martensite ageing *(Russian)* 77—66660
- steel, stainless, Cs enhanced corrosion, Te influence 78—23866
- steel, stainless, ferritic, corrosion in formic acid at 70°C, effect of Mo additions 78—35551
- steel, stainless, ferritic, corrosion resistance improvement by Mo and Ti additions 77—90505
- steel, stainless, ferritic, Ni-free, effect of V, Ti addition on ductility 79—79048
- steel, stainless, intercrystalline corrosion, effect of alloying elements, thermodynamic anal. 77—90504
- steel, stainless, oxidation resistance, effect of C, Zr, Ti and Nb 80—35394
- steel, stainless, recrystallisation texture, effect of Cu, Ti additions on development *(Japanese)* 78—80558
- steel, stainless, resulphurated, Cr-Mo (18,2 wt.%), Mo effect on corrosion resistance *(French)* 77—63830
- steel, stainless, surface oxide characterisation by Raman spectroscopy 80—50308
- steel, stainless AISI 316, Si and Ti effect in phase stability and swelling behaviour 79—78972
- steel, stainless austenitic, low alloy 316, high temp. plasticity, B addition effects *(Russian)* 77—28852
- steel, stainless complex alloy, hot ductility, B effect 80—30038
- steel, stainless type 316 80—108646
- steel, structural, addition of solid SiO, effect on ductile fracture 80—16465
- steel, structural, effect of rare earth metals on cold temper brittleness 79—29202
- steel, temper embrittlement and embrittling intergranular segregates, Mo effects *(French)* 79—91788
- steel, transformer, texture formation tendency *(Russian)* 77—59803
- steel, ultrahigh strength, Si addition and retain austenite effect on SCC, quenched and tempered 78—48567
- steel, V high strength low-alloy, low temp. use, $VC_{0.75}$ and VN solubility 79—70118
- steel, WC reinforced surface layer, serviceability improvement by Ni, Cu-Ni, V alloying additions 77—21290
- steel *(French)* 80—66670

alloying additions continued
steel 23K2G2T, corrosion cracking susceptibility, C and Cr effects 78—19952
steel 35GS and 20GS, thermally strengthened rolled, H$_2$ embrittlement and cracking resistance *(Russian)* 78—35479
steel 40 khNMS, high temp. thermomechanical treatment, Cr effects on props. 77—12651
steel casting surface alloying feasibility trials 79—83395
steel creep resistant, rare earth metal effect on inclusion charact. *(Czech)* 77—86134
steel electrode, erosion resist., influence of C and carbide-forming elements *(Russian)* 78—11389
steels, nuclear reactor pressure vessel steels, optimum chem. comp. rel. to props. 80—93517
steels, secondary hardened, microstruct. rel. to mech. props. 80—25851
superalloy, microstructure resulting from alloying and heat treatment, effect on creep, fatigue, fracture strength 78—11246
surface layer alloying effect on electroerosion working *(Russian)* 78—64760
Ticonal, effect of rare earth metals on mag. props., struct., and phase transformations 79—99732
transition metal amorphous alloys with metalloid elements, embrittlement/crystn. relationship *(Japanese)* 79—96134
transition metal silicides, struct. and supercond., Cu influence 80—50592
transition metal-Si-B ternary and quaternary amorphous alloys, effect of comp. on crystn. *(Japanese)* 79—94910
Zircaloy-4, elastic props., O additions effect 80—66565
Ag-Cu-Sn(Zn)(Au), effect of additions on eutectic and peritectic temp., of binary alloys 78—84801
Ag-Sb (1.16 wt.%), Sb effect on sintering kinetics in early stages 79—52137
Ag-Sn-Au, dental amalgams, effect of small additions of Au, struct. and corrosion study 79—20718
Ag-Zn, internally oxidized, elec. contact characts., alloying additions effect *(Japanese)* 80—88619
AgZn, $\beta'\rightarrow\zeta$ transformation, effect of additional elements 80—66507
Al alloy, 51S, modified by misch metal, for space appl. 80—55466
Al alloy, fracture toughness and struct. *(Russian)* 77—25134
Al alloy 7075, CrAl$_7$ form., effect of V and Zr 78—44132
Al alloys, columnar struct. of alloys solidified in flowing melt in centrifugal casting 80—71640
Al alloys, Cu interdiffusion with sintered Al powder, struct. effect at high press. 78—60606
Al alloys, effect of alloying elements on cond. 80—3205
Al bronze, G, Si additions, corrosion resistance 77—16714
Al conductor alloys, subgrain-strength relationship, effect of alloying and processing 77—32606
Al foil, alloying additions (Si, Mg, Y, Se, Sc) effect, on tensile strength, weldability 80—55475
Al substitutional solid solution alloys, volumetric effect and props. *(Russian)* 80—39293
Al, thin film resistor, rare earth alloying effects *(Russian)* 79—78211
Al-(Mn), effects of Mn on electrode or free corrosion potentials 80—100942
Al-Ag (up to 4 wt.%), creep, 570-630°C, influence of Ag addition *(Russian)* 79—5003
Al-Ag(Cu), alloying effect on phonon spectrum and lattice heat cond. 77—62695
Al-Cr, quench hardened, Cr effects on resoftening 77—66657
Al-Cu-Mg (2.6, 0.4 wt.%), Fe, Si, Mn and Ti addition effects on age-precipitation *(Japanese)* 80—20937
Al-Cu-Mg alloy, extruded, press forming in liquid/solid coexisting state, mech. props., Mg effects 78—11151
Al-Cu-Mg-Si-Fe-Mn-Ti, Si, Fe, Mn and Ti effect on precipitation in solid soln. *(Korean)* 79—66064
Al-Cu-Mg-Zn, Mg and Zn addition effects on dendrite struct. and mech. props. *(Korean)* 77—28796
Al-Cu-Mg-(Ag), effect of addition on fatigue microstructure relationships 80—40483
Al-Cu-Mn (1-5.2, 0-0.6 wt.%), N alloying and comp. effect on mech. props. *(Bulgarian)* 80—71719
Al-Cu-Sn, ageing process, effect of Sn atoms, ^{119}Sn Mossbauer spectra obs. 80—7598
Al-Cu(Zn-Mg), age hardening, conditions leading to localised plastic deform. and fracture in slip bands during fatigue 78—64670
Al-Fe, cast, influence of Zr on precipitation, solidification and grain size *(Rumanian)* 78—84813
Al-Fe (0.5 wt.%)-Ti-Cr, Ti, Cr addition effects on toughness/microstruct. relationship *(Japanese)* 77—48525
Al-Mg, influence of Mg, Si, Fe, Mn on homogenisation process *(Polish)* 79—78949
Al-Mg, Mg effect on ductility, 25 to 250°C 79—100214
Al-Mg, plastic deform., separation of internal friction components *(Russian)* 79—52282
Al-Mg$_2$Si (0.95 wt.%), excess Si effect on ductility 78—27580
Al-Mg-Ag, age effect on age hardening *(Japanese)* 78—52831
Al-Mg-Bi -Na, Bi additions to prevent Na embrittlement 77—86153
Al-Mg-Fe-Mg-Si-Cr, alloys, dendritic segregation with Fe, Mg, Si and Cr additions *(Polish)* 79—56980
Al-Mg-Si, dil. alloy, Mn additions and heat treatment effect on $\beta\rightarrow\alpha$ transformation 80—7566
Al-Mg-Si alloy, Mn additions, effect on deform. 77—8876
Al-Mg-Si-Mn, Mn addition effects on fracture 78—60791
Al-Mg-(Ag), effect of addition on fatigue microstructure relationships 80—40483
Al-Mn (0.35 wt.%), quenched exam. of Mn-vacancy interaction 78—76676
Al-Mn(0.6 wt.%), supersat. solid solns., isothermal decomp., Zr addition effects 77—63626
Al-Si (35 wt.%), Cr, Co, Si addition effects on strength of powder 77—24983
Al-Si eutectic, Na, Sb and Sr alloying addition effects on microstructure *(French)* 78—64548
Al-Si-Mg alloys, and Si content and Mg addition effect on mech. props., Na treatment *(Korean)* 79—38901
Al-Si(Mn)(Ti)(Cr)(Ni)(Cu)(Fe), liq., dissoln. and diffusion of alloying components, 700-1000°C *(Russian)* 80—15275
Al-Sn, Sn effect on electrochemical behaviour in acetate buffer 78—19927
Al-TiB$_2$-Si, Si effect on grain refinement *(German)* 79—91656

alloying additions continued
Al-water vapour reaction, stress corrosion susceptibility STEM study, Mg addition effect 80—3247
Al-Zn, GP zones, effect of Si, Ag, Mg on transport props. 77—16588
Al-Zn-Fe-Si, Fe and Si effects on precip., TEM and X-ray diffr. obs., ageing at 90°C 77—48439
Al-Zn-Mg alloy, Ag addition and pre-precipitation treatment, influence on GP zone growth 80—71658
Al-Zn-Mg-Cu type 7XXX, Cu effect and recrystallisation, low cycle corrosion fatigue 79—91852
Al-Zn-Mg-Cu-Cr-Zr, high strength Cr and Zr addition effects 77—59820
Al-Zn-Mg-Ti, Ti effect on microstructure during ageing 78—64568
Al-Zn-Ti(Mn), mech. props., Ti or Mn addition effect *(Korean)* 80—93613
Au-Fe-Ni layer coating, Fe and Ni conc. meas. by X-ray diffr. *(German, English)* 80—34330
CC Fe-Ni-Cr (35, 15 wt.%): Nb(Ti)(Mo), corrosion in HTGR He environment 80—61021
Cd-Sn(-Pb) liquid (0.03 to 0.10 at.% Cd), Cd activity coeffs., interaction parameters, EMF depend. on temp. 80—49383
Co alloys, dil., factors affecting high-temp. oxidation behaviour, alloying effects 77—77638
Co vacuum condensates, Cr alloying addition effect on texture characts. *(Russian)* 80—108471
Co-based amorphous alloys, effect of alloying additions on corrosion resistance *(Japanese)* 79—96215
Co-Cr-Al-Y(Hf), high temp. oxidation 78—11432
Co-Ni-Cr-Nb, effect of Fe addition on precipitation behaviour 80—29962
Co-transition metal, transition metal additives influence on struct., specific resistance, microhardness, mech. props., magnetic props. 79—29078
Co-W(25 wt.%), cellular decomposition, third element effects *(Russian)* 77—1837
Co-X-Co (X=Cr,Mo,W) systems, crystn. temp. and hardness 79—77529
Co-Zr-Er alloys, mag. annealing effect, effect of Er on induced uniaxial mag. anisotropy 80—39771
CoCrAl-Y(Hf), Y and Hf effects on oxidative behaviour 78—44275
(Co$_{0.93}$Fe$_{0.07}$)$_{75-x}$Cr$_x$Si$_{15}$B$_{10}$ amorphous alloy, thermal stability, Cr conc. effects, DTA expts. 80—59395
β-CoGa, Cu addition effects on defect struct. *(German)* 77—11546
Cr, and Cr alloys, cast, B additions effect on struct. and props. *(Russian)* 78—19891
Cr, optimum alloying with rare earth metals, Ti, Zr, Hf, Nb, Ta 78—68651
Cr, thin film resistor, rare earth alloying effects *(Russian)* 79—78211
Cr-C facing alloys, effect of B on phase composition and facings props. during abrasive wear 80—21117
Cr-Ce-N, Ce and N effects in ductile-brittle transition, microstruct., hardness, *(Russian)* 78—35497
Cr-Fe base ternary alloys, 4d transition metal additions, magnetically insensitive Invar production 77—28026
Cr-La-V-Nb-Ta, La, V, Nb Ta effect on hardness and strength *(Russian)* 79—34050
Cr-Sm-Pr, Sm and Pr additions and plastic deform. effects on texture *(Russian)* 77—55983
Cr-V-Ce-N, (2.4 to 2.6, 1.7 to 2.3, 0.005 to 0.23 wt.%) V effect on hardness, and ductile to brittle transition temp. *(Russian)* 79—34138
Cr-X-C amorphous alloys, (X=Fe, Co, Ni, Nb, Mo and Ta), crystn. temp. and hardness 79—73133
Cr$_3$C$_2$ fibre reinforced Ni-based composite, oxidation and creep, Y additions effect 80—66685
γ-γ'-Cr$_3$C$_2$-Y eutectic, Y addition effect on oxidation during thermal cycling 79—74310
Cr$_2$O$_3$, effect of oxide additions on sintering in air and reducing atm. 77—59729
Cu alloy, mobility of boundaries, transition metal addition effects *(Russian)* 77—21160
Cu alloy solid solution condensed films, influence of alloying components on phase composition and lattice spacing *(Russian)* 80—20047
Cu alloy vacuum condensed films, alloying addition influence on electrophysical props., elec. cond. *(Russian)* 80—34529
Cu and Cu-Sn(Zn)(Al) alloys, wear, effect of Mn$_5$Si$_3$ content *(Japanese)* 78—35525
Cu, cold work, P effect on annealing 79—47707
Cu, corrosion, noble metal additions effect, Auger spectra 78—35579
Cu melts, pure and alloyed, supercooled, influence of impurities on crystallisation 79—29042
Cu, microalloyed with B, elec. cond. and strength props. *(Polish)* 80—89285
Cu powder, flowability, apparent density and comp., effect of Na, Mg and Al additions 79—28986
Cu-Ag(Mn)(Ni)(Si)(Zn), alloying effect on embrittlement of stainless steel during soldering 79—47773
Cu-Ag(Se)(Sn)(Ag-SeSn), Ag, Se, and Sn effects, singly and together, on recrystallisation 79—100164
Cu-Al-Fe (11, 2 and 1 wt.%), Fe effects on microstruct. and mech. props. *(Korean)* 77—28807
Cu-Al-Ni, mixed powder compacts, Ni content influence in sintering behaviour *(Japanese)* 80—35130
Cu-Al-Ni(Mn), duplex shape memory effect after nonuniform plastic deform. *(Russian)* 80—25759
Cu-Al-Si, Si effect on mech. props. and microstructure *(Korean)* 79—38903
Cu-Al(Sn), effect of Al and Sn on friction and wear 78—11348
Cu-Be (2 wt.%), alloying addition effects on grain boundary reaction *(Japanese)* 80—49236
Cu-Be-Ni-Ti-Mg bronze, alloying element influence on minimum thermo EMF, cold working *(Russian)* 80—34426
Cu-Bi-Fe, Fe effects on embrittlement 77—28900
Cu-Ce(Y)(In), effect of alloying additions on electrical cond., and mech. strength 78—44233
Cu-Cr-Zr-Ti-B alloy system, solidification cracks formed during welding, reduction by microalloying with B 79—96148
Cu-In(Sb), growth kinetics, of discontinuous precipitation, third element effects 77—36511
Cu-Mn(Fe)(Ni)(Zn)(Ge), effect of impurities on Cu recrystallisation 78—52836
Cu-Ni, cast, strength and hot ductility, alloying and residual elements effect 80—66595
Cu-Ni alloys, alloying additions effect on thermal conductivity, 20-400°C *(Russian)* 77—59159

alloying additions continued
Cu-Ni cast alloy, effect of addition of Ni, Mn, Si, Al, and Fe 78−85033
Cu-Ni-Al, cast, strength and hot ductility, Al effect 80−66595
Cu-Ni-Be-(Al) (30,0.5,(0.2-2) wt.%), Al addition effect on grain boundary reaction *(Japanese)* 80−54254
Cu-Ni-Fe, cast, strength and hot ductility, Fe effect 80−66595
Cu-Ni-Mn, cast, strength and hot ductility, Mn, effect 80−66595
Cu-Ni-Si, cast, strength and hot ductility, Si effect 80−66595
Cu-Sb solid soln., finely lamellar discontinuous precipitation, ternary addition effects 77−36510
Cu-Sn alloy system, long period superlattice obs. and impurity effects 80−103297
Cu-Ti, Zr effects on cellular precipitation 77−16587
Cu-Zn, cyclic stress/strain curves in monocrystalline and polycrystalline samples, cold work and Zn addition effects 78−95786
Dy-Sm, magnetic moment growth due to Sm addition *(Russian)* 80−34608
α-Fe, 0.14 wt.% P addition effect on creep 77−90420
Fe alloy, martensitic transform., critical driving force, effect of alloying elements 77−48437
Fe alloy, molten, N_2 diffusion, effect of Si, P, Al and B *(German)* 77−20099
Fe alloy, oxide dispersed, mech. alloying, microstruct. 77−25063
α-Fe, alloying with Ti, V, G, Mo, W and Mn, effect on dislocation mobility *(Russian)* 77−31671
Fe alloys, CC distribution ability of alloying elements *(Czech)* 80−29047
Fe base amorphous alloys, alloying element role in improving corrosion resist., ESCA study 80−50754
Fe base binary alloys, thermoelectric force caused by internal adsorption *(Russian)* 78−95288
Fe based amorphous alloys, delayed fracture in atmosphere, effect of alloying additions *(Japanese)* 79−96212
Fe, cast, C and Si effect on spheroidal graphite *(Korean)* 79−38839
Fe, cast, cast Fe, spheroidal graphite, rare earth treated, nodularizing element distrib. *(Chinese)* 80−11653
Fe, cast, electron probe determ. of traces of modifying agents in spheroidal graphite 79−52814
Fe, cast, ferritic, Ce addition effect on impurity distrib. Mossbauer study *(Russian)* 78−18673
Fe, cast, grey, fracture surface after dynamic fracture, Mg conc. effect 80−100909
Fe, cast, H_2 charging effect on nodularizing efficiency of Ce-La additions 78−27544
Fe, cast, mech. props., demodification influence of isothermal holding and Mg additions *(Bulgarian)* 79−15707
Fe cast, Mg, austenite isothermal transform., Sn addition effect 79−87611
Fe, cast, Mg micro distrib., microprobe anal., electron fractography 77−70373
Fe, cast, modular graphite form., Ce effect *(Japanese)* 77−56000
Fe, cast, nodular graphite formation, Mg and S effects *(Japanese)* 77−56001
Fe, cast, nodular graphite form. by Bi and Pb additions *(Japanese)* 77−63693
Fe, cast, nodularization efficiency of rare earth alloy treatment, charging effect 79−91714
Fe, cast, P and Ce effect on struct. *(Russian)* 79−52224
Fe, cast, Si, ferrite heterogenisation, phase separation and embrittlement, Si effects 79−96125
Fe, cast, Sn additions 78−48347
Fe, cast, spheroidal graphite, Mn effects *(Korean)* 77−8841
Fe, cast, spheroidizing effect of Mg and Ce modifiers 80−35193
Fe, cast, tensile strength, Al addition effects *(Korean)* 80−71736
Fe, cast, unalloyed and alloyed, addition effects on struct., thermodynamics of microsegregation 79−8305
Fe, cast, white, high Cr, phase composition, B effect 80−104172
Fe, cast, Y effect on struct. 80−29967
Fe, cast nodularisation of graphite by Ce, Y, La, Ti, and Zr additions *(Japanese)* 77−55999
Fe, cast-Mg, 78−44149
Fe, grey cast, corrosion resist., Cu alloying additions effect *(Russian)* 78−56807
Fe, grey cast, P effect on distrib. of alloying elements 77−12634
α-Fe, irradiation induced void swelling, Cr additions effect 80−55408
Fe, liq., viscosity, effect of C, O, S, P additions *(Russian)* 77−59134
Fe, liquid, alloying element effect on H_2 diffusion *(Russian)* 79−69270
Fe, liquid, N solubility depend. on added elements, mechanism *(Russian)* 80−65223
Fe, segregation of impurities, physico-chemical aspects *(Czech)* 80−60866
Fe solid solution, substitution strengthening by Cr and Mo *(Czech)* 80−30080
Fe, solubility of P, alloying element effects *(Russian)* 79−69248
α-Fe-(Ni,Mn,Cr,Mo,W)-P (1 wt.%). grain boundary segregation, temper brittleness, AES study *(Japanese)* 79−78981
Fe-Al, Al effect on softening in solid soln. *(French)* 79−52226
Fe-Al-Ni-Co-Cu alloys, Ti alloying and deoxidising addition *(Russian)* 78−80181
Fe-As melts, influence of Sn, Si, Mn and Cr additions on surface tension and density *(Russian)* 80−15337
Fe-As-Su-Si (Cr)(Mn) melts, As and Sn distrib., Si, Cr, and Mn influence *(Russian)* 80−16274
Fe-B-Mo-Cr, amorphous, Mo and Cr addition effect on corrosion behaviour 80−16568
Fe-based metallic glasses, effect of metalloidal elements on thermal stability, crystn. temp. *(Japanese)* 79−94909
Fe-C amorphous alloys, corrosion resistance improvement by Cr and/or Mo addition 79−66211
Fe-C-Mn-Si (4, 2, 1.5 wt.%), cast wire, influence of B addition on struct. and elec. cond. *(Russian)* 80−55391
Fe-C-Ni-Cr(Cu), dynamically hot pressed, mech. props., additives effect 78−60620
Fe-C-Pb, sintered, antifriction props., Pb introduction effect 79−96155
Fe-C-S-Mg melt, S and Mg effect on graphite growth shape 79−38817
Fe-C-Si(Co), eutectoid alloy, Si and Co addition effects on pearlite growth rate 77−16575
Fe-CR (26 wt.%), role of C and N in brittle fracture 80−16456
Fe-Co (25-35%), ordering, Cr addition effects, Mossbauer expts. *(Russian)* 78−19741

alloying additions continued
Fe-Co alloy, V addition effect on atomic order parameters, dislocation struct., mechanical props. 79−91762
Fe-Co-Cr, Cr effect on struct. *(Russian)* 78−27535
Fe-Co-Cr, Cr effect on struct. of ordering 78−35407
Fe-Co-Ni-Al, Si alloying of mag. hard alloys *(Russian)* 79−73765
Fe-Co-V alloys, effect of V on struct., electron diffr. and Mossbauer meas. *(Russian)* 77−77507
Fe-Cr, irradiation induced void swelling, Cr additions effect 80−55408
Fe-Cr (20 wt.%), high temperature oxidation resistance, effect of rare earth and reactive element additions *(Japanese)* 79−20271
Fe-Cr (20 wt.%), role of rare earths and reactive elements in high-temp. oxidation 79−79178
Fe-Cr (20 wt.%) high temp. oxidation behaviour with small La additions (0 to 1.3 wt.%) *(Japanese)* 78−85039
Fe-Cr-A1 (14, up to 2 wt.%), Al effects on high temp. oxidations *(Japanese)* 79−15865
Fe-Cr-Al, Al addition effect on oxidation, 900 to 1200°C 79−66222
Fe-Cr-Al, Al effect on high temp. oxidation in wet O_2 79−66223
Fe-Cr-Al, elec. heating alloy, effect of rare earth additives on quality *(Chinese)* 78−84825
Fe-Cr-Al-Ce, Ce effect on high temp. oxidation 79−100301
Fe-Cr-Al-Ce, high temp. oxidation *(Japanese)* 78−11413
Fe-Cr-Al-Y, influence of Y additions on oxide-scale adhesion 77−8993
Fe-Cr-B, B inhibition of oxidation, AES study 79−61785
Fe-Cr-Co ductile magnet alloys, phase diagram and mag. props., V or V+Ti addition effects 77−8959
Fe-Cr-Co-V-(Ti) hard magnets, V and V-Ti effects on mag. and mech. props. 79−91810
Fe-Cr-La(Y)-Al, La or Y with Al addition effect on high-temp. oxidation 79−100302
Fe-Cr-Mn, Cr and Mn effect on N_2 solubility above 1000°C *(Bulgarian)* 79−65203
Fe-Cr-Mn, influence of alloying with Ni, Mo, N on defect conc. energy *(Russian)* 80−54241
Fe-Cr-Ni (12, 15 wt.%) austenitic alloy, Ni^{6+} irradiated, void swelling and phase stability, Si and Ti effects 80−65055
Fe-Cr-Ni-Cu-Sn, Cu and Sn effect on Cr and Ni segregation *(German)* 78−72777
Fe-Cr-Ni-Mo-V, Mo and V effects on segregation *(German)* 77−55942
Fe-Cr-Ni-Ti-Al, superalloy, Ti, Ni, Al, H_2 variations effect on mech. props. 78−3188
Fe-Cr-Pd, Pd alloying effects on passivation 80−35373
Fe-Cr-Si, oxidation resist. in high pressure CO_2, Si effect 80−66704
Fe-Cr-Y, Y addition effect on high temp. oxidation resistance *(Japanese)* 79−70223
Fe-Cr(W)-M, (M=Si,Mo,Ni,Mn,P,Cr), cellular growth of S-pearlite formed by carburisation 80−108486
Fe-Cu-Ni, Ni effect on austenite decomposition 80−3048
Fe-Cu-Ti, improvement of irradiation-enhanced Cu embrittlement by Ti addition 79−43393
Fe-Hl (Si) (Ti) (V), molten, gaseous O_2 absorption 80−11836
Fe-Mn, struct. and props., effect of Nb, C and Si alloying *(Russian)* 77−90360
Fe-Mn-B, B effect on intergranular embrittlement 80−108555
Fe-Mn-C-Si alloy G20, effect of Si and Mn additions on phase composition in multiple $\gamma\rightleftarrows\varepsilon$ transitions *(Russian)* 78−95743
Fe-Mn-Cr(Ni), mag. and crystallographic transformation depend. on Cr-Ni addition *(Russian)* 79−83334
Fe-Mn-Cu-C, Cu effect on ε'-martensite, X-ray obs. of heating effects *(Russian)* 79−87667
Fe-Mn(Sb)(Sn), additive effect, on eutectoid transformation of Fe 78−52799
Fe-Mn(Si)(Cr)(Ni), effect of alloying additions on magnetoelastic effects 78−43624
Fe-Mo (0 to 6 wt.%), alloys, in chloride solns., role of Mo as localised corrosion inhibitor 79−20255
Fe-Mo-C amorphous alloys, Mo effect corrosion resistance in HCl *(Japanese)* 79−96214
Fe-Mo-P, P-induced temper embrittlement, Mo role 80−35316
Fe-Ni, crystallization texture, rolling, effect of impurities 78−15425
Fe-Ni, reactive metal alloy, effects of thermomechanical processing on strength and toughness 79−70112
Fe-Ni (3 wt.%), grain boundary segregation of Sn and P embrittling additions, STEM microanal. 78−76654
Fe-Ni austenitic, effect of Al and Ti on relaxation resist. 80−20993
Fe-Ni system, Ni addition effects on activated sintering of Fe powder compacts 77−4756
Fe-Ni-Al-Co-Cu-Sn alloy YuNDK35T5, Sn addition effects on physicomechanical and magnetic props. and workability *(Russian)* 77−70101
Fe-Ni-Al-Cu (25, 14, 4 wt.%), alloy YuND4, effect of Ti addition on structure, mag. props. 80−15714
Fe-Ni-Al-(Cu) (12, 0.5, 0.5 to 3 wt.%), Cu addition strengthening at 77K, mech. props. 80−60875
Fe-Ni-Al(Ti)(Nb)(V), cryogenic toughness, strength, rel. to reactive metal addition 78−39885
Fe-Ni-B-Mo, crystn. temp. and elec. cond. correl., Mo effect 80−75179
Fe-Ni-C, C effect on recrystallisation and reversion *(French)* 77−81282
Fe-Ni-C martensite morphology, butterfly-lenticular transition temp., Cr addition effect *(Japanese)* 80−81053
Fe-Ni-Cr (35, 15 wt.%), high temp. alloys, for HTR primary components, alloying additions for carburisation protection 80−5243
Fe-Ni-Cr (35, 15 wt.%) superalloy, stress rupture and tensile props., C and B additions effect *(Chinese)* 80−104244
Fe-Ni-Cr alloy 800, minor alloying element effect on creep, ageing microstruct. 78−27572
Fe-Ni-Cr-Al-Y, oxidation mechanism, Y addition effect on kinetics and oxide adherence 80−97623
Fe-Ni-Cr-Mn-Al-Ti Incoloy 800, exam. of scale morphology, alloying element distrib. after oxidation 78−80677
Fe-Ni-Cr-Si, superalloy, Cr and Si effect on mech. props. and microstruct. *(Chinese)* 79−100207
Fe-Ni-Cr-Si alloy 800, Si effect on creep and age hardening 77−48444
Fe-Ni-Cr-Ti-Al, Ti and Al effect on microstruct. and mech. props. *(Chinese)* 79−74130
Fe-Ni-Cr-Y, Y addition effect on selective oxidation/diffusion phenomena relationship *(French)* 80−108623
Fe-Ni-Mo(Si), austenite, annealing effect on atom redistrib., Mossbauer anal. *(Russian)* 80−66529
Fe-Ni-Ta (-Co), alloys, Co effect on martensite ageing at 300-600°C *(Russian)* 80−20972

alloying additions continued
Fe-Ni-Ti-(Cu) (12, 0.25, 2 wt.%), Cu addition strengthening at 77K, mech. props. 80−60875
Fe-Ni-V-Co, Co influence on age hardening *(Russian)* 78−68703
Fe-Ni-V-(Cu) (12, 2, 2 wt.%), Cu addition strengthening at 77K, mech. props. 80−60875
Fe-Ni-(Cu) (12, 0.5 to 3 wt.%), Cu addition strengthening at 77K, mech. props. 80−60875
Fe-P-C amorphous alloys, corrosion resistance by alloying with metallic elements 79−66212
Fe-P(S) sintered materials, antifriction props. 79−24626
Fe-Si (3 to 5 wt.%) sinters, mag. props., Si and Fe-Si additions effect 80−71104
Fe-Si (6.5 wt.%), ductility and mag. props., Ni and Mn addition effects 78−76704
Fe-Si (6.5 wt.%), Ni, Al and Mn additions effect on mech. and mag. props. 77−12667
Fe-Si-Al (6,4 wt.%), Sendust alloy, effect of Ni content on mag. props. 78−72897
Fe-Si-B, high induction alloy, improving mag. props. by adding B to coating 79−83338
Fe-Si-B-N-S, B, S, N effects on grain boundary segregation and grain growth inhibition, review 80−3047
Fe-Si-Mn, effect of Mn addition on mag. props. and elec. resist. 78−91890
Fe-Si-Mn (3, 0.004 to 0.1 wt.%), Mn effect on oxidation in H_2O-H_2 atmos. 78−31560
Fe-Si-Mn-C, east, Ce additions, nonmetallic inclusions *(Russian)* 78−19710
Fe-Si-MnS-Al, Al effect on hot rolling struct., recrystallization, texture magnetic props. *(Chinese)* 78−11237
Fe-Ti, Ti as H trap for embrittlement control 80−66662
Fe-TiB_2, eutectic alloy, high temp. props. 78−84931
Fe-Zn, coating on low C rimming steel, effect of addition of Al on phase composition and morphology *(Polish)* 78−53014
Fe-Zn, layer formed in diffusion couple, effect of small alloying element addition *(French)* 77−43388
$Fe_{82}B_{14}Si_4$, chill block melt-spinning process, geometry depend. 80−97448
Fe_3C, cementite, modified by rare earth metal and alloying additions, thermal stability *(Russian)* 78−56663
$Fe_{65.4}Cr_{20.5}Al_{10.7}V_{3.4}$, effect of Al and V on form. of $L2_1$ superstructure and stratification 77−77474
$(Fe_{100-x}Ni_x)_{83}B_{17}$, amorphous, crystn. 80−75176
$(Fe_{100-x}Ni_x)_{83}B_{17}$ glassy alloys, Ni content influence on crystn., and bend ductility changes, during annealing 79−73103
ε-FeTi, Ce addition effect on H_2 absorption capacity 79−61899
ε-FeTi, effect of Ce on H_2 absorption 79−73315
Ga-Al, effect of Al on solidification kinetics, and morphology of Ga 78−56628
Ge-Al(Cu), alloying effects on elec. transport props. of amorphous and crystalline Ge films 79−51689
$(Hf_xZr_{1-x})_{80}Nb_{20}$, influence of Hf additions to $Zr_{80}Nb_{20}$, beta decomposition anal. 79−8304
Ho-Dy-Sm, magnetic moment growth due to Sm addition *(Russian)* 80−34608
Ho-Sm, magnetic moment growth due to Sm addition *(Russian)* 80−34608
Ir-W (0.3 wt.%): Al(Fe)(Th)(Ni)(Rh), effect of additions on grain boundary composition 79−83309
Ir-W (0.3%), grain boundary comp., trace element additions effect 80−66661
La-Al(Ge)(Au), amorphous, alloying effect on supercond. props. 79−60951
La-Ni(-Ce)(-Co), H absorption for storage appls. 80−45790
La_3In, supercond. T_c. alloying effects 79−38227
$LaNi_5$-H, with small Cr additions, NMR parameters *(Russian)* 80−29637
$LaNi_4Al$, solubility and sorption props. of H_2, effect of Al 80−103482
$LaNi_{5-x}Al_x$ ternary alloys, Al addition effects on structural and H_2 absorpt. props. 79−52761
$LaNi_{5-x}Fe_x(Cr_x)$, Fe and Cr electron hydride formation, X-ray and SEM obs. *(Japanese)* 79−43202
MO-B, B effects, rolled, segregation of implanted elements, Auger spectroscopy exam. *(Russian)* 78−35389
Mg-Ni-W-Co-Al-Cr alloy KhN56VMKYu, Al effect on excess Mg phase 80−29926
Mg-Y-Zn-Nd-Cd alloys, influence of Zr addition on struct. and mech. props. *(Russian)* 80−40370
Mn cast Fe, W effect on transform. in thin surface layers during dry sliding friction 77−21289
Mn-Cu, alloying addition and heat treatment effects on damping capacity 78−3165
$Mn_{2-x}V_xSb$, $0.08 \leq x \leq 0.25$, mag. props. modification by V 77−36071
Mo alloy:Re, effect of Re on mechanical props. 80−35196
Mo alloys, dil. additions, HVEM bombarded, neutron damage simulation, defect cluster and dislocation obs. 80−107330
Mo, cast state, interaction nature between C, O_2 and N_2 *(Russian)* 79−70114
Mo, powder sintering, transition metal activators, 1000-1350°C, heterodiffusion model 78−44044
Mo, recrystallised sintered sheet, C addition effect on ductility 79−8319
Mo, segregation of impurities and alloy elements at surface *(French)* 79−47697
Mo-B, Mo-B-Fe(Ni), microalloying influence on mechanical props., cold rolling, plasticity *(Russian)* 80−40502
Mo-C(Ti)(B)(Zr)(Ru)(Pt), electron beam melted, alloying addition effects on brittleness and ductility 79−61728
Mo-Cr, powder mixture, activating effect of Group VIII metals on alloy form. during sintering 77−59728
Mo-Fe metalloceramic alloy, brittle fracture investigation, segregation, morphology, struct. *(Russian)* 80−55503
Mo-Mn metalloceramic alloy, brittle fracture investigation, segregation, morphology, struct. *(Russian)* 80−55503
Mo-Nb-C, mech. props., effect of alloying and Mo cryst. orientation *(Russian)* 80−71706
Mo-Ni-Fe-Co-Zn alloys, Ni, Fe, Co and Zn distrib. using neutron-activation anal. 79−52531
Mo-O-C system, grain boundary segregation and intergranular fracture 80−55516
Mo-TiN (3.5 vol.%), failure characts. exam. 78−68788

alloying additions continued
Mo-Zr-Nb-C alloys, phase diagram and comp., Zr and Nb influence *(Russian)* 79−52167
Nb, and Nb-V alloy, supercond. T_c and H_{c2}, effect of purity and alloying with Ta, Cr, Mo or Re 77−85375
Nb, effect on transformation and strength of hot rolled medium C steel 80−7607
Nb-C alloys, alloyed with Mo, Ti, and Zr, phase comp. and precip. after heat treatment 79−57020
Nb-Cr, diffusion of N, effect of Cr and struct. defects 79−55938
Nb-Fe(Co)(Ni)(Os), alloying element influence on strength, ductility, surface and grain boundary energies *(Russian)* 79−74234
Nb-Ge-Si, Si effect on raising superconducting transition temp. in pelicular specimens *(Russian)* 78−23188
Nb-Mo, diffusion of N, effect of Mo and struct. defects 79−55938
Nb-Mo-Al-(Cr), eutectic, heat resist. increase by Cr substitution *(Russian)* 80−40481
Nb-Mo-Zr-Ti, Zr and Ti effects on struct. and mech. props. 77−70061
Nb-Sn-Cu, Cu effect on Nb solubility and peritectic transform. temp. in Sn bath *(Czech)* 77−59754
Nb-V-Cr, Nb-V, and Nb-Cr, oxidation resist., Cr and V effects *(Russian)* 80−40585
Nb-W, diffusion of N, effect of W and struct. defects 79−55938
Nb-Zr, diffusion of N, effect of Zr and struct. defects 79−55938
Nb_3Sn, alloying agent influence on struct. and supercond. props. *(Russian)* 80−39698
Nb_3Sn strip, made by diffusion method, crit. curent anisotropy, Zr alloying addition effects *(Russian)* 78−47921
Nb_3Sn superconductors, bronze-processed, effect of Ta additions 78−95404
Nb_3Sn, ternary additions effect on upper crit. field at 4.2K 77−28316
Nb_3Sn, Zr alloy element effect on growth kinetics *(Chinese)* 79−90579
$(Ni,Co)_3Ge$, Co effect on temp. depend. of yield stress 78−31487
$(Ni,Co)_3Ge$, single cryst., Co effects on temp. depend. of yield stress 77−4812
Ni alloy, heat resistant, optimum alloying 77−55904
Ni alloy IN-738, Y_2O_3 (1.5 wt.%) addition, mechanical alloying 77−40427
Ni, alloying, influence on recrystn. and grain growth *(Russian)* 80−81071
Ni, alloying effect of magnetostriction and rolling texture *(Russian)* 77−32229
Ni alloys, aluminising, thermodynamic anal. of phase transforms. 80−76413
Ni alloys, dil., factors affecting high-temp. oxidation behaviour, alloying effects 77−77638
Ni based superalloys 713C and Mar-M200, Si effect on oxidation, hot corrosion and mech. behaviour 78−39950
Ni, thin film resistor, rare earth alloying effects *(Russian)* 79−78211
Ni, yield point, effect of alloying elements *(Russian)* 80−50670
Ni-Al (0.5 wt.%), microstruct. formation during internal oxidation, effect of additional microalloying *(Russian)* 77−80650
Ni-Al-Cr_3Cr_2, eutectic alloy, directionally solidified, oxidation resistance, influence of Y 80−89409
Ni-Al-Si, β-phase stability *(Russian)* 78−39738
Ni-Al(-Si), diffusion, lattice parameter, microhardness, and constitution, effect of Si additions *(Russian)* 80−84316
Ni-B, hydrogen embrittlement, effect of B additions *(Japanese)* 78−84973
Ni-based superalloys, hot workability, effect of S, Ca, Mg, Y and Zr minor elements 80−66552
Ni-Be bronze, Fe and Si alloying addition effect on phase composition *(Russian)* 78−15360
Ni-Co-Cr-Mb-W-Ta, Cr, Mb, W, Ta effects on σ phase occurrence 77−36507
Ni-Co-H system, phase transform. under high H_2 press., Co additive effects *(Russian)* 78−60645
Ni-Co-Mo-Al-Cr, melt, effect of Al, Cr on O_2 activity, electrochemical determ. 79−11556
Ni-Cr, surface oxide characterisation by Raman spectroscopy 80−50308
Ni-Cr (20 wt.%), Al and Ti containing, oxidation, effect of dispersal oxides 77−44404
Ni-Cr wires, added metals effect on sublimation behaviour in vac. *(German)* 79−90775
Ni-Cr-Ce, Ce effect on oxidation 79−43484
Ni-Cr-Co, Mo, Ti, Y and R alloying additions influence on oxidation *(Russian)* 80−40587
Ni-Cr-Co-Al-W-Mo-Ti-Ta, heat resist. and struct., Ta effect 80−76312
Ni-Cr-M alloys, M=minor alloying addition Y, La, Ce, Sm, Th, U, Zr, V, corrosion rates 77−16750
Ni-Cr-Mn alloy solidification, effects of Si, Mo and Co alloying 79−83193
Ni-Cr-Si (10, 1.8 wt.%), Zr, Hf, La or Sm alloying additions effect on oxidation resist. 77−63831
Ni-Cr-W-Mo-Al-Ti (15,6,3,2,2, wt.%), wrought, Si effect on transition brittleness *(Chinese)* 80−55491
Ni-Cr-W(Mo)(Ti)(Al), long range ordering of matrix of complex heat resistant alloys *(Russian)* 77−77509
Ni-Cr-Y, Y addition effect on intergranular and volumetric diffusion, oxidation reduction *(French)* 79−83382
Ni-Fe-Ce superalloy, vacuum melted, Ce effects on microstruct. 77−36552
Ni-Fe-Cr base superalloy, addition effect on mech. props. *(Chinese)* 80−20998
Ni-Mo-MoS_2 composite, Mo alloying effect on physicochem. interactions 80−7692
Ni-Ta-Al-Fe, Al and Fe effect on precipitation kinetics 79−20054
Ni-Ti-Co, Co effect on martensitic transform. temp. and low temp. props. *(Korean)* 78−11224
Ni_3Al, room temp. ductility improvement by ternary trace element addition *(Japanese)* 79−52315
Ni_3Al, substitutional soln. and defect hardening mechanisms 77−21155
Ni_3Al-B, $L1_2$ type intermetallic cpd. room temp. ductility improvement by B addition *(Japanese)* 80−35263
Ni_3Al-Fe, Fe effect on Mossbauer effect study 77−32298
Ni_3Fe, transport props. and magnetisation, effect of alloying with Cr, Mo, W or Cu *(Russian)* 78−39095
NiTaC, eutectic alloys, chem. incompatibility of ceramic nitrides for directionally solidifying 80−81046
NiTiCu, shape memory alloys, electron microscope and X-ray diffr. study of struct. 79−82179

alloying additions continued

- Pb, grain refinement, and structural stability by S, Se and Te additions *(German)* 80−55387
- Pb melts, As and Sn distrib., Si, Cr, and Mn influence *(Russian)* 80−16274
- Pb-Ca-Sn, effect of Sn additions on precipitation behaviour, of Pb-Ca alloys *(German)* 78−52821
- Pb-Cu, hypoeutectic, grain refinement, and structural stability by S, Se and Te additions *(German)* 80−55387
- Pb-Sb-Te-Cu-Sn, influence of specimen and grain size on mech. props. *(Russian)* 77−81297
- Pb-Sn microduplex eutectic, cavitation during superplastic flow due to hard particles 77−36575
- Pb(Ag) alloys, effect of Ag content on yield strength 80−76322
- Pb−(Au) (0.1 and 0.2 wt.%), single crysts., yield strength depend. at 77K on Av conc. 80−55479
- Pt alloys, influence of Rh, Au, Mo, W, Zr, Hf alloying elements on creep activation energy at high temp. *(Chinese)* 80−66573
- Pt-Au, dil., recovery spectrum after thermal neutron irrad., Au effect and defect conc. depend. 80−65057
- Pu binary alloys, periodical depend. of equilibrium distrib. coeffs. of Pu admixtures on atomic number of admixture 80−18419
- Sc alloying behaviour, C and B stabilising effect, lattice parameters and at. radius 77−36454
- Si, amorphous, CVD, retarding crystn. by alloying with C,N,B or Ge 80−44129
- Si, in Ni solidified from supercooled condition, Si conc. influence on struct. *(Russian)* 77−16567
- Si, nitridation, effect of Fe alloy additions 78−48650
- Si, nitridation, metal additives effects, comparative study 77−44511
- SiC fibre reinforced Ti, effect of Al, Zr and Mo alloying additions on reaction rate of Ti with fibres 80−16249
- SiC fibre reinforced Ti-Al-Mo-Zr composites, matrix selection *(Russian)* 80−35192
- $Sm_2(Co, Cu, Fe, M)_{17}$, M=Nb, V, Ta, Zr, effect of M on mag. props. 77−89978
- Ta, sintering with transition metal additions 78−15335
- Ta(C,N)-Ni-VC, sintering behaviour, VC effect 80−93520
- Tb-Sm *(Russian)* 80−34608
- Ti alloy, hardening heat treatment, alloying element effects development trends 78−95759
- β-Ti alloy, metastable, alloying element effects on phase equilib. 79−56975
- Ti alloy, microstructure resulting from heat treatment, alloying, effect on creep, fatigue, fracture strength 78−11246
- Ti alloys, heat-resistant, mech. props., alloying addition effects *(Russian)* 77−59861
- α-Ti alloys, plastic deforms ands rupture mechanisms, depend on B additives *(Russian)* 79−61650
- Ti alloys with eutectoid-forming elements, mech. props. 77−44313
- Ti and Ti alloys, struct. sensitivity of mech. props., alloying influence *(Russian)* 79−47748
- Ti, commercial, creep behaviour, 25 to 400°C, role of impurities and/or alloying elements *(French)* 80−45354
- Ti, surface layer alloying element distrib. *(Russian)* 78−19934
- Ti, X-ray $K_{\beta5}$ emission band, effect of struct. change on alloying *(Russian)* 77−59645
- Ti-Al, Al effects on susceptibility to salt corrosion *(Russian)* 77−25185
- Ti-Al, elec. spark Al doping of VT-18, surface struct. and props. *(Russian)* 80−76398
- Ti-Al, hardening of Ti by addition of Al *(French)* 78−23715
- Ti-Al (Sn), porous, effect of Al and Sn on sintering 80−20830
- Ti-Al (14.7 wt.%), sintered, mech. props., effect of alloying and dispersed ZrO_2 phase 77−12636
- Ti-Al-H, H effect on mech. props. and lattice constants 80−21036
- Ti-Al-Mo-Cr-Fe, distrib. of Sn, Zr between phases, temp effect. 80−55357
- Ti-Al-O, V effect on thermal stability and mech. props. 77−21171
- Ti-Al-Sn-Zr-Mo-Si-O-H, Si, O, H effects on fatigue, fracture and creep charact. 79−11697
- Ti-Al-Zr (3,3 wt.%), W alloying addition effects on mech. props. *(Russian)* 77−59860
- Ti-Cu-Al(Zr)(Sn)(Nb)(Mo), heat treatable alloys, effect of alloying on strength, tensile props. 78−56671
- Ti-Er(Y), effects of Er and Y additives on deformation behaviour 80−81121
- Ti-Fe-Al(Mn), homogeneity and lattice parameters, Mn and Al effect on hydriding cmpd. FeTi 80−108400
- Ti-Nb alloys, Fe, Mo, V, Ta alloying additions on microstruct. after combined treatment *(Russian)* 77−59826
- Ti-Nb alloys, Ta and Zr additions effect on supercond. props. 80−93059
- Ti-Nb-Zr-Fe, supercond. and paramag. props., effect of Fe additions *(Russian)* 80−65730
- Ti-Ni, effect of alloying on crit. points and martensitic transform. hysteresis 80−20935
- Ti-Ni-Co(Fe) alloys, shape memory temp., alloying effect 79−38912
- Ti-Ni-Mo (1.5, 2 wt.%), Mo effect on microstructure 77−36536
- Ti-transition metal, transition metal additive effect on struct., specific resistance, microhardness, mech. props. 79−29078
- Ti-V-Mo-Cr system, β-phase stability 80−55353
- Ti-V-Si, Si effects on precipitation and strengthening 77−55970
- βTi-V-Si (40, 1 at.%), Si effect of precipitation and age hardening 77−63676
- α-Ti-Zr-W, effect of W impurity on mech. preps. 80−16392
- Ti_3Al, Cu, Fe, Mo (1 at.%) additions, oxidation resistance, 700 to 800 degrees C 77−12744
- Ti_3Al-Sn-Zr, alloy, Sn and Zr alloying influence on creep and scaling resist. *(Russian)* 79−52302
- TiC-(Mo-Cr-Ni-Mn) steel alloy, optimum comp. and manufacture conditions, Mn effect 80−84896
- TiC-steel cermet with Cu additions, precip. hardening and ht. treatment temp. 77−40414
- TiC-steel composite, effect of method of Cr additions on props. 78−15341
- TiNi alloys, structural transform., physical props. and memory effects *(Russian)* 79−1856
- (V,Ti)C+(Ni,Mo) cermet systems, effect or V/Ti ratio or Mo partitioning 79−79099
- V and V-Mo, mechanical properties, O, N_2 and C addition effects 79−52356
- V, and V-Nb alloy, supercond. T_c and H_{c2}, effect of purity and alloying with Ta, Cr, Mo or Re 77−85375
- V_3Ga superconducting multifilamentary wire, crit. current props. with third element additions 79−61013
- W alloys, recrystallisation alloying effects of ThO_2, Mo-Re, HfC, NbC 77−70083
- W, cast state, interaction nature between C, O_2 and N_2 *(Russian)* 79−70114
- W fibre, KAl, KSi, KSiAl and KSiGa, addition effects on workability *(German)* 78−64557
- W fibre reinforced Al, alloying element effect on interface form. *(Czech)* 77−85963
- W-C(0.01 to 0.2 wt.%), C effect on high temp. strength 77−16614
- W-Cr-Pd, Pd effects on diffusion 77−24445
- W-Cu-Co(Ni), electrical contact material, comparison of Co and Ni effects *(Korean)* 78−10539
- W-Cu-Ni(6), contact materials, activated sintering, Ni and Co effects 79−95967
- W-Ni (0.5, 2 and 5 wt.%), Ni effect on shrinkage anisotropy during sintering 77−21056
- W-Re(Mo)(Cr), powder mixture, activating effect of Group VIII metals on alloy form. during sintering 77−59728
- W-ThO_2 fibre reinforced Ni base alloys, powdered matrices, fibre/matrix interaction above 1300°C, alloying effects *(Russian)* 78−95755
- W-Ti, Ti addition effect on heat resistance and radiative props. *(Russian)* 80−25515
- W-Zr, Zr addition effect on heat resistance and radiative props. *(Russian)* 80−25515
- W-Zr-C, Zr and C addition effect on heat resistance and radiative props. *(Russian)* 80−25515
- W-ZrC(-Re) eutectic alloy, Re effect on breaking stress, lattice parameters, electron struct. *(Russian)* 79−1845
- WC-Co alloys, P additions, effect on hot pressing, hardness and wear resist. 78−11162
- $YNi_{5-x}Al_x$ ternary alloys, Al addition effects on structural and H_2 absorpt. props. 79−52761
- Zn-Al-Cu-Mg-Pb-Sn, Cu, Mg, Pb, Sn effects on corrosion in wet steam 77−48585
- Zn-Al-Cu-Mg-Pb-Sn (12, 1, 0.02, 0.01, 0.015, wt.%), combined effects of Pb and Sn additions on corrosion, in wet steam 78−39952
- Zr-Al-Fe (8.9, 0.001 to 0.006 wt.%) Fe partitioning to Zr_2Al during peritectoid transformation 78−39784
- Zr-Mo(-Al) (3, 1 wt.%), β-phase stability 78−39742
- Zr-Nb-Mo-Re, alloying effect on dislocation core struct., determ. by discrete lattice modelling 78−30618
- α-Zr-Sn(Mo), creep characts., influence of Sn and Mo *(Czech)* 80−81119

alloys

alloys such as Au-Cu, Au-Cu-Zn are indexed under components of the named elements i.e. gold alloys; copper alloys; zinc alloys in these examples

see also actinide alloys; alkali metal alloys; alkaline earth alloys; alloying additions; aluminium alloys; antimony alloys; arsenic alloys; bismuth alloys; boron alloys; cadmium alloys; dilute alloys; eutectic alloys; gallium alloys; germanium alloys; indium alloys; lead alloys; liquid alloys; mercury alloys; rare earth alloys; selenium alloys; silicon alloys; solid solutions; superalloys; tellurium alloys; thallium alloys; tin alloys; transition metal alloys; zinc alloys

- AB_2 Friauf-Laves phases, atomic sites and H absorpt. 80−24406
- AB alloy, equilib. props. by Markovian simulation 78−91302
- activity coefficient and short-range order, correl. *(Russian)* 78−56614
- activity coefficient of nonmetallic solutes in liquid metals and binary alloys 78−52766
- AES, quantitative analysis *(Polish)* 78−76967
- aged, with correlated system of second phase particles, X-ray and electron scatt. *(Russian)* 77−59738
- alloy, production using electrodeposition and heating in reducing atm. 79−100079
- alloys, X-ray fluoresc. anal. using matrix correctional procedure 78−80817
- amorphous, electronic struct. 78−72062
- amorphous, exhibiting Mossbauer spectra, elec. props. *(French)* 80−80244
- amorphous, hole struct. of computer models 80−49109
- amorphous, mag. props. and appls. 78−95475
- amorphous, magnetic, transport props. 79−73485
- amorphous, mangetic bubble memory material, ^{85}Kr waste encapsulation appl. 80−47589
- amorphous, Mossbauer spectrometry *(French)* 80−80660
- amorphous, struct. determ. by energy dispersive X-ray diffraction 80−84063
- amorphous, struct. relax., compositional SRO 78−79538
- amorphous alloys, cold rolling 80−55423
- amorphous alloys, density of states of n-components 80−80153
- amorphous alloys, transport props., thermopower 80−34411
- amorphous intertransition metal alloys, short-range struct. 79−50995
- antiferromagnetic, nesting type model, spin fluctuations 78−84435
- antiferromagnetic alloy, stoichiometric depend. of elec. resist. 77−69312
- atom-probe field ion microscopy, relationship between results of analysis and structure of sample *(French)* 80−55732
- atomic absorption spectrometric analysis, of laser-vaporised solid samples 78−7252
- atomic diffusion when exposed to liquid Na 77−7899
- atomic ordering, statistical theory 77−15542
- atomic rearrangements, radiation induced, in ordering and clustering alloys, conf. Atlanta, GA, USA (March 1977) 79−42099
- austenitic alloys, neutron irradiation induced embrittlement, review 79−65120
- austenitic alloys in hot water, low cycle fatigue, appl. to nuclear reactors 77−4871
- axial shadow pattern, width and shape, thermal and static displacements effect *(Russian)* 80−107024
- B2 structure, relationship between enthalpy of form. and disorder parameter 77−7878
- B-32 superstructure, instability in absence of many-particle interactions 77 58972
- BCC, glide and work hardening, review *(German)* 79−29089
- BCC, glide and work hardening, review *(German)* 79−34067
- BCC, low temp. softening 79−34113

alloys continued
BCC, order-disorder transform. in surface layers, theory *(Russian)* 78—19739
BCC, ordered, implanted atom redistrib. at octahedral and tetrahedral interstitial sites *(Russian)* 78—34533
BCC, plastically deformed, electron microscopy *(French)* 77—44299
BCC lattice, crit. embrittlement temp., struct. parameters effect *(Russian)* 80—66618
BCC metals and alloys, review of plastic deformation and work hardening *(German)* 78—84946
BCC single crystals, plastic deformation localisation 80—54303
BEC binary alloys, order-disorder transformation kinetics 79—20040
binary, 50-50, singularities at metal-insulator transition, CPA calc. 80—84428
binary, activity of most oxidizable element *(French)* 79—61868
binary, atomic misfit effect on coexistence and spinodal transform. boundary 78—60644
binary, atomic roughness and chemical adsorption at solid-liquid interface *(French)* 78—51787
binary, BCC, order-disorder transform., three-body interaction effects 80—39257
binary, calibration line introduction for comp. determ. by AES 79—56892
binary, charge transfer and alloy binding, Thomas-Fermi-Dirac approx. 77—76775
binary, completely disordered, position of electronic energy bands, CPA calc. *(French)* 78—22999
binary, computer experiments on phase separation 79—43198
binary, constitution diagrams, computer calc. *(Russian)* 80—84909
binary, crystallisation kinetics, temperature dependence, kinetic phase diagrams 80—16294
binary, crystallisation under parabolic stability *(Russian)* 79—70054
binary, Debye temp., simple relation for additivity 80—10627
binary, diffused layer growth kinetics, effect of interphase reaction rate 77—7888
binary, elec. resist. depend. on LRO, SRO and composition, inhomogeneous order effects 79—60781
binary, elec. resist. due to crit. fluctuations near order-disorder temp., theory 77—40071
binary, elec. resist. near crit. point 80—96847
binary, electrical conductivity of disordered systems, tight binding approx. in Kubo formalism 79—60778
binary, electrodeposition, recent developments, review 77—81233
binary, electron localisation, self-consistency theory *(French)* 79—42480
binary, electronic density of states, generalized cluster-Bethe-lattice approach 79—42432
binary, electronic density of states in Bethe lattice, using Weaire-Thorpe Hamiltonian 78—51870
binary, estimation of electron backscattering factor 78—72649
binary, generalised coarsening theory 78—39778
binary, Hall coeff. sign change origin 77—69302
binary, HCP struct., influence of spatial nonuniformity of short-range order on interdiffusion *(Russian)* 78—6187
binary, interdiffusion coeff. and Matano interfaces *(Japanese)* 78—14516
binary, interdiffusion theory allowing for nonuniformity of inert marker displacement *(Russian)* 77—7889
binary, intrinsic diffusion coeffs. meas. method *(German)* 77—28036
binary, kinetic behaviour of vacancies and atoms 79—28129
binary, kinetic conditions for two phase zone form. *(Russian)* 77—66633
binary, kinetics of nuclei coalescence by reactive diffusion *(Russian)* 79—42398
binary, magnetic, interface struct., Monte Carlo simulation 80—60317
binary, magnetic moment determ. from neutron scatt. 77—73011
binary, marker displacements as result of diffusion 80—92724
binary, model substitutionally disordered, electron momentum density 78—56061
binary, multicritical phenomena at surfaces 77—32208
binary, nonequilib. crystn. dynamics, eqns. for supercooling, supersaturation of melt *(Russian)* 78—95736
binary, nonstoichiometric, mean field theory, improved approx. 80—79910
binary, one-dimens., appl. of density-of-states theory for disordered system with short range order 78—23000
binary, one-dimens., embedded-cluster calcs. of phonon spectra 79—77703
binary, order-disorder transition kinetics, computer simulation 80—92643
binary, ordered, self-diffusion kinetics 80—10698
binary, ordered and disordered, transfer of charge 77—15785
binary, ordering, residual resist. in CPA *(Russian)* 77—24545
binary, oxidation, solid solution scale formation, approx. calc. of O_2 activity profile 78—88577
binary, phase boundary effect on isothermal transform *(Russian)* 79—1857
binary, quenched, computer simulation of cluster dynamics of two dimensional model systems 78—31434
binary, quenched, time evolution, computer-simulation of three-dimensional model system 77—48422
binary, quenching, cluster growth, first order phase transition, computer simulation anal. 79—34039
binary, region of metastability in normal growth 79—87613
binary, relative sensitivity for quantitative Auger analysis 77—32861
binary, segregating alloy, theory of surface effects 79—19435
binary, selective oxidation with quasiparabolic kinetics, fixed alloy-scale boundary soln. 78—72930
binary, short range order calc. using equilib. diagram *(Russian)* 79—87610
binary, simultaneous mag. and spatial long-range order 77—69491
binary, single phase, empirical relationship for homogenization 79—55892
binary, solid state second phase redistribution in applied field 78—51721
binary, solidification, predicted volume changes 77—28802
binary, solidification calc. using compensation system *(Russian)* 80—16292
binary, structural aspects of energy 77—39556
binary, supercond. transition temp. lowering by nonmagnetic impurities 80—100546
binary, surface composition, regular soln. theory 78—10265
binary, surface composition determ., review 79—90849
binary, surface dehomogenisation during evaporation and ion sputtering 77—73207

alloys continued
binary, surface phase diagram, electron spectroscopy 77—24469
binary, surface segregation kinetics 80—80044
binary, surface segregation prediction using bulk alloy variables 79—65300
binary, theory for initial stage of grain growth and unmixing kinetics 78—19714
binary, thermal cond. conc. depend., irreversible processes, thermodynamic calcs. *(Russian)* 80—39550
binary, thermal EMF, short-range order effects *(Russian)* 77—15835
binary, thin layer electrodeposition 78—3067
binary, vaporisation kinetics from one source with feed maintenance *(Russian)* 79—37824
binary, vol. changes during sintering, inter-ion interaction influence 79—28982
binary, with arbitrary mole fraction, order disorder transition in case of FCC lattice 80—88295
binary, with curved solid-liq. interface, lateral solute segregation during unidirectional solidification 79—47692
binary, with mixed ferro- and antiferromag. exchange, magnetisation, phenomenological theory *(German)* 78—56297
binary alloy, atomic ordering and ferromagnetism 79—87278
binary alloy, concept of partial elastic energy in anal. of surface segregation *(French)* 79—77884
binary alloy, density of states, CPA with nonretracing paths 77—31924
binary alloy, electron localisation, self-consistent theory *(French)* 78—60088
binary alloy, electron theory of short range order 78—10390
binary alloy, normal growth on an atomically rough boundary 79—94934
binary alloy, numerical calc. and simulation of nonsteady mass transfer by moving phase boundaries *(German)* 77—8811
binary alloy, ordered, electronic struct. in Bethe lattice, exact analytic treatment 80—49582
binary alloy, ordered BCC to disordered FCC transition 77—43327
binary alloy, phenomenological theory of interdiffusion, role of nonequilib. vacancies *(Russian)* 78—59966
binary alloy, quenched, time evolution of struct. function free energy 78—55937
binary alloy, random, wavelength localisation 78—34795
binary alloy, solidification chemical inhomogeneity *(Russian)* 80—75335
binary alloy, time const. for preferential sputtering 80—2912
binary alloy freezing, non-equilibrium thermodynamic processes 80—34167
binary alloy single crysts., dilute, morphological stability of unidirectional growth, thermodynamic study *(French)* 79—86727
binary alloy with BCC type lattice, order-disorder transition 79—78957
binary alloys, acoustic modes in random and correlated alloys, order-disorder transform. 80—65189
binary alloys, BCC lattice, ordered structs. of interstitial solutes 79—82196
binary alloys, charge transfer and transport props. in tight-binding model 79—82577
binary alloys, density of states in CPA 77—51633
binary alloys, diagrams of state, component interaction parameters *(Russian)* 80—55354
binary alloys, diagrams of state, component interaction parameters, computer calcs. *(Russian)* 80—55355
binary alloys, diffusion-controlled growth of solid soln. scales 77—70232
binary alloys, directional solidification, theory of dendritic growth 80—70145
binary alloys, FCC, with short-range order, electron theory, pair interaction and third-order perturbation theory 79—69404
binary alloys, ferromagnetism and spatial long-range order 80—60159
binary alloys, form factors of pseudopot., OPW calc. *(Russian)* 79—19498
binary alloys, initial transient segregation during unidirectional solidification in a furnace with thermal damping 80—70146
binary alloys, isothermal phase transformations, impingement and impoverishment effect 79—51234
binary alloys, kinetic nucleation model 77—85118
binary alloys, mag. interactions effects on phase separation 78—27047
binary alloys, preferential sputtering with diffusion, equilib. distrib. 78—68592
binary alloys, quenched, vacancy concs. 80—107212
binary alloys, random, dielec. matrix and related props. 78—51916
binary alloys, relative sensitivity factors by quantitative Auger analysis 77—60151
binary alloys, simple model to describe isothermic phase transform. 78—75832
binary alloys, surface conc. profile and surface energy 80—84350
binary alloys, two phase region calcs. in solidifying melt *(Russian)* 80—65195
binary and ternary, interdiffusion parameters, possibility of correl. with solidus temp. *(Russian)* 77—24426
binary conc., with short and long range order, computer simulation of diffusion 78—30778
binary disordered, effective periodic pot. 78—10325
binary disordered, electronic density of states, optical theorem and multiple scatt. theory 79—4500
binary disordered alloy with long range order, elec. cond., single band model 77—28154
binary ferromagnetic, electron interactions and spin-wave stiffness const. 77—1548
binary internal oxidation beneath external scales, onset criteria 79—5074
binary linear chain, electronic props., short-range order effects 80—96769
binary metal alloys, surface segregation correlation with bulk diffusion 80—54388
binary metallic alloys, cathodic deposition and characterisation 79—69998
binary metallic solid solns., thermodynamic quantities rel. to vacancy and diffusion characts. 79—95204
binary metallic system, conc. profiles across solid-liq. interfaces 80—55382
binary metallic systems, calc. of isomorphous and simple eutectic phase diagrams 79—11570
binary narrow-band, metal-dielectric transition, off-diagonal disorder *(Russian)* 79—4512
binary ordering alloy, theory of surface effects 79—19434
binary random Heisenberg ferromagnet transition temp. crit. conc., RKKY model 78—52266

alloys continued
binary solidification, transition from diffusion controlled to diffusionless solute drag treatment 77—16563
binary substitutional, determ. of local atomic configurations 79—86739
binary substitutional, short-range ordering kinetics, vacancy behaviour 78—55867
binary substitutional alloy, with long range order, electron energy spectrum *(Russian)* 78—84121
binary substitutional alloy with long range order, electron energy spectra *(Russian)* 78—75974
binary systems, alloying tendencies and impurity heats of soln. 79—28102
binary thermodynamic data 80—104121
binary with long and short range order, electron energy spectrum calcs. *(Russian)* 79—99471
brittle and plastic, energetic strength theories *(Bulgarian)* 80—38296
carburising, process parameters and gas conditions 79—96208
cemented carbide, porosity 77—59722
cemented carbides, hardmetal, bending strength and fracture toughness 79—20181
cemented carbides, indentation fracture, surface fracture toughness nature 78—60849
chemical bonds in metal phases *(Russian)* 79—73131
chemical induced segregation, obs. by Auger fine struct. anal. 78—15416
chemicothermal treatment, mathematical modelling 80—100955
chemicothermal treatment, process kinetics 80—35415
cleaved alloys, electronic theory, off-diagonal disorder 79—4596
close-packed, temp. depend. of stacking, fault energy 79—19266
coarsening by temp. cycling 79—29111
cohesive energy, semiempirical model, heat of form. expressions 80—70160
cold worked, internal friction peak rel. to back reaction annealing kinetics 78—3161
colour and colour stability as alloy design criteria 80—101005
complex, phase stability diagram 77—90322
composite alloys, two-phase systems, deformation textures 79—83219
compositional changes due to removal of one constituent by surface reaction 77—8996
compositional modulation spectra, line shape 78—76491
concentrated, vacancy formation energies determ. 78—63756
concentrated alloys, excess vibr. entropy and local environment effects 77—76498
conduction electrons mag. susceptibilty 79—87230
conference, condensed matter physics, Sarajevo, Yugoslavia (Oct. 1976) 77—51629
continuous plastic cracks in ordered alloys, discrete dislocation analysis 78—80625
corrosion, potential-pH diagrams for interpretation in high salinity geothermal brines 79—96191
corrosion conditions simulation in crack-like defects using electrochemical cell *(Russian)* 79—52445
corrosion resistance in geoethermal brine environments 78—85032
corrosion resistant surface alloy, form. by ion implantation 78—88569
corrosion testing under stress, unit for producing biaxial tensile stresses 79—57174
covalent alloys, amorphous, dimensionality of subnetworks 80—28916
Cowley short-range order parameters, distance dependence restrictions 80—103294
crack growth, subcritical, in high-strength alloys 79—43494
crack resistance, aggressive environment influence *(Russian)* 79—52434
creep, in single and two-phase power law representations, deviations at high strain rates 77—48504
creep and stress relaxation curves, phenomenological description 79—100231
creep cavitation control, intergranular precipitates role 80—66664
creep conditions at high temp. 77—77550
creep elongation, modification of Monkman-Grant relation *(Czech)* 77—63726
creep failure criteria for high temperature alloys 80—65150
creep rupture like improvement mechanism, reheat treatment 78—64666
criteria of chemical inhomogeneity 80—59670
critical shear stress, for alloys with ordered domains and disordered regions *(Russian)* 80—107237
critical temperatures determination, elec. resist. method, IMASh-5S-69 installation 80—71827
cryogenic, creep, review 80—104222
cryogenic structural materials 77—17989
crystal growth mechanism, stat. modelling of binary melt-cryst. phase transform. kinetics 80—24389
crystallisation, apparatus for decanting solid and liquid phases 78—56597
crystallisation, kinetic diagram appl. *(Russian)* 78—15384
crystallisation, variational approach to continuum theory 80—1951
crystallisation process, X-ray fluoroscopic obs. 80—50620
crystallising, impurity distrib. under suppressed natural convection temp. *(Russian)* 77—28795
cubic, computer simulation of formation of tweed and modulated structs. 79—96029
cubic alloys, anisotropic hyperfine interactions, Mossbauer spectra 80—15854
cubic metal binary alloys for H energy storage 80—45787
cutting alloy detonation coating, struct. and friction *(Russian)* 78—15537
de Haas-van Alphen effect 79—99473
Debye temperature, determ. from elec. resist. meas. *(French)* 77—4322
deep-drawing curves, cryst. microstruct. during deform. *(French)* 79—20066
deformation, alloy with two ductile phases of unequal strength *(Japanese)* 78—11284
deformation of two phase alloy 77—8893
deformation process, stage-by-stage nature investigation using acoustic emission *(Russian)* 80—40434
deformation strengthening and anisotropy prediction *(Russian)* 78—27533
density of electronic states, dressed-cluster approx. 78—95249
density of states, numerical result for three-dimens. alloy with site diagonal disorder 78—30858
design by automatic modelling, CAD system *(Japanese)* 77—52607
development of intermetallic compounds, 20-years research results 77—7843
diagonally disordered binary alloy, mass operator 80—52140

alloys continued
diffusion, meas. of conc. profile by changes in polarisation current density 77—89584
diffusion controlled stress rupture 77—32681
diffusion layers, effect of chemicothermal treatment on struct., surface energy, and bulk props. 79—96207
diffusion of implanted atoms, free energy calc. for any conc. of implanted atoms, diffusion current in chem. pot. gradient *(Russian)* 78—34657
diffusion rate in Al melts, meas. apparatus 79—86913
diffusional crystal growth mechanisms 80—3059
diffusive creep, theory *(Russian)* 80—40437
digital electronic control system for co-evaporation prep. of two component alloys 79—24457
dilatometric method for study of dimensional anomalies in metallic materials rel. to crystal struct. *(French)* 79—52563
dilatometric methods *(French)* 79—5100
dilute magnetic alloys moment-conserving decoupling scheme 79—61048
discontinuous precipitation in binary metallic systems, review 80—3060
dislocation bowing computed from Orowan relations 77—19949
dislocation climb, in modulated structs. under irradiation conditions 80—70195
dislocation movement, in volume dispersion of obstacles, stochastic model, low temp. anomalies rel. to yield stress 79—60367
dislocation pile-up model, fatigue crack nucleation at intermetallic particles 79—69189
dislocation stress-velocity depend. 80—96537
dislocation structure in precipitation hardened alloys *(Hungarian)* 79—55746
dislocations and operative slip systems, correl. for CsCl-type intermetallics 79—10852
disordered, binary decoupling schemes for many site correlation functions 78—18984
disordered, bulk and surface density of states, effect of surface segregation 77—15729
disordered, charge density function calculation method 79—42433
disordered, density of states, and their moments 77—11837
disordered, electron correls. and ferromagnetism 78—43548
disordered, electron localisation, temp. depend. 80—80219
disordered, influence of strong hybridization on elec. cond. 79—11097
disordered, interatomic distances, coord. numbers, and mean relative displacements, EXAFS anal. 80—89087
disordered, IR absorption spectra, chem. bond. *(Russian)* 77—90155
disordered, muffin-tin model, electronic struct. and density of states, theory 80—29301
disordered, off-diagonal randomness, phonon-modulated electronic transport 77—15813
disordered, optical absorpt., at high temp., CPA calc. *(Russian)* 77—44028
disordered, orbital mag. susceptibility of conduction electrons CPA calc. 78—76217
disordered, spectral functions, augmented space formalism 78—84126
disordered, temp. depend. of elec. resist., force-correlation functions 79—51542
disordered, with strong impurity scatt., adiabatic approx. 77—66161
disordered alloy, residual resistivity due to clustering, ageing effects 80—65521
disordered alloys, band edge position, tight-binding Hamiltonian *(French)* 78—10324
disordered alloys, electronic density of states in muffin tin model 80—88467
disordered alloys, electronic struct., CPA calcs., short-range order 78—63964
disordered alloys, temp. depend. of elec. resist., elastic electron-phonon scatt., CPA calcs. 79—56185
disordered alloys, transport phenomena theory, coherent pot. approx. 78—87958
disordered and binary alloys, Hubbard III approx. numerical results 77—51874
disordered binary, crit. US attenuation 79—99272
disordered binary, electron-electron correl., T-matrix approx. 79—78026
disordered binary, electronic structure 77—15755
disordered binary alloys, three-dimens. model, density of states calcs. 77—43469
disordered binary alloys, X-ray diffuse scatt., effect of correlation 78—71640
disordered binary alloys of ferromag. crystals, mag. dipole fields at interstitial sites 80—97176
disordered ferromagnetic, magnetooptic effects, theory 77—12366
disordered ferromagnetic alloys, even magneto-optical effects, light cond. tensor 79—4792
disordered metal ribbon production by ultrarapid quenching 80—71612
disordered muffin tin type, coherent pot. approx. appl. 79—15062
disordered substitutional alloy, mag. props., Heisenberg model 79—38342
disordered substitutional alloys with strong electron correl., elec. cond. 77—62885
disordered system with short range order, elementary excitations 77—47709
disordered ternary, DC elec. cond. calc. 77—15812
disperse state formation *(Russian)* 78—52757
dispersion hardened, friction stress for high-temp. creep 78—11289
dispersion hardened, particle size effect on fracture 79—43418
dispersion hardened, temp. depend. of work-hardening due to Orowan loops 79—91668
dispersion hardened, work hardening due to Orowan loops, temp. depend. *(Japanese)* 80—66534
dispersion hardened alloys, strengthening theories 80—97498
dispersion hardened load type effect on yield stress 78—35458
displacement determination in special alloys by holographic and speckle interferometric methods 78—27688
dissolution controlled cracking mechanism, repassivation effects 78—64772
divalent metal alloy, solid solubility 79—60514
DO$_{22}$ and L1$_0$ superstructures, atomic ordering, multicluster approx., order-disorder transition 80—38990
Drucker postulate verification at high temp. 80—30025
ductile fracture surfaces, statistical characts. of microcracks *(Russian)* 78—23807
durability during random loading, approx. determ. method 77—48610
dynamic hardness testing of metallic materials 80—21241
Earth lower crust, metal alloys rel. to Curie isotherms in deep mag. anomalies 78—44805

alloys continued
elastic const. meas. technique 78—7164
elastic constants determ. by resonant vibr. in thin disk, apparatus 77—56182
electric power industry uses, high temp. phase diagram phenomena 79—11575
electrical resistance meas. at increased temp. under stress. 77—56147
electrodeposition theories, review 80—11581
electrodes, high-β electron emission sites 79—61502
electron beam irradiated, influence of created pulsed press. on struct. and props. *(Russian)* 78—34539
electron diffraction and imaging, at high resoln., characterisation of alloys and ceramics 80—104050
electron irradiated, temp. depend. spall threshold 78—48504
electron irradiation in HVEM, solute redistrib. calcs. 80—107324
electron microprobes and scanning electron microscopy, conf., Orsay, France, Dec. (1978) 80—11979
electron momentum density, positron annihilation meas., book contrib. 79—99976
electron spectroscopy of crystals, book 80—36786
electronic characts. from thermomodulation spectra 79—87421
ELN-1 alloy, prestrain effects on strength *(Russian)* 78—11267
EM acoustic reson. for elastic moduli meas. 80—15573
embrittling residuals categorisation by Auger electron spectroscopy 80—66739
emissivity determination, using low-inertia opt. dilatometry 80—59684
emissivity measurement of small specimens at high temperatures, structural materials appl. 79—7281
engineering, intergranular fragility index 80—66637
enthalpy of mixing, 'const. vol. alloy' formulation 79—28111
environmental fatigue crack propag., texture influence 79—91802
fabrication of metallic, ceramic alloys by laser, theory, appls. 77—2639
fatigue behaviour of metals and alloys, vacuum effect, review 80—35309
fatigue crack growth at low stress intensities 77—86167
fatigue life distrib. theoretical obs. near fatigue limit 80—59569
fatigue limit, static and cyclic loading 80—71755
fatigue-strength at const. and variable temps., cycle period effect of high temp. alloy 78—7127
FCC, anisotropic ordering of interstitial impurities *(Russian)* 77—76389
FCC, binary, on Ising system, sublattice magnetisation, tricrit. point, simulation 79—33491
FCC, closed packed, ordering-type transitions 80—2140
FCC, CuAu type, interstitial, atom redistrib. in octahedral and tetrahedral interstices *(Russian)* 77—55280
FCC, deform. behaviour 77—8892
FCC, fracture mechanism maps and construction 79—61693
FCC, grain boundary energy and self-diffusion, effect of solute segregation 78—15412
FCC, hardening by spinodal modulated structure 80—60874
FCC, impurity atom position determ. from ion-excited characteristic X-ray emission *(Russian)* 78—47408
FCC, interstitial diffusion, theory *(Russian)* 80—65296
FCC, macroscopic shear band contrib. to rolling texture 77—86056
FCC, model for form. of annealing twins 78—59818
FCC, Monte Carlo simulation of surface segregation 78—31413
FCC, plastically deformed, electron microscopy *(French)* 77—44301
FCC, quenched, form. of prismatic loops 77—65979
FCC, stacking faults, long-range oscillatory interactions and stability 80—65012
FCC, tensile fracture mechanism, review of pressure effects 77—70155
fcc alloy, A_3B ordering process time evolution, Monte Carlo simulation 79—86869
FCC alloys, theory of interphase and antiphase boundaries 79—83174
FCC alloys, with multiatom interactions, ground state derivation 79—83173
FCC base hard materials, low temp. toughness *(Japanese)* 80—100916
f.c.c. rolling texture *(Russian)* 77—1843
FCC texture transitions, computer simulation 79—90666
Fermi surface, high resolution high intensity apparatus for positron annihilation meas. 78—23008
Fermi surface and phase stability 77—77459
ferrimagnet, amorphous, dipolar mechanisms for mag. anisotropy 78—64233
ferromagnetic, binary, anomalous Hall effect *(Russian)* 79—42521
ferromagnetic, coercive force, automatic meas. by remote means 79—24690
ferromagnetic, disordered cryst. and amorphous, mag. dipolar field distrib., computer simulation 80—65790
ferromagnetic, hyperfine field systematics of nonmag. ions 78—60093
ferromagnetic, itinerant electron model, spin wave stiffness const. calc. 80—34613
ferromagnetic, partially ordered, spin wave stiffness const. 79—24150
ferromagnetic, temp. depend. of mag. props. and sp. ht., mag. phase transition region 78—64207
ferromagnetic alloy, binary ordered, dynamic mag. susceptibility, spin wave stiffness constant 79—38307
ferromagnetic alloys, conc., spin fluctuations, SCR theory and CPA calcs. 78—64290
ferromagnetic alloys, itinerant electrons, magnon stiffness const. 77—63155
ferromagnetic alloys, surface spin waves, cluster Bethe lattice approach 80—70983
ferromagnetic amorphous alloys, temp. depend. of mag. hystersis props. 79—61186
ferromagnetic binary alloy, atomic and mag. ordering, critical slowing down 78—14915
ferromagnetic binary alloys, narrow-band with random hopping, spin wave stiffness const. 79—56524
ferromagnetic binary alloys, strictly regular, quasi chemical model 78—39316
ferromagnetic disordered alloys, spin wave and ferromag. reson. linewidth 80—66045
ferromagnetic disordered binary alloy, CPA theory of magnetoabsorption, electron scatt. mechanisms *(Russian)* 77—8549
ferromagnetic exam. of atomic ordering mech., when in mag. field *(Russian)* 79—11609
ferromagnetic hyperfine field 77—24537
ferromagnetic random binary alloys, elastic neutron scatt. cross section 78—91845
ferrous and nonferrous. air-plasma cutting 79—8401
fibre reinforced metals and alloys 77—21060

alloys continued
film, rate controlled deposition using electron impact emission spectroscopy based instrument *(German)* 80—89152
film, vacuum deposition, monitoring and controlling techniques, review 78—11113
films, deposition processes, rate controlling and composition analysis by electron impact emission spectroscopy 77—44165
fine structure effect on stress corrosion cracking in 01420 *(Russian)* 78—35571
finishing, use of ion implantation technique, affect on wear and corrosion props. 79—34204
fisson reactor materials, irradiation induced creep, fundamental mechanisms *(Italian)* 80—55457
force-and-mass disordered alloys, vibrs., average local-information transfer approx. 80—88290
fracture mechanism maps for materials which cleave 79—91774
fracture toughness, micromechanical modelling *(Russian)* 78—31504
fracture toughness and fatigue crack growth data, of metallic alloys, compendium of sources 78—84963
fracture toughness and impact strength, correl. breakdown 80—55523
fracture toughness determ. in conditions of similarity to local fracture *(Russian)* 78—31505
fracture toughness determ. of alloy B95T1 with surface cracks *(Russian)* 77—25141
fracture toughness rel. to microstruct. characts., alloy design 79—43423
friction and wear, effect of oxides 79—20203
fusion reactor metals, He embrittlement, grain boundary cavity model 80—34075
gas solutions in alloys, due to impurity-deoxidising element interactions, thermodynamic analysis *(Russian)* 79—34347
gas turbine engine, substitution of ceramics for high temp. alloys 80—97678
Gibbs equilibrium thermodynamic pot. second derivatives, discontinuity surfaces rel. to phase boundaries of q-component systems 79—82304
glass forming ability of metallic alloy, prediction 79—23524
grain and phase boundary model *(German)* 79—99216
grain boudnary drag 78—51550
grain boundary relax., model *(Russian)* 80—39107
group VIII and nearly related elements, cmpd. and superlattice form. 79—94955
Guinier-Preston zones, role of anisotropy in elec. resist. 77—36515
hard, binary carbide with Ni-Mo binder, physicomech. props. 77—90461
hard, powder mixtures, porosity and hardness during pressing, u.s. vibration effects 77—1821
hard alloy bar, slide rule for calc. transverse rupture strength 80—40530
hard alloy coatings, detonation deposition from fine powder mixtures 79—100078
hard alloy insert jig brushes, wear resist. *(Russian)* 80—60977
hard-alloy powder mixtures, compressibility in hydrostatic working 78—68645
hardfacing alloys in impact abrasive loading, wear resistance, temp. effects 79—87737
Hastelloy X, crevice corrosion by water vapour and methane in Ar at 1 and 25 atm. 77—25203
HCP, low temp. interstitial struct., statistical-thermodynamic theory *(Russian)* 79—51100
HCP, plastically deformed, electron microscopy *(French)* 77—44300
HCP, stacking faults, long-range oscillatory interactions and stability 80—65012
heat of formation within density functional formalism 79—57283
heat resistance under one sided loading 77—1872
heat resistant KhN80TBYuA and KHN62VMkYu, microscopic intergranular crack form. prediction in high temp. deform. 77—81325
heat treating and melting with scanning laser or electron beam 78—11406
heat treatment, chem., principles and practical procedures *(Russian)* 79—52260
heat-resistant, alloying and heat treatment effects on struct. and strength 78—95758
heat-resistant, thermal stress cracking resist. evaluation method 80—3260
heat-resistant alloys, fatigue under conds. of mech. and thermal stress loading 79—87726
heat-resistant alloys, installation for mech. tests under superplasticity conditions 80—55603
Heisenberg antiferromagnetic alloy, critical behaviour *(Russian)* 78—88128
Heisenberg ferromagnetic alloy, critical behaviour *(Russian)* 78—88127
heterogeneous nucleation activity, and melting point ratio correlation 78—92255
heterogeneous nucleation during solidification 79—28077
heterogeneous with coarse microstruct., steady state power law creep 79—61644
Heusler, order-disorder transitions, intermediate model 80—54341
Heusler, ternary, order-disorder transitions, Bragg-Williams approx. 79—90755
Heusler, ternary order-disorder transitions, Bragg-Williams approx. 79—90756
Heusler alloy with nonmagnetic impurity, transferred hyperfine field using volume overlap model 79—78054
Heusler alloys, hyperfine fields at sp sites, spin echo NMR meas. 78—19371
Heusler alloys, ionic spin distribution and RKKY interactions 78—27028
hexagonal crystal structure, anisotropy of elastic props. calc. *(Russian)* 78—23749
high strength, marine corrosion fatigue crack growth rate, bulk soln. chemistry condition effect 79—83373
high temperature, mechanical, thermal and corrosion props. 78—95763
high temperature alloys, quantitative anal. by ion microanalyser *(Japanese)* 78—7291
high-concentration alloy analysis by optical emission spectrometers 80—104477
high-temperature alloys, hot corrosion, book contrib. 78—11444
highly resistive, temp. depend. on elec. resist. 78—91657
homovalent disordered solid alloy, entropy-vol. correlation 78—63868
hot plastic strain, stress- strain-time dependences *(Russian)* 80—40430
hot twisting, differential method of shear stress determ. 77—56026
HTR material, oxidation and carburization in He 80—108645
Hume-Rothery Phases, electronic struct., main features 79—23883
hydride forming phase hardening 78—52833
hyperplastic, diffusion coeffs. determ. during deform. 79—51298

alloys continued
- III-V ternary alloy, intrinsic bowing parameters of indirect energy gap 79−99469
- impurity diffusion and distrib. 79−33118
- inclusions behaviour, during processsing, effects on directionality 80−55345
- intergranular precipitate effect on diffusion growth of creep voids 79−34041
- intermetallic cmpd., monovacancy form. enthalpy 79−90649
- intermetallic compounds, correl. between interstitial hole sizes and hydride thermodyn. props. 78−18798
- intermetallic compounds, review 78−15333
- intermetallic phases, B2 struct., substitutional and triple defects, enthalpies of formation 80−96520
- intermetallic phases, struct. description *(German)* 80−88090
- intermetallic phases, technical superconductor applications *(German)* 78−27005
- intermetallic phases with $L1_2$ and $D0_{19}$ struct., atom incompressibility, lattice parameter approach 78−91294
- intermetallic powder, spark erosion prep. 78−27452
- internal friction, amplitude depend., for polycryst. specimens *(Russian)* 79−90726
- interstitial, storage of H_2, review 79−10956
- interstitial alloys, interstitial atomic arrangement and mobility at high degrees of interstice filling *(Russian)* 80−107223
- interstitial atoms, distrib. and kinetics of redistrib. in interstices *(Russian)* 77−43207
- interstitial solid solns., HCP, ordering type transitions within thermodynamics theory framework 80−49162
- ion bombardment, surface composition changes 80−2913
- ion implantation in tribology and corrosion science, overview 79−14830
- ion-implanted, annealing behaviour and appls. 79−14829
- ion-implanted, integral Gaussian profile determ. method 80−107313
- ion-implanted alloys, surface props. effects and appls. 80−79824
- irradiated, effect of defect trapping and solute segregation, on defect recombination rates and void swelling 78−47369
- irradiated, segregation, inverse Kirkendall effect, effect of constitution on void swelling 78−91472
- irradiated, solute segregation and precipitation effects on void swelling 78−67741
- irradiated dilute alloys, kinetic model for solute redistrib. to sinks and void growth 79−78973
- irradiation induced precipitation, thermodynamic approach 79−78975
- Ising ferromagnet, annealed, of binary alloys 77−59368
- itinerant electron ferromagnetic alloys, magnon energy, effect of ordering 79−7986
- Johnson-Mehl-Avrami (JMA) formula, appl. to alloy decomposition kinetics 80−16263
- $L1_2$ and $L1_0$ superstructure atomic ordering phase diagrams, order-disorder transition 80−38989
- $L1_2$ ordered, temp. depend. of hardness 80−30104
- $L1_2$ ordered alloys, latent hardening 77−16676
- $L1_2$-type superstructure, anomalous temp. depend. of deform. characts. *(Russian)* 79−20109
- lamellar multiphase, struct. and spatial comp. variation, analytical STEM 78−24011
- laser erosion, influence of metallic target temp. *(Russian)* 79−39028
- laser irradiated, time-resolved specular reflectivity 79−69819
- laser surface melted, heat transfer props. and microstructs. 79−70085
- laser surface melting 77−90492
- latent cold work heat release kinetics meas. using adiabatic elec. heating 77−52344
- lattice defects, positron annihilation study, book contrib. 79−99977
- Laves phase AB_2 intermetallic compounds, H_2 sorption, capacity and preferred location 79−43791
- liquid metal embrittlement 79−52421
- liquidus and solidus temperatures, determ. by γ-ray method 80−65193
- local composition determ., assessment of TEM direct lattice imaging technique 78−53294
- local concentration, short-range order, clustering and microstruct., definition for arbitrary duration and expt. temp. 79−51267
- local density of states and local environment 79−82509
- machining damage, depth of surface layers determ. 80−85094
- magnetic, amorphous, manufactured by special quenching, magnetic strip appl. *(German)* 77−16700
- magnetic, binary, spinodal decomp., computer simulation study of interface behaviour 80−84913
- magnetic, highly concentrated, Kondo effect 79−24134
- magnetic, Lifshitz point occurrence, reviews 78−52265
- magnetic alloys, conc., density of states, Kondo effect, theory 80−65780
- magnetic anisotropy, influence of local symmetry *(Russian)* 80−93109
- magnetic binary alloy, computer simulation, time evolution 79−56488
- magnetic binary alloys, phase separation, double Ising system 78−91835
- magnetic localisation and charge oscillations, spin glasses 80−75781
- magnetic properties from Rhodes-Wohlfarth plot 78−52190
- magnetic ternary alloys, statistical theory of electrical resistivity 78−87969
- magnets, mixed, competing spin glass and mag. order, phase diagrams, crit. points 80−39802
- many-body atomic correlations, Mossbauer spectroscopy study 80−15934
- martensitic phase transition in β-phase alloys 80−108444
- martensitic transitions accompanied by interactions between phases *(Russian)* 80−7568
- mathematical models of disordered systems, book 80−1878
- mechanical properties, electric current effect, test device for 4.2-300K 80−66719
- melting line slope 77−15553
- memory alloy engine, efficiency 80−71648
- metal metal system, glass formation 80−64921
- metal-H alloys, phonon dispersion relation, neutron scatt. studies, review 79−60451
- metal-H system, electro- and thermotransport of H, book contrib. 80−24644
- metal-H system study by neutron scattering, review *(French)* 80−34226
- metal-H systems, appl. oriented props., book 80−22154
- metal-H systems, heat transformer for energy cascading, book contrib. 80−26151
- metal-H systems, solvus line interpretation, enthalpy change 79−15655
- metal-H systems at high H press., physicochemical props., book contrib. 80−24535

alloys continued
- metal-hydrogen system, 2-dimens., elastic interaction, spinodal temp. and density modes 77−69072
- metal-hydrogen system, electronic sp. ht. meas. 80−49378
- metal-semimetal alloy, phase diagram computation from thermodynamic functions 80−40329
- metastable, determination and representation of phase diagram features 79−11568
- metastable microalloys, equilib. form. criteria 78−30762
- metastable phase formation by ion implantation, reviews 80−49254
- microstructural instabilities, review 78−35348
- mictomagnet props. review 79−24183
- modulated structures, conference, Kailua Kona, Hawaii, USA (March 1979) 79−94928
- multicomponent, optimal composition determ., mathematical-statistical methods *(Czech)* 79−15624
- multicomponent, thermodynamic partial molar quantities, calc. from known quantity of one component 77−72703
- multicomponent alloy, phase diagram calc., computerised data bank 79−1848
- multicomponent alloy films, struct. form. laws and elec. prop. changes obs. during vacuum condensation 78−6850
- multicomponent alloy phase diagrams, calc. methods used at National Physics Laboratory 79−11569
- multicomponent alloys, phase diagram calc. program from thermodynamic data 80−3008
- multicomponent phase diagram calc., NPL alloy data bank 78−92243
- multinary alloy, X-ray small-angle scattering, rel. to elec. resist. 79−19125
- mutual alloying behaviour of later transition and early B subgroup elements, graphical rep. 77−19895
- mutual alloying behaviour of the elements straddling the line Li-Mg-Cu-Au in the long periodic table 78−84769
- nearly and weakly ferromagnetic, mag. clusters, unpolarised neutron diffuse scatt. 78−39297
- nearly-free-electron, random, charge transfer rel. to stability 78−6316
- nitriding methods and programmed control system 78−95857
- NMR results, metals and alloys, brief survey 79−73830
- non-ferrous, exam. of props. with aid of phase diagrams 79−11573
- nonfissile irradiation creep 77−42072
- nonlinear anelasticity and the martensitic transformation 79−61634
- nonlocality and energy of form. 79−20459
- nontransition metals, binary alloying tendencies 78−2261
- nontransition metals, electronegativity parameters of theory of heats of alloy form. 79−74412
- nuclear reactor materials developments for advanced HTR systems 77−46297
- nuclear reactor plant materials developments for HTGR systems 77−46298
- off-diagonal disordered alloys, density of states and cond., CPA calc. 80−24780
- omega forming, internal friction 78−19796
- one-dimensional, electronic struct. 79−69391
- optical constants determ., review 79−33655
- order strengthening as method of reducing irradiation creep 77−48485
- order-disorder transformation kinetics 80−2138
- ordered, conservative jog slip on superpartial screw dislocations, work hardening 77−7731
- ordered, cryst. struct. and phase transforms. *(Russian)* 79−29047
- ordered, Cu_3Au-type struct., redistribution of interstitial atoms after temp. change *(Russian)* 77−62523
- ordered, eqn. of state, applicability of semiempirical function of binding energy *(Russian)* 77−15533
- ordered, $L1_2$, yield stress 77−52392
- ordered, mechanical properties *(Czech)* 77−1854
- ordered, spinodal decomposition, theoretical basis 80−60862
- ordered, superlattice fringe images, computer simulation 80−103296
- ordered, with $L1_2$ structure, dissociation of superdislocations and plastic deform. mech. *(Russian)* 78−52909
- ordered alloy, noncoaxial dislocation loop behaviour 77−11549
- ordered alloys, long period antiphase structs. 79−95027
- ordering, atomistic approach 79−94947
- ordering, BCC lattice, diffusion of insterstitial atoms *(Russian)* 79−19400
- ordering, improved variant of quasi-chemical theory *(Russian)* 78−22685
- ordering, nonlinear critical relaxation of the Ginzburg Landau field coupled to a conserved density 80−90803
- ordering, variation in interatomic interaction and lattice parameters *(Russian)* 77−81255
- ordering alloys, effect of press. on phase diagrams and order-disorder transforms. 78−52797
- oxidation, alloy depletion profiles resulting from preferential removal of less noble metals 79−11728
- oxidation, Auger spectra 78−14600
- oxidation, high temp., obs. using $^{18}O(p,\gamma)^{15}N$, ^{18}O distrib. determ. 79−87912
- oxidation behaviour in the environment, appl. to GCFR fuel claddings 80−104350
- oxidation mech., exam. using autoradiography 79−20326
- oxidation resistance, high-temp., improvement by alloying additions 80−66702
- oxidised, heat resistant, radiation emission props. depend. on oxidation conditions 77−43358
- passivatable, role of oxide films in stress corrosion cracking initiation 80−50762
- passivity, in metals and alloys 80−50750
- pewter, English and Scottish measures, X-ray fluoresc. anal. 78−347
- phase analysis by Mossbauer spectra 80−15922
- phase diagrams, exam. of compilation activity 79−8274
- phase diagrams, prediction using non thermodynamic approaches 79−8281
- phase stability, computer calc. using modified pair potentials 78−35352
- phase transformations, role of phase boundaries 78−72772
- phase transformations in metals and alloys, thermodynamic and mechanistic classification, review 80−2995
- phase transforms. 79−2771
- phase transition premonitory phenomena, exam. by electron diffr. and microscopy *(French)* 80−59651
- physical props., correl. with outer electron density of state *(Chinese)* 79−51466

alloys continued
- polycomponent metallic solid soln., creep and diffusion of vacancies *(Czech)* 79—43340
- polycrystalline, LF viscosity meas. 78—80576
- polyhedrisation of quinary metallic systems with isomorphic intermediate phases *(Russian)* 80—45270
- positron annihilation, CPA calc. for spatial and momentum distrib. 77—80720
- positron annihilation, theoretical and expt. techniques, book 79—99975
- positron annihilation and charge transfer in simple alloys 78—31274
- positron annihilation technique in Fermiology 79—69902
- positron localisation in ordered and disordered alloys 78—79962
- powder metallurgy techniques applied to superalloys 78—3073
- powder resistive foils, manufacture and props. of multicomponent alloys *(Polish)* 80—35131
- powders, production using electrodeposition and heating in reducing atm. 79—100079
- precipitate dimensions, annealing temp. depend. *(Russian)* 78—15399
- precipitate distribution in subscales forming in dilute alloys 79—38834
- precipitated phases, size, shape, distrib., diffusion controlled changes 80—3072
- precipitation hardened, containing narrow soft zones at grain boundaries, fracture toughness 77—77553
- precipitation hardening, yield stress *(Russian)* 79—56990
- production process strength *(Russian)* 77—21152
- pseudobinary, use of parallel and monochromatic beams for comp. determ. by X-ray fluorescence 79—48000
- pseudopotential investigation of phys. props. 77—43526
- PWR boiler tubes, corrosion risk reduction by material selection, evaluation 79—39045
- quasiequilibrium crystallisation in rotating systems *(Russian)* 80—16293
- quaternary, order-disorder transition using classical fluctuation theory and correl. functions 79—73288
- quenched, binary, time evolution, computer simulation of three-dimensional model system 78—31433
- quenched binary alloy at low temps., time evolution, phase separation 78—68670
- quenched model binary alloy, time evolution in nucleation region, computer simulation 79—82344
- quenched random, phase diagrams, multicritical points, mixed anisotropies 79—38343
- quenched to sufficiently low temp., struct. function, long time behaviour 77—84886
- radiation damage prediction and measurement 78—75693
- radiation effects on ageing and precipitation, review 80—29956
- radiation-induced segregation in binary and ternary alloys 79—78970
- random, binary, diffusion correlation factors calc., comparison of matrix inversion, Monte Carlo and diffusion of probability techniques 78—30779
- random, elementary excitations 77—4278
- random, equilib. and transport props., single-site approxs. 80—92801
- random, with short-range order, iterative calc. of energy levels 77—66104
- random alloys, CPA calcs. cluster extensions, appraisal of applicability 79—15063
- random binary, Anderson localization, equation-of-motion method 79—42482
- random binary, single-particle Hamiltonian and self-consistency 79—37953
- random binary, with partial order, electronic struct., self-consistent approx. 77—62796
- random binary alloys, electronic struct., Mott-Anderson model 80—49671
- random binary alloys, quantum percolation 80—80156
- random magnetic alloys, mean field effective medium theory, Ising model appl., phases 78—84438
- random metal alloy, electron-phonon dynamics and resistivity anomalies 80—10958
- rapid hardening from liquid state, apparatus 80—76275
- rapidly quenched crystalline, struct., and heat treatment effects 80—76292
- rapidly quenched metals, conf., Brighton, England (July 1978) 80—67934
- rapidly solidified powder, nucleation, undercooling and homogeneous struct. 79—11598
- recoil implantation and ion-beam-induced comp. changes 80—34021
- refractory, creep mechanism and struct. changes *(Russian)* 79—52299
- refractory, safe-life testing *(Russian)* 79—52476
- refractory, spectrochem. anal. using high-voltage unipolar spark discharge *(Russian)* 78—15750
- refractory, surface investigation by FIM and atom probe *(German)* 79—55623
- refractory metal alloy, heat resistance and cold brittleness, achievements and trends 78—95718
- refractory metal solid solutions, thermodynamic study *(Ukrainian)* 79—37845
- refractory metal-H alloy prep. technique for TEM studies 77—90544
- refractory metals and alloys, processing by powder and vacuum melting techniques 79—33966
- relaxation, rel. to defect struct. *(Russian)* 78—19801
- relaxation resistance testing using constantly loaded sample 78—39965
- resistivity evolution during decomposition, theory *(French)* 80—75546
- rotated remelted ingots, macrosegregation 79—52196
- s-d alloys, density of states calc. using coherent potential approx. *(Japanese)* 77—76721
- SCC, book 79—100303
- segregating phases identification, single crysts., radiographs computer calc. 80—84934
- segregation, non-equilib., review 80—66516
- segregation, radiation-induced, theory 79—77633
- segregation studies by imaging atom probe microscopy 80—66911
- selection for cryogenic resistors with low temp. coeff. 80—98922
- selective stripe alloy electrodeposition and hot flow techniques, metallurgical characteristics 80—50567
- self-consistent cluster theories for diagonal and off-diagonal disorder 79—37950
- shape memory alloy, martensite boundaries, lattice imaging study 80—107359
- shape memory alloy, recovery stress determ. 79—15665
- shape memory alloys temperature entropy diagram of solid state engines and solid state heat pumping system 77—7785
- shape memory effect, device for testing in bending 80—66723
- shape memory effect alloy connector for optical fibres 80—53475

alloys continued
- shape-memory alloys, practical appls. 80—45307
- shock wave effect on martensitic transform. *(Russian)* 80—96595
- short-range order, electronic theory using pseudopot. approx., reveiw 79—47004
- sigma phase structure, ionicity modified pair pot. model anal. 78—51466
- simple metal alloys, electronic theory for metal-non-metal transition 78—47702
- single phase, annealing of diffusion layer 78—14518
- sintered mats., complex diffusion alloying 78—68650
- solid soln., grain boundary mobility 79—46676
- solid soln. strengthening, HTR appl. 79—15688
- solid solution, large grained, creep ductility 78—48479
- solid solution alloys, creep behaviour at intermediate stresses and creep power law breakdown 79—57058
- solid state reactions, effect on microstruct. 79—29015
- solid substitutional soln., diffusive creep *(Russian)* 79—55816
- solid-liquid metallic binary alloy, interfacial tension, chem. adsorption and temp. depend. 80—59777
- solidification, kinetic model, appl. to liquisol quenching 78—44116
- solidification, multidimensional three-phase free boundary problems 80—75340
- solidification, planar interface stability *(Czech)* 80—89212
- solidification, review of theory, industrial techniques *(French)* 77—73268
- solidification mechanisms, contribution of microgravity expts. 78—88457
- solidification models for high cooling rates 79—91639
- solidified, thermophysical charact. in region of special points of phase diagram *(Russian)* 78—44082
- solidus temperature determ. by method of moving specimen boundary projected on screen 78—35353
- space environment, metallurgical studies in Skylab and Apollo-Soyuz 79—47700
- space lattice types A_1, A_2 and A_3, strain hardening function *(German)* 80—20955
- spherical monocrystals for X-ray work obtained by plasma remelting of alloy powder 78—47205
- spinodal decomposition, review 80—96657
- spinodally decomposed, interfacial energy effect on mech. strength, theoretical estimation 79—38790
- splat-quenching device, refractories in magnetic levitation furnace *(Croatian)* 79—11639
- spring alloys, microplastic deform. and endurance limit 80—81197
- sputtering, non-elemental solid surface, surface composition, yields, desorption effects, review 77—44111
- sputtering, surface binding and mass difference effects 79—83077
- sputtering characteristics, transient, glow discharge optical spectroscopy meas. 77—44156
- sputtering of metal alloys containing second-phase precipitates, glow-discharge optical spectra 78—48264
- sputtering process and sputtered ion emission, models 80—35044
- stabilisation of long-period superlattices 79—95348
- stability and structure, pseudopotential calcs. *(German)* 80—38913
- strain hardening criteria eval. 77—55982
- strain rate history, endochronic theory of viscoplasticity 80—65122
- strain rate sensitivity rel. to ductility, anomalies 77—36590
- strength/ductility relation *(Japanese)* 79—29145
- strengthening mechanism anal. by thermal activation theory 79—78987
- stress ageing embrittlement, under short term thermally stressed cycle *(Russian)* 80—60885
- stress corrosion cracking *(Japanese)* 78—56820
- stress corrosion cracking testing, for coal gasifiers appl. 80—7726
- stress-strain time dependence based on nonlinear heredity, delayed yielding 78—48452
- structural, fracture at temps. approaching absolute zero 78—72877
- structural, time-depend. fatigue, nuclear reactor materials 79—1909
- structural transformations during ageing, book contrib. 78—11199
- structure and thermodynamic properties at high temperatures, microscopic theory *(Japanese)* 80—29191
- structure determ. by Mossbauer effect in high-temp. chamber 77—17982
- substitutional, electrical resist., long and short range orders effect 80—107761
- substitutional, self consistent cluster theory for off diagonal disordered systems 80—84272
- substitutional alloy, disorder description within supercell model 78—26479
- substitutional alloys, conditions for appearance of striations in stress/strain curves *(French)* 77—44319
- substitutional alloys of intermediate valence systems, static mag. susceptibility con. and temp. depend. 80—84586
- substitutional alloys with large mass disorder, phonon modes 78—95122
- substitutional solid soln., irradiated creep rate enhancement theory 77—63739
- substitutionally disordered, optical cond., intraband transitions 80—103933
- sulphidation mechanisms, review *(Polish)* 80—45413
- superalloys, cast, phase volume fraction determ. using manual point count practice 78—53052
- superalloys, phase extraction, chemical and X-ray diffr. anal. 78—72951
- superalloys, phases *(Chinese)* 78—95728
- superconducting, metallurgical factors influencing T_c 79—38225
- superplastic, grain size effect on maximum strain rate sensitivity 79—100227
- surface, free energy of segregation 80—29256
- surface, theory of segregation 79—77886
- surface alloys, metastable, prod. by ion implantation, empirical rules for substitutionality 79—14832
- surface composition after fabrication by SIMS 80—65351
- surface composition modification by high-power CW lasers 80—93699
- surface disorder, source of magnetism 79—56487
- surface layer alloying effect on electroerosion working *(Russian)* 78—64760
- surface layer anal. with emission spectrochemical anal. *(Japanese)* 78—92570
- surface layer effects on bulk props. 78—85049
- surface rippling induced by surface tension during laser melting and alloying 78—11405
- surface segregation, appl. of quantification of atom-probe FIM data 78—62263
- surface segregation, existence of surface miscibility gaps within regular soln. theory 78—71909
- surface segregation, miscibility gaps, reg. soln. theory 78—18882

alloys continued
  - surface segregation prediction from bulk melting curve shape 77-12597
  - temper embrittlement, impurities and alloying elements role, review 80-66649
  - temper embrittlement kinetics, ternary and binary alloys, computer simulation 78-84953
  - tenacity parameters 80-60973
  - tensile failure prediction for fission reactor components 80-5241
  - ternary, A-15 phase, Cr_3Si type, atomic volumes deduced 78-22690
  - ternary, density of states, CPA calc., off-diagonal disorder 78-22998
  - ternary, disordered, elec. cond. and density of states, CPA calc. *(Russian)* 79-47072
  - ternary, interdiffusion coeffs., expt. determ. 79-95221
  - ternary, metastable miscibility gap determ. by small angle scatt. 77-28780
  - ternary, ordered, Green's function treatment, disorder transition 77-15540
  - ternary, phase diagram, general theory 77-32558
  - ternary, phase equilibria calc., line compounds 80-10638
  - ternary, transition of univariant form. equiliv. into decomposition equilib. *(German)* 79-43196
  - ternary alloy ordering, correlation effects, Kirkwood method calcs. *(Russian)* 79-66038
  - ternary alloy with three-body potentials, transition temp. calc. using correl. function approach 79-69451
  - ternary alloys, AB-AC quasi-binary sections of order-disorder phase diagram 78-88463
  - ternary alloys, vibr. freq. distrib. spectra, small cluster statistical theory 79-24317
  - ternary and binary, phase diagrams and transition temp., correl. function approach 79-95164
  - ternary and multicomponent systems, partial molal props. calc. 78-79784
  - ternary BCC alloys, ordering process, effect of short-range order *(Russian)* 80-84908
  - ternary systems, high temp. adsorption 79-77914
  - ternary systems, triangulation parameters correl. with isomorphic intermediate phases *(Russian)* 79-52203
  - thermal cycling fracture 78-60839
  - thermal expansion characts. determ. using strain gauges 78-81942
  - thermal expansion coefficient, and volume effect anomalies during transformations, review of differential dilatometric error sources *(Russian)* 79-34223
  - thermal fatigue testing, installation for −180 to 1100°C 80-3266
  - thermobalance for studying high-temp. sulphidation kinetics of metals 78-23876
  - thermochemical treatment, surface layer form. *(German)* 78-15598
  - thermodynamic and structural changes in deform. twinning 78-2139
  - thermodynamic computation data bank, appl. to inorganic and metallurgical systems 77-59100
  - thermodynamic functions calc., ternary alloy of quasi-binary cross sections 80-16265
  - thermodynamic study of corrosion 79-57161
  - thermoelectric power measurements, use in study of alloys *(French)* 79-69497
  - thermoelectric properties, effect of interference between electron-impurity and electron-phonon interactions 79-33282
  - thermoemission props. determ., meas. instrument based on scanning electron beam 78-74025
  - thermophysical charact., peculiarities of temp. depend., dimensional change meas. *(Russian)* 78-95868
  - thermostress treatment of thin rolled sheets 79-52273
  - thin film, thickness depend. of CPA electronic densities of states 80-65644
  - thin film alloys, surface magnetism props., Curie temp., Ising model 80-108039
  - three component, conditions for mass transfer, diffusion processes 80-54445
  - torsion pendulum for damping capacity meas. and related phenomena 77-77687
  - trace element detection by atom probe microanalysis 80-66910
  - transfer matrix approx., dispersion relations and transport props. 79-42524
  - with twinned martensite, crystallog. singularities in reverse martensitic tranform. *(Russian)* 77-32571
  - twinning, HCP struct., relative orientation of cryst. lattices 80-84181
  - two component, powder sintering 80-20847
  - two phase, hardening by second phase particle coalescence 80-7591
  - two phase microstrct. revealed by selective sublimation 79-24698
  - two-band model, self-consistent cluster Bethe lattice study 80-29303
  - two-component layered system, with interpenetrating components, thermoelec. and galvanomag. props. 78-79982
  - two-phase, alloys, coarse microstructs., structural approach to yield strength 80-7634
  - two-phase, deform. struct. and recrystallisation, review 79-34061
  - two-phase, recrystallisation mechanisms 79-47708
  - type A15 structure, Czochralski growth, supercond. behaviour 79-74080
  - undersaturated, irradiated, solute segregation kinetics, via drift and defect-solute complexes 80-60872
  - unidirectional memory effect *(French)* 80-66606
  - vacancies and lattice elec. cond. determ. method at high temp. 79-37695
  - vacancy formation energy, new method for determining 78-47345
  - vacuum coating deposition by vaporisation *(Russian)* 79-74093
  - vacuum rolling at high temp. *(Russian)* 79-15708
  - valence bond test for validity of structure 79-10830
  - vaporisation kinetics in vacuum *(Russian)* 77-72683
  - vapour deposited coatings, mech. props. 78-6247
  - void swelling depth distribution produced by 5 MeV Ni ions 77-7771
  - void swelling under irradiation, theory 78-75692
  - wear resistant, hardfacing, review 78-72937
  - weldable clad metal interlayer growth kinetics model 79-24493
  - welding parameters in variable composition alloys, errors in deriving empirical relationships, using accelerated methods 80-25980
  - work hardening phenomena and screw dislocation dipole clusters 80-100845
  - X-ray analysis, energy selective, TEM appls. 80-84036
  - X-ray analysis methodology appl., wide-angle *(German)* 80-3283
  - X-ray fluorescence correction in thin foil analysis 80-85256
  - X-ray line shapes for core levels, phonon broadening 77-12464

alloys continued
  - X-ray microanalysis, thin foils, data correction for absorpt. effects 80-85255
  - X-ray self-absorption spectroscopy method for unoccupied valence states obs. *(Russian)* 77-81175
  - X-ray spectroscopy 77-55849
  - XPS, asymm. of core electron lines *(Ukrainian)* 78-2982
  - yield criterion, rheological interpretation *(Russian)* 80-21014
  - yield limit theory for alloy with dispersion precipitate of ordered phase *(Russian)* 77-1855
  - cemented carbide tool, wear when turning grey cast Fe 79-43442
  - CsCl type, nearest neighbour distance and atomic props. 78-51465
  - H storage, effect of the interstitial hole size and electron concentration on complex metal hydride formation [for H storage] 80-45789
  - H_2, embrittlement, mechanisms *(Russian)* 77-25128
  - NiAs crystal lattice alloys and cpds., mag. transitions, mag. field and high press. effects 79-82780

alnico alloys *see iron alloys*

Al_2O_3 *see alumina*

Al_2O_3-α *see corundum*

α-Al_2O_3 *see corundum*

alpha-decay
  - *see also alpha-decay theory; alpha-particle spectra*
  - $^{260}104$, detection methods, comparison of reactions $^{246}Cm+^{18}O$, $^{248}Cm+^{16}O$, $^{249}Bk+^{15}N$ 77-23106
  - $^{263}106$, identification from alpha-decay chain $^{263}106 \rightarrow {}^{259}Rf \rightarrow {}^{255}No \rightarrow {}^{251}Fm$ 77-26637
  - $^{294}110$, naturally occurring superheavy element search, alpha emission half-life 80-63139
  - $^{298}114$, high spin pot. energy surfaces, fission barrier, α-, γ-decay half lives, yrast spectrum 80-73764
  - $A=149$-155, systematics of α-particle energies of isotopes, $N=84$-87, $59 \leq Z \leq 76$ *(Russian)* 77-14071
  - $A=215$, nuclear data sheets, decay characteristics and level struct. 78-58224
  - $A=219$, nuclear data sheets, decay characts. and level struct. 78-58225
  - $A=223$, nuclear data sheets, decay characts. and level struct. 78-58226
  - $A=227$, nuclear data sheets, decay characts. and level struct. 78-58227
  - $A=354$, $Z=126$, spontaneous fission, α-decay, β-decay half-lives calc. 77-6469
  - actinoid elements, current state of results 78-17159
  - CANDU fuel radioactive decay props., natural uranium fuel cycle 77-71655
  - CANDU reprocessed fuel and high level waste radioactive decay props. 77-71656
  - cluster role in natural α-decay 79-6519
  - coherent rotational states, alpha decay, α-emission probability 80-102155
  - compound highly excited states populated in (n,α) *(Russian)* 78-29472
  - Conway granite, reinvestigation of 4.4 MeV alpha-activity 78-57210
  - determ. of bulk α and β radioactivity *(Rumanian)* 79-88346
  - energies of separation and alpha- and beta-decay, 1977 at. mass evaluation tables 78-4895
  - explosive r process cooling process 78-69791
  - fission method study *(French)* 79-93565
  - fisson-emitted alpha particles, energy spectrum, fission fragment shape and orientation depends. 78-74346
  - giant halo radioactive inclusions in minerals 80-94524
  - giant resonances, cluster emission decay 79-26413
  - heavy nuclei, $Z=68$-72, nucleon separation, pairing and decay energies and mass defect 77-79301
  - history of alpha particles, 1903-1977, discovery, props., alpha decay 77-78942
  - inner shell electron rearrangements in radioactive decay 77-18881
  - lifetimes, comparison of calc. methods 78-78325
  - liquid drop model decay periods *(Russian)* 80-32246
  - mica, giant haloes, cleavage cracks enhancing radiation damage 78-7623
  - monazite, α-spectra evidence for natural activity at 6.52 to 9.07 MeV 80-67363
  - natural, $E>11$ MeV emulsion and counting techniques 78-8785
  - natural substances *(Rumanian)* 77-49067
  - near Pb region, α-decay peculiarities and shape staggering effects 79-49611
  - neutron-deficient isotopes at ISOLDE, CERN 77-22967
  - phenomenological pot. and folding model results relation for nuclear α-clustering 78-78289
  - pre-compound decay into complex particle channels 79-6456
  - prep. and chem. charact. for half-life meas. 79-26404
  - probabilities of α-, β- and γ-transitions accompanied by changes in nuclear shape *(Russian)* 78-89820
  - radioactive nuclide decay data for reactor calcs., activation products and related isotopes 78-82426
  - radiotracer diffusion rates in ionic solid, influence of transmutation products 77-89568
  - rare earth nuclei, high spin isomer α-decay search 80-102158
  - rocks, Scandinavian, giant and dwarf haloes rel. to unknown radioactivity 78-81157
  - serial decay, transient equilib. and secular equilib. 79-80901
  - Sp(6,R) symmetry, α-breakup amplitudes, of giant E2 excitations in light nuclei 78-29435
  - spectroscopic information from nuclear reactions: applications 79-459
  - spectroscopic information from nuclear reactions: theory 79-458
  - spectroscopic information from nuclear reactions 79-6455
  - spherical nuclei, probabilities of α-transitions, effect of higher configs. of α-particle internal waves functions 78-17155
  - superheavy elements, search for high-energy α-particles 79-59040
  - superheavy nuclei in $Z=126$ region, α-particle stability 77-300
  - total α-widths of neutron resonances, nuclei from ^{64}Zn to ^{177}Hf 77-26708
  - weak interaction between nuclear particles, parity violation, review 77-6295
  - $Z=114$-126, nuclear stability reexamination using deformed Woods-Saxon pot. lifetimes level density 79-3094
  - α-emission probability at very high ang. momenta, shape change effects 79-89229
  - $(d,{}^6Li)$, $A=144$-238, alpha-cluster transfer from alpha-decaying nuclei 80-91166
  - ^{109}Ag (^{40}Ar, X), α-decay amplification in superdeformed nuclei, high ang. momentum deexcitation 80-22776

alpha-decay continued
^{27}Al+^{14}N, 100 MeV, α preequilibrium decay 79−6666
^{27}Al(^{16}O,^{12}Cα)^{27}Al, 65 MeV, pre-equilib. α-decay obs. 77−61390
^{231}Am alpha decay, ^{237}Np γ-ray transitions *(French)* 79−492
^{232}Am, absolute γ yields 78−86516
^{241}Am, α-decay low-energy γ-radiation *(French)* 78−74342
^{241}Am, γ-ray spectrum above 600 keV, Ge(Li) detector, ^{237}Np states 79−6480
^{243}Am half life and α-activity 80−102159
^{A}At, A=198m,198g,199, alpha branching ratios 80−99154
^{211}At half life, branching ratio of electron capture and α decay modes 78−58253
^{212}At, relative α-decay width and excited levels, nuclear field theory 80−47437
Au+^{86}Kr, 724 MeV, coincidence meas., pre-equilibrium α-emission 78−33208
^{A}Au, A=181, 182, alpha decay, half lives, decay energies and branching ratios 79−45215
^{6}Be, α+p+p decay, α spectrum meas. 77−74813
^{9}Be, disintegration obs. in ^{9}Be(γ,n) and (γ,α) reacts. 78−37327
^{9}Be, molecular model, n and α-particle decay widths, charge form factors 78−46015
Bi isotopes, neutron deficient, anal. of α decay in terms of surface probabilities of α-particle formation *(Russian)* 79−9527
^{188}Bi alpha decay half lives 80−57749
^{210}Bi→^{210}Po→^{206}Pb, decay chain, L-shell ionisation investig., X-ray emission during β, α decay 77−18891
^{210}Bi→^{210}Po→^{206}Pb, L-shell auto -ionisation 77−6739
^{212}Bi, isomeric states from α-activities 78−82282
^{12}C α-decay, (d,d′) excited, 4π ang. pattern meas., DWBA anal. 79−67720
^{12}C, positive-parity states, anomalous α-decay props. 78−62511
^{12}C, radiative transitions and isospin mixing 77−38242
^{12}C(1^{+}) decay to 3 α-particles, final-state interactions, spectra calc. 77−88086
^{40}Ca, α-and p-spectra from giant reson. region via ^{40}Ca(α,2α) and ^{40}Ca(α,αp) 77−30523
^{40}Ca, isoscalar multipole resonances 78−66190
^{246}Cf, α-decay meas., daughter energy levels *(Russian)* 77−82882
^{249}Cf, α-decay, ^{245}Cm level scheme 79−6477
^{252}Cf effective half-life 77−22966
^{242}Cm, α-activity, half-life 77−54193
^{245}Cm decay, ^{241}Pu level structure and γ-transitions 80−105980
^{248}Cm, α-decay meas., daughter energy levels *(Russian)* 77−82882
Cs, A=114-118, neutron deficient isotopes, half lives, β^{+},γ, delayed p and α meas. 78−70489
^{114}Cs, neutron deficient isotopes from ^{58}Ni(^{58}Ni,xpyn), alpha decay studies 79−93567
^{116}Cs, delayed particle emission in β^{+} decay 78−8778
^{118}Cs, delayed particle emission in β^{+} decay 78−8778
^{251}ES decay, ^{247}Bk proton states, transitions and spectroscopic factors 79−89224
^{253}Es, coupled-channel α-decay theory 78−17156
^{255}Fm, coupled-channel α-decay theory 78−17156
^{A}Fr, A=201-203, alpha decay, branching ratios, mass excess and half life 80−99154
^{146}Gd region, proton subshell effects from α-decay and spectroscopy, self-consistent study 80−57748
Hf, alpha decay studies of the isotope 79−63636
^{178}Hf, decay of highly excited states using (n,α) reacts. *(Russian)* 79−9526
^{A}Hg, A=177-183, 188, alpha decay, half lives, decay energies and branching ratios 79−45215
^{A}Hg, A=181-185, α-decay, Pt rot. states and moments of inertia staggering 78−89779
^{A}Hg, A=182-184, alpha decay branching ratio 80−57749
^{185}Hg decay, ^{181}Pt ground state spin 77−22968
^{152}Ho α-decay and branching ratio 79−89241
^{A}I, A=110-113, neutron deficient isotopes from ^{58}Ni(^{58}Ni,xpyn), alpha decay studies 79−93567
^{A}Ir, A=169, 170, decay characteristics 79−503
^{170}Ir, prod. in Cu induced reacts., decay characteristics 77−82961
^{7}Li→αt virtual decay vertex constant from (d,t), (p,α) 80−78231
^{8}Li(β)^{8}Be*(α)α, obs. of ^{8}Be state at ~6 MeV 78−93938
^{A}Lu, A=158, 159, alpha decay and gamma transitions 80−73827
^{157}Lu, short lived α emitter, α energy, $T_{1/2}$ and branching ratio 80−501
Mg, giant quadrupole resonance states α decay to ^{20}Ne ground state 78−37323
^{24}Mg 6_3^{+} level, α and γ decays, branching ratios from ^{12}C(^{16}O,α) 79−75901
Na neutron rich isotopes, β-delayed emission of n, 2n, α, t 78−74343
^{20}Na, positron decay, β-α ang. correl. meas. 77−46138
^{20}Ne, α decay from 8p-4h O^{+} state, branching ratios 78−50132
^{20}Ne cluster struct., coupled channel orthogonality condition model, α-decay, excited states, transitions 79−97681
^{20}Ne high spin states, J$^{\pi}$ and α-decay branching ratios from ^{16}O(^{12}C,^{8}Be) 80−18166
^{20}Ne→α_0+^{16}O, exam. of high spin states in ^{20}Ne 78−50066
^{58}Ni, isoscalar giant quadrupole reson., decay modes 79−63649
^{58}Ni(e,e′α), electric quadrupole giant resonance α-decay *(Russian)* 79−85434
^{237}Np α-decay, ^{233}Pa excited level scheme and γ-transitions 79−80876
^{237}Np, quasi-stationary state decay through two bump barrier *(Russian)* 80−13420
^{16}O, α-decay from excited states produced in ^{16}O(^{12}C,^{12}Cα)^{12}C 78−50189
^{16}O high spin states, J$^{\pi}$ and α-decay branching ratios from ^{12}C(^{12}C,^{8}Be) 80−18166
^{16}O highly excited states from ^{12}C(^{6}Li,d), spin, parity, decay into α+^{12}C 77−79395
^{16}O isoscalar giant quadrupole resonance, α-decay dominance from ^{16}O(α,α'+charged particle) 78−46035
^{16}O+^{58}Ni, 6 MeV/N, pre-equilib. α-emission 77−82883
^{16}O→α_0+^{12}C, exam. of high spin states in ^{16}O 78−50066
^{17}O α-cluster states, α-decay orbital momenta and parities from ^{13}C(^{6}Li,d) and α-decay *(Russian)* 78−86486
^{171}Os, alpha decay, half lives, decay energies and branching ratios 79−45215
^{A}Pa, A=215-218, 222, α-decay half life and energies from ^{151}Ta+^{40}Ar and ^{184}W+^{40}Ar 79−45216

alpha-decay continued
^{231}Pa α-decay, γ-rays and internal conversion spectrum, ^{227}Ac levels and bands 79−45217
Pb region, comparison with α-transfer data 77−334
^{A}Pb, A=183,184, alpha decay half lives 80−57749
^{192}Pb anomalous α-decay rate 79−67721
^{208}Pb(^{16}O,^{12}C)^{212}Po and α-decay, comparison for α-transfer reaction mechanism 79−6652
^{208}Pb(^{6}Li,d), 90 MeV, alpha-cluster transfer from alpha-decaying nuclei 80−91166
^{208}Pb(d,^{6}Li) ^{204}Mg, SS MeV, levels and spectroscopic factors, α clustering, DWBA anal. 79−67694
Po in mica, anomalous haloes origin 79−44186
Po light isotopes, α-decay width calcs., Feshbach theory 78−89829
^{194}Po, prod. in ^{182}W(^{20}Ne,xn) reactions 78−8835
^{208}Po, L-shell ionisation in α-decay 78−78324
^{210}Po, alpha-decay, population of 0^{+} of ^{206}Pb 80−22775
^{210}Po, α-decay inner shell ionis., L-electron-alpha ang. correlation 77−34267
^{212}Po, isomer with spin and parity 8^{+}, α- and γ-decay 78−82283
^{212}Po, surface α-clustering and α-decays 79−75926
^{214}Po, half life of α-emitting excited 0^{+} state 79−45205
^{A}Pt, A=173-179, 188, alpha decay, half lives, decay energies and branching ratios, rot. struct. 79−45215
^{A}Pt, A=178,179, alpha decay branching ratio 80−57749
^{188}Pt α-decay energy and branching ratio 79−22237
Pu, alpha-energy and mass analyses, using single sample mount 78−15744
^{237}Pu α-decay, ^{233}U levels, bandheads, total α-branching and transitions 79−93516
^{238}Pu, α-activity, half-life 77−54193
^{238}Pu half-life determ. 77−22965
^{239}Pu, α-decay half-life by two independent methods 77−82881
^{239}Pu, calorimetric determ. of half-life 79−26405
^{239}Pu, cross sections for α-decay and neutron induced fission *(Russian)* 79−17944
^{239}Pu, half life determ. by isotope dilution mass spectroscopy of ^{235}U 79−26409
^{239}Pu half life meas. by calorimetry, mass spectrometry and α-particle counting 79−26403
^{239}Pu, half-life determ. from α-emission rates 79−26407
^{239}Pu, half-life determ. specific activity meas., mass spectroscopy of ^{235}U daughter growth 79−26408
^{239}Pu, half-life determ. using isotope dilution mass spectroscopy and α-specific activity meas. 79−26410
^{239}Pu, specific power and half-life, calorimetric determ. 79−26406
^{239}Pu, subparticle formation expt. 79−6520
^{239}PuO$_2$, fragmentation of respirable particles in water by alpha decay 77−56487
^{240}Pu, α-decay meas., daughter energy levels *(Russian)* 77−82882
^{240}Pu, half life and specific activity by α-counting 79−502
^{241}Pu half life from α-spectrometry and ^{241}Am ingrowth 80−68609
^{242}Pu half life relative to ^{238,239}Pu, α-activity and atom ratios 80−5100
^{242}Pu, half-life meas. 78−17154
^{242}Pu halflife from precise low-temp. heat capacity meas. on PuF$_3$, PuF$_4$, PuO$_2$ 77−2952
^{244}Pu, in minerals, haloes prod. by alpha particles 77−29300
^{223}Ra decay chain, precise γ-ray spectroscopy 77−54175
^{225}Ra rotational band level diagram from α-decay and conversion electrons 80−18156
^{228}Ra-Be (α,n) source, neutron spectrum calc. from angular distrib. and cross-section data 78−41882
Re, alpha decay studies of the isotope 79−63636
^{A}Re, A=166, 167, 168, α-branching ratios, decay characteristics 79−503
Rn, meas. with electronic cups, U exploration appl. 78−7781
^{199}Rn and ^{199}Rn^{m} alpha decay signatures from ^{169}Tm(^{35}Cl,5n) 80−68610
^{28}Si α-doorway states in α-decay to ^{24}Mg low lying K-band 80−47438
Ta, alpha decay studies of the isotope 79−63636
^{A}Te, A=107-110, neutron deficient isotopes from ^{58}Ni(^{58}Ni,xpyn), alpha decay studies 79−93567
^{A}Te, A=108,109, neutron deficient isotopes, new island of α-emission 79−6521
^{A}Th, A=212, 213, 214, decay energies and half lives from ^{176}Hf(^{40}Ar,X) 80−47440
^{230}Th alpha-decay half life from specific activity method 80−102157
^{230}Th α-decay, search for the K$^{\pi}$=0^{+} excited states in ^{226}Ra 78−86504
^{231}Th, rotational band level diagram from α-decay and γ-transitions 80−18156
^{232}Th, α-decay half-life, liq. scintillator expt. for students 78−12496
^{44}Ti, lowest T=2 state decay, branching ratios from ^{46}Ti(p,t) 42 MeV 78−78304
^{186}Tl, α-decay, half-life meas. 77−79343
^{153}Tm, short lived α emitter, α energy, $T_{1/2}$ and branching ratio 80−501
U and Th in rocks, abundances via fission/α technique 77−29497
U in natural samples, alpha-emitting nuclei recoil rel. to U series disequilibrium 79−16466
U, thick target corrections for charged particle spectra 80−37714
^{230}U decay chain, γ-ray single and coincidence meas., internal conversion spectra obs. 77−6319
^{232}U half-life from specific and relative activity methods 80−9270
^{232}U→^{212}Pb decay chain, obs. of collective states fed by weak α-transitions 78−8786
^{233}U alpha-decay, γ-spectra and ^{229}Th levels 77−26636
^{235}U α decay and ^{231}Th β decay, γ-radiation study, energy level scheme *(Russian)* 78−17160
^{235}U, cross sections for α-decay and neutron induced fission *(Russian)* 79−17944
^{235}U, radioactive series decay, computer simulation 80−102160
^{238}U, radioactive series decay, computer simulation 80−102160
W, alpha decay studies of the isotope 79−63636
^{260}X$_{105}$, prod., L X-ray spectra, decay 78−8780
$^{228}_{126}$X, primordial and other nuclei, shell model calc. 78−8752
^{A}Xe, A=111-113, neutron deficient isotopes from ^{58}Ni(^{58}Ni,xpyn), alpha decay studies 79−93567
Yb, A=153-158, neutron deficient isotopes, daughter products, α-decay, halflives 78−21533
^{A}Yb, A=158, 159, alpha decay and gamma transitions 80−73827
Zn to Ni even isotope transition, α-particle spectroscopic factors, shell model calcs. 79−6385

alpha-decay theory
see also alpha decay
A=16-40, α-spectroscopic factors between ground states, shell model prediction 79−13204
antisymmetrisation in α-decay and α-transfer based on cluster representation 78−86514
bound α-particle motion in α-decay, comment on various functions 78−86515
cluster preformation coeffs. and level densities 77−71579
complex energy eigenvalue theory 78−41678
conference on nuclear physics, Mikolajki, Poland (2-14 Sept. 1979) 80−101662
consistent theory for nuclear α-decay, appl. to Po isotopes 77−61389
Coulomb repulsive energy, as cause of or barrier to α-decay 78−66253
decay widths, alpha particle struct. effect 78−62513
α-decay without tunnelling, α-decay radius, even-even α-emitters 77−74812
deformed and superdeformed nuclei from heavy ion reactions, α-decay amplification 80−102156
even-even nuclei with collective oscillations, surface probabilities of α-particle formation *(Russian)* 78−41677
exchange effects in radioactive decay theory based on many body scatt. 79−9525
exclusion principle effects, significant separation distance 79−6518
Feshbach theory of nuclear reactions, α-decay width calcs., light Po isotopes appl. 78−89829
generator coord. method, Gamov states 77−14075
heavy nuclei, alpha cluster formation at and outside nuclear surface 80−63138
heavy spherical nuclei, choice of density depend. interaction and α-decay *(Russian)* 78−46010
internal pair production, probability 79−71821
light nuclei, α-spectroscopic amplitudes, jj coupling and isotopic spin formalism 77−14072
one-body alpha-decay widths and resonance states 79−13259
pair production probability estimate 78−13036
parity nonconservation, asymmetric α-emission in polarised nuclei decay 79−6379
preformation of α's in even-even nuclei, without tunnelling approach 77−30524
preformation probability, even-even nuclei, comparison of expt. and theoretical results 78−8784
Q-value and half-life calc. based on alpha decay as a fission-like process 79−93566
quantum mechanics, α-particle emission as violation of usual interpretation 78−62108
review *(Russian)* 79−49612
rotation signatures, rel. to nuclear deform. changes 79−13258
scission α-particles, emission mechanism 77−18516
sensitivity of alpha-decay to the real alpha-nucleus potential 79−97714
spectroscopic factors, coupled channel problem, local pots. justification 80−47439
spherical nuclei, α-decay widths calc., nuclear shell model *(Rumanian)* 77−46145
spherical nuclei, absolute α-decay widths, renormalised effective interaction contrib. in shell model 79−75925
spheroidal nuclei, barrier penetration theory in more than one dimension *(Russian)* 77−33879
spontaneous fission character of α-decay 77−79344
statistical model calcs. of α-emission from excited nuclei 78−17157
superheavy and heavy nuclei, absolute decay probability, four projectors theory, plateau model 77−14074
superheavy nuclei, α-decay lifetimes 79−36203
superheavy nuclei, alpha half-lives, alpha particle struct. effects 78−17158
superheavy region, neutron drip line, energy density mass formula extrapolation 78−93932
two-centre shell model, alpha decay widths calcs. 77−71593
width calc. in meth. not involving arbitrary channel radii 77−54192
α-preequilibrium decay, emission rate, α-preformation factor 78−41676
α-transfer to α-decaying nuclei 77−79396
e^+e^- pair production probability determ. 78−50133
^{27}Al(p,α_0), E_p=887.8 keV, blocking lifetime meas. comparison 79−59041
^{241}Am, e^+e^- pair production probability determ. 78−50133
^{212}At, ^{212}At^m, configuration mixed shell model, α-decay rate calc. 77−74814
^{212}At, nuclear field theory approach to alpha-decay, calc. of relative α-decay rates 79−45218
^{12}C, 3α system, resonating group method, α-decay width 78−50108
^{12}C, excited state struct., anomalous α-decay props. 3-cluster GCM model 79−6399
^{20}Ne, coexistence of shell struct. and cluster struct. 78−78279
^{56}Ni from HI reactions, superdeformed nucleus decay, α-decay amplification 80−68608
^{16}O, α-spectroscopic amplitudes, jj coupling and isotopic spin formalism 77−14072
^{16}O, α-spectroscopic amplitudes anal. using shell model based calc. 79−13203
^{16}O, parity violating alpha decay width 77−14073
^{16}O$\rightarrow$^{12}C+α, alpha spectroscopic factors, K-harmonics method 78−62512
^{209}Po, 125-neutron isotone, shell model alpha decay theory 77−18483
^{210}Po effect of renormalisation of effective interaction on ground state wave functions *(Russian)* 77−284
^{210}Po, nucl. alpha decay, electron inner shell vacancy creation, semi quantal approach 80−68607
^{212}Po, shell model α-spectroscopic factors 80−32245
^{213}Ra, 125-neutron isotone, shell model alpha decay theory 77−18483
^{211}Rn, 125-neutron isotone, shell model alpha decay theory 77−18483
^{149}Tb from HI reactions, superdeformed nucleus decay, α-decay amplification 80−68608
Z, from ^{12}C(^{6}Li, d)^{16}O(α)^{12}C 77−82880

alpha-particle absorption
fusion plasma prod. by laser, penetration length of alpha particles 77−15214
range-energy relations and stopping power in tissue equivalent liquid 80−23275
stopping power of liquids for alpha particles, meas. apparatus 80−88224

alpha-particle absorption continued
water, ice and vapour, stopping cross section, 0.3 to 2.0 MeV 77−55313
Al, cross-section of alpha particles slowing down, stopping power *(Russian)* 77−80560

alpha-particle angular distribution
see also alpha-particle spectra
α-clustering studies, role of angular correl. anal. 78−634
elastic scatt. at 100, 140 MeV, Fraunhofer diffr. oscills., refractive damping anal. 77−61445
fusion reactors, blister-induced first wall erosion, alpha incident velocity and poloidal angle distribs. 80−37583
laser fusion targets, spatially resolved α-emission 77−68811
light nuclei, backward scatt. and heavy-particle stripping 78−13107
(α,α), critical energies, ang. distrib. energy depend. semiclassical theory 79−76007
(α,α'), γ-α ang. correls., theoretical description including delay effects *(Russian)* 77−34329
^{18}0(γ,σ_0), 19-32 MeV, E1 and E2 cross section, E1-E2 phase difference 80−63172
^{27}Al(α,α'), 145 MeV, excitation energy anal., octupole strength conc. 78−21584
^{197}Au+^{32}S, 373 MeV, in-plane ang. correls. between α and residue heavy ions 78−46101
^{10}B(t,α)^{10}B, 0.5 to 1.25 MeV, excitation functions and ang. distribs. 78−17216
^{10}B(t,α)^{9}Be, 0.5 to 1.25 MeV, excitation functions and ang. distribs. 78−17216
^{11}B(n,α)^{8}Li, 14.4 MeV, spectra and ang. distribs., recoil nucl. transitions 78−17193
^{11}B(p,3α), E_p=2 to 4 MeV, energy depend. of interference phenomena 78−13084
^{9}Be(^{3}He,α)^{8}Be(O), reaction mechanism and isoscalar giant resonances in C^{12} *(French)* 78−78341
^{9}Be(d,α_0)^{7}Li, 0.9 to 2.5 MeV, ang. distribs. 77−18573
^{9}Be(d,α_1)^{7}Li*, 0.9 to 2.5 MeV, ang. distribs. 77−18573
^{9}Be(d,α)^{7}Li 12.17 to 14.43 MeV, α ang. distribs., excitation functions 78−54770
^{9}Be(p,α)^{6}Li, α ang. distrib. determ. by Doppler γ-line broadening method 77−61407
^{209}Bi(α,X), 69.2, 140 MeV, scatt. and fission reaction mechanisms, cross sections 80−18350
^{12}C(^{16}O,α)^{24}Mg, 13.7, 14.2, 14.7 MeV, ang. distribs., intermediate resonance struct. 79−13331
^{12}C(^{3}He,α)^{11}C, 11 MeV, multistep mechanism, CCBA calcs. 78−41734
^{12}C(^{9}Be,α) at 11.4 MeV c.m. energy 80−9302
^{12}C(α, $\alpha'\gamma$) γ angular correlation function obs. *(Russian)* 79−13246
^{12}C(α,α), 2$^+$ collective level excitation, microstruct. of diffr. ang. distrib. 77−61440
^{13}C(^{6}Li,α)^{15}N, 32 MeV, ang. distrib. meas., zero-range DWBA calc. 78−13155
^{A}Ca(α,α), 40-62 MeV, A=40,44, elastic and inelastic, ang. distribs. and collective state excitation 79−6650
^{40}Ca(α,α), 36-61 MeV, large angle struct. 78−41743
^{40}Ca(α,α), E_α=27.2 MeV, ang. distrib. meas. 78−13120
^{44}Ca(α,α), 36-61 MeV, large angle struct. 78−41743
^{54}Fe, surface structure analysis using Blair phase shifts 78−12959
^{56}Fe, surface structure analysis using Blair phase shifts 78−12959
^{56}Fe(α,α), 2$^+$ collective level excitation, microstruct. of diffr. ang. distrib. 77−61440
^{58}Fe, surface structure analysis using Blair phase shifts 78−12959
^{3}He(^{4}He,^{4}He)^{3}He, 20-26 MeV, elastic scatt., ang. distribs. and excitation functions *(Russian)* 77−327
^{180}Hf(α,α'), 21, 24 MeV, ang. distrib. meas., sensitivity to excited-state quadrupole moments 77−88158
^{42}K, levels, studied by ^{44}Ca(d,α)^{42}K reactions, 11 MeV, DWBA analysis 78−8723
^{6}Li(d,α), (d,p), simultaneous determ. of p and α particle ang. distribs., cellulose nitrate detector 79−737
^{6}Li(n,α)^{3}H, 23 keV cross section, absolute meas., ang. distribs. 80−18305
^{7}Li(α,α), microscopic study of elastic scatt. 77−88156
^{7}Li(α,α) at 2, 4 and 7 MeV, ang. distribs. calcs., 2α+t system model 78−50110
^{24}Mg(α,α), 2$^+$ collective level excitation, microstruct. of diffr. ang. distrib. 77−61440
^{15}N(α,α), E_α=16-23.7 MeV, differential cross sections, ang. distribs. and excitation functions 78−13121
^{20}Ne states, J^π, differential cross sections and ang. distribs. from ^{16}O(α,α') 80−18203
^{60}Ni(e,α)e$'$X, alpha particle spectra, statistical model calc., direct reaction component 78−41704
^{16}O+α nucleon exchange and backangle anomaly 79−6638
^{208}Pb(^{3}He,α)^{207}Pb, 70 MeV, deephole states, $T_>$=45/2 components 78−82362
^{208}Pb(α,α'), 96 MeV, ang. distribs., breathing mode states, DWBA calcs. 78−50183
^{208}Pb(p,α), 20 MeV, ^{3}H pick-up, $^{205}\pi$ transition strengths and ang. distribs. 79−13271
^{210}Po, α-decay inner shell ionis., L-electron-alpha ang. correlation 77−34267
^{192}Pt(α,α'), 24 MeV, α-angular distrib. for 0^+, 2^+, $2^{+\prime}$, 4^+, $4^{+\prime}$ and 3^- state excitation 78−70550
^{34}S(p,α)^{31}P, 35.5 MeV, DWBA, coherence effects 77−38271
Sb(t,α), A=121, 123, ang. distrib. at 12 MeV, DWBA anal. 78−62546
^{80}Se(d,α)^{78}As, 16.0 MeV, levels of ^{78}As 78−8827
Si, ang. distribs. of 6.6 MeV protons, 12.5 MeV deuterons, and 24 MeV α-particles 78−29720
^{28}Si(α,α), elastic and inelastic scatt., compound nucleus contrib. anal. 78−37356
^{144}Sm(α,α'), 96 MeV, ang. distribs., breathing mode states, DWBA calcs. 78−50183
^{147}Sm(n, α)^{144}Nd, 12 to 18 MeV, energy and angular distribution of α-particles, statistical, pre-equilibrium and knock-on models 80−13477
^{159}Tb(^{14}N,X), 95 MeV, fast α-particle ang. distribs. 80−63207
^{173}Tm level and band struct., spin assignments, ang. distribs. from ^{176}Yb(p,α), 16 MeV, ^{173}Tm level and band struct., spin assignments, ang. distribs. 79−474
^{233}U(α,X), 28-140 MeV, scatt. and fission reaction mechanisms, cross sections 80−18350

alpha-particle angular distribution continued
^{236}U fission, quasistatic scission configurations obtained from long range particle accompanied fission distributions 78—74411
^{A}Zn(α,α'), 18 MeV, A=64,66,68,70, compound and precompound α emission spectra 78—82367
^{A}Zn(p,α), 12.5 MeV, A=64,66,68,70, compound and precompound α emission spectra 78—82367
^{68}Zn(α,α), 2^{+} collective level excitation, microstruct. of diffr. ang. distrib. 77—61440

alpha-particle attenuation *see alpha-particle absorption*

alpha-particle detection and measurement
see also alpha-particle spectrometers; radioactivity measurement
air ionisation probe for α, β, γ hand and shoe monitor 80—58084
air monitoring system for α-activity and nuclide specific noble gas meas. 80—63408
air pollution control at Nuclear Research Institute *(Czech)* 78—88906
air-luminescence in liquid scintillation spectrum 79—36479
airborne radioactivity meas. in HFEF/N 80—18687
alpha spectral line intensity gauge using semiconductor detector *(Italian, Spanish)* 78—86716
angular distrib. meas. with positron sensitive detector 80—27899
bidimensional spectra and ang. correlation for the ^{7}Li(d,$\alpha\alpha$n) reaction, 7.0 MeV 78—82357
biological and ecological samples *(French)* 78—5052
cellulose acetate solid state track detectors, catalytic oxidation sensitization *(Chinese)* 80—102399
cellulose acetate solid state track detectors, swelling sensitisation *(Chinese)* 80—99422
cellulose nitrate, detection efficiency and alpha-particle range 77—10540
cellulose nitrate, energy loss critical rate 80—74082
cellulose nitrate, sensitivity to α-particle registration 78—17498
cellulose nitrate α-particle detector for Rn short lived daughters, results and calibration *(Czech)* 78—62663
cellulose nitrate emulsion, sensitivity and efficiency for α-particle detection 78—13380
cellulose nitrate emulsion for α-particle track relocalisation 78—17480
cellulose nitrate layer, α-particle autoradiography 78—17499
cellulose nitrate nuclear track detectors, energy resolution enhancement for alpha particle detection 80—91392
cellulose nitrate thin foil manufacture for α particle track detector *(Spanish)* 80—74091
cellulose nitrate track detector, simultaneous determ. of p and α particle ang. distribs., (d,α) and (d,p) reactions 79—737
cellulose nitrate track detectors, CA80-15 and LR-115, etch pits due to Rn and Tn alpha particles 78—855
cellulose nitrate track detectors, detect. of efficiency and range meas. of alphas and protons 78—17524
cerenkov counter for spacecraft application 78—86734
cloud chamber, low-pressure tissue-equivalent gas for α-particle tracking 80—9462
coincidence meas. of α, X, and γ-rays 79—26851
computer program for α-spectrum anal. 78—29692
condenser microphone as ionisation chamber for intense α fluxes 77—79506
controllable secondary electron emission method for particle detection 77—30711
coral, alpha emitter analysis by solid-state track detect., Bikini lagoon 78—53661
corona flow counter, multi-filament *(Slovak)* 78—55094
corona streamer counter appl., performance appl. 78—25402
corona-streamer counter, performance characts. 79—9962
counting chamber, for use with surface barrier detectors 78—873
detection probabilities using surface barrier detectors for alpha-decay-chain members 79—76315
determ. of bulk α and β radioactivity *(Rumanian)* 79—88346
diacel plastic track detector, threshold energy for alpha-particles 79—59312
diacel solid state track detector 79—750
diamond, elec. props and performance for α- and β-particles 79—36481
diamond detector use as immersed α counter 77—54461
diamond detectors, use as immersed alpha-counters 77—54432
dosimeter, aq. coumarin soln. response to high LET radiation from ^{10}B(,nα)^{7}Li reaction 78—24149
dosimetry, ion pair formation, depend. of average energy on atomic number 80—18695
drift chamber with thin foil cathodes 77—83463
electronic alpha cups for U exploration 78—7781
emulsion layers, α-irradiated, processing by iron oxalate developer *(Russian)* 78—50443
energy loss measurements for slow particles, 0.01 to 1.0 MeV, multiple scatt. corrections 80—95511
fission product and actinide adsorption on silica gel, for urinary gross α activity determ. 79—88155
free air ionisation chamber, mean level response for α-rays 78—90024
glass detectors, appl. to α-particle and fission fragment ranges in air 79—45597
heavy element superficial mass meas. by elastic α-particle scatt. *(French)* 79—61927
imaging alpha detector, radioactive contamination monitoring appl. 80—102384
ionisation chamber with solid Ar 77—30720
IR spectroscopy appl. to charged part. dose meas. in cellulose triacetate 78—94145
Kodak LR 115 dielec. track detect., applicability as α-particle detector *(Czech)* 79—8711
laser-produced thermonuclear alpha particle pinhole imaging 77—67934
liquid scintillation alpha counting and spectrometry , appl. to bone and tissue samples 77—25617
liquid scintillation alpha-particle assay with energy and pulse shape discrimination 77—23350
low energy α and proton spectra, simultaneous detect. *(Russian)* 77—50332
magnetic spectrom. with position- and cutting angle-sensitive detectors, ang. distrib. reconstruction 78—70687
Makrofol-E polycarbonate detectors, liq. N_2 enhancement of α-particle tracks 77—67946
mean ionising cross-section and charge produced, meas. method 78—78577
microprocessor controlled long lived alpha emitter monitor 80—58069
minerals, radiography of geological specimens for determ. of α- and fission-activity 78—20540
modern atomic and nuclear physics (book) 80—11
monitoring system for alpha-in-air, real-time 80—23155
multielement α-spectrometry for individuals and environment monitoring 80—58024
NE-111 thin homogeneous scintillator foils, alpha particle energy loss and straggling 77—83472
nuclear reactor irradiated fuel, anal. of α-emitting isotopes through laser micro-boring 80—37444
on-line radiation monitoring at a nuclear fuel reprocessing plant 80—95469
parallel plate avalanche counters, simple accurate method for bidimens. position readout 78—21822
parallel plate avalanche counters for registration of light charged particles 80—91369
personal dosimetry instrument for airborne radon daughter meas. *(French)* 80—57989
phosphate fertilizer, specific activity of U and Th rel. to particle size 80—106244
plastic detectors, appl. to α-particle and fission fragment ranges in air 79—45597
plastic foils, automatic spark counting of α-tracks 77—79524
plastic scintillator, in nanosecond time of flight system for fast neutron scatt. expts. 77—6604
polycarbonate foil, α-particle track prod., electrochemical etching 80—52825
portable alpha survey instrument 79—22535
position-sensitive detectors, use of the SnO_2-Si heterotransition 80—91375
pressure gauge, exptl. accuracy *(Japanese)* 78—58537
proportional low-pressure chamber with high space resolution 78—870
pulse shape discrimination for alpha-gamma separation with trans-stilbene 78—13386
radionuclide radiation precision spectrometry using semiconductor detectors *(Russian)* 79—31305
range, energy and range straggling, stopping power meas. 78—73815
range-energy relations and stopping power in tissue equivalent liquid 80—23275
real-time environmental α-β-γ radiation monitoring system 78—94152
REM ratemeter for direct reading of dose equivalent rate 78—53502
scintillation counters, temperature characteristics of α-datum stabilizers 79—26808
scintillation kinetics in condensed Xe 79—26828
self-scanning photodiode array for fast ion detection 80—87018
self-triggered liquid xenon drift chamber by the use of proportional ionization or proportional scintillation 79—45562
self-triggering wide-gap spark chambers for recoil alpha-particles 77—30710
semiconductor, ion-doped, coordinate detector 79—26825
semiconductor radiometer-spectrometer for meas. of surface contamination by α-radioactive materials 77—38423
smear samples, simple and rapid meas. of α-rays using air luminesc. 80—106243
solid state nuclear track detectors, ^{222}Rn and ^{220}Rn meas. 78—25396
solid state nuclear track detectors, alpha sensitive plastic films for Rn gas conc. meas. 80—94618
solid state track detector for differential alpha radiography of actinide solutions 80—71932
solid state track detectors in solutions of actinides, α track registration 80—63486
solid-state track detectors, international α-particle registration intercomparison 78—17497
solutes in liquids, conc. determ. by (n,α) and (n,γ) reacts., scintallation counting 80—35602
spark counting of α-radiograms recorded on LR-115 strippable cellulose nitrate film 79—26859
SSNTD, alpha sensitive plastic detectors for Rn gas conc. meas. 80—94617
stack monitoring of long-lived α-emitters, review of meas. techniques 79—48195
stopping cross-sections determ. for N_2, H_2, CH_4, C_4H_{10}, C_3H_6 79—49917
superheavy elements, search for high energy α-particles 79—59040
surface-barrier Au(Si) detectors, protective glass walls 80—91374
thick sample total counting, review 79—36488
thick target corrections for charged particle spectra 80—37714
thin dielectric track detector as particle discriminator, α dosimetry appl. 78—17511
TOF spectra using channel plates 77—14305
TOF spectrom., intrinsic time resolution of detectors 78—849
trajectory detector for meas. of short lived activity by decay in flight 80—27867
transuranic aerosol measurement system and its field results 80—58068
working level survey meter 3R-WL, meas. of α-particles from ^{218}Po and ^{214}Po 78—25330
Z>103 transactinides, method for rapid separation and identification 77—26952
α-emitting effluents from nuclear processing plant, detection and meas. 80—95468
Ar gas, high press., recombination luminescence in scintillation induced by alpha particles 78—50441
Ar, liquid, scintillation decay due to α-particles and electrons 78—55099
Ar+10% CH_4, Fano factor determ. from α-particle pulse height distribs. 79—76284
$CaSO_4$:Dy, α and γ thermoluminescence response comparison 79—85814
$CaSO_4$:Dy thermoluminescence sensitivity and glow curves, 700° to 1300°C 79—85815
Cu foils, activation by p, d, ^{3}He, ^{4}He from cyclotron beam, monitoring props. 77—38578
D(^{3}He, α)H, background reduction in depth profiling expts. using electrostatic deflector 79—14841
GaAs radiation detector, characteristics 79—68139
Li isotope composition determ., α prod. by d bombardment 79—7029
LiF thin layers, effect of LET on thermolum. props. 78—73255
Ni foils, activation by p, d, ^{3}He, ^{4}He from cyclotron beam, monitoring props. 77—38578
Pb poisoning in human teeth, determ. using alpha-sensitive plastic track detector 80—94433

alpha-particle detection and measurement continued

- ^{210}Po determ. in air, radiochem. separation and α-counting method 78-73113
- Pu, alpha-energy and mass analyses, using single sample mount 78-15744
- Pu low-background assay equipment, liquid scintillation detector, sample changer, electronics 77-54474
- Pu-Am survey instrument, β-α-γ-X-ray scintillation detect. probe 78-33376
- ^{239}Pu alpha particle tracks on polycarbonate foils 79-76310
- ^{239}Pu, half-life determ. from α-emission rates 79-26407
- ^{239}Pu, half-life determ. using isotope dilution mass spectroscopy and α-specific activity meas. 79-26410
- ^{226}Ra, alpha scintillation counter for determ. of low natural conc. 80-9456
- ^{226}Ra, determ. of tap water pollution *(Czech)* 79-34675
- ^{226}Ra source leakage testing by mailed track detector method 77-60264
- Rn daughter airborne conc. meas. in atmosphere 80-37636
- Rn daughter products, ionisation large area gridded chamber appl. 78-49128
- Rn daughter time-integrating environmental TLD dosimeter 79-67962
- Rn daughters in air, conc. meas. by α-spectrom. 78-32218
- Rn daughters in air, precision alpha counting methods 77-57841
- Rn detection, effect of humidity 77-6647
- ^{222}Rn, alpha scintillation counter for determ. of low natural conc. 80-9456
- ^{222}Rn concentration meas. by plastic detectors to determ. environmental α-emitters from natural sources 80-91292
- ^{222}Rn gas detection using Track Etch system for U exploration 80-98488
- ^{222}Rn low conc. meas. in air, α-scintillation method 78-92970
- ^{222}Rn progeny, air conc. meas. by α-particle spectrometric counting 79-68171
- Si detector, α-particle dense track charge losses 77-3233
- Si detector, energy response differences for p and α particles 79-6805
- Si detector, ionisation energy for channelled 160 MeV α-particles 78-62680
- Si diffused junction detector for alpha air monitoring instrumentation 80-58083
- Si diode with pulse height analyser as alpha-detector *(Danish)* 77-18732
- Si gate spectrum, alpha lines, empirical eqn. for broadening and asymmetry *(Spanish)* 79-63859
- Si heavy ion surface barrier detector, plasma delay times, electron backscattered from fission fragment or alpha particle 80-58095
- Si junction detectors, low noise, fabrication 80-52820
- Si surface barrier detectors, dE/dx thin detector technology, n$^+$ layer electrolytic removal *(Russian)* 77-57823
- Si surface barrier detectors, direct meas. of plasma delays due to fission fragments and α-particles 78-58546
- Si surface barrier detectors, meas. of plasma delay differences due to ^{252}Cf fission fragments and α-particles 78-58547
- p-Si surface barrier detectors, charact. meas. *(Bulgarian)* 78-82592
- Si surface barrier detector, operation in nitrate solns. 79-63873
- Si:P, B, α-particle spectrum fabrication by ion implantation 78-33373
- $ThBr_4$, inorganic scintillator, use in nucl. and accelerated particle detection 78-58540
- Tn daughter products, ionisation large area gridded chamber appl. 78-49128
- U activity, liquid scintillation counting 80-27873
- U content in solid waste mats. using α-particle detectors, two layer proportional counter *(Russian)* 80-27904
- U ore detection, using trace detection sensitive to ^{222}Rn α-particles *(Hungarian)* 78-77339
- U, specific α radioactivity meas. rel. to size using aerosol centrifuge 79-76255
- Xe filled proportional scintillation detector for charged particles 80-32572
- ZnS scintillator, field monitoring of alpha-emitting contaminants in environment 78-70646

alpha-particle effects

- A-15 compounds, effect on critical temp. for supercond. of disorder, induced by α-particles 78-47897
- aerosol particle charging by α-ionizing radiation in electric field 78-11566
- alcohols, α-particle impact, 0.3-2.0 MeV, O stopping cross-sections 78-17753
- alpha-particle damage, quadrupole nucl. interactions on ^{73}A nuclei, TDPAC meas. 77-36160
- anthracene:tetracene crysts., mag. field modulation of scintillation under α-irrad. 77-48256
- anthracene, α-particle tracks, excited states, creation and evolution 78-43934
- anthracene, dissolved in toluene and cyclohexane, scintillation from α-particles, time depend. *(Spanish)* 79-99950
- anthracene, exciton sounding of α-particle induced radiation defects 77-12423
- anthracene crystals, α-particle induced scintillation, mag. field effects 80-40161
- aqueous tissue equivalent soln., alpha particle stopping power, 0.5-8 MeV 78-40334
- bacterial cells, heavy ion irrad., long range effects, comparison with γ-irrad 80-101236
- barium aluminosilicate glass coating on NbZr, d and He ion irrad., blistering 77-35605
- benzene, soln., fluoresc., quenching in pulsed proton and alpha particle irrad., radiation quality effects 80-66259
- benzophenone, aqueous system, LET depend. of transient yields in deuteron and alpha pulse radiolysis 77-63940
- bone cancer induction 78-15871
- breeding performance of female mice, comparative effects of ^{60}Co γ-rays and ^{239}Pu α-particles 80-72231
- bronchial cancer induction by α-emitting warm particles 78-96078
- t-butanol, aqueous system, LET depend. of transient yields in deuteron and alpha pulse radiolysis 77-63940
- carcinogenesis, beagle dogs exposed to ^{226}Ra and ^{90}Sr 79-66487
- carcinogenicity of inhaled air-oxidised ^{239}PuO$_2$, rat obs. 79-66492
- cell survival following multiple-track irradiation 79-66488
- charge exchange in solids, studies with Van de Graaff tandem *(French)* 79-4339

alpha-particle effects continued

- Chinese hamster cells, enhanced killing by ^{238}Pu α-particles in the presence of cordycepin 80-72233
- chromatographic support materials decomposition by ionising radiation *(German)* 78-92587
- chromosome aberrations, dose-effect relationship, population exposed to increased natural radioactivity 80-72254
- creep, irrad. induced, 60 MeV alpha particles 80-92597
- cytogenetic dosimetry, human, dose response relationship for ^{241}Am α-particle 80-30895
- diacel solid state track detector, characts. for α-particle detect. 79-750
- diamond, light ion damage, channelling investigation 80-65068
- E. coli, value of photoreactivable component after exposure to ionising radiation 80-72224
- environmental actinides, pot. carcinogenic effects 80-30780
- Escherichia coli K-12 rec and uvr mutants, LET-depend. radiosensitivity 78-15874
- ethers, α-particle impact, 0.3-2.0 MeV, O stopping cross-sections 78-17753
- fusion reactor, sputtering erosion of cavity walls, comput. procedure 77-38410
- fusion reactor brittle materials, swelling, blistering by 140 keV p, d and He ion irrads. 77-35603
- fusion reactor metals, irradiated, defect cluster nucleation, He injection effect 80-34091
- fusion reactors, blister-induced first wall erosion, alpha incident velocity and poloidal angle distribs. 80-37583
- glass, blister formation by 150 keV He$^+$ irrad., effects of gas diffusivity 77-35604
- glass for radioactive waste containment *(French)* 77-26849
- graphite, permeable, 0.6, 3.5 MeV He$^+$ irrad., surface erosion, porosity effects 77-35602
- graphite, radiation damage effect on erosion by H 78-21640
- graphite, surface erosion by 100 keV ^{4}He$^+$ and 200 keV H$_2{}^+$ 78-23569
- inhalation carcinogenesis of high-fired ^{244}CmO$_2$ in rats 80-21502
- n-InSb, surface recomb. vel., repeated cyclic surface treatment effects 77-32065
- intratrajectory reacts. in radiolysis of aq. solns. by recoil particles from ^{10}B(n,α)^{7}Li *(French)* 77-12812
- ionic crystal, ionis. energy losses and ranges of α-particles 77-47501
- IR emission under α-irrad. *(Russian)* 77-85811
- light atoms in crystal lattices, position determ. by α-particle channelling and backscatt. 79-65113
- lung, carcinogenic effect of localised fission fragment irrad., rat expts. 80-81656
- lung, late effects of inhaled ^{253}Es(NO$_3$)$_3$ in rats 80-30781
- lung, Syrian hamster, tumourigenic hazard of particulate α-activity 80-41133
- lung parenchyma irradiated by inhaled ^{238}PuO$_2$ particles, collagen localisation, Syrian hamsters 80-72252
- Makrofol-E polycarbonate detectors, liq. N$_2$ enhancement of α-particle tracks 77-67946
- mammalian cells, lethally damaged, proliferation obs. after irrad. by various particles 80-108971
- mammalian cells, transformation by α-particles 80-45968
- mammary tumour, mouse, interstitial ^{226}Ra irradiation 79-57716
- metals, stopping power for 28 MeV α-particles, re-evaluation 78-79651
- metals, stopping powers for 28.8 MeV α-particles 77-80556
- metals, stopping powers for 8.78 MeV α-particles 77-80557
- mica, alpha-particle tracks, prompt process and post effect 78-43053
- mica, giant haloes, cleavage cracks enhancing radiation damage 78-7623
- naphthalene single crystal, 4.50 MeV α bombardment, scintillation response, planar channelling, blocking *(German)* 78-6780
- PBD, dissolved in toluene and cyclohexane, scintillation from α-particles, time depend. *(Spanish)* 79-99950
- phage ϕX 174 inactivation by accelerated ions, enhancement by δ-ray effect 80-36008
- plagioclases, volcanic, α-particle dose evaluation rel. to thermoluminescence dating 80-98475
- POPOP, dissolved in toluene and cyclohexane, scintillation from α-particles, time depend. *(Spanish)* 79-99950
- PPO, dissolved in toluene and cyclohexane, scintillation from α-particles, time depend. *(Spanish)* 79-99950
- quartz, alpha particle induced radiation defects, EPR and thermoluminescence study 80-20461
- quartz, E$_1'$ centre formation and regeneration, α and γ radiation efficiency 79-32992
- quartz resonator, irradiated by alpha particles, frequency change 77-16253
- radioactive waste, Magnox, development and radiation stability of glasses for vitrification 77-61554
- rare-earth metals and oxides, very-short-lived radiation effects following Coulomb excitation 79-60411
- skin, α-irradiation, possibility of late effects, U miners 79-20584
- soft errors and oxide damage induced in LSI/VLSI cells, geometric anal. 80-59528
- steel, 0Kh16N15M3B type, He ion irradiation effect on struct. and mech. props. 78-19848
- steel, austenitic stainless, embrittled by α-particle irrad. 77-69015
- steel, stainless, He ion irrad., fracture behaviour, in-situ HV electron microscopy 80-29089
- stopping power data, air/nitrogen gaps, graphite-tissue and polythene tissue interfaces 80-26353
- superconducting films of A15 materials, α-particle induced defects 77-32101
- surface processes investigated by alpha-particle effect on electron work function 78-2547
- tissue-equivalent gases, Rossi-type, ionisation, energy dependance of $\bar{W}$ 79-6999
- tissuelike medium α trajectory heavy secondary ion ejection 80-9466
- tissuelike medium α trajectory production of δ-rays 80-9465
- Tokamak reactor, fusion-product bombardment of first wall 77-38409
- VMOS dynamic memory, 65536-bit, investigation of alpha-particle induced soft errors 80-88223
- water, liq. and vap., alpha particle stopping power, 0.5-8 MeV 78-40334
- yeast cells, elevated temp. effect on radiation sensitivity 79-79610
- Ag-In, dil., interaction between recoil implanted impurities and lattice defects, TDPAC meas. 78-39467
- Ag-Pd(Pt), dil., TDPAC exam. of radiation damage 78-39464

alpha-particle effects continued
  Al, 20 keV He^+ implantation, gas re-emission, critical dose, temp. effects 77–35596
  Al and SaP 930, 300 keV He irrad., blistering, flaking, gas re-emission 77–35601
  Al, α-particle bombarded, He bubble growth mech. 77–7774
  Al, blocking of α-particles from $^{27}Al(p,\alpha)^{24}Mg$ reaction, nuclear lifetime meas. problems 77–47500
  Al, dechannelling of α-particle by dislocation loops *(French)* 79–95056
  Al foil, irrad. under fusion reactor conditions, He bubble alignment during deform. 80–107345
  Al, foil, secondary electron emission due to α-particle irrad. *(Russian)* 80–66344
  Al foils, energy straggling, 5.486 MeV alpha-particles 77–80550
  Al sintered powder, 100 keV He ion irrad., surface erosion due to blistering 77–35600
  Al, vacancy distribution, interbonding atoms, heat peaks in scattered cascades *(Russian)* 80–39169
  Al, with He-bubbles, TEM obs. 77–4132
  Al-Ag (0.10 at.%), channelling meas. of trapping efficiencies of solute atoms for self-interstitials 79–86829
  $(Am,Cm)O_2$ solid soln., struct. changes under self- and reactor irrad. 77–27927
  $^{241}Am(OH)_3$, cryst., self-irrad. effects 77–69013
  ^{241}Am, α-radiation self-damage effect on hyperfine interaction and Debye-Waller factor, Mossbauer meas. 80–7230
  Ar, condensed, luminescence decay under α- and β-particle excitation 79–38678
  Ar, liq., α-irrad., free-ion yield, geminate recomb., track model 80–24983
  Ar, liq., α-irrad., geminate recomb. of charges, hot electron thermalization length 80–20266
  Ar, liq., α-particle excited carriers, geminate recombination 78–34876
  Au, foil, electron spectra from α-particles and fission products 77–24918
  $BaTiO_3$, ferroelectric semicond. anomalous photovoltaic effect due to ionising radiation 80–29437
  Be sintered powder, 100 keV He ion irrad., surface erosion due to blistering 77–35600
  C, pyrolytic, 0.6, 3.5 MeV He^+ irrad., surface erosion, porosity effects 77–35602
  $^{13}C/^{12}C$ isotope fractionation of organic matter assoc. with U ores induced by alpha irradiation 79–57932
  $CaTiSiO_5$, sphene, α decay radiation damage, effect on track etching characts. 78–65435
  cancer risk from $^{239}PuO_2$, max. permissible conc. in air 79–25108
  Cd, recovery after 6.1 MeV α-particle irradiation at 4.2K 78–47441
  Cd, stage III recovery, after α-particle irradiation 77–27924
  Cd:^{116}Sn, quadrupole interaction, radiation damage effects 78–43752
  CdTe, thin film, stopping power for protons and alpha particles, proton energy straggle values 77–89489
  CmO_2, struct. changes under self- and reactor irrad. 77–27927
  $^{244}Cm(OH_3)$, cryst., self-irrad. effects and lattice parameters 77–69013
  Cu, irradiated with protons, α-particles and C ions, increase of elec. resist. meas. 77–84808
  Cu surface, 1-25 keV irrad., range profiles, reemission, blistering 78–38758
  Cu-Be (0.25 at.%), channelling meas. of trapping efficiencies of solute atoms for self-interstitials 79–86829
  Cu_2O, radiation damage 77–84809
  $ErRh_4B_4$, superconducting and mag. transitions, alpha particle irradiation damage effects 79–60954
  Fe-Cr-Ni, α-particle induced precip. and phase instability 79–1470
  Fe_3C, alpha-particle irrad., Mossbauer study of nucl. reaction aftereffects 80–40015
  Ge, in mag. field, radiative electromagnetic effect 78–10434
  Ge single cryst., radiation piezoelec. effect 78–19419
  Ge:O ion implanted, O localisation determ. 79–95040
  He^{2+} 650 MeV beam relative biological effectiveness as function of depth 80–26281
  n-InSb, surface recomb. velocity, temp. and α-bombardment dose effects 77–8173
  KCl, ion bombard., damage profiles, track effect anal. 77–15465
  KCl:Tl and KCl, F-centre production by positive ions and X-rays 78–38760
  LiF, high-energy particle bombard., F-centre creation, optical meas. and model 77–47497
  Mg-Ag (0.18 at.%), channelling meas. of trapping efficiencies of solute atoms for self-interstitials 79–86829
  MnO, alpha-particle irrad., Mossbauer study of nucl. reaction aftereffects 80–40015
  Mo, 29 MeV α-particle irrad. in He, micropore and dislocation loops form. 79–14859
  N_2, electric breakdown in long high-voltage gaps with gamma and alpha particle irrad. 79–18993
  $NH_4H_2PO_4$, α-particle bombard. effects, circular crater form. 77–59051
  NaOH, aqueous system, LET depend. of transient yields in deuteron and alpha pulse radiolysis 77–63940
  $Na_2ZrSiO_5:Ln^1,Ln_2$, scintillation, α-excited *(Russian)* 79–28841
  Nb, blistering *(Russian)* 78–18686
  Nb blistering by 5-15 keV He ions, dose rate and temp. effects 77–35595
  Nb, polycrystalline, 10 to 1500 keV $^4He^+$ irrad., blister skin thickness, meas.-calcs. correl 77–35597
  Nb, stress distrib. from He ion irrad., vol. expansion, calcs. 77–35599
  Nb, swelling correlation with local gas concentration following He irrad. 80–70271
  Nb-Zr (1 wt.%), He bubble growth, α-particle effects 78–67749
  Nb_3Ge, α-particle irrad., relationship between density of states and supercond. transition temp. 79–42684
  Nb_3Ge, irrad., supercond. transition width 78–23193
  Nb_3Ge, low fluence alpha irradiation, behaviour of supercond. transition temp. 78–43510
  $Nb_3Ge(Sn)$, electron irradiation at cryogenic temps., effect on T_c and transport props. 78–52122
  Nb_3Sn, A-15 struct. Nb based superconductors, irrad. type influence on radiation defects 80–15093
  Nb_3Sn, α-particle irrad., relationship between density of states and supercond. transition temp. 79–42684
  Nb_3Sn, effect on critical temp. for supercond. of disorder, induced by α-particles 78–47897

alpha-particle effects continued
  Nb_3Sn, low fluence alpha irradiation, behaviour of supercond. transition temp. 78–43510
  Nb_3Sn, radiation damage effect on superconducting props. 78–52127
  Ni, alpha-particle irrad., Mossbauer study of nucl. reaction aftereffects 80–40015
  Ni, exfoliation depth and damage energy distrib., range 80–29075
  Ni, stress distrib. from He ion irrad., vol. expansion, calcs. 77–35599
  Ni-Cr-Fe (75, 35, 12 wt.%), electron and α-particle irrad., positron annihilation and elec. resist. meas. 79–83054
  Ni-Cr-Fe alloys, radiation enhanced precip. and dissolution of precipitates, point defect kinetics and dislocation obs. 80–108467
  PdO, irrad., black form., adsorpt. props. 77–11796
  ^{210}Po, inner shell electron ejection in α-decay 77–79342
  Pt alloy, fission-fragment-induced He blistering 78–86601
  Pt-In, dil., radiation damage heating, TDPAC exam. 78–39466
  PtO, irrad., black form., adsorpt. props. 77–11796
  PuO_2 pellets, control of microstructural damage caused by He release 79–67926
  PuO_2, radiation damage, point defect ingrowth and annealing behaviour 77–27926
  PuO_2, struct. changes under self- and reactor irrad. 77–27927
  ^{238}Pu 4.4 MeV α-particles, mutagenicity and cytotoxicity rel. to X-rays 80–72265
  Si, 5 MeV α-particle irrad., X-ray exam. of surface layer struct. changes 78–6114
  Si, energy loss and multiple scattering of non-channelled α-particles *(German)* 80–59544
  Si, p^+-n junction, irrad. with α-particles, defect form 80–24509
  Si, p-n junction, alpha-particle effects, photoelec. parameters determ. *(Russian)* 77–31702
  Si, postimplantation damage profiles, backscatt. meas. 78–47402
  Si radiation detectors ion-doped, effects of 5.5 MeV α-particle irradiation 77–65397
  SiC, 0.6, 3.5 MeV He^+ irrad., surface erosion, porosity effects 77–35602
  SiC, 10 keV H^+ irrad., C deposition, surface swelling, surface morphology changes 77–35608
  Sn, supercond. tunnel junction, quasiparticle excitation by α-particles 80–103791
  steel, stainless, He cavitation, rel. to TiC precipitation 80–45399
  Ti, 300 keV He^+ irrad., exfoliation, flaking, blistering, in-situ SEM obs. 77–35598
  UO_2, radiation damage, point defect ingrowth and annealing behaviour 77–27926
  ^{238}U complex, α-induced defects, vibronic luminesc. band fine struct. 79–87489
  V, 80 keV ^4He irrad., depth profiles, migration, release, surface effects, blistering 77–35606
  V, blister behaviour during 200, 2000 keV He irrad, temp. depend. 77–35607
  V, ion implanted with 2 MeV He under pulsed conditions, microstructure obs. 80–29088
  VTi alloys, blister behaviour during 200, 2000 keV He irrad. temp. depend. 77–35607
  Zn, 6.1 MeV α-particle irrad., stage III and IV recovery kinetics, defect diffusion 77–76474
  Zn, α-irradiation damage and stage I recovery 78–38759
  Zn, quadrupole interaction of ^{67}Ge and ^{71}Ge, TDPAC meas. 78–43740
  Zn, recovery after 6.1 MeV α-particle irradiation at 4.2K 78–47441
  ZnTe, thin film, stopping power for protons and alpha particles, proton energy straggle values 77–89489
  $Zr(HPO_4)_2H_2O$, ^6Li loaded, α-radiation damage, X-ray Guinier powder reflection study *(German)* 78–47437

alpha-particle interactions *see alpha particle-nucleus reactions*

alpha-particle model *see nuclear cluster model*

alpha particle-nucleus reactions
  for inelastic alpha particle-nucleus scattering, see "alpha particle-nucleus scattering"
  0.7-8 GeV, scaling and nonscaling of inclusive π prod. 79–22296
  $^{209}Bi(\alpha,f)$, search for near threshold asymmetrical fission *(Russian)* 78–33233
  (α,f) on preactinide nuclei Hf-Bi 30-50 MeV, ang. anisotropy 77–18637
  A=12 to 40, $(\alpha,^2He)$ reaction, high spin state transition cross sections in 1p and 2s1d shell 79–6644
  alpha-particle breakup on various nuclei at 140 MeV 78–46080
  compound nucleus (α,p) cross-sections in Ni region, 15 and 18 MeV 77–74864
  conference on nuclear interactions, Canberra, Australia (Aug.-Sep. 1978) 80–4476
  correlations between secondary particles in interactions at 4.2 GeV/c *(Russian)* 77–46181
  emulsion nuclei, g-proton energy and ang. characteristics *(Russian)* 79–40937
  FFTF fuel, neutron source strength as function of irradiation 80–22929
  fissionability, target mass depend. for π, γ, α, p, cascade-evaporation and liquid drop calcs. *(Russian)* 80–106089
  fragmentation at 100 MeV, fireball and coalescence model anal. 79–93642
  fusion, α-induced, γ-ray spectra calcs. 79–36291
  high-energy, at Saturne I, five years of expts. *(French)* 79–3262
  laboratory apparatus 77–28
  light relativistic ion-target interactions, particle emission 80–102193
  multi-nucleon transfer and direct reactions, nuclear struct., review 78–50060
  multiple collision model anal., at high and relativistic energies 78–86542
  multiplicity distribution, shape, and low-fold coincidence probabilities 78–54779
  nucleus properties from scatt. studies *(Hungarian)* 80–18159
  nucleus-nucleus total cross section energy depend. 80–106071
  optical potential as three body problem, microscopic description 79–6536
  optical potential parameters of α, elimination of discrete multivaluedness 77–6333
  primary cosmic ray interactions with photoemulsion nuclei using satellite Intercosmos-6 *(Russian)* 78–93063
  relativistic nuclear collisions, p, d, and t inclusive energy spectra 80–63199
  target nucleon$+\alpha$ potential, microscopic model with antisymmetrisation effects 78–62516

alpha particle-nucleus reactions continued
- thermonuclear reaction rate data for intermediate mass nuclei 80−31427
- $(\alpha,2\alpha)$, 90 MeV, strong absorption diffraction model, spectroscopic factors 79−22306
- $(\alpha,2\alpha)$, A=9, 12, 16, 20, 22 80−68629
- $(\alpha,2\alpha)$, pole peripheral model, ang. correl. functions calc. for ^{6}Li, ^{9}Be, ^{12}C 77−6328
- $(\alpha, 2\alpha)$ 700 MeV, cross section, effective cluster number from PWIA, momentum distrib. 79−40940
- $(\alpha,2\alpha)$ comparison with $(p,p\alpha)$ reactions, antisymmetrisation effects 79−6575
- $(\alpha,2\alpha)$ reacts., three-body anal. 78−13126
- $(\alpha,2n\gamma)$ studies of vibr. and other side bands in ^{162,164,166}Er 77−2893
- $(\alpha,3n)$ reaction producing ^{105}Pd, level scheme 77−82849
- (α,α), critical energies, ang. distrib. energy depend. semiclassical theory 79−76007
- $(\alpha,\alpha'X)$, 4.5 GeV/c/N, secondary charged particles azimuthal correlations *(Russian)* 80−27651
- $(\alpha,\alpha'X)$, isoscalar giant quadrupole resonance decay props. 80−22792
- $(\alpha,\alpha'X)$, inelastic interaction cascade model for Z=3-13, 29-82 80−106064
- $(\alpha,\alpha X)$, 1 GeV/N, inclusive hadron-nucleus cross-sections, multiple scatt. series 80−13519
- $(\alpha,^{12}C)$, 90.3 MeV, cross sections and systematics multi-α-cluster transfer implications 80−42675
- $(\alpha,^{12}C)$, 90.3 MeV, multi-α-cluster transfer and direct pickup cross sections 80−57760
- (α,d), double stripping core independ. 2-nucleon transfer, Tang-Herndon effective interactions 80−73836
- (α,f) 140, 150 MeV, fission cross sections and probabilities, isomeric yield ratio 79−45308
- (α,γ), direct and resonance capture, giant dipole and quadrupole resonances 80−37385
- $(\alpha,^{2}He)$, 55 and 65 MeV, on 1p and 2s1d shell nuclei, A=12 to 40 78−82365
- $(\alpha,^{2}He)$ reaction in 1p- and 2s1d-shell nuclei, A-depend. of neutron binding energy 78−74379
- $(\alpha,^{3}He)$ absolute normalisation const. meas. from $^{48}Ca(^{3}He,\alpha)$ and ^{48}Ca(d,t) 77−54234
- $(\alpha, ^{3}HeX)$, 1 GeV/N, momentum distribs. after high energy fragmentation, spectator peak 80−99164
- $(\alpha, ^{3}Me)$, composite particle scatt. breakup mechanism 80−83105
- (α,n), A=88 to 124, reaction rates of reaction important to nucleosynthesis 79−45253
- (α, N), DWBA finite range calc. 79−9541
- (α,N), microscopic finite-range anal. 80−63181
- (α,n), mixture and compound neutron yield from separate component thick target yields 80−37414
- (α,n), on B, C, N, Mg, Al, P, activation anal. appl. 80−61206
- (α, n), spin alignment attenuation factors in mass 61-67 nuclei 79−26390
- (α,n) cross-sections and α-stopping power in light elements 77−74862
- (α, n) excitation functions, non-statistical reaction contribs. 77−82939
- (α,n) for Fe group elements, Hauser-Feshbach theory, He prod. in fusion reactors 77−23100
- (α,n) reactions, black and grey neutron detectors 79−9971
- (α,n) thick target yields for Li, ^{9}Be, B, $Pb^{19}F_2$, $Zn^{19}F_2$, Mg, ^{27}Al, Si, and $^{28}SiO_2$ 79−71860
- $(\alpha, n(p))$ recoil-distance lifetime meas. in ^{22}Ne, ^{22}Na, ^{27}Al 77−30510
- (α,p), on B, C, N, Mg, Al, P, activation anal. appl. 80−61206
- (α, p), spin alignment attenuation factors in mass 61-67 nuclei 79−26390
- (α,p) direct 3-nucleon transfer reactions, microscopic approach review 79−6545
- (α,p) reactions, medium nuclei, calc. of α strength factors 77−18454
- (α,π), 700 MeV, backward π^{+} prod., momentum depend., scaling, Monte Carlo calcs. 79−13305
- (α,t), 20-50 meV 80−42670
- (α,X), 140 MeV, inclusive spectra, 'quasi-two-body scaling' and 'hot spots' 80−5142
- (α,X), 1.6 GeV, in-beam nuclear γ-rays from Na, S, Ca 79−6483
- (α,X), complete fusion barrier and evaporation from ^{194}Hg 80−68715
- (α,X), relativistic collisions, slow and fast fragment correlations, multiplicity association 80−86886
- (α,X) on light nuclei, 1.55, 2.89 GeV/c, total and inelastic cross sections 79−6610
- (α,xn), 640, 710 MeV, n ang. and energy distribs., intranuclear cascade model 80−83109
- $(\alpha,xn\gamma)$, rare earth nuclei, complete fusion process n and γ multiplicity 80−18363
- (α,xy), projectile fragmentation processes at 35 MeV/amu, absorptive breakup 80−27653
- α-α, pot. calc. appl. to even-even N=Z nuclei 79−6661
- α-α and α-nucleus calcs. using effective pot. interaction, ^{8}Be rot. levels. 77−22915
- $(\gamma, \pi X)$, 4.2, 4.5 GeV/N, pion multiplicities and theoretical models, review 80−42657
- γ spectra of millisecond isomers, 38 MeV α-induced reactions, abs. cross-section determ. 79−9502
- π multiplicity dispersion in nuclear collisions *(Russian)* 79−54443
- $^{48}Ca(\alpha,2n\gamma)^{50}Ti$, high spin states in ^{50}Ti 78−54675
- 90 MeV, α-n coincidence ^{5}He breakup kinematics 77−6419
- Ag (α,x), 0.2-4.2 GeV/N, compression phenomena and Mach shock waves 80−22851
- Ag+α, 720 MeV, correlated energy spectra of light fragments, fireball and coalescence models 78−62555
- $AgBr(^{4}He,X)$, 2.1 GeV, central collisions, Maxwell-Boltzmann distrib. anal. 78−66315
- $^{107}Ag(\alpha, 2n\gamma)$ 20-30 MeV, ^{109}In high spin states, transitions, isomeric state, negative parity bands 80−451
- $^{107}Ag(\alpha,f)$, 640MeV 80−95329
- $^{109}Ag(\alpha,2n\gamma)$, ^{111}In $21/2^{+}$ isomeric state g-factor and relaxation time 80−73794
- $^{109}Ag(\alpha,2n\gamma)$, γ studies, ^{111}In level struct., spin, parity 78−58249
- $Ag(\alpha,X)$, 16.5 GeV/c, inelastic cross sections, multiplicity, ang. and momentum distribs. 78−82359
- $Ag(\alpha,X)$, 720 MeV, nuclear fragment prod. thermodynamic evaporation and firestreak description, pre-equilibrium emission 79−54426
- $Ag(\alpha,X)$ X=p,d,t,^{3}He,^{4}He, 720 MeV, back-angle prod. of light ions, model calcs. 79−45280

alpha particle-nucleus reactions continued
- $Ag(\alpha,f)$, fission fragments tracklength and ang. distribs., fission moment of inertia 77−50182
- Al+α, 720 MeV, correlated energy spectra of light fragments, fireball and coalescence models 78−62555
- $^{27}Al (\alpha, ^{8}B)$, 109 MeV, ^{23}Ne structure, differential cross sections 80−5153
- $^{27}Al(\alpha, p), (\alpha, d), (\alpha, t)$, 50 MeV, reaction mechanism determ. *(Russian)* 78−54778
- $^{27}Al(\alpha,^{7}Be)^{24}Na$, up to 156 MeV, excitation functions 77−3021
- $^{27}Al(\alpha,X)$, 140 MeV, nonequilibrium light charged particle yield, energy spectra and ang. distribs. 79−40942
- $^{27}Al(\alpha,X)$, 20, 40 MeV/N, α breakup yield, fragment yield ratios 80−9300
- $^{27}Al(\alpha,3p)$ ^{28}Mg radionuclide yield 80−32290
- $^{27}Al(\alpha,\alpha)$, x=p,d,t,h,α' and x-γ, 140 MeV, reaction mechanism characts. for deformed ^{27}Al 79−63682
- $^{27}Al(\alpha,d)$, 27.2 MeV, ^{29}Si levels and ang. distribs., DWBA anal. 80−78157
- $^{27}Al(\alpha,d)^{29}Si$, d ang. distrib. corrections for finite interaction radius 79−9597
- $^{27}Al(\alpha,n)$, ^{30}P high spin states, recoil dist. lifetime meas. 78−74386
- $^{27}Al(\alpha,n)$, 10-18 MeV, ^{30}P spin cutoff parameters, spectral distrib. calc. and meas. comparison 79−6382
- $^{27}Al(\alpha,n)^{30}P$ short-lived positron emitter production obs. 79−76236
- $^{27}Al(\alpha,t)$, 25 MeV, DWBA anal. of triton ang. distrib. meas. 78−54776
- $^{27}Al(\alpha,t)^{28}Si$, 27.2 MeV, transitions to ground and $2^{+}{}_{1}$ states *(Russian)* 77−34328
- $^{27}Al(\alpha,x)$, 140 MeV, mass fragment meas., reaction mechanism models 79−63683
- $^{27}Al(\alpha,xp+yn)$, up to 156 MeV, excitation functions 77−3021
- $^{27}Al(\alpha,xp)$, up to 156 MeV, including prod. of ^{28}Mg, excitation functions 77−3021
- $Al(\alpha,X)$ 720 MeV, nuclear fragment prod. thermodynamic evaporation and firestreak description, pre-equilibrium emission 79−54426
- $Al(\alpha,X)$ X=p,d,t,^{3}He,^{4}He, 720 MeV, back-angle prod. of light ions, model calcs. 79−45280
- $Al(\alpha, \chi\pi)$, 18 GeV, π multiplicity distrib. 79−97713
- $^{241}Am(\alpha,n)$, neutron yield in AmO_2 79−17912
- $^{243}Am(\alpha,f)$, fragment mass distrib., and yield, statistical anal. *(Russian)* 80−5183
- $^{38}Ar(\alpha,n)^{41}Ca$ in early solar system, search for ^{41}K anomaly in Allende meteorite 78−49398
- $^{38}Ar(\alpha,n\gamma)$, ^{41}Ca, spin and parity from angular distrib. and linear polarisation of γ 80−63079
- $^{38}Ar(\alpha,n\gamma)^{41}Ca$, high-spin positive parity states of ^{41}Ca anal. 77−38224
- $^{38}Ar(\alpha,p)$, ^{41}K l-forbidden M1 decay from 1st excited state 78−13024
- $^{38}Ar(\alpha,p\gamma)^{41}K$, level props. of ^{41}K below 3.3 MeV 78−62588
- $^{40}Ar(\alpha,n\gamma)$, struct. of high spin positive parity states in ^{43}Ca 78−46025
- $^{40}Ar(\alpha,n\gamma)^{43}Ca$, γ-ray spectroscopy, levels and decay scheme deform. of ^{43}Ca 79−80896
- $^{40}Ar(\alpha,p)^{43}K$, 15 MeV, ^{43}K 738 keV state g-factor, PAC technique 77−6227
- $^{40}Ar(\alpha,p\gamma)$, 7-17 MeV, ^{43}K high spin states, J^{π} and lifetimes 79−67621
- $^{40}Ar(\alpha,p\gamma)^{43}K$, 10.4 MeV, lifetime of 738 keV level of ^{43}K, M2 transition strength meas. 77−65226
- $^{75}As(\alpha, 3n\gamma)^{76}Br$, 30 to 55 MeV, study of ^{76}Br level structure 77−54174
- $^{75}As(\alpha,2n)^{77}Br$ production excitation curves 79−85468
- $^{75}As(\alpha,3n)$, ^{76}Br long-lived positive parity isomer 79−54375
- $^{75}As(\alpha,4n\gamma)$, 30-55 MeV, obs. of ^{75}Br levels and prolate deform. 78−50088
- ^{73,74}As, yields in α, d and p interactions on Ge, Ga and As 77−54223
- Au, binary fission characts. induced by α-particle bombardment of 0.65 to 4.12 GeV 78−13169
- ^{197}Au, (α,p), (α,d) and (α,t) reactions, 50.5 MeV, particle spectra 77−6405
- $^{197}Au(\alpha, 3n)$, simple formula for excitation functions 78−93978
- $^{197}Au(\alpha, 3n)^{198}Tl$, 30 to 55 MeV, study of ^{198}Tl rotational structure 77−54130
- $^{197}Au(\alpha, p), (\alpha, d), (\alpha, t)$, 50 MeV, reaction mechanism determ. *(Russian)* 78−54778
- $^{197}Au(\alpha,2n)$, prod., best conditions, medical appls. 80−51245
- $^{197}Au(\alpha,2n)$, simple formula for excitation functions 78−93978
- $^{197}Au(\alpha,5n)$, 65 MeV, ^{196}Tl high spin states, γ-decay and rot. structs. 79−440
- $^{197}Au(\alpha,f)$, 640MeV 80−95329
- $^{197}Au(\alpha,xn)$, 16-27 MeV, ^{199,200}Tl cross section and excitation function statistical anal. *(Rumanian)* 80−22846
- $^{207}Au(\alpha,f)$, 640MeV 80−95329
- $Au(\alpha,f)$ 0.65, 1.74, 4.12 GeV, and using polycarbonate detector 78−13178
- $Au(\alpha,f)$, fission fragments tracklength and ang. distribs., fission moment of inertia 77−50182
- B+α, gamma-ray spectra from elements within $^{241}Am(n,\alpha)$ source 79−3269
- $^{10}B(\alpha,d)^{12}C$, 40 MeV, ratio of isospin forbidden/allowed yield 77−18385
- $^{10}B(\alpha,n_0)^{13}N$, 18-20 MeV, neutron ang. distribs. multi-nucleon transfer mechanism 77−14144
- $^{10}B(\alpha,n_1)^{13}N^{*}$, 18-20 MeV, neutron ang. distribs., multi-nucleon transfer mechanism 77−14144
- $^{11}B, (\alpha,\gamma_0)$, 15.5-19.5 MeV, excitation curve ang. distrib., cross section, ^{15}N resonances 78−94019
- $^{11}B(\alpha,\gamma_0)^{15}N$, giant dipole reson. region 77−26777
- $^{11}B(\alpha,n)^{14}N$, n polarisation ang. distrib., R-matrix anal., ^{15}N excited states 78−4937
- $^{11}B(\alpha,p)^{14}C$, 4.4-6.7 MeV, absolute differential cross-section meas. 78−46054
- $^{11}B(\alpha,p)^{14}C$, subsurface production of ^{14}C, groundwater dating 80−85690
- $^{10}Ba(\alpha,p)^{13}C$, appl. to B predeposited Si wafer anal. by combined ion beam techniques and X-ray microanal. 79−5238
- $Ba(\alpha,xn)Ce$ reactions, study of ^{138}Ce, ^{139}Ce high-spin states, lifetime meas. 77−18476
- Be+α, gamma-ray spectra from elements within $^{241}Am(n,\alpha)$ source 79−3269
- $^{9}Be(\alpha, ^{3}He)$, 65 MeV, ^{10}Be levels and differential cross sections, DWBA and coupled channel anal. 80−102121
- $^{9}Be(\alpha, n)$, 100 MeV, neutron polarisation meas. 78−70726
- $^{9}Be(\alpha,n,\gamma)$, secondary reaction yield for meas. of Be coating thickness 78−82600

alpha particle-nucleus reactions continued
^{9}Be(α,n) 6.5 MeV, ^{13}C, T=3/2 resonance parameters, ground state γ-decay width 79−3123
^{9}Be(α,n)^{12}C, appl. to Be determ. in metals using nuclear microprobe anal. 79−5204
^{9}Be(α,nγ)^{12}C, ^{12}C gamma line Doppler broadening at 4438 keV 80−91147
^{9}Be(α,t), 65 MeV, ^{10}B levels and differential cross sections, PWBA and coupled channel anal. 80−102121
Be(α,n), neutron spectrum of ^{228}Ra-Be source 78−41882
Bi, binary fission characts. induced by α-particle bombardment of 0.65 to 4.12 GeV 78−13169
^{201}Bi (α,f), 23-140 MeV, l_{crit} from fragment ang. distribs. anal. 80−106087
^{209}Bi(α,^{3}He), 172.5, 140 MeV, plane wave spectator model anal. n momentum distrib. in α 79−54445
^{209}Bi(α,X), 140 MeV, nonequilibrium light charged particle yield, energy spectra and ang. distribs. 79−40942
^{209}Bi(α,X), 20, 40 MeV/N, α breakup yield, fragment yield ratios 80−9300
^{209}Bi(α,X), 69.2, 140 MeV, scatt. and fission reaction mechanisms, cross sections 80−18350
^{209}Bi(α,f), 640MeV 80−95329
^{209}Bi(α,n), excitation functions and isomer ratios of ^{212}At 80−83039
^{209}Bi(α,np), excitation functions and isomer ratios of ^{211}Po 80−83039
^{209}Bi(α,p), excitation functions and isomer ratios of ^{212}Po 80−83039
^{209}Bi(α,t), 40 MeV, effective residual interaction matrix elements, spectroscopic factors, cross sections 80−99134
Bi(α,f), 0.65, 1.74, 4.12 GeV, and using polycarbonate detector 78−13178
^{79}Br(α,2n)^{81}Rb-^{81m}Kr production excitation functions and thick target yield curves 80−12253
^{79}Br(α,3n) 30-55 MeV, populating ^{80}Rb 77−88028
^{79}Br(α,xn)$^{83-x}$Rb, radioisotope selective production *(Croatian)* 78−44608
^{81}Br(α, 2n), 23 MeV, ^{83}Rb high spin states, positive and negative parity bands 80−18178
^{81}Br(α,2n), 19-25 MeV, ^{83}Rb band struct., spin assignments and transitions 80−73774
^{81}Br(α,2n), 19-25 MeV, ^{83}Rb high spin states, Jπ and transitions 80−105949
^{81}Br(α,3n), 30-55 MeV, ^{82}Rb, level structure, gamma angular and time distribs. 80−52583
^{81}Br(α,xn)$^{85-x}$Rb, radioisotope selective production *(Croatian)* 78−44608
Br(α,X) 80−22851
Br(α,X), 16.5 GeV/c, inelastic cross sections, multiplicity, ang. and momentum distribs. 78−82359
C, 180° prod. of protons in high-energy reacts. 78−8816
^{12}C+α, 100-160 MeV, ^{10,11}B prod., cosmic-ray propag. appl. 77−79380
^{12}C+α, 2.5 GeV-nucleon, nuclear fragmentation meas. *(Russian)* 78−54773
^{12}C+α, spallation fragments $6 \leq A \leq 11$ yields, nucleosynthesis interest 79−30845
^{12}C+p(d)(α), transparency in composite particle reactions 80−9273
^{12}C(^{4}He,π^{0}), 710 MeV, inclusive neutral pion prod. cross section 77−6410
^{12}C(α,^{5}He), 90 MeV, α-n coincidence, ^{5}He breakup kinematics 77−6419
^{12}C(α,^{6}Li), 46 MeV, finite range DWBA anal. 77−14142
^{12}C(α,Li*), unbound Li, relative energy distrib. of correlated decay products 79−13274
^{12}C(α,X), 4.2 GeV/c, multitudes of secondary negative particles, momentum distrib. ratios *(Russian)* 80−63178
^{12}C(α,α), 1.37-2.55 GeV, microscopic anal. 80−47490
^{12}C(α,γ_n), excitation function meas. in vicinity of 12.44 and 13.1 MeV levels of ^{16}O 77−6413
^{12}C(α,γ)^{16}O cross-section, K-matrix parametrisation 77−6411
^{12}C(α,p_0), 17.5-18.7 MeV, p ang. distribs. and integrated cross section 79−30846
^{12}C(α,p), comparison with ^{16}O(α,p), direct evidence for 3p-4h excitations 79−67659
^{12}C(α,p)^{15}N, 50 MeV, proton spectra, excitation of high-spin states *(Russian)* 77−6209
^{12}C(α,p)^{15}N ($3/2^{-}$, 6.328 MeV) transition, giant resonance effects 79−9601
^{13}C(α,n)^{16}O, 0.60-1.15 MeV, astrophysical appls. 77−13230
^{13}C(α,n)^{16}O, widths of isospin forbidden decays of ^{17}O T=3/2 levels 77−6321
^{13}C(α,n)^{16}O process, 0.60 to 1.15 MeV, reaction rate 77−45300
^{14}C(α,γ)^{18}O and onset of core He flash in low-mass stars 80−51735
Ca+α, 100 MeV, fireball and coalescence model anal. 79−93642
^{A}Ca(α,X), 10-27 MeV, A=40,44, fusion cross sections, anomalous large angle scatt. 79−80966
^{A}Ca(α,p)$^{A+3}$Sc, 25 MeV, population of $f_{7/2}{}^{4}$ states 79−59077
^{14}Ca(α,α), 1.37-2.55 GeV, microscopic anal. 80−47490
^{40}Ca+α, core-like pot., resonating group anal. 78−4922
^{40}Ca+p(d)(α) transparency in composite particle-nucleus reactions 80−9273
^{40}Ca(α,^{6}Li), 46 MeV, finite range DWBA anal. 77−14142
^{40}Ca(α,αp), 96.8 MeV proton pickup by α-particles to unbound states DWBA anal. 79−22305
^{40}Ca(α,d)^{42}Sc, 40 MeV ang. distribs. meas., Sc levels anal. 78−21579
^{40}Ca(α,γ), ^{44}Ti lowest T=2 state isospin forbidden γ-decay from resonances 79−22228
^{40}Ca(α,γ)^{44}Ti, 2.75-4.00 MeV, γ-ray ang. distrib. of reson. for spin parity values 77−65230
^{40}Ca(α,γ)^{44}Ti, lifetimes and spins of ^{44}Ti levels meas. 77−79328
^{40}Ca(α,n) 20 MeV, ^{43}Ti positive parity states, mean lifetimes, quasirotational band 79−6415
^{40}Ca(α,nγ) 20 MeV, ^{43}Ti, lifetime and γ decay of isomeric $19/2^{-}$ state 78−70486
^{41}Ca(α,p)^{44}Sc, 25 MeV, population of $(f_{7/2})^{4}$ states, relative transition strengths, semi-microscopic model calcs. 79−6645
^{42}Ca(α,n)^{45}Ti, 5.41-10.95 MeV, cross sections 79−85470
^{42}Ca(α,n)^{45}Ti, integral rot., hyperfine field and g-factor of Ti $3/2^{+}$ state 77−50052
^{42}Ca(α,n)^{45}Ti, reaction rates in stars 80−82183
^{43}Ca(α,nγ), 8-15 MeV, ^{46}Ti deduced levels, spin assignments and γ-decay, band struct. 78−78302
^{44}Ca(α,n)^{47}Ti, integral rot., hyperfine field and g-factor of Ti $7/2^{-}$ state 77−50052

alpha particle-nucleus reactions continued
^{48}Ca(α,2nγ), 24-33 MeV, ^{50}Ti high spin states, transitions and J^{π} values 80−455
C(α,X), 16.5 GeV/c, inelastic cross sections, multiplicity, ang. and momentum distribs. 78−82359
C(α,X), 4.2 GeV/N, multiple π^{-} prod., mean multiplicity *(Russian)* 80−27647
C(α,χα), 18 GeV, π multiplicity distrib. 79−97713
C(α,d)N for ^{12,13}C isotopes, 50 MeV, deuteron energy spectra *(Russian)* 77−6209
Cd even-mass isotopes, vibr. excitations 77−54129
Cd, isotopes A=109, 106, 105, 104, high spin states excited by (α,xnγ) *(French)* 78−29394
^{108}Cd(α,2np), 44 MeV, ^{109}In high spin states, γ-transitions, ang. distribs. 80−73783
^{110}Cd(α,2nγ), ^{112}Sn 6^{+} isomeric state, g-factor and relaxation time 80−73794
Cd(α, 2nγ), 17-33 MeV, ^{A}Sn, A=112, 114, 116, 118, positive parity band heads, excitation energies and transitions 79−45136
Cd(α,2nγ), 17-33 MeV, ^{112,114,116,118}Sn collective bands, spin, parity, γ meas. 78−54719
Cd(α,xn), 30-67 MeV, ^{A}Sn, A=109,111,113,115,117, level scheme, J^{π} assignments, high spin states 79−45168
^{140}Ce(α, xn), 85 MeV, ^{138,139}Nd high spin states, J^{π}, γ-cascades and shape transition 80−102090
^{140}Ce(α, xn), 86 MeV, ^{A}Nd, A=138,139, high spin states, isomers and γ-cascade 80−78120
^{142}Ce(α,2n)^{144}Nd, high-spin states of ^{144}Nd anal. 77−82940
Ce(α,xn)Nd, reactions, lifetime meas. of ^{141,142}Nd high-spin states 77−18476
^{250}Cf(α,t) 28 MeV, ^{251}Es level struct. and p states, level transitions 78−78268
^{35}Cl(α, pγ), 18 MeV, ^{38}Ar yrast levels, J^{π} assignments, transitions, branching and mixing ratios 79−67625
^{35}Cl(α,pγ), 16 MeV, ^{38}Ar high spin state density, γ-decay mode, deformed states 80−32168
^{37}Cl(α,d), 27 MeV, spectra, ang. distribs., ^{39}Ar low lying states, spins 78−25212
^{37}Cl(α,γ), 2.9-5.2 MeV, excitation function competition cusps, Mauser-Feshbach calcs. 80−13404
^{35,37}Cl(α,d), 40 MeV, populating high-spin states, L-transfer 77−74865
^{246}Cm (α,t), 28, 29 MeV, ^{247}Bk proton states, transitions and spectroscopic factors 79−89224
^{59}Co(α, p), (α, d), (α, t), 50 MeV, reaction mechanism determ. *(Russian)* 78−54778
^{59}Co(α,n)^{62}Cu, 6-11 MeV, gamma transitions from ^{62}Cu excited levels obs. *(French)* 77−26615
^{59}Co(α,p)^{62}Ni, 6-11 MeV, ^{62}Ni energy levels determ. *(French)* 77−26615
^{59}Co(α,pγ), 10 MeV, ^{62}Ni level struct. and decay scheme, shell model calcs. 79−3085
^{59}Co(α,pγ)^{62}Ni, lifetime meas. of excited states in ^{62}Ni 79−3115
^{59}Co(α,t), 25 MeV, DWBA anal. of triton ang. distrib. meas. 78−54776
^{59}Co(α,t), 27.2 MeV, cross sections, optical potential, spectroscopic factors *(Russian)* 77−38290
^{59}Co(α,xnyp), 20-172.5 MeV, cross sections excitation functions, hybrid model, preequilib. effects 80−57784
^{50}Cr(α,p)^{53}Mn, cyclotron preparation of ^{53}Mn, extraction, anal. 77−61441
^{50}Cr(α,pγ)^{53}Mn, ^{53}Mn lifetimes meas. *(French)* 79−67711
^{52}Cr(α,Znγ), 24-33 MeV, ^{54}Fe high spin states, transitions and J^{π} values 80−455
^{52}Cr(α,2nγ)^{54}Fe, high spin states in ^{54}Fe 78−54675
Cr(α,p), 18, 26 MeV, levels in ^{53,55,57}Mn, J-depend., spins, parities 78−78397
^{133}Cs(α,2n)^{135}La, band struct. of ^{135}La, in-beam γ-ray spectroscopy 78−4951
^{133}Cs(α,pn)^{135m}Ba, ^{135m}Ba yield depend. on energy of bombarding particle 80−5151
^{63}Cu(α,nγ), 18 MeV, ^{66}Ga high spin states, shell model interpretation *(French)* 79−3086
^{63}Cu(α,p)^{66}Zn, proton polarisation calc., distorted wave method 77−6404
Cu(α, χπ), 18 GeV, π multiplicity distrib. 79−97713
Cu(α,π), 0.7-8 GeV, scaling and nonscaling of inclusive π prod. 79−22296
D(^{3}He,H)^{4}He, determ. of D adsorption coverage on W (001) 79−23835
^{A}Dy(α,xnγ), A=162,164, Er yrast levels, spin alignment 80−52557
^{164}Dy(α,4nγ), 51 MeV, ^{164}Er high spin props. in multiple band crossing region 80−83023
^{164}Dy(α,α′), 11.5-12 MeV, E_2 and E_3 transition strengths meas. 77−26618
^{164}Dy(α,xnγ), x=6-11, 120 MeV, pre-equilibrium n emission, deexcitation mechanism 79−93641
Dy(α,t) ^{A}Ho single proton states, A=157, 159, 161, 163 78−489
Dy(α, xn γ) equilib. and pre-equilib. reactions, ang. momentum transfer, ground state bands 79−45277
Dy(α, xn γ)Er, 90 MeV, preequilibrium and equilibrium de-excitation processes 78−50185
^{164}Er(α,2n), gamma deexcitation mechanism of rot. levels 79−26442
^{166}Er (α,α′), 11.5-12 MeV, E_2 and E_3 transition strength meas. 77−26618
^{166}Er(^{4}He,xnαγ), angular momentum effects in pre-equilibrium processes 78−50208
^{166}Er(^{4}He,xnγ), angular momentum effects in pre-equilibrium processes 78−50208
^{168}Er(α,2n), 27 MeV, ^{170}Yb negative parity yrast band, rot. aligned n, deformation coupled bandhead 79−93489
^{170}Er(α,Zn), 27 MeV, ^{172}Yb octupole band, particle vibrational alignment 80−13351
^{170}Er(α,2n) 27 MeV, ^{172}Yb levels, bands, J^{π} and $T_{1/2}$ 80−91127
^{170}Er(α,4n), 50 MeV, ^{170}Yb negative parity yrast band, rot. aligned n, deformation coupled bandhead 79−93489
^{151}Eu(α,4n), 45-55 MeV, ^{151}Tb 11/2 isomer, high spin few-particle states, in beam study 79−17805
^{151}Eu(α,xn), 68-110 MeV, ^{A}Tb, A=147, 148, high spin particle-hole states, octupole M2/E3 isomers 80−18171
Eu(α, 2n) and (α, 4n), ^{153}Tb excited states, rot. bands, spin, parity 78−62552
F+α, gamma-ray spectra from elements within ^{241}Am(n,α) source 79−3269
^{19}F(α, t), 25 MeV, DWBA anal. of triton ang. distrib. meas. 78−54776

alpha particle-nucleus reactions continued
^{19}F(α,αp), 140 MeV, quasifree p knockout, spectroscopic factors, DWIA anal. 79−67650
^{19}F(α,n), 5.4 MeV, ^{22}Na 0^+ level mean life, isovector mag. dipole transition 80−68595
^{19}F(α,n)^{22}Na, 2.3-4.7 MeV, populating ^{23}Na reson. levels 77−65199
^{19}F(α,n)^{22}Na, 2.6-5.1 MeV, cross sections, excitation function 78−54777
^{19}F(α,n)^{22}Na, 5.5 MeV level lifetimes, instrument testing 78−13375
^{19}F(α,n)^{22}Na, isoscalar M2 transition in ^{22}Na obs. 77−10363
^{19}F(α,p)^{22}Ne, E=5.31 MeV, 3.34 MeV lifetime meas. 77−38245
^{19}F(α,pγ)^{22}Ne, 2.3-4.7 MeV, populating ^{23}Na levels 77−65199
^{54}F(α,2p), side feeding to ^{56}Fe 6^+ doublets 78−13014
Fe+α, 7-24 MeV, ^{59}Ni formation cross section, poss. prod. in cosmic dusts 78−78399
^{54}Fe(α,^{8}He), 110 MeV, ^{50}Fe proton rich nucleus, Q values, mass excesses 77−88162
^{54}Fe(α,γ)^{58}Ni, 7.6 to 12.8 MeV, giant electric resonances in ^{58}Ni 78−41739
^{54}Fe(α,nγ), 18-27 MeV, ^{57}Ni high spin yrast cascade, decay modes J assignment 80−68514
^{54}Fe(α,p), 12-24 MeV, high spin states in ^{57}Co anal. 77−46115
^{54}Fe(α,p), 5.3-9.06 MeV, excitation functions, resonance struct., α-widths of ^{58}Ni states 77−30617
^{56}Fe, (α,p), (α,d) and (α,t) reactions, 50.5 MeV, particle spectra 77−6405
^{56}Fe(α,γ), 4.2-7.1 MeV, reaction cross section, statistical model anal. 79−45278
^{56}Fe(α,pγ), ^{59}Co level energies, branching ratios lifetimes and spins 80−63093
^{57}Fe(α,pγ), 13 MeV, ^{60}Co low lying states, spin constraints, γ mixing ratios 78−29487
^{58}Fe(α,nγ), 9.0 MeV, determ. of lifetime of ^{61}Ni low lying levels 77−88078
^{58}Fe(α,nγ), spectroscopy of ^{61}Ni levels below 2 MeV 77−6289
^{69}Ga(α,3n), 30-55 MeV, ^{70}As states, excitation functions, spin and halflifes 79−6414
Ga(α,p), 25 MeV, ^{72,74}Ge $0_2{}^+$ levels, struct. transition between N=40 and 42 80−73800
Gd (α, xn) Dy, K-shell ionisation cross-sections meas. 80−78687
^{A}Gd+α, A=154,160, reaction cross section meas., in beam γ-spectrometric technique 79−26445
^{152}Gd (α,4n), 60 MeV, ^{152}Dy 60 ns isomer deexcitation E2 x- (orΔ) transition, half life, $\gamma\gamma$-coincidence 80−86859
^{152}Gd(α,3nγ)^{153}Dy, 35-45 MeV, collective band struct. of ^{153}Dy anal. 77−61342
^{152}Gd(α,5N), ^{151}Dy high spin yrast isomers, shell model configs. 79−49573
^{154}Gd (α, xn), 47-130 MeV, reaction cross section 80−22844
^{154}Gd (α,xn), deformed Dy quasicontinuum spectrum, M1, E1, E2 components 80−498
^{154}Gd(α,6n), obs. of ^{152}Dy high-spin isomer at high excitation energy 77−22841
^{158}Gd(α,4n), 40 MeV, fusion and neutron evaporation, ^{158}Dy γ-spectrum 79−36291
^{158}Gd(α,xn) 47-130 MeV, Dy atom K-shell ionisation and X-rays 79−93960
^{160}Gd(α, xn), 40-110 MeV, ^{A}Dy A=158,160, quasi-continuum γ-ray cascades, neutron drip line 79−75903
^{160}Gd(α,4n) 40, 49 MeV, fusion and neutron evaporation, ^{160}Dy γ-spectrum 79−36291
^{160}Gd(α,4n)^{160}Dy, quasi-continuum transitions multipolarities from ICC 77−82945
^{160}Gd(α,xn), 40-110 MeV, Dy equilibrium and pre-equilibrium decay, α-multiplicities, energies and entry lines 79−93549
^{160}Gd(α,xn), 47-130 MeV, reaction cross section 80−22844
^{160}Gd(α,xnγ), compound and precompound γ-ray entry lines from measured multiplicities and energies 79−6649
Gd(α,α'), 11.5-12 MeV, E_2 and E_3 transition strengths meas. 77−26618
Gd(α,xn), 47-130 MeV, Dy K-shell internal conversion yields, gamma transition multipolarities 80−78215
Gd(α, xn)Dy, K-shell ionisation cross-sections meas. 80−78687
Gd(α, xnγ), 67-100 MeV, ^{A}Dy, A=152, 153, isomeric states and complex band structs. 79−67624
^{70}Ge(α, nγ) 10-18 MeV populating ^{73}Se high-spin states 77−10324
^{72}Ge(α,npγ)^{74}As, 30 to 50 MeV, level structure of ^{74}As 77−10357
^{76}Ge(α,mγ), 12 MeV, ^{79}Se high spin levels, transitions, J^π assignments 80−459
^{76}Ge(α,p), 26 MeV, ^{79}As levels, J^π and ang. distribs. 80−78161
^{1}H(α,^{3}He)^{2}H, 3.98 GeV/c, ang. distrib. meas., comparison with DWBA 77−61416
^{1}H(α,α'X), 1.74, 2.57 GeV, low mass πN enhancement, cross section t-depend. 80−63193
^{2}H(^{2}H,p)^{3}He, appl. to effective ion temp. determ. in plasma focus *(Russian)* 79−27824
^{2}H(α, αn)p, 28.3 MeV, ^{5}Li ($3/2^-$) tensor polarisation 80−13450
^{2}H(α, n), 100 MeV, neutron polarisation meas. 78−70726
^{2}H(α,^{5}He(g.s.))p tensor polarisation ang. distribs. from sequential decay ^{2}H(α,p)^{5}He(α)n reaction 77−82899
^{2}H(α,^{5}Li)n, ^{5}Li tensor polarisation and cross sections 79−75967
^{2}H(α,α)np, 20-28 MeV, total reaction cross section 79−89317
^{2}H(α,αn), quasi-elastic scatt., direct reaction unitarised impulse approx. 80−42674
^{2}H(α,αn)^{1}H, 27.2 MeV, absolute differential cross sections 79−9599
^{2}H(α,αp), 140 MeV, quasifree p knockout, spectroscopic factors, DWIA anal. 79−67650
^{2}H(α,αp), 9.22-11.3 MeV, ^{6}Li excited states, final state interactions, three-body force effects 80−57692
^{2}H(α,αp)n, 15 MeV, semiphenomenological impulse approx. anal. 77−82943
^{2}H(α,αp)n, 15 MeV, six-body effects, Faddeev anal. 79−76008
^{2}H(α,αp)n, 15-42 MeV, ^{6}Li 1^+ resonance and breakup amplitude, three body model 79−75954
^{2}H(α,αp)n, 15-42 MeV, three body calc., reaction mech. 78−70546
^{2}H(α,αp)n, 42 MeV, observation and comparison to theoretical calcs. 77−82942
^{2}H(α,n)αp, 100 MeV, differential cross-section and polarisation meas. 77−88157
^{2}H(α,np)^{4}He, differential cross section and polarisation, three body model 80−47460
^{2}H(α,pα) 22.5 MeV, tensor polarisation ang. distribs. in ^{2}H(α,^{5}He(g.s.))p 77−82899

alpha particle-nucleus reactions continued
^{2}H(α,pα)n, 18 MeV, cross section, ang. depend. meas., semiphenomenological anal. 78−58292
^{2}H(α,pα)n, 18 MeV, obs. of n-p final state interaction 77−6414
^{2}H(α,pα)n, 7.5-7.9 MeV, modified impulse approx. anal. 79−6648
^{2}H(α,pα)n, Coulomb interaction effects, ^{5}He(g.s.) resonance energy and width 77−71615
^{3}H(^{4}He,d), reaction mechanism, effect of Pauli principle and channel coupling 77−65219
^{3}H(α,^{6}Li)n, 11.3-12.0 MeV, excitation functions 78−621
^{3}H(α,n)^{6}Li cross section, exptl. data base for ^{7}Li system 79−9584
^{3}H(α,t)^{4}H, 11.3-12.0 MeV, excitation functions 78−621
^{3}H(α,t)n, 11.3-12.0 MeV excitation 78−621
H(α,X), 16.5 GeV/c, inelastic cross sections, multiplicity, ang. and momentum distribs. 78−82359
H(α,α), 1.37-2.55 GeV, microscopic anal. 80−47490
Hd(α,t), ^{A}Pm, A=143-153, odd-A, spectroscopic factors, shell model anal. 80−78137
^{3}He(D,p)^{4}He, appl. to effective ion temp. determ. in plasma focus *(Russian)* 79−27824
(^{4}He,^{8}Be), A=9-16, 65-72.5 MeV, α-cluster pickup DWBA anal. 77−6418
(^{4}He,2nf), statistical model anal. of fission isomer production Pu, A=235, 237 78−66326
(^{4}He,xnf)^{239}Am, statistical model anal. of fission isomer production 78−66326
^{4}He-^{4}He, possible ^{8}Be high-lying reson. below α-α* threshold 77−82840
^{4}He+^{4}He, microscopic description of nuclei collisions, GCM and RGM framework 77−34272
^{4}He+α, 103 MeV, exptl. study of ^{6,7}Li and ^{7}Be prod. 79−45279
^{4}He+α, 75.2 MeV, TDHF calcs. using separable three dimens. wavefunctions 78−50111
^{4}He+α break-up reactions, 130 MeV, continuous energy spectra of emitted particles 79−76013
^{4}He+$\alpha$$\rightarrow$^{6}He, ^{6}Li, ^{7}Li, ^{7}Be, 61.5-158.2 MeV, Li nucleosynthesis 79−17886
^{4}He(α,αX), 4,5 GeV/c, Thomas Reiche Kuhn sum rule appl., mean energy losses 80−91192
^{4}He(α,α), 1.37-2.55 GeV, microscopic anal. 80−47490
^{4}He(α,α), nonlocal and separable complex path *(Russian)* 77−306
^{4}He(α,αd), 119 MeV, excited states, J^π and γ-ang. correlations 80−86809
^{4}He(α,γ), 32-36 MeV, ^{8}Be isovector radiative decay, E2-M1 mixing ratio, conserved vector currents 79−6488
^{4}He(α,n)^{7}Be, ^{4}He(α,p)^{7}Li, α-α scatt. phase shifts, cross sections near threshold 79−3163
^{4}He(α,n)^{7}Be, differential cross sections meas., 39 to 50 MeV 78−25207
^{4}He(α,p)^{7}Li, differential cross sections meas., 39 to 50 MeV 78−25207
^{174}Hf(α,2n), gamma deexcitation mechanism of rot. levels 79−26442
^{177}Hf(α,3nγ), 38 MeV, ^{178}W high spin rot. levels and bands 79−26359
^{180}Hf(α,2nγ), 26 MeV, rot. and intrinsic struct. of ^{182}W determ. 77−41914
^{A}Hg(α,f) (A=198 to 204), 41 and 65 MeV, cross section, fragment mass distrib. 77−38307
^{198}Hg(α,2n), 30 MeV, levels of ^{200}Pb and isomers 78−66192
^{202}Hg(α,3nγ), 38.2 MeV, γ-spectra obs., ^{203}Pb decay scheme determ. 78−29489
^{204}Hg (α,4n), yrast levels in ^{204}Pb, spin, parity, γ spectra 78−12954
^{204}Hg(α,5n), 53-5 MeV, ^{203}Pb in-beam electron conversion from high spin states 79−93554
^{62}Hi(α,^{3}He), 172.5, 140 MeV, plane wave spectator model anal. n momentum distrib. in α 79−54445
^{165}Ho(α,2n)^{167}Tm, levels and transitions 80−73766
^{165}Ho(α,2nγ), 21-27 MeV, ^{167}Tm rotational bands, J^π, γ-transitions and branching ratios 80−86781
^{165}Ho(α,2nγ)^{167}Tm, energy level scheme *(German)* 80−68576
^{165}Ho(α,6n)^{163}Tm, high spin rot. levels in ^{163}Tm 78−8722
^{165}Ho(α,t)^{166}Er, 2-quasiparticle states obs. 80−18198
I+α, ^{127,129}Cs yield 79−67760
^{127}I(α,2n), ^{129}Cs $11/2^-$ isomer, g-factor and lifetime in CsI cubic environment MeV, ^{129}Cs $11/2^-$ isomer, g-factor and lifetime in CsI cubic environment 79−6394
^{127}I(α,2n)^{129}Cs, band struct. of ^{129}Cs, in-beam γ-ray spectroscopy 78−4951
^{127}I(α,4n), ^{127}Cs collective quadrupole dynamics, band struct., transitions, collective model anal. 80−78112
I(α, 2n), ^{A}Cs A=127, 129, 131, 133, high spin states and collective properties 79−22170
^{113}In(α, 2nγ)^{115}Sb, 20-30 MeV, high-spin states in ^{115}Sb anal. 77−41982
^{115}In(α,2nγ), 22 Mev, ^{117}Sb M2, E3 transition reduced matrix elements, EM core polarisation 79−17847
^{115}In(α,4n), 48 MeV, ^{115}Sb g-factor of $19/2^-$ and $11/2^-$ isomers 79−40845
^{115}In(α,xn), 16-38 MeV, Sb isomer ratio, high spin trapping 80−22655
Ir(α,xn), ^{A}Au A=190, 192, 194, levels, J^π, isomers and rot, aligned bands 80−9215
Ir(α,xnγ), 51, 77 MeV, ^{A}Au, A=189, 191, 193, high spin states and transitions, isomeric states 80−5038
^{39}K(α,p), 9.5, 16 MeV, ^{42}Ca high spin states, lifetimes, multipole mixing ratios 78−50186
^{39}K(α,pγ), 15.1 MeV, ^{42}Ca high spin state density, γ-decay mode, deformed states 80−32168
^{41}K(α,d)^{43}Ca, 40 MeV, four-particle one-hole states 78−21580
^{41}K(α,n)^{44}Sc, 5-11 MeV, ^{44}Sc mean lifetimes deduced 77−6299
^{82}Kr(α,n), 14-21 MeV, in-beam γ-ray spectra, high-spin states of ^{85}Sr obs. 77−41915
^{84}Kr(α,3n), 35-45 MeV, in-beam γ-ray spectra, high-spin states of ^{85}Sr obs. 77−41915
Kr(α,xn), ^{81,83}Sr yrast and high spin states of neutron deficient isotopes 80−73776
Kr(α,xn), 16-45 MeV, ^{83}Sr high spin states, J^π and de-excitation 80−42516
^{16}L(α,d)^{18}F, 29.8 MeV, cluster form factors, DWBA calcs. 79−6643
^{139}La(α,4n), ^{139}Pr medium spin states, J^π, transitions and shape 80−86779
Li+α, gamma-ray spectra from elements within ^{241}Am(n,α) source 79−3269
^{6}Li, 180° prod. of protons in high-energy reacts. 78−8816
^{6}Li+α, 18 GeV/c, π^- multiplicity distribs. *(Russian)* 78−41742
^{6}Li+α system, exchange effects, resonating-group study 80−9240
^{6}Li(α, $\chi\pi$), 18 GeV, π multiplicity distrib. 79−97713

alpha particle-nucleus reactions continued
^{6}Li(α,αd)α, 42 MeV, α-α final state interaction 77−61442
^{6}Li(α,αp), 140 MeV, quasifree p knockout, spectroscopic factors, DWIA anal. 79−67650
^{6}Li(α,γ), 1140-1250 keV, ^{10}B 1175 keV level resonance strength 79−45228
^{6}Li(α,γ), 1.02-1.18 MeV, ^{10}B T=1 states, γ-transition strengths, lifetimes, branching and mixing ratios 80−27594
Li(α,γ), 0.96 MeV, ^{11}B analog of ^{11}C 6478 keV state, lifetime 80−5092
^{176}Lu(α, 2n), 23-27 MeV, ^{178}Ta level properties, rot. bands, transitions and level lifetimes 79−36158
Mg, α capture, giant quadrupole resonance strength 78−37323
^{24}Mg (α,Li*), unbound Li, relative energy distrib. of correlated decay products 79−13274
^{24}Mg (α,α^{1} ^{12}C), 120 MeV, symmetric fission, resonances and average partial widths 80−42714
^{24}Mg(α, ^{12}C)^{16}O, 12.7-17.4 MeV, quasimol. resonance in excitation function, ^{12}C+^{16}O system, spins 78−54775
^{24}Mg(α, n)^{27}Si, threshold to 27 MeV, excitation functions, non-statistical reaction contribs. 77−82939
^{24}Mg(α,^{12}C)^{16}O, 22-26 MeV, intermediate resonances in ^{12}C+^{16}O system, J$^{\pi}$ assignments 79−17880
^{24}Mg(α,^{12}C)^{16}O, E$_{\alpha}$=90 MeV, reaction mechanism 79−6646
^{24}Mg(α,^{6}Li), 46 MeV, finite range DWBA anal. 77−14142
^{24}Mg(α,α'), 120 MeV, ground and gamma band excitation, coupled channel calcs. in rotational model 79−89315
^{24}Mg(α,γ), 1.5-3.8 MeV, determ. of ^{28}Si levels and resonances 78−66205
^{24}Mg(α,n)^{27}Si, threshold to 13.1 MeV, total cross section 78−618
^{24}Mg(α,nγ)^{27}Si, 12.60-16.35 MeV, ang. correl. and lifetime meas. 78−17224
^{24}Mg(α,p)^{27}Al, 25-26 MeV, high spin selectivity 77−23097
^{24}Mg(α,p)^{27}Al, 3.38 to 3.52 MeV, test of detailed balance at isolated resonances and time reversibility 79−45260
^{26}Mg(α,^{6}He), ^{24}Mg ground and γ-bands, direct and multistep processes 80−102094
^{26}Mg(α,2p), ^{28}Mg radionuclide yield 80−32290
^{26}Mg(α,xp), up to 156 MeV, including prod. of ^{28}Mg, excitation functions 77−3021
^{55}Mn(α,α), 4.5 to 7 MeV, Coulomb excitation, search for 1.29 MeV 1/2^{-} level 78−82360
^{55}Mn(α,pγ), 10 MeV, ^{58}Fe energy level lifetimes up to 4213 keV 79−17853
^{55}Mn(α,pγ), 12 to 24 MeV, ^{58}Fe high spin states, decay props., γ-γ coincidence 78−21515
Mo, activation in cyclotron by p, d, α, ^{3}He 79−30839
Mo bombardment, yields of Tc isotopes, energy depend. 77−23098
Mo+α, A=92,96,100, isobaric yield curves at A=72 from high energy spallation 78−25211
^{92}Mo(α,nγ), ^{95}Ru level scheme, low lying states, g-factor 77−88071
^{92}Mo(α,p2n) 43 MeV, ^{93}Tc 17/2^{-} isomer, internal conversion coeffs., parity mixing search 78−78255
^{100}Mo(α,4n)^{100}Ru, 45 MeV, negative parity bands obs. in ^{100}Ru 77−6291
Mo(α, xn)^{97}Ru, in compact cyclotron, ^{97}Ru chem. separation 77−37054
^{14}N+α, spallation fragments 6$\leq$A$\leq$11 yields, nucleosynthesis interest 79−30845
^{14}N(α,d), determ. of widths of the 14.32 and 14.40 MeV levels in ^{16}O 79−93513
^{14}N(α,γ), 1.51-1.62 MeV, populating ^{18}F 5603 keV level, isospin mixing 78−543
^{14}N(α,γ), 2.35-2.53 MeV, ^{18}F J$^{\pi}$=3 doublet at 6241 keV, isospin mixing 80−511
^{14}N(α,γ)^{18}F, hadronic nuclear-parity violation with change of isospin, γ spectrum search 78−94018
^{15}N(α,γ), 1.68-1.85 MeV, ^{19}F low lying band state lifetimes, stopping power, transition strengths 80−42585
^{15}N(α,γ)^{19}F, 2.8 to 4.0 MeV, ^{19}F reson. strengths and ang. distrib. 77−65211
^{15}N(α,γ)^{19}F, 5.2 to 8.4 MeV, resonances and gamma decay schemes 78−37358
^{15}N(α,γ)^{19}F, energy levels from α-^{15}N and t-^{16}O coupled channel orthogonality condition model 80−37326
^{60}N(α,pnγ), 22-35 MeV, ^{62}Cu high spin states, level scheme *(French)* 78−21496
^{64}N(α,nγ), 8.2 MeV, ^{67}Zn, γ spectroscopy of low spin states 78−78303
Nb bombardment, yields of Tc isotopes, energy depend. 77−23098
^{93}Nb(α, X), 15-72 MeV, excitation functions and spallation cross-sections 80−18274
^{93}Nb(α,2n), 23-7 MeV, proton-neutron excitations in high-spin states of ^{95}Tc 78−17225
^{93}Nb(α,2nγ)^{95}Tc, 17 to 27 MeV, band struct. of high momentum states in TC 78−33109
^{93}Nb(α,n) 13-27 MeV, ^{96}Tc, high spin states, γ-energy, intensity, coincidence, ang. distrib. and electron conversion 80−52554
^{93}Nb(α,n)^{96}Tc 10.8, 14.0 MeV populating ^{96}Tc low-lying levels 77−2931
^{93}Nb(α,xn) (x=1 to 4), $^{93-96}$Tc excitation functions and isomer ratios 80−492
^{A}Nd(α,xn), A=144,146, 20 to 43 MeV, ^{146,147}Sm excited states, energy levels, spin, parity, shell and cluster-vibration models 80−57683
^{142}Nd(α,4n), 60 MeV, ^{142}Sm isomers, lifetimes and transitions 80−78122
^{146}Nd(α,4n), 47.9 MeV, ^{146}Sm, high spin states and transitions 79−6423
^{146}Nd(α,pn), 29-59 MeV, ^{148}Pm^{m,g} isomeric pair prod. 77−88144
^{148}Nd(α,3nγ)^{149}Sm, 35-45 MeV, collective band struct. of ^{149}Sm anal. 77−61342
^{150}Nd(α,4n), 45 MeV, fusion and neutron evaporation, ^{150}Sm γ spectra 79−36291
^{150}Nd(α,4n)^{150}Sm, 45 MeV, yrast bands in Sm anal. in interacting boson approx. 78−13124
^{150}Nd(α,α'), 11.5-12 MEV, e$_{2}$ and E$_{3}$ transition strengths meas. 77−26618
^{150}Nd(α,n)^{153}Sm, 14 to 22 MeV, theoretical and expt. study of ^{153}Sm 79−58999
^{150}Nd(α,xn), 40-110 MeV, Sm, equilibrium and pre-equilibrium decay, α-multiplicities, energies and entry lines 79−93549
Nd(α,X), 20-37 MeV, ^{A}Sm, A=148,9, structural connections, levels, bands, J$^{\pi}$, transitions and mixing ratios 79−63576
^{20}Ne+α, 18 GeV/c, π^{-} multiplicity distribs. *(Russian)* 78−41742
^{20}Ne(^{4}Ne, ^{8}He), 117 MeV, ^{16}Ne mass excess and diproton decay width 78−78245

alpha particle-nucleus reactions continued
^{20}Ne(α, γ), 2.7-6 MeV, ^{24}Mg radiative decays of unbound high spin states, resonance J$^{\pi}$ assignment 79−67701
^{20}Ne(α,2α)^{16}O, DWIA 77−34273
^{20}Ne(α,γ), ^{24}Mg, K$^{\pi}$=0 , K$^{\pi}$=3^{-} bands, radiative and α-widths 80−18173
^{20}Ne(α,γ), 3.0-6.0 MeV, ^{24}Mg radiative decays of unbound high spin states 79−6484
^{20}Ne(α,γ), 4-16 MeV, ^{24}Mg Coulomb matrix elements, isospin mixing in giant dipole resonance 79−93507
^{20}Ne(α,γ)^{24}Mg, radiative width of 8^{+} member of 2^{+} band in ^{24}Mg meas. 77−71613
^{20}Ne(α,p), 39.5 MeV, ^{23}Na levels and spectroscopic amplitudes, J$^{\pi}$ assignments, high spin states 79−75848
^{22}Ne(α,n)^{25}Mg neutron source effects in red giants and planetary nebulae 78−49430
^{22}Ne(α,nγ)^{25}Mg, particle-gamma and gamma-gamma coincidence, energies and branching ratios 77−22892
Ne(α, $\chi\pi$), 18 GeV, π multiplicity distrib. 79−97713
Ni+α, 100 MeV, fireball and coalescence model anal. 79−93642
^{A}Ni(α,γ), A=62, 64, 4.5-8.6 MeV, excitation function competition cusps, Mauser-Feshbach calcs. 80−13404
^{A}Ni(α,n), A=62, 64, 5.3-8.7 MeV, excitation function competition cusps, Mauser-Feshbach calcs. 80−13404
^{58}Ni, (α,p), (α,d) and (α,t) reactions, 50.5 MeV, particle spectra 77−6405
^{58}Ni(α,^{8}He), 110 MeV, ^{54}Ni proton rich nucleus, Q values, mass excesses 77−88162
^{58}Ni(α,X), 140 MeV, nonequilibrium light charged particle yield, energy spectra and ang. distribs. 79−40942
^{58}Ni(α,X), 20, 40 MeV/N, α breakup yield, fragment yield ratios 80−9300
^{58}Ni(α,α'c), 150 MeV, c=charged particle, particle decay from isoscalar giant resonance region 80−13439
^{58}Ni(α,p), 6.26-9.12 MeV, excitation functions, resonance struct., α-widths of ^{62}Zn states 77−30617
^{58}Ni(α,pγ), 17 and 19.5 MeV, ^{61}Cu γ-cascade multiplicities, entry state depend. on excitation energy 78−82311
^{58}Ni(α,tp), double differential cross section, t-p ang. correlation function, direct breakup 80−22797
^{60}Ni, (α,p), (α,d) and (α,t) reactions, 50.5 MeV, particle spectra 77−6405
^{60}Ni(α,2n)^{62}Zn excitation function, and prod. of ^{62}Zn-bleomycin 78−28067
^{60}Ni(α,2nγ), 28-35 MeV, in beam gamma spectroscopy of ^{62}Zn 77−6297
^{60}Ni(α,nγ), 10-14 MeV, ^{63}Zn level scheme, spin and parity assignments 79−465
^{60}Ni(α,nγ), 9.5-19.0 MeV, ^{63}Zn EM decay transitions, level J$^{\pi}$ assignments, level lifetimes 79−85402
^{60}Ni(α,nγ)^{63}Zn, 8-16 MeV, low-lying negative parity states of ^{63}Zn anal. 78−21521
^{60}Ni(α,pγ), 10 MeV, ^{63}Cu low excitation states, level struct. and lifetimes 80−86813
^{60}Ni(α,pγ), 9.5-19.0 MeV, ^{63}Cu EM decay transitions, level J$^{\pi}$ assignments, level lifetimes 79−85402
^{60}Ni(α,pnγ)^{62}C, mag. hyperfine interaction, ^{62}Cu 390 keV isomeric state 77−2903
^{61}Ni(α,X), 35.5 MeV, ^{66}Zn* composite particle emission, ang.-distribs., exciton-coalescence model 80−78265
^{61}Ni(α,X), X=p, d, t, ^{3}He, α, 35.5 MeV, continuous spectra and ang. distribs. meas. 77−3016
^{61}Ni(α,nγ), 8.6, 9.35 MeV, ^{64}Zn high spin states, J$^{\pi}$, T$_{1/2}$, γ-decays 80−73767
^{61}Ni(α,nγ)^{64}Zn, 7.8 MeV, γ-ray spectroscopy Zn levels below 3.1 MeV 78−21514
^{62}Ni(α, nγ), 8-14 MeV, γ ray study of ^{65}Zn odd-parity states, energies, transitions 78−50120
^{62}Ni(α,nγ), 8.2 MeV, ^{65}Zn lifetimes 77−74804
^{64}Ni(^{4}He,^{6}He), 80 MeV, spectroscopy to determine ^{8}He mass 78−25106
^{64}Ni(^{4}He,^{8}He), 80 MeV, spectroscopy to determine ^{8}He mass 78−25106
^{64}Ni(^{4}He,^{8}He)^{60}Ni, angular distrib., evidence of direct process in (^{4}He,^{8}He) reaction 78−29488
^{64}Ni(α,n), (α,2n), 17-25 MeV, level struct. of ^{66}Zn, ^{67}Zn determ. 77−46178
^{64}Ni(α,n)^{67}Zn, 6.5 to 17.0 MeV, γ ray studies of levels below 2.0 MeV in ^{67}Zn 78−62483
Ni(α,^{3}He), 172.5 MeV, double-differential cross-sections determ. 78−82363
Ni(α,X)Zn, α spectroscopic factors in shell model 79−45158
Ni(α,nγ)Zn, 6.5-17 MeV, particle-vibr. coupling in ^{65,67}Zn 77−38241
^{237}Np(^{4}He,f), (^{4}He,n), (^{4}He,2n), E=17.5-22.5 MeV excitation function meas. 78−656
^{237}Np(α,f), fragment mass distrib., and yield, statistical anal. *(Russian)* 80−5183
Np(α,xn) ^{241}Am, neutron emission probability and fissionability energy depend. 78−655
^{16}O (α, 2α), DWIA calc., cross section and spectroscopic factors 79−63681
^{16}O+^{4}He, 3-D TDHF calcs. 78−54781
^{16}O+^{4}He, group theory appl. to reaction studies 80−9276
^{16}O+α, spallation fragments 6$\leq$A$\leq$11 yields, nucleosynthesis interest 79−30845
^{16}O+α nucleon exchange and backangle anomaly 79−6638
^{16}O+p(d)(α) transparency in composite particle reactions 80−9273
^{16}O(^{4}He,^{8}He), 117 MeV, ^{12}O mass excess and diproton decay width 78−78245
^{16}O(α,2α), determ. of spectroscopic factors by DWIA 79−6639
^{16}O(α,2α)^{12}C, DWIA 77−34273
^{16}O(α,α'+charged particle), 155 MeV, α-decay dominance in ^{16}O isoscalar giant quadrupole resonance 78−46035
^{16}O(α,α'), inelastic scatt. from 8.88 MeV 2^{-} state, magnitude and ang. distribs. of cross sections at 40.5 and 65 MeV 79−49631
^{16}O(α,α')^{16}O, 3.05 MeV elastic scatt. reson., appl. to O concentration determ. in Au-Si contacts 79−4482
^{16}O(α,d), 1.12 MeV, forward peaking variation, DWBA with optical pots., ang. distribs. 80−13488
^{16}O(α,d)^{18}F, 28 to 33.6 MeV, forward angle yield, optical potential of incident channel 78−58291
^{16}O(α,d)^{18}F production on SiO$_{2}$ target 79−79650
^{16}O(α,γ), 10.27 MeV, radiative widths of T=1,2^{+} state of ^{20}Ne 78−549

alpha particle-nucleus reactions continued
^{16}O(α,γ), 3.0-9.5 MeV, ^{20}Ne levels, J^{π}, branching ratio and EM transition rates 80−42540
^{16}O(α,γ), CC ^{20}Ne 8^{+} level radiative width, resonance strength 80−83065
^{16}O(α,γ), uncorrelated target, optical pot. unitary content, DWIA and Glauber theory 80−105947
^{16}O(α,γ) 8.18 MeV 79−22189
^{16}O(α,γ)^{20}Ne, 6.9-10.2 MeV, level and isospin mixing parameters 78−66292
^{16}O(α,p), 20.1 MeV, level struct. of ^{19}F, spin, parity *(Spanish)* 77−67756
^{16}O(α,p), comparison with ^{12}C(α,p) direct evidence for 3p-4h excitations in ^{15}N 79−67659
^{16}O(α,p)^{19}F, 40 MeV, populating ^{19}F levels, J^{π}, spectroscopic factors 77−14140
^{17}O(α,d)^{19}F, 47.5 MeV, population of positive parity states, DWBA anal. 78−70548
^{17}O(α,n), 1.4-2.3 MeV, decay width of lowest $T=3/2$ level of ^{21}Ne 77−6322
^{18}O(α,γ), 0.6 to 2.3 MeV, props. of ^{22}Ne compound states, astrophys. reaction rate 78−57545
^{18}O(α,nγ)^{21}Ne, 4.3-6.5 MeV, excitation functions meas. 78−8833
O(α,X), 16.5 GeV/c, inelastic cross sections, multiplicity, ang. and momentum distribs. 78−82359
O(α,n), exam. of neutron yield 80−86912
^{182}Os(He,xnγ), K-isomer population levels 78−93927
^{189}Os(α,2n), 23-27 MeV, ^{191}Pt level scheme, γ, conversion electron spectra, spins, parities 78−25149
^{31}P(α,n), 14.4 MeV, obs. of ^{34}Cl high spin states 78−82289
^{31}P(α,n), high spin negative parity states in ^{34}Cl, lifetime meas. 78−74327
^{31}P(α,n) 13.0, 14.6 MeV, ^{34}Cl negative parity high spin states, ang. distribs. and lifetimes 79−17812
^{31}P(p,γ)^{32}S resonances below $E_p=1.5$ MeV 77−50141
Pb, binary fission characts. induced by α-particle bombardment of 0.65 to 4.12 GeV 78−13169
^{208}Pb(α,4n), 41-51 MeV, yrast states in ^{208}Po anal. 78−78307
^{208}Pb(α,αp) 96.8 MeV, proton pickup by α-particles to unbound states DWBA anal. 79−22305
^{208}Pb(α,d)^{210}Bi, 33 and 48 MeV, two-step contrib. in two-nucleon transfer reactions 78−82364
^{208}Pb(α,n), excitation functions and isomer ratios of ^{211}Po 80−83039
^{208}Pb(α,t), 40 MeV, effective residual interaction matrix elements, spectroscopic factors, cross sections 80−99134
Pb(α,X), 3.6 GeV proton emission invariant cross sections *(Russian)* 80−13500
Pb(α,X), 3.6 GeV/N, secondary particle ang. and vel. distribs., π,p,d,t prod. *(Russian)* 80−63194
Pb(α, $\chi\pi$), 18 GeV, π multiplicity distrib. 79−97713
Pb(α,d)Bi, 48 MeV, spectra and ang. distrib. obs., Bi two-particle states anal. 77−38289
Pb(α,f), 0.65, 1.74, 4.12 GeV, and using polycarbonate detector 78−13178
Pb(α,f), 0.65, 1.74, 4.12 GeV, fission fragment recoil characts. 78−89925
Pb(α,p), 35.5 MeV, DWBA anal. of ^{211}Bi 410 keV state single particle component 77−88034
Pb(α, p), 3.6 GeV, max. in p ang. distrib. *(Russian)* 79−36253
^{102}Pd(α,2nγ), 20-27.5 MeV, ^{104}Cd quasirot. ground state band and γ-transition 80−105955
^{102}Pd(α,2nγ)^{104}Cd, high-spin states in ^{104,105}Cd anal. 78−62484
^{102}Pd(α,nγ)^{105}Cd, high-spin states in ^{104,105}Cd anal. 78−62434
^{104}Pd(α,3nγ)^{105}Cd, high-spin states in ^{104,105}Cd anal. 78−62484
^{104}Pd(α,pnγ), ^{106}Ag low-lying excited states 80−57693
^{105}Pd(α,2n)^{107}Cd, g-factor of 845.6 keV state, differential PAC 77−6225
Pd(α,3nγ), 35-44 MeV, obs. of high spin states in Cd nuclei 80−450
Pd(α,d)Bi, 48 MeV, mass excess of Bi calc. 77−10312
^{141}Pr(α,2n), 22.7-77 MeV, ^{143}Pm high spin states, J^{π}, transitions, isomer g-factors 80−32154
^{141}Pr(α,4n), ^{141}Pm medium spin states, J^{π}, transitions and shape 80−86779
^{195}Pt(α,2n), 23-27 MeV, ^{197}Hg level schemes, γ and conversion electron spectra, spins, parities 78−25149
Pt(α,d), A=194, 196, 198, 35.1 MeV, stripping strength, Au excitation energies, high spin states 78−78398
Pt(α,xn), Hg isotopes, level energies, B(E2) values, rot. aligned bands 78−70483
^{239}Pu(α,f), 19-27 MeV, integral and differential cross sections, anisotropy energy depend. *(Russian)* 80−37407
^{242}Pu(α,f), fragment mass distrib., and yield, statistical anal. *(Russian)* 80−5183
Pu(α,n), determination system by passive neutron counting 79−40985
^{85}Rb(α,2nγ), 24-36 MeV, ^{87}Y level struct., γ-spectroscopy and J^{π} 80−83040
^{87}Rb(α,2nγ), ^{89}Y high spin states and decay scheme 80−32166
^{87}Rb(α,2nγ), 30-55 MeV, ^{89}Y high spin states from γ-ang. distribs. 78−93941
^{87}Rb(α,3n), 40.1 MeV, ^{88}Y 14 ms 8^{+} isomeric state, g-factor 80−63080
Re(α,xn)^{185}Ir, levels of ^{185}Ir excited in reaction 80−9231
^{103}Rh, (α,p), (α,d) and (α,t) reactions, 50.5 MeV, particle spectra 77−6405
^{103}Rh(α, 2nγ), 17-32 MeV, ^{105}Ag high spin states and bands, g-factor and isomeric state 79−36125
^{103}Rh(α, 3nγ), 33-55 MeV, ^{104}Ag levels, J^{π}, $T_{1/2}$, bands and transitions 80−102093
^{103}Rh(α, 4nγ), 35-52 MeV, ^{103}Ag high spin states, bands transitions, intermediate deformation Coriolis coupling 80−105944
^{103}Rh(α,2n), obs. of ^{105}Ag high spin states 77−22936
^{103}Rh(α,nγ), ^{106}Ag low-lying excited states 80−57693
Rh(α,^{5}He), 90 MeV, α-n coincidence, ^{5}He breakup kinematics 77−6419
^{98}Ru (α,pn), ^{100}Rh short lived isomer, decay scheme 79−75920
^{33}S levels, excited by α-capture reactions 78−33124
^{34}S(A,p), 16-22 MeV, ^{37}Cl high spin state decay, spin assignments, yrast level lifetime 79−6490
^{34}S(α,Γ)^{38}Ar, 2-3.5 MeV, reson. levels, mixing ratio 79−71859
^{36}S(α,nγ), 6.0-7.8 MeV, ^{39}Ar, energy level spin and parity assignments, level spectroscopy 78−93943
^{32,33,34}S(α,d), 40 MeV, populating high-spin states, L-transfer 77−74865
Sb(α,2nγ), collective excitations in ^{123,125}I, spin, parity, level schemes 78−4891

alpha particle-nucleus reactions continued
^{45}Sc(α,p), 26 MeV, ^{48}Ti levels and transition ang. distribs., form factors, DWBA anal. 79−45202
^{45}Sc(α,pγ), ^{48}T excited states, level struct., lifetimes, from DSA and pγ coincidence meas. 78−74326
^{45}Sc(α,pγ), 11, 12, 13 MeV, ^{48}Ti high spin states, γ-decay, J^{π} assignments, lifetimes 80−13356
^{45}Sc(α,pγ), 11 MeV, high spin states in ^{48}Ti 78−74378
^{45}Sc(α,t), 27.2 MeV, cross sections, optical potential, spectroscopic factors *(Russian)* 77−38290
^{77}Se(d,2np), ^{78}Br high-spin states, decay into isomers 80−52569
^{28}Si(α,^{2}He)^{30}Si, 65 MeV, spectrum ang. distrib. meas. 78−29492
^{28}Si(α,^{8}He), ^{24}Si, Q value and mass excess 80−86795
^{28}Si(α,α'c), c=charged particle, 150 MeV, isoscalar giant quadrupole resonance struct. 80−13438
^{28}Si(α,dγ), 50 MeV, ^{30}P high spin two nucleon states decay props. 80−13402
^{28}Si(α,γ), 4-16 MeV, ^{32}Si Coulomb matrix elements isospin mixing in giant dipole resonance 79−93507
^{28}Si(α,γ)^{32}S resonances below $E_{\alpha}=3.83$ MeV anal. 77−50141
^{28}Si(α,n)^{31}S, cross sections and thermonuclear reaction rates 80−73852
^{28}Si(α,p)^{31}P, proton polarisation calcs., distorted wave method 77−6404
^{30}Si(α,n), threshold to 6.3 MeV, total n prod. cross sections, statistical model parameters, nucleosynthesis 79−9602
Si(α,γ), 4-16 MeV, ^{A}S, A=32,34, E1 and E2 strength, E1 giant resonance decay, isospin 79−89266
Sm (α, xn), ^{A}Gd, A=146.7, particle hole yrast states and Z=64 shell closure 79−49571
^{144}Sm(α,2np), 50 MeV, ^{145}Eu high spin levels, isomers and in-beam γ-spectroscopy 80−78124
^{144}Sm(α,2npγ), 50 MeV, ^{145}Eu high spin and isomeric states, transitions, weak coupling 80−13348
^{144}Sm(α,3n), 50 MeV, ^{145}Gd levels, J^{π} and transitions, neutron hole coupling to ^{146}Gd core 80−78164
^{144}Sm(α,4nγ), 60-110 MeV, ^{144}Gd level scheme, delayed transitions, in-beam study 79−17809
^{148}Sm(α,t), 27 MeV, ^{149}Eu proton states and transitions shell model anal. 79−30781
^{148}Sm(α,xn)^{146}Gd, high multiplicity yrast isomers prod. 78−41666
^{149}Sm(α,xn)^{147}Gd, high multiplicity yrast isomers prod. 78−41666
^{150}Sm(α, 2n), 19, 27 MeV, ^{152}Gd β- and octupole bands, downbending moments of inertia 80−91131
^{150}Sm(α,3nγ)^{151}Gd, 35-45 MeV, collective band struct. of ^{151}Gd anal. 77−61342
^{150}Sm(α,4n), obs. of ^{150}Gd negative parity yrast states 77−88033
^{150}Sm(α,xn) reactions, γ-ray multiplicities meas. at beam energies 40 to 140 MeV 78−21585
^{152}Sm(α,2n), gamma deexcitation mechanism of rot. levels 79−26442
^{152}Sm(α,2nγ), 24 MeV, ^{154}Gd levels from γ ang. distribs. 79−442
^{152}Sm(α,6n), obs. of ^{150}Gd negative parity yrast states 77−88033
^{154}Sm (α,^{6}He), ^{152}Sm ground and γ-bands, direct and multistep processes 80−102094
^{154}Sm(α,t), 25 MeV, ^{155}Eu single proton states, spins and parity, rot. bands 79−30766
Sm(α,α'), 11.5-12 MeV, E_2 and E_3 transition strengths meas. 77−26618
Sm(α,xnγ), 28,50 MeV, ^{152}Gd N=88 nuclei quasirot. bands and J^{π} 80−83025
^{A}Sn(α,2n)$^{A+2}$Te, A=115,117,119, $\Delta J=1$ band structures on ns isomeric states in odd mass 79−54382
^{112}Sn(A,n)^{115}Te, nuclear alignment of ^{115}Te temp. depend. 78−41720
^{116}Sn(α,p), 35.6 MeV, ^{119}Sb intrinsic high spin state population, cluster DWBA anal. 79−67630
^{118}Sn(α,2nγ), ^{120}Te quasi-rot. band based on proton 4p-2h state, level scheme, transitions 80−78119
^{118}Sn(α,n), 24 MeV, ^{121}Te isomeric state, spin, lifetime and mag. moment 80−47387
^{120}Sn(α, p), semi-microscopic spectator model 77−26779
Sn(α,α'), even-even isotopes, nuclear struct. effects in microscopic theory 80−37391
Sn(α,pn), 16-38 MeV, Sb isomer ratio, high spin trapping 80−22655
Sn(d, 2n), 19.8-27 MeV, ^{A}Te, A=117, 119, 121, collective excitations, high spin states and transitions 80−13346
^{84}Sr(α, n)^{87}Zr, in-beam γ-ray spectroscopy of excited states of ^{87}Zr 79−17852
^{84}Sr(α,nγ), 16.7 MeV, high spin states in ^{87}Zr 78−74383
^{84}Sr(α,p), 18 MeV, low-lying states of ^{87}Y anal. 78−17228
^{86}Sr(α, 2nγ)^{88}Zr, study of ^{88}Zr high spin states above 8^{+} isomer 79−40848
^{86}Sr(α, 3n)^{87}Zr, in-beam γ-ray spectroscopy of excited states of ^{87}Zr 79−17852
^{86}Sr(α, nγ), ^{89}Zr high spin states, J values, γ ang. distrib. 79−89217
^{88}Sr(α, 2nγ), ^{89}Zr high spin states, J values, γ ang. distrib. 79−89217
Sr(α,2nγ), 28, 35 MeV, high spin states in ^{86,88}Zr 78−74383
Sr(α,xn), ^{85}Zr yrast and high spin states of neutron deficient isotopes 80−73776
Ta, 180° prod. of protons in high-energy reacts. 78−8816
Ta+α, 720 MeV, correlated energy spectra of light fragments, fireball and coalescence models 78−62555
Ta(A,X), 720 MeV, nuclear fragment prod. thermodynamic evaporation and firestreak description, pre-equilibrium emission 79−54426
Ta(He,X), 4.2 GeV.c^{-1}, inelastic cross section meas. and multiplicities obs. *(Russian)* 79−9580
^{181}Ta+α, 4.2 and 5.15 GeV, central nuclear collisions, pion multiplicity calc. *(Russian)* 79−59079
^{181}Ta(α,X), 4.2 GeV/c, multitudes of secondary negative particles, momentum distrib. ratios *(Russian)* 80−63178
Ta(α,X), 4.2 GeV/N, multiple π^{-} prod., mean multiplicity *(Russian)* 80−27647
Ta(α,X) X=p,d,t,^{3}He,^{4}He, 720 MeV, back-angle prod. of light ions, model calcs. 79−45280
^{159}Tb(α,4nγ)^{159}Ho, use in determ. ^{159}Ho energy levels 77−26556
^{159}Tb(α,5n)^{158}Ho, isomeric state and rotational band in ^{158}Ho 77−2890
^{A}Te(α,nγ)Xe, 16 MeV, A=126, 128, props. of low-lying levels of Xe 80−464
^{A}Te(α,t)I, 36 MeV, A=124 to 130, comparative study of $^{121\text{ to }131}$I proton states 79−63572
^{124}Te(α, 3n), ^{125}Xe $11/2^{-}\rightarrow9/2^{-}$ transition in odd parity band 80−9203
Te(α,f), fission fragments tracklength and ang. distribs., fission moment of inertia 77−50182
Te(α,t) 35 MeV, ^{A}I, A=121, 123, 125, mass excesses, ^{121}I energy levels 78−78246

alpha particle-nucleus reactions continued
Te(α, xn)^{125}Xe, prod. of ^{125}Xe for medical use using natural Te 78−3604
^{232}Th, ^{4}He ion-induced fission, ^{148m}Pm, ^{148g}Pm independent form. cross-sections 78−33228
^{232}Th(α,X), 140 MeV, nonequilibrium light charged particle yield, energy spectra and ang. distribs. 79−40942
^{232}Th(α,4nγ), 40 MeV, ^{232}U high spin states and ground state rot. band 80−47349
^{232}Th(α,f), 19-27 MeV, integral and differential cross sections, anisotropy energy depend. *(Russian)* 80−37407
^{232}Th(α,f), 25.8-41.4 MeV, fragment ang. momentum determ. 77−82975
^{232}Th(α,f), 640MeV 80−95329
^{232}Th(α,x), 140 MeV, spallation and fission product yields 80−13512
Th(α,f), 0.65, 1.74, 4.12 GeV, fission fragment recoil characts. 78−89925
Th(α,f), 0.65-4.11 GeV, cross sections for binary and ternary fission 77−3055
^{46}Ti(α,nγ)^{49}Cr, gamma-ray ang. distrib., ang. correlation, linear polarisation and Doppler-shift attenuation meas. 77−82941
^{47}Ti(α,p), 15.35 MeV, level density parameters, statistical model anal. 78−13130
^{47}Ti(α,pγ), 10 MeV, ^{50}V excited states, lifetimes 78−21583
^{48}Ti(α,pnγ)^{50}V, high-spin levels obs. by in-beam γ-spectroscopic technique *(French)* 78−21572
^{48}Ti(γ,nγ), 8.08 MeV, ^{51}Cr bands, levels, EM transitions, J^π, branching and mixing ratios 80−52606
^{50}Ti(α,Znγ), 24-33 MeV, ^{52}Cr high spin states, transitions and J^π values 80−455
^{50}Ti(α,2nγ), ^{52}Cr high spin states, spectroscopic meas. 77−65190
^{50}Ti(α,2nγ)^{52}Cr, high spin states in ^{52}Cr 78−54675
^{50}Ti(α,n), 9,11 MeV, ^{53}Cr excited state lifetimes 79−26392
^{203}Tl(α,4n), 46-55 MeV, ^{203}Bi high spin states, halflives 78−29485
^{205}Tl(α,2n), 30-43 MeV, ^{207}Bi high spin states, level decays, three particle interactions 79−49567
^{205}Tl(α,2n)^{207}Bi, spin and parity assignment of ^{207}Bi levels 78−89788
^{205}Tl(α,3n), 35-51 MeV, ^{206}Bi high-spin states anal. 78−82368
Tl(α,xn)^{205}Bi, population of high spin states, γ and conversion electron spectra 77−30616
^{169}Tm(α,6n), 72 MeV, interpretation with level scheme of ^{167}Lu 77−88026
U+^{4}He, 400 MeV nucleon^{-1}, inclusive proton production, classical many-body calc. 79−17918
UO$_2$(α,n), 3.6 to 8 MeV, neutron yields 79−6651
^{A}U(^{4}He,xn) A=233-235, x=1-4, cross sections, fission evaporation competition in Pu isotopes 78−66325
^{A}U(α,f), A=235,238, 19-27 MeV, integral and differential cross sections, anisotropy energy depend. *(Russian)* 80−37407
^{233}U(α,X), 28-140 MeV, scatt. and fission reaction mechanisms, cross sections 80−18350
^{234}U(α,t), 30 MeV, ^{235}Np deduced levels and Nilsson band configurations 79−468
^{236}U(α,α'f), 50 MeV, total KE release 78−78426
^{238}U+^{4}He, expt. and relativistic two fluid model energy spectra 78−78298
^{238}U(α,f), 23 to 115 MeV, interpretation of fragment anisotropies 77−30644
^{238}U(α,f), 640MeV 80−95329
^{238}U(α,f), fragment mass distrib., and yield, statistical anal. *(Russian)* 80−5183
^{238}U(α,xnf), 50 MeV, post and prefission neutron meas. 79−76042
U(α,^{5}He), 90 MeV, α-n coincidence, ^{5}He breakup kinematics 77−6419
U(α,f), 0.65, 1.74, 4.12 GeV, fission fragment recoil characts. 78−89925
U(α,f), 0.65-4.11 GeV, cross sections for binary and ternary fission 77−3055
U(α,xn) ^{238,239}Pu, neutron emission probability and fissionability energy depend. 78−655
^{50}V(α,d), 14 MeV, ^{52}Cr 4.57 MeV excited state, 8^+ assignment 78−74380
^{51}V(α,n), 9,11 MeV, ^{54}Mn excited state lifetimes 79−26392
^{51}V(α,nγ)^{54}Mn, Doppler shift attenuation meas. of ^{54}Mn excited state lifetimes 78−17141
^{51}V(α,pγ), 10 MeV, ^{54}Cr levels, transitions, $T_{1/2}$, J^π, shell model anal. 80−47381
^{51}V(α,t), 25 MeV, DWBA anal. of triton ang. distrib. meas. 78−54776
^{51}V(α,t), 27.2 MeV, cross sections, optical potential, spectroscopic factors *(Russian)* 77−38290
^{51}V(α,t), absolute normalisation from spin depend. sum rule anal. 80−27652
W, activation in cyclotron by p, d, α, ^{3}He 79−30839
^{A}W(α,f) (A=182 to 186), 41 and 65 MeV, cross section, fragment mass distrib. 77−38307
^{187}W+α, 2 to 5 GeV/nucleon, multiplicities of secondary particles *(Russian)* 78−46066
W(α,2nγ), 28 MeV, ^{A}Os, A=186, 188, 7^- isomeric state lifetime 79−17854
W(α,α'e^+e^-), 1.0-2.5 MeV, e^+e^- pair prod. search 80−27637
^{89}Y(α,2nγ)^{91}Nb, g-factor of $21/2^+$ state in ^{91}Nb 77−30487
^{89}Y(α,2nγ)^{91}Nb at 24.0, 35.7 MeV, high spin states in ^{91}Nb 79−93514
^{64}Zn(α,n), ^{67}Ge, EM transition, gamma ray and internal conversion electron meas. 78−89823
^{64}Zn(α,nγ), ^{67}Ge, mass excess and low lying states, comparison with ^{63,65}Ni, ^{65,67}Zn and ^{69}Ge 78−66213
^{64}Zn(α,nγ), 9-15 MeV, ^{67}Ge excited state decay scheme, mean lifetimes 79−26393
^{64}Zn(α,pγ), 7-16 MeV, ^{67}Ga level struct. 77−88042
^{64}Zn(α,pnγ), 30 MeV, ^{66}Ga high spin states, shell model interpretation *(French)* 79−3086
^{66}Zn (α, ^{8}B), 109 MeV, ^{62}Co differential cross section 80−5153
^{66}Zn(α,nγ), 11.8-16.5 MeV, ^{69}Ge excited states, lifetimes and J^π assignments, mixing ratios 79−63629
^{67}Zn(α,2nγ), ^{70}Ge level spin and parity assignments 79−3081
^{68}Zn(α,2nγ), ^{70}Ge level spin and parity assignments 79−3081
^{68}Zn(α,nγ)^{71}Ge, 8-10 MeV, statistical compound nuclear model anal. 78−8742
^{68}Zn(α,pnγ)^{70}Ga, high spin levels of ^{70}Ga 77−30611
^{70}Zn(^{4}He, ^{7}Be) pick-up reaction, ^{67}Ni mass excess 79−9452
^{70}Zn(α,2nγ)^{72}Ge, 30 MeV, determ. of high spin levels for ^{72}Ge with $J^\pi=11^-$, 12^+ *(French)* 79−22304
^{70}Zn(α,p), 26 MeV, ^{73}Ga levels, J^π and ang. distribs. 80−78161

alpha particle-nucleus reactions continued
Zn(α,p), A=64-70 even, 18 MeV, compound and pre-compound processes 77−34296
^{90}Zr (α,Zn), ^{92}Mo in beam γ-spectroscopy, level, lifetimes and excitation functions 79−13240
^{90}Zr(α,X), 140 MeV, nonequilibrium light charged particle yield, energy spectra and ang. distribs. 79−40942
^{90}Zr(α,X), 20, 40 MeV/N, α breakup yield, fragment yield ratios 80−9300
^{90}Zr(α,2nγ), 28 MeV, high spin states above 8^+ isomer in ^{92}Mo 78−89786
^{90}Zr(α,αp) 96.8 MeV proton pickup by α-particles to unbound states DWBA anal. 79−22305
^{91}Zr(α,t), 35.4 MeV, ^{92}Nb low lying multiplets, DWBA anal. for spectroscopic factors 80−57685
^{96}Zr(α,n), 20 MeV, ^{99}Mo first excited state g factor 79−17801

alpha particle-nucleus scattering
2d-1s shell, optical model and coupled-channel anal., 24.2 MeV 77−6407
A=50 to 89, α-particle elastic scatt., neutron shell sensitivity, optical model parameters 79−6642
A≤28, giant quadrupole resonance, E2 intensity distrib., from (α, α'), DWBA anal. *(Hungarian)* 80−52642
alpha-alpha interaction for coupled channels 77−18489
antisymmetrization effects in alpha-nucleus scattering 79−71826
back-angle anomalies, S-matrix continuation to complex l-plane 77−30613
backscattering by light nuclei, heavy particle transfer mechanism 77−6420
backward glory 79−71866
Brueckner-generator-coord. method, α-α scatt. 78−62487
cluster scatt. process in (2,α'), quasi-free model 77−14139
critical radii for α-particle elastic scatt., correl. with nuclear matter distribs. 79−45148
differential cross sections meas. by SPES I 79−75983
effective surface potential for α particles and its OCM justifications 79−97715
eikonal approx. and distortions in heavy particle stripping mechanism *(Russian)* 78−78337
Fraunhofer diffr. oscills. at 100, 140 MeV, refractive damping anal. 77−61445
gamma-ray line emission from nucleus de-excitation following energetic particle reactions 80−18219
giant quadrupole resonances in light nuclei excited by α or p inelastic scatt. 78−624
high-energy elastic and inelastic scatt. by light nuclei, mechanism and struct. determ. *(French)* 79−534
inelastic reactions at 3.6 GeV/nucleon 78−82358
internal S-matrix dynamics and internal deflection function 80−78307
laboratory apparatus 77−28
light ion scatt., optical pot. and proximity pot. comparison 79−3121
light nuclei, backward scatt. and heavy-particle stripping 78−13107
monopole excitations in heavy nuclei, hadron induced 78−86471
N=85 isotones, bands and transitions from α and HI excitation, in-beam study 80−78123
nucleon-alpha particle, two-channel potl., exact method for calc. 77−18488
optical model analysis of α-nucleus elastic scatt. 78−41737
phenomenological-potential constant, from phase shift, theory of complex orbital momentum 77−14145
potential scatt. at large angles 77−71614
Rutherford experiment, computer programs for high-school expts. 78−86094
Rutherford scattering, analogous demonstration by mech. expt. using mag. disc *(German)* 78−81778
sensitivity of alpha-decay to the real alpha-nucleus potential 79−97714
two-channel nucleon-alpha potential, exact method for calc. 77−18488
Z=50-83, K-X-ray nuclear satellites, by α-bombard., 17.5-22.5 MeV 80−42984
(α,α), antisymmetrisation effects, α pot. form factor, optical model anal. 78−82366
(α,α), elastic scatt. critical radius, single particle anal. 80−13490
(α,α), folding potentials, Woods-Saxon and squared Woods-Saxon parametrisations 80−102195
(α,α), total reaction cross section of ^{197}Au, ^{206}Pb, ^{209}Bi, ^{208}Pb 78−25209
(α,α) anomalous large angle scatt., optical model sensitivity 79−13309
(α,α) elastic and inelastic, by heavy nuclei, Glauber amplitude approx. scheme 79−40939
(α,α) scatt. near Coulomb barrier and matter distribs. of medium and heavy nuclei 78−66291
(α,α) scatt. on ^{12}C, ^{13}C, ^{15}N and ^{16}O, forward differential cross sections 78−25210
(α, α) scatt. on A=40 nuclei, accurate optical pots. 79−97718
(α,α'), A=40-208, low energy octupole resonances, 96 and 115 MeV 79−511
(α,α'), γ-α ang. correls., theoretical description including delay effects *(Russian)* 77−34329
(α,α') spectra of light nuclei, multipole giant resonances 78−86462
(α,n,p) elastic scatt., ^{6}Li structure three body model 79−75875
α-α, appl. of generator coordinate formalism 77−18584
α-α, pot. calc. appl. to even-even N=Z nuclei 79−6661
α-α interaction, consistent calc. by resonating group method 77−18491
α-α scatt., 75.2 MeV, TDHF calcs. in 2 and 3 dimensions 78−78401
α-α scatt., quasi-mol. struct. model of ^{8}Be 79−6397
α-α scatt. phase shift calc., microscopic wave function of ^{8}Be 78−62503
α+nucleus real pot., energy and target depend. 79−36251
$\alpha\alpha$ and NN scatt. analogies, quark struct. and clustering connections 79−6442
$\alpha\alpha$ scattering system, microscopic nucl. cluster model of ^{8}Be 78−54703
^{6}Li(α,α), resonant-group kernel function, analytical computation 79−40941
NN interaction, local density dependence, double-folding calcs. 80−83114
^{232} Th(α, α'), coupled channel Born anal. of deformation correl 80−5149
^{12}(α, α), 1.37 GeV, microscopic anal. using modified Glauber model 78−617
^{27}Al(α, α), 120-172.5 MeV, optical pot. uniqueness and shape 79−97719
^{27}Al(α,α'), 106, 120, 145, 172.5 MeV, giant quadrupole reson. obs. 77−6415
^{27}Al(α,α'), 145 MeV, excitation energy anal., octupole strength conc. 78−21584

alpha particle-nucleus scattering continued
^{27}Al(α,α')^{27}Al, 126 MeV, GQR, DWBA anal. 77−74826
^{27}Al(α,α), 41 MeV, elastic and inelastic, ang. distribs., optical and DWBA anal., scatt. pots. 79−556
^{27}Al(α,α), x=p,d,t,h,α' and x-γ, 140 MeV, reaction mechanism characts. for deformed ^{27}Al 79−63682
^{27}Al(α,x), 140 MeV, mass fragment meas., reaction mechanism models 79−63683
^{A}Ar(α,α), A=36,40, 29 MeV, energy and mass depend. of extracted optical potentials 79−49632
^{40}Ar(α,α_1), 12-15 MeV, J^π assignments for deduced levels 79−89232
^{40}Ar(α,α'), 172.5 MeV, isoscalar giant quadrupole resonance 79−45231
^{197}Au(α,α'), 120 MeV, isoscalar resonance excitation, low lying transitions, DWBA calc. 80−512
^{197}Au(α,α'), 120 MeV, new giant resonance at 80 $A^{-1/3}$ MeV 77−41939
^{10}B(α,α), 5-50 MeV, optical and Inopin-Ericson model anal. 77−3025
^{A}Ba(α,α') A=135,137, 9.7-12.2 MeV, Coulomb excitation, transition probabilities, γ-rays and level collectivity 80−78201
^{135}Ba(α,α'), 8-10 MeV Coulomb excitation, reduced E2 transition probabilities 78−13127
^{138}Ba+α, closed shell 82 neutron nucleus, B(E2)-values 78−66296
^{8}Be(α,α)^{8}Be elastic scatt. generalised optical potentials, three-body approximation *(Russian)* 79−13313
^{9}Be+^{4}He, microscopic ion-ion spin-orbit pot. 78−17163
^{9}Be(α, α'), 65 MeV, levels and differential cross sections, optical anal. 80−102121
^{9}Be(α,α'), 6.5 MeV, ^{13}C, T=3/2 resonance parameters, ground state γ-decay width 79−3123
^{9}Be(α,α)^{9}Be, 40 MeV, anomalous effects and cluster behaviour 78−615
^{209}Bi(α,X), 69.2, 140 MeV, scatt. and fission reaction mechanisms, cross sections 80−18350
^{209}Bi(α,α'), 120 MeV, isoscalar resonance excitation, low lying transitions, DWBA calc. 80−512
^{209}Bi(α,α'), 120 MeV, new giant resonance at 80 $A^{-1/3}$ MeV 77−41939
^{209}Bi(α,α), elastic and total reaction cross sections, absolute α widths 79−67762
Br(α,α), 12.5-15.0 MeV, total reaction cross section determ. 79−93638
CC ^{12}C(α, α), 1.37 GeV, elastic and inelastic, Glauber multiple scatt. theory 79−3161
^{12}C (α,α), ang. distrib., microscopic anal., Pauli principle, excitation effects 78−33198
^{12}C, penetration range, 200 MeV to 2 GeV *(French)* 78−4964
^{12}C(^{4}He,^{4}He), incident ion binding energy effects on scatt., qualitative anal. 79−9600
^{12}C(α, α'), 40.2 MeV branching ratio of 7.654 MeV state, rate of stellar He burning 77−2941
^{12}C(α, $\alpha'\gamma$) γ angular correlation function obs. *(Russian)* 79−13246
^{12}C(α, α), 120-172.5 MeV, optical pot. uniqueness and shape 79−97719
^{12}C(α,α'), 38-50.5 MeV, sign of nuclear deform. from Blair phase shift 77−61439
^{12}C(α,α'), 60 MeV, high lying continuum states, multipolarities, strengths 77−82925
^{12}C(α,α'), generator coordinate multichannel calc., levels and resonances 80−78149
^{12}C(α,α')^{12}C*, 45 MeV, ang. correls., ^{12}C 14.08 MeV J^π assignment 77−82819
^{12}C(α,α'c), 104 MeV, CC ^{12}C, isoscalar giant quadrupole resonance 78−78238
^{12}C($\alpha,\alpha'\gamma$)^{12}C, 17.6 to 21.8 MeV 'rotation' of ang. correl. function 77−6406
^{12}C(α,α), 150 MeV, isoscalar giant quadrupole reson. 77−307
^{12}C(α,α), 17.9 GeV/c, Glauber model rigid projectile approx. 79−63685
^{12}C(α,α), 1.37 GeV, modified eikonal multiple scattering theory 78−21576
^{12}C(α,α), 1.37 GeV, S-matrix expansion from Glauber multiple scatt. theory 80−91191
^{12}C(α,α), 2^+ collective level excitation, microstruct. of diffr. ang. distrib. 77−61440
^{12}C(α,α), 20 to 24 MeV, optical model anal. 77−65228
^{12}C(α,α), 2.8-6.5 MeV, anal., global pot. 78−21577
^{12}C(α,α), 9-11 MeV, elastic and inelastic, resonances and ang. distribs., orthogonality condition model 79−6637
^{12}C(α,α), α-particle elastic scatt. excitation functions, α-cluster state energies 79−63688
^{12}C(α,α), exchange process calc. in impulse approx. *(Russian)* 77−74819
^{12}C(α,α), excitation function anal. with allowance for exchange processes 79−9596
^{12}C(α,α), generalised optical potentials 80−22781
^{12}C(α,α), generator coord. method anal. 78−12960
^{12}C(α,α), spectra and widths of quasistationary α-cluster states *(Russian)* 77−46180
^{12}C(α,α)^{12}C, differential cross section calc. with hard core potential 77−30614
^{12}C(α,α)^{12}C, elastic and inelastic, 1.37 GeV, multiple diffr. model, eikonalised DWIA 77−34326
^{13}C(α,α'), 22, 36 MeV, resonant state line shapes 80−91148
^{A}Ca (α,α') A=40, 44, nuclear level mag. moments, ^{40}Ca 2_1^+ level, ^{44}Ca 3_1^- level 79−85368
^{A}Ca(α,α'), 24,29 MeV, A=40,42,44,48 backward ang. distrib. anomaly, coupled and channel anal. 80−86911
^{A}Ca(α,α'), A=40, 42, 44, 1.37 GeV, low lying state ang. distribs., Glauber rigid body approx. 79−54394
^{A}Ca(α,α), 40-62 MeV, A=40,44, elastic and inelastic, ang. distribs. and collective state excitation 79−6650
^{A}Ca(α,α), A=40, 42, 44, 48, 104 MeV, cross sections and optical pots., nuclear size 80−68524
^{A}Ca(α,α), A=40, 42, 44, 48, 104 MeV nuclear size and density distrib. from folding model anal. 80−68525
^{A}Ca(α,α), A=40, 48, 104 MeV, refined folding model validity 79−509
^{A}Ca(α,α), A=40, 48, nuclear matter density distrib., saturation effect, optical potential 80−63115
^{A}Ca(α,α), A=42,44,48, 29 MeV, energy and mass depend. of extracted optical potentials 79−49632
^{A}Ca(α,α) and (α,α'), (A=40,42,44,48), single pole dominance 77−41985
^{40}Ca (α, α), velocity of refined folding model approaches 80−541
^{40}Ca (α,α'), 104 MeV, giant resonance ang. distribs., L-transfer contribs. 80−27610
^{40}Ca, anomalously small absorption of α-particles 79−93640
^{40}Ca, penetration range, 200 MeV to 2 GeV *(French)* 78−4964

alpha particle-nucleus scattering continued
^{40}Ca(α, α), generator coordinate method for arbitrary cluster widths 77−18581
^{40}Ca($\alpha,2\alpha$), 115 MeV, GQR decay spectra 77−30523
^{40}Ca(α,α')^{40}Ca, medium energy, DWBA calc. 77−6380
^{40}Ca($\alpha,\alpha'\gamma$), 16.17 MeV, mag. moment of 3 level meas. 77−10314
^{40}Ca(α,α), 104 MeV, ^{48}Ca-^{40}Ca radius difference, optical model calcs. 79−454
^{40}Ca(α,α), 104 MeV, density depend. of N-N interaction 79−6660
^{40}Ca(α,α), 104 MeV, optical model analysis 78−41737
^{40}Ca(α,α), 1.37 GeV, S-matrix expansion from Glauber multiple scatt. theory 80−91191
^{40}Ca(α,α), 22 to 142 MeV, energy and mass depend. of extracted optical potentials 79−49632
^{40}Ca(α,α), 26 to 47 MeV, large angle scatt., differential cross section 78−46082
^{40}Ca(α,α), 27-9 MeV, anomalous large-angle scatt. 77−18583
^{40}Ca(α,α), 29 MeV, optical pot., double folding model for anomalous large angle scatt. 78−70551
^{40}Ca(α,α), 36-61 MeV, large angle struct. 78−41743
^{40}Ca(α,α), 6-18 MeV, resonances, anomalous large angle scatt. and quasi-molecular states 80−27613
^{40}Ca(α,α), $<$85.6 MeV, energy depend. of optical model params. 77−3024
^{40}Ca(α,α), back-angle anomaly, semi-microscopic absorpt. pot. 78−616
^{40}Ca(α,α), backward angle anomaly, resonating group method macroscopic study 78−74382
^{40}Ca(α,α), E_α=27.2 MeV, ang. distrib. meas. 78−13120
^{40}Ca(α,α), entrance channel resonances, backward angle scatt., elastic scatt. enhancement 80−27612
^{40}Ca(α,α), giant isoscalar quadrupole resonance, α-over p-decay ratio, SU(3) and shell model 80−27608
^{40}Ca(α,α), optical pot., nuclear glory effect 78−21578
^{40}Ca(α,α) 140 MeV, modified optical pot., folding pots. and energy depend. 78−70549
^{40}Ca(α,α)^{40}Ca, 166 MeV, matter density determ. from model-independ. anal. 77−38285
^{40}Ca(α,α)^{40}Ca, semiclassical anal., backward glory 79−71866
^{40}Ca(α,αp), 115 MeV, GQR decay spectra 77−30523
^{40}Ca($\alpha\alpha$), 104 MeV, Fourier-Bessel anal. of optical pots. and nucl. matter densities 79−97716
^{42}Ca(α,α'), mirror state EM decay rates, multipole matrix element isospin decomposition 79−36190
^{44}Ca(α,α), 36-61 MeV, large angle struct. 78−41743
^{48}Ca (α, α), 104 MeV, Fourier-Bessel anal. of optical pots. and nucl. matter densities 79−97716
^{48}Ca(α, α), velocity of refined folding model approaches 80−541
^{48}Ca(α,α), 104 MeV, ^{48}Ca-^{40}Ca radius difference, optical model calcs. 79−454
Ca(α,α), 1.37 GeV, differential cross sections meas. on A=40, 42, 44, 48 isotopes 77−41984
Ca(α,α), (α,α'), 1.4 GeV, theoretical anal. 78−66293
Ca(α,α), large angle scatt., cluster exchange and one-nucleon exchange 77−88152
Ca(α,α'), 1.37 GeV, differential cross sections meas. on A=40, 42, 44, 48 isotopes 77−41984
C(α,α')C, A=12,13, 65 MeV, monopole excitation of ^{4}He, DWBA calc. 77−10419
^{114}Cd(α,α) (elast. and inelast.), 21 MeV, Coulomb-nuclear interference calcs. 79−26444
^{116}Cd($\alpha,\alpha'\gamma$), 8.5 MeV, quadrupole moments determ. 77−41887
^{140}Ce, hexadecapole motion obs. from α-scatt., EM transitions and conversion electron spectra 78−25097
^{140}Ce+α, closed shell 82 neutron nucleus, B(E2)-values 78−66296
^{52}Cr(α,α'), 8-18 MeV, cross sections, search for giant dipole resonance 80−9281
^{52}Cr(α,α), 15-19 MeV, inelastic scatt. form factors, Coulomb-nuclear interference region 78−66288
Cr(α,α), A=50,2,3, 25 MeV, back-angle elastic scatt. 77−18582
^{133}Cs(α,α'), 161 keV state magnetic moment and B(E2) values, Coulomb excitation 79−45159
^{65}Cu(α,α), 27-9 MeV, anomalous large-angle scatt. 77−18583
Cu(α,α), A=63 and 65, 48 MeV, I.L. potential depth, optical model anal. 78−50187
^{A}Dy(α,α), A=161,163, 9.0-13.5 MeV, B(E2) values, rigid rotor model validity 79−494
^{163}Dy(α,α'), E2 and E4 transition moments, rotational states 78−41740
Dy(α,α'), A=156,8, E=12-13 MeV, E2, E4 transition matrix elements determ. 78−33202
^{A}Er, A=166-170, α-particle Coulomb excitation of octupole vibr. states 78−41618
^{166}Er, Coulomb excitation with ^{4}He and ^{16}O ions 78−8839
^{166}Er(α,α'), 11.25 to 12 MeV, elec. moment, charge deform. parameters 77−54233
^{167}Er(α,α), 9.0-13.5 MeV, B(E2) values, rigid rotor model validity 79−494
^{167}Er(α,α), E2 and E4 transition moments, rotational states 78−41740
Er(α,α'), A=162, 4, E=12-13 MeV, E2, E4 transition matrix elements determ. 78−33202
^{A}Fe(α,α'), A=54,58, 8-18 MeV, cross sections, search for giant dipole resonance 80−9281
^{54}Fe, surface structure analysis using Blair phase shifts 78−12959
^{54}Fe(α,α'), coupled channels calc., capture cross section, GQR decay modes 80−27654
^{56}Fe, surface structure analysis using Blair phase shifts 78−12959
^{56}Fe(α,α), 15-19 MeV, inelastic scatt. form factors, Coulomb-nuclear interference region 78−66288
^{56}Fe(α,α), 2^+ collective level excitation, microstruct. of diffr. ang. distrib. 77−61440
^{56}Fe(α,α), side feeding to ^{56}Fe 6^+ doublets 78−13014
^{58}Fe, surface structure analysis using Blair phase shifts 78−12959
$^{154\text{-}160}$Gd(α,α'), 11-17 MeV Coulomb excit. of vibrational levels 77−74803
^{A}Gd(α,α'), 30 MeV, A=144,146,147,148, high spin isomer g-factors yrast traps 80−78146
^{154}Gd(α,α'), 11.8 MeV, charge deform. parameter determ. 78−33201
^{155}Gd(α,α), 9.0-13.5 MeV, B(E2) values, rigid rotor model validity 79−494
^{156}Gd(α,α'), 11.25 to 12 MeV, elec. moments, charge deform. parameters 77−54233

alpha particle-nucleus scattering continued
Gd(α,α'), 11.8 MeV, A=154, 156, electric quadrupole and hexadecapole moments, charge deform. parameters 77–30489
Gd(α,α'), A=154,156,158,160, E2 and E4 reduced matrix elements 78–29490
^{1}H+α, interaction potential from inverse scatt. problem method *(Russian)* 78–46068
^{1}H(α,α)p, in mica, giant halos round α-emitting inclusions containing water 77–51420
^{2}H, elastic scatt. of protons and α-particles *(Russian)* 78–21566
^{2}H(α,α), 17.9 GeV/c, Glauber model rigid projectile approx. 79–63685
^{2}H$(\alpha,\alpha)^{2}$H, 6 to 14 MeV, cross section meas. 80–27655
^{2}H$(\alpha,\alpha)^{2}$H, three body calcs., Pade technique 78–46074
^{2}H$(\alpha,\alpha)^{2}$H, up to 14 MeV, elastic and inelastic cross sections, phase shift anal. 77–22996
^{2}H(α,α)H, cross-section measurement, ^{6}Li excited states from $\alpha d \rightarrow \alpha d$ 80–47491
^{3}H+α, elastic scatt., orthogonality condition model derived from parity energy surfaces 78–29432
^{3}H$(\alpha,\alpha)^{3}$H, up to 14 MeV, elastic and inelastic cross sections, phase shift anal. 77–22996
^{4}H(α,α) intermediate energies, Glauber analysis 78–46077
H(α,α), 4.00, 5.08. 6.90 GeV/c, cross-section meas. 77–6416
He+nuclear emulsion, 1.05 GeV/amu, scatt. const. 78–13151
^{3}He(^{4}He,^{4}He), local pot. theory for phase shifts and reson. 77–34270
^{3}He(^{4}He,^{4}He)^{3}He, 20-26 MeV, elastic scatt., ang. distribs. and excitation functions *(Russian)* 77–327
^{3}He(α,α), 24.5 to 42.0 MeV, meas. of polarisation analysing power 77–3026
^{4}He deduced monopole excitation to O^{+} state DWBA anal. from (α,α') 79–22226
^{4}He-^{4}He effective interaction, energy density formalism *(Russian)* 77–46119
^{4}He+^{4}He, Hill-Wheeler eqn. direct soln. 78–4956
^{4}He+^{4}He, reson. excit., ^{8}Be α-cluster, coupled channel calcs. 78–529
^{4}He+^{4}He, resonating-group method anal. 77–82886
^{4}He+^{4}He elastic scattering, barrier penetration effects, semiclassical theory 77–34339
^{4}He+α scattering, generator coord. method, Kohn-Hulthen variational principle 77–2957
^{4}He(^{4}He,^{4}He), local pot. theory for phase shifts and reson. 77–34270
^{4}He(α,α), ^{8}Be isospin mixed 2^{+} doublet, level parameters 80–27556
^{4}He(α,α), 158.2 MeV, differential cross sections, optical model anal. 79–22307
^{4}He(α,α), 17.9 GeV/c, Glauber model rigid projectile approx. 79–63685
^{4}He(α,α), 4.32, 5.07 GeV/c, Glauber multiple scatt. theory comparisons 80–63192
^{4}He(α,α), 5.05, 4.30 GeV/c, high energy multiple diffraction theory 78–29486
^{4}He(α,α), composite particle scatt., generator coordinate and natural boundary condition methods 80–13489
^{4}He(α,α), large amplitude collective motion, adiabatic TDHF calcs. 80–86786
^{4}He(α,α), natural boundary condition methods for the microscopic treatment of composite-particle scattering 79–63680
^{4}He(α,α), nuclear separable plus Coulomb interaction 80–83106
^{4}He(α,α), s-wave, Coulomb amplitudes from generator coordinate theory 80–83107
^{4}He(α,α), size change of α effect on phase shift, generator coordinate and variational methods *(Chinese)* 80–68683
^{4}He(α,α), time dependent HF calcs. reaction cross sections 79–26443
^{4}He(α,α) anal. to study direct part of N-N potential 77–10420
^{4}He(α,α) elastic scatt. 32.6 to 35.4 MeV, ^{8}Be levels by double resonance formalism 78–62553
^{4}He(α,α) microscopic optical pot. for elastic scatt. in terms of nuclear density 79–54444
^{4}He$(\alpha,n)^{7}$Be meas. and α-α elastic phase-shift calcs. 77–50143
$^{176\text{-}180}$Hf(α,α'), 11-17 MeV Coulomb excit. of vibrational levels 77–74803
^{180}Hf(α,α^{1}), 21 and 24 MeV, nonrotational interpretation of E$_4$ matrix element in ^{180}Hf 78–33111
^{180}Hf(α,α'), 21, 24 MeV, ang. distrib. meas., sensitivity to excited-state quadrupole moments 77–88158
Hf(α,α'), A=176,8,180, E2 and E4 reduced matrix elements 78–29490
^{A}Hg(α,α'), A=198, 200, 204, 16-27 MeV backward scatt., collective states 80–13365
^{201}Hg (α,α), missing f$_{5/2}$ state Coulomb excitation, level scheme, J$^{\pi}$, transitions 80–47386
^{6}Li (α,α), 59 MeV, elastic and inelastic, differential cross section systematic anal. 80–22845
^{6}Li(α,α) 5-15 MeV, calc. illustrating generator coordinate amplitudes 77–54194
^{6}Li$(\alpha,\alpha)^{6}$Li, cross section using var. calcs. in generator coordinate method 78–13122
^{7}Li(α,α), low energy elastic and inelastic scatt., Pauli principle effect 78–4953
^{7}Li(α,α), microscopic study of elastic scatt. 77–88156
^{7}Li(α,α) at 2, 4 and 7 MeV, ang. distribs. calcs., 2α+t system model 78–50110
^{7}Li$(\alpha,\alpha)^{7}$Li, ^{11}B excited states parameters *(French)* 79–93637
^{7}Li$(\alpha,\alpha)^{7}$Li elastic scatt. generalised optical potentials, three-body approximation *(Russian)* 79–13313
^{175}Lu(α,α), 9.0-13.5 MeV, B(E2) values, rigid rotor model validity 79–494
Mg isotopes, optical model and coupled-channel anal., 24.2 MeV 77–6407
^{24}Mg $(\alpha,\alpha'\gamma)$ 104 MeV, nuclear deformation from ang. correlations, coupled channel anal. 78–78301
^{24}Mg(α,α), 120-172.5 MeV, optical pot. uniqueness and shape 79–97719
^{24}Mg(α,α_0), 5.9-6.25 MeV, ^{28}Si lowest T=2 resonance α-width, observed narrow resonances 79–45236
^{24}Mg$(\alpha,\alpha_1\gamma)$, 104 MeV, alpha-gamma ang. correl., quadrupole deform. 77–88155
^{24}Mg(α,α'), 1.37 GeV, low lying state ang. distribs., Glauber rigid body approx. 79–54394
^{24}Mg(α,α'), 22-26 MeV, intermediate resonances in ^{12}C+^{16}O system, J$^{\pi}$ assignments 79–17880
^{24}Mg(α,α'), 28, 40 MeV, lowest 3^{+} state population, compound nucleus formation 78–33197

alpha particle-nucleus scattering continued
^{24}Mg(α,α'), 38-50.5 MeV, sign of nuclear deform. from Blair phase shift 77–61439
^{24}Mg(α,α'), excitation of low-lying 0^{+} states, indirect processes 77–6417
^{24}Mg$(\alpha,\alpha')^{24}$Mg, 126 MeV, GQR, DWBA anal. 77–74826
^{24}Mg$(\alpha,\alpha')^{24}$Mg, 16.7-20 MeV, quasimol. intermediate resons., statistical anal. 78–41741
^{24}Mg$(\alpha,\alpha')^{24}$Mg, exptl. evidence of intermediate resonances, alpha-particle doorway states 79–13314
^{24}Mg(α,α), 2^{+} collective level excitation, microstruct. of diffr. ang. distrib. 77–61440
^{26}Mg $(\alpha,\alpha'\gamma)$ 104 MeV, nuclear deformation from ang. correlations, coupled channel anal. 78–78301
^{26}Mg (α,α), 104 MeV, oblate-prolate effects in struct. and reactions 80–9225
^{26}Mg(α,α_1), 15 MeV, anal. of α-γ angular correlations 77–74866
^{26}Mg(α,α'), mirror state EM decay rates, multipole matrix element isospin decomposition 79–36190
Mg(α,α'), A=24,5,6, 106, 120, 145, 172.5 MeV, giant quadrupole reson. obs. 77–6415
Mg(α,α'), giant quadrupole resonance strength, p- and α-inelastic scatt. and α capture 78–37323
^{98}Mo$(,\alpha,\alpha')$, 8 MeV, multiple Coulomb excitation, fast $2^{+} \rightarrow 0^{+\prime}$ transition 79–17846
^{98}Mo(α,α'), 8 MeV, static quadrupole moment of first 2^{+} state 80–5061
^{100}Mo$(\alpha,\alpha'\gamma)$, 8.5 MeV, quadrupole moments determ. 77–41887
Mo(α,α') A=94-100, 8 MeV, static quadrupole moment determ. 77–6226
^{14}N$(\alpha,\alpha_1)^{14}$, 7.6 to 16.9 MeV, study of isospin-mixed ^{18}F states 77–14029
^{14}N(α,α), 1.5, 1.6 MeV, ^{18}F resonances, α-widths, isospin and parity mixing, R-matrix anal. 80–91162
^{14}N(α,α), 20 to 24 MeV, optical model anal. 77–65228
^{14}N(α,α), 23.7 MeV, cross sections, 20 to 170° 78–13118
^{15}N$(\alpha, \alpha)^{15}$N, backscatt., heavy particle transfer mechanism 77–6420
^{15}N(α,α), ^{19}F levels, resonances and phase shifts, resonating group calcs. 80–32189
^{15}N(α,α), E$_{\alpha}$=16-23.7 MeV, differential cross sections, ang. distribs. and excitation functions 78–13121
^{142}Nd+α, closed shell 82 neutron nucleus, B(E2)-value 78–66296
^{150}Nd(α,α'), 11.5 MeV, electric quadrupole and hexadecapole moments, charge deform. parameters 77–30489
^{3}Ne(α,α), antisymmetrisation effects on the effective internuclear potential 79–59085
^{20}Ne$(\alpha,\alpha'\gamma)$, 3.0-6.0 MeV, ^{24}Mg radiative decays of unbound high spin states 79–6484
^{20}Ne(α,α), 20 to 24 MeV, optical model anal. 77–65228
Ne(α,α), A=20, 22, 150 MeV, isoscalar giant quadrupole reson. 77–307
Ne(α,α), A=20,22, large angle elastic scatt., 24.6-31.7 MeV, single Regge pole anal. 78–70547
^{14}Ni(α, α), A=58-64, 120-172.5 MeV, optical pot. uniqueness and shape 79–97719
^{58}Ni(α,α') 1.37 GeV, low lying state ang. distribs., Glauber rigid body approx. 79–54394
^{58}Ni(α,α), 139 MeV, optical model analysis 78–41737
^{58}Ni(α,α), 27 to 49 MeV, cross sections, optical model anal. 79–85483
^{58}Ni(α,α), <85.6 MeV, energy depend. of optical model params. 77–3024
^{58}Ni(α,α), elast. and inelast., 29-58 MeV, coupled channels anal. 78–66289
^{58}Ni(α,α), radial sensitivity of optical pot. 80–86869
^{58}Ni(α,α) 140 MeV, modified optical pot., folding pots. and energy depend. 78–70549
^{58}Ni$(\alpha,\alpha)^{58}$Ni, 104 MeV, calc. of S-matrix oscillations and differential cross section 77–6333
^{58}Ni$(\alpha$-$\alpha)$, 50.2 MeV, composite particle optical pot. discrete ambiguities, partly Pauli-forbidden states 80–86870
^{60}Ni, hexadecapole motion obs. from α-scatt., EM transitions and conversion electron spectra 78–25097
^{60}Ni(α,α'), 8-18 MeV, cross sections, search for giant dipole resonance 80–9281
^{60}Ni(α,α), 15-19 MeV, inelastic scatt. form factors, Coulomb-nuclear interference region 78–66288
^{60}Ni(α,α), elast. and inelast., 29-34 MeV, coupled channels anal. 78–66289
^{61}Ni$(\alpha,\alpha\gamma)^{61}$Ni, 4.5-5.5 MeV, low-lying levels study 77–26610
Ni(α,α), A=62 and 64, 48 MeV, I.L. potential depth, optical model anal. 78–50187
^{16}O+α scattering generator coord. method, Kohn-Hulthen variational principle 77–2957
^{16}O+light ion scatt., exchange Coulomb kernel in resonating group formulation 79–6531
^{16}O$(\alpha, \alpha)^{16}$O, backscatt. heavy particle transfer mechanism 77–6420
^{16}O$(\alpha, \alpha)^{16}$O, one-channel scatt., nonlocal potential 79–9621
^{16}O(α,α'), 14.6-20.4 MeV, ^{20}Ne states, J$^{\pi}$, differential cross sections and ang. distribs. 80–18203
^{16}O(α,α'), 3.0-9.5 MeV, ^{20}Ne levels, J$^{\pi}$, branching ratio and EM transition rates 80–42540
^{16}O(α,α'), 60 MeV, giant dipole and quadrupole 77–2965
^{16}O(α,α'), hyperfine dynamic mag. field effects 80–68689
^{16}O$(\alpha,\alpha')^{16}$O, 65 MeV, monopole excitation of ^{4}He, DWBA calc. 77–10419
^{16}O(α,α), 20 to 24 MeV, optical model anal. 77–65228
^{16}O(α,α), 23.7 MeV, cross sections, 20 to 170° 78–13118
^{16}O(α,α), 25 MeV, macroscopic description of exchange effects 77–57635
^{16}O(α,α), 28 to 33.6 MeV, optical potential of incident channel 78–58291
^{16}O(α,α), 28-33.6 MeV, forward peaking variation, DWBA with optical pots., ang. distribs. 80–13488
^{16}O(α,α), antisymmetrisation effects on the effective internuclear potential 79–59085
^{16}O(α,α), α-particle elastic scatt. excitation functions, α-cluster state energies 79–63688
^{16}O(α,α), effect of Pauli principle on optical potl. 77–6412
^{16}O(α,α), giant isoscalar quadrupole resonance, α-over p-decay ratio, SU(3) and shell model 80–27608
^{16}O(α,α), spectra and widths of quasistationary α-cluster states *(Russian)* 77–46180

alpha particle-nucleus scattering continued

- ^{16}O(α,α), uncorrelated target, optical pot. unitary content, DWIA and Glauber theory 80−105947
- ^{16}O(α,α) 17 to 27 MeV, backscatt., dynamic deformation and excitation functions, optical anal. 80−18227
- ^{16}O(α,α)^{16}O, 20 to 25 MeV, backward angle anomaly, α-cluster states in ^{20}Ne 77−38287
- ^{16}O(α,α)^{16}O, 3.045 MeV, O distrib. profiles, from emitted α-particle energy anal. 79−5213
- ^{16}O(α,α)^{16}O, 6.9-10.2 MeV, level and isospin mixing parameters 78−66292
- ^{16}O(α,α)^{16}O, differential cross section calc. with hard core potential 77−30614
- ^{16}O(α,γ_1), obs. of gamma decays of some T=0, 1 and 2 states above 9.5 MeV in ^{20}Ne 77−34244
- ^{17}O(α, α)^{17}O, backscatt., heavy particle transfer mechanism 77−6420
- ^{A}Os(α,α') A=188,190,192, 4_3^+ level population, hexadecapole vibrs. 78−89780
- ^{31}P, optical model and coupled-channel anal., 24.2 MeV 77−6407
- Pb+α, 3.6 GeV, emitted proton vel. spectra max. *(Russian)* 79−9571
- ^{A}Pb(α,α'), A=204, 206, 208, 16-27 MeV backward scatt., collective states 80−13365
- ^{A}Pb(α,α), A=206, 208, 120 MeV, isoscalar resonance excitation, low lying transitions, DWBA calc. 80−512
- ^{206}Pb(α,α'), 120 MeV, new giant resonance at 80 $A^{-1/3}$ MeV 77−41939
- ^{208}Pb (α,α^1), 100-172 MeV, giant monopole resonance evidence from strong energy depend. 80−13432
- ^{208}Pb(α, α'), neutron collectivities, E2 giant resonance excitation 77−26558
- ^{208}Pb(α,α'), 120 MeV, new giant resonance at 80 $A^{-1/3}$ MeV 77−41939
- ^{208}Pb(α,α'), 172 MeV giant monopole and quadrupole resonances, multipole excitations 80−106031
- ^{208}Pb(α,α'), 65 MeV, inclusive reaction, giant resonance background, heavy ion model anal. 80−5150
- ^{208}Pb(α,α'), 96 MeV, ang. distribs., breathing mode states, DWBA calcs. 78−50183
- ^{208}Pb(α,α'), 96 MeV, obs. of isoscalar breathing mode state 78−17086
- ^{208}Pb(α,α'), cross section calc. using microscopic wave functions 78−50142
- ^{208}Pb(α,α'), levels, B(E3), transition density and nuclear pot., folding model anal. 80−86812
- ^{208}Pb(α,α'), RPA calcs., existence of breathing mode 78−25163
- ^{208}Pb(α,α), 104 MeV, optical model analysis 78−41737
- ^{208}Pb(α,α), 172 MeV, giant resonance structures 80−91163
- ^{208}Pb(α,α), 172 MeV, strongly excited giant monopole resonance 80−18273
- ^{208}Pb(α,α), elastic and total reaction cross sections, absolute α widths 79−67762
- ^{208}Pb(α,α), elastic ang. distrib., nuclear contributions, Born approx. validity 79−36252
- ^{208}Pb(α,α), optical model parametrization, cross section, energy depend. 78−33196
- Pb(α,α), 104 MeV, A=204,206,208, neutron density RMS radii 78−17088
- Pb(α,α), 104 MeV, nucl. matter sizes and isoscalar octupole transition rate 77−6422
- Pb(α,α'), A=204,206,208, 13.8 MeV, quadrupole moment and B(E3) values 79−17797
- ^{192}Pt(α,α'), 24 MeV, α-angular distrib. for 0^+, 2^+, $2^{+\prime}$, 4^+, $4^{+\prime}$ and 3^- state excitation 78−70550
- ^{194}Pt(α,α'), 7-17.5 MeV, Coulomb excitation, low lying collective state reduced matrix elements, triaxiality 78−82269
- Pt(α,α')Pt, 14.9 MeV, A=192, 194, 2^+ and 3^+ state Coulomb excit. 78−622
- ^{239}Pu(α,α), 19-27 MeV, differential cross section, transmission coeffs. for fission cross section *(Russian)* 79−67800
- ^{A}Ru(α,α'), 8.5-9.5 MeV, A=96, 98, 100, 102, 104, first 2^+ excited state quadrupole moment 80−47374
- ^{102}Ru(α,α), 8.5, 9.0 MeV, Coulomb excitation, 2^+ state electric quadrupole moment 80−73793
- ^{102}Ru(α,α), 8.5-9 MeV, 2^+ state quadrupole moment, reorientation effects and multiple Coulomb excitation 80−5063
- S isotopes optical model and coupled-channel anal., 24.2 MeV 77−6407
- ^{A}S(α,$\alpha'\gamma$), 8-9 MeV, A=32, 34, 2_1^+ state transient field g-factor meas. 79−36151
- ^{45}Sc+^{4}He, low-lying negative parity levels, Coulomb excitation 79−93552
- ^{45}Sc(α,α'), levels, J^π, transitions and lifetimes 80−63091
- ^{45}Sc(α,α), 25 MeV, back-angle elastic scatt. 77−18582
- ^{45}Sc(α,α), 27-9 MeV, anomalous large-angle scatt. 77−18583
- ^{45}Sc(α,α), 27.2 MeV, elastic scatt. differential cross section 78−13116
- ^{74}Se(α,α'), 7.3 MeV, first excited state, static quadrupole moment, deformation evidence 79−17802
- ^{82}Se(α,α), 7.3 MeV, static quadrupole moments of first 2^+ excited states 77−65197
- Si, energy loss and multiple scattering of non-channelled α-particles *(German)* 80−59544
- ^{A}Si(α,α), 41 MeV, A=28-30, ang. distribs., optical and DWBA anal., scatt. pots. 79−556
- ^{28}Si (α,$\alpha'\gamma$) 104 MeV, nuclear deformation from ang. correlations, coupled channel anal. 78−78301
- ^{28}Si(α,α'), excitation of low-lying 0^+ states, indirect processes 77−6417
- ^{28}Si(α,α') 120 MeV, giant reson. multipolarities 77−54201
- ^{28}Si(α,α')^{28}Si, 126 MeV, GQR, DWBA anal. 77−74826
- ^{28}Si(α,$\alpha'\gamma$), 104 MeV, ang. correl. meas., sensitivity to quadrupole deform. 78−54774
- ^{28}Si(α,α), 150 MeV, isoscalar giant quadrupole reson. 77−307
- ^{28}Si(α,α), elastic and inelastic scatt., compound nucleus contrib. anal. 78−37356
- Sm, A=152, 154, electric quadrupole and hexadecapole moments, charge deform. parameters, Coulomb excitation expts. 77−30489
- ^{144}Sm+α, closed shell 82 neutron nucleus, B(E2)-value 78−66296
- ^{144}Sm(α,α'), 96 MeV, ang. distribs., breathing mode states, DWBA calcs. 78−50183
- ^{144}Sm(α,α'), 96 MeV, obs. of isoscalar breathing mode state 78−17086
- ^{154}Sm(α,α), 50 MeV, long range absorption and optical model effects from strong inelastic coupling 80−535
- Sm(α,α'), 11.25 to 12 MeV, a=152,156, elec. moments, charge deform. parameters 77−54233
- ^{116}Sn(α,α'), 96, 129 MeV, giant resonance excitation, isoscalar breathing mode state, nuclear incompressibility 80−68620

alpha particle-nucleus scattering continued

- ^{124}Sn(α,α'), ang. distrib. meas. and DWBA anal. 78−13125
- ^{124}Sn(α,α), optical model parametrization, cross section, energy depend 78−33196
- ^{124}Sn(α,α) (elast. and inelast.), 19.5 MeV, Coulomb-nuclear interference calcs. 79−26444
- ^{A}Te(α,α) A=122,124 (elast. and inelast.), 19.3 MeV, Coulomb-nuclear interference calcs. 79−26444
- ^{122}Te, backscatt. of ^{4}He, ^{14}N, ^{16}O, and ^{18}O, reorientation effect meas 78−50209
- ^{122}Te(α,α'), ang. distrib. meas. and DWBA anal. 78−13125
- ^{124}Te(α,α'), ang. distrib. meas. and DWBA anal. 78−13125
- ^{128}Te backscatt. of ^{4}He, ^{14}N, ^{16}O, and ^{18}O, reorientation effect meas. 78−50209
- Te(α,α) A=122-128, 8-18 MeV, optical model and deform. parameters 77−34221
- ^{232}Th+α, 19.8 to 27.2 MeV, elastic scatt. or capture and fission, optical model pots. 77−88181
- ^{232}Th(α,α'), 120 MeV, isoscalar giant resonances, DWBA anal. 80−42621
- ^{232}Th(α,α'f), total kinetic energy release 80−27682
- ^{233}Th(α,α') 120 MeV, isoscalar giant quadrupole resonance fission decay channel inhibition 79−54419
- ^{A}Ti(α,α), A=46,48,50, 140 MeV, nuclear size comparison, optical model pot. 79−17913
- ^{47}Ti(α,α'), 15.35 MeV, level density parameters, statistical model anal. 78−13130
- ^{49}Ti(α,α') 5.2-5.8 MeV, B(E2) value meas. for 3/2 to $7/2^-$ transition 78−82308
- ^{50}Ti(α,α), 140 MeV, model independent description limits from local optical pots. 80−102196
- Ti($\alpha\alpha$), A=49,50, 25 MeV, back-angle elastic scatt. 77−18582
- ^{A}U(α, α'), A=234, 236, 238, coupled channel Born anal. of deformation correl 80−5149
- ^{233}U(α,X), 28-140 MeV, scatt. and fission reaction mechanisms, cross sections 80−18350
- ^{235}U(α,α), 19-27 MeV, differential cross section, transmission coeffs. for fission cross section *(Russian)* 79−67800
- ^{236}U(α,α'f), total kinetic energy release 80−27682
- ^{51}V(α,α), 27.2 MeV, elastic scatt. differential cross section 78−13116
- V(α,α), A=50,1, 25 MeV, back-angle elastic scatt. 77−18582
- W isotopes, A=182, 184, 186, Coulomb excitation with ^{4}He and ^{16}O ions 78−8839
- ^{183}W(α,α'), 15 MeV, level and band Coulomb excitation, B(E2) values 80−32233
- W(α,α'), 13.5 MeV, anal. of deexcitation γ-rays, quadrupole moment determ. 78−12968
- ^{168}Yb(α,α'), 12-13 MeV, E2, E4 transition matrix elements determ. 78−33202
- ^{176}Yb(α,α), rot. state excitation, coupled-channel and adiabatic calc. 77−50094
- ^{A}Zn(α, α'), A=64, 66, 129 MeV, isoscalar giant monopole resonances, nuclear incompressibility 80−83083
- ^{A}Zn(α,α'), 18 MeV, A=64,66,68,70, compound and precompound α emission spectra 78−82367
- ^{64}Zn(α,α), 15-19 MeV, inelastic scatt. form factors, Coulomb-nuclear interference region 78−66288
- ^{68}Zn(α,α), 2^+ collective level excitation, microstruct. of diffr. ang. distrib. 77−61440
- ^{68}Zn(α,α), 38 MeV, correls. of optical pot. parameters for elastic scatt. 78−13117
- Zn(α,α), A=64 and 66, 48 MeV, I.L. potential depth, optical model anal. 78−50187
- ^{40}Zr(α, α), energy depend. of phenomenological optical pot. 79−97717
- ^{90}Zr (α,α) 40 to 140 MeV, modified optical pot., folding pots. and energy depend. 78−70549
- ^{90}Zr(α,α'), 96, 129 MeV, giant resonance excitation, isoscalar breathing mode state, nuclear incompressibility 80−68620
- ^{90}Zr(α,α), E=26.2-166 MeV, antisymmetrisation effects, α pot., form factor, optical model anal. 78−82366
- ^{90}Zr(α,α), form factor, coupling between real and imaginary optical potential 80−68680
- Zr(α,α), A=90, 92, optical model parametrization, cross section, energy depend. 78−33196
- Zr(α,α), A=90,2, E=40-120 MeV, form factors, optical model anal. 78−13123

alpha-particle scattering *see alpha particle-nucleus scattering*

alpha-particle spectra

see also alpha-particle angular distribution

- actinoid element alpha-decay, current state of results 78−17159
- alpha lines, empirical eqn. for broadening and asymmetry *(Spanish)* 79−63859
- automatic evaluation of isotope anal. of nuclear fuels, isotope dilution, mass and α spectrometry 78−55120
- complex alpha-spectra evaluation using program ALFUN 78−74552
- computer program for α-spectrum anal. 78−29692
- computer program to determ. average FWHM in background-free spectra 79−31349
- diffusion coefficients evaluation, numerical algorithm for using α spectrometry 80−34223
- emulsion nuclei, He nuclei emission in 7.5 to 200 GeV hadron interactions *(Russian)* 80−9325
- fission-emitted alpha particles, energy spectrum, fission fragment shape and orientation depends. 78−74346
- heavy element superficial mass meas. by elastic α-particle scatt. *(French)* 79−61927
- inner radiation belt, Prognoz 5 meas. 79−84587
- laser-produced thermonuclear alpha particle pinhole imaging 77−67934
- LWR spent fuel, alpha spectrometric meas. for SNM verification 80−78424
- massive transfer in heavy ion reactions on rare-earth targets, α-γ coincidence 78−70556
- monazite, α-spectra evidence for natural activity at 6.52 to 9.07 MeV 80−67363
- monazite mineral, high-energy alpha emitters, $E \geq 10.6$ MeV 79−48467
- nuclear π^- capture, p, d and α inclusive prod. spectra 79−22338
- odd-odd neutron deficient nuclei, spectra of delayed protons and α-particles in β^+ decay *(Russian)* 78−46034
- sediments, α-spectrometric dating method, using ^{210}Po 78−28350

alpha-particle spectra continued
- spectral line intensity gauge using semiconductor detector *(Italian, Spanish)* 78–86716
- student experiments, alpha spectroscopy equipment and techniques *(Danish)* 77–49529
- (α,α') spectra of light nuclei, multipole giant resonances 78–86462
- β-delayed α-particle emission, α-strength function below Coulomb barrier 78–37318
- (e^-,$\alpha\nu$) on heavy nuclei, peripheral model 80–37369
- (n,α) resonance neutron reactions, α-widths from statistical relationships, deviations 78–33173
- (p,α), continuous α-spectra, meas. and anal. 79–6585
- ^{235}U(n,f), thermal to 1.75 MeV, energy spectra and yields of alpha-particles 77–26805
- Ag (π,αX), 70 MeV, α cross sections and energy spectra, intranuclear cascade calcs. 79–575
- Ag+α, 720 MeV, correlated energy spectra of light fragments, fireball and coalescence models 78–62555
- ^{107}Ag(e,α), 100 MeV, energy spectra, cross sections 77–18529
- Al+α, 720 MeV, correlated energy spectra of light fragments, fireball and coalescence models 78–62555
- ^{27}Al+n, 15 MeV, sub-Coulomb-barrier spectra 77–23007
- ^{27}Al(^{6}Li,d)^{31}P, 36 MeV, absolute cross sections, ang. distribs. 79–89321
- Al(π,αX), 70 MeV, α cross sections and energy spectra, intranuclear cascade calcs. 79–575
- ^{40}Ar+^{58}Ni, deep inelastic collision at 280 MeV, fragment energy and spin 78–21599
- Au (π,αX), 70 MeV, α cross sections and energy spectra, intranuclear cascade calcs. 79–575
- Au+^{86}Kr, 724 MeV, coincidence meas., pre-equilibrium α-emission 78–33208
- ^{197}Au(^{22}Ne,αX), 178 MeV, max. α-particle energy at forward angles 80–68698
- ^{197}Au(p,αx), 72 MeV, pre-equilibrium α-emission 79–26440
- ^{10}B(t, α)^{9}Be*(2s$_{1/2}$), resonant spectra 80–22691
- ^{11}B(n,α)^{8}Li, 14.4 MeV, spectra and ang. distribs., recoil nucl. transitions 78–17193
- ^{11}B(p,α)^{8}Be, continuous energy spectra of α-particles 77–30567
- ^{138}Ba+α, closed shell 82 neutron nucleus, B(E2)-values 78–66296
- ^{209}Bi+^{14}N, 85 and 95 MeV, preequilibrium α spectra, statistical treatment 78–41750
- ^{12}C, photodisintegration induced by 40 MeV γ-rays, correl. spectroscopy 77–6345
- ^{12}C+n, 18.2 MeV, multiparticle breakup, three-α correl. spectra 77–6364
- ^{12}C(^{16}O, α)^{24}Mg, population of resonant ^{12}C+^{12}C states 78–62563
- ^{12}C(^{6}Li,α)^{14}N, α-particle spectrum sharp lines observation, originating from ^{16}O decay *(Russian)* 78–29495
- ^{12}C(1$^+$) decay to 3 α-particles, final-state interactions, spectra calc. 77–88086
- ^{14}C, photodisintegration induced by 40 MeV γ-rays, correl. spectroscopy 77–6345
- ^{40}Ca, α-and p-spectra from giant reson. region via ^{40}Ca(α,2α) and ^{40}Ca(α,αp) 77–30523
- ^{140}Ce γ-spectra, E1 and M1 hindrance factors from ^{143}Nd(n,$\gamma\alpha$) 80–37386
- ^{140}Ce+α, closed shell 82 neutron nucleus, B(E2)-values 78–66296
- ^{252}Cf fission, scission point config., α-particle trajectories 77–82974
- C(π,αX), 70 MeV, α cross sections and energy spectra, intranuclear cascade calcs. 79–575
- Cs, A=114-118, neutron deficient isotopes, half lives, β^+,γ, delayed p and α meas. 78–70489
- CsI crystal, neutron bombardment, p and α emission spectra, yields, preequilib. mech. 77–50139
- ^{63}Cu(e,α), 100 MeV, energy spectra, ang. distribs. 77–18529
- D-T plasma, Monte Carlo anal. of particle spectra 79–72992
- Dy(n,α)Gd, A=161, 163, at 14.1 and 18.2 MeV, α-emission energy spectra 77–65224
- ^{166}Er(α,α'), 11.25 to 12 MeV, elec. moment, charge deform. parameters 77–54233
- ^{253}Es, separation and α-spectra identification following neutron irradiation of Cf 78–17435
- ^{19}F(p,α)^{16}O, 1.5 to 2 MeV, [211] quartet state in ^{20}Ne 78–46006
- ^{156}Gd(α,α'), 11.25 to 12 MeV, elec. moments, charge deform. parameters 77–54233
- ^{4}He(d,pα)n, at E_d=8.9 MeV, absolute cross-section meas. 77–34317
- ^{165}Ho(e,α), 100 MeV, energy spectra, cross sections 77–18529
- ^{74}Kr, charged particle evaporation following form. from ^{58}Ni+^{16}O 80–47453
- ^{6}Li(d,α)^{4}He*, 13.6 MeV, α spectra, excited state of ^{4}He, spin, parity 78–54771
- ^{14}N-induced reactions energy relax. during fusion determ. by preequilib. α emission 79–26446
- ^{142}Nd+α, closed shell 82 neutron nucleus, B(E2)-value 78–66296
- Ni-Cr thin film resistors, α-particle elastic scatt. and PIXE anal. 79–48022
- ^{A}Ni(p,α), A=58, 60, 30 MeV, α-particle angular distrib. 79–6588
- ^{58}Ni+^{16}O, deep-inelastic collisions, light particle pre-equilibrium emission 78–54786
- ^{58}Ni+p, 1 GeV, alpha-particle decay channels 80–22826
- ^{58}Ni(d,$\alpha\gamma$), 7 MeV, mean lifetimes of ^{56}Co levels 78–4950
- ^{60}Ni(e,α)e′X, alpha particle spectra, statistical model calc., direct reaction component 78–41704
- Ni(π,αX), 70 MeV, α cross sections and energy spectra, intranuclear cascade calcs. 79–575
- ^{31}P(^{6}Li,d)^{35}Cl, 36 MeV, absolute cross sections, ang. distribs. 79–89321
- ^{208}Pb(^{3}He,α)^{207}Pb, 70 MeV, deephole states, $T_>$=45/2 components 78–82362
- Pb(d,α)Tl, A=208,206,204 at 80 MeV, high-spin states, α-spectra 78–504
- Pu isotopes, in soil, determination using alpha-spectrometry 80–45601
- ^{242}Pu, half-life meas. 78–17154
- ^{213m}Ra, 2.1 msec. isomer, gamma and alpha decay meas. 77–14067
- ^{221}Rn, decay scheme, α-, β-, γ-spectra meas. 79–6507
- ^{222}Rn progeny, air conc. meas. by α-particle spectrometric counting 79–68171
- ^{36}S(d,α) 3.05-3.26 MeV, α-spectrum, ^{34}P mass and energy levels 79–6632
- ^{80}Se(d,α)^{78}As, 16.0 MeV, levels of ^{78}As 78–8827
- ^{29}Si(^{6}Li,d)^{33}S, 36 MeV, absolute cross sections, ang. distribs. 79–89321
- ^{144}Sm+α, closed shell 82 neutron nucleus, B(E2)-value 78–66296

alpha-particle spectra continued
- ^{148}Sm compound states partial α-widths, α-spectra of ^{147}Sm(n,α) 80–47392
- Sm(α,α'), 11.25 to 12 MeV, a=152,156, elec. moments, charge deform. parameters 77–54233
- ^{120}Sn γ-spectra, E1 and M1 hindrance factors from ^{123}Te(n,$\gamma\alpha$) 80–37386
- ^{84}Sr(^{3}He,α)^{83}Sr, 18 MeV, ^{83}Sr levels, DWBA calcs. using optical model 78–41738
- Ta+α, 720 MeV, correlated energy spectra of light fragments, fireball and coalescence models 78–62555
- ^{181}Ta(e,α), 100 MeV, energy spectra, cross sections 77–18529
- ^{159}Tb(e,α), 100 MeV, energy spectra, cross sections 77–18529
- ^{44}Ti, α-particle spectroscopic factors, two-oscill. shell model calcs. 79–6386
- ^{46}Ti, ^{48}Ti+n, 15 MeV, sub-Coulomb-barrier spectra 77–23007
- ^{47}Ti(α,α'), 15.35 MeV, level density parameters, statistical model anal. 78–13130
- ^{169}Tm(e,α), 100 MeV, energy spectra, ang. distribs. 77–18529
- U, A=233,5, thermal neutron fission with alpha-particle emission *(Russian)* 77–46198
- U isotopes, in soil, determination using alpha-spectrometry 80–45601
- ^{230}U, production, tracer appls., α-spectra 77–61644
- ^{233}U(ρ,f), alpha-particle angular and energy spectra, cross-section anisotropy 80–57809
- ^{234}U spectrum, surface barrier detectors, charact. meas. *(Bulgarian)* 78–82592
- ^{235}U, thermal-neutron induced fission, scission point configuration determ. 77–82973
- ^{235}U(γ,f), 20 MeV, long range α-particle spectrum 80–47516
- ^{235}U(n,α), thermal, α-particle spectra 78–78425
- ^{235}U(n,f), thermal, α-particle spectra 78–78425
- ^{238}U(e,α), 40 MeV, isoscalar E2 giant resonance α particle search 79–9549
- ^{238}U(e,α)e′^{234}Th, cross section, α-spectra, γ-spectra of ^{234}Th decay 78–58262
- ^{50}V(p,α), 13.85 MeV, level density parameters, statistical model anal. 78–13130
- Zn to Ni even isotope transition, α-particle spectroscopic factors, shell model calcs. 79–6385

alpha-particle spectrometers
- *see also alpha-particle spectra*
- ARS-1 attachment, for radiometry of samples containing alpha-radioactive isotopes 77–75022
- cellulose nitrate, He (A=3, 4) energy spectroscopy 78–13377
- cellulose nitrate film, pinhole imaging of laser-prod. thermonucl. alpha particles 77–67934
- complex alpha-spectra evaluation using program ALFUN 78–74552
- counting system with Si surface barrier detector 78–82565
- immersible Si Li-drift alpha- and beta-radiation detector, fabrication 77–65386
- immersible Si spectrometric alpha-particle detector, fabrication 77–65385
- ionisation large area gridded chamber, atmospheric radioactivity meas. 78–49128
- liquid scintillation alpha counting and spectrometry , appl. to bone and tissue samples 77–25617
- liquid scintillation alpha particle spectroscopy, pulse-shape discrimination cct. 78–21823
- liquid scintillation alpha-particle assay with energy and pulse shape discrimination 77–23350
- liquid scintillation high resolution alpha spectroscopy, optimisation of detector and electronics 78–13370
- magnetic α spectrograph performance 79–31316
- magnetic analysis of charged particles, α-, β- and mass spectrometers *(Russian)* 80–87011
- one-arm magnetic spectrometer, Alfa facility, description and characts. 79–26809
- portable, single-channel, for meas. of Rn daughter product concs. 77–30702
- scintillation, liquid, of low alpha activities *(Slovak)* 77–83453
- scintillation, liquid, radiometric determ. of U content *(Czech)* 78–69487
- semiconductor radiometer-spectrometer for meas. of surface contamination by α-radioactive materials 77–38423
- SKM-200 installation with 2 m streamer chamber in mag. field 80–23241
- stabilisation using ^{148}Gd source, multichannel analyser 79–22523
- trajectory detector for meas. of short lived activity by decay in flight 80–27867
- Si semiconductor detect., stopping power and straggling in liqs. 78–82563
- Si, stopping power and straggling in water and tissue-equivalent liquid 80–23274
- p-Si surface barrier detectors, charact. meas. *(Bulgarian)* 78–82592
- Si:P, B, fabrication by ion implantation 78–33373
- U analysis in phosphate fertilisers and other materials using liq. scintillation spectrometry 78–53280

alpha-particles
- *see also cosmic ray alpha-particles and helium nuclei*
- alpha reduced widths, point approx., higher order corrections 79–13213
- direct breakup, t-p ang. correlation function from ^{58}Ni(α,tp) 80–22797
- fusion reactor, time-dependent tandem mirror confinement, start-up and alpha particle build-up 80–10419
- fusion-generated alpha particles driven plasma transport 78–83533
- fusion-produced, interaction with mag. plasma fluctuations in D-T reactor 80–24204
- history of alpha particles, 1903-1977, discovery, props., alpha decay 77–78942
- plasma, laser-fusion, α-emission recoil force effect on confinement 80–6275
- plasma, neutral beam injection, charge exchange and ionis. rate coeffs., analytical approx. 79–86590
- solar wind alpha particle component, results of Prognoz satellite meas. 77–53385
- stellarator geometry, superbanana orbits for 3.5 MeV alpha particles 80–24231
- stopping power in H_2, He, N_2, O_2, CO_2, Ne, Ar, Kr, Xe 80–14057
- Tokamak, fusion reactor, axisymmetric, slowing-down alpha particle loss, Monte-Carlo calc. 78–59653

alpha-particles continued
Tokamak fusion reactor, ignited operation regimes 80−10423
Tokamak reactors, role of α-particles review 80−86971
transport in hot, dense D-T plasma, moment method calc. 78−22458
^{12}C(^{12}C,xα), 12-31.5 MeV, inclusive α-particle yield, resonant like structs. 80−42691
Ge, stopping power for fast channelled α-particles 78−79654
^{4}He, reaction matrix equation, Brueckner calcs. in harmonic oscill. basis 79−59015
^{4}He$_{\Lambda}$-^{4}H$_{\Lambda}$ binding energy difference, exact 4-body calc. 79−63622
^{58}Ni(^{40}Ar,X), 280 MeV, deep inelastic, light fragments, thermal equilib., ang. momentum transfer 80−63203
^{16}O, α-cluster model, clustering and nuclear forces in terms of quark struct. 79−6443
^{16}O(^{12,13}C,αX), 140 MeV, fast α prod. and molecular resonance search 80−106066

alpha-radiation *see alpha-particles*

alpha-rays *see alpha-particles*

alpha-rhythm *see bioelectric potentials*

alpha-rhythm measurement *see electroencephalography*

alternators
1000-2000 MVA turboalternators, for LWR power station, design *(French)* 77−3153
fusion reactor, TEXT, motor-generator power supply system 80−99292
linear, Stirling free-piston engine/alternator power conversion system, 1978 development status 79−48178
linear, Stirling free-piston engine/alternator system, demonstrator engine design 79−48175
superconducting, 50 MVA thermal design of cryogenic rotor 79−58710
superconducting, design and test of liquid He rotating cryostat 77−26309
superconductive, with rotating field windings, research using rotating He rig 79−58719

altimeters
see also radioaltimeters
balloon ascent meter *(Japanese)* 78−61567
NS LX1600A pressure transducer, use as short-range altimeter 78−28344
satellite, GEOS-3, for remote sensing of ocean surface topography 79−39882

altitude measurement *see height measurement*

alumina
see also corundum
α-phase, growth and microstruct. on Ni-Al alloys 80−108626
β-phase, stoichiometric, Raman and IR spectra, Frenkel defects, order-disorder transition and cation cond. 80−55086
γ-irrad., hole centres, luminesc. and EPR obs. 77−32256
γ-type, adsorbed benzene high-temp. IR spectra *(German)* 79−28757
abrasive, wear in simulated hot grinding 78−56784
abrasive grains, single, wear on steel, exam. *(Japanese)* 78−44230
absorption of Fe(CN)$_6$, tunnelling spectra, isotope shifts 80−29262
absorptive laser damage of thin film coated sample, Weibull distrib. analysis 80−33061
activators for cementation at Zr/graphite *(French)* 77−52552
addition to molten PbO-SiO$_2$ system, effect on PbO activity 78−60663
additive for Pb(Zn$_{1/3}$Nb$_{2/3}$)O$_3$-PbTiO$_3$-PbZrO$_3$ ceramics, HF filters appl. *(Japanese)* 80−60507
additive for sintered TiO$_2$ ceramics, effect on props. 78−35329
additive modified, charact. by NMR 78−10785
additive to Cr$_2$O$_3$-Mo$_2$O$_3$ catalyst, effect on activity in oxidation of methanol to formaldehyde *(Russian)* 79−66346
adherence to Ni-Cr-Al alloy, improvement by addition of Pt and Rh 77−8995
adhesion of thick films, destructive and nondestructive meas. 80−50809
adsorbed 1-butene isomerisation, IR study 80−76554
adsorbed H$_2$ submonolayer, ortho-para separation coeff., mol. alignment and rot. levels 77−7971
adsorbed layers of methane, γ-radiolysis 80−3375
adsorbed molecules, Raman spectroscopy study 80−65358
adsorption and orientation of sulphonic acids, tunnelling spectroscopy obs. 78−34707
adsorption of 1-butene, microgravimetric-IR study 80−75432
adsorption of 2-butanol, PMR spectra 79−19457
adsorption of benzoic acid, benzoate ion binding energy 79−60629
adsorption of CO$_2$ on η-Al$_2$O$_3$, IR and microgravimetric meas. 78−14578
adsorption of Cs, Sr, Eu, Co, and Cd 80−99240
adsorption of electron acceptors, strength and distrib. of electron donor sites, ESR meas. 78−84055
adsorption of electron acceptors 77−48681
adsorption of ethanol, acetic acid and acetaldehyde, inelastic electron tunnelling spectra, surface vibr. struct. determ. 80−35572
adsorption of ethylene clycol, inelastic electron tunnelling spectroscopic study rel. to lubrication 80−70302
adsorption of H$_2$, diffusive motion, neutron scatt. study 79−42394
adsorption of H$_2$O, energetics, effects of adsorption temperature on surface processes 78−60028
adsorption of HCl and water vapour 79−73398
adsorption of isobutyl alcohol, gravimetry, IR investigs. 79−1546
adsorption of linoleic acid, under carbon tetrachloride immersion, IR obs. 79−24822
adsorption of NH$_3$, KVV Auger spectra, deconvoluted spectra 80−50508
adsorption of saturated hydrocarbons, gas-solid chromatography based on compensation effect 80−26053
adsorption of TCNQ anion radical salts, EPR and electronic spectra 77−72776
adsorption of thioindigo, photoisomerisation 80−89503
β''-Al$_2$O$_3$, Mg- and Li-stabilized, high electron microscopy images of defects 79−73135
β-Al$_2$O$_3$-Ag$_2$O, antiferroelectric transformation, Potts' model universality class 80−50277
β-Al$_2$O$_3$-Cu$_2$O, phys. and chem. props., use in determ. of thermodynamics of Cu-Sn alloys 80−107502
β-Al$_2$O$_3$-Na$_2$O, diffusion and ionic cond. meas. 80−6542
β- and β''-Al$_2$O$_3$-Na$_2$O, fast ion conductors, TFM obs. 79−86920
β-Al$_2$O$_3$-Na$_2$O, IR high temp. amplitude-phase spectroscopy 79−35860
β-Al$_2$O$_3$-Na$_2$O, mechanism of diffusion 80−2202
β-Al$_2$O$_3$-Na$_2$O, Monte Carlo calc. of Na diffusion 77−89579
Al$_2$O$_3$-SiO$_2$ refractories, using neutron-2 equipment 80−45612

alumina continued
alkaline earth glasses, 45RO.5Al$_2$O$_3$.50P$_2$O$_5$, (R=alkali earths), electron beam irrad., exam. of charge accumulation and light-sum kinetics 79−4336
alkaline earth glasses, 45RO.5Al$_2$O$_3$.50P$_2$O$_5$, (R=Mg,Ca,Sr,Ba), electron beam irrad., temporal change in electric field produced 79−4760
alkaline earth glasses, RO-Al$_2$O$_3$, -P$_2$O$_5$, R=Mg, Ca, Sr, Ba, exam. of electron beam irradiation effects 79−4253
alkaline earth phosphate (MO-Al$_2$O$_3$-P$_2$O$_5$) irradiated electret glasses, relax. of external field intensity on heating 80−25282
alumina based ceramics containing Mn and Ti compounds, sintering and paramag. props. 77−21069
alumina gel, hydrated, prep. by homogeneous precipitation method, phase change by heating *(Japanese)* 77−25046
alumina-acrylic composite bone cement 79−79689
aluminophosphate glass, multicomponent, 3.2 micron broad absorption band computer anal., residual H$_2$O vibr. 78−52478
aluminosilicate refractory, wetting by molten steel 79−82415
ambipolar diffusion in deformation mechanism maps 78−48454
amorphous, energy level schemes, Fermi level-electrochemical potential level coincidence, quantum yield spectrum 79−69400
amorphous, implanted ion detection by X-ray emission anal. in TEM 78−51575
amorphous, range of ^{29}Si meas. by (p,γ) reson. broadening 77−69023
amorphous anodic film, struct. anal. 79−51452
amorphous film, high temp., transport props., prep. conditions effect 77−12040
amorphous film, non-thermal switching in Al-Al$_2$O$_3$-Al struct. *(Russian)* 78−80069
amorphous films, struct., electron diffr. investigation 80−20046
amorphous layers for MIS structs., prep. and props. *(Slovak)* 78−64122
angular particle impact erosion of reaction-bonded SiC 80−89362
annealing, stable hardened subsurface layer form. 77−56128
anode film, galvanoluminesc. during pulsed excitation 79−74006
anodic, growth on GaAs 79−83344
anodic, Ni-pigmented, for selective absorpt. of solar energy, optical and struct. props. 80−55892
anodic, on Al alloy, characteristic emission of negatively charged particles during tensile deform. 78−92179
anodic, passified, inhibition of reaction with water 80−89390
anodic barrier film characts., ISS/SIMS 78−53021
anodic film, behaviour of emulsion particles during electrodeposition 80−104357
anodic film, complex TSC pattern analysis 78−23104
anodic film, gas emission, mass spectrometer study *(Polish)* 77−9157
anodic film, transient pitting during film growth 78−56817
anodic film, trapped O$_2$ and effect on dielec. stability 80−100634
anodic film growth, on high purity Al, luminesc. during growth 77−48589
anodic film in MIM struct., elec. props. obs. 79−99646
anodic film on Al, strain to failure, failure characts. 77−12734
anodic films, formed on Al, optical reflectance method anal. 80−37073
anodic films, trapping levels study using TSC 80−103768
anodic layer, thickness meas. by elliposmetry 78−171
anodic layer formation in H$_3$PO$_4$ solns., surface charact. 78−15603
anodic oxide film colour and structure obs. 78−11450
anodic oxide films, luminesc., breakdown and colouring 78−19528
anodic oxide films on superpure Al, growth kinetics and UV radiation effect 79−34190
anodisation for surface passivation of GaAs and InP, MIS characts. 80−93004
anodised film, arc cathode root initiation, electron emission, UV radn. effects 78−2985
anodised film, charge storage, UV radn. effect on electron emission arc roots 78−6827
anodised film, surface impregnated by organic phosphors, fluoresc. spectrum *(Japanese)* 80−55170
anodised film conduction and internal field obs. 80−15639
anomalous absorpt. in far IR region 78−56464
antireflection coating, 100 ns pulsed laser damage at 2.7 and 3.8 μm 80−33057
aqueous acid slip, casting in gypsum mould 79−83165
arc spot heat impact degradation *(Japanese)* 78−39819
atomic capture ratio for μ-transferred from μp to Al$_2$O$_3$ 79−10236
atomic disorder, dominant type 78−63757
atomically sharp cracks, TEM study 80−71729
Auger peaks, bremsstrahlung-induced, utility in spectroscopy 79−30618
barrier layer, for good high-temp. stability, BN in contact with W 79−70194
bauxite, Si, Al, Fe determ., neutron activation anal. 79−24858
bending strength, surface roughness effect at high temp. *(Japanese)* 79−70131
biaxially stressed, exam. of localised impact damage 78−72846
blister formation in anodised Al, pitting precursor 78−27678
bone bioceramic implants, surface structure *(German)* 79−44057
brittle, non metallic materials, wear chart, exam. *(German)* 78−35521
brittle ceramic fracture toughness meas. notch requirements *(German)* 77−59937
cabal glass:SiO$_2$(TiO$_2$), microheterogeneity, and elec. cond. 78−83997
cable insulation, resistance to high-temp. and intense gamma radiation 78−25332
calcined, exam. of morphological changes during calcination by SEM, exam. of sintering behaviour *(German)* 79−4931
catalyst pellets, porous, thermal cond. 79−86936
cathode, production of D ion beam impurities 79−86592
cathodic luminescence of oxide covering on Al electrode in electrolyte soln. 77−69915
cement grog bodies, high Al$_2$O$_3$ content, creep characts. obs. 80−66578
ceramic, delayed fracture 77−44342
ceramic, subcritical crack extension and crack resist. 77−8911
ceramic artificial hip joint wear tests *(German)* 79−8567
ceramic bars, fired, high Al$_2$O$_3$, modulus of rupture, relative humidity depend. 80−40473
ceramic Sinoksal, strength variation dependence on type of loading and temperature 79−57080
ceramic-metal composite using metal-coated alumina powder 77−21081
ceramics, elastic props. meas. in 100 to 300°C range 80−55445
ceramics, high rate reactive ion etching 80−85070
ceramics, ladder structures, interference phenomena explanation 78−72898
ceramics, sintering condition effects on props. *(German)* 78−56604

alumina continued
ceramics, sintering mechanism and kinetics, glass-forming additives effect 80—89187
ceramics, with thermoplastic bond, prep. 80—45254
cermet, protective coating for blast furnace tuyeres *(German)* 79—66193
channelling of He ions in α-phase 78—38764
chemical reduction by atomic hydrogen 79—93830
chemically-strengthened polycryst. mat., flexural strength at high temps. 77 21302
chemisorbed aromatic molecules, radiative and non-radiative transitions 79—36686
chemisorbed formic acid, effect of formate ion conc. on conductance of MIM struct. 79—15233
chemisorption, of formic acid, electron tunnelling spectra study 78—84049
chemisorption of monocarboxylic acids, tunnelling spectroscopy 78—91545
chemisorption of propylene by η phase, desorption and D exchange obs. 78—51827
chemisorption of water electron binding energies, UPS, SCF-Xα-SW calcs. 77—69169
circuit substrate, TiO_2 doped PbO-ZnO-B_2O_3 glass corrosion protection 79—29236
clay, Al_2O_3 and SiC recovery by C reduction 80—108704
coated TiO_2 powder, thickness meas., XPS and ion sputtering 79—88913
coating, half-wave, for (Al,Ga)As CW long-life laser 77—23688
coating, pore size distrib. and permeability 79—24641
coating for Al mirrors, highly efficient refl. type polarisers for 10.6 μm laser radiation 78—71177
coating on Al anode, anodic spark deposition 78—11382
coating on Cu, thermal shock performance 78—7081
coating on refractory fibre, effect on high-temp. strength *(Russian)* 77—52536
coating on Ti, detonation deposition, impact interaction parameters 80—40602
coating produced from separated flow vacuum arc plasma *(Russian)* 78—31548
coating protective, on SiC fibres in Ni-Cr alloy based composites, IR investigation 78—60623
coatings, detonation deposited on steel, prep., wear resist., antifriction props. 78—60877
coatings, form. and behaviour under particle bombard. 80—35029
coatings, on Ni-Al-Cr_3C_2 eutectic alloy, for oxidation resist. 80—50776
column for radioactive Sr adsorption, ^{82}Rb generator 80—12257
commercial, Na_2O impurity removal and modifier incorporation 79—43183
compact, morphological investigations significance 79—33988
compatibility with BN at high temp. 77—24995
complex glow spectra, improvement of fractional glow technique, thermally stimulated exoelectron emission 79—65984
composite film, barrier layer, ellipsometric meas. 78—67918
composite films, elec. instability 78—68452
compressive stress state strength determ. in brittle material 77—16757
concentration determ. in electrolyte of Al cells, semicontinuous 77—48713
conduction and dielec. loss mechanisms, paired interstitialcy model 80—107468
confined arc, ablation-induced effects 80—70073
cordierite glass ceramics, effect of TiO_2 and ZrO_2 content on phase sequence during heat treatment 78—48381
corrosion resistance of phosphate bonded castable, and dense fired types in steam CO at 199°C 79—20222
corundum refractories, dense production and performance 80—20866
crack detection caused by thermal shock, AE technique *(Japanese)* 80—21248
crack resist. and sub-crit. crack extension 78—19874
crack resistance and crack velocity, evaluation using controlled fracture expts. 78—72881
creep and grain boundary sliding 77—36576
creep and long term strength 78—23802
creep in pure and Fe or Cr doped polycryst. mat., diffusion mechanisms 78—11272
cryolite melts saturated with alumina, interfacial tension between Al and melt 78—38913
crystal subgrain misorientations, X-ray diffr. microscopy technique 77—70272
crystallisation of γ-phase from reactive pulse plasma 78—31308
crystallite size and lattice distortion, determination using X-ray line broadening analysis, appl. to ceramic powders 79—8261
cutting tool, performance relationships, porosity determ. 78—11169
cutting tools, effect of acid etching on cutting performance 79—96169
CVD and Czochralski grown crysts., imperfection anal. comparison 79—78868
CVD facet coating for GaAs-g$\rightarrow$Ga$_{1-x}$Al$_x$As laser, effect on degradation 78—13722
CVD-grown α-Al_2O_3, cryst. perfection by transmission X-ray diffr. topography 79—65337
cyclic fatigue in direct push-pull, exam. 78—56746
cylindrical cavity effect on fracture 79—66144
cylindrical voids, exam. of instability 78—79603
Czochralski bulk flow, in microgravity, digital simulation 80—28934
defect microstructure due to ion bombardment, TEM study 80—34100
deformation mechanism map 79—34109
deformed by prismatic slip, HV TEM obs. of dislocations 80—108517
dense, effect of oxide sintering additions on strength *(German)* 77—1866
dense, exposed to steam, influence of Ca migration on strength reduction 80—11797
dense, steam-enhanced Ca segregation, AES and SEM obs. 79—83352
deposition by activated reactive evaporation, struct. obs. 77—44176
derived from gels, sintering 80—20875
detonation coating, porosity, electrical strength, phase anal. *(Russian)* 77—69204
detonation deposited coatings, porosity and adhesion, processing parameters effects 79—70227
diametral compression test, parametric study 78—44282
dielectric and thermophysical props. 77—52009
dielectric breakdown mechanism determ. using acoustic signature anal. techniques 80—11337
dielectric hard transparent coatings 77—36678
diffusion creep activation energy 78—11274

alumina continued
diffusion of moisture 78—10219
discharge tube for cataphoresis lasers 77—75551
dislocation creep, creep deform. predictions 78—19815
dispersed particles in Cu, effect on H-embrittlement *(Russian)* 78—3207
dispersed particles in CuCl, effect on ionic cond. 80—24649
dispersion hardened by Ba mica, thermal diffusivity 80—25713
dispersion in polycryst. NaCl, diffusive creep 80—97531
dispersion strengthened Fe condensates, struct., mech. props. 77—90361
dispherse speres in KCl, cooling crystal dislocation mechanism for stress relaxation *(Russian)* 80—54347
on , dissolution and corrosion in high temp. water and moisture 77—48564
dissolution in Na_3AlF_6 *(French)* 77—51297
dopant effect on resistivity of $(Ba_{1-x}Y_x)TiO_3$ ceramic 79—65474
dynamic deformation, stress-wave response 80—21020
effect on carbothermic reduction of Cr_2O_3, to metallic Cr *(Japanese)* 78—48651
effect on thermal oxidation of Si 77—12722
elastic behaviour, finite element anal. model, thermal props. 78—31449
elastic moduli measurement, US method for up to 2000K *(French)* 80—104373
electric field effect on α to γ transform. 79—52209
electrical conductivity near melting point 77—28176
electrical properties under isentropic compression up to 500 GPa 78—71789
electro-erosional prep. *(Russian)* 80—81297
electroceramic, Al_2O_3 based, thermal expansion coefficient, linear, low-temp. meas. 79—60526
electrolyte, polycryst., impedance of electrochem. cells, cond. relax. 79—100401
electron beam deposition, heating of multiple layer structs. *(Russian)* 78—92192
electron slowing-down flux spectrum, due to β-decay of neutron-activated ^{164}Dy 78—10108
electron tunnelling spectroscopy, inelastic, of adsorbates, MgO comparison 80—88686
electronic struct., XPS meas. 77—73217
electrophotography, for radiographic imaging, thermocurrent and radiocond. meas. 78—35936
emissivity from bed of coarse particles 78—47542
enstatite content as geobarometer for plagioclase and spinel lherzolite 77—2142
epoxy-Al_2O_3 mixture, acoustic wave prop. characts., using differential-path US technique 79—42151
erosion impact of annealed 310 stainless steel, SEM and TEM study 78—64725
exoelectron emission, energy and ang. distrib. anal. *(German)* 78—92180
explosively compacted powder, struct. and annealing 77—55926
extraction and prep. for technical ceramics *(German)* 78—53200
extraction from coal wastes, sinter process investigation 77—28769
fabrication methods, new, of β-form 79—78916
facet coating, effect on degradation behaviour of Ga$_{1-x}$Al$_x$As buried heterostruct. injection laser 79—50313
fast ion transport and electrochem. storage in beta aluminas 80—61324
fatigue, static and dynamic in moist air 79—39002
femoral cement-free implant, mechanical strength tests *(German)* 79—8570
fibrous, thermal diffusivity and conductivity 78—10232
filled epoxy composite, shock wave compression, 0.4-3.7 GPa 78—59856
film, γ-phase, enhanced activated reactive evaporation process, ion effect 79—66013
film, anodic, dielec. breakdown 77—1637
film, anodic, H conc. profiles meas. 80—75261
film, anodic, trapping of ^{3}He and ^{4}He ions at room temp. 80—84221
film, anodised, in strong elec. field, pulsed V-I characteristics *(Russian)* 78—64156
film, CVD, props. rel. to deposition parameters 78—92197
film, CVD on Si, chem., phys. and elec. props. 77—12543
film, DC reactive sputtering prep., IR spectra characterization 79—11513
film, DC reactively sputtered, in MIS structs., effects of annealing on C-V characts. 77—51822
film, dielec. const. and resist., thickness depend. 78—39502
film, dielec. props., AC and DC elec. characts. 78—68445
film, effective electron mass determ. from current-voltage characts. in thermionic region 77—85135
film, elec. breakdown during anodic growth 80—55034
film, electrical breakdown by impact ionisation, models compared with expt. 79—91373
film, etching in carbon tetrachloride plasmas 80—76407
film, form., cross-sections, struct. obs. 78—67917
film, form. in discharge, IR absorpt. spectra *(Russian)* 77—12461
film, growth by anodisation of sintered Al, and elec. props. 79—95964
film, low energy electron absorpt., struct. and absorpt. centres 79—7763
film, MBE-growth on GaAs, MOS GaAs capacitor appl. 79—77943
film, MOS gate insulator, photoconductive processes 77—8216
film, on Al, IR refl. obs. 78—35591
film, on GaAs, prep. and surface states 77—85336
film, props., rel. to deposition conditions, appl. in semicond. devices 78—23612
film, refr. index and struct., deposition temp. depend. 79—4857
film, refr. index determ. by Nomarski differential interference contrast microscopy 78—24849
film, RF sputtered, stability 78—22993
film, RF sputtered, transient currents 78—23184
film, RF sputtered by planar magnetron, phys. props. 77—43448
film, self drifting of ionic charges, detection by surface potential decay method 78—72295
film, single-layer, 2.8 μm and 3.8 μm absorpt. meas. 78—90463
film, sputtered, form. by oxidation of Al magnetron sputtering target in Ar/O_2 mixtures 80—55291
film, stability, high temp. and electron irrad. effects 77—39747
film, switching times and arc cathode emitting site lifetimes 80—59332
film coating for GaAlAs DH laser diode 79—50321
film deposition from pyrolysis of Al acetylacetonate 77—85943
film for Si devices, surface and bulk elec. conduction obs. 77—43761
film form. by reactive HF sputtering with voltage bias 78—3045
film growth on MBE GaAs 78—39706

alumina continued

film on Al, particle and photon emission during tensile deform. 78—39672
film on Al substrate, IR photoacoustic spectra 80—13163
film on GaAs, elec. props. 79—66189
film on metal, IR refl.-absorpt. spectra *(Russian)* 78—11014
film on stainless steel in water, Gaussian ultrasonic beam refl. 78—67896
film pore size distribution meas., adsorpt.-desorpt. vs. TEM methods 77—74357
film prep. by pyrolysis of Al acetylacetonate 77—85098
film properties, form. by water reaction and anodic oxidation 78—15606
film thickness meas. by IR refl. spectroscopy *(German)* 79—58671
films, amorphous, self-supporting, vac.-tight, from electrochem. oxidation of Al in $(NH_4)_2CO_3$ solns. 80—16177
films on Al, photoacoustic refl.-absorption spectroscopy 78—31264
fireproof ceramic, direct energy conversion appl. *(Czech)* 79—70455
floating zone melting, forced and free convection, computer simulation 78—88423
floating zone melting, forced convection, computer simulation 78—88422
fluorided γ-phase, appl. of XPS method for surface anal. 78—40104
formation and dissolution on Al in oxalic acid bath, pH and conc. effects 77—16754
formation of $Al-SiO_2$ film-substrate interface 78—91571
fracture, multiaxial, general approach to statistical anal. 78—90785
fracture probability under static bending and tensile loading at 800°C *(German)* 78—23806
fracture resistance, exam. 78—76826
fracture stress, rel. to flaw and fracture mirror sizes, comment 79—11689
fracture toughness and acoustic emission rel. to microstructure, temp. depend. 80—11745
fracture toughness determ. using four-point-bend specimens 80—108536
fracture toughness meas. using Knoop indentation method *(German)* 80—25830
fracture toughness specimen, appl. of wedge indentation technique for precracking 78—85087
fracture toughness testing by AE *(German)* 79—70234
fusion reactor material, chem. interaction with H plasma discharge impurity ions 77—35357
gamma irradiated single crystal, defect centres 79—65117
gas phase equilibria, high temp., mass spectra 78—23925
gel particles, ultrafine, form. from NH_3-AlCl_3 soln. 80—93807
glass resistant, plasma coating props. 79—34164
glass-Al_2O_3 seals, diffusion of Al, electron microprobe study 80—107577
glazed, cement, as vacuum chamber material 79—40585
grain boundary thickness obs. using electron diffr. techniques 80—79811
grain orientation, permeable pressing effect *(Japanese)* 78—15349
grain size and fracture toughness, effect of fracture toughness test methods 78—72883
grain structure of notched substrate, SEM obs. *(German)* 80—33860
grinding and polishing, quantitative control and optimization *(German, English)* 80—35460
grinding material, grain shape optimization *(Polish)* 80—29916
growth in Ni-Al, morphology and spalling model 78—53030
Haynes Stellite 6B, Al_2O_3 particle erosion of surface, SEM obs. 78—88545
heat capacity laser-flash calorimetry 80—4716
heat of formation 79—91982
heat treated, adsorpt. of SO_2 79—56070
heat treatment rel. to texture of γ-Al_2O_3 78—72789
high alumina cement pastes, accelerated conversion, acoustic emission 77—36726
high temperature interactions with Re 80—16665
high-alumina materials, X-ray fluoresc. analysis accuracy 77—60163
high-frequency phonon lifetimes 80—70338
hot isostatic press. 80—108377
hot pressed, crack-growth boundaries, subcritical, fractographic criterion 79—100243
hot pressed, fracture stress-reflecting spot relations 80—71731
hot pressing, microstruct., texture 80—40299
hot pressing, role of polymorphic transform. 77—63612
hot pressing characts. 78—27456
hot-pressed, transparent and translucent properties 80—60533
hydrated gel synthesis by homogeneous precip. method using $NaAlO_2$, phase change by heating *(Japanese)* 78—68937
impact fatigue 77—56048
inclusion in steel, effect of high temp. heating on size, number and distrib. 78—44145
initial layer on Al-Mg alloy, role in growth of MgO film with high secondary electron emission 78—35590
initial sintering, method for obtaining surface diffusion coeffs., appl. to shrinkage data 78—95713
insulator, electrical puncture strength at high temps. *(German)* 79—70175
integrally coloured oxide films on Al, optical properties 80—93420
intense proton beam, effect, bonding methods 79—63261
interface of γ-phase with electrolyte solns., adsorption of ions, surface conductance, ion mobility and surface pot. 80—75622
interference filter, solar radiation resistance 77—39015
ion condensing metal plasma stream, coating microhardness, chemical reactions 79—42426
ion plated films on stainless steels and Inconel 77—40476
IR absorpt. spectra of OH^-, OD^-, and OT^- 80—55145
IR laser window materials, absorption props. 77—46770
IR spectra, comparison to inelastic electron tunnelling spectra *(French)* 78—68489
IR transparent materials, forward and backward scatt. data 78—59099
irradiated, displacement function calc. 80—34047
irradiation stability obs. using X-ray emission meas. *(Russian)* 80—66326
kaolinite to mullite reaction series, reexam. of solid state phase transformations 78—64535
kyanite-sillimanite concentrate, sintering and mullitisation of basic minerals 77—59726
laminated coatings, for fuel confinement, fusion reactor target appls. 78—60883
laser coating, UV damage obs. 80—33056
laser drilling and cutting, anal. of results using computer model 79—70180
laser window material, surface and bulk absorpt., photoacoustic meas. 78—25912

alumina continued

layer, obtained by reactive evap., surface struct. and morphology *(Polish)* 79—28242
layer on Mo film, passivation against IR reflectance losses caused by oxidation 79—3758
layer on stainless steel in water, leaky wave generation 80—75419
layer prep. by reduction by carbon in vacuum 77—8757
limiter and liner, results in Tokamak Petula 79—655
liquid, exam. of diffusion parameters, using Al^{26} 79—1518
liquid, sp. ht. eqn. for high temp. 77—51510
liquid, viscosity determ., oscill. cup technique 79—23758
low solubility in $Mg_2Si_2O_6$, enstatite, rel. to palaeogeotherm uncertainties 78—65283
luminescence of α-phase, additively coloured crystals *(Russian)* 80—55169
Madelung pot. determ. by Ewald method 80—92475
magnetically quenchable positronium-like systems, obs. in γ-phase 79—87065
MAOS memory element, stored charge volatility 78—52100
MAOS structure, for memory appl., cond. and charge storage 78—52099
mechanical props. charact. by dynamic elastic modulus meas. up to 1400°C *(German)* 79—70101
melt growth, influence of cooling rate on nucleation *(German)* 78—38638
melting speed, effect of struct. and grain shape *(Polish)* 79—29002
metal layer interdiffusion, Rutherford backscatt. 77—85000
MIS capacitor, Al_2O_3 gate insulator, low temp. radiation response 78—26960
MIS Schottky structures, photovoltaic response 80—101115
modulus of rupture, expt. test of Weibull scaling theory 77—21258
moisture sensor for sealed hybrid packages 77—87754
Mollwo-Ivey relation between peak-colour absorption energy and average O ion spacing 77—90179
molten, specific elec. cond. up to 3000K 78—2273
molten particles, complex refractive index *(Russian)* 77—55766
molten structural, conform. and solidification 77—36491
monolayer, core excitons and inner well resonances in surface soft X-ray absorpt. spectra 80—40187
mullite, crystallisation from $SiO_2-Al_2O_3$ melts 78—47243
mullite, quantitative X-ray anal., standardisation, texture *(German)* 78—11176
mullite fibre reinforced mullite, in vitro degradation, bending strength, Young's modulus, density meas. 78—85011
muonium and positronium form. 79—56679
β-$Na_2O-Al_2O_3$ low temp. ultrasonic vel. meas., temp. depend. 80—79885
neutron irrad., EPR spectra, F^+-centres 77—4558
NMR, multi-level, of ^{27}Al, obs. of two-quantum rotary echoes 77—63316
NMR, multilevel, spin-locking, spin-locked echo and rotary saturation associated with two-quantum transition 78—80245
NMR of ^{27}Al, quadrupole splittings, strain meas. of US modulation 79—28636
noncrystalline films, opt. and elec. props. 77—51627
optical absorption and external photoeffect 6-40 eV 77—55802
optical constants, high-temperature determination method 77—85680
optical props. of F-centre 79—43003
optical waveguide, fabrication by reactive Al sputtering in O_2-Ar atm. 80—33262
particles, influence of ionic treatment on formation of Al coatings *(Russian)* 80—50552
particles embedded in surface of amorphous Co-Si-B-Fe magnet, mag. anal. by electron diffr. 79—56568
particulate emission from calcining of clay, removal using electrostatic precipitator 79—24925
permeability and solubility of H_2, 1200-1450°C 80—39351
phase diagram calc. quasibinary and quasiternary oxide systems 79—96006
phase transformations, γ to α, produced by shock wave working 80—16305
phase transformations and microstruct., in boehmite derived transition Al_2O_3 80—60857
phonon spectra using freq. crossing techniques 78—14415
phonon spectroscopy of transition metal ion doped samples using freq. crossing techniques 79—42193
phosphate glasses, $P_2O_5-Al_2O_3$-Mg(Ba)(Sr)(Ca)O, struct. energetics and charging under irrad. *(Russian)* 77—84791
phosphor, thermolum. induced by 254 nm UV photons 80—55204
phosphors, photon multiplication and secondary electron-hole pairs generation *(Russian)* 80—66262
photocathode, for windowless XUV photodiode, photoefficiency 20 to 250 eV 78—65963
plasma anodised film, dielec. props., high field cond. *(Japanese)* 78—23185
plasma heating, alumina loaded antenna for lower hybrid wave heating 79—4159
plasma interactions in PETULA Tokamak *(French)* 77—62372
plasma sprayed, struct. and thermal diffusivity 79—86932
plasma-anodised, current efficiency 78—91797
plasmochemical synthesis, oxidised from metals, exam. of props. 80—2984
polarised luminescence in neutron- and proton-irradiated single crystals of α-phase 80—66271
polyamide, Al_2O_3 filled, low temp. thermal and mech. props. 80—25816
polycrystalline, compressive strength, microplasticity 77—36620
polycrystalline, conditions for formation of anion vacancies 79—10844
polycrystalline, effects of space charge, grain-boundary segregation and mobility differences on conductivity 80—79979
polycrystalline, on Si, anodisation, MAOS struct. form. and elec. props. 77—48563
polycrystalline, stress-strain data up to 1.25 GPa 80—100899
polyethylene based compositions, filled with Fe, Al_2O_3 powder, effect of filler particle size on wear resistance 78—44226
polymorphic transitions during heat treatment at 900-1500°C 79—11607
porcelain, crack propag. data applicability to failure prediction 80—81154
porcelain for high voltage insulators, increased mech. strength 78—11269
porous, anodic, growth, ionic cond. 78—48663
porous, anodic, growth, physical model 78—48662
porous, sintered, delayed failure, static fatigue in distilled water 78—64750
porous, validity of high pressure Hg intrusion porosimetry 79—24697

alumina continued
porous anodic films formed on Al, cell walls anal. by STEM and energy dispersive X-ray anal. 79−19476
porous anodic films on Al, nucleation and growth 78−44273
porous film, elec. cond. charact. 78−76179
porous refractories, production 80−35149
porous transparent films as antirefl. coatings for glass surfaces, low refr. index 80−74448
powder, active, sintering 80−20870
powder, disintegration of powder particle agglomerates under the action of an alternating electric field 78−68642
powder, injected into induction plasma, particle temp. and trajectory 78−59607
powder, NMR expts. on confined liq. ^3He 79−51371
powder, particle size analysis, using centrifugal sedimentation *(German)* 78−57890
powder, tensile and compressive strength meas. *(Japanese)* 80−25780
powder grains, melting, in plasma flame 79−60200
powder sinterability, prep. history effects *(Japanese)* 77−66616
powder sintering, isochronal temp. depend. data interpretation 77−77453
powder support for MnO_2 catalyst, N adsorption obs. of dispersion modes 80−81363
powder synthesis rel. to prod. of transparent ceramic 77−52270
prefired substrate, acid treatment, improvement in as-fired surface finish 79−24636
preparation, purification of technical gibbsite *(German)* 79−100091
pressing method, for the telecommunication industry *(Hungarian)* 78−52728
prismatic slip dislocations in single crystals, obs. *(French)* 77−59016
production rel. to props. of dense corundum refractories 80−25627
protective coating for Al mirror, refl. depend. on angle of incidence, 8 to 12 μm 78−37960
quench hardening, effect on mech. strength for various quenching mediums *(German)* 78−35403
radiation damage in HVEM, at high temp. and high dose in α-phase 79−46707
radiation damage in HVEM, temp. depend. of displacement threshold in α-phase 79−46706
rapid firing, XPS study of cryst. struct. 78−68663
reactions with Ti-Al-Cr-Mo alloy VT3-1 80−16585
reactive hot pressing, exam. of pressing characteristics 78−80499
recombination luminescence mechanism 80−71477
reduction cells, electrolytic, instabilities of metal surface, computer simulation 78−39720
reduction in Li vapour, 1800-2500K, thermodynamics 77−90595
reflective coatings, refr. index, UV polariser mirror coating appl. *(Russian)* 77−34928
refractories, fracture, J-integral meas. 80−108537
refractories, stability of refractory bond phases in steam-CO atmosphere 79−24634
refractory ceramic, deform. test apparatus and method *(Russian)* 78−35613
refractory metal-Al_2O_3 systems, vaporis. at elevated temp., mass spectrometric obs. 79−29388
RF sputtered film, transient current meas. 78−52113
rod, damaged, mech. strength, surface defects effect, appl. as insulators *(German)* 80−76330
rods, quenched, exam. of contact induced strength degradation 78−76731
sapphire filaments in Al_2O_3:MgO matrix, single cryst. boundary migration 80−44369
scales on Pt-Al alloy, elec. props. 79−20282
semisintered, shear strength at high press. 80−76308
shrink-free high Al_2O_3 compounds, prod. method using slips made from clay, orthophosphoric acid 80−66460
β-Sialon, high strength, reaction sintering 80−7525
silica, vitreous, effects on viscosity of impurity alkali oxide, OH, Al_2O_3 and Ga_2O_3 78−64580
silica-alumina hard coating for magnetic surfaces 80−7715
simultaneous reduction with Nb_2O_5 by CaH_2, Nb_3Al prep. 80−100809
single cryst., self-diffusion of O, isotope exchange investig. 80−100348
single crystal, fracture mirror formation, anisotropy of fracture surface energy and elastic constants 78−68824
sinterability, $NH_4AlO(OH)HCO_3$ crystallinity effect *(Japanese)* 78−52711
sinterability, $NH_4AlO(OH)HCO_3$ synthesis conditions effect *(Japanese)* 78−52710
sinterability dependence on crystallinity at $NH_4AlO(OH)HCO_3$ parent salt *(Japanese)* 78−6883
sintered, comparison with hard metal alloys, of stress intensity factor depend. on notch base dia. *(German)* 78−35470
sintered, containing $MgAl_2O_4$ precipitates, Mg distribution at grain boundaries 78−80498
sintered, correlation between wear, crack resistance and stress intensity factor *(German)* 77−36666
sintered, electron microprobe anal. of impurity and additive distribs. 80−40359
sintered, MgO-enhanced densification, test of second phase and impurity segregation models 78−64511
sintered, residual stress meas., piezospectroscopic technique 78−52704
sintered, strength, effects of moisture-assisted slow crack growth 78−27593
sintered, TEM obs. of K containing β''' precipitates 78−27522
sintered, wear and friction of MgO single crystal in vacuum 77−12710
sintered or hot-pressed, porosity effect on positron mean lifetime 78−27463
sintered surfaces, premetallizing with Mo-Mn-SiO_2 79−47792
sintered tubes, H_2 permeability 80−24675
sintered with Cu powder, props. 77−55909
sintering, calcination cond. effect *(German)* 80−16251
sintering, effect of furnace atmosphere 79−20010
sintering, effect of SrO, MgO and Y_2O_3 additives on α-Al_2O_3 mineralisation 80−89186
sintering, impurity effects, analysis *(German)* 78−6881
sintering, initial phase kinetics, model with diffusion *(French)* 78−35328
sintering, isothermal, surface area reduction 77−8779
sintering, rate controlled 80−20871
sintering, role of MgO 80−81010
sintering and props., glass forming additive effect 79−61544
sintering as function of phase comp. 80−66464

alumina continued
sintering at Si_3N_4-Al_2O_3-Y_2O_3 *(Japanese)* 78−19703
sintering behaviour, effect of calcination with mineralisers *(German)* 80−25622
sintering behaviour and props. of 24 aluminas *(German)* 79−4932
sintering in liq. phase presence, particle rearrangement 79−29004
sintering in reducing atmosphere, Na effect on density and strength 77−63613
sintering of single phase and multiphase components *(German)* 78−80494
sintering response with const. rate of heating, depend. on processing related pore distrib. 79−28992
sintering temperature effect of titanate additions 80−60808
sintering under press., survey *(Polish)* 78−31368
sintering with admixtures of titanates *(Polish)* 79−100096
sintering with $SrTiO_3$ admixture *(Polish)* 78−19699
slip band form. under fatigue stress, Schmid factor effect *(Korean)* 78−44199
smelter, crusting behaviour 77−73432
soft X-ray absorption and EXAFS on K edge 79−99981
solid electrolyte, beta phase, optimisation of fabrication process, for Na/S load levelling batteries 80−72035
solid electrolyte β- and β''-phases, defect struct. obs. by high resolution TEM, battery ageing relevance 80−107501
solid electrolyte based Na/S traction batteries, development progress and problems, review 80−61326
solid electrolyte for Na/S battery, GEC development program 80−61327
solid electrolytes, β- and β''-type, resist. obs. 200-1000°C 80−107500
solid electrolytes, elec. cond. and activation energy *(Chinese)* 80−79987
solid solubility in MgO 80−15247
solubility in orthopyroxenes in spinel and plagioclase peridotites and spinel pyroxenite 77−5186
solubility of α-Fe_2O_3, Mossbauer studies 77−7867
solution of single crystals in M_2O-V_2O_5 (M=Li, Na, K) and $NaVO_3$-KVO_3 melts 80−20910
spalling and cracking by compression 77−81313
spark source mass spectrometric study of species 79−29423
spatial distrib. of β- and β''-phases 79−66045
spectral emittance meas. at temp. up to 3000°C 77−22550
spectrographic determ. enhancement using alumina cup electrode *(Japanese)* 77−86418
sphere packed bed thermal storage analysis 79−57486
spray coated, reaction with Si, IR investig. 79−39197
spray dried agglomerates, compaction response, fracture, deform. 79−43172
sputter deposited, struct. and heat treatment charact. 78−15307
sputtered film, static compression to 1.2 Mbars, elec. resist. 79−55822
sputtered insulating film contouring over substrate topography 77−8752
steel, stainless types 321-SS and 430-SS, alumina coated, H_2 permeation 80−34244
steel against Al_2O_3, elastohydrodynamic contact, lubricated by naphthenic hydrocarbon, IR meas. of surface temp 79−15807
steel fibre reinforced Al_2O_3-Al, production and mech. props. 80−11619
STEM, Pt on Γ-Al_2O_3, atomic number contrast, supported catalyst particles 80−79651
stopping power, influence of chem. effect 80−47830
stopping power and energy straggling meas., Li ion backscatt. anal. 79−3328
strength-size relation 77−21255
stress value determination by bending tests, comparison with crack tip theory 78−67154
substrate, adherence of Ti and Cr films 80−7496
substrate, influence on adherence fracture energy of glass bonded Pt-Au thick film conductor 77−56075
substrate, quantitative electron microprobe analysis for Si, MnBi and CoPt films 77−9150
substrate, tape-casted, fracture strength analysis 80−60948
substrate for W-Al_2O_3 composite films, oxide evaporation deposited, struct., props. 80−25581
substrate material requirements for GaN VPE *(Polish)* 77−43440
substrates, grain growth during sintering 80−40302
substrates for Ni-Cr/Au films, interdiffusion processes and oxidation phenomena 80−59735
superionic conductor, Haven ratio, temp. depend., correl. effects role 80−107504
supermicrogrid preparation and props. for use as support film in high resolution electron microscopy 80−99010
supported catalysts, X-ray fluoresc. anal. using matrix correctional procedure 78−80817
supported metal catalysts, particle growth, obs. of Pt on alumina 77−8831
supported Ni catalyst, CO adsorpt. in H_2-He, effect of H_2S on IR spectrum 78−71945
supported Rh-Cu catalyst, chemisorbed CO, IR spectra *(French)* 80−60559
supporting film prep. by Al evaporation 77−67538
surface, $(10\bar{1}2)$, effect of multiple binding states on desorption and decomposition of Ga_2O 78−44406
surface, acidity, rel. to topochem., IR determ., adsorption method 80−35611
surface, adsorption effects during inelastic electron tunnelling spectroscopy *(French)* 79−822
surface, crystalline, mass transport mechanisms at high temperatures *(Japanese)* 80−54479
surface, laser Raman fluoresc. background, OH^- excitation, in η-phase 78−10875
surface, mass spectroscopic investig. of chem. reactions between adsorbed species 77−40600
surface, of γ-Al_2O_3, physisorption and reaction of $Mo(CO)_6$, IR spectra obs. 80−80064
surface, SiO deposited film, SiH bond form., inelastic electron tunnelling spectra 79−69375
surface, solar radiation absorpt., comparison with Planckian black body *(German)* 77−35026
surface analysis, quantitative, comparison of XPS results with model 78−40091
surface blistering, SEM and TEM obs., ion energy, dose and target temp. depends., review 77−43261
surface diffusion coefficient obtained by free sintering 77−72765
surface electrical resistivity in Cs vapour 77−51802

alumina continued
- surface electron donor sites and acid-base props., adsorbed radical ESR 77—21417
- surface energy measurement by const. temp. method data for liquid Cu-Sn and Au-Ag 78—6208
- surface of γ-Al_2O_3, OH layer, IR spectra, outgassing temp. effects 80—66175
- surface smoothness and densification, effects of SiO_2 additive 78—27462
- surface spark discharge, channel spreading and substrate vaporisation 77—89336
- surface structure of γ phase, hydrate adsorption, IR spectral study 77—89622
- surface tension and wetting by liquid Ni-O *(Japanese)* 79—99398
- surface treatment of insulators with Mn-Ti, effect on voltage-holdoff in vacuum 79—24261
- surface $Zr(BH_4)_4$ catalytic reactions, inelastic electron tunnelling spectra 80—75425
- suspended particles, behaviour on solidification of Al-Cu (33%) under reduced gravity *(German)* 80—60853
- suspension, mobility and zeta potential meas. in various solvents 77—36761
- suspensions, grinding method influence on rheology and suitability for high-density sintering 79—29001
- targets manufacture for vacuum thin film deposition, by powder metallurgy *(German)* 80—11586
- temperature drop parameter when testing with const. thermal flux 78—51049
- tensile failure of unflawed polycryst. samples, SEM and acoustic emission expts. 78—27598
- thermal anal. using solar heating *(Ukrainian)* 79—77725
- thermal characts. using constant power source method 79—95222
- thermal conductivity and diffusivity meas. by scanning temperature method 77—45831
- thermal etching of α-phase *(German, English)* 78—60934
- thermal expansion, 20-100-1700°C, as standard samples for dilatometry 78—26699
- thermal-sprayed coating on steeel, acoustic emission 80—21247
- thermally shocked, strengthening kinetics 77—8920
- thermally stressed insulator surfaces, behaviour under vacuum 80—18652
- thermodynamic props., calc. for liq. and solid phases 77—43348
- thermoluminescence, in H_2O vap. atm., temp. depend., time decay *(Russian)* 77—44074
- thermoluminescence, optical bleaching/stimulation effects following irrad. 78—43940
- thermoluminescence glow curves and emission spectra, 90-500K, for UV dosimetry grade Al_2O_3 78—72615
- thermoluminescent phosphor, annealing characts. and nature of traps 77—85817
- thermoluminescent trap stability, 450 to 1400°C 79—24372
- thick vacuum condensates, electron microscopy struct. investig. *(Russian)* 78—95242
- thin film used in inelastic electron tunnelling spectroscopy, X-ray photoelectron spectrum 80—108319
- thin films, electron trapping due to neutron irradiation 80—2505
- TLD for dosimetry after accidental gamma radiation release 78—57076
- TLD material, kerma for monoenergetic neutrons, theory, expt. comparison 77—5086
- TLD phosphor for gamma-rays 77—6637
- translucent, fabrication by high press. sintering 78—11167
- transparent, evaluation of freeze drying and spray drying for prep. 77—4761
- transparent, polycrystalline, prep. by sol-gel method *(Japanese)* 78—19698
- transparent ceramic manuf., characts. of powder and process 77—48383
- transparent film on Al, refr. index, thickness, ellipsometric meas. 77—52195
- twinning and microcrack nucleation during indentation 77—63793
- ultrafine powder, prod. by cryochemical, freeze drying, spray drying or soln. techniques 80—55336
- UV visible absorpt. by laser calorimetry, wavelength modulation spectroscopy 78—66876
- vacuum compacted using $MgCl_2$ soln. moistener and MgO additive 79—61546
- vacuum condensate, Mo-Al_2O_3, prod. by simultaneous condensation from 2 sources, growth direction *(Russian)* 77—21026
- vacuum condensate, struct. and mech. props., second phase effect *(Russian)* 80—71705
- vacuum vessel for Petula Tokamak RF hating expts. 78—70634
- valence band density of states from self-deconvolution of L_{23}VV Auger spectrum 79—47561
- vaporisation process, mass spectrometric exam. 77—1220
- vapour grown, single crystal, self diffusion coeff. of O 78—30792
- void formation by fast neutron irradiation, TEM exam. 78—51591
- VPE growth by photochemical reaction by Al and O_2 under UV excitation, MOS struct. characts. 79—60927
- waveguide for CW CO_2 laser 78—55376
- weakly emitting overlayer on Al surface, Fourier transform IR emission study 79—67399
- wear, effect of liquid environment, use of pendulum scratching sclerometer *(Russian)* 77—16693
- wear resistant coatings on cemented carbide machine tools *(German)* 79—74297
- wettability of single crysts. by liq. metals *(Russian)* 77—43408
- wetting by Cu-Sn-Ti alloys 78—71904
- wetting by Cu-Ti ternary alloys 80—107617
- whiskers growth by hydrolysis of AlF_3 79—28260
- X-ray induced desorption of gases from surface 77—35813
- X-ray Kα satellite struct., target chem. effects, 38 MeV F ion bombardment 77—24910
- XPS examination of interatomic Auger transitions 77—8692
- Zircon ceramic, exam. of development and fabrication 80—11608
- $2ZrSiO_43Al_2O_3$, identification of stages in reactive hot-pressing 79—11542
- $33K_2O.7Al_2O_3.60P_2O_5$, high expansion glass, chemical durability improvement by ion exchange 79—66180
- $3Al_2O_3$-GeO_2-SiO_2, reduction by C, mixed diffusional-kinetic regime *(Russian)* 80—66771
- $3CaO.Al_2O_3$, hydration retardation by $CaSO_4$ 79—61856
- $3Y_2O_3.5Al_2O_3$, garnet, synthesis by firing mixed oxides 79—61545
- adsorption of epoxy system, inelastic electron tunnelling spectra 79—15952

alumina continued
- Ag impregnated, appl. in radioactive methyl iodide removal 79—85638
- Ag-Al_2O_3-Al junction, internal photoemission 79—82683
- Ag-Al_2O_3-Al structure, photoinduced currents, UV detection characts., 325 nm 77—53979
- Ag-Al_2O_3-Au structure, electrorefl. meas. *(French)* 80—50366
- Ag-β-Al_2O_3, test for solid electrolyte by EMF meas on Ag/Au couples *(German)* 80—104307
- Ag_2O-Al_2O_3-MgO-Na_2O, β''-alumina, structure, X-ray determ. 80—107148
- Ag_2O-MgO-Al_2O_3, ionic cond. 80—107480
- $(Al,Fe)_2O_3$ on Al containing dispersed Al_3Fe, anodic film struct. and stability 78—11449
- Al, anodic film, formed in H_2SO_4, electron microscopy 78—68843
- Al/(Al_2O_3)-BaSt/Sn struct., internal voltage temp. variation 80—20326
- Al/Al_2O_3/Al, dielec. props. 80—80404
- Al/Al_2O_3/Al structures with organic monomolecular layer, cond. at high elec. fields 80—80402
- Al/Al_2O_3/CdS, junction characts. 79—82481
- Al-Al oxide-Pd tunnel junctions, exposed to H_2, inelastic electron tunnelling spectra 80—20327
- Al-Al_2O_3, dispersion hardened, creep *(Czech)* 80—108463
- Al-Al_2O_3, local struct. and interface states using surface soft X-ray absorpt. and photoemission spectroscopy 79—69595
- Al-Al_2O_3, recrystallisation nucleation in drawn wires, optical and TEM obs. 79—47709
- Al-Al_2O_3, supercond. granular film, mag. penetration depth, depend. on normal state resist. and temp. 79—56378
- Al-Al_2O_3 alloys, dilatometric method for studying relaxation of conc. of defects 77—55288
- Al-Al_2O_3 composite, brittle zone on fibre surface deform. and fracture 77—56104
- Al-Al_2O_3 electron transport in very thin multilayers 79—4602
- Al-Al_2O_3 films, coincidence energy spectra for (e, 2e) reaction 79—69936
- Al-Al_2O_3 thin film system, electrical conductivity and I-V characts. meas. *(Polish)* 79—56310
- Al-Al_2O_3:Mn-electrolyte, yellow electrolum. during anodisation of Al-Mn (1 wt.%) 77—63464
- Al-Al_2O_3-Ag structure, electron bombard, charge accumulation kinetics, exoelectron emission obs. 77—51825
- Al-Al_2O_3-Ag tunnel junction, surface plasmon excitation 78—10578
- Al-Al_2O_3-Ag tunnel junction, 4-pyridine carboxaldehyde-doped, surface enhanced Raman spectra, surface plasmons 79—98111
- Al-Al_2O_3-Al, oxide film prod. by pulsed evap., capacitor prod. and characts. *(Russian)* 78—60584
- Al-Al_2O_3-Al, thin film capacitors, dielec. losses 78—76382
- Al-Al_2O_3-Al, tunnelling junctions *(Russian)* 78—60232
- Al-Al_2O_3-Al junctions, Dy doped at Al_2O_3-Al interface, electron transport mechanisms and barrier height 78—91778
- Al-Al_2O_3-Al MIM struct., photocond. anal. *(French)* 77—72921
- Al-Al_2O_3-Al MIM struct., elec. cond., island metal struct. 79—15231
- Al-Al_2O_3-Al structure, elec. cond. 261 to 418K *(Russian)* 78—64144
- Al-Al_2O_3-Al(Au), thin films, elec. props. *(Czech)* 78—76159
- Al-Al_2O_3-Au device in Cl_2 atmosphere, current-voltage characts., press. depend. 80—65704
- Al-Al_2O_3-Au sandwich conduction props. 78—2580
- Al-Al_2O_3-Au structure, conduction props. in O_2 atmosphere 78—26971
- Al-Al_2O_3-CdS diodes fabricated by MBE, junction characts. 79—65550
- Al-Al_2O_3-Dy junctions, steady state and nonsteady state behaviour 79—78205
- Al-Al_2O_3-Dy thin junctions, Poole-Frenkel effect obs. and cause 80—80398
- Al-Al_2O_3-GaAs backwall MIS Schottky barrier solar cell, anal. model 80—85289
- Al-Al_2O_3-GaAs MOS struct., mol. beam reaction growth of Al_2O_3 film, C-V characts. 80—11095
- Al-Al_2O_3-Hg systems, I-V characts. at room temp. for different thicknesses 79—47172
- Al-Al_2O_3-In_2O_3:Sn tunnel junction, light emission via inelastic tunnelling effect 79—24076
- Al-Al_2O_3-InP MIS struct., elec. props. 79—78184
- Al-Al_2O_3-InSb MIS structures, recomb. processes and carrier lifetimes 79—38177
- Al-Al_2O_3-M, thin film sandwich, leakage current and dielec. relax., 80-500K 78—76158
- Al-Al_2O_3-Nb, quantitative proximity tunnelling spectroscopy 79—91193
- Al-Al_2O_3-Pb, oxide-layer chemisorbed phenols, electron tunnelling spectra, 2K 77—62736
- Al-Al_2O_3-Pb contacts, tunnelling spectroscopy, band struct. of Pb 80—80169
- Al-Al_2O_3-Pb structure, traps in Al_2O_3 detected by tunnelling 77—8202
- Al-Al_2O_3-Pb tunnel junction, Pb supercond. film behaviour in mag. field 78—14894
- Al-Al_2O_3-Pb(Au), solid-state anodisation of Al by vapour infusion, oxide growth rate 80—11830
- Al-Al_2O_3-Pd diodes, resonant tunnelling via localized inpurity states 79—28416
- Al-Al_2O_3-Si structure, study of charge trapping 80—60097
- Al-Al_2O_3-SiO_2-Si capacitors, physical and elec. props. of RF plasma grown Al_2O_3 80—100530
- Al-Al_2O_3-SnTe, junction, tunnelling, Fermi level depend. on carrier conc., influence of surface states 80—25016
- Al-Al_2O_3-SnTe structure, tunnelling characts., model anal. 80—29480
- Al-Al_2O_3-(a-Ge)-Al, electron tunnelling into a-Ge, press. effect 80—49938
- Al-Al_2O_3-electrolyte, electroluminesc., nondestructive electronic avalanche 78—68563
- Al-Al_2O_3-electrolyte system, electrolum. theory, thickness depend. 80—3358
- Al-Al_2O_3-metal capacitors, elec. props. interrelations 80—54801
- Al-Al_2O_3-metal capacitor, capacitance and power factor rel. to voltage and temp. changes 80—54802
- Al-Al_2O_3-p-GaAs MOS diode, capacitance-voltage characts. 80—107914
- Al-AlO_x-Pb, tunnel junctions, aromatic ring compound absorption, inelastic electron tunnelling 79—59521
- Al-Mg/Al_2O_3 composites, interface phase, Auger and electron diffr. study 80—25646
- Al-oxide-electrolyte system, luminesc. spectra *(Russian)* 78—76539
- β-Al_2-O_3-Ag_2O, sp. ht. 0.1-1 K, evidence for localised low-energy excitations 78—34632

alumina continued
(Al-Mg-Si)-Al_2O_3, SAP type, ageing 79–96055
$Al_{2x}Ga_{2(1-x)}O_3$:Cr^{3+}, luminesc., lifetime, 77 and 4K, struct., energy transfer 79–28798
β-$Al_{11-y}Mg_yO_{16}$, X-ray diffuse scatt. obs. of struct. 80–107186
AlN-Al_2O_3 composites, phys. and mech. props. of hot-pressed 77–52275
AlN-Al_2O_3 powders, hot pressing, crystalline phase obs. 78–95720
β-AlO_3-$(Na,Li)_2O$, NMR, Raman and IR spectra, and X-ray diffr., heat treatment induced changes 80–107508
$Al_{2+x}O_3$, nonstoichiometric, DC and AC cond., 20 to 1200°C 77–51740
$Al_{2+x}O_3$, sintered, elec. cond. temp. and comp. depend., thermoelec. power 80–2438
β-Al_2O_2-Na_2O, between metal electrodes, cell complex admittance diagrams, grain boundary effect *(French)* 80–45653
β-Al_2O_3, ^{22}Na labelled monocrystals, radiochemical anal. by isotope dilution method 80–11976
Al_2O_3 (96 wt.%), fractographic criteria for subcritical crack growth boundaries 80–81155
Al_2O_3, acceptor-dominated polycrystn., cond. and creep 79–78109
α-Al_2O_3, adsorption of $H(H_2)$, microweighing and X-ray obs. *(German)* 78–51825
γ-Al_2O_3, adsorption of methane, γ-radiolysis, reaction kinetics 78–95940
β-Al_2O_3, alkali-free water containing, cryst. struct. determ. *(German)* 77–47416
Al_2O_3, anodic, passified, inhibition of reaction with water 80–89390
Al_2O_3, anodic oxide film, field assisted pore form. 77–81336
γ-Al_2O_3 as intermediate cubic phase in kaolinite-mullite thermal sequence 80–25652
Al_2O_3, band structure and stored charge 80–49589
Al_2O_3 bicrystals, grain boundary obs. 80–39106
Al_2O_3 bioceramic synthesis, for orthopedic purposes, props. *(Polish)* 80–66465
Al_2O_3 ceramic, thermal expansion coeffs., represented by Gaussian spline polynomials 80–44341
Al_2O_3, coating, wear characteristics, comparison or coated and uncoated WC hard metals 78–92365
Al_2O_3, composite base ceramic coating, hot pressed, H_2 permeability 77–56164
β-Al_2O_3 compounds, stoichiometry, phase transition and conductivity 79–23773
α-Al_2O_3, computed X-ray powder diffr. patterns and densities 77–43172
β''-Al_2O_3, conductive, Li_2O stabilised, sintering and annealing 77–59724
α-Al_2O_3, cryst. struct. determ. at 2170K 80–39015
Al_2O_3, DC reactively sputtered, in MIS structs. optical and elec. props. 79–19486
β-Al_2O_3, defect props. and ionic transport 80–107486
Al_2O_3, dense, surface segregation of Ca under exposure to steam and steam-CO 78–85013
Al_2O_3, derived from metalalkoxides, sintering behaviour 79–29005
Al_2O_3, effect on elastic modulus temp. depend. of silicate glass 79–61637
γAl_2O_3, electronic struct., determ. by X-ray spectroscopy 79–8210
β-Al_2O_3, field assisted bonding to metals 80–45474
Al_2O_3 film, Al embedded, non-ohmic conduction behaviour 78–64157
Al_2O_3, fine grained, basal slip and nonaccommodated grain boundary sliding 80–60916
Al_2O_3, fine grained, interface-controlled diffusional creep 80–60915
Al_2O_3, fine powder, prep. by evaporative decomposition of solns. 78–39725
Al_2O_3, fusion cast ceramics, crystn., microstructures rel. to conditions 80–11638
Al_2O_3 gel, prep. of ultra-fine particles, from $Al(OH)_3$ colloidal soln. 79–74431
α-Al_2O_3, grain boundary segregation, electron microscopy 80–103361
Al_2O_3 hot pressed, high density, effect of grain size on grinding 78–39723
Al_2O_3 humidity sensor, ageing improvement *(Japanese)* 80–100863
γ-Al_2O_3, hydrotreating catalyst, oxidic precursory state of Co-Mo 79–61898
α-Al_2O_3, impurity energy levels, uniaxial stress effects 80–54642
β-Al_2O_3, internal friction and Na transport 80–59578
β-Al_2O_3, ionic superconductors *(French)* 80–39346
β''-Al_2O_3, Li_2O stabilised, hot-pressed and sintered, fracture props. 77–36626
β''-Al_2O_3, Li_2O-stabilised, hot-pressing 80–40298
β''-Al_2O_3, Li_2O-stabilised, deterioration under electrolytic conditions 80–40592
β-Al_2O_3, long-period structs., electron microscope obs. 80–92501
β''-Al_2O_3, Mg- and Li-stabilised, high-resoln. electron microscopy images 80–107277
Al_2O_3, microhardness as function of grain size 79–79084
Al_2O_3, Mo-refined single crysts., fabrication 80–16250
β-Al_2O_3, Na, K and Ag substitued, lattice vibrs., ion transport spectra 77–20121
Al_2O_3, neutron irradiated, electron centres, optical spectra exam. 77–63440
β-Al_2O_3, new slip casting technique for fabrication of ceramics 78–84745
α-Al_2O_3, noncubic cryst., axial-to-planar channelling transition 79–4367
Al_2O_3 on Al, anodic oxide film, effect of interface roughness on cracking 78–76755
η-Al_2O_3 outgassed at 400, 650°C, heat of adsorpt. of pyridines from soln., surface acidity 80–61154
β-Al_2O_3 phases, synthesized, effect of starting Al_2O_3 composition and halogen ion additions, on structural state 78–76620
β-Al_2O_3, polycryst. with preferred grain orientation, hot pressing of gibbsite and Na_2CO_3 *(Japanese)* 79–56948
Al_2O_3, polycrystn., high-temp. fatigue and strength 80–60954
β-Al_2O_3, polycrystn., with preferably orientated grains, prep. *(Japanese)* 80–81012
β''-Al_2O_3, polycrystn. electrolyte tubing, prepilot process for fabrication 79–87597
Al_2O_3, powder, phase composition, sintering, effect of explosive treatment 77–21079
η-Al_2O_3, prep. and struct. *(Japanese)* 77–55930
Al_2O_3 production, removal of S compounds in Na_2O-CaO sintering *(Chinese)* 80–55323
α-Al_2O_3 protective scale, influence of Pt 77–16749
α-Al_2O_3, pure and doped, rapid sintering 79–74123
Al_2O_3 rich substrate, surface smoothness and metallization props. *(German)* 78–19906

alumina continued
α-Al_2O_3 scales, early stages of development on Fe-Cr-Al and Fe-Cr-Al-Y alloys at high temp. 80–89413
Al_2O_3, single cryst., O self diffusion, ion-probe meas. 80–59701
β-Al_2O_3 structures, superionic props., IR spectra 80–107483
Al_2O_3, surface energy meas. by temp. variant method for liquid metals 78–6209
Al_2O_3, temp. distribution in growth from Czochralski method 79–65998
Al_2O_3, thermoluminescence, effect of heat treatment following gamma irradiation 77–59624
α-Al_2O_3, trigonal crystal, optical heterodyne detection using collinear acousto-optic interaction 78–66927
β- Al_2O_3 type compounds, microsyntactic intergrowth 79–99149
Al_2O_3, vitreous-bonded, eval. of proof testing to assure against delayed failure 78–84954
Al_2O_3, vitreous-bonded, mech. behaviour under various stress-time schedules 79–38968
Al_2O_3, X-irrad., electron and hole traps, TSC and optical bleaching meas. 79–28356
α-Al_2O_3:Ca(Ce), semicond. props. 80–54684
Al_2O_3:Co, spectra, heat treatment and irrad. effects 77–4659
Al_2O_3:Cr, Mg, stabilisation of Cr^{5+}, thermal cond. meas. 78–22905
Al_2O_3:Cr, pure and doped, electron irrad. induced cond., TSC and EPR study 80–80277
Al_2O_3:Cr photoexcited crystals, cooperative thermoluminescence quenching *(Russian)* 80–80881
Al_2O_3:Cr^{2+}, HF phonon spectroscopy using supercond. tunnel junctions 80–65178
Al_2O_3:Cr^{2+}, Jahn-Teller study, EPR data anal. 78–84172
Al_2O_3:Cr^{2+}, multiple-ion phonon absorpt. 79–82971
α-Al_2O_3:Cr^{3+}, electronic Raman transition from optically pumped excited state 78–39531
Al_2O_3:Cr^{3+}, impurity centre interaction with external elec. field 77–89727
Al_2O_3:Cr^{3+}, Jahn-Teller system, zero-phonon line broadening due to nonradiative transitions 80–108258
Al_2O_3:Cr^{3+} crystal, radiationless relax., photoacoustic spectra 78–27264
Al_2O_3:$CrCl_3$, calcination, mag. and optical studies of CrO_n 79–24736
α-Al_2O_3:Cr(Ti)(V), impurities effect on thermoluminesc. 80–40170
Al_2O_3:Cr(V)(Mn), phonon spectroscopy in supercond. tunnel junctions 79–90738
α-Al_2O_3:Er(Cr), crystal defects from X-ray irradiation, F-centres, X-ray luminesc. obs. 80–55176
Al_2O_3:Eu, surface luminesc. centres excitation characts. 78–52560
Al_2O_3:Fe, pore form. during oxidative annealing, grain growth slowing 80–100856
Al_2O_3:Fe^{2+}, phonon spectroscopy using superconducting tunnel junctions 78–91389
Al_2O_3:Fe^{3+}, mag. susceptibility, cryst. field calc. 78–76035
β-Al_2O_3:Gd^{3+}, EPR, ion site occupancy 77–81003
Al_2O_3:Gd^{3+}, mag. susceptibility, cryst. field calc. 78–76035
Al_2O_3:Li, TSEE, Li doping effects 80–80953
α-Al_2O_3:Mg, defect. struct., cond. and optical absorptiob 77–55279
Al_2O_3:Mg, pure and doped, recombination luminesc. spectra 79–83021
Al_2O_3:MgO, diffusion creep examined under three-point bending *(Japanese)* 79–96104
Al_2O_3:MgO, grain boundary segregation of Ca and Mg X-ray spectrosc. and STEM study 80–107269
β-Al_2O_3:MgO, strength and delayed fracture behaviour 80–35290
Al_2O_3:Mn, appl. of differential method for low temp. thermal cond. meas. 79–63227
Al_2O_3:Mn^{2+}, EPR meas., comparison with theory of EPR of S-state ions 77–1587
α-Al_2O_3:Mn^{2+}, intensity of forbidden $\Delta m=2$ EPR lines of S-state ions with axial cryst. environments 77–77090
Al_2O_3:Mn^{3+}, electronic and vibronic Raman scatt. 78–2839
Al_2O_3:Mn^{3+}, Jahn-Teller Mn^{3+} ions, phonon spectroscopy and thermal cond. meas. 80–88282
Al_2O_3:Mn^{3+} under uniaxial stress, Jahn-Teller model 80–88521
β-Al_2O_3:Mn(Co)(Ni), absorpt. and emission spectra, mag. susceptibility 79–87471
β-Al_2O_3:$NH_4^+(Nd_4^+)$, polarised Raman scatt. 80–103947
Al_2O_3:Ni, γ-irrad., thermoluminesc. 78–2925
Al_2O_3:Ni, heat transfer at low temp. 78–38888
Al_2O_3:Ni anodised films, electrolytically coloured, spectrally selective surface 80–11490
Al_2O_3:Ni^{3+}, effect of uniaxial stress on EPR spectra 79–82862
Al_2O_3:Ni^{3+}, heat transfer at low temperatures 78–91493
Al_2O_3:Ni^{3+}, Jahn-Teller effect for Ni^{3+}, EPR 79–82564
Al_2O_3:Ni^{3+}, phonon-spin interaction study by thermal cond. meas. 79–82395
Al_2O_3:Ni(Cr), thermally detected EPR of Ni^{3+}, Cr^{2+}, Cr^{3+} and Cr^{4+} ions 77–63273
α-Al_2O_3:Pb, implantation, lattice disorder 77–80525
Al_2O_3:Si, Ti, pure and doped, luminescence, optical absorpt. and colour centres 79–87501
Al_2O_3:Si,Ti photostimulated thermolum., and appl. to UV dosimetry 78–53511
Al_2O_3:Si(Ti), sensitised TLD phosphor, photon energy dependence 80–78498
α-Al_2O_3:Ti, defect struct., electronic and ionic cond., optical absorption meas. 78–30603
Al_2O_3:Ti^{3+}, dynamic Jahn Teller effect, role of nonadiabatic operators 77–59270
Al_2O_3:V, V^{3+} pairs studied by phonon freq.-crossing spectroscopy 78–39068
Al_2O_3:V, valency changes of V ions, γ irradiation, thermal cond. optical absorption and EPR meas. 77–80541
Al_2O_3:V^{3+}, frequency crossing signals of V^{3+} ions, conc. depend. study using thermal phonons 78–95115
Al_2O_3:V^{3+}, $g_\perp/g_\parallel$ determ. by freq. crossing spectroscopy using thermal phonons 78–23055
Al_2O_3:V^{3+}, Jahn-Teller effects, ground state 80–75528
Al_2O_3:V^{3+}, magnetocaloric effect in high magnetic fields 80–25140
α-Al_2O_3:V^{3+}, near IR spectra, line lifetime, 2, 10, 77K 78–10972
Al_2O_3:V^{3+}, phonon scattering, comparison between theory and experiment 78–95116
Al_2O_3:V^{3+}, phonon spectroscopy study of V^{3+} ion pairs 79–87068
Al_2O_3:V^{3+}, spin-phonon coupling, rot. mode role 80–70329
Al_2O_3:$V^{3+}(Fe^{2+})$, hyperfine splitting and magnetoelastic consts., freq. crossing spectroscopy 80–107392

alumina continued
α-$Al_2O_3{:}V^{3+}(V^{4+})(Co^{3+})(Co^{2+})$, optically and thermally stimulated reactions, absorpt. spectra 80—80825
$Al_2O_3{:}V^{4+}$, dil. solution, stimulated phonon emission 78—63817
$Al_2O_3{:}Zr$ ceramic, elec. props., additives effect, and interaction with steel melt 80—104305
Al_2O_3/Al clad powder prep. and physicomech. props. 79—29010
Al_2O_3/Al soldered samples, UTS and fracture surface comp., 20 to 500°C 79—38941
Al_2O_3/CuO, thin film interaction, $CuAl_2O_4$ form. *(Russian)* 78—52697
Al_2O_3/Nb, fracture mech. parameter determ. at high temps. *(German)* 79—70136
Al_2O_3/Nb laminates, metal to ceramic joints, adherence props. 80—45386
$Al_2O_3/Nb/Al_2O_3$ joint, solid state bonded, exam. of bond fracture strength 78—76826
Al_2O_3/stainless steel, adhesive energy, meas. techniques 80—50803
Al_2O_3-$4SiO_2$-H_2O, pyrophyllite, thermal diffusivity meas. using const. rate heating method *(Japanese)* 77—87759
β-Al_2O_3-$(K,Li)_2O$, ionic cond. and Raman spectra 80—107509
β-Al_2O_3-$(K,Sn)_2O$, ionic cond. and Raman spectra 80—107509
β-Al_2O_3-$(Na,K)_2O$, equil. distrib. of ionic species 80—107511
β-Al_2O_3-$(Na,K)_2O$, model calcs. of cond. anomalies, pot. energies of cation arrangements 80—107510
β-Al_2O_3-$(Na,Li)_2O$, first-order quadrupole NMR obs. of cation distrib. and ion motion 80—108113
β-Al_2O_3-$(Na,Li)_2O$, ionic cond. and Raman spectra 80—107509
β-Al_2O_3-$(Na,Li)_2O$, ionic motion obs. using NMR and internal friction 80—108099
β-Al_2O_3-$(Na,Li)_2O$ solid electrolyte, Li motion and activation obs. using ^7Li NMR 80—108100
β-Al_2O_3-Ag_2O, cryst. structs. of stoichiometric and non-stoichiometric phases by X-ray diffr. *(French)* 80—28987
β-Al_2O_3-Ag_2O, Haven ratio, temp. depend., Ag diffusivity and ionic cond. 80—107503
β-Al_2O_3-Ag_2O, low temp. dielec. susceptibility meas. 79—82911
β''-Al_2O_3-Ag_2O, Raman scatt. from mobile cations 80—11394
β-Al_2O_3-Ag_2O, stoichiometric and nonstoichiometric, structure comparison, phase transitions in stoichiometric compound *(French)* 80—60856
β-Al_2O_3-Ag_2O, stoichiometric A phase, X-ray diffuse scatt. obs., sublattice phase transition 80—64944
β-$11Al_2O_3$-Ag_2O, sublattice phase transition, stoichiometric 79—42241
β-Al_2O_3-Ag_2O, superionic conductor, microwave absorption spectrum 80—11515
β-Al_2O_3-Ag_2O, thermal cond. below 300K 77—24454
β-Al_2O_3-Ag_2O, with mobile ion species, dielec. relax. 79—91351
β-Al_2O_3-$Ag_2O{:}Cu^{2+}$, EPR of Cu^{2+} ions in conduction plane 77—69678
β-Al_2O_3-$Ag_2O(D_2O)(NH_4{}^+)$ 80—107512
β''-Al_2O_3-$Ag_2O(H_3O)(K_2O)(Li_2O)(NH_4{}^+)(Na_2O)$, ionic cond. at room temp. 80—107513
β-Al_2O_3-$Ag_2O(K_2O)(Li_2O)(Na_2O)$, low-energy excitation spectra, localised modes 80—59606
β''-Al_2O_3-$Ag_2O(K_2O)(Li_2O)(Na_2O)(Rb_2O)$, single cryst. Raman scatt., cond. mechanism and cryst. struct. 80—66209
Al_2O_3-Ag(Au)(Cr)(Cu) cermet selective surfaces for evacuated solar collectors 79—43785
Al_2O_3-Al, disordered, energy diagram model 79—56110
Al_2O_3-Al, multiphase thin films, correlation between optical props. and chemical/metallurgical constitution 78—19588
Al_2O_3-Al, sintered, plastic props. *(Russian)* 80—58923
Al_2O_3-Al interface, AES depth profiling, appl. of tailored modulation techniques 77—15702
Al_2O_3-Al triple-barrier structure, negative resist. caused by resonant tunnelling 78—14819
Al_2O_3-AlN, creep 77—21235
Al_2O_3-AlN phase diagram and reaction sintering of transparent cubic ALON spinel 80—25669
Al_2O_3-Au, cermet coatings, solar energy photothermal conversion, Bruggeman effective medium theory 79—83627
Al_2O_3-Au cermet, optical constants, incl. proximity effects 78—56446
Al_2O_3-B_2O_3 system, phase comp. and sorption props., Al salts chem. nature influence 79—51426
Al_2O_3-B_2O_3-P_2O_5 glasses, formation and props. 78—83737
Al_2O_3-B_2O_3-P_2O_5 system, glass formation by laser melting 78—44074
Al_2O_3-B_2O_3-RO, glass, (R=Ba,Ca,Cd,Mg,Sr,Zn), ionic and DC cond., comp. effects 77—31804
Al_2O_3-B_2O_3-SiO_2 system, liq. phase calc. for commercial quartzite powders 80—25671
Al_2O_3-B_4C, behaviour as control rod in commercial reactor 78—8918
Al_2O_3-BaO, fracture *(German)* 77—28882
Al_2O_3-bone composites, fracture toughness 77—37108
Al_2O_3-Ca (0.6 to 1.6 at.%), fracture behaviour, Ca segregation effect 80—40504
Al_2O_3-Ca_3SiO_5, solid solution, exam. of lattice defects 79—95167
Al_2O_3-CaF_2, phase relns. 78—23700
Al_2O_3-Cr (III), radiationless relax., heat-pulse meas. technique 77—36277
Al_2O_3-Cr cermet, Ti effect on sinterability 79—61552
Al_2O_3-Cr_2O_3, crystalline soln., microstrain rel. to lattice energy and strain energy 77—24411
Al_2O_3-Cr_2O_3, microstrain correction 78—59852
Al_2O_3-Cr_2O_3, solid soln., thermal expansion anisotropy, lattice consts. 80—54411
Al_2O_3-Cr_2O_3 melt, exam. of surface tension and density 79—1541
Al_2O_3-Cr_3, surface spark discharge, channel spreading and substrate vaporisation 77—89336
Al_2O_3-Cr(Re)(Nb)(Ta)(Ti)(V) heterophase films, elec. props. rel. to Al_2O_3 content 77—15969
Al_2O_3-Cu composite, dispersion-strengthened, hardness, tensile strength and struct. 77—70063
Al_2O_3-Cu composite, vapour deposition, microstruct., texture and surface topography 77—70001
β-Al_2O_3-D_2O, anhydrous, prep. and struct. of $DAl_{11}O_{17}$ 80—107187
β-Al_2O_3-D_3O^+, anhydrous, cryst. struct. from powder neutron diffr. 80—1983
Al_2O_3-Dy_2O_3, phase diagram at high temps. *(Japanese)* 79—38810
Al_2O_3-Dy_2O_3, phase diagram at high temps. *(Japanese)* 80—50619
Al_2O_3-epoxy mechanical mixtures, stress-wave propag. model, dynamic response expts. 79—1477
Al_2O_3-Er_2O_3 system, high temp. phase diagrams 80—40340

alumina continued
Al_2O_3-Eu_2O_3 system, phase diagram at high temp. *(Japanese)* 80—40339
Al_2O_3-$Eu_2O_3(Gd_2O_3)$, phase diagrams at high temps. exam. 78—44114
Al_2O_3-Fe cermet, microstruct. and physical props. 79—42279
Al_2O_3-$Fe_2O_3{:}Cr^{3+}$, dil. paramag. system, Cr^{3+} conc., effect on cross relax. 79—15387
Al_2O_3-$Fe_2O_3({:}Cr^{3+})$ paramag. system, cross relax. temp. and mag. field effects on Mossbauer spectra 79—33576
Al_2O_3-GaAs interface, elec. props., rel. to MESFET passivation 80—49934
Al_2O_3-GaAs interface, fabricated by interactive oxidation, props. 80—49935
Al_2O_3-Gd_2O_3 system, phase diagram at high temp. *(Japanese)* 80—45290
Al_2O_3-glass mixture, microstructural changes and shrinkage during sintering 80—25640
β-Al_2O_3-H_2O, H^+ and H_3O^+ conduction, dehydration effect 78—51726
β-Al_2O_3-H_2O, stability and dehydration 78—51693
β-Al_2O_3-H_3O, with mobile ion species, dielec. relax. 79—91351
Al_2O_3-H_3O^+, β and β'' phases, protonic, conductance and spectroscopy 80—70450
β-Al_2O_3-H_3O^+, ESR of paramag. defects in cond. planes 80—29617
β-Al_2O_3-H_3O^+, high press. thermal stability 79—23678
β-Al_2O_3-H_3O^+, ionic conductivity at 25°C, obs. 78—22893
β-Al_2O_3-H_3O^+, pulsed ^1H NMR study, 77 to 440K 79—87329
β-Al_2O_3-H_3O^+ protonic cond., struct. investig. 79—19213
β''-Al_2O_3-$H_3O^+(Na_2O)$, struct. basis for superionic cond. 80—107498
β-Al_2O_3-$H^+(H_2O)_n$, IR and Raman spectra, OH stretching freqs., struct. and cond. 78—27210
β''-Al_2O_3-$H^+(H_2O)_n$, IR study 80—16037
β-Al_2O_3-$H^+(H_2O)_n$, p-type conductor, stability *(French)* 79—38063
Al_2O_3-Ho_2O_3 system, high temp. phase diagrams 80—40340
β-Al_2O_3-K_2O, ESR of paramag. defects in cond. planes 80—29617
β-Al_2O_3-K_2O, K-content determ., ave. backscatt. spectra anal., rot. sample technique 79—5208
β-Al_2O_3-K_2O, low temp. dielec. susceptibility meas. 79—82911
β-Al_2O_3-K_2O, sp. ht. 0.1-1 K, evidence for localised low-energy excitations 78—34632
β-Al_2O_3-K_2O, thermal cond. below 300K 77—24454
β-Al_2O_3-K_2O, with mobile ion species, dielec. relax. 79—91351
β''-Al_2O_3-K_2O 80—11394
β-Al_2O_3-K_2O/K ferrite, interfaces and solid soln., thermal expansion and lattice parameter variations 78—55959
β-Al_2O_3-K_2O-MgO, cryst. struct., nonstoichiometry, ion-ion correlations 80—88129
Al_2O_3-$La_2O_3{:}Eu^{3+}$ system, optical and struct. exam. 77—4674
β-Al_2O_3-Li_2O, low temp. dielec. susceptibility meas. 79—82911
β-Al_2O_3-Li_2O, Raman scatt. from $^6Li^+$ and $^7Li^+$ ions 79—28766
β-Al_2O_3-Li_2O, sp. ht., 0.1-1 K, evidence for localised low-energy excitations 78—34632
β-Al_2O_3-Li_2O, thermal cond. below 300K 77—24454
β-Al_2O_3-Li_2O, with mobile ion species, dielec. relax. 79—91351
β-Al_2O_3-Li_2O-Na_2O, solid electrolytes, elec. props., stability 77—84978
β-Al_2O_3-Li_2O-Na_2O, spin-lattice relaxation and Li motion 80—70451
β-Al_2O_3-M_2O, M=Ag, K, Rb, Na, Eu, X-ray diffuse scatt. 78—71725
B-Al_2O_3-M_2O, M=Na, Ag, Rb, K, far IR absorption and ionic cond. 78—72512
β-Al_2O_3-M_2O, M=monovalent metal, superionic cond., phonon spectra and sp. ht. calc. 77—24368
Al_2O_3-martensitic steel, mag. and dielec. emulsion, prep. by abrasion of steel surface 78—27826
Al_2O_3-MgO, MgO addition role in sintering 79—91608
β-Al_2O_3-MgO ceramic, formation and structure of atomic scale cracks 80—45395
Al_2O_3-MgO spinel, 9.4 GHz US wave damping, defect and phonon scatt. 77 39637
Al_2O_3-MgO/ZrO_2-CeO_2/MgF_2 triple layer antirefl. coating for crown glass in visible region 78—13777
Al_2O_3-MgO-Cr_2O_3, effect of Cr_2O_3 on surface grain growth 79—23815
Al_2O_3-MgO-H_2O fast proton conductor 78—91480
Al_2O_3-Mo, dielectric cermet, thermophysical props. 77—51557
Al_2O_3-Mo (20 wt.%) cermet, ZrO_2 crystal addition effect on thermal fatigue resistance 80—40528
Al_2O_3-Mo cermets, effect of processing factors on props. 79—100103
Al_2O_3-Mo cermets, ZrO_2 and mullite whisker reinforced, strength var. with temp. 80—104232
Al_2O_3-$MoSi_2$, for use as heating element, fabrication method and prop. *(Japanese)* 79—95989
β-Al_2O_3-$NH_4{}^+$, high press. thermal stability 79—23678
β-Al_2O_3-$NH_4{}^+$, $NH_4{}^+$ jump diffusion and rotational tunnelling, proton NMR, spin isomerism theory 79—99778
β-Al_2O_3-$NH_4{}^+$, p-type conductor, stability *(French)* 79—38063
β-Al_2O_3-$NH_4{}^+$, PMR relax. time obs. of ionic motion 80—71213
β-Al_2O_3-$NH_4{}^+$, protonic cond., struct. investig. 79—19213
β-Al_2O_3-$NH_4{}^+$, single cryst. characts. and AC cond. obs. 80—107514
β-Al_2O_3-$NH_4{}^+$, single cryst. PMR and proton motion 80—108101
β-Al_2O_3-$NH_4{}^+$ proton dynamics neutron scatt. study 80—59408
β''-Al_2O_3-$NH_4{}^+$-H_3O^+, single cryst. PMR and proton motion 80—108101
β- Al_2O_3-Na_2-CaO, microstruct. and ionic resistivity 80—44357
β-Al_2O_3-Na_2O, ^{23}Na NMR spectrum, correl. effects 78—76324
β''-Al_2O_3-Na_2O, ^{23}Na NMR obs. of ionic diffusion, 180 to 800K, attempt freq. 80—108097
β-Al_2O_3-Na_2O, ^{23}Na NQR and two-dimens. diffusion, model analysis 80—108111
β-Al_2O_3-Na_2O, ^{23}Na nucl. spin-lattice relax., barrier height distribs. and diffusion processes 77—55720
β-Al_2O_3-Na_2O, ^{27}Al NMR obs., Na motion and cond. characts. 80—108096
β-Al_2O_3-Na_2O, AC impedance, microstruct. and strength 80—100349
β-Al_2O_3-Na_2O, AC ionic cond., dielec. and NMR relax. 80—59713
β-Al_2O_3-Na_2O, AE during breakdown under Na^+ transport 78—67860
β''-Al_2O_3-Na_2O, absorbed water effect on NMR lineshape and spin-lattice relax. time 80—108098
B-Al_2O_3-Na_2O, adsorbed of Na, surface electronic struct. calcs. 80—75431
β-Al_2O_3-Na_2O, anomalous Na behaviour obs. using pulsed and CW NMR 80—108095
B″-Al_2O_3-Na_2O, bulk and grain boundary ionic cond. from conductance and capacitance meas. 80—2204

alumina continued
Al_2O_3-Na_2O, β and β'' phases, stability, cond., paramag. impurity effects obs. 77—84976
Al_2O_3-Na_2O, β and β'' phases, formation by solid state reaction between $NaAlO_2$ and γ-Al_2O_3 80—29912
Al_2O_3-Na_2O, β' and β'' phases, engineering props. data compilation, rel. to energy storage 80—49415
β-Al_2O_3-Na_2O, calculation of simultaneous ionic cond. and tracer diffusion 78—43178
β-Al_2O_3-Na_2O, cation vibrations, disorder and hydration, IR and Raman spectra *(French)* 80—7343
β-Al_2O_3-Na_2O, ceramic and powder specimens, various Na_2O content, NMR study 79—61240
β-Al_2O_3-Na_2O, colour centers, AES, electron energy loss, and optical spectroscopy obs. 78—35176
β-Al_2O_3-Na_2O, colour centre ESR by localised tunnelling states 80—108073
β''-Al_2O_3-Na_2O, computer simulation of ionic conductivity 77—89580
β-Al_2O_3-Na_2O, cond. plane struct. and energetics 80—92715
β-Al_2O_3-Na_2O, conductivity dispersion in single crystal 77—28037
β-Al_2O_3-Na_2O, development for Na/S battery 80—71615
β-Al_2O_3-Na_2O, diffusion of Na^+, effect of path tortuosity and anisotropy 79—28140
β-Al_2O_3-Na_2O, ENDOR meas. of defects 80—66074
β-Al_2O_3-Na_2O, EPR and optical absorpt. studies of X-ray produced defects 78—95517
β-Al_2O_3-Na_2O, ESR of paramag. defects in cond. planes 80—29617
β-Al_2O_3-Na_2O, electrolytes, electric modulus spectroscopy 77—84974
β-Al_2O_3-Na_2O, fracture stress, effect of microstruct. defects 77—44338
β-Al_2O_3-Na_2O, grain boundaries and ionic cond. 79—23620
β-Al_2O_3-Na_2O, H_2O effect on Na^+ diffusivity 77—31806
β-Al_2O_3-Na_2O, H_2O intercalation effect on ionic cond. 79—99364
β-Al_2O_3-Na_2O, hot pressing and phys. props. 79—4940
β-Al_2O_3-Na_2O, ionic cond. temp. depend., comparison with NASICON 80—107520
β-Al_2O_3-Na_2O, layered material, contact free conductivity 80—2195
β''-Al_2O_3-Na_2O, Li_2O stabilized β'' phase, texture conductivity relationship 79—47788
β-Al_2O_3-Na_2O, low freq. Raman scatt. from NH_4^+ ions 78—43878
β-Al_2O_3-Na_2O, low temp. dielec. susceptibility meas. 79—82911
β-Al_2O_3-Na_2O, low-temp. ^{23}Na satellite spectra, Na ion motion 80—108112
β-Al_2O_3-Na_2O, MgO stabilised sintering *(German)* 78—19696
β-Al_2O_3-Na_2O, microwave absorpt., low-temp. dielectric props. anomalies, ion tunnelling states 78—92013
β-Al_2O_3-Na_2O, motion of charge carrying ions, mol. dynamics simulation 80—107506
β''-Al_2O_3-Na_2O, NMR of ^{23}Na, elec. quad. interaction, 185 to 419K, ion motion obs. 80—108110
β-Al_2O_3-Na_2O, non-stoichiometric, amorphous, US attenuation and velocity 80—39228
β''-Al_2O_3-Na_2O, nonstoichiometric, correl. effects in diffusion, Haven ratio, point defect interactions 80—107505
β-Al_2O_3-Na_2O, nucl. double reson. interferometry, satellite spectrum 78—31123
β-Al_2O_3-Na_2O, planar [00.l] disorder, TEM obs. 77—31680
β''-Al_2O_3-Na_2O, polycryst., Na^+ ion diffusion rel. to cond. 77—72715
β''-Al_2O_3-Na_2O, polycryst., ionic cond., 25-800°C 77—80645
β-Al_2O_3-Na_2O, potential energy distrib. and ionic motion 80—70455
β-Al_2O_3-Na_2O, preferable orientation for Na^+ cond. 80—35144
β-Al_2O_3-Na_2O, protonic, conductance and spectroscopy 80—70450
β''-Al_2O_3-Na_2O, Raman scatt. from mobile cations 80—11394
β''-Al_2O_3-Na_2O, rapid ion conductor, Na penetration 80—24653
β-Al_2O_3-Na_2O, single cryst. and polycryst., elec. props. 77—72714
β-Al_2O_3-Na_2O, single crystal ionic conductor, migration losses 77—80643
β-Al_2O_3-Na_2O, single cryst., non-Debye capacitance 80—107497
β-Al_2O_3-Na_2O, solid electrolyte, battery appl. *(Polish)* 80—12005
β''-Al_2O_3-Na_2O, solid electrolyte, behaviour at high current density, sodium heat engine mode 80—61330
β-Al_2O_3-Na_2O, sp.ht., 0.1-1 K, evidence for localised low-energy excitations 78—34632
β''-Al_2O_3-Na_2O, spinel formation, TEM obs. 77—76423
β-Al_2O_3-Na_2O, superionic anisotropic ceramic, prod. by microwave sintering *(French)* 78—52742
β-Al_2O_3-Na_2O, superionic conductor, microwave absorption spectrum 80—11515
Al_2O_3-Na_2O, syntaxy between β and β'' structures, TEM 77—20075
β-Al_2O_3-Na_2O, synthesis, ceramic form., sintering, cond. 79—11537
β-Al_2O_3-Na_2O, synthesis by chem. methods 77—24993
β-Al_2O_3-Na_2O, thermal cond. below 300K 77—24454
β-Al_2O_3-Na_2O, thermal desorption of ions 77—7973
β-Al_2O_3-Na_2O, thermal etching *(German, English)* 78—60934
β-Al_2O_3-Na_2O, thermal expansion 79—55910
β-Al_2O_3-Na_2O, tunnelling states, electron spin relax. 79—78518
β-Al_2O_3-Na_2O, vacuum hot pressed, densification kinetics 78—72758
β-Al_2O_3-Na_2O, with mobile ion species, dielec. relax. 79—91351
β-Al_2O_3-Na_2O, X-ray induced defects, EPR and ENDOR study 80—60456
β-Al_2O_3-Na_2O, Young's modulus and internal friction obs. 77—35624
β-Al_2O_3-Na_2O 79—19396
β-Al_2O_3-Na_2O ^{23}Na asymmetry parameter, temp. variations 80—6540
β-Al_2O_3-Na_2O doped with transition metal ions, complex plane anal. of impedance and admittance 80—70452
β-Al_2O_3-Na_2O electrolyte development for Na-S battery 79—29461
Al_2O_3-Na_2O solid electrolytes phase composition 77—36468
β''-Al_2O_3-Na_2O solid electrolyte, tube fabrication from cast ceramic tape 80—60819
β''-Al_2O_3-Na_2O solid electrolyte, processing and phys. props. 80—60820
β''-Al_2O_3-Na_2O solid electrolyte, strength degradation under electrolytic conditions 80—61329
β''-Al_2O_3-Na_2O solid electrolyte, heat treatment effects on ionic cond. and microstruct. 80—65293
β-Al_2O_3-Na_2O tube life determ. for Na-S battery 79—29462
β-Al_2O_3-Na_2O:Ba(Ti), dopant effect on ionic cond. and phase comp. 79—65242
β-Al_2O_3-Na_2O:Cr, absorpt. and emission spectra, mag. susceptibility 79—15495
β-Al_2O_3-Na_2O:Cu^{2+}, EPR of Cu^{2+} ions in conduction plane 77—69678
β-Al_2O_3-Na_2O:Fe, coordination site, oxidation state, Mossbauer, absorpt., emission spectra, mag. susceptibility meas. 78—68431

alumina continued
β-Al_2O_3-Na_2O:Mg, ionic cond., effect of microstruct. and phase composition 78—67859
β-Al_2O_3-Na_2O:Mg, with and without Co co-doping, ionic cond. and cryst. struct. 78—26723
β-Al_2O_3-Na_2O:Mn^{2+}, EPR of Mn^{2+} 78—6569
β-Al_2O_3-Na_2O:Mn^{2+}, ESR exam. 78—19313
β-$''$-Al_2O_3-Na_2O:Na^+,Ca^{2+}, charge compensation mechanism, Na^+ and Ca^{2+} ion movement 78—22891
β-Al_2O_3-Na_2O_3:Ag^{2+}, EPR measurements 78—95515
β-Al_2O_3-Na_2O-K_2O, cation interstitial pair modes in vibr. spectra 79—37788
β-Al_2O_3-Na_2O-Li_2O, ^7Li NMR 79—15361
Al_2O_3-Na_2O-Li_2O, phase transformations during firing 80—3036
β-Al_2O_3-Na_2O-Li_2O, struct. determ. by powder neutron diffr. 79—46623
β''- Al_2O_3-Na_2O-Li_2O (8.85, 0.75 wt.%) pressing powders, prep. by spray drying 80—40294
β-Al_2O_3-Na_2O-Li_2O membranes from Na-S cells, failure anal. 80—12003
Al_2O_3-Na_2O-LiO_2 (8.8, 0.75 wt.%) exam. of Na^+ resistivity as function of temp. grain size model 78—80654
β''-Al_2O_3-Na_2O-MgO, blocking defects observed by high resolution electron microscopy 78—55879
β-Al_2O_3-Na_2O-Rb_2O, cation interstitial pair modes in vibr. spectra 79—37788
β-Al_2O_3-Na_2O-SiO_2, solid electrolytes, exam. of microstruct. ionic resistivity 78—80566
β-Al_2O_3-Na_2O(Ag_2O), Raman scatt., 12-400K, 2nd order phase transition 77—81091
β''-Al_2O_3-NaO-LiO_2, stabilised, effect of phase composition, grain size, on Na ion cond. 78—47582
Al_2O_3-Nb, cermet thin film, electrical transport and thermoelectric power 77—20462
Al_2O_3-Nb, dielectric cermet, thermophysical props. 77—51557
Al_2O_3-Nb composites, influence of gas impurities on solid-state bonding on annealing 80—11739
Al_2O_3-Nb_2O_5-MgO, solid state equilibria at 1400°C phase diagram *(Italian)* 78—23671
Al_2O_3-Nb_2O_5-NiO, isothermal phase sections, 1100, 1250, 1400°C *(Italian)* 79—20032
Al_2O_3-Nd_2O_3, optical absorpt. spectrum and struct. of β-phase *(French)* 77—69848
Al_2O_3-Nd_2O_3, phase diagram at high temps. *(Japanese)* 77—63649
Al_2O_3-Nd_2O_3, phase-diagram at 1100°C *(Japanese)* 78—79747
Al_2O_3-Ni cermets, prep. and props. *(French)* 80—20877
Al_2O_3-NiCr composite, plasma sputtering of electroheating coatings, elec props. *(Russian)* 80—108350
Al_2O_3-NiO reaction at substrate-film interface, Rutherford backscatt. obs. 80—59733
Al_2O_3-Ni(Pt), composite solar selective absorbers optical props. 79—52037
β-Al_2O_3-OH_3^+, proton dynamics neutron scatt. study 80—59408
Al_2O_3-P_2O_5 glass, electron bombard. induced elec. discharge, electromech. effects *(Russian)* 77—32324
Al_2O_3-P_2O_5:Cr^{3+} glass, absorpt. spectra, Fano antireson. and vibronic Lamb shift 80—71458
Al_2O_3-P_2O_5:Nd^{3+} glass, high Nd conc., spectroscopy and lasing obs. 78—46609
Al_2O_3-P_2O_5-H_2O system, phase diagram 80—3014
Al_2O_3-P_2O_5-Mg(Ca)(Sr)O glasses, Na^+, Sr^{2+} diffusion coeffs. rel. to temp. 78—30787
Al_2O_3-polymethylsiloxane composite, thermoreactive compaction 80—20879
Al_2O_3-Pr_2O_3, phase diagram at high temps. 77—63648
Al_2O_3-Pr_2O_3, phase diagram at high temps. *(Japanese)* 78—88449
Al_2O_3-Pt metal-ceramic reaction, micro/macro obs. 80—66467
Al_2O_3-Si, alternating layers, dielec. facet reflector for semiconductor lasers 78—66841
Al_2O_3-Si boundaries, insulator charges evaluation *(German)* 79—82682
Al_2O_3-Si_3N_4 preparation, compressive strength 80—25634
Al_2O_3-Si-Te-Al_2O_3 layered apertured facet reflector, for lateral mode stabilisation of diode lasers 80—23708
Al_2O_3-SiO_2, derived from metalalkoxides, sintering behaviour 79—29005
Al_2O_3-SiO_2, mullite, powder, synthesis using silicic acid, clay and $AlCl_3$ *(German)* 79—4933
Al_2O_3-SiO_2, sillimanite, lattice defects, crystallo-chemical model, TEM obs. *(French)* 78—26570
Al_2O_3-SiO_2, thermomech. props., dependence on struct. and composition 78—84748
Al_2O_3-SiO_2 (3 wt.%), J-integral meas. at high temps. *(German)* 80—93624
Al_2O_3-SiO_2 fibre/mineral wool fibre composites, exam. of strength and shrinkage characts. rel. to Al_2O_3-SiO_2 fibre content effects 79—20105
Al_2O_3-SiO_2 heat insulating refractories, prep., physical, thermal, structural props. 78—68662
Al_2O_3-SiO_2 melt, exam. of surface tension and density 79—1541
Al_2O_3-SiO_2 powder, plasma-prepared, glass form. and phase transforms 77—44208
Al_2O_3-SiO_2 refractory, creep, viscosity, resist. to inelastic deform. 80—89309
Al_2O_3-SiO_2 refractory concrete, elastic props. 80—89280
Al_2O_3-SiO_2 system, evidence for metastable miscibility gap 80—71632
Al_2O_3-SiO_2 system, solid state transform. of andalusite to mullite 80—16281
Al_2O_3-SiO_2-CaO-B_2O_3(1,1,1 wt.%) chemical analysis by photocolorimetry and titration 79—20483
Al_2O_3-SiO_2-Fe_2O_3-CaO-MgO-TiO_2, refractory, corrosion and mech. behaviour correlations 80—40563
Al_2O_3-SiO_2-MgO, cordierite, powder, synthesis using silicic acid, clay and $AlCl_3$ *(German)* 79—4933
Al_2O_3-SiO_2-MgO-CaO, blast furnace slag, viscosity, MP *(Russian)* 77—25039
Al_2O_3-SiO_2-Si boundaries, insulator charges evaluation *(German)* 79—82682
Al_2O_3-SiO_2-TiO_2-B_2O_3-Fe_2O_3, exam. of porous structure, using a combinational method 79—29303
Al_2O_3-SiO_2-ZrO_2, liquidus surface, discussion 77—44231
Al_2O_3-SiO_2-ZrO_2 refractories, corrosion behaviour in glassmelting furnaces *(Polish)* 80—71783
Al_2O_3-Sm_2O_3, phase diagram at high temps. *(Japanese)* 78—19732
Al_2O_3-Sm_2O_3, phase diagram at high temp. *(Japanese)* 78—92253

alumina continued
- Al_2O_3-Ta system, phase comp. of solid products formed in vacuum heating *(Russian)* 77—44185
- Al_2O_3-TiC, composite, fracture behaviour in three-point bending 80—60951
- Al_2O_3-TiC, multiphase ceramics, mech. strengthening due to dispersion of non-metallic particles *(German)* 78—60674
- Al_2O_3-TiO_2, coatings, detonation deposited on steel, prep., wear resist., antifriction props. 78—60877
- Al_2O_3-TiO_2 (1 wt.%), with and without α-Al_2O_3 laminar crystals, bend tests 77—16531
- Al_2O_3-TiO_2 (1 wt.%), with and without α-Al_2O_3 laminar crystals, heat resistance 77—16532
- Al_2O_3-TiO_2 coating, prep. by plasma arc spraying and characterisation 79—23873
- Al_2O_3-TiO_2 powder, plasma-prepared, morphology and phase constitution 80—100833
- Al_2O_3-TiO_2 thermal-sprayed coating on steel, acoustic emission 80—21247
- Al_2O_3-TiO_2-MgO.$2TiO_2$, exam. of solid solutions by X-ray phase analysis 79—95981
- β-Al_2O_3-Tl_2O:Cu^{2+}, EPR of Cu^{2+} ions in conduction plane 77—69678
- Al_2O_3-V_2O_3-VO_2 system, phase equil. at 1273K *(French)* 77—35668
- Al_2O_3-W, dielectric cermet, thermophysical props. 77—51557
- Al_2O_3-W cermet, phase bonding 78—52745
- Al_2O_3-W cermet, sintered pressed compact, compressive and transverse rupture strength 78—19850
- β-Al_2O_3-X_2O, (X=Na,K,Rb,Ag,Tl), infrared and Raman spectra 79—1761
- Al_2O_3-Y_2O_3, melting behaviour and metastability determ. by optical DTA 80—92648
- Al_2O_3-Y_2O_3, plasma spraying, microstruct., porosity and adhesion 77—32710
- Al_2O_3-Y_2O_3, sintering kinetics, influence of minor additions of Y_20_3 80—84868
- Al_2O_3-Y_2O_3 ceramics, corrosion protective W coating 80—35367
- Al_2O_3-ZnO, surface spark discharge, channel spreading and substrate vaporisation 77—89336
- Al_2O_3-ZrO_2, dispersion hardened, fracture toughness improvement by induced microcracking *(German)* 78—31501
- Al_2O_3-ZrO_2, microstructure effect on friability 78—64515
- Al_2O_3-ZrO_2, tetragonal to monoclinic transform. of ZrO_2 particles *(German)* 79—43240
- Al_2O_3-ZrO_2 composite, fracture toughness increase by microcracking in energy dissipative zone near crack tip 79—20156
- Al_2O_3-ZrO_2 dispersed system, thermal diffusivity/conductivity, effect on microcracking resulting from phase transform. 78—10231
- Al_2O_3-ZrO_2 dispersed system, fracture toughness, inclusion induced microcracking effect 78—11296
- Al_2O_3-ZrO_2 mixture, stress induced transformation of tetragonal ZrO_2, exam. 78—48392
- Al_2O_3-ZrO_2-SiO_2, fusion cast refractory, effects of glassy phase on thermal cycling resist. 78—84956
- Al_2O_3-$ZrSiO_4$ mixture, reaction sintering, correlation between densification and reaction 80—29911
- Al_2O_3+ethanol, surface reaction, 295-575K, surface species study 79—100435
- Al_2O_3+tetrafluoroethylene, AlF radical, form. in arc plasma, spectra 77—28989
- Al_2O_3+TiC system, elastic and fracture charact. at elev. temp. *(German)* 79—43299
- Al_2O_3+TiO_2, reaction on sintering in reducing media 78—27457
- Al_2O_3+W(WO_2) reacts. in H_2, vacuum, high temps., reduction, oxidation conditions 77—16518
- Al_3O_3:^{57}Co, Mossbauer study of the charge state and symmetry of $^{57}Fe^m$ in diverse cobalt spinels *(Spanish)* 79—69754
- Al_xO_y, Raman spectra using pulsed laser and gated detection 77—74529
- (Al_2O_3-Fe_2O_3):Cr^{3+}, (0.04 mol.% Fe_2O_3), paramag., cross relax., annealing temp. effect from Mossbauer meas. 80—44983
- $Al_2O_3(H_2O)_3$, gibbsite, synthetic, crystallinity and topotactic reactions, X-ray diffr. obs. 78—63851
- $Al_2O_3(H_2O)_n$, uniform colloidal dispersion, prep. by chem. reactions in aerosols 80—97735
- $(Al_2O_3)_n$MgO, n=1.1, high temp. creep, dislocation behaviour 78—80593
- $(Al_2O_3)_n$MgO, spinel composition, dislocation climb, mass transport 79—32996
- β-$Al_2O_3Na_2O$, H-exchanged, effect of moisture, on H_2 activity changes and thermal stability 78—47580
- β-Al_2O_3.Ag_2O, low temp. sp. ht., tunnelling states and diffusion theory 77—43345
- β-Al_2O_3.$(K_xNa_{1-x})_2O$, anomalous behaviour in ionic cond. obs. 78—87818
- β-Al_2O_3.K_2O, low temp. sp. ht., tunnelling states and diffusion theory 77—43345
- β-Al_2O_3.Li_2O, low temp. sp. ht., tunnelling states and diffusion theory 77—43345
- β-Al_2O_3.$(NH_4)_2O$, neutron scatt. study of NH_4^+ motion 78—30785
- β-Al_2O_3.Na_2O, ceramic tube fabrication, crystallite preferred orientation, ionic cond. 77—8781
- β-Al_2O_3.Na_2O cryst. or sintered disc, Au electrode interface impedance rel. to roughness 77—4437
- β-Al_2O_3.Na_2O, low temp. sp. ht., tunnelling states and diffusion theory 77—43345
- β-Al_2O_3.Na_2O, single cryst. and polycryst., anisotropic cond., low temp. modulus spectra 77—4217
- β-Al_2O_3.Na_2O type compounds, struct. and stoichiometry by TEM 77—11521
- β-Al_2O_3.Na_2O:Cu, EPR, localisation of Cu^{2+} and linewidth effect 78—39395
- β-Al_2O_3.Rb_2O, low temp. sp. ht., tunnelling states and diffusion theory 77—43345
- Al_2O_3.SiO_2.H_2O, new materials from pianlinite minerals *(Chinese)* 79—95982
- $3Al_2O_3$.$2SiO_2$ as intermediate cubic phase in kaolinite-mullite thermal sequence 80—25652
- $3Al_2O_3$.$2SiO_2$, mullite, synthesis by freeze drying 80—16252
- $3.5Al_2O_3$.$2SiO_2$, mullite, decomposition by SiO_2 volatisation 80—61082
- $3Al_2O_3$.$2SiO_2$-ZrO_2 composites, sintered, in situ-reacted, fracture props. 80—81158
- Al_2O_3.$3H_2O$-H_3PO_4-CaO(ZnO), phase equilib., $AlPO_4$ solid soln. 79—11586

alumina continued
- $AlPO_4$-Al_2O_3 system, oxyorthophosphates form. 79—78942
- Au to Al_2O_3 solid state reaction bond, effect of ambient atmosphere 78—67914
- Au-Al_2O_3 cermet film, dense regular, optical props., rel. to appl. as selective solar absorber 79—79408
- Au-Al_2O_3-Al system, influence of mech. modulation on elec. transport 80—2481
- Au+Al_2O_3, solid-state reaction, bonding, temp. depend. 78—48695
- B_2O_3-Na_2O-SiO_2-Al_2O_3, effect of alumina dispersions on the thermal cond./diffusivity/stress resist. 80—39368
- BaO-Al_2O_3-B_2O_3:Ce^{3+} glass, EPR spectra, before and after X-irrad. 78—19320
- BaO-Al_2O_3-B_2O_3:Ag, X-ray irrad., atomic centre interactions, EPR spectra 80—25207
- BaO-Al_2O_3-B_2O_3-V_2O_5 glass, spectra, oxidation-reduction behaviour, DC cond. 77—76814
- BaO-Al_2O_3-GeO_2-MF_2 (M=0.45 CaF_2+0.55MgF_2), MgF_2 and CaF_2 effect on physicochem. props. 80—34876
- BaO-Al_2O_3-SiO_2-H_2O system, phase transitions during hydrothermal treatment 79—43216
- BaO-TiO_2-Al_2O_3 system, subsolidus equilibria, X-ray powder diffr. 80—108413
- $BaPO_3F$-Al_2O_3-B_2O_3 glasses, viscosity in the softening region and crystn. range 80—29105
- $BaPO_3F$-Al_2O_3-B_2O_3 system, liq. phase separation, IR spectra, microstruct. 80—29940
- BeO-Al_2O_3 V_2O_5, mixture kinetics and mechanism of formation of cryosoberyl 79—11535
- $CaAl_2O_4$ cement bond phases, corrosion in steam-CO at 199°C 79—29234
- $CaAl_2O_4$, fine powder, prep. by evaporative decomposition of solns. 78—39725
- $CaAl_2O_4$-$SrAl_2O_4$-BaA_2O_4, binary and ternary systems, solid solubility *(Japanese)* 80—35174
- $CaAl_2O_5$, form by interdiffusion of CaO and Al_2O_3 79—28998
- $CaAl_2O_5$, form. by solid state reaction of CaO and Al_2O_3, electric field effects 79—28997
- CaF_2-AlF_3-Na_3AlF_6(-Al_2O_3), phase equilibria, X-ray diffr. and DTA meas. 80—108409
- CaF_2-CaO-Al_2O_3, phase diagram contribution *(German)* 80—100830
- CaO-(CaF_2)-Al_2O_3, IR absorption spectra and X-ray emission spectra obs. *(Japanese)* 77—52075
- CaO-Al_2O_3, binary slag, reduction of Al_2O_3 by C saturated Fe *(Japanese)* 79—24733
- CaO-Al_2O_3, molten binary slag, dissolved C study *(Japanese)* 78—60662
- CaO-Al_2O_3 melt, solubility of H_2O at 1600°C 78—51687
- CaO-Al_2O_3 melts, density, atm. comp. effect 78—22624
- CaO-Al_2O_3 melts in presence of graphite, solubility of C and N 78—38850
- CaO-Al_2O_3-CaF_2, electroslag remelting slag, solubility of N_2 and C, equilibria 78—44110
- CaO-Al_2O_3-Fe_2O_3, and resonance spectroscopy study *(Russian)* 77—55733
- CaO-Al_2O_3-H_2O system, chemical degradation under high gaseous pressure and temp. 79—20464
- CaO-Al_2O_3-P_2O_5, sub-solidus relationships 79—66046
- CaO-Al_2O_3-SiO_2 80—89187
- CaO-Al_2O_3-SiO_2 glass, remanent magnetisation, log t low 78—68300
- CaO-Fe_2O_3-Al_2O_3 system, solid soln. of $Ca_2Fe_{2(1-x)}Al_{2x}O_5$ *(Russian)* 80—16284
- CaO-MgO-Al_2O_3-Cr_2O_3-Fe-O_2-SiO_2 system, exptl. determ. of periclase and spinel comps. 78—6906
- CaO-MgO-Cr_2O_3-Al_2O_3-ZrO_2-SiO_2 system, subsolidus region characts. 80—97466
- CaO-Nd_2O_3-Fe_2O_3-Al_2O_3 system, solid-state reactions 80—35173
- CaO-SiO_2-Al_2O_3, slag phase, activity of components at 1873K *(Polish)* 78—52775
- CaO-SiO_2-Al_2O_3, wollastonite, low dielec. loss factors, fabrication *(Japanese)* 80—55032
- CaO-SiO_2-Al_2O_3-Fe_2O_3 mix, liquid phase sintering 79—91610
- CaO-SiO_2-Al_2O_3-MgO, phase equilibria 77—86011
- β-CaO.Al_2O_3, onset temp. of decomp. 77—81244
- CaO.Al_2O_3, thermal expansion 77—84953
- 3CaO.Al_2O_3-$CaSO_4$.$2H_2O$-CaO-H_2O, citric acid effect on reactions 78—27725
- CaO.$6Al_2O_3$, thermodynamic stability, reaction with Ti, Cr and Zr oxides 80—92687
- Ca_3SiO_5-Al_2O_3 solid soln., elec. cond., 800-1000°C, hydration 80—54683
- CdO-Al_2O_3-P_2O_5 glass, γ-irrad., EPR study 80—84639
- CdO-Bi_2O_3-Al_2O_3, glass formation and IR transmission *(Japanese)* 80—54146
- Cl_2O_3:Ni^{3+}, EPR spectra anal. using dynamic Jahn-Teller model 79—82863
- Co/γ-Al_2O_3 catalyst, ESCA and EPR meas. after hydrodesulphurization reaction *(French)* 79—52755
- Co-Al_2O_3 catalysts, reducing and sulphiding treatments, XPS obs. 78—85196
- CoMo/γ-Al_2O_3 catalyst, ESCA and EPR meas. after hydrodesulphurization reaction *(French)* 79—52755
- CoO-Al_2O_3, isoelectric point meas. 80—88609
- CoO.Al_2O_3, prep. from film forming soln. 80—60811
- CoO.Al_2O_3-Al_2O_3, solid soln. *(Japanese)* 77—32567
- Cr-Al_2O_3 powder targets for plasma-ion spray deposition of resistance films 80—84897
- α-$Cr_xAl_{2-x}O_3$ solid soln., catalysis of H-D exchange 77—52631
- Cr_2O_3-Al_2O_3 solid solution, electrochemical determ. of activity 78—44391
- Cr_2O_3-Al_2O_3 solid solns., effect of Cr on point of zero charge 78—61021
- Cr_2O_3-Al_2O_3 solid soln., Vickers micro-hardness 80—66629
- Cr_2O_3-Al_2O_3-$ZrSiO_4$, exam. of microstructure by optical microscopy 79—29073
- Cr_2O_3-Al_2O_3-$ZrSiO_4$ system, electrosmelted refractories, phase comp., corrosion and glass resist. Cr^{3+} conc. depend. 79—33982
- $CrPO_4$-Al_2O_3 system, oxyorthophosphates form. 79—78942
- Cs-SiO_2-Al_2O_3 system interactions, getter development for radiocaesium 80—83208
- Cs_2O.Al_2O_3.$4SiO_2$ (pollucite) for long term-storage of ^{137}CsCl 80—37467
- Cu, with Al_2O_3 inclusions, breakdown and emission props., effect of inclusions 79—87389

alumina continued
Cu-Al_2O_3, composite coatings, prep. by precip., props. 78—23841
Cu-Al_2O_3, dispersion hardening single crystal, cyclic deform. *(French)* 79—1893
Cu-Al_2O_3, dispersion strengthened, plasticity qualities, fractographical analysis *(Czech)* 80—50680
Cu-Al_2O_3, dispersion-strengthened, vapour-deposited, tensile creep 78—11115
Cu-Al_2O_3, sinterec, deform., temp. and loading rate effects 77—77548
Cu-Al_2O_3 (1 vol.%), effect of second phase particles on diffusional creep 78—31472
Cu-Al_2O_3 alloy, internally oxidised, plastically deformed, influence of particle form on primary loop nature *(French)* 80—103344
Cu-Al_2O_3 cermet film, solar absorbing, production by dual cathode DC magnetron sputtering 80—16186
Cu-Al_2O_3 cermet films, temp. depend. of AC and DC cond. 79—87166
Cu-Al_2O_3 coatings, electrodeposited, dispersion hardened, exam. of props. 79—34181
Cu-Al_2O_3 composite coating, codeposition kinetics from $CuSO_4$ plating bath 78—15555
Cu-Al_2O_3 composite coating, electrodeposited, exam. of particle-cathode adhesion during formation 79—33954
Cu-Al_2O_3 disperse phase alloy oxidation kinetics 77—48584
Cu-Al_2O_3 dispersed composite, electron beam deposition, struct. characterisation 77—44197
Cu-Al_2O_3 dispersion hardened wires, drawn, substruct. and strength 78—35405
Cu-Al_2O_3 electrodeposits, dispersion hardened, props. 79—28258
Cu-Al_2O_3 extruded bars, strength anisotropy 77—16597
Cu-Al_2O_3 powder, electrolytic deposition 78—84743
Cu-Al_2O_3 thin film ceramets, TEM study of composition and struct. 79—99437
Cu_3Al-Al_2O_3 dispersion hardenend, short range order, quenching effect on yield stresS 78—35399
D plasma interaction, surface structure, chemistry and resistivity changes 78—53010
Fe/Al_2O_3 composite film, optical props., rel. to solar collector appls. 78—72622
Fe-Al oxide system, depth profile anal. by secondary ion mass spectra *(Japanese)* 78—7290
Fe-Al_2O_3, dispersion strengthened, thick vacuum condensate, control of struct. and mech. props. 80—16324
Fe-Al_2O_3 condensate, struct. and mech. props., disperse particle content depend. *(Russian)* 78—19772
Fe-Al_2O_3 granular film, interface props., Mossbauer spectroscopy 80—34336
Fe-Al_2O_3 granular films, superparamag., Mossbauer effect 80—7131
Fe-Al_2O_3 granular films, superparamagnetism and relax. effects 80—71118
Fe-Al_2O_3-MoS_2, self lubricating coatings, exam. of props. 79—96217
Fe-SiO_2-Al_2O_3 Lisakovskii concentrate mixture, sintering process, temp. thermal treatment *(Russian)* 80—55317
FeO-Fe_2O_3-SiO_2 -Al_2O_3-$CuO_{0.5}$/Cu slag-metal system, distrib. equilib. of Sn, Se, Te 78—44111
Fe_2O_3-Al_2O_3, solid solns., effect on Fe on point of zero charge 78—61021
Fe_2O_3-Al_2O_3 mixed oxide, X-ray diffr. and elec. cond. 80—79954
films, DC reactively sputtered, struct. 80—96764
GaAs-Al_2O_3 MIS struct., interface props. and MISFET fabrication 79—65557
Gd_2O_3-Al_2O_3 glasses, crystallization 79—50998
$HAl_{11}O_{17}$, H β-alumina, IR absorpt. study 80—100655
HF adsorption, by smelter-grade aluminas, during Al smelting 80—80075
β-$H_2O.11Al_2O_3$, conversion from β-$Na_2O.11Al_2O_3$ and characterization 78—3069
HfO_2-Al_2O_3, phase diag., 1500-2250°C 77—85998
InP-Al_2O_3 MIS struct., interface props. and MISFET fabrication 79—65557
K^+ ion nonuniformity, in contact with $NaNO_3$ and Na_xS_y melts 78—10215
K-β-Al_2O_3, far IR absorpt., Beevers-Ross sites, interstitials 80—66240
β-K_2O-Al O$_3$, cation distrib. 77—80487
β-K_2O-Al_2O_3, synthesis 77—81238
K_2O-Al_2O_3 system, high temp. thermodynamics and phase equilibria 78—80521
K_2O-Al_2O_3-B_2O_3, subsolidus compatibility relations determ. *(Japanese)* 79—4957
K_2O-Al_2O_3-B_2O_3:Fe_2O_3, glasses, liq.-liq. phase separation, Fe^{3+} ions rel. to mag., optical props. 77—15322
K_2O-Al_2O_3-P_2O_5 glass, low-temp. viscosity 80—39198
K_2O-MgO-Al_2O_3, ionic cond. 80—107480
L_2O-Al_2O_3 quenched glasses, crystn. and ionic cond. 80—33899
La_2O_3-Al_2O_3 system, alumina rich phase, X-ray obs. 79—29030
LiF-AlF_3-Na_3AlF_6-Al_2O_3 system, phase equilibrium, X-ray diffr., DTA, quenching, optical microscopy study 80—50610
LiF-Li_2O-Al_2O_3-P_2P_5 glass, ionic cond., transport numbers determ. 79—28143
LiI:α-Al_2O_5, model for fast ionic cond. 79—77811
Li_2O-Al_2O_3-Cr_2O_3 system, subsolidus equilibria 80—60843
Li_2O-Al_2O_3-P_2-O_5:V^{4+}, glass exam. of ESR spectrum of V^{4+}, optical spectra, and structure 78—88180
Li_2O-Al_2O_3-SiO_2 glass, crystn. aggregation and migration of ion-implanted Ag 77—55240
Li_2O-Al_2O_3-SiO_2 glass, He migration, struct. effects 77—55389
Li_2O-MgO-Al_2O_3 system, subsolidus phase equilibria 80—81036
(Li_2O-Al_2O_3-SiO_2):Fe_2O_3, glass, pyroceramic form., colour centres, magnetochem. investig. 77—16537
100($Li_2O.2SiO_2$).$3Al_2O_3$, directionally solidified, thermal and mech. props. *(Japanese)* 80—16295
MgO:nAl_2O_3 spinel, plastic deformation at T<1000°C, slip systems 80—108505
MgO-Al_2O_3 spinel crysts., thermolum. spectra 79—65938
MgO-Al_2O_3 system, surface microphases investigation by X-ray electron spectral anal. 79—51269
MgO-Al_2O_3 transparent spinel ceramic, fabrication by reactive hot pressing *(Japanese)* 77—77454
MgO-Al_2O_3-Cr_2O_3, vacuum vaporisation, Langmuir method 78—95149
MgO-Al_2O_3-Cr_2O_3 refractory system, phase conversion and props., X-ray anal. 77—90336
MgO-Al_2O_3-CuO, phase relations and microstruct. 79—74140

alumina continued
MgO-Al_2O_3-Fe_2O_3-SiO_2, cordierite, in ceramic, effect of heat treatment on cordierite content 79—20039
MgO-Al_2O_3-P_2O_5 system glass, heat treatment of aluminium metaphosphate influence on thermolum. 80—108285
MgO-Al_2O_3-SiO_2, exam. of microstructure and crystallisation kinetics 78—80501
MgO-Al_2O_3-ZrO_2, wetting with liquid Fe and Al 78—22936
MgO-CaO-Fe_2O_3-Al_2O_3-SiO_2, clinker production from dolomite and magnesite 80—55339
MgO-CaO-SiO_2-Al_2O_3-$Na_2O.P_2O_5$, effect of $NaPO_3$ on phase composition rel. to basic refractories 78—80528
MgO-P_2O_5-Al_2O_3-$3P_2O_5$ glass, absorpt. shift, electron and hole traps, thermolum. meas. 79—65897
$(MgO)_x$-$(Al_2O_3)_y$ formation of nonstoichiometric spinel on heating hydrous $MgAl_2O_4$ 78—76672
MgO$(Al_2O_3)_{1.8}$, spinel, X-ray refl. topography, dislocation substructures during creep form. *(French)* 78—68737
MgO.1.1 Al_2O_3 spinel, high temp. deform., cryst. orientation effect 80—107263
MgO.3.5Al_2O_3, precipitation during creep experiments 79—47694
MnO-Al_2O_3-SiO_2 glass, optical spectra 78—68528
MnO_2 porous powders, Al_2O_3 and SiO_2 coated, changes in surface free energy for N adsorption 80—84363
MnO.Al_2O_3.SiO_2, spin glass materials, mag. field dependence of susceptibility peak 80—103840
Mo-Al_2O_3, catalysts, reducing and sulphiding treatments, XPS obs. 78—85196
Mo-Al_2O_3 based hydrosulphurisation catalyst, used, ESR of SO_2^- and Mo^{5+} 77—70342
Mo-Mn-Fe-Si/Al_2O_3 ceramic seal, interfacial phases 78—72011
MoO_3/Al_2O_3, catalyst support system, Raman obs. 79—28734
MoO_3-Al_2O_3 catalyst, state during thiophene hydrogenolysis 77—86359
Mo_2O_3-Al_2O_3, reduced catalyst, adsorption of O_2, O^- form. 78—85197
β-Na, O-Al_2O_3, onset temp. of decomp. 77—81244
Na-βAl_2O_3 ceramics, synthesis 80—40305
Na_2-β-Al_2O_3, far IR absorpt., Beevers-Ross sites, interstitials 80—66241
Na_3AlF_6-LiF-CaF_2-AlF_3-Al_2O_3, electrolyte, exam. of phase equilibria, review 79—11590
$NaAl_{11}O_{17}$, local electroneutrality 79—65054
NaCl-Al_2O_3, threshold stress in particle inhibited diffusive creep 79—38922
NaF-Al_2O_3, β-Al_2O_3 form. *(Japanese)* 78—6912
β-Na_2O-Al_2O_3, isomorphous replacement of Al^{3+}, solubility of Cr^{3+}, Ti^{3+}, Fe^{3+} 77—85926
β-Na_2O-Al_2O_3, thermal dissoc. at high press. 77—36435
Na_2O-Al_2O_3-B_2O_3 glasses, kinetic study of Cu^+-Cu^{2+} equilib. 79—8448
Na_2O-Al_2O_3-B_2O_3-Fe_2O_3 glass, Mossbauer expts., 85-500K 78—80260
Na_2O-Al_2O_3-B_2O_3-SiO_2, glass, ESR exam. of paramagnetic centres formed during mech. destruction by grinding 78—88188
Na_2O-Al_2O_3-P_2O_5, exam. of subsolidus structure 79—4954
Na_2O-Al_2O_3-P_2O_5 glass, low-temp. viscosity 80—39198
Na_2O-Al_2O_3-P_2O_5:Eu glasses, fluorescence line narrowing meas. *(French)* 80—34975
Na_2O-Al_2O_3-$SiO_2.xH_2O$, fibrous crystal growth in silica gel, X-ray, electron probe and IR spectra obs. 80—25541
β-Na_2O-CaO-Al_2O_3, impurity conc. at grain boundaries, AES obs. 77—35570
Na_2O-Li_2O-Al_2O_3, local electrode current density and flow decoration 80—100935
Na_2O-Li_2O-β-$Al_2O_3.H_2O$, water mol. vibrs., IR and Raman spectra 80—89006
Na_2O-MgO-Al_2O_3, β'''-alumina, high-resolution electron microscopy 80—75208
Na_2O-MgO-Al_2O_3, ionic cond. 80—107480
β''-Na_2O-MgO-Al_2O_3, thermal dissoc. at high press. 77—36435
Na_2O-NaF-Ca_xZnO_{1-x}-Al_2O_3-SiO_2, opal glasses, strength, surface composition 80—30066
β and β-Na_2O_3-Na_2O, selection rules for spinel-block modes 79—19332
β-$Na_2O.Al_2O_3$, high-field ^{23}Na NMR 78—64284
$Na_2O.Al_2O_3.10TiO_2$, crystallized bronze, chem. comp., morphology, optical and thermal props. *(Japanese)* 80—16172
$Na_2O.Li_2O.Al_2O_3$, comp. and props. for use in Na-S battery 79—87745
$Na_2O.11Al_2O_3$, Cr, impurity ion struct., ESR study 80—80605
$Na_2O.5Al_2O_3$, diffusion of Na, computer simulation based on Monte Carlo method 77—24431
$Na_2O.y(Al_{1-x}Fe_x)_2O_{3-m}$, β''-Al_2O_3 phase stability, lattice constants 80—45283
β''-$Na_20.6Al_2O_3$, polycrystalline Na^+ ion drift and diffusion anomalies in elec. field 77—43372
Nb-Al_2O_3 cermet-type film, thermoelec. power and annealing effects 77—47911
Nb_3Sn-Al_2O_3 composite, electron beam deposited, microstruct., rel. to supercond. props. 79—37935
Ni dispersed epitaxial layer, textural effects on catalyst, ferromag. reson. 78—23963
Ni/Al_2O_3 catalysts, coprecipitated methanation type, metal-support interaction, XPS obs. 80—80936
Ni/Al_2O_3 composite film, optical props., rel. to solar collector appls. 78—72622
Ni/Al_2O_3 methanation catalysts, nonreduced, IR spectra 78—88288
Ni-Al_2O_3, composite coating, electrodeposited, exam. of particle-cathode adhesion during formation 79—33954
Ni-Al_2O_3, dispersion strengthened, thick vacuum condensate, control of struct. and mech. props. 80—16324
Ni-Al_2O_3 alloy, electron beam evaporated, struct. and mech. props. 78—11114
Ni-Al_2O_3 cermet, fabrication and mech. characts. 79—38781
Ni-Al_2O_3 composite film, selectively absorbing, optical props. 78—6798
Ni-Co-Cr/Al_2O_3 catalyst, IR spectra of adsorption and interaction with pyridine 80—71946
Ni-Cr-Al_2O_3 powder targets for plasma-ion spray deposition of resistance films 80—84897
β-NiAl, oxidation, α-Al_2O_3 growth and microstruct. 80—108627
NiO-Al_2O_3, Verneuil-grown crysts., phase comp. 77—66586
NiO-Al_2O_3 powders, coprecipitated particle-size distrib. meas. 78—39726
NiO-Al_2O_3 system, concurrent meas. of vol., grain boundary and surface diffusion coeff. 77—55399
NiO-$NiAl_2O_4$-Al_2O_3, heterogeneous solid state reactions, role of phase boundaries, dynamic equilib. at interfaces 78—71848

alumina continued

- P_2O_5-Al_2O_3-Na_2O-K_2O-Li_2O-(CaO+MgO) glass system, ion exchange effect on mech. props. 80—30229
- P_2O_5-MO-Al_2O_3, (M=MgO, CaO, SrO, BaO) (45, 5 wt.%) glass, electron irradiation effect on dielec. props. 80—29056
- Pb-Al_2O_3 composites, mech. alloyed, hot hardness meas. *(Japanese)* 78—84830
- Pb-Al_2O_3-HgSe junction, asymmetry of tunnelling characts. 79—47169
- PbO-Al_2O_3-B_2O_3 vitreous system with relaxation structure, spinodal decomposition 78—75553
- PbO-B_2O_3-Al_2O_3 glass, spinodal decomp. during continuous cooling, theoretical anal. 80—1935
- PbO-B_2O_3-Al_2O_3 system melts and glasses, viscosity, phase separation, and supercritical fluctuations effects 79—65235
- PbO-B_2O_3-SiO_2-LiO_2-Al_2O_3, glass enamel, chemical durability and microstruct., Al_2O_3 addition effect 79—29255
- PbO-Bi_2O_3-Al_2O_3, glass formation and IR transmission *(Japanese)* 80—54146
- Pd, catalyst hollow cone dark field microscopy on γ-alumina substrates 78—61049
- Pd on Al_2O_3, surface atomic composition by AES 77—86377
- Pd/Al_2O_3, adsorption of CO, IR study 80—108193
- Pd/Al_2O_3 catalyst, contact poison 2-methylthiophene damage reduction by neutron irrad. *(Russian)* 79—20467
- Pt/Al_2O_3, electron accepting sites by pyridine absorpt. 80—71947
- Pt-Sn/Al_2O_3 catalyst, Mossbauer effect, reactivity 80—11298
- Re/Al_2O_3, catalyst, Re-O_2 surface interactions; 77 to 773K 79—79286
- Rh/Al_2O_3 catalysts, surface interaction between NO and CO, IR study 79—70369
- Rh/γ-Al_2O_3 disperse δ-phase, chemisorpt. of CO, IR spectra, site distrib., mol. mobility 78—72496
- Si-Al_2O_3, MIS structure, with dielectric film, from UV irradiation converted metalorganic compounds *(Russian)* 80—45245
- Si-Al_2O_3 interface, charge injection from surface depletion region 80—54797
- Si-Al_2O_3-SiO_3 in MIS struct., charge accumulation and spreading *(Russian)* 78—64116
- Si-Al-O-N, mullite like cpd. comp., EPMA, X-ray and chem. anal. obs. *(Japanese)* 80—35175
- Si-Al-O-N sintered ceramic, microstruct., phase composition and transformation mech., mech. props. 80—40309
- α-SiC-Al_2O_3, sintering 80—11611
- Si_3N_4:(MgO+Al_2O_3)(Y_2O_3), hot-pressed and sintered, microstruct. and impurity distrib. 80—49261
- Si_3N_4-Al_2O_3, hot-pressed with crystn. grain boundary phases, prep. 78—95715
- Si_3N_4-Al_2O_3, Sialon, pressure sintering 77—55919
- Si_3N_4-Al_2O_3-Y_2O_3, sintered, observation of a noncrystalline phase 78—64536
- Si_3N_4-Al_2O_3(25.5, 37.0, 47.8 and 57.8 mol.%) thermal diffusivity 77—7913
- β-Si_3N_4-AlN-Al_2O_3-MgO, insolubility of Mg in β-Si_3N_4 79—10953
- Si_3N_4-AlN-Al_2O_3-SiO_2-Y_2O_3, phase equilibrium study by X-ray diffr. and optical microscopy 80—50614
- Si_3N_4-AlN-SiO_2-Al_2O_3 solid-liquid equilibria 78—92247
- Si_3N_4-Y_2O_3-Al_2O_3-SiO_2, X-ray diffr. exam., phase equilib. at 1400 degrees C *(Japanese)* 78—44113
- Si_3N_4-Y_2O_4-Al_2O_3 (4-17, 4 wt.%), sintering 80—81009
- Si_3N_4AlN-Al_2O_3 system, reaction sintering forming β-Si_3N_4 solid solns. 80—50585
- Si_2N_2O-Al_2O_3, solid soln., prep., effect of Si_3N_4 powder reactivity 80—45256
- SiO_2 coated and pure, surface props., catalytic activity 79—79287
- SiO_2:Al_2O_3, ultrafine and ultrapure powder prep., SEM study 79—70025
- SiO_2/Al_2O_3 ratio in zeolite containing catalysts, IR spectra, struct. 79—42958
- SiO_2-Al_2O_3, (Al_2O_3)(ZrO_2), noncrystalline film form., IR study *(Japanese)* 77—59634
- SiO_2-Al_2O_3, calculated thermodynamic data and metastable immiscibility 78—27495
- SiO_2-Al_2O_3, minerals, phase equilibrium *(German)* 77—73261
- SiO_2-Al_2O_3, mullite, sintering behaviour and microstruct. 80—20876
- SiO_2-Al_2O_3, refractory fibrous heat insulating material 78—6990
- SiO_2-Al_2O_3, sintering theoretical treatments and exp. procedure 78—44067
- SiO_2-Al_2O_3, surface electron donor sites and acid-base props., adsorbed radical ESR 77—21417
- SiO_2-Al_2O_3 (36.6 wt.%) plasma prep. powder, metastable immiscibility and microstruct. during sintering 80—35143
- SiO_2-Al_2O_3 based minerals, phase equilib., struct., comp. *(French)* 78—60659
- SiO_2-Al_2O_3 glaze, adhesive behaviour of metallic cation glaze exchanged on acid site struct. on steel *(Japanese)* 79—66216
- SiO_2-Al_2O_3 melts, densities 79—99259
- SiO_2-Al_2O_3 mixture, depend. of phase comp. on nuclei available 79—11584
- SiO_2-Al_2O_3 porous catalysts, EPMA quantitative anal., new correction calc. method, modified ZAF method *(Japanese)* 80—93822
- SiO_2-Al_2O_3 refractories, thermal shock props., fracture mech. appl. *(French)* 79—96109
- SiO_2-Al_2O_3 system, phase equilibria 79—77724
- SiO_2-Al_2O_3-CaO-MgO, liq. silicic and slag, struct, density, surface tension *(Polish)* 78—83711
- SiO_2-Al_2O_3-CaO-MgO-NaO-K_2O-B_2O_3-ZrO_2, glaze, exam. of zircon crystallisation 79—19155
- SiO_2-Al_2O_3-CaO-MgO-B_2O_3, E-glass, acid resist. studies 80—60991
- SiO_2-Al_2O_3-Fe_2O_3-K_2O, form. of Al-Fe leucite, inversion temp. *(Japanese)* 77—62481
- SiO_2-Al_2O_3-Fe_2O_3-CaO-MgO-Na_2O-SO_3 glass, thermophysical props. 78—18849
- SiO_2-CaO-Na_2O-TiO_2 system, water, alkali, acid resist., chem. durability 79—34162
- SiO_2-TiO_2-Al_2O_3-SrO(BaO), glasses, ceramic form. rel. to Al_2O_3 content 77—25005
- Si_2ON_2-Y_2O_3-Al_2O_3 phase relations at 1400°C *(Japanese)* 79—38811
- SnO_2-Cu_xS-ZnS:Mn,Cu-Al_2O_3-Al, light-emitting struct., cond. and electrolum., heat treatment 80—97345
- SrO-Al_2O_3-B_2O_3-SiO_2, glass, corrosion by Cs vapour or liq. 77—16706
- T diffusion 77—55391
- Ti-Al_2O_3 system mixed films, prep., phase comp., struct. and elec. props. 79—37930

alumina continued

- $(Ti_{1-x}Al_x)_2O_3$, crystal struct. determ., metal-metal distance, effect on electronic struct. 77—47431
- TiB_2-Al_2O_3, thermal stability of composite materials 78—60638
- TiB_2-Al_2O_3 system-based composites 77—85979
- TiN-Al_2O_3, exam. of sintering and densification kinetics, and physical props. 79—95986
- TiO_2:Al_2O_3, in purity influence on polymorphic crystn. 79—78858
- TiO_2-Al_2O_3 system, dislocation mechanism of diffusion processes 79—77837
- TiO_2-Al_2O_3-P_2O_5 glass, ESR of Ti^{3+}, exam. 78—88181
- Ti_2O_3, Al_2O_3 doping effects on struct. changes 77—55276
- β-Tl_2O-Al_2O_3, cation distrib. 77—80487
- V/Al_2O_3 composite film, optical props., rel. to solar collector appls. 78—72622
- $V_{1-x}Al_xO_{2\pm y}$, mag. and struct. props. meas. 78—2658
- W-Al_2O_3 cermet films, oxide evaporation deposited on Mo, Ti, Al_2O_3 substrates, struct., props. 80—25581
- W-Al_2O_3 granular film, percolation conductivity 78—84319
- YAG, production of densely sintered ceramic, exam. of recrystallisation during sintering 80—11609
- Y_2O_3, reduction in Li vapour, 1800-2500K, thermodynamics 77—90595
- Y_2O_3-2Y_2O_3.Al_2O_3 two-phase refractory, fracture 80—21080
- Y_2O_3-Al_2O_3, thin film, electron diffraction exam. of phase transformations *(Russian)* 79—34025
- Y_2O_3-AlN, creep 77—21235
- YPO_4-Al_2O_3 system, oxyorthophosphates form. 79—78942
- $(Zn_{0.2}Co_{0.8}(Ni_{0.8}))O.Al_2O_3$, ZnO evaporation in vac. 80—59640
- ZnO/Al_2O_3, microstratified mixing of suspensions, viscosity dependence 79—70023
- ZnO-Al_2O_3, isoelectric point meas. 80—88609
- Zr-Al_2O_3 couple, diffusion welding, 1000 to 1300°C *(German)* 79—28155
- ZrN-Al_2O_3, effect of N on sintering 79—33991
- ZrN-Al_2O_3, exam. of sintering and densification kinetics, and physical props. 79—95986
- ZrN-Al_2O_3, sintering reaction thermodynamics 80—2989
- ZrN-Al_2O_3 composites, strength rel. to solid-, liquid-phase sintering 80—100823
- ZrO_2-Al_2O_3-SiO_2 fusion cast ceramics, crystn., microstructures rel. to conditions 80—11638
- ZrO_2-$ZnAl_2O_4$ transparent glass-ceramic, microstruct. and props. 78—59960
- $ZrSiO_4$-Al_2O_3 mixture, reaction hot pressing 79—38775
- $ZrSiO_4$-Al_2O_3 suspensions for slip casting, prep. and props. 80—104103
- $ZrSiO_4$-Al_2O_3 system, particle rearrangement kinetics due to densification 80—25626

aluminium

- *see also nuclei with ......*
- (100), oxidised surface structure anal., extented appearance potential fine struct. study. 80—75411
- (111) surface, Pb, Sn monolayer, double layer growth, struct. 80—70567
- 6061-T6, plastic conical shell buckling under axial compression 77—72197
- ^{26}Al in seawater rel. to oceanic residence times of dissolved Al 79—34856
- $^2P_{3/2}$, at. quadrupole shielding factor 79—10222
- abrasion, low speed, strain rate effects 79—20208
- absorber, bremsstrahlung from β-rays in thick target, 30-1300 keV 79—83049
- abundance in cool halo stars implications for galaxy abundance 80—105232
- AC anodizing in H_2SO_4 79—96229
- accelerator coils, Al strips used instead of Cu 79—72126
- acoustic emission energy release, grain size and flow stress depend. of polycrystalline samples 80—11722
- acoustic emission from moving dislocations during tensile tests 77—19964
- acoustic emission power, strain rate depend. 77—4808
- acoustic emission signals in plastic deform., amplitude distrib. *(Japanese)* 78—6978
- acoustic emission under plastic deform., appl. of spectral anal. energetic anal. of moving US source *(French)* 77—77543
- acoustic emission under plastic deform., spectral anal., dislocation mean free path 78—84934
- acoustic NMR saturation studies 79—73835
- acoustic non-linearity parameter in cubic cryst. 77—51444
- acoustic velocity, shock-compressed uniform solid, lateral discharge ang. semiempirical formula *(Russian)* 78—55910
- acoustic wave drag, acousto-elec.-mag. effects *(Russian)* 79—19638
- acoustoelastic stress field imaging technique, stress field contour plots 79—77033
- acoustomagnetic effect, temp. depend. acoustomag. effect. temp. depend. *(Russian)* 77—72941
- addition to Si killed steel, effect of Al addition to Zn on phase composition and morphology of products of Fe-Zn reaction *(Polish)* 78—85021
- additive to fluoride-oxide slags, influence on elec. cond. *(Russian)* 80—39572
- adhered lap-shear and double cantilevered beam specimens, cyclic stress testing 79—15820
- adhesion of epoxy resins to surface 77—4888
- adhesion of polycaprolactam, effect of crystallisation 77—66742
- adhesive bond system, US determ. of bond strength due to surface prep. variations 77—21336
- adhesive bonds with polymers, shear resist., polymer crystn. effect 80—89462
- adhesively bonded and weldbonded aircraft struct. subjected to acoustic excitation, determ. of sonic fatigue life 78—92351
- adion-surface interaction energy, density formalism calcs. for alkali metal ions 78—68069
- adsorbed Ar, differential refl. spectroscopy, local field effect 80—80811
- adsorbed Na, adatom valence-level position variation 80—88611
- adsorbed on Si, thermal expansion and at. vibr. singularities 77—89635
- adsorption, of O_2 (NO), 80 to 290K, 10^{-6} to 10^{-2} Pa, XPS study 78—95657
- adsorption and decomp. NH_3 and hydrazine XPS obs. 80—92783
- adsorption and decomp. of methanol, UPS, XPS and thermal desorption obs. 79—82441
- adsorption of NH_3, KVV Auger spectra, deconvoluted spectra 80—50508
- adsorption of O_2, AES, XPS, and LEED obs. 79—46938

aluminium continued

adsorption of O_2, intrinsic and extrinsic plasmon coupling, XPS of adsorbed atoms core states 78−10278
adsorption of O_2, relation between energy-band and cluster model 78−52048
adsorption of O_2 and CO, interatomic Auger transition spectroscopy 80−11521
adsorption of propane, SIMS and EID obs. 77−69167
adsorption of S(O)(N)(C), internal and external sources of electrons 77−44097
adsorption of small molecules, photoelectron spectra, surface plasmon spectroscopy 79−47148
adsorption on cleaved Si (111) surfaces, effect on electronic structure 80−75610
adsorption on Si (111) 7×7 surface, electron energy loss spectroscopy and LEED 77−43432
AES, backscattering factor, Monte Carlo method calc. 80−7449
AES, obtaining density of states information from self-deconvolution of Auger band-type spectra 78−92150
AES, role of inelastic refl., expt. check of model 78−11027
air pollution neutron activation anal. using 14 MeV neutrons 77−91257
albedo number meas. using ^{60}Co, ^{137}Cs sources 79−26768
alkali halide, PO_4^{3-}-Al^{3+} anion-cation impurity mol. complex, IR absorpt. obs. *(Russian)* 77−16317
alloys, Cu determ. by at. emission spectroscopy with spark source, photodiode array detector *(German)* 79−87926
alpha particle energy loss straggling 80−42902
alpha-particle slowing down, cross-section and stopping power *(Russian)* 77−80560
alternating bending of single crysts., shear strain accumulation and microstrain distrib. *(Russian)* 78−60706
aluminisation of Ni-Cr type alloys, Co surface pretreatment 80−40612
amorphous, heavy ion ranges, He^+ backscatt. obs. 78−63796
anharmonic effects associated with ⟨110⟩ screw dislocations 78−30625
anharmonic lattice dynamics, computer simulation of dynamical struct. factor 78−6130
anisotropic electron scatt. on defects in quenched and irradiated material 79−95397
anisotropic electron scattering, Hall coefficient, path integral calc. 79−91027
anisotropic Fermi vel., surface Landau level reson. 78−10333
annealed, subjected to torsional impact loading strain-rate effects 78−92303
annealed and neutron irrad., exam. of positron lifetimes in voids and other defects 78−47426
annealing in moist atm., causes and kinetics of H_2 blister form. *(German)* 80−25923
annealing of lightly deformed samples, effect of press. *(Russian)* 78−39795
annealing twin growth, obs. by synchrotron radiation X-ray topography 79−55753
annihilation spectrum, narrow component, Fermi impulse of electrons, plastic deform. recovery *(Czech)* 78−64591
anode, implanted in heart-blocked dog, AC impedance and corrosion investig. 77−60297
anode, with Al_2O_3 coated by anodic spark deposition 78−11382
anode spot of vacuum arc 80−107006
anodic attack in chloride medium, passivation *(French)* 79−96224
anodic barrier film characts., ISS/SIMS 78−53021
anodic behaviour in NO_3^-/Cl^- solns., electrochemical and XPS meas. 80−16694
anodic coated, and free anodic film, deformation-strength props. *(Russian)* 77−69203
anodic film, formed in H_2SO_4, electron microscopy 78−68843
anodic film, H profile meas. by SIMS 78−27847
anodic film formed in H_2SO_4, thin film TEM obs. by direct vertical sectioning 78−7106
anodic films, acoustic and electron-emission during deform. 80−80143
anodic films, flaw obs. 80−93696
anodic films, formed on Al, optical reflectance method anal. 80−37073
anodic layers, coloured, prep. by ultramicrotome without embedding for TEM and X-ray obs. 79−39074
anodic oxidation, effect of vacuum and heat treatment *(German)* 79−96225
anodic oxidation, in H_2SO_4, pH-values effect *(German)* 80−76419
anodic oxidation, in phosphoric, sulphuric and tartaric acids, barrier layer growth study 77−8983
anodic oxidation, ion movement study by O^{18} and MeV ion beam techniques 78−15604
anodic oxidation, mobility of implanted As, Sb, Bi, Se and Te 77−90494
anodic oxide coating, comparison of water or steam sealing 79−96228
anodic oxide coatings, characteristics by tribostimulated exoemission 79−91829
anodic oxide coatings, quality testing *(German)* 77−28943
anodic oxide film, field assited pore form. 77−81336
anodic oxide film, porosity determ. by pore filling method 79−47848
anodic oxide film arborescent structure formation *(Russian)* 80−35409
anodic oxide films, space charge, TSC obs. 77−32326
anodic oxide layers, meas. of growth by photoluminescence, description of equipment 79−52511
anodic oxide superficial layer, X-ray emission spectrometry and ion backscattering *(French)* 80−49482
anodic polarisation, charge transfer processes 77−16736
anodisation, 'flaw-free' film growth and luminesc. characterisation 78−15605
anodisation, barrier and porous layer regions of Al_2O_3, eqn. 79−5089
anodisation, behaviour of maleic acid 78−44262
anodisation, high voltage barrier, Cl^- ion effects 80−104327
anodisation, impedance meas. during 80−3236
anodisation, in phosphoric, sulphuric and tartaric acids, theory and expt. 77−25271
anodisation, influence of substrate orientation 78−88581
anodisation, intensity of luminesc. and film thickness 78−80413
anodisation in CrO_3 solns, film colour/structure relationship *(Russian)* 79−91851
anodisation in H_2PO_4, irregular film formation obs. 80−30153
anodisation in $SnSO_4$ soln., state of Sn 78−35582
anodisation nucleation and growth of porous anodic films 78−44273
anodised, adsorption of ^{90}Sr and ^{90}Y, oxide layer thickness, Al purity, temp. depend. studies 79−82458
anodised, electrolytic colouring, improvements 79−15870

aluminium continued

anodised, electrolytic treatment *(German)* 80−45243
anodised, IR reflectance, use as cryogenic material 79−71458
anodised, photostimulated exoelectron emission, effect of oxide thickness 78−80461
anodised layer, exam. of factors affecting abrasion resistance 79−34207
anodised layer bonding, depend. on prep. conditions *(Japanese)* 77−25195
anodised oxide films, for adhesive bonding appls., AES and SEM study 80−66689
anodised surface, neutral particle emission during tensile deform. 79−78856
anodised thick films, O conc. determ. using non Coulomb H ion backscatt. 80−55753
anodising, AC, in H_2SO_4 79−52465
anodising, behaviour of emulsion particles during electrodeposition 80−104357
anodising, coloured coatings prod. in AC electrolysis, thick coatings case 80−25908
anodising, coloured coatings prod. in AC electrolysis, thin coatings case 80−21176
anodising, porous films formed in chromic acid 80−100966
anodized, as cryogenic material, IR reflectance 79−61387
anodized, inorganic glass coating, solution deposited, environmental protection 79−34205
anodizing, hard, high temp. 79−96230
anomalous intensity ratios in H like L_α doublet in optically thick laser prod. plasmas 80−103186
atmosphere, Al particles from space rocket launching 80−81503
atom, $4s^2S_{1/2}$ reson. level, mean life 79−59400
atom, and isoelectronic ions, excited-state energy level k-ordering, l-patterns 77−88406
atom, autoionisation reson. determ. from photoelectron polarisation meas. 80−58221
atom, beam-foil populations, charge state distribs., independent electron model 77−19035
atom, chem. environent effect on $K\alpha$ satellites intensity, heavy-ion collision 77−54527
atom, Compton profile asymmetry obs., Al, Ti, Fe, Cu, using $K\alpha$ fluoresc. 77−57937
atom, Compton profiles using Gaussian expansion of at. orbitals 80−945
atom, electron impact excitation cross sections 79−54972
atom, electron scatt., transitions, oscill. strengths, config. superposition calcs. 77−6732
atom, fast electron beam scatt. calcs. 77−65534
atom, incoherent scatt. factors calc. by direct integration over impulse approx. Compton profiles 80−102475
atom, ion beam bombardment, $(1s^{-1}2p^{-1})^1P_1$ state nonstatistical population, X-ray spectrum 78−62894
atom, $K\alpha$ and $K\beta$ X-ray spectra induced by 84 MeV N^{4+} 77−50517
atom, K-shell hole production by light ions, hydrogenic and Hartree-Fock model of target 77−83715
atom, K-shell ionisation by ultrarelativistic electrons, density effect 80−99576
atom, lowest S-state lifetime meas. 77−65436
atom, photoelectric cross section, derived from total absorpt. cross sections 77−10646
atom, photoelectron ang. distrib. of 3s subshell 79−76397
atom, photon-bound-electron scatt. meas. 77−14394
atom, Raffenetti-type atomic basis set calcs. 79−97974
atom, s-shell spin polarisation calcs. 77−75318
atom, SCF electron-gas local-spin-density model including correlation 80−9488
atom, spectral anal. in HV impulse discharge sensitivity limit 79−29420
atom, Stark broadening of reson. lines, 3961.5 and 3944 Å 78−58622
atom, static quadrupole polarisability and shielding factor, Hartree-Fock calc. 78−41950
atom, transitions, Stark broadening and oscillator strengths 78−29761
atom + halogen chemiluminescent reactions 77−9086
atom + heavy ion, X-ray spectra, one-photon two-electron rearrangements 77−6712
atom in metal-halide arc, laser Raman scatt. determ. of local density 77−11424
atom resonance line profiles, influence of boundary layer of Al-seeded shock heated plasma 80−43876
atomic electron impact excitation cross sections calc. *(Russian)* 78−55240
atomic gas, Raman transitions, active reson. spectroscopy 77−27003
atomic oscillator strengths and radiative lifetimes 79−54811
atomic structure factor calc. 78−6030
atomic-transition lasers based on two-photon dissociation of metal-triiodide vapors 80−23679
atomistic images of field ion microscopy at high temps. 78−55792
atomized powder, metallic contact for hot rolling in air 77−73294
atoms and ions, regularities within Stark widths and reson. lines 78−78662
Auger, RHEED and TEM combined obs., specimen transfer device 80−70093
Auger electron microscopy, edge effect, Monte Carlo simulation 79−1801
Auger electron prod. by Ne^+ bombard., origin of Ne Auger peaks *(French)* 80−7461
Auger electron prod. by Ne^+ bombard. 80−7460
Auger electron production by noble gas ion bombardment 77−1778
Auger electrons, proton-excited, attenuation lengths of low-energy electrons 78−11058
Auger emission target, contrib. of reflected electrons 78−92152
Auger spectra, KLL and KLV, screening effects and plasmon gains 80−80913
Auger spectra induced by 100 keV Ar^+ impact 80−84820
Auger spectrometric characterisation of anodic oxide films *(French)* 77−36324
Auger spectroscopy produced in glow discharge *(Russian)* 78−14545
Auger spectrum, KLL, plasmon gain satellite obs. 78−76562
Auger spectrum, meas. by new retarding field spectrometer 78−23564
backscattering of fission products 80−16138
band structure, pseudopot. calc. 79−56119
band structure, self-consistent calculations 78−6266
band structure and density of states, calc. using model pot. method 77−76742
band structure effects on transport 78−34820

aluminium continued
bar, shear modulus meas. using holographic interferometry 77—31073
barrier film growth in soln. of film promoting and aggressive ions 77—8975
Bauschinger AE peak detection of back stress component in flow stress *(Japanese)* 78—6977
Bauschinger effect, orientation depend. 77—21237
Bauschinger effect, temp. influence, combined tension-torsion testing machine 80—45453
beam, creep rupture under variable load, rupture life lower bound 77—3785
beam, exam. of elastoplastic contract strength law, using impact bending *(German)* 79—43365
beam-foil spectra, Al V-VII, between 85 and 135 Å 78—9134
bend contours, obs. using correction of Mollenstedt filter images by auxiliary lenses 77—39520
beta-ray backscattering variation with target thickness, self-absorpt. coeff., Z depend. 79—78801
bicrystal, {100⟩ oriented, plastic deform. 78—19812
bicrystal, faceting of migrating ⟨110⟩ coincidence boundaries 79—46680
bicrystal, fatigue crack initiation, crystal boundary effects *(Japanese)* 78—92328
bicrystal, fatigue crack initiation along crystal boundaries *(Japanese)* 79—70163
bicrystal, high resolution electron microscopy obs. of dislocations 80—103347
bicrystal, liquid metal induced grain boundary fracture, relative orientation effects 77—36690
bicrystal, migration of special ⟨110⟩ tilt boundary 79—46670
bicrystal, plastically deformed, slip heterogeneities 80—79858
bicrystal, tensile and creep deform. obs. by holographic interferometry *(Japanese)* 77—56197
bicrystal, varying purity, breakaway of grain boundary from adsorbed impurity 77—31678
bicrystal having $\Sigma 7$ and $\Sigma 21$ coincidence tilt boundary, plastic deform. *(Japanese)* 79—66116
bicrystalline, RF size effect at intercryst. boundary *(Russian)* 80—29431
bicrystals, faceting of migrating ⟨110⟩ coincidence boundaries 80—34013
bicrystals, fatigue crack initiation, cryst. boundary effect 80—55537
bicrystals, isoaxial, fatigue crack initiation in grain boundary affected regions *(Japanese)* 80—89338
bicrystals, stress induced migration of ⟨112⟩ symmetric tilt boundaries *(Japanese)* 80—15311
bicrystals, [011] low angle tilt boundaries, high resolution electron microscopy 80—34012
bimetal film with Cu, Ti(V,Ni) and alloy MLT(RS-3710), struct. and macroscopic defects *(Russian)* 79—1555
binding energy and compressibility, model pot. calc. 79—99650
blanket/shield designs, minimum-activity, for D-T and D-^{3}He fusion blankets 79—85796
blazed grating, MgF$_2$ coated, complete absorpt. of P-polarised specific wavelength light 78—25957
blistering and exfoliation by 2 MeV He$^+$ beam 79—46722
blistering by plasma focus discharge deuterons, statical anal., plasma diagnostics 77—35351
Bloch electron system, exchange correction to dielec. function, local exchange approx. 77—1384
blocking of α-particles from ^{27}Al(p,α)^{24}Mg reaction, nuclear lifetime meas. problems 77—47500
bombardment by Ar ions, impact-parameter depend. of K- and L-X-rays 79—76501
bonded Al-CFRP single lap joint strength 79—29328
bonding onto Fe, with O and N impurities, growth of intermediate phases 78—27680
Bordoni effect during recrystallisation 77—90388
Bordoni relaxation, microdeform. 80—104204
borsic fibre reinforced Al, hot pressed forged, plasma sputtered *(Russian)* 78—35330
boundary dislocations gliding, on coincidence boundaries, TEM study 79—82224
boundary lubrication, inelastic electron tunnelling spectroscopic study 80—70302
Bragg diffraction, anharmonic contributions, Mossbauer study 78—76358
bremsstrahlung, β generated, spectral shape depend. on target thickness 78—56545
Bremsstrahlung distrib. from 22 MeV electron irradiation 78—59840
bremsstrahlung isochromat beyond Duane Hunt limit 77—73188
bremsstrahlung spectra, 10 to 30 keV, thick target expts. 77—8687
Brillouin scattering from surface waves, appl. of surface Green's function mapping method 80—40125
Brillouin spectra, light scatt. cross section for surface ripples 80—71434
buckling and structural efficiency of open-section stiffened compression panel 77—35061
bulk and plasma-sprayed coating, D$_3{}^+$ trapping meas. 80—20754
bulk superconducting fluctuations in elec. resist. 80—49995
burst acoustic emission during Bauschinger effect 77—48475
caesiated thin film, surface plasma wave excitation by polarised light, photoemission obs. 80—50518
cantilever beams, nonlinear damping for nonsinusoidal strain 79—47762
capture radius of impurities 80—20110
cast, strength and plasticity under hydrostatic pressure 78—56694
cast, US and X-ray testing of castings, moulds and die-casting machines 78—53097
cast and directionally solidified, porosity 79—74145
cathode, production of D ion beam impurities 79—86592
cathodes for glow discharge and hollow cathode spectroscopic light sources 78—82047
cathodic polarization 80—21153
Cauchy relations, violation for elastic moduli 79—69179
cavitation erosion considering bubble collapse and pulse height spectra 80—16503
cavitation erosion in water flow, initial stage 78—27648
cell structures produced by cycling and monotonic creep, comparison 80—55452
ceramic oxidation behaviour, effect of Al on oxidation behaviour of MoSi$_2$, Si$_3$N$_4$ *(German)* 78—31587
CESR at 60 GHz, plastic surface coating effect 77—32259
CESR due to edge dislocations 78—19328
CESR lineshape and A/B and g-values 77—63284
CESR linewidth, freq. effects 78—10775

aluminium continued
CESR linewidth and g-shift in presence of spin-orbit perturbation, spin-phonon scatt. 77—63285
chain of Al rings, plastic extension due to axial impact load 79—18737
charge-exchange effects in energy-loss straggling for low mass particles, $A<16$ 80—65104
chemical polishing, electrochem. props. of soln. 79—29282
chemisorbed monolayer on Si (111) surface, local density of states 79—47142
chemisorbed O layer on (111) surface, angle-resolved photoemission, band struct. 80—40229
chemisorbed on GaAs, surface barrier formation, localised orbital theory 79—51671
chemisorbed on Si (111), electronic struct., self-consistent pseudopotential calc. 78—34880
chemisorbed ordered O overlayer on (111) surface, angular resolved photoemission 79—82462
chemisorption, charge-density maps 79—19453
chemisorption, of formic acid, electron tunnelling spectra study 78—84049
chemisorption, of O$_2$, orbital resons., $X\alpha$ cluster model calcs. 77—72774
chemisorption of CO, interatomic Auger transition spectroscopy 79—7747
chemisorption of H$_2$, adatom geometry and binding energy 77—66093
chemisorption of H$_2$, calc. of adsorption sites and binding energy 79—46953
chemisorption of O$_2$, on (111) and (100) faces, AES and work function obs. 77—35822
chemisorption of O$_2$, photon and electron emission as indicators of intermediate states 80—39439
chemisorption of O, on (100), mol. orbital cluster calc. 78—14582
chemisorption of O, site determ. by LEED 80—39421
chemisorption of O, unoccupied extrinsic surface resonances and site struct. determ. by soft X-ray absorpt. 79—73403
chemisorption of O on (100), overlayer electronic struct. 77—85058
chemisorption of O on (111) surface 78—14593
chemisorption on GaAs (110), ab initio theory 80—75612
chemisorption on GaAs (110), electronic struct., tight binding calc. 80—49842
chemisorption site geometry and interface electronic struct. on GaAs (110), photoelectron spectra 80—49843
circular plate perforation and deformation by square section punch 79—34100
circular tube, forming limit of free bulge-forming *(Japanese)* 80—55477
cladding of Al$_2$O$_3$ and ZrO$_2$ 79—29010
classical plasma frequency in long-wavelength limit, quantum correction 80—107728
clay-Al floc, physical characts., density function 79—100454
clay-Al floc physical characts., floc strength determ. 79—100455
cluster, growth and composition on NaCl substrate 77—89677
coated by phosphosilicate glass film, corrosion in high temp. water and moisture 77—48564
coated C fibre, stress rupture 78—80628
coated diffraction gratings, UV light polarisation at grazing incidence 78—87129
coated IN-100, microstruct. degradation, influence of corrosioin protective coating 80—40611
coated Na$_2$O-CaO-SiO$_2$ glass, electron bombarded, SIMS anal. 79—66376
coated Ni-Cr-(Co) alloys, microstruct. and chem. 80—76189
coated Si planar diode, binary memory device, laser writing 79—69593
coated steel, porosity evaluation, micro X-ray spectral anal. *(Russian)* 80—35389
coated steel Kh25N20S2, structural transformations, oxidation effect 79—57154
coated with polyethylene, in vac., adhesion 79—61793
coating, on steel, produced by thermal decomposition of alkyls 78—15590
coating, plasma sprayed on steel substrate, microstructural investigation and oxidation effects 78—11426
coating, surface implantation of Y and Ce, effect on oxidation resistance at high temp. 77—8977
coating for optical fibres, empirical formula for induced excess loss 79—46074
coating of particles by polymer film, oxidation protection *(Russian)* 77—86232
coating of Pt and Pt coated Ni-Co-Cr alloy IN 738 78—31583
coating on directional Ni$_3$Al-Ni$_3$Nb eutectic alloy, microstruct. exam. 78—15593
coating on Ni alloys, spontaneous form. of diffusion barrier *(German)* 78—71886
coating on steel, thickness meas. using radioisotope thickness gauge *(Russian)* 78—56582
coating prod. by thermal decomp. of Al alkyls 80—104076
coating reflectivity in vacuum UV, heating effect 80—95981
coating thickness determ. H$_2$ generating method *(German)* 79—35660
coatings on polyethylene terephthalate, thickness determ. using photometry 80—62626
coatings on superalloys, improvement by sputtering *(French)* 79—29278
cohesive properties, augmented-spherical-wave calcs. 79—94952
coincidence site lattice and DSC dislocation network model of high angle grain boundary structure 80—54260
cold rolled, annealed, fatigue crack propag. rate, temp. effect 78—39904
cold rolled, commercial purity, initial stages of recrystallisation, TEM obs. 79—56999
cold rolled, weak beam method appl. to dislocation obs. *(German)* 77—84757
cold rolled, X-ray diffr. and optical microscope exam. of fatigue damage *(Japanese)* 78—84976
cold rolled and annealed, substruct., near fatigue crack tip, X-ray microbeam technique exam. *(Japanese)* 78—64621
cold rolled bicrystal, plane grain growth anisotropy 79—91686
cold rolling, inhomogeneous texture 80—89251
cold rolling of 1100 plates, substruct. development 80—108476
cold worked, effect of bias stress on US attenuation induced by geometrical kinks mobility *(French)* 77—31728
cold worked, internal friction peaks 80—97520
cold worked, reverse polar figure const. using linear eqn. system 77—73488
cold-worked, plastically deformed, internal friction spectrum, Hasiguti peaks associated with dislocations 80—7618
cold-worked, transport props., 1.5-8.5K 78—7059

aluminium continued
collective properties of degenerate electron gas, (e, 2e) technique *(Russian)* 79—56149
combustion in water vapour, thermodynamic calc., 0.1 to 40 MPa *(Russian)* 79—39148
commercial purity, density changes, void growth in biaxial stress fields, plastic deformation 80—71692
commercially pure, prestrained, yield criteria and stress-strain relations anal. 79—57051
composite, C fibre reinforced, formed by ion plating and vacuum hot pressing, mech. strength 78—11165
composite, SiC fibre reinforced, plasma-formed semifinished products, props. 80—84890
composite superconductors design in elasto-plastic region 77—28851
compressed, nucleation and recrystallisation study by electron microscopy and Kikuchi diffr. 79—52236
compression, effect of press. on lattice defects up to 90 kbar *(Japanese)* 77—72654
Compton defect calcs. in Born impulse approx. atom 77—88427
Compton profile, 59.54 keV γ-rays 79—91520
Compton profile, multiple scatt. correction 79—61456
Compton profile from 662 keV γ-ray spectroscopy 78—56539
Compton profile from X-ray Ag K_α fluorescence radiation 78—48257
Compton profiles for liq. and solid phases 79—91519
computer simulation of tilt grain boundaries 78—30642
concentration in atmospheric sedimentable powder, in Vizcaya, Spain *(Spanish)* 78—57265
condensate, effect of growth conditions on critical thickness 79—69985
condensed film, phase and struct. nonuniformity *(Russian)* 80—54536
conduction electron spin relax. and g-factor, plastic surface coating effect 77—32258
conduction-electron spin flip by phonons, expt. data anal. 79—61219
constitutive equation for porous materials with strength, press. effects 80—79875
contact area, effect of loading time *(Japanese)* 78—6230
contact for n-type Si, current load capacity meas. *(Czech)* 77—89846
contact junction formation by ion evaporation 77—90285
contact resistance against metals, for high compressive stress and high current density 77—59324
content in Fe ores and coal, nuclear activation logging 79—80042
conversion coating formed in chromate/fluoride soln., TEM obs. 79—74289
convoy electrons from solids, ion vel. and Z and target material depend. 78—84692
core and valence electron enhancement factors from positron annihilation-correlation curves 80—25479
core electron expansion, kinetic energy in Compton profiles 78—72628
core level XPS energy loss study, angle and energy dependence 78—23582
corrosion, general and pitting, Mo and Ar ion implantation effects 80—71794
corrosion, localised, blister form. in oxide film as pitting precursor 78—27678
corrosion, monitoring using polarisation resistance meas., techniques and correlations 77—16711
corrosion and anodic polarization in NaOH soln., effect of aldehydes 78—19923
corrosion by carbon tetrachloride, IETS obs. 80—81230
corrosion characteristics in ethylene glycol-water mixtures 78—7095
corrosion during 10 years at coastal site at Alicante 79—20244
corrosion in chloroacetic acids, 2-mercaptobenzothiazole inhibitor effectivenes 79—57148
corrosion in uninhibited ethylene glycol-water solutions 79—70222
corrosion inhibition of liq. Li cooling system of fusion reactor by Al addition 80—108646
corrosion rate of Al tube, drag-reducing polyethylene oxide as corrosion inhibitor 80—45445
corrosion resistant pure metal, passivity and pitting in chloride solutions 78—44258
corrosion resistant surface alloys, form. by ion implantation 78—88569
corrosion-protective chromate coatings, characterisation 79—47798
crack resistance, J-integral approach, crack line wedge loaded specimen 78—35513
crack resistance, J-integral approach 77—66699
creep, grain boundary, role of dislocations 78—43065
creep, grain size effect on rate at 408K 77—52428
creep, high temp., in high-purity sample, approx. determ. of parameters *(German)* 80—50688
creep, low-temp., during dynamic relaxation, effect of dislocation struct. *(Russian)* 77—25103
creep, press. effect *(Russian)* 79—29134
creep, rel. to radiation swelling and stacking fault energy *(Russian)* 78—27562
creep, stationary, in HVEM, cell struct. evolution 80—104242
creep, threshold stress importance in anal. of data 80—64389
creep, transient, effect of pre-torsional deform., dislocation glide and density 77—4147
creep activation energy at low temp., thermoactivation anal. *(Russian)* 77—31717
creep and dislocation distribution, influence of electron irradiation *(Russian)* 78—95775
creep and dislocation struct., electron irrad. effects 80—49268
creep and rupture, 77 to 273K *(Russian)* 79—43386
creep and rupture, in torsion, mech. *(Russian)* 79—5030
creep at intermediate temps., in situ study of cell boundary evolution HVEM 78—48480
creep behaviour, 3D presentation of deformation mechanism diagrams 80—3141
creep behaviour, at high temp., influence of oxidation 80—97538
creep behaviour, precipitate form. 80—7646
creep data anal. at very low stresses 78—27570
creep strength and rupture under combined stresses 79—20133
creep under step stress changes, viscous viscoelastic model for type 2618 80—81138
critical pitting potential meas., review 79—43501
critical resolved shear stress, orientation depend. 80—21001
critical stress intensity factor determ., antibuckling constraint effect 77—40502
critical temp. determ. by exploding wires method, liquid metal enthalpy 78—6149

aluminium continued
cryolite melts saturated with alumina, interfacial tension between Al and melt 78—38913
crystal, lattice rotation during tensile deform., X-ray diffr. meas. 80—49231
crystal defects, study with muon probes 78—47314
crystal growth, large perfect single crysts., by isothermic recrystallisation after small deform. *(Czech)* 77—63688
crystal growth from melt, different orientations of crystallisation front *(Russian)* 77—55881
crystal orientation effect on their cutting mechanism in single crystals 79—34193
crystal potential, low-order Fourier coeff., modified thickness fringe method 80—75130
crystal structure, computed X-ray powder diffr. patterns and densities 77—43172
crystallisation thermokinetics calc. of pure cylindrical specimen *(Czech)* 77—63654
cumulative damage in creep 79—70140
cutting, temp. effect on built-up edge behaviour *(Japanese)* 78—7083
cutting mechanism, anisotropy effects 79—11760
cutting of bicrystal to compare mechanism for large crystals and polycrystals *(Japanese)* 78—60871
CVD coating on Ni base alloys, transport agent comparison 78—11429
cyclic loading, change in mech. props. rel. to heat treatment 80—104282
cyclic torsional deformation, final texture 80—7595
cylindrical metal liners, explosion-accelerated, form stability anal. 78—83425
cylindrical rod, stress wave propag. from electrical discharge 78—59866
Debye temp., X-ray diffr. determ., anharmonic parameters of pot. function 80—100320
Debye temperature correlations at high temp. 80—15210
Debye Waller determ. from modified Cheveau model 78—59918
Debye-Waller factor temp. parameter 78—30725
Debye-Waller factors, modified ang. force model 77—66013
dechannelling of α-particle by dislocation loops *(French)* 79—95056
deep planar diffusion in Si 79—69290
defect annealing during plastic deform. 78—88478
defect annealing study by positron annihilation, and elec. resistivity meas. 78—51584
defect structure after plastic deformation, X-ray investigation 78—31467
defects due to neutron irrad., muon probes study 79—56701
defects formed during cryst. growth or by plastic deform., X-ray transmission topography obs. *(Russian)* 80—25761
deformation, in situ, of [111] single crystal, HVEM obs. 78—52886
deformation, internal friction, dynamic modulus and creep meas. 79—91727
deformation and recrystallisation, Rowland transform. model *(French)* 77—77498
deformation enhanced photoemission meas. 77—32511
deformation mechanism map 79—34109
deformation parameters, ultrasonically induced resonance, new technique 80—97676
deformation sub-struct., effect on tensile props. *(Japanese)* 78—11279
deformation temperature effect, on stage IV deform. in ⟨100⟩ single crysts. *(Japanese)* 80—66587
deformed, efficiency of dislocation as sink for vacancies, resist. obs. 77—36570
deformed, nucleation and recrystallisation at second phase particles 78—6941
deformed, positive muons diffusion and trapping 79—11372
deformed, recrystallisation, orientation relations, hard-sphere model for Rowland transform. *(French)* 77—77497
deformed, resist. decay. meas. of initial stages, method and results 79—49256
deformed, struct. and recrystallisation, transmission Kossel diffr. obs. 77—52340
deformed, thermal recovery, microstruct. and stress-strain relations 80—16325
deformed in tension, elec. cond. changes at 78 and 283K, grain boundary effect *(Japanese)* 80—30029
deformed in uniaxial and equibiaxial tension, dislocation arrangements 80—108516
deformed surface layer, block misorientation 79—99405
dendritic solidification, fluid flow effect 78—11215
deposited on InP surfaces, Schottky barrier formation 80—39671
deposition by ion beam sputtering, composition and stress state 77—89674
depth profiling of ^{3}He ion implantation 78—59830
depth resolution for MeV $^4He^+$ backscattering in C, Al, Cu 79—14840
determ. by atomic absorption, using low temp. flames 80—30307
determination, by neutron activation anal., 14 MeV *(Czech)* 79—24862
determination, in archaeological bone, using neutron activation anal. 79—52847
determination, in Bayer liquors by elect. cond. meas. 77—73493
determination by activation anal. (α,n), (α,p) reacts. investig. 80—61206
determination by spark-source mass spectroscopic anal., sensitivity calibration 78—68962
determination in bauxite by neutron activation anal. 79—24858
determination with Si in atmospheric aerosols by neutron activation anal. 80—72116
diagnostic radiography, diffr. phenomena on using Al attenuation-equalising filters 79—39486
diamond surface interaction with gases and metals 77—72758
diamond-turned, surface reflectivity meas. 1 to 12 μm 80—1298
dielectric function, wave-vector and freq. dependence, energy loss spectra 77—1385
dielectric function pseudopot. theory, vol. plasmon dispersion 79—23917
dielectric screening function and effective interaction strength 79—33387
diffraction grating, concave, Al-coated, polarisation anomalies 80—69519
diffraction grating, MgF_2 coating effects on efficiency 77—39064
diffusion, of Cu(Zn), isotope effect 78—84006
diffusion and dissolution of alloying components in liq. Al, 700-1000°C *(Russian)* 80—15275
diffusion and solubility in Be 77—35758
diffusion and solubility of H_2 *(Japanese)* 79—99370
diffusion bonding with Cu and Fe 77—62687
diffusion coating of steel, circulation method, thermodynamics 80—30163
diffusion coefficients of Zn, Co, and Ni, resistometric determ. 79—51313
diffusion in Ge single cryst., effects of ultrasound 77—69119
diffusion in Hg, diffusion coeff. meas. 80—24627

aluminium continued
- diffusion in migrating interfaces 79—19390
- diffusion into Si_3N_4 film, AES and depth profiling 78—51744
- diffusion into Si, in open tube, high vacuum system 78—91349
- diffusion of ^{28}Mg 77—20127
- diffusion of ^{65}Zn, 165 to 645°C 77—11743
- diffusion of ^{85}Kr *(Russian)* 79—65258
- diffusion of Ag in polycryst. sample in temp. gradient 77—76619
- diffusion of Hg, Tl, Pb *(Japanese)* 79—19403
- diffusion of Zn along grain boundaries, effect of grain boundary struct. *(Japanese)* 77—15628
- diffusion thermopower, inelastic electron-phonon interaction 80—96851
- discharge, hollow cathode with pulse feeding, spectroscopic study 78—34377
- dislocation activation, using UHV electron microscope const.-load tensile device 78—11462
- dislocation and point defect interactions, US study under quasistatic stress *(French)* 80—2061
- dislocation behaviour at melting, HV electron microscope in-situ obs. *(Japanese)* 77—43216
- dislocation density, prep. of high-purity cryst. by strain-anneal method 78—48314
- dislocation dynamics study by current noise measurements 79—14813
- dislocation interactions with grain boundaries, in annealed and creep polycryst. specimens 79—42067
- dislocation line movement at low temp., obs. by US meas. *(French)* 79—95025
- dislocation loops, interstitial, size distrib. for metal irradiated in high voltage electron microscope *(Russian)* 80—103335
- dislocation loops, mechanical multipole moments determ. 78—55868
- dislocation loops, multiple-faulted, in quenched material, TEM obs. 77—27887
- dislocation loops and pores due to 23 MeV proton irrad. *(Russian)* 80—54235
- dislocation struct. change during cyclic straining at high temps. 78—44218
- dislocation substructure formation under hydrostatic extrusion 78—56696
- dislocation velocity, from amplitude-dependent internal friction 79—11653
- dislocation-pinning defects in cold-worked Al, US attenuation obs. 77—31673
- dispersed in epoxy resin RDGE MPDA hardened, holographic correlometer study 80—74321
- dispersion hardened, mech. props., effect of strain rate *(Czech)* 77—59865
- dispersion hardening Al_4C_3 77—55978
- dissolution in HCl soln., inhibition by hydrazine derivatives 80—50759
- dissolution of amorphous Si into Al at Si-Al interface 78—95188
- dissolved Al concs. in French hot spring water *(French)* 79—74913
- Duralumin D16T, creep, energy variant of theory expt. verification 78—6993
- dynamic compaction, mixture theory of porous solids 78—63315
- dynamic screening of ions passing through solids 78—10379
- dynamic strength and logarithmic modulus of plasticity 77—16655
- dynamical factors calcs., by multi-slice dynamical diffr. methods 79—23505
- elastic constants, temp. depend. 80—2109
- elastic constants, third-order 79—51184
- elastic consts., third order, pseudopotential calc. by method of homogeneous deformation 80—29106
- elastic grain boundary responses, thermodynamic props., computer calc. 77—39593
- elastic properties *(Russian)* 78—56678
- elastic strain wave generation, by electron beam pulse *(Russian)* 77—76463
- elastoplasticity, dislocation model, work hardening, tensile tests, stress/strain curves *(Japanese)* 77—52410
- electrical and thermal transport props. at low temp., Matthiessen's rule breakdown 78—26847
- electrical conductivity temp. depend., inelastic electron scatt. by dislocations *(Russian)* 77—69315
- electrical resistance and magnetoresist., 2 to 40K, Matthiessen rule deviations *(Russian)* 77—31996
- electrical resistivity and magnetoresist., anisotropic temp. depend. *(Russian)* 79—11103
- electrical resistivity of ultra pure samples at low temp. 79—60794
- electrically exploded foils, heating and burst phenomena 77—39488
- electro-plastic stress curve propag. *(Czech)* 80—108507
- electrochemical anode, oxide film growth accompanied by luminesc. 79—57236
- electrochemical displacement reactions, electron microscope obs. of nucleation and growth, comparison of Cu/Fe and Cu/Al cementation systems 79—47939
- electrochemical nucleation and growth, of Cu, TEM 80—104451
- electrode, electrical breakdown of water in μs region 80—103917
- electrode, in high repetition rate spark switches, surface ageing 80—106997
- electrode, porous disc, prep. by powder metallurgy, performance in LiAl/FeS_x cell 80—26130
- electrode for SAW transducers, micro-fabrication technique 77—80042
- electrode material, influence on electric breakdown in dielectric liquids *(Russian)* 80—50265
- electrodeposition, chemical factors 80—16207
- electrodeposition, cyclic reaction mechanism 79—83143.
- electrodes, charge effects on insulating films obs., PET and SiO_2 80—75625
- electrodes, use of soluble corrosion inhibitors to suppress electrode dissolution 78—88565
- electrolysis units, air washing tests *(French)* 79—29493
- electrolytic bath in plants, power consumption limitation method *(Russian)* 80—3366
- electrolytic capacitors effect of electrical parameters of Al foil capacitors *(Polish)* 80—30245
- electromagnetic wave propagation, demonstration 80—73149
- electromigration of Cu, apparent effective charge, 325-500°C 77—39695
- electron backscatter fractions, exptl. determ. 80—18617
- electron backscattering, X-ray prod., energy distrib. calc. 79—38698
- electron backscattering by bulk target, theoretical model *(French)* 80—60722
- electron beam deposition on SiO_2 in FET, effect on electron trapping 78—80060

aluminium continued
- electron beam evaporation, high rate deposition on strip steel 79—24440
- electron beam impact, measurement of dynamic response using laser interferometer 79—42102
- electron beam irradiation, 2.3 MeV, positron annihilation exam. of radiation defects *(Russian)* 78—34542
- electron beam plasma sputtered coating on Si substrate, islet struct. *(Russian)* 80—39460
- electron beam reflection, high current *(Russian)* 78—84690
- electron diffraction, medium energy 78—83682
- electron dose distribs. from plane infinite oblique sources, Monte Carlo calcs. 77—65339
- electron drag on mobile dislocations at low temps., strain rate, temp., and field depend. 80—19808
- electron emission, optically stimulated, fatigue enhancement 77—4719
- electron emission induced by low energy light ions 79—61482
- electron emission spectra produced by exploding wire photon sources, yield and energy meas. 78—31299
- electron energy deposition and transmission coeffs., Monte Carlo calcs. 80—49269
- electron energy loss meas., direct nonvertical interband transitions at large wave vectors 78—34759
- electron energy loss spectra, appl. of cylindrical electrostatic analyser *(French)* 77—55856
- electron energy loss spectra, incoherent multiple scattering, uniqueness and inversion problem 80—7455
- electron energy loss spectra, microanal. appl. 77—44099
- electron energy loss spectra 78—34560
- electron inelastic mean free paths and energy losses, electron gas model 79—46732
- electron inelastic mean free paths and energy losses, electron gas statisitcal model 79—46733
- electron irradiated, di-interstitial formation within small defect clusters 78—26566
- electron irradiated, interstitial loop nucleation at impurity site *(Japanese)* 77—43247
- electron irradiated, selfinterstitial atomic defect interaction radii, recovery expts. and error sources 80—65049
- electron irradiated, stage I_E recovery, interstitial trapping 77—15405
- electron irradiation damage 77—19988
- electron irradiation induced aqueous corrosion 77—81343
- electron liquid, excitation spectrum, memory-function approach 77—39791
- electron liquid, plasmon dispersion 78—56099
- electron mean free path, stopping and straggling 78—91367
- electron mean free paths and stopping powers calc. using statistical model 77—19996
- electron MFP determ. by depth and ang. depend. of inelastically scatt. electron spectra 78—92154
- electron microprobe local anal. of light elements, ultrasoft X-ray spectroscopy 80—99027
- electron microscopic images, bend contour, n-slice approx., calc. of inelastic scatt. effect 77—62455
- electron range, low-energies continuous-slowing-down approx. and range straggling calcs. 80—39183
- electron scattering cross sections, 300 to 1200 keV 78—9922
- electron spatial absorbed-dose distrib. for 25 MeV beam 77—88289
- electron spectroscopy, energy loss and photoemission 78—72682
- electron stopping power, 2-10.9 keV 78—43055
- electron transmission, secondary electron emission, appl. of Boltzmann equation *(French)* 80—20740
- electron transmission and absorpt. in bulk solids, 5 to 30 keV 77—89491
- electron transmission and absorption, massive target 77—65990
- electron-irradiated, anelastic relax. due to clustered self-interstitial atoms 77—39628
- electron-irradiated, anelastic relax. due to single self-interstitial atoms 77—39627
- electron-phonon enhancement of electron-electron scatt., elec. and thermal cond. 80—49326
- electron-phonon interaction, press. depend., rel. to supercond. transition temp. 79—95106
- electron-phonon interaction, press. depend. rel. to normal state resist. 79—28063
- electron-phonon scattering rates, anisotropic, meas. on Fermi surface 78—87753
- electronic characteristic, thermomodulation spectra 79—87421
- electronic charge density, OPW-based pseudopot. calc. 78—87896
- electronic density of levels, singular struct. 79—77997
- electronic Gruneisen parameter in shock Hugoniot equation of state 80—10635
- electronic momentum densities by two-dimensional angular correlation of annihilation radiation 78—91605
- electronic states, model pseudopotential 78—91582
- electronic stopping function for He^+ and Li^+, 50-300 keV 79—69169
- electronic stopping power of H_2^+ 79—10888
- electronic structure exam. by soft X-ray and X-ray photoelectron spectroscopy 77—85136
- electronic thermal cond. in metal and dil. alloys 78—47764
- electrons around vacancies, electron density calc. 78—64003
- electroplastic effect 80—7647
- electroplating on brass from $AlCl_3$/NaCl melt 77—77434
- electroslag welding, using plate electrodes for Al busbar component parts welding 80—81083
- EM excitation in metals with anisotropic Fermi surface 77—39768
- EM generation of ultrasound, obs. of anomalies 78—84131
- emissivity, 140-300K 77—35729
- emissivity, 335-1100K, polishing effect 77—39682
- emissivity, total hemispherical, temp decay method meas. 78—26708
- empirical potential methods, use of Wedepohl pot., vacancy form. energy 80—39230
- encapsulation of GaAs, surface effects, RHEED 77—1883
- endochronic theory of viscoplasticity, steady waves in impacted plate, Al numerical calc. 78—83282
- energy and elastic constants 80—59435
- energy bands, densities of states and X-ray spectra, superposed self-consistent pots. 78—39010
- energy loss of 120 keV heavy ions, range and range straggling determ. 79—45595
- energy losses and straggling for H^+ and He^+ beams *(Russian)* 80—84226

aluminium continued
- energy losses on C contaminated surfaces, secondary electron spectra, AES, and EELS 79—99997
- energy release during annealing, Bragg diffr. expt. with Mossbauer γ rays 79—24546
- environmental fatigue crack propag., texture influence 79—91802
- epitaxial film, resist. vs. grain diameter curves, theory and expt. 77—76961
- epitaxial film growth on MgO, effect of weak interfacial interactions 77—1325
- epitaxial films, grain boundary struct. evolution during recrystn., interface energy effect *(Russian)* 80—15387
- epitaxial growth, on alkali halide substrates, role of phase interaction, TEM study 79—46979
- epitaxial growth on GaAs (001) 80—24757
- epitaxial growth on Pd, alloying effects 77—62785
- epitaxial layers, elec. props. 79—42671
- epoxide resin, self-toughening mechanism on Al substrate 79—70293
- epoxy Al bonded, adhesive joints under complex loading, development of failure criterion 78—92344
- epoxy bonded joint, determ. and appl. of COD 80—30078
- epoxy-Al composite, thermal conductivity 77—76630
- epoxy-Al composite, thermal conductivity model 77—76629
- equation of state for all press. between 300-200000K, numerical calcs. *(French)* 77—72672
- equation of state from statistical electronic free energy 79—99495
- equation of state under very high dynamic load *(German)* 78—59858
- erosion by coal ash particles 79—61745
- erosion by solid particle impingement at normal incidence, SEM obs. 80—104304
- etched, electronic props. of surface *(Russian)* 78—15569
- etching of high purity single cryst., etch pit morphology and their correl. with microstruct. *(French)* 79—69106
- etching surfactant evaluation 77—77646
- etching technique for revealing plastic zones 78—72955
- etching wastes, appl. to corundum ceramics prod. 80—108376
- ethylene-O_2-N_2-Al particle mixture, two-phase detonation and combustion *(French)* 80—61097
- evaporated layer, on Si film, solid-phase crystn. of Si 77—85100
- evaporated layer, secondary electron energy distrib. and work function *(French)* 79—99993
- evaporation filament/strip source improved version for deposition on glass plate 77—85941
- exoelectron emission under recrystallisation annealing 77—90412
- exoelectron emission under tensile deform. and fracture *(Japanese)* 77—55870
- exoelectron photoemission enhanced by slip steps, plasmon reson. theory 78—15300
- expansion, isentropic, vaporisation and condensation kinetics anal. 77—66623
- explosion product accelerated plate, shock wave diagnostics using laser interferometer 79—64814
- explosive compaction of metal powders 78—64501
- extrusion, pick-up form. on surface 78—39882
- extrusion, plastic flow pattern smoothing 80—7625
- failure under hydrostatic press., kinetics 78—52944
- fast electron multiple scattering, and inner secondary electron generation 77—1160
- fast neutron irradiated, struct. of defect cascades, diffuse X-ray scatt. study 80—39167
- fatigue, effect of active media on struct. and stress condition *(Russian)* 77—28929
- fatigue, effect of pre-existing subgrains 79—5041
- fatigue, environmental, mean strees effect on commercial purity 77—86227
- fatigue, grain size effects *(Japanese)* 77—59911
- fatigue, high temp., cyclic grain boundary migration phenomena 80—85053
- fatigue, struct. changes during cyclic deform. *(Russian)* 77—25127
- fatigue characteristics, low-cycle, theoretical predictions and expt. 78—27641
- fatigue crack initiation, model using probabilistic technique 78—68800
- fatigue crack initiation, pre-existing subgrain effect 80—97565
- fatigue crack propag., grain size effect *(Japanese)* 78—39889
- fatigue crack propagation, quantifying the parameters 80—100891
- fatigue crack propagation rates, stress intensity factors *(French)* 77—25154
- fatigue cracks, microwave detection of third-order nonlinearities 80—55594
- fatigue damage, test temp. effects *(Japanese)* 77—52475
- fatigue damage detection by exoelectron emission meas. *(Japanese)* 77—55871
- fatigue hardening at various test freqs. 79—24539
- fatigue induced dislocation struct. and hardening, exam. *(Japanese)* 78—64624
- fatigue life, influence of cyclic loading conditions 80—76350
- fatigued, inhomogeneous positron trapping 77—90216
- faulted defects, two- and three-layer, two-Shockley unfaulting 77—55292
- FCC, atomic defects, computed electron microscope images 78—26392
- FCC, dynamical study for Gruneisen parameters 77—47594
- FCC, Gruneisen parameters, effect of temp. variation 78—22812
- FCC, polycrystalline, deformation-strain curve description using substruct. parameters *(Russian)* 79—87690
- FCC, props. of vacancies and divacancies 80—10545
- FCC, stacking fault, antiphase boundary energies, investig. methods, review *(French)* 79—42080
- FCC, strain hardening and recovery by pure metal mode, high temp. deform. *(Japanese)* 78—52843
- FCC crystals, compressively activated slip, theoretical latent hardening 80—65128
- FCC single crystal, crystal rotation accompanying scratch deform. *(Japanese)* 79—15733
- Fermi momentum, for solid and liq. phases, temp. variation, Compton scatt. obs. 80—50451
- Fermi surface, de Haas van Alphen technique 78—2412
- Fermi surface, electron-phonon collision frequencies, RF size effect 79—90945
- Fermi surface, positron annihilation study 79—4869
- Fermi surface, scattering anisotropy of conduction electrons on dislocations *(Russian)* 78—60051

aluminium continued
- Fermi surface under homogeneous strain, local pseudopot. model 80—29308
- fibre, micron sized, light scatt. 77—65571
- fibre reinforced by SiO_2, thermal degradation kinetics 77—44194
- fibre reinforced plastic/Al/adhesive laminate, interlaminar behaviour under thermal loading 77—81309
- fibrous heat treated composites, thermal stress anal. 77—46943
- filings, interrelation between dynamic and static distortions, X-ray diffr. meas. *(Russian)* 77—43305
- film, (e, 2e) reaction, ang. correlation functions, plasmon satellites 79—19955
- film, absolute work function meas. by field-emission retarding-pot. device 77—59322
- film, adsorption of O_2 and N_2 77—24486
- film, air corona discharge, thermal energy positive ion extraction 80—38801
- film, Al/copper phthalocyanine/Au cell, photoexcitation, doping, energy loss mechanisms 79—99573
- film, anodisation rate and augmentation factor, oxidation in ammonium tartrate 79—79152
- film, beam splitter phase coatings, for producing phase quadrature interferometer outputs 78—77974
- film, bleaching possibility by laser pulse, liq. metal-insulator transition 77—43498
- film, caesiated, photoelectron escape length, 1.5-4 eV *(French)* 79—47585
- film, colour anodised, selective surfaces for solar collectors *(Japanese)* 80—55893
- film, condensate obtained in electric field, anisotropy of elec. props. 80—44743
- film, condensation from partially ionised vapour flow, peculiarities of form. and struct. 79—28252
- film, condensed and fused, on Ge, press. and residual gas comp. influence on struct. 77—16497
- film, damage production rates of 5 MeV Al^{2+} ions, exam. 78—47444
- film, deform. under He ion bombardment 80—65073
- film, deposition on grooves of grating-polariser for IR spectral region, optimisation 79—55221
- film, diffusion of Cu 78—2303
- film, dislocation observation by electron microscope using convergent beam *(French)* 80—96532
- film, dispersion curve of surface plasma waves, rel. to refl. power minimum curve *(French)* 78—88372
- film, effect of annealing of electrode films on elec. resist. 78—23179
- film, electromigration, AC and DC studies 77—24424
- film, electromigration under pulsed current conditions, calcs. 77—1495
- film, electron beam evaporation, on Kapton laminates, and characterisation 78—11373
- film, electron beam transmission, reflection, and absorp., $35 \leq E \leq 70$ keV 77—39754
- film, electron energy-loss spectrum, wavelength depend. fine struct. 77—11609
- film, electron transmission, 1-5 keV, electron MFP 77—15472
- film, electron transmission, ang. aspects *(French)* 80—49284
- film, electron transmission, calc. 80—60724
- film, electron transmisson less than 3 keV *(French)* 78—10109
- film, electron transport, grain boundary scatt. 79—60937
- film, energy losses of 20-40 keV electrons 78—92153
- film, energy losses of electrons, microcalorimetric meas. 80—59543
- film, energy straggling of H^+ and He^+ ions in 0.1 to 1.2 MeV range 77—80559
- film, enhanced mirror, high-rate sputtering, reflectance and dispersion 77—42636
- film, Er impurity, spin-flip scatt. and supercond. order parameter dynamics 79—78267
- film, etching in carbon tetrachloride plasmas 80—76407
- film, evaporated, adhesion meas. 80—50822
- film, evaporated, corrosion in distilled water, ellipsometric obs. 77—48590
- film, evaporated, interaction with BCl_3, HCl, adsorpt. 78—75945
- film, evaporated, oxidation resistivity change meas. *(Japanese)* 79—11723
- film, fine particles, supercond. transition temp. meas. 77—12044
- film, five atomic layers, electronic band struct. using linearised APW method 79—69393
- film, getter sputtered at low temp. 78—35305
- film, granular, transition to localisation, elec. resist. 80—70877
- film, growth by vacuum deposition, impurity presence, effect *(Hungarian)* 80—7495
- film, He^+ irrad., overpressurised bubble obs. 79—51165
- film, inelastic-elastic scatt. ratio of 80 keV electrons use for radiation damage monitoring 77—4127
- film, influence of predeposited island film on crystallisation of continuous films 78—18930
- film, initial oxidation, AES, work function and gravimetric meas. 78—7087
- film, initial oxidation, electron energy loss spectra 78—7088
- film, internal stress, effect of residual gas press. 77—66100
- film, intrinsic stress meas. 80—71696
- film, ion plated, morphology exam. by SEM 79—28251
- film, ion plating, through mask hole, thickness nonuniformity *(Japanese)* 79—19999
- film, ion plating deposition system using electron beam evaporation *(French)* 80—20802
- film, ion-beam-activated vacuum deposition, struct. and props. 80—15422
- film, lattice and bulk heat capacity meas. for normal and supercond. states 80—92684
- film, Maxwell stresses at charged surface from elastoresistance 80—49957
- film, MBE and field emission deposition on III-V semiconductors, comparative study 79—87016
- film, mean free path for plasmon excitation, 1.5 to 10.9 keV 78—51915
- film, microwave induced supercond. above crit. temp. 79—56364
- film, neutron irradiated, increase of elec. resist. 78—26973
- film, nonlinear elec. props., paramag. admixture effects *(Russian)* 77—24624
- film, nucleation and growth on C layers, adsorption energy and surface diffusion 79—99451
- film, nucleation-grown, RF sputtered, Mayadas-Shatzkes cond. 77—1498

aluminium continued
  - film, on amorphous C and Si substrates, dispersion force contrib. to adhesion *(French)* 80−59842
  - film, on CdS, bonding and interdiffusion, XPS obs. 80−80000
  - film, on fused quartz, threshold adhesion failure, meas. by stylus method 80−50806
  - film, on simple cryst. Si slices, long-term tests 79−33346
  - film, optical cond., energy derivative spectrum 77−66551
  - film, optical dielec. const. in visible region, 300 to 1.5K 77−90211
  - film, Pb$^+$ implanted, ion scatt. erosion rate, Rutherford backscatt. 79−74038
  - film, photoelectron-grain boundary scatt. in MOS struct. 78−64120
  - film, plasma anodisation to exhaustion on Si 80−7722
  - film, plasma anodisation to exhaustion on Si and GaAs substrates 79−83388
  - film, polycryst., chemisorpt. of O_2, synchrotron radiation photoemission expts., 70-150 eV 78−95228
  - film, polycryst., heat conductivity depend. on thickness, block boundary density *(Russian)* 79−82689
  - film, polycrystalline, analytical approx. eqns. for resist. and its temp. coeff. 77−85346
  - film, polycrystalline, trapping of ^{3}He and ^{4}He ions at room temp. 80−84221
  - film, porous anodisation, initial stages of oxide growth and pore initiation, ellipsometry obs. 77−1888
  - film, quench-condensed, disorder effect on optical cond. and band struct. 77−1746
  - film, reflection coeff., effects of plasma bursts prod. 78−56547
  - film, RF impedance temp. and freq. depend. 77−4453
  - film, RF sputtered, resist. recovery obs. 77−8207
  - film, RF sputtered, TCR, calc. and expt. 77−76960
  - film, room temp. oxidation, scanning HEED expts. 78−91567
  - film, simulation of transmission of 1 keV electrons 77−12475
  - film, single cryst., defects, residual gas effects, TEM obs. 77−39587
  - film, single cryst., elastoresist. effect 78−84321
  - film, sputtered, effects of sputter etching and process technology on props. 79−83122
  - film, sputtered, physical props. 79−77938
  - film, struct. and props., effect of ion implantation 79−77936
  - film, supercond., meas. of effective quasiparticle recombination times, density of electronic states at Fermi level 79−38264
  - film, supercond. crit. field, spin-polarized tunnelling meas., test of high-field supercond. theory 79−87220
  - film, superconducting, metastable current states 79−15265
  - film, superconducting transition temp. and lattice dynamics 80−93028
  - film, surface resist. freq. depend. in range 7.7 to 37 GHz 77−20468
  - film, thermomodulation of Al $L_{2,3}$ absorption edge 79−91533
  - film, thickness determ. using ^{63}Ni radioactive source 78−22989
  - film, thickness measurement using Talbot effect 78−9321
  - film, transparent, secondary electron emission of 10-100 keV electrons 77−32477
  - film, transport equation treatment of transmitted electrons *(French)* 77−80558
  - film, transversal magnetoresist. meas. 77−72925
  - film, two photon photoelectron effect in surface plasma reson. 77−69962
  - film, ultrathin, quench-condensed, two-dimensional elec. cond. 78−39233
  - film, underlayer for Ni-Fe-Co film, effect of deposition parameters on ferromag. props. 77−77078
  - film, vacuum deposited, 7 to 65 μ thick, morphology and purity determ. 77−76699
  - film, vacuum deposited, O_2 contamination effect on form. 79−82487
  - film, vacuum deposited, rate and press. depend. of contamination 78−72732
  - film, vacuum deposited, structural changes during annealing at temp. near melting point 78−84096
  - film, vapour deposited on polymer, ageing, adhesion, elec. cond., electrochem. pot. *(Russian)* 79−33362
  - film, vol. plasmon dispersion and damping, electron energy loss spectra 79−7797
  - film, wave front reversal, holography applications *(Russian)* 80−58483
  - film, XPS lineshapes, many body processes 78−39663
  - film and polished bulk specimens, initial stages of oxidation obs. using SIMS 80−81239
  - film deposition, by cathode sputtering in enriched plasma *(Czech)* 77−63557
  - film deposition, step coverage optimisation by computer simulation and SEM 78−51838
  - film deposition, using pulsed ruby laser *(Czech)* 79−52126
  - film deposition from metal plasmas 78−6859
  - film deposition on Kapton laminates by electron beam evaporation 78−76603
  - film evaporated on quartz substrate, surface irregularities 79−90920
  - film growth on C, conductance meas. 79−82495
  - film in microwave radiation field, resistive state transition *(Russian)* 80−93038
  - film on α-quartz, SAW velocity/temp. dependence 77−31861
  - film on Cr-Mo aircraft steels, vacuum deposited 79−70231
  - film on Fe foil, EM excitation of sound, Mossbauer study *(Russian)* 79−99795
  - film on Si(111) substrate, struct., props. depend. on vapour flow, ionisation *(Russian)* 80−75453
  - film on Si substrate, eutectic point displacement on annealing *(Russian)* 80−100850
  - film pulse biased sputter deposited, Kr entrapment 79−28255
  - film reaction with vitreous silica substrate 77−86380
  - film strips, freq. depend. of microwave-enhanced supercond., and local injection of electrons 78−6492
  - film strips, radiation stimulated supercond. 77−28298
  - film strips, thermal emissivity, appl. of distant-focused IR radiometer system 77−169
  - films, action of plasma in capacitive electrode HF discharge *(Russian)* 78−95818
  - films, Al^{2+} irrad., increase of resist. and supercond. transition temp. 80−7027
  - films, deposited on calcite substrate, grain boundary scattering, elec. resistivity meas. 79−65096
  - films, integral radiation ability determ. by electron diffr. *(Russian)* 80−54413
  - films, plasma etching, MOS processing appl. 80−40577
  - films, resistance changes due to bombardment by N, C, or Ar ions 80−103670

aluminium continued
  - films, struct. induced electromigration failure, Monte Carlo calcs 80−49405
  - films on Si substrates, electromigration and diffusion of Cu 79−77820
  - fine particles, prep. by gas evaporation technique, crystal habit 77−52239
  - fission product ranges and kinetic energies 78−94037
  - flat plate, yield surface, biaxial testing machine *(Japanese)* 77−70268
  - flow mechanism in cutting, crystal orientation effects in single crystal 79−100300
  - flow stress during cutting 77−59881
  - fluxural oscillations in longitudinal mag. field, sound attenuation, magnetoelasticity *(Russian)* 80−54844
  - foil, 150-400 keV electron transmission coeffs. Monte-Carlo calc. continuous deceleration model 77−50604
  - foil, 8 ns laser pulse-target interactions, ion-expansion struct. 79−14575
  - foil, α-particle irrad. under fusion reactor conditions, He bubble alignment during deform. 80−107345
  - foil, alloying additions (Si, Mg, Y, Se, Sc) effect, on tensile strength, weldability 80−55475
  - foil, anodic oxidation, characterisation by nucl. methods *(French)* 77−73378
  - foil, Au implanted, positive-ion SIMS analysis 80−52377
  - foil, burn-through by laser-driven ablation 80−33794
  - foil, CESR at 20.98 and 9.27 GHz 77−28445
  - foil, deformation, laser optical scanning obs. 80−100995
  - foil, elec. explosion, dielec. breakdown 78−67388
  - foil, elec. explosion, immersion medium effects 78−67389
  - foil, electrical conduction, electron mean free path, surface scatt. 80−88535
  - foil, electron diffr. effects and images from inclined grain boundaries 79−82241
  - foil, electron scatt., appl. of Monte Carlo type calc. *(French)* 77−7636
  - foil, electron scattering, most probable transmitted scatt. angle calc. *(French)* 77−68901
  - foil, electron-irradiated, interstitial trapping on impurities 79−99242
  - foil, electrostatic spray painting using Van de Graaff generator, teaching demonstration 78−54136
  - foil, etching by negative air ions from corona 80−40593
  - foil, exploding, atomic emission spectroscopy appl. 77−12840
  - foil, flaw detection using proton radiography 79−15939
  - foil, influence of O_2-pressure on oxidation rate, TEM study 80−104355
  - foil, interaction between ^{57}Co atoms and quenched-in vacancies, Mossbauer meas. 80−7234
  - foil, internal friction changes during low temp. plastic deform. *(Russian)* 80−100304
  - foil, large M0 K X-ray, anisotropy from Ne on Al foil 78−55254
  - foil, laser irrad., fracture props. *(Russian)* 80−108523
  - foil, low-temp. on-line Mossbauer meas. of implanted ^{83m}Kr 78−35071
  - foil, modification of texture by fatigue, X-ray diffr. exam. 78−88477
  - foil, naturally passivated, ESCA, sputter etching 77−70218
  - foil, partially stripped $^{12}C^{n+}$ energy straggling 3-36 MeV 79−41237
  - foil, quenched, anomalous annealing phenomena, quantitative study 78−80565
  - foil, secondary electron emission due to α-particle irrad. *(Russian)* 80−66344
  - foil, solar wind ion bombardment, lunar surface modification 80−109325
  - foil, sputtering with ^{252}Cf fission products, desorbed secondary ions 78−68596
  - foil, straggling of relatively electrons, 0-4000 eV 78−14393
  - foil, surface pretreatment of polyethylene by melting against Al 77−32700
  - foil, transparency, UV laser irrad. effects *(Russian)* 77−1768
  - foil, with Au overlay, impedance-match expts. using laser-driven shock waves 80−29119
  - foil, X-ray induced electron emission, secondary electron energy distrib. 77−59669
  - foil + Ne, projectile K-vacancy production cross section, X-ray production rel. to target thickness 77−19059
  - foil anodes, effect of AC component in etching process on specific capacitance, electrolytic capacitors appl. *(Polish)* 80−35420
  - foil electrolytic perforation, surface film phase composition obs. *(Russian)* 80−61004
  - foil explosion caused by electric discharge, cylindrical foil, obs. 79−55597
  - foil fuse, electrically exploded, surrounding medium effect 80−103207
  - foil in quartz dust, electrical explosion for accelerator application 80−6314
  - foil-excited ion, X-ray spectra and satellite classification 80−95567
  - foils, energy straggling, 5.486 MeV alpha-particles 77−80550
  - foils, high strength, vapour deposited on curved surfaces, quantitative characterisation 80−80144
  - foils, thickness uniformity determ. from proton backscatt. yield 77−10510
  - fracture, high temp. SEM obs. 77−59918
  - fracture character and time-to-rupture, near MP *(Russian)* 77−21245
  - fracture due to shock waves leaving surface, shear stresses 78−51128
  - fracture mechanics for impact penetration damage, probability approach, appl. to Al panels 78−1606
  - fracture mechanism, plastic strain role 79−38977
  - fracture mechanism 80−100903
  - fracture speed during phase explosion due to electron beam irrad. *(Russian)* 80−76336
  - fracture toughness, of type 6061-T651 80−35301
  - fracture toughness and struct. *(Russian)* 77−25134
  - fracture toughness testing, plane strain, simple meas. method 77−73381
  - fracture under influence of high power US waves *(Russian)* 79−5034
  - Frenkel pair formation due to passage of relativistic electrons, computer simulation *(Russian)* 80−6402
  - friction stress method for cyclic inelastic behaviour of metals 77−4855
  - frictional behaviour, effect of mechanical properties 80−55548
  - fusion reactor, Al min. activity blanket design for TFTR upgrade 78−58460
  - fusion reactor blanket/shield design 78−54899
  - fusion reactor material, 100 keV He ion irrad., surface erosion due to blistering 77−35600
  - fusion reactor material, 20 keV He$^+$ implantation, gas re-emission, critical dose, temp. effects 77−35596
  - fusion reactor materials, 300 keV He irrad., blistering, flaking, gas re-emission 77−35601

aluminium continued
- galvanic corrosion, anal. for coplanar electrodes with one electrode infinitely large 79—8398
- galvanoluminescence during anodisation in non-dissolving electrolytes 79—52680
- galvanomagnetic properties, low-field, Fermi surface and defect struct. effects 77—4323
- galvanostatic anodising of high purity samples, galvanolum. obs. 77—90488
- galvanostatic anodising of high purity sheet, galvanolum. obs., cryst. orientation effect 77—90489
- gamma photon backscattering, energy dependence *(Rumanian)* 79—76316
- gamma photons penetration, 6 MeV, expt. benchmark data and computed data comparison 80—5256
- gamma-ray attenuation coeff. meas., 1115, 1173, 1332 keV 77—55303
- gamma-ray buildup factors 80—27822
- gamma-ray impact, absolute pair production cross-section meas. 78—43958
- gamma-ray scattering, incoherent, total at. cross section 79—13679
- gases in metals, detection by vacuum spark technique, appl. to Al wire 78—61094
- glass fibre reinforced plastic/polyurethane foam/Al sandwich, flexural props. *(Japanese)* 78—56707
- glass-Al, layered target, reduced thermal cond., X-ray meas. 77—31523
- glass-fibre reinforced Al, highly deformed, microstruct. and mech. props. *(German)* 80—55489
- grain boundaries, periodic struct., computer simulation 77—89448
- grain boundaries, periodic struct., geometrical anal. 77—89449
- grain boundaries energy evaluation in dangling-bond approx. 80—54256
- grain boundaries in equilib. struct. of annealed polycryst. Al *(Russian)* 80—29982
- grain boundaries movement, 3-fold nodes, in high temp. creep. 80—89317
- grain boundary behaviour, validity of coincidence site lattice model of grain boundary struct. 79—51120
- grain boundary diffusion of Zn, nonvacancy mechanism *(Russian)* 80—24669
- grain boundary energy calcs. 77—27892
- grain boundary internal friction after recrystn. annealing *(Russian)* 80—66561
- grain boundary migration, TEM obs. on mechanism 80—79812
- grain boundary orientation in pure, cubic, lattice *(Russian)* 77—11567
- grain boundary sliding and deformation mechanism maps 80—3128
- grain growth 77—36520
- grain refinement, effect of Al_3Ti, TiC and B 78—52828
- grain refinement by α-Al nucleation on dissolving $TiAl_3$ crystals 80—35178
- grain refinement during unidirectional solidification, effects of addition of powdered cpds. *(Japanese)* 78—35395
- granular, hopping cond., supercond., magnetoresist., Zeeman splitting 78—60243
- granular bridges, with different thicknesses and widths, crit. current, temp. depend. 80—88688
- granular films, inhomogeneous supercond. transitions, microwave meas. 80—103789
- granular films, self-ion implantation supercond. transition temp. enhancement 80—103774
- granular films, vortex noise at supercond. transition 80—84530
- granular supercond., normal state cond. 80—88529
- granular superconducting bolometer as mol. beam detector 80—73524
- granules, hot rolling, angle parameters and forward slip 80—25601
- graphite composite, mech. props., effect of thermal exposure 77—36629
- graphite fibre reinforced, temp. and press. effect on interface chemistry mech. prop. meas. 78—64595
- graphite fibre reinforced Al, mech. props., comparison with B-Al composite 77—52470
- graphite reinforced Al, wear volume/sliding time relationship 79—61743
- graphite reinforced epoxy/Al laminate, cantilever shells and late, natural modes 79—91737
- graphite-Al composite development using liquid infiltration technology 77—24986
- PAN graphite-Al composites, fracture characteristics and props. 80—11779
- graphitisation of phenolic resin carbon, catalytic mechanism 77—28734
- grinding wheel loading meas. using neutron-activated workpieces 79—5070
- ground state, momentum representation of generalised hydrogen-type wave functions 77—6674
- Gruneisen coeff. depend. on specific volume, phonon spectra calcs. 79—65165
- Gruneisen coefficient, dynamic determ. 77—24418
- Gruneisen parameter, behaviour at high press. 78—83899
- Gruneisen parameter determ. using thermoelastic effect 79—28068
- Gruneisen parameters, dynamical study using modified Bhatia model 79—37797
- Gruneisen parameters, low temp. 79—23694
- hadron cascades prod. by 300 GeV protons on target inside magnet 77—10566
- hard anodic coatings, effects of cellular structures 78—11448
- He bubble behaviour during high plastic deform. 80—29087
- heat capacity of granular film 0-4.5K, crit. coupling between grains 78—84348
- heat of soln. of H, electron charge distrib. calc. 78—51689
- heat of soln. of H, spherical model 80—96656
- heat transfer during cooling with water *(German)* 80—23873
- heavy ion ranges, 120 keV Pb ions backscatt. obs. 80—19855
- helicon attenuation below 1K, metal with diamag. domains *(Russian)* 77—85254
- hermetic jacketing on SiO_2 fibres, reductions in static fatigue 79—43448
- high β-plasma in spindle-cusp mag. container, laser produced 78—59650
- high intensity US absorpt. 79—86845
- high purity, cyclic torsional deform., factors influencing ductility 77—56031
- high purity, development of rolling and recrystallisation textures 77—25070
- high purity, spectrographic determination of trace impurities *(Polish)* 80—35603
- high-density quantum statistical model 79—55824
- holographic, nondestructive testing of brazed, and epoxy bonded honeycomb panels 78—40017

aluminium continued
- hot and cold deformation drawing strengthened, thermal EMF study *(Russian)* 80—54674
- hot extrusion, nonsteady state temp. distrib., numerical method 80—60886
- Hugoniot curves of third and fourth order for cubic crystals *(French)* 77—11634
- hydration, in vap. phase, rel. to upper atmosphere chemiluminesc. 79—29362
- hydroextrusion, effect of longitudinal US oscills. *(Russian)* 79—34071
- hyperfine interactions of implanted Fe, conversion electron Mossbauer spectroscopy 78—52391
- ice detection using surface acoustic waves, testing on Al substrate 78—18129
- imaging by FIM 78—30526
- immersion plating of Au on Al, adhesion and contact resist. 79—39033
- impact strength, exam. with pulsed drop impact loading 78—84944
- implantation into Cu for corrosion protection 80—71789
- implantation of Si, Al, Hf, Ta into InP and GaAs, form. of protective oxide 78—79622
- implantation on Cr-Ni Nb stabilized austenitic stainless steel surface, effect on oxidation behaviour 80—71791
- implanted ^{119m}Sn, Mossbauer spectroscopy, isomer shift and Debye-Waller factors 79—24240
- implanted Li atoms, depth profiles and sputtering anal. by optical spectra 77—35579
- implanted Xe behaviour during anodic oxidation 80—71800
- implementation of Fe-Cr-Al Fecralloy stainless steel surface, effect on oxidation behaviour 80—71790
- impurities heat of solution, pseudopot. calc. 77—51393
- impurity diffusion 78—47595
- impurity influence on superplasticity, elongation decrease at rupture *(Russian)* 79—91735
- impurity low-field galvanomag. coeffs., 4 OPW calcs. 77—69304
- impurity-vacancy binding energy clustering effect calc. 78—47411
- inclusion, in Si, behaviour during annealing in elec. field *(Russian)* 79—23779
- industrial, depth profiling by ion microprobe with high mass resolution 79—46894
- ingot solidification by HV pulses, impurity distrib. and conc. region formation *(Russian)* 80—20919
- ingot struct., effect of mould rotation and electromagnetic stirring *(Japanese)* 77—63652
- inhomogeneous granular, superconductivity 80—103795
- initial interaction of O with single cryst. faces, LEED, AES and work function study 80—84392
- initial oxidation, interatomic Auger transition spectroscopy 79—7746
- instantaneous plastic strain associated with stress increments during steady state creep 78—48478
- interatomic potentials from phonon spectra 80—19744
- interface, Al(111)-Al(111), local and nonlocal contribs. to adhesive energies 77—85085
- interface, Al (111)-Al (111), self-consistent electronic densities and adhesive energies 78—72005
- interface reactions with polyurethane adhesive, surface treatment effects 77—81384
- internal friction, dislocation glide and jog climbing *(French)* 78—11261
- internal friction, strain amplitude dependent, hydrostatic press. effect 77—77520
- internal friction, strain amplitude dependent damping at 8.3×10^{-3} Hz 77—1172
- internal friction and elastic constants, reson. vibrs. of metal spheres 78—15443
- internal friction at medium temps. *(French)* 78—39826
- internal friction due to dislocation-loop interaction *(French)* 79—79017
- internal friction peaks at high temps., deformation and annealing effects 77—32615
- interstitial clustering following electron irradiation at low temp. 79—19243
- interstitial loop form., effects of repeated electron irrad. 80—75220
- interstitial trapping configuration study by ion channelling 78—47455
- interstitial waters of recent marine sediments 79—92524
- interstitials, displacement field calc. using discrete lattice model 77—1122
- intrinsic stacking fault energy, effect on cyclic hardening 79—11638
- ion beam milling, amomalous sputter yield behaviour 80—108624
- ion bombarded, L_{23} shell ionisation cross section, Auger spectra obs. *(French)* 77—69956
- ion bombarded, L_{23} shell ionisation cross-section under H^+, heavy-ion impact, Auger spectra *(French)* 79—24406
- ion bombarded, photon and ion emission, simultaneous meas. 78—15276
- ion bombardment, energy distrib. of positive secondary ions and sputtered atoms 77—32485
- ion bombardment, sputtering, re-emitted kinetic energy ang. distrib. 80—2910
- ion impact excited, ang. resolved Auger emission 79—61475
- ion implantation, oxidation mechanisms study 77—8980
- ion implanted, ^{29}Si ion range meas. by (p,γ) reson. broadening, 20-100 keV 77—69023
- ion implanted, electron beam annealing, ion backscatt. and TEM meas. 80—59500
- ion implanted, ranges of implanted 10-30 keV D^+ 78—83858
- ion irradiated, Auger electron spectra struct., possible surface diagnostic methods 79—69946
- ion irradiated with Al ions, void swelling and annealing of voids, electron microscopy study 80—88216
- ion laser, CW, in HV hollow cathode discharge 78—9371
- ion plated coating on steel *(Japanese)* 78—80477
- ion plating, low friction wear-resist, surface form. on Ti 78—11442
- ion range of 100 keV Pr^{2+} and Tb^{2+}, M-shell X-ray cross-sections 77—35614
- ion recombination laser 78—17923
- ion stopping power systematics, Z_1-oscills. 79—65130
- ion-excited Auger emission from sample trays in Auger-sputter profiling study 78—52607
- ion-implanted, 40-60 keV, up to 5×10^{15} ions cm^{-2}, for implantation ref. standard 79—69140
- ion-implanted, dechannelling by dislocations, backscatt. expts. 79—7642
- ion-induced Auger electron emission, depend. on ion energy 79—78814
- ion-induced electron emission, ion charge depend. 80—108315
- ions, $2s^22p^53l$ and $2s^22p^63l$ configs., excited state energy levels 79—54781

aluminium continued

- ions, 720 keV beam foil spectra 1800 to 7000 Å, excited state cascades and lifetimes 77—23450
- ions, He-like, satellite lines to higher-order reson. series lines in laser-prod. plasma 79—85930
- ions, in plasma, spectral line intensity rel. to composition *(Russian)* 77—36851
- ions, two vacancies in K shell, 2 electron 1 photon, and hypersatellite transition probabilities 78—46294
- IR laser reflectance, anomalous absorpt., plasma ignition 80—7439
- irradiated, containing self-interstitials and vacancies, electronic transport props. 78—60105
- irradiated with electrons and neutrons, positron annihilation meas. *(German)* 77—62563
- irradiation defects, intrinsic thermal expansion meas. 79—95186
- irradiation with 100 and 400 keV Al ions, obs. and analysis of damage struct. 77—4133
- isoaxial bicrystal, deformation behaviour, study by photoelastic coating and moire methods *(Japanese)* 78—11294
- isoaxial bicrystal, Moire investigation of mechanical behaviour 77—16647
- isothermal compression curves to 120 kbar, X-ray diffr. study 78—83876
- isotropic, Brillouin scatt. 78—80367
- joints glued with reaction resinous mortar, photoelastic exam. *(German)* 78—76825
- junction growth, expt. anal. with junction model 79—47783
- K X-ray absorption, K-emission spectrum, band struct. using APW method 80—97380
- K-shell X-ray production, by 0.4 to 2.4 MeV ^{4}He and ^{1}H ions 79—47550
- kaolinite-mullite reaction sequence, spectroscopic anal. of Al coordination changes 78—48719
- Kapitza conductance, heat transport through subcooled He II 79—23794
- Kapitza resistance of interfaces with liq. ^{3}He and ^{4}He, 0.3-1.4K 77—24475
- kinematic viscosity temp. depend. porosity, H solubility, supercooling *(Russian)* 80—54425
- kinetic friction re-examination using modified pin and disc machine 80—55547
- Kovar-silicon oxynitride-aluminium cathode, local electron emission and electroluminesc. patterns obs. 80—108327
- L-shell ionisation by 80 keV electrons, transmission electron energy loss spectrometry 80—60721
- laminate, free-free plates, predicted and expt. natural modes 79—10520
- laminate with polyethylene, flexural fatigue props. *(Japanese)* 78—56751
- laminated, creep, comparison with B-Al composite 77—36587
- laminated coatings, for fuel confinement, fusion reactor target appls. 78—60883
- laser, 7.84 Å, travelling wave source pumping, numerical anal. 77—83864
- laser action in Al II slot cathode discharge 77—61943
- laser damage threshold at 10.6 μm, up to 10^{10} W/cm^2 77—50707
- laser driven shock waves vel., risetime, luminosity struct. meas. using shocks own luminosity 78—59857
- laser fusion target simulation, press. ionisation 80—63374
- laser impact, multiple crater refl., effect on refl. props. 78—52596
- laser irradiated, charged particle emission from back side of target 78—2949
- laser irradiated, conditions for appearance of bleaching 78—35228
- laser irradiated, thermal response and plasma characts. 79—86595
- laser microprobe emission spectroscopy, matrix effects 77—16870
- laser plasma, high-Z, temp. meas. from bremsstrahlung emission 80—87914
- laser power meter, Al slab, for output meas. from high power CW CO$_2$ laser 79—59739
- laser produced plasma, momentum transfer, cratering, and blow-off plasma ang. distrib. 78—5898
- laser produced plasma, X-ray spectroscopy 77—72502
- laser pulse damage at 10.6 μm, single cryst. target in vac. 77—50706
- laser pulse irrad. of Al targets, absorpt. studies 80—79455
- laser radiation absorptance at 1.064μm 79—87528
- laser radiation absorption in craters on metal targets 80—97386
- laser strengthening, struct., hardness and dislocation density *(Russian)* 80—76399
- laser target, multiple-pulse thermal coupling at 3.8 μm wavelength 80—96371
- laser-produced plasma, momentum transfer and interaction phenomena of high power CO$_2$ laser 80—48921
- laser-produced plasma, X-ray bremsstrahlung and fast ion meas. 78—5936
- latent hardening in single cryst. *(Japanese)* 78—44135
- lateral spread distribution widths MeV He ions in C, Al, Cu from energy spectra 79—14860
- lattice atom displacements near end of implanted μ^+ tracks 78—55890
- lattice dimensions, difference between vacuum condensates and massive specimens *(Russian)* 77—31912
- lattice dynamics, modified Bhatia model, phonon dispersion, Debye-Waller factor temp. depend. 77—31729
- lattice resistance stress, Bordoni relax., microdeform. and US attenuation results 80—25747
- lattice thermal cond., 1.5-15K 78—30904
- lattice thermal cond., low temp., comparison with dil. Al-Cu alloys 77—62889
- lattice thermal cond. at low temps., Ashcroft pseudopotential method 80—19897
- lattice vibrations, seven parameter non-central force model 80—44270
- layer covered Si n-p planar diode, laser beam produced alloy areas, characterisation 79—69594
- layers on Si or GaAs, ellipsometric anal. methods, correl. between optical props., thickness and surface roughness meas. *(German)* 80—55215
- LEED, high temp. limit Debye model 77—1207
- Lifshitz constant for calc. of van der Waals force between two solids *(French)* 80—107658
- light interaction with solid at extreme intensities 77—80328
- liquid, asymptotic form of structure factor 77—7651
- liquid, atomic radial distrib. curve anal. *(Russian)* 80—14996
- liquid, bulk modulus, calc. using press. fluctuation in microcanonical ensemble 80—2106
- liquid, charge density fluctuations in surface layer *(Russian)* 80—15580
- liquid, coordination numbers, calc. in microinhomogeneous struct. model *(Russian)* 80—38902

aluminium continued

- liquid, density fluctuations 78—55806
- liquid, diffusion interaction with solid W *(Russian)* 78—26735
- liquid, diffusion of W under low gravity *(Russian)* 78—22875
- liquid, dissolution of Co and Fe, kinetics, 700-900°C *(Russian)* 77—59119
- liquid, dynamical struct. factor 78—71667
- liquid, dynamical struct. factor calc. 80—64880
- liquid, effect of treatment on dissociation of solid solns. of alloys *(Russian)* 78—15353
- liquid, electron component of entropy *(Russian)* 79—23747
- liquid, electron correlations, evidence 78—55805
- liquid, electron momentum density, perturbed Green's function method 78—60052
- liquid, energy moments and longit. freq. dispersion 79—60262
- liquid, interaction potential 77—58945
- liquid, isothermal compressibility, harmonic pot. model calc. 79—14870
- liquid, kinematic viscosity temp. depend., porosity, H solubility, supercooling *(Russian)* 80—54425
- liquid, longit. current spectra calc. 79—82143
- liquid, molecular dynamic simulation of static and dynamic structural factors *(Russian)* 79—69005
- liquid, momentum density of electron 78—6309
- liquid, neutron scattering experiments up to 1900K using sapphire container 79—63215
- liquid, pair correl. function, Monte Carlo calc., with pseudopot. 77—15300
- liquid, pair interaction pot., struct. factor calcs. 77—51298
- liquid, phase form. and diffusion interaction with W-Re alloy, under weightlessness *(Russian)* 78—22876
- liquid, pure, surface tension meas. *(German)* 77—35799
- liquid, radial distrib. function calc., pseudopot. method *(Russian)* 79—19138
- liquid, resist. and thermo-electric power using corrected parameters of Shaw model 79—19566
- liquid, second and fourth order moments temp. depend. 77—72545
- liquid, short-wavelength density fluctuations 79—46550
- liquid, spreading behaviour on Fe-Si 80—84345
- liquid, structural details, molecular dynamics calcs. *(Russian)* 80—64879
- liquid, structure factor and radial distrib. function, neutron diffr. 77—47334
- liquid, thermoelectric power, pseudopotential calc. 80—59959
- liquid, viscosity, 600-1000°C *(Russian)* 77—59133
- liquid, viscosity calc. using microinhomogeneous struct. model *(Russian)* 80—15284
- liquid, X-ray diffraction analysis 79—4232
- liquid and polycryst., density fluctuations, neutron scatt. anal. 80—70349
- liquid film, electron diffr. 78—83721
- liquid impact erosion and cavitation erosion comparison 80—104302
- liquid inclusion in Si, migration in temp. gradient field 78—18842
- liquid inclusions, thermal migration, dislocation drag 77—7911
- liquid metal embrittlement, by Ga 80—7675
- liquid metal embrittlement by Ga 78—64653
- liquid metals, structure factor modelling using quasi-crystallised model *(Russian)* 80—54118
- liquid structure factor, 680 to 840°C, neutron diffr. study 79—46552
- lithographic sheet, AC etching 80—35547
- load relaxation, plastic deform. theory and plastic eqn. of state 78—27554
- longitudinal compressive impact test, comparison of expt. and calc. results *(Japanese)* 79—96119
- longitudinal magnetoresistance anisotropy, high purity single cryst. 77—76793
- low temperature lattice parameters and Gruneisen parameter 78—38658
- low vacuum condensates, struct., IR refl. obs. *(Russian)* 78—30850
- lunar basalts and regolith, anal. of var. in Al, Mg and Si abundances 78—16320
- magneotresistance, mag. breakdown, open trajectories, temp. depend. *(Russian)* 77—35921
- magnetic breakdown, quantum phenomena *(Russian)* 78—43290
- magnetic breakdown, transverse magnetoresist. meas. 77—47795
- magnetic susceptibility, model pot. theory 80—75710
- magnetomorphic oscillations, magnetoresist. and Hall coeff. meas. 77—28159
- magnetoplastic effect and eddy current heating *(Russian)* 77—43858
- magnetoresistance, elec. field distrib. in strong mag. fields *(Russian)* 79—11104
- magnetoresistance, field strength function, electrodeless methods 79—91026
- magnetoresistance, longitudinal, meas. on single crystals 80—75550
- magnetoresistance, path integral method calc. 80—65537
- magnetoresistance, temp. depend., impurity effects 80—70682
- magnetoresistance and Matthiessen's rule departure, temp. depend., linear lattice defects role *(Russian)* 80—84456
- magnetoresistance oscillations near [001] axis 79—56197
- magnetoresistance size effect, effect of cyclotron orbit nature 78—47767
- magnetoresistivity, linear growth, in strong mag. fields *(Russian)* 78—51972
- magnetoresistivity, low temp., anomalous behaviour *(Russian)* 77—31998
- magnetothermopower, low-temp. electron-diffusion, meas. 77—15834
- magnetron sputtering in Ar and Ar/O$_2$ mixtures, discharge characts. 80—89145
- mean excitation energies from α-particle stopping power meas. 79—13615
- mechanical deformation with superimposed insonation, volume effects 78—60723
- mechanical properties, 20 to 300°C *(French)* 77—56018
- melt, adhesive props. on Ti and graphite, 300 to 1200K *(Russian)* 77—15663
- melt, environment for Ti ductility testing at 700-900°C *(Russian)* 77—52537
- melt, exam. of H$_2$ bubble origin, using first bubble technique 78—85115
- melt, structural factors, at. distrib. curves, thermodynamic and neutron diffr. study *(German)* 80—19687
- melt, wettability of ZrO$_2$ melt 77—89619
- melt, wetting of MgO-Al$_2$O$_3$ ZrO$_2$ refractory 78—22936
- melt density, temp. depend. *(Russian)* 79—69174
- melt-NaF filter material interaction mechanism *(Russian)* 80—108743
- melting, existence of before and after effects, neutron scatt. 77—84895

aluminium continued
melting curve and Gruneisen coeff. at high press. 80—65200
melting of semiinfinite solid, nonFourier heat cond. temp. distrib., interface location, small times 77—58542
melting theory for small particles, Helmholtz free energy 80—59629
melting transition, TEM 77—80603
melts, metallic materials diffusion rate, meas. apparatus 79—86913
membrane, lifetime prediction and design 80—71752
membranes, circular, plastic deform. under impulsive loading by underwater wire explosion 79—100208
membranes, life testing 79—70256
membranes in pulsed electron beam, temp. and ultimate load calcs. 79—45484
metal, Auger spectra, plasmon satellite intensity 78—64432
metal, B determ., spark source mass spectrometric method 79—74479
metal beam epitaxy, high temp. high purity sources 79—43156
metal-poor stars, spectra and Al/Fe ratios 78—57549
metallic, phonon freq., binding energy, compressibility, elastic const. and energy band gap calcs., linear pot. 80—88284
metallic compressibilities, general pseudopotential approach 80—54631
metallisation of B, borsic, SiC fibres by continuous coating *(Russian)* 78—35538
metallisation of quartz and $LiNbO_3$ SAW resonators 77—39147
metallisation on ⟨100⟩Si, Si epitaxial regrowth and grain struct. 78—79901
metallised amorphous GeSe junctions, electrical contact effects on properties *(German)* 80—93010
metallised coating on polyethylene terephthalate film, fracture under laser irrad. *(Russian)* 80—76333
metallization of semiconductor devices by high rate magnetron/plasmatron sputtering 79—28919
MHD laminar flow, longitudinal dynamic effects determination for Al *(Rumanian)* 80—64792
microcrack propagation and plastic strain 80—81187
microdeformation associated with double kink formation *(French)* 77—28873
microdisc targets for single beam laser expts., prod. method 78—1865
microhardness under high hydrostatic press., meas. by microindentation 80—3182
microrupture singularities in low stress range at elevated temp. *(Russian)* 79—29172
microstructure inhomogeneities, cold neutron small angle elastic scatt. 77—84736
microvoid form., gaseous impurity atom effects, positron annihilation study 80—49275
mirror, acted on by laser radiation, reflectivity meas. 79—10342
mirror, Al_2O_3 coated, highly efficient refl. type polarisers for 10.6 μm laser radiation 78—71177
mirror, Al_2O_3 protected, refl. depend. on angle of incidence, 8 to 12 μm 78—37960
mirror, polarisation effects by overcoatings 77—72055
mirror, SiO_x protected, far UV refl., UV irrad. effects 79—7191
mirror, spherical, generation with single point diamond cutting tool 80—33249
mirror film, ultraclean DC sputtered, optical props. 77—50748
mirror IR reflectance at 45° incidence, obs. 79—14074
mirror reflectance 8 to 12 μm, normal to high incident angles, Y_2O_3, HfO_2 protective layers 78—79090
mirror surfaces for solar power stations, specular reflectance obs. 78—13786
mirror with MgF_2 coating, AES, UV irrad. effect 77—72047
mirrors, on metal substrates, resistance to heat and radiation 79—94319
mobile dislocation density determ. from sound velocity 79—19258
molten, determination of H content, using electrochemical probe 79—11843
molten, dissoln. kinetics and diffusion coeffs. of Fe, Co and Ni 80—59666
molten, dissolution of Fe and Fe alloys *(Japanese)* 78—71858
molten, graphite wetting, effects of US 79—15629
molten, interface with halides, liquid-liquid interfacial tension meas. 80—10750
molten, Na determ. using β-Al_2O_3 probe 77—48714
molten, showering cryst. form. in mould cooled from top *(Japanese)* 80—66498
molten, thermal expansion meas. to 1300K 80—65254
molten, viscous flow, H dissolution temp. depend. X-ray anal. 79—91628
molten fine wires, migration in thin Si wafer, vertical p-n junction fabrication 78—68077
molten reactor fuel-coolant interaction simulation, water-molten Al reaction 78—58363
monolayer, effect on atomic modulation of interdiffusion at Au-GaAs interface 80—49432
monovacancy formation parameters, temp. depend. 78—75658
monovacancy thermodynamic parameter calcs., temp. dependence 78—2114
multiple plasmon excitation, in energy loss spectrum 79—4872
multiple scattering, relativistic cross section for double scatt. 79—69898
muon$^+$ spin resonance, diffusion, temp. depend. 78—39490
muon$^+$ trapping at vacancies in quenched samples, compared with positron annihilation 80—15937
muon diffusion, μSR 79—56696
muon diffusion, impurities effect *(Russian)* 78—35077
muon diffusion, LAMPF results 80—71285
muon diffusion at low temp., effect of nuclear elec. field gradients 77—52005
muonic atoms, Lyman series, muon transfer effect 79—7040
muonic atoms formed by muon transfer free μp and μd systems, isotope effect on Lyman series 79—86090
muonic K-shell X-ray transitions, nuclear charge radius 78—66195
narrow superconducting bridges, microwave radiation stimulated T_c enhancement 80—84537
Nernst-Ettingshausen coeff., electron-phonon Umklapp scatt. 78—26848
Nernst-Lindemann equation, validity over temp. range 293 to 925K 77—72695
neutron activation analysis, trace element removal technique 79—57309
neutron damage, positron annihilation 80—65056
neutron irradiated, direct obs. of radiation induced coated cavities 77—47493
neutron irradiated, phonon dispersion curves, neutron scatt. meas. 77 43290
neutron irradiated, void annealing kinetics 80—44234
neutron irradiated, void surface props. determ. anisotropic small-angle neutron scatt. 78—10095
neutron irradiation, mobile interstitials production 80—34080
neutron radiotherapy, 14 MeV, skin-sparing, effect of metal sheets 78—35923
neutron yield calcs., electron beam incidence 78—95622
neutron-irrad., void annealing, positron annihilation obs. 77—76469
Nimonic alloy reinforced laminate composites, low-temp creep singularities, structural defect changes *(Russian)* 80—11696
non-elastic deformation, phenomenological model with solute strengthening effect incorporation 78—39832
non-pair inter ion interaction through cond. electrons, inelastic neutron scatt. study *(Russian)* 79—46773
nonequilibrium superconductivity in microwave field 79—42695
nonlinear conductivity of thin films in mixed state *(Russian)* 80—80464
nonlinear helicon resonance *(Russian)* 77—28208
nonlinear skin effect at 4.2K, surface resist. determ. *(Russian)* 79—87122
nonlinear sound wave interactions, sound attenuation in weak superconducting state *(Russian)* 80—75310
normal metal-superconductor boundary excess resist. temp. depend., quasi-particle Andreev reflection *(Russian)* 79—73640
notched bars, deform. behaviour and strength having biaxial state of stress at notch root *(Japanese)* 80—81116
nuclear acoustic resonance, influence of longitudinal and transverse magnetoresistivity 79—24222
nuclear acoustic resonance 77—20732
nuclear acoustical reson., 20-80K 79—8058
nuclear paramagnet for thermometry 77—26292
nuclear paramagnetism, used for calibration of SQUID magnetometer 79—67358
nuclear reactor fuel tubes, proton activation determ. of impurities 80—27741
nuclear spin lattice relaxation measurements in small superconducting particles. 80—88681
nucleosynthesis, isotopic yields from C and Ne zones in explosion of massive star 80—90406
in oceanic phosphorites, Fe, Ti and Al behaviour during initial form. stages 80—31029
optimised model potential parameters Hartree-Fock-Slater procedure for calc. 77—69214
orientation distribution function determ. using one pole figure *(German)* 77—25242
oriented single crystal, plastic deform. *(Japanese)* 79—43336
orthogonal cut surface, effect of cutting condition on residual stress *(Japanese)* 78—85035
orthogonal cut surface, relations between residual stress and moire strain, exam. *(Japanese)* 78—85036
overlay film on quartz for SAW device temp. compensation 80—79043
overlayer on GaAs (110), O_2 adsorption 80—50740
overlayer on Si (111) surface, electronic states 80—11061
overlayers on GaAs (110), interfacial electron states, UPS and LEED obs. 80—80377
overlayers on Si (111), theoretical study 78—95366
overlayers on Si (111) surface, surface electronic struct., self-consistent pseudopotential method 79—4595
oxalic acid bath, pH and conc. effects on form. and dissolution of Al_2O_3 77—16754
oxidation, direct obs. in TEM 79—61789
oxidation, influence on deformation map 80—40599
oxidation, IR refl. obs. of oxide film 78—35591
oxidation, meas. using quartz oscillator microbalance 77—70219
oxidation by exposure to O_2 and H_2O, soft XPS exam. 78—80683
oxidation examination by inter-atomic Auger yield spectroscopy 78—11419
oxidation in $(NH_4)_2CO_3$ solutions, to form amorphous self-supporting vac.-tight Al_2O_3 films 80—16177
oxidation in hot water, electron microscope obs. of initial stages 79—11718
oxidation in water, oxide growth rate and struct. 78—76783
oxidation of (111) surface, initial stages, LEED anal. 80—80082
oxidation of magnetron sputtering target in Ar/O_2 mixtures 80—55291
oxidation states, multiple, obs. by photoelectron spectra of core level shifts 77—8720
oxidative vaporisation, thermochemical analysis 78—11447
oxide coated, inhibitive and aggressive ion effects, secondary ion mass spectrometry 77—8974
oxide covered, tensile deform. in high vac., particle and photon emission 78—39672
oxide film characterisation, using low energy electron induced X-ray spectroscopy *(French)* 78—41386
oxidised surface, EXAFS in soft-X-ray region 79—37921
oxidised surface, light emission from sputtered O atoms or ions 80—58199
pack aluminisation of Ni based Rene 80 superalloy 80—76188
pair potentials calc., appl. to point defect props. 80—19798
particles prepared by evaporation in clean Ar atm., cryst. morphology 77—62494
particulate combustion process model *(Russian)* 78—85164
phase comparisons for Sondheimer size effect oscills. 78—34823
phase layer growth during aluminide coating of Ni 78—27682
phonon anharmonic response, neutron-scatt. test of computer calcs. 80—44281
phonon density of states by neutron scatt., sp. ht. and Debye temp. 80—2132
phonon dispersion curves, lattice dynamics unpaired forces 79—42170
phonon dispersion relations and Debye-Waller factor calcs. 78—51630
phonon dispersion relations and lattice heat capacity, modified Bhatia model 77—20024
phonon dispersion relations and lattice heat capacity calc. 77—20023
phonon scattering surfaces, obs., by neutron film methods 79—46761
photionisation and electron impact ionisation relationship, mean free paths 79—22672
photoacoustic effect from thermally thin solid 80—75304
photocathode in X-ray detector photoelec. diode, calibration 77—54033
photoelectric cross sections, from total absorption cross sections, 5 to 130 keV 79—26947
photoelectron spectral yields from monochromatic soft X-radiation 79—22757
photoemission, influence of oxide films *(Russian)* 77—81194

aluminium continued
photoemission, primary and secondary yields using low-energy monochromatic X-rays 80−35053
photoemission cross-sections fpr 2s and 2p levels 80−93453
photoemission from (100), (110), and (111) cryst. faces, surface states 79−4893
photoemission spectrum for exploding wire radiator source, Boltzmann eqn. soln. 79−26949
photoemission study of energy depend. of bulk plasmon loss intensity 79−47035
photoemission theory, book contrib. 80−16159
photon absorption and photoelectric cross-sections calcs. 79−31486
photon penetration, photon backscatt. incidence angle depend. 80−104008
photoneutron yields released by incident electrons, improved calc. 80−27630
physicomechanical and wear props., influence of ion implantation and overlay coatings 80−40603
pion$^-$, in vivo dosimetry using Al activation 80−46060
pionic atom, 2p level shifts and widths 78−46469
pipe diffusion along segment of faulted dislocation loops during annealing 80−107256
pitting, potentiostatic, anode current oscillations 77−90496
pitting corrosion in Cl solns., electrochemical exam. 79−20248
pitting mechanism, obs. using Engell-Stolica potentiostatic method 80−25905
PIXE anal., conc. profile determ. using beam energy variation 78−76965
PIXE anal. of Ar implantation by Ar ion excitation 80−45609
planar target, CO$_2$ laser irrad., 10^6-10^8 W cm^{-2}, diagnostics 77−89281
plane coalescence, at grain boundaries 80−70221
plane stress calc. with two dimensional elastic-plastic computer program 78−35465
plasma, CO$_2$ laser produced, fast particle emission 78−42805
plasma, dense, nondegenerate, electron transport, thermal cond. *(Russian)* 79−98865
plasma, evap. by long pulse Nd laser, spectroscopy 78−14201
plasma, expanding, high power CO$_2$ laser radiation interaction 78−47138
plasma, hot, dense, line emission obs. 80−79456
plasma, hot dense homogeneous, X-ray production rate and ionisation state density, calc. 78−71458
plasma, hot spot distribution, significance interpretation of laser produced plasma expts. 79−98945
plasma, laser prod., expsn., X-ray meas. 77−80326
plasma, laser produced, momentum and energy transfer pulse duration/polarisation depend., torsion pendulum diagnostics 80−43952
plasma, laser produced, origin of K$_\alpha$ radiation 78−9833
plasma, laser produced, reflectance meas. 80−79568
plasma, laser-heated, Al(XII) and (XIII) reson. line trapping, source distrib. diagnostics 78−42730
plasma, laser-heated, reson. line emission, spatial and spectral intensities 77−39460
plasma, laser-prod., space-resolved extreme UV emission 80−54015
plasma, laser-prod., X-ray spectrum time depend. *(Russian)* 77−55173
plasma, laser-produced, high-Z, X-ray diagnostics 80−75074
plasma, laser-produced, population inversion between Al^{11+} levels, X-ray lines obs. 78−38539
plasma, laser-produced, X-ray line emission spatial resolution, shadow technique 77−35400
plasma, photon reabsorption attenuated radiation emission 80−64776
plasma, simplified spectra obtained by electro-optic gating of radiant emission 78−22561
plasma, transfer eqn. soln. using freq. and angle averaged photon escape probabilities 80−64688
plasma, X-ray photoabsorpt. coeff. 79−27754
plasma anodisation current efficiency *(Japanese)* 79−24655
plasma anodisation forming voltage limitation mechanism *(Japanese)* 80−16579
plasma anodization kinetics 77−77630
plasma etching, undercutting phenomena 80−97635
plasma etching in CCl$_4$, end point determ. by spectroscopy 78−76786
plasma formation, CO$_2$ laser pulse interaction with Al target in air 80−96374
plasma parameters, Al target bombardment in vacuum by microsecond laser pulses 79−64884
plasma sprayed coating, effect of Si substrate surface conditions and impact velocity of sprayed particles 80−21145
plasma sprayed coating adhesion to mild steel, substrate pretreatment effect 79−83391
plasma vapour surrounding plane target, light propag. in plasma vapour, 10.6 μm laser 79−23435
plasmon dispersion, dynamical exchange effects 79−51509
plasmon dispersion, effect of band struct., dielec. function calc. 78−26825
plasmon dispersion in polycryst., pseudopotential method 78−23039
plasmon line width, k-depend., pseudopot. theory 77−85169
plasmon loss intensities in XPS, Auger and electron energy loss spectra 79−38012
plasmon sideband exam. by synchrotron radiation tuning of electron escape depths, UPS 77−47755
plasmon struct. obs. in K photoabsorpt. spectra 79−38693
plasmon-dislocation interactions, electron microscope investig. 77−15421
plasmons, long-wavelength, interband damping, imaginary part of dielec. const. 77−85165
plastic anisotropy of textured sheet *(Japanese)* 79−34103
plastic deform., strain rate history and temp. effects depend. 79−11684
plastic deform. and prominent cross slip of ⟨100⟩ oriented single crystal 78−19851
plastic deform. build-up during low cycle fatigue *(Russian)* 77−25207
plastic deform. effect on third-order elastic moduli, dislocation anharmonism *(Russian)* 80−50786
plastic deform. of poly- and single-crystals, AE study 79−24579
plastic deformation, appl. of current noise technique for dislocation processes 80−35442
plastic deformation, energy storage efficiency 77−4807
plastic deformation, initial stages *(Japanese)* 80−93618
plastic deformation, thermoactivated creep and stress relax. 79−87692
plastic deformation and prominent cross slip in ⟨100⟩ oriented single crysts. *(Japanese)* 77−8889
plastic deformation depend. on mag. field at 4.2K *(Russian)* 79−91754

aluminium continued
plastic deformation meas. in normal and supercond. states, down to 0.4K *(Russian)* 79−11658
plastic deformation thermal activation parameters from creep kinetics and stress relaxation 80−71717
plastic flow in plain strain extrusion, photographic appl. 80−7626
plastic flow under torsion, thermoactivation parameters *(Russian)* 79−38926
plastic props., room temp., to recrystallisation temp., stress/strain relations, computer program 77−1865
plastic strain in tension, effect of strain rate 77−32654
plastic stress-strain rels. under proportional loading 77−32627
plastically deformed, influence of microstruct. on energy stored 78−84894
plastically deformed, spreading of extrinsic grain boundary dislocations 78−43023
plastically deformed, X-ray diffr. and diffuse scatt. techniques to study defect structure 77−68976
plastically deformed by pulsed mag. field, mobility of Fe atoms, radiotracer profiles 79−28584
plastically deforming at high strain rates, distrib. of temp., strain rate and strain 79−19311
plastically prestrained, dynamic props. 79−15743
plasticity, temp. and rate dependence for different rigidities of stressed state *(Russian)* 79−29139
plasticity variations rel. to heat treatment *(Russian)* 79−57050
plate, defect location by natural frequency meas. method 80−30191
plate, explosive hardening of one end 77−36531
plates, exam. of stress conc. around conical cutouts, using strain gauges 79−41639
plates, oblique perforation by projectiles 77−62141
plates with air gap, temp. field for microplasma welding of edge joints *(Russian)* 80−7755
plating, new method 79−70228
polished, target in air, refl. of CO$_2$ laser radiation, plasma layer form. 80−25500
polishing, electrolytic and chemical, SEM exam. of gassing defects 79−34206
polishing for optical appl. 78−5587
polishing in H$_3$PO$_4$ and HClO$_4$+methanol, polarisation curves 78−56851
polycrystalline, abrasion, deform., fatigue, study by exoelectron microscope *(Japanese)* 78−74108
polycrystalline, elastic consts., inelastic coherent neutron scatt. meas. 80−34122
polycrystalline, implanted with Cu(Pb), doping profile after laser pulse irradiation 80−88194
polycrystalline, probabilistic micromech. theory 77−863
polycrystalline, recrystallisation, synchrotron X-ray topography dynamic expts. 78−67621
polycrystalline, secondary ion emission angle, energy distrib. depend. 78−76569
polycrystalline, X-ray attenuation and photoelec. coeffs. in range 0.3 to 1.3 Å 79−99979
polycrystalline aggregate, various grain sizes, specimen thickness effect on mech props. 79−61645
polyethylene contact charging, electron transfer mechanism, PES characts. 80−35055
polygon construction via diamond cutting 78−33919
polygonisation at high press., kinetic regularities, dislocation struct. at 140°C 79−66070
porosity, secondary H, development and pore growth *(Russian)* 80−19946
porosity determ. in ingot, US signal integration technique 77−44430
porous, Hugoniot synthesis at high pressures 79−95080
porous anodic films on Al, ion beam thinned, electron microscope exam. 78−92390
position annihilation radiation, two-dimensional ang. correlation, momentum density meas. 78−10331
positron annihilation, ang. correl. meas., electronic momentum density calcs. 77−4284
positron annihilation, angular distrib., Umklapp effects *(French)* 80−50454
positron annihilation, detection of N impurities 79−65777
positron annihilation, effects of quenching, annealing and neutron irrad. 80−20732
positron annihilation and residual resistivity, effect of microvoid size 77−48272
positron annihilation and vacancy formation, Doppler broadening study 80−60708
positron annihilation ang. correl., trapping by mono- and multi-vacancies 77−32466
positron annihilation characteristics, effect of temp. 78−64427
positron annihilation in small voids, self consistent calc. 77−20952
positron annihilation momentum profiles, core contrib. and independent particle model 77−24908
positron annihilation momentum spectra, low temp depend. 79−19948
positron annihilation radiation, ang. correl. shape, deform. effects 77−85831
positron annihilation rel. to thermocyclic treatment 79−52040
positron annihilation studies using high-density proportional chambers 80−25478
positron annihilation with high-momentum core electrons, vacancies study 80−25481
positron penetration depth and energy loss 80−92578
positron trapping, defect specific temp. depend. 78−47336
positron trapping at voids, temp. depend. 79−61464
positron-vacancy interactions, equilib. temp. depend. of positron annihilation 78−76547
positronium formation at surface, positron beam irrad. 79−13845
positrons around vacancies 77−40297
powder, disintegration of powder particle agglomerates under the action of an alternating electric field 78−68642
powder, gas suspension, critical spark ignition conditions 79−100373
powder, liq.-solid phase transforms. *(French)* 80−45294
powder, liquid phase sintering, solid-state solubility effect on vol. change 78−35332
powder, nonuniformity of stress and strain distrib. over width of rolled powder strip 77−12577
powder, protective coatings of Ni, Cu, Fe and their alloys *(Russian)* 78−60881

aluminium continued
powder, X-ray at. scatt. factors at 80K 78—2065
powder fusion under weightlessness conditions *(Russian)* 78—31357
powder reaction with N, in low-temp. plasma 80—16257
powder reduction of $CaO.V_2O_5$ 78—44049
powder thin foil, prep. for TEM study 80—42310
powder-based composite, hydrostatic pressing 77—63593
powder-epoxy mixtures, cryo-tip refrigerator appl., heat transport 78—37013
powders, electric-pressure sintering onto cylindrical parts in fluidised bed 80—100960
powders, grain size determ. by sedimentation, automatic recording system 78—60897
prep. by evap. and ion plating, AES determ. of comp. profiles 77—89675
pressure effect on diffusion, theoretical study 78—47566
pressure shear impact in transverse displacement interferometer, plastic flow in 6061-T6 Al 80—81137
pressure-mode soft-metal vacuum seal, for glass and ceramics 80—17952
pressure-shear waves due to oblique plate impact 77—65713
prestrained, isotropic hardening rule, rel. to stress/strain curve 78—23772
primary electron backscatter yield using material model parameters 80—39184
prismatic dislocation loops, (g.b)s product sign determ. *(Russian)* 78—38705
prismatic displacement rings, plane normals determ. *(German)* 77—86118
production, kaolinic clay chlorination 78—6878
projected range distrib. of 5-25 keV $^4He^+$ 80—65094
protection potential 79—52427
proton beam dosimetry, miniature Si dosimeter 80—47733
proton energy stagggling in ion backscatt. expt. 79—37750
proton irradiated, muon spin rotation study at low temps. 78—92011
proton irradiation, Al atomic displacement position study 80—103401
pseudo-brittle fracture, aspect of impact testing 79—79111
PTFE-Al, adhesion joints, effect of Cu and CuO 78—53183
pure, hydroextrudates, incomplete axial orientation *(Russian)* 80—20949
pure, neutron irradiated, suppression of radiation damage microstruct. by trace impurities 79—77643
quantum oscillations of thermal EMF under mag. breakdown conditions *(Russian)* 77—69305
α-quartz:Al, Ag, EPR of Al-Ag centres 78—88186
α-quartz:Al, thermal cond. below 10K 79—51320
quasi-particle properties, anisotropic, electron-phonon interaction study 77—43480
quenched, diffusion solution for point defects in stress field, steady state and transient 78—30780
quenched, irradiated, and quenched plus irradiated, grain boundary hardening 80—3162
quenched, positron annihilation obs. of vacancy clustering 78—27348
quenched, vacancy agglomeration, elec. resist., splat-cooling effects 77—51365
quenched, vacancy annihilation at surface and dislocation loops 79—60351
quenched, vacancy annihilation to non-uniformly distributed dislocations 78—6096
quenched, vacancy-Fe interactions 78—47412
quenched-in lattice defects, Mossbauer anal. of associated ^{57}Co 78—39820
radiation damage due to protons, μSR 79—56702
radiation damage with radioactive probes, TDPAC meas. 77—24336
radiographic testing of parts *(German)* 77—1900
rapid melting and solidification of surface layer, exam. using computer heat flow model 78—83228
reaction kinetics of liquid with B_4C 80—84344
reaction with H_2, influence of surface reactions on rate *(Russian)* 80—66863
reactive electro-erosion under pulse electric discharge 79—52686
reactive etching in RF plasma containing halogen species 78—72923
reactive ion etching, preferential lateral chemical etching 79—83371
reactive ion etching by discharge impedance monitoring, end-point determ. 79—83372
reactor irradiated, neutron inelastic scattering meas. of phonon dispersion curves 78—75758
recovery annealing, exam. using in situ high voltage electron microscopy 80—7596
recovery during stress relaxation testing at 298K 77—8872
recovery features, TEM and positron lifetime meas. examination 78—80611
recovery from coal combustion wastes, using combustion sinter-dilute acid leach methods 79—48063
recrystallisation and recovery during temperature strain *(Czech)* 77—70071
recrystallisation and recovery during temperature strain *(Czech)* 77—73287
recrystallisation dislocations formation, during recrystn. in single crysts., study by X-ray synchrotron topography 79—38849
recrystallisation kinetics after small deform. and grain growth *(Czechoslovakian)* 77—32592
recrystallisation nuclei form. and well defined deform. band struct. 79—20136
recrystallised, substructure strengthened, long-term strength 77—21173
recycling, effect on comp. 80—66455
reduction cell, C cathode intercalation props. 79—43559
reflection coefficients, changes at high temps. 78—19440
reflective coating, reflectance in UV and visible 80—28307
reflectivity at high temps., pulsed laser heating 77—63388
relativistic electron beam impact, vac. UV emission 77—47263
relief of residual quenching stresses *(Korean)* 79—70091
remanent supercond., effect on temp. depend. of normal phase resist. 79—56362
remanent superconductivity, temp. depend. elec. resistivity meas. 79—99529
resistance welding, apparatus using C rod electrodes 77—79077
resistive layer microstructure on superconducting Al surface *(Russian)* 80—34567
resistivity, press. depend., calc. 80—20151
resistivity and thermoelec. ratio, electron-electron scatt. contrib. 80—70670
resistivity decrement under torsional deform., impurity segregation at moving dislocations 77—4321

aluminium continued
resistivity temp. depend., evidence for electron-electron scatt. 79—69488
resistivity well above T_c, supercond. effect up to $2T_c$ 80—6810
reverse finish cutting, exam. *(Japanese)* 78—85034
review *(Spanish)* 80—84544
rhodamine 6G laser radiation interaction with Al 80—97387
ring, ultrahigh accel., pulsed mag. field 78—5386
rings, deformation modes under static axial compression 80—25768
rolled, analytical vectorial method for crystallographic texture *(French)* 80—20956
rolled sheet, transverse US wave attenuation, thickness meas. 79—52573
rolled single crystal, annealing texture 79—91678
rolled strip from granules, coeff. of deform. 77—90422
rolling discs, coeff. of friction 79—14360
ruby:Al, ^{27}Al NMR line width, charact. features of behaviour 79—69734
sacrificial anode dissolution, Hg effect study using ion implantation 79—39016
sapphire-Al interface barrier, transport and trapping obs. 77—76921
SAW attenuation coeffs. and wave speeds 79—46903
scanning Auger electron microscopy, Monte Carlo calc. 78—19610
SCF $X\alpha$ scattered wave calc. for clusters up to 43 atoms 78—10323
screening of light impurities 77—85177
screw dislocation core, atomic struct. calc., modified lattice-statics approach 78—75669
seawater, Al conc. from clay minerals dissolution 77—66928
seawater Al content controlled by inorganic processes 80—61815
seawater concentration and distrib., control by biological activity 78—61437
secondary electron emission, Monte Carlo calc. 79—69933
secondary electron emission, on proton and deuteron irrad., 0.5-2.5 MeV 77—63512
secondary electron emission, role of plasmon decay 77—81186
secondary electron emission 2-12 MeV electron impact, Monte Carlo calc. 79—28868
secondary electron emission anisotropy for (001) and (110) faces, Monte Carlo calc. 79—99996
secondary electron emission by reflection, Boltzmann eqn. resolution method 80—45178
secondary electron emission from (001) and (110) surfaces, ang. depend., model 77—73197
secondary electron spectrum, EELS and AES, comparison, for clean and oxidised surfaces 80—55237
secondary ion emission, energy spectra, 0-55 eV, contamination levels 79—15573
secondary recrystallization *(Czech)* 79—70080
secondary-electron energy distribution in high-energy photoemission 77—48305
selective coating electrodeposition on Al substrates for solar collectors 79—62079
self-consistent spin density functional calcs. for 3d impurities 80—70635
self-interstitial interaction with solutes, resistivity meas. 78—47331
SEM, contrast of electron channelling patterns, estimation from low index refl. 78—9921
SEM, electron channelling patterns 78—83697
SEM exam., ultra-high vacuum secondary electron emission dependence on electron beam density dose, surface interactions from AES and ELS 80—61209
shear constants, press. effect up to 2500 atm., —196 to 25°C 77—31710
shear modulus and internal friction under press., EM reson. technique 77—31709
shear-band temp. meas. of type 2014-T6 80—48655
shearing, scissors type process, ductile sheet Al 78—19816
sheet, in-plane stretching, limit strain meas. 78—80573
sheet, recrystallization, DSC eval. 80—3105
sheet, stainless steel wire reinforced, prod. by explosive compaction, and mech. props. 77—32542
sheet, strain-induced changes in mech. props. and press formabilities 78—19781
sheet D16AT, plastic strain distrib. at crack tip by coordinate-grid method 80—16400
sheet metal, texture heterogeneity, numerical simulation *(French)* 78—92274
sheets, dislocations obs. at high temp., annealing effect *(Japanese)* 80—34003
shell, explosive expansion, rupture behaviour 80—85063
shield, thick-walled, conducting, for biomag. expts. 80—104845
shielded room for biomag. meas. 80—104846
shock adiabatics at ultrahigh press. *(Russian)* 77—27941
shock compressed, thermal energy relaxation 77—69043
shock compression at high press., neutron irrad. *(Russian)* 80—88264
shock compression at high press. *(Russian)* 80—92608
shock pulse attenuation in rods 78—55503
shock transition rise-time meas., limiting viscosity coeffs. 79—77680
shock wave data, 'solid Hugoniot' rel. to 'fluid Hugoniot' 80—65155
shock-waves, ultrahigh-press., laser-driven 79—55823
short range order amongst cond. electrons 80—107040
n^+-Si-Al ohmic contacts, metallisation structs. for very shallow n^+/p junctions 80—60084
single cryst., latent hardening in tension 80—60878
single cryst., primary knocked-out atom, energy of spatial distrib., modelling of 0.2 MeV proton trajectories 79—14864
single crystal, deformation behaviour during cold rolling 79—47751
single crystal, nonstop uniaxial tensile tests, electro-optical image intensifier 79—34277
single crystals, effect of environment on liquid-metal embrittlement, stress corrosion cracking and corrosion fatigue 78—64676
single crystals, relation between axial orientation rotating and deform. banding 80—104206
single vacancy formation energy, determ. using energy bands and wave functions, from LCAO calc. 78—47348
single vacancy formation energy calc., SCF-LCGO modified solid state scatt. theory 80—54637
sintered powder, heat resistance increase method 77—90292
sintered powder, interdiffusion with Cu, struct. effect at high press. 78—60606
sintered powder coatings, form. and behaviour under particle bombard. 80—35029
sintering, activated, under thermal cycling 77—21053
sintering, low temp., form. of interparticle metallic contacts 80—20844
sintering in vacuum and O_2, room temp. 80—7512
sintering mechanism and sintered body anodization 79—95964

aluminium continued

- slab, fast electrons slowing down, Monte Carlo transport simulation *(French)* 78—26610
- sliding behaviour, against polymers laminates and coated surfaces at cryogenic temps. 80—66671
- sliding wear in NaCl of varying pH 78—3240
- slip, work of C. Crussard 80—62443
- slip systems in high purity single crystals 78—47387
- small particle, NMR study, Knight shift, spin-lattice relax. time, supercond. effects 80—39710
- small spheres, bulk plasmons damping 80—75561
- smelting, bench scale prebaked anode fracture, coke and formulation variables effect 79—52371
- smelting cell, effect of anthracite calcination and formulation variables 78—39719
- soft, type 1100-0, erosion tests in cavitating venturi 80—35347
- soft X-ray absorption and EXAFS on K edge 79—99981
- soft X-ray emission and absorpt. edges, self-absorpt. studies 80—40183
- soft X-ray emission edge, temp. depend. 80—89090
- Soft X-ray emission edge self absorption and effect of exciting voltage 77—90220
- soft X-ray spectrum, Al core state transition probabilities, band struct. calc. 77—77325
- soil Al leaching response to acid precip., effects on high-elevation watersheds in NE. United States 80—12442
- solar energy concentrators, metallised polymer films and Al coatings, spectral characteristics 79—96422
- solar selective absorbers, Si on Al, interf. films deposited on diffr. gratings 79—14103
- solid cylinder, annealed, dynamic forming by compression *(Japanese)* 77—70267
- solid electrolytic capacitors, pit etching method for improving freq. and temp. characts. 80—100944
- solidification, apparent solid region *(Japanese)* 77—63653
- solidification, high press. effects 80—66499
- solidification, stability of spherical particle growing from stirred melt 77—47365
- solidification of castings, electrical modelling study *(Rumanian)* 79—74142
- solubility in $BaTiO_3$, estimation by conductivity meas. 79—69250
- solubility in surface water on granite *(French)* 77—41029
- Sondheimer oscillation 79—87085
- Sondheimer size effect, phonon-limited mean path, 1.8-12K 80—49698
- spark gaps with Al parallel plane electrodes, erosion characts. 80—70076
- spark-source mass spectrometry, relative sensitivity coeffs. 79—92045
- specific entropy, and surface heat determ. as function of temp. *(German)* 80—6619
- specific heat, 0-100 kbar, press. depend. 77—51512
- spectrophotometric determination, in aq. organic medium using eriochrome cyanine R 77—36829
- specular reflectance standards for visible and infrared region using thin Al film vacuum deposited on optical flats *(Japanese)* 80—102789
- spin wave excitations, CESR expts., 79 GHz 77—40128
- splat cooled, vacancy transformations, resist. meas. 77—59770
- spraying Si semiconductor plates, for control of quality of surface treatment 80—60989
- spreading kinetics on Ni 80—24717
- spreading of high-press. polyethylene melt, index 79—37902
- sputter deposit PIXE expt. 80—61196
- sputtered and electron gun evaporated films, grain size and orientation obs. 78—10308
- sputtered coating development, porosity, durability temp. depend., electric arc metallisation regime *(Russian)* 80—39402
- sputtered excited Al particles, effect of O during ion bombardment on spectra 79—38703
- sputtered film, compressive stress transition 78—10310
- sputtered film, thermal ageing, thickness dependent effects 78—6462
- sputtering, planar magnetron, H_2 effect on Ar discharge 80—80970
- sputtering, reactive, in O_2-Ar atm., Al_2O_3 optical waveguide fabrication 80—33262
- sputtering, under D^+ and He^{4+} bombardment, microstruct. effects study 80—84821
- sputtering and chem. attack by H ions of 100 eV energy 78—95635
- sputtering by 10 keV inert gas ions, angular distrib. 79—52061
- sputtering by 15 keV Ar^+ ions, microroughness 79—91556
- sputtering by He^+, photon emission, dose depend. 77—8695
- sputtering in inert atm., with uncooled cathode, oxidation of metallic coatings, X-ray diffr. obs. 78—3041
- sputtering process study on Au, Al, Si targets, Rutherford backscatt. technique 77—8703
- sputtering rate on Ar ion bombard. 80—55245
- SQUID, granular supercond. characterisation 79—28489
- stabilised superconducting solenoid, design and construction, for CERN intersecting storage rings 77—46428
- stabiliser for fusion reactor supercond. mag., neutron irrad. effects on magnetoresistance 80—34062
- stability and strength of FCC metal using Morse pot. 80—59430
- stacking fault energy and delamination wear, single phase FCC 78—3239
- steel, Al content determ. by fast neutron radiation *(Hungarian)* 78—92586
- steel, fibre reinforced Al, fracture mechanics under fatigue *(Czech)* 78—64629
- steel, reinforced, fatigue strength, surface layer effects 77—12697
- steel, stainless, clad Al, sandwich sheet material, forming limits 80—3131
- steel, stainless, fibre reinforced Al, CC strengthened by lattice transformations, mech. props. study *(Japanese)* 79—43332
- steel, stainless brittle zone Al 3 component composites deform. and fracture 77—56104
- steel, stainless/Al laminate, sandwich sheet material, plane strain compression and rolling 79—57062
- steel, stainless/Al laminate, sandwich sheet materials, deform. in uniaxial tension 79—57061
- steel fibre reinforced, role of brittle layers at elevated temps. 79—96135
- steel fibre reinforced, vacuum hot pressing, strength *(Czechoslovakian)* 77—32543
- steel fibre reinforced Al_2O_3-Al, production and mech. props. 80—11619
- steel fibre reinforced Al, fatigue strength *(Czech)* 78—60748
- steel fibre reinforced Al, fibre orientation effect on strength *(Korean)* 80—30027
- steel fibre reinforced Al, thermophys. props. 80—59745

aluminium continued

- steel-Al bimetallic wire for overhead lines, manufacturing methods 80—16247
- steel-Al-steel plate, fatigue damage analysis and life predictor 77—25120
- steel-aluminium plates, exam. of adhesion strength by impulse loading 78—84943
- stiffness and damping in creep 78—23780
- stopping power and energy straggling meas., Li ion backscatt. anal. 79—3328
- stopping power for 0.3-1.5 MeV protons 79—55801
- stopping power for 28 MeV α-particles, re-evaluation 78—79651
- stopping power for 6.75 MeV protons 80—34107
- stopping power for MeV H^+, D^+, $^4He^{2+}$, $^7Li^{3+}$ ions, deviations from Bethe formula 78—26612
- stopping power meas. for 4-5 MeV/N ^{16}O, ^{40}Ar, ^{65}Cu, and ^{84}Kr 78—70720
- stopping power of valence electrons, Monte Carlo calcs. 79—10886
- stopping powers, low energy, determ. by TOF techniques 79—45594
- stopping powers for 28.8 MeV α-particles 77—80556
- stopping powers for 8.78 MeV α-particles 77—80557
- stopping ratios of 50-300 keV H^+, He^+, $^7Li^+$, and $^8Be^+$ 80—42903
- storage ring vacuum chambers, glow discharge processing versus bakeout 78—70658
- strain rate sensitivity and ductility, trace element conc. effect 80—66597
- strained, anisotropic electron scatt. in elec. resist. 78—91656
- strained, localised corrosion on slip steps 79—20265
- strength changes on US treatment during programmed loading *(Russian)* 77—32583
- strength differential effect, temp. and strain rate sensitivity in saturation cycling 79—66094
- stress corrosion susceptibility, water vapour reaction, STEM study 80—3247
- stress induced ordering of self-interstitial clusters 78—47358
- stress relaxation test, appl. to discerning frictional and internal stresses 77—63712
- stress wave propag., transmitted wave profile 77—80578
- stress-strain curve from continuous indentation test 77—90396
- stress-strain curves, cyclic loading initial stage, commercial purity *(Japanese)* 80—93617
- stress/strain constitutive equation, constitutive eqn. covering wide range of strain rates *(Japanese)* 80—79862
- strips, supercond., order-parameter relaxation meas. 79—47207
- structure changes in single cryst. under influence of static and dynamic stresses *(Russian)* 78—92300
- structure sensitive props., temp. hysteresis after melting and crystallisation *(Russian)* 79—29036
- structure stability 77—8015
- subgrain coalescence, grain boundary recrystallisation nucleation 80—3094
- subgrain growth during annealing after cold work 78—56656
- substrate, adhesion and hydrophilicity of glow-discharge-polymerised propylene coating 79—15829
- substrate, Au film, optical reflectance and absorpt. obs. 80—7426
- substrate, porous anodic film form. in H_3PO_4 79—70229
- substrate for Ag films deposited from hot hollow-cathode source, adhesion 77—8754
- substrate for polystyrene film, electrode effect on carrier injection, TSC, I-V characts. 80—34463
- substrate for Zn film deposition, TEM and electron diffr. obs. 80—75460
- substruct. developed during recrystallisation, exam. *(Japanese)* 78—64566
- substructural developments, during recovery, Sandstrom's model validity 79—74187
- subsurface flaw detection by photoacoustic microscopy 80—66725
- supercond. film, resistance, effective medium approach 78—60249
- superconducting, an anomalous strain-rate sensitivity of flow stress 79—43313
- superconducting, crystalline and granular, tunnelling meas. 78—84355
- superconducting, energy gap enhancment by tunnelling extraction 80—34564
- superconducting, order parameter, spatial var. near Anderson impurity 79—60962
- superconducting, phonon absorption and pair breaking at 35 GHz 77—32120
- superconducting, phonon mechanism for sound-affected energy gap *(Russian)* 77—43781
- superconducting, quasiparticle charge distrib. due to tunnel injection 80—44771
- superconducting, tunnelling characts., phonon struct. enhancement by high energy spectral weight 79—60984
- superconducting Al heat switch and plated press-contacts 78—54377
- superconducting and normal state, anisotropic impurity scatt. and EM surface resist. 78—30970
- superconducting bolometer, free floating sensitive heat pulse detection 77—79149
- superconducting bridges, nonequilibrium phenomena under microwave radiation 79—56420
- superconducting cylinder, order parameter enhancement by microwave irrad. 80—70896
- superconducting film, 2 GHz SAW attenuation meas. of mean free path 77—39999
- superconducting film, anomalous resistive state due to light pulse 78—52157
- superconducting film, cylindrical, granular, crit. currents and electron mean free paths 80—7057
- superconducting film, deviations of equilib. order parameter from mean field theory 77—69453
- superconducting film, dielectric coating effect on superconductivity and normal resistance 80—7026
- superconducting film, granular, crit. field anisotropy and fluctuation cond. 78—26994
- superconducting film, granular, edge pinning in perpendicular mag. fields 79—4633
- superconducting film, granular, O content and oxide barrier thickness, transition temp. meas. 79—15250
- superconducting film, implanted at low temp. by H or D, critical temp. enhancement *(French)* 77—8237
- superconducting film, intrinsic and expt. quasiparticle recomb. times 77—15999
- superconducting film, metastable current states, mean free path variation *(Russian)* 80—2538

aluminium continued
superconducting film, microwave enhanced critical current, charact. time const. meas. 79—24102
superconducting film, new supercond. state obs. at high quasiparticle injection 77—72949
superconducting film, order-parameter variation meas. 80—103797
superconducting film, perforated, crit. currents associated with interaction of commensurate flux-line sublattices 78—34937
superconducting film, perforated with triangular lattice of 1 μm holes, critical currents 77—28332
superconducting film, permanent resistive states created by light pulses 79—56450
superconducting film, precursor diamagnetism, magnetisation meas. 77—32115
superconducting film, quasiparticle branch mixing rates 79—78269
superconducting film, quasiparticle injection, tunnel junction characts. 78—76193
superconducting film, resistive states, voltage switching effect in tunnelling systems *(Russian)* 79—7938
superconducting film, self-heating effects in long thin film over wide temp. range 79—51717
superconducting film, supercooling mag. field and thermal fluctuations 78—34925
superconducting film, transition to zero vorticity, long-range topological order 80—93039
superconducting film in presence of Formvar, excess elec. cond. above T_c 78—60250
superconducting film with magnetically weakened section, Josephson effect 77—28302
superconducting films, thick, phonon damping of virtual levels 79—4626
superconducting films, tunnelling with spin polarised electrons 79—4627
superconducting granular film, vortex chain size effect and negative resist. 77—80888
superconducting granular films as weak link in Josephson devices 80—88685
superconducting microbridges, non-equilibrium phenomena 79—56410
superconducting order parameter, relax. time, temp. depend. 77—77011
superconducting particles, nucl. relax. and supercond. fluctuations 78—60251
superconducting particles, Zeeman crit. field, NMR spin echo meas. 79—56453
superconducting point contact, microwave-enhanced critical currents 77—8242
superconducting small particles, Josephson-coupled, local fluctuation effects 78—72308
superconducting state parameters, dielectric screening functions effect 77—4471
superconducting strips, on Si substrates, microwave-enhanced crit. currents, phonon effects 79—56451
superconducting strips, with local injection of electrons, microwave-enhanced crit. currents 77—63044
superconducting surface, layer struct. and dynamics on switching off mag. field 79—60998
superconducting thin film, crit. temp. enhancement *(Russian)* 80—93021
superconducting thin film, evidence for Kosterlitz-Thouless transition 80—39721
superconducting transition, effect on jump-like deform. *(Russian)* 80—34538
superconducting transition edge bolometer 77—71371
superconducting transition temp., electron-phonon mass enhancement, pseudopot. calcs. 78—2604
superconducting transition temp., perturbative corrections, direct and indirect ladder diagrams 80—49979
superconducting tunnel junction, quasiparticle recomb. times and electronic density of states at Fermi level 79—56414
superconductive fixed points for temperatures above 0.5K 79—63221
superconductivity, microwave-enhanced, strip meas. 80—2509
superconductivity, stimulation and enhancement by external micropower irradiation *(Russian)* 78—95394
superconductor, appl. of non-local extension to Gaspari-Gyorffy theory 78—80093
superconductor, microwave enhanced energy gap, tunnelling meas. 77—51853
superconductor, order-parameter relax. time calc. 79—4618
superconductor, quasiparticles, nonequilib. distrib. function 78—91810
superplastic deformation depend. on subgrain struct. electron microscope study *(Russian)* 79—83257
superplasticity, single and polycrystals in torsion *(Russian)* 78—3180
superplasticity in single crystals 79—1901
superpure, anodic oxide film growth kinetics, UV radiation effect 79—34190
superpure, creep, rate-controlling processes 80—85009
surface, 10-30 keV H ion bombardment, energy refl. meas. 78—27359
surface, ^{4}He backscatt., Rutherford scatt. cross section correction test 80—66369
surface, α-cyanoacrylate in first monolayer, IR spectra, H-bond form., stretching vibr. 80—87119
surface, (001), enhanced photoexcitation 80—80937
surface, (001), scatt. matrix method for surface states 79—60894
surface, (001) and (110), LEED intensities 77—47656
surface, (100), 9-23 eV photoionis., spatially-varying photon field effects 80—2921
surface, (100), angular resolved photoemission from intrinsic surface states 78—39665
surface, (100), chemisorbed O, photoemission ang. depend., MO cluster model calc. 78—76576
surface, (100), inelastic LEED at beam emergence condition 78—83690
surface, (100), overlayer covered systems, angle-resolved UPS, substrate effects 78—84694
surface, (110), prep. and props. of Pb and Sn monolayers 79—15018
surface, (110) and (100), MEED intensity calc. using chain method 77—20169
surface, (111), adsorbed O, surface struct., LEED and SEXAFS data 80—92782
surface, (111), adsorption of O_2, possible ordered struct. 80—44412
surface, (111), electron density profiles, pots. and charge overlap forces 77—32061
surface, (111), interlayer spacing, LEED data anal. 80—54484
surface, (111), ordered O overlayer associated with chemisorption state 78—47665

aluminium continued
surface, ang. depend. of plasmon loss features in XPS 78—43987
surface, Ar^+ and e^- excited Ar Auger electron emission 79—47560
surface, chem. anal., low energy ISS compared with SIMS 78—64908
surface, chemisorption of O, O-Al and O-O bond lengths, surface extended X-ray absorpt. fine struct. 80—29267
surface, Cl_2, CO_2, NH_3 and alkanes thermal accommodation coeffs., translational (internal) gas-solid energy exchange 78—92506
surface, CO_2 laser beam-irrad., shielding time 79—55530
surface, CO_2 laser energy coupling into ionised blowoff material 78—72641
surface, effect of melting polyethylene, XPS meas. on polymer surface 78—15556
surface, electronic surface resonances of crystals, Al(001) 79—95464
surface, $H^+(H_2{}^+)$ ion impact, energy refl. coeffs. 78—54969
surface, He atom scattering pot., surface electron density depend. 80—104027
surface, incident H^+ beam, plasma form., plasma radiative and gasdynamic processes 80—53946
surface, ion impact, mol. effects in electron emission 78—80446
surface, laser supported detonation waves, initiation 78—63568
surface, light diffr., photon excitation of compound plasmon resonances 79—28307
surface, luminesc. accompanied by ion implantation 80—60683
surface, mol. chemisorption, self-consistent calc. 79—95260
surface, multiply charged ion interactions, laser plasma 80—70007
surface, nearly-free-electron metal, origin of surface reson. states 78—95322
surface, negative affinity, narrow beam emission of slow positrons 80—89091
surface, O_2 layer thickness, reson. α-scatt. from ^{16}O 78—64778
surface, obs. of positron Bragg refl. 80—103221
surface, oxidation, synchrotron radiation photoelectron obs. 78—52634
surface, plasma cleaning and etching, removal of C 80—97645
surface, plasmons, mean free path of electrons, charact. energy loss spectra determ. 77—51800
surface, porous anodic films, cell walls anal. by STEM and energy dispersive X-ray anal. 79—19476
surface, positronium emission 80—80897
surface, prepared for adhesive bonding, oxide morphologies 79—70203
surface, proton bombarded at 450 keV, X-ray bremsstrahlung, 2.5-8.5 keV 78—80436
surface, proton or α-particle bombarded, secondary electron emission 77—36346
surface, pulsed CO_2 laser interaction at oblique incidence 80—48916
surface, pulsed ruby laser irrad., noncryst. phase form 80—35012
surface, pure, oxidised element determ. by SIMS 78—85247
surface, rough, liq. spreading 80—39389
surface, rough, reflection loss for s and p polarised waves near surface plasmon freq. *(French)* 80—97225
surface, single cryst. unoccupied surface resonances, surface soft-X-ray absorption spectroscopy 79—28862
surface, slow-positron emission 78—95079
surface, supercond., layer struct. arising after mag. field $H>Hc$ is switched off 79—61000
surface, thermal activation meas. of positron binding energies 79—95371
surface, thermal and impulse coupling by pulsed KrF laser 80—45171
surface, thermal desorption of oxide film, influence of grain boundaries and recrystn. 80—61023
surface, US cleaning process 78—11417
surface (001), 100-2000 eV electron backscatt., surface and bulk plasmon losses 77—32480
surface (100), photoemission, ang. terms in optical pot. 80—55269
surface (100), with adsorbed O, $X\alpha$-scatt. wave cluster approach 80—49851
surface (110), relax., LEED results and anal. by convolution-transform method 77—89624
surface (111), adsorption and condensation of O_2 at 30K, UPS obs. 79—60635
surface (111), angle-resolved UPS obs. of 2-dimens. band structs. of S, Se and Te 80—60059
surface (111), bonding of O, electronic struct. calcs., rel. to UPS data 80—59801
surface (111), chemisorpt., of O_2, SCF X_α scatt. wave MO calc. 79—42374
surface (111), LEED Kikuchi pattern, contrast change due to plasmon excitation 78—34686
surface (111), O-induced band dispersion and symmetry, photoelectron spectrosc. obs. 79—61490
surface (111), oxide layer amorphous to cryst. surface transition, slow positron obs. 80—75417
surface Ar^+ ion bombard., photon and secondary ion emission, single cryst. struct. effect 77—59660
surface bombardment by fast H^+ 80—66376
surface broadening of 2p core level photoemission spectra 80—25524
surface chemical characterisation, by SIMS glow discharge spectrometry and other techniques 80—66907
surface contamination by exposure to DC-704 silicone liq., IR refl. spectra anal. 77—59630
surface cracks, small, size estimation using SAW 78—76793
surface crater form., by laser pulse, frontal method, approx. soln. 77—77327
surface cratering by microparticle impact, viscous effects 79—66255
surface damage, meas. and detect. after static contact loading 80—64495
surface deformation, He implanted, integrated lateral stress 77—31697
surface deformation and wear track obs. using analytical electron microscope 80—108687
surface diffusion on Si (111) 79—28184
surface effects on X-ray level widths 79—47147
surface electron density crimping, Ashcroft potential, density functional calcs. *(Russian)* 79—82653
surface energy, self-consistent calc. including ion pot. perturbation effect 77—8166
surface energy and adhesion props. 80—10774
surface erosion due to US activation *(German)* 79—57122
surface exfoliation and blistering induced by He ion bombard. in energy range 10-80 keV 80—39173
surface fatigue damage meas. by photostimulated exoelectron emission 78—19876
surface film electronoptical exam., appl. of ultramicrotomy to specimen prep. 79—47847

aluminium continued
surface films, Cr^{6+}/Cr^{3+} colloidal SiO$_2$, TEM/XPS studies 80−85090
surface hydrous, oxide film formation 78−15602
surface ionisation, elemental anal. of sputtering products *(French)* 80−50905
surface laser impact, 30-350 MW cm^{-2}, surface press. meas., atm. depend. *(Russian)* 77−77328
surface layer structure in magnetic field *(Russian)* 78−56268
surface oxidation reaction, surface chemiluminesc. study 80−55708
surface oxide layer, Fourier-transform IR emission studies of overlayers on metal surfaces 79−67399
surface photoelec. effect, surface photoemission spectroscopy on jellium 79−4900
surface photoelectric effect, optical excitation using synchrotron radiation 79−4892
surface plasmon dispersion, high-energy electron loss spectroscopy obs. 77−20390
surface plasmon dispersion curves, splitting by Ag surface layers 78−60178
surface props., Rayleigh-Ritz variational calcs. 79−69570
surface relaxation using surface EXAFS 79−23816
surface resonances and oxidation 78−72225
surface roughness effects on the energy dispersion of backscattered protons 79−24403
surface roughness meas. using Rutherford backscattering of protons 79−51400
surface sliding damage, no lubrication, materials depend. *(Japanese)* 78−56780
surface strengthening in single crysts. on coating with evaporated films 77−8972
surface subjected to friction, wear, exoelectron emission, rel. to O$_2$, H$_2$O, gaseous adsorpt. 79−1816
surface wave scatt. from elliptical cracks for failure prediction 80−55608
surface-barrier diode, ageing of Al contact to p-type Si 77−32077
surfaces, Au-coated and diamond-turned, EUV reflection efficiencies 79−14073
surfaces, interaction with O$_2$, work function changes and ellipsometric parameters 79−47831
surfaces, machined, X-ray diffr. residual stress meas. methods, comparison 77−56212
surfaces, Van der Waals forces computation 79−15204
surfaces (001) and (110), angular resolved Auger emission, expt. results and predictions from simple model 78−39635
surfaces (111) and (100), initial interaction with O$_2$, LEED and AES meas. 79−83383
suspension in Ar stream, Nd laser radiation interaction, spark form., breakdown intensity *(Russian)* 77−35435
Swift effect, dynamic and static response to simple compression, tension and torsion 77−28858
Swift effect, in twisted tubes 77−28859
Swift effect, rel. to stress/strain behaviour in simple compression, tension and torsion 77−28860
symmetrical high angle boundaries computer simulation 77−51389
target, nanosecond laser pulse-target interactions, prepulse effects 77−89280
target, spatial distrib. of heating by laser-ignited air plasmas 79−23433
target interaction with pulsed CO$_2$ laser beam, pulse shape importance 80−108307
TEM, excess vol. of grain boundaries 80−15111
TEM of He-bubbles 77−4132
tensile curve and specific value of anisotropy coefficient *(French)* 77−28867
tensile deformed single crystal, form. of recrystallisation textures 77−12647
tensile flow stress at room temp., grain size and strain effect 77−77528
tension-torsion impact testing, instantaneous plastic property 79−52474
tensioned sheet with edge slot, buckling load 77−54909
texture correlability, with formability parameters, influence of solid soln. elements 79−91696
texture evolution, effect of rolling or tensile deform., rel. to strain ratio 79−91672
texture influence on stress/strain curves, prestrain, solid soln. and particle hardening effect on inhomogeneous deform. *(German)* 80−30014
texture variation during rolling 77−70066
thermal conductivity, min. 78−76050
thermal conductivity, press. depend. up to 2.5 GPa 77−85195
thermal conductivity maximum, temp. range 4.2 to 70K, plastic deform. influence 78−76049
thermal conductivity minimum, effect of lattice component 80−15500
thermal cyclic annealing of single crystal, subboundary obs. 77−55992
thermal diffusivity meas. by flash with negative pulse, plasma jet heating 79−37888
thermal emissivities and diffusivities, expt. transient technique and theory for foils 78−43353
thermal expansion meas., 5 to 320K, using dilatometer of parallel-plate capacitor type 77−51523
thermal expansivity, simple eqn. of state appl. 77−27970
thermal generation of vacancies involving dislocation climb 77−59808
thermal neutron cross sections, in single crysts. 80−19672
thermal sprayed coating on steel substrate, cavitation and corrosion resist. in sea water 80−35427
thermal strain meas. in Al plate, one-beam laser speckle interferometry method 80−103005
thermoelectric power and Nernst-Ettingshausen effect 78−56134
thermoelectric props., giant quantum oscills. 79−65453
thermomechanical treatment 77−44277
thermopower, Hall effect and magnetoresist. in samples containing point defects 79−65458
thermopower, low-temp., of Frenkel defects 78−19024
thermopower and thermal conductivity, simultaneous meas., method and apparatus 77−72854
thick film, supercond., tunnelling characts., geometrical reson., in Al-Pb struct. 79−38260
thick probes, subthermal neutron transmission curves for grain size and texture eval. *(German)* 80−71667
thin conducting film, electromigration under superimposed DC and noise powers 80−107879
thin crystal foil, large angle electron scattering by dependent Bloch wave model 79−99257
thin film, elec. resist., effect of annealing In electrodes 80−80416

aluminium continued
thin film, K X-ray production due to ^{16}O ions, 0.25-2.25 MeV/amu 79−69906
thin film, micrometeroid penetration expts. performed in laboratory 80−77292
thin film, thermal cond. meas., size effect 80−65715
thin film deposited on Si, work function *(French)* 80−80353
thin film deposition using solar furnace 80−89148
thin film resistor, rare earth alloying effects *(Russian)* 79−78211
thin film stripes, electromigration lifetimes width depend. 80−92799
thin films, discontinuous, thickness meas., electron mode microanalyser 79−2744
thin films, H incorporation effects on stress and electromigration 80−80139
thin films, spontaneous destruction by atmospheric pressure, electron microscopy *(Croatian)* 77−76711
thin films, vacuum deposited, crystal growth in presence of O$_2$ and Ni 80−15409
thin films, vacuum deposited, influence of film thickness on internal stresses magnitude *(Russian)* 79−37938
thin films evaporated on rough quartz substrates, surface irregularities, light scattering measurements *(Polish)* 80−88450
thin filters, for use on Apollo Telescope Mount XUV spectrograph, fabrication 77−60602
thin foil, adhesion and friction, rel. to observed dislocation density 78−64706
thin foil, electron irrad., observation of triangular loops at twin boundaries 80−34005
thin foil, Monte Carlo calcs. of electron transmission 77−80555
thin foil thickness meas. using ^{148}Gd and ^{241}Am alpha-particles 79−30417
thin solid target, proton bombarded, secondary electron bremsstrahlung, directional anisotropy 77−69953
tilt boundaries ⟨110⟩, computer simulation, struct. and symmetry 79−37713
tilt boundaries kinetic properties 78−34522
tilt boundary, $\Sigma=5$, struct. and atomic vibr., computer simulation 80−70223
Tokamak fusion reactor low activity blanket 77−6560
Tokamak toroidal field coil shielding calc. 79−31212
torque and length change during fracture in torsion test *(German)* 79−24611
torsional fatigue and bending tests 79−43521
total backscatt. coeffs., MeV electrons obliquely incident on target 77−63508
transfer etch control in chemical polishing 80−16599
transient reflectivity at 10.6 μm 79−11408
treated steel for sulphide corrosion resistance 77−63826
trial cuts at low speeds in relation with traction trials *(French)* 80−24448
tribological investigation using two-cylinder tribometer *(German)* 77−25164
tribomechanically activated, optically stimulated exoelectron emission *(German)* 78−48290
tribomechanically activated, photostimulated electron emission 79−33905
tube, large deform. under transverse loading 77−36567
tube, thin-walled, statically pre-tensioned, torsional impact loading 78−27557
tubes, liquid filled Al and PMMA longitudinal wave experiments, laminar flow 79−64604
tubes, type HT30, crushed between rigid plates, large deformation compression 80−66579
tunnel junction, barrier layer structure, mol. adsorption mechanisms *(Russian)* 79−31634
tunnel junctions, superconductivity enhancement by microwaves 80−107956
twin and stacking fault energies 79−38018
two-parameter dynamical model appl., sp. ht. and Debye-Waller factor calc. 80−10597
type Al2N5, impurity influence on spreading temp. of grain boundary dislocations 79−77609
type Al6N, impurity influence on spreading temp. of grain boundary dislocations 79−77609
ultimate tensile strength for brief impact 80−70309
ultrafine particle, positron annihilation exam. 78−56542
ultrafine particle film, size effects in optical absorption 79−99965
ultrafine particles, far IR absorpt. 77−52084
ultrafine particles, optical props., 0.3-2.5 μm 80−76020
ultrahigh vacuum behaviour, ISABELLE intersecting storage ring vacuum component performance at 1×10^{-11} Torr operation 79−81105
unpaired ion-ion interaction, transverse phonon branch, neutron scatt. expt. *(Russian)* 78−87751
US amplitude distrib. generated by direct EM method 78−2526
US attenuation, precrack damage and crack propag. study 80−40656
US effects, high-power, measurements using multiparameter system 80−7742
US fatigue crack propagation obs. 77−40451
US hardening kinetics rel. to dislocations 80−50644
US inspection of purity and dislocation struct. in A999 79−70286
US quantum oscillation exam. of third-zone Fermi surface 78−47695
US scattering and vel. determ. 77−84848
US soldering, industrial applications 77−58499
US torsional vibrations in metals, measurement of absorpt. 80−58856
US velocity, anomalous response to applied stress 78−63811
US velocity, depend. of applied stress and third order elastic const. *(Japanese)* 79−29124
US velocity, meas. method for isotropic nondispersive solids 80−69616
US velocity, temp. depend., stress effects 80−75307
US vibrations, damping under high hydrostatic press. 77−55324
US wave excitation by electron beam 79−14888
UV emission under inert gas ion bombard. 78−84664
vacancy, mechanical multipole moments determ. 78−55868
vacancy and divacancy diffusion 79−82377
vacancy annihilation to dislocations, annealing profiles 77−80536
vacancy charact. study by electrical resistance derivative method, rel. to temp. 78−47361
vacancy diffusion along single edge dislocations, computer modelling *(Russian)* 77−47612
vacancy distribution, interbonding atoms, heat peaks in scattered cascades *(Russian)* 80−39169
vacancy double jumps and atomic diffusion 78−6175

aluminium continued
- vacancy double jumps at high temp. 78—47569
- vacancy electron density, local electronic struct. theory 79—1580
- vacancy electron density distrib. using Thomas-Fermi eqns. 77—15791
- vacancy electronic struct. LCGO calcs., solid state scattering theory 79—78044
- vacancy form. energy, math. model 77—51369
- vacancy form. energy from positron annihilation meas. 78—47340
- vacancy form. enthalpy, simultaneous positron lifetime and momentum meas. 78—47335
- vacancy formation energy, thermal expansion meas. 79—14798
- vacancy formation energy and entropy, migration, quenched-in resist. meas. 77—11540
- vacancy formation energy calc. within density functional and second order perturbation formalisms 78—67975
- vacancy formation enthalpy, positron annihilation spectroscopy 78—67707
- vacancy formation volume, temp. depend. 78—47350
- vacancy loop formation, quenched-in vacancy clustering, continuum model 79—77594
- vacancy migration energy at high temp. 78—43010
- vacancy-solute interaction 78—47413
- vacuum arc, excited state density from line intensities 80—96404
- vacuum arc, excited state density theory 80—100107
- vacuum condensate, struct. and mech. props. depend. on deposition conditons 80—15417
- vacuum deposited, solar radiation props., grey-reflector appl. 77—20098
- vacuum deposited, structural singularities and porosity *(Russian)* 78—75950
- vacuum deposited metal film, elec. field effect on residual struct. 78—51836
- vacuum deposition on GaAs (001), perfect and facetting growth 79—47632
- vacuum evaporation appl. of TiB$_2$-TiC and TiB$_2$-BN for crucibles 79—74094
- vacuum-condensed film, structural changes under glow discharge *(Russian)* 79—15852
- valence band Auger spectra, surface effect 80—80915
- vaporisation of cone, solution by wave front method 78—5640
- vapour deposited on NaCl, defects and their effect on props. 80—39474
- vapour deposition on substrates, splash-free, using modified W helix 78—52689
- VLSI metallisation, Al and Al alloy metallisation sputter deposition 80—66429
- voids, neutron radiation induced, in US and in 80US-10UC-10UC$_2$ 79—50951
- volume contraction accompanying solidification 78—52791
- water/Al/adhesive/Al/water five layer struct., time domain anal. of US propag. 79—20319
- wave propagation, weak, in elastic-plastic and elastic viscoplastic solids with interfaces, Al calcs. 78—18216
- wear, recrystallisation as controlling process, FCC metals 77—56117
- wear particles, spheroid form. by cavitation erosion 79—52382
- wear under reversed friction, temp. effect 80—108588
- wear volume/sliding time relationship 79—61743
- wetting of fused silica 77—15664
- whisker, diffusion of Zn, temp. depend. 77—85122
- windows, unbacked, for He discharge lamps directly mountable as part of Cu seal between UHV flanges 79—97397
- wire, appl. of subgrain control 77—86060
- wire, determ. of incomplete axial texture by X-ray diffr. 78—23720
- wire, specimen preparation for TEM by ion beam thinning *(German, English)* 80—11861
- wire, spurious ringing in pulse NMR 79—93187
- wire, torsion fatigue strength and fibre texture 77—48549
- wire drawing plastic deform. in Al and dil. alloys 80—108508
- wire fibre reinforced Al, stress-deformed state, elastic, strength props. *(Russian)* 80—76303
- wire gaskets for demountable, bakeable ultrahigh vac. seals *(Japanese)* 79—93154
- wires, eddy current effects on NMR 80—2645
- work function temp. depend. 79—78154
- work function temp. depend. at low temp. 77—47928
- work hardening, waveform variation of reflected acoustic shock pulse 77—21167
- work softening, microstruct. interpretation 77—32593
- workhardened thin specimens, fracture, anisotropy coeff. role *(French)* 80—104276
- X-ray absorption, emission, and photoemission spectroscopies, compatibility of many-body response 80—16124
- X-ray absorption, shock wave compression meas. *(German)* 78—95618
- X-ray absorption and emission edges, one-electron and many-body effects 80—25484
- X-ray appearance pot. spectrum, 1s soft, struct. 79—33862
- X-ray attenuation, 5-40 MV, rel. sensitivities of materials for half-value-layer meas. 77—45927
- X-ray continua emission, proton and ^{14}N bombard. 78—23559
- X-ray Debye-Waller factors, CGW vs. DAF models 79—37794
- X-ray diffraction, energy-dispersive, preferred orientation influence 78—22603
- X-ray emission, incomplete phonon relax. calc. 77—52202
- X-ray emission from laser irrad. Al target in presence of high elec. field 79—94818
- X-ray emission spectra, high energy plasmon satellite intensities 78—64430
- X-ray emission spectra of CO$_2$ laser-irrad. targets, nonlinear processes 80—33793
- X-ray Huang diffuse scatt. from dislocation loops on {111} planes 80—79797
- X-ray Kα satellite struct., target chemical effects, 38 MeV F ion bombardment 77—24910
- X-ray line radiation from laser produced plasma, ang. distrib. 77—15238
- X-ray photoemission, electron yield, 30-90 keV 77—8726
- X-ray spectra, temp. broadening 77—69936
- X-ray threshold anal. 78—31281
- XPS, achromatic X-ray source, spectrum iterative deconvolution 2p spectrum 78—72689
- XPS, angle-resolved, from valence levels, Brillouin zone averaging 78—48285
- XPS, plasmon struct. of core lines 77—63530
- XPS angular depend. *(Russian)* 79—38722

aluminium continued
- XPS core line asymmetries in muffin tin approximation 79—69953
- XPS from core levels, electron energy loss spectra, intrinsic and extrinsic plasmons 77—63532
- XPS theory, core level spectra, plasmon creation 78—72701
- XPS theory, valence band spectra band struct. 78—72702
- yield condition for isotropic hardening 79—61653
- yield surface motion and loading surface 78—15449
- yield surfaces from dislocation mechanics 77—14917
- Young's modulus changes after plastic deforms. at room and cryogenic temps. 78—23747
- Z dependence of thick target β-ray backscattering 80—76118
- zero-temperature equation of state, statistical model with density gradient correction 80—15215
- zone refining 77—8750
- α-particle bombarded, He bubble growth mech. 77—7774
- μ^+ localisation in Cu, Al and Al-Mn, temp. depend. 80—44993
- Ae-GaAs (110), XPS study of interface interaction, Al proximity effects and replacement reaction 79—100019
- Ag:Al$_2$O$_3$:Al tunnel-junction struct., surface polariton mean free path, roughness 80—93008
- Ag/Al thin film couples, diffusional alloying, Kiessig X-ray interf. obs. 80—10713
- Ag-Al polycryst. thin-film couples, interaction process 79—51443
- Ag-Al$_2$O$_3$-Al junction, internal photoemission 79—82683
- Ag-Al$_2$O$_3$-Al structure, photoinduced currents, UV detection characts., 325 nm 77—53979
- Ag-BN-Si-Al sandwich, humidity sensitive threshold switching 78—88046
- Al bicrystal, estimation of grain boundary torque 77—7736
- Al castings, grain refinement by gas-generating mold coatings containing hexachloroethane 79—83355
- Al coated glass microballoon targets for laser implosion expt., search for shell disintegration 80—33792
- Al, cryst. and polycryst., inhomogeneity effects on galvanomagnetic props. 78—60109
- Al film, magnetron sputtered deposition, characts. 79—91587
- Al films, N$_2^+$ and O$_2^+$ ion bombardment, structural and phase changes 80—2094
- Al, high purity, deformed at 573K, stress reductions effect on creep behaviour 79—74216
- Al I, 1932 and 1936 Å autoionisation lines in solar flare, Skylab obs. 80—26829
- Al I, electron impact line broadening in arc spectra 79—26919
- Al I, fine struct. splittings in some highly ionized $n=3$ doublets 80—43200
- Al I, II, III, photon emission from secondary ions 77—59660
- Al I, laser stimulation optimisation for intraresonator spectroscopy 80—77881
- Al I, perturbed HFS, interconfiguration interaction calc. 80—9523
- Al I, relativistic and cancellation effects in line strength ratios 78—82689
- Al I, resonance level, radiative lifetime, dye laser excitation 78—46300
- Al I isoelectronic sequence, forbidden transition probabilities for ground terms 77—2376
- Al I line broadening and shifts by van der Waals interaction with Ar and He atoms 79—6912
- Al I line profiles, Stark broadening meas. 78—9115
- Al I to XIII, energy levels and ionisation energies, data compilation 80—14100
- Al II, ^{3}F^0 Rydberg series, energy levels, multiconfigurational HF procedure 80—47882
- Al II, energy levels, spectrum obs. 8640 to 683 Å 79—54797
- Al II line profiles, Stark broadening meas. 78—9115
- Al II near IR laser transitions, large diameter hollow cathode Ne-Al discharge 80—102715
- Al II to Al VI, beam-foil obs. from 1100 to 1900 Å, lifetimes and oscillator strengths 80—14108
- Al II to Al VI, beam-foil obs. from 300 to 2000 Å, mean lives and oscillator strengths 80—14109
- Al II-VII, radiative lifetimes, beam-foil spectra 79—49986
- Al IV, autoionising transitions ns^{2}np^6—nsnp^{6}mp 77—88419
- Al IV, independent particle pots. comparison 80—52846
- Al IV, lifetimes of $n=3$ and 4 levels meas. and calc. *(French)* 80—9554
- Al IV, Ne-like, atomic lifetimes, second order calc. and beam-foil meas. 79—59422
- Al IV, transition probabilities and radiative lifetimes 79—76372
- Al IV, V, beam foil spectra, 1100-1900 Å, lifetime meas. 78—70919
- Al IX to Al XI, beam-foil obs. of lifetimes and oscillator strengths, 300 to 1000 Å 80—14110
- al, liq., sticky hard sphere pot., stuct., function evaluation 80—33869
- Al, molten, impurity diffusion of fourth period solutes and homovalent solutes *(Japanese)* 80—70436
- Al, neutron irrad., μ^+ mobility and trapping by vacancies, muon spin rot. meas. 79—4757
- Al, oxide films, metal and O$_2$ transport, AES and inert marker, techniques 80—97641
- Al, plastic flow, role of osmotic forces in low angle fatigue, vacancy generation *(Russian)* 79—60430
- Al, polycrystn., HVEM in-situ investigation of creep mechanism 80—104214
- Al powder, particle nonequiaxiality effect on size distrib. meas. in pulse conductometeric anal. 80—20833
- Al, pure, polycryst., steady-state flow, stress and temp. depend. 80—45341
- Al, rigidity modulus, neutron irrad. and quenched, point defects 78—27546
- Al sequence, 4s^{2}S-4p^{2}P transition, f-values 78—78651
- Al, splat-cooled, grain-size distrib. function, TEM study 80—40396
- Al, US and X-ray testing of castings, moulds and die-casting machines 78—53097
- Al vacuum deposited coating on glass, strength 80—55505
- Al X, beam-foil obs. of oscillator strengths for E1 transitions 80—14112
- Al XII, electron density meas. using Stark profiles 79—81181
- Al XII, He-like ion, oscillator strengths of transitions between low-lying S and P states 78—13470
- Al XII, He-like ion resonance line satellites 79—10064
- Al XII, intercomb. line obs., in laser-produced plasma 78—9106
- Al XIII, 1s2p^{3}P$_2$ and 1s2p^{3}P$_0$ levels, radiative lifetimes and hyperfine induced decay 80—74149
- Al XIII, H-like ion, anal. of satellites to reson. lines in X-ray region 77—88421

aluminium continued
- Al XIII, hot pinched plasma, Lyman series Stark profiles, electron density determ. 78−51348
- Al^-, metastable, electron affinity calcs. 79−31439
- Al^+, reson. line regularities in plasma Stark widths and shifts 80−43881
- Al^+, static dipole quadrupole polarisabilities and shielding factors calc. using HF scheme 80−99450
- Al^{10+}, $^4P^0{}_{5/2}$ state excitation energy, X-ray spectra 77−27017
- Al^{10+}, partial photoionis. cross-sections and radiative recomb. rate coeffs. 80−52951
- Al^{2-}, parameters for analytical radial orbitals, total and binding energies 77−6668
- Al^{3+} ion, plasma in fast evolution, time-resolved soft X-ray absorpt. transitions 77−18827
- Al^{3+}, ionic size rel. to Koopmans' ionisation pot. 79−85892
- Al^{5+}, $2s2p^5$-$2s2p^4 3s$ transition, spectroscopic investig. 79−59384
- Al^{7+}, $2s2p^3$ terms, mean lives, from beam-foil spectra 78−37601
- Al:^{111}In, electron irrad., defect trapping at impurities 78−55892
- Al:^{12}B, relax. mechanism for polarised implant 78−87693
- Al:^{24}Na, diffusion of Na, determ. of diffusion coeff. and activation energy 78−51746
- Al:^{57}Fe study via conversion electron Mossbauer spectroscopy 77−55735
- Al:Ca (Ga), ion implantation, defect structures obs. 80−59494
- Al:Er(Dy), orbit-lattice coupling, nonuniform strain effects 78−88182
- Al:Fe(Cu), CESR, effect of ion implantation 77−20701
- Al:Ga, pulsed electron-beam annealing, lattice site location improvement 80−107303
- Al:H, impurity energies and geometrics, self-consistent jellium calc. 79−99507
- Al:H(He), interaction energy of two H(He) atoms, Hohenberg-Kohn-Sham density functional formalism 79−51519
- Al:He, excited He atom lifetime, optical absorption 79−38578
- Al:He, pseudopotential calc. of screening of He atom 78−51917
- Al:O, $^{18}O^+$ ion implantation in channelling directions, expt. conditions and range profile obs. 80−65022
- Al:O, perforated supercond. film, RF resist. in mag. field, pinning force const. 79−56471
- Al:O single crystal, $^{18}O^+$ ions implantation in channelling directions, stopping power meas. from max. range 80−65078
- Al:O supercond. film, RF complex impedance meas., dynamic pinning 80−84573
- Al:Si, film deposition by reactive sputtering 79−66005
- Al:WO_3 films, resistive state, effect of UHF rad. on dynamic cond. *(Russian)* 78−52154
- Al/(Al_2O_3)-BaSt/Sn struct., internal voltage temp. variation 80−20326
- Al/(Zn-)phthalocyanine/Au, photovoltaic effects, illuminated thin-film cell props. 79−4605
- Al/(Zn-)phthalocyanine/Au, photovoltaic effects, dark elec. props. of rectifying cells 79−4604
- Al/Ag interface, interface energy and charge oscills. 77−62984
- Al/Al_2O_3/Al, dielec. props. 80−80404
- Al/Al_2O_3/Al structures with organic monomolecular layer, cond. at high elec. fields 80−80402
- Al/Al_2O_3/CdS, junction characts. 79−82481
- Al/Al_xO_y vacuum deposited laminates, struct. and mech. props. 79−28219
- Al/Al-Mg filler welds, weld fusion boundary structure 80−39459
- Al/$AlCl_3$-NaCl/FeS_2 secondary cell, preliminary study 80−108793
- Al/AlO_x/La-rare earth metal tunnel junctions, cond. meas., cryst. field effects 80−88694
- Al/As_2SeTe_2/Sb structures, rectifying effects 80−75654
- Al/Au/Al layer configuration, electron energy deposition meas. 77−24338
- Al/brass/Al bimetal, three layers, formed by cold rolling, exam. of formation of intermetallic phases at interface 78−56658
- Al/Cr thin films, interdiffusion meas. 79−82391
- Al/Cu laminates, vapour deposited, strength enhancement 79−24576
- Al/Cu thin film couples, interfacial reactions, low temp. contact resist. meas. 80−44709
- Al/Cu thin film couples, TEM study of intermetallic nucleation at interface 80−65305
- Al/GaAlAs, film, epitaxial growth on (100) GaAs by hot vac. deposition and characterisation 79−56085
- Al/GaAs contacts, metallization of surfaces covered with absorbed S *(French)* 80−107909
- Al/Ge multilayered superconducting films, crit. fields and crit. temps. 79−7945
- Al/Ge thin film couples, accel. ageing 80−44726
- Al/Ge/Al sandwich structs., interdiffusion effect on Ge film conductivity 79−23788
- Al/III-V interfaces, photoemission 80−25526
- Al/metal-free phthalocyanine Schottky barrier solar cells, photovoltaic props. 79−100527
- Al/Mg soldered samples, UTS and fracture surface comp., 20 to 500°C 79−38941
- Al/Nb superimposed layer anodic oxidation, ion movement study by O^{18} and MeV ion beam techniques 78−15604
- Al/NiSi/Si system, high temp. interaction study, elec. and struct. characts. 79−24075
- Al/Pb two-layer target, moderate energy electron interactions, direct statistical modelling *(Russian)* 77−66561
- Al/Pd thin film couples, thermal reactions 80−59830
- Al/Si thin film couples, accel. ageing 80−44726
- Al/SiO_x/p-Si contacts for IMS solar cells, high temp. lifetesting 79−87988
- Al/SiO_x/pSi MIS solar cells, stability 80−85287
- Al/SiO-B_2O_3/Au, emitted electron energy distrib. *(French)* 80−39681
- Al/Sn, composite, kinetics of adsorption softening of solid interface *(Russian)* 79−61619
- Al/Sn interface, effect of plastic deformation on structure and adhesion strength of interface *(Russian)* 79−28218
- Al/Ta double layer on Si, anal. by low energy ion scatt. *(French)* 77−59663
- Al/tetracene/neutron cell, electroabsorption and electrorefl., interfacial elec. fields 79−65548
- Al-304 stainless steel laminate composite, fatigue crack nucleation and propagation 79−100244
- Al-adsorbed monolayer-Al junction, elec. cond. mech. 78−95386
- Al-Ag, struct. of two-layer film 79−23851
- Al-Ag, thin-layered laminates, yield strength rel. to dislocation generation and motion 79−20137

aluminium continued
- Al-air, seawater activated secondary cell 80−26128
- Al-air batteries, mechanically rechargeable, for automotive propulsion 79−48103
- Al-Al oxide-$Bi_{1-x}Pr_x$ tunnel junction, cryst. field struct. obs. in conductance 78−84358
- Al-Al oxide-Pd tunnel junctions, exposed to H_2, inelastic electron tunnelling spectra 80−20327
- Al-Al_2O_3, dispersion hardened, creep *(Czech)* 80−108463
- Al-Al_2O_3, local struct. and interface states using surface soft X-ray absorpt. and photoemission spectroscopy 79−69595
- Al-Al_2O_3, recrystallisation nucleation in drawn wires, optical and TEM obs. 79−47709
- Al-Al_2O_3, sintered, plastic props. *(Russian)* 80−58923
- Al-Al_2O_3, supercond. granular film, mag. penetration depth, depend. on normal state resist. and temp. 79−56378
- Al-Al_2O_3 composite, brittle zone on fibre surface deform. and fracture 77−56104
- Al-Al_2O_3 electron transport in very thin multilayers 79−4602
- Al-Al_2O_3 films, coincidence energy spectra for (e, 2e) reaction 79−69936
- Al-Al_2O_3 superconducting granular film, crit. current density 77−40013
- Al-Al_2O_3 triple-barrier structure, negative resist. caused by resonant tunnelling 78−14819
- Al-Al_2O_3-Ag structure, electron bombard, charge accumulation kinetics, exoelectron emission obs. 77−51825
- Al-Al_2O_3-Ag tunnel junction, surface plasmon excitation 78−10578
- Al-Al_2O_3-Ag tunnel junction, 4-pyridine carboxaldehyde-doped, surface enhanced Raman spectra, surface plasmons 79−98111
- Al-Al_2O_3-Al, non-thermal switching in Al_2O_3 amorphous film *(Russian)* 78−80069
- Al-Al_2O_3-Al, thin film capacitors, dielec. losses 78−76382
- Al-Al_2O_3-Al junctions, Dy doped at Al_2O_3-Al interface, electron transport mechanisms and barrier height 78−91778
- Al-Al_2O_3-Al MIM struct., photocond. anal. *(French)* 77−72921
- Al-Al_2O_3-Al MIM struct., elec. cond., island metal struct. 79−15231
- Al-Al_2O_3-Al structure, elec. cond. 261 to 418K *(Russian)* 78−64144
- Al-Al_2O_3-Al structure, tunnel I-V characts., transmission coeffs. 78−80068
- Al-Al_2O_3-Al(Au), thin films, elec. props. *(Czech)* 78−76159
- Al-Al_2O_3-Au device in Cl_2 atmosphere, current-voltage characts., press. depend. 80−65704
- Al-Al_2O_3-Au sandwich conduction props. 78−2580
- Al-Al_2O_3-Au(Al), capacitance, water sorption effects 77−43738
- Al-Al_2O_3-CdS diodes fabricated by MBE, junction characts. 79−65550
- Al-Al_2O_3-Dy junctions, steady state and nonsteady state behaviour 79−78205
- Al-Al_2O_3-Dy thin junctions, Poole-Frenkel effect obs. and cause 80−80398
- Al-Al_2O_3-GaAs backwall MIS Schottky barrier solar cell, anal. model 80−85289
- Al-Al_2O_3-GaAs MOS struct., mol. beam reaction growth of Al_2O_3 film, C-V characts. 80−11095
- Al-Al_2O_3-Hg systems, I-V characts. at room temp. for different thicknesses 79−47172
- Al-Al_2O_3-In_2O_3:Sn tunnel junction, light emission via inelastic tunnelling effect 79−24076
- Al-Al_2O_3-InP MIS struct., elec. props. 79−78184
- Al-Al_2O_3-InSb MIS structures, recomb. processes and carrier lifetimes 79−38177
- Al-Al_2O_3-M, thin film sandwich, leakage current and dielec. relax., 80-500K 78−76158
- Al-Al_2O_3-Nb, quantitative proximity tunnelling spectroscopy 79−91193
- Al-Al_2O_3-Pb contacts, tunnelling spectroscopy, band struct. of Pb 80−80169
- Al-Al_2O_3-Pb Josephson junction, nonuniform, paracond., fluctuation effects 77−59359
- Al-Al_2O_3-Pb tunnel junction, Pb supercond. film behaviour in mag. field 78−14894
- Al-Al_2O_3-Pb tunnel junction, depend. of conductance corres. on chemisorbed ion conc. in barrier 79−15233
- Al-Al_2O_3-Pb(Au), solid-state anodisation of Al by vapour infusion, oxide growth rate 80−11830
- Al-Al_2O_3-Pd diodes, resonant tunnelling via localized inpurity states 79−28416
- Al-Al_2O_3-SiO_2-Si capacitors, physical and elec. props. of RF plasma grown Al_2O_3 80−100530
- Al-Al_2O_3-SnTe, junction, tunnelling, Fermi level depend. on carrier conc., influence of surface states 80−25016
- Al-Al_2O_3-SnTe structure, tunnelling characts., model anal. 80−29480
- Al-Al_2O_3-(a-Ge)-Al, electron tunnelling into a-Ge, press. effect 80−49938
- Al-Al_2O_3-electrolyte, electroluminesc., nondestructive electronic avalanche 78−68563
- Al-Al_2O_3-electrolyte system, electrolum. theory, thickness depend. 80−3358
- Al-Al_2O_3-metal capacitors, elec. props. interrelations 80−54801
- Al-Al_2O_3-metal capacitor, capacitance and power factor rel. to voltage and temp. changes 80−54802
- Al-Al_2O_3-p-GaAs MOS diode, capacitance-voltage characts. 80−107914
- Al-Al_2O-Al tunnel junction, Fe doped, Kondo-type zero-bias conductance 78−56237
- Al-Al_3Ni two-phase matrix, Al electrolytic etching in $AlCl_3$ molten salts 78−3280
- Al-Al_xO_y-Pb tunnel junction, thermal annealing effects 80−49952
- Al-Al-PbBi double tunnel junction structs., quasiparticle relax. times, energy and temp. depend. 79−56412
- Al-AlF_3-Al MIM struct., dielec. props. temp. irreversibility *(Czech)* 80−15616
- Al-AlF_3-Al thin film structures, dielec. and elec. props. *(Slovak)* 80−100536
- Al-AlN-Au, voltage controlled negative resist., O_2 press. effect 78−72281
- Al-AlN-SiO_2-Si capacitors, physical and elec. props. of RF plasma grown AlN 80−100530
- Al-AlO_x-Pb junctions, organic ring cpd. doped, asymmetries in elastic and inelastic tunelling 79−95549
- Al-AlO_x-PbBi tunnel junction, quasiparticle energy distrib. in nonequilib. supercond. 77−80881
- Al-amorphous Ge-nSi, photoelectric props. 80−70822

aluminium continued
Al-amorphous GeSe-Al structs., AC cond. and capacity, thickness depend. 79—65566
Al-amorphous Se-Al struct., capacitance variation with illumination 79 87165
Al-anodic oxide-n-GaAs MOS struct., elec. instabilities and annealing effects 79—60928
Al-anodised Ta_2O_3/native oxide-n-GaAs MOS structure evaluation 80—84514
Al-As_2Se_3-Al, photographic process based on electrochem. reactions *(Russian)* 79—6213
Al-As_2Se_3-Al layers, photoelectrochem. process 77—76953
Al-Au bimetal thin film interdiffusion zone, intermetallic phase form kinetics, 70-160°C 78—75891
Al-Au couple, electroformed, nonohmic characts. and electron emission 80—60066
Al-B fibre-D16 alloy welded composites, structure, strength and fracture props. *(Russian)* 80—108524
Al-Ba stearate-Sn struct., internal voltage, thickness depend. 77—72920
Al-barium stearate-Al struct., intrinsic voltage in insulating film 78—72277
Al-barium stearate-Al symmetric junction, internal voltage due to Al_2O_3 film on electrodes 79—78202
Al-Be, two-layer foils, mech. props. *(Russian)* 78—51858
Al-brass, clad sheet metal, optimum combination of composing sheets for deep drawing 77—81241
Al-brass tubes, passivation treatment for atmospheric corrosion protection during storage and transport 80—85079
Al-C-Al sandwich, microwave irradiated, superconductivity at room temp. *(Russian)* 80—11138
Al-C-silaceous sand mixture in N_2 atmos., weight loss during heating, compaction *(Japanese)* 80—35151
Al-CdS-Au structure, interfacial phenomena, complex impedance meas. *(French)* 79—42668
Al-CdS(Se) function formation, coupled interface plasmons, low energy electron energy loss spectra 77—24621
Al-CdSe, Schottky barrier diode, I-V and C-V characts. 78—10555
Al-CdSe-Ag dry air stabilised struct., elec. cond. mechanism, breakdown phenomena 80—34527
Al-CdTe Schottky barriers, defect effects 79—60921
Al-CdTe-Al thin film VLF dielectric props. *(Slovak)* 79—7907
Al-CeF_3-Al(Au) MIM struct., dielec. props. temp. irreversibility *(Czech)* 80—15616
Al-chalcogenide glass thin layer struct., EMF in elec. field *(Russian)* 77—39936
Al-copper phthalocyanine-Ag diode struct. with Schottky barrier 77—43740
Al-Cr, thin film metal contact, sheet resistance changes 80—80356
Al-Cr thin film interdigital transducers for SAW devices at GHz freqs. form. by electron beam lithography 80—4702
Al-Cu, thin-layered laminates, yield strength rel. to dislocation generation and motion 79—20137
Al-Cu thin film couple, interdiffusion, AES obs. 80—6569
Al-$CuAl_2$ lamellar composite, creep, microstruct. obs. 79—8331
Al-dimethyl terephthalate contacts, effect of elec. field on contact electrification 79—19660
Al-epoxy adhesive joints, cohesive-interfacial mixed-mode fracture 79—39110
Al-epoxy adhesive systems, opening and edge-sliding fracture toughness 78—95805
Al-Fe bimetal, O_2 effect on diffusion inhibition 77—89597
Al-Fe interface, O_2 content, reson. α-scatt. from ^{16}O 78—64778
Al-Fe_2O_3-Al, space charge limited current, current density as function of elect. field and temp. 79—51688
Al-Fe_3O_4 binary thermite powder mixture, compaction 79—74125
Al-$Fe_{78}Mo_2B_{20}$ wire composite, mech. props. 80—40441
Al-formvar superconductive junction, Ginzburg's generalised jellium model 80—15663
Al-Formvar-Pb junction electron tunnelling, phonon spectrum 77—59080
Al-Formvar-Sn coupled films, Ginzburg's excitonic supercond. model 80—97039
Al-formvar-Sn junction, supercond. order parameter fluctuations below T_c 77—66227
Al-Formvar-Sn tunnel junction, mode propag. in dirty type I supercond. 80—15662
Al-fuchsin-SnO_2 MSM structure, field depend. of electroabsorption spectra 77—40263
Al-GaAs, surface reactions and interdiffusion, photoemission study 80—49532
Al-GaAs (110), Schottky barrier form., defect mechanism 80—49902
Al-GaAs interface, struct. study by X-ray total-external-refl.-Bragg diffr. 80—34321
Al-GaAs interface, thermal ageing of Al film, optical microscopy and SEM obs. 77—20203
Al-GaAs interfaces, chemically induced charge redistrib. 79—33342
Al-GaAs Schottky barrier diode, Richardson const. 77—20424
Al-GaAs Schottky barrier diode, prep. by MBE on GaAs, and characts. 78—72257
Al-GaAs-$Al_xGa_{1-x}As$ Schottky barrier diodes, prep., characts. 80—6948
Al-GaAs(110) structure, interface states, photoemission study 78—95359
Al-Ge, amorphous, junction, current-voltage charact. 80—44725
Al-Ge (100) interfaces, MBE prep. and geometrical struct., total refl. X-ray diffr. study 80—49531
Al-Ge photovoltaic cell, charact. 79—40612
Al-Ge-Al(Cr)(Au), study of metal contact resistance and microstruct. 77—89880
Al-Ge-Ge_3N_4-Al structure, V-I and V-C characts. *(Russian)* 78—47893
Al-GeS-Al, dielectric relax. currents, pot. distrib. in amorphous GeS layer 77—16250
Al-GeS-Al structure, current-voltage characts., thermionic electron emission model 77—28260
Al-GeS-Al system, Schottky and Poole-Frenkel cond. mechanisms 80—54799
Al-GeSe-Al(Mo)(Au)(C), effect of contact material on DC and AC behaviour of sputtered amorphous GeSe film 79—95513
Al-Ge(001) interface, struct., total-reflected X-ray diffr. 80—88441
Al-gelatin-GaAs, capacitance-voltage characts. after and before incorporation of $AgNO_3$ 79—51684
Al-graphite adhesion and contact angle, effects of metal additives *(Japanese)* 78—60008
Al-graphite two-dimensional shield, neutron penetration meas. 79—3245

aluminium continued
Al-I-Pb tunnel junction, clean and doped, tunnelling conductance 79—15232
Al-In multicomponent binding layers, acoustic light modulator 80—87546
Al-In_2S_3-Si layered struct., Hall effect, I-V characts., surface states *(Russian)* 80—97001
Al-InP Schottky barrier, increase 80—15603
Al-insulator-Al(Au) diodes, elastic tunnelling current 79—42666
Al-insulator-$In_{1-x}Mg_x$ film tunnel junction, resistance zero-bias anomalies 80—107925
Al-insulator-Pb, clean and doped tunnel junctions, barrier profiles 79—56445
Al-insulator-Pb tunnel junction doped with m-cresol, asymm. in tunnel spectra 77—6782
Al-KCl composite, far IR absorption 78—56466
Al-lead stearate-Hg, transient and alternating electric currents 78—84311
Al-matrix, composites preparation by Na-process, interface reactions 78—84742
Al-Mg (4 wt.%), struct. and strengthening in hot working 80—84968
Al-MgF_2, reflective multilayer coatings for far UV 77—758
Al-MgF_2 coatings for UV reflecting mirrors for space appls. *(French)* 77—67022
Al-MgF_2 layers on transparent substrates for making scales 77—798
Al-Mn(0.6 wt.%), supersat. solid solns., isothermal decomp., Zr addition effects 77—63626
Al-MoO_3-Al structure, current-voltage characts., 251K-301K 79—91156
Al-monolayer-Pb, supercond. junction, electron tunnelling meas. 79—28482
Al-n-GaAs surface barrier diodes, influence of exciton effects on photo-EMF spectrum 78—10557
Al-nSi-Al, p^+np^+ reach through structs., electronic cond. mechanism 78—64103
Al-NaCl(F) adhesion 78—18914
Al-Nb, tunnelling expts. on normal metal backed by Al 80—65751
Al-Nb superimposed metallic layers, ionic movements during anodization, Rutherford backscatt. and nuclear microanal. 80—71913
Al-O (100), extended appearance potential fine struct. anal., LEED study 80—50467
Al-octaethylporphin-Ag, electroluminesc. 77—59615
Al-Ox-Ag-Cu-Pb and Al-Ox-Cu-Ag-Pb trilayer junctions, tunnelling characts. 79—87208
Al-oxide-Mg-Al, thin proximity effect sandwiches, spin-polarised tunnelling obs. 80—50007
Al-oxide-Pb tunnel junction, clean and doped, cond. 77—59335
Al-oxide-electrolyte system, luminesc. spectra *(Russian)* 78—76539
Al-oxidised Al-Pb tunnel junction, nature of oxide barrier for IETS 77—72922
Al-PMMA laminated composites, shock wave propag., flash radiographi obs. 79—4370
Al-PTFE, spacecraft surface material performance modelling 78—4061
Al-Pb junction, intensity and line-shape measurements in inelastic electron tunneling spectroscopy 79—24104
Al-Pb proximity sandwiches, Josephson and quasi-particle tunnelling expts. 79—65616
Al-Pb:Bi, tunnel-junction relax. oscillator, appl. to thermometry 79—85138
Al-PbBi superconducting tunnel junction as phonon spectrometer 78—47477
Al-PbBi superconducting tunnel junctions, optically illuminated, quasiparticle energy distribution 80—75688
Al-PbS coatings, absorptivity, emissivity as function of PbS thickness 78—46731
Al-PbS selective surfaces for solar photothermal conversion, prep., emissivity, absorptivity 80—12030
Al-Pd_2Si contacts on Si, elec. and structural characterisation 77—43695
Al-Permalloy two-layer films, mag. anisotropy, grain boundary diffusion *(Russian)* 80—71122
Al-Plexiglas, double layer barrier, deform. of electron spectra *(Russian)* 78—84292
Al-poly-Si Schottky-barrier solar cells, grain boundary effects on electrical behaviour 80—85279
Al-polyacrylonitrile-Al films, current-voltage characteristics 80—11125
Al-polyferrocene-Al structure, I-V and I-d characts. 78—80064
Al-polymer contacts, charge transfer and contact charge spectroscopy 79—56305
Al-polymer joint, meas. of temp. dependence of joint strength 80—50824
Al-polymer-Au, short circuit current with temp. variation 77—32090
Al-Pt catalyst, deep oxidation of benzene, kinetic model depend. of reaction rate 77—90583
Al-Pt film sandwich, interdiffusion and intermetallic form. 77—24448
Al-sapphire-Si capacitor, effect of electron-beam aluminisation on Si-sapphire interface 77—89856
Al-Sb_2O_3-In films, negative resistance characts. 80—11103
Al-Si, contact resist. response surface of sintered Al film on Si (100) 79—78175
Al-Si, ion plated contacts *(Rumanian)* 78—88029
Al-Si contacts, effect of vacuum ambience 77—43718
Al-Si interface, solid phase epitaxial growth of Si 80—34324
Al-Si MIS solar cells, depth conc. profiles, elec. and optical props. of Al films 80—94076
Al-Si Schottky barrier solar cell, metallurgical reactions 77—72914
Al-Si Schottky diodes, with Ti contact, voltage-current characts., appl. to ignition circuits 80—11088
Al-Si structure, contact resist. and bulk resist. of Si, pulse method 78—52083
Al-Si system, Si regrowth minimisation through overlying Al or Al alloy film 80—70569
Al-Si_3N_4-Al cathode, fluctuation noise 78—2998
Al-Si_3N_4-Al thin film cathode, pulsed emission obs. 77—8728
Al-Si_3N_4-Al thin-film cold cathode, electrical forming, expt. 78—76160
Al-Si_3N_4-Ge, thermally stimulated depolarisation current meas. 80—88643
Al-Si_3N_4-Si, electrical strength effect of struct. defects in Si_3N_4 *(Russian)* 78—26955
Al-Si_3N_4-Si struct., surface energy bands under step function illumination 80—49840
Al-Si_3N_4-SiO_2-Ge structure, small signal HF photo EMF meas. 78—52097
Al-Si_3N_4-SiO_2Si, MNOS structures degradation under UV irradiation effect 80—107923

aluminium continued

- Al-$Si_xN_yO_z$-Al structure, electron microscope obs. of irreversible changes *(Russian)* 77—85342
- Al-$Si_xN_yO_z$-Al thin film cathode, physical model from expt. study 80—100535
- Al-Si_xNyO$_z$-Al systems, mechanism of current transfer *(Russian)* 77—69427
- Al-Si-Al contact current response to 100 keV neutron irrad. *(Russian)* 80—49956
- Al-Si-Al(Mo), sputtered Si film, photovoltaic props. 77—24623
- Al-SiC cermet elasticity, porosity meas. by US means 80—81101
- Al-SiO_2, Al-SiO_2(SiO)-Si, solid-state reaction mechanism 77—52623
- Al-SiO_2, film system, kinetics of interaction 77—44459
- Al-SiO_2, surface reactions and interdiffusion, photoemission study 80—49532
- Al-SiO_2 (2wt.%), dispersion hardened particulate composite, prep. 80—7588
- Al-SiO_2 film-substrate interface, obs. of Al_2O_3 and free Si 78—91571
- Al-SiO_2 interface, chem. struct., deposition conditions depend. 78—72007
- Al-SiO_2 interface, internal photoemission, phonon scatt. effects 77—85315
- Al-SiO_2 interface, internal photoemission and photon-assisted tunnelling 80—6982
- Al-SiO_2 interface, stress and microstruct. via TEM 78—26797
- Al-SiO_2 interface in MOS capacitors, conductivity effects of oxidation temperatures 80—100518
- Al-SiO_2 layered system, complete absorpt. of transverse mag. waves 78—39615
- Al-SiO_2-Au, thin layer struct., electroluminesc. *(French)* 78—76531
- Al-SiO_2-Si, charge measurement in MIM and MIS struct., MOS system appl. 78—2572
- Al-SiO_2-Si, MIS diode, neutralisation of mobile ions in insulating film *(Japanese)* 79—73591
- Al-SiO_2-Si, MOS struct., lateral photovoltaic effect 79—4601
- Al-SiO_2-Si, pyroelectricity 80—100524
- Al-SiO_2-Si, void form. in Al interconnection lines at Si-SiO_2 boundaries 80—2476
- Al-SiO_2-Si capacitors, transient capacitance temp. depend., −40 to 70°C 79—47167
- Al-SiO_2-Si MOS structures, charge motion, TSC meas. 80—100534
- Al-SiO_2-Si Schottky barrier solar cells, recomb. effects 79—39310
- Al-SiO_2-Si struct., mobile ion neutralisation in SiO_2 layer, TSC and C-V characts. meas. 79—95503
- Al-SiO_2-Si structs., implanted B^+ ions, high-freq. CV characts. *(Russian)* 78—80056
- Al-SiO_2-Si structure, Auger depth profiling and ion sputtering of interfaces 77—20200
- Al-SiO_2-Si structure, location of positive trapped charge by internal photoemission 77—51820
- Al-SiO_2-Si structure, photon-assisted tunnelling 77—89865
- Al-SiO_2-Si structure, photocurrents, 1.4 to 3.1 eV 79—65514
- Al-SiO_2-Si structure, positive interface charge, exciton and H diffusion models 80—2471
- Al-SiO_2-Si structure, small signal HF photo EMF meas. 78—52097
- Al-SiO_2-Si system, EMF origin in pulsed UHF field 77—4448
- Al-SiO_2-Si system with reactively sputtered SiO_2, work functions difference 80—6987
- Al-SiO_2-Si:B ions, annealing effect on energy spectrum of radiation defects *(Russian)* 78—88488
- Al-SiO_2-Si-Pb, MIS system, photocurrent, effect of supercond. to normal transition in Pb 78—72271
- Al-SiO_2-TiO_2 interference mirror coatings, high mech. strength 78—30043
- Al-SiO_2-p-Si solar cells, comparison of majority- and minority-carrier silicon MIS solar cells 80—85280
- Al-SiO_2Si, mobile ion kinetic behaviour 79—56315
- Al-SiO_x-Al structure with evap. amorphous films, threshold and memory switching 77—76945
- Al-SiO_x-Au, MIM struct., electroformed, struct. and elec. props., 4-300K 79—78206
- Al-SiO_x-Au cathode, emitted electron energy distrib. 78—52645
- Al-SiO_x-GaAs, C-V characteristics 79—65553
- Al-SiO_x-Si, experimental verification of theoretical predictions 80—29485
- Al-SiO_x-Si MIS solar cells, short-wavelength response 79—57428
- Al-SiO_x-Si MIS solar cells, I-V characts. temp. depend. 80—7935
- Al-SiO_x-Si MOS solar cells, open-cct. voltage var. with oxide layer thickness 80—81434
- Al-SiO_x-Si minority-carrier MIS photodiodes, elec. characts. 79—51676
- Al-SiO_x-(p-)Si barrier structs., minority carrier injection ratio meas., MIS solar cell model 80—93007
- Al-SiO_x-p-Si MIS solar cells with back surface fields 80—12006
- Al-SiO_x(+SiO_2)-Si structures, I-V and C-V characts., current and capacitance kinetics 78—88043
- Al-SiO-Al structure, tunnel I-V characts., transmission coeffs. 78—80068
- Al-silicide-Si systems with $CoSi_2$, $Pt_xNi_{1-x}Si$, and $MoSi_2$ as silicide, diffusion, compound form., and microstructure 80—34253
- Al-silicide-n-Si systems with $CoSi_2$, $MoSi_2$, and $Pt_xNi_{1-x}Si$ as silicide, Schottky-barrier height 80—34520
- Al-silicon oxynitride-Al cathode, LF noise sources and reduction 80—108328
- Al-Sio-Al structure, with amorphous SiO, VLF behaviour 77—76946
- Al-stearic acid-Al, low-loss thin film capacitor 80—71317
- Al-steel mixture, wear resistant, produced by compaction by discrete shock waves 80—84882
- Al-steel profiled composite, pulling from melt, mech. props. 78—3075
- Al-steel radiation shields, build-up factors for 6.2 MeV photons 79—81093
- Al-Ta_2O_5-Al, healing of defects in dielec. film by anodisation 80—65406
- Al-Ta-poly-Si interdiffusion, Ta barrier effect, Auger anal. 78—71888
- Al-TeO_2-Al, field-assisted cond. mechanism 80—11105
- Al-tetracene-Au cell, depletion layer, LF capacitance meas. 79—56328
- Al-$TiSi_2$-n-Si struct., elec. props., charge transfer mechanism across $TiSi_2$-Si interface *(Russian)* 80—34515
- Al-V-Ti junction, spin-dependent electron tunnelling 79—19700
- Al-vitreous C composite, microchem. inhomogeneity of transition zone 77—24985
- Al-Xe film, ion implanted radiation enchanced Xe outdiffusion, Rutherford backscatt. 77—76609
- Al-ZnO-SiO_2-Si monolithic MIS struct., charge-transfer device using SAW 79—11229

aluminium continued

- Al+Al, (Cl)(F), molecular K X-ray transitions, mol. radiative electron capture effect 78—58802
- $Al+CO_2 \rightarrow AlO+CO$, HTFFR kinetics obs., 300 to 1900C 77—90596
- $Al+H^+$, K-shell ionis., impact parameter depend., 90-200 keV 78—17775
- $Al+H^+$, K-shell ionisation cross sections for 15-65 keV protons 78—90284
- $Al+H^+$, K-shell ionisation 0.5 to 40 MeV, meas. and PWBA-BEA calcs. 80—78699
- $Al+H^+(^3He)$ ion collisions, K-shell ionisation cross sections 77—23555
- Al+H(D)(He)(Li) ions, K-shell ionis., universal cross sections 78—62895
- $Al+He^+$, X-ray spectra, two-electron one-photon transition in solid target, 2 MeV 78—94209
- $Al+He^+(H^+)$, 1.9 MeV, Kα X-ray polaris. and line strengths 77—30983
- Al+He(C)(N)(O), inner-shell multiple ionisation systematics, X-ray obs. 80—63790
- Al+He(C)(O)(Ne), K-shell ionising collisions, average L-shell ionisation probability, K_α spectra 79—72408
- $Al+N^{n+}(O^{n+})(F^{n+})$, X-ray prod. and electron transfer cross-section 79—45790
- $Al+NO_3^-$, reactions between metal and aq. nitrate solns., XPS 77—12825
- $Al+NO+Ar \rightarrow AlNO+Ar$, rate coeff., 600K, fluoresc. and absorption spectrum obs. 77—40521
- Al+Ne, recoil effects on molecular-orbital X-ray spectra in solid targets 80—25510
- $Al+O_2 \rightarrow AlO+O$, product. rot., vibr. translational energy, AlO fluoresc. 78—23928
- $Al+O_3 \rightarrow AlO+O_2$, chemiluminesc., $A^2\pi$-$X^2\Sigma^+$ transition obs. 78—31639
- $Al+SO_2$, high temp. fast flow reactor obs. of kinetics 80—30226
- $Al+Si^{n+}(Al^{n+})(Cl^{n+})(Ar^{n+})$, K-shell vacancy sharing ratio 78—42198
- (Al+Si)-Si thin films, struct. transitions and phase comp. 80—49537
- $Al^+ +Al$, 25 MeV, K-shell double ionis., K$\alpha\alpha$ and K$\alpha\beta$ obs. 77—57918
- $Al^+ +N_2(O_2)(N_2O)$, reaction cross sections 77—29000
- Al^{n+} +S(Ar)(Al)(Cu), K-shell vacancy sharing ratio, foil or gas target 78—42198
- Al_2, repulsive region ground state pot. curves, SCF with STO basis set calc. 80—14188
- Al_2^{6+}, repulsive region ground state pot. curves, SCF with STO basis set calc. 80—14188
- Al_5, chemisorpt. of Na, Si and Cl, core hole induced electronic relax. 79—90874
- $Al_2^-(Al_2^-)(Al_2^+)$ configurations, ab initio study, LCAO, STO, MO-SCF and CI calcs., binding energy *(French)* 80—91447
- $AlCl_3$-Al chemically deposited photosensitive cells, photovoltaic characts. 79—39303
- $AlGe_3N_3$-GaAs structures and MISFETs based on them 79—60932
- AlIX-XII, plasma, X-ray line radiation, radiation transport eqns., calc. method 80—64777
- $Al_xMo_6S_8$ Chevrel phase, synthesis, stability and characts. 80—71608
- α-Al_2O_3 fibre FP reinforced Al and Mg composites, fabrication and props. 80—81004
- Al_2O_3/Al soldered samples, UTS and fracture surface comp., 20 to 500°C 79—38941
- Al_2O_3-Al, disordered, energy diagram model 79—56110
- Al_2O_3-Al, multiphase thin films, correlation between optical props. and chemical/metallurgical constitution 78—19588
- Al_2O_3-Al interface, AES depth profiling, appl. of tailored modulation techniques 77—15702
- Al_2O_3-ZrO_2, multiphase ceramics, mech. strengthening due to dispersion of non-metallic particles *(German)* 78—60674
- Al(^{2}P) isoelectronic series, Sternheimer valence shielding and antishielding factors 80—18807
- ^{26}Al activity in ureilitic meteorite Kenna 77—41368
- ^{26}Al and partial ionization of solar nebula 79—58282
- ^{26}Al content of Dalgety Downs meteorite 79—75167
- ^{26}Al content of stony meteorites with gas losses 78—32418
- ^{26}Al, cosmogenic, in stony meteorites *(Russian)* 77—9719
- ^{26}Al from meteorites, possible 'record' of solar wind action and luminosity variations 78—61830
- ^{26}Al from red giant stars 80—67712
- ^{26}Al in early solar system, fossil or fuel 77—17387
- ^{26}Al in Fe meteorites and past cosmic ray intensity 79—44422
- ^{26}Al in N.Pacific deep sea sediments, rel. to prod. by cosmic rays in atm. 77—5181
- ^{26}Al isotopic anomalies in solar system, local proton irradiation model 78—93128
- ^{26}Al nucleosynthesis in novae and supernovae outbursts 80—62143
- ^{26}Al, prod. from stellar evolutionary sequence 79—5809
- ^{26}Al, search for effects in Allende meteorite FUN inclusion Cl 79—16896
- ^{26}Al, separation from ^{26}Mg isobar via negative ion mass spectroscopy 80—31146
- ^{26}Al, solar system synthesis limits from carbonaceous chondrites B concs. 79—16897
- ^{26}Al, synthesis in explosive H burning 80—85929
- ^{26}Al, use in meas. Mn nodule growth rate 78—40537
- ^{27}Al in aqueous soln., quadrupolar relax., motions of hydration water mols. 78—64291
- ^{27}Al, in minerals, use as probe nucleus in NQR techniques appl. to geosciences 80—67426
- ^{27}Al ion damage rates in Al 77—84810
- $^{27}Al^+$ ion ranges in Ti(Ni)(Cu)(Mo)(Ag)(Ta)(W)(Au)(Pb), meas. by (p,γ) reson. broadening 79—46729
- Al(111)-Al(111), metallic adhesion 79—73463
- Al|chlorophyll-a|Hg/In, sandwich cell, photovoltaic, rectifying and tunnelling effects 79—1628
- Au/Al thin film, Al diffusion studied by attenuated total reflection method 80—92722
- Au-Al thermocompressional contacts, diffusional zones, phase growth during annealing *(Russian)* 80—75389
- Au-Al/GaAs interfaces, atomic interdiffusion, soft XPS studies 80—65302
- Au-Si-Al structure electrode mass transfer and switching with memory 78—95389
- Au-tetrathiotetracene-Al systems, dark cond., photocond. mechanisms rel. to contact phenomena *(Russian)* 78—52103
- B determ. in high purity Al 77—90707

aluminium continued
B fibre reinforced, fibre/matrix interface reaction during prep. 80—25619
B fibre reinforced, hot pressed forged, plasma sputtered *(Russian)* 78—35330
B fibre reinforced Al, crack tip damage and fracture toughness 79—57093
B fibre reinforced Al, dynamic Young's modulus and internal friction 80—25754
B fibre reinforced Al, fracture toughness 77—70157
B fibre reinforced Al, fracture propag. 78—23823
B fibre reinforced Al, fracture mechanical study, unidirectional composites 78—88520
B fibre reinforced Al, fracture 79—57092
B fibre reinforced Al, hot reverse moulding of tubes, calc. of process optimum parameters *(Russian)* 78—15344
B fibre reinforced Al, impact behaviour under fatigue 80—7661
B fibre reinforced Al, impact damage tolerance and reliability 80—81177
B fibre reinforced Al, interaction between fibre and matrix 80—10712
B fibre reinforced Al, orthotropic elastic stiffness consts., US vel. meas. 80—49289
B fibre reinforced Al, prep. by reaction sintering 79—38769
B fibre reinforced Al, residual stress, internal friction anal. 80—45339
B fibre reinforced Al, stress redistrib. anal., upon brittle fibre breakage 78—48527
B fibre reinforced Al, stress redistribution in fibre elastic deformation failure *(Russian)* 79—47740
B fibre reinforced Al, stressed state nondestructive testing method *(Russian)* 80—40631
B fibre reinforced Al, tensile strength and brittle fracture 80—11707
B fibre reinforced Al, thermal expansion 77—51525
B fibre reinforced Al, thermal degradation of tensile strength, due to fibre strength degradation 78—39861
B fibre reinforced Al, thermophys. props. 80—59745
B fibre reinforced Al, unidirectional, K-calibration and compliance curves 78—88518
B fibre reinforced Al, X-ray investigation of internal stresses *(Russian)* 77—73290
B fibre reinforced Al alloy 6061, cross plied laminate, tension-compression fatigue 79—38940
B fibre reinforced Al composites, corrosion, electrochem. behaviour 79—20225
B fibre reinforced Al composite, strength of fibre-matrix interface and tensile strength *(Russian)* 80—21005
B fibre reinforced Al laminate with discontinuities, fracture 78—19877
B fibre reinforced Al laminate, unidirectional, interlaminar shear strength exam. 78—35434
B fibre reinforced Al laminate, effect of ply by-up sequence on fracture toughness 78—35492
B fibre reinforced matrix, matrix-fibre interaction depend. on metallic dopants *(Russian)* 80—76479
B fibre reinforced strength determ. procedure in annular specimens *(Russian)* 78—95864
B fibre reinforced tensile and compressive strength, prior thermal treatment effect 78—11264
B fibre/Al laminates, use in neutron collimators 79—45506
B reinforced Al laminates, applic. of linear elastic fracture mechanics 77—28893
B-Al, fibre reinforced composite, transverse creep, comparison with laminated Al 77—36587
B-Al cast braid, crystallisation and structuring of Al matrix *(Russian)* 78—52725
B-Al composites, B filament CVD technology, book contrib. 78—48352
B-epoxy-Al sandwich laminate. influence of residual stresses on tensile strength 78—60703
B-fibre reinforced Al, elastic props., 300-4K 77—86066
B-fibre reinforced Al, with imperfect separation boundary, material stability *(Russian)* 80—54307
$BaTiO_3$:Al, 0.05-0.3 wt.%, ceramic dielectric, dielec. and mech. props. 79—8091
C fibre reinforced Al, interaction between components and compatibility, mech. props. effect 80—11761
C fibre reinforced Al, matrix-fibre interaction depend. on metallic dopants *(Russian)* 80—76479
C fibre reinforced Al, mech. props. 80—11708
C fibre reinforced Al composite, CVD fibre coating, diffusion barrier and wetting agent 77—40458
C fibre reinforced Al composite, C-Al contact interaction kinetics 79—20007
CO_2 laser bimetallic mirror coating vacuum sputtering technology 80—35086
CaO:Al, phosphon, luminesc., electron-hole recombination processes 79—65919
CaO:Al, X-ray and UV luminesc., electron-hole recombination processes *(Russian)* 78—76528
$Cd_{1-x}Mg_xTe$:Al, donor-acceptor pair and self-activated luminesc. 77—52161
CdS:Al, cathodolum. on diffusion front 77—32447
CdS:Al photoelectric props., optical absorption vacuum deposited film 78—60162
CdS-Al, ohmic contact stability improved by annealing 78—6443
CdSb:Al, p-n junction formation by laser emission, photoelectric effects *(Russian)* 80—70815
CdSb:Al, p-n junction formation by laser radiation 80—96983
$CdSnAs_2$-Al, surface barrier junction, elec. props., temp. depend. 80—65686
CdTe:P,Al, IR absorpt. investig. of localised vibr. modes of impurity centres 77—52136
Co implantation, replacement collision probability at 4.2K 80—70237
Co_3O_4:Al, elec. cond. and thermo-EMF 80—20231
Cr powders (60 to 70%), spectral determination of Al and Fe 77—90679
Cu, positive muon spin rotation meas. 78—10819
Cu/Al film system, interdiffusion and phase growth kinetics 77—69122
Cu-Al composites, laminar, polycryst., electron diffr. proportional anal. 77—44444
Cu-Al powder mixture, elec. discharge reaction sintering 78—64507
Cu-Al thin film multistructure, Xe^+ ion beam cratering 80—66708
$Cu+X^{n+}$, X=F, Al, Si, S, K X-ray production, target thickness depend. 77—75280
$CuAl_2$ and Al crystals, mutual orientations in terms of lattice disorientations 80—28936

aluminium continued
$DyFeO_3:Al^{3+}$, Morin transition, mag. vacancies effect *(Russian)* 78—27039
$(Eu,Lu)_3Fe_5O_{12}$:Ga(Al)(Ca,Ge), bubble material, dynamic characterisation, comparison between transport and FMR methods 80—39833
EuIG:Al, mag. anisotropy, magnetisation meas. 80—60240
Fe-Ni-Al, cryogenic toughness, strength, rel. to reactive metal addition 78—39885
α-Fe_2O_3:Al, hematite, spin reorientation, Mossbauer spectra obs. 78—72356
α-$Fe_2O_3:Al^{3+}$, substitution effect on Morin transition, neutron diffr. study 80—44827
film, meas. of stress gradients generated by electromigration, X-ray topography and SEM 77—51541
Ga/Al ratio vars. along Reykjanes Ridge and Iceland 79—8617
Ga-Al and Ge-Si fractionation in Hawaiian volcanic rocks 79—12112
GaAs:Al, optical detection of NQR 79—69752
GaAs-Al interdiffusion, 250-450°C, AES meas. 77—1263
GaAs-Al interface, metal overlayer effect on semicond. (110) surface states 77—4441
p-GaAs-Al interface, produced by diffusion method using heavily doped GaAs, rectifying props. 79—28409
n-GaAs-Au(Al) Schottky diodes, interface state density model 77—80840
GaN:Al, VPE grown, luminesc. and elec. props. depend. on doping conc., bound excitons 80—20688
Ge, high-purity, with Al, B and P, residual impurities, photothermal cond. 80—24965
Ge:Al, acceptor levels, Zeeman splitting, far IR photoconductivity spectrum 78—43444
Ge:Al, excitation spectra of shallow acceptors, Zeeman effect, expt. 80—7381
Ge:Al, impurity ground state levels from photo-thermal cond. in mag. field 77—51699
Ge:Al, limiting solubility, rel. to charge carrier conc. 80—24596
Ge:Al, polycrystalline film, electron transport props. 79—99642
Ge:Al, shallow acceptor spectral line intensities 80—88517
Ge:Al, solid solns. decomp. 80—15249
Ge:Al, uniaxially stressed, photoionisation of acceptors, impurity photocond. meas. 78—10509
Ge:Al, Zeeman effect in excitation spectra, photoelectric spectroscopy 79—82633
Ge:Al film, amorphous, ion implantation, effect on cond. 78—83839
GeO_2:Al, Ga, EPR, transferred hyperfine interactions of impurity-related trapped hole centres 77—85568
GeO_2:Al, tetragonal, $[Al]^0$ centre, nuclear Zeeman and quadrupole effects 78—35035
H impurity detection by $^1H(^{15}N,\alpha\gamma)$ reaction 80—55767
H_2 diffusion, desorption meas. 78—30797
H_x^+ + Al surface, x=1,2,3, relative K X-ray yields 77—75282
HF adsorption, by smelter-grade aluminas, during Al smelting 80—80075
He injected, tracing bubble evolution by positron annihilation 77—19992
He, Ne isotopes and radionuclides prod. cross sections induced by 12-45 MeV protons 77—17310
$Hg_{1-x}Cd_xTe$:Al, ion implanted, damage and lattice location study 80—103381
In-ZnO-Al metal-semicond. diode, electrolum. and photoluminesc. spectra 79—99948
n-InP-Al, Schottky barrier height and stability characterisation 80—54786
InP-Al interface struct., low temp. interaction, AES study 80—107661
KCl-Al composite, optical and IR reflectance 78—56465
$KNbO_3:Al^{3+}$, dopant effect on domain struct., etching study 79—56749
$KNbO_3:Ba^{2+}$, dopant effect on domain struct., etching study 79—56749
Li ions stopping power and straggling 80—42908
Li, one-electron calcs. of X-ray absorpt. and emission, jellium model 78—56543
Li-Al-FeS, high temp. battery, ceramic powder, as electrode separators 79—61966
$Li_2SO_4:Al^{3+}$, monoclinic-cubic transform., effect of impurities 79—52744
liquid, calc. of neutron scatt. law 77—47330
Mg positron trapping and bound states 80—2367
MgF_2-Al, flashlamp for I photodissoc. laser 77—79848
MgF_2-Al film substrate tunable external-reflector retarder, computer based anal. 80—53407
MgO:Al, and nominally pure single crystal, thermally stimulated luminesc. rel. to temp., and EPR *(Russian)* 80—84789
MgO:Al, exciton, electron hole energy transfer 78—10998
MgO:Al, hole processes in photostimulated luminesc., electron emission, X-ray irrad., ESR relaxation 79—69889
MgO:Al, impurity-induced UV luminesc. 79—83037
$MgO:Al^{2+}$, short-wave luminesc., V-centre electron recomb., impurity effects *(Russian)* 77—20921
$MgO:Al^{3+}$, defect struct., shell model calcs. 79—99180
$MgO:Al^{3+}$, positron annihilation meas. 77—8681
Mn_3O_4:Al elec. cond. and thermo-EMF 80—20231
Mo fibre reinforced, SEM study *(Slovenian)* 78—84923
Mo reinforced, fatigue strength. surface layer effects 77—12697
Mo-Al, thin film system, phase growth kinetics *(Russian)* 77—43390
Nb reinforced, fatigue strength, surface layer effects 77—12697
Nb-Al proximity sandwiches, supercond. transition temp. and tunnelling meas. 80—7045
Nb-Al-Ge-Cu, rapidly quenched, comp. and phase equilib. 80—76235
Nb-NbO_x-Al/Pb supercond. proximity function, production by RF sputtering and photolytographic techniques 77—43787
NbTi-Al-(Cu-Ni) multifilamentary composite supercond. wire, stability, AC losses 77—76998
Ne-Al^+, hollow-cathode laser, five Al II transitions 358 to 747 nm 77—58316
NiO:Al, Ni self-diffusion, vacancy-impurity complex effects 80—107493
O^+ + Al, Al K-vacancy cross sections, 0.15 to 91 MeV, recoil effects and mechanisms 77—19033
$^{16}O^{x+}$ + Al, energy-loss straggling, charge exchange effects 78—58799
Pb/Bi-I-Al tunnel injected nonequilibrium supercond. struct., diffusive quasiparticle instability, multiple gap states 80—50005
Pb-Al radiation shields, build-up factors for 6.2 MeV photons 79—81093
$Pb_{1-x}Sn_xTE$:Al, elec. props., dopant influence 79—51599
Pd-Al metallisation on Si, Cr thin film used as barrier to interaction of Pd_2Si with Al 77—43724
powder, resist.-sintability *(Japanese)* 80—16228

aluminium continued
Pt-Al, Fermi energy influence on thermodynamic props. *(German)* 80—24619
sheet, speed effects in deep drawing *(Japanese)* 79—52241
Si, nitridation, effects of Fe and Al additions 77—16708
Si particle reinforced Al, internal stresses, X-ray diffr. meas. *(Russian)* 78—23765
Si:Al, absorpt. line broadening 78—95594
Si:Al, acceptor levels, IR spectra 78—67972
Si:Al, binding energy, excited state spectra, photolum., semi-empirical short range pot. 80—44534
Si:Al, bound exciton and bound multiexciton complexes, electronic structure, luminesc. obs. 79—56139
Si:Al, bound exciton and multiple bound electron luminesc., fine struct. 77—48221
Si:Al, bound exciton lifetimes for acceptors 77—80738
Si:Al, bound multiexciton complexes, work function thermodynamic determ. 78—72078
Si:Al, bound-exciton absorption 78—56507
Si:Al, CC Si:Al(Ga), O_2 diffusion, conc. profile meas. 80—79990
Si:Al, compensated substrates for solar cells, effects of Fe and Al 80—94009
Si:Al, diffusion, open-tube high-vacuum method 78—6084
p-Si:Al, diffusion and incorporation of dopant in closed system, elec. props. 77—59026
Si:Al, edge luminesc. spectra of acceptors, multiexciton complexes 78—56517
Si:Al, electron excited, recomb. radiation, high resolution investigation 78—15233
Si:Al, electron irrad. induced defects, transient capacitance study 80—59516
Si:Al, extrinsic detector material props. 77—89797
Si:Al, ion implanted film, elec. prop. impurity depend. 80—24467
Si:Al, localised exciton bound to isoelectronic trap 80—66283
Si:Al, MBE, growth, struct. and elec. props. 77—89458
Si:Al, P-diffused, recomb. centres, thermally stimulated capacitance meas. 77—72834
Si:Al, polycryst. film, grain boundary diffusion, Auger sputter profiling 80—75388
Si:Al, recomb. enhanced migration of interstitial Al 79—82201
Si:Al, spreading resist. calibration using Si:B 80—103690
Si:Al, thermally induced deep levels, TSC meas. 77—31974
Si:Al, valley-orbit splitting of bound exciton states 79—28290
Si:Al effect of dopants on grain growth 80—54575
Si:Al epitaxial layers, nuclear microanalysis of Al impurities $^{27}Al(d,\alpha)^{25}Mg$ 80—61193
Si:Al film, amorphous, ion implantation, effect on cond. 78—83839
Si:Al film, low-temp. diffusion of Al 78—38878
Si:Al p-n lamellar structures, processing by molten Al rich wire thermomigration 78—10068
Si:Al ribbon, edge-defined film-fed growth, Al redistrib. 80—29873
Si:Se,Al, diffusion of Se, solubility and ionization levels, Hall effect and photocond. meas. 79—42486
Si/Al interfaces, chemical bonding states, low energy AES 80—6985
Si-Al, film, quantitative anal. by DC arc optical emission spectroscopy 78—68940
p-Si-Al, ohmic contacts, Si dissoln. and recrystn. effects, computer calc. 80—103749
Si-Al CC Si n-p junction vertical solar cells, Al-plated, photovoltaic effect variation with impurity conc. 79—100522
Si-Al devices, thickness meter for Al contacting layers *(Russian)* 80—36980
Si-Al interface, barrier height anal. including virtual surface states 77—69416
Si-Al interface, electron energy loss spectra of Schottky barrier 77—48290
Si-Al interface in semiconductors, electronic parts, electromigration aspects 80—39355
Si-Al optically thick, plasma, use of multiple photoexcitation to obtain lasing at 44 Å 79—3684
Si-Al Schottky diode, type II localised interface states, Si surface prep. effects 78—39210
Si-Al solid-phase epitaxial growth, substrate effects, SIMS and backscatt. spectra 79—42421
Si-Al system, Si regrowth minimisation methods in Al films 80—15384
Si-Al-Al_2O_3 system, solid phase Si regrowth on sapphire 80—100413
Si-Al-Si, isothermal version of the moving solvent method 79—1824
Si-Cr_2O_3Al, current-voltage characts., oxide film effects 80—70841
Si-Ge:Al, hot-pressed alloy, thermoelec. props. 78—91711
Si-Si_3N_4-Al, photoexcitation of emission currents, I-V characts. *(Russian)* 77—72917
Si-SiO_2-Al, interface barrier energies for tunnel oxides, internal photoemission meas. 80—84512
Si-SiO_2-Al, internal photoemission, pot. barrier height determ. 80—65699
Si-SiO_2-Al MOS surface channel influence on channel-to-contact diode charact. 80—92994
Si-SiO_2-Al structure, mechanical stress at Si(111) surface 78—63921
Si-SiO_2-Al with thick dielec. layer, photoelec. props. 80—92979
n-Si-SiO_2-ZnO-Al, SAW convolver in monolithic MIS struct. 77—23791
Si-TiO_2-Al, current-voltage characts., oxide film effects 80—70841
Si-V_2O_5-Al, current-voltage characts., oxide film effects 80—70841
SiC fibre reinforced Al interaction between components and compatibility, mech. props. effect 80—11761
SiC fibre reinforced Al, thermophys. props. 80—59745
SiC fibre reinforced Al, synthesis by liquid pressing method 80—100816
B SiC, sintered, effect of Al trace amounts on specimen props. 79—83289
SiC:Al, 4H-, 6H- and 3C-polytypes, melt growth and photoluminesc. 77—24885
SiC:Al, g-values, spin temp., determ. from Raman spectra 78—43856
B-SiC:Al, ion implanted, elec. props. and luminesc. meas. 77—12443
SiC:Al,N, blue cathodolum. spectra obs. 78—19574
SiC:Al,N (6H), ODMR for effective-mass-like acceptor 80—93213
SiC:Al (6H), photoluminesc., site-depend. donor and acceptor levels 79—61421
SiC:Al (6H) LEDs, fabrication by rotation dipping technique, electrolum. mechanisms 80—50426
α-SiC:Al diodes, ion implanted, transient characts. of electrolum. 79—24369
SiC:Al epitaxial layers, growth, Al distrib. and solubility 80—15391
$SiC:Al^+$ p-n junctions, elec. props., defect effects 80—15594

aluminium continued
4H-SiC:Ga(Al), photoluminesc. spectra 77—66530
SiC-coated C fibre, compatibility with Al *(Japanese)* 80—71700
$Si_{1-x}H_x$:Al, amorphous, co-sputtered Al modification, electronic and optical props. 80—100461
SiO-Al multilayer capacitors and inductors, heat treatment effect on elec. props. 77—32082
SiO_2, Al implantation, in MOS struct., trapped charge location, using photo I-V technique 79—15227
SiO_2 film, Al implantation, in MOS struct., electron traps characts. obs. 79—15226
SiO_2:Al, vitreous state, EPR of Al defects 78—91951
SiO_2:Al film, ion-implanted, electron trapping behaviour 78—67729
SiO_2:Al gel, gamma rad. effects, depend. of H_2 adsorption and colour centre form. on Al content 79—69156
Si⟨111⟩/Al/Si, growth kinetics of ⟨111⟩ Si through Al layer by solid phase epitaxy 79—28236
Sn diffusion, and surface segregation in limit of small conc., AES study 79—82384
SnO_2-Cu_xS-ZnS:Mn,Cu-Al_2O_3-Al, light-emitting struct., cond. and electrolum., heat treatment 80—97345
Ti-Al diffusion coatings on C steel, struct. and props. 79—57156
Ti-Al-Mo-Sn-Si, type IMI 680 and 551, stability of martensitic phases 80—7574
Ti-Al-V (6, 4 wt.%), type IMI 318, stability of martensitic phases 80—7574
Ti-anodic oxide-Al, electronic cond. *(French)* 79—95512
Ti-W/Au metallisation on Al, temp. stability, barrier props. 79—23868
Ti+Al coating on steel 45, failure during high temp. creep in NH_3 79—11731
TiC coating on C fibre, by CVD TiC coated C fibre compatibility with Al *(Japanese)* 79—78898
TiO_2:Al, polycrystalline photoanode, improved solar efficiency 79—96479
U_3O_8-Al cermet fuel for research reactors 79—9835
V/Al-Al_xO_y-Pb tunnel junction, superconducting transition, critical currents, Josephson effect *(Russian)* 80—29507
V-Al junction, spin-dependent electron tunnelling 79—19700
VO_2:Al, phase transforms., influence of nonstoichiometry 77—85274
VO_2:Al, photoacoustic effect study of phase transitions 80—69615
VO_2:Al, thin layer prep. by reactive DC sputtering, doping effectiveness *(German)* 78—6847
VO_2:Al layers, liq. phase prep., resist.-temp. behaviour *(German)* 77—77435
V_2O_3:Al, struct., props., rel. to V_2O_3:Cr, X-ray diffr. and elec. resist. obs. 78—2531
vacancy, electron and positron densities and temp. depend. of positron lifetime 78—19001
W fibre reinforced Al, alloying element effect on interface form. *(Czech)* 77—85963
W reinforced Al, melting under weightlessness *(Russian)* 78—23691
W:K-Al-Si, state of bonding, distribution of impurities 78—92212
W-Al fibrous heat treated composites, thermal stress anal. 77—46943
YIG:Al, diamagnetically substituted, annealing effects on cation distrib. 79—1455
(Zn,Cd)S:Cu,Al, luminesc. efficiency deterioration due to surface oxidation by $(NH_4)_2Cr_2O_7$ thermal decomp. 80—29810
Zn diffusivity along grain boundaries, grain boundary struct. effects 77—20128
Zn:Al, ion implantation, temp. and time depend. 80—65013
Zn:Al, ion implantation of Al, defect flow induced outdiffusion 78—63779
Zn:Al, residual resistivity, numerical calc., Fermi surface and multiple plane wave band struct. 77—51722
Zn_3P_2-Al, diode, spectra response meas. of minority carrier diffusion length 79—78131
ZnS:Ag, Al and ZnS:Cu, Al, LV cathodoluminesc. 79—33844
ZnS:Ag, Al(Cu), trap parameters, thermostimulated luminesc. and cond. meas. *(Russian)* 77—72868
ZnS:Ag,Al, computer calc. of band model for luminesc. and photocond. *(Russian)* 78—52542
ZnS:Al, IR studies of Al complexes 79—33741
ZnS:Al, luminesc., exciton struct. 79—33801
ZnS:Al, signal enhancement by field modulation, ODMR expts. 78—56406
ZnS:Al, UV spectra 77—12404
ZnS:Al,Cu(Ag)(Au) phosphors, luminesc. excitation spectra and exciton struct. 80—55164
ZnS:Al phosphors, luminesc. excitation spectra and exciton struct. 80—55165
$ZnS:Al^{3+}$, $Cu^+(Ag^+)$, interimpurity luminesc. at high press. 78—19532
ZnS:Cu, Al phosphors, mechanism of IR stimulated and quenching 77—69881
ZnS:Cu,Al phosphor, shallow hole traps 78—31237
ZnSe:Al, current switching mechanism *(German)* 79—28385
ZnSe:Al, defect struct., Hall effect and Zn self-diffusion meas. 79—1427
ZnSe:Al, effect of thermal treatment and doping on elec. props. 77—85223
n-ZnSe:Al, free carrier absorpt., 80-300K 77—63432
ZnSe:Al, high temp. electron mobility, lattice scatt. and ionized impurity scatt. 79—91042
ZnSe:Al, Schottky diode, direct impact excitation of luminescent centres 79—7900
ZnSe:Al, single cryst., diffused, blue luminesc. 78—39584
ZnSe:Al, thermally stimulated transients, new approach 79—38086
ZnSe:Al, vapour phase doped, thermodynamics 79—90686
ZnSe:Al single crysts., photoluminescence spectra *(Russian)* 77—28627
ZnSe:Al(Mn), elec. and luminesc. props. 77—39844
ZnSe:Cu, Al, single cryst., low-voltage red cathodolum. 78—80423
ZnSe:Cu,Al, LV cathodoluminesc. 79—33844
ZnTe:Al, ion implanted and annealed, photoluminesc. meas. 78—15208
ZnTe:Al, pure and doped, Zn vacancy energy levels, elec. and optical props. 79—4827
ZnTe:Al,Cl, photolum., complex acceptor, ionization energy 80—20693
Zr/Al, getter for TFTR Flexibility Modification, in-torus surface pumping 80—95451

aluminium alloys
see also aluminium compounds
1201, preliminary forging effects on struct. and mech. props. of extruded sections *(Russian)* 78—80564

aluminium alloys continued
2017A, low-cycle fatigue, effect of direction of first half-cycle *(French)* 77—25236
2024, shock-loaded, recovery of Young's modulus 78—23751
2618 A, Al alloy, crack closure effect *(French)* 79—20172
6061-T6, thickness depend. of G_c for shear lip propag. from single crack propag. 78—11305
7039 alloy, high strain rate compression 79—29137
7075-T6, H_2 effects and Cd segregation to grain boundaries 78—84764
accelerated fatigue-resistance evaluation by programmed stress-amplitude increase 77—73386
accumulation of damages in stress concentration zones in alternating creep and fatigue 79—100261
acoustic emission power, strain rate depend. 77—4808
acoustic emission response in type 7075-T6 79—87801
acoustic investigation of ageing 79—34083
acoustic stress wave emission during plastic deform., dislocation motion explanation 77—36697
acoustic-emission signals, rel. to struct. of D16T alloy 79—52297
adhesion with Ni-SiC coating, metal interdiffusion *(Russian)* 80—66697
adhesive bonded multi-ply laminate of 2024-T81, effective remote stresses and stress intensity factors 77—73328
adhesive laminate, fatigue crack growth 80—16424
AE spectra, laboratory comparisons 80—108658
age hardening AZ5G, heat treatment effect on mech. props., microstruct. *(French)* 77—52370
age-hardenable, extraction of precips., electrochem. method 77—32735
aged, local plastic strain distrib. by selected area channelling patterns 77—44349
ageing, high temp. effect on endurance of thin walled joints of alloy AK4-1T1 78—80570
ageing effect on hardness and tensile props. rel. to delay time till quenching, in alloy 7001 78—92286
AK4-1, preliminary forging effects on struct. and mech. props. of extruded sections *(Russian)* 78—80564
AK4-1 alloy, sheet mat., fatigue and corrosion fatigue strengths, coatings effects *(Russian)* 78—11397
AK7, AK5M2, AK5M7 liquid, kinematic viscosity temp. depend., porosity, H solubility, supercooling *(Russian)* 80—54425
Al alloy, welded, behaviour in sea water desalting conditions, corrosion behaviour of welded alloys *(Japanese)* 77—25192
Al-Cu(4wt.%), θ' precipitation, effect on Young's modulus, electron microscope obs. *(French)* 79—47689
Al-Mg alloy N4, irradiation with 100 and 400 keV Al ions, obs. and analysis of damage struct. 77—4133
Al-Si (2.4 wt.%), liq. fluidity, solid-liq. coexisting zone *(Japanese)* 80—15175
Al-Zn-Mg (5,1 wt.%), decomp. process, TEM study 80—71660
Al-Zn-Mg (6, 3 wt.%), water vapour embrittlement and H_2 bubble form 78—15564
Alclad, 2024-T3, dimpled loaded-hole fatigue strength, effect of interf. 78—72948
Alinco 5, thermal treatment in mag. field, mag. props. 78—91905
alloying additions, effects on cond. 80—3205
Alnico, 5 and 8, spinel type permanent magnet, magnetic aftereffect 77—16118
Alnico, domain struct., variation under influence of heat treatment *(Russian)* 78—23292
Alnico, high-energy magnetic materials technology developments and props. *(Italian)* 80—54914
Alnico 5 alloy, S and Ti additions effect rel. to non-metallic inclusions, coercive force and grindability 80—89375
Alnico 5 and 8, spinodally decomposed magnetic alloy, magnetic flux temp. coeff. *(Japanese)* 78—35006
Alnico 8, permanent magnetic alloy, topography of precipitate phase *(Chinese)* 80—66512
Alnico alloy, C addition effects on struct. and mag. props. 78—23835
Alnico alloys, effect of Ce addition on mag. props. 78—2699
Alnico type YuNDK25DA alloy permanent magnets, thermal mag. hysteresis 80—75818
alumel, B versus H measurement from 25 to 180°C 78—23297
Alumel, thermocouple alloy, heat treatment effects on thermoEMF and mag. flux 77—63235
alumel-chromel, thermocouples, neutron irradiation effects *(Russian)* 77—82515
aluminides of non-magnetic transition metals, atomic volumes deviation from additivity 79—82178
analysis by ion microprobe, quantitative, using matrix ion species ratios 78—61070
annealed alloy 1100, thick walled cylinder, finite strain pressure-tension loading 77—32632
anodic dissolution in $NaClO_3$ and NaCl solutions compared *(Russian)* 80—21290
anodic finish exam. by SEM and electron probe micro anal. obs. 79—96278
anodic oxidation, direct coloured oxide layer *(Rumanian)* 78—23852
anodic oxide film arborescent structure formation *(Russian)* 80—35409
anodic oxide film hardness, effect of pH and metallic additives *(Japanese)* 77—56146
anodic oxide mechanical properties and influence on fatigue behaviour 77—44408
anodisation in CrO_3 solns, film colour/structure relationship *(Russian)* 79—91851
anodised 2024-T351 rods, humidity and coating thickness effects on fatigue in reversed torsion 77—25205
anodised oxide films, for adhesive bonding appls., AES and SEM study 80—66689
anodized, corrosion fatigue endurance *(Russian)* 77—16724
Auger spectroscopy produced in glow discharge *(Russian)* 78—14545
axial load, asymmetrically applied, sensitivity of strength 79—66126
beam, higher modal plastic response 77—50948
binary, rapid quenching, struct. and decomp. 80—76244
binary alloys, exam. of dislocation structure, using diffraction electron microscopy *(Russian)* 79—10857
binary dilute alloys, neutron irradiated, suppression of radiation damage microstruct. by trace impurities 79—77643
α-brass, Al bearing, high temp. relief cavitation, SEM, STEM, TEM, SIMS and EDX anal. 79—5039
brass condenser tubes, XPS study of protective layers 80—35383
brass leaded, effect of Al, Sn, Fe on solidification, differential thermal analysis exam. *(Russian)* 79—29041

aluminium alloys continued
Br.AZhNMts 7-2.5-1.5-9 bronze, Mg-Al, type, fatigue and stress corrosion cracking, welding effects 80—3233
bronze, Al, wear on 13% Cr steel in presence of aviation fuel 80—11781
bronze, Al and Ti, sintered frictional material, wear resistance, effect of matrix struct. 77—28911
bronze, creep forging 77—59848
bronze, electrode strip, short-time sintering 77—1824
bronze, O free, annealing in photoemission electron microscope, twin density recrystallised grain size relation *(German)* 78—52850
bronze, superplastic, low cycle fatigue 78—27632
bronze plasticity of two-phase coarse microstruct.-material *(German)* 77—59882
buckling under axial compression on circ. integrally stringer-stiffened shell 78—63346
burst acoustic emission during Bauschinger effect in 6061 and 2024 77—48475
calorimetric studies of 7000 series, comparison of 7075, 7050 and RX720 77—86037
calorimetric studies on 7000 series, matrix precipitate charact. of 7075 77—86036
cast, forging and heat treatment effects on diamond planishing treatment 79—43237
cast AL15V, brittle, strength in three axial stress state 79—66134
cast struct form. in continuous casting *(German)* 78—92256
cathodic protection in seawater, sacrificial anode performance 79—57246
cavitation-erosion by hydraulic liquids, assessment using ultrasonic dispergator 80—71832
Cb Tb-Cu-Al, mag. props. *(Russian)* 77—51905
charge perturbations around impurities, NMR anal. 77—85582
chevron fracture in tube reduction by spinning in alloys 7178 and M580 78—64664
chromel-alumel thermocouple readings, stability prediction 77—87760
circular plates with work hardening, nonlinear behaviour, experimental deflection and strain data 79—38893
coated, filled fluoroplastic coating effect on fretting corrosion resistance *(Russian)* 77—59972
coatings, for high temp. alloys, process development and props. 80—40614
coldworked fastener holes, elastic-plastic boundary layer determ. in type 7075-Tb 79—34066
coloured anodisation without organic dyes 79—79176
columnar to equiaxed transition on solidification 77—63655
commercial, slow fatigue crack growth and threshold behaviour in air and vacuum 80—30062
compacts, specific press. for extrusion 79—20070
composite matrix, reinforced with fibrous and particulate nonmetals, wear friction 77—4758
contamination, automated nondestructive inspection 80—16629
continuous precipitation, nucleation, spinodal decomposition 80—3061
corrosion, monitoring using polarisation resistance meas., techniques and correlations 77—16711
corrosion behaviour evaluation, for heat exchanger appls. 80—85092
corrosion characteristics in ethylene glycol-water mixtures 78—7095
corrosion fatigue strength, influence of surface layer *(Japanese)* 80—16574
corrosion fatigue strength, tensile prestrain effects *(Japanese)* 78—56819
corrosion fatigue testing, galvanostatic vs. potentiostatic control 77—40467
corrosion in uninhibited alcohol/water coolants 78—44248
corrosion inhibition by organic dyes, protective compound form. 78—44255
corrosion monitored by acoustic emission 77—90499
corrosion potential/time, and potentiostatic polarisation curves as a method of predicting corrosion 80—45419
corrosion studies of materials for nucl. reactor applic. 77—34402
corrosion testing in industrial atmos. of O1920 *(Russian)* 77—70205
crack arrest toughness, used to estimate plane strain fracture toughness 77—63863
crack closure during fatigue crack growth, for two thicknesses of alloy BS 2L71 78—68792
crack closure in 2219-T851 specimen 78—7012
crack growth rate prediction under creep conditions 80—85107
crack initiation at high strain rates, uniaxial and biaxial tests 80—85141
crack opening displacement, expt. and FEM study 78—68811
crack opening stress level in fatigue, determ. by eddy current technique 80—16617
crack propag. toughness testing 77—44449
crack propag./wear rate relationship 78—3232
crack propagation, part through, by alternating bending stress in 2017-T3 *(Japanese)* 78—27607
crack propagation and closure, tensile overloads effects in 7050 79—43384
crack propagation rate and crack closure, mean stress effects in 7050-T76 79—52336
crack tip closure assessment by electron fractography, in type 2124 T351 80—19875
crack tip opening under cyclic loading, effect of environment and R ratio *(French)* 80—65145
crack tip opening under cyclic loading, environment and R-ratio effects 80—45377
crack tip studies, stretched zone and COD 78—68812
crack-closure in single overload in single-edge-notched specimens of 7075-T6 77—56066
creep and recovery under combined stress, viscous-viscoelastic model representation in type 2618 79—34117
creep bahaviour prediction, physically consistent method for type 2618-T61 80—66610
creep crack growth 80—60976
creep crack growth rate, temp. and cyclic load effect in type 2024 *(Japanese)* 79—83302
creep curve scatter in alloys D16T and AMg6 77—63762
creep deformation investig. using method of precision lattices 77—86250
creep life, remaining estimation from creep crack density meas., for alloy RR58 78—44194
creep of materials with different properties in tension and compression 80—81129
creep rate and fracture, effects of prior stress history 77—4829
creep rupture props. of A356-T61 78—27612
creep rupture testing, metallographic studies of fracture test specimens 77—63862

aluminium alloys continued
creep-rupture tests over long-times 80—76434
critical pitting potential meas., review 79—43501
critical stress intensity factor determ., fatigue tests on notched specimens *(French)* 78—35502
cryogenic, 1201 and 01381, fracture toughness and structural strength 77—59927
cryogenic, mech. props. of AMg5 and AMg6 at −196°C 77—63748
cryogenic constructing material, far IR spectral refl. 77—24855
cryogenic welded vessels, type D20, structural strength 80—16477
Cu-Al, FCC, study of dipoles using weak-beam electron microscopy 78—22724
Cu-Al (24.0 at.%), eutectic systems, specific phase boundary enthalpy, calorimetric study *(German)* 79—29016
Cunial MNA13-3, Mn addition effect on props. 80—21035
cyclic and monotonic crack propag. in high toughness type 7010-T7651 80—108528
cyclic plastic strain damage eval. and summation in high strength alloys 79—57060
cyclically deformed, high strength, hydrogen embrittlement 78—31584
cylindrical parts, crack detection by two channel eddy current inspection unit 78—72998
cylindrical specimens with crack. fracture characts. in inelastic strain, test methodology 80—25839
D16, Fe and Si impurity effects on K_{Ic} 78—84990
D16, preliminary forging effects on struct. and mech. props. of extruded sections *(Russian)* 78—80564
D16 alloy, sheet mat., fatigue and corrosion fatigue strengths, coatings effects *(Russian)* 78—11397
D16 alloy rod, wave profiles generated by short shock pulse 78—6125
D16 extruded rod, substruct, anisotropy and decomp. at subboundaries *(Russian)* 77—25095
deformation at ageing temp., effect on struct. and props. of type 2036 80—7605
deformation at large plastic strains, work hardening rate 79—20065
deformation processes in sheet materials, application of failure maps 78—56718
delayed retardation phenomena of fatigue crack growth, exam. 78—56745
desorption of neutral mols. by electron and ion bombardment of vacuum material 6061 78—95229
determination by spark-source mass spectroscopic anal., sensitivity calibration 78—68962
die casting, heat transfer coeff. 79—81685
die casting, steel mould thermal fatigue 79—24619
dilute, cold worked, internal friction peaks 80—97520
dilute, depend. of electron scatt. rate on lattice relax. 77—69311
dilute, diffusion thermopower, inelastic electron-phonon interaction 80—96851
dilute, elec. transport and deviations from Matthiessen's rule 80—65524
dilute, Hall coeff., calc. by 4-OPW approx. 78—76052
dilute, Matthiessen's rule deviations in strong mag. field 80—44571
dilute, neutron irradiation 78—22766
dilute, quenched, foreign element effects on dislocation loop form. 80—54239
dilute, recrystallisation during hot rolling 79—47732
dilute, size effect, valency factor and point defect interactions 79—51143
dilute, size effect of impurity atoms rel. to trapping radii for migrating self-interstitials 78—75690
dilute, with 3d or 4f elements, XPS, virtual bound state 78—15285
dilute alloys, elec. resist., impurity and temp. depend. 80—65526
dilute binary alloy, residual resistivity 77—1406
disc, quality factor of vibr. rel. to gravit. radiation detector 78—75093
dislocation dynamic props., investigation by impact loading for alloy D16 *(Russian)* 78—85069
dislocation loops, multiple-faulted, in quenched material, TEM obs. 77—27887
dispersion hardened with refractory carbides, sintering 79—74118
dispersion strengthened, made by mech. alloying 78—3136
dispersion-hardening, AK4-1, US effects on ductility and thermal resist. *(Russian)* 77—32582
double ligament tensile test in deformation processing 77—32753
drilling accuracy *(Japanese)* 79—100181
ductile erosion, prediction, mechanistic model 77—12709
ductile fracture, microvoid effects in type 2024-T4 *(Japanese)* 80—108542
ductility effects during plastic deform., rel. to struct. changes and hot forming 78—23770
Duralumin, adsorpt. of Hg, effect on mech. strength, creep, fatigue, embrittlement *(Russian)* 79—29267
Duralumin, attenuating shock waves, following meteoroidal impact *(Russian)* 77—71068
Duralumin, contact angs. meas., aq. ethanol (glycerine) solns., 20-70°C 78—56025
Duralumin, contact resist. against metals, for high compressive stress and high current density 77—59324
Duralumin, D16AT alloy, residual stresses in samples with hole in static and cyclic tension 80—3149
Duralumin, effect of alloy purity and ageing on fracture mechanism, and resultant toughness 79—5049
duralumin, elastic-plastic stress anal. by photoelasto-plastic method and X-ray method *(Japanese)* 78—13978
Duralumin, endurance limit and corrosion resistance *(Russian)* 77—16720
Duralumin, fatigue cracks development, intermetallic inclusion influence 79—38962
Duralumin, gas evolution obs. under electron bombardment *(Russian)* 79—1460
Duralumin, lifetime after preliminary plastic deform., kinetic theory of strength 79—43395
duralumin, shock-compressed, compression and rarefaction waves obs., 150-250 kbar 77—77535
Duralumin 2017, superplasticity *(Korean)* 79—38902
Duralumin rod, dynamic bending and residual deformation *(Russian)* 80—75293
Duraluminium, surface erosion due to US activation *(German)* 79—57122
Duraluminium rings, stress/strain relations, compression and tension tests, rigid plastic theory 79—34098
dynamic material behaviour under nearly uniaxial strain conditions, modified Kolsky apparatus 78—85070

aluminium alloys continued
elastic moduli, temp. depend., −196 to 1000°C 80—6451
elastic moduli, temp. depend. *(Japanese)* 77—59840
elastoplastic bending of beams of various cross section 78—3196
electric connectors, Al/Cu bimetal, galvanic corrosion elimination 80—35387
electric field effect on strength, hardness 80—50714
electrode, corroding, acoustic emission 80—60997
electroforming, study of process variables in the electromagnetic bulging of tubes 78—80582
electron beam welding, glow discharge appl. 79—73052
electronic charge density around 3d-transition metal impurities 78—34799
embrittlement by cathodic H_2, surface film effect 78—64643
endurance at elev. temp, of strip with loaded hole, alloy AK4-1T1 77—86181
endurance determ. method over wide range of load asymmetry 78—56836
energy absorption during uniaxial tension and axial compression, geometric and heat treatment effects 77—73312
energy dispersive X-ray fluoresc. spectrometry, computer directed optimisation 80—45585
engineering problem solution, review 77—66605
epoxy bonded sheet, fatigue crack initiation, propagation 79—15776
epoxy resin-Al alloy 5086, scarf joint test specimen, mixed mode adhesive fracture, bond angle effect 78—68768
erosion by ball bearing impact 79—61740
erosion damage, temp. effects 79—34156
eutectic alloys, unidirectionally solidified, solidification and morphology relationship 80—25684
extrusion, purity effect on fracture props. 79—100248
extrusion type 7050, corrosion fatigue crack growth tests 77—36703
failure kinetics, method for investigating under long-term static loading in corrosive medium 80—85110
fatigue, alloy 2024, loading sequence, normal and reversed sequence effect 78—68791
fatigue, effect of intermediate thermomech. treatments, in 7050 79—8352
fatigue, low cycle, prior treatment effect on type RR58 at 423K 80—104254
fatigue, low-cycle, of types 2017A, 2014, 2618A, 7049A, 7050, 7075, under applied stress and strain *(French)* 79—74250
fatigue, mechanoenvironment effects 77—32717
fatigue, microcrack development, acoustic SHG study 80—35440
fatigue, total life estimation of notched and cracked members 79—77015
fatigue and failure mechanisms in modified type 7075 79—100252
fatigue crack, low growth rate 78—64701
fatigue crack, microfractographic charact., low temp. effects *(Russian)* 77—70147
fatigue crack arrest, corrosive environment, at low stress intensities 78—92415
fatigue crack closure, and delay effects under mode I spectrum loading, elastic-plastic anal. 80—19282
fatigue crack closure 80—16420
fatigue crack closure determ. using elec. pot. method, cf compliance method 78—5701
fatigue crack closure for 2024-T3 alloy 78—72833
fatigue crack closure in vacuum and air in type 7175 80—21065
fatigue crack closure with negative stress ratio, following single tensile overloads in alloy 2024-T3 78—64687
fatigue crack delay behaviour, alloy 2024-T3, effect of stress level 78—68790
fatigue crack growth, crack closure 78—80650
fatigue crack growth, delayed retardation phenomena, stress ratio at baseline loading effect 79—79065
fatigue crack growth, delayed retardation phenomenon, from single overload in A2017, A5083 78—92317
fatigue crack growth, effect of frequency changes 78—64693
fatigue crack growth, environment effect in types RR58 and LM30 79—79171
fatigue crack growth, exam. of some aspects 78—56772
fatigue crack growth, Paris's law 78—39902
fatigue crack growth, R-curve concept appl. in types 2024-T3 and 2219 79—61733
fatigue crack growth, stage I, effect of liquid environment 77—86164
fatigue crack growth and fracture resistance meas., at 295, 111, 76 and 4K 78—35509
fatigue crack growth data, three component model anal. 80—3161
fatigue crack growth in D16AT and V95A sheets *(Russian)* 77—52463
fatigue crack growth in type BS2L71, effect of mean stress and thickness 79—61710
fatigue crack growth in ultrahigh vacuum *(Japanese)* 77—56088
fatigue crack growth model, notch analysis of fracture approach, Al 2024-T3 and Al 7075-T6 78—52984
fatigue crack growth rate, kinetic eqns. of temp. depend. *(Russian)* 77—25136
fatigue crack growth rate change on decreasing temp. in D16AT and V95A sheets *(Russian)* 77—59894
fatigue crack growth testing, A356 T6 and 2219-T851, decreasing stress intensity technique, computer-controlled 78—72949
fatigue crack initiation, computer simulation 80—100893
fatigue crack initiation, effect of intermetallic comp. and microstruct. 79—5054
fatigue crack propag., 293 to 463K, alloy RR58 77—16672
fatigue crack propag., effect of overloads *(French)* 78—19892
fatigue crack propag., load interaction effects 77—56055
fatigue crack propag., mechanism of overload effect 78—56730
fatigue crack propag., plastic work role in types 2024-T4, 2219-T861, overaged 2219 79—79070
fatigue crack propag., statistical nature in type 2024 T3 80—35330
fatigue crack propag., stress ratio effect in 7075-T6 *(Japanese)* 79—38946
fatigue crack propag. and closure, repeated loading under low stress intensity *(Japanese)* 80—30077
fatigue crack propag. and fatigue life, shallow notch effect *(Japanese)* 79—29199
fatigue crack propag. and fractography under periodic overstressing, exam. *(Japanese)* 78—52958
fatigue crack propag. at low ΔK of types 2024-T3 and 7075-T6 79—83291
fatigue crack propag. in air and vacuum *(French)* 78—15518

aluminium alloys continued
fatigue crack propag. near threshold conditions, environment and load ratio effects 80—55522
fatigue crack propag. rate and stress intensity factor at varying stress ratio 78—7049
fatigue crack propag. rate rel. to accumulated plastic strain rate, cold work effect *(Japanese)* 79—96115
fatigue crack propag. under periodic overstressing, design criterion *(Japanese)* 79—20166
fatigue crack propagation, in alloy BS1477 NP8 80—40538
fatigue crack propagation, in alloys 2024-T3, 7475-T761 80—21105
fatigue crack propagation, stress ratio effect in types L73 and L88 80—71733
fatigue crack propagation, under variable stresses *(Japanese)* 80—86028
fatigue crack propagation in AU2GN under alternating shear load *(French)* 78—44191
fatigue crack propagation rates, stress intensity factors *(French)* 77—25154
fatigue crack propagation under repeated two-step loadings above and below threshold condition *(Japanese)* 79—38945
fatigue crack retardation in vacuum in type 2024-T351 79—79069
fatigue cracked alloy 7075 T6, repair machining and inspection of components 78—80689
fatigue cracking diagrams *(Russian)* 79—29301
fatigue cracks, propagation, model, low cycle, cyclic stress-strain response determinations, for 2024-T351 79—68653
fatigue cracks propagation in type 2024-T351 79—70146
fatigue damage, sum distribs. during programmed tests at 120°C 78—23809
fatigue damage detection by optical correlation in alloy 2024 78—27717
fatigue damage detection in alloy 2024-T3, optical correlation technique 78—35511
fatigue damage in D20 Al alloy, possibilities of inspection on basis of change of natural oscillations freq. 79—57116
fatigue deformation and crack growth, holographic study in type 2024-T3 80—25836
fatigue endurance scatter in transitional region of fatigue curve *(Russian)* 78—56738
fatigue life, effect of stress cycle asymmetry, shape of fatigue curves 77—1873
fatigue life, struct. and microhardness, working conditions effect on alloy D76AT 80—55525
fatigue life distrib., statistical anal., mixed Weibull distrib. *(Japanese)* 78—72841
fatigue life estimation from creep rupture data *(Japanese)* 79—79089
fatigue life prediction, X-ray diffr. method, in type 2024 80—25837
fatigue of fillet welds, peening effect 79—91853
fatigue props. eval. 79—15750
fatigue resistance, low-cycle, in internally heated type AK4-1-T1 80—21077
fatigue resistance improvement by laser shock 80—93654
fatigue strength, low-cycle, isothermal hardening effect 79—38863
fatigue test method, accelerated 80—100981
fatigue testing, exam. of scale relationship of endurance limit 78—60914
fatigue testing, low cycle, effect of testing method on fatigue on type D16 79—52515
fatigue tests with axial and diametral extensometers 78—85062
films, struct. induced electromigration failure, Monte Carlo calcs. 80—49405
FIM and microanalysis, developments 80—100155
FIM and microanalysis developments 78—35782
flexural vibration of beam, forced vibration technique for meas. of material damping 78—19964
foils, preparation for electron microscope exam. by electrospark cutting 77—52590
forge-rolled AK4-1T1 alloy slabs, fracture toughness scatter assoc. with plane deform. 78—7014
forgings, unhealed porosities and crystalline steps *(Chinese)* 79—74178
fracture, dynamic, of Al alloy 6061-T6 cylinder, expt. rel. to Mott's theory 78—64651
fracture, grain size effect 78—60781
fracture analysis of exfoliation 79—43464
fracture anisotropy of OT4-1u and VT14, with varying H_2 content, rel. to loading condition *(Russian)* 77—70148
fracture initiation and propagation during strip drawing 78—64663
fracture mechanics, K_{1c} values determ. in elastic-plastic material behaviour range 80—45376
fracture mechanisms review 80—35296
fracture micromechanisms, fracture toughness, exam. 78—56766
fracture of large second phase particles 78—7010
fracture props., effect of thermomechanical treatment 78—60793
fracture relief formed in fatigue crack growth, rel. to failure mechanism 80—76347
fracture toughness, cyclic *(Russian)* 79—52343
fracture toughness, cyclic and static, low temp. effect in alloy D16 *(Russian)* 79—52344
fracture toughness, effect of specimen thickness 77—70151
fracture toughness, split Hopkinson pressure bar application 80—85140
fracture toughness anisotropy and struct. *(Russian)* 77—25139
fracture toughness determ., dynamic mode II 77—36720
fracture toughness determ., rel. to mech. props. 77—21277
fracture toughness determ. of alloy AK4-1 with surface cracks *(Russian)* 77—25141
fracture toughness of 7075 Al alloy, hydrostatic press. depend., tensile ductility 78—3209
fracture toughness rel. to acoustic emission, 2124-T851 specimens 78—7109
fracture toughness testing, acoustic emission, inspection technique 78—68860
fracture toughness testing with eddy current sensor 80—45459
fracture toughness under plane stress 78—92316
fracture toughness values, wide range specimen thicknesses, new rig design 77—60011
fretting corrosion, exam. of secondary structures 79—100292
fretting fatigue crack form. in type 7075-T7351 80—35344
fretting fatigue cracks, earth growth in type 7075-T7351 80—35345
fretting fatigue tests, effects of environmental H_2O, O_2 78—92407
fusion welding of Al alloys, weld susceptibility to hot cracking 80—81143
galvanic corrosion in tap and artificial sea water of type 1050, 5086, 2024 and 7075 alloys 80—21162

aluminium alloys continued
galvanic couple with Cu, steels, Zn and Ti-Al-V, velocity effect on corrosion 78—35566
gas desorption coeffs., electron- and ion-induced, bakeout temp. effect 79—65329
glass fibre reinforced Al alloy, formed by hot extrusion, heat-treatment 77—24988
glass fibre reinforced Al alloy, formed by hot extrusion, mech. props. 77—24987
glass fibre reinforced epoxy/Al bonded joint, mean strength, moisture effects 79—20106
grain refinement, effect of Al_3Ti, TiC and B 78—52828
granule size distribution, centrifugally atomised melts 79—100080
granules, hot rolling, angle parameters and forward slip 80—25601
granules, lubricants for rolling 80—60980
granules of AK5M2, rolling speed effects 78—60604
graphite dispersed casting, damping capacity *(Japanese)* 79—96059
graphite particle-Al alloy composite, improved damping capacity and machinability 77—4786
graphite particle-Al alloy composite, prod. by pellet method, and mech. props. 78—27454
Gruneisen coefficient, dynamic determ. 77—24418
hardness testing, depth of impression meas., automated 79—15892
heat treatment of semifinished products of alloy 01420 before cold deformation 78—84873
Hiduminium, shallow spherical cap buckling under uniform external press. 77—23902
high strength Al-Zn-Mg-Cu alloys, mechanical props. *(Japanese)* 79—91654
high strength alloy bar stress wave propagation, finite element analysis *(Japanese)* 79—79030
high strength structural mats., microstruct. influences on fatigue and fracture resist. 78—56728
high-strength, quenching using water-soluble polymers 79—38862
high-strength alloy constitutive eqns. and high-velocity deformation *(Japanese)* 79—79029
hot working, struct. states and recrystn. of alloy AK4-1 *(Russian)* 78—19778
HYCSOS chemical heat pump, low grade heat enhancement using $LaNi_{5-x}Al_x$ 80—61467
hydrogen embrittlement of 7075 78—15523
hydrogen induced fracture 79—91837
impact wear, microstruct. effect 80—11791
Indal 3S, corrosion behaviour evaluation, for heat exchanger appls. 80—85092
inelastic cyclic deform. and fatigue 77—63795
inelastic electron scattering by dislocations *(Russian)* 78—79988
ingot, dendrite arm spacing through heat flow control 77—73267
ingots, crystallisation condition effects on fan-shaped zone struct. *(Russian)* 78—3114
interdiffusion, evaporated couple with Cu alloys *(Russian)* 77—43389
internal fatigue crack growth in vacuum 78—56729
K_{1c} determ. method, results scatter *(French)* 77—70167
laminated sheet material, adhesive bonded, fatigue props. 80—50695
laminates, adhesively bonded, axial fatigue 80—40491
laminates, fracture of bonded 2024-T3/7075-T6 78—56722
laser generated stress waves, effect on microstruct. hardness and strength 79—69192
laser surface melted, topographical characts., for 2024 T-351 79—70200
laser surface method, porosity form. 78—44279
limiting plastic props. *(Russian)* 78—88504
loading freq. effect on fatigue growth rate 78—83873
lug, fatigue crack growth 80—30061
Magnico alloy, with Si, Nb, Ti and La, low-temp. thermomag. treatment 77—63812
Magnico alloy, with Si, Nb, Ti effect of Ub on mag. props. and grindability 77—63811
marine atmosphere stress corrosion tests on precracked specimens, corrosion product wedging effect 78—88570
mechanical anisotropy evaluation, using hardness test *(Polish)* 78—48575
mechanical properties, correlation with elect. cond. 79—34114
mechanical props. at 4.2K, reflecting shield appl. *(German)* 80—3081
mechanical props. at cryogenic temps. 79—29206
melt, contact reactions with Fe group metals 78—60879
melt, Ti alloy dissolving, reaction zone formation, component interaction *(Russian)* 80—54377
melt-treatment with granules, effect on mech. props. and microstruct. *(Russian)* 77—44190
melting line slope of Al alloy 2024 77—15553
membrane, lifetime prediction and design 80—71752
metallisation of B, borsic, SiC fibres by continuous coating *(Russian)* 78—35538
microcrack closure load development for stage I and II cracking in Al 7075-T651 77—86150
microcrack closure phenomena in type 2219-T851 79—57097
microcrystalline, rapidly quenched particulates, appl. 80—84887
microfracture characts., failure in repeated loading 77—40490
microstruct. effects on strength, fracture toughness, fatigue cracks 79—43434
mischmetal-$Ni_{5-x}Al_x$ ternary alloys, Al addition effects on structural and H_2 absorpt. props. 79—52761
mischmetal-Ni-Al alloys, H_2 absorpt.-desorpt. characts. 79—95168
molten, determination of H content, using electrochemical probe 79—11843
multicomponent alloy optimum composition for high-strength *(Bulgarian)* 79—15628
multilayer shells, stress-strain state and stability at high temps. 77—54903
multiple notched specimens, fatigue props. of type JIS A5083-0 79—61729
neutron irradiation effects, on microstruct., mech. props. and swelling 79—65121
Ni_3Al-Ni_3Nb eutectic alloy, aluminide coating microstruct. exam. 78—15593
β_1-Ni-Al, premartensitic transformation 78—76645
Nimonic, IN100, γ' precipitates, casting conditions effect on morphology 80—7548
Nimonic 80A, stress dip creep tests 79—74223
Nimonic 90, creep rate stress exponents and friction stress, comparison with Lagneborg particle by-passing model 80—55481

aluminium alloys continued

- Nimonic alloy, effect of annealing on hardness, carbide phase strengthening *(Russian)* 79—34137
- Nimonic PE16, neutron irradiated after heat treatment, solute segregation to pt.-defect sinks 79—78976
- Nimonic type, elastic interphase strains on ageing effects on extinction *(Russian)* 77—66646
- NK, thermocouple alloy, heat treatment effects on thermoEMF and mag. flux 77—63235
- non-transition metal alloying effect on Landau diamag. susceptibility 77—63075
- noncontinuum crack tip deform. of surface cracks 80—104273
- notch sensitivity in fatigue 78—60757
- notch sensitivity in static and repeated loading of high strength V93 78—27639
- notched, cyclic stress/strain behaviour, random fatigue life *(German)* 80—100907
- notched sheet under tensile loaded, notch tip opening/contraction, J-integral relationship *(Japanese)* 77—4840
- optical contrast enhancement by vacuum deposited ZnTe interference layers 78—44301
- overageing effects at 175°C on fatigue crack growth rate in alloy 7075 *(French)* 77—56010
- oxide-covered, characteristic emission of negatively charged particles during tensile deform. 78—92179
- particle strengthened, yield drop and creep minimum *(German)* 78—39881
- phosphor bronzes, surface Cs$^+$ impact, 5.5 keV negative secondary ion emission obs., rel. to Cu *(French)* 77—66562
- pipe, creep-resistant, influence of chem. comp. on formability *(German)* 78—84900
- pit initiation mechanism, alloy type 7075 77—12733
- pit propagation, influence of anions 78—72917
- pitting, rotation effects 79—100281
- pitting corrosion rel. to load-carrying capacity of sheets *(Russian)* 78—56806
- pitting resistance, short duration test and new characterization test 77—90513
- plastic, anisotropic hardening pot., stress/strain relation under combined axial load/torsion 78—52896
- plastic anisotropy of textured sheet in 5052 *(Japanese)* 79—34103
- plastic deform., accelerated yielding of H$_2$ 77—36594
- plastic deform. of 7075, acoustic emission sources 78—27573
- plastic deformation under abruptly changing loading or strain paths 78—56700
- plastic flow in plain strain extrusion, photographic appl. 80—7626
- plastic stress/strain curve, in reverse loading process *(Japanese)* 80—7622
- plastic zone form. and fatigue crack growth 78—64702
- plastically anisotropic, non-associated flow law *(Polish)* 78—80603
- plasticity due to superimposed macrosonic and static strains 78—60719
- plasticity variations rel. to heat treatment *(Russian)* 79—57050
- plate shaped precipitates, growth kinetics 80—3065
- plates with cut, stability loss critical stresses for AMg-6M.D16, AMtsM alloys 80—11690
- post-shock temp. meas. in type 2024 79—92527
- powder, erosion resist. to hot propellant gases 77—56165
- powder metallurgy technology innovations, 1978 status 79—47646
- precipitate free zones, X-ray microanal. 80—108768
- precipitation hardened 2014 and 2219, temp. depend. of elastic constants 77—66673
- precipitation hardening, creep deform. effect 77—16601
- precipitation hardening, effect on dynamic strain ageing and jerky flow 80—20945
- precipitation hardening, positron annihilation investig. by X-ray Doppler broadening 77—81174
- precipitation hardening, prior strain and ageing effect in high purity 6061 77—66651
- precipitation hardening, toughness and microstruct. *(Japanese)* 78—15509
- pressure vessel material, delay effects 78—35515
- prestrain effect on fatigue crack growth and crack closure 77—56049
- pseudoelastic single crystal fatigue 79—52364
- punch stretching, strain and strain rate hardening effects at elev. temps. in type 5182-0 79—56998
- pyrochlore struct. and its relatives 79—14773
- quenching rate rel. to mech. props., residual stresses, optimum quench coolings *(French)* 78—64562
- radiography with gamma rays, using Se electroradiographic plates, comparison with X-ray plates 78—72978
- rare earth alloys, RAl$_2$, ordered, NMR determ. of hyperfine fields 78—84180
- rare earth alloys, RCoAl, mag. props. 78—2659
- rare earth alloys, RCu$_4$Al$_8$, mag. struct. and interactions 80—25092
- rare earth alloys, RFe$_4$Al$_8$, cryst. struct. mag. props. and hyperfine interactions 78—87648
- rare earth alloys, RFe$_4$Al$_8$, mag. props., Mossbauer spectra, ordering effects 77—63179
- rare earth aluminium Laves phase cpds., RAl$_2$, anisotropic magnetostriction, temp. depend. 80—39841
- rare earth intermetallic, RCu$_4$Al, struct. 78—30587
- rare earth intermetallics, RAl$_2$, cryst. field volume magnetostriction calc. 79—8029
- rare earth intermetallics, RAl$_2$, exchange modification of cond. bands 79—82568
- rare earth intermetallics, RAl$_2$, orbital and spin polarisations of cond. electrons 80—65791
- rare earth intermetallics, RAl$_2$-Gd(Er)(Dy)(Nd), dil., (R=La, Yb, Lu), EPR and mag. susceptibility 80—15797
- rare earth trialuminides, long period polytypes, electron diffr., high resolution imaging 78—83781
- rare earth-Al$_2$, cubic Laves phases, prep. and phys. props. *(German)* 78—23075
- rare earth-Al$_2$, mag. coupling mechanism 79—4655
- rare earth-Al, RAl$_2$, spontaneous cell distortion due to cryst. field, magnetoelastic consts. 77—63255
- rare earth-Al Laves phase intermetallics, RAl$_2$, R=Gd, Ho, Dy, Tb, cubic Laves phase compounds, exchange striction determ. 80—44895
- rare earth-Co$_2$-Al, dil., nonmag. impurities effect on ordering temp. 78—84427
- rare earth-Fe-Al alloys, RFe$_4$Al$_8$, mag. props. 78—52250

aluminium alloys continued

- rare earth-transition metal alloys, RM$_{4+x}$Al$_{8-x}$, magnetism and hyperfine interactions, magnetisation and Mossbauer effect studies 80—75892
- rare earth-transition metal-aluminium intermetallics, RT$_6$Al$_6$, T=Cr, Mn, Fe, Cu, cryst. struct. 80—107110
- Rayleigh waves, laser-induced 79—51407
- reactive etching in RF plasma containing halogen species 78—72923
- reactive ion etching, preferential lateral chemical etching 79—83371
- recrystallisation during hot deform. and after cold working 79—47715
- Rene 41, volatilisation of oxides during oxidation at 1200°C 78—23873
- residual stress change in conc. zone in cyclic loading in AMg6 78—3224
- residual stress gradient meas., modified hole-drilling technique 79—29300
- residual stress relax. rel. to temp., load cycling, aircraft struct. appl. 78—7053
- rods axisymmetric motions, experimental assessment of Mindlin-McNiven rod theory 78—1595
- rolled sheet, transverse US wave attenuation, thickness meas. 79—52573
- rolling of granules, temp. and speed effects 79—70015
- SA, thermocouple alloy, heat treatment effects on thermoEMF and mag. flux 77—63235
- SAP 895 (Al-Al$_2$O$_3$) alloy containing ^{4}He and ^{3}H, tensile props. 80—34129
- SAP (Al$_2$O$_3$-Al) alloy, effect of high He$^+$ and H$_2^+$ conc. on microstruct. 80—34098
- saturation of Ti alloys with A and Cr, powder method 77—21052
- SCC, subcritical flow growth, comparison of aircraft alloys in NaCl soln. 78—53028
- screening charge anisotropy around impurities, nucl. quadrupole couplings meas. 77—32286
- seals with phosphate glass, elec. and mech. props., glass transition 80—81018
- selection using fracture mechanics 78—56725
- SEM characterization of surfaces anodized in phosphoric acid 80—81241
- semiquantitative anal. with SIMS, AES and wet chemical anal. 77—48291
- Sendust alloy, magnetic head wear resistance and surface characts. against mag. tape *(Japanese)* 80—35335
- serrated flow and thermomechanical treatment in type 7075 *(Korean)* 80—30026
- sheet, anisotropic, yield strsses and plastic strain rates, directionality correl. 78—23760
- sheet, fatigue tested, fracture surface rotation mechanism 80—11764
- sheet materials, attachment for testing during sign alternating loading 77 -52579
- sheet materials, D16AT, regression anal. of critical stages of fracture process 79—15786
- sheets, type 7004, asymmetrical solidification structures, fluid flow, in W arc welds 78—84794
- shell, cylindrical, buckling under combined axial preload, nonuniform heating and torque 80—53662
- shock-compressed 6061-T6, reshock and release 77—32732
- Silumin, AlSi10Mn, struct. and mech. props., Na modification effects 77—63786
- Silumin, CsSi phase form. due to Cs diffusion 79—38798
- sintering, physical and chemical phenomena *(Italian)* 79—83147
- sintering of powder metallurgy parts, metallographic exam. and hardness testing 77—4752
- slip deformation and low-cycle fatigue damage 77—73301
- solar water heaters, aluminium alloy rolled-welded heating panels production and use 79—96421
- solidification, method for evaluating influence of each element on microsegregation *(French)* 79—74159
- solidification of castings, electrical modelling study *(Rumanian)* 79—74142
- space application, of Al alloy 51S modified by misch metal 80—55466
- specimen preparation for electron microscopy 80—40636
- spectrochemical analysis with glow-discharge lamp *(Japanese)* 78—85262
- spherical shell, three layer, stress/strain relations *(Russian)* 80—3122
- standard resistance, low temp., appl. in resistors and strain gauges 77—17997
- statistical fatigue props. of A5083 and A7075 79—5060
- steel, Al, quenched, tempered, orientation of precipitated Fe$_x$C particles, X-ray obs. *(Russian)* 79—29063
- steel, Al, relax. twins in martensite, electron diffr. and electron microscopy *(Russian)* 78—47391
- steel, Al alloying addition effect on resistance to hydrogen embrittlement 77—59925
- steel, Al-Ti-(Mo), Al-Ti-V-(Mo), Al-Ti-Nb-(Mo) and Al-V-(Mo) low-alloy, toughness improvement through Ti additions 80—66525
- steel, alloy, Fe-Cr-Ni-Mo-Al, (13, 8, 2, 1, wt.%), H$_2$ effects on fracture, exam. 78—60809
- steel, aluminising, thermodynamic anal. of phase transforms. 80—76413
- steel, austenite, martensite cryst. struct. changes on γ irrad. 79—90699
- steel, austenitic, Al-C, microstruct., Mossbauer obs. *(Russian)* 80—29655
- steel, austenitic, Mn-Al, low temp. appl. explosion test of fracture mode *(Chinese)* 78—31496
- steel, cementite isolation, Mossbauer anal. 80—93225
- steel, deformation and fracture resistance due to low-cycle fatigue in plane bending 79—66166
- steel, Fe-Cr-Al, sulphidation behaviour, 750°C, preoxidation effect *(French)* 78—15566
- steel, fine grained C-Mn-V-Al-N, relationship between ferrite and austenite grain size 80—3001
- steel, low C, Al killed, improvement in Al control using rings 77—21049
- steel, low C, Al-killed, effect of V on mag. props. 79—83339
- steel, low C hot rolled sheet, drawability improvement by Al addition *(Ukrainian)* 79—78996
- steel, low-C, Al-stabilised, texturing during annealing *(Russian)* 78—19777
- steel, Mn-Nb-Al-C, crack progag. and hot ductility during straightening concast strand 80—66646
- steel, Mn-Ni-Al, nonmagnetic, carbide-intermetallic strengthening 79—83208
- steel, Nb,(V),(Al), hot-rolling, laboratory simulation, recrystn. of austenite 80—97512
- steel, Ni-Ti-Al, 36NTYu, heavily deformed, subgrain struct. due to discontinuous precipitation of γ' phase *(Russian)* 79—52218
- steel, Si (6.5 wt.%) Mn, Ni and Al additions influence obs., on mech. and magnetic props. *(Slovak)* 79—5064

aluminium alloys continued
steel, Si-Al, non-oriented elec., internal oxidation and nitridation effects on mag. props. 79−83336
steel, stainless, austenitic, CC Ni-Al, γ-phase, fracture mechanical aspects of abrasive friction, wear, chip formation 78−72865
steel, stainless, Fecralloy, creep-rupture props., 650-800°C 80−97535
steel, stainless, fibre reinforced Al alloy, exam. of deformation, fracture and forging behaviour 80−11681
steel, stainless, fibre reinforced Al alloy, tensile props., cryogenic cooling effect 79−61623
steel, stainless wire reinforced Al-Zn-Mg system, resistance to crack propagation 79−43409
steel fibre reinforced Al alloy, corrosion resistance, electrochemical characts. 80−11806
steel fibre reinforced Al alloy, stressed state, NDT method *(Russian)* 80−40631
steel fibre reinforced Al alloy D16T, sheet reinforced by Ti alloy butt straps, fatigue 79−100262
strain distribution near notch tip under mixed plane stress-plane strain condition of 7076-T6 *(Japanese)* 77−8891
strain response to acoustic excitation, statistical props., comparison with C fibre reinforced plastic 79−43502
strength contribution of particles and dislocations *(German)* 79−29080
stress concentration under creep, two dimensional problem solution 77−56044
stress corrosion crack growth 78−19930
stress corrosion cracking, active path form., electrolytically notched specimens 77−16713
stress corrosion cracking, active path formation 80−85077
stress corrosion cracking, of AA7075 effect of orientation and loading history 78−95835
stress corrosion cracking, role of H_2, state of art review 80−61017
stress corrosion cracking control measures 77−90509
stress corrosion cracking protection, by γ_1-Al_2O anodic film 78−95836
stress corrosion cracking testing 79−20296
stress corrosion susceptibility, water vapour reaction, STEM study 80−3247
stress depend. of US velocity, in alloy A3B2 *(Japanese)* 78−26629
stress intensity factor specimen design, constant factor for crack length range 77−73380
stress measurement, US method, calibration expt. results *(German)* 80−53725
stress relaxation in cyclic deformation, in type 6351 and 6061 80−3119
stress-rupture data correlation 77−44346
stress-strain behaviour at large strains 77−52442
stress-strain diagrams, for complex cyclic loading of alloy PA6 80−16372
stress-strain state after treatment by pressure, moire strip method appl. *(Russian)* 80−40648
structural alloys for superconducting magnets in fusion energy systems, props. at 4K 80−86976
subgrain-strength relationship, effect of alloying and processing 77−32606
substitutional solid solution alloys, volumetric effect and props. *(Russian)* 80−39293
substrate, Cu plated, for Antares CO_2 laser mirrors 80−14349
substrates for Ni coatings, adhesion strength, meas. using microindentation method 80−40640
superplastic eutectics, tensile deform. behaviour *(Japanese)* 78−27558
superplasticity of V96Ts alloy 79−52326
supersaturated solid soln., decomp. process, electron microscope obs. and acoustic anal. *(Russian)* 79−15650
surface, electron beam impact, time-varying evaporation 79−10942
surface chemical cleaning, Pourbaix diagrams appl. 79−83380
surface composition of 2024-T3 adherend surface, chem. and thermal treatment effects 78−39939
surface corrosion effect on fatigue resistance in clad D16ATV *(Russian)* 78−31576
surface layers, cross-sectional struct., appl. of cryogenic fracturing technique 77−30219
surface preparation for adhesive bonding, surface characteris. techniques 77−56132
surface shot blasting, prep. for plasma deposition 80−16586
Swift effect, dynamic and static response to simple compression, tension and torsion 77−28858
Swift effect, in twisted tubes 77−28859
Swift effect, rel. to stress/strain behaviour in simple compression, tension and torsion 77−28860
Temp-1 system for the ultrasonic inspection of bulky aluminium alloy plates 80−66755
tensile deformation, influence of strain path on mech. props., orthogonal tensile paths 80−30035
texture correlability, with formability parameters, influence of solid soln. elements 79−91696
thermal force surface, of creep process in AK4-1T bar 79−87695
thermal force surface in process of damage and time until failure in alloy D16T and AK4-IT 80−35324
thermally activated deformation, exam. of hypothesis 78−72820
thermoelasticity, retardation time effects on heat pulse propagation 79−18725
thermomechanical parameters, effect on struct. and props. on type VAD23 80−20988
thermomechanical treatment on struct. and props. of alloy 2036 79−29109
thermomechanical treatments, effects on microstruct. 80−100858
thermomechanical working effect on mech. props. *(Russian)* 77−21181
thermomechanically treated 6061, elev. temp. mech. props. 79−8310
thixoforging into net-shapes, of type 2024 80−16339
threshold stress intensity range, physical interpretation during fatigue loading *(German)* 78−19888
Ticonal, domain struct., variation under influence of heat treatment *(Russian)* 78−23292
Ticonal, effect of rare earth metals on mag. props., struct., and phase transformations 79−99732
ticonal, grindability improvement, thermomagnetic and heat treatments 77−16625
Ticonal, two- and one-dimens. modulated struct. after thermomag. treatment and water quenching *(Russian)* 80−29983
Ticonal strength, effect of thermal stresses and phase transforms. 79−87721
Ticonal with magnetic texture, struct. damages during ageing 77−16626

aluminium alloys continued
Ticonal with Sm, magnetic props., phase transform. after thermomagnetic treatment 78−3155
Ticonal-type alloys, struct. after quenching from 800-850°C *(Russian)* 77−59822
time and spatially resolved at. absorpt. anal. 80−40760
transition metal group VIII aluminide, NMR near equiatomic composition *(Russian)* 80−20479
transition metal impurities, 3d, influence of multiple scatt. effects on residual resist. 79−19570
transition metal-Al, X-ray spectra, electronic structure 79−78793
TsM-10 alloy, fatigue fracture mechanism, dislocation struct. *(Russian)* 77−32674
type 2024-T4, fatigue crack initiation and microcrack growth 79−79100
type 2036-T4, in-plane deformation, correlation with Hill's theory 79−83260
type 2124-T4, fatigue crack initiation and microcrack growth 79−79100
type 6061, A356, forging of liquid and partially solid alloys 78−80569
type 7075-T6, effect of shot peening on fatigue behaviour 79−79102
Udimet 700, Ni-Co-Cr-Al-Ti (18.8, 15.2, 4.5, 3.39 wt.%) exam. of high temp. creep 79−61684
Udimet 700, Ni-Co-Cr-Al-Ti (18.8, 15.2, 4.5, 3.39 wt.%) exam. of high temp. creep, viscoplastic flow 79−61685
UHV bakeable vacuum chamber, use of Al alloy *(Japanese)* 80−52248
ultrasonic application influence on creep during multistage ageing of AL22 *(Russian)* 79−91708
US characts., change with stress appl., exam. 78−48579
US flaw detection of ingots, struct. effect 80−66722
US inspection of overheating in parts 79−52607
US response of machined slots and fatigue cracks in 7075 77−40506
US structure monitoring of parts of AK4-1 and D16 78−53082
US testing of cold worked surface, quality evaluation 78−48602
viscoplastic deformation, adiabatic, at high strain rate, negative strain hardening *(French)* 77−21212
void form. in defeated targets 77−15403
VT22, hot deform., microstruct. form. and mech. props. *(Russian)* 77−28830
waffle cylindrical shell, technological charact. and bearing capacity 79−3936
wall and limiter material for Tokamaks, induced desorption diffusion and gas production by 100 eV electrons and ions 79−675
weld at cryogenic temps., mech. props. 79−66136
weld metal structure and hot cracking susceptibility 79−24595
welded joint, microstructural and chemical heterogeneity 79−29096
welded joint fatigue life improvement, vacuum annealing appl. in type 01420 80−7597
welded joints, hot cracks in mutual solidification zone 79−24594
welded joints in dissimilar Al alloys, fishbone testpiece axis of symmetry, residual stress investigations 80−7725
wire drawing plastic deform. in Al and dil. alloys 80−108508
work hardening in surface layers and bulk during fatigue in 2024-T3 78−48428
X-ray fluoresc. anal., interelement correction, models, computer program 77−56315
X-ray spectral microanalysis by accel. voltage variation method *(Bulgarian)* 79−16093
yield, discontinuous, under tensile strain in liquid He, governing laws 77−63760
yield surface, effect of 2-D cyclic loading 79−34097
yield surface after proportional preloading, Tresca-type stress-strain rel. 77−32628
yield surface of material subjected to combined cyclic loadings 78−84905
yield surfaces, effect of preloading under combined axial load and torsion 77−25091
yielding of tubing under dynamic biaxial loading of 6061-T6 80−16377
Young's modulus of 2024 alloy under shock loading, heat treatment effects 77−32611
Zircaloy, in-pile temp. depend of yield strength and growth, under neutron irrad. 79−73219
Zircaloy pressure tubes, effect of microstruct. on irradiation creep 79−74208
Zircaloy-4, ^{51}Cr bulk diffusion 79−73347
Zircaloy-4, creep rupture at monotonous stress and temp. ramp loading 79−74241
Zircaloy-4, fuel cladding, steady-state creep from 940 to 1873K 79−74206
Zircaloy-4 cladding, creep transients, plastic hoop strain meas. 79−57068
β'-NiAl, Ni rich, electron diffr. pattern anomalies, rel. to martensitic transform. and short range ordering 78−6926
Ag-Al, dil., temp. depend. of elec. field gradient, impurity mass and conc. effects 78−48085
Ag-Al, dislocation interactions with migrating interphase boundary electron microscope obs. 77−55963
Ag-Al, electric field gradient temp. depend., nearest neighbour mass effect, TDPAC meas. 78−6612
Ag-Al, plastic flow enhancement during massive transformations 78−48468
Ag-Al, short-range order, X-ray and electron diffr. study 80−54173
α-Ag-Al, superconducting transition temp. depend. on electron per atom ratio, lattice deform. 77−8222
Ag-Al, ζ-phase, short range order *(Japanese)* 80−15256
Ag-Al (26 at.%), massive transform, $\beta \to \zeta$, crystallography and morphology 80−97475
Ag_xAl_y, TDPAC meas. of ^{111}Cd 77−28492
Al, alloy, laser surface melting 78−48557
Al alloy, semifinished materials, fracture toughness determ. after tempering 78−7128
Al alloy 2024-T4, compact shear specimen, finite element anal. rel. to fracture 80−16423
Al alloy 7050, crack propagation and closure, tensile overloads effects 79−43384
Al alloy AMg6, preliminary plastic deform., effect on stability of compressed rods 77−81305
Al alloy AU2GN, variation of crack opening-load diagram with fatigue crack growth rate 77−66691
Al alloy blend 6061, isostatically computed powder, effect of heat treatment temp. on tensile strength and hardness 79−61720
Al alloy D16T, acoustic emission temp. depend. 78−53136

aluminium alloys continued

- Al alloy sheets, type 7075-T6 used in aircraft, early detection of fatigue cracks 80—66730
- Al alloy-mica particle composite, cast prep. and mech. props., bearing appl. 80—71613
- Al alloys, columnar struct. of alloys solidified in flowing melt in centrifugal casting 80—71640
- Al alloys, steady-state fatigue crack growth rate behaviour 79—43432
- Al bronze, anisotropic bend ductility in single phase alloys 78—60726
- Al bronze, BA 1032, deformation at high temp. *(Polish)* 79—79023
- Al bronze, duplex alloy, corrosion fatigue behaviour 79—70218
- Al bronze, elastic limit after repeated transverse deformation *(Russian)* 77—66668
- Al bronze, G, Si additions, corrosion resistance 77—16714
- Al determination, in presence of V *(Polish)* 80—35605
- Al-2024-T351 alloy, precipitation hardening, thermal cond. 78—91661
- Al-3d transition metal, dil., transport props., sp. ht. and supercond. ant. temp. calcs. 77—1393
- Al-3d transition metal, dil. alloy, preasymptotic charge oscillations around 3d impurities 77—36055
- Al-3d transition metal, dil., localisation of additional screening charge 79—47051
- Al-3d transition metal, dil., electronic states, reson. model pot. method 79—77995
- Al-3d transition metal, dil., pre-asymptotic charge oscills. 80—20099
- Al-(Mn), effects of Mn on electrode or free corrosion potentials 80—100942
- Al-A$_3$Ni eutectic, effect of some thermal parameters on the directional solidification process 78—88456
- Al-Ag, alloying effect on phonon spectrum and lattice heat cond. 77—62695
- Al-Ag, dil., deviation from Matthiessen's rule at high temps. 77—69294
- Al-Ag, dil., electron irrad., stage I_E recovery, interstitial trapping 77—15405
- Al-Ag, dil., radiation damage by channelled and random He$^+$ ion beams 79—46719
- Al-Ag, discontinuous decomposition *(Polish)* 78—52808
- Al-Ag, electrical resist. of Guinier-Preston zones during age hardening 77—72848
- Al-Ag, force-and-mass disordered alloys, vibrs., average local-information transfer approx. 80—88290
- Al-Ag, low-conc. alloy, spinodal curve and metastable miscibility gap 77—63680
- Al-Ag, nonhomogeneity of deform. 78—84888
- Al-Ag, precipitation kinetics and coarsening, effect of interfacial props. 79—91651
- Al-Ag, precipitation study by internal friction *(French)* 80—35190
- Al-Ag, resonance splitting of phonons 78—75759
- Al-Ag, thin foil, X-ray microanalysis, surface film effect 78—44428
- Al-Ag, type-II superconductor, torque oscillations in mag. field *(Russian)* 80—103800
- Al-Ag (0.10 at.%), channelling meas. of trapping efficiencies of solute atoms for self-interstitials 79—86829
- γ'-Al-Ag (15 wt.%), dislocation splitting mechanism, cessation above critical temp. 78—26572
- Al-Ag (15 wt.%), precipitate growth kinetics 77—28817
- Al-Ag (15 wt.%), precipitation hardenend cyclic stress-strain response 78—35412
- Al-Ag (16 wt.%), quenched, early stages of decomposition, small-angle X-ray scatt. meas. 77—59740
- Al-Ag (1.03 at.%) alloy elec. resist. meas. above room temp., Ag atom configuration correlation 78—35534
- Al-Ag (4 wt.%), scattering of conduction electrons, effect of size and internal struct. of GP zones *(Japanese)* 77—21149
- Al-Ag (40 wt.%), deformed, free energy changes in process of discontinuous precipitation 80—3054
- Al-Ag (40 wt.%), plastic deform. effect on discontinuous precipitation 80—3053
- Al-Ag (5 wt.%), Guinier-Preston zone struct., correl. function *(Russian)* 77—12627
- Al-Ag (7.27 wt.%), peculiarities exhibited during fatigue loading *(Chinese)* 80—71723
- Al-Ag (up to 4 wt.%), creep, 570-630°C, influence of Ag addition *(Russian)* 79—5003
- Al-Ag (up to 40 at.%), exam. of anelastic phenomena and structural state 78—76693
- Al-Ag alloy, ageing exam. by X-ray electron spectroscopy and electron diffr. exam. *(Russian)* 78—60685
- Al-Ag alloy, second ageing stage, diffuse electron and X-ray scatt. *(Russian)* 78—68711
- Al-Ag alloy, thin foil, X-ray microanalysis 77—81439
- Al-Ag alloy precipitation and heat of evolution, microcalometric obs. *(Japanese)* 78—15406
- Al-Ag alloys, critical resolved shear stress 80—49296
- Al-Ag alloys, dilute, electrical magnetoresist., temp. depend., mag. breakdown 79—99532
- Al-Ag mirror for use as solar reflector, co-sputtering 80—20789
- Al-Ag$_2$Al, eutectic alloy, exam. of terminal solid solubility limits 78—76633
- Al-Ag-Cu alloy precipitation and heat of evolution, microcalometric obs. *(Japanese)* 78—15406
- Al-Ag-Si alloys, phase equilibria at 500°C *(Russian)* 78—56612
- Al-Ag-Zn, ring diffuse X-ray scatt. phenomena *(Russian)* 77—16538
- Al-Ag(Au)(Cu), electronic structure exam. by soft X-ray and X-ray photoelectron spectroscopy 77—85136
- Al-Ag(Au)(Cu), growth kinetics of plate precipitates 77—66649
- Al-Ag(Cu)(Mg)(Si)(Zn), dil., μ^+ depolarisation 79—56697
- Al-Ag(Ga)(Ge) dil. alloys, Hall coeff., residual resist., and relax. times 79—11107
- Al-Ag(Ge)(Mg)(Zn), dil., electron-irradiated, impurity-interstitial interaction 77—15449
- Al-Ag(Mg)(Zn)(Ga)(Ge), dil., deviations from Matthiessens's rule, 4-OPW approx. calc. 79—19574
- Al-Ag(10 at.%), supercond., flux pinning, torque meas., decomp. effect 77 1525
- Al-Al$_2$ eutectic, abrasive fragmentation *(Czech)* 78—64715
- Al-Al$_{21}$Pt$_5$ eutectic alloys, unidirectionally solidified, struct. study 80—108394
- Al-Al$_2$Cu, aligned eutectic, precipitation, TEM and microhardness meas. 78—27529

aluminium alloys continued

- Al-Al$_2$Cu, eutectic composite, abrasive fragmentation *(Czech)* 80—30110
- Al-Al$_2$O$_3$ alloys, dilatometric method for studying relaxation of conc. of defects 77—55288
- Al-Al$_3$Fe, anodic film struct. and stability 78—48564
- Al-Al$_3$Ni, aligned, eutectic alloy, mech. behaviour at high strain rates 78—39855
- Al-Al$_3$Ni, eutectic, creep model 77—36588
- Al-Al$_3$Ni, eutectic composite, directionally solidified, thermal cycling induced distortion 78—39899
- Al-Al$_3$Ni, eutectic composite, abrasive fragmentation *(Czech)* 80—30110
- Al-Al$_3$Ni directionally solidified eutectic, microstructural degradation in temp. gradient 78—3145
- Al-Al$_3$Ni directionally solidified eutectic alloy, struct. and mech. props. *(Korean)* 80—29944
- Al-Al$_3$Ni eutectic, cryst. struct., orientation, electron microscopy, computer calcs. *(German)* 77—72582
- Al-Al$_3$Ni eutectic, temp. gradients, microstructural changes 80—84971
- Al-Al$_3$Ni eutectic, thermal stability in temp. gradient 79—61611
- Al-Al$_3$Ni eutectic alloy, electrolytic prep. of Al$_3$Ni fibres, SEM and anodic polarisation studies 80—100817
- Al-Al$_3$Ni eutectic composite, substructural matrix hardening *(Russian)* 77—21162
- Al-Al$_3$Ni eutectic composite, structural response to shape variations 79—83190
- Al-Al$_3$Ti, directionally solidified, thermal stability during annealing, 435-660°C 80—108393
- Al-Al$_3$Ti, peritectic transform. 77—16564
- Al-Al$_4$C$_3$, dispersion hardened physical props. meas. *(German)* 78—31415
- Al-Al$_4$Ca, eutectic alloy, unidirectionally solidified, exam. of growth and crystallography 78—72771
- Al-Al$_4$Cin eutectic alloy, extruded and unidirectionally solidified, corrosion a neutral NaCl soln. 80—21154
- Al-Al$_6$Fe, fibre reinforced eutectic, deformation behaviour by rolling, TEM and SEM study 79—29129
- Al-Al$_6$Fe eutectic, thermal stability rel. to soaking times 77—21131
- Al-AlN, disperse system prep. by heterogeneous reaction in molten metal *(Czech)* 77—85964
- Al-alloys, biaxial prestrain influence on tensile props. 80—30036
- Al-Au, interdiffusion *(Czech)* 77—62684
- Al-Au (0.2 wt.%), precipitation mechanism and creep behaviour 80—3058
- Al-Au bimetal thin film interdiffusion zone, intermetallic phase form kinetics, 70-160°C 78—75891
- Al-Au melt, Si solubility *(Russian)* 77—66024
- Al-Au(Cu), growth kinetics of plate shaped precipitates 78—6932
- Al-Au(Cu), growth kinetics of plate shaped precipitates 78—6933
- Al-Au(Cu), growth kinetics of plate-shape precipitates 78—6934
- Al-Au(Cu), growth kinetics of plate-like precipitates, vol. diffusion controlled growth 78—6935
- Al-B, dil., diffusion of ^{12}B 79—60541
- Al-B, enthalpies and free energies, effusion and mass spectra, phase diagram 78—23665
- Al-B, manufacture, use of NaBF$_4$, transfer of B 78—27453
- Al-B$_4$C, neutron shielding materials, long term radiation effects 80—9413
- Al-based 3d-transition metal alloys, soft X-ray absorpt., electronic struct. 79—38690
- Al-Be-Mg (30, 5wt.%) alloy, weld solification parameters 79—24511
- Al-Bi-(Fe), directionally solidified monotectic, growth parameters for aligned microstructs. 79—43236
- Al-Bi(Cd)(Pb)-Ti, containing low-melting pt. inclusions, mech. props. 80—93632
- Al-Bi(In)(Pb), monotectic system, rapid cooling from melt, effect on struct. *(Russian)* 79—70053
- Al-bronze, input energy, hysteresis, and fracture in low cycle buckling fatigue, superelastic range 78—31527
- Al-bronze, single crystal rod, energy dissipation, deformed by cyclic buckling in superelastic range 78—31479
- Al-C, coupled phase diagrams and thermochemical data 79—66036
- Al-C, dispersion hardened, effect of processing parameters on mech. props. 80—20826
- Al-C alloys, dispersion hardened exam. of production method using pressed powders 80—16244
- Al-C interstitial solid solns., atomic static displacements and deform. interaction *(Russian)* 80—64953
- Al-C(Si)(Ge) film, ion-implanted, enhancement of supercond. transition temp. 77—32103
- Al-Ca-Zn (5,5 wt.%) superplastic sheet alloy, mechanical properties, superplastic forming behaviour 80—60920
- Al-Cd hypomonotectic alloy, rapid solidification and decomposition 80—50638
- Al-Ce, very dil. alloy, low temp. sp. ht. 79—51745
- Al-Ce (0.06 at.%), rapidly quenched from melt, vacancy loops and precipitates, TEM 77—59769
- Al-Co, defect structs. introduced by electron irrad., Mossbauer study 80—7239
- Al-Co, dil., binding and caging of impurities and trapped interstitials 78—39462
- Al-Co, dil., electron and neutron irradiation, interstitital atom clustering at ^{57}Co impurity, Mossbauer meas. 78—30607
- Al-Co, electron irradiated, self-interstitials trapped at Co impurities, Mossbauer line shape anal. 78—6615
- Al-Co, electron irradiated, quadrupolar relaxation effect in Mossbauer effect 78—39459
- Al-Co dil., fast neutron irradiation, Mossbauer spectra, interstitial atom trapping 77—27914
- Al-Co(Ni)(Ru)(Rh)(Pd)(Ir), composite, paramagnetic resonance and electron-positron annihilation *(Russian)* 79—87314
- Al-Cr, Al-Mn, Al-Cr-Mn, dil. alloys, Hall coeff. and elec. resist. 77—11898
- Al-Cr, cold-worked and homogenised, precipt. kinetics, impurity resist. and TEM meas. 77—16596
- Al-Cr, dil., supercond., nucl. spin relax. and quasiparticle excitations 80—88680
- Al-Cr, dilute, morphological stabilities of planar solid-liquid interfaces during unidirectional solidification 79—4960
- Al-Cr, dilute, vacancy-impurity interaction investig. by tempering method *(French)* 77—68995

aluminium alloys continued
Al-Cr, Kondo alloys, spin and phonon resistivity independ. 78—47777
Al-Cr, magnetic susceptibility, single impurity and interaction effects 77—63093
Al-Cr, neutron irrad., Cr atom distribution NMR study 80—54957
Al-Cr, quench hardened, Cr effects on resoftening 77—66657
Al-Cr, rapidly solidified, crystalline and amorphous structures 77—44274
Al-Cr (0.1 wt.%), exam. of pre precip. behaviour, by elec. resistivity meas. and TEM exam. 78—48406
Al-Cr (3 to 11 at.%), cooling rate effect on solidification struct. and mech. props. *(Japanese)* 78—39755
Al-Cr alloys, corrosion inhibition by o-substituted phenols in NaOH soln. 78—44250
Al-Cr-Zn (2.5, 1.5 wt%), phase equilibrium, solubility *(Russian)* 78—19723
Al-Cr-Zr(Nb), calc. of phase equilibria 79—11569
Al-Cr(Mn), anisotropic electron scattering, Hall coefficient, path integral calc. 79—91027
Al-Cr(Mn), struct. form. and phase transform. kinetics *(Russian)* 78—15359
Al-Cr(Ti), electron irradiated, interstitial trapping and detrapping at undersized impurity atoms 78—47424
Al-Cr(V)(Ti), dil., electron irradiated, interaction of self interstitials with undersized solute atoms 78—63789
Al-Cr(Zr), simultaneous recrystallisation and precipitation *(French)* 80—16313
Al-Cu, age hardened, coherency stresses, composition and dislocation interactions for θ'' precipitates 77—36525
Al-Cu, alloying effect on phonon spectrum and lattice heat cond. 77—62695
Al-Cu, anal. of electron diffr. micrographs using Patterson function *(French)* 79—20044
Al-Cu, Bauschinger effect 79—61646
Al-Cu, bicrystals, neutron irrad. effects on grain boundaries, intergranular fracture and precip. 77—48520
Al-Cu, binary, solidification, predicted volume change 77—28802
Al-Cu, cast, chilled zone composition and thickness obs. *(Japanese)* 80—7541
Al-Cu, cast and directionally solidified, porosity 79—74145
Al-Cu, cathodes for He-Ne lasers, cold, vapour deposited 80—5748
Al-Cu, condensed films, metastable states 79—15046
Al-Cu, crack advance during fatigue, effect of cyclic hardening and COD 77—16675
Al-Cu, decomposition of Guinier-Preston zones *(German)* 80—30014
Al-Cu, dendritic solidification, fluid flow effect 78—11215
Al-Cu, diffuse light scattering method for in situ obs. of pitting corrosion 80—25930
Al-Cu, dil., anisotropic scattering of conduction electrons on dilute Cu impurities 79—47082
Al-Cu, dil., core and valence band spectra, XPS study 80—84837
Al-Cu, dil., pulsed ruby laser irrad., noncryst. phase form 80—35012
Al-Cu, dil., virtual bound states 77—43528
Al-Cu, dil. alloy, quench condensed thin films, supercond. and struct. from electron diffr. patterns 78—47901
Al-Cu, disordered, electron energy struct. and X-ray emission bands, average t-matrix approx. *(Russian)* 80—24779
Al-Cu, effect of alloy purity and ageing on fracture mechanism, and resultant toughness 79—5049
Al-Cu, elastic interaction energy calcs. for Guinier-Preston zones 79—11617
Al-Cu, electric discharge sintering of powder mixtures 78—60605
Al-Cu, electrical resist. of Guinier-Preston zones during age hardening 77—72848
Al-Cu, epitaxial film, vac. deposited on NaCl(001), orientation obs. *(French)* 79—95294
Al-Cu, evaporation, successive dilution method for reproducible control 77—69994
Al-Cu, film, prep. by planar magnetron sputtering *(Japanese)* 80—16184
Al-Cu, flow stress, origin of high strain rate sensitivity 78—44186
Al-Cu, high strength, type 2024-T3, crack growth, fatigue induced surface deform., holographic detect. 80—85120
Al-Cu, high temp. internal friction peaks 77—48470
Al-Cu, implanted metal system, Cu redistrib. after laser irrad. 79—69163
Al-Cu, intergranular morphology of θ' precipitates, angle between grain boundary/precipitate plane 78—48413
Al-Cu, isothermal coarsening of liquid inclusions 77—21166
Al-Cu, lattice thermal cond. at low temps. 77—62889
Al-Cu, liq. alloys, surface tension meas. *(French)* 78—18875
Al-Cu, liq. alloys, with zero superheat, fluidity 80—70289
Al-Cu, liq. diffusion coeff. meas. using temp. gradient zone melting 78—26710
Al-Cu, liquid, surface tension model using surrounded atom concept 77—15665
Al-Cu, melt near solid-liquid interface, diffusion during crystallisation *(German)* 79—29046
Al-Cu, molten, showering cryst. form. in mould cooled from top *(Japanese)* 80—66498
Al-Cu, O transport during fatigue crack growth 78—52981
Al-Cu, partially solidified, viscosity and struct. *(Japanese)* 79—14950
Al-Cu, precipitation hardened, hysteretic plastic work as failure criterion in Coffin-Manson type relation 77—32657
Al-Cu, single and two phase, superplastic behaviour 80—11709
Al-Cu, solidification, solid-liq. interface, solute conc. effects 80—59632
Al-Cu, solidification, stability of spherical particle growing from stirred melt 77—47365
Al-Cu, splat quenched, amorphous regions 77—4047
Al-Cu, splat quenched, amorphous regions, comment 77—4048
Al-Cu, splat quenching, electron transparent area prod. 77—4754
Al-Cu, splat-quenched, microstruct. thickness and comp. depend., TEM 77—8863
Al-Cu, stir cast microstructure, turbulent flow and solidification 79—20036
Al-Cu, superconducting amorphous films of high stability 80—70889
Al-Cu, surface enrichment of Cu due to Xe sputtering, AES and He ion backscatt. meas. 77—4250
Al-Cu, thermal conductivity, data anal. and synthesis 78—95284
Al-Cu, type 1100, synchrotron radiation microradiography 80—85121
Al-Cu, type 2024, fractography of fatigue 80—40488

aluminium alloys continued
Al-Cu, type 2036-T4, plane-strain work hardening, meas. and anal. 80—81073
Al-Cu, type 2219-T851, fracture mechanics and surface chemistry of fatigue crack growth 80—81168
Al-Cu, US wave propag. velocity, exam. 78—72982
Al-Cu, vertically solidified, effect of fluid flow on solidification struct., and macrosegregation *(Japanese)* 78—48391
Al-Cu, work hardening under tension at 1.6-900K 79—38842
Al-Cu (Ag)(Au), precipitate plate growth kinetics 79—15679
Al-Cu (Mg)(Zn), corrosion of chill zone, solidification microstruct. effect 77—36687
Al-Cu (0.1 wt.%) alloy, unidirectional solidification, stability of planar solid liquid interface 77—86020
Al-Cu (0.5, 2 and 4.5 wt.%), solidification, apparent solid region *(Japanese)* 77—63653
Al-Cu (0.5 to 40 wt.%), morphology of quenched solid-liquid interface *(Czech)* 77—86021
Al-Cu (0.5 to 4.6 wt.%), cathode foil for electrolytic capacitors, relationship between comp., struct., and etchability 79—74314
Al-Cu (0.5 wt.%), evaporated layers, electromigration, linewidth depend. 80—65277
Al-Cu (1 to 10 wt.%), vapour deposited films, ion scattering spectrometry characterisation 80—15386
Al-Cu (1 wt.%), electron irradiated, dislocation damage, HVEM study 80—103389
Al-Cu (1 wt.%) alloy, plasmon-dislocation interactions, electron microscope investig. 77—15421
Al-Cu (10 wt.%), inverse segregation 78—52819
Al-Cu (1.5 at.%), vacancy charact. study by electrical resistance derivative method, rel. to temp. 78—47361
Al-Cu (1.7 at.%), age-hardening, resistivity charge by low temp. deform. *(Japanese)* 78—84831
Al-Cu (1.7 at.%), EXAFS study of precipitation 79—100151
Al-Cu (1.9 at.%), solute fluctuations, EXAFS study 80—79949
Al-Cu (2-5 wt.%), precipitation total surface influence on resistivity *(French)* 80—71650
Al-Cu (2%), metallisation for SAW devices 80—23856
Al-Cu (2.12 at.%), irradiated by 8J CO$_2$ laser pulses, metastable precipitate and amorphous phase *(French)* 78—80552
Al-Cu (2.6 wt.%), sheets, effect of strain path changes on formability 79—43347
Al-Cu (3 wt.%), stress aged, GP zone struct. by X-ray diffuse scatt. meas. *(Japanese)* 80—71653
Al-Cu (3 wt.%) single cryst., stress aging, oriented precipitation *(Japanese)* 80—71652
Al-Cu (33 wt.%) eutectic, superplasticity, in-situ obs. by TEM 77—28876
Al-Cu (33 wt.%) eutectic, solidification under reduced gravity, behaviour of suspended Al$_2$O$_3$ particles *(German)* 80—60853
Al-Cu (3.5 wt.%), precipitation on stationary and non-stationary grain boundaries 78—84820
Al-Cu (3.71 wt.%), stress oriented precipitation of Guinier-Preston zones and θ' 78—52809
Al-Cu (3.93 wt.%), planar defects within theta precipitates 77—16583
Al-Cu (3.97 wt.%), containing Guinier-Preston zones, high resolution lattice images 80—107114
Al-Cu (4 wt.%), AE during deform., effect of ageing at 170°C 78—64597
Al-Cu (4 wt.%), aged to contain Guinier Preston zones, crystallographic fatigue crack growth 78—60832
Al-Cu (4 wt.%), effect of semicoherent precipitation on void swelling, when neutron irradiated 79—42115
Al-Cu (4 wt.%), elastic accommodation of semicoherent θ' 78—64543
Al-Cu (4 wt.%), enhanced precipitation under electron irradiation in HVEM 78—52818
Al-Cu (4 wt.%), fatigue crack propag. role of adsorption in H$_2$S, Hg and moist air *(French)* 78—15580
Al-Cu (4 wt.%), high temp. cyclic deform., θ' particle dissolution obs. 80—108515
Al-Cu (4 wt.%), interparticle spacing influence on cyclic deformation and fatigue crack propag. 79—61717
Al-Cu (4 wt.%), naturally aged, early stages of G.P. zone form. 77—90355
Al-Cu (4 wt.%), neutron irrad., weak-beam dark-field obs. of dislocations near θ' precipitates 80—107333
Al-Cu (4 wt.%), non IPS geometric surface relief effects associated with diffusional phase transform. 77—32575
Al-Cu (4 wt.%), precipitation sequence of metastable phases, NMR meas. 78—23713
Al-Cu (4 wt.%), precipitation hardened and fatigued alloys, solute loss at fracture surface, EPMA exam. 78—39893
Al-Cu (4 wt.%), relationship between enthalpy, yield strength, and size of Guinier-Preston zone *(French)* 78—19767
Al-Cu (4 wt.%), reversion charact. *(Japanese)* 77—21150
Al-Cu (4 wt.%), reversion process of Guinier-Preston zones, ^{63}Cu NMR obs. 80—60871
Al-Cu (4 wt.%), single crystal, anisotropy in plane strain compression 77—36599
Al-Cu (4 wt.%), single cryst., small angle X-ray scatt. map after spinodal decomp. 79—15645
Al-Cu (4 wt.%), size distrib. and form. mechanism of GP zones *(Japanese)* 77—25054
Al-Cu (4 wt.%), stress corrosion cracking, effect of cold reduction *(Japanese)* 77—48580
Al-Cu (4 wt.%), supersaturated and aged conditions, high strain deform. 80—60907
Al-Cu (4 wt.%), TEM obs. of intergranular corrosion 79—91835
Al-Cu (4 wt.%), θ' phase coalescence 79—56985
Al-Cu (4 wt.%), θ'-phase precipitation, characterisation of stages 79—56984
Al-Cu (4 wt.%), with θ' precipitates, relation between elastic limit and hardness *(French)* 79—5018
Al-Cu (4 wt.%) alloy, coherency loss of θ'-phase due to deform. 77—15424
Al-Cu (4 wt.%) alloy, precipitation hardened, single crystal, directional plastic behaviour, exam. 78—39788
Al-Cu (4 wt.%) alloy, θ' precipitate growth kinetics, electron microscope obs. *(French)* 77—44253
Al-Cu (4 wt.%) fractography *(German)* 78—19982

aluminium alloys continued
- Al-Cu (4 wt.%) partially coherent precipitation hardened alloy, high temp. cyclic deform. 80–25710
- Al-Cu (4% wt.), single crystals, positron trapping at precipitates 78–76554
- Al-Cu (4.2 wt.%), precipitation strengthened, solute depletion at fatigue facets, AES study 79–38973
- Al-Cu (4.3 wt.%), containing Guinier-Preston zones, high resolution lattice images 80–107115
- Al-Cu (4.3 wt.%) alloy, lattice electron micrograph interpretation 79–86659
- Al-Cu (4.5 wt.%), cast alloy, ductile intergranular fracture 77–28908
- Al-Cu (4.5 wt.%), growth structs. with dendrite growth directions differing from heat flow direction during solidification 79–43235
- Al-Cu (4.5 wt.%), volume contraction accompanying solidification 78–52791
- Al-Cu (4.5 wt.%) alloy, controlled electropotential corrosion in NaCl soln., microstruct. exam 78–39948
- Al-Cu (4.5 wt.%) cast alloy, press. effect during solidification on struct. and mech. props. *(Korean)* 77–77469
- Al-Cu (4.5% at.wt.), laser surface melting and subsequent solidification, computer heat flow models 79–69916
- Al-Cu (4.6 wt.%), cold work and ageing influence on ductility and fracture behaviour *(Japanese)* 80–89295
- Al-Cu (4.8 wt.%), homogenization, temp. gradient driver process 77–52362
- Al-Cu (4.8 wt.%), secondary arms in dendritic growth, solidification effects *(Japanese)* 78–15387
- Al-Cu (4wt.%), elastic limit, precipitation effects *(French)* 79–47738
- Al-Cu (5 wt.%), ageing, extinction effects *(Russian)* 77–81283
- Al-Cu (5 wt.%), ageing during relax. of elastic stresses, X-ray diffr. expts. *(Russian)* 77–59821
- Al-Cu (5 wt.%), fatigue strength, coarse precipitation effect *(German)* 79–91660
- Al-Cu (5.7wt.%), unidirectionally solidified, dendritic morphology and dendrite arm spacing 79–29043
- Al-Cu (6.3 wt.%), fatigue crack propag., plastic work role 79–79070
- Al-Cu (96.5, 3.5 wt.%), characts. of disappearance of excess vacancies on dislocations 80–33991
- Al-Cu (up to 0.5 at.%), neutron damage rate, interpretation of results 78–63794
- Al-Cu alloy, deposition from RF induction source, onto laminated polyimide substrates and characterisation 80–16535
- Al-Cu alloy, microsegregation *(Japanese)* 77–16589
- Al-Cu alloy, nonstationary mass transfer in front of moving phase boundaries in mormal freezing *(German)* 77–44238
- Al-Cu alloy, Portevin-Le Chatelier effect, influence of specimen dimensions and machine stiffness 77–70128
- Al-Cu alloy, press-forming under coexisting state of liquid and solid, mech. props. 77–81240
- Al-Cu alloy, vacuum deposited thin film, abnormal grain growth before melting transition and subsequent struct. change 79–60663
- Al-Cu alloy 1201, thermomech. treatment effect on strength characts. and fracture toughness *(Russian)* 80–40391
- Al-Cu alloy D16, riveted, low-cycle fatigue strength 80–30097
- Al-Cu alloy dendritic solidification kinetics 80–81041
- Al-Cu alloy in NaOH, aminophenols as corrosion inhibitors 80–30136
- Al-Cu alloy metallisation sputter deposition for VLSI 80–66429
- Al-Cu alloy precipitation and heat of evolution, microcalometric obs. *(Japanese)* 78–15406
- Al-Cu alloy prod., Cu interdiffusion with sintered Al powder, struct. effect at high press. 78–60606
- Al-Cu alloy RR58, high strain fatigue life, prior treatment effect 78–60835
- Al-Cu alloys, anisotropy function determ. 77–43565
- Al-Cu alloys, coarsening mechanisms of secondary dendrite arm, and organic analogue 80–81049
- Al-Cu alloys, Cu precipitate detect. by positron annihilation, GP zone development 80–3051
- Al-Cu alloys, dil., EXAFS spectra 80–2898
- Al-Cu alloys, Guinier-Preston zones study by stress ageing 79–100152
- Al-Cu alloys, hypo- and hyper-eutectic, dendrite coarsening during solidification 77–63651
- Al-Cu alloys, positive muons diffusion and trapping 79–11372
- Al-Cu alloys, quenched rapidly, microstruct. 78–56668
- Al-Cu dil. alloys, elec. resist. temp. depend. 77–8068
- Al-Cu dilute alloys, vein closing mechanism in fluidity tests 80–84924
- Al-Cu edges in Permalloy conductor crossing effect on bubble propagation margins 80–29588
- Al-Cu eutectic, mechanism of lamellar spacing adjustment 78–31395
- Al-Cu eutectic alloy, cooling rate in rapid solidification, estimation from cell spacing 80–50623
- Al-Cu eutectic melts, struct. determ. *(Russian)* 77–80408
- Al-Cu film, anodic oxidation, corrosion props. 78–35581
- Al-Cu film, galvanostatic formation anodic oxide, Rutherford backscattering and depth profiling 78–92395
- Al-Cu film, magnetron sputtered deposition, characts. 79–91587
- Al-Cu film bilayers, growth kinetics of θ phase, He$^+$ backscatt. and X-ray exam. 78–84105
- Al-Cu films, DC sputtered, Cu distrib. 80–80113
- Al-Cu films, deposition rate, mol. beam incidence angle influence on struct., film props. *(Russian)* 79–60646
- Al-Cu full coherent precipitation hardened alloy, high temp. cyclic deform. 80–25711
- Al-Cu hypoeutectic, solidification cycle, thermal anal. 80–29945
- Al-Cu layer, photolithographically patterned, separation from substrate using plasma etching *(Slovak)* 80–45405
- Al-Cu liquid alloys, rapid quenching prep. of metastable solids, apparatus *(German)* 79–28990
- Al-Cu samples (0.5, 2.0 and 4.0 wt.%) polycryst., precipitation, positron annihilation and TEM 80–50639
- Al-Cu single cryst., hardening due to oriented GP zones 80–55414
- Al-Cu solid soln., supersaturated, plastic deform. effects *(French)* 79–91748
- Al-Cu thin films, microstruct. rel. to electromigration 80–44355
- Al-Cu type 2024 alloy, erosion in cavitating venturi 80–108602
- Al-Cu-Fe, liquid, mag. moment and transition from mag. to nonmag. state 79–24132
- Al-Cu-Fe alloys, solid and liquid, exam. of constitution and mag. props. *(German)* 78–52206
- Al-Cu-Mg, acoustic emission power, strain rate depend. 77–4808

aluminium alloys continued
- Al-Cu-Mg, acoustic emission during tensile testing 80–7632
- Al-Cu-Mg, aged, stress corrosion cracking in NaCl soln. 80–7709
- Al-Cu-Mg, alloy 2124-T351, crack tip closure assessment by electronfractography 80–16427
- Al-Cu-Mg, alloy Al2048, early stages of fatigue crack propag. 77–63780
- Al-Cu-Mg, alloys A-U4, A-U4G1, A-U2GN, effect of environment on fatigue crack growth 78–64677
- Al-Cu-Mg, cold plastic deformation, stress/strain relations 79–56991
- Al-Cu-Mg, dil. alloys, ageing response *(Korean)* 77–28832
- Al-Cu-Mg, rolled plate fatigue charact. *(Russian)* 80–16437
- Al-Cu-Mg, string ghost form. during solidification *(Japanese)* 79–100130
- Al-Cu-Mg, tpye RR55, high strength, creep behaviour, effect rel. to anodic coatings, SEM study 80–97542
- Al-Cu-Mg, tube drawing, tensile forces, plastic deformation *(French)* 79–70130
- Al-Cu-Mg, type D16 alloy, stress intensity coeff. determ. 79–87711
- Al-Cu-Mg, type D16T, thin-wall cylinder cold rolling method 80–66535
- Al-Cu-Mg (1.3, 1.3 at.%) alloy, natural ageing, meas. of quenching vacancy dislocation loops 79–15704
- Al-Cu-Mg (2.0, 1.1 wt.%), Ostwald ripening of S' precipitates *(Korean)* 79–38831
- Al-Cu-Mg (2.6, 0.4 wt.%), Fe, Si, Mn and Ti addition effects on age-precipitation *(Japanese)* 80–20937
- Al-Cu-Mg (4, 1.5 wt.%), mica dispersed, wear characts. and bearing performance 80–108591
- Al-Cu-Mg (4,1 wt.%), behaviour during ductile fracture, SEM *(Rumanian)* 80–21062
- Al-Cu-Mg alloy, extruded, press forming in liquid/solid coexisting state, mech. props., Mg effects 78–11151
- Al-Cu-Mg alloy, influence of plastic deformation on fatigue limits, for prestrained components 78–68799
- Al-Cu-Mg alloy, struct. of Guinier-Preston zones *(Russian)* 79–1870
- Al-Cu-Mg alloy D16T, fatigue cracking under cyclic bending *(Russian)* 78–31506
- Al-Cu-Mg alloy RR58, comparison of methods of correlating creep crack growth 78–60826
- Al-Cu-Mg type 2036, thermomech. treatment, flow stress anal., effect in mech. props. 80–93584
- Al-Cu-Mg/mica particulate composite mech. props. 80–100919
- Al-Cu-Mg-Ag casting alloy, precipitation hardening in artificially aged condition 79–1874
- Al-Cu-Mg-Fe-Ni, Hiduminium RR58, crack propag. rates in air and salt soln. 80–21063
- Al-Cu-Mg-Li alloy extrusions, microstruct., embrittlement and fracture props. 80–60965
- Al-Cu-Mg-Mn, shot peened, positron annihilation meas. 77–63833
- Al-Cu-Mg-Mn (4.5, 1.5, 0.6 wt.%), alloy 2024-T3, exam. of residual strength of plate containing crack, fracture anal. 78–90792
- Al-Cu-Mg-Mn (4.5, 1.5, 0.6, wt.%), alloy 2024-T81, plates, adhesively bonded, exam. of fatigue crack growth 78–92349
- Al-Cu-Mg-Mn (4.5, 1.5, 0.6 wt.%), thin sheet, exam. of fracture toughness, and fatigue crack growth 78–92353
- Al-Cu-Mg-Mn-Fe-Si, alloy D16, effect of mechanisothermal treatment on mech. props. 78–56674
- Al-Cu-Mg-Mn-Si-Fe, endurance with cyclic bending, effect of loading conditions 80–50724
- Al-Cu-Mg-Mn-Si-Fe, subcritical crack growth under static plane stress 80–55528
- Al-Cu-Mg-Mn-Si-Fe, torsional vibrations decrement, deformed vol. effect 80–76326
- Al-Cu-Mg-Mn(-Zn-Cr), low temp. deformed, ageing and mech. props. 79–1881
- Al-Cu-Mg-Ni-Fe alloy RR 58, creep resistance at elevated temps., thermomechanical treatment effects 77–59836
- Al-Cu-Mg-Si-Fe-Mn-Ti, Si, Fe, Mn and Ti effect on precipitation in solid soln. *(Korean)* 79–66064
- Al-Cu-Mg-Si-Mn (2.5, 0.7, 0.7, 0.5 wt.%), alloy AK6, US inspection of heat treatment quality 78–76681
- Al-Cu-Mg-Si-Mn alloy AK8, fatigue strength, effect of residual stresses and cold working 77–56101
- Al-Cu-Mg-Zn, Mg and Zn addition effects on dendrite struct. and mech. props. *(Korean)* 77–28796
- Al-Cu-Mg-(Ag), effect of addition on fatigue microstructure relationships 80–40483
- Al-Cu-Mg(:Fe,Si) alloys, double-ageing, resist., hardness meas. 77–28822
- Al-Cu-Mg(-Si), inclusions, oriented distrib. metallography and effects on anisotropy *(Russian)* 78–80589
- Al-Cu-Mn, long term strength and creep 80–60925
- Al-Cu-Mn, type 2219, edge effects of fatigue crack closure 80–3189
- Al-Cu-Mn, type 2219, synchrotron radiation microradiography 80–85121
- Al-Cu-Mn (6.3, 0.3 wt.%), Al 2219-T851, fatigue crack initiation and early propag. 77–32684
- Al-Cu-Mn (6.3, 0.3 wt.%), alloy Al 2219-T851, crack closure load meas. during fatigue 77–63870
- Al-Cu-Mn (6.3,0.3 wt.%), alloy Al 2219-T851, crack closure load development for surface microcracks 77–86226
- Al-Cu-Mn alloys, effect of comp. and N alloying on mech. props. *(Bulgarian)* 80–71719
- Al-Cu-Mn-Mg alloy D16, sheet, corrosion fatigue strength, with anodised and painted surfaces *(Russian)* 78–35575
- Al-Cu-Mn-Mg-Fe-Si, corrosive environment effect on fatigue crack growth rate 80–55584
- Al-Cu-Mn-Mg-Fe-Si (4.48, 0.66, 1.55, 0.43, o.23 wt.%), alloy D16, relationship between intercrystallite corrosion depth, and elec. cond. 79–20220
- Al-Cu-Mn-Mg-Fe-Si-Zn alloy D16, surface layers chem. composition rel. to fatigue resist., corrosion-fatigue resist. 79–29275
- Al-Cu-Mn-Zr, type 2219, particle, coarsening of disk shaped Θ' particles 80–45315
- Al-Cu-Mn-Zr-Fe-Si (6,0.3,0.18,0.3,0.1 wt.%) experimental evidence of Mn enrichment in Al_2Cu precipitates by EDS in TEM 78–15415
- Al-Cu-Ni, alloy RR 350, θ'-hardened, deform. induced microstructural instability, high temps. 80–16321
- Al-Cu-Ni, directionally solidified, exam. of struct. of two phase alloys 78–80537

aluminium alloys continued
Al-Cu-Ni, vacancy ordering, electron microscope and electron diffr. obs. 79—27954
Al-Cu-Si, Al rich, unidirectionally solidified, microstruct. 79—34021
Al-Cu-Si, effect of sample conditions on sputtering and intensities, emission spectrochem. anal. using glow discharge *(Japanese)* 80—21349
Al-Cu-Si-Mg, deform. simulation using torsional test, elastoplastic constitutive eqn. 80—93594
Al-Cu-Si-Mg (4, 0.8, 0.8 wt.%), GPB zone formation during room temp. ageing 77—44263
Al-Cu-Si-Mn, type 2017S-T4, crack initiation at root of circumferential notch of round bar specimens *(Japanese)* 80—60947
Al-Cu-Sn, ageing process, effect of Sn atoms, ^{119}Sn Mossbauer spectra obs. 80—7598
Al-Cu-Sn (3.4, 0.28 wt.%), Mossbauer anal. of Sn behaviour during ageing 78—31431
Al-Cu-Zn alloy, ageing, X-ray and electron diffr. meas. *(Russian)* 78—39806
Al-Cu-Zn system, solid-phase reactions, phase diagram 80—50603
Al-Cu-Zr, superplastic alloy Supral, solidification and recrystallisation 80—7550
Al-Cu-Zr (6, 0.3 wt.%), superplastic, texture studies 79—83210
Al-Cu-Zr (6, 0.3 wt.%), superplastic, mech. anisotropy and deformation mechanisms 79—83254
Al-Cu-Zr (6, 0.4 wt.%), superplastic flow activation energy 80—11701
Al-Cu-Zr (6, 0.4 wt.%), superplastic deformation characts. 80—16387
Al-Cu-(Mg), precipitation strengthened, Bauschinger effect 77—36585
Al-CuAl$_2$, directionally solidified eutectic alloy, effect of heat treatment 77—55977
Al-CuAl$_2$, directionally solidified eutectic, structural changes during strength tests *(Russian)* 80—7543
Al-CuAl$_2$, eutectic system, interlamellar spacing meas. 77—36492
Al-CuAl$_2$, interface undercooling-growth vel. relationship, horizontal and vertical solidification 79—8294
Al-CuAl$_2$ aligned, fracture, effect of growth speed, orientation, environment 77—28907
Al-CuAl$_2$ eutectic, deformed, thermal stability 77—52348
Al-CuAl$_2$ eutectic, heat treatment and interlamellar spacing effect on tensile deformation 80—29979
Al-CuAl$_2$ eutectic, superplastic behaviour during compressive deform. 77—52429
Al-CuAl$_2$ eutectic, thermal instability in temp. gradient 78—52851
Al-CuAl$_2$ eutectics, microstruct. after solidification, heat pipe influence 80—76243
Al-CuAl$_2$ lamellar composite, creep, microstruct. obs. 79—8331
Al-CuAl$_2$ lamellar composite, stress and temp. depend. of creep 79—52330
Al-CuAl$_2$ lamellar eutectic, computer simulation of two dimensional Zn diffusion 78—30799
Al-Cu(Ag), tensile ductility, effect of ageing and impact velocity *(Japanese)* 78—15465
Al-Cu(Ag)(Ge), dil., deviation from Matthiessen's rule at high temps. 78—64025
Al-Cu(Mg), age-hardenable, US cavitation erosion mechanisms, effects of comp. and heat treatment 78—53002
Al-Cu(Mg), comparison of liquid impact erosion and cavitation erosion 80—104302
Al-Cu(Mg), dil. binary alloy, planar interface stability during solidification *(Slovak)* 80—108424
Al-Cu(Mg), liquid impact erosion 80—108598
Al-Cu(Mg), low freq. internal friction during plastic deform. *(Chinese)* 80—103420
Al-Cu(Mg), macrosegregation during solidification *(Japanese)* 79—100150
Al-Cu(Mg)(Cu-Mg), normal and gravity segregation in ingots, expt. study *(Japanese)* 79—24526
Al-Cu(Mg)(Zn), cold working causing preprecipitation, thermoelec. power *(French)* 79—8306
Al-Cu(Si)(Mg) binary and ternary alloys, dimensional changes in heat treatment. 80—89271
Al-Cu(Si)(Zn)(Mg)(Cr), recrystallization texture 79—91679
Al-Cu(Zn, Ag, Mg$_2$Si), intermediate precipitates, stability, X-ray, elec. resist. and hardness study 80—3063
Al-Cu(Zn-Mg), age hardening, conditions leading to localised plastic deform. and fracture in slip bands during fatigue 78—64670
Al-Cu(0-10 wt.%) sintered alloys using composite powder 80—76210
Al-Cu(4 wt.%), alloy AU4, θ' precipitation, apparent hardening maxima *(French)* 77—16598
Al-Cv (0.3 wt.%), moving solid-liq. interface, diffusion in liq. 80—107456
Al-Dy, dil., ion implanted, crystal hyperfine field interaction, Mossbauer spectroscopy study 80—44968
Al-Er, dil., lattice location of ^{169}Er ions after implantation, Mossbauer effect of ^{169}Tm 78—39460
Al-Er, dil., supercond., order parameter dynamics and collective modes, pair tunnelling meas. 79—56409
Al-Er(Tm)(Lu), dil., transmission ESR expts 77—20704
Al-Fe, alloy with mixed types of order, uniform mag. phase diagram 79—78368
Al-Fe, cast, influence of Zr on precipitation, solidification and grain size *(Rumanian)* 78—84813
Al-Fe, dil., annealing after cold working, impurity-vacancy interactions, Mossbauer meas. 80—7236
Al-Fe, dil., defects and phases, Mossbauer studies 80—40004
Al-Fe, dil., Mossbauer spectra of implanted ^{57}Fe, ageing behaviour 80—7233
Al-Fe, dil., phase analysis by Mossbauer spectra 80—15922
Al-Fe, dil., quenched, secondary defects, Mossbauer spectroscopy 77—28491
Al-Fe, dil. solid soln., vacancy-trapped Mossbauer impurity Debye Waller factor 80—60468
Al-Fe, electron irradiated, interstitial-solute complexes, internal friction spectra 78—92289
Al-Fe, spectrophotometric determ. of Al content *(Polish)* 80—35604
Al-Fe (0.02 at.%), rapidly quenched, ^{57}Fe Mossbauer spectrum associated with vacancy 78—23378
Al-Fe (0.02 wt.%), Mossbauer spectrum of ^{57}Fe associated with vacancies 77—85636
Al-Fe (0.5 wt.%)-Ti-Cr, Ti, Cr addition effects on toughness/microstruct. relationship *(Japanese)* 77—48525
Al-Fe (1 wt.%), depth resolved ^{57}Fe conversion electron Mossbauer spectra 79—38413

aluminium alloys continued
Al-Fe (49 at.%) quenched alloy, neutron diffuse scatt., diffuse ω phase obs. 80—84141
Al-Fe alloys containing dispersed Al$_3$Fe phase, anodic film structure and stability 78—11449
Al-Fe dil., magnetisation, 2-0.01K 79—4652
Al-Fe dil. alloy, bamboo struct., grain boundary internal friction peak 79—43306
Al-Fe-Ni, influence of strain path on mech. props., orthogonal tensile paths 80—30035
Al-Fe-Ni, oxidation in hot water, electron microscope obs. of initial stages 79—11718
Al-Fe-Si, eutectic alloy growth, by twinning plane propagation *(French)* 78—60667
Al-Fe-Si, Fe phase form., solidification condition effects *(French)* 77—70030
Al-Fe-Si commercial alloy, elevated temp. low cycle fatigue behaviour under rotating bending 79—47766
Al-Fe-Si(0.5, 0.2 wt.%), cast, phase determ. 77—70032
Al-Fe-X-Si (X=transition metal), struct. and comp. by electron microscopy 80—88093
Al-FeAl$_3$, unidirectionally solidified eutectic, α-liq. interface stability 77—63650
Al-Ga, dil., low-temp. electron-diffusion magnetothermopower meas. 77—15833
Al-Ga, dil., neutron irrad., 4.2K, defect prod., recovery 77—1155
Al-Ga, electrical resist. and magnetoresist., 2 to 40K, Matthiessen rule deviations *(Russian)* 77—31996
Al-Ga, face centred cubic struct. stability, melt equilib., α-Ga effects 78—18766
Al-Ga, internal friction and shear modulus, temperature and concentration dependence 77—86077
Al-Ga (10 wt.%), exam. of ^{27}Al diffusion by NMR technique 78—87813
Al-Ga-Ge, liq., enthalpy of form., direct reaction calorimetry, 713-1230K *(French)* 79—66336
Al-Ga-Ge, thermodynamic props. of mixing of binary systems, phase diagram 80—45275
Al-Ga-In, liq. alloys, excess Gibbs functions 633 to 1173K 78—60655
Al-Ga-In system, thermodynamic anal. 79—60512
Al-Ga(-Ge), and Al-Ge, Al activity, EMF study, phase diagrams 79—83175
Al-Ga(Ag), dil., Hall coeff. by OPW Fermi surface model 80—6816
Al-Ga(Ge)(Mg)(Si)(Zn)(Ag), dil., Dingle temp. calc. 78—39005
Al-Ga(In) systems, thermodynamic anal. 79—60512
Al-Ga(In)(Sn), interpretation of metallic phase diagrams, entropy of mixing 79—42274
Al-Ga(In)(Tl), enthalpy of mixing, 'const. vol. alloy' formulation 79—28111
Al-Ga(Sn), ab initio calcs. of partial enthalpy and result for enthalpy of mixing 79—43197
Al-Ge, and Al-Ga(-Ge), Al activity, EMF study, phase diagrams 79—83175
Al-Ge, dil., magnetoresist., temp. depend. 80—70682
Al-Ge, directionally solidified lamellar eutectics, specimen prep. for TEM *(German, English)* 78—95885
Al-Ge, film, double supercond. transition in resistance-temperature and current-voltage characts., percolation theory 79—56365
Al-Ge, galvanomag. transport coeffs., Hall effect 79—91029
Al-Ge, internal friction and shear modulus after neutron irrad. at 80K 79—1468
Al-Ge, liq., enthalpy of form., direct reaction calorimetry, 713-1230K *(French)* 79—66336
Al-Ge, structural changes during superplastic deformation, grain boundary porosity *(Russian)* 79—83258
Al-Ge (0 to 8 wt.%), superplastic props. *(Russian)* 80—45345
Al-Ge (0.1 wt.%), channelling meas. of Al interstitial atom trapping by Ge atoms 80—59537
Al-Ge (0.2 at.%), exam. of interstitial trapping by X-ray diffuse scatt. 78—47363
Al-Ge (2 wt.%), averaged, plastic flow mechanism 77—48507
Al-Ge (2 wt.%), quenched and aged, deform. slip line obs. 78—51544
Al-Ge (4 wt.%), superplasticity exam. *(Russian)* 78—39836
Al-Ge (6.8 at.%), quenching from mushy state for production of metastable phases 80—35223
Al-Ge alloy, effect of high press. on phase equilibrium *(Russian)* 79—1844
Al-Ge alloy, Ge particle size, determ. by small- and wide-angle X-ray scatt. 78—19966
Al-Ge alloy, Ge precip., ion irrad., dose rate and temp. depend. 78—79642
Al-Ge eutectic alloy, X-ray spectral exam. *(Russian)* 77—63489
Al-Ge film, random percolation, elec. resist. meas. 79—28418
Al-Ge thin film alloy, critical currents near metal-insulator transition 79—65626
Al-Ge-Sn, thermodynamic props. of mixing of binary systems, phase diagram 80—45275
Al-Ge(Mg)(Zn)(Ga), dil., electronic transport coeffs. for point defect scatt., 4-OPW calc. 79—42531
Al-In, dil., vacancy trapping and detrapping at ^{111}In, PAC spectra 78—39461
Al-In (40, 70 wt.%), liq. phase immiscible system, solidification in microgravity 78—84770
Al-In alloy, dilute, electron irradiation, interstitial dislocation loop obs. 78—18681
Al-In alloys within miscibility gap, agglomeration in space environment 79—47672
Al-In emulsion, solidification mechanisms at zero gravity, review 78—88458
Al-In(0.1 wt.%), neutron radiation induced voids in US and in 80US-10UC-10UC$_2$ 79—50951
Al-La, thermodynamic interaction in liquid phase *(Russian)* 78—44080
Al-Li, ageing mechanism, metastable δ' phase and stable δ phase precip. *(Russian)* 77—8858
Al-Li, annealing of vacancies and ageing, resist. and TEM obs. 77—21172
Al-Li, cold worked neutron irrad. alloys, He bubble behaviour, microstruct. changes 77—54359
Al-Li, diffusion coeff. determ. during hydriding *(German)* 79—29288
Al-Li, dil., quenched and irrad., recovery, resist. and internal friction obs. 78—52848
Al-Li, dil. alloy, cold-worked, annealing spectrum 78—39801

aluminium alloys continued
Al-Li, dilute substitutional alloy, impurity Knight shift and electric field gradient 80—44940
Al-Li, Fermi surface impurity scatt. 79—56114
Al-Li, microvoid form., gaseous impurity atom effects, positron annihilation study 80—49275
Al-Li (10 at.%), struct. changes on annealing, 25-500°C, Li atoms role 80—35183
Al-Li (1.3 wt.%), prismatic dislocation loop rows due to precipitation *(Japanese)* 79—52220
Al-Li (2.8 wt.%), ageing in US field, precip. hardening *(Russian)* 80—29968
Al-Li (6.72 at.%), δ' coherent solvus determ. on ageing at 20 to 200°C, X-ray scatt. 77—25056
Al-Li ageing, δ-′-phase precip., effect of quenching conditions *(Russian)* 78—19761
Al-Li alloy, thermal anal. of precipitation 78—15417
Al-Li alloys, precipitating, annealing spectrum 78—31429
Al-Li solid soln., decomposition exam. by secondary ion ion emission *(Russian)* 78—68696
Al-Li system, δ' coherent miscibility gap determ. by small-angle X-ray scatt. 77—77483
Al-Li-Mg, estimation of isothermal sections of phase diagram 79—11567
Al-Li-Mg system, isothermal sections comput. 78—6896
Al-Li-Mg-Be alloys, phase composition of surface films, oxidation protection mechanism *(Russian)* 80—65417
Al-Li-Mn (2.8, 0.3 wt.%), recrystallised sheet, fracture behaviour, SEM and TEM study 80—97566
Al-M, dil. alloy, electronic states of 3d-transition metal (M) impurities 78—64005
Al-Mg, AMg6, US vibr. during superplastic deform. effect on struct. 79—38911
Al-Mg, AMg6 alloys, effect of chem. comp. on strength and ductility at low temps. 80—3148
Al-Mg, acoustic emission during tensile testing 80—7632
Al-Mg, acoustic emission power, strain rate depend. 77—4808
Al-Mg, ageing process, effects of Ag additions and pressure *(Russian)* 80—45321
Al-Mg, alloy, surface activity of Mg, XPS and AES meas. 79—86975
Al-Mg, alloy 5083, effect of environmental factors on stress corrosion cracking 78—80684
Al-Mg, alloy A5083-O, fatigue crack propag. and crack closure behaviour under plain strain conditions *(Japanese)* 80—81160
Al-Mg, cast, chilled zone composition and thickness obs. *(Japanese)* 80—7541
Al-Mg, cold plastic deformation, stress/strain relations 79—56991
Al-Mg, cold-worked, transport props., 1.5-8.5K 78—7059
Al-Mg, creep behaviour in broad stress interval at 623K 80—30044
Al-Mg, crystallization interface *(Slovak)* 79—78951
Al-Mg, deformation, tension, torsion compression test exam. *(Russian)* 78—31455
Al-Mg, determ. of distortion field, induced by substitutional defect 80—44536
Al-Mg, dil., ang. correlation of annihilation radiation from impurity trapped positrons 80—104010
Al-Mg, dil., electron irrad., stage I_E recovery, interstitial trapping 77—15405
Al-Mg, dil., form of distortion field produced by Mg substitution, elastic neutron scatt. meas. *(German)* 79—42092
Al-Mg, dil., long-range solute-host interactions 78—95062
Al-Mg, dil., neutron irrad., 4.2K, defect prod., recovery 77—1155
Al-Mg, dil., thermal generation of vacancies involving dislocation climb 77—59808
Al-Mg, dil. alloy, ^{65}Zn diffusion 77—51540
Al-Mg, dil. alloy, residual resistivity, model pseudopot. form factors 77—8062
Al-Mg, dilute, dislocation loops, interstitial, size distrib. for metal irradiated in high voltage electron microscope *(Russian)* 80—103335
Al-Mg, discontinuous deform. under various conditions 77—63716
Al-Mg, dynamic uniaxial tension and compression curves 80—100884
Al-Mg, effect of Ag addition on ageing and related props. 77—36522
Al-Mg, elastic and anelastic props. in relation to Guinier-Preston zones, US investigation *(French)* 79—38833
Al-Mg, electrical resist. and magnetoresist., 2 to 40K, Matthiessen rule deviations *(Russian)* 77—31996
Al-Mg, foil, oxidation in O_2 atm., TEM study 80—104356
Al-Mg, fracture during superplastic flow 78—60729
Al-Mg, fracture resistance at low temps. 80—104284
Al-Mg, grade 5083, superplastic, interaction effects during growth of drilled holes 79—38923
Al-Mg, grain boundary dislocation identification, TEM obs. 77—62534
Al-Mg, Guinier Preston zone study by neutron diffr. *(French)* 77—28819
Al-Mg, homogenisation process, effect of solidification rate and alloying *(Polish)* 79—78949
Al-Mg, liquid alloy energy of soln. pseudopotential calcs. *(Russian)* 79—66330
Al-Mg, Mg effect on ductility, 25 to 250°C 79—100214
Al-Mg, new metastable phase 78—52772
Al-Mg, oxidation control study, electron opt. techniques eval. 80—85089
Al-Mg, oxidation induced stresses, dislocation network form., HVEM obs 80—14978
Al-Mg, plastic deform., separation of internal friction components *(Russian)* 79—52282
Al-Mg, rapidly solidified, metastable phases *(German)* 79—34011
Al-Mg, recrystallised, grain boundary dislocation identification by computer simulation of TEM image *(Japanese)* 77—47457
Al-Mg, relationship between props. and nonequilib. phase diagram 79—96000
Al-Mg, Si alloy, void form. under different precip. conditions, after Al ion irrad. 80—59529
Al-Mg, single crystal, elastic consts., ultrasonic meas. during ageing 78—11263
Al-Mg, solidification, solid-liq. interface, solute conc. effects 80—59632
Al-Mg, subcritical crack growth under static plane stress 80—55528
Al-Mg, superconducting, an anomalous strain-rate sensitivity of flow stress 79—43313
Al-Mg, thermal conductivity, data anal. and synthesis 78—95284
Al-Mg, thermodynamic props. *(German)* 79—29027
Al-Mg, type AMg6, cryogenic welded vessels, structural strength 80—16477

aluminium alloys continued
Al-Mg, type AMg6, pool metal solidification kinetics in welding with electromag. stirring 80—71636
Al-Mg, type A5083P-0 effects of anisotropy in cutting mechanism *(Japanese)* 80—89232
Al-Mg, vapour press. temp. depend., 1104 to 1637K 80—24576
Al-Mg, work hardening under tension at 1.6-900K 79—38842
Al-Mg 0.1 at.%, neutron-irradiated, dislocation loop characterisation by TEM 79—23614
Al-Mg (0.1 at.%), neutron damage, positron annihilation 80—65056
Al-Mg (0.3 wt.%) single cryst., dislocations obs. by high voltage electron microsc. 80—79796
Al-Mg (1 to 11 wt.%), alloy A99, dissociation in solid soln., effect of treatment of liquid Al *(Russian)* 78—15353
Al-Mg (1 to 14 wt.%), oxidation in air, O_2, CO_2 and flue gas 77—73374
Al-Mg (1 wt.%), behaviour during ductile fracture, SEM *(Rumanian)* 80—21062
Al-Mg (1 wt.%), mechanisms of dynamic strain ageing and jerky flow 79—79024
Al-Mg (13 wt.%), aged single crysts., small angle neutron scattering 80—1961
Al-Mg (2 wt%), high temp. creep, effect of cold working on mechanism 79—43351
Al-Mg (2 wt.%), exam. of Harper-Dorn creep 79—5026
Al-Mg (2 wt.%), hardening and fracture characts., β-phase dissolution role 80—81178
Al-Mg (2 wt.%), steady creep characts., precip. effect 80—35189
Al-Mg (2 wt.%) subgrain formation at low stresses 78—84928
Al-Mg (2.2 at.%), creep at 573K 79—20145
Al-Mg (2.2 at.%), high temp. creep mech. determ. by stress-relaxation 77—12670
Al-Mg (2.4 wt.%) alloy, solution-treated, grain size effects on fatigue strength 77—4839
Al-Mg (2.5wt.%) sheet, surface oxide state and weldability 80—59769
Al-Mg (3 and 7 at.%) alloys, plasmon-dislocation interactions, electron microscope investig. 77—15421
Al-Mg (33 at.%), liquisol quenched, decomposition 79—61622
Al-Mg (4 wt.%), enhanced ductility at elevated temps. 77—63740
Al-Mg (4 wt.%), struct. and strengthening in hot working 80—84968
Al-Mg (4.4 and 6 wt.%), for liquefied natural gas appls., material and weld props. 79—61736
Al-Mg (4.4 and 6 wt.%) for liquefied natural gas appls., material and weld props. 79—61735
Al-Mg (4.4 wt.%), Burgers' vector of boundary dislocation, electron microscope obs. 78—43025
Al-Mg (4.6 wt.%) alloy, mech. effects during static or cyclic creep 78—39865
Al-Mg (5 wt.%), hardness-flow stress rel. during strain-controlled bending fatigue 79—74245
Al-Mg (5 wt.%), recovered dislocation substruct. during plastic flow 79—83273
Al-Mg (5 wt.%), serrated flow 79—43343
Al-Mg (5 wt.%), static strain ageing at low temp. 79—29116
Al-Mg (5 wt.%) deformed bars, cold rolled, exam. of microstruct. by thin foil TEM 78—88502
Al-Mg (5.5 at.%), applied stress change effect in creep *(Czech)* 79—70126
Al-Mg (5.5 at.%), internal stress during creep at high temp. 79—91749
Al-Mg (5.5 at.%), stress change expt. on creep 79—24584
Al-Mg (5.5 at.%), theory of internal stress for class I high temp. creep 78—19807
Al-Mg (5.5 wt.%), effect of stress changes during creep on dislocation struct., TEM study 79—74214
Al-Mg (5.5 wt.%), instantaneous plastic strain associated with stress increments during steady state creep 78—48478
Al-Mg (5.5%), creep, absence of instantaneous plastic strain upon stress changes 78—75718
Al-Mg (5.7 at.%), stress relaxation test, appl. to discerning frictional and internal stresses 77—63712
Al-Mg (5.7 wt.%) alloy, pre-precipitation, elec. resist. investig. 77—32601
Al-Mg (6 wt.%), liq., environment for Ti ductility testing at 700-900°C *(Russian)* 77—52537
Al-Mg (7 wt.%), bare surface reaction rates in aq. solns. 80—101022
Al-Mg (7 wt.%), β-phase soln. behaviour and mech. props. *(Korean)* 78—11277
Al-Mg (7 wt.%), corrosion cracking, exam. of slip dissolution and hydrogen embrittlement mechanisms 78—72852
Al-Mg (7wt.%), corrosion fatigue crack propag. 80—30145
Al-Mg alloy, AL24M, decomp. kinetics and ageing mechanism *(Russian)* 80—45269
Al-Mg alloy, charge transfer, X-ray emission spectra exam. 77—47774
Al-Mg alloy, creep rate, effect of dislocation pinning by impurity atoms *(Russian)* 78—38719
Al-Mg alloy, crystallisation front form. props., casting in EM field *(Russian)* 80—55384
Al-Mg alloy, disperse β-phase, kinetic laws of coagulation *(Russian)* 78—27518
Al-Mg alloy, nitridation process study 80—61013
Al-Mg alloy, superplastic behaviour, effects of bidirectional twisting 77—70129
Al-Mg alloy AMg5, welded structures, machine for fatigue life investigation 79—52566
Al-Mg alloy AMg6, deform. in plane stress at low temps. 78—39873
Al-Mg alloy AMg6, fatigue, random process effect on life 79—66160
Al-Mg alloy AMg6, mech. props. of welded joints, impurity effects 78—95789
Al-Mg alloy A99, intercrystalline fracture during US treatment 79—15795
Al-Mg alloy Al27-1, corrosion cracking behaviour and fine struct. *(Russian)* 79—52438
Al-Mg alloys, 3004 and 5182, oxide films, IR refl. spectra characterisation 77—77644
Al-Mg alloys, AC colour anodisation 79—20283
Al-Mg alloys, distrib. of liquid Mg at liquid-solid interface *(Slovak)* 79—91637
Al-Mg alloys, initial decomposition exam. by X-ray diffr. *(Russian)* 77—77482
Al-Mg alloys, overheating effects on microstruct. and props. 77—63698
Al-Mg cold drawn wires with FCC lattice, texture and structure 77—70067

aluminium alloys continued
- Al-Mg sheet, artificial stress raiser effect on strength and local plasticity of weld joint 80—81130
- Al-Mg single crystal, fatigue deform. 79—91747
- Al-Mg solid soln., AE during plastic deform. 78—64592
- Al-Mg solid solns., decomposition studied by ultrasonic meas. of elastic props. 80—35184
- Al-Mg spherical shell with reinforced holes, local stability 80—50686
- Al-Mg supersaturated solid soln., spinodal decomposition at 20°C *(French)* 77—85987
- Al-Mg surface, growth of MgO film with high secondary electron emission 78—35590
- Al-Mg weldment, US testing, defect acceptance criteria, electron strength 77—70239
- Al-Mg/Al$_2$O$_3$ composites, interface phase, Auger and electron diffr. study 80—25646
- Al-Mg$_2$Si, ageing sequence study by electron microdiffr. 80—81068
- Al-Mg$_2$Si, STEM microdiffr. obs. of precip. struct. 80—104167
- Al-Mg$_2$Si (0.95 wt.%), excess Si effect on ductility 78—27580
- Al-Mg$_2$Si (1 wt.%), precipitation reactions 80—11652
- Al-Mg$_2$Si (1 wt.%) secondary recrystallisation by grain boundary unsewing 79—1886
- Al-Mg$_2$Si (1.7 wt.%), impurity influence on spreading temp. of grain boundary dislocations 79—77609
- Al-Mg$_2$Si(1.42 wt.%), aged, dislocation structs. caused by plastic deformation 80—25786
- Al-Mg-Ag, age effect on age hardening *(Japanese)* 78—52831
- Al-Mg-Be, solid soln. decomposition, metallographic study 77—16577
- Al-Mg-Bi -Na, Bi additions to prevent Na embrittlement 77—86153
- Al-Mg-Cr, tube drawing, tensile forces, plastic deformation *(French)* 79—70130
- Al-Mg-Cu-Si-Cr (1,2.7,0.6,0.2wt.%), laser shock hardening of weld zones 78—39800
- Al-Mg-Fe-Mg-Si-Cr, alloys, dendritic segregation with Fe, Mg, Si and Cr additions *(Polish)* 79—56980
- Al-Mg-Li, subboundary brittleness due to horophilic Na *(Russian)* 77—21244
- Al-Mg-Li alloy, 01420, surface layer props. *(Russian)* 78—80674
- Al-Mg-Li alloy, metastable S′-phase, struct. *(Russian)* 80—103291
- Al-Mg-Li alloy 01420, riveted, low-cycle fatigue strength 80—30097
- Al-Mg-Li-Si system, phase diag. *(Russian)* 78—80515
- Al-Mg-Li-Zr alloys, struct., mech. props. 79—24498
- Al-Mg-Mn, with high Al content, resist., 1.5 to 4.2K 78—26841
- Al-Mg-Mn alloy, disperse β-phase, kinetic laws of coagulation *(Russian)* 78—27519
- Al-Mg-Mn alloy AMG-6M, endurance determ. by dimensionless damageability curves 79—96141
- Al-Mg-Mn-Cr (4, 0.45, 0.15 wt.%), laser shock hardening of weld zones, exam. 78—39800
- Al-Mg-Si, brittleness and heat treatment, statistical design of expts. 77—73349
- Al-Mg-Si, cast, precip.-rich zones on grain boundaries, soln. heat treatment conditions effect on mech. props. 80—104176
- Al-Mg-Si, DTA exam. after small and medium deform. 80—21002
- Al-Mg-Si, deformed, orientation of recrystallisation nuclei 79—91681
- Al-Mg-Si, dendritic non-homogeneity 78—56641
- Al-Mg-Si, dil. alloy, Mn additions and heat treatment effect on $\beta \rightarrow \alpha$ transformation 80—7566
- Al-Mg-Si, dispersoid effect on fatigue crack propag. 79—43420
- Al-Mg-Si, effect of quenching on recrystn. after hot working 79—43289
- Al-Mg-Si, electron probe microanalysis, depleted zone formation in air and vacuum 79—57013
- Al-Mg-Si, Guinier-Preston zones, inception and effect on ageing, review *(Hungarian)* 79—11627
- Al-Mg-Si, heavily rolled, electron microscope obs. of cube oriented region, rolling texture 79—29093
- Al-Mg-Si, heterogeneous precipitation studies using differential scanning calorimetry 80—3062
- Al-Mg-Si, Mg loss, mass spectrometry/thermogravimetry 77—16620
- Al-Mg-Si, nucleation and precipitation growth on dislocations, electron microscope studies 80—3064
- Al-Mg-Si, Portevin-Le Chatelier effect, effect of precipitation hardening 77—32585
- Al-Mg-Si, precipitation of cube-shaped phases, electron diffr. study using TEM *(Japanese)* 79—43251
- Al-Mg-Si, thermomechanically treated, age-hardening 78—11236
- Al-Mg-Si, type 6010, microstruct. characts. influence on formability, heat treatment 80—81090
- Al-Mg-Si, type 6061-T6, 6063-T6, effective stress range factor in fatigue 80—100924
- Al-Mg-Si, under ion irradiated, modification of precipitate interface and effect of precipitates stability 79—77651
- Al-Mg-Si (Alcan 6351), plastically deformed, influence of microstruct. on energy stored 78—84894
- Al-Mg-Si (0.52, 0.58 wt.%), ductile fracture intergranular mechanism 79—15784
- Al-Mg-Si (0.7, 0.4 at.%), effect of precipitation hardening on strain rate behaviour and yield behaviour 79—29075
- Al-Mg-Si alloy, descriptive method for alloy creep tests by nonstationary loadings 78—23759
- Al-Mg-Si alloy, dispersion hardened, concentrators, US waveguides appl. *(Polish)* 80—89237
- Al-Mg-Si alloy, Mn additions, effect on deform. 77—8876
- Al-Mg-Si alloys, DTA exam. of zone form. and other solid phase conversions 77—86057
- Al-Mg-Si alloys, DTA meas. of struct. changes in zones after quenching and isothermal heat treatment 79—52248
- Al-Mg-Si alloys, effects of dispersoids upon micromechanism of crack propagation 79—83286
- Al-Mg-Si core, deformation behaviour contrib. in rod drawing *(German)* 80—11684
- Al-Mg-Si liquid alloy, exam. of thermodynamic props at 780-820°C *(Czech)* 79—91626
- Al-Mg-Si rod, extruded and cold drawn, annealing *(German)* 78—39804
- Al-Mg-Si solid solution under stress, solute atom clustering during ageing 78—31430
- Al-Mg-Si-Cu, cold plastic deformation, stress/strain relations 79—56991
- Al-Mg-Si-Cu, tube drawing, tensile forces, plastic deformation *(French)* 79—70130
- Al-Mg-Si-Mn, Mn addition effects on fracture 78—60791
- Al-Mg-Si-Mn foil, planar defect spacing meas. by TEM 78—2135

aluminium alloys continued
- Al-Mg-Ti-Zr alloy AL23-1, nucleating cellular dendritic crystallisation *(Russian)* 79—70055
- Al-Mg-Ti(Zr), struct. and factors determining brittle intermediate compound form. 78—52817
- Al-Mg-Zn, granulated, degassing atm. effect on mech. props. of semifinished products 80—7720
- Al-Mg-Zn, interdiffusion 78—51751
- Al-Mg-Zn, neutron small angle scatt. study 79—43255
- Al-Mg-Zn, O$_2^+$ ion bombard., SIMS and photon emission spectra, local thermodynamic equilib. model 80—20751
- Al-Mg-Zn alloy, surface Be migration, depth profiling by ion microprobe with high mass resolution 79—46894
- Al-Mg-Zn alloy 7179-T651, reduced ductility under tensile after exposure to water 80—11835
- Al-Mg-Zn alloys, Al-rich, weld metal comp. effect on microsegregation and eutectic phase segregation *(German)* 80—108455
- Al-Mg-Zn alloys, evaporation effect of alloying elements Mg and Zn in in-situ EM studies 80—103388
- Al-Mg-Zn alloys, liq./solid phase equilibria determ. *(German)* 80—50601
- Al-Mg-Zn solid solution, thermophysical props., 0-400°C *(Russian)* 77—89548
- Al-Mg-Zn-Cu, type 7050, calorimetric study of fatigue induced microstructural changes 80—85034
- Al-Mg-Zr, phase diagram *(Russian)* 78—11205
- Al-Mg(-Zn)(-Zn-Cu), exam. of precipitation struct. by neutron scattering 78—92270
- Al-Mg(Cu)(Si), (5.0(4.5)(11.8) wt.%), ingots, vibr. effect during solidification on porosity formation 80—108426
- Al-Mg(Mg-Cu)(Cu), Al$_2$O$_3$ fibre reinforced, exam. of interface interactions during fabrication 78—76616
- Al-Mg(Si), acoustic emission signals in plastic deform., amplitude distrib. *(Japanese)* 78—6978
- Al-Mg(Zn-Mg), long term strength and creep 80—60925
- Al-Mg(Zn), electron probe microanalysis, depleted zone formation in air and vacuum 79—57013
- Al-Mg(Zn)(Cu), pitting potential 78—35550
- Al-Mn, anodisation, intensity of luminesc. and film thickness 78—80413
- Al-Mn, cold-worked and homogenised, precip. kinetics, impurity resist. and TEM meas. 77—16596
- Al-Mn, cooling after recrystallisation, phase transform., X-ray and thermal anal. *(Russian)* 77—66663
- Al-Mn, dil., ^{54}Mn Knight shift meas. using nucl. orientation 78—68396
- Al-Mn, dil., coherent propag. and strain-induced localisation of muons 78—95537
- Al-Mn, dil., core and valence band spectra, XPS study 80—84837
- Al-Mn, dil., magnetisation, 2-0.01K 79—4652
- Al-Mn, dil., magnetoresist. meas. 77—28160
- Al-Mn, dil., magnetoresist. meas. 77—62900
- Al-Mn, dil., supercond., nucl. spin relax. and quasiparticle excitations 80—88680
- Al-Mn, dil., superconducting and normal state, ^{27}Al spin-lattice relax. rates 79—60977
- Al-Mn, dilute, NMR investig. of spin density oscills. around Mn impurities 77—4570
- Al-Mn, direct chill-cast, struct. changes during heat treating *(German)* 80—40408
- Al-Mn, Kondo alloys, spin and phonon resistivity independ. 78—47777
- Al-Mn, magnetic susceptibility, single impurity and interaction effects 77—63093
- Al-Mn, metastable L1$_0$ phase, transformations, mag. struct., TEM study 80—3029
- Al-Mn, Mn impurity displacement during He irradiation, computer simulation 77—80563
- Al-Mn, μ^+ localisation temp. depend. 80—44993
- Al-Mn, splat cooling and heat treatment effect on struct. and props. *(Russian)* 77—48456
- Al-Mn (0.35 wt.%), quenched exam. of Mn-vacancy interaction 78—76676
- Al-Mn (0.55-5 at.%), magnetoresist. depend. on mag. field and impurity conc. 77—62896
- Al-Mn (1 wt.%), anodisation, yellow electrolum. from Al-Al$_2$O$_3$:Mn-electrolyte system 77—63464
- Al-Mn (1 wt.%), commercial, recrystallisation 79—47710
- Al-Mn (1 wt.%), single crysts., rolled to (123)[41$\bar{2}$], recrystn. textures 80—104183
- Al-Mn (1 wt.%), subgrain growth during annealing after cold work 78—56656
- Al-Mn (1 wt.%) corrosion in uninhibited ethylene glycol-water solutions 79—70222
- Al-Mn (1.3 wt.%), corrosion inhibition in trichloroacetic acid using chloroanilines 79—83389
- Al-Mn (1.8 wt.%), cold-rolled, precipitation and recrystallisation 78—27540
- Al-Mn alloys, study of solidification by rapid cooling *(Japanese)* 78—88459
- Al-Mn profiled alloy components pulled from melt, physicomech. props. 78—3175
- Al-Mn sheet, artificial stress raiser effect on strength and local plasticity of weld joint 80—81130
- τ-Al-Mn-C, permanent magnetism and microstruct. 80—75811
- Al-Mn-Fe(Co)(Ni)(Cu), permanent magnetic materials, grain struct. effect *(Rumanian)* 79—73773
- Al-Mn-Mg laminated composite, fatigue fracture, fatigue strength enhancement 79—87725
- Al-Mn-Si, recrystallisation and precipitation 78—52824
- Al-Mn-Zn, fatigue cracks, in NaCl, oil and water vapour *(Japanese)* 78—11414
- Al-Mn-Zr (0.9, 0.4%), strain induced continuous recrystn., rel. to superplastic behaviour 78—84915
- Al-Mn(Cr), dil. alloys, single impurity and interaction effects in susceptibility 77—8269
- Al-Mn(Cu)-Zr, particle stabilized structures, hot deform. 79—47733
- Al-Mn(Cu)(Ag), solute atom displacement in mixed dumbbell interstitials for FCC lattice 78—79631
- Al-Mn(Fe)(Ce)(Ni)(Cu), dil., electronic states, XPS meas. 77—44117
- Al-Mn(Fe)(Co)(Ni), liquid alloys, thermodynamic charact. calc. *(Russian)* 78—27475
- Al-Mn(G), quenched, thermal stability *(Russian)* 80—20976

aluminium alloys continued
Al-Mn(0.6 wt.%), supersat. solid solns., isothermal decomp., Zr addition effects 77−63626
Al-Mo, struct. and props. of alloys obtained from granules 80−50717
Al-Nb, struct. and props. of alloys obtained from granules 80−50717
Al-Nb-R system, R=rare earth, X-ray diffr. obs. of phase equil. *(Ukrainian)* 77−32560
Al-NbTi solenoid magnet for high energy particle detector, conductor and cryostat design 79−31319
Al-Ni, dil., core and valence band spectra, XPS study 80−84837
Al-Ni, interdiffusion and intrinsic diffusion in NiAl δ phase 79−10988
Al-Ni, positive muon trapping at vacancies 79−56704
Al-Ni, solidification in mag. field, crystallite obs. *(Russian)* 77−4770
Al-Ni, thermoelastic phase transform., acoustic emission 80−3039
Al-Ni (10 to 70 at.%). NMR of ^{27}Al *(French)* 77−51974
Al-Ni (2 at.%), rapidly quenched from melt, vacancy loops and precipitates, TEM 77−59769
Al-Ni (3-18wt.%), gun-quenched from melt, struct. 80−76225
Al-Ni (3.6 at.%), quenched from melt, distortion of matrix caused by coherent precipitates, electron diffr. meas. 77−59791
Al-Ni (6 wt.%), fine-grained, deform. in tension and torsion 80−85008
Al-Ni (6 wt.%) misorientation between subgrains, second-phase particles role, STEM microdiffr. obs. 80−104415
Al-Ni (63.6 at.%), elastic softening and electron diffr. anomalies prior to martensitic transform. 77−86078
Al-Ni alloys, solid and liq. mag. susceptibility, 600-1650°C *(Russian)* 80−15685
Al-Ni eutectic, mechanism of lamellar spacing adjustment 78−31395
Al-Ni eutectic alloy, directional solidification using electroslag remelting 79−61578
Al-Ni foil, vapour deposited, multiply twinned particles, electron microscopy 77−28083
Al-Ni mixed-powder-based plasma-sprayed coatings, strength characts. 77−12548
Al-Ni multiphase system, simultaneous diffusion in cylindrical symm. *(Russian)* 80−100357
Al-Ni solid, liquid mixture, diffusion processes *(Russian)* 80−107563
Al-Ni system, Knight shift, NMR line widths determ. *(French)* 77−77113
Al-Ni with multiple layer plasma coating, exam. of cohesion strength *(Russian)* 80−7714
Al-Ni-Co, directionally solidified ternary eutectic morphology *(Czech)* 77−59772
Al-Ni-Co(Si), directionally solidified eutectic, morphological and mech. props. *(Russian)* 80−30057
Al-Ni-Si, eutectic, unidirectional solidification 77−16565
Al-Ni-Si sintered SAS-1 alloy, struct. *(Russian)* 79−52135
Al-Ni-Ti, calc. of phase equilibria using thermodynamic values from different models 78−60646
Al-Ni-(Mg) (6, 0.3 wt.%), fine grained, Luders' band deform. 77−77527
Al-Ni(Ca)(6 and 7.6 wt.%), polycrystalline containing coarse particles, Bauschinger effect 77−48480
Al-Ni(Cd)(Fe)(Si), cold worked, struct. and props. 80−71666
Al-Ni(Fe,Co,Cr,Ti) powder based composite, high temp. strength of W reinforcing fibres 79−70021
Al-Ni(Pt)(Zn), rapidly solidified, twinned dendrites 80−70572
Al-Ni(Si), liquid, thermodynamic props. 79−91619
Al-Ni(Si), optical emission spectrographic analysis of some binary alloys by a glow discharge of Grimm lamp *(Japanese)* 79−99015
Al-Pb, dil., pulsed ruby laser irrad., noncryst. phase form 80−35012
Al-Pb, with isolated liq. phase inclusions, recrystn. *(Russian)* 80−20970
Al-Pb solid solution, thermal expansion, 10-55K *(Russian)* 77−80635
Al-Pb(Bi)(Cd), containing low melting point inclusions, impact props., temp. depend. 78−60792
Al-Pb(Bi)(Sn) liquid alloy, surface tension and surface adsorpt. determ. *(French)* 79−69325
Al-Pb(Sn), liquid, surface tension, size effect *(French)* 80−15341
Al-Pd, preferred sputtering on surface, mass difference and chemical bonding difference effects, AES obs. 79−83078
Al-Pd, rapidly solidified, new ordered phase, electron microscope obs. 79−11645
Al-Pd (6 at.%), metastable Al_2Pd phase formed by rapid quenching, electron diffr. obs. 79−51054
Al-Pd eutectic, microstruct. morphology 80−3018
Al-Pd_2Si-Si junction thermal stability improvement 79−78186
Al-Pd(Si) film, preferred sputtering on surface, mass and bonding difference effects, AES obs. 79−87552
Al-Pr (16 wt.%), resist. depend. on temp. and hot rolling *(Polish)* 80−39555
Al-Pt (2 at.%), splat cooled, $AlPt_2$ phase, electron diffr. obs. 79−15657
Al-Pt (2 wt.%), rapidly solidified alloy, metastable phase formation and decomposition 79−52194
Al-PtSi-Si junction thermal stability improvement 79−78186
Al-rare earth alloys, granules, rolling to form foil, exam. 80−20825
Al-Sb, ion-implanted, precipitation form. and evolution TEM obs. 79−55766
Al-Sb, laser induced surface alloy formation and Sb diffusion 80−54439
Al-Sc, dil., thermomigration of Sc 79−69280
Al-Sc, elec. resist. determ. 80−92876
Al-Sc, solid solubility and residual resist. 79−51265
Al-Si, AC colour anodisation 79−20283
Al-Si, and Al-Si-Na eutectic melts, struct. determ. *(Russian)* 77−80408
Al-Si, DC magnetron-sputtered, residual gas influence on props. 80−80968
Al-Si, deformed, local lattice rotations at second phase particles 80−25709
Al-Si, dil., mechanism of dissolution of Si 79−19375
Al-Si, dilute, anomalous primary creep behaviour, precipitate form. 80−7646
Al-Si, effect of irrad. on the nucleation of incoherent precipitates 79−8303
Al-Si, enhanced interdiffusion during Ar ion bombardment 79−99353
Al-Si, eutectic, quasiisotropic, rheological deformation theory 80−79165
Al-Si, eutectic colonies morphology by stereometric microanal. *(Russian)* 77−81247
Al-Si, graphite dispersed, wear characts. *(Korean)* 80−93658
Al-Si, hypereutectic Ostwald ripening of Si crystals during solidification *(Japanese)* 79−4962
Al-Si, hypereutectic silumins, P and Na modification 78−84792
Al-Si, inoculated with NaCl+KCl+NaF, effect on morphology of eutectic columns *(Russian)* 79−15684

aluminium alloys continued
Al-Si, internal friction and Si precipitate nucleation 78−60690
Al-Si, liq. alloy, chem. diff. coeff. determ. 77−1249
Al-Si, liquid alloy, compressibility and struct. factors at zero wavevector 79−23515
Al-Si, magnetic susceptibility and elect. resistivity, 500 to 1000°C, struct. sensitive props. *(Russian)* 78−15550
Al-Si, molten, Na determ. using β-Al_2O_3 probe 77−48714
Al-Si, neutron small angle scatt. study 79−43255
Al-Si, off-eutectic alloy growth from stirred melt 77−8809
Al-Si, penetrability coeffs. for two-phase zone of solidifying castings *(Russian)* 77−55956
Al-Si, preferred sputtering on surface, mass difference and chemical bonding difference effects, AES obs. 79−83078
Al-Si, thermal control of interphase microstresses and mech. props. 77−12654
Al-Si, three dimensional dry cutting, with sintered diamond tool *(Japanese)* 80−25917
Al-Si, unidirectionally solidified eutectic alloy grow at different rates, Vickers hardness 77−36654
Al-Si (0.57 at.%), Si precipitate dissolution kinetics 80−84935
Al-Si (0.6, 0.9, 1.19 wt.%), interdiffusion coeffs. determ. by Matano's method 79−42295
Al-Si (1 wt.%) hardness-flow stress rel. during strain-controlled bending fatigue 79−74245
Al-Si (16 wt.%) melt, fivefold twinned Si cryst. growth, crytallographic study 80−2942
Al-Si (1.2 and 0.6 wt.%), single crystal, dispersion hardened with SiC, Bauschinger effect and work hardening 79−43360
Al-Si (1.2 wt.%), dispersion hardened, temp. depend. of work-hardening due to Orowan loops 79−91668
Al-Si (1.2 wt.%), dispersion hardened, work hardening due to Orowan loops, temp. depend. *(Japanese)* 80−66534
Al-Si (25.4 wt.%), solidification, high press. effects 80−66499
Al-Si (2.4 wt.%), liq. fluidity in solid-liq. zone 80−108429
Al-Si (35 wt.%), Cr, Co, Si addition effects on strength of powder 77−24983
Al-Si (8 wt.%), threshold H_2 for pore form. during solidification 78−52794
Al-Si (9 wt.%), precipitation hardening during isothermal ageing 80−29969
Al-Si alloy, as-cast binary, wear characteristics against steel 79−96156
Al-Si alloy, compression, effect of press. on lattice defects up to 90 kbar *(Japanese)* 77−72654
Al-Si alloy, dilute, electron irradiation, interstitial dislocation loop obs. 78−18681
Al-Si alloy, hot shortness, rheological model *(Russian)* 77−56072
Al-Si alloy, rod, tensile loaded, internal friction and Young's modulus measuring equipment, inelastic phenomena exam. *(Hungarian)* 79−52546
Al-Si alloy metallisation by rate controlled dual electron beam gun evaporator 79−11516
Al-Si alloy metallisation sputter deposition for VLSI 80−66429
Al-Si alloys, modification by Na-containing agents, ^{24}Na radioisotope investigation *(Russian)* 77−40567
Al-Si alloys, neutron irrad., precip. processes, neutron small-angle scatt. obs. 77−4131
Al-Si alloys, phosphorus content determ. by neutron activation anal. *(Russian)* 77−40614
Al-Si alloys, surface tension *(Czech)* 79−77865
Al-Si cast alloy, flank wear of carbide tool during machining *(Japanese)* 78−19900
Al-Si casting alloys, graphite-dispersed, mech. props. and wear resist. 77−4857
Al-Si coatings, form. and behaviour under particle bombard. 80−35029
Al-Si crystals, work hardened, softening and creep rates on annealing 80−11663
Al-Si eutectic, depend. between min. creep rate and time of beginning of secondary creep *(Czech)* 80−35267
Al-Si eutectic, directionally solidified, tensile props. 78−64531
Al-Si eutectic, high temp. creep, two regimes of flow, modified Dorn eqn. anal. 79−74215
Al-Si eutectic, irregular, branching limited growth 80−81042
Al-Si eutectic, Na, Sb and Sr alloying addition effects on microstructure *(French)* 78−64548
Al-Si eutectic, pressure effect on metal-die heat transfer coeffs. during solidification 80−7544
Al-Si eutectic alloy, banded struct., SEM and optical microscopy 80 - 104144
Al-Si eutectic alloy, hardness rel. to tensile and compressive strength 79−52354
Al-Si eutectic alloys, superplasticity 80−11710
Al-Si eutectics and hypoeutectics, mech. props. and thermal cond., P impurity effect 79−83271
Al-Si film, magnetron sputtered deposition, characts. 79−91587
Al-Si hypereutectic alloy, dissolution and primary crystallization of Si *(French)* 77−59832
Al-Si hypereutectic alloy, wear resistance 77−77593
Al-Si melt, microheterogeneity *(Russian)* 80−103238
Al-Si melts, hypoeutectic, eutectic, hypereutectic structural factors, atomic radial distrib. functions *(Russian)* 79−73091
Al-Si melts, spreading behaviour on Fe 80−84345
Al-Si melts, struct. factors, at. distrib. curves, thermodynamic and neutron diffr. study *(German)* 80−19687
Al-Si-Cn-Mg, alloy AL32, ageing of castings produced by pressure die castings 78−56650
Al-Si-Cu, fracture resistance at low temps. 80−104284
Al-Si-Cu, granules, energy conditions of rolling 77−12578
Al-Si-Cu, LM30, crack propag. rates in air and salt soln. 80−21063
Al-Si-Cu alloy metallisation sputter deposition for VLSI 80−66429
Al-Si-Cu casting alloy, optimum selection of chem. contents for optimum strength *(Czech)* 79−15625
Al-Si-Cu-Be alloys, phase equilib. *(Russian)* 77−59748
Al-Si-Cu-Mg-Ni, piston, depend. between min. creep rate and time of beginning of secondary creep *(Czech)* 80−35267
Al-Si-Cu-Mg-Ni cast alloy, fractography *(German, English)* 79−87809
Al-Si-Cu-Ni alloy casting, thermal props. 78−95814
Al-Si-Cu-Zr, ageing kinetics *(Russian)* 80−76274
Al-Si-Li system, Al-rich, phase comp., limits of solid solubility *(Russian)* 77−21097
Al-Si-Mg, corrosion inhibition in 0.1 N NaOH soln. 78−19924

aluminium alloys continued
Al-Si-Mg, Si content and Mg addition effect on mech. props., Na treatment *(Korean)* 79—38901
Al-Si-Mg alloy metallisation sputter deposition for VLSI 80—66429
Al-Si-P (19, 0.02 wt.%), primary Si crystals in Al melt, Ostwald ripening and solidification growth 80—35179
Al-Si-Sr phase diagram *(Russian)* 78—15363
Al-Si-Y alloy, phase equilibria in Al rich region *(Russian)* 80—93537
Al-Si-Zn alloy, creep rates, pre-torsional deformation effect 79—96096
Al-Si(Cu)(Zn-Mg-Cu), extraction and phase anal. 79—15673
Al-Si(Ge) eutectic alloys in screened ohmic contacts for solar cells 80—94090
Al-Si(Ge) film, ion-implanted, percolation and superconductivity 78—26982
Al-Si(Mn)(Ti)(Cr)(Ni)(Cu)(Fe), liq., dissoln. and diffusion of alloying components, 700-1000°C *(Russian)* 80—15275
Al-Si(0.4 wt.%), voids, neutron radiation induced, in US and in 80US-10UC-10UC$_2$ 79—50951
Al-Si(7 wt.%), anodically oxidised, sunlight absorber, struct. and thermal efficiency 77—125
Al-Si(9.3, 12) with graphite particles seizure resistance study using Hohman wear tests 80—89360
Al-Sn, (<0.28 wt.%) corrosion behaviour in 16% HCl 78—85054
Al-Sn, conc. profiles across solid-liq. interfaces 80—55382
Al-Sn, dil. alloy, vacancy-impurity interaction, exam. by electrical resistivity meas. at 77K *(German)* 78—83846
Al-Sn, discrete eutectic formation mechanism *(Russian)* 77—66634
Al-Sn, liq. alloy, chem. diff. coeff. determ. 77—1249
Al-Sn, Sn effect on electrochemical behaviour in acetate buffer 78—19927
Al-Sn alloys, heat treatment effect on ^{119}Sn Mossbauer spectrum 80—7228
Al-Sn dil. alloy, cube orientation texture development 79—96040
Al-Sn liquid alloys, heats of mixing and activities calcs. 79—42264
Al-Sn-U alloy, phase equilib. exam. by metallographic and X-ray anal. 77—21102
Al-Sn(Ag) liquid alloys, diffusion of Ge, mechanism *(Russian)* 80—15276
Al-Sn(Ag)(Cu)(Au), liquid alloys, exam. of Si diffusion *(Russian)* 79—28118
Al-Sr-Nd phase diagram *(Russian)* 80—20893
Al-T alloys, relationship between struct. and thermodynamic props. *(German)* 78—91307
Al-Ti, dilute, morphological stabilities of planar solid-liquid interfaces during unidirectional solidification 79—4960
Al-Ti, manufacture, use of Na$_2$TiF$_6$, transfer of Ti 78—27453
Al-Ti, mechanical props. improvement, by work hardening *(French)* 80—97502
Al-Ti, molten, showering cryst. form. in mould cooled from top *(Japanese)* 80—66498
Al-Ti, solid soln., unidirectionally solidified, segregation patterns revealed by etching 79—47693
Al-Ti alloy spark alloying, cathode weight change and hardened layer obs. *(Russian)* 80—61005
Al-Ti alloy target in surface anal. by XPS 79—43682
Al-Ti alloys, growth crystallography and morphologies of Al$_3$Ti primary dendrites 79—43230
Al-Ti dilute alloys, solute distribs. during unidirectional solidification 79—4961
Al-Ti system, interdiffusion coeffs. determ. 80—70477
Al-Ti-B, liquidus surface at Al corner *(Japanese)* 77—55948
Al-Ti-B alloys, phase comp. and distrib. of components, X-ray obs. *(Russian)* 79—52164
Al-Ti-B alloys, segregation of Ti, electron microscope exam. 78—52820
Al-Ti-C, grain refinements study using centrifugal force *(Japanese)* 79—20035
Al-Ti-Fe, ternary phase diagram, computer calculations 80—45274
Al-Ti-Si phase diagram, calc., interpretation of grain refinement results 78—84781
Al-TiB$_2$-Si, Si effect on grain refinement *(German)* 79—91656
Al-Ti(-Si), nucleation entropy and grain refinement 79—91627
Al-Ti(Mn)(Ni)(Cu), couple phase diagrams and thermochemical data 79—66037
Al-transition metal, dil., residual resist. of 4d and 5d impurities 77—28155
Al-transition metal, impurity binding energies 79—42096
Al-transition metal, residual resistivity, effect of 4d and 5d transition metal impurities 79—60791
Al-transition metal alloys, anomalous sp. ht. and nuclear spin-lattice relax. 79—46814
Al-V, dil., supercond., nucl. spin relax. and quasiparticle excitations 80—88680
Al-V, dil., superconducting and normal state, ^{27}Al spin-lattice relax. rates 79—60977
Al-V-Ti, SiC coated B fibre reinforced, tensile and compressive strength, prior thermal treatment effect 78—11264
Al-V(Ti)(Fe), dil., screening charge around 3d impurities, NQR meas. 77—32287
Al-W, struct. and props. of alloys obtained from granules 80—50717
Al-Y, dil., hyperfine interactions, ^{87}Y^{m} nuclear orientation meas. 78—43715
Al-Y, specific elec. resist., variation with Y conc. 80—84455
Al-Zn, age hardenable precipitation and dissolution, positron annihilation and X-ray scatt. 80—16314
Al-Zn, ageing alloy, zonal decomposition stage, new effects in X-ray diffr. anal. *(Russian)* 79—4982
Al-Zn, coating on mild steel, interface struct. 79—52466
Al-Zn, comparison between very-slow-neutron transmission and small-angle neutron scatt. expts. 80—19677
Al-Zn, dil., grain boundary diffusion 78—91475
Al-Zn, dil., magnetoresist., temp. depend. 80—70682
Al-Zn, dil. alloy, ^{65}Zn diffusion 77—51540
Al-Zn, dil. alloy, ageing and reversion, annealing curves, X-ray obs. 78—88485
Al-Zn, discontinuous decomposition *(Polish)* 78—52808
Al-Zn, effects of temp. on order-depend. elec. resist. 77—31992
Al-Zn, electrical resist. and magnetoresist., 2 to 40K, Matthiessen rule deviations *(Russian)* 77—31996
Al-Zn, electrical resist. of Guinier-Preston zones during age hardening 77—72848
Al-Zn, flow stress, Zn content effect 79—38913

aluminium alloys continued
Al-Zn, formation of Guinier-Preston zones, and their limit temp. *(Japanese)* 78—84861
Al-Zn, GP zones, effect of Si, Ag, Mg on transport props. 77—16588
Al-Zn, G.P. zone form., temp. limit 80—16317
Al-Zn, grain boundary reaction sites, determ. of struct. aspects, by electron microscopy 80—103359
Al-Zn, Guinier-Preston ellipsoidal zone model of X-ray scatt. *(French)* 77—84568
Al-Zn, Guinier-Preston zone form. kinetics study using linear localisation probe *(French)* 78—15413
Al-Zn, Guinier-Preston zone reversion, thermoelectric power meas. *(French)* 79—20058
Al-Zn, Guinier-Preston zone struct., absolute SAXS meas. *(Japanese)* 79—70072
Al-Zn, interdiffusion meas. by elec. resist. 80—49433
Al-Zn, isothermal preprecipitation, small angle X-ray scatt. expts. 80—35186
Al-Zn, liq., physical props. study by electrodiffusion method *(Czech)* 77—84956
Al-Zn, liq. solutions, thermodynamic properties *(Polish)* 80—49380
Al-Zn, low temperature lattice parameters 78—38658
Al-Zn, metastable phases formed at 200°C, room temp. stability 80—16315
Al-Zn, metastable solvus curve, struct. changes 77—55950
Al-Zn, miscibility gap, spinodal region, thermodynamic data transferability *(German)* 79—20027
Al-Zn, neutron small angle scattering from above critical point 79—1840
Al-Zn, neutron small angle scatt. study 79—43255
Al-Zn, nonhomogeneity of deform. 78—84888
Al-Zn, plastic deform. effect on struct. transform. at elev. temp. *(Czech)* 79—79044
Al-Zn, precipitation struct. and phys. props. effect of miscibility gap *(German)* 78—92265
Al-Zn, resistivity anomalies in Guinier Preston zones *(French)* 78—6937
Al-Zn, resistivity calc. for age-hardened alloy 77—73284
Al-Zn, short range order, many electron effects, pseudopotential method 78—79954
Al-Zn, short-range order, electronic theory, pseudopotential approach 77—80717
Al-Zn, small-angle neutron scatt. in crit. point regions, 324-435°C *(German)* 77—85993
Al-Zn, solid soln., exam. of evolution by thermo EMF meas. *(French)* 78—52862
Al-Zn, spinodally decomposing, main wavelength of conc. fluctuations calc. 80—97459
Al-Zn, tension deformed superplastic specimens, instantaneous strain rate variation *(Russian)* 79—79033
Al-Zn, type 7075-T6, coldworked hole specimens, residual stresses, fracture mech. anal. 80—97587
Al-Zn, work hardening under tension at 1.6-900K 79—38842
Al-Zn, X-ray diffr. after omnidirectional compression *(Russian)* 80—88262
Al-Zn 6.8 at.%, Guinier-Preston zones *(French)* 79—87640
Al-Zn (0.041 to 4.4 at.%), clusters, electrical resistivity meas. *(Japanese)* 77—21168
Al-Zn (0.14 at.%), nuclear acoustic reson., 20-80K 79—8058
Al-Zn (10 at.%), ring diffuse X-ray scatt. phenomena *(Russian)* 77—16538
Al-Zn (10 at.%), short-range order parameter calc. in pseudopot. approx. *(Russian)* 80—49183
Al-Zn (10 wt.%), ageing at low temp., solute conc. fluctuation effects *(Japanese)* 79—4969
Al-Zn (10 wt.%), ageing at low temp., effects of fluctuation of solute conc. 80—76287
Al-Zn (10 wt.%), ageing at low temp., effects of fluctuation of solute conc. 80—76288
Al-Zn (10 wt.%), ageing behaviour, calorimetric study 80—45328
Al-Zn (10 wt.%), solid soln., decomposition meas. by resistivity meas. under isothermal conditions *(French)* 79—20025
Al-Zn (10 wt.%), solute conc. fluctuation effects on ageing at low temp. 79—57023
Al-Zn (11 wt.%), stress depend. of strain rate at elev. temps. 78—23757
Al-Zn (11.8 at.%), growth and dissolution of metastable precipitates, neutron scatt. study 79—15671
Al-Zn (12.5 wt.%) retardation of precip. reaction by DC stress 77—55969
Al-Zn (15,16,18 at.%) alloys, coherency spinoidal curve position determ. 77—52281
Al-Zn (15 at.%), structural changes during post ageing between 125°C to 215°C 80—40399
Al-Zn (15 at.%), supersaturated alloy, growth and decomposition kinetics 80—29965
Al-Zn (15 wt.%), calorimetric ageing study 80—45330
Al-Zn (18 at.%), position of coherency spinodal curve 78—23660
Al-Zn (1.9 at.%), 1 MeV electron irradiated, induced homogeneous precipitation 79—77638
Al-Zn (2 and 4 wt.%), ageing and elec. cond. reversion *(Japanese)* 79—4983
Al-Zn (20 (30) (35) (40) (60) at.%), effect of UTS on cyclic creep strength *(Korean)* 80—25778
Al-Zn (21.8 at.%), elec. conductivity and α'-precipitates, 276-302°C 77—80758
Al-Zn (22 at.%), X-ray scatt. obs. of segregation *(French)* 79—96032
Al-Zn (22 wt.%), superplastic strain rate sensitivity, rel. to ductility 78—31478
Al-Zn (30 wt.%), metastable phases, transformation kinetics, quenching rate effects meas. 77—55960
Al-Zn (30 wt.%), precipitation sequences and transformation kinetics, X-ray diffr. and TEM obs. 77—55959
Al-Zn (30 wt.%), precipitation ageing plastic deform. effects 77—66645
Al-Zn (38 at.%), alloy, TEM study of precipitation processes or different microstructures during ageing 80—93561
Al-Zn (3.9 wt.%), single crysts., fatigued age-hardenable, dislocation structure *(German)* 80—54247
Al-Zn (40 at.%), resistance of homogenization in micro-segregation 79—100180
Al-Zn (40 wt.%), grain refinement by thermal cycling 78—3149
Al-Zn (40 wt.%), mechanical properties after thermal cycling 78—3150
Al-Zn (40(50)(65) wt.%), deformed, free energy changes in process of discontinuous precipitation 80—3054

aluminium alloys continued
  Al-Zn (40(50)(65) wt.%), plastic deform. effect on discontinuous precipitation 80—3053
  Al-Zn (4.5 at.%), age-hardening, resistivity charge by low temp. deform. *(Japanese)* 78—84831
  Al-Zn (5.05 at.%), comparison of X-ray and neutron small-angle scatt. 79—15647
  Al-Zn (60 or 71 wt.%), natural ageing *(Russian)* 78—48367
  Al-Zn (6.5 at.%), fatigue props., effect of ageing and thermomech. treatment 78—27620
  Al-Zn (6.8 at.%), decomposition, electron microscope study *(French)* 77—40422
  Al-Zn (6.8 at.%), hardening during spinodal decomposition *(French)* 79—66035
  Al-Zn (6.8 at.%), neutron small angle scatt., interparticle interference 77—77514
  Al-Zn (6.8 at.%), synchrotron radn. use in X-ray scatt. *(French)* 79—47723
  Al-Zn (6.8 at.%) alloy, elec. resist. temp. depend. rel. to ageing processes 77—77486
  Al-Zn (6.8 wt.%), effects of ageing temps. on microhardness and resistivity *(Japanese)* 78—35408
  Al-Zn (6.8 wt.%), Guinier Preston zones internal struct., study by X-ray diffusion, α_R phase comparison *(French)* 80—66472
  Al-Zn (7 at.%), liquid quenched, early stage phase separation, exam. 78—68698
  Al-Zn (70, 30 wt.%), decomp. study, 25-160°C *(Czech)* 80—89225
  Al-Zn (8-25 wt.%), solid solns., residual resist. during clustering 80—97483
  Al-Zn alloy, resist. and X-ray small angle scatt. during GP zone form., theory *(French)* 79—29070
  Al-Zn alloy, solid state eutectoid transformation 79—74146
  Al-Zn alloy, type 7010, die-forged, tensile props. after heat treatment, stress corrosion 79—66103
  Al-Zn alloy cladding materials, corrosion behaviour under vacuum heating *(Japanese)* 79—91845
  Al-Zn alloys, anisotropy function determ. 77—43565
  Al-Zn alloys, cast, Zn diffusion during homogenization *(Polish)* 79—33108
  Al-Zn alloys, interfacial stability of planar solid-liq. interface during solidification 80—104145
  Al-Zn alloys, interfacial holes distrib. at beginning of interfacial instability in solidification 80—104146
  Al-Zn alloys, preprecipitation, elec. resist., microhardness meas., dislocation-growth distortion interactions *(Japanese)* 77—25053
  Al-Zn alloys, recrystallisation and superplasticity, HVEM straining 80—39207
  Al-Zn alloys, relation between microhardness and average radius of Guinier-Preston zones 78—95811
  Al-Zn alloys, room temp. decomp. of metastable phases precipitated at 200°C 78—84814
  Al-Zn alloys, spinodally decomposing, resistivity behaviour 80—45271
  Al-Zn changes in inner-electron binding energies during ageing, electronic spectra study 77—28816
  Al-Zn coated steel sheet, chromate passivation protection against wet-storage stain 78—95854
  Al-Zn eutectic, mechanism of lamellar spacing adjustment 78—31395
  Al-Zn eutectoid, superplastic, fracture, electron microscope obs. 78—31533
  Al-Zn eutectoid, superplasticity, test machine rigidity effect 79—70250
  Al-Zn eutectoid alloy, sensitivity analysis of torsion method in evaluating superplasticity indicators 77—56179
  Al-Zn melt, electrotransfer *(Russian)* 77—66034
  Al-Zn solid soln., controlling creep mechanisms, role of diffusion 78—31469
  Al-Zn solid soln., controlling creep mechanisms role of diffusion 78—31470
  Al-Zn system, R-phase, mixing free enthalpy approx. calc. 77—1832
  Al-Zn thin film, prep. using Sn-Zn evaporant source 80—100789
  Al-Zn-Cu (22, 0-3 at.%) alloys, coherent spinodal curve 79—87605
  Al-Zn-Cu-Mg (V95T1), subcritical crack growth under static plane stress 80—55528
  Al-Zn-Fe-Si, Fe and Si effects on precip., TEM and X-ray diffr. obs., ageing at 90°C 77—48439
  Al-Zn-Hg alloy, cathodic protection characts., surface free energy, lattice struct. 79—29281
  Al-Zn-In-Mg, substitution for Mg in Mg-MnO_2 short-circuited cell, performance 79—61964
  Al-Zn-Mg, acoustic emission meas. during tensile testing, reproducibility of results 80—50782
  Al-Zn-Mg, age-hardenable, precipitation and dissoluton processes, positron annihilation and X-ray small-angle scattering comparison 80—89238
  Al-Zn-Mg, atmosphere effect on fatigue crack propag. *(Japanese)* 80—81161
  Al-Zn-Mg, cavitation during superplastic deform. *(Japanese)* 78—15464
  Al-Zn-Mg, crack-arrest markings on integranular stress corrosion fracture surfaces 80—89405
  Al-Zn-Mg, decomp. kinetics and ageing mechanism *(Russian)* 80—45269
  Al-Zn-Mg, decomposition calorimetric study *(German)* 79—74165
  Al-Zn-Mg, ductile intercrystalline fracture obs. 77—77554
  Al-Zn-Mg, duplex ageing effect on tensile props. 79—91721
  Al-Zn-Mg, effect of microstruct. on localised shear failure 78—52996
  Al-Zn-Mg, effect of microstruct. and corrosive environments on stress corrosion cracking *(Japanese)* 79—79159
  Al-Zn-Mg, elec. resist. of η' precipitates 77—48441
  Al-Zn-Mg, electron probe microanalysis, depleted zone formation in air and vacuum 79—57013
  Al-Zn-Mg, fatigue crack propag., stage I 77—36653
  Al-Zn-Mg, fractographic stage I fatigue facets 77—16680
  Al-Zn-Mg, grain boundary surfaces, plasmon loss satellites in Auger spectra 78—15261
  Al-Zn-Mg, grain boundary segregation, AES meas. 78—72781
  Al-Zn-Mg, Guinier-Preston zones, comp. and contrib. to elec. resist. 80—16316
  Al-Zn-Mg, heat treatment and inversion processes, elec. resist. study *(Hungarian)* 77—25078
  Al-Zn-Mg, metastable miscibility gap determ. by small angle scatt. 77—28781
  Al-Zn-Mg, O transport during fatigue crack growth 78—52981

aluminium alloys continued
  Al-Zn-Mg, oriented growth of precipitates on dislocations, model 80—108448
  Al-Zn-Mg, plastic deform. influence on structural transform. and mechanical props. *(Russian)* 80—7623
  Al-Zn-Mg, plastic instability rel. to grain boundary failure at low temps. 78—56702
  Al-Zn-Mg, polygonized struct. in extrusions, thermal stability and mech props. 80—50659
  Al-Zn-Mg, precipitation mechanism, effect of Mg additions *(French)* 77—52330
  Al-Zn-Mg, precipitation of η' phase, heat treatment, electron microscope obs. 78—68699
  Al-Zn-Mg, precipitation strengthened, Bauschinger effect 77—36585
  Al-Zn-Mg, role of dispersed transition metal intermetallic compounds 79—96088
  Al-Zn-Mg, solid soln. decomp., 20 to 200°C 79—38830
  Al-Zn-Mg, steel wire reinforced, tensile strength depend. on angle of reinforcement *(Russian)* 78—15452
  Al-Zn-Mg, stress conversion cracking based on micromech. surface reactions 80—7716
  Al-Zn-Mg, TEM and calorimetric study 80—76290
  Al-Zn-Mg, TEM characteris. of precipitates 80—104166
  Al-Zn-Mg, thermomechanically treated, precip. behaviour 78—84856
  Al-Zn-Mg, type 7075, edge effects of fatigue crack closure 80—3189
  Al-Zn-Mg, type 7075, fractography of fatigue 80—40488
  Al-Zn-Mg, type 7075, strain rate effects on H embrittlement 80—3190
  Al-Zn-Mg, type 7075-T651 plate, thickness direction inhomogeneity of mech. props. and fracture toughness 80—100892
  Al-Zn-Mg, type V-95, ultimate tensile strength for brief impact 80—70309
  Al-Zn-Mg, weldable, microstruct. and intercrystalline fracture 77—48550
  Al-Zn-Mg, welded section stress in rolled plate edges, mechanical surface treatment and environment effects 80—21193
  Al-Zn-Mg, zone composition change during ageing 79—29110
  Al-Zn-Mg (Fe), dil. alloy, ^{65}Zn diff. 77—51540
  Al-Zn-Mg (2.1, 1.3 wt.%), single crysts., fatigued age-hardenable, dislocation structure *(German)* 80—54247
  Al-Zn-Mg (2.64, 1.40 at.%), age-hardening, resistivity charge by low temp. deform. *(Japanese)* 78—84831
  Al-Zn-Mg (3,1.5 wt.%), precipitation hardened and fatigued alloys, solute loss at fracture surface, EPMA exam. 78—39893
  Al-Zn-Mg (3.2, 2.2 wt.%) alloy, GP zone reversion, η' of formation, quant. investig. 77—4784
  Al-Zn-Mg (3.6, 1.95 wt.%), ageing and plastic deform., effect on structure, electron microsc. and X-ray diffr. study *(Russian)* 80—81108
  Al-Zn-Mg (3.87, 1.79 wt.%) TEM exam. of early stage precipitation, on dislocation lines 79—4972
  Al-Zn-Mg (3.87, 1.79 wt.%), oriented growth of precipitates on dislocations, TEM obs. 80—108447
  Al-Zn-Mg (4.5, 2 to 3 at.%) solid state reactions by interrupted continuous heating 80—25737
  Al-Zn-Mg (4.5, 2 wt.%), stress corrosion resist., vac. heat treatment effect 79—96203
  Al-Zn-Mg (4.5, 2.5 wt.%), fatigue crack propag. 77—86171
  Al-Zn-Mg (4.5, 2.5 wt.%), composition effect on stress corrosion and mech. behaviour 78—27684
  Al-Zn-Mg (4.5 at.%, 2 or 3 at.%), decomposition behaviour during continuous cooling, XSAS and TEM examination 80—16264
  Al-Zn-Mg (4.5 at.%, 2 to 3 at.%), decomp. behaviour during continuous heating 80—29922
  Al-Zn-Mg (4.8, 1.1 wt.%), second phase dissolution, calorimetry study 79—100193
  Al-Zn-Mg (4.8, 1.2 wt.%), quenched, Guinier Preston zones formation 80—45273
  Al-Zn-Mg (5, 1 wt.%), relation between mech. props., SCC and dislocation struct. *(German)* 77—81345
  Al-Zn-Mg (5, 2 wt.%), diffusion of ^{65}Zn, 165 to 560°C 77—11743
  Al-Zn-Mg (5,2 wt.%), TEM of early stages of precipitation 77—40423
  Al-Zn-Mg (5,2.5 wt.%) observation of stress corrosion cracking 78—60868
  Al-Zn-Mg (5.9, 2.9 wt.%), ageing effects on microstruct. 80—16306
  Al-Zn-Mg (6, 2.5 wt.%), fracture toughness-transgranular fracture relation 77—52447
  Al-Zn-Mg (6, 2.5 wt.%) alloy, intergranular fracture mechanism due to ledge formation 79—57089
  Al-Zn-Mg (6,1.5%), influence of ageing and cold work on tensile and fracture props. *(Japanese)* 78—52842
  Al-Zn-Mg (6,3 wt.%), hydrogen embrittlement and trapping 80—55490
  Al-Zn-Mg (6,3 wt.%) high-strength alloy, dislocations distrib., corrosive environment influence *(Russian)* 79—52442
  Al-Zn-Mg (6.0, 2.5 wt.%), aged, grain, size depend. of fracture toughness 78—48495
  Al-Zn-Mg (6.27, 2.94 wt.%), single crystals, effect of environment on liquid-metal embrittlement, stress corrosion cracking and corrosion fatigue 78—64676
  Al-Zn-Mg (9, 1 wt.%), superplastic flow, relative motion of grains 77—52426
  Al-Zn-Mg (91, 6, 3, wt.%), H embrittlement and trapping, HVEM obs. 80—76364
  Al-Zn-Mg alloy, Ag addition and pre-precipitation treatment, influence on GP zone growth 80—71658
  Al-Zn-Mg alloy, microstruct. obs. by optical and electron microscopy *(German, English)* 77—52601
  Al-Zn-Mg alloy, stress corrosion cracking, exam. *(Japanese)* 78—53026
  Al-Zn-Mg alloy, thermomech. treatment, precipitation and strengthening 79—24527
  Al-Zn-Mg alloy, welded, solute profiles at weld bead/parent metal interface 78—19942
  Al-Zn-Mg alloy 1915, stress corrosion cracking, protective anodic film *(Russian)* 78—35572
  Al-Zn-Mg alloy 7075, effect of thermal and mechanical pretreatments, on Guinier-Preston zone 78—39817
  Al-Zn-Mg alloy 7075, unstable shear failure 77—48516
  Al-Zn-Mg alloy (6, 3 wt.%), grain boundary segregation, AES exam. 78—39783
  Al-Zn-Mg alloy AA-7039, stress corrosion cracking, SEM obs. 80—104323
  Al-Zn-Mg alloy V95, two-stage ageing kinetics, mech. props. effects 79—83238

aluminium alloys continued
Al-Zn-Mg alloys, decomp. kinetics from Young's modulus obs., microprocesses *(German)* 78—64522
Al-Zn-Mg alloys, decomposition kinetics, resistivity meas., extended jump model 78—84766
Al-Zn-Mg alloys, extra-resistivity of coherent precipitates calc. using X-ray small angle scattering intensities 80—3050
Al-Zn-Mg alloys, grain boundary segregation, implications to stress corrosion cracking 80—84936
Al-Zn-Mg alloys, H_2 bubbles in embrittlement 78—19868
Al-Zn-Mg alloys, precipitation behaviour *(German)* 78—39780
Al-Zn-Mg alloys, stress corrosion cracking *(Japanese)* 77—25194
Al-Zn-Mg alloys stress corrosion 80—35395
Al-Zn-Mg and Al alloy 7050, age hardenable, microstruct., effect of monotonic and cyclic straining 77—36633
Al-Zn-Mg granules and bands rolled from them, heat treatment 80—100862
Al-Zn-Mg plasma sputtered, mech. props. rel. to heat treatment *(Russian)* 80—40387
Al-Zn-Mg powder, selected-area electron diffr. ring patterns 80—50642
Al-Zn-Mg superplastic alloy, cavity growth under creep conditions 80—60940
Al-Zn-Mg type 7N01-T4, weld, SCC in NaCl-H_2O_2 soln. *(Japanese)* 80—108631
Al-Zn-Mg type 7017 and 7018 alloy plate, fractographic study of stress-corrosion crack propag. 79—57158
Al-Zn-Mg/Al-Mg filler welds, weld fusion boundary structure 80—39459
Al-Zn-Mg-Ag, detection of small amounts of Ag by energy dispersive X-ray anal. 77—60154
Al-Zn-Mg-B fibre reinforced composite, packet rolling, thermodeform. process parameters *(Russian)* 80—55433
Al-Zn-Mg-Co, crazing tendency *(Russian)* 80—30068
Al-Zn-Mg-Cu, age hardened, effect of strain rate, temp. and environment on ductility 80—45368
Al-Zn-Mg-Cu, alloy 7075, hydrostatic pressure effects on ductile fracture 78—60779
Al-Zn-Mg-Cu, alloy 7075, fatigue, loading sequence, normal and reversed sequence effect 78—68791
Al-Zn-Mg-Cu, alloy 7075, effect of purity level, dispersoid type, heat treatment, on fracture toughness 78—80636
Al-Zn-Mg-Cu, alloy 7075-T6, corrosion in halide solutions, exam. of anion dependency 78—60867
Al-Zn-Mg-Cu, alloy 7075-T6, fatigue crack closure with negative stress ratio, following single tensile overloads 78—64687
Al-Zn-Mg-Cu, flaw growth in stress corrosion environment 79—66198
Al-Zn-Mg-Cu, fracture toughness 78—7044
Al-Zn-Mg-Cu, inclusions, oriented distrib. metallography and effects on anisotropy *(Russian)* 78—80589
Al-Zn-Mg-Cu, optimum treatment combination for thermochemical processing 77—44278
Al-Zn-Mg-Cu, type 7075, microstruct. role in hydrogen assisted fracture 80—30091
Al-Zn-Mg-Cu (6, 2.5, 1.5 wt.%), deform. simulation using torsional test, elastoplastic constitutive eqn. 80—93594
Al-Zn-Mg-Cu (6,2, xwt.%) type alloy, fatigue crack propag., Cu content and recryst. effect 80—60960
Al-Zn-Mg-Cu (6.76, 2.37, 1.80 wt.%), cyclic SCC in salt water *(Japanese)* 80—45435
Al-Zn-Mg-Cu age-hardened alloys, fatigue crack propagation rel. to grain size in vac. and NaCl soln. 80—16538
Al-Zn-Mg-Cu alloy, laminated, adhesively bonded alloy 7075-T6, exam. of fracture resistance 78—76754
Al-Zn-Mg-Cu alloy, stress corrosion cracking mechanisms, rel. to micrographic obs. *(French)* 77—73376
Al-Zn-Mg-Cu alloy, type 7050 and AZ 74.61, engineering props. 79—70219
Al-Zn-Mg-Cu alloy, X-ray microanalysis in scanning transmission electron microscope, limitations 78—20122
Al-Zn-Mg-Cu alloy 7075, SCC from T6 to overaged T7X 77—90487
Al-Zn-Mg-Cu alloy 7075, overaged, precracked stress corrosion specimen, incubation effects 79—91832
Al-Zn-Mg-Cu alloy 7075-T651, adiabatic shear localisation and erosion 79—96157
Al-Zn-Mg-Cu alloys, effect of alloying elements as stress corrosion failure using regression analysis 78—80669
Al-Zn-Mg-Cu foil, STEM-microanal., specimen thickness effect on X-ray count rates 77—70374
Al-Zn-Mg-Cu type 7XXX, Cu effect and recrystallisation, low cycle corrosion fatigue 79—91852
Al-Zn-Mg-Cu type 7075, heat treatment optimisation 80—60888
Al-Zn-Mg-Cu-Co (6.5, 2.5, 1.5, 0.4 wt.%), fatigue crack propag. 80—55521
Al-Zn-Mg-Cu-Co-Fe-Si, powder alloy, fatigue crack tip plasticity, from load interactions 80—21066
Al-Zn-Mg-Cu-Cr, (5.6, 2.5, 1.6, 0.3 wt.%), laminates, 8 and 22 layers, adhesively bonded exam. of fatigue crack propag. 78—92345
Al-Zn-Mg-Cu-Cr, (5.6, 2.5, 1.6, 0.3 wt.%), alloy 7075, plates, adhesively bonded, exam. of fatigue crack growths 78—92348
Al-Zn-Mg-Cu-Cr, shot peened, positron annihilation meas. 77—63833
Al-Zn-Mg-Cu-Cr-Zr, high strength Cr and Zr addition effects 77—59820
Al-Zn-Mg-Li alloys, effect of Li on thermal props. 79—24515
Al-Zn-Mg-Mn, correlation of microscopic features, with macroscopic crack propagation 78—60800
Al-Zn-Mg-Ti, Ti effect on microstructure during ageing 78—64568
Al-Zn-Mg-Zr (6.45, 2.08, 0.11 wt.%), exam. of cyclic stress strain response in corrosion fatigue 78—64788
Al-Zn-Mg-(Zr), low cycle fatigue, grain refinement effect 77—44345
Al-Zn-Mg-(Zr) alloy, microstruct. effect on fatigue crack growth 80—3164
Al-Zn-Mg(Mg-Ti), TEM exam. of early stage ageing behaviour, exam. of precip. kinetics 78—56645
Al-Zn-Mg(3.2, 2.2 wt.%), deform. strengthened by Guinier Preston zones 77—52343
Al-Zn-Si, thermodynamic props., meas. by EMF method *(Czech)* 77—59753
Al-Zn-Ti(Mn), mech. props., Ti or Mn addition effect *(Korean)* 80—93613
Al-Zn-(Mg), age hardenable single crystal, fatigue and fatigue cracks *(German)* 77—16689
Al-Zn(Ag)-Mg, metastable T′ phase 77—21151

aluminium alloys continued
Al-Zn(Cu)(Ni), ingots, solidified, formation of equiaxed eutectic grains *(Japanese)* 78—39756
Al-Zn(Sn), binary metallic melt, deviation from the Kopp law, specific heat *(Russian)* 80—39305
Al-Zn(10 at.%), supersaturated solid soln., structural charact. of decomposition 77—70027
Al-Zn(11 wt.%), dynamic recovery during and after steady state deform. 77—1842
Al-Zr, cast, precipitation and solidification *(German)* 77—36519
Al-Zr, dilute, vacancy-impurity interaction investig. by tempering method *(French)* 77—68995
Al-Zr, interphases, formed during precipitation and solidification *(German)* 79—29062
Al-Zr, solidification and precipitation, Zr effect on cast struct. *(German)* 77—36518
Al-Zr (0.22 wt.%), hardness and struct. changes during prolonged ageing at 350, 400 450°C *(Japanese)* 79—52281
Al-Zr (0.8 and 1.5 wt.%), hyperperitectic, non equilibrium solidification 78—3113
Al-Zr (1-13 wt.%), rapidly quenched, extended solid solubility, grain refinement and age-hardening 80—76266
Al-Zr solid soln., discontinuous precipitation of metastable Al_3Zr 78—3130
Al-ζ(AlAg) eutectic and off-eutectic alloys, thermal stability 77—25077
(Al-Cu)/Si system, Si regrowth minimisation through overlying Al or Al alloy film 80—70569
(Al-Mg-Si)-Al_2O_3, SAP type, ageing 79—96055
(Al-Si)/Si system, Si regrowth minimisation through overlying Al or Al alloy film 80—70569
(Al-Zn):Cd eutectic system, cellular growth, unidirectional solidification investig. *(Korean)* 77—28805
AlAg, Auger spectra, 4d bandwidth effect 80—89093
$Al_{0.965}Ag_{0.035}$, reson. splitting of phonons 77—59086
AlB_2, thermochemistry and stability 80—97723
$Al_{1.1}Be_{0.6}B_{22}$, metal distrib., X-ray diffr. study 80—75204
AlBi, X-ray fluorescence analysis *(Japanese)* 78—88663
$Al_4C_3.3Be_2C$, X-ray difr. and TEM study 80—14973
Al_4Ca, phase transformation, struct. and orientation relationships 79—78963
Al_2Ce, Al_3Ce, nucl. orientation exam. of Ce ground state at very low temp. 78—67999
Al_3Ce and $Al_{11}Ce_3$, Kondo cpds., mag. behaviour obs. by neutron diffr. 80—50049
Al_3Ce, thermal expsn. below 1K 79—90803
AlCu, electron microscope spot prep. of deform. bands 79—15922
AlCu-NiCo (5 at.%), Θ′ hardened, creep mechanism 80—85013
Al_2Cu crystal, Young's modulus, Poisson ratio, elastic consts. determ. by extensometry and US meas., anisotropy discussion *(French)* 79—50683
Al_2Cu, de Haas-van Alphen effect and LMTO band struct. 79—69396
Al_2Cu, single cryst. elastic consts., 4.2-300K 78—72803
Al_4Cu_9, rhombohedral γ-brass, direct imaging of struct. and structural defects 80—15115
AlCuMgPb, microstruct. and flow stress during deform. at 573K 77—81307
$Al_{20}Cu_{25}Zr_{55}$ metallic glass, inelastic deform., free energy spectra 80—71699
α-AlFeSi, crystal struct., anomalous dispersion methods 78—9998
$Al_{10.4}Ga_{0.08}V$, low temp. thermal expansion 78—95167
AlGd alloys, μ^+ depolaris. rate 79—56695
AlGe (4 wt.%), struct. peculiarities of superplastic behaviour due to porosity 79—34111
AlH_x, electronic struct. and electron-phonon interaction, hydrogenation effect, rel. to supercond. 80—107694
$Al_2La_xCe_{1-x}$, low temp. mag. props. 80—20564
AlMg, high pressure nitriding 77—70336
Al_3Mg_2, diffusionless phase transformation 80—104150
Al_cMg_{1-c} liquid alloys, vols. and entropies of mixing, calc. 80—75363
$AlMg_2Mn$, H impurity detection by $^1H(^{15}N,\alpha\gamma)$ reaction 80—55767
AlMgSi, adhesive jointing, acoustic anal. *(German)* 78—7168
AlMg5, memory effect of plastically deformed alloy under complex loading 79—38891
$AlMn_x$, muon diffusion, μSR 79—56696
$Al_{45}Mn_{55}$, pure and C doped, phase transforms. 79—96022
Al_8Mn_5, rhombohedral γ-brass, direct imaging of struct. and structural defects 80—15115
$Al_4(Ni, Co)_3$ ternary phase in Al-Ni-Co system, cryst. struct., vacancy controlled phase *(Chinese)* 80—70164
Al_3Ni, cryst., theoretical morphology and comparison with observed habits *(French)* 80—79732
Al_3Ni dendrite facets, determ. cryst. direction by SEM *(French)* 78—87893
Al_3Ni-Al two-phase matrix, Al electrolytic etching in $AlCl_3$ molten salts 78—3280
AlPb alloy prod. under microgravity *(German)* 79—38766
AlSc, lattice parameter changes in Al 3d alloys 77—62504
AlSi alloys, X-ray spectrometric anal. method *(Dutch)* 79—96394
Al_3Ti, effect on grain refinement in Al 78—52828
Al_3Ti, precipitate shape, and distribution in chill-cast Al-14 wt.% Ti alloy 80—16310
$Al_{10}V$, low temp. thermal expansion 78—95167
$Al_{10}V$, supercond. transition temp. determ., localised phonon modes 77—63016
$Al_{10}V$, well defined local modes 78—26648
$Al_{10}V$-Ga, dil., well defined local modes 78—26648
AlZn alloys, ageing zone stage duration depend. on quenching temp. *(Russian)* 77—55993
AlZn, disordered, residual resistivity due to clustering, ageing effects 80—65521
AlZn, homogenization processes, dendritic struct. 79—15700
AlZnMg alloy, precipitation hardened, strength 78—39786
AlZnMg, corrosion cracking *(Czech)* 79—43478
AlZnMgCuO.5, crack propag. under monotone and cyclic load 78—7006
AlZnMgCuO.5, static crack growth, stress state effect, elec. pot. meas. 78—7007
$AmAl_2$, crystal structure and mag. props. of Laves phases 77—27851
Au-Al, liq. alloy, thermodynamic activities and enthalpies 80—19960
Au-Al system, influence of current on phase form. in diffusion layer *(Russian)* 78—52826
Au-Al-In solid soln., elastic strain energy depend. of supercond. T_c 79—38229

aluminium alloys continued

- Au-Cu (4 wt.%), fatigue crack propag., environmental effects *(French)* 77-66711
- AuAl formation by thin film interactions, identification by X-ray diffraction 79-99442
- $AuAl_2$, core-level binding energy shifts and charge transfer 80-25268
- $AuAl_2$ superconductive device to provide reference temps. below 0.5K 79-63220
- Au_2MnAl, Heusler alloy, Mossbauer, determ. of Au hyperfine field 77-4586
- Au_2MnAl, Heusler alloy, ferromag., NMR meas. 78-76320
- $Au_2(MnAl)_2$, Heusler alloy, magnetic order and coupling 79-38303
- B fibre reinforced 6061 alloy, fracture 80-11773
- B fibre reinforced Al alloy, influence of bond strength on failure *(Russian)* 79-43387
- B fibre reinforced Al alloys, hot compression moulding, optimum parameter calc. by pipe piercing *(Russian)* 79-66027
- B fibre reinforced Al alloy D16T, sheet reinforced by Ti alloy butt straps, fatigue 79-100262
- B fibre reinforced Al alloy, corrosion resistance, electrochemistry 80-11806
- B fibre reinforced Al-Cr(Mg)(Mn)(Si), calc. of thermodynamic interaction potential between B fibre and matrix 80-11627
- B fibre reinforced Al-Mg, heat treatment effect on struct., tensile strength 80-55487
- B fibre reinforced AlB_2, fibre coating effect on strength *(Russian)* 80-40426
- B-Al coating on steel 45, effect of abrasive particle size on wear 78-44225
- Ba-Al-Si, exam. of phase diagram, confirmation of $BaAl_2Si_2$ and $Ba(Al,Si)_2$ *(Russian)* 79-29019
- Ba-Al-Si system, phase diagrams construction by simplex designing method 78-6899
- $BaAl_4$ type structure, role of elongated rhombic dodecahedron in alloy structs. 79-32946
- Be-Al, plastic deform., flow stresses, fracture *(Russian)* 80-108496
- Be-Al, solubility of Cu at low temps. 77-62646
- Be-Al-Fe, phase equilibria and diffusion using high energy ion beams 77-16542
- Be-Al-Fe system, phase equilibria using high energy ion beams 79-43203
- C fibre reinforced Al alloy, corrosion resistance, electrochemistry 80-11806
- CC Al-Zn-Mg (4.5,1(2)(3) at.%), decomposition during ageing, preageing and cooling rate influence 80-20938
- CC Ni_3Al, refractory transition metal alloying effects on ht. capacity 78-26691
- Ca-Al, metallic glass, stability, microscopic calcs. 79-32914
- $CaAl_2$, Laves phase, soft X-ray spectrum, band struct. calc. 77-77325
- $(Ce,La)Al_2$, collective phenomena 80-65933
- $(Ce, La)Al_3$, near stabilisation of Ce moment upon dilution 79-91209
- $(Ce,Y)Al_2$, collective phenomena 80-65933
- Ce-Al, liquid, solubility and thermodynamic props. *(Russian)* 78-19717
- Ce-Al, XPS valence band spectra meas. 77-48306
- Ce-Co-Al (0-33.3 at.% Ce), isothermal section, X-ray study *(Ukrainian)* 80-39002
- CeAl, mag. props. and mag. struct. 78-6517
- $CeAl_2$, and $CeAl_3$, magnetisation and sp. ht. 80-20418
- $CeAl_2$, Anderson lattice system, volume collapsed strongly mixed valent state 79-38033
- $CeAl_2$, Anderson lattice system, thermal expansion meas. 1.5 to 10K 79-37860
- $CeAl_2$, Anderson lattice system, ground state props. 80-20443
- $CeAl_2$, anisotropic magnetostriction near antiferromagnetic transition 78-88157
- $CeAl_2$, antiferromag. ordering between 4f shells, Kondo effect 80-20417
- $CeAl_2$, antiferromag. ordering and Kondo behaviour, ^{27}Al NQR study 80-71231
- $CeAl_2$, $CeAl_3$, Kondo lattice theory 80-20380
- $CeAl_2$, collective phenomena 80-65933
- $CeAl_2$, conf. Kondo system, sp. ht. meas. 78-52210
- $CeAl_2$, dynamic Jahn-Teller effect, neutron energy loss obs. 79-78060
- $CeAl_2$, electronic transition under pressure, resist. meas. 79-33311
- $CeAl_2$, low temp. mag. behaviour, neutron diffr. 78-84395
- $CeAl_2$, low temp. mag. props., Kondo effect 80-20381
- $CeAl_2$, mag. anisotropy, transition, crystal field splitting 78-52243
- $CeAl_2$, mag. behaviour 2.5 to 300K, neutron scatt. meas. 77-63110
- $CeAl_2$, mag. ordering, neutron diffr. meas. 78-6518
- $CeAl_2$, mag. ordering and anomalous ground state, neutron diffr. obs. 79-78331
- $CeAl_2$, magnetic ordering, 24 component Ginzburg-Landau model 80-97095
- $CeAl_2$, magnetisation curves under high mag. field and hydrostatic press. 77-63233
- $CeAl_2$, magnetoelasticity, rot. invariance and magnetoacoustic birefringence 79-87304
- $CeAl_2$, mode softening due to magnetoelastic interaction, elastic consts. meas. 1.5 to 280K 77-32233
- $CeAl_2$, multiple q mag. struct. 79-78330
- $CeAl_2$, multiple-q mag. struct. 80-25100
- $CeAl_2$, multiple-*q* structure or coexistence of different mag. phases, neutron diffr. study 80-107985
- $CeAl_2$, NMR, cryst. field effects and mag. order in low temp. phase 78-68391
- $CeAl_2$, neutron diffr. at low temp., magnetism 80-20383
- $CeAl_2$, press.-induced electronic transition 80-20147
- $CeAl_2$, resistivity and volumetric meas., phase diagrams, comparison with CeS 80-107789
- $CeAl_2$, skew scatt., evidence of cryst. field effect, Hall effect meas. 78-2466
- $CeAl_2$ sound vel. in high mag. fields 79-78500
- $CeAl_2$, sp. ht. in high mag. fields, Kondo effect 78-52284
- $CeAl_3$, anomalous resistivity maxima in metallic magnetic system 78-79977
- $CeAl_3$, cryst. field effects, inelastic neutron scatt. meas. 77-51710
- $CeAl_3$, effect of disorder on cond. transition into ground state 77-89755
- $CeAl_3$, inelastic neutron scatt. meas. 79-47066
- $CeAl_3$, magnetic susceptibility, dense Kondo system 77-63087
- $CeAl_3$, singlet ground state at T=0, mag. ordering 2.5-6K 78-84388
- $CeAl_3$, sp. ht., Kondo effect and ferromag. order coexistence 80-65927
- $CeAl_3$, sp. ht. anomalies due to presence of $CeAl_{11}$ 79-19745

aluminium alloys continued

- $CeAl_3$, valence mixed state, Kondo lattice, Anderson localisation models *(Japanese)* 78-51945
- Ce_3Al_{11}, competition between ferro- and antiferromag. interactions 80-60258
- Ce_3Al_{11}, mag. ordering at low temps. under press., relation to $CeAl_3$ props. 79-19745
- Ce_3Al_{11}, sp. ht., Kondo effect and ferromag. order coexistence 80-65927
- $CeCoAl_4$, X-ray anal. of crystal struct. *(Russian)* 77-55263
- $Ce_{1-x}La_xAl_2$, extraordinary Hall effects, 4.2-300K, cryst. field interaction 78-79980
- $(Ce_xLa_{1-x})Al_2$, inelastic neutron scatt. cross-section, effect of cryst. field 79-65642
- $Ce_xLa_{1-x}Al_3$, Kondo system, mag. susceptibility, 1.5 to 20K 79-78310
- $Ce_x(La_yY_{1-y})_{1-x}Al_2$, local mag. moments, neutron scatt. study 79-61058
- $CeNi_4Al$, mag. susceptibility, H adsorption-desorption cycle effects 80-107990
- $Ce_{1-x}Pr_xAl_2$, mag. struct., comp. depend., neutron diffr. and mag. susceptibility meas. 80-50054
- $Ce_{1-x}Pr_xAl_2$, mixed mag. phase at low temp. 78-68228
- $Ce_{1-x}Sc_xAl_2$, fluctuating valence system, quadrupole interaction temp. depend. 80-54972
- Co-Al, band model of high temp. magnetism 78-26809
- Co-Al, band struct. and density of states, KKR method and X-ray meas. 80-10863
- Co-Al, couple phase diagrams and thermochemical data 79-66037
- Co-Al, deformed, mag. props., positron annihilation *(Russian)* 77-85416
- Co-Al, dendritic segregation 80-76260
- Co-Al, gas corrosion, in composite atmospheres *(Polish)* 79-79142
- Co-Al, mag. struct. of Co rich intermetallic cpd., neutron scatt., cluster model 78-80130
- Co-Al, multilayer martensite phases, illustration of polytype structures 80-84932
- Co-Al, positron lifetime and angular correl. curves 79-47538
- Co-Al, X-ray K-absorption spectrum 80-97378
- Co-Al coating, low temp. hot corrosion, Na_2SO_4-induced, mechanism, burner rig tests 80-40610
- Co-Al solid soln., lamellar spacing in discontinuous precipitation, expt. proof of Gaussian distrib. *(German)* 77-36517
- Co-Al system, nucl. spin relaxation exam. 79-19798
- Co-Al-Cr(Nb)(Ta), eutectic alloys, charact. by melting, oxidation resistance and composition 78-52768
- Co-Al-Nb, monovariant directionally solidified eutectics, struct. and mech. props. *(Russian)* 78-92254
- Co-based Heusler alloys, Co_2TAl, (T=Ti, Zr, Hf), paramag. state NMR and susceptibility meas. 79-65643
- Co-CoAl, two phase, interaction between deform., fracture initiation and propag. 80-85006
- Co-CoAl eutectic, invariant composition redeterm. 78-3099
- Co-Cr-Al, eutectic alloy, unidirectional solidification, oxidation and tensile tests 78-52790
- Co-Cr-Al, exam. of cyclic oxidation resistance at 1100 and 1200°C, comparison with Ni-Cr-Al system 78-88572
- Co-Cr-Al, high temperature wear resistant coatings, CrO_2 hardened 79-24677
- Co-Cr-Al, oxidation at 1000°C 77-59963
- Co-Cr-Al, protective coating, exam. of interdiffusion kinetics, development of analysing procedure 79-5085
- Co-Cr-Al, ternary system, interdiffusion, electron probe anal. 80-34256
- Co-Cr-Al based coating, electron beam evaporation of low vapour press. elements 80-40613
- Co-Cr-Al-C eutectic alloy, thermal cyclic loading, exam. 78-48496
- Co-Cr-Al-Y, low temp. hot corrosion, Na_2SO_4-induced, mechanism, burner rig tests 80-40610
- Co-Cr-Al-Y, turbine blade coating, hot corrosion by Na_2SO_4 and vaporous NaCl 78-19941
- Co-Cr-Al-Y coated turbine airfoils, effect of electron beam deposition rate on struct. 79-23870
- Co-Cr-Al-Y coating, Pt-modified, oxidation and hot corrosion resist. 78-11437
- Co-Cr-Al-Y coatings, hot corrosion resist., thermal expansion coeffs. 79-24674
- Co-Cr-Al-Y protective coating for combustion turbines, hot corrosion evaluation 80-40608
- Co-Cr-Al-Y(Hf), high temp. oxidation 78-11432
- Co-Cr-C-Al (39, 2.2, 2 wt.%), directionally solidified eutectic alloy, Larson Miller C const. 79-70162
- Co-Cr-Ni-Ta-Al-Y (25, 10, 5, 3, 0.5 wt%), exam. of hot corrosion 79-20251
- CoAl, bonding, self-consistent energy bands 78-91610
- CoAl, electronic struct., cluster calc. 77-69209
- $Co_{1-x}Al_x$, ordered β-phase, enthalpy of formation are defect struct. descript. 80-89519
- $Co_{49\,6}Al_{50\,4}$, Compton scatt., 59.54 keV γ-rays, charge transfer study 78-68578
- CoCrAl alloy, Al_2O_3 forming, oxidation resistance improvement by dispersed oxide addition 79-83379
- CoCrAl-Y(HF), Y and HF effects on oxidative behaviour 78-44275
- Co_2HfAl, ferromag., hyperfine fields meas. by NMR 77-63315
- Co_2HfAl, hyperfine fields of Fe impurities, Mossbauer spectra 80-71255
- $Co_{1-x}Ni_xAl$, Knight shift and mag. susceptibility study, electron struct. peculiarities *(Russian)* 80-15814
- $(Co_{1-x}Ni_x)_{75}(PBAl)_{25}$, amorphous, high-field magnetoresist. meas. 80-34423
- $CoTi_{1-x}Al_x$, form. of mag. moment of Co atom, X-ray diffr., mag. meas. and NMR 77-43819
- $CoTi_{1-x}Al_x$, mag. and electronic props., ferromag. and paramag. state 80-65814
- Co_2TiAl, ^{59}Co NMR, above and below Curie temp. 78-2760
- Co_2TiAl, ferromag., hyperfine fields meas. by NMR 77-63315
- Co_2TiAl, hyperfine fields of Fe impurities, Mossbauer spectra 80-71255
- Co_2VAl, ferromag., hyperfine fields meas. by NMR 77-63315
- Co_2VAl, hyperfine fields of Fe impurities, Mossbauer spectra 80-71255
- Co_2ZrAl, ferromag., hyperfine fields meas. by NMR 77-63315
- Cr-Al, abnormal thermal cond., 5 to 100K 79-19573
- Cr-Al, antiferromag., charge and spin density, neutron and X-ray diffr. 77-31971
- Cr-Al, antiferromag., transport props., anomalous crit. behaviour 79-61108

aluminium alloys continued
  Cr-Al, band struct. and density of states, KKR method and X-ray meas. 80—10863
  Cr-Al, couple phase diagrams and thermochemical data 79—66037
  Cr-Al, disordered alloy, effect of high press. on resistivity 78—95286
  Cr-Al, effect of Al concentration and hydrostatic press. on Neel temp. 79—33482
  Cr-Al, elementary excitations, exchange stiffness const., inelastic neutron scatt. study 79—47294
  Cr-Al, mag. excitation, neutron spectrometry 79—4654
  Cr-Al, spin density wave, neutron diffraction studies 79—1664
  Cr-Al, temp. depend. of Hall coeff. 79—33280
  Cr-Al alloy KH40NYu3, microplastic deform. *(Russian)* 77—66681
  Cr-Al-C, ternary system, phase relationships 80—76230
  Cr-AlN, dispersion hardened, erosion resistance 77—12637
  Cr-AlN, dispersion strengthened, hardness and oxidation rate, 1000 to 1500°C *(Russian)* 78—15574
  CrAl coating on Ti alloy, electrospark applied, friction and wear resistance obs. *(Russian)* 79—1916
  CrAl, semicond. solid solns., temp. depend. of elec. resist. at high temp. 78—67941
  $CrAl_7$ form. in alloy 7075, effect of V and Zr 78—44132
  Cr_5Al_8, 26R cryst. struct., unit cell parameters 77—19904
  γ-Cr_5Al_8, γ-brass, cryst. struct. redeterm. 77—47377
  Cr_5Al_8, γ-phase, microstruct., transform. strains, TEM obs. 79—11614
  $Cr_{99\,94}Al_{00.6}$, thermal and elec. transport coeffs. near Neel temp. 79—78075
  α_2-Cu-Al, antiphase period and tetragonality 78—15374
  Cu-Al, α_2 phase, config. of periodic antiphase boundaries 79—95029
  Cu-Al, α_2 phase form. process 77—48464
  α-Cu-Al, binary substitutional, short-range ordering kinetics, vacancy behaviour 78—55867
  Cu-Al, change in force constant due to volume effects 78—75778
  Cu-Al, chemical emission by Ar^+ ion bombardment *(French)* 77—86410
  Cu-Al, cold worked solid soln., anneal hardening, grain boundary effects 78—48420
  Cu-Al, critical voltage effect *(Japanese)* 78—91206
  Cu-Al, diffusive redistrib. during friction *(Russian)* 78—52999
  Cu-Al, dil., optical props. and electronic struct. 78—35164
  Cu-Al, dil., thermal expansion *(French)* 79—95185
  Cu-Al, directionally solidified eutectic composite alloy, form. and strength 77—90294
  Cu-Al, dislocation core cut-off parameter, estimation from stacking fault nodes 80—103370
  Cu-Al, dislocation core energy, core tension, Peierls model 79—27984
  Cu-Al, dislocations, dissociated, climb mechanism, nucleated loops, Burgers vectors 80—65002
  Cu-Al, disordered alloys, interatomic distances, coord. numbers, and mean relative displacements, EXAFS anal. 80—89087
  Cu-Al, dispersion hardening by internal oxidation 78—56649
  Cu-Al, effect of Al on friction and wear 78—11348
  Cu-Al, effect of original grain size on struct. and props., after deformation and annealing 78—44178
  Cu-Al, eutectic composition, exam. of high temp. mechanical behaviour *(French)* 78—72818
  Cu-Al, explosive loading, depend. of struct. on deform. *(Russian)* 78—3177
  α-Cu-Al, FCC, fractographic obs. of SCC 78—64786
  Cu-Al, fatigue cracks, propagation, model, low cycle, cyclic stress-strain response determinations 79—68653
  Cu-Al, faulted dipoles, geometry and form. 78—59809
  Cu-Al, fission under weightlessness conditions *(Russian)* 78—31357
  α-Cu-Al, fracture behaviour, effect of deform. temp. and alloying content *(Japanese)* 79—20159
  Cu-Al, gamma-2 phase intermetallic cpd., mech. props., effect of inversion domains 79—61599
  Cu-Al, HV electron microscopy, crit. voltages depend. on comp., temp. and short-range order 80—100146
  Cu-Al, heat capacity of phases, 233 to 800K, heat of transform. and entropy 77—47589
  Cu-Al, heavily deformed martensites, annealing 79—38873
  Cu-Al, impurity concentration effects 78—75777
  Cu-Al, internally oxidised, elec. resist. meas. 77—35753
  Cu-Al, internally oxidised, structural, elec. and mech. characts. 78—60761
  Cu-Al, intrinsic temp. depend. of stacking-fault energy 78—51564
  Cu-Al, irrad. in HVEM, climb of dissociated dislocations and point defect absorpt. 80—107257
  α-Cu-Al, kinetic behaviour of vacancies and atoms 79—28129
  Cu-Al, lamellar eutectoids, calorimetric determ. of interfacial enthalpy 78—60668
  Cu-Al, lattice thermal cond. meas., 0.06-2K 77—15822
  Cu-Al, linear dislocation multipoles, weak-beam TEM 80—75233
  Cu-Al, liq., elec. cond., temp. and conc. depend., model interpret. and alloy struct. *(Russian)* 80—88528
  Cu-Al, low temp. deform., heating of dislocation sources 78—18660
  Cu-Al, magnetic susceptibility, comp. and temp. depend., melting effects 78—52202
  α-Cu-Al, mechanical twinning characts., 4.2 to 300K *(Russian)* 79—37714
  Cu-Al, morphological stability study, phase transformations, two phase structure 78—11231
  Cu-Al, negative muon capture ratios 80—55007
  Cu-Al, optical composition modulation spectra, dielec. const. var., Fermi surface and electronic level shifts 80—6707
  Cu-Al, ordered, superlattice fringe images, computer simulation 80 103296
  Cu-Al, planar faults, faint electron microscopic image contrast obs. 80—107283
  Cu-Al, plasticity, athermal and thermal *(Russian)* 79—11685
  Cu-Al, positive muon trapping at vacancies 79—56704
  Cu-Al, preferred crystallographic orientation of melt grown single crystals *(Czech)* 79—43134
  Cu-Al, preferred crystallographic orientation of unidirectionally solidified polycrystals *(Czech)* 79—43233
  Cu-Al, short range order and static distortion contribution to residual elec. resistivity *(Russian)* 80—70672
  α-Cu-Al, short range order effect, atomic potential appl. 77—27850
  α-Cu-Al, short range ordered, struct. and new superlattice phase 78—52756

aluminium alloys continued
  Cu-Al, single crystal, dislocation velocity meas. 78—3171
  Cu-Al, single crystal, dislocation velocity meas. 78—3172
  α-Cu-Al, single crystal, low cycle fatigue 79—43405
  α-Cu-Al, single crysts., deformed and annealed, neutron small angle scattering 79—82127
  Cu-Al, single crysts., hysteresis behaviour implications rel. to fatigue, plastic strain cycling 80—3191
  Cu-Al, sintering, reduction processes, resist. meas. *(German)* 80—25597
  α-Cu-Al, solid soln., ductility, comp. effect *(Japanese)* 79—43334
  Cu-Al, solid soln., intermediate temp. embrittlement *(Japanese)* 79—20158
  α-Cu-Al, solid soln., residual elec. resist. *(Russian)* 79—51547
  Cu-Al, strength and substruct., strain point influence *(Russian)* 79—52233
  α-Cu-Al, stress-strain behaviour, effect of grain size and composition 77—56038
  Cu-Al, study of internal oxidation using central diffusion of X-rays *(French)* 79—37839
  Cu-Al, sulphurisation solid state phenomena 78—64781
  Cu-Al, surface ionisation, elemental anal. of sputtering products *(French)* 80—50905
  Cu-Al, surface segregation during adsorption and low pressure oxidation *(French)* 78—75932
  Cu-Al, two-phase Cu-rich alloy, influence of microstruct. on stress-strain behaviour 80—7631
  Cu-Al, vacuum condensate, struct. and mech. props. depend. on deposition conditons 80—15417
  Cu-Al, wear, effect of Mn_5Si_3 content *(Japanese)* 78—35525
  Cu-Al (0.05 wt.%), dil. alloy, anisotropic oxidation, electron microprobe Auger spectroscopy 77—12748
  α-Cu-Al (0.5 to 10 at.%), latent hardening and dislocation density 78—19853
  Cu-Al (0.5-17.6 at.%), mol. ions in spark source mass spectra 78—44427
  Cu-Al (10, 16 at.%), dislocation interactions, influence of jogs on extension of dislocation nodes 80—84176
  Cu-Al (10 at.%), dislocation glide source, TEM obs. 77—19958
  Cu-Al (10 at.%), single crystal, orientation depend. of work hardening near [111] axis 77—12646
  Cu-Al (10 at.%), single crystal, variation of flow stress after changes in strain rate 77—28879
  Cu-Al (10 at.%) alloy, work hardening at high temp. 77—32589
  Cu-Al (10 wt.%), annealed, tensile fatigue strength at high temp. in vacuum *(Japanese)* 78—35493
  Cu-Al (10 wt.%), deformed and tempered transform. during heat treatment of β' martensite *(Rumanian)* 79—34031
  Cu-Al (10 wt.%), water-quenched, tensile fatigue strength at high temp. in vacuo *(Japanese)* 78—72837
  Cu-Al (10 wt.%), wear, recrystallisation as controlling process, FCC metals 77—56117
  Cu-Al (10.4%), creep, absence of instantaneous plastic strain upon stress changes 78—75718
  Cu-Al (10.5 at.%), dislocation generation and displacement in single crystal in bending 79—60368
  Cu-Al (11 at.%) single cryst., dislocation reactions during deform. twinning 80—79795
  Cu-Al (11.47 wt.%), high temp. phase transforms., effect of pre-exposure to neutrons 79—20045
  Cu-Al (11.6 wt.%), mech. props., tempering temps. effects 78—76669
  Cu-Al (12 wt.%), acoustic emission related to props. 79—34032
  Cu-Al (13 at.%), polycryst., effect of grain size, specimen thickness, on mech. props. 78—84945
  Cu-Al (13 at.%), polycrystalline aggregate, various grain sizes, specimen thickness effect on mech props. 79—61645
  Cu-Al (13wt.%), polycrystn. rod specimens; effect of specimen size on flow stress 79—79051
  Cu-Al (14.3 wt.%), ^{110}Ag diffusion in β/γ_2 interphase boundary 80—79989
  Cu-Al (14.8 at.%), vacancy formation energy determ. 78—63756
  Cu-Al (15 at.%), CC Cu-Al(Si), single crysts., latent hardening study by meas. of flow stress on secondary systems *(Japanese)* 79—24538
  Cu-Al (15 at.%), FCC, dislocations, elastic instability 79—82235
  α-Cu-Al (15 at.%), low temp. neutron irrad. induced point defects behaviour 77—43251
  Cu-Al (15 at.%), rolled single crysts., metallographic study of deformation struct., orientational change, shear bonds *(Japanese)* 79—24582
  Cu-Al (15 at.%), single crystal, steady state deform. with ⟨001⟩ axis at high temp. *(Japanese)* 78—6980
  Cu-Al (15 at.%), vacancy migration, and short range ordering, comparison of exp. results with theory 78—47356
  Cu-Al (15 wt.%), residual resistivity, influence of short range order and size effect *(Ukrainian)* 79—99528
  Cu-Al (15 wt.%) single crystal, steady state deform. at high temps. *(Japanese)* 78—19833
  Cu-Al (15.8 at.%), extension of jogs on dissociated dislocations, electron microscopy obs. 79—95017
  Cu-Al (2, 6.8 and 15 at.% Al), electron irrad. at 300 and 575 kV, exam. of damage rate 78—47425
  Cu-Al (21 at.%) transition state, tempered and quenched alloy *(French)* 80—55392
  Cu-Al (25 at.%), BCC β phase, high temp. creep, existence of master curve 80—55473
  Cu-Al (2.2 or 4.9 at.%), stacking fault energies, weak beam method of electron microscopy 77—19971
  Cu-Al (2.5 at.%), single crystal, steady state deform. at high temps. *(Japanese)* 77—52415
  Cu-Al (3 wt.%), annealing twins density, photoemission microscopy 80—35208
  Cu-Al (4 at.%), anneal hardening mechanism 80—60879
  Cu-Al (4.5 at.%), dislocation recovery anomalies *(Russian)* 77—21163
  Cu-Al (5 wt.%), subjected to tension-compression fatigue, deform. and fracture strength *(Japanese)* 80—93644
  Cu-Al (5.5, 7.3, 6.3 and 2.5 wt.%), Hg embrittlement under cyclic loading 77—86225
  Cu-Al (5.8 at.%) dislocation multipoles, weak-beam electron microscope obs. 79—73171
  α- Cu-Al (6 to 17 at.%), short-range order investigated by diffuse X-ray scatt. *(Russian)* 80—104187
  Cu-Al (6.4 wt.%), rolled low stacking fault energy alloy, struct. and texture 78—52844
  Cu-Al (7.5 at.%), single crystal, etched under load, slip bands 77—89446

aluminium alloys continued
Cu-Al (7.9 wt.%), burst acoustic emission during Bauschinger effect 77—48475
Cu-Al (8 at.%), coplanar slip, related with specimen size and axis *(Japanese)* 78—34518
Cu-Al (8 wt.%) single crystal, surface dissolution effect on fatigue damage and crack nucleation 78—39936
Cu-Al (9 wt.%), deformed, fatigue crack propag. 78—27621
Cu-Al (9 wt.%), sudden mean stress variations during fatigue crack propag. 80—7668
Cu-Al (9 wt.%) deformed, dispersed, ordered, microcalorimetry of plastic zones during fatigue crack propag. 79—47769
α-Cu-Al (9.13, 13.56, 14.76, wt.%) short-range ordered, characterisation of locally ordered regions 80—79747
Cu-Al (9.3 wt.%), in torsion, deformation temp. depend., superplasticity due to grain size, dislocation density *(Russian)* 79—74200
Cu-Al (<3 at.%), new type of discontinuous slip at low temps. 77—12676
Cu-Al alloy, dil., lattice expansion and localised vibr. mode 79—37789
α- Cu-Al alloy, short range order structure 78—91303
Cu-Al alloy, vacancy formation energy, determ., using new method, elect. cond. meas. 78—47345
Cu-Al alloy, vibrs., average local information transfer approx. 79—46774
Cu-Al alloy film, electron transport props. 77—76955
Cu-Al alloy UA10, heat treatment *(French)* 80—35225
Cu-Al alloys, laser microprobe emission spectroscopy, matrix effects 77—16870
Cu-Al alloys, spark-source mass spectrosc. chem. anal., using mol. ions 79—92031
Cu-Al alloys, strain hardening parameters, conc. and temp. depend., 4.2 to 300K *(Russian)* 79—20063
Cu-Al bulk and thin-film forms, reflecting surface absorpt. coeffs. at 10.6 μm 80—95984
Cu-Al composite, simulation of tensile behaviour and fracture void initiation *(Japanese)* 78—52948
Cu-Al dil. alloy crystal, dislocation etch pits on {111} surfaces *(Japanese)* 77—62536
Cu-Al dil. alloys, dislocation etch pit obs. on {111} surfaces 79—10861
Cu-Al electrode, photopotentials, rel. to corrosion 79—24648
Cu-Al eutectic alloy, unidirection transform. controlled by heat flow *(Japanese)* 78—15386
Cu-Al film, electron energy loss spectra meas., optical functions calc. 78—19618
Cu-Al film, thermoelec. power, 80-350K 78—68096
Cu-Al films, elec. cond. of vacuum condensates depend. on composition, annealing *(Russian)* 80—65709
β'Cu-Al martensite, stacking order, disorder anal. by continuous Fourier transformation of diffracted intensities 80—39115
Cu-Al martensite, temper hardening, study by TEM, DTA, microhardness and yield strength meas. 79—43260
Cu-Al powder compacts, elec. resist., temp. depend. 80—49690
α-Cu-Al single crystal, strain burst during low cycle fatigue 80—25866
Cu-Al solid soln., internally oxidised, mech. props. *(Japanese)* 77—52411
Cu-Al system, high temp. lattice parameters by X-ray diffr. 80—28950
Cu-Al_2O_3 and Cu-$NiAl_2O_4$, internally oxidised, orientational relationships of precip. oxide phase 77—4783
Cu-Al-Co, precipitate-free zones near grain boundaries, growth kinetics, TEM obs. 80—40368
Cu-Al-Co liquid alloys, constant Co-content of 5 wt.%, mag. props. *(German)* 80—88720
Cu-Al-Fe, dil. liq. alloy, localised mag. state interactions *(German)* 77—1539
Cu-Al-Fe, mech. props. rel. to heat treatment 80—50682
Cu-Al-Fe, strength increase from intermediate annealing determ. of annealing temp. by recrystallisation 78—44136
Cu-Al-Fe (11, 2 and 1 wt.%), Fe effects on microstruct. and mech. props. *(Korean)* 77—28807
Cu-Al-Fe-Mn, phase transform. during continuous cooling *(German, English)* 79—70044
Cu-Al-Fe-Mn (10,3,2 wt.%), phase comp. struct., continuous cooling from β-phase effect 79—24499
Cu-Al-Mn, Heusler alloy, magnetic prop. investig. of struct. transitions *(German)* 77—8289
Cu-Al-Mn, partial decomp. of β_1 phase, effect on mag. props. and martensitic transform. *(Russian)* 80—45306
Cu-Al-Mn liq. alloys, susceptibility behaviour 80—93077
Cu-Al-Mn spin glass, field depend. suscept. 79—73739
Cu-Al-Mn(Ni)(Fe)(Co), hypereutectic, martensitic transform., effect of β_1-phase decomposition *(Russian)* 78—23705
Cu-Al-Ni, 2H to 6R lattice restructurization during deform., anomalous elasticity 78—19753
Cu-Al-Ni, elastic const. behaviour near Ms 77—12623
Cu-Al-Ni, formation of martensitic phases during deform. by extension 79—20048
Cu-Al-Ni, habit plane for SIM $\gamma'\rightleftarrows\beta_1'$ transform. 78—56640
Cu-Al-Ni, heredity of martensitic transformations 79—47688
Cu-Al-Ni, long period martensite phases, X-ray diffr obs. 80—7571
Cu-Al-Ni, mixed powder compacts, Ni content influence in sintering behaviour *(Japanese)* 80—35130
Cu-Al-Ni, phase diagram associated with stress induced martensitic transform. 79—8272
Cu-Al-Ni, positron annihilation study of vacancies before and after martensitic transform. 79—99971
Cu-Al-Ni, quenched, complex martensite form. 79—56977
Cu-Al-Ni, rubber like behaviour 77—86114
Cu-Al-Ni, single variant twinned martensites, pseudoelasticity 77—28849
Cu-Al-Ni, sintered, internal friction after heat treatment *(Japanese)* 80—11686
Cu-Al-Ni, stress induced martensite 77—36500
Cu-Al-Ni, struct. anal. of stress induced β_1'' martensite by neutron diffr. 79—60308
Cu-Al-Ni (13.8, 7.9 wt.%), cooling rates effect on internal friction *(Japanese)* 80—39217
Cu-Al-Ni (14, 2.5 wt.%). thermodynamics of thermoelastic martensitic transform. 79—61585
β-Cu-Al-Ni (14, 3 wt.%), single cryst., thermal effect due to stress induced martensite formation 80—81059
Cu-Al-Ni (14, 4.5 wt.%), premartensitic alterations 77—12655
Cu-Al-Ni (14, 8 wt.%), γ'-martensitic, sintered high damping 80—50577
Cu-Al-Ni (14.0 4.2 wt.%), two stage superelasticity, successive martensite to martensite transform. 77—8826
Cu-Al-Ni (14.1, 3 wt.%), autooscillations and nonlinear anelasticity 80—70307
β_1-Cu-Al-Ni (14.2, 4.3 wt.%), quenched, metastable 2H type phase characts., TEM and electron diffr. study 79—74149
Cu-Al-Ni (14.3, 4 wt.%), ω-phase form. during quenching and ageing *(Russian)* 80—25686
Cu-Al-Ni (14.5, 3 wt.%), polycrystalline, pseudoelastic, cyclic stress strain response 77—86144
Cu-Al-Ni (14.5, 3 wt.%), fatigued, polycrystn., pseudoelastic, dislocation and martensite substructs. 79—82223
Cu-Al-Ni alloy, thermoelastic transformation hysteresis loop width strain rate depend. *(Russian)* 79—100138
Cu-Al-Ni alloy single crystals, anomalous elasticity orientation depend., martensitic phase struct. during strain 79—87634
Cu-Al-Ni alloys, deformed, fine struct. of martensite *(Russian)* 78—6923
Cu-Al-Ni alloys, successive stress-induced martensitic transformations and associated transformation pseudoelasticity 79—43245
Cu-Al-Ni Marmen alloys, rapid solidification and ageing 80—76245
β-Cu-Al-$Ni_3(DO_3)$, nonradial diffuse streaks and complex diffuse scatt. patterns of electrons 79—7527
Cu-Al-Ni-Fe, (10, 5, 5 wt.%), cast microstruct. 78—80535
Cu-Al-Ni-Fe system, corrosion behaviour in sea water 80—45421
Cu-Al-Ni-Fe-Mn, cast Ni-Al bronze, fracture metallography 78—27597
Cu-Al-Ni(Mn), duplex shape memory effect after nonuniform plastic deform. *(Russian)* 80—25759
Cu-Al-Si, Si effect on mech. props. and microstructure *(Korean)* 79—38903
Cu-Al-Si-C (95, 2.8, 1.8, 0.4 wt.%) fracture characts. of superplastic single phase, exam. 78—48500
Cu-Al-Si-Co (2.8, 1.8, 0.4 wt.%), superplastic phase, exam. of mech. props. 78—52891
Cu-Al-Sn system, coexistence of different and brass like phases 80—89206
Cu-Al-Ti, formation of modulated structure rel. to barrier nucleation of new phase *(Russian)* 77—32580
Cu-Al-Ti-Zr, internally oxidized, morphology of precipitates and dispersion hardening *(Russian)* 79—52217
Cu-Al-Zn, period of periodic antiphases, quant. metallography *(French)* 79—100111
Cu-Al-Zn, structural phenomena preceding martensitic transform. 77—12624
Cu-Al-Zn martensites, internally faulted, shape memory mechanism 80—30010
α-Cu-Al(Fe) dil. alloys, Al ion charge screening, elec. resist. obs. 77—4500
Cu-Al(10 at.%) foils, trapezoidal splitting of partial dislocations 77—51376
Cu-Al(23.5 at.% and 25.3 at.%), martensitic transform., positron annihilation meas. 77—16578
Cu-Al(8 at.%), single crystal, twinning deform. 77—21236
Cu-Mn-Al, constricted hysteresis loop rel. to microstruct. 78—19273
Cu-Mn-Al, Heusler alloy, single cryst. and polycryst., martensitic transform. *(Russian)* 78—48398
Cu-Mn-Al, Heusler alloys, ferromag. inclusions, mag. props. and struct. study *(Russian)* 80—80570
Cu-Mn-Al, mag. props. and atomic ordering 79—24139
Cu-Mn-Al alloys, displaced hysteresis loop and microstructure obs. 80—84613
Cu-N, quenched, complex martensite form. 79—56977
Cu-Ni alloys, alloying additions effect on thermal conductivity, 20-400°C *(Russian)* 77—59159
Cu-Ni-Al, ageing charact., optical TEM, X-ray, hardness obs. 79—29079
Cu-Ni-Al, cast, strength and hot ductility, Al effect 80—66595
Cu-Ni-Al, grain boundary reaction under isothermal ageing at 623 to 973K *(Japanese)* 79—70090
Cu-Ni-Al, review 80—7564
Cu-Ni-Al (5, 2.5 at.%), precip. hardening *(Japanese)* 80—71663
Cu-Ni-Be-(Al) (30,0.5,(0.2-2) wt.%), Al addition effect on grain boundary reaction *(Japanese)* 80—54254
Cu-Ni-Nb-Al, correlation of γ' and γ'' precipitates phase stability 80—25704
Cu-Ni-Nb-Al, formation of γ' and γ'' precipitates 78—76655
Cu-Sn-Al, deform at high temps. *(Polish)* 80—89284
Cu-Sn-Al, quenched and aged, struct. of phases *(Russian)* 80—49184
Cu-Ti-Al, wetting of Al_2O_3, alloying effects 80—107617
Cu-Zn-Al, β_1' martensite crystal crossing rel. to reversible shape memory effect *(Japanese)* 80—108499
β-Cu-Zn-Al, diffr. effects., obs. and interpretation of extra maxima 80—44173
β-Cu-Zn-Al, electron microscope exam. of premartensitic state 78—72801
Cu-Zn-Al, internal friction, temp. and amplitude depend. 78—11262
Cu-Zn-Al, internally faulted martensite, TEM obs. 78—3124
Cu-Zn-Al, martensitic phase transformation effect on low cycle fatigue behaviour 80—7666
Cu-Zn-Al, martensitic transform., short range order effect 79—61586
Cu-Zn-Al, memory alloy wire and ribbon reversible martensitic transformation, ageing effect, review 80—7564
β-Cu-Zn-Al, ordering, TEM obs. 78—39768
β-Cu-Zn-Al, ordering 78—68687
Cu-Zn-Al, polycrystn., β-phase, fatigue life, intergranular cracking 79—38974
Cu-Zn-Al, pseudoelastic alloy, exam. of fatigue props. 78—76744
Cu-Zn-Al, reversible shape memory effect associated with $\beta_1\rightleftarrows\beta_1'\rightleftarrows\alpha_1'$, transform. *(Japanese)* 79—43242
Cu-Zn-Al, reversible shape memory effect obtained by heating under constraint *(Japanese)* 79—43335
Cu-Zn-Al, reversible shape memory effect *(Japanese)* 80—108500
Cu-Zn-Al, single cryst., stress induced martensitic transformation 80—45308
Cu-Zn-Al, TTT diagrams *(German)* 79—43208
β-Cu-Zn-Al, US elastic const. meas. near martensitic transform. temp. 78—39827
Cu-Zn-Al, Zener relaxation *(Russian)* 77—21198
α-Cu-Zn-Al (18, 7 at.%), deform. and mech. props. 79—29159
Cu-Zn-Al (19.3, 13.0 wt.%), effect of hydrostatic or uniaxial stress on elastic consts., near martensitic transformation point 78—76697

aluminium alloys continued

- Cu-Zn-Al (19.5, 6.35 wt.%), martensitic, static stresses influences on damping behaviour 80−10594
- Cu-Zn-Al (26, 4 wt.%), martensitic transform. temp. variation after low temp. ageing 79−15666
- β-Cu-Zn-Al (27.5, 4.0 wt.%), strain induced martensite, exam. of structure, microstructure 80−7648
- Cu-Zn-Al (35.45, 1.72 wt.%), memory effect and martensitic transform. *(Russian)* 79−43320
- Cu-Zn-Al alloy, lattice dynamical study of premartensitic state, phonon meas. 79−77696
- Cu-Zn-Al alloys, dendritic struct. obs. 77−8810
- Cu-Zn-Al cubic alloy, phonon sp. ht. near martensitic transform. 79−60521
- Cu-Zn-Al Marmem alloy, β_1 phase superstruct. obs., rel. to transform. mode 78−39776
- Cu-Zn-Al martensite, β-phase, single cryst., elastic waves behaviour as function of temp. 79−55807
- Cu-Zn-Al martensite, lattice dynamics, neutron scatt. meas. 80−88286
- Cu-Zn-Al martensite, the rubber effect 79−47684
- Cu-Zn-Al martensites, model for rubber like behaviour 79−47685
- β-Cu-Zn-Al pseudoelasticity 79−29126
- Cu-Zn-Al wire, made from pendant drop melt extraction technique from bulk material, X-ray diffr. and thermal anal. 79−43227
- α-CuAl, kinetic study of short-range ordering 78−23726
- $CuAl_2$ and Al crystals, mutual orientations in terms of lattice disorientations 80−28936
- $CuAl_2$, chemical effects on Al and Cu AES 77−59651
- $CuAl_2$, constitutional defect struct., from X-ray and density meas. proposed substitutional-vacancy model 79−37696
- $CuAl_2$, Kossel interferences of proton-induced AlK_α radiation 77−43112
- $CuAl_2$, single cryst., embrittlement and subboundary hardening via interstitial segregation *(Russian)* 77−12679
- $CuAl_2$, topological evolution during soln. heat treatment 77−32607
- $Cu_{0.7}Al_{0.3}$, chemical effect on valence electronic states, AES and SXAPS meas. 79−47558
- γ-Cu_9Al_4, struct. refining from diffr. meas. 78−55834
- $CuMnAl_x$, hysteresis, spin orbit scattering effect on anisotropy in spin glass state, rel. to Al impurity conc. 80−71095
- Cu_2MnAl, alloy, energy band calc. by nonrelativistic SAPW method 79−4507
- Cu_2MnAl, dislocation structure, antiphase boundary energies, deformation behaviour prediction *(Russian)* 79−65085
- Cu_2MnAl, dynamical mag. susceptibility, spin waves, calc. from band struct. 80−54871
- Cu_2MnAl, ferromag. Heusler alloy, polarised neutron study of mag. moment density 78−84391
- Cu_2MnAl Heusler alloy, inelastic magnon scatt. of neutrons 77−4509
- Cu_2MnAl, Heusler alloy, single crystal, plastic deform. 77−44308
- Cu_2MnAl, Heusler alloy, spin waves, neutron inelastic scatt. meas. 77−80921
- Cu_2MnAl, Heusler alloy, magnetisation mag. anisotropy, magnetostriction and elastic consts. 78−23318
- Cu_2MnAl Heusler alloy, elec. resistivity 79−91020
- Cu_2MnAl, Heusler alloy, decomposition at 360°C 80−7536
- Cu_2MnAl, plastically deformed, domain struct., X-ray diffr. and electron microscope obs. *(Russian)* 79−20110
- Cu_2MnAl superparamagnetic particles in Cu_3Al lattice, magnetic moment ferromagnetic ordering *(Russian)* 79−78444
- Cu_2MnAl-Pd_2 MnAl mixed Heusler alloys, mag. props. 80−60269
- $Cu_2Mn_{0.863}Al_{1.057}$, Heusler alloy, mag. moment distrib., polarised neutron study 79−47247
- $Cu_2Mn_{0.98}Al_{1.02}$, Heusler alloy, hyperfine fields at sp elements, spin echo NMR meas. 78−84496
- $Cu_{2+x}Mn_{1-x}Al$, omega phase, roles of electron microscopy and electron diffraction *(French)* 78−27524
- $Cu_{3-x}Mn_xAl$, and $Cu_2Mn_{2-y}Al_y$, Heusler alloys, order-disorder transitions 80−59619
- $Cu_2Mn(Al_{1-x}Sn_x)$, Heusler alloys, thermal effects, saturation magnetisation 77−85499
- $Cu_2MnAl_{1-x}Sn_x$, Mossbauer effect study 80−60473
- Cu(Sn)/Nb(Al), composite superconductor fabrication and characts. 77−81242
- CuZnAl, martensitic, ordering effect on yield stress 79−100133
- CuZnAl single crystal, thermodynamic anal. of martensitic transform. under stress 79−87635
- Dy-Fe-Al, pseudobinary alloy, struct. exam. 77−58979
- Dy-Fe-Al, pseudobinary alloys, mag. props. 77−59397
- $DyAl_2$, conduction electron spin and orbital polarisation effects 78−80228
- $DyAl_2$, first order transition and tricrit. points, three-state Potts model 78−43589
- $DyAl_2$, sp. ht. and thermal props., 5 to 300K 77−43342
- $DyAl_3$, polytypism, high resolution microscopy and electron diffr. obs. *(French)* 77−11503
- $DyCo_2$-$DyAl_2$ system, mag. and structural studies 80−108006
- $Dy(Fe,Al)_2$, saturation and remanent magnetostriction meas. 77−63256
- $Dy_{1-x}Gd_xAl_2$, ferromag, easy axis rot., ^{163}Dy NMR obs. 79−78562
- $Dy_{1-x}Gd_xAl_2$, ordered alloys, ^{163}Dy NMR, hyperfine field 78−10801
- $Dy_{1-x}Gd_xAl_2$, ordered alloys, hyperfine field, anomalous con. depend. NMR 80−75868
- $Dy_{0.9}M_{0.1}Al_2$, (M=Sc, Y, La, Lu), hyperfine field, NMR spectra 80−15811
- $Dy_{1-x}Y_xAl_2$, cryst. field quenching of Dy^{3+} 4f shell, Mossbauer effect meas. 78−39480
- $Dy_{1-x}Y_xAl_2$, ordered alloys, ^{163}Dy NMR, hyperfine field 78−10801
- $Dy_xY_{1-x}Al_2$, domain wall dynamics, NMR 77−69614
- Er-Fe-Al, cryst. struct. and H_2 capacity 77−89543
- $ErAl_2$, conduction electron spin and orbital polarisation effects 78−80228
- $ErAl_2$, sp. ht. and thermal props., 5 to 300K 77−43342
- $ErAl_3$, 15 layer rhombohedral struct., mag. struct. 77−63104
- $(ErCo_2)_x(ErAl_2)_{1-x}$, mag. and struct. investigations of intermetallic systems 78−95440
- $ErFe_4Al_8$, neutron diffr. exam., mag. struct. 78−10656
- $Er_{1-x}Gd_xAl_2$, effective mol. field at ^{167}Er, NMR meas. 80−71197
- $Er_{1-x}Gd_xAl_2$, nuclear hyperfine field, quadrupolar splitting, NMR study 80−39888
- $(Er_xY_{1-x})Al_2$, cryst. field splitting, inelastic neutron scatt. data 80−44551
- $Er_xY_{1-x}Al_2$, mag. props. meas. and neutron diffr. data 80−7126

aluminium alloys continued

- $EuAl_2$, and $EuAl_4$, hyperfine interactions, high press. Mossbauer expts. 78−43714
- $EuFe_4Al_8$, mag. ordered, mixed valency of Eu, X-ray, susceptibility and Mossbauer spectra studies 79−19728
- $Eu_xLa_{1-x}Al_2$, binding energy and workfunction charges using XPES 80−33928
- $Eu_xLa_{1-x}Al_2$, cryst. fields and exchange parameters, ESR meas. 80−71175
- $Eu_xLa_{1-x}Al_2$, dil. EPR, cryst. fields and effective exchange interaction 80−66029
- (Fe,Co)PBAl, metallic glass, viscous flow, alloying effect 78−79793
- Fe, cast, grey Al-Si, eutectoid decomp. of austenite 80−29951
- Fe, cast, tensile strength, Al addition effects *(Korean)* 80−71736
- α-Fe-Al, ⟨111⟩ fibre texture development through diffusion process without α-γ transform 79−100170
- Fe-Al, Al effect on softening in solid soln. *(French)* 79−52226
- Fe-Al, antiphase boundary motion, microscopic diffusional theory, appl. to domain boundary coarsening 79−61563
- Fe-Al, atom-probe field ion microscopy obs. *(French)* 78−86389
- Fe-Al, band struct. and density of states, KKR method and X-ray meas. 80−10863
- Fe-Al, chemical emission by Ar^+ ion bombardment *(French)* 77−86410
- Fe-Al, cold-worked, Mossbauer study of recovery 80−7593
- Fe-Al, conduction band states, X-ray spectra obs. *(Russian)* 80−29317
- Fe-Al, couple phase diagrams and thermochemical data 79−66037
- Fe-Al, deformed, low temp. recovery of elec. resist. *(Russian)* 80−7697
- Fe-Al, dil., film, NMR spin echo, rel. to struct. inhomogeneities *(Russian)* 80−29644
- Fe-Al, dil., mag. hyperfine fields, Curie temp. and Mossbauer meas. 77−63190
- Fe-Al, dil., XPS meas. 77−63538
- Fe-Al, dil. alloy, temp. depend. of ^{27}Al hyperfine field 78−47972
- Fe-Al, directional Compton profiles, self-consistent APW band struct. calc. 80−25476
- Fe-Al, disordered, obs. of Kohn singularities in X-ray diffuse scatt. 79−27874
- Fe-Al, domain struct. and magnetostriction, heat treatment effect 80−60398
- Fe-Al, electron density distrib. vs. at. order 79−60309
- Fe-Al, electron-beam-induced surface oxidation, HVEM obs. 80−14978
- Fe-Al, equilibria of Fe, Al ordered phase *(Japanese)* 79−70042
- Fe-Al, ferromag.-mictomag. transition, intermediate superparamag. 77−12140
- Fe-Al, gas corrosion, in composite atmospheres *(Polish)* 79−79142
- Fe-Al, hardness after nitriding, metallographic, electron microscopic and microprobe anal. 78−51608
- Fe-Al, high temp. Mossbauer study of order-disorder transform. 79−100137
- Fe-Al, hot- and cold-rolled, texture form., pole figures method *(Russian)* 80−45317
- Fe-Al, hyperfine field meas. using muon-spin-rotation method 80−10933
- Fe-Al, ion-implanted, depth profile and diffusion coeff. 80−54277
- Fe-Al, liq., thermodynamic characts. calc. *(Russian)* 80−15264
- Fe-Al, local ordering, neutron scatt. study 78−64193
- Fe-Al, low energy Stoner excitations, spin wave obs. in neutron scatt. study 79−51770
- Fe-Al, mag. aftereffect meas., phenomenological description 80−88835
- Fe-Al, magnetic moment determ. from neutron scatt. 77−73011
- α-Fe-Al, migration of C, mag. permeability disaccommodation meas. 77−36100
- Fe-Al, morphological stability study, phase transformations, two phase structure 78−11231
- Fe-Al, Mossbauer spectra, local mag. moments 80−15861
- Fe-Al, Mossbauer study of ordering *(Japanese)* 79−19822
- Fe-Al, O containing, mag. aftereffect and disaccommodation meas., time depend., activation energy, and ageing props. 80−88836
- Fe-Al, optical props., comp. and order-disorder transform. depend. *(Russian)* 79−28852
- Fe-Al, optical props. rel. to order-disorder transformations 80−29736
- Fe-Al, ordered, superlattice fringe images, computer simulation 80−103296
- Fe-Al, ordering and phase separations *(Japanese)* 80−50595
- Fe-Al, ordering studied by Mossbauer effect 77−63342
- Fe-Al, oxide layer form. during annealing, AES in-depth anal. *(German)* 80−16576
- Fe-Al, paramag. props., T_c to 1500K 78−68153
- Fe-Al, planar faults, faint electron microscopic image contrast obs. 80−107283
- Fe-Al, positron lifetime and angular correl. curves 79−47538
- Fe-Al, rate of form. and thickness of diffusion layer, 200 to 600°C 80−15315
- Fe-Al, residual elec. resist., contrib. from static lattice distortions and short-range parameters *(Russian)* 79−51548
- Fe-Al, short range order, neutron scatt. meas. 77−19907
- Fe-Al, single crystal, twinning and pseudoelasticity 79−15718
- Fe-Al, single crystals, deform. at high temps. 80−81125
- Fe-Al, sintered and worked alloy, nonmetallic inclusion identification by quantitative metallography 77−77701
- Fe-Al, soft X-ray emission 77−32471
- Fe-Al, solid and liq. paramag. props. *(Russian)* 77−66247
- Fe-Al, spin glass transition, Monte Carlo study 80−39801
- β-Fe-Al, struct. defect obs. 78−14337
- Fe-Al, vacancy formation energy 78−18638
- Fe-Al, variation in absolute thermoelec. power under heat/treatment *(Ukrainian)* 79−38051
- Fe-Al, X-ray emission spectra 80−25489
- Fe-Al, X-ray exam. of dynamic characts. *(Russian)* 77−62608
- Fe-Al (0.069 and 0.158 wt.%), internally oxidised, low temp. deform. *(Japanese)* 78−52876
- Fe-Al (0.27 to 0.50 at.%), spin glass behaviour, microscopic model, Ising lattice, exchange and superexchange 80−39800
- Fe-Al (1 to 4 wt.%), effect of nitriding on surface structure and props., and on diffusion layer *(Russian)* 79−34197
- Fe-Al (12 wt.%) alloy 23 kHz US transducer piezomagnetic props. 78−59240
- Fe-Al (15 at.%), short range order form. kinetics *(Russian)* 78−3146
- Fe-Al (16 wt.%), improvement of certain props. discussion *(Chinese)* 78−84826
- Fe-Al (16 wt.%), prop. improvement *(Chinese)* 77−73280
- Fe-Al (25 at.%), anomalous magnetic behaviour *(Japanese)* 77−48011

aluminium alloys continued
Fe-Al (25 at.%), double Curie point phenomena 77—73030
Fe-Al (25 at.%), long-range ordered, compression induced mag. anisotropy 77—69546
Fe-Al (30 or 45 at.%) film, elec. resist. and magnetoresist., atomic ordering effects *(Russian)* 77—80853
Fe-Al (38.5-47 at.%), type B_2 ordered alloys, elec. resist. recovery stages after neutron irrad. *(French)* 77—69010
Fe-Al (4 wt.%), mag. anisotropy induced by cold rolling *(Russian)* 80—84595
Fe-Al (4 wt.%) single crystals, rolling induced mag. anisotropy and its removal by annealing treatment *(Russian)* 79—61746
Fe-Al (40 at.%), ordered, plastically deformed, neutron irrad. damage and recovery, resist. meas. 77—19993
Fe-Al (40 at.%) and Fe-Al (50.5 at.%) ordered alloys, 20K neutron irrad. effects, stoichiometry depend., resist. obs. *(French)* 80—84215
Fe-Al (40 at.%) B_2 type ordered alloy, C migration, resistivity meas. *(French)* 78—52868
Fe-Al (40 wt.%), defect elimination by laser irradiation *(French)* 79—65960
Fe-Al (45%), ordered and disordered states, optical and elec. props. 77—85826
Fe-Al (50.5 at.%), ordered, neutron irrad. enhanced defect diffusion, resist. meas. 77—11598
Fe-Al (51 at.%), crystal vacancies, dilatometric and field ion microscopy exam. 78—47346
Fe-Al (8 at.%), XPS investig. of cond. band region 77—16456
Fe-Al (up to 7.2%), oxidation process 78—85022
Fe-Al alloy, antiphase boundary energies 77—36460
Fe-Al alloy, B_2-type, electrical resist. meas. 78—30917
Fe-Al alloy, C saturated, at 1873K, activity meas. with Knudsen cell-mass spectrometer 78—39745
Fe-Al alloy, γ-ray effect on resistivity and configuration struct. *(Russian)* 78—43049
Fe-Al alloy layers, formed by reaction of Fe alloy with molten Al *(Japanese)* 78—72926
Fe-Al alloys, pairwise interaction energy 77—36461
Fe-Al alloys, powdered composites, metastable gamma-phase decomp. *(Russian)* 77—59741
Fe-Al alloys, rapidly quenched, mag. props. 80—29579
Fe-Al alloys, X-ray fluoresc. spectra, cond. electron wave function, lattice symm. depend. 77—85844
Fe-Al alloys with Fe_3Al order, phase separation 77—73258
Fe-Al α phase solid solution, interdiffusion coeff. depend. on ordering *(Russian)* 79—99373
Fe-Al compounds, X-ray emission investig. of electron localisation in valence zone *(Russian)* 77—48277
Fe-Al eutectic alloy, duplex crystals, unit cell parameters, appl. of Weissenberg technique 78—67684
Fe-Al liquid alloys, apparatus for viscosity meas. *(Czech)* 80—29103
Fe-Al powder composite, phase composition, produced in low-temp. plasma 77—90295
Fe-Al powder cpds., prep. in low-temp. plasma, struct. props. 77—44192
Fe-Al systems, band struct. and cluster calcs. 79—51480
Fe-Al-C, gamma irrad., crystal lattice parameter reversible changes *(Russian)* 80—10576
Fe-Al-C, low C, precip. of carbides and cementite after quenching and ageing 78—52814
Fe-Al-C, mag. permeability disaccommodation 78—88141
Fe-Al-C alloys, C migration and mag. aftereffect, mag. permeab. disaccommodation and long-range order meas. 79—8020
Fe-Al-Co-Ni, Alnico alloys, irreversible remagnetisation processes in rotating fields *(Russian)* 79—8015
Fe-Al-Cr (10, 5 to 10, wt.%), corrosion by coal char, SEM and X-ray diffr. exam. 78—88573
Fe-Al-Fe, phase diagram, microscopic model 80—34630
Fe-Al-N alloy, precipitation and coarsening of AlN *(Korean)* 79—91652
Fe-Al-Ni-Co-Cu alloys, Ti alloying and deoxidising addition *(Russian)* 78—80181
Fe-Al-Si, bending test, mech. props. under high press. and temp. *(Japanese)* 78—76711
Fe-Al-Si (6.22, 9.63 wt.%), bending test under high press., high temp. 80—85057
Fe-Al-Si alloy, order-disorder transform. exam. by Mossbauer spectroscopy 77—63334
Fe-Al-(Nb), fatigue deform. 77—44350
Fe-Al(V)(Ti), nitrided, struct. and props. 78—19950
Fe-Al(16 wt.%), ordered, antiphase region obs. cooling rate effects *(French)* 77—59834
Fe-Al(24.3 at.%)-C alloy, magnetic permeability disaccommodation, 260-400K 80—93144
Fe-Al(25 at.%), mag. anisotropy induced by plastic deform., dislocations, long-range order 77—4544
Fe-Al(4 wt.%), ferromag. alloy, mag. anisotropy induced by cold rolling 80—30114
Fe-C-Al, electronic structure, thermodynamics of structure formation 79—99475
Fe-C-Al system, liq.-solid equilib. at high press., influence of graphitising elements *(Russian)* 78—56613
Fe-C-Mo-Nb-Al-Ti-B (0.015, 5.75, .7, 1.6, 2.5, 0.1 wt.%), TZM sheet, wear resistance, effect of surface hardening 77—59985
Fe-Co-Al-Cu-Ti (40, 14, 7.5, 4.5 wt.%), metastable equilibrium, high coercive state *(Russian)* 80—66476
Fe-Co-Ni-Al, Si alloying of mag. hard alloys *(Russian)* 79—73765
Fe-Co-Ni-Al (35, 14.5, 7.2 wt.%), high-coercivity, substructure and texture change during bending and upsetting 80—21037
Fe-Co-Ni-Al-Cu, polycryst. hard mag., C diffusion 79—77827
Fe-Co-Ni-Al-Nb (15-20, 14, 9, 0.1-5.5 at.%), Nb effect on magnetic props., lattice parameter *(Russian)* 77—55689
Fe-Co-Ni-Al-Zr magnetically hard alloys, reduction *(Russian)* 78—43614
Fe-Co-Ti-Al alloy type YuNDK magnets, metallographic method of distinguishing cracks 80—85096
Fe-Cr-Al (14, up to 2 wt.%), Al effects on high temp. oxidations *(Japanese)* 79—15865
Fe-Cr-Al, Al addition effect on oxidation, 900 to 1200°C 79—66222
Fe-Cr-Al, Al effect on high temp. oxidation in wet O_2 79—66223
Fe-Cr-Al, attenuation and vel. of acoustic shock waves, amplitude depend. 78—63810
Fe-Cr-Al, blackness change in air, 1-8 micron, 1200°C, film props. depend. 77—66033

aluminium alloys continued
Fe-Cr-Al, corrosion by coal char at 871° and 982°C 80—3237
Fe-Cr-Al, elec. heating alloy, effect of rare earth additives on quality *(Chinese)* 78—84825
Fe-Cr-Al, electrical heating material, SEM obs. and surface analysis of oxide films formed at high temps. 77—16738
Fe-Cr-Al, HOS 875, oxidation, cyclic, role of thermal shock 80—97640
Fe-Cr-Al, Kanthal films, vac. deposited, evaporation characts., comp., struct. and elec. props. 80—88646
Fe-Cr-Al, kinetics and mechanism of high temp. S corrosion 80—25911
Fe-Cr-Al, scale and spalling resist. determ., appl. of cyclic oxidation method 77—77695
Fe-Cr-Al, scales, α-Al_2O_3, early stages development at high temp. 80—89413
Fe-Cr-Al (0.3 wt.%), oxidation behaviour at high temps. *(Japanese)* 80—35404
Fe-Cr-Al (12, 3 wt.%), internal friction and rigidity modulus, strain amplitude depend. *(Japanese)* 80—92606
Fe-Cr-Al (14, 0.1 to 2 wt.%), oxidation at high temps. *(Japanese)* 78—60872
Fe-Cr-Al (17, 4 or 6 wt.%), high temp. corrosion in S vapour 80—40591
Fe-Cr-Al (7, 5 wt.%), expt. stainless alloys, phys. and mech. props. 80—97637
Fe-Cr-Al alloys, localised mag. moment determ. and electron struct. 77—66268
Fe-Cr-Al alloys, low temp. sp. ht., resistivity and coercive force 78—63866
Fe-Cr-Al film heater, lifetimes for 800 to 1000°C temp. range 78—215
Fe-Cr-Al liquid alloy, thermodynamical anal. of O_2 solubility *(Russian)* 80—92676
Fe-Cr-Al-Ce, Ce effect on high temp. oxidation 79—100301
Fe-Cr-Al-Ce, high temp. oxidation *(Japanese)* 78—11413
Fe-Cr-Al-TaC (13.5, 3.7, 9 wt.%) eutectic alloy, directionally solidified, thermal cycling effects on microstruct. 77—32686
Fe-Cr-Al-Ti-Y_2O_3 (20, 4.5, 0.5, 0.5) type MA956, strain rate effect on fracture behaviour at 1366K 80—16458
Fe-Cr-Al-Y, high temp. corrosion depend. on Y, oxidation, stress growth *(Russian)* 80—40588
Fe-Cr-Al-Y, influence of Y additions on oxide-scale adhesion 77—8993
Fe-Cr-Al-Y, oxidation resistance, heat treatment and Al^+ ion implantation 80—71785
Fe-Cr-Al-Y, scales, α-Al_2O_3, early stages development at high temp. 80—89413
Fe-Cr-Al-Y (Y-Al_2O_3)(Y_2O_3), preparation and exam. of mech. props. 78—52720
Fe-Cr-Al-Y-C, GE-1541, volatilisation of oxides during oxidation at 1200°C 78—23873
Fe-Cr-Al(-Y), isothermal oxidation behaviour at 1200°C, SEM 80—50755
Fe-Cr-Al(-Y), oxide grain morphology and growth mechanism 80—3239
Fe-Cr-Al(-Y), thermal cycling influence on oxidation behaviour at 1200°C, SEM 80—50756
Fe-Cr-Co-Al (27.5, 17.5, 0.5) alloy, magnetic props. and microstructure 78—72367
Fe-Cr-Co-Al (27.5, 17.5, 0.5 wt.%) alloy, induced anisotropy 78—76239
Fe-Cr-Co-Al-(Nb), phase equilib., X-ray diffr. meas. *(Russian)* 79—47658
Fe-Cr-La(Y)-Al, La or Y with Al addition effect on high-temp. oxidation 79—100302
Fe-Cr-Ni-Al alloys, 25 keV ion implanted, metallic corrosion behaviour 79—52447
Fe-Cr-Ni-Ti-Al, superalloy, Ti, Ni, Al, H_2 variations effect on mech. props. 78—3188
Fe-Cr(Cr-Ni)(Cr-Ni-Mo)-Al, liquid, N solubility, AlN precipitation 79—11630
Fe-Hl (Si) (Ti) (V), molten, gaseous O_2 absorption 80—11836
Fe-Mn-Al-C, hardening during ageing, 450-750°C *(Russian)* 78—3135
Fe-Mn-P-B-Al metallic glass, exchange anisotropy 77—16068
Fe-Mn-PBAl, amorphous mixed mag. system, resist. minima 79—60784
Fe-Mn-Ti-Al, magnetic texture rel. to annealing temp., Mossbauer investig. 77—28499
Fe-Ni-Al, correlation of microscopic features, with macroscopic crack propagation 78—60800
Fe-Ni-Al, Curie temp. depend. on ordering, antiferromag. ordering *(Russian)* 79—61101
β_2-Fe-Ni-Al, diffusion 77—24449
Fe-Ni-Al, liq. alloys, N solubility and AlN precipitation 80—11648
Fe-Ni-Al, magnetic anisotropy form. and struct. changes by annealing, Mossbauer obs. 80—39994
Fe-Ni-Al, Mossbauer spectra, strong elastic stress effects 77—90084
Fe-Ni-Al, oxidation in O_2 at 600 to 800°C 79—83376
Fe-Ni-Al, struct. of aged austenite *(Russian)* 77—52357
Fe-Ni-Al, type YuN14DK25BA, thermomag. treatment 80—16512
Fe-Ni-Al (10, 0.1 wt.%), clustering of Al_2O_3 inclusions 79—83205
Fe-Ni-Al (18.2 wt.%) aged, fracture toughness and mode, grain size depend. 77—12700
Fe-Ni-Al (30, 4wt.%), ageing, peculiarities of struct. state *(Russian)* 79—57008
Fe-Ni-Al alloy, metastable equilib. in its high-coercivity state *(Russian)* 79—52161
Fe-Ni-Al alloys, ordering X-ray and neutron diffr. obs. *(Russian)* 79—20038
Fe-Ni-Al alloys, phase diagram, miscibility gap, DTA meas. 78—92237
Fe-Ni-Al austenite, high N content, cryst. struct. electron diffr. and electron miscroscope anal. *(Russian)* 79—24490
Fe-Ni-Al system, multiphase diffusion at 1000°C, diffusion structs. and props. 80—19995
Fe-Ni-Al system, multiphase diffusion at 1000°C, interdiffusion coeffs. for β and γ alloys 80—24684
Fe-Ni-Al-Co-Cr-Ti, YuNDK35T5BA, exam. of hypodissociation process *(Russian)* 79—11547
Fe-Ni-Al-Co-Cu alloy, sintered single-crystal mag. prod., props. 77—66709
Fe-Ni-Al-Co-Cu-Sn alloy YuNDK35T5, Sn addition effects on physicomechanical and magnetic props. and workability *(Russian)* 77—70101
Fe-Ni-Al-Co-Cu-Ti, 38 to 40 wt.% Co, 8 to 8.5 wt.% Ti, alloy YuNDKT tempering and thermomagnetic treatments 78—3154
Fe-Ni-Al-Co-Cu-Ti alloy YuNDKT, nature of X-phase heat treatment effect on microstruct. 77—90380
Fe-Ni-Al-Co-Cu-Ti magnetic alloy electrolytic treatment with programmed pulse current *(Russian)* 79—100282

aluminium alloys continued
Fe-Ni-Al-Co-Cu-Ti YuNDK type, S effect on mech. props. 80—60927
Fe-Ni-Al-Co-Ti base alloys, highly coercive, phase comp., Mossbauer meas. 80—39996
Fe-Ni-Al-Cu (25, 14, 4 wt.%), alloy YuND4, effect of Ti addition on structure, mag. props. 80—15714
Fe-Ni-Al-Ti, N27Yu2T2, aged austenite, diffuse electron scatt. distrib. during martensitic deform. *(Russian)* 78—60669
Fe-Ni-Al-(Cu) (12, 0.5, 0.5 to 3 wt.%), Cu addition strengthening at 77K, mech. props. 80—60875
Fe-Ni-Al(2.5, 7.5 at.%), fracture surface morphology, ageing temp. effects 77—16600
Fe-Ni-Cr-Al-Ti-W-Mo (35, 15, 2.4, 2.3, 2.2 wt.%) wrought superalloy, freckles *(Chinese)* 80—104137
Fe-Ni-Cr-Al-Y, oxidation mechanism, Y addition effect on kinetics and oxide adherence 80—97623
Fe-Ni-Cr-Mn-Al-Ti Incoloy 800, exam. of scale morphology, alloying element distrib. after oxidation 78—80677
Fe-Ni-Cr-Ti-Al, ausaging alloy, cellular precipitate indentification *(Chinese)* 78—11225
Fe-Ni-Cr-Ti-Al, Ti and Al effect on microstruct. and mech. props. *(Chinese)* 79—74130
Fe-Ni-Cr-Ti-Al, with thermoelastic control coeff., comp. and heat treatment influence on props. *(French)* 80—81074
Fe-Ni-Cr-Ti-Al Elinvar alloys, dispersion-hardened, structural transform. *(Russian)* 79—1872
Fe-Ni-Ti-Al, martensite, nature of tetragonality 79—32936
Fe-Ni-Ti-Al-Nb, struct. mechanism for inverse $\alpha \rightarrow \gamma$ transform. *(Russian)* 80—40351
Fe-Ni(Mn)-Al-C, form. of ductile Ni_3Al by split quenching, mech. props. 79—100197
Fe-P-Al, amorphous alloy, anelastic relaxation 79—4997
Fe-P-B-Al, amorphous, magnetostriction as function of glass formers 78—19299
Fe-P-Cu-SiO_2-$FeAl_3$-asbestos composite, thermal and elec. conds., temp. and composition depends. 77—66609
Fe-Si (3 wt.%), Al-bearing, grain-oriented, N_2-H_2 annealing effect on texture, mag. props. 77—12714
Fe-Si-Al, high temp. oxidation resist., comp. depend. 77—12739
Fe-Si-Al, Sendust, 12 μ thick film prep. by sputtering, mag. and other props. 77—55888
Fe-Si-Al, Sendust, ribbon-form, prep. by rapid quenching, mech. and mag. props. 80—71611
Fe-Si-Al, surface oxide layer struct., AES study 80—89396
Fe-Si-Al (2.8-3.4, 0-0.86 wt.%) oxidation, annealing 80—89395
Fe-Si-Al (5,10 wt.%) struct. anal. by electron microscopy and electron diffr. *(Chinese)* 79—11618
Fe-Si-Al (6,4 wt.%), Sendust alloy, effect of Ni content on mag. props. 78—72897
Fe-Si-Al (6.5 wt.%, up to 0.5 wt.%), elongation, cold workability and mag. permeability meas. 77—12667
Fe-Si-Al (9.6, 5.4 wt.%), ribbon-form Sendust alloy, mag. props., annealing effects 80—88800
Fe-Si-Al alloy, cryst. lattice deform. at antiphase boundaries, theoretical electron images exam. 77—11448
Fe-Si-Al ribbon-form Sendust alloy made by rapid roll quenching, mag. props., recording head appls. 80—81001
Fe-Si-Al Sendust alloy ribbon form, rapid quench prepared, elec. cond., coercive field, permeability 79—83151
Fe-Si-Al sendust type alloys, Co preferred substitution sites, Mossbauer spectra 79—91328
Fe-Si-Al-Ni alloy, Super Sendust, Ni content and thermomag. treatment effects 77—4861
Fe-Si-MnS-Al, Al effect on hot rolling struct., recrystallization, texture magnetic props. *(Chinese)* 78—11237
Fe_2-Mn-Al alloys, Fe-rich, disordered, local moments on Fe and Mn 77—43811
Fe_3-Al, solid soln., rheological study of crystallographic order on creep *(French)* 80—97548
FeAl B2 struct., band struct. and density of states, KKR calc. 78—63969
FeAl, bonding, self-consistent energy bands 78—91610
FeAl, electronic struct., cluster calc. 77—69209
ε-FeAl, eutectoid, directional decomp. rate rel. to lamellar period 77—4773
ε-FeAl, eutectoid, directional decomp. rate, reply to comments 77—4775
ε-FeAl, eutectoid directional decomp. rate, comment 77—4774
FeAl intermetallic, constitutional vacancies, lattice parameter and thermal vacancy conc. obs. 79—23599
FeAl, isomer shift, electronic charge density 78—80264
FeAl, order parameter, atomic scattering factor, thickness fringes in electron micrographs 79—10832
FeAl, positron localisation in metallic alloys 78—79962
FeAl single crystal, compressed, dislocation arrangement 78—14354
$FeAl_x$, ferromag. to mictomag. transition, Mossbauer meas. 77—24692
$Fe_{0.7}Al_{0.3}$, local environment effects and magnetic clustering 78—10658
Fe_2Al, mag. moment determ., role of local environment, self consistent calcs. 80—44815
Fe_3Al, alloys, superlattice-fringe imaging theory, images formed from two beams 80—79649
Fe_3Al, computer simulation of energy dissipation from near threshold knock-ons 78—30666
Fe_3Al, containing C in solid solution., mag-permeability disaccommodation *(Polish)* 79—95613
Fe_3Al, Cu^+ (Au^+) ion-bombarded 80—15167
Fe_3Al, elec. resist. due to crit. fluctuations near order-disorder temp., theory 77—40071
Fe_3Al, electrical resistivity and LRO, energy gap formation in Fermi surface 80—88533
Fe_3Al, electronic structure, X-ray spectra comparison with band struct. calcs. 80—97383
Fe_3Al, electronic structure, magnetic moments 80—107695
Fe_3Al, exam. of hyperfine field variations with order state 80—6800
Fe_3Al, long-range order parameter from electron micrograph thickness fringes 77—65938
Fe_3Al, magnetic form factor 78—76222
Fe_3Al, magnetoresistance tensor depend. on degree of ordering, −196 to 650°C *(Russian)* 77—31997
Fe_3Al, order-disorder transform. effect on optical and elec. props. *(Russian)* 77—39820
Fe_3Al, order-disorder transition, elec. resistance meas. 79—42518

aluminium alloys continued
Fe_3Al, order-disorder transition effect on low energy spin waves 79—47271
Fe_3Al, ordered, magnetostriction and thermal expansion 80—39842
Fe_3Al, ordered alloys, atomic order parameters from topology of electron-microscope diffr. contrast from antiphase boundaries, quantitative determ. 78—95016
Fe_3Al, partly disordered B2 struct., spin wave dispersion relation 78—64201
Fe_3Al, phase separation 77—63664
Fe_3Al, roll magnetic anisotropy and dislocations *(Japanese)* 77—80930
Fe_3Al, slip geometry and pseudoelastic behaviour, effect of crystal orientation *(French)* 78—87681
Fe_3Al, super-lattice, band theory 77—15758
Fe_3Al, vacancy conc. and ordering conc. 78—18639
Fe_3Al-M, ternary ordered solid solns. with M=Ti, Mn, Ni, Cu, Ge substituent 77—43177
$Fe_{49.7}Al_{50.3}$, Compton scatt., 59.54 keV γ-rays, charge transfer study 78—68578
$Fe_{70.8}Al_{29.2}$, meas. of ordering instability 79—38818
$Fe_3Al_xSi_{1-x}$, DO_3 structured, ferromag., lattice parameters 79—42010
$Fe_{73}Al_xSi_{27-x}$, DO_3 structured, ferromag., lattice parameters 79—42010
$Fe_{80}B_{20-x}Al_x$ glass, magnetisation, Curie and crystn. temps. 79—87289
$Fe_{1-x}Co_xAl$, Knight shift and mag. susceptibility study, electron struct. peculiarities *(Russian)* 80—15814
$Fe_{3-x}Co_xAl$, site preference and local environment effects, Mossbauer and NMR meas. 80—71264
$Fe_{35}Co_{32}B_{20}Si_{10}Al_3$, stress-induced variation in magnetisation and dynamic magnetostrictive charact. 80—88855
$Fe_{65.4}Cr_{20.5}Al_{10.7}V_{3.4}$, effect of Al and V on form. of $L2_1$ superstructure and stratification 77—77474
$(Fe_{1-x}Mn_x)_3Al$ alloys, disordered, mag. moments and distrib. on lattice sites 77—63112
$(Fe_{1-x}Mn_x)_3Al$, local Mn moment distrib., neutron scatt., nucl. spin echo *(Russian)* 77—12091
$(Fe_{1-x}Mn_x)_3Al$, mag. moments determ. from magnetisation and neutron and electron diffr. expts. 79—56520
Fe_2MnAl, dislocation structure, antiphase boundary energies, deformation behaviour prediction *(Russian)* 79—65085
Fe_2MnAl, plastically deformed, domain struct., X-ray diffr. and electron microscope obs. *(Russian)* 79—20110
$Fe_{3-x}Mn_xAl$, ordering of Fe atoms, X-ray diffr. meas. and mid gamma reson. anal. *(Russian)* 80—96469
$(Fe_xMn_{1-x})_{75}P_{16}B_6Al_3$, amorphous, mag. ordering temp., hyperfine field distrib., elec. resist. 80—34633
$(Fe_xMo_{1-x})_{75}P_{16}B_6Al_3$, amorphous, effects of Mo on mag. props., Mossbauer meas. 79—73859
$Fe_{1-x}Ni_xAl$, Knight shift and mag. susceptibility study, electron struct. peculiarities *(Russian)* 80—15814
$(FeNi)_{80}Bi_{17.5}Al_2Si_{0.5}$, stress-induced variation in magnetisation and dynamic magnetostrictive charact. 80—88855
FeNiCrAlLi alloy, γ' hardened, noncellular mech. for form of lamellar η phase morphology 77—28824
$(Fe_{0.3}Ni_{0.7})_{0.75}P_{0.16}B_{0.06}Al_{0.03}$, amorphous, spin wave spectrum, neutron scatt. 77—16064
$(Fe_{0.5}Ni_{0.5})_{75}P_{16}B_6Al_3$ glass, struct. relax. as origin of Curie temp. ageing 78—84418
$(Fe_{1-x}Ni_x)_{75}(PBAl)_{25}$, amorphous, high-field magnetoresist. meas. 80—34423
$(Fe_{1-x}Ni_x)_{75}P_{16}B_6Al_3$, amorphous alloy, low temp. elec. resist. saturation 78—68005
$(Fe_{65}Ni_{35})_{75}P_{16}B_6Al_3$, amorphous ferromag., high temp. spin dynamics 78—47965
$(Fe_{65}Ni_{35})_{75}P_{16}B_6Al_3$, amorphous ferromagnet, mag. excitations 79—7984
$(Fe_{65}Ni_{35})_{75}P_{16}B_6Al_3$, amorphous, crystn. temp., press. and heating rate depend. 80—70132
$(Fe_xNi_{1-x})_{0.75}P_{0.16}B_{0.06}Al_{0.03}$, metallic glass, thermal expansion 78—43151
$(Fe_xNi_{1-x})_{75}P_{16}B_6Al_3$, amorphous, spin wave excitations and low temp. magnetisation 79—33468
$(Fe_xNi_{1-x})_{75}P_{16}B_6Al_3$, magnetisation temp. depend., spin wave theory 80—44927
$Fe_{75}P_{16}B_6Al_3$, aged metallic glass, Mossbauer effect 79—91318
$Fe_3Si_{1-x}Al_x$, hyperfine interactions and structural disorder, spin echo, X-ray and magnetisation meas. 77—32289
$Fe_3Si_{1-x}Al_x$, hyperfine-field distrib. 79—69732
$Fe_3Si_xAl_{1-x}$-Co, dil., site preference of ^{57}Co impurities, Mossbauer study 80—39999
$Fe_xSi_yAl_z$ ribbon, magnetostriction exam. 79—73794
Ga-Al, amorphous, mag. and elec. props. 80—80499
Ga-Al, effect of Al on solidification kinetics, and morphology of Ga 78—56628
Ga-Al alloys, solubility of GaAs, in multilayer LPE of $Ga_xAl_{1-x}As$ 78—52690
$(Gd,Dy)Al_2$, spin adjustment, NMR spin echo obs. 78—15058
Gd-Al, amorphous alloy, mag. coupling 78—88108
Gd-Al, amorphous alloy films, mag. phase diagram, spin glass and ferromag. regions 78—68234
Gd-Al, amorphous film, microwave mag. reson. 78—91948
Gd-Al, XPS valence band spectra meas. 77—48306
Gd-Al sputtered amorphous films, spin glass state 77—66393
Gd-Al-Co, H sorption props. for H storage, influence of Al 80—45794
Gd-Ni-Al, (Gd<33.3 at.%), isothermal section, 800°C, X-ray and microscopic anal. *(Russian)* 79—27950
$GdAl_2$, amorphous, mag. heat capacity 77—89969
$GdAl_2$, anisotropy and magnetostriction 78—10741
$GdAl_2$, anomalous change of Curie temp. 78—47976
$GdAl_2$, ferromag., spin reorientation 78—39334
$GdAl_2$, ferromagnetic, extraordinary Hall effect 80—39560
$GdAl_2$, H_2 sorption props. 79—86980
$GdAl_2$, hyperfine fields, ferromagnetic coupling between rare earth spins, NMR study 80—39880
$GdAl_2$, spin reorientation, NMR features rel. to preferred magnetisation direction change 77—63213
$GdAl_2$, spin reorientation 78—39335
$GdAl_2$-$GdCo_2$ system, EPR and mag. props. 79—33478
$GdAl_3$ thin films, polytypism 79—99446
$GdAl_4$, mag. props., mag. exchange strength 77—85440
$Gd_{0.37}Al_{0.63}$, amorphous film, anomalous resonance field shift 79—73821
$Gd_{0.37}Al_{0.63}$ film, amorphous, spin-glass order parameter meas. 77—28396

- **aluminium alloys** continued
  - $Gd_{0.37}Al_{0.63}$ sputtered film, amorphous, conc. spin glass, microwave reson. spectrum obs. 78—15018
  - Gd_2Al, magnetic properties, 4.2 to 400K, metamagnetism 77—32193
  - $Gd_{37}Al_{63}$ amorphous film, spin glass, microwave mag. resonance, freq. dependence 80—39798
  - $Gd(Al_{1-x}Cu_x)_2$, C15 struct., elec. resist., comp. depend. 78—14705
  - $Gd(Al_{1-x}Cu_x)_2$, thermoelec. power, exchange interactions 80—24881
  - $Gd(Al_xFe_{1-x})_2$, intermetallic compounds, pseudobinary, Mossbauer studies 80—75887
  - $Gd(Al_{1-x}Mn_x)_2$, alloys soft X-ray emission spectra investigation 79—91537
  - $Gd(Al_{1-x}Mn_x)_2$, ordering on crystallographic sites, X-ray diffr. 78—38662
  - $Gd_{1-x}Ca_xAl_2$, mag. props. and phase relations 80—107991
  - $Gd_2Co_6Al_{11}$, NMR and mag. susceptibility 79—15367
  - $Gd_2Cu_6Al_{11}$, NMR and mag. susceptibility 79—15367
  - $Gd_{1-x}Dy_xAl_2$, EPR bottleneck, Dy substitution effect 77—63281
  - $Gd(Fe_{1-x}Al_x)_2$, magnetisation, Curie temps., and mean mag. moments 79—51817
  - $Gd(Fe_xAl_{1-x})_2$, magnetic behavior 80—108079
  - $Gd_{0.9}La_{0.1}Al_2$, ferromag., NMR of ^{139}La 78—52377
  - $Gd_xLa_{1-x}Al_2$ ($x<0.05$), Hall effect measurements 80—44569
  - $Gd_xLa_{1-x}Al_2$, cryst. fields and exchange parameters, ESR meas. 80—71175
  - $GdMn_2$-$GdAl_2$ intermetallics, mag. props., 80-650K 78—60282
  - $GdMn_2$-$GdAl_2$ system, mag. and structural studies 80—108006
  - $(GdMn_2)_x(GdAl_2)_{1-x}$, mag. and struct. investigations of intermetallic systems 78—95440
  - $Gd_2Ni_{17-x}Al_x$, cryst. struct., X-ray obs. 79—65034
  - $Gd_2Ni_{17-x}Al_x$, EPR of Gd^{3+} ions 80—97139
  - $Gd_2Ni_{17-x}Al_x$, mag. behaviour in paramagnetic region 79—73675
  - $Gd_xY_{1-x}Al_2$ ($x<0.05$), Hall effect measurements 80—44569
  - $(Gd_xY_{1-x})Al_2$, ferromag. and spin glass like behaviour, magnetisation meas. 80—75734
  - Ge-Al, alloying effects on elec. transport props. of amorphous and crystalline Ge films 79—51689
  - Ge-Al (1.15 wt.%), US wave vel. meas. for anal. of solid soln. breakup 78—23887
  - Ge-Al film, amorphous, EPR meas. 78—80212
  - Ge-Al film, codeposited, amorphous and polycryst., struct. and elec. props. 80—24766
  - Ge-Al film, elec. resist. and IR transmission, comp. and substrate temp. depend. 78—52112
  - Ge-Al film, polycryst., struct. props. determ. 79—4494
  - H assisted cracking, mechanisms, review 80—50721
  - H impurities, improving productivity and detection threshold, by removing moisture with light pulse 80—26076
  - Hf-Al-C, phase diagram and lattice constants, X-ray diffr. method 80—89207
  - $HfAl_3$, anomalous growth in thin films, AES, TEM and He backscatt. meas. 77—43462
  - $HoAl_2$, biquadratic pair coupling from mag. anisotropy 77—28383
  - $HoAl_2$, heat capacity, 1.5-12K, magnetocryst. anisotropy effects 78—68236
  - $HoAl_2$, Ho moment reorientation, polarized neutron diffr. study 79—42761
  - $HoAl_2$, magnetisation and neutron diffr. meas., cryst. field and exchange 77—63163
  - $HoAl_2$, magnetisation reorientation 79—87291
  - $HoAl_2$, magnetoelastic effects on elastic consts., 4.2-280K 78—72385
  - $HoAl_2$, single cryst., redeterm. of Ho neutron scattering length 79—99032
  - $HoAl_2$, spin reorientation, sp. ht. meas. 79—73724
  - HoAlGa, mag. props. and struct. 78—39302
  - $HoAl_xGa_{2-x}$, mag. props. and phase transitions 80—25133
  - $LIAl_{1-x}In_x$, thermal expansion, comp. depend. 78—22869
  - $(La,Ce)Al_2$ and $(La,Gd)Al_2$, magnetic impurity effect on thermal cond., normal and supercond. states 77—63027
  - $(La,Ce)Al_2$, conf. Kondo system, sp. ht. meas. 78—52210
  - $(La,Er)Al_2$, cryst. field parameters, inelastic neutron scatt. study 79—23937
  - $(La,Gd)Al_2$, dil. alloy, magnetoresistivity determ. 79—73495
  - $(La,Gd)Al_2$, mag. props. 78—52299
  - $(La,Gd)Al_2$, normal and supercond. state, US attenuation, freq. depend. and mechanisms 80—49992
  - $(La,Gd)Al_2$, reverse Kondo alloy, transport props. at finite mag. field 80—6812
  - $(La,Gd)Al_2$, spin glass, cluster glass and magnetisation characts. for different comps. 77—69585
  - $(La, Gd)Al_2$ spin glass, suscept. and sp. ht., mag. field depend. 79—61173
  - $(La,Gd)Al_2$, spin glass materials, mag. field dependence of susceptibility peak 80—103840
  - $(La,Gd)Al_2$ spin glasses, reversible and irreversible mag. susceptibility 80—15738
  - $(La,Gd)Al_2$ spin glasses, time depend. mag. props. 80—65909
  - $(La,Gd)Al_2$, very dil., resist. 79—23958
  - La-Al, amorphous, alloying effect on supercond. props. 79—60951
  - La-Al, XPS valence band spectra meas. 77—48306
  - La-Al amorphous alloys, internal friction, relaxation process 80—92607
  - La-Ce-Al_2, dilute alloy, cryst. fields and Kondo effect 77—43809
  - $LaAl_2$, calc. of energy band-structure and Fermi surface by APW method 80—70590
  - $LaAl_2$, cryst. field splitting and spin-spin interaction of Eu^{2+} and Gd^{3+}, ESR meas. 78—68370
  - $LaAl_2$, de Haas-van Alphen effect, Fermi surface 80—15436
  - $LaAl_2$, doped with Tb, Nd, or Pr, crystal field effects, tunnelling within mK range 80—70907
  - $LaAl_2$, electronic struct., APW method and local-spin-density approx. 80—65434
  - $LaAl_2$, H_2 sorption props. 79—86980
  - $LaAl_2$, inelastic neutron scatt. 80—11165
  - $LaAl_2$, magnetoresist. and de Haas-van Alphen effect, Fermi surface model 79—15069
  - $LaAl_2$, rare earth ion impurities, mag. moments 78—6515
  - $LaAl_2$, supercond. and normal states, anomalous US attenuation and velocity change 80—80446
  - $LaAl_2$, Tb and Pr substituted, superconductors, cryst. field transitions linewidths 80—24854
  - $LaAl_2$:$Gd^{3+}(Eu^{2+})$, cryst. field parameters, relax. rates 78—84482
- **aluminium alloys** continued
  - $LaAl_2$:Gd(Ce), supercond., electronic thermal cond. 77—12063
  - $LaAl_3$-Ce, dil., linewidth of cryst. field excitations 78—67988
  - $(LaCe)Al_2$, unstable valence system, model for thermodynamic props. 77—69487
  - $La_{1-c}Ce_cAl_2$, Kondo superconductor, self-consistent theory of pairbreaking 78—26989
  - $(La_{1-n}Ce_n)_3Al$, mag. impurity effects in normal and supercond. state, NMR 78—2622
  - $(La_{1-x}Ce_x)Al_2$, Kondo supercond., tunnelling density of states 78—14900
  - $(La_{1-x}Ce_x)Al_2$, Kondo supercond., tunnel junction fabrication with wax barriers, tunnelling meas. 78—19191
  - $La_{1-x}Ce_xAl_2$, Kondo system, mag. susceptibility calc. in Anderson model 77—55661
  - $La_{1-x}Ce_xAl_2$, Kondo system, low temp. thermal expansion behaviour 79—19382
  - $(La_{1-x}Ce_x)Al_2$, Kondo system, antiferromag., specific heat 79—24179
  - $La_{1-x}Ce_xAl_2$, supercond., nucl. relax. and impurity magnetism 77—20495
  - $LaCoAl_4$, X-ray anal. of crystal structure *(Russian)* 77—55263
  - $(La_{1-n}Gd_n)_3Al$, mag. impurity effects in normal and supercond. state, NMR 78—2622
  - $(La_{1-x}Gd_x)Al_2$, dil., reverse resistance anomaly 78—76054
  - $(La_{1-x}Gd_x)Al_2$, spin glass, susceptibility maximum freq. depend. 79—61172
  - $La_{1-x}Gd_xAl_2$, spin glass, thermoremanent and isothermal remanent magnetisation 79—87276
  - $La_{1-x}Gd_xAl_2$, supercond., nucl. relax. and impurity magnetism 77—20495
  - $LaNi_4Al$, solubility and sorption props. of H_2, effect of Al 80—103482
  - $LaNi_{5-x}Al_x$, Al addition effects on structural and H_2 absorpt. props. 79—52761
  - $LaNi_{5-x}Al_x$, use in hydride conversion and storage system chemical heat pump 80—72077
  - $LaNi_{5-x}Al_x$, versatile alloy system for metal hydride appls. 77—86308
  - $LaNi_{5-y}Al_y$ alloys and related hydrides, thermodynamic and struct. props. for H_2 storage appl. 80—16847
  - $LaNi_{5-y}Al_y$ alloys and their hydrides, for H storage appls. 80—45816
  - β-$LaNi_{5-y}Al_y$ hydrides, H diffusion, NMR studies 80—15298
  - $La_{1-x}Tb_xAl_2$, competing paramag. anisotropy from cryst. field and indirect quadrupolar coupling 80—60180
  - $La_{1-x}Tb_xAl_2$, paramag. anisotropy of Tb^{3+} in cubic cryst. field 80—15687
  - $La_{1-x}Tb_xAl_2$, supercond., 0.6 meV cryst. field transitions, neutron spectroscopy 78—67991
  - $La_{1-y}Tb_yAl_2$, neutron spectroscopy of 0.6 meV cryst. field transitions 78—30894
  - $(La_{1-x}Y_x)_{1-y}Ce_yAl_2$, resistivity meas., Kondo temp. enhancement 77—62917
  - Li Al, electronic struct., mol. cluster calc. 78—14649
  - Li-Al, equiatomic, B-32 superstruct. instability in absence of many-particle interactions 77—58972
  - β-Li-Al, lattice parameters, density, defect struct. 80—24440
  - Li-Al, sorption of tritium, appl. as thermonuclear reactor material 77—1301
  - Li-Al alloy electrode performance, effects of metal additives 78—23953
  - Li-Al electrode performance In and Mg surface additives effect 80—40698
  - Li-Al system, Li solubility and chem. diffusion in Al, electrochem. study 80—107432
  - Li-Al-Mg alloy electrodes, polarisation behaviour and struct. 79—43588
  - LiAl, anomalous elec. resistivity near critical composition 80—103673
  - LiAl, β phase thermodynamic props., chem. diffusion coeff., electrochem. meas. 80—39308
  - 7LiAl, cryst. growth, Stockbarger method, struct. and homogeneity 80—89137
  - LiAl, elastic moduli and Debye temp., US meas. 79—91724
  - LiAl, NMR relax. investig. of ^7Li self-diffusion 77—12217
  - β-LiAl, optical dispersion, room temp. reflectance spectra 80—66195
  - LiAl, pseudopotential method and ordering problem 77—35500
  - LiAl, semimetallic, B32 struct., electronic props. 78—56062
  - LiAl single crystals, growth by Tamman technique 80—66422
  - LiAl, transport props., rel. to semimetallic band struct. 80—88581
  - LiAl/FeS, battery system research developments at ANL 80—61323
  - LiAl/FeS experimental cells with molten salt electrolyte, self-discharge behaviour 80—104501
  - LiAl/FeS_x cell with negative electrode prep. by powder metallurgy, performance 80—26130
  - LiAl/$FeS(S_2)$ battery developments for electric vehicle propulsion and load levelling appls. 80—61325
  - $LuAl_2$, sp. ht. and thermal props., 5 to 300K 77—43342
  - Mg-Al, dil. alloy, residual resistivity, model pseudopot. form factors 77—8062
  - Mg-Al, unidirectional solidification, method for determ. of diffusion and thermal diffusion coeffs. in molten Mg 78—30772
  - Mg-Al (0.8 wt.%), grain-boundary sliding component in high temp. fatigue 80—50706
  - Mg-Al (18.4 wt.%), damping capacity 77—48474
  - Mg-Al (25 wt.%) powder, reaction with high press. H_2, MgH_2 form. and decomposition *(Korean)* 78—11554
  - Mg-Al (5, 7, 9 and 11 at.%,) discontinuous precipitation growth kinetics 77—63677
  - Mg-Al (9 wt.%), ageing via cellular reaction, microanal., cell boundary vel. meas. 78—11230
  - Mg-Al cylindrical shells, loading history, effect on plastic buckling *(Russian)* 79—14288
  - Mg-Al single crystal growth, specimen for tensile testing in corrosive medium *(Russian)* 80—20774
  - Mg-Al-Tl(Pb) systems, phase diags., electrode pots. *(Russian)* 78—80516
  - Mg-Al-Zn, anelastic creep and recovery 77—63709
  - Mg-Al-Zn (3, 1 wt.%), alloy AZ31, mech. props. of extruded and welded pipe and sheet, optical microscopy exam. 79—34065
  - Mg-Al-Zn (94.3, 3.9, 1.8 wt.%), pricip. on dislocations, weak-beam TEM 80—76264
  - Mg-Al-Zn (9wt.%Al), sand cast, preferred orientation and mechanical props. *(Japanese)* 80—20979
  - Mg-Al-Zn-Mn (8, 0.5, 0.3 wt.%) casting alloy, penetration resistance 80—100901
  - Mg-Al(-Zn), solute-vacancy binding energies from hardness meas. 78—39789
  - Mg-Li-Al, phase diag. *(Russian)* 77—59746

aluminium alloys continued
Mg-Li-Al (31, 1 at.%), heat treated, precipitation 80—40364
Mg-Li-Sn-Al, investigation in Mg rich region *(Russian)* 78—15364
Mg-Ni-W-Co-Al-Cr alloy KhN56VMKYu, Al effect on excess Mg phase 80—29926
Mg-Y-Al alloys, phase equilib. *(Russian)* 80—20890
$MgCu_2$-$MgAl_2$, Friauf-Laves phase, long-period stacking variants, electron conc. depend. 77—80444
$Mg(Cu_{0.535}Al_{0.465})_2$, 2D lattice images of Friauf-Laves phase and defect type 80—24324
$Mg(Cu_{1-x}Al_x)$ with $x=0.465$, Friauf-Laves phase, electron microscope obs. 77—19908
Mn content determination *(Polish)* 80—31889
Mn-Al, vacuum codeposited, disorder of $MnAl_6$ phase in recovery process 78—51854
Mn-Al alloy, domain struct., cryst. defect effects 77—69609
Mn-Al alloys, permanent magnet material development 78—91895
Mn-Al permanent magnets, defect structure, mag. props. TEM obs. 78—91902
Mn-Al-C, ferromag., transform. kinetics 80—34627
Mn-Al-C, ferromag. alloy, transform. kinetics 80—76229
Mn-Al-C, fine-grained cast struct., remanence and coercive force 80—60365
Mn-Al-C, metallic magnets investigations, present state *(Polish)* 80—107987
Mn-Al-C, permanent magnet, mag. props., machinability 77—85505
Mn-Al-C (70, 29.5 wt.%) alloy magnet, Almax, anisotropic, mag. props. *(Japanese)* 80—60371
Mn-Al-C alloy, anisotropic, permanent magnet appl., properties and production *(German)* 79—8309
Mn-Al-C anisotropic permanent mag., cryst. orientation and form., X-ray diffr. anal. 79—82778
Mn-Cu-Al alloy under torsion, anomalous elasticity and transformation plasticity obs. *(Russian)* 78—75834
Mn-Ni(V)(Fe)(Ti)-Al, phase stability 77—48397
Mn-V-Al, magnetic props., heat treatment effects 79—29233
τ-MnAl, estimated theoretical limit of mag. moment 80—97072
$Mn_{1.11}Al_{0.89}$, crit. behaviour, neutron diffr. meas. 78—34982
$Mn_{1.11}Al_{0.89}$, neutron diffr. investig. of mag. struct., degree of order 77—55662
$Mn_{1.11}Al_{0.89}$, unit cell parameters, temp. depend. 79—55697
Mn_4Al_{11}, X-ray cryst. struct. 80—38999
$Mn_{55}Al_{45}$ alloy, permanent mag. props., depend. on particle size 78—91899
MnAlGe film, mag. domains and amorphous to cryst. phase transition, electron microscopy obs. 80—71129
Mo fibre reinforced, SEM study *(Slovenian)* 78—84923
Mo fibre reinforced AlMg, SEM study *(Slovenian)* 78—84923
Mo-Al, amorphous supercond. alloy, produced by coevaporation, struct. and supercond. 79—91179
Mo-Al, couple phase diagrams and thermochemical data 79—66037
Mo-Al-Ge, new compounds, structure and props. 80—39003
Mo-Al-Ge, phase equilibria, X-ray and microstructural anal. 80—93536
Mo-AlN, dispersion hardened, erosion resistance 77—12637
Mo-B-Al-C, alloy TsM-10 rolled, recrystallised, deformed system, behaviour under cyclic loading 79—91795
Mo-B-Al-C, stress cycling at room temp. *(Russian)* 77—25148
Mo-Co-Al, phase diagram *(Russian)* 78—19722
Mo-Cu-Al, phase equilibrium *(Russian)* 78—15361
NI_3Al, structural order and homogeneity, X-ray, mag. susceptibility and Mossbauer meas. 77—63663
Na_3AlFe_6 coatings, transmission and refraction dispersion spectra *(Russian)* 77—48264
Nb-Al, A-15 struct., influence of composition on supercond. transition temp. 77—20486
Nb-Al, A15 and σ-phases, supercond. and normal state electronic props. 77—43765
Nb-Al, couple phase diagrams and thermochemical data 79—66037
Nb-Al, diffuse electron scatt. *(Russian)* 80—103438
Nb-Al, fast quenching of A15-phases *(German)* 77—36014
Nb-Al, prep. from gaseous phase *(Russian)* 78—27451
Nb-Al, supercond., high press.-high temp. treatment, phase props. 77—28746
Nb-Al (20 at.%), diffuse scatt. before Nb_3Al phase form., unstable phase *(Russian)* 78—3131
Nb-Al film, Josephson junction, tunnelling exam. 79—38257
Nb-Al σ- and A15-phases, Knight shift and supercond. 77—15984
Nb-Al-C, phase diagram and lattice constants, X-ray diffr. method 80—89207
Nb-Al-C, phase equilib. and supercond. 80—50593
Nb-Al-Ir A-phase, crystal struct. determ., $MgZn_2$-Laves C14 type 77—1099
Nb-Al-Si, supercond. transition temp., Si conc. depend. 78—84339
Nb-Al-(Ge) film, superconductor, high rate sputter deposition and heat treatment 77—36399
Nb-Mo-Al-(Cr) eutectic directionally crystallised alloy, heat resistance, alloy struct. *(Russian)* 80—40481
Nb-Nb_3Al superconductor, fabrication by quench-age method 77—40403
Nb-Nb_3(Al,Ge) multifilamentary supercond., fabrication and props. 77—20480
Nb-Nb-Al-(Cr), γ/γ'-δ type eutectic, fatigue, effect of composition and microstruct. 78—48520
Nb-Ni-Al, cryst. struct. and defects, high resolution electron microscopy obs. 79—94961
Nb-Ti-Al alloy, effect of heat treatment on strength and elastic props. 77—55976
Nb-Zr-Al, superconductor, struct. determ. by optical microscopy and electron diffraction *(Russian)* 77—16628
Nb_3(Al,Ge) and Nb_3(Al,Si), liq. quenched, supercond. props. 80—84580
Nb_3(Al,Ge) supercond., diffused layer critical current depend. on Cu before and after annealing *(Russian)* 79—69643
Nb_3(Al,Ge) superconducting wire, improved fabrication method 77—28763
Nb_3(Al, Ge) tape, effect of thermal treatment on superconducting props. 79—61016
NbAl, α phases, lattice parameter and order 77—76359
Nb_2Al, $NbAl_3$, supercond. and mag. props. 77—47922
Nb_3Al, A-15 struct., converted from cold worked BCC struct., crit. currents 80—75697
Nb_3Al, A15 cpd., normal state, low temp. resist. 80—107762

aluminium alloys continued
Nb_3Al, and $Nb_3Al_{0.76}Ge_{0.24}$, supercond. props. of cold worked core wires an basis of A15 phases 77—85369
Nb_3Al, anomalous resistivity, insight from band theory 78—60106
Nb_3Al, BCC struct., cold working and converting to A-15 struct. 78—64553
Nb_3Al base ternary solid solns., supercond. T_c, dopant depend. 77—1510
Nb_3Al based ternary solid solns., supercond. transition temp., paramag. susceptibility and lattice parameters meas. *(Russian)* 77—43766
Nb_3Al, complex refractive index meas. 80—93264
Nb_3Al, composition effects on T_c 77—76993
Nb_3Al core wires and pressed powder compacts, supercond. transition 80—34541
Nb_3Al, electron energy loss spectra, AES and HEED investig. of surface 77—24635
Nb_3Al, electron-phonon coupling and supercond. crit. temp. 79—33379
Nb_3Al, electronic struct. calcs. 79—47005
Nb_3Al, electronic struct., electron-phonon interactions, and low temp. anomalies 79—60701
Nb_3Al film, electron-beam coevaporated, prep. and characts. 80—76187
Nb_3Al film, quasiamorphous, supercond. phase formation by heat pulse 77—63017
Nb_3Al, high-T_c supercond., apparent T^2-depend. of normal-state resist. and lattice sp. ht. 77—47921
Nb_3Al, liq.-quenched, crit. current density and T_c 77—72957
Nb_3Al, mechanical and supercond. props. 79—38214
Nb_3Al, metallic bonding, electronic states calcs. 78—79916
Nb_3Al multifilamentary composite, metallurgy, fabrication and supercond. props. 77—28764
Nb_3Al, multifilamentary wires, supercond. props. 78—64175
Nb_3Al, NMR of ^{93}Nb and spin-lattice relax. time at low temp. 77—85388
Nb_3Al, NQR freq. temp. depend., supercond. transition temp. 80—93207
Nb_3Al, neutron irrad. effects on transition temp. *(Japanese)* 79—82707
Nb_3Al, neutron irradiated, A15 compound, recovery of T_c by annealing 78—52132
Nb_3Al, nuclear magnetic relaxation, near T_c *(Russian)* 79—42852
Nb_3Al, obs. of shear struct., electron microscopy *(Russian)* 78—6938
Nb_3Al, phonon density of states, temp. depend. 79—42183
Nb_3Al, prep. by reduction of Nb_2O_5 and Al_2O_3 by CaH_2, thermodynamic calc. 80—100809
Nb_3Al, quantum interference and Josephson effect *(Russian)* 78—56259
Nb_3Al, quasi-one-dimensional supercond., giant enhancement of nucl. relax. rate near T_c 78—56257
Nb_3Al, supercond., fast neutron irrad. effects on T_c 77—55633
Nb_3Al, supercond. props. and lattice parameter, comp. and neutron irrad. effects 80—70880
Nb_3Al, supercond. transition temp., rel. to A15 phase stability 78—52137
Nb_3Al, superconductivity, crit. temp., paramag. susceptibility comp. depend. *(Russian)* 77—66219
Nb_3Al superconductors, sputter deposited, BCC to A15 transition, microstruct. investig. 78—27512
Nb_3Al tape, effect of thermal treatment on superconducting props. 79—61016
Nb_3Al, temp-depend. of elec. resist. 80—103675
Nb_3Al:^{93}Nb, NQR spectra, NQR signal disappearance in supercond. state 78—19369
Nb_3Al-Nb_3Ge-Nb_3Ga system, supercond. crit. temps. 77—8218
Nb_3Al-Ni(Cr)(Fe) mag. impurities effect on supercond. props. 77—1524
$Nb_3Al_{0.8}Ge_{0.2}$, supercond., sp. ht. meas. 77—28296
$Nb_3Al_{0.83}Ge_{0.21}$, A-15 phase, sp. ht. meas. 79—19689
$Nb_3Al_{1-x}Ge_x$, RF sputtering synthesis, supercond. transition temp. variation 77—81216
NbAlIr A′ phase, struct. 78—18587
Nb_3(AlSi), electronic characts. from thermomodulation spectra 79—87421
Nb_3(AlSi) film, thermomodulation spectra, 1.1-2.8 eV 78—48250
Nb_3(AlSi), ternary supercond. alloy films, T_c, props. *(Russian)* 78—88055
$Nb_3Al_{0.2}Si_{0.8}$, A-15 alloy synthesis by ion implantation 78—80489
$Nb_3Ge_xAl_{1-x}$, ternary supercond. alloys, comp. variations 80—97022
Nb_3(Sn-Al) system, X-ray spectroscopic studies of electronic struct. of A15 cpds. 80—2900
Nd-Ni-Al, isothermal section, 600°C, X-ray struct. anal. *(Ukrainian)* 80—33929
NdAl, ferromagnetic, extraordinary Hall effect 80—39560
$NdAl_2$, conduction electron spin and orbital polarisation effects 78—80228
$NdAl_2$, elastic constants, 4.2K to 280K, crystal field effects 77—11615
$NdAl_2$, ferromag., cryst. field excitations, neutron inelastic scatt. meas. 77—63154
$NdAl_2$, mag. excitation spectrum, neutron inelastic scatt. 78—10673
$NdAl_2$, mag. form factor, diffuse moment density, polarised neutron meas. 77—63108
$NdAl_2$, magnetostriction in high mag. fields 79—99745
$NdAl_3$, cryst. field effects, inelastic neutron scatt. meas. 77—51710
$Nd_2Co_{17-x}Al_x$, magnetisation, Curie temp., anisotropy 77—89947
Ni alloys, aluminising, thermodynamic anal. of phase transforms. 80—76413
Ni base alloy IN792, carbide morphology 77—36508
Ni superalloy Mar-M200, slow fatigue crack propagation rate meas. using high freq. resonant technique 78—52983
Ni/Ni_3Al-Ni_3Nb, directionally solidified lamellar eutectic alloy, deform. anisotropy and fracture 77—36604
Ni/Ni_3Al-Ni_3Nb eutectic, directionally solidified, plastic deformation *(Russian)* 78—39843
Ni/Ni_3Al+Ni_3Nb, directionally solidified eutectic alloy, crack growth rate under creep fatigue conditions 79—52361
Ni-A-Ti (6,1 wt.%), γ' phase precip., deform. effects *(Russian)* 78—48404
Ni-Al, (2 and 6 wt.%), oxidation, α-Al_2O_3 growth, microstruct., precip. 80—108626
Ni-Al, B2 type, vacant sites on Ni sublattice and p-d stabilization energy 79—60357
Ni-Al, band model of high temp. magnetism 78—26809
Ni-Al, band struct. and density of states, KKR method and X-ray meas. 80—10863
Ni-Al, CC Ni-Al (42 at.%), Al_2O_3 growth, morphology and spalling model 78—53030
Ni-Al, cohesive props., augmented-spherical-wave calcs. 79—94952
Ni-Al, dil., oxidation mech. at 800 to 1200°C 77—90483

aluminium alloys continued
- Ni-Al, effect of solute misfit and temp. on irradiation induced segregation 78—72779
- β_2-Ni-Al, elastic consts., supersaturated thermal vacancy effects 80—54298
- β_1-Ni-Al, elastic softening and electron diffr. anomalies prior to martensitic transform. 77—8825
- Ni-Al, electronic, mag., and cohesive props. 80—44491
- Ni-Al, ferromag. solid sol., electronic struct., X-ray absorpt. spectra meas. 79—69653
- Ni-Al, gas corrosion, in composite atmospheres *(Polish)* 79—79142
- Ni-Al, grain boundary diffusion in migrating boundaries 79—46830
- Ni-Al, intercrystalline creep rupture *(Czech)* 77—86135
- Ni-Al, ion irradiated, dendritic growth of voids 77—11605
- Ni-Al, ion irradiation induced void swelling and defect microstruct., TEM obs. 79—51164
- Ni-Al, itinerant electron ferromagnet, magnetovolume effects 80—60397
- Ni-Al, liquid, diffusion coeff. differences, rotating-disc determ. 80—39330
- Ni-Al, melt, short-range order and microinhomogeneity, rel. to NiAl form. 77—35466
- Ni-Al, neutron irradiated, rel. between irradiation induced swelling and shear modulus 80—15157
- Ni-Al, order hardening, comparison between revised theory and expt. 80—93565
- β'-Ni-Al, precipitation studies 80—3067
- Ni-Al, Raney nickel catalyst, surface texture studied by N_2 adsorption and ESCA *(French)* 79—69348
- Ni-Al, solid soln., rheological study of crystallographic order on creep *(French)* 80—97548
- Ni-Al, solid soln. and solid soln. hardened, stead state creep 78—27578
- Ni-Al, spinodal decomposition, atom probe field ion microscopy study 80—3028
- Ni-Al, with large volume fraction of γ', precipitation hardening 77—36524
- β-Ni-Al, X-ray absorpt. spectra meas., Fermi level location 80—35005
- Ni-Al (0.5 wt.%), microstruct. formation during internal oxidation, effect of additional microalloying *(Russian)* 77—80650
- Ni-Al (12.8 at.%), irradiation enhanced coarsening 79—66060
- Ni-Al (12.8 at.%) foil, ion irrad., surface effects on precip. morphology 80—104168
- Ni-Al (12.8 wt.%), Ni^+ ion irradiation, precipitate restructuring, mechanisms and kinetics 79—77650
- Ni-Al (14 at.%), two stage ageing effect on spatial distrib. of γ'-phase particles *(Russian)* 78—39805
- Ni-Al (15 wt.%) single crystals, morphological changes of γ' precipitates during uniaxial stress-annealing 79—83236
- Ni-Al (1.18 wt.%), substruct. hardening effect, depend. on mechanism controlling creep rate, 700°C 79—20144
- Ni-Al (36 at.%) martensite, ordering obs. *(Russian)* 77—80446
- β_2-Ni-Al (47.6 to 60.5 at.% Ni), elastic stiffnesses -196 to 400°C 78—27556
- Ni-Al (51 to 55 at.%), vacancy defective, TEM exam. of structure 78—76677
- Ni-Al (6.05 wt.%), prediction and meas. of precipitate number density 78—19756
- Ni-Al (6.2 wt.%), high temp. creep *(Czech)* 77—63727
- Ni-Al (6.3 at.%), influence of localised order on thermo-EMF and Hall-EMF *(Russian)* 78—6951
- Ni-Al (6.35 wt.%) foil, radiation-induced precipitate redistrib. 78—30681
- Ni-Al (6.35 wt.%) precipitate coarsening, redistribution and renucleation during ion irradiation 78—23709
- Ni-Al (7.2 wt.%), fatigue crack propag., plastic work role 79—79070
- Ni-Al alloy, solid phase reaction kinetic parameter calcs., defect formation *(Russian)* 80—54399
- Ni-Al alloys, effects of electron irradiation in precipitation, nucleation and dislocation loop growth, TEM study 79—42106
- γ,γ'-Ni-Al alloys, irrad. effects on precip. 77—8829
- Ni-Al alloys, XPS for band struct. 79—33889
- Ni-Al base ageing alloys, single cryst., deform. and hardening 78—23716
- Ni-Al bronze, fracture resistance of tubes 78—19867
- Ni-Al bronze, fracture toughness 77—81312
- Ni-Al coating, low temp. hot corrosion, Na_2SO_4-induced, mechanism, burner rig tests 80—40610
- Ni-Al film, co-evaporated, comp.-depend. struct. and morphological changes 79—87020
- Ni-Al film, high-temp. condensed, electron diffr. and elec. resist. *(Russian)* 79—4485
- Ni-Al films, evaporated, grain size and microstruct. 80—15423
- Ni-Al solid solns., N_2^+ irrad., void ordering 78—79644
- Ni-Al solid solutions, Ni-rich, phase transforms. during quenching 77—32577
- Ni-Al spraying powders, alumina and aluminide formation 80—25920
- Ni-Al system, calculating interdiffusion coefficient in case of cylindrical symmetry *(Russian)* 79—69297
- Ni-Al system, Mossbauer spectroscopy investigation *(Russian)* 80—20523
- Ni-Al system, ordering and instability of β phase near martensitic transform. *(Russian)* 80—45304
- ζ Ni-Al system, solid soln., interdiffusion *(Japanese)* 80—70476
- Ni-Al thermally reactive powder, particle heating dynamics during plasma deposition 80—16179
- Ni-Al-Cr, ageing kinetics and γ'-phase particles spatial distrib. under applied load *(Russian)* 77—32598
- Ni-Al-Cr, IN-100, growth geometry of carbides in dendritic monocrystals, solidification effects 79—11597
- Ni-Al-Cr, precipitation-strengthened, mechanical props. 78—84968
- Ni-Al-Cr, strain hardening, participation of various slip systems *(Russian)* 79—24536
- Ni-Al-Cr alloy Ehi 826 77—86120
- Ni-Al-Cr alloy IN 100 powder, rapidly solidified, effect of high melt superheat on microstructure 79—52195
- Ni-Al-Cr superalloy IN-100, crack retardation at elev. temp., hold time effect of single overload 79—79068
- Ni-Al-Cr_3C_2, eutectic, directionally solidified, high-temp. oxidation 80—50775
- Ni-Al-Cr_3C_2, eutectic, Al_2O_3 coatings for oxidation resist. 80—50776
- Ni-Al-Cr_3Cr_2, eutectic alloy, directionally solidified, oxidation resistance, influence of Y 80—89409
- Ni-Al-Cr-Co-Ti, Waspaloy, exam. of dislocation-precipitate interaction, cyclic stress-strain behaviour 78—84925

aluminium alloys continued
- Ni-Al-Cr-Mo-Ti-W-(Co) alloys EhI 826 and EhI 929, reverse elastic after effect under loading 78—39829
- Ni-Al-Cr-Ti-W-Mo, US vibration applied during solidification, improved strength, corrosion resistance *(Russian)* 78—15382
- β'-Ni-Al-Fe, mag. impurity states, resist. meas. 77—55519
- Ni-Al-Fe system, order-disorder phase transform., Gorskii-Bragg-Williams approx. *(Russian)* 79—29048
- Ni-Al-Fe(Co), electrical and mag. anomalies due to substitutional atoms 77—15839
- Ni-Al-Mn alloy system, oxidation resist. 79—24661
- Ni-Al-Mo, eutectic form., struct. and mech. props. *(Russian)* 77—21129
- Ni-Al-Mo (12.7, 21.6 wt.%), directionally solidified eutectic composite, precipitation 80—108454
- γ-αNi-Al-Mo eutectic, γ' precipitation 77—12629
- γ/γ-Ni-Al-Nb, aligned eutectic alloy, H_2 embrittlement 77—8951
- Ni-Al-Nb, eutectic form., struct. and mech. props *(Russian)* 77—21129
- Ni-Al-Nb ternary system, electron microprobe analysis of nickel-rich region at 1473K 80—71631
- Ni-Al-Si, β-phase stability *(Russian)* 78—39738
- Ni-Al-Ta, solvus surface determ. using precipitation method 79—15674
- Ni-Al-Ta (7.5, 2.0 wt.%), dendritic monocrystal, microsegregation and nonhomogenisation 79—37940
- Ni-Al-Ta dendritic monocrysts., directionally solidified, coarsening kinetics 80—108425
- Ni-Al-Ti, ageing kinetics and γ'-phase particles spatial distrib. under applied load *(Russian)* 77—32598
- Ni-Al-Ti, eutectic alloy charact. by melting temp., composition and oxidation resistance 78—52771
- Ni-Al-Ti, soln. temp. of hardening intermetallic phase in heat resistant alloys 78—52865
- Ni-Al-Ti cast superalloy, eutectic transform. on ageing *(Chinese)* 79—100110
- Ni-Al-Ti ferromagnetic non-homogeneous alloy, composition determination by Curie temp. meas. 80—11196
- Ni-Al-Ti protective coating, on Ni-Al alloy IN 100, Ti content influence, oxidation behaviour *(French)* 78—3258
- Ni-Al-Ti-Cr superalloys, estimation of conjugate γ and γ' compositions 79—8282
- Ni-Al-Ti-(W) (Cr) (Co) (Mo) (Ta) (Nb), heat resist., solidification range 80—35177
- Ni-Al-Ti(Nb), heat-resisting dispersion-hardening alloys, props. and struct., γ'-phase comp. influence *(Russian)* 80—20943
- Ni-Al(-Si), diffusion, lattice parameter, microhardness, and constitution, effect of Si additions *(Russian)* 80—84316
- β-Ni-Co-Al, martensitic transform., metallographic, X-ray diffr., and elec. resist. obs. *(Russian)* 78—19748
- Ni-Co-Al (1, 35.2 at.%), tempered martensite, new ordered phase 79—11560
- Ni-Co-Al alloys, continuous precip., SEM, TEM, X-ray diffr. study 80—89220
- Ni-Co-Cr-Al-Ti-Mo superalloy IN738, casking porosity removal using hydrostatic press. sintering 80—55322
- Ni-Co-Cr-Al-Y, plasma-arc-sprayed, metallurgical characts. and oxidation behaviour 80—40618
- Ni-Co-Cr-Al-Y coating, electron beam evap., low press. gas scatt. 77—40474
- Ni-Co-Cr-Al-Y coating, electron beam deposited, for Ni-base superalloy, fatigue crack initiation and propag. 78—11438
- Ni-Co-Cr-Al-Y protective coating for combustion turbines, hot corrosion evaluation 80—40608
- Ni-Co-Cr-Mo-Al, Astroloy, extruded powder metallurgy superalloy, recrystallisation study 79—4976
- Ni-Co-Cr-Mo-Al-Ti (17.5, 15.1, 4.9, 4.15, 3.25 wt.%), creep and stress rupture behaviour in air and vacuum 80—60918
- Ni-Co-Cr-Mo-Ti-Al Nimonic 105, loading frequency and environmental effects on high temp. fatigue crack growth 78—64675
- Ni-Co-Cr-Ta-Al-W-Mo-Ti, cast, phase volume fraction determ. using manual point count practice 78—53052
- Ni-Co-Mo-Al-Cr, melt, effect of Al, Cr on O_2 activity, electrochemical determ. 79—11556
- Ni-Cr-Al, effect of ultrasound on crystallisation, dendritic structure, and plasticity *(Russian)* 80—11637
- Ni-Cr-Al, hot corrosion resist. of Na_2SO_4 cooled specimens 78—44264
- Ni-Cr-Al, oxidation, NaCl vapour effects on microstruct. 78—44274
- Ni-Cr-Al, oxidation at 850°C in air containing HCl gas 79—8396
- Ni-Cr-Al, oxide dispersion strengthened, creep and tensile props. 77—86042
- Ni-Cr-Al, oxide dispersion strengthened materials, effect of prior creep at 1365K on room temp. tensile props. 78—39857
- Ni-Cr-Al, protective coating, exam. of interdiffusion kinetics, development of analysing procedure 79—5085
- Ni-Cr-Al, resist. to cyclic oxidation at 1100 and 1200°C 77—77641
- Ni-Cr-Al, shape of γ'-precipitates on surface after sublimation *(German)* 77—81266
- Ni-Cr-Al (15, 5 wt.%), oxide dispersion strengthened, effect of dispersoids on oxidation 78—80679
- Ni-Cr-Al (20, 4 wt.%), tensile stress effect on high temp. oxidation *(Japanese)* 80—89393
- Ni-Cr-Al alloy, Al_2O_3 adherence, improvement by addition of Pt and Rh 77—8995
- Ni-Cr-Al alloy, scale behaviour in carbonaceous gas atmos. 77—36693
- Ni-Cr-Al aluminised coating, diffusion paths for formation and degradation of oxidation resistant coatings 78—11431
- Ni-Cr-Al coatings, corrosion and thermal shock resist. in diesel engines 79—24675
- Ni-Cr-Al coatings Ni eutectic alloys in gas turbines, use of diffusion barrier 79—24673
- Ni-Cr-Al sintered alloy, hot vac. pressure, fracture and mech. characts. 80—66667
- Ni-Cr-Al-Cu, Evanohm, Kapitza conductance meas. using superconducting current comparator 77—41645
- Ni-Cr-Al-TaC, eutectic composite, microstructure, fatigue props. 80—85038
- Ni-Cr-Al-ThO_2, hot corrosion, cyclic oxidation depth of attack determinations 80—11837
- Ni-Cr-Al-Ti, KhN78TYu, heavily deformed, subgrain struct. due to discontinuous precipitation of γ' phase *(Russian)* 79—52218
- Ni-Cr-Al-Ti, stress corrosion cracking, factors influencing susceptibility 80—97617

aluminium alloys continued
- Ni-Cr-Al-Ti (Ti-Co), exam. of back stress role in creep behaviour of particle strengthened alloys 78−52889
- Ni-Cr-Al-Ti alloy type ZhS6U, effects of heat treatment in high vel. gas streams on props. 79−57025
- Ni-Cr-Al-Ti-Mo, low temp. mech. behaviour, precipitation 78−39860
- Ni-Cr-Al-W-Ti alloy MA 6000E, mechanical alloying for high temp. appl. 78−44046
- Ni-Cr-Al-Y coating for oxidation protection of Ni base TaC eutectics 77−40475
- Ni-Cr-Al-Y/ZrO_2-Y_2O_3, NASA two-layer thermal barrier coating, for gas turbine engines, test results 80−40617
- Ni-Cr-Al-Y_2O_3 superalloy, recrystn. and texture development 80−16328
- Ni-Cr-AlPt, exam. of phase diagram 79−8276
- Ni-Cr-Co-Al alloy IN-738, uniaxial damage accumulation law for time depend. loading with creep-fatigue interaction 79−83324
- Ni-Cr-Co-Al-Ti-W-Ta-Mo, IN 738 LC, loading frequency and environmental effects on high temp. fatigue crack growth 78−64675
- Ni-Cr-Co-Al-W-Mo-Ti-Ta, heat resist. and struct., Ta effect 80−76312
- Ni-Cr-Co-Mo-Al-Ti (10, 15, 3, 5.5, 4.5 wt.%), superalloy, exam. of creep and fracture behaviour 78−48464
- Ni-Cr-Co-Mo-Al-Ti alloys, Waspaloy, Astroloy, exam. of microstruct. effect on crack growth 78−52977
- Ni-Cr-Co-Mo-Ti-Al, powders, HCl surface treatment to prevent TiC precipitation, fracture props. 79−8397
- Ni-Cr-Co-Ti-Mo-W-Al (14, 9.8, 5, 4, 3.9, 3 wt.%), low cycle fatigue, prior heat treatment effect 80−60962
- Ni-Cr-Mo-Ti-Al, quenching and ageing effects on props. of type 36NkhTYuM8 79−52275
- Ni-Cr-Mo-W-Al-Ti, heat-resist., phase comp. 80−76250
- Ni-Cr-Nb-Al eutectic alloys, sulphidation/oxidation at high temps., corrosion mechanism 78−72934
- Ni-Cr-Ti-Al, precipitation of γ' phase during single and combined ageing treatment *(Russian)* 77−52328
- Ni-Cr-Ti-Al/Au-Ni brazed joint, high temp., AE under elev. temp. and loading *(German)* 78−31597
- Ni-Cr-Ti-Al-Fe-Co (19.65, 2.40, 1.37, 0.78, 0.52 wt.%), strength of γ' hardened alloy, ageing exam. 78−88501
- Ni-Cr-Ti-Al-Mo-Nb-Fe (13-16, 2.35-2.75, 1.3-1.7, 2.8-3.2, 1.8-2.2, 2.0 wt%), heat resistant props, mech props. struct., stepwise ageing effects *(Russian)* 78−76666
- Ni-Cr-Ti-Co-W-Al-Mo alloys AF-115 and AF2 1DA, superalloy powder compacts, fatigue origins 78−48521
- Ni-Cr-W-Co-Al, high-temp. sulphide corrosion 80−76408
- Ni-Cr-W-Mo-Al-Ti (15,6,3,2,2, wt.%), wrought, Si effect on transition brittleness *(Chinese)* 80−55491
- Ni-Cr-W-Mo-Ti-Al, heat-resist., recovery and recrystn. 80−76268
- Ni-Cr-W-Mo-Ti-Al alloy KhN67MVTYu, heat treatment effect on mech. props. 77−70082
- Ni-Cu-Al (36.8, 7.6 at.%), spinodal decomposition, morphology of microstructure, elastic strain energy anisotropy effect 78−15354
- Ni-Fe-Al type B2 lattice alloys, Fe atom distribution, Mossbauer study *(Russian)* 79−99796
- Ni-Fe-Cr-Mo-Ti-Al, PE 16, thermally activated domain wall motion 80−88777
- Ni-Fe-Nb-Al, mag. props. and struct. *(Chinese)* 78−84450
- Ni-Fe-Nb-Al (11.2, 8.09, 79.66 wt.%), modulated struct. growth process rel. to ageing *(Chinese)* 80−66541
- Ni-Fe-Nb-Al(-Mo), wear resisting mag. head material, mag. props. and struct. 80−35350
- Ni-Fe-Nb-Mo-Al, head material for mag. recording, DC and AC mag. props. 80−88812
- Ni-Mn-Al-Si-Co, Alumel, Ettingshausen-Nernst coeff. and transport props. from 200 to 473K 80−44573
- Ni-Mo-Al and Ni-Mo-Al-V, high-resist., struct. transforms., TEM *(Russian)* 78−19762
- Ni-Mo-Al eutectics, unidirectional solidification 77−4769
- Ni-Nb-Al, eutectic, thermal cycling effect on strength and ductility *(Russian)* 79−24601
- Ni-Nb-Al, unidirectionally solidified γ/γ'-δ eutectic, fatigue crack propag. 79−29184
- Ni-Nb-Al (21,2.5 wt.%), eutectic aligned alloy, mech. behaviour at high strain rates 78−39855
- Ni-Nb-Al (25, 2.5 wt.%), directionally solidified γ/γ'-δ eutectic, growth conditions on struct. 80−11639
- Ni-Nb-Al-Cr, directionally solidified, exam. of growth and morphology 79−11601
- Ni-Nb-Al-(Cr), eutectic, mech. props., high press. H_2 effects 77−63779
- Ni-Nb-Cr-Al, directionally solidified eutectic superalloy, high temp. oxidation resistant coatings 78−39937
- γ/γ'-δ-Ni-Nb-Cr-Al (20, 6, 2.5 wt.%), growth kinetics of γ' precipitates 77−40424
- Ni-Ni_3Al-Cr_3C_2 eutectic composite, creep 77−40431
- Ni-Ni_3Al-Ni_3Nb, directionally solidified, role of twinning in cyclic stress strain behaviour 78−80605
- Ni-NiAl solid soln., high temp. transforms *(Russian)* 79−56973
- Ni-$NiAl_2O_4$, internally oxidised, orientational relationships of precip. oxide phase 77−4783
- Ni-Si-Al alloy system, oxidation resist. 79−24661
- Ni-Ta-Al system, phase equilibria and diagram, electron probe, X-ray diffr. anal. 80−29927
- Ni-Ta-Al-Fe, Al and Fe effect on precipitation kinetics 79−20054
- Ni-Ti-Al, martensitic, coherent γ'-phase particles and influence on $\alpha \rightarrow \gamma$ transformation *(Russian)* 79−29056
- Ni-Ti-Al superalloy, pendant drop melt extracted, struct. and props. 80−76242
- Ni_2 (Al, Nb) single crystals, orientation and temp. depend. of yield stress 80−25791
- Ni_3 (Al.Ti), flow stress and work hardening, exam. of temp. depend. by tensile tests 78−84839
- Ni_3(Al, Nb) single crystal, yield stress, orientation and temp. depend. 80−108511
- Ni_3(Al,Ti), deformation characts., temp., strain rate and orientation depend. 77−44320
- γ'-Ni_3(Al,Ti), single crystal, dislocation movement, HVEM obs. *(Japanese)* 80−108503
- Ni_3(Al,W), yield strength, temp. and orientation depend. 77−28857
- Ni_3(Al,W), yield stress, orientation depend. 78−39830
- β-NiAl alloy, elastic soft modes preceding martensitic phase transition 79−4388

aluminium alloys continued
- β_2-NiAl alloys, Young's modulus, −196 to 800°C, effect of martensitic transforms. 79−83253
- NiAl, annealed near stoichiometric, elec. resist. meas. 77−8071
- β'-NiAl B2 phase, mag. aftereffect 80−34700
- NiAl, bonding, self-consistent energy bands 78−91610
- NiAl coating on Ti alloy, electrospark applied, friction and wear resistance obs. *(Russian)* 79−1916
- NiAl, compositional depend. of oxidation rates 79−8393
- β'-NiAl, density of states, XPS meas. 78−48284
- β'-NiAl, dislocation climb, hot stage TEM 77−24318
- NiAl, electronic struct. by cluster calc., comparison with self-consistent APW method 77−69209
- β'-NiAl, electronic struct. and optical props. 80−97228
- NiAl martensite, Ni-rich, precip. of Ni_3Al, mechanism 77−86033
- NiAl, nonstoichiometric, interstital defect cluster obs. 80−107226
- β-NiAl, omega-like structural defects, diffuse X-ray scatt. obs. 79−95005
- β'-NiAl, ordered, hardness after-effect studied by anelastic relaxation 80−66570
- β-NiAl, oxidation, α-Al_2O_3 growth and microstruct. 80−108627
- NiAl, oxidation, effect of gaseous NaCl 78−95853
- β-NiAl, oxide films, metal and O_2 transport, AES and inert marker, techniques 80−97641
- NiAl precipitation hardening of medium C steel, fatigue behaviour 78−84983
- NiAl, quenched and annealed, void formation 79−46652
- β'-NiAl, self-consistent embedded-cluster model for mag. impurities 78−67973
- β'-NiAl, single cryst., quenched and annealed, ω-like diffr. effects, TEM and X-ray diffr. study 79−60216
- NiAl, sputtered in vacuum, struct. *(Russian)* 77−69986
- NiAl, thermal defects, dilatometric study *(Japanese)* 80−15092
- NiAl, vapour phase mass spectra, correl. between bond strengths in liq. and gas phases 77−35466
- NiAl-Cr, eutectic, directionally solidified, temp. behaviour of misfit dislocations *(German)* 78−3119
- NiAl-Cr eutectic alloy, directional solidification singularities *(Russian)* 78−68678
- NiAl-V join, phase relations and eutectic directional solidification 78−31396
- $NiAl_3$, quantitative STEM chem. anal. using standard and standardless programs 79−17578
- $Ni_{1-x}Al$ solid solution, vacancy ordering exam. by electron diffr. after annealing 78−3123
- β-$Ni_{1\pm x}Al_{1\pm x}$, defect struct. and Debye Waller factors vs. composition 77−31658
- γ'-Ni_3Al and β-NiAl, pure and alloyed environmental resistance 77−59962
- Ni_3Al and Ni_3(Al, Ti), S segregation to grain boundaries 78−48410
- Ni_3Al, at. displacements, characteristic temp. and lattice spacing, temp. depend. *(Russian)* 79−90598
- Ni_3Al based alloys, mean square atomic displacements 79−28053
- Ni_3Al, cold-worked, substruct., X-ray diffr. obs. 77−59806
- Ni_3Al, deformation characts., temp., strain rate and orientation depend. 77−44320
- Ni_3Al, dissociation of superdislocations and plastic deform. mech. *(Russian)* 78−52909
- Ni_3Al, ductility, tensile and compressive tests *(Japanese)* 77−52414
- Ni_3Al, ductility in poly- and single crystals, compressive and tensile tests 78−56715
- Ni_3Al, elastic moduli changes at Curie point 77−66406
- Ni_3Al, itinerant ferromagnet, magneto-volume expt. 77−66404
- Ni_3Al, itinerant ferromag., Fermi surface and single particle excitations 80−34350
- Ni_3Al, long-range order parameter, temp. depend. 77−27849
- Ni_3Al, magnetovolume effects near crit. conc. for ferromag. 79−56591
- Ni_3Al, Mossbauer experiments on homogeneity 78−48395
- Ni_3Al, Mossbauer spectra, exam. of struct., superlattice population anal. 78−88240
- Ni_3Al, noncoherent second phase particle effect on strain-hardening parameters *(Russian)* 79−47703
- Ni_3Al, off-stoichiometric alloy, inverse mag. susceptibility rel. to defect conc. 80−60216
- Ni_3Al, overshooting while testing in tension 78−44189
- Ni_3Al, room temp. ductility improvement by ternary trace element addition *(Japanese)* 79−52315
- Ni_3Al, substitutional soln. and defect hardening mechanisms 77−21155
- Ni_3Al, thermal expansion, mag. contribs. 77−43355
- Ni_3Al, unpaired spin density distrib., polarised neutron diffr. 78−10659
- Ni_3Al/Ni_3Nb, DSC-1 and DSC-2 lattices, coincident and near coincident cells for two lattices 77−84746
- Ni_3Al-B, $L1_2$ type intermetallic cpd. room temp. ductility improvement by B addition *(Japanese)* 80−35263
- Ni_3Al-Fe, Fe effect on Mossbauer effect study 77−32298
- Ni_3Al-Fe (10 at.%), activation anal. of plastic deform. 79−1900
- γ'-Ni_3Al-Fe (10 at.%) alloy, steady-state creep 78−15460
- Ni_3Al-Ni_3Nb, directionally crystallised, thermal and electric cond., emissivity 77−43556
- Ni_3Al-Ni_3Nb, directionally crystallised eutectic, influence of prolonged annealing on microstructs. and props. *(Russian)* 79−74182
- Ni_3Al-Ni_3Nb, eutectic, temp. and thermal cycling influence on oxidation 80−45417
- Ni_3Al-Ni_3Nb, eutectic alloy, crack development, failure energy capacity *(Russian)* 80−40480
- Ni_3Al-Ni_3Nb directional eutectic, oxidation and interaction with protective coatings *(Russian)* 77−52526
- Ni_3Al-Ni_3Nb eutectic, directionally solidified, high-temp. oxidation mechanism 80−16544
- Ni_3Al-Ni_3Nb eutectic alloy, ^{63}Ni diffusion rate rel. to struct. defects *(Russian)* 78−2288
- Ni_3Al-Ti(Cr)(Fe)(Zr)(Mo)(W), powder, X-ray spectral analysis exam. 80−16239
- β'-$Ni_{48}Al_{52}$, 3d transition metal impurities, elec. resist. meas. 77−69295
- $(NiAl)_{1-x}M_x$, $M = 3d$ transition metal, elec. resist. and magnetoresist. 77−43580
- Ni_3(Al.Ti), single crysts., flow and fracture behaviour tested in tension 79−79075
- $Ni_3Al(\gamma')$-$Ni_3Nb(\delta)$, directionally solidified, deformation substruct. and slip systems 79−8326

aluminium alloys continued
$Ni_{62}Co_4Al_{34}$, fine struct. of martensite, electron microscopy obs. *(Russian)* 79−46672
$Ni(Cr)/Ni_3Al$-Ni_3Nb directional eutectic, oxidation and interaction with protective coatings *(Russian)* 77−52526
NiCr-AlY sintered fibre metal struct. abradable seal material, friction and wear 78−56785
NiCr-MoAl-ThO_2 (13,3 wt.%), powder, mech. alloying 78−84744
NiCrAlY, mechanically alloyed, maintaining elongated grain struct. after deform. 77−36534
Ni_3(Mn, Al), ordering process mechanism by neutron diffr. *(Russian)* 77−55961
NiPBAl, metallic glass, viscous flow, alloying effect 78−79793
$(Ni_{1-y}Y_y)_3Al_{1-x}Sc_x(Ti)_x$, quarternary gamma prime ($L1_2$) pseudobinary props. revealed by ionicity modified pair model 78−19725
$NpAl_4$ clusters, band struct., variational Xα calc. 79−4508
$NpAl_4$, clusters, X_α calculations *(Japanese)* 79−82519
Pd-Al alloys, Fermi level position rel. to mixing behaviour, Al activity, thermodynamic props. *(German)* 78−75835
Pd-Al appl. of quasichem. method of cluster components *(Russian)* 77−80623
PdAl-Fe(Ni), phase diagrams, eutectic points and solubility *(Russian)* 80−40333
$PdAl_x$ hydrides, supercond. transition temp. 79−47188
Pd_2AlCu-PdAl system, interactions and solid-state transforms *(Russian)* 80−16272
$PdAl_xH_y$ films, ion implantation prop., supercond. crit. temp. 79−87182
PdAl.r, cryst. struct. determ. 77−84700
Pr-Al liquid alloys, atomic interactions, thermodynamic props. *(Russian)* 80−39307
Pr-Cu-Al system, X-ray and microscopic anal. *(Ukrainian)* 78−84774
Pr-Ni-Al system, Pr (0 to 33.3 at.%), isothermal section at 800°C *(Ukrainian)* 79−34002
PrAl, annealed, mag. props. and mag. struct. 78−6517
$PrAl_2$, cryst. field interpretations of inelastic neutron scatt. meas. and mag. props. 79−56174
$PrAl_2$, cryst. field splitting of Pr^{3+}, inelastic neutron scatt. exam. 77−20275
$PrAl_2$, crystal field splitting, inelastic neutron scatt. study 79−47067
$PrAl_2$, elastic constants, 4.2K to 280K, crystal field effects 77−11615
$PrAl_2$, ferromagnetic, extraordinary Hall effect 80−39560
$PrAl_3$, crystal-field effects, inelastic neutron scatt. meas. 77−8268
Pr_3Al, crystal field splitting, inelastic neutron scatt. study 79−47067
$PrAl_{2-x}Ag_x$, cryst. field and exchange interactions 77−63076
$Pr_{1-x}Ca_xAl_2$, mag. props. and phase relations 80−107991
$PrCoAl_4$, X-ray anal. of crystal struct. *(Russian)* 77−55263
$Pr_{1-c}La_cAl_2$, mag. props. 79−65658
$Pr_xLa_{1-x}Al_3$, cryst. elec. field 80−24856
Pt-Al, development, growth and adhesion of Al_2O_3 77−8994
Pt-Al, solid soln., magnetic props. and lattice parameters *(German)* 79−87236
Pt-Al (22 wt.%), elec. props. of growing alumina scales 79−20282
Pt-Al melts, surface tension and density *(Russian)* 80−39388
Pt_3Al, Ll_2 ordered alloy, positive temp. depend. on strength, phase destabilization 80−81203
$Pt_{53}Al_{47}$, ordered BCC phases at high temp. 79−32948
Pu-Al-Ga system, phase diagram 77−21108
$PuAl_2$, low temp. sp. ht., spin fluctuation phenomena 77−28405
$PuAl_4$ clusters, band struct., variational Xα calc. 79−4508
$PuAl_4$, clusters, X_α calculations *(Japanese)* 79−82519
RFeAl, scatter order cpds., mag. props. 77−51891
Re-Al-Si , X-ray determ.of system *(Russian)* 78−19763
Re-Al-Si system, phase equilibria, $ReAl_{1.2}Si_{0.8}$, $ReAl_{1\ 25}Si_{0.75}$ prod., struct. 78−35357
Re-Cu-Al phase diagram, X-ray structural and microscopic anal. *(Russian)* 80−20895
Re-Fe-Al, physical-chemical investigation *(Russian)* 78−15362
Rh_2MnAl, mag. and cryst. props. 77−20568
$ScAl_2$, density of states, ^{45}Sc NMR 77−63276
$ScAl_2$-Er(Dy)(Nd), dil., EPR and mag. susceptibility 80−15797
$ScAl_2$-Eu, intermediate valence on Eu ions, Mossbauer isomer shift 80−84587
$ScAl_2$-Gd, dil., EPR, comparison with YAl_2, La Al_2, $LuAl_2$ 77−63276
$ScFe_{2-2x}Al_{2x}$, mag. props., composition depend. 77−20593
Si/Al-Si systeym, vacuum deposition, rate controlling and composition anal. by electron impact emission spectroscopy 79−91591
Si-Al, composite, simulation of tensile behaviour and fracture void initiation *(Japanese)* 78−52948
Si-Al, silumin, crystn. of eutectic phases *(Russian)* 80−29942
Si-Al C fibre composite technological coatings, liquid phase method preparation *(Russian)* 80−108375
Si-Al electrical steel, surface oxidation during annealing 78−68838
$Si_{100-x}Al_x$, RF sputtered, amorphous, props. 80−34754
SiC fibre reinforced Al-Si alloy, liq. phase process prep. effect on mech. props. 79−70020
SiC fibre reinforced Al-Mg, heat treatment effect on struct., tensile strength 80−55487
SiC fibre reinforced Ti, effect of Al, Zr and Mo alloying additions on reaction rate of Ti with fibres 80−16249
$SmAl_2$, exchange and cryst. field effects 80−24857
$SmAl_2$, hyperfine field exam. by NMR spin echo 78−23365
$SmAl_2$, hyperfine fields, ferromagnetic coupling between rare earth spins, NMR study 80−39880
$Sm_2(Co_{1-x}Al_x)_{17}$ *(Russian)* 78−64202
$Sm_2Co_{17-x}Al_x$, magnetisation, Curie temp., anisotropy 77−89947
$Sm_{1-x}Gd_xAl_2$, hyperfine fields, ferromagnetic coupling between rare earth spins, NMR study 80−39880
$SmNi_4Al$, intrinsic mag. hardness 77−85506
Sn-Al melt, reaction with Nb for protective coating prod. *(Russian)* 79−70221
Sr-Al-Nd phase diagrams *(Russian)* 78−27480
Sr-Al-Si system, phase diagrams construction by simplex designing method 78−6899
Ta-Al-C, phase diagram and lattice constants, X-ray diffr. method 80−89207
Ta-Cr-Si-Al, heat resistive films prepared by sputtering, lifetime meas. 80−80132
TaAl, α phases, lattice parameter and order 77−76359
TbAl-NdAl, existence of high-temperature superconducting phase *(Russian)* 79−42685

aluminium alloys continued
$TbAl_2$, conduction electron spin and orbital polarisation effects 78−80228
$TbAl_2$, ferromagnetic, extraordinary Hall effect 80−39560
$TbAl_2$, hyperfine field exam. by NMR spin echo 78−23365
$TbAl_2$, origin of magnetostriction 79−78499
$TbAl_3$, polytypism occurrence 80−44164
TbAlGa, mag. props. and struct. 78−39302
$TbAl_xGa_{2-x}$, mag. props. and phase transitions 80−25133
$TbFe_{1.5}Al_{0.5}$, crystalline, small angle neutron scatt. study of mag. order and mag. microstruct. 79−15283
$TbFe_4Al_8$, commensurate-incommensurate modulated mag. struct., neutron diffr. obs. 79−95576
$TbFe_4Al_8$, neutron diffr. exam., mag. struct. 78−10656
$Tb_{1-x}Gd_xAl_2$, effective mol. field at ^{159}Tb, NMR meas. 80−71197
$Tb_xGd_{1-x}Al_2$, magnetic anisotropy, magnetostriction 78−56364
$ThAl_4$ clusters, X_α calculations *(Japanese)* 79−82519
$ThCo_{5-x}Al_x$, homogeneity regions, X-ray powder diffr. study 79−77554
$ThFe_{5-x}Al_x$, homogeneity regions, X-ray powder diffr. study 79−77554
$ThMn_{5-x}Al_x$, homogeneity regions, X-ray powder diffr. study 79−77554
$ThNi_{5-x}Al_x$, absorption of H, form. of hydride 77−84932
(Ti,Al)Co, magnetovolume effects near crit. conc. for ferromag. 79−56591
Ti alloy OT4, high plasticity effect 80−35272
Ti alloy VT3-1, large forgings, heat treatment, struct. and mech. props. 78−52864
$\alpha+\beta$ Ti alloy VT9, influence of phase comp. on fracture *(Russian)* 78−56665
Ti-6Al-4V, oxidation kinetics, water vapour, comparison with pure Ti 77−21321
Ti-6Al-4V, stress distrib. for steady axisymmetric extrusion 80−3103
Ti-A-V (6, 4 wt.%), castings, fatigue crack initiation 79−29186
Ti-Al, age-hardened, deform., order effects in Ti_3Al and temp. effects 77−25111
Ti-Al, Al effects on susceptibility to salt corrosion *(Russian)* 77−25185
Ti-Al, α_2 phase obs. using microscopy and X-ray diffr. 79−52497
Ti-Al, elec. spark Al doping of VT-18, surface struct. and props. *(Russian)* 80−76398
α-Ti-Al, H_2 diffusion *(Korean)* 78−30794
Ti-Al, H_2 diffusion at room temp. *(Japanese)* 80−19987
Ti-Al, hardening of Ti by addition of Al *(French)* 78−23715
Ti-Al, interaction with N_2 at elevated temp., nitridation behaviour 77−12742
Ti-Al, microprobe anal. of alloying addition distrib. 80−55358
α-Ti-Al, Mossbauer spectra, metastable θ- and ω-phases 80−20556
Ti-Al, phase diagram in Ti rich region *(Russian)* 77−25013
Ti-Al, porous, effect of Al and Sn on sintering 80−20830
α-Ti-Al, slip band spacing, correlation with β-Ti-Mn 79−99211
α-Ti-Al, stress/strain curves 77−63738
Ti-Al, structural and phase changes due to annealing *(Russian)* 80−55440
Ti-Al, surface segregation, AES exam. *(French)* 78−22941
Ti-Al, Ti-Al-Sn, specific heat and thermal expansion, 4-290K *(Russian)* 79−51276
Ti-Al, VT5, solid solutions, heat cond. at low temps. *(Russian)* 79−82574
Ti-Al, VT5-1, strength variation under influence of shock waves *(Russian)* 78−92299
Ti-Al (14.4 at.%), void form. and solute segregation under Ni ion irradiation 79−42122
Ti-Al (14.7 wt.%), sintered, mech. props., effect of alloying and dispersed ZrO_2 phase 77−12636
Ti-Al (27.3 wt.%), arc melted, microstruct. 79−61577
Ti-Al (30 to 57 wt.%), phase equilibria from mag. susceptibility studies 79−60483
Ti-Al (4,6,9 wt.%) X-ray line profile analysis 77−47459
Ti-Al (4 to 5.5 wt.%), alloy VT5 with WC-Co coating appl. by detonation, antifriction props. 80−21188
Ti-Al (4 wt.%), sintered, long-time strength 80−40529
Ti-Al (40 wt.%), TiAl plate dissolution 79−66055
Ti-Al (6 wt.%), D profiles after $D_3{}^+$ implantation 80−37581
Ti-Al (6.1 wt.%), hot rolled sheet, ductile fracture nuclei, SEM obs. 78−64654
Ti-Al (6.6 wt.%), hydride habit planes, H_2 embrittlement, slip 77−36648
Ti-Al (7.4 at.%), swaged and recrystallized, grain growth 80−3092
Ti-Al age-hardened alloys, fatigue crack propagation rel. to grain size in vac. and NaCl soln. 80−16538
Ti-Al alloys, Mossbauer effect, comp. depend. *(Russian)* 78−6611
Ti-Al film, evaporated, anodisation, anodic voltage-time dependence obs. *(Polish)* 80−55574
Ti-Al film, struct. and elec. props. 80−7002
Ti-Al system, compact growth in liquid phase sintering 80−20835
Ti-Al system, quenched from β-region, struct. obs. *(Russian)* 77−21146
Ti-Al type VT5-1, describing cyclic-creep processes with parametric eqn. 79−57074
Ti-Al-C, ternary system, phase relationships 80−76230
Ti-Al-Cr-Fe-Si alloy AT6, and weldments, mech. and corrosion props. 77−90409
Ti-Al-Cr-Mo (6, 2.0, 2.5 wt.%), microstructural changes and mech. props. 77−25080
Ti-Al-Cr-Mo alloy VT3-1, reactions with some refractory compounds 80−16585
Ti-Al-Cr-Mo system, VTZ-1 alloy, microstruct. influence on fatigue characts. 80−3195
Ti-Al-Cr-Mo-Fe(V)(Zr), effect of structure and heat treatment on tensile strength, ductility, fatigue limit and notch sensitivity 78−56711
Ti-Al-Cr-Mo-U, alloy VT22, phase composition and fatigue strength 78−3219
Ti-Al-Cr-Mo-V, alloy VT22M, exam. of ageing and phase transitions *(Russian)* 79−11641
Ti-Al-Cr-Mo-V, VT22 alloy, metastable β-phase decay under continuous heating, plastic strain effect *(Russian)* 80−71656
Ti-Al-Cr-Mo-V alloy VT-22, effect of heating rate on phase recrystallisation *(Russian)* 79−34077
Ti-Al-Cr-Mo-Zr hard alloy VK15, shot blasting in strength improvement 77−81272
Ti-Al-H, H effect on mech. props. and lattice constants 80−21036
Ti-Al-Kh18 steel, O_2 solubility thermodynamical anal. *(Russian)* 80−92676
Ti-Al-Mn, endurance with cyclic bending, effect of loading conditions 80−50724

aluminium alloys continued

- Ti-Al-Mo, type BT22, phase transformations under step-by-step heat treatment *(Russian)* 80—108436
- Ti-Al-Mo, type Ti-6242S, irrad. induced creep 80—39163
- Ti-Al-Mo (31, 13 wt.%), transform. microstruct. 78—48394
- Ti-Al-Mo alloy VT-14, spherical pressure vessel, correlation between fracture stresses and mech. laboratory characts. 80—25838
- Ti-Al-Mo alloy VT14, fracture anisotropy, with varying H_2 content, rel. to loading condition *(Russian)* 77—70148
- Ti-Al-Mo-Cr, weldment containing orthorhombic martensite, autotempering behaviour and alpha precip. strengthening 80—84976
- Ti-Al-Mo-Cr (4.5, 5, 1.5 wt.%), CORONA-5, effect of microstructure and heat treatment on fracture 78—60805
- Ti-Al-Mo-Cr (4.5, 5, 1.5 wt.%), weld metal, α/β interace sliding 80—108512
- Ti-Al-Mo-Cr-Fe, distrib. of Sn, Zr between phases, temp effect. 80—55357
- Ti-Al-Mo-Cr-Fe (6.4, 2.7, 1.6, 0.4 wt.%), quenched VT3-1, decomposition kinetics of α'' and β in annealing *(Russian)* 77—66662
- $(\alpha+\beta)$-Ti-Al-Mo-Fe alloy VT-22, behaviour during creep testing, solid soln. dissoc. *(Russian)* 80—40346
- Ti-Al-Mo-Sn alloy, elastically and plastically deformed, positron annihilation meas. of deformation 80—21038
- Ti-Al-Mo-Sn-Si, type IMI 680 and 551, internal friction study of martensitic transformations 80—7573
- Ti-Al-Mo-Sn-Si(4,4,2,0.5 wt.%), fracture toughness and crack propag. 78—39892
- Ti-Al-Mo-V, crack resistance in chloride soln., electrochem. protection, polarization effect 80—55589
- Ti-Al-Mo-V (8, 1, 1 wt. %), stress corrosion cracking and slow strain rate H_2 embrittlement 78—48569
- Ti-Al-Mo-V (8, 1, 1 wt.%), environmental fatigue crack propag., texture influence 79—91802
- Ti-Al-Mo-V (8, 1, 1 wt.%), Widmanstatten colonies, fracture toughness 80—85031
- Ti-Al-Mo-Zr, compressor disk, surface plastic deform., optimal method 80—60924
- Ti-Al-Mo-Zr, type VT-9, creep eqns. rel. to extension and compression props. 80—100875
- Ti-Al-Mo-Zr (Cr-Fe), effect of heating on thermal stability of phases, lattice constants and chem. comp. 78—56672
- Ti-Al-Mo-Zr alloy, VT9, decomp. kinetics of metastable β-phase, X-ray and mech. props. obs. *(Russian)* 78—48368
- Ti-Al-Mo-Zr alloy VT9, Cu-Cr(Ni) coated, plastic deform. and diffusion annealing effect on props. *(Russian)* 78—35425
- Ti-Al-Mo-Zr SiC fibre reinforced composites, matrix selection *(Russian)* 80—35192
- Ti-Al-Mo-Zr-Si (6.6, 3.3, 1.8, 0.3 wt.%)-SiC fibrous composite, component interaction kinetics *(Russian)* 80—55364
- Ti-Al-Mo-(Cr), etching as a function of struct. *(Russian)* 78—15568
- Ti-Al-Mo(Cr)(Fe), thermomechanical treatment effect on mech. props., strengthening mechanisms 80—55441
- Ti-Al-Nb-Ta-Mo (6, 2, 1, 0.8 wt.%), elevated temp. flow strength, creep resist., diffusion welding characts. 80—30033
- Ti-Al-O, V effect on thermal stability and mech. props. 77—21171
- Ti-Al-Sn, alloy 6242, dynamic effects of flow and fracture during isothermal forging 80—76343
- α-Ti-Al-Sn, alloy Ti-679, electron diffr. anal. of Ti_3Si phase *(Chinese)* 80—64845
- Ti-Al-Sn, type Ti-5621S, irrad. induced creep 80—39163
- Ti-Al-Sn, VT5-1, solid solutions, heat cond. at low temps. *(Russian)* 79—82574
- Ti-Al-Sn (3.7, 0.8 at.%) alloy, specific heat, 4 to 290K *(Russian)* 79—14938
- Ti-Al-Sn (5, 2.5 wt.%), annealing of near-basal hydrides 80—20989
- Ti-Al-Sn (5, 2.5 wt.%), ductile fracture at low temps. 78—64659
- Ti-Al-Sn (5, 2.5 wt.%), electron microscope and X-ray diffr. exam., of basal and near basal hydrides 78—80550
- Ti-Al-Sn (5, 2.5 wt.%), fracture mechanism at cryogenic temps. 78—64642
- Ti-Al-Sn (5, 2.5 wt.%) alloy, fatigue under combined alternating bending and torsional stresses 77—8923
- Ti-Al-Sn (5, 2.5%) cryogenic constructing material, far IR spectral refl. 77—24855
- Ti-Al-Sn-Zr, Ti-680, O contamination under high temp. *(Chinese)* 80—66688
- Ti-Al-Sn-Zr (6.19, 1.92, 1.43 wt.%), fatigue cracking characteristics of β annealed microstruct. 79—5051
- α-βTi-Al-Sn-Zr-Mo (6, 2, 4, 6 wt.%), interface struct. 77—44212
- α-βTi-Al-Sn-Zr-Mo (6, 2, 4, 6 wt.%), deformation associated with surface cracks and α particles 79—79107
- Ti-Al-Sn-Zr-Mo (6,2,4,6 wt.%), α-β type 6246, fusion zone fracture behaviour in weldments 80—30093
- Ti-Al-Sn-Zr-Mo (6,2,4,6 wt.%) fusion weldment, substruct. characts. 80—84183
- Ti-Al-Sn-Zr-Mo (6,2,45 wt.%), surface cracking under unidirectional loading 78—56753
- Ti-Al-Sn-Zr-Mo alloy, Ti-6242, $\alpha+\beta$, creep property improvement by Pt ion plating 80—16408
- $\alpha+\beta$-Ti-Al-Sn-Zr-Mo-Cr, low cycle fatigue crack nucleation and early growth 79—8354
- Ti-Al-Sn-Zr-Mo-Si (6, 2, 4, 2, 0.1 wt.%), effect of elevated temperature and environment on fatigue crack growth 80—40486
- Ti-Al-Sn-Zr-Mo-Si-O-H, Si, O, H effects on fatigue, fracture and creep charact. 79—11697
- Ti-Al-Sn(V), corrosion resist. in marine environments *(French)* 80—50767
- Ti-Al-Sn(V)(V-Cr)(Mo-V), electrochemical behaviour under tensile stress in boiling H_2SO_4 and acidic chloride solns. 78—95851
- Ti-Al-U (6,4 wt.%), low and high cycle fatigue rupture at same load 78—3217
- Ti-Al-V, (6,4 wt %), fracture mode, tearing topography surface fracture 80—7670
- Ti-Al-V, (6,4 wt.%), history dependent steady state creep rate 78—39866
- Ti-Al-V, (6,4 wt.%), single and dual ion irrad., microstruct. studies 80—29077
- Ti-Al-V, (6.7, 4.3 wt.%), fatigue crack growth and fracture resistance enhancement, due to annealing 78—35510
- Ti-Al-V, alloy 685, fatigue life, creep and dynamic strain ageing effect, 25 to 400°C *(French)* 80—45384

aluminium alloys continued

- β-Ti-Al-V, annealed, differing interstitial O content, fatigue crack propag. resist. 79—11696
- Ti-Al-V, containing 0-6000 ppm ^3He, sensitivity of tensile props. 80—39197
- Ti-Al-V, erosion resistant boride coating 79—20290
- Ti-Al-V, friction coeff. reduction on injection with TiC particles 80—85086
- Ti-Al-V, fusion reactor blanket structures, radiation resistance 80—63379
- Ti-Al-V, irrad. induced creep 80—39163
- Ti-Al-V, long-term corrosion stability rel. to use in joint endoprostheses 78—36059
- Ti-Al-V, oxidation by water vapour *(French)* 78—76787
- Ti-Al-V, plane strain toughness and resistance to crack propagation *(French)* 78—23813
- Ti-Al-V, rolled, elastic stiffness and Bauschinger effect accompanying anisotropic hardening *(Russian)* 80—40435
- Ti-Al-V, VT6 alloy, butt welded joints, electron beam welding conditions effecting interstitial impurities distribution 80—39136
- Ti-Al-V (Mo-Sn)(Zr), environmental effects in alloy fretting, effect on fatigue props. 78—56787
- Ti-Al-V (4.7, 2 wt.%) pseudo alpha alloy, laminar struct. singularities, β to α transformation *(Russian)* 80—7552
- Ti-Al-V (6, 4, wt.%), delayed retardation phenomena of fatigue crack growth, exam. 78—56745
- Ti-Al-V (6, 4, wt.%), texture influence on fracture toughness and deformation 79—91801
- Ti-Al-V (6, 4 wt.%), annealed and rolled plate, elevated temp. plastic anisotropy 79—61663
- Ti-Al-V (6, 4 wt.%), α-β anneal, recrystn. anneal, β-anneal, room temp. creep 79—61662
- Ti-Al-V (6, 4 wt.%), cavitation induced erosion, under mill annealed, soln. treated and aged, and beta annealed conditions 79—8371
- Ti-Al-V (6, 4 wt.%), compliance calibration results 78—19798
- Ti-Al-V (6, 4 wt.%), deform. charact. under isothermal forging conditions 77—36600
- Ti-Al-V (6, 4 wt.%), dynamic crit. stress intensity vs. crack vel. 80—2115
- Ti-Al-V (6, 4 wt.%), fatigue crack growth data 77—73332
- Ti-Al-V (6, 4 wt.%), fatigue crack propag. under dwell time conditions 78—80639
- Ti-Al-V (6, 4 wt.%), fretting corrosion of orthopaedic implant materials by bone cement 80—104813
- Ti-Al-V (6, 4 wt.%), friction characts. improvement by O_2 dissolution and controlled surface hardening *(French)* 80—45401
- Ti-Al-V (6, 4 wt.%), gust spectrum fatigue crack propag. 80—21105
- Ti-Al-V (6, 4 wt.%), high temp. cyclic oxidation, AE monitoring 79—83413
- Ti-Al-V (6, 4 wt.%), hot isostatically pressed casting, fatigue crack initiation 79—79078
- Ti-Al-V (6, 4 wt.%), improvement of props. by ion implantation 80—16601
- Ti-Al-V (6, 4 wt.%), repassivation and pitting corrosion 80—30143
- Ti-Al-V (6, 4 wt.%), ring test, evaluation for strain rate sensitive materials 78—39991
- Ti-Al-V (6, 4 wt.%), solution treatment temp. effect on fracture morphology 79—61620
- Ti-Al-V (6, 4 wt.%), stress corrosion cracking, composition, microstruct. and texture effects 79—11725
- Ti-Al-V (6, 4 wt.%), superplastic, mech. behaviour and hardening characts. 79—83269
- Ti-Al-V (6, 4 wt.%), targets, metallographic features after ballistic tests 79—79046
- Ti-Al-V (6, 4 wt.%), temp. distrib. for steady axisymmetric extrusion 80—11670
- Ti-Al-V (6, 4 wt.%), temp. distrib. for steady axisymmetric extrusion numerical results 80—11671
- Ti-Al-V (6, 4 wt.%), texture effect on fatigue crack path 78—27633
- Ti-Al-V (6, 4 wt.%), textured, anisotropy of fracture toughness over various specimen orientations 79—8353
- Ti-Al-V (6, 4 wt.%), texture depend. stress corrosion cracking 80—104334
- Ti-Al-V (6, 4 wt.%), type IMI 318, internal friction study of martensitic transformations 80—7573
- Ti-Al-V (6, 4 wt.%), void formation and growth, tensile fracture, exam. 78—80637
- Ti-Al-V (6, 4 wt.%), Widmanstatten, microstructurally sensitive fatigue crack growth obs. 78—27627
- Ti-Al-V (6, 4 wt.%) cylinders, residual stresses introduced by quenching elastoplastic anal. *(French)* 80—45355
- Ti-Al-V (6, 4 wt.%) effect of high temp. oxidation on eddy current conductivity 78—76770
- Ti-Al-V (6, 4 wt.%) slow crack growth in air and fracture toughness, H content effect *(French)* 80—45385
- Ti-Al-V (6,4 wt %), superplasticity, effect of temp. 80—7639
- Ti-Al-V (6,4 wt%), cyclic temp. creep, transition effect 80—97539
- Ti-Al-V (6,4 wt.%), age hardened, deform. charact. 77—36608
- Ti-Al-V (6,4 wt.%), alloy plate, fatigue crack propag. under in-plane loading, expts. 79—52337
- Ti-Al-V (6,4 wt.%), alloy plate, fatigue crack propag. under in-plane loading, anal. 79—52338
- Ti-Al-V (6,4 wt.%), α/β interface phase, formation characts. 79—52272
- Ti-Al-V (6,4 wt.%), α/β interface phase influence on tensile props. 80—30034
- Ti-Al-V (6,4 wt.%), β-annealed, subsurface fatigue crack initiation 80—108553
- Ti-Al-V (6,4 wt.%), corrosion fatigue behaviour, surgical implant material 79—39027
- Ti-Al-V (6,4 wt.%), cyclic stress-strain response 77—21170
- Ti-Al-V (6,4 wt.%), D profiles after D_3^+ implantation 80—37581
- Ti-Al-V (6,4 wt.%), D trapping in fusion reactor materials, temp. dependence 80—37577
- Ti-Al-V (6,4 wt.%), effect of air exposure on fracture characts. 80—100890
- Ti-Al-V (6,4 wt.%), fatigue crack growth, influence of dwell-time 79—43380
- Ti-Al-V (6,4 wt.%), fretting fatigue resistant coating, for steel/Ti-Al-V mating surfaces 78—64721
- Ti-Al-V (6,4 wt.%), fretting fatigue behaviour of temps. up to 600°C 80—21104
- Ti-Al-V (6,4 wt.%), H related fatigue fracture 80—76344

aluminium alloys continued
Ti-Al-V (6,4 wt.%), heat treated and rolled, texture instability 77—63689
Ti-Al-V (6,4 wt.%), heavy ion irrad. effect on microstructure 79—10884
Ti-Al-V (6,4 wt.%), high temp. fretting fatigue, fatigue and fretting wear 80—3197
Ti-Al-V (6,4 wt.%), improved toughness from prior β-grains 78—15522
Ti-Al-V (6,4 wt.%), ion irradiated, microstruct. study using TEM 80—96572
Ti-Al-V (6,4 wt.%), laser surface melted, topographical characts. 79—70200
Ti-Al-V (6,4 wt.%), metallogaphically prepared, fracture surface, phase anal. by energy dispersive X-ray microanal. *(German, English)* 77—48606
Ti-Al-V (6,4 wt.%), microstruct. improvement by cyclic heating *(Japanese)* 79—100185
Ti-Al-V (6,4 wt.%), microstruct. effect of base metals on diffusion welding *(Japanese)* 80—89296
Ti-Al-V (6,4 wt.%), phase transformation after hydrogenation 80—7560
Ti-Al-V (6,4 wt.%), plastic flow instability and multiple necking during superplastic flow 77—8896
Ti-Al-V (6,4 wt.%), porous compacts, determ. of effective stress in hot pressing 80—100807
Ti-Al-V (6,4 wt.%), quenched, struct. and age hardening rel. to treatment temp. 80—11657
Ti-Al-V (6,4 wt.%), strongly textured, influence of cryst. orientation on fracture toughness 78—84951
Ti-Al-V (6,4 wt.%), strongly textured, influence of crystallographic orientation on tensile behaviour 80—7633
Ti-Al-V (6,4 wt.%), superplasticity microstructural influences 79—52323
Ti-Al-V (6,4 wt.%), surface cracking under unidirectional loading 78—56753
Ti-Al-V (6,4 wt.%), surface and grain boundary free energy, zero-creep determ. 79—4313
Ti-Al-V (6,4 wt.%), surface residual stresses, surface topography, fatigue behaviour 79—52366
Ti-Al-V (6,4 wt.%), surgical implant ion beam textured, stress/strain relations, fatigue characts. 78—73297
Ti-Al-V (6,4 wt.%), sustained loading charact. and H_2 effects 78—48515
Ti-Al-V (6,4 wt.%), to H effect on fracture props. and microstruct. 80—40512
Ti-Al-V (6,4 wt.%) alloy, fatigue crack closure eval. with electric potential method 79—50678
Ti-Al-V (6,4 wt.%) alloy foil, substrate temp. effect on struct. 80—7497
Ti-Al-V (6,4 wt.%) for TiC reactively sputtered coatings, adherence, XPES and wear study 80—25565
Ti-Al-V (6,4 wt.%) superplastic deform. 78—31471
Ti-Al-V (6,4 wt.%) superplastic alloy, maximum attainable ductility 80—60919
Ti-Al-V (6,4wt.%), galvanic couple with Al alloys, velocity effect on corrosion 78—35566
Ti-Al-V (6.4 wt.%), electron beam melting for scrap recycling 77—66604
Ti-Al-V (6.4 wt.%) cast alloy, with improved microstruct., mech. props. *(Japanese)* 80—71701
Ti-Al-V alloy, thermophysical meas. above 1450K, using subsecond transient technique 78—95161
Ti-Al-V alloys, 17.5 MeV Cu ion irradiation, resistance to void damage 79—55795
Ti-Al-V-Be-B, melt-extracted polycryst., mech. props. 80—76360
Ti-Al-V-Cr-Mo-Zr (3,8,6,4,4 wt.%), beta-C, microstruct. effect on mech. props. 78—27577
Ti-Al-V-Cr-Zr-Mo (3, 8, 6, 4, wt.%), phase transforms. 79—100113
Ti-Al-V-Cr-Zr-Mo-Fe (3.4, 8.3, 5.8, 3.9, 4.2, 0.06 wt.%), shock loaded, residual strength 77—36589
Ti-Al-V-Fe-Cu, melt-extracted polycryst., mech. props. 80—76360
Ti-Al-V-Fe-Si, alloy VT6, phase transform. kinetics and Young's modulus *(Russian)* 77—81258
Ti-Al-V-Sn (5.5, 5.3, 2.3 wt.%) fatigue crack growth and fracture resistance enhancement, due to annealing 78—35510
Ti-Al-V-Sn (5.5, 5.5, 2 wt%), crack growth, slow, H-induced 80—104272
Ti-Al-V-Sn (6, 6, 2 wt.%) weldments, heat treated, transangular fracture 80—40524
Ti-Al-V-Sn (6, 6, 2 wt.%), fatigue crack growth, cyclic freq. and microstruct. influence 80—55515
Ti-Al-V-Sn (6,6,2 wt.%), H_2 induced crack growth, in-situ scanning Auger anal. 79—8355
Ti-Al-V-Sn (6,6,2 wt.%), α-β type 662, fusion zone fracture behaviour in weldments 80—30093
Ti-Al-V-Sn (6,6,2 wt.%), depend. of K_{ISCC} on loading rate and crack orientation 80—45427
Ti-Al-V-Sn (6,6,2 wt.%) solid metal embrittlement by Cd, Ag and Au 80—16551
Ti-Al-V-Sn (6,6,2 wt.%) fusion weldment, substruct. characts. 80—84183
Ti-Al-V-Sn-Zr alloy TS5, annealing effect on ductility and strength *(Russian)* 78—35427
Ti-Al-V-Sn(Mo-Fe), heavy section extrusion, fabrication and mech. props. 78—6985
Ti-Al-V-(Mo), Widmanstatten, quantitative anal. of microstruct. effect on fatigue crack growth 79—79071
Ti-Al-V-(Sn), SCC, subcritical flow growth, comparison of aircraft alloys in NaCl soln. 78—53028
Ti-Al-V-(Sn), surface finishing effect on internal stresses, X-ray study *(German)* 79—34210
Ti-Al-V(Sn) alloys, plastic deformation and fracture characts. at low temps. *(Russian)* 80—7624
Ti-Al-V(6,4 wt.%), electrical potential method, unusual potential drop 77—16761
Ti-Al-V(6,4 wt.%), environmental fatigue crack propag. 77—36632
Ti-Al-V(6,4 wt.%), partially ordered, i.r. absorptance, 0-600°C 77—4632
Ti-Al-Zr, TA6Zr5D, oxidation at high temp. *(French)* 78—23860
Ti-Al-Zr (3,3 wt.%), W alloying addition effects on mech. props. *(Russian)* 77—59860
Ti-Al-Zr (6,5 wt.%), alloy IMI 685, SEM exam. of crack growth 78—72849
α-Ti-Al-Zr (6.16, 5.23 wt.%), alloy IMI 685, electron microscope observations of strain induced hydrides 78—72828
Ti-Al-Zr alloy, TA6Zr5D, structural evolution during continuous cooling at different rates *(French)* 80—45300
Ti-Al-Zr system, room temp. elec. resist. and thermal EMF *(Russian)* 77—20290
Ti-Al-Zr-Mo alloy 685, phase at α/β interface *(French)* 80—25661

aluminium alloys continued
Ti-Al-Zr-Mo-Si (6, 5, 0.5, 0.25 wt.%), β-processed, fatigue props., hold time effect 80—60961
Ti-Al-Zr-Mo-Si (6,5,0.5,0.25 wt.%) fracture toughness and crack propag. 78—39892
Ti-Al-Zr-Si (5, 5, 0.5 wt.%), creep 77—36595
Ti-Al-Zr-W, phase struct. and props. *(Russian)* 80—16270
Ti-Al-(Mo), phase relations 80—108398
Ti-Al-(V) (6,4 wt.%), hot salt stress corrosion susceptibility, microstruct. effects 77—36688
αTi-Al-(Zr), embrittlement due to ageing 78—56673
Ti-Al(—V)(Mo), impact strength anisotropy, influence of texture *(Russian)* 80—20952
Ti-Al(0.5 to 2 at.%), thermal and athermal solid solution strengthening 77—4787
Ti-Co-Al, Th_6Mn_{23} type struct., mag. susceptibility *(Russian)* 79—42736
Ti-Cu-Al, heat treatable alloys, effect of alloying on strength, tensile props. 78—56671
Ti-Fe-Al, homogeneity and lattice parameters, Al effect on hydriding cmpd. FeTi 80—108400
Ti-Fe-Al, Th_6Mn_{23} type struct., mag. susceptibility *(Russian)* 79—42736
Ti-M-V-Cr-Mo, RMI 38644, shock loaded, age hardening 79—29112
Ti-Mo-Al, determ. of interaction parameters from EPMA data 77—63635
β-Ti-Mo-Cr-Al (8, 4.5, 2.5 wt.%), metastable, tensile ductility, α-phase morphology and distrib. effect 77—86098
Ti-Mo-Fe-Cr-Al, alloy VT3-1, influence of constitution on fracture toughness *(Russian)* 77—77559
Ti-Mo-V-Al-Cr-Fe (4.8, 4.7, 5.2, 1.1, 1.0 wt.%), structural changes during heating up to 1000°C, DTA study *(Russian)* 80—93552
β-Ti-Mo-V-Fe-Al (8, 8, 2, 3, wt.%), exam. of stress induced H_2 migration 78—87823
Ti-Mo-V-Fe-Al (8,8,2,3, wt.%), exam. of stress controlled fatigue response 79—61734
β-Ti-Mo-V-Fe-Al (8,8,2,3 wt.%), metastable, high cycle fatigue crack initation, grain size effect 77—86145
β-Ti-Mo-V-Fe-Al (8,8,2,3 wt.%), metastable alloy, microstruct. and mech. props. ageing time and temp. effect 78—64569
β-Ti-Mo-V-Fe-Al(8,8,2,3 wt.%), metastable factors affecting stress corrosion cracking 77—28928
Ti-Mo-Zr-Al (15, 5, 3 wt.%), quenched and aged metastable β-phase, crystallography, morphology and decomposition 80—76262
Ti-Mo-Zr-Al (15,5,3 wt.%), phase transform. kinetics study by X-ray diffr. 79—56960
Ti-Nb-Al, decomposition during isothermal annealing 80—25653
Ti-Ni-Al, Th_6Mn_{23} type struct., mag. susceptibility *(Russian)* 79—42736
Ti-V-Cr-Al (13, 11, 3 wt.%) alloy spring wire, torsional fatigue props. 77 77649
Ti-V-Cr-Al (13, 11, 3 wt.%), stress corrosion cracking in methanolic solutions 80—50752
Ti-V-Fe-Al (10, 2, 3 wt.%), fracture toughness and stress corrosion resistance 80—100904
Ti-W-Al, mech. props. and heat treatment 80—35274
TiAl, coatings, electrospark applied, friction and wear resistance obs. *(Russian)* 79—1916
TiAl, manufacture by extrusion of blended elemental powders 77—28750
TiAl, Mossbauer effect on impurity nuclei of ^{57}Fe *(Russian)* 77—1621
TiAl, Ti_3Al, ordered alloys, Fe impurity atoms distrib. *(Russian)* 77—35584
TiAl, Ti_3Al-(Nb) dynamic elastic moduli 77—86070
α-β TiAl-Sn-Zr-Mo (6,2,4,6 wt.%), age hardening 79—61604
$TiAl_3$ crystals dissolution in pure Al liq., grain refinement of α-Al solid-solution by Ti addition 80—35178
Ti_3Al, Cu, Fe, Mo (1 at.%) additions, oxidation resistance, 700 to 800 degrees C 77—12744
Ti_3Al, cyclic deform., dislocation struct. 78—7003
Ti_3Al, oxidation *(Russian)* 78—19939
Ti_3Al, phase transitions and physical props. 77—25068
Ti_3Al-(Mo) (0.5 at.%), ordering, Mo effects 77—28841
Ti_3Al-(Nb), ordering transform. and mech. props. 78—31402
Ti_3Al-Sn-Zr, alloy, Sn and Zr alloying influence on creep and scaling resist. *(Russian)* 79—52302
$Ti(Al_xB_{1-x})_2$ (B=Cr, Mn, Fe, Co), $0<x<0.4$, influence of Al on H sorption props. X-ray cryst. struct. determ. 79—28198
$Ti_{0.75}Al_{0.25}H_x$, $x<1.5$, metastable hydride form. 78—51682
TiN coated, tribological anal. 80—108600
$(Tm,La)Al_2$ disordered alloys, cryst. field transitions, inelastic neutron scatt. obs. 80—50055
$TmAl_2$, ferromagnetic structs., elastic neutron scatt. obs. 80—50055
TmS(Se)(Te), Mossbauer expt. in ^3He-^4He dilution refrigerator 78—27127
U-Al, storage of unirradiated fuel in borated concrete, criticality safety anal. 80—13608
U-Al, transform. and struct. changes, cooling, cooling rate effect *(Korean)* 77—63660
U-Al (0.78 at.%), behaviour of metastable phases under neutron irrad., application of model 78—48408
U-Al alloy components, process control analysis of ^{235}U during fuel element manuf., neutron absorpt. method 79—85720
U-Cr-Al (0.2, 0.1 at.%) fuel elements with high swelling resistance for KS-I5O reactor 78—78471
UAL_2, band magnetism due to f-electrons, T_{sf} 77—73039
UAl_2, dynamical susceptibility, diffuse neutron scatt. study 79—24138
UAl_2, elastic consts., temp. and mag. field depend. 80—55450
UAl_2, high field, high press. mag. props. 80—11172
UAl_2, inelastic neutron scatt. 80—11165
UAl_2, low temp. mag. susceptibility 79—38301
UAl_2, low temp. sp. ht., spin fluctuation phenomena 77—28405
UAl_2, spin fluctuations, mag. field effect, electronic sp. ht. and elec. resist. 80—108026
UAl_2, surface comp. and electronic struct., photoemission study 80—66382
UAl_2, transport props., susceptibility and sp. ht. 80—11174
UAl_2-UNi_2, phase relationships, thermal, microscopic and X-ray exam. *(German)* 78—88447
$UAl_2+2Al \rightarrow UAl_4$, effect on Young's modulus and rupture strength in dispersion reactor fuel *(German)* 78—62596
UAl_3, thermoelectric power, 5-300K 79—65444
UAl_4, clusters, band struct., variational Xα calc. 79—4508

aluminium alloys continued
  UAl_4, clusters, X_α calculations *(Japanese)* 79—82519
  UAl_x dispersion nuclear fuels, development and irrad. performance 80—78368
  UAl_x plate-type reactor fuel element fabrication 79—49822
  UAl_x-Al dispersion fuel for thermal high flux reactors, irradiation 77—18660
  $U_{1-x}Th_xAl_2$, ferromag. spin fluctuation system, sp. ht. and elec. props. 77—20604
  ^{235}U-Al castings in water, pulsed reactivity meas., Monte Carlo anal. 79—26522
  ^{235}U-Al castings in water moderated lattices, pulsed reactivity meas. 79—26529
  V-Al, band struct. and density of states, KKR method and X-ray meas. 80—10863
  V-Al, conduction band states, X-ray spectra obs. *(Russian)* 80—29317
  V-Al thin film system, phase growth kinetics, electrochemical anode etching 77—72805
  V-Al/Cu-Ge composite superconductors, transition temp. and upper crit. field, heat treatment effects 79—38268
  V-Al/Cu-Ge composite tape, transition temp., upper crit. field 78—68126
  V-Al-C, phase equilib. and supercond. 80—50593
  V-Al-C, ternary system, phase relationships 80—76230
  V-Ni-Al, phase equilib., elect. cond., hardness *(Russian)* 77—66627
  V_3Al, electronic struct., electron-phonon interactions, and low temp. anomalies 79—60701
  V_3Al, electronic struct. calcs. 79—47005
  V_3Al film, quasiamorphous, supercond. phase formation by heat pulse 77—63017
  γ-V_5Al_8, γ-brass, cryst. struct. redeterm. 77—47377
  V(Nb)-Al-Cu, rapidly quenched, comp. and phase equilib. 80—76235
  V_3Si-Al solid soln., supercond. T_c and paramag. susceptibility *(Russian)* 77—59348
  $V_3Sn_{0.5}Al_{0.5}$, elec. resist., temp. depend., T_c to 300K 79—65426
  W-Al, couple phase diagrams and thermochemical data 79—66037
  W-Al, phase formation in diffusion layers between solid and liquid metals *(Russian)* 79—69257
  W-K-Si-Al doped wires, heavily drawn, fibre struct., annealed 79—56993
  W-Ru-Al-B glass, struct. obs. 80—1938
  $(Y,Er)Al_2$, cryst. field parameters, inelastic neutron scatt. study 79—23937
  Y-Ni-Al ternary system, 800°C isothermal section in range 0 to 33.3 at.% Y *(Russian)* 77—70028
  YAl_2, de Haas-van Alphen effect 78—91590
  YAl_2-Er, dil., EPR, $Er^{3+}\Gamma_8$ ground state 80—15798
  YAl_2-Er(Dy)(Nd), dil., EPR and mag. susceptibility 80—15797
  $Y_2(Co_{1-x}Al_x)_{17}$, low-temperature sp. ht. meas. 79—56541
  $Y_2(Co_{1-x}Al_x)_{17}$, single crystal, mag. props. 77—47993
  $Y_xEr_{1-x}Al_2$, paramag. anisotropy 80—39737
  $Y(Fe_{1-c}Al_c)_2$, local model for mag. behaviour 77—63135
  $Y(Fe_{1-c}Al_c)_2$, mag. and Mossbauer study, local environment effects 78—27033
  $YFe_{2-x}Al_x$, magnetisation behaviour, mag. scatter order 77—28373
  $Y(Fe_cAl_{1-c})_2$, mag. props. 79—38308
  $Y(Fe_xAl_{1-x})_2$, mag. order in pseudobinary systems down to millikelvin temps. 78—19251
  $Y(Fe_xAl_{1-x})_2$, Mossbauer spectra and mag. props. 80—39950
  $Y_6(Fe_{1-x}Al_x)_{23}$, cryst. struct. and mag. props. 79—82180
  $YNi_{5-x}Al_x$, Al addition effects on structural and H_2 absorpt. props. 79—52761
  Yb-Al, valence changes during autoionisation and Auger electron emission 80—50475
  Yb-Al mixed valent film form., XPS study 80—80943
  $YbAl_2$, $YbAl_3$ and YbCuAl, intermediate valency cpds., paramag. susceptibility, 1.4 to 1060K 77—63079
  $YbAl_3$, Mossbauer effect obs. of induced hyperfine field 78—52396
  $YbAl_3$, susceptibility, sp. ht. and magnetisation 79—28512
  $YbAl_3$, unstable valence system, model for thermodynamic props. 77—69487
  $YbAl_3$, valence instabilities 79—78546
  $YbAl_3$, XPS studies, valence band, 4-f region 78—6831
  YbCuAl, intermediate-valent, nucl. reson. and relax. 79—78550
  YbCuAl, mixed valence behaviour, mag. props. 78—68150
  YbCuAl, mixed valence cpd., dynamic susceptibility, neutron inelastic scatt. 80—65807
  YbCuAl, mixed-valence behaviour, mag. susceptibility and sp. ht. 77—80939
  YbCuAl, mixed-valent cpd., thermal expansion and magneto-volume effects 80—66005
  YbCuAl, phase diagrams, lattice props., electron hole symmetry 79—91002
  YbCuAl, susceptibility, sp. ht. and magnetisation 79—28512
  $Yb_{0.99}Gd_{0.01}CuAl$, intermediate Yb valence states, mag. props. 79—51743
  $Yb_xSc_{1-x}Al_3$, valence fluctuation system, suscept. meas. 78—68149
  $Yb_{1-x}Y_xCuAl$, disordered extended Anderson model, CPA-alloy analogue treatment 80—65506
  $Yb_{1-x}Y_xCuAl$, intermediate Yb valence states, mag. props. 79—51743
  Zn-22 wt.% Al superplastic eutectoid alloy tensile deformation obs. *(Japanese)* 79—90714
  Zn-Al, dil., impurity quasi-particle lifetimes and pseudopotential form factor 78—47734
  Zn-Al, dil., isotherm of internal adsorption at dislocations 79—37733
  Zn-Al, dil. alloy, creep ductility 79—38899
  Zn-Al, dislocation slip peculiarities during superplastic deform. 79—20102
  Zn-Al, electroless plating of Ni, baths and activating solns. *(Japanese)* 80—71604
  Zn-Al, high strength superplastic alloy, exam. of precise forging method 79—4929
  Zn-Al, impure and pure, as cast, endogenous-exogenous freezing 78—19736
  Zn-Al, liq., partial interference functions, short range chem. order effects 79—7541
  Zn-Al, near eutectoid alloy, deformation kinetics analysis 79—29161
  Zn-Al, splat quenched and bulk specimens, eutectoid decomposition 77—63628
  Zn-Al, unidirectional eutectic, FCC phase, preferred orientation 80—29973
  Zn-Al, unidirectionally solidified eutectic, morphology and crystallography 77—48421

aluminium alloys continued
  Zn-Al (0.4 wt.%), grain size effect on acoustic emission generated during plastic deformation 78—80609
  Zn-Al (0.4 wt.%), intergranular slip during in situ superplastic deform. 80—96538
  Zn-Al (10,22,50wt.%), low temp. mech. props. plastic deformation, glissile dislocation nucleation *(Russian)* 80—11695
  Zn-Al (15 wt.%), thermal sprayed coating on steel substrate, cavitation and corrosion resist. in sea water 80—35427
  Zn-Al (1.1 wt.%) superplastic alloy, grain size determ. *(Czech)* 80—81118
  Zn-Al (20 wt.%) superplastic alloys, Zn diffusion, strain influence *(Russian)* 79—37870
  Zn-Al (22 at.%), heat treatment and straining effect on fracture and corrosion 79—87672
  Zn-Al (22 at.%) eutectic, superplastic, microscopic examination of internal void formation 80—16383
  Zn-Al (22 wt.%), activation energy for superplasticity 77—86112
  Zn-Al (22 wt.%), eutectoid, low stress and superplastic creep behaviour 80—81120
  Zn-Al (22 wt.%), meas. of plasticity parameters under superplastic flow 78—60710
  Zn-Al (22 wt.%), positron diffusion and trapping at grain boundaries 80—39157
  Zn-Al (22 wt.%), superplastic eutectoid cavitation evidence 77—63741
  Zn-Al (22 wt.%), superplastic deform. mechanism, electron microscope obs. 78—3167
  Zn-Al (22 wt.%), superplastic deform. rate rel. to flow stress, determ. methods 78—60709
  Zn-Al (22 wt.%), superplastic, eutectoid alloy, ductility and fracture 78—60819
  Zn-Al (22 wt.%), superplastic, of very high purity, cavitation 79—24586
  Zn-Al (22 wt.%), superplastic eutectoid, concurrent grain growth and deformation mechanism 79—74222
  Zn-Al (22 wt.%), texture effect on superplasticity 79—20103
  Zn-Al (22 wt.%) eutectoid, superplastic, factors affecting ductility 77—86097
  Zn-Al (22 wt.%) eutectoid, superplastic, grain size effect on plastic deform. at room temp. *(Japanese)* 78—31462
  Zn-Al (22 wt.%) superplastic alloy, cavitation and neck form. 80—30022
  Zn-Al (22 wt.%) superplastic alloy, grain growth texture 80—81075
  Zn-Al (40 wt.%), superplastic deform., dislocation effects 77—48515
  Zn-Al alloys, comp. effects on intergranular slip during superplastic deform. *(Russian)* 77—32633
  Zn-Al alloys, dislocations obs. in superplastic deformation 78—51549
  Zn-Al dilute alloy, Kondo effect anisotropy 77—43578
  Zn-Al eutectic alloy, uni-directionally solidified, damping capacity *(Japanese)* 80—16364
  Zn-Al eutectoid, superplasticity, study by electron microscopy 77—48479
  Zn-Al eutectoid alloy, straining at elev. temp., whisker crystal 79—29087
  Zn-Al eutectoid alloy sheets, creep bulging 80—1439
  Zn-Al eutectoid superplastic alloy, fatigue, microstruct. obs. and frequency effect 77—36659
  Zn-Al superalloy, transform. kinetics 79—100114
  Zn-Al superplastic eutectoid alloy, low strain rate behaviour 80—40458
  Zn-Al-Cu (18, 4 wt.%), plastic deform. at room temp., superplastic props., tensile strength *(Czech)* 80—45360
  Zn-Al-Cu (18, 5 wt.%) alloy, superplasticity *(Russian)* 77—59856
  Zn-Al-Cu casting alloys, mech. props. and dendritic morphology, Al content effect *(Korean)* 80—93612
  Zn-Al-Cu-Mg (22, 0.5, 0.01 wt.%), superplastic alloy, strengthening mechanism *(Japanese)* 77—55975
  Zn-Al-Cu-Mg (4.1, 3.1, 0.05 at.%), thermal cond. and sp. ht. meas. below 4.2K 77—20081
  Zn-Al-Cu-Mg-Pb-Sn, Cu, Mg, Pb, Sn effects on corrosion in wet steam 77—48585
  Zn-Al-Cu-Mg-Pb-Sn (12, 1, 0.02, 0.01, 0.015, wt.%), combined effects of Pb and Sn additions on corrosion, in wet steam 78—39952
  Zn-Al-Mg alloy, annealed, recrystallised, influence of strain and purity on orientation *(Russian)* 79—52234
  Zn-Al(Cu), mech. and technological props. *(Polish)* 80—89286
  Zn-Al(Mg) alloys, cold-rolled, texture formation rel. to Zn purity *(Russian)* 77—59804
  Zn-Al(22 wt.%), alloy sheet, superplastic, cold-rolling effects on mech. props. and microstructure *(Japanese)* 80—71671
  Zn-Cd liquid/Fe-Ni-Al mag. powder, effective viscosity of composites *(Russian)* 80—54424
  ZnAl (18.75 wt.%), supercooling phase β break up kinetics *(Polish)* 80—25654
  Zr-Al, diffusion welding with Al_2O_3 and ZrO_2, 1000 to 1300°C *(German)* 79—33122
  Zr-Al (14 at.%), martensitic, discontinuous precipitation, TEM obs. 79—34040
  Zr-Al (14 wt.%), transformation sequence from Zr-Al martensite to Zr_3Al phase 80—3027
  Zr-Al (4.6 wt.%), microstruct. effect on mech. props. 79—20080
  Zr-Al (4.6 wt.%) martensite, precipitation of Zr_3Al_2, TEM study 79—74156
  Zr-Al (8.0 wt.%), tensile props. and fracture toughness after fast neutron irradiation 80—3198
  Zr-Al (8.6 wt.%), dimensional stability struct. and mech. props, effects of neutron irrad. 80—92563
  Zr-Al (8.6 wt.%), effect of fast neutron irradiation on irradiation growth of Zr_3Al 78—55896
  Zr-Al (8.6 wt.%), fast neutron irradiated, tensile props. and fracture toughness 80—84994
  Zr-Al (8.6 wt.%), neutron irradiation effect on tensile props., swelling 77—7768
  Zr-Al alloy, selective gettering action for partial H_2 press. meas. 77—87775
  Zr-Al getter modules, transient getter scheme for Tokamak fusion test reactor 80—79584
  Zr-Al getter pump, for fusion reactor 77—57748
  Zr-Al getter pumping in beam driven Tokamaks 78—50401
  Zr-Al intermetallic compounds in SAES ST101 getter, surface anal. during stimulated pumping 79—67945
  Zr-Al martensite, DO_{19} phase formation, selected area diffr. obs. 78—84779
  Zr-Al-C, phase diagram and lattice constants, X-ray diffr. method 80—89207
  Zr-Al-Cr H sorption props. for H storage, influence of Al 80—45794

aluminium alloys continued
- Zr-Al-Fe (8.9, 0.001 to 0.006 wt.%) Fe partitioning to Zr_2Al during peritectoid transformation 78—39784
- Zr-Al-V, H sorption props. for H storage, influence of Al 80—45794
- Zr-Al-(Fe,Co), H sorption props. for H storage, influence of Al 80—45794
- Zr-Al(8.6 wt.%), mech. props., corrosion and fast neutron irrad. influence 78—84948
- Zr-Al(8.6 wt.%), neutron irradiated, irradiation growth and recovery, annealing 80—15162
- Zr-Mo-Al (3, 1 wt.%), β-phase stability 78—39742
- β-Zr-Mo-Al-(La), metastable, deform. induced transform. 78—52805
- Zr-Nb-V-Al alloys, decomp. of β solid soln., metastable and equilib. phases 79—11632
- Zr-Zr_2Al_3, diffusion weldings between 1000 and 1300°C, electron microprobe anal. *(German)* 78—84011
- $ZrAl_2$, X-ray energy spectrum of valence electrons *(Russian)* 80—108304
- Zr_2Al, X-ray energy spectrum of valence electrons *(Russian)* 80—108304
- Zr_3Al, Ar^+ ion and electron irradiation, irradiation swelling, lattice parameter changes 79—65123
- Zr_3Al base alloy, forming press. tubes 77—8784
- Zr_3Al, cold worked, annealing effects 77—36535
- Zr_3Al, deformed and irrad., lattice defects obs., superlattice dislocations and defect clusters 80—107261
- Zr_3Al, disordering by 1 MeV electron irradiation 78—51583
- Zr_3Al, hyperperitectoid, tensile strength, effect of fast neutron irrad. 77—52408
- Zr_3Al, ion beam prod. damaged regions 79—60409
- Zr_3Al, irradiation 78—6111
- Zr_3Al, $L1_2$ phase, work hardening 78—23718
- Zr_3Al, $L1_2$ phase yield strength 78—19811
- Zr_3Al, neutron irrad. effect on tensile props. 80—3156
- Zr_3Al, ordered, elec. resist. of LI_2 phase as function of temp. 79—19572
- Zr_3Al, ordered, exam. of Young's modulus and thermal expansion coeff. 78—72805
- Zr_3Al, ordered, notch sensitivity, neutron suppression 78—23779
- Zr_3Al, ordered, oxidation, weight gain and metallography 80—89398
- Zr_3Al, ordered, review of physical metallurgy 78—15419
- Zr_3Al, ordered, strengthening by fast neutron irrad. 78—84838
- Zr_3Al ordered alloy, ion bombardment damage, TEM 80—100287
- Zr_3Al, ordered polycrystals, hardness and flow stress relationship 77—44309
- Zr_3Al, ordered polycrystals, ductile fracture 78—64641
- Zr_3Al, tensile props., surface preparation depend. 80—3155
- Zr_4Al_3, X-ray energy spectrum of valence electrons *(Russian)* 80—108304
- $Zr(Al_xCo_{1-x})_2$, Laves phase, H_2 absorption capacity meas. 78—87866
- $Zr(Al_xFe_{1-x})_2$, Laves phase, H_2 absorption capacity meas. 78—87866
- $Zr(Fe,Al)_2$, weak itinerant ferromag., mag. anisotropy effects on mag. isotherms 80—11187
- $Zr(Fe_{1-x}Al_x)_2$, Curie temp., magnetisation, and cryst. struct., conc. depend. 80—75730
- $Zr(Fe_{1-x}Al_x)_x$, transition region, spin glass or long range mag. order 80—44841
- $Zr(V,Al)_2$, struct., supercond. props., elec. resist. and mag. susceptibility, 4.2 to 300K *(Russian)* 79—15246

aluminium compounds
- *see also alumina; aluminium alloys*
- β-eucrypite, glass-ceramics, internal stresses 79—15770
- $Al_5(BO_3)O_6$ synthetic, interplanar distances, struct. 79—86775
- n-$Al_xGa_{1-x}As$, large-lattice relax. model for persistent impurity photocond. 77—85261
- allophane, synthetic, amorphous mineral struct. obs. using ^{57}Fe Mossbauer effect 80—34836
- aluminas, surface modified, DTA and TGA exam., gas chromatographic eval. 77—36785
- aluminate phosphors, energy transfer models 79—43019
- aluminates and aluminosilicates, thermodynamic props. determ. by Monte Carlo calc. 77—47597
- aluminates with tetrahedrally coordinated Al atoms, normal vibs. 77—51456
- aluminium methylammonium selenate alum, effect of hydrostatic pressure on dielec. props., near transition pt. 79—56712
- alumino-chromo-phosphate adhesive, chem. interaction with α-Fe substrate, Mossbauer obs. 80—40596
- alumino-silicate melt, Monte Carlo calc. of ionic struct. 79—60256
- aluminophosphate adhesive, chem. interaction with α-Fe substrate, Mossbauer obs. 80—40596
- aluminophosphate melts with V, Cr, Fe and Co oxides, resistivity, 800-1200°C 77—39903
- aluminosilicate refractories, X-ray struct. determ. of quantitative phase contents 77—52707
- aluminosilicates, quantitative anal. by XPS 78—35742
- aluminous porcelain, electrical conductivity of function of O_2 partial press. *(German)* 77—1419
- anadalusite, thermal expansion and cell parameters 79—90801
- anodic films, influence of substrate orientation 78—88581
- $Ba(PO_3)_2$-AlF_3-BaF_2 (SrF_2) 79—95215
- bauxite, determ. of Sr, Y, Zr, Ga, X-ray fluoresc. method 77—36849
- bauxite, Fe-containing, Mossbauer analysis 78—44806
- bauxite reduction at 800-1800°C, corundum recrystallization 77—86296
- bauxites, analysis, comparison of atomic absorpt., X-ray fluoresc. and other classical methods 80—89551
- binary, with chalcogenides and pnictides, at. vol. and semicond. props. 77—20089
- borates, synthesis, thermal anal. and micrography *(French)* 77—85967
- carnegieite, metastable cathodochromic, prep. by zeolite decomposition *(French)* 79—95719
- chalcogenate and chalcogenite double salts, form. laws and acid-base props. 80—101070
- chloroaluminium phthalocyanine, sublimed layer, IR absorption, vibr. assignments 78—55174
- cordierite, dense ceramic prep. with sintered condition over 300°C interval 79—33983
- cryolite, molten, struct. charact. by IR spectroscopy and splat cooling *(French)* 79—69835
- eucryptite-cordierite binary system, sintering of polycrystalline bodies *(Japanese)* 77—12588

aluminium compounds continued
- feldspar, crystalline track detector, etching characts. anisotropy 77—46465
- GaAs-$Al_xGa_{1-x}As$ strip buried heterostructure laser densely packed monolithic linear array 79—45956
- GaAs-$Ga_{1-x}Al_xAs$, ultrathin layer heterostruct., pseudopot. calcs. 78—95343
- gibbsite purification, to produce pure Al_2O_3 *(German)* 79—100091
- graphite-$AlCl_3$, well-staged, Raman and IR spectra 80—50339
- guanidine aluminium sulphate, lattice charge contribution to coordination polyhedron cryst. potential 80—103651
- guanidine aluminium sulphate hexahydrate:Cr^{3+}, ESR spectra fine struct. 80—93169
- guanidinium aluminium sulphate hexahydrate:Fe^{3+}, EPR spectra, angular var. calc. 80—54940
- guanidinium aluminium sulphate hexahydrate, ESR of V^{3+}, 21.5 GHz, 4.2K 78—91942
- guanidinium aluminium sulphate hexahydrate, surface obs., SEM and AES expts. 80—71362
- hexaurea aluminium perchlorate:VO^{2+}, single cryst. ESR 77—16158
- kaolinite:C, high temp. reduction reactions, thermodynamic anal. 80—104426
- kaolinite, optical spectroscopy study of structural changes at 700-1000°C 79—65193
- kaolinite rare-earth complexes, relax., molar free energy of activation for dipole relax. 80—88919
- kyanite, deformed, defect struct. 77—31668
- laterites, Venezuelan, analysis, comparison of atomic absorpt., X-ray fluoresc. and other classical methods 80—89551
- methylammonium aluminium selenate dodecahydrate, dielec. dispersion and relax. 77—28515
- methylammonium aluminium sulphate, third order elastic consts. from stress shifted reson. freqs. 78—55905
- methylammonium aluminium sulphate dodecahydrate, ferro to paraelectric transition, low freq. dielectric behaviour 79—4770
- methylammonium aluminiumselenate:Cr^{3+}, EPR and linewidth anomaly 77—12191
- montmorillonite, Co^{2+} form, optical spectroscopy study of structural changes at 700-1000°C 79—65193
- mullite-based dispersed refractory system, rheological props. at high temp. 77—16629
- $NH_4Al(SO_4)_2.12H_2O$:MnO_4^-, visible and UV absorpt. spectra interpretation 80—45116
- oxide film, anodic, colloidal metal, origin of colour, optical props. meas. 78—68571
- oxide film, anodic, photodepolarisation *(Russian)* 77—32316
- oxide thickness measurements up to 120 Å on silicon and aluminium using the chemically shifted Auger spectra 78—23586
- oxides, morphologies, on Al prepared for adhesive bonding 79—70203
- oxides and hydroxides, electro-erosional prep. *(Russian)* 80—81297
- pseudoboehmite, exam. of structure, using radial electron distrib. method, and X-ray diffraction 80—1977
- rare earth aluminium borates, thermal stability, X-ray struct. anal., refractive indices 79—4297
- rare earth halide-Al halide system, potential R ion laser, spectroscopic props. 78—66812
- sialon, oxidation 77—56126
- Sialon, prep. and charact. of ultrafine powders 80—11604
- β'-Sialon, sintering kinetics and rates of microstructural changes 79—100102
- β'-sialon compositions, reaction sintering obs. 80—55337
- SiAlON X-phase, X-ray diffr. data 80—49198
- silicaalumo gels, Na-K, crystn. and characts. of A-type zeolites 79—52780
- sillimanite-mullite intermediate phase, crystallisation under hydrothermal conditions 77—44137
- tourmaline, resonator, electroelastic constants, elec. field induced freq. shift study 80—20597
- turquoise, crystalline, Nogales Mexico, SEM and TEM study 79—29760
- ultramarine, catalyst struct., binding energies, ESCA 77—21420
- vanadate polystyrene based membranes, parameters, biionic pot. 79—57294
- YAG synthetic, cryst. growth, review *(German)* 79—33926
- zeolite, new crystal phosphors *(Russian)* 78—2903
- zeolite A, synthetic, with salt inclusions, elec. and thermal props. 79—55925
- zeolite inclusion complexes, $LiA.LiNO_3$ and $LiX.LiNO_3$, ^7Li NMR motional line narrowing 79—56618
- zeolite interface, ionic conduction bands 77—35745
- zeolite surfaces, bonding of Cu^{2+}, Cr^{3+}, Co^{2+} ions, EPR, optical spectroscopy investig. *(German)* 79—95266
- zeolite-water desorption, complex reaction interphase boundary kinetics 79—57203
- zeolites, coordination of Al and Si from X-ray spectra 78—11021
- zeolites, synthetic, effect of sintering on elec. cond., porosity and microstruct. 79—29009
- ALF_3, evaporated layers DC props. and α-particle scatt. 78—14845
- ALN, O_2 effects on sintering 77—77451
- Ag_2^+/AlO_4 paramagnetic centre in X-irrad. α-quartz, EPR obs. 79—28612
- (Al,B)N, production by nitriding AlB_{12} powder 77—12560
- (Al,Ga)As, CW long-life laser, use of half-wave Al_2O_3 facet coatings 77—23688
- (Al,Ga)As, channelled substrate planar struct. injection lasers 77—71996
- (Al,Ga)As DH diode laser, double-dovetail constricted, single mode CW operation 79—22949
- (Al,Ga)As DH injection lasers, internal quantum efficiency, algorithm for meas. 78—66822
- (Al,Ga)As DH injection lasers, sustained oscills. depend. on DC current bias 79—68392
- (Al,Ga)As DH laser, effect of mounting on pulsed threshold 78—13711
- (Al,Ga)As DH laser, pulsations produced by saturable absorber Q-switching, possible model 79—81426
- (Al,Ga)As, DH laser, stripe geometry, threshold for amplitude-stabilised oscill. 77—7084
- (Al,Ga)As DH laser degradation, facet oxide formation 79—86185
- (Al,Ga)As DH lasers, temp. accelerated ageing and degradation characts 78—22130
- (Al, Ga)As DH lasers, water role in gradual degradation 80—74379
- (Al,Ga)As DH lasers, superlinear emission characts., negative resist. obs 80—95895

aluminium compounds continued
(Al,Ga)As, DH stripe-geometry CW laser, junction voltage saturation 77—23675
(Al,Ga)As DH wafer, Al distrib. meas. 77—7994
(Al,Ga)As double heterostructure laser, comparison of deep and shallow proton bombardment fabricated devices 80—99724
(Al,Ga)As double-heterostructure lasers degraded, deep-level changes during accelerated ageing at high temps. 80—74356
(Al,Ga)As injection lasers, pulsations and adsorbing defects 79—94234
(Al,Ga)As laser, ageing-induced self-pulsation stabilisation and initial degradation elimination by facet coatings 80—43347
(Al,Ga)As, laser, DH, threshold current var., optical scatt. losses 77—3588
(Al,Ga)As long-lived DH injection lasers for fibre optic communication, degradation exam. 78—50778
(Al,Ga)As proton-bomard. stripe-geometry DH lasers, optical nonliniarities and optical spikes 79—55138
(Al,Ga)As:Zn planar stripe lasers with deep Zn diffusion, guiding mechanisms controlled by impurity concs. 80—78853
(Al,Ga)As/GaAs, LPE grown heterostructures, X-ray diffr. exam. of interfacial elastic strains 78—72019
(Al,Ga)As-GaAs laser, transverse junction stripe, high temp. single mode CW operation 78—74918
Al complex, Al $urea_6(ClO_4)_3:Cr^{3+}$ structural phase transition, ESR meas. 77—20681
Al complex, carboxylate-Al (III), surface alignment of liq. cryst. 80—1924
Al electrolytes, X-ray determ. of cryolite ratio 78—3417
Al ion, effect on Fe_3O_4 formation and structure *(Japanese)* 77—59727
Al saponite, evidence for inclusion in chlorite-like mineral group, X-ray and chem. anal. 79—12108
Al/Al_xO_y vacuum deposited laminates, struct. and mech. props. 79—28219
$Al/AlCl_3$-$NaCl/FeS_2$ secondary cell, preliminary study 80—108793
Al/AlO_x/La-rare earth metal tunnel junctions, cond. meas., cryst. field effects 80—88694
Al/GaAlAs, film, epitaxial growth on (100) GaAs by hot vac. deposition and characterisation 79—56085
Al-Al_2O_3 superconducting granular film, crit. current density 77—40013
Al-Al_2O_3-Au(Al), capacitance, water sorption effects 77—43738
Al-Al_xO_y-Pb tunnel junction, thermal annealing effects 80—49952
Al-AlF_3-Al MIM struct., dielec. props. temp. irreversibility *(Czech)* 80—15616
Al-AlN-Au, voltage controlled negative resist., O_2 press. effect 78—72281
Al-AlN-SiO_2-Si capacitors, physical and elec. props. of RF plasma grown AlN 80—100530
Al-AlO_x-Pb junctions, organic ring cpd. doped, asymmetries in elastic and inelastic tunelling 79—95549
Al-AlO_x-PbBi tunnel junction, quasiparticle energy distrib. in nonequilib. supercond. 77—80881
Al-B(-C) system, synthesis and struct. of boride phases 80—45282
Al-Ga-As, light emitting heterojunction diode, $\eta_e \approx 40\%$ *(Russian)* 77—81157
Al-Ga-As heterostruct. with confined current flow, fabrication 78—68081
Al-Ga-As heterostructure formation by LPE 77—32517
Al-Ga-As heterostructure photocell with a transition layer 79—19655
Al-Ga-In-P(As)(Sb), III-V quaternary alloy, $A_xB_yC_zD$ or $AB_xC_yD_z$, energy band gap and lattice constant 79—4296
Al-Ga-Sb, ternary phase diagram, appl. to LPE growth 77—59761
Al-Ga-Sb system, ternary phase diagram and appl. to soln. growth 79—74135
Al-Ga-Sb ternary phase diagram, calc., DTA and LPE expts. 80—29931
Al-GaAs-$Al_xGa_{1-x}As$ Schottky barrier diodes, prep., characts. 80—6948
Al-Ge-SiO solar selective absorber surfaces, optical behaviour at high temp. 80—101130
Al-H_2O, mol. complex, electronic struct. calcs. 78—66465
Al-P-As-Sb, III-V quaternary alloy, $A_xB_yC_zD$ or $AB_xC_yD_z$, energy band gap and lattice constant 79—4296
Al-Si-N-O system, comps. corresponding to β'-sialon phase reaction hot-pressing 80—84891
$Al(Al_{1+2x}Si_{1-2x})O_{5-x}$, mullite, X-ray diffr. structural model 80—49191
AlAs, APW calc. of electronic structure and optical props. 79—99479
AlAs, chem. transport equilib. with I_2 in gaseous phase *(French)* 77—55876
AlAs, chem. transport equilib. with I_2 in gaseous phase *(French)* 77—55877
AlAs epilayers, MBE growth on GaAs, self-terminating thermal oxidation 78—92374
AlAs, gas phase dissoc. energy, mass spectrometric determ. 79—81301
AlAs, oxidised, as multidielectric for GaAs MIS devices 79—65333
p-AlAs, saturation characts. over CO_2 laser spectrum 80—83646
n-AlAs, VPE on GaAs, for heterojunction devices 77—1814
n-AlAs/p-GaAs, VPE growth for solar cells 77—77391
AlAs-GaAs, binary heterostruct. LED, external quantum yield *(Russian)* 77—8661
AlAs-GaAs, heterostructure electroluminesc. characts., active region electron density depend. 77—12446
AlAs-GaAs, strip heterolaser, O^+ implantation optimisation, relative threshold current density *(Russian)* 78—1230
AlAs-GaAs (001) interface and superlattice, electronic props., band struct. 79—95485
AlAs-GaAs (100) interface, tight binding calc. of electronic struct. 78—95342
AlAs-GaAs (100) superlattices, band struct. 78—30868
AlAs-GaAs (110) interface, self-consistent calc. of interface states and electronic struct. 78—52066
AlAs-GaAs abrupt (110) interface, electronic struct. 78—95339
AlAs-GaAs double heterostructure, effective lifetime of nonequilibrium carriers 78—6435
AlAs-GaAs film heterojunction, VPE growth and characts. 78—6439
AlAs-GaAs heterojunctions, on graphite substrate, props., solar cell appls. 78—91760
AlAs-GaAs heterostructure, fabrication by selective liq.-phase epitaxy 79—15618
AlAs-GaAs LEDs, Ge or Zn-doped, mechanism of degradation 77—76911
AlAs-GaAs monolayer crystal, two-photon absorpt. spectrum 78—52589
AlAs-GaAs monolayered periodic cryst., optical props. 77—81079
AlAs-GaAs multipass heterostructure, spectral and ang. charact. of luminesc. 77—20418

aluminium compounds continued
AlAs-GaAs multipass heterostructures, external quantum efficiency of luminesc. 77—20419
AlAs-GaAs solid solution, quantitative analysis, use of internal calibration technique developed by AES 77—36834
AlAs-GaAs stripe heterojunction laser, O^+ implantation effect on threshold characts. 79—41383
AlAs-GaAs:Ge double heterojunctions, efficiency of radiative recombination 77—77286
$AlAsO_4$, XPS of cryst., inner shell binding energies of elements 79—43092
$AlAsO_4.2H_2O$, XPS of cryst., inner shell binding energies of elements 79—43092
AlAs(Sb), fine structure of lowest exciton state *(Russian)* 80—96801
$Al_{.20}As_{.40}Te_{.40}$, amorphous alloy, radial distribution function anal., X-ray diffr. *(Spanish)* 80—28915
AlB_{12}, abrasive, effect on machinability of Ti alloys *(Russian)* 80—97593
AlB_{12}, α- and β-forms, elec. props. at high temps. and in strong elec. fields, thermistor appls. 80—92903
α-AlB_{12}, cryst. struct. 77—43197
α-AlB_{12}, cryst. struct. and refinement 77—15376
α-AlB_{12}, cryst. struct. related to β-tetragonal B 79—77551
α-AlB_{12}, heavily doped, elec. props. 78—10446
α-AlB_{12}, hopping cond., book contrib. 78—47797
AlB_{12}, powder, production of nitride materials by nitriding 77—12560
α-AlB_{12}, prep. and electrothermal props. 80—20863
AlB_{12}, preparation of single crystal 78—43997
γ-AlB_{12}, struct. rel. to isohedral B framework 78—2086
α-AlB_{12}, valence electron distrib. deform. 79—65042
AlB_2, band struct. and density of states, metallic behaviour 77—59249
AlB_2 electronic struct. calcs. 78—2417
AlB_2 flakes, reinforcing props., composite prep., props., book contrib. 78—48366
AlB_2, structure types, coordination 77—19913
AlB_2-$ThSi_2$, struct., symm. and rel. to other linear structs. 77—11525
$AlBO_3$, crystal atomic struct., B-O bond length determ. 78—10010
$AlBeB_{24}$, and β-$(Al,Be)B_{12}$, prep. and struct., book contrib. 78—47277
$Al_{1.0}Be_{0.7}B_{22}$, cryst. struct. by X-ray diffr. 80—15069
$Al_2Be_3(Si_6O_{18})$, beryl single crysts., dislocations obs., X-ray topography *(French)* 79—37709
$Al_2Be_3Si_6O_{18}:Cu^{2+}$, synthetic beryl, ESR, optical spectra and X-ray diffr. meas. 77—16166
$Al_2Be_4(Si_6O_{18})$, beryl single crysts., growth defects study using X-ray topography *(French)* 79—37710
AlBi, possibility of existence with sphalerite struct. 80—33950
$Al_4Bi_2O_9$, single cryst., struct., X-ray obs. 77—43191
AlBr solution, in propylene carbonate, dissociation, radius and number of ion solvation *(French)* 79—70319
AlBr, UV emission spectrum, vibr. consts., isotope displacement and dissoc. energies 77—3381
$AlBr_2$, IR spectra in Ar matrix, struct. 79—31520
$AlBr_3$, Raman IR spectra, organic solvent effect *(German)* 77—3370
$AlBr_3$, specific and equivalent cond. of aq. solns., viscosity 77—35736
Al_2Br_6, Br_2Al-Br-$AlBr_3$, vibr. obs., normal coordinate anal. *(German)* 79—26967
$AlBrCl_2$, matrix isolated, vibr. spectrum, struct., vibr. freqs. 78—46339
$AlBr_2Cl$, matrix isolated, vibr. spectrum, struct., vibr. freqs. 78—46339
$Al_{10}Br_3(OH)_{27}(H_2O)_{13\pm2}$, cryst. struct., X-ray powder diffr. obs. *(French)* 78—2084
$Al_{10}Br_4(OH)_{26}(H_2O)_{13\pm2}$, cryst. struct., X-ray powder diffr. obs. *(French)* 78—2084
$AlBr_3.NH_3$, mol. struct., vap. phase electron diffr. obs. 77—65541
$AlBr_3.SrBr_3$, $AlBr_3.BiBr_3$ complexes, NQR 77—20747
AlC, precipitates in Ni-base superalloy, STEM microanal. 80—81067
Al_4C_3, solid-state ^{13}C NMR spectra 79—24220
Al_4C_3, stability at 1873K, Gibbs energy of formation determ. 78—39745
Al_4C_3, vaporis. thermodynamics, 1321-1607K 80—66859
Al_4C_3-Be_2C-SiC system, phase equilibria 80—45284
Al_4C_3-Be_2C-SiC system, phase analysis and TEM struct. obs. 80—108420
AlC_xN_y, refractory deposit, prep. by thermal decomp. of Al dialkylamides and characterisation 80—11572
AlCl, A-X system, vibr. anal. 80—23394
AlCl, ionisation energies, self-consistent-charge Hartree-Fock-Slater calcs. 77—6687
AlCl, pseudopot. calcs. 80—91446
AlCl+HCl, matrix reaction, $HAlCl_2$ IR spectrum *(German)* 79—11786
$AlCl_3$, aq. soln., HCl additive effects on ^{27}Al spin-lattice relax. 80—66058
$AlCl_3$, aq. solns., order phenomena, X-ray diffr. obs. 80—1915
$AlCl_3$ aqueous soln., quasi-elastic neutron scatt. study 78—26425
$AlCl_3$, force and compliance consts., OVFF, UBFF and GVFF models 78—50663
$AlCl_3$ intercalation of C cathode in Al reduction cell 79—43559
$AlCl_3$, matrix isolated, vibr. spectrum, struct., vibr. freqs. 78—46339
$AlCl_3$, soln., IR spectra 78—74649
$AlCl_3$, use in radioactive source prep. for $4\pi\beta$-γ coincidence counting 78—838
$AlCl_3$-Al chemically deposited photosensitive cells, photovoltaic characts. 79—39303
$AlCl_3$-alkali chloride, molten mixture, vap. pres. meas. 78—87779
$AlCl_3$-graphite intercalation compound, electrochem. characterisation method 80—55666
$AlCl_3$-LiCl, molten mixtures, specific cond. meas., comp. and temp. depend. 80—15279
$AlCl_3$-N-alkylpyridium halides, molten mixtures, density, elec. cond. and viscosity meas. 80—24630
$AlCl_3$-NH_3 system, supersaturation calc. during AlN epitaxial growth 77—8758
$AlCl_3$-NaCl melt, n-TiO_2 electrode, electrochem. and photoelec. props. 80—81328
$AlCl_3$-$TbCl_3$, vap., high-energy laser medium props., for fusion ignition 78—63075
$AlCl_4$, distortion from T_d symm. 78—63706
$AlCl_4^-$, IR spectra in $AlCl_3$-MCl (M=Li, Na, K) melts 79—806
Al_2Cl_6, ab initio LCAO SCF minimal basis set calc., struct. 79—49943
Al_2Cl_6, matrix isolated, vibr. spectra, isotopic fine struct. and valence force field calcs. 80—58258
Al_2Cl_6 molten, nuclear mag. relax., mol. rot. 80—71209
AlClBr, IR spectra in Ar matrix, struct. 79—31520

aluminium compounds continued
$AlCl_2Br$, IR spectra in Ar matrix, struct. 79−31520
$Al_{10}Cl_3(OH)_{27}(H_2O)_{13\pm2}$, cryst. struct., X-ray powder diffr. obs. *(French)* 78−2084
$Al_{10}Cl_4(OH)_{26}(H_2O)_{13\pm2}$, cryst. struct., X-ray powder diffr. obs. *(French)* 78−2084
$1.5Al_2Cl_6(g)+GdCl_3(s)=GdAl_3Cl_{12}(g)$, entrainment quenching and chem. transport, rel. to appl. for GdIG CVD 80−24750
α-$Al_2(CrO_4)_2Cr_2O_7.4H_2O$, cryst. struct. determ. 78−6038
$AlCuCl(SO_4)_2.14H_2O$, aubertite, X-ray cryst. struct. determ. *(French)* 80−33932
AlD, $A'\pi$, spectral lifetime and predissociation 79−59515
AlF, $a^3\Pi$-$X^1\Sigma^+$ transition, rot. anal. 77−18938
AlF, hyperfine structure simulated by computer programme 78−50538
AlF, in sunspots, prediction of line intensities 78−20803
AlF, pseudopot. calcs. 80−91446
AlF, radical, form. in arc plasma, spectra 77−28989
AlF_3, $^4He^+$ ion scatt. spectrometry below 5 keV 80−108313
AlF_3, $L_{II,III}$ fine struct. of XAS 80−11508
AlF_3 based glasses, chem., thermal and optical props. *(French)* 80−70139
AlF_3, disordered film, optical transitions as function of prep. conditions 78−27340
AlF_3, enthalpy of fusion from meas. of mixing with liq. Li_3AlF_6 and Na_3AlF_6 77−40569
AlF_3 film, dielec. characts. 77−85650
AlF_3 film, optical absorption meas. rel. to prep. conditions *(French)* 77−44078
AlF_3 film, RF sputtered, dielec. props. meas. 77−36173
AlF_3 film, refr. index and struct., deposition temp. depend. 79−4857
AlF_3 films, electronic transitions near optical absorpt. edge, depend. on prep. conditions *(French)* 77−63429
AlF_3 in Al-AlF_3-Al MIM thin film structures, dielec. and elec. props. *(Slovak)* 80−100536
AlF_3, localised electronic levels, thermoluminesc. and thermally stimulated current exam. 78−11001
AlF_3, single crysts., vapour phase chem. transport prep. *(French)* 79−69971
AlF_3-$Li_3AlF_6(Na_3AlF_6)$, solid-liquid and liquid-liquid enthalpy of mixing meas. 77−40569
AlF_3-M_2F glasses, M=alkaline earth, density-of-states and structural forms, Raman spectra study 80−97255
AlF_3-MF(M=Li, Na, K, Rb or Cs), ion-molecule equilibria studied by mass spectrometric method, heats of dissoc. and form. calc. 80−104479
AlF_6^{3-}, octahedral complex, ionis. energy, SCF-Xα study 78−70967
AlF_6^{3-}, SCF Xα SW calcs., ionis. pot. 79−26887
Al_2F_6, ab initio LCAO SCF minimal basis set calc., struct. 79−49943
$AlFeF_5.7H_2O$, Mossbauer spectra, thermal decomp. products 78−80258
Al_xGa_{1-x}-GaP structure, LPE, double heterostruct. light modulator appl. 79−28963
AlGaAs buried heterostructure lasers, gain and absorpt. spectra meas. 80−91792
AlGaAs CW heterolaser, hysteresis of output radiation power 79−64230
AlGaAs CW injection heterostructure laser, with second order distributed Bragg reflectors, exam. 78−37907
(AlGa)As, CW laser diodes, long-term lifetests at room temp. 79−22963
(AlGa)As CW narrow stripe injection laser with induced waveguide, expt. props. 80−32988
AlGaAs CW oxide defined stripe laser, optical feedback effects 78−79045
(AlGa)As CW oxide-defined stripe laser, reliability statistical study 79−76687
AlGaAs constricted DH diodes, stable single filament laser action obs. 78−55358
AlGaAs constricted DH laser with large optical cavity, CW high-power single-mode operation 80−48276
(AlGa)As DH, proton-striped, proton-induced defects, photoluminesc. study 80−48251
AlGaAs DH, temp. depend. of intensities and times of radiative transitions 79−38660
(AlGa)As DH CW laser diodes modulation characts. 77−38965
AlGaAs DH injection phase-locked laser, coherence 80−102726
(AlGa)As, DH junction laser, stripe geometry second derivatives of elec. characts. obs. 77−10923
(AlGa)As DH laser, insulating C film deposition to prevent facet deterioration 78−87049
AlGaAs DH laser, self-pulsations due to proton bombarded region self-annealing during ageing 80−99728
(AlGa)As, DH laser, threshold current temp. depend. 79−81431
(AlGa)As DH laser degradation due to facet oxidation 78−42336
AlGaAs DH laser epilayer struct. optimization for integrated optical circuits 80−99879
AlGaAs DH laser mirror degradation mechanism and lasing characts. changes 80−9919
AlGaAs DH laser preamplifier to improve optical receiver sensitivity 80−53316
AlGaAs DH laser with external grating oscillation properties 80−48247
(AlGa)As DH lasers, catastrophic optical damage generation mechanism, TEM obs. of dark line defects 80−100239
(AlGa)As DH lasers, comparison of 'normal' lasers and lasers exhibiting light jumps 80−106519
(AlGa)As DH narrow stripe injection laser with rigid waveguide, expt. props. 80−32987
AlGaAs DH short wavelength lasers, internal stress and degradation 79−68393
AlGaAs DH stripe geometry lasers, spontaneous radiation, carrier conc., and threshold current, luminesc. meas. 79−36898
AlGaAs DH stripe laser, spontaneous emission factor 77−75514
AlGaAs DH stripe laser, side lobe suppression by Te facet coating 80−5744
AlGaAs double heterostruct. laser, 'window-stripe', high power emission 79−72566
AlGaAs electroluminescent heterostructures, LPE, appl. to LED fabrication 80−55308
AlGaAs, heteroepitaxial waveguides for image transmission *(Russian)* 77−11037
AlGaAs, heteroepitaxial waveguides, far radiation field characts. *(Russian)* 77−11038
AlGaAs heterojunction laser, single transverse and longit. mode operation 78−37887

aluminium compounds continued
AlGaAs heterojunction laser diodes for optical analogue link, evaluation 79−68395
AlGaAs heterojunction diode as light source for fibre optical communication 80−58653
AlGaAs heterojunction laser, lightwave sources and detectors 80−64068
AlGaAs heterojunctions, nonradiative recomb. vel. estimate from edge luminesc. props. 80−65668
AlGaAs heterojunction photocell with luminesc. wavelength converter 80−108800
(AlGa)As heterostruct., proton irrad., photoluminesc. 80−29808
AlGaAs heterostructures in integrated optics 77−75713
AlGaAs high-power constricted DH diode laser, for optical recording 80−43351
AlGaAs injection lasers, undoped, estimation of intra-band relax. time 80−43335
AlGaAs injection laser, large optical cavity, with multiple active regions 80−106538
AlGaAs integrated twin guide laser with distributed Bragg reflectors 77−88744
AlGaAs junction laser, with optical waveguiding 77−42540
AlGaAs, LPE layers, growth initiation and cathodoluminesc. irregularities 79−87010
(AlGa)As laser, CW, accelerated ageing effect on optical props. 77−38898
AlGaAs laser, monolithic integration with amplifier/detector by twin-guide struct. 78−42466
AlGaAs laser array on Si heat sink, optical power detection 80−74383
AlGaAs laser array with Si detector array for stabilization 80−58817
AlGaAs laser diode, interference and polarisation characts., using single mode fibre cable 79−81535
AlGaAs laser mode, fractional spontaneous emission coupling, power fraction, expt. evaluation 79−959
(AlGa)As laser system, VPE growth and degradation mechanisms 80−99748
AlGaAs lasers, CW high-power single-mode constricted DH lasers with large optical cavity 80−64076
(AlGa)As lasers, facet protection using SiO_2 sputter deposition 79−81444
AlGaAs lasers, relaxation oscillation rel. to carrier diffusion length, spontaneous emission 80−32986
AlGaAs layer, epitaxial, grown from pre-heated Ga soln., photolum. study 78−39591
AlGaAs leaky-mode buried heterostruct. injection lasers 77−68209
AlGaAs mode-locked diode laser, optical pulse generation 80−95907
AlGaAs multimode laser, longitudinal modes intensity fluctuations effect on high bit-rate optical transmission 79−68415
(AlGa)As oxide-defined strip lasers, self-sustained oscillations, ageing effects 80−32991
AlGaAs p-n diodes, I-V characts., tunnelling 80−100510
AlGaAs pulse modulate DH laser, oscillatory longitudinal mode competition 79−81427
AlGaAs resonant laser amplifier, gain and saturation power 80−53315
AlGaAs rib waveguides, characts. 80−33177
(AlGa)As self-pulsing junction laser, saturable absorpt. effects 79−72568
AlGaAs semiconductor lasers, single-mode stabilisation by traps 80−95893
AlGaAs, strip buried heterostruct. laser, linear light-current characts. 78−37908
(AlGa)As strip buried heterostructure lasers, mode locking using external cavity 80−91791
(AlGa)As, stripe geometry DH laser, emission nonlinearities 77−685
(AlGa)As stripe geometry, proton-bombardment delineated DH laser, lifetime 80−106520
AlGaAs stripe-geometry DH laser, filament displacement and refr. losses 80−58536
AlGaAs transverse junction stripe lasers, single longit. and fund. transverse mode oscill. 78−22124
(AlGa)As, transverse junction stripe single mode oscillating laser, gain spectra 78−55356
AlGaAs transverse junction stripe laser with distributed Bragg reflector 80−106535
AlGaAs tunnel diode, fabrication and appl. in cascade solar cell struct. 80−35682
AlGaAs twin guide struct., monolithic integration of laser and laser amplifier or detector 78−38082
(AlGa)As, visible CW heterojunction laser diodes, room temp. operation 77−38895
AlGaAs, Zn diffused window structure laser, high optical power density emission 79−98394
p- (AlGa)As:Zn, MBE grown, elec. props., shallow junction solar cell use 79−91175
AlGaAs/GaAs monolithic series-connected solar cell arrays 80−97794
(AlGa)As-GaAS DH lasers prep. by new LPE technique 77−40358
AlGaAs-GaAs, DH laser material, singular instabilities of LPE growth surface 77−24969
AlGaAs-GaAs, DH laser, with bent guide of planar struct. 78−1256
AlGaAs-GaAs, DH semiconductor laser, influence of struct. parameters on lasing characteristics 79−45942
AlGaAs-GaAs, double heterostructure, optically induced dislocation glide, cooperative phenomena 78−74911
(AlGa)As-GaAs, large area high efficiency solar cell fabrication, LPE process 77−36410
AlGaAs-GaAs, TJS laser, single-mode oscill. with low threshold currents, optical communication appl. 80−14355
AlGaAs-GaAs CW injection heterolaser, single freq., tunable by external dispersive resonator 80−28236
AlGaAs-GaAs cascade solar-cell structure, fabrication and characteristics 79−43758
AlGaAs-GaAs concentrator solar cells of high-efficiency characts. 79−48125
AlGaAs-GaAs DH injection laser, emission energy, wavelength depend. in strong mag. fields 80−48248
AlGaAs-GaAs DH laser, bent-guide struct. 77−75544
AlGaAs-GaAs DH lasers, accel. life test 77−79828
AlGaAs-GaAs DH laser, impurity effects on relaxation oscillations 78−13710
AlGaAs-GaAs DH laser, impedance meas. 78−17939
AlGaAs-GaAs DH lasers, multipeak freq. response obs. 78−17940

aluminium compounds continued
AlGaAs-GaAs DH laser, carrier leakage, physical mechanisms 78−66824
AlGaAs-GaAs DH lasers, accelerated life test 78−66830
AlGaAs-GaAs DH lasers, coupling efficiency between gain-induced guides 79−23094
AlGaAs-GaAs double heterostructure laser lifetime, point defect generation model calcs. 80−32992
AlGaAs-GaAs heteroepitaxial wafers, Mg doping, surface morphology and photoluminesc. props. laser applics. 77−3591
AlGaAs-GaAs heterostructure, minority carrier lifetime, photon recycling effect *(Japanese)* 79−42556
AlGaAs-GaAs heterostructures, luminescent characts., efficiency and radiative lifetime conc. depend. 80−55151
AlGaAs-GaAs injection laser, spectral band homogeneous broadening and narrow band emission 79−98364
AlGaAs-GaAs lasers, defects and degradation *(Japanese)* 79−31899
AlGaAs-GaAs lasers for optical fibre transmission, defects and degradation 79−41382
AlGaAs-GaAs multimode laser, intensity fluctuations in each longit. mode 77−75512
AlGaAs-GaAs proton irradiated solar cells, deep level defects and recombination parameters 80−94032
AlGaAs-GaAs remote junction heterostructure laser, recomb. enhanced annealing effect 79−98355
AlGaAs-GaAs ring laser, injection type, laser oscill. 77−75570
(AlGa)As-GaAs solar cells, theoretical perform. of multi-layer grid patterns 80−55846
AlGaAs-GaAs transverse mode stabilised plano-convex waveguide laser made by single step LPE 80−48274
AlGaAs-GaInAs cascade solar cells, AM 0-AM 5 spectra, anal. 79−79396
$Al_{0.25}Ga_{0.75}As$, optically oriented electron, nuclear spin systems, local anisotropy effects on states, resonances *(Russian)* 78−43679
n-$Al_{0.3}Ga_{0.7}As$, layer of (AlGa)As DH laser, deep levels 78−46605
$Al_{0.3}Ga_{0.7}As$:Te(SN), impurity effects on interface morphology of LPE films on corrugated GaAs substrates 78−88435
$Al_{0.3}Ga_{0.7}As$-GaAs DH mesa stripe laser, metalorganic VPE growth and characterisation 79−98391
$Al_{0.35}Ga_{0.65}As$-GaAs cascade solar cell structs., spectral response and junction characts. 80−93926
$Al_{0.35}Ga_{0.65}As$-GaAs N-p heterojunction diodes, current suppression by cond. band discontinuity 80−80362
$Al_{0.36}Ga_{0.64}As$, LPE films, Te-induced defects 78−43037
$Al_{0.4}Ga_{0.6}As$:Te, saturable optical absorpt. of deep Te-complex centre 79−99917
$(Al_{0.42}Ga_{0.58})As$, LPE grown layer, optical absorpt. coeff. meas. 78−6801
$Al_{0.42}Ga_{0.58}As$-GaAs-$Al_{0.42}Ga_{0.58}As$, etalon, optical bistability and modulation 80−58628
$Al_{0.5}Ga_{0.5}As$, first order phonon spectrum replicas 78−60467
$Al_{0.5}Ga_{0.5}As$:O insulator layers on GaAs, meas. of MIS capacitors 78−95371
$Al_{0.5}Ga_{0.5}As$:O surface layer, on GaAs p-n junction, surface recomb. current reduction 80−49878
$Al_{0.5}Ga_{0.5}As$-GaAs heterojunction phototransistors, growth by metalorganic vapour deposition 79−67380
$Al_{0.5}Ga_{0.5}As$-GaAs minimum heterojunction width determ. by sputter Auger techniques, interface broadening 79−69586
$Al_{0.7}Ga_{0.3}As$ layers, diffusion of Zn, comparison with GaAs 78−26589
$Al_{0.93}Ga_{0.07}As$-GaAs monolithic series-connected solar cell array 80−7939
$Al_{1-x}Ga_xAs$ laser, transverse junction stripe, with low threshold current and high efficiency 78−82985
$Al_{1-x}Ga_xAs$, transient-mode LPE on GaP 78−72746
$Al_xGa_{1-x}As$ CSP laser, analytical waveguide study 79−10302
$Al_xGa_{1-1}As$ heterojunction LED monolithic matrix fabrication 79−56301
$Al_xGa_{1-x}As$, analytic approx. for Fermi energy 78−63973
$Al_xGa_{1-x}As$ and GaAs planar local struct. synthesis by LPE 79−56097
n-$Al_xGa_{1-x}As$, Au-based ohmic contacts TEM obs. 80−34509
$Al_xGa_{1-x}As$ buried heterostruct. laser, fabrication, optical props. and reliability 80−53322
$Al_xGa_{1-x}As$ CW heterolaser, 10000 hr. lifetime tests, degradation of mirror surfaces 80−106542
$Al_xGa_{1-x}As$, CW low threshold, high efficiency injection laser props. 78−22126
$Al_xGa_{1-x}As$ CW multiwavelength TJS laser, MBE, single-longitudinal modes 80−64049
$Al_xGa_{1-x}As$, compensated, electron mobility temp. depend. 80−96868
$Al_xGa_{1-x}As$, cryst. growth by MBE 78−39707
$Al_xGa_{1-x}As$, DH, defect generation in active regions at high optical excitation rates 79−23845
$Al_xGa_{1-x}As$ DH, origin of $n \simeq 2$ injection current, photolum. expts. 78−14799
$Al_xGa_{1-x}As$ DH laser, threshold current, stripe width influence 77−61952
$Al_xGa_{1-x}As$ DH laser, linear light output power depend. on effective gain width 77−75553
$Al_xGa_{1-x}As$ DH laser, accelerated ageing and uniform mode of degradation 77−83874
$Al_xGa_{1-x}As$ DH laser, with constricted active region, fabrication and characts. 78−37895
$Al_xGa_{1-x}As$ DH laser, rake-line form. in LPE growth, doping effects 80−2287
$Al_xGa_{1-x}As$ DH laser diodes, temp. rise under transient state conditions 77−68211
$Al_xGa_{1-x}As$ DH laser material, Ar laser induced catastrophic damage 79−86178
$Al_xGa_{1-x}As$ DH lasers, deep-level luminesc. 79−65913
$Al_xGa_{1-x}As$ DH lasers continuously operated, with 70°C lifetimes as long as two years 78−17952
$Al_xGa_{1-x}As$ DH p-n junction, surface recomb. effects on current, luminesc. expts. 78−72246
$Al_xGa_{1-x}As$ DH stripe-geometry lasers, degraded, capacitance spectroscopy 77−14715
$Al_xGa_{1-x}As$ DH superluminesc. diode, with unpumped region, time-delayed laser oscill. 77−54711
p-$Al_xGa_{1-x}As$, DH under optical orientation conditions, diffusion of spin labelled electrons 77−8189

aluminium compounds continued
$Al_xGa_{1-x}As$, DX photocond. centres, photocapacitance and DLTS meas. 80−11044
$Al_xGa_{1-x}As$, defect state identification associated with Ga vacancy 77−69269
$Al_xGa_{1-x}As$, dependence of energy spectrum of levels introduced by electron irrad. on composition 79−60766
$Al_xGa_{1-x}As$ double heterostructure laser, CW optical power 77−14716
$Al_xGa_{1-x}As$ double heterostruct. lasers, optical pulsations 79−98354
n-$Al_xGa_{1-x}As$, electrical props. 78−6381
$Al_xGa_{1-x}As$, electron mobility illumination, compensation, space charge regions, carrier scatt. 80−70691
$Al_xGa_{1-x}As$, energy band struct. calc. 78−23019
n-$Al_xGa_{1-x}As$, epitaxial, photolum. emission and excitation spectra 78−76526
$Al_xGa_{1-x}As$ epitaxial diode, neutron and γ-irrad. effects on cathodolum. in SEM 79−11473
$Al_xGa_{1-x}As$ epitaxial film, LPE growth and semi-insulating props. 77−44179
$Al_xGa_{1-x}As$ epitaxial films, microanal. in photoemissive electron microscope 79−16068
n-$Al_xGa_{1-x}As$ epitaxial films, elec. cond. press. depend. 79−56337
$Al_xGa_{1-x}As$ epitaxial film, microstruct., effect on elect. characts. of Schottky diode *(Russian)* 80−107671
$Al_xGa_{1-x}As$, epitaxial growth, orienting substrates effects 77−43444
$Al_xGa_{1-x}As$, epitaxial growth from limited vol. melt 79−70005
$Al_xGa_{1-x}As$, epitaxial layer struct., dislocation etching obs. 77−85095
$Al_xGa_{1-x}As$, epitaxial layer crystn. from soln. in melt, diffusion limited 78−35321
$Al_xGa_{1-x}As$, epitaxial layer, distribution of Te and Ge impurities 78−43046
$Al_xGa_{1-x}As$ epitaxial layers on GaAs, struct. study by scanning Auger electron microscopy 80−80110
$Al_xGa_{1-x}As$, fabrication of mesa-type waveguides by laser irrad. 80−5849
$Al_xGa_{1-x}As$ film, hot photoluminescence spectrum, polarisation depend. 78−31254
p-$Al_xGa_{1-x}As$ film, variable-gap photo-EMF 80−65626
$Al_xGa_{1-x}As$, graded band-gap heterostruct., photo-EMF 79−24072
$Al_xGa_{1-x}As$, graded-gap crystal, voltage-current characteristics 79−69613
$Al_xGa_{1-x}As$ grown by organometallic VPE, luminesc. efficiency 79−78892
$Al_xGa_{1-x}As$, growth of high-resistivity layers by liquid-phase epitaxy 79−70008
$Al_xGa_{1-x}As$, growth of uniform epitaxial layers 77−40393
$Al_xGa_{1-x}As$, Γ-X intervalley junctions 77−4433
$Al_xGa_{1-x}As$, Hall effect measurements to 40 kbar under hydrostatic pressure in piston-cylinder device, 150 to 300K 79−67337
$Al_xGa_{1-x}As$, Hall effect, press. temp. and composition depend. 80−49775
$Al_xGa_{1-x}As$, hetero junction light-emitting diode, construction and performance characts. *(Russian)* 77−85808
$Al_xGa_{1-x}As$ heterojunction laser diode, technology and spectral characts. 77−38885
$Al_xGa_{1-x}As$ heterojunction laser diode, accelerated step-temperature ageing 78−46599
$Al_xGa_{1-x}As$ heterojunction LED, fabrication by negative profiling of substrate and characts. 78−56523
$Al_xGa_{1-x}As$ heterojunction LED 79−28403
$Al_xGa_{1-x}As$ heterostructure laser, improved light-output linearity by antireflective coating 78−17953
$Al_xGa_{1-x}As$ heterostructures, photoelectric convertors of conc. solar radiation 80−12015
$Al_xGa_{1-x}As$, indirect, exciton-phonon coupling, photolum. meas. 79−47511
$Al_xGa_{1-x}As$, indirect-gap, laser oscill. involving N isoelectronic impurities 77−10919
$Al_xGa_{1-x}As$, injection laser, transmitter for fibre optical transmission lines 77−7134
n-$Al_xGa_{1-x}As$, ion implanted films, optical and luminesc. props. 80−60699
p-$Al_xGa_{1-x}As$, LED in red and IR region, multiple-pass heterostruct. 79−19653
$Al_xGa_{1-x}As$, LPE, cathodoluminesc. obs. 78−68565
$Al_xGa_{1-x}As$, LPE, effect of doping on interface morphology 77−81231
$Al_xGa_{1-x}As$, LPE, quantitative analysis by AES 77−89667
$Al_xGa_{1-x}As$, LPE layer, deep levels, photocapacitance obs. 77−15790
$Al_xGa_{1-x}As$, laser, spectral, threshold, power and time characts. 77−715
$Al_xGa_{1-x}As$ laser diode, reliability 80−53320
$Al_xGa_{1-x}As$ laser-alloyed stripe-geometry lasers 80−5745
$Al_xGa_{1-x}As$ layer, LPE, graded bond gap solar cell, composition profile, Rutherford backscatt. 78−76612
$Al_xGa_{1-x}As$ layers, graded band gap, growth and properties 79−60645
$Al_xGa_{1-x}As$, lower conduction band struct. 78−6270
$Al_xGa_{1-x}As$, MBE grown film, in situ surface characterisation by RHEED, SIMS and AES 77−43410
$Al_xGa_{1-x}As$ MBE layers, ionized beam doping, elec. and optical characts. 79−37721
$Al_xGa_{1-x}As$, metalorganic-CVD, photopumped laser operation meas. GaAs quantum well 79−10303
$Al_xGa_{1-x}As$, method for determ. of liquidus surfaces in Ga-Al-As phase diagram 77−28787
$Al_xGa_{1-x}As$, mode-stabilised injection laser, longitudinal-mode behaviour 79−962
$Al_xGa_{1-x}As$, modified-strip buried-heterostructure lasers, CW electro-optical properties 80−74359
$Al_xGa_{1-x}As$, monolithic optical integration for new devices 77−75714
$Al_xGa_{1-x}As$ native oxide, low leakage, MOS characterisation 78−91795
n-$Al_xGa_{1-x}As$, nonradiative donor related defect centre obs. 78−23497
$Al_xGa_{1-x}As$, optically magnetised, luminescence polarisation anisotropy, hysteresis effect symmetry props. 80−34982
$Al_xGa_{1-x}As$, organometallic VPE growth, and characterisation 79−78899
$Al_xGa_{1-x}As$ oxidised AlAs as multidielectric for GaAs MIS devices 79−65333
$Al_xGa_{1-x}As$, p-n homojunction, hot carrier recomb., overheating luminesc. 78−92122
$Al_xGa_{1-x}As$ p-n junction, photolum. and current, interface recomb. effects 78−95346

aluminium compounds continued

- $Al_xGa_{1-x}As$, p-n junction solar cells, effect of interface recombination on photoluminescence and current 80—93893
- $Al_xGa_{1-x}As$, point defects, recomb. enhanced interactions with dislocation networks 79—60398
- $Al_xGa_{1-x}As$, press. coeff. of direct band gap from optical absorpt. meas. 80—11430
- $Al_xGa_{1-x}As$ pulsating DH laser, spectral broadening 80—23686
- $Al_xGa_{1-x}As$, pure and Ge doped, shallow acceptor photoluminescence 80—76064
- $Al_xGa_{1-x}As$, Raman spectroscopy, characterisation of thin films and heterostructures 78—76439
- $Al_xGa_{1-x}As$, resistor pressure sensors 79—2756
- $Al_xGa_{1-x}As$ semitransparent photocathode, LPE, quantum efficiency spectrum 80—76153
- $Al_xGa_{1-x}As$ solar cell, intermediate wavelength conversion for operation with concentrators 79—70451
- $Al_xGa_{1-x}As$, solid soln., controlled electrochemical and selective etching, integrated optics appl. 77—14814
- $Al_xGa_{1-x}As$ solid soln., epitaxial layer growth on GaAs by zone recrystallisation with temp. gradient 77—16510
- $Al_xGa_{1-x}As$, solid soln., synthesis by ion implantation Al^+ ions 78—38741
- $Al_xGa_{1-x}As$ stripe geometry DH lasers, proton bombarded, intensity pulsations 79—94235
- $Al_xGa_{1-x}As$, temp. coeff. of resistance of pressure sensors 79—6108
- $Al_xGa_{1-x}As$ thick epitaxial layer production, by zone recrystn. in temp. gradient 79—15619
- $Al_xGa_{1-x}As$ thin graded band-gap layers, isothermal LPE growth 80—34325
- $Al_xGa_{1-x}As$, transverse mode stabilized injection lasers 78—29964
- $Al_xGa_{1-x}As$ triggerable semiconductor lasers made by deep proton bombardment 80—69408
- $Al_xGa_{1-x}As$, VPE, recent advances, book contrib. 79—66011
- $Al_xGa_{1-x}As$, VPE and LPE growth, electron mobility 79—91165
- $Al_xGa_{1-x}As$, VPE growth and characterisation 78—35315
- $Al_xGa_{1-x}As$, valence and core level photoemission spectra 79—19973
- $Al_xGa_{1-x}As$ variable gap junction, photosensitivity 78—39204
- $Al_xGa_{1-x}As$ variable gap thin structs., radiative recomb. photoluminesc. spectra 79—43036
- n-$Al_xGa_{1-x}As$, variable-gap crystal, magnetoresistance 78—34850
- n-$Al_xGa_{1-x}As$, variable-gap solid solns., diffusion length, photolum. meas. 79—38659
- $Al_xGa_{1-x}As$, waveguide heterostruct. epitaxial growth with gradual composition change 79—42416
- $Al_xGa_{1-x}As$:Sn(Te), persistent photocond., due to donor-related centres, symmetry 80—15558
- p-$Al_xGa_{1-x}As$:Be layer, MBE growth, Be doping and diffusion 77—51397
- $Al_xGa_{1-x}As$:Cr, deep level props. 79—69465
- $Al_xGa_{1-x}As$:Cr, exptl. verification of Cr^{2+} models of photoluminescent transitions 78—27320
- $Al_xGa_{1-x}As$:Cr, high resist. film, photolum. and photocond. meas. 78—72596
- $Al_xGa_{1-x}As$:Cu, variable-gap semicond., impurity props., carrier recomb. 80—96907
- $Al_xGa_{1-x}As$:Cu(Ag)(Au), LPE film, impurity levels, elec. and optical props. meas. 78—26862
- p-$Al_xGa_{1-x}As$:Ge layer on GaAs substrate, Hall and elec. cond. meas., Hall mobility 80—2402
- p-$Al_xGa_{1-x}As$:Ge-p-GaAs:Ge-n-GaAs:Sn heterostructure solar cells, LPE growth techniques 80—66977
- $Al_xGa_{1-x}As$:Ge(Te)(Zn), photo- and cathodolum., comp. depend. *(Russian)* 77—48215
- $Al_xGa_{1-x}As$:Mg doping characteristics, elec. props., effective hole masses 79—78117
- $Al_xGa_{1-x}As$:Mn epitaxial layers, Mn-O association, EPR meas. 77—69677
- $Al_xGa_{1-x}As$:N, indirect band-gap, visible laser oscill. at 77K 77—79820
- $Al_xGa_{1-x}As$:N, ion implantation, in situ annealing photoluminesc. obs. 80—10567
- $Al_xGa_{1-x}As$:N, luminescent material, appl. in optically pumped lasers and electrolum. diodes *(Japanese)* 77—44069
- $Al_xGa_{1-x}As$:N, photolum. excitation spectra 77—63451
- $Al_xGa_{1-x}As$:N, photoluminesc. and optical absorpt. spectra of N impurity bound-excitons 79—47496
- $Al_xGa_{1-x}As$:N^+, (x=0.58), laser annealing of optically active impurities, photolum. charact. 80—20682
- $Al_xGa_{1-x}As$:O, appl. as insulating layer in MIS struct. 78—64115
- $Al_xGa_{1-x}As$:O-n-GaAs heterojunction for MIS device, capacitance voltage meas. 79—87157
- $Al_xGa_{1-x}As$:Si, charge state of impurity atoms, positron annihilation meas. 78—39062
- $Al_xGa_{1-x}As$:Sn(Te)(Ge), anneal-induced defects, photoluminesc. obs. 79—61422
- $Al_xGa_{1-x}As$:Te, epitaxial film, elec. cond. and Hall coeff. rel. to donor levels 77—24630
- $Al_xGa_{1-x}As$:Te, persistent photocond. trapping centre, donor complex model, photocapacitance meas. 79—65517
- $Al_xGa_{1-x}As$:Zn DH laser, stripe geometry, horizontal transverse mode stabilisation, lasing characts. 77—19313
- $Al_xGa_{1-x}As$:Zn epitaxial layers, composition and Zn carrier conc. 80—25585
- $Al_xGa_{1-x}As$/$Al_yGa_{1-y}As$ heterostructure lasers, prep. characts., and CW reliability 80—58586
- $Al_xGa_{1-x}As$/GaAs heterojunction laser, appl. of stress distrib. calc. for multilayer heteroepitaxial struct. 77—72798
- $Al_xGa_{1-x}As$-$Al_yGa_{1-y}As$ DH superluminesc. diode, for Nd:YAG laser pumping, room temp. CW operation 77—7122
- $Al_xGa_{1-x}As$-Al_yGa_{1-y} DH laser, threshold current temp. depend., potential barrier height influence 80—53296
- $Al_xGa_{1-x}As$-$Al_yGa_{1-y}As$ DH IR-visible (0.89-0.72 μm) MBE grown lasers 80—64058
- $Al_xGa_{1-x}As$-Au interface, Auger depth profiling 77—89657
- $Al_xGa_{1-x}As$-GaAs, CW 300k quantum-well heterojunction laser, optical and injection pumping operation 80—5735
- $Al_xGa_{1-x}As$-GaAs, carrier transport across heterojunction interfaces 79—47158
- $Al_xGa_{1-x}As$-GaAs, DH laser, lateral current confinement by reverse biased junction 77—58339
- $Al_xGa_{1-x}As$-GaAs, DH integrated optics development 80—33240

aluminium compounds continued

- $Al_xGa_{1-x}As$-GaAs, diode pump system for YAG:Nd^{3+} laser 79—41396
- $Al_xGa_{1-x}As$-GaAs, epitaxial heterostructure, influence of defects on diffusive distrib. of group I impurities 78—43045
- $Al_xGa_{1-x}As$-GaAs, heterojunction, interface width, AES obs. 80—20290
- $Al_xGa_{1-x}As$-GaAs, p-n heterojunction laser, low temp. operation 80—1204
- $Al_xGa_{1-x}As$-GaAs, p-n heterostruct. laser, tunnel injection and phonon-assisted recomb. 80—5733
- $Al_xGa_{1-x}As$-GaAs, quantum-well MO-CVD heterostructure lasers, band-filling props. 79—22954
- $Al_xGa_{1-x}As$-GaAs, quantum-well heterostructure laser diode, temp. depend. of threshold current 80—87395
- $Al_xGa_{1-x}As$-GaAs abrupt LPE heterojunction, Auger profiling 77—85101
- $Al_xGa_{1-x}As$-GaAs DH injection laser, active region internal parameters determ., composite resonator use 80—106548
- $Al_xGa_{1-x}As$-GaAs DH laser, short cavity, performance characts. 77—83889
- $Al_xGa_{1-x}As$-GaAs DH lasers, metalorganic CVD growth and performance characts. 80—53312
- $Al_xGa_{1-x}As$-GaAs DH laser diode, I-V characts., variation of ideality factor 80—64027
- $Al_xGa_{1-x}As$-GaAs DH laser operation, phonon contrib. 80—102724
- $Al_xGa_{1-x}As$-GaAs DH photodetector, optical power conversion at 8500 Å and I-V characts. 77—87833
- $Al_xGa_{1-x}As$-GaAs differentially doped heterojunction interface, two-dimens. electron gas obs. 80—49886
- $Al_xGa_{1-x}As$-GaAs heterostructure superlattice, construction of bound states in continuum 77—32076
- $Al_xGa_{1-x}As$-GaAs heterostructure, effect of photon recycling on diffusion length and internal quantum efficiency 77—39929
- $Al_xGa_{1-x}As$-GaAs heterostructure photoluminesc., origin of large dark spots 77—85763
- $Al_xGa_{1-x}As$-GaAs heterojunction, MBE, diffusion across interface, optical annealing expts. 78—2305
- $Al_xGa_{1-x}As$-GaAs heterostructure, nonradiative large dark spots rel. to minority carrier transport 78—9378
- $Al_xGa_{1-x}As$-GaAs heterostructures, nonradiative large dark spots exam. 78—23149
- $Al_xGa_{1-x}As$-GaAs heterojunction photodiodes, high-efficiency fast-response 78—52073
- $Al_xGa_{1-x}As$-GaAs heterostructures, MO-CVD, phonon assisted recomb. and stimulated emission 80—1205
- $Al_xGa_{1-x}As$-GaAs heterostruct. lasers, metallorganic CVD 80—23692
- n-$Al_xGa_{1-x}As$-GaAs heterojunctions, selectively doped, FET 80—80364
- $Al_xGa_{1-x}As$-GaAs heterostructure, quantum-well, hot electrons and phonons 80—84505
- $Al_xGa_{1-x}As$-GaAs heterostruct., varizonal, parameter determ. by photoluminescence method *(Russian)* 80—108291
- $Al_xGa_{1-x}As$-GaAs interface, Auger depth profiling 77—89657
- $Al_xGa_{1-x}As$-GaAs large-quantum-well heterostructures, induced phonon-sideband laser operation 80—95888
- $Al_xGa_{1-x}As$-GaAs laser, made by organometallic CVD, continuous room temp. operation 80—1201
- $Al_xGa_{1-x}As$-GaAs linear-gradient heterostruct., photoelec. props. 79—11205
- $Al_xGa_{1-x}As$-GaAs long life laser, initial degradation, minority carrier lifetime reduction 77—71984
- $Al_xGa_{1-x}As$-GaAs multilayer heterostructures, optical birefringence 78—64422
- $Al_xGa_{1-x}As$-GaAs multilayers, LPE, using addition of GaCl vapour and new boat struct. 79—33950
- $Al_xGa_{1-x}As$-GaAs multiple-quantum-well injection lasers grown by metal-organic CVD, room temp. continuous operation 80—1218
- $Al_xGa_{1-x}As$-GaAs n-n heterojunction, LPE, Auger profiling and absence of rectification 78—95349
- $Al_xGa_{1-x}As$-GaAs n-n heterojunction, interface width determ. 80—49887
- $Al_xGa_{1-x}As$-GaAs phonon-sideband metalorganic-CVD quantum-well heterostructure laser 79—64244
- $Al_xGa_{1-x}As$-GaAs photopumped quantum-well heterostructure lasers grown by metalorganic CVD 79—98390
- $Al_xGa_{1-x}As$-GaAs quantum-well heterostructure laser, metalorganic CVD growth, CW operation 300 to 337K 79—10304
- $Al_xGa_{1-x}As$-GaAs quantum-well heterostructure laser diode, threshold current temp. depend. 80—43331
- $Al_xGa_{1-x}As$-GaAs quantum well heterostructure lasers, operation 80—53292
- $Al_xGa_{1-x}As$-GaAs quantum-well heterostructures, phonon-assisted recomb. and stimulated emission 80—74358
- $Al_xGa_{1-x}As$-GaAs quantum-well heterostruct., exciton in recomb. 80—103990
- $Al_xGa_{1-x}As$-GaAs single-quantum-well heterostructure laser diodes grown by metalorganic CVD, continuous 300K operation 79—50309
- $Al_xGa_{1-x}As$-$GaAs_{1-y}Sb_y$ solar cells, appl. of recomb. vel. at III-V cpd. heterojunctions *(Korean)* 80—54771
- $Al_xGa_{1-x}As$-GaAs-$Al_xGa_{1-x}As$ photopumped quantum-well laser, room temp. CW operation 78—74908
- $Al_xGa_{1-x}As$-GaAs-$Al_xGa_{1-x}As$ quantum well, carrier collection 79—15211
- p-$Al_xGa_{1-x}As$-n-$Al_yGa_{1-y}As$ junction, electrolum. spectra at high press. 77—48246
- p-$Al_xGa_{1-x}As$-n-GaAs heterojunction solar cells, optical characts. study 77—24609
- p-$Al_xGa_{1-x}As$-p-GaAs-n-GaAs heterophotocells, optimal parameters for high solar-excitation level 80—93872
- $Al_xGa_{1-x}As_x$-GaAs, heterojunction photodiode, electric and photoelectric characts. 77—55604
- $Al_xGa_{(1-x)}As$-$Al_yGa_{(1-y)}As$ DH optically pumped laser, room temp. single pass gain 77—75511
- $Al_yGa_{1-y}As$-$Al_xGa_{1-x}As$ laser struct., for integrated optics, MBE 78—13817
- $Al_yGa_{1-y}As$-$Al_xGa_{1-x}As$, electrooptic rib waveguide modulators and switches 78—38046
- AlGaAsP/GaAs heterojunction, X-ray characterisation of defects 78—95239
- AlGaAsP(Sb), compositional grading by LPE 80—10844
- AlGaAsSb LPE growth, lattice-matched to GaSb, characterisation 80—60794
- AlGaAsSb, photodiode, lattice-matched to GaSb 79—71527

aluminium compounds continued
AlGaAsSb-GaSb heterojunction injection laser, radiative props. 1.4 to 1.8 μm range 80—91798
n-AlGaAsSb-GaSb-p-AlGaAsSb binary heterostructure injection laser, room temp. operation 78—9381
$Al_xGa_{1-x}As_ySb_{1-y}$, heterostructure composition profile by photoemission microanalysis 80—44717
$Al_yGa_{1-y}As_{1-x}Sb_x$ heterostructure, electroluminesc., appl. to LED's 77 8663
$Al_yGa_{1-y}As_{1-x}Sb_x$ LPE phase diagram 78—11137
$Al_yGa_{1-y}As_{1-x}Sb_x$, LPE, strain effects near miscibility gap, importance 79—7759
$Al_yGa_{1-y}As_{1-x}Sb_x/GaAs_{1-x'}Sb_{x'}$, buried heterojunction electroabsorption modulator, report of operation 78—38044
$Al_yGa_{1-y}As_{1-x}Sb_x$-$Ga_{1-z}Sb_z$ buried heterojunction electroabsorption modulation 78—55439
$Al_xGa_{1-x}AsZn$-GaAs solar cells by LPE, open circuit voltage, fill factor 80—101108
$Al_xGa_{1-x-y}In_yAs$, LPE on InP, solid-liq. equilib. calcs. 78—84083
$Al_xGa_{1-x}N$ epitaxial layers, growth and props. 79—11522
$Al_{2x}Ga_{2(1-x)}O_3$:Cr^{3+}, luminesc., lifetimes 79—33784
$Al_{1-x}Ga_xP$, IR phonons, lattice reflection spectra 78—51626
$Al_xGa_{1-x}P$, LPE, crystallographic obs. and electrolum. 80—88445
$Al_xGa_{1-x}P$, photoluminescence excitation spectra, bound excitons, Al conc. depend. 80—20687
$Al_xGa_{1-x}P$, proportional ingredient content determ. by X-ray fluoroscopy 80—97747
$Al_xGa_{1-x}P$, solid solutions, refr. index dispersion characts. *(Russian)* 77—81080
$Al_xGa_{1-x}P$, Zn diffusion behaviour, device appls. 77—11741
$Al_xGa_{1-x}P$(:Zn), solution-grown single crysts., photo- and electrolum. at 77K 79—52004
AlGaSb, growth and characts. for 1.0-1.8 μm heterojunction devices 78—6870
p-$Al_xGa_{1-x}Sb$ epitaxial layers, cathodoluminescence. investig. for varying x *(Russian)* 77—20931
$Al_xGa_{1-x}Sb$, LED, 1.54 μm efficient emission at 300K reproducible fabrication 79—42636
$Al_xGa_{1-x}Sb$, method for determ. of liquidus surfaces in Ga-Al-Sb phase diagram 77—28787
$Al_xGa_{1-x}Sb$ mixed crystal, two-phonon absorption meas., 15-48 μm 77—1682
$Al_xGa_{1-x}Sb$, photolum. intensity increase due to composition variation 79—15528
$Al_xGa_{1-x}Sb$, solid soln., epitaxial layer growth from liq. phase 77—85089
$Al_xGa_{1-x}Sb$, solid soln., depend. of forbidden-band width on composition 78—39602
$Al_xGa_{1-x}Sb$ solid soln., electrochem. deposition of Ni and Pd 80—93505
$Al_xGa_{1-x}Sb$ solid solns., freq. dependences of form of luminesc. spectra 80—40160
$Al_xGa_{1-x}Sb$, soln.-grown, photolum. 80—71476
$Al_xGa_{1-x}Sb$, surface flatness depend. on LPE condition 79—15042
$Al_xGa_{1-x}Sb$, vibr. spectra, Raman light scatt. study 80—45080
$Al_xGa_{1-x}Sb$:Zn, impurity diffusion, p-n junction depth 80—24678
$Al_xGa_{1-x}Sb$:Zn(Si)(Ge)(Sn)(Pb), doping of solid solns. during LPE *(Russian)* 77—85087
$Al_xGa_{1-x}Sb$-Pd contacts, struct., preparation elec. props. 80—65684
$Al_xGa_{1-x}Sb$-Pd contacts, band gap depend. of barrier height 80—65685
AlGaSbAs heterostructures and LED's luminesc. props. in 1-2 micron band 78—10988
$Al_2Ge_2O_7$ reduction by C, gaseous and metallic Ge yields *(Russian)* 80—40737
$Al_2Ge_2O_7$, reduction processes by C, kinetic analysis, reaction products *(Russian)* 80—55644
$Al_xGe_{1-x}Sb$, photolum. spectra 78—95602
AlH, (1,1)-band emission of $b^3\Sigma$-$a^3\Pi$ system 78—42092
AlH, $A'\pi$, spectral lifetime and predissociation 79—59515
AlH, pseudopot. calcs. 80—91446
AlH, SCF pot. curves, 0.1-10 Bohr, ground and excited states 78—58610
AlH, valence excited states, pot. curves 78—41973
AlH, vibr. consts. of electronic states, calc. method 79—93967
AlH, $X^1\Sigma^+$ states, many body effects, diagrammatic perturbation theory 77—79547
AlH^+, PNO-CI and CEPA calcs. of electron correl. effects 77—34561
AlH^+ radical cation, EPR matrix isolation obs., hyperfine components calcs. 80—14158
AlH^+, SCF pot. curves, 0.1-10 Bohr, ground and excited states 78—58610
AlH^+, spectrum at 3632 Å, rot. anal. 80—78632
AlH_3, AlH_3^-, ground electronic states and geometries, ab initio calcs. 77—57863
AlH_3, covalent nature of chem. binding, positron annihilation obs. 78—18581
AlH_3, dark electrical cond., exam. 80—39624
AlH_3, effect of 1 MeV Co^{60} γ-irrad. on isothermal decomp. 78—92472
AlH_3, elec. cond. meas., V/I characts. *(Russian)* 77—51752
AlH_3, I-V and relax. characts. in dark cond. 77—85235
AlH_3, localised states spectrum, photosensitivity 79—78135
AlH_3, nucl. spin-spin coupling consts., ab initio calcs. 80—95647
AlH_3, photo-and thermochem. reactions, 200-350K, UV Induced local states 78—31667
AlH_3, photocond., photocurrent carrier-type 78—34855
AlH_3, photocond., reversible processes 79—65516
AlH_3, photoelectric effect spectra and kinetics, photochem. mechanism colour centres 78—56506
AlH_3, photographic processes, thermo- and electrochemical transformations 78—89576
AlH_3, photolysis, luminesc. spectra of adsorbed rhodamine dyes 80—55171
AlH_3, photolytic decomp. using high-intensity UV light 78—92472
AlH_3, polycrystalline, photoconductivity and photochemical decomp. 80—44638
α-AlH_3, prep., thermal decomposition, transform., struct. *(French)* 80—3326
AlH_3, spectral distrib. of photoconductivity and condensed photoeffect before and after illumination *(Russian)* 77—72889
AlH_3, synchronous photochem. processes in lattice 80—101029
AlH_3, thermo-EMF meas. 80—39617
AlH_4^-, AlD_4^-, intramol. force fields, F_2 vibrs., isotope shifts 77—3336

aluminium compounds continued
Al_2H_6, electron density distrib., reaction channels and bonding characts., electrostatic mol. pot. CNDO/2 calc. 80—23309
$Al^{3+}(H_2O)n$ (n=1,2,4,6), FSGO-pair-pot. calcs. *(German)* 80—74278
$AlH(SO_4)_2.H_2O$, cryst. parameters and X-ray powder diffr. data *(French)* 79—14765
$Al(HSeO_3)_3$, synthesis under hydrothermal conditions 77—85918
$AlHfTaO_6$, powder X-ray diffr. data 79—99155
AlI, electronic spectrum, Franck-Condon factors, r-centroids 78—62817
AlI_3, molten, electrical cond., press. effect, 0-1 kbar 78—55963
AlI_3, UV absorbance, dimer-monomer dissoc. equilib., vap. press. of solid 78—13511
$Al(IO_3)_3.8H_2O$, crystal structure, thermal vibr. parameters, X-ray study 80—64979
$AlInS_3$, X-ray cryst. struct. determ. 80—28968
$Al_2In_{12}S_{21}$, dielec. const., temp. depend. 79—82909
$Al_2In_{12}S_{21}$, preparation, struct. and elec. props. 77—59685
$Al_2In_{12}S_{21}$, thermal decomposition 78—20016
$(Al_xIn_{1-x})_2S_3$, x=0-0.33, cryst. struct., X-ray diffr. 79—55710
$Al_xIn_{1-x}Sb$, DC sputtering and struct. 78—52674
$Al_2In_{12}Se_{21}$, cryst. growth from melt, elec. props. 79—56922
$AlK(SO_4).12H_2O$, growth and dissoln. rates 80—50545
$AlM_xH_{1-x}(SeO_3)_2.nH_2O$, M=alkali metal, hydrothermal crystallization, thermal decomp. 77—90265
$AlMgB_{14}$, prep. and electrothermal props. 80—20863
Al_2MgO_4, spinel, dislocations, dissociated, weak-beam technique, appl. *(French)* 79—42070
$Al_3Mg_2[Si_5AlO_{18}]$, cordierite cryst., effect of face symmetry on structural ordering of Al 78—22703
$Al_2Mn_3Si_3O_{12}$ amorphous spin glass, spin dynamics, neutron scatt. meas. 80—15741
$Al_2Mn_3Si_3O_{12}$, amorphous insulating spin glass, susceptibility and magnetisation meas. 80—88765
$Al_2Mn_3Si_3O_{12}$ glass, mag. ordering effects at low temps., Mossbauer and neutron diffr. meas. 77—16047
AlN, $(^2P)Al$-$(^4S)N$, $(^2P)Al$-$(^2D)N$, nonempirical pseudopotential, configuration interaction calcs. 79—93930
AlN, absorpt. edge shape interpretation, Wannier excitons absorpt. in charge impurity elec. field 80—66233
AlN, activating sintering process 80—25639
AlN, asymmetry in displacement energy for Frenkel-pair prod., n-type to p-type conversion 78—2116
AlN, CVD from $AlCl_3/NH_3$, calc. of equilibrium yields 79—52121
AlN, condensates, growth from vapour, morphological comparison with, ZnO, MgO 78—34450
AlN, cpd. form. reaction in reactive evaporation, quadrupole mass analysis *(Japanese)* 78—23628
AlN, creep during hot pressing 78—23650
AlN, cryst. struct. refinement 77—84731
AlN, crystn. from reactive pulse plasma 78—31308
AlN, effect of valence states on X-ray Compton line shapes 77—8682
AlN, epitaxial, refl. spectra, 5-12.5 eV 79—99967
AlN, epitaxial film growth by MBE, physical and optical props. 80—2293
AlN epitaxial films, optical props. in vac. UV region 79—56872
AlN, epitaxial growth, by ammonolysis of $AlCl_3$, thermodynamics 77—8758
AlN, excitation, luminescence, reflection spectra in fund. absorpt. region 78—10956
AlN filamentary crystal reinforced mullite-corundum ceramics, filaments strength, eval. 80—104230
AlN film, CVD, characterisation of film props. 78—43496
AlN film, chemical and plasmachem. vapour deposition, optical and other props. 77—28727
AlN film, epitaxial growth by reactive evaporation *(Japanese)* 78—23629
AlN film, nonlinear optical susceptibility SHG expts. 78—30012
AlN film, optical consts., thickness and surface roughness determ. *(German)* 77—41670
AlN film, oriented c-axis, low temp. deposition by reactive magnetron sputtering 80—76180
AlN film, reactive ion beam sputtering deposition, form. and characterisation 80—44452
AlN film, Si doping by DC glow discharge 78—19674
AlN film, thermodynamics and kinetics of CVD 80—108354
AlN film on Si and Ge, growth, struct. and props. 77—55468
AlN films, RF glow discharge deposited, current-voltage characts. 80—84515
AlN films, RF reactive ion-plating, struct. and morphology 80—104074
AlN films on glass substrate, prep. by reactive DC magnetron sputtering technique, c-axis orientation 80—89146
AlN foil, thickness determ. by TEM using diffr. and energy loss anal. 78—29088
AlN, heteroepitaxial, for SAW and electro-optic device appl., prep. and props., book contrib. 79—83134
AlN, hot pressed, effect of O_2 content on flexural strength and compact density 79—11668
AlN, impurity-doped film, cathodoluminescence spectra 79—83038
AlN, inelastic scattering probabilities for fast electrons in single cryst., orientation depend. 80—2905
AlN, interatomic interactions from XPS 80—49171
AlN, K-shell cross section for 80 kV electrons 79—55798
AlN, luminesc. excitation spectrum and band struct. 80—84783
AlN, nonlinear susceptibilities 79—27312
AlN, photocond., 6-12 eV, prior UV illum. effect, mechanism 77—89796
AlN, physical props. and appls. in integrated optics *(Czech)* 80—28355
AlN, piezoelectric film, low temp. growth by RF reactive planar magnetron sputtering method 80—76175
AlN, plasmochemical synthesis, powder dispersion control 80—55332
AlN, polycrystalline, stress-strain data up to 1.25 GPa 80—100899
AlN powder, effect of O impurity on sintering and thermal cond. *(Japanese)* 79—20017
AlN powder, plasma synthesized, sintering behaviour, props. and struct. 79—100097
AlN powder, plasma-chem. and self-propag. high-temp. thermoplastic slips, synthesis 80—25633
AlN powder, production using Al powder in N plasma with electric discharge 79—33990
AlN powder, synthesis, in low-temp. plasma 80—16257
AlN, powder shock wave compression prior to sintering 77—66615
AlN powders, synthesis and impurities 80—55329

aluminium compounds continued
- AlN, precipitation from gas phase 78—6025
- AlN, precipitation in steel, Fe-Si and Fe-Ni *(French)* 78—23711
- AlN, prep. and charact. of ultrafine powders 80—2983
- AlN preparation technology, powder, thin film and volume crystals *(Czech)* 78—3037
- AlN, reactively sputtered, on GaAs, $Ga_{1-x}Al_xAs$ and $GaAs_{1-x}P_x$ *(French)* 78—23849
- AlN, single cryst. growth by sublimation-recondensation technique 78—31310
- AlN, sputtered deposit, encapsulation of preliminary heated GaAs *(French)* 77—32714
- AlN sputtered layer, GaAs:Si encapsulation, photolum., annealing effects 80—20681
- AlN synthesis, temp. distrib. in plasma-chemical reactor 77—59730
- AlN, thermal cond. and stability at high temp. 78—47610
- AlN thread-like crystals reinforced mullite-corundum ceramics, props. 80—108525
- AlN, ultradispersed powder, IR spectra 80—50312
- AlN, VPE by closed space vapour process, and optical absorpt. edge 78—88371
- AlN, wetting by Ni alloys 78—80710
- AlN whiskers, strength rel. to growth conditions using vapour-liquid-solid method 79—11052
- AlN, X-ray diffuse scattering 80—14964
- AlN, X-ray Kα satellite struct., target chemical effects, 38 MeV F ion bombardment 77—24910
- AlN:Mn, vol. and surface excited luminesc. 79—38630
- AlN:Mn(Eu), luminescence at high excitation levels with and without doping 77—1721
- AlN:O, deep impurity states, orbital spectra, CNDO/2 calcs. 78—6319
- AlN:O, energy spectrum of deep impurity 79—83035
- AlN:O, influence of O on luminesc. excitation spectrum in interband transition range 77—8644
- AlN:O, thermolum. mechanism, 80-420K 79—78761
- AlN:O, UV spectra of deep impurity centres, radiative recombination 79—87490
- $AlN-Al_2O_3$ powders, hot pressing, crystalline phase obs. 78—95720
- $AlN-Al_2O_3$ solid solution, quantitative analysis, use of internal calibration technique developed by AES 77—36834
- AlN-Mo cermets, ZrO_2 and mullite whisker reinforced, strength var. with temp. 80—104232
- $AlN-Si_3N_4$ CVD film preparation and props. 77—77408
- $AlN-Si_3N_4$ mixture film, CVD, characterisation of film props. 78—43496
- $AlN-Si_3N_4-Be_3N_2$ system, phase equilibria 80—60844
- AlN-SiC, solid solns. series rel. to new materials in Si-C-Al-O-N system 78—95159
- AlN+Ni(Co)(Fe), reactions at sintering temps. 79—74377
- Al_3N_4, dispersion in transformer steel for cubic texture formation *(Russian)* 78—80557
- $AlNH_4HP_3O_{10}$, cryst. struct. determ. *(French)* 77—47408
- $AlNH_4(SO_4)_2{:}Cr^{3+}$, optical spectral, crystal field, spin orbit and exciton interactions 80—34958
- $Al(NO_3)_3$, additive to $Cr_2O_3-Mo_2O_3$ catalyst, effect on activity in oxidation of methanol to formaldehyde *(Russian)* 79—66346
- $Al(NO_3)_3$, aq. soln., X-ray diffr. obs. 77—72541
- $Al_{10}N_8O_3$, sublimation growth, cryst. struct. determ. 80—19751
- $Al_9N_7O_3$, sublimation growth, cryst. struct. determ. 80—19751
- $Al(NO_3)_3.9D_2O$, X-irradiated, ENDOR and ESR of radicals 77—50455
- $Al(NO_3)_3.9H_2O$, cryst., deuteration rel. to NO_3^- ion vibr. spectrum *(Russian)* 77—40240
- $Al(NO_3)_3.9H_2O{:}Fe^{3+}$, nucl. level hyperfine struct., reson. RF field effect *(Russian)* 77—77133
- $AlNbO_4$, diffuse refl. and luminesc. spectra 78—56516
- $AlNbO_4$, polycrystalline, thermal diffusivity, effect of microcracking 78—26743
- $Al_2Nb_2O_7$, new phase of mixed oxide 78—59787
- AlO, A-X transition, Franck-Condon factors computation, iterative method compared with Langer's method 78—86762
- AlO, $B^2\Sigma-X^2\Sigma$, Einstein A coeffs., band strength and band oscillator strength 80—43113
- AlO, $D^2\Sigma-X^2\Sigma$, Franck-Condon factors and V-centroids *(Russian)* 78—74642
- AlO, Franck-Condon factors, rot. quantum number effect 79—31613
- AlO, Franck-Condon factors and r-centroids for $D^2\Sigma-X^2\Sigma$ transition 79—94037
- AlO, ground state, pot. energy curve, dissoc. energy 78—46286
- AlO, ground state dissoc. energy, normalised temp. method *(German)* 77—476
- AlO, in $Al+O_3(N_2O)$ chemilum., perturbations and vibr. population anomalies obs., mechanism 77—63917
- AlO, in arc, normalised temperature, localised emission, aureoles *(German)* 77—62413
- AlO radical, ground state dissoc. energy 80—53159
- AlO, spectra, vibr. consts., pot. curves, Franck-Condon factors and r-centroids 78—42243
- AlO stellar IR bands rel. to Mira phenomena 78—69801
- AlO_2 molecule, mass spectrometric study 80—89563
- Al_2O_2, thermochem. evidence rel. to mol. structure 77—38738
- $Al_2O_2-SiO_2$, mullite 2:1 cryst., dielectric tensor components 77—48142
- Al_2O_3 anodic film peak voltage rel. to ellipsometric thickness 77—77597
- Al_2O_3, ion implantation for radiation damage studies 77—80530
- Al_2O_3-AlN phase diagram and reaction sintering of transparent cubic ALON spinel 80—25669
- $Al_2O_3-Ln_2O_3$, Ln=La,Ce,Pr,Nd,Sm,Gd,Tb, struct. and thermal characts. of amorphous phases *(French)* 77—72558
- $Al_2O_3-SiO_2$ system, andalusite and kyanite powders, shock induced transformations 80—45301
- Al_2O_3-TiC sinter products, grain size meas. by combination etching process 79—74331
- $Al_2O_3-UO_2$, differential thermal anal. of irradiated material 79—62484
- AlOH→HAlO system, intramol. rearrangement, ab initio calc. of pot. surfaces and min. energy paths, geom. parameters 80—32623
- $Al(OH)_3$, (gibbsite), crysts., vibr. spectra, approx. calc. method *(Russian)* 78—35148
- $Al(OH)_3$ based ceramics containing Mn and Ti compounds, sintering and paramag. props. 77—21069
- $Al(OH)_3$, coprecipitated with $Cr(OH)_3$ gel, magnetic, optical studies, calcination 79—47995
- $Al(OH)_3$, derived from metalalkoxides, sintering behaviour 79—29005

aluminium compounds continued
- $Al(OH)_3$, from Al etching wastes, firing to prod. corundum ceramics 80—108376
- $Al(OH)_3$, precip. from solns. containing Li ions, X-ray diffr. patterns and comp. determ. 80—76502
- $Al(OH)_3$, unit cell, determinantal eqns. for scale factor, temp. factors, quantitative chem. contents 78—75609
- $Al(OH)_3{:}Fe^{3+}$, thermal decomposition, EPR obs. 78—40047
- $Al_x(OH)_y$, Raman spectra using pulsed laser and gated detection 77—74529
- $Al(OH)_xCl_{3-x}$, soln., IR spectra 78—74649
- $Al_2O_3(H_2O)_3$, gibbsite, synthetic, crystallinity and topotactic reactions, X-ray diffr. obs. 78—63851
- $Al_2(OH)_4(SO_4).7H_2O$, aluminite, cryst. struct. determ. and refined 78—83782
- AlO_xN_y spinel, crystal struct. model 78—91333
- γ-AlOOD, boehmite, hydrogen bond, neutron profile refinement of struct. 78—71701
- γ-AlOOH and γ-AlOOD, IR and Raman spectra obs., struct. and $D_{2h}{}^{17}$ space group anal. 80—89000
- γ- AlOOH, boehmite, dehydration to γ-Al_2O_3 80—21277
- γ-AlOOH, boehmite, lattice vibrs., evidence for $C_{2\nu}{}^1{}_2$ space group 79—28756
- γ-AlOOH, boehmite, proton pair obs. from NMR absorpt. spectra 80—75866
- γ-AlOOH, boehmite, structural variability 78—38681
- AlOOH, diaspore, cryst. struct. refinement and electron density distrib. 80—79758
- Al-AlOOH, disapore, superstructure form. on dehydration, electron microscopy obs. 80—3327
- $Al(OOH)_3$, formed by reaction of methyl esters and $Na_2Al_2O_2$, exam. of props. 78—48346
- Al_2O_3.Si kyanite, dislocation dissociation 77—76412
- $Al_2O_3.3P_2O_5.5H_2O-SiO_2$ composite, binding and struct. 79—66030
- AlP, APW calc. of electronic structure and optical props. 79—99479
- AlP, ground state of electron subsystem, quasimolecular model 79—69055
- AlP, multiple pulsed double NMR and nucl. spin dynamics 77—16208
- AlP, semicond., ^{31}P nuclear mag. shielding 79—33549
- AlP(As)(Sb), avalanche breakdown voltage for p-n junction, calc. 78—88020
- AlP(As)(Sb), refractive index dispersion 79—24280
- AlP(As)(Sb), surface (110), energy distrib. of dangling-orbital surface states 80—80347
- AlPO cristobalite form, polymorphic transform. investig., X-ray diffr. and IR spectra 77—4199
- $Al(PO_3)_2$, vitreous, microhardness 80—25864
- $Al(PO_3)_3$, vitreous struct. 78—26443
- $Al(PO_3)_3-BaF_2-Al_3$ glasses, opt. props., group I-III fluorides effect 80—66143
- $Al(PO_3)_3$-NaF system, glasses, IR spectra and struct. 79—65882
- $Al(PO_3)_3$-NaF system glasses, microhardness and US vel. 79—99274
- $Al(PO_3)_3$-NaF-LiF glasses, mixed-alkali effect 80—19715
- $AlPO_4$, amorphous, struct. determ. by radial distrib. functions derived from X-ray diffr. 77—43151
- $\alpha AlPO_4$ as SAW substrate material, piezoelec. props. 80—80710
- $AlPO_4$, α-β cristobalite phase transition, Raman meas. 79—4799
- α-$AlPO_4$, berlinite, H_2O conc. determ. by Raman scatt. 80—76572
- $AlPO_4$, berlinite, material for SAW devices 79—56735
- $AlPO_4$, berlinite, piezoelectric coupling for SAW applications 79—56055
- α-$AlPO_4$, berlinite, SAW props. 78—79871
- α-$AlPO_4$, berlinite, SAW velocity and piezoelec. coupling obs. 79—56056
- α-$AlPO_4$, berlinite, surface skimming bulk wave theory 79—56064
- α-$AlPO_4$, berlinite, temperature-compensated surface and pseudo-surface acoustic wave props. 77—51584
- $AlPO_4$, berlinite, temperature-compensated cuts for SAW devices 78—60018
- α-$AlPO_4$, berlinite, X-axis boule cut SAW props. 79—56061
- $AlPO_4$ crystal, P K-band X-ray emission spectra, state anal. 80—40190
- α-$AlPO_4$ crystal, totally symm. high-freq. fund. vibrs., identification refinement 80—100656
- $AlPO_4$ high piezoelectric coupling temp. compensated cuts for SAW devices 78—13869
- $AlPO_4$, high temp. behaviour up to liq. state, phase relations, X-ray diffr. and therm. anal. study *(French)* 80—10660
- $AlPO_4$, high-low cristobalite transitions, DTA meas. 79—82335
- $AlPO_4$, hydrothermal synthesis 78—48297
- $AlPO_4$ hydrothermal synthesis 78—60562
- α-$AlPO_4$, IR and Raman spectra, optical phonons 80—2767
- $AlPO_4$, low quartz struct., charge density refinement, use of elec. field gradient calcs. 79—73480
- $AlPO_4$, negative muon capture, rel. probability meas. 77—50550
- $AlPO_4$ solubility, in H_3PO_4 hydrothermal soln., conditions for cryst. growth *(French)* 79—77539
- $AlPO_4$, synthetic berlinite, electron irrad. effects, ESR, ENDOR, optical spectral study 80—80608
- $AlPO_4$, twinning and phase transform., X-ray diffr. obs. 77—47466
- $AlPO_4$, vibr. normal modes, rel. to α-quartz phonon dispersion curve 78—75750
- $AlPO_4$, XPS of cryst., inner shell binding energies of elements 79—43092
- $AlPO_4{:}Fe^{3+}$, EPR, α-β phase transition 77—90016
- $AlPO_4{:}Fe^{3+}$, luminesc. emission and excitation spectra 79—69873
- $AlPO_4-Al_2O_3$ system, oxyorthophosphates form. 79—78942
- $AlPO_4-Cr_2O_3$, system, oxyorthophosphates form. 79—78942
- $AlPO_4-Y_2O_3$, system, oxyorthophosphates form. 79—78942
- $AlPO_4.2H_2O$, XPS of cryst., inner shell binding energies of elements 79—43092
- $AlPO_4.2H_20$, cryst. struct., X-ray diffr. 77—19924
- AlS, $B^2\Pi-X^2\Sigma^+$ transition, assignment of UV bands, vibr. and rot. anal. 80—58278
- Al_2S_3, as ice nucleating material 78—49093
- α-Al_2S_3, prep. by direct sulphidation, chem. vapour transport and AlI_3 flux growth 79—43118
- Al_2S_3, X-ray Kα satellite struct., target chemical effects, 38 MeV F ion bombardment 77—24910
- $Al_2(SO_4)_2\ (NH_4)_2SO_4.24H_2O$, crystn. kinetics in an MSMPR crystalliser 80—100185
- $Al_2(SO_4)_3$, decomposition, charact. of gaseous and solid products 78—44374
- $Al_2(SO_4)_3\ K_2SO_4.24H_2O$, formation, survival and growth of nuclei from secondary nucleation 80—50540

aluminium compounds continued
$Al_2(SO_4)_3$ soln., adiabatic and apparent molal compressibility determ. from US vel. meas. 78—63797
$Al_2(SO_4)_3+Sc_2(SO_4)_3$ aq. solns., complex form. reacts., kinetics, US relax. investig. 79—1942
$Al_2(SO_4)_3K_2SO_4.2H_2O$, growth and growth dispersion 80—49148
$Al_2(SO_4)_3K_2SO_4.2H_2O_7$ small cryst. growth 80—50543
$Al_2(SO_4)_3K_2SO_4.24H_2O$, secondary nucleation rate under agitation 80—50541
$Al_2(SO_4)_3(NH_4)_2SO_4$ or $AlNH_4(SO_4)_2.12H_2O$, size dependent growth systems, effective nucleation rate 80—38972
$Al_2(SO_4)_3.K_2SO_4.24H_2O$, spirals, growth and dissolution from liq. state 80—15027
$Al_2(SO_4)_3.17H_2O$, precipitated from acetic acid soln., thermal decomposition 79—91934
AlSb (110), surface struct., EPR meas. and elastic energy minimisation calcs. 79—51405
AlSb (110), wave functions and surface struct. 78—91519
AlSb, APW calc. of electronic structure and optical props. 79—99479
n-AlSb, acoustoelectric effect due to piezoelectrically active wave 80—80331
AlSb, amorphous, localised gap states, hopping cond. and chem. bonding 78—23052
AlSb as high-energy photon detector 77—75026
AlSb film, laser-induced metal-semicond. transition in Al-Sb mixed film 80—6661
AlSb, gravitational influences on liquid-state homogenisation and solidification 79—78864
AlSb, indirect exciton dispersion, ‘camel’s back’ 79—73447
AlSb, laser pulse annealing, induced nucleation, crystal growth 80—84966
n-AlSb, many-valley semicond. anisotropic acoustoelectric effect, thermo-EMF anisotropy fluctuation depend. on ultrasound freq. 79—69562
AlSb, molten, temp. depend. of vel. of sound and adiabatic compressibility 77—27944
p-AlSb, saturation characts. over CO_2 laser spectrum 80—83646
AlSb Schottky barrier solar cells, characteristics and efficiency of Czochralski-grown crystals 80—61366
AlSb solar cell material, epitaxy, ionicity and bond struct. 80—61367
AlSb, thin film growth on insulating substrates, by metal organics CVD 80—60786
AlSb-Bi system, molten, enthalpy change due to mixing *(German)* 79—86892
AlSb-CdTe, phase diag. 77—52299
AlSb-InSb(GaSb), liq., mixing enthalpies *(German)* 79—77755
$Al_{1-x}Sb_x$, amorphous, localised gap states, variable range hopping 77—72866
$(AlSb)_x(GaSb)_{1-x}$, solid soln., LPE 77—40392
AlSe, $A^2\Sigma^+$-$X^2\Sigma^+$ transition, rot. anal. 79—72325
$Al_2(SeO_3)_3.6H_2O$, synthesis under hydrothermal conditions 77—85918
α-Al_4SiC_4, $Al_4Si_2C_5$, X-ray crystallographic data 80—49197
$Al_4Si_2C_5$, synthesis, X-ray diffraction pattern, lattice constants 80—50581
Al_2SiO_5, andalusite, phonon spectra and rigid-ion model calcs. 80—11391
Al_2SiO_5, EPR of Fe^{3+} at V-band and the pair spectra 78—80204
Al_2SiO_5, kyanite, sillimanite, mullitisation, effect of gaseous atm. 79—11604
Al_2SiO_5 polymorphs (sillimanite-andalusite-kyanite), thermal expansion and high-temp. cryst. chemistry 80—39319
Al_2SiO_5, sillimanite and andalusite, elastic constants, cryst. struct. 79—60422
Al_2SiO_5, solid state reaction with $Ca_2P_2O_4$ *(Japanese)* 78—19702
Al_2SiO_5:Fe^{2+}, andalusite travelling wave maser in 40 to 46 GHz freq. range *(Ukrainian)* 80—53246
Al_2SiO_5:Fe^{3+}, spin lattice relax. 77—73076
Al_2SiO_5:Fe^{3+} appl. of sensitive EPR spectrometer to zero field splitting determ. *(Russian)* 77—57372
Al_2SiO_5:Fe^{3+} crystals, andalusite, spin-lattice relaxation, lattice oscillator heating 78—23329
$Al_6Si_2O_{13}$, mullite, crystal growth by floating zone method using thermal imaging system 77—77373
$Al_6Si_2O_{13}$:Fe^{3+}, mullite:Fe^{3+}, Mossbauer exam. of relaxation behaviour of Fe^{3+} 77—1620
$Al_2SiO_4F_2$, topaz, thermolum. props., dosimeter appl. 78—35957
$Al_4Si_4O_{10}(OH)_8$, kaolinite dispersion, adsorbed water, PMR exam. *(Russian)* 78—35058
$AlSiP_2$, wurtzite-pyrite intergrowth struct. 79—60328
$Al_{0.23}Te_{0.77}$, amorphous semicond., radial distrib. anal. by X-ray diffr. 78—71678
$Al_{23}Te_{77}$ glasses, crystallization 79—51000
Al_2TeO_6:U^{6+}, luminesc. spectrum 79—56845
Al_2TiO_5, eutectoid decomposition, kinetic study *(Japanese)* 77—55941
Al_2TiO_5, grain size pseudobrookite oxide, microcracking relations 79—29194
Al_2TiO_5 powders, decomposition kinetics using nucleation and growth-rate constants *(Japanese)* 80—35156
Al_2TiO_5, sinterability improvement by partial decomposition 79—28994
Al_2TiO_5, sintering and annealing effect on decomposition *(Japanese)* 79—87606
$AlTiTaO_6$, powder X-ray diffr. data 79—99155
$AlVO_4$, luminesc. spectrum 79—56846
θ-$Al_{0.35}V_2O_5$, NMR of ^{51}V 80—71232
$Al_{0.35}V_2O_5$, spin glass phase, low temp. mag. susceptibility meas. 80—29565
Al_xVO_2, reduced, microstruct., crystallographic shear planes, electron microscope obs. 79—1443
$(Al_xV_{1-x})_2O_3$, heat capacity anomalies, metal-insulator transition, phase diagram 77—11701
$(Al_xV_{1-x})_2O_3$, impurity doping effects, elec. props. obs. 80—75609
$AlWO_4$, form., struct. 77—16518
$Al_2(WO_4)_3$:Cr(Eu), and undoped crystals, luminesc. obs. 80—89047
AlX_3^- (X=Cl, Br, I), pseudo-exact force consts. 77—31022
$Al_2[(OH)_2(PO_4)_2(UO_2)_3].(OH)_4.10H_2O$, phuralumite, X-ray cryst. struct. determ. 79—90606
$Al[(PO_4)_2(UO_2)_2].OH.8H_2O$, threadgoldite, X-ray cryst. struct. determ. 80—28969
Au-$Al_{0.5}Ga_{0.5}As$ -GaAs heterojunction Schottky-barrier solar cells, barrier height enhancement 80—85284
Au-$Ga_{1-x}Al_xSb$ Schottky barriers, barrier height 80—96986

aluminium compounds continued
Au-n-$Al_xGa_{1-x}As$-n-GaAS Schottky barrier solar cells, prep. and props. 80—26140
Au-n-AlGaAs-n-GaAs Schottky-barrier solar cells, band readjustment effect 80—81458
Au-n-$Ga_{1-x}Al_xAs$-n-GaP narrow-band variable-gap surface-barrier photoedetector 80—96944
BN-AlB, cubic phase solid soln., crystallographic and metallographic study, thermal resist. *(Russian)* 78—30599
BPO_4-$AlPO_4$, non-equil. phase diagram, electron microscope obs. 79—43225
$BaAl_2Ge_2O_8$, feldspar, crystal atomic struct. 78—14312
$Ba(PO_3)_2$-AlF_3-CaF_2, glass, elec. cond. and IR spectra 80—89005
$Ba(PO_3)_2$-AlF_3-MgF_2, glass, elec. cond. and IR spectra 80—89005
(Be, Al)B_{12}, wide-gap semicond., elec. cond., refl. and absorpt. spectra 80—20188
$Be_3Al_2Si_6O_{18}$:Cr^{3+}, EPR spectra, exchange-coupled pairs 79—28596
$Be_3Al_2[Si_6O_{18}]$:Cr^{3+}, artificial emerald, distrib. of Cr^{3+} impurity 80—59505
BeF_2-KF-CaF_2-AlF_3:Nd^{3+} (Er^{3+}) glass, multiphonon relax., fluoresc. obs. 78—15219
BeF_2-KF-CaF_2-AlF_3-EuF_3 fluoroberyllate glass, Eu^{3+} fluoresc. linewidth 80—66285
Bi_2O_3-$AlPO_4$, phase equilib. 80—35168
$C(NH_2)_3Al(SO_4)_2.6H_2O$, temp. depend. quadrupole coupling const. for $^{27}Al^{3+}$ and $^{71}Ga^{3+}$ 78—19368
$Ca_2Al_2GeO_7$, gehlenite struct., synthesis and physicochem. props. 79—43181
$CaAl_2Si_2O_8$-$NaAlSi_3O_8$ (anorthite-albite) system, crystal growth rates and processes 80—4010
$Ca_3Al_2Si_3O_{12}$, garnet, thermophysical props., 5 to 600K 79—60517
CaF_2-AlF_3, phase equilibria, DTA and X-ray diffr. study 78—27493
CaF_2-AlF_3-Na_3AlF_6(-Al_2O_3), phase equilibria, X-ray diffr. and DTA meas. 80—108409
CaO-Al_2O_3, binary slag, reduction of Al_2O_3 by C saturated Fe *(Japanese)* 79—24733
CaO-Al_2O_3-Fe_2O_3-SiO_2, phase relations 77—12610
CaO-Al_2O_3-SiO_2 diffusion triangular diagram, diffusion between lime and sintered kaolinite *(French)* 79—69296
CaO-SiO_2-Al_2-O_3, 1500°C, ion transport coeffs., interdiffusivities 77—11718
CaO-SiO_2-Al_2O_3, metallurgical slag, dissolution of N_2 77—21109
$12CaO.7Al_2O_3$, composition of gases released on heating, crystallisation *(Russian)* 80—93820
$Ca_x(Si,Al)_{12}(O,N)_{16}$, α'-Sialon ceramics, prep. and characterisation 78—84750
CoO-MgO-Al_2O_3-Cr_2O_3-TiO_2, form. and colour of spinel solid soln. *(Japanese)* 77—32550
CoO-ZnO-Al_2O_3-Cr_2O_3-TiO_2 system, form. and colour of spinel solid soln. *(Japanese)* 77—25001
$(Cr,Al)_2O_3$-$ZrSiO_4$ refractories, glass resist. and corrosion mechanism 79—61757
$CrAl_3Cl_{12}$, gas, mol. struct., ligand field spectrum *(German)* 78—37762
$Cr(H_2PO_4)_3$-$Al(H_2PO_{43})$-H_2O system, IR spectra 79—87428
Cr_2O_3-Al_2O_3, antiferromag. cluster stability, 300-5200K 77—20683
$CsAl(SO_4)_2.12H_2O$, third order elastic consts. from stress shifted reson. freqs. 78—55905
$CsAl(SO_4)_2.12H_2O$:Cr^{3+}, ESR spectra 78—91944
$CsAlSiO_4$, prep. and X-ray characterisation 78—39728
$CsLi_{0.5}(Al,Fe)_{1.5}F_6$ pyrochlore, Mossbauer contrib. to exam. of cationic order *(French)* 80—93224
$Cs_2SO_4.Al_2(SO_4)_3.24H_2O$, $^{53}Cr^{3+}$ ENDOR Lines, RF ENDOR power and modulation freq. effects 80—75884
Cu-Al ferrite films, LPE growth 80—96752
Cu-Al_2O_3 dispersed system, electron beam evaporated thick film, struct./prop. relations 77—44198
$CuAl_{1-x}Fe_xS_2$ system, delocalisation of d-electrons, mag., elec. and optical obs. 78—34804
emerald:Cr^{3+}, spin-lattice coupling consts. 79—99761
$Er_3Al_{5-x}Ga_xO_{12}$, LPE, spectroscopic props. 80—93419
$Fe_{1-x}Al_xBO_3$, synthesis, cryst. chem. and mag. props. 78—31058
$FeAl_{2-x}Cr_xO_4$, spinel, elec. cond. behaviour during oxidation 79—19593
γ-$(Fe_{1/3}Al_{2/3-y}Cr_y)_2O_3$, lacunar spinels, elec. cond. behaviour during oxidation 79—19593
$(Fe_{1-y}{}^{3+}Al_y{}^{3+})_2O_3{}^{2-}$, γ to α transform. elec. cond. study, oxidation initial stage kinetics, lacunar spinel form. 78—92384
$(Fe_{6-y}Al_y)O_9$, IR spectra, lacunar γ-phase to corundum α-phase transform. 80—108199
$Fe_{1-x}Al_xOOH$, Mossbauer study, determ. of Al content and mag. props. 80—39938
$(Fe_2Cr_{4-y}Al_y)O_9$, IR spectra, lacunar γ-phase to corundum α-phase transform. 80—108199
FeO-Fe_2O_3-SiO_2-Al_2O_3-$CuO_{0.5}$ slag, and Cu, distribution equilibria of Sn, Se, Te 77—51502
$Fe_{2.6-x}Ti_{0.4}Al_x O_4$, $Fe_{2.4-x}Ti_{0.6}Al_xO_4$, titanomagnetite, monodomain, mag. props. 78—56346
(Ga, Al, As) heterostructures and compounds, electronic props., empirical pseudopot. calc. 80—80366
(Ga,Al)As CW diode laser, L(J) charact., external cavity induced nonlinearities 77—79824
(Ga,Al)As DH lasers used for optical recording, hole machining in Te films 79—89954
(Ga,Al)As injection laser parameters, homogeneous degradation calc. from initial rates 79—22951
(Ga,Al)As, LPE growth of multilayered struct., explanation for meniscus lines on surfaces 77—76681
(Ga, Al)As laser diode, operation and gain meas., importance of gap shrinkage effects 80—66257
(Ga,Al)As narrow double-current-confinement channelled-substrate planar laser fabrication, double etching technique 80—74371
(Ga,Al)As transverse mode stabilised laser, direct obs. of saturation behaviour of spontaneous emission 78—46600
(Ga,Al)As:Si, Ge, epitaxial layers, radiative recomb., compensation, cathodolum. study 80—66307
Ga complex, $Gaurea_6(ClO_4)_3$:Cr^{3+} structural phase transition, ESR meas. 77—20681
Ga-Al-Sb, liq. phase epitaxy, phase diagram, X-ray microanal. 79—19491
Ga-AlSb-GaSb, phase diagram, LPE of $(AlSb)_x(GaSb)_{1-x}$ solid soln. 77—40392

aluminium compounds continued
- $Ga_{1-x}Al_x$ As, metal-gap channel waveguides, intensity modulation 78−66899
- Ga_xAl_{1-x} melt, solubility of Si, ternary phase diagram *(French)* 77−51498
- GaAlAs actively mode-locked laser, bandwidth limited picosecond pulses 80−95905
- (GaAl)As buried-heterostructure laser with buried optical guide, highly efficient operation 80−1219
- GaAlAs CW DH diode lasers, 1/f noise behaviour 78−1226
- (GaAl)As CW DH lasers with stripe geometry, LF intensity noise obs. 77−38887
- GaAlAs CW diode laser, external cavity control, 32 MHz single axial mode 78−1271
- GaAlAs DH, optically-pumped, degradation at elevated temps. 79−50295
- GaAlAs, DH CW diode laser, picosecond pulse generation 78−83002
- (GaAl)As DH diode laser, microscale degradation absorpt. centres 78−13704
- GaAlAs DH injection laser, half-ring, room temp. operation 80−58558
- (GaAl)As DH laser, gradual degradation accel. as exponent of driving current value 80−32990
- GaAlAs DH laser, In solder deterioration, Au diffusion in In 80−33019
- (GaAl)As, DH laser, LPE growth, meniscus lines as nucleation sites 77−15706
- (GaAl)As DH laser, low-current, proton-bombarded, design and characts. 78−87059
- GaAlAs DH laser, narrow stripe geometry, spontaneous carrier lifetime 80−87392
- GaAlAs DH laser, optimum p-n junction depth, photoluminesc. method 79−4598
- GaAlAs DH laser, stripe geometry, spatially resolved emission 79−27257
- (GaAl)As DH laser, threshold current density, growth terraces effect 80−99723
- GaAlAs DH laser diode, deep level associated with slow degradation 78−87050
- GaAlAs DH laser diodes, catastrophic degradation 79−50290
- GaAlAs DH laser diodes, long-lived high-power at 70°C, using Al_2O_3 film coating 79−50321
- GaAlAs DH laser diodes, small signal modulation, junction capacitance effect 80−83625
- GaAlAs DH laser diode, edge coupling to planar $LiNbO_3$:Ti waveguide 80−87559
- (GaAl)As DH laser wafer, photoluminesc. improvement with buffer layer 80−64014
- GaAlAs DH laser-diode-to-diffused-waveguide coupling calcs., Gaussian beam model 79−94372
- (GaAl)As, DH lasers, degradation mechanisms, temp. depend. 78−66825
- GaAlAs DH lasers, electron-hole recomb. effects 79−45944
- GaAlAs DH lasers, nonlinearity, second and third harmonic distortion 79−31898
- GaAlAs DH lasers, proton-bombard., nonradiative recomb., luminesc. time-response meas. 79−98371
- GaAlAs DH lasers, SiO_2 insulated, characts. and near field 80−64019
- GaAlAs DH lasers, self-sustained pulsation suppression, effect of SiO_2 facet coating films 80−95894
- GaAlAs DH p-n junction laser, construction and operating characts. 78−9377
- GaAlAs DH photovoltaic detectors, high efficiency 79−11198
- (GaAl)As DH stripe contact injection lasers, local attached data fibre link appls. 80−19044
- GaAlAs DH stripe geometry lasers, degradation phenomena 80−53290
- GaAlAs, diode laser, CW radiation, intensity noise spectra of axial mode groups 77−34890
- (GaAl)As heterojunction laser with distributed Bragg refl., mode switching 80−43336
- GaAlAs, heterostruct. formed by LPE, growth and dissolution kinetics 79−99439
- (GaAl)As high performance diode laser, high-reflectivity cavity mirrors 78−82994
- (GaAl)As injection lasers, optimisation of power efficiency 77−42539
- (GaAl)As injection lasers, self-pulsations, Q-switching and mode-locking effects 78−66827
- GaAlAs injection lasers, AM characts. 79−50330
- GaAlAs injection laser, long wavelength radn. spatial distrib. 79−76686
- GaAlAs injection lasers, stability in single transverse mode operation 80−38027
- GaAlAs injection laser, monolithic integration with Schottky-gate FET 80−48275
- (GaAl)As injection laser operating in external cavity, intensity self-pulsations 80−64013
- (GaAl)As injection lasers operating with optical fibre resonators 80−91812
- (GaAl)As, LPE, GaAs dissolution kinetic in undersaturated isothermal solns. in Ga-Al-As system 80−80106
- (GaAl)As laser, stripe struct. for horizontal transverse mode stabilisation 77−79859
- GaAlAs laser diode, CW, ps pulse generation 79−50329
- GaAlAs laser nonlinearities, harmonic distortion 80−74357
- GaAlAs laser transmitters using optical tap for feedback control, output power stability 79−64241
- (GaAl)As lasers, low threshold proton isolated, spectral and transient response 78−87052
- GaAlAs lateral injection laser, low threshold, single mode operation 77−75545
- GaAlAs light intensity modulators using p-n junctions 80−99871
- (GaAl)As low-beam-divergence CW DH laser, grown by low press. metallorganic CVD 80−74376
- GaAlAs, luminescence circular polarisation, electron optical orientation resonant variation *(Russian)* 80−84782
- GaAlAs mode stabilised separated multiclad layer stripe geometry DH laser, optical waveguide 80−64051
- GaAlAs mode-stabilised semiconductor lasers 78−46638
- GaAlAs, native defects, stoichiometry, doping effect 77−11541
- GaAlAs novel DH lasers fabrication 78−50803
- GaAlAs on GaAs thin film stacked multiple-bandgap solar cell structs., prep. using CVD techniques 80−94083
- (GaAl)As oxide-stripe geometry DH laser, cavity length effect on output 79−50323

aluminium compounds continued
- GaAlAs, p-n and heterojunctions, superinjection coeffs., luminesc. obs. 80−50427
- GaAlAs p-n heterostructures, current-flow mechanisms, luminesc. spectra 80−20298
- GaAlAs plasma grown oxide film, anal. by combined ion beam techniques 79−7760
- GaAlAs, SEM defect study, transmission cathodoluminescence 79−64964
- GaAlAs solar cells, appl. for navigational satellite power systems 80−35694
- GaAlAs stripe laser, longit. and transverse mode dynamics on junction plane 77−38890
- GaAlAs, surface vacancies, bound state energy levels calc. 80−80340
- (GaAl)As system, automated system for growth of multilayered structs. by LPE 79−38752
- GaAlAs terraced substrate laser, visible-light-emitting, characts. 80−106523
- (GaAl)As, Zn diffused DH laser with twin transverse junctions, low threshold current 79−98393
- (GaAl)As, Zn diffused proton bombarded stripe laser 79−98392
- (GaAl)As:Be implanted DH stripe geometry laser 80−64044
- n-GaAlAs:Sn LED DH donor-level analysis, DLTS obs. 79−47040
- GaAlAs/GaAs, n-p-n heterojunction transistor, elec. props. 79−87149
- GaAlAs/GaAs heterostructures, ellipsometric assessment of epitaxial layer during growth in organometallic VPE system 79−37933
- GaAlAs/GaAs solar cells, efficiency optimisation at high and low current levels *(French)* 80−61348
- GaAlAs/GaAs solar cells, Be and Zn behaviour 80−101111
- (GaAl)As/GaAs-heterostructure lasers, degradation studies of sawn cavity lasers under pulsed operation 78−29953
- (GaAl)As-GaAs, DH laser, degradation in water due to facet deterioration 79−22970
- (GaAl)As-GaAs, double heterostructure laser, TEM study of dark line defect growth from dislocation clusters 79−33206
- (GaAl)As-GaAs, long life lasers, initial degradation mode 77−14712
- GaAlAs-GaAs (100) interfaces, carrier transport coeffs., tight binding calc. 80−49889
- (GaAl)As-GaAs concentrator solar cells, series resistance effects 79−57427
- GaAlAs-GaAs DH injection laser, external cavity operated angled-stripe geometry, CW operation 80−64078
- (GaAl)As-GaAs DH laser, anomalous emission intensity, cavity competition 77−79823
- GaAlAs-GaAs DH lasers, degradation caused by growth of dislocation networks 80−53289
- GaAlAs-GaAs double heterostructure, interfacial recomb. velocity, photolum. meas. 78−68075
- GaAlAs-GaAs epitaxial heterostructures for integrated optics functional elements 78−50948
- GaAlAs-GaAs heteroface solar cells, 1 MeV electron irrad., analytical and expt. study 79−70450
- GaAlAs-GaAs heteroface solar cells, high open-cct. voltage, full-factor and efficiency 80−94081
- GaAlAs-GaAs heterojunction prep., Zn conc. effect in epitaxial layer, high-power IR emission *(Spanish)* 77−39932
- GaAlAs-GaAs heterojunction solar cells, high temp. props. 25 to 300°C 80−94035
- (GaAl)As-GaAs heterostruct. lasers, factors affecting catastrophic degradation 77−75524
- GaAlAs-GaAs heterostructures, electronic excitation effects on mobility of point defects and dislocations 78−2561
- (GaAl)As-GaAs heterostructure lasers, factors affecting catastrophic degradation 78−17942
- GaAlAs-GaAs heterostruct. solar cells, Al, P, Zn incorporation by LPE *(French)* 79−24899
- GaAlAs-GaAs heterostruture, optical waveguide characteristics, mode spectrum, universal dispersion curves 79−72706
- (GaAl)As-GaAs laser, low temp. threshold behaviour 78−46604
- GaAlAs-GaAs lasers, channelled substrate, prepared by combination of organometallic pyrolysis and LPE 80−99745
- GaAlAs-GaAs n-n heterojunction, rectification 79−28402
- (GaAl)As-GaAs narrow stripe laser, improved optical communication system performance 80−102733
- GaAlAs-GaAs solar cell structs., photolum. props. 80−50958
- (GaAl)As-GaAs twin-transverse-junction stripe laser with linear light/current characteristic and low threshold 79−36893
- GaAlAs-GaAs-GaAlAs etalon, optical bistability 80−5781
- (GaAl)As-heterostruct. stripe lasers, light/current characts. and near field shifts, waveguide self focusing effects 78−29952
- $GaAl_xAs_{1-x}$, ion beam synthesis for photodetector fabrication 79−46688
- $Ga_{0.1}Al_{0.9}As$ LPE layers containing low-cond. regions, charging effects in SIMS anal. 80−66348
- $Ga_{0.5}Al_{0.5}As$, heterostructure, cation order, effect on energy bands 79−1570
- $Ga_{0.5}Al_{0.5}As$-GaAs, DH, interfacial recomb., photolum. time decay meas. 78−95347
- $Ga_{0.5}Al_{0.5}As$-GaAs(:Ge) DH structure, minority carrier lifetime and internal quantum efficiency of surface-free GaAs 79−43013
- $Ga_{0.64}Al_{0.36}As$, plasma grown oxide, phys. and elec. props. 78−48550
- $Ga_{0.65}Al_{0.35}As$ epitaxial layer on GaAs, two-dimensional lattice mismatch parallel to interfacial boundary 79−51439
- $Ga_{0.65}Al_{0.35}As$, LPE growth, wave morphologies on surface 77−40396
- $Ga_{0.7}Al_{0.3}As$ epitaxial film, inclusion-generated dislocation clusters 77−89445
- $Ga_{0.7}Al_{0.3}As$-GaAs chemically etched mirror lasers, optical coupling effect 77−72000
- $Ga_{0.7}Al_{0.3}As$-GaAs n-n heterojunction, LPE, rectification 80−49888
- $Ga_{0.9}Al_{0.1}As$, nucleation morphologies on $Ga_{0.65}Al_{0.35}As$ surfaces grown by LPE 78−15323
- $Ga_{0.9}Al_{0.1}As$:Ge(Si) epitaxial layers, defect obs. by TEM 77−51618
- $Ga_{1-x}Al_xAs$ DH injection laser diode, long-term-degraded, TEM obs. 78−71102
- $Ga_{1-x}Al_xAs$-GaAs DH lasers, very low threshold, grown by metalorganic CVD 78−55365
- $Ga_{1-x}AlAs$ (110) oxide-free Schottky barriers, surface comp. and characts., AES obs. 79−82661
- $Ga_{1-x}AlAs$, LPE layers, electron mobility, scatt. processes 80−84519
- $Ga_{1-x}AlAs$:Zn, acceptor energy level and elec. props. 80−65482
- $Ga_{1-x}Al_xAs$, alternate monolayer crysts., MBE and props. exam. 78−10289

aluminium compounds continued

$Ga_{1-x}Al_xAs$, appl. of theory of electroepitaxy of multicomponent systems 80—65396
$Ga_{1-x}Al_xAs$, band struct. from I-V, C-V meas. on Schottky diodes 80—96989
$Ga_{1-x}Al_xAs$ based layer structures, optimum growth conditions, comp. and struct. perfection 80—104069
$Ga_{1-x}Al_xAs$ buried heterostruct. injection laser, degradation rate, optical flux density depend. 79—50313
$Ga_{1-x}Al_xAs$, channelled substrate, planar struct. and DFB lasers 78—79032
$Ga_{1-x}Al_xAs$ DH catastrophically degraded laser, TEM obs. of defects 80—32989
$Ga_{1-x}Al_xAs$ DH injection laser, FM at microwave freq. rates 80—58610
$Ga_{1-x}Al_xAs$ DH laser, accelerated ageing test 79—76688
$Ga_{1-x}Al_xAs$ DH laser diode, long-lived, high-power, facet coated 80—58564
$Ga_{1-x}Al_xAs$ DH laser hybrid device, reliability 79—27281
$Ga_{1-x}Al_xAs$, DH stripe geometry laser, lasing-induced change in differential resistance 79—45943
$Ga_{1-x}Al_xAs$, deep level-dislocation interactions, DLTS meas. 80—29357
$Ga_{1-x}Al_xAs$, deep levels, pressure effects 80—49651
$Ga_{1-x}Al_xAs$, degraded DH LED, defect struct. by electrolum. topography and TEM obs. 79—60369
$Ga_{1-x}Al_xAs$ double heterostruct. lasers, aging characts. 79—72569
$Ga_{1-x}Al_xAs$ electrodes, interface capacitance meas., flatband pot., conduction and valence band boundaries *(French)* 79—33339
$Ga_{1-x}Al_xAs$, electrolum. study using high-gain image intensifier 80—55193
$Ga_{1-x}Al_xAs$, epitaxial, radiative deep states 80—76061
$Ga_{1-x}Al_xAs$, epitaxial layers, reflectivity meas. by wavelength modulation spectroscopy *(French)* 77—59632
$Ga_{1-x}Al_xAs$, epitaxial layers, on GaAs substrates, X-ray double-cryst. diffractometry, state of strain 79—19480
$Ga_{1-x}Al_xAs$ epitaxial layer, absorpt. and transmission coeffs. *(French)* 80—2887
$Ga_{1-x}Al_xAs$ epitaxial layer, elec. cond., Hall effect, band struct. 80—49964
$Ga_{1-x}Al_xAs$ heterostructure, LPE prep., growth and dissolution kinetics, thermodynamic and kinetic models 80—75456
$Ga_{1-x}Al_xAs$, hot electron distrib. meas. and calc. 78—27318
$Ga_{1-x}Al_xAs$, IR refl. spectra and Raman spectra 80—20623
$Ga_{1-x}Al_xAs$ injection laser automatic bias control cct. 78—5498
$Ga_{1-x}Al_xAs$, intervalley energy gaps, temp. junction, exptl. determ. 80—80179
$(Ga_{1-x}Al_x)As$ LOC DBR laser integration with p-n junction detector 78—38066
$Ga_{1-x}Al_xAs$, LPE, growth mechanism and morphology on channelled substrates 79—28960
$Ga_{1-x}Al_xAs$ LPE crystals for DH laser, LEDs, TEM obs. of Ge, Si-doped epitaxial layers 79—1556
$Ga_{1-x}Al_xAs$, LPE growth and characterisation 80—50566
$Ga_{1-x}Al_xAs$, LPE layer thickness depend. on soln. comp. 78—10295
$Ga_{1-x}Al_xAs$, LPE layers, grown under const. cooling rate conditions, cryst. composition 78—39710
$Ga_{1-x}Al_xAs$ LPE layers, diffusion limited growth, thickness comparison with GaAs 78—87892
$Ga_{1-x}Al_xAs$ LPE layer on GaAs, lattice mismatch using X-ray source 79—82470
$Ga_{1-x}Al_xAs$ LPE layers, comp. and refr. index, ellipsometry meas. 79—87011
$Ga_{1-x}Al_xAs$ laser, buried heterostruct., stable operation during accelerated ageing at 70°C 79—7125
$Ga_{1-x}Al_xAs$ laser, DH, enhanced localised degradation and anomalous emission spectra 77—680
$Ga_{1-x}Al_xAs$ laser, SHG with $KNbO_3$ 80—74431
$Ga_{1-x}Al_xAs$ laser, stripe-geometry DH, improved light output linearity 77—682
$Ga_{1-x}Al_xAs$, laser, temp. sensitive, enhanced degradation rates 77—79825
$Ga_{1-x}Al_xAs$ lasers, processing stresses effect on residual degradation 79—72567
$Ga_{1-x}Al_xAs$ layer, surface conc. x determ. by rapid localised non-destructive optical method *(French)* 77—62725
$Ga_{1-x}Al_xAs$ layer form. on GaAs during dissolution in Ga-Al-As soln. 80—10799
$Ga_{1-x}Al_xAs$, liquid and solid comp. variations during LPE growth 79—99445
$Ga_{1-x}Al_xAs$ low threshold stripe geometry DH laser, Be implanted, on semi-insulating substrate 80—69409
$Ga_{1-x}Al_xAs$, MBE, state-of-the-art 79—24450
$Ga_{1-x}Al_xAs$ n-p_3-p_2-p_1-p_0 struct., degradation electrolum. 80—50428
$Ga_{1-x}Al_xAs$, NMR of optically oriented nuclei, quadrupole effects *(Russian)* 77—85592
$Ga_{1-x}Al_xAs$, non-shallow levels and cond. band struct. from Hall carrier conc. meas. 80—39607
$Ga_{1-x}Al_xAs$, ohmic contacts, metallisation systems 80—25010
$Ga_{1-x}Al_xAs$, optical detection of CESR 77—36155
$Ga_{1-x}Al_xAs$, p^+-n-n^+ heterostructure, distrib. of injected carriers, forward V-I characts. *(Russian)* 80—6973
$Ga_{1-x}Al_xAs$ p-i-n structure photoelectric props. 78—95353
$Ga_{1-x}Al_xAs$ p-n structure, charge-storage diode, variable-gap 80—11076
$Ga_{1-x}Al_xAs$, Peltier LPE, absence of electromigration of As and Al 77—81230
$Ga_{1-x}Al_xAs$, photoluminescence, deep level trap emission capture 80—29805
$Ga_{1-x}Al_xAs$, point defects and dislocation climb, interaction with deep level donor 79—82209
$Ga_{1-x}Al_xAs$, protection by reactively sputtered AlN *(French)* 78—23849
$Ga_{1-x}Al_xAs$, quantum magnetoresist. results, using pulsed fields up to 35 T 79—73528
$Ga_{1-x}Al_xAs$, rapidly degraded LED, defect struct. of ⟨100⟩ dark lines 78—10052
$Ga_{1-x}Al_xAs$ Schottky barrier, oxide free, surface composition and fabrication 78—68084
$Ga_{1-x}Al_xAs$ Schottky directional coupler switch, construction and operation 78—25960
$Ga_{1-x}Al_xAs$, Se ion implantation *(French)* 77—68986
$Ga_{1-x}Al_xAs$, self-aligned three dimensional struct. MBE growth 77—59697

aluminium compounds continued

$Ga_{1-x}Al_xAs$, semiconductor defects, spectroscopic study of electronic props. 80—84446
$Ga_{1-x}Al_xAs$, Shubnikov-de Haas oscillation, in semiconductor superlattice 77—62947
$Ga_{1-x}Al_xAs$, solid solution, synthesized by ion implantation, Raman scattering 79—42972
$Ga_{1-x}Al_xAs$ structures, STEM and scanning deep level transient spectroscopy in defect centre anal, cathodoluminesc. techniques 80—103642
$Ga_{1-x}Al_xAs$ superlattices, multilayers, periodic and near-periodic, small-angle interferences of reflected X-rays 79—94846
$Ga_{1-x}Al_xAs$, surface phonon polaritons, frustrated total internal refl. expts. 78—47656
$Ga_{1-x}Al_xAs$ symmetrised epitaxial variable-gap waveguide, coherent radiation generation 80—38018
$Ga_{1-x}Al_xAs$ transparent LED, optical wavelength multiplex transmission system appl. 78—30063
$Ga_{1-x}Al_xAs$, VPE, on-time comp. depend. 78—67915
$Ga_{1-x}Al_xAs$ VPE layers, X-ray diffr. 80—29296
n-$Ga_{1-x}Al_xAs$, variable gap photodetector, quantum efficiency 79—7903
$Ga_{1-x}Al_xAs$, variation of optical transitions *(French)* 79—60708
$Ga_{1-x}Al_xAs$, varizone layer photoelectron yield depth estimation 80—100745
$Ga_{1-x}Al_xAs$, velocity saturation and cond. band struct. under press. 78—26863
$Ga_{1-x}Al_xAs$ visible diode lasers, transverse-mode stabilised, nonstigmatic laser beams 79—76694
$Ga_{1-x}Al_xAs$ visible diode lasers, degradation 80—43330
$Ga_{1-x}Al_xAs$ visible diode lasers, degradation mechanisms 80—64026
$Ga_{1-x}Al_xAs$ visible diode lasers, degradation due to macroscopic defects (<730 nm) and facet oxidation (>740 nm), life tests 80—99729
$Ga_{1-x}Al_xAs$:Si, LPE, phase diagram, Hall effect meas., carrier conc., donor ionisation energies 77—72803
$Ga_{1-x}Al_xAs$:Si, linear-gradient p-n junction, barrier capacitance 77—43705
n-$Ga_{1-x}Al_xAs$:Si, room-temp. cond. and band struct. 80—96869
$Ga_{1-x}Al_xAs$:Si p-n junction, reemission effects 78—15230
$Ga_{1-x}Al_xAs$:Si p-n junction, doping in LPE, elec. and luminesc. props. *(Czech)* 78—47851
$Ga_{1-x}Al_xAs$:Si photoelectric convertors, broadband varizone creation 80—40856
$Ga_{1-x}Al_xAs$:Sn, layer Schottky barrier, deep level spectroscopy 80—49666
$Ga_{1-x}Al_xAs$:Te, plasmon-LO-phonon coupling, IR refl. obs. 80—50335
n-$Ga_{1-x}Al_xAs$-Au, Schottky barrier height as function of AlAs content 79—65535
$Ga_{1-x}Al_xAs$-Au variable-gap surface-barrier struct., photoelec. effect 80—39634
$Ga_{1-x}Al_xAs$-$Ga_{1-y}Al_yAs$ p-n heterojunction, minority carrier lifetime, elec. characts. and electrolum. meas. 78—2554
$Ga_{1-x}Al_xAs$-$Ga_{1-y}Al_yAs$ DH laser, grown by organometallic CVD, room temp. operation 78—29950
$Ga_{1-x}Al_xAs$-GaAs, abrupt quantum-well heterostruct. grown by metalorganic chemical vapour deposition 79—56933
$Ga_{1-x}Al_xAs$-GaAs, CVD laser diodes, operation and growth processes 78—46598
$Ga_{1-x}Al_xAs$-GaAs, DH laser, curved stripe, operation and appl. 78—42341
$Ga_{1-x}Al_xAs$-GaAs, grown by LPE, direct obs. of dislocations 79—65087
$Ga_{1-x}Al_xAs$-GaAs, injection lasers, defects, TEM anal. 79—23866
$Ga_{1-x}Al_xAs$-GaAs channel guide laser grown by metalorganic CVD 79—10317
$Ga_{1-x}Al_xAs$-GaAs DH injection lasers grown by metalorganic CVD, props. 80—99751
$Ga_{1-x}Al_xAs$-GaAs DH lasers grown by metalorganic CVD, room temp. operation 78—1248
$Ga_{1-x}Al_xAs$-GaAs heterostructure lasers grown by metalorganic CVD, prep. and props. 79—36918
$Ga_{1-x}Al_xAs$-GaAs heterostruct. superlattice, props. in high mag. fields 79—73570
$Ga_{1-x}Al_xAs$-GaAs heterojunctions grown by metallorganic CVD 80—15599
$Ga_{1-x}Al_xAs$-GaAs injection laser, branching waveguide coupler fabrication by LPE 78—63202
$Ga_{1-x}Al_xAs$-GaAs LPE multilayer heterostructure photovolt. solar cells, fabrication and performance 79—48128
$Ga_{1-x}Al_xAs$-GaAs laser, degradation, appl. of dislocation climb model 77—1125
$Ga_{1-x}Al_xAs$-GaAs laser, DH, grown by metalorganic CVD, room temp. operation 78—13702
$Ga_{1-x}Al_xAs$-GaAs laser, distributed Bragg confinement, room temp. operation 78—74907
$Ga_{1-x}Al_xAs$-GaAs p-n and p-p-n heterojunction solar cells, high efficiency, prep., eval. and characters *(Japanese)* 80—61342
$Ga_{1-x}Al_xAs$-GaAs p-n structures, variable-gap front layer, photoelec. props. 79—7884
$Ga_{1-x}Al_xAs$-GaAs p-n solar cell, with thin variable gap layer, high efficiency 79—24064
$Ga_{1-x}Al_xAs$-GaAs solar cell, deep level obs. 77—89834
$Ga_{1-x}Al_xAs$-GaAs solar cells, photoluminesc. characterisation 80—3512
$Ga_{1-x}Al_xAs$-GaAs solar cell, radiation resist., theoretical evaluation and optimisation 80—35681
$Ga_{1-x}Al_xAs$-GaAs solar cells, computer anal. of cell characts. incl. band gap variation 80—55866
$Ga_{1-x}Al_xAs$-GaAs:Si, momentum distrib. of valence electrons, positron annihilation meas. 79—51530
$Ga_{1-x}Al_xAs$-GaAs-GaAs, p-p-n junctions, variable gap solar photocell with coordinate depend. band gap gradient 79—11213
$Ga_{1-x}Al_xAs$-Ge, MBE of ultra thin film superlattices on GaAs substrates, TEM study 79—37932
$Ga_xAl_{1-x}As$ channelled-substrate planar struct. injection laser 77—88742
$Ga_xAl_{1-x}As$ DH laser, suppression of output nonlinearities by use of misaligned mirrors 78—17954
$Ga_xAl_{1-x}As$ diode laser, modulation characts. 77—83903
$Ga_xAl_{1-x}As$ embedded stripe DH laser monolithically integrated with strip waveguide 78—59025
$Ga_xAl_{1-x}As$ injection heterojunction distributed output laser, exptl. study 80—43369
$Ga_xAl_{1-x}As$, LPE, GaAs solubility in Ga-Al alloys investig. 78—52690
$Ga_xAl_{1-x}As$ layer, optical guiding in Bragg configuration 78—1431

aluminium compounds continued
- $Ga_xAl_{1-x}As$, optically oriented electron, nuclei spin instability *(Russian)* 80−70660
- $Ga_xAl_{1-x}As$, Schottky barrier, effect of oxide composition on elec. behaviour, AES meas. 79−87141
- $Ga_xAl_{1-x}As$ stripe-geometry laser, current carrier conc. distrib. and threshold props. 77−68212
- $Ga_xAl_{1-x}As$:Cu epitaxial layers, spatial distrib. of nonradiative defects, STEM imaging spectroscopic technique 77−89438
- $Ga_xAl_{1-x}As$-GaAs DH laser, degraded, nature of ⟨110⟩ dark-line defects, TEM 77−89439
- $Ga_xAl_{1-x}As$-GaAs DH laser, continuous room temp. operation 78−55363
- $Ga_xAl_{1-x}As$-GaAs DH laser material crystal cathodoluminescence, SEM analysis 80−97349
- $Ga_xAl_{1-x}As$-GaAs double heterostructure laser diode, temp. depend. of photolum. 80−5734
- $Ga_xAl_{1-x}As$-GaAs heterostructure laser, suppression of internally circulating modes, effect on catastrophic degradation and efficiency 77−83896
- $Ga_xAl_{1-x}As$-GaAs heteroepitaxial layer distortion characterisation by X-ray multiple diffr. 80−96754
- $Ga_xAl_{1-x}As_x$ photodetector diode on GaAs substrate dark currents, tunnelling, energy gaps, effective masses 80−70805
- GaAlAsP-GaAs T-Q DH laser, light induced misfit dislocation motion 77−75518
- $Ga_{1-x}Al_xAs_{1-y}P_y$ epitaxial film, nonradiative recomb. at dislocations 80−44213
- $Ga_{1-x}Al_xAs_{1-y}P_y$ epitaxial layer heterojunction, nonradiative recombination at misfit dislocations 80−96901
- $Ga_{1-x}Al_xAs_{1-y}P_y$ layer of uniform composition grown on GaAs by LPE, temp. diff. method appl. 79−23864
- $Ga_{1-x}Al_xAs_{1-y}P_y$-GaAs quaternary heterojunction strains and IR laser diode performance 78−9385
- $Ga_{1-x}Al_xAs_{1-y}P_y$-GaAs quaternary heterojunction, misfit dislocation charact. by synchrotron radiation white beam topography 78−63771
- $Ga_{1-x}Al_xAs_{1-y}P_y$-GaAs heterojunctions, light-induced misfit dislocation motion, photoluminesc. and X-ray diffr. meas. 79−11200
- GaAlAsSb/GaSb alloys, prep. and optoelectronic device appl. 80−25587
- GaAlAsSb-GaSb low bandgap solar subcell for high efficiency multibandgap convertors, LPE growth 80−93927
- $Ga_{1-x}Al_xN$ heteroepitaxial films, photoluminesc., cathodoluminesc. 80−66292
- $Ga_{1-x}Al_xN$, VPE growth on sapphire, RHEED obs.of orientation rels. 77−20208
- $Ga_xAl_{1-x}N$ film, growth and props. 78−39702
- $Ga_{1-x}Al_xP$, bending parameters calc. by pseudopot. method 78−26813
- $Ga_{1-x}Al_xP$, LPE grown, green electroluminescence 78−19571
- $Ga_{1-x}Al_xP$, long-wavelength optic phonons, IR reflectance meas. 77−7804
- $Ga_{1-x}Al_xP$, two-phonon optical absorpt. 78−88341
- $Ga_{1-x}Al_xP$ varigap structs., crystallation 80−80993
- $Ga_{1-x}Al_xP$:N epitaxial films, ion implanted, cathodoluminescence study 80−60684
- $Ga_{1-x}Al_xP$-GaP-GaP n-n-p struct., electrolum. spectra 79−24368
- $Ga_xAl_{1-x}P$ high-temp. solar cell with 0.3 eV band gap 80−21400
- $Ga_{0.5}Al_{0.5}Sb$, surface cleaning by sputter-etch technique 77−48560
- $Ga_{0.72}Al_{0.28}Sb$ avalanche photodiodes, ionization coeff. 79−17488
- $Ga_{1-x}Al_xSb$, dispersive energy and energy gap calcs. *(French)* 79−99478
- $Ga_{1-x}Al_xSb$, LPE growth and phase diagram *(French)* 77−24974
- $Ga_{1-x}Al_xSb$, melt growth and elec. props. 79−65999
- $Ga_{1-x}Al_xSb$ p-n homojunction LPE and photovoltaic effect obs. *(French)* 78−64108
- $Ga_{1-x}Al_xSb$ p-n structure, variable-gap, elec., photoelec. and electrolum. props. 77−11996
- $Ga_{1-x}Al_xSb$ p-n structure, variable-gap, electroluminescence 78−52582
- $Ga_{1-x}Al_xSb$, second order Raman spectra, photon combinations *(French)* 80−34912
- $Ga_{1-x}Al_xSb$, small wave vector modes 78−75785
- $Ga_{1-x}Al_xSb$, surface oxidation, Raman spectra, residual Sb layers 80−71419
- n-$Ga_{1-x}Al_xSb$, transport phenomena in low and high mag. fields 78−80007
- $Ga_{1-x}Al_xSb$ variable-gap p-n struct., selective photoelec. effect 77−76912
- $Ga_{1-x}Al_xSb$ variable-gap p-n structures, wide-band photoelec. effect 79−42635
- $Ga_{1-x}Al_xSb$, variation of optical transitions *(French)* 79−60708
- $Ga_xAl_{1-x}Sb$, VPE, closed tube transport technique 79−28935
- $Ga_xAl_{1-x}Sb$, VPE with I_2 as transport agent 78−48325
- GaAs:Zn-$Al_{0.5}Ga_{0.5}As$ p-n junction, surface layer effect on surface recombination current 79−69585
- GaAs/$Al_xGa_{1-x}As$ heterostruct., anomalous elec. and optical characts. 80−2865
- GaAs/AlGaAs, DH laser, degradation under Ar laser irrad. 79−98375
- GaAs/AlGaAs DH wafers and lasers, defect struct., X-ray topography 79−50312
- GaAs/AlGaAs integrated twin guide injection lasers prepared by LPE, coupling coeff. and coupling length meas. 79−81458
- GaAs-(Ga,Al)As heterostructure transmission photocathodes, characts. and epitaxial growth *(French, English)* 78−52616
- GaAs-(Ga,Al)As light modulators and distributed Bragg reflector laser, monolithic integration 78−50944
- GaAs-(GaAl)As channelled substrate buried heterostruct. injection laser, fabrication 77−7087
- GaAs-(GaAl)As DH lasers, automated LPE growth, CW reliability tests 80−20804
- GaAs-(GaAl)As epitaxial layers and DH lasers, deep centre 1.02 eV luminesc. 78−80387
- GaAs-(GaAl)As injection lasers with circular resonator 80−74377
- GaAs-(GaAl)As terraced-substrate injection lasers, fabrication and output characts. 79−50310
- GaAs-(GaAl)As terraced substrate laser, fundamental transverse and longit. mode oscill. 79−98357
- GaAs-$Al_{0.2}Ga_{0.8}As$ periodic layered media, optical surface waves 78−43946
- p-GaAs-$Al_{0.3}Ga_{0.7}As$, cladded dielec. waveguide, loss meas. using Raman scatt. 79−81539
- GaAs-$Al_{0.3}Ga_{0.7}As$ n-N heterojunction, LPE grown, cond. band discontinuity, C-V profiling meas. 80−70801

aluminium compounds continued
- GaAs-$Al_{0.4}Ga_{0.6}As$, p-n heterojunction, quantum confinement and compositional grading effects on band struct. 79−87151
- GaAs-$Al_{1-x}Ga_xAs$ lar, PbO-SiO_2 glass optical coating 78−71113
- GaAs-$Al_xGa_{1-x}As$, optically pumped multilayer struct. and DH, laser oscillations 77−3589
- GaAs-$Al_xGa_{1-x}As$, single mode optical rib waveguides, MOS control of switches 78−1432
- GaAs-$Al_xGa_{1-x}As$, optically pumped taper coupled laser, second order Bragg reflector 78−50788
- GaAs-$Al_xGa_{1-x}As$, DH laser, effect of bulk nonradiative recombination 78−82967
- GaAs-$Al_xGa_{1-x}As$, film waveguide, heterojunction lasers with Bragg mirrors, threshold characts. 79−23095
- GaAs-$Al_xGa_{1-x}As$, negative differential resist., real-space electron transfer 80−6958
- GaAs-$Al_xGa_{1-x}As$, heterojunction and superlattice, magnetophonon reson., polaron mass 80−44715
- GaAs-$Al_xGa_{1-x}As$, current transverse junction lasers, low threshold, MBE prep. 80−83614
- GaAs-$Al_xGa_{1-x}As$ buried-heterostructure lasers, current injection confinement, MBE/LPE hybrid technique 80−74374
- GaAs-$Al_xGa_{1-x}As$ CW-diode laser, coupled to freq.-selective external cavity, self-pulsing 77−61982
- GaAs-$Al_xGa_{1-x}As$ channelled-substrate-planar-struct. laser with lateral-evanescent-field distributed feedback 79−98398
- GaAs-$Al_xGa_{1-x}As$ current injection multi-quantum-well heterostructure lasers, MBE grown 80−19042
- GaAs-$Al_xGa_{1-x}As$ DH laser structures, high-resolution composition profiling with photolum. 78−71101
- GaAs-$Al_xGa_{1-x}As$ DH laser, room temp. threshold current 78−79019
- GaAs-$Al_xGa_{1-x}As$ double heterojunctions, dark-line defects and recomb. centres, scanning photocurrent microscopy 79−35822
- GaAs-$Al_xGa_{1-x}As$ DH lasers, MBE grown, low current threshold, high lasing uniformity 79−64223
- GaAs-$Al_xGa_{1-x}As$ DH broad contact pulse lasers, second-order coherence props. 80−23685
- GaAs-$Al_xGa_{1-x}As$ DH lasers, very low current threshold, MBE grown 80−43353
- GaAs-$Al_xGa_{1-x}As$ DH lasers, MBE grown, substrate temp. effect on current threshold 80−48243
- GaAs-$Al_xGa_{1-x}As$ DH laser, MBE grown, CW electro-optical props. 80−102725
- GaAs-$Al_xGa_{1-x}As$ electro-optic frequency- and polarisation-modulated injection laser 80−91810
- GaAs-$Al_xGa_{1-x}As$ films for optical devices, masked MBE 78−38100
- GaAs-$Al_xGa_{1-x}As$ heterojunction, avalanche phototransistors, detectivity and noise 78−2558
- GaAs-$Al_xGa_{1-x}As$ heterojunctions, MBE grown, photocollection efficiency and interface charges 79−11199
- GaAs-$Al_xGa_{1-x}As$ heterostruct., photon recycling, diffusion length and lifetime determ. 79−47499
- GaAs-$Al_xGa_{1-x}As$ heterojunctions, LPE grown, 2D electron gas obs. 79−99606
- GaAs-$Al_xGa_{1-x}As$ heterojunction interface, two-dimensional hole gas obs., Shubnikov-de Haas meas. 80−80357
- GaAs-$Al_xGa_{1-x}As$ heterostructures, real-space electron transfer by thermionic emission, analytical model 80−100512
- GaAs-$Al_xGa_{1-x}As$ integrated injection lasers and detectors with etched reflectors 77−62074
- GaAs-$Al_xGa_{1-x}As$ LPE heterojunction, interface states 78−19128
- GaAs-$Al_xGa_{1-x}As$ multilayer struct., MBE, selective area growth using Si shadow masks 77−85946
- GaAs-$Al_xGa_{1-x}As$ modulation-doped heterojunction superlattices, electron mobilities 79−7877
- GaAs-$Al_xGa_{1-x}As$ multilayer, photoluminesc., electron spin orientation 80−25453
- GaAs-$Al_xGa_{1-x}As$ MOS rib waveguide polarizers 80−64207
- GaAs-$Al_xGa_{1-x}As$ MOS rib waveguide polariser, modulator and isolator 80−64217
- GaAs-$Al_xGa_{1-x}As$ multilayers, two-dimens. transport at high mag. fields 80−65724
- GaAs-$Al_xGa_{1-x}As$ single heterostructure laser diode, pulse operating, anal. of temp. decrease in active region 78−13706
- GaAs-$Al_xGa_{1-x}As$ stripe geometry DH laser, threshold current density, effect of optical mode losses 78−59008
- GaAs-$Al_xGa_{1-x}As$ superlattice, mag. field induced dimensionality change 78−64381
- GaAs-$Al_xGa_{1-x}As$ structures for DH lasers, LPE *(Polish)* 79−4922
- GaAs-$Al_xGa_{1-x}As$ strip-buried heterostruct. laser with distributed feedback 79−76696
- GaAs-$Al_xGa_{1-x}As$ strip buried heterostructure lasers 79−81425
- GaAs-$Al_xGa_{1-x}As$ system, injection layers with double heterostruct., injection lasers, amplified luminesc. 80−2824
- GaAs-$Al_xGa_{1-x}As$ superlattice, electronic props. 80−11080
- GaAs-$Al_xGa_{1-x}As$ strip buried heterostructure laser with passive DBR 80−14352
- GaAs-$Al_xGa_{1-x}As$-GaP photocathodes, minority carrier diffusion length determ. by photoluminesc. 80−103992
- GaAs-AlAs, alternate monolayer single cryst., optical waveguides 77−72065
- GaAs-AlAs, epitaxial layer, partition coefficients of impurities 77−15443
- GaAs-AlAs, epitaxial struct. with alternate layer comp. modulation, fabrication and characterisation 77−1322
- GaAs-AlAs, heterolight diodes, mesoconstruction, output *(Russian)* 77−12441
- GaAs-AlAs, heterostructure, effects of cation order on energy bands 80−11081
- GaAs-AlAs, large area p-n heterojunctions, vapour phase epitaxially grown, elec. characterisation 77−11990
- GaAs-AlAs, one-dimensional superlattice, X-ray diffr. 77−27860
- GaAs-AlAs, pseudobinary alloy, phase diagram calc. 78−52786
- GaAs-AlAs alternating monolayers, zone folding effects on phonons 78−72510
- GaAs-AlAs and related monolayer heterostructures, pseudopot. calc 78−60198
- GaAs-AlAs heterojunction, recombination currents 78−14806
- GaAs-AlAs layered films, MBE prep., struct., rel. to optical props. 79−77950
- GaAs-AlAs layered superlattices, deposited by MBE, exam. of crystal growth kinetics 78−72739

aluminium compounds continued
GaAs-AlAs mixed crystal, optical obs. of multiple-photon absorpt. NMR *(Russian)* 77−90073
GaAs-AlAs mixed crystals, valence charge distrib. and elec. field gradients 80−80239
GaAs-AlAs multilayer heterostructure laser, power and photoelectroluminescence characts. 80−53297
GaAs-AlAs superlattice, folded acoustic phonons obs., Raman scatt. 80−88996
GaAs-AlAs system, diffuse scatt. of X-rays by single crysts. *(German)* 78−30517
GaAs-AlGaAs DH, improved LPE growth, lasing characts. 77−81229
GaAs-AlGaAs DH injection laser with stripe contacts, radiation pulse stepped shape 80−91799
GaAs-AlGaAs DH laser, rapid degradation caused by process-induced defects 77−71985
GaAs-AlGaAs DH laser, improved lifetime by defects reduction during LPE 77−75547
GaAs-AlGaAs DH laser with buried facet 78−55373
GaAs-AlGaAs DH laser, degradation rate rel. to photocurrent 80−28233
GaAs-AlGaAs DH laser structure, defect assessment by differentiated cathodolum. topography 80−59819
GaAs-AlGaAs DH layers, tapered growth by wipingless LPE 77−66594
GaAs-AlGaAs half-ring laser, fabrication by deep Zn diffusion 78−17960
GaAs-AlGaAs heterojunction superlattices, electron mobilities 80−29473
GaAs-AlGaAs heterojunction superlattices, obs. of intersubband excitations in multilayer two dimensional electron gas 80−29753
GaAs-AlGaAs heterojunction superlattices, inelastic light scatt. by two-dimens. electron gas 80−93360
GaAs-AlGaAs heterostructure thyristors, operation and elec. characts. 79−7891
GaAs-AlGaAs high-radiance LED for optical communication systems, power and modulation bandwidth 78−42416
GaAs-AlGaAs LPE growth, wipinglass method for DH laser *(Japanese)* 78−48304
GaAs-AlGaAs LPE layers, baking effect on surface morphology 78−14625
GaAs-AlGaAs multilayer stack, optical surface wave propag. 78−38090
GaAs-AlGaAs photoelectroluminescent diodes, characts., radiant power 80−6972
GaAs-AlGaAs solar cells *(Rumanian)* 80−93877
GaAs-AlGaAs superlattice, selective transmission of HF phonons 80−34154
GaAs-AlGaAs transverse junction stripe laser, single mode behaviour after 12000 hr ageing test 78−66831
GaAs-AlGaAs:Si heterojunction interface, two-dimens. electron gas, Hall effect and cyclotron reson. meas. 79−65530
GaAs-Ga$_{0.7}$Al$_{0.3}$As (001), (211), threading dislocation in single layer heteroepitaxial struct., bowing 79−65341
GaAs-Ga$_{0.8}$Al$_{0.2}$As layered struct., LPE, optical surface waves 78−48244
GaAs-Ga$_{1-x}$Al$_x$As, DH, dark line defects induced by mech. bending 77−683
GaAs-Ga$_{1-x}$Al$_x$As, monolithically integrated DFB diode laser, freq. multiplexing 77−702
GaAs-Ga$_{1-x}$Al$_x$As, n$^+$-i-n heterojunction, radiative recombination under double injection *(Russian)* 77−77298
GaAs-Ga$_{1-x}$Al$_x$As, superlattice umklapp processes in resonant Raman scattering 78−64362
GaAs-Ga$_{1-x}$Al$_x$As, single-heterostructure laser diode with short current pulses, heat spreading analysis 79−76690
GaAs-Ga$_{1-x}$Al$_x$As, variable band gap, photo-EMF 80−20296
n-GaAs-Ga$_{1-x}$Al$_x$As, heavily doped superlattice, electronic props., perpendicular low temp. mobility 80−65660
GaAs-Ga$_{1-x}$Al$_x$As DH lasers, long-term degradation due to facet erosion 77−50672
GaAs-Ga$_{1-x}$Al$_x$As DH injection laser, curved junction stabilized filament, struct. and characts. 78−33744
GaAs-Ga$_{1-x}$Al$_x$As half-ring laser, fabrication by LPE over chemically etched channels 77−684
GaAs-Ga$_{1-x}$Al$_x$As heterostructures, quantum size effect in superlattices, electronic props. 80−29471
GaAs-Ga$_{1-x}$Al$_x$As laser, low threshold room temp. embedded DH, fabrication and characts. 77−681
GaAs-Ga$_{1-x}$Al$_x$As laser, optically pumped, longit. mode broadening due to transient heating 77−61953
GaAs-Ga$_{1-x}$Al$_x$As multilayer struct., growth over preferentially etched channels, MBE 77−40388
GaAs-Ga$_{1-x}$Al$_x$As n$^+$-ν-n junction, avalanche carrier multiplication *(Russian)* 78−76140
GaAs-Ga$_{1-x}$Al$_x$As repeated monolayer heterostructure, electronic struct. 77−66197
GaAs-Ga$_{1-x}$Al$_x$As red LED, 4% quantum yield *(Russian)* 77−85809
GaAs-Ga$_{1-x}$Al$_x$As single heterostructure laser diode, anal. of temp. rise under transient-state conditions 77−61949
GaAs-Ga$_{1-x}$Al$_x$As superlattices, resonance enhanced Umklapp Raman process 78−39547
GaAs-Ga$_{1-x}$Al$_x$As superlattice, sub-band dimensionality 78−63981
GaAs-Ga$_{1-x}$Al$_x$As stripe geometry lasers 79−94245
GaAs-Ga$_{1-x}$Al$_x$As superlattice, Raman scatt., polar phonon anisotropy 80−45052
GaAs-Ga$_{1-x}$Al$_x$As variable gap p-n junction, variable gap and photo EMFs 80−15596
GaAs-Ga$_{1-x}$Al$_x$As-Ga$_{1-y}$Al$_y$As n$^+$-i-n heterostructure, electroluminesc. characts., 80 to 330K *(Russian)* 79−28404
GaAs-Ga$_{1-x}$Al$_x$GaAs heterostructure, electron tunnelling theory 78−47861
GaAs-Ga$_{2.2}$Al$_{0.8}$As:Be, LPE, diffusion of Be into GaAs substrate 80−103517
GaAs-Ga$_x$Al$_{1-x}$As, injection laser with external resonator, mirrors of Michelson interferometer 79−81455
GaAs-Ga$_x$Al$_{1-x}$As DH diode lasers, single longitudinal mode operation 78−1243
GaAs-Ga$_x$Al$_{1-x}$As double heterojunction laser structures, LPE growth with double source method 79−28962
GaAs-Ga$_x$Al$_{1-x}$As DH laser wafers, active layer inhomogeneities 79−74106
GaAs-Ga$_x$Al$_{1-x}$As DH lasers, dislocation effects 79−82221
GaAs-Ga$_x$Al$_{1-x}$As heterostructure, depend. of efficiency of radiative transitions on composition 78−2909

aluminium compounds continued
GaAs-Ga$_x$Al$_{1-x}$As injection laser, large-optical-cavity, with low-loss distributed Bragg reflectors 78−1244
GaAs-Ga$_x$Al$_{1-x}$As laser, degradation, TEM obs. 77−51625
GaAs-Ga$_x$Al$_{1-x}$As superlattice, photoconductor with high sensitivity and reduced dark current appl. 79−7881
GaAs-GaAlAs, DH laser material, LPE grown, obs. of melt carryover 78−91553
GaAs-GaAlAs, heterostructure laser diode, lasing threshold calc. 80−28232
GaAs-GaAlAs, inverted-ridge-waveguide DH injection laser with current and lateral optical confinement LPE growth 77−75540
GaAs-GaAlAs, superlattice, subband related anisotropy in negative magnetoresistivity 80−11082
GaAs-GaAlAs (100) abrupt interface, carrier transmission and refl. coeffs. 79−69588
GaAs-GaAlAs bipolar transistor and heterostruct. laser, monolithic integration 80−102858
GaAs-GaAlAs CW diode laser, lateral mode stabilization using apertured facet reflectors 80−23708
GaAs-GaAlAs CW injection laser, stripe geometry DH, temporal coherence 80−38016
GaAs-GaAlAs channelled-substrate narrow-stripe lasers, low threshold currents 80−23706
GaAs-GaAlAs DH CW laser, growth by Peltier effect induced LPE 77−48357
GaAs-GaAlAs DH LEDs, with thin active layer, Burrus type, internal interference in emission spectrum 78−27325
GaAs-GaAlAs DH LED, transient current trap spectroscopy 78−80049
GaAs-GaAlAs DH laser on semi-insulating substrate using carrier crowding 77−83886
GaAs-GaAlAs DH laser diode, lateral modes 78−59009
GaAs-GaAlAs DH laser, beam scanning with twin-stripe injection lasers 79−10334
GaAs-GaAlAs DH laser with low threshold current, metalorganic CVD 79−50293
GaAs-GaAlAs DH lasers, strain-enhanced luminesc. degradation, photoluminesc. obs. 80−69392
GaAs-GaAlAs DH laser, O$^+$ isolation compared with SiO$_2$ isolation 80−74382
GaAs-GaAlAs double heterostruct., self-absorpt. effects on radiative lifetime 77−39928
GaAs-GaAlAs embedded stripe DH laser with polycryst. GaAsP, cleaved mirrors 77−75548
GaAs-GaAlAs embedded stripe DH laser with polycryst. GaAsP, etched mirrors 77−75549
GaAs-GaAlAs grating coupled lasers, output power efficiency 77−79858
GaAs-GaAlAs heterostructures, growth by metal-alkyl hydride process 78−15313
GaAs-GaAlAs heterostructure, GaAs preferential etching, using O$_2$ and CCl$_2$F$_2$ 79−8373
GaAs-GaAlAs injection lasers, on semi insulating substrates, using laterally diffused junctions 78−37910
GaAs-GaAlAs injection laser, branching waveguide directional coupler, fabrication and operation 78−38047
GaAs-GaAlAs injection lasers on semi-insulating substrates using laterally diffused junctions 78−55364
GaAs-GaAlAs injection laser sources for fibre optic communications, design 79−31923
GaAs-GaAlAs injection lasers, narrow-stripe proton-implanted, high bit-rate modulation 80−91824
GaAs-GaAlAs LEDs, deep levels *(French)* 78−56218
GaAs-GaAlAs laser, degraded, characterisation by selective etching and photoetching 80−48252
GaAs-GaAlAs laser, optical repeater using PFM at 1 GHz 79−98395
GaAs-GaAlAs multilayer struct., Hall mobility enhancement 80−100511
GaAs-GaAlAs multiple-stripe phase-locked laser array, behaviour 79−45955
GaAs-GaAlAs nonplanar large optical cavity laser, pulsed room temp. operation 80−28244
GaAs-GaAlAs planar stripe DH laser, origin of dark line defects 77−75510
GaAs-GaAlAs room temp. DBR lasers, highly collimated broadside emission 78−1428
GaAs-GaAlAs superlattices, metalorganic VPE growth, in sites ellipsometry monitoring 80−70547
GaAs-GaAlAs TJS lasers, high power density single mode operation, Si$_3$N$_4$ facet coating 79−86186
GaAs-GaAlAs wafers, defects and degradation, transmission cathodolum. evaluation 80−65395
GaAs-GaAlAs-GaAs rectifying semicond. struct., prep. by MBE and characts. 80−65657
n-GaAs-n-Al$_x$Ga$_{1-x}$As rectifying heterojunction, cond. props. study 80−88626
(GaAs)$_n$-(AlAs)$_n$, multilayer heterostructure, cation order, effect on energy bands 79−1570
GaAs$_{0.84}$Al$_{0.16}$As, surface processing, residual film monitoring by ellipsometry 80−13124
(GaAs)$_n$(AlAs)$_m$ multilayers, MBE, interdiffusion, X-ray diffr. study 80−70474
GaAsSb/GaAlAsSb DH lasers, growth and props. 80−69412
GaAs$_{1-x}$Sb$_x$-Al$_y$Ga$_{1-y}$As$_{1-z}$Sb$_z$, DH laser, threshold characts. and extended wavelength operation 78−9379
GaN-AlN, solid solution, epitaxial growth and electrical props. 77−73236
GaP-Al$_x$Ga$_{1-x}$P, DH electrooptical strip modulator *(Russian)* 78−1344
GaP-AlGaP, stripe-geometry electrooptical modulator 80−23798
GaP-GaAlP, heterojunction cold cathode 79−69965
p-GaSb−n-Ga$_{1-x}$Al$_x$Sb, photodiode, LPE, spectral response, quantum efficiency 78−47850
Ge-Al$_2$O$_3$ composite film, optical props., appls. 77−754
Ge$_x$Al$_{1-x}$ amorphous film junction, I-V and C-V characts. 77−85307
n-Ge$_{1-x}$Al$_x$As:Te, long-lifetime photocond. effect obs., Hall effect meas. 77−89795
HgCr$_{2-x}$Al$_x$Se$_4$, temp. depend. of ESR linewidth, 105-300K 80−71161
HoAlO$_3$, neutron diffr. at 0.04K, mag. ordering *(French)* 78−10653
In$_{1-x}$Al$_x$As, band gap, IR absorpt. spectra meas. 80−66205
In$_x$Al$_{1-x}$P, proportional ingredient content determ. by X-ray fluoroscopy 80−97747
InAs-Al$_x$Ga$_{1-x}$Sb heterojunctions, elec. and photoelec. props. 79−11206

aluminium compounds continued
- InAs-AlAs, phase diagram plotting by DTA and thermodynamic calc. 77—86016
- InGaAsSb-AlGaAsSb DH laser, room temp. operation at 1.8 μm wavelength 80—43358
- $KAl(CrO_4)_2.2H_2O$, cryst. struct. *(French)* 77—80478
- $KAl(SO_4)_2.12H_2O$, single cryst., Raman spectra, temp. depend., SO_4^{2-} site dynamic disorder 77—40219
- $KAl(SO_4)_2.12H_2O$, occlusion formation during dendritic crystal growth, expt. 78—38993
- $KAl(SO_4)_2.12H_2O$, third order elastic consts. from stress shifted reson. freqs. 78—55905
- $KAl(SO_4)_2.12H_2O$, secondary nucleation, origin, nuclei size distrib. 79—94933
- $KAl(SO_4)_2.12H_2O{:}MnO_4^-$, visible and UV absorpt. spectra interpretation 80—45116
- $K_2Al_2(SO_4)_4.24H_2O$, temp. depend. curves of quadrupole interaction parameter for $^{27}Al^{3+}$ 77—55727
- $KAlSiO_4$ metastable polymorph, prep. by ion exchange with $RbAlSiO_4$, struct. 78—79585
- $KAlSi_3O_8$, orthoclase, impact structs., peak shock press., X-ray diffr. investig., lunar rock bombard. appls. 78—7002
- $K_xAl_xTi_{8-x}O_{16}$, ionic cond., K mobility rel. to struct. and bonding *(French)* 77—76594
- $K_xAl_xTi_{8-x}O_{16}$, ionic cond., rel. to struct. and chemical bonding *(French)* 78—18824
- $KAl[Fe(CN)_6]$, isomer shift of Mossbauer spectra 80—29662
- $KCr_xAl_{1-x}(SO_4)_2.12H_2O$, EPR of single crystals, zero-field splitting of Cr^{3+} 80—66015
- $KO_{0.5}$-$AlO_{1.5}$-SiO_2 system, activities calc. from vapour press. meas. and known data 79—91985
- K_2O-Al_2O_3-P_2O_5-TiO_2, structural role of Ti, kinetic study of chem. destruction 80—88055
- K_2O-AlF_3-B_2O_3 glass, Al atom bonding mode, optical absorption of VO^{2+} and AlK_α spectrum *(Japanese)* 78—11023
- $KPO_3.Al(PO_3)_3{:}U$, vibronic excitation, absorption and emission spectra 78—52524
- K_2S-Al_2S_3, prep., phase props. and elec. cond. 79—96010
- $K_2SO_4.Al_2(SO_4)_3.24H_2O$, stirring effect on crystalline quality of soln. grown crystals 78—91281
- $LaAl_{0.85}Mg_{0.15}O_{2.925}\square_{0.075}$, $LaAl_{0.8}Mg_{0.2}O_{2.9}\square_{0.1}$, ionic conductivity 77—20119
- $LaNi_5H_6$ sponges, Al substitution, neutron diffr. 80—24427
- Li-Al-Cl system, thermodynamic props., phase equilib. 80—89211
- Li-Al-borophosphate glass, activated with Ag, in-reactor dosimetry *(Russian)* 77—83113
- LiAl ferrite, substituted ferrospinel, spin configuration determ. *(Russian)* 77—32162
- $Li_{0.5}Al_xFe_{2.5-x}O_4$, polycrystalline, ferromag. reson. absorpt. curves, stress effects *(Russian)* 77—20713
- $Li_{0.5}Al_xFe_{2.5-x}O_4$, polycrystalline ferromagnetic reson. theory applicability limits *(Russian)* 77—55709
- $LiAlSiO_4$, β-eucryptite one-dimens. fast ion cond., temp. depend. of cryst. struct. 80—107191
- β-$LiAlSiO_4$, eucryptite, one-dimensional ionic conductor, neutron scatt. study 80—49361
- β-$LiAlSiO_4$, superionic cond., NMR relax. 77—12220
- $LiAlSiO_4{:}Cu$, β-eucryptite solid electrolyte, Cu^{2+} EPR obs. of ion exchange props. 80—108056
- $LiAlSi_2O_6$, IR refl. spectra dispersion anal. 79—99877
- $LiAlSi0_4$, β-eucryptite, superionic conductor, order-disorder transition, microwave impedance obs. 79—14966
- $LiBaAlF_6{:}Eu^{2+}$, luminesc., band emission and line emission 79—28810
- $LiCl$-$AlCl_3$, phase diagram determ. by DTA and X-ray anal. *(Japanese)* 78—92250
- $LiCl$-$NaCl$-$AlCl_3$ melt, elec. cond., 800 to 1200K *(Japanese)* 80—24633
- $LiCl$-$NaCl$-$AlCl_3$ ternary melt, density as function of temp. and composition, meas. by macrometric method *(Japanese)* 79—42130
- LiF-AlF_3, mixture at 1293K, thermodynamic function 80—104134
- LiF-AlF_3-Na_3AlF_6-Al_2O_3 system, phase equilibrium, X-ray diffr., DTA, quenching, optical microscopy study 80—50610
- LiF-$NaPO_3$-AlF_x glasses, IR spectroscopy study 80—16042
- $Li_{0.5}Fe_{2.17}Al_{0.33}O_4{:}Co$, single cryst., domain struct., mag. annealing effect depend. on induced anisotropy 78—68290
- Li_2O-Al_2O_3-GeO_3, glass, interdiffusion coeffs. of Li and Na 80—88369
- $Li_2O.nAl_2O_3(7.3\text{-}n)SiO_2$, metastable solid soln., Al^{3+} vacancy incorporation 77—12593
- $LiPO_3$-$Al(PO_3)_3{:}Ag$ glass, ionic motions, thermally stimulated depolarisation study 79—65239
- $LiPO_3.Al(PO_3)_3{:}U$, vibronic excitation, absorption and emission spectra 78—52524
- Li_2S-Al_2S_3, prep., phase props. and elec. cond. 79—96010
- $Li_x(Si,Al)_{12}(O,N)_{16}$, α′-Sialon ceramics, prep. and characterisation 78—84750
- Mg-Al spinel, hot pressed ceramic, annealing effect on transparency and microstruct. *(Japanese)* 79—74188
- Mg-Al spinel, non-stoichiometric, climb dissociation of network dislocations 80—2031
- Mg-Si-Al-O-N, grain boundary segregation, combined X-ray microanal. and lattice fringe imaging determ. 79—15681
- $MgAl_xFe_{2-x}O_4$, comp. effects on ferrite characts. 78—52305
- $MgAl_2O_4$, composition rel. to ceramic microstruct. form., light transmission 79—43188
- $MgAl_2O_4$, IR spectrum exam. 78—76454
- $MgAl_2O_4$, transverse elastic wave damping at 36.5 GHz 77—80583
- $Mg_{0.7}Na_{0.9}K_{2.0}Ca_{2.4}Al_{9.1}Si_{26.9}O_{72}.xH_2O$, erionite, cryst. struct. exam., stacking faults 78—2083
- $2MgO$-$2Al_2O_3$-$5SiO_2$, cordierite, synthesis rel. to WC addition 77—8787
- MgO-$CaMgSiO_4$-Al_2O_3, spinel phase, phase equilibrium relations and spinel bonding 80—55376
- MgO-$CaMgSiO_4$-$(Al_{0.5}Cr_{0.5})_2O_3$, spinel phase, phase equilibrium relations and spinel bonding 80—55376
- MgO-CaO-FeO-Fe_2O_3-SiO_2-Cr_2O_3-Al_2O_3 spinel refractories, physicochem. prod. conditions 80—89185
- MgO-Nd_2O_3-$Al(Cr)_2O_3$, reactions kinetics in mixtures of components and phases 77—40523
- $MgO.Al_2O_3$-$MgO.nAl_2O_3$ spinel, coordination state of atoms, charact. X-ray emission *(Japanese)* 78—6816
- $MgO.nAl_2O_3$, nonstoichiometric spinel, DTA 77—28791
- NH_3-$AlCl_3$ solution, Al_2O_3 ultrafine gel particle form. 80—93807

aluminium compounds continued
- $NH_4Al(OH)_2CO_3$, NH_4-dawsonite, cryst. struct., X-ray powder diffr. *(Japanese)* 79—69096
- $(NH_4)_2Al(SO_4)_2$, ^1H spin-lattice relax., 100-500K 79—38398
- $NH_4Al(SO_4)_2.12H_2O$, third order elastic consts. from stress shifted reson. freqs. 78—55905
- $NH_4Al(SO_4)_2.12H_2O$, dielectric losses, proton spin lattice relaxation by NH_4^+ hopping 79—56721
- $NH_4Al(SO_4)_2.12H_2O$, CrO_4^{3-} centres, EPR and optical absorption spectra 79—91475
- $NH_4Al(SO_4)_2.12H_2O{:}Mo^{3+}$, EPR, X-band, ion position and spin-Hamiltonian parameters 77—48042
- $NH_4Al(SO_4)_2.12H_2O{:}Fe^{3+}$, spin-lattice relax. of paramag. ions, Mossbauer effect 79—95688
- $(NH_4)_2SO_4.Al_2(SO_4)_3.24H_2O$, temp. depend. curves of quadrupole interaction parameter for $^{27}Al^{3+}$ 77—55727
- $(NH_4)_2SO_4.Al_2(SO_4)_3.24H_2O{:}Cr^{3+}$, and deuterated derivative, structural transition studied by EPR 77—85553
- $NaAl(CO_3)(OH)_2$, cryst. struct., IR spectral investig. 77—8567
- $NaAlCl_4$, relative enthalpy to 573K and standard enthalpy of form., molar enthalpy of fusion 80—50878
- $NaAl(CrO_4)_2.2H_2O$, cryst. struct. *(French)* 77—80478
- Na_3AlF_6, molten, structure *(French)* 77—51297
- Na_3AlF_6-LiF-CaF_2-AlF_3-Al_2O_3, electrolyte, exam. of phase equilibria, review 79—11590
- $Na_8Al_6Ge_6O_{24}.CO_3.2H_2$, cryst. struct. 78—83805
- $NaAl(MoO_4)_2$, domain struct., phase transition, and dielec. props. 79—56748
- $NaAl(MoO_4)_2$, ferroelastic, domain struct. obs. 77—15483
- $Na_{0.91}Al_2(Si_{3.09}Al_{0.91})O_{10}(OH)_2$, paragonite 1M, cryst. struct. determ., electron diffr. 78—26547
- $NaAlSi_3O_8$, cryst., Al-Si order-disorder, electroneutrality effects in model 79—90593
- $Na_6Al_6Si_6O_{24}(NaX)_{2n}$, X=Cl, Br or I, sodalites, thermal destruction of colour centres *(Russian)* 80—84169
- $Na_6Al_6Si_6O_{24}.NaX_{(2-n)}$, (X=Cl, Br, I), X-ray irrad., thermal-erase cathodochromism and dihalide mol. centres *(Russian)* 80—66236
- $Na_3Al_3Si_3O_{12}.2H_2O$, cryst. struct. determ. 79—90625
- $Na_2Al_2Ti_6O_{16}$ bronze, synthesis in $NaBO_2$, growth conditions *(French)* 78—43998
- $NaCl$-$AlCl_3$, phase diagram determ. by DTA and X-ray anal. *(Japanese)* 78—92250
- $NaCl$-$AlCl_3$ melt mixtures, viscosity meas. 79—82368
- $NaCl$-$AlCl_3$-$CrCl_3$, molten, electrochemical exam. of Cr 78—56939
- NaF-AlF_3 binary melt, density and elec. cond. *(Japanese)* 78—18814
- NaF-AlF_3 melt mixture, viscosity meas. 79—82369
- NaF-AlF_3 system, thermodynamics, solid soln. in cryolite 79—52183
- β-Na_2O-Al_2O_3, single cryst. Czochralski growth 77—77367
- Na_2O-Al_2O_3-TiO_2 ternary systems, X-ray investigation 79—51067
- Na_2O-K_2O-$Al_2O_3SiO_2$-H_2O system A-type zeolites, crystn. from Na-K silicaalumo gels, and characts. 79—52780
- $NaPO_3$-$AlF_3(\text{-}NH_4HF_2)$ glasses, synthesis, chem. thermal and optical anal. *(French)* 79—100104
- $NaPO_3.Al(PO_3)_3{:}U$, vibronic excitation, absorption and emission spectra 78—52524
- Na_2S-Al_2S_3, prep., phase props. and elec. cond. 79—96010
- Nb-Al_2O_3 composite, semicond. films, cond. on localised states 77—24628
- Nd-Al-Cl complex, Nd^{3+} vapour phase laser expts. 78—66813
- $Nd(Al,Cr)_3(BO_3)_4$, CW laser action, CR^{3+} cross pumping, Nd^{3+} direct pumping 79—64231
- $NdAl_3(BO_3)_4$, cw laser action at 1.3 μm 79—27258
- $NdAl_{2.07}(B_4O_{10})O_{0.6}$ nonstoichiometric, crystal struct. by X-ray spectral microanalysis 79—77582
- $NdAl_3[BO_3]_4$, luminescence and lasing characts., solubility 79—31910
- $NdAl_3[BO_3]_4$, single phase crystallisation region from solvent melt 80—38977
- $NdCl_3$-$AlCl_3$ vap. complexes, Nd^{3+}, $^4F_{3/2}$ level deactivation 77—61786
- $NdCl_3$-$AlCl_3$ vapour complex, optical gain at 1.06 μm 78—33742
- OAlCl and OAlF, IR matrix spectra, vibr. freqs. *(German)* 79—11785
- $Pb_{1-x}Al_xF_{2+x}$, ionic cond. of quenched and annealed specimens, interstitial cond. mechanism 80—2199
- PbF_2-AlF_3, ionic cond., characts., effect of trivalent cations 77—89576
- PbF_2-AlF_3 glass, optical props., crystn. and thermal expansion 80—48367
- PbF_2-AlF_3 glass, prep. and props. 80—49120
- α-$Rb_5Al(MoO_4)_4$, cryst. struct. 79—19219
- $RbAl(SO_4)_2.12H_2O$, ENDOR of $^{57}Fe^{3+}$ in trigonally distorted octahedral sites 79—38405
- $RbAl(SO_4)_2.12H_2O$, spin-Hamiltonian with trigonal S^3I terms for describing $^{57}Fe^{3+}$ ENDOR spectra 80—75885
- $RbAl(SO_4)_2.12H_2O{:}Cr^{3+}$, high order EPR transitions 79—22736
- $SbCl_3/AlCl_3$ molten mixtures, Raman spectra 80—93305
- (Si,Al)N, vapour deposition, feasibility of fusion reactor first wall regeneration in situ 77—18701
- Si-Al-B-O-N, calc. of phase diagrams from data set 80—55362
- Si-Al-Be-C-N system, phase equilibria 80—60839
- Si-Al-O-N, ceramics, thermal decomposition 79—91936
- Si-Al-O-N, compression creep, comparison with SiC and Si_3N_4 79—15728
- Si-Al-O-N ceramic, grain boundary desegregation and intergranular cohesion 80—100872
- Si-Al-O-N ceramic, single phase form. using hot pressing *(Japanese)* 79—70031
- Si-Al-O-N ceramic systems, layer struct. 80—6382
- Si-Al-O-N ceramics, grain boundary segregation determ. by X-ray microanal. and lattice fringe imaging 79—15681
- Si-Al-O-N composites, dense direct prep. from naturally occurring SiO_2 and Al powder 78—11187
- Si-Al-O-N polytypes, direct lattice resolution using high resolution electron microscopy 78—38682
- Si-Al-O-N system, exam. of compounds and properties 78—48387
- Si-Al-O-N system, ionic cond. from 850 to 1400°C 80—2203
- Si-Al-O-N system, phase analysis and TEM struct. obs. 80—108420
- Si-Al-O-N system, stable phase cryst. struct. and microstruct. obs. using TEM 80—108421
- Si-Al-O-N system, TEM exam. of X phase structure 78—56606
- Si-Al-Zr-O-N, calc. of phase diagrams from data set 80—55362
- Si_5-Al-O-N_7, hot pressed, exam. of fracture mechanisms 78—72879
- SiAlON ceramic, pressureless sintering 78—27449
- SiAlON powder, prod. by reaction clay+C+N_2 80—40295

aluminium compounds continued
SiAlON, prepared from siliceous sand and Al powder, hot pressing, steatite contamination effects *(Japanese)* 80—93528
SiAlON system, β', 15 R phases, oxidation resist. *(French)* 78—72899
$Si_{6-x}Al_xO_xN_{8-x}$, x=1.5, 3, 4, Sialon ceramics, elec., thermal cond. 79—33124
$Si_{6-z}Al_zO_zN_{8-z}$, hot pressed, DC elec. props., 18-500°C, fields up to 1.1×10^4 V cm^{-1} 78—26860
$Si_{(6-Z)}Al_ZO_ZN_{(8-Z)}$ 78—39136
$SiC\text{-}Al_2O_3$, hot pressing, role of grain boundaries 77—24999
Si_3N_4/Al_2O_3, powder compact, electron microprobe investigation of reactions *(French)* 80—26009
$Si_3N_4\text{-}Al_2O_3\text{-}AlN$, isothermal sections, free energy of formation 80—55363
$Si_3N_4\text{-}Al_2O_3\text{-}AlN$, Sialon, fabrication and reaction sintering 77—44201
$\beta\text{-}Si_3N_4\text{-}AlN\text{-}Al_2O_3\text{-}MgO$, insolubility of Mg in $\beta\text{-}Si_3N_4$ 79—10953
$Si_3N_4\text{-}AlN\text{-}Al_2O_3\text{-}SiO_2\text{-}Y_2O_3$, phase equilibrium study by X-ray diffr. and optical microscopy 80—50614
$Si_3N_4\text{-}AlN\text{-}SiO_2\text{-}Al_2O_3$ solid-liquid equilibria 78—92247
$Si_3N_4\text{-}SiO_2\text{-}AlN$ mixture, reaction sintering forming $\beta\text{-}Si_3N_4$ solid soln. 79—52145
$Si_3N_4\text{-}SiO_2\text{-}AlN$ system, β-Sialon form. *(Japanese)* 80—45261
$Si_3N_4AlN\text{-}Al_2O_3$ system, reaction sintering forming $\beta\text{-}Si_3N_4$ solid solns. 80—50585
$SiO_2\text{-}Al_2O_3$, coprecipitated gel, Si-Al spinel formation during transformation on heating 79—78958
$SiO_2\text{-}Al_2O_3$ system, location of metastable immiscibility gap 79—77521
$SiO_2\text{-}Al_2O_3\text{-}Si_3N_4$, isothermal sections, free energy of formation 80—55363
$SiO_2\text{-}AlN$ mixture sintering, form. of $\beta\text{-}Si_3N_4$ solid solns. 78—23655
$SiO_2\text{-}Al(OH)_3$, derived from metalalkoxides, sintering behaviour 79—29005
$Sr_2Al_2GeO_7$, gehlenite struct., synthesis and physicochem. props. 79—43181
$SrAl_2Si_2O_8$, TEM obs. of feldspar aand hexacelsian polymorphs 78—83827
Ta-Al-N thin film resistors with improved elec. props. 80—100544
Tb-Al-Cl vapour complex, fusion laser gain medium 78—63073
$TbCl_3\text{-}AlCl_3$ complex, fluoresc. spectrum and gas-phase lasing 77—83861
$TbCl_3\text{-}AlCl_3$ vap. complex, kinetics and laser fusion pot. 79—98343
$TbCl_3(AlCl_3)_x$ complex, potential Tb^{3+} vapour laser system, fluoresc. obs. 78—66812
Ti-Al-C(N) system cpds., abrasive power, glass grinding 77—63820
Ti_2AlC, Ti_3AlC, TiC, phys. props. 77—43602
TiN-AlN, composite, erosion resist. in electron stream 78—11365
TiN-AlN composites, struct. and props. 77—40413
$Ti_3O_5\text{-}Al_2TiO_5$, solid solubility, X-ray phase and optical microscopic exam. 80—59657
$V/Al\text{-}Al_xO_y\text{-}Pb$ tunnel junction, superconducting transition, critical currents, Josephson effect *(Russian)* 80—29507
$V_{0.985}Al_{0.015}O_2$, insulating T-phase cation disproportionation and V-V pairing 77—62825
$V_{1-x}Al_xO_2$, phase diag. 77—52308
$V_2O_3\text{-}Al_2O_3$ solid soln., interactions between V atoms, comp. and temp. depend. of mag. susceptibility 77—8056
$V_2O_5\text{-}AlNbO_4$ system, interfacial reactions, efficient boundary conditions and solid state reactivity 80—76542
Y-Si-Al-O-N solid soln., based on $\alpha\text{-}Si_3N_4$ struct., comp. and struct. 79—74136
YAG, optical films, high quality growth 79—46984
$YAl_3(BO_3)_4$, and $(Y,Er)Al_3(BO_3)_4$, crystallisation and growth characts., density and composition 80—35080
$YAl_3(BO_3)_4$, cryst. growth rate determ. 79—86731
$YAl_3(BO_3)_4$, crystallisation from solution in a melt, solvent composition 80—38976
$YAl_3(BO_3)_4$, thermolum. anal. 79—87514
$YAl_3B_4O_{12}{:}Bi^{3+}$, luminesc., vibr. struct., energy transfer 79—38584
$Y_2O_3\text{-}AlN\text{-}SiO_2$ oxynitride glasses, elec. props. 80—80267
$Y_2O_3\text{-}SiO_2\text{-}Al_2O_3$ system, composition depend. of refractive index in vitrification region 77—24812
$Y_x(Si,Al)_{12}(O,N)_{16}$, α'-Sialon ceramics, prep. and characterisation 78—84750
$Y_{1-x}Tb_xAl_3B_4O_{12}$ phosphors, cathodoluminesc. 77—73177
$ZnS\text{-}Al_2S_3$, phase relationships, 720 to 1110°C 79—1852
Zr-Al-O system, diffusion welding, 1000 to 1300°C, Al_2O_3-(Zr-Al) alloy, ZrO_2-(Zr-Al) alloy, $Al_2O_3\text{-}ZrO_2$ couples *(German)* 79—33122
ZrN-AlN, composite, erosion resist. in electron stream 78—11365
ZrN-AlN composites, struct. and props. 77—40413

aluminosilicate glasses
β-spodumene, glass-ceramics, internal stresses 79—15770
alkali, acid resistance 80—21140
alkali aluminosilicate melt, wetting of graphite materials 77—1831
alkali boroaluminosilicate system, self-focusing fibres with aperture of 0.18 80—87548
alkali oxide-$Al_2O_3\text{-}SiO_2$ glass, EPR 78—91930
aluminoborosilicate, working props. during microfibre and ultrafine fibre prod. 79—24486
aluminosilicate glass:Co (14.3 wt.%), AC susceptibility meas. 80—88771
annealed and tempered, fracture strength studies under dynamic conditions 79—96132
barium aluminosilicate glass coating on NbZr, d and He ion irrad., blistering 77—35605
boroaluminosilicate glasses, alkali free, density calc. *(Chinese)* 78—14396
ceramic surface streaks and blisters, UV fluoresc. study 80—84347
diffusion of Sn(IV) 80—49417
fibres, crystn. during heat treatment 79—52258
fibres clad with $B_2O_3\text{-}SiO_2$ effect of drawing tension on residual stresses 78—64554
fluorophlogopite mica, glass-ceramic, thermal diffusivity, crystallisation effects 78—6190
gehlenite, crystallisation kinetics 79—4251
holograms, photoinduced anisotropic recording media 79—41354
machinable glass ceramic, elastic moduli, press. and temp. derivatives 78—52873
manganese aluminosilicate glass, insulating spin glass, exchange dipole optical transition 80—40136
$MgO\text{-}Al_2O_3\text{-}SiO_2$: ZrO_2, TiO_2, glass phase separation *(German)* 80—38932
mullite crystallisation from glass powder, during hot pressing 78—60639

aluminosilicate glasses continued
nitrides formed by reduction with C *(Japanese)* 78—68929
particles, new method for X-ray micro-anal., based on peak to background meas. 79—24881
petrological melts and glasses, Fe-containing, structural transformations 80—34170
phase separated, phase characterization by STEM and X-ray microanal. 80—50643
polishing, surface characts. using X-ray reflection grazing *(French)* 80—65353
sital, structural glass component, strength in complex stress state 79—91763
sitall cylindrical shell reinforced with internal stiffening ribs, stress-strain state under external press. 80—71684
Sitalls, soln. rate in alkali soln. 80—16531
sitalls, synthesis based on elec. power plant residues 80—40314
sodium-alumoborosilicate photochromic glasses, Weigert effect *(Russian)* 77—68250
spin-lattice relaxation times of paramag. hole and E_1'-centres 80—39871
tensile and impact strength, effect of surface damaging and annealing *(Czech)* 79—74227
thermally toughened, residual compressive stresses evaluation 78—31523
vibrational spectra and glass structure 80—84732
X-ray irradiated, high-dose, and reactor radiation effects 80—19838
X-ray spectral fluorescent analysis, standard function method, chemical analysis of glasses 79—52822
$40CaO.20Al_2O_3.40SiO_2$ slag glass, self-diffusion of Ca^{2+} ions *(Japanese)* 78—6173
Ag halide photochromic glass, darkening mechanisms under pulsed laser excitation 78—25938
Ag halide photochromic glasses, optical properties, effect of Cu ions 80—93364
$Al_2Mn_3Si_3O_{12}$, amorphous spin glass, spin relax. 79—65685
$Al_2Mn_3Si_3O_{12}$ glass, mag. ordering effects at low temps., Mossbauer and neutron diffr. meas. 77—16047
$Al_2Mn_3Si_3O_{12}$, spin correlations and phase transitions, neturon diffr. exam. 78—84390
$Al_2O_3\text{-}B_2O_3\text{-}SiO_2$, alkali glasses, granulating mechanism for medical use 80—40315
$Al_2O_3\text{-}B_2O_3\text{-}SiO_2$ glasses, elec. cond. study, 700-1900°C 79—65487
$Al_2O_3\text{-}B_2O_3\text{-}SiO_2$ sheet glass, solar energy appl., optical and mech. props. 80—87447
$Al_2O_3\text{-}B_2O_3\text{-}SiO_2$ system, metastable liq.-liq. phase separation 79—42263
$Al_2O_3\text{-}BaO\text{-}SiO_2$ glass coatings in fission and fusion reactors, permeation, elec. cond. and dielectric breakdown 80—18439
$Al_2O_3\text{-}CaO\text{-}SiO_2(\text{-}B_2O_3)(\text{-}Na_2O)$ composite glasses, high strength, prod. by overlayering 80—89193
$Al_2O_3\text{-}CoO\text{-}SiO_2$, spin correls., neutron diffr. meas. 80—15694
$Al_2O_3\text{-}MgO\text{-}SiO_2$, S-glass, solvent effect of water 77—4889
$Al_2O_3\text{-}MnO\text{-}SiO_2$, spin correls., neutron diffr. meas. 80—15694
$Al_2O_3\text{-}SiO_2$, struct., localised radiation centres, spectroscopic investig. *(Russian)* 77—69844
$Al_2O_3\text{-}SiO_2$ glasses, phase decomp., small-angle X-ray and neutron scatt. study 79—14688
$Al_2O_3\text{-}SiO_2$ powder, plasma-prepared, glass form. and phase transforms 77—44208
$Al_2O_3\text{-}SiO_2$ refractory, SiO_2-rich glassy phase, deconvolution of microprobe conc. profiles 77—52606
$Al_2O_3\text{-}SiO_2\text{-}Cu_2O$ glasses, Grueneisen's constant of low expansion 79—77779
$Al_2O_3\text{-}SiO_2\text{-}MO\text{-}Fe_2O_3$ glass, M=Ca, Mg, Ba, Sr, UV and EPR absorpt. spectra 80—89018
$Al_2O_3\text{-}SiO_2\text{-}MgO\text{-}CaO\text{-}Fe_{(l)}$, heterogeneous equilib. calcs. *(Russian)* 77—59093
$Al_2O_3\text{-}SiO_2\text{-}MnO\text{-}Cr_2O_3\text{-}B_2O_3$ system, additive in sintering of high-alumina ceramic 79—61544
$Al_2O_3\text{-}SiO_2\text{-}Na_2O\text{-}CaO\text{-}MgO\text{-}Fe_2O_3\text{-}SO_3$ glass, thermal capacity meas. at low temps. 80—44334
$Al_2O_3\text{-}SiO_2\text{-}Na_2O(Li_2O)$, coordination number study by AlK_α fluorescence X-ray spectra *(Japanese)* 77—73190
$Al_2O_3\text{-}SiO_2\text{-}P_2O_5$, refractory glasses, exam. of liquid immiscibility and crystallisation 78—55814
$Al_2O_3\text{-}Y_2O_3\text{-}SiO_2$ containing TiO_2, La_2O_3, exam. of elastic moduli and refractive indices 78—80502
$(Al_2O_3)_{0.2}(Ho_2O_3)_{0.2}(SiO_2)_{0.6}$, amorphous low temp., AC susceptibility, freq. depend. of spin freezing temp. 79—82808
$BaO\text{-}Al_2O_3\text{-}SiO_2$ ceramic, chem. resist. and struct. 79—61756
$BaO\text{-}Al_2O_3\text{-}SiO_2\text{-}TiO_2$ system glass-crystal material, elec. cond. 79—60876
$BaO\text{-}Al_2O_3\text{-}SiO_2\text{-}Ta_2O_5\text{-}Mo$ glass ceramic metal composites, cermet prep. 80—11618
$BaO\text{-}Al_2O_3\text{-}TiO_2\text{-}SiO_2$, glass formation, structure of cations *(Russian)* 80—38933
$BaO\text{-}SrO\text{-}Al_2O_3\text{-}TiO\text{-}SiO_2$ glass ceramics, cryst. phases form., BaO/SrO ratio influence 80—19705
$BaO.Al_2O_3.2SiO_2$, hydrothermal synthesis, phase transitions 77—48378
$BeO_2\text{-}Al_2O_3\text{-}SiO_2\text{-}MF_2$ (MF) glasses, M=Mg, Ca, Sr, Ba, Li, Na, fluoride ion role during crystn. 79—65176
Ca aluminophosphate foam glasses, for prosthetic appl., porosity and mech. props. 79—74128
$CaAl_2Si_2O_8\text{-}CaSiO_3\text{-}CaMgSi_2O_6$, exam. of glass forming regions and properties of glasses 79—4958
$CaO\text{-}Al_2O_3\text{-}B_2O_3\text{-}SiO_2\text{-}FeO$, glass, IR spectra at room and melt temp. 80—88986
$CaO\text{-}Al_2O_3\text{-}SiO_2$, glass ceramic prod. by TiO_2 nucleating agent 78—11189
$CaO\text{-}Al_2O_3\text{-}SiO_2$ additive to zircon ceramic, sintering and mech. props. 80—60814
$CaO\text{-}Al_2O_3\text{-}SiO_2$ based glasses, kinetic parameters of glass ceramic form. 77—24385
$CaO\text{-}Al_2O_3\text{-}SiO_2$ ceramic, chem. resist. and struct. 79—61756
$CaO\text{-}Al_2O_3\text{-}SiO_2$ glass-$MoSi_2$ filler, vitreous composite prod. 77—90313
$CaO\text{-}Al_2O_3\text{-}SiO_2$ glass, remanent magnetisation, log t low 78—68300
$CaO\text{-}Al_2O_3\text{-}SiO_2$ glasses, density-of-states and structural forms, Raman spectra study 80—97255
$CaO\text{-}Al_2O_3\text{-}SiO_2$ melt, at 1723 to 1823K, determ. of inter diffusivities matrix 78—43161
$CaO\text{-}Al_2O_3\text{-}SiO_2\text{-}TiO_2$ system glass-crystal material, elec. cond. 79—60876
$CaO\text{-}Al_2O_3\text{-}SiO_2\text{-}ZnO$, continuous unidirectional crystn. of fibrous metasilicates from melt 78—95739

aluminosilicate glasses continued
$CaO-Al_2O_3-TiO_2-SiO_2$, glass formation, structure of cations *(Russian)* 80−38933
$CaO-Li_2O-Al_2O_3-SiO_2:Nd^{3+}$, CaO enriched, laser-type glasses, spectroscopic behaviour 78−60497
$CaO-MgO-Al_2O_3-SiO_2$, glass-ceramic prep. by hot pressing and crystallisation of powder 78−11192
$CaO-MgO-Al_2O_3-SiO_2$, glass ceramic, prep. by hot pressing and crystallisation, mech. props. 78−15351
$CaO-MgO-Al_2O_3-SiO_2$, shale glass, glass forming and dielec. props. 78−22660
$CaO-MgO-Al_2O_3-SiO_2$, shale glass, crystn. behaviour 78−22661
$CaO-MgO-Al_2O_3-SiO_2-ZnO$, continuous unidirectional crystn. of fibrous metasilicates from melt 78−95739
$CaO-MgO-Al_2O_3-SiO_2$, quartz sand-dolomite-magnesia-clay based glasses, crystn. 80−20915
$CaO-MgO-Al_2O_3-SiO_2$, glass formation, at molar ratio CaO: MgO=1 *(Russian)* 80−39269
$CaO-SiO_2-Al_2O_3$, effect of Al_2O_3 on viscosity if ternary aluminosilicates *(Japanese)* 78−83989
$CaO-SiO_2-Al_2O_3-Na_2O-CaF_2$ melts, surface tension and limit wetting angle in contact with C and CrNi steels *(Czech)* 79−37908
$Ca_2O-Al_2O_3-SiO_2$, rain erosion mechanisms 79−34154
$CdO-ZnO-Al_2O_3-Fe_2O_3-SiO_2$ system glass, ESR spectra 79−65711
$CoO-Al_2O_3-SiO_2$, amorphous, remanent magnetisation short time depend. 80−65919
$CoO-Al_2O_3-SiO_2$, spin glasses, low-field susceptibility, freq. depend. 78−47981
$CoO-Al_2O_3-SiO_2$, spin glass, magnetic aftereffects 79−61176
$CoO-Al_2O_3-SiO_2$ glass, mag. ordering, Mossbauer exam. 77−24764
$CoO-Al_2O_3-SiO_2$ spin glass, new state in very weak mag. field 79−78416
$Cu_2O-Al_2O_3-SiO_2$ glass, thermal expsn. coeff. 79−51284
$Cu_2O-Al_2O_3-SiO_2$ glasses, strengthening by alkali-Cu ions exchange 80−55467
$CuO.Al_2O_3.2SiO_2$, hydrothermal synthesis, phase transitions 77−48378
$Fe_2Ca_3Si_3O_{12}$ glass, mag. ordering effects at low temps., Mossbauer and neutron diffr. meas. 77−16047
$KAlSi_3O_8$:rare earth ion, glass, nonradiative energy transfer and fluoresc. quenching 77−20905
$K_2(F,O)-Al_2O_3-B_2O_3-SiO_2$, props. 78−63677
$K_2O-Al_2O_3-B_2O_3-SiO_2$, glass, ESR exam. of paramagnetic centres formed during mech. destruction by grinding 78−88188
$K_2O-Al_2O_3-SiO_2$ system, crystallisation of glasses in primary phase field of leucite 78−67658
$K_2O-Al_2O_3-2SiO_2-BaO$ plasma emitter 80−96368
$K_2O-CaO-Al_2O_3-SiO_2$ glass, exam. of liquid phase separation phenomena 79−4417
$K_2O-SiO_2-Al_2O_3$ glasses, Raman spectra 79−73925
$La_2O_3-Al_2O_3-SiO_2:Sm^{3+}$, luminesc. selective laser excitation line narrowing 80−25434
$La_2O_3-Y_2O_3-Al_2O_3-SiO_2$, coloration by transition metal oxides, absorpt. bands *(Japanese)* 80−55148
Li aluminosilicate, formation of glass-ceramic in $LiCl_3$ vapour 77−16536
Li aluminosilicate glasses, variation of refractive index during ion-exchange diffusion from molten salts *(Russian)* 77−28539
Li, containing Cu and halogen impurities, ESR spectra 80−66027
$LiAlSiO_4$, crystalline, glass and glass-ceramic form, effect of composition changes, substitutions and press. on ionic cond. 78−43172
$LiAlSiO_4$ glass-ceramics, percolative ionic cond. 77−76605
$LiAlSiO_4$ glass-ceramic, fracture phenomena as function of initial flaw size and temp. 78−95797
$LiO_2-Al_2O_3-SiO_2$, bonding of Si-O exam. by X-ray emission spectra 78−52594
$LiO_2-Al_2O_3-SiO_2$, anal. of composition by IR reflection spectra 80−40783
$LiO_2-Al_2O_3-SiO_2$, containing ZrO_2, cryst. process 80−103253
$LiO_2-Al_2O_3-SiO_2-TiO_2:Sn^{3+}$, ESR and X-ray phase anal. 79−99752
$LiO_2-Na_2O-MgO-TiO_2-Al_2O_3-SiO_2$, exam. of specific heat and thermal conductivity *(Russian)* 79−55898
$Li_2O-Al_2O_3-SiO_2$, crystn., aggregation and migration of ion-implanted Ag 77−55240
$Li_2O-Al_2O_3-SiO_2$, effect of ZrO_2 on crystn. 77−16534
$Li_2O-Al_2O_3-SiO_2$, glass ceramic form. obs. using positron annihilation 77−7762
$Li_2O-Al_2O_3-SiO_2$, glassy and polycryst., interdiffusion coeffs. for ion exchange 78−26738
$Li_2O-Al_2O_3-SiO_2$, glass ceramic, elastic props. at high press., US meas. 78−83863
$Li_2O-Al_2O_3-SiO_2$, glass-ceramic, crystallisation mechanism 79−90559
$Li_2O-Al_2O_3-SiO_2$, He migration, struct. effects 77−55389
$Li_2O-Al_2O_3-SiO_2$, kinetics of glass-ceramic formation, by modified broken total internal reflection method 77−36444
$Li_2O-Al_2O_3-SiO_2$, phase separation of initial stages of sitallisation 80−88053
$Li_2O-Al_2O_3-SiO_2$, study of elastic props. 80−104205
$Li_2O-Al_2O_3-SiO_2$, $Tb^{3+}(^5D_3)$ luminesc., cross-relax. quenching *(Russian)* 79−33836
$Li_2O-Al_2O_3-SiO_2$, with refractive index gradient, produced by ion exchange diffusion, exam. of refractive index and concentration changes 79−4782
$Li_2O-Al_2O_3-SiO_2$ C→:C Cd^+, γ-irrad., EPR study 80−84639
$Li_2O-Al_2O_3-SiO_2$ ceramic, chem. resist. and struct. 79−61756
$Li_2O-Al_2O_3-SiO_2$ glasses, viscosity, thermal expansion, glass transform. temp., and refr. index 79−42282
$Li_2O-Al_2O_3-SiO_2$ glass, aq. corrosion 79−61753
$Li_2O-Al_2O_3-SiO_2$ glass ceramic, fracture initiation, influence of temperature and composition 79−100246
$Li_2O-Al_2O_3-SiO_2$ glass-ceramic, near-zero thermal-expansion heat treatment effect in fracture behaviour 80−66537
$Li_2O-Al_2O_3-SiO_2$ glass, crystallised, grain size and internal strain 80−103259
$Li_2O-Al_2O_3-SiO_2$ system melts, alkali ions interdiffusion coeffs., conc. depend. 79−65231
$Li_2O-Al_2O_3-SiO_2$:Cu, Cu film self-generation for low-expansion IR laser mirrors 79−14127
$Li_2O-Al_2O_3-SiO_2:Cd^+$, ESR study 80−103879
$Li_2O-Al_2O_3-SiO_2-TiO_2$ system glasses, Raman spectra obs. of glass-ceramics form. 80−60825
$Li_2O-Al_2O_3-4SiO_2$, glass-ceramic, tensile creep and high temp. fracture 78−52914

aluminosilicate glasses continued
$Li_2O-BaO-Al_2O_3-SiO_2-xTiO_2$ glass, X-ray spectra, Ti ion electron config. *(Russian)* 77−8674
$Li_2O-MgO-Al_2O_3-SiO_2$, effect of ZrO_2 on crystn. 77−16534
$Li_2O-MgO-Al_2O_3-SiO_2$ glass scintillator for pulsed neutron detection 80−87019
$Li_2O-Na_2O-B_2O_3-Al_2O_3-SiO_2$ glass, Young's modulus and density, ion exchange effects 80−84982
Li_2O-SiO_2, effect of ZrO_2 on crystn. 77−16534
$Li_2O-TiO_2-Al_2O_3-SiO_2$ glass, γ-irrad., struct. position of Ti, EPR study 80−84644
$(Li_2O-Al_2O_3-SiO_2):Fe_2O_3$, glass, pyroceramic form., colour centres, magnetochem. investig. 77−16537
$19Li_2O.19Al_2O_3.62SiO_2$ glass, ionic cond. meas. 79−33110
$LiTaO_3-SiO_2-Al_2O_3$, transparency in relation to microstruct. 78−53005
$MgO-Al_2O_3-SiO_2$, exam. of microstructure and crystallisation kinetics 78−80501
$MgO-Al_2O_3-SiO_2$, glass ceramics, phase transformation processes 80−3025
$MgO-Al_2O_3-SiO_2$, glass ceramic, structure and props. *(German)* 80−38927
$MgO-Al_2O_3-SiO_2$, melt and glass crystn. with ZrO_2-TiO_2 nucleants 77−31599
$MgO-Al_2O_3-SiO_2$, metastable liq. phase separation region, electron microscope exam. 78−88451
$MgO-Al_2O_3-SiO_2$, sintered, cordierite, mineralogy and props. 80−60827
$MgO-Al_2O_3-SiO_2$ based cordierite glass-ceramic, strength and thermal shock, surface treatment effect 80−25884
$MgO-Al_2O_3-SiO_2$ glass ceramic, nucleation, effect of electric fields 78−83742
$MgO-Al_2O_3-SiO_2$ glass, features of crystallisation, in the presence of the thermal decomposition of tetrabutoxytitanium 78−87627
$MgO-Al_2O_3-SiO_2$ glass/polysulphone adhesive failure, ISS and SIMS obs. 80−55626
$MgO-Al_2O_3-SiO_2$ system glasses and glass ceramics, EPR obs. of transition elements, crystn. effects 78−23332
$MgO-Al_2O_3-SiO_2:Ce^{3+}$ scintillator, energy transfer, luminesc. efficiency under UV and charged-particle excitation 79−95821
$MgO-Al_2O_3-SiO_2-NiO$ glass, gamma ray irradiated, exam. of ESR spectrum of Ni(I) 79−4719
$MgO-Al_2O_3-TiO_2-SiO_2$, glass formation, structure of cations *(Russian)* 80−38933
$MgO-BaO-Al_2O_3-SiO_2$, glass, IR absorpt. spectra and solid struct. exam. 78−88314
$MgO-CaO-Al_2O_3-SiO_2(-TiO_3)$ systems, glass-ceramics, crystn. kinetics *(Russian)* 79−37626
$MgO-CaO-FeO(Fe_2O_3)-Al_2O_3-SiO_2$ glass, X-ray spectra Fe ion electron config. *(Russian)* 77−8674
$MgO-TiO_2-Al_2O_3-SiO_2$, γ-irrad., struct. position of Ti, EPR study 80−84644
$MgO.Al_2O_3.2SiO_2$, hydrothermal synthesis, phase transitions 77−48378
$Mn_3Al_2Si_3O_{12}$, amorphous, spin-glass, insulating, Mn^{2+} mag. reson. 80−65918
$MnO-Al_2O_3-SiO_2$, amorphous, spin glass like behaviour at low temp. 79−61177
$MnO-Al_2O_3-SiO_2$, amorphous, remanent magnetisation short time depend. 80−65919
$MnO-Al_2O_3-SiO_2$, amorphous spin glass, AC susceptibility 80−80520
$MnO-Al_2O_3-SiO_2$, spin glasses, low-field susceptibility, freq. depend. 78−47981
$MnO-Al_2O_3-SiO_2$ glass, spin freezing, muon spin depolarisation 78−39491
$MnO-Al_2O_3-SiO_2$ glass, spin freezing, muon spin depolarisation, superparamag. domain model 78−68272
$MnO-SiO_2-Al_2O_3$, effect of Al_2O_3 on viscosity if ternary aluminosilicates *(Japanese)* 78−83989
$NaAlSi_2O_6$ melts quenched at high press., struct. from IR and Al K-radiation data 79−32907
$Na_2O-Al_2O_3-B_2O_3-SiO_2-AgBr(Cl)$, photochromic glass, exam. of role of O and Cu ions, using luminescence spectra 79−4849
$Na_2O-Al_2O_3-B_2O_3-SiO_2$, CuCl crystal activated photochromic glasses, absorpt. spectra 79−27353
$Na_2O-Al_2O_3-B_2O_3-SiO_2-AgCl(Br)$, photochromic glass, kinetics of thermal decolorisation 80−103931
$Na_2O-Al_2O_3-SiO_2$, formation from alkoxides phys. and chem. evolution 78−80503
$Na_2O-Al_2O_3-SiO_2$, glass, nucleation, crystn., ceramic form. 80−84082
$Na_2O-Al_2O_3-SiO_2$, interaction with aq. salt solns., alkali ions distrib. in surface layers 80−21142
$Na_2O-Al_2O_3-SiO_2$, leaching in HCl solns., Na conc. distrib. in surface layers 80−21141
$Na_2O-Al_2O_3-SiO_2$, porous, crack shape, US fractography obs. 77−44336
$Na_2O-Al_2O_3-SiO_2$, surface charge in aqueous electrolyte soln. 79−29245
$Na_2O-Al_2O_3-SiO_2$ glass, composition-density relationship 77−90326
$Na_2O-Al_2O_3-SiO_2$ glasses, elec. cond. and cation mobility 78−59973
$Na_2O-Al_2O_3-SiO_2$ glass, diffusion of Ca and Mg, SIMS study 79−82387
$Na_2O-Al_2O_3-SiO_2$ system melts, alkali ions interdiffusion coeffs., conc. depend. 79−65231
$Na_2O-Al_2O_3-SiO_2-TiO$, effect of Cr_2O_3, NiO, and MgO additions on crystallisation 78−87626
$Na_2O-Al_2O_3-SiO_2-TiO_2-NiO$ glass, paramagnetic centres, form. during crystn., ESR study 79−65710
$Na_2O-Al_2O_3-SiO_2(-K_2)$ glasses, ion exchange kinetics and interdiffusion mechanisms 80−80003
$Na_2O-Al_2O_3-SnO_2-SiO_2$, chemical stability in NaOH and Na_2CO_3 solns. 80−16532
$Na_2O-Al_2O_3-ZrO_2-SiO_2$, chemical stability in NaOH and Na_2CO_3 solns. 80−16532
$Na_2O-BaO-Al_2O_3-SiO_2$, glass, nucleation, crystn., ceramic form. 80−84082
$Na_2O-CaO-Al_2O_3-SiO_2-Cr_2O_3$, Raman spectra obs. of Cr^{VI} 77−52076
$Na_2O-CaO-Al_2O_3-SiO_2$ glass, exam. of liquid phase separation phenomena 79−4417
$Na_2O-CaO-Al_2O_3-SiO_2-F-B_2O_3-ZrO_2$ glaze, crystallisation, MgO, ZnO, BaO and SrO effects 79−60279
$Na_2O-CaO-Al_2O_3-SiO_2$ glass, crystn. for the purpose of obtaining vitroceramics *(French)* 80−75163
$Na_2O-CaO-MgO-Al_2O_3-SiO_2$ glasses, ternary and quaternary, struct., Raman spectra obs. 77−36229
$Na_2O-CaO-MgO-Al_2O_3-SiO_2$, corrosion and microhardness, effect of detergents 80−16518

aluminosilicate glasses continued
Na_2O-K_2O-Al_2O_3-SiO_2 glasses, effect of Al_2O_3 on elec. cond. 77—8104
Na_2O-K_2O-Al_2O_3-SiO_2, mixed alkali effect, nonbridging O content effects 78—18827
Na_2O-K_2O-Al_2O_3-SiO_2, structure of modified surface layer, internal friction method 80—103258
Na_2O-MgO-Al_2O_3-SiO_2, chemical durability at different pH values 78—72902
Na_2O-NaF-CaO_xZnO_{1-x}-Al_2O_3-SiO_2, opal glasses, strength, surface composition 80—30066
Na_2O-SiO_2-Al_2O_3, effect of Al_2O_3 on viscosity if ternary aluminosilicates *(Japanese)* 78—83989
Na_2O-SiO_2-Al_2O_3 glasses, Raman spectra 79—73925
Na_2O-SiO_2-B_2O_3-Al_2O_3, comp. changes as evidence for spinodal decomposition 79—11549
Na_2O-SiO_2-Ga_2O_3-Al_2O_3-B_2O_3-SnO_2, ion exchange reactions with $NaNO_3$ and KNO_3 melts 80—16673
Na_2O-SiO_2-Ga_2O_3-Al_2O_3 in mixed $AGNO_3$-$NaNO_3$ melts, ion exchange 80—21282
Na_2O-TiO_2-Al_2O_3-SiO_2, γ-irrad., struct. position of Ti, EPR study 80—84644
$Na_2O_3(CaO)$-Al_2O_3-SiO_2, effect of composition on mechanical props. 78—48435
Nd_2O_3-Al_2O_3-SiO_2 glass, exam. of spectroscopic and luminescent props. 78—88364
PbO-B_2O_3-SiO_2-Al_2O_3-ZnO-CuO-Bi_2O_3 solder glass, crystallisation prevention by Cu addition 80—11654
PbO-SiO_2-Al_2O_3, effect of Al_2O_3 on viscosity if ternary aluminosilicates *(Japanese)* 78—83989
PbO-SiO_2-$Al_2O_3(-K_2O)$, corrosion in acid, leaching kinetics 78—92378
Si-Y-Al-O-N glasses, compositional anal., hardness depend. on N_2 content 79—34129
Si_3N_4-Al_2O_3-SiO_2 systems, glass forming regions 80—84070
SiO_2 fabric, prep. from E-glass, structural stability rel. to brittleness, X-ray diffr. and IR spectrosc. studies 80—96634
SiO_2-Al_2O_3, vitreous US vel. and absorption 80—107380
SiO_2-Al_2O_3 (8 mol.%) glass, heat treated, devitrified phases 80—66469
SiO_2-Al_2O_3 glass, Raman spectra and refr. index meas. 77—24836
SiO_2-Al_2O_3 system, location of metastable immiscibility gap 79—77521
SiO_2-Al_2O_3 system, phase equilibria 79—77724
SiO_2-Al_2O_3-B_2O_3, glass fibre, water and acid resistance 80—11799
SiO_2-Al_2O_3-B_2O_3 glass mech. strength increased by etching 80—97609
SiO_2-Al_2O_3-B_2O_3-LiO_2 ($LiO_2.Na_2O$) (Na_2O) glass exam. of optical props. 78—88277
SiO_2-Al_2O_3-B_2O_3-MgO-CaO-Na_2O, strengthened by ion exchange, exam. of internal stresses using polarising microscope 78—88549
SiO_2-Al_2O_3-B_2O_3-CaO-Na_2O-K_2O system glasses, relax. of struct. stresses rel. to forming process 79—34088
SiO_2-Al_2O_3-CaO-BaO-SrO-ZnO-Na_2O-K_2O-B_2O_3, glaze effect of P_2O_5 additions 80—60824
SiO_2-Al_2O_3-CaO-K_2O system, phase separation and crystn., F catalytic effect 79—60280
SiO_2-Al_2O_3-CaO-MgO-TiO_2 system glasses, phase separation and crystn. 77—24384
SiO_2-Al_2O_3-CaO-MgO-Na_2O (1.58, 7.16, 3.59, 14.9 mole.%), polished sheet, strength in commercial state and after strengthening by ion exchange 79—1904
SiO_2-Al_2O_3-CaO-MgO-Na_2O, ion exchange and electrodiffusion of Li ions in surface layer 79—20227
SiO_2-Al_2O_3-CaO-MgO, crystallized, prod. from inorganic waste *(Japanese)* 79—69017
SiO_2-Al_2O_3-CaO-MgO-Na_2O-K_2O effect of partial substitution of Na_2O by K_2O, on crystallisation 80—10499
SiO_2-Al_2O_3-CaO-MgO-FeO-Fe_2O_3 glasses, struct. transforms during heating 80—15014
SiO_2-Al_2O_3-CaO-MgO-B_2O_3, E-glass, acid resist. studies 80—60991
SiO_2-Al_2O_3-CaO-Na_2O:Fe^{3+}, optical absorpt. due to Fe^{3+} ligand field and charge transfer 80—89020
SiO_2-Al_2O_3-Cr_2O_3 system, KT-11 type, chromia-containing material production based on high-silica glass fabric 80—45266
SiO_2-Al_2O_3-Cu_2O glass alkaline durability, corrosion rate, heat capacity and elastic moduli 80—93673
SiO_2-Al_2O_3-Fe_2O_3-K_2O, form. of Al-Fe leucite, inversion temp. *(Japanese)* 77—62481
SiO_2-Al_2O_3-Fe_2O_3-CaO-MgO-Na_2O-SO_3 glass, thermophysical props. 78—18849
SiO_2-Al_2O_3-Fe_2O_3-CaO-MgO-Na_2O-B_2O_3-SO_3, exam. of white flaky inclusions, causes and formation time 79—29237
SiO_2-Al_2O_3-Fe_2O_3-CaO-MgO, basalt glass, AES obs. 79—91543
SiO_2-Al_2O_3-Fe_2O_3-CaO, basalt glass ceramics, crystallite form. due to heat treatment 80—38917
SiO_2-Al_2O_3-Fe_2O_3-Na_2O-K_2O-CaO-MgO glasses, Mossbauer spectra study 80—39967
SiO_2-Al_2O_3-FeO-CaO-MgO pyroxene glasses, phase changes 80—15013
SiO_2-Al_2O_3-K_2O glass ceramic interaction with Pb borosilicate glaze 80—84398
SiO_2-Al_2O_3-K_2O-Na_2O, exam. of leucite crystal growth 79—19496
SiO_2-Al_2O_3-Li_2O glass ceramic, crystn., microstructures rel. to conditions 80—11638
SiO_2-Al_2O_3-$Li_2O(MgO)(Na_2O)$, paramagnetic defect formation, ESR study during crystn. of TiO_2, Cr_2O_3 and Nb_2O_5 containing glasses 79—65739
SiO_2-Al_2O_3-MgO-CaO-Fe_2O_3, glass ceramic, crystn., microstructures rel. to conditions 80—11638
SiO_2-Al_2O_3-MgO-TiO_2, internal friction during crystn. 79—52285
SiO_2-Al_2O_3-MgO-TiO_2 devitrificates, microstruct. and props. *(Polish)* 80—70141
SiO_2-Al_2O_3-$MgO(-K_2O-F)$, glass ceramics, crystn., microstructures rel. to conditions 80—11638
SiO_2-Al_2O_3-Na_2O-BaO-TiO_2, glass ceramic interaction with Pb borosilicate glaze 80—84398
SiO_2-Al_2O_3-R_2O_3-MgO-TiO_2, T=rare earth of Ce group, glass-ceramic permittivity comp. depend. 77—43928
SiO_2-Al_2O_3-RO-R_2O type glass additions, sintering of porcelain bodies 80—45265
SiO_2-Al_2O_3-Y_2O_3-La_2O_3-TiO_2 glasses with high elastic moduli, alkaline durability 80—85071
SiO_2-B_2O_3-Al_2O_3-$Na_2O(K_2O)$ glasses, Ag interdiffusion, optical and NMR studies 80—24683
SiO_2-B_2O_3-Li_2O-Al_2O_3 (28, 2, 1 wt.%) glass, dielec. const. at 3 GHz 80—93233

aluminosilicate glasses continued
SiO_2-CaO-Na_2O-TiO_2 system, water, alkali, acid resist., chem. durability 79—34162
SiO_2-Li_2O-Al_2O_3-K_2O:$Ag_2O(-CeO_4)$ $(-Sb_2O_3)$, surface resist. meas. 80—44700
SiO_2-LiO_2-Al_2O_3 glass, luminesc., polarisation degree distrib. 80—108257
SiO_2-MgO-CaO-Al_2O_3:Ce,Fe, redox equilib., expt. 80—85171
SiO_2-Na_2O-CaO-MgO-Al_2O_3, toughening by electrochemical treatment in Sn melt 80—11800
SiO_2-Na_2O-CaO-MgO-Fe_2O_3-Al_2O_3-SO_3-Sn thermally polished, exam. of strength of surfaces 80—25887
SiO_2-Na_2O-K_2O-CaO-MgO-Al_2O_3 glass melt, anodic dissolution of Ti 80—19949
SiO_2-$NaAlSiO_4$ glasses and devitrificates, prep. and vibr. spectroscopy study *(Polish)* 80—93530
SiO_2-NaO-K_2O-CaO-MgO-Al_2O_3 melt, anodic dissolution of Co and Ni in melt 78—88582
SiO_2-PbO-B_2O_3-Al_2O_3-CaO-Na_2O-K_2-O glaze, interaction with aluminosilicate glass-ceramics 80—84398
SiO_2-TiO_2-Al_2O_3-$SrO(BaO)$, glasses, ceramic form. rel. to Al_2O_3 content 77—25005
SiO_2-ZrO_2-Al_2O_3-CaO-Na_2O-K_2O-Li_2O, chemical resistant glass for glass fibres 80—21128
SiO_3-Na_2O-CaO-MgO-Al_2O_3 charge, silicate formation during heating 80—55342
$SiO_2B_2O_3$-K_2O-Al_2O_3-As_2O_3 glass fibres containing metallic granules, tensile strength, Young's modulus, DC conductivity 80—30023
SrO-Al_2O_3-SiO_2-TiO_2 system glass-crystal material, elec. cond. 79—60876
SrO-Al_2O_3-TiO_2-SiO_2, glass formation, structure of cations *(Russian)* 80—38933
SrO-Li_2O-Al_2O_3-SiO_2:Tb^{3+}, energy transfer, luminesc. efficiency under UV, neutron and charged-particle excitation 79—95822
TiO_2-Al_2O_3-SiO_2 system, ternary glass-forming region and phys. props. 80—84919
TiO_2-containing slag-glasses, phase separation and glass-ceramic formation 78—51424
Y-Si-Al-O-N glass, prep. and props. 80—25647
$Y_2O_3.2SiO_2.Al_2O_3$ glass, thermal stability 77—44502
ZnO-Al_2O_3-SiO_2, transparent glass-ceramics, EPR obs. of glass crystallisation 78—80507
ZnO-Al_2O_3-SiO_2 glass, crystalline phase precipitation, crystallisation *(Japanese)* 79—32916
ZnO-Al_2O_3-SiO_2:Cu, Cu film self-generation for low-expansion IR laser mirrors 79—14127
ZnO-Al_2O_3-SiO2, transparent glass ceramics, heat treatment effect on microstruct. 78—56667
ZnO-$Al_2O_3SiO_2$, transparent glass-ceramic, microstruct., physical props., crystallisation ht. treatment depend. 78—80506
ZrO_2-Al_2O_3-SiO_2, subsolidus equilibria and stabilization of tetragonal ZrO_2 78—27497

a.m. (modulation) *see amplitude modulation*

ambient temperature *see temperature*

americium
see also nuclei with ......
5f-electron delocalisation 80—70595
after-effects of ^{241}Am α-decay, ^{237}Np Mossbauer spectra obs. 79—61271
atom, isotope shifts rel. to $|\psi(0)|^2$ 78—17580
build-up in Trino Vercellese PWR fuel rods 79—85754
Debye-Waller factor, temp. depend., Mossbauer effect meas. 78—83902
determination in biological samples by solvent extraction and liquid scintillation counting 79—53260
dilatometry and thermal anal., melting point, transformation regions 79—43241
electrical resistivity and sp. ht. 78—47762
electrical resistivity of ^{241}Am metal, 3.6-300K 78—6345
high pressure form, cryst. struct., X-ray diffr. obs. up to 14 GPa 80—24399
ions, electronic props., Dirac-Fock studies 78—60094
isotope separation, chemical treatment of irrad. targets *(French)* 77—26883
magnetic susceptibility meas., Faraday method 77—28369
movement through food chain 78—61264
oxalate precipitation for separation of Am, Cm, and trivalent lanthanides 80—83202
phase transformation at high press., X-ray diffr. obs. 80—107422
polymorphic transform. exam. by hot stage X-ray diffr. anal. *(Russian)* 79—24518
polymorphic transformations obs. *(Russian)* 78—6153
production by US irrad. in reactor, chem. separation yield 77—63986
radioactive effluent, Pu and Am inventory of ecosystem near a nuclear facility 80—97820
radioactive target preparation and characterisation 80—18734
radioactive waste, low conc. meas. in earth samples, appl. of Si(Li) X-ray detector 78—58505
radioactive waste storage, Am sorption on major rock-forming minerals 80—13716
radioactive waste storage, mineral-contributed anion effects on the retention of trivalent actinides in the environment 80—13717
release into estuarine-coastal sea ecosystem, assessment methodology 79—70471
skin transport, role of diffusion 78—20158
specific heat, Debye temp. 80—15258
superconducting critical field, sp. ht. 80—11136
superconductivity, discovery of, up to 0.79K 79—11262
target prpe. for synthesis of transactinide elements 80—23206
vapour pressure, 1200-1600K, heats of vap. and La mixing 80—15232
waste disposal, retention by rock 77—71679
$^{241}Am^{3+}$, diffusion in ion exchange membrane, autoradiographic obs. 77—90637
Am-Be, neutron fluence-to-dose conversion factors 79—6771
$^{240}Am^{m}$, spontaneously fissioning isomer optical shift in pumped $^8S_{7/2}\rightarrow{}^{10}P_{7/2}$ transition, nuclear deformation 80—27971
^{241}Am and Pu/^{241}Am ratios, environment meas. using X-ray spectrometry 77—60265
^{241}Am, α-radiation self-damage effect on hyperfine interaction and Debye-Waller factor, Mossbauer meas. 80—7230
^{241}Am, biological availability, influence of DTPA at soil-plant and plant-animal interfaces 78—73264

americium continued
^{241}Am, conc. in thermonuclear test debris, collected near Bikini Atoll 78—96103
^{241}Am concentrations concs. in drinking water and organic fertiliser 77—56488
^{241}Am, concs. in sediments from coastal basins off California and Mexico 80—98303
^{241}Am, environmental pollution, biophysical aspects 79—39530
^{241}Am, gamma-ray meas. of Pu and Am in molten salt residues for nuclear materials safeguards 80—83165
^{241}Am, gastrointestinal absorpt. in hamster 79—39520
^{241}Am, high purity solid, vapour pressure 77—28011
^{241}Am III retention and distrib. in neonatal beagle 78—28094
^{241}Am, in English Channel, transfer into S.North Sea 79—48519
^{241}Am, in-situ anal. of radioactive waste 79—85715
^{241}Am metal, specific heat, 15 to 300K 77—28019
^{241}Am metallic film, elec. resist. meas., 3.6 to 300K 77—28263
^{241}Am, radioactive waste, sorption in igneous rocks 80—95367
^{241}Am removal, Ca-DTPA vs. Zn-DTPA in beagles 77—73599
^{241}Am soil concs., in situ gamma anal. and sampling data comparison, Nevada 77—64143
^{241}Am sorption on USA subsoils from differing weathering intensity areas, ^{241}Am, ^{237}Np and ^{99}Tc 78—16014
^{241}Am source ingestion, case report 78—28088
^{241}Am spectrometer for Compton scatt. studies 79—2899
^{241}Am thin source preparation 80—18730
^{241}Am, vertical distribution in Mediterranean Sea 79—84301
^{241}Am-^{239}Pu monitor for in situ soil surface and pond bottom assay 77—9546
^{241}Am^{3+} ion diffusion in ion-exchange membrane, autoradiographic method 78—35721
^{241}Am(n,X)Cm, Japan Material Testing Reactor, separation of transuranium elements from fission products and cladding *(Japanese)* 80—52731
^{242}Am/$^{239+240}$Pu activity ratio rel. to global fallout 78—57263
Pu-Am survey instrument, β-α-γ-X-ray scintillation detect. probe 78—33376

americium compounds
aqueous solution, electrochem. props., thermodynamic props., radiopolarography 77—29040
in phosphoric and soln., prep. and stability of highest oxidation states 77—29029
(Am,Cm)O_2 solid soln., struct. changes under self- and reactor irrad. 77—27927
Am-Pt intermetallics, after-effects of ^{241}Am α-decay, ^{237}Np Mossbauer spectra obs. 79—61271
AmAs magnetic susceptibility meas., Faraday method 77—28369
$AmCl_3$, vapour phase hydrolysis using ^{241}Am and ^{243}Am, heat of formation of AmOCl 77—29037
α-$Am_2(MoO_4)_3$, cryst. struct., lattice parameters 79—14774
AmN magnetic susceptibility meas., Faraday method 77—28369
AmO, and AmO_2, electronic struct. and chem. bonding and XPS line shape calcs. 79—33264
AmO_2, Am_2O_3, after-effects of ^{241}Am α-decay, ^{237}Np Mossbauer spectra obs. 79—61271
AmO_2, IR spectra, values of transverse vibr. frequencies 77—28585
AmO_2, XPS meas. 77—48314
$^{243}AmO_2$, neutron diffraction study, possible occurrence of antiferromagnetism 79—78332
AmO_2-UO_2, target possibilities for waste incineration, simulation study 80—32419
AmOBr, cryst. struct. from powder patterns 79—46617
AmOCl heat of formation, vapour phase hydrolysis of $AmCl_3$ using ^{241}Am and ^{243}Am 77—29037
$^{241}Am(OH)_3$, cryst., self-irrad. effects 77—69013
AmSi, $AmSi_2$, prep. and cryst. struct. 78—18607
$AmTe_{1.73(2)}$, X-ray single cryst. struct. determ. and refinement 79—19201
Am(VI) formation in molten salts 77—29039
α-$Am_2(WO_4)_3$, cryst. struct., lattice parameters 79—14774
α-$LiAmO_2$, prep. and crystallographic data *(French)* 78—47290
Li_xAmO_{1+x}, after-effects of ^{241}Am α-decay, ^{237}Np Mossbauer spectra obs. 79—61271

ammeters
1 nA meter, voltmeter conversion circuit using RCA CA3130 devices 77—37928
calibration method at 1 MHz for RF ammeters 79—88905
circular-scale 240° moving-iron AC ammeters and voltmeters 77—57360
DC, for up to 50 kA, using Hall pickups 80—31793
DC and AC, calibration using digital voltmeter *(Polish)* 78—45655
DC nanovoltammeter based on modem 80—31797
DC picoammeter, 10^{-5} to 10^{-11} A range, portable 79—17441
DC picoammeter, digital *(Spanish)* 79—88980
demonstration apparatus, forces between parallel wires, calibration 77—33757
F136 DC microvolt nanoammeter 78—24780
frequency error determination over wide range 80—4734
high speed pico-ammeter, design and construction *(Japanese)* 80—17960
in-circuit DC current measurement device for PCBs 77—18009
maintenance, renovation and repair procedures for multimeters including Avo model 8 79—35795
measurement techniques for minute currents *(German)* 79—54153
microammeter testing installation adaptation for $<30\ \mu$A 78—45653
milliammeter with decatron light-spot display 78—24779
pick-up for titrimetric chem. analyser *(Russian)* 80—71984
picoammeter for atmospheric measurement of elec. cond. and small ion mobility, pollution aspects 78—92931
picoammeter with adjustable input pot. 77—141
servo-controlled balance, absolute ampere determ. 78—82003
Tesla-ammeter (F4354/1), improvement for investigation of const. mag. fields 77—26364

ammonia
abundance determ. for Jupiter from 2 μ spectrum 79—35182
abundance on Jupiter and Saturn from visible obs. 80—82269
adsorbed, effect on elec. cond. of amorphous Si:H film 78—88048
adsorbed gas, on glassy AsSe, surface cond., photocond. 78—80038
adsorbed on amorphous silica surface, Raman scatt. obs. 80—11948
adsorbed on $CaCl_2$ and $CaBr_2$, IR and far IR spectra 77—24478
adsorbed on graphite, NMR pulsed field gradient method, diffusion coeff. meas. 80—15362

ammonia continued
adsorbed on graphite, struct. and dynamics, neutron diffr. and inelastic scatt. 78—87869
adsorbed on irrad. SiO_2 gel, neutron scatt. 79—33194
adsorbed on quartz, effect on surface cond. 77—85297
adsorbed on Si (111) surface, electron energy loss spectroscopy 78—2374
adsorbed on silica gel, neutron scatt. investig., mol. vibrs., rots. 77—51608
adsorption, on Al(Fe), thermal accommodation coeffs., translational (internal) gas-solid energy exchange 78—92506
adsorption and cryogenic refrigeration systems 79—58722
adsorption and decomp. on stepped Pt surface, LEED, AES and desorption expts. 78—38943
adsorption and decomposition on Fe(110) surface, identification of surface species using SIMS 79—90862
adsorption and decomposition on Fe (110) surface 79—69345
adsorption and desorption on Ru (0001), effects of electron beam 78—38955
adsorption of NH_3 and ND_3 on $CaCl_2$ and $CaBr_2$, complex formation, IR and far IR spectra obs. 80—80063
adsorption on Al_2O_3, KVV Auger spectra, deconvoluted spectra 80—50508
adsorption on Al, KVV Auger spectra, deconvoluted spectra 80—50508
adsorption on Al surface, NH_3 decomp., XPS obs. 80—92783
adsorption on Cu, photoelectron spectra 78—6830
adsorption on Fe, 80-290K, XPS and UPS obs. 77—31901
adsorption on Ge (111) surface, surface recomb. centre neutralization 79—38147
adsorption on Ir, field emission energy distrib. spectra 80—25535
adsorption on Mo, and catalytic decomposition, field emission study 78—14596
adsorption on Mo (111) planes, preferential nitriding, FEM study 80—66877
adsorption on Pd surface, hydrogenation and dehydration, AES meas. 77—1315
adsorption on plasma deposited a-Si:H, effect on cond. 80—49749
adsorption on Pt, surface composition, AES and temp. programmed desorption meas. 80—34313
adsorption on Ru (0001) surface, AES, LEED and thermal flash desorption meas. 78—38954
adsorption on W, thermal desorption and pulsed time of flight mass spectra anal. 80—30285
aerosol, possible presence in Uranus clouds 80—31253
affinities for $H^+(Li^+)(K^+)(CH_3{}^+)$, ab initio SCF calculations 80—102443
affinity for $Li^+(Na^+)(K^+)$, ab initio SCF calcs. 80—58125
air pollution, microdeterm. by ring oven technique 77—45164
air pollution conc. determ. on long path from CO_2 laser radiation reson. absorpt. 79—29904
alkali metal-ammonia solns., elec.-cond. and thermopower 77—1370
alkali metal-ammonia solns., metal-insulator transition, h.f. and u.s. props. 77—1369
alkali metal-ammonia solns., spin site exchange mechanism for electron relax. times 78—27077
alkali metal-ammonia solutions containing cryptands, metal anion and trapped electrons form. by evap. 79—100340
alkali metal-NH_3 solution, Hall effect and cond. at metal-nonmetal transition 78—2530
alkali metal-NH_z solutions, metal-nonmetal transition Hall mobility, electrodeless meas. 78—56194
ammoniated electrons, reaction rate consts. with hydroquinone, phenol, propionamide 77—9043
aqueous soln., stripping by sieve plate column without downcomers 78—22430
associated, struct. and dynamics, atom-atom pots., gas, solid and liq., props. 80—23487
atmosphere, acid sulphate aerosols existence and NH_3 gas conc. 77—81998
atmosphere, aircraft meas. of NH_3 budget contribs. 78—73469
atmosphere, NH_3 ν vibr.-rot. band identification in ground level solar spectra 78—81287
in atmosphere, NH_3 and particulate $NH_4{}^+$ fluxes evaluation over W.Germany 80—94132
atmosphere, NH_3 from undisturbed land 77—81967
atmosphere composition, Southern Ocean air 80—61871
atmosphere concentration measurement, ring oven technique 80—81507
atmospheres of Uranus and Neptune, estimation of ammonia and water vapour contents 80—90366
atmospheric, photoacoustic spectroscopy at 9 μm, 10 μm $^{12}C^{16}O_2$ laser wavelengths 79—21014
atmospheric cycles 79—48562
atmospheric gas complex analysis method, resonance absorption with pulsed laser light *(Japanese)* 80—36421
atmospheric NH_3 determ., method 80—56614
atmospheric pollution detection, high sensitivity, using tunable diode laser 78—57373
atmospheric pollution resulting from accidental spills of liquid anhydrous NH_3 onto water 77—73846
atmospheric remote sensing by multiphoton sequential photodissociative excitation 79—48199
atmospheric trace gases and pollutants, data compilation on mag. tape 78—44995
Auger electron spectrum for gas-phase 77—31005
catalytic decomposition of single pulses on W, mol. beam relax. spectrometry 80—21321
catalytic synthesis on Fe, promoter action of K 79—29390
cell, incavity, technique for obtaining CW CO_2 sequence laser lines 79—18438
chemisorbed on Ir (111), mol. adsorbate structs. from angular-resolved photoemission 80—76141
chemisorption, on W, decomposition mechanism, isotope effect 79—29409
chemisorption and decomposition on clean and N-covered Fe (111) and Fe (100) 78—40077
chemisorption on clean Fe (100) and (111) surfaces, LEED and thermal desorption 78—71996
chemisorption on Fe(111) clean single crystal surface, of N_2, NH_3, H_2, photoelectron spectroscopy, LEED studies 77—66087
chemisorption on Ni (111) and reaction, LEED, desorption and photoemission expts. 80—59799
chemisorption on ZnO, differential heat 79—52759

- **ammonia** continued
  - collisionally induced transition rates, estimation from lab. data, rel. to interstellar mols. 79—45787
  - compressed gas, electron drift vel., density depend. 78—63534
  - concentrations in wastewater, simultaneous automated determ. 77—29511
  - condensation by homogeneous nucleation in supersonic nozzles 77—11230
  - continuous absorption cooling flat plate collector design and optimisation 79—62081
  - Coriolis and l-type interactions, ν_2, $2\nu_2$ and ν_4 states, IR spectra 80—47993
  - crystal, and deuterated crystal, atom-atom and multipole-multipole pot. lattice dynamics calc. 79—1479
  - crystal, radiolysis yield, temp. effects, Arrhenius depend. 77—48662
  - crystal, rotation mol. motion *(Russian)* 78—87762
  - decomposition, on supported FE catalyst, kinetics, IR obs. 79—11792
  - decomposition by Re filament at low press. above 500K 79—61906
  - decomposition kinetics on Pt plane 77—1948
  - dense vapour, electron localisation 80—44558
  - depletion in atmosphere of Uranus, theory and obs. 78—53870
  - detection of extragalactic ammonia 79—48886
  - diamond surface interaction with gases and metals 77—72758
  - dimer, $(NH_3)_2$ intermol. pot. calc. 78—58764
  - dimer, inversion, influence of H-bond, SCF calc. 77—50556
  - dipole moment derivatives, polar tensors, effective charges, CNDO calcs. 77—38613
  - dissociating gas in pipe flow, heat transfer crisis, flow laminarisation 79—1265
  - dissociation monitoring in nitriding process 79—52556
  - dissolved in poly-γ-benzyl-L-glutamate-chloroform, NMR study 80—34805
  - Earth's early atmosphere, NH_3 photochemically produced in small quantities 80—109208
  - Earth atmosphere, spectral line meas. using 10μm superheterodyne receiver 78—16335
  - effect on low-cycle fatigue of bronze 80—104348
  - electron Coulomb profile beyond impulse approx. 80—87083
  - electronic Compton profile beyond impulse approx. *(French)* 80—53057
  - emission and absorption at 23 GHz toward radiosource W3(OH) 78—36714
  - emission lines obs. from galactic regions 78—28780
  - epitaxial film, on metal (111) substrates, surface struct., LEED obs. 79—86969
  - equation of state, perturbed-hard-sphere, applicable to sub- and supercritical temps. 79—19350
  - excitation in interstellar Kleinmann-Low nebula 79—5878
  - far IR emissions by IR pumping using N_2O laser 80—74345
  - film, on metal substrate, surface struct. using LEED 79—77879
  - flow in steel tubes, wall heat transfer with catalytic dissoc. 78—14099
  - fluid, second dielec. virial coeff. calc. 78—22449
  - fluorobenzene in liq. NH_3, solvated electrons reaction kinetics 77—73434
  - frost, near IR refl. spectra, appl. to Saturn upper clouds 79—8135
  - frosts, Na and K doped, reflectance spectra and implications for Io surface 78—84561
  - fuel cell, high temperature solid electrolyte, overpot. and product selectivity characts. 80—104504
  - gas, 2nd and 3rd coeffs. calc., including nonadditive interactions 77—76013
  - gas, electron-ion recombination, at 292K, three-body interaction 79—46418
  - gas, ion mobility meas. 79—23393
  - gas, monitoring by Pd gate MOSFET 78—44645
  - gas, phase conjugation via degenerate four-wave mixing 80—106566
  - gas, sensing probe, potentiometric, micro-size 78—61071
  - gas, weak IR absorpt. meas. using double-beam Fourier spectrometer 80—105725
  - gas, with variable physical props., pipe flow, turbulent momentum and heat transfer calc. 78—90869
  - gas phase proton solvation energetics, mol. beam-photoionis. obs. 79—29345
  - gaseous, IR obs. spectra meas. using $Pb_{1-x}Sn_xTe$ diode laser *(Japanese)* 79—49306
  - gaseous ammonia in Saturn troposphere 80—94748
  - glow discharge, electron energy distrib. and negative ions *(Russian)* 79—7499
  - H-bonded dimers, PCILO calc., energies, geometries 78—37557
  - hot band lasing transitions 80—1191
  - hyperfine quadrupole coupling, ro-inversional levels, inversional depend. 80—27961
  - impurity in H_2-air-H_3PO_4 fuel cells, effect on performance 80—108795
  - intercalated in TaS_2, press. induced diffusion effects, NMR study 79—19797
  - intercalation complexes, wideline NMR obs., translational and reorientational effects 77—1602
  - intercalation compound with TaS_2, kinetic study of NH_3/ND_3 exchange by neutron diffr. 79—29350
  - intercalation reaction with TaS_2 (2H), reaction rates, X-ray diffr. expts. 77—12828
  - interstellar, absorpt. in Sagittarius B2 direction 79—35341
  - interstellar, obs. in DR 21, NGC 1333 and NGC 6334 N 79—17044
  - interstellar, obs. in Kleinmann-Low Nebula 77—13440
  - interstellar, obs. in Orion Molecular Cloud 80—36687
  - interstellar, obs. in southern H II regions 78—69863
  - interstellar, radio survey of dark clouds 78—49507
  - interstellar emission lines in direction of T Tauri stars, radio obs. 79—25662
  - interstellar NH_3, in dark clouds, hyperfine struct. 77—78852
  - interstellar NH_3, nonmetastable levels obs. 79—25665
  - interstellar NH_3, obs. in mol. cloud near (S106) 79—84840
  - interstellar NH_3, obs. in Taurus Molecular Cloud 2 (TMC-2) 80—26957
  - interstellar NH_3 emission in Heiles 2 dust cloud, distrib. rel. to cyanobutadiyne emission 80—17641
  - interstellar NH_3 in Taurus dark cloud, line widths rel. to gas temps. and motion 77—78851
  - inverse level doubling mol., space and combined parity nonconservation *(Russian)* 80—52879
  - inversion lines from nonmetastable rotational levels, SHF obs. of Kleinmann-Low nebula 80—73016
  - inversion spectra, ν_4 state 80—47965
  - ionisation coefficients and dissociative electron attachment 80—43833
  - IRC+10216, C star, NH_3 obs. in circumstellar envelope 79—48793

- **ammonia** continued
  - Jupiter, atmospheric methane and ammonia abundance photoelectric obs. 77—33397
  - on Jupiter, longitudinal variability in atm. visible spectra 80—82270
  - Jupiter, NH_3 1.56 μ band study 77—17422
  - Jupiter, NH_3 6450 A absorption band obs. 77—33396
  - Jupiter, spectral line meas. using 10μm superheterodyne receiver 78—16335
  - Jupiter, thermal profiles and NH_3 distribs. from IR spectral meas. 79—40126
  - Jupiter atmos. comp., IR spectral obs., 800-1000 cm^{-1} 78—16336
  - in Jupiter atmosphere, abundance deduced from absorpt. bands in refl. sunlight 80—56758
  - Jupiter NH_3 distrib. and photochemical products 77—67063
  - laser, 12.08 μm emission, CO_2 laser pumped, temp. depend. 78—46582
  - laser, 1 mJ output energy at 16 μm, optical excitation of mol. levels 77—88707
  - laser, compact, high-efficiency, optically pumped 78—5492
  - laser, CW far IR emissions, CO_2 laser pumping and Stark tuning 80—106508
  - laser, efficient energy extraction by superradiant emission 80—53271
  - laser, far IR cascade emission 77—38867
  - laser, far IR emissions from forbidden transitions, using Stark effect with CO_2 laser pumping 79—86168
  - laser, fine temporal structure and power 77—79806
  - laser, for 16 μm range, review *(Rumanian)* 80—87408
  - laser, high energy density, using unstable resonator CO_2 laser pump 80—53327
  - laser, high energy output in 13 μm region, CO_2 laser pump 79—89927
  - laser, high power, 12.08 μm, optically pumped, for appl. to UF_6 isotope separation 78—74923
  - laser, high power, improved optical pumping geometry in Littrow cavity config. 79—22973
  - laser, high power pulse, pumped optically by CO_2 laser radiation 78—46631
  - laser, high-power efficient optically pumped, tunable over 770 to 890 cm^{-1} range 80—91780
  - laser, multiline IR emissions, appl. for InSb Raman laser pumping 79—94216
  - laser, optical pumping by HF laser, press. and temp. depends. 78—29939
  - laser, optically pumped, freq. tuning 80—28208
  - laser, optically pumped, multi-line, 9.3-13.8 μm 77—14751
  - laser, optically pumped, multiwatt, laser operation in 12-13 μm range 79—7141
  - laser, optically pumped, wide range line-tunable oscill. 80—53267
  - laser, optically pumped 12 μm, for UF_6 isotope separation, parametric study *(Japanese)* 79—81414
  - laser, optically pumped by CO_2 laser, high power emission at 12.812 μm 77—38864
  - laser, resonantly pumped, for spectroscopy 80—48277
  - laser, sub mm, Michelson interferometric output coupling, optical pumping 77—14744
  - laser, subMM 81.5 μm, freq. meas. by CO_2 laser difference freq. comparison 80—74415
  - laser, synchronous pumping, ultrashort pulse generation at 151 μm 80—102705
  - laser, two-photon-excited, 16μm emission, wavelength meas. technique 78—71085
  - laser, waveguide cavity, efficient CW far IR output 77—72001
  - laser 12.8 μm source, 60% efficient SHG in Te cryst. 80—83640
  - laser action 11-13 μm, optical pumping by continuously tunable CO_2 laser 80—83596
  - laser action without population inversion, Raman type transitions 77—10891
  - laser emission, far IR, from $^{15}NH_3$, optical pumping by CO_2 laser 78—46578
  - laser emission, far IR CW, by optical pumping 79—3687
  - laser emission, IR and far IR, using TE CO_2 laser pump 79—934
  - laser emission at 16 μm by two-quantum excitation of $2\nu^{-}{}_{2}(7,5)$ state 79—86165
  - laser generation on two-photon excitation, 6 to 35 μm 77—10890
  - laser irradiated, by HF laser, visible luminesc. 77—46593
  - laser lines, CW far IR, CO_2 laser pumping and Stark tuning 80—69382
  - laser lines, far IR, optical pumping by CO_2 laser 78—90415
  - laser pumped by two CO_2 lasers *(Russian)* 79—68386
  - laser submillimetre with optical pumping energy yield, emission pulse delay time depend. on pumping pulse *(Russian)* 78—71088
  - laser transitions, CW, two-photon pumped 80—99702
  - laser with focusing-prism raster and light-guide pump system 80—9905
  - lasing, two-photon generated, effect of press. variation 77—88703
  - lasing lines, CW far IR, using Stark tuning 79—81407
  - LCAO-MO-SCF calcs., analysis of Gaussian basis sets rel. to one-electron props. 78—55122
  - liquid, acidic solns., anodic behaviour of Fe 78—27671
  - liquid, CC ^{15}N NMR chem. shift references evaluation 78—24835
  - liquid, computer simulation, intermolecular potentials 80—38890
  - liquid, contraction phenomenon in DNMR spectra, simulation obs. 77—88469
  - liquid, electron injection from semicond. electrodes 80—6977
  - liquid, irradiated, solvated electron yield, partially diffusion-controlled ion recomb. 79—100409
  - liquid, localised excess electrons, semicontinuum models 78—73129
  - liquid, longitudinal proton and deuteron relaxation rates, press. and temp. depend. 80—44941
  - liquid, mol. correlation functions 77—62459
  - liquid, photoelectron emission of immersed electrode 79—60868
  - liquid, relax. time and activation energy 79—91335
  - liquid, solvated electron optical absorpt. spectra anal., method of moments 77—50436
  - liquid, superheated, boiling kinetics 80—15231
  - liquid, vapour press., isotope effect, relevance to isotope exchange reaction calcs. 80—39272
  - liquid and crystal, IR spectra 77—32360
  - liquid intermol. force model, used to compare Monte Carlo and mol. dynamics calc. methods 80—14984
  - liquid NH_3-GaO junctions, elec. characts. *(French)* 80—2460
  - liquid properties representation, by modified Redlich-Kwong eqn. of state 78—34590
  - low lying states, generalised VB and CI calcs., vertical excitation energies 77—30789
  - marine pollution in Kuwait, meas. 79—5510

ammonia continued
maser, injection priming of pulsed molecular-beam maser oscillator 79—27226
maser with 8 NH$_3$ beams, behaviour study using Fabry-Perot resonator *(French)* 78—42315
metal-ammonia soln., ionis. equilib. instability of weakly-ionised 3-component plasma 80—10877
metal-NH$_3$, soln., thermophysical props. review 79—77758
metal-NH$_3$ mixture, attractive electron-electron interaction from molecular tunnelling mode 79—37793
metal-NH$_3$ solid solutions, phase comp., dissoc. *(Russian)* 77—35665
metal-NH$_3$ solutions, metal-nonmetal transition 77—51789
metal-NH$_3$ solutions, optical and microwave props. of microscopically inhomogeneous materials 77—77161
mixing ratio in Jupiter stratosphere 79—16874
molecular, ab initio calcs., appl. of convergent SCF procedure 80—47875
molecular alignment relaxation rate, laser saturation reson. technique 78—25755
molecular beam, electrostatic space focusing 80—28118
molecular beam, IR-IR double reson., laser spectroscopic method appl. 79—68243
molecular beam apparatus, appl. as target for storage ring 77—6586
molecular beam maser with semi-confocal cavity, output power spectra distrib. 80—43311
molecular cloud in NGC 2264, NH$_3$ line emission mapping, SHF and UHF 80—94847
molecular energy quantities from localised charge densities, dependence on geometry and basis set 80—63525
molecular groups in solids, stochastic jumps, group theoretical method 80—79714
molecular photodissoc. ionis., 16-41 eV 77—18995
molecular rotational transition, collision induced shift 77—484
molecule, 10.6 μm region absorption lines, diode laser meas. 78—58689
molecule, 2sQ(1,1) meas. in $2\nu_2$-ν_2 band, using heterodyne spectrometer 79—75626
molecule, 35 keV electron elastic differential cross section, bond formation, independent atom model 79—31683
molecule, 9.5 μm region diode laser spectra 78—58688
molecule, ^{14}N quadrupole coupling consts., ab initio calcs. 80—58283
molecule, ν_2 band as R(1, 1) line self-broadening coeff. 79—98158
molecule, ν_2 IR band, vibr.-rot. lines, self-broadening and intensities 77—34635
molecule, ab initio SCF calcs., force consts., vibrs., pot. energy surface 78—5209
molecule, absorpt. coeffs. meas. in Nd laser emission band 80—78620
molecule, absorpt. cross sections at CO$_2$ laser wavelengths, temp. and press. depend. 80—78613
molecule, absorption line profile at 10 μm, high resolution meas. 77—42359
molecule, absorption spectra, 6000-6500 Å, intracavity laser detection 79—89684
molecule, and -d$_n$ IR matrix isolation spectra, rotation and inversion 78—5218
molecule, and ND$_3$, new electronic state, multiphoton ionis. obs. 78—74717
molecule, anharmonic pot., determ. of zeroth approx. 77—75255
molecule, Auger spectrum, resolved peak assignments 77—42362
molecule, Balmer radiation production by electron impact 0-2000 eV 79—76521
molecule, beam state selection and focusing, hyperfine spectrum 80—28119
molecule, bond bending, bond orbitals rel. to nucl. motion 80—95513
molecule, bond dissociation, MCSCF LMO calcs. 77—57886
molecule, bonding electron pairs, size and shape parameters, Gaussian basis set MO calcs. 80—27935
molecule, collisional broadening, vel. depend., IR optical saturable absorpt. technique book contrib. 78—9201
molecule, Compton profile asymmetry, 35 keV electron impact spectroscopy 79—7025
molecule, computer controlled CARS spectra of Q branches 78—62241
molecule, core 1s shakeup study, XPS and Xalpha calcs. 80—69064
molecule, core ionis., single orbital relax., LCAO MO SCF calcs. 78—29739
molecule, correl. energy, fourth order diagrammatic, many body Rayleigh Schrodinger perturbation theory 80—63556
molecule, CW and pulsed Pb$_{1-x}$Sn$_x$Se diode laser spectroscopy 79—26980
molecule, decay of saturation reson., IR ν_2 as Q(8,7) transition 78—25609
molecule, dipole oscill. strength distribs., sums 78—21975
molecule, dipole oscill. strengths for excitation, ionisation and fragmentation by 5-60 eV electrons 77—68129
molecule, dipole properties and dispersion energies additivity, using atoms and small mol. models 80—53091
molecule, direct and dissociative electron impact cross-sections 77—61864
molecule, Doppler free coherent two-photon transients, collision induced relax. time, meas., Stark switching 78—90249
molecule, double min. vibr. pot., FORMAC program 77—23444
molecule, dynamic Stark effect obs. at mircowave freq. in mol. beam maser 77—83648
molecule, dynamic Stark shift, microwave obs. 79—72352
molecule, elec. dipole polarisability, coupled and uncoupled Hartree-Fock calcs. 77—34539
molecule, electron correl., quadrupole excitation in correl. energy theories 79—36538
molecule, electron excited Auger emission 77—88518
molecule, electron impact, 35 keV, Bethe surface and Compton profile 80—87235
molecule, electron impact, dissoc. excitation cross-sections, fragment obs. 78—62936
molecule, electron impact, H,D(2s,2p) prod. 78—42230
molecule, electron impact dissoc., H atom sublevel excitation 77—14593
molecule, electron impact dissoc. excitation cross sections 77—61861
molecule, electron impact ionisation, threshold to 180 eV, mass spectrometric obs. 78—13615
molecule, electron impact ionisation, total and partial cross sections meas. 80—95729
molecule, electron impact partial absolute ionis. cross section, 20-350 eV, rel. to H$_2$ and H$_2$O *(French)* 79—861
molecule, electron pair interactions calcs. 80—23298
molecule, electron scatt., 35 keV, Compton defect 79—27092

ammonia continued
molecule, electrostatic force theory appl. to mol. geometry ab initio verification 79—98002
molecule, energy functional, direct minimisation in LCAO-MO density matrix formalism 78—5118
molecule, ESCA and soft X-ray emission, vibr. excitation 80—23433
molecule, excited state population decay time meas., press. depend. 77—75489
molecule, excited states, pot. energy curves w.r.t. bond ang., one-centre expansion approx. 79—6886
molecule, excited vibr. states, transition dipole moments, laser Stark spectrosc. 79—68261
molecule, expansion cooled, mol. photoionisation, rot. struct., rot. predissoc. of excited states 80—91611
molecule, field ionis., critical energy deficits, field depend. 78—82852
molecule, first triplet state, photodissoc. and Rydbergisation investig. 80—53067
molecule, forbidden vibr.-rot. transitions, ν_2 band, IR-microwave two-photon spectra 77—3428
molecule, force consts., vibr. freqs., CNDO/2 and MINDO calcs. 77—14607
molecule, fragment ion formation on photoionisation, energetics and mechanism 77—501
molecule, Franck-Condon factors calcs. 78—17723
molecule, freq. depend. hyperpolarisability, time-depend. Hartree-Fock calcs. 79—36559
molecule, Gaussian lobe orbitals, symmetry defects 79—9990
molecule, geometry changes during inversion, ab initio calcs. 78—5154
molecule, geometry optimisation, using bond function augmented basis sets 78—905
molecule, GO AO exponents optimisation and scaling effects on mol. props. 77—65424
molecule, ground state, analytical pot. function 78—1050
molecule, ground state, microwave inversion lines 80—87098
molecule, H-X bond position, correlation with electronegativity 78—9069
molecule, Hartree-Fock perturbation theory, first-order, symmetry calcs. 79—6854
molecule, heavy nucleus isotope shift calcs. 78—86917
molecule, HF geometry calcs. and SCF calcs. 80—47877
molecule, Hg-photosensitised luminesc. at low press., isotope effects 78—13542
molecule, high-resolution absorpt. spectra obs. using pressure-tuned diode laser 80—82835
molecule, high-resolution polarisation spectroscopy in 10 μm region 79—6196
molecule, high-resolution spectroscopy using pulsed Pb$_{0.955}$Sn$_{0.045}$Se laser 79—64252
molecule, intermolecular interaction energies calcs. using minimal basis sets 80—78681
molecule, interstellar emission line in Orion, 23 GHz obs. 79—30109
molecule, inversion, one-electron props. variation, electronic and nuclear components partitioning 77—83491
molecule, inversion, transfer reaction theory calcs. 78—44364
molecule, inversion spectrum, reson. half-widths calcs. 77—75221
molecule, inversion spectrum collisional line broadening, general theory 80—87184
molecule, inversion spectrum press. broadening by He and Ar, linewidths calc. 80—95599
molecule, inversion splitting calc., variable pot. barrier 79—18177
molecule, inversion-vibration interactions, pot. energy function calcs., isotope effects 78—33567
molecule, ionisation pots. and excitation energies, correl calcs. 77—26986
molecule, IR absorption band integrated intensities, ab initio and LMO studies 80—23458
molecule, IR absorption spectra in 800-1200 cm^{-1} region 79—98086
molecule, IR intensity anal. 77—58081
molecule, IR intensity formulations 77—58004
molecule, IR multiphoton dissoc., laser fluoresc. and chemiluminesc. obs. 79—68276
molecule, IR spectra, $\nu_3+\nu_4$ band anal. 77—75154
molecule, IR spectra, fine struct. of rot.-vibr. bands 80—102504
molecule, IR spectra, line intensities in 2 μ band, Doppler broadened lines 77—75155
molecule, IR spectrum, use of Pb$_{1-x}$Sn$_x$Te injection laser 79—76714
molecule, IR-microwave double reson., rot. and vibr. relax., inversion layers 78—86902
molecule, IR-microwave double resonance, book contrib. 80—54997
molecule, IR-microwave double resonance 79—81221
molecule, laser photochemistry 79—43604
molecule, laser saturation spectroscopy in time delayed mode 78—86976
molecule, laser-induced excitation at 1076 cm^{-1} in megawatt region 80—10354
molecule, linear response function, diagonal ARPA calcs. 78—74594
molecule, linewidth parameter $\Delta\nu/p$ for the J=13, K=13, inversion line *(French)* 78—42131
molecule, LMO population calc. method appl., from given SCF eigenvector matrix 80—14063
molecule, localisability in MO calcs., measured by absolute overlap and 2nd moment dispersions 78—74557
molecule, lone pair contributions to infrared intensities, ab initio calculations 80—63630
molecule, lone pair orbital explicit representation, augmented contracted Gaussian basis set 78—25423
molecule, lowest triplet excitation, electron energy loss spectra 77—71880
molecule, lowest triplet state geometry, SCF and CEPA-PNO calc. 80—914
molecule, mag. shielding consts., coupled HF perturbation theory 79—6863
molecule, mag. susceptibility, HF perturbation method 77—79702
molecule, magnetic relaxation rates for microwave spectrum and contributions to linewidth 80—5564
molecule, mapping in L 183 (L 134 N) dust cloud high density core, SHF obs. 80—105307
molecule, mean amplitude of mol. vibration, approx. calc. method 79—13697
molecule, microwave absorpt. coeff. 77—64378
molecule, microwave spectra, press. shift of inversion lines 79—31615
molecule, microwave spectrum, width and shift parameters 77—18985
molecule, microwave-microwave double resonance 80—53029
molecule, minimal basis set localised orbitals, conjugate gradients method calcs. 79—6849

ammonia continued
- molecule, mol. Rydberg $S \leftarrow S$ and $S \leftarrow T$ transitions, semi-empirical SCF MO calc. 80−91453
- molecule, mol. vibr., G-intensity sum rule 78−74632
- molecule, multipole expansion of diatomic overlap, MEDO calcs. 78−46264
- molecule, ND_3, Einstein A coeff. for $A \rightarrow X$ transition 77−27127
- molecule, nucl. elec. shielding tensor calcs. 80−83296
- molecule, nuclear spin-spin coupling, ab initio SCF perturbation theory 78−33525
- molecule, nuclear spin-spin coupling consts., finite perturbation-CI calcs. 80−5563
- molecule, on Pt surface, heterogeneous reaction of decomp., stimulation by CO_2 laser 78−61052
- molecule, one-electron props. in terms of localised mol. orbital components 79−6840
- molecule, orbital relax. energy for single and double ionis. from valence shells 80−106253
- molecule, photoabsorpt. cross section, 10 to 50 nm 77−61797
- molecule, photodissoc., ab initio SCF and CI calcs. 78−21984
- molecule, photodissoc., NH $c^1\Pi$ state anomalous population 79−10133
- molecule, photodissociation in $A \leftarrow X$ absorption region, D isotope effects 77−77790
- molecule, photodissociation to NH_2 ground state, off-reson. multiphoton absorption 77−14501
- molecule, photoelectron spectra, 21.2-151.4 eV and soft X-ray, ionis. cross-section 78−37683
- molecule, photoionis. cross section calc., for $YM\zeta$ line, HF vs OPW methods 77−42353
- molecule, photoionisation branching ratios and partial oscill. strengths 78−5303
- molecule, photolysis, $NH(X^3\Sigma^-)$ radical form., detect. and reactions 79−64036
- molecule, photosensitisation by Hg, fluoresc. spectrum 78−90198
- molecule, polarisability, elec. dipole, near Hartree-Fock value, using EFV GTOs 77−88591
- molecule, pot. energy surface by MS $X\alpha$ method and mol. geometry 79−13656
- molecule, predissociation of A''_2 state from UHF calcs. of potential energy surface 80−1034
- molecule, proton mag. shielding const., HF perturbation theory 78−46258
- molecule, pseudospectral dipole oscillator strength distribs. 78−50503
- molecule, relaxation by IR and microwave coherent transients 80−28092
- molecule, rot. spectrum 20 to 120 cm^{-1}, Fourier transform spectrometry meas. method 77−45902
- molecule, rot.-inversion Raman spectra, K-splitting 80−9611
- molecule, saturated absorpt. at 888 cm^{-1} using tunable diode laser 78−94239
- molecule, selective two-step dissoc. by laser, ^{14}N, ^{15}N separation, book contrib. 78−9208
- molecule, self assoc., intermolecular interactions, matrix isolation vibr. spectra obs. Raman and IR spectra 80−52995
- molecule, self-assoc., matrix isolation vibr. spectroscopy, complex form. studies 78−62952
- molecule, self-assoc., matrix isolation vibrational spectra, appls. 78−46416
- molecule, separated electronic pair functions, direct minimisation of energy functional, LCAO-MO SCF, density matrix formalism 79−31392
- molecule, sextic centrifugal distortion consts., Watson Hamiltonian, perturbation method 77−10785
- molecule, spectral line breadth, $S^RR(8,3)$ transition of ν_4 band 79−54916
- molecule, spectral parameters, Lamb dip method investig. 78−89560
- molecule, symmetric bending mode, Raman intensity, electrolyte solvent effects 77−34638
- molecule, three photon transitions in gases at microwave freqs. 78−9211
- molecule, time-resolved four-level double-reson. signal, coherent transients effects 78−78732
- molecule, transverse relax. time, T_2, of inversion doublets from free induction decay 80−58281
- molecule, triple-dipole energy calcs. using pseudo-spectral theory 78−46418
- molecule, two-photon population inversion, adiabatic rapid passage 78−78763
- molecule, two-photon transition, collisional dephasing time meas. by Stark switching 77−75248
- molecule, UV laser photodissoc., NH_2 internal energy distribs., NH states 80−11901
- molecule, vibr. excitation in soft X-ray emission and core ESCA spectra 80−69163
- molecule, vibr. levels of inversion splitting, generalised WKB method 80−9585
- molecule + H(2S), collisional quenching, mass spectral obs. 78−25685
- molecule + He, rot. excitation, IOS approx. calcs. 79−45801
- molecule + molecule, vibr. and rot. energy transfer, IR-microwave double reson. study 78−46432
- molecule + radical ion, thermal energy charge transfer, reaction mechanism 77−16796
- molecule + Rydberg atom, reaction channels, expt. vs. theory 80−63755
- molecule in inert solvents, far IR absorpt., free rotational models 77−450
- molecule nonlinear optical polarisability meas. 79−54991
- molecules, dispersion energy consts., dipole oscill. strength, refractivity 77−50492
- moleucle, $\tilde{C}'$-state, 3-photon gas phase spectroscopy obs. 79−89715
- monitor using Stark microwave cavity resonator 80−61500
- multiple photon dissociation, NH_2 fragments, laser-excited fluoresc. obs. 80−11938
- nitrided steel surface wear-related topography 78−60847
- non-metastable absorption at 23.1 GHz, first obs. towards compact H II region W3 (OH) 78−65677
- ocean-atmosphere-continent system, N compounds exchange 78−3794
- olefin + NH_3, gas mixtures, γ-radiolysis over whole composition range *(Japanese)* 79−5172
- optical spectrum, band strengths, curves of growth and NH_3 spatial distrib. on Jupiter 80−46386
- optical two-photon coherent transients, expts. 80−19073
- oxidation, Pt catalyst surface morphology and faceting obs. 77−52669
- oxidation, rel. to amino acid photodegradation in presence of TiO_2 78−11531

ammonia continued
- oxidation in nonurban troposphere 78−32183
- oxidation leaching of chalcopyrite, reaction kinetics 77−52639
- oxidation leaching of chalcopyrite, surface deposit effects 77−48643
- parametric upconversion, resonantly enhanced 26 GHz, of CO_2 laser 79−23020
- partial pressure over ammonium sulphates, nucleation of new particles in atmosphere 79−81708
- pellet generation system for Baseball II-T target plasma expt. 77−39444
- phase conjugation in an inhomogeneously broadened medium 80−83642
- phenol NH_3, intermolecular H-bond, semi-empirical CNDO/2 78−13427
- phonon dispersion curves, phonon lifetimes, anharmonic effects 80−15202
- photochemistry in Jupiter's atm. 77−45354
- photodissoc. in discharge, spectra of metastable NH radicals, rot., vibr. consts. determ. *(German)* 77−34642
- photodissociation in $A \leftarrow X$ absorption region, translational excitation of H atoms and predissociation mechanism 77−77791
- photolysis and greenhouse effect in primordial atmosphere 79−39864
- photooxidation mechanism, computer simulation 77−32810
- photorespiratory cycling, reassimilation involving glutamine synthetase 79−2011
- plasma, surface treatment of polyester fabric, effect on surface struct., props. 78−95831
- plasticisation of nylon 6, deformation by solid-state extrusion 80−25736
- positive glow discharge, N_2^{2+} radiation intensity distrib. obs. *(Russian)* 78−30512
- production by ocean thermal energy conversion 80−66988
- proton-bound dimers, form. in ion-mol. assoc. reactions, rates analysis 77−60054
- pure gas, enthalpy, Carlson-Thodos van der Waals eqn. calcs. 80−83878
- Raman lasing, far IR CW 80−83595
- Raman scatt., high press., high temp. 77−27077
- reaction with Si (111) surface, 1225 to 1380°C 79−100441
- resonantly enhanced four-wave parametric generation of 823 cm^{-1} radiation 78−63151
- Saturn, far IR spectrum, PH_3 and NH_3 absorpt. lines 78−12147
- Saturn, outer atmosphere obs. and model of NH_3 abundance *(Russian)* 77−33406
- Saturn NH_3 1.56 μ band study 77−17422
- semiconductor-NH_3 electrolyte, interface, photo-assisted electron injection 79−87152
- sensing probe, potentiometric, micro-size 78−61071
- sensitiser, excitation in MW region using CO_2 laser, pumping models 80−11911
- solar energy storage system, ammoniated salt heat pump using $MgCl_2$, $CaCl_2$, NH_4Cl 80−81484
- solar thermochemical cavity absorber based on NH_3 dissociation, design and cost anal. 80−81489
- solid, AES excited by X-rays 79−33894
- solid, electron-irrad., cluster-ion prod., lattice and fragmentation energies 77−4911
- solid, gamma-irrad., cryostats development 77−45856
- solid, IR and Raman intensity of lattice vibrs., theory 80−11381
- solid, lattice dynamics, atom-atom model of intermol. forces 78−75751
- solid, lattice vibrs., group theoretical anal. by computer 77−80590
- solid, melting curves, Lennard-Jones Devonshire theory 80−65201
- solid, proton irradiated, dynamic nucl. polarisation below 0.5K 79−78569
- solid, UPS, valence band struct. 79−33890
- solid and liquid, IR spectra 77−32360
- solid film, absorpt. coeffs. determ. 50 to 7000 cm^{-1} 80−97356
- solid film, contaminant on cryocooled Ge optical window, IR transmission 79−32007
- solid-^{57}Fe, Mossbauer study of iron bonding to solid ammonia and its photofragments 80−15833
- solutions, in benzene(CCl_4)(pentane) Fermi resonance, solvent and phase depend. 80−47960
- solutions, UV absorpt. of solvated electron 79−87935
- solvated electron, polaron coupling const. from dipolar plasmon freq. 77−89720
- solvated electrons, optical spectra and model potentials 80−30318
- special-purpose frequency standard and clock 78−57913
- spectral lines near 11 μm, precise meas. using IR heterodyne technique 78−5230
- spectrophotometer, IR, effective spectral slit width determ. using NH_3 absorpt. line 80−95167
- Stark cell for wideband modulation of CO_2 laser R(18) line 77−23704
- Stark effect modulation at 2.2 μm *(French)* 78−50912
- Stark shift, microwave Σ-transitions in presence of strong elec. fields 78−90213
- Stark tuned 26 GHz parametric upconversion at 10.8 μm 77−88845
- stimulated hyper-Raman scattering in a molecular gas via a three-photon process to obtain IR and far IR radiation 80−58633
- stratosphere, NH_3 injection detected from change in nature of aerosol 78−28286
- surface water continuous analysis by NH_4^+-sensitive plastic membrane electrode 80−89701
- synthesis, industrial, using N_2 reducing solar cells 80−89632
- synthesis, sintering of catalyst based on Fe_2O_3 79−61551
- synthesis catalysts, XPS studies 79−70370
- thermodynamic props., anal. of data tables 78−93636
- troposphere, vertical distrib. by photochem. model 80−85701
- troposphere vertical profile, daily and seasonal variation 80−85700
- turbine flowmeter for high press. 79−55431
- turbulent flow in tube, heat transfer 79−14395
- two photon excited 16 μm laser 78−58986
- two-photon pumping, of four-level system, to obtain 12.16 μm radiation for isotope separation 78−90414
- vapour, supercrit. and subcrit., 80−59162
- vertical density profiles in Jupiter and Saturn atm. from emissivity data 80−82267
- viscosity measurements using oscillating disc type viscometer 78−51273
- Ag(I) reduction by tartrate in HN_3 solns. *(Russian)* 79−47976
- $AlBr_3.NH_3$, mol. struct., vap. phase electron diffr. obs. 77−65541
- $AlCl_3$-NH_3 system, supersaturation calc. during AlN epitaxial growth 77−8758
- Ar-NH_3 mixtures, viscosity under press., density depend. and mol. assoc. 80−1727
- C-H-O(-N) gas mixtures, high temp. emissivity, 4.8 μ region, shock waves 77−76027

ammonia continued
CO-H_2O-NH_3-methanol, solid mixture vibr. modes, IR spectra 80—90504
$CO_2+H_2(CO_2)(Ne)(NH_3)(CH_3F)$, rot. transfer collisions, momentum transfer distributions 77—523
$CaCl_2$-NH_3 dry absorption for solar refrigeration 80—61310
$CaCl_2+8NH_3$ coolant for solar refrigeration *(French)* 79—24911
$Cl+NH_3$, reaction rate consts., flash photolysis-reson. fluoresc. obs. 78—3327
Cs-NH_3, Cs-ND_3, solns., US absorption, metal-nonmetal transition 79—69194
Cs-NH_3 solution, metal-nonmetal transition, cond. density and Hall coeff. meas. 77—51789
$GaBr_3.NH_3$, mol. struct., vap. phase electron diffr. obs. 77—65541
H-bonded dimers involving H_2O and HF, PCILO study 79—72238
H_2-NH_3 mixture, viscosity meas., 25-100°C, up to 120×10^5 Pa 79—32731
$H^+(NH_3)_n$, secondary electron emission from charged clusters on 2.4 keV Ar bombarded surfaces 79—15580
$He+NH_3$, rot. excitation rate consts., semiclassical method 79—3538
$Hg+2NH_3 \rightarrow HgNH_3+NH_3$, photosensitised, $HgNH_3$ complex lifetime 78—53193
$Hg+NH_3$, excited UV luminesc., low press., $HgNH_3$* form. 77—21388
$HgNH_3$ complex, fluoresc., lifetime meas. 78—53193
Hg^*+NH_3, UV emission at low press., pulsed excitation, relax. meas. 77—79570
$K+NH_3$, rot. inelastic, time-of-flight spectra 78—5325
Li:NH_3, soln., free MHD convection near horizontal cylinder *(Russian)* 77—7467
Li-ND_3, near liq.-liq. crit. point, conc. fluctuations, neutron diffr. long wavelength thermodynamic limit 79—10948
Li-NH_3, conc. solns., elec. cond. and thermoelec. power 79—19640
Li-NH_3 concentrated solution, NMR relaxation of ^7Li 80—108084
Li-NH_3 solution, metal-nonmetal transition, US absorption coeff. 77—51443
Li-NH_3 system, inhomogeneous, numerical simulations of Hall effect 77—43551
molecule, IR-microwave two-photon spectra using CO_2 lasers 78—37664
N_2-NH_3 mixture, viscosity measurements using oscillating disc type viscometer 78—51273
$NCl_3.NH_3$, force const. calcs. 79—36603
ND_3, adsorbed on graphon, neutron scatt. study 79—60640
ND_3, chemisorbed on W, decomposition mechanism, isotope effect 79—29409
ND_3, effect of phase density on ionisation process and electron localisation 77—89731
ND_3, Hg-photosensitised luminesc. at low press. 78—13542
ND_3, hyperfine structure of inversion transitions, molecular beam electric resonance 79—98071
ND_3, in $TaS_2(TiS_2)$, intercalation system, wideline NMR, temp. effects 77—16184
ND_3, inversion-vibration interactions, pot. energy function calcs., isotope effects 78—33567
ND_3, photodissoc. in discharge, spectra of metastable ND radicals, rot., vibr. consts. determ. *(German)* 77—34642
ND_3, predissoc. mol., rot. resolved IR reson. scatt. 77—30882
ND_3, relax. rates determining the inversion spectra 77—454
ND_3, sub mm beam maser spectrum, D hyperfine splitting 77—61874
NH, ND, vib. relax. in amorphous solid inert gas systems 77—7817
NH_3, $(\bar{A}\,^1A_2'')$ predissoc., vac. UV photolysis, NH_2 form. 78—13547
NH_3, aqueous solution, fluorescence by Nd laser radiation *(Russian)* 77—54753
NH_3 H-bonded dimers, PCILO calc., energies, geometries 78—37557
NH_3, relax. rates determining the inversion spectra 77—454
$NH_3{}^+$, fast mol., dissoc. in thin C foils, Doppler broadening obs. 78—22019
$NH_3{}^+$ ion, electrostatic force theory appl. to mol. geometry ab initio verification 79—98002
$NH_3{}^+$, ionisation pot. of ^2E state, Jahn-Teller effect 78—62948
$NH_3{}^+$ radical, EPR in X-irrad. $K_2SO_4:(NH_4)SO_4$ 80—11272
$NH_3{}^+$, two-mode Jahn-Teller effect calcs. 80—83297
$^{14}NH_3$, $^{15}NH_3$, electric dipole moment, vibr. depend. 79—59598
$^{14}NH_3$, $^{15}NH_3$, submm-wave rot.-inversion transition, ν_2 state 77—75138
$^{14}NH_3$, $^{15}NH_3$ and $^{14}NH_2D$, IR laser Stark spectroscopy 80—47978
$^{14}NH_3$, Doppler free spectroscopy, 16 micron generation applications 79—94049
$^{14}NH_3$, IR saturated absorpt. spectra, vibr. depend. of hyperfine quadrupole const. 77—27072
$^{14}NH_3$, inversion spectrum 79—3438
$^{14}NH_3$, J=13, K=13 inversion line displacement as function of pressure *(French)* 78—70815
$^{15}NH_3$ far IR laser emission at 153, 375 μm, optically pumped by $^{13}C^{16}O_2$ laser 80—58507
$^{15}NH_3$, IR-IR double resonance, ν_2 vibr. state, electric dipole moment 77—83626
$^{15}NH_3$, inversion doublets, T_1 and T_2 M depend. 78—13489
$^{15}NH_3$, modulated coherent Raman beats 80—23464
$^{15}NH_3$, nucl. spin-spin coupling consts. calc., vibr. averaging effects 78—33521
$^{15}NH_3$, two-photon spectroscopy, double resonance studies with a new coincidence 78—70888
NH_3-$AlCl_3$ solution, Al_2O_3 ultrafine gel particle form. 80—93807
NH_3-Ar mixture, thermal cond., viscosity, Senftleben-Beenakker effect 80—100054
NH_3-CO_2 gas mixture, thermal diffusion const. 78—67300
NH_3-$CaCl_2$, isothermal dissociation and regeneration, appl. to solar refrigeration *(French)* 80—61300
NH_3-ethylene (propylene) mixtures, crit. curves at high-press. 79—23715
NH_3-H_2 solid mixture, compressibility rel. to possible existence of metallic ammonium 80—24567
NH_3-H_2O, solar absorption refrigeration system, Seoul, Korea *(Korean)* 78—51052
NH_3-HCl, assoc., matrix isolation vibrational spectra, appls. 78—46416
NH_3-He mixture, viscosity, Senftleben-Beenakker effect 80—100054
NH_3-LiF adduct, mol. consts., ab initio SCF LCAO MO calcs. *(French)* 78—13423
NH_3-LiH, struct. and props., SCF ab initio calcs. 80—106250
NH_3-Li(Na) solution, small angle X-ray scatt. meas. 79—14667
NH_3-lithium halide complex, ab initio calcs., Li bond rel. to H bond 77—14343
NH_3-methane, mol. relax., optoacoustic reson. meas. 80—27351

ammonia continued
NH_3-$N_2(H_2)(Ne)(Ar)(Kr)(Xe)$, as R(1,1) vibr-rot. line parameters, ν_2 band, using CO_2 laser light 79—3444
NH_3-ND_3, electron impact ionisation, threshold to 180 eV, mass spectrometric obs. 78—13615
NH_3-NO mixtures, combustion emission spectra, identification of NH_2, NH, OH, NO by rapid scanning spectra *(French)* 79—52665
NH_3-water system, vapour-liquid equilib., thermodynamics 79—42246
NH_3+2H_2, triplet n3S Rydberg state, ab initio UHF CI SCF calc. 80—53095
NH_3+Ar^{12+}, N K-shell Auger effect 77—6908
NH_3+BP, dissoc. reacts. 79—43627
NH_3+Br_2, gas phase reaction, $NHBr_2$ identified by ESCA 79—31599
$NH_3+C^+(CH_n{}^+)$, rate coeffs., ionised product distribs. 77—40522
$NH_3+CH_3{}^+$, condensation reactions mechanism 80—25996
$NH_3+CO_2(N_2)$, collisional broadening of NH_3 inversion spectrum lines 80—99521
NH_3+Cl^+, reactions at room temp. 80—93749
$NH_3+D_3O^+(D_2O)_n$, binary reactions, rate coeffs. and product ion distributions determ. 80—81305
NH_3+Fe interaction, chemical species formed studied by Mossbauer effect 80—43080
NH_3+formaldehyde, cross sections meas. *(French)* 79—76487
NH_3+H_2, NH_3 inversion transition, linewidths and T_1/T_2 ratio 80—99499
NH_3+H_2 collisions, semi-empirical non-Lorentzian line shape determ. 77—34699
$NH_3+H_2{}^+(He^+)$, dissociative charge transfer reactions, energy transfer depend. 77—25258
NH_3+H_2O, collision-induced energy transfer, IR-microwave double reson. obs. 78—42171
NH_3+H_2O coolant for solar refrigeration *(French)* 79—24911
$NH_3+H_3O^+(H_2O)_n$, binary reactions, rate coeffs. and product ion distributions determ. 80—81305
$NH_3+HNO_3 \rightleftharpoons NH_4NO_3$ equilib. in atmosphere 79—88389
$NH_3+Hd \rightleftharpoons NH_2D+H_2$, deuterium separation factors, calc. 80—3310
NH_3+He, differential scatt. cross-section, intermol. pot. 79—36728
NH_3+He, interaction potentials, ghost orbital SCF and Gordon-Kim calcs. 79—94057
$NH_3+He(Ar)$, ammonia inversion spectrum press. broadening 78—86915
$NH_3+He(H_2)$, rot. relax. double and triple reson. obs. 78—66570
$NH_3+He(H_2)$, rot. relax., double and triple reson. obs. 78—90196
$NH_3+He(Ne)(Ar)(Kr)$, pure rot. line, press. broadening calcs. 80—78656
$NH_3+Hg(^3P_1)$, quenching rate constants determ. with nanosecond light pulser with Hg vapour 80—100111
NH_3+methyl cation, reaction kinetics, 0.04-1 eV *(French)* 80—66768
NH_3+N_2, spectral broadening of line in $_4\nu$ band in NH_3 79—54916
NH_3+N^+, 35-200 keV, X-ray spectrum, rel. to N^++N mechanism 78—42183
$NH_3+N^+(O^+)(Ne^+)$ symmetric collisions, double K-shell ionisation, two-electron-one-photon transitions 77—19067
$NH_3+NH_3(He)(Ar)(N_2)(O_2)$, ν_2 state vibr. relax., laser induced vibr. fluoresc. obs. 79—18269
$NH_3+NH_3(He)(Ar)(N_2)(O_2)$, vibr. energy transfer temp. depend. 80—63763
$NH_3+NH_3(ND_3)(HCl)(H_2O)$, inversion relax., isotope effects, beam-maser ang. resolution effects 77—30964
NH_3+NO_2, continuum quenching in upper atmosphere 79—88520
$NH_3+NaSCN$, coolant for solar refrigeration *(French)* 79—24911
NH_3+Ne^+, thermal energy, reaction rate coeffs. and product distrib. 79—29333
NH_3+Ne^*, quenching rate const. for metastable $Ne(^3P_2)$, flowing afterglow 78—46295
NH_3+O, rot. excitation, classical Monte Carlo calcs. 77—34727
NH_3+O_2, flash photolysis, NH_2+HO_2 rate const. 79—47943
NH_3+OH, rot. inelastic collision, microwave spectra 79—45806
$NH_3+OH^+(H_2O^+)(H_3O^+)$, bimolecular reactions, product. distrib., rate consts. 78—11513
$NH_3+O(^1D)$, rate consts., temp. depend. 78—27747
NH_3+SO_3, donor-acceptor adduct form., ab initio calcs. 78—82612
NH_3+X^{n+}, (X=Ar,Kr,Xe,U), Auger emission line shape after dissoc. 78—86838
$NH_3{}^++H_2O$, bimolecular reactions, product. distrib., rate consts. 78—11513
$NH_3{}^{\cdot+}+H_2O \rightarrow NH_4{}^++OH^{\cdot}$, statistical phase space theoretical anal., vibr. depend. cross section 78—15660
$NH_3{}^{\cdot+}+NH_3 \rightarrow NH_4{}^++NH_2$, statistical phase space theoretical anal., vibr. depend. cross section 78—15660
$(NH_3)_3$, open-chain and cyclic structs. 80—45480
$(NH_3)_n$, (n=1-6), mol. beam elec. deflection obs. 79—72371
$NH_4{}^+$, libration and tunnelling freq. rot. heat capacity, hindered rot. energy level calcs. 79—98058
$^{13}NH_4{}^+$, for myocardial imaging, prod., distrib. and imaging characts. 77—40752
NH_4-^{15}N, absorpt. and transfer to amino-N, rat small intestinal sac 80—16909
$NH_4{}^++H_2O$, supermolecule calcs. with additive procedure, intermolecular interactions and binding energy 80—52880
NH_3BF_3 and d_3, polycryst., for IR spectra, lattice vibrs., cryst. and mol. struct. interpret. 80—2771
$NH_4Cl:NH_3$, TSC obs. of polarisation 79—78618
NHD_2, inversion-vibration interactions, pot. energy function calcs., isotope effects 78—33567
NH_2D, dipole moments effects of RF elec. field modulation on IR stark spectroscopy 80—52989
NH_2D, heat cond. gas, nonequilib. vel. distrib. function, laser absorption obs. 78—22448
NH_2D, inversion-vibration interactions, pot. energy function calcs., isotope effects 78—33567
NH_2D, mixing of CO_2 laser radiation with 4 GHz microwaves, Stark-induced three-wave mixing, expt. 77—10974
NH_2D, mixing of CO_2 laser radiation with 4 GHz microwaves, Stark-induced three-wave mixing, calc. 77—14774
NH_2D Stark active mol., cavity dumping for CO_2 laser pulse generation 77—88800
NH_2D Stark cell noise reduction for CO_2 laser beam 78—59059
$(NH_3)_nH^+$, n=1-9, detected in photoionisation of supersonic mol. beam mass spectra, H-bonding 79—74356

ammonia continued
- $NH_3(ND_3)$ in solid Ar, UV absorption spectra, temp. depend. of matrix spectra 80—63652
- $NH_3(ND_3)$, photolysis, excited NH(ND) prod., collisional quenching 77—19018
- $NH_3(ND_3)+Hg$, photosensitised luminesc., phase shift anal. 79—15966
- $NH_3(ND_3)(NT_3)$, harmonic force fields, equal coord. method calcs. 77—30845
- NH_2T, β-decay, ab initio SCF MO calcs. 77—71842
- NH_2TNH_3, β^- decay effect on H-bond, ab initio LCAO SCF MO calc. 78—76894
- NOCl, optically pumped laser, 11-17 μm 78—46581
- ^{13}N labelled NH_3 production for medical appl. 80—72327
- $^{13}NH_3$ intravenous injection, absorbed radiation dose calcs. 80—94375
- $^{14}NH_2D$, i.r. absorption coeff., press. broadening 77—464
- $^{14}NH_3$, ν_2-band Doppler-free two-photon resons. in Stark field 77—23527
- $^{14}NH_3$ gas absorption spectrum, microwave power meas. appl. 77—18013
- $^{15}N/^{14}N$ isotope ratios in atm. aerosols and precip. 78—44896
- $^{15}NH_3$, and $^{14}NH_3$, laser-microwave two-photon spectroscopy, appl. of tunable source 79—30579
- $^{15}NH_3$, Doppler-free optical double reson. spectroscopy using single-freq. laser and modulation sidebands 80—68274
- $^{15}NH_3$, interstellar detection at 23 GHz 79—44590
- $^{15}NH_3$, $\nu_2R(2,0)$ line freq. coincidence with R(42) CO_2 laser line collisional relax., double reson. obs. 77—46562
- $^{15}NH_3$, T_2/T_1 determ. for inversion transitions, power-broadened line shape 77—38654
- $^{15}NH_3$ far IR CW laser, optically pumped with $^{13}C^{16}O_2$ laser 80—78866
- $^{15}NH_3$ frequency standard, 22.79 GHz, feasibility study 79—71418
- Na-NH_3, nonmetal-metal transition, thermodynamics 78—18964
- Na-NH_3, solns., US absorpt. and vel. near crit. point 79—28047
- Na-NH_3 film, quench-condensed, anomalous elec. cond. obs. 77—32057
- Na-NH_3 film, vapour deposited, elec. resistivity, metal-nonmetal transition 78—84317
- Na-NH_3 solid mixture, cond., three component reactive percolation model 78—68003
- Na-NH_3 solns., UV absorpt. *(German)* 77—24869
- $O(^1D_2)+NH_3 \rightarrow OH(v,N)+NH_2$, bimodal OH rot. distrib. obs. and energy disposal 80—76501
- SO_2+NH_3, atmospheric aerosols direct form. 77—29377
- TaS_2 intercalated with NH_3, charge transfer, PAC meas. 78—76366
- $TaS_2:NH_3$, mol. motion, neutron quasielastic scatt. obs. 79—90827
- $Xe+NH_3(H_2S)(SO_2)(HCl)$, ionis. cross sections calc. 77—68103
- Xe(nf)+NH_3, at. Rydberg state further excitation by rot. transfer, field ionis. obs. 78—58795
- Xe(nf Rydberg state)+NH_3, n- and l-changing and ionising collisions 80—58360

ammonia clocks *see atomic clocks*

ammonium compounds
- alkali halide:NH_4^+, hindered rot. energy levels calc. 80—10514
- alkali halides:NH_4^+, inelastic neutron scatt. 78—14407
- alunite-jarosite, spcae group refinement by means of vibr. spectroscopy 79—94981
- ammonia Rochelle salt, temp. depend. of optical axis angle, phase transitions *(Russian)* 80—97216
- ammonium bioxalate monohydrate spontaneous parametric scatt. spectra, polariton wave vector and Stokes lines analysis 78—43885
- ammonium hydrogen chloracetate, order disorder type transition 79—47399
- ammonium hydrogen oxalate hemihydrate, low temp. dielec. and thermal props. 77—28510
- ammonium hydrogen oxalate hemihydrate, single cryst., DNMR obs., elec. field gradients, reorientation 77—85618
- ammonium oxalate monohydrate, Raman spectrum, internal and external vibrs. 79—73924
- ammonium Rochelle salt, cryst. with modulated struct., neutron scatt. obs. 79—95713
- ammonium Rochelle salt, first order phase transition 78—43818
- ammonium Rochelle salt, incommensurate phase transitions under existence of Lifshitz invariant 79—15416
- ammonium Rochelle salt, incommensurate phases and ferroelectricity 78—52455
- ammonium Rochelle salt, thermodynamics of ferroelec. transition 80—84702
- amonium alginate, aq. solns., laminar flow heat transfer in helical coils 80—59030
- aryl ammonium hydrogen difluorides, IR vibr. spectra and NMR reson. obs. 80—34788
- d-10-camphorsulphonic acid ammonium salts, characts. rel. to spectropolarimetry 77—24816
- CD NH_4^+, rot. states, coherent neutron scatt. 77—84678
- dialkyl ammonium manganese chloride, phases and structural phase transitions, DSC and X-ray diffr. meas. 77—47574
- double salts, NH_4 MBX_4, (M=alkali metal; $BX_4=SO_4$, SeO_4, BeF_4, etc.), theory of phase transitions 79—99837
- fertilizers, nitrogenous and phosphate, pollution problems from manufacture 79—34450
- halides, acoustic anomalies above critical temps., volume magnetostriction type terms 80—2123
- halides, anomalous sound attenuation above lambda point 78—51617
- halides, cryst., H bonding, order-disorder phenomena 80—6379
- halides, phase transitions by Monte Carlo method using cubic Ising model 80—70408
- halides, phonon dispersion, cohesive and dielec. props. in three body force shell model 80—79892
- halides, simple, complex, polycryst., hydrogen bonding, NH_3D^+ probe ion IR spectra 79—82966
- halides, sound attenuation near lambda point 77—66002
- hexahalometallate (IV) complexes, A_2MX_6, A=alkali metal or ammonium, M=lanthanide or actinide, X=F or Cl, lattice energies and thermochem. 79—60307
- isopropyl ammonium chloroplatinate and chlorostannate, ferroelastic transition, thermal, optical, and elastic meas. 79—28096
- lithium ammonium tartrate, piezoelec., proper ferroelastic transition 78—2812
- lithium ammonium tartrate dihydrate, ferroelectric-elastic phase transition. theoretical model and expt. *(Russian)* 80—75961
- lithium ammonium tartrate monohydrate, isostructure with lithium potassium tartrate monohydrate: Mn^{2+}, EPR obs. 80—29607

ammonium compounds continued
- lithium ammonium tartrate monohydrate, Raman spectra, anomalous low-lying response 80—2746
- lithium ammonium tartrate monohydrate, spontaneous shear strain, X-ray obs. 78—56433
- lithium ammonium tartrate monohydrate, struct. phase transitions, light scatt. meas. 79—95774
- $M^IM^{IV}IO_6$, vibr. spectra (M^I=Na,K,Rb,Cs,NH_4; M^{IV}=Ge,Sn,Pb) 77—42325
- malate, SHG, 492-640 nm, phase matching, refr. index and nonlinear susceptibility 77—72031
- metallic ammonium, possible existence, equation of state 80—24567
- methyl sulphite, IR spectra of NH_3D^+ ion, mol. motion 77—36232
- methylammonium bromide, solid, phase transitions, PMR, DTA study 80—107421
- $(NH_4)_2SO_4:Mn^{2+}$, ferroelec. phonon driven phase transform., reduction of spin Hamiltonian consts. 78—92033
- $NH_4Al(SO_4)_2.12H_2O:MnO_4^-$, visible and UV absorpt. spectra interpretation 80—45116
- NH_4Cl, PMR free induction decay shape and moments 78—68394
- $NH_4H_2PO_4$, cryst. growth from aqueous solns., dislocation groups in (100) faces, kinetics 79—74072
- NMR lineshape rel. to ion reorientation 77—48074
- nuclear fuel fabrication, low level radioactive waste solns. containing NH_4NO_3, spray tower treatment *(German)* 79—93798
- oxalate monohydrate: Mn^{2+}, ESR, 77-345K 79—19768
- oxalate monohydrate, IR refl. and Raman spectra, internal and external modes *(French)* 77—36231
- oxide reactor fuel pellets, ammonium polyuranate precipitation, continuous, particle size distrib. and agglomeration control 79—93804
- photographic emulsions, preparation, explosion hazard of ammoniated silver salt solns. 78—4727
- PMR absorption of tetrahedrally coordinated four-spin-$^1/_2$ system 77—8425
- proton spin relax. and phonons in ammonium salts 78—84493
- proton spins, relaxation time of dipolar energy 78—76333
- reorientation of NH_4^+, PMR relax. and inelastic neutron scatt. 79—82167
- Rochelle salt, dipole interaction symm. aspect 77—20805
- Rochelle salt, incommensurate ferroelectricity 79—61311
- (Rochelle salt)$_{1-x}$(ammonium Rochelle salt)$_x$, phase transitions, hydrostatic press. effects 80—93246
- Rochelle salt-ammonium Rochelle salt mixed cryst., elastic props., piezoelec. reson. method 78—76390
- rotational tunnelling, temp. dependence 80—38970
- salt-containing liq. NH_3 solns., electrochem. behaviour of Fe electrodes, impurities effect 80—50857
- sodium ammonium tartrate, crysts., temp. depend. of elastic compliances at phase transition 79—15409
- sodium ammonium tartrate, ferroelec., thermodynamic theory of phase transitions 77—90112
- sodium ammonium tartrate, improper ferroelec. transition anomalies 78—19430
- sodium ammonium tartrate, polarisation, improper ferroelec. transition 78—72477
- steel, mild, cyclic strain enhanced dissolution in NH_4NO_3, corrosion fatigue props. 80—85083
- sulphates, vapour pressure, nucleation of new particles in atmosphere 79—81708
- tartrate, triboluminescence and cryst. fracture dynamics 80—50437
- tetraalkylammonium halides, mol. reorientation, spin lattice relax. time study 80—18875
- tetrachloroaluminate, vapor characterisation by photoelectron spectrosc. 80—81388
- tetraphenylboride, IR spectra of NH_3D^+ ion, mol. motion 77—36232
- thermal decomposition, appl. to solar storage 80—76656
- trimethylammonium chloride and deuterated forms, cryst., inelastic neutron scatt. H bond vibr. obs. 77—7796
- trisoxalatoferrate complexes, Mossbauer studies of electronic relax. phenomena 80—44973
- tunnelling frequency of NH_4 ion in crystals, cubic and noncubic 78—38633
- Tutton's salts, $(NH_4)_2M(SO_4)_2.6H_2O$, IR spectra, correl. of vibr. freq. and N...O distance for NH_3D^+ 78—92066
- uranyl nitrate, IR spectra, force const., bond orders 77—30873
- ADP-type crystals, electrooptic effect in ultraviolet region 78—76431
- $AlNH_4HP_3O_{10}$, cryst. struct. determ. *(French)* 77—47408
- $AlNH_4(SO_4)_2:Cr^{3+}$, optical spectral, crystal field, spin orbit and exciton interactions 80—34958
- β-Al_2O_3-NH_4^+, high press. thermal stability 79—23678
- β-Al_2O_3-NH_4^+, NH_4^+ jump diffusion and rotational tunnelling, proton NMR, spin isomerism theory 79—99778
- β-Al_2O_3-NH_4^+, neutron diffr. obs. of struct. 80—107512
- β-Al_2O_3-NH_4^+, PMR relax. time obs. of ionic motion 80—71213
- β-Al_2O_3-NH_4^+, protonic cond., struct. investig. 79—19213
- β-Al_2O_3-NH_4^+, single cryst. characts. and AC cond. obs. 80—107514
- β-Al_2O_3-NH_4^+ and β''-Al_2O_3-NH_4^+-H_3O, single cryst. PMR and proton motion 80—108101
- β-Al_2O_3-NH_4^+ proton dynamics neutron scatt. study 80—59408
- β''-Al_2O_3-NH_4^+-H_3O, ionic cond. at room temp. 80—107513
- β-$Al_2O_3.(NH_4)_2O$, neutron scatt. study of NH_4^+ motion 78—30785
- $Al_2(SO_4)_2$ $(NH_4)_2SO_4.24H_2O$, crystn. kinetics in an MSMPR crystalliser 80—100185
- $CH_3NH_3Ga(SeO_4)_2.12H_2O$, dielec. relax. near transition temp. 80—60493
- $CaNH_4HP_2O_7$, monoclinic, crystal struct. exam. 78—2070
- $CaNH_4NaP_2O_7.3H_2O_7$, crystal data *(French)* 78—14316
- $Cd(NH_4)_2(Cr_2O_7)_2.2H_2O$, chemical prep. and crystal data *(French)* 80—24416
- $CdNH_4NaP_2O_7.3H_2O$, crystal data and crystal struct. *(French)* 78—14316
- $Cd(NH_4)_2(SeO_4)_2.6H_2O:Mn^{2+}$, EPR of Mn^{2+}, spin-Hamiltonian parameters 79—33528
- $CeNH_4P_4O_{12}$ and $Ce(NH_4)_2(PO_3)_5$, synthesis by solid-phase reaction, characts. 80—60778
- $Co(NH_4)_2(BeF_4)_2.6H_2O$, cryst. struct. refinement by X-ray diffr., comparison with neutron diffr. *(French)* 77—47387
- $Co(NH_3)_6Cl_3$, proton second moment meas., 96 to 404K 79—95652
- $Co(NH_4)_2(SO_4)_2.6H_2O$, LF relax. meas. 78—15012
- $Co(NH_3)_6X_3$, (X=Cl, Br, I), internal and lattice vibr. normal coordinate anal. 79—69203

ammonium compounds continued
Cs_2SO_4-$(NH_4)_2SO_4$ mixed cryst., ferroelec. transition, structural and dielec. props., proton spin-lattice relax. 78—39512
$Cu(NH_4)_2Br_4.2H_2O$, Heisenberg ferromag., corrections to scaling in sp. ht. 77—66328
$Cu(NH_4)_2Br_4.2H_2O$, Heisenberg ferromag., mag. props. at high press. 77—69512
$Cu(NH_4)_2Br_4.2H_2O$, uniaxial ferromag. insulator, influence of press. on magnetisation 77—69661
$Cu(NH_4)_2Br_4.2H_2O$ Heisenberg ferromagnet, mag. props. in mag. field 80—34637
$Cu(NH_3)_4PtCl_4$, $Cu(NH_3)_4^{2+}$ cation mol. orbital parameters 78—64011
$Fe(NH_4)_2(SO_4)_2.4H_2O$, rehydration kinetics, Mossbauer effect study 80—61081
$Fe(NH_4)_2(SO_4)_2.6H_2O$, Mohr salt, elec. field gradient determ., appl. of intensity tensor to thick single cryst. 80—44966
HN_4^+, in crystalline cpds., tunnelling, PMR, generalised line shape, theory 79—73827
H_3N-BH_3, cryst., electronic struct., ab initio, MO calcs., fractional charge model 77—34547
$HO_2.H_2O(NH_3)$ complex form., ab initio calcs., min. energy configs. 77—14340
$HgI_2:NH_4I$, cryst. growth from soln., doping rel. to elec. cond., phase transitions 77—55880
$HgNH_3^*$, excited complex photosensitised luminesc. and fluoresc. phase shifts 78—33535
$KH_2PO_4:NH_4H_2PO_4$, EPR of arsenic and phosphorus oxyradicals 77—77102
$K_2SO_4:(NH_4)SO_4$, X-irrad., EPR of NH_3^+ 80—11272
$K_2SnF_6.H_2O$, crystallographic characts. *(French)* 78—10011
$LiND_4SO_4$, ^7Li and ^2D NMR exam. of high-pressure phase 79—11396
$LiNH_4SO_4$, atomic struct. exam. 79—37678
$LiNH_4SO_4$, DC elec. cond. 80—88603
$LiNH_4SO_4$, ferroelect. and press. induced phase transitions 79—38473
$LiNH_4SO_4$, ferroelectric phase transition, lattice parameters and thermal expansion coeffs. 80—40074
β-$LiNH_4SO_4$, lattice modes and phase transition, polarised Raman meas. 77—20859
$LiNH_4SO_4$, phase transitions, temp. depend. of NMR, spontaneous polarisation, birefringence and SHG 78—10191
$Mg(NH_3)_6(ClO_4)_2$, solid, mol. rot., Raman contour, quasielastic neutron scatt., and PMR obs. 79—87444
$Mg(NH_4)_2(SO_4)_26H_2O:VO(H_2O)_5^{2+}$, proton ENDOR meas. used to determine hyperfine coupling tensors 80—66075
$Mg(NH_4)(SO_2)_4.6H_2O:Cu(H_2O)_6^{2+}$, ^1H ENDOR 79—73854
$Mg(NH_4)_2(SO_4)_2.6H_2O:VO^{2+}$, polycryst., struct., EPR 78—15014
$Mg(NH_4)_2(SO_4)_2.6H_2O:Cr_2O^{2-}$, optical absorption study, $Cr_2O_7^-$ and CrO_4^{3-} centres 80—55128
$Mg(NH_4)_2(SeO_4)_2.6H_2O:Mn^{2+}$, EPR spectra 80—100608
$Mg(NO_3)_2.6H_2O$-NH_4NO_3 system, molten, elec. cond. 79—51288
$Mg_2S_2O_3$-$(NH_4)_2$ S_2O_3-H_2O system, 20°C isotherm *(French)* 78—52506
$Mn(NH_3)_2.Ni(CN)_4.(benzene)_2$, antiferromag. ordering, mag. susceptibility, sp. ht. and Neel temp. meas. 77—12128
ND_4^+, NMR in lyotropic systems 79—22732
$(ND_4)_2BeF_4$, cryst. with modulated struct., neutron scatt. obs. 79—95713
$(ND_4)_2BeF_4$, ferroelec. transition, Raman spectra obs. *(Russian)* 78—23408
$(ND_4)_2BeF_4$, incommensurate-commensurate phase transition and spontaneous polarisation 77—40192
$(ND_4)_2BeF_4$, incommensurate phase, ^9Be NMR study 80—75973
β-ND_4Br, ND_4^+ orientational fluctuations, neutron scatt. obs. 79—7557
ND_4Br, neutron diffr. exam. of P-T phase diagram 77—7861
$ND_4Br:Cu^{2+}$, pseudo-Jahn-Teller effect manifestation in ESR spectrum 80—71168
ND_4Cl, order-disorder transformation, elasticity and heat capacity temp. depend., US obs. 78—71851
ND_4Cl, ordered phase, Raman spectrum, dipole and polarisability derivatives 77—52072
ND_4Cl, sp. ht. at high press. meas., near order-disorder transition 77—84944
ND_4Cl, ultrasonic exam. near order-disorder transition, elastic consts. 79—46799
$ND_4Cl:Cu^{2+}$, high-press. EPR, order-disorder transitions 78—19310
ND_4ClO_4, level-crossing relax. study of MD_4^+ ion tunnelling freq. 80—7185
ND_4ClO_4, librational tunnelling and proton relax. temp. 80—38969
$(ND_4)_2Cu(OD_2)_2Cl_4$, Raman spectra, order-disorder transition *(French)* 79—91436
$(ND_4)_2CuX_4.2D_2O$, $X=Cl$, Br, quadrupolar interaction, 4-300K, reorientation 79—73848
$ND_4D_2AsO_4$, ND_4 role in antiferroelec. transitions, D NMR 77—52025
$ND_4D_2AsO_4$, protonic cond. near antiferroelec. Neel temp. 80—59703
$(ND_4)_2D_3IO_6$, neutron diffr. study 80—88098
$ND_4D_2PO_4$, cryst., transverse and longit. elec. susceptibilities, modified Ising model calcs. 80—97203
$ND_4D_2PO_4$ type ferroelecs., distrib. functions and thermodynamic props. 78—76409
$ND_4D_2PO_4:AsO_4^{4-}(SeO_4^{3-})$, antiferroelec., low freq. fluctuations, isotope effects, EPR, ENDOR, ESCA 77—73118
ND_4DS, polycryst., vibr. spectrum, lattice dynamics 77—90138
$(ND_4)_3D(SO_4)_2$, ferroelectricity and isotope effect on ferroelec. activity 77—85660
$(ND_4)_3D(SO_4)_2$, press.-temp. phase diagram 78—38834
ND_4DSeO_4, crystals, struct., IR spectra, dielec. props. 80—75919
$(ND_4)_3D(SeO_4)_2$, phase transitions, isotope effect, dielectric and dilatometric meas. 79—38500
ND_4I, librational motion of ND_4^+ ion, far IR spectra obs. *(Japanese)* 79—8142
ND_4I, Raman spectra at high press. 79—47459
ND_4I, Raman spectrum, press. effects 80—97261
ND_4IO_4, NQR freq. in cryst. 79—65756
ND_4IO_4, Raman spectra, libration lattice modes 80—60575
ND_4NO_3, low temp. phase, Raman scatt. meas. 78—84568
ND_4NO_3, Raman spectra meas., 250-420K 77—20845
ND_4PF_6, tunnelling ND_4^+ ion, deuteron NMR lineshape computations, first order quadrupolar interactions 79—15362
$(ND_4)_2PbCl_6$-ND_4Cl polycryst. mixture, D spin-lattice relax. times, ND_4^+ reorientation activation energies 78—6587
$(ND_4)_2PtCl_6$, level-crossing relax. study of MD_4^+ ion tunnelling freq. 80—7185

ammonium compounds continued
$(ND_4)_2PtCl_6$, ND_4^+ ion, deuteron NMR lineshape computations, first order quadrupolar interactions 79—15362
ND_4ReO_4, ^{187}Re NQR temp. and press. depend., deuteration shift 79—65756
ND_4ReO_4, nuclear electric hexadecapole interactions of ^{185}Re and ^{187}Re 79—1722
$(ND_4)_2(SO_4)_3$, ferroelec. langbeinites, Raman scattering 80—34926
$(ND_4)_2Zn(SO_4)_2.6D_2O:Cu^{2+}$, EPR exam. 77—24735
NG_4HgCl_3, NQR freq. anomalous temp. depend., reorientation 80—54976
$(NH_4,Cs)Cl$, negative isotope effect on II-III phase transition *(German)* 78—95155
$(NH_4,Rb)Cl$, negative isotope effect on II-III phase transition *(German)* 78—95155
NH_3-$(HF)(F_2)$ complexes, CNDO/2 calcs. for electronic struct. and props. 78—25442
NH_3-CO_2 complex, matrix isolation IR spectrum, struct., ab initio SCF calcs. 78—5209
NH_4,AlF_4, single cryst., prep. and struct. *(French)* 80—79762
NH_4 Br single cryst., low temp. PMR lineshapes of tunnelling NH_4^+ ions 80—25223
(NH_4), CO_3, reactions with Fe-Mn powders 80—11597
NH_4 ReO_4, explanation of ^{187}Re NQR freq. anomalous behaviour 78—48075
(NH_4), SO_4, nonclassical ferroelectricity, phase transitions 80—25320
NH_4^+, contrib. to acidity of rain 79—2327
NH_4^+, exchange in ocean-atmosphere-continent system 78—3794
NH_4^+, hindered rot. effects in nuclear spin-lattice relax. 77—8433
NH_4^+, hindered rot. energy levels in trigonal field 77—7678
NH_4^+, in afterglow, electron recomb. coeffs. mass spectrometric meas. 77—6927
NH_4^+, in crystal lattice, tunnelling effect on proton spin-lattice relax. time 79—61252
NH_4^+, in Greenland snow and ice, natural and anthropogenic origins 79—70815
NH_4^+, in rain water collected at Julich, Germany, N isotope comp. 78—57284
NH_4^+, ion rot. states in $(NH_4)_2SnCl_6$, inelastic neutron scatt. 78—30552
NH_4^+, mol. consts. and mean vibr. amplitudes calcs. 80—106318
NH_4^+ motion in solids, nucl. spin-lattice relax. exam. 78—56388
NH_4^+, mutual neutralisation, with simple and clustered positive (negative) ions 78—44372
NH_4^+, ND_4^+, in lyotropic mesophase, ^{14}N NMR, and quadrupole splitting 78—17690
NH_4^+, NMR line shapes at low temp., composite tunnelling, reorientation 78—48054
NH_4^+, nuclear dipolar relaxation in four-spin-1/2 tetrahedral group 79—24225
NH_4^+, nuclear quadrupole coupling and mol. deformations 78—90191
NH_4^+, particulate, fluxes into free atmosphere over W.Germany evaluation 80—94132
NH_4^+, proton-proton dipolar coupling in nematic soln. using high resolution NMR 77—3387
NH_4^+, reactant ions, appls. to plasma chromatography 78—44419
NH_4^+, removal of, using Itaya-zeolite *(Japanese)* 78—95951
NH_4^+, solvation in water, discrete, continuum and discrete-continuum models 78—73130
NH_4^+, Sternheimer shielding, perturbing elec. field and field gradient effects 77—88403
NH_4^+, tetrahedron, hindered rot. energy levels in orthorhombic crystalline field, rot. heat capacity 77—76332
NH_4-ion rotation, quantum effect on spin-lattice relax. time 80—75875
$NH_4^+ + Ca$, proton transfer reaction cross sections, 1-6 eV 78—20003
$NH_4^+ + e$, dissociative recomb. reaction in interstellar clouds, products, statistical theory 78—57604
$NH_4^+ + LiH(H\ \ )$, substitution and abstraction reactions, ab initio calcs. 77—48624
$(NH_4)_2,SO_4$, ferrielectricity, triple 60 Hz D-E hysteresis loops 80—71364
$(NH_4)_2$ $Zn(SO_4)_2.6H_2O:VO^{2+}$, γ-irradiated NH_3^+ ESR, N hyperfine coupling tensor 79—69722
NH_5^+, stability, ab initio calcs. 77—23419
$(NH_3$-$(CH_2)_2$-$NH_3)Cd_{1-x}Mn_xCl_4$, Mn^{2+} single ions, clusters and layers, ESR study 79—78507
$NH_4Ag_4I_5$, ionic conductivity and heat capacity near T_c 78—47584
$NH_4Ag_4I_5$, Raman spectra, internal vibrs. of NH_4^+ ions 78—72497
$NH_4Ag_4I_5$, solid electrolyte, Raman spectra 79—73934
$NH_4Ag_4I_5$, superionic solid film, prep. and elec. cond. 80—54431
$NH_4Ag_4I_5$, superionic cond., pressure effect on phase transitions 80—70405
$NH_4Ag_4I_5$, superionic solid film, surface diffusion coeff. 80—92709
$NH_4Ag_4I_5$, superionic phase transition, dynamical and crit. pt. props. 80—107535
$NH_4Ag_4I_5$, thin film solid state battery 78—76876
$NH_4Al_2Br_7$, ^{81}Br NQR and ^{27}Al NMR 78—6597
NH_4AlCl_4, crystal struct., X-ray, Raman, IR and NMR 78—63720
NH_4AlF_3, hydrothermal growth method in presence of hydrofluorhydric acid *(French)* 80—25543
$(NH_4)_2AlF_6$, proton NMR lineshapes of NH_4^+ undergoing slow tunnelling rotations 79—90576
$NH_4Al(OH)_2CO_3$, NH_4-dawsonite, cryst. struct., X-ray powder diffr. *(Japanese)* 79—69096
$NH_4AlO(OH)HCO_3$ parent salt for α-AL_2O_3, crystallinity effect on sinterability *(Japanese)* 78—6883
$(NH_4)_2Al(SO_4)_2$, ^1H spin-lattice relax., 100-500K 79—38398
$NH_4Al(SO_4)_2.12H_2O$, third order elastic consts. from stress shifted reson. freqs. 78—55905
$NH_4Al(SO_4)_2.12H_2O$, dielectric losses, proton spin lattice relaxation by NH_4^+ hopping 79—56721
$NH_4Al(SO_4)_2.12H_2O$, CrO_4^{3-} centres, EPR and optical absorption spectra 79—91475
$NH_4Al(SO_4)_2.12H_2O:Cr^{3+}$, zero-field fluctuations in Cr^{3+} near phase transition 77—28435
$NH_4Al(SO_4)_2.12H_2O:Mo^{3+}$, EPR, X-band, ion position and spin-Hamiltonian parameters 77—48042
$NH_4Al(SO_4)_2.12H_2O:Fe^{3+}$, spin-lattice relax. of paramag. ions, Mossbauer effect 79—95688
NH_4AsO_2, struct. characterisation, monoclinic cell, $P2_{1/c}$ space group *(French)* 78—22697
$(NH_4)_3AsO_4.3H_2O$, cryst. struct. 78—18600

ammonium compounds continued
- NH_4BF_4, H^+ relax. and tunnelling, nucl. spin-lattice relax. obs. 79−51876
- NH_4BF_4, IR spectra of NH_3D^+ ion, mol. motion 77−36232
- NH_4BF_4, ionic radii and chem. shifts, correl. with electronegativity 80−66054
- $(NH_4)_2BeF_2$, paraelec. phase, cryst. struct. 78−95025
- $(NH_4)_2BeF_4$ crystal, macroscopic quadrupole moment anomalies in incommensurable phase *(Russian)* 79−65808
- $(NH_4)_2BeF_4$ crystals, incommensurate-commensurate phase transitions, optical props. 79−95733
- $(NH_4)_2BeF_4$, effect of surface layer on spontaneous polarisation 79−38445
- $(NH_4)_2BeF_4$, elastic compliance, US attenuation and piezo-coeffis., 170 and 190K 79−51918
- $(NH_4)_2BeF_4$, elastic props., US damping 80−84229
- $(NH_4)_2BeF_4$, far-infrared and submillimetre dielectric response 80−80782
- $(NH_4)_2BeF_4$, ferrielectricity, triple 60 Hz D-E hysteresis loops 80−71364
- $(NH_4)_2BeF_4$, ferroelec. transitions into inhomogeneous modulated phase, Landau theory analysis 77−8527
- $(NH_4)_2BeF_4$, ferroelec. transition, Raman spectra obs. 77−85705
- $(NH_4)_2BeF_4$, ferroelectric, Brillouin scattering study 79−15470
- $(NH_4)_2BeF_4$, ferroelectric, cryst. struct., phase transition, X-ray study 79−28689
- $(NH_4)_2BeF_4$, ferroelec., incommensurate struct., dynamic props. *(Russian)* 80−11373
- $(NH_4)_2BeF_4$, ferroelectric, incommensurate phase, nonlinear optical props., SHG study *(Russian)* 80−33089
- $(NH_4)_2BeF_4$, γ-irrad., trapped H atoms, ferroelec. transition, EPR meas. 79−4724
- $(NH_4)_2BeF_4$, γ-irrad. cryst., F_2^- ions, ESR meas. 80−34770
- $(NH_4)_2BeF_4$, improper ferroelec., incommensurate-commensurate transitions 78−60404
- $(NH_4)_2BeF_4$, incommensurate-commensurate phase transition 78−87760
- $(NH_4)_2BeF_4$, incommensurate phase transitions under existence of Lifshitz invariant 79−15416
- $(NH_4)_2BeF_4$, incommensurate phase, Mossbauer spectrum 79−61276
- $(NH_4)_2BeF_4$, incommensurate phase superstructure, linear and nonlinear cryst. optics *(Russian)* 80−14387
- $(NH_4)_2BeF_4$, incommensurate phase, ^{9}Be NMR study 80−75973
- $(NH_4)_2BeF_4$, linear and nonlinear optical props. in incommensurate phase 80−69452
- $(NH_4)_2BeF_4$, Mandelstam-Brillouin and US exam. of phase transitions 77−12347
- $(NH_4)_2BeF_4$, order-disorder phase transitions with many-minimum potential, thermodynamic props. 80−96623
- $(NH_4)_2BeF_4$, paraelec. and ferroelec. phases, X-ray diffuse scatt. and superlattice struct. *(Japanese)* 77−43189
- $(NH_4)_2BeF_4$, paraelec. phase, X-ray and neutron diffr. cryst. struct. anal. 80−84159
- $(NH_4)_2BeF_4$, phase transition at 185K, X-ray scatt. obs. 77−36186
- $(NH_4)_2BeF_4$, polycrystalline, surface layer effects on dielec. behaviour 78−39494
- $(NH_4)_2BeF_4$, powder, IR spectra, assignments, mol. libration, in paraelec. and ferroelec. phases 78−88299
- $(NH_4)_2BeF_4$, unmatched phase, second optical harmonic generation *(Russian)* 78−79073
- $(NH_4)_2BeF_4$, X-ray cryst. struct. determ. 79−69072
- $(NH_3)_nBi^+(Rb^+)(K^+)$, gas phase clusters, relative bond strengths, thermodynamic props. 78−35649
- NH_4Br, ^{14}N NMR obs., rel. to structural transforms. 79−15368
- NH_4Br and NH_4I, Raman scatt., 1 bar-7 kbar, 86-295 K 80−34909
- NH_4Br, anisotropy of T_{1D} and $T_{1\rho}$ 79−38393
- NH_4Br, aq. soln., IR reflectivity spectra, Kramers-Kronig anal. 78−68500
- NH_4Br, birefr. and opt. rot. near structural phase transition points 78−75823
- NH_4Br, β-γ phase transition, critical anomalies, phenomenological eqns. 80−39275
- NH_4Br, cubic-tetragonal transition, macroscopic quadrupole moment meas. *(Russian)* 77−62642
- NH_4Br, heat capacity meas. near order-disorder transition 80−88332
- NH_4Br, λ-type phase transition, Brillouin scattering 78−79725
- NH_4Br, NH_4^+ rot. motion, quasielastic neutron scatt. obs. 80−96492
- NH_4Br, NMR under high press. 78−84485
- NH_4Br, neutron diffr., exam. of P-T phase diagram 77−7861
- NH_4Br, order-disorder phenomena, high press. US investigation 79−37835
- NH_4Br, partially disordered, librational modes below 235K, Raman scatt. obs. 78−72500
- NH_4Br, partially disordered, librational modes below disorder-order phase transition temp. 78−79680
- NH_4Br, phase diagrams, from Raman meas. under high press. 78−52776
- NH_4Br, proton spin-lattice relax. time up to 2200 bar, phase transitions 77−63307
- NH_4Br, proton spin-lattice relax., temp. depend. 79−42859
- NH_4Br, self-polarisation at order-disorder transition 78−52432
- NH_4Br, solid, discontinuous orientational phase transitions, thermodynamics, isotope effects 80−6590
- NH_4Br soln., conductance and viscosity, temp. and concentration depend. 80−6531
- NH_4Br, supercooled, polymorphic transform., struct. correspondences and mechanisms 80−107097
- NH_4Br, thermorefl. spectra, band energy anal. 77−12402
- $NH_4Br:Cl^-$, impurity mode, far IR transmission obs. 77−16308
- $NH_4Br:Cu^+$, luminesc., orientation phase transition 80−100687
- $NH_4Br:Cu^{2+}$, ESR and absorpt. spectra, 300-1500 nm 78−60492
- NH_4Br:Tl, absorption, excitation and fluorescence spectra 79−33824
- NH_4Br:Tl, and pure crystals, luminesc., VUV irradiated at 80K *(Russian)* 80−84763
- NH_4Br-NH_4I mixed crysts., far IR spectra, phase transition and NH_4^+ libration 77−85719
- $NH_4Br(Cl)$, dynamic crit. phenomena 79−77690
- $NH_4Br_xCl_{1-x}$, cryst., order-disorder phase transitions, US investig. 80−6378
- $NH_4Br_xCl_{1-x}$, heat capacity meas. near order-disorder transition 80−88332

ammonium compounds continued
- NH_4CNS, kinetic-morphological types of polymorphic transform., relax. theory 78−9993
- NH_4CNS-polyethylene oxide complexes, order-disorder transformations 78−47251
- $(NH_4)_2Ca_2(SO_4)_3$, phase transitions, dielec. props. obs. 78−6643
- NH_4CdCl_3, X-ray cryst. struct. refinement by blocked least-squares method 79−1404
- $(NH_4)_2Cd_5Fe_3Al(SO_4)_{12}.18H_2O$, EPR above ferrimag. transition 78−10762
- $(NH_4)_2Cd_2(SO_4)_3$, dielec. and spontaneous polarisation, −195 to −180°C, particle size depend. 80−97200
- $(NH_4)_2Cd_2(SO_4)_3$, ferroelec. langbeinites, Raman scattering 80−34926
- $(NH_4)_2Cd_2(SO_4)_3$, structural phase transition, phenomenological theory 79−7693
- $(NH_4)_2Cd_2(SO_4)_3:Mn^{2+}$, UO_2^{2+}, luminesc., vibr. modes 79−38629
- $(NH_4)Cd[PO_3OH](OH)$, cryst. struct. of second modification 77−1115
- $(NH_4)Cd_6[P_2O_7]_2[P_3O_{10}]$, with mixed anion radical, cryst. struct. by X-ray anal. 79−86771
- $(NH_4)Cd[PO_4].H_2O$, B phase, cryst. struct. refinement, X-ray diffr. meas. 78−2095
- $(NH_4)_2Ce(NO_3)_6$, acid soln. photolysis, NO_3 radical study 79−52717
- $(NH_4)_2Ce(NO_3)_6$, proton tunnelling frequencies from nuclear spin-lattice relaxation 78−6591
- $(NH_4)_2Ce(NO_3)_6$, proton relax. by tunnelling at low temp. 78−43666
- $(NH_4)_2Ce(NO_3)_6$, proton spin-lattice relax., temp. depend. 79−42859
- $(NH_4)_2Ce(NO_3)_6$, proton NMR lineshapes of NH_4^+ undergoing slow tunnelling rotations 79−90576
- NH_4Cl, ^{15}N zero point vibr. energy from nuclear photon scattering 80−59593
- NH_4Cl, acoustic absorption by soft modes of defects 80−59584
- NH_4Cl, activation coefficients and solvation numbers in mixed methanol solvents 80−81334
- NH_4Cl, anisotropy of T_{1D} and $T_{1\rho}$ 79−38393
- NH_4Cl, aq. soln., dynamical props., mol. dynamics simulation 80−1918
- NH_4Cl, aq. soln., IR reflectivity spectra, Kramers-Kronig anal. 78−68500
- NH_4Cl, aq. soln., pulsed limiter discharge, nonideal plasma chem. composition 80−19657
- NH_4Cl, aq. soln., struct. props., mol. dynamics simulation 79−82142
- NH_4Cl, CC ^{15}N NMR chem. shift references evaluation 78−24835
- NH_4Cl, coexistence states during first order transition, optical obs. 80−75350
- NH_4Cl, crit. behaviour near tricritical point, phenomenological interpretation 80−70389
- NH_4Cl, cryst., impurity overtone states, interference two-photon spectrum *(Russian)* 79−24344
- NH_4Cl, cryst. nucleation, growth rates from organic media, outline meas. technique 79−38730
- NH_4Cl crystal, polariton light scattering spectra in zone of dissociated states 79−47029
- NH_4Cl, dendrite development and growth in very small crystals, Monte Carlo study 80−107683
- NH_4Cl, dendrite growth at very low supersaturation 78−43277
- NH_4Cl, dispersion of vibrational excitations, Raman scatt. 78−84588
- NH_4Cl, doped and undoped, spontaneous polarisation at order-disorder phase transition 80−25281
- NH_4Cl doped ice microcrystals, activation energy of Debye's dipolar relax., influence of salt content *(French)* 78−56424
- NH_4Cl, electro-optical props. near order-disorder transition 78−31173
- NH_4Cl, ferroelastoelectric poling, differing piezoelec. props. of domain states 77−16102
- NH_4Cl, gas $^1A_1$ ground state, pot. surface 80−32626
- NH_4Cl, heat capacity from AC calorimetry at high press. 77−41616
- NH_4Cl in RbCl(KCl), NH_4^+ motion, PMR, proton spin-lattice relax. time temp. depend. 78−27104
- NH_4Cl, λ-type phase transition, hypersonic study using Brillouin scatt. 80−34165
- NH_4Cl, molar heat capacity near order-disorder transform. under high press. 78−51697
- NH_4Cl, NH_4^+ dynamics in disordered states, neutron scatt. exam. 78−26459
- NH_4Cl, NH_4^+ ion rotation, near order-disorder transition, quasielastic neutron scatt. obs. *(German)* 77−84679
- NH_4Cl, NMR under high press. 78−84485
- NH_4Cl, obs. of Raman scatt. by Cu vapour laser 78−95586
- NH_4Cl, order parameter, electro-optic measurement 78−88280
- NH_4Cl, order parameter variation near multicritical pt., SHG 79−81484
- NH_4Cl, order-disorder transition, slip bands 78−22848
- NH_4Cl, order-disorder transition exam. by optical second harmonic generation 78−51671
- NH_4Cl, order-disorder phase transition, type of multicritical point, nonlinear quadratic susceptibility 78−83947
- NH_4Cl, order-disorder phase transform., effect of plastic deform. and electrooptic effect 79−33672
- NH_4Cl, ordered phase, press. depend. of Raman scatt. meas. 77−12388
- NH_4Cl, ordered phase Raman spectrum, dipole and polarisability derivatives 77−52072
- NH_4Cl, orientational disorder, Raman and far IR spectra 78−23447
- NH_4Cl, piezoelec. effect near nonferroelastic phase transition 80−66116
- NH_4Cl, polariton Raman spectra, bound and many particle states 77−32372
- NH_4Cl, powder, adsorpt. of H_2O vapour 79−1545
- NH_4Cl, proton spin resonance relaxation time near ordering transition 79−61251
- NH_4Cl, pure and NH_3 and $NiCl_3$ doped, TSC obs. of polarisation 79−78618
- NH_4Cl, Raman scatt. at polarons near intramol. vibrs. 77−44003
- NH_4Cl, Raman scatt. of light on limiting and nonlimiting dipole vibr. 80−11402
- NH_4Cl Raman spectra, pressure effects 80−97268
- NH_4Cl, reactions with Fe-Mn powders 80−11597
- NH_4Cl, self-polarisation at order-disorder transition 78−52432
- NH_4Cl single crystals, quasielastic neutron scattering expts. near order-disorder phase transition 79−4410
- NH_4Cl smoke, natural sedimentation, visual, photogrpahic, and laser sonde obs. *(Russian)* 78−32216
- NH_4Cl, solid phase, resonant transfer of nucl. spin dipolar order in rotating frame 79−33564
- NH_4Cl soln., crystal growth under press. *(Korean)* 77−73266

ammonium compounds continued
NH_4Cl, sp. ht. at high press. meas., near order-disorder transition 77−84944
NH_4Cl, specific heat, thermal cond. simultaneous meas. method, 90-300K, near phase transition 77−37892
NH_4Cl, submicron particles, density, morphology 80−61166
NH_4Cl, surface roughening transition in vapour phase growth 78−2044
NH_4Cl, thermal cond. and heat capacity of solid phases under press. 80−2225
NH_4Cl, thermal conductivity, crystal transformation 78−2310
NH_4Cl, thermorefl. spectra, band energy anal. 77−12402
NH_4Cl, transitional plasticity, light scatt. study 79−77674
NH_4Cl transparent soln., basaltic equiaxed solidification, visualisation of convection *(French)* 80−44297
NH_4Cl, vibrations of isotopic impurities, IR reflection and Raman spectra meas. 77−51465
$NH_4Cl:[MoOCl_5]^{2-}$, single cryst., struct. investigations 77−66524
$NH_4Cl:Cr^{3+}$, ESR of Cr^{3+} centres, room temp. 78−91943
$NH_4Cl:Ni^{2+}$, EPR spectrum, spin Hamiltonian, zero-field splitting effects 80−97135
$NH_4Cl:Tl$, phosphoresc. decay rates obs., pretreatment effects 79−4853
NH_4Cl-H_2O, binary dendritic system, exam. of solidification 79−11599
NH_4Cl-H_2O, solidification microstructs., effect of reduced gravity 80−96632
NH_4Cl-H_2O solidification model for showering cryst. form. in molten metal cooling *(Japanese)* 80−66498
$NH_4Cl-TlCl$, mixed phosphors, diffuse absorption spectrum 79−24342
$NH_4Cl(Br)$, effect of NH_4^+ internal motion on elec. and optical props. 80−100454
$NH_4Cl(Br):Cu^{2+}$, compressed D_{4h} cluster, g_{zz}-g_0 value 77−80756
$NH_4Cl_{1-x}Br_x$, dielectric const. meas. at 1 MHz 77−16238
$NH_4Cl_{1-x}Br_x$, dielectric const. meas. at 1 MHz by immersion method *(Japanese)* 77−90087
$NH_4Cl_{1-x}Br_x$ mixed cryst., phase diagram and characts. of phase transitions 77−62637
$NH_4Cl_{1-x}Br_x$, phonon dispersion 78−75760
$NH_4Cl_{1-x}Br_x$, US exam. of order-disorder phase transform. 78−38841
$NH_4Cl(Br)(I)$, dielectric const. meas. at 1 MHz by immersion method *(Japanese)* 77−90087
$NH_4Cl(Br)(I)$, proton NMR lineshapes of NH_4^+ undergoing slow tunnelling rotations 79−90576
NH_4ClO_4, AC elec. cond. temp. and freq. depend., obs. and unified defect struct. model 80−88554
NH_4ClO_4, DC elec. cond. meas. 77−84984
NH_4ClO_4, elec. field effect on decomp. 79−15987
NH_4ClO_4, formation of colour center by X-irradiation, optical absorption spectra 79−19247
NH_4ClO_4, γ-irrad., trapping and motion of NH_3^+ radical in cryst. lattice 79−33538
NH_4ClO_4, γ-irrad., motions of trapped NH_3^+ radical, ESR study 79−95648
NH_4ClO_4, γ-irrad. single cryst., NH_3^+ EPR obs., g-tensor, hyperfine splitting 78−2739
NH_4ClO_4, IR spectra of NH_3D^+ ion, mol. motion 77−36232
NH_4ClO_4, incomplete thermal decomp. 79−91939
NH_4ClO_4, instantaneous jump reorientations, neutron scatt. study 79−41990
NH_4ClO_4, NH_4 ion rot. tunnelling splitting, inelastic neutron scatt. 77−15325
NH_4ClO_4, photothermochemical process, influence of phase transition 79−24770
NH_4ClO_4, photothermochemical process 79−24769
NH_4ClO_4, polymorphous phase transition mechanism 80−79737
NH_4ClO_4, proton relax. by tunnelling at low temp. 78−43666
NH_4ClO_4, proton spin relax. and phonons 78−84493
NH_4ClO_4, proton tunnelling frequencies from nuclear spin-lattice relaxation 78−6591
NH_4ClO_4, single ion props. by lattice energy minimisation 78−83769
NH_4ClO_4, with 0.015% and 0.1% D, proton Zeeman relaxation 78−6592
NH_4ClO_4, X-ray data collection and estimation of intensities variations 79−60312
$NH_4^+ClO_4^-$, X-ray cryst. struct. refinement with multipole deformation density functions 79−60313
$NH_4ClO_4:Co^{2+}$, optical absorpt. spectra 77−66523
$NH_4ClO_4:Cu^{2+}$, dislocation etch pits exam., rel. to thermal decomp. 77−11555
$NH_4ClO_4:SO_4^{2-}(CrO_4^{2-})$, thermal depolarisation, relax. parameters 78−43779
$NH_4Cl.3NH_3-NH_4Cl$, solar energy storage system heating and cooling 80−81484
NH_4CoF_3, sp. hts., librational and reorientational 77−84946
NH_4CoF_3, susceptibility and magnetisation meas. 77−85432
$(NH_4)_2Co(SO_4)_2.6H_2O$, sbumillimeter ESR meas., SH^3 term of effective spin Hamiltonian 78−64264
$(NH_4)_2Co(SO_4)_2.6H_2O$, submillimetre ESR meas. using pulsed high mag. field 80−44905
$(NH_4)_2Co(SeO_4)_2.6H_2O:Mn^{2+}$, EPR 77−90017
$(NH_4)_2CrO_4$, investig. by diffuse reflectance spectroscopy 78−88326
$(NH_4)_2Cr_2O_7$ crystal hypomorphism and hypermorphism 80−59427
$(NH_4)_2Cr_2O_7$, proton spin-lattice relax., temp. depend. 79−42859
$(NH_4)_2Cr_2O_7$, proton tunnelling frequencies from nuclear spin-lattice relaxation 78−6591
$(NH_4)_2Cr_3O_{10}$, hexagonal form, cryst. data *(French)* 80−24418
$(NH_4)_2Cr_3O_{10}$, X-ray cryst. struct. determ. *(French)* 80−28974
$(NH_4)_2Cr_4O_{13}$, cryst. data *(French)* 80−28980
$(NH_4)_{1-x}Cs_xCl(Br)$, and $(ND_4)_{1-x}Cs_xCl(Br)$, phase diagrams, DTA and birefr. obs. *(German)* 79−83185
$((NH_4)_{1-x}Cs_x)_2SO_4$ mixed cryst., EPR of NH_3^+ and SeO_3^- radicals 80−50190
$(NH_4)_2CuBr_4.2H_2O$, ferromag., static and dynamic mag. props. 80−50074
$(NH_4)_2CuBr_4.2H_2O$, ferromag., hyperfine and exchange interactions, NMR study 80−50208
$(NH_4)_2CuBr_4.2H_2O$, hyperfine and super-exchange interactions 80−103654
$NH_4Cu_4Cl_3(I_{2-x}Cl_x)$, highly conducting solid electrolyte 80−65280
$(NH_4)_2CuCl_4.2\ H_2O$, lattice dynamics, anal. of Raman scatt. measurements 80−34149
$(NH_4)_2CuCl_4.2H_2O$ and $(NH_4)_2$, $CuBr_4.2H_2O$, exchange anisotropy by NMR 77−55714

ammonium compounds continued
$(NH_4)_2CuCl_4.2H_2O$, HDO and NH_3D^+ species, IR spectrum, low-temp., phase transitions 77−77182
$(NH_4)_2CuCl_4.2H_2O$, Raman sepctra, dynamics, struct., phase transition 79−47434
$(NH_4)_2CuCl_4.2H_2O$, Bloch-wall NMR, anisotropic hyperfine interaction 79−51864
$(NH_4)_2CuCl_4.2H_2O$, order-disorder transition, Raman spectra obs. 79−61357
$(NH_4)_2CuCl_4.2H_2O$, submillimetre ESR meas. using pulsed high mag. field 80−44905
$(NH_4)_2CuCl_4.2H_2O$, ferromag., hyperfine and exchange interactions, NMR study 80−50208
$(NH_4)_2CuCl_4.2H_2O$, hyperfine and super-exchange interactions 80−103654
$(NH_4)_2(Cu(H_2O)_6)(CuSO_4)_4$, cryst. struct. determ. by X-ray diffr. 78−55839
$(NH_{4(1-x)}D_{4x}H_{2(1-x)}D_{2x}AsO_4)$, crystal growth of para- and antiferroelectric phases 78−48300
$NH_4D_2PO_4:Cr_2O_7^{2-}$, optical absorpt. spectra, mol. orbital calcs. 79−15491
NH_4F, cryst. struct., mol. wavefunction calcs. of struct. factors 77−62507
NH_4F, electron distribution and charge transfer in NH_4^+ ion 78−91291
NH_4F, thermal cond. of four solid phases, rel. to H_2O 78−38887
$NH_4F.H_2O_2$ crystals, X-ray structural study 80−44188
$(NH_4)_4Fe(CN)_6.1.5H_2O$, cryst. struct., and possible ionic transport mechanism 79−14758
α-$NH_4Fe(CrO_4)_2$, cryst. struct. *(French)* 77−47398
$(NH_3)_2FeF_5$, one-dimensional antiferromag. systems, Mossbauer studies 80−71266
$(NH_3)_2FeF_5$, quasi two-dimens. antiferromagnet, Mossbauer study 80−39947
NH_4FeF_4, mag. and Mossbauer obs. *(French)* 78−19389
NH_4FeF_4, Mossbauer and optical evidence for crystallographic transition 79−14931
NH_4FeF_4, two-dimens. antiferromagnetism 77−66444
$NH_4Fe_2F_6$, hydrothermal growth method in presence of hydrofluorhydric acid *(French)* 80−25543
$(NH_4)_2GaF_6$, proton NMR lineshapes of NH_4^+ undergoing slow tunnelling rotations 79−90576
$(NH_4)_2GaF_5.H_2O$, crystal struct., water coordination by Ga, valence angles, cell parameters 79−77584
$(NH_4)GeF_6$, IR absorpt. spectra, integrated intensity temp. depend. 79−73946
$(NH_4)_2GeF_6$, A=Si, Ge, Sn, IR absorpt. spectra, integrated intensity 79−73944
$(NH_4)_2GeF_6$, cryst., highly bent H bonds, IR spectrosc. investig. 80−93292
$(NH_4)_2GeF_6$, H^+ relax. and tunnelling, nucl. spin-lattice relax. obs. 79−51876
$(NH_4)_2GeF_6$, NMR, nuclear dipolar energy relax. 79−42853
$(NH_4)_2GeP_4O_{13}$, cryst. struct. determ. *(French)* 77−51358
$NH_4H_2ASO_4-NH_4H_2PO_4$, EPR spectra of central peak fluctuations 78−91932
$(NH_4)_2HAsO_4$, hydrogen bonded, ^{75}As NQR study 79−38399
$(NH_4)_2HAsO_4$, molecular motion, PMR meas. 77−85591
$(NH_4)_2HAsO_4$, Zeeman perturbed NQR spectra, EFG tensors and antiferroelectric ordering 77−43898
$(NH_4)H_2AsO_4$ and deuterated analogues, low temp. transition, thermal hysteresis, Cr impurity effect on transition temp. 80−2705
$NH_4H_2AsO_4$, and $ND_4D_2AsO_4$, IC spectra and phase transitions, under pressure 78−31180
$NH_4H_2AsO_4$, doubling crystal for ring dye laser 79−41392
$NH_4H_2AsO_4$, freq. doubling of CW tunable dye laser 78−17965
$NH_4H_2AsO_4$, H positions, paraelectric phase 79−19210
$NH_4H_2AsO_4$, microhardness, expt. determ. 79−24603
$NH_4H_2AsO_4$, paraelec. phase, ^{75}As NMR linewidth, near transition temp. 77−36184
$NH_4H_2AsO_4$, protonic conduction and electrolysis investig. 77−35749
$NH_4H_2AsO_4$, SHG, CW UV radiation prod. 78−46712
$NH_4H_2AsO_4$, tunable UV generation by freq. doubling 77−42571
$NH_4H_2AsO_4:Cr^{5+}$, fast and slow dynamic reorientation 78−80306
$NH_4H_2AsO_4:Cr^{5+}$, ENDOR spectra 78−88224
$NH_4H_2AsO_4:Cr^{5+}$, antiferroelec. phase transition, EPR intensity and linewidth meas. 79−4721
$NH_4H_2AsO_4-NH_4H_2PO_4$ solid soln., Curie temp. and permittivity comp. depend. 77−59533
$NH_4H_2AsO_4-NH_4H_2PO_4$, AsO_4^{4-} centre, EPR central peak dynamics 79−33523
$NH_4H_2AsO_4-NH_4H_2PO_4$ antiferroelectric solid solution, soft-mode and energy calcs. 79−56743
$(NH_4)_4H_6(As_6V_4O_{13}).4H_2O$, cryst. struct. determ. by X-ray diffr. *(French)* 79−69076
$NH_4HC_2O_4$, hemihydrate, ^{14}N NMR, high resolution spectra, elec. field gradient tensor 77−81018
$NH_4HC_2O_4.1/2H_2O$, X-ray TDS effects on at. parameters and electron density distribs. 77−19819
$(NH_4)_2HCr_3AsO_{13}$, prep. and cryst. struct. *(French)* 79−1415
$(NH_4)_2HCr_3AsO_{13}$, X-ray cryst. struct. determ., existence of a new anion (Cr_3AsO_{13}) *(French)* 79−4295
NH_4HF_2, ^{19}FNMR 78−2754
NH_4HF_2, powder, proton and fluorine 2nd moments meas., 77-395K 80−34803
$(NH_4)_2H_3IO_6$, paraelec. and antiferroelec. phases, IR vibrational study 77−85697
$(NH_4)_2H_3IO_6$, Raman spectra and phase transition 77−77196
$(NH_4)_x^+(H_2O)_y[NbS_2]^{x-}$, hydrate layered chalcogenide, anisotropic mobility of water, NMR 79−65744
$(NH_4)_x^+(H_2O)_y[TaS_2]^{x-}$, hydrate layered chalcogenide, anisotropic mobility of water, NMR 79−65744
$NH_2H_2PO_4$, temporal power variation of fourth harmonic generation of Q-switched YAG laser radiation 78−25922
$(NH_4)_2HPO_4$, molecular motion, PMR meas. 77−85591
$(NH_4)_2HPO_4$, NH_4^+ motions, PMR relax. times obs., 77-430K, struct. transition 77−85599
$(NH_4)_2HPO_4$, nonexponential proton relaxation 77−69716
$(NH_4)_2HPO_4:KH_2AsO_4$, EPR of arsenic and phosphorus oxyradicals 77−77102
$NH_4H_2PO_4$, ^{1}H spin-lattice relax. in paraelec. and antiferroelec. phases 79−33555

ammonium compounds continued
$NH_4H_2PO_4$, 90° phase matching temp., refr. index freq. and temp. depend. 78—46720
$NH_4H_2PO_4$, {100} faces cryst. growth kinetics, low supersaturations range, dislocations 79—56047
$NH_4H_2PO_4$, acoustooptical and photoelastic props. 78—27181
$(NH_4)H_2PO_4$ and deuterated analogues, low temp. transition, thermal hysteresis, Cr impurity effect on transition temp. 80—2705
$NH_4H_2PO_4$, and $ND_4D_2PO_4$, IC spectra and phase transitions, under pressure 78—31180
$NH_4H_2PO_4$, antiferroelec., positron lifetime meas. during phase transitions 78—6644
$NH_4H_2PO_4$, α-particle bombard. effects, circular crater form. 77—59051
$NH_4H_2PO_4$, blue tunable picosecond pulse generation by synchronous mixing of Nd:glass laser with sideband radiation 80—87431
$NH_4H_2PO_4$, correlation between cryst. perfection and refl. intensity for analyser cryst. 78—48259
$NH_4H_2PO_4$, cryst., cascade UV generation, by harmonic generation, temp. stabilisation calcs. 78—66868
$NH_4H_2PO_4$, cryst., transverse and longit. elec. susceptibilities, modified Ising model calcs. 80—97203
$NH_4H_2PO_4$, cryst. growth, pH effect, H_3O^+ inclusions 79—55682
$NH_4H_2PO_4$, cryst. growth in presence of Mn ions 80—93468
$NH_4H_2PO_4$, crystal, and deuterated cpd., optical meas. of phase transition point by domain obs. 77—40187
$NH_4H_2PO_4$ crystal, ferroelectricity, spontaneous polarisation obs. 79—28687
$NH_4H_2PO_4$, crystal-solution interfacial tension, from crystn. meas. 79—69045
$NH_4H_2PO_4$ crystals, plastic deform. and mech. props. 79—79035
$NH_4H_2PO_4$, crystal growth kinetics, in situ X-ray topography study 80—76167
$NH_4H_2PO_4$, crysts., mechanism of habit change due to Fe^{3+}, Mossbauer study 79—19821
$NH_4H_2PO_4$, defects, X-ray topographic study 78—26580
$NH_4H_2PO_4$, dislocation obs. using electron microscopy and replica method 77—59013
$NH_4H_2PO_4$, efficient generation of tunable UV radiation down to 2400 Å 79—55182
$NH_4H_2PO_4$, elec. cond. and diffusion, Co dopant effects 77—72716
$NH_4H_2PO_4$, electronic struct., UV reflection spectra and XPS 79—38558
$NH_4H_2PO_4$, ferroelec., electronic struct. study *(Japanese)* 79—87463
$NH_4H_2PO_4$, filiform crystals at low temp., tensile strength determ. 80—100877
$NH_4H_2PO_4$, focused beam SHG, temp., wavelength and angle bandwidths 79—50343
$NH_4H_2PO_4$, harmonic and sum freq. generation, tunable CW UV radiation prod. 78—46712
$NH_4H_2PO_4$, high temp. phase transition, IR spectra, differential 80—25319
$NH_4H_2PO_4$, IR overtone spectra and temp. depend. 79—47456
$NH_4H_2PO_4$, improper antiferroelec. phase transition, elastic props., free energy, thermodynamic theory 78—80299
$NH_4H_2PO_4$, magnetoelectric susceptibilities, phenomenological rules for computation 80—55068
$NH_4H_2PO_4$, microhardness, expt. determ. 79—24603
$NH_4H_2PO_4$, Mn^{2+}, Mn^{3+} and MnO_4^- ions effect on cryst. habit 77—58992
$NH_4H_2PO_4$, Mn^{3+} doping effect on Curie temp. and dielec. permittivity 77—59532
$NH_4H_2PO_4$, N_2 and dye laser pulses mixing 0.68-1.1 μm output 77—27314
$NH_4H_2PO_4$, optical parametric amplifier, gain limitations 79—55177
$NH_4H_2PO_4$ parametric amplifier, rhodamine laser light shifting into blue-green 79—18471
$NH_4H_2PO_4$, parametric excitation of continuously tunable visible picosecond pulses 79—18482
$NH_4H_2PO_4$, parametric superluminesc., picosec. spectroscopy 79—55187
$NH_4H_2PO_4$, phase transition, phonon echo method *(French)* 78—6640
$NH_4H_2PO_4$, phonon echos in SiO_2, ADP, KDP, and Rochelle salt *(Japanese)* 79—51213
$NH_4H_2PO_4$, Pockels effect in UV region 77—12398
$NH_4H_2PO_4$, polycrystalline materials; pyroelec. temp. anal. as method for studying ferroelec. transitions 79—38502
$NH_4H_2PO_4$, powder sample, pyrocharge temp. depend. near phase transition 79—87399
$NH_4H_2PO_4$, rods, longitudinally vibrating, polarizing effect and electrostatic tensor 77—7278
$NH_4H_2PO_4$, ruby SHG, comparison with RbH_2AsO_4 78—50856
$NH_4H_2PO_4$, SHG efficiency, 532 to 266 nm 77—23710
$NH_4H_2PO_4$, SHG method pulse width meas. of Nd:YAG laser *(Chinese)* 80—87432
$NH_4H_2PO_4$, SHG of rhodamine 6G laser, tunable UV source 77—42565
$(NH_4)H_2PO_4$, single cryst., X-ray diffr. contrast at twin boundaries, computer simulation 79—33000
$NH_4H_2PO_4$, single cryst., thermal depolarisation current 79—51303
$NH_4H_2PO_4$ single crystal evidence for spiral growth on pyramidal faces 80—84120
$NH_4H_2PO_4$, solution growth mechanism investig., growth spiral interactions 77—58963
$NH_4H_2PO_4$, surface effects on strength of whiskers and microcrysts. *(Russian)* 78—51864
$NH_4H_2PO_4$ thin crystal, intracavity SHG of synchronously mode-locked CW dye laser 80—95945
$NH_4H_2PO_4$ total internal reflection intercavity laser switch 77—38955
$NH_4H_2PO_4$, total internal refl. diffr.-type modulator as laser cavity switch 78—5511
$NH_4H_2PO_4$, tunable coherent radiation generation below 250 nm at MW power levels 78—59080
$NH_4H_2PO_4$, two photon absorption at 266.1 nm 77—88844
$NH_4H_2PO_4$, two-stage internal SHG in coupled resonators of Nd:YAG laser *(German)* 79—98438
$NH_4H_2PO_4$, two-step polishing process 79—64363
$NH_4H_2PO_4$, UV radiation prod., intracavity freq. doubling of rhodamine 6G laser 77—3628
$NH_4H_2PO_4$, unstable growth features and mechanisms of inclusion formation 79—99090
$NH_4H_2PO_4$, vac. UV transmission 77—73150
$NH_4H_2PO_4$, X-ray interference fringes due to diffraction effect at grown-in twin boundary 78—38728
$NH_4H_2PO_4$, Z-cut, SAW props. 80—84358

ammonium compounds continued
$NH_4H_2PO_4$:^{57}Fe, Mossbauer study, Fe^{3+} effect in habit 80—100627
$NH_4H_2PO_4$:AsO_4^{4-} (SeO_4^{3-}), antiferroelec., low freq. fluctuations, isotope effects, EPR, ENDOR, ESCA 77—73118
$(NH_4)H_2PO_4$:Cr^{3+}, EPR exam. above and below T_c 78—68363
$NH_4H_2PO_4$:CrO_4^{2-} (CrO_7^{2-}), electrical cond., thermal depolarisation studies 79—95212
$NH_4H_2PO_4$:VO^{2+}, EPR of VO^{2+} ions in antiferroelec. cryst. 79—47329
$NH_4H_2PO_4+La_2O_3 \rightarrow La(PO_3)_3$, solid phase reaction 79—79235
NH_4HS, polycryst., vibr. spectrum, lattice dynamics 77—90138
NH_4HSO_4, dielectric relax. in ferroelectric and paraelectric phases 77—16246
NH_4HSO_4, ferroelec. Brillouin shifts and linewidths 77—16322
NH_4HSO_4, ferroelec., press.-temp. phase diagram 77—85663
NH_4HSO_4, ferroelec., critical slowing down of dielec. relax. *(Japanese)* 77—90109
NH_4HSO_4, ferroelectric powder dielectric behaviour particle size depend. 80—55046
NH_4HSO_4, movement of NH_4^+ in all phases over 77 to 388K, NMR study 77—28524
NH_4HSO_4, volume expansion, spontaneous strain, second order phase transitions 79—65224
NH_4HSO_4:VO^{2+}, ferroelastic, inernal strains, ferroelec. transitions, EPR 79—47400
NH_4HSO_4-type crystal, ferroelectric phase transform. model, SO_4 group ordering 77—77156
$(NH_4)_3H(SO_4)_2$, movement of NH_4^+ in all phases over 77 to 388K, NMR study 77—28524
$(NH_4)_3H(SO_4)_2$, phase transitions, sp. ht. meas. 80—2157
$(NH_4)_3H(SO_4)_2$, phase transitions, dielec. study at low temps. 80—88902
$(NH_4)_3H(SO_4)_2$, press.-induced ferroelectricity, dielec. const. meas. 77—12328
$(NH_4)_3H(SO_4)_2$, press.-temp. phase diagram, dielec. and DTA meas. 77—81067
$(NH_4)_3H(SO_4)_2$, pressure-induced ferroelectricity, dielec. const. meas. 78—23412
$(NH_4)_3H(SO_4)_2$, room temp. phase, cryst. struct. 78—42965
$(NH_4)_3H(SO_4)_2$, successive phase transitions, dilatometric and X-ray expts. 80—11348
$((NH_4)_3H(SO_4)_2)_{1-x}[(ND_4)_3D(SO_4)_2]_x$ system, ferroelectric transitions 80—108160
NH_4HSeO_4, cryst. struct., dielec. and ferroelec. props. 80—60528
NH_4HSeO_4, ferroelec. phase transition, pyroelec. props. 80—60513
NH_4HSeO_4, ferroelec. props. rel. to struct. 80—71345
NH_4HSeO_4, ferroelec., phase transitions, permittivity and pyroelectricity meas. 80—71350
NH_4HSeO_4, para- to ferroelectric transition obs. by permittivity meas. 79—51916
$(NH_4)_3H(SeO_4)$, ferroelec. transition, press. and temp. effects on dielec. props. 78—23413
$(NH_4)_3H(SeO_4)_2$, ferroelec. phase transition, dielec. meas. 77—63376
$NH_4H_3(SeO_3)_2$, Raman spectra meas. 78—10899
$NH_4H_3(SeO_3)_2$, single crystal, ^{77}Se magnetic shielding, chemical shift tensors 80—71207
$NH_4H_3(SeO_3)_2$, X-ray crystal struct. refinement at −150°C 77—4090
$(NH_4)_6H_6W_{12}O_{42}.10H_2O$, X-ray cryst. struct. determ. *(French)* 79—77560
$(NH_4)_4Hf(C_2O_4)_4.nH_2O$, electric field gradient at metal site, γ-ray perturbed ang. correlation meas. 78—52380
$(NH_4)_3HfF_7$, longitudinal decoupling of quadrupole interaction 78—39456
NH_4HgCl_3, high resolution heat capacity meas. *(Japanese)* 80—52218
α-NH_4HgCl_3, NQR freqs., anomalous temp. depend. NH_4^+ ion reorientation 79—56624
αNH_4HgCl_3 quasione dimensional type cryst., phase transition statistics, molecular field approx. calcs. 80—34190
α-NH_4HgCl_3, thermal expansion, lattice constants between 302 and 364K 80—15268
α-NH_4HgCl_3. Raman study of phase transition *(French)* 80—11378
NH_4I, ^{14}N NMR obs., rel. to structural transformations 79—15368
NH_4I, $(NH_4)_{0.16}K_{0.84}I$ and $(NH_4)_{0.16}K_{0.84}Br$, reorientation motion of NH_4^+ 78—79542
NH_4I, coexisting phases and NH_4^+ dynamics, neutron scatt. exam. 79—42158
NH_4I, cryst., Debye characteristic temp. calcs. 79—37796
NH_4I, cubic NaCl-type cryst., Debye temp. 80—54333
NH_4I, dielectric const. meas. at 1 MHz 77—16238
NH_4I, ND_4I, lattice dynamics calcs. 78—6133
NH_4I, NMR, spin-torsional spectra 79—15363
NH_4I, NMR under high press. 78—84485
NH_4I, orientational disorder, Raman and far IR spectra 78—23447
NH_4I, phase diagrams, from Raman meas. under high press. 78—52776
NH_4I, powder, adsorpt. of H_2O vapour 79—1545
NH_4I, Raman spectra at high press. 79—47459
NH_4I, Raman spectrum, press. effects 80—97261
NH_4I, reorientation dynamics of NH_4 ions, quasielastic neutron scatt. obs. 77—31610
NH_4I, reorientational motion of ammonium ions in octahedral environments, neutron scatt. exam. 79—42159
NH_4I, thermorefl. spectra, band energy anal. 77—12402
NH_4I, torsional spectroscopy by NMR in rotating frame 78—27119
NH_4I_3, NQR freq. anomalous temp. depend., reorientation 80—54976
$NH_4I(ND_4I)$.dioxane complexes, Raman spectra, vibrs., H-bonding 78—25544
NH_4IO_3, effect of hydrostatic press. on ferroelec. phase transition 79—51917
NH_4IO_3, ferroelec., structural phase transition 80—7308
NH_4IO_3, new ferroelectric materials *(Japanese)* 77—28529
NH_4IO_3, phase transitions, SHG obs. 78—76398
NH_4IO_3, static electrooptic coeffs., temp. depend. 77—28547
NH_4IO_4, ^{127}I NQR rel. to thermal expansion 79—4742
NH_4IO_4, chem. shift, NMR obs. 80—48015
NH_4IO_4, dynamics of IO_4^- vibr. in lattice 79—42157
NH_4IO_4, high order phase transition, quadrupole coupling temp. depend. 80—54371
NH_4IO_4, Raman spectra, libration lattice modes 80—60575
$NH_4IO_3.2HIO_3$, dielec. constant, elec. cond. phase transition and cryst. struct. 80—1999
$(NH_4)_2InCl_5$:Fe^{3+} EPR, site g-tensor, spin Hamiltonian factors 77—63270

ammonium compounds continued
$(NH_4)_3In(SO_4)_3$, low temp. form, cryst. and powder diffr. data *(French)* 80—28981
$NH_4In(SO_4)_2.4H_2O$, cryst. struct. 79—19231
$NH_4In(SO_4)_2.4H_2O$, H-bond system, X-ray diffr. obs. 80—6395
$(NH_4)_2IrCl_6$, mag. susceptibility in ordered and paramag. phases 79—73759
$((NH_4)_{1-x}K_x)_2$ $CuCl_4.2H_2O$, Raman scatt. spectra 79—15459
$(NH_4)_{0.16}K_{0.84}I(Br)$, reorientation motion of ammonium ions in octahedral environments, neutron scatt. exam. 79—42159
$((NH_4)_{0.16}K_{0.84})_2SO_4$, reorientational relax. times, quasielastic neutron scatt. obs. 78—55821
$((NH_4)_xK_{1-x})_2SO_4$, NH_4^+ dynamics, neutron scatt. study 79—42167
$((NH_4)_xK_{1-x})_2SnCl_6$, mixed cryst., spectroscopic study 79—33712
$((NH_4)_xK_{1-x})_2SnCl_6$, mixed cryst., NQR relax. and reson. 80—54990
NH_4LiSO_4, ferroelec., phase transition points, hydrostatic press. effect 77—77155
NH_4LiSO_4, ferroelec., PMR line shape and spin-lattice relax. 78—88205
NH_4LiSO_4, ferroelec., hydrostatic press. effect on I-II phase transition, dielec. meas. 79—38496
NH_4LiSO_4, high press. phase, point group symmetry 79—51039
NH_4LiSO_4, I-II phase transition in improper ferroelec., hydrostatic press. effects 78—84533
NH_4LiSO_4, new ferroelectric materials *(Japanese)* 77—28529
NH_4LiSO_4, phase transforms., SHG obs. 78—76398
NH_4LiSO_4, point group symm. at high press. phase 80—70150
$(NH_4)_2MCl_6$, (M=Pd, Pt, Te, Ru, Ti, Ir and Re), proton relaxation and tunnelling 79—4737
$(NH_4)_2M(SO_4)_2.6H_2O$, M=Ni, Co, Mg, IR spectra 80—97280
$(NH_4)_2Mg(CO_3)_2.4H_2O$, cryst. and powder diffr. data 80—24420
$(NH_4)_2Mg_2(SO_4)_3$, phase transitions, dielec. props. obs. 78—6643
$(NH_4)_2Mg(S_2O_3)_2.6H_2O$, isolation, struct., decomposition *(French)* 78—52506
NH_4MnCl_3, X-ray single crystal analysis, phase transitions, Mossbauer effect 79—19366
$(NH_4)_6MnMo_9O_{32}.8H_2O$, mag. susceptibility, rel. to EPR, zero field splitting parameter 77—36122
$(NH_4)_5Mo_2Cl_9.H_2O$, resonance Raman spectra, $MO_2Cl_8^{4-}$ vibrs. 78—64350
$(NH_4)_2MoO_4$, ^1H spin-lattice relax., 100-500K 79—38398
$(NH_4)_4Mo_8O_{26}.4H_2O$, Lindqvist octamolybdate, cryst. and mol. struct. 77—76373
$(NH_4)_4Mo_8O_{26}.4H_2O$, X-ray cryst. struct., Fourier and Patterson synthesis *(French)* 79—42032
$(NH_4)_2MoS_4$, aq. soln., Raman intensity, scatt. frequency depend. 79—28747
$(NH_4)_2MoS_4$, cryst. struct. refinement, X-ray diffr. meas. *(French)* 77—4076
$(NH_4)_2MoS_4$, electronic struct., XPS and X-ray emission spectra 77—42336
NH_4N_3, cryst. struct. determ. by neutron diffr. 78—79574
NH_4N_3, diamag. susceptibility, rel. to cryst. struct. 79—24127
NH_4NBeF_4, successive phase transitions, dielec. and optical props. obs. 80—50275
$NH_4(NH_3)_n^+$, n=0 to 4, gas phase IR spectra 80—43044
$NH_4NH_2SO_3$, ^1H spin-lattice relax., 100-500K 79—38398
NH_4NO_2, thermal anal. by energy-dispersive X-ray diffr. 78—91440
NH_4NO_3 aqueous solution, enthalpies of dilution and relative apparent molar enthalpies, dissociated soln. case 80—50876
NH_4NO_3, CC ^{15}N NMR chem. shift references evaluation 78—24835
NH_4NO_3 conc. aqueous soln., X-ray scatt., NO_3^--H_2O interactions 78—42881
NH_4NO_3 crystals, NH_4^+ ion symmetry in phases II-V, Raman spectra obs. 80—66200
NH_4NO_3, elastic growth of cryst. during IV to x polymorphic transitions 79—46593
NH_4NO_3, IR spectra study of shear-stress-induced phase transitions at high press. 77—32368
NH_4NO_3, IR spectra and vibr. bands 80—69144
NH_4NO_3, intrinsic electroluminescence obs. 78—80420
NH_4NO_3, low temp. phase, Raman scatt. meas. 78—84568
NH_4NO_3, molten, countercurrent electromigration cell, isotope separation appl. 78—47547
NH_4NO_3, NMR double resonance *(Rumanian)* 79—58763
NH_4NO_3, phase II, cryst. struct., neutron diffr. study, profile refinement method 79—60314
NH_4NO_3, phase III, cryst. struct., neutron powder diffractometer study 80—107134
NH_4NO_3, phase transition, IR spectra 80—7350
NH_4NO_3, proton NMR lineshapes of NH_4^+ undergoing slow tunnelling rotations 79—90576
NH_4NO_3, proton spin-lattice relax., temp. depend. 79—42859
NH_4NO_3, Raman scatt. in region of extended IV-V phase transition 79—99887
NH_4NO_3, Raman spectra meas., 250-420K 77—20845
NH_4NO_3, Raman spectra of low temp. phases 78—92081
NH_4NO_3, shock-induced intramol. bond breaking, XPS and EPR study 80—76512
NH_4NO_3, solid, nuclear double reson. cross-relax. 79—15379
NH_4NO_3 soln., Raman spectral studies of NO_3^- motion and interaction 78—92067
NH_4NO_3 solution cathodic gas evolution rate rel. to electrode material *(Russian)* 80—26020
NH_4NO_3, standard enthalpy of soln. in water, standard thermodynamic state search 80—50877
NH_4NO_3-$LiNO_3$-NH_4Cl-water system, cond. and viscosity *(French)* 79—51286
$NH_4NO_3 \rightleftharpoons NH_3+HNO_3$ equilib. in atmosphere 79—88389
$(NH_4)Na_2Cd(P_2O_7)_2Cl$, crystal struct. determ. 77—84732
$(NH_4)_2Ni(BeF_4)_2.6H_2O$, X-ray cryst. struct. determ. 80—107137
$(NH_4)_2Ni(CrO_4)_2.6H_2O$, X-ray single cryst. struct. determ. 79—19207
$(NH_4)_2Ni_3(P_2O_7)_2.nH_2O$, thermal dehydration 80—35513
$(NH_4)_{0.8}Ni_{1.1}PO_4.xH_2O$, ion exchange props., Cs^+ ion sorpt., struct., IR spectra 77—9121
$(NH_4)_2Ni_2(SO_4)_3$, phase transitions, dielec. props. obs. 78—6643
$(NH_4)_2Ni(SeO_4)_2.6H_2O$, X-ray cryst. struct. determ. 80—39027
NH_4OCN formation, in interaction of CO, NO and H_2 over Pt, Rh, Ru and Os 78—73082
NH_4OH, aerosols existence in planetary atms., IR reflectivity spectra, Kramers-Kronig anal. 78—68500
NH_4OH, IR reflectivity spectra, Kramers-Kronig anal. 78—68500

ammonium compounds continued
$5(NH_4)_2O.12WO_3$, thermal decomp. 100-500°C 77—56223
$NH_4P_3Be_2O_{10}$, cryst. struct., X-ray diffr. *(French)* 77—19920
$(NH_4)_3PCr_4O_{16}$, cryst. struct., $(PCr_4O_{16})^{3-}$ anion geometry 80—107157
NH_4PF_6, H^+ relax. and tunnelling, nucl. spin-lattice relax. obs. 79—51876
NH_4PF_6, IR spectra of NH_3D^+ ion, mol. motion 77—36232
$(NH_4)_2PO_3F$, H_2O, X-ray diffraction and Raman spectra struct. determ., external mode temp. depend. *(French)* 78—52507
$(NH_4)_2PO_3F.H_2O$, cryst. struct. comparison with $(NH_4)_2SO_3.H_2O$ *(French)* 77—47404
$(NH_4)_2PbCl_6$, inelastic neutron scatt. and pot. shape 80—1946
$(NH_4)_2PbCl_6$, librational tunnelling and proton relax. temp. 80—38969
$(NH_4)_2PbCl_6$, temp. depend. of tunnel freq. 80—1947
$NH_4Pb_2Cl_5$, cryst. struct., X-ray diffr. 77—19923
$NH_4PbI_3.2H_2O$, X-ray cryst. struct. determ. 80—64958
$(NH_4)_2PdCl_6$, inelastic neutron scatt. and pot. shape 80—1946
$(NH_4)_2PtBr_6$, cubic to tetragonal phase transitions 79—1500
$(NH_4)_2PtCl_6$, inelastic neutron scatt. and pot. shape 80—1946
$(NH_4)_2PtF_6$, X-ray cryst. struct. determ. 80—107125
$(NH_4)_2PtI_5$, synthesis and cryst. struct. *(German)* 78—79588
$(NH_4)_2PtI_6$, crystal symm., struct. phase transition, ^{127}I NQR freq. 80—34815
$(NH_4)_xRb_{1-x}Al(SO_4)_2.12H_2O:Cr^{3+}$ EPR study, effect of monovalent ions on trigonal distortion 80—11255
$(NH_4)_{1-x}Rb_xCl(Br)$, and $(ND_4)_{1-x}Rb_xCl(Br)$, phase diagrams, DTA and birefr. obs. *(German)* 79—83185
$((NH_4)_{1-x}Rb_x)_2SO_4$, isomorphic impurity effect on dielec. and nonlinear optical props. 80—88911
$((NH_4)_{1-x}Rb_x)_2SO_4$ mixed cryst., EPR of NH_3^+ and SeO_3^- radicals 80—50190
$(NH_4)_{2(1-x)}Rb_{2x}SO_4$, mixed crystal, dielectric and US meas. of ferroelec. phase transition *(Japanese)* 80—7305
$(NH_4)_{2(1-x)}Rb_{2x}SO_4$, stoichiometry defects, electron probe microanal. 80—39143
$(NH_4)_2ReCl_6$, neutron diffr. study of cryst. struct. 79—55701
$(NH_4)_2ReCl_6(IrCl_6)$, proton relaxation near antiferromagnetic phase transitions 80—80640
NH_4ReO_4, ^{187}Re HQR freq. temp. depend. 80—25245
NH_4ReO_4 (ND_4ReO_4), nuclear electric hexadecapole interactions 80—65513
NH_4ReO_4, cryst. struct. at 295 and 135K 78—26521
NH_4ReO_4, heat capacity and thermodynamic props., 8 to 304K 80—100335
NH_4ReO_4, high order phase transition, quadrupole coupling temp. depend. 80—54371
NH_4ReO_4, ND_4ReO_4, Raman spectrum, temp. depend. 78—80335
NH_4ReO_4, ND_4ReO_4, external lattice vibr. modes and elastic wave vels., dispersion relations 79—33050
NH_4ReO_4, NQR and thermal expansion investig. 77—12229
NH_4ReO_4, NQR and thermal expansion 77—20745
NH_4ReO_4, NQR freq. of $^{185,187}Re$, temp. depend. 77—12228
NH_4ReO_4, NQR freqs., anomalous temp. depend. NH_4^+ ion reorientation 79—56624
NH_4ReO_4, NQR freq. anomalous temp. depend., reorientation 80—54976
NH_4ReO_4, nuclear electric hexadecapole interactions of ^{185}Re and ^{187}Re 79—1722
NH_4ReO_4, nuclear quadrupole coupling, NQR temp., press. depend., continuous phase transition 78—27109
NH_4ReO_4, PMR, NH_4^+ tunnelling, ground torsional level struct. 78—27097
NH_4ReO_4, polycryst., ^1H spin-lattice relax. by mech. sample rot. 77 16200
NH_4ReO_4, proton absorpt. lineshape and spin-lattice relax., ^{187}Re anomalous temp. depend. 78—48067
NH_4ReO_4, quadrupole coupling, cation electric field gradients 78—35060
$(NH_4)_2(RuCl_5NO)$, polarised Raman and IR spectra, vibr. anal. 77—69819
$(NH_4)_2S_5$, Raman spectra, vibrs. and rot. isomers of Sn^2 (n=4-8) *(German)* 78—13504
NH_4SCN, charge distrib., deform. density, cryst. struct. determ. by X-ray and neutron diffr. 77—47415
NH_4SCN, polymorphous structural-kinetic transformations, phase orientational relation 79—90590
NH_4SCN, proton NMR lineshapes of NH_4^+ undergoing slow tunnelling rotations 79—90576
NH_4SCN, proton spin-lattice relax., temp. depend. 79—42859
$(NH_4)_2SO_4$ aerosol production under elevated temp. inversion in Cleveland Country, model 78—81397
$(NH_4)_2SO_4$, aqueous solns. and cryst., optical consts. meas. rel. to atm. aerosol props. 77—52034
$(NH_4)_2SO_4$, aqueous soln., SO_4^2 -H_2O interaction, X-ray scatt. 79—77479
$(NH_4)_2SO_4$, atm. dust, imaginary refr. index rel. to particle size 78 7763
$(NH_4)_2SO_4$, atm. particles conc. and size distrib., rural conditions 79—74564
$(NH_4)_2SO_4$, Brillouin scatt. from room temp. to −70°C 78—52517
$(NH_4)_2SO_4$, dielec. props., 210-250K, 1 MHz-25 GHz, ferroelec. transition obs. 77—59541
$(NH_4)_2SO_4$, ESR study of NH_3^+ radicals 79—38367
$(NH_4)_2SO_4$, e.s.r., of NH_3^+ and SeO_3^- radicals, ferroelec. transition obs. 77—16180
$(NH_4)_2SO_4$, ferrielec., dielec. behaviour and nature of phase transition 78—88262
$(NH_4)_2SO_4$ ferrielectric, X-ray anal. of sub-lattice order parameters 78—92035
$(NH_4)_2SO_4$, ferroelec., ion group reorientation temp. and press. depend., PMR obs. 78—72470
$(NH_4)_2SO_4$, ferroelec. transition, EPR study 79—38472
$(NH_4)_2SO_4$, ferroelec. dispersion in microwave region, transition to ferrielectric structure 80—45016
$(NH_4)_2SO_4$, IR photoacoustic spectra 80—13163
$(NH_4)_2SO_4$, intrinsic electroluminescence obs. 78—80420
$(NH_4)_2SO_4$, irrad., −50°C transition, librational mode softening, paramag. NH_3^+ probe obs. 77—20037
$(NH_4)_2SO_4$, mechanically twinned, orthorhombic, search for antiphase boundaries 79—37715
$(NH_4)_2SO_4$, microscopic model for ferroelectric phase transition 78—6641

ammonium compounds continued
- $(NH_4)_2SO_4$, NH_4^+ dynamics, neutron scatt. study 79–42167
- $(NH_4)_2SO_4$, optical SHG expts. on microscopic origin of permanent dipoles 78–1299
- $(NH_4)_2SO_4$, order-disorder phase transitions with many-minimum potential, thermodynamic props. 80–96623
- $(NH_4)_2SO_4$, paraelec. phase, X-ray diffuse scatt., soft mode model 77–31744
- $(NH_4)_2SO_4$, paraelectric to ferroelectric phase boundaries 78–19426
- $(NH_4)_2SO_4$, paraelectric, N-quadrupole coupling meas. by proton-N double resonance 80–60459
- $(NH_4)_2SO_4$, phase transition mechanisms by optical spectroscopy 79–15411
- $(NH_4)_2SO_4$, phase transition theory 79–24275
- $(NH_4)_2SO_4$, polycrystalline materials; pyroelec. temp. anal. as method for studying ferroelec. transitions 79–38502
- $(NH_4)_2SO_4$ polydisperse aerosol number and mass conc. meas. by elect. aerosol anal. 80–108753
- $(NH_4)_2SO_4$ powder and aqueous soln., photoacoustic spectra in middle IR 77–81101
- $(NH_4)_2SO_4$, powder sample, pyrocharge temp. depend. near phase transition 79–87399
- $(NH_4)_2SO_4$, pure and Rb doped, ferroelec. transition, light scatt. meas., dielec. and elastic props. 78–43822
- $(NH_4)_2SO_4$, reorientational relax. times, quasielastic neutron scatt. obs. 78–55821
- $(NH_4)_2SO_4$ rounded particles, Mueller scatt. matrices 78–90366
- $(NH_4)_2SO_4$, single crystal growth from aq. soln. *(Japanese)* 78–92182
- $(NH_4)_2SO_4$, solid-to-solid transition temperature under hydrostatic pressures to 0.6 GPa 80–24586
- $(NH_4)_2SO_4$, static and dynamic dielec. behaviour 80–71337
- $(NH_4)_2SO_4$:Cd^+, ferroelec. transition, soft mode contrib., EPR obs. 78–72469
- $(NH_4)_2SO_4$:Cr^{5+}, EPR study of ferroelec. phase transition 78–64337
- $(NH_4)_2SO_4$:Cu^{2+}, ESR parameters, effect of pH of mother soln., trapping sites 80–15791
- $(NH_4)_2SO_4$:Cu^{2+}, ferroelec., ESR, Cu^{2+} in trigonal bipyramidal coord. 78–23330
- $(NH_4)_2SO_4$:Cu^{2+}, ferroelec. transition, ESR study 79–91286
- $(NH_4)_2SO_4$:MnO_4^-, X-ray irrad. damage, optical absorpt. spectra study 80–66246
- $(NH_4)_2SO_4$:SeO_3^-, γ-irrad., hyperfine interaction, ferroelec. transition effects, EPR expt. 78–15024
- $(NH_4)_2SO_4$:VO^{2+}, EPR spectrum, temp depend. 110-300K 80–11249
- $(NH_4)_2SO_4$:VO^{2+}, ferrielectric phase transition, two-sublattice model, EPR of polar VO^{2+} probes 78–48127
- $(NH_4)_2SO_4$-ethanol-benzene-water, liq. mixture, near tricrit. pt., thermodynamic model and sum rules 80–34196
- $(NH_4)_2SO_4$-ethanol-benzene-water, liq. mixture, near tricrit. pt., light scatt. and sum rules 80–34933
- $(NH_4)_2SO_4$-H_2O-ethanol-benzene, tricritical mixture, light scatt. 79–15473
- $(NH_4)_2SO_4$-K_2SO_4 mixed crystal, cryst. struct., X-ray diffr. meas. 77–80484
- $(NH_4)_2SO_4$-type crystals, ferroelastic, ferrielectric, and incommensurate phase transitions *(Japanese)* 79–65811
- $(NH_4)_2S_2O_3$, cryst. and X-ray powder data 79–51074
- $(NH_4)_2S_2O_3$, X-ray crystal and powder diffr. data 79–14766
- $(NH_4)_2S_2O_3$, X-ray cryst. struct. determ. 79–77562
- $(NH_4)_2S_2O_7$ etchant, for NbC, TaC and HfC 80–85097
- $(NH_4)_2S_2O_8$, proton spin-lattice relax., temp. depend. 79–42859
- $(NH_4)_2S_2O_8$-HCl-H_2O dislocation etchant for β-brass crysts. 80–65004
- NH_4SO_3F, IR spectra of NH_3D^+ ion, mol. motion 77–36232
- $(NH_4)_2SO_4.Al_2(SO_4)_3.24H_2O$, temp. depend. curves of quadrupole interaction parameter for $^{27}Al^{3+}$ 77–55727
- $(NH_4)_2SO_4.Al_2(SO_4)_3.24H_2O$:$Cr^{3+}$, and deuterated derivative, structural transition studied by EPR 77–85553
- $(NH_4)_2SO_4.Al_2(SO_4)_3.24H_2O$:$Cr_2O_7^{2-}$, optical absorpt. spectra, mol. orbital calcs. 79–15491
- $(NH_4)_2SO_3.H_2O$, S^{IV} lone pair, stereochem. role in struct. *(French)* 77–47404
- NH_4SbF_5, dielectric props. and structural phase transitions *(German)* 80–25274
- $(NH_4)Sb_{0.5}M_{0.5}{}^{IV}Cl_6$, ($M^{IV}$=Se, Te, Sn), ^{121}Sb Mossbauer effect 78–84506
- $(NH_4)_6Sb_4(SO_4)_3F_{12}$, dielec. props. and phase transitions 79–69765
- $(NH_4)_3Sc(SeO_4)_3$, cryst. struct. determ. 78–26524
- $(NH_4)_3Sc(SeO_4)_3$, cryst. struct. 79–99122
- $(NH_4)_2SeO_4$, cryst. struct. 77–24299
- $(NH_4)_2SeO_4$, detect. in subway air 78–36273
- $(NH_4)_2SeO_4$:Mn^{2+}, single cryst., EPR and phase transition 79–73805
- $(NH_4)_2SeO_4$:VO^{2+}, EPR spectrum 79–61207
- $(NH_4)_2Se_2O_5$, X-ray cryst. struct. determ. 80–54189
- $(NH_4)_2SeO_4.2NH_4HSeO_4$, cryst. struct. 78–71715
- $(NH_4)SiF_6$, IR absorpt. spectra, integrated intensity temp. depend. 79–73946
- $(NH_4)_2SiF_6$, A=Si, Ge, Sn, IR absorpt. spectra, integrated intensity 79–73944
- $(NH_4)_2SiF_6$, cryst., highly bent H bonds, IR spectrosc. investig. 80–93292
- $(NH_4)_2SiF_6$, cryst. phases, Raman obs. 20-290K 77–66495
- $(NH_4)_2SiF_6$, cubic and trigonal, proton tunnelling frequencies from nuclear spin-lattice relaxation 78–6591
- $(NH_4)_2SiF_6$, elastic constants, softening of acoustic modes, obs. by Brillouin scattering 80–71440
- $(NH_4)_2SiF_6$, low-temp. dielec. loss maxima in cubic and trigonal crysts. 79–19831
- $(NH_4)_2SiF_6$, proton NMR lineshapes of NH_4^+ undergoing slow tunnelling rotations 79–90576
- $(NH_4)_2SiF_6$, proton relax. by tunnelling at low temp. 78–43666
- $(NH_4)_2SiF_6$, trigonal, proton and ^{19}F relax, 30 to 200K 77–76549
- $(NH_4)_2SiP_4O_{13}$, cryst. struct. determ. *(French)* 77–4070
- $(NH_4)_2SnBr_6$, structural phase transitions study by Raman scatt. 80–93318
- $(NH_4)_2SnCl_6$, ^1H spin-lattice relax., 100-500K 79–38398
- $(NH_4)_2SnCl_6$, $^{35,37}Cl$ NQR, Raman spectra and spin lattice relax., hindered rot. 80–54974
- $(NH_4)_2SnCl_6$, elastic constants, softening of acoustic modes, obs. by Brillouin scattering 80–71440
- $(NH_4)_2SnCl_6$, inelastic neutron scatt. and pot. shape 80–1946

ammonium compounds continued
- $(NH_4)_2SnCl_6$, NH_4^+ ion rot. states, inelastic neutron scatt. obs. 78–30552
- $(NH_4)_2SnCl_6$, NH_4^+ libration and tunnelling freq. rot. heat capacity, hindered rot. energy level calcs. 79–98058
- $(NH_4)_2SnCl_6$, proton relax. by tunnelling at low temp. 78–43666
- $(NH_4)_2SnCl_6$, proton tunnelling frequencies from nuclear spin-lattice relaxation 78–6591
- $(NH_4^+)_2SnCl_6^{2-}$, torsional ground state splitting in cryst. field, energy level press. depend. 80–15019
- NH_4SnF_3, cryst. struct. *(German)* 78–34480
- $(NH_4)_2SnF_6$, A=Si, Ge, Sn, IR absorpt. spectra, integrated intensity 79–73944
- $(NH_4)_2SnF_6$, cryst., highly bent H bonds, IR spectrosc. investig. 80–93292
- $(NH_4)_2Sn_{1-x}Sb_xCl_6$ (x=0.13, 0.21, 0.28, 0.33), mixed valence compound, ^{121}Sb Mossbauer spectroscopy 79–51890
- NH_4TaWO_6, rapid ionic motion, spin-lattice and spin-spin relax. times meas. 79–38396
- $(NH_4)_2TcCl_6$, X-ray single cryst. struct. determ. 79–19197
- $(NH_4)_2(TeBr_6)$, far IR and Raman spectra and phase transitions 80–11376
- $(NH_4)_2(TeCl_6)$, IR and Raman spectra, lattice and internal modes, phase transition 78–6659
- $(NH_4)_2TeCl_6$, inelastic neutron scatt. and pot. shape 80–1946
- $NH_4TeO_3(OH)$, cryst. struct., Patterson and Fourier synthesis *(French)* 80–33942
- $(NH_4)_2TeO_2(OH)_4$, X-ray cryst. struct. anal. 79–77563
- $(NH_4)_2Te_3O_8(OH)_4$, synthesis and crystallochem. study *(French)* 80–1990
- $(NH_4)_2TiF_6$, ^1H-^{19}F coupled NMR, line shapes, spin-lattice relax. 79–73839
- $(NH_4)_2TiF_6$, cryst., highly bent H bonds, IR spectrosc. investig. 80–93292
- $(NH_4)_2TiF_6$, H^+ relax. and tunnelling, nucl. spin-lattice relax. obs. 79–51876
- $(NH_4)_2TiF_6$, Raman spectra, internal and lattice vibrs. 77–8569
- $(NH_4)_xTl_{1-x}Al(SO_4)_2.12H_2O$:$Cr^{3+}$, zero field splitting, g-values, EPR spectra obs. 80–50169
- $(NH_4)_{1-x}Tl_xCl(Br)$, and $(ND_4)_{1-x}Tl_xCl(Br)$, phase diagrams, DTA and birefr. obs. *(German)* 79–83185
- $NH_4Tl(SeO_4)_2$, $(NH_4)_3Tl(SeO_4)_3$, and $(NH_4)_5Tl(SeO_4)_4$, cryst. struct. *(French)* 80–84148
- $(NH_4)_3UO_2F_5$, normal coordinate anal. 79–22596
- $(NH_4)_2UO_2(HPO_3)_2$, synthesis and comp. 80–35516
- $NH_4UO_2(NO_3)_3$, fluoresc. decay rates, temp. depend. 80–25429
- $NH_4UO_2(NO_3)_3$, Raman spectra 6-293K, phase transition 78–27220
- $(NH_4)_2(UO_2)_4O_2(OH)_2Cl_4(H_2O)_6$, cryst. data 77–76366
- NH_4VO_3, cryst. struct. 78–6043
- NH_4VO_3, polycryst., quadrupole coupling const., asymmetry parameter, chem. shift, NMR computer calcs. 78–6584
- $(NH_4)_{0.33}WO_3$, supercond. and special phonons, neutron scatt. obs. 80–15643
- NH_4X, (X=Cl, Br, I), tricritical points 79–7695
- $(NH_4)_2ZnCl_4$, commensurate-incommensurate phase transition, ^{35}Cl NQR study 80–75966
- $(NH_4)_2ZnCl_4$, ferroelectricity and incommunsurate-commensurate phase transitions 80–60523
- NH_4ZnF_3, hindered rot. sp. ht. of NH_4^+, 2.5-300K 77–62648
- NH_4ZnF_3, rot. motion of NH_4^+ in lattice, neutron scatt. 79–37773
- NH_4ZnF_3, sp. hts., librational and reorientational 77–84946
- $(NH_4)_2Zn(SO_4)_2$:Ni^{2+}, optical absorpt. spectrum, room and liq. air temp. 79–15499
- $(NH_4)_4[Bi_2Br_{10}].4H_2O$, cryst. struct. 77–58988
- $(NH_4)_2[Co(NCS)_4]$, X-ray Co K absorpt. edge struct. meas. 77–20956
- $NH_4[NbO(C_2O_4)_2(H_2O)_2].3H_2O$, cryst. struct. neutron diffr. obs. 77–24306
- $(NH_4)_2[Pt(CN)_4]Cl_{0.42}.3H_2O$ quasi one dimensional conductor, physical props., cond. freq. depend. 79–95393
- $(NH_4)_2[Pt(CN)_4].2H_2O$, DC elec. cond. props. 79–51582
- $(NH_4)_2[Pt(CN)_4].2H_20$, energy band calcs. 77–39780
- $NH_4[TcO_4]$, X-ray cryst. struct. determ. 80–39016
- $NH_4[Te^{IV}Te^{VI}O_5(OH)]$, 5 coordination of Te^{IV} atom by O atoms, cryst. struct. *(French)* 79–99130
- $(NH_4)_2[VF_4O]$, X-ray cryst. struct. determ. 80–107128
- $(NH_4)_{10}[W_{12}O_{40}(OH)_2].H_2O$, thermal polycondensation 79–14924
- $(NH_4)_2[ZnCl_4]$, X-ray cryst. struct. determ. 80–107138
- $NH_4^+.(NH_3)_n$, in afterglow, electron recomb. coeffs. mass spectrometric meas. 77–6927
- NaH_2PO_4-NH_4Cl-$NiCl_2$, soln., Ni yield, factors affecting, pot. use as radiographic media 79–52702
- $NaND_4C_4H_2D_2O_6.4D_2O$, ferroelec. phase, incommensurate satellite refls. 78–84531
- $NaNH_4SO_4.2H_2O$, ferroelec. and thermal props. 78–83968
- $NaNH_4SeO_4.2H_2O$, model of ferroelec. phase transition 78–19433
- $NaNH_4SeO_4.2H_2O$, ferroelectric crystal, effect of hydrostatic pressure on phase transition 78–52453
- $NaNH_4SeO_4.2H_2O$, atomic struct. exam. and phase transition 79–37678
- $NdNH_4P_4O_{12}$, isotypism with $PrNH_4P_4O_{12}$ *(French)* 77–24301
- $NiCl_26NH_3$, low temp. sp. ht. and mag. ordering 80–75784
- $Ni(NH_3)_6I_2$, EPR of Ni^{2+} ion near structural phase transformation 80–11248
- $Ni(NH_4)_2(SO_4)_2.10H_2O$, precipitation, supersaturation, cryst. size distrib. changes 77–72573
- $Ni(NH_3)_6X_2$, X=Cl,Br,I, rotational tunnelling by inelastic neutron scatt. 78–30553
- $PrNH_4P_4O_{12}$, cryst. struct. determ. *(French)* 77–24301
- $RbMnP_2O_7.3H_2O$, physicochem. characts. 77–39562
- $RbNH_4SO_4$, ferroelec., ion group reorientation temp. and press. depend., PMR obs. 78–72470
- Rb_2SO_4-$(NH_4)_2SO_4$ mixed cryst., ferroelec. transition, structural and dielec. props., proton spin-lattice relax. 78–39512
- $Tb(NO_3)_3$-$Fe(NO_3)_3$-$(NH_4)_2CO_3$-H_2O system, cpd. form., comp. and props. 80–100832
- $Te(OH)_6.2(NH_4)_2HAsO_4$, synthesis and cryst. data *(French)* 80–33948
- $(Tl,NH_4)_2Cd_2(SO_4)_3$, langbeinite type mixed cryst., ferroelec. transitions, dielec. and elastic meas. 78–2810
- $Tl_{0.33}(NH_4)_{0.67}H_2PO_4$, X-ray crystallographic investig. *(French)* 80–49192

ammonium compounds continued
- $Zn(NH_3)_4(ClO_4)_2$:Mn, EPR study of Mn^{2+} detection of structural transition 79—87308
- $Zn(NH_4)_2(SeO_4)_2.6H_2O:Mn^{2+}$, EPR spectra 80—100608

amorphisation
- amorphisation due to ion bombardment, SRO struct. 80—79844
- asbestos, chrysotile, crushed, temp.-induced changes in struct. 77—24305
- diamond, amorphisation during ^{133}Xe implantation, Mossbauer effect study 80—40010
- Heisenberg model, amorphisation *(Russian)* 78—80118
- high pressure effect on formation of amorphous state *(Chinese)* 80—28917
- ion bombardment induced amorphisation, energy spike generation and quenching processes 78—47448
- ion implantation, target heating, temp. measurement 80—34032
- metal ribbon, amorphous, fluid-flow-temp. model for casting by melt extraction 79—56942
- metal ribbons, amorphous Newtonian-quenched, formed by melt spinning and melt extraction, dimens. variations 79—56943
- metal-metalloid amorphous alloys produced by ion implantation, TEM 80—15128
- metals, ion-induced amorphisation, review 79—14686
- polyethylene, single, polycryst., ^{60}Co-γ irrad., effect on melting behaviour 77—15548
- pyrographite, surface struct., amorphisation, secondary electron spectra and AES 79—43077
- α-quartz, electron irrad., defect struct. and radiolysis 80—107321
- quartz surface, oscillation ground, amorphous zone distribution *(German)* 79—64995
- semiconductor, amorphous zone accumulation under ion irrad., composite model 79—51169
- semiconductor, radiation dose for amorphisation, max. point defect conc. 77—55301
- semiconductor monocrystal-amorphous radiation-induced transitions 77—80554
- semiconductors, amorphisation by high-energy ion irrad. 79—51172
- semiconductors, ion irradiation produced amorphisation, disorder-ion fluence functions, disorder mechanisms 80—29090
- Al, and Al-Cu(Pb) dil. alloys, pulsed ruby laser irrad., noncryst. phase form 80—35012
- Au/Si films, laser-irrad., phase transform. study 80—49536
- Au-Si system, transition layer struct. form. and heat treatment influence, amorphisation obs. 80—54529
- $BeAl_2O_4$, chrysoberyl, kinetics and mechanism of formation, in presence of V_2O_5 79—11535
- D_2O with soluted NaOD, collective excitations in liquid and amorphous state, 77 to 300K 80—92636
- GaAs, amorphous layer formation, ion implantation, IR spectra 78—95063
- GaAs, optical modulation spectra, proton damage effect 78—76487
- GaAs:Cr pulsed electron beam induced recrystallisation and damage, amorphous layer formation 80—34052
- Ge film, radiation damage in electron microscope 77—84794
- Ge, ion bombardment-induced photon emission as function of target temp. 80—100698
- Ge surface, (111), ion-bombarded and annealed, spectroscopic ellipsometry study 80—103543
- In, amorphization by ion implantation 78—52135
- Nb-Ni, amorphous thin film, vapour quenched, elec. resistivity and thermoelectric power 79—33275
- Ni-Dy, annealing behaviour of implantation damage, Dy outdiffusion, TEM obs. 77—77505
- P, crystalline to amorphous transition, thermodynamic functions 80—54354
- Se, acoustic props. near first-order phase transition 77—20014
- Si, amorphisation by $^{31}P^+$ ion irrad. 79—51172
- Si, amorphisation by ion implantation, homogeneous or heterogeneous nucleation 77—11578
- Si, amorphisation due to irradiation with heavy ions 77—11606
- Si, amorphised by ion irrad., doping effects on cond. in hopping transport regime 79—28424
- Si, amorphous, substrate orientation effect on regrowth by laser pulses, channeling, backscatter 80—84409
- Si, by ion implantation, energy depend. 77—7769
- Si, crystalline, repeatable transformation using intense laser beam 80—39150
- Si, energy depend. of amorphisation by ion implantation 78—2175
- Si film, ion bombarded, crystalline-to-amorphous transition, defect-rich film prep. 80—65071
- Si, form. of amorphous surface layers after irrad. with Cr^+ 79—90707
- Si, implantation induced strains, X-ray interferometry and topography 78—43039
- Si, implanted annealed layers, amorphised structure formation mechanism and crystallographic nature 80—29091
- Si, ion bombard. effect on surface struct., RHEED and Au decoration 80—2096
- Si, ion bombard. induced residual stress in amorphous implanted surface layers 77—35610
- Si, ion bombardment induced buildup of disordered material, model 77—47496
- Si, ion implanted, EPR line shape exam. of amorphous centres 79—28587
- Si, ion-implanted, cryst. to amorphous transform., ESR expts. and composite model 78—59825
- Si layers amorphized by molecular ions, laser annealing 80—103379
- Si, order-disorder transformation, pulsed UV laser induced 79—60400
- Si, polycrystalline film, amorphisation after ion implantation 80—2054
- Si, post-annealed amorphous layer, twinning struct. by transmission electron diffr. 77—76685
- Si:N(P), ion implanted, IR transmission and rel. spectra study 80—108244
- Si:P, amorphised by Ne^+ implantation, high fluence P implants, plasma region obs. 79—86807
- p-Si:P, random and aligned implants, Rutherford backscatt. and TEM exam. 78—47454
- Si:Pb, lattice location of dopant and amorphous zones, by Rutherford backscatt. 77—68990
- SiC, amorphisation induced by ion bombardment, Raman spectroscopy 77—80551

amorphisation continued
- SnO_2:P, CVD films, elec. props., cryst. to amorphous transition effects 80—107933
- SnO_2:P, CVD growth and etching characts., doping effects 80—107667
- ZnS ion beam etching, topographic changes, amorphisation, luminescence study 80—76078
- Zr_3Al, irradiation 78—6111
- Zr_3Al ordered alloy, ion bombardment damage, TEM 80—100287
- $ZrSiO_4$, heavy ion irrad., metamict zircon form. 80—2088

amorphous magnetic materials *see magnetic properties of amorphous substances*

amorphous semiconductors
- *see also chalcogenide glasses; electrical conductivity of amorphous semiconductors and insulators; insulators*
- absorption edges, temp. depend. 77—77160
- amorphous, EXAFS, evidence for inequivalent environments of Ga and As 79—15558
- amorphous, high field transport, impact ionisation, carrier mobility 80—80286
- amorphous, photogeneration, thermalisation model calcs., band gap *(French)* 80—75595
- amorphous film, glow discharge deposited, for low cost solar cells 80—61355
- amorphous layer, crystallisation anal. by cond. meas. *(French)* 77—72599
- amorphous semiconductor, switching effect, anomalous temp. depend. 78—26927
- amorphous semiconductors, dispersive charge transport 80—39585
- Anderson transition, electron localisation in disordered systems, review 80—29361
- anthracene-tetracene amorphous films, host-guest energy transfer 78—60505
- applications in electrophotography, thin film electronics and solar cells 80—107693
- band structure and forbidden gap in glasses and amorphous semiconductors, review 78—75987
- barrier controlled charge carrier transport in structures, props. *(German)* 79—47162
- bonding and transport properties 79—90950
- β-carotene, hole mobility meas. by transient photocond., Poole-Frenkel effect 77—11957
- carrier mobility and transient pulse dispersion for hopping mechanisms 80—44586
- carrier pulse propagation, macroscopic theory 78—72154
- carrier recombination and trapping, exponential trap distrib. case 78—14760
- carrier transport in p^+-ν junction, theory 79—60914
- chalcogenide switching device, on-state behaviour and degradation effects 77—11967
- characterisation for solar cell applications 79—61983
- characteristics, review *(Croatian)* 77—39771
- charge transport behaviour, model 79—91048
- classification into structurally ‘soft’ and ‘hard’, thermoelectric approach 78—42908
- conductivities, drift and diffusion 79—95413
- conductivity, thermopower and statistical shift 79—95434
- conference, Balatonfured, Hungary (Sept. 1976) 77—76802
- conference, Cambridge, MA, USA (Aug. 1979) 80—41933
- conference, Masnuy-St-Jean, Mons, Belgium, Oct. 1979 80—82570
- conference on noncrystalline solids, Clausthal, Germany (Sept. 1976) 78—22654
- configuration-coordinate model, Urbach rule 80—34948
- copper phthalocyanine-iodine, amorphous cpd. prep. by I_2 diffusion in polycrysts., triplet EPR signals obs. *(Russian)* 80—66016
- Coulomb gap occurrence *(Russian)* 78—14658
- covalent, choice and fabrication for switching applications 78—2415
- covalent, local struct., bonding and electronic props. 78—51882
- covalent, localised electronic states, Hubbard model calcs. 77—89732
- covalent, random two-band Weaire model, localisation theory 77—15788
- crystallisation, elec. cond. determ. model and its verification for Ge 77—20475
- crystallisation and decomposition 79—41959
- current fluctuations and switching 79—87133
- defect centres, cooperative charge disproportionations 80—54649
- defect chemistry and states in gap, models 79—38030
- defects, band gap states 80—80215
- density of states determ. from field effect data 80—107688
- diamagnetic, photostructural changes, mechanism 80—92557
- diamagnetic glassy semiconductors, at. tunnelling states, dielec. and elastic losses 79—87385
- diamagnetic susceptibility enhancement 79—65640
- dielectric relaxation current meas. methods and uses 77—77141
- diffusion phenomena, mechanisms and meas. 77—76608
- disordered and amorphous semiconductors, band conduction mech. 79—95414
- disordered hopping systems, AC and DC conductivity theory 80—54698
- disordered semiconductor, high-field cond. in random field 79—65489
- disordered semiconductor, possibility of density of state determ. by tunnel spectroscopy *(Russian)* 77—47713
- disordered system in mag. field, frequency dependence of conductivity tensor, theoretical investigation 80—70725
- dispersive charge transport 80—39585
- dispersive hopping transport, Monte Carlo calcs., variable range percolation 80—44587
- dispersive transport, trap-limited model 78—6378
- doped, electronic props. 78—19030
- doped, electronic props. 80—80283
- doping effect and nature of localised states 78—14696
- doping of tetrahedrally bonded cpds. 80—2361
- drift effect on carriers in amorphous semiconds. *(Russian)* 78—47789
- drift mobility, size and field variation of activation energy 80—49769
- electrical and optical props., w.r.t. electronic band states *(Japanese)* 79—23979
- electrical conduction mechanisms, review 79—56214
- electrical conductivity, super-linear freq. depend. 79—28348
- electrical conductivity and threshold switching by computer simulation 78—88002
- electrical conductivity at strong elec. fields and high hydrostatic press. *(Czech)* 77—24560

amorphous semiconductors continued
  electrical properties, containing transition metal ions *(Rumanian)* 78—47791
  electrical properties, DC and AC cond., high field effects, magnetoresist., EPR, carrier transport, review *(Japanese)* 77—35943
  electrical switching, aggregated electrons emulsion inversion as possible mechanism 79—38139
  electron-hole recombination, mech. 78—72196
  electronic devices appl. 79—57431
  electronic phenomena, book 80—77551
  electronic properties and localised states, review 77—62871
  electronic properties and structure *(Japanese)* 79—47179
  electronic states, effect of local rearrangement modes 78—47696
  electronic states, theoretical methods 80—80167
  electronic structure, chem. bond approach 79—65374
  elemental, struct. models 79—37628
  elemental, vibr. props., review 77—84873
  enhanced diffusion mechanisms, review 78—67847
  epitaxial polySi and amorphous Si photovoltaic thin film developments 79—74524
  exciton effects on absorpt. spectra for Gaussian random pot. solid 77—16273
  field effect and capacitance-voltage meas. anal., localised density of states 80—103686
  film, density of localised band tail states, transient photoconductivity 77—15898
  film, hologram recording 77—88677
  film, ion bombardment effect on electronic props. 79—65125
  film, laser induced nucleation, long wavelength instability 80—84126
  film formation by vacuum deposition review *(Japanese)* 77—66590
  fluctuations and non-randomness in continuous network models 80—49112
  galvanomagnetic phenomena, model, transport phenomena in presence of medium range disorder *(French)* 78—56162
  gap states, electronic behaviour 78—2452
  glass, Anderson model, thermoelectric power 78—84241
  glasses containing V_2O_5, small polaron cond. *(French)* 77—72867
  glassy semiconductors, neutron irradiated, paramag. centres 79—82872
  glassy-crystalline, with switching channel, electrothermal instability 80—15576
  graphite, layered, electronic band struct., direct evaluation by angle resolved photoemission 77—51652
  group V, defect states 79—87057
  group V, trends in defect controlled electronic props. 80—49658
  Hall effect, review of expt. data 79—51606
  Hall effect, two-carrier one-dimens. transport anal. 80—44614
  Hall effect in disordered systems, conf., Cambridge, England (May, 1978) 79—51604
  Hall effect in noncrystalline systems, theory 79—51610
  Hall mobility by modified relaxation time approx. 80—24950
  heavily doped, impurity bands, review of expt. results 79—95367
  hole structure of computer models 80—49109
  hopping carriers, AC cond. and DC Hall mobility 80—44585
  hopping conduction, freq. depend., two-site model 77—76825
  hopping conductivity, rate eqn. formulations, quantum transport approach 77—15841
  hopping conductivity in ordered and disordered solids, review 77—1420
  hopping mechanism of dispersive transport 80—10971
  hopping transport, microscopic rate equations 80—39580
  hopping transport for random spatial distrib. of localised sites 79—23971
  II-IV p-n amorphous heterojunction, phenomenological model 80—54769
  II-IV-V_2, solid-state inductance, theory and expt. 78—56138
  II-IV-V_2 semiconductors, amorphous, SRO 77—84653
  II-VI amorphous semiconductors, electronic states, sublattice one-band Hamiltonian transform. 80—59861
  III-V, electronic local density of states, cluster Bethe lattice method 77—11868
  III-V, tetrahedrally bonded, electronic density of states and optical spectrum 77—62797
  III-V amorphous semiconductors, electronic states, sublattice one-band Hamiltonian transform. 80—59861
  ill-condensed matter, summer school, Les Houches, France (July-Aug. 1978) 80—82561
  impurity control *(Japanese)* 79—37722
  injected charge drift and localisation in amorphous and organic layers *(German)* 78—91794
  internal friction and relaxation in vitreous solids *(French)* 77—72651
  ion implantation formation of amorphous layer *(Japanese)* 78—22746
  ion transport, field-depend. packet dispersion at low temps. 80—19981
  ionicity and struct., interrelation, appl. to zincblende, rocksalt and wurtzite structs. and amorphous semiconductors 77—1093
  ionised centre diffusion accel. by electrostatic fields 80—70473
  laser crystallisation, for production of large grained sheets for solar cells 80—93570
  lattice dynamics of disordered or unstable lattices 78—75790
  light irradiation, nonequilib. electron distrib. function in forbidden gap *(Russian)* 78—75988
  local order as determined by electronic and vibrational spectroscopy 79—37627
  local rearrangement mode model for pair and single particle localised states 77—76773
  localised gap states, chemical trends 78—39067
  localised gap states, hopping cond. and chem. bonding 78—23052
  localised singly occupied gap states, variable range hopping, susceptibility and EPR 77—72866
  localised states and cond. mechanism *(Japanese)* 80—84467
  lone-pair, effect of electronegativity difference on defect chemistry 78—72063
  lone-pair semiconductor, defects, valence-alternation model and new directions 80—54646
  low-temperature, elementary excitations, struct. 80—49577
  luminescence 80—80862
  luminescence and absorption spectra calcs. 79—99938
  metal-amorphous Si barrier, electronic props. 80—11089
  mobility gap, phononless hopping 77—55527
  mobility gap temp. derivative calc., polar contrib. 78—26861
  model amorphous semiconductor struct., electronic props. 79—65974
  modulated photoconductivity anal. 80—44650
  modulated photocurrent, analysed for trap-limited case *(Japanese)* 80—60030
  monocrystal-amorphous radiation-induced transitions 77—80554

amorphous semiconductors continued
  Mossbauer effect, props. and investigation methods *(French)* 80—80652
  non-polar, mobility gap temp. variation calcs. 78—10339
  noncrystalline, mag. freeze out effect 78—43281
  ohmic contacts to semicond. based on graded amorphous-cryst. junction, model 77—76923
  optical absorption, interband transitions 77—90167
  optical absorption, theory 80—80818
  optical information media role of amorphous materials 77—54764
  optical props. and densities of states *(French)* 77—72809
  optically induced changes, ps. spectroscopy 80—48326
  oxide glasses, elec. cond., polaronic hopping model 79—65479
  oxide semiconducting glass, structural energy characteristics, rotational isomerism, mol. motion *(Russian)* 79—56602
  oxide semiconducting glasses, electronic cond. mechanism 80—65562
  phase-grating formation, phenomenological model 77—10989
  phonon-assisted interband optical absorption 80—34947
  phosphate glasses:Cu^{2+}, EPR, optical spectra 78—72399
  phosphate glasses:V^{4+}, EPR, optical spectra 78—72399
  phosphate-tungstate semicond. glass, W (V) complex, EPR and electronic spectra interpretation 77—69682
  photocurrent spectral distribution 79—56259
  photoelectric properties in ionic contact regime 77—76873
  photoluminescence props., review 79—56862
  photostimulated processes in inorganic materials and optical information storage, review 78—82926
  photovoltaic effects *(Japanese)* 80—54737
  poly-N-vinylcarbazole-polycarbonate mixture, hole drift mobility and photosensitivity 77—85260
  polyacetylene:I, electric props. in semicond. and metallic regions 80—29432
  polyacetylene, doped, p-n junction, elec. props., review *(Japanese)* 80—29410
  polyacetylene and polyacetylene: AsF_5, one-dimens. spin diffusion, NMR T_1 and dynamic nuclear polarisation meas. 80—44946
  polybisaminophosphazenes, elec. cond. 77—32016
  polycarbonate: tri-p-tolylamine, chemical control of conductivity 80—59984
  polycarbonate:tri-p-tolylamine amorphous film, elec. and mag. props 80—49959
  Poole-Frenkel conduction, screening effects 77—43606
  Poole-Frenkel conduction for centres with screened Coulomb pot. 78—19044
  random field acting on charge carriers 80—44580
  random field parameters and pseudopotential calc., amorphous, liquid and glassy semiconductors 80—29316
  RC network model, based on percolation theory 79—4560
  recombination processes, review 79—38088
  review, properties, principles, appls. 77—4287
  review of properties, current and potential applications 78—30539
  review of structural and electronic props. 80—64901
  role in photovoltaic and solar thermal conversion 79—61981
  scattered electrons emission angle and energy distribution 79—91545
  Schottky barrier, capacitance-voltage meas., localised density of states determ. 80—49900
  secondary electron emission, universal yield curve verification 80—45179
  semiconductor, amorphous zone accumulation under ion irrad., composite model 79—51169
  semiconductor epitaxial regrowth, ion implantation induced defects, annealing 80—24479
  semiconductors, compensated and amorphous, hopping cond. and density of localised states 77—89763
  short-range order, theory and probes 80—79698
  a-Si:H_x structure, effect of H-Ar plasma contact on elec. props., and optical gap 80—34533
  solar cell applications 79—48130
  solid-state inductance, theory and expt. 78—56138
  sputtered amorphous film heterostructure solar cell and laser fabrication 78—64472
  stereochemistry, shape of disorder 79—64994
  structural disorder effects, pseudopot. theory *(German)* 78—30581
  structural models 79—37628
  structure of semiconds. in noncryst. states, diffr. investigations review 77—72559
  structure of simple inorganic amorphous solids, review 80—15004
  superconducting properties, laser induced 77—72960
  superconductivity feasibility model *(Russian)* 78—80092
  switching device, transient on characts., filament model 77—15917
  switching initiation, Anderson model 78—10524
  TCNQ salts organic semiconducting polymers, electron transfer mechanisms 79—42544
  tetracene, amorphous film, TSC meas., carrier traps 80—2496
  tetrahedral glasses, disorder 78—51423
  tetrahedrally bonded, As(P) doped, gap density of states 79—19545
  tetrahedrally bonded, effects of quantitative disorder on electronic struct. 79—47003
  tetrahedrally bonded, electronic density of states cluster calc., size effects 77—8002
  tetrahedrally bonded, random stacking model, X-ray scatt. intensity 78—9953
  tetrahedrally bonded solid, theory of fluctuations and localised states 78—10405
  tetrahedrally co-ordinated, random stacking model 77—62479
  tetrahedrally coordinated, pnictide and chalcogenide, defect energies 80—54647
  thermoelectric generators, utilisation of amorphous semiconductors 80—35704
  thermoelectric power and transport models 78—10482
  thermoelectric power transport coeff. calc. by quasiclassical approx. 80—20230
  thermopower, conductivity, statistical shift, doping effects 79—69537
  threshold switching, Mott model 80—29447
  transition metal phosphate glasses, ohmic contact and dielectric. relax. 79—65795
  trap-controlled transient current injection 79—23984
  trapping, photo-stimulated and thermally-stimulated current obs. 77—28192
  Urbach tail, rel. to Mott-Street model 77—47771
  very far IR properties 78—80344
  vibrational properties, effects of topology versus disorder 77—69063

amorphous semiconductors continued
violanthrene-A film, amorphous and crystalline, carrier mobility differences 78−60125
Wannier excitons, single-site theory in disordered semiconductors, general consideration 79−99486
wave packet propagation in random struct. at crit. energy 78−26855
Wiedemann-Franz law in semiconductor and metal glasses 79−65422
a-Si:H, effect of H conc. on photovoltaic props. 79−99577
Ag_2S, nonlinear V-I characts. obs. at low temp. *(Japanese)* 78−34866
Al-amorphous Ge-nSi, photoelectric props. 80−70822
Al-amorphous Se-Al struct., capacitance variation with illumination 79−87165
$Al_{0.23}Te_{0.77}$, amorphous semicond., radial distrib. anal. by X-ray diffr. 78−71678
amorphous, Raman scatt. investig. of irreversible thermostruct. transform. 77−48163
As, AC cond. and photo-induced states 79−87128
As, amorphous, absence of photodarkening 80−103970
As, amorphous, effect of high press. on elec. props. 77−59309
As, amorphous, photoluminescence, bulk and sputtered thin films 80−25457
As, amorphous, short-range order, theory and probes 80−79698
As, amorphous, theoretical calc. of defect states 80−49657
As, defects, band gap states 80−80215
As, electronic and phonon densities of states 77−8001
As, electronic struct. of even-ring network model 79−23884
As film, interference enhanced Raman scatt. 80−50326
As, intermediate range order from polarised features of Raman spectrum 80−49113
As, NQR for tunnelling modes and local struct. order 79−61261
a-As, opt. and elec. props. 77−39894
As, optical, vibr., transport and defect-related props., review 79−51935
As, refr. index meas. near absorpt. edge 78−2819
As, vibr. excitations at defect sites, IR and Raman spectra calc. 80−49329
As, vibrational excitations of defect sites 80−49332
As:Ni(Ge)(S)(Se)(Te) film, amorphous, chemical modification of props. 80−49250
As-S, film, photoinduced RI changes, heterodyne interferometry 77−3639
As-Se-Ge, amorphous film, relief-type hologram mode, hologram replication *(Japanese)* 78−78959
As-Se(Te)-Ge, fabrication of amorphous semicond. thin films with graded band struct. *(Japanese)* 77−55623
AsGe amorphous film, far IR absorpt. spectra, refractive index 80−80785
$As_4Ge_{15}Te_{81}$, crystal-glass transition influence on local struct. 77−36163
As_2O_3 crystalline and amorphous, EXAFS study of struct. 80−19776
As_2S_3, amorphous, struct. determ. by electron diffr. 77−11485
As_2S_3, amorphous film, light enhanced vaporisation, photolithographic process, photographic appls. 77−5949
As_2S_3, crystalline and amorphous, surface charging effects on valence band spectra in XPS 77−8725
As_2S_3, elec. cond. mech. obs., in bulk material and evaporated thin films *(Japanese)* 80−11028
As_2S_3 film, evaporated, switching effects 80−96952
As_2S_3, kinetics of photoconductivity, near fundamental absorption edge *(Russian)* 79−56263
As_2S_3 layered crystal and amorphous analogues, XPS valence band spectra, electronic struct. 77−52218
As_2S_3, photoacoustic spectroscopy, app. of expt. system for powdered samples 77−87846
As_2S_3, photodissolution of Ag, elec. resist. meas. 77−62786
As_2S_3, XPS, electronic struct. calcs. using scattered wave method 79−11502
As_2S_3-Ag interface, photodissolution kinetics of Ag in amorphous films 77−15955
AsS(Se)I and $As_4Te_5I_2$, crystal-glass transition influence on local struct. 77−36163
$As_2S_3(Se_3)(Te_3)$ and $As_2Se_3.As_2Te_3$, crystal-glass transition influence on local struct. 77−36163
As_2Se_3, struct. determ. in amorphous and liq. state using EXAFS meas. 77−89366
As_2Se_3, vitreous, short-range structure obs. in high momentum transfer region 77−4045
As_2Se_3:Ag, doping effect of gap states and elec. cond., dielec. relax. and DC cond. meas. 79−47098
As_2Se_3:Cu, diffusion, electrodiffusion profile determ., migrating impurities charge determ. 78−6185
As_2Se_3-Au sandwich cell, origin of dark currents 77−76920
As_7Se_3 amorphous films, thermal relax. processes determ. by optical props. 77−15716
As_2Te_3, amorphous struct. determ. by electron diffr. 77−11485
As_2Te_3-GaAs, amorphous-monocrystalline heterojunctions, space charge limited conduction 78−64099
$As_{50}Te_{50}$, amorphous semicond., elec. props. after heavy-ion irrad. *(French)* 77−72639
$As_{10}Te_{75}Ge_{15}$, dielec. props. 77−63355
$As_{0.3}Te_{0.48}Ge_{0.1}Si_{0.12}$, amorphous film, transient switching processes 78−84232
B amorphous film, elec. cond. in strong elec. field 77−11928
B film, interference enhanced Raman scatt. 80−50326
B prep. methods, review, book contrib. 78−48358
B:H CVD films, IR, visible, and near UV optical props. 80−50442
BaO-Al_2O_3-B_2O_3-V_2O_5 glass, spectra, oxidation-reduction behaviour, DC cond. 77−76814
BaO-CaO film, Cu-electrodes, electrical props. 77−35997
BaO-V_2O_5-CuO semiconducting glasses, impurity effects, elec. resist. and EPR study 80−103692
C, film, amorphous, two-dimensional variable range hopping cond. 80−10977
C film, elec., struct. and optical props. 77−20474
C film, elec. transport props. and atomic comp. 78−6457
C film, hopping cond., thickness depend. 77−89887
C film, struct. and semicond. props. and heterojunction form. with single cryst. Si 80−25002
C, glassy, prep. and DC cond. at low temps. 79−95404
C, prepared by glow discharge method, elec. and optical props. 77−21036
C:H films, amorphous, elec. props., chem. modifications 80−84523
CC NiO, amorphous, charge transport in band tails 78−76026

amorphous semiconductors continued
CaO-B_2O_3-Fe_2O_3 glass, electronic and dielec. props. meas. 77−24574
CaO-B_2O_3-Fe_2O_3 glasses, effect of heat treatment on electronic props. 78−2480
a-CdAs thin film fabrication for switching applications 78−2415
$CdAs_2$ based glasses, AC cond. 78−39109
$CdAs_2$ based glasses, cond. and permittivity, freq. depend. 77−76859
$CdAs_2$, elec. cond. and thermopower 80−49722
$CdAs_2$ glasses, covalently bonded, energy gap correl. with average atomisation enthalpy 77−76740
Cd_3As, film, amorphous, crystallisation effects 77−35482
Cd_3As_2, amorphous to crystalline transform. 79−77519
Cd_3As_2, film, transmission spectra. 0.6-15 μm, and band struct. 78−11013
Cd_3As_2 film on NaCl substrate, vacuum deposition, growth morphology, microstructure 80−75479
Cd_3As_2 films, elec. resist., Hall mobility, temp. depend., cond. mechanism 77−76982
$CdB^4C^5_2$, chalcopyrite struct., surface energy and compressibility, rel. to glass form. 79−51417
$CdGa_2Te_4$ film, effect of thermal annealing on struct., optical absorpt. and photocond. 79−65342
$CdGeAs_2$, glassy, structural model 77−35490
$CdGeAs_2$, short-range order, Mossbauer expts. 78−22648
$Cd_{23}Ge_{12}As_{65}$, amorphous, threshold switching, expt. 80−49830
$Cd_6Ge_3As_{11}$, band gap, DC cond., elastic consts., and glass transition temp., pressure depend. 78−72064
$(CdGeAs_2)_{1-x}D_x$ amorphous films, property control in common target sputtering, elec. cond. 80−7494
$CdGe_{1-x}M_xAs_2$ (M=Si,Sn,Pb), (x=0.0,0.1,0.2), amorphous struct. 78−22651
$CdGeP_2$, electronic struct. at cryst./vitreous transition, X-ray K-absorpt. and emission 78−15248
$CdGe_{1-x}Sb_xAs_2$ glass, DTA, microhardness meas. *(French)* 77−72564
$CdGe_{1-x}Sb_xAs_2$ system, amorphous and cryst. phases, DTA and microhardness obs. 78−22835
$CdGe_{1-x}Sm_xAs_2$, radial distrib. anal. and mag. susceptibility meas. 77−43152
a-CdS film, DC cond. Seebeck data 77−24626
CdS film, growth by chem. bath deposition, photocond. props. 77−59703
CdS(Se)(Te), determ. of wurtzite, zincblende and rocksalt phases 80−100219
CdSe-Sb_2Se_3 heterojunction, photoelec. props. 80−70816
$CdSiAs_2$ chalcopyrite photovoltaic material 79−74526
$CdSn(Ge)As_2$, amorphous, SRO 77−84653
CdTe, amorphous, photocond., effective density of localised states 77−28210
$Cd_{1-x}Zn_xS$, film, technical data, for low cost solar cell 79−48127
Cu-CdP_2-Cu diode structure, switching effect obs. 77−4452
$CuInSe_2$ amorphous thin film, flash evaporation, struct., stoichiometry 80−89150
$CuInTe_2$, vac. deposited film, growth, struct. and elec. characts. 77−69995
Cu_2O, switching channel electron probe microanalysis, switching cycle number (life) 77−32056
Cu_2O, thermal breakdown mechanism of switching process, expt. obs. *(German)* 77−28225
EuS, on W, memory effect in field emission 80−89126
FeO-P_2O_5 glasses, electrical and mechanical losses 78−80283
FeO_x-P_2O_5 glass, dielec. props., thermally stimulated depolarisation meas. 79−95704
Fe_2O_3-B_2O_3-PbO glass, semicond., elec. resist. meas. 78−95300
FeO.Fe_2O_3.MgO.P_2O_5 glass, conversion electron Mossbauer anal. of surfac struct. and chem. state 77−63333
$Fe_{80}P_{13}C_7$, amorphous and crystalline, electrochemical and semicond. behaviour *(Russian)* 80−101021
α-GaAs, amorphous, mobility gap temp. derivative calc., polar contrib. 78−26861
GaAs amorphous film, effective medium theory and freq. depend of conductivity 79−24090
GaAs amorphous film/cryst. junctions, optical and elec. props. 79−99611
GaAs, amorphous layer formation, ion implantation, IR spectra 78−95063
GaAs, amorphous layers, ion-implanted, low-temp. epitaxial regrowth 80−92790
GaAs, amorphous state, thermal stability, elec. cond. obs. 80−33888
GaAs, epitaxial film, amorphous and polycrystalline, vol. plasmon energy and linewidth, electron scatt. obs. 80−50482
GaAs, film, composition, study by nondispersive X-ray anal. *(French)* 79−8457
GaAs, optical absorpt. edge shape, band edge fluctuations 77−20880
GaAs, sputtered films, hydrogenated, photoinduced optical absorpt. 80−50362
GaAs:Te, amorphous, ion implanted layers, optical refl., 1.5-7.0 eV 79−8152
GaAs:Te, ion implanted optical transitions in modulated reflectivity spectrum 79−73972
$GaAs_{1-x}H_x$, amorphous, vib. props., Raman and IR meas. 80−50322
GaP, effects of hydrogen incorporation during deposition by sputtering 79−69981
GaP, optical absorpt. edge shape, band edge fluctuations 77−20880
GaP/GaAs and GaP:H/GaAs amorphous film/cryst. junctions, optical and elec. props. 79−99611
GaSb amorphous film, elec. props. *(French)* 78−14843
GaSb, optical absorpt. edge shape, band edge fluctuations 77−20880
GaSe-InSe, heterostructure, optical crystallisation of amorphous films 79−73580
Ga_2Se_{1-x}-SnO_2 heterostruct., amorphous, photovoltaic effect 78−14803
$Ga_{0.25}Te_{0.75}$, film, off-state recovery after nonosecond switching 80−44681
$Ga_{1-x}Te_x$ amorphous films, elec. cond., optical absorpt. and transparency, band gap energy 79−56335
Ge, 1 MeV electron irrad. influence on kinetics of crystallisation 77−89476
Ge alloys, amorphous film, crystn. transform. kinetics 78−22653
Ge, amorphons, appl. of theory of AC and DC hopping cond. 80−54698
Ge, amorphous, -metal junction, current-voltage charact., contact material effect 80−44725
Ge, amorphous, anomalous magnetoresistance 80−687
Ge, amorphous, EPR expts. 78−88167

amorphous semiconductors continued
Ge, amorphous, ESR and DC cond. 77—48032
Ge, amorphous, far IR absorption 78—88306
Ge, amorphous, growth rate of crystallisation, Raman spectroscopy study 80—44227
Ge, amorphous, ionisation enhanced crystallisation, elec. cond. meas. 77—35481
Ge, amorphous, molecular liquid model and electronic structure 80—54133
Ge, amorphous, possible ABB-type excitonic superconductor *(Chinese)* 80—7029
Ge, amorphous, pure and H doped, voids, atom probe FIM 80—49107
Ge, amorphous, scatt. of 2 MeV He$^+$ 77—69954
Ge, amorphous, struct., dislocation model 78—42911
Ge, amorphous, thermoelec. power in phonon-assisted hopping regime, Coulomb effects 78—76097
Ge, amorphous, tunnelling states simulation and sp. ht. 79—37791
Ge, amorphous and crystalline, hopping conduction, semiclassical theory 79—91052
Ge, amorphous and crystn. films, contamination behaviour, XPS examin. 79—1815
Ge, amorphous and polycryst. layers, sputtered, elec. cond. and thermoelec. power 78—2586
Ge amorphous evaporated film, to metal contact resist. diffusion and microstruct. 77—89880
Ge amorphous film, AC conductivity, anomalous freq. depend. 77—4456
Ge, amorphous film, annealing, effect on localised states 79—4535
Ge amorphous film, bright-field hollow cone images 80—75136
Ge amorphous film, crystn. front velocity during scanned laser crystn. 80—107662
Ge, amorphous film, DC sputter deposited, effect of trapped Ar on minimum temp. for impulse stimulated explosive crystallisation 80—100422
Ge amorphous film, disorder induced phonon absorpt. meas. using double beam Fourier spectrometer 80—105725
Ge amorphous film, effective medium theory and freq. depend of conductivity 79—24090
Ge amorphous film, effects of ion implantation on structure 78—55881
Ge amorphous film, high freq. phonon scatt. 80—49328
Ge, amorphous film, ion-implanted, regrowth 79—15043
Ge, amorphous film, large aligned grain solid-phase growth during scanned laser crystallisation 80—49100
Ge amorphous film, O depth profiling by SIMS 80—39480
Ge, amorphous film, optical consts. in near IR range *(Korean)* 79—8137
Ge, amorphous film, persistent photoconductivity, dangling bonds 80—84487
Ge, amorphous film, post nucleation growth, computer simulation 78—34729
Ge, amorphous film, temp. thermal conductivity 78—22994
Ge amorphous films, structural relaxation and crystallisation 80—100170
Ge, amorphous layer, comparison of laser and electron beam pulsed annealing 79—69374
Ge, amorphous layer, on single cryst. Si, heteroepitaxy by laser annealing 79—77952
Ge, amorphous layer on Ge bulk, photoemission during X-ray Bragg diffr. 78—47209
Ge, amorphous overlayer on ultrathin Pt film, effect on cond. 78—72284
Ge amorphous solid dielectric loss meas. by submillimetric waveguide laser 79—33603
Ge amorphous thin films prepared by vac. evaporation, density meas. 77—80714
Ge, amorphous whisker growth 78—2400
Ge, amorphous/cryst. interface, supercond. mechanism 80—44783
Ge, annealing effect on absorpt. edge *(Korean)* 79—15142
Ge, anomalous magnetoresist., hopping model 78—23117
Ge black, selective absorber characterisation 80—80112
Ge, crystallisation study 80—33889
Ge, DC hopping, analytical formulae, degenerate hopping in wide bands 77—89761
Ge, defects, band gap states 80—80215
Ge, dislocation model 80—1929
Ge, dislocation model 80—1930
Ge, doping, Schottky barrier and p-n junction form. by RF sputtering 77—8187
Ge, elastic moduli, random network model, calc. 78—6119
a-Ge, elastoresistive effects 79—60838
Ge, elec. and opt. props., review 78—23094
Ge, electrodeposited, X-ray, electrochem., and electrorefl. characterisation 78—14624
Ge, electron energy loss spectra, appl. of cylindrical electrostatic analyser *(French)* 77—55856
Ge, electron scattering, inelastic, 70-1400 eV, mean free path 78—84696
Ge, electronic density of states, mol. liq. model 80—49581
Ge, epitaxial and amorphous film growth, low energy ion beam deposition 77—28729
Ge film, ^{74}Ge ion implanted, defect struct. obs. 78—51848
Ge, film, amorphous, contamination anal. by AES 77—36828
Ge film, amorphous, LF vel. of sound for Young's modulus mode 77—35636
Ge film, amorphous, O implantation effects on absorpt. edge and elec. cond. 77—39970
Ge film, amorphous, thermally induced reversible switching, effect of change in thermal resist. 77—20371
Ge film, amorphous, two-dimensional variable range hopping cond. 80—10977
Ge film, amorphous, vac. deposited, XPS and elec. props., evidence for polycryst. phase 77—28691
Ge film, amorphous and crystalline, optical props. 77—16412
Ge film, amorphous to crystalline transform. 77—20206
Ge film, complex refractive index and reflectance 77—52121
Ge film, crystn. kinetics, elec. cond. obs. 77—62767
Ge film, elec. cond. obs. of crystn., expt. verification of model 77—20475
Ge, film, electronic struct. charge on ordering, double beam photoemission 78—19634
Ge film, evap., structural aspects in electronic transport data interpret. 77—76977
Ge film, evaporated, non-destructive density meas. 80—6680
Ge film, evaporated amorphous, angle of deposition effects, electron microscopy 77—43451
Ge film, high resolution electron microscopy, digital processing use 78—37116

amorphous semiconductors continued
Ge film, hopping cond., thickness depend. 77—89887
Ge, film, in situ meas. of thermal EMP, by ultrahigh vacuum electron microscopy 79—26184
Ge film, influence of deposition parameters on e.p.r. 77—1586
Ge, film, laser pulse annealing 80—15006
Ge film, prep. conditions influence on supernetwork struct. 77—76709
Ge film, thermoelec. power and structural investigs. using in-situ electron microscopy 77—76983
Ge film, vac. evaporated, density meas., microcrystalline model of struct. 80—2313
Ge, first order transition to metallic liquid, calc. of transition temp., enthalpy and entropy 79—69227
a-Ge, Ge-O removal in pre-crystallisation annealing 78—9957
Ge, high-press. expts., quenchable products. 77—19874
Ge, hydrogenated amorphous and cryst., IR spectra 79—61359
Ge, IR absorpt., first-order effective charges due to at. displacements 77—48164
Ge, ideal network struct., electronic struct., tight-binding model 80—44485
Ge, ideal surface, definition and characts. 80—107623
Ge, interface structural model between amorphous and crystalline phase 78—63941
Ge, ion-implanted amorphous, epitaxial regrowth on Ge 77—35835
Ge, ion-implanted amorphous layers, melting model for pulsing-laser annealing 79—56080
Ge, laser recording of implanted amorphous layer 79—19270
Ge, localised states, Cayley trees appl. 79—65373
Ge, nearest-neighbour atom mean-square relative displacements, EXAFS spectra 79—91532
Ge, nucleation, growth and transform. of amorphous and crystalline solids condensing from gas phase 80—24745
Ge, O$_2^+$ ion implanted, influence on electrical and optical props. 77—89891
Ge, optical absorpt. edge shape, band edge fluctuations 77—20880
Ge, optical and microwave props. of microscopically inhomogeneous materials 77—77161
Ge, pure and hydrogenated, Raman spectra 79—61358
Ge, sputtered films, hydrogenated, photoinduced optical absorpt. 80—50362
Ge, sputtered hydrogenated amorphous, steady-state and transient photocond. meas. 78—10506
Ge, struct. and growth kinetics, topological principles 80—49123
Ge, substitutional doping, electronic props. 77—1418
Ge, thin film, fast crystn. and void precipitation in laser pulse annealing, TEM exam. 79—56086
Ge thin films, crack networks of voids 78—2399
Ge, two-band model, Thorpe-Weaire type, localisation near band edges 78—23050
Ge, vibrational spectra, struct. model calcs. 78—22806
Ge:Al(Sb) film, amorphous, ion implantation, effect on cond. 78—83839
n-Ge:As closely compensated, photolum. of charge carriers localised in trails of density of states 77—77294
Ge:Fe, amorphous film or ion-implanted, comparison of ^{57}Fe Mossbauer data 77—40159
Ge:Fe, implanted, Mossbauer spectra, conversion electron, temp. dependence 80—40025
Ge:H, H content determ. by IR absorpt., gas evolution and nuclear reaction methods 80—44130
Ge:H films, photoemission spectra 80—50517
Ge:inert gas, ion implantation, UV photoemission exam. 78—80457
Ge:Mn, amorphous, cond. increase by Mn doping 78—72155
Ge:Mn, amorphous, EPR meas. 77—85559
Ge:O, Cu, amorphous thin film, impurity effects on struct. 80—107054
Ge:P, amorphous, electronic transport and photocond. 79—60834
Ge:Sb(Ga), amorphous, doping effects on Fermi level, electrical meas. 79—42546
Ge:Sb(In), film, electronic props. 78—84330
Ge:transition metal, amorphous, impurity effects on hopping conductivity 79—65485
Ge-Al (Sb) film junction, I-V and C-V characts. 77—85307
Ge-Fe system, amorphous films, mag. and elec. props. 79—51695
Ge-Ga amorphous alloy, co-evaporated elec. and optical props. 80—70860
Ge-Mo amorphous semicond.-granular metal film system, elec. transport and thermopower 77—76984
Ge-Pb$_{1-x}$Sn$_x$Te, amorphous/crystalline heterojunction, rectification props., IR detector appl. *(Japanese)* 78—60197
Ge-S film, amorphous, photo-induced ESR and optical absorption edge shift 78—88374
Ge-Se-Fe films, metallic and semicond., amorphous, mag. and elec. props. 78—52319
Ge-Si, amorphous, freshly-evap. and ion-bombarded, struct. differences 79—55666
Ge-Si amorphous film, ferromagnetic interaction between spins 78—2710
a-Ge-Si crystal interface, low resist. elec. behaviour 77—89843
Ge-SiO$_2$-p$^+$Si tunnel junctions, for determ. of AC cond. of amorphous Ge 77—24608
Ge$_{1-x}$H$_x$, amorphous, atomic struct., X-ray study 80—49106
GeO amorphous film, hologram recording, photochem. props. 79—64186
GeO amorphous semicond. films, photostructural changes by photomodulation ellipsometry 79—71510
GeO$_2$-SiO$_2$, pyrolytic film prep. 77—81223
GeP, thin films, vacuum-deposited, struct. characterisation 77—47691
GeS$_x$, neutron irrad., thermal and elec. conductivity and heat capacity 78—2165
Ge$_2$S$_3$, photoenhanced diffusion of Ag 79—65257
GeSe, amorphous film, photocond. meas. 77—43647
GeSe amorphouse sputtered film, DC and AC behaviour, effect of contact material 79—95513
GeSe$_2$ amorphous film, laser induced oscillatory phenomena 80—84711
GeSe$_2$, exciton absorpt., transmission spectra of cryst., glasses and amorphous samples 79—15485
Ge$_{0.5}$Sn$_{0.5}$Te film, elec. and optical props. 77—12028
GeTe, amorphous film, annealing effects on resistivity, comparison with SnTe 77—66212
GeTe amorphous films, annealing effect on optical props. 77—72931
GeTe film, amorphous and crystalline, electron diffr. meas. 77—39748
Ge$_{15}$Te$_{85}$, crystal-glass transition influence on local struct. 77—36163
Ge$_x$Te$_{1-x}$ amorphous matrix with Te crystallites, effect of annealing 77—24274

amorphous semiconductors continued
$Ge_{15}Te_{81}X_4$ amorphous semicond. switches, fabrication technology *(German)* 80-7493
H_xWO_y film, effect of struct. on optical and electrical props. 78-84671
(In, Ga)Sb, sputter deposited amorphous film, impulse stimulated explosive crystallisation 78-84098
InAs amorphous film, DC sputtered, optical absorpt. 78-19589
InSb amorphous film, AC conductivity, anomalous freq. depend. 77-4456
InSb amorphous film, effective medium theory and freq. depend of conductivity 79-24090
InSb, epitaxial film, amorphous and polycrystalline, vol. plasmon energy and linewidth, electron scatt. obs. 80-50482
InSb, optical absorpt. edge shape, band edge fluctuations 77-20880
InSb, pressure induced struct. transform., X-ray diffr. obs. 77-11690
InSb, sputtered NaCl-type compression 79-46751
InSe film, structure, influence of laser beam 79-7761
In_xSe_{1-x}, amorphous film, in metal-In_xSe_{1-x}-SnO_2 system, photovoltages 77-28215
In_xSe_{1-x}-SnO_2 amorphous film-SnO_2 system, photovoltic spectra, annealing effect *(Japanese)* 80-92926
$In_{0.25}Te_{0.75}$, film, off-state recovery after nonosecond switching 80-44681
$In_{1-x}Te_x$ amorphous films, elec. cond., optical absorpt. and transparency, band gap energy 79-56335
MoO_3-P_2O_5 glass, thermoelec. power meas. 78-84242
Na_2O-B_2O_3-SiO_2-$As_2O_3(As_2O_5)$ glasses, DC and AC resist., bipolaronic hopping cond. 80-88558
Na_2O-K_2O-Al_2O_3-SiO_2 glasses, effect of Al_2O_3 on elec. cond. 77-8104
Nb_2O_5 amorphous films, switching phenomena and dielec. breakdown 77-24594
NiO electrode for photolysis 80-40696
P, amorphous, red, far IR absorpt. spectra 80-34923
P, red, photolum. props. and band gap 80-50403
P, red, Raman scattering 80-11416
P, vibrational excitations of defect sites 80-49332
P_2O_5-FeO glass, electrical cond., nonadiabatic hopping of small polaron 77-1417
PbO-SiO_2-Fe_2O_3(0,2,10 wt.%), conduction process 77-8096
$Pb_{1-x}Sn_xTe$-PbTe, amorphous/crystalline heterojunction, rectification props., IR detector appl. *(Japanese)* 78-60197
Pd-amorphous Si thin film interaction, metal rich Pd-silicide formation 80-2284
S-based amorphous semicond. film, prep. by plasma decomp. of H_2S-N_2-NH_3, and characterisation 80-80422
SSe_x (x=10, 15, 40), amorphous crystal transition, appl. of Kolmogorov-Avrami equation 78-67649
Sb electrodeposit, explosive crystn., semicond-semimetal transition and IR absorpt. 78-51849
Sb, vibrational excitations of defect sites 80-49332
Sb_2S_3:Ag, sensitised photolysis and structure of latent photographic image 78-89574
SbSBr glass, IR reflectivity spectra 80-71403
SbSI, cryst. and vitreous, nonlinear light absorpt., effect of temp. and phase transitions 77-75604
$(Sb_2S_3)_{0.95}(Na_2S)_{0.05}$, condensate, local states and switching effect 80-20336
Se, 2p photoabsorpt. spectra 78-23551
Se, acoustic props. near first-order phase transition 77-20014
Se, acousto-optic props., 10.6 μm 77-43966
Se, amorphous, AC cond. magnitude and variation *(French)* 79-47095
Se, amorphous, bulk, Raman scatt. near Tg 80-60596
Se, amorphous, bulk, reson. Raman scatt. 80-60597
Se, amorphous, diffusion and electrodiffusion of Ag and its role in switching effect 78-19163
Se, amorphous, effect of doping on mol. struct. and valence alternation states 80-49249
Se, amorphous, electronic struct. and optical props., pseudopot. calc. 80-65428
Se, amorphous, friction and wear under lightly loaded contact 78-64740
Se, amorphous, kinematic transform. study by DTA 79-27921
Se, amorphous, O impurity addition rel. to elec. cond. 79-38067
Se, amorphous, sound propag. at low temps. 77-72657
Se, amorphous, struct. relax. effects, obs. by mech. props. *(French)* 79-51201
Se, amorphous, theoretical calc. of defect states 80-49657
Se, amorphous, theory of anomalous dispersion of photocurrent transients 78-6412
Se, amorphous, trap-limited model for dispersive transport of holes 78-6378
Se, amorphous, trigonal and α-monoclinic, positron annihilation 79-11484
Se, amorphous, US attenuation at low temp., internal friction peak 80-65152
Se, amorphous, US wave attenuation and vel., near glass transition 77-89501
Se, amorphous electrophotographic layers, resolution parameters 80-31926
Se, amorphous film, AC conductivity at radio and microwave frequencies 79-11248
Se, amorphous film, dark and photoconductivities 79-87173
Se, amorphous film, dielec. activity obs. near glass transition temp. 80-75933
Se, amorphous film, highly disordered, UPS study 80-76148
Se, amorphous film, inverse/combined photoadsorption and photodeposition, light-temp. interference 79-46977
Se amorphous film, stabilisation by thermal treatment *(French)* 79-47176
Se, amorphous films, evaporated, ageing and crystn., DTA 80-65413
Se amorphous layer structure, influence of vacuum deposition conditions *(German)* 78-63957
Se amorphous thin film photodeposition from hydrosols 78-11109
Se, appl. to xerography 80-57415
Se, carrier lifetime and drift mobilities 78-87985
Se, conducting channel temp., time depend., under monostable switching conditions 78-19109
Se, correl. between mol. struct. and props. 77-11484
Se, crystallisation kinetics correlation with molecular structure 78-94998
Se, crystn., elec. field effect 77-15318
Se, density of surface states 77-76897

amorphous semiconductors continued
Se, dipolar activity at glass transition temp., AC method 77-66454
Se, elastic props. at high press. 79-37753
Se, electrical transport, activation energy 79-95406
Se, electronic props. rel. to xerography, defects 79-97454
Se, evap. layers, electrophotographic props. depend. on thermal treatment of initial material 77-76978
Se, evaporated films, structural relax., viscosity, creep, heat capacitors, and IR spectra meas. 79-42424
Se, evaporated layers, struct. inhomogeneities due to prep. technology fluctuations 77-76710
Se, far IR investigation of structure, ring and polymeric chain components *(Japanese)* 77-76311
Se film, amorphous, crystallisation induced by corotron charging 77-35832
Se film, amorphous, empirical formula for temp. depend. of dielec. loss peaks 80-97197
Se film, block formation during crystn., electron microscope obs. 79-11030
Se film, controlled vapour deposition, crystn., and optical props. 78-39696
Se, film, crystn., thermal and photo-effects 77-47692
Se film, density of localised states 78-34742
Se, film, effect of thermal history and substrates or crystn. by vac. condensation 77-15713
Se, film, influence of wavelength on optical quenching of photoconductivity 80-60046
Se film, interference enhanced Raman scatt. 80-50326
Se, film, photodeposition by Selor process struct. 78-75962
Se, film, photodeposition by Selor process, kinetics 78-75963
Se, film, photodeposition by Selor process, struct. and kinetics 78-75964
Se film, spherulite formation and role of stresses due to volume changes in crystallisation 77-1083
Se film, struct. and crystn., far IR transmission spectrum on DSC obs. 77-85106
Se film, substrate effects on crystn. kinetics 77-1337
Se film, thermo-crystn. obs. 77-11810
Se film, threshold and memory switching 79-82651
Se film, vac. evaporated, density meas., microcrystalline model of struct. 80-2313
Se, film-metal system, contact pot. distrib. and photo-EMF, work function 77-76925
Se, Fourier-transformed Compton profile as microstruct. probe 77-59636
Se, glass transition temp., enthalpy rel. to annealing, DSC 77-15561
Se, glassy, pure and K-doped, photolum. and optically induced ESR 80-50398
Se, Hg activated amorphous film, anomalous photocond. 77-43658
Se, influence of O_2 on phase separation 77-47354
Se, layer, localised states in band gap 80-59928
Se layer crystallinity meas., combination microwave resonator method *(Russian)* 78-22652
Se layers, amorphous, steady-state photocond. meas. 77-35961
Se layers, dielectric relax. in glass transition range, ageing 79-82923
Se layers, substrate range depend. on dielec. relax. in glass transition temp. 79-69773
Se, liq. and amorphous, struct. by pulsed neutron diffr. using an electron LINAC 77-51307
Se, localised electronic states, photoluminesc. and ESR studies 80-65501
Se, luminescence 80-80862
Se, memory and threshold switching effects 78-14774
Se, modulated photocurrent, analysed for trap-limited case *(Japanese)* 80-60030
Se, mol. structure, local atomic arrangement at intrinsic bonding defects 80-59374
Se, monostable switching, current noise 80-44682
Se, photoconductivity quantum yield, experimental validation of fund. theory 80-6909
Se, photoinjection of holes onto triphenylamine doped bisphenol-A-polycarbonate polymer 78-72191
Se, press. depend. of AC cond. 77-76858
Se, Raman scatt. meas., comparison with liq. spectra 80-50328
Se, Raman spectra, crystn. processes 80-60608
Se, red amorphous film, textural change, thermal and photo effects 78-63951
Se, relax of sound velocity, struct. determ. 78-38786
Se, Se:Te, negative magnetoresist., doping depend. 78-56161
Se, struct., DSC and X-ray diffr. expts. 78-22662
Se, struct. and elec. cond. transitions under high press. 79-42237
Se, TSC, dielec. relax. modes 77-90090
Se, thermal quenching of photocond. 78-23137
Se, trigonal, vitreous and red amorphous, phonon density of states comparison 80-54329
Se, trigonal and amorphous, Compton profiles 77-32464
Se, trigonal and amorphous, electronic struct. and nonempirical calc. of struct. props. 80-59866
Se, trigonal and amorphous, positron lifetimes, positronium form. 80-60711
Se, trigonal or amorphous, thermal expansion and Gruneisen coeffs., 10-300K 78-22870
Se, US relaxation and retardation of deform. near T_g point 80-84256
Se, vac. deposited on polymeric substrates, with dynamic coating device 80-100792
Se, viscosity meas. using holographic technique 79-37263
Se, vitreous, crystn., optical microscope obs. 77-84659
Se, vitreous, mech. props. at temps. <300K, uniaxial compression tests *(French)* 78-55908
Se, vitreous, time dependent thermal expansion 78-14485
Se, X-ray K-shell absorpt. discontinuity 79-61467
Se:As, amorphous, pure and doped, photoelectronic preps. in glass transition region 79-4583
Se:As, amorphous film, dielec. activity obs. near glass transition temp. 80-75933
Se:As X-ray plates, electronic transport *(German)* 80-80290
Se:Ge(Si)(Sn), vitreous, crystn. kinetics study by elec. cond. meas. 79-65526
Se:Hg amorphous film, photocond. anomaly due to HgSe layer form. 77-66183
Se:Hg film, anomalous photocond. and residual interelectrode photo-EMF 77-69376

amorphous semiconductors continued
- Se:I, vitreous, crystn, kinetics determ. *(German)* 80—79936
- Se:O, photocond. spectrum, impurity effect 77—76862
- Se:O(Cl)(K) amorphous, elec. cond. increase on impurity addition 77—11920
- Se:P, vitreous, crystn. kinetics study by elec. cond. meas. 79—64998
- Se:Te(Ag), amorphous film, elec. cond., 300 to 350K, transition 77—4454
- Se:U, cryst. and amorphous, impurity conc. and distrib., solid state nuclear track detection 79—46694
- Se-As, dipolar activity at glass transition temp., AC method 77—66454
- Se-As 36.4 at % amorphous alloy, heat treatment effect on acoustic props. 79—86843
- Se-As alloys, appl. to xerography 80—57415
- Se-poly-N-vinyl carbazole, photoinsulator-air gap-dielectric system, charges on surface 79—67407
- Se-polystyrene hexylmethacrylate, interface photocurrent studies, charge transfer mechanism 79—99627
- $Se_{1-x}Ge_x$, amorphous, IR absorption spectra *(French)* 77—73146
- $Se_{1-x}Ge_x$ amorphous film, photocontraction effect 79—46975
- $Se_{1-x1}Te_{x1}$-$Se_{1-x2}Te_{x2}$ heterostructure, amorphous, rectification phenomena and photovoltaic effects 79—99610
- Si, absorber, high efficiency, for solar energy utilisation 77—39907
- Si, amorphisation by bombardment with O ions 78—10098
- Si, amorphisation by ion implantation energy depend. 77—7769
- Si, amorphisation by ion implantation, homogeneous or heterogeneous nucleation 77—11578
- Si amorphisation dependence on low-energy irrad. conditions 79—60408
- Si, amorphisation due to irradiation with heavy ions 77—11606
- Si, amorphised by ion implantation, EPR obs. of mag. ordering 79—24186
- Si, amorphised by ion implant., localised states and cond., irrad. and heat treatment, doping 80—39529
- Si, amorphous, anomalous magnetoresistance 80—6877
- Si, amorphous, as photo-receptor for electrophotography 80—47126
- Si, amorphous, chemical effects on freq. of Si-H vibrations 79—51227
- Si, amorphous, clean and O_2 adsorbed, light sensitive electron laser meas. 79—24396
- Si, amorphous, dissolution with Al 78—95188
- Si, amorphous, doped, drift and Hall mobility, photocond. 79—65477
- Si, amorphous, doped, electronic props. 80—80283
- Si, amorphous, doped, photoconductivity and recomb. meas. 77—89800
- Si, amorphous, EPR expts. 78—88167
- Si, amorphous, ESR and DC cond. 77—48032
- Si, amorphous, electron and hole drift mobility meas. 78—19027
- Si, amorphous, epitaxial regrowth by pulsed laser beam 78—91554
- Si, amorphous, film, hydrogenation by H diffusion, effect on elec. cond., band gap *(Korean)* 80—45326
- Si, amorphous, glow discharge produced, defect creation, high optical excitation 80—97327
- Si, amorphous, hopping conduction, semiclassical theory 79—91052
- Si, amorphous, hydrogenated, spin depend. photoluminesc. 78—72589
- Si, amorphous, hydrogenated, diffusion of D_2, SIMS anal. 78—75877
- Si, amorphous, hydrogenated, pure and B doped, annealing effect on cond. and band gap states *(Korean)* 79—15142
- Si, amorphous, hydrogenated film, struct. determ. using electron microscopy 80—10806
- Si, amorphous, hydrogenated, small angle X-ray scatt., void distrib. 80—15087
- Si, amorphous, hydrogenated, soft H plasma effect, IR absorpt. *(French)* 80—45054
- Si, amorphous, hydrogenated, electronic struct., SCF Xα calc. 80—49580
- Si, amorphous, hydrogenated, electronic density of states determ. from Schottky diode meas. 80—49907
- Si, amorphous, hydrogenated, stacked solar cells 80—55842
- Si, amorphous, hydrogenated, electron drift mobility meas. 80—75565
- Si, amorphous, hydrogenated film, electroreflectance study 80—88967
- Si, amorphous, hydrogenated and deuterated, struct. 80—103245
- Si, amorphous, hydrogenation using DC and HF plasma treatment 80—59497
- Si, amorphous, implanted, recrystn. induced by scanning CW laser, reaction rates, analytical model 80—66334
- Si, amorphous, in contact with electrolyte, Schottky barriers at interface 79—78169
- Si amorphous, ion bombardment, controlled hydrogenation at low temps. 79—69119
- Si, amorphous, ion implantation method, B and P ions 80—100274
- Si, amorphous, ion implanted, laser annealing, reflectivity meas. 80—29039
- Si, amorphous, ion-implanted, hopping parameter at natural phonon freqs. 79—15152
- Si, amorphous, mag. field depend. of luminesc. 79—43034
- Si, amorphous, molecular liquid model and electronic struct. 80—54133
- Si, amorphous, opaque, surface phonon attenuation, Brillouin scatt. 80—80808
- Si, amorphous, optically detected ESR obs. 78—84500
- Si, amorphous, photo-induced changes in elec. props., defect states 79—82553
- Si, amorphous, photostructural changes, photodarkening 80—49121
- Si, amorphous, photovoltaic diodes, influence of mag. field on charge transport 80—49891
- Si, amorphous, possible ABB-type excitonic superconductor *(Chinese)* 80—7029
- Si, amorphous, prep. by RF sputtering, photoconductivity determ. 77—73231
- Si, amorphous, prep. by reactive RF sputtering in Ar-silane mixtures, undoped, n-type and p-type targets 80—76182
- Si, amorphous, production by glow-discharge method *(Japanese)* 77—90283
- Si, amorphous, pure and H doped, picosecond relax. of optically induced absorption 80—97302
- Si, amorphous, pure and hydrogenated, far IR absorption coeff. meas. 80—108213
- Si, amorphous, Raman spectra, vibrational properties 79—99881
- Si, amorphous, reduced intensity functions, thermal vibr. coupling 78—42910
- Si, amorphous, scanning TEM studies of cryst. inclusions 80—79699
- Si, amorphous, Schottky barrier solar cell, large-area RF sputtered, contact form, scaling and optimisation 80—45679
- Si, amorphous, Si implanted, substrate-orientation depend. of epitaxial regrowth rate 78—79900

amorphous semiconductors continued
- Si, amorphous, solar cell appl. *(Chinese)* 80—45671
- Si, amorphous, solar cell construction and performance *(German)* 79—61970
- Si, amorphous, spin-depend. photocond. 77—59302
- Si, amorphous, sputter-deposited electrical and optical props. 79—47181
- Si, amorphous, structural defects EPR 80—25208
- Si, amorphous, substrate orientation effect on regrowth by laser pulses, channeling, backscatter 80—84409
- Si, amorphous, thermoelec. power in phonon-assisted hopping regime, Coulomb effects 78—76097
- Si, amorphous, time-resolved ODMR and luminesc. 80—25254
- Si, amorphous, topological and electronic struct. 77—28102
- Si, amorphous, tunnelling states simulation and sp. ht. 79—37791
- Si, amorphous, UHV evaporated, annealing behaviour of spin density 80—93163
- Si, amorphous, undoped, photocond., continuous illum. effect 80—84486
- Si, amorphous 79—28103
- Si, amorphous and cryst., electronic and optic props. 78—39013
- Si, amorphous and cryst., optical absorpt. at $\lambda = 1.06\ \mu m$, temp. depend. 79—82939
- Si, amorphous and cryst. K X-ray spectra of band struct. 79—87525
- Si, amorphous and crystalline, hydrogenation and dehydrogenation 78—51677
- Si, amorphous and crystalline, heating by Q-switched laser radiation 80—84963
- Si, amorphous and crystalline, ion implanted, UPS meas. 80—97411
- Si, amorphous CVD film photodetector for picosecond pulses 80—47101
- Si, amorphous CVD films for high temp. solar photothermal conversion 80—26161
- Si, amorphous deposited, laser induced epitaxy 79—69372
- Si, amorphous discharge produced, electronic density of states 79—46992
- Si, amorphous evaporated, picosecond optoelectronic detect., sampling and correlation meas. 80—100478
- Si amorphous evaporated film, doping 79—51127
- Si amorphous film, AC conduction 77—66213
- Si amorphous film, anisotropic etching phenomenon, appl. as solar selective absorber surfaces 80—72054
- Si, amorphous film, drift mobility and photocond. 79—15143
- Si amorphous film, EPR rel. to elec. cond. 77—69692
- Si, amorphous film, ESR, cond. secular change on annealing *(Japanese)* 79—15238
- Si, amorphous film, epitaxial laser crystallisation 78—84078
- Si, amorphous film, Fermi energy shift with substitutional doping 79—46998
- Si, amorphous film, glow discharge deposition, rate enhancement by mag. field 80—65412
- Si amorphous film, heavy doping by alkali ion implantation 80—2045
- Si amorphous film, hole carrier transport 80—2500
- Si, amorphous film, hole drift mobility, temp. depend. 79—23973
- Si amorphous film, ion-implanted, regrowth 79—15043
- Si amorphous film, optical props., electronic states 80—25475
- Si, amorphous film, oxidised, vacuum deposited, cond. change due to electron irrad. 78—10089
- Si, amorphous film, plasma-deposited, photoluminesc. and EPR meas. 79—4864
- Si, amorphous film, RF plasma deposition from $SiCl_4$-H_2, characterisation 80—66435
- Si amorphous film, saturation meas. on ESR signals 79—33535
- Si, amorphous film, selective laser recrystn. over heavily doped lines 80—84947
- Si, amorphous film, sputtering by 0.5 to 5 keV Ar^+ ions 79—91550
- Si amorphous film, vacuum deposited, microscopic voids, gas absorpt., crystn. study 80—49534
- Si, amorphous film deposition from silane glow discharge plasma 77—44173
- Si, amorphous film prepared by CVD, optical props. and struct., solar absorber appl. 79—52035
- Si, amorphous films, characterisation by Rutherford backscatt. spectrometry 80—50498
- Si amorphous films, laser beam annealing, optical information storage possibilities 79—87515
- Si, amorphous films, RF sputtering prep. at high Ar press., props. obs. 80—80418
- Si amorphous films, switching, electrothermal model 80—80407
- Si, amorphous hydrogenated solar cells, field depend. quantum efficiency, electron-hole recombination 80—66971
- Si, amorphous laser effects 79—69921
- Si, amorphous layer, comparison of laser and electron beam pulsed annealing 79—69374
- Si amorphous layer, inhomogeneity formed by ion bombardment 77—69017
- Si amorphous layer, ion-beam induced epitaxial regrowth 79—69378
- Si, amorphous layer, ion-implanted, spatially controlled cryst. regrowth by laser irradiation 78—55810
- Si amorphous layer, solar furnace annealing to induce solid-phase epitaxy 80—2277
- Si, amorphous layer crystn., effect of ^{16}O, ^{12}C, ^{14}N and inert gases 78—14623
- Si amorphous layer recrystallisation by laser beam 80—93566
- Si amorphous layers, glow-discharge, laser-annealed, elec. props. 80—75661
- Si, amorphous layers, laser induced As profile broadening 79—95045
- Si amorphous layers, on Si substrates, deposited and ion-implanted, laser-annealing behaviour 79—69373
- Si, amorphous layers, RF-sputtered on sapphire, crystallisation by CW ion laser annealing 80—80109
- Si amorphous p-n junctions, high current, characts. 80—70807
- Si, amorphous presence of acceptor states around Fermi level 78—2445
- Si, amorphous sputtered thin film, US anomalies, 0.5-300K 80—34145
- Si, amorphous thin films, appl. in solar cells, recent developments 78—80016
- Si, amorphous/cryst. interface, supercond. mechanism 80—44783
- Si, and Si:H, ps. relax., optically induced absorpt. 80—48325
- Si and Si:H amorphous films, porosity and oxidation of evap., sputtered and plasma-deposited films 80—10838
- Si, anomalous magnetoresist., hopping model 78—23117
- Si, asymmetrical profile of ion implanted P 79—46693
- Si based alloys, amorphous, photovoltaic behaviour, solar cell appl. 80—94051
- Si, CVD, retarding crystn. by alloying with C,N,B or Ge 80—44129

amorphous semiconductors continued
Si, CVD layers, change of etch rate associated with amorphous to crystalline transition 78—7064
Si, CVD prepared solar thermal absorber, temp. variation of absorpt. edge 80—12028
Si, co-sputtered doped, photovoltaic material appl. 80—93488
Si, control of dihydride bond density using RF sputtering 80—34327
Si, Coulomb gap and hopping cond. 80—44583
Si, cryst. and amorphous surface layers, ruby laser pulse effects 79—69920
Si crystallisation study 80—33890
Si, defects, band gap states 80—80215
Si, diamagnetism temp. depend. 78—47940
Si, discharge produced, optical and photocond. props. 78—39147
Si, discharge produced, reversible cond. changes 77—85256
Si, doped amorphous, transport props., conductivity, thermopower, temp. depend. 79—73512
Si, doping, Schottky barrier and p-n junction form. by RF sputtering 77—8187
Si, doping and absorption edge 80—29042
Si, EPR and spin-dependent effects 80—80592
Si, EPR of radiation defects, temp. depend. 78—15023
Si, ESR linewidth, exchange interaction effect 79—61216
Si, effect of disorder on H content 80—75258
Si, effective mass theory, impurity states in band gap 79—77992
Si, elastic moduli, random network model, calc. 78—6119
Si, elec. and opt. props., review 78—23094
Si, electrical conduction in amorphous semiconductors, mechanisms 79—56214
Si, electron-hole recombination, mech. 78—72196
Si, electronic density of states, mol. liq. model 80—49581
Si, electronic props. and localised states, review 77—62871
Si, electronic struct. and optical dielec. function, LCAO calc. 79—42478
Si, energy depend. of amorphisation by ion implantation 78—2175
Si, epitaxial and amorphous film growth, low energy ion beam deposition 77—28729
Si, epitaxial regrowth, structure and impurities effect 80—84401
Si, epitaxial regrowth of thin amorphised layers by laser annealing, absorpt. coeff. influence 79—46968
Si film, acoustic study using Rayleigh waves 80—75312
Si film, amorphous, formed by CVD, crystallisation 77—39746
Si film, amorphous, LF vel. of sound for Young's modulus mode 77—35636
Si, film, amorphous, two-dimensional variable range hopping cond. 80—10977
Si film, amorphous and crystalline, optical properties 77—24906
Si film, amorphous and polycrystallised, localised states, elec. and optical props. 78—64008
Si film, analytical techniques, review 80—80120
Si film, annealing behaviour of void network 78—18551
Si film, CVD, microscopic surface roughness, effective-medium models, ellipsometric expts. 80—24756
Si film, CVD or evaporated, covered with Al layer, solid-phase crystn. obs. 77—85100
Si film, crystn. on annealing at low temps. in contact with Al 80—24765
Si film, dangling bond ESR, light-induced quenching 80—50162
Si, film, EELS microanalysis 80—100722
Si film, effect of gas exposure on EPR signal 78—84475
Si film, evap., structural aspects in electronic transport data interpret. 77—76977
Si film, glow discharge deposited, refl. spectra and dielec. function 80—50360
Si, film, glow-discharge, optical props. *(Japanese)* 79—65946
Si film, glow-discharge, optically detected mag. reson., annealing and substrate temp. effects 80—20519
Si film, high resolution electron microscopy, digital processing use 78—37116
Si film, hopping cond., thickness depend. 77—89887
Si film, hydrogenated, preparation by SiH_4 decomposition 80—80956
Si film, hydrogenated amorphous, Brillouin scatt. 78—72538
Si film, IR and Raman spectra of Si-H bonds 78—19482
Si film, ion bombarded, crystalline-to-amorphous transition, defect-rich film prep. 80—65071
Si film, low press. CVD prep., struct., elec. and optical props. 80—70548
Si, film, optical absorption at high press. 78—35216
Si film, plasma preparation 78—72740
Si film, plasma-deposited, H_2 evolution, mass spectrometry and RHEED obs. 78—72050
Si film, prep. conditions influence on supernetwork struct. 77—76709
Si film, sputtered amorphous, P and B doped, elec. cond. and thermopower meas. *(French)* 78—47403
Si film, structural comparison of evaporated and glow discharge samples 77—62778
Si film prepared from glow discharge, qunatitative H anal. 77—69188
Si films, crystallisation kinetics and morphology, TEM obs. 78—84093
Si films, laser annealing, photoluminesc. study 80—2049
Si, first order transition to metallic liquid, calc. of transition temp., enthalpy and entropy 79—69227
Si foil, electronic energy, straggling of light ions, at. number depend. 77—11612
Si, glow discharge, fatigue effect in luminesc., recovery by annealing 80—50416
Si, glow discharge amorphous film, reflectance and transmittance *(Japanese)* 80—34995
Si, glow discharge deposited, photolum. decay 78—72590
Si, glow discharge deposited, mobility edge calc. 80—80220
Si, glow-discharge deposited, ODMR spectrum, deposition temp. and annealing effects 80—50229
Si, heavy ion ranges, He^+ backscatt. obs. 78—63796
Si, hopping model for activated charge transport 79—87099
Si, hydrogenated, amorphous, theoretical calc. of defect states 80—49657
Si, hydrogenated, H configs., Cayley trees appl. 79—65373
Si, hydrogenated, use as solar cell material 78—2565
Si, hydrogenated, work function and Auger spectroscopy of initial oxidation 78—76132
Si, hydrogenated amorphous, laser annealing 80—100713
Si, hydrogenated amorphous, gap states, comparison of photoemission and photocond. results 80—103724
Si, hydrogenated amorphous film, XPS and UPS 78—19636
Si, hydrogenated photolum., heating effects 78—15204
Si, hydrogenation and density of defect states, hopping cond. 79—60757

amorphous semiconductors continued
Si, IR absorpt., first-order effective charges due to at. displacements 77—48164
Si, ideal network struct., electronic struct., tight-binding model 80—44485
Si, ideal surface, definition and characts. 80—107623
Si, implanted, struct. transition under laser irrad. 79—50992
Si, implanted ion trajectory and spatial distrib., Monte Carlo simulation 77—11611
Si implanted with ^{31}P, ^{75}As, ^{11}B, amorphous layer reordering 78—14622
Si, interface structural model between amorphous and crystalline phase 78—63941
Si, interface with V, V silicide formation, backscattering, diffraction meas. 80—2285
Si, ion bombardment induced buildup of disordered material, model 77—47496
Si, ion implantation, negative magnetoresist., localised mag. states 80—70731
Si ion implanted, amorphous to crystalline transition due to laser irrad. 80—103451
Si, ion implanted, difference between ruby and Nd:YAG laser annealing 79—37723
Si, ion implanted, EPR line shape exam. of amorphous centres 79—28587
Si, ion implanted amorphous layers, free carrier plasma effects 77—73133
Si, ion irrad., temp. and dose depend. of defect profiles 80—29097
Si, ion irradiated, elec. cond. 79—11127
Si, ion penetration, computer program 80—88185
Si, ion-implanted, laser epitaxial recrystallisation threshold energy 80—70571
Si, ion-implanted amorphous layers, melting model for pulsing-laser annealing 79—56080
Si, large vacancy cluster annealing by ion bombard., EPR investig. 77—68965
a-Si, laser induced crystallisation mechanism, epitaxial regrowth 80—84962
Si, laser pulse induced amorphous to cryst. transition, thickness depend. 78—47678
Si, laser-induced epitaxial regrowth, substrate and doping effects 79—56082
Si, Lifshitz constant for calc. of van der Waals force between two solids *(French)* 80—107658
Si, luminesc. of diode structures 77—8656
Si, luminescence 80—80862
Si, MIS diode I-V characts. 78—43485
Si MIS solar cells, spectral response and diffusion length 79—92077
Si, monolithic solar cell appl. 80—45666
Si, neutron irradiated, heavily disordered, electronic excitation bands 78—2448
Si noncrystalline film, struct., interatomic distances, SRO 80—107053
Si, optical absorpt. edge shape, band edge fluctuations 77—20880
a-Si p-i-n and c-Si p-n junction solar cells, design concept differences 80—94031
Si, p-n junction devices, barrier profile effect on elec. props. 80—49890
Si, p-n junction preparation, by SiH_4 decomposition *(Czech)* 77—63560
Si, phonon interaction in luminescence 78—43927
Si, phonon spectroscopy, amorphous versus crystalline material 78—83898
Si, photoconductivity, mag. field depend. 78—80023
Si, photogeneration of charge carriers and recomb. 77—81147
Si, photoluminesc. and radiative lifetimes 79—61419
Si, photoluminesc. spectra from 77K to room temp. 77—20916
Si, photoluminescence, fast radiationless recombination 79—99939
Si, photovoltaic cell, plasma deposited, horizontally multilayered struct. 80—50964
Si, photovoltaic characts., rel. to appl. in solar cells 78—84253
Si plasma deposited amorphous hydrogenated film, optical props., annealing effect 79—56874
Si, position of Fermi level, spectroscopic and transport determ. 80—6706
Si, post-annealed amorphous layer, twinning struct. by transmission electron diffr. 77—76685
Si, postimplantation defect annealing in samples heavily damaged by 140 keV Si^{2+} ions 77—11602
Si, prep. by glow discharge decomposition method *(Japanese)* 77—81226
Si, pure and doped amorphous photolum. meas. 77—36285
Si, pure and hydrogenated, Raman spectra 79—61358
Si, RF sputtered amorphous film, high temp. metal induced crystn. 77—11825
Si, radiative and non-radiative tunnelling, photoluminesc. decay meas. 79—83026
Si, radiative recomb. obs. as efficient luminesc. 78—2914
Si, random-network model, charge-density variation 80—80165
Si, recomb. centre study by spin-depend. photocond. 80—49805
a-Si, resonant and non-resonant photoconductivity changes 80—49814
a-Si, resonant and non-resonant luminesc. changes theory 80—50410
Si, scatt. intensity and radial distrib. function, random stacking model 79—27919
Si, Schottky barrier and p-n junction props. 79—28407
Si, Schottky barrier solar cells, deep hole traps, spectral response and TSC meas. 80—50962
Si, Schottky diodes on sputtered amorphous Si:H, light induced ageing effects, interpretation of photovoltaic stability 80—54780
Si, self-ion implanted, amorphous to polycrystalline transition induced by laser beam 77—84771
Si, small dia. laser beam annealed, temp. distrib. and microstructure 79—73098
Si solar cell production, Union Carbide Corporation Silane Process, cost analysis 80—21403
Si, solar cells, and photovoltaic devices *(Japanese)* 80—50965
Si solar cells, barrier props. determ. by differential I-V characts. meas. 80—94053
Si solar cells, current collection and electrical shorting problems 80—93969
Si solar cells, design considerations 80—85277
Si solar cells, efficiency, transport props. 80—50961
Si, solar cells, glow discharge produced 80—12013
Si solar cells, perform. parameters of amorphous and polycryst. thin film cells 80—93882
Si, solar cells *(Japanese)* 79—57430

amorphous semiconductors continued
Si, solid-state epitaxial growth of amorphous layer 80—10803
Si, spin depend. recomb., luminesc. and light induced ESR 80—50393
Si, spin-pairing at defect centres, mechanism in terms of chem. bonding 79—23928
Si, sputter deposited, O_2 incorporation during and after fabrication 80—49541
Si, sputtered, Auger surface spectroscopy 80—50472
Si, sputtered, resist. control by ion implantation 80—100262
Si, sputtered amorphous film, photocond. and electronic props., effects of annealing in plasma gas 80—44644
Si, sputtered film, in Al-Si-Al(Mo), photovoltaic props. 77—24623
Si sputtered film, solar energy selective absorber, spectral emissivity 78—83045
Si, sputtered films, hydrogenated, photoinduced optical absorpt. 80—50362
Si, sputtering with keV Ar^+ ion, meas. and Monte Carlo calc. of sputtering yield 79—95886
Si, struct. and growth kinetics, topological principles 80—49123
Si, structural and electronic props., review 80—64901
Si, structural disorder rel. to electronic props. 78—34756
Si, substituted doping, electronic props. 77—1418
Si surface, amorphous and hydrogenated, AES and LEED, comparative study *(French)* 80—44398
Si, thin film, evaporated amorphous, hydrogenation by plasma treatment 78—91555
Si, time resolved photoluminesc. near band gap 80—25445
Si, transient electrical transport, general and unified treatment 80—59977
Si, undoped and B doped, ESR-linewidth temp. depend. meas. 80—20459
a-Si, vapour species rel. to amorphous film deposition 78—14641
Si wafer, thin surface layers, amorphous to cryst. transform., obs. technique 80—107288
Si whisker, amorphous, meas. of Young's modulus 78—83865
Si, whisker, growth method for field desorption mass spectrometry 79—28262
Si, whisker growth characts. by SiH_4 thermal decomposition 80—34342
Si, whisker growth in amorphous state, in SiH_4-Ar atmosphere, visual obs. 78—84112
Si whiskers, polytypism and amorphousness 78—26801
Si:^{11}B, amorphous, calc. of implanted-ion range and energy-deposition distrib. 77—7748
Si:Al(Sb) film, amorphous, ion implantation, effect on cond. 78—83839
Si:Ar, ion implanted, amorphous, epitaxial regrowth 79—10868
Si:Ar, ion-implanted, epitaxial regrowth by laser annealing, microstruct. 80—84404
Si:As, amorphous, field effect and thermoelectric power 79—33289
Si:As, appl. of EXAFS methods for struct. determ. 79—37624
Si:As, CW laser annealing mechanism, annealed spot size, solid phase epitaxial regrowth 79—78798
Si:As, H, amorphous system, struct. and defects, Raman and EPR meas. 80—49103
Si:As, ion implanted, amorphous-cryst. transition induced by multiple-pulsed ruby laser 79—90555
Si:As, ion-implanted, laser recrystallisation by freq.-doubled Nd:YAG laser 79—77613
Si:As, melting by high power ns laser pulsing, As diffusion 78—79789
Si:As,Sb, amorphous, damage depend. of epitaxial regrowth during annealing 78—47679
Si:$As^+(P^+)$ ion implanted, laser annealed, correlation of struct. and elec. props 80—70855
Si:Au, O(H), film, amorphous, elec. cond. meas. 80—80423
Si:B amorphous film, CVD prep., EPR, elec. and optical props. 79—4558
Si:BF_2^+, recrystallisation of implanted amorphous layers, F migration 79—55763
Si:$BF_2^+(Si^+,B^+)$, recrystallisation of implanted amorphous layers, elec. props. 79—55762
Si:B(P), amorphous, photo- and dark conductivity 77—28216
Si:B(P), ion implanted crystalline and amorphous laser annealing 80—97509
Si:D, thermal stability, comparison with Si:F 80—49542
Si:F, amorphous, heat resistant, prep., elec. cond., IR absorpt., annealing 80—65719
Si:F, amorphous film, effect of F on elec. cond. 80—34444
Si:F, H amorphous films, optical props., photoconductivity, photostructural changes 80—11034
Si:F, pure and doped, vibr. excitations at defect sites, IR and Raman spectra calc. 80—49329
Si:F, thermal stability, comparison with Si:D 80—49542
Si:F,H, amorphous, elec. and optical props. 80—60031
Si:F,H, amorphous efficient carrier generation for solar photovoltaic energy conversion 80—92906
Si:F(,H), electronic struct., orthogonalised LCAO calc. 80—44486
Si:Fe, implanted, Mossbauer spectra, conversion electron, temp. dependence 80—40025
Si:Ga^+, influence of recrystallisation of amorphous layers on impurity distrib. during annealing 79—69152
Si:Ge, regrowth behaviour from backscatt. and channelling meas. 80—2300
Si:H, amorphous, 2p level shift, XPS obs. 80—97401
Si:H, amorphous, Auger electron spectrosc. obs. 80—76112
Si:H, amorphous, band tail absorpt., photocurrent meas. for Schottky barrier solar cell 80—60032
Si:H, amorphous, defect photoluminesc. meas. 80—97334
Si:H, amorphous, doped, Fermi level position, photoelectron spectra 79—47592
Si:H, amorphous, effect of gap state density on photocond. and photolum. 79—91096
Si:H, amorphous, electronic states of hydrogenated Si, theory 79—42494
Si:H, amorphous, exodiffusion of H, EPR expts. 80—49102
Si:H, amorphous, geminate recombination model for photoluminescence decay 80—71481
Si:H, amorphous, glow discharge deposited, thermal dehydrogenation, IR spectra 80—44442
Si:H, amorphous, glow discharge deposited, laser annealing 80—49104
Si:H, amorphous, HV photovoltaic cells, design parameters 80—101105
Si:H, amorphous, horizontal cascade type integrated photovoltaic cell module 80—94091
Si:H, amorphous, image pickup devices 80—100481
Si:H, amorphous, luminesc., band tail states and thermalization 80—25455

amorphous semiconductors continued
Si:H, amorphous, optical studies of excess carrier recomb., evidence for dispersive diffusion 80—76059
Si:H, amorphous, p^+-i-n^+ struct. solar cells, material parameters and deposition condition optimisation study for higher efficiencies 80—45676
n-Si:H, amorphous, photoelectromagnetic effect 80—107845
Si:H, amorphous, plasma-deposited, effect of DC elec. field superimposed during deposition 80—44643
Si:H, amorphous, Pt film growth, AES and LEED study 80—88447
Si:H, amorphous, RF sputtered, suitability as solar cell material 80—40864
Si:H, amorphous, RF sputtered, Schottky barrier solar cells, photovoltaic props. and capacitance-voltage charact. 80—45678
Si:H, amorphous, radiative recomb. and luminescent processes 80—55152
Si:H, amorphous, Schottky diode, spectral response and hole drift mobility 80—39673
Si:H, amorphous, Schottky barrier solar cell, degradation mechanisms affecting stability and operation 80—45680
Si:H, amorphous, Schottky barrier solar cell, deposition parameter effects on elec. props. 80—45681
Si:H, amorphous, Schottky diodes, elec. props., light-induced effects 80—103741
Si:H, amorphous, short-range order, theory and probes 80—79698
Si:H, amorphous, solar cells using ultrathin active layer to increase conversion efficiency 80—94030
Si:H, amorphous, solar cells, trap spectroscopy using transient current techniques 80—104508
Si:H, amorphous, solar-cells, charge collection and spectral response 80—85275
Si:H, amorphous, sputtered on $Gd_2(MoO_4)_3$, ferroelec. domain wall motion, image scanning 80—83663
Si:H, amorphous, sputtered Schottky barrier solar cells, conduction mechanism 80—104506
Si:H, amorphous, stacked solar cells, development 80—94050
Si:H, amorphous, surface activated, photoemission spectra, minority carrier diffusion length 80—40235
Si:H, amorphous, surface states distribution using MOS tunnel junctions 80—103735
Si:H, amorphous, temp. depend. of photolum. 80—89063
Si:H, amorphous defect model 80—24363
Si:H, amorphous field induced and quenched-in excess cond. 80—24968
Si:H, amorphous film, anal. of intrinsic photocond. spectrum 79—73541
Si:H, amorphous film, prep. by plasma decomp. of SiH_4 under mag. field, and characterisation 80—45239
Si:H, amorphous films, plasma-deposited, defect states, IR, ESR, and refractive index meas. 79—65944
Si:H, amorphous hydrogenated film, decomp. kinetics 79—100342
Si:H, amorphous Schottky solar cells, prep. and characts. of diode RF reactive cathodic sputtered films *(French)* 80—61347
Si:H, amorphous thin film, ion plating, IR absorpt. meas. 80—84857
Si:H, amorphous thin film solar cells 80—81478
Si:H, amorphouse film, optical and elec. props. 79—82694
Si:H, Brillouin scattering from acoustic bulk and surface waves 80—11425
n-Si:H, bulk density of deep states, DLTS meas. 80—88518
Si:H, control and anal. of deposition, using plasma spectroscopy 80—45230
Si:H, defect creation and H evolution 80—50392
Si:H, defect states, luminesc. and ESR obs. 80—76075
Si:H, depletion width determ. by analytical model 80—100445
α-Si:H, discharge produced, electronic props. rel. to solar cell characts. 79—15241
Si:H, dopant conc., glow discharge optical spectroscopy 80—49546
Si:H, electronic struct. calc., rel. to UPS data 80—39527
Si:H, evaporated amorphous film, prep. elec. cond. and photocond. 79—38201
Si:H, excess carrier thermalisation and recomb., luminesc. decay and photocond. 80—50397
Si:H, H content determ. by IR absorpt., gas evolution and nuclear reaction methods 80—44130
Si:H, H^+ sputtered as result of ion bombardment, ionis. mechanism 79—100009
Si:H, hydrogenation and dehydrogenation, luminesc. spectra 80—11477
Si:H, in p^+-i-n^+ struct., hole diffusion length meas. 80—44712
a-Si:H, influence of H on optical props., H conc. and H bonds 80—76098
Si:H, light-induced ESR and photoluminesc., dangling bonds with positive correl. energy 80—50161
Si:H, mobility edge position using continuous random network model for struct. 80—44544
Si:H, model for variable gap intrinsic semiconductor 80—10988
Si:H, photoelectrochem. behaviour 80—81480
Si:H, photoinduced optical absorpt. and photocond. 80—50361
Si:H, plasma-deposited amorphous film, proton mag. reson. 80—44931
Si:H, prep. from SiH_4 and characts. 78—48326
Si:H, prod. by high temp. thermal decomp. of SiH_4, and photocond. 79—87585
Si:H, radiative recomb. by diffusion and tunnelling, photocond. quantum efficiency 80—50394
Si:H, refr. index, temp. depend., implications for thermoreflectance and electroreflectance 80—50290
Si:H, rehydrogenation, photoluminesc. recovery 78—72571
Si:H, Schottky barrier solar cells, depletion region, capacitance study 80—50963
Si:H, solar cell struct., photocurrent meas., absorpt. coeff. 80—50960
a-Si:H, spin defect and recombination influence on electronic transport 80—50409
Si:H, sputter deposited, O_2 incorporation during and after fabrication 80—49541
Si:H, sputtered, Auger surface spectroscopy 80—50472
Si:H, sputtered, excitation spectra and photoluminesc. 80—50396
a-Si:H, structural interpretation of vibr. spectra 79—69864
Si:H, structural model 80—49105
Si:H,F,O amorphous, plasma deposited, comp. and optical props. 80—50441
Si:H,Li, amorphous, photoluminescence obs. 80—66280
Si:H,P, amorphous, in MOS tunnel junction, electron tunnelling characts. 79—73592
Si:H amorphous, plasma-deposited, luminesc. decay 79—73989
Si:H amorphous, solar cell structure, optical absorption by gap states 80—94052

amorphous semiconductors continued
Si:H amorphous film, H quantitative depth profiling by nuclear reactions and SIMS 78—14373
Si:H amorphous film, plasma-deposited, growth morphology and defects 80—44128
Si:H amorphous film, plasma-deposited, elec. and comp. heterogeneity 80—44745
Si:H amorphous film, prop. by glow discharge deposition, and plasma parameter effects on props. 80—45240
Si:H amorphous film, sputtered in Ar-SiH_4 mixtures, props. 79—87023
Si:H amorphous film, sputtered IR vibr. spectra and photolum., effects of partial evolution of H 80—44413
Si:H amorphous films, effects of glow-discharge prep. conditions on H content 79—46969
Si:H amorphous films, IR spectrum and struct. 80—97277
Si:H amorphous films, role of Ar in deposition process, IR absorpt. and photocond. meas. 80—50321
Si:H amorphous glow discharge film, optical absorpt., near IR region 79—87518
Si:H amorphous layer as passivant for p-n junction in crystalline Si 79—47155
Si:H amorphous MIS solar cell, loss mechanisms and photovoltaic parameters, overview 80—93923
Si:H amorphous sputtered film, photoluminesc., photocond. 80—20729
Si:H amorphous sputtered films, optical gap, IR absorpt. meas. 80—50320
Si:H film, amorphous, bombarded, defects, luminesc. and ESR meas. 80—34977
Si:H film, amorphous, photocond. imaging 80—1300
Si:H film, amorphous, plasma-deposited, small angle X-ray and neutron scatt. studies 80—59826
a-Si:H film, glow discharge deposited, H profiles, doping level 80—84202
Si:H film, H-associated disorder modes, PMR spin-lattice relax. time meas. 80—93202
Si:H film, interference enhanced Raman scatt. 80—50326
Si:H film, prep. by RF glow discharge decomp. of SiH_4, optical props. and H conc. 80—15416
Si:H films, optoelectronic behaviour depend. on impurity incorporation during plasma deposition 80—49804
Si:H films, photovoltaic and photocond. spectra, photoluminesc. 80—44645
Si:H films, reactively sputtered, prep. and characterisation 80—100785
a-Si:H highly homogeneous, for low-cost solar cell fabrication 80—72053
Si:H layers, ion bombard., AES study, $L_1L_{23}V$ Coster-Kronig transition 79—99992
Si:H plasma deposited film, amorphous, microstruct., TEM and SEM obs. 80—10801
a-Si:H Schottky barrier diodes, capacitance studies 80—49908
Si:H solar cells, carrier generation, recombination, and transport 80—55844
Si:H solar cells, photovoltage source in photocond. materials due to comp. and doping var. 80—7938
a-Si:H sputtered films, ohmic contacts by H depletion, H diffusion 80—34511
Si:H:F, depletion width determ. by analytical model 80—100445
a-Si:H/Pt, Schottky diode, influence of prep. conditions on forward bias currents 79—78171
Si:H(B)(P), amorphous, UV absorpt. spectra 80—25420
Si:H(D), amorphous films, CVD, post-hydrogenation 80—54552
Si:H(F), Schottky barrier profiles, depletion region width 80—49871
Si:In(Sb), incorporation of implanted impurities during amorphous layer regrowth 79—55761
Si:Li, amorphous, elec. cond. and thermopower 79—73537
Si:Li, interstitial doping by in-diffusion and implantation and elec. characterisation 78—26585
Si:Mn, amorphous, cond. increase by Mn doping 78—72155
Si:Mn, amorphous, EPR meas. 77—85559
Si:N, amorphous, DC sputtered, enhanced, photocond. 78—56183
Si:N, amorphous, prep. by RF sputtering and props. 80—44229
Si:Na(K)(Cs), ion implanted, control of cond. 79—60835
Si:Ne(Ar)(Kr), amorphous, implanted and sputtered, epitaxial regrowth, influence of noble gas atoms 80—2289
Si:Ne(Kr), ion implanted, amorphous, epitaxial regrowth 79—10869
Si:O, evaporated amorphous film, effect of O_2 on props., ESR spectra 80—11265
Si:O,H, plasma-deposited, electronic and struct. props. 80—50391
Si:O,H amorphous, time resolved luminesc. 80—66288
Si:P, amorphised by Ne^+ implantation, high fluence P implants, plasma region obs. 79—86807
Si:P, amorphous, CVD, substitutional doping, electronic props. 79—23923
Si:P, amorphous, elec. cond. and thermoelectric power 77—89783
Si:P, amorphous, substitutionally doped CVD, electrical props. 79—99566
Si:P, amorphous, thermoelectric power and conductivity 77—89782
Si:P, CVD amorphous film, electronic density of states 79—46993
Si:P, heavily doped, glow-discharge-produced, elec. and optical props 80—2497
Si:P, ion implanted, regrowth of damage structs. by laser annealing 80—107289
Si:P,B, amorphous, localised level density 79—56168
Si:P CVD films, doping and annealing effects on localized states, ESR meas. 79—38380
Si:P film, amorphous, unusual temp. depend. of thermoelec. power 77—59343
Si:P(B), film, electronic props. 78—84330
Si:transition metal, amorphous, impurity effects on hopping conductivity 79—65485
a-Si/Au barrier, capacitance and cond. 80—2469
Si/In_2O_3-SnO_2 thin film junctions, polarity dependent memory switching effects 80—70814
Si/Pd system, solid phase epitaxial growth control by C ion implantation 80—75466
Si/Si-Ge solar cell, multijunction structure, increased conversion efficiencies, low cost 80—45677
Si-Au amorphous film, metal-nonmetal transition, elec. cond., thermoelectric power meas. 79—47132
Si-Au amorphous system, optical absorpt., IR photocond. 79—42582
Si-Au Schottky barrier solar cell fabrication, doping of a-Si 80—50969
Si-Au(Cr)(Pd), contact reactions between amorphous Si and metallic films, TEM, transmission electron diffr. obs. 79—23846
Si-B amorphous film, plasma deposited, characterization 79—69828

amorphous semiconductors continued
Si-C amorphous wear-resistant coating 79—34165
Si-C:H, film, vibr. spectrum 79—61450
Si-F-H amorphous alloy for electronic appls. 79—15627
Si-F-H amorphous solar cells, DC glow discharge fabrication 80—72041
Si-Ge alloy, hot-pressed, thermal cond., effect of grain size 77—31813
Si-Ge amorphous films, effects of annealing and crystn., ESR microstruct. and elec. meas. 78—26790
Si-Ge film, ESR line intensity anal., rel. to cond. mechanism 78—43645
Si-Ge solar cells, tandem multiple gap 80—94029
Si-Ge:As,P, heavily doped, electron scatt., Hall coeff., Seebeck coeff. and resist. meas., 4-300K 77—4379
Si-H, amorphous, energy gap negative-U states, Si-H-Si three centre bond model 78—91606
Si-H, amorphous, H three-dimens. distrib., ion-induced AES and Rutherford backscattering 80—44132
Si-H, amorphous, on Nb or W, spectrally selective absorber, IR spectra 80—26164
Si-H, amorphous, plasma-deposited, H evolution and defect creation 80—44914
Si-H, amorphous, random network model 80—1932
Si-H, amorphous, sputtered, photolum. obs. 80—80856
Si-H, amorphous, struct. anomalies, theoretical interpretation 79—90556
Si-H, amorphous film, in situ prepared, photoemission studies 80—35060
Si-H, amorphous plasma deposited film, H content and density 79—82472
Si-H, RF sputtered amorphous alloy, influence of Ar press. on elec. props. and photoluminesc. 79—91585
Si-H, structural and electronic props., review 80—64901
Si-H, thermal stability and decomp. kinetics 80—24758
Si-H (up to 15 at.%), amorphous, ion implanted, laser annealing obs. 79—69133
Si-H amorphous film, reactively sputtered, prep. and props. 79—78889
Si-H sputtered film, luminesc. and non-radiative decay 80—50395
a-Si-H sputtered solar cells, temp. depend. of Schottky barrier characts. 80—45669
Si-H:As alloy, amorphous film, coordination of impurities, EXAFS of data 77—84780
Si-H:P amorphous film, dark cond., struct., Raman scatt. 80—88588
Si-H(-D), film, IR and Raman spectra, H bonding effects 78—72515
a-Si-metal Schottky barrier, I-V characts., barrier heights 77—8191
Si-O-C , product quenching, mol. dynamics 78—39711
Si-TiO_x-Ni, MIS amorphous solar cell, increase in open-circuit voltage and short-circuit current on addition of TiO_x layer 79—57425
Si(-H), amorphous, H atom effect on Si-Si atomic short-range order, X-ray diffr. obs. 79—64996
Si_xAs_{1-x}:H, amorphous system, struct. and defects, Raman and EPR meas. 80—49103
$Si_{1-x}Au_x$ amorphous films, IR absorpt. spectra 80—16034
SiC film, elec. props. and hopping transp. 77—66211
SiC film, reactively sputtered, effects of S/C ratio and H content on elec. and optical props. 79—90906
SiC film synthesis by plasma deposition process 78—11127
SiC, sputtered amorphous film, struct., elec. and optical props. 79—78236
SiC:H amorphous reactively sputtered film, H content effect on film props. 80—75459
$Si_{1-x}C_x$:H glow discharge films, local atomic struct., XPS and AES study 80—93448
Si_xC_{1-x}, luminescence 80—80862
Si_xC_{1-x}, photoluminesc., comp. depend. 78—68541
Si_xC_{1-x}:H reactive sputtering deposition, compositional and structural props. 79—99077
$Si_{1-x}Ge_x$ amorphous, ESR centres, effect of annealing 77—55701
Si_xGe_{1-x}, vibr. props. 77—4176
Si_xGe_{1-x}(H) amorphous alloys, from glow discharge, optical properties 78—19510
$SiH_{0.16}$ amorphous films, optical props. and photocond. near optical gap 80—50443
SiH_x, amorphous, solar cells, short circuit-currents and collection efficiencies 80—94028
SiH_x amorphous reactively sputtered films, in Pd Schottky barrier devices, photovoltaic props. 80—49910
SiH_x amorphous reactively sputtered films, optical props. 80—50444
SiH_x discharge produced amorphous film, gap state role in carrier transport 79—73608
SiH_x polymer film, struct. rel. to amorphous solid 78—72048
$Si_{1-x}H_x$, amorphous, atomic struct., X-ray study 80—49106
$Si_{1-x}H_x$, amorphous, gap states, DLTS 80—49656
$Si_{1-x}H_x$ amorphous sputtered films, IR vibr. spectra 79—43051
$Si_{1-x}H_x$ film, RF sputtered, pure and P(B) doped, optical consts. 79—95866
a-$Si_{1-x}H_x$, oxygenated thin film, sputtered, elec. cond. and optical props. 79—15239
$Si_{1-x}H_x$:Al, amorphous, co-sputtered Al modification, electronic and optical props. 80—100461
Si_3N_4, amorphous, charge transport in band tails 78—76026
SiO_2, amorphous, temp. below 1K, props., tunnelling 80—49576
SiO_2, amorphous and α-cristobalite cryst., band struct., photoelectron and X-ray spectra interpret. 80—24787
$Si_{12}Te_{48}As_{30}Ge_{10}$, amorphous film, elec. cond. mechanisms, temp. depend. *(Japanese)* 78—80078
Si(111):Pb ion implanted amorphous layers, recrystallisation, impurity out-diffusion model *(Chinese)* 80—88363
Sn-Se-P system, glasses, comp. depend. 77—84658
SnO_2, film, effects of Sb and In additions on struct. and resist. 77—20469
SnO_2:Sb film, electrotransport phenomena obs., under DC electric field 80—59840
SnO_2-Sb_xS_{1-x}Sn structures, photovoltaic effects *(Korean)* 80—44647
TE, Rayleigh scatt. of Mossbauer radn., lattice dynamics 80—15845
Te, amorphous, electronic struct. and optical props., pseudopot. calc 80—65428
Te, film, electronic struct. charge on ordering, double beam photoemission 78—19634
Te film in Sn/Te/electrolyte system 77—63923
Te, Raman spectra, crystn. processes 80—60608
Te, trigonal and amorphous, electronic struct. and nonempirical calc. of struct. props. 80—59866
TeO_2-V_2O_5 glass threshold devices, reversible monopolar switching 80—2434

amorphous semiconductors continued
- TiO_2-P_2O_5 reduced glasses, prep., elec. transport, chem. anal., DC, AC cond., seebeck coeff. 78—30924
- TiO_2-SiO_2, semicond. glass, small polaron hopping cond. 78—60126
- TiO_2-SiO_2, semicond. glass, optical props. 78—60412
- TiO_2-Ti_2O_3-P_2O_5, glass form., struct. and elec. props. 80—44592
- TlS_2, optical consts, 79—11400
- TlS_2, spectral depend. of absorpt. and refr. indices 77—77222
- VO_2, amorphous thin films, phase transition, resistivity and opt. transmission discontinuities 77—47871
- VO_2, film, IR induced metal-semicond. phase transition *(Russian)* 77—15769
- VO_2, film, semicond.-metal transition, carrier density, mobility and Hall meas. 77—43751
- VO_2, metal-semiconductor transition, effect of deviations from cryst. lattice periodicity 79—23898
- V_2O_5 amorphous film, photochromism and thermochromism 80—93254
- V_2O_5, amorphous semicond., solubility and fibrous texture 80—75162
- V_2O_5 film, CVD prep. method 80—55299
- V_2O_5, hydrated amorphous, EPR, struct. and electron mobility *(French)* 77—15319
- V_2O_5 layer, photocond. investig. using V_2O_5-n-Si system 77—76875
- V_2O_5 thin film, thickness, density and refr. index determ. from reflectance interference spectra 80—55206
- V_2O_5-B_2O_3-ZnO semiconductivity glasses, optical and modulated absorpt. spectra in band gap region 77—48189
- V_2O_5-based glasses, amorphous and crystallized electronic cond. and related props. 79—99547
- V_2O_5-GeO_2 glass, effect of thermal processing on elec. and thermal props. *(Russian)* 77—63814
- V_2O_5-GeO_2-PbO glasses, memory and threshold switching 78—23142
- V_2O_5-MoO_3, solid soln. thermogravimetric anal., ion formation on crystallisation 77—20076
- V_2O_5-MoO_3-P_2O_5 glass, DC cond., dielec. props 79—91044
- V_2O_5-$NaPO_3$-P_2O_5 threshold switches, elec. props. 77—35974
- V_2O_5-P_2O_5 (70-30), electrical cond. and thermoelectric meas., Au-glass-Au sandwich 80—29403
- V_2O_5-P_2O_5 glass, EPR investig., samples with varying V^{4+} content and cond. 77—8389
- V_2O_5-P_2O_5 glass, electrical 1/f noise and DC cond. 79—91109
- V_2O_5-P_2O_5 glass, in metal-semicond.-metal struct., TSC of dielec. relax. *(Russian)* 77—35998
- V_2O_5-P_2O_5 glass, in SnO_2/V_2O_5-P_2O_5/Si heterojunction, static optoelectronic characts. 79—87146
- V_2O_5-P_2O_5 glass, splat-cooled, EPR of V^{4+}, polaron hopping and carrier localisation 77—28436
- V_2O_5-P_2O_5 glass, switching and memory behaviour, Pt point contact effects 77—11970
- V_2O_5-P_2O_5 glass, thermoelec. power meas. 78—84242
- V_2O_5-P_2O_5 glasses, Raman spectra 79—78667
- V_2O_5-P_2O_5 glasses, secondary electron emission 79—87534
- V_2O_5-P_2O_5 glasses, threshold and memory switching 77—76887
- V_2O_5-P_2O_5 glasses containing metallic particles, elec. props. 79—42547
- V_2O_5-P_2O_5-CaO glass with metal electrodes, elec. characts., thermal conditions effect *(Russian)* 78—47884
- V_2O_5-P_2O_5-$Cs_2O(Na_2O)$ glasses, enhanced secondary electron emission yield 80—93441
- V_2O_5-P_2O_5-MO system glasses, (M=Ba,Ca,Cu and Mg), phase separation, crystn. and EPR spectra 77—76321
- V_2O_5-P_2O_5-Nb_2O_5 glasses, switching 80—88604
- V_2O_5-TeO_2 glasses, ESR spectra 78—10755
- V_2O_5-WO_5, solid soln. thermogravimetric anal., ion formation on crystallisation 77—20076
- V_2O_5-ZnO-B_2O_3 glass, sputtered, optical absorpt., band gap and Urbach tail 77—8597
- $mV_2O_5.(100\text{-}m)P_2O_5$, (m=100-2), V(IV) complexes conc., absorpt. and ESR spectra 78—64266
- $V_{1+x}P_{1-x}O_{5-x/2}$ glasses, structure, adiabatic hopping conduction model 77—43588
- WO_3-B_2O_3-ZnO glasses, DC cond. and optical absorpt. 80—107783
- WO_3-MnO-P_2O_5 system, glass form. and memory effects 77—76888
- WO_3-P_2O_5 glass, thermoelec. power meas. 78—84242
- $ZnB^4C^5_2$, chalcopyrite struct., surface energy and compressibility, rel. to glass form. 79—51417
- ZnO ceramic containing rare earth metal oxides and Co_3O_4, non-ohmic props. 77—76833
- ZnO film, CVD growth and elec. props. 77—76973
- ZnS film, evaporated amorphous, mechanism of memory phenomena *(Japanese)* 78—23140
- ZnSe, amorphous thin film, prep. and electronic props. 77—85350
- a-ZnSe, elec. and optical meas., Mott-type model for amorphous semicond. 78—2414
- a-ZnSe, low temp. photocond., increase of activation energy as temp. decreases 78—26902

amorphous state
- *see also electrical conductivity of amorphous metals and alloys; electrical conductivity of amorphous semiconductors and insulators; electron energy states of amorphous solids; magnetic properties of amorphous substances; vitreous state*
- acids, conc. aqueous, amorphous protonic conductors, DC cond., glass transition and elec. relax. meas. 78—2290
- acoustic props. at low temps., ultrasonic attenuation, dielec. props. *(French)* 77—72658
- alkyl halide, amorphous, depolarisation thermocurrents and dielectric relaxation time distrib. *(French)* 80—60490
- allophane, synthetic, amorphous mineral struct. obs. using ^{57}Fe Mossbauer effect 80—34836
- alloy, and metastable phases, cryst. kinetics, review *(Japanese)* 80—38912
- alloy, struct. relax., compositional SRO 78—79538
- alloys, cold rolling 80—55423
- alloys, stability and structure, pseudopotential calcs. *(German)* 80—38913
- alloys, struct. determ. by energy dispersive X-ray diffraction 80—84063
- alloys, struct. end plastic flow, review 80—84090
- alloys, vibr. props., appl. to Si_xGe_{1-x} 77—4176
- amorphous ferromagnets, spatial fluctuations of magnetisation 79—19727
- amorphous-crystalline substances, high temp. plastic deform. interpret. 77—35627
- anomalous transient-time dispersion 78—31155

amorphous state continued
- anthracene, noncryst. solid, excimers, time resolved fluoresc. obs. 79—52006
- binary alloys, disordered, electronic struct. 77—15755
- bisphenol A-phthallic anhydride epoxy resin, diglycidyl ether, Rayleigh scatt., Brillouin and IR spectra 80—66211
- cation subsystem in binary cpd., amorphous state by rapid cooling 77—51322
- chain molecular amorphous solids, stat. thermodynamics and mol. theory 78—26442
- charge transport, continuous time random walk, simple approx. solns. 77—43584
- chlorobenzene-cis-decalin mixtures, phase transitions and dielec. behaviour study in 77-330K 80—29680
- trans-1,4-chlorobromocyclohexane, liquid, crystalline and amorphous state, conformation and vibr. spectra, IR obs. 80—60568
- trans-1,4-chloroiodocyclohexane, liquid, crystalline and amorphous state, conformation and vibr. spectra, IR obs. 80—60568
- conference on noncrystalline solids, Clausthal, Germany (Sept. 1976) 78—22654
- covalent alloys, amorphous, dimensionality of subnetworks 80—28916
- dark field speckle patterns in high resolution electron microscopy 78—34402
- Debye solid, amorphous and disordered harmonic, struct. factors 78—9954
- deformation, computer simulation 79—7647
- deformation processes 77—4813
- dielectric and US dispersion at low temps. freq. and temp. depend. 79—95092
- dielectric anomalies at very low temps., acoustic anomalies analogy 78—31146
- dielectric film, covalent, disruption of stationary state and electrical breakdown 77—20332
- dielectric film, ionic, disruption of stationary state and electrical breakdown 77—20333
- dielectric ribbon-form material, rapid quenching from melt *(Japanese)* 78—92210
- dielectric solids, molecular optics model, electrodynamic eqns. derivation 78—27151
- diffusion of nonspherical particles in amorphous solids, correl. effects 80—39337
- digital simulation using parallel computers in University research 79—54114
- dislocation model *(Japanese)* 79—42065
- disordered alloys, density of states, and their moments 77—11837
- disordered materials, inhomogeneous, numerical simulations of Hall effect 77—43551
- disordered metals, incipient Anderson localisation role in resistivity 80—49687
- disordered structure, deviations of polaron hopping mobility from Mott law 77—8095
- disordered system, electron density of states asymptote in a random field 80—44489
- disordered system, electron mobility in Gaussian random pot. 77—24543
- disordered system, ensemble averaged Green function, analytic approx. 77—11842
- disordered system, four-dimensional, electrons 77—8039
- disordered system, freq. depend. of hopping cond. 77—28174
- disordered systems, static. cond. at zero temp. and localisation of states 77—51715
- disordered systems, theory of Hall effect in hopping region 77—47836
- disordered systems, two dimensional, localisation of p-electrons 77—15784
- elastometric glasses and porous network polymers, review of future developments 78—22657
- electron localisation theory 77—1391
- electron microscopy, dose minimisation as criterion for selection of imaging modes 77—55220
- electron microscopy, high resolution imaging of amorphous materials 79—99039
- electron scattering, 1.2 to 3 MeV, Monte-Carlo method *(French)* 79—99037
- element, local fields coeffs. for classical electrostatic pot. calc. 78—34808
- entropy, excess, compared to ordered crystalline form 80—38914
- ethylene-propylene copolymer, melt struct., X-ray diffr. obs. *(Russian)* 79—23533
- EXAFS, determ. of struct. of disordered regions *(French)* 80—80905
- extended X-ray absorption fine structure using real space transform, struct. determ. technique 78—23553
- Fermi glass, theory for localised electrons 77—39807
- film, anomalous scatt. of photoinjected electrons *(Russian)* 78—52642
- film, surface phonon assisted tunnelling at low temp. 77—4421
- film, thickness meas. in electron microscope 79—26186
- film, tunnelling states, at low temps., thermal and acoustical props. 77—24500
- formation criteria *(Chinese)* 80—19702
- glass transition temp. rel. to low temp. phonon mean free path 79—51226
- glassy-amorphous structures, obs. by laser scatter light *(German)* 79—69015
- Hall effect in disordered and ordered systems, theoretical view 79—51605
- hard sphere model of noncrystalline solids, homogeneous and isotropic appl. to metallic glasses 78—83731
- high dielectric materials *(Japanese)* 79—73876
- high pressure effect on formation of amorphous state *(Chinese)* 80—28917
- high resolution dark-field images 78—26398
- implanted ion ranges and standard deviations 78—30656
- inorganic amorphous solids, struct., review 80—15004
- insulators, noncryst., electron density captured at traps, liberated to conduction band 78—87946
- interstellar amorphous ice grains, H_2 form. and importance for planetary atmospheres 80—26933
- ion implantation formation of amorphous layer *(Japanese)* 78—22746
- ion range in amorphous target, Lindhard-Scharff-Schiott theory refinement 77—15473
- ion scattering, lateral, in amorphous and polycryst. solids *(German)* 80—24508
- ion-implanted alloys, surface props. effects and appls. 80—79824
- IR absorption spectra, chem. bond. *(Russian)* 77—90155

amorphous state continued
irradiation induced crystalline to amorphous transition, Gibbs energy 80—70371
light scattering in amorphous media, object wave and its coherence 78—25799
liquid and amorphous metals, electronic states, optical theorem, multiple scatt. theory 80—49578
liquids and amorphous solids, similarity and short range order parameters 78—83730
low energy atomic motions and anomalies at low temps. 78—30724
low-energy excitations of phonons, magnons, electrons rel. to struct. factor 80—44488
lubricant, shear rheological behaviour at high press. 80—35342
magnetic material used in bubble memory devices, ^{85}Kr waste encapsulation appl. 80—47589
magnetic materials prep. techniques *(Japanese)* 79—43169
magnetic powder, prep. by atomisation technique 78—92213
mathematical models of disordered systems, book 80—1878
metal, amorphous struct., simple computer modelling 79—19154
metal, deformation mechanisms *(Japanese)* 79—42136
metal, elec. resistivity temp. depend. calc. 78—6342
metal, electron-phonon interaction effect on thermopower 80—29393
metal, electronic density of states 78—51868
metal, icosahedral microclusters as possible structural unit 78—34439
metal, ion implantation studies, review 77—43236
metal, struct. model and SRO characts. *(Japanese)* 77—84654
metal film, disordered and amorphous, quench-condensed, optical cond. and band struct. 77—1746
metal-metalloid amorphous systems, thermal instability, crystn. characts. 77—4044
metallic disordered systems, effect of nonorthogonality in density of states 77—59243
metallic glasses, amorphous, Young's modulus, using impulse induced resonance method 80—30008
metallic glasses, production and properties, technological appl. 80—71105
metallic glasses, structure, stability, phys. characts., prod. principles *(Hungarian)* 77—84656
metallic glasses props., development and appl. 80—19710
metallic thin films, optical props., effect of quench condensation 79—78773
metals, amorphous and liquid, electronic states, average spectrum 80—49579
metals, computer simulations of tensile deformation and radiation damage *(Japanese)* 79—42137
metals, geometric struct. models and diffraction exam. techniques 80—79700
metals, positron annihilation studies, book contrib. 79—99977
metals, superconducting properties rel. to ordering 80—65735
Metglas 2826 ribbon, voids formation during crystallisation 80—108428
MgSiO$_3$, Mg$_2$SiO$_4$, vapour condensed, mid IR optical props. 80—31337
minerals, irradiated, differential thermal anal. 79—62484
mixed system, correlation of Tg, glass transition 80—24574
mobility edge properties for disordered system 77—4330
models and exptl. methods, review 78—22655
molecular crystal, exciton density of states, effect of struct. disorder 79—28288
Mossbauer effect, props. and investigation methods *(French)* 80—80652
Mossbauer effect appl., conference, Kyoto, Japan (Aug.-Sept. 78) 80—7199
Mossbauer spectra of amorphous materials, anal. 77—20762
neutron diffraction, struct. investigations of melts and amorphous substances *(German)* 80—44108
neutron induced at. cascades, slowing down 77—1156
non-Markov carrier diffusion 80—6841
noncrystalline materials, personal review by Sir Nevill Mott 78—55811
olivine, IR extinction with appls. to interstellar dust 79—53873
one-dimens. disordered solid, anomalous specific heat 79—23746
optical oscillator strengths and excitation energies in liquids, solids and mols. 78—6648
organic glass, creep under shear with superposition of hydrostatic press. 78—31482
organic solids, cryst. and amorphous, optical spectra, Urbach rule, struct. disorder effect 78—23479
origin of thermal anomalies, struct. model 78—91256
pentacene, disordered solid layer, absorpt. spectra 80—93417
phonon echo *(Russian)* 77—80596
phonon scattering by density fluctuations and thermal conductivity 80—10626
physical structure, of amorphous state, conf., Atlantic City, USA (Sept. 1974) 77—76327
PMMA, amorphous, electron microscope and small angle X-ray studies 77—84666
PMMA, amorphous, reorientational relax., 6-165°C, polarised laser beam scatt. correlation 78—2864
PMMA, amorphous, tunnelling models and thermal expansion below 4K 79—73326
PMMA, amorphous polymer, Rayleigh scattering of Mossbauer γ-rays 80—39926
PMMA, visoelastic props., γ-irrad. influence *(Russian)* 78—88492
poly(ethyleneterephthalate)-p-hydroxybenzoic acid copolyester, liquid crystalline, X-ray scatt. obs. 78—9949
poly-N-n-alkylmaleimides, glass transition temp. 77—65956
polyalkylene tetephthalates, amorphous and cryst., durability under stretching *(Russian)* 78—88511
polyamide chain, conformational freedom above MP 77—55344
polycarbonate, amorphous, electron microscope and small angle X-ray studies 77—84666
polycarbonate, amorphous, yield behaviour in oriented and unoriented condition, effect of temp. 80—97537
polycarbonate, TSC anal. by activation energy spectra 80—20579
polydimethyl siloxane, Brillouin scatt. and hypersonic relax. 77—55795
polyethylene, amorphous fraction determ., multiple pulse NMR 77—77107
polyethylene, glass temp. 77—66017
polyethylene, high density, effects of draw rate and temp. on necking stress *(Japanese)* 79—91757
polyethylene, irrad., thermophys. characts. of amorphous phase, effects on crystallinity 77—7870
polyethylene, linear, quenching of thin films to amorphous state 80—28929

amorphous state continued
polyethylene, melt crystallized, amorphous phase, IR spectrum 78—76463
polyethylene, melt struct., X-ray diffr. obs. *(Russian)* 79—23533
polyethylene, MP, heat of fusion, degree of crystn. determ. by differential scanning calorimetry *(Russian)* 77—62489
polyethylene, stress rel. to draw ratio during ultra draw *(Japanese)* 79—91759
polyethylene, struct. from NMR line shape analysis and MAR-NMR 80—28931
polyethylene, terephthalate, amorphous, electron microscope and small angle X-ray studies 77—84666
polyethylene, ultradrawing, effects of temp. and drawing rate *(Japanese)* 79—91760
polyethylene film, melt-cast, deform. in equatorial region of spherulites, electron diffr. 77—25115
polyethylene terephthalate, amorphous state change by heat treatment below glass transition temp. 78—30550
polyethylene terephthalate, film, two-stage orientation in monoaxial extension *(Russian)* 77—62488
polyethyleneterephthallate, sorption of low MW solvents on struct. and mech. props. *(Russian)* 78—11358
polyisobutylene, Brillouin scatt. and hypersonic relax. 77—55795
polymer, amorphous, domain struct. determ. by electron microscopy and electron diffr. 77—84667
polymer, amorphous, enthalpy relax. rel. to T$_g$ 77—52278
polymer, amorphous, high temp. thermal transport, phonon modes 77—62691
polymer, amorphous, segmental distrib., light-, neutron- and X-ray scatt., piezooptical and dielec. meas., review 78—51444
polymer, amorphous, struct. determ. by small-angle X-ray and neutron scatt. 77—84668
polymer, bulk, structure models and exptl. methods, review 78—22671
polymer, chain conform., small-angle neutron scatt. obs. *(Polish)* 80—10511
polymer, crystn. rate eqn., effect of vol. relax. of amorphous material 77—62482
polymer, mag., suscept. and neutron scatt. function 77—12099
polymer, molecular origin of relaxations 78—26058
polymer, oriented, amorphous-crystalline low ang. X-ray diagrams, supermol. struct. models, schematic representation *(Russian)* 78—87630
polymer, rubberlike, time-temperature-pressure superposition phenomena, free volume theory 78—26059
polymer, stress-optical investig. of short-range order 78—22672
polymer, super-glass transition processes, damping process 80—24573
polymer, translational motion and lattice vibr. obs. by Raman scatt., T$_g$ phenomena 78—23469
polymer matrix, amorphous, stressed, thermodynamics of embedded crystallite deform. *(Polish)* 77—52424
polymer multiple dielectric relaxation, time-correlation function representation 80—15951
polymer solutions, conc., Adam-Gibbs theory, for viscoelasticity and glass transition 78—83353
polymeric noncrystalline chain orientation evaluation, with polarised fluorescence method *(Japanese)* 80—6368
polymers, hydrostatic extrusion effects on subsequent mechanical behaviour 77—90392
polymers, localised low-energy excitations 79—73322
polymers, semi-crystalline, dynamical mech. props., relaxation *(French)* 77—72653
polymethylpentene, visoelastic props., γ-irrad. influence *(Russian)* 78—88492
polypropylene, amorphous, ^{13}C NMR spin-lattice relaxation times of isotactic, syndiotactic sequences 77—4572
polypropylene, atactic, Brillouin scatt. and hypersonic relax. 77—55795
polystyrene, amorphous, failure in methanol and ambient air 80—3165
polystyrene, amorphous, low temp. sp. ht. calcs. 77—28014
polystyrene, atactic, chain length depend. of hypersonic relax., Brillouin spectra 77—55797
polystyrene, oriented amorphous, supermol. structures rel. to mech. behaviour 78—22673
polystyrene, press. effect on glass transition and glassy state 78—26674
polystyrene, T$_{||}$ relax. above glass transition 79—4259
polystyrene films, amorphous, X-ray small angle scatt. near glass transition, struct. *(Russian)* 77—31606
polyvinyl acetate, Brillouin scatt. and hypersonic relax. 77—55795
polyvinylacetate films, amorphous, X-ray small angle scatt. near glass transition, struct. *(Russian)* 77—31606
quartz, amorphous and crystalline, surface polaritons and splitting of optical frequencies 78—72090
quartz, piezoelectric layer, non-crystalline characteristics after ion implantation *(French)* 77—73117
radial distribution functions, for liqs. and amorphous substances, analytical computation method 80—24301
radiation suppression *(Russian)* 78—30686
Raman intensities, connection with EXAFS Debye-Waller factors in amorphous solids 80—108214
rapid quenching, techniques for determ. very short room temp. lifetimes of amorphism 80—84981
rare earth amorphous alloys, cryst. field, nonaxial elec. field gradient 80—20138
rare earth-3d transition metal amorphous alloys, crystallisation behaviour 80—49116
recrystallisation kinetics, system of eqns. 78—22650
refractory films, stability, high temp. and electron irrad. effects 77—39747
RHEED patterns from amorphous surface, refr. correction 78—71646
s-p superconductor, Eliashberg function, phonon spectrum 78—88066
semiconductor, electronic props. and struct. *(Japanese)* 79—47179
silicates, IR extinction meas., rel. to interstellar dust 77—12352
soft-core amorphous system, mol. dynamics 80—6359
solid, abnormal bonding and electronic states in forbidden energy gap 78—51942
specific heat at low temps. 77—11703
specific heat of disordered solid, linearity at low temp. 77—69097
sputtering of amorphous target, ang. distrib. of sputtered atoms 79—69947
steel, alloy high-C, amorphous, mech. props. and thermal stability 80—76361
stochastic geometry, review, book contrib. 80—73269

amorphous state continued
  structure determination by diffraction methods, philosophical aspects 78−50665
  structured defects, computer simulation study 80−88040
  summer school on ill-condensed matter, Les Houches, France (July-Aug. 1978) 80−82561
  superconducting amorphous metals, mag. impurity interactions 80−44777
  surface, energy profile and binding energy, computer simulation 80−100381
  surface phonons, tunnelling states and propagation characts., low temps. 79−69337
  surface-gas interaction, model potential 79−46919
  swollen rubber network, stress-optical coeff. and amorphous order 77−77169
  symmetry of short-range order, polyhedra model 78−42913
  TEM, filtered electron image contrast for elastic scatt., calc. 80−107026
  TEM, tilting and defocus effects in high resolution dark field images 80−79652
  tetracene, disordered solid layer, absorpt. spectra 80−93417
  tetrahedrally-bonded solid, electronic struct., theoretical approach 80−29315
  thermally stimulated creep method for mol. motions investig. 78−22787
  thermoluminescence, traps and emission centres 79−24373
  thin films condensed onto cold substrate, prism-film coupler for in vacuo investigation 78−24873
  transition metal alloys, disordered, formation energy of vacancies 77−27876
  transition metal binary alloy, amorphous and crystalline, superconducting transition temp. correlation with solute conc. 78−52139
  transition metals, amorphous, prep. and struct., rel. to liq. struct. 77−51323
  transition metals, amorphous, superconducting transition temp. *(Chinese)* 80−54817
  transition metals, liq. and amorphous, elec. transport 77−51720
  trap-controlled transient current injection 79−23984
  TSC calculations for amorphous materials 80−7284
  two dimensional random lattice, struct. and vibr. props. 77−7820
  vacancies and vacancy clusters, stability under relaxation 80−15005
  vapour quenching techniques, high-rate, use in amorphous phase prep. 80−80977
  very far IR props. of amorphous solids 78−80344
  X-ray diffraction, extremely asymmetric Laue case, small incidence angle 77−84567
  X-ray K-absorption edge chemical shifts 80−80904
  AgI film, crystallisation, exciton absorption spectra meas. 77−35483
  Ag$_{83.3}$Nd$_{16.7}$ amorphous alloy, EPR of Nd^{3+} 79−65727
  Al-Cu, splat quenched, amorphous regions 77−4047
  Al-Cu, splat quenched, amorphous regions, comment 77−4048
  Al-polymer joint, meas. of temp. dependence of joint strength 80−50824
  Al$_2$O$_3$ amorphous layers in MIS structures, prep. and physical props. *(Slovak)* 78−64122
  Al$_2$O$_3$, range of ^{29}Si meas. by (p,γ) reson. broadening 77−69023
  Al$_2$O$_3$-Ln$_2$O$_3$, Ln=La,Ce,Pr,Nd,Sm,Gd,Tb, struct. and thermal characts. of amorphous phases *(French)* 77−72558
  β-Al$_2$O$_3$-Na$_2$O, non-stoichiometric, amorphous, US attenuation and velocity 80−39228
  As, amorphous, bonding coordination defects, Raman scatt. and IR absorption meas. 78−60498
  As, amorphous, effect of high press. on elec. props. 77−59309
  As, amorphous, electron and phonon density of states calcs., comp. to XPS 78−56066
  As, amorphous, electronic struct. of defects using cluster-Bethe-lattice method 79−73471
  As, amorphous, thermally generated paramagnetism 79−19720
  As, amorphous, US attenuation and sound vel. meas., 4.2 to 300K; 80−49308
  As, amorphous and cryst., phonon density of states calc., comp. to IR absorpt. and neutron scatt. data 78−55924
  As amorphous solid dielectric loss meas. by submillimetric waveguide laser 79−33603
  As, condensed layers, low temp. allotropic phase transition *(Russian)* 80−54553
  As, low temp. thermal cond. and sp. ht. 79−28161
  As, phonon frequency distrib. 78−30723
  As, phonon states 79−60464
  a-As, second and third order elastic consts., ultrasonic velocity meas. 80−103408
  As, sp. ht. and thermal cond. at low temp. 79−65213
  As, spontaneous crystallisation temp. determ. 77−27833
  As$_2$S$_3$, amorphous film, photodissolution of Ag, struct. changes 77−11815
  Au amorphous film, getter sputtering at 25K 79−38741
  Au, bombard. by Au ions, collision cascades, computer simulation 79−46731
  Au$_{35}$Ni$_{65}$, vapour quenched amorphous alloy, atomic arrangements 80−100173
  Au$_{1-x}$Si amorphous metallic films, optical props. as function of composition 79−95865
  Au$_{1-x}$Si$_x$, amorphous film, spectra 0.01-6.2 eV, $0.13 \leq x \leq 0.5$ 78−68574
  Au$_x$Si$_{1-x}$ amorphous alloy, crystallisation, elec. cond. study 80−103246
  B, amorphous film, Raman scatt. exam. 78−39545
  B, struct. changes on Zn incorporation 78−79596
  B, X-ray Raman scatt. 78−48157
  B:C,H amorphous film, IR absorpt. spectra 77−77312
  B-transition metal, amorphous thin film, crystallisation, TEM obs. 79−19483
  B-transition metal thin films, amorphous to cryst. transformation 80−7563
  B$_2$O$_3$, amorphous, acoustic props. at 20 GHz, Brillouin scatt., 3-300K 80−24536
  BaCl$_2$, non-crystalline film, disorder-induced Raman scatt. 80−11387
  BaFCl, non-crystalline film, disorder-induced Raman scatt. 80−11387
  BaFe$_2$O$_4$ amorphous film, prep. by RF sputtering, crystallisation 80−76183
  BaPb$_{1-x}$Bi$_x$O$_3$ film, RF sputtered, T$_c$ as function of comp. and annealing conditions 79−24100
  BaTiO$_3$ ceramics, PTC-type, grain boundary study using TEM 80−107267
  BaTiO$_3$, phonon spectroscopy, amorphous versus crystalline material 78−83898

amorphous state continued
  Be, amorphous, reflection of D and T, Monte Carlo study 80−40197
  Bi, amorphous films, supercond. fluctuation effects in perpendicular mag. fields 79−60980
  Bi, amorphous metal films, crystallisation with and without mag. field 80−70570
  Bi film, supercond. fluctuation effects in resist. transition 78−10609
  C, amorphous, diffraction intensities, chem. bonding effects 77−72557
  C, amorphous, inelastic electron scatt., valence electron contrib. 80−55240
  C, amorphous, X-ray and electron diffr. intensities, model struct. 78−26441
  C, amorphous film, spin resonance, IR spectra, microhardness 80−71157
  C, amorphous film, vac. evaporated, density meas., microcrystalline model of struct. 80−2313
  C, electron energy loss spectra 79−47566
  C film, adsorpt., atomic imaging using the dark-field annular detector in the STEM 80−6331
  C film, amorphous, surface plasmon dispersion, electron energy loss spectra meas. *(French)* 77−63504
  C film, growth under ion impact in butane plasma, and IR transparency 78−52688
  C film, prepared by vac. evaporation, density meas. 77−80714
  C foil, electronic energy straggling of light ions, at. number depend. 77−11612
  C foil, influence of detector geometry on STEM image props. 77−56554
  C, glass tip, field emission current stability 80−11544
  C, glassy, surface erosion by ion bombardment crystal anisotropy effect 78−23845
  C, Lifshitz constant for calc. of van der Waals force between two solids *(French)* 80−107658
  C, ranges of implanted 10-30 keV D$^+$ 78−83858
  C substrate, cluster migration in early stages of Au film growth 79−77964
  C, tip, field emission characts. 80−11543
  Cd-Mn, dil., lattice state effects on pair breaking 77−8219
  Cd-Sb alloy condensate film, phase transform. kinetics 77−15721
  Co, amorphous and liquid, density of electronic states 79−23881
  Co, amorphous and liquid states, electronic states and transport 79−99474
  Co, random close packed, normal Hall effect meas. 77−35924
  Co, resist. calc. using t-matrix approach 77−55510
  Co-Ar film, struct., electron diffr. meas., rel. to metal-nonmetal transition 77−51626
  Co-Fe-B, amorphous, crystn. and thermal stability 80−107057
  Co-Gd film, prep. conditions influence on supernetwork struct. 77−76709
  Co-Ni-Mo-C, amorphous alloys, med. props. and thermal stability *(Japanese)* 80−85049
  Co-P foil, complex permeability and eddy currents, annealing induced short-range order 77−8360
  Co-Si-B-Fe amorphous alloy, electron diffr., mag. anal. *(German)* 79−61182
  Co-Ti (22 at.%), amorphous eutectic phase 80−55360
  Co-X-Co (X=Cr,Mo,W) systems, crystn. temp. and hardness 79−77529
  Co$_{70}$Fe$_5$Si$_{15}$B$_{10}$, amorphous, crystn. and thermal stability 80−107057
  Co$_2$Ge$_3$, CoGe$_2$, amorphous film, annealing effects on struct. and elec. resist. 77−85099
  Co$_5$Ge$_3$ amorphous film, elec. resist., microstruct. and annealing 77−85188
  Co$_4$P, amorphous ferromag., mag. excitations calc. in Heisenberg model 77−1546
  Co$_{75}$Si$_{15}$B$_{10}$, amorphous, crystn. and thermal stability 80−107057
  Cr, resist. calc. using t-matrix approach 77−55510
  Cr-Ge liquid and amorphous alloys, struct. props., cond., viscosity, surface tension *(Russian)* 80−54119
  Cr-X-C amorphous alloys, (X=Fe, Co, Ni, Nb, Mo and Ta), crystn. temp. and hardness 79−73133
  Cr$_{11}$Ge$_8$, CrGe, and Cr$_{11}$Ge$_{19}$ films, short-range order, electron diffr. obs. *(Russian)* 78−56050
  Cr$_3$Ge amorphous films, short range order struct. *(Russian)* 78−30841
  Cs amsorphous film, catalytic crystallization by Ni particles 79−14683
  Cu, amorphous, sputtering, computer simulation in binary collision approx. 79−56900
  Cu, bombard. by Au ions, collision cascades, computer simulation 79−46731
  Cu, metastable alloy form. by ion implantation 79−82252
  Cu-Ag-P amorphous alloys, strain gauge factor and elec. props. *(Japanese)* 79−79130
  Cu-Sn alloys, electron-phonon interaction effect on thermopower 80−29393
  Cu-Zr alloys, amorphous, struct. X-ray scatt., rel. to Ni-P alloys 77−51324
  CuCl, disordered, diamag. transition 80−34636
  Cu$_{0.57}$Zr$_{0.43}$, partial struct. factor, TOF pulsed neutron diffraction 79−14684
  Cu$_{57}$Zr$_{43}$, amorphous alloy, computer simulation of atomic structure 80−70125
  DyCo$_{3.4}$, amorphous, mag. props. 77−32177
  Fe, amorphous, realistic structural model, search for Bernal holes 78−83734
  Fe, amorphous, reflection of D and T, Monte Carlo study 80−40197
  Fe amorphous film, getter sputtering at 25K 79−38741
  Fe base amorphous alloys, Ni addition effect on corrosion resistance 77−4869
  Fe base amorphous alloys, alloying element role in improving corrosion resist., ESCA study 80−50754
  Fe based amorphous alloys, Invar effects, mag. and elastic props. *(Japanese)* 79−20100
  Fe, chain of Bernal holes, dislocation model 79−4249
  Fe, liquid and amorphous states, electronic states and transport 79−99474
  Fe, metastable alloy form. by ion implantation 79−82252
  Fe, radiation damage simulation 80−34045
  Fe, resist. calc. using t-matrix approach 77−55510
  Fe, short-range order, comparison with liquid state 77−1069
  Fe, struct. model, polyhedron and cavity anal. 79−50994
  Fe, structure factor of liquid near transform. to amorphous solid, X-ray diffr. *(Russian)* 77−31579
  α-Fe, vibrational states, phonon dispersion, phonon softening 80−88289

amorphous state continued
Fe^{3+} ions, in frozen aq. solns., spin-spin relax., Mossbauer obs. of effect of paramag. impurity ions 79—33573
Fe:Ti, C induced amorphous surface layers 80—107287
Fe-B, amorphous, crystn., metal or metalloid exchange influence 80—75172
Fe-B amorphous ribbons formation, high-speed photography investigation 80—76216
Fe-base amorphous alloys, embrittled by H and heat-treatment 80—55518
Fe-C (4.3 wt.%), splat cooled, amorphous phase form. and crystn. 77—15323
Fe-C-Mn-Si (4, 2, 1.5 wt.%), cast wire, influence of B addition on struct. and elec. cond. *(Russian)* 80—55391
Fe-Co-Mo-C, amorphous alloys, med. props. and thermal stability *(Japanese)* 80—85049
Fe-Ni-Mo-C, amorphous alloys, med. props. and thermal stability *(Japanese)* 80—85049
Fe-Ni-P-B amorphous ribbons, form. by melt spin technique 80—76215
Fe-P-B, amorphous alloy, Mossbauer effect and short-range order 80—2675
Fe-P-C, amorphous alloy, Mossbauer effect and short-range order 80—2675
Fe-rare earth, amorphous thin film, crystallisation, TEM obs. 79—19483
Fe-Si amorphous film, conversion electron Mossbauer effect 78—72440
Fe-Si amorphous film, crystallisation, Mossbauer studies 80—33900
Fe-Si amorphous film, Hall const. and magnetoresistive effect 78—52105
Fe-Y(Th)(Zr), amorphous, charge transfer and mag. props., ^{57}Fe Mossbauer spectra 79—19719
Fe_{40} $Ni_{40}B_{20}$, amorphous alloy, ductile-brittle transition temp., relation to composition 78—52972
$Fe_{80}B_{20}$ amorphous ribbon, initial susceptibility time lag 80—100579
$Fe_{80}B_{20}$, amorphous to cryst. transorm. 80—34188
$(Fe_{0.05}Co_{0.95})_{78}Si_8B_{14}$ amorphous ribbon, anomalous mag. aftereffect 80—100602
$FeGe_2$, amorphous film, annealing effects on struct. and elec. resist. 77—85099
Fe_3Ge films, short-range struct., electron diffr. obs. 77—24267
Fe_5Ge_3, amorphous film, elec. resist., microstruct. and annealing 77—85188
Fe_5Ge_3 film, electron diffr. study of struct. and microheterogeneity 77—85108
Fe_xGe_{1-x}, amorphous alloy, short range order anal. 77—80423
FeNi amorphous films, fast phase transition investigation by TEM method 80—107029
$Fe_{40}Ni_{40}C_{14}P_6$ amorphous film, dislocation and mag. struct., neutron diffr. study 80—70956
$Fe_{40}Ni_{40}P_{20}$, amorphous alloy, ductile-brittle transition temp., relation to composition 78—52972
(FeNi)PB amorphous wires, surface oxidation and annealing influence on induced anisotropy 80—100957
$Fe_{40}Ni_{40}P_{14}B_6$, amorhpous ribbon, influence of torsion on mag. props. 80—7138
$Fe_{40}Ni_{40}P_{14}B_6$, amorphous alloy, ductile-brittle transition temp., relation to composition 78—52972
Fe_2O_3, plasma sputtered coatings, oxide dissociation, coating props., struct. and composition *(Russian)* 80—54577
FePC molten and amorphous alloys, struct. factors 80—79674
FeSb alloy films, vapour-deposited, formation of metastable phase 80—44437
Ga, amorphous metal films, crystallisation with and without mag. field 80—70570
GaAs, implanted amorphous layer reordering 77—76435
Gd-Co amorphous films, correlation between struct. and mag. props. *(Chinese)* 80—54532
Gd-Co amorphous films, mag. struct., mag. bubbles, electron diffr. study *(Chinese)* 80—71126
Gd-Co amorphous thin films, crystn. process and domain struct. *(Chinese)* 80—54533
Gd-Co thin films sputtered from mosaic target, thickness and composition distrib. 80—6676
$Gd_{0.37}Al_{0.63}$ film, amorphous, spin-glass order parameter meas. 77—28396
a-GdCo film, magneto-optical Kerr effect spectra 77—12458
$(Gd_{1-x}Co_x)_{1-y}Ar_y$ amorphous mag. film, elec. and mag. prop. depend. on Ar 80—80410
$Gd_{0.27}Co_{0.64}Kr_{0.09}$, amorphous film, thermal release of Kr and H, meas. using UHV mass spectrometric technique 80—3439
Ge alloy, amorphous film, formation and stability criteria 79—10799
Ge alloys, amorphous film, crystn. transform. kinetics 78—22653
Ge-Ga alloys, amorphous, far IR absorption 78—88306
GeO_2, phonon frequency distrib. 78—30723
GeS layers, between Al electrodes, dielec. relax. currents, pot. distrib. 77—16250
H_2O ice, interstellar, as source of 3.1 μm absorpt. in mol. clouds 80—26956
H_xWO_3, amorphous, Anderson transition, disorder depend. and optical detection 78—47840
H_xWO_3 films, proton diffusion coeffs. 80—6548
In_2S_3, film struct. and props. 77—80706
IrO_2 anodic amorphous film, electrochromism isotherms, internal entropy 80—50300
$KFeF_4$, amorphous, Mossbauer study 80—39970
La-Al amorphous alloys, internal friction, relaxation process 80—92607
La-Al(Ge)(Au), alloying effect on supercond. props. 79—60951
La-B, amorphous, B-rich, low freq. modes, Raman scatt. obs. 80—108202
La-Ni-H compounds, prep. by gas absorpt. in La-Ni system, struct. 77—9078
La-Sm-Au, amorphous, surface effects on Sm valence, XPS and X-ray absorption meas. 80—108325
$La_{18}Au_{22}$, amorphous, evidence for short wavelength cutoff in fluctuation spectrum 78—68113
$La_{76}Au_{24}$, disordered ribbons, production of quenched samples using arc furnace 80—71612
$La_{70}Cu_{30}$, disordered ribbons, quenched samples production using arc furnace 80—71612
$La_{1-x}Ga_x$, amorphous foil, Hall coeff. meas. 80—20153
$La_{1-x}Ga_x$ foils, amorphous, splat cooled, calorimetric and resistive meas. 79—33417

amorphous state continued
$LiNbO_3$, amorphous ribbons, prep., electron and X-ray diffr. obs., dielec. const. temp. depend. 79—50993
$LiNbO_3$, piezoelectric layer, non-crystalline characteristics after ion implantation *(French)* 77—73117
Mn, resist. calc. using t-matrix approach 77—55510
Mn-Bi film, form. and crystn. 79—28923
Mn_3Ge_2, $Mn_{11}Ge_8$, amorphous thin films, quasieutectic model, electron diffr. investigation of short range order 79—69013
Mo, amorphous, reflection of D and T, Monte Carlo study 80—40197
Mo, amorphous thin films, for photothermal conversion, CVD fabrication 80—7503
Mo superconducting film, amorphous and crystalline, transition temp. exam. by UPS 79—28433
Mo:N film, high T_c amorphous phase stabilisation by interstitial nitrogen 78—23622
Mo-Ge(Bi) amorphous films, supercond. transition temp. and residual elec. resist. *(Russian)* 79—19680
MoO_3 amorphous films, EPR of Mo^{5+} centres 80—34771
MoO_3, film, colour centre studies, optical absorpt. spectra 78—71724
$(Mo_{0.5}Ru_{0.5})_{80}P_{20}$, amorphous normal and mixed supercond. state, ^{31}P NMR 79—87193
MoS_2, amorphous, cathode, electrochem. props. rel. to secondary Li battery 80—40851
MoS_3, amorphous struct., X-ray radial distrib. anal. and XPS 80—49115
Na-A zeolite, struct. obs. by high-resolution electron microscopy 80—84175
$NaFeF_4$, amorphous, Mossbauer study 80—39970
Nb-Ge, amorphous supercond. alloy, resistivity, transition temp. 80—60126
Nb-Si amorphosamorphous thin film tunnel junctions 79—28473
Nb-Si liquid quenched alloy, metastable A-15 and amorphous phases, interstitials 80—54394
Nb_3Ge, amorphous nongranular thin superconducting film, thermodynamic and resistive transitions 80—34571
Nb_3Ge, ordered and disordered A15 phases, energy gaps, tunnelling 77—8235
Nb_3Ge, supercond. film, amorphous content, X-ray diffr. study, rel. to transition temp. 80—75668
Nb_3Ge, superconducting hybridisation and bonding, XPS exam. 78—2988
$Nb_3Ge(Si)$, RF sputtered films, amorphous atomic scale struct. 80—84064
$Nb_{50}Ni_{50-x}Fe_x$, mag. interactions 78—95432
Nb_2O_5 film, in MIM struct., Schottky barrier effects on dielec. props. 77—8203
Nb_3Si A15 phase from amorphous Nb-Si alloys, high-press. synthesis 80—93516
Ni, amorphous and liquid states, electronic states and transport 79—99474
Ni, amorphous film, getter sputtered at 25K, resistivity, Curie temp. 78—52673
Ni, amorphous film, getter sputtering at 25K 79—38741
Ni films, RF sputtered, O_2 incorporation, ESCA obs. 80—10832
Ni, metastable alloy form. by ion implantation 79—82252
Ni, resist. calc. using t-matrix approach 77—55510
Ni-Au film, ferromagnetic, anomalous Hall resist. 77—15832
Ni-B amorphous alloy film, atomic and electronic transport *(French)* 78—84325
Ni-Co-P, electrical and mag. props. 78—95281
Ni-Cr-P, amorphous, corrosion behaviour, immersion tests and electrochem. meas. *(Japanese)* 80—85085
Ni-Mn alloy, disordered FCC, stiffness const., single cryst. neutron inelastic scatt. meas. 77—20558
Ni-P, amorphous, electrical transport, appl. of extended Ziman theory 77—47787
Ni-P, amorphous, low P, struct. study using high-angle X-ray diffr. 80—107055
Ni-P, amorphous, prod. by ion implantation 80—75257
Ni-P, amorphous, struct., X-ray scatt., rel. to Cu-Zr alloys 77—51324
Ni-P, amorphous electrodeposited alloys, phase-separation *(Japanese)* 80—54140
Ni-P, amorphous metallic, sound attenuation and rel. meas. 77—31722
Ni-P, amorphous metallic, logarithmic temp. depend. of sound vel. 77—31725
Ni-P, metallic glass, acoustic wave vel. log. temp. depend. *(French)* 77—72659
Ni-P amorphous alloy, positron annihilation exam. of crystallisation 79—43061
Ni-P amorphous alloy prep. by ion implantation 78—22748
Ni-P amorphous thin films, crack networks of voids 78—2399
Ni-Ti-P, amorphous, corrosion behaviour, immersion tests and electrochem. meas. *(Japanese)* 80—85085
$Ni_{66}B_{34}$, morphological, structural and phys. props. *(French)* 80—44444
$Ni_{0.625}GE_{0.375}$, film, crystn. mechanism *(Russian)* 77—51623
NiGe, and Ni_2Ge, amorphous film, electron diffr. exam. of struct. 77—35828
Ni_3Ge, amorphous film, electron diffr. exam. of struct. 77—35827
Ni_5Ge_3, amorphous film, elec. resist., microstruct. and annealing 77—85188
$Ni_{80}P_{20}$ amorphous alloy, liquid-quenched structure 77—1082
$NiSi_2$, amorphous, crystallisation by energy beam annealing 79—69012
P, amorphous, NMR studies 79—69740
P, amorphous, stability in air, XPS study, comparison with cryst. polymorphs 80—25517
P, amorphous, struct. by electron microscopy 80—84065
P, amorphous, US attenuation and sound vel. meas., 4.2 to 300K; 80—49308
P, amorphous film, prepared by chemical transport in glow discharge, electronic props. 79—24011
P, bulk red amorphous, Raman scatt. and IR absorption 79—24323
P, prepared by chem. transport in low-press. H_2 plasma, radial distrib. function 80—64899
P, XPS anal. of stability, form. of oxidised layer *(German)* 79—11496
Pb film, amorphous, nucleated with Mo, supercond. and normal elec. cond. 77—24633
Pb microclusters, mol. beam electron diffr., amorphous struct. 78—66703
Pb-Ar (Xe) film, struct., electron diffr. meas., rel. to metal-nonmetal transition 77—51626
Pb-Ar films, atomic arrangements, high energy electron energy diffractogram study, Ar conc. depend. 79—99444

amorphous state continued
- Pb-Bi film, amorphous and polycrystalline, specific heat meas. 77—80715
- Pb-Ga(Ge)(Si)(Mo)(Bi) amorphous films, supercond. transition temp. and residual elec. resist. *(Russian)* 79—19680
- $PbTiO_3$, $(PbTiO_3)_{0.9}(B_2O_3)_{0.1}$ amorphous ribbons, prep., electron and X-ray diffr. obs., dielec. const. temp. depend. 79—50993
- $PbTiO_3$, amorphous, crystallisation process, DTA and Raman spectroscopy meas. 80—75161
- Pd-Au-Si, amorphous films, RF sputter deposition, composition and thermal behaviour 80—55292
- Pd-Ni-Si amorphous alloys, crystn. process during isothermal ageing 80—89275
- Pd-Si, amorphous, US velocity, freq. and temp. depend. 78—63812
- Pd-Si, amorphous metallic, sound propag. at low temps. 77—72656
- Pd-Si, amorphous thin films, laser irrad., metastable phases 80—96622
- Pd-Si amorphous alloy, positron annihilation exam. of crystallisation 79—43061
- Pd-Si amorphous films, RF and DC sputter deposition, composition and thermal behaviour 80—55292
- Pd-Si-H(D) alloys, superconductivity in solid solution and amorphous phase regions, isotope effect 79—56347
- $Pd_{78}Ag_4Si_{18}$, amorphous, crystallisation kinetics 77—35487
- $Pd_{82-x}Ag_xSi_{18}$, amorphous, roller-quenching conditions determ. 77—21051
- $Pd_{70}Fe_{10}Si_{20}$ alloy, amorphous to cryst. transition, 350 to 450°C, Mossbauer spectra 78—59758
- $Pd_{60}Ni_{20}Si_{20}$, amorphous, struct., high resolution electron microscopy 80—1969
- PdSi alloys, amorphous thermal behaviour and crystallisation kinetics 78—26446
- $Pd_{0.8}Si_{0.2}$ alloy, short-range order, comparison with liquid state 77—1069
- a-$Pd_{0.8}Si_{0.2}$ alloy, struct. factor determ. rel. to short-range correlations 77—1060
- $Pd_{0.8}Si_{0.2}$, amorphous, He^{2+} ion irradiation effect on structure 79—42120
- Pd_4Si and Pd_2Si, amorphous, crystallisation by energy beam annealing 79—69012
- $Pd_{80}Si_{20}$, amorphous, structural changes by neutron irradiation, X-ray scatt. meas. 78—6104
- $Pd_{80}Si_{20}$, vapour quenched amorphous alloy, atomic arrangements 80—100173
- $Pd_{100-x-y}Si_xFe_y$, amorphous, ^{57}Fe Mossbauer spectra, X-ray diffr., ageing behaviour 79—28651
- PdZr, amorphous, supercond., US props. 80—44765
- $Pr_xLa_{80-x}Au_{20}$, amorphous, low temp. excitations, specific heat 80—100337
- Pt-Au, amorphous struct. produced by Au implantation, spinodal decomp. TEM obs. 78—31379
- Pt-Si, amorphous thin films, laser irrad., metastable phases 80—96622
- Pu-transition metal alloys, prod. by high rate sputter deposition 77 -21025
- $R_{1-x}Co_x$, rare earth amorphous alloys, thermal stability, elec. cond. enthalpy 80—100172
- S, amorphous and monoclinic transform. kinetics *(German)* 79—42239
- Sb, amorphous film on glass substrate, effect of substrate temp. on crystallisation 80—39468
- Sb, critical thickness observations for crystallisation in amorphous thin films 79—69379
- Sb electrodeposit, explosive crystn., semicond-semimetal transition and IR absorpt. 78—51849
- Sb-Au amorphous film, quench condensed, struct. and stability 79—99459
- Sb-Au amorphous films quench-condensed, resistivity and Hall effect meas. 79—99638
- Sb_2S_3-SbI_3, amorphous phase formation in vacuum condensates, TEM study 79—86712
- Se, amorphous, acoustic behaviour in terms of model involving stochastic reson. 79—23681
- Se amorphous solid dielectric loss meas. by submillimetric waveguide laser 79—33603
- a-Se, hole form. energy, heating time and cooling rate depend. 79—41958
- Se, liquid and amorphous, struct. modelling using Monte Carlo method 80—59391
- Se, vacuum evaporated film, photoinduced amorphous-crystalline transition obs. *(German)* 79—82156
- Se:Tl, and undoped material, dielec. losses and permittivity meas. 77—28518
- Si amorphous, diffraction intensities, chem. bonding effects 77—72557
- Si, amorphous CVD fabrication for solar photothermal conversion appl. 80—7504
- a-Si, Ar^+ bombardment induced ripple topography 77—77336
- Si, CVD amorphous films, effect of surface characts. on visible and UV optical props. 80—60698
- Si-Au, ESR linewidth var. with temp. and comp. 77—48033
- Si-H amorphous, defect model, light-induced ESR obs. 79—69721
- Si-SiO_2 interface struct. by cross-sectional TEM, amorphous oxide layer 77—24487
- $Si_{100-x}Al_x$, RF sputtered, amorphous, props. 80—34754
- $Si_{100-x}Au_x$, amorphous, dielec. anomaly, rel. to nonmetal-metal transition 78—2791
- $Si_{1-x}C_x$ protective coating for GaAs laser 80—5753
- SiH_x amorphous films, internal photoemission, metal contacts 80—96964
- Si_3N_4, amorphous, $L_{2,3}$ threshold spectra 77—69934
- Si_3N_4 amorphous films, CVD mech. and thermal props. *(Japanese)* 77—90280
- Si_3N_4 amorphous films, struct., short-range order, and crystn. kinetics 79—28240
- Si_3N_4, CVD, structural props., effect of deposition parameters 77—55272
- Si_3N_4, CVD, Vickers microhardness, effect of deposition parameters 77—56079
- Si_3N_4, CVD prep., struct. characts. by pulsed neutron diffr. 80—33891
- Si_3N_4 film, amorphous, optical props., band gap and surface roughness 77—32396
- Si_3N_4 film, high temp. annealing effect on struct. and comp. 77—15714
- Si_3N_4, Si(LVV) Auger spectra, ion bombardment, electron energy loss spectra 80—80911
- Si_3N_4, thin intergranular phase, imaging by high-resolution electron microscopy 79—90895
- Si_3N_4:H, amorphous, ion induced H transfer from N to Si, band passivation, elec. props. 78—47439
- SiO amorphous film, high freq. phonon scatt. 80—49328

amorphous state continued
- SiO, amorphous film, vac. evaporated, density meas., microcrystalline model of struct. 80—2313
- SiO, condensed amorphous, valence states, photoelectron spectra meas. 77—36353
- SiO film, prepared by vac. evaporation, density meas. 77—80714
- SiO_2, amorphous, ^{30}Si diffusion *(French)* 80—59696
- SiO_2, amorphous, chemical effects on freq. of Si-H vibrations 79—51227
- SiO_2, amorphous, fast-time heat capacity, heat pulse propagation 78—51700
- SiO_2, amorphous, $L_{2,3}$ threshold spectra 77—69934
- SiO_2, amorphous, surface phonon theory 78—84044
- SiO_2, amorphous, time-resolved hole transport, small polaron model 77—43598
- SiO_2, amorphous, tunnelling models and thermal expansion below 4K 79—73326
- SiO_2, amorphous and crystalline, with O vacancy, cathodolum. meas. 77—24901
- SiO_2, amorphous and crystalline, surface polaritons and splitting of optical frequencies 78—72090
- SiO_2, amorphous and cryst., Compton profile study 78—88378
- SiO_2, amorphous and cryst., neutron irrad. and unirrad., intrinsic defect photolum. 80—50401
- SiO_2, amorphous anodic layer on Si, MeV light ion multiple through-scatt., backscatt. obs. 79—86828
- SiO_2, amorphous charge transport and storage 80—6864
- SiO_2, amorphous estimate valence alternation pairs 80—54132
- SiO_2 amorphous film, Si(LVV) Auger spectra, ion bombardment, electron energy loss spectra 80—80911
- SiO_2, amorphous layer in multilayer target for channelled ion stopping power meas. 80—63431
- SiO_2, and $SiO_{0.7}$, amorphous sputtered thin film, US anomalies, 0.5-300K 80—34145
- SiO_2 CVD layer, high current injection from Si rich SiO_2 film 80—80430
- SiO_2, cryst. and amorphous, laser-induced breakdown, electron avalanche damage mechanism 80—100711
- SiO_2 crystal and amorphous modifications, structural defect model 80—38915
- SiO_2, defect-controlled carrier transport 79—91049
- SiO_2, diffusion of ^{30}Si, SIMS *(French)* 80—107482
- SiO_2 fibres, LF optical phonons, Raman spectra 80—80789
- SiO_2 film, amorphous, shock crystn. obs. 80—10828
- SiO_2 film, IR spectra and elec. props., influence of prep. conditions 79—87176
- SiO_2 films, amorphous to cryst. transform. induced by diethyl ether vapour 79—55667
- SiO_2, glassy-amorphous, light scatt. exam. 78—14281
- SiO_2, IR optical props. 79—56780
- SiO_2 in MOS struct., interface states 77—28254
- SiO_2, low temp. acoustic absorpt., 9 to 20K and 15 to 65 MHz, Anderson model interpret. 78—26633
- SiO_2, P-doped amorphous, porous and hydrophilic, water adsorpt. and IR spectra obs. 80—80061
- SiO_2, phonon spectroscopy, amorphous versus crystalline material 78—83898
- SiO_2, phonons, cluster-Bethe lattice approach 78—10150
- SiO_2 RF sputtered film, Na^+ motion, small-voltage elec. response 79—90822
- SiO_2, silica, amporphous, acoustic absorpt. in range 1 to 20K and 15 to 65 MHz 77—24357
- SiO_2, small amorphous particles, high resolution TEM 79—82157
- SiO_2, sp. ht., time-dependent, 0.1 to 1K 80—100338
- SiO_2, struct. and chem. bonding 78—51422
- SiO_2-water system, inorg. polymer struct. form., globular crystn. 80—101042
- SiO_x, amorphous and recrystallised layer, optical props. 80—25474
- SiO_x amorphous films, acoustic study using Rayleigh waves 80—75312
- SiO_x film, dispersion of refr. index and chem. comp. 80—7429
- SiO_x system, cluster plus effective medium tight-binding study 79—33216
- $Si_xO_yN_z$ film, amorphous, shock crystn. obs. 80—10828
- Sm-Au, amorphous, surface effects on Sm valence, XPS and X-ray absorption meas. 80—108325
- Sn-Au(Cu), amorphous film, optical props. 79—69895
- Sn-Cu(Au) films, amorphous and polycrystalline, thermopower meas. *(German)* 77—80857
- $SrCl_2$, non-crystalline film, disorder-induced Raman scatt. 80—11387
- $Sr_2Nb_2O_7$, sputtered films, amorphous, dielec. props. 80—54573
- Ta_2O_5, range of ^{27}Al meas. by (p,γ) reson. broadening 77—69023
- Ti-Nb-Si, amorphous alloy, supercond. props. and crystn. behaviour, TEM and DTA study *(Japanese)* 80—84536
- TiO_2 amorphous film, alkali resistance, refractive index, IR spectra *(Japanese)* 78—23546
- TiO_2 films, deposition by electron beam evap. chem. comp., refr. index, struct. *(Japanese)* 77—62777
- TiO_2, phonon spectroscopy, amorphous versus crystalline material 78—83898
- TiO_2-ZrO_2-SiO_2 amorphous film, alkali resistance, refractive index, IR spectra *(Japanese)* 78—23546
- $Ti(OH)_x$, amorphous, dehydration and crystallisation 77—43150
- Tl_xSe_{1-x}, amorphous and cryst., IR transmission spectra and struct. interpret. 78—23471
- V, amorphous film, supercond. props., gaseous impurities effect *(Russian)* 78—72301
- V-Ti(Cr) amorphous films, supercond. transition temp. 79—60953
- V_2O_5 amorphous films, CVD prep., structural characts. 80—49114
- V_2O_5, electronic cond., effect of random glass struct. 79—23972
- V_2O_5, splat-cooled, crystallisation, high-press. effects 78—9956
- V_2O_5-n-Si system, carrier transport mechanisms 77—62999
- V_2S_5, amorphous, electrochemistry in Li cells 80—76626
- W, amorphous, reflection of D and T, Monte Carlo study 80—40197
- WO_3 amorphous anodic film growth on W in acidic soln. 80—81232
- WO_3, amorphous coloured film, charge transfer, XPS 77—12491
- WO_3, amorphous film, vac. evaporated, density meas., microcrystalline model of struct. 80—2313
- WO_3 electrochromic absorption dependence on crystallinity 77—77314
- WO_3 electrochromic cell, deposited Cr_2O_3 as barrier 78—15147
- WO_3 electrochromic films, bleaching by electric fields 79—99852
- WO_3 film, amorphous, electrochromism and local order 77—59553
- WO_3 film, evaporated, mech. of elec. cond. 80—44747

amorphous state continued
- WO_3 film, struct. and crystn., TEM obs. 80—103606
- WO_3 layers, electrochromic absorpt. depend. on crystallinity and electron localisation 77—59589
- WO_5 film, amorphous, band structure and colour-centre band, fast electron energy loss spectrum 77—55478
- WS_3, amorphous struct., X-ray radial distrib. anal. and XPS 80—49115
- WSi_2, amorphous, crystallisation by energy beam annealing 79—69012
- Y-B, amorphous, B-rich, low freq. modes, Raman scatt. obs. 80—108202
- Y_2GdIG film, amorphous, mag. bubbles obs. and structural transformation 80—75824
- Yb, amorphous metal films, crystallisation with and without mag. field 80—70570
- Zr-Co, amorphous and crystalline, d-band struct., alloying effects 80—59862
- Zr-Co(Ni) amorphous alloy, thermal stability and electronic props. 79—73487
- Zr-Ni, amorphous and crystalline, d-band struct., alloying effects 80—59862
- Zr-Rh alloys, amorphous, thermal relax. effects on electronic and supercond. props. 79—65575
- ZrC-C, disordered, Hall const. anomalies 79—56277
- $Zr_{40}Cu_{60-x}M_x$, (M=Gd, Tb, Fe or Mn), mag. interactions 78—95432
- $Zr(HPO_4)_2$, amorphous, crystalline, enthalpy of formation 80—6518
- ZrO_2 amorphous film, alkali resistance, refractive index, IR spectra *(Japanese)* 78—23546
- $Zr_{75}Rh_{25}$, amorphous, evidence for short wavelength cutoff in fluctuation spectrum 78—68113
- $ZrSiO_4$, mechanochemical effect by mechanical grinding *(Japanese)* 78—84754

amorphous state structure *see noncrystalline state structure*

amplification
- *see also acoustic wave amplification; amplifiers*
- 6.6 kHz magnetospheric transmission linear and nonlinear amplification 78—40771
- acoustic array gain, rel. to correl. coeffs. and patch size 77—31158
- acoustic focusing systems, nonlinear effects 79—32126
- acoustic parametric sources, parametric gain and beam patterns 77—46836
- antiferromagnetic semiconductor, spin-wave amplification 80—7099
- BBOT dye vapour single-pass gain obs. 79—55136
- biomembranes, low noise amplification of voltage and current fluctuations 78—44741
- dense gas nanosecond discharge, cathode region field amplification 80—38855
- drifting hot carriers, EM wave amplification, linear theory *(Russian)* 79—69539
- e.m. waves reflected by rotating cylinder, calc. *(Russian)* 77—3523
- ferrite-semiconductor structure, EM wave excitation and amplification 80—6891
- ionography, high-press. gas, amplification and resolution degradation 77—70532
- laser beam, saturation parameter from gain meas. 78—66797
- magnetic field amplification during radiation era 78—96577
- magnetoelastic Love waves by interaction with carrier waves in layered composite 79—28577
- monochromatic Langmuir wave amplification by electron beam in nonlinear plasma *(Russian)* 77—76112
- optical beam, lateral wave amplification through refl. from active medium 78—78987
- photomultiplier arrays, efficient alignment procedure using standard dynode resistor chain 77—3229
- plane axial-shear wave, amplification by circular semiconducting piezoelectric cylinder 78—2806
- radial-mode disc concentrators, reson. dimens. and gain 77—68301
- shock waves, astrophysical, post-collisional propag. and amplification *(Russian)* 79—44360
- spectrometer output amplification, single peak distortion due to electronic time consts. 77—2667
- superconductor-semiconductor contact amplification props. 79—7941
- supersonic flow of inverted population gas flow round blunt bodies, amplification factor 78—5828
- thin-film multimode waveguides, higher order mode amplification 80—96012
- Ge p-n junctions with hot carriers, current amplification, elec. domain form. 80—6966
- InSb optical signal amplification and bistability 80—9937
- Na beam, optical amplification without population inversion 77—50645
- YIG-semiconductor coupled systems, energy anal., magnetostatic surface wave amplification 77—55699

amplification measurement *see gain measurement*

amplifiers
- *see also amplification; audio-frequency amplifiers; d.c. amplifiers; differential amplifiers; fluidic amplifiers; high-frequency amplifiers; intermediate-frequency amplifiers; microwave amplifiers; operational amplifiers; parametric amplifiers; power amplifiers; preamplifiers; pulse amplifiers; radiofrequency amplifiers; ring lasers; ultra-high-frequency amplifiers; wideband amplifiers*
- amplifier-discriminator for magnetostriction spark chambers 78—868
- back diode amplifier, use at low temp. 80—57324
- bioelectrode motion artefact model and artefact reduction by amplifier input stage design 80—56261
- biomedical amplifier-electrode hybrid module for surface EMG pots. meas. 80—41294
- blood pressure instruments, direct systolic/diastolic meas., review 78—69234
- bolometer, IR spectrometer for Meteor artificial satellites *(German)* 78—28484
- composite amplifier-discriminator cct., RMS noise meas. 77—54473
- correcting, bolometer frequency characteristics 80—52305
- current, for 100 ps risetime pulse drive cct. for GaAs laser 77—7149
- current, temp. signals in presence of EM disturbances appl. *(German)* 78—86267
- degenerate, swept-gain, steady-state pulse behaviour 78—87033
- dual channel microphone amplifier, for Macquarie University lectures tape recording 79—71210
- dynamic load line construction amplifiers, tutorial 80—67963
- ECG amplifiers, instruments and maintenance, review 78—69232
- electrode amplifier, fast recovery, for electrophysiology 79—70654

amplifiers continued
- electrolyte electrical conductivity meas., voltage amp. for temp. compensation *(German)* 78—54399
- electrometers, errors and nonlinearity in low-current meas. 79—6142
- electronics for the physicist with applications, book 80—62403
- gravitational wave detector, resonant transducer matching between cryogenic antenna and low-noise amplifier 80—46949
- high sensitivity, LF operation of millivoltmeters appl. *(German)* 78—74032
- high-rate amplifier-digitiser for liq. Ar calorimeter 78—46230
- HV transistor nanosecond amplifier for unipolar pulse signals amplification 78—12720
- hybrid fast instrumentation, photometric signal processing unit 78—41342
- IC, muscle potential monitor applic. 77—40899
- input, 43dB, blocking filter, biofeedback appl. *(Dutch)* 77—37100
- interplanetary plasma meas. by modulation method, amplifiers sensitivity increase 79—92676
- intracellular potential amplifier input capacitance determ. errors 77—60320
- length meas., capacitive transducer method, precision, procedure and instruments *(German)* 79—26024
- with level independent phase shifts, for H_2 maser tuning 77—19223
- lock-in, AC voltmeter appl., for small voltages C below *(Czech)* 77—13779
- lock-in, Auger spectra phase sensitive detect., tailored waveform modulation calc. 77—32860
- lock-in, high sensitivity time-domain reflectometer applic. 77—18016
- lock-in amplifier, for measurements when signal-to-noise ratio is less than unity 78—29134
- lock-in amplifier with synchronous filter, construction *(Japanese)* 80—28362
- locked-in type, for NQR spectrometer 78—256
- logarithmic amplifier, schematic diagram 80—57047
- logarithmic detection of signals with high noise background, luminesc. spectra recording *(German)* 77—37904
- longitudinal thermomagnetic amplifier using Bi or InSb-NiSb 77—47838
- low-noise broadband amplifier system with low input impedance 77—22569
- magnetometer output amp., improving accuracy of pulse magnetometer meas. 79—2793
- membrane potentials tracing system, using amplifier for voltage clamping *(German)* 78—61285
- MOSFET amplifier, fabrication on Si wafer, integrated acoustic transducer arrays 80—74683
- negative feedback for passive value parameter transducer error correction *(Russian)* 78—49819
- Nernst amplifier, feasibility with heat sink and magnet winding at liq. N_2 temp. 77—53932
- noise figure, measurement by connecting source resistance between input and output *(French)* 80—68214
- noise thermometry system, features, design aspects *(German)* 79—30478
- normalising, modulation spectroscopy and other meas. appl. 80—73470
- nuclear acoustic resonance spectrometer, amplifier-generator 80—27324
- phase sensitive amplifiers, appl. to interference suppression and light detection *(Czech)* 78—86331
- phase-stable amplifier, with automatic gain control, input stage 78—4633
- photodetector low-noise amplifiers using J-FETs for optical fibre receivers 78—37997
- programmable gain amplifier, for chem. anal. instruments 79—43644
- sample and hold, for stimulus artifact suppression in bioelectric recordings 78—77163
- segmented bidirectional amplifier SAW oscillator 78—1528
- selective limiter-amplifier, high phase-amplitude stability 78—4632
- shaper amplifier for proportional chambers, logical microcircuits and high time resolution 78—5103
- solid state, linear, high input/low output impedances, nucleonics appls. 80—5451
- spectrophotometers appl., SF-4 and SF-4A, improved design 80—31882
- spike train special purpose amplifier, insect taste cells 80—72394
- superconducting chopper amplifier for resistance meas., sensitivity and noise calc. 79—12817
- unity gain follower with buffer for electrophysiological meas. 79—12048
- voltage, temperature signals in presence of EM distrurbances appl. *(German)* 78—86267
- wattmeter calibration, (3+3)-phase voltage and current source of high stability 77—18038
- $LiNbO_3$-InSb amplifier production, role of protective films 78—95220
- ZnO/SOS monolithic SAW amplifier 78—6205

amplifying *see amplification*

amplitude limiting circuits *see limiters*

amplitude modulation
- *see also pulse amplitude modulation*
- 4-bit digitally driven integrated optical amplitude modulator for data processing 80—53476
- acoustic tone, human auditory assessment of modulation freq. 78—3515
- afferent elec. nerve stimulation with ref. to prosthesis sensory feedback 77—90962
- auditory system, pitch of amplitude-modulated low-pass noise and predictions by temporal and spectral theories 80—67095
- carrier for phase measurement in transmission acoustic microscopy 80—74665
- complex system characteristic derivative meas. by input deep modulation *(Russian)* 78—45588
- dispersive modulator using Stark effect system, for optical pulse compression 77—54793
- dye CW lasers, RF tuning 80—1243
- electrooptic radiation modulators utilizing semiconductor ridged waveguides 80—91925
- EMG signal nonstationary model 77—86481
- far IR spectrometer with interference selective AM 78—86362
- ferromagnet light modulation by microwave using magnetodynamic resonance 80—71393
- galvanomagnetic effects meas., magnetoresistance and Hall EMF, of low-resistance materials 80—52278
- injection lasers, harmonic distortion in direct modulation 79—68411
- ionosphere, pulsation excitation by 4.61 MHz transmitter action *(Russian)* 78—4026
- ionosphere radio wave, modulation trough of small-scale plasma scatt intensity 79—58159

amplitude modulation continued
Lamb wave device using interdigital transducer, influence of electrical termination 79—41549
laser interferometers, AM and FM operation and applications *(German)* 80—86389
laser scanned acoustical imaging systems, demodulation scheme 79—59826
magnetised semiconductor plasma, EM wave amplitude modulation and demodulation 80—84482
magnetooptic bounce-cavity modulator, direct AM 80—5769
microwave backscatter modulation by shoaling ocean waves 78—57212
moderate-resolution spectrometer with interf. selective amplitude modulation, construction of prototype 79—30588
multichannel audio monitor for detecting electrical signals, neurophysiological expt. appl. 79—20694
multifrequency Bragg acousto-optic deflector, laser beam AM suppression 80—53426
multimode optical fibre phase modulators and discriminators, theory 78—55446
multimode optical fibre phase modulators and discriminators, expts. 78—55449
NMR, amplitude-modulated DNMR in two-spin system with chem. exchange 79—93194
optical diffraction pattern and AM sideband parallelism *(German)* 79—89854
optical second harmonics 80—78908
optical video disc, acoustooptic travelling wave transcription signal recording 79—36986
radio signal diffraction in homogeneous dispersive medium, space time geometric theory 79—4149
ruby laser, ultrashort pulse generation by internal phase and amplitude modulation 80—106551
SAW devices based on interaction of SAW with electrons in semicond. 77—80025
sound modulation detect. by trained musicians 78—3517
strong radio wave, amplitude modulation effects on upper ionosphere disturbance 79—12330
temporal modulation transfer functions based upon modulation thresholds 80—21478
thin-film waveguide with liq. cryst. boundary modulation of refr. index, mode switching 80—23800
tones, dependence of fluctuation strength on sound parameters *(German)* 79—34569
total internal reflection modulator, small glancing angles 78—74987
$Ba_2NaNb_5O_{15}$ crystal domains, amplitude modulation of light by diffr. 79—59832
CO_2, fast flow discharge laser, amplitude modulation in stable, unstable resonators 77—75478
CO_2, TEA laser, pulse-forming and line-broadening in AM mode locking 77—54743
GaAlAs injection lasers, AM characts. 79—50330
He-Ne ring laser beat frequency deviation rel. to dispersion and modulation 79—68410
Nd:YAG, actively AM mode-locked Q-switched laser, pulse compression by liq. Kerr cell 79—22990

amplitude selectors *see limiters*

analogue computer applications *see analogue simulation*

analogue computer circuits
see also function generators; operational amplifiers
electrophysiological average transients computer, 200 point 80—12284
LF function generator/controller using X-Y recorder 78—21108
plasma diagnostics, Thomson scatt. system, analogue data processing circuits 78—87488
response linearisation using programmable multifunction module 78—45604
subtraction circuits, for thermoelectric power meas. 78—244
vented box loudspeaker analogue model using operational amplifiers 80—92015
wattmeter, differential, adiabatic calorimeter and liquid chromatograph appl. *(Czech)* 78—23979

analogue computer methods *see analogue simulation*

analogue computer programming
response linearisation using programmable multifunction module 78—45604

analogue computers
see also analogue-digital conversion; analogue storage; differential analysers; digital-analogue conversion
auditory evoked cortical potential online detector 78—31952
Heath valve unit, conversion to linear IC op-amp 77—13549
matrix multiplying optical system resolution calc. *(Russian)* 79—98456
optical analogue computer performance advantages 78—78949
radiation exposures from film dosimeters, analogue computer anal. *(Bulgarian)* 79—85877

analogue differential analysers *see differential analysers*

analogue digital computers *see hybrid computers*

analogue-digital conversion
see also digital-analogue conversion
$3^1/_2$-digit voltmeters using new A/D convertors *(French)* 78—21114
12 kHz IC resistance-frequency convertor *(Russian)* 78—81963
16-channel analog store and multiplexer unit 79—45614
A/D convertor with special appl. to medium precision Pt resist. thermometry 80—86297
analog signal processing, book 80—86047
angle digitiser, for ang. displacement control via fast error-signal transducer 78—186
angle transducer, conversion error evaluation using probability precision model 77—82498
astronomical images, interactive program for digital display *(Italian)* 80—98559
astronomical instrumentation, X-ray XUV telescope/white light coronagraph expt., quadratic A/D converter 80—62024
astronomy, photon counting and analogue TV systems with digital real time image processing 78—96402
atmosphere acoustic forecasts production, method using digital computer 79—79960
atomic absorption spectrophotometer, analogue-digital convertor taking into account nonselective absorption 79—57331
audio signal processing, spurious signals and their suppression *(Czech)* 79—98555

analogue-digital conversion continued
automatic measuring-limit selecting devices in multi-channel systems 79—71397
BEBC pictures, automatic anal. using flygin spot digitiser 77—88342
Brilliant ADC, semi-autonomous controller for data acquisition 78—46245
bubble chamber pictures, compact digitiser 77—83452
calibration of mechanical meas. values *(German)* 79—67247
charge to time convertor, gated seven channel 78—13388
chart recorder information translation into digital form 77—22537
chromosome analysis, automatic, specialised image treatment equipment *(French)* 77—37111
circular magnetoelectric convertors, angle-of-rotation conversion errors 77—17968
coherent optical image processing, halftone screen techniques 77—75434
color map automatic digitisation, spectral classification scanner technique 80—17424
colorimetry appl., description *(French)* 77—5882
contracted orbital formulation of many-body perturbation theory 80—87026
CRO storage, Gould Advance OS4000 using A/D and D/A convertors 78—93673
CRO with digital storage, OS4000, features *(Spanish)* 79—6116
CRT screen image distortion corrections in R7912 transient digitiser, FORTRAN programs 79—30440
current digitiser, 2×10^{-15} A to 2×10^{-10} A, ion chamber currents meas. appl. 77—61666
current-to-frequency transducer systematic error and sensitivity threshold 77—79117
cycle scale compensated converters 80—14039
data acquisition module for microprocessor systems, high-speed, multiple channel 77—57304
delay line digitizer 78—46249
differential fluid viscometer *(Russian)* 79—90355
digital colorimeter appl. *(Russian)* 77—37963
digital multimeter, hand-held instrument with liquid crystal display 77—74423
digital plot system developed for nondestructive materials testing exam. 78—53067
digital recording of analogue voltage on stereo cassette recorder 77—61061
digital storage instrum. and function generator electronic modelling appls. 78—77937
digital thermocouple cold junction compensation methods *(Italian)* 78—37002
digital thermometer, using LSI ADC 79—44907
digital voltmeter accuracy eval. *(Czech)* 77—57361
digital voltmeter SM 215, portable transfer standard 78—41325
digitisers, nonlinear clock 79—18091
digitisers of time and pulse height, monolithic flash A/D convertor 80—63475
digitising error from period and freq. counting techniques 78—61570
digitizer and image analyzer, microcomputer-controlled 80—86270
digitizer for generating computer readable chem. data 79—74454
digitizer for use with pulsed depth sounders 79—21065
displacement A/D convertor with multichannel phase shifter 77—5823
DVMs, DMMs and counter-timers, review 77—37913
ECG, long-term recordings, rapid computer analysis system Argus/H 78—36002
ECG, meas. changes due to precision level 77—40865
ECG digital voltmeter with output to punched tape 77—21646
ECG processing A/D convertor control by microprocessor *(Bulgarian)* 79—25123
ECG/VCG minicomputer digitising and preprocessing system 77—40863
EEG data, low cost microcomputer system 77—40881
electro-optic A/D conversion using channel waveguide modulators 78—66898
electro-optic guided-wave A/D convertor, high speed 80—33234
electrocardiographic data processing, filtering and sampling 78—24162
electron beam fusion accelerators, data acquisition and processing 78—37469
electrooptic analogue-digital conversion, using channel waveguide modulators 78—38051
Electrophysiological Data Interface 79—79677
evoked potential multi-channel data acquisition system, microprocessor controlled 78—11750
fast event recorder utilizing a CCD analog shift register 79—45578
fast sampling, for DVM line shared display 77—74424
fibre and integrated optical devices for signal processing 80—33233
Fourier transform IR spectroscopy and gain ranging, digitisation noise 79—97448
fusion reactor, diagnostics of radial plasma transport rate, data acquisition and handling system 78—54937
gas chromatography mass spectrometry appls. of wide dynamic range system 80—62788
geometric reconstruction of bubble chamber events meas. on HPD 79—753
graphic materials, aided-track cursor for improving digitising accuracy 79—29899
graphics calculator system using X-Y recorder and computer as digitiser 80—13046
high rate liquid Ar calorimeter electronic systems, design and operating experience 80—58087
home-made IC digital voltmeter *(German)* 77—10062
Hough-Powell digitizer for processing film from bubble chamber Mirabelle in K^+p expt. at 32 GeV/c 80—69040
hydrometeorological information, optimum conversion to digital form 79—29903
ICL 7109 12 bit convertor, three-chip digital scale zeroes tare weight, appl. 80—27282
IEEE 488-1975 interface bus, high speed ADC and addressable trigger generation 80—41283
image digitizer system design considerations 80—10025
image processing, digital, parallel logic device and half-adder circuit 80—10027
immunity noise abatement methods *(Russian)* 77—54838
integrated electro-optical A/D convertor, using branching waveguide modulator channels 78—42474
integrated optics A/D convertor based on bulk acousto-optic interaction 80—69552
integrating recorder of a slowly varying voltage 79—93124

analogue-digital conversion continued

- interferometer signals processing, far IR, use of microcomputer 77—2689
- klirr-factor unit dimension meas., errors evaluation 80—98873
- laboratory microcomputer and A/D convertor interfacing 80—22337
- large scale digitiser system for charge and time digitisation in high energy physics exptl. 77—54489
- light beam deflector, electrooptic phased array, application to analogue-digital conversion 78—38052
- linearised NTC circuits with A/D convertor for temp. meas. *(German)* 79—80619
- liquid level meter, using conversion in binary-decimal refl. code *(Polish)* 77—17949
- logarithmic A/D convertor for light control unit *(German)* 79—93117
- magnetotelluric signals digitization equipment *(French)* 77—87092
- marine seismic survey, modified integrating A/D convertor *(Russian)* 78—49142
- mass spectrometer to multichannel analyzer interface 80—27916
- measurement systems, errors in derivative determ. 79—80567
- meteorological satellite data *(Japanese)* 78—7711
- METEOSAT synchronisation and image channel system *(Italian)* 77—82110
- micromanometer, conversion to large range digital readout 77—2716
- microprocessor based data acquisition and exptl. control system 78—36086
- microprocessor controlled dual parameter ADC system with CAMAC interface 79—3337
- miniature pressure-frequency convertor with pulse output 78—57926
- minicomputerised pressure transducer data logging system *(Russian)* 79—6102
- modular 125 ps resolution time interval digitizer for 10 MHz stop burst rates and 33 ms range 79—45591
- Mossbauer spectra, active data acquisition 80—9079
- MTI filter, with inherent A/D, for US blood flow velocimeter 79—16263
- multi-parameter CAMAC compatible ADC scanner 79—31350
- multichannel, without timing skew, for LF biological signals 78—61271
- multichannel complex for hydrophysical data conversion for computer anal. *(Russian)* 78—65427
- multichannel digitizer for routine monitoring of ion emission from laser-driven implosions 80—57268
- multichannel pulse height analyser adaptation for 4096×4096 two-parameter meas. 77—14316
- multitrack pulse height electronics 79—3325
- neutron-gamma pulse shape discrimination, liquid scintillators 77—403
- nonlinear optical processing with Fabry-Perot interferometers containing phase recording media 80—48158
- operation and performance, multimeter design appl. *(German)* 77—34007
- ophthalmological tissue differentiation, digitisation of HF US signals 78—80935
- optical, using single half-tone photograph 77—5936
- optical A/D conversion and page composition for holography 78—5436
- optical A/D conversion using single halftone photograph 78—78919
- optical A/D convertor using channel waveguide modulators, design and analysis 79—55249
- optical fibre laser plate for digital image processing, all-optical parallel logic operation 80—106463
- optical method, direct, using coherent or incoherent light 79—22908
- optical parallel A/D conversion, real time, using liq. cryst. light valve 80—53451
- optical spectra, direct encoding using computer interfaced vidicon TV camera 77—10114
- PACE ADC system, CAMAC interface module 77—34534
- particle detectors, large-scale digitiser system, analogue convertors 77—54427
- peak height digitiser for autoanalyser charts 78—44431
- power and energy meas., digital, errors sources and suppression *(Rumanian)* 80—47078
- precision convertors for data meas. systems 78—8387
- precision gated current integrator and live time meter system 79—9973
- printing scalar, single channel, for photon counting 77—5919
- proportional step size tracking A/D convertor 80—57269
- proton storage ring, NAP-M conversion equipment in supervisory system 77—65365
- prototype CCD system for the time projection chamber 79—45575
- pulse height store 80—14054
- pulse sequence fast A/D conversion 78—55119
- pulsed data A-D acquisition system 79—22572
- pulsed light source with thin-film modulator, fabrication and characts. 80—43467
- punched register for astronomical elec. photometer *(Russian)* 78—93117
- pyroelectric detector array for IR and far-IR studies, improvement of sensitivity using digital averaging technique 79—49290
- quantiser algorithm for real-time block quantising 79—64449
- radar meteor A/D filter characts. *(Italian)* 79—80032
- recorders, transient, 1024-point, circuits, operation 77—53868
- renal histopathological section image dissection and analysis 79—79679
- resistance thermometer, novel circuit *(German)* 77—74394
- rhythm analysis, long-term ECG data storage and multipass scanning 79—39578
- Royco aerosol particle counter 225, data processing system and modified system props. 80—37005
- satellite IR pictures, automatic digital techniques for oceanic features enhancement and extraction 79—5682
- SAw/CCD accumulating correlator for analogue signal processing 79—72757
- scanning image digitizer, playback corrections 77—83816
- seismic observations digital processing, steady numerical solns. *(Russian)* 79—53317
- seismology common depth point data digital processing technique *(Russian)* 79—74875
- selsyn rotor angle-to-digital code convertor, design *(Russian)* 78—65915
- signal interface element survey, low cost quantisers, fast ADC's, high energy physics appl. 79—45584
- signal processing, fibre and integrated optics techniques 77—27379
- signal processing fibre and integrated optical devices 79—76887
- solar spectrum, analogue-digital conversion via automation system *(Russian)* 80—12659
- sonic digitizer, 2-sensor, accuracy obs., radiation therapy appls. 80—30806
- spectrophotometer (UR-20), digital output of experimental data 77—26409

analogue-digital conversion continued

- SQUID, A/D conversion, conditions for countable pulse train 79—91191
- SQUID magnetometer, broadband and higher-power, for small signal A-D convertor 78—62211
- stellar magnitude, colour index and position meas. from astronomical photographs, automated technique 79—21194
- stereo image digitiser for automatic feature extraction 80—106614
- structure model, photograph to digital convertor 79—60213
- successive approx. convertors, reduction of differential nonlinearity 77—79517
- successive approximation A/D convertor for pulse height analyser, rapid coding 77—23386
- temperature meas. by compensated thermocouples *(German)* 78—41304
- temperature measurement, using A/D convertors TL505/507 and TMS 1000 microprocessor *(French)* 80—57290
- temperature sensor, electronic, with 4-bit words output *(German)* 78—12693
- Texas Experimental Torus, data acquisition and processing system 77—24217
- thermal diffusivity meas. by laser-pulse technique, instrumental recording and data processing 77—45846
- thermographic image digitisation and anal. 77—16960
- time digitiser for laser ranging, ps. resolution, built in CAMAC minicrate 78—36301
- time digitiser in CAMAC format 77—10558
- time interval digitiser *(French)* 79—76309
- time projection chamber multichannel ADC and readout system 79—45590
- time to amplitude converters, precision 1 GHz time calibration 80—27903
- time-pulse, multichannel analyser applic. 77—18752
- transcriptor F595 control unit for measurement and recording of strain parameters *(Russian)* 79—88945
- transducer, pulsed frequency, continuous random signals errors evaluation, by means of computer simulation 77—74386
- two channel boxcar integrator with A/D conversion for pulsed NMR spectrometer 79—80657
- two-phase A/D convertor processes small analogue signals *(German)* 78—61572
- US digitiser/processor for extraction of clinical parameters from Doppler-shift waveforms 80—36042
- US time-coordinate convertors for distance meas., design aspects *(Russian)* 78—77857
- video image digitiser, interactive, appl. to interferogram anal. 78—58021
- vidicon systems, time digitiser in CAMAC format 80—14062
- vocoders for present day and for mid 1980s, practical implementation 80—33357
- Wilkinson type, speed increase and differential nonlinarity improvement 77—57832
- X-ray picture transmission over voice grade telephone channels 78—44607

analogue memories *see analogue storage*

analogue simulation

- acoustic defectoscopes, low freq., elec. simulation of compound piezoelec. transducers 80—102956
- aortic dynamics in man, analogue simulation model 78—80903
- artificial heart, atrial charact. estimation using analogue simulation 77—44846
- axially symmetric form of biharmonic eqn., elec. analogue technique for approx. soln. 77—27502
- bar magnet field, analogue simulation by electrostatic field, boundary conditions 77—61892
- betatron, electron beam rapid extraction by parametric reson., analogue computer anal. 77—18731
- biophysics, teaching appls. of analogue computers 79—84890
- breathing process analogue model *(German)* 79—16228
- cardiac output flow wave calculator *(Japanese)* 77—70489
- cardiovascular system, analogue circuit and compartmental model, normal and defective states 79—57700
- cavity-coupled Josephson device, parametric dependences, I-V characts. 80—20356
- coherent optical feedback analogue computer for partial differential eqns. with inhomogeneous terms 79—76870
- complex ECG and triaxicardiometric recording and analogue processing 79—44023
- coronary haemodynamic parameter estimation using elec. analogue 77—37092
- data logger mean square error minimisation *(Russian)* 77—9994
- dielectric solid, space charge problems by analogue modelling on field analyser 80—40058
- diesel engine pistons, simulation of slap at TDC 77—72222
- diffusion eqn., using variable-element networks *(French)* 77—5653
- diffusion process, by means of electric analogies *(Hungarian)* 79—17361
- DTA apparatus, modelling, elec. analogue approach 80—3270
- Earth EM fields, analogue model meas. for horizontal mag. dipole embedded in conducting medium 79—12068
- ECG recovery after defibrillation, anal. and simulation 77—40910
- education, diffraction grating and interference effects, electronic cct. analogue 79—9052
- effective annealing time determ. 78—88475
- electrets, meas. of charge distrib. 77—30184
- electrochemical impedance simulation, by AC ladder networks 77—12806
- electrode, disc type, current distrib., analogue model investig. 79—34321
- electrometer, for apparent power meas. *(Czech)* 77—5859
- eye movement, gaze-evoked nystagmus 78—27938
- geomagnetic variations induced by ocean waves, analogue model 77—49003
- groundwater flow simulation with computer-controlled RC network 77—45045
- heat conduction, difference eqns. appl. *(Japanese)* 78—1664
- heat conduction, inverse nonlinear problems, simulation methods 78—94513
- heat conduction, inverse problems using analogue computer 79—37121
- heat conduction of metallic joints, using electrolytic tank 78—83207
- Hilbert transformation of phase object, optical simulation 78—1174
- hot film transmitters, thermal processes, Beuken method appl. *(German)* 78—55546
- hot strip rolling simulation, by hot torsion technique 80—29990
- hydrodynamic flow modelling by AC induced electric fields *(German)* 77—57200

analogue simulation continued
joint-simulating machines, prosthesis wear meas. 79—20716
Josephson junction phase-locked loop analogue to study effects of thermal noise 77—47939
kidney preservation, analogue model of perfusion dynamic changes 79—83724
laser beam heat flux and power profiling, using swept null point calorimetry 80—69439
linear array, far-field directivity patterns, electrical analogue simulation 77—804
liquid flow, incompressible, electro-hydrodynamic analogy, design 77—27627
locomotion, analogue simulation of swing phase 78—31827
locomotion of human leg, swing phase anal. 78—3531
magnetic fields induced by ocean waves, laboratory analogue model study 79—66807
measuring equipment and testing means 79—80564
muscle length reflex control, servosystem simulation 79—57639
muscular fatigue, EMG meas. and analogue model *(Japanese)* 79—8498
MWPC with analogue read-out, high energy e^-/γ detection 79—13593
myocardial perfusion index calculator for prediction of subendocardial ischaemia in cardiac surgery 77—40915
natural channel flow simulation by computer-controlled RC network 77—45046
neuron model of burst generation, FET analogue 77—44630
nonhomogeneous ventilatory mechanics 79—79575
nonlinear direct and inverse heat and mass transfer, analogue and hybrid simulation 77—53767
nonlinear heat conduction simulation by analogue and hybrid computers 77—53768
nonstationary heat transfer through walls, elec. analogy *(Slovene)* 77—39191
nonsteady heat conduction in solid cylinder, analogue computer soln. *(Rumanian)* 77—68362
nuclear fuel production, continuous gas flow control simulation *(German)* 80—78416
nuclear reactor neutron field, one-group difusion approximation and finite difference methods appl. *(Russian)* 78—74416
optical computing, past, present and future 78—46531
phenazine, triplet formation kinetics temp. depend., analogue computer anlaysis 77—58058
plasma electron energy determ. using analogue computer and Langmuir probe 78—14212
plasma probe, spherical, slightly ionised continuum, current-pot. curves 77—72494
polymerisation kinetics 77—36754
polymers, contract electrification, analogue model 79—51655
power spectra for chaotic transitions in Rossler dynamical system 80—53898
projectile motion, teaching to sixth-form level 77—60862
pulmonary arterial compliance effect on pulmonary blood flow distrib. 78—44553
pulmonary resistance measurement by forced oscill. technique 77—40877
PWR power plant modelling and simulation 79—9828
quantum chemistry, analogue computer appls. *(German)* 78—28903
quasilinear parabolic eqns. by networks of FETs 77—50854
real time interferogram simulation by analogue device, aberration generation, CRT display 79—54181
renal autoregulation, math. model of transient adjustments 77—90842
room acoustics and subjective sound perception *(Polish)* 79—7258
semiconductor charge flow, attenuation-free upwind difference formula 77—28241
soap film simulation of phase changes, catastrophes, teaching appl. 79—62974
solar energy systems, electrical analogue simulator development 80—30382
specific heat meas., precise method using analogue simulator 77—49721
steam drum dynamics, nuclear power plants 77—71645
Stirling cycle machines, comparison with expt. simulation and theoretical analysis 79—48169
suspension, rheological thixotropy analogue simulation study with plane-cone Ferranti-Shirley viscometer *(French)* 77—65725
synthetic aperture radar image coherent-optical simulation 77—50632
temperature distribution in turbine and torsional stresses in non-circular shaft *(German)* 77—68551
thermal contacts fluxes modelling, electrolytic *(Italian)* 77—24504
thermal diffusivity automatic meas. by pulse method using analogue computer *(Japanese)* 80—27294
thermoelectric coolers, electrical analogue simulation of transient behaviour 78—21140
thermonuclear device self-adjusting system automatic feedback parameter search 78—26336
three-dimensional analogue reactor simulation with allowance for heat transfer 79—63739
TV-optical analogue computer soln. of partial differential eqns. 79—76869
vented box loudspeaker analogue model using operational amplifiers 80—92015
ventilatory phonetics, analogic 80—51131
ventricle, pneumatically driven, sac-type, dynamic model 78—15925
vestibular nystagmus, Alexander's law model 80—35878
Al-Mg, recrystallised, grain boundary dislocation identification by computer simulation of TEM image *(Japanese)* 77—47457

analogue storage
see also sample and hold circuits
16-channel analog store and multiplexer unit 79—45614
capillary and clad acoustic fibre delay line storage 78—9504
charge-coupled analogue memory, nucl. data acquisition 78—46250
complex ECG and triaxicardiometric recording and analogue processing 79—44023
ferroelectric memory, matrix-addressed analogue, on $Gd_2(MoO_4)_3$ cryst. 80—103926
multichannel analog memory, using MOS transistors for data transmission to M6000 computer 79—26043
multichannel analyser, random signal flow intensity levelling using analogue memory device 77—18752
photoferroelectric image storage in antiferroelectric-phase PLZT ceramics 80—71353
sample-and-hold voltmeter for time-related meas. 77—57347

analogue storage continued
sampling instrum. for recording/meas. instantaneous values of periodic events, oscilloscope appl. *(German)* 77—53876
SEM colour images, electronic adding-up and storing 79—21879
small-area ultrasonotomogram magnification and smoothing 77—86572
wideband chirp and Barker code correlations with storage convolver 77—23832

analogues, direct *see direct analogues*

analysers, differential *see differential analysers*

analytical chemistry *see chemical analysis*

anaphoresis *see electrophoresis*

AND gates *see logic gates*

Anderson model
adsorption of isolated atoms, quantum theory 78—22957
alkali halides, U-centre, electronic struct., self-consistent model 79—65406
alloy, random binary, Anderson localization, equation-of-motion method 79—42482
alloys, dil., mag. field and impurity interaction effects on resist. 79—51554
alloys, random binary, electronic struct., Mott-Anderson model 80—49671
amorphous semiconductor or insulator, optical absorption 77—90167
amorphous solid, frozen liquid phonons disorder parameter, Anderson localisation 78—75784
amorphous system, theory of electron localisation 77—1391
asymmetric, ground state, perturbation approach, w.r.t. s-d mixing integral 80—54582
asymmetric Anderson Hamiltonian, ground state 80—65503
asymmetric Anderson Hamiltonian, perturbation expansion 80—6687
asymmetric Anderson model, ground state, perturbation approach 80—65504
asymmetric Anderson model, scaling theory 78—34807
asymmetric model, ground state fundamental nature 79—90932
atomic limit, perturbation expansion in infinite conduction bandwidth limit, Kondo temp. 79—28506
BCS-superconductor with mag. impurities, transition temp. in spin fluctuation limit 77—32104
binary alloy, density of states, CPA with nonretracing paths 77—31924
binary alloy type of disorder, numerical study of localisation 78—64009
Bose glass, marginal fluctuations 80—2586
chemisorbed atoms, spatial variation of extraorbital screening charge 79—60886
chemisorption on metal, intra-adsorbate Coulomb correl. and surface struct. roles 78—71979
chemisorption on metal, intra-adsorbate Coulomb correl. and surface struct. roles 78—71980
correlation corrections to the chemisorption energy in the Anderson model 79—19538
critical dimensionality in Anderson-Mott transition 80—10876
degenerate Anderson model, Fermi liq. theory 79—19715
degenerate Anderson model, fermi liq. theory 79—90935
degenerate d-electron alloys, dilute, local moment and ferromagnetic state formation 79—51748
demagnetisation through level crossing, effect of charge fluctuations 78—52193
diagonal vertex approx. for Gaussian random systems 78—23003
diamond cubic lattice, Anderson localisation in presence of off-diagonal disorder 77—85179
diamond lattice, Anderson localisation, real-space renormalisation study 79—28324
dilute alloy, impurity electron states, method of orthogonal operators 79—33254
dilute alloy, perturbation expansion for the asymmetric Anderson Hamiltonian 80—80202
dilute magnetic alloy, configuration fluctuations 79—33449
dilute magnetic alloys, asymmetric Anderson model, renormalisation-group approach, static props. 80—44802
dilute magnetic alloys, symm. Anderson model, renormalisation-group approach, static props. 80—44801
dilute magnetic alloys moment-conserving decoupling scheme 79—61048
dilute nearly magnetic alloys, magnetoresist. calc. LSF approx. of Anderson model 77—62901
disorder parameter for Anderson transition in three dimensions, crit. strength 77—59256
disordered alloy, electron localisation, temp. depend. 80—80219
disordered electronic systems, low-dimensionality, Anderson localisation, resist. 80—84491
disordered extended Anderson model, CPA-alloy analogue treatment 80—65506
disordered metals, incipient Anderson localisation role in resistivity 80—49687
disordered molecular insulators, Anderson localisation of mol. excitons 77—89733
disordered semiconductor, mobility edge exam. by new perturbation theory 78—47790
disordered system, Anderson localisation, numerical study *(Japanese)* 78—30890
disordered system, Anderson localised states, intra- and inter-state interactions 80—44543
disordered system, conductivity and mobility edge, square and diamond lattice calc. 78—43347
disordered system, conductivity near mobility edges 78—76038
disordered system, electron localisation, spatial extension of wavefunction 77—80752
disordered system, particle diffusion in Anderson model 79—33273
disordered systems, Anderson localisation, appl. of recursion method 80—107744
disordered systems, Anderson localisation theory in two dimens., real space scaling method 80—44540
disordered systems, electron localisation, Anderson transition, review 80—29361
doped semiconductors, correlation effects on Anderson localised states 79—95337
double exchange, infinitely strong s-d coupling *(Russian)* 77—8264
dynamical susceptibility of impurity electrons 77—12090
electrical resistivity, for wide range of Coulomb coupling parameters 80—2373
electron correlation effects on Anderson localized states 79—23919

Anderson model continued
- electron gas, orthogonality catastrophe due to local electron correlation 78−43320
- electron gas, screening of proton, Anderson model calc. 80−59895
- electron localisation in systems with purely off-diagonal disorder, Anderson transition 79−19518
- electron systems, 2D disorderd, transport props. in strong mag. fields 78−95318
- electron-electron interaction effects on Anderson transition 80−65453
- Fano effect theory, electronic structure, d band metals and alloys 78−2402
- fermion gas moving in strong three-dimens. random pot., conductivity 79−56130
- ferromagnetism, basic models, classification of theories *(Rumanian)* 78−91840
- glasses, low temp. props., two-electron excitons 77−15786
- ground state, t-matrix approx. 80−20061
- ground state, var. trial function approach 80−59913
- ground-state energy 79−99511
- heterojunction theory, proposal for new approach 80−6961
- II-VI compounds, acceptor state model 80−2059
- impurities, direct interaction 80−54681
- impurity conduction phenomena, review of exptl. work *(Japanese)* 80−49737
- impurity pair interactions, local moment form., var. method 80−92854
- inflowing structure, Anderson localisation, elec. cond. temp. depend. *(Russian)* 80−103639
- interacting Anderson impurities, pair, Fermi-liq. theory 80−44803
- intermediate valence, phase diagram and Kondo behaviour 80−29366
- intermediate valence compound, pressure-temperature phase diagram 79−28283
- intermediate valence compounds, dynamic susceptibilities 80−70653
- intermediate valence compounds, mag. susceptibility and sp. ht., mean-field theory of periodic Anderson model 78−47937
- intermediate valence compounds, phonon produced instabilities, periodic Anderson model 78−79964
- intermediate valence cpds., phonon effect on press.-temp. phase diagram 80−24849
- intrastate and interstate interactions 80−20113
- isotopically mixed crystals, electronic energy transfer, crit. conc. 77−76771
- Kondo alloy, dil., thermoelec. power in asymmetric single-orbital Anderson model, perturbation calc. 79−99534
- Kondo alloy, low temp. props. 80−2569
- local densities of states near a crystal surface with disordered overlayer 79−15201
- local electron interaction, orthogonality catastrophe, overlap integral, Anderson theorem in general case 78−67962
- local moment magnitude 77−77022
- local moments and localised states, review of early work on Anderson model 78−72327
- local moments and localized states, theory, review 79−23935
- localisation, mean field theory and ε-expansion 80−80203
- localisation, real-space renormalisation approach 80−2364
- localisation, study by continued-fraction method 79−4534
- localisation and recursion method 78−84167
- localisation edges and critical exponents 79−90986
- localisation problem, anal. of time depend. of randomly specified wavefunction 77−47761
- localisation problem, numerical results 78−23040
- localised electronic system, sp. ht., singularity at Anderson-Mott transition 80−34381
- localised magnetic impurity problem, functional-integral approach, sp. ht. calc. 77−77026
- magnetic alloys, dil., spin correlation 78−84385
- magnetic alloys, dil., transition metal hosts, props. review 78−84417
- magnetic alloys, dilute, static suscept., Anderson model, functional integral approach 80−50050
- magnetic alloys, dilute, thermopower 79−65455
- magnetic ions in metals, Friedel-Anderson VBS and ionic approaches, compatibility 79−61051
- magnetoresistance, negative, electron correlations effect 79−65499
- many body systems, localisation phenomena, state variable randomness, perturbation theory 80−29297
- metal, local moments and localised states *(Czech)* 80−2353
- metal, review of chemisorption 79−42377
- metal, with mag. impurities, inc. local coupling to boson field, HF approx. and RPA 77−40033
- metal inhomogeneous granular, superconductivity 80−103795
- metal surface, electron correl. in chemisorbed H atom, friction coeff. 78−60026
- metal surface, ionisation of atoms 79−68310
- metal surface, tight-binding, dissociative chemisorption of molecule 78−2368
- metal-semiconductor disordered interface, supercond. transition temp. enhancement by bipolaron interface centres 80−84528
- metals, indirect mag. coupling between local moments 78−52207
- metals, Kondo effect, Anderson hamiltonian 80−60187
- metals, localised mag. moment magnitudes of transition or rare earth impurity, Anderson model 80−25086
- metals, localised moment interaction, Alexander-Anderson model, perturbation expansion 80−29524
- mixed organic solids, Anderson transition, electronic energy transfer in impurity bands 79−99502
- mixed organic solids, triplet exciton transport at crit. conc., Anderson localization or delocalization 79−15087
- mixed valence compounds, dynamic susceptibility, RPA study of Anderson lattice 80−97075
- mixed valence compounds, periodic Anderson model self-consistent treatment, specific heat, susceptibility 79−99514
- mixed valence compounds, phase diagrams, lattice props., electron hole symmetry 79−91002
- mixed valence compounds, structural phase transitions, effect of electron-phonon coupling 79−33265
- mixed valence cpds., elec. cond., periodic Anderson model, memory function approach 80−84458
- mixed valence cpds., electron-hole symmetry, phase diagrams, and lattice props., periodic Anderson model 80−15481
- mixed valence cpds., mag susceptibility and sp. ht., periodic Anderson model, CPA alloy analogue method 80−15474
- mixed valence problem, renormalisation group approach 77−89734

Anderson model continued
- MOS inversion layer, 2-dimens. disordered electron systems in strong mag fields 77−76930
- naphthalene, in naphthalene-d_8, Anderson-Mott transition model for excitation transport 80−96812
- naphthalene, in naphthalene-d_8, energy trapping from localised states 80−100440
- naphthalene-betamethylnaphthalene, mixed cryst. $(C_{10}H_8/C_{10}D_8)$, luminesc., test of excitation transport model 79−65914
- nearly magnetic impurities in non-mag. host 78−2647
- negative magnetoresistance 79−28357
- non-orthogonal elec. resist. 80−59947
- noncrystalline system, continuous and discontinuous metal insulator transitions 78−56076
- noninteracting electron gas, dynamical conductivity, Anderson transition 79−28279
- numerical methods in Anderson transition 79−60767
- off-diagonal disorder, exact solutions 77−15739
- off-diagonal disorder, exactly solvable 77−80719
- one dimensional disordered system, cond. and electron localisation 80−103658
- one dimensional site disordered lattice, AC conductivity 78−84199
- orbitally degenerate, exchange coupling in atomic limit 80−108000
- organic solid, isotopically mixed, electronic energy transfer, Anderson localisation model 79−19557
- organic solid, isotopically mixed, electronic energy transfer, Anderson transition 80−44545
- orthogonality catastrophe due to local electron correlation in asymmetric Anderson model 79−60745
- orthogonality catastrophe due to local electron interaction 79−1566
- orthogonality catastrophe for a system of interacting electrons 79−1576
- periodic Anderson Hamiltonian, alloy analogy treatment for mixed valence states 80−75527
- perturbation theory of asymmetric model 80−6766
- phonon assisted DC hopping conductivity, Anderson localised electronic states 77−32010
- quantal spin system, classical representation and scaling props. of spin Hamiltonians 78−14919
- quasiparticle lifetimes 80−44532
- random alloys, CPA calcs. cluster extensions, appraisal of applicability 79−15063
- random lattice with off-diagonal disorder, absence of Anderson's transition 78−30889
- random systems, localisation 80−80218
- rare earth alloys and cpds., intermediate valence, models for anomalous systems 80−96827
- rare earth compounds, spinless periodic Anderson model with phonons, appl. to mixed valence systems 78−84153
- rare earth compounds, valence mixed state, Kondo lattice, Anderson localisation models *(Japanese)* 78−51945
- rare earth metal impurity in metallic host, exchange interaction, electrical resistivity 80−84453
- rare earth metals, alloys and cpds., susceptibility for high mag. impurity conc. 77−63069
- rare earth sesquioxides, cubic, indirect exchange interactions Anderson model 79−95585
- rare earth systems, Kondo singularity, Anderson-Smith model 80−80479
- real-space renormalisation group theory, decimation method 80−88461
- renormalisation group study of Anderson localisation in random system 80−39530
- sealing theory based on renormalisation group ideas 80−70646
- second-order self-energy, analytical results 79−51463
- self-consistent diagrammatic theory 80−107746
- semiconductor:transition metal, Anderson model localised impurity states *(Russian)* 80−6788
- semiconductor, chemisorption of H_2, Anderson model including correlation and overlap effects 77−76662
- semiconductor, doped, metal-insulator transition, anal. 80−88478
- semiconductor with transition metal impurity states, EPR linewidth calc. 80−80599
- semiconductors, amorphous, electronic states, theoretical methods 80−80167
- semiconductors, doped, shallow impurity states, Hubbard bands and donor excitonic states, HF calc. 80−100443
- simple averaged DC conductivity, numerical calc. 79−99522
- slow ion secondary emission model, rel. to Anderson model *(French)* 79−56902
- soluble local moment problem 78−52194
- solution for $U=0$ limit 78−19205
- spatially disordered systems, Anderson localisation and metal-insulator transition 80−59926
- spin glass, Luttinger and Edwards-Anderson models, equivalence 77−80951
- spin polarisation and spin correl. densities, local singlet state 77−63068
- strongly disordered electronic system, DC cond., Anderson's tight binding model, numerical calcs. 80−49673
- substitutional alloys of intermediate valence systems, static mag. susceptibility con. and temp. depend. 80−84586
- superconducting alloy, transition metal impurities, described by Anderson model, Josephson tunnel effect 77−16000
- superconducting order parameter, spatial variations in presence of impurity near transition temp., Anderson model calcs. 79−38245
- superconducting proximity effect sandwiches, appl. of Anderson theorem to elastic scatt. 80−84568
- superconductivity, magnetic impurity effects, Anderson model 78−52148
- superconductor, effect of mag. impurities with high Kondo temp., in Anderson model 77−63023
- switching initiation, Anderson model 78−10524
- T-matrix approximation, self-consistent soln. 78−43330
- thin wires, exptl. study of Anderson localisation 80−96849
- three-dimensional disordered lattice, numerical simulation of diffusion 79−78092
- transition element cpds. and their dil. alloys, supercond. crit. temp., s-d Coulomb interaction 78−31012
- transition in mag. field, weak field cond. and Hall effect 80−6726
- transition metal, chemisorption of H_2, Anderson model including correlation and overlap effects 77−76662
- transition metal alloys, volume anomalies 79−56490
- transition metal magnetic alloys, dilute, props., review of theory 79−15282

Anderson model continued
- transition metal oxides, sulphides, and selenides, Mott transition electronic and mag. phase diagrams 78—51894
- transition metals, d-band superconds., s-electron current density calc. 77—47926
- transition metals, mag. ordered state, interacting virtual state approach 77—69464
- transition metals, magnetism, interacting virtual state approach 77—72987
- two-dimensional electron system in strong mag. field, Anderson localisation 77—15929
- two-dimensional localisation, real-space scaling study 79—65416
- valence fluctuation system, ground state and elementary excitations, Anderson lattice model Hamiltonian, dense Kondo problem 80—54656
- wavefunctions on long finite random chains 78—47726
- zero-component classical field, electron localisation and statistical mechanics 78—30855
- Al, superconducting, order parameter, spatial var. near Anderson impurity 79—60962
- Al-3d transition metal, dil. alloy, preasymptotic charge oscillations around 3d impurities 77—36055
- Al-Cu-Fe, liquid, mag. moment and transition from mag. to nonmag. state 79—24132
- Al-Mn, dil., coherent propag. and strain-induced localisation of muons 78—95537
- As, liq., Anderson transition, cond., at high temp. and supercrit. press. 78—34869
- Ce alloys, Kondo system, mag. susceptibility calc. in Anderson model 77—55661
- Ce compounds, Anderson model, exchange parameter, Kondo temp., mag. susceptibility 79—1656
- CeAl$_2$, Anderson lattice system, volume collapsed strongly mixed valent state 79—38033
- CeAl$_2$, Anderson lattice system, thermal expansion meas. 1.5 to 10K 79—37860
- CeAl$_2$, Anderson lattice system, mag. moment reduction, press. effects 80—7093
- CeAl$_2$, Anderson lattice system, ground state props. 80—20443
- Cu-Al-Co liquid alloys, constant Co-content of 5 wt.%, mag. props. *(German)* 80—88720
- Cu-Al-Fe, dil. liq. alloy, localised mag. state interactions *(German)* 77—1539
- Eu-alloys, mixed valence, role of phonons and Coulomb interactions 79—38032
- Fe-V-C melts, electron struct., mag. susceptibility meas. *(Russian)* 78—47729
- FeSi$_2$ films, structural and Anderson transitions, cond. and IR reflectance meas. 79—15200
- 1T-Fe$_x$Ta$_{1-x}$S$_2$, Anderson localisation, elec. resist. and magnetoresist. meas. 80—44596
- GaAs-Al$_x$Ga$_{1-x}$As heterojunctions, MBE grown, photocollection efficiency and interface charges 79—11199
- H chemisorption on metal substrate, model including image charge effects 79—73405
- H$_x$WO$_3$ bronzes, Anderson transition, XPS 80—107705
- InAs, two dimensional accumulation layer, Anderson localisation 80—107871
- KMnF$_3$, exchange interaction of excited Mn^{2+}(^{4}A$_1$) ions, Anderson model 80—25124
- La$_{1-x}$Sr$_x$VO$_3$, semiconductor-metal transition, Anderson localisation, Hall mobility and 1/f noise meas. 79—78142
- Na$_x$WO$_3$, degenerate electron gas, Friedman effect, review 77—20242
- Ni, chemisorbed H$_2$ photoemission spectrum, Anderson model parameterisation 77—40334
- β'-Ni-Al-Fe, mag. impurity states, resist. meas. 77—55519
- NiFe$_2$O$_4$, electronic phase transition 80—65640
- Se, liq., Anderson transition, cond., at high temp. and supercrit. press. 78—34869
- Si, dangling bonds, EPR, localised states and unpaired electrons on microcrack surfaces 78—52351
- Si inversion layers, Anderson transition, random field origin, substrate bias effect 77—28255
- Si MOS devices, Anderson localisation in Landau level tails, anal. of Shubnikov-de Haas cond. minima 77—76947
- Si MOS inversion layer, Anderson localisation and Wigner crystal form. *(Japanese)* 77—69425
- Si vacancy, electron states, Anderson negative-U system 80—96820
- Si, vacancy, possible Anderson negative-U system 80—2358
- Si:P, electronic states, NMR of metallic and intermediate samples 79—4511
- Si:P, heavily doped, mag.-field depend. of sp. ht., rel. to metal-nonmetal transition 80—29183
- Si:P, metal-nonmetal transition, Anderson localisation 79—95335
- SiO$_2$, amorphous, low temp. acoustic absorpt., 9 to 20K and 15 to 65 MHz, Anderson model interpret. 78—26633
- TaS$_2$ (1T), low temp. elec. props., Anderson localisation by random impurity pot. 77—85205
- 1T-TaS$_2$, and 1T-TaS$_{2-x}$Se$_x$, Anderson localisation, elec. resist. and magnetoresist. meas. 80—44596
- Ta$_{1-x}$Ti$_x$S$_2$ (1T), magnetoresistance in the Anderson localized states near the metal-nonmetal transition 80—88479
- Ta$_{1-x}$Ti$_x$S$_2$ (1T), magnetoresist. near metal-nonmetal transition at ultra low temps. 80—88600
- TmSe, Anderson lattice resist. for antiferromag. ordering 80—65556
- WV$_2$O$_6$, magnetic susceptibility, behaviour in terms of quasi-isolated binuclear units 80—97073
- Yb$_{1-x}$Y$_x$CuAl, disordered extended Anderson model, CPA-alloy analogue treatment 80—65506
- Zn-Mn(Cr), dil, mag. anisotropy, Hartree-Fock calcs. 80—11162

anechoic chambers
- 3 GHz surface and lateral EM wave meas. 80—103742
- absorption coefficient of wall covered with sound-absorbing cubes *(German)* 77—84081
- acoustical enclosure, airtight, methods for predicting the insertion loss 79—18607
- bat's sonar system simulation, coherent processor performance estimation appl. *(French)* 80—56072
- design principles 78—51007
- EM wave scatt., echo width meas. 79—3614

anechoic chambers continued
- large chamber for road vehicles and large machines, instrum. room and services room *(German)* 77—72121
- loudspeaker, frequency response measurment in echo chamber *(German)* 77—75762
- music reproduction in small rooms, theory *(Spanish)* 78—38155
- National Bureau of Standards, acoustic props. 78—87217
- noise source investigation, industrial acoustic problems appl. 77—75742
- reverberation chamber design, constr., loudspeaker performance measurement appl. *(Italian)* 78—26013
- semianechoic chamber sound power meas. by traversing microphone 77—62116
- testing rooms for analysis of engines 77—84084
- thin ferrite tiles properties *(Japanese)* 78—46861
- waterfilled US testing tanks, appl. of filled rubber material system to echo absorpt. 80—96059
- wedge lined free field rooms, HF performance 78—33962

anelastic relaxation
- *see also Bordoni effect; creep; elastic aftereffect; internal friction; Snoek effect; stress relaxation; Zener relaxation*
- alkali borate and phosphate glasses, mech. and dielec. relaxs. and interpet. 78—27159
- alkali silicate glass, isothermal mech. loss spectrum, appl. of Rheovibron 80—88260
- alkali silicate glasses, secondary relax. transitions 80—88261
- BCC metals, HF mech. relax. peak 78—91379
- borate glasses, mechanical relax. in transition range 78—80575
- butadiene styrene elastomers, cross-linked, mech. relax. behaviour *(German)* 80—84986
- butadiene styrol rubber, effect of polyfunctional nitro-oligomers on relaxation *(German)* 78—31441
- cellulose, mech. relaxation at low temps. rel. to adsorbed H$_2$O 77—43277
- Debye relax. eqns. for stand. solid with high relax. strength 77—20011
- density matrix formalism for anelastic relaxation 79—14880
- dicyclohexyl phthalate, plasticiser for PVC, effect on secondary relax. 79—4995
- dispersions, thixotropic, mech. props., structural hysteresis, statistical thermodynamic anal. 77—46978
- elastic amorphous medium, relax. by defect diffusion 80—58925
- elastomers, soot filled, mech. relax. behaviour *(German)* 80—84985
- epoxy resin with various fillers, filler effect on relaxation time spectra 77—52390
- general linear response analysis of anelasticity 79—10895
- glass, network forming, oxide, internal friction *(Japanese)* 77—70096
- glass, relaxation phenomena and Raman spectroscopy, review of developments 78—22665
- high polymers, solid, mech. energy relax., linear response theory 77—89387
- ice:HF, I$_c$, Bjerrum defects *(French)* 78—6122
- inelastic solids, anelastic relaxation anal., extended to creep at high temp., appl. to internal friction *(French)* 78—63806
- internal stress measurement, in creep, anelasticity influence 80—70306
- LF fluctuation, dissipation and relaxation properties, universality 80—84687
- long-range diffusion, review 80—60904
- low-frequency fluctuation, dissipation and relaxation properties 80—39661
- 3-lumped parameter vibrational mdoel, anal. for dynamic characteristics of materials of relaxation type 79—72827
- material anelastic behaviour, anal. using 3-lumped vibr. model *(Japanese)* 78—47473
- measurement of mag. aftereffect, high time const. relax. processes meas. 78—29129
- metal-H system, elastic interaction and phase transition, book contrib. 79—83178
- metal-H systems, anelastic and plastic props., review 80—49298
- metals, Snoek-Koster relaxation, theory 80—16369
- noncrystalline solids, thermally stimulated creep method for mol. motions investig. 78—22787
- phenolformaldehyde resin moulding compounds, dynamic testing *(German)* 78—76699
- plastic powder compact rheological characteristics *(Japanese)* 78—95770
- polycarbonate, glassy, temp. drop during deform. 78—15456
- polycrystalline materials, effect of grain boundary sliding on anelasticity 80—96592
- polydecamethylene-oxide, dynamic mechanical measurements using a dynamic viscoelastometer *(Spanish)* 79—61636
- polyethylene, γ-ray polymerised, cold compacted films, mech. relaxations, mechanism 77—16631
- polyethylene films, two-layer, elongation, recovery rates meas., relaxational props. *(Russian)* 77—32663
- polyethylene melt, rheology and molecular struct., melt identification from mech. props. 77—11490
- polyethylene terephthalate, thermally stimulated creep method for mol. motions investig. 78—22787
- polyethylene terephthalate, TSC and thermally stimulated creep, dielec. and mech. retardation modes 79—78613
- polymer, amorphous, molecular origin of relaxations 78—26058
- polymer, crystallising, defects and mech. relax. *(Russian)* 78—22789
- polymer blends, viscoelastic props. *(Russian)* 78—72808
- polymer network formation, relaxational props. variation 80—38961
- polymer relaxation, computer used to calculate mech. charact. 77—52388
- polymers, amorphous, semi-cryst., mech. motions, review 77—32616
- polymers, highly elastic state, mechanical losses and relaxation processes *(Russian)* 78—76698
- polymers, semi-crystalline, dynamical mech. props. in amorphous phase *(French)* 77—72653
- polyphenylquinoxaline cyclotriphosphazine hexaisothiocyanate networks, dynamic mech. props. *(Russian)* 78—72809
- polypropene-alt-1,4-butadiene and hydrogenated derivative, mol. relaxations in glassy state 80—53177
- polypropylene, cold-drawn isotactic bars and thin films, microstruct. and annealing 78—95760
- polystyrene-b-isoprene and hydrogenated derivative, mol. relaxations in glassy state 80—53177
- PTFE, partially crystalline, time-temp. superposition 77—4801
- refractory, rheological behaviour at high temp. *(French)* 77—56016
- steel, C, relax. resist. rel. to struct. 78—23788
- stress relaxation theory, for plastic deform. *(Hungarian)* 80—97661
- styrene-isoprene triblock copolymer, mol. relax. in glassy state 80—53177

anelastic relaxation continued
- sugar crystal, triboluminesc. kinetics and mech. relax. 77—73178
- thermotropic liquid crystals, anomalous rheological responses, spectrometer study 80—6358
- urethane elastomer, temp. strain relaxation investigation by opticomechanical method and IR spectroscopy 77—4805
- vitreous solids, internal friction and relaxation *(French)* 77—72651
- Ag-Zn, vacancy prod. rate by displacement cascades, anelastic meas. during neutron irrad. 80—19794
- Al, electron-irradiated, anelastic relax. due to single self-interstitial atoms 77—39627
- Al, electron-irradiated, anelastic relax. due to clustered self-interstitial atoms 77—39628
- Al, stress wave propag., transmitted wave profile 77—80578
- Be, internal friction, temperature spectrum and dislocation damping, anelastic relaxation *(Russian)* 80—2118
- Fe, US velocity anomalies at elevated temp. 78—75830
- Fe:C(N), small concs. determ., mag. and mech. relax. methods 80—7879
- Fe-B(-Si)(-Ni), amorphous alloy, anelastic relaxation 79—4997
- Fe-Ni-P-B(C), amorphous alloy, anelastic relaxation 79—4997
- Fe-P-Al(Si)(B), amorphous alloy, anelastic relaxation 79—4997
- $Fe_{40}Ni_{40}P_{20-x(B)}B_{x(B)}$, ferromagnetic metallic glass, thermal and mech. stability 77—66698
- $Fe_{83}P_{17-x(B)}B_{x(B)}$, ferromagnetic, metallic glass thermal and mech. stability 77—66698
- Ge:Cu, anelastic relax., internal friction temp. depend. meas. 79—65143
- MgF_2:LiF crystal, defect struct., anelastic and dielec. relax. meas. 77—27938
- MgO:Li, internal friction, mech. and dielec. relax. *(German)* 80—34135
- MnF_2:LiF, anelastic relax. of Li^+-Li^+ split interstitial defect 79—77678
- Na_2O-B_2O-SiO_2 glasses, high temp. mech. relax. 79—96071
- Nb, cold-worked, Snoek-Koster relaxation transient period, comparison with Schoeck's theory 79—34086
- Nb, solute trapping of H, symmetry of O-H pair 80—108488
- Nb, theory of Gorsky effect of interstitial diffusion, for low interstitial H concs. 79—10896
- Nb-H(D) system, anelastic behaviour, 0.5-15K 80—49300
- $Nb_{53}Ta_{47}$, elastic const. charge caused by H addition, hydrostatic press. effect 80—75287
- Ni cold worked, annealed, exam. of anelastic relaxation at low temp. 78—84877
- Ni, hardness after-effect studied by anelastic relaxation 80—66570
- Ni, pure and doped, mech., mag. relax. meas. dumb-bell self-interstitital reorientation *(German)* 78—52879
- β'-NiAl, ordered, hardness after-effect studied by anelastic relaxation 80—66570
- $Pb_{0.84}Sn_{0.16}Te$ solid soln., single cryst. *(Russian)* 77—51437
- Pd-H system, α and $\alpha+\beta$ phases, annealed and deformed, anelastic effects 80—66567
- Ta-H(D), anelasticity due to long-range diffusion 80—60904
- Ti, irradiated and cold worked, internal friction pdaks 77—86074
- V, elastic const. charge caused by H addition, hydrostatic press. effect 80—75287
- V-H(D), anelasticity due to long-range diffusion 80—60904
- α-Zr, anelastic relaxation and O_2 diffusion 77—4219
- α-Zr, internal friction and O_2 pair diffusion 77—16634

anelasticity
- *see also anelastic relaxation*
- acceleration waves in anelastic bodies, propag. conditions 77—1169
- amorphous materials, deform. processes 77—4813
- anisotropic point defects, influence on anelasticity of crystals 78—14403
- austenitic stainless steel, type 316, anelasticity and creep transients 78—84880
- bone, anelastic deform. and friction stress 78—19871
- α-brass, electron irradiated, vacancy migration props., effect on enhanced atomic mobility 79—46829
- causal absorption, effect on synthetic seismograms 79—92486
- collagen film, dynamic mech. props., β-galactosidase impregnation effects 79—11885
- creep, contrib. of climb rate of dislocation links and config. 77—52431
- creep, fluctuation-dissipation theorem derivation for linear anelasticity 78—43066
- creep, high temp., steady state, anelasticity and measured internal stress 78—35456
- damaged body, unknown boundary value problem explicit solution *(French)* 80—79166
- deformation body anelastic hysteresis determ. and error formula *(German)* 77—80123
- deformation kinetics analysis of stress sensitivity 77—3737
- Earth, surface waves phase vel. and attenuation simultaneous inversion, Love waves appl. 78—85491
- Earth crust and upper mantle, inversions of high freq. Q_γ^{-1}(f) 77—33000
- Earth mantle beneath Japanese Arc, anelastic props. from multiple ScS waves attenuation 79—92508
- fibre reinforced composite, anelastic behaviour using continuum theory of internal separation 77—46907
- filled polymers, US study of internal damage, nonlinear elastic effects, theory 80—49307
- glass, internal friction 79—52286
- internal stress, stochastic model for dip test in steady-state creep 80—58915
- internal stress measurement, in creep, anelasticity influence 80—70306
- isotropic media, linear dynamical equations of state 80—22314
- metal, anelastic study of intrinsic point defects, irradiation effects 78—47323
- metals and alloys, nonlinear anelasticity and the martensitic transformation 79—61634
- nonlinear anelasticity, and autooscillations 80—70307
- nonlinear theory of simple dipolar elastic solid, successive approx. method 77—39221
- peridotite, high-temp. anelasticity and elasticity 80—17256
- piezoelectric solid, anelastic loss, specimen geometry effect 79—78624
- polycarbonate, anelastic component of strain *(Japanese)* 77—8870
- polyethylene, linear role of recovery forces in deformation 78—48459
- polymeric glasses, non-elastic deformation, thermodynamic and kinetic anal. 78—64604
- polymers, temp. depend. under dynamic conditions, linear theory of thermoviscoelasticity 79—61642

anelasticity continued
- polypropylene, glassy state, macrodeformation stresses, anelastic characteristics 79—52289
- polystyrene, glassy state, macrodeformation stresses, anelastic characteristics 79—52289
- PVC, glassy state, macrodeformation stresses, anelastic characteristics 79—52289
- quartz, electron irradiated, optical and anelastic absorptions and resonator freq. 78—64385
- rubber, synthetic, nonlinear anelastic behaviour at finite strains 79—3923
- steel, austenitic, measured internal stress and anelasticity in creep *(Czech)* 79—38909
- steel, austenitic, Ni-Cr, precipitation strengthened, anelasticity, plastic creep limit, 823K 79—1899
- steel, stainless, anelastic and nonlinear viscoplastic behaviour relations at low homologous temps. 77—63742
- steel, stainless, type 316, cyclic creep behaviour, as func. of max. applied stress 78—48460
- string vibrating against rigid wall, partially elastic or anelastic impact, energy calcs. 78—67028
- sugar, mechanical relax. time, determ. from tribolum. 77—1173
- Ag-Cu, highly deformed eutectic composite wire, anomalous props., fibre diameter and foreign atom effects *(German)* 77—36566
- Ag-Zn (24 at.%), γ-irradiated, directional order by in-flux anelasticity meas. *(French)* 79—10877
- Al, dislocation line movement at low temp., obs. by US meas. *(French)* 79—95025
- Al-Ag (up to 40 at.%), exam. of anelastic phenomena and structural state 78—76693
- Al-Mg, elastic and anelastic props. in relation to Guinier-Preston zones, US investigation *(French)* 79—38833
- Cu-Al-Ni (14.1, 3 wt.%), autooscillations and nonlinear anelasticity 80—70307
- Cu-Ge (8 wt.%), anelastic effect due to deform. twins *(Japanese)* 79—20095
- Fe, inelastic deformation, mech. eqn. of state, stress relax. 77—56047
- Fe-Co-V, anelastic phenomena, related to atomic order, exam. of magnetostriction *(French)* 78—80579
- Fe-V(Nb)-N, precipitation study, 550 to 600°C *(German)* 77—90350
- Mg single crystal, anelastic internal stress field in easy glide region 78—48442
- Mg-Al-Zn, anelastic creep and recovery 77—63709
- Mn-Cu alloys, mechanical damping at 40 kHz 78—23755
- $Mn_{0.82}Fe_{2.18}O_4$, anelasticity, 280 to 730K, 125 kHz vibr. study 78—87740
- Ni-Cr base alloy, strain relaxation, effect of grain size, particle size, γ' vol. fraction 79—47741
- Pb-Sn eutectic, superplastic, anelasticity effect on stress relaxation 78—31443
- $Pd_{80}Si_{20}$, plastic flow, fracture, slanted necking and elongation at high temps. 79—57057
- Se, vitreous, micromech. props., anelastic behaviour, internal friction *(French)* 77—72652
- Sn-Pb eutectic alloy, inelastic behaviour 77—48471
- Ta, proton implanted, anelasticity, internal friction meas. 79—24560
- Ti β III alloy, elastic and anelastic phenomena associated with α and ω phase isothermal precipitation *(French)* 79—52288
- UO_2, config. and climb rate of dislocation links, contrib. to anelastic creep 77—52431
- V-O solid soln., BCC, modelling of interstitial solute behaviour 79—77748
- Zr, amplitude depend. damping 77—32617
- α-Zr, anelastic relaxation and O_2 diffusion 77—4219

anemometers
- *see also laser velocimeters*
- acoustic anemometer based on turbulent pressure fluctuations 78—16179
- acoustic optic cells, appl. *(Portuguese)* 77—89217
- air flow meas. in tunnel using anemometers and pitot tubes 79—41779
- anemograph data quality control 80—56642
- bivane anemometer, Reynolds stress defl. and elevation angle sensing 80—109265
- boundary layer meas. system for wind and temp. obs. *(German)* 80—94616
- bubble-flow regime, two-phase laser Doppler anemometry 77—39366
- catalytic error with anemometer for gaseous mixture conc. fluctuation meas. 77—26291
- coherent structure in flow fields anal. using laser Doppler anemometry 80—10339
- commercial LDA instruments *(Czech)* 79—46409
- conduction type, with external mag. field, turbulence spectrum correction 78—1766
- conference, fluid flow research instrumentation, Saint-Louis, France, May 1976 77—35271
- constant resistance hot wire, flow average temp. variations, reading effects *(Russian)* 78—88925
- constant temp. wire, thermal inertia 77—31401
- constant-temperature hot-wire anemometer evaluation for respiratory gas flow meas. 79—83967
- crossed hot-film, wind velocity meas., compensating for non-ideal geometry 80—31122
- cup, rain-induced errors in mean wind speed meas. in surface layer at sea 78—61485
- cup type, appl. to wind vel. spectra determ. *(Russian)* 77—13102
- cups, propellers and lasers for wind speed and direction meas. 80—90264
- cylindrical hot-wire for power station dust-laden gas flow meas., characts. 77—27632
- deep ocean current meas. system 77—5382
- digital anemograph, for wind direction and average speed meas. *(Czech)* 80—77174
- Digital Anemograph Logging Equipment 77—82036
- dual-beam laser Doppler anemometer, beam waist location and meas. 78 37931
- electrogasdynamic spectral anemometer 78—87422
- electrolyte soln. flow, transducer-electrode freq.-ampl. characts. 77—76001
- errors in rotational anemometers, wind tunnel tests 77—29454
- Fabry-Perot spherical mirror interferometer for wind velocity meas. *(Chinese)* 79—77308
- flow meas., laser Doppler anemometry, practical considerations 79 27725

anemometers continued
flowpath velocity meas., semiconductor hot element anemometer 80—48823
fluid anemometric microthermistor sensor sensitivity curves *(Russian)* 78—34219
four wire probe for turbulent flow temp. and vel. meas. 78—67290
frequency shift laser meas. of water and wind velocities 77—39385
frequency tracker for laser Doppler anemometry 79—72968
Gill UVW 3-dimens. anemometer with propellers, correction method *(French)* 78—3987
heat waves, appls. in flow metrology 79—68879
holographic interferometry methods and applications *(French)* 79—7099
hot film, calibration and use in fluids at varying background temp. 78—1767
hot film and hot wire anemometers, signal-to-noise ratio 78—94861
hot film in reversing shear flow, heat transfer 77—15014
hot film probe, wedge shaped, theoretical performance 77—31403
hot wire, comments on 'squared signals' analysis technique and reply 80—28581
hot wire, comparison of dynamic and static calibrations for vel. perturbation meas. 77—19644
hot wire, const. current, response to temp. fluctuations 78—94860
hot wire, probes, X-configuration dynamic testing device 78—87421
hot wire, single rotating slanting, meas. of Reynolds stress tensor in curved duct expt. 80—75006
hot wire, supersonic rarefied gas flow vel. meas. 80—100040
hot wire and hot film temperature compensating circuits, temp. probe appl. 78—59510
hot wire anemometer response in a flow with acoustic disturbances 78—63517
hot wire anemometers, appl. as particle vel. detector in standing sound waves 77—62124
hot wire anemometry, calibration at low vel., wire support correction 79—60077
hot wire anemometry method for the flow patterns in an array of heat exchanger tubes 79—90357
hot wire anemometry of turbulent spot interaction with turbulent boundary layer 78—90858
hot wire dynamic behavior, CSIRO liquid water probe, freq. response 80—12562
hot wire technique for simultaneous nonisothermal flow vel. and temp. meas. *(Japanese)* 78—38421
hot wire transducer, use for vel. meas. in fluids of variable press. and temp. *(Rumanian)* 78—34212
hot-film, appl. to blood flow velocity meas. *(Japanese)* 79—29678
hot-film, turbulence meas. in gas-liquid two-phase flow *(German)* 77—11254
hot-film anemometer, calibration of low-vel., flow direction 78—91043
hot-film anemometer for cylinder wake pattern with spray cooling 78—34238
hot-film anemometers, freq. optimisation theory 78—26218
hot-film probe, calibration in liquids 79—27723
hot-film probe velocity measurements in liquid metal MHD duct flow experiments 80—75009
hot-film type, signal anal. method for two-phase flow 79—32639
hot-film wall shear probes, miniature, for biomedical appls., method for alignment 79—53262
hot-film wall-shear probes in liquids, calibration device 79—50823
hot-wire, analysis of signals of multidimensional turbulent flow field 79—27720
hot-wire, appl. to temp. meas. in transient gas flow 77—82508
hot-wire, calib., for temp. and vel. meas., low-freq. effects 79—50825
hot-wire, computerised, for vel.- and temp.-meas. in heat turbulent flow 78—91040
hot-wire, const. temp., comments on determination and optimization of freq. response in supersonic flows 80—87832
hot-wire, const. temp., dynamic characts. using shock tube and electronic testing 79—72974
hot-wire, constant-temp., effect of varying resistance ratio on behaviour 80—59141
hot-wire, constant-temperature anemometer, freq. response and electronic testing 77—58820
hot-wire, constant-temperature anemometer, nonlinear theory 77—58821
hot-wire, error reduction in supersonic thin turbulent layer meas. 78—34235
hot-wire, fluctuation data anal. with end-loss correction for supersonic flow 78—55703
hot-wire, for air flow measurements, calibration at low vels. 79—27724
hot-wire, for atmospheric turbulence meas. in marine environment, freq. response 77—33214
hot-wire, for liquid N_2 flow rate meas. 77—31409
hot-wire, freq. response of constant temp. anemometers in supersonic flow 80—59149
hot-wire, influence of humidity changes 80—75007
hot-wire, linearised, with bridge circuit, for turbulence research, characts. 77—55118
hot-wire, meas. of turbulence fluctuation in nonisothermal jet 77—35189
hot-wire, modification for meas of turbulence in supersonic flows 79—90356
hot-wire, response to stream temp. perturbations 78—83503
hot-wire, sensitivity to stream temp. fluctuations, end cond. effects 78—34215
hot-wire, slanting, flow velocity in pipe meas. 77—62313
hot-wire, spatial vorticity distrib. meas. technique 78—67289
hot-wire, temp. compensation errors estimation *(Russian)* 78—57345
hot-wire, transonic flow, boundary layer turbulence 78—14103
hot-wire, use of triple-sensor probes for turbulent flow-field investigations 80—100043
hot-wire, very low velocity calibration 80—75008
hot-wire, wall proximity meas. corrections 80—74841
hot-wire and hot-film probes, response to passage through air-water interface 78—22438
hot-wire anemometer, static and total press. probes turbulence effects 78—34240
hot-wire anemometer, turbulent flow near 400°C, sensitivity and temp. fluctuations *(French)* 78—42684
hot-wire anemometry combined with smoke flow visualisation, technique, appl. to turbulent boundary layer 78—91044
hot-wire anemometry in transonic flow, fluctuation anal. 77—65817
hot-wire anemometry used in subsonic airflow measurement, interpretation of probe signals 80—14857

anemometers continued
hot-wire direction sensitive probe for flow reversal detection in unsteady flow 80—10333
hot-wire freq. response to heating current fluctuations 77—39369
hot-wire measurement errors in shear flows 77—55119
hot-wire measurements in the wall vicinity, anal. of errors 78—34220
hot-wire probe, simultaneous, instantaneous, temp. and vol. component meas. in turbulent flow 78—34236
hot-wire probes in low speed flow 79—82010
hot-wire sensor, effect of centrifugal and Coriolis forces on rotating probe 78—94862
hot-wire system for turbulence quantities meas. in two-stream mixing layer 79—32488
hydroresistor thermoanemometer, empirical heat exchange eqn. 80—21852
inclined hot-wire response equations, for flow field having dominant tangential velocity component 78—14105
indoor climate research, anemometers modification and calibration 77—3897
inside-out type, constructional details 78—59516
integrated direction sensitive flowmeter 77—7484
internal combustion engine efficiency studies using laser anemometer 80—53307
Joint North Sea Wave Project anemometer, development and appls. *(Dutch)* 78—3785
laer Doppler anemometry meas. in water flows 77—58818
laser, for periodic fluid flow measurement, periodic sampling 80—64657
laser, gas-solid suspension flow meas. 77—35268
laser, IR heterodyne detect. of aerosols *(French)* 77—37991
laser, Reynolds stress expt. analysis appl., turbulent flow in rectangular channel *(Italian)* 79—4094
laser anemointerferometer, for simultaneous velocity and density meas. 79—18976
laser anemometer, appl. to investigation of supersonic shock-wave boundary-layer interaction 77—35275
laser anemometer, with differential optical arrangement, instrum. function 77—959
laser anemometer elements, Gaussian beam transform. 79—45991
laser anemometry, flow statistics retrieval via photon correl. 77—3896
laser anemometry, fringe-type, review of high-speed wind tunnel appl. in France and Germany 77—35272
laser anemometry, fundamental limitation and accuracy 80—87829
laser Dopper, photon correl., laminar flow autocorrel. 79—50826
laser Doppler, acousto-optical modulator using TeO_2 78—83082
laser Doppler, analogue, photon correl. and rate. correl. techniques 79—50828
laser Doppler, dual-beam, coincidence of beam waist and crossover region 80—14377
laser doppler, feasibility assessment method *(Russian)* 79—98832
laser Doppler, for meas. of solids vel. in air 77—84379
laser doppler, microprocessor-based autocorrelator 77—72396
laser Doppler, principles and status, survey *(German)* 78—9738
laser Doppler, sensing volume and biasing corrections for dual counter processors 79—77314
laser Doppler and time of flight combined anemometer 79—55434
laser Doppler anemometer, digital signals processing via SAW spectrum analyser 78—26007
laser Doppler anemometer, directionally sensitive two-component 80—75004
laser Doppler anemometer, flow field meas. in wake of blunt body, effect of chem. reaction 77—35262
laser Doppler anemometer, flow meas. in fluidic amplifiers *(German)* 77—961
laser Doppler anemometer, meas. of turbulent vortex flow 80—79412
laser Doppler anemometer, S/N, detector influence *(German)* 77—19651
laser Doppler anemometer, two-component, using rotating radial diffr. grating 77—3898
laser Doppler anemometer measurements, bias correction 80—24114
laser Doppler anemometer system, influence of Gaussian beam props. 79—41406
laser Doppler anemometer with microscopic intersection volume 79—94750
laser Doppler anemometery digital data acquisition system 77—80253
laser Doppler anemometry, instrumentation, appls., explanation using Moire patterns 77—7490
laser Doppler anemometry in internal combustion engine cylinder 79—77296
laser Doppler anemometry of high-temp. industrial gas flow *(German)* 79—10618
laser Doppler anomemeter for velocity fields meas. near prosthetic heart valves 79—57814
laser Doppler system, optics and signal processor for turbulent low speed flows *(French)* 78—59521
laser fibre-optic Doppler 78—30373
laser for powder electrodeposition particles flow meas. 78—18364
laser fringe anemometers, light scatt. aspects, particle size meas. appl. 78—83020
laser signals, visibility characts., particle sizing appl. 77—42482
laser transit anemometer signals, semiclassical processing 80—59145
laser-Doppler anemometry and photon correlation for turbulence length scales 80—87828
laser-Doppler microprocessor-based signal processing system 77—89218
liquid flow rates through pipes, applicability of experimental meas. methods 80—100044
low and high turbulence flows, hot wire measurement based analysis 78—59511
low-speed anemometer, with const. temp. thermistor *(French)* 77—21922
low-speed thermoanemometers testing apparatus 79—77311
lung model, human, velocity distrib. and pressure drop. expt. 79—96602
meteorological Gill propeller anemometer, for medium and high winds 80—26618
microprocessor-based, features 79—60087
miniature drag force anemometer 78—14117
multicomponent frequency shifting self-aligning laser velocimeters 78—87423
ocean surface meteorological buoy and aircraft VHF link 80—46298
opticomechanical anemometer for flow vel. meas. of optically transparent material 77—68718
overspeeding of cup anemometer rel. to turbulence intensities 77—53241
paired Gill-type propeller, effective dynamics response 77—70846

anemometers continued
photon correlation anemometer, differential Doppler system, appl. supersonic flow 77—35277
pneumatic type, operational description and calibration *(Russian)* 77—37420
pocket air flow anemometer with built-in calculator, appls. *(German)* 78—75242
posistor element for improved linearity *(Russian)* 77—15139
probe calibration device, operational principle *(Polish)* 77—72391
propeller anemometer and thermistor meas., meas. interpretation *(French)* 79—16708
propeller vane devices, dynamic props. 80—31138
pulse height analyser for wind speed and direction meas., automatic distrib. meas. system 79—96839
pulsed-wire, for low velocity air flow meas. *(Japanese)* 77—62319
pulsed-wire, randomly triggered, turbulence spectra meas. 77—15141
pulsed-wire and hot-wire, turbulent wake meas. 77—11288
Rayleigh interferometer, two-freq., performance as refractometer and anemometer 79—75579
reflected-beam laser anemometry using photon correlator 80—106861
reverse flow sensing hot-wire probe 79—98838
rotating hot wire single inclined type, characts. anal. and obs. 77—51146
rotating sphere in still fluid, velocity meas. *(Japanese)* 77—35112
shipboard meteorological data system 80—46299
simple linearised hot wire anemometer, performance characts. 80—53904
solid-state cupless anemometers 79—96832
sonic anemometer for boundary layer eddy correl. 80—56637
sonic anemometer-thermometer, phase-locked loop CW system 80—41565
spatial flow field determination, hot wire anemometry based analysis 78—59512
spectral analysis of signals from a laser Doppler anemometer operating in the burst mode 80—100041
speed meas. devices survey, industrial appl. *(French)* 79—93105
tethered aerodynamically lifting anemometer for WTG siting meas. 80—48830
thermistors, thermally compensated, math. models *(French)* 80—90227
thermoanemometer, influence of probe filament aspect ratio and diameter 80—19532
thermoanemometers using single-crystal p-type Si whiskers 78—3975
thermocouple hot-wire anemometer for boundary layer meas. with free convection in liquids *(German)* 80—10329
thermocouple-anemometer, mass flow meas. in shock tube 79—77300
thermosyphon solar water heaters, transient flow meas. using laser doppler anemometer 80—61413
three dimensional anemometers, feasibility of use in simulated tornado flow meas. 77—17244
three-axis thermal anemometers, eddy correlation flux meas., turbulence effects 80—17401
time-of-flight laser anemometer, for velocity meas. in atm. 78—69469
time-of-flight laser anemometer 77—39383
transistor use, wind sensor for portable battery operated instrument 79—71420
turbulence characts. meas. using 45° slant hot-wire probe 79—72967
turbulence measurement by laser Doppler anemometers, book contrib., review 80—19538
turbulent and high frequency fluctuating flow, mean static pressure measurement, hot wire anemometer and Pitot tube combined appl. 78—57889
turbulent flow, developing, in rectangular duct, laser Doppler anemometer obs. 77—14995
turbulent flow measurement by laser Doppler anemometry, concentration and size of tracer particles, theoretical limits 78—59514
two dimensional laser Doppler anemometer, turbulent jet flow field meas. 80—28582
two-wire probe in nonisothermal flow, simultaneous vel. and temp. meas. 78—91042
upper atmosphere wind, meas. with airglow Fabry-Perot spectrometer 80—77156
velocimeter based on CO_2 laser for long-range anemometry 78—36333
vertical Gill anemometer meas. of boundary layer parameters 80—56618
video equipment for remote meas. of wind velocity for pollution monitoring *(French)* 80—7990
vortex anemometers, second-generation 77—78436
wind data acquisition and processing for wind power site evaluation 79—66400
wind energy survey anemometer and recording instrumentation 77—33222
wind gust recorder, digital 77—56762
wind-tunnel laser anemometer photon correlation techniques 77—80256
X-hot wire probe, procedure for symmetric orientation 79—68835
CO_2-air, heat transfer from cylindrical anemometer probe 77—84256
Na vapour, particle size meas. using anemometer 80—13195

angle measurement *see angular measurement*

angle modulation
see also frequency modulation; phase modulation
optical signals, parameter meas. *(Russian)* 78—37047

angular correlation techniques
annihilation radiation, automatic installation 77—6648
bovine carbonic anhydrase, γ-ray perturbed directional correl. obs. of conform. change, active site ^{111}In ions 79—83700
charged particle pairs, correlation techniques 77—18762
chemistry applications of γ-γ perturbed ang. correl. meas. *(Japanese)* 78—40098
clustering studies, ang. correl. anal. 79—6547
curved plunger for TDPAC meas. on recoil into gas 79—76313
fission products, complementary, ang. correlations anal. 79—76311
gamma spectroscopy, source activity calculation from counting rates in single and coincidence photopeaks 78—13371
gamma-gamma, Ge(Li)-NaI(Tl) and NaI(Tl)-NaI(Tl) meas. *(Spanish)* 79—89525
gamma-ray angular correlation, intrasource absorpt. and scatt. effects 79—97958
heavy ion induced transfer reactions, new methods using particle ang. correls. *(French)* 79—558
high density proportional counter, medical imaging of e^+ radioisotope distrib. 79—5399
Institut Laue-Langevin, on-line ang. correl. system 80—52615
molecular biophysics, conformational changes and mol. dynamics in bovine serum albumin 80—81538

angular correlation techniques continued
moment method in stochastic perturbation of angular correlations 77—3268
multidetector meas. of ang. correl. 79—41084
oriented nuclei, β-γ ang. correl., G-parity nonconservation 78—54723
oriented radioactive nuclei, JINR investigs. using SPIN equipment *(Czech)* 77—42220
parity assignments, ang. correl. method, model independ. technique 78—21827
particle+gamma angular correlations in (a,bγ) type reactions, phase, sign conventions 77—26641
particle diagnosis of fusion plasma 77—35397
particle-gamma ang. correls. meas. 77—10567
particle-particle angular correl. study of $^{12}C(^6Li,d)^{16}O\rightarrow\alpha+^{12}C$ 77—79395
particle-particle correlation experiment, on-line four parameter anal. system *(Chinese)* 80—42910
positron annihilation ang. correl. curves anal. using ANNIH program 80—37709
random sampling of scattering angle in neutron transport 79—85574
review of apparatus and meas. at KURRI 77—42219
scattering set-up for many particle correlation expts. at Hamburg Isochronous Cyclotron 80—37711
statistical theory of asymmetry detection 79—26853
TDPAC, appl. to chemistry and solid state physics, review 79—75665
three body sequential decay processes, α-transfer reaction studies 79—6526
three body sequential decay X(a,b)Y(c)Z processes, parity, spin, reaction mechs. info. from ang. correl. method 78—50222
windowed ang. correl. method for positron annihilation params. meas. 77—34528
e^+ annihilation in solids, angular correl. meas. by proportional counter 79—4869
e^+e^- annihilation $\gamma\gamma$ angular correlation measurement, design and construction of liquid He cryostat 79—93148
γ-γ technique, meas. of physics params. of fission reactors 77—14212
pN, 400 GeV, study in nuclear photoemulsion *(Russian)* 79—93475
$^{111}Cd^m$ bound on DNA, perturbed, γ-γ ang. correlations 79—79457
^{154}Gd, 2^+ rot. states, time integral perturbed angular correl., meas. method 77—9154
In, positron annihilation, Fermi momentum and core electron contribution 77—81173
^{138}La, magnetic moment of the first excited state, meas. using TDPAD 79—63589
$^{16}O(^6Li,d\gamma)^{20}Ne$, d$\gamma$ ang. correl. reaction strength comparison, DWBA anal. 79—26452
Pb-Ni-Si, metallic glass, electron irrad., positron annihilation radiation, angular correlation study 78—84678
^{152}Sm, 2^+ rot. states, time integral, perturbed angular correl., meas. method 77—9154
Sn, positron annihilation, Fermi momentum and core electron contribution 77—81173
^{181}Ta, 133-482 keV cascade, effect of source preparation technique on differential ang. correl. 77—71711
^{160}Tb, perturbed ang. correl. determ. by one ang. meas. 79—17851
^{235}U(n,f), time correlated associated particle method, CAMAC experiment 80—52702
Xe, γ-γ PAC following nucl. electron capture, cascades perturbed by hyperfine coupling 78—37303

angular measurement
see also angular velocity measurement
acoustic passive bearing estimation, removal of bias and 2π ambiguities 78—38150
adaptive industrial robot, calc. method *(Russian)* 80—42192
angle etalon constr., angular scale, polygon calibration appl. *(German)* 78—77852
angle interferometer with 90° range, system set-up, calibration *(German)* 78—165
angular stresses of spindle with air bearings 79—35678
auto-collimating telescope calibration methods *(German)* 78—77848
butterfly-valve inductive orientation detector 80—68193
capacitance-based micropositioning system for X-ray rocking curve measurements 80—205
capacitive position indicators *(German)* 80—57256
circular magnetoelectric convertors, angle-of-rotation conversion errors 77—17968
circular scale calibration by reflection grating polygon *(German)* 80—86250
coherent light source angular coordinates using received wave phase front 78—46526
contact angle, for sessile drop on horizontal surface, projected image magnification 77—55421
counting interferometer, for angles in range 70° *(German)* 77—10095
cutoff angle of piezoelec. quartz wafers using X-ray comparator 80—105755
diffraction grating used for angle measurement between edges of distant objects 80—86259
digital method using photoelectric angular transducer with unstable datum, increasing accuracy 80—17920
dimensions, classification and symbols for means of meas. 79—6081
disc rotation meas. from elliptical projection, appl. to eye movements 78—15931
displacement, digital, magnetic scale recording system 77—2635
displacement angle monitoring using diffr. gratings 77—33973
dragline bucket inclination system *(Russian)* 80—22325
dynamic angular displacement measurements by interferometry 79—49276
eddy-current angle displacement transducer for 213-473K temp. range, types *(Russian)* 77—33974
education, holographic double exposure interferometry for small rot. meas. 78—36758
electroless Ni deposits from Ni/P and Ni/B plating solutions, solderability by contact angle meas. study 79—88910
electrooptical meter for rotation angle meas. 79—88908
error anal. method *(Russian)* 79—97345
feedback monitoring, normal conditions for linear and angular measurements 79—75492
flotation integrating gyroscope, dynamic errors 79—93135
Fraunhofer diffraction pattern appl. *(Japanese)* 80—52159

angular measurement continued

- galaxies, equidensitometric determ. of angular diameters of compact objects 78—16308
- goniometry, from photographs or angle-true sketches 79—55619
- in-plane motion measurements with Fourier lensless holography 80—77746
- instrument for checking autocollimators 80—77832
- interferometer for 90° angle meas. of transparent- and opaque-materials *(German)* 78—164
- interferometers appl., light *(Czech)* 78—49794
- interferometric angle meas., 30°-60° range, calibration, accuracy *(German)* 77—79051
- joint angle of limbs in two-dimensional movement, linear RF transducer appl. 77—90938
- large-scale angle inspection unit 78—77864
- laser beam meas. of surface profile and angular deflection 79—85125
- laser interferometer appl., built-in system for machine tools *(German)* 80—9022
- laser interferometer for autocollimating telescope calibration *(German)* 78—77853
- laser interferometer for small angle meas., description, operation, resolution *(Chinese)* 77—49768
- laser interferometric auto-correcting system of high precision thread grinder 80—90830
- laser interferometric method, errors 80—42196
- laser interferometry measurement system 79—6171
- light beam deflection angle determ. from holographic shear interference patterns 80—95848
- limb 'diameter' setting errors 79—71416
- linear and angular microdisplacement instrument *(Japanese)* 79—21728
- machine tool industry, angle measurement, automatic testing of precision dividing heads *(German)* 80—82740
- magnetic angle convertor accuracy test method 78—77948
- method *(Russian)* 79—30413
- microcomputer based laser interferometer for instrument graduation *(Polish)* 80—90816
- moire fringe properties and appls. with regular interval spiral gratings *(Japanese)* 80—53434
- multiblade-tool angles meas. using shadow-section method 79—71410
- multifaceted prism test automation 79—72724
- non-contacting transducer, IR source and fibre optic probe 80—86257
- optical instrum. in engineering 80—13119
- optical instrument, target position meas., statistical model 80—101778
- optical rotating table eccentricity error compensation 79—71415
- opticoelectronic phase goniometers compared to opticoelectronic amplitude goniometers 79—71412
- optoelectronic meas. devices, error anal. method *(Russian)* 80—95066
- optoelectronic meas. methods appl., with twin diodes *(German)* 80—13064
- orientation angle calc. using image matrix transformation *(Russian)* 80—73314
- orientation of vibration test-bed, dynamic meas. using system of He-Ne laser and photodiode 77—49712
- out of plane tilts measurement, Fourier speckle technique 77—13735
- pendulums, random interactions, error anal. *(Russian)* 80—73313
- photodetector freq. doubler nonlinear distortions effect on meas. errors 78—36968
- photoelectric angular-displacement transducer, accuracy 80—8977
- point-source image energy centre of gravity, location accuracy, aberrations effect 79—27192
- polyhedral prisms checking instrument, unit of plane angle transmission 77—7221
- radiointerferometric frequency and coordinate meas. accuracy, tropospheric fluctuation constraints 79—8848
- repeater gyrocompass, digitiser construction principle *(Russian)* 80—73311
- ring laser method, meas. principle 78—16777
- ring laser output characteristic coefficient determ. 77—7123
- rotary encoder appl. *(Japanese)* 77—22523
- rotatable sample holder with voltage readout, angle sensing mechanism 78—13873
- rotated image correlation by gradient vector sum histograms 79—75647
- rotating ring laser appl. *(Russian)* 77—38942
- rotation-angle pickup, for goniometer, using precision variable resistor 80—47047
- selsyn rotor angle-to-digital code convertor, design *(Russian)* 78—65915
- sine bar devices application, meas. errors anal. 78—81944
- sine cosine rotating transformer, measurement apparatus *(Russian)* 79—97344
- Soviet (Ukrainian) developments 80—52162
- Soviet instruments and meas. systems exhibition 80—52161
- standards reproduction, autocollimating telescopes appl. *(German)* 78—77851
- stepping motor for timber volumetric meter *(Russian)* 80—57253
- surveying, precise direction measurement by laser, techniques and instruments *(Czech)* 79—30414
- telescopes appl., auto-collimating, absolute calibration methods *(German)* 78—86239
- testing of meas. instrument for errors 80—42186
- tilt of diffusely reflecting surfaces, real-time measurement by electronic speckle correlation 80—57252
- tiltmeter, stability and thermal compensation of a test-cell for a Hg-level tiltmeter 80—36978
- tiltmeter, using optical fibres 80—8958
- torque generated by an angle sensor with a short-circuited-coil rotor *(Russian)* 79—26025
- tribometric meas., angle detector *(French)* 78—92434
- units, rel. to time meas., history 78—20931
- US device for precision measurement *(German)* 79—80572
- USSR All-Union State Standard for linear and angular meas. 77—17946
- vernier resolvers, angle measuring and coding transducers *(French)* 80—37022
- very small angles, meas. by constant inclination interference *(Chinese)* 79—30419
- wind direction measurement, electronic method *(Croatian)* 77—41181
- He-Ne ring laser, experimental appl. *(Japanese)* 79—71408

angular momentum

- astronomical systems, ang. momenta mass depend. rel. to self-similarity 80—36490

angular momentum continued

- atmosphere, angular momentum advection by axisymmetric motions 77—87039
- atom+atom collisions, intense laser irradiation effects, ang. momentum approx. 79—94058
- atomic scattering theory, diffraction and angular momentum effects 79—89734
- beam-target interaction, atomic orientation prod. by electron capture, semiclassical model 80—9723
- binary system, close, with mass and ang. momentum loss, period changes 80—72998
- black hole, rotating, interaction with weak mag. field, ang. momentum changes 77—74080
- black hole ang. momentum reduction in dense stellar system 77—29874
- Bodewadt flow, spin-up, angular momentum adjustment 80—28511
- close binary stars, ang. momenta rel. to fission origin 79—5859
- close binary stars, orbital ang. momentum loss by gravit. radiation, mass transfer rates 78—40991
- conservation, rel. to springboard divers, gymnasts and trampolinists 79—84884
- contact binary stars, solar type, ang. momentum controlled evolution 80—36670
- cylindrical gas system, rotating and self gravitating, thermodynamic instability 80—82191
- Dirac equation generalized total ang. momentum operator in curved space time 79—49128
- Earth atmosphere, angular momentum fluctuations and day length changes 80—85715
- education, gyroscopes, rolling and suspended, ang. momentum demonstration 79—9061
- Einstein-Podolsky-Rosen gedankenexperiment *(German)* 77—41508
- Einstein-Podolsky-Rosen paradox, contradiction between classical quantum theory of meas. and total ang. momentum conservation *(French)* 80—52042
- EM field, static, angular momentum 80—46771
- finite rotations and angular velocity 80—46766
- free relativistic spin-1/2 particle energy-momentum invariants and kinetic moment *(French)* 78—62287
- galaxies, ang. momenta rel. to form. by gravit. instability 80—98722
- galaxies, distrib. of ang. momenta 78—20886
- galaxies, mass and ang. momentum, statistical relations 80—8689
- galaxies, masses and ang. momenta anal. rel. to morphological types *(Chinese)* 79—17097
- galaxies, tidal hypothesis for ang. momentum origin 79—48927
- galaxies in Local Group 78—93400
- hadrons, uncharmed, rotational states 80—22596
- inert gases, photoabsorption to bound state and photoabsorption to continuum state (ionisation), comparison, HF calcs. 80—47910
- interstellar clouds angular momentum problem and mag. braking, time independent soln. 79—62884
- ion+polar molecule collisions, average dipole orientation theory, ang. momentum conservation 78—92466
- late-type stars, ang. momentum loss rel. to mag. dynamo 78—45331
- long jump take off, angular momentum considerations 78—20204
- mass relationship for cosmic objects, Ambartsumian's proto-matter hadronic nature determ. 80—77528
- meteoroids, orbital ang. momentum and Earth's atmosphere 77—56877
- minimum uncertainty states of angular momentum system 78—93559
- multiply charged ions, $2p_{1/2}3p_{3/2}$ config., level widths, relativistic calc., S-matrix method 80—63546
- N-body isolated system, ang. momentum flux in higher multipole moments 79—80474
- nonaxial quantum mech. top, coherent states *(Russian)* 77—45739
- nonholonomic system, motion eqns. derivation *(Russian)* 78—20956
- orbital angular momentum transfer to nucl. spin polarisation in external mag. fields 80—14217
- oscillator, reson. interaction with harmonic oscill., exact soln. by means of Taylor expansion 77—33902
- particles, angular momentum in centre-of-mass frame, teaching 80—90631
- planetary systems, ang. momenta rel. to fission origin 79—5859
- planets spin angular momentum distrib. explanation 80—41741
- potential scattering, partial waves with nonzero ang. momentum, zero range pot. method *(Russian)* 78—29006
- predictive relativistic mechanics, two particle case 77—2540
- protoplanetary cloud, ang. momentum transfer by meridional currents 77—53436
- rigid body with fixed point, angular velocity hodographs *(Russian)* 77—62144
- rotating black hole perturbations, ang. momentum 77—53623
- rotating gas cloud collapse, equatorial ring formation, Lagrangian method 78—12628
- seasonally condensing atmospheres, appl. to Mars 80—26735
- solar nebula/giant gaseous protoplanets ang. momentum transfer rel. to protoplanet evolution 80—56727
- solar system, angular momentum distrib. and formation *(Chinese)* 77—67049
- star cluster, spherically symmetric, total ang. momentum rel. to struct. and dynamics 80—62215
- star collapsing core, neutrino ang. momentum losses 77—56916
- star formation, angular momentum considerations 78—69781
- star formation protostellar cloud ang. momentum problem, mag. breaking 80—82342
- stars, ang. momentum transfer during steady disc accretion 78—65609
- stars, pre main sequence, effect of ang. momentum on evolution in gravit. contraction phase 80—62133
- stars in close binaries, rotational angular momenta 77—57057
- static EM angular momentum, in vacuo obs. 80—73631
- stellar orbits in Galaxy, ang. momenta rel. to applicability of approximate third integral of motion 80—67798
- Sun, ang. momentum outward transport by gas convection rel. to equatorial accel. 77—53531
- Sun, differential rotation rel. to turbulent transport of angular momentum 78—16372
- superfluid, anisotropic, BCS ground state ang. momentum 79—90840
- thermal conductivity of gases, ang. momentum polarisation contrib. 79—37435
- two-centre integrals calculation method including ang. momentum in chem. shift determ. *(French)* 80—32601
- Ar+N_2 rotational excitation, differential cross sections and orientation effects, classical trajectory method 80—23523

angular momentum continued
- ^{3}He, superfluid A-phase, mass current, intrinsic orbital angular momentum 80—84338
- I_2, angular momentum transfer, elastic, inelastic collisions, orientation and polarised fluoresc. 78—90271
- Ne, doubly excited energy levels, subshell ang. momenta coupling, frozen core superposition of config. method 80—52874

angular momentum theory
- *see also quantum theory; Regge poles and trajectories*
- 3-j symbols, general set of relns. 78—41183
- 3j and 6j coefficients, symmetries 80—62506
- 3j and 6j coeffs., recursive computation 77—5687
- 3j coeff., symmetries 79—305
- 3j coefficients, computation 79—49076
- 3j symbols, T coeffs. and D function *(Russian)* 77—30055
- 3j-coeff., symmetries 78—41181
- 6-j and 9-j symbols, special relations, appl. in nuclear physics 77—17838
- Abraham-Minkowski controversy, EM momentum in static fields, teaching 80—101678
- addition of identical angular momenta 77—71228
- Airy functions, asymptotic behaviour of derivatives 80—17830
- angle-angular momentum variables in quantum mechanics, commutation relations 80—86112
- angular structure of unique spherical shells, appl. to ang. momentum quantisation 78—73873
- angular velocity vector, attached to moving reference frame, time variation 80—41986
- asymptotic behaviour and defn. of ang. momentum in general relativity 77—49650
- atom, transition metal Racah parameters, atomic screening parameter Slater and Clementi-Raimondi values 80—69071
- atom-diatom collisions, total body frame radial wavefunction, coupled states and infinite order approxs. 78—25641
- atomic hyperfine struct. quantum beats, intensity profile, ang. momentum theory graphical method 78—25497
- atoms, P-state collisions, quantum mechanical treatment, angular momentum coupling 80—99541
- axisymmetric spacetime, ang. momentum and Dirac charge quantisation 78—70045
- body-fixed frames and angular momentum projection operators 80—86122
- calculation program ANGMOM 78—89359
- cascade quantum beats, intensity profile calculation 79—89630
- Clebsch-Gordan coefficients for meson sector in SO(8) model of elementary particles 78—58135
- complex angular momentum theories, background integral evaluation 79—6986
- conjugate momentum of ang. momentum modulus 78—16673
- coupling and Clebsch-Gordan coeffs., calc. method 77—9895
- cubic harmonics computation, using point groups and an algorithm 78—20994
- differential equations satisfied by Fredholm determinants, appl. to inversion formalism for parameter depend. potentials 77—22437
- dimuon energy asymmetries in neutral heavy lepton decay, ang. momentum constraints 77—38155
- dipole sum rules for products of 3-j symbols 78—65803
- double groups and projective representations, Clebsch-Gordan coeffs. calcs. 79—92977
- double groups and projective representations 79—88833
- DWBA computer program for heavy-ion transfer reactions 78—50145
- education, angular momentum operators, derivation in spherical polar coords. 77—78932
- education, rotations, Lorentz transformations, and arbitrary axes 79—97155
- electrodynamics, interaction of elec. and mag. charges 78—8253
- electron in magnetic field, induced angular momentum, classical and quantum calcs. 78—86060
- equivalent electrons, J allowed values in jj coupling, teaching 80—90624
- even-even nuclei, excited states, angular momentum projection method, appl. to ^{162}Er 0^- band 79—3069
- extremum uncertainty product and sum states 78—24687
- four-body problem, ang. momentum reduction anal. 77—37767
- fractional parentage coeffs. and ang. momentum projection operators, simplification 78—16681
- fusion reactions, critical angular momentum phenomenological approach 78—33203
- gauge theories, exact gauge symm. group, ang. momentum operator, mag. monopole props. 77—2764
- Gaussian orbitals, multi-centre integrals, Racah algebra, Talmi transformation 79—45626
- generalised 3j symbols 78—36876
- generalised 6-j symbols 80—31557
- generalised equivalent operator products 79—49071
- generalised hydrogen-type wave functions, momentum representation 77—6674
- generating invariants for Clebsch-Gordan coeffs., nontrivial selection rules 77—82414
- geometry of the quantization of angular momenta (l,s,j) in fields of central symmetry 80—105530
- graphical evaluation of relativistic matrix elements 79—58586
- graphical spin algebra, differential operators 77—60964
- graphical technique for angular momentum expressions reduction, computer method, perturbation calcs. 77—26126
- harmonics on 3-sphere, Lie group SU(2) 78—57813
- Hartree Fock problem with angular momentum projection, soln. using variational principle 79—93537
- Helmholtz theorem, decomposition of solenoidal vectors 77—2556
- hidden couplings and relationships 78—88
- Hill-Wheeler integral for rotational energies, polynomial expansion 79—95
- integral transformation describing Clebsch-Gordan coefficients, d-function SU(2) and their symmetry *(Russian)* 79—2665
- isotropic harmonic oscillator in ang. momentum basis, algebraic formulation 80—94983
- j symbols and jm factors for all dihedral and cyclic groups 79—92968
- KMS states and ang. momentum, extension 79—75439
- kq representations in quantum mechanics 79—84990
- linear invariance and virial theorem in classical mechs. 77—74214
- magnetothermoelastic continua, macroscopic nonlinear theory 77—83775

angular momentum theory continued
- matrix diagonalisations via reduced characteristic eqns., appl. to ang mom. coupling 80—17828
- monopoles harmonics 78—8720
- multiparticle scattering operators, cluster decomp. 80—22592
- multipole states, tensor struct., transition operator 80—36907
- neutrino orbital angular momentum 77—50038
- nonAbelian gauge field monopole, ang. momentum operator *(Chinese)* 79—58865
- nonAbelian gauge field theories, flux quantisation and angular momentum 77—74594
- nondegenerate decay system, anal. 78—447
- nuclear rotation, zero point energy 78—25101
- nuclear struct. theory, angular momentum projection 77—50066
- O(3) shift operators, general anal. 79—94
- off-diagonal operator equivalents, closed polynomial formula in terms of two-dimensional harmonic oscilltor 79—67186
- operator equivalents, polynomial formula, derivation in terms of ang. momentum operators 79—6014
- operator product of traces, derivation from operator identities 80—73202
- operator props. through three-dimens. rot., teaching 80—105469
- orbital angular momentum and parity 80—77564
- orthonormalization method, angular momentum coupling of fermions in single j-shell 78—50100
- path integrals with a periodic constraint: entangled strings 79—2651
- Pauli equation with differential operators for the spin *(German)* 79—2664
- projection of angular momentum 77—5689
- projection of wave functions on states with definite ang. momentum 78—12590
- projection operator, finite sum representation 79—92993
- quantum mechanical addition, statistical distribs. 80—22274
- quarks, four, angular momentum group 78—16980
- Racah U(3) coeffs., canonical resolution of multiplicity problem, constructive soln. 77—17874
- radiating point charge, energy and ang. momentum splitting 78—69996
- reactance matrices, fine struct. cross sections, JAJOMPRE program 78—90312
- recoupling coefficients, subgroup factorisation 78—66
- recurrence relations for angular momentum traces 80—98816
- recursion relations for traces of products of angular momentum operators in the spherical basis 78—65805
- relativistic atomic structure, ang. momentum coeffs., Fortran program MCP75 77—10605
- rotating chair, quantitative ang. momentum expt. 77—75789
- rotation aligned coupling, ang. momentum projection method, odd-A La isotopes 77—2921
- scalar field, reln. of spin and orbital angular momenta 79—67170
- scalar isodoublet angular momentum in magnetic monopole field 78—41428
- Schwinger boson representation for the quantized rotator 78—93602
- Schwinger representation of SU(2), coupling of ang. momenta 78—41196
- spherical harmonic gradient formula, generalisation 79—17271
- spherical top molecule, triply degenerate fundamentals, line freq. expression for lage ang. momentum 79—36614
- spin permutation group representations, transformation matrices, graphical approach 77—71224
- spins, arbitrary no., quantum mech. vector addition 80—57134
- SU_3 group, Wigner-Racah algebra construction 79—58903
- SU(2), eigenstates of complex linear combinations of J_1, J_2, J_3 78—58139
- superheavy nuclei, stability and fission barriers, crit. ang. momentum depend. 80—32262
- tensor harmonics in the helicity basis 79—49080
- tensor spherical harmonics and multipoles in Euclidean space 77—2515
- trace problem, use of ang. momentum operators between ladder and rot. operators 80—62533
- traces of products of ang. mom. operators in spherical basis 78—32705
- traces of products of angular momentum operators 79—75382
- two-body system average ang. momentum, lower bound, hadron collision appls. 77—57514
- U(n), multiplicity free Wigner and Racah coeff. 80—31556
- vector addition of identical ang. momenta, multipliciaty formula 77—17839
- vector coupling coeffs., exact and approx. formulas 80—4564
- vector invariants method, use in anal. of physical symmetries 77—79003
- vortices, quantised, ang. momentum, creation and significance 78—24675
- Wigner 12j symbols of first kind, calcs. 77—60953
- Wigner 12j symbols of second kind, calcs. 77—60954
- Wigner 9-j symbol 79—97229
- Wigner operators in phase space 78—4511
- Wigner rotations for zero mass particles *(French)* 77—41783
- Wigner-Eckart theorem for an arbitrary group of Lie algebra 80—86124
- Ω^- spin, centrifugal barriers, quantisation of $l=0$ baryon levels 77—18221
- Co^{2+} in crystals, Racah parameter 78—56110
- HBr, photoelectron angular distrib. 80—58318
- HI, photoelectron angular distrib. 80—58318
- IrF_6, ligand field theory analysis of spectra 79—72248

angular velocity measurement
- 6 to 30 r.p.m.; using magnetic tape recording/reproduction 77—9990
- bacterial cells, tethered, rot. rate and direction detect. apparatus 77—73620
- centrifugal-pendulum system parameters selection *(Russian)* 79—97364
- centripetal force apparatus, modifications 77—71171
- contactless devices survey, industrial appl. *(French)* 79—93105
- DC motor, contactless method *(Russian)* 80—73329
- differential frequency angular rate and displacement sensor, construction *(Russian)* 78—70106
- differential optical polarisation device appl., expt. *(Russian)* 78—29093
- fibre optic rotation sensor with low drift 80—69530
- fluctuation of measured values of a constant velocity using a Doppler laser velocitometer *(Japanese)* 80—6179
- frequency-voltage convertor appl. *(Polish)* 78—70101
- gas in rot. cylinder, velocity profile meas. 79—50737
- gyrotachometers and gyroscopes parameter meas., mechanical spring simulation under working conditions 79—67263
- induction motors, piezoelectric pick-up appl. *(Russian)* 78—65911
- induction tachometer for measuring speed of rotating rolling mill rollers 79—80584

angular velocity measurement continued
  instantaneous, method *(Russian)* 79—30428
  laser gyroscope, passive ring resonator, for inertial rot. meas. 77—58352
  linear rotary convertor, measuring transducer *(Russian)* 79—63192
  low speed rotating table of gear hobbing machine, error meas. *(Japanese)* 77—53867
  Mach-Zehnder heterodyne interferometer as gyroscope 77—82594
  machine coil planetary motion, method 80—42202
  neutral fraction of unmagnetized plasma, 6MKh1S mechanotron meas. 78—5925
  non-contact rotational speed measurement and integrated spatial filter detector *(Japanese)* 79—93107
  nonuniformity, magnetic resonance appl. *(Russian)* 80—62637
  optoelectronic revolution counter for X-ray tube anodes *(German)* 78—12678
  photoelectric meter using ring lighting devices *(Russian)* 77—37863
  precision increase, using structural redundancy *(Russian)* 78—49804
  ring laser, solid state, beat regime with nonlinear absorber, appl. to ang. vel. sensor *(Russian)* 78—1273
  ring laser gyroscope, accuracy limit, model calc. 80—1241
  ring laser output characteristic coefficient determ. 77—7123
  rotary tachometers appl. 79—63198
  rotating optical fibre ring interferometer, Fresnel-Fizeau effect 78—4685
  rotation sensor using EM-SAW transduction 77—31194
  rotational angular acceleration and velocity meas. by miniature linear accelerometers 78—12679
  shaft, using digital tachometer 79—6101
  strobe light with variable pulse length over 22-360 Hz frequency range 80—58716
  tachometer, light activated, non-contact, with 0 to 20000 and 10000 to 30000 RPM ranges 79—80602
  transducer, transformer-type for low rotational spaced meas. *(Polish)* 79—2752
  USSR State Standard 1976-77 79—30429
  viscosity meas. using Couette-type viscometer, capacitor assembly for meas. small rotational vels. 80—100046
  vortex flow rotational speed meas. instrument 77—80247
animal communication *see biocommunications*
anisotropy, magnetic *see magnetic anisotropy*
anisotropy, magnetocrystalline *see magnetic anisotropy*
annealing
  see also graphitising; magnetic annealing; recrystallisation annealing; solution annealing; stress relaxation
  A15 compounds, disordered, reordering kinetics 80—96678
  acoustic emission during tensile tests, H$_2$ assisted fracture 79—100257
  acrylic plastic, deform. of rigidly clamped specimens subject to one sided cyclic heating 77—59932
  adamantine ceramic, structural, thermophysical and electrophysical props. 80—6918
  age temperature shifting rel. to phenomenological theory of annealing and precipitation hardening 78—15428
  alkali halide, F-centre, stabilisation process in first colouring stage, thermal-annealing-curves 79—19246
  alkali halide, thermal annealing of colour centres, monomolecular and bimolecular sequence of kinetics 78—47373
  alkali halides, divalent metal impurities, aggregation process, order of reaction, fractional time conc. depend. 80—107308
  alkali metal halides, irradiated 78—92494
  alkaline earth fluorides, F-centre annealing and intrinsic luminesc. 79—65937
  alloy, cold worked, internal friction peak rel. to back reaction annealing kinetics 78—3161
  alloy, precip. dimensions, annealing temp. depend. *(Russian)* 78—15399
  alloy, single phase, annealing of diffusion layer 78—14518
  alloy, solid state reactions, effect on microstruct. 79—29015
  alloy, two-phase, recrystallisation mechanisms 79—47708
  alloys, disordered binary, crit. US attenuation 79—99272
  alloys, ion-implanted, annealing behaviour and appls. 79—14829
  alloys, supplementary annealing during rapid hardening from liquid state, apparatus 80—76275
  Alumel, thermocouple alloy, heat treatment effects on thermoEMF and mag. flux 77—63235
  aluminosilicate glass, diffusion of Sn(IV) 80—49417
  amethyst, Fe^{3+} diffusion, associated phenomena 77—36269
  amorphous, vac. evaporated, doping, transport and optical props. 80—49715
  amorphous alloy, struct. relax., compositional SRO 78—79538
  amorphous metals, low-temp. annealing, geometrical relaxation model on struct. charge and kinetics *(Japanese)* 79—94908
  amorphous semiconductor characterisation for solar cell applications 79—61983
  amorphous semiconductor film, laser induced nucleation, long wavelength instability 80—84126
  anodic oxide film, exam. using SIMS and ellipsometry 79—61770
  anthracene, single cryst., X-radiation damage recovery, using triplet state exciton probe 78—75694
  anthracene, ultrathin films on fused quartz and sapphire 80—59812
  apatite, influence of crystallographic struct. on annealing of fission fragment tracks 77—38577
  Astroloy, grain coarsening by critical strain annealing 79—47711
  baddeleyite-corundum refractories, creep and annealing 78—84907
  BBB polybisbenzimidazobenzophenanthroline-dione, films, dynamic mechanical investig. at high temps. 77—4800
  bent single crystal, equilib. face, surface relief form. during annealing 78—47651
  binary alloy, annealed Ising ferromagnet 78—47927
  biotite, thermal decomposition, stability of ferromag. products 78—57195
  borosilicate glass, phase separated, depolarised light scatt. in terms of Rayleigh-Gans theory 79—87452
  α-brass, 70:30, cold-worked, recrystallised grains nucleation on heating 80—29998
  brass, 70:30, rolled, nucleation and annealing texture development 80—45320
  brass, α and $\alpha+\beta$ type, positron annihilation, short-range order, clustering and lattice defects influence 79—29107
  α-brass, dislocation structure around crack tips in early stage of fatigue 78—60830
  α-brass, drawability correlation with sheet metal texture 78—60683
  α-brass, electron irradiated, defect production and interdiffusion [illegible]

annealing continued
  β' brass, eutectoid, microstruct. obs. 77—36553
  α-βbrass, exam. of creep fracture by tensile tests 78—88531
  α-brass, FCC, fractographic obs. of SCC 78—64786
  α-brass, polycrysts., deformed in tension or rolling, anneal hardening *(Japanese)* 80—93564
  αbrass, single cryst., yielding behaviour rel. to low temp. annealing treatment *(Japanese)* 80—93582
  α-brass, single crystal, obstacle strength variation during stress relaxation 78—68723
  α-brass, thin sheet, plastic anisotropy 77—63683
  brass (70/30), interaction of annealing twins in fcc metals and alloys 78—68712
  brass formation by diffusion in multilayer Cu-Zn condensates 78—43186
  α-brass sheets, earing, R-values and 3-D orientation distrib. functions, comparisons 79—91702
  brass/water interface leaky Rayleigh wave reflectivity loss meas. 78—59187
  α-brasses, cold worked, atomic diffusion kinetics to stacking faults, Laplace transformation method 80—19977
  bronzite, influence of crystallographic struct. on annealing of fission fragment tracks 77—38577
  calcic plagioclase, ordering and antiphase boundaries 79—95032
  [CC] Ag—(100)InP, metal-semicond.cathode contact, metallurgical, physical, chemical processes 80—107911
  cellulose acetate, reverse osmosis membranes, ion mobility, diffusion coeff., elec. resist. obs. 80—45550
  cellulose acetate membranes, modified, tensile props., desalination performance 79—11818
  cellulose nitrate track detectors, CA80-15 and LR-115, etch pits due to Rn and Tn alpha particles 78—855
  ceramics, archaeological, dating by alpha-recoil tracks in mica 78—70237
  chalcogenide amorphous semiconductors, ESR studies of doped Mn, review *(Japanese)* 77—90019
  chalcogenide glasses, O-free, cooling rate influence on optical consts. 80—88952
  chlorite, fission track annealing and age determ. 78—36307
  Chromel, thermocouple alloy, heat treatment effects on thermo EMF and mag. flux 77—63235
  Cl (Co$_{100-x}$Fe$_x$)$_{83}$B$_{17}$, $1\leq x\leq 30$, annealing embrittlement and crystn. 80—45329
  Co, influence of annealing time on mech. props. 79—47677
  conference, Masnuy-St-Jean, Mons, Belgium, Oct. 1979 80—82570
  contact film absorption on plastic deform. of contacting bodies *(Russian)* 80—93596
  copolyester, melting temperature changes due to heat treatment *(Japanese)* 79—70096
  corundum large optical crystal production with zero orientation 79—50457
  crystal growth by solid state techniques review 77—85935
  crystalline samples, temp. control system design *(Spanish)* 80—73362
  cylindrical tubes or shells, mild steel, quasi-static piercing 80—45351
  defect prod. and annealing, radiation-induced, computer expts. 78—87710
  diacel plastic track detector, track diameter meas. of alpha particles, influence of annealing 79—49911
  diamond:^{111}In, ion implanted, intrinsic limitations of doping 80—34019
  diamond: Sb, ion implanted, defect study using optical absorpt. and EPR 80—24480
  diamond:Sb, implanted, radiation damage and annealing study 80—100263
  diamond, amorphization process, ^{133}Cs Mossbauer spectra 79—99809
  diamond, B doped, electron irradiated, defects at low temps., elec. resist. meas. 77—11593
  diamond, high temp. ion implantation 79—23623
  diamond, low-temp. electron-irrad., EPR 77—59045
  diamond, natural, high conc. of implanted Si ions, He backscatt. and IR absorption 77—89466
  diamond, natural, topography of impurity distrib. and neutron-induced colouring 77—39613
  diamond, natural semicond., isothermal annealing of electron radiation damage 77—7764
  diamond, thermal conductivity, high temp., electron irrad. effects 80—65318
  diamond, transformation of type IB dispersed N into type IA aggregate N 78—6089
  diamond, type IIa, electron irradiated, annealed to high temps., EPR spectrum 77—90034
  diamond, type-I, electron irrad., annealing at 800-1500°C 80—24500
  diamond, type-IIa, electron irrad., EPR spectrum 80—25210
  dicalcium lead propionate, ferroelec., annealed, crit. exponents, dielec. const. temp. depend. 80—55050
  diffusion-controlled defect annealing, theory 80—92520
  displacement spike annealing, Mont Carlo method computer expteriments 78—30672
  ductile fracture, strain hardening and damage relationship 80—108564
  effective annealing time determ. using analogue computer 78—88475
  elastic properties measurement, apparatus for elevated temps. *(Polish)* 79—96279
  elasticity, annealing and deformation effects, with and without texture 79—52274
  electrode films, effect of annealing on elec. resist. of Al films 78—23179
  electroluminescent films, activating impurity diffusion coeff. *(Russian)* 77—84995
  electrotechnical steel, quality significance on energy and materials savings in magnetic circuits *(Czech)* 80—20947
  Elinvar, γ to γ' transformation and γ' phase form. kinetics, lattice consts. 80—35191
  Elinvar, Curie point, magnetisation and susceptibility, heat treatment effects *(Russian)* 78—47973
  epoxy polymers, dense-network, elastic deform. rel. to props. *(Russian)* 80—40468
  epoxy resin, crack propagation, photoelasticity investig. 79—8341
  epoxy system, rubber-modified and unmodified, sub-T$_g$ annealing expts. 79—11643
  ethanol-water system, metastable states, hydrates existence and props., low temp. 78—71835
  ethylene-vinyl alcohol copolymer, drawn samples, annealing effect around T$_g$ temps. on shrinkage and mol. orientation 80—79712
  eutectoid thermomechanically treated, textural studies 80—29978
  exploding wire, structural inhomogeneity and MHD sausage instability, arc chains, grain size and annealing 79—41904

annealing continued
  - externally stimulated interstitial release followed by vacancy-interstitial annihilation, kinetics 78—34535
  - fatigue, dislocation substructure effects 77—86140
  - faulted dislocation loops induced by elastic interaction, climbing motion 80—75227
  - FCC lattice, computer simulation of low energy displacement cascade 78—47367
  - FCC metal, Frenkel pair annihilation, discrete lattice model *(Russian)* 78—10042
  - Fe-SiO_2 cermet film, solar absorbing, production by dual cathode DC magnetron sputtering 80—16186
  - ferrite, 350 NNI, for use in superhigh vacuum systems 80—108478
  - ferritic alloy, reinforced by dispersed oxide, mech. props., modification by recovery heat treatment *(French)* 77—59837
  - ferroelectrics, domain structure as outcome state for poling procedure 80—80728
  - ferromagnetic alloy, 35KFN10, X-ray diffr. investig. after thermomech. treatment *(Russian)* 77—48457
  - film on Si substrate, eutectic point displacement on annealing *(Russian)* 80—100850
  - fission track annealing characteristics of epidote, appls. to geochronology, geol. 78—94038
  - fission track annealing characts. in crystals 79—26863
  - float glass, heat transfer and temp. control in annealing, computer appl. 78—27543
  - fluorophosphate laser glass, highly homogeneous, production 80—14411
  - fluorophosphate optical glass development 80—106588
  - fluorphlogopite, valence transition of Ti impurity, ESR and optical absorption data 77—16155
  - furnace O_2 gettering by NiSi or Pd_2Si 79—100160
  - fusion reactor, first wall, life extension by periodic annealing 80—102344
  - fusion reactor metals and alloys, microvoid form., gaseous impurity atom effects, positron annihilation study 80—49275
  - n-GaAs, neutron irrad. and thermally induced defects, annealing stages 77—51409
  - garnet, epitaxial film, mag. bubble props., permanent local modification by laser annealing 80—2612
  - garnet epitaxial layer, decomposition caused by annealing 78—18918
  - garnet film, bubble, anisotropy field and nonmagnetic regions in implanted layers, ferromag. reson. study 79—99774
  - garnet film, mag. bubble domain, annealing by laser pulse 80—15769
  - glass, annealed and tempered, impact damage, strength 80—85025
  - glass, flat, horizontal annealing process, math. model 79—61615
  - glass, optical grade, refractive index-density relationship changes assoc. with reannealing 78—27175
  - glass, refractive index during annealing, nonlinear structural relaxation model 78—44234
  - glass, tensile and impact strength, effect of surface damaging and annealing *(Czech)* 79—74227
  - glass, toughened, stress relax. at temp. below annealing range *(Czech)* 79—43305
  - glass articles, optimum temp. curve, analogue model *(Polish)* 79—52279
  - glass blank for primary mirror for large azimuthal telescope 77—72101
  - glass strip, surface temp. field during annealing in tower of vertical drawing system 78—11242
  - glass track detectors, effects of pre-irradiation and conditions on etching 80—37702
  - glass transition, soft-sphere model, mol. dynamics study 80—49343
  - graphite, fast neutron irrad. damage, chem. rate theory applic. effect of annealing and thermal equilib. defect concs. 77—67804
  - graphite, fusion reactor first wall appl., radiation damage 79—86822
  - graphite, irradiated, stored at room temp., neutron damage annealing and C_{44} shear modulus 80—2080
  - graphite, microhardness changes, effect of annealing and neutron irradiation 77—8861
  - graphite, neutron induced changes, exam. of lattice consts., elastic modulus, elec. cond 79—95053
  - graphite, neutron irrad., annealing of radiation damage 79—1465
  - graphite, neutron irrad., microporosity, elec. resist., length, struct. changes 78—43051
  - graphite, neutron irradiated, thermoelec. and thermomag. effects 77—59296
  - graphite, neutron irradiation, electron transport, annealing study 80—39165
  - graphite, polycryst., reactor-grade, neutron-irradiated, cryst. struct. recovery, ESR obs. *(Japanese)* 77—43254
  - graphite, pyrolytic, neutron irrad., Raman spectra, point defects 77—69834
  - graphite, surface morphology changes after irrad. with energetic He ions 78—21767
  - graphites, pyrolytic, compressed, annealed, low temp. electron irrad., elastic const. meas. *(French)* 78—43050
  - Hastelloy C-276, cold worked, annealed, surface segregation, Auger spectroscopy study 79—83204
  - heat treatment, struct. and mech. props. 78—52864
  - high-temp. behaviour of inelastic metals 77—4830
  - ice, edge dislocation dipole form. by heat treatment, X-ray diffr. topography 79—99203
  - Incoloy 800, oxidation resistance, alloy depletion effect 77—8989
  - Incoloy 800, steam oxidised, oxide coating anal. 80—89399
  - Incoloy 800 in 50% NaOH, stress corrosion cracking, slow strain rate method *(Japanese)* 80—55575
  - Inconel, caustic stress corrosion cracking resistance, processing variables effect 80—71796
  - Inconel, type 706, precipitation and creep rupture behaviour, optical and TEM study 79—74158
  - Inconel 600, thermal treatment, grain boundary microstruct. and SCC resistance 80—71675
  - Inconel 600 in 50% NaOH, stress corrosion cracking, slow strain rate method *(Japanese)* 80—55575
  - Inconel 625, creep rupture behaviour in Ag environment 80—25853
  - n-InSb, surface recomb. vel., repeated cyclic surface treatment effects 77—32065
  - insulating film for semicond. devices, props., rel. to deposition conditions 78—23612
  - Invar, mag. susceptibility in technical saturation region and internal stress 77—85429
  - ion implantation damage, laser annealing 77—25308
  - iron, pure, tensile deformation behaviour under high pressure *(Japanese)* 80—16381

annealing continued
  - iron phthalocyanine, annealed, elec. cond., daylight exposure and thickness effect *(French)* 80—84484
  - Ising model, restricted annealing of random models 78—80154
  - laser, Au diffusion barrier formation, at metal-semiconductor on metal-metal interface 80—80373
  - laser annealing, conference on laser-solid interactions and laser processing, Boston, MA, USA (Nov. 1978) 79—69911
  - laser annealing for improved stacked-struct. oxide quality 80—65386
  - laser annealing mechanisms, continuous and pulsed laser impact, melting 80—84964
  - laser annealing of ion-implanted surfaces 79—69912
  - laser annealing parameters, in thermal working *(Russian)* 80—100848
  - laser applications in materials processing, seminar, San Diego, CA, USA (Aug. 79) 80—90609
  - laser technology, parallel plate, polarisation problems obs. and solution 80—1225
  - latent cold work heat release kinetics meas. using adiabatic elec. heating 77—52344
  - lehr, position of radiation burners *(Polish)* 77—65036
  - low-alloy steel, abrasive wear resistance, effect of C content, annealing quenching 77—56115
  - lunar fines, effect of annealing temp. on reactivity towards adsorbed water 77—60632
  - LWR pressure vessels, guidelines for thermal annealing to correct radiation embrittlement 79—22435
  - magnetite nodules, from superconcentrates, strengthening annealing and reduction *(Russian)* 80—16333
  - measurement, transfer cryostat from liquid N_2 to He 77—45855
  - metal, annealing, struct. and grain boundary mobility 79—47728
  - metal, annealing embrittlement, AES study *(Chinese)* 79—38982
  - metal, defect annealing study by positron annihilation, and elec. resistivity meas. 78—51584
  - metal, degree of deform. effect on thermophys. props. at high temps. 78—26694
  - metal, FCC, irrad., annealing, Frenkel pair annihilation in discrete mattice model 77—59009
  - metal, irradiated, determ. of time threshold energy for Frenkel pair creation 77—47444
  - metal, vacancy defect mobilities and binding energies obtained from annealing studies 78—47325
  - metal colloid, irradiation-induced defects in alkali halide crystals 80—107316
  - metal film, disordered and amorphous, quench-condensed, optical cond. and band struct. 77—1746
  - metal powder mixture with decomposing oxide, growth kinetics of surface film during annealing 79—96216
  - metal sheet, recovery strain during unloading in tensile test, roll-forming appl. *(Japanese)* 79—100182
  - metal surface, near point-defect, annealing, diffusion theory and Monte Carlo anal. 78—47646
  - metal surfaces for laser mirrors, ion polishing and vac. annealing 78—5588
  - metal-metalloid amorphous systems, thermal instability, crystn. characts. 77—4044
  - metal-tunnel oxide-Si junctions, processing condition depend. 80—80380
  - metallic glass, annealing, struct. relax. and crossover effect 79—86715
  - metallic glass, current exptl. data on struct., review 80—88058
  - metallic glasses, aged, atomic clustering exam. using positron annihilation methods 77—84655
  - metallic glasses, annealing behaviour, thermal stability and crystn. 80—75167
  - metallic glasses, struct., stability and prod., elec., mag. and mech. props. 80—44134
  - metallic glasses, structure, stability and prod., elec., mag. and mech. props., review 80—44134
  - metals, irradiated, solute segregation and annealing kinetics at sinks 79—23640
  - metals, plant deform. and recrystallisation textures 78—68708
  - metals, radiation defect treatment at annealing stages V and VI *(Russian)* 80—71676
  - metals, thermal instabilities due to recomb. of radiation-induced Frenkel pairs 79—23597
  - metals and alloys, FCC, model for form. of annealing twins 78—59818
  - Metglas 2826 ribbons, ferromagnetic resonance and SEM obs. 80—15804
  - methane, effects of impurities and annealing on triple point 78—83919
  - ^{13}C-methane-d_1:O, annealed, spin conversion and proton 2nd moment time-depends. 80—11283
  - 2-methyltetrahydrofuran-methanol mixed glasses, annealed, γ-ray produced electrons transfer from IR to bisible traps 80—11440
  - mica, natural, high γ- and electron-irrad. doses effect on annealing behaviour, thermal decomp. resist. 80—60897
  - microcomputer precision regulator, electron field emitters and multiple multichannel analyser 78—86384
  - migration of implanted species during annealing and oxidation, small angle Rutherford backscatt. obs. review 77—44108
  - MIM, sandwich sputtered film, interfacial effects characterisation 79—82685
  - mineral fission fragment track annealing characteristics for geochronology 79—100827
  - minerals, thermal annealing of ion tracks 78—20604
  - MIS dielectrics, charge centre removal, low press. RF annealing technique 78—56230
  - MIS dielectrics, charge centres, removal by RF annealing 78—88035
  - MIS structure, radiation induced charge storage 80—6997
  - MIS structure, RF annealing method for removing radiation damage 78—39224
  - MIS structures, electron-beam irrad., RF annealing effect 79—91152
  - MNOS capacitor, HCl annealing of memory oxide, effect in memory window size and location 79—70079
  - MNOS capacitors, retention and endurance characts., annealing and oxidation effects 79—74274
  - MNOS device, high temperature annealing, effect on Si_3N_4 stress, interface charge density and memory props. 79—87158
  - MNOS devices, transient behaviour of electron-beam-induced current 79—99630
  - MNOS p-channel transistor, memory characts., H_2 anneal effects 80—80388
  - MNOS structures, electron-beam-irrad., interface defects, high temp. H_2 anneal 80—96745

annealing continued
- MNOS structures, high temp. H anneal, effects of fast surface states 79—38178
- Monel, in thermoluminesc. dosimeter, low dose meas. *(Japanese)* 78—86696
- MOS capacitor, polycryst. Si gate, surface state annealing 77—39946
- MOS capacitor, SiO_2 precipitation in Si, effect on generation currents 79—78188
- MOS device, transient behaviour of electron-beam-induced current 79—99630
- MOS diodes defects elimination, due to electron beam lithography *(Japanese)* 80—54787
- MOS structure, B ion implanted, form. and annealing of radiation damage 79—56321
- MOS structure, effect on surface and bulk generation currents 78—47883
- MOS structure, slow-trapping instability, effect of high temp. H_2 annealing 78—47880
- MOS structures, radiation-induced positive charge, thermal annealing 80—75648
- MOSFETs, short channel, fabrication by ion implantation and laser annealing 80—20312
- Mossbauer effect exam. of annealing effect on struct. 78—19396
- muscovite, fission track etching and annealing anal., dating appl. 78—32036
- muscovite mica, annealing of latent tracks of heavy ions *(French)* 79—19290
- n^+-p-p^+ bifacial back surface field solar cells, optimisation of p^+ doping level by ion implantation 80—97784
- Nafion, densities and expansion coeffs. as function of various parameters 80—79711
- neutron-irrad., void annealing, positron annihilation obs. 77—76469
- new materials properties achievable by ion implantation doping and laser processing 79—69127
- Nimonic alloy, effect of annealing on hardness, carbide phase strengthening *(Russian)* 79—34137
- NK, thermocouple alloy, heat treatment effects on thermoEMF and mag. flux 77—63235
- nodular graphite, annealed, fracture behaviour at low temps. 78—72875
- nuclear reactor fuel elements, annealing apparatus and tests up to 2500°C *(German)* 79—3228
- nylon 66, annealed in glycerol, stepwise lamellar thickening 77—86059
- nylon 66, doubly oriented, annealing of drawn and rolled samples, struct. 78—52859
- nylon 66, filament, heat setting and thermomechanical behaviour 78—15435
- nylon 6, relationship between morphology and dynamic mech. props. 79—4992
- Nylon 6, small-angle X-ray scatt. struct. changes w.r.t. thermal and mech. history 79—41976
- Nylon 6 fibre, shrinkage, influence of chain rupture during tensile deform. 79—34055
- nylon 6 fibres, struct. changes due to strain annealing 79—15692
- Nylon 6 gut yarn, fine struct. change in twisting, annealing and untwisting, microbeam X-ray obs. 80—81026
- Nylon 6 gut yarn, fine struct. change in twisting, annealing and untwisting, X-ray and electron microscopy obs. 80—84904
- Nylon 6 yarns, NMR, fibre struct. rel. to annealing, drawing *(Japanese)* 77—32269
- nylon-11, folded-chain crystal, pressure-induced crystallisation from melt, annealing 77—84671
- nylon-12, folded-chain crystal, pressure-induced crystallisation from melt, annealing 77—84672
- nylon-6, chain extension mechanism during crystallisation under press. 77—56008
- Nylon-6 fibre, crystal struct., WAXS obs. 80—15015
- nylon-6 pressure-crystallised, annealing under pressure 77—84670
- olivine, naturally deformed, recovery process, rel. to Earth upper mantle mech. state 78—96202
- omphacite, Mossbauer spectra study 79—65771
- optical component blank pressure shaping, semiautomatic apparatus 79—72731
- optical fibre, γ-ray irrad., damage recovery by annealing 79—23078
- organic crysts., γ-irrad., positron lifetime rel. to free radical conc. 78—72635
- p-n junction diode, electron-beam annealing of ion-implantation damage 79—77622
- $Pb_{80}In_{20}$ foil, flux-flow crit. freq. and generalised bundle size depend. on fluxoid traversal distance and length 80—7054
- pearlite spheroidization, quantitative meas. 77—44275
- Permalloy, 50NP, and 79NM, magnetic properties and structure, environment effect during annealing 80—60366
- Permalloy, FCC, mag. anisotropy induced by cold rolling 80—11188
- Permalloy film, obliquely deposited, mag. anisotropy, annealing and deposition parameter effects *(Russian)* 77—80971
- PET, densification, cryst. perfection, mechanism 79—66082
- PET, thermodynamic equilib. melting parameters, effect of annealing 78—71837
- phase diagrams, ion beam determination of phase boundaries, exam. of techniques 79—8418
- phenolformaldehyde resin, sp. ht. obs. *(German)* 78—75845
- phlogopite, fission track etching and annealing, chronological application 79—84230
- phosphosilicate glass flow mechanism, and appl. in MOS devices 77—77393
- pigeonite, annealing expts. rel. to antiphase domains exptl. coarsening 80—81886
- plasma torch with magnetically traversed arc for surface heat treatment 79—32832
- plate, numerical solutions of nonlinear problems of heat conduction 77—50857
- PMMA, biaxially oriented, shrinking kinetics in transform. range 78—27588
- PMMA, optical damage threshold, alteration methods 80—99814
- PMMA organic glass shell, circular, cylindrical, under combined twisting moment/axial load buckling 79—100220
- poly(1-butene), melting and annealing behaviour, X-ray diffr. and DTA 79—28083
- poly(vinylidene fluoride) film, strong piezoelec. under high press. annealing 80—11344

annealing continued
- β-poly(vinylidene fluoride) films, single cryst. orientation, piezoelec. 80—20591
- poly 2,3-dichlorobutadiene, struct., morphology, polymorphism 79—65008
- poly-1,6-di-N-carbazolyl-2,4-hexadiyne, synthesis, thermal expansion, photocond., optical transition 78—76858
- poly-1-butene, annealing and melting behaviour 79—38871
- poly-γ-methyl-D-glutamate, α-helical form, annealing effect, morphology 79—14702
- poly-m-phenylene isophthalamide-ε-caprolactam, complex polymer cryst. 78—9967
- polyamide-6, fibrillar struct. and annealing, small-angle X-ray diffr. 78—75565
- polybutylene terephthalate, semicryst., mech. props., effect of annealing below glass temp. 77—25066
- polybutyleneterephthalate, drawn annealed, struct. and props., X-ray scattering 79—7552
- polycaprolactam, crystallisation effect on adhesion to Al 77—66742
- polycarbonate, dielec. relax. and ductile brittle transition 78—52438
- polycarbonate, effect of thermal treatment on strength, TSC meas. 77—52368
- polycarbonate, glassy state, enthalpy relax., thermal density fluctuations 80—59678
- polycarbonate, glassy state, rel. between thermal pre-treatment and viscoelastic behaviour 79—79038
- polycarbonate, impact behaviour, effects of thermal pre-treatment and mol. wt. 78—95798
- polycarbonate, struct. ordering changes after annealing 79—94921
- polycarbonate fibre, highly-oriented, drawing behaviour and mech. props. 78—76708
- polyether ester-PVC blends, annealed, dynamic mechanical and sonic velocity behaviour 80—25740
- polyethylene, γ-ray polymerised, cold compacted films, mech. relaxations, mechanism 77—16631
- polyethylene, annealed, crystallinity effect on mech. props. *(German)* 80—35230
- polyethylene, branched, annealing effect on lattice consts. 79—14698
- polyethylene, chain-extended, oriented, microindentation hardness 78—76728
- polyethylene, crystallisation of thick film from glassy state by annealing 80—54151
- polyethylene, dielectric props., investigation for morphology changes created by mechanical drawing and annealing 80—84697
- polyethylene, doubly oriented, low density, deformation and structure, exam. 80—11705
- polyethylene, high-density, dielec. loss, below 4.2K, antioxidant, annealing and drawing effects 78—84518
- polyethylene, linear, films, elec. cond. rel. to drawing, annealing *(Japanese)* 79—15817
- polyethylene, low density, with a single texture, oriented crystallisation of biphenyl 78—9966
- polyethylene, microstruct. obs., variation during drawing and annealing, electron microscopy *(German)* 80—38944
- polyethylene, microwave dielec. losses variation rel. to different sample treatments 80—25881
- polyethylene, mol. conformations after recrystallisation or annealing at high press. 77—88612
- polyethylene, oriented, elastic stiffness constants, US meas. 78—76690
- polyethylene, oriented, shear strain, effect on stuct., props. *(Russian)* 80—7656
- polyethylene, oxidised, paraelectricity, dielec. relax. obs. 77—48123
- polyethylene, polyethylene-D_4, migration and copolymerisation at high press. with shearing stress 78—51678
- polyethylene, single crystal, structural changes due to electron irrad. 80—29053
- polyethylene, sp. ht. after annealing at low temps. 77—39679
- polyethylene, ultradrawn, electron microscope exam. of struct. after annealing 80—11662
- polyethylene, ultrahigh modulus linear, annealing effects on mech. stiffness and struct. 79—91717
- polyethylene, ultraoriented high-density, annealing characts. 77—8852
- polyethylene films, uniaxially and doubly oriented, crystallite size determ., microparacrystallite lamellar surface identification 78—48431
- polyethylene oxide, nascent and annealed, X-ray study of crystal structure 80—64922
- polyethylene oxide, solid state relaxation, DSC study 78—9962
- polyethylene terephthalate, β relax., dynamic mech. and dielectric loss data 79—15399
- polyethylene terephthalate, effect of excess thermodynamic props. versus struct. form. on dynamic moduli 77—86053
- polyethylene terephthalate, filament, heat setting and thermomechanical behaviour 78—15435
- polyethylene terephthalate, oriented, amorphous, stress-induced crystn., shrinkage meas. 80—92466
- polyethylene terephthalate yarns, NMR, fibre struct. rel. to annealing, drawing *(Japanese)* 77—32269
- polyethylene terephthalate-p-oxybenzoate, nematic→isotropic transition loss 80—44300
- polymer, amorphous, enthalpy relax. rel. to T_g 77—52278
- polymer, fibrous, drawing and annealing 78—15458
- polymer crystal growth, during annealing 78—14300
- polymer crystallisation, growth rates, nucleation, annealing and random copolymer crystallisation 78—51435
- polymer dielectric nuclear track detector, particle stopping power depend. on preirrad. annealing 79—72185
- polymer film, conformational transitions, activation energy determ. *(Russian)* 78—48186
- polyolefine, liq., memory effect 80—103268
- polyoxymethylene, drawn, extra meridional reflections 80—24376
- polyoxymethylene, LF Raman band shifting on annealing 77—59572
- polyoxymethylene-copolyamide blend melt, viscoelastic peculiarities *(Russian)* 78—38263
- polyphenylacetylene, crystallizable, DC cond., annealing and defect effects 77—62923
- polypropylene, cold-drawn isotactic bars and thin films, microstruct. and annealing 78—95760
- polypropylene, electron bombarded electret, trapped charges ESR study 80—7170
- polypropylene, isotactic, low temp. annealing, differential scanning calorimetry obs. 80—60895
- polypropylene, oriented, annealing, mol. mechanisms 77—12642

annealing continued
- polypropylene isotactic, LF Raman band shifting on annealing 77–59572
- polypropylene nonfilaments, highly drawn, plastic deform. 78–44174
- polystyrene, annealed, enthalpic retardation times 80–19959
- polystyrene, atactic, effect of excess thermodynamic props. versus struct. form. on dynamic moduli 77–86053
- polystyrene, atactic, indentation recovery 80–84988
- polystyrene, compressed, TEM obs. of coarse shear bands, annealing of coarse bands 79–70117
- polystyrene, isotactic, normal vibrational anal. 78–43869
- polystyrene, shear bands, morphology and annealing behaviour 80–100873
- polystyrene, shrinkability, orient. 79–11660
- polystyrene, soln. grown isotactic crystals, degree and distrib. of crystallinity, thermal stability 78–9964
- polystyrene, solution grown isotactic crystal, thermal change kinetics study by X-ray diffr. 78–9965
- polystyrene+poly(2,6,-dimethyl phenylene oxide), isotactic, crystallisation and melting 78–18554
- polystyrene filament, melt spun, struct. and mech. props., effect of drawing, twisting, annealing, untwisting 80–45331
- polystyrene-poly(styrene-b-butadiene-b-styrene) polyblends, electron micrographs for struct. 78–51442
- polystyrene-tetrachloroxylene(tetrachlorobenzene) glassy solns., additive morphology rel. to mech. props. 79–65007
- polyurethane, segmented, time depend. struct. changes on annealing, X-ray meas. 77–4052
- polyvinyl fluoride film, pure and vanadyl ion doped, elec. cond., annealing 78–26859
- polyvinylidene fluoride films, corona-poled, piezoelectricity *(Japanese)* 80–55040
- porphyrin films, methine bridge substituted, surface photovolt. depend. on fabrication method 80–60119
- positron studies of annealing in cold worked state, review 79–100163
- post irradiation annealing facility 78–70649
- power satellite solar cell array conception and efficiency analysis 79–96464
- properties of high-conductivity copper and copper alloy wires *(Japanese)* 79–91665
- PTFE, annealing effect on melting and crystallisation *(Japanese)* 80–20980
- pulsed irradiation, annealing and accumulation of defects 78–47419
- PVC, amorphous, orientation study by creep thermomechanical method, computer anal. 78–75561
- PVC, highly syndiotactic, X-ray diffr. and IR studies of annealed material, crystallinity 78–2022
- PVC, oriented mouldings, struct. order 80–60896
- PVC, rigid, microdomains, small angle X-ray scattering study 80–28930
- PVC, rigid, viscoelastic props. rel. to thermal, mech. history 79–5016
- PVC, thermally induced conformational changes, Fourier transform. IR spectroscopy 78–9287
- PVC-Cu composite, annealing effects on elec. resist. 78–68060
- PVDF, film, polymorphism induced by poling and annealing 80–24372
- pyrocarbon, diffusion coeff. of Cs and Ag by post irradiation annealing of coated 78–13247
- pyrocarbon coated particles, influence of fast neutrons on transport behaviour of solid fission products *(German)* 79–13427
- pyrocarbon coatings for Biso fuel, permeability 77–79433
- quartz, electron irradiation effects on optical, dielec., elastic props. 80–59521
- quartz, electron-hole centres, activation energy determ. by isothermal annealing 200 to 550°C 79–32991
- quartz, He$^+$ ion implanted, SAW velocity, influence of annealing 79–14996
- quartz, irrad., annealed optical absorpt. power *(Russian)* 77–36273
- quartz, neutron irradiated, annealing effect on optical props. *(Russian)* 77–32381
- quartz, OH$^-$ impurity IR absorpt., electron irrad. effects 79–99913
- quartz, plant deform. and recrystallisation textures 78–68708
- α-quartz, Raman FTIR spectra, surface layer and vol. spectra comparison 78–52491
- quartz, synthetic, annealed, light scatt. centres 77–11586
- quartz, synthetic, electron beam irrad., defect form., annealing and migration effects, ESR obs. 80–50180
- quartz, track retaining props. for high temp. in-core neutron fluence meas. 77–75032
- α-quartz, uncompensated Ti^{3+} centre, X-irrad., EPR meas. 79–65731
- α-quartz and quartz glass, neutron irradiated struct., neutron diffr. meas. 78–22769
- quartz powdered, thermal effects of Fe contamination, adsorbed H$_2$O, annealing on DTA 79–100161
- quartz radiation defects, effect of annealing on absorpt. spectrum *(Russian)* 77–47495
- α-quartz seed plate fracture strength, etching and annealing effects 77–36661
- radiation enhanced, dose rate dependent effects of total ionising dose irradiation 80–70249
- rare earth oxide film, short-range order to long-range order transition 78–10288
- rare-earth dihydride epitaxial films, growth and struct. 79–37936
- recovery recrystallisation and grain growth in materials, conf., Chicago, USA (Oct. 1977) 79–97122
- recrystallisation, conf., Leeds, England (April 1978) 79–47706
- rolling, critical reduction, effect on chemicothermal treatment processes 77–70073
- ruby, cryst., optical properties, effect of annealing near melting point 78–90419
- ruby colouring due to specific growth, annealing and irrad., exam. of visible, infrared and UV spectra 79–11440
- S glass-Ni sphere composite, exam. of crack shape and fracture toughness 78–72886
- SA, thermocouple alloy, heat treatment effects on thermoEMF and mag. flux 77–63235
- sapphire, neutron bombard., F-centre fluorescence, photoluminescence 80–100676
- seals, glass-metal and glass-ceramic, annealing effect on internal stresses 80–40389
- semiconductor, dynamics of surface melting and resolidification during laser annealing 79–69918
- semiconductor, ion implanted, laser annealing 79–69124
- semiconductor, ion implanted, laser annealing *(Japanese)* 80–19821

annealing continued
- semiconductor, ion implanted, pulsed laser and electron beam annealing comparison 80–92547
- semiconductor, kinetics of defect cluster annealing 80–84209
- semiconductor, laser annealing of ion-implanted defects 80–55431
- semiconductor, radiation damaged, residual defects rel. to back reaction annealing kinetics 78–3161
- semiconductor, surface melting during laser annealing 79–74023
- semiconductor background heating for laser annealing 79–96047
- semiconductor layer, implanted, effectiveness of annealing by millisecond laser pulses 78–55885
- semiconductor with inhomogeneous impurity distrib., irrad. effects, annealing effects 79–10875
- semiconductors, annihilation processes of radiation-produced vacancies and interstitials 77–89432
- semiconductors, ion implanted, laser annealing 80–65023
- semiconductors, laser annealing after ion implantation, temp. distrib. 80–54265
- semiconductors, laser beam annealing of ion implanted layers 80–24469
- semiconductors, laser processing, bibliography 79–74028
- semiconductors, pulsed electron beam processing 79–69159
- sheet-metal laminate effect of interstage annealing on stretch formability 77–55917
- shells of revolution, thin, numerical anal. thermal stress relief 77–89041
- n-Si:B, ion implanted, rapid identification of faulted loops 79–19254
- Si:P$^+$, ion-implanted, annealing characts., X-ray diffr. exam. 78–14372
- Si, As segregation, TEM obs. 77–63674
- silicate glaze, diffusion of Sn(IV) 80–49417
- silicide fabrication, surface resist. meas. for control 77–89854
- silicide formation in Mo-W bilayer films on Si substrates 79–99376
- silicone-clad silica low-loss fibre radiation response obs. 78–1397
- solar cells, ion implantation and annealing technology 80–93996
- SOS, gettering effect by O implantation, Hall and Rutherford backscattering meas. 79–65103
- SOS films, cryst. quality improvement by Si ion channelling, annealing 80–44222
- sphene, fission track annealing, fission track age-temp. relationship 80–98316
- spin glasses, annealing and mag. remanence 80–60308
- sputter ion pumped system for annealing of metal wire, operation aspects 77–26318
- stainles steel, type 316, irrad. in simulated environment, tensile props. 80–34076
- stainless steel, machine faceted, low-energy ion erosion studies 80–80923
- stainless steel, type 316, irradiated cladding, second-phase precipitation 79–54501
- steel, 0.45% C, annealed, roller, macroscopic and microscopic changes in surface layer due to rolling contact 77–77518
- steel, 0.45% C, annealed, roller, rolling contact fatigue life, effect of changing rolling direction 77–77519
- steel, 0.54% C, fatigue crack accel. and closure in rotating bending tests, in annealed or quenched/tempered state 79–43383
- steel, 08Yu, annealing effect on texture, microstruct., and mech. props. 78–44138
- steel, 40Kh, heat-treated, wear during friction under extreme conditions 78–85007
- steel, 45 and U7, deform. microheterogeneity and ductility 77–73309
- steel, Al killed, cold rolled and recrystallised grain shape anisotropy 79–34064
- steel, Al-stabilised, texture formation in continuous annealing, effect of coiling temp. of hot strip 79–91688
- steel, alloy, 08kp, denitriding annealing, affect on mech. props. 79–52461
- steel, alloy, cluster formation susceptibility in 40 KhN, influence of isothermal working in H$_2$ *(Russian)* 78–56643
- steel, alloy, deep drawing sheet, annealing effect on coercive force *(German)* 80–29573
- steel, alloy, forgings, H precipitation kinetics, diffusion to voids, effect on shattercrack formation 80–16344
- steel, alloy, high speed, R12, R18, R6M5, R9K5, R14F4, annealing effect on props. 77–90373
- steel, alloy, high speed, rapid stepless cyclic method 80–16352
- steel, alloy, low C, effects of pre-treatment on graphitisation behaviour *(Japanese)* 78–84860
- steel, alloy, structure and properties after nitriding in molten salts, steel 08kp with Al diffusion coating 80–35418
- steel, alloy, type 25Gs, increasing fatigue resistance by surface plastic deformation 78–88530
- steel, alloy, uphill diffusion during homogenization 77–90381
- steel, anisotropic rolled plate, fatigue crack growth, rel. to laminated struct. and inclusions 78–92313
- steel, anisotropic rolled plate, torsional fatigue in middle and high cycle fatigue ranges *(Japanese)* 77–12691
- steel, austenitic, Cr-Mn-N, plastic deformation influence on internal friction, relaxation processes *(Russian)* 80–100870
- steel, austenitic, creep exposure, partial recovery of mech. props. by subsequent annealing *(German)* 77–59886
- steel, austenitic, high-speed, austenite grain growth, W addition effects 79–20085
- steel, austenitic, neutron irradiated, He absorption 77–51414
- steel, austenitic, Ni-Ti, alloy N35T5, ageing, magnetisation and Curie temp. depend. on plastic deform., Mossbauer studies *(Russian)* 79–69669
- steel, austenitic, supercooled, decomposition by heat treatment, carbide particle morphology *(Russian)* 77–70076
- steel, austenitic, supercooled ShKh15, stability, effect of spheroidising carbides *(Russian)* 77–25074
- steel, austenitic, thermonuclear reactor walls, ferromagnetic layer form. magneto-optical testing method 80–35465
- steel, austenitic stainless, aged and deformed, growth and dissolution of NbC particles 78–39782
- steel, austenitic stainless, extrinsic grain boundary dislocation spreading 79–57004
- steel, austenitic stainless, FCC, fractographic obs. of SCC 78–64786
- steel, austenitic stainless, fusion reactor first-wall and blanket material, mech. props. 80–34074
- steel, austenitic stainless, grain boundary struct. changes during initial stages of recrystallisation 77–36559
- steel, austenitic stainless, grain size effect on softening *(Russian)* 78–23731

annealing continued
steel, austenitic stainless, interaction of annealing twins in fcc metals and alloys 78−68712
steel, austenitic stainless, intergranular corrosion evaluation 77−16741
steel, austenitic stainless, recrystallization after hot rolling 79−47734
steel, austenitic stainless, supercond. magnets, mech. and phys. props. at 4K 80−86976
steel, austenitic stainless, tensile fracture, phase transform. effect, comparison of stable and metastable phases 78−60798
steel, austenitic stainless, tensile stress effect on He bublbe growth 79−87684
steel, austenitic stainless, texture influence as through thickness strength 79−91771
steel, austenitic stainless, type 316, hydrogen embrittlement, tensile testing 80−7671
steel, austenitic stainless, type 321S12, fatigue cycling in R=−1 loadings 80−35317
steel, austenitic stainless recrystallisation *(Japanese)* 77−52346
steel, austenitic stainless types 304 and 316, environment effect on crack growth, under creep and fatigue conditions 80−85035
steel, bright strip, light oil annealing, mathematical simulation 77−77512
steel, C, coarsening of dispersed particles, in solid matrices 78−56651
steel, C, cold rolled St3Kp, annealed, mag. nondestructive inspection of strip and ribbon 78−60913
steel, C, crack propag. and sealing, effect of thermal working *(Russian)* 79−34078
steel, C, decomposition of supercooled austenite, exam. of carbide formation *(Russian)* 78−35388
steel, C, S15C, S35C, S55C, rotating bending fatigue strength, annealing in vacuum effects *(Japanese)* 78−11314
steel, C, wire, drawing effect on spheroidization *(Korean)* 77−66656
steel, C content effect on annealing texture, plastic anisotropy and mechanical props. 80−29976
steel, C type U10A, X-ray diffr. investig. of carbide residues after deform. and tempering *(Russian)* 77−81275
steel, C-Mn-(Cr), structural changes during stress cycling after heat treatment and cold rolling *(Russian)* 78−19787
steel, carbide phase determ. by annealing in moist H_2 *(German)* 79−39231
steel, carbide phases formation during annealing, of lower bainite *(Russian)* 78−6930
steel, CC Cr-Mo (2.25, 1 wt.%) effect of heat treatment on tensile props. 78−23745
steel, CC Cr-Ni, soaking at forging temp., effect on struct. and mech. props. *(Czech)* 78−64628
steel, cementite coarsening in type 1080 in a temp. gradient 78−88486
steel, cementite migration in temp. gradient 78−44151
steel, cementite phase evolution during annealing *(Russian)* 77−32836
steel, cold rolled, deep drawing, continuous annealing effect on mech. props. *(German)* 77−90362
steel, cold rolled, high strength, mech. props. 77−36527
steel, cold rolled high strength sheet, with high drawability, fabrication process 77−73288
steel, cold strained, defects interaction with carbide strengthening phases, carbide decomp. degree *(Russian)* 80−84955
steel, cold worked, original struct. effect on softening during heating 80−60882
steel, cold-rolled, recovery of lattice defects in cementite 77−90370
steel, constructional, struct., props., isothermal thermomechanical working *(Russian)* 77−25076
steel, continuously cast, optimum conditions for annealing castings during dynamic working *(Russian)* 78−44134
steel, Cr, H-dislocation interaction 79−8307
steel, Cr, high C, ingot, macrostruct., effect of diffusion annealing, solidification condition *(Chinese)* 78−15429
steel, Cr (12wt.%), mech. props, carbide phase struct. 79−15702
steel, Cr modified, heat resist. rel. to thermomech. treatment 79−20084
steel, Cr-Mn, annealing effect on mech. props. for cryogenic appl. *(Russian)* 78−19788
steel, Cr-Mn, unstable austenite, martensitic transform., effect of alloying, heat treatment, and deform. 78−19751
steel, Cr-Mo, annealed, creep and rupture, heat treatment effects 79−24548
steel, Cr-Mo (2.25, 1 wt.%), annealed, heat treatment effect on tensile props. 78−11243
steel, Cr-Mo (2.25, 1 wt.%) annealing, high strain rate tensile props. 77−25117
steel, Cr-Mo-V, excessive temp. effect on creep behaviour, structure and hardness *(German)* 80−30054
steel, Cr-Ni (32,8), two phase austenite-ferrite alloy, fatigue behaviour *(Japanese)* 79−79091
steel, Cr-Ni-Mo, resistometric study of austenitization and carbide dissolution preliminary annealing *(Czech)* 77−59829
steel, Cr-Ni-Mo-V, Mossbauer austenitometry and mag. props. 80−40003
steel, Cr-Si-Mn-ΔV-Ti-Nb-Mo, effect of V, Ti, Mo, Nb additions on substructure, mech. props. *(Russian)* 79−34108
steel, CrMoV, low alloy, coarsening rate and activation energy of M_4C_3 and M_7C_3 carbides *(Czech)* 80−108480
steel, Cu, fission reactor vessels, neutron embrittled, exam. of technique for in situ thermal annealing 79−29114
steel, deep drawing, texture control as affected by processing variables 79−91689
steel, deep-drawing, texture problem after processing through continuous annealing 79−87659
steel, deformed eutectoid C_2 back stress decrease on annealing and H embrittlement 80−20981
steel, duplex ferritic/ martensitic, design for improved mech. props., heat treatment, TEM obs. 77−63697
steel, eutectic 1080, fatigue life improvement by thermomech. processing 80−25732
steel, eutectoid, mech. behaviour, thermomech. treatment effects 80−84970
steel, failure and radiation damage *(Czech)* 80−619
steel, Fe-Mn, improvement of cryogenic mech. props. through thermal/mech. treatments 79−79098
steel, ferritic, Cr-Mo (2.25, 1 wt.%), annealed, time depend. strain controlled fatigue, nuclear steam generator appl. 77−8915
steel, ferritic martensitic, effect of ductility of second phase on ductile fracture 78−19847

annealing continued
steel, ferritic stainless, embrittlement 80−85041
steel, ferromagnetic, U8, magnetic method of martensite transform. study *(Russian)* 79−87631
steel, heat resisting, type 15Kh1M1F, exam. of structural stability and props. *(Russian)* 79−29104
steel, high C, high alloy, $M_{23}C_6$ type carbides, effect of alloying elements on defect struct. and hardness 80−16481
steel, high hardenability carburising, accelerated annealing technique 78−84857
steel, high Ni (19 wt.%), thermal stabilisation of austenite 78−15397
steel, high speed, cast R6M5, carbide transform. during high temp. treatment 77−90375
steel, high speed, R18 and R6M5, rolled and annealed carbide phase investigation 77−90374
steel, high speed R8F8K7M6, cast, forged, sintered, struct. and props. 77−77516
steel, high strength, failure stress, structural relationships 80−81190
steel, high-C, ShKh15, interaction with controlled atmospheres during annealing 77−44269
steel, high-speed, low temp. mag. cycling effects on ferromag. struct. 80−100928
steel, high-speed, N effects on struct. and props. 77−59799
steel, hypoeutectoid, morphology and stability of Widmanstatten struct. *(Slovak)* 79−70094
steel, low alloy, rel. between over-heating embrittlement and behaviour of S, Auger spectroscopy anal. *(Japanese)* 79−79088
steel, low alloyed (Mo,Cr,B), structural and mech. props., report *(French)* 80−25691
steel, low C, Al-killed, effect of V on mag. props. 79−83339
steel, low C, alloy, structural transform. during deform. and annealing *(Russian)* 79−91707
steel, low C, brittle fracture susceptibility, low temp. deform. effects 77−56103
steel, low C, capped, cold rolled sheet, deep drawability, effect of carbide size, cold reduction annealing 78−64559
steel, low C, cold rolled, graphite precip. and S segregation, AES investigation *(Japanese)* 80−89222
steel, low C, cold swaged, exam. of H_2 attack mechanisms 78−76791
steel, low C, containing P, Mg effect on annealing texture, mech. props. and plastic anisotropy 78−27536
steel, low C, crack propagation energy rel. to temp., time factors 79−29179
steel, low C, cyclic loading, change in mech. props. rel. to heat treatment 80−104282
steel, low C, fatigue crack tip, observation of crack closure phenomena, by electron microscopy 78−68794
steel, low C, ferrite grain nuclei form. during polymorphic transform. *(Russian)* 80−50626
steel, low C, high cycle fatigue, crack initiation model *(Japanese)* 80−104258
steel, low C, hot rolling effects on struct. *(Russian)* 78−19793
steel, low C, Mn effect on recrystallisation and texture *(French)* 80−3110
steel, low C, pressurised, strain rate sensitivity prior to serrated yielding onset 78−48482
steel, low C, struct. changes during decarburisation in intercritical temp. interval *(Russian)* 77−25075
steel, low C, Ti-stabilized, recrystn. texture development 79−83231
steel, low C (0.01-0.05 wt.%), structural and mech. props., report *(French)* 80−25691
steel, low C sheets, effect of N_2 content on recrystn. texture 79−83233
steel, low-alloy 12GN2MFAYu, heat treated, testing temp. influence on fatigue strength *(Russian)* 80−40501
steel, low-C, phosphorus effect on annealing texture, plastic anisotropy and mech. props. 77−25069
steel, maraging, ageing study by internal friction meas. 77−12660
steel, maraging, Ni-Co-Mo (18, 8, 5 wt.%), fatigue strength charact. *(German)* 77−21241
steel, maraging, thermally embrittled, TiC precipitation 77−25055
steel, martensitic, low C wire, strain tempering by rapid heating *(Japanese)* 78−31428
steel, martensitic-aged, plastic deformation influence in type N17K12M5T steel on mech. props. *(Russian)* 80−76305
steel, mild, annealed, fatigue crack init., microstructure and strain ageing effect 77−86162
steel, mild, cold-deformed, struct. changes during annealing, electron microscope obs. *(Russian)* 78−23722
steel, mild, implantation of Cu(Cr), annealing and rolling behaviour of conc. profiles 78−75684
steel, mild, sheet, with low Al content, annealing, AlN recrystn., precipitation kinetics *(French)* 79−20083
steel, mild, solderability, annealing effect *(Japanese)* 80−89244
steel, mild, surface analysis rel. to annealing *(French)* 77−32857
steel, mild, tensile deformation, behaviour under high pressure *(Japanese)* 80−16381
steel, Mn, tempered, sementite crystals, carbide phase segregation, X-ray study *(Russian)* 78−35391
steel, Nb-stabilised, orientation depend. of cell size and recrystallisation texture development 79−91682
steel, Nb-V, cold rolled, HSLA, prod. by precipitation hardening, annealing 78−88471
steel, neutron irradiated press. vessel material, small angle neutron scatt. meas. 79−13428
steel, Ni and W, recrystallisation mech. during laser treatment 80−50658
steel, Ni-(Cr)-Ti, thermomechanical and heat treatment effects on retained austenite *(Russian)* 77−66661
steel, Ni-Cr, case hardened rollers, macroscopic and microscopic changes in surface layer due to rolling contact 77−77518
steel, Ni-Cr, case-hardened roller, rolling contact fatigue life, effect of changing rolling direction 77−77519
steel, Ni-Mn directional martensitic transform expt. 79−11613
steel, P, deep-drawing, spatial orientation distrib. of crystallites in cold-rolled and in annealed sheets 80−81079
steel, plastic loosening and deform. defect healing during recovery annealing of 12Kh18N10T *(Russian)* 80−66530
steel, pressure tank, heat-treatment effects and mech. props. *(German)* 80−40409
steel, rimming, shape change and pore form. during multiple polymorphic transform. *(Russian)* 77−25044

annealing continued
- steel, ShKh15, carbide particle size and pearlite grain size changes *(Russian)* 78−6946
- steel, Si, nonoriented sheet prod. with texture of {100} ⟨ovw⟩ 80−89246
- steel, Si, textured, alloying addition inhibition effects on grain orientation and growth *(Japanese)* 79−43270
- steel, Si (3 wt.%), struct. and preferred orientation, annealing parameters influence *(Czech)* 80−89248
- steel, Si-Cr-Mo-W-V (2,4,1,3,2 wt.%), heat treatment and props. 80−16349
- steel, Si-Mn, 27SG, heat treated sheets, underwater explosive forming *(Polish)* 79−34052
- steel, Si-P-C, low C, varying Si content, cold rolled annealing 80−3090
- steel, sintered, mech. props., effect of small cold reduction 79−39048
- steel, sintered type M2 high speed, heat treatment response and cutting props. 78−15336
- steel, spring leaf retainer with variable ductility, processing error, cold working error *(German, English)* 79−70267
- steel, stainless, 0Kh16N15M3B *(Russian)* 80−39170
- steel, stainless, 15Kh25T, embrittlement at 400 to 550 degrees C, grain size and cooling rate effects 78−44203
- steel, stainless, 18-8, stress corrosion cracking, in H_2SO_4-NaCl soln. *(Japanese)* 77−21315
- steel, stainless, 304, deformed in torsion, annealed, static recrystallization and restoration after hot deform. 79−47735
- steel, stainless, 316, 304, LMFBR primary piping materials, mech. props., review 77−25151
- steel, stainless, austenitic, deform. substruct. and annealing, stacking fault tetrahedra form 80−107282
- steel, stainless, austenitic grain growth, annealing twins role 79−57016
- steel, stainless, austenitic high Mn, thermally induced segregation 79−4971
- steel, stainless, blistering owing to He^+ bombard., 2 MeV 80−49279
- steel, stainless, C heterogeneities demonstration by high-resolution autoradiography *(French)* 77−66729
- steel, stainless, Cr (17 wt.%), recrystallisation texture, effect of N *(Japanese)* 79−4978
- steel, stainless, Cr-Ni-Mo, phase anal. of carbide phases after isothermal annealing *(Czech)* 80−89224
- steel, stainless, electrode material, annealing temp. cycle which improves emission props. 78−95858
- steel, stainless, fatigue crack morphology of type 304 cycled at const. stress amplitude at elev. temps. 78−64671
- steel, stainless, ferritic, 430 Zr, oxidation, forming and mech. props. 80−11680
- steel, stainless, ferritic, Cr-Mo-Ni (29,4,2 wt.%) 77−44276
- steel, stainless, Frank-Read dislocation source obs. in grain boundary 77−84756
- steel, stainless, fusion reactor He embrittlement simulation, splat cooling in development of B doping 80−30072
- steel, stainless, grain boundaries, electron microscope obs. *(Russian)* 79−4311
- steel, stainless, highly protective film development by surface treatment 80−66699
- steel, stainless, hot rolled texture, effect on cold rolled and annealed textures *(Japanese)* 78−48425
- steel, stainless, microduplex, austenite/ferrite, recrystallisation, annealing and cold work effects 79−47713
- steel, stainless, neutron irrad., pore annealing kinetics 77−72638
- steel, stainless, neutron irradiated, stress effects on microstruct. 77−47490
- steel, stainless, O_2 desorpt. during laser irrad., etching, AES study 80−66338
- steel, stainless, prestrained, heat treatment effect on fatigue strength *(Czech)* 78−60747
- steel, stainless, sensitization, C content and ferrite morphology effect 80−89400
- steel, stainless, stress corrosion cracking, prestrain effect, stress relaxation study 80−35384
- steel, stainless, surface chem. rel. to metallurgical props., SIMS, XPS and AES *(French)* 80−80045
- steel, stainless, surface morphology of H ion eroded samples 79−86968
- steel, stainless, two phase, variation of tensile and impact strength with heat treatment 79−34085
- steel, stainless, type 07Kh16N6, heat treatment 79−66158
- steel, stainless, type 304, effect of cold work as sensitization 79−66071
- steel, stainless, type 304, exam. of H_2 induced cracking 78−76738
- steel, stainless, Type 304, surface analysis by SXAPS *(Japanese)* 77−70231
- steel, stainless, type 304, viscoplastic behaviour, strain rate sensitivity, creep, relaxation, tensile tests 80−66727
- steel, stainless, type EP838 ion irradiated, surface structure changes during post-irradiation heating *(Russian)* 80−75272
- steel, stainless 18KhNMA, microplastic deform. *(Russian)* 77−66681
- steel, stainless 304, recrystallisation, effect of dislocation structure 77−32595
- steel, stainless 310, proton induced radiation damage investigation by Mossbauer effect 79−1735
- steel, stainless 316, recovery by annealing of creep produced dislocations 80−11702
- steel, stainless 316, stress-strain behaviour of micron thickness foils 79−52327
- steel, stainless type 304, shock hardening, anomalous residual, at short pulse duration 80−20942
- steel, stainless type 316, neutron irradiated, or themally aged diamond-cubic η phase formation, TEM study 79−99249
- steel, steam pipes, 12Cr1MoV, selection of allowable stresses based on minimum possible strength data 80−104237
- steel, structural changes after deformation and annealing, Mossbauer spectroscopic exam. *(Russian)* 78−35446
- steel, tempered, kinetics of solution of Mn in precipitated cementite *(Russian)* 78−6891
- steel, Ti-V, Ti and V effects on precipitation, hardness and annealing *(German)* 77−55968
- steel, tool, NC6, carbide lattice, kinetics of its destruction *(Polish)* 78−92280
- steel, transformer, textural barriers to grain growth after cold rolling and annealing *(Russian)* 78−39796
- steel, TRIP, strengthened by hydrostatic extrusion, struct. and mechanical props. *(Russian)* 78−76647

annealing continued
- steel, tufftrided, residual stress and fatigue crack propag. *(Japanese)* 77−48536
- steel, type A508, Cl 2, microcrack formation during stress-relief annealing of a weldment 78−80629
- steel, type AISI 316, thermal passivation in controlled vacuum 80−76276
- steel, types 60G, ShKh15, structural changes near holes and inclusions due to pulsed currents *(Russian)* 80−108459
- steel, US attenuation sorting of normally and partially annealed sheet *(German)* 77−77692
- steel, very low C, delamination study by impact testing 78−3218
- steel, W, high C, amorphous, rapidly quenched from melt, mech. and thermal props. 79−38874
- steel, W-Mo, high speed, hot deform. and heat treatment effect on props. 77−90372
- steel, X5CrNiTi26.6, ferrite-austenitic struct., optical and electron microscopy 78−84848
- steel, Zi, high permeability grain-oriented, AlN precip. study 79−83337
- steel, Zi, nonoriented elec. sheet, solute oxidation effect on mag. props. 79−83335
- steel 12Kh1MF, fine struct., effect of isothermal transform. temp. 77−21137
- steel 40 khNMS, high temp. thermomechanical treatment, Cr effects on props. 77−12651
- steel 40 KhSN2MVF, chemical micro-inhomogeneity recovery during thermal working *(Russian)* 78−15442
- steel bearing rings, optimisation of thermomechanical working parameters *(Russian)* 80−93579
- steel fibre reinforced Ag, exam. of recrystallisation behaviour *(German)* 78−84849
- steel fibre reinforced Pb, fabrication, mech. props. *(Korean)* 77−12579
- steel high strength X 3 CrNiMoNbN 2317, Bauschinger effect and creep at room temp., effect of heat treatment *(German)* 77−36543
- steel low C, fatigue strength of notched specimen, low-temp. quenching and quench ageing effects 79−100173
- steel low C, Mn surface segregation during annealing, kinetic studies 78−27528
- steel low C, surface segregation of Mn during annealing 77−36555
- steel N22, crack movement rate during cyclic deform., internal microstress effects 78−3225
- steel nitride phase hardening, precipitation and solution kinetics after heat treatment 78−95756
- steel sheets, surface composition, degreasing and batch annealing effects 80−66700
- steel St.3kp, ductile-brittle transition temp., variation with grain size 78−27640
- steel stainless, solar energy collector optical props. rel. to heat treatment 78−94455
- steel strips, elec., grain-oriented, effect on stress-relief annealing treatments on permeability and ageing 78−23832
- steel transformer, Mossbauer atomic struct. anal., decarburising annealing, cold rolling *(Russian)* 80−11294
- steel wires, drawn and annealed, tensile fatigue and tensile strength under cyclic stress *(Japanese)* 78−15507
- steels, tempered with different Ni contents, scaling behaviour obs. 80−71817
- steels for nuclear reactor pressure vessels, neutron irrad. embrittlement, temp. effects, annealing *(German)* 77−34384
- strengthening phase particle distrib., quantitative analysis 78−15629
- substitutional solid solutions, new phase nucleation mechanism 80−61135
- surface cleaning techniques review, atomically clean surfaces preparation 80−11804
- surface discontinuity, annealing by surface diffusion 79−23812
- surfaces, laser-annealed, characterisation by ellipsometry 80−103544
- technical superconductor radiation damage obs. 79−33422
- Teflon, non-destructive charge release 80−24946
- Teflon, phosphor embedded, fast neutron dosimetry using S activation 78−70648
- Teflon FEP, annealed electret, charge stability 80−6943
- terephthalate copolyester, heat treatment effect on melting point *(Japanese)* 80−40400
- TGS:Cr^{3+}, EPR and spontaneous polarisation stabilisation during annealing 77−4610
- TGS, autostabilised state, elec. second harmonic generation 80−103921
- TGS, domain nucleation in AC elec. fields 80−34867
- TGS, internal bias field, hysteresis loops *(Chinese)* 80−84705
- TGSSe, autostabilised state, elec. second harmonic generation 80−103921
- thermo-plasticity of irradiated metals 77−4146
- thin-film reactions, solid phase, laser annealing 79−51438
- titanomagnetites, temp. depend. cation distrib., mag. prop. obs. 80−85647
- TLD, effect of post irradiation annealing on fading characteristics 78−90030
- TLD cards based on $CaSO_4$:Dy Teflon discs, annealing and repeated readout 80−3812
- TLD fading charactristics effect of post irradiation annealing 78−90029
- TLD-600, activation and damage effects after neutron pre-exposure 79−13540
- tourmaline, fission track etching and annealing, thermal retention 77−82042
- transition metal carbides, elastic moduli, scratch geometry, micromech. tests 78−35416
- transition metal hydrides and deuterides, conc.-temp. depend. of mag. susceptibility 80−29523
- transmutation doped, stabilisation 78−10449
- TTF-TCNQ, and related compounds, low temp. irrad. effects 80−24906
- twin form., statistical anal. *(French)* 77−81281
- vermiculite, fission track annealing and dating 80−81885
- vibrational spectra crystals with split configuration interstitial *(Russian)* 78−76450
- void size distribution during irradiation and annealing, time depend. computation 78−30674
- web dendrites, dislocations, stacking faults, X-ray topographic study *(Chinese)* 80−88148
- Zircaloy, deformed, positron annihilation and electron microscopy 77−8898
- Zircaloy, irradiated spent fuel cladding, annealing effects 79−89382
- Zircaloy, unirrad., stress corrosion cracking, I_2-induced, effect of test temp., alloy comp. and heat treatment 80−97632

annealing continued
zircaloy 2, annealed, corrosion fatigue in aqueous soln. at 575K 78—64789
Zircaloy 4 tubing, cold-worked and annealed, stress relaxation behaviour 77—57717
Zircaloy cladding, irrad., tensile props., effects of temp., strain rate and annealing 77—48463
Zircaloy for reactor fuel pin cladding, metallurgical processing, transient temperature distribution 80—47573
Zircaloy-2, effect of simulated fission products on elongation fractography and metallography 80—649
Zircaloy-2, neutron irrad., low temp. deform. studies 79—47757
Zircaloy-2 cladding, creep and creep rupture props., 1000 to 1500°C, effect of annealing 78—78470
Zircaloy-2 cladding tubes, heat treatment influence on texture and mech. anisotropy 79—91694
Zircaloy-4, strain ageing 77—25071
Zircaloy-4, stress relaxation specimens, thermally induced strain recovery causing microstruct. changes 77—25057
Zircaloy-4 spent fuel cladding, tensile props. and annealing characts. 79—22392
Ag, dislocation recovery *(Russian)* 77—65980
Ag, electron irradiated, exam. of vacancy migration energies, and annealing kinetics 78—47571
Ag, electron irradiated, thermal variation of dislocation pinning by point defects 79—51150
Ag, fatigued single crystal, annealing of deform. struct. 78—3204
Ag film, annealing study of elec. resist. and defect density 78—76167
Ag film, hole formation and hillock growth after heating in O_2 atmosphere 79—65345
Ag film, sputtered, hillock growth and agglomeration by annealing, SEM obs. 80—2309
Ag film, vacuum deposited on NaCl, microstructure and orientation, surface condition influence 79—82486
Ag film, void growth, TEM obs. 80—59833
Ag films, hillock form. hole growth and agglomeration 80—44455
Ag, production and annealing of radiation defects 78—47362
Ag, surfaces, dislocation climbing, etch pit investig. 79—19260
Ag, tensile deformed single crystal, recrystallisation texture 79—91685
Ag thin films, deposited by cathodic sputtering using high-resolution electron microscopy, voids obs. 80—49557
Ag:^{111}Cd, hyperfine interaction, dose-rate depend. and annealing props. rel. to PAC obs. 77—27920
Ag:He, implanted films, solid solutions radiation induced polymorphism 79—86810
Ag/Au thin film couple, interdiffusion mechanism 77—20132
Ag/$Na_2SO_4(WO_4)$, and Ag/$Ag_2SO_4(WO_4)$ solid cell systems interface form., intergrain contact growth 77—16827
Ag-Au alloy, ion irrad., surface segregation and selective sputtering, AES expts. 79—7740
β'-Ag-Cd (45 at.%), growth kinetics of bainite plates and Widmanstatten needles 77—36551
Ag-Cd alloys, internally oxidised, thermal stability of CdO, exam. of particle coarsening 78—76789
Ag-Cu couple, grain boundary diffusion of Ag through Cu film, Rutherford backscattering obs. 80—34252
Ag-Cu metastable solid soln., form. by ion-beam mixing 80—75244
Ag-Fe, implanted, Mossbauer conversion electrons spectroscopy, rel. to dose and annealing temp. 78—52397
Ag-Ga (27 at.%), cooling rate depend. of thermal arrest, transform. temp. 79—29053
Ag-Ga solid soln., internally oxidised, hardness *(Japanese)* 78—60744
Ag-Ni, two ductile phase alloy, exam. of softening behaviour after cold rolling 78—72847
Ag-Pd alloy, for use as wire-spring relay contact material 79—52278
Ag-Pu alloys, metastable, high rate sputter deposition, annealing behaviour of deposits 77—21025
Ag-Sn (0 to 6 wt.%) exam. of bulk diffusion of ^{113}Sn and ^{110}Ag 78—75864
Ag-Sn (6,11 at.%) alloy, splat-quenched, X-ray diffr. study of microstruct. 77—8860
Ag-Te amorphous films, effect of annealing on elec. resist., phase transitions 79—11241
Ag-Zn(Cd), production and annealing of radiation defects 78—47362
$AgAsS_2$-$AgSbS_2$ system, thermal, microstructural X-ray phase anal. 77—32565
AgBr:Sr, stress induced anomalies in internal friction, logarithmic decrement 79—66095
$AgGaSe_2$, growth by Bridgman method, optical characts. 77—69980
Ag_2O, film, photocond., annealing and time effects *(French)* 78—23135
Al 2024 alloy, Young's modulus under shock loading, heat treatment effects 77—32611
Al, Al ion irradiated, void swelling and annealing of voids, electron microscopy study 80—88216
Al alloy, recrystallisation during hot deform. and after cold working 79—47715
Al alloy 01420, welded joint fatigue life improvement, vacuum annealing appl. 80—7597
Al alloys, (5083, 6061, 2219), supercond. magnets, mech. and phys. props. at 4K 80—86976
Al and Al-Mg alloys, thermal generation of vacancies involving dislocation climb 77—59808
Al and Al-Mn (1 wt.%), subgrain growth during annealing after cold work 78—56656
Al, annealed, positron annihilation momentum spectra, low temp depend. 79—19948
Al, annealed, subjected to torsional impact loading strain-rate effects 78—92303
Al, annealed and neutron irrad., exam. of positron lifetimes in voids and other defects 78—47426
Al, annealing in moist atm., causes and kinetics of H_2 blister form. *(German)* 80—25923
Al, annealing of lightly deformed samples, effect of press. *(Russian)* 78—39795
Al, annealing twin growth, obs. by synchrotron radiation X-ray topography 79—55753
Al, α-particle bombarded, He bubble growth mech. 77—7774
Al bimetal film with Cu, Ti(V,Ni) and alloy MLT(RS-3710), struct. and macroscopic defects *(Russian)* 79—1555
Al bronze, O free, annealing in photoemission electron microscope, twin density recrystallised grain size relation *(German)* 78—52850

annealing continued
Al, cold rolled, annealed, fatigue crack propag. rate, temp. effect 78—39904
Al, cold rolled and annealed, substruct. near fatigue crack tip, X-ray microbeam technique exam. *(Japanese)* 78—64621
Al, cold rolled bicrystal, plane grain growth anisotropy 79—91686
Al, cold-worked, plastically deformed, internal friction spectrum, Hasiguti peaks associated with dislocations 80—7618
Al, cold-worked, transport props., 1.5-8.5K 78—7059
Al, condensed film, phase and struct. nonuniformity *(Russian)* 80—54536
Al, cyclic loading, change in mech. props. rel. to heat treatment 80—104282
Al, deformation enhanced photoemission meas. 77—32511
Al, deformed, efficiency of dislocation as sink for vacancies, resist. obs. 77—36570
Al, deformed, struct. and recrystallisation transmission Kossel diffr. obs. 77—52340
Al, dislocation density, prep. of high-purity cryst. by strain-anneal method 78—48314
Al, dynamic defect annealing during plastic deform. 78—88478
Al, electron and neutron irrad., Doppler broadened positron annihilation meas. *(German)* 77—62563
Al, electron-irrad., NQR, EFG around vacancies and interstitials 78—88220
Al, electroplastic effect 80—7647
Al, energy release during annealing, Bragg diffr. expt. with Mossbauer γ rays 79—24546
Al, fatigue, effect of pre-existing subgrains 79—5041
Al, fatigue induced dislocation struct. and hardening, exam. *(Japanese)* 78—64624
Al film, polycryst. heat conductivity depend. on thickness, block boundary density *(Russian)* 79—82689
Al film, vacuum deposited, structural changes during annealing at temp. near melting point 78—84096
Al films, Al^{2+} irrad., increase of resist. and supercond. transition temp. 80—7027
Al foil, alloying additions (Si, Mg, Y, Se, Sc) effect, on tensile strength, weldability 80—55475
Al foil, electron-irrad., interstitial trapping on impurities 79—99242
Al foil, quenched, anomalous annealing phenomena, quantitative study 78—80565
Al, fracture mechanism, plastic strain role 79—38977
Al, He injected, tracing bubble evolution by positron annihilation 77—19992
Al, high purity, neutron irradiated, void annealing kinetics 80—44234
Al, high-temp. internal friction peaks, deformation and annealing effects 77—32615
Al, internal friction, dislocation glide and jog climbing *(French)* 78—11261
Al, neutron damage, positron annihilation 80—65056
Al, pipe diffusion along segment of faulted dislocation loops during annealing 80—107256
Al, polycryst., annealed, special grain boundaries in equilib. struct. *(Russian)* 80—29982
Al, polycryst. in annealed and creep conds., dislocation interactions with grain boundaries 79—42067
Al, positron annihilation, effects of quenching, annealing and neutron irrad. 80—20732
Al, positron annihilation rel. to thermocyclic treatment 79—52040
Al, pure elec. cond. grade, substructural developments during recovery, Sandstrom's model validity 79—74187
Al, quenched, irradiated, anisotropic electron scatt. on defects 79—95397
Al, quenched, irradiated, and quenched plus irradiated, grain boundary hardening 80—3162
Al, quenched, positron annihilation study, isochronal annealing effect 78—27348
Al, quenched, vacancy annihilation to non-uniformly distributed dislocations 78—6096
Al, quenched, vacancy-Fe interactions 78—47412
Al, quenched-in lattice defects, Mossbauer anal. of associated ^{57}Co 78—39820
Al, radiation damage with radioactive probes, TDPAC meas. 77—24336
Al, recovery annealing, exam. using in situ high voltage electron microscopy 80—7596
Al, recovery features, TEM and positron lifetime meas. examination 78—80611
Al, recrystallisation kinetics after small deform. and grain growth *(Czechoslovakian)* 77—32592
Al, recrystallisation nuclei form. and well defined deform. band struct. 79—20136
Al rods, waveform variation of reflected acoustic shock pulse due to work hardening 77—21167
Al, rolled single crystal, annealing texture 79—91678
Al, self-interstitial interaction with solutes, resistivity meas. 78—47331
Al sheets, dislocation obs. at high temp., annealing effect *(Japanese)* 80—34003
Al single crystal, polygonisation at high press. kinetic regularities, dislocation struct. at 140°C 79—66070
Al, subgrain coalescence, grain boundary recrystallisation nucleation 80—3094
Al, substruct. developed during recrystallisation, exam. *(Japanese)* 78—64566
Al, thermal cycle annealing of single crystal, subboundary obs. 77—55992
Al, zone refined, vacancy annihilation to dislocations, annealing profiles 77—80536
Al:Ga, pulsed electron-beam annealing, lattice site location improvement 80—107303
Al:Sb(Zn), ion implanted electron beam annealing, ion backscatt. and TEM meas. 80—59500
Al/brass/Al bimetal, three layers, formed by cold rolling, exam. of formation of intermetallic phases at interface 78—56658
Al/Cu thin film couples, interfacial reactions, low temp. contact resist. meas. 80—44709
Al/Pd thin film couples, thermal reactions 80—59830
Al/Sn, composite, kinetics of adsorption softening of solid interface *(Russian)* 79—61619
Al/Sn interface, effect of plastic deformation on structure and adhesion strength of interface *(Russian)* 79—28218
Al-^{57}Co, implanted, Mossbauer effect obs. of annealing 80—39126

annealing continued

Al-Ag (16 wt.%) alloy, quenched, early stages of decomposition, small-angle X-ray scatt. meas. 77—59740
Al-Ag(Ge)(Mg)(Zn) alloy, dil., electron-irradiated, impurity-interstitial interaction 77—15449
Al-Al$_2$O$_3$ alloys, dilatometric method for studying relaxation of conc. of defects 77—55288
Al-Al$_3$Ti, directionally solidified, thermal stability during annealing, 435-660°C 80—108393
Al-Al$_x$O$_y$-Pb tunnel junction, thermal annealing effects 80—49952
Al-alloy plates, type VAD23, thermomech. parameters effect on struct. and props. 80—20988
Al-anodic oxide-n-GaAs MOS struct., elec. instabilities and annealing effects 79—60928
Al-Au(Cu), growth kinetics of plate shaped precipitates 78—6932
Al-Au(Cu), growth kinetics of plate shaped precipitates 78—6933
Al-Co, dil., electron and neutron irradiation, interstitital atom clustering at ^{57}Co impurity, Mossbauer meas. 78—30607
Al-Co alloy, dil., fast neutron radiation damage, interstitial trapping, Mossbauer spectra and elec. resist. meas. 77—27914
Al-Cr, thin film metal contact, sheet resistance changes 80—80356
Al-Cr (0.1 wt.%), exam. of pre precip. behaviour, by elec. resistivity meas. and TEM exam. 78—48406
Al-Cr(Mn), struct. form. and phase transform. kinetics *(Russian)* 78—15359
Al-Cu, crack advance during fatigue, effect of cyclic hardening and COD 77—16675
Al-Cu, implanted metal system, Cu redistrib. after laser irrad. 79—69163
Al-Cu, isothermal coarsening of liquid inclusions 77—21166
Al-Cu alloy, vacuum deposited thin film, abnormal grain growth before melting transition and subsequent struct. change 79—60663
Al-Cu alloys, condensed films, metastable states 79—15046
Al-Cu alloys, Cu precipitate detect. by positron annihilation, GP zone development during thermal annealing 80—3051
Al-Cu films, DC sputtered, Cu distrib. 80—80113
Al-Cu samples (0.5, 2.0 and 4.0 wt.%) polycryst., precipitation, positron annihilation and TEM 80—50639
Al-Cu thin film couple, interdiffusion, AES obs. 80—6569
Al-Cu-Sn, ageing process, effect of Sn atoms, ^{119}Sn Mossbauer spectra obs. 80—7598
Al-Cu-Sn (3.4, 0.28 wt.%), Mossbauer anal. of Sn behaviour during ageing 78—31431
Al-CuAl$_2$ eutectic, deformed, thermal stability 77—52348
Al-CuAl$_2$ eutectic, thermal instability in temp. gradient 78—52851
Al-Fe, dil., annealing after cold working, impurity-vacancy interactions, Mossbauer meas. 80—7236
Al-Fe, dil., defects and phases, Mossbauer studies 80—40004
Al-Fe (0.02 wt.%), Mossbauer spectrum of ^{57}Fe associated with vacancies 77—85636
Al-Fe alloys, dil., quenched, secondary defects, Mossbauer spectroscopy 77—28491
Al-Ge (0.1 wt.%), channelling meas. of Al interstitial atom trapping by Ge atoms 80—59537
Al-Ge (0.2 at.%), exam. of interstitial trapping by X-ray diffuse scatt. 78—47363
Al-Li, cold worked neutron irrad. alloys, He bubble behaviour, microstruct. changes 77—54359
Al-Li, dil. alloy, cold-worked, annealing spectrum 78—39801
Al-Li (10 at.%), struct. changes on annealing, 25-500°C, Li atoms role 80—35183
Al-Li alloy, annealing of vacancies and ageing, resist. and TEM obs. 77—21172
Al-Li alloy, dil., quenched and irrad., recovery, resist. and internal friction obs. 78—52848
Al-Li alloys, precipitating, annealing spectrum 78—31429
Al-Mg (0.1 at.%), neutron damage, positron annihilation 80—65056
Al-Mg (33 at.%), liquisol quenched, decomposition 79—61622
Al-Mg alloys, cold-worked, transport props., 1.5-8.5K 78—7059
Al-Mg$_2$Si (1 wt.%), precipitation reactions 80—11652
Al-Mg-Si, deformed, orientation of recrystallisation nuclei 79—91681
Al-Mg-Si, Guinier-Preston zones, inception and effect on ageing, review *(Hungarian)* 79—11627
Al-Mg-Si, heavily rolled, electron microscope obs. of cube oriented region, rolling texture 79—29093
Al-Mg-Si rod, extruded and cold drawn, annealing *(German)* 78—39804
Al-Mn (0.35 wt.%), quenched exam. of Mn-vacancy interaction 78—76676
Al-Mn (1 wt.%), commercial, recrystallisation 79—47710
Al-Mn (1 wt.%), single crysts., rolled to (123)[41$\bar{2}$], recrystn. textures 80—104183
Al-Mn (1.8 wt.%), cold-rolled, precipitation and recrystallisation 78—27540
Al-Ni (3.6 at.%) alloy, quenched from melt, distortion of matrix caused by coherent precipitates, electron diffr. meas. 77—59791
Al-Ni multiphase system, simultaneous diffusion in cylindrical symm. *(Russian)* 80—100357
Al-Pt film sandwich, interdiffusion and intermetallic form. 77—24448
Al-sapphire-Si capacitor, effect of electron-beam aluminisation on Si-sapphire interface 77—89856
Al-Sc, dil., thermomigration of Sc 79—69280
Al-Si crystals, work hardened, softening and creep rates on annealing 80—11663
Al-Si eutectic alloy, banded struct., SEM and optical microscopy 80—104144
Al-Si$_3$N$_4$-SiO$_2$Si, MNOS structures degradation under UV irradiation effect 80—107923
Al-SiO$_2$-Si:B ions, annealing effect on energy spectrum of radiation defects *(Russian)* 78—88488
Al-Sn, dil. alloy, vacancy-impurity interaction, exam. by electrical resistivity meas. at 77K *(German)* 78—83846
Al-Sn dil. alloy, cube orientation texture development 79—96040
Al-Zn, dil. alloy, ageing and reversion, annealing curves, X-ray obs. 78—88485
Al-Zn, plastic deform. effect on struct. transform. at elev. temp. *(Czech)* 79—79044
Al-Zn, precipitation struct. and phys. props. effect of miscibility gap *(German)* 78—92265
Al-Zn (0.041 to 4.4 at.%), clusters, electrical resistivity meas. *(Japanese)* 77—21168

annealing continued

Al-Zn (12.5 wt.%) alloy, retardation of precip. reaction by DC stress 77—55969
Al-Zn (2 and 4 wt.%), ageing and elec. cond. reversion *(Japanese)* 79—4983
Al-Zn (22 wt.%), superplastic strain rate sensitivity, rel. to ductility 78—31478
Al-Zn (40 wt.%), grain refinement by thermal cycling 78—3149
Al-Zn (40 wt.%), mechanical properties after thermal cycling 78—3150
Al-Zn (70, 30 wt.%), decomp. study, 25-160°C *(Czech)* 80—89225
Al-Zn alloys, cast, Zn diffusion during homogenization *(Polish)* 79—33108
Al-Zn-Mg, zone composition change during ageing 79—29110
Al-Zn-Mg alloys, role of dispersed transition metal intermetallic compounds 79—96088
Al-Zn-Mg plasma sputtered, mech. props. rel. to heat treatment *(Russian)* 80—40387
Al-Zn(10 at.%), supersaturated solid soln., structural charact. of decomposition 77—70027
(Al+Si)-Si thin films, struct. transitions and phase comp. 80—49537
AlAs-GaAs LEDs, Ge or Zn-doped, mechanism of degradation 77—76911
AlAs-GaAs stripe heterojunction laser, O$^+$ implantation effect on threshold characts. 79—41383
AlGaAs DH laser, self-pulsations due to proton bombarded region self-annealing during ageing 80—99728
AlGaAs-GaAs remote junction heterostructure laser, recomb. enhanced annealing effect 79—98355
Al$_x$Ga$_{1-x}$As:N, ion implantation, in situ annealing photoluminesc. obs. 80—10567
Al$_x$Ga$_{1-x}$As:N$^+$, (x=0.58), laser annealing of optically active impurities, photolum. charact. 80—20682
Al$_x$Ga$_{1-x}$As:Sn(Te)(Ge), anneal-induced defects, photoluminesc. obs. 79—61422
β-AlO$_3$-(Na,Li)$_2$O, NMR, Raman and IR spectra, and X-ray diffr., heat treatment induced changes 80—107508
α-Al$_2$O$_3$, annealing, stable hardened subsurface layer form. 77—56128
Al$_2$O$_3$, composite base ceramic coating, hot pressed, H$_2$ permeability 77—56164
β''-Al$_2$O$_3$, conductive, Li$_2$O stabilised, sintering and annealing 77—59724
α-Al$_2$O$_3$, crystal defects from X-ray irradiation, F-centres, X-ray luminesc. obs. 80—55176
Al$_2$O$_3$, crystallite size and lattice distortion, determination using X-ray line broadening analysis, appl. to ceramic powders 79—8261
Al$_2$O$_3$, cylindrical voids, exam. of instability 78—79603
Al$_2$O$_3$, defect microstructure due to ion bombardment, TEM study 80—34100
Al$_2$O$_3$, explosively compacted powder, struct. and annealing 77—55926
Al$_2$O$_3$ film, DC reactively sputtered, in MIS structs., effects of annealing on C-V characts. 77—51822
Al$_2$O$_3$, γ-irrad., hole centres, luminesc. and EPR obs. 77—32256
α-Al$_2$O$_3$, ion bombard., vol. expansion, annealing compaction, surface props. 78—67748
β''-Al$_2$O$_3$, Li$_2$O-stabilised, hot-pressing 80—40298
Al$_2$O$_3$ phase transformations, γ to α, produced by shock wave working 80—16305
Al$_2$O$_3$ plasma-sprayed, struct. and thermal diffusivity 79—86932
Al$_2$O$_3$, polycrystalline, conditions for formation of anion vacancies 79—10844
Al$_2$O$_3$ porous refractories, production 80—35149
Al$_2$O$_3$, sintered, electron microprobe anal. of impurity and additive distribs. 80—40359
Al$_2$O$_3$ substrates, grain growth during sintering 80—40302
Al$_2$O$_3$, thermoluminescence, effect of heat treatment following gamma irradiation 77—59624
Al$_2$O$_3$:Co, spectra, heat treatment and irrad. effects 77—4659
α-Al$_2$O$_3$:Er(Cr), crystal defects from X-ray irradiation, F-centres, X-ray luminesc. obs. 80—55176
Al$_2$O$_3$:Fe, pore form. during oxidative annealing, grain growth slowing 80—100856
Al$_2$O$_3$:Si thermoluminescent phosphor, annealing characts. and nature of traps 77—85817
Al$_2$O$_3$:Ti(Si), annealing, electron irrad., absorpt. spectra 77—20890
Al$_2$O$_3$-Cu composite, dispersion-strengthened, hardness, tensile strength and struct. 77—70063
Al$_2$O$_3$-Nb composites, influence of gas impurities on solid-state bonding on annealing 80—11739
Al$_2$O$_3$-SiO$_2$, fracture strength studies under dynamic conditions 79—96132
(Al$_2$O$_3$-Fe$_2$O$_3$):Cr^{3+}, (0.04 mol.% Fe$_2$O$_3$), paramag., cross relax., annealing temp. effect from Mossbauer meas. 80—44983
AlSb, laser pulse annealing, induced nucleation, crystal growth 80—84966
Al$_2$TiO$_5$, eutectoid decomposition, kinetic study *(Japanese)* 77—55941
Al$_2$TiO$_5$, sintering and annealing effect on decomposition *(Japanese)* 79—87606
AlZn, homogenization processes, dendritic struct. 79—15700
As, film A1-type supercond. vapour-quenched transition temp., A7-type phase transition 78—52145
As-Ge-S(Se), glass films, photostruct. changes 77—85822
As-S amorphous film, photo-induced optical changes, annealing effect 78—27345
As-S chalcogenide glass holographic recording efficiency, photocond. and annealing effects *(Russian)* 80—15556
As-S glass media, temp. control of hologram props. 78—17883
As-Se amorphous film, density of upper valence band states, annealing effects, UPS obs. 80—29845
As-Te-Ge chalcogenide films, thermally induced transformations, TEM obs. 79—94917
As$_2$S$_3$ (Se$_3$), electron irradiated, effects on elec., photoelec. and optical props. 80—49806
As$_2$S$_3$, amorphous, acousto-optical effects *(Japanese)* 79—82946
As$_2$S$_3$ and As$_4$S$_4$ vapour-deposited films, valence states, thermal and photo-induced changes UPS study 80—93459
As$_2$S$_3$ film, amorphous, deposited at different temps., IR spectra 80—40102
As$_2$S$_3$ film, effect of light exposure and heat cycling 78—94417
As$_2$S$_3$ film, vacuum deposited, selective etching characts. obs. *(Russian)* 80—3207
As$_2$S$_3$ glass, at. struct. changes due to irrad., comp. variations and annealing 77—76323

annealing continued

- As_2S_3 glass, melt-quenched, reversible photostruct. change 77−68925
- As_xS_{100-x} amorphous film, composition depend. of photo-induced refr. index changes 79−78644
- $As_2S_3(Se_3)$ evaporated films, optical absorpt. and thermally induced effects 79−42989
- $As_2S_3(Se_3)$ evaporated films, struct. and thermally induced effects 79−41963
- As_2Se_3, amorphous, hole emission defect states 80−49759
- As_2Se_3 amorphous film, comp. ratio variation by annealing and laser irrad., ESCA meas. 79−99447
- As_2Se_3, and As_4Se_5Ge glasses, struct. changes, Mn^{2+} EPR expts. 78−79534
- a-As_2Se_3 chalcogenide glass, influence of thermally induced defects on transport props. 80−49766
- As_2Se_3 glass, heat capacity and struct. relaxation of enthalpy 77−55360
- As_2Se_3:Bi, annealing kinetics, cond. activation energy and density 79−73503
- As_2Se_3-As_2Te_3 glasses, crystallisation 77−43156
- As_3Se_2, electron irradiated, effects on elec., photoelec. and optical props. 80−49806
- As_4Se_5Ge, glass, light irrad. induced changes in optical and elec. props. *(Japanese)* 78−68031
- $AsTeCu_x$ $(0 \leq x \leq 0.4)$ glass, effect of Cu on elec. cond. and thermoelectricity, 100 to 370K 78−87978
- $AsTeE_x$, E=S, Se, Sb, Bi, annealing effects on elec. cond. of films 77−43594
- $As_4Te_5Ge(Si)$ glass, struct. changes, Mn^{2+} EPR expts. 78−79534
- Au, deformed, annealing kinetics of vacancies, elec. cond. meas. and computer simulation 78−47353
- Au, deformed, annealing kinetics of vacancies *(Japanese)* 80−88139
- Au, electron irradiated, exam. of vacancy migration energies, annealing kinetics 78−47571
- Au, electron irradiated, interstitials and their clusters, diffuse X-ray scatt. study 80−33997
- Au film, adatom surface diffusion at low temps., elec. resist. study *(French)* 80−65376
- Au film, annealing curves, size effect parameter determ. from Mayadas Shatzkes theory 77−76962
- Au film, interface reaction with n-type $Ga_{0.7}Al_{0.3}As$ and GaAs 80−39482
- Au film bicrystals, exam. of low energy planes for tilt grain boundaries 78−51551
- Au films on Si substrate, solid-solid reactions 78−95369
- Au, hardening mechanisms, grain size effect 80−35302
- Au, magnetoresist of quenched and annealed metal, defect scatt. 79−4981
- Au polycrystalline wire, internal oxidation of impurities 78−83842
- Au, proton irrad. at 0.3K, resistivity annealing 77−76475
- Au, quenched and annealed, cond. electron scatt., de Haas-van Alphen Dingle temp. meas. 77−89688
- Au, quenched and annealed, conduction electron scattering 78−47774
- Au quenched single crysts., vacancies, diffuse scatt. and resist. obs. 80−33994
- Au, thin film bicrystal, annealing twin form. by boundary dissociation 79−47729
- Au, thin foil, growth of stacking fault tetrahedra 80−19815
- Au/Sn films, evaporated, microstructure and texture, TEM obs. 80−39481
- Au/Ti thin film, temp. and humidity effect on interdiffusion 79−51317
- Au-Ag, mech. damping 78−31444
- Au-Al thermocompressional contacts, diffusional zones, phase growth during annealing *(Russian)* 80−75389
- Au-As, system interactions due to heat treatment, backscattering anal. 79−91719
- Au-Cd (47.5 at.%), effect of cooling rates on stress-strain behaviour 78−76721
- Au-Co, electron scatt., spin-orbit effects 80−65533
- Au-Co electrodeposits, heating effect on microstruct. and surface topography 77−43456
- Au-Cr alloy pressure gauges, annealing effects 78−49854
- Au-Cu, dil., electron irradiated, interstitials and their clusters, diffuse X-ray scatt. study 80−33997
- Au-Fe, polygonisation, recrystallisation, precipitation microstruct. without external plastic deform. 79−43276
- Au-Pd (1(50) wt.%), quenched, vacancy annihilation and short-range order formation, elec. resist. 80−108487
- Au-Pd alloy, on rock salt, epitaxial growth and struct. 77−20211
- Au-Sb, system interactions due to heat treatment, backscattering anal. 79−91719
- Au-Si interface, valence band and core levels, Si diffusion, alloy form., photoelectron spectra obs. 80−45205
- Au-Si system, transition layer struct. form. and heat treatment influence, amorphisation obs. 80−54529
- Au-Si-Mn, amorphous spin glass film, mag. susceptibility 79−42775
- Au-Sn evaporated films, comp. and annealing behaviour, 20-400°C 77−76695
- Au-$Ti_{0.3}W_{0.7}$, thermal annealing study of metallisation on Si 80−80134
- Au-W-GaAs Schottky barrier, elec. and chem. props., AES 80−96973
- AuAl formation by thin film interactions, identification by X-ray diffraction 79−99442
- AuCu-Al thin film bilayer system, phase formation, backscattering spectra 80−96728
- AuFe alloy films, mag. susceptibility, Fe concentration and annealing depend. 79−61119
- $Au_{11}Mn_4$ ordered phase formation, electron diffr. and microscopy study 80−107418
- Au_4Mn, high resolution dark field electron microscopy exam. of ordering 79−7615
- Au_5Mn_2, monoclinic, ordering, high resolution electron microscopy 79−43290
- Au(111) and polycrystalline surfaces, O_2 adsorption, LEED, AES and energy loss spectra 80−34310
- B fibre reinforced Al-Mg, heat treatment effect on struct., tensile strength 80−55487
- β-B, rhombohedral, dielec. loss temp. depend., −196 to 350°C 80−20585
- BC, sintered, struct. and props. 80−104181
- B_4C, FBR control rod elements, neutron damage and post-irrad. annealing 80−13581
- BN films, optical and electrophysical props. *(Russian)* 77−20941

annealing continued

- B_2O_3, glassy, influence of annealing on transition region 80−44145
- BP:Zn(Se)(Cd), epitaxial layers, ion implantation, defects and lattic locations, channelling obs. 80−88179
- Ba ferrite powder, effect of lattice defects on coercivity *(German)* 79−24194
- BaF_2, formation and growth of oxidation centres result of O^{2-} diffusion 80−7706
- BaF_2, thermoluminesc. and F-centre annealing, after neutron irrad. 80−7422
- $BaF_2:La^{3+}$, relaxation processes, studies by ionic-thermocurrent techniques 79−69769
- BaFCl crystals, F-centres, X- and γ-irradiation, thermoluminescence and optical absorption spectra 80−45155
- $BaFe_{12}O_{19}$, powder, milled and annealed, phase composition, lattice conts. and crystallite size 80−71677
- $BaPb_{1-x}Bi_xO_3$ film, RF sputtered, T_c as function of comp. and annealing conditions 79−24100
- Ba_2RF_7, (R=Dy, Ho, Er, Tm, Yb, Lu, Y), superstructure phases, prep., thermal characterisation and X-ray powder diffr. 80−96494
- $BaSO_4$, X-ray irrad., electron and holes traps, g-factors, ESR obs. 80−50183
- $BaTiO_3$, acceptor doped, exam. of electrical conductivity 130 to 300°C 79−33286
- $BaTiO_3$, ferroelec., reduction of hysteresis losses 79−42926
- $BaTiO_3$ film, dielectric props. depend. on sinusoidal elec. field 80−71318
- $BaTiO_3$, unipolar cryst., topography of defect. and thermodepolarisation currents 77−43954
- $BaTiO_3$:Mn, polycrystn., annealing effect on transition temps. 80−3100
- $BaTiO_3$:X(X=Cr, Mn, Fe, Co, Ni, Zn, Ga), annealed in H_2 and O_2, valence change in phase stability 80−20600
- $BaVS_3$, annealing influence on lattice constants, neutron diffr. profile anal. 80−1976
- Be bronze BrB2, quenched deformed, substruct. and props., effect of prerecrystallisation annealing *(Russian)* 78−60677
- Be, low oxide, isostatically pressed block, factors affecting tensile strength, elongation, impact resistance 77−16610
- Be, neutron irradiated, annealed, tensile props. and swelling, effect of He bubbles 78−22765
- Be-Al-Fe, phase equilibria and diffusion using high energy ion beams 77−16542
- Bi film, adatom surface diffusion at low temps., elec. resist. study *(French)* 80−65376
- Bi film, evaporated, lattice distortion spectrum, elec. resistance temp. variation 80−54806
- Bi film, vap. deposited, effect on deposition parameters and substrate condition on crystallinity 78−10290
- Bi, film A1-type supercond. vapour-quenched transition temp., A7-type phase transition 78−52145
- Bi, quenching and annealing of defects, elec. resist. meas. 78−87973
- Bi, superconducting ultrathin film, metastable, supercond. props. *(Russian)* 79−7917
- Bi, US attenuation, annealed sample, 0.6 kbar, 25-120°C 78−47474
- Bi:Sb(Te), quenching and annealing of defects, elec. resist. meas. 78−87973
- Bi-MnBi, directionally solidified composite, processing parameter role on mag. props. 80−35352
- Bi-MnBi directionally solidified eutectic alloys, struct. and mag. props. 79−51815
- Bi-MnBi eutectic composites, microstructure and mag. props., annealing effect 79−82827
- Bi-Te thin thermoelectric films prep. by solid state reaction method 80−108361
- Bi_2O_3, thermally-grown capacitor-film, dielec. props. 80−2480
- Bi_2S_3-Bi_2Se_3 and Bi_2Te_3-Bi_2Se_3 systems, thermal cond. change during phase transitions 80−100368
- $Bi_{1-x}Sb_x$ film, evaporated, cross-sectional struct., electron microscopy and replica technique study *(German)* 78−22977
- Bi_2Te_3-Sb_2Te_3 solid soln., deviation from stoichiometric cross section 78−35362
- Bi_2Te_3-$SbTe_3$, ordered structure formation, heat treatment effect on thermal cond. 80−54448
- n-$Bi_2Te_{2.88}Se_{0.12}$, extrusion deformed, powder dispersion degree influence on thermal and elec. props. *(Russian)* 80−39366
- C, amorphous, diamond-like 3-fold coord. 80−50323
- C, amorphous film, struct. props., Raman scatt. study 80−11417
- C fibre reinforced Ni, hot pressed and electrodeposited, strength 79−38898
- C fibre reinforced Ni, struct. and strength change at high annealing temp. *(Russian)* 79−66076
- C fibres, Al coated, effect of annealing on ultimate tensile strength and fracture 78−56744
- C films, surface struct., graphitisation, secondary electron spectra and AES 79−43077
- C steel, abrasive wear resistance, effect of C content, annealing, quenching 77−56115
- C steel, fatigue crack propagation, effect of mean stress on crack closure 77−73315
- C steel, superplasticity due to successive deformations *(Russian)* 80−55464
- CC Si:P, secondary defect generation suppression and diffusivity restraint by HCl oxidation 79−70191
- CU-Zr-(Cr), powder metallurgical alloys, thermomech. treatment effect on props. 80−50660
- $Ca_5(F, Cl)(PO_4)_3$, apatite, Indian, fission track dating and annealing, U content determ. 79−57891
- CaF_2, (n,γ) induced lattice defect annealing, polarised ^{20}F NMR 77−20725
- CaF_2, additively coloured, Ca colloid form. and size evolution during annealing 77−20895
- CaF_2, thermolum., F-centre annealing after neutron irrad. at 20K 79−55787
- CaF_2, thermoluminesc. and F-centre annealing, after neutron irrad. 80−7422
- CaF_2:Er, defect structure, quenching effect, dielec. relax. and optical absorption 80−65031
- $CaF_2:Er^{3+}$, fluorite, defect equilibria cluster control 79−99231
- CaF_2:Eu, CaF_2:Eu,Mn(Gd), single crystal predisintegration phenomena, SEM cathodolum. obs. 80−59502
- CaF_2:Mn, CaF_2:Eu,Mn, single crystal predisintegration phenomena, SEM cathodolum. obs. 80−59502

annealing continued
$CaF_2:Mn^{3+}$, fluorite, radiation and thermal redox processes 80−55678
$CaF_2:O_2^-$, OH^-, ion incorporation by reaction with surrounding atm. 80−55143
CaF_2-YF_3, fluorite- and tysonite-related ordered phases *(German)* 79−23725
CaO, neutron irrad., MCD, optical absorpt. lines 77−77255
CaO:Li, thermally quenched, generation of Li^0 centres 80−50382
$Ca_{10}(PO_4)_6X_2$, halophosphate luminophor, forming during annealing of briquetted mixture 78−11173
CaS:Bi as UV dosimeter 80−34991
$CaSO_4$:Dy, fast neutron dosimetry using S activation 78−70648
$CaSO_4$:Dy, TLD phosphor, gamma-ray induced sensitisation 78−74542
$CaSO_4$:Dy, TLD-900, thermolum. stability at low radiation doses 80−101272
$CaSO_4$:Dy, thermoluminescent glow peaks, post γ-irrad. annealing study 80−89077
Ca_2SiO_4-FeO, conditions and mechanism in cryst.-chemical stabilisation of unstable phases 80−39302
Ca_2SiO_4-MgO, conditions and mechanism in cryst.-chemical stabilisation of unstable phases 80−39302
$CaTiSiO_5$, sphere, effects of thermal annealing on track etching rate 78−65435
Cd, film, freshly deposited, 77K, refl., annealing effect, thickness depend. 77−16413
Cd, lattice defects studied by gamma ray angular correlation 79−51895
Cd, loading and annealing, dislocation struct. control *(Russian)* 78−3142
Cd, stage III recovery, after α-particle irradiation 77−27924
Cd-Ag, polycryst. quenched foil, the influence of Ag on the recovery spectrum 78−76661
Cd-Ag, polycryst. wire, cold worked, resistivity changes 78−68827
Cd-Co(-Mo), amorphous films, thermal stability of mag. props. *(Japanese)* 79−47307
Cd-Ge-As system, quenched samples, phase diagram, DTA after annealing 79−69226
Cd-Sn alloy, superconductivity and microstructure 80−107949
Cd-Zn, polycryst. wire, cold worked, resistivity changes 78−68827
Cd-Zn (Ag), annealed, work softened, exam. of crystallographic texture, hardness 78−80559
Cd-Zn eutectic, microstruct. degradation, role of temp. fluctuations 77−4766
Cd_3As_2, effect of annealing on elec. transport props. 80−49739
$Cd(ClO_3)_2$, irrad., bleaching and annealing expts., EPR and optical absorpt. 79−91476
$Cd(ClO_3)_2$ irradiated single crystal, ESR and annealing, trapped defect centre 80−55141
$CdCr_2Se_4$, ferromagnetic semiconductor, P_{Se}-T phase diagram, where $Se=Se_2$, near peritectoid reaction temps. *(Japanese)* 77−52290
$CdCr_2Se_4$, Se_2 and Cd vapour, P-T phase diagram between 600 and 964°C 77−63636
$CdCr_2Se_4$:Ag, mag. anisotropy, effect of annealing in vacuum 77−80929
$CdCr_2Se_4$:Ag, magneto-optical effects in impurity spectral region 80−97313
$CdCr_2Se_4$:In, elec. cond., annealing effect 79−87102
CdF_2:Eu, role of solution and precipitation phenomena on ITC spectra 80−7265
$CdF_2:Eu^{3+}$, luminesc. spectra conc. and annealing depend. 79−65917
$CdGa_2Te_4$ film, effect of thermal annealing on struct., optical absorpt. and photocond. 79−65342
$Cd_{0.2}Hg_{0.8}Te$, annealing in saturated Hg vapour *(German)* 79−43447
p-$Cd_xHg_{1-x}Te$, Hall const. variation with comp. after annealing in Hg vapour 77−15868
$Cd_xHg_{1-x}Te$ magnetoresistor prep. and props. 79−7844
$Cd_xHg_{1-x}Te$, precip. 77−90352
$Cd_xHg_{1-x}Te$, vacancy mech. of resorption of Hg droplets 80−39070
CdO-SnO_2 film, DC reactively sputtered, transparent electrode props., optimum sputtering conditions 80−11116
CdP_2:Cu, photoluminescence and photocond. characts., interimpurity recomb. of carriers 77−8637
CdS, 200 keV electron induced defects, low temp. annealing 77−80796
CdS, chemically precipitated film, optical spectra, annealing effects *(Russian)* 79−11424
CdS, elec. cond., plastic deform. and annealing effects 77−55534
CdS film, chemically deposited, cond. depend. on thickness, grain size, annealing time *(Russian)* 77−8210
CdS film, electrolessly deposited, annealing effect on optical spectra 80−2884
CdS films, photosensitive, growth by reactive RF sputtering, props. *(French)* 78−35308
CdS films, precip. from soln., phase comp. change during annealing in air at 200-600°C 80−15393
CdS, high-energy electron irrad., photoluminescence spectra, course of annealing 77−90198
CdS, single cryst., effects of annealing in Cd or S vapour on photoelectric props. 77−16370
CdS, single cryst., surface treatment effects on photoluminesc., struct. and optical props. *(Russian)* 78−15224
n-CdS single crystals, effect of high-temp. annealing on electrical transport props. 79−78098
CdS sprayed films, elect. and optical props. 78−39241
CdS, surface energy struct. changes during ion cleaning and thermal annealing 80−92962
CdS, thin film, dark- and photo-currents, annealing time effect 79−38199
CdS:Li, thermochemical changes in microstructure of anisotropic centres, polarisation modulation method meas. 79−38027
CdS:Li film, photocond., effects of annealing, S vacancies, and O_2 adsorption 78−34854
CdS:Na, Hagemark theory, green edge emission line intensity 80−75517
CdS:Na, thin film, dark- and photo-currents, annealing time effect 79−38199
CdS-Al, ohmic contact stability improved by annealing 78−6443
CdSb, self-diffusion of Cd, radioactive tracer investig. 77−24428
CdSe, comp. and evap. kinetics on vacuum heating, effects on deposited film characts. 77−85940
CdSe crystals, photocurrent and electrorefl. spectra, stoichiometry defects revealed by annealing *(Russian)* 77−52134
CdSe film, laser annealing effects on surface struct. and elec. characts. 79 73605
CdSe film, stimulated recrystallisation 77−4272

annealing continued
CdSe film, vac. deposited, stabilisation by heat treatment in vac. *(French)* 79−95532
CdSe film, vac. deposited, elec. resist. and surface changes by laser annealing 80−2491
CdSe film polycryst., thermal diffusion of Cr, 240-400°C 80−80001
CdSe films, effect of annealing on resistivity and charge carrier mobility 77−8209
CdSe, Se-annealed and Cu-diffused, photocond. props. 79−99580
CdSe, single cryst. elec. props., annealing in Se atm., expt. *(Japanese)* 77−1423
CdSe thin film transistor and MISM struct., effect of annealing on electron mobility and conc. 79−78198
CdSe thin film transistor on Cr substrate, cryst. struct., substrate defect effects 80−70563
CdSe:Ar(N)(P), implanted, electroreflection obs. 80−40089
CdSe:Cl(In), photoluminesc. props. near fund. absorpt. edge, impurity conc. effects 79−52003
p-$CdSiAs_2$, electron irrad. elec. props. annealing, lattice defects 80−100465
$CdSiP_2$, PAC examination of deuteron irrad. damage, annealing effects 78−47446
CdTe detectors, gamma and electron irradiation effects 78−41893
CdTe, growth on Te substrate by solid-state reaction 79−95287
CdTe, high-resistivity, irradiation effects on carrier transport and trapping process 78−2164
CdTe, influence of heat treatment on carrier lifetime, photoelectromagnetic effect meas. 77−55576
CdTe, laser annealing, surface layer temp. distrib. 79−74029
CdTe, laser annealing of ion bombardment damage 80−25502
p-CdTe, nondoped, heat treatment in vacuum, dissoc. obs. effects on struct. and props. *(Japanese)* 80−60662
CdTe, single cryst. IR laser window, low absorption at 10.6 μm 78−79081
CdTe, Yb^{3+} implantation, nonstoichiometry effect 77−15440
CdTe:As(P), ion implanted, elec. props. 80−65021
CdTe:Cu, doping effects on evaporation kinetics and electronic props. during high-temp. annealing in vacuum 78−22743
CdTe:Fe(Ni), luminesc. and refl. spectra, high temp. annealing effects 80−24472
CdTe:In precipitation and out-diffusion of solute during cooling 80−100840
CdTe:P, annealing induced lattice defects, TEM obs. 80−2010
$CdTl_2Se_4$:Au, solubility meas. by microhardness method 80−96650
$CdTl_2Te_4$, Hall and thermo-EMF coeffs., in solid, liquid states 80−54704
Cds, pure and Na doped, chemical bath deposited, photothermoelectric effect 80−6906
$(Co, Cu, Fe)_5Ce$, sintered permanent magnets, magnetic charact. 78−60608
$(Co,Cu,Fe)_5Ce$, sintered, mag. props. 78−68302
$(Co,Fe)_{0.75}B_{0.25}$ metallic glasses, annealed, equilib. crystalline phases 80−3019
$(Co,Fe)_{80}B_{20}$ glass, induced anisotropy and time changes of permeability 80−75815
Co allotropic transformation, X-ray diffr., analysis exam. *(Russian)* 79−34027
Co, deformed and annealed, mechanism and kinetics of polymorphic transformations *(Russian)* 78−35381
Co ferrite film prep. by vac. evaporation and annealing 77−85939
Co-B-Si amorphous alloy, liq. quenched, elec. resist. and cyclic deform. 80−59949
Co-Cr, fibrous eutectic, thermal stability 77−36547
Co-Cr-Al, protective coating, exam. of interdiffusion kinetics, development of analysing procedure 79−5085
Co-Cr-NiTaC eutectic, directionally solidified, microstructural stability 79−38815
Co-Fe alloys effect on magnetostrictive vibrs. 78−6558
Co-Fe amorphous alloys, high permeability props. *(Japanese)* 77−51927
Co-Fe-Nb, heavily cold worked, magnetic hardening 79−20073
Co-Fe-V-Ni, mag. and mech. props., heat treatment and stress effects 80−60363
Co-Ga β' quenched single crystals, annealing-out of point defects 80−55426
Co-Gd-Mo amorphous films, resist. and extraordinary Hall effect, thermal annealing effect 80−70852
Co-Gd-Mo films, sputtered, O effects on mag. props. during annealing 80−89374
Co-Nb-C, obtained by liq. quenching, superconductivity 80−75699
Co-Ni, deformed and isochronally annealed, positron lifetimes, annihilation at dislocation trapped monovacancy 80−55221
Co-P, amorphous alloy, domain struct., effect of annealing 78−60304
Co-P, amorphous foil, complex permeability and eddy currents, annealing induced short-range order 77−8360
Co-Pt, struct. and mag. props. rel. to degree of order 78−72368
Co-Pu alloys, metastable, high rate sputter deposition, annealing behaviour of deposits 77−21025
Co-V (12.4-18.7 at.%), ferromag. behaviour 79−24163
$Co_{100-x}B_x$, amorphous alloys, saturation magnetostriction and annealing behaviour 80−34739
Co(Cr,Ni)-TaC fibrous eutectic, deformed, thermal stability of microstruct. *(Russian)* 79−1895
$Co_{70.4}Fe_{4.6}Si_{15}B_{10}$, amorphous, mag. aftereffect spectra and annealing props. 80−88831
Co_2Ge_3, $CoGe_2$, amorphous film, annealing effects on struct. and elec. resist. 77−85099
Co_5Ge_3 amorphous film, elec. resist., microstruct. and annealing 77−85188
Co_5Ge_3, phase and struct. characts. 77−36450
$Co_x(Ni_{0.5}Cu_{0.5})_{1-x}Fe_2O_4$ ferrite, relation between elec. cond. and mag. anisotropy 80−75548
CoNiZn ferrites, Fe excess, complex permeab. var. with annealing temp. 77−89979
CoP amorphous alloy, heat treatments influence on opt. props., struct. and DC resist. obs. 80−80892
CoP metallic glasses, elec. and optical props., annealing effects 79−38565
CoPr, coercive force variation as function of annealing temp. *(Japanese)* 79−47787
$Co_{74}Si_{10}B_{16}$, amorphous ferromagnetic alloy, isothermal annealing effect on static magnetic props. *(Japanese)* 79−52398

annealing continued
Co$_5$Sm, coercive force variation as function of annealing temp. *(Japanese)* 79−47787
Cr black solar selective absorbers, thermal degradation 80−61417
Cr film, obtained by thermo ionic precipitation, phase composition, lattice parameters *(Russian)* 80−96756
Cr, internal friction and segregation effects *(Russian)* 77−66669
Cr, specific heat of strained and annealed samples 79−38331
Cr-(Pd$_2$Si)-Si, CrSi$_2$ form. kinetics 77−24492
Cr-Al alloy KH40NYu3, microplastic deform. *(Russian)* 77−66681
Cr-Co-Fe permanent magnet anisotropic alloys, plastic deform., ageing, particle alignment temp. 80−35254
Cr-Cr$_2$O$_3$, black, electrolytic deposited, characterisation and thermal stability *(French)* 80−55898
Cr-Fe-Ni, γ-solid soln., thermodynamic activity determ. at 1500K 80−108397
Cr-Ge amorphous films, annealing effect on elec. resistance and struct. 80−54667
Cr-Nb, dislocation cell growth kinetics by TEM during annealing *(Russian)* 79−65084
Cr-Si interfaces, metallurgical and electrical props. 80−60081
Cr-SiO cermet thin films, thickness effect on density, resist., adhesion and annealing coeff. 77−69432
Cr-SiO films, sputtered, elec. and struct. props. 80−39694
Cr-SiO$_2$-Si structure, solid-phase interaction between Cr and SiO$_2$, X-ray spectral obs. 78−10560
Cr$_2$O$_3$-Fe$_2$O$_3$ solid soln., completely annealed, reclustering of Fe^{3+} ions 79−33578
CsI, and Na doped sample, elastically loaded, effect of annealing on optical absorption 77−44034
CsI, annealing effects on mech. and microstruct. props. 77−66686
Cs$_2$O-MgO-SiO$_2$ system, glasses, crystn. prods., composition, props. 79−41961
Cu, annealed, cyclic plasticity under cyclic nonproportional strain histories, cyclic hardening, memory erasure, strain hardening 78−88510
Cu, annealed, plastic strain during non-proportional loading 80−89291
Cu annealed and cold rolled, with bamboo structure, exam. of grain boundaries as vacancy sources in diffusional creep 78−88508
Cu, annealing of lightly deformed samples, effect of press. *(Russian)* 78−39795
Cu based materials, sputter deposited at high rate, microstruct. and props. 78−22988
Cu coating, vacuum-deposited, separation from leucosapphire substrate during annealing *(Russian)* 77−7997
Cu, cold rolling, mechanical props., ageing, annealing, recrystallisation, plastic strain *(Russian)* 80−35202
Cu, cold work, P effect on annealing 79−47707
Cu, cold worked, determ., of dislocation pinning and unpinning stages, using internal friction meas. 78−92278
Cu, continuously cast, O free, effect of nonmetallic inclusion on microstruct. and props. 77−81280
Cu, cyclic loading, change in mech. props. rel. to heat treatment 80−104282
Cu, cyclic strain hardening under deform. at various temps. 79−43273
Cu, defect annealing around stage III, $\gamma\gamma$ ang. correlation expt. 79−14846
Cu, defect clusters, electron microscope exam. 78−47380
Cu, deuteron bombarded, annealing elec. resist. changes freq. factors, activation energy distrib. 79−77648
Cu, electrical conductivity, effect of cyclic strains and work hardening at 4.2K 78−91655
Cu, electrodeposited coating, annealing effect on struct. and microhardness *(Russian)* 78−76668
Cu electrolytically deposited on Al, annealing, ring-like pattern *(Japanese)* 78−44139
Cu, electron and neutron irrad., Doppler broadened positron annihilation meas. *(German)* 77−62563
Cu, electron irrad., migration and thermal conversion of defects, 100 to 330K 80−59519
Cu, electron irrad., positron lifetime exam. of annealing recovery 78−47354
Cu, electron irrad. at 100K, comparison of irrad. hardening with dislocation vel. 80−54284
Cu, electron irradiated, evidence for vacancy migration in stage III 78−38693
Cu, electron irradiated, exam. of vacancy migration energies, and annealing kinetics 78−47571
Cu, electron irradiated, small-angle X-ray scatt. investig. of stage III recovery 77−7763
Cu, electron irradiated, thermal variation of dislocation pinning by point defects 79−51150
Cu, electron-irrad., stage III recovery kinetics 78−63792
Cu, electron-irradiated, monovacancy migration during stage III annealing, NQR study 80−107576
Cu, electron-irradiation internal friction behaviour, shear modulus and damping meas. 80−55444
Cu, evaporated film, effect of annealing on surface roughness amplitude 79−69381
Cu, filament produced by glass-coated melt spinning, tensile strength 77−48508
Cu film, annealing effect on grain size 78−72015
Cu film, diffuse optical scattering from variable roughness surfaces 80−100704
Cu film, electrodeposited, recrystallisation kinetics, X-ray scatt. *(Russian)* 78−60045
Cu film, electron transport props., struct. defects role 77−40117
Cu film, partially oxidised, oxide removal and O$_2$ desorption on vac. annealing 77−12738
Cu film, vacuum-deposited, interrelation between dynamic and static distortions, X-ray diffr. meas. *(Russian)* 77−43305
Cu film on Mo substrates, film stability on reinforced fibre substrates *(Russian)* 80−39462
Cu foi.foil, interstitial impurity interaction investigation by stage II isochronal recovery expts. 78−47423
Cu foil, electron irradiated at low temps., annealing, form. of clusters of atomic defects 77−15416
Cu foil, electron-irrad., interstitial trapping on impurities 79−99242
Cu, foil recrystallisation during annealing in high voltage electron microscope, grain growth *(Russian)* 79−100159
Cu foils, electron-irradiated, point defect agglomerates, HVEM invest. during in-situ annealing 80−84213

annealing continued
Cu, grain boundary character, revealed by etching and slip line continuity 79−33001
Cu, He defect complexes and depth distribution, production theory 77−31686
Cu, He-vacancy clusters, computer simulation 77−39583
Cu, heavily drawn ETP wire, secondary recrystallisation 77−36537
Cu, heavily rolled, electron microscope obs. of cube oriented region, rolling texture 79−29093
Cu, high purity crystal, resistivity changes with deform., subsequent recovery 77−52397
Cu, interaction of annealing twins in fcc metals and alloys 78−68712
Cu, irradiation with O$_2$ ions, defect production and annealing 80−88214
Cu, isochronal recovery of high energy d-Be neutron damage 78−51592
Cu, near Σ9 grain boundary properties, boundary dissociation 80−100251
Cu, O free, annealing in photoemission electron microscope, twin density recrystallised grain size relation *(German)* 78−52850
Cu, oxidation kinetics, influence of intermediate annealing treatment 80−89412
Cu, plastically deformed, recovery, isochronal annealing, positron lifetime meas. 77−59807
Cu, polycryst., grain size and high-temp. yield strength 80−7641
Cu, polycryst., low temp., plastic deform., structural defects, elec. resist. meas. *(Russian)* 78−39844
Cu, polycrystalline, recovery and recrystallization after hot working 79−91661
Cu, prestrained, tough pitch and sintered, ductile fracture, voids *(Japanese)* 77−52472
Cu, proton irradiation, 10 to 16 MeV, isochronal annealing meas. 80−2083
Cu, quench-condensed thin film, annealing effect on resistivity 78−43488
Cu, radiation damage with radioactive probes, TDPAC meas. 77−24336
Cu, recrystallisation kinetics after small deform. and grain growth *(Czechoslovakian)* 77−32592
Cu, recrystallization diagram for fine grained metal in region of small deform. *(Czech)* 77−59811
Cu, self-interstitial interaction with solutes, resistivity meas. 78−47331
Cu sheets, earing, R-values and 3-D orientation distrib. functions, comparisons 79−91702
Cu single crystal, weakly deformed, elec. resist. recovery, annealing effect 77−81304
Cu single crystals Au ion implanted, pulsed electron beam irrad. 80−65019
Cu, single crysts., deformed and annealed, neutron small angle scattering 79−82127
Cu single crysts., deformed, HVEM study of recrystn. texture 80−104179
Cu, solderability, annealing effect *(Japanese)* 80−89244
Cu, stress removal during annealing after hydrostatic extrusion 79−83215
Cu, surface tension at intermediate and high temps., influence of additional elements 78−15476
Cu, very low atomic displacement threshold energy obs. 78−95078
Cu, well annealed crystal, etch pit technique refinement, dislocation config. study *(Japanese)* 79−4307
Cu wire, residual elec. resist., size effect and grain boundary contribs., heat treatment effects *(Russian)* 78−56126
Cu, wire, residual resistivity reduction by internal oxidation 79−87747
Cu, yield stress of electron irrad. cryst., isochronal annealing effects 79−79037
Cu:Co precipitates, mag. anisotropy, precipitate shape, coercive force 80−80500
Cu:In, He, lattice defect struct., PAC meas. 80−70190
Cu/Cu system, explosive cladding, TEM obs. and thermomech. model 79−96041
Cu-AL(Zn), effect of original grain size on struct. and props., after deformation and annealing 78−44178
Cu-Ag film, amorphous resistivity, Hall coeff., thermopower and annealing kinetics 77−43744
α_2-Cu-Al, antiphase period and tetragonality 78−15374
α-Cu-Al, binary substitutional, short-range ordering kinetics, vacancy behaviour 78−55867
Cu-Al, cold worked solid soln., anneal hardening, grain boundary effects 78−48420
α-Cu-Al, disordered by plastic deform. and ordered by heat treatment, effect of annealing on residual elec. resist. *(Russian)* 79−51547
α-Cu-Al, FCC, fractographic obs. of SCC 78−64786
Cu-Al, heavily deformed martensites, annealing 79−38873
Cu-Al, short range order and static distortion contribution to residual elec. resistivity *(Russian)* 80−70672
α-Cu-Al, single crysts., deformed and annealed, neutron small angle scattering 79−82127
Cu-Al (10 wt.%), annealed, tensile fatigue strength at high temp. in vacuum *(Japanese)* 78−35493
Cu-Al (15 at.%), vacancy migration, and short range ordering, comparison of exp. results with theory 78−47356
α-Cu-Al (9.13, 13.56, 14.76, wt.%) short-range ordered, characterisation of locally ordered regions 80−79747
Cu-Al alloy, vacancy formation energy, determ., using new method, elect. cond. meas. 78−47345
Cu-Al alloy UA10, heat treatment *(French)* 80−35225
Cu-Al films, elec. cond. of vacuum condensates depend. on composition, annealing *(Russian)* 80−65709
Cu-Al$_2$O$_3$ cermet film, solar absorbing, production by dual cathode DC magnetron sputtering 80−16186
Cu-Al$_2$O$_3$ cermet films, temp. depend. of AC and DC cond. 79−87166
Cu-Al$_2$O$_3$ coatings, electrodeposited, dispersion hardened, exam. of props. 79−34181
Cu-Al$_2$O$_3$ dispersed system, electron beam evaporated thick film, struct./prop. relations 77−44198
Cu-Al$_2$O$_3$ electrodeposits, dispersion hardened, props. 79−28258
Cu-Al-Fe, strength increase from intermediate annealing determ. of annealing temp. by recrystallisation 78−44136
Cu-Al-Si-Co (2.8, 1.8, 0.4 wt.%), superplastic phase, exam. of mech. props. 78−52891
Cu-Al-Zn, structural phenomena preceding martensitic transform. 77−12624
Cu-Al(Au)(Ga)(Ni)(Pd)(Rh)(Zn) (4 at.%), anneal hardening mechanism 80−60879
Cu-Au, (0.02-5 at.%), cold worked, internal friction peaks 79−11652

annealing continued
Cu-Au, dose depend. of recovery after thermal neutron irrad. 77—69011
Cu-Au alloys, vacancy and divacancy migration activation energies, elec. cond. meas. 80—88140
Cu-base alloy formed by high rate sputtering 78—11368
Cu-Be-Ni-Zr, anodic behaviour of intermetallic phase 78—72895
Cu-Bi alloys, embrittled grain boundary obs. using STEM, Cu-SiO_2 comparison 78—38730
Cu-Cd (0.03 at.%), single cryst., deformed, dislocation arrangement 79—10856
Cu-Cr, dil. alloys, Frenkel defects, effects on anomalous resistivity and thermopower 77—8084
Cu-Cr (0.75 wt.%), deformation characts., fully reversed cyclic strain with fatigue cracks and dislocation struct. 80—81148
Cu-Fe, dil. alloy, anomalous thermoelec. power, sensitivity to defects, annealing effect 77—51728
Cu-Fe, dil. alloy, quench-condensed thin film, annealing effect on resistivity 78—43488
Cu-Fe, implanted, Mossbauer study, rel. to annealing temp. 78—31135
Cu-Fe, precipitation kinetics study by thermoelectric power measurement *(French)* 79—20050
Cu-Fe, precipitation processes during aging, TEM, resistivity, hardness study *(Japanese)* 80—35221
Cu-Fe system, ageing and reversion phenomena study 80—89274
Cu-Ga (17 wt.%), elec. resist. and TEM studies 80—108604
Cu-Ge (2 wt.%), positron annihilation, photon ang. distrib. meas. effect of deformation, annealing temp. *(Russian)* 78—35220
Cu-Ge(Sn)(Sb) alloys, stress removal during annealing after hydrostatic extrusion 79—83215
Cu-In, thermally cycled, effect on mech. props. and microstruct. 79—4987
β-Cu-In eutectic, unidirectionally decomposed discontinuous coarsening reaction 78—27472
Cu-MgO, dispersion hardened, prep. by milling Cu and Mg oxidising atmos. *(German)* 78—64509
Cu-Mn (3, 5, 10 at.%) alloys, surface segregation of Mn and oxide film form., AES study *(French)* 79—66065
Cu-Nb multifilamentary composite, dislocation resistivity 80—70671
Cu-Nb_3Sn, in situ formed multifilamentary composite, supercond. and mech. props. 78—39279
Cu-Nb(Nb_3-Sn) composite wires, powder metallurgy prod., supercond. props. and annealing 79—33428
Cu-Ni, annealing effect on oxidation kinetics, reduction in vacancy level 80—50760
Cu-Ni, bimetallic film, exam. of diffusion by electrical resistivity meas. *(Russian)* 79—14970
Cu-Ni film, (001), in situ oxidation, TEM obs. 78—23874
Cu-Ni-Fe alloys superparamag. early stages of decomp. *(Russian)* 78—6890
Cu-Ni-P, precipitation hardening 77—12633
Cu-Ni-Sn, thermal decomposition after prior cold work 78—15427
Cu-O, effect of Se, S, Pb impurities on annealability and resistivity 77—28834
Cu-plated C fabric, plasma sputtering influence on strength and elec. cond. *(Russian)* 80—21008
Cu-Sb, peculiarities in temp. behaviour of internal adsorption *(Russian)* 79—55890
Cu-Sc alloy, dil., impurity effects on annealing and resist., vacancy-Sc interaction 79—51142
Cu-Si, reaction diffusion, effect of compressive stress 77—28050
Cu-SiO_2 (0.0052 vol. fraction), work hardened, low temp. softening, particle size effects 77—52342
Cu-SiO_2 single crystals, dispersion hardened, exam. of yield stress between 77 to 1200K 78—76720
Cu-Sn (25 wt.%), struct. changes with ageing *(Russian)* 77—40421
Cu-Sn(5 wt.%), electrical resistivity, annealing, cold rolling 77—8070
Cu-Ti, ageing effect on internal friction and elastic props. *(Russian)* 77—28842
Cu-Ti (Zr), strength improvement by thermomechanical treatment *(Japanese)* 78—48426
Cu-Ti(0.7 at.%), plastic deform. and precip. hardened, annealing time 78—48446
Cu-V-Si, two-step supercond. transition 80—34539
Cu-Zn (30 wt.%), slip band growth, thermally activated 80—40457
β-Cu-Zn(-Ni)(-Mn), order-disorder transformation temperature effect on quench hardening 78—95745
α-CuAl, kinetic study of short-range ordering 78—23726
$CuCr_2Se_4$, magnetic properties obs. 78—76227
$CuCr_2Se_4$ single crystal, magnetic props. *(Japanese)* 78—6520
CuFe film, metastable polycrystalline optical props. 79—83044
$CuGaS_2$, crystal growth by solid phase crystallisation 80—25556
$CuGaS_2$, ESR assessment of S diffusion behaviour on annealing 78—35036
$CuInS_2$ films, RF sputtered, growth and props. 80—80124
$CuInS_2$, homogeneity region and intrinsic dopant mechanism 78—34630
$CuInTe_2$ single crystals, directional freezing growth and doping, resist. changes on annealing 80—60768
$CuInTe_2$:Zn, donor impurity in diffusion, elec. and optical props. 78—68504
CuMn, acceleration of coarsening by temp. changes, study by resistivity meas. 79—47718
r-CuMn, annealing ordered phase study by neutron diffr. 80—89265
$Cu_2MnIn_{1-x}Sn_x$ alloy, compositional SRO, hyperfine interactions 80—71065
$Cu_{40}Nb_{30}X_{30}$ (X=Ti, Zr, Hf), superconductors with metastable ordered structs. 80—108484
Cu_2O, Cu inclusions and annealing, optical and IR absorpt. obs. 80—60630
Cu_2O, epitaxial, on Cu(111), misfit dislocation annealing, TEM obs. 79—82228
$Cu_2O:Cd^{2+}$ implanted, reson. Raman scatt., annealing effect 77—24838
Cu_2O:He(Na)(Cd), ion-implanted, resonance Raman studies of annealing 79—55765
Cu_2O:Mn, photomemory mobility components, charged centre conc. 80—103725
CuPt alloy, equiatomic, ordering processes, anisothermal annealing exam. *(Japanese)* 78—39765
CuPt equiatomic alloy, effects of quenching temp. on ordering, study by elec. resistivity meas. *(Japanese)* 79—43285
Cu_2S(Te), microstructure, work hardening in polymorphic transform. and subsequent annealing effect 79—52199

annealing continued
ε-(Cu_3Sn)-Cu diffusion couples, growth of intermediate phase layers *(Japanese)* 80—49431
Cu_2TE, annealing and deform. of defects induced by phase work hardening during thermal cycling 79—52230
Cu_2Te, microstructure, work hardening in polymorphic transform. and subsequent annealing effect 79—52199
CuZn32 bands, mechanical props. anisotropy after annealing at variable heating rates 77—90364
$Cu_{60}Zr_{40}$, amorphous, ductility and stress relief, low-temp. annealing effects 80—76296
Dy, electron irradiated, defect annealing, recovery spectra 79—23648
DyIG, thermoelectric power, elec. cond. charge carrier conduction mechanism 80—34441
Dy_2O_3 film, phase transforms. on annealing 79—95285
DySe, formation and crystallographic charact. of thin film phase 78—91574
Er, electron irradiated, defect annealing, recovery spectra 79—23648
$Er_2EuFe_{5-x}Ga_xO_{12}$, rag-domain garnet film, controlled variation of props. under O_2 annealing 79—15328
ErO, vac. deposited films, struct. changes due to annealing 79—77741
Eu-Te, chalcogenides, exam. of crystal-chemical characts. 79—1407
Eu_xO_y film, dielec. props. rel. to annealing 79—99636
EuS, ferromag., on W, electron field emission 79—8230
EuS film, struct., elec. and opt. prop. changes during annealing in air 77—7983
EuSe, polarisability of shallow donors, permittivity meas. 80—24833
α-Fe, 0.14 wt.% P addition effect on creep 77—90420
Fe alloy, (110) [001] texture development by recrystallization and normal grain growth 77—32594
Fe alloys, ion-implanted, depth profile and diffusion coeff. 80—54277
Fe and Fe-C, (0.8 wt.%), sintered, hot forging ahd chemicothermal treatment, effect on wear resistance 80—25606
Fe, annealed, and deformed, exam. of immobile dislocation distrib. *(Russian)* 79—32995
Fe, Armco, flat-rolled and annealed, dislocation struct. and mech. props. *(Russian)* 79—20062
Fe, Armco, microstruct., effect of strain rate on change, due to tension-compression 78—80614
Fe based binary alloys, intercrystalline internal adsorption, effect of annealing temp. *(Russian)* 78—35390
Fe based metallic glasses, Curie temp., struct. relax. effects 77—8313
Fe, cast, air-atomized powder, effect of particle size on C and O contents 78—15340
Fe, cast, atomised powder, reduction and decarburisation annealing in converted gas 79—24463
Fe, cast, atomised powder, reduction-decarburisation annealing with converted gas, optimum conditions 79—24465
Fe, cast, austenitic grain size determ. 80—81255
Fe, cast, ferritic grey, exam. of ordering kinetics by elastic modulus meas. 79—100136
Fe, cast, graphite content determ. by X-ray diffr. method 80—100977
Fe, cast, grey, fracture surface after dynamic fracture, Mg conc. effect 80—100909
Fe, cast, high Cr, phase composition, mech. props. rel. to heat treatment 79—29108
Fe, cast, homogenization of property difference due to mass effect by repeated heat treatment *(Japanese)* 79—38857
Fe, cast, inoculated with Ce, exam. of phase composition 78—56620
Fe, cast, malleable, with divorced pearlite, structural strength improvement by annealing 79—96049
Fe, cast, mech. props., effect of repeated heating and cooling *(Japanese)* 77—59907
Fe, cast, P, powder, H annealing 79—66025
Fe, cast alloyed, struct., props., heat treatment 77—16623
Fe, cast grey, effect of quenching conditions, on elastic modulus 78—56675
Fe, cast powder, exam. of reaction between C and O, before and after annealing in converted gas 79—33973
Fe, cold rolled, struct., transmission Kossel patterns obs. 77—48451
Fe, commercial, ductile-brittle transition temp., variation with grain size 78—27640
Fe, creep at 77, 295K, formation of five struct. 80—60926
Fe, deformation twin form. during high temp. creep *(Russian)* 79—24573
Fe dilute alloys, irradiation softening, isochronal annealing of yield stresses 80—76319
α-Fe, electron irradiated, vacancy annealing 79—55785
α-Fe, exam. of structural defects due to shock waves, and induced hardness 78—48427
α-Fe, FIM specimens annealed at $0.5T_m$, surface energy anisotropy 77—20181
Fe, fatigue fracture strength and failure, at 77K after cyclic loading at room temp. 78—84996
Fe, filament produced by glass-coated melt spinning, tensile strength 77—48508
Fe film, amorphous and polycrystalline, Hall effect, resistivity and mag. moment 78—91786
Fe, film mag. structures and stresses, ferromagnetic resonance 78—72375
Fe foil, electrodeposited, phys. and mag. props. 79—91275
Fe, grain boundaries, electron microscope obs. *(Russian)* 79—4311
Fe, grain growth, normal and abnormal, statistical distrib. of linear grain sizes 80—93581
Fe, heavy impurity implanted, relation between hyperfine field and lattice-location meas., influence of radiation damage 80—6794
Fe, high purity, boriding with cryst. B powder 80—84951
Fe, high purity, single crystal prep., by strain-anneal technique *(German)* 77—48326
Fe, high purity large single crystal sheet prep. method *(French)* 77—77375
Fe, internal friction in plastic deformation process *(Chinese)* 80—88259
Fe, irradiated with electrons then annealed, magnetoresistance at 20K *(French)* 80—103677
Fe, isochronous annealing recovery, in cold rolled and explosively formed samples 79—100166
α-Fe, laser irrad., Mossbauer effect and positron annihilation *(Russian)* 78—19390
α-Fe, mag. aftereffect spectrum after low temp. electron irrad. 78—2704
α-Fe, magnetic aftereffect disaccommodation between 30 and 300K after low-temp. neutron-irrad. 80—29585

annealing continued
  α-Fe, neutron irradiated, mobile C atom trapping, anelastic and magnetic relaxations 80—100306
  α-Fe, point defects due to radiation, short term annealing computer simulation 80—54282
  Fe polycrystals, grain misalignment, electron microscope determ. *(Russian)* 80—103358
  Fe powder, final reduction annealing in vibrating bed 80—84883
  Fe, powder, reduction annealing, thermodynamic anal. 78—60597
  Fe powder, reduction annealing, comminution of sintered cakes 80—66456
  Fe, powder preforms., hot consolidated rolled strip, mech. props. 78—15338
  Fe, proton irradiation, 10 to 16 MeV, isochronal annealing meas. 80—2083
  Fe, pure, effect of H_2 on relaxation 77—52391
  Fe, pure, grain growth, abnormal, kinetics 79—24537
  Fe, pure, initial grain boundaries effect on cold-rolling and annealing textures *(Japanese)* 80—35205
  Fe, radiation induced defects, annealing exam. using channelling tech. 78—47316
  γ-Fe, S diffusion, grain size effect 79—86930
  Fe, segregation of S, O_2 and P at (100) surface in single crystal *(Japanese)* 79—61591
  Fe, sintered, produced by dynamic hot pressing, recrystn. diagram 79—70017
  Fe, static loading over wide deform. and temp. range, acoustic emission, fracture, plastic flow 77—90425
  Fe, stress relaxation in high purity single crystal with controlled amounts of C *(French)* 79—70105
  Fe, surface chemistry during annealing of soft magnet 78—48546
  Fe, under US vibrs., initial struct. effect on C diffusion *(Russian)* 78—38876
  α-Fe, vacancy migration, annealing expt. study, irradiation induced defects 78—6956
  Fe, vacancy mobility determ., HVEM expts. 80—33993
  Fe waisted cylinders, fatigue, exam. of Miner's rule 78—64689
  Fe:^{129}Te, implanted atom sites, Mossbauer obs. 77—20756
  Fe:^{133}Xe, heavy ion implantation, recovery, Mossbauer effect meas. 78—52393
  Fe:^{169}Tm(^{175}Lu), radiation-damage evolution influence on hyperfine interaction 80—6793
  Fe:^{169}Yb, lattice location and hyperfine field of implanted Yb, annealing temp. depend. 77—48100
  Fe:C, neutron irradiated at low temp., mag. disaccommodation 80—44881
  Fe:N, ion implanted foil, Mossbauer effect study, annealing effect on nitride stability 78—27149
  Fe:Yb(Au), radiation-damage evolution, influence on lattice-location meas. 80—6426
  Fe-Al, single crystal, twinning and pseudoelasticity 79—15718
  Fe-Al (4 wt.%) single crystals, rolling induced mag. anisotropy and its removal by annealing treatment *(Russian)* 79—61746
  Fe-Al (40 at.%), ordered, plastically deformed, neutron irrad. damage and recovery, resist. meas. 77—19993
  Fe-Al (40 at.%) B_2 type ordered alloy, C migration, resistivity meas. *(French)* 78—52868
  Fe-Al (40 wt.%), defect elimination by laser irradiation *(French)* 79—65960
  Fe-Al (51 at.%), crystal vacancies, dilatometric and field ion microscopy exam. 78—47346
  Fe-Al alloys, cold-worked, Mossbauer study of recovery 80—7593
  Fe-Al-C alloys, C migration and mag. aftereffect, mag. permeab. disaccommodation and long-range order meas. 79—8020
  α-Fe-Al(Zn), $\langle 111 \rangle$ fibre texture development through diffusion process without α-γ transform 79—100170
  Fe-B, amorphous alloy, mag. props. 80—84618
  Fe-B, rapidly solidified, metastable phases *(German)* 79—29045
  Fe-B amorphous alloy, annealed, microstruct. and mag. domain changes 80—75790
  Fe-B glass, crystallisation kinetics, elec. resist. meas. 79—4254
  Fe-B metallic ribbons, correl. between quenching temp. and mech. and mag. props. 80—89373
  Fe-B ribbon, microhardness, and static coercive force, melt overheating effect 80—84978
  Fe-B-C, amorphous, effects of replacement of B by C on mag. props. 80—84621
  Fe-B-C amorphous alloys, room-temp. saturation induction over 17.5 kG 79—47300
  Fe-B-C system, phase composition, morphology after heat treatments, $Fe_{23}B_5C$ struct. 77—28779
  Fe-B-Si amorphous alloy, liq. quenched, elec. resist. and cyclic deform. 80—59949
  Fe-B-Si amorphous alloys, crystallisation temp., Curie temps., saturation magnetisation 79—82820
  Fe-B-Si amorphous ribbons, effect of annealing conditions on magnetomechanical props. 80—34740
  Fe-base wear resistant dispersion hardened electrolytic coating, annealed and sintered 78—35593
  Fe-BeO, dispersion hardened alloy, struct.-props. relationships 77—66652
  Fe-C (0.64 wt.%), quasicleavage during fatigue crack propag., pearlitic microstruct. effect 79—11702
  Fe-C alloy, oxidation at 500°C cold work and annealing effects 78—44276
  Fe-C single crystals, effect of heat treatment prior to cold rolling on recrystn. texture 79—83232
  Fe-C-Cu (0.21, 0.2 wt.%), neutron irradiated, torsional props. effect of Cu additions and annealing temp. 78—56699
  Fe-C-N, annealing in dry H_2, below 1180K, to purify to low C and N concs. 78—3072
  Fe-C-Si, cast, graphite nodularization during annealing, Mg and S effects *(Japanese)* 80—81087
  Fe-C-Si, S effect on graphite morphology, formed during annealing *(Japanese)* 78—15434
  Fe-C-X (X=Cr, Mn, Mo, Ni), lattice parameters of cementite, annealing effect 80—29007
  Fe-Ci (3 wt.%), commercially produced, grain-oriented, mag. props., stress coating effects 80—34727
  Fe-Co, damping capacity of Gentalloy, internal friction meas., mech. and mag. depend. *(Japanese)* 78—52875

annealing continued
  Fe-Co (35 wt.% and 52 wt.%), heat treated, decrease in sensitivity of mag. props. to mech. stresses *(Russian)* 78—56363
  Fe-Co (5 to 25 wt.%), exam. of damping capacity of Gentalloy 78—72800
  Fe-Co-Cr, 25KKh15 alloy, nuclear γ-reson. investig. of atomic redistrib. during annealing *(Russian)* 77—12640
  Fe-Co-Cr, alloy K25Kh15, phase tranforms., nucl. gamma reson. and X-ray diffr. meas. *(Russian)* 77—44241
  Fe-Co-Cr, Cr effect on struct. *(Russian)* 78—27535
  Fe-Co-Cr, solid state phase equilib., isothermal sections determ. 800-1300°C 79—91623
  Fe-Co-Cr-W-Ni-C, alloy KKhVN, transforms. during annealing and nature of hardening *(Russian)* 78—56653
  Fe-Co-Ni-Si-B amorphous alloy, magnetostriction and permeability, effect of annealing 79—1701
  Fe-Co-Si (4,1.5 wt.%), textured, mag. props. 80—35200
  Fe-Co-V(-Ni), annealing effect on microstruct. rel. to mag. and mech. props. 80—89267
  Fe-Co(Al), B_2 superlattices, point defect investigations 78—47357
  Fe-Cr, influence of annealing on hyperfine interaction parameters, Mossbauer effect 80—71263
  Fe-Cr, oxidation, in H_2/H_2O vapour mixtures, epitaxial oxide phase formation, effect on oxidation 78—88568
  Fe-Cr-Co, effect of heat treatment on strain gauge factor 78—72802
  Fe-Cr-Co, heat treatment effect on strain gauge factor *(Japanese)* 78—6954
  Fe-Cr-Co (28, 10.5 wt.%) ductile magnet alloy, humidity-induced H_2 embrittlement 80—89406
  Fe-Cr-Co-Mo, melted in open induction furnace, microstruct. and magnetic props. 79—61626
  Fe-Cr-Ni, α-particle induced precip. and phase instability 79—1470
  Fe-Cr-Ni, electron irradiated, resistivity during annealing, 4.2-1300K 78—87962
  Fe-Cr-Ni, textured $(\alpha+\gamma)$ alloy, α' lath martensite formation 78—95749
  Fe-Cr-Ni alloy 800, sensitization times for intergranular corrosion 77—16746
  Fe-Cr-(C), oxidation, grain size and growth effects *(Japanese)* 77—48583
  Fe-Cu (1.2 wt.%) effect of precipitation on recrystallisation, texture 78—88476
  Fe-Cu-C-O(-Ni) powder, atomized, reduction and decarburizing annealing parameters 80—25603
  Fe-Ge (10 to 50 at.%), phase diagram rel. to heat treatment, supercooling diagram *(German)* 78—92240
  Fe-Mn cast alloys, homogenisation annealing and chemical diffusion *(Czech)* 80—66551
  Fe-Mn-Ti-Al, magnetic texture rel. to annealing temp., Mossbauer investig. 77—28499
  Fe-Mo, damping capacity *(Japanese)* 78—11259
  Fe-N, neutron irrad. effects on mech. props. 79—4338
  Fe-Ni, austenite formed from martensite during annealing in $(\alpha+\gamma)$ region, crystallographic study 78—19782
  Fe-Ni, Invar, Curie point, annealing effects and time depend. 80—80508
  Fe-Ni, reactive metal alloy, effects of thermomechanical processing on strength and toughness 79—70112
  Fe-Ni (29.3%), N29, martensitic tranform. kinetics and morphology, ordering role 77—63673
  Fe-Ni alloy, effect of electron irradiation and deform. on martensitic transform. 77—16581
  Fe-Ni alloys, enthalpy change between $\alpha' \rightarrow \gamma$ and $\alpha \rightarrow \gamma$ transformations 80—93550
  Fe-Ni alloys, heat treatment variations effect on surface conditions and on Hg wetted switch behaviour 80—66547
  Fe-Ni alloys, ordering on annealing and electron irrad., mech. props. change *(Russian)* 80—29981
  Fe-Ni base amorphous alloy, crystallisation 77—84660
  Fe-Ni base amorphous alloys, effect of annealing on Curie temp. 80—34632
  Fe-Ni base metallic glass, annealing embrittlement 78—64635
  Fe-Ni base metallic glasses, microhardness charact. of stability under annealing 79—57011
  Fe-Ni heterogeneous alloys, ferrite, martensite and austenite phase distrib., effect on mech. props. 80—45363
  Fe-Ni Invar alloys, Mossbauer spectra, heat treatment effect 80—15855
  Fe-Ni Invar alloys, splat quenched, mag. props. 80—75799
  Fe-Ni single crystals, stress induced martensite 77—8827
  Fe-Ni two-phase films, alloy component redistrib. during annealing, electron diffr. anal. *(Russian)* 79—20053
  Fe-Ni-Al, magnetic anisotropy form. and struct. changes by annealing, Mossbauer obs. 80—39994
  Fe-Ni-Al(Ti)(V)(Nb), cryogenic toughness, strength, rel. to reactive metal addition 78—39885
  Fe-Ni-C, atomized, O/C ratio effect, particle size on annealing kinetics, physicotechnological props. 80—20832
  Fe-Ni-C, model alloy, intercrystalline brittleness caused by segregation and precipitation in austenite *(Slovak)* 79—70073
  Fe-Ni-C, quenched martensite, annealing during cathodic hydrogenation, 200°C *(French)* 80—93573
  Fe-Ni-C, single crystal, form. and strength of strain-induced martensite 79—100225
  Fe-Ni-C, thin foil, high voltage TEM exam. of martensitic form. 78—92264
  Fe-Ni-C (24, 0.45 wt.%), single crystal, plastic deform. effect on martensitic burst transform. 79—15695
  Fe-Ni-C-Mn (3.56, 3.25, 0.6 wt.%), solid soln., quenched, changes during annealing to crystal structure, mech. props. *(Russian)* 79—34076
  Fe-Ni-Co, texture form. after cold working and annealing *(German)* 80—3089
  Fe-Ni-Cr, at. distrib. effect on mag. props. *(Russian)* 78—2657
  Fe-Ni-Cr (30.6, 21.3 wt.%), Alloy 800, high temp. oxidation at low O_2 press., SEM, AES and electron probe microanal. study 80—93688
  Fe-Ni-Cr (40, 15.8 wt.%), precipitation and creep rupture behaviour, optical and TEM study 79—74158
  Fe-Ni-Cr-Ti-Al, with thermoelastic control coeff., comp. and heat treatment influence on props. *(French)* 80—81074
  Fe-Ni-Mn(Mo) alloys, two-stage martensitic transformation kinetics, depend. on austenite initial state *(Russian)* 79—74151
  Fe-Ni-Mo, inhomogeneous solid solns., annealed and work hardened states, X-ray K-absorption spectra *(Russian)* 78—56544

annealing continued
Fe-Ni-Mo, martensitic transformation, annealing, influence on struct. of austenite *(Russian)* 80—81057
Fe-Ni-Mo(Si), austenite, annealing effect on atom redistrib., Mossbauer anal. *(Russian)* 80—66529
Fe-Ni-P-B, metallic glasses, struct. relax., annealing effects on mag. props. 80—89261
Fe-Ni-Ti martensitic alloy, γ' particle effect on crystallisation struct. *(Russian)* 78—44129
Fe-P-S composite sintered bearing materials manufacture, wear intensities 80—20881
Fe-P-Si alloys, electrothermal-grade, thermoelec. characts. in region 273 to 573K 78—23834
Fe-rare earth, amorphous thin film, crystallisation, TEM obs. 79—19483
Fe-S system, segregation kinetics *(Japanese)* 79—61592
Fe-Sb system, α-phase, interdiffusion 79—73349
Fe-Si, internal friction, domain boundary area *(Russian)* 79—24562
Fe-Si, mag. props., stress and reannealing effects 80—88844
Fe-Si (3 wt.%), (110)[001] oriented single crystal, form. of rolling and annealing texture 77—16608
Fe-Si (3 wt.%), Al-bearing, grain-oriented, N_2-H_2 annealing effect on texture, mag. props. 77—12714
Fe-Si (3 wt.%), grain growth inhibition by MnS spherical particles with size distrib. 80—35218
Fe-Si (3 wt.%), high induction grain oriented, metallurgical treatment and mag. props. 77—86044
Fe-Si (3 wt.%), secondary recrystn., role of solutes 77—86043
Fe-Si (3 wt.%) locally deformed, EM loss depend. on cryst. struct. and orientation *(Russian)* 80—7694
Fe-Si (3% wt.), increase in effectiveness of thermomagnetic treatment due to low temp. annealing *(Russian)* 79—51772
Fe-Si (3.25 wt.%), mag. props., influence of struct. and chemical composition of surface oxide layer 78—2700
Fe-Si (6.5 wt.%), ductility and mag. props., Ni and Mn addition effects 78—76704
Fe-Si (6.5 wt.%), effect of ordering on mag. props. 79—51833
Fe-Si (6.5%) alloy, struct. and rolling texture 79—79006
Fe-Si amorphous film, struct. and crystallisation, Mossbauer study 80—11300
Fe-Si cast alloy with spheroidal graphite, transform. investigation during tempering *(Russian)* 80—97479
Fe-Si steel, high permeability, processing effect on recrystn. and deform. 77—12716
Fe-Si-Al, Sendust, ribbon-form, prep. by rapid quenching, mech. and mag. props. 80—71611
Fe-Si-Al, surface oxide layer struct., AES study 80—89396
Fe-Si-Al (2.8-3.4, 0-0.86 wt.%) oxidation, annealing 80—89395
Fe-Si-Al (6,4 wt.%), Sendust alloy, effect of Ni content on mag. props. 78—72897
Fe-Si-Al (9.6, 5.4 wt.%), ribbon-form Sendust alloy, mag. props., annealing effects 80—88800
Fe-Si-Al Sendust alloy ribbon form, rapid quench prepared, elec. cond., coercive field, permeability 79—83151
Fe-Si-Al-Ni alloy, Super Sendust, Ni content and thermomag. treatment effects 77—4861
Fe-Si-B amorphous films, mag. props. 80—34710
Fe-Si-B ferromagnetic amorphous alloys, Young's modulus and delay time characts. *(Japanese)* 77—85543
Fe-Si-Mn-C, east, Ce additions, nonmetallic inclusions *(Russian)* 78—19710
Fe-Si(Al), oxide layer form. during annealing, AES in-depth anal. *(German)* 80—16576
Fe-Si(6.5 wt.%) ribbon, prep. by rapid quenching and mag. props. 80—45251
α-Fe-Ti, ion implanted, microstruct., ion beam anal. and TEM study 80—107294
α-Fe-Ti, ion implanted, with C impurity, microstruct. of TiC precips. 80—66513
α-Fe-Ti, ion-implanted and annealed, microstruct. evolution 80—15132
Fe-Ti(Nb), internally nitrided, mech. props. 77—44307
Fe-V (1 wt.%), nitrided and annealed, struct. 77—8998
Fe-V(Cr)(Mn)(Ni), unlimited component solubility, intercrystallite internal adsorption *(Russian)* 80—39294
Fe-Zn, homogeneous intermetallic cpd., synthesis and charact., δ_1-phase 79—87616
Fe_3Al, containing C in solid solution., mag-permeability disaccommodation *(Polish)* 79—95613
Fe_3Al, phase separation 77—63664
Fe_3Al, vacancy conc. and ordering conc. 78—18639
$Fe_{1-x}B_x$ amorphous films, mag. props. and thermal stability 79—78446
$Fe_{100-x}B_x$, amorphous alloys, saturation magnetostriction and annealing behaviour 80—34739
$Fe_{80}B_{20}$, amorphous, crystallization 78—42917
$Fe_{80}B_{20}$, amorphous, crystn. 80—75187
$Fe_{80}B_{20}$, amorphous, deform. and annealing effects on mag. and mech. props. 77—12717
$Fe_{80}B_{20}$, amorphous, fast neutron and fission fragment irrad., effect on elec. resist., annealing effects 80—19846
$Fe_{80}B_{20}$, amorphous, mag. permeability aftereffect during annealing 80—88834
$Fe_{80}B_{20}$ amorphous ribbon, initial susceptibility time lag 80—100579
$Fe_{80}B_{20}$ amorphous wire, crystn. by annealing at 780°C 80—100177
$Fe_{80}B_{20}$, crystallisation of amorphous alloys, TEM and X-ray diffr. exam. of struct., growth characts. 78—79539
$Fe_{80}B_{20}$ metallic glass, crystn. and struct. relax., Mossbauer effect study 80—75182
Fe_xB_{100-x}, amorphous, stress relax. after annealing 80—55447
$Fe_{80}(B_{1-x}P_x)_{20}$ amorphous alloys, isothermal crystallisation kinetics 80—33895
$Fe_{40}B_{40}P_{14}B_6$ and $Fe_{80}B_{20}$, Metglas 2826 and 2605, amorphous ribbon, power loss variation with freq. and applied stress 80—88849
$Fe_{78}B_{12}Si_{10}$, amorphous, Mossbauer study of hyperfine interaction and mag. anisotropy 80—40027
FeCo, isothermal annealing effect on lattice const. *(Japanese)* 79—20076
FeCo, ordered and disordered alloy, annealing of point defects created by neutron irrad. at 20K *(French)* 79—1467
$(Fe_{0.06}Co_{0.94})$-B, amorphous, ferromag., mag. instability rel. to struct. 79—99729
$Fe_{3-x}Co_xO_4$, effect of Fe^{2+} content on coercivity instability 79—51820

annealing continued
$(Fe_{1-x}Co_x)_yPBAl$ metallic glasses, influence of composition and ageing on Curie temps. 77—85445
$(Fe_{1-x}Co_x)_{78}Si_{10}B_{12}$, amorphous alloys, magnetic anisotropy meas., effect of high temp. annealing 80—2570
$(Fe_{1-x}Co_x)_{78}Si_{10}B_{12}$, amorphous, roll mag. anisotropy 80—75757
$Fe_5Co_{70}Si_{15}B_{10}$, amorphous, change of mag. props. by low temp. annealing 78—27058
$Fe_5Co_{70}Si_{15}B_{10}$, amorphous ferromagnetic alloy, isothermal annealing effect on static magnetic props. *(Japanese)* 79—52398
$Fe_5Co_{70}Si_{15}B_{10}$, amorphous, crystn. effect on mag. props. *(Russian)* 80—44858
$FeCo_2V$, ordered and disordered alloys, annealing of point defects created by neutron irrad. at 20K *(French)* 79—1467
$Fe^{2+}Cr_x{}^{3+}Al_{2-x}{}^{3+}O_4{}^{2-}$, finely divided, oxidation kinetics 80—50848
$Fe_xCu_{1-x}Cr_2Se_4$, crystallographic and image props. 80—39049
$FeGe_2$, amorphous film, annealing effects on struct. and elec. resist. 77—85099
Fe_5Ge_3, amorphous film, elec. resist., microstruct. and annealing 77—85188
$Fe_{78}Mo_2B_{20}$, amorphous, fast neutron and fission fragment irrad., effect on elec. resist., annealing effects 80—19846
$Fe_{40}Ni_{38}$-Mo_4B_{18} amorphous alloys, compatibility of DC and AC mag. props. 80—34695
Fe_xNi_{1-x}, amorphous films, crystallisation, effect of codeposited O_2, N_2 or Kr gases 80—10807
$(Fe_{100-x}Ni_x)_{83}B_{17}$, amorphous, crystn. 80—75176
$(Fe_{100-x}Ni_x)_{83}B_{17}$ glassy alloys, Ni content influence on crystn., and bend ductility changes, during annealing 79—73103
$Fe_{40}Ni_{40}B_{20}$, amorphous, resist. min. disappearance on annealing 79—60786
$Fe_{40}Ni_{40}B_{20}$, amorphous, casting conditions effect on mag. props. *(Japanese)* 80—34698
$Fe_{40}Ni_{40}B_{20}$, amorphous, phase transforms., resistometric anal. 80—75538
$Fe_{40}Ni_{40}B_{20}$, amorphous ribbon, power loss variation with freq. and applied stress 80—88849
$Fe_{40}Ni_{40}B_{20}$ and $Fe_{40}Ni_{40}P_{14}B_6$, amorphous, mag. aftereffect spectra and annealing props. 80—88831
$Fe_{50}Ni_{30}B_{20}$, crystallisation of amorphous alloys, TEM and X-ray diffr. exam. of struct., growth characts. 78—79539
$(Fe_xNi_{1-x})_{80}B_{20}$, amorphous alloys, engineering mag. props. 79—51832
$Fe_{32}Ni_{36}Cr_{14}P_{12}B_6$, metallic glass, changes in Curie temp., physical dimensions and mag. anisotropy during annealing 77—85446
$Fe_{32}Ni_{36}Cr_{14}P_{12}B_6$, Metglas 2826A, Hall resistivity, effect of thermal cycling and annealing 78—56125
$Fe_{40}Ni_{38}Mo_4B_{18}$ ribbon, magnetic characterisation 80—34680
(FeNi)PB amorphous wires, surface oxidation and annealing influence on induced anisotropy 80—100957
$Fe_{27}Ni_{53}P_{14}B_6$, amorphous, Hall resist. and mag. props., short range order effects 80—34422
$Fe_{27}Ni_{53}P_{14}B_6$, metallic glass, changes in Curie temp., physical dimensions and mag. anisotropy during annealing 77—85446
$Fe_{40}Ni_{40}P_{14}B_6$, amorphous ribbon, cold rolling, annealing mag. props. 77—8958
$Fe_{40}Ni_{40}P_{14}B_6$, amorphous, deform. and annealing effects on mag. and mech. props. 77—12717
$Fe_{40}Ni_{40}P_{14}B_6$, amorphous alloy, small angle X-ray scattering 77—65953
$Fe_{40}Ni_{40}P_{14}B_6$, amorphous alloy, structural relaxation kinetics, X-ray diffr. exam. 78—38627
$Fe_{40}Ni_{40}P_{14}B_6$, amorphous, annealed and unannealed, temp. depend. of flow stress and ductility 79—29119
$Fe_{40}Ni_{40}P_{14}B_6$, amorphous, resistometric study of short-range ordering rel. to heat treatment 80—70140
$Fe_{40}Ni_{40}P_{14}B_6$ amorphous alloy, temper embrittlement 80—76295
$Fe_{40}Ni_{40}P_{14}B_6$, amorphous, mag. polarisation in approach to ferromag. saturation 80—80560
$Fe_{40}Ni_{40}P_{14}B_6$, amorphous, steady-state creep rate, cryst. effect 80—81102
$Fe_{40}Ni_{40}P_{14}B_6$, amorphous, mag. permeability aftereffect during annealing 80—88834
$Fe_{40}Ni_{40}P_{14}B_6$ glass, positron lifetimes in as-received, cold-rolled, embrittled and crystallized samples 79—74177
$Fe_{40}Ni_{40}P_{14}B_6$, metallic glass, cryst., isothermal annealing behaviour 80—6367
$Fe_{40}Ni_{40}P_{14}B_6$ metallic glass, ferromag. reson., spin waves, thermal ageing and long-range order effects 80—25214
$Fe_{40}Ni_{40}P_{14}B_6$, metallic glass, bending tests, evidence of ideal elastic-plastic deform. 80—97543
$Fe_{40}Ni_{40}P_{14}B_6$, metglas 2826, amorphous, Hall resistivity, thermal cycling and annealing effects 79—38050
$Fe_cNi_{80-c}P_{14}B_6$, amorphous, annealing effects on mag. props. 79—78383
$Fe_xNi_{80-x}P_{14}B_6$, and $Fe_xNi_{80-x}B_{20}$ glass, microhardness, correl. with mag. props. 79—57085
$Fe_{29}Ni_{49}P_{14}B_6Si_2$, metallic glass, changes in Curie temp., physical dimensions and mag. anisotropy during annealing 77—85446
$Fe_{1-x}O$, quenched, decomposition and ordering, electron diffr. and microscopy 77—31635
γ-Fe_2O_3 acicular particles, coercivity increase by Co ferrite surface crystn. 80—44866
Fe_2O_3 films, DC reactively sputtered, for selectively semitransparent photomasks, deposition conditions and optical props. 80—60782
Fe_2O_3, haematite, annealing of nonequil. defects 79—43283
Fe_2O_3, haematite, single domain, defect moment components coercivities 79—16438
Fe_3O_4, partial thermal dissociation in air, using solar concentrator *(French)* 79—20015
$2Fe_2O_3.3H_2O$, bog Fe ore, Mossbauer effect exam. of annealing effect on struct. 78—19396
$Fe_{75}P_{16}B_6Al_3$, aged metallic glass, Mossbauer effect 79—91318
$Fe_{75}P_{15}C_{10}$ foils, amorphous, ferromag. domain orientation, Mossbauer study 78—15000
$Fe_{80}P_{13}C_7$, amorphous, rapidly quenched, magnetic props., effect of annealing 77—16701
$Fe_{80}P_{13}C_7$, amorphous ferromagnetic alloy, isothermal annealing effect on static magnetic props. *(Japanese)* 79—52398
Fe_3Pd, quenched, or annealed exam. of magnetostriction, galvano- and thermomagnetic props. *(Russian)* 79—19757
Fe_3Pt austenites, ordering kinetics 80—104155
Fe_3Pt:Sn Invar alloy, Mossbauer shift temp. depend. 80—100626
$Fe(Sb_{1-x}Te_x)_3$ system cpds., prep., cryst. struct., elec. and mag. characteris. 80—108349

annealing continued
FeSi-Fe$_2$Si$_5$ eutectic, FeSi$_2$ formation, annealing temp. and time effects 79—24512
Fe$_{75}$Si$_{15}$B$_{10}$, amorphous ferromagnetic alloy, isothermal annealing effect on static magnetic props. *(Japanese)* 79—52398
FeTi, hydrogen storage, annealing effects *(Japanese)* 79—100542
FeTi, positronium form. after hydrogenation-dehydrogenation cycling and annealing 80—18947
Ga, film, freshly deposited, 77K, refl., annealing effect, thickness depend. 77—16413
Ga, films, distorted, crit. mag. fields *(Russian)* 78—39273
Ga-As-O, equilib. phase diagram, GaAs oxidation 80—104130
Ga-As-Sb system, two- and three-phase fields obs. 80—55373
Ga-Cu-Sn solders, exam. of structural transformations due to hardening, heat treatment *(Russian)* 80—7578
GaAS, semiinsulating, heat treatment effects 78—6382
GaAs, (100) surfaces, reconstructed, ang. resolved photoemission from surface states, adsorption and annealing effects 80—16143
GaAs, annealing rel. to stoichiometry deviation, Hall effect, electron microscope meas. 77—24410
GaAs, annealing with Si$_3$N$_4$, Cr profiles meas. 79—90693
GaAs, anodic oxidation and MOS devices 77—80845
GaAs, anodic oxide, loss of As during annealing 79—66190
GaAs, anodic oxide film, annealing effect on carrier density profile 78—88040
n-GaAs, anodic oxide film, exam. using SIMS and ellipsometry 79—61770
GaAs, defect cluster annealing, pot. barrier height determ. 80—84209
GaAs, degraded layer form. by annealing, photolum. obs. of defects 78—10968
GaAs, electroluminescent study of irrad. induced struct. damage, athermal annealing 80—108280
n-GaAs, electron and gamma ray irradiated, introduction and annealing of defects 78—67736
GaAs, electron beam induced defect annealing 77—80790
n-GaAs, electron irrad. defects, carrier removal rate, annealing effects 80—75269
GaAs, electron irrad. induced defect levels, hydrostatic press. effect 80—92858
GaAs epitaxial layers, surface impurity gradients, Schottky barrier capacitance meas. 80—70782
GaAs, epitaxial layers, electron irrad. deep level trap energy depend. 80—80205
p-GaAs, field electron emission current-voltage characts., annealing effect 80—45219
GaAs for MOSFETs, native oxides, annealing effects and inversion layer mobilities 78—6452
GaAs, growth of noncrystalline Si$_3$N$_4$ layers by CVD for encapsulation 79—19994
n-GaAs, heat treatment effect on electron traps 78—6396
GaAs, implantation disorder, flux and fluence depend., electrorefl. expts. 78—83833
GaAs, implanted amorphous layer reordering 77—76435
GaAs, implanted p-n junction form. using laser pulse annealing 77—15946
GaAs, ion beam induced annealing effects 80—59530
GaAs, ion damage, TEM study of laser annealing 80—88215
GaAs, ion implantation, review 78—6080
GaAs, ion implantation with proximity cap annealing 80—24475
GaAs, ion implanted, capless annealed and dielectrically annealed, comparison of doping profiles 80—100278
GaAs, ion implanted, diffusion of Zn and Ag, profiles 80—24681
GaAs, ion implanted, laser annealing 79—69124
GaAs, ion implanted, laser pulse annealing 80—19825
GaAs, ion implanted, laser annealing 80—107296
GaAs, ion-implanted, capless anneal, effect of As partial press. 80—29038
GaAs, ion-implanted layers, close contact capless annealing, elec. props. 80—84192
GaAs, ion-implanted semiconductor, annealing, crystallisation, laser pulse energy depend. 78—34528
GaAs, laser annealed, Ga precipitation, Rutherford backscattering and TEM study 79—79127
GaAs, laser annealing, optical refl. meas. of melted layer 79—78796
GaAs, laser annealing of ion bombardment damage 80—25502
GaAs, laser-annealed ohmic contacts for microwave devices 79—73584
GaAs, laser-annealing behaviour, Si$_3$N$_4$ encapsulation effect forming n-type layers 79—79131
GaAs, luminescence due to deep centres, annealing effect on quantum efficiency 77—55825
In-GaAs, MOS capacitor struct., elec. props., annealing effects 80—34519
GaAs, melt grown, improve elec. and luminesc. props. after short time heat treatment 77—63452
n$^+$-GaAs, multiple energy proton bombard. effects on elec. characts. 77—39853
GaAs, native vacancies study using positron lifetime technique 79—83052
n-GaAs ohmic planar contacts formation and elec. props. on basis of Au and Au-Ge alloys 79—15223
GaAs, oxide, charge density and breakdown voltage, depend. on annealing 79—66189
GaAs oxide films, anodically and thermally grown, XPS study 80—16141
GaAs, oxide layers prepared by anodic, thermal and plasma oxidation, in-depth profiles and annealing effects 79—61768
GaAs passivated and unpassivated surfaces, heat treatment effects 79—73383
GaAs, plasma-grown oxides, physical props., Auger and IR spectral anal. 79—91821
GaAs, point defects, laser annealing 80—107224
GaAs, radiative yield improvement by laser annealing 80—45128
GaAs, reactor irrad., opt. props. 77—90137
GaAs, reactor-irradiated, anisotropy in diffuse small angle neutron scatt. 78—51598
GaAs Schottky barrier with Au and Au-Ga contacts, high temp. annealing behaviour 77—43725
GaAs, semi-insulating, thermal conversion, Hall effect and luminesc. meas. 78—6405
GaAs, Si ion implantation and annealing, damage recovery, surface carrier profile 77—4119

annealing continued
GaAs, SiO$_2$ and Si$_3$N$_4$ encapsulants for annealing, photolum. and AES evaluation 78—27657
GaAs, solar cells, electron-irrad., annealing kinetics 80—7937
GaAs solar cells, electron and proton radiation damage 80—94034
GaAs solar cells, ion-implanted and laser-annealed 79—79390
GaAs solar cells, simultaneous radiation damage and annealing 80—94033
GaAs, sputtered-etched surface, Schottky contact characterisation and its recovery by annealing 79—99603
GaAs, stoichiometry meas. by 15 MeV He^{2+} backscattering 79—99330
GaAs, surface cryst. regularity by X-ray photoelectron diffr. 80—89112
GaAs thin film polycrystalline solar cells, props. and prep. 80—81437
GaAs, transmutation doping by thermal neutrons 80—10581
GaAs, undoped epitaxial layer growth from nonstoichiometric solns., O$_2$ contamination sources 80—108362
GaAs VPE layers, electron irrad., electron traps 80—25026
GaAs vaporisation during laser annealing 80—25495
GaAs:^{119}Sn^{m}, Mossbauer spectra 80—29667
GaAs:Au, back surface gettering 80—10758
GaAs:Be, annealing effect during MBE 78—79898
GaAs:Be, implantation and annealing, elec. props. 79—99540
p-GaAs:Be, ion implanted, annealing characts., defect cond. profiling, electron diffr. obs. 79—4318
GaAs:Be, ion-implanted, IR refl. and transmission meas. 80—34908
p-GaAs:C, ion implantation efficiency, elec. profile and compensation level meas. 77—27880
GaAs:Cr, Be$^+$ implantation, atomic conc. and defect density profiles after annealing 80—39123
GaAs:Cr, Cr$^+$ and Cr^{2+} centres, thermal treatment effects, EPR 80—65492
GaAs:Cr, gettering by back surface mech. damage 80—10759
GaAs:Cr, implantation depth profiles of S$^+$ and S$_2$$^+$ using AES, annealing effects 79—55774
GaAs:Cr, ion implanted, implantation damage profiles, laser annealing, ellipsometry study 80—79819
GaAs:Cr, low temp. gettering 80—96549
GaAs:Cr, Mg, ion implanted, elec. meas. and optical activation studies 79—86806
GaAs:Cr, redistrib. of Cr during laser annealing 80—88192
GaAs:Cr, Se implantation, carrier conc. and mobility profiles depend. on dose and annealing temp. 77—47479
GaAs:Cr, Se layers, ion implanted, ohmic contact form., contact resist. meas. 79—91158
GaAs:Cr, semi-insulating, defect chemistry, EPR study 79—99754
GaAs:Cr, semi-insulating, thermal conversion suppression by arsine-controlled capless-anneal, ion implantation 80—49245
GaAs:Cr, semi-insulating, Cr redistrib. during thermal annealing as function of encapsulant and implant fluence 80—84199
GaAs:Cr, semi-insulating, damage gettering of Cr during annealing of Cr and S implants 80—107304
GaAs:Cr, Te implantation, electron conc. and mobility profiles depend. on dose and annealing temp. 77—39607
GaAs:Cr, Zn(Se) shallow impurity implantation, elec. props. after annealing 80—24465
GaAs:Cr,Se, ion-implanted, semi-insulating effects of Cr redistrib. on elec. characts. 80—59982
GaAs:Cr,Zn, implanted, doping profiles after laser annealing, elec. props. 80—2058
GaAs:Cr capless annealed, under As press., Cr redistrib., SIMS obs. 80—59503
GaAs:Cr substrates and LPE layers, Au film deposition and annealing, Cr redistrib. 80—15312
GaAs:Ge, cryst. and epitaxial layers, ion-implanted, elec. props. 79—99542
GaAs:Li diffused, lattice imperfections, TEM 77—80521
GaAs:Mg ion implanted, photoluminesc. and annealing characts. 77—16361
GaAs:Mg(C)(Te)(Ge), ion implanted, laser annealing, ellipsometric and Hall meas. 79—73193
GaAs:O, annealing effects, optical absorpt. and I-V characts. 80—29037
GaAs:S(Si), ion-implanted, capless anneal in As controlled vapour 79—55767
GaAs:Se, and undoped sample, annealed, surface cond. change, n-p double layer 78—64095
GaAs:Se, Ga, dual species ion implantation, elec. characts. 80—103377
GaAs:Se, implantation and laser annealing 80—24476
GaAs:Se, implanted, annealing with O-free CVD Si$_3$N$_4$ encapsulant 78—83834
GaAs:Se, ion implanted, Cr redistrib. during annealing, SIMS anal. 80—10570
GaAs:Se, ion implanted, laser annealing 80—24482
GaAs:Se, low dose Se$^+$ ions implanted, DLTS study of laser annealing 80—80204
GaAs:Se, pulsed electron beam annealing, doping profiles 80—6421
GaAs:Se ion implanted samples, Q-switched ruby laser annealing, improvement in elec. props. 80—100460
GaAs:Se ohmic contacts, pulsed electron beam annealing donor density, mobility 80—65678
GaAs:Se$^+$, implanted semi-insulating, pulsed electron and laser beam annealing effects on elec. characts. 79—73196
GaAs:Se$^+$, TEM structural study, surface and interior damage 80—34025
GaAs:Se(Si), ion-implanted, capless annealing by melt-controlled ambient technique 80—75251
GaAs:Se(Sn), annealing kinetics of implanted donor ions 78—6079
GaAs:Se(Te), laser annealed, donor implanted, elec. props. 79—4556
GaAs:Si, activation by multiply scanned electron beams 80—75246
GaAs:Si, donor-acceptor pair defects absorpt. bands 80—16064
GaAs:Si, ion implantation, thermal annealing, Hall meas., SIMS atomic profile meas. 80—75243
n-GaAs:Si, ion implanted and/or annealed, As vacancy form., photolum. line 77—27875
GaAs:Si, ion implanted effect of anneal ambient and occurrence of compensated regions in Si implants 77—51394
GaAs:Si, ion-implanted, elec. props. 79—46686
GaAs:Si, ion-implanted, annealing with Nd:glass laser 79—73194
GaAs:Si, pulsed laser annealing of implanted layers, defect structure and Hall effect meas. 79—69118
n-GaAs:Si, thermally treated, photolum., acceptor levels obs. 79—38587

annealing continued
GaAs:Si,Cr, under layer of SiO_2, effect of annealing, on electron concentration and mobility, and impurity distrib. 79−4323
GaAs:Si encapsulated with AlN, Si_3N_4 layers, photolum., annealing effects 80−20681
GaAs:Si(Se), ion implanted, laser annealing, microwave device appl. 79−69139
GaAs:Si(Sn), ion implanted, laser annealed, high doping levels 80−88181
n-GaAs:Si(Te), radiative transitions induced by modest annealing, photoluminesc. spectra 80−55158
GaAs:Sn, implantation, annealing, impurity-defect struct., Mossbauer study 80−54269
GaAs:Sn, proton implantation and annealing behaviour *(Chinese)* 80−44224
GaAs:Sn thermal diffusion from spin-on SnO_2/SiO_2 source 80−96691
GaAs:Te, heavily-doped, annealing-induced prismatic dislocation loops and elec. changes 78−51546
GaAs:Te, implanted and laser annealed, surface crystallinity, refl. and channelling meas. 79−95036
GaAs:Te, ion implanted, laser annealing 79−73192
GaAs:Te, ion implanted, surface crystallinity and stoichiometry of laser annealed samples 79−73198
GaAs:Te, laser annealing of implanted Te 78−35400
GaAs:$Te^+(Se^+)(Sn^+)(Ge^+)$, ion implanted, laser annealing effect on elec. characts. 79−73195
GaAs:Te-implanted by laser-annealing, ohmic contacts 79−19658
GaAs:Zn, diffusion during LPE, impurity gradients and annealing effects 80−29882
GaAs:Zn, implanted, furnace annealed, electrical, Rutherford backscattering and TEM meas. 80−100272
GaAs:Zn, implanted, laser annealing, elect., Rutherford backscattering and SEM meas. 80−100273
GaAs:Zn, ion implanted, TEM study after laser and furnace annealing 80−70234
GaAs:Zn, laser annealing of implanted layers 77−55296
p-GaAs:Zn, luminescent, ion doped MBE growth 80−44436
GaAs:Zn, pulsed laser annealing, expt. 78−34828
GaAs:Zn ion implanted ionic alloy, electrophysical props., annealing 80−39133
GaAs:Zn(Se), recrystn. of implanted amorphous layers, TEM and channelling obs. 77−89459
GaAs-Al_2O_3 MOS struct. capacitance-voltage and conductance-voltage characts. before and after annealing in H_2 79−60927
GaAs-Al_xGa_{1-x}As heterojunction, MBE, diffusion across interface, optical annealing expts. 78−2305
GaAs-metal junctions, thermal stability improvement, with and without near noble metals 79−7143
GaAs-plasma grown oxide interface, new resonant ellipsometric technique for characterisation 79−40606
GaAs-Si ion implanted, impurity profiles elec. props. 80−96550
GaAs(-GaP) single cryst., defect distrib. near abraded surface 80−92533
$GaAs_{1-x}H_x$, amorphous, vib. props., Raman and IR meas. 80−50322
n-$GaAs_{0.6}P_{0.4}$, anodic oxide film, exam. using SIMS and ellipsometry 79−61770
$GaAs_{0.6}P_{0.4}$:N, isoelectronic tape by ion implantation and CO_2 laser annealing 80−24464
$GaAs_{1-x}P_x$, diffusion of implanted Zn ions, ion microbe analysis 78−95190
$GaAs_{1-x}P_x$, electron irrad., radiation defects annealing 80−29059
$GaAs_{1-x}P_x$, N implantation, characterisation by photolum. and channelling 80−54262
$GaAs_{1-x}P_x$, N^+ implantation, annealing props. 77−68988
$GaAs_{1-x}P_x$, solid state diffused, conc. distrib. obs., electroreflectance and tracer sectioning obs. 80−54389
$GaAs_{1-x}P_x$, thermal oxide, dielec. leakage current and C-V hysteresis effects, effect of annealing 79−61772
$GaAs_{0.6}P_{0.4}$P:Be, differential resistivity, Hall effect and secondary ion mass spectrometry meas. 78−84213
Ga_xIn_{1-x}Sb p-n junction photodiode fabrication, sensitivity as 1 to 2.5 μm detectors *(Japanese)* 80−52311
GaN:Zn epilayers, growth parameters effect on props., device struct. 78−26975
Ga_2O_3-Fe_2O_3 system, anomalous Mossbauer lineshapes, incomplete annealing 77−51998
GaP, anodic oxidation and MOS devices 77−80845
GaP, complex ^{119}Sn impurity-defect, Mossbauer study 80−75898
GaP crystal, structure defect formation due to annealing and stress, dendrites, slip, dislocations 80−29026
GaP crystals, radiation defects, TSC obs. 80−65588
GaP, electron irrad., radiation defects annealing 80−29059
GaP, epitaxial growth from Sb and Bi melts 79−52131
p-GaP, field electron emission current-voltage characts., annealing effect 80−45219
GaP LED degradation, effect of γ-irradiation 78−95610
GaP single cryst., defect distrib. near abraded surface 80−92533
GaP:Mg, ion implanted, elec. profiles 79−77628
GaP:N(Te), ion implanted at 40 keV, refl. spectra, 210-2000 nm, annealing *(Russian)* 78−80386
GaP:s, elec. props. following 1.7 MeV electron irradiation 78−80005
GaSb amorphous film, elec. props. *(French)* 78−14843
p-GaSb, electron irrad., annealing 77−51407
GaSb films, amorphous and cryst., vac. evaporated, Elec. cond. thermoelec. power and optical absorpt. 80−2504
GaSb-Au contacts, interface struct., technology rel. to elec. props. *(German)* 77−72915
$(GaSb)_{1-x}Ge_x$ films, single-cryst. metastable semicond., growth and phase stability 80−80115
Gd, electron irradiated, defect annealing, recovery spectra 79−23648
Gd-Co, and Gd-Co-Mo films, amorphous, mag. props., annealing effects 78−64235
Gd-Co, film, evaporated and sputtered, struct. and mag. anistoropy, electron microscopy 79−56578
Gd-Co amorphous films, annealed, short-range order and perpendicular mag. anisotropy 80−15765
Gd-Co amorphous films, mag. anisotropy, static and ferromag. reson. expts. 79−33477
Gd-Co films, amorphous, mag. anisotropy from torque meas. 77−47987
Gd-Co-B system, phase composition, struct., phase equilibria 78−35355
Gd-Co(Fe) amorphous films, microstruct. and mag. anisotropy 79−82838

annealing continued
Gd-Fe film, amorphous, mag. props., annealing effects 78−64235
GdCo film, amorphous, sputtered, in-plane anisotropy induced by rare gas annealing 78−84458
Gd_xCo_{1-x} annealing amorphous film, ferromag. reson. 77−85580
$(Gd_{1-x}Co_x)_{1-y}Ar_y$ amorphous mag. film, elec. and mag. prop. depend. on Ar 80−80410
$(Gd_xCo_{1-x})_{1-y}Ar_y$ amorphous films, effective anisotropy field, ferromag. reson. obs. 80−71123
$Gd_{0.27}Co_{0.64}Kr_{0.09}$, amorphous film, thermal release of Kr and H, meas. using UHV mass spectrometric technique 80−3439
GdFe, amorphous films, thermal stability of mag. props. *(Japanese)* 79−47307
GdO film, new reduced variant due to annealing 77−89660
Ge (111) surface, 500 eV Ar^+ bombard., high temp. annealing, recovery, RHEED obs. 78−87723
Ge, (111) surface, clean and O_2 adsorbed, photoemission yield spectroscopy of electronic surface states 79−91122
Ge, acceptor complex spectra, tunnelling H systems 80−89036
Ge alloys, amorphous film, crystn. transform. kinetics 78−22653
Ge, amorphous, annealing effect on absorpt. edge *(Korean)* 79−15142
Ge, amorphous, Mott's parameters for hopping cond., effect of annealing 77−69324
Ge, amorphous and crystn. films, contamination behaviour, XPS examin. 79−1815
Ge, amorphous and polycryst. layers, sputtered, elec. cond. and thermoelec. power 78−2586
Ge, amorphous film, annealing, effect on localised states 79−4535
Ge, amorphous film, laser pulse annealing 80−15006
Ge amorphous films, high elec. field cond. and magnetoresist. at 4.2K 80−49748
Ge amorphous films, structural relaxation and crystallisation 80−100170
Ge, amorphous layer, comparison of laser and electron beam pulsed annealing 79−69374
Ge, amorphous thin films, fast crystn. and void precipitation in laser pulse annealing, TEM exam. 79−56086
Ge, cross-slip of single dissociated screw disclocations, double etching and X-ray topography studies 80−15104
Ge crysts., electron beam induced changes of real struct., HVEM 80−103390
Ge, defects, radiation effects 80−29016
Ge, deformation, annealing characts., X-ray study 78−75713
Ge, dislocation motion near surface 79−82219
Ge, electron irrad., light-sensitive defects 80−24498
n-Ge, electron irradiated, annealing at 6K, Watkins model explanation 78−47427
n-Ge, electron irradiated, high temp. annealing, nonequilibrium carrier lifetime and Hall effect 77−4370
Ge, electron irradiated in HV electron microscope, defect form. and interaction with dislocation 77−19990
Ge epitaxial film, ion implantation and electron beam anneal effects on carrier conc. 80−75255
Ge epitaxial film, vac. deposited on GaAs, doping effect of annealed GaAs surface 80−65718
Ge, fast and slow quenching defects 78−39052
Ge film, amorphous, influence of deposition parameters on e.p.r. 77−1586
Ge, film, electronic struct. charge on ordering, double beam photoemission 78−19634
a-Ge, Ge-O removal in pre-crystallisation annealing 78−9957
Ge, heavily-doped single cryst., macroinclusions, annealing in elec. field 77−47474
Ge, high parity detectors, 6 GeV/c proton irradiation 78−37508
Ge, ion bombarded, radiation defect formation, atom-atom collision cascades modelling 80−10582
Ge, ion irrad., accumulation and annealing of struct. defects, secondary emission obs. 78−2167
Ge, ion-implanted amorphous layers, melting model for pulsing-laser annealing 79−56080
Ge, irradiated and annealed, cyclotron reson. linewidth investig. of electron scatt. 77−55707
Ge, irradiation at about 6K, low temp. annealing of defect 78−2162
Ge, irradiation by 3.5 MeV electrons at high temp., carrier density and lifetime changes 77−4128
Ge, laser annealing, optical refl. meas. of melted layer 79−78796
Ge, laser pulse annealing, induced nucleation, crystal growth 80−84966
Ge, n- and p-type, fast neutron irrad. at low temp., resistivity, annealing characts. 77−89481
Ge, neutron irrad., absorpt. edge 80−93320
p-Ge, neutron irrad. quenched sample, lattice defects 79−19284
Ge, neutron irradiated, capture of positrons by radiation defects 78−38756
Ge, neutron irradiated, positron annihilation, ESR and resist. meas. 80−15160
Ge, neutron-irradiated, positron lifetime 80−97374
Ge, on Si(111), solid phase heteroepitaxy 80−6670
Ge, quenched, defect annihilation process near 100°C 79−95047
Ge, quenched n- and p-type, intrinsic defects migrating near 100°C 77−62670
Ge, quenching temp. effect on annealing rate of quenched-in acceptors 79−82590
Ge radiation detectors, high-purity, ion implanted n-type contact 77−54416
Ge, reactor irrad., opt. props. 77−90137
Ge, screw dislocation loops, shrinkage vel. and cross slip freq., activation energies *(German)* 78−43028
Ge, shrinkage of single dislocation loops during annealing 79−82212
Ge surface, (111), ion-bombarded and annealed, spectroscopic ellipsometry study 80−103543
Ge, surface recomb. before and after laser annealing, 10-μm transmission meas. 80−1247
Ge thin films on glass substrates, annealing by Ar ion bombardment 80−80136
Ge, trapping defects, deep level transient spectroscopy 79−47045
Ge^+, low energy mass analysed ion beam deposition on Ge and Si substrates 79−33946
Ge:^{57}Co, ion-implanted, Mossbauer study, annealing effects 80−7231
Ge:Al, solid solns. decomp. 80−15249
n-Ge:As(Sb)(Bi), irradiated with fast electrons at 77K, investigation of 300K annealing stage 79−51155

annealing continued
p-Ge:Au, interaction of primary radiation defects with Au atoms, after irrad. and annealing 79—51145
p-Ge:Cd,Sb, electron irrad. at 300K, elec. props. 80—6435
n- Ge:Cu, characts. of radiation defects 78—55893
Ge:Cu, quenched, energy levels of thermal acceptors, annealing effect 78—34798
Ge:Ga, cryst. defects due to neutron irrad., elec. cond. and annealing 79—55789
Ge:P, solubility and segregation of electrically active P 77—15442
Ge:Sb, annealing stages of thermal defects, elec. meas. 77—55282
p-Ge:Sb, cryst. defects due to γ-irrad. 79—55779
Ge:Sb, cryst. defects due to neutron irrad., elec. cond. and annealing 79—55789
n-Ge:Sb, fast electron irrad. at 77K, radiation defect changes by annealing at 220K 79—37737
n-Ge:Sb, fast neutron irrad. effects on donor conc., and annealing 78—56107
n-Ge:Sb, γ-irrad. effects on donor conc. and compensation by acceptors 78—56106
Ge:Sb, solid solns. decomp. 80—15249
Ge:Sb, thermal defects, influence on radiation defect formation and annealing 77—55281
Ge:Sb(As)(P), implantation doping, annealing and doping profile determ. 77—19972
Ge:Te, ion-implanted, thermally assisted Xe-flash annealing, Rutherford backscatt. meas. 79—10881
Ge-Al (1.15 wt.%), US wave vel. meas. for anal. of solid soln. breakup 78—23887
Ge-Au-Ni(Pd)(Pt), trilayer film, interdiffusion obs. 78—2308
Ge-Au-Ni(Pt)(Pd) trilayered films, annealing, interdiffusion 78—22902
Ge-Bi-Te system, thermal cond. change during phase transitions 80—100368
Ge-Cu (0, 23, 40 at.%), amorphous film struct. *(German)* 78—95391
Ge-Fe, laser annealing of implanted ^{57}Co sources, Mossbauer obs. 80—39139
Ge-Ga (1.13 wt.%), US wave vel. meas. for anal. of solid soln. breakup 78—23887
Ge-S, Ge-S-Ag, amorphous prop. and origin of paramagnetic defects 79—10801
Ge-S film, amorphous, photo-induced ESR and optical absorption edge shift 78—88374
Ge-S glass, melt-quenched photoinduced ESR, annealing behaviour and glass comp. depend. 80—71156
Ge-Sb, chemical diffusion *(Japanese)* 78—14515
Ge-Sb, eutectic alloy, exam. of morphology during solidification *(Russian)* 79—34022
Ge-Si, electron irradiation and annealing 77—55305
Ge-Si alloys, n-type, phosphorous doped, precipitation effects due to heat treatment 80—107833
Ge-SiO$_2$-p$^+$Si tunnel junctions, for determ. of AC cond. of amorphous Ge 77—24608
Ge-ZnSe heterojunction, change in interfacial microstruct. on high temp. annealing 77—28242
GeS_2 glass, melt quenched, reversible photostructural change, optical transmission spectra obs. 80—45109
Ge_2S_3, electron irradiated, effects on elec., photoelec. and optical props. 80—49806
GeSe, amorphous, film, thermally induced effects, UPS study 80—104042
$GeSe_2$, amorphous, film, thermally induced effects, UPS study 80—104042
$GeSe_2$ evaporated films, struct. and thermally induced effects 79—41963
$GeSe_2$ evaporated films, optical absorpt. and thermally induced effects 79—42989
Ge_xSe_{1-x}, $0<x<0.2$, crystallisation in amorphous bulk and thin films 78—55813
Ge_xSe_{1-x}, amorphous, AC cond. *(Korean)* 80—44591
$Ge_{20}Se_{40}Te_{40}$ amorphous alloys, thermal crystn. study 78—26789
$Ge_{1-x}Si_x$, with Si implanted ions, optical and photoelec. props. 79—24014
GeTe, amorphous film, annealing effects on resistivity, comparison with SnTe 77—66212
GeTe amorphous films, annealing effect on optical props. 77—72931
GeTe films, elec. props. and struct., influence of annealing and condensation conditions 80—15388
GeTe, machining effects on electrophys. props. 77—86199
$GeTe_x$ cermet specimens, density, 25 to 412°C, depend. on nonstoichiometry and annealing temp. 77—25004
Ge_xTe_{1-x} amorphous matrix with Te crystallites, effect of annealing 77—24274
HBr, and DBr, in monatomic matrices, near IR spectra and aggregate structs. 79—89667
HCl, and DCl, in monatomic matrices, near IR spectra and aggregate structs. 79—89667
H_xWO_y film, effect of struct. on optical and electrical props. 78—84671
^{4}He, solid, boundary limited thermal cond., Poiseuille phonon flow 80—2241
Hf-Ge-B system, phase equilibria 78—35356
Hf-Mo-C, isothermal section of phase diagram at 1400°C, X-ray phase analysis determ. 79—34006
$HfAl_3$, anomalous growth in thin films, AES, TEM and He backscatt. meas. 77—43462
HfO_2, monoclinic, microcracking, elasticity, internal friction, thermal expansion meas. 79—29195
HfO_2 single crystals, y_2O_3 stabilised, optical props., impurities and annealing conditions influence 79—52399
HfO_2:M^{n+}, M=Ce, Pr, Tb, Eu impurity valence transitions 77—51694
HfO_2-Cr_2O_3 system in Ar medium, phase equilibria, 1600-2500°C *(Russian)* 77—55953
Hg electric field gradients at different Be lattice sites, gamma-spectral study 80—80224
Hg-Ar quench condensed system, annealing effects on elec. cond. 79—60880
$Hg_{0.6}Cd_{0.4}Te$, annealing temp. effect on carrier conc. 78—72167
$Hg_{0.79}Cd_{0.21}Te$, ion implanted, elec. props. 80—20184
$Hg_{1-x}Cd_xTe$, epitaxial layers, elec. properties in the range 4.2 to 300K *(French)* 80—65721
$Hg_{1-x}Cd_xTe$, grown from melt, Kirkendall and Frenkel effects 80—100365
annealing continued
$Hg_{1-x}Cd_xTe$, implanted with Hg, Al, damage and lattice location study 80—103381
$Hg_{1-x}Cd_xTe$, segregation, compositional characterisation 80—107434
$HgCr_2Se_4$, electronic props. rel. to departure from stoichiometry 80—100472
HgTe, vacancy doping by off-stoichiometry, influence on transport props. 78—55862
HgTe, vacancy mech. of resorption of Hg droplets 80—39070
HgTe:Cu, effect of prep. conditions on impurity distrib., hole conc. 77—8743
HgTe:Cu(In), dopant interactions 77—47834
Ho, elastic consts., 80-140K, 95K anomaly and annealing 79—46734
Ho, electron irradiated, defect annealing, recovery spectra 79—23648
Ho-Co film, evaporated, struct. and mag. anistoropy, electron microscopy 79—56578
HoCo film, amorphous, sputtered, in-plane anisotropy induced by rare gas annealing 78—84458
Ho_xCo_{1-x} amorphous films, microstruct. and mag. anisotropy 79—82838
In electrode, annealing, effect on elec. resist. of metallic thin film 80—80416
In, film, freshly deposited, 77K, refl., annealing effect, thickness depend. 77—16413
In-Sb-Bi system, solid solns., solubility limits, microhardness, microstruct. investig. 78—35368
n-InAs, electron irrad., carrier introduction rate, annealing 80—24948
InAs, exam. of decomposition of donors 79—1605
InGaAsP:Be, avalanche photodetectors annealing temp. effect on photolum. spectra 79—69872
$In_{0.3}Ga_{0.7}P$, N free and implanted, photoluminescence study 80—97322
$In_xGa_{1-x}Sb$, influence of annealing on microstruct., exam. 78—56669
In_2O_3-SnO_2, X-ray and optical meas. of solubilities 79—55894
In_2O_3-SnO_2 thin film, Hall mobility, temp. depend., grain boundary effects 80—75658
InP (110) surfaces, cleaved and polished-sputtered-annealed, LEED and AES study 80—103550
InP, critical implantation temp. and annealing 79—90691
InP film, electron-beam annealed, surface conduction 80—84500
n-InP, γ-ray and electron irrad., annealing of radiation point defects, elec. cond. and Hall coeff. meas. 80—65051
n-InP, heat treatment in controlled P vapour 80—88137
InP, ion-implanted layers, close contact capless annealing, elec. props. 80—84192
InP, plastic deform. and scratch microhardness meas. 78—27583
InP:Be, ion implantation, hole conc. and mobility, junction depth 79—46685
InP:S^+(Se^+), ion-implanted VPE layers, laser annealing, elec. and struct. anal. 79—73199
InP:Se, implantation and laser annealing 80—24476
InP:Si, pulse electron annealing, carrier activation and mobility 80—15124
InP:Si(Mg), ion implantation and PH_3 ambient annealing under VPE conditions 79—42085
InP-Au contacts, conditions of fabrication that control interfacial microstruct. 79—42643
InSb, absorpt. edge, exciton struct. 80—93321
n-InSb, elec. props. changes during ht. treatment 77—85213
InSb film, prep. by rotary type flash method *(Japanese)* 77—40372
InSb, galvanomagnetic props. of annealed single crystals 80—96909
InSb, high-purity specimen irradiated at 80K, transport prop. and defect annealing 78—95307
InSb, ion bombard. and defect annealing, n- and p-type cond. layer prod. 78—26606
p-InSb, ion bombardment using 30-80 keV ions, isochronous annealing, elec. props. obs. 79—19295
InSb, ion implantation at elevated temps. 79—10870
InSb, ion irrad., isothermal annealing effects 80—6424
InSb, low-temp. annealing effect on elec. props. 77—8091
InSb, radiation defect annealing following 50 MeV electron beam irrad. 80—15154
InSb, Raman scattering study of unoxidised Sb in anodic oxide films 80—88985
InSb:Ge annealing effect on electrical parameters, absorption spectra and photocond. 77—11939
InSb:Ge(Zn)(Mn)(Cd), heat treatment effects on elec. props. 78—43411
n-InSb:Zn, Zn diffusion out of implanted layers, annealing effects 79—10984
h-InSb-oxide system, interface recombination activity variation on annealing *(Russian)* 79—78199
$InSb_{1-x}Bi_x$ films, single-cryst. metastable semicond., growth and phase stability 80—80115
α-In_2Se_3, far infrared optical study of ordered and disordered forms 78—84572
In_xSe_{1-x}-SnO_2 amorphous film-SnO_2 system, photovoltic spectra, annealing effect *(Japanese)* 80—92926
In_2SnO_3 film, effect of ambient atmosphere during annealing, elec. props. 80—97510
InTe thin films, flash evaporation, electrical props. 80—65722
Ir oxidation and vaporisation of the volatile oxides, gravimetric exam. comparision with losses due to vacuum annealing *(Russian)* 79—57136
Ir-W (0.3 wt.%), P segregation to grain boundaries, effect on high temp. ductility 78—95754
IrSi, Schottky barrier height meas. 79—47160
KBr crystal, cordlike defects and countermeasures 79—72636
KBr in contact with KCl, mutual diffusion, development of relief on contact surfaces 78—22964
KBr, stored energy after X-irrad. at low temp., 10-50K 77—76459
KBr, X-irradiated, at 80K, interstitial K ions associated with interstitial Br ions *(Russian)* 78—75655
KBr:Li(Na), low temp. radiation hardening mechanism, single halogen interstitials as hardening agent, Ha annealing 79—23634
KBr:Rb, H-centre interaction with Rb^+ ion 78—75662
KBr-KCl, birefringence, annealing effects, photoelasticity 78—72483
KBr(Cl):OH , cc U_2 to H_2O^- defects conversion after UV photodecomp. 80—107230
$KCaCl_3$ impurity in NaCl cryst., precipitation and dissolution 79—42259
KCl, annealed in KBr vapour, crack and pore formation, diffusionally induced stress relaxation *(Russian)* 80—40388
KCl birefringence, annealing effects, photoelasticity 78—72483
KCl, electron-irrad., positron-capture centres, thermal annealing kinetics 79—95875

annealing continued
- KCl, gamma-irradiated crystal, interrelation between V_2 and V_3 centres *(Russian)* 79−69862
- KCl, irradiated crystal, determ. of oscillator strength of V_3-centre *(Russian)* 78−92095
- KCl, thermal and photothermal conversion of colour centres, after high-dose electronic interaction *(Russian)* 80−39156
- KCl, thermal annealing of F, V_2-, V_3-centres *(Russian)* 80−54229
- KCl:Ba^{2+}, localised stress relaxation in excess vacancy system, prismatic loops *(Russian)* 80−88160
- KCl:Br^{2+}, solid solution periodic precipitation in inhomogeneous conc. field 80−103485
- KCl:Ca^{2+}, Z_3-centre thermolum. 80−80879
- KCl:$Ca^{2+}(Sr^{2+})$, impurity precip., flotation density obs. 78−51690
- KCl:Li, X-irrad., F_A centres, thermolum. studies 80−80878
- KCl:Pb, lead aggregation effect on yield stress, incoherent precipitates, solubility determ. method 80−50645
- KCl:Pb exam. of simultaneous effect of heat treatment, Pb concentration on state, phase diagram construction 79−96008
- KCl:Pb^{2+} crystals, precipitation, density changes, nucleation mode, lattice relaxation, heat treatment 79−66066
- KCl:$SnCl_2$, X-ray irrad., polarised luminesc. and EPR study of Sn^{3+} centres 80−39868
- KCl:Sr, Ca, simultaneous diffusion, coefficients meas. 78−79813
- KCl:$SrCl_2$, H_{Na} annealing, X-ray irrad., H centre capture by IV dipoles 78−10927
- KCl:$SrCl_2$, thermal depolarisation 77−28514
- KCl:TlCl, lattice defects, X-ray line profile obs. 80−24455
- KCl-CuCl solid solution supersaturated, precipitation, impurity aggregation 80−29174
- $K(H_{1-x}D_x)_2PO_4$, single cryst., 77K, γ-radiation damage centres, and EPR obs. 78−68379
- KH_2PO_4, soft branch Brillouin specta, quasielastic central peak suppression by annealing 78−95588
- $KMgF_3$:Co^{2+}, γ-irrad. single cryst., visible and IR absorption, MCD, annealing data 78−10926
- La-N-C system, metallographic investigation *(German, English)* 77−52600
- La-Re-B, annealed and quenched, X-ray structural and phase anal. 78−11207
- $La_{100-x}Au_x$, amorphous film, phase stability determ. 79−4636
- LaF_3-$La(OH)_3$, high pressure phases, X-ray diffr. and IR spectroscopic anal. 79−47679
- $(La_2O_3)_{1-x}$-$(CeO_2)_x$:Mn, valence state of Mn, effect of annealing in H_2 atm., ESR obs. *(French)* 80−71164
- $LaSi_2$, thin film, exam. of phase transitions during vacuum annealing 79−95281
- La_5Si_3 thin film, exam. of phase transitions during vacuum annealing 79−95281
- Li-Na ferrite powders, props. rel. to Fe_2O_3 chem., thermal, mech. historical 79−11539
- Li_5AlO_4, Li_5FeO_4 and Li_5GaO_4, additives and moisture effect on ionic cond. 80−107523
- $Li_2B_4O_7$ thermoluminescent dosimeters, high dose characteristic 78−35966
- LiF (TLD-100), thermoluminescent response to 0.1-5 keV electrons 79−95852
- LiF, annealing effects on thermoluminescence, dipoles and dimers 77−12452
- LiF, γ-irrad. induced defects, positron capture and annealing obs. 80−60707
- LiF, irrad. at pile temp., higher F aggregate centres produced during thermal annealing 77−43212
- LiF single crystals, dislocation motion and generation on plate impact 79−95011
- LiF single crystals, exam. of void morphology effects on their disappearance kinetics 79−10843
- LiF TLD phosphor, γ-irrad. induced sensitisation, UV effects 80−108286
- LiF TLD phosphor, residual thermoluminescence effect on sensitisation 80−108287
- LiF, TLD phosphor, Z_3 centre, thermolum. and optical absorption spectra 79−24374
- LiF TLD-100, thermolum. response to 5 to 30 keV electrons effect of annealing atm. 77−86638
- LiF TLD-100 material, long term recycling characts. 78−11737
- LiF TLD-100 phosphor, sensitisation mechanism study, thermolum. glow peak intensity obs. 80−55202
- LiF, thermoluminescence mechanisms following gamma irradiation 77−59625
- LiF, thermoluminescence response to gamma rays 77−59626
- LiF, thermoluminescent dosimeters, high dose characteristic 78−35966
- LiF:Be(Mg), Maxwell-Wagner relax. induced by impurity clouds around dislocations, ionic thermocond. meas. 80−7281
- LiF:Mg, thermal annealing effects on sensitivity and fading of dosimeter 78−82522
- LiF:Mg, Ti TLD long-term annealing at 400°C, radiation and thermally induced damage, recovery 77−5085
- LiF:Mg, X-ray irrad., trapping processes, Z-centres and dipoles, two models 80−49222
- LiF:OH crystals, X-irradiated, H centres formation and annealing 80−54226
- LiF-PTFE TLD performance, influence of heating element design 78−25333
- $LiFe_5O_8$, vacuum annealed, tetragonal γ-phase obs. with TEM 80−11661
- Li_4GeO_4-Zn_4GeO_4, solid electrolyte system, phase diagram 80−66489
- $LiInS_2$, blue-band emission 80−76062
- Li_3N, ionic cond., annealing, trans- and intercryst. resist. 78−43176
- $LiNbO_3$, γ-irradiated and annealed, elastic and piezoelectric props. 78−2807
- $LiNbO_3$, spontaneous elec. breakdown 77−66458
- $LiNbO_3$, waveguide and modulator form. by ion implantation 80−48469
- $LiNbO_3$:Fe, characts. for holographic storage appls. 77−23630
- $LiNbO_3$:Fe, origin of photoelectrons and conc. of point defects 77−43645
- $LiNbO_3$:Fe, state of impurity Fe cation, nucl. gamma reson. study 80−40014
- $LiNbO_3$:Ti optical waveguide, technique for suppressing Li_2O out-diffusion 78−18040

annealing continued
- Li_2O-Al_2O_3-P_2-O_5:V^{4+}, glass exam. of ESR spectrum of V^{4+}, optical spectra, and structure 78−88180
- Li_2O-Al_2O_3-SiO_2 glass-ceramic, near-zero thermal-expansion heat treatment effect in fracture behaviour 80−66537
- $(LiPO_3)_x.H_2O$, intramolecular rearrangement on annealing 79−19179
- $LiTaO_3$, spontaneous elec. breakdown 77−66458
- $Li_{1+x}Ti_{2-x}O_4$, high temp. spinel-Ramsdellite transform. 80−70407
- Lu, electron irradiated, defect annealing, recovery spectra 79−23648
- Lu, low-temp. electron-irradiated, recovery 78−6102
- Mg alloy, MA12, structural state effect on life and in fatigue crack generation in air and in vacuo 79−87728
- Mg and Mg-Fe films, defect energy distrib., elec. resist. meas. during annealing 80−54808
- Mg cast iron, effect of heat treatment on phase comp., microstruct., wear resistance 77−56006
- Mg cast iron, microstruct. of spheroidal graphite, rel. to polishing and annealing treatments 77−56160
- Mg ferrite, crystal lattice defectiveness and degree of inversion, effect of synthesis temp. 77−11501
- Mg, recrystallisation after cold rolling 78−72790
- Mg, SiO_4:Th TLD phosphor, γ-ray induced sensitisation and phototransfer 79−33851
- Mg-Ag, ion implanted, recovery stage characterisation by electron irrad. 80−107295
- Mg-Al spinel, hot pressed ceramic, annealing effect on transparency and microstruct. *(Japanese)* 79−74188
- Mg-Al spinel ceramics, mech. strength, non-stoichiometry and microstruct. *(Japanese)* 80−21054
- Mg-Fe, dil. alloy, elec. resist., var. with annealing temp. *(French)* 79−60815
- Mg-Fe alloy film, quench-condensed, resistance meas. 79−15235
- Mg-Mn, dil. alloy, elec. resist., var. with annealing temp. *(French)* 79−60815
- Mg-Y-Nd-Zn-Zr (2,2,0.3, 0.7 wt.%), heat treatment effect on casting dimensional stability, alloy mech. props. 78−44146
- $MgAl_2O_4$, radiation damage, optical absorpt., F-centres 80−64994
- $MgAl_2O_4$, thermochemical coloration and annealing 79−91468
- Mg_3Cd, effect on order, of compression deformation 78−52924
- MgF_2 obs. of radiation induced point defects, cross-relaxation processes, polarised β-active nuclei 80−60431
- $Mg_{0.8}Mn_{0.2}Fe_{1.8}Al_{0.2}O_4$, grade 6SChl ferrite, milling conditions effect on fine cryst. struct. and activity 79−24483
- MgO, cryst. preliminary processing rel. to deform. curve parameters, slip line struct. 77−52421
- MgO, electron irradiation induced mobility of substitution H 77−55390
- MgO film, IR spectroscopy and RHEED analysis 77−89664
- MgO irradiated with Li^+ and K^+ ions, optical props. of metal aggregates 79−65907
- MgO, Li precipitates orientation and struct. *(French)* 79−86888
- MgO, neutron irrad., MCD, optical absorpt. lines 77−77255
- MgO, orientation relationship and struct. of Li precipitates 79−82342
- MgO, plastically deformed, recovery of internal friction at room temp. *(French)* 78−80577
- MgO polycrystals, hot-pressed, effect of annealing on props. 79−34073
- MgO, single crystal, effect of heat treatment on mechanical props. 77−70070
- MgO, thermochemical coloration and annealing 79−91468
- MgO:Li, oxidation and reduction up to 1700K, defect prod. 79−39013
- MgO:$Li^+(Na^+)$, precipitation rel. to dislocations *(French)* 79−51163
- MgO-NiO, solid soln. formation, initial stage obs. 77−81243
- Mn film, heat treated, lattice distortion energy, resist. meas. 79−19492
- Mn film, resistivity-temperature variation 79−24085
- Mn thin film, DC resist., activation energy, thickness depend. 80−84518
- Mn-Al-C, ferromag., transform. kinetics 80−34627
- Mn-Al-C, ferromag. alloy, transform. kinetics 80−76229
- Mn-Cu, mag. and cryst. struct., neutron and X-ray diffr. meas. *(Russian)* 78−22694
- γ-Mn-Cu, metastable, structural aspects of decomposition 79−1871
- Mn-Cu alloy, volume effect, paramagnetic-antiferromagnetic and structural transition, lattice consts. 80−39007
- Mn-Cu-Zn system, optimum heat-treatment routine for max. damping 79−87670
- Mn-MgF_2 cermet, heat treated, lattice distortion, resist. meas. 79−19492
- Mn-MgF_2 cermet film, resistivity-temperature variation 79−24085
- Mn-Ni, thermal expansion, mag. susceptibility, lattice consts. 80−100341
- Mn-Ni-Ti (Zr) systems, and mech. props. thermal expansion for different heat treatments *(Japanese)* 79−29123
- Mn-Ni-Ti(Zr), non-ferromagnetic Elinvar-type alloys 79−24566
- Mn-Ni-V(Nb)(Ta), nonferromagnetic Elivar type, mech. props. meas. 77−48473
- Mn-SiO, annealed cermet films, elec. resist., composition depend. 80−97007
- Mn-SiO cermet films, elec. resist., annealing behaviour 80−54803
- Mn-SiO cermet thin film, DC resist., activation energy, thickness depend. 80−84518
- Mn-Y-Zn-Cd alloy,phase equilibria, plastic deformation, microhardness *(Russian)* 80−40334
- MnBi film, electrical props., in situ annealing effect 80−65708
- MnBi films, prep. by ionised-cluster beam deposition technique, magnetooptical props. 80−100790
- $MnCo_2O_4$ DC sputtered films, struct. and elec. props. 80−54812
- $Mn_xCr_{3-x}O_4$ spinels, miscibility gap boundaries, annealing expts. 77−86012
- Mn_3Ga, formation of DO_{22} superstruct. and para-antiferromag. transition 79−19737
- MnZn ferrite, O_2 stoichiometry effect on fracture 80−25826
- $Mn_{1-x}Zn_xFe_2O_4$, prepared by wet method, neutron diffr. and high field Mossbauer expts. 80−75719
- Mo alloy, finely dispersed precipitate distrib. change due to homogenisation annealing 77−70056
- Mo, annealing in stage I, dose depend. and radiation doping defects 78−47422
- Mo, CVD films of high IR reflectance 79−52119
- Mo, desorption of He, during stage III annealing, vacancy model 77−1123
- Mo, effect of microvoid size on positron annihilation and residual resistivity 77−48272
- Mo, electron beam melted with C additions, mech. props. *(Japanese)* 77−48449

annealing continued
Mo, electron irradiated, recovery studies of pure and radiation doped crystals 79—19280
Mo, fatigue charact., effect of Ni and Re surface doping on mech. props. *(Russian)* 80—7660
Mo film, evaporated, annealing behaviour, SEM obs. 80—65397
Mo film, sputtered, elec. resist., annealing and struct. effects 80—60109
Mo film, sputtered on Si, annealing effect on uniform and nonuniform strains 79—82504
Mo film on Si surface, MoSi$_2$ form. conditions *(French)* 78—43270
Mo, gamma irradiated defects, interaction with positrons *(Russian)* 80—97372
Mo, gamma-ray irrad. positron annihilation during radiation defect annealing *(Russian)* 79—99970
Mo, grain boundaries, electron microscope obs. *(Russian)* 79—4311
Mo, H and D trapping, enhancement due to He ion damage, annealing and cold work effects 77—31698
Mo, hardened sub-structure, high-temp. radiation resist. *(Russian)* 78—56654
Mo, high-temp. neutron irradiated, annealing study by positron lifetime 77—51413
Mo, internal friction and segregation effects *(Russian)* 77—66669
Mo, irrad., defect configurations, PAC study 79—86817
Mo, irrad.-induced voids and dislocations, annealing, theory *(Russian)* 78—47418
Mo, irradiated with fission fragments, creep, 20-30K *(French)* 77—48493
Mo, neutron irrad., radiation anneal hardening mechanism 80—71678
Mo, neutron irradiated, radiation softening and hardening 80—34083
Mo, neutron irradiated extended low temp. annealing 79—79014
Mo, neutron irradiated single crystals, vacancy reactions in III recovery 79—73220
Mo, neutron-irradiated, positron lifetime study 79—23654
Mo, oxidation kinetics, Mossbauer study 80—40005
Mo, plastically deformed single cryst., mag. susceptibility *(Russian)* 80—93074
Mo, point defect migration, stage III annealing 77—80548
Mo polycrystals, grain misalignment, electron microscope determ. *(Russian)* 80—103358
Mo powder, influence of powder reduction processes on props. 80—89175
Mo, proton irradiated, annealed and rolled, void form. 78—22774
Mo, rolled and annealed, zone-refining effect on recryst. grain orient. 77—36532
Mo, secondary recrystallisation grain structure, effect of conditions of annealing *(Russian)* 78—6945
Mo sheet, conc. of interstitial elements on lamination surface 77—86038
Mo, single crystal, ductility and high temp. strength in routine tests 77—90427
Mo, stress-to-rupture strength at high temps., struct. effect 77—70175
Mo, vaporisation, influence of inert gases on losses *(Russian)* 79—55878
Mo, voids, effect of impurities on positron lifetime 77—15453
Mo:N, ion implanted proton-irradiated, annealing behaviour 78—91362
Mo:Xe, BCC, heavy ion implanted, vacancy recovery, Mossbauer spectroscopy 79—82896
Mo-B, Mo-B-Fe(Ni), microalloying influence on mechanical props., cold rolling, plasticity *(Russian)* 80—40502
Mo-C-Zr (0.03, 0.17 wt.%), thermal treatment effect on yield drop 77—90382
Mo-C-Zr-B (0.004, 0.12, 0.002 wt.%) effect of grain size, cellular dislocation structure, on mech. props. *(Russian)* 79—34105
Mo-permalloy, magnetic permeability and order form. kinetics under annealing, conc. depend. 77—8356
Mo-Re, solid soln., dislocation internal friction *(Russian)* 78—23748
Mo-Re(Os)(Ru), recovery after deform. and annealing, destrengthening mechanism *(Russian)* 80—97546
Mo-Si sputtered contacts, contact resistance 80—92970
Mo-SiO$_2$-Si, Mo-Si pelicular structures, struct. transitions during vacuum thermal treatment *(Russian)* 78—95238
Mo-SiO$_2$-Si, R/MOS struct., heat treatment effects 78—76683
Mo-W (50 wt.%), emissivity, 1200-3000K, effects of annealing and surface treatment 78—43154
Mo-W-Mo (4.74, 2.17 wt.%), creep resistance in ultrahigh vacuum 79—5027
Mo-W-N system, nitrided annealed samples, W replacement of Mo 80—76227
Mo-Zr, interaction with MoSi$_2$ diffusion coating, at elevated temps. *(Russian)* 79—28150
Mo-Zr alloys, TsM-6, Zr segregation at grain boundaries, carbide precipitation, X-ray spectral anal. *(Russian)* 79—74154
Mo-Zr-B-C, dil. alloy, struct. changes under prolonged high temp. annealing *(Russian)* 78—6944
Mo-Zr-C alloys, carburising and annealing effects *(Russian)* 77—59828
Mo-Zr-Ti-C(0.1, 0.15, 0.004 wt.%), alloy TsM2A, cavitation failure mechanism 77—70169
MoS$_2$, homogeneity size estimation, stacking fault conc. effect 80—96661
MoS$_2$ on Mo, cryst. struct. and thermal stability 77—52539
MoSe$_2$ coating, on Mo, support annealing influence on orientation, texture and hardness *(Russian)* 80—20961
MoSi$_2$, integrated intensities and lattice parameters, X-ray anal. 78—63733
MoSi$_2$ refractory formation by As$^+$ ion beam bombardment 80—107286
Mo$_5$Si$_3$ based coating, interaction with Mo alloy substrate *(Russian)* 80—21167
NI$_3$Al, structural order and homogeneity, X-ray, mag. susceptibility and Mossbauer meas. 77—63663
Na$_6$Al$_6$(Si$_{0.99}$Ge$_{0.01}$)$_6$O$_{24}$.2NaBr, Ge-doped sodalite powders, UV absorpt. band 80—71452
NaBrO$_3$, single crystals, thermolum., optical absorpt., X-ray effect 79—95858
NaCl, (100), (110) and (111) surfaces annealed in vac. 400-800°C, evap. struct. 77—15572
NaCl, bent single crystal, equilib. face, surface relief form. during annealing 78—47651
NaCl crystal, annealed near thermodynamic equilib. of cryst. and vapour, {110} surface struct. and coarsening 77—28067
NaCl crystals irrad. by high electron doses, annealing, colour centre prod 80—2074
NaCl, effect of annealing and neutron irrad. on block struct. 80—29061
NaCl, hydrostatically compressed crysts. in easy glide stage, plastic deformation 80—7630

annealing continued
NaCl, monocrystalline, defect struct. and intrinsic ionic cond. relationship 79—95211
NaCl, plastically deformed, recovery of work hardening *(German)* 77—35626
NaCl, reduction of dislocation density during isothermal annealing *(Russian)* 79—4303
NaCl, single cryst., crack healing at low temp. 77—36622
NaCl:Ag$^+$, X-irrad., B-centres, thermal annealing, monomolecular and bimolecular sequence of kinetics 78—47373
NaCl:Ca, precipitate form., transform. after annealing, critical flow stress 78—38848
NaCl:Ca^{2+}, highly doped, aggregation of point defects, NMR and dielec. loss meas. 79—10847
NaCl:Eu, secondary Eu phase dissolution, EPR and optical absorpt. study 80—96655
NaCl:Mn^{++}, Mg^{++}, doubly doped, ionic thermocurrent study of linear dimer 80—79977
NaCl:Mn^{2+}, radiation-induced colouring, room temp. kinetics 79—55736
NaCl:NaOH, NaNO$_3$, oxygen colour centres, spectral absorpt. rel. to annealing 200-600°C 77—69862
NaCl:Ni^{2+}, kinetics of impurity precipitation 77—69090
NaCl:Sr, dimer and trimer aggregate formation by NMR, ionic cond. and dielectric losses 80—15094
NaCl+Pb, Pb aggregation effect on yield stress, incoherent precipitates, solubility determ. method 80—50645
NaCl(:Ca), irrad. at room temp., stored energy rel. to thermolum. 80—10574
NaClO$_3$, X-irrad., thermal stability of radiation damage products 79—34324
NaNO$_3$, pure and Ca^{2+} doped, γ-irrad., damage species annealing 79—66324
Na$_2$O-Al$_2$O$_3$-P$_2$O$_5$, exam. of subsolidus structure 79—4954
Na$_2$O-B$_2$O$_3$ glass, γ- or UV-irrad., laser and thermal bleaching of colour centre, absorpt. spectra 79—33744
Na$_2$O-B$_2$O$_3$ glass, mag. susceptibility, annealing and base comp. effect 79—91811
Na$_2$O-CaO glass, impacted with sharp SiC particles, strength degradation of annealed surfaces 79—61760
Na$_2$O-CaO-SiO$_2$ glass, annealed and tempered, fracture strength studies under dynamic conditions 79—96132
Na$_2$O-K$_2$O-SiO$_2$ glasses, optical absorption of Ni (II) complex, complex co-ordination change, annealing effects 79—69870
Na$_2$O-SiO$_2$, effect of annealing on absorbed H$_2$O action on temp. spectra of internal friction 78—88487
Na$_2$O-SiO$_2$ glass, microcracking about NiS inclusions, fracture mech. description 80—89333
Na$_2$O.SiO$_2$ fibre, reactivity to atmospheric moisture below annealing range, internal friction measurement 78—92288
Nb alloys, cold worked, chemicothermal strengthening, internal oxidation 80—35229
Nb, anomalous slip of single crystal, obs. 77—8900
Nb, blister diameter and blister skin thickness correl. under He ion irrad. SEM obs. 79—82266
Nb, blister form. on single crystal under Ne$^+$ ion bombardment 78—71772
Nb CVD coatings on graphite, grain struct. depend. on temp. 80—25574
Nb, defect annealing in 7 MeV-irrad. samples, positron annihilation obs. 80—24497
Nb, depth profiling of Li ions using ^{7}Li(p,n) reaction 77—80534
Nb, effect of O ion irradiation on supercond. 78—52131
Nb film, superconducting tunnelling, meas. of annealing characteristics 79—7944
Nb films, ion beam sputtered, supercond., laser annealing effects 80—97024
Nb, H$_2$ diffusion, low temp. recovery 79—73342
Nb, H$_2$ loaded, cold worked, plastic deformation, exam. of α internal friction peak 78—92307
Nb, high purity, faceting of boundaries 78—83826
Nb, isochronal recovery of high energy d-Be neutron damage 78—51592
Nb, low temp. annealing effect, precip. of Nb$_2$O$_5$ *(Russian)* 77—52456
Nb, low temp. neutron irradiation 77—27915
Nb, neutron induced defect structs., TEM exam. 77—84802
Nb, neutron irrad., microvoid form., ang. correl. and yield strength meas., TEM obs. 78—88381
Nb, neutron irradiated, radiation anneal hardening *(Japanese)* 80—89243
Nb, neutron irradiation, low temp., 15 MeV, effect on superconducting props. 78—52179
Nb, plastic deformation effects on superconducting specific heat transition 80—20352
Nb, radiation damage in fusion reactors, computer expts. 80—13839
Nb, residual resistivity, effect of interstitial atoms of O, N and C *(German)* 77—11895
Nb, resistivity variations caused by H and D interstitials, isotope effects 77—89750
Nb single crystals, for tunnel meas., annealing in ultra high vac. device *(German)* 80—89169
Nb, supercond. surface resistance derivative meas. for annealed and unannealed crysts. 79—33395
Nb, superconductor, neutron irradiation, low temp., effect on critical current 78—52180
Nb, trapped He, temp. depend. 77—31685
Nb, US attenuation, hysteresis near and below H$_{c1}$, annealing effects 80—75676
Nb, vaporisation, influence of inert gases on losses *(Russian)* 79—55878
Nb wire drawing, NbFe$_2$ layers form. by diffusion 79—28153
Nb wires, neutron irrad., radiation anneal hardening 200 to 700°C 79—70077
Nb:He, implant saturation and annealing, effect on struct. and supercond. props. *(Russian)* 78—43538
Nb-Al$_2$O$_3$ cermet-type film, thermoelec. power and annealing effects 77—47911
Nb-Ga-Cu, phase diagram, metallographic and X-ray study, annealed and as-cast supercond. crit. temp. *(Russian)* 78—56617
Nb-Ge, A15 struct. superconductor, high field transport props. TEM study 80—34574
Nb-Ge, supercond. A-15 phase, supercond. transition temp. after ion implantation 80—49972
Nb-Ge film, phase transformations due to annealing, electron diffr. study 80—54551

annealing continued
- Nb-Ge-Si, A15 struct. superconductor, high field transport props. TEM study 80−34574
- Nb-H system, temp.-stimulated acoustic emission, hydride precip. 80−3044
- Nb-Pt alloy, superconducting parameters of A15- and σ-phases 78−39242
- Nb-Pt-O system, phase equilibria, diagram, unit cell parameters, supercond. 80−55352
- Nb-Si(−V)(Zr)(Mo)(Ta)(W)(C)(B)(Ge), ductile amorphous, superconductivity 80−60131
- Nb-Sn(Ge), A-15 compound formation by ion implantation 78−51572
- Nb-Ti, metallurgical treatment, effects on props. 79−38846
- Nb-Ti, superconductivity after heavy ion irradiation at low temps. and high fluence 77−69437
- Nb-Ti-Al alloy, effect of heat treatment on strength and elastic props. 77−55976
- Nb-Ti-Ti_3O system, phase analysis, struct. stabilization 77−90330
- Nb-Zr (1 at.%), He irregular bubble growth by ion implanatation, TEM investig. 80−15164
- Nb-Zr (1 wt.%), He bubble growth, α-particle effects 78−67749
- Nb-Zr-C alloys, plastic deform. and annealing, dislocation struct. *(Russian)* 80−20951
- Nb-Zr-N, deformed and annealed, internal friction, rel. to structural state *(Russian)* 78−6957
- Nb-Zr-O, corrosion resistance in molten Li *(Russian)* 78−31567
- Nb-Zr(Nf)(Mo)(W)(Rh), dil., neutron irradiation at 4.6K, influence of impurities on defect prod. 79−55790
- Nb_3(Al,Ge) supercond., diffused layer critical current depend. on Cu before and after annealing *(Russian)* 79−69643
- Nb_3Al, BCC struct., cold working and converting to A-15 struct. 78−64553
- Nb_3Al, complex refractive index meas. 80−93264
- Nb_3Al, mechanical and supercond. props. 79−38214
- Nb_3Al, supercond. props. and lattice parameter, comp. and neutron irrad. effects 80−70880
- Nb_3Al-Nb_3Ge-Nb_3Ga system, supercond. crit. temp., composition determ., effect of annealing 77−8218
- Nb_3(AlSi), ternary supercond. alloy films, T_c, props. *(Russian)* 78−88055
- $Nb_3Al_{0.2}Si_{0.8}$, A-15 alloy synthesis by ion implantation 78−80489
- $NbC_{0.89}$, implantation or diffusion of C rel. to supercond. transition temp. 77−69442
- NbC_x (x=0.868, 0.834, 0.766), single crysts., thermomech. behaviour during annealing 80−3104
- NbC_x, reactor irrad. effects on elec. resist. and supercond. props. *(Russian)* 78−47895
- NbC_x, self diffusion, near surface effect 79−42303
- Nb_3Ga, comp. and LRO effects on supercond. T_c 77−39992
- Nb_3Ga, supercond. crit. temp. and struct., heat treatment and stoichiometry effects 77−43769
- $Nb_{78}Ga_{22-x}Mn_x$, supercond. props., influence of Mn mag. impurities 80−54825
- $Nb_{80}Ga_{20-x}Mn_x$, supercond. props., influence of Mn mag. impurities 80−54825
- Nb_3Ge amorphous films, X-ray diffr. analysis of microstruct. 78−72035
- Nb_3Ge, DC sputtered films, annealing and mech. deform. effects on struct. and supercond. props. 79−38217
- Nb_3Ge, neutron irradiated, A15 compound, recovery of T_c by annealing 78−52132
- γ-NbN, single crystal growth by annealing, NbN in nitrogen gas pressure 79−8246
- $4NbO_{0.76}$ thin film, FCC cell struct. investigation 80−92796
- Nb_3Pt, neutron irrad. effects on supercond. props. 79−38224
- $NbSe_x$, nonstoichiometric, thermodynamic props. and crystal struct. *(Japanese)* 78−11206
- $NbSe_x$, x=1.48-2.0, nonstoichiometric, press.-comp.-temp. rel. determ. by annealing 79−74139
- Nb_3Si A15 phase from amorphous Nb-Si alloys, high-press. synthesis 80−93516
- Nb_3Si, ion implantation synthesis, supercond. transition temp. optimization 79−38218
- Nb_3Sn, critical current enhancement by low temp. fast neutron induced flux pinning centres 78−52177
- Nb_3Sn, effect of O ion irradiation on supercond. 78−52131
- Nb_3Sn, filamentary conductors, type-II, low temp. 30 GeV proton effects on critical props. 78−52178
- Nb_3Sn multifilamentary composite superconductor, effect of heat treatment on supercond. props. 79−33376
- Nb_3Sn, O^{4+} bombarded, Mossbauer studies 80−2672
- Nb_3Sn, radiation damage effect on superconducting props. 78−52127
- Nb_3Sn strip, made by diffusion method, crit. curent anisotropy, Zr alloying addition effects *(Russian)* 78−47921
- Nb_3Sn, supercond. tape, crit. current, effect of Sn-Nb phase, annealing 79−24119
- Nb_3Sn supercond. tape substrate structural changes 79−33373
- Nb_3Sn superconductor, low temp. deuteron irradiation 78−52182
- Nb_3Sn-Cu composite superconductors, in-situ, AC losses 79−38283
- Nb_3Sn-Zr (0.8%), supercond. tape, crit. current, two stage annealing effect *(Russian)* 77−63046
- Nb_3Sn(Al), neutron irradiated, A15 compound, recovery of T_c by annealing 78−52132
- Nb_3Sn(Ge), resistivity and T_c measurement after low temp. neutron irradiation 78−52123
- NbTi, filamentary conductors, type-II, low temp. 30 GeV proton effects on critical props. 78−52178
- NbZr(Hf)-C(N) alloys, phase comp. after casting and annealing, precip. 79−56983
- Nd-Co film, amorphous, exam. of domain struct. 78−68336
- $Nd_xPr_ySm_zCo_5$ permanent magnets, coercive force, low-temp. annealing influence *(Russian)* 80−39812
- Ni (111), adsorption and decomp. of hydrocarbons, high resolution EELS study 80−40739
- Ni alloy, rolled, annealing texture *(Russian)* 77−21159
- Ni alloy 718, intermetallic second phase obs. using electrolytic extraction and SEM 79−34074
- Ni alloy EhI867, effect of structural state on fatigue and heat resistance *(Russian)* 79−34140
- Ni alloy IN-738, Y_2O_3 (1.5 wt.%) addition, mechanical alloying 77−40427

annealing continued
- Ni and Ni-Co, recovery of single crystal after varying amounts of cold work 79−100162
- Ni based superalloy, interaction of annealing twins in fcc metals and alloys 78−68712
- Ni, cathodically H charged, isothermal ageing 79−15703
- Ni, cold rolled, influence of impurities on recovery and recrystallisation, positron annihilation meas. 79−15696
- Ni cold worked, annealed, exam. of anelastic relaxation at low temp. 78−84877
- Ni, cold-worked, impurity-induced vacancy clustering 79−99972
- Ni, creep at 77, 295K, formation of five struct. 80−60926
- Ni, deformed, struct. form. during annealing, Ni_3Al type ordered phase precipitation *(Russian)* 80−45325
- Ni, deformed by filing, fine struct. obs. *(Russian)* 77−21309
- Ni, dislocation intersection and solution strengthening, effect of solute on obstacle profiles 80−7590
- Ni electrodeposits, fibre textures before and after thermal treatment 79−91693
- Ni, electroplated, fuchsin additive effect on low-temp. annealing characts., resist. meas. 77−32725
- Ni, electroplated layers, internal friction and ΔG effect, rel. to bath comp. and annealing 78−19296
- Ni ferrite, quenched, Neel temp. and initial susceptibility 80−75762
- Ni film, electrodeposited, recrystallisation kinetics, X-ray scatt. *(Russian)* 78−60045
- Ni film, evaporated, galvanomag. and mag. props. 78−23180
- Ni film, mag. structures and stresses, ferromag. resonance 78−72375
- Ni film, vac. deposited on liquid-He-cooled sapphire, galvanomag. props. 79−95519
- Ni film on leucosapphire, island growth as annealing in Ag vapour *(Russian)* 78−51830
- Ni films, adhesion on graphite 80−80141
- Ni films, HCP and amorphous, RF sputtered, O_2 incorporation, ESCA obs. 80−10832
- Ni, foil, electron bombard., impurity redistrib. during third stage of annealing, residual resist. meas. 80−6434
- Ni, grain boundary ledge density, effect on flow stress 78−48465
- Ni, H diffusion in H_2 quenched sample, elec. resist. recovery 78−2299
- Ni, H diffusion in imperfect lattice, annealing and cold rolling effect 80−49425
- Ni, high-purity, softening of strained single crystals *(Russian)* 80−40499
- Ni, Hopkinson effect, mag. field depend. *(Russian)* 79−4657
- Ni, integranular precipitation after annealing, ion imaging microanalysis *(French)* 79−61594
- Ni, laser irrad., elec. cond. recovery *(Russian)* 77−55512
- Ni, O free, annealing in photoemission electron microscope, twin density recrystallised grain size relation *(German)* 78−52850
- Ni, oxidation kinetics, influence of intermediate annealing treatment 80−89412
- Ni, plastically deformed, recovery stages III and IV investig. by positron annihilation 77−31715
- Ni, polygonisation, high press. grain growth, dislocation struct., electron microscopic obs. 77−16613
- Ni precipitates, isothermal annealing influence on structural state, X-ray diffr. anal. *(Russian)* 80−100849
- Ni, push-pull fatigued polycrystals, point defects, elec. excess resist. meas. 80−100910
- Ni, self-ion irradiated, defect clusters, annealing 78−18687
- Ni, shock hardening, anomalous residual, at short pulse duration 80−20942
- Ni single crystals, cyclically deformed, effect on domain patterns and dislocations 78−71740
- Ni, sputtered, on Si, annealing effects on transmission electron diffr. patterns, silicide form. 78−91562
- Ni, thin film, size depend. electronic cond., annealing effects 79−47174
- Ni thin films, annealing and oxidation effects in stress, Michelson interferometer meas. 77−2650
- Ni, void annealing and void formation energy 77−68962
- Ni, volume strained, sintered, porous, physicomechanical props., electrical resistivity 77−12572
- Ni, volume-strained sintered porous, physicomech. props., u.s. vibration propag. velocity 77−1823
- Ni:^{129}Te, implanted atom sites, Mossbauer obs. 77−20756
- Ni:In, He, lattice defect struct., PAC meas. 80−70190
- Ni/Au-Ge/GaAs contact system, alloying behaviour, microprobe AES and X-ray diffr. 80−54548
- Ni/Cr-Fe-C, Inconel, dislocation intersection and solution strengthening, effect of solute on obstacle profiles 80−7590
- Ni-A-Ti (6,1 wt.%), γ' phase precip., deform. effects *(Russian)* 78−48404
- Ni-Al (15 wt.%) single crystals, morphological changes of γ' precipitates during uniaxial stress-annealing 79−83236
- Ni-Al (51 to 55 at.%), vacancy defective, TEM exam. of structure 78−76677
- Ni-Al (6.3 at.%), influence of localised order on thermo-EMF and Hall-EMF *(Russian)* 78−6951
- ζ Ni-Al system, solid soln., interdiffusion *(Japanese)* 80−70476
- Ni-base wear resistant dispersion hardened electrolytic coating. annealed and sintered 78−35593
- Ni-Co, dislocation intersection and solution strengthening, effect of solute on obstacle profiles 80−7590
- Ni-Co films, electron-beam evaporated, magnetoresist. anisotropy, deposition temp. effect 80−34528
- Ni-Co-Cr superalloy, powder produced, necklace struct. development 80−40395
- Ni-Cr, (30 wt.%), collective dislocation movements, in situ study 80−100243
- Ni-Cr, deformed, struct. form. during annealing, Ni_3Al type ordered phase precipitation *(Russian)* 80−45325
- Ni-Cr, heat resisting, dispersion hardened, electrical resistance meas. *(Russian)* 77−66708
- Ni-Cr, solubility limit determ., X-ray method 79−43199
- Ni-Cr (0-35 at.%), neutron irrad. at 25K, damage, elec. resist. obs. *(French)* 80−54286
- Ni-Cr alloys, crystallisation anomalies *(Russian)* 78−19719
- Ni-Cr-Al, protective coating, exam. of interdiffusion kinetics, development of analysing procedure 79−5085
- Ni-Cr-Fe, Inconel, effects of heat treatment on surface segregation, Auger spectroscopic exam. 80−7602

annealing continued

- Ni-Cr-Fe (75, 35, 12 wt.%), electron and α-particle irrad., positron annihilation and elec. resist. meas. 79—83054
- Ni-Cr-Fe alloys, radiation enhanced precip. and dissolution of precipitates, point defect kinetics and dislocation obs. 80—108467
- Ni-Cr-W (20, 10 to 40 wt.%), phase composition, struct. and props. 80—21034
- Ni-Cr-W-Co-Ti heat resistant alloy ZhS6K, fatigue resistance, heat treatment and protective coating effects 77—81320
- Ni-Cr-ZrO_2, dispersion hardened, sintered, rupture 77—21272
- Ni-Cr(Mo), oxidation effect on magnetic props. *(Russian)* 78—23868
- Ni-Cu, electron-irrad., neutron-scatt. studies 80—75268
- Ni-Cu (30 wt.%), cast cold- and warm-worked, recrystallization 79—29092
- Ni-Cu alloys, short-range atomic clustering, residual resist. meas. 80—29386
- Ni-Fe, epitaxial thin film, mag. structures and stresses, ferromag. resonance 78—72375
- Ni-Fe, influence of atomic ordering on spin waves 79—7987
- Ni-Fe-Mo, K-effect, Mossbauer study 80—39998
- Ni-Fe-Nb, Hardperm alloy, sheets, effect of sheet thickness, and annealing, on mag. props. 78—76772
- Ni-Ge (2 wt.%), positron annihilation, photon ang. distrib. meas. effect of deformation, annealing temp. *(Russian)* 78—35220
- Ni-HfO_2 (3 wt.%), dispersion hardened alloy VDU-2, thermal and mech. treatment 77—90376
- Ni-In, ion-implanted, impurity defect interaction and diffusion, Rutherford backscatter and TDPAC expts. 80—34039
- Ni-Mo, and Ni-Mo-V alloys, struct. changes on annealing *(Russian)* 77—21145
- Ni-Mo (20.8 wt.%), order, heat treatment effects 80—40406
- Ni-Mo-W, type N55M20V25, quenched at various cooling rates, phase transformations *(Russian)* 79—66052
- Ni-Nb amorphous alloy, transformation to crystalline state, ion emission microscope study *(Russian)* 79—82158
- Ni-Nb-C, obtained by liq. quenching, superconductivity 80—75699
- Ni-P, struct. obs. by X-ray diffr., low temp. annealing and deform. effects 79—56995
- Ni-P amorphous alloy prep. by ion implantation 78—22748
- Ni-ThO_2, irradiated with 5 MeV Ni^{++}, ThO_2 redistrib. 78—71771
- Ni-ThO_2 (2.51 wt.%), dispersion hardened, high temp.-strength, deform. method and annealing effects 79—1882
- Ni-ThO_2(HfO_2) dispersion hardened alloys, recrystallisation during annealing, O_2 partical press. effects *(Russian)* 78—3140
- β-Ni-Ti, struct. changes during annealing, TEM and selected area diffr. 79—34081
- Ni-Ti (48 at.%), annealed and rolled electron microscope and probe analysis of structure 79—100189
- Ni-Ti/Cu composite, plastic deform. influence on internal friction *(Russian)* 80—100871
- Ni-W (20 to 50 at.%), phase distrib. var. with annealing time, metastability of hexagonal phase *(Russian)* 77—8851
- α-Ni-Zn, solid soln. diffusion annealing effect *(Japanese)* 80—34255
- Ni-Zn diffusion couple, annealing and reaction diffusion *(Japanese)* 78—51749
- Ni-ZrO_2, dispersed inclusions, effect on recovery and recrystallisation 77—25064
- Ni-ZrO_2, electron-beam-evaporated condensate, cold deform. and annealing effects on microstruct. 80—16331
- NiAl, annealed near stoichiometric, elec. resist. meas. 77—8071
- NiAl, quenched and annealed, void formation 79—46652
- β'-NiAl, single cryst., quenched and annealed, ω-like diffr. effects, TEM and X-ray diffr. study 79—60216
- $Ni_{1-x}Al$ solid solution, vacancy ordering exam. by electron diffr. after annealing 78—3123
- Ni_3Al, Mossbauer spectra, exam. of struct., superlattice population anal. 78—88240
- Ni_3Al-Ni_3Nb composite, long term annealing effect on impact strength and long-term strength *(Russian)* 79—74182
- $NiClO_4$, neutron activated, radiation annealing 80—93569
- Ni_2Cr, neutron irrad., point defect prod. and annealing 78—87718
- NiCrAlY, mechanically alloyed, maintaining elongated grain struct. after deform. 77—36534
- $Ni_{0.75}Fe_{0.25}$, influence of atomic ordering on spin waves, inelastic neutron scatt. 77—69516
- Ni_3Fe, change of H_2 diffusivity with order-disorder transformation 80—59729
- Ni_3Fe, compression induced mag. anisotropy and superlattice dislocations, annealing effect 78—31067
- Ni_3Fe, compression induced magnetic anisotropy, annealing effect 80—93112
- Ni_3Fe, magnetocryst. anisotropy, annealing temp. depend. 80—103828
- Ni_3Fe, short range order determ. after heat treatments 79—96044
- Ni_3Fe-Sn, dil., atomic order detection by ^{119}Sn spectroscopy 80—39993
- $Ni_{36}Fe_{32}Cr_{14}P_{12}B_6$ metallic glass, mech. props. and thermal stability 80—76362
- $NiFe_2O_4$ ferrite, mag. props., neutron irrad. 80—103858
- $Ni_{40}Fe_{40}P_{14}B_6$, amorphous alloy, microstruct. study of crystallisation 77—86062
- NiGa, point defects, lattice parameter determ. 78—38695
- Ni_5Ge_3, amorphous film, elec. resist., microstruct. and annealing 77—85188
- $Ni_{98}M_2$, M=impurity metal, formation of MH(D)-complexes 80—65236
- Ni_3Mn, change of H_2 diffusivity with order-disorder transformation 80—59729
- Ni_4Mo, domain struct. on annealing, and dislocation struct. during deform. *(Russian)* 77—16640
- $Ni_{65}Mo_2Fe$, O_2 effect on secondary recrystallisation and mag. props. 80—35201
- NiO, single crysts., TEM of dislocations 79—4306
- NiP amorphous alloy, heat treatments influence on opt. props., struct. and DC resist. obs. 80—80892
- Ni_3Pt, change of H_2 diffusivity with order-disorder transformation 80—59729
- NiSb, dilute alloy, impurity-induced vacancy clustering 79—99972
- $Ni_{0.96}Sb_{0.04}$, surface segregation, XPS and AES obs. 80—76135
- NiSe film, vac. deposited, phase transformation, electron microscope studies 80—2302
- NiSe, thin film phases, struct. and resist. 78—39236
- $NiSi_2$, amorphous, crystallisation by energy beam annealing 79—69012
- NiTa, exam. of oxidation 79—96221

annealing continued

- $Ni_{0.36}Zn_{0.64}Fe_2O_4$, normal grain growth 78—72796
- $Ni_{100-x}Zr_x$, (x=34-40) metallic glass, cryst., isothermal annealing behaviour 80—6367
- PLZT, RF sputtered thin film, ferroelectric props. 79—69780
- Pb, anomalous grain growth 77—8855
- Pb, effect of O ion irradiation on supercond. 78—52131
- Pb, electron irradiation at 4.7K and below 3K, annealing expts. 77—11595
- Pb film, amorphous, nucleated with Mo, supercond. and normal elec. cond. 77—24633
- Pb, film, deposited on Si substrate, residual strains 78—18915
- Pb, high purity, polycrystalline, Bordoni relaxation peak high vacuum annealing effect 78—39828
- Pb, O ion irradiated, damage rate decrease 78—26604
- Pb, plastically deformed, annealed, positron trapping rate, 4-100K 78—31275
- Pb, positron annihilation, Doppler broadening, 4.2 to 600K 79—47540
- Pb, sample length effect on plasticity 78—44179
- Pb, superconducting film, radiation induced critical temp. 79—87179
- Pb, vacancy and divacancy props., exam. via quenching and annealing 78—47343
- Pb-Au (0-0.0918 at.%), lattice parameter changes due to Au dissolution 79—77558
- Pb-Bi, supercond. tunnelling, effect of phase composition and press. 79—15261
- Pb-Fe, supercond. films, modification of props. by Fe grains *(French)* 79—60957
- Pb-Sn (62 wt.%), superplastic eutectic, exceptional ductility 78—27579
- $Pb_{1-x}Al_xF_{2+x}$, ionic cond. of quenched and annealed specimens, interstitial cond. mechanism 80—2199
- PbF_2-AlF_3, ionic cond., characts., effect of trivalent cations 77—89576
- PbI_2, first-order 2H-4H polytype transition, exciton spectroscopic study 80—59647
- $Pb_{0.8}In_{0.2}$, superconducting, flux-flow noise 79—95556
- $Pb_{80}In_{20}$ foil, deformed, annealed, correlation between pinning strength and flux flow noise charges 77—43792
- $Pb_{1-x}Mn_xTe$ (x=0.005, 0.001, 0.05), solid solns., exam. of electrical and thermal props. 79—1599
- $PbNb_2O_6$, O defects and elec. props. anomalies 79—42898
- PbO-B_2O_3, solder glass, thermal reduction of Cu^{2+} and Cu^+:Cu^{2+} effect on thermal props. 78—15350
- PbO-Bi_2O_3-GeO_2, exam. of glass forming and liquid phase separation regions, and optical props. 78—88453
- PbS epitaxial layers, ion bombardment effects on struct., and annealing 79—10882
- PbS, low carrier conc., prep. and props. 77—39846
- PbS, surface defect annealing *(Russian)* 77—47658
- PbS:Tl, Hall and Seebeck coeffs., Hall mobility, impurity states 80—15545
- $Pb_xSn_{1-x}I_2$, thin films, photosensitivity, ageing and annealing effects *(Russian)* 78—6804
- $Pb_{1-y}Sn_ySe$, electron irrad., isochronous annealing of cond., Hall mobility and recomb. lifetime 79—56227
- $Pb_{0.8}Sn_{0.2}Te$:In, implanted thin epitaxial films, laser annealing 79—65104
- $Pb_{1-x}Sn_xTe$ (x=0.15 to 0.20), SEM study, dislocation density, and carrier density and mobility 79—69107
- $Pb_{1-x}Sn_xTe$, electron irrad., isochronous annealing stage of Hall mobility, cond. and recomb. lifetime 79—56227
- $Pb_{1-x}Sn_xTe$:Cd, deep energy level, temp. depend. of elec. cond. 78—18994
- $Pb_{1-x}Sn_xTe$:Cd, long-wavelength photosensitivity shift on annealing, Cd influence 78—26912
- $Pb_xSn_{1-x}Te$, RF sputtered film IR detector, photocond. response speed improvement by annealing 79—58790
- $Pb_{0.95}Sr_{0.05}(Zr_x, Ti_{1-x})O_3$-$Nb_2O_5$, phase coexistence range, lattice consts. 80—92680
- PbTe, carrier conc. inhomogeneity 78—52019
- PbTe, epitaxial film on fluorphlogopite, effects of annealing in Te vapour 77—80709
- n-PbTe, low temperature electrical transport, Hall effect 80—84478
- PbTe:Ga, location, behaviour of Ga, electrophysical props. meas. 79—38016
- PbTe-Ga_2Te_3, phase interaction, DTA, XPA and microstructural anal. 80—96625
- $PbTiO_3$, amorphous, crystallisation process, DTA and Raman spectroscopy meas. 80—75161
- $PbTiO_3$-$Pb(Fe_{1/2}Nb_{1/2})O_3$-$PbZrO_3$, with additions, exam. of electrical characteristics 80—2698
- Pd, annealed, cold worked, H_2 diffusion effect on mech. props. *(Japanese)* 78—10222
- Pd film, VPE growth on Au(111), interface struct. 79—95297
- Pd film on Si, Xe ion beam induced form. of PdSi 80—10800
- Pd films, evaporated, and thermoelec. power, annealing effects 80—39684
- Pd, H phase hardened, recrystallisation study 80—60883
- Pd, silicide formation due to laser and electron beam annealing 80—84849
- Pd, transport props. 40 mK-6K 78—51968
- Pd-Ag microwires, electrical resistance, influence of gaseous environment in heat treatment *(Russian)* 80—20146
- Pd-Ag-Si alloys, amorphous, crystn. kinetics, DSC meas. 80—1933
- Pd-amorphous Si thin film interaction, metal rich Pd-silicide formation 80—2284
- Pd-Cu-Ga, cold work and annealing-induced hardening, X-ray diffr. anal. and metallographic exam. *(Russian)* 79—38844
- Pd-Ni bilayers, on single cryst. Si, vacuum annealing, silicide form. 79—51444
- Pd-Pt bilayers, on single cryst. Si, vacuum annealing, silicide form. 79—51444
- Pd-Si, struct. obs. by X-ray diffr., low temp. annealing and deform. effects 79—56995
- Pd-Si structure, epitaxial silicide growth, LEED and AES study 80—103590
- Pd-W, elect. resist., mag. susceptibility, Hall coeffs., in plastically deformed state and after annealing *(Russian)* 79—66174
- $(Pd_{80}Au_7Si_{13})/Fe_{30}$, compositionally modulated amorphous film, diffusion, struct. relax. 80—103518
- $Pd_{77.5}Cu_6Si_{16.5}$ metallic glass, diffusion of Au 78—55983
- β-PdDx (x=0.710, 0.742, 0.754, 0.780), structural changes in temp. region of 50K anomaly 80—100131

annealing continued
  Pd_2Ge, PdGe, growth kinetics on single cryst. and evaporated Ge 78—22985
  α-PdH_x, impurity motion, neutron scatt. obs. 80—24682
  α-PdH_x, local mode intensity var. with conc., temp., direction and annealing 77—11653
  PdH_x, PdD_x, ordering, resistivity, annealing and neutron diffr. obs. 79—34030
  PdSi alloys, amorphous thermal behaviour and crystallisation kinetics 78—26446
  PdSi, amorphous, structural relaxation enhancement following stress reduction 80—3118
  Pd_2Si, on Si substrate, thermally induced Si accumulation, AES study 80—24718
  Pd_4Si and Pd_2Si, amorphous, crystallisation by energy beam annealing 79—69012
  $Pd_{80}Si_{20}$, amorphous alloy crystn., high press. effect 78—95001
  $Pd_{82}Si_{18}$ glassy, long term creep tests, isoconfigurational viscosity rel. to annealing treatment 79—66122
  $(Pd_{85}Si_{15})_{61}/(Fe_{85}B_{15})_{39}$, compositionally modulated amorphous film, diffusion, struct. relax. 80—103518
  $Pd_{77}Si_{17}Cu_6$, amorphous, struct. changes due to cold rolling and low temp. annealing 79—66072
  $Pd_{1-x}W_x$, calc. of short-range order parameters from X-ray scatt. data *(Russian)* 80—75367
  Pt (997) surface, partial facetting, He beam scatt. and LEED study 80—103547
  Pt, deuteron irrad., energy release and resist. recovery, self-interstitial-atom interaction energies 79—95002
  Pt, elec. cond., impurities on grain boundaries 79—87076
  Pt, electron and deuteron irrad., close Frenkel pair recomb. during annealing 78—87716
  Pt, electron irradiated, interstitials activation vol. 79—51154
  Pt foil, quenched, 1.2 MeV electron irrad., subthreshold irrad. effects 78—51585
  Pt, Frenkel defect migration and reactions, by subthreshold recoil events, exam. 78—47364
  Pt, interstitial thermal conversion study by elec. cond. meas. 80—15096
  Pt, isochronal recovery of high energy d-Be neutron damage 78—51592
  Pt, neutron damage, positron annihilation 80—65056
  Pt, quenched, deviations from Matthiessen's rule 77—69289
  Pt, radiation damage with radioactive probes, TDPAC meas. 77—24336
  Pt, recovery of thermal-neutron-irradiated samples 78—95081
  Pt, silicide formation due to laser and electron beam annealing 80—84849
  Pt wire, cold worked, recovery of elec. resist. 77—12643
  Pt:^{181}Hf, interaction of implanted impurity with radiation induced lattice defects, TDPAC meas. 80—24494
  Pt-Cu, surface composition, XPS *(Portuguese)* 80—24722
  Pt-Fe alloy foils prep. by electrodeposition of Fe 80—35113
  Pt-Mo(Re), and Pt-(Re-Mo) bimetal sheet specimens, interdiffusion, 1500°C *(Russian)* 77—62683
  Pt-Ni bilayers, on single cryst. Si, vacuum annealing, silicide form. 79—51444
  Pt-Rh alloy, on rock salt, epitaxial growth and struct. 77—20211
  Pt-Si contact, annealed in H_2 ambient, elec. props. 78—64110
  Pt-Si contact, silicide layer struct. and elec. props. sputter etching and annealing ambient effects 77—62991
  Pt-Si Schottky barriers on Si, laser formation and characts. 80—60079
  PtSi, epitaxial film, cryst. perfection and thermal stability, channelling and backscatt. meas. 79—99255
  PtSi film formation by ion sputtering and annealing, form. and exam. problems 80—100782
  PtSi, growth under protective layers on Pt covered Si substrates, X-ray diffr. and Rutherford backscattering anal. 78—22965
  Pu, oxidation, binding energies, Auger and X-ray photoelectron spectra study 80—76550
  PuO_2, alpha radiation damage, point defect ingrowth and annealing behaviour 77—27926
  Re, metal losses during annealing in O_2, air, water vapour, high temp., low press. *(German)* 77—8856
  Re-Fe-Al, physical-chemical investigation *(Russian)* 78—15362
  Re-Ir (1 wt.%), positron annihilation, photon ang. distrib. meas. effect of deformation, annealing temp. *(Russian)* 78—35220
  Re-Mo bimetal sheet specimens, interdiffusion, 1500°C *(Russian)* 77—62683
  Rh, film, annealing effect on struct., TEM, electron diffr. study 78—76682
  Ru (~001) stepped surface, O_2 chemisorption, LEED and AES obs. 80—11947
  RuS_2 amorphous, prep. at ambient temp., magnetic structure 80—35119
  S:P, ion implanted, defect annealing 450-800°C, deep-level transient spectroscopy 79—47042
  $(SN)_x$ films, influence of annealing on thermopower and conductivity 78—91782
  Sb film A1-type supercond. vapour-quenched transition temp., A7-type phase transition 78—52145
  Sb, Mossbauer radiation, Rayleigh scatt., Debye-Waller factor determ., annealing effect 80—39963
  Sb:^{111}Cd,In, elec. field gradient, TDPAC expts. 80—55002
  p-$Sb_{1.48}Bi_{0.52}Te_3$, extrusion deformed, powder dispersion degree influence on thermal and elec. props. *(Russian)* 80—39366
  $Sb_{1.48}Bi_{0.52}Te_3$, obtained by zone crystallisation, effect of extrusion and annealing on elec. props. 79—96038
  Sb_2Te_3 epitaxial films, growing conditions effect on elec. cond., thermo-EMF 80—39687
  Sb_2Te_3, Mossbauer radiation, Rayleigh scatt., Debye-Waller factor determ., annealing effect 80—39963
  Sb_2Te_3-Bi_2Te_3 and Sb_2Te_3-Sb_2Se_3 systems, thermal cond. change during phase transitions 80—100368
  Sb_2Te_3-Sb_2Se_3, ordered structure formation, heat treatment effect on thermal cond. 80—54448
  Sc, strength and plasticity 77—90429
  Sc-H, conc.-temp. depend. at room temp. of elec. resist. thermo-EMF, mag. susceptibility, and Hall coeff. 80—29382
  Sc_2O_4, polycryst., form. conditions of anion vacancies, phase comp. 80—54220
  Se, amorphous, evap. layers, electrophotographic props. depend. on thermal treatment of initial material 77—76978
  Se, film, effect of thermal history and substrates or crystn. by vac. condensation 77—15713

annealing continued
  Se, glass transition temp., enthalpy rel. to annealing, DSC 77—15561
  Se powder compacts, sintered, electrical cond. 80—70693
  Se, single crystals, fast neutron irradiated, annealing expts., dark conductance, reflectivity spectra 77—85266
  Se-As-Ge, glass alloy system, light irradiated, annealed, photoinduced absorption change, random network model predictions 79—59773
  $Se_{75}Ge_{25}$, obliquely deposited amorphous films, photo-induced optical effects, effect of postannealing and preannealing 79—56871
  Si, ^{75}As implantation, scanned CW electron beam annealing 79—99225
  Si, ^{75}As implanted, comparison of effects of pulsed ruby laser and pulsed electron beam annealing 79—69135
  Si (001) wafer, pyramidal hillocks, TEM obs. during chemical etching 80—70508
  Si (100), self-ion implanted, laser annealing, channelling and TEM meas. 80—24466
  Si (111) surface, 500 eV Ar^+ bombard., high temp. annealing, recovery, RHEED obs. 78—87723
  Si, (111) surface, annealing of scratches 79—60609
  Si (111) surfaces, 2×1 to 7×7 struct. transition during annealing, LEED obs. 79—42352
  Si, ambient effect of O precipitation, self interstitial mechanisms, IR spectra, TEM study 80—66510
  Si, amorphised by ion implant., localised states and cond., irrad. and heat treatment, doping 80—39529
  Si, amorphous, film, hydrogenation by H diffusion, effect on elec. cond., band gap *(Korean)* 80—45326
  Si, amorphous, glow discharge, fatigue effect in luminesc., recovery by annealing 80—50416
  Si, amorphous, glow-discharge deposited, ODMR spectrum, deposition temp. and annealing effects 80—50229
  Si, amorphous, hydrogenated, photolum., heating effects 78—15204
  Si, amorphous, hydrogenated, pure and B doped, annealing effect on cond. and band gap states *(Korean)* 79—15142
  Si, amorphous, ion implanted, laser annealing, reflectivity meas. 80—29039
  Si, amorphous, large vacancy cluster annealing by ion bombard, EPR investig. 77—68965
  Si, amorphous, small dia. laser beam annealed, temp. distrib. and microstructure 79—73098
  Si, amorphous, sputtered, resist. control by ion implantation 80—100262
  Si, amorphous, substrate orientation effect on regrowth by laser pulses, channeling, backscatter 80—84409
  Si, amorphous, UHV evaporated, annealing behaviour of spin density 80—93163
  Si, amorphous, undoped and B doped, ESR-linewidth temp. depend. meas. 80—20459
  Si amorphous film, annealing behaviour of void network 78—18551
  Si amorphous film, crystn. on annealing at low temps. in contact with Al 80—24765
  Si amorphous film, glow-discharge, optically detected mag. reson., annealing and substrate temp. effects 80—20519
  Si, amorphous film, heavily doped, glow discharge, AC cond. 80—49718
  Si, amorphous films, hopping conduction, dangling bond generation by high temp. annealing 80—60115
  Si amorphous films, laser beam annealing, optical information storage possibilities 79—87515
  Si, amorphous layer, comparison of laser and electron beam pulsed annealing 79—69374
  Si amorphous layer, ion-beam induced epitaxial regrowth 79—69378
  Si amorphous layers, glow-discharge, laser-annealed, elec. props. 80—75661
  Si amorphous layers, on Si substrates, deposited and ion-implanted, laser-annealing behaviour 79—69373
  Si, amorphous layers, RF-sputtered on sapphire, crystallisation by CW ion laser annealing 80—80109
  Si, annealed, electron irradiated, positron annihilation 78—87713
  Si, annealed, ion-implanted, in MOSFET, defect spatial distrib. 77—11973
  Si, annealed, neutron-irradiated, EPR centre (S=1), characts. 80—71177
  Si, annealed, photoluminesc. anal. of defects 80—80836
  Si, annealing, impurity film form., energy loss anal. 77—31916
  Si, annealing, using laser pulses, impurity incorporation at melt-cryst. interface 80—59504
  Si, annealing during Czochralski growth, influence on defect density 80—60769
  Si, annealing of vacancy clusters produced by ion bombardment 77—89485
  Si, As segregation, TEM obs. 77—63674
  Si, B implanted, enhanced annealing behaviour, p-n junction formation 77—43233
  Si bridging epitaxy from Si windows onto SiO_2, ruby laser pulse annealing 80—44441
  Si, CW laser annealed, defect luminesc. 80—50388
  Si, cast polycryst., laser annealed for solar cells 80—93918
  Si, compressed, polycrystalline, deform. and recrystallisation texture 78—27538
  Si, cross-slip of single dissociated screw disclocations, double etching and X-ray topography studies 80—15104
  Si, cryst. and amorphous surface layers, ruby laser pulse effects 79—69920
  Si, crystal defects and impurities interaction obs. by electron microscopic methods 80—65003
  Si crysts., deformed, strain distrib. characterisation, annealing response 77—70140
  Si, Czochralski grown, inhomogeneous O precip. and stacking fault form. 79—14820
  Si, Czochralski grown, oxide precip. homogeneous nucleation 80—65221
  Si, Czochralski grown, oxide precipitates, diffusion-limited growth 80—97484
  Si, Czochralski grown crystal, O precip., nucleation behaviour and dislocation loop form. *(Japanese)* 80—59664
  Si, Czochralski-grown crysts., thermally induced microdefects, annealing temp. and starting material effects 80—49141
  Si, defect generation and annealing by intense subthreshold electron beam bombardment 79—51149
  Si, deformation, annealing characts., X-ray study 78—75713
  Si, deformed, defect states associated with dislocations, capacitance transient spectroscopy 79—42483
  Si, deformed crystal, Czochralski and float zone growth, Luder's bands 79—79025

annealing continued
Si, dense plasma dynamics during pulsed laser annealing, carrier density, recombination 80−84479
Si, diffusion of nitrogen during annealing, effects on ion implanted layers 77−24436
Si, dislocation defect states, capacitance transient spectroscopy 79−82549
Si, dislocation free, C and O impurity clouds, heat treatment influence on light scatt. 80−6427
Si, dislocation loops, creation in region of interface, after annealing 79−82210
Si, dislocation motion near surface 79−82219
Si, dislocation structure, effect of induction heating *(Russian)* 77−21180
Si, dislocation-free, O_2 precip., IR and TEM obs. 80−29173
Si, dislocationless plates, microdefect dissolving due to high temp. annealing *(Russian)* 80−54378
Si, divacancies due to proton irrad., IR absorpt., annealing effects 80−20673
Si, divacancy charge states, photoconductivity spectra 77−15899
p-Si divacancy charge transfer during annealing after fast neutron bombard., piezo-spectroscopic study *(Russian)* 77−28607
Si, dopant segregation by pulsed-laser annealing, test case for thermal melting concept 80−24489
Si doping by thermal neutron irrad., annealing characts. of bulk electron traps obs. 80−49244
Si dosimetry diode, irrad. by γ-rays and fast neutrons, lattice defect annealing *(Czech)* 79−45570
Si, elec. props., plastic deform. and annealing temp. depend., dislocation effects *(Russian)* 77−89765
p-Si, elec. props. and thermal defects, influence of high temp. treatment 79−69531
Si, electron beam annealing, beam voltage effect modeling 80−75275
Si electron beam deposited film, epitaxy by pulsed laser annealing 78−56055
Si, electron beam scan annealed, deep levels 80−65481
Si, electron irrad., effect on positron annihilation 78−76552
p-Si, electron irrad. induced defects, thermally stimulated capacitance 77−11933
Si, electron irrad. induced defect form., annealing effect, carrier parameter changes 77−43250
n-Si, electron radiation defect annealing, negative stage, Hall coefficient, defect levels 79−90701
Si, electronic defect levels in self-implanted CW laser annealed samples 79−87053
Si epitaxial layer regrowth due to laser annealing mechanism, liquid and solid phase regimes 80−100712
Si, epitaxial layers, cryst. quality improvement by ion implantation, backscatt. and TEM obs. 79−42397
Si, epitaxial regrowth of thin amorphised layers by laser annealing, absorpt. coeff. influence 79−46968
Si, epitaxial wafer, saucer pit microdefects reduction by intrinsic gettering 80−75450
Si film, amorphous, effects of annealing of gap states 78−72115
Si film, amorphous, plasma-deposited, H_2 evolution, mass spectrometry and RHEED obs. 78−72050
Si film, amorphous and polycrystallised, localised states, elec. and optical props. 78−64008
Si films, polycryst., annealing of paramag. vacancy-type defects, EPR obs. 79−10848
Si, floating zone structural perfection changes by high temp. treatment, dendrites, dislocation interactions 80−29049
Si, form. of carbonaceous layer during high dose ion implantation, removal by cleaning, annealing and oxidation 79−70374
n-Si, gamma ray irrad., impurity composition influence on recombination centre formation 80−6872
Si, glow discharge deposited, optical spectra, reflectance, dielectric function and oscillator strength 80−11492
Si, graphoepitaxy on fused SiO_2 using surface micropatterns and laser crystn. 80−70554
Si, heavily damaged ion implanted (100) and (111), development of secondary defects 79−51166
Si, heavily doped implantation layers, laser beam annealing 78−88481
Si, heavily implanted, lattice defects and strains after high temp. annealing 78−10077
Si, heavily irrad., ESR study of annealing characts. 78−10771
Si, high dislocation density crystals, photoelectret state investigation 80−97191
Si, high dose self-irrad., spatial correl. between primary and secondary defect profiles 80−59536
Si, hydrogenated amorphous, laser annealing 80−100713
Si, implantation induced strains, X-ray interferometry and topography 78−43039
Si, implanted amorphous, comparison of laser and thermal annealing 79−70084
Si, implanted and annealed, misfit dislocations removal by laser irrad. 79−83063
Si, implanted annealed layers, amorphised structure formation mechanism and crystallographic nature 80−29091
Si, implanted crystal, laser induced annealing and diffusion behaviour 80−88202
Si implanted layers, interaction of defects and impurities stimulated by induced ionisation, ESR 80−11270
Si implanted layers, utilisation coefficient of impurities after laser annealing 77−76437
Si, implanted semiconductors, laser annealing, review 80−107301
Si, in elec. field, behaviour of second phase inclusions *(Russian)* 79−23779
n-Si, influence of deform. on capture of electrons by divacancies 77−1449
Si, ion bombarded, radiation defect formation, atom-atom collision cascades modelling 80−10582
Si, ion damage TEM study of laser annealing 80−88215
Si, ion implantation, investigation of radiation damage by pendellosung topography 79−51125
Si, ion implantation damage, annealing, role of stresses 78−75679
Si, ion implantation-induced damage after Ar and P implantation, defect density and distrib. *(German)* 77−24337
Si ion implanted, amorphous to crystalline transition due to laser irrad. 80−103451

annealing continued
Si, ion implanted, annealing of heavy ion cascade damage, channelling meas. 80−89255
Si, ion implanted, annealing by ion beam heating 80−103382
Si, ion implanted, damage struct. obs. using TEM and cross section specimens 80−107298
Si, ion implanted, difference between ruby and Nd:YAG laser annealing 79−37723
Si, ion implanted, dynamic behaviour of pulsed-laser annealing, time depend. optical reflectance meas. 79−60393
Si, ion implanted, extent of annealed or melted regions as function of pulsed laser irrad. energy 79−74025
Si, ion implanted, interstitial generation and loop form. during annealing in oxidising medium 80−107225
Si, ion implanted, laser annealing, periodic regrowth phenomena 78−67724
Si, ion implanted, laser annealing 79−69124
Si, ion implanted, laser annealing 79−69126
Si, ion implanted, laser annealed, elec. characterization 79−69137
Si, ion implanted, laser annealed, deep levels study 79−69457
Si, ion implanted, laser annealed, elec. props. and annealing kinetics 79−69508
Si, ion implanted, laser-annealed, theoretical anal. of thermal and mass transport 78−91364
Si, ion implanted, photovoltaic effect related to annealing 78−76111
Si, ion implanted, pulsed electron beam annealing 79−52254
Si, ion implanted, pulsed electron and laser beam annealing, comparison 79−52256
Si, ion implanted, pulsed ruby laser annealing 79−52255
Si, ion implanted, scanning CW and pulsed laser annealing 80−92549
Si, ion implanted, self implanted, self annealing using high ion current density treatment 80−89254
Si, ion implanted, SiO_2 antireflection coating effect on CW laser annealing 80−49242
Si, ion implanted, spin density effect on laser annealing 80−11517
Si, ion implanted and laser annealed, characterisation 80−29043
Si, ion implanted Kr migration during anneal 78−18834
Si ion implanted layers, pulsed electron beam annealing, TEM and particle backscatt. meas. 79−69134
Si, ion-implanted, disorders, nature and annealing behaviour, review 78−83836
Si, ion-implanted, effect of free-carrier absorpt. on annealing by pulsed laser 79−55757
n-Si, ion-implanted, elec. characts. after laser annealing 80−88562
Si, ion-implanted, impurity activation monitoring by SAW techniques 80−65020
Si, ion-implanted, laser annealing at 1.06 μm, computer simulation 79−47556
Si, ion-implanted, laser annealing, appls. 79−73202
Si, ion-implanted, laser irrad., characterisation by X-ray topography 79−74026
Si, ion-implanted, period surface struct. in laser annealing, new expt. evidence 80−29836
Si, ion-implanted, pulsed-laser annealing, dynamic behaviour by optical reflectance meas. 79−69122
Si, ion-implanted amorphous layers, melting model for pulsing-laser annealing 79−56080
Si ion-implanted dopant redistribution under laser annealing 80−70242
Si ion-implanted laser-annealed solar cells 80−93881
Si, ion-implanted layers, impurity profile meas. after laser annealing 78−87702
Si, ion-implanted layers, residual defects after high temp. annealing 78−87695
Si, ion-implanted semiconductor, annealing, crystallisation, laser pulse energy depend. 78−34528
Si ion-implanted solar cells, factors controlling efficiency 80−81451
Si ion-implanted structure annealing, defect behaviour obs. *(Russian)* 80−49281
Si, irrad. with Cr^+, form. and annihilation, of defects, ESR investigation 79−90707
n-Si, irradiated with large neutron doses, defect annealing 80−19849
Si, junction FET, annealing of neutron induced defects, transductance meas. 78−43052
Si, laser annealed, charge collection microscopy, carrier lifetime determ. 79−69136
Si, laser annealed, EPR and cyclotron resonance 80−34773
Si, laser annealed, elec. props. 79−69609
Si, laser annealed, solubility of impurities 79−69247
Si, laser annealed ion implanted, elec. props., melting threshold 80−10969
Si, laser annealing, nonequilib. incorporation of impurities during rapid solidification 80−55286
Si, laser annealing, nonlinear dynamic transport processes 80−93437
Si, laser annealing, optical refl. meas. of melted layer 79−78796
Si, laser annealing, surface layer temp. distrib. 79−74029
Si, laser annealing after ion implantation, temp. distrib. 80−54265
Si, laser annealing at 1.06 μm, free carrier absorpt. role 80−24964
Si, laser annealing mechanisms, disordered overlayers, crystalln. 80−84967
Si, laser annealing of ion bombardment damage 80−25502
Si laser annealing of SiO_2 layers 80−97505
a-Si, laser induced crystallisation mechanism, epitaxial regrowth 80−84962
Si, laser irradiated, positron annihilation crystal struct. imperfection monitoring 80−11506
Si, laser pulsed annealing, carrier diffusion role in lattice heating 80−45172
Si, lattice damage, influence of laser annealing 79−23608
Si layer, on buried SiO_2 layer formed by high-dose, O ion implantation, TEM, AES, and XPS obs. 80−88172
Si layers, ion implanted, pulsed electron beam annealing, He^+ backscatt. and TEM study 79−51152
Si layers amorphized by molecular ions, laser annealing 80−103379
Si, local mechanical defects, annealing and effect on autoepitaxial growth *(Russian)* 80−7701
Si materials, advanced, preliminary evaluation for space solar cells 80−94006
Si, n^+-p diode, γ-radiation defects, annealing and recomb. props. 80−65045
Si n^+p solar cells, effect of elec. bus during 1 MeV electron irrad. and isochronal annealing, elec. characts. and deep level pop. 80−94086

annealing continued
Si, n-type, with ^{11}B implanted ions, high-temp. treatment effect on distrib. profile *(Russian)* 77—89454
Si, near (III) surface, dislocation movement at annealed scratches, X-ray topography obs. 80—2029
n-Si neutron and electron irrad., isochronous annealing influence on edge absorpt. 80—11449
Si, neutron irrad. effects on lattice parameter and anomalous X-ray transmission 79—86821
n-Si, neutron irradiated, annealing behaviour characterisation by electrochem. meas. 80—19847
p-Si, neutron irradiated, elec. props. 78—51939
Si, neutron transmutation doping, annealing, lattice damage 80—15163
Si, neutron transmutation doped, isochronal annealing of resistivity 80—19828
Si, neutron transmutation doping, annealing, deep defect levels 80—20123
Si, neutron-transmutation doped, annealing behaviour, EPR obs. 79—86804
Si, new materials properties achievable by ion implantation doping and laser processing 79—69127
Si, non thermal laser induced ordering, plasma life time, phonon interactions 80—84481
Si on sapphire, laser annealing dynamics epitaxial regrowth, optical reflectivity 80—29285
Si on sapphire film, laser annealing non-thermal theory expt. test 80—89273
Si, oxidation stacking faults and microdefects, growth behaviour during high temp. annealing 78—72901
Si, oxidation stacking faults, shrinkage and growth, bulk O_2 effects 80—96546
Si, oxidation-induced stacking faults, control by Cl implantation 79—46682
Si, oxidation-induced stacking faults, influence of annealing ambient on shrinkage kinetics 80—29035
Si, P diffused sample, stacking faults and dislocations formation from interstitials 78—95059
Si, P implanted, low temp. annealing characts. 77—11576
Si, P implanted low pressure CVD polycryst. films, elect. characts. 80—60114
Si p-n junction, negative annealing of γ-radiation defects 77—43246
Si, packing defects, change in size during heat treatment 80—39079
Si, photoacoustic signal changes assoc. with crystallinity, recrystallisation after laser annealing 80—16127
Si, photoluminescence of annealed cryst., defect anal. 79—87500
Si, photoluminescence of thermal donors after annealing 79—87499
Si, planar technology, insulating thin film preparation and props. 78—10589
Si plasma deposited amorphous hydrogenated film, optical props., annealing effect 79—56874
Si, plasma effects during pulsed laser annealing 80—84480
n-Si, plastically deformed, donor action of dislocations, elec. props. 79—11126
Si, point defects, laser annealing 80—107224
Si, polycryst, CVD, electron beam recrystn. 80—24759
Si polycryst. film, ion-implanted, pulsed laser annealing 79—77612
Si, polycrystalline, As segregation at grain boundaries, elec. props. meas. 80—75259
Si, polycrystalline, recrystn. after plastic deform. and annealing 80—3145
Si polycrystalline film resistivity reduction by Nd:YAG laser annealing 80—100539
Si, polycrystalline solar cells, fabricated from metallurgical grade Si 80—81441
Si polycrystalline solar cells fabricated from refined metallurgical-grade Si, impurity gettering 80—94011
Si, postimplantation defect annealing in samples heavily damaged by 140 keV Si^{2+} ions 77—11602
Si, precipitation of O, 1000°C TEM, IR absorpt. and X-ray studies 80—34194
Si, precipitation of O, annealing, IR spectra meas. 80—24606
Si processing technology, appls. of scanning CW lasers and electron beams 80—100932
Si, proton irrad., efficiency of form. and nature of defects, Hall meas. 80—6444
p-Si, proton irrad. magnetiodiode effect, heat treatment, photocond. spectra 79—69591
Si, proton irradiated and annealed, hydrogen containing radiative recomb. centres 77—24896
Si, pulsed laser annealing, nonthermal, plasma annealing 80—25498
Si, pulsed laser annealing, mechanism 80—25739
n-Si, quenched, fast electron irradiated, annealing of defects 80—89259
Si, RF sputtered amorphous film, high temp. metal induced crystn. 77—11825
p-Si, radiation defects by annealing, kinetics anal. 79—33018
Si, radiation-doped and annealed, carrier density and mobility meas. 78—56145
Si, reflectivity time dependence during pulsed laser annealing 80—66214
Si, screw dislocation networks, TEM study 80—70204
Si, self-implanted, ⟨100⟩ and ⟨111⟩, crystallised layers by laser annealing, struct. 78—47644
p-Si, self-interstitials, influence of white light on annealing process *(German)* 79—19245
Si, shrinkage of single dislocation loops during annealing 79—82212
Si, single crystal, kinetics of annealing of vacancy complexes 78—87666
Si, single crystal solar cell manufacturing process, laser annealing of implanted area, energy saving 80—97791
Si, slip dislocation nucleation during laser annealing 80—84179
Si, snowflake defect due to annealing in H at 1000°C, X-ray topography study *(Chinese)* 80—49227
Si solar cell processing, pulsed laser techniques for annealing ion-implantation damage 80—81453
Si solar cells, high open circuit voltage, P implantation 80—89642
Si solar cells, ion implanted grating type 80—101102
Si solar cells, ion-implanted, furnace annealing 80—81452
Si solar cells, ion-implanted, expt. study of efficiency controlling factor 80—93997
Si solar cells, laser annealing, conversion efficiency improvement *(French)* 80—66976
Si solar cells, n$^+$-p, Li-counterdoped, radiation damage 80—94000
Si solar cells, radiation damaged, origin of reverse annealing 80—76630

annealing continued
Si solar cells, radiation damage annealing mechanisms and low temp. annealing 80—94003
Si solid phase grown, structural obs. 78—2397
Si, sputtered amorphous film, photocond. and electronic props., effects of annealing in plasma gas 80—44644
Si, stacking fault formation, elimination by preoxidation annealing in N_2/HCl/O_2 mixtures 78—88550
Si, surface, pulsed electron beam processing, doping, annealing 80—75254
Si, surface, stacking fault generation due to mech. damage, preoxidation annealing influence 80—54261
Si, surface structures after pulsed laser annealing, LEED obs. 80—54494
Si, surface topography changes due to pulsed laser annealing 80—84348
Si, TEM and EELS identification of oxide precipitates 80—100723
Si, temperature during CW laser heating, Raman scatt. meas. 80—76109
Si, V-grooves formed by etching, phosphosilicate glass bridge struct. 80—104312
Si, wafer, Cu-decoration technique for lattice imperfection characterisation *(Japanese)* 79—65069
Si wafer, ion implanted, electron beam annealing, computer simulation 80—96569
Si wafer, shrinkage and annihilation of stacking faults 77—39598
Si, wafer, suppression of oxidation stacking fault generation by preannealing in N_2 atm. 78—30648
Si wafers, Czochralski-grown, lifetime improvement by two-step annealing 80—49916
Si wafers, dislocation dynamics during annealing, X-ray topography system obs. 77—76261
Si with thermal defects, photocond., effect of annealing on elec. resist. 80—6837
Si, X-irrad., photocond. spectrum 77—15903
p-Si, X-ray bombard. effects on elec. resist., and carrier density, annealing effect 77—4125
Si, X-ray channeling technique anomalous transmission, appl. to microdefects induced by heat treatment 79—19124
Si: As(Pb), high-dose ion implanted and annealed, implant redistribution 80—107309
Si:^{119}Te(^{119}Sb), implanted atom site changes with time, Mossbauer obs. 77—20757
Si:^{31}P$^+$, implanted layers, characterisation by ellipsometry 79—90683
Si:^{57}Co, ion-implanted, Mossbauer study, annealing effects 80—7231
Si:^{57}Co/^{57}Fe, Mossbauer spectra, deep level Co impurity study 80—29666
Si:Al film, low-temp. diffusion of Al 78—38878
Si:Ar, As, ion implanted, laser annealing, doping profiles, channelling 80—97506
Si:Ar, ion implant gettering of MOS capacitors using linear voltage ramp and N$^+$ backscattering 79—95502
Si:Ar, ion implanted, amorphous, epitaxial regrowth 79—10868
Si:Ar(Ne)(O)(N), ion-implanted, defect reverse annealing, 550-650°C 80—88875
Si:As, CW CO_2-laser annealing, comparison with thermal annealing 80—84193
Si:As, CW laser annealing mechanism, annealed spot size, solid phase epitaxial regrowth 79—78798
Si:As, diffused, laser irrad., stability study 80—65547
Si:As, dual wavelength, laser ion implantation damage annealing 79—69117
Si:As, effects of recoil-implanted O on elec. activation of As 79—99227
Si:As, elec. activation of implanted As during low temp. anneal, Hall effect meas. 78—51571
Si:As, electron irrad. induced defect levels, annealing, deep level transient spectroscopy obs. 77—59044
Si:As, electron irradiated, majority carrier trap prod., effect of O_2 enhanced annealing 77—1151
Si:As, high-dose implanted, irrad. time and subsequent heat treatment effects on laser annealing 80—29041
Si:As, implanted, residual defects after one- and two-step annealing 78—6083
Si:As, implanted, spatially varied activation during regrowth of amorphous layers, sheet resist. and backscatt. obs. 78—71749
Si:As, implanted As redistrib. during annealing in oxidising ambient, carrier distrib. meas. 79—19275
Si:As, implanted through SiO_2 films, elec. props., defect struct. 80—54264
Si:As, ion implanted, annealing characts., elec. props. 77—19974
Si:As, ion implanted, beam techniques 80—24474
Si:As, ion implanted, laser scanning apparatus for annealing 78—34526
Si:As, ion implanted, laser annealed, lattice defects, epitaxial regrowth 80—103334
Si:As, ion implanted, low temp. thermal annealing 80—96552
Si:As, ion implanted, pulsed ion beam annealing 80—103395
Si:As, ion implanted, scanning-electron-beam annealing 79—60391
Si:As, ion implanted, two-step annealing 78—18664
Si:As, ion implanted, two-step annealing, TEM study 79—82249
Si:As, ion implanted layers in device structures, boundary effects in laser annealing 79—73188
Si:As, ion-implanted, CW IR laser annealing 80—34022
Si:As, ion-implanted, channelling anal. of CW Ar laser annealing 79—73186
Si:As, ion-implanted, laser annealing, channelling obs. of As cluster form. 79—69128
Si:As, ion-implanted and post-annealed, dislocation loops, TEM obs. 77—84776
Si:As, ion-implanted layers, ellipsometric anal. of laser annealing 79—73190
Si:As, laser annealing, channelling, optical obs., and resist. meas. 79—1444
Si:As, laser annealing of implanted layers 77—55296
Si:As, p-n junction form. by laser annealing, space charge region, effects on reverse current 80—54772
Si:As, scanning electron beam annealing, spreading resistance, junction depth 80—75267
Si:As, shallow junctions by high-dose implants 80—96694
Si:As, solid solubility and thermal behaviour of metastable 80—75359
Si:As, solid solubility of As determ. by ion implantation, CW laser annealing 80—6517
Si:As high-dose implanted single crysts., pulsed electron-beam annealing 80—103373
Si:As ion implanted, laser induced diffusion modelling 80—24672

annealing continued
Si:As ion implanted layers, annealing by CO_2 laser, doping profile shift 80—84965
Si:As wafers, laser annealing, Rutherford backscatt., optical, and TEM obs. 79—1445
Si:As$^+$, implanted, CW laser annealing, electron-beam induced current 80—100709
Si:As$^+$ sheet resistivity rel. to isochronal annealing and defect structures 77—76443
Si:As$^+$(P$^+$) ion implanted, laser annealed, correlation of struct. and elec. props 80—70855
Si:As(B), implanted CW laser annealing, elec. props., cryst. struct. and limitations 80—39131
Si:As(B), ion implanted, pulsed laser annealing appl. to device fabrication 79—73180
Si:As(B)(P), ion-implanted polycrystalline films, laser annealing 79—73181
Si:As(P), ion implanted, TEM study after laser and furnace annealing 80—70234
Si:As(P) film, polycryst. laser annealed, resistivity changes during thermal annealing 79—91163
Si:As(Sb), implanted, pulsed ruby-laser annealing, Rutherford backscatt., TEM and ion channelling study 79—86805
Si:As(Sb), ion implant lattice location after pulsed ruby laser annealing 79—73204
Si:As(Sb), ion implanted, lattice location of impurities after pulsed laser annealing 80—88196
Si:As(Sb), ion-implanted, CO_2 laser annealing 79—73183
Si:B, annealing mechanism of radiation change and dopants in pulsed laser irrad. ion implanted layers 79—46691
Si:B, conc. profile of implanted cryst., by ^{11}B(p,α) chem. anal., annealing *(German)* 78—83843
p-Si:B, defect energy levels with 1 MeV electron irrad. and annealing, transient capacitance spectra 77—62860
Si:B, distrib. profiles, high temp. treatment effects 79—69150
Si:B, heavily doped, annealing characteristics obs. *(Japanese)* 78—18666
Si:B, high conc. effects in ion implantation 80—75245
p-Si:B, high temp. treatment, effects on ion implanted impurity distrib. profile 78—79625
Si:B, implanted, shrinkage of rod shaped defects 78—6061
Si:B, implanted laser annealed, lattice strain, X-ray study 80—96554
Si:B, implemented laser annealed samples, unidirectional contraction 78—71747
Si:B, ion implanted, laser annealing 78—34525
Si:B, ion implanted, laser and thermal annealing compared, TEM obs. 78—75681
Si:B, ion implanted, laser annealed, thermal annealing effect 79—73191
Si:B, ion implanted, laser annealed, IR and Raman spectra 79—73914
Si:B, ion implanted, laser annealed, Raman scatt., Fano interactions, lattice damage 79—78711
Si:B, ion implanted, radiation defect accumulation and annealing, X-ray diffr. obs. 79—37726
Si:B, ion implanted, structure defects formation and behaviour under annealing in various ambients 80—65033
Si:B, ion-implanted, annealing by incoherent light source 79—19267
Si:B, ion-implanted, dislocation climb, TEM obs. 78—6062
Si:B, ion-implanted, rod-like defects, TEM obs. 77—68975
n-Si:B, ion-implanted damage, positron annihilation and sheet resist. meas. 80—35003
Si:B, ionisation-assisted annealing 79—23628
Si:B, layer resist. depend. on implanting and annealing conditions *(German)* 80—96551
Si:B, P, high temp. diffusion, effects of laser irrad. on diffused layer 79—14834
Si:B, p-n junction diodes, scanning-electron-beam annealing, elec. characts. 79—79128
Si:B, polycryst., effect of laser annealing on struct. and elec. props. 79—11243
Si:B, solubility and precip., and supersat. resulting by thermal predeposition 78—11232
Si:B, TEM study of stacking fault form. and annealing 78—51566
Si:B, with insulating coating, mechanical stress influence on B diffusion, strained surface layers 80—29224
Si:B,P, double implanted layer, n-p-n struct., single pulse laser annealing 80—49247
Si:B (0.2 wt.%) ion implanted, B atom displacement due to low temp. irrad. 80—88234
p-Si:B epitaxial layer, proton-implanted, annealing characts., carrier conc. profiles 77—32097
Si:B film, sputter-deposited, elec. props., struct., SEM and TEM obs. 79—95298
Si:B radiation damage and minority carrier lifetime, SEM-EBIC obs. 80—96573
Si:BF$_2^+$, ion implantation appl. in semicond. device production 80—103383
Si:BF$_2^+$, ion implanted, arc annealing by flash lamp 80—44223
Si:BF$_2^+$, recrystallisation of implanted amorphous layers, F migration 79—55763
Si:BF$_2^+$ implanted, low-temp. annealing characts. 79—55759
Si:B(Al), (P)(As)(In), ion implanted film, elec. prop. impurity depend. 80—24467
p-Si:B(Al), radiation defect form. and annealing study using Hall effect, cond. and carrier diffusion length 80—84214
Si:B(P), diffusion induced imperfections, laser annealing, rel. to junction characts. 78—75678
Si:B(P), ion implanted, polycryst., elec. props. and recrystn. 77—24324
Si:B(P), ion implanted crystalline and amorphous laser annealing 80—97509
Si:B(P) polycrystalline thin film, plasma annealing, effect on elec. props. 80—7005
Si:B(P)(As)(Cu)(Fe), dopant profile changes induced by laser irrad. using SIM and backscatt. meas. 79—69148
Si:B(P)(As)(Sb), ion implanted, redistrib. of dopants by pulsed laser annealing 79—7620
Si:B(P)(As)(Sb)(Cu)(Fe), ion implanted, doping profile, pulsed laser annealing effects 80—88197
Si:Be, ion implanted, correl. of atomic distrib. and implantation induced damage profiler 80—88199
Si:Bi, ion implanted, channelling obs. of pulsed Q-switched ruby laser annealing 80—59542

annealing continued
Si:C, disorder profiles by proton backscattering, proton bombardment annealing 78—47449
Si:C, H$^+$ and He$^+$ beam impact phemomena, damage annealing rates 78—47450
Si:Co, high-temp. ion-implanted and diffused samples, Mossbauer spectra of ^{57}Co 79—51891
Si:Co, implanted or diffused, and annealed, localisation of Co atoms, Mossbauer obs. 80—39140
n-Si:Cs, ion implanted, minority carrier lifetime and defect struct., annealing effect 78—6395
Si:Cu, interaction between vacancy emitting absorbing precipitates and dislocations, TEM obs. 78—71755
Si:D, amorphous, thermal stability, comparison with Si:F 80—49542
Si:F, amorphous, heat resistant, prep., elec. cond., IR absorpt., annealing 80—65719
Si:F, amorphous, thermal stability, comparison with Si:D 80—49542
Si:Fe, B, Fe reaction with ion implanted B 79—77620
Si:Fe, implanted, annealing and stripping, Mossbauer expts. 80—39141
Si:Fe, ion implanted, laser annealing studies using Mossbauer spectroscopy 80—79827
Si:Fe, laser annealing of implanted ^{57}Co sources, Mossbauer obs. 80—39139
n-Si:Ge, electron induced defects, room temp. instability 80—29052
Si:H, amorphous, defect creation and H evolution 80—50392
Si:H, amorphous, discharge prod., optically induced cond. changes 80—96937
Si:H, amorphous, glow discharge deposited, laser annealing 80—49104
Si:H, amorphouse film, optical and elec. props. 79—82694
Si:H, ion-implanted, photoluminesc. spectrum 80—45129
a-Si:H, spin defect and recombination influence on electronic transport 80—50409
Si:H amorphous films, IR spectrum and struct. 80—97277
Si:H amorphous films, role of Ar in deposition process, IR absorpt. and photocond. meas. 80—50321
Si:H film, amorphous, bombarded, defects, luminesc. and ESR meas. 80—34977
Si:In, C, 0.111-eV acceptor level, X-level defect conc. from IR absorpt. and Hall meas. 79—51512
Si:In, implanted, laser annealing 79—52050
p-Si:In, ion implanted, doping profiles from capacitance-voltage characts. 80—88203
Si:In, ion implanted, time differential PAC obs. of annealing behaviour 77—89455
Si:In(Sb), incorporation of implanted impurities during amorphous layer regrowth 79—55761
Si:Ir, precipitation of solid soln., photocapacitance, electrical resistivity meas. 78—47833
Si:K, ion implanted, influence of doping and annealing on carriers 78—38742
Si:Li, precipitation centres, elec. cond., Hall effect meas. 78—48417
Si:Li(Na)(K)(F)(Cl), amorphous, implantation effects on elec. props. 80—49716
Si:N, laser-annealed, Jahn-Teller distorted donor, EPR meas. 80—84642
Si:N wafers, Si_3N_4 layer growth by high dose implantation and annealing, elec. props. 80—70227
p-Si:N$_2^+$ implanted, anneal behaviours of lateral photovoltaic method 79—14825
Si:N(P), ion implanted, IR transmission and rel. spectra study 80—108244
Si:Na ion implanted, Hall effect temp. depend., electron surface density and mobility 80—11018
Si:Ne(Ar)(Kr), ion implantation damage, annealing, comparative study 79—10867
Si:Ne(Kr), ion implanted, amorphous, epitaxial regrowth 79—10869
Si:O, annealed, minority carrier lifetime 79—23985
Si:O, annealed, precipitates, dislocation and stacking fault loops, TEM characterisation 77—4111
Si:O, annealing behaviour of O donor, conc. reductions via resistivity meas. 79—51129
Si:O, CVD layer, RHEED study of surface crystallinity, annealing effect on structure 79—69371
Si:O, cryst., annealed, struct. defects 78—75673
Si:O, cryst., donor form. during annealing, elec. resist. study 80—49653
Si:O, effect of interstitial O on elec. props. 77—76846
Si:O, high temp. annealing effect on impurities 78—38745
Si:O, specific resist. rel. to annealing, Si-O complex form., O_2 distrib. *(German)* 77—72863
Si:O film, thermally deposited, semi-insulating, crystallographic study 78—75954
Si:O wafer, annealed, surface- and inner-microdefects, TEM obs. 80—54236
Si:O(C), implant redistribution, annealing effects, SIMS meas. 80—96561
Si:P, amorphised by Ne$^+$ implantation, high fluence P implants, plasma region obs. 79—86807
p-Si:P, annealing behaviour, recovery, surface carrier density and Hall mobility meas. 77—32012
Si:P, defect annealing, ionisation effects, DLTS meas. 80—24483
Si:P, effect of annealing on charge carrier conc. on floating zoned crystals 78—47805
Si:P, heavily ion implanted, polycrystalline, grain growth 79—19477
Si:P, implantation damage of channelled P ions, elec. activity recovery stages 77—59034
Si:P, implanted, pulsed electron beam annealing, Hall effect and sheet resist. meas. 80—34467
Si:P, implanted, SiO_2-film-covered, laser annealing behaviour 79—86808
Si:P, implanted, two-stage laser annealing of lattice disorder 79—1452
Si:P, implanted layers, ionisation-enhanced crystallisation 79—51151
Si:P, implanted low temp. annealed, elec. activation, damage depend. 80—88182
Si:P, incoherent light flash annealing, elec. props., backscattering spectra 80—97504
Si:P, ion implantation defect annealing investig. by CESR 77—8404
Si:P, ion implantation doped, positron annihilation meas. 78—14380
Si:P, ion implanted, damage layer props. obs. using ellipsometric parameters *(Russian)* 77—43234
Si:P, ion implanted, ionisation enhanced annealing, resist. changes meas. 78—30667
Si:P, ion implanted, irrad. by laser of different wavelengths, annealing behaviour 79—69132

annealing continued
Si:P, ion implanted, laser and thermal annealing, elec. cond. and Hall effect meas. 79—69145
Si:P, ion implanted, regrowth of damage structs. by laser annealing 80—107289
Si:P, ion implanted with small doses, defect annealing by nanosecond laser pulses 80—107297
Si:P, ion-implanted, damage-dependent elec. activation 79—55793
Si:P, ion-implanted, laser annealing 80—10564
Si:P, ion-implanted and unimplanted, laser annealing, photoluminesc. study 80—2049
Si:P, neutron transmutation doped, electron trap annealing, deep level transient spectra 78—14368
Si:P, neutron transmutation doped, EPR obs. of annealing behaviour 79—1453
Si:P, neutron transmutation doped, EPR, electron trapping 79—73179
Si:P, polycryst., CVD, elec. activation of impurities, EPR obs. 80—34774
p-Si:P, random and aligned implants, Rutherford backscatt. and TEM exam. 78—47454
Si:P, thermally annealed, high dose, ion-implanted, dislocation array prevention by prior laser annealing 79—73187
Si:P, through-oxide implanted samples, anomalous residual defects after annealing 77—76432
Si:P amorphous films, doping and annealing effects on localized states, ESR meas. 79—38380
Si:P CVD films, ion-implanted, doping effect on elec. props. 80—2495
Si:P film, polycryst. pulsed electron beam annealing 80—10566
Si:P implanted, multiscanning electron beam annealing 80—75242
Si:P solar cell, minority carrier lifetime degradation during ion implanted processing, surface photovoltage 79—39305
Si:P^+, highly implanted, two step annealing effect on crystallinity 77—31683
Si:P^+, misfit dislocation net propagation due to osmotic forces 79—65108
Si:P^+ ion implanted single crysts., secondary defects development during annealing 80—44228
Si:P(As)(B), nonequilibrium solid solutions obtained by heavy ion implantation and laser annealing 80—92544
Si:Pb, diffusion behaviour of Pb in high dose implanted Si layers during isothermal annealing 79—1525
Si:Pb, implanted, laser annealing 78—75685
Si:Pb, implanted and annealed, impurity redistrib. 78—75689
Si:Pb, ion-implanted and annealed, dose depend. of residual lattice disorder 77—43228
n-Si:Re diode photocapacitance spectra, Re centre dissociation 79—90997
Si:Sb, high dose implanted, orientation dependent annealing effects 78—18665
Si:Sb, high dose Sb ion implantation, buried layer appls. 80—88186
Si:Sb, ion implanted, annealing behaviour of stress 78—63778
Si:Sb, ion implanted and annealed, influence of implantation temp. on dislocation generation 80—88158
Si:Sb, redistribution of thin impurity layers after laser annealing, theoretical model and expt. results 79—69147
Si:Sb,P, double implants, residual defect reduction after damage anneal 80—88170
Si:Sb vacuum deposited coating, p-n junction, pulsed electron beam annealing doping, diffusion 80—75480
Si:Sb wafers, laser annealing, Rutherford backscatt., optical, and TEM obs. 79—1445
Si:Sb(Ga)(Bi)(In), dopant solubility limit, laser irrad. effects 80—84295
Si:Te implanted, laser annealing, Mossbauer obs. 80—39127
Si:Zn, implanted atom diffusion during laser annealing 79—37725
Si/Pd system, solid phase epitaxial growth control by C ion implantation 80—75466
Si/Pd-W, contact reactions, backscattering, X-ray diffr. meas. 80—20040
Si-Au system, ion implanted induced giant gettering, annealing effects 80—88221
Si-Ge, heavily doped, reversal of precip. 80—2409
Si-Ge amorphous films, effects of annealing and crystn., ESR microstruct. and elec. meas. 78—26790
Si-H, amorphous, plasma-deposited, H evolution and defect creation 80—44914
Si-metal thin film reactions, laser annealing 79—70364
n-Si-Ni, Schottky barrier, thermal annealing effect on props. 79—69596
n-Si-Ni surface barrier junction, rectifying, struct. and elec. characts., effect of low temp. annealing 78—14821
Si-Ni surface barrier struct., surface electronic states, annealing effects *(Russian)* 78—6441
Si-$Pd_{80}Si_{20}$, amorphous, Pd_2Si layer form., shallow contact 80—103586
Si-saphhire, Si ion implanted wafer, laser annealing 79—99989
Si-sapphire, interface radiation induced charge trapping, rapid anneal phenomena 79—19666
Si-SiO_2, Al-implanted, low-temp. annealing effect on charge and surface state density 77—85337
Si-SiO_2, ESR centres, interface states and oxide fixed charge 80—2474
Si-SiO_2, electron-beam annealing of ion-implantation damage 79—77622
Si-SiO_2, ion bombardment by $H_2{}^+$, $D_2{}^+$, changes in annealing behaviour 79—78185
Si-SiO_2, ion implantation through SiO_2 film, recoil implantation of O, EPR study 80—88180
Si-SiO_2, surface state annealing 77—39946
Si-SiO_2, surface states, oxide charge centres, annealing effects 78—2570
Si-SiO_2, two layer system, P^+-ion penetration tails, expt. and computer anal. 80—75249
Si-SiO_2 interface, effect of N_2 annealing on electron scatt. 79—42660
Si-SiO_2 interface, effect of high-temp., post-oxidation annealing on elec. props. 79—82673
Si-SiO_2 interface, N_2 gas reaction, elec. and structural characts. 77—39950
Si-SiO_2 interface, rad. hardness, carrier localisation in inversion layer 77—85332
Si-SiO_2 interface, stacking fault-free region formation by annealing 78—51561
Si-SiO_2 interface in MOS solar cells, operational characts. and struct. 80—93901
Si-SiO_2 interface state density, dependence on thermal oxidation process variables 80—15607
Si-SiO_2 interface states, deposition of H containing layers and annealing 80—92991
Si-SiO_2 layer formation by $O_2{}^+$ ion implantation, interface struct. and C-V characts. 77—1142

annealing continued
Si-SiO_2 MOS capacitors, relationship between trapped holes and interface states 80—70830
Si-SiO_2 structures, B ions implanted, energy spectra of shallow traps at various implantation energies 80—80392
Si-Te, laser and thermal annealing, Mossbauer resonance lines 79—99810
Si(:Au), gamma-induced trapping levels 79—87059
SiC, amorphisation induced by ion bombardment, Raman spectroscopy 77—80551
SiC base material, electrical props., heat treatment effect 77—12645
SiC, diffusion coeff. of Cs and Ag by post irradiation annealing of coated 78—13247
SiC fibre reinforced Al-Mg, heat treatment effect on struct., tensile strength 80—55487
SiC fibre reinforced Ni-Cr alumina coated fibres, hot pressed, annealed, IR study 78—60623
SiC fibre reinforced Ti, effect of Al, Zr and Mo alloying additions on reaction rate of Ti with fibres 80—16249
SiC fibres reinforced Ni complex alloy, influence of TiN coating on fibre matrix interaction *(Russian)* 78—95820
SiC, fusion reactor first wall appl., radiation damage 79—86822
SiC ion implanted, laser induced ordering and defects 80—84754
SiC, radiation defect annealing, recovery of LEED maxima 80—65075
α-SiC, single crysts. phase struct. rel. to heat treatment, nucleation 80—38991
SiC, surface defect annealing, following Ar ion and electron irrad. 80—7603
SiC:H amorphous reactively sputtered film, H content effect on film props. 80—75459
SiC-Si struct. formation on ^{12}C ion implantation in Si, optical and photoelectric props. 79—91136
$Si_{1-x}Ge_x$ amorphous, ESR centres, g-shift rel. to annealing 77—55701
$Si_{1-x}H_x$ film, amorphous, RF sputtered, pure and P(B) doped, optical consts. 79—95866
SiN_x film, plasma deposited, comp. and characterisation, optical and elec. props. 80—15401
Si_3N_4, CVD, chem. bound H, NH_3/SiH_4 ratio and annealing depend. 77—76680
Si_3N_4 degradation due to high-temp. processing 78—6454
Si_3N_4, dielectric films made by NH_3-silane reaction, TEM study 80—84413
Si_3N_4 film, CVD, ion implanted, compressive stress buildup, annealing effects 77—89456
Si_3N_4, film, H_2 concentration profile, chem. bonding 79—33205
Si_3N_4 film, high temp. annealing effect on struct. and comp. 77—15714
Si_3N_4 film formation by $^{14}N_2{}^+$ ion implantation into Si 79—99455
Si_3N_4, films, ion-beam synthesis, IR spectra, struct., crystallisation on annealing 77—16705
Si_3N_4, hot pressed, crack healing *(German)* 79—24599
Si_3N_4, hot-pressed, fracture in bending *(Japanese)* 79—79113
Si_3N_4, hot-pressed with crystn. grain boundary phases, prep. 78—95715
Si_3N_4, mechanism of α-β transition under annealing 79—87629
Si_3N_4, N ion implantation synthesis, struct. and resonance mechanism of α-β transition during annealing 80—33981
Si_3N_4 powder, high press. hot pressing 79—38772
Si_3N_4-Al_2O_3, hot-pressed with crystn. grain boundary phases, prep. 78—95715
Si_3N_4-MgO, compressive creep, source of viscoelastic effect 80—50675
Si_3N_4-Y_2O_3 ceramic, thermal degradation, C impurity effect 80—50708
Si_3N_4-Y_2O_3-Al_2O_3-SiO_2, X-ray diffr. exam., phase equilib. at 1400 degrees C *(Japanese)* 78—44113
SiO_2, As-implanted, electron trapping and detrapping characts. 80—65692
SiO_2 film, Al implanted, in MOS struct., electron traps characts. obs. 79—15226
SiO_2 film, attenuated total reflectance study, impurity spectra 80—97311
SiO_2 film, on n-GaAs, Ga content after annealing at 730-940°C neutron activation anal. 78—43255
SiO_2 film, spin-on oxide, phys. and cond. meas. 77—43762
SiO_2 film on Si, negative bias instability 78—91773
SiO_2 films, Si-rich, amorphous Si region obs. 80—84400
SiO_2 films, stabilised by ion bombardment and heat treatment, crystn. and phase separation 79—77931
SiO_2, fused, surface crystn. by Li^+ ion implantation and annealing 80—89383
SiO_2, ion implanted, fused, refr. index profiles 80—54272
SiO_2 ion implanted, radiation defects and optical props. 80—107293
SiO_2 layer used for MOSFETs, electron trapping behaviour 80—92981
SiO_2 layers, in MOS struct., hole trapping induced by ion implantation and annealing at room temp. 80—54792
SiO_2 MOS structures, removal of electron traps by RF annealing 80—44728
SiO_2, reactive ion etching damage, electron trapping characts. in MOS struct. 79—90704
SiO_2, vitreous, Raman active defects, thermal equilibration 80—55092
SiO_2:Al film, ion-implanted, electron trapping behaviour 78—67729
SiO_2:As^+ implanted layers in MOS struct., electron trapping and detrapping characts. 80—92982
SiO_2:Ga film, impurity distrib. after annealing, neutron activation anal. 80—24484
SiO_2-Al_2O_3-CaO-MgO-NaO-K_2O-B_2O_3-ZrO_2, glaze, exam. of zircon crystallisation 79—19155
SiO_2-M_2O (M=Na,K) glasses, temp. depend. of elastic modulus 80—40410
SiO_2-Si, P ion implantation, electrical transport props. 80—39130
SiO_2-Si inversion layer solar cells, radiation effects 77—43244
SiO_2-Si MOS system, ion irrad. effects on struct. and electrophysical props. 80—6995
SiO_2-Si:A, effects of recoil-implanted O on elec. activation of As 79—99227
SiO_x, amorphous and recrystallised layer, optical props. 80—25474
$^{30}Si(n,\beta)^{31}P$ transmutation doping and electrical characterisation 78—10071
Si(111), water vap. and O_2 interactions, EELS 78—14571
Sm, electron radiation damage, elec. resistivity change rates 80—59954
Sm-Co-Cu-Fe, single phase 2-17 sample, hard mag. props. 77—8349
$SmCo_5$ based alloys, dissociation process *(Russian)* 78—27542
$SmCo_5$ magnets, effect of heat treatment on coercive force *(Russian)* 79—1684
Sm_2Co_{17}, coercive force depend. on annealing temp. 80—65964

annealing continued

Sm_2Co_7 sintered magnets, coercive force and constitution, annealing temp. depend. *(Russian)* 80–88786

$Sm(Co_{1-x}Cu_x)_{7.8}$ alloys, coercive fields, domain wall energies, mag. and metallographic exam. 78–91897

SmO film, new reduced variant due to annealing 77–89660

SmSe, formation and crystallographic charact. of thin film phase 78–91574

Sn, effect of O ion irradiation on supercond. 78–52131

Sn film, evaporated on cooled substrate, influence of annealing temp. on elec. resist. and struct. 79–65561

Sn film, polycrystn., elec. props., internal size effect rel. to annealing temp. 79–65560

Sn, film, superconducting fluctuations, transition temp. *(Russian)* 80–65740

Sn, single crystal, dislocation walls consisting of double arrays 79–46664

Sn, superconducting film, radiation induced critical temp. 79–87179

Sn-Ni, equiatomic, metastable, transformation kinetics, Avrami parameters calc. method 78–92239

Sn-Sb (0.57 at.%) solid soln., yield point for cold-worked and annealed specimens *(Russian)* 78–48448

Sn-Sb (10 wt.%), decomposition of supersaturated solid soln. 80–29960

Sn-Zn (0.4 at.%) solid soln., yield point for cold-worked and annealed specimens *(Russian)* 78–48448

$Sn_{1-x}Pb_xSe(Te)$ films, oxidation rel. to annealing temp. and time, Mossbauer spectra, X-ray and microstruct. obs. 80–104311

$SnS(Se)(Te)(S_2)(Se_2)$, oxidation, thermal decomp., Mossbauer spectra 79–11713

SnSb film, defect density variation with deposition rate, annealing, elec. resist. meas. 77–21027

SnTe, annealed, iodide method of prep., props. meas. 80–71591

p-SnTe, cathodoluminescence and Fermi level hole effective mass 80–25467

SnTe, film, heat treatment in air, effect on struct., props. 79–11037

SrF_2, neutron irrad., role of F-centres in thermoluminesc. 79–19941

SrF_2, thermoluminesc. and F-centre annealing, after neutron irrad. 80–7422

$Sr_2Nb_2O_7$, sputtered films, amorphous, dielec. props. 80–54573

SrO:Co, noncentral and interstitial ion complexes, ESR obs. 80–71169

Ta, elastic moduli, effect of H and UHV annealing 77–90389

Ta, low temp., diffusion of H and D from quenching and annealing study 80–6555

Ta, low temp. diffusion of H and D from quenching and annealing study 80–6555

Ta, resistivity variations caused by H and D interstitials, isotope effects 77–89750

Ta, rolled and annealed, zone-refining effect on recryst. grain orient. 77–36532

Ta, rolled single crystal, recovery and recrystallization 80–3093

Ta, vaporisation, influence of inert gases on losses *(Russian)* 79–55878

Ta-8W-2Hf wt.% (t-111) alloy, dissolution kinetics of small amounts oxygen, internal oxide disp. reactions, annealing 77–16612

Ta-Ir (1 wt.%), positron annihilation, photon ang. distrib. meas. effect of deformation, annealing temp. *(Russian)* 78–35220

Ta-O, steady state O_2 solubility *(German)* 80–44322

Ta-Pu alloys, metastable, high rate sputter deposition, annealing behaviour of deposits 77–21025

Ta-T(D), diffusion and resistivity at low temps. 78–14511

Ta_2N, and TaN_x, films, thermal oxidation and resist. 80–60125

$2Ta_2O_3$ thin film, FCC cell struct. investigation 80–92796

$TaSi_2$ refractory formation by As^+ ion beam bombardment 80–107286

Tb, electron irradiated, defect annealing, recovery spectra 79–23648

Tb-Fe amorphous film, thermomag. contact printing 77–89986

Tb-Ho, single cryst., annealed, thermal expansion 78–47541

$TbAl_3$, polytypism occurrence 80–44164

TbSe, formation and crystallographic charact. of thin film phase 78–91574

Te, cryst., effect on Hall coeff. and conductivity 79–7847

Te, elec. props. anisotropy, influence of deform. and annealing 77–15859

Te film, annealing effect on elec. cond. and Hall effect 77–8213

Te, film, electronic struct. charge on ordering, double beam photoemission 78–19634

Te film, evaporated, crystallinity and electronic props., annealing effect 77–85107

Te, hexagonal film vac.-evaporated at normal incidence, X-ray Fourier line shape anal. 79–99454

Te, thin film, piezoresistance 79–95524

Te thin film, thermoelec. EMF, Seebeck coeff., elec. cond. structural depend. 79–78230

Th, ion irrad., surface C and O, AES obs. 78–71775

Th_3As_4, prep. and semicond. props. 78–23087

(Ti,V)C, activated reactive evaporation deposited films, annealing study, microstructure 80–24762

Ti, (0.9998), positron lineshape parameter and hardness rel. to annealing temp. 80–3281

α-Ti alloy, VT1-1, cold rolled, recrystn. texture and prop. anisotropy 78–52846

Ti alloy, X-ray diffr. anal. of hydrides 77–12628

Ti alloy 685, β-processed, fatigue behaviour 77–90453

Ti alloy AT-3, crack development in air, H_2, aq. H_2SO_4, electrochem. charact. *(Russian)* 77–70209

Ti alloy VT23, quenched decomposition of metastable phases during heating *(Russian)* 78–15432

Ti alloy VT3-1, fracture toughness, rel. to struct. 79–79105

Ti alloy VT5-1, annealed, plastic deform. nonuniformity depend. on stressed state and test temp. 79–57071

Ti alloys, AT3 and AT6, tensile props. prolonged oxidation effects 78–85050

β-Ti alloys, annealed, faceted fracture 79–57102

Ti alloys, β-annealing and controlled rate quenching effects 78–80568

Ti alloys, pseudo-α, salt-corrosion effects on long-term strength, vacuum annealing and stress concentrators effects *(Russian)* 78–11392

Ti, and alloys, intergranular precipitation after annealing, ion imaging microanalysis *(French)* 79–61594

Ti, cold rolled, transcrystalline SCC in methanol-bromine soln., crystallographic texture effect 79–15872

Ti, cold worked, annealed, internal friction meas. of H degassing *(French)* 79–43304

Ti, commercial, texture depend. stress corrosion cracking 80–104334

Ti, commercial purity, cyclic behaviour and delayed softening 77–36641

annealing continued

Ti, D profiles after D_3^+ implantation 80–37581

Ti, dynamic annealing, effect on dynamic strain ageing phenomena 80–7594

Ti, exam. of whether interstitial O can cause internal friction 78–48537

Ti, IMI-125, strain rate effect on mech. behaviour 80–3153

Ti, industrial grade structural changes during polygonization *(Russian)* 78–19779

Ti, irradiated and cold worked, internal friction pdaks 77–86074

Ti, neutron irrad., low temp. deform. studies 79–47757

Ti powder, physical props., effect of prep. methods *(Russian)* 77–66603

Ti sheet, anisotropy and texture, effect of plastic deform., recovery and recrystallisation *(Russian)* 77–8850

α-Ti sheet, texture dependent stress corrosion cracking in Br_2-methanol soln. 80–71803

Ti, sheets, porous, production and props. 78–60602

Ti, strip prod. by powder rolling 78–80493

Ti, type 70A, containing 0-6000 ppm ^3He, sensitivity of tensile props. 80–39197

Ti-Al, structural and phase changes due to annealing *(Russian)* 80–55440

Ti-Al (6 wt.%), D profiles after D_3^+ implantation 80–37581

Ti-Al (6.1 wt.%), hot rolled sheet, ductile fracture nuclei, SEM obs. 78–64654

Ti-Al alloy film, evaporated, anodisation characts. obs. *(Polish)* 80–55574

Ti-Al-Cr-Mo (6, 2.0, 2.5 wt.%), microstructural changes and mech. props. 77–25080

Ti-Al-Cr-Mo-U, alloy VT22, phase composition and fatigue strength 78–3219

Ti-Al-Mo, type BT22, phase transformations under step-by-step heat treatment *(Russian)* 80–108436

Ti-Al-Mo, type Ti-6242S, irrad. induced creep 80–39163

Ti-Al-Mo-Cr-Fe (6.4, 2.7, 1.6, 0.4 wt.%), quenched VT3-1, decomposition kinetics of α'' and β in annealing *(Russian)* 77–66662

Ti-Al-Mo-Zr alloy VT9, Cu-Cr(Ni) coated, plastic deform. and diffusion annealing effect on props. *(Russian)* 78–35425

Ti-Al-O, V effect on thermal stability and mech. props. 77–21171

Ti-Al-Sn, type Ti-5621S, irrad. induced creep 80–39163

Ti-Al-Sn (5, 2.5 wt.%), annealing of near-basal hydrides 80–20989

Ti-Al-Sn (5, 2.5 wt.%), ductile fracture at low temps. 78–64659

Ti-Al-Sn (5, 2.5 wt.%), electron microscope and X-ray diffr. exam., of basal and near basal hydrides 78–80550

Ti-Al-Sn-Zr (6.19, 1.92, 1.43 wt.%), fatigue cracking characteristics of β annealed microstruct. 79–5051

Ti-Al-V, containing 0-6000 ppm ^3He, sensitivity of tensile props. 80–39197

Ti-Al-V, irrad. induced creep 80–39163

Ti-Al-V, VT6 alloy, butt welded joints, electron beam welding conditions effecting interstitial impurities distribution 80–39136

Ti-Al-V (6, 4 wt.%), annealed and rolled plate, elevated temp. plastic anisotropy 79–61663

Ti-Al-V (6, 4 wt.%), α-β anneal, recrystn. anneal, β-anneal, room temp. creep 79–61662

Ti-Al-V (6, 4 wt.%), texture depend. stress corrosion cracking 80–104334

Ti-Al-V (6, 4 wt.%), Widmanstatten, microstructurally sensitive fatigue crack growth obs. 78–27627

Ti-Al-V (6,4 wt.%), age hardened, deform. charact. 77–36608

Ti-Al-V (6,4 wt.%), cyclic stress-strain response 77–21170

Ti-Al-V (6,4 wt.%), D profiles after D_3^+ implantation 80–37581

Ti-Al-V (6,4 wt.%), heat treated and rolled, texture instability 77–63689

Ti-Al-V (6,4 wt.%), microstruct. effect of base metals on diffusion welding *(Japanese)* 80–89296

Ti-Al-V-Sn-Zr alloy TS5, annealing effect on ductility and strength *(Russian)* 78–35427

Ti-Al-Zr (3,3 wt.%), W alloying addition effects on mech. props. *(Russian)* 77–59860

Ti-Al(Fe) microprobe anal. of alloying addition distrib. 80–55358

Ti-Al(Mo), swaged and recrystallized, grain growth 80–3092

Ti-B-W(Mo), annealed at 1400°C, exam. of phase diagram, using X-ray phase and metallographic analysis 79–1847

Ti-Cu-Al(Zr)(Sn)(Nb)(Mo), heat treatable alloys, effect of alloying on strength, tensile props. 78–56671

Ti-Fe, corrosion, effect of microstruct. caused by casting, annealing, beating *(Russian)* 79–57140

α-βTi-Mn (4.3 wt.%), interface phase struct. 77–44212

Ti-Mo (Zr) (Nb), sintered, manufacture and exam. of props. 79–95975

β-Ti-Mo-Cr-Al (8, 4.5, 2.5 wt.%), metastable, tensile ductility, α-phase morphology and distrib. effect 77–86098

Ti-Mo-V (8 wt.%, 8 wt.%), FCC phase, decay of β-solid soln., electron microdiffr. 79–15670

Ti-Mo-Zr-Sn (11.5, 6, 4.5 wt.%), metastable beta III phase, recrystallization and grain growth 80–3091

Ti-Mo-Zr-Sn-Fe-C-Si alloy, β-III, cold deform. and annealing, effect on struct. and mech. props. *(Russian)* 79–24533

Ti-Nb, phase transformation due to shock wave treatment *(Russian)* 79–91641

Ti-Nb-Al, decomposition during isothermal annealing 80–25653

Ti-Ni, eutectoid decomposition, effect of interphase boundary struct. on mech. 79–4952

Ti-Ni, multiplicity of structural transitions, phase diagrams, elec. cond. meas. 80–71649

Ti-Ni (48 to 53 at.%), heat treatment and deviation from stoichiometry 80–104192

Ti-Ni-Fe, multiplicity of structural transitions, phase diagrams, elec. cond. meas. 80–71649

Ti-Pd (0.15 wt.%), IMI-260, strain rate effect on mech. behaviour 80–3153

Ti-Permalloy thin film diffusion couples, low temp. interdiffusion interdiffusion 78–71889

Ti-Ru (0.05 to 90 wt.%) hardness, thermal EMF, electrical conductivity, in annealed or quenched state *(Russian)* 77–55998

Ti-V-Cr, type Ti-15-333, irrad. induced creep 80–39163

Ti-W/Au, metallisation on Al, temp. stability, barrier props., annealing effects 79–23868

Ti-Zr-Mo alloy, effect of O_2 on elec. resistivity, microhardness, mech. props. 77–56092

Ti_3Al, phase transitions and physical props. 77–25068

Ti_3Al-(Mo) (0.5 at.%), ordering, Mo effects 77–28841

annealing continued
Ti_3Al-(Nb), ordering transform. and mech. props. 78–31402
TiB_2 coatings for Tokamaks, H trapping and re-emission, annealing effects 80–37582
TiB_2, low-temp. neutron irrad., electrical resistance and stored energy 78–67744
TiC, activated reactive evaporation deposited films, annealing study, microstructure 80–24762
TiC, low-temp. reactor irrad., calorimetric investig. 77–80547
TiC-steel composite, effect of method of Cr additions on props. 78–15341
TiC_x, effect of structural vacancies on neutron radiation damage 77–35591
TiN, highly dispersed, metallic thermo-EMF 78–43363
TiN, precipitation of ordered δ'-phase *(Russian)* 78–6929
TiN-AlN composites, struct. and props. 77–40413
$Ti_{55}Nb_{45}$, supercond., anomalous phonon thermal resist. 77–69451
TiNi-TiCu, exam. of shape memory effect, specific work 79–100216
TiO_2 (rutile), (001) and (110) faces, UPS and LEED obs. 80–45206
TiO_2 film deposited on Si, SiO growth under film during postdeposition high temp. annealing 80–15400
TiO_2, iron bearing, exsolution of Fe_2O_3 79–61597
TiO_2-Ni (100) interface, electronic props., struct., comp., chemical bonding 80–84499
TiO_{2-x} reduced, crystallographic shear planes, dislocation struct. 80–107175
TiOy, annealed, lattice const. meas., thermal expansion coeffs. calc. 79–55906
$TiSi_2$, crystal atomic struct., X-ray diffr. exam., lattice parameters and integrated intensities 78–75647
$TiSi_2$, TiSi, Ti_5Si_3, formed by solid state reaction of Ti film on Si, backscattering anal., of layer structure 79–69377
$Ti0_2$ electrodes, effect of processing variables on photoelectrochem. props 80–6975
Tl-B-Se system, vitrification region, primary crystallisation fields 77–15321
Tl_2O_3, single crystal, elec. cond., annealing at 923K in O_2 effects 77–85220
TlP_3, elec. cond. temp. depend., 77-590K 77–51743
Tl_2S-SnS, phase equilibria exam. 80–55369
Tl_2Se, fused, diffusion of ^{204}Tl, ^{110}Ag, ^{112}Sn impurities 80–54415
Tl_5Te_3-Tl_4SnTe_3-Tl_4PbTe_3, phase equilib., DTA, SPA and microhardness meas. 80–96628
Tm, electron irradiated, defect annealing, recovery spectra 79–23648
Tm_2O_3 film, between Al electrodes, prep. and elec. props. 80–60103
α-U, strain rate effect on tensile flow and fracture 80–84992
U-alloys, thermal creep and swelling, characterisation 79–74226
U-Mo (1.5 wt.%) metallurgical study of forging *(French)* 78–21737
U-Mo(Nb) and U-Mo(Nb)-Zr alloys, shear martensitic transform. during quenching, plastic deform. and annealing 77–28815
U-Nb (14 at.%), exam. of shape memory effects 78–76694
U-Re-C, crystalline struct. of a compound 77–25023
$UAl_2(Co_2)$, surface comp. and electronic struct., photoemission study 80–66382
UC-UC_2, alloyed, electron bombarded, enhancement of U_2C_3 deposition 77–27911
UO_2, alpha radiation damage, point defect ingrowth and annealing behaviour 77–27926
UO_2, grain growth, in-reactor and lab. testing 79–74184
UO_2 grain growth studies, grain size and activation energy meas., rel. to nuclear fuel evaluation 79–93808
UO_2, irradiated, intergranular fission gas bubbles 78–21651
UO_2, sintered pellet, isothermal grain growth kinetics 77–18663
$US_xN_yO_z$, neutron diffraction exam. of structure 78–79777
V,V-Zr (2 wt.%), internally oxidised, neutron irradiated, annealing effect on mech. props., elec. cond. and electron microscope obs. *(Japanese)* 79–15701
V, annealing after irradiation with 210 keV He at 625°C at high fluences 78–67751
V, blister form and stress build-up, under the bombardment, surface prep. effects 78–95094
V, blistering after Ar^+ ion bombard., irrad. mode effect 80–39176
V, dehydrogenation by annealing with Zr foils, internal friction meas. 80–96736
V, effect of O ion irradiation on supercond. 78–52131
V, electron-irradiated, positron annihilation study 80–70259
V film, vac. evaporated, elec. props. 80–80414
V, first wall fusion reactor material, anneal-blistering 78–55897
V, internal friction α-peak origin 78–95773
V, resistivity variations caused by H and D interstitials, isotope effects 77–89750
V, supercond., influence of plastic deform. 77–85378
V, superconductor, neutron irradiation, low temp., effect on critical current 78–52180
V thin film-amorphous Si interface, V silicide formation, backscattering diffraction meas. 80–2285
V-C alloys, low carbides struct. rel. to ht. treatment 77–48458
V-C-O, phase relations 79–96012
V-N α-solid solution, struct. transform. during annealing and quenching *(Russian)* 77–81257
$V_{0.75-x}Ga_{0.25+x}$ ^{51}V, nucl. spin-lattice relax. time, annealing and neutron effects 79–82710
V_3Ga, filamentary conductors, type-II, low temp. 30 GeV proton effects on critical props. 78–52178
V_3Ga, LRO rel. to supercond. T_c 77–11504
V_3Ga, neutron irradiation and annealing 78–52130
V_3Ga, supercond., neutron-induced disorder revealed by isochronal annealing 77–72938
V_3Ga, supercond. transition temp., as-cast and annealed *(Russian)* 78–56618
V_3Ga, superconducting transition temp., metallurgical processing, struct. 77–63019
δ-VN, cryst. growth by floating zone and zone annealing techniques 77–69983
VO_2, amorphous thin films, phase transition, resistivity and opt. transmission discontinuities 77–47871
VO_2 film, ion bombard. effect on metal-dielec. phase transition, optical props. meas. 79–90963
V_2O_5-P_2O_5-CaO glass with metal electrodes, elec. characts., thermal conditions effect *(Russian)* 78–47884

annealing continued
VSi_2 thin film growth rel. to annealing environment and interposed layers 78–2395
V_3Si, neutron irradiated, A15 compound, recovery of T_c by annealing 78–52132
W (100), clustering of Kr, He desorption spectrometry 80–77908
W (110), O_2 and WO_2 adsorption by LEED AND AES 80–34317
W alloys, deformed, vacuum technology appl., mech. props. *(German)* 79–57046
W, defect recovery following neutron irrad., annealing effect 79–77642
W, doped wire, secondary recrystallisation temp., bubble parameter effects 77–32596
W, drawn wire, microstruct. effect on fracture 80–3177
W, electron irradiated, or quenched, point-defect mechanism for Stage III recovery, field ion microscope study 79–60403
W fibre reinforced Ni, high temp. stability 77–48372
W fibre reinforced Ni-Cr steel, TiN coated fibre, protective props. *(Russian)* 79–66201
W, Frenkel pair creation and stage I recovery of electron irrad. cryst. near threshold 79–1463
W, grain boundary migration initiated by high hydrostatic press. 78–51554
W, implantation effects of ^{133}Xe, annealing behaviour, Mossbauer study 80–40011
W, incoherent twin boundary microfaceting on annealing, field ion microscope determ. 79–77608
W, metal-ceramic, mech. props. and structural nonuniformity 79–15705
W, neutron irrad., at thermal energies, annealing exam. of recovery 78–47355
W, neutron irrad., recovery of defects, isochronal and isothermal annealing 79–46712
W, neutron irradiated, FIM obs. of radiation damage 79–7632
W, O_2 chemisorption hysteresis effect, SIMS 77–72771
W, plastically deformed single cryst., mag. susceptibility *(Russian)* 80–93074
W, polygonisation critical stage in single crystals deformed in compression 79–4979
W, recrystallisation of commercially pure and doped wire drawn to high strain 79–100165
W, structural defect recovery after irradiation and cold work 78–47429
W, substruct. stability of single crysts. on high temp annealing *(Russian)* 77–66666
W, surface cleanness control using secondary electron spectroscopy *(Russian)* 79–90858
W surface wetting by liquid Cu depend. on preliminary surface treatment *(Russian)* 80–35388
W, thermal neutron irradiated, radiation damage and stage III defect annealing 78–51586
W, vacancies, quenching and recovery invest., resist. and TEM study 80–39074
W, vacancy-defect clustering, due to annealing and quenching, TEM and elec. cond. exam. 78–47344
W, vaporisation, influence of inert gases on losses *(Russian)* 79–55878
W wire, AKS-doped, second phase particle obs. by TEM, SEM and atom probe microanalysis 80–108457
W, with impurities, grain boundaries, effect on high temp. plasticity *(Russian)* 79–79057
W:K-Al-Si, state of bonding, distribution of impurities 78–92212
W:Re, polygonisation in diffusion process, glide dislocation interactions 80–38998
W:Xe, BCC, heavy ion implanted, vacancy recovery, Mossbauer spectroscopy 79–82896
W/EuS field emitters, electron emission current depend. on annealing temp., mag. props. 80–16160
W-C(0.01 to 0.2 wt.%), C effect on high temp. strength 77–16614
W-Cr-Pd, Pd effects on diffusion 77–24445
W-Fe, dil., spin glass props., DC mag. susceptibility meas. 78–68283
W-Ir (1 wt.%), positron annihilation, photon ang. distrib. meas. effect of deformation, annealing temp. *(Russian)* 78–35220
W-K-Si-Al doped wires, heavily drawn, fibre struct., annealed 79–56993
W-Ni liquid alloys, sintered, coarsening of W grains, exam. 78–56598
W-Re alloy, effect of thermal prehistory on resistivity meas. 78–3241
W-Re alloy, elec. resistivity meas. near conc. anomaly, 300 to 1200K 77–35911
W-Re alloy, substruct. stability of single crysts. on high temp. annealing *(Russian)* 77–66666
W-Re alloys, anomalous conc. depend. of elec. resistivity 77–35917
W-Re fibre-reinforced Ni-base refractory alloy, struct. and props. *(Russian)* 77–59721
W-Zr (2.92, 7.42 and 10.02 wt.%), and W_2Zr, thermal expansion, elec. resistance, 100-900°C, crystallisation 78–91455
W-Zr field emitter, time-of-flight atom-probe study 80–80949
WC-Co (10 wt.%), elevated temp. bend deform. and fracture, effect of C 77–59877
WC-Co hard alloys, hot-pressed, wear resist. under abrasive friction, heat treatment effect 80–66555
WO_3 amoprhous film, sublimed under different conditions, elec. transport props. 80–7015
WSi_2, amorphous, crystallisation by energy beam annealing 79–69012
WSi_2 refractory formation by As^+ ion beam bombardment 80–107286
WSi_2, sputtered, props. for MOS IC appl. 80–70831
W(111) surface, effect on ethane chemisorption obs., AES and LEED pattern exam. 79–15005
$(Y,Eu,Tm,Ca)_3(Fe,Ge)_5O_{12}$ garnet film coercivity, new annealing method 78–84459
$(Y,Sm,Ca)_3(Fe,Ge)_5O_{12}$ epitaxial films, mag. props., growth condition effects 80–97124
$(Y,Sm,Lu,Ca)_3(Fe,Ge)_5O_{12}$ garnet film coercivity, new annealing method 78–84459
$(Y,Sm)_3(Ga,Fe)_5O_{12}$ epitaxial layers, annealing effect on mag. props. 79–61191
Y, electron radiation damage, elec. resistivity change rates 80–59954
Y-Er, surface, high-freq. elec. cond. dispersion function, effects of polishing and annealing 78–19506
Y-Re-B, annealed, and quenched X-ray structural and phase anal. 78–11207
YAG laser trimmer for wafer level products 80–87428
YAG:Ce^{3+} luminesc., efficiency reduction after annealing 79–61443
YAG:Nd,Ce,Cr, effect of γ-rays, fast electrons on optical props., annealing and colour centre destruction 77–8608
YAG:Ti, growth conditions from melt 79–95924

annealing continued

$Y_3Al_5O_{12}$ crystals, variation of microhardness anisotropy with heat treatment 79−56053
YCo_3 amorphous films, ^{59}Co spin echo study 80−80636
YCo_3 film, amorphous, sputtered, in-plane anisotropy induced by rare gas annealing 78−84458
Y_xFe_{1-x} amorphous films, microstruct. and mag. anisotropy 79−82838
$YFe_{5-x}Al_xO_{12}$, impurity redistrib. kinetics, temp. depend., vacancy effects 80−75263
$YFe_{5-x}Ga_xO_{12}$, impurity redistrib. kinetics, temp. depend., vacancy effects 80−75263
YIG, diamagnetically substituted, annealing effects on cation distrib. 79−1455
YIG, electron and γ-irrad., photomagnetic effect 80−103877
YIG, film, LPE, annealing-induced relief of compressive misfit strain 78−2386
YIG:Ca, oxidising effects of high temp. annealing in reducing atmosphere 80−66696
Y_2O_3-Fe_2O_3 systems, solid-phase reacts., $Y_3Fe_5O_{12}$ form. 78−44062
$Y_{2.6}Sm_{0.4}Fe_{5-x}Ga_xO1_2$, epitaxial, domain wall crit. vel., effect of material parameters 79−99740
$(YSmLuCa)_3(FeGe)_5O_{12}$, epitaxial films, LPE grown, annealing effects on mag. anisotropy 80−66548
$(Y_{1-x}2Co_x)Co_5$, anisotropy fields, coercivities, annealing effects 78−91898
Yb, electron radiation damage, elec. resistivity change rates 80−59954
YbSe, formation and crystallographic charact. of thin film phase 78−91574
zircalloy-2, annealed, neutron irradiated, 573 to 923K, damage struct. 79−99247
Zn, dislocation struct. stability, effect of deformational and thermal annealing 78−64567
Zn, highly perfect crysts., Bridgman growth, dislocation density rel. to annealing *(Japanese)* 80−40252
Zn, hot rolled, grain boundary fine structures, TEM exam. 78−76680
Zn, isothermal annealing effect at 400-410°C, on dislocation struct. in monocrystals *(Russian)* 79−20082
Zn, loading and annealing, dislocation struct. control *(Russian)* 78−3142
Zn, thermal recovery and stress-strain relations 78−11266
Zn-Al (1.1 wt.%) superplastic alloy, grain size determ. *(Czech)* 80−81118
Zn-Al (22 at.%), heat treatment and straining effect on fracture and corrosion 79−87672
Zn-Al (22 wt.%), superplastic eutectoid cavitation evidence 77−63741
Zn-Al eutectic alloy, uni-directionally solidified, damping capacity *(Japanese)* 80−16364
Zn-Al eutectoid alloy, straining at elev. temp., whisker crystal 79−29087
Zn-As system, homogeneity range of $ZnAs_2$ and electrophys. props. 80−60833
Zn-Ga-P-S quaternary system, p-type conductive alloys 78−39105
Zn-Sb diffusion couple, ZnSb phase layer growth kinetics, 240-320°C, up to 30 kbar 78−10229
$Zn_xHg_{1-x}Te$, vacancy mech. of resorption of Hg droplets 80−39070
$ZnIn_2S_4$, III(a) polytype, absorpt. spectrum tail changes due to microstresses 80−2788
ZnMn ferrites, prepared by wet chemical and ceramic methods, comparison of struct. and mag. props. *(German)* 79−24470
ZnO (0001), $(000\bar{1})$ and $(10\bar{1}0)$, UPS rel. to elec. struct. 78−15288
ZnO, adsorpt. of H_2O vapour, annealing and grinding effects 78−68656
ZnO, ellipsometric spectroscopy of nonpolar $(1\bar{1}00)$ surface 79−33651
ZnO, polar $(000\bar{1})$ surface, annealing and Ar^+ bombard. effects on conductivity, LEED obs. 79−51653
ZnO RF sputtered films, post deposition annealing behaviour 80−100416
ZnO-Bi_2O_3-CoO-MnO-Sb_2O_3 (97.5, 0.5, 0.5, 1.0 mole%), exam. of elec. props. at different annealing temps. 80−3099
Zn_3P_2, elec. cond., Hall effect, P interstitial effects 80−84465
Zn_3P_2 photovoltaic material and Schottky diode characteristics 78−64066
ZnS, defect form. in single crysts. during implantation of Zn, S, and Ar *(Russian)* 78−14369
ZnS, high temp. annealing effects on photoluminescence 78−19564
ZnS, ion implantation effects on luminesc., thermo-EMF 80−88178
ZnS, S annealed, IR enhancement and quenching of photocond. 78−14763
$ZnS:Er^{3+}$, ion-implanted, annealing, cathodolum. obs. 80−2868
ZnS:Mn, electrolum. films, activating impurity diffusion coeff. *(Russian)* 77−84995
ZnS:Ne, implanted single crysts., photolum. and bombardment effect, thermolum. curve obs. 80−55166
ZnS-Mn sublimated phosphor films, annealing effects *(Russian)* 78−43949
ZnSb, epitaxial films, growing conditions effect on elec. cond., thermo-EMF 80−39687
ZnSe cryst., IR absorpt., annealing effect 80−80774
ZnSe, electron irrad., dislocation climb, TEM obs. 79−1461
ZnSe, in liq. Pb, photoluminescence 80−60661
ZnSe, reactor irrad., opt. props. 77−90137
ZnSe:I, I vapour transport prep., conductive and photolum. cryst. 79−100035
ZnSe:In, heavily compensated, negative magnetoresistance 79−91079
ZnSe:In elec. transport props., effect of Zn-annealing, 300 to 77K 78−76075
ZnSe:N, ion implanted cond. type conversion on annealing *(Korean)* 78−18668
ZnSe(:Ga)(Al), effect of thermal treatment and doping on elec. props. 77−85223
p-$ZnSiAs_2$, electron irrad. elec. props. annealing, lattice defects 80−100465
$Zn_2Ta_2O_6$, metastable orthorhombic variety, crystallographic characts. *(French)* 79−82185
ZnTe, dominant acceptors, annealing and quenching 80−24463
ZnTe, effects of Zn anneals in 400-550°C range on acceptor conc. 80−10571
ZnTe, elec., SEM and TEM studies of impurity segregation during long annealing 80−30001
ZnTe, ion implantation defect introduction, cathodolum. studies 80−75250
ZnTe, irradiation induced radiative centers obs. 80−66290
ZnTe, TEM obs. of precipitates, shape of Te solidus line 80−25703

annealing continued

ZnTe:Bi, laser annealing, channelling, reflectivity spectra 80−66215
ZnTe:Li, impurity segregation during short annealing and quenching, SEM, TEM and elec. meas. 80−10676
ZnTe:Li, Li in Te precipitates, diffusion during thermal anneal 80−39358
ZnTe:Li(Cl)(Al)(In), ion implanted and annealed, photoluminesc. meas. 78−15208
ZnTe:O, electronic and optical parameters of O related centre 77−24534
ZnTe:P(As), ion implanted, cathodoluminescence emission spectrum 80−108281
ZnTe-Ga_2Te_3, phase diagram 78−35360
Zr, 10 keV deuteron irradiated, retention and precipitation 80−34099
Zr alloys, irradiation growth, influence of microstructure and test conditions 80−92561
Zr alloys, neutron irrad., yield strength changes and radiation hardening, damage annealing *(Italian)* 77−65269
Zr, annealed, neutron irradiated, 573 to 923K, damage struct. 79−99247
Zr base alloys, irradiation growth, dislocation model 78−51595
β-Zr, Cr diffusion rates in temp. range 914 to 1240°C 80−15304
Zr, H(D) implanted, superconductivity enhancement obs. 80−70884
Zr, irradiation growth, influence of microstructure and test conditions 80−92561
Zr, neutron irrad., low temp. deform. studies 79−47757
Zr polycrystalline, low-temp. alternating deformation and annealing, yield stress, elec. cond. variation *(Russian)* 79−74199
Zr, proton irradiation, 10 to 16 MeV, isochronal annealing meas. 80−2083
Zr-Al(8.6 wt.%), neutron irradiated, irradiation growth and recovery, annealing 80−15162
Zr-Au (0.3 and 0.2 wt.%), irradiated, backscattering meas. of Zr self-interstitial atom trapping by Au 77−69014
Zr-B (1.3 wt.%), investigation of swelling due to neutron irrad. *(Russian)* 79−60404
Zr-base alloys, annealed specimens, irradiation growth 80−49276
Zr-Cu-Ti (2.5, 0.15 wt.%), indentation irregularity at elastic limit after heat treatment *(French)* 79−79004
Zr-Fe, amorphous alloy quenched by levitation method, crystallisation 79−55669
Zr-Ge-B system, phase equilibria 78−35356
Zr-Nb (1 and 2.5 wt.%), annealed, thermal expansion, α/β transition *(Russian)* 78−26702
Zr-Nb (2.5 wt.%), neutron irradiated, 573 to 923K, damage struct. 79−99247
Zr-Nb (2.5 wt.%), transforms. during annealing of welded joint, after thermal cycling *(Russian)* 80−29984
Zr-Nb (2.5 wt.%) pipe, fracture resistance, hydrogenation effect 80−104279
Zr-Nb-Fe (13 wt.%, 5 wt.%), struct. changes during decay of BCC β solid solution 79−15669
Zr-Nb-V-Fe (12 wt.%, 6 wt.%, 4 wt.%), struct. changer during decay of BCC β solid soln. 79−15669
β-Zr-Nb(Cb) alloys, anneal hardening and flow softening 79−78993
Zr-Ni, surface layer, segregation of ferromag. Ni, magnetooptic investigation 80−2256
Zr-Ni-H_x($x=2.8$ to 3), surface layer, segregation of ferromag. Ni, magnetooptic investigation 80−2256
Zr-Rh alloys, amorphous, thermal relax. effects on electronic and supercond. props. 79−65575
Zr-Ru(Pd), heat treated, mech. props. and struct. 78−80571
Zr_3Al, cold worked, annealing effects 77−36535
Zr_3Al, ordered polycrystals, hardness and flow stress relationship 77−44309
ZrC, low-temp. reactor irrad., calorimetric investig. 77−80547
ZrCu, constitutional and struct. studies, by mag. susceptibility, metallography and X-ray diffr. 80−70166
$ZrH_{1.8}$, radiation-induced defects in hydrogen sublattice 79−37739
$ZrH_{1.9}$, neutron irrad. induced defects, nature and thermal stability 77−50246
ZrN-AlN composites, struct. and props. 77−40413
ZrO_2 1.6H_2O, anion defect formation and annealing during thermal decomp. in vacuum 77−51366
ZrO_2 single crystals, Y_2O_3 stabilised, optical props., impurities and annealing conditions influence 79−52399
ZrO_2-based solid solutions, effect of added B_2O_3 and Nb_2O_5 on sintering and stability 77−40410
ZrO_2-Cr_2O_3 system, react., phase diagram 1600-2400°C 79−11580
$ZrSiO_4$, natural zircon, nucl. radiation effect on elastic moduli 77−11616
$ZrSiO_4$, zircon, Indian, fission track dating and annealing, U content determ. 79−57891

annealing, magnetic *see magnetic annealing*

anodes

arc, high current, anodes processes, plasma pot., probe meas. 77−19801
arc, vac., anode spot and ion form., review 77−80382
arc, vac., anode spot form., threshold current time depend. 78−87515
arc discharge, high current, anode near-electrode layer, spot formation and sheath breakdown 80−38835
cathodic protection in seawater, sacrificial anode performance 79−57246
contraction region modeling in high intensity arcs 80−103210
cylindrical proportional counter, gas multiplication factor dependence on anode wire attachment 78−78560
dielectric coated, surface and excess vol. charge meas. in presence of flare discharge 77−11426
diffuse discharge, HV, anode drop meas. in transverse air flow 77−39483
diffuse discharge, HV, anodic region anal. at 10 to 400 mm Hg 77−43094
electron accelerator with inductive energy accumulator 79−26785
energy balance of anode in low-pressure heavy-current discharge with hollow cathode *(Russian)* 78−51369
foilless anode electron-beam laser with chopper-wheel gas pulser 78−63122
Geiger counter, self-quenching, anode surface changes with ageing 80−58025
graphite arc, in Ar flow, meas. of anode voltage drop 80−84022
high-current, low/intermediate press. arc, anode sheath and pot. drop 79−41901
high-current arc, negative anode pot. drop, existence region for ignition 77−55187

anodes continued
- high-current arc, positive anode pot. drop 79—41902
- high-speed rotating anode disc, spot motion and erosion calc. 78—71498
- HIP-1 hot ion plasma, effect of anode-cathode geometry on performance characts. 77—24112
- ion beam extraction, computer simulation, finite element method 80—96387
- low-pressure discharge anode sheath in crossed fields, electron density distrib. 78—75424
- material effects, switching in high-resistance layers of ZnSe 79—65549
- metal anode, hot electron emission from NaCl single-crystal film, anode damage 79—15244
- microchannel plates, low distortion resistive anodes 80—886
- multiwire gas counter for VUV region coordinated meas. 79—67384
- optoelectronic revolution counter for X-ray tube anodes *(German)* 78—12678
- pacemaker, Ti as anode and container, passivation and muscle twitch 77—40934
- photoelectrochemical cells, cathodes and anodes for splitting of water 77—44484
- plasma accelerator, end-fire type, high-current discharge effects, anode damage 79—27839
- plasma electron emitter with constricted arc discharge, characts., anode spots effects 80—70040
- plasma triode ion beam production, anode design for reflex operation without impedance collapse 78—9862
- porous Ti-MnO_2 anodes for matrix-type electrochemical cell 77—81414
- potential drop, calorimetric meas. 77—35433
- rotating-anode X-ray tube apparatus 78—58100
- tetrode, reflex, unidirectional ion flow, with additional aluminised mylar anode 78—37473
- Trichel corona negative ion transit times 79—19115
- triggered vacuum gap, anode spot formation, characts. 77—39485
- X-ray, rotating, temperature distribution, various types comparison 79—2901
- X-ray tube, high continuous power, with Rh-W disc bonded to graphite *(German)* 80—105760
- X-ray tube rotary anode, by transition metal carbides *(German)* 80—105759
- X-ray tube rotating anodes, temperature distribution, physical props. 78—29222
- Al anode spot of vacuum arc 80—107006
- Al, implanted in heart-blocked dog, AC impedance and corrosion investig. 77—60297
- Ar arc plasma, circuit-breaking, anode layer, optical diagnostics 77—80351
- Au anode, chem. dissolution in aq. alkaline cyanide, electron stoichiometry 80—40697
- C fibre layers on arc anodes props. and cooling behaviour 79—52245
- Cd_2GeO_4 anode for H_2O photoelectrolysis 80—108716
- $CdIn_2O_4$ anode for H_2O photoelectrolysis 80—108716
- CdSe photoanodes, S substitution during operation and mech. of surface protection 80—107906
- Cd_2SnO_4 anode for H_2O photoelectrolysis 80—108716
- Co_3O_4 anode, wear-resistant, use in applied electrochem. 80—40701
- Cu electrode, cryogenic, multiple anode spots during arc discharge 79—90485
- Fe, rotating disc, partially passivated, pot. and current distrib. calcs. 80—35545
- Ga, liquid point anodes, field-ion emission 80—2928
- n-GaAs photoanodes for water photoelectrolysis 77—77789
- Kr water-cooled arc lamp, anode, temp. distrib. along length, anode geometry effects 80—106994
- Ni-Fe alloy, Ni base cathodes, powder metallurgy technique 80—29903
- Pb battery anode reverse polarisation corrosion test method *(Bulgarian)* 80—50950
- Pb-(Sb)(Sn)(Ag) anodes, film behaviour for Cr electroplating 80—35115
- Pt, anode, impedance behaviour study in β-ZnS suspension-electrolysis leaching in 1N H_2SO_4 soln. *(Japanese)* 79—24754
- Pt black anode of implantable fuel cells, effect of O_2 77—60309
- Pt, oxide film growth in H_2SO_4 solns., temp. study 80—71802
- Pt-Ti bielectrode use as insoluble anode in electroplating 77—44490
- RuO_2-TiO_2 anode, wear-resistant, use in applied electrochem. 80—40701
- S-tolerant components development for molten carbonate cell 80—89611
- Si-SiO_2 interface props., electrolyte anode polarisation effect 77—80849
- Ta powder, particle shape effect on parameters of vol.-porous anodes of electrolytic capacitors 79—61539
- Ti, heart pacemaker appl. 79—44052
- Ti in acidic chloride solns., anodic dissolution and passivation 80—35541
- Ti, Pt-Ir coated, corrosion and passivation behaviour in Cu electrowinning appl. 80—55573
- TiO_2:H photoanodes, diffusion and surface chemistry 80—35546
- TiO_2-RuO_2 anode, wear-resistant, use in applied electrochem. 80—40701
- W, anode, dendritic growths during prebreakdown conditions in organic residual gas, electron microscope obs. 78—44383
- W monocrystals in alkaline electrolyte, surface orientation, effect on anode current *(Russian)* 80—75360
- WC, performance in fuel cells with H_2SO_4 electrolyte 80—21293

anodes, electrochemical *see electrochemical electrodes*

anodic machining *see electrolytic machining*

anodisation
- anodic activation of passive metals, theory 80—25918
- anodic oxidation technique, carbide determ. in annealed high speed steels *(Japanese)* 78—85040
- brass, admiralty, anodic dissolution as stress corrosion cracking mechanism 78—27592
- chalcopyrite oxidation, in acidic chloride medium electrochem. study 78—95817
- concrete, cracking in seawater due to embedded metal corrosion 80—30116
- dielectric films on semiconductor devices, review of deposition techniques 78—23611
- Fe, strengthening in H_2S04, H_2 hardening rel. to struct., anodic behaviour *(Russian)* 79—15855
- GaAs, anodic oxidation mechanism, temp. and electrolyte comp. effects 80—3220
- graphite intercalation cpds. with H_2SO_4 and sulphuric oleums, elec. resist. evolution 80—45518
- Hastelloy B-2, decomposition of metal oxide films under electron bombardment 78—19928

anodisation continued
- high space charge conditions in large elec. field, single carrier steady state theory 77—48561
- III-V semiconductor, anodic oxide film formation, current flow mechanism 77—90479
- III-V semiconductor anodic oxidation and applications 77—77598
- III-V semiconductors, film, sample preparation for TEM studies 78—14258
- Incoloy 800, stress corrosion cracking and anodisation during straining in boiling NaOH soln. 80—30140
- Inconel 600, stress corrosion cracking and anodisation during straining in boiling NaOH soln. 80—30140
- ion-to-electron conversion dynodes, prep. by plasma anodisation 77—1887
- isopropanol, anodic oxidation *(Rumanian)* 78—19907
- layered semiconductor, anodisation as layer counting method 78—76776
- layered semiconductor, constant current anodisation, representation of layer periodicity 80—3218
- metals, corrosion in marine atm., potentiometric technique, appls. 79—24693
- metals and semiconductors, plasma anodisation, model 79—28952
- open-circuit transient method for overpotential anal., technique and appl. to Ta 78—27776
- plasma anodisation, mass transfer from cathode to anode, Auger spectra 78—35583
- semiconductor, anodic etching, physicochemical parameters for maximum resolution 79—74276
- semiconductor, n-type, thermodynamic pot. for anodic dissolution, rel. to photoelectrochem. cell efficiency 78—26948
- steel, austenitic stainless, anodic polarization, Cr content effect 80—35382
- steel, austenitic stainless, current maxima in passivity range 79—66200
- steel, high speed, annealed, carbide determ. by anodic oxidation technique *(Japanese)* 78—85040
- steel, mild, anodic polarisation behaviour in hot alkaline sulphide solns. 80—100949
- steel, stainless, passive state breakdown, and repassivation 79—39031
- steel, stainless, stress corrosion cracking and anodisation during straining in boiling NaOH soln. 80—30140
- steel, stainless 304, sensitized electrochemical polarisation in high temp. water *(Japanese)* 79—15868
- valve metal thin films, deposited on dielectric supports, exam. of anodisation kinetics *(Russian)* 80—7702
- wetting by molten silicate, applied polarization potential effect *(Japanese)* 79—51394
- Zircaloy-2, cladding appl. 77—81341
- Zircaloy-2, electrochemical pitting in alkaline chloride soln., H_2 evolution and anodic disintegration 80—16553
- Ag, corrosion in marine atm., potentiometric technique, appls. 79—24693
- Ag, surface roughness induced electronic Raman scatt. 80—50347
- Ag-Pd-Ni, corrosion in marine atm., potentiometric technique, appls. 79—24693
- Al, AC anodizing in H_2SO_4 79—96229
- Al alloy, anodic oxidation, direct coloured oxide layer *(Rumanian)* 78—23852
- Al alloy anodic oxide film hardness, effect of pH and metallic additives *(Japanese)* 77—56146
- Al alloy coloured anodisation without organic dyes 79—79176
- Al and Al/Nb superimposed layer, anodic oxidation, ^{18}O and MeV ion beam obs. of ion movement 78—15604
- Al and alloy anodic oxide film arborescent structure formation *(Russian)* 80—35409
- Al, anode, with Al_2O_3 coated by anodic spark deposition 78—11382
- Al, anodic attack in chloride medium, passivation *(French)* 79—96224
- Al, anodic layers, coloured, prep. by ultramicrotome without embedding, for TEM and X-ray obs. 79—39074
- Al, anodic oxidation, effect of vacuum and heat treatment *(German)* 79—96225
- Al, anodic oxidation, mobility of implanted As, Sb, Bi, Se and Te 77—90494
- Al anodic oxidation fabrication of Al/Al_2O_3/p-GaAs MOS diodes 80—107914
- Al, anodic polarisation, charge transfer processes 77—16736
- Al anodisation, 'flaw-free' film growth and luminesc. characterisation 78—15605
- Al, anodisation, behaviour of maleic acid 78—44262
- Al, anodisation, high voltage barrier, Cl ion effects 80—104327
- Al, anodisation, impedance meas. during 80—3236
- Al, anodisation, intensity of luminesc. and film thickness 78—80413
- Al, anodisation in H_2PO_4, irregular film formation obs. 80—30153
- Al anodised layer, exam. of factors affecting abrasion resistance 79—34207
- Al, anodised layer bonding, depend on prep. conditions *(Japanese)* 77—25195
- Al, anodized, inorganic glass coating, solution deposited, environmental protection 79—34205
- Al, barrier and porous layer regions, eqn. 79—5089
- Al, behaviour of emulsion particles during electrodeposition 80—104357
- Al, characterisation by nucl. methods *(French)* 77—73378
- Al, coated with anodic oxide, characterisation by tribostimulated exoemission 79—91829
- Al, coloured coatings prod. in AC electrolysis, thin coatings case 80—21176
- Al, coloured coatings prod. in AC electrolysis, thick coatings case 80—25908
- Al, compact anodic oxide film, field assited pore form. 77—81336
- Al, corrosion and anodic polarization in NaOH soln., effect of aldehydes 78—19923
- Al electrochemical electrode, oxide film growth accompanied by luminesc. 79—57236
- Al, electrolytic colouring of anodised layers, improvements 79—15870
- Al, electrolytic treatment and Cu electrodeposition *(German)* 80—45243
- Al film, plasma anodisation to exhaustion on Si and GaAs substrates 79--83388
- Al film, plasma anodisation to exhaustion on Si 80—7722
- Al film for solar collectors, colour-anodised, with selective characts. *(Japanese)* 80—55893
- Al films, anodisation rate and augmentation factor, oxidation in ammonium tartrate 79—79152
- Al, formation of Al_2O_3 on GaAs, interface props. 80—49935
- Al, galvanostatic anodising of high purity samples, galvanolum. obs 77—90488

anodisation continued
Al, galvanostatic anodising of high purity sheet, galvanolum. obs., cryst. orientation effect 77—90489
Al, high temperature hard anodizing 79—96230
Al, implanted Xe behaviour during anodic oxidation 80—71800
Al, in H_2SO_4, AC 79—52465
Al, in phosphoric, sulphuric and tartaric acids, theory and expt. 77—25271
Al, in $SnSO_4$ soln., state of Sn 78—35582
Al, influence of substrate orientation and anodising conditions 78—88581
Al, localised corrosion, blister form. in oxide film as pitting precursor 78—27678
Al, nucleation and growth of porous anodic films 78—44273
Al plasma anodisation current efficiency *(Japanese)* 79—24655
Al plasma anodisation forming voltage limitation mechanism *(Japanese)* 80—16579
Al, plasma anodization kinetics 77—77630
Al, porous anodisation, initial stages of oxide growth and pore initiation, ellipsometry obs. 77—1888
Al, sacrificial anode dissolution, Hg effect study using ion implantation 79—39016
Al, sintering mechanism and sintered body anodization 79—95964
Al, substrate, porous anodic film form. in H_3PO_4 79—70229
Al, superpure, anodic oxide film growth kinetics, UV radiation effect 79—34190
Al, surface energy and adhesion props. 80—10774
Al-Al_2O_3-Pb(Au), solid-state anodisation of Al by vapour infusion, oxide growth rate 80—11830
Al-Al_2O_3-electrolyte system, electrolum. theory, thickness depend. 80—3358
Al-Al_3Fe, anodic film struct. and stability 78—48564
Al-Cu film, anodic oxidation, corrosion props. 78—35581
Al-Cu film, galvanostatic formation anodic oxide, Rutherford backscattering and depth profiling 78—92395
Al-Cu-Mn-Mg alloy D16, sheet, corrosion fatigue strength, with anodised and painted surfaces *(Russian)* 78—35575
Al-Mg (7 wt.%), bare surface reaction rates in aq. solns. 80—101022
Al-Mg alloys, AC colour anodisation 79—20283
Al-Mn, anodisation, intensity of luminesc. and film thickness 78—80413
Al-Mn (1 wt.%), yellow electrolum. from Al-Al_2O_3:Mn-electrolyte system 77—63464
Al-Nb superimposed metallic layers, ionic movements during anodization, Rutherford backscatt. and nuclear microanal. 80—71913
Al-Si alloys, AC colour anodisation 79—20283
Al-Si(Cu)(Zn-Mg-Cu), extraction and phase anal. 79—15673
Al-Sn, Sn effect on electrochemical behaviour in acetate buffer 78—19927
Al-Ta_2O_5-Al, healing of defects in dielec. film by anodisation 80—65406
Al-Zn-Mg alloy 1915, stress corrosion cracking, protective anodic film *(Russian)* 78—35572
Al_2O_3, anodic, passified, inhibition of reaction with water 80—89390
Al_2O_3 composite films, elec. instability 78—68452
Al_2O_3, polycryst. on Si, anodisation, MAOS struct. form, and elec. props. 77—48563
Au, anodic dissolution in H_2SO_4, current-potential curves 79—70344
Bi, anodic oxide film capacity in various soln. 80—104320
Bi, anodic oxide film preparation, dielec. props. 77—20794
Bi anodisation, electric breakdown 79—20377
Bi surface, anodic oxide film, nucleation and growth 77—59966
Bi_2Te_3, anodic film form., in situ ellipsometric study 80—104318
Bi_2Te_3, anodic oxide films, two-dimens. nucleation and growth 80—11807
Bi_2Te_3, constant current anodisation, representation of layer periodicity 80—3218
CdS, semicond. film, contoured anodic photodissolution 79—74277
CdTe, anodic oxidation as thin-layer removal technique for impurity distrib. profile determ. 79—34169
Co, anodic dissolution into silicate glass melt 78—88582
Co, anodic oxidation in neutral and basic soln. 79—39032
Cr, anodic behaviour in methanolic solns. 77—73368
Cu, (100) plane, anodic dissolution in acidic $CuSO_4$ soln., caffeine additive effects 78—27672
Cu anode, passivating behaviour and illum. effects in alkaline soln. 80—104449
Cu, friction under electrolyte immersion condition 78—64738
Cu, in NaOH soln., Cu_2O form., chronopotentiometry, SEM and TEM obs. 77—48573
Cu, stress reduction of straining single crystal due to anodic dissolution *(Japanese)* 78—15579
Cu-Hg, dil., pool electrodes, passivation in alkaline soln. 79—70214
Cu_xO film, growth by anodisation, switching characts. 77—55898
$Cu_{50}Ti_{50}$, amorphous and cryst. alloy, corrosion rates and anodic polarisation curves 79—24650
$Cu_{50}Zr_{50}$, amorphous and cryst. alloy, corrosion rates and anodic polarisation curves 79—24650
Fe, anodic behaviour, in acidic solns. of liq. NH_3 78—27671
Fe, anodic behaviour in 1M H_2SO_4, influence of straining 80—97612
Fe, anodic dissolution in acidic chloride solns., exam. 78—92389
Fe anodic polarisation in H_2SO_4, current and potential oscillation *(Japanese)* 78—11412
Fe, cast, anodic polarisation in slag melt *(Russian)* 80—45513
Fe, cast, anodic protection under boiling H_2SO_4 in industrial conditions 79—20245
Fe powder, passivating oxide layer comp. 78—31558
Fe, two phase film form., overpot. anal. 77—16737
Fe-Cr, grain-boundary segregation of carbon, electrochemical study 79—100147
Fe-Cr (28 wt.%), intergranular corrosion and anodic polarization at grain boundary groove *(Japanese)* 79—15869
Fe-Cr surface alloy formed by ion implantation, anodic polarisation 78—48561
Fe-Ni surface alloy formed by ion implantation, anodic polarisation 78—48562
Fe-Ni-Cr (10, 6 to 14 wt.%), electrochemical polarisation in high temp. water *(Japanese)* 79—15868
Fe-Si binary alloys, anodic behaviour using cyclic voltammetry 79—52417
Ga film, on GaAs or Si, Ga_2O_3 film prep. 77—81338
GaAS, anodic oxide film growth, in situ differential refl. obs. 77—73354
n-GaAS, initial film form. in tartaric acid-water-propylene glycol 77—21301

anodisation continued
GaAS(P)(Sb)-anodic oxide MOS struct. oxide and interface props. 79—60929
n-$GaAs_{0.6}P_{0.4}$, anodic oxide film, exam. using SIMS and ellipsometry 79—61770
GaAs, anodic native oxides for MOS devices, quality assessment 79—61767
GaAs, anodic oxidation 77—16710
GaAs, anodic oxidation in nonaqueous electrolyte and MOS characts. 79—38183
GaAs, anodic oxidation in O plasma 79—66188
GaAs, anodic oxidation under dark and illuminated conditions, behaviour of cell voltage 77—16826
GaAs, anodic oxidation using O plasma, and oxide layer evaluation 78—85015
GaAs anodic oxide, analysis using low-energy ion scattering spectrometry *(French)* 79—52845
n-GaAs, anodic oxide film, exam. using SIMS and ellipsometry 79—61770
GaAs anodic oxide film prep. by plasma anodisation of O-sputtered surfaces, MOS device characts. 79—66176
GaAs anodic oxide films, composition meas. by ion scatt. spectrometry, influence of current density 80—11802
GaAs, anodic oxide for device application, crystallisation dynamics 79—66190
GaAs anodic oxide growth rate in mixed electrolyte 77—44382
GaAs, anodically oxidised, etch pits, defect characterisation 77—56122
GaAs anodisation, ellipsometric study *(Japanese)* 80—97610
GaAs, anodisation, O incorporation at oxide-electrolyte interface, ion microprobe mass anal. 77—25273
GaAs, anodisation at low substrate temp. by low pressure O_2 plasma 80—104314
GaAs, anodisation in HF O_2 plasma, oxide film form. mechanism and kinetics *(Japanese)* 80—93667
GaAs, anodisation obs. by in situ differential refl. 80—50732
GaAs, anodised, interfacial reactions, Raman scatt. obs. 80—49544
GaAs, DC plasma anodisation, and elec. props. of oxide 78—35535
GaAs, device compatible anodic oxidation technique 78—44236
GaAs, epitaxial and metallic thin-films, anodic oxidation anal. 78—80673
GaAs, for MAOS diode with stable charge storage 77—15960
GaAs interface with anodic and thermal oxides, comparison of AES and ESCA 78—95980
GaAs MOS solar cells by anodisation in active region 80—101107
GaAs MOS structures, native oxide growth by wet anodisation 80—70832
GaAs, multiple insulator layers studied by Auger anal. 79—83345
GaAs, oxidation, initial process and oxide/semicond. interface formation 80—50739
GaAs, oxide layers prepared by anodic, thermal and plasma oxidation, in-depth profiles and annealing effects 79—61768
GaAs, plasma anodisation in DC discharge, AES and MIS diode expts. 78—95826
GaAs, shallow-homojunction solar cell by MBE, conversion efficiency 80—30476
GaAs surface, low temp. thermal nitridation 80—97607
GaAs/anodic oxide interface, characterisation of proposed model 80—103754
GaAs-anodic oxide solar cell structs., photolum. props. 80—50958
$GaAs_{0.1}P_{0.9}$:Zn, shallow Zn diffusion profile determ. using anodic oxidation and double radioactive tracer method 77—43239
$GaAs_{0.6}P_{0.4}$, anodic oxide, electronic props. 79—61771
$GaAs_{1-x}P_x$ epi-wafer, comp. profile of heterogeneous struct., anodisation-electrorefl. meas. 78—26782
$GaAs_{1-x}P_x$, heterogeneous struct. obs. by anodisation-electrorefl. technique 78—84088
$Ga_xIn_{1-x}As_yP_{1-y}$, anodisation, effect of pH, current density and illumination 78—95823
n-GaP, anodic oxide film, exam. using SIMS and ellipsometry 79—61770
GaP:Zn, implanted, elec. profiling using anodic oxidation in N-methylacetamide 80—54690
GaP:Zn, shallow Zn diffusion profile determ. using anodic oxidation and double radioactive tracer method 77—43239
GaSe, anodic film form., in situ ellipsometric study 80—104318
GaSe, anodic oxide films, two-dimens. nucleation and growth 80—11807
GaSe, constant current anodisation, representation of layer periodicity 80—3218
InGaAsP. anodic oxidation, refractive indices 80—97601
InP, anal. of anodically oxidised (111) layers by MeV $^4He^+$ channelling effect meas. and AES 79—4492
InP, anodisation, effect of pH, current density and illumination 78—95823
InP interface with anodic and thermal oxides, comparison of AES and ESCA 78—95980
InP, MIS diode prep. by anodic oxidation 79—74270
InP/anodic oxide interface, Auger analysis 77—90478
InSb, anode oxide film coated, ellipsometric and interferential study, optical parameters *(Russian)* 80—50449
InSb MIS diode, anodised, C-V characts., effect of high elec. field pulse 80—60092
InSb-oxide-electrolyte interface, electroluminesc. in anodic oxidation *(Russian)* 77—90201
Li, anodic behaviour in aq. LiOH solns. 78—39941
Mn, in solns. of Mn salts, anodic oxidation *(French)* 78—11520
Mo, anodic behaviour in methanolic solns. 77—73368
Mo, oxide struct., electronic current, and const. current efficiency 78—15575
Nb, anodic oxidation, open circuit transient anal., dielec. and elec. props. of oxide film 80—3245
Nb, anodic oxide layers, depth profiling by sputtered neutral mass spectroscopy 77—77833
Nb, mono- and polycrystn., crystallographic orientation, etching technique determ. 80—71814
Nb-Al superimposed metallic layers, ionic movements during anodization, Rutherford backscatt. and nuclear microanal. 80—71913
Nb-Ta superimposed metallic layers, ionic movements during anodization, Rutherford backscatt. and nuclear microanal. 80—71913
Nb_3Sn, AC losses, surface effects 78—64171
Ni alloys, anodic charact. meas. by AC impedance method *(Japanese)* 79—70224
Ni amalgam, anodic polarisation in alkaline soln. 80—11823
Ni, anodic dissolution into silicate glass melt 78—88582

- **anodisation** continued
  - Ni, anodic oxidation in neutral electrolyte, ellipsometric obs. 78—27673
  - Ni, anodic oxidation kinetics, electrochem. props. 79—15861
  - Ni, electrochem. oxidation and reduction, arrest struct. 77—12735
  - Ni, oxide film form. by electropolishing or anodising, open circuit breakdown 77—90495
  - Ni, role of oxide defects in anodic oxidation 80—76403
  - Ni-Ag, corrosion in marine atm., potentiometric technique, appls. 79—24693
  - Ni-Pd, anodic behaviour, potentiodynamic current density and impedance potential meas. *(German)* 80—25925
  - NiCoPd, anodic dissolution, SFE effect *(German)* 80—25924
  - $Ni_{35}Fe_{30}Cr_{15}P_{14}B_6$, amorphous, anodic polarisation and localised corrosion 77—21310
  - O_2 sensing electrode stability 77—60268
  - Pb, chill cast and wrought, cyclic voltammetry and electrochemical meas. of anodic activity, PbO_2 form. 78—31582
  - Pb electrode, in situ surface phase study by laser Raman spectroscopy 80—103542
  - Pb, passivation in H_2SO_4 soln. 78—76871
  - Pb-Ca-Sn, chill cast and wrought, cyclic voltammetry and electrochemical meas. of anodic activity, PbO_2 form. 78—31582
  - Pb-In film, RF sputter anodisation, Josephson junction form., ellipsometry anal. 79—29258
  - Pb-Sb, chill cast and wrought, cyclic voltammetry and electrochemical meas. of anodic activity, PbO_2 form. 78—31582
  - PbO_2 α- and β-phases prep. by anodic oxidation, electrochem. behaviour *(French)* 79—83460
  - $Pb_{1-x}Sn_xTe$ anodic oxide film form. conditions, IR absorpt. spectra 80—11494
  - Pt, preanodised or passivated, DTA, Pt-O system 77—16733
  - Si, anodic oxidation at constant voltage, mechanism 79—70184
  - Si, anodic oxidation in RF induced O plasma 80—100931
  - Si, anodisation at low substrate temp. by low pressure O_2 plasma 80—104314
  - Si film removal using anodic oxidation, determination of active impurity distrib. 80—40583
  - Si, form. of carbonaceous layer during high dose ion implantation, removal by cleaning, annealing and oxidation 79—70374
  - Si, high electronic current density in anodic oxidation 80—89386
  - n-Si, high resistivity wafer, oxide layer anodically grown, improved homogeneity 79—24642
  - Si, mobile ion identification, Rutherford backscatt. analysis 77—44381
  - Si, p-n junction, electrolytic anodic oxidation method of decoration 80—60069
  - Si, porous, form. during anodic treatment in aq. HF 80—35369
  - Si, porous layer, oxidation, and oxide film props. 80—55556
  - Si, profile anal. using anodisation and stripping, computer algorithm 77—43241
  - n-Si, selective anodic oxidation after P implantation *(German)* 79—52411
  - Si solar cells for cathode protection of submerged marine structures 80—40859
  - Si, thin sheet, Sb impurity profile eval. in p-n diffusion junction by anodisation and resist. meas. 79—46695
  - Si:B(P) impurity conc. profile determ. by anodic oxidation 79—28010
  - n-Si-electrolyte boundary, selective anodic oxidation 78—15563
  - $Si-Si_3N_4$ system, into SiO_2, charge in electrophysical props. 78—2574
  - $Si-SiO_2$ interface formation, F^- and Cl^- ions effect obs. 79—15842
  - SiC polytypes, electrolum. in anodic oxidation, band model *(Russian)* 80—50429
  - SiO_2 films, DC plasma Si anodisation, dielectric const., O_2 pressure influence 80—70564
  - SiO_2 grown anodically over Si, optical and electrophys. props. 77—72934
  - Sn, anodic behaviour in neutral phosphate soln. 79—96187
  - Sn electrodes, potentiostatic polarisation in NaOH soln., XPS 77—90608
  - T, anodic oxidation, ion implanted impurities effects 77—90502
  - Ta, anodic oxide layers, depth profiling by sputtered neutral mass spectroscopy 77—77833
  - Ta, anodisation consts., for oxide thickness prediction 77—48574
  - Ta film, anodisation voltage relationship to oxide thickness *(German)* 78—11443
  - β-Ta film, Ta^{n+} transport number during anodic oxidation 79—39036
  - Ta, formation of Ta_2O_5 on GaAs, interface props. 80—49935
  - Ta on Nb duplex layers, cation-transport processes during anodic oxidation, Rutherford backscatt. and nucl. microanal. 79—20264
  - Ta, open-cct. transient method for overpotential anal. 78—27776
  - Ta-Nb superimposed metallic layers, ionic movements during anodization, Rutherford backscatt. and nuclear microanal. 80—71913
  - Ta_2O_5 anodic films, reanodisation effect on exoelectron emission 79—43110
  - Ti alloy, TA6V, struct. and growth of anodic oxide film 78—23861
  - Ti, anodic behaviour, steady-state, in conc. HCl 80—45515
  - Ti, anodic film structure, intensiostatically formed, pH and current density influence, TEM study *(French)* 79—66217
  - Ti, anodic oxidation kinetics, electrochem. props. 79—15861
  - Ti, anodic oxidation under high voltage, porous layers *(French)* 80—54574
  - Ti anodic oxide film growth kinetics *(French)* 78—23864
  - Ti in perchloric acid-acetic acid soln., AES study of anodic films 79—5072
  - Ti, in perchloric acid-acetic acid soln., polarisation behaviour, stoichiometry 79—5073
  - Ti, passive oxide layer form. in H_2SO_4, ageing with and without photoexcitation *(French)* 80—45432
  - Ti, plasma-anodisation, surface film comp. determ. 77—48591
  - Ti, struct. and growth of anodic oxide film 78—23861
  - Ti, thick anodic oxide film struct., thick *(Russian)* 78—35577
  - Ti-Al alloy film, evaporated, anodic voltage-time dependence obs. *(Polish)* 80—55574
  - Ti-Fe, corrosion, effect of microstruct. caused by casting, annealing, beating *(Russian)* 79—57140
  - Ti-Ni, anodic oxidation kinetics, electrochem. props. 79—15861
  - V, oxide struct., electronic current, and const. current efficiency 78—15575
  - V, source of O in oxide film 79—100389
  - V, use of nucl. reactions to trace source of O in anodisation 79—52683
  - V_2O_5 electrode, anodic dissolution in aq. acid soln. *(German)* 79—91826
  - W, anodic behaviour in methanolic solns. 77—73368
  - W, anodic oxidation, open circuit transient anal., dielec. and elec. props. of oxide film 80—3245
- **anodisation** continued
  - W, anodic oxidation in aq. base 77—77627
  - W dendritic surface anodisation for solar absorptance enhancement 79—34440
  - W electrolytic anodisation, production of WO_3 electrochromic elements 80—25921
  - W, in acidic chloride solns., formation and breakup of anodic oxide films 77—16719
  - W, oxide struct., electronic current, and const. current efficiency 78—15575
  - W solar absorbing surfaces improvement, by anodised interference coating 78—13815
  - WO_3 amorphous anodic film growth on W in acidic soln. 80—81232
  - Zn alloys, anodic corrosion in seawater 77—77628
  - Zr, anodic oxidation, growth stresses of ZrO_2 film 77—16716
  - Zr, anodic oxidation, growth and morphology of ZrO_2 films 77—16717
  - Zr, anodic oxidation, typical valve and behaviour 77—21311
  - Zr, electrochemical pitting in alkaline chloride soln., H_2 evolution and anodic disintegration 80—16553
  - Zr, use of nucl. reactions to trace source of O in anodisation 79—52683
- **anodised coatings** *see anodised layers*
- **anodised layers**
  - AK4-1 alloy, sheet mat., fatigue and corrosion fatigue strengths, coatings effects *(Russian)* 78—11397
  - alumina, anodic, dielec. breakdown 77—1637
  - barrier oxide films, elec. breakdowns, theory 78—11391
  - blackened optical surfaces, IR absorpt. rel. to stray light reduction, spectral emittance meas. 79—61449
  - coloured coatings on Al, prod. in AC electrolysis, thick coatings case 80—25908
  - coloured coatings on Al, prod. in AC electrolysis, thin coatings case 80—21176
  - D16 alloy, sheet mat., fatigue and corrosion fatigue strengths, coatings effects *(Russian)* 78—11397
  - electrolytic colouring, improvements 79—15870
  - ellipsometer obs. interpretation using film form. models 80—101828
  - ellipsometric observation of anodic film growth, automated interpretation 78—56902
  - Hastelloy B-2, corroded surface, electron bombardment effect during Auger electron anal. 80—61014
  - III-V semiconductor anodic oxidation and applications 77—77598
  - ionic conduction determination, open-circuit transient method, rel. to other techniques 80—24650
  - nucleation, growth rel. to electrode pot. variation 78—68634
  - optical reflectance method, for anal. of anodic films on Al 80—37073
  - oxide coating effects on mechanical behaviour of Nb and Ta 77—32659
  - oxide film, photodepolarisation *(Russian)* 77—32316
  - oxide films, ionic conduction 80—34224
  - oxide films, space charge, TSC obs. 77—32326
  - oxide films on Al, heat treatment effect on photoluminesc. props. 77—28610
  - oxides on Al alloys, mech. props. and influence on substrate fatigue 77—44408
  - oxides produced during Al anodisation, thickness meas. by ellipsometry 78—171
  - refractory films, stability, high temp. and electron irrad. effects 77—39747
  - solar photothermal non-selective and energy control films coatings 80—26157
  - space charge effects on steady-state transport in oxide films 80—11124
  - strong elec. field, pulsed V-I characteristics *(Russian)* 78—64156
  - AL, AC anodisation in H_2SO_4 79—52465
  - $(Al,Fe)_2O_3$ on Al containing dispersed Al_3Fe, anodic film struct. and stability 78—11449
  - Al, 1100, anodic barrier film characts., ISS/SIMS 78—53021
  - Al, adsorption of ^{90}Sr and ^{90}Y, oxide layer thickness, Al purity, temp. depend. studies 79—82458
  - Al alloy, anodic finish exam. by SEM and electron probe micro anal. obs. 79—96278
  - Al alloy anodic oxide film hardness, effect of pH and metallic additives *(Japanese)* 77—56146
  - Al alloy surfaces anodized in phosphoric acid, SEM characterization 80—81241
  - Al alloys, contamination, automated nondestructive inspection 80—16629
  - Al alloys, oxide-covered, characteristic emission of negatively charged particles during tensile deform. 78—92179
  - Al and Al alloy anodised oxide films, for adhesive bonding appls., AES and SEM study 80—66689
  - Al and Al/Nb superimposed layer, anodic oxidation, ^{18}O and MeV ion beam obs. of ion movement 78—15604
  - Al, anodic film, formed in H_2SO_4, electron microscopy 78—68843
  - Al, anodic film formed in H_2SO_4, thin film TEM obs. by direct vertical sectioning 78—7106
  - Al anodic films, acoustic and electron-emission during deform. 80—80143
  - Al anodic films, flaw obs. 80—93696
  - Al, anodic oxide film, porosity determ. by pore filling method 79—47848
  - Al anodic oxide films, AES exam. *(French)* 77—36324
  - Al, anodic oxide layers, meas. of growth by photoluminescence, description of equipment 79—52511
  - Al, anodic oxide superficial layer, X-ray emission spectrometry and ion backscattering *(French)* 80—49482
  - Al anodisation in CrO_3 solns, film colour/structure relationship *(Russian)* 79—91851
  - Al, anodised, cryogenic material, IR reflectance 79—71458
  - Al, anodised, photostimulated exoelectron emission, effect of oxide thickness 78—80461
  - Al, anodised in phosphoric, sulphuric and tartaric acids, barrier layer growth study 77—8983
  - Al anodised layer, exam. of factors affecting abrasion resistance 79—34207
  - Al, anodised layer bonding, depend on prep. conditions *(Japanese)* 77—25195
  - Al, anodised surface, neutral particle emission during tensile deform. 79—78856
  - Al anodising, porous films formed in chromic acid 80—100966
  - Al, anodized, as cryogenic material, IR reflectance 79—61387
  - Al, coated with anodic oxide, characterisation by tribostimulated exoemission 79—91829
  - Al, electrolytic treatment and Cu electrodeposition *(German)* 80—45243

anodised layers continued
Al film for solar collectors, colour-anodised, with selective characts. *(Japanese)* 80−55893
Al films on Cr-Mo aircraft steels 79−70231
Al, influence of substrate orientation 78−88581
Al oxide anodic film, colloidal metal, origin of colour, optical props. meas. 78−68571
Al, oxide coating, comparison of water or steam sealing 79−96228
on Al, photoluminesc. obs. 77−1729
Al, porous anodic film, ion beam thinned, electron microscopy 78−92390
Al rods, humidity and coating thickness effects on fatigue in reversed torsion 77−25205
Al, substrate, porous anodic film form. in H_3PO_4 79−70229
Al-Cu-Mg, tpye RR55, high strength, creep behaviour, effect rel. to anodic coatings, SEM study 80−97542
Al-oxide-electrolyte system, luminesc. spectra *(Russian)* 78−76539
Al_2O_3, amorphous, self-supporting, vac.-tight, from electrochem. oxidation of Al in $(NH_4)_2CO_3$ solns. 80−16177
Al_2O_3, amorphous anodic film, struct. anal. 79−51452
Al_2O_3 amorphous films, struct., electron diffr. investigation 80−20046
Al_2O_3 anode film, galvanoluminesc. during pulsed excitation 79−74006
γ_1-Al_2O_3, anodic film, stress corrosion cracking protection of Al alloys 78−95836
Al_2O_3, anodic film, trapped O_2 and effect on dielec. stability 80−100634
Al_2O_3, anodic film on Al, strain to failure, failure characts. 77−12734
Al_2O_3 anodic film peak voltage rel. to ellipsometric thickness 77−77597
Al_2O_3, anodic film transient pitting during film growth 78−56817
Al_2O_3 anodic films, formed on Al, optical reflectance method anal. 80−37073
Al_2O_3 anodic films, H conc. profiles meas. 80−75261
Al_2O_3 anodic films, trapping levels study using TSC 80−103768
Al_2O_3 anodic layer formation in H_3PO_4 solns., surface charact. 78 15603
Al_2O_3, anodic oxide film, field assisted pore form. 77−81336
Al_2O_3 anodic oxide film colour and structure obs. 78−11450
Al_2O_3, anodic oxide films, luminesc., breakdown and colouring 78−19528
Al_2O_3, anodised film, arc cathode root initiation, electron emission, UV radn. effects 78−2985
Al_2O_3, anodised film, charge storage, UV radn. effect on electron emission arc roots 78−6827
Al_2O_3, composite film, barrier layer, ellipsometric meas. 78−67918
Al_2O_3 composite film props., form. by water reaction and anodic oxidation 78−15606
Al_2O_3, elec. breakdown during anodic growth 80−55034
Al_2O_3 film pore size distribution meas., adsorpt.-desorpt. vs. TEM methods 77−74357
Al_2O_3 films, barrier and porous layer regions, eqn. 79−5089
Al_2O_3, films, form., cross-sections, struct. obs. 78−67917
Al_2O_3, form. and behaviour under particle bombard. 80−35029
Al_2O_3, growth of anodic layers on GaAs 79−83344
Al_2O_3 hard anodic coatings, effects of cellular structures 78−11448
Al_2O_3, integrally coloured oxide films on Al, optical properties 80−93420
Al_2O_3, luminesc. during growth on high purity Al 77−48589
Al_2O_3, Ni-pigmented, for selective absorpt. of solar energy, optical and struct. props. 80−55892
Al_2O_3, O conc. determ. using non Coulomb H ion backscatt. 80−55753
Al_2O_3 plasma anodised films, dielec. props. and high-field cond. *(Japanese)* 78−23185
Al_2O_3, plasma-anodised, current efficiency 78−91797
Al_2O_3 supermicrogrid preparation and props. for use as support film in high resolution electron microscopy 80−99010
Al_2O_3, surface impregnated by organic phosphors, fluoresc. spectrum *(Japanese)* 80−55170
Al_2O_3 thin anodised film conduction and internal field obs. 80−15639
Al_2O_3:Ni anodised films, electrolytically coloured, spectrally selective surface 80−11490
Be, anodised, emissivity, in 400-1000K range on function of oxide layer struct. 77−35726
Bi_2O_3, anodic film, dielec. props. 77−20794
Bi_2O_3 anodic film form. on Bi, electric breakdown 79−20377
Bi_2O_3 anodic films, struct. and electronic props., photoeffects 80−44749
CoO_2, anodically formed, emission Mossbauer studies 79−61268
Co_xO_y, comp. of layers formed by anodic oxidation of Co in neutral and basic soln. 79−39032
Cu_2O, form. on Cu electrodes immersed in NaOH, chronopotentiometry, SEM and TEM obs. 77−48573
Fe oxide films, anodically formed, compositions 79−90898
Fe-Cr, surface covered with anodic oxide film, in-depth composition profiles 80−10763
Fe-Ni alloy, anodic oxide film formed in H_3BO_3-$Na_2B_4O_7$ soln., exam. of in depth profile by AES and sputter etching 79−20247
FeO_x on Fe, semicond. props. 77−36003
FeS amorphous films, on mild steel during anodic polarisation in alkaline sulphide solns. 80−100949
$Ga_{1-x}Al_xAs$, anodic oxide films, ellipsometric anal. 79−20234
GaAs anodic films, XPS study 80−71562
GaAs anodic MIS system, dynamic props. of interface state bands 80−49933
GaAs anodic MOS structure, small signal admittance study 80−2478
GaAs anodic MOS structs., interface-state band model 80−11093
GaAs, anodic native oxides for MOS devices, quality assessment 79−61767
GaAs, anodic oxidation in O plasma 79−66188
GaAs anodic oxide, multiple angle incidence ellipsometry, meas. at $\lambda=632.8$ nm 79−63294
GaAs anodic oxide, quantitative chem. depth profiles 77−72799
GaAs anodic oxide, states, electrochemical meas. 80−80176
GaAs anodic oxide chem. depth profiles, neutron activation analysis and Auger spectroscopy 77−77619
GaAs anodic oxide film, self drifting of ionic charges, detection by surface potential decay method 78−72295
GaAs anodic oxide film, optical props. 78−72626
GaAs, anodic oxide film, annealing effect on carrier density profile 78−88040
n-GaAs, anodic oxide film, exam. using SIMS and ellipsometry 79−61770
GaAs anodic oxide film, ellipsometric and IR spectroscopic studies 80−11493

anodised layers continued
GaAs, anodic oxide film comp. profile anal., radioactive tracer technique 77 59956
GaAs, anodic oxide for device application, crystallisation dynamics 79−66190
GaAs anodic oxide formation, galvanostatic obs. 77−77620
GaAs, anodic oxide layers, chem. depth profiles, XPS determ. 80−3222
GaAs anodisation, ellipsometric study *(Japanese)* 80−97610
GaAs, film, selective anodisation, grain boundary edge passivation 79−11711
GaAs, MIS struct., with natural anodic oxide elec. props. 79−99634
GaAs oxide, growth rate in mixed electrolyte, and struct. 77−44382
GaAs oxide, growth-induced damage from photolum. expts. 78−75953
GaAs oxide, heat treatment temp. effects, optical props. obs. 78−27658
GaAs oxide, in-depth profiles, XPS expts. 78−84086
GaAs oxide, optical props., 1.5-6.0 eV 77−90209
GaAs oxide, passivated layers, quantitative in-depth profile, AES-SIMS thermal, anodic and plasma oxidations 78−84087
GaAs oxide, prep. by low pressure O_2 plasma, refractive index and elec. props. 80−104314
GaAs oxide, refl. and transmission, 0.01-6 eV 78−95613
GaAs oxide, refr. index meas., sellmeier eqn. 77−12454
GaAs oxide films, anodically and thermally grown, XPS study 80−16141
GaAs, oxide layers prepared by anodic, thermal and plasma oxidation, in-depth profiles and annealing effects 79−61768
GaAs, surface passivation using composite Al_2O_3 and native oxide, MIS characts. 80−93004
GaAs/oxide interface, interface states obs. by electrochem. method 79−99626
GaAs-anodic oxide interfaces, struct. and chem. props., Raman scatt. obs. 79−47168
n-GaAs-anodic oxide MIS devices, inversion and accumulation layer form. at elevated temps. 79−60934
n-GaAs-anodic oxide-Al MOS struct., elec. instabilities and annealing effects 79−60928
n-$GaAs_{0.6}P_{0.4}$, anodic oxide film, exam. using SIMS and ellipsometry 79−61770
$GaAs_{0.6}P_{0.4}$, anodic oxide, electronic props. 79−61771
$GaAs_{1-x}P_x$, anodic oxide films, ellipsometric anal. 79−20234
GaP anodic MOS structs., interface-state band model 80−11093
n-GaP, anodic oxide film, exam. using SIMS and ellipsometry 79−61770
GaP, anodic oxide film comp. profile anal., radioactive tracer technique 77−59956
GaP anodic oxide system, multiple angle incidence ellipsometry, meas. at $\lambda=632.8$ nm 79−63294
GaP, anodically grown insulating layers, prep. and props. *(German)* 78−64158
GaP oxide, optical props., 1.5-6.0 eV 77−90209
GaP, single-crystal, anodically oxidised layers, AES measurements 78−91556
GaSb oxide, optical props., 1.5-6.0 eV 77−90209
H_xWO_3, formation on Na_xWO_3 surface 80−71767
InAs anodic oxide films prep. and props. 80−55553
InGaAsP/InP, native oxide stripe laser 79−68405
InP anodically grown native oxide, antirefl. coating for InGaAsP-InP photodiode 80−13137
InP oxide, anal. by MeV $^4He^+$ channelling effect meas. and AES 79−4492
InP, surface passivation using composite Al_2O_3 and native oxide, MIS characts. 80−93004
InSb, anode oxide film coated, ellipsometric and interferential study, optical parameters *(Russian)* 80−50449
InSb, n-type, anodic oxide film dielectric, MOS structure *(Russian)* 77−89874
InSb-anodic oxide MIS struct., electrophys. props. *(Russian)* 77−39961
IrO_2 anodic amorphous film, electrochromism isotherms, internal entropy 80−50300
IrO_2 anodic films, electrochromium, on transparent substrates 79−19861
IrO_2 heat-treated anodic films, pH depend. of electrochromism 79−8120
IrO_x anodic film electrochromics in nonaqueous acid soln. 80−2722
IrO_x, anodic film electrodes in electrochromic cell 80−7329
IrO_x anodic film electrochromic cell, fabrication and display device use 80−61320
IrO_x, anodic films, electrochem. characts., electrochromic system 78−80316
IrO_x anodic films, electrochromism and ionic cond., model 80−59706
IrO_x anodic films, electrochromic props. and device uses 80−61319
IrO_x anodically grown film as electrochromic material 80−71377
IrO_x, electrochromic, oxidation state changes and struct. 80−100950
IrO_x film, anodic, electrochromism, pH effects on corrosion stability, coloration and bleaching mech. 80−2726
on Mo, structure and stoichiometry, thickness effects 77−77634
Mo_xO_6, struct. and stoichiometry 78−15575
Nb anodic oxide films, reversible optical changes 78−35580
on Nb, structure and stoichiometry, thickness effects 77−77634
Nb-Ta-N sputtered films and their anodic oxides, elec. props. of resist. and dielec. films 80−11126
Nb_2O_5 anodic coatings, refr. index and spectral phase change, reflectance meas. 79−43052
$(Nb_{1-x}Zr_x)_3$ Sn, bronze-processed tape, AC losses between 5 and 16K after anodising 79−82727
Ni, anodic passive film form. in NaOH soln., refl. and ellipsometric study 80−104447
Ni, anodically oxidised, 100 keV proton channelling investig. of oxide layer struct. 77−84820
NiO film, formed by Ni galvanic oxidation in borate buffer soln., struct. 80−100948
NiO films, on Ni (100) electrodes, oxide defect sites role in breakdown 79−43587
Rh oxide film, anodic, two-colour electrochromic system 80−66150
Sb_2O_3 anodic layers on Sb, semicond. props. 79−56303
Si, anodic oxidation in RF induced O plasma 80−100931
Si, anodic oxide superficial layer, X-ray emission spectrometry and ion backscattering *(French)* 80−49482
Si oxide film, prep. by low pressure O_2 plasma, refractive index and elec. props. 80−104314
Si, porous, formation during anodic treatment in HF aq. soln., growth kinetics and density 80−20059
Si, porous layer form. mechanism by anodisation in HF soln. 80−71769
SiC, surface luminesc. in presence of anodisation 78−52579

anodised layers continued

- SiO_2, amorphous anodic layer on Si, MeV light ion multiple through-scatt., backscatt. obs. 79—86828
- SiO_2, ellipsometry of anodised layers on clean and ion bombarded Si surfaces *(Russian)* 79—24382
- SiO_2 layers, anodic oxidation growth on p-Si, transmission electron diffr. obs. 79—28241
- SiO_x, on SiC, IR spectra *(Russian)* 78—11376
- Sn, anodically treated in borate buffer, passive film form., Mossbauer meas. 80—39990
- Sn mixed oxide film formation and meas. 77—77622
- Ta, anodic barrier film characts., ISS/SIMS 78—53021
- on Ta, electrochem. reactions by tunnel current 77—81340
- on Ta, structure and stoichiometry, thickness effects 77—77634
- Ta, valve metal deposited on dielectric supports, exam. of anodisation kinetics *(Russian)* 80—7702
- TaO_n, combined SIMS, AES and XPS investigation 79—33199
- Ta_2O_5, adhesion, ductility and fracture, spectrophotometric thickness meas. and SEM obs. 79—99460
- Ta_2O_5, anodic, sputtered, equilib. surface comp., mass and energy depend. 79—19472
- Ta_2O_5 anodic film, scintillation 79—91500
- Ta_2O_5, anodic film, thermally stimulated exo-electron emission 80—11546
- Ta_2O_5, anodic film on Al, strain to failure, failure characts. 77—12734
- Ta_2O_5 anodic film with Au counterelectrodes, conduction process 78—84312
- Ta_2O_5 anodic films, elec. cond. mechanism, admittance meas. 80—70705
- Ta_2O_5 anodic films, reanodisation effect on exoelectron emission 79—43110
- Ta_2O_5, anodised film, nonuniformities, optical props., spectrophotometric obs. 78—2933
- Ta_2O_5, elec. breakdown during anodic growth 80—55033
- Ta_2O_5 film, atomic composition depth distrib. by energetic ion anal. 80—35617
- Ta_2O_5, film, dielec. props. meas., two layer Maxwell-Wagner model 78—76373
- Ta_2O_5 films, Poole-Frenkel effect and cond., effect of heat treatment in oxygen and in vacuum 80—39693
- Ta_2O_5, on sputtered Ta_2N, dielec. props., 20-10^5 Hz, 150-500K 79—87386
- Ta_2O_5/Ta, heat treated, exoelectron emission and radiation dosimetry *(Japanese)* 79—83110
- Ta_2O_5-TiO_2, Rutherford backscatt. 77—16734
- Ti alloy, TA6V, struct. and growth of anodic oxide film 78—23861
- Ti anodic oxide film growth kinetics *(French)* 78—23864
- Ti anodic oxide films, reversible optical changes 78—35580
- Ti, anodic oxide superficial layer, X-ray emission spectrometry and ion backscattering *(French)* 80—49482
- Ti, growth kinetics, determ. *(French)* 78—76788
- Ti, struct. and growth of anodic oxide film 78—23861
- Ti-anodic oxide-Au(Al), electronic cond. *(French)* 79—95512
- Ti-Mo alloy, thin anodic oxide, AES depth profile 80—71801
- Ti-O, anodic film structure, intensiostatically formed, pH and current density influence, TEM study *(French)* 79—66217
- TiO_2, anodic films on Ti, struct. *(French)* 77—56154
- TiO_2, anodically formed layers, film instability obs. 78—72916
- TiO_2 films, in Ti-TiO_2-electrolyte system, electroreflectance response 79—42945
- TiO_2 layer form. by anodic oxidation, characterisation using ^{4}He backscatt. *(French)* 80—45433
- TiO_2:Cu, anodic, effect of Cu on optical props., rel. to possible appl. in solar energy conversion 80—16115
- TiO_x, surface film on plasma anodised Ti, comp. determ. 77—48591
- on V, structure and stoichiometry, thickness effects 77—77634
- VO_x, anodic film, optical anisotropy 77—20942
- V_xO_y, struct. and stoichiometry 78—15575
- on W, structure and stoichiometry, thickness effects 77—77634
- WO_3, antirefl. coating on textured W surface, for solar absorber appl., props. 78—63157
- WO_3 electrochromic elements, prod. by electrolytic anodisation of W, and characterisation 80—25921
- WO_3 electrodes, electrochromic processes, digital simulation model 80—76518
- WO_3 electrodes, vac. evaporation and anodic oxidation prep., electrochromic process kinetics 79—100390
- WO_3 film, anodically formed, electrochromism 79—1752
- WO_x, anodic oxide films, quadratic electro-optic and electrostrictive effects, ellipsometry 80—108184
- W_xO_y, struct. and stoichiometry 78—15575
- Y_2O_3 film in Y-Y_2O_3-metal junction, electroforming and conduction 78—26969
- ZnO microcrystals, morphology, formed by Zn anodic electrocrystn. 77—80432
- ZnO solar absorber surface spectral selectivity rel. to temp. and UV ageing 79—62027
- ZrO_2 anodic film, ionic incorporation 79—57160
- ZrO_2, anodic films, growth stresses 77—16716
- ZrO_2, anodic films, growth and morphology 77—16717

anodised thin films *see anodised layers*

anolytes *see electrolytes*

anomalous skin effect

- conducting ferromagnets, surface impedance resonance depend. *(Russian)* 79—91089
- cyclotron resonance, retarded, effect of electron-phonon coupling *(Russian)* 79—8051
- difference between normal and abnormal skin effects *(Russian)* 77—11953
- diffuse boundary plasma, ordinary wave excitation under anomalous skin effect conditions 77—15204
- diffusive electron reflection, anomalous EM wave penetration *(Russian)* 77—28209
- metal, anomalous microwave penetration for near-specular electron refl. *(Russian)* 77—89785
- metal, cyclotron reson. on open electron orbits *(Russian)* 80—88878
- metal, EM props., general lecture 78—26901
- metal, field distrib. under anomalous skin-effect conditions 77—15887
- metal, in mag. field normal to surface, reson. singularities of surface impedance 78—10495

anomalous skin effect continued

- metal, nonlinear second harmonic refl., cyclotron reson. *(Russian)* 77—28449
- metal, surface electrons, reson. and cyclotron waves *(Russian)* 77—73081
- metal, surface impedance near anomalous skin-effect limit, electron-electron N processes 80—100497
- metal, surface roughness effect on light absorptivity 78—80314
- metal, US generation by EM radiation, surface scatt. effects 80—24973
- metal electrodes, plasma-type electroreflection, mechanisms 77—1659
- metal film, Umklapp processes of charge carriers and anomalous transmittance in RF range *(Russian)* 80—70851
- metals, cyclotron resonance depend. on surface, anomalous skin effect *(Russian)* 80—75860
- metals, cyclotron resonance in weak mag. fields surface impedance, current density asymptotic *(Russian)* 80—2641
- metals, cyclotron wave excitation, diffuse boundary scatt. *(Russian)* 80—54729
- plasma, cylindrical, elec. and mag. wave propag., absorbed power-freq. rel. *(Russian)* 77—3942
- plasma anomalous skin effect conditions 78—67544
- plasma column, free, HF, electron distrib., anomalous skin effect *(Russian)* 80—1741
- plasma cylinder, anomalous skin effect, surface impedance, energy loss calc. 78—47098
- plasma with diffuse boundary in mag. field *(Russian)* 77—51195
- plasmas, hot with sharp electron reflecting boundaries 80—24173
- RF anomalous penetration in collisionless plasma 80—64730
- superconductors, type I, surface impedance, anomalous skin effect, surface supercond. regime *(Russian)* 80—80459
- transition metal, optical consts. 12 to 24 μm, anomalous skin effect region 77—20842
- unmagnetised plasma column, anomalous skin effect, finite element calc. 79—14552
- Au, thermal radiative props. at cryogenic temps., comparison with model predictions 77—15604

antenna accessories

see also antenna feeders; directional couplers

- artificial cold resistors, gravitational radiation antenna transducer appl. 78—32750
- Cassegrain radiotelescope prism beamswitch 79—21186
- coupling efficiencies for surface EM waves 77—19391
- coupling to edge metal-oxide-metal junction 79—87161
- EM wave diffraction by plane angular sector, geometrical theory 79—45896
- paraboloidal reflector backward diffraction suppression by corrugated cylinder 77—75383
- radiotelescope for amateur, electronic components 79—21189
- radome and backstructure design improvements 78—57449
- radome for ground station, SIRIO satellite down link propagation expts. in Finland 79—84338
- VHF phase difference meter *(Polish)* 77—87779

antenna arrays

see also antenna phased arrays; directional couplers; microwave antenna arrays

- acoustic, underwater, optimization technique 79—64405
- acoustic, underwater focused nonuniformly spaced 2-dimensional, minimax optimization 79—59897
- acoustic adaptive array processing, time and frequency domains 79—59874
- acoustic arrays, underwater acoustics, review 79—64467
- acoustic parametric sources, parametric gain and beam patterns 77—46836
- acoustic sounder, design from loudspeaker elements for atmospheric appls. 78—87226
- Australian synthesis telescope, design, array config. 78—69690
- biomedical telemetry, transmission and reception with embedded antennae 78—77125
- circular waveguide system, large antenna array, radioastronomy appl. 78—24465
- correlator interferometer, theory, radiotelescopes appl. 80—12670
- cylindrical arrays, vertical sidelobe suppression 77—46848
- EM scattering by array of conducting cylinders, finite difference technique 77—54656
- HF receiving array, for spatial phase structure meas. of ionospherically reflected waves 79—84505
- hydrophone array, for deep ocean submersions 77—62087
- IEE antennas and propag. international conf., London, England, 1978, Nov. 79—12342
- Ionospheric Sounding Satellite, command system, transmitting/receiving antennas *(Japanese)* 77—78609
- large-aperture radio system for meteor studies 80—85870
- linear array, electrical analogue simulation of directivity patterns 77—804
- microwave arrays for localised tumour heating 80—94308
- microwave holography using quadratically spaced linear antenna array 80—32938
- MM wave arrays, surface to volume wave conversion 79—86114
- optical heterodyne receiver arrays, partial tracking, operating in turbulent atm. 79—41345
- passive, tracking continuous-wave transmitting projectiles 80—94955
- radio antenna arrays, incoherent optical 1-bit cross-correlators, radioastron. appls. 80—98555
- radiotelescope transmission lines, antenna arrays and impedance transformation 78—96399
- resonant antenna system, anomalous radiation and electrodynamic characts. 80—69302
- space-time signal processing, optimal versus conventional detectors 79—27467
- T-type correlation antennas, optical image forming system 79—27180
- three-ring antenna, radiation characts. when used for electron plasma waves excitation 78—91107
- two-element array of insulated antennas in relatively dense medium 77—25794
- ULF wave generation by peninsular loop currents 80—90247
- Very Large Array, phase switching, Walsh function appl. in radioastronomy 78—81539

antenna components *see antenna accessories*

antenna feeders

- compact dual-hybrid-mode feeds with low crosspolar radiation 80—12662

antenna feeders continued
IEE antennas and propag. international conf., London, England, 1978, Nov. 79—12342
planar dielectric waveguide, interacting discontinuities, anal. 79—27445
quasioptical feed system for millimetre wavelengths, 7 m Cassegrain radiotelescope 78—32343
radiotelescope, chromatism due to blocking and feed scatt. 78—73630
radiotelescope VLPA FIAN, two wire feed lines, characts. *(Russian)* 77—22066
Very Large Array waveguide transmission system for radiotelescope 77—5444
VHF/UHF with switching of polarisation *(Russian)* 77—22090

antenna lobe patterns *see antenna radiation patterns*

antenna patterns *see antenna radiation patterns*

antenna phased arrays
acoustic, multi-mode operation using noise signals 80—96157
ground-to-satellite power transfer by laser beam 79—62724
IR phase conjugation adaptive array 77—46790
Mills' cross array antenna, digital baseband processing 80—36500
periodic structure of conducting semiplanes of finite structure, diffr. *(Russian)* 77—31049
radiotelescope VLPA FIAN, antenna phased array equipment, characts. *(Russian)* 77—22065
radiotelescope VLPA FIAN, two wire feed lines, characts. *(Russian)* 77—22066
reflector phased array aberration effects, optical modelling *(Russian)* 78—16290
sonar Doppler phased array coherent imaging and processing by metaxial optics 79—72521
space antenna, self-deploying large parabolic antenna and array design 78—57450
UTR-2 radiotelescope, expt. techniques, data processing, for decametric survey of discrete northern sources 78—57461

antenna radiation patterns
acoustic parametric sources, parametric gain and beam patterns 77—46836
array directivity patterns, electrical analogue simulation 77—804
axisymmetric spherical acoustic radiator with mixed boundary conditions, directivity 77—46827
brightness temps. estimates from scanning radiometer data 78—85716
Cassegrain reflector antennas, double knife-edge diffraction for curved screens 80—14273
circular plate electron plasma wave antennas, exact directional patterns 78—30449
compact dual-hybrid-mode feeds with low crosspolar radiation 80—12662
current loop radiation pattern in inhomogeneous plasma column 77—76102
dielectric spherical radiator, horn-fed, near field characteristics 77—56543
dipole antenna in magnetoactive plasma EM field distrib. 80—100079
dipole antennas entering planetary atmosphere, plasma wake model and radiation patterns 79—48647
echosonde antenna, effects of phase-front distribs. on radiation patterns 77—39123
electric field intensity and power density, conversion equations for meas. 77—26332
elevation patterns computation, piecewise homogeneous ground models appl. 79—66774
EM scattering by array of conducting cylinders, finite difference technique 77—54656
EM wave source in composite media, air and three-layered earth 78—22076
far-field of blocked circular aperture, example of 100 m radiotelescope, Effelsberg *(German)* 77—2341
helical antenna in compressible electron plasma, radiation resistance 78—38503
heterodyne receivers of CO_2 laser emitters, antenna characts. meas. 77—67498
horizontal dipole, subsurface geophysical probing, of a two layered medium 78—7788
horizontal electric dipole, quasi-static subsurface-to-subsurface and subsurface-to-air 78—73375
impurity photoresistor in interferometer, threshold charact. 80—31856
initial value problem, soln. *(Chinese)* 78—9294
ion wave antennas in plasma, reciprocity reln. 77—3952
IR and submillimetric-wave antenna design and simulation 79—30552
IR antenna characts. of W-Ni point contact diode 77—49772
laboratory plasma in whistler wave regime 77—27685
loop antenna, electron plasma wave radiator and detector, exptl. obs. 77—51198
magnetoplasma immersed antenna, radiation patterns 80—43933
meteor recording freq., influence of form and orientation of antenna directivity diagram *(Russian)* 80—67665
microwave horn aerial, 3.2 cm, circular scanning indicator *(Russian)* 77—26328
Mills' cross array antenna, digital baseband processing 80—36500
near zone field of circular apertures calc., using geometrical theory of diffraction *(French)* 78—5398
non-planar dipole antenna in weakly ionised plasma, radiation pattern 77—3944
Ondrejov meteor radar, antenna radiation pattern 77—78634
open-structure submillimetric-wave mixer props. 79—30551
optical waveguide directional couplers, parameter meas. using radiation patterns 79—3771
opto-acoustic antenna, floating, acoustic field statistical characts., surface waviness depend. *(Russian)* 78—1536
plasma, cyclotron harmonic wave propag. 79—4152
plasma antenna system: dual-integral-equation method 78—75361
plasma antenna system, multilayered, electronically scannable, for space communication 79—4151
plasma antenna system, radiation from plasma column in glass tube excited by waveguide 79—50860
plasma drifting, cold or hot, radiation potential of immersed point antenna, DRFT computation 80—14906
plasma immersed antenna, EM fields meas. techniques, results 77—24095
point source in magnetoplasma, cyclotron harmonic waves and reson. cone 78—91098
radioastronomical antenna systems with complex aperture form, optical modelling *(Russian)* 77—22095

antenna radiation patterns continued
radiotelescope, Effelsberg 100 m, large dynamic range obs. 78—96391
radiotelescope optical modelling using coherent optics and holographic methods, expt. *(Russian)* 77—22096
resonant antenna system, anomalous radiation and electrodynamic characts. 80—69302
Seasat scanning multichannel microwave radiometer, antenna pattern corrections error analysis algorithm 80—94683
semiconductor plasma containing system, cylindrical, with ring source of magnetic current 77—3951
solar radio emission centre displacement measurement using alignment of antennas *(Russian)* 77—22089
sonar, directional characts. of cylindrical receiving arrays with nonuniform hydrophone response 77—88979
sonar cylindrical arrays, vertical sidelobe suppression 77—46848
source radiation in presence of smooth convex bodies, theory 79—64151
spherical, calc. of radiating field *(Chinese)* 79—10243
symmetry analysis of scattering and antenna pattern problems 77—75388
three-ring antenna, radiation characts. when used for electron plasma waves excitation 78—91107
transform-pair relationship between incident and scatt. fields from arbitrary reflector 79—7058
transmitting antennas, body-mounted, biotelemetry appl., design 77—90927
troposphere communication, effect of beam with on energy spectrum of delays *(Russian)* 79—2329
UHF antennas, improved optical simulator appl. 80—26742
underwater horns, directivity 78—18138
underwater transducers, directivity gain using attached horns 78—18138
wave radiation by oscillating electric dipole in moving warm plasma 80—87868
whip antenna coupling with human body *(Czech)* 79—43958

antenna reflectors
bivariate beamshaping in elliptic case, numerical method for reflector surface design 77—27225
EM wave scatt. by plane grating with reflector, point matching soln. 79—45894
radiotelescope, surface meas. with two feeds 79—12403

antenna theory
antenna in magnetoplasma, radiation patterns 80—43933
Babinet's principle, extensions inc. concepts of resistive and conductive sheets 77—54651
boundary value problem, null field approach, computational approach 79—13877
circular aperture antenna immersed in plasma, induced HF thermal noise 78—87496
circular aperture J^2 supersynthesis, radioastronomy meas. appl. 78—40835
circular aperture near zone field calc., using modified geometrical theory of diffraction *(French)* 78—5399
circular apertures near zone field calc., using geometrical theory of diffraction *(French)* 78—5398
coherent microwave imaging of limited fields of view, angular and aperture noise, optimum procedure 77—67045
diffraction coefficient for cylindrically truncated planar surface, ray optical techniques appl. 80—9782
dipole antenna buried in stratified anisotropic media, electromag. field 79—94128
dipole antenna in magnetoactive plasma EM field distrib. 80—100079
dipole field diffraction by perfectly conducting thick half-plate 78—46488
double knife-edge diffraction for curved screens, Cassegrain reflector antennas appl. 80—14273
doubly orthogonal function construction 80—32888
electric dipole in isotropic plasma, low-freq. radiation 79—46436
EM coupling, between two short circuited flat dipoles *(French)* 79—81320
EM field of dipole above layered anisotropic medium 77—10812
EM fields, in inhomogeneous axially symmetric media, coupled azimuthal potentials 77—54650
EM scattering by array of conducting cylinders, finite difference technique 77—54656
EM wave diffraction problem solution using antenna potential method *(Russian)* 80—63899
EM wave generated by long-narrow slit, EM field estimation 78—46494
EM waves and antennas above and below Earth surface, theory 79—66620
embedded bare and insulated receiving antennas, design for biotelemetry appls. 77—40947
field problems, Green function selection and effects on matrix condition 80—14271
finite antenna, EM radiation calcs. 77—68149
finite elements in electrical and magnetic field problems, book 80—62399
Fredholm eqn. of the second kind for current distrib. in antenna theory *(Chinese)* 78—66708
Gaussian beam modes by multipoles with complex source points 77—68171
gravitational antenna sensitivity, quantum mech. anal. *(Russian)* 79—75436
gravity antenna small perturbation meas., optimum strategy 77—82438
hemispherical monopole surrounded by plasma layer, Tonks-Dattner reson. and input admittance 80—87887
HF diffraction of arbitrary incident field by half plane, asymptotic techniques 78—42264
horizontal antennas above infinite plane Earth, input imepdance and current distrib. 80—90259
horizontal electric dipole antenna, quasi-static range propag. within conducting slab 79—48515
IEE antennas and propag. international conf., London, England, 1978, Nov. 79—12342
infinite horizontal wire, current excitation by vertical electric dipole 77—14642
LF noise induced in dipole antenna in ionospheric plasma 79—80072
LF source localization and polarization determination using satellite radioastronomy *(French)* 79—70940
long thin wire scattering widths, meas. using open resonator 78—46489
Maxwell-Vlasov equations, in region exterior to perfectly cond. infinite cylindrical antenna 78—1843
metal whisker diode, with thermally enhanced field emission, elec. fields, calc. by antenna theory 77—47889

antenna theory continued
  microstrips, asymptotic expansion for Sommerfeld integrals 80—14272
  microwave antenna in plasma, radn. patterns *(Russian)* 78—38504
  Mills' cross array antenna, digital baseband processing 80—36500
  monopole immersed in lossy medium, effect of finite size of ground plane on impedance 80—12205
  moving collisional plasma and moving plasma with intrinsic spatial dispersion, emission of longit. waves 80—87848
  multichannel reflector radiotelescope, factors affecting noise interference, anal. *(Russian)* 77—22067
  natural noises detected by antennas in plasmas 80—24181
  natural VLF antenna, Deception Island, impedance meas. 79—48399
  non-planar dipole antenna in weakly ionised plasma, radiation pattern 77—3944
  nonlinear interference, theory of EM scatt. by vibrator with nonlinear contact 80—1110
  optical analogue processing system, antenna systems design appl. *(Spanish)* 80—95822
  parabolic aerial with monopulse exciter for meteorological satellite S-band reception *(German)* 79—92628
  periodically loaded wire grid, EM scatt. theory 77—42467
  plane strip source antennas, doubly orthogonal function construction 80—32888
  plasma antenna system, multilayered, electronically scannable, for space communication 79—4151
  plasma immersed antenna of revolution, current distribution and impedance 77—24096
  plasma layer covered spherical antenna, radiation characts. 80—14907
  pulsed field, due to electric dipole and perfectly conducting wedge 77—54652
  radiation and scatt. from wires and surfaces, free space impedance functions 78—86999
  radiocommunication, propag. problems connected with special source structs. 80—87272
  radiotelescope rotational aperture synthesis, tangent-plane aberration 79—8847
  receiving optical antenna, sensitivity to scatt. aerosol particle, laser location of atm. aerosols 77—70847
  ring aperture antenna in plasma, input admittance anal. 78—38542
  solar power satellite design, use of nomograph 79—70433
  Sommerfeld integral, numerical approximations for fast convergence 78—66727
  sphere with circular opening, radiation form, diffr. field *(Russian)* 77—58238
  superconducting microbridges, basic props. and appls. 77—26400
  surface reactance of corrugated planes, rigorous soln. 80—9775
  surface scattering integrals, asymptotic approx. 77—42468
  thin wire antenna coupling with human body 77—21563
  transfer functions, space-variant, for inhomogeneous scatt. media characterisation 78—71012
  transform-pair relationship between incident and scatt. fields from arbitrary reflector 79—7058
  transponder dipole antennas in and near three-layered body 80—98181
  travelling wave arc antenna in a warm plasma 79—82071
  two-element array of insulated antennas in relatively dense medium 77—25794
  ULF wave generation by peninsular loop currents 80—90247
  wide-angle spherical mirror under oblique illum., EM diffr. in focal region 78—58888
  wire antennas impedance in magnetoplasma, transmission line theory 77—39429
  wire cross, plane wave incident at an angle, induced currents 78—5391
  wire loop laid on ground, radiation resistance calc., antenna for parametric depth sounding *(Chinese)* 78—61565
  Yagi antenna, satellite telecommand transmission, design 77—45286

antennas
  see also active antennas; antenna radiation patterns; dipole antennas; directive antennas; microwave antennas; mobile antennas; radar antennas; receiving antennas; reflector antennas; scanning antennas; television antennas
  acoustic, parametric, radiation, approx. soln. *(French)* 77—42680
  acoustic, sound propagation conf., France (May 76) *(French)* 77—42638
  antenna concepts, for interstellar search systems for extraterrestrial intelligence 78—28545
  antennas and propagation, symposium, Amherst (1976) 77—14633
  antennas and propagation, symposium, Stanford (1977) 77—75378
  automobile whip antenna, first overtone vibrational mode obs. 80—17747
  calibration, radioastronomical methods, standard sources *(Russian)* 78—4103
  circular aperture immersed in plasma, induced HF thermal noise calc. 78—87496
  circular plate electron plasma wave antennas, exact directional patterns 78—30449
  conical slow wave antenna, plasma source using electron cyclotron resonance heating 78—42775
  Debye screening and electron conc. nonuniformity effects on cylindrical antenna on satellite 78—69563
  Doppler sodar antenna configs. for horizontal wind meas. 78—65410
  electric current collection, by long wire in near-Earth orbit 79—25438
  electric dipole in isotropic plasma, low-freq. radiation 79—46436
  ELF, ferrite rod, for Magion satellite for 0.1 to 16 kHz freq. range *(Czech)* 80—85775
  EM field strength meas., broadband antenna probes *(Polish)* 79—21722
  EM waves and antennas above and below Earth surface, theory 79—66620
  gravitation antenna, quantum interferometer as recording element *(Russian)* 78—45557
  gravitational, design for use at 3 mK 77—82435
  gravitational radiation detection method, elastooptical antenna, photoelastic effect 80—46947
  gravitational wave antennas, magnetic pick-up transducer theory 79—85052
  gravitational wave antennas, with and without piezoelectric ceramics, elec. equivalent circuits 78—73915
  gravitational-wave antenna, small, cryogenic, meas. at 1.5K 79—21646
  gravitational-wave resonant antennas, optimum filtering and sensitivity 80—8545
  gravitoelectric antennas, direction sensitive, using uniformly moving charged particle beam 79—9164

antennas continued
  HELIOS command station, correction factors for main transmission axis determining *(German)* 78—4116
  horizontal electric dipole antenna, quasi-static range propag. within conducting slab 79—48515
  IEE antennas and propag. international conf., London, England, 1978, Nov. 79—12342
  ionospheric research, optimum types *(Polish)* 77—45252
  IR antenna characts. of W-Ni point contact diode 77—49772
  monopole mounted on conic frustum, HF scattering 79—76552
  natural VLF antenna, Deception Island, impedance meas. 79—48399
  oblate spheroidal, radiation and reception characts. for electron plasma waves 78—42765
  oceanography buoy transmitting antennas, selection criteria *(Russian)* 80—109253
  optical antennas combined with laser beam, parameters optimisation 79—81475
  orbital antenna farm, concept 80—8514
  passive antenna system for atmosphere elec. cond. meas., comparative study 80—85762
  piezoelectric gravitational antenna for use at 3 mK 78—58103
  plasma, whistler wave ducting caused by antenna actions 78—59586
  plasma heating, alumina loaded antenna for lower hybrid wave heating 79—4159
  plasma immersed antenna, EM fields meas. techniques, results 77—24095
  plasma immersed antenna of revolution, current distribution and impedance 77—24096
  plasma ringing with localised antenna, pulsed reson. cone 77—58866
  printed resonant antenna, for monolithic Schottky diode submillimetre wave detector 77—34025
  prototype Nb gravitational radiation antenna 79—44841
  quartz gravitational wave antenna, Q-factor 79—35623
  quasi-static potential oscillations of thin conductor, instability 80—87900
  radiotelescope, antenna design for amateur equipment 79—88597
  radiotelescope with two antennae, phase-switched between 160 and 190 MHz *(Italian)* 79—12402
  ring aperture antenna in plasma, input admittance anal. 78—38542
  safety, biological effects of 10MHz to 1GHz radiation, ANSI and EPA recommendations 80—30765
  small thin wire, coupling with biological body, impedance and induced current effects 78—3548
  spacecraft communication antennas, composite material for fabrication 78—4063
  Sun, gravitational lens for interstellar radiocommunication 80—62040
  supersonic optoacoustic antenna, acoustic field 78—1540
  troposphere random inhomogeneities, effect on operation, statistical anal. 77—13111
  variable profile for RATAN-600 (Soviet) radiotelescope *(Czech)* 78—53824
  VLF wave measurement at ground station, antenna pickup for vertical elec. field 80—105063
  whip, radiation effect on human body *(Czech)* 79—43958
  wire antenna resonance near lower hybrid freq. in RF-generated magnetoplasma 79—55516
  Yagi antenna, satellite telecommand transmission 77—45286
  W-Ni, MBM diode, resist. depend. of detected signals 80—2482

antibaryons *see baryons*

anticorrosion coatings *see corrosion protective coatings*

antiferrimagnetism
  two-sublattice, spin waves, magnetocaloric effect 78—31073
  vivianite type spin structure model, mol. field approx. 77—66232

antiferroelectric materials
  see also antiferroelectricity; ferroelectric materials
  β-Al$_2$O$_3$-Ag$_2$O, antiferroelectric transformation, Potts' model universality class 80—50277
  copper formate tetradeuterate, deuterated, paraelec. and antiferroelec. phases, neutron diffr. obs. of struct. 79—87404
  copper formate tetrahydrate, antiferroelec., dielec. anisotropy 78—43768
  copper formate tetrahydrate, dielec. anisotropy and dimer theory 79—38427
  copper formate tetrahydrate, dielec. props. under hydrostatic press. 77—20789
  copper formate tetrahydrate, ferrielectricity 80—2706
  copper formate tetrahydrate, stress effect on antiferroelec. phase transition, dielec. meas. 79—38498
  critical points and transitions, in phase diagram, geometrical relation *(Japanese)* 80—24568
  cupric formate tetrahydrate, dielec. props. under hydrostatic press. 77—12343
  cupric formate tetrahydrate, pressure effect on dielectric props. *(Japanese)* 79—65787
  cupric formate tetrahydrate, uniaxial stress effect on dielec. props. 78—48125
  noncentrally symmetric phase identification using SHG 78—74947
  orthovanadates, centrosymmetric exhibiting cooperative Jahn-Teller effect, dielec. props. 79—28694
  perovskite crystals, static and dynamic aspects of PAC meas. 78—88241
  perovskite structure, semiconductor props., review *(Polish)* 78—56437
  photoferroelectric image storage in antiferroelectric-phase PLZT ceramics 80—71353
  praseodymium ethyl sulphate, cooperative Jahn-Teller antiferroelec. ordering 77—66144
  SHG determ. of ferroelec. and antiferroelec. props. 78—74947
  squaric acid, ^{13}C chemical shift tensor study of antiferroelec. second order phase transition 78—52462
  squaric acid, antiferroelec., struct. phase transition mechanism 80—75969
  squaric acid, critical slowing down of fluctuations at phase transition, ^{13}C spin-lattice relax. 80—44948
  squaric acid, dielec. props., press. and temp. depend. 79—99815
  squaric acid, H-bonded antiferroelec., cluster form., NMR obs. 79—28628
  squaric acid, layered, phase transition mechanism 80—97210
  squaric acid, sp. ht. near phase transition 79—91389
  squaric acid, two dimensional antiferroelec., Brillouin scatt. at structural phase transition 80—71430
  squaric acid, two-dimens. antiferroelec., temp. depend. of order parameter, birefr. obs. 80—11351
  squaric acid, two-dimens. phase transition, Raman scatt. study 80—71401

antiferroelectric materials continued
- squaric acid-d_0,-d_2, 2-dimens. antiferroelec., dielec. props. and phase transitions, press. effects 79—95700
- stibiotantalite type structure ferro- and antiferroelectrics, props. and crit. points 79—38460
- thiourea, dielec. const. and IR spectra in ferroelec. and antiferroelec. phases 79—33589
- thiourea, IR reflectivity study of ferroelec. and antiferroelec. phases, dielec. function model 79—33686
- TTF-TCNQ, antiferroelectric ordering of TCNQ ion elec. polarisation 80—20598
- TTF-TCNQ crystal, antiferroelec. ordering of electronic polarisation, simple model anal. 78—92028
- $Ag_2H_3IO_6$, antiferroelec. phase transition investig., Landau anal. 77—1644
- $Ag_2H_3IO_6$, paraelec. and antiferroelec. phases, IR vibrational study 77—85697
- $(AsO_4)_2H_2(UO_2)_2.8H_2O$, point group symmetry for ferroelec., antiferroelec. and paraelect. phases 78—42983
- $BaBiLiTeO_6$, $BaBiNaTeO_6$, $BaLaLiTeO_6$, $BaLaNaTeO_6$, synthesis and charact. 77—55758
- $Ba(H_2PO_4)_2$, dielectric const. and polarisation, antiferroelectricity 77—59526
- $Ba(H_2PO_4)_2$, phonon spectra above and below transition temp. 77—62592
- $BaMnF_4$, anomalous acoustic phonon dispersion 77—47523
- $BaMnF_4$, dielectric props. near 250K phase transition 77—12335
- $BaMnF_4$, phase transitions, review 79—78378
- $BaMnF_4$, spectroscopy, ferroelectric/ferromagnetic coupling, antiferroelectric props. 79—19845
- Ba_2MnReO_6, seignettomagnets with perovskite struct. 79—38459
- Bi complex oxides, antiferroelec. and ferroelec., pyrochlore struct., dielec. and structural study 79—38488
- $Bi_2B'_xB''_{2-x}O_7$, pyrochlore-structured compounds, diffuse transition 77—36182
- $BiFeO_3$-$LaFeO_3$, solid solns., antiferroelec.-antiferromag., magnetoelectric effect at antiferroelec. transition 80—100637
- $BiTaO_4$, X-ray and ESR study of phase changes 78—72476
- $CdFe_{1/2}Nb_{1/2}O_3$, high temp. X-ray exam. 77—11527
- CsD_2PO_4, pseudo-one-dimensional ferrolec. and antiferroelec. transitions, phase diagram obs., soft modes 80—93245
- CsH_2PO_4, and deuterated phase, press. induced antiferroelec., switching behaviour 79—78634
- CsH_2PO_4-d, antiferroelec. under hydrostatic press. 79—91384
- $CsH_3(SeO_3)_2$, paraelec. phase, struct. determ. by neutron diffr. 78—34472
- $CsPbCl_3$, high-resolution elastic neutron diffr. study 80—28984
- $CsPbCl_3$, lattice thermal expansion, X-ray powder technique 80—19965
- $DyAsO_4$, first-order cooperative Jahn-Teller phase transition, dielec. suscept. studies 80—19940
- $DyVO_4$, dielec. anomaly and improper antiferroelectricity at Jahn-Teller transition 77—24802
- $DyVO_4$, electric field influence on elastic props., electron state initial splitting 80—34123
- $DyVO_4$, Jahn-Teller phase transition and improper antiferroelectricity *(Japanese)* 78—80294
- $HUO_2AsO_4.4H_2O$ and $HUO_2PO_4.4H_2O$ layered cpds., struct. investigs. below antiferroelec. transition temps., H bond ordered structs. 80—107416
- $HUO_2AsO_4.4H_2O$ and $HUO_2PO_4.4H_2O$ layered cpds., single and polycryst., proton cond. behaviour w.r.t. antiferroelec. transition temps. 80—107481
- KCN, antiferroelectric phase, 83K phase transition based on model Hamiltonian 79—15418
- KCN, dynamics of CN^- ions near phase transitions at 83K 80—80717
- KCN, F-centres, optical props. 78—2892
- KCN, lattice dynamics and order-disorder transitions, neutron scatt. expts. 78—14434
- KCN, optical F centres and phase transitions 78—56504
- $KCN{:}H^-$, U-centre, local mode meas. 77—1199
- KH_2PO_4, low temp. transition, thermal hysteresis, Cr impurity effect on transition temp. 80—2705
- KNO_3, press. induced II to IV phase transition, Raman scatt. 78—15161
- $(Li_{0.5}La_{0.5})_xBa_{1-x}TiO_3$, cryst. struct., dielec. and IR spectral meas. 79—46614
- $LiNH_4SO_4$, atomic struct. exam. 79—37678
- $ND_4D_2AsO_4$, ND_4 role in antiferroelec. transitions, D NMR 77—52025
- $ND_4D_2AsO_4$, protonic cond. near antiferroelec. Neel temp. 80—59703
- $ND_4D_2PO_4$, cryst., transverse and longit. elec. susceptibilities, modified Ising model calcs. 80—97203
- $(NH_{4(1-x)}D_{4x}H_{2(1-x)}D_{2x}AsO_4)$, crystal growth of para- and antiferroelectric phases 78—48300
- $NH_4H_2ASO_4$-$NH_4H_2PO_4$, EPR spectra of central peak fluctuations 78—91932
- $(NH_4)_2HAsO_4$, $(NH_4)_2HPO_4$, molecular motion, PMR meas. 77—85591
- $(NH_4)_2HAsO_4$, hydrogen bonded, ^{75}As NQR study 79—38399
- $(NH_4)_2HAsO_4$, Zeeman perturbed NQR spectra, EFG tensors and antiferroelectric ordering 77—43898
- $(NH_4)H_2AsO_4$, $(NH_4)H_2PO_4$ and deuterated analogues, low temp. transition, thermal hysteresis, Cr impurity effect on transition temp. 80—2705
- $NH_4H_2AsO_4$, microhardness, expt. determ. 79—24603
- $NH_4H_2AsO_4$, paraelec. phase, ^{75}As NMR linewidth, near transition temp. 77—36184
- $NH_4H_2AsO_4{:}Cr^{5+}$, fast and slow dynamic reorientation 78—80306
- $NH_4H_2AsO_4{:}Cr^{5+}$, ENDOR spectra 78—88224
- $NH_4H_2AsO_4{:}Cr^{5+}$, antiferroelec. phase transition, EPR intensity and linewidth meas. 79—4721
- $NH_4H_2AsO_4$-$NH_4H_2PO_4$ solid soln., Curie temp. and permittivity comp. depend. 77—59533
- $NH_4H_2AsO_4$-$NH_4H_2PO_4$ antiferroelectric solid solution, soft-mode and energy calcs. 79—56743
- $(NH_4)_2H_3IO_6$, paraelec. and antiferroelec. phases, IR vibrational study 77—85697
- $NH_4H_2PO_4$, ^1H spin-lattice relax. in paraelec. and antiferroelec. phases 79—33555
- $NH_4H_2PO_4$, antiferroelec., positron lifetime meas. during phase transitions 78—6644
- $NH_4H_2PO_4$, cryst., transverse and longit. elec. susceptibilities, modified Ising model calcs. 80—97203

antiferroelectric materials continued
- $NH_4H_2PO_4$, crystal, and deuterated cpd., optical meas. of phase transition point by domain obs. 77—40187
- $NH_4H_2PO_4$, defects, X-ray topographic study 78—26580
- $NH_4H_2PO_4$, improper antiferroelec. phase transition, elastic props., free energy, thermodynamic theory 78—80299
- $NH_4H_2PO_4$, microhardness, expt. determ. 79—24603
- $NH_4H_2PO_4$, Mn^{3+} doping effect on Curie temp. and dielec. permittivity 77—59532
- $NH_4H_2PO_4$, phase transition, phonon echo method *(French)* 78—6640
- $NH_4H_2PO_4$, single cryst., thermal depolarisation current 79—51303
- $NH_4H_2PO_4{:}AsO_4^{4-}(SeO_4^{3-})$, antiferroelec., low freq. fluctuations, isotope effects, EPR, ENDOR, ESCA 77—73118
- $NH_4H_2PO_4{:}VO^{2+}$, EPR of VO^{2+} ions in antiferroelec. cryst. 79—47329
- $(NH_4)_3H(SO_4)_2$, movement of NH_4^+ in all phases over 77 to 388K, NMR study 77—28524
- $(NH_4)_2SeO_4.2NH_4HSeO_4$, cryst. struct. 78—71715
- $NaBiMgTeO_6$, $NaBiCoTeO_6$, $NaBiCdTeO_6$, $NaBiCaTeO_6$, antiferroelectric, synthesis and charact. 77—55758
- NaCN, lattice dynamics and order-disorder transitions, neutron scatt. expts. 78—14434
- NaCN, optical F centres and phase transitions 78—56504
- $NaNO_2$, adiabatic and isothermal elastic compliances, critical behaviour 78—92031
- $NaNO_2$, antiferroelec. phase, struct. anal. by neutron diffraction 80—24410
- $NaNO_2$, complex dielectric constant, sinusoidal phase in ferroelectric material 79—11376
- $NaNO_2$, elastic constants and US attenuation coeffs., anisotropic charact. 78—63809
- $NaNO_2$, electrostrictive constants, isothermal and adiabatic, in antiferroelec. transition region 77—12317
- $NaNO_2$, incommensurate-and-antiferroelectric phase transition, amplitude mode, ultrasonic study 80—39227
- $NaNO_2$, incommensurate antiferroelec. phase, Brillouin scatt. freq. shift 80—93349
- $NaNO_2$, modulation of intermediate antiferroelectric phase 79—38462
- $NaNO_2$, NQR of ^{14}N at ferroelec. transition, order-disorder fluctuations 77—63311
- $NaNbO_3$, antiferroelec., primary order parameter, X-ray scatt. 79—51919
- $NaNbO_3$, thermoelec. effect and phase transitions 78—48123
- PLZT, effect of ageing on temp. depend. of permittivity, for ferroelectric and antiferroelectric compositions 78—48121
- PLZT, ferroelectric phase transitions, phase state identification 80—45018
- PLZT, Sn substituted, antiferroelectric ceramics research and their applications *(Chinese)* 79—33617
- Pb compounds, perovskites, polymorphic transformations possibility, mag. anal. elec. ordering effects 80—55389
- Pb ternary oxides, antiferroelec., growth and props. 79—38461
- $PbBiLiTeO_6$, $PbBiNaTeO_6$, $PbLaLiTeO_6$, $PbLaNaTeO_6$, antiferroelectrics, synthesis and charact. 77—55758
- Pb_2CoReO_6, seignettomagnets with perovskite struct. 79—38459
- $PbCo_{1/2}Te_{1/2}O_3$, antiferroelec., high-frequency permittivity, temp. depend. 80—71325
- Pb_2CoWO_6, antiferroelectric substruct. 79—38489
- Pb_2CrO_5, thermal X-ray and dielec. investigations, antiferroelec. phase transition 79—47403
- Pb_2FeReO_6, seignettomagnets with perovskite struct. 79—38459
- $Pb(Fe_{2/2}U_{1/3})O_3$-$PbZrO_3$ solid solns., phase transition 77—48138
- Pb_3GeO_5 antiferroelectric, cryst. struct. 79—19233
- Pb_3GeO_5, single crystal, props., grown by hydrothermal method 79—11504
- $PbHfO_3$, antiferroelectric-ferroelectric phase transition in strong elec. field 80—15990
- $PbHfO_3$, elec. quadrupole interaction, temp. depend., DPAC meas. 79—51884
- $PbHf_{1-x}Ti_xO_3$, phase diagram, influence of poling treatment, ferroelec. antiferroelec. transition *(French)* 77—63374
- $Pb_2Li_{1/2}Nb_{3/2}O_6$, antiferroelec. cryst. growth and props. 77—36189
- $PbMg_{1/3}Nb_{2/3}O_3$-$BiMg_{2/3}Nb_{1/3}O_3$, dielectric polarisation of solid solutions 78—43776
- $Pb(Mg_{1/3}Nb_{2/3})O_3$-$Pb(W_{1/2}Mg_{1/2})O_3$, struct. and dielec. props. 80—25312
- Pb_2NiReO_6, seignettomagnets with perovskite struct. 79—38459
- $4PbO.GeO_2$, X-ray phase and thermal anal., new antiferroelectric 79—1744
- $PbTi_{1-x}Zr_xO_3$, low freq. vibrational modes and ferroelec. transitions 79—33637
- Pb_2WMO_6, M=Cd, Mg, synthesis, struct., phase transitions 77—84715
- $Pb(Zr,Ti,Ge)O_3$, antiferro-ferroelectric transition 78—95565
- $Pb(Zr,Ti)O_3$, doped, Goldschmidt factors and ferroelec. antiferroelec. transition 77—12332
- $PbZrO_3$, antiferroelectricity, survey *(Japanese)* 79—65803
- $PbZrO_3$ based ferroelec. ceramic, pressure-temp. phase diagrams 79—24273
- $PbZrO_3$, Clausius-Mossotti formula and irreducible susceptibility *(Japanese)* 79—65802
- $PbZrO_3$ crystal, structural phase transitions in very high elec. fields 80—15987
- $PbZrO_3$, lattice distortion, X-ray diffr. profiles 79—55712
- $PbZrO_3$-monocryst., elec. cond., permittivity, polarisation, para- and ferro-to antiferroelec. phase transistions 78—60402
- $PbZrO_3$-$PbCd_{0.5}W_{0.5}O_3$, phase transitions 78—43817
- $PbZr_{0.95}Ti_{0.05}O_3$, soft mode dielec., anomalous low temp. sp. ht. 78—14423
- $PrBr_3(Cl_3)$, cooperative Jahn-Teller antiferroelec. ordering, struct. phase transition 77—66144
- $PrCl_3$, cooperative Jahn-Teller ordering of elec. dipoles in non-Kramers doublets 78—15115
- $PrCl_3$, one and three dimensional antiferroelec. ordering 77—4607
- $RbNO_3$, permittivity and dielec. cond. press. up to 5 kbar, antiferroelec. transition obs. 77—36183
- $SbNO_4$, ferro- and anti-ferroelec., crit. points and props. 79—38460
- $SnCl_2.2H_2O$, layered, dielectric anomaly calc. using Ising model, possibility of antiferroelectricity 77—12341
- $SrBiLiTeO_6$, $SrBiNaTeO_6$, $SrLaLiTeO_6$, $SrLaNaTeO_6$, antiferroelectric, synthesis and charact. 77—55758
- Sr_2MnReO_6, seignettomagnets with perovskite struct. 79—38459

antiferroelectric materials continued
- $Sr_x(Na_{0.5}Bi_{0.5})_{1-x}$ solid solutions, piezoelec. and ferroelec. props. *(French)* 80—108158
- $Sr_5TiNb_4O_{17}$, layer perovskite-like struct., physical props. 78—10854
- $Tb(MoO_4)_3$ cryst. struct. in ferroelec., ferroelastic, antiferroelec. and paraelastic phases 80—75205
- $TiSe_2$, optical refl. spectra obs., suppression of antiferroelectricity by excess carriers 77—59536
- TlD_2PO_4, antiferroelectricity, permittivity, electric field double hysteresis loops 80—60512
- TlH_2PO_4 and TlD_2PO_4, dielec. props. under hydrostatic press. up to 7 kbar 80—29696

antiferroelectricity
- *see also antiferroelectric materials*
- dynamics, order-disorder transition, correl. functions and polarisation waves *(Russian)* 80—50282
- electron-hole pairing systems, current states and domains 80—54614
- ferrites, coupled magnetoelec. oscills. and high freq. susceptibility tensor *(Russian)* 80—93152
- ferroics, secondary, polycryst., poling effects 77—16102
- gamma-rays generation by fast electrons travelling through antiferroelectric or antiferromagnetic crystalline structures 78—76545
- Ising model, with transverse field 77—77016
- Ising model with dipole interaction, crit. behaviour 78—48133
- low-lying vibrational modes and theory of local and transport props. at transitions 78—14425
- modified antiferroelectric six-vertex model 79—93050
- order-disorder antiferroelectric, simple model dynamics, diagram method formulation *(Russian)* 80—40070
- orthophosphates, dynamics of ferroactive cryst. 79—37801
- paraelectric-ferroelectric-antiferroelectric phase transitions, electrostrictive effects 80—97209
- phenomenological theory of antiferroelectric transition 79—4771
- transition, bias effect 77—81066
- vibronic theory, developments 79—33620
- $Ag_2H_3IO_6$ crystal, growth, specific heat, antiferroelec. transition 77—69781
- CsH_2PO_4, ferroelec., press. induced antiferroelectricity 79—4774
- CsH_2PO_4, press.-induced antiferroelectricity *(Japanese)* 80—15992
- $DyVO_4$, Jahn-Teller phase transition and improper antiferroelectricity *(Japanese)* 78—80294
- KD_2PO_4, ferroelectric, longit. and transverse props., Monte Carlo study 79—51912
- $ND_4D_2AsO_4$, ND_4 role in antiferroelec. transitions, D NMR 77—52025

antiferromagnetic Curie temperature *see Curie temperature*

antiferromagnetic-ferromagnetic transitions *see ferromagnetic-antiferromagnetic transitions*

antiferromagnetic-paramagnetic transitions *see paramagnetic-antiferromagnetic transitions*

antiferromagnetic properties of substances
- *see also antiferromagnetism; magnetic semiconductors*
- actinide compounds, mag. and structural props. review 77—63132
- actinide dioxides, low temp. lattice parameters, Neel pt. behaviour 77—27867
- actinide elements and compounds, mag. props., book contrib. 80—75727
- alkali bromide-VBr_2 systems, cryst. struct., DTA investig. *(German)* 78—72766
- alkali hyperoxides, ionic π-electron systems, magnetogyration 80—93155
- alkaline earth transition metal ternary and quaternary oxides, ATO_3, $ATi_{1-x}T_xO_3$, and $AZr_{1-x}T_xO_3$, prep., mag. props. and struct. 79—15277
- alkyl ammonium manganese chloride, birefringence, two-dimens. mag. behaviour, magneto-optical meas. 78—31175
- alloy, stoichiometric depend. of elec. resist. 77—69312
- anisotropy energy in basal plane, temp. dependence 78—2673
- BCC magnetically ordered alloys, effects on at. ordering-spontaneous magnetisation reln. *(Russian)* 78—19261
- bis(diethylammonium) copper tetrachloride, mag. susceptibility, EPR spectra 78—68193
- α-bis(N-methylsalicylaldiminato) copper II, dynamic behaviour of antiferro- to ferromagnetic transition 79—73715
- α-bis (N-methylsalicylaldiminato) copper II, one-dimens. spin-$^{1}/_{2}$ Heisenberg antiferromag., high-field spin dynamics 80—71224
- 1,3-bisdiphenylene-2-phenyl allyl benzene complex, free radical, EPR, antiferromag. long range ordering 79—47335
- Brillouin-Mandelstam scattering from thermal and excited magnons 80—70980
- calcium copper acetate hexahydrate, $CaCu(CH_3COO)_4.6H_2O$ anc $CaCu(CD_3COO)_4.6H_2O$, T_N, susceptibility meas. 78—2680
- calcium copper acetate hexahydrate, mag. susceptibility behaviour at low temp. 77—24679
- calcium copper acetate hexahydrate, mag. susceptibility field depend. 79—87241
- chalcogenide spinels, ACr_2X_4 ($A=Zn$, Cd, Hg), mag. exchange interactions 77—24690
- chromium phosphinate polymer, one-dimensional antiferromagnet, spin-flop 80—50131
- cobalt formate dihydrate, mag. relax. phenomena near T_N 79—65656
- cobalt formate dihydrate, mag. struct., antiferromag. mode 79—99678
- cobalt formate dihydrate, ordered state, paramag. cross relax. *(Japanese)* 77—43873
- cobaltous acetate tetrahydrate, weak ferromag. obs. below 85 mK 79—73695
- complex, $Mn(C_5H_5NO)_6(BF_4)_2$, mag sp. hit below 1K 77—89968
- copper, benzoate, one-dimens. antiferromag., heat capacity, field-induced crossover of spin-dimensionality 80—97099
- copper acetate, deuterated, dimeric, single crysts., inelastic neutron scatt. 80—92867
- copper acetates, antiferromag. exchange coupling, superexchange mech. 78—39310
- copper benzoate, antiferromag., spin dynamics at low temp. 77—32278
- copper benzoate, antiferromag. reson. below 1K, Neel temp. determ. 78—39407
- copper benzoate, low-dimensional Heisenberg antiferromag., high field magnetisation 80—80558
- copper benzoate, mag. heat capacity and Neel temp. in mag. field 79—61147
- copper complex $CuBr_2$ (pyrimidine)$_2$, mag. susceptibility and magnetisation curve, 1.2-4.2K 80—11177

antiferromagnetic properties of substances continued
- copper dichloride dipyridine, ground state wave function and superexchange interaction 79—42752
- copper dipyridine dichloride, antiferromag. reson. below 1K 79—28619
- copper dipyridine dichloride, dynamic shift of the ESR field 80—2630
- copper formate.$4D_2O$, field-induced antiferromag. order above T_N 78—84389
- copper formate bisurea dihydrate, magnetisation curves 78—23298
- copper formate tetradeuterate, paramag., induced staggered magnetisation, NMR 77—12212
- copper formate tetrahydrate, antiferromag. phase, neutron diffr. study 80—93085
- copper formate tetrahydrate, two-dimens. spin 1/2 Heisenberg antiferromag., phase transition characts. 77—66352
- copper formate urea hydrate, two dimens. antiferromagnet, EPR, temp. depend. 80—54937
- copper oxalate, two dimens. antiferromag., proton reson. exam. 77—28453
- copper tetraamine sulphate, two-dimensional Heisenberg antiferromag., high field magnetisation 80—80558
- copper tetrammine sulphate monohydrate, evidence for exchange coupled quadratic nets 77—24705
- Cr-Au alloys, dil., elec. resist., 77-700K 78—64035
- di(ethyleneammonium) manganese tetrachloride, 2-dimens., EPR linewidth and spin-dimens. crossover 77—69670
- dialkylammonium iron tetrachloride, antiferromag., mag. susceptibility meas. 80—60220
- dialkylammonium manganese tetrachloride, quasi two-dimensional antiferromag., temp. depend. of absorption spectra 78—43894
- diammonium layer compound, $(CH_2)_2(ND_3)_2MnCl_4$, mag. and optical props. 79—51760
- diammonium layer compound, $(CH_2)_n(NH_3)_2CuCl_4$, mag. and optical props. 79—51760
- diammonium layer compound, $Mn(NH_3)_2(CN)_42C_{12}H_{10}$, mag. susceptibility and sp. ht. meas. down to antiferromagnetic state 79—7999
- diammonium layer compound, ND_3-$(CH_2)_2$-ND_3CuCl_4, antiferromag., magneto-optical meas. birefringence 78—68483
- diammonium layer compounds $(CH_2)_n(NH_3)_2MnCl_4$, quasi-two-dimens. antiferromag., magnetis., spin-flop and crit. exponents 77—66311
- diammonium layer cpds., $(CH_2)_4(NH_3)_2MnCl_4$, EPR linewidth and spin-dimens. cross-over 77—69670
- diethylammonium copper tetrachloride, antiferromag. mode excitation in EPR spectra 78—56373
- diethylammonium manganese chloride, 20 spin diffusion, EPR linewidth meas. 79—47289
- diethylammonium manganese chloride, antiferromag., low temp. luminesc. spectra, magnetoelastic effect 80—2810
- diethylammonium manganese chloride, antiferromag., magnon sideband exam. by absorpt. spectra 77—12108
- diethylammonium manganese chloride, Heisenberg magnet, spin diffusion, EPR study 80—66019
- diethylammonium manganese chloride, planar Heisenberg magnet, spin diffusion, EPR study 80—15793
- diethylammonium manganese tetrachloride, quasi two-dimensional antiferromag., magnon sideband in absorption spectra 78—43895
- diisopropylammonium copper chloride, mag. interactions, susceptibility, 2-230K 80—60237
- dimethyl ammonium manganese chloride, quasi one-dimensional mag. systems, impurity effects 80—71015
- dimethyl ammonium manganese chloride, sp. ht., quasi-one dimens. behaviour 78—52293
- dimethyl ammonium manganese trichloride, NMR for mag. ordered state at 3.6K 79—47340
- dimethylamine iron tetrachloride, antiferromag., mag. susceptibility meas. 80—60220
- dimethylammonium copper chloride, magneto-optical props., 0.03-13.5 eV 77—52132
- dimethylammonium copper chloride bromide, mag. props., pulsed NMR expts. 80—11292
- dimethylammonium copper manganese chloride, two-dimens. mixed magnet, EPR 80—66030
- dimethylammonium copper tetrabromide, quasi two-dimensional antiferromag., mag. behaviour 80—97098
- dimethylammonium copper tetrachloride-tetrabromide mixed cryst., mag. transition 80—65874
- dimethylammonium iron bromotrichloride, canted spin system, mag. susceptibility meas. 78—39303
- dimethylammonium iron chloride, two-dimens. antiferromag., ^{57}Fe Mossbauer obs., sublattice magnetis. 77—66443
- dimethylammonium iron tetrachloride, Mossbauer study of struct. phase transition 80—39278
- dimethylammonium manganese chloride, antiferromag., low temp. luminesc. spectra, magnetoelastic effect 80—2810
- dimethylammonium manganese chloride, perovskite-type layer structure submillimetric-wave spectroscopy 79—33540
- dimethylammonium manganese tetrachloride, antiferromag. and spin-flop resonance obs., 70 to 100 GHz 80—71190
- dimethylammonium manganese tetrachloride, H-bonding, struct. transition, neutron diffr. study 79—42004
- dimethylammonium manganese tetrachloride, Heisenberg ferromag., spin wave anal. 79—61237
- dimethylammonium manganese trichloride:Cd(Cu), impurities in quasi-one-dimens. Heisenberg systems, anisotropy effect 80—80502
- dimethylammonium manganese trichloride, antiferromag. props. 79—73694
- dimethylammonium manganese trichloride, pseudo one-dimens. Heisenberg antiferromag., phase diagrams 79—61148
- dipropylammonium coppertetrabromide, Faraday effect obs. of mag. struct., and domains 77—63399
- dipropylammonium manganese tetrachloride, and tetrabromide, two-dimens. antiferromagnet, spin canting and exchange 80—34620
- dipropylammonium manganese tetrachloride, two-dimens. weak ferromagnet, AC susceptibility 80—65823
- dislocations producing domains and disclinations *(Russian)* 77—32213
- DPPH-benzene, organic radical, pressure induced mag. ordering *(Russian)* 78—88120
- electrical resistivity of antiferromagnetic metals 78—14720
- Eu-Ag alloy, amorphous, formation and mag. props. 79—91216
- ferrous oxalate dihydrate, Mossbauer spectrum, hyperfine fields 78—39483

antiferromagnetic properties of substances continued
- garnet, specific heat meas., elastic type of antiferromag. ordering *(Russian)* 77—55686
- garnets, crystal and static mag. props. 79—99166
- GdH$_3$, mag.-ordering at 1.8K 80—50062
- graphite-FeCl$_{3-x}$ intercalation compounds, Mossbauer spectra 80—20538
- guanidine aluminium sulphate hexahydrate type ferroelectrics, ESR of Fe^{3+} exchange pairs 77—90022
- guanidinium vanadium sulphate hexahydrate, mag. behaviour in applied fields below 1K 77—66376
- guanidinium vanadium sulphate hexahydrate, singlet ground state system, low temp. mag. props. 80—44843
- guanidinium vanadium sulphate hexahydrate, susceptibility meas. spin-lattice relax. effects 77—66279
- Heisenberg open finite chains, mag. and thermodyn. props. 77—72971
- hexagonal antiferromagnet, light interaction *(Russian)* 77—36257
- ilvaites, Mossbauer spectra and mag. features 80—7248
- interstitial compounds, electronic structure and useful phys. props. 77—89683
- Invar, antiferromagnetic Cr-Fe-Mn alloy, Elinvar charact., US wave propag. charact. 77—11640
- Invar, ferromagnetism and antiferromagnetism coexistance at low temp. 77—66320
- Invar, local moment model 79—56505
- Invar, ternary alloys based on Cr-Fe and 4d transition metals, magnetically insensitive 77—28026
- Invar alloys elastic and magnetoelastic effects 79—56589
- Invar problem, conf., Nagoya, Japan (Sept. 78) 79—56481
- ionic crystals, transition metal doped, optical spectra *(Rumanian)* 79—87474
- iron formate dihydrate, higher order term of uniaxial anisotropy *(Japanese)* 80—2571
- itinerant electron antiferromagnet, effects of paramagnetic impurities on Neel temperature 79—4678
- KFeF$_5$, one dimensional antiferromagnets, field depend. spin reduction temp. variation, spin flopping 79—78586
- magnetic crystal, sound velocity temp. depend. anomaly 77—72891
- magnetic phase diagram in external mag. field, spin reorientation curve, critical point coordinates *(Russian)* 80—29548
- manganese acetate, crit. slowing down, 180-350 MHz 77—16083
- manganese acetate tetrahydrate, crit. relax. studied by HF mag. susceptibility 78—39299
- manganese formate dihydrate, 2-D Heisenberg antiferromag., sp. ht. 78—14965
- manganese formate dihydrate, Zn- and Mg-substituted, anomalous crit. phenomena 80—60316
- manganese zinc formate dihydrate, two-dimens. antiferromag., anomalous crit. phenomena, neutron scatt. and PMR obs. 80—50104
- metallic rare earths, conference, St. Pierre-de-Chartreuse, France (Sept. 1978) 80—12844
- metallic very small particles, mag. ordering temps., ferro- and antiferromag. spin structures 77—73027
- α-bis(N-methylsalicylaldiminato)-copper (II), ^{1}H NMR spin-lattice relax. time, spin dynamics 79—99786
- Mn$_{1.98-x}$Cr$_x$Fe$_{0.02}$Sb, Mossbauer effect exam. 78—68432
- Mossbauer spectra, struct., electronic and mag. props. 79—91320
- NiWO$_4$, antiferromag., low symmetry exhibited during spin-flop phase transition 80—60263
- NMP-TCNQ, Peierls insulator and antiferromagnetic mixed phase, mean field approx. 77—20626
- orthoferrites, magneto-optical refl. spectra by equatorial Kerr effect *(Russian)* 77—32400
- oxovanadium carboxylates, near one-dimensional antiferromagnetism, thermal and mag. props. calc. 77—20602
- perovskite-like oxides, ACu$_3$B$_4$O$_{12}$ subseries, synthesis, struct. and mag. props. 77—68960
- perovskites, ordered, mag. props. *(French)* 78—95434
- phase transitions, in systems with competing interactions 78—14963
- polyvinyl alcohol film containing Cu^{2+} complexes, photoconductivity 80—107849
- praseodymium ethyl sulphate, one-dimensional X-Y model, hyperfine contrib. to specific heat 79—1678
- press. depend. of effective mag. fields on ^{57}Fe nuclei 78—52383
- 1,3-propanediammonium MnCl$_4$, 2-dimens. antiferromagnet, with dipolar broadening, spin diffusion, EPR obs. 79—38371
- 1,3-propanediammonium tetrachloromanganate(II) mag. props. 4.2-220K 77—20567
- pyridinium manganese trichloride, pseudo one-dimens. Heisenberg antiferromag., phase diagrams 79—61148
- quinolinium (TCNQ)$_2$, random exchange Neisenberg antiferromag. chain, intermediate field magnetisation meas. 80—103857
- quinolinium manganese (II) chloride monohydrate, crystal struct. and mag. susceptibility 79—19239
- rare earth alloys, amorphous, magnetoresistivity, exchange scatt. model 78—95287
- rare earth alloys, amorphous, random anisotropy antiferromag. model 78—95428
- rare earth alloys, RFe$_4$Al$_8$, cryst. struct. mag. props. and hyperfine interactions 78—87648
- rare earth amorphous alloys, antiferromagnetism, mol. field approx. 78—80142
- rare earth amorphous alloys, random anisotropy antiferromag. model 80—20399
- rare earth amorphous alloys, random anisotropy magnetism 80—65853
- rare earth amorphous alloys, random mag. anisotropy, antiferromag., Monte Carlo calcs. 79—33471
- rare earth arsenides, microwave resist. meas. 77—4383
- rare earth cobalt alloy, RCo$_2$, itinerant system, weak ferromagnetism 78—52191
- rare earth compound, R$_{1-x}$Mo$_6$S$_8$, magnetically ordering, supercond. props. 79—56373
- rare earth compounds, R$_x$Mo$_6$S$_8$ mag. susceptibility meas., 1.3-300K 78—14936
- rare earth compounds, RMo$_6$X$_8$, X=S,Se, coexistence of supercond. and antiferromag. order 79—65579
- rare earth compounds, RRh$_4$B$_4$, supercond. and long range mag. order coexistence 80—15642
- rare earth cpds., RRh$_4$B$_4$ and RMo$_6$X$_8$ (X=S, Se), mag. order and supercond., neutron scatt. studies 80—44807
- rare earth germanides, RMn$_2$Ge$_2$, magnetisation, 4.2-1200K 77—8285

antiferromagnetic properties of substances continued
- rare earth intermetallic, RCu$_4$Ag (R=Nd,Sm,Gd,Tb), mag. props. and cryst. struct. 77—20562
- rare earth intermetallics, RAu$_3$ (R=Gd, Tb, Dy, Ho, Er, Tm), mag. props. *(German)* 79—51761
- rare earth intermetallics, RGa$_2$, mag susceptibility, 1.5-300K and Neel temp. 78—68184
- rare earth intermetallics, RM$_{12}$, mag. interactions, mag. meas. and neutron diffr. 77—63103
- rare earth metal, muon spin relax. meas. of Neel temp. and antiferromag. transitions *(Russian)* 79—87369
- rare earth molybdenum sulphides, R$_{1.2}$Mo$_6$S$_8$, low temp. magnetisation meas., and supercond. props. 79—8018
- rare earth orthochromites, mag. interactions and weak ferromagnetism 78—52220
- rare earth orthoferrite, stripe domain struct. near spin-reorientation points 77—24707
- rare earth orthoferrites, Neel point, cation depend. *(Japanese)* 77—43834
- rare earth orthovanadites, phase transitions and Jahn-Teller distortions 79—28548
- rare earth orthovanadites, RVO$_3$, magnetic and cryst. struct., Jahn-Teller effect 77—32169
- rare earth palladinides, R$_3$Pd$_4$, mag. props. 77—47980
- rare earth perovskites, prep. and props. book contrib. 80—44193
- rare earth sesquioxides, cubic, indirect exchange interactions Anderson model 79—95585
- rare earth silicides, RMn$_2$Si$_2$, magnetisation, 4.2-1200K 77—8285
- rare earth strontium vanadates, R$_{1-x}$Sr$_x$VO$_{3.01x}$, elec. cond. and mag. susceptibility, temp. depend., 77-300K 77—47816
- rare earth systems with singlet ground states, low freq. modes 78—68131
- rare earth ternary compounds, supercond. and antiferromag. coexistence 80—25030
- rare earth tetraborides, mag. and elec. props., metallic character 80—20386
- rare earth vanadites, mag. ordering, susceptibility meas., 60-300K 77—32190
- rare earth Y alloys, Neel temps., mag. susceptibility meas. 77—73025
- rare earth-copper intermetallic cpds., RCu$_2$, metamag., mag. props. 79—87242
- rare earth-copper intermetallic cpds., RCu$_2$, metamag., mag. props. 79—87243
- rare earth-Cu intermetallic compds. single crysts., mag. props. 80—54892
- rare earth-Ga$_2$ intermetallics, mag. structs. 78—84394
- rare earth-gold intermetallics, RAu$_2$, mag. props., 4.2-300K 79—7972
- rare earth-Mg, magnetisation and neutron diffr. meas. 77—63105
- rare earth-transition metal alloys, amorphous, ferrimag., spin arrangements in large fields 80—75718
- rare earth-transition metal hydrides, magnetic props., book contrib. 79—82754
- rare earth-Zn$_{12}$, mag. props. and structs. 78—84393
- rare-earth alloy, RSb, (R=Er, Ho, Dy, Tb, Nd, Gd), mag. props., hydrostatic press. depend. 77—80918
- rare-earth compounds, antiferromag., mag. props., cryst. field theory 78—27006
- rare-earth compounds, antiferromag., mag. props., cryst. field theory 78—27007
- semiconductors, magnetic, spin wave electron amplification theory 80—97083
- semiconductors, magnetic, static magnetic properties, mean field approach 80—7090
- spin glasses, one-dimens., with antiferromag. exchange 80—25231
- steel, stainless, Cr-Mn, N strengthened, anomalous low temp. elastic behaviour 77—77524
- steel, stainless, Cr-Ni-Mn, N-strengthened, low temp. elastic props., correl. with mag. props. 79—70109
- steel, stainless, type 310, antiferromag. ordering, press. depend., Mossbauer meas. 79—73861
- TANOL, free radical, spin flopping transition, temp. depend., mag. anisotropy energy 80—54890
- TANOL, linear chain antiferromagnet, long-range order, magnetisation, PMR 78—23266
- TCNQ complexes, disordered, thermodynamics of random exchange models 80—103826
- TCNQ salt, acridinium (TCNQ)$_2$ low temp. heat capacity, Debye temp. 80—2180
- TCNQ salt, dibenzo-TTF-TCNQCl$_2$, one-dimens. mag. semicond., mag. and elec. props. 80—88601
- TCNQ salt, Mn(TCNQ)$_2$, mag. props. 77—85558
- TCNQ salt, N-methyl-N-ethyl-morpholinium-(TCNQ)$_2$, spin-Peierls transition 79—82803
- TCNQ salt, NMP$_{0.63}$phenazine$_{0.37}$TCNQ, mag. susceptibility, 0.03-4.2K 80—25191
- TCNQ salt, Qn(TCNQ)$_2$, Heisenberg antiferromag. chain for low temp. thermometry and cooling, EPR expts. 79—63217
- TCNQ salt, Qn(TCNQ)$_2$, one-dimens. spin glass with antiferromag. exchange, Knight shift meas. 80—25231
- TCNQ salt, quinolinium, electron spin location, elec., mag., and thermal props. 80—25189
- TCNQ salt, quinolinium (TCNQ)$_2$, random-exchange Heisenberg antiferromag. chain, sp. ht., 0.07-5K 78—14976
- TCNQ salts, Mn(TCNQ)$_2$ and hydrates, mag. and elec. props. 79—82767
- TCNQ salts, n-methylacridium (TCNQ)$_2$, 2,2′bipyridinium (TCNQ)$_2$ and Qn(TCNQ)$_2$, with asymmetric donors, mag. susceptibility, 0.035-4.2K 80—25190
- TCNQ salts, Rb^{+}TCNQ^{-}, and TMB^{+}TCNQ^{-}, triplet exciton dipolar splitting tensors rel. to mag. susceptibility 77—62839
- tetrabutylammonium iron tetraiodide, structural and mag. props., ^{57}Fe and ^{129}I Mossbauer spectra 79—61282
- tetraethylammonium iron tetraiodide, structural and mag. props., ^{57}Fe and ^{129}I Mossbauer spectra 79—61282
- tetrathiotetracenenickel bis(ethylene-1,2-dithiolene), one-dimens. cond., preparation and props. 77—85201
- TMMC:Cu, EPR linewidth freq. depend., spin dynamics 80—15794
- TMMC:Cu, random one-dimens. Heisenberg antiferromag., spin fluctuations 79—61140
- TMMC:Cu(Ni)(Cd), mag. and non-mag. impurity effects on suscept. and Neel temp. 77—66312
- TMMC:M, impurity (M) effects on Neel temp. and low temp. mag. susceptibility 78—88113

antiferromagnetic properties of substances continued
TMMC, 1-D antiferromag., excitation linewidths, temp. depend. 77—20574
TMMC, 3d ordering, effect of mag. field, PMR meas. 77—4569
TMMC, antiferromag., nuclear spin-lattice relax. by solitons 80—97159
TMMC, antiferromag. coupling in linear chains, molecular orbital approach 78—52239
TMMC, antiferromag. reson. below 1K 78—39408
TMMC, classical Heisenberg antiferromagnet, one-dimens., dynamic props., review 80—15737
TMMC, crossover transition, effects on susceptibility and EPR shift 80—71047
TMMC, Cu-substituted, spin dynamics, neutron scatt. cross section 80—60312
TMMC, effect of impurity spins on three-dimensional ordering 79—24159
TMMC, EPR lines in one-dimensional mag. systems, dynamic effect of low-symmetric spin distrib. 80—39853
TMMC, exchange-narrowed EPR linewidth, temp. depend. 78—52292
TMMC, field-suppression of spin fluctuations, NMR obs. 78—91971
TMMC, Heisenberg antiferromagnet, magnetism in one dimension, mag. behaviour 79—28495
TMMC, impurity doped, antiferromag. three-dimensional ordering, proton NMR meas. 79—78414
TMMC, linear antiferromag., 3D ordering and spin correlations, mag. field effect 78—19262
TMMC, linear antiferromag., energy gaps in spin-wave dispersion, neutron inelastic scatt. 79—91223
TMMC, linear antiferromag., mag. field effect on nucl. spin-lattice relax. time, 2 to 4.2K 79—61255
TMMC, linear antiferromag., mag. phase diagram, expt. and theoretical study 80—71038
TMMC, linear Heisenberg antiferromag., effect of mag. field on 3d ordering and spin correlations 78—68229
TMMC, linear Heisenberg antiferromagnet, EPR half-field transitions 80—15792
TMMC, low-symmetry spin distrib. effect on EPR line 80—66018
TMMC, mag. heat capacity and Neel temp. in mag. field 79—61147
TMMC, Neel temp. in large mag. fields 77—89953
TMMC, neutron scatt. obs. of mag. behaviour 77—66254
TMMC, one dimens. antiferromag., neutron scatt. exam. of impurity effects 78—43598
TMMC, one dimens. Heisenberg system, shift of half-field EPR line 78—23325
TMMC, one dimensional antiferromagnet, EPR expts. 80—20454
TMMC, one-dimens. antiferromag., nonlinear dynamics 80—80521
TMMC, one-dimens. antiferromag., spin wave line widths, neutron scatt. study 79—51767
TMMC, one-dimens. Heisenberg magnet, EPR sidebands 78—88163
TMMC, one-dimens. magnet, local magnon modes 80—65829
TMMC, one-dimensional antiferromag., solitons, neutron inelastic-scatt. meas. 80—44810
TMMC, quasi-1D antiferromag., mag. phase diagram 80—2573
TMMC, spin dynamic exam., effect of mag. field at low temp. 79—73733
TMMC, symmetry crossover in spin dynamics, proton spin lattice relax. calc. 77—40147
TMMC, XY-Ising crossover transition, quasi-elastic neutron scatt. obs. 80—44826
TMMC linear chain antiferromag., optical absorption, magnon sideband intensities calc. 77—59569
TMMC one-dimens. antiferromagnet, effect of mag. field on correl. length 79—91244
transition metal, 3d, localised moments, detection by electron energy loss spectra 77—69949
transition metal 3d monoxides, specific vol. and mag. moment calcs. 80—65822
transition metal alloy, electronic structure, mag. props. 78—95254
transition metal alloys, mag. props. *(Japanese)* 78—47935
5d-transition metal antifluorite crystal, struct. props. and lattice dynamics, mag. struct. 80—44268
transition metal chalcogenides, MU_8X_{17}, (χ=S or Se), mag. susceptibilities 79—61073
transition metal complexes with 1,2,4-triazole, mag. susceptibility, 2-300K, struct., antiferromag. props. 77—77045
transition metal compounds, antiferromag. ordering of cation spin ang. momenta due to 90° exchange interactions 79—69666
transition metal compounds and dil. alloys, mag. ordering phenomena in high mag. fields 80—50075
transition metal diiodides, (V, Cr, Mn, Fe, Co, Ni, Cd), Mossbauer spectrum, electronic and mag. props. 77—32302
transition metal intercalates of Ni and Ta dichalcogenides, Hall coefficient and resistivity 80—39610
transition metal intercalates of Ni and Ta dichalcogenides, magnetic susceptibility, function of temp. 80—39756
transition metal pyrites, mag. and elec. props., review *(Japanese)* 78—47941
transition metal salts, ^{111}Cd hyperfine fields, PAC meas. 77—48104
transition metal vanadates, elec. and mag. props. 79—78094
transition metals and alloys, superconductivity, relevance of mag. interactions 80—100545
3d-transition-metal dichalcogenides, mag. props. rel. to Hubbard model 79—78373
trimethyl ammonium cobalt chloride dihydrate, antiferromag., ^{59}Co NMR 77—77124
trimethylammonium cobalt trichloride, mag. heat capacity and Neel temp. in mag. field 79—61147
trimethylammonium cobalt trichloride, metamagnet, AC susceptibility and exchange consts. 80—70961
trimethylammonium manganese bromide, mag., anisotropy, biquadratic exchange 78—14952
trimethylammonium manganese heptachloride(-bromide), antiferromag. chain systems, high-field magnetisation meas. 79—61187
trimethylammonium manganese trichloride, Heisenberg antiferromag. chain, specific heat and EPR 80—65931
TTF-BDT(M), BDT=$S_4C_4(CF_3)_4$, M=Cu, Au, spin-Peierls transition, sp. ht. meas. 77—28401
TTF-bis-dithiolene metal complex compounds, donor-acceptor type, one-dimens. mag. variety and props. 77—66271
TTF-bisdithiolene metal complexes, spin Peierls transition 77—4523

antiferromagnetic properties of substances continued
TTF-CuBDT, inter- and intra-chain exchange couplings, proton spin-lattice relax. time meas. 80—71220
TTF-$CuS_4C_4(CF_3)_4$, quasi-one-dimens. antiferromag., spin-lattice dimerisation, X-ray scatt. obs. 77—85464
TTF-TCNQ, Peierls insulator and antiferromagnetic mixed phase, mean field approx. 77—20626
TTF-TCNQ and related cpds., magnetic props., press. effects 77—47981
type II antiferromagnet with bilinear and biquadratic coupling, magnetic excitons in cubic cryst. field 79—78353
vanadyl carboxylates, EPR and mag. susceptibility, near one-dimens. antiferromagn. 77—63265
weak ferromagnet, domain wall dynamics, nonlinear waves, mag. solitons *(Russian)* 80—75793
$Al_2La_xCe_{1-x}$, low temp. mag. props. 80—20564
Au-Mn alloys, equiatomic region of phase diagrams crystallographic and mag. exam. 78—52755
AuMn, mag. struct., phase transition, and magnon spectrum, random anisotropy effects 80—88722
$B_2O_3.Fe_2O_3.2CoO$, mag. props. up to 1200K transitions and magnetisation curves 77—36069
$B_2O_3.Fe_2O_3.2MgO$, mag. props. up to 1200K transitions and magnetisation curves 77—36069
$B_2O_3.Fe_2O_3.nMO$ (M=Fe, Co, Ni, Cu, Mg), synthesis and mag. props. 80—20384
$B_2O_3.Fe_2O_3.nMO$, (n=2 or 4, M=Mg, Co, Ni, Cu), mag. props., transitions 80—75763
$BaCoF_4$, low temp. magnon effects on polarisation 79—42905
Ba_2CoReO_6, seignettomagnets with perovskite struct. 79—38459
Ba_2CoS_3, linear chain antiferromag., mag. susceptibility meas. and Mossbauer spectra 80—107992
$Ba_3Fe_{2-x}Ho_xUO_9$, $0 \leq x \leq 1.2$, perovskites, struct. and mag. props. *(French)* 78—18612
$Ba_2Fe_7O_{11}$, antiferromagnet, exam. of mag. props. by mag. meas., and Mossbauer spectroscopy 78—52256
Ba_2FeS_3, linear chain antiferromag., mag. susceptibility meas. and Mossbauer spectra 80—107992
$BaLa_2Fe_2O_7$, Mossbauer exam. of mag. struct. 77—40157
$BaLaMRuO_6$, (M=Mg, Fe, Co, Ni, Zn), cubic ordered perovskites, Mossbauer and mag. susceptibility meas. 80—75889
$BaMnF_4$, antiferromag., dielec. anomalies at low temp. obs. 77—20791
$BaMnF_4$, dielec. anomaly, mechanism, spin canting 78—10744
$BaMnF_4$, mag. and structural phase transitions, neutron scatt. obs. 79—87259
$BaMnF_4$, phase transitions review 79—78378
$BaMnF_4$, pure and Co doped, ferroelec. antiferromag., dielec. anomalies 80—71288
$BaMnF_4$, spectroscopy near ferroelec. transition, dielec. anomalies near mag. ordering temp. 80—75965
$BaMnF_4$, struct. and mag. transitions, magnon dispersion curves, nearest neighbour exchange consts. 79—42760
$BaMnO_4$, ferroelectrically induced ferromagnetism 77—73067
Ba_2MnS_3, linear chain antiferromag., mag. susceptibility meas. and Mossbauer spectra 80—107992
$BaNiF_4$, low temp. magnon effects on polarisation 79—42905
$BaNiF_4$, obs. of anomalous pyroelec. behaviour due to cooperative mag. singularity 77—59517
Ba_2NiF_6, obs. of short range order by optical birefringence 79—11318
Ba_2NiF_6, quadratic layer antiferromag., optical spectra obs. 77—16326
Ba_2NiF_6, specific heat capacity, critical amplitude, cross-over from 2-D Ising to Heisenberg behaviour 80—39791
$Ba_2Ni_3F_{10}$, cryst. struct. and antiferromag. props. 80—107153
$BaNi_2(PO_4)_2$ and $BaNi_2(AsO_4)_2$, mag. props., neutron diffr. and sp. ht. meas. 80—70948
Ba_2NiReO_6, mag. and cryst. struct. 77—20554
$BaO-Fe_2O_3-B_2O_3$ glass system, mag. struct., Mossbauer study 78—39485
$BaO-Fe_2O_3-B_2O_3$ glass, Mossbauer study of struct. and mag. props. 79—47369
$BaO-Fe_2O_3-B_2O_3$ glass, struct. and mag. props., Mossbauer spectra 80—7226
$BaSr_xCa_{1-x}Fe_4O_8$, substituted hexagonal ferrites, mag. split Mossbauer spectra obs. and X-ray struct. data 80—71250
$BaTiO_3-BiFeO_3$ solid solns., ferroelec.-antiferromag., magnetoelectric effect at ferroelec. transition 80—100637
$BaVS_3$, elec. resist., mag. susceptibility, structural transition amd Mossbauer effect meas. 77—84923
$BaVS_3$, exam. of ferromagnetic, antiferromagnetic behaviour, depending on stoichiometry 78—52233
$BaVS_3$, mag. and elec. props. 79—91214
Ba_2XRuO_6(X=La,Eu), ^{99}Ru Mossbauer spectra and other techniques 80—29659
$BiFeO_3$, ferroelec., antiferromag., cryst. and mag. struct., neutron diffr. study 80—65786
$BiFeO_3$, pyroelectric-antiferromag., magnetoelectric effect *(Russian)* 78—43625
$BiFeO_3-LaFeO_3$, solid solns., antiferroelec.-antiferromag., magnetoelectric effect at antiferroelec. transition 80—100637
$BiFeO_3-Pb(Fe_{0.5}Nb_{0.5})O_3$, ferroelec., magnetoelec. obs. temp. and conc. depend. 80—50156
$Bi_2Fe_4O_9$, antiferromag., mag. glass props. *(Russian)* 77—4519
$Bi_2Fe_4O_9$, mag. struct., neutron diffr. meas. 78—91844
$Bi_9Ti_3Fe_5O_{27}$, combined hyperfine interaction 79—28663
$Bi_7Ti_{2.5}Sn_{0.5}Fe_3O_{21}$, layered ferroelec. antiferromag., superparamagnetism, Mossbauer spectra obs. 77—51999
$(CH_3NH_3)_2FeCl_2Br_2$, two-dimensional antiferromag., field depend. of susceptibility meas. 77—63130
$Ca_3Cr_2Ge_3O_{12}$, and $Ca_3Cr_2Si_3O_{12}$, absorpt. and luminesc. spectra, cryst. field and exchange interactions 77—73154
$CaCu_3Ti_4O_{12}$, mag. struct. and props. *(French)* 77—69495
$CaCu_3Ti_4O_{12}$, mag. struct., neutron diffr. powder data, 27K T_N 77—69502
$Ca_3Fe_xCr_{2-x}Ge_3O_{12}$, antiferromagnetic order below 12K, Mossbauer study 80—39945
$Ca_3Fe_2Ge_3O_{12}$, antiferromagnetic reson., anisotropy and magnetoelastic interaction effects *(Russian)* 77—69712
$Ca_3Fe_2Ge_3O_{12}$, antiferromag. single crystal garnet, magnetostriction *(Russian)* 79—8027
$Ca_3Fe_2(Mn_2)Ge_3O_{12}$, single magnetic sublattice antiferromagnetic garnets 78—52652
$CaFeO_3$, preparation, cryst. struct., mag. and elec. props. 78—44066

antiferromagnetic properties of substances continued

- $CaLaFeO_4$, two-dimens. mag. ordered, structural and mag. props. *(French)* 80—70173
- $CaLaFeO_4$, two-dimens. mag. props. rel. to cryst. struct. 80—75776
- $Ca_3Mn_2Ge_3O_{12}$, antiferromagnetic garnet, neutron diffr. study in mag. field 80—50060
- $Ca_3Mn_2Ge_3O_{12}$ garnet, metamagnetic transition, high anisotropy peculiarities *(Russian)* 80—60274
- $Ca_3Mn_2Ge_3O_{12}$, highly anisotropic garnet, neutron diffr. obs. of mag. struct. 78—68168
- $Ca_3Mn_2Ge_3O_{12}$, mag. struct. study 80—2554
- $Ca_3Mn_2Ge_3O_{12}$, neutron diffr. in mag. field, metamagnetism, antiferromag. ordering 79—65651
- $Ca_3Mn_2Ge_30_{12}$, mag. field induced transition 80—50094
- $Ca_2Mn_3O_8$, mag. props. 79—78339
- $Ca_2Mn_3O_8$, mag. props. and EPR 79—91215
- $Ca_2MnO_{4-x}F_x$, antiferromagnetic props. and elec. cond. *(French)* 80—29526
- $Ca_2Ti_{2-2x}Fe_{2x}O_{6-x}$, antiferromag. phases, Neel temp. variation, vacancy long-range order *(French)* 78—34979
- Ca_2XRuO_6 (X=Y,La,Eu), ^{99}Ru Mossbauer spectra and other techniques 80—29659
- $Cd_{1-x}Ag_xCr_2Se_4$, Ag acceptor states effect on exchange interaction 80—20397
- $Cd_3Cr_2Ge_3O_{12}$, absorpt. and luminesc. spectra, cryst. field and exchange interactions 77—73154
- $Cd_3Cr_2Ge_3O_{12}$, antiferromagnetic ordering of Cd^{3+}, sp. ht. and mag. susceptibility meas. 77—16062
- $Cd_3Cr_2Ge_4O_{12}$, antiferromagnetic reson., anisotropy and magnetoelastic interaction effects *(Russian)* 77—69712
- $CdCr_2Se_4$-$ZnCr_2Se_4$, single cryst., mag. props. 79—28526
- $Cd_2Mn_3O_8$, mag. props. 79—78339
- $Cd_2Mn_3O_8$, mag. props. and EPR 79--91215
- $Cd_{1-x}Mn_xTe$, semimagnetic, exchange interactions between localised and delocalised electrons 80—97245
- CdS, amorphous antiferromag., mag. props. of dilute neutral donors 79—78367
- CdS, model $S={}^1/_2$ amorphous antiferromagnet, spin polarisation 78—52288
- Ce binary and pseudobinary intermetallics, struct. and mag. data 80—20129
- Ce compounds with group V elements, temp.-renormalised longit. mag. excitations 77—51862
- Ce cubic intermetallics, interconfig. fluctuations 80—20130
- Ce monochalcogenides, cryst. field effects, phase transitions 80—24853
- Ce monopnictides, cryst. field effects, phase transitions 80—24853
- β-Ce, susceptibility meas., 2-300K 77—4320
- CeAg(Mg)(Zn), magnetic struct. and cryst. field, neutron diffr. exam. 78—72328
- CeAl, mag. props. and mag. struct. 78—6517
- $CeAl_2$, and $CeAl_3$, magnetisation and sp. ht. 80—20418
- $CeAl_2$, Anderson lattice system, thermal expansion meas. 1.5 to 10K 79—37860
- $CeAl_2$, Anderson lattice system, ground state props. 80—20443
- $CeAl_2$, anisotropic magnetostriction near antiferromagnetic transition 78—88157
- $CeAl_2$, antiferromag. ordering between 4f shells, Kondo effect 80—20417
- $CeAl_2$, antiferromag. ordering and Kondo behaviour, ^{27}Al NQR study 80—71231
- $CeAl_2$, conf. Kondo system, sp. ht. meas. 78—52210
- $CeAl_2$, low temp. mag. behaviour, neutron diffr. 78—84395
- $CeAl_2$, low temp. mag. props., Kondo effect 80—20381
- $CeAl_2$, mag. anisotropy, transition, crystal field splitting 78—52243
- $CeAl_2$, mag. ordering, neutron diffr. meas. 78—6518
- $CeAl_2$, mag. ordering and anomalous ground state, neutron diffr. obs. 79—78331
- $CeAl_2$, magnetic ordering, 24 component Ginzburg-Landau model 80—97095
- $CeAl_2$, multiple q mag. struct. 79—78330
- $CeAl_2$, multiple-q mag. struct. 80—25100
- $CeAl_2$, multiple-q structure or coexistence of different mag. phases, neutron diffr. study 80—107985
- $CeAl_2$, neutron diffr. at low temp., magnetism 80—20383
- $CeAl_2$, specific heat between 0.02 and 1K 79—1680
- Ce_3Al_{11}, competition between ferro- and antiferromag. interactions 80—60258
- $Ce_{80}Au_{20}$, metallic glass, mag. ordering and cryst. field effects, speromagnetism 80—80531
- CeB_6, resist. anomaly and mag. ordering obs. 79—61110
- CeBi(Sb), enhanced lattice-displacement effects on cryst. field and anomalous mag. anisotropy 79—73477
- CeC_2, mag. props. 80—108008
- $CeCl_3(Br_3)$, interaction parameters, high freq. meas. of adiabatic differential susceptibility 78—68211
- $Ce_xDy_{1-x}C_2$, mag. props. 80—108008
- $CeIn_3$, mag. struct., neutron diffr. study 80—80481
- $CeIn_3$, magnetisation and sp. ht. 80—20418
- $CeIn_3$, Neel temp., hydrostatic press. depend. 80—29549
- $CeIn_{3-x}Sn_x$, scaling behaviour near valence instability, mag. susceptibility and mag. transitions 80—25111
- $Ce_x(La,Y)_{1-x}Sb$, and $Ce_x(La,Y)_{1-x}Bi$, antiferromag. spin arrangement, neutron diffr. obs. 77—63106
- $Ce_{1-x}La_x$, thermoelectric power, mag. transition temps. 80—20154
- $Ce_xLa_{1-x}B_6$ solid solutions, Weiss const. antiferromagnetic ordering calcs., mag. props. *(Russian)* 79—91212
- $Ce_x(La_{0.76}Y_{0.24})_{1-x}Bi$, mag. phase diagrams 79—56535
- $CeMn_2Si_2$, cryst. and mag. struct. determ. 78—52225
- $CeMn_2(Si_xGe_{1-x})_2$, $Ce(Mn_{1-x}M_x)_2Si_2$, (M=Fe, Cu), mag. props. 80—25134
- CeP(As), single crystals, low temp. thermal, electrical and mag. props. meas. 78—27051
- CeP(As)(Sb), microwave resist. meas. 77—4383
- $Ce_{1-x}Pr_xAl_2$, mag. struct., comp. depend., neutron diffr and mag. susceptibility meas 80—50054
- CeS, mag. props., sp. ht. and thermal expansion 78—60292
- CeSb, antiferromag., first-order transitions, mag. phase diagram 80—60252
- CeSb, commensurate-commensurate transitions, devil's stairs theory 79—19740
- CeSb, mag. phase diagram and mag. struct., neutron diffr. determ. 77—63182

antiferromagnetic properties of substances continued

- CeSb, mag. phase transitions, zero applied mag. field 78—31070
- CeSb, mag. transition, effect of applied mag. field 78—43590
- CeSe, mag. ordering, ε expansion predictions, neutron diffr. obs. 79—61060
- CeSe, mag. props., sp. ht. and thermal expansion 78—60292
- CeTe, mag. ordering, ε expansion predictions, neutron diffr. obs. 79—61060
- CeTe, mag. props., sp. ht. and thermal expansion 78—60292
- $CeTl_3$, mag. susceptibility, magnetisation, neutron diffr., elec. resist., and sp. ht. meas. 80—75733
- CeZn, cryst. field and exchange effects, inelastic neutron scatt. study 80—24855
- CeZn, mag. struct. and cryst. field effects 78—52223
- Cm, antiferromag. state, paramag. suscept. meas., electronic struct. *(Czech)* 78—80133
- Cm, mag. structure, neutron diffr. meas., antiferomag. below 52K 77—63101
- ^{244}Cm, electrical resistivity and mag. ordering 77—80760
- Co complex, $CoCl_2.2$ pyrazine, mag. sp. ht. below 2K 79—61152
- Co complex, $Co(C_5H_5NO)_6(ClO_4)_2$ and $Co(C_5H_5NO)_6(BF_4)_2$, $S={}^1/_2$ XY magnet, sp. ht. below 1K 77—55682
- Co complex, Co(II)(1,2,4-triazole$\}_2$(NCS)$_2$ quasi two-dimens. canted S=1/2 antiferromag. 80—70976
- Co complex, tetra-μ-benzoato-bis(4-methylquinoline)dicobalt II, triclinic cryst., antiferromag. exchange 78—39309
- Co-CoO films, evaporated, exchange anisotropy 80—88841
- $CoAl_xGa_{2-x}O_4$, mag. interactions, susceptibility obs., 4.2 to 300K 79—15294
- $Co_2(AsO_4)Cl$, temp. depend. of mag. susceptibility 80—70962
- $Co_3B_7O_{13}Cl$, polydomain ferroelec., magnetoelec. effect below Neel temp. 78—10745
- $Co_3B_7O_{13}I$, neutron diffr. investig. of mag. and cryst. struct., ferro- and paraelec. phases 77—32170
- $CoBr_2,6[xD_2O(1\text{-}x)H_2O]$, mag. order investig. by neutron diffr. 77—66310
- $CoBr_2$, lamellar, field depend. of uniform magnon. energies, antiferromag. reson. meas. 77—73086
- $CoBr_2$, magnon Raman scatt. 79—15462
- $CoBr_2$, paramag. and antiferromag., Raman scatt. from electronic excitations and phonons 79—69826
- $CoBr_2.2H_2O$, metamagnetic, relax. phenomena at phase transitions 79—24164
- $CoBr_2.6D_2O$, crystallographic and mag. struct. determ. 77—8278
- $CoBr_2.6(0.48D_2O, 0.52H_2O)$ spin-flop system, intermediate phase existence, sublattice magnetisation reorientation 80—80510
- $CoBr_2.6[(D_2O)_{0.48}(H_2O)_{0.52}]$, antiferromag. ordering, quasi-elastic neutron scatt. study 79—61068
- $CoBr_2.6[(1-x)H_2O.xD_2O]$, mag. intermediate phase, magnetisation and neutron scatt. meas. 80—60195
- $Co(C_5H_5NO)_6(ClO_4)_2$ $[(BF_4)_2]$, X-Y antiferromagnet, Neel temp., spin correlation functions 80—60345
- $CoCO_3$, antiferromag., Raman spectra, 2-300K 77—32380
- $CoCO_3$, Brillouin-Mandelstam light scatt. obs. of spin wave spectra 80—93358
- $CoCO_3$, exciton and magnon excitation spectra *(Russian)* 78—23467
- $CoCO_3$, LF exciton and Raman spectra, one-magnon and two-magnon scatt. 80—93333
- $CoCO_3$, light interaction with spin system at antiferromag. reson. 77—69707
- $CoCO_3$, light scatt. by thermal magnons and magnons excited by antiferromag. reson. 79—82965
- $CoCO_3$ light scatt. from parametric magnons and phonons *(Russian)* 80—34937
- $CoCO_3$, light scatt. from magnons and phonons excited by microwave pumping 80—66213
- $CoCO_3$ light scattering on spin waves *(Russian)* 77—4650
- $CoCO_3$, linear magneto-optical effect, birefr. 80—66155
- $CoCO_3$, mag. props., microscopic level calcs. *(Russian)* 80—97078
- $CoCO_3$, spin excitation energies, quantum theory *(Russian)* 80—88735
- $CoCO_3$, spin wave excitation by uniform precession of magnetisation due to two magnon scatt. 78—68207
- $CoCO_3$, spin wave spectra light scatt. expts., review 80—50081
- $CoCO_3$, two-sublattice noncollinear antiferromag., exciton-magnon light absorpt. mechanisms *(Russian)* 80—89017
- $CoCO_3$, weak ferromag., antiferromag. reson., phenomenological theory 78—60339
- $CoCO_3$, weak ferromagnet, light absorpt. dichroism and mag. config. *(Russian)* 79—87457
- $CoCO_3$, weak ferromagnet, antiferromag. reson. and two-magnon absorpt. *(Russian)* 80—29627
- $CoCO_3$, weakly ferromagnetic, light scatt. accompanying spin system excitation by high microwave power *(Russian)* 78—2745
- $CoCO_3$, weakly ferromag., light scatt. on spin waves *(Russian)* 78—72419
- $CoCO_3$, weakly ferromag., light absorpt. dichroism and mag. config. 80—66223
- $CoCl_2$, antiferromag., elec. field effect in NMR 77—28459
- $CoCl_2$, antiferromag., elementary excitations 77—69519
- $CoCl_2$, antiferromag., mag. excitations, mag. neutron inelastic-scatt. meas. 77—85437
- $CoCl_2$, antiferromag., phase diagram, heat capacity meas. 80—93126
- $CoCl_2$, elementary excitations, electronic Raman scatt. meas. 77—80922
- $CoCl_2$, lamellar, field depend. of uniform magnon. energies, antiferromag. reson. meas. 77—73086
- $CoCl_2$, one-magnon Raman scatt. 78—43877
- $CoCl_26H_2O$, g-tensor and exchange parameters, mag. reson. studies 79—87324
- $CoCl_2.2H_2O$, antiferromag., light scatt. from phonons and magnons 80—40104
- $CoCl_2.2H_2O$, Ising antiferromag., high field transverse magnetisation meas. 80—93143
- $CoCl_2.2H_2O$, magnon-phonon interactions and two-magnon Raman scatt., magnetoelastic waves and selection rules 80—34917
- $CoCl_2.2H_2O$, metamagnetic transition, microscopic dynamics 77—16073
- $CoCl_2.2NC_5H_5$, quasione dimens. Ising system, thermodynamic props. 78—27042
- $CoCl_2.6D_2O$, crystallographic and mag. struct. determ. 77—8278
- $CoCl_2.6D_2O$, neutron diffr. study, cryst. and mag. struct. *(French)* 78—42946

antiferromagnetic properties of substances continued
$CoCl_2.6H_2O$, antiferromag., spin flop and paramag. resons. at very low temp. 77–66426
CoF_2, 180-degree antiferromag. domain obs. by new magnetooptical effect 80–44855
CoF_2, antiferromag. crit. props., neutron scatt. obs. 80–88749
CoF_2, deformed, magnetoelastic interactions and single-domain antiferromag. state 77–43849
CoF_2, domain formation in staggered field induced by uniaxial stress, neutron diffr. exam. 78–76289
CoF_2, linear magneto-optical effect, birefr. 80–66155
CoF_2, phase transition in transverse mag. field, magnetoelastic interactions 79–65676
CoF_2 plate, antiferromag. reson. in transverse mag. field 78–2749
CoF_2, spin excitations in longitudinal mag. field 79–69657
CoF_2, visual obs. of 180° antiferromag. domains, mag.-optical effect *(Russian)* 79–61349
$CoF_2:Mn^{2+}$, spin impurity approx. *(Russian)* 79–87253
$Co_xFe_{1-x}Cl_2.2H_2O$ solid soln., mag. props. and phase diagram 79–78346
$CoGa_2O_4$, mag. props. 78–23254
Co_2GeO_4, crystal growth by Czochralski method under 4 atm N_2 77–77368
$Co_{1-p}Mg_pCl_2$, magnetic excitations, antiferromagnetic resonance spectra response simulation 79–99775
$Co_{1-c}Mn_cF_2$, antiferromagnet mag. impurities, spin excitation spectrum collective rearrangement in external mag. field 80–50199
$CoNb_2O_6$, Co^{2+}-Co^{2+} interaction, susceptibility and magnetisation, 3.3-300K 77–8282
$CoNb_2O_6$, magnetic struct., neutron diffr. and mag. susceptibility meas. 80–15693
$CoNb_2O_6$, ordered state, field induced mag. transitions 77–16074
$Co_{1/3}NbS_2$, intercalate, metallic cond., Hall effect and mag. props. 77–76789
$Co_xNi_{1-x}Cl_2.6H_2O$, calorimetry, γ-type transitions of sp. ht. 78–68256
$Co_xNi_{1-x}Cl_2.6H_2O$, solid solution, mag. props. and phase diagram, calc. 80–7104
$Co_xNi_{1-x}O$, neutron diffr. study of mag. struct. 80–34595
CoO, antiferromag. mag. excitations, spin wave model, neutron scatt. study 79–51766
CoO, antiferromagnetic, ^{59}Co NMR and hyperfine field 77–77109
CoO, collinear antiferromag., equiv. type-II mag. struct. 78–56296
CoO, mag. excitations, neutron scatt. expts., 13K 79–61092
CoO, non-stoichiometry and temp.-depend. mag. susceptibility 79–82768
CoO, paramag. shifts of ^{19}F at O 78–43719
CoO, relax. valence averaging, Mossbauer spectra evidence 77–1626
$CoO:Ni^{2+}$, far IR absorpt. by impurities and collective antiferromag. reson. mode 77–8576
$CoRh_xGa_{2-x}O_4$, mag. interactions, susceptibility obs., 4.2-1000K 79–15293
$CoSe_{1.95}$, NMR and susceptibility meas., absence of antiferromag. 77–16060
$Co_{1-x}Te$, fluctuating localised mag. moments, d band motion, Mossbauer study 80–65768
$CoTiO_3$, antiferromag., mag. anisotropy, magnetisation meas. 80–65856
CoU_2S_5, mag. struct., exchange energy, magnetisation and neutron diffr. expts. 78–68170
CoU_2S_5, mag. struct. and props. 80–11166
CoZn, complex, $Co_pZn_{1-p}(C_5H_5NO)_6(CPO_4)_2$, dilute simple-cubic antiferromag., sp. ht. near crit. conc. 79–38336
$Co_{1-x}Zn_xF_2$, antiferromag. crit. props., neutron scatt. obs. 80–88749
$Co_xZn_{1-x}Rh_2O_4$, mag. props., EPR spectra, antiferromag. order 80–75736
$Co_xZn_{1-x}Rh_2O_4$ spinel, crit. conc. for long range mag. order, expt. evidence 79–47239
$CoZnSnO_4$, paramagnetic props. and short-range ordering 77–32155
$Co_{2-y}Zn_yTiO_4$, spinel series, exchange integrals, mag. struct. and coercive force, magnetisation meas. 77–69507
$Co_{1-x}Zn_x$hexa(pyridine-N-oxide)$(ClO_4)_2$, dilute cubic S=1/2 XY antiferromag., sp. ht. data 77–66358
$Co(urea)_2Cl_2.2H_2O$, two-dimens. mag. props., cryst. struct., specific heat 80–75777
$(Cr, Mn)_2As$, mag. props. and struct. 78–64190
Cr alloy, localised magnetic moments in band antiferromagnets, impurity interactions *(Russian)* 80–54888
Cr alloyed with d-transition elements, magnetic transformations, triple point *(Russian)* 80–88747
Cr and alloys, itinerant antiferromagnetism and density waves at surface 79–82743
Cr, antiferromag., mag. and non-mag. impurities, hyperfine interactions, ^{181}Ta and ^{100}Rh TDPAC meas. 78–43704
Cr, antiferromag., muon depolarisation, mag. anisotropy determ. *(Russian)* 79–61290
Cr, antiferromag., nature of spin-flip transition 77–63186
Cr, antiferromag., stress depend. of Fermi surface 77–11846
Cr, antiferromag., stress depend. of spin density wave state 77–63257
Cr, antiferromagnetic, mixed state, mag. torque and magnetostriction meas. 77–89909
Cr, antiferromagnetic, muon diffusion, spin relax. and coherent motion 80–71281
Cr, antiferromagnetic, phase fixation, excitonic and spin superfluidity of electron-hole pairs 78–30872
Cr, antiferromagnetic, polarisation domain effects on US velocity 78–52329
Cr, antiferromagnetic, positive muons as light isotopes of H, book contrib. 79–82907
Cr, antiferromagnetic, pressure effect on Fermi surface by de Haas-van Alphen effect *(Russian)* 80–6701
Cr, antiferromagnetic, surface Raman scatt., calc. 80–45069
Cr, antiferromagnetic, US attenuation and phase diagram 80–103831
Cr, antiferromagnetic spin-density-wave domain and size and behaviour, X-ray and neutron topography 79–42793
Cr, antiferromagnetic structure, mag. field effect, spin density wave model *(Russian)* 80–70953
Cr, antiferromagnetic transition, first order, crit. neutron scatt. obs. 79–33480
Cr antiferromagnetic with nonmagnetic impurities, mag. susceptibility using two band model 80–2559
Cr complex, dinuclear, exchange interactions, neutron inelastic scatt. obs. 77–55502
Cr complex, trimeric clusters, low temp. mag. props. 78–76261
Cr, critical coeff. of resistivity near Neel temp. 77–59417

antiferromagnetic properties of substances continued
Cr, deformation waves and spin density waves, electron diffr. obs. *(Russian)* 79–19721
Cr, EM absorpt. 79–51925
Cr, elec. resist. near Neel temp. 79–33278
Cr, electron interference oscills. and spin-density-wave energy gaps at Fermi surface 80–49574
Cr, electronic structure model, Invar effect, antiferromagnetic-non mag. transitions 80–20370
Cr, Fermi surface, stress depend., from quantum oscill. effects, rel. to itinerant antiferromagnetism 78–91597
Cr, Fermi surface under press., de Haas-van Alphen effect meas. 80–75499
Cr, ferromagnetic surface layer on antiferromag. bulk, determ. by surface magnetoplasma wave detect. 78–68356
Cr film, size effects on spin density waves, struct. and elec. props. 77–80973
Cr, giant internal mag. press. and compressibility anomalies, itinerant model 77–16034
Cr, Hall coeff., mag. field depend. at low temp. 77–20296
Cr, hyperfine interactions on ^{111}Cd-probe nuclei, TDPAC meas. 80–75904
Cr hyperfine particles, surface magnetisation, explanation of expt. work 78–23303
Cr, incommensurate antiferromag., inelastic neutron scatt. meas. 80–25088
Cr, inelastic neutron scatt. expts., spin density waves 80–44818
Cr, mag. phase diagram, near, spin-flip temp., US attenuation 80–60267
Cr, mag. struct., effect of mag. field direction, neutron diffr. obs. 77–63121
Cr, mag. struct., phase transition, and magnon spectrum, random anisotropy effects 80–88722
Cr, mag. susceptibility calc. two band model for electronic spectrum 78–10663
Cr, magnetic excitations of incommensurate spin density wave 80–11183
Cr, magnetic phase transition at Neel temp. 78–2681
Cr, magnetic torque anal. in thermally activated domain model, near spin-flip temp. 77–63229
Cr, magnetisation process *(Russian)* 78–15007
Cr, μ^+ depolarization and diffusion 77–59500
Cr, μSR meas. 79–56667
Cr, Neel temperature and Fermi energy, nonmag. impurity effects 80–65888
Cr, phase transition at T_N 79–4676
Cr, Q-vector locking, press. induced hardening 80–103870
Cr, single cryst., mag. hysteresis, neutron diffr. obs. 79–15327
Cr, single modulation state, temp. limits of cryomagnetic method 78–72374
Cr, single Q-state, antiferromag. phase, rel. to band struct. 77–15759
Cr, specific heat of strained and annealed samples 79–38331
Cr, spin density wave, Nambu-Eliashberg eqns. for k-state electron-hole pairing 80–97050
Cr, spin density wave, stress and impurity conc. depend. 77–73029
Cr, spin density wave, temp. depend. of second and third harmonics 77–12094
Cr, spin density wave phases, domains 80–103871
Cr, spin density wave Q vector, vel. depend. 79–4669
Cr, spin density wave Q-vector, temp. and press. depend. 80–11167
Cr, spin density wave state, phenomenological free energy density description 80–75720
Cr, spin density waves, interacting virtual states 77–72987
Cr, spin density waves detected by Ta mag hyperfine field meas. 78–60364
Cr, spin relaxation of μ^+-mesons *(Russian)* 79–8083
Cr, spin-density-wave antiferromagnet, uniaxial anisotropy 78–10640
Cr, spin-flip transition temperature, press. depend. from elastic const. meas. 80–65944
Cr, strain and spin-flip transition, Landau theory 78–39318
Cr, surface electronic struct., tight-binding approx. calcs. 78–64090
Cr, transverse magnetoresist. meas. in antiferro- and paramag. states, 15 to 80°C 77–85197
Cr, transverse magnetoresist., electron interference oscills. 80–65534
Cr, transverse spin-density-wave phase, absence of neutron diffr. line broadening due to polarisation domains 77–24677
Cr, US velocity and damping in Neel temp. range, thermocyclic treatment effect *(Russian)* 79–91282
Cr-Al, abnormal thermal cond., 5 to 100K 79–19573
Cr-Al, antiferromag., charge and spin density, neutron and X-ray diffr. 77–31971
Cr-Al, antiferromag., transport props., anomalous crit. behaviour 79–61108
Cr-Al, disordered alloy, effect of high press. on resistivity 78–95286
Cr-Al, effect of Al concentration and hydrostatic press. on Neel temp. 79–33482
Cr-Al, elementary excitations, exchange stiffness const., inelastic neutron scatt. study 79–47294
Cr-Al alloys, antiferromag., charge and spin density, neutron and X-ray diffr. 77–31971
Cr-Co, dil., antiferromag., elec. resist. min., press. and impurity effects 80–59970
Cr-Co, dil., Neel temp., impurity conc. depend. calc. 78–68232
Cr-Co, phase transformations and magnetostriction *(Russian)* 80–103869
Cr-Co (4.0 at.%) alloy, antiferromag., disappearance of resist. min. under press., and press. coeff. of T_N 80–10960
Cr-Co (up to 8 at.%), antiferromagnetic, resist. minimum, Kondo effect by pairs of Co atoms 80–39566
Cr-Co alloys, dil., with local mag. moments, Neel temps. 79–73713
Cr-Co-V alloys, dil., elec. resist. min. 80–54680
Cr-Fe, antiferromag. phase boundary, neutron diffr. meas. 78–95437
Cr-Fe, antiferromag. sp.ht. around Neel point 79–73750
Cr-Fe, antiferromagnetic, effect of press. on hyperfine mag. fields at Fe nuclei *(Russian)* 80–15936
Cr-Fe, dil., antiferromag., elec. resist. min., press. and impurity effects 80–59970
Cr-Fe, dil., magnetisation, Fe local moments 80–60215
Cr-Fe, dil., Neel temp., impurity conc. depend. calc. 78–68232
Cr-Fe, dilute, localised moment cluster model, ferromagnetic exchange coupling 80–39774
Cr-Fe, low conc. alloys, coexistence of itinerant antiferromagnetism with paramagnetism 78–84386

antiferromagnetic properties of substances continued
Cr-Fe, magnetically insensitive Invar-type alloys *(Japanese)* 79—8034
Cr-Fe (0.6 at.%), antiferromag., anomalous press. effect on resist. minimum 79—15138
Cr-Fe (0.8-8 at.%) alloy, mag. phase transforms, sp. ht. obs. *(Russian)* 77—80941
Cr-Fe (14 wt.%), spin density wave and spin glass ordering coexistence at low temps. 79—61059
Cr-Fe (6.5 wt.%), atomic clustering and mag. defects, mag. moments 80—60246
Cr-Fe alloy, dil., mag. incoherent elastic neutron scatt. 79—73678
Cr-Fe alloys, elec. resistivity, Kondo effect 79—60812
Cr-Fe alloys, itinerant antiferromag. effect of mag. impurities 77—32186
Cr-Fe alloys, polycrystalline, antiferromag., elastic moduli and thermal expansion meas. 77—43860
Cr-Fe_x (x=0.5, 1.5 and 3.5 at.%), antiferromag., Kondo anomaly 80—11163
Cr-Fe-Si alloy, sp. ht., 1.4-4.2K 77—20079
Cr-Fe-V, effects of V on mag. transition, elec. and mag. props. 77—69554
Cr-Fe(Co) alloys dil., exchange interactions 77—47986
Cr-Fe(2.8 at%), antiferromag., meas. of incoherent elastic neutron scatt. cross section 79—19723
Cr-Ga alloys, dil., Neel temp., elec. resist. and thermal expansion meas. 79—51778
Cr-Mn, order of mag. transitions in antiferromag. alloys 79—4677
Cr-Mn (0.5 at.%) alloy, mag. phase transforms, sp. ht. obs. *(Russian)* 77—80941
Cr-Mn alloy, strain wave and spin density wave intensities, neutron diffr. 78—60266
Cr-Mn alloys, antiferromag. and weak ferromag., elec. props. 79—56514
Cr-Mn alloys, elec. resist. near T_N 77—69313
Cr-Mn alloys, magnetisation process, magnetisation in 90-300K range *(Russian)* 78—15007
Cr-Mo, behaviour of mag. impurities 79—4672
Cr-Mo-Fe (2, 14 wt.%), spin density wave and spin glass ordering coexistence at low temps. 79—61059
Cr-Ni(V), dil., mag. susceptibility, 77 to 400K *(Russian)* 80—50066
Cr-Os, magnetic transition T-P-C diagram, triple points *(Russian)* 80—54895
Cr-Pd dilute alloys, itinerant antiferromag., neutron diffr. meas. 77—77032
Cr-Pt, dil., effect of Pt on itinerant antiferromagnetism 78—64191
Cr-Pt alloy, mag. props., effect of atomic environment 78—23247
Cr-Pt alloys, neutron diffraction study, (100) magnetic peak, magnetic structure transitions 79—56506
Cr-Re, dil. alloy, mag. susceptibility temp. depend., thermal expansion coeff. *(Russian)* 78—76225
Cr-Re, mag. excitations in commensurate antiferromag. phase 80—50079
Cr-Re, phase transformations and magnetostriction *(Russian)* 80—103869
Cr-Re, surface spin-density wave near T_N 79—91238
Cr-Re (0.18 wt.%), mag. excitations in longitudinal and transverse SDW phases 80—70946
Cr-Rh, dil., hyperfine fields meas. 79—47056
Cr-S system, mag. props. *(Japanese)* 77—43825
Cr-Sb alloy, dil., mag. phase diagram, elec. resist. and thermal expansion obs. 79—1669
Cr-Si, dilute alloy, mag. susceptibility and Neel temp. meas. 80—71017
Cr-Si (1.37 at.%), thermal and elec. props. 79—78071
Cr-Si alloys, antiferromag.-ordering, neutton diffr. 77—69492
Cr-Si alloys, press. depend. of Neel temp. 77—69555
Cr-Si-V, (2, 0.1 at.%), paramag. to commensurate spin density wave transition 80—65875
Cr-Ta, mixed SDW and Zeeman hyperfine interactions, TDPAC calc. 79—99797
Cr-V, itinerant electron antiferromag., spin fluctuations, low temp. specific heat 80—107439
Cr-V alloy, strain wave and spin density wave intensities, neutron diffr. 78—60266
CrAl, semicond. solid solns., depend. of energy gap 78—67941
$Cr_{99.94}Al_{00.6}$, thermal and elec. transport coeffs. near Neel temp. 79—78075
CrAs, anisotropy of compressibility 79—7648
CrAs, antiferromag.-paramag. transition up to 5 kbar 79—87256
CrAs, heat capacity, enthalpy increments, thermodynamic props., 5 to 1280K 78—91450
CrAs, high press. paramag. antiferromag. transitions, elec. props., band model development *(Russian)* 80—60277
CrAs, mag. transition under press., volume striction mechanism 77—24696
CrB_2, CrB, and Cr_5B_3, mag. and thermal props. at low temps. 80—20385
CrB_2, crystal growth by floating-zone method, elec. and mag. props. 77—1801
CrB_2, itinerant antiferromag., sping fluctuations, NMR study 80—108119
CrB_2, NMR of ^{11}B meas. 78—56397
Cr_2BeO_4, magnetoferroelectricity, weak pyroelectric effect 79—42914
CrCo, dil., low temp. specific heat meas., 1.5 to 4K 80—60328
CrF_2, heat capacity, entropy, 10-300K, mag. ordering effects 79—87264
$Cr_{1-x}Fe_x$, Mossbauer spectra, mag. behaviour 80—20532
$Cr_xFe_{3-x}O_4$, spin and charge density oscillations due to impurities *(Korean)* 80—20565
$Cr_{1-x}Fe_xOOH$, $0 \leq x \leq 10$, prep., Mossbauer effect, Neel temp. 80—108134
$(Cr_{1-x}Fe_x)_{1+\delta}Sb$, interstitial occupancy, Cr:Fe distrib., X-ray and neutron diffr. study 79—42012
$Cr_{0.6}Mn_{0.4}$, mag. moment, neutron diffr. study 79—33459
$Cr_{0.98}Mn_{0.02}$, spin dynamics and spin wave form factor, neutron scatt. expt. 77—40047
$Cr_{995}Mn_{005}$, spin density wave Q vector, vel. depend. 79—4669
$Cr_xMn_{1-x}As$, antiferromagnetic-ferromagnetic transition, mag. moment and elec. resist. meas. 80—15718
$Cr_xMn_{1-x}As$, mag. susceptibility anomaly at displacive phase transition 80—93091
$Cr_{1-x}Mo_xCo$, $x \lesssim 0.25$, nucl. mag. relax. 78—6590
CrN, antiferromagnetic EPR spectra, binding energy, isotropic exchange and ordering *(German)* 80—80604
CrN, mag. struct. and first-order antiferromag. transition 79—61132

antiferromagnetic properties of substances continued
$Cr_{0.5}NbSe_2$, cryst. struct., metallic cond., mag. and phys. props. *(French)* 80—33956
Cr_2O_3, antiferromag., muon spin rotation *(German)* 80—54877
Cr_2O_3, antiferromag. reson. and mech. of parallel magnetoelectric effect 79—47337
Cr_2O_3, dielec. const. in mag. field, nonlinear magnetoelec. effect in Neel pt. region 80—66006
Cr_2O_3, EPR linewidth, near Neel temp. 78—23327
Cr_2O_3, elastic consts., distance depend. of mag. interactions, US vel. meas. 77—4539
Cr_2O_3, exchange parameters including temp. effects 79—24153
Cr_2O_3, mag. phase boundaries near bicrit. and Neel points 78—34980
Cr_2O_3, magnetic susceptibility, near Neel temp. 79—56509
Cr_2O_3, magnetoelec. effect, SQUID magnetometer meas. 79—87302
Cr_2O_3, magnetostriction anomalies near mag. field induced transitions 77—66315
Cr_2O_3, magnon energy temp. renormalisation calc. 77—1531
Cr_2O_3, muon spin rotation expts. 80—71282
Cr_2O_3, muon states, local mag. fields 80—75911
Cr_2O_3, μSR meas. 79—56666
Cr_2O_3, paramagnetic-antiferromag. transition temp. increase in mag. field 77—12121
Cr_2O_3, specific heat near. Neel temp. 77—63207
Cr_2O_3, thermal magnetoresist., 0.1 to 100K, magnon-phonon interactions 79—65266
Cr_2O_3:Ga_2O_3 EPR, antiferromagnetic coupling energy temp. depend. *(German)* 78—10766
β-CrOOH, neutron diffr. exam., cryst. and magnetic struct. *(French)* 78—2654
$CrPS_4$, phys. props. and Li intercalates 79—19788
$Cr_{0.995}Pt_{0.005}$ alloy, mag. struct., neutron diffr. study 80—60198
CrS, magnetic struct. from neutron diffr. meas., Neel point 77—32164
$CrS_{1-x}Se_x$, antiferromag. props., struct., variations near Neel temp. 78—64199
CrS_xTe_{1-x} (x=0 to 0.2), magnetic props. study 80—11194
$CrSb_2$, heat capacity and thermodynamic props., mag. transition, enthalpy of decomposition 78—43591
$CrSb_{1-x}As_x$, exchange striction and press. effect on Neel temp. 77—63189
$CrSb_{1-x}As_x$ press. effect on Neel point 80—71147
$Cr_{3\pm x}Se_4$, struct., elec. and mag. props. 80—107160
Cr_3Se_4, mag. susceptibility and sp. ht. meas. *(French)* 79—56507
$Cr_3Se_xS_{4-x}$, mag. susceptibility and sp. ht. meas. *(French)* 79—56507
$Cr_2Se_{3-x}Te_x$, mag. props. and lattice parameters, comp. depend. 77—66263
$Cr_3Se_{4-x}Te_x$, mag. props. and lattice parameters, comp. depend. 77—66263
CrTe, mag. ordering under high-press., ferromag. transition, ESR and neutron diffr. *(French)* 78—31053
CrTe, neutron diffr. at high press., mag. transition *(Russian)* 79—38326
Cr_2TeO_6, CC ^{57}Fe Mossbauer spectrum, hyperfine field, Neel temp. 79—56636
$Cr_{1-x}Ti_xN$, cryst. and mag. struct., at low temps. *(French)* 80—29005
$CrTiNdO_5$, distrib. of Cr^{3+} and Ti^{4+} ions, Mossbauer spectrum 77—69747
$Cr_{1-x}V_x$, nucl. spin relax., spin fluctuation effect 80—34811
$Cr_{1-x}V_xCo$, $x \lesssim 0.5$, nucl. mag. relax. 78—6590
$Cr_{1-x}V_xN$, solid soln., mag. struct. *(French)* 78—6519
$CrVO_4$, Neel temp., mag. susceptibility meas. 80—29550
$CsCdBr_3$:Gd^{3+}, EPR of coupled pairs of Gd^{3+} ions 78—19322
$CsCoBr_3$, ID Ising antiferromagnet, spin dependent Raman scattering from phonons and electronic excitations 80—103948
$CsCoBr_3$, quasi ID Ising antiferromag., polarised Raman scatt. from mag. excitations 80—66182
$CsCoBr_3$, quasi one dimensional antiferromag., magnon Raman scatt. 80—11395
$CsCoCl_3$,$2H_2O$, pseudo one-dimens. Ising-like system, mag. heat capacity and metamag. transitions 77—66351
$CsCoCl_3$, ^{59}Co NMR spectrum obs. by spin echo method 79—51881
$CsCoCl_3$, 1-D Ising antiferromag., mag. phase transitions 79—51779
$CsCoCl_3$, 1D Ising antiferromag., mag. excitations, electronic Raman and IR absorption spectra 78—2668
$CsCoCl_3$, anisotropic antiferromag., inelastic neutron scatt. study 78—60274
$CsCoCl_3$, Ising antiferromagnet, electronic Raman scatt. on Co^{2+} 78—10878
$CsCoCl_3$, Ising like antiferromag., mag. phase transition, ^{133}Cs NMR 80—7184
$CsCoCl_3$, Ising-like antiferromag., spin dynamics 79—42747
$CsCoCl_3$, Ising-like antiferromag., instantaneous spin correlations 79—42746
$CsCoCl_3$, mag. excitation spectrum, spin-wave response, neutron scatt. study 80—50080
$CsCoCl_3$, mag. struct., neutron diffr. meas. 78—43563
$CsCoCl_3$, one-dimensional antiferromag., neutron scatt. investig. of spin waves 77—47982
$CsCoCl_3$ spin dynamics, neutron scatt. study 80—80493
$CsCoCl_3$, spin wave spectrum 79—28514
Cs_2CoCl_4, mag. susceptibility and magnetisation curve meas. 80—11176
$CsCoCl_3.2D_2O$, metamag., thermodynamic props. near multicrit. pt. 77—66305
$CsCoCl_3.2H_2O$ interchain exchange low temp. susceptibility 78—19240
$Cs_2Co_{1-x}Zn_xCl_4$, mag. sp. ht., effect of dilution, comparison with linear XY antiferromag. 77—66354
$CsCrCl_3$, mag. structure and excitations, neutron diffr. and susceptibility meas. 80—44806
$CsCrI_3$, Mossbauer spectra, struct., electronic and mag. props. 79—91320
$CsCuBr_3$, quasi-1-dimens., NQR obs. 80—54987
$CsCuCl_3$, one-dimensional antiferromag., ^{63}Cu NMR mas. 78—2756
$CsCuCl_3$, quasi-1-dimens., NQR obs. 80—54987
$Cs_2FeCl_5.H_2O$, cryst. struct., superconducting susceptometer mag. meas. 79—73717
$Cs_2FeCl_5.H_2O$, mag. phase boundaries, susceptibility, 3D Heisenberg antiferromag. behaviour 78—84420
Cs_2FeF_5, mag. struct. and one-dimens. antiferromagnetism 80—60209
$CsLi_{0.5}(Al,Fe)_{1.5}F_6$ pyrochlore, Mossbauer contrib. to exam. of cationic order *(French)* 80—93224
$CsLi_{0.5}Fe_{1.5}F_6$ pyrochlore, Mossbauer contrib. to exam. of cationic order *(French)* 80—93224

antiferromagnetic properties of substances continued
$CsMnBr_3$, quasi-one-dimens. antiferromagnet, inelastic neutron scatt. 78 14929
$CsMnBr_3$, triang. antiferromagnet, spin wave theory 79−7978
$CsMnBr_3.2D_2O$, extended scaling in spin flop system 79−73737
$CsMnBr_3.2D_2O$, mag. phase diagram near bicrit. point 79−15302
$CsMnBr_3.2D_2O$, spin-flop systems, neutron scatt. expts. 79−61109
$CsMnBr_3.2D_20$, spin-flop system, extended scaling near bicrit. pt. 79−51752
$CsMnBr_3.2H_2O$, pseudo-one-dimensional mag. system, low-temp. sp. ht. 77−85471
$CsMnCl_3$, antiferromagnetic resonance, parametric spin wave excitation *(Russian)* 80−93183
$CsMnCl_3$, mag. anisotropy measurement 79−11310
$CsMnCl_3(Br_3)$, rare earth doped, energy transfer, emission spectra obs. 80−20684
$CsMnCl_3.2H_2O$, antiferromag. resonance and two-magnon absorpt. *(Russian)* 77−81014
$CsMnCl_3.2H_2O$, antiferromag. reson. and two-magnon absorpt. 79−61234
$CsMnCl_3.2H_2O$, antiferromag. reson. temp. depend. *(Russian)* 79−87321
$CsMnCl_3.2H_2O$, antiferromag. insulator, self-trapping of excitons 80−70619
$CsMnCl_3.2H_2O$, Heisenberg antiferromag., linear mag. birefringence meas. 77−16277
$CsMnCl_3.2H_2O$, linear antiferromagnet, specific heat, exchange interactions and anisotropy effects 77−1556
$CsMnCl_3.2H_2O$, luminesc., electronic excitations localisation *(Russian)* 79−87492
$CsMnCl_3.2H_2O$, mag. phase diagram near bicritical point 80−71021
$CsMnCl_3.2H_2O$, nonequilibrium magnon population obtained by optical pumping *(Russian)* 80−11457
$CsMnCl_3.2H_2O$, pseudo-one-dimensional mag. system, low-temp. sp. ht. 77−85471
$CsMnCl_3.2H_2O$, quasi-onedimens., microwave absorpt. and antiferromag. reson. *(Russian)* 77−51962
$CsMnCl_3.2H_2O$, quasi-one-dimensional antiferromag., luminesc. enhancement in mag. field *(Russian)* 79−91487
$CsMnCl_3.2H_2O$, quasi-one-dimensional antiferromag., phase diagram *(French)* 80−20405
$CsMnCl_3.2H_2O$, quasi one-dimensional mag. systems, impurity effects 80−71015
$CsMnCl_3.2H_2O$, spin wave anal. 77−8292
$CsMnCl_3.2H_2O$, subthreshold two-magnon absorpt., depend. on freq., temp. and mag. field, exchange coupling const. *(Russian)* 80−71184
$CsMnCl_3.2H_2O$, thermal cond. in mag. field 80−70481
$CsMnCl_3.2H_2O:Cu$, parallel susceptibility, impurity effect on spin-flop field *(French)* 78−43569
$CsMnCl_3.2H_2O:Cu(Co)$, mag. impurity effect on Neel temp. and spin-flop field 79−61099
$CsMn_{1-x}Co_xCl_32H_2O$, random mag. mixture, oblique-antiferromag. phase obs. 80−93142
$CsMn_{1x}Co_xCl_3.2H_2O$, random mag. mixture, mag. torque and sp. ht. expts. 80−60323
$CsMn_{1-x}Cu_xCl_3.2H_2O$, impurities in quasi-one-dimens. Heisenberg systems, anisotropy effect 80−80502
$CsMnF_3$, antiferromag., variation of spin wave spectrum in interaction between magnons 80−65841
$CsMnF_3$, exciton migration, excitation and luminesc. study *(Russian)* 80−66264
$CsMnF_3$, exciton-magnon interactions in optical transition, absorpt. and emission spectra meas. 80−70981
$CsMnF_3$, hexagonal antiferromagnet, light interaction *(Russian)* 77−36257
$CsMnF_3$, isotropic antiferromag., crossover behaviour of mag. phase boundaries 79−78370
$CsMnF_3$, light absorpt. spectrum in mag. fields up to 300 kOe *(Russian)* 77−52115
$CsMnF_3$, mag. phase boundaries, XY to Ising crossover, virtual bicritical point 80−50095
$CsMnF_3$, mag. struct., phase transition, and magnon spectrum, random anisotropy effects 80−88722
$CsMnF_3$, magnon absorption and luminesc. 80−7400
$CsMnF_3$, NMR saturation, nuclear spin wave excitation, large freq. shifts *(Russian)* 80−50207
$CsMnF_3$, new types of nuclear spin echo, single pulse and parametric echo 77−69726
$CsMnF_3$, optical investig. of spontaneous tilt of mag. sublattices *(Russian)* 77−40215
$CsMnF_3$, ordering temp., virtual bicritical pt. 79−61128
$CsMnF_3$, parametric excitation of magnons, effect of RF modulation of mag. field 80−65842
$CsMnF_3$, parametric magnon excitation, relaxation *(Russian)* 78−23352
$CsMnF_3$, parametric nuclear magnon excitation, mag. field modulation *(Russian)* 80−107999
$CsMnF_3$, RF modulation effect on parallel microwave pumping threshold *(Russian)* 80−29628
$CsMnF_3$, specific heat, crossover from Heisenberg to XY like behaviour 77−85461
$CsMnF_3$, spin wave propag. 77−63159
$CsMnF_3$, spin wave spectrum obs., review 80−50081
$CsMnF_3$, spin waves excitation 79−82772
$CsMnF_3$, spin-wave dispersion relations, neutron inelastic scatt. obs. 77−51895
$CsMnF_3$, struct. with compensated magnetisation in noncollinear phase *(Russian)* 78−88095
$CsMnF_3$, suscept. oscillations beyond threshold for parametric excitation of electronic magnons *(Russian)* 77−59398
$CsMnFeF_6$, neutron scatt. and magnetisation meas. 77−66258
$CsMnI_3$, Mossbauer spectra, struct., electronic and mag. props. 80−15908
$CsMnX_3.2H_2O$ ($X=Cl,Br$), pseudo one-dimens. Heisenberg antiferromag., phase diagrams 79−61148
$CsNiBr_3$, nearly one-dimensional antiferromag., thermal and mag. props. meas. 77−77041
$CsNiCl_3$, antiferromag. coupling in linear chains, molecular orbital approach 78−52239
$CsNiCl_3$, linear chain antiferromag., mag. props., 1.1 to 7K 79−61076
$CsNiCl_3$, linear-chain antiferromag., low temp. thermal expansion 80−39326

antiferromagnetic properties of substances continued
$CsNiCl_3$, mag. props. 79−73736
$CsNiCl_3$, nearly one-dimens. antiferromag., mag. sp. ht. determ. 77−24702
$CsNiCl_3$, nearly one-dimensional antiferromag., spin-flop transition 78−6527
$CsNiCl_3$, nuclear spin-lattice relax., temp. depend., anisotropic effects 78−64293
$CsNiCl_3$, one-dimens. antiferromag., US attenuation, crit. behaviour 77−66308
$CsNiCl_3$, one-dimens. antiferromag., US attenuation 78−88156
$CsNiF_3$, demagnetising effects on antiferromag. reson. 80−15803
$CsNiF_3$, field depend. mag. behaviour, mag. linear dichroism 79−73903
$CsNiF_3$, one-dimensional mag., Young's modulus softening along linear-chain direction 77−62578
$CsNiF_3$, quasi-one-dimens. Heisenberg system, reaction field approx. and dipolar interaction 77−36088
$CsNiF_3$, quasielastic neutron scatt. around Neel-point 80−75768
$CsNiFeF_6$ pyrochlore, Mossbauer contrib. to exam. of cationic order *(French)* 80−93224
CsO_2, low temp. phases, mag. order, EPR and antiferromag. reson. 79−95630
$Cs_{1-x}Rb_xMF_3$ ($M=Mg$, Co, Ni, Zn), hexagonal fluoride perovskite structural evolution by cationic substitution *(French)* 80−24430
$CsVCl_3$, antiferromag. coupling in linear chains, molecular orbital approach 78−52239
α-Cs_xVF_3, mag. props. *(French)* 77−80933
$CsVI_3$, Mossbauer spectra, struct., electronic and mag. props. 79−91320
$Cs_{0.35}V_3O_7$, cryst. struct., semicond. and antiferromag. behaviour 77−35515
$CsVX_3$, $X=Br$, Cl, I, mag. props. *(French)* 77−16059
Cu complex, 1,2-ethanediammonium tetrachlorocuprate, layered struct. mag. susceptibility 80−7094
Cu complex, $Cu_3Cl_6(H_2O)_2.2$ tetramethylsulphone, mag. interactions, susceptibility, 2-230K 80−60237
Cu complex, dichloro-bis-pyridine copper II, one-dimens. antiferromagnet, dynamic props., review 80−15737
Cu complex, dichloro(dimethylnitrosamine) Cu II, mag. props., ^{14}N NQR obs. 80−54988
Cu complex, hexa(pyridine-N-oxide)$(ClO_4)_2$, Heisenberg antiferromag., mag. props. and sp. ht. 78−23287
Cu complex with adenine, powder, physical properties obs. *(Japanese)* 77−43878
Cu, nuclear antiferromagnetism, NMR obs. 79−78538
Cu, nuclear antiferromagnetism, low temp. NMR study 80−66049
Cu, nuclei, antiferromag. ordering, mean field theory 79−78333
Cu, spin density wave fluctuations in nuclear spins, susceptibility, internal energy 80−50115
Cu-Mn, mictomag., massive short-range antiferromagnetism 77−12139
Cu-Mn (7 at.%), magnetic susceptibility, clustering, band model of heterogeneous magnetics 77−43823
Cu-Mn (8 to 75 at.%), spin correl., neutron polarisation anal. study 80−65905
$Cu_2(AsO_4)Cl$, temp. depend. of mag. susceptibility 80−70962
$CuBeF_4.5H_2O$, NMR, interactions between paramag. ion system and antiferromag. linear chains 77−63295
$CuBr_2$, quasi-1-dimens., NQR obs. 80−54987
$Cu(C_5H_5NO_6)(BF_4)_2$, sp. ht. and susceptibility, comparison with quadratic spin 1/2 Heisenberg antiferromag. calcs. 77−66353
$CuCl_2$, anhydrous, mag. phase transition 80−80506
$CuCl_2$, anhydrous, single cryst., mag. behaviour in low temp. ordered phase 79−7974
$CuCl_2$, quasi-1-dimens., NQR obs. 80−54987
$CuCl_2.CuCl_2.2D_2O$, neutron scatt. aspherical effects, mag. form factor 78−27017
$CuCl_2.2D_2O$, cryst. struct., mag. and reson. props. 80−60424
$CuCl_2.2D_2O$, staggered magnetisation, neutron diffr. obs. 78−39296
$CuCl_2.2H_2O$, antiferromag. reson. in tilted mag. fields *(Russian)* 77−51961
$CuCl_2.2H_2O$, antiferromagnetic relax., autocorrel. function time evolution 77−59464
$CuCl_2.2H_2O$, antiferromag. to paramag. transition, high field magnetisation meas. 78−64204
$CuCl_2.2H_2O$, EPR linewidth and relax., effect of antisymmetric exchange 77−59448
$CuCl_2.2H_2O$, effect of press. on mag. phase transition, NMR meas. 78−19253
$CuCl_2.2H_2O$, energy gaps mag. field depend., antiferromag. reson. 79−87320
$CuCl_2.2H_2O$, flop of sublattice moments and Neel temp., press. effects, NMR obs. 77−40058
$CuCl_2.2H_2O$, influence of high hydrostatic press. on intermediate state associated with spin flopping 78−35020
$CuCl_2.2H_2O$, magnetoelastic props. under press., antiferromagnetic resonance, lattice parameters 80−29598
$CuCl_2.2H_2O$, NMR, high press. effect on existence domain width of intermediate state 79−87255
$CuCl_2.2H_2O$, range of existence of intermediate state, NMR expt. 77−59410
$CuCl.2N(C_5D_5)$, one-dimens. antiferromag., mag. excitation line-shape, field depend., neutron study 79−38314
$CuCl_2.2NC_5H_5$, antiferromag. spin dynamics at low temp. 77−32278
$CuCrS_2$ single cryst., spectral study and phys. props. *(French)* 80−29002
$CuCrSe_2$, influence of excess Cu on physical props. 80−103836
$Cu_{1-x}Cr_2Se_4$, influence of excess Cu on physical props. 80−103836
CuF_2, heat capacity, entropy, 10-300K, mag. ordering effects 79−87264
$CuFeS_2$, antiferromag., NQR local mag. field effects 80−71234
$CuFe_2S_3$, cubanite, spontaneous magnetisation, polarised neutron obs. *(French)* 78−23245
Cu_5FeS_4, mag. ordering and vacancy clustering, mag. susceptibility and Mossbauer spectra meas. 77−85625
$Cu_{0.5}Ga_{0.5}Cr_2S_4$, mag. struct. determ. 77−8272
γ-$Cu(IO_3)_2$, cryst. struct. and mag. behaviour 78−79571
$Cu_{1-x}In_xCr_2S_4$, light induced magnetisation 78−76275
γ-$Cu_{15}Mn_{85}$, antiferromag., neutron diffr. 80−2550
$Cu(NH_3)_4(NO_3)_2$, single cryst., low temp. susceptibility and sp. ht., 10 behaviour 77−89929
$Cu(NH_3)_4SO_4.H_2O$, interface with liq. ^3He, Kapitza resist. anomaly near T_N 77 -69139

antiferromagnetic properties of substances continued
$Cu(NH_3)_4SO_4.H_2O$, submillimetre ESR meas. using pulsed high mag. field 80—44905
$Cu(NO_3)_2.2^1/_2H_2O$, ^1H spin-lattice relax. time, 4.2K, 5-60 kOe 79—15371
$Cu(NO_3)_2.2^1/_2H_2O$, high field phase transition, susceptibility and NMR meas. 77—69559
$Cu(NO_3)_2.2^1/_2H_2O$, long-range ordered state, mag. props. 78—39417
$Cu(NO_3)_2.2^1/_2H_2O$, singlet ground-state system, mag. props., short-range ordered state 78—23289
$Cu(NO_3)_2.2^1/_2H_2O$, singlet ground state system, mag. props. 80—44850
$Cu(NO_3)_2.2.5\ D_2O$, magnetic ordering, neutron diffr. meas., 0.08-0.25K 80—39749
$Cu(NO_3)_2.2.5H_2O$, linear Heisenberg antiferromag., mag. and thermodynamic props. 79—61136
$Cu(NO_3)_2.2.5H_2O$, linear Heisenberg antiferromag., proton spin-lattice relax. times 79—61257
$Cu(NO_3)_2.2.5H_2O$, single cryst., $S={}^1/_2$ alternating linear antiferromag. spin dynamics 79—51793
$Cu(NO_3)_2$(pyrazine), single cryst. PMR 78—2761
$Cu_4NiSi_2S_7$, X-ray cryst. struct. determ., mag. props. 80—107172
Cu_2O-CuO-MoO_3, subsolidus phase diagram, mag. props. 80—50615
$CuSO_4.5H_2O$, $CuSeO_4.5H_2O$ and $CuBeF_4.5H_2O$, mag. ordering in external field, NMR obs. 77—66350
$CuSO_4.5H_2O$, low freq. spin dynamics, proton relax. study 80—71218
$Cu_{2-x}Se$, electric, thermal and magnetic props. investigation in low temp. phase *(Croatian)* 79—11299
$CuSeO_4$, $S={}^1/_2$ Heisenberg antiferromag. linear chain, proton spin-lattice relax. 78—39433
$CuSe_2O_5$, strongly antiferromag. coupled Cu linear chain, orbital props. 80—100580
CuSeO4.5H_2O, $S=1/2$ antiferromag. chain, proton relax. near saturation field 79—15370
$CuSeO_4.5H_2O$, antiferromag. chain system, proton spin-lattice relax. near saturation field 79—61256
$CuSeO_4.5H_2O$, $CuSO_4.5H_2O$ and $CuBeF_4.5H_2O$, linear-chain antiferromag., mag. phase transition investig. 77—55684
$CuWO_4$, elec. cond., thermoelectric power and dielectric constant temp. depend. 80—96886
dimethylammonium manganese tetrachloride, 2D Heisenberg antiferromag., spin wave anal. 80—54879
Dy, anomalous thermal expansion, interferometric meas. 78—52333
Dy, antiferromagnetic, thermal expansion, US attenuation anomalies 79—47319
Dy, basal plane mag. anisotropy constant, field depend. meas., 4.2-120K 77—63165
Dy, critical exponents and amplitude ratios from elec. cond. data, theoretical model 80—50126
Dy, elec. resist. and mag. struct. near Neel point *(Russian)* 79—47074
Dy, helical antiferromagnetic phase, basal plane anisotropy 78—84412
Dy, magnetic domain structure, hysteresis, thermal modulation study 80—71082
Dy, magnetic phases, US study 78—31101
Dy, magnetocaloric effect and mag. phase transitions, 80 to 300K 80—60279
Dy, magnetocaloric effects between 84 and 280K 79—73721
Dy, magnetoelastic effects in mag. ordered regime 78—15003
Dy, μSR in ferro- and antiferromag. phases, local fields 78—43763
Dy, resistivity anomalies at mag. transitions, sp.ht. 80—39785
Dy, US attenuation in mag. field 77—40104
Dy:^{181}Ta, ferro- and antiferromag. phases, temp. depend. of mag. hyperfine field, TDPAC obs. 77—36165
Dy-Fe-Al, pseudobinary alloys, mag. props. 77—59397
Dy-Pr(Nd) alloys, mag. struct. and ordered moments, neutrons diffr. data 77—66252
Dy-Sm alloys, elec. resist. singularities and mag. transitions *(Russian)* 79—47075
Dy-Th, single cryst., mag. susceptibility, transitions, anisotropy 80—54873
Dy-Y, magnetisation and hysteresis, temp., depend. 79—69673
DyAG, adiabatic magnetisation, optical obs. 78—88283
DyAG, antiferromag., induced staggered mag. fields 80—65810
DyAG, antiferromag., induced staggered magnetic fields, microscopic mech. 80—80527
DyAG, cubic antiferromagnet, multiaxis phase transitions 79—78377
DyAG, forced magnetostriction meas. 78—68349
DyAG, light scatt. from metamag. domains, crit. exponent determ. 77—66482
DyAlG, tricrit. wing exam. 77—73026
$Dy_3Al_5O_{12}$, antiferromag., optical birefringence in fields along [111] meas. 77—28540
$Dy_3Al_5O_{12}$, magnetostriction, role of order parameter 79—73796
$DyAsO_4$, phase transitions obs. 80—70412
$DyAu_2$, long-duration pulsed mag. field appl. to magnetisation meas. 79—61183
$DyAu_{3.6}$, ordering temps. and effective moments 78—60283
DyB_4 *(French)* 77—20566
DyB_4, cryst. and mag. struct., neutron diffr. meas. 80—15692
DyC_2, mag. susceptibility, temp. depend. 79—87239
$DyCo_2Si_2$, mag. props. 80—107988
$DyCrO_3$, Cr^{3+} exciton-Dy^{3+} spinflip absorpt. 77—73153
$Dy_xEr_{1-x}FeO_3$, transition to antiferromag. state, Dy^{3+} conc. effects 77—66319
$DyFe_{0.998}Co_{0.002}O_3$, mag. transition, NMR meas. 78—27036
$DyFe_{1-x}Co_xO_3$, magnetostriction, thermal expansion and elastic moduli near Morin point 77—8383
$DyFeO_3$, field induced spin reorientation, Mossbauer spectroscopy 80—65878
$DyFeO_3$, mag. field induced intermediate state, magneto-optical effect meas. 77—55672
$DyFeO_3$, magnetic intermediate state at antiferromag. to weakly ferromag. transition *(Russian)* 77—40059
$DyFeO_3$, non Heisenberg R-Fe exchange interaction, behaviour in mag. field *(Russian)* 80—2568
$DyFeO_3$, phase domains, polarisation microscope obs. 77—28407
$DyFeO_3$, spin reorientation near Morin temp., magnetooptical exam. 78—68284
$DyFeO_3$, spin reorientation transitions induced by magnetic fields, Mossbauer study 80—71246
$DyFeO_3$, weak ferromagnet, μSR study 80—93226

antiferromagnetic properties of substances continued
$Dy_3Ga_5O_{12}$, sp. ht. meas., 37 mK-2K, antiferromag. ordering obs. 77—85476
DyH_2, mag. and crystal field props. from ^{161}Dy Mossbauer studies 79—95692
$DyIn_3$, magnetisation 80—25106
Dy_2In, mag. props., 4.2 to 270K 79—56512
DyMg, mag. props., neutron diffraction and magnetisation meas. 77—16045
$DyMo_6S_8$, long range mag. order in supercond. state 79—65653
$DyMo_6S_8$, supercond. and antiferromag. coexistence, neutron study 78—95401
$DyMo_6S_8$, superconductor, neutron scatt. exam. of mag. phase 79—73680
$Dy_{1.2}Mo_6S_8$, long-range mag. order and supercond., neutron diffr. obs. 79—78320
$Dy_{1.2}Mo_6S_8$, low temp. heat capacity anomaly rel. to antiferromag. transition in supercond. state 80—25044
$DyNi_2Si_2$, mag. props., 4.2-200K 80—84602
$Dy_2O_2SO_4$, antiferromag., specific heat, 0.6 to 30K 79—33487
$Dy_2O_2SO_4$, antiferromag., mag. props. and Zeeman effect meas. 79—33464
$Dy_2O_2SO_4$, mag. ordering, magnetisation, AC susceptibility and Zeeman effect meas. 80—60205
$Dy_2O_2SO_4$, magnetic struct. in antiferromag. and ferrimag. states 80—15695
DyO_2X, X=S,Se,Te, mag. and quadrupole hyperfine interactions 77—63336
$DyPO_4$, mag. phase diagram and crit. exponents, MCD obs. 77—66307
$DyPO_4$, mag. transitions under hydrostatic press., neutron diffr. study 80—71030
$DyPO_4$, metamagnet, mag. phase transitions, elastic neutron scatt. study 79—78371
$DyPO_4$, metamagnet, phase diagram, influence of internal strains 79—28544
$DyPO_4$, susceptibility near mag. phase boundaries 78—52258
DySb, biquadratic exchange interactions, magnetisation above Neel point 77—69533
DySb, magnetic excitations 79—78358
DySb, magnetisation study, intermediate metamagnetic phase transitions 79—99698
DySb, quadrupole interactions above T_N 79—78304
$Dy_{1-x}Sm_x$, magnetoresist. of polycryst. specimens in fields up to 44 kOe *(Russian)* 80—92880
$Dy_xTb_{1-x}FeO_3$ orthoferrites, Dy^{3+} and Tb^{3+} contribs. to anisotropy const. *(Russian)* 77—89946
$Dy_xTm_{1-x}FeO_3$, transition to antiferromag. state, Dy^{3+} conc. effects 77—66319
$DyVO_4$, basal plane magnetisation anisotropy under Jahn-Teller distortion 78—68222
$DyVO_4$, phase transitions obs. 80—70412
Dy_2ZrS_5, mag. and sp. ht. meas. on polycrystalline samples 78—23253
Er, elastic constants, magnetoelastic contrib. 80—15777
Er, paramagnetic and antiferromagnetic states, optical absorption *(Russian)* 78—56497
$ErAl_3$, 15 layer rhombohedral struct., mag. struct. 77—63104
ErB_4 *(French)* 77—20566
ErB_4, cryst. and mag. struct., neutron diffr. meas. 80—15692
ErB_4, mag. phase diagram, neutron diffr. study 80—50091
$ErCo_2Si_2$, mag. props. 80—107988
$ErCrO_3$, dynamic spin reorientation process, magneto-optical meas. 77—69590
$ErCrO_3$, field-induced spin reorientation relax. 79—78402
$ErCrO_3$, mag. field induced spin reorientation, optical Zeeman absorpt. spectra 79—61398
$ErCrO_3$, magnetisation, NMR freq. temps. depend. weak ferromagnetic-antiferromagnetic spin reorientation transition 80—29631
$ErCrO_3$, phonon Raman spectra rel. to mag. ordering 77—52100
$ErCrO_3$, spin-reorientation, optical obs. 77—63201
ErCu, cubic antiferromag., mag. excitations inelastic neutron scatt. meas. 78—72341
ErCu, magnetic excitations 80—25115
$ErFe_3$, 47K magnetic anomaly, point charge crystal field model 77—20517
$ErFe_3$, mag. anomalies at 47 and 131K 77—63134
$ErFe_3$, Mossbauer and magnetisation investig. of 47K mag. anomaly, atomic rearrangement 77—20766
$ErFe_4Al_8$, neutron diffr. exam., mag. struct. 78—10656
$ErFeO_3$, field induced spin reorientation, Mossbauer spectroscopy 80—65878
$ErFeO_3$, weak ferromag., high freq. props. in ordering region of spin system, antiferromag. reson. study *(Russian)* 80—2644
$ErFeO_3$, weak ferromagnet, μSR study 80—93226
ErGa, antiferromag., mag. props., 4.2 to 350K 77—63230
ErH_3, cryst. fields and mag. props. 78—68181
$ErH_2(D_2)$, mag. props., 1.5 to 10K, Mossbauer meas. 79—78578
$Er_xLa_{1-x}Cu$, and $Er_xY_{1-x}Cu$, antiferromag., mag. and resist. behaviour 80—34412
$ErMo_6S_8$, long range mag. order in supercond. state 79—65653
$Er_xMo_6Se_8$, long-range antiferromag. order and supercond. coexistence 78—10715
Er_2O_3, mag. susceptibility, elec. cond. and dielectric const., hopping cond. 77—12083
$Er_2O_2SO_4$, antiferromag., mag. props. 1.6 to 40K 79—33464
$Er_2O_2SO_4$, antiferromag., specific heat, 0.6 to 30K 79—33487
$ErVO_3$, produced by $Er_2O_3+VO_2$ high-press. reaction, cryst. struct. and mag. props. meas. 80—19773
Er_2ZrS_5, mag. and sp. ht. meas. on polycrystalline samples 78—23253
Eu, antiferromag., thermal cond., elec. and thermal magnetoresist., at low temps. 77—69301
Eu, band struct. and Fermi surface 77—62814
Eu chalcogenide, spin-disorder Raman scatt., mag. phase depend., theory 78—10887
Eu, elec. resist., effect of mag. field near Neel point 77—8073
Eu, elec. resistance anomaly below Neel temp. 77—11889
Eu, mag. and struct. transitions, X-ray K-line shift, 77-1000K *(Russian)* 77—4518
Eu, mag. anisotropy of helicoidal struct., magnetisation, 4.2-300K *(Russian)* 79—56499
Eu, magnetoresist., irreversible component rel. to antiferromag. struct. *(Russian)* 77—35920
EuB_6, correlation between mag. struct. and elec. props. 77—63192

antiferromagnetic properties of substances continued
- EuB_6, ferromag. and antiferromag. sp. ht meas., 1.8-77K 80–65948
- EuB_6, single and bulk polycryst., EPR, temp. and freq. depend. 79–28606
- $EuB_{6-x}C_x$, magnetisation, effects of C 80–25163
- $EuB_{6-x}C_x$, Mossbauer spectra, cond. electrons effect 80–20545
- $EuCrO_3$, long term mag. ordering, antiferromagnetic resonance study *(Russian)* 80–54953
- $EuFe_4Al_8$, mag. ordered, mixed valency of Eu, X-ray, susceptibility and Mossbauer spectra studies 79–19728
- $Eu_{1-x}Gd_xS$, concentrated system with ferromag. and antiferromag. interactions, spin-glass props. 80–34639
- $Eu(Lu_{0.5}Ta_{0.5})O_3$, mag props. 77–4587
- $Eu(Lu_{0.5}Ta_{0.5})O_3$, mag. props. 77–4587
- EuM_2Ge_2, M=Mn, Fe, Co, Ni, Cu, magnetism and hyperfine interactions 78–76228
- $EuMg_2$, cryst. and mag. props., ordering 78–68185
- $Eu(Mg_{0.5}W_{0.5})O_3$, mag. props. 77–4587
- EuS, thermo- and magnetorefl. spectra, dynamical spin fluctuation effect on exciton state 77–52126
- $EuSO_4$, sp. ht. and susceptibility meas. 78–14977
- $EuS_{1-x}Se_x$, mag. phase diagram, from temp. depend. of magnetisation 80–7105
- $EuSb_2$, cryst. struct. and antiferromag. props. 79–32973
- Eu_2Sb_3, cryst. struct., elec. and mag. props. 80–33958
- EuSe, mag. phase depend. Raman scatt. 78–10886
- EuSe, mag. phase stability, theory 77–63183
- EuSe, mag. struct. and transition temp., indirect exchange 78–91860
- EuSe, microwave and DC cond., dielec. const., 1.7 to 300K 77–20347
- EuSe, MnO-type antiferromag. spin order, Faraday rotation obs. 77–47974
- EuSe, spin assisted Raman scatt. theory 78–43866
- EuSe(Te), cryst. and electronic struct., mag., elec., and optical props., book contrib. 80–39760
- EuSe(Te), magnetic phase transitions, thermal modulation spectroscopy study *(French)* 80–97301
- EuSe(Te), phase transition spectroscopy 77–63426
- $EuSe_{1-x}Te_x$, transferred hyperfine fields at Eu nuclei, NMR meas. 80–71195
- $Eu_5Sn_3S_{12}$, mag. and thermodynamic props., metamagnetism 80–60273
- EuTe, antiferromag. FCC lattice of second kind, surface magnons and mag. structs. 78–23261
- EuTe, antiferromag. semicond., Raman scatt., spin-phonon interactions 80–66185
- EuTe, exchange and superlattice band splittings, magneto-optical meas. in high mag. fields 79–61342
- EuTe, exchange interaction mechanisms, theory compared with expt. *(Russian)* 78–39312
- EuTe, field depend. correl. function theory of Raman scatt. near antiferromag.-paramag. transition 78–68490
- EuTe, mag. 'Bragg' scatt. obs. through Raman scatt. 80–66179
- EuTe, mag. struct. and transition temp., indirect exchange 78–91860
- EuTe, Neel temp. and hyperfine interactions, press. depend. up to 60 kbar, ^{151}Eu Mossbauer obs. 77–63181
- EuTe, optical absorpt. in high mag. field 79–28726
- EuTe, phonon Raman scatt. from spin superstructures 80–16030
- EuTe, spin alignment, high field Faraday rotation expt. 77–63401
- EuTe, spin order and fluctuations, Raman scatt. study 80–97273
- EuTe, spin-dependent Raman scattering 79–95782
- EuTe, superexchange interaction parameters, many-electron model calc. 79–7988
- Eu_4Y_2X, (Y=pnictogen, X=chalcogen), anti-Th_3P_4 type struct. 79–65048
- $Eu_{1-x}Yb_xTe$, ($0<x<1$), mag. semicond., elec., mag. and optical props. 80–97070
- Fe complex, bis(N,N-dialkyldithiocarbamato) iron III halides, short range antiferromag. coupling, Mossbauer spectra 77–90076
- Fe complex, Fe(III) Schiff-base complexes, mag. relax., Mossbauer spectra 80–15897
- Fe complex, $Fe(1,2,4\text{-triazole})_2(NCS)_2$, quasi-2-dimens. $S={}^1/_2$ antiferromag., mag. props., hidden canting 80–107986
- Fe complex, tris(1-pyrrolidinecarbodithioato)iron(III), and related cpds. mag. props., struct. 77–89933
- Fe complex (2, 9-dimethylphenanthroline) sulphate, mag. props., Mossbauer spectra 80–66081
- Fe complexes, S-bridged binuclear, orbitally dependent exchange 77–24688
- Fe film, antiferromagnetic ordering, Mossbauer spectroscopy 78–14990
- Fe, film, FCC, antiferromag. ordering, Mossbauer expts. 77–85508
- Fe, Neel temp. 78–88124
- γ-Fe precipitates, antiferromag. ordering, press. depend., Mossbauer meas. 79–73861
- γ-Fe precipitates in Cu, Invar related system, high press. Mossbauer spectra 79–56642
- Fe-Cr, mag. props. of Fe, local coupling with spin modulation of matrix 79 15299
- Fe-Cr (70-92 at.%), coexistence of ferro- and antiferromagnetism *(Russian)* 78–47955
- Fe-Cr alloys, mixed ferro-/antiferromag. interactions *(Russian)* 77–32173
- Fe-Cr-Ni, spin system, relaxation props. at low temp. 79–82758
- Fe-Cr-Ni alloys, linear expansion, 4.2-300K rel. to antiferromag. rearrangement 78–43146
- Fe-Mn, annealed, α-γ phase transformation obs. 78–75831
- Fe-Mn (14.1 wt.%), G14, α-martensite formation in mag. field 79–91648
- γ-Fe-Mn alloys, antiferromag., mag. and crystallographic transformations 77–55964
- Fe-Mn alloys, elasticity modulus anomaly and magnetoelastic effect *(Russian)* 79–28578
- Fe-Mn alloys, mag. susceptibility and conc. depend. of Neel point *(Russian)* 79–47279
- Fe-Mn-Co-Ni-Cr, antiferromag. props., Neel temp. determ. 78–88124
- Fe-Mn-Cr(Ni), mag. and crystallographic transformation depend. on Cr-Ni addition *(Russian)* 79–83334
- Fe-Mn-Ni antiferromag. alloy, neutron scatt. exam. of antiferromagnons 77–66283
- Fe-Nb alloys, mag. and Mossbauer meas. 77–63133
- Fe-Ni, $Fe_{65}(Ni_{1-x}Cr_x)_{35}$, low-temp. elec. and galvanomag. props. rel. to mag. boundaries *(Russian)* 77–35910

antiferromagnetic properties of substances continued
- Fe-Ni-Al, Curie temp. depend. on ordering, antiferromag. ordering *(Russian)* 79–61101
- Fe-Ni-Cr, mag. props. in weak mag. fields *(Russian)* 80–75771
- Fe-Ni(-Al)(Mn) Invar alloys, mag. heterogeneities *(Russian)* 77–66251
- Fe-Ni(-Mn)(Cr)(V), concentration ferromag. antiferromag. phase transition and mag. state diagram. *(Russian)* 80–20401
- Fe-Ni(Cr), Invar, exchange interactions between ferromag. and antiferromag. components 80–29545
- Fe-Pt, high mag. field phase transition 77–66301
- Fe-Pt alloy, ordered, anisotropy of mag. props. *(Russian)* 78–60280
- Fe-Rh, mag. phase transitions, triple point 79–1672
- Fe-Rh alloy, nonmag. and mag., band theory 79–37973
- Fe-Rh alloys, spin wave spectrum in antiferromag. and ferromag. phases, inelastic neutron spectrometry 77–63158
- Fe-Rh(Os), mag. hyperfine interactions Mossbauer effect meas. 77–66442
- Fe-Ru (30-60 at.%) alloy, mag. ordering, Mossbauer obs. 77–4585
- Fe-Ru(Os), CC hexagonal phase, ^{57}Fe Mossbauer study, saturated hyperfine fields and Neel temp. determ. 79–91321
- Fe-Ru(Os) alloys, antiferromag. ordering, hyperfine fields 80–15867
- Fe-Y(Th)(Zr), amorphous, charge transfer and mag. props., ^{57}Fe Mossbauer spectra 79–19719
- $Fe_{1-x}Al_xOOH$, Mossbauer study, determ. of Al content and mag. props. 80–39938
- FeAs, Mossbauer spectra of paramag. and ferromag. states, helimagnetic spin ordering 80–7197
- Fe_2As, antiferromagnet, Mossbauer spectra determ. 77–8480
- Fe_2As, mag. props., Mossbauer study 80–88897
- $FeBO_3$, antiferromag., vibr. spectra, 6000-30 cm^{-1} 78–19473
- $FeBO_3$, antiferromag., optical absorpt. spectra, role of local mag. mode 79–28785
- $FeBO_3$, antiferromag., two magnon reson. Raman scatt. 79–33703
- $FeBO_3$, crit. behaviour, Mossbauer and magnetisation meas. *(Russian)* 79–61106
- $FeBO_3$, Curie temp. displacement under press. up to 3 kbar 77–20603
- $FeBO_3$, mag. linear dichroism and absorpt. spectra, exciton-magnon absorpt. mechanism 80–66160
- $FeBO_3$, magnetisation near crit. temp., up to 3 kbar hydrostatic press., scaling theory 77–8316
- $FeBO_3$, photoinduced linear birefringence *(Russian)* 78–52469
- $FeBO_3$, spin-reorientation phase transition *(Russian)* 80–93122
- $FeBO_3$, weak ferromag., mag. field influence on crit. behaviour of susceptibility 78–14942
- $FeBO_3$, weak ferromag., FMR instability, parametric excitation of phonons, Brillouin scatt. obs. 79–78529
- $FeBO_3$-MBO_3 solid soln., (M=Mn, Cr, Al, Ga, In), synthesis, crystal chem. and mag. props. 78–31058
- $FeBO_6$, critical indices splitting of sublattice magnetisation *(Russian)* 78–60299
- Fe_3BO_6, canted mag. struct. near Neel point, Mossbauer meas. 78–35073
- Fe_3BO_6, polarised absorpt. spectra in range of $^6A_1 \rightarrow {}^4T_1$, $^4T_2$ transitions 77–52092
- Fe_3BO_6, spin reorientation by mag. field, Mossbauer meas. 78–35074
- Fe_3BO_6, weak ferromag. state, Mossbauer determ. of mag. struct. 77–40164
- Fe_3BO_6, weak ferromag. and antiferromag. reson. modes obs. 77–69706
- Fe_3BO_6, weak ferromagnetism and spin reorientation, antiferromag. reson. spectra 78–6580
- $Fe_3B_7O_{13}Br$, $Fe_3B_7O_{13}Cl$, polydomain ferroelec., magnetoelec. effect below Neel temp. 78–10745
- $Fe_3B_7O_{13}I$, ferroelec., mag. ordering, neutron diffr. meas. 78–72331
- $FeBr_2$, dynamic Jahn-Teller system, Raman scatt. from electronic excitations and phonons 78–56474
- $FeBr_2$, Faraday rot., optical absorption, multicrit. behaviour 77–4627
- $FeBr_2$, hyperfine interaction, ^{57}Fe Mossbauer expts., mag. transition obs. 78–43720
- $FeBr_2$, optical props. around Neel temp. 79–78658
- $FeBr_2$:Mn^{2+}, impurity spin reson. 77–43876
- $FeBr_2$:Mn^{2+}, layered antiferromag., infinity mode NMR study 79–38390
- $FeBr_2$:$MnBr_2$, magnon modes and impurity spin reson. 79–15501
- $FeBr_2(Cl_2)(I_2)$, far IR antiferromag. reson. 77–36138
- $FeCO_3$, antiferromag., siderite, Raman spectra obs. 77–85708
- $FeCO_3$, mag. field drawn destruction of antiferromag. destruction, light depolarisation at mag. transform. *(Russian)* 78–23432
- $FeCO_3$, mag. neutron scatt., spin orbit coupling effects 77–85419
- $FeCO_3$, metamagnetic insulator Neel temp. anal. by model including spin fluctuations *(Russian)* 80–15715
- $FeCO_3$, siderite, Fe^{2+} Mossbauer spectrum, ligand field theory 77–16212
- $FeCO_3$, vibronic coupling at Neel temp. 80–15491
- $FeCO_3$:Mn^{2+}, far IR host and impurity excitations, antiferromag. and paramag. temp. ranges 77–52140
- $FeCl_2$, antiferromag., magnon-phonon interactions in thermal cond. 80–65315
- $FeCl_2$, antiferromag. reson., temp. depend. 78–68384
- $FeCl_2$, antiferromag. reson., 2-D Ising model interpretation 79–47323
- $FeCl_2$, collinear metamag., mag. phase diagram 80–71035
- $FeCl_2$, dynamic Jahn-Teller system, Raman scatt. from electronic excitations and phonons 78–56474
- $FeCl_2$, electron-phonon coupling, Raman spectra change at antiferromagnetic ordering temp. 79–15451
- $FeCl_2$, in transverse mag. field, magnetoelastic coupling effect on mag. props. 79–28582
- $FeCl_2$, light scatt., metamagnetic transition effects 77–4513
- $FeCl_2$, magnetic transition and sublattice mag. moment rotation nonequivalence *(Russian)* 80–100586
- $FeCl_2$, magnon-phonon hybridisation, inelastic neutron scatt. study 79–47272
- $FeCl_2$, metamagnet, one-magnon light scatt., effect of anisotropy 79–33678
- $FeCl_2$, metamagnetic hysteresis, magnetooptical rot. meas. 77–40057
- $FeCl_2$, mixed antiferromag.-paramag. state, light scatt. in mag. field 77–40069
- $FeCl_2$, one-magnon Raman scatt. 78–43877
- $FeCl_2$, optical props. around Neel temp. 79–78658
- $FeCl_2$, reorientation of mag. moments under mech. stresses at 0K 80–93153
- $FeCl_2$, tricritical dynamcis, model 77–39719

antiferromagnetic properties of substances continued
$Fe_{1-x}Cl_2:Cd_x$, randomly disordered, tricrit. behaviour, light scatt. 78−68255
$FeCl_2.2H_2O$, and $FeCl_2.2D_2O$, Raman scatt. at metamagnetic phase transitions, mag. hysteresis 78−14958
$FeCl_2.2H_2O$, antiferromag. metastable state obs. in metamag. transition 77−66314
$FeCl_2.2H_2O$, magnon-phonon interactions and two-magnon Raman scatt., magnetoelastic waves and selection rules 80−34917
$FeCl_2.2H_2O$, metamagnetic, resonant magnon-optical phonon coupling 79−28773
$FeCl_2.2H_2O$-$CoCl_2.2H_2O$ random mixture, phase diagram 79−73748
$FeCl_2.2H_2O$-$CoCl_2.2H_2O$, random mixture with competing spin anisotropies, tetracrit. transition, neutron diffr. obs. 80−2575
$FeCl_2.4H_2O$, antiferromag., Mossbauer exam. 77−16221
$Fe_{1-x}Co_xCl_2$, mag. phase diagram 80−11198
$Fe_xCo_{1-x}Cl_2$, metamagnet, mag. phase diagram by mag. induced light scatt. 80−65883
$Fe_{1-x}Co_xCl_2.2H_2O$, random mixture with competing spin anisotropies, tetracrit. behaviour 80−60324
$Fe_{(1-x)}Co_xCl_2.2H_2O$, random mixture of anisotropic antiferromags., isotropic state obs. 78−84396
$Fe_{(1-x)}Co_xCl_2.2H_2O$, antiferromag. random mixture, sp. ht. meas. 79−65678
$FeCoCrO_4$, Mossbauer study, cation distrib. and Neel temp. determ. 79−33571
$Fe_{1-x}Co_xGe_2$ solid solns., mag. susceptibilities, multiple stages in mag. transitions, effective mag. moment 77−8286
$Fe_xCo_{1-x}Rh_2S_4$, spinel struct., X-ray, mag., elec. and Mossbauer spectra meas. 77−12278
$FeCr_{2-x}In_xSe_4$, struct. and mag. props., comp. depend. 77−66262
$(Fe_{1-x}Cr_x)_2O_3$, Mossbauer exam. of mag. struct. 77−24694
$(Fe_xCr_{1-x})_2O_3$ corundum-type solid solution single crystal growth, chem. vapour transport 80−93465
$Fe_xCu_{1-x}Rh_2S_4$, mag. tetrahedral intrasublattice interaction, X-ray, magnetisation and Mossbauer expts. 78−52241
FeF_2 antiferromag., anomalous anti-Stokes/Stokes Raman scatt. intensity ratio 80−66177
FeF_2, antiferromag. spin flop boundary 78−84419
FeF_2, antiferromagnet, fourth-order spin Hamiltonian terms for Fe^{2+} 78−10628
FeF_2, interacting phonon-magnon states, theory of Raman scattering and IR obs. 80−71426
FeF_2, mag. sp. ht. near Neel temp. mag. susceptibility meas. 80−60341
FeF_2, magnon-acoustic phonon hybridisation in far IR absorpt. spectra 78−60271
FeF_2, one-magnon Raman scatt., anomalous behaviour of anti-Stokes-Stokes intensity ratio 80−40115
$FeF_2:Co^{2+}$, impurity-induced magnon, influence of localisation 80−11182
FeF_2:Mn, antiferromag., NMR relax., impurity bonding 80−66061
FeF_2:Mn, antiferromag. reson. and local magnon mode, FIR laser study 80−66042
FeF_2:Mn, Heisenberg antiferromagnet, impurity thermodynamics, NMR meas. 79−61098
FeF_2:Mn, Heisenberg antiferromag., impurity banding and mag. reson., theory 80−93181
FeF_2:Mn, Heisenberg model, impurity band resonance at 0K, theory 80−66041
FeF_3, amorphous, characterisation by thermal, mag. and Mossbauer study 79−42782
FeF_3, amorphous, noncryst. magnet with antiferromag. interactions 79−91228
FeF_3, amorphous, struct. and mag. props., computer model 80−96446
FeF_3, canted antiferromag., spin echo spectra of ^{57}Fe and ^{19}F nuclei 80−2662
FeF_3, magnetic susceptibility near Neel point 77−55670
FeF_3, Mossbauer spectrum, effect of mag. hyperfine struct. at low temps. 79−28662
FeF_3, thin film, optical absorpt. meas. 79−15546
FeF_3, weak ferromag., NMR of ^{57}Fe nuclei 79−95676
FeGe, hyperfine interactions of ^{119}Sn atoms, Mossbauer spectra *(Russian)* 80−29665
$FeGe_2$, antiferromag., biquadratic exchange 80−2371
$FeGe_2$, antiferromag., Fermi surface, stress effects, oscillatory magnetostriction and torque meas. 80−103616
$FeGe_2$, antiferromagnet, de Haas-van Alphen effect 79−4505
$FeGe_2$ canted antiferromagnet, mag. susceptibility anisotropy and temp. dependence 80−25112
$FeGe_2$, collinear and canted antiferromag. structures 77−51887
$FeGe_2$, mag. struct., Mossbauer method 78−60268
FeI, magnon energies, phase transitions of eight sublattice model 77−59463
FeI_2, antiferromag. struct., four spin exchange interaction 78−14948
FeI_2, eight sublattices model, antiferromag. reson. uniform modes and metamag. behaviour 77−69498
FeI_2, far IR magnetoabsorption, excitation of two spin deviations 78−80339
FeI_2, hyperfine interaction, ^{57}Fe Mossbauer expts., mag. transition obs. 78−43720
FeI_2, neutron inelastic scatt. from mag. excitations 80−50078
FeI_2, spin waves and two magnon bound states, mag. field IR absorption meas. 80−65840
Fe_xI_y cyclodextrin, quasi-one-dimens. cpd., synthesis, elec. and mag. props. 80−2380
Fe(III) compounds, $A_2FeX_5.H_2O$, (A=alkali ion, X=Cl or Br), antiferromag. props. and struct. 78−31056
$Fe_{1-x}M_xCl_2$, disordered, Mn spin excitations by microwave absorption at high freqs. 80−34759
$(Fe_{1-x}M_x)_2O_3$, yH_2O, M=Cr,Cu,Ni, crystal growth, characterisation by Mossbauer spectroscopy, mag. meas. and electron microscopy *(French)* 80−80655
$FeMO_2S_4$, Mossbauer investigation, Neel point, superparamag. effects 80−97170
$Fe_{1-p}Mg_pCl_2$, magnetic excitations 78−91852
$Fe_xMg_{1-x}Cl_2$, metamagnet, mag. phase diagram by mag. induced light scatt. 80−65883
γ-FeMn, alloys, itinerant antiferromag., spin dynamics, neutron scatt. meas. 77−12105
FeMn hydrated oxides, ferromanganese freshwater nodules, antiferro- to speromag. order 77−70649

antiferromagnetic properties of substances continued
$Fe_{1-x}Mn_x$, elec. resist., anomalies in temp. depend. 79−23942
$(Fe_{1-x}Mn_x)_3Al$, mag. moments determ. from magnetisation and neutron and electron diffr. expts. 79−56520
$Fe_{2.1-x}Mn_xAs$, $0 \leq x \leq 2.1$, mag. phase transitions 78−2679
$Fe_{1-x}Mn_xCl_2$, disordered, Raman scatt. from Fe^{2+} and Neel temp. 80−60579
$Fe_{1-x}Mn_xCl_2$, low-lying electronic excitations in antiferromag. and paramag. phases Raman scatt. study 80−71414
$(Fe_{1-x}Mn_x)_3P$, cryst. struct. and mag. props. 78−19222
$Fe_{2-x}Mn_xP_{1-y}As_y$, mag. props., Mossbauer obs. 77−40156
$(Fe_{1-x}Mn_x)_{75}P_{15}C_{10}$, amorphous, mag. ordering, Mossbauer study 80−39747
$Fe_xMn_{1-x}Pt_3$, ferro-antiferromag. transform. at 4.2K *(Russian)* 78−88117
$(FeMn)_3Si$ alloys, antiferromag. props. rel. to Mn conc. 77−59393
$(Fe_{1-x}Mn_x)_3Si$, sp. ht. at low temps., mag. transitions *(Russian)* 77−32189
Fe_2MnSi, antiferro- and ferromag. props. 77−12104
$Fe_{1-x}Mn_xSn$, spin reorientation, Mossbauer study, 77 to 400K 80−97172
Fe_2MoO_4, electron exchange between $Fe^{2+}-Fe^{3+}$ ions on tetrahedral and octahedral sites, Mossbauer spectra 79−78585
Fe_2MoO_4, magnetic struct. of low and room temp. by neutron diffr. 77−63100
$(Fe_xMo_{1-x})_{75}P_{16}B_6Al_3$, amorphous, effects of Mo on mag. props., Mossbauer meas. 79−73859
$FeMo_2S_4$, cryst. struct., mag. struct. and props., neutron diffr. meas. *(French)* 77−47971
$FeMo_2S_4$, Mossbauer spectra, 79-300K, Neel pt. determ. 78−60360
$FeNb_2O_6$, low temp. Mossbauer exam. 79−28659
$FeNb_2O_6$, magnetisation, 1.4-80K, antiferromag. ordering 78−10666
$Fe_{1/3}NbS_2$, intercalate, metallic cond., Hall effect and mag. props. 77−76789
Fe_xNbSe_2 (2H), mag. susceptibility meas., 1.3-300K 80−39740
Fe_xNbSe_2, transport props. and mag. ordering 80−65527
$Fe(Nb_{1-x}W_x)O_4$, mag. and elec. props. and Mossbauer effect 79−78590
$FeNiBO_4$, mag. and Mossbauer studies 79−65661
$FeNi_2BO_5$, mag. and Mossbauer studies 79−65661
$Fe_{0.5}(Ni_xMn_{1-x})_{0.5}$, antiferromag. ground state, elec. resist., anomalies in temp. depend. 79−23942
$Fe_{65}(Ni_{1-x}Mn_x)_{35}$, magnetic struct. and inhomogeneities by neutron scatt. and Mossbauer effect *(Russian)* 77−63122
$Fe_{0.5}Ni_{0.5}S_2$, hyperfine field at ^{57}Fe, Mossbauer effect *(Japanese)* 77−43916
$Fe_{1-x}O$, low-energy mag. excitation dispersion curves 79−4665
$Fe_{1-x}O$, wustite, phonon and magnon props., inelastic neutron scatt. 78−52236
Fe_2O_3 amorphous film, Mossbauer spectra, mag. props. 80−15851
Fe_2O_3 amorphous RF sputtered thin films, Mossbauer and mag. study 80−34711
α-Fe_2O_3 and α-Fe_2O_3:Mn, linear mag. birefringence near Morin transition 77−52052
α-Fe_2O_3, antiferromag., muon spin rotation meas. 78−48106
α-Fe_2O_3, antiferromag., muon spin rotation *(German)* 80−54877
α-Fe_2O_3, antiferromag., reson. two magnon Raman scatt. obs. 77−63417
α-Fe_2O_3, antiferromag., two magnon reson. Raman scatt. 79−33703
α-Fe_2O_3, antiferromag. reson. in absence of external field, 150 and 320K *(Russian)* 79−4730
α-Fe_2O_3, Bragg diffr. of 14.4 keV reson. γ-quanta in inclined mag. field *(Russian)* 78−2784
α-Fe_2O_3, exchange parameters including temp. effects 79−24153
α-Fe_2O_3 film, prep. by reactive condensation and mag. props. 78−64241
α-Fe_2O_3, H-T phase diagram 79−87258
α-Fe_2O_3, haematite, birefr. under uniaxial stress in mag. field *(Russian)* 78−88285
α-Fe_2O_3, haematite, linear mag. birefr., Morin transition 77−8309
Fe_2O_3, haematite, mag. domain distrib., appl. of mag. Laue neutron diffr. method 78−95455
Fe_2O_3, haematite, mag. field induced phase transition meas. by magneto-optic methods 78−10686
α-Fe_2O_3, haematite, mag. susceptibility meas. near Morin temp. 77−59404
α-Fe_2O_3, haematite, mag. susceptibility, near high temp. mag. phase transition 79−56510
Fe_2O_3, haematite, optical indicatrix deform. and rot. during field induced phase transition 78−68482
Fe_2O_3, haematite, SHG, acoustic detect. of modulated sound wave *(Russian)* 78−43623
Fe_2O_3, haematite, single domain, defect moment origin and props. 79−16438
α-Fe_2O_3, haematite, substituted, Morin transition, neutron diffr. study 80−54897
α-Fe_2O_3, haematite, temp. mag. hysteresis near Morin temp. 79−56566
Fe_2O_3, haematite, weak ferromag., Hall effect mag. field depend. *(Russian)* 77−11937
Fe_2O_3, haematite, X-ray diffr. of high temp. anomalous behaviour of cryst. lattice 77−58991
α-Fe_2O_3, hematite, field-induced domain struct., neutron diffr. meas. *(German)* 77−16101
α-Fe_2O_3, hematite, high temp. anomalous behaviour of cryst. lattice 77−69087
α-Fe_2O_3, hematite, interdomain phase transition 79−65675
α-Fe_2O_3, hematite, Morin transition, Mossbauer mag. diffr. spectra 80−20562
α-Fe_2O_3, hematite, surface magnetism, magneto-optical meas. 77−20831
α-Fe_2O_3, hematite, weakly ferromag. domain struct., X-ray topography obs. 79−28551
Fe_2O_3, hematite, weakly ferromag., transverse galvanomag. parity effects anisotropy *(Russian)* 80−49770
α-Fe_2O_3, magneto-optical meas. of orientation of antiferromag. vector accompanying phase transition *(Russian)* 78−14961
α-Fe_2O_3, magneto-optical refl. spectra by equatorial Kerr effect *(Russian)* 77−32400
α-Fe_2O_3, magnetoelastic coupling in nonlinear acoustic phenomena, exchange interaction effects *(Russian)* 77−90010
α-Fe_2O_3, Morin transition, Mossbauer spectra meas. 78−31071
α-Fe_2O_3, Mossbauer spectra near Neel temp., critical indices, magnetisation *(Russian)* 80−66094
α-Fe_2O_3, muon spin rotation above and below Morin transition 78−43762

antiferromagnetic properties of substances continued
α-Fe_2O_3, muon spin rotation expts. 80−71282
α-Fe_2O_3, muon states, local mag. fields 80−75911
α-Fe_2O_3, μSR meas. 79−56666
Fe_2O_3, natural haematite, weakly ferromag., magnetoresist. *(Russian)* 78−23110
α-Fe_2O_3, neutron Laue diffr. investig. of domain distrib. 77−24712
γ-Fe_2O_3, prep. from thermal decomp. of $[Fe_3(HCOO)_6(OH)_2]HCOO.4H_2O$ and characterisation 78−80741
α-Fe_2O_3, pure and Mn doped, characts. of Morin phase transition, linear mag. birefringence meas. 77−69560
Fe_2O_3, shocked hematite, Mossbauer exam. 78−64304
α-Fe_2O_3:$Al^{3+}(Ga^{3+})(Cr^{3+})(In^{3+})$, substitution effect on Morin transition, neutron diffr. study 80−44827
α-Fe_2O_3:Sn, Mossbauer investig. of mag. hyperfine interactions 77−32306
α-Fe_2O_3:Sn^{4+}, antiferromag. reson. *(Russian)* 80−7175
Fe_2O_3-BaO-B_2O_3, magnetic props. of Fe-rich amorphous oxide *(French)* 80−80511
Fe_2O_3-Bi_2O_3 system, mag. props., hyperfine parameters, Mossbauer spectrum 77−69746
Fe_2O_3-Dy_2O_3-Na_2O-B_2O_3 glass, AC mag. susceptibility, antiferromag. interactions 77−32179
Fe_3O_4, muon states, local mag. fields 80−75911
Fe_3O_4, nuclear gamma reson. investig. of high temp. electronic struct. 77−20751
Fe_3O_6, O_2 annealed, optical absorpt., spin struct., polaronic absorpt., cryst. field transitions 78−68493
Fe_xO, surface magnetism probe by photoelec. currents 77−73214
Fe_zO, non-stoichiometric, mag. struct., neutron diffr. exam. 79−42737
$FeOHSO_4$, mag. structure, modulation of moments, neutron diffr. meas. 77−69499
FeOOH, high-pressure phase, neutron diffraction study 78−52212
ϵ-FeOOH, synthesis, mag. struct. 78−34961
β-FeOOH, ultrafine particles, mag. struct., Mossbauer spectroscopy 78−72372
α-FeOOH ultrafine particle NGR spectra, size distrib. and surface effects 80−11299
α-FeOOH.nH_2O, hydrogoethites, weak ferromag. props. 77−53042
FeP, mag. suscept., resistivity and thermal expansion meas. 78−2661
$Fe_2(PO_4)Cl$, Mossbauer study of mag. ordering and local co-ordination 80−39972
$Fe_2(PO_4)Cl$, temp. depend. of mag. susceptibility 80−70962
$FePS_3$ and $FePSe_3$, mag. props., NMR meas. 79−24223
$Fe(Pd_{1-x}Au_x)_3$, mag. struct. ferro-antiferromagnetism coexistence *(Russian)* 79−82759
$FePt_3$, metamagnetic transitions in external fields 80−60272
$FePt_3$, neutron scattering study of spin waves 78−91856
FeRh, antiferromag., band structure and effect of Fe impurity on mag. props. 77−28377
FeRh, antiferromag., band struc., off-stoichiometry effects 78−10341
$Fe_{48}Rh_{52}$, hyperfine mag. field at ^{57}Fe and ^{119}Sn nuclei, press. depend. *(Russian)* 78−80266
FeS, zinc blende type, mag. struct. *(French)* 78−91846
$Fe_{0.9}S$, ferrimag. transition, mag., thermodynamic props., kinetics 79−47280
$Fe_{0.996}S$, antiferromag., energy dispersion of spin waves, inelastic neutron scatt. meas. 77−69522
Fe_9S_{10}, antiferro- to ferrimag. transition, Mossbauer and mag. exam., diffusion of Fe during transition 79−73716
Fe_9S_{10}, polytypism, Fe diffusion near antiferromag. to ferrimag. transition 80−44830
$FeSO_4$, α- and β-forms, magnetic interactions, neutron inelastic scatt. study 80−107980
β-$FeSO_4$, high-temp. polymorph, stability, mag. struct., mag. props. 77−43815
$Fe_{1+\delta}Sb$, nonstoichiometry influence on mag. props. *(Russian)* 80−65813
$Fe_{1+x}Sb$, Mossbauer meas. of lattice and interstitial Fe atom mag. ordering 79−99807
$Fe_{1+x}Sb$-CoSb solid soln., mag. props., Mossbauer spectra, solubility limits, and lattice consts. *(Russian)* 77−59394
$Fe_{1+x}Sb$-NiSb solid soln., mag. props., Mossbauer spectra, solubility limits, and lattice consts. *(Russian)* 77−59394
$FeSb_xO_{4-y}$, defect struct. and mag. transition, elec. transport and Mossbauer expts. 78−59803
$FeSn_2$, hyperfine mag. fields at ^{57}Fe, ^{119}Sn nuclei, under press. *(Russian)* 78−39486
$FeSnO(OH)_5$, mag. props. and cryst. struct. 78−43574
$FeTe_2$, Mossbauer spectroscopy and nonstoichiometry 78−31125
$FeTe_x$, Mossbauer spectra, 80 to 750K, quadrupole splitting and isomer shift 77−4590
$Fe_{1-x}Te$, fluctuating localised mag. moments, d band motion, Mossbauer study 80−65768
Fe_2TeO_5, mag. struct. 78−27020
Fe_2TeO_6, CC ^{57}Fe Mossbauer spectrum, hyperfine field, Neel temp. 79−56636
$FeTiNdO_5$, isomer shift, hyperfine field and distrib. of Fe^{3+} ions, Mossbauer spectrum 77−69747
$FeTiO_3$, ilmenite, lunar and terrestrial, cell dimensions and antiferromagnetism 77−21764
Fe_2TiO_4, ulvospinel, mag. props. weak ferromag. in 4-200K temp. range 78−56351
$Fe_{3-x}Ti_xO_4$, $0.5\leq x\leq 1$, mag. props. of antiferromag. phase 80−70960
FeU_2S_5, mag. struct., exchange energy, magnetisation and neutron diffr. expts. 78−68170
$FeVO_4$, Neel temp., mag. susceptibility meas. 80−29550
$Fe_xV_{1-x}O_2$, mag. props. and Mossbauer spectra meas., exchange-coupled Fe^{3+} clusters at lower temp. 78−31136
$(Fe_xV_{1-x})V_2S_4$, and $(Fe_xV_{1-x})V_4S_8$, mag. props. 78−27034
$Fe_{1-x}Zn_xF_2$, dil. antiferromag., Raman scatt. expts. 79−78666
$Fe_{1-x}Zn_xF_2$, dil. antiferromag., electronic and mag. props., Raman scatt. and optical absorpt. study 80−108207
$Fe_{1-x}Zn_xF_2$, electronic Raman scatt., mag. anisotropy 80−66184
$Fe_xZn_{1-x}F_2$, Neel point and short range order, dilution effects, mag. birefr. obs. 80−71019
Ga_2O_3-Fe_2O_3 system, anomalous Mossbauer lineshapes, incomplete annealing 77−51998
Gd compounds, NaCl type, exchange striction 78−84409
Gd Ni_2Si_2, mag. props., 4.2-200K 80−84602

antiferromagnetic properties of substances continued
Gd-Y (40 wt.%) alloy, magnetic phase transitions, elastic consts. meas. 78−14957
Gd-Y alloy, anomalous thermal expansion, interferometric meas. 78−52333
Gd-Y alloys, mag. crit. temp. gap 80−60260
$Gd_{54}Ag_{46}$, amorphous, susceptibility and magnetisatiom, 6-300K *(French)* 77−36060
$GdAlO_3$, ^{155}Gd excited states, determ. of nuclear parameters using Mossbauer effect 79−28646
$GdAlO_3$, bicrit. and tetracrit. behaviour, susceptibility obs. 77−47992
$GdAlO_3$, canted antiferromagnetic, Mossbauer meas. 80−97171
$GdAlO_3$, crossover effects near spin-flop multicritical point 78−68245
$GdAlO_3$, magnetoelec. susceptibility, mag. struct., mag. phase diagram and crit. coeffs. 77−66303
$GdAlO_3$, magnetoelectric susceptibility, crit. behaviour 78−10743
$GdAlO_3$, spin-flop bicritical line obs. 77−66306
$GdAlO_3$:La, antiferromag., random-field crit. and multicritical behaviour 80−65939
$GdAlO_3$:La, random antiferromagnets, crit. and multicritical props. 80−60332
GdAs(Sb)(Bi), antiferomag., EPR meas., Neel temp. determ. 77−32242
GdAuSn, mag. props. 77−85439
GdB_4 *(French)* 77−20566
GdB_6 single crystals, mag. behaviour and structure change at low temp. 80−71018
GdC_2, mag. susceptibility, temp. depend. 79−87239
$GdCl_3$, interaction parameters, high freq. meas. of adiabatic differential susceptibility 78−68211
$GdCo_2Si_2$, mag. props. 80−107988
$GdCrO_3$, EPR linewidth, Neel point to 700K 80−39849
$GdCrO_3$, Faraday rot. and linear birefr. meas., 0.8 to 2 μm 77−77180
GdCuGe, $Gd_6Cu_8Ge_8$ and $GdCu_2Ge_2$, magnetic props. 77−32180
$GdCu_2Si_2$/Mo, point contact spectroscopy of magnons 79−38312
GdCuSn, mag. props. 77−85439
$GdCu_{1-x}Zn_x$, mag. struct. determ. 79−87238
$Gd_xDy_{1-x}C_2$, solid soln., mag. susceptibility, temp. depend. 79−87239
$GdFe_2Ge_2$, magnetisation, 4.2-273K, and Neel temp. 77−8310
$Gd_3Ga_5O_{12}$, mag. phase diagram, AC susceptibility meas. 80−60265
$Gd_3Ga_5O_{12}$, magnetic interactions and short range order 79−78401
GdH_3, magnetisation and mag. suscept. 77−43821
$GdIn_3$, magnetisation 80−25106
Gd_2In, mag. props., 4.2 to 270K 79−56512
$Gd_{1-x}M_x$, M=Co, Ni, Fe, temp. depend. of magnetisation 77−77043
GdM_2Ge_2, M=Mn, Fe, Co, Ni, Cu, magnetism and hyperfine interactions 78−76228
$GdMg_3$, mag. props., Mg conc. depend. 78−84392
β-$Gd_2(MoO_4)_3$, antiferromag., polarised ferroelec., ferroelastic, magnetothermodynamics 79−7996
$GdMo_6S_8$, coexistence of antiferromagnetism and superconductivity, neutron diffraction study 79−99685
$GdMo_6S_8$, long range mag. order in supercond. state 79−65653
$Gd_{1.2}Mo_6S_8$, low temp. heat capacity anomaly rel. to antiferromag. transition in supercond. state 80−25044
$Gd_{1.2}Mo_6Se_8$, coexistence of supercond. and long range antiferromag. order 80−84534
GdN, and $GdN_{1-x}O_x$, mag. interactions 80−60218
$GdN_{1-x}O_x$, magnetic interaction and carrier conc. 80−71005
$Gd(Ni,Cu)_2$, spin disorder resist. evaluation, influence of antiferromagnetic order 77−73035
Gd_2O_3, C-phase, specific heat, 1.4 to 18K, antiferromag. ordering 79−38351
$Gd_2O_2SO_4$, antiferromag., specific heat, 0.6 to 30K 79−33487
$Gd_2O_2SO_4$, antiferromag., mag. props. 1.6 to 40K 79−33464
GdP, electronic struct., mag. exchange and elec. transport props. 78−87974
GdP-GdS systems, mag. exchange interactions, free carrier conc. 78−60278
GdS, electronic struct., mag. exchange and elec. transport props. 78−87974
GdS, low temp. phase transitions, mag. moment orientation, spin flip 79−99700
GdS, meas. of opto-magnetic interactions at low mag. fields 80−2735
GdS, metallic FCC antiferromag., phonon Raman scatt. 78−60458
Gd_2S_3, antiferromag. to ferromag. and semiconductor to metal transitions *(Russian)* 79−33485
Gd_xS_y, nonuniform ferro-antiferromag. ordering, 1.6 to 300K range obs. *(Russian)* 77−69504
GdS(Se), antiferromag., EPR meas., Neel temp. determ. 77−32242
GdSe, low temp. phase transitions, mag. moment orientation, spin flip 79−99700
$GdSn_3$, Neel temp., hydrostatic press. depend. 80−29549
GdTe, low temp. phase transitions, mag. moment orientation, spin flip 79−99700
$GdVO_4$, ^{155}Gd excited states, determ. of nuclear parameters using Mossbauer effect 79−28646
$GdVO_4$, antiferromag., US attenuation at 9 GHz 77−24728
$GdVO_4$, hyperfine field and exchange interactions, Mossbauer meas. 79−47370
$GdVO_4$:Ho^{3+}, optically excited doublet splitting in magnetically ordered state 78−19238
Gd_2ZrS_5, mag. and sp. ht. meas. on polycrystalline samples 78−23253
$GeFeO_3$, field induced spin reorientation temp. depend. 77−63200
$GeFe_2O_4$, single crysts., elec. and mag. props, optical absorpt. spectra 80−54719
GeSe, antiferromagnetic behaviour, res. to negative magnetoresistance effect 79−73719
H, atomic crystalline phase, ground state energy calc. *(Russian)* 79−19426
^{3}He adsorbed layers, antiferromag. indirect exchange 79−99389
^{3}He, BCC, first-neighbour mag. interaction sign 78−14538
^{3}He, BCC, four-spin interaction effects on ordering processes 77−39721
^{3}He, BCC lattice, quadruple exchange in Heisenberg antiferromagnet 77−89616
^{3}He, BCC solid, nucl. mag. order and paramag. susceptibility 80−59757
^{3}He, FCC, vacancy induced spin polarons 80−59756
^{3}He, liq., exchange model 80−88387
^{3}He liquid, exchange model, antiferromagnetic exchange field, susceptibility-specific heat ratio *(French)* 80−80019
^{3}He, solid, antiferromag. spin Hamiltonian with four spin interactions for BCC, lattice, mean field theory 79−1652

antiferromagnetic properties of substances continued
^{3}He, solid, deform.-assisted pairing, magnetic transition interpreted 78—2334
^{3}He, solid, mag. ordering, NMR study 80—54470
^{3}He, solid, mag. susceptibility near ordering temp., pulsed NMR meas. 78—18869
^{3}He, submonolayer on Grafoil, vacancy induced ferromag. 78—14536
^{3}He with C particles, pulsed NMR, mag. susceptibility surface induced ferromagnetism, antiferromagnetic exchange interaction 78—79844
$Hg_{1-x}Fe_xTe$ mixed crystals, zero gap, magneto-optical evidence of exchange interactions 80—45045
$Hg_{1-x}Mn_xTe$, antiferromag. exchange interaction and mag. susceptibility meas. 77—4508
$Hg_{1-x}Mn_xTe$, indirect exchange interaction 79—61094
$Hg_{1-x}Mn_xTe$, mag. props., self-consistent two spin cluster model 80—54874
$Hg_{1-x}Mn_xTe$, non-parabolic zero-gap semicond., indirect exchange interaction 80—80498
$Hg_{1-x}Mn_xTe$, semimagnetic, exchange interactions between localised and delocalised electrons 80—97245
$Hg_xZn_{1-x}Cr_2Se_4$, absorption spectra near the absorption edge 78—80340
Ho, magnetoelastic interactions 78—64252
Ho, phase transition along mag. field, X-ray obs., 77-292K *(Russian)* 77—4504
Ho, sp. ht., using lattice dynamical model for HCP metals 79—51273
Ho-Ag, crystal field parameters from neutron spectra, rel. to mag. props. in ordered state 77—43546
Ho-Cu, crystal field parameters from neutron spectra, rel. to mag. props. in ordered state 77—43546
Ho-Pr(Nd) alloys, mag. struct. and ordered moments, neutron diffr. data 77—66252
Ho-Sn, dil. alloy, hyperfine interaction of ^{119}Sn, Mossbauer meas. 78—91998
HoAlGa, mag. props. and struct. 78—39302
$HoAl_xGa_{2-x}$, mag. props. and phase transitions 80—25133
$HoAlO_3$, electronic and nucl. mag. ordering, mol. field approx. 80—60157
$HoAlO_3$, neutron diffr. at 0.04K, mag. ordering *(French)* 78—10653
$HoAu_3$, mag. phase diagram 80—75761
HoB_4 *(French)* 77—20566
HoB_4, antiferromag. props. *(French)* 77—20566
$HoCo_2Ge_2$, crystal and magnetic structure obs. 80—64976
$HoCo_{5-x}Ni_x(Cu_x)$, lattice parameters and mag. props. 79—82817
$HoCrO_3$, cryst. field levels and mag. interactions, inelastic neutron scatt. study 77—69277
$HoCrO_3$, mag. form factor of Ho^{3+}, inelastic neutron scatt. meas. 77—16050
$HoCrO_3$, magneto-optical investig. of Ho-Cr and Ho-Ho interactions 77—52055
HoCu, resist. and magnetoresist., mag. ordering obs. 80—70677
$HoCu_2$, mag. struct. and elec. resist., neutron diffr. obs. 80—60206
$HoCu_2$, resist. and magnetoresist., mag. ordering obs. 80—70677
$Ho_{0.5}Dy_{0.5}FeO_3$ orthoferrite, domain wall struct., stability conditions, Morin transition, anisotropy const. 80—34684
$HoFeO_3$, field induced spin reorientation, Mossbauer spectroscopy 80—65878
$HoFe_2O_4$, magnetic props., 77-300K 80—11225
$Ho_3Ga_5O_{12}$, hyperfine interac. induced antiferromag. order *(French)* 77—59392
Ho_5Ge_4, mag. struct., neutron diffr. study 80—25093
$HoH_2(D_2)$, mag. props., 1.5 to 10K, Mossbauer meas. 79—78578
$Ho(Ir_xRh_{1-x})_4B_4$ pseudoternary system, supercond. and mag. ordering 80—70876
$Ho_{1.15}Lu_{0.05}Mo_6S_8$, long range mag. order in supercond. state 79—65653
$HoMo_6S_8$, long range mag. order in supercond. state 79—65653
$HoNi_{0.7}Cu_{0.3}$, mag. behaviour 79—99688
$Ho_2O_2SO_4$, antiferromag., mag. props. and Zeeman effect meas. 79—33464
$Ho_2O_2SO_4$, antiferromag., specific heat, 0.6 to 30K 79—33487
$Ho_2O_2SO_4$, mag. ordering, magnetisation, AC susceptibility and Zeeman effect meas. 80—60205
$Ho_2O_2SO_4$, magnetic phase diagram, magnetisation and mag. susceptibility meas. 80—15720
$Ho_2O_2SO_4$, magnetic struct. in antiferromag. and ferrimag. states 80—15695
$HoPO_4$, metamagnet, mag. phase transitions, elastic neutron scatt. study 79—78371
HoSb, mag. phase diagram, quadrupolar interactions 80—65820
HoSm elec. props. in temp. range near zero to 150K *(Russian)* 79—11098
Ho_xTe, mag. ordering, neutron diffr. meas. 78—2649
$HoTiO_3$, magnetic structure determination, neutron scatt. study 80—65809
$HoVO_3$, at. and mag. struct., neutron diffr. meas. 79—24142
$HoVO_4$, enhanced nuclear cooling and antiferromagnetism 79—61070
$HoVO_4$, NMR predictions of properties, dipolar interactions and antiferromagnetic exchange 80—50203
$Ho_cY_{1-c}Sb$ system, magnetisation, elec. resist., and sp. ht. meas. 80—60213
$Ho_xY_{1-x}Sb$, mag. props. 80—34634
p-InSb, negative piezomagnetoresist. and Hall effect meas., antiferromag. order form. 78—19061
p-InSb, uniaxially deformed, mag. field induced semicond.-metal transition 79—95457
$KCoF_3$, antiferromag., obs. of domains by X-ray topography 78—14981
$KCoF_3$, antiferromag., ^{59}Co NMR exam. 78—76332
$KCoF_3$, antiferromag. domains obs. by cryogenic X-ray topography 77—39507
$KCoF_3$, antiferromag. domain wall motion under external stress 80—80583
$KCoF_3$, $KFeF_3$ and $KNiF_3$, crystal growth from flux, degree of perfection and dislocation density 77—77359
$KCoF_3$, mag. form factor calc. for Co^{2+} 77—20555
$KCoF_3$, mag. suscept. and Neel temp. determ. 77—77044
$KCoF_3$, magnon-phonon interaction mechanism 77—20019
$KCoF_3$, NMR, magnon-phonon interaction contribution to nuclear spin-lattice relax. 78—88207
$KCoF_3$, single crystal, mag. susceptibility, ^{19}F NMR and static measurements 79—11301
$KCoF_3$, strain sensitive props., Mossbauer spectra obs. 77—20765
$KCoF_3$, with residual orbital moment, nucl. mag. relax. 80—71215

antiferromagnetic properties of substances continued
K_2CoF_4, 2-dimens. Ising antiferromag., mag. excitons, Raman scatt. obs. 80—66181
K_2CoF_4, neutron scatt. obs. of mag. behaviour 77—66254
K_2CoF_4, pseudo Ising antiferromag., inelastic light scatt. by mag. excitons 80—11377
K_2CoF_4, specific heat capacity, critical amplitude, cross-over from 2-D Ising to Heisenberg behaviour 80—39791
K_2CoF_4, two-dimens. Ising antiferromag., nearest neighbour correl. function, birefr. expts. 80—71386
K_2CoF_4, two-dimensional Ising-like antiferromag. birefringence, short-range order effect 77—81081
K_2CoF_4, two-dimensional antiferromag., one- and two-magnon Raman scatt. 79—51945
$K_2CoF_4:Mn^{2+}$, impurity induced mag. excitations, magnon gap mode, far IR spectra obs. 80—44821
$K_2Co_2(SO_4)_3$, cubic langbeinite struct., low temp. mag. susceptibility 78—56299
$KCrO_2$, two-dimens. mag. order, neutron powder diffr. obs. 80—44805
$KCrO_2$, two-dimensional antiferromag., mag. props. *(French)* 78—23251
$KCuF_2$, linear chain Heisenberg antiferromag., nearest neighbour correl. function, birefr. expts. 80—71386
$KCuF_3$, antiferromag., low-dimensional susceptibility 79—28513
$KCuF_3$, chain-like antiferromag., sublattice magnetisation temp. depend. 77—51892
$KCuF_3$, chain-like antiferromag., parallel susceptibility 78—80137
$KCuF_3$, nearly 1-D spin-$^1/_2$ antiferromagnet, spin wave energy dispersion 80—2551
$KCuF_3$, one-dimens. antiferromag., spin waves, neutron scatt. study 80—65848
$KCuF_3$, one-dimensional $S=1/2$ Heisenberg antiferromag., mag. energy, optical birefringence meas. 78—52467
$(KF)_n$-FeF_3, dimensionality and spin reduction effects, Mossbauer study 80—39947
$K_3Fe(CN)_6$, electronic struct., electron density, elec. field gradient, mag. susceptibility and g-tensor 79—91006
$K_3Fe(CN)_6$, mag. ordering and spin struct., Mossbauer obs. 77—40038
$K_2FeCl_5(H_2O)$, antiferromag., press. depend. on spin-flop transition 80—80505
$K_2FeCl_5(H_2O)$, phase diagram, antiferromag., paramag. and spin flop phases 80—44831
$K_3Fe(Cn)_6$, mag. and thermodynamic props. below 0.4K in mag. fields 79—56542
$KFeF_3$, magnetisation density of Fe^{2+} 79—78313
$KFeF_3$, strain sensitive props., Mossbauer spectra obs. 77—20765
K_2FeF_4, antiferromagnet, two-dimensional, mag. excitations 80—80492
K_2FeF_4, Mossbauer study of mag. ordering 79—28655
K_2FeF_4, Raman scatt. in two dimens. antiferromagnet 78—19488
K_2FeF_4, two dimensional planar antiferromag., mag. excitations, Raman and far IR spectra obs. 78—72343
K_2FeF_4, two dimensional easy plane antiferromag., neutron scatt. expts. 80—65838
K_2FeF_4, two-dimensional antiferromag., with easy-plane anisotropy, mag. excitations and two-magnon Raman scatt. 80—65839
K_2FeF_4, two-dimensional antiferromag., cryst. field effects, Mossbauer spectroscopy 80—71254
K_2FeF_5, mag. struct. and one-dimens. antiferromagnetism 80—60209
K_2FeF_5, Mossbauer spectra, 1D antiferromag. 80—15886
K_2FeF_5, one dimens. antiferromag., zero point spin reduction 77—85456
K_2FeF_5, one dimensional antiferromagnet, Mossbauer effect, mag. and electric field gradient axes 79—78587
K_2FeF_5, one-dimens. antiferromag., single cryst. Mossbauer spectra 78—23376
K_2FeF_5, one-dimensional antiferromag., neutron diffr. and mag. meas. *(French)* 79—47241
K_2FeF_5, one-dimensional antiferromag. systems, Mossbauer studies 80—71266
$K_3Fe_2F_7$, two-dimensional antiferromag., cryst. field effects, Mossbauer spectroscopy 80—71254
$KFeO_2$, cryst. and mag. struct., neutron and X-ray powder diffr., and Mossbauer effect meas. 77—84722
KFe_2O_3, β'' phase, mag. props., hyperfine interactions, Mossbauer study 80—20524
K_2FeO_4, antiferromag., critical fluctuations obs. using Mossbauer spectroscopy 80—39955
K_2FeO_4, crit. slowing down of spin fluctuations, Mossbauer spectra and relax. theory 80—65882
$KFeS_2$, cryst. struct. and mag. ordering, neutron diffr. and mag. susceptibility meas. 80—54867
$KFeS_2$, spin analogue of active sites of ferrodoxins, mag. struct., neutron diffr. exam. 79—73688
K_2IrCl_6, mag. susceptibility in ordered and paramag. phases 79—73759
K_2IrCl_6, sp. ht. meas. at low temp. 80—7119
K_2IrCl_6, thermal expansion meas. near antiferromag. transition 77—20610
$KMgF_3$:Ni, Co, emission from Ni-Ni and Ni-Co pairs, exchange coupling const. 79—33788
$KMnCl_3$, rare earth doped, energy transfer, emission spectra obs. 80—20684
$KMn_{1-x}Co_xF_3$, Raman scatt. by mag. excitations 77—55775
$K_2Mn_{1-x}CoF_4$, mag. and neutron scatt. exam. 79—33466
$KMnF_3$, acoustic nucl. spin echo *(Russian)* 77—48088
$KMnF_3$, antiferromag., multi-magnon luminesc. sidebands 78—76525
$KMnF_3$, antiferromag. cryst., luminesc. enhancement in mag. field, exciton model *(Russian)* 77—48214
$KMnF_3$, antiferromagnetic resonance in strong mag. field *(Russian)* 79—8054
$KMnF_3$, EPR antiferromag. reson. linewidths near Neel point, exchange interactions *(Russian)* 77—8386
$KMnF_3$, exchange interaction of excited $Mn^{2+}(^4A_1)$ ions, Anderson model 80—25124
$KMnF_3$, exciton line and magnon satellite in UV spectrum at high press. *(Russian)* 79—4517
$KMnF_3$, mag. props. and struct. transitions, antiferromag. reson. meas. 79—8052
$KMnF_3$, Mossbauer effect in ^{57}Fe, struct. and mag. transition investig. 77—20779
$KMnF_3$, optically detected antiferromag. reson. 78—15029
$KMnF_3$, specific heat near Neel temp. *(Russian)* 80—100340
$KMnF_3$, spin density parameters at ^{19}F nuclei 78—68001
$KMnF_3$, stress-induced phase transition, optical props. meas. 77—20067

antiferromagnetic properties of substances continued
$KMnF_3$, width of central peak in crit. scatt. of γ-rays 77−1623
K_2MnF_4, 2-dimens. antiferromagnet, with dipolar broadening, spin diffusion, EPR obs. 79−38371
K_2MnF_4 and K_2NiF_4, two-dimens. antiferromag., two-magnon Raman scatt. linewidth, finite temp. 77−66508
K_2MnF_4, EPR g-shift and anisotropic mag. susceptibility 77−85546
K_2MnF_4, Heisenberg antiferromag., magnon renormalisation 78−23259
K_2MnF_4, nucl. spin-magnon relax. time, temp. depend., NMR study 80−25117
K_2MnF_4, ordered quadratic-layer Heisenberg antiferromag., nucl. spin-magnon relax. 80−71217
K_2MnF_4, quadratic layer antiferromag., intrinsic emission obs. 77−20906
K_2MnF_4, quadratic layer antiferromag., field induced two magnon nuclear spin-lattice relax. 79−61258
K_2MnF_4, specific heat capacity, critical amplitude, cross-over from 2-D Ising to Heisenberg behaviour 80−39791
K_2MnF_4, two dimens. Heisenberg system, shift of half-field EPR line 78−23325
K_2MnF_4, two-dimens. antiferromag., diffusion-controlled mode coupling, EPR linewidth 79−51844
K_2MnF_4, two-dimens. Heisenberg antiferromag., field and temp. depend. of magnetic 77−66272
K_2MnF_4, two-dimensional antiferromag., NMR, magnetisation field-depend., spin-wave theory 77−63294
K_2MnF_4, two-dimensional antiferromag., crit. behaviour, quasielastic neutron scatt. 77−85468
K_2MnF_4:Co^{2+}, Raman spectra meas. 77−12389
K_2MnF_4:Ni^{2+}, and undoped, magnon spectra, Raman and far IR spectra meas. 77−20573
K_2MnF_4:Zn(Mg)(Ni), mag. effects of impurities 80−65869
K_2MnF_4:Zn(Mg)(Ni), local magnetisation, NMR and Green's function study 80−65870
$K_3Mn_2F_7$, antiferromagnet, two magnon Raman scatt. 78−15164
$K_3Mn_2F_7$, crit. EPR line broadening near Neel temp. 80−71165
$K_3Mn_2F_7$, double layer antiferromagnet, susceptibility 77−16061
$K_3Mn_2F_7$, double-layer antiferromag., mag. prop. meas. and calc. 77−55666
$K_3Mn_2F_7$, double-layer antiferromag., mag. ordering, neutron scatt. meas. 79−61062
$K_3Mn_2F_7$, quadratic double-layer antiferromag., NMR, spin-wave anal. of sublattice magnetisation 77−63293
$K_3Mn_2F_7$, quadratic double-layer Heisenberg antiferromagnet, sublattice magnetis., NMR obs. 77−66270
$K_3Mn_2F_7$, quadratic double layer antiferromag., two-magnon Raman scatt. 80−66183
$K_3Mn_2F_7$, two magnon Raman scatt., magnon dispersion, susceptibility, Green's function methods 80−50340
$K_3Mn_3F_7$, Heisenberg double-layer antiferromag., neutron scatt. 79−61065
$K_2Mn_{0.987}Fe_{0.022}F_4$, antiferromag., mag. field induced transitions, neutron scatt. meas. 79−82782
$K_2Mn_{1-x}Fe_xF_4$, anisotropy on two and three dimens. mag. order 77−66259
$K_2Mn_{1-x}Fe_xF_4$, layered antiferromag., anisotropy effects on mag. ordering, neutron diffr. study 79−47254
$K_2Mn_{1-x}Fe_xF_4$, mag. and neutron scatt. exam. 79−33466
$K_2Mn_{1-x}Fe_xF_4$, mag. ordering, neutron scatt. expt. 79−42789
$K_2Mn_{1-x}Fe_xF_4$, tetracrit. line in x-H-T phase diagram, neutron scatt. exam. 78−47977
$K_2Mn_{1-x}Fe_xF_4$, vs. transition temperature, phase diagram, critical lines crossing tetracritical point, discussion 78−39326
$K_2Mn_xM_{1-x}F_4$, (M=Mg,Zn,Cd), 2-dimens. antiferromag., sidebands on EPR lines 78−56370
$K_2Mn_cMg_{1-c}F_4$, EPR spectra 78−76298
$K_2Mn_cMg_{1-c}F_4$, impurities effect on EPR spectra 79−91283
$K_2Mn_xMg_{1-x}F_4$, two-dimensional antiferromag., ESR meas. 77−36121
$KMn_{1-x}Ni_xF_3$, antiferromag. crit. props., neutron scatt. obs. 80−88749
$K_2Mn_{1-x}Ni_xF_4$, antiferromagnets, impurity associated and host magnetizations, NMR exam. 78−10800
$K_2Mn_2(SO_4)_3$, cubic langbeinite struct., low temp. mag. susceptibility 78−56299
$KMn_{0.18}Zn_{0.82}F_3$, excitation of Mn^+ clusters, neutron scatt. 78−68200
$KMn_xZn_{1-x}F_4$, three dimens. Heisenberg antiferromag., fluctuations near percolation threshold 79−78390
$KNiF_3$, ^{19}F spin-lattice relaxation 80−93211
$KNiF_3$ and K_2NiF_4, MCD and stress linear dichroism on double excitonic transitions 77−52051
$KNiF_3$, and K_2NiF_4, double-excitonic optical transition intensity, exchange and dimensionality effects 77−69591
$KNiF_3$, antiferromag., obs. of domains by X-ray topography 78−14981
$KNiF_3$, antiferromag. domains obs. by cryogenic X-ray topography 77−39507
$KNiF_3$, antiferromag. domain behaviour 77−69607
$KNiF_3$, antiferromag. domain wall motion obs. by X-ray synchrotron topography 78−88139
$KNiF_3$, electronic UV laser excited Raman, scatt. by mag. excitons 78−68492
$KNiF_3$, field-induced domain reorientation, NMR obs. 79−82816
$KNiF_3$, isotropic antiferromag., phase diagrams, US meas. 78−68350
$KNiF_3$, isotropic antiferromag., crossover behaviour of mag. phase boundaries 79−78370
$KNiF_3$, K_2NiF_4, two-exciton transition 77−32398
$KNiF_3$, low anisotropy antiferromag., phase boundary crossover behaviour 79−38324
$KNiF_3$, mag. form factor calc. for Ni^{2+} 77−20555
$KNiF_3$, magnetostriction, X-ray diffractometry and strain gauge meas. 80−65997
$KNiF_3$, nonlinear optical effects, spin wave contrib. 77−10987
$KNiF_3$, refr. index, isotropic exchange contrib. 77−69808
$KNiF_3$, spin density parameters at ^{19}F nuclei 78−68001
$KNiF_3$, spin-lattice relax. exam. 79−73838
K_2NiF_4, 2D antiferromag., volume depend. of superexchange, US velocity meas. of T_N 78−19237
K_2NiF_4, antiferromag., one-magnon light scatt., effect of anisotropy 79−33676
K_2NiF_4, antiferromag., one-magnon light scatt. from spin-flop and paramag. regions, effect of anisotropy 79−33677
K_2NiF_4, electronic UV laser excited Raman, scatt. by mag. excitons 78−68492
K_2NiF_4, neutron scatt. obs. of mag. behaviour 77−66254

antiferromagnetic properties of substances continued
K_2NiF_4, nucl. spin-magnon relax. time, temp. depend., NMR study 80−25117
K_2NiF_4, ordered quadratic-layer Heisenberg antiferromag., nucl. spin-magnon relax. 80−71217
K_2NiF_4, quadratic layer antiferromag., optical spectra obs. 77−16326
K_2NiF_4, quadratic layer antiferromag., field induced two magnon nuclear spin-lattice relax. 79−61258
K_2NiF_4, specific heat capacity, critical amplitude, cross-over from 2-D Ising to Heisenberg behaviour 80−39791
K_2NiF_4, two-dimensional antiferromagnet, fine struct. obs., 4.2K *(Russian)* 77−59587
K_2NiF_4, two-dimensional antiferromag., crit. behaviour, quasielastic neutron scatt. 77−85468
$K_3Ni_2F_7$, quadratic double layer antiferromag., two-magnon Raman scatt. 80−66183
$KNi_xMn_{1-x}F_3$, mixed antiferromagnet, light scatt. meas. 80−16025
$KNi_xMn_{1-x}F_3$, two-magnon Raman scatt. 77−66509
$K_2Ni_2(SO_4)_3$, cubic langbeinite struct., low temp. mag. susceptibility 78−56299
KO_2, low temp. phases, mag. order, EPR and antiferromag. reson. 79−95630
$K_2PbCu(NO_2)_6$, antiferromagnetic Heisenberg linear spin 1/2 chain, mag. and caloric meas. 79−78397
K_2ReCl_6, sp. ht. meas. at low temp. 80−7119
K_2ReCl_6, thermal expansion meas. near antiferromag. transition 77−20610
KVF_3, antiferromag. ordering points, thermal anal. and X-ray diffr. meas. *(French)* 78−84421
α-K_xVF_3, mag. props. *(French)* 77−80933
(La,Ce)Al_2, conf. Kondo system, sp. ht. meas. 78−52210
$(La_{1-x}Ce_x)Al_2$, Kondo system, antiferromag., specific heat 79−24179
La_2CoO_4, mag. behaviour obs. 80−70971
$LaFe_{1-x}D_xO_3$:Sn, D=Al, Ga or Sc, Mossbauer effect, hyperfine mag. fields at Sn 77−24772
$La_{1-x}Gd_xAg$, spin echo NMR anal. 80−15821
La_2MnFeS_5, antiferromag., mag. props. and mag. struct., neutron diffr. and magnetisation meas. 80−65801
$LaMnO_3$, monoclinic and cubic perovskite struct., mag. props., neutron diffr. meas. 78−27022
$LaMnO_3$, orthorhombic lattice distortions, mag. props. rel. to prep. conditions 77−20592
$La_2(MnO_3)_3$, hydrostatic press. effect on mag. struct., neutron diffr. 77−51886
La_2MnZnS_5, antiferromag., neutron diffr. study 80−25099
$La_{1-x}Na_xFeO_{3-x}$, defect perovskite system, Mossbauer effect 77−36159
La_2NiO_4, La_2CuO_4, magnetic properties obs. 80−70937
$LaRu_xFe_{1-x}O_3$ perovskites, cryst. struct., elec., mag. and Mossbauer behaviour 77−55274
$La_{2-x}Sr_xCoO_4$, mag. behaviour obs. 80−70971
$LaV_{1-x}M_xO_3$ (where M=Cr or Fe), solid solns., elec. and mag. props 79−23967
$LiCrO_2$, EPR of Cr^{3+} ion, g-factor and effective mag. moment 77−73073
$LiCrO_2$, two-dimens. mag. order, neutron powder diffr. obs. 80−44805
$LiCrO_2$, two-dimensional antiferromag., mag. props. *(French)* 78−23251
$LiCuCl_3.2H_2O$, antiferromagnetic relax., autocorrel. function time evolution 77−59464
$LiCuCl_3.2H_2O$, EPR linewidth and relax., effect of antisymmetric exchange 77−59448
$LiErF_4$, EPR studies, lowest levels of rare-earth ions, submillimetre freq. 80−39865
$LiErF_4$, low-temp. mag. susceptibility, evidence of antiferromag. ordering 78−23249
$LiFeS_2$, magnetic hyperfine interactions, Mossbauer spectra and mag. susceptibility meas. 80−29658
LiH, antiferromagnetism, neutron diffraction study, appl. to polarised targets 79−68065
LiH, mag. domains and nucl. mag. ordered phases, antiferromag. and ferromag. neutron diffr. obs. 80−50051
LiH, mag. ordering in nucl. antiferromag. state, neutron diffr. obs. 79−65654
LiH, neutron diffr. evidence of nuclear antiferromagnetism 79−61066
LiH, nucl. antiferromag. struct., neutron diffr. and dynamic polarisation *(French)* 78−88226
LiH, nuclear antiferromagnetism, dynamic nuclear polaris., NMR 79−1724
LiH, nuclear antiferromagnetism studied by neutron diffr. 79−11358
LiH, nuclear ordered ferromag. and antiferromag. phases, neutron diffr. study 80−50052
$Li_2Mn_xTi_{1-x}O_3$, EPR exam. of antiferromag. props. 78−15015
Li_xNiPs_3, mag. props. and ionic mobility, NMR mag. 79−24223
$LiRF_4$, R=rare earth, low-temp. magnetically ordered states 77−63098
$Ls_6Fe_4S_{14}$, antiferromag., neutron diffr. study 80−70954
$LuCrO_3$:Er^{3+}, doping effect on ^{53}Cr NMR in domain walls 80−71219
Ma-Cu (10 at.%), antiferromag. defect scatt., neutron polarisation anal. 78−2652
$Mg_{1-x}Mn_xTe_2$, random dil. antiferromagnet, mag. props. 80−54870
MgU_8X_{17}, (χ=S or Se), mag. susceptibilities 79−61073
β-Mn alloys, weakly antiferromag., hyperfine fields, NMR meas. 78−39441
Mn, antiferromag., spin wave mode, wave function calcs. 80−20098
Mn, antiferromagnetic, NMR exam. 77−16193
γ-Mn, antiferromagnetic, self-consistent bandstructure calcs. 80−88475
γ-Mn, collinear spin structure stability 80−107984
Mn complex, manganese (II)(1,2,4-triazole)$_2$(NCS)$_2$, 2-dimens. Heisenberg antiferromag., mag. props. 78−72336
Mn compound crysts. with spin-forbidden transitions, two-photon light absorption *(Russian)* 77−48185
α-Mn, electronic structure model, Invar effect, antiferromagnetic-non mag. transitions 80−20370
Mn, FCC, itinerant antiferromag., spin susceptibilities and collective excitations, many band effects 77−63140
α-Mn film, low temp. resist., rel. to deposition conditions 79−78223
Mn, giant internal mag. press. and compressibility anomalies, itinerant model 77−16034
Mn hyperfine particles, surface magnetisation, explanation of expt. work 78−23303
α-Mn, magnetoresist., temp. and field depend. 78−2464
δ-Mn, paramag., antiferromag. and ferromag., magnetic moment calcs. 80−60223

antiferromagnetic properties of substances continued

- α-Mn, spin fluctuations, temp. depend. of elec. resist. 77−62913
- β-Mn, spin fluctuations effect on sp. ht. 79−82788
- Mn ternary nitrides, Mn_3MN, M=metal, mag. props. 77−63116
- γ-Mn-Au(Pd), magnetic struct. for compositions near onset of antiferromag. ordering 77−63111
- γ-Mn-Cu, antiferromag. defect neutron scatt. study 79−47252
- Mn-Cu, mag. and cryst. struct., neutron and X-ray diffr. meas. *(Russian)* 78−22694
- Mn-Cu, shape-memory effect at martensitic transform., cryst. and mag. struct. 77−36610
- γ-Mn-Cu (10 at.%), spin wave studies using neutron diffraction 80−70991
- Mn-Cu (9.3 wt.%), cryst. struct. at FCC to FCT transform. *(Russian)* 80−11643
- Mn-Cu alloy, plastic deform. mechanism and shape-memory effect, mag. struct. obs. *(Russian)* 78−60705
- Mn-Cu alloy, volume effect, paramagnetic-antiferromagnetic and structural transition, lattice consts. 80−39007
- Mn-Cu alloys, stressed, diffuse neutron scatt. exam. 78−47950
- γ-Mn-Fe, FCC→FCT transform. temp. and Neel temp., X-ray and neutron diffr. expts. *(Russian)* 78−84797
- β-Mn-Fe-Sn alloys, weak itinerant electron antiferromagnetism, Mossbauer spectra meas. 77−36158
- α-Mn-Fe(Cr), influence of Fe and CR on Neel point *(Russian)* 77−1554
- Mn-Ga, Elinvar charact. *(Japanese)* 79−61638
- Mn-Ga, mag. and cryst. struct. in conc. region of gamma phase, temp. depend. *(Russian)* 79−65649
- Mn-Ge, antiferromagnetic, NMR exam. 77−16193
- Mn-Ni, single cryst. or polycryst., elastic anomalies at antiferromag. transition 78−14972
- Mn-Ni, thermal expansion, mag. susceptibility, lattice consts. 80−100341
- γ-Mn-Ni (15 at.%), antiferromag. defect scatt., neutron polarisation anal. 80−50056
- Mn-Ni alloys, antiferromag., Invar-like thermal expansion and spontaneous volume magnetostriction 77−69654
- Mn-Ni alloys, γ-phase, lattice distortion and elastic props., ΔE effect interpret. 77−20671
- Mn-Ni alloys, Mn-rich, structural changes associated with antiferromag. ordering 77−69085
- γ-Mn-Ni-C, elastic anomalies, martensitic transformation in Mn rich alloys 78−84807
- Mn-Ni-Ti (Zr) systems, and mech. props. thermal expansion for different heat treatments *(Japanese)* 79−29123
- Mn-Ni-Ti(Zr), non-ferromagnetic Elinvar-type alloys 79−24566
- γ-Mn-Pd, antiferromag. defect neutron scatt. study 79−47252
- Mn-Pd (10 at.%), antiferromag. defect scatt., neutron polarisation anal. 78−2652
- Mn-Pt, Elinvar props., −150 to 500°C *(Japanese)* 77−52385
- Mn-Pt (<29 at.%), eutectoid transform., antiferromag. struct. transform. *(French)* 78−92259
- Mn-Pt alloys, mag. struct., neutron diffr. study 79−91210
- β-Mn-Sn, Mossbauer and neutron diffr. exam. 77−66253
- Mn-V(Cr)(Fe)(Co)(Ni), spin fluctuations effect on sp. ht. 79−82788
- Mn-ZnF_2, crit. neutron scatt. 78−52249
- Mn^{2+}-Cu^{2+} coupled pair, ESR spectrum, strong isotropic exchange model 80−29606
- $MnAs_{0.925}P_{0.075}$, low spin state electron config. *(Japanese)* 77−43813
- $MnAs_{0.97}P_{0.03}$, orthorhombic, mag. anisotropy 77−43832
- $MnAs_{1-x}P_x$, mag. and crystallographic anal. 79−47257
- $MnAs_{1-x}P_x$, mag. susceptibility anomaly at displacive phase transition 80−93091
- $MnAs_{1-x}P_x$ mixed crystals, metallic magnetically ordered, Hall effect 80−65536
- $MnAs_{1-x}P_x$ whiskers, thermoelectric power, 5 to 350K, phonon drag effects and mag. transitions 79−28363
- $MnAs_{1-x}Sb_x$, mag. and crystallographic anal. 79−47257
- γ-MnAu, phase diagram, X-ray diffr. and Young's modulus meas. 80−71024
- $MnAu_2$, helical antiferromagnetic compound, optical props. and electronic struct., visible and IR obs. *(French)* 80−45101
- $MnAu_2$, helical antiferromag., optical absorpt., density of states 80−66224
- MnB_2, polycryst., magnetoresist. and mag. props. *(Russian)* 80−92907
- $Mn(Br_{1-x}Cl_x)_24H_2O$, antiferromagnetism, controllable anisotropy 80−93116
- $MnBr_2.4H_2O$, high-resolution sp. ht. meas. near Neel temp. 77−28393
- Mn_3C, Mn_5C_2, $Mn_{15}C_4$, Mn_7C_3 and $Mn_{23}C_6$, mag. susceptibility temp. depend. 79−51754
- $Mn(CN)_3.(H_2O)_{0.57}$, mag. interactions, theory 80−97085
- $MnCO_3$, antiferromag. reson. linewidth due to relax. processes 77−24750
- $MnCO_3$, NMR saturation, nuclear spin wave excitation, large freq. shifts *(Russian)* 80−50207
- $MnCO_3$, new types of nuclear spin echo, single pulse and parametric echo 77−69726
- $MnCO_3$, parametric excitation of magnons, effect of RF modulation of mag. field 80−65842
- $MnCO_3$, parametrically excited antiferromagnetic, possible maser effect 78−48051
- $MnCO_3$, RF modulation effect on parallel microwave pumping threshold *(Russian)* 80−29628
- $MnCO_3$, relax. of nuclear spin waves, temp. and wave vector depend. *(Russian)* 77−90042
- $MnCO_3$, spin wave spectrum obs., review 80−50081
- $MnCO_3$, spin waves excitation 79−82772
- $Mn_xCd_{1-x}(NH_3)_2.Ni(CN)_4.2C_6H_6$, Hofmann type mixed cryst., mag. props. 79−4659
- $MnCl_2$, $MnBr_2$, mag. phase diagram, optical absorption meas. 77−4514
- $MnCl_2.2H_2O$, magnetically ordered phase, $^6A_{1g}$ to $^4T_{2g}$ transition absorpt. lines, Zeeman effects 78−6699
- $MnCl_2.2H_2O$, magnetisation and mag. resonance 79−11349
- $MnCl_2.2H_2O$, ordered, paramag. phases, optical absorpt. spectra, V-lines, Zeeman effects 78−6698
- $MnCl_2.2H_2O$, paramag. phase, external mag. field depend. of $^4T_{2g}$(II) Kramer doublets of Mn^{2+} 78−6700
- $MnCl_2.4H_2O$, antiferromag., magnetic and thermal props. 78−14937
- $MnCl_2.4H_2O$, antiferromagn., nucl. orientation 78−43652
- $MnCl_2.4H_2O$, antiferromag., low temp. thermal cond. 80−65320
- $MnCl_2.4H_2O$, biaxial antiferromag., bicritical region, sp. ht. meas. 78−68246

antiferromagnetic properties of substances continued

- α-$MnCl_2.4H_2O$, crossover from divergent to non-divergent nature of paramag. transition 79−73735
- $MnCl_2.4H_2O$, isothermal and adiabatic susceptibilities near field depend. anitferromag. phase transitions 77−69561
- $MnCl_2.4H_2O$, single cryst., mag. phases, obs. by ^{54}Mn nucl. polarisation 77−81031
- $MnCo_3$, parametric nuclear magnon excitation, mag. field modulation *(Russian)* 80−107999
- $MnCo_3$, weak ferromag., antiferromag. reson., phenomenological theory 78−60339
- $Mn_{0.27}Co_{0.73}Cl_2.6H_2O$, antiferromag., sp. ht. meas., phase transition obs. 79−78415
- $Mn_{1-x}Co_xF_2$, Raman scatt. by mag. excitations 77−55775
- $MnCrF_5$, antiferromag., mag. struct. *(French)* 78−52211
- $Mn_3Cr_2Ge_3O_{12}$ garnet, antiferromag. ordering *(Russian)* 78−80146
- $Mn_{1-x}Cr_xP$, mag. susceptibility and transitions 79−47256
- $Mn_{1.88}Cr_{0.12}Sb$, antiferromag.-ferrimag. transition, neutron crit. scatt. and crossover effect 80−71023
- $Mn_{1.88}Cr_{0.12}Sb$, magnetic phase transition effect on magnon renormalisation 77−59405
- $Mn_{1.88}Cr_{0.12}Sb$, magnon renormalisation 77−69520
- $Mn_{1.88}Cr_{0.12}Sb$, thermomagnetic props., antiferromag. to ferrimag. transition 77−63194
- $Mn_{2-x}Cr_xSb$, exchange-inversion interaction and acoustical magnon soft mode 77−40049
- $Mn_{2-x}Cr_xSb$, sintered, intrinsic coercivity 77−89983
- $(Mn_{0.95}Cr_{0.05})_3Si$, sp. ht. at low temps., mag. transitions *(Russian)* 77−32189
- γ-MnCu crystals, antiferromag. Czochralski growth 80−97420
- MnCu, neutron scatt. near crit. comp., effects of stress and ageing 79−19722
- γ-MnCu, stressed, mag. defects meas. by neutron polarisation anal. 80−50076
- MnF_2, antiferromag., magnetocryst. anisotropy, susceptibility, static torque meas. 77−69545
- MnF_2 antiferromag., mag. space groups, Clebsch-Gordan coeff. calcs. 80−79731
- MnF_2, antiferromag., multi-magnon luminesc. sidebands 78−76525
- MnF_2, antiferromag. and piezomag. domain struct., neutron topography study 80−71088
- MnF_2, antiferromag. domains, obs. using neutron technique 78−64213
- MnF_2, antiferromagnetic phase stability limit near spin-flop boundary 78−10683
- MnF_2, heat capacity and entropy, 10 to 300K, mag. ordering contrib. 77−16080
- MnF_2, heat transport by magnons, effect of magnon-phonon thermal relax., calc. 77−39705
- MnF_2, Heisenberg antiferromag., props. calc. 77−85406
- MnF_2, inelastic light scatt. from antiferromag. polaritons, theory 77−73144
- MnF_2, local mag. ordering above Neel point, EPR *(German)* 77−36125
- MnF_2, MCD spectrum, Zeeman splitting of purely excitonic lines 77−40262
- MnF_2, macroscopic quadrupole field meas. with SQUID magnetometer, order determ. 79−24140
- MnF_2, mag. anisotropy at OK 79−33473
- MnF_2, mag. susceptibility, crit. behaviour near Neel point 79−91217
- MnF_2, magnetic, thermal, elastic refraction of light, mag. order influence on refractive index *(Russian)* 80−34880
- MnF_2, magnon-photon interaction for EM wave vector perpendicular to sublattice magnetisation 79−69662
- MnF_2, nuclear spin lattice relax. exam. 78−76331
- MnF_2, nuclear spin-lattice relax. and magnon lifetime near spin-flop transition 77−69721
- MnF_2, one-magnon luminesc. sidebands of excitonic transition 78−60517
- MnF_2, parallel pumping studies of magnon damping 80−70990
- MnF_2, reson. NMR near phase transition 78−76265
- MnF_2, resonant phonon-magnon scatt., phonon spectroscopy obs. 79−65150
- MnF_2, specific heat, Heisenberg to Ising crossover near Neel temp. 78−47980
- MnF_2 spin wave lifetime, theory compared with expt. 80−60228
- MnF_2, spin-flop bicritical point, susceptibility and RF absorpt. meas. 79−87277
- MnF_2, spin-flop transition obs. by neutron diffr. 79−73734
- MnF_2, surface spin-flop and antiferromag. spin-flop transition 78−52257
- MnF_2, thermal cond., mag. field effects, magnon contrib. 78−38890
- MnF_2, thermal cond., temp. depend., role of reson. scatt. of phonons by OH^- defects 78−38889
- MnF_2, two-exciton light absorption, with four-photon excitation *(Russian)* 78−35186
- MnF_2, two-exciton many photon absorption, effect of statistical props. of light on intensity *(Russian)* 78−95589
- MnF_2, two-magnon Raman scatt., temp. effects 77−48179
- MnF_2, uniaxial antiferromag. anisotropy in paramag. susceptibility, cluster variation theory 78−52200
- MnF_2:Fe^{2+}, temp. depend. of magnon pair-mode energies, Raman scatt. meas. 77−20577
- MnF_2:Ni^{2+}, IR fluoresc., field depend., exchange energy 78−68543
- $Mn_{1-x}Fe_xP$, magnetisation, susceptibility and mag. transitions 79−47256
- $Mn_{1-c}Fe_cPt_3$, noncollinear mag. structs., neutron diffr. anal. *(Russian)* 80−25087
- $Mn_{2-x}Fe_xSb$, Mossbauer effect exam. 78−68432
- $Mn_{5-x}Fe_xSi_3$, elec. resist. and mag. susceptibility, ferromag. to antiferromag. transition 80−80504
- Mn_3Ga, formation of DO_{22} superstruct. and para-antiferromag. transition 79−19737
- Mn_3GaN, sp. ht., 6 to 350K, mag. and crystallographic phase transitions 80−71060
- Mn_3Ge, elec. and mag. props. *(Russian)* 77−76792
- Mn_3Ge_2, textured, thermal expansion, 158K transformation *(Russian)* 77−32196
- Mn_5Ge_3-Mn_5Si_3, electrical resistivity meas., order-disorder transition 80−10945
- Mn_3In, mag. susceptibility, X-ray and neutron diffr. 79−11314
- $Mn_xMg_{1-x}S$, mag. props. 77−66244
- $Mn_{1-x}Mg_xSe$, mag. and struct. phase transitions, mag. susceptibility and X-ray diffr. study 80−71022
- $Mn_2N_{0.86}$, cryst. and mag. struct. at low temps. *(French)* 77−73003

antiferromagnetic properties of substances continued
$Mn(NH_3)_2Ni(CN)_42C_{12}H_{10}$, phase transition, mag. susceptibility, sp. ht. 79−91234
$Mn(NH_3)_2.Ni(CN)_4.(benzene)_2$, antiferromag. ordering, mag. susceptibility, sp. ht. and Neel temp. meas. 77−12128
$Mn(Nb_{0.5}Ta_{0.5})_2O_6$, nonuniaxial spin-flop magnet, bicrit. lines, crossover 78−14973
$Mn(Nb_{0.5}Ta_{0.5})_2O_6$, spin flop magnet, four dimens. phase diagram and multicrit. phenomena 79−15304
$Mn_{73}Ni_{27}$, generalised susceptibility, spin wave contrib., inelastic mag. neutron scatt. 79−47262
$Mn_{3-x}Ni_xB_4$, mag. props. *(Russian)* 77−51923
$Mn_{3-x}Ni_xB_4$, with onset of spontaneous magnetisation below T_N, singularities of mag. props. *(Russian)* 77−59427
$Mn_xNi_{1-x}Cl_2.nH_2O$, antiferromag., sp. ht. meas. 79−91226
MnO, absorption line shape, magnon sidebands 77−52128
MnO, antiferromag., magnon lifetime and its effect on magnon sideband 77−12106
MnO, antiferromag., temp. depend. of elastic consts., US study 80−79854
MnO, antiferromag. reson., press. depend., and magnetostriction consts. 78−19339
MnO, antiferromagnetic-paramagnetic phase transiton at high press. 80−39778
MnO, cubic antiferromag., magnon-phonon sideband in fine-struct. of optical absorption 77−59590
MnO, Hall mobility of photoelectrons 77−69352
MnO, Jahn-Teller effect on optical absorption spectra 78−52484
MnO, linear optical anisotropy meas. at antiferromag. transition 77−36205
MnO, mag. phase transition, first-order 77−47988
MnO, magneto-elastic coupling by dipolar interactions and spin orientation 79−78494
MnO, magnon lifetime 77−69518
MnO, magnon-sideband lineshape, exciton-phonon interaction effects 80−65846
MnO, multidomain single cryst. and monodomain cryst., crit. and elastic behaviour, T_N to 300K 77−66407
MnO, muon probe expts. 77−63351
MnO, neutron diffr. meas., 100 to 700K, spin correls, above and below T_N 77−59390
$MnO:Mn^{2+}$, EPR, antiparallel spin coupling above Neel point, antiferromagnetic clusters *(German)* 77−16168
$MnO-B_2O_3$, polycryst. cpds., mag. susceptibility and ^{11}B NMR 79−8056
γ-MnOOH, antiferromag., prep. and mag. props., EPR meas. 79−87310
$x.MnO.(1-x)[19TeO_2.PbO]$, glass, antiferromag. behaviour, mag. props. 80−50072
Mn_2P, heat capacity, mag. entropy and thermodynamic functions 77−80630
$MnPS_3$ and $MnPSe_3$, mag. props., NMR meas. 79−24223
MnS, crit. behaviour, neutron diffr. exam. 78−80169
α-MnS, polycryst. and oriented single cryst., phase transition at 131K 78−6157
MnS, thermal cond., temp. depend., paramag.-antiferromag. transition effects 80−65321
MnS_2, first order antiferromag. phase transition 77−8317
$MnSO_4$, mag. struct. and phase transitions, neutron diff. study 80−60208
$MnS_2(Se_2)(Te_2)$, antiferromagnetic ordering, effective electron model 77−47975
$MnS_2(Se_2)(Te_2)$, mag. ordering, 2 cation, 2-anion indirect exchange interactions *(French)* 78−43566
Mn_2Sb, Bi-modified, mag. first order phase transition 79−51777
Mn_2Sb, hyperfine fields of ^{121}Sb in several mag. phases 79−28650
$Mn_2Sb_{1-x}Bi_x$, temp. depend. of magnetisation *(Japanese)* 79−78375
$Mn_2Sb_{1-x}Sn_x$, mag. transitions, Mossbauer meas. 78−52406
α-MnSe, mag. and struct. phase transitions, mag. susceptibility and X-ray diffr. study 80−71022
MnSe, mag. suscept., thermal expansion and elec. resist. meas. 78−34964
MnSe, thermal hysteresis, ESR spectra 79−99758
$MnSe_2$, IR lattice vibrs., dielectric dispersion 79−28735
β-$MnSeO_4$, mag. interactions 79−78361
α-$MnSeO_4$, magnetic interactions, neutron inelastic scatt. study 80−107980
MnSi, crit. transverse US attenuation, spin fluctuations 78−48022
MnSi, itinerant electron helical mag., ESR 77−59446
MnSi, itinerant electron system, neutron scatt. 78−68194
MnSi, low field mag. studies 78−23255
MnSi, mag. anisotropy exam., ferromag. to antiferromag. transition 79−73708
MnSi, weak itinerant ferromag., mag. excitations, neutron scatt. obs. 78−34969
Mn_3SnN, perovskite type struct., mag. props., neutron and Mossbauer meas. 77−32159
α-$MnSo_4$, mag. interactions 79−78361
MnTe, effect of press. on Neel temp. and lattice parameter 79−95594
MnTe, resistivity anomalies at mag. transitions, sp.ht. 80−39785
$MnTe_2$, Mossbauer spectra, hyperfine field 80−15866
$MnTe_2$, pyrite struct., susceptibility, 4.2-450K, exchange consts. 77−77040
$MnTiNdO_5$, distrib. of Mn^{3+} and Ti^{4+} ions, Mossbauer spectrum 77−69747
$MnTiO_3$, quasi-two dimens. antiferromag., mag. crit. behaviour 77−32191
$Mn_{2-x}V_xSb$, $0.08 \leq x \leq 0.25$, mag. props. modification by V 77−36071
$Mn_{1-c}Zn_cF_2$, Heisenberg antiferromag., linear mag. birefringence meas. 77−16277
$Mn_{1-x}Zn_xF_2$, antiferromagnetic reson. freq. from far IR transmittance spectra 77−69695
$Mn_{1-x}Zn_xF_2$, linear mag. birefr., crit. behaviour 77−52061
$Mn_{1-x}Zn_xF_2$, randomly diluted uniaxial antiferromagnet, CPA theory 79−78388
$Mn_cZn_{1-c}F_2$, crit. neutron scatt. near percolation threshold 78−2693
$Mn_xZn_{1-x}F_2$, antiferromag. spin flop crit. field 79−24218
$Mn_xZn_{1-x}F_2$, CPA estimate for Neel temp. 78−76245
$Mn_xZn_{1-x}F_2$, Neel point and short range order, dilution effects, mag. birefr. obs. 80−71019
$Mn_xZn_{1-x}F_2$, three dimens. Heisenberg-Ising antiferromag., fluctuations near percolation threshold 79−78390

antiferromagnetic properties of substances continued
$Mn_{0.510}Zn_{0.417}Fe_{2.073}O_{4+\delta}$ relationship between magnetic permeab stoichiometry 79−42799
Mn_3ZnN, sp. ht., 6 to 350K, mag. and crystallographic phase transit 80−71060
NH_4CoF_3, sp. hts., librational and reorientational 77−84946
NH_4CoF_3, susceptibility and magnetisation meas. 77−85432
$(NH_3)_2FeF_5$, one-dimensional antiferromag. systems, Mossbauer studies 80−71266
$(NH_3)_2FeF_5$, quasi two-dimens. antiferromagnet, Mossbauer study 80−39947
NH_4FeF_4, mag. and Mossbauer obs. *(French)* 78−19389
NH_4FeF_4, two-dimens. antiferromagnetism 77−66444
$N_2H_6FeF_5$, Mossbauer spectra, 1D antiferromag. 80−15886
$N_2H_6FeF_5$, one-dimens. magnetism, mag. suscept. and Mossbauer reson. exam. 77−51893
$N_2H_6FeF_5$, one-dimens. antiferromagnetism 77−66444
$N_2H_6FeF_5$, one-dimensional antiferromagnetism, Mossbauer study 80−65872
$(NH_4)_2IrCl_6$, mag. susceptibility in ordered and paramag. phases 79−73759
$(NH_4)_2ReCl_6(IrCl_6)$, proton relaxation near antiferromagnetic phase transitions 80−80640
$NaCa_2Mn_2V_3O_{12}$, antiferromag., spin wave contrib. to sp. ht., λ-anomaly at 25.05K T_N 77−77068
$NaCeS_2$, mag. susceptibility, 3.7 to 297K, extended mol. field model 79−87227
$NaCrO_2$, two-dimens. mag. order, neutron powder diffr. obs. 80−44805
$NaCrO_2$, two-dimensional antiferromag., mag. props. *(French)* 78−23251
$NaCrS_2$ antiferromag. reson. meas. 77−69705
$NaCrS_2$, antiferromag. semicond., Raman and far-IR spectra 79−47454
$NaCrS_2$, rhombohedral, antiferromag. reson. meas. 77−20717
$Na_2(Fe,Mg)_5Si_8O_{22}(OH)_2$, riebeckite, low temp. Mossbauer obs. of oriented single cryst. behaviour and mag. props. 80−84674
$NaFeF_2$, Mossbauer and low-temp. dilatometry study *(French)* 80−80662
$NaFeF_4$, two-dimens. antiferromagnetism 77−66444
α-$Na_3Fe_2(PO_4)_3$ orthophosphate, cryst. and vitreous, Mossbauer spectroscopy and mag. susceptibility *(French)* 80−80657
$NaMnCl_2$, mag. susceptibility, 4.2-350K, quasi-two-dimens. antiferromagnetism 77−59399
$NaMnCl_3$, antiferromag. insulator, self-trapping of excitons 80−70619
$NaMnCl_3$, exciton self-localisation, luminesc. and excitation spectra *(Russian)* 80−11456
$NaMnCl_3$, mag. props., 2-25K, antiferromag.-paramag. transition *(Russian)* 78−88125
$NaMnCl_3$, mag. struct. and spin-flip transition, powder neutron diffr. exam. 80−60210
$NaNiF_3$, electronic UV laser excited Raman, scatt. by mag. excitons 78−68492
$Na_2O-Fe_2O_3-SiO_2$ glass, partially crystallised 78−23302
Na_3RuO_4, ^{99}Ru Mossbauer spectra, antiferromag. order, mag. relax. 80−50234
$NaUO_3$, anomaly in mag. susceptibility-temp. curves 77−32152
β-$Na_xV_2O_5$, antiferromag. props. and weak ferromagnetism 79−78337
Na_xVS_2, Na_xVSe_2, charge density waves, electron localisation 79−47038
Nb_3Ge film, superconductivity, relevance of mag. interactions, EPR study 80−100545
$NbS_2(Se_2)$ intercalation complexes with 3d transition metals, mag. and metallic transport props. 80−44814
Nd, antiferromag., thermal cond., elec. and thermal magnetoresist., at low temps. 77−69301
Nd, mag. ordered, single cryst. elastic consts. meas., 4-50K 77−63249
Nd, magnetic structure, 2D modulated 80−15697
Nd, magnetic-structure, neutron and X-ray diffr. study 80−60197
Nd, single cryst. elastic consts., 4.2 to 300K, mag. ordering effects 77−15477
Nd, sp.ht., 1.5-10K, in applied fields 0-1.3T 79−61158
Nd-Dy(Ho)(Tb), HCP struct., mag. props. 77−63177
Nd-Y alloy, mag. character of stable and metastable phases 79−38329
$NdAg_x$, low temp. mag. meas. 80−107989
$Nd_xEu_{1-x}B_6$ solid solution, mag. susceptibility, lattice parameters, Weiss temp. 80−29535
$NdFeO_3$, mag. transition, NMR meas. 78−27036
$NdFeO_3$, magnetic struct., time of flight neutron diffr. method 77−8280
$NdFeTiO_5$, mag. susceptibility, 4.2-77K, antiferromag. ordering obs. 78−68186
$NdFeTiO_5$, magnetic props. and crystal growth 78−92185
$NdIn_3$, magnetisation 80−25106
$Nd_{1-x}La_x$, thermoelectric power, mag. transition temps. 80−20154
$Nd(Mn_{1-x}Cr_x)_2Si_2$, mag. and structural props. 79−78342
Nd_2NiO_4, Nd_2CuO_4, magnetic properties obs. 80−70937
NdP-UP solid soln., cryst. field parameters 80−10927
$Nd_{1-x}S$, grown-in defect exam. 78−43014
NdSb, mag. excitation spectrum, neutron inelastic scatt. 77−63152
$NdSn_3$, magnetoresistance 80−24877
$NdSn_3$, Neel temp., hydrostatic press. depend. 80−29549
$NdVO_3-CaVO_3$ solid solns., mag. props. rel. to cryst. struct. 78−43571
Ni complex, $(Ni(C_2H_5NO)_6)(NO_3)_2$, field induced level crossing and cryst. struct. 79−47070
Ni complex, hexa(pyridine-N-oxide)$(ClO_4)_2$, field-induced mag. ordering in S=1 singlet ground-state 78−23288
Ni complex, $Ni(C_5H_5NO)_6(ClO_4)$ field-induced mag. phase transition obs. 77−36072
Ni complex, $Ni(C_5H_5NO)_6(ClO_4)_2$, field induced antiferromag., magnetocaloric effect 80−29551
Ni complex, tris(ethylenediamine)nickel(II) nitrate, mag. props. from susceptibility and sp. ht. meas., 0.3-3.0K 78−91877
Ni complex, with 1,2,4-triazole, mag. susceptibility, 2-300K, struct., antiferromag. props. 77−77045
Ni ferrite, quenched, Neel temp. and initial susceptibility 80−75762
Ni I_2, neutron diffr. and sp. ht. meas. 77−55663
Ni, stress induced cross-over effect near Curie point *(German)* 80−103873
Ni, stress induced crossover effect near Curie point *(German)* 80−103874
Ni-Fe film, unidirectional anisotropy by exchange coupling, appl. to biasing of magnetoresist. read head 78−91907
Ni-I single crystals, mag. and dielectric props. 80−93095

antiferromag **rties of substances** continued
α-Mn, ered, exchange-anisotropy field, magnetisation curves
β-Mr red, mag. struct., high field twist deform. 78–68166
Mg lec. and structural props. meas. 77–85447
transition and accompanying struct. transition
ıan spectrum, 88-295K, vibr. anomalies 78–76479
ctric tensor component detection 79–95625
phase transition, X-ray diffr. obs., 77-300K, rel. to mag. susceptibility anomaly 77–47573
$Ni_3B_7O_{13}I$, struct. and mag. transitions, light scatt. study 79–24308
$NiBr_2$, ^{1}Eg spin-forbidden transition, temp. depend. and magnetoabsorpt. 78–48151
$NiBr_2$, commensurate and incommensurate mag. struct., neutron diffr. study 80–97067
$NiBr_2$, low-temperature magnetic phase, incommensurate spin structure 80–93082
$Ni(BrO_3)_2.6H_2O$, tetrahedral antiferromag. at very low temps., EPR meas. 77–81001
$NiBr_2.6H_2O$, antiferromag. transition, susceptibility and sp. ht. meas. 77–69587
$NiBr_2.6H_2O$, antiferromag. ordering and paramag. behaviour 78–14941
$Ni(C_5H_5NO)_6(ClO_4)_2$, susceptibility and magnetisation meas., field, freq. and temp. depend. 77–66279
$NiCO_3$, crystal growth by counterflow diffusion and temp. drop hydrothermal synthesis 77–4731
$Ni_xCd_{(1-x)}(NH_3)_2$. $Ni(CN)_4.2C_6H_6$, mag. susceptibility meas. 77–63126
$NiCl_2$, Raman spectrum at and below antiferromagnetic ordering temp. 79–99871
$NiCl_26NH_3$, low temp. sp. ht. and mag. ordering 80–75784
$NiCl_2.2H_2O$, mag. phase diagram and exchange parameters 77–77054
$NiCl_2.6H_2O$, antiferromag., phase diagram, low temp. canted paramag. boundary, bicritical point 79–47282
$Ni_xCo_{1-x}Cl_2.6H_2O$, mixed uniaxial planar antiferromag., magnetisation process 80–88788
$Ni_{1-x}Co_xF_2$, Raman scatt. by mag. excitations 77–55775
$Ni_{1-x}Co_xO$, LF magnons, inelastic neutron scatt. exam. 77–66288
$Ni_{1-x}Co_xO$ mixed crystal, lowest mag. excitation, antiferromag. reson. meas. 77–69704
$Ni_xCo_{3-x}O$, composition depend antiferromagnetic-ferrimagnetic ordering, mag. susceptibility meas. 80–70973
NiF_2, antiferromag. reson., Lagrange and nonequilib. thermodynamics descriptions 79–15357
NiF_2, electronic UV laser excited Raman, scatt. by mag. excitons 78–68492
NiF_2, magnetisation and antiferromagnetic resonance freq. in mag. field *(Russian)* 80–34781
NiF_2, thermal expansion and magnetostriction, 55K to room temp. 80–80586
NiF_2, weak ferromag., antiferromag. reson., phenomenological theory 78–60339
$Ni_{0.6}Fe_{2.4}B_7O_{13}I$, boracite, mag. hyperfine interactions, Mossbauer study 80–39935
$(Ni_{1-x}Fe_x)S$, solid solns., electronic props., X-ray, thermal and Mossbauer study 79–78376
$Ni_{1-x}Fe_xS_2$ ($x=0$ to 0.075), weak ferromag. exam. 79–51755
$Ni_{1-x}Li_xO$, $0.01 \leq x \leq 0.08$, mag. susceptibility in region 80 to 800K *(Russian)* 78–2664
$Ni_pMg_{(1-p)}(OH)_2$, random magnet, AC susceptibility 79–47258
$Ni_xMg_{1-x}(OH)_2$, random magnet, magnetisation 79–24195
Ni_xMn_{1-x} disordered alloy, mag. interactions exam. 77–24687
$Ni_xMn_{1-x}Cl_2$, sp. ht., 2-28K, anomalies *(Russian)* 77–89970
NiMnGe, crystal and spiral mag. struct., Neel temp., X-ray and neutron diffr. 77–16052
NiMnGe, mag. struct., and mag. phase transitions 77–63187
$Ni_2Mn(Mn_xSn_{1-x})$, Heusler alloy, antiferromagnetic order, X-ray and neutron diff. 78–64189
$Ni(NH_3)_2Ni(CN)_4.2C_{12}H_{10}$, mag. susceptibility, sp. ht., spin arrangements and transition obs. 77–20590
$Ni(NO_3)_26NH_3$, specific heat discontinuity at Neel point 77–51912
$Ni(NO_3)_2.6H_2O$, susceptibility and specific heat meas., spin ordering, antiferromag. spin pair coupling 80–7084
$NiNb_2O_6$, antiferromag., principle mag. susceptibility and field induced magnetisation meas. 77–20589
$NiNb_2O_6$, magnetisation and susceptibility, antiferro-paramag. transition, expt. and theory 77–43822
$Ni_{1/3}NbS_2$, intercalate, metallic, cond., Hall effect and mag. props. 77–76789
NiO (001), surface layers, sublattice magnetisation temp. depend., LEED exam. 78–27018
NiO (100), LEED calcs. of exchange refls. 78–14949
NiO (111) platelets, antiferromag. S domains, optical obs., spin flop 80–54915
NiO (111) platelets, magnetic anisotropy investigation by torque and mag. susceptibility meas. 80–54885
NiO (111) surfaces, antiferromag., mag. scattering by polarised LEED, spin polarisation effect in theory 80–29529
NiO, antiferromag., one-magnon light scatt. from spin-flop and paramag. regions, effect of anisotropy 79–33677
NiO, antiferromag., one-magnon light scatt., effect of anisotropy 79–33676
NiO, antiferromag., two magnon reson. Raman scatt. 79–33703
NiO, antiferromag. domains, obs. using neutron technique 78–64213
NiO, antiferromag. domains exam. by magnetic neutron Laue diffr. 79–51806
NiO, antiferromag. ordering, mag. transition-state approach 80–80507
NiO, bulklike powder, sp. ht., 14-280K 79–69260
NiO fine particles, mag. props. rel. to physicochem. props. 78–52315
NiO, linear birefringence in S-domains near antiferromag. phase transition 80–60261
NiO, mag. struct., neutron Laue diffr. method 80–70951
NiO, mag. transition, neutron scatt. exam. 78–56313
NiO, magnetic susceptibility, near Neel temp. 79–56509
NiO, multidomain mat., opt. anisotropy meas. at T_N 77–16279
NiO, paramag. shifts of ^{19}F at O 78–43719
NiO, relax. valence averaging, Mossbauer spectra evidence 77–1626
NiO, superexchange interactions, models, prospects for ab initio calcs. 77–69281
NiO, surface sublattice magnetis., temp. depend., determ. using low energy electron exchange scatt. *(Japanese)* 77–55700

antiferromagnetic properties of substances continued
NiO, thermal expansion, birefringence, AC susceptibility, temp. depend. 78–10664
NiO, thin plate, antiferromag. domain obs. by neutron diffr. topography 77–32209
NiO, transport props., temp. and stoichiometry depend., antiferromag. T-domain influence 77–8332
$NiO:^{67}Zn$, perturbed ang. correl. 78–95535
NiO:Cr, effect of Cr additives on structure parameters *(Bulgarian)* 80–44319
NiO:Fe, exchange anisotropy of Ni-ferrite precipitates 79–28520
$Ni(OH)_2$, quasi-two-dimensional antiferromagnet, specific heat 79–11317
$NiPS_3$, mag. props., NMR meas. 79–24223
$NiPtCl_6.6H_2O$, singlet-ground-state magnets, ESR at low temps. 80–97132
$Ni_{1-x}Rh_xS$, nonvolume effect of Rh substitution on paramag. metal-antiferromag. nonmetal transition 79–28277
NiS, antiferromag., press. effect on metal-nonmetal transition 77–69229
NiS, high energy spin waves, neutron scatt. study 79–51765
NiS, metal-nonmetal transition under press. 77–69228
NiS, spin polarons exam. and metal-insulator transition 78–10377
NiS_2, antiferromag. metallic state, neutron diffr. study 79–38325
NiS_2, antiferromag. struct., effects of four spin interactions 77–51885
NiS_2, high press. effect on mag. transition temps. 78–91866
NiS_2, hyperfine parameters and quadrupole splitting determ., ^{57}Fe Mossbauer spectra 77–77131
NiS_2, mag. struct. at 5K, polarised neutron study 78–80131
NiS_2, mag. torque curve 79–47305
NiS_2, neutron diffr. anomaly at Curie temp., antiferromag. refl. 78–76260
NiS_2, pyrite type, mag. struct., antiferromag. refl. of neutron diffr., susceptibility meas. 77–69497
NiS_2, spin struct. and mag. props. 78–39300
NiS_2, thermal expansion and cryst. distortion below antiferromag. Neel and weak ferromag. Curie temps. 77–15579
NiS_2, weak ferro- and antiferromag., magnetisation and neutron diffr. meas. 80–65794
NiS_2, weak ferromagnet, galvanomagnetic effect 79–11148
NiS_2, weak ferromagnetic semiconductor single crystal, elec. and magnetic props. 77–85226
$Ni_{0.991}S$, sublattice magnetisation temp. var., neutron diffr. 77–40077
$Ni_{1-x}S$, and $Ni_{1-x}S_{1-y}O_y(Se_y)$, mag. state in metal-semicond. transition region, neutrnon diffr. obs. *(Russian)* 77–89926
$NiS_{2-x}Se_x$, elec. resistivity temp. depend., pressure depend., paramagnetic-antiferromagnetic transition 78–10690
$NiS_{2-x}Se_x$, mag. struct., ^{57}Fe Mossbauer study 78–56409
$NiS_{2-x}Se_x$, sp. ht. and elec. resist. in metallic regime 77–69589
NiS_yTe_{1-y}, mag. susceptibility, correl. with metal-insulator transition data 79–24145
Ni_2Sc_2W, mag. order 77–63120
$NiSnCl_6,6H_2O$, singlet-ground-state magnets, ESR at low temps. 80–97132
$NiSnCl_6.6H_2O$, ESR line shift at very low temps. 78–56375
$Ni_{1-x}Te$, fluctuating localised mag. moments, d band motion, Mossbauer study 80–65768
$NiTiO_3$, antiferromag., mag. anisotropy, magnetisation meas. 80–65856
$NiWO_4$, AC elec. conductivity, thermoelec. power and dielec. const. 80–70736
$NiWO_4$ monoclinic antiferromagnet, orientational phase transition and intermediate state *(Russian)* 80–15725
$NiWO_4$, monoclinic antiferromag., domain struct. induced by strong mag. field 80–44856
$Ni_{1-x}Zn_xFe_2O_4$, polycryst., domain wall energy rel. to anisotropy 80–71090
Np intermetallics, NpM_2Si_2, ($M=Cr$, Fe, Co, Ni, Cu), Mossbauer and magnetisation expts. 78–31138
$NpAs_2$, magnetic props., 4.2 to 77K, Mossbauer study 80–39937
$NpCo_2Si_2$, mag. props., high press. studies with ^{237}Np(60)-resonance 80–39924
$NpCo_2Si_2$, mag. struct., neutron diffr. determ. 80–93084
$NpFe_{2-x}Co_xSi_2$, mag. and hyperfine props. 79–51887
$NpFe_{2-x}Co_xSi_2$, mag. and hyperfine props. 80–7247
$NpIr_2$, itinerant antiferromagnetism 79–61154
NpM_2Ge_2 ($M=Cr$, Fe, Co, Ni, Cu), Mossbauer and magnetisation meas. 77–1555
$NpRe_2$, mag. susceptibility 78–68182
$NpSn_3$, band magnetism due to f-electrons, T_N 77–73039
$NpSn_3$, itinerant f-electron antiferromag. obs. 77–8315
O, solid, magnetic props. theory for Heisenberg system *(Russian)* 80–54900
O_2, adsorbed layer on graphite film, mag. susceptibility 78–43241
O_2 adsorbed layer porous Vycor glass, props. characteristic of amorphous antiferromag. obs. 78–10665
O_2 adsorbed monolayers, antiferromag. struct. obs. by neutron diffr. 77–66257
α-O_2, antiferromagnetic polycrystal, splitting of exciton absorpt. lines in mag. field *(Russian)* 80–103943
α-O_2, cryst., exciton, exciton-magnon, and biexciton absorpt. at 1.5K 80–84750
α-O_2 crystals, spin ordering effect on light absorpt. *(Russian)* 80–89029
α-O_2, elementary excitations, effect of mag. anisotropy *(Russian)* 78–76317
O_2 monolayers, on graphite, mag. α-phase and α-β-phase transition 80–70530
O_2, solid, internal sublattice fields, nucl. heat capacity meas. of ^{17}O 79–95597
β-O_2, solid, possible mag. struct. *(Russian)* 79–56500
α-O_2, solid, quasi 2D antiferromag., magnon and libron excitation spectra *(Russian)* 77–36067
O_2, solid, struct. elementary excitation spectrum and thermodynamic props. *(Russian)* 79–55696
O_2, solid, susceptibility, temp. depend. as function of press. and mag. field, α-β transition obs. 77–47991
$2PbFe_{1/2}Nb_{1/2}O_3$-Pb_2FeReO_6, comp., struct., dielec. and mag. props. 80–2704
$Pb_2Fe_2O_5$, IR absorpt., Mossbauer spectra, Neel temp., cryst. cell *(French)* 79–42759
$Pb(FeTa)_{1/2}O_3$, Mossbauer spectra, 78-480K 79–51885

antiferromagnetic properties of substances continued
- $2PbFe_{1/2}Ta_{1/2}O_3$-Ba_2FeReO_6, comp., struct., dielec. and mag. props. 80—2704
- $2PbFe_{1/2}Ta_{1/2}O_3$-Pb_2FeReO_6, comp., struct., dielec. and mag. props. 80—2704
- $PbFe_{2/3}W_{1/3}O_3$-$BaTiO_3$ system ferroelec., antiferromag., ESR and dielec. props. meas. 77—40172
- Pb_2MnF_6, antiferromag. and superionic conductor, EPR and NMR meas. 79—99366
- Pd, magnetic properties in para-process region *(Russian)* 78—2672
- PdF_2 flourite-type form, mag. props., structure studies *(French)* 80—34187
- $(Pd_{0.9965}Fe_{0.0035})_{1-x}Mn_x$, mag. behaviour at Fe sites, Mossbauer effect meas. 80—66085
- Pd_2MnIn, Cd impurities, hyperfine field meas. 78—15074
- $Pd_2MnIn_{1-y}Sb_y$, Heusler alloy, mag. order obs. 80—29528
- $Pd_2MnIn_{1-x}Sb_x(Sn_x)$, Heusler alloy, Mossbauer effect exam., mag. coupling 79—69755
- $Pd_2MnIn_{1-x}Sn$, and $Pd_2MnIn_{1-y}Sb$, Heusler alloys, mag. order, disorder effects 80—88723
- $Pd_2MnIn_{1-x}Sn_x$-Cd, dil., Heusler alloy, hyperfine mag. field on Cd, TDPAC obs. 79—8075
- $Pd_2MnIn_{1-x}Sn_{1-x}$, mag. order exam. 77—40036
- $(Pd_xPt_{1-x})_3Fe$ atomically ordered alloy, thermoelectric power, carrier energy spin shift, mag. props. 80—29394
- $(Pd_xPt_{1-x})_3Fe$, magnetisation intensity and coercive force, antiferro- to ferromag. transition *(Russian)* 77—48008
- Pr, antiferromagnetic ordering 80—15709
- Pr, magnetic form factors, polarised neutron diffr. meas. 80—50057
- Pr, magnetic ordering, stress induced 80—15776
- Pr, magnetic ordering due uniaxial stress, mag. excitons by neutron scatt. 78—84467
- Pr, magnetoelastic effects, zero field single cryst. elastic consts. meas. 77—66403
- Pr-Dy(Ho)(Tb), HCP struct., mag. props. 77—63177
- Pr-Eu, dil., magnetisation, Mossbauer spectra 80—15928
- Pr-Nd alloy, elec. resist. and magnetisation 77—66367
- PrAl, annealed, mag. props. and mag. struct. 78—6517
- Pr_2C_3, cryst. struct., mag. struct. and props., 1.6 to 300K 79—11296
- $PrCo_2Ge_2$, crystal and magnetic structure obs. 80—64976
- $PrCu_2Ge_2$, magnetic props. 77—32180
- $PrFe_2Ge_2$, magnetisation, 4.2-273K, and Neel temp 77—8310
- $PrFeO_3$, magnetic struct., time of flight neutron diffr. method 77—8280
- Pr_2NiO_4, Pr_2CuO_4, magnetic properties obs. 80—70937
- PrSb, mag. excitations, press. depend., inelastic neutron scatt. meas. 78—10699
- PrSb, neutron scatt., press. induced antiferromag. 80—15699
- PrSb, pressure-induced antiferromag., neutron scatt. study 80—39750
- $PrSn_3$, magnetoresistance 80—24877
- $PrSn_3$, Neel temp., hydrostatic press. depend. 80—29549
- Pt-Fe alloy, ordered, T-c phase diagram, antiferro- and ferromagnetism *(Russian)* 80—65871
- Pt-Fe ordered alloy, multiply mag. phase transitions 80—60264
- $Pt_{0.72}Fe_{0.28}$, isomer shift and effective mag. field at ^{57}Fe, press. depend. 77—16232
- Pt_3Fe, transport and mag. props. near Neel temp. 79—7976
- PuC_x (x=0.8, 1.44, 1.67), low temp. sp. ht., mag. ordering obs. 80—49372
- PuN, heat capacity, at low temps. 79—24168
- RM_4Al_8 (M=Cr, Mn, Fe, Cu), magnetism and hyperfine interactions 80—25256
- $RbCoCl_3.2D_2O$, metamagnetic phase transition, crystallographic and mag. struct., neutron diffr. meas. 80—44174
- $RbCoF_3$, antiferromag., anisotropic exchange, dispersion relations of mag. excitations 77—69532
- $RbCoF_3$, mag. space group and Raman tensors in antiferromag. phase 79—82760
- $RbCoF_3$, single oriented antiferromag. domain, polarised Raman scatt. under uniaxial stress 78—23463
- $RbCoF_4$, 2-dimens. Ising antiferromag., mag. excitons, Raman scatt. obs. 80—66181
- Rb_2CoF_4, pseudo Ising antiferromag., inelastic light scatt. by mag. excitons 80—11377
- Rb_2CoF_4, two dimens. Ising like antiferromag., spin wave excitations 78—72342
- Rb_2CoF_4:^{57}Fe, Ising antiferromag., Mossbauer spectra, critical dynamics 80—15884
- Rb_2CoF_4:^{57}Fe, Mossbauer spectra, critical region anal. 80—15888
- $Rb_2Co_{0.95}Mg_{0.05}F_4$:$^{57}Fe$, Mossbauer spectra, critical region anal. 80—15888
- $Rb_2Co_cMg_{1-c}F_4$ mag.-nonmag. two-dimens. antiferromag. Ising system, spin fluctuations 80—80545
- $Rb_2Co_cMg_{1-c}F_4$, random 2D antiferromag., neutron inelastic scatt. 79—28505
- $Rb_2Co_cMg_{1-c}F_4$, random two-dimens. Ising antiferromag., unstable mag. long-range order, neutron scatt. obs. 80—44839
- $Rb_2Co_pMg_{1-p}F_4$, dilute antiferromag. two dimens. Ising system, phase boundary effective medium theory 80—50130
- $Rb_2Co_xMg_{1-x}F_4$, neutron scatt. exam., obs. of two dimens. mag. long range order 78—56295
- $Rb_2Co_xMg_{1-x}F_4$, static critical phenomena, neutron diffr. obs. 79—56528
- $Rb_2Co_xMg_{1-x}F_4$, two-dimens. Ising antiferromag., fluctuations near percolation threshold 79—78390
- $Rb_2Co_{0.5}Mn_{0.5}F_4$, two dimens. random antiferromag., excitations 80—107997
- $RbCuCl_3$, quasi-1-dimens., NQR obs. 80—54987
- $(RbF)_n$-FeF_3, dimensionality and spin reduction effects, Mossbauer study 80—39947
- $RbFeCl_3$, $2H_2O$, pseudo one-dimens. Ising-like system, mag. heat capacity and metamag. transitions 77—66351
- $Rb_2FeCl_5.H_2O$, cryst. struct., superconducting susceptometer mag. meas. 79—73717
- $RbFeCl_3.2H_2O$, 2D Ising system, crit. fluctuations, Mossbauer spectra study 80—44842
- $RbFeCl_3.2H_2O$, pseudo-one-dimens. canted Ising antiferromag., spin-cluster reson. 79—61233
- $RbFeCl_3.2H_2O$, pseudo-one-dimensional canted Ising antiferromag., spin-cluster excitations 80—70989
- $RbFeCl_3.2H_2O$, spin cluster excitation expts. 80—66039
- $RbFeF_3$, antiferromag., Mossbauer study of mag. axis 79—4752
- $RbFeF_3$, magnetisation density of Fe^{2+} 79—78313

antiferromagnetic properties of substances continued
- $RbFeF_5$, one dimensional antiferromagnets, field depend. spin re temp. variation, spin flopping 79—78586
- Rb_2FeF_4, antiferromagnet, two-dimensional, mag. excitations 80—
- Rb_2FeF_4, two dimensional planar antiferromag., mag. excitations, Ra and far IR spectra obs. 78—72343
- Rb_2FeF_4, two-dimensional antiferromag., with easy plane anisotropy, mag excitations and two-magnon Raman scatt. 80—65839
- Rb_2FeF_5, 1D antiferromagnetic system, Mossbauer investigation 78—95533
- Rb_2FeF_5, mag. struct. and one-dimens. antiferromagnetism 80—60209
- Rb_2FeF_5, Mossbauer spectra, 1D antiferromag. 80—15886
- Rb_2FeF_5, one-dimensional antiferromag. systems, Mossbauer studies 80—71266
- $RbMnCl_3$, antiferromag. static mag. props. *(Russian)* 78—60270
- $RbMnCl_3$, high-pressure cubic phase, mag. props. 79—47260
- $RbMnCl_3$, specific heat near Neel temp. *(Russian)* 80—100340
- $RbMnCl_3$, twinning struct., cryst. domains, orientation mag. transition *(Russian)* 80—107275
- $RbMnCl_4$, changes in birefr. due to spin flopping 79—73910
- $RbMnCl_4$, quadratic layer antiferromag., intrinsic emission obs. 77—20906
- Rb_2MnCl, optical absorpt., temp. and mag. field depend. 80—20661
- Rb_2MnCl_4, 2D Heisenberg antiferromag. spin wave analysis 80—54879
- Rb_2MnCl_4 antiferromagnet, spin flopping of sublattice mag. moments in mag. fields 79—69687
- Rb_2MnCl_4, Heisenberg antiferromag., spin wave anal. 79—61237
- Rb_2MnCl_4, rare earth doped, energy transfer, emission spectra obs. 80—20684
- Rb_3MnCl_4, quasi-2D-antiferromag., linear birefr. and optical absorpt. spectra 80—71385
- $Rb_3Mn_2Cl_7$, two dimens. double layer antiferromag., neutron diffr. exam. 77—8277
- α-$RbMnCl_3.2H_2O$, pseudo-one-dimensional mag. system, low-temp. sp. ht. 77—85471
- $RbMn_{1-x}Co_xF_3$, Raman scatt. by mag. excitations 77—55775
- $RbMnF_3$, ^{19}F spin-lattice relax., 0.1-3K 77—20743
- $RbMnF_3$, acoustic nucl. spin echo *(Russian)* 77—48088
- $RbMnF_3$, antiferromag., temp. depend. of NMR linewidth 77—63292
- $RbMnF_3$, antiferromag., multi-magnon luminesc. sidebands 78—76525
- $RbMnF_3$, antiferromag., mag. props. 79—8032
- $RbMnF_3$, antiferromag., spin-wave lifetimes calc. 79—7980
- $RbMnF_3$, antiferromagnetic resonance, optical detection, luminescence 80—7174
- $RbMnF_3$, domain struct. in fields exceeding spin-flop value 79—69693
- $RbMnF_3$, Heisenberg antiferromagnet, paramag. region, NMR, spin pair correl. 78—15032
- $RbMnF_3$, Heisenberg antiferromagnet, spin diffusion below T_N 78—34968
- $RbMnF_3$, isotropic antiferromagnetic, T-H phase diagram as test of theory 77—32192
- $RbMnF_3$, isotropic antiferromag., phase diagrams, US meas. 78—68350
- $RbMnF_3$, isotropic antiferromag., crossover behaviour of mag. phase boundary, US meas. 78—80145
- $RbMnF_3$, isotropic antiferromag., crossover behaviour of mag. phase boundaries 79—78370
- $RbMnF_3$, NMR, modes interaction *(Russian)* 77—59468
- $RbMnF_3$, nucl. spin waves *(Russian)* 78—34973
- $RbMnF_3$, nuclear spin echo of ^{55}Mn, freq. pulling 77—69727
- $RbMnF_3$, nuclear spin waves spectra, relaxation, parametric excitation, NMR dynamic shift *(Russian)* 80—11180
- $RbMnF_3$, pure and Fe, Co or Ni doped, thermal cond., spin wave and mag. impurity contribs. 77—40046
- $RbMnF_3$, spin wave lifetime, theory compared with expt. 80—60228
- $RbMnF_3$, spin wave widths 80—97081
- $RbMnF_3$, triplet states, piezospectroscopy 79—38562
- $RbMnF_3$, two-spin Raman scatt. at high temp. 77—40225
- $RbMnF_3$ universal relations among crit. amplitude, calc. up to order ε^2 for systems with continuous symm. 77—17936
- $RbMnF_3$, zone-boundary magnon energy and damping, Raman scatt. meas. 78—31202
- $RbMnF_3$:Ni, antiferromag., exchange splitting of $^3T_{2g}E$ state, fluorescence meas. 77—12419
- $Rb_3Mn_2F_7$, double-layer antiferromag., mag. prop. meas. and calc. 77—55666
- $RbMn_{1-x}Mg_xCl_3$, dilute pair antiferromag., mag. susceptibility and ESR meas. 79—78338
- $Rb_2Mn_{0.5}Mg_{0.5}F_4$ and $Rb_2Mn_{0.5}Ni_{0.5}F_4$, neutron scatt. obs. of mag. behaviour 77—66254
- $Rb_2Mn_cMg_{1-c}F_4$, dil. antiferromag., mag. correlations, neutron scatt. meas. 77—66356
- $Rb_2Mn_cMg_{1-c}F_4$, two-dimens. antiferromag., spin fluctuations, neutron diffr. study 80—44846
- $Rb_2Mn_xMg_{1-x}F_4$, random magnetic-nonmagnetic 2-dimens. antiferromag., spin fluctuation dynamics 77—63147
- $Rb_2Mn_xMg_{1-x}F_4$, spin dynamics near percolation threshold, EPR study 80—39859
- $Rb_2Mn_xMg_{1-x}F_4$, two dimens. Heisenberg-Ising antiferromag., fluctuations near percolation threshold 79—78390
- $Rb_2Mn_{0.5}Ni_{0.5}F_4$, site-random two-dimensional antiferromag., crit. behaviour, quasielastic neutron scatt. 77—85468
- $RbNiCl_3$, cryst., ^{35}Cl and ^{87}Rb NMR down to 1.3K 79—42848
- $RbNiCl_3$, mag. props. 79—73736
- $RbNiCl_3$, nearly one-dimensional antiferromag., spin-flop transition 78—6527
- $RbNiF_3$ spin lattice, susceptibility, Heisenberg model *(Russian)* 80—65893
- Rb_2NiF_4, MCD and stress linear dichroism on double excitonic transitions 77—52051
- Rb_2NiF_4, planar antiferromagnet, cluster-Bethe-lattice method 80—22306
- Rb_2NiF_4, quadratic layer antiferromag., optical spectra obs. 77—16326
- Rb_2NiF_4, specific heat capacity, critical amplitude, cross-over from 2-D Ising to Heisenberg behaviour 80—39791
- $RbNi_xMn_{1-x}F_3$, powder, mag. props. 80—2560
- RbO_2, low temp. phases, mag. order, EPR and antiferromag. reson 79—95630
- $RbVCl_3$, mag. props. *(French)* 77—16059
- $RbVF_3$, antiferromag. ordering points, thermal anal. and X-ray diffr. meas. *(French)* 78—84421
- α-Rb_xVF_3, mag. props. *(French)* 77—80933

antiferromag ties of substances continued
α-Mn, rnary oxides, prep., cryst. struct. and mag. props.
β-Mr)−15707
Mg ordering of holes, recombination radiation
) 80−45121
transition *(Russian)* 79−32937
ansitions, X-ray K-line shift, 77-1000K *(Rus-*
with ferromag. impurities, mag. props., 1.5-300K
9947
SmAs, low temp. props. 79−28528
SmAu$_{3.6}$, ordering temps. and effective moments 78−60283
SmB$_4$ *(French)* 77−20566
SmBi, low temp. props. 79−28528
SmCrO$_3$, spin reorientation phase transition, second order nature 77−80950
Sm$_2$CuO$_4$, magnetic properties obs. 80−70937
Sm$_{1-x}$Gd$_x$S, metal-insulator transition, induced by temp. and press. *(Japanese)* 79−51488
SmH$_2$, low temp. sp.ht., antiferromag. ordering and cryst. field splitting effects 78−84439
SmMg$_2$, cryst. and mag. props., ordering 78−68185
SmP, low temp. props. 79−28528
SmRh$_4$B$_4$, coexistence of supercond. and antiferromag. order 80−11140
SmS$_{1-x}$As$_x$ solid solns., intermediate valence phase, lattice const. and mag. susceptibility meas. 79−87245
SmSb, low temp. props. 79−28528
SmSb$_{1-x}$S$_x$, magnetic ordering and configuration mixing 78−68179
Sm$_2$ZrS$_5$, mag. and sp. ht. meas. on polycrystalline samples 78−23253
(SrCaR)$_2$(Cr$_x$Ga$_{1-x}$)O$_4$, R=La or Sm, mag. 2-D oxide, phys. props. 78 47974
Sr$_2$CoReO$_6$, seignettomagnets with perovskite struct. 79−38459
SrEuFeO$_4$, Neel temp. and spin reorientation, Mossbauer study 80−39934
SrEu$_2$Fe$_2$O$_7$, ferrite, Mossbauer effect study of hyperfine interactions, spin reorientation 78−19383
SrFeO$_{3-x}$, neutron diffr. exam. of mag. struct. 77−20553
Sr$_7$Fe$_{10}$O$_{22}$, mag. props. and spin order 78−52232
Sr$_2$Fe$_x$Ru$_{1-x}$O$_4$ solid soln., Mossbauer spectrosc. study 80−50235
Sr(Fe$_{0.766}$W$_{0.234}$)O$_3$, cryst. growth, mag. and Mossbauer studies 79−42743
SrGdFeO$_4$, Neel temp. and spin reorientation, Mossbauer study 80−39934
SrLaFeO$_4$, mag. and cryst. struct. determ. *(French)* 80−54866
SrLaFeO$_4$, two-dimens. mag. props. rel. to cryst. struct. 80−75776
Sr$_{0.5}$La$_{1.5}$Li$_{0.5}$Fe$_{0.5}$O$_4$, high spin configuration stabilisation for Fe^{4+} *(French)* 80−88519
SrMCrO$_4$, M=La, Nd, mag. struct. determ. by neutron diffr. *(French)* 79−28507
SrNd$_2$Fe$_2$O$_7$, mag. struct., neutron diffr. determ. *(French)* 78−52224
SrO-Fe$_2$O$_3$, EMF meas. with solid state cell, Mossbauer effect and magnetic props. *(Korean)* 77−28493
SrO.R$_{1-x}$Sr$_x$VO$_{3-0.1x}$, R=Nd, Eu, Gd, solid solns., elec. and mag. props. 77−89819
SrRFeO$_4$, R=La, Pr, Nd, Sm, Eu, Gd, Mossbauer effect, Neel temp. and internal mag. field 77−12284
SrR$_2$Fe$_2$O$_7$, (R=Pr,Nd,Sm,Eu,Gd or Tb), Mossbauer exam. of mag. struct. 77−40157
SrR$_2$Fe$_2$O$_7$ series, mag. struct. and spin reorientation, neutron diffr. and Mossbauer meas. 77−69503
SrTb$_2$Fe$_2$O$_7$, ferrite, Mossbauer effect study of hyperfine interactions, spin reorientation 78−19383
SrTb$_2$Fe$_2$O$_7$, Mossbauer spectra, hyperfine parameters, ordering temp. 77−90079
Sr$_2$YRuO$_6$, ^{99}Ru Mossbauer spectra and other techniques 80−29659
TMMC, 3-D ordering temp. controlled by solitons and defects, mag. field depend. 80−60275
TTF.CuS$_4$C$_4$(CF$_3$)$_4$, spin-Peierls system, nucl. spin-lattice relax. process 78−19361
TaS$_2$ intercalation complexes with 3d transition metals, mag. and metallic transport props. 80−44814
Tb alloy, antiferromag. state, decrease in stability 77−20556
Tb, critical magnetic studies 80−15745
Tb, elastic modulus in mag. field, US meas. using CdS transducer 77−11151
Tb, magnetic phase diagram, US meas. of elastic const. 80−15721
Tb, magnetisation intensity in antiferromag. state and mag. field induced phase transforms. *(Russian)* 80−65811
Tb, sp. ht., using lattice dynamical model for HCP metals 79−51273
Tb-Cu-Ag, mag. props. *(Russian)* 77−51905
Tb-Er alloy, magnetisation process of helical spin struct., neutron diffr. and magnetisation meas. 77−43850
Tb-Ho, US attenuation and elastic consts. in 3 mag. phases, 4.2 to 300K 77−72645
Tb-Ho (50%), antiferromagnetic, thermal expansion, US attenuation anomalies 79−47319
Tb-Ho (50%), hexagonal anisotropy effect on thermal expansion 79−51283
Tb-Ho alloy, influence of internal strain on Neel temp., thermal expansion and elastic const. meas. 77−63176
Tb-Pr(Nd) alloys, mag. struct. and ordered moments, neutrons diffr. data 77−66252
Tb-Sc(Y)(La)(Lu)(Yb)(Mg)(Th), mag. ordering temps., susceptibility meas. 80−25136
Tb-Sn, effective field at diamag. Sn impurities, 4.2 to 235K *(Russian)* 77−69549
Tb-Tm alloys, mag. struct., neutron diffr. 77−8273
Tb-Y, Fermi surface topology var., mag. and elec. props. *(Russian)* 77−80723
Tb-Y, helicoid antiferromag. ferromag. transition, magnetostriction and magnetocaloric effect *(Russian)* 77−80937
Tb-Y, magnetostriction, mag. and elec. props. 78−27068
TbAg, hyperfine field exam. by NMR spin echo 78−23365
TbAg$_{1\ \ x}$In$_x$, mag. and transport props. 78−43572
TbAg$_{1-x}$Zn$_x$ solid solns., mag. props. *(Russian)* 77−77049
TbAlGa, mag. props. and struct. 78−39302
TbAl$_x$Ga$_{2\ \ x}$, mag. props. and phase transitions 80−25133
TbAsO$_4$, mag. ordered, neutron diffr. study 79−47238
TbAu$_3$, mag. phase diagram 80−75761
TbAu$_{3.6}$, ordering temps. and effective moments 78−60283

antiferromagnetic properties of substances continued
TbB$_4$ *(French)* 77−20566
TbBe$_{13}$, magnetic structure at low temps., antiferromagnetic, neutron diffraction study *(French)* 80−39743
TbBi, type II antiferromag., trigonal lattice distortion, temp. depend. 79−23732
TbD$_2$, mag. struct., neutron diffr. study 77−85421
TbD$_2$, sublattice magnetisation, cryst. elec. field effects 78−39295
TbD$_x$, non-stoichiometric, complex antiferromag. struct., neutron diffr. study 80−50061
TbF$_3$, mag. phase diagram, crit. and tricrit. behaviour 78−14959
TbFe$_4$Al$_8$, commensurate-incommensurate modulated mag. struct., neutron diffr. obs. 79−95576
TbFe$_4$Al$_8$, neutron diffr. exam., mag. struct. 78−10656
TbFe$_2$Ge$_2$, magnetisation, 4.2-273K and Neel temp. 77−8310
TbFeO$_3$, mag. phase transitions, Van Vleck interaction and R-Fe exchange *(Russian)* 79−61105
Tb(Fe$_{1-x}$Rh$_x$)$_2$, Fe sublattice spin reorientation possibility, Mossbauer spectra *(Russian)* 79−78335
TbGa$_2$, mag. props. and struct., neutron diffr. patterns at 4.2, 300K 77−63109
Tb$_3$Ga$_5$O$_{12}$, hyperfine interac. induced antiferromag. order *(French)* 77−59392
Tb$_5$Ge$_4$, mag. struct. and mag. transitions, neutron diffr. expts. 78−43564
TbH$_{2-x}$, TbD$_{2-x}$, mag. susceptibility conc. depend. 80−70968
Tb$_2$In, mag. props., 4.2 to 270K 79−56512
TbMg$_3$, antiferromagnetic struct. 78−14930
TbMg$_3$, mag. props., Mg conc. depend. 78−84392
TbMnO$_3$, mag. struct., ordering of Mn^{3+}, Tb^{3+} moments, neutron diffr. expt. 77−69500
TbMo$_6$S$_8$, long range mag. order in supercond. state 79−65653
TbMo$_6$S$_8$, superconductor, neutron scatt. exam. of mag. phase 79−73680
Tb$_{1.2}$Mo$_6$S$_8$, long-range mag. order and supercond., neutron diffr. obs. 79−78320
Tb$_{1.2}$Mo$_6$S$_8$, low temp. heat capacity anomaly rel. to antiferromag. transition in supercond. state 80−25044
TbNi$_2$Si$_2$, mag. props., 4.2-200K 80−84602
Tb$_2$O$_2$S, tunnelling effect and mag.-cryst. transition, neutron diffr. expts. 77−63180
Tb$_2$O$_2$SO$_4$, antiferromag., mag. props. 1.6 to 40K 79−33464
Tb$_2$O$_2$SO$_4$, antiferromag., specific heat, 0.6 to 30K 79−33487
TbP (As)(Sb)(Bi), mag. transitions, quadrupolar interaction effects 80−80512
TbP, singlet-groundstate magnetism, static mag. props. 80−7109
TbPO$_4$, anomalous magnetostriction at low temp. 78−84470
TbPO$_4$, linear optical birefr. meas. near bicritical point 80−15719
TbPO$_4$, phase transitions at low temp. 80−15237
TbPO$_4$, sp. ht., 0.5-10K 78−52298
TbPO$_4$, specific heat from 1.2 to 6K 78−14475
TbS, type II antiferromag., trigonal lattice distortion, temp. depend. 79−23732
Tb$_x$S, mag. ordering, neutron diffr. meas. 78−2649
TbSc, crit. scatt. of electrons near antiferromag. transition temp. 79−69505
TbSe, type II antiferromag., trigonal lattice distortion, temp. depend. 79−23732
TbTe, type II antiferromag., trigonal lattice distortion, temp. depend. 79−23732
Tb$_x$Te, mag. ordering, neutron diffr. meas. 78−2649
Tb$_p$Y$_{1-p}$AsO$_4$, crystallographic, mag. phase transition as function of temp. and Tb conc. 78−43334
Tb$_c$Y$_{1-c}$Sb, elec. resist., cryst. field and exchange interaction contribs. 80−39556
Tb$_2$ZrS$_5$, mag. and sp. ht. meas. on polycrystalline samples 78−23253
TeCr$_2$O$_6$, exchange interactions within binuclear entity (Cr$_2$O$_{10}$)$^{14-}$ 80−60236
(Ti,V)$_2$O$_3$, magnetisation, field and temp. depend., down to 1.6K 77−8284
TiBe$_2$, cubic Laves compound, sp. ht. rel. to intinerant antiferromag. 79−82356
TiBe$_2$, itinerant antiferromag., mag. susceptibility and elec. cond. meas. 79−19726
TiBe$_2$, itinerant antiferromagnetism, mag. susceptibility obs. 79−15288
TiBe$_2$, weak itinerant magnetism as inhibited superconductivity 79−51715
TiO$_2$-P$_2$O$_5$ glasses, reduced, mag. susceptibility, 1 to 400K, mag. exchange between Ti^{3+} ions 79−73691
(Ti$_{1-x}$V$_x$)$_2$O$_3$, spin glass to antiferromag. regime 78−52276
(Ti$_{1-x}$V$_x$)$_2$O$_3$, spin glass and metallic antiferromagnetism 78−68268
(Ti$_{1-x}$V$_x$)$_2$O$_3$, spin-glass props., 0.05-300K 80−25149
(Ti$_{1-x}$V$_x$)$_2$0$_3$, metallic antiferromag. struct., neutron studies 80−65797
TlBr-VBr$_2$ system, cryst. struct., DTA investig. *(German)* 78−72766
TlMnCl$_3$, antiferromag., absorpt. spectrum, excitation-magnon-phonon process 79−87461
TlMnCl$_3$, specific heat near Neel temp. *(Russian)* 80−100340
TlMnCl$_3$, weak ferromag. and mag. struct., temp. depend. 78−19219
Tm, magnetisation, uniaxial anisotropy, mean field model 78−2660
TmCrO$_3$, temp. and field-induced spin reorientation, magnetisation meas. 77−69588
TmFeO$_3$, acoustic vel. and attenuation shifts at spin reorientation phase transition 80−65986
TmFeO$_3$, domain struct. in spin reorientation region, Faraday effect obs. 77−20835
TmFeO$_3$, magnetoelastic props. at spin reorientation region 77−8382
Tm$_2$O$_3$, susceptibility, 4.2-270K 77−12081
Tm$_2$O$_2$SO$_4$, antiferromag., specific heat, 0.6 to 30K 79−33487
Tm$_2$O$_2$SO$_4$, antiferromag., mag. props. 1.6 to 40K 79−33464
TmS, antiferromag. struct. below 8.9K, neutron diffr. obs. 79−78318
TmSe, Anderson lattice resist. for antiferromag. ordering 80−65556
TmSe, elec. resist. under press. at very low temp. 80−96878
TmSe, intermediate valence state, resistivity of magnetically ordered ground state 79−1683
TmSe, intermediate valence cpd., susceptibility, single-ion approach 80−70935
TmSe, mag. neutron scatt. 80−25096
TmSe, mag. ordering under press., neutron diffr. obs. 80−70947
TmSe, mag. props. and struct. 80−25109
TmSe, mixed valence systems, spin dynamics and mag. ordering 78−68162
TmSe, mixed-valent, field-depend. mag. phase transitions 78−10657

antiferromagnetic properties of substances continued
TmSe, susceptibility, Tm^{2+} and Tm^{3+} characts. 80−25110
Tm_xSe, $0.87<x<1.05$, mag., thermal and transport props., comp. depend. 78−68239
Tm_xSe, magnetoresist. and Hall effect, stoichiometry effects 80−65597
Tm_xSe, valence instabilities, antiferromag. order 80−20128
$TmZn_2$, Mossbauer effect meas. in antiferromag. and paramag. states 80−71265
U dipnictides, elec. and mag. props. 78−84399
U sesquichalcogenides, mag. props. temp. depend. 77−8287
U tetragonal compounds, mag. props. 80−15704
UAs, anisotropic susceptibility 79−42754
UAs, anisotropic susceptibility 80−7087
UAs, magnetic struct. in high mag. fields, neutron diffr. study 80−34597
UAs, magnetisation, ferrimag. spin struct. 80−7088
UAs, search for lattice distortions at low temps. 80−79759
UAs, sp. ht. meas., 5-300K, mag. transition obs. 80−50101
U_3As_4, mag. struct., mag. refls. in paramag. state 77−20559
UBr_3, cryst. field levels, neutron scatt. determ. 80−65509
UGeS(Se)(Te), mag. susceptibility, struct. in temp. range 4.2 to 300K 78−10667
UGeY, (Y=S, Se, Te), mag. ordering, neutron diffr. obs. 78−72329
UN, antiferromag., mag. susceptibility, elec. resist. and elastic consts. meas. 77−69510
UN, cubic antiferromag., anisotropic critical neutron scatt. behaviour 79−61112
UN, mag. inelastic scatt. 80−7079
UN, mag. susceptibility under press. 80−7086
UN, magnetisation, in fields up to 40 T 79−33505
UN, phonon dispersion relation near Neel temp., neutron coherent inelastic scatt. 78−59900
UN, search for lattice distortions at low temps. 80−79759
UN, single crystal, electronic props. 77−77061
UN, single crystal, mag. props. 77−77042
UN, sound velocity temp. depend. anomaly 77−72891
UN, sound velocity temp. depend. anomaly in elastic consts. determ. 77−72892
UN-ZrN, Young's modulus antiferromagnetic anomaly 80−92583
$U_2N_2As(P)(S)(Se)$, susceptibility, 4.2-1000K, cryst. field and exchange interactions 77−20569
UO_2, electronic transitions, crystal field effects and phonons, phase transition 80−97303
UO_2, new type of mag. domains *(Russian)* 77−59430
UO_2, phase transition crossover from first- to second-order in symmetry-breaking field 79−82805
UO_2, spin wave spectrum, mag. susceptibility, sp. ht. *(Russian)* 79−33470
UO_2, symmetry changes in mag. phase transitions 77−20597
UO_2, temp. depend. of 5f to $6de_g$ absorption edge and intra-5f transitions 79−24314
UP, anisotropic susceptibility 80−7087
UP, vol. changes at mag. transitions 80−7107
UP-PrP (NdP) systems, mag. phase diagrams 78−84424
UPb_3, crystal field energy levels, magnetisation and susceptibility, neutron spectra obs. 80−50064
USb, anisotropic susceptibility 80−7087
USb, antiferromag., neutron diffr. exam. of ordered state 77−20557
USb, collective elementary magnetic excitation, neutron inelastic scatt. obs. 79−24141
USb, crit. neutron scatt. 77−24674
USb, magnetisation, in fields up to 40 T 79−33505
USb, neutron inelastic scatt. from collective excitation 80−7080
USb, neutron inelastic scatt. meas., phonon spectra, mag. response, anisotropy 80−50065
USb, search for lattice distortions at low temps. 80−79759
USb, short-range spin correlations, neutron study 78−39293
$USb_{0.9}Te_{0.1}$, multiaxial mag. structure 80−15696
$USb_{1-x}Te_x$, mag. struct. and mag. phase diagram, neutron diffr. study 80−50059
$U_xTh_{1-x}As$, mag. phase diagram, magnetisation meas. 80−60271
V-Cr, elastic moduli, US pulse echo meas. 78−84881
V-Mn-Cr, disordered BCC state, mag. phase diagram, mag. and elec. props. 77−63185
$V_{1-x}Al_xO_{2\pm y}$, mag. and struct. props. meas. 78−2658
VF_2, prep., struct., heat capacity 5-300K, mag. ordering 79−86746
$V_{1-x}Ga_xO_2$, phase transitions, semicond. metal transition, antiferromag. props. 77−11969
VI_2, antiferromag., zone-boundary phonon Raman scattering, modulation of exchange interaction 80−11386
VI_2, MCD spectra, interpretation rel. to mag. struct. 80−66222
VI_2, mag. 'Bragg' scatt. obs. through Raman scatt. 80−66179
VI_2, phonon Raman scatt. from spin superstructures 80−16030
VI_2, spin-dependent Raman scatt. from phonons 80−97274
V_2O_3, insulating phase, mag. struct. 79−38305
V_2O_3 insulating phase, realistic Hartree-Fock calc. 79−38306
V_2O_3, low temp. antiferromag. phase, mag. struct. 78−52213
V_2O_3, phase transitions, Raman scatt. expts., 20-300K 78−39538
V_2O_3, pure and Cr doped, metal-insulator transition 79−37989
V_2O_3-Al_2O_3 solid soln., interactions between V atoms, comp. and temp. depend. of mag. susceptibility 77−8056
V_2O_3-M_2O_3, M=Ti, Cr, struct. and mag. props. 78−27041
V_2O_{3+x}, $0\leq x\leq 0.08$, mag. and elec. props. 80−49833
V_2O_{3+x}, nonstoichiometric, microscopic mag. props., NMR and inelastic-spin-flip neutron scatt. 79−38323
V_3O_5, electrical, thermodynamic and mag. props. at metal-semicond. transition, homogeneity range 77−4413
V_3O_5, mag. anisotropy 77−85441
V_3O_5, spin order, one-dimensional, Neel transition 80−39799
V_3O_7, hyperfine interactions, inelastic spin flip neutron scatt. 77−28372
V_3O_7, microscopic mag. props., NMR 80−7177
V_4O_7, sublattice magnetisation temp. depend., ^{51}V NMR 79−91301
V_6O_{11}, sp. ht., 0.4-50K 78−72358
V_nO_{2n-1}, Magneli phases, sp. hts. 0.4 to 50K 79−42774
V_xO_y, metal-insulator transition, external mag. field effects 80−92819
VOCl, and $Li_{0.8}VOCl$ intercalation cmpd., magnetic, optical and electrical props. 79−95402
$V_{1+x}S_2$, local moment formation, X-ray, mag. susceptibility and NMR meas. 77−69511
V_3S_4, and V_5S_8, itinerant antiferromag. spin fluctuations, NMR studies 80−93198

antiferromagnetic properties of substances continued
V_3S_4, antiferromag. order, ^{51}V NMR spectrum 79−56625
V_5S_8, antiferromag., NMR meas. 77−36140
V_5S_8, single cryst., mag. props. 78−88098
$V_{2-x}Sb_xO_4$, defect struct. exam., temp. depend. 78−18635
V_3Se_4, antiferromag. order, ^{51}V NMR spectrum 79−56625
V_3Se_4, itinerant antiferromag., spin fluctuations, NMR study 80−75874
V_5Se_8, itinerant antiferromag., spin fluctuations, NMR study 80−75874
VTe, mag. and elec. transport props. 80−92897
$(V_{1-x}Ti_x)_2O_3$:Fe, metallic antiferromagnetism, Mossbauer spectra 80−15881
WCr_2O_6, exchange interactions within binuclear entity $(Cr_2O_{10})^{14}$ 80−60236
WV_2O_6, exchange interactions within binuclear entity $(V_2O_{10})^{14-}$ 80−60236
WV_2O_6, magnetic susceptibility, behaviour in terms of quasi-isolated binuclear units 80−97073
Y-rare earth metal, mag. susceptibility, 4.2 to 300K, Neel temps. 79−19735
YC_2-DyC_2, solid solution, antiferromag. props. 79−91230
$Y_{1-x}Co_x$, temp. depend. of magnetisation 77−77043
$YCrO_3$, antiferromag., exciton absorption lines obs. during field induced spin-reorientation 77−63397
$YCrO_3$, EPR linewidth, Neel point to 700K 80−39849
$YCrO_3$, mag. circular dichroism and Faraday rotation in R-lines region 79−28725
$YCrO_3$, mag. domain walls, ^{53}Cr NMR study 79−11327
$YCrO_3$, magnetisation, NMR freq. temps. depend. weak ferromagnetic-antiferromagnetic spin reorientation transition 80−29631
$YFe_{1-x}Mn_xO_3$ orthoferrite, spin reorientation, mag. torque meas. 78−47979
$YFeO_3$, mag. domain walls, photomagnetic effects, ^{57}Fe NMR obs. 78−95464
$YFeO_3:Co^{2+}$, weak ferromagnetism, single ion anisotropy contrib. 80−25126
YFe_2O_4, low temp. phase transitions and mag. props. 80−7106
YFe_2O_4, Mossbauer spectra of ^{51}Fe in antiferromag. and paramag. states 80−15834
YFe_2O_4, parasitic ferrimagnetism 79−4703
$Y_3Fe_5O_{12}$, amorphous, mag. moments, susceptibility, Mossbauer studies 79−78345
YM_4Al_8 (M=Cr, Mn, Fe, CU), magnetism and hyperfine interactions 80−25256
YRh_4B_4, supercond., anomalous cond.-electron polaris. 80−25047
$Y_{1-x}Th_xFe_3$, saturation magnetisation, fields up to 120 kOe, comp. depend. 77−8283
$YV_{1-x}M_xO_3$ (where M=Cr or Fe), solid solns., elec. and mag. props 79−23967
Yb, FCC phase, low temp. mag. props., impurity effects 80−20387
$YbAlO_3$, and mag. ordering 79−8078
$YbBe_{13}$, mag. props. and EPR meas. 80−11175
$YbFe_xMo_6S_8$, singularities in mag. and supercond. props. 79−51710
$YbFeO_3$:Co, mag. struct. factors, neutron diffr. study 79−47248
$Zn_{1-x}Co_xF_2$, Raman scatt. by mag. excitations 77−55775
$ZnCr_2O_4$, mag. phase with short range order *(French)* 77−63203
$ZnCr_2Se_4$, magnetoelastic coupling, mag. suscept. meas. 78−76288
$ZnCr_2Se_4$, screw spin struct., neutron diffr. exam. 78−27019
$ZnCr_2Se_4$, screw spin structure, method of controlling the sense, polarised neutron diffr. study 80−70944
$ZnCr_2Se_4$, screw spin structure, magnetoelectric effect 80−75827
$ZnCr_2Se_4$:In, magnetoresist. and elec. resist. above and below Neel temp. *(Russian)* 80−88576
$Zn_xFe_{0.85-x}O$, prep. and struct., mag. and semicond. props. *(French)* 78−51506
$ZnGa_2O_4:Cr^{3+}$, weak exchange interaction determ., ESR study 80−93107
$Zr(Fe,Al)_2$, weak itinerant ferromag., mag. anisotropy effects on mag. isotherms 80−11187
$(Zr_{1-x}Nb_x)Fe_2$, antiferromag. spin struct., Mossbauer effect study 80−66086

antiferromagnetic resonance
antiferromagnet, effect of external stress on AFMR and other spin wave frequencies 79−61230
1,3-bisdiphenylene-2-(p-chlorophenyl)-allyl, antiferromag. resonance, antiferromag. phase transition 78−6579
Brillouin-Mandelstam scattering from thermal and excited magnons 80−70980
copper benzoate, antiferromag. reson. below 1K, Neel temp. determ. 78−39407
copper dipyridine dichloride, antiferromag. reson. below 1K 79−28619
cubic crystal, magnetoelastic interaction effect on antiferromag. reson. freq. *(Russian)* 77−69711
dimethylammonium manganese chloride, perovskite-type layer structure submillimetric-wave spectroscopy 79−33540
dimethylammonium manganese tetrachloride, antiferromag. and spin-flop resonance obs., 70 to 100 GHz 80−71190
dimethylammonium manganese tetrachloride, Heisenberg ferromag., spin wave anal. 79−61237
disordered media, ferro- and antiferromag., and spin glasses, dynamic props. *(Russian)* 78−39350
easy plane antiferromagnets, mag. props. 79−1665
easy-plane antiferromagnet, coupled spin wave branches *(Russian)* 80−93096
easy-plane magnet, antiferromag. reson. linewidth and relax., theory 80−71189
film, surface spin waves and surface anisotropy effects at finite temp. 79−78452
Heisenberg antiferromagnet, AFMR freq. temp. depend., integral peak intensities *(Russian)* 80−54951
Heisenberg impure antiferromagnetic, impurity banding and mag. reson., theory 80−93181
Heisenberg magnet, impurity band resonance at 0K, theory 80−66041
high-frequency props. of weak ferromagnets and antiferromagnets, singularities *(Russian)* 80−50196
linewidth theory, multimagnon processes contrib. 77−69708
magnetodielectrics, magnetoelastic coupling 79−87300
multimagnon processes, temp. depend., relax. rate 77−4564
NMR, resonant, near mag. transition 78−76265
nonlinear dynamics of electron-nuclear spin system 77−66438

antiferromagnetic resonance continued
- parametrically excited antiferromagnetic, possible maser effect 78−48051
- quasi-two-dimensional antiferromagnet, nonreson. HF field absorpt. *(Russian)* 77−63287
- random antiferromagnets, theory of mag. excitations, antiferromag. reson. 80−97146
- relaxation mechanism 77−12204
- relaxation processes, spin-sound wave coupling 78−60340
- review of magnetic resonance, book contrib. 80−11242
- semiconductors, antiferromagnetic resonance rel. to surface impedance, magnetoelastic contrib. 80−50200
- spin wave relaxation in strong mag. field 78−2747
- spin waves in antiferromagnets, microwave and optical expts., review 80−50081
- spin waves studied by microwave absorpt. 78−91960
- spin-spin resonance in antiferromagnet under press., theory *(Russian)* 77−20712
- stationary and transition processes in region of identical nucl. and electron mag. reson. freqs. *(Russian)* 78−80225
- submillimetric spectroscopy appl. to mag. excitations 77−40135
- TMMC, antiferromag. reson. below 1K 78−39408
- TMMC, one-dimens. antiferromag., spin wave line widths, neutron scatt. study 79−51767
- TMMC, one-dimensional, EPR at HF and low temp. 78−80205
- uniaxial antiferromagnet, mag. polaritons in spin-flop phase 78−23349
- uniaxial antiferromagnets in transverse mag. field, quantum theory, spin configuration 79−69647
- weak ferromagnet, collective excitations in transverse mag. field, AFMR spectrum 80−93100
- $Ca_3Fe_2Ge_3O_{12}$, antiferromagnetic reson., anisotropy and magnetoelastic interaction effects *(Russian)* 77−69712
- $Cd_3Cr_2Ge_4O_{12}$, antiferromagnetic reson., anisotropy and magnetoelastic interaction effects *(Russian)* 77−69712
- $CoBr_2$, lamellar, field depend. of uniform magnon. energies, antiferromag. reson. meas. 77−73086
- $CoCO_3$ far IR spectrum, HF antiferromag. resonance and two-magnon absorption 77−40136
- $CoCO_3$, light interaction with spin system at antiferromag. reson. 77−69707
- $CoCO_3$, light scatt. by thermal magnons and magnons excited by antiferromag. reson. 79−82965
- $CoCO_3$ light scatt. from parametric magnons and phonons *(Russian)* 80−34937
- $CoCO_3$, light scatt. from magnons and phonons excited by microwave pumping 80−66213
- $CoCO_3$ light scattering on spin waves *(Russian)* 77−4650
- $CoCO_3$, long wave IR spectrum, high freq. antiferromag. reson. *(Russian)* 78−31115
- $CoCO_3$, spin wave spectra light scatt. expts., review 80−50081
- $CoCO_3$, weak ferromag., antiferromag. reson., phenomenological theory 78−60339
- $CoCO_3$, weak ferromagnet, antiferromag. reson. and two-magnon absorpt. *(Russian)* 80−29627
- $CoCO_3$, weakly ferromagnetic, light scatt. accompanying spin system excitation by high microwave power *(Russian)* 78−2745
- $CoCO_3$, weakly ferromag., light scatt. on spin waves *(Russian)* 78−72419
- $CoCl_2$, antiferromag., elementary excitations 77−69519
- $CoCl_2$, antiferromagnetic resonance, effect of hydrostatic pressure *(Russian)* 78−35042
- $CoCl_2$, lamellar, field depend. of uniform magnon. energies, antiferromag. reson. meas. 77−73086
- $CoCl_2 6H_2O$, g-tensor and exchange parameters, mag. reson. studies 79−87324
- $CoCl_2.6H_2O$, antiferromag., spin flop and paramag. resons. at very low temp. 77−66426
- CoF_2, phase transition in transverse mag. field, magnetoelastic interactions 79−65676
- CoF_2 plate, antiferromag. reson. in transverse mag. field 78−2749
- $Co_{1-p}Mg_pCl_2$, magnetic excitations, antiferromagnetic resonance spectra response simulation 79−99775
- $Co_{1-c}Mn_cF_2$, antiferromagnet mag. impurities, spin excitation spectrum collective rearrangement in external mag. field 80−50199
- $CoO:Ni^{2+}$, far IR absorpt. by impurities and collective antiferromag. reson. mode 77−8576
- Cr_2O_3, antiferromag. reson. and mech. of parallel magnetoelectric effect 79−47337
- Cr_2O_3, magnetoelectric effect mechanism, magnetoelec. susceptibility and antiferromag. reson. elec. shift meas. 80−44894
- $CsMnCl_3$, antiferromagnetic resonance, parametric spin wave excitation *(Russian)* 80−93183
- $CsMnCl_3.2H_2O$, antiferromag. resonance and two-magnon absorpt. *(Russian)* 77−81014
- $CsMnCl_3.2H_2O$, antiferromag. reson. and two-magnon absorpt. 79−61234
- $CsMnCl_3.2H_2O$, antiferromag. reson. temp. depend. *(Russian)* 79−87321
- $CsMnCl_3.2H_2O$, quasi-onedimens., microwave absorpt. *(Russian)* 77−51962
- $CsMnCl_3.2H_2O$, subthreshold two-magnon absorpt., depend. on freq., temp. and mag. field, exchange coupling const. *(Russian)* 80−71184
- $CsMnF_3$, parametric magnon excitation, relaxation *(Russian)* 78−23352
- $CsMnF_3$, RF modulation effect on parallel microwave pumping threshold *(Russian)* 80−29628
- $CsMnF_3$, spin wave spectrum obs., review 80−50081
- $CsNiF_3$, demagnetising effects on antiferromag. reson. 80−15803
- $CsNiF_3$, subthreshold parallel pumping of magnons and antiferromag. reson. 80−71185
- CsO_2, low temp. phases, mag. order, EPR and antiferromag. reson. 79−95630
- $CuCl_2.2D_2O$, cryst. struct., mag. and reson. props. 80−60424
- $CuCl_2.2H_2O$, antiferromagnetic relax., autocorrel. function time evolution 77−59464
- $CuCl_2.2H_2O$, antiferromag. reson. temp. depend., spin-flop phase *(Russian)* 78−23348
- $CuCl_2.2H_2O$, energy gaps mag. field depend., antiferromag. reson. 79−87320
- $CuCl_2.2H_2O$, HF spectrum, press. and temp. depend. *(Russian)* 77−36137
- $CuCl_2.2H_2O$, in tilted mag. fields *(Russian)* 77−51961

antiferromagnetic resonance continued
- $CuCl_2.2H_2O$, magnetoelastic props. under press., antiferromagnetic resonance, lattice parameters 80−29598
- dimethylammonium manganese tetrachloride, 2D Heisenberg antiferromag., spin wave anal. 80−54879
- $ErFeO_3$, weak ferromag., high freq. props. in ordering region of spin system, antiferromag. reson. study *(Russian)* 80−2644
- $EuCrO_3$, long term mag. ordering, antiferromagnetic resonance study *(Russian)* 80−54953
- EuTe, mag. semicond., antiferromag. reson. meas. 80−44926
- $FeBO_3$, basal mag. anisotropy, antiferromag. reson. *(Russian)* 79−47338
- $FeBO_3$, dynamic NMR frequency shift for ^{57}Fe *(Russian)* 78−43677
- $FeBO_3$, magnetoelastic coupling, antiferromag. reson. deform. depend. meas. 77−73069
- Fe_3BO_6, weak ferromag. and antiferromag. reson. modes obs. 77−69706
- Fe_3BO_6, weak ferromagnetism and spin reorientation, antiferromag. reson. spectra 78−6580
- $FeBr_2(Cl_2)(I_2)$, far IR antiferromag. reson. 77−36138
- $FeCl_2$, antiferromag. reson., temp. depend. 78−68384
- $FeCl_2$, antiferromag. reson., 2-D Ising model interpretation 79−47323
- FeF_2:Mn, antiferromag. reson. and local magnon mode, FIR laser study 80−66042
- FeF_2:Mn, Heisenberg model, impurity band resonance at 0K, theory 80−66041
- FeF_2:Mn, mag. polariton, impurity mode enhancement and superradiance effects 79−28622
- FeI, magnon energies, phase transitions of eight sublattice model 77−59463
- FeI_2, eight sublattices model, antiferromag. reson. uniform modes and metamag. behaviour 77−69498
- $Fe_{1-p}Mg_pCl_2$, magnetic excitations 78−91852
- α-Fe_2O_3, antiferromag. reson. in absence of external field, 150 and 320K *(Russian)* 79−4730
- α-$Fe_2O_3:Sn^{4+}$, antiferromag. reson. *(Russian)* 80−7175
- ^{3}He, solid, nuclear antiferromag. reson. 80−54471
- K_2CoF_4, two-dimensional antiferromag., one- and two-magnon Raman scatt. 79−51945
- $KMnF_3$, antiferromagnetic resonance in strong mag. field *(Russian)* 79−8054
- $KMnF_3$, EPR antiferromag. reson. linewidths near Neel point, exchange interactions *(Russian)* 77−8386
- $KMnF_3$, mag. props. and struct. transitions, antiferromag. reson. meas. 79−8052
- $KMnF_3$, optically detected antiferromag. reson. 78−15029
- $K_2MnF_4:Ni^{2+}$, and undoped, magnon spectra, Raman and far IR spectra meas. 77−20573
- KO_2, low temp. phases, mag. order, EPR and antiferromag. reson. 79−95630
- $LiCuCl_3.2H_2O$, antiferromagnetic relax., autocorrel. function time evolution 77−59464
- $MnCO_3$, antiferromag. reson. linewidth due to relax. processes 77−24750
- $MnCO_3$, nuclear spin waves from antiferromag. reson. line temp. depend. *(Russian)* 78−48050
- $MnCO_3$, RF modulation effect on parallel microwave pumping threshold *(Russian)* 80−29628
- $MnCO_3$, relax. of nuclear spin waves, temp. and wave vector depend. *(Russian)* 77−90042
- $MnCO_3$, spin wave spectrum obs., review 80−50081
- $MnCO_3$, weak ferromag., antiferromag. reson., phenomenological theory 78−60339
- $MnCl_2.2H_2O$, magnetisation and mag. resonance 79−11349
- MnF_2, reson. NMR near phase transition 78−76265
- MnF_2 spheres, magnetostatic modes 77−1599
- MnO, antiferromag. reson. linewidth below and above T_N 77−40133
- MnO, antiferromag. reson., press. depend., and magnetostriction consts. 78−19339
- MnO, low freq. branch gap due to magnetoelastic interaction 77−40134
- $Mn_{1-c}Zn_cF_2$, far IR spectrum, CPA calc. 77−20716
- $Mn_{1-x}Zn_xF_2$, antiferromagnetic reson. freq. from far IR transmittance spectra 77−69695
- $Mn_{1-x}Zn_xF_2$, randomly diluted uniaxial antiferromagnet, CPA theory 79−78388
- $Mn_xZn_{1-x}F_2$, antiferromag. spin flop crit. field 79−24218
- $NaCrS_2$ antiferromag. reson. meas. 77−69705
- $NaCrS_2$, rhombohedral, antiferromag. reson. meas. 77−20717
- $Ni_{1-x}Co_xO$ mixed crystal, lowest mag. excitation, antiferromag. reson. meas. 77−69704
- NiF_2, antiferromag. reson., Lagrange and nonequilib. thermodynamics descriptions 79−15357
- NiF_2, magnetisation and antiferromagnetic resonance freq. in mag. field *(Russian)* 80−34781
- NiF_2, weak ferromag., antiferromag. reson., phenomenological theory 78−60339
- α-O_2, elementary excitations, effect of mag. anisotropy *(Russian)* 78−76317
- $RbFeCl_3.2H_2O$, spin cluster excitation expts. 80−66039
- Rb_2MnCl_4, 2D Heisenberg antiferromag. spin wave analysis 80−54879
- Rb_2MnCl_4, Heisenberg antiferromag., spin wave anal. 79−61237
- $RbMnF_3$, antiferromagnetic resonance, optical detection, luminescence 80−7174
- RbO_2, low temp. phases, mag. order, EPR and antiferromag. reson. 79−95630

antiferromagnetism
- *see also antiferromagnetic properties of substances; exchange interactions (electron); metamagnetism*
- acoustic nuclear resonance, self-induced transparency *(Russian)* 79−91304
- acoustic wave nonlinear self-interaction in antiferromag. with easy plane anisotropy *(Russian)* 78−80187
- alloy, binary, with mixed ferro- and antiferromag. exchange, magnetisation, phenomenological theory *(German)* 78−56297
- alloy, FCC, binary, on Ising system, sublattice magnetisation, tricrit. point, simulation 79−33491
- alloy, spin disorder resistivity, coherent potential approx. 78−14722
- alloy between ferromag. and antiferromag. species, competing order parameters, Bethe-Peierls approx. 77−48003
- alloys, Lifshitz point occurrence, review 78−52265
- alloys, nesting type model, spin fluctuations 78−84435
- amorphous, spin waves, exchange fluctuations, calc. 80−65847

antiferromagnetism continued
amorphous antiferromagnet, spin waves, semiclassical theory 77—36064
amorphous Heisenberg and Ising chains, thermodynamics 80—108022
amorphous Heisenberg magnet, antiferromag. coupling, ground state and frustration, theory 80—65766
amorphous Ising antiferromagnetic model, frustration effects 80—103838
amorphous Ising chain, finite, thermodynamic behaviour 79—61028
amorphous magnet, Bethe-Peierls-Weiss approx. 78—76263
anisotropic antiferromagnet, correction to scaling in specific heat 78—80168
anisotropic antiferromagnet, phase transition, with external mag. field 79—11316
anisotropic antiferromagnet mixture with different easy axes, theory 79—42717
anisotropic antiferromagnets, mixture of two, with different easy axis, oblique antiferromag. phase 77—59408
anisotropic chain, spin wave spectrum 78—60273
anisotropic Fermi liquid, mag. order and transitions, phenomenological theory *(Russian)* 77—36038
anisotropic magnet, low-temperature properties 79—65633
anisotropic magnet mixture, Heisenberg spin system by Monte Carlo simulation 79—78408
antiferromagnet, magnetoelectric susceptibility crit. behaviour, renormalisation group theory 78—48023
antiferromagnetic biexcitons in critical temp. range 79—95601
antiferromagnetic resonance, effect of external stress 79—61230
band theory, electron orbital ordering 77—89923
band theory *(Russian)* 78—2646
BCC Ising model with competing interactions, fluction-induced first-order transition 80—20424
Berezinski transition, effective temp. *(Russian)* 80—65889
biaxial antiferromagnet, spin configuration in longitudinal mag. field *(Russian)* 79—7998
biaxial low-dimensional antiferromagnet, two-magnon absorpt. in collinear phase *(Russian)* 77—69803
birefringence of antiferromagnetic crystal, optical class lowering induced by longitudinal mag. field *(Russian)* 79—8127
Blume-Capel model for plane-triangular and FCC lattices 78—80114
bond-diluted antiferromagnetic triangular cactus tree, ordered phase 80—71037
Bravais lattice, ferromagnetic ground state conditions in Ising and Heisenberg models 80—50129
chain compound, Peierls distortion energy, exact limit, renormalisation calc. 79—4643
chains of classical spins, weak ferromagnetism, antiferromag. even and odd chains 79—15268
classical mag. moment system, antiferromag. phase transition, secular dipole interactions 80—80551
cluster approximation, Neel temp. and specific heat calc. 80—54901
conference on magnetism, Munster, Germany (Mar. 1977) 78—10626
critical behaviour of three-dimensional antiferomagnet, fluctuation-induced first-order phase transitions, Monte Carlo calc. 77—85465
critical dynamics above crit. temp., dipolar coupling 78—52286
critical resistivity of antiferromagnets below T_c 78—68004
critical thermodynamics of antiferromagnet with two pairs of mag. sublattices *(Russian)* 78—60300
crossover, field-induced, in mag. chain, scaling theory 80—54904
cubic antiferromagnet, applied stress effects on equilib. config. 78—56365
cubic antiferromagnet, with exactly-known ground state 78—43540
cubic antiferromagnetic, first to second order transition crossover 78—10709
cubic flopped antiferromagnet, nuclear magnon relax. rates 77—63149
cubic spin model, one-dimens., ground states and magnetization in mag. field 79—78372
cylindrical magnetic domains, statistical props. 77—40080
de Haas-van Alphen effect, field depend. spin-splitting zero 80—84450
degenerate semiconductor, antiferromag., thermal and mag. props. 78—19224
dielectric, crit. behaviour of exciton relaxation consts. 78—84442
dilute antiferromagnet, ground state energy 77—40027
dilute antiferromagnet, impurity-induced mag. susceptibility *(Russian)* 77—32172
dilute Heisenberg antiferromagnet, mean spin on finite clusters 78—68139
dilute Heisenberg magnet excitations near percolation threshold 79—87270
dilute magnetic systems, with nearest-neighbor and next-nearest neighbour interactions, crit. temp. 79—61121
dilute paired antiferromagnet, bond dilution problem, CPA theory 79—78389
diluted antiferromagnet, linear spin-wave theory, effective medium approach 80—20393
diluted Ising and Heisenberg magnets with competing interactions, phase diagrams and mag. props. 80—34672
dislocation slowing down due to spin waves *(Russian)* 79—95584
disordered anisotropic antiferromagnet. random field effects 80—2580
disordered binary alloy, mag., with mixed exchange interaction, crit. behaviour *(Russian)* 79—1675
disordered linear chain, exchange probability distrib., Hubbard model 78—10641
disordered media, ferro- and antiferromag., and spin glasses, dynamic props. *(Russian)* 78—39350
disordered metamagnets, random field effects 80—60318
disordered one-dimensional system, Hubbard model 78—10642
disordered spin flop, bicritical behaviour, critical experiments 80—65899
disordered spin-flop antiferromagnets, random-field effects 80—11208
domain boundary movement, thickness depend. *(Russian)* 78—43611
domain structure of antiferromagnets in high-freq. mag. field 79—65694
domain structure theory, for antiferromagnet with weak ferromagnetism 78—47997
domain theory, intermediate state *(Russian)* 77—69616
domain wall eqns. of motion *(Russian)* 78—27054
domains, ferromagnetic and antiferromagnetic, neutron techniques for obs., review 78—64213
domains, indirect evidence, direct obs. methods, wall motion, review 79—51799
domains, rel. to dislocations *(Russian)* 77—51919
dynamic scaling deviation 77—31820
dynamical critical properties, using light scatt. as probe 79—15314
easy plane type anisotropy antiferromagnets, specific props. 79—1665

antiferromagnetism continued
easy-plane, coupled spin wave branches *(Russian)* 80—93096
easy-plane antiferromagnet, acoustic wave damping, effective phonon-phonon interactions 79—73797
easy-plane antiferromagnet, NMR under magnon bottleneck conditions, eqns. of motion 77—66429
effective spin 1/2 system correlated effective field theory 79—73759
elastic properties of magnetic materials, review 80—7142
electric dipole absorption of light, new mechanism *(Russian)* 77—32406
electron liquids, temp. mag. transitions 77—69563
electron-hole pairing systems, current states and domains 80—54614
EM and acoustic energy attenuation in many-domain magnets 80—7140
EM and acoustic response echoes of nuclear spin system *(Russian)* 79—69747
exchange-coupled one-dimens. anisotropic chain with $S=1/2$, comparison with expts. 77—20530
exciton motion in antiferromagnets, magnon approx. 80—70617
excitons, in magnetically ordered dielectric, review *(Russian)* 77—80943
extended Hubbard chain, excitonic effects on optical absorption 79—61323
extended Hubbard model, antiferromagnetic solution 78—19208
FCC alloys, atomic ordering and antiferromagnetism 78—72330
FCC lattice of second kind, surface magnons and mag. structs. 78—23261
FCC lattices, ordered superstruct., phase diagrams, cluster variation calc. 80—39256
Fermi liquid, critical phenomena, neutron scatt., Neel point *(Russian)* 80—71077
Fermi liquid model in external mag. field *(Russian)* 77—47952
ferroelectric antiferromagnet, coupled ferroelec.-magnetoelastic waves 77—51935
ferroelectric antiferromagnet, damping of spin waves and 'hard' excitation effect 79—28518
ferroelectric antiferromagnetics, spin wave fluctuations in strong mag. fields *(Russian)* 79—82773
ferroelectric antiferromagnets, exchange enhancement of the magnetoelectric coupling 78—88159
ferroelectric antiferromagnets, phase transformations *(Russian)* 80—93114
ferroelectric ferro- and antiferromagnet, energy gap in spin wave spectrum 78—91858
ferroelectroantiferromagnetics, spin wave spectrum and exchange amplification of magnetoelectric correlation 79—38311
ferroics, secondary, polycryst., poling effects 77—16102
ferromagnet-antiferromagnet alloys, phase diagrams and multicrit. points in random mixed magnets 79—73756
ferromagnets and spin glasses, supercond. and mag. order 80—93029
field-theory renormalization and critical dynamics above T_c: helium, antiferromagnets, and liquid-gas systems 78—87767
film, surface spin waves and surface anisotropy effects at finite temp. 79—78452
first order orientational transition, sound propag. anomalies 77—1580
first-order orientational phase transition in antiferromagnet, second acoustic-harmonic generation 78—27067
gamma-rays generation by fast electrons travelling through antiferroelectric or antiferromagnetic crystalline structures 78—76545
garnets, review of experimental data 77—80952
ground state energy, renormalisation procedure 79—40486
ground state energy for linear antiferromagnetic Heisenberg chain, neighbour interactions 80—84606
ground states, phase transitions and spin wave spectra 79—87246
heavily doped semiconductor, stability of canted antiferromag. order 77—12095
Heisenberg, spin $^1/_2$ dil. magnet, crit. props. 80—15733
Heisenberg and biquadratic exchange, eigenstates of short chains of spin-1 atoms 77—55652
Heisenberg anisotropic antiferromag., spectrum and correlation functions 79—28499
Heisenberg anisotropic linear chain, spectral density method 79—47222
Heisenberg antiferromagnet, ABX_3-type, exchange interaction and zero-point spin reduction 77—12080
Heisenberg antiferromagnet, AFMR freq. temp. depend., integral peak intensities *(Russian)* 80—54951
Heisenberg antiferromagnet, anisotropic, excitations at finite temp., CPA calcs. 79—95562
Heisenberg antiferromagnet, anisotropic, spectrum and correl. functions in spin-flop phase in generalized HF approx. 78—39283
Heisenberg antiferromagnet, dil. two dimensional, mean spin per site in linearised spin-wave theory 78—39304
Heisenberg antiferromagnet, dil. with random first- and second-neighbour exchange bonds, CPA theory 78—52187
Heisenberg antiferromagnet, disordered, magnetic atom-conc. near percolation threshold, mag. props. *(Russian)* 78—80171
Heisenberg antiferromagnet, exchange interaction, kinetic, in narrow S-band 77—55655
Heisenberg antiferromagnet, excitations at finite temp. using CPA 79—56554
Heisenberg antiferromagnet, Green function theory 80—107975
Heisenberg antiferromagnet, isotropic, hydrodynamic spectrum at low temp. 79—73663
Heisenberg antiferromagnet, light scatt. off surface 78—23475
Heisenberg antiferromagnet, magnon renormalisation, two-magnon Raman scatt., kinematic interaction 78—23228
Heisenberg antiferromagnet, magnon renormalisation 78—23259
Heisenberg antiferromagnet, one dimens., spin-flop transition 79—73723
Heisenberg antiferromagnet, one-dimens., autocorrelation function, low freq., temp. and field depend. 80—65929
Heisenberg antiferromagnet, one-dimens., Friedel type oscills. 78—60296
Heisenberg antiferromagnet, one-dimens., impure, mag. susceptibility 80—60168
Heisenberg antiferromagnet, one-dimens. spin 1/2 dimerised, renormalisation group and other calcs. 79—78393
Heisenberg antiferromagnet, one-dimensional, spin waves in spin-flop phase 80—44817
Heisenberg antiferromagnet, phase transitions in quantum spin systems 78—84434
Heisenberg antiferromagnet, quadratic spin 1/2, sp. ht. and susceptibility, comparison with $Cu(C_5H_5NO)_6(BF_4)_2$ data 77—66353
Heisenberg antiferromagnet, randomly dilute, mag. transitions, MFA-VCA theory 77—63219

antiferromagnetism continued
Heisenberg antiferromagnet, randomly diluted, field-induced phase transitions 77—36089
Heisenberg antiferromagnet, s=$^1/_2$ linear, zero-temp. dynamics in mag. field 80—65764
Heisenberg antiferromagnet, uniaxial, props. by Green's function method 77—85406
Heisenberg antiferromagnetic alloy, critical behaviour *(Russian)* 78—88128
Heisenberg antiferromagnetic alternating spin 1/2 chains, susceptibility calcs., spin-Peierls transition 79—78394
Heisenberg antiferromagnetic chain, random, low temp. thermodynamic props. in zero mag. field 80—34657
Heisenberg antiferromagnetic chain, spin dynamics, quantum effects 80—34651
Heisenberg antiferromagnets, relax. functions, method for calc. transport coeffs. 77—69474
Heisenberg antiferromagnets, S=∞ two-dimensional, approx. to susceptibility 77—80905
Heisenberg bicritical points in antiferromagnets, universality tests 80—84604
Heisenberg chain, alternating, appl. of zero temp. quantum renormalisation group 80—80526
Heisenberg chain, classical, nearest-neighbour, low temp. dynamics 80—80524
Heisenberg chain, dimerised, spin dynamics 77—20528
Heisenberg chain, first-order Peierls transition 78—34986
Heisenberg chain, nonsinglet excitations 77—4491
Heisenberg chain, one-dimens. spin 1/2 dimerised, spectral excitations, renormalised group calc. 79—78295
Heisenberg chain, spin 1/2, excitations energy 78—6503
Heisenberg chains, antiferromag., ground state energies 78—23230
Heisenberg classical nearest-neighbour chain, dynamics, exact perturbative results 78—10700
Heisenberg classical spins on triangular cactus tree, random ordered phase 79—87265
Heisenberg dilute systems, computer simulation, mag. conc. of clusters, linearised eqns. of motion 79—78409
Heisenberg exchange integral, in nonorthogonal basis, for anti- and ferromag. systems 78—2641
Heisenberg impure antiferromagnetic, impurity banding and mag. reson., theory 80—93181
Heisenberg linear chain, dynamical correl. functions 77—63221
Heisenberg linear chain, spectral density approach 77—40023
Heisenberg linear chain, spectral density approach decoupling effect 77—80903
Heisenberg linear spin systems, dynamical spin correlation functions 78—31035
Heisenberg magnets, with two kinds of exchange interactions, surface magnons and surface spin arrangements 77—36043
Heisenberg model, 1-dimens., two-spin IR absorpt., Green's function and classical moments theories 77—40025
Heisenberg model, anisotropic, finite cell calcs. 80—60164
Heisenberg model, classical, low temp. spin wave dynamics 78—6501
Heisenberg model, classical antiferromag. chain, low temp. dynamics 80—39803
Heisenberg model, dil, CPA calc. 78—68263
Heisenberg model, ground state energy, pair correl. 78—72321
Heisenberg model, ground state energy, renormalisation calc. 79—61150
Heisenberg model, helical spin chains, static and dynamic props. 79—73661
Heisenberg model, phase diagram and multicrit. behaviour 78—56337
Heisenberg model, quasilow dimensional, small dilution perturbation theory at 0K 78—56281
Heisenberg model, randomly dil., excitations 78—23258
Heisenberg model, second order Green's function 78—43545
Heisenberg model, second order self-energy 78—56279
Heisenberg model, short range order effects on EPR frequencies 77—69669
Heisenberg model, specific heat, high-temp. expansions, numerical investigation *(German)* 77--59420
Heisenberg model, spin waves at finite temp., CPA calc. 79—73728
Heisenberg model, square lattice, ground state energy 77—80904
Heisenberg model, zero temp. props. in 3 dimens. 79—61032
Heisenberg one-dimensional magnet, classical, nonlinear dynamics 80—71056
Heisenberg quantum chain near T=0, exact results 79—78291
Heisenberg randomly dil., antiferromag., spin wave excitation exam. 77—24665
Heisenberg S=1/2 antiferromagnet, ground state props. 79—15274
Heisenberg theory, spin wave exam. *(Dutch)* 79—1663
Heisenberg two-dimens. S=1/2 model, excitation spectra numerical exam. 77—36044
Heisenberg-Ising magnets, random, critical temps., binary mixture, amorphous magnet and spin glasses 80—54911
hexagonal antiferromags., ground states antiferromag. vectors, ferromag. moments *(Russian)* 78—27040
high frequency properties, spin wave spectra corrections, magnon interactions *(Russian)* 80—54876
high-frequency props. of weak ferromagnets and antiferromagnets, singularities *(Russian)* 80—50196
honeycomb lattice, real space renormalisation, ferromag. (antiferromag.) appls. 80—11200
Hubbard antiferromag. semiconductor, electron correlations, weak coupling 78—67969
Hubbard antiferromagnetic semiconductor, collective excitations, weak coupling limit 78—19210
Hubbard chain, half-filled band, strong coupling, low temp. absorpt. lineshape 77—59546
Hubbard chain, interband absorpt., Peierls dimerisation, excitonic effects 80—25072
Hubbard linear chain, disordered, arbitrary filling case 78—31043
Hubbard model, antiferromagnetic ground state 79—82742
Hubbard model, antiferromagnetic ordering onset, alloy analogy approx. 77—36049
Hubbard model, antiferromagneiism onset 78—19206
Hubbard model, cluster-variation method in two-site approx. at high temp. 80—7071
Hubbard model, degenerate, charge-ordered soln. 78—39284
Hubbard model, degenerate in mag. field, appl. to Jahn Teller systems 77—28358

antiferromagnetism continued
Hubbard model, doubly degenerate, functional integral approach 79—99711
Hubbard model, effects of four spin interactions 77—51885
Hubbard model, electron struct. in mag. field *(Russian)* 78—60287
Hubbard model, FCC, fourth order interaction effects 78—23235
Hubbard model, FCC lattice, mag. and elec. props. 78—56334
Hubbard model, half-filled, ground-state energy and momentum distrib. 77—47961
Hubbard model, half-filled s-band 77—63070
Hubbard model, itinerant antiferromagnetism 78—91841
Hubbard model, Mott metal-insulator transition, ten-fold spin-orbital degeneracy 78—52285
Hubbard model, one-dimensional, with nearest and second nearest neighbour hopping in Hartree-Fock approx. 77—32149
Hubbard model, static approx., mag. phase transitions 77—1558
Hubbard model, transforms 77—72972
Hubbard model, two band, mag., orbital and charge ordered states 78—27012
induced staggered magnetic fields in antiferromagnets, microscopic mech. 80—80527
inelastic light scattering from antiferromag. polaritons, theory 77—73144
insulating systems, magnetic, review of expts. 78—68240
insulator, antiferromag., light scatt. in strong mag. field 78—72523
insulator, impurity doped, spin glass 79—51796
insulator, magnetothermal resist. 77—35767
insulator, strongly anisotropic, spin config. and magnon spectrum 77—8279
insulators, lattice thermal cond. 80—65319
intermediate state, stability in HF mag. field *(Russian)* 79—95591
intermediate valence compounds, phonon produced instabilities, periodic Anderson model 78—79964
interphase boundary dynamics, domain wall motion and scatt. *(Russian)* 80—108032
intrinsic magneto-optical effects, phenomenological anal. 79—33679
intrinsic semiconductors, indirect exchange interaction, finite temp., valence bands and energy gaps effect 80—59943
IR absorption on impurity excitations near upper edge of spin-wave band of antiferromagnet 80—80829
Ising, 2- and 3-dimens. lattices, appl. of Kadanoff's variational approx. 80—2583
Ising, spin $^1/_2$ dil. magnet, crit. props. 80—15733
Ising antiferromag. phase boundaries, hard-core lattice gas calcs. 80—80542
Ising antiferromagnet, crit. props., calc. 80—65946
Ising antiferromagnet, FCC, nearest neighbour interactions, Monte Carlo method 80—80544
Ising antiferromagnet, finite field, second-order phase boundary, series investigation 79—42777
Ising antiferromagnet, induced staggered mag. fields, g-factor mechanism 77—55676
Ising antiferromagnet, nonlinear response to high freq. mag. field, quantum theory *(Russian)* 80—93066
Ising antiferromagnet, phase boundary, crit. temp. field depend., Monte Carlo anal. 78—34995
Ising antiferromagnet, square lattice, interface free energy and transition temp. 77—73041
Ising antiferromagnet, triangular, improved mol. field approach 79—73745
Ising antiferromagnet, two-dimens., mag. susceptibility calc. 80—60225
Ising antiferromagnet, with nearest neighbour ferromag. interaction, tricrit. behaviour 77—40062
Ising antiferromagnet with next-nearest-neighbour interactions, tricritical exponents and crossover behaviour 77—16089
Ising chain in 3-dimensional phonon field, rel. to spin-glass models 79—56540
Ising FCC antiferromagnet, mag. phase diagram, ordering, Monte Carlo calc. 80—103833
Ising ferro and antiferromagnet random bond mixture, on s.c. lattice, phase transition 77—12131
Ising ferro- and antiferromagnet, quenched random mixture, Bethe approx. for phase transition 77—16082
Ising ferromagnet and antiferromagnet, two-dimens. square, ground state, apparent 3-spin interactions 80—88709
Ising lattice, degeneracy at crit. mag. field and zero temp. 79—8007
Ising mixed ferromagnetic-antiferromagnetic systems with arbitrary spin, critical temp. 79—78407
Ising mixture, quenched random, on Cactus tree 77—16081
Ising model, 3-dimens., with finite entropy at zero temp. 77—40021
Ising model, antiferromag. case, modified Kadanoff variational renormalisation method 80—88710
Ising model, antiferromagnet, phase boundary determ. by real space renormalisation group methods 78—88134
Ising model, BCC, crit. behaviour in mag. field, Monte Carlo calc. 78—31088
Ising model, BCC, in mag. field, Monte Carlo calcs. 78—31032
Ising model, bond random, ferromagnetic-antiferromag. mixture, triangular cactus tree, statistical theory 80—75702
Ising model, dilute-bond, spin-glass phase transition 77—69569
Ising model, disordered, thermodynamic pot., ferro-and antiferromagnetic bonds, mag. moment and entropy *(Russian)* 79—19714
Ising model, ferromag. and antiferromag. in mag. field, new perturbation approach 78—56336
Ising model, free energy and susceptibility inequalities, phase transition 78—43541
Ising model, in mag. field 80—11203
Ising model, spin-glass, renormalisation group calc. for two dimens. models 78—14968
Ising model, three-dimensional, two-spin correlation function, method for phase diagram 78—56323
Ising model, Toulouse frustration effect 79—24167
Ising model, triangular, mag. field depend. transition temp. 77—8323
Ising model, triangular, with transverse field, zero temp., ground-state props. 80—7115
Ising model, tricritical phenomena, nearest neighbour and next nearest neighbour interactions 77—69566
Ising model, two-dimens., interface free energy 78—60261
Ising model, with transverse field, ferromagnetic and antiferromagnetic susceptibilities 80—60160
Ising model, with transverse field 77—77016
Ising model, with zero field splitting, multicritical behaviour 77—12136

antiferromagnetism continued
Ising model on triangular lattice, phase diagram, free energy 78—23283
Ising model with competing interactions, critical properties and exact results 80—93129
Ising model with random exchange bonds, phase diagram 78—43604
Ising $S=1$, $^1/_2$ mixture, one-dimens., random, mag. props., spin distrib. 78—95407
Ising site model, random mixtures, Monte Carlo simulation 78—73935
Ising site model, random mixtures, Monte Carlo simulation 78—73936
Ising spin glass, d-dimensional, frustration effect 80—108019
isotropic antiferromagnet, magnetic moment and sp. ht. fluctuations near critical temp. 78—91867
isotropic antiferromagnets, anal. by equivalent Hamiltonian method 79—82734
isotropic antiferromagnets, crit. dynamics using renormalisation group methods 79—8006
isotropic antiferromagnets, crossover behaviour of mag. phase boundaries 79—78370
isotropic linear chain, antiferromag., ground state, spectral density method 77—85407
itinerant, effect of imperfect nesting of band struct. 78—31045
itinerant, s-band Hubbard model, zero temp. props. 77—4493
itinerant antiferromag., partially disordered, electronic density of states 77—4494
itinerant antiferromagnet, paramag. impurity effects on Neel temp., calc. 80—60257
itinerant electron, dynamic magnetisation as internal Josephson effect 78—47931
itinerant electron, mag. excitations 78—56305
itinerant electron antiferromag., localised mag. states 79—28500
itinerant electron antiferromagnet, localised spin coupling 78—68142
itinerant electron antiferromagnet, spin wave spectrum calc. 77—36063
itinerant electron antiferromagnetic matrix, local moments, spin Hamiltonian 80—34626
itinerant electron ferro- and antiferromagnetism, spin fluctuations 79—7961
itinerant electron model, effect of mag. field 78—27013
itinerant electron model, susceptibility, local exchange approx. calc. 80—60169
itinerant electron model for ferro- and antiferromag. systems, dynamic susceptibility 77—72988
itinerant electron system, antiferromagnetism model 80—2547
itinerant electron system, coexistence of antiferro- and ferromagnetism 78—2645
itinerant electron system, cond. transition to antiferromag. metallic phase 77—72980
itinerant electron theory, spin susceptibilities 78—6504
itinerant magnetic-systems, general alloy analogues 77—85410
itinerant magnets and superconductors, structural instabilities, phase diagrams 78—14922
itinerant model, antiferromag. instability and energy gap 78—31044
itinerant model, spin density wave transition, impurities effect 77—72986
itinerant-electron, possible coexistence with itinerant-electron ferromagnetism 78—39286
itinerant-electron antiferromagnet, effect of mag. field on crit. temp. 78—60293
itinerant-electron antiferromagnet elec. resistivity near Neel temp. 79—42742
Kadanoff's variational approximation applied to the 2-D antiferromagnetic Ising lattice 79—73659
kinetic exchange interaction, doubly degenerate narrow bands 78—23263
Kondo Hamiltonians with non-zero ground-state spin 79—51746
Krieger-James approx. of short range order effects, antiferro- and ferromag. 78—56276
lattice, ground-state energy calc., Kadanoff cells renormalisation procedure 77—77015
lattice spin model with multicrit. pt., soln. in spherical model limit 77—66338
lattice systems with short-range and Coulomb interactions 80—82715
layer systems, mag. polaritons 78—31060
light absorption in antiferromag. 77—48149
linear chain, biquadratic exchange interaction effects 77—63062
linear chain, disordered, q-depend. mag. susceptibility 78—27010
linear chain, ground state energy upper bound from trial functions 79—78293
linear chain antiferromagnet, interface with liq. ^{3}He, anomalous thermal behaviour and nucl. spin relax. of ^{3}He 79—56002
linear Heisenberg antiferromagnet, $S={}^1/_2$ zero temp. dynamics 79—73741
linear-chain antiferromagnet, sine-Gordon solitons 80—80543
local field at positive muon 78—92010
localised magnetic moments in band antiferromagnets, impurity interactions *(Russian)* 80—54888
localised model for systems with double-exchange coupling 79—38318
low crystal anisotropy, nuclear spin waves spectra, relaxation, parametric excitation, NMR dynamic shift *(Russian)* 80—11180
low-dimensional susceptibility 79—28513
Lu-tinger-Tisza method generalisation, appl. to highly anisotropic dipole-dipole interactions 77—20514
macroscopic quadrupole field meas. with SQUID magnetometer, order determ. 79—24140
magnetic and thermal props. of antiferromagnets 78—14937
magnetic dipoles on a lattice, theory at low temps. 80—50082
magnetic dislocation domains, mag. moment distribution 80—2601
magnetic excitations within local exchange approx. 77—69517
magnetic impurity levels, standard basis operator method *(Russian)* 80—11192
magnetic materials, μSR meas. 79—56660
magnetic ordering in antiferromagnets without spatial struct., phase transitions *(Russian)* 80—50134
magnetic phases, spin configurations in external field 80—70955
magnetic semiconductor, light scatt. by magnons, appl. to $CdCr_2Se_4$ and EuTe 77—69805
magnetic susceptibilities in Heisenberg and Ising models 79—24185
magnetisation, crit. spin-flop angle, temp. and field depend. *(Russian)* 80—7111
magnetisation density waves, weakly linear 77—51888
magnetisation fluctuations of first-order spin-flop phase transition near crit. point 77—24708
magnetisation nonlinear waves *(Russian)* 79—91251
magnetoacoustic resonance of domain boundaries *(Russian)* 80—65636

antiferromagnetism continued
magnetoelastic coupling in nonlinear acoustic phenomena, exchange interaction effects *(Russian)* 77—90010
magnetoelastic soliton propag. 80—66003
magnetoelasticity, exchange enhancement 79—87299
magnon and phonon damping, effect of intermediate state lifetime 79—24151
magnon damping, influence of magnetoelastic interaction 79—28517
magnon damping due to impurity scatt. 78—68206
magnon damping due to magnon-phonon interactions *(Russian)* 79—11305
magnon damping in zero external mag. fields, magnon-magnon interactions 80—70988
magnon parametric generation with impulses at Brillouin zone boundary *(Russian)* 80—29540
magnon-photon interaction for EM wave vector perpendicular to sublattice magnetisation 79—69662
many-valley semiconductors, antiferromagnetic or atomic ordering effects on conduction electrons 80—2329
metal, antiferromag., magnetoresistance, two band model 78—79979
metal, antiferromag., thermoelec. power in mag. field 80—70686
metal, antiferromagnetic, nesting type model, spin fluctuations 78—56329
metal, electron scatt. features, s-d exchange model 77—8085
metal, magnetoelastic coupling effect on magnetoelec. reson. 80—75837
metal, with paramag. impurities, Neel temp., impurity conc. depend. calc. 78—68232
metal antiferromag. critical resistivity, appl. to Dy 79—47077
metals, magnetic, Seebeck coefficient anomaly near spin ordering temp. 77—20302
metals, Neel temp. and crit. exponents determ. from electronic transport coeffs. 77—69556
metamagnetic phase transitions, theory 78—39327
metamagnetic transitions, theory 77—16076
mixed magnets, competing spin glass and mag. order, phase diagrams, crit. points 80—39802
mixture of two antiferromag. with different easy axis, mag. props. 79—4660
Mott insulator, magnetism and charge ordering 79—60751
Mott-Hubbard insulator, one-dimens., charge transfer absorpt. 79—37958
moving dislocations, interactions with spin waves in antiferromagnet *(Russian)* 78—56303
narrow band gap semiconductor, antiferromag. in strong mag. field *(Russian)* 77—28387
Neel temperature of low-dimensional antiferromag. in mag. field 77—32200
neutron optical activity in helicoidal antiferromagnetic materials 78—74419
neutron scattering studies of one- and two-dimens. mag. systems, review 77—66254
NMR frequency, amplification and dynamic shift, rel. to local mag. props. *(Russian)* 77—20722
noncollinear, exciton-magnon light absorpt. at $T\neq O$ *(Russian)* 78—23482
nonlinear waves in antiferromags., domain boundary description 80—84612
nonsymmetry distrib. of parametrically excited waves *(Russian)* 78—47967
nuclear magnetic relax. of two-dimens. antiferromagnet *(Japanese)* 78—19364
nuclear magnetisation, temp. dependence 79—33462
nuclear magnetisation motion under parametric influence of longitudinal RF field *(Russian)* 79—82880
nuclear magnetism 77—63124
nuclear orientation in antiferromagnets 78—43652
nuclear secondary echo in ferromagnets and antiferromagnets 79—73852
nuclear spin lattice relaxation, field depend. of dipolar-induced two-magnon process 78—6593
nuclear spin oscillations, interaction with lattice vibrs. 80—70996
nuclear spin wave relax. 80—65850
nuclear spin-lattice relaxation, possible magnon bottleneck 77—32283
one dimensional anisotropic Heisenberg model, spin 1/2, Ising like antiferromag., dynamic correlation function 80—75704
one dimensional system, Kondo lattice and weak antiferromagnetism 77—73038
one-dimensional, thermodynamically stable long-range order *(Russian)* 79—27946
one-dimensional antiferromagnet, interchain coupling, effect on US attenuation 80—19880
one-dimensional antiferromagnet, nonlinear dynamics 80—80521
one-dimensional antiferromagnet, renormalisation group nearest neighbour interactions 80—60357
one-dimensional antiferromagnet, with antisymmetric exchange, Green's function theory 79—15290
one-dimensional dilute Heisenberg system, mag. props. 78—64179
one-dimensional disordered spin system with isotropic antiferromag. interaction, susceptibility and Knight shift *(Russian)* 78—88202
one-dimensional disordered systems, magnetism 80—25152
one-dimensional electron system, generalised susceptibilities in mag. field *(Russian)* 77—80750
one-dimensional Heisenberg antiferromag., dynamic struct. factor 79—28497
one-dimensional Heisenberg antiferromagnet, spin wave theory 79—91222
one-dimensional Hubbard model, antiferromag. and Peierls instability 78—23233
one-dimensional magnetic systems, sound attenuation at finite temp. 77—63247
one-dimensional organic semiconductors, resonant states, mag. excitations and impurities 80—24839
one-dimensional system, correl. functions, limiting relationships 77—62790
one-dimensional system obeying third law of thermodynamics, exact theory of mag. cooling 77—66321
one-magnon light scatt. from antiferromag., effect of anisotropy 79—33676
one-magnon light scatt. from metamagnetic phase effect of anisotropy 79—33678
one-magnon light scatt. from spin-flop and paramag. regions, effect of anisotropy 79—33677
one-magnon states in BCC Heisenberg antiferromag., spectral density near stepped surfaces 80—20396

antiferromagnetism continued
- pair interaction and arbitrary fields, correlation inequalities, Ginibre-Percus double variables method 80—68147
- parallel susceptibility of chain-like antiferromagnets 78—80137
- parametric excitation of sound near phase transition point 79—69710
- parametric excitation on spin waves in the induced magnetoelastic crystals *(Russian)* 78—60272
- Peierls antiferromagnet, and exciton ferromag., two-parameter Landau expansion 79—23907
- Peierls-Hubbard model, antiferromag. and lattice-distortion 77—47964
- Peierls-Hubbard model, antiferromagnetism and lattice distortion 77—55656
- Peierls-Hubbard model, quasione dimens., antiferromagnetism and Peierls distortion 78—67931
- phase transformations in strong mag. fields, mag. moments collapse, strengthened magnetoelastic links *(German)* 78—68227
- phase transition crossover from first- to second-order in symmetry-breaking field 79—82805
- phase transitions, Landau Ginzburg Wilson Hamiltonian for n=4 type II antiferromagnets 80—15735
- phase transitions in antiferromagnets with order parameters of dimension six and three 79—42762
- phonon relaxation in antiferromagnets with dislocations 79—69216
- phonon-magnon relaxation times, external mag. field depend. 80—44898
- Poisson brackets, nonlinear hydrodynamics eqns. in condensed matter physics 80—54296
- polarisation analysis of diffuse neutron scattering from magnetic systems 80—25098
- polaritons, antiferromag., dispersion relation and light scatt. 77—35871
- Potts model, three-state 78—23279
- pseudo-one-dimensional antiferromagnets, thermodynamic variables 80—65935
- quadratic antiferromagnet, with easy-plane anisotropy, spin wave theory 78—91855
- quantum anisotropic antiferromag. Heisenberg model, Gibbs state limitation 80—50027
- quantum critical dynamics with mode coupling 80—108024
- quantum spin systems, ground state energies, renormalisation techniques appls. 80—93132
- quantum spin systems, renormalisation group transformation 78—47984
- quasi one-dimensional spin lattice coupled system, collective modes 80—24896
- quasi-one-dimens. system, Peierls insulator and antiferromagnetic mixed phase 77—20626
- quasi-one-dimensional electron systems, instabilities, mean field approx. 78—23036
- quasi-two-dimensional antiferromagnet, nonreson. HF field absorpt. *(Russian)* 77—63287
- radiation problem of parallel pumping, magnon-photon interaction 79—51934
- random annealed one-dimensional Ising spin system, site model, specific heat, susceptibility 77—32139
- random antiferromagnetic chain, quantum spin-1/2 Heisenberg soln. 80—11148
- random antiferromagnets, crit. and multicritical props. 80—60332
- random binary magnetic systems, quenched, Neel temp. calc. 77—89963
- random exchange Heisenberg antiferromagnetic chain, exchange-coupled pair model 80—20423
- random exchange interactions, and 'frustration effect' 78—68212
- random ferromagnetic-antiferromagnetic alloy, elementary excitations 79—8001
- random mixture of ferro- and antiferromag. exchange interactions, high temp. expansion 78—23280
- random ordered phase in site model, statistical theory 79—47218
- random quenched mixtures, ferro- and antiferromagnetic exchanges 77—51864
- random quenched site model, competing exchange energies and competing anisotropy energies 80—29552
- rare earth alloys, amorphous, study of hysteresis effects using Monte Carlo technique 79—1686
- rare earth antiferromagnet, magnetic excitation, appl. to DySb 79—78358
- relaxation processes in antiferromagnet, theory 77—24750
- residual stress induced domains in antiferromags., specific heat meas. anal. 78—60286
- resistance critical behaviour, temp. and mag. field depends. 77—73037
- resistive anomalies at mag. crit. points, effect of inelastic scatt. 77—55675
- resistivity of magnetic systems, critical behaviour 78—87955
- rhombohedral antiferromagnet, spin-reorientation phase transition *(Russian)* 80—93122
- S=1, singlet ground state systems, mag. props. 80—11157
- s-f model with electron-hole reson., antiferromag. behaviour and phonon spectrum 78—47992
- scaling and multiplicative renormalising in solid state physics *(Hungarian)* 79—11289
- screw spin ordered state through dipole-dipole interaction 78—39337
- second-order phase transition, weakening of effect of fluctuation in order parameter near crit. point 79—15316
- semiconductor, antiferromag., ferron-polaron states of carriers 77—69257
- semiconductor, antiferromag., magnon-spin flip excitations in Raman scatt., g-factors 77—66494
- semiconductor, conductive electron spectrum, influence of nonlinear spin waves 79—28270
- semiconductor, double exchange and small-polaron hopping 79—19591
- semiconductor, magnon-plasmon interaction and its effect on Raman scatt., theory 78—56302
- semiconductor, sound propagation 78—72211
- semiconductor, spin-magnetomagnon resonance 80—2566
- semiconductor, theory of Raman scatt. due to magnon-spin flip excitation 77—36209
- semiconductors, antiferromagnetic, magnetoelec. effect, magnetization and ferroelec. props. 80—25180
- semiconductors, heavily doped, Faraday light depolarisation in mixed mag. states 80—29726
- singlet ground state system, mag. props. 80—44850
- singlet ground state system in mag. field, anisotropic exchange interaction effect on props. 79—91224
- sound absorption in low temp. antiferromagnets 79—69711
- sound damping by phonon-magnon interaction, high Neel temp. *(Russian)* 78—43626

antiferromagnetism continued
- spherical model, eqn. of state near phase boundary 77—55681
- spin arrangement of field-induced phases, mag. space groups 77—32166
- spin density wave antiferromagnet, neutron scatt. by magnons, modulated spin amplitudes 80—75722
- spin density waves, mag. anisotropy 77—69540
- spin dynamics near bicrit. points in uniaxial antiferromag. 77—16090
- spin fluctuation resistivity near T_N, theory 77—40071
- spin glass, antiferromagnetic clusters, mean-field approx., static props. 79—4689
- spin glasses, dilute ferromagnets, ferromagnetic modes 80—93133
- spin Hamiltonian with four spin interactions for BCC, lattice, mean field theory 79—1652
- spin one Heisenberg antiferromagnet, with uniaxial anisotropy, thermodynamic props. 79—56539
- spin wave parametric excitation by noise pumping *(Russian)* 80—34617
- spin wave relaxation in strong mag. field 78—2747
- spin waves, mechanism for hard excitation *(Russian)* 78—19235
- spin waves, microwave and optical expts., review 80—50081
- spin waves, parametric instability *(Russian)* 78—34971
- spin waves in absorptive mag. material, light scatt. lineshape 78—23476
- spin waves in weak antiferromagnetic exchange field system 78—43577
- spin-1, with biquadratic exchange, sublattice magnetisation and Neel temp., RPA 77—47953
- spin-1/2 cubic lattice, with anisotropic exchange, configs. 80—65926
- spin-flop multicritical points in systems with random fields and in spin glasses 79—33495
- spin-one Ising system, phase diagram 78—95441
- spin-Peierls transition, dynamic struct. factor 78—14964
- spin-Peierls transition in mag. field, phonon freq., Heisenberg model calcs. 80—25151
- spin-wave spectrum in antiferromagnet Heisenberg 1-dimens. chain, external mag. field effect 77—89943
- square-lattice Ising antiferromagnet, interface props. and transition temp. 79—42787
- staggered magnetisation in antiferromagnets, crit. fluctuations, AC susceptibility meas. 80—60219
- static properties of spin systems with truncated secular dipolar coupling 78—88130
- statistical models, thermodynamic properties, variational calc. 77—85405
- strongly correlated electrons in narrow bands 78—76218
- sublattice magnetisation temp. depend., appl. to $KCuF_3$ 77—51892
- sublattice metamagnet, temp. dependent anisotropy, magnetisation curves, mag. transitions, classical approx. 80—39795
- substrate for ferromag. film, parametric reson. in film *(Russian)* 77—90043
- superconductor, antiferromag., isolated vortex line 80—70912
- superconductor, magnetic, Fermi surface nesting effect on mag. instability 80—54831
- superconductor, surface impedance 79—82709
- superconductor, uniaxial antiferromag., depend. of crit. field on supercond. order parameter 79—87219
- superconductors, antiferromag., new pairing state, pair destruction, theory 80—54847
- superexchange antiferromag., charge transfer light absorpt. 78—34975
- superfluid flow states, existence from Ginzburg-Landau theory *(Russian)* 78—72085
- surface, itinerant antiferromagnetism and density waves 79—82743
- surface, ortho to para H_2 conversion 79—34362
- surface magnetic moment, induced, effect on spin-wave spectrum 78—19234
- surface spin-waves, long-wavelength 80—88737
- surface structure, adatoms, electron state at high coverages 79—28400
- susceptibilities of S=1/2 XY model on the square lattice at T=0 80—88732
- susceptibility, parallel, ferromag. and anti-ferromag., graphical illustration, for teaching 78—41118
- susceptibiltiy and sp. ht., reln. between temp. depend. *(German)* 77—69567
- TCNQ alkali salt, spin-Peierls transition, 1-D antiferromag. Heisenberg model 80—29395
- tetragonal XY-like antiferromagnet, multicritical behaviour, global phase diagrams 79—42779
- thin films, two dimens. spin-wave theory, spontaneous magnetisation parameter depend. 80—34714
- transition metal fluorides, magneto-optical effect in longitudinal mag. field *(Russian)* 77—85694
- transition metals, conf., Toronto, Canada (Aug. 1977) 78—91577
- transition to superconductivity, model 79—82706
- transverse dynamical susceptibility within the local exchange approx. 78—76229
- transversely anisotropic antiferromagnets, spin-wave theory of paramag. phase boundary 77—69552
- triangular antiferroamgnetic lattice, ground state energy, upper bound determ. using renormalisation 78—76212
- triangular antiferromagnet, spin wave theory 79—7978
- triangular Ising lattice with small second neighbour interaction crit. temps. 78—56331
- triangular Ising model with anisotropic interactions, phase diagram 79—51798
- two-dimens. XY magnet and Heisenberg antiferromagnet, ground state anal. 79—42728
- two-dimensional antiferromagnet, with easy-plane anisotropy, mag. excitations and two-magnon Raman scatt. 80—65839
- two-dimensional antiferromagnets, approx. to susceptibilities 78—47928
- two-dimensional antiferromagnets, diffusion-controlled mode coupling, EPR linewidth 79—51844
- two-dimensional antiferromagnets, expansion for suceptibilities 80—70963
- two-dimensional Ising antiferromagnet, neutron scatt., review 80—50103
- two-dimensional Ising antiferromagnet, transition temp., appl. of real space renormalisation techniques 79—78420
- two-dimensional lattice, cluster expansion method 78—34942
- two-magnon Raman scattering, temp. effects 77—48178
- two-spin light scattering, disordered phase rutile antiferromags., MnF_2, NiF_2 78—80336
- two-sublattice Neel-type, stable spin configurations, external mag. field and single-ion orthorhombic anisotropy effects 80—60249
- type I and type II antiferromagnets, first-order phase transition 78—39332
- type II antiferromagnet with bilinear and biquadratic coupling, magnetic excitons in cubic cryst. field 79—78353

antiferromagnetism continued
uniaxial antiferromagnet, crit. dynamics at bicritical points 80−15321
uniaxial antiferromagnet, effect of magnetostriction on reorientation phase transitions 79−69674
uniaxial antiferromagnet, influence of field direction and single-ion anisotropy on phase diagram 77−16072
uniaxial antiferromagnet, mag. polaritons in spin-flop phase 78−23349
uniaxial antiferromagnet, nonuniform spin configurations 80−97109
uniaxial antiferromagnet, spin configuration in ferromag. phase, field and temp. depend. 79−38321
uniaxial antiferromagnetic, phase diagram, spin flop transition *(Russian)* 80−100587
uniaxial antiferromagnets, crystalline anisotropy energy determ. from low field torque data 78−19245
uniaxial antiferromagnets in transverse mag. field, quantum theory, spin configuration 79−69647
uniaxial Heisenberg antiferromagnet, phase diagrams 80−15730
uniaxial Lifshitz point, Monte Carlo calcs. 78−39353
uniaxial S=1 antiferromagnet, effect of cryst. field anisotropy 77−28344
vacancy distribution along mag. sublattices in β-brass type ferro and antiferromagnetic alloys *(Russian)* 80−79783
weak ferromagnet, paramagnons and phase transitions 77−61015
weak metamagnets, novel multicritical points 79−78398
weakly anisotropic, effective anharmonicity of elastic subsystem 77−69658
Wolff model, effective mag. interactions between impurity and conduction electrons 78−68143
X-Y antiferromagnet, one-dimens., Friedel type oscills. 78−60296
X-Y model, ground state energy, renormalisation calc. 79−61150
X-Y model, spin Peierls transition in mag. field 79−56537
X-Y quasi-one-dimens. system anisotropic, spin-Peierls phase transition, tricritical point 80−25142
Cu_3Au type antiferromagnet Ising lattice, finite entropy at T=0, phase transition 77−89958
$CuSO_4.5H_2O$, $S={}^1/_2$ antiferromag. Heisenberg chain, spin dynamics 80−11285
$K_2BaCu(NO_2)_6$, antiferromagnetic Heisenberg spin 1/2 simple quadratic lattice, mag. and caloric meas. 79−78397

antihyperons *see hyperons*

antimony
see also nuclei with ......
4d subshell, photoionisation partial cross-section, energy depend. meas. 80−29850
abundance in ordinary chondritic meteorites 80−8595
adsorption on GaAs, surface state exam. by energy loss spectra 77−15935
AES and characteristic energy loss spectra, expt. and interpretation 78−27354
alkali halide, $PO_4{}^{3-}$-Sb^{3+} anion-cation impurity mol. complex, IR absorpt. obs. *(Russian)* 77−16317
amorphous, defect controlled electronic props. 80−49658
amorphous, sputter-deposited film, vibr. props., Raman spectra meas. 77−63411
amorphous, vibrational excitations of defect sites 80−49332
amorphous film, elect. resist. 78−95390
amorphous film on glass substrate, effect of substrate temp. on crystallisation 80−39468
amorphous layer crystallisation *(German)* 77−69196
amorphous semiconductor, defect states 79−87057
anodic layers, of Sb_2O_3, semicond. props. 79−56303
Atlantic Ocean waters, As and Sb content *(Russian)* 77−60428
atom, excited state lifetimes, crossed at. electron beams obs. 79−790
atom, Franck-Condon factors and r-centroids for ${}^1\pi-X^1\Sigma$ of p^{121} Sb and p^{123} Sb 80−42992
atom, GTO basis sets, Hartree-Fock-Roothaan calcs. 79−97973
atom, integral K-shell Compton scattering, cross-section, for 1250 keV photons 78−90128
atom, ionisation cross sections for L_1 and L_2 subshells by 250-500 keV protons *(Russian)* 77−6918
atom, $K\beta_3/K\beta_1$ and $K\beta_2/K\beta_1$ relative intensities 77−75088
atom, new autoionised series, flash pyrolysis IR absorption obs. 79−85937
atom, $np^2(n+1)s$ excited-state config. quadrupole moments, Sternheimer shielding factor 80−37755
atom, XPS and XES, dynamical effects 80−52924
Auger electron spectra, solid state effects 80−20739
band structure on Jones zone boundary, pseudopot. calc. 80−54603
carrier density at press. up to 80 kbar, magnetoresist. and Hall effect obs. 79−73534
carrier energy spectrum, effect of hydrostatic pressure 78−87903
carrier transport, magnetoresistivity, field-dependent tensor study 80−39609
chemical bonding in group V and VI elements and compounds with tetradymite structure 80−15036
cleavage faces, evaporation pattern determ. by decoration method in electron microscopy *(German)* 80−107626
clusters, 2 to 500 atoms, nucleation, mass spectra 80−102596
coated thick Fe films, surface magnetism 80−7196
compressive stress-strain curves in single crystals, device *(French)* 79−47852
conduction-electron elec. field gradient, probe valence effects 78−47749
contact charge density, press. depend., trends for Ag-Te 78−39077
core level binding energies 80−71564
crystal structure to 26 kbar meas. via diamond anvil cell and X-ray diffractometer 77−31560
crystallisation in amorphous Sb thin film, critical thickness observations 79−69379
current carrier concentration charge, under pressure *(Russian)* 79−7824
de Haas-van Alphen effect, effective mass, Fermi levels 78−75982
Debye-Waller factors and thermal expansion 78−43089
deformed in compression, secondary slip system *(French)* 79−66120
desorption properties on GaAs (100), AES obs. 80−80074
determination, in combustible municipal solid waste, by AAS 78−85229
determination by at. emission from static induction plasma, anal. curves, detection limits 79−87919
determination in Cu alloys, inverse voltamperometry method 78−61099
diamond: Sb, ion implanted, defect study using optical absorpt. and EPR 80−24480
diamond:Sb, implanted, radiation damage and annealing study 80−100263

antimony continued
diamond:Sb, ion implanted under channelling conditions, depth profile, distribution tail 80−2057
diffused Ge-Si alloy p-n junction, TSC 80−20289
diffusion, in Si, from doped oxide source, masking effects 77−15437
diffusion along dislocations in Si, 1165-1320 °C 77−15631
diffusion and solid solubility in Fe, 773-873K, ion backscatt. anal., rel. to intergranular embrittlement 78−71880
diffusion in α-Fe single cryst., dislocation struct. 78−30798
diffusion in liquid Bi, 713-853K *(Russian)* 77−15611
diffusion in liquid Cu *(Japanese)* 78−10204
diffusion in Si, implantation damage effects 78−55988
diffusion in steel, glass fusion treatment *(Russian)* 78−35585
diffusion of ^{124}Sb in Cu 79−77828
discontinuous thin films, cluster shape models 80−100419
dislocation drag constant temp. depend. 77−11565
dislocation internal friction changes due to high-amplitude US oscills. *(Russian)* 80−10556
dislocation internal friction depend. on high amplitude US vibrations *(Russian)* 79−90727
dislocations, contrast simulation *(French)* 79−60374
elastic moduli, calc. from interatomic forces 79−95071
electrical resist., thermal cond. and thermopower, low temp. transport props. 80−49708
electrical resistivity and anisotropy coeff. at press. up to 80 kbar 77−43554
electrode, thin film, pH sensitivity and electrode potential *(Japanese)* 79−39159
electrodeposit, amorphous, explosive crystn., semicond-semimetal transition and IR absorpt. 78−51849
electron density at nucleus, press. depend., Hartree SCF calcs., Mossbauer shift press. depend. 78−56411
electron mean free path, stopping and straggling 78−91367
electron microscope irradiation effects, agglomeration of point defects, dislocation climb and loops *(French)* 80−59518
electronic band struct. changes due to plane straining effects *(Russian)* 80−54602
electronic struct., depend. on hydrostatic pressure 80−80158
electronic structure change with press., pseudopot. calcs. *(Russian)* 79−47006
energy spectrum variation under strong uniaxial tension 79−73432
entropy of fusion, vibr. contrib. 77−47601
epitaxial growth, of electrodeposits on oriented single cryst. surfaces of CU, electron diffr. study 79−66016
epitaxial growth of electrodeposits on oriented single crystal Au and Ag 78−43267
epitaxial growth on Bi substrate 78−95246
evaporated film crystallisation rel. to substrate temp., −50° to 170°C 78−47680
Fermi levels of electrons and holes, press. depend. 77−43490
Fermi surface, tension effect *(Russian)* 78−75980
filamentary crystals, growth from gaseous state 77−40339
film, elec. cond. and struct., thickness depend. 78−26974
film, electron microscopy, identification criteria of dislocations *(French)* 77−76411
film, electroreflectance effects 79−43055
film, evaporated, crystallite struct., texturisation 77−7991
film, initial stages of growth and orienation, TEM study 79−28237
film, liquid and vapour quenched, metastable struct. 79−56974
film, Maxwell stresses at charged surface from elastoresistance 80−49957
film, MBE deposited, struct. by RHEED obs. 79−82491
film, microrelief, electron microscope obs., grain size and condensation rate 77−55469
film, thermoelec. power, thickness depend. 77−1501
film, X-ray diffr. anal., {001} textured growth 78−72016
film A1-type supercond. vapour-quenched transition temp., A7-type phase transition 78−52145
film growth mechanism, action of residual gases rel. to deposition conditions 79−23850
film with epitaxial thin Fe film 78−56572
films, splat-cooled and vapour-deposited, metastable structs. 79−87018
foil, traversed by $H^+(He^+)$, energy loss and straggling meas. 78−95100
fused, solubility of GaP, thermodynamics, rel. to epitaxial growth 78−34721
high-pressure polymorphism, phase diagram 77−43324
ideal electrical and thermal resistivities, mutual drag effect 79−73507
impurities in low alloy steels, effect on neutron irrad. embrittlement 80−85055
impurity in Cr-Mo-V low-alloy steel, effect on high-temp. ductility and crack growth 80−66652
impurity migration from doped Si sources in epitaxial layers *(Russian)* 80−107570
interlattice displacement and second-order elastic consts. 80−34121
ion bombardment, energy distrib. of positive secondary ions and sputtered atoms 77−32485
ion implantation, combined with Si vacuum deposition *(Japanese)* 78−88428
ion implanted in semiconductors, Mossbauer spectroscopy exam. of radiation damage 78−2176
ion source, high current, characts. 79−17561
L-shell fluorescence yield, L_2L_3 average yield 80−47936
liquid, diffusion of O_2, activity coeff. 80−65267
liquid, O_2 activity from electrochem. meas. 80−55695
liquid, self-diffusion, long capillary method obs., using radioactive Sb 77−89564
liquid, solubility and activity of O_2 *(German)* 79−90793
liquid, struct. model, using interference functions *(German)* 77−58946
liquid, structure factor shoulders and interatomic pot. rel. to electron theory 77−7658
liquid, thermoelec. power meas. 79−40591
magneto-quantum oscillations obs., new method 77−62946
magnetoreflection of circularly polarised IR radiation, band struct 77−52094
magnetoresistance, superficial cond. effects 77−28235
magnetoresistence, effect of surface layer current, and meas. of Kapitza resist. 77−69348
magnetoresistivity, mutual drag effect, temp. depend 78−52012
magnetosonic waves propagating in Voigt configuration obs. 78−23126
metalliferous sediments in Pacific Ocean, Sb content 77−78156

antimony continued
microsegregation in faceted (nonfaceted) Si Czochralski cryst. growth 80—45227
Mossbauer radiation, Rayleigh scatt., Debye-Waller factor determ., annealing effect 80—39963
muon precession freq., anomalous shift 78—39488
muonic Knight shift, temp. and mag. field depend. 79—56659
muonic Knight shift, temp. and mag. field depend. 79—91331
natural waters, radiotracer methods for speciation study 79—88490
neutron activation anal. in biological and environmental samples 79—53008
neutron rich isotopes, half-lives, fission yields, and neutron emission probabilities 77—67721
NQR, nucl. spin-lattice relax., 4.2K 78—91984
optical phonon anharmonicity and melting, light scatt. study 80—60621
optical phonon temp. depend., Raman scatt. meas. 77—76509
phase transformation due to high press. and shear stress 80—75357
phosphate glass:Sb^{3+},Dy^{3+}, fluorescence and energy transfer obs. 78—6778
polymorphism at high press., temp. hysteresis, DTA *(Russian)* 79—82328
positron lifetime meas., comparison with theory 77—63483
powder production,, β-Sb_2O_3 reduction atomic H effect 80—2978
production by H_2 reduction of stibnite 79—66023
quadrupole interaction of ^{69}Ge, TDPAD expts. 78—48089
quantum oscillations of vel. of sound meas. in mag. field 78—39004
rhombohedral crystals, slip dislocations and slip systems 79—23617
separation from fission products, fast chem. methods 77—16856
spin splitting meas. from de Haas-van Alphen effect, g-factors 78—51881
superconductor, A1-type, critical mag. field 79—69638
surface decoration, with epitaxial Bi condensates 79—28227
surface relaxation in CESR, evidence of spin lattice character 79—28615
texture of deformed polycryst. 77—59809
thermal diffusivity by laser flash technique 78—6189
thermoelectric figure of merit, 1-12 kbar, 100K 78—80013
thermoelectric props., press. effects up to 90 kbar 78—47818
thin film, elec. cond., grain boundary scatt. effects 80—103766
thin films, IR absorpt. and intraband transitions 80—16114
thin films, vacuum deposited on Si, solar cells prep. by laser induced diffusion 80—93998
thin plates, electron conduction, 4-293K, surface reflection ang. depend. *(Russian)* 78—19170
tree rings, long term environmental pollution histories, neutron activation analysis 79—92107
twinning dynamics of single crystal 77—4115
vaporisation behaviour, transpiration and boiling temp. studies 80—29161
volume diffusion in Ni, activation energies, expt. and by Le Claire method *(Russian)* 79—99369
whisker crystals, magnetoresist., size effects *(Russian)* 79—7821
whiskers, quantum oscills. of magnetoresist. *(Russian)* 78—60145
XPS, electronic struct. 80—7464
zone centre phonons and elastic consts., hydrostatic press. depend. 78—59905
Al:Sb, anodic oxidation, mobility of foreign atoms 77—90494
Al:Sb, ion implanted, electron beam annealing 80—59500
Au-Sb thin film interdiffusion 77—59152
Bi:Sb, mag. field dependent electron and hole scatt., quantum limit 77—15878
Bi:Sb, quenching and annealing of defects, elec. resist. meas. 78—87973
Bi:Sb, solid soln. struct., growth rate effects 77—52246
Bi:Sb polycrystal elastic constants for US velocity obs. 79—69180
Bi-Sb, bicrystal rearrangement of grid of nonconformity dislocations on (111) interface during heating 79—28215
Bi-Sb interface, film, thermoelectricity, ageing differential efficiency *(German)* 78—60146
$Ca_2P_2O_7$:Sb, (Sb,Mn), luminesc., activation, colour centres *(Russian)* 78—92123
$Ca_2P_2O_7$:Sb(,Mn), luminesc., colouration 80—2828
$Ca_3(PO_4)_2$:Sb,(Sb,Mn), luminesc., activation, colour centres *(Russian)* 78—92123
β-$Ca_3(PO_4)_2$:Sb(,Mn) 80—2828
$Ca_5(PO_4)_3OH$:Sb^{3+}, thermolum. props. 80—2877
$Ca_{10}(PO_4)_6X_2$:Sb, halophosphate luminophor, causes of Sb loss during synthesis 78—11172
Cd-Sb diffusion couple, layer growth of CdSb phase at high press. 80—2217
Cd-Sb diffusion couple, layer growth of CdSb phase at high press., elec. meas. 80—2218
Cd-Sb system, contact fusion in complex metallic systems 78—26664
CdS:N, P, As, Sb, Bi photoluminescence obs. 78—10965
Cu-Sb thin film couples, room temperature interactions 80—96699
Cu_2Sb-Sb, contact fusion in complex metallic systems 78—26664
EuIG:Sb(Ca)(Ti), growth from PbO-B_2O_3 based flux, prop. depend. on Pb content 80—39824
in Fe meteorites, concs. rel. to chemical classification and nebular condensation 80—36594
GaAs:Sb, resonance levels of isoelectronic impurities 80—107740
GaAs:Sb (100) surface, Sb-induced surface states 78—10529
GaN-Sb contact, using GaN made by oxidation and subsequent nitridation of GaAs, I-V characts. 77—20436
GaP:Sb, gap vibrs. and impurity conc. determ. 79—69869
GaP:Sb, lattice location of implanted atoms, ion backscatt. and ion-induced X-ray obs. 77—84785
GaP-Sb, Sb solubility in region of GaP primary crystn. 79—86891
GaSe:Cu(Cd, Sb), photovoltaic spectra 80—20240
$GdPO_4$:Sb^{3+}, Dy^{3+}, energy transfer from sensitiser to activator, intermediate role of Gd^{3+} 80—50389
p-Ge:Ag, Sb, electron beam irradiation cond. characts. 80—19842
Ge:Au, Sb, Hall mobility, temp. dependence 80—96919
Ge:Au, Sb 79—69577
Ge:Au,Sb, electron irradiated, Hall effect, photocond., and photomagnetic effect meas. 77—4369
p-Ge:Au,Sb,Hg(Zn), radiation-defect form., Au influence 80—92911
p-Ge:Cd,Sb, electron irrad. at 300K, elec. props. 80—6435
Ge:Ga,Sb, compensated, low temp. props. rel. to appl. in bolometry 80—31867
Ge:Hg, Sb, influence of electron irradiation on elec. props. 77—20318
Ge:Mn, Sb, recombination waves, convective instability development 80—70721
n-Ge:Ni,Sb, transient response at 4K, nonequilib. carrier recomb. 77—43659

antimony continued
p-Ge:Nz, Sb, influence of electron irradiation in elec. props. 77—20318
Ge:S film, amorphous, ion implantation, effect on cond. 78—83839
Ge:Sb, 2.5 MeV electron irradiated, cond. switching effect 77—89820
Ge:Sb, acoustic attenuation, uniaxial stress effects 78—59863
Ge:Sb, amorphous, doping effects on Fermi level, electrical meas. 79—42546
Ge:Sb, amorphous, electronic transport props. 80—44589
Ge:Sb, annealing stages of thermal defects, elec. meas. 77—55282
Ge:Sb, bolometer element, absorpt. spectra, bias depend. 79—30553
Ge:Sb, cleaved surface, influence of impurities on local surface states 79—78150
p-Ge:Sb, cryst. defects due to γ-irrad. 79—55779
Ge:Sb, cryst. defects due to neutron irrad., elec. cond. and annealing 79—55789
Ge:Sb, Czochralski growth, orientation depend. of impurity distrib. coeff. 79—69976
Ge:Sb, D^- states in mag. fields, photocond. spectra, and far IR absorption spectra 79—95370
Ge:Sb, D^-states investigated by long wavelength photoconductivity 78—6323
n-Ge:Sb, deep levels obs., freq. depend. of capacitance of p-n junctions 77—4315
Ge:Sb, dopant distrib. rel. to direction of cryst. growth 77—51400
Ge:Sb, effect of degree of doping on surface state charact. 79—69577
Ge:Sb, electron irradiation effects on elec. props. 78—6103
Ge:Sb, electron-hole drop lifetime, quenching temp. influence 80—59889
Ge:Sb, excited donor states, double optical transitions, reson. absorpt. meas. 80—93371
n-Ge:Sb, exciton absorption 78—6688
n-Ge:Sb, far IR absorpt. spectra 79—91469
n-Ge:Sb, fast electron irrad. at 77K, radiation defect changes by annealing at 220K 79—37737
n-Ge:Sb, fast electron radiation defects, 0.52 eV absorpt. band, impurity photocond. and Hall effect meas. 78—27273
n-Ge:Sb, fast neutron irrad. effects on donor conc., and annealing 78—56107
Ge:Sb, fast-neutron irradiated, shallow radiation defect levels, electronic props. 78—23049
Ge:Sb, growth atm. effect on struct. microdefect form. 80—20779
Ge:Sb, γ-irrad., carrier trapping and recomb. at point radiation defects 80—107810
Ge:Sb, γ-irrad., electron capture mechanism by radiation defects 78—26885
n-Ge:Sb, γ-irrad. effects on donor conc. and compensation by acceptors 78—56106
Ge:Sb, heavily doped, anomalous magnetoresist., metallic impurity cond., down to 5 mK 79—65502
Ge:Sb, heavily doped, mass anisotropy, and multiple scattering effects 80—107802
Ge:Sb, heavily doped, scatt. of electrons 77—59283
Ge:Sb, heavily doped semicond., scatt. mechanism, resist, and Hall coeff. maxima 80—75586
n-Ge:Sb, high-field Hall effect spectroscopy 80—65600
Ge:Sb, implantation doping, annealing and doping profile determ. 77—19972
Ge:Sb, impurity photocond. spectra under uniaxial compression 80—44656
n-Ge:Sb, irradiated with fast electrons at 77K, investigation of 300K annealing stage 79—51155
Ge:Sb, kinetics of strain-confined large electron-hole drop and its clinging exciton system 80—75508
Ge:Sb, lattice thermal resist. due to bound state electrons 79—46850
Ge:Sb, limiting solubility, rel. to charge carrier conc. 80—24596
Ge:Sb, low temp. anomaly of impurity cond. 79—95428
Ge:Sb, low-freq., low temp. dielec. behaviour below metal-insulator transition 80—50250
n-Ge:Sb, magnetothermal cond., 4.2K 80—24688
Ge:Sb, moderately heavily doped, electron-hole drops photoluminesc. 80—7417
Ge:Sb, neutron irrad., carrier mobility theory and expt. 78—56166
Ge:Sb, neutron irradiated, hopping cond. between shallow defect levels 77—4347
n-Ge:Sb, neutron-irradiated, paramag. defects, analysis of EPR spectra 77—55703
Ge:Sb, Ni(Mn), recombination wave spectrum, two-level traps 80—96906
Ge:Sb, phonon thermal cond. calc. 78—71893
Ge:Sb, phonon-bound donor resonance scatt., donor-electron radius mag. field depend. 79—77847
Ge:Sb, shock polarisation anisotropy in elastoplastic compression range 77—16244
Ge:Sb, solid solns. decomp. 80—15249
Ge:Sb, thermal defects, influence on radiation defect formation and annealing 77—55281
Ge:Sb, thermal phonon scatt., piezo-thermal cond. 80—70482
Ge:Sb, Zn(Hg), photoelec. props., 70 to 300K 80—65621
Ge:Sb,Au, photoelectronoc exam. of multilevel gold structure 77—69272
Ge:Sb,Cu, exactly compensated, impurity absorpt. and photocond. spectra 78—56189
n-Ge:Sb,Cu, exactly compensated, static photocurrent-voltage characts. 79—38131
n-Ge:Sb,Cu, exactly compensated, unipolar injection influence on photoconductivity 79—42592
Ge:Sb,Cu, high resist. compensated, impurity of photocond., pulsed unipolar injection carriers 80—92935
Ge:Sb,Cu, photoelec. props., fast electron irrad. effects 80—60036
Ge:Sb,In, lightly doped semicond., low temp., phonon cond., electron-phonon scatt. 79—60456
Ge:Sb (As), isolated D^- states and D^- complexes in mag. fields 80—15473
Ge:Sb crystals, purification by zone recrystallisation with temp. gradient 79—4916
Ge:Sb film, electronic props. 78—84330
Ge:Sb semiconductors, inhomogeneously strained, phonon resonance scatt., Kwok's theory method 79—60455
Ge-Sb, D^- complexes and band form., photocond. 78—84251
Ge-Sb, far IR emission stimulation by impact ionisation 80—66301
Ge-Sb, meas. of electron-hole drop size by light scatt. 80—44515
Ge-Si:Sb, energy spectrum of Sb 80—34382
Ge-Si:Sb, prepared in Universal Furnace expt. in Soyuz-Apollo programme, melting and crystn. 80—19737

antimony continued
InAs:Sb (100) surface, Sb-induced surface states 78—10529
Li/Sb interface, CESR meas. 78—80218
Mn-Sb two layer film, cpd. formation kinetics, ion backscatt., X-ray diffr. and mag. meas. 77—72801
Ni-Si:Sb, implanted dopant redistrib. after silicide form., appl. to ohmic contacts 79—37729
Pb-Si:Sb Schottky tunnel junction, variable range hopping assisted tunnelling 80—39670
$Pb_xSn_{1-x}O_2$:Sb films, DC sputtered, elec. props. 80—80426
PbTe:Sb, thermoelec. props., thermal and elec. cond. 79—82616
Pd-Si:Sb, implanted dopant redistrib. after silicide form., appl. to ohmic contacts 79—37729
Pt-Si:Sb, implanted dopant redistrib. after silicide form., appl. to ohmic contacts 79—37729
Sb I, ratio of oscillator strengths for 217.6 and 231.1 nm lines *(Russian)* 79—31457
Sb II, radiative lifetimes meas. 79—54813
Sb III, radiative lifetimes, calcs. and beam-foil spectra 77—75223
Sb, liquid-quenched, stabilisation and transformation kinetics of metastable phases 80—3022
Sb negative ion source 78—4734
Sb VI, $4d^95d$ and $4d^96s$ configs., UV spectrosc. obs. 80—18817
Sb VI, $4d^95s$-$4d^95p$ transitions, UV spectra 79—93942
Sb VI, reson. lines, UV spectra 77—46515
Sb VI, spectra, ionisation limits 79—54794
Sb VII, $4d^9$-$4d^85p$ transitions, spectra, least squares calc., Hartree Fock calcs. 79—54794
Sb VII, $4d^9 \rightarrow 4d^85p$ transitions, UV spectra 77—46515
Sb VII, spectrum obs. 600 to 2100 Å, analysis of $4d^85s$-$4d^85p$, $4d^9$-$4p^54d^{10}$ transitions 80—102471
Sb_2^-, photodetachment cross-section meas., crossed beam expt. 77—61723
Sb^{2+}, and isoelectronic ions, excited-state energy level k-ordering, l-patterns 77—88406
Sb:^{111}Cd, quad. interac. temp. depend. 77—59487
Sb:^{111}Cd,In, elec. field gradient, TDPAC expts. 80—55002
Sb:Cd, electric field gradient temp. depend. for ^{111}Cd 79—51894
Sb:Te, de Haas-van Alphen effect, effective mass, Fermi levels 78—75982
Sb:Te vapour saturation, diffusion zone struct. crystallisation orientation *(Russian)* 80—54438
Sb/As_2SeTe_2/Al structures, rectifying effects 80—75654
Sb-Bi film thermopiles for radiation pyrometry 78—214
Sb-Hg, quadrupole interaction, time differential perturbed ang. correl. and nucl. orientation 79—24250
Sb-I-Ca process for thermochem. H_2 prod. by H_2O dissoc. 80—16824
Sb-Sb_2O_3 pH electrode improvement 79—53270
Sb+Ar^{x+}(Cl^{x+}), vacancy sharing between K and L shells in 3dσ mol. orbital 79—22807
Sb^-+He, term parameters, electron spectra and scatt. cross sections 77—27148
Sb_4, gaseous, atomisation enthalpy and enthalpy of form., mass-spectroscopic Knudsen cell method 78—80780
Sb_4, vap., $M_{4,5}N_{4,5}N_{4,5}$ Auger electron spectra 79—50089
SbI, ^2D state radiative lifetimes 79—3381
SbII, ^3P, ^3D state radiative lifetimes 79—3381
Sb_2Se_3-Sb, liq. semicond., thermal cond. meas., resistive probe method 77—15636
^{A}Sb, A=121, 123, elec. and mag. hfs. 79—10224
^{121}Sb, Mossbauer isomer shifts, book contrib. 79—87360
^{124}Sb, diffusion coeff. in liq. Cu 79—95196
^{124}Sb, diffusion in Cu 80—65301
^{125}Sb, in HCl solns., valency states investig., radioanal. tracer preparation, stability 77—63943
Sb($5^4S_{3/2}$)+NO(O_2), rate consts., time-resolved reson. fluoresc. meas. 78—27732
Si epitaxial layers, grown in vac. at low temps. P and Sb doping 80—88189
Si n/n^+ epitaxial layers, anomalies of Sb distrib. 80—65035
Si:As,Sb, amorphous, damage depend. of epitaxial regrowth during annealing 78—47679
n-Si:P, Sb, reson. four wave mixing, valley orbit splitting 79—89960
Si:P,Sb, impurity implantation effect on CESR, spin-orbit interactions 77—36133
Si:Sb, amorphous, electronic transport props. 80—44589
Si:Sb, appl. of ion implantation systems, high throughput 80—34029
n-Si:Sb, arbitrary doping profiles produced by MBE 79—7617
Si:Sb, bound excitons and bound multiexciton complexes for shallow donors, luminesc. meas. 79—24363
n-Si:Sb, characts. of piezoresist. 77—51750
Si:Sb, deform. coeff. due to impurity diffusion 78—18671
Si:Sb, diffusional doping by doped oxide method 80—15127
Si:Sb, donor-polarizability enhancement as the insulator-metal transition is approached from the insulating side 80—80184
Si:Sb, dopant implantation, activation analysis errors due to isotope comp. *(German)* 80—34037
Si:Sb, dopant microsegregation rel. to crystal and crucible rotation 78—11106
Si:Sb, dopant solubility limit, laser irrad. effects 80—84295
Si:Sb, electron irrad. damage, electron trapping centres 77—39798
Si:Sb, electron-nucl. interaction under optical pumping, ^{29}Si optical polarisation meas. 79—95680
Si:Sb, epitaxial film, growth by mol. beam technique 80—2292
Si:Sb, epitaxial layers, doping profile techniques 80—44231
Si:Sb, epitaxial regrowth of amorphous layers created by high-dose Sb implantation 78—30654
Si:Sb, heavily doped, TEM obs. of impurity effects in dislocation motion 77—43220
Si:Sb, high dose implanted, orientation dependent annealing effects 78—18665
Si:Sb, high dose Sb ion implantation, buried layer appls. 80—88186
Si:Sb, high resolution study of group V impurities absorption 80—7388
Si:Sb, implantation damage removal by laser irrad. and its thermal stability, TEM study 79—74024
Si:Sb, implantation of Sb for buried layers appl. *(French)* 77—80527
Si:Sb, implanted, pulsed ruby-laser annealing, Rutherford backscatt., TEM and ion channelling study 79—86805
Si:Sb, in solar cell struct., heavily doped, dopant striation, SEM 79—39312
Si:Sb, incorporation of implanted impurities during amorphous layer regrowth 79—55761

antimony continued
Si:Sb, ion implant lattice location after pulsed ruby laser annealing 79—73204
Si:Sb, ion implantation and pulsed laser annealing, supersat. alloy form. 80—54267
Si:Sb, ion implantation combined with vacuum deposition of Si 79—47631
Si:Sb, ion implanted, annealing behaviour of stress 78—63778
Si:Sb, ion implanted, annealing of heavy ion cascade damage, channelling meas. 80—89255
Si:Sb, ion implanted, doping profile, pulsed laser annealing effects 80—88197
Si:Sb, ion implanted, lattice location of impurities after pulsed laser annealing 80—88196
Si:Sb, ion implanted, redistrib. of dopants by pulsed laser annealing 79—7620
Si:Sb, ion implanted, Sb diffusion during oxidation, snow-plough effect 80—88366
Si:Sb, ion implanted and annealed, influence of implantation temp. on dislocation generation 80—88158
Si:Sb, ion implanted doping, isotopic composition shifts on neutron activation determination 80—24487
Si:Sb, ion-implanted, CO_2 laser annealing 79—73183
Si:Sb, ion-implanted, thermally assisted Xe-flash annealing, Rutherford backscatt. meas. 79—10881
Si:Sb, laser doping, evaporation loss and diffusion of Sb, under pulsed laser irrad. 80—59508
Si:Sb, low energy ion implantation, profile determ. 80—88176
Si:Sb, low energy ion implantation Schottky barrier diodes and resistors 80—88177
Si:Sb, luminescence associated with transitions from bound exciton excited states 78—23534
Si:Sb, MBE, evaporation for n-type doping 80—15126
Si:Sb, MBE, on n^+ Si, with wide range doping control 78—27402
Si:Sb, MBE film, doping technique 80—79821
Si:Sb, Mossbauer spectra of ^{119}Sn defect struct. 80—97174
Si:Sb, multiparticle impurity complexes *(Russian)* 78—72601
Si:Sb, polarisability of Sb donors in mag. field 79—95368
Si:Sb, produced by ion implantation and laser annealing, Sb behaviour above solid solubility 80—88200
Si:Sb, redistribution of thin impurity layers after laser annealing, theoretical model and expt. results 79—69147
Si:Sb, shallow donor electrons, hyperfine interactions, reply to Onffroy's calcs. 78—51934
Si:Sb, shallow donor states with strong central cell perturbation theory 78—51933
Si:Sb, single cryst., transmission characts. for IR optical components 77—27325
Si:Sb, striated impurity distrib. calc. in melt-grown crystals 80—24488
Si:Sb, temp. depend. of irradiation induced displacement of Sb, backscattering meas. 78—26605
Si:Sb, vacuum deposition combined with ion implantation *(Japanese)* 79—28005
Si:Sb,As, autodoping effect of Sb-As simultaneous diffusion 77—80522
Si:Sb,P, double implants, residual defect reduction after damage anneal 80—88170
Si:Sb crystal Czochralski growth, radial microsegregation analysis 78—11105
Si:Sb device, anal. using SEM-AES-IMA combination with SIM spectrometer *(Japanese)* 78—85249
Si:Sb epitaxial film, doping efficiency *(Japanese)* 79—73201
Si:Sb film, amorphous, ion implantation, effect on cond. 78—83839
Si:Sb film, homoepitaxial interpretation of temp. depend. of partition and sticking coeffs. 77—7756
Si:Sb film, implanted, elec. cond., sheet resist. as function of ion dose and temp. 79—78235
Si:Sb vacuum deposited coating, p-n junction, pulsed electron beam annealing doping, diffusion 80—75480
Si:Sb wafers, laser annealing, Rutherford backscatt., optical, and TEM obs. 79—1445
Si:Sl, mean square dynamic displacement of atoms, effect of electron-phonon interactions *(Russian)* 78—10145
Si-Sb, microdefect formation depend. on doping, Cu decoration, X-ray transmission topography, preferential etching 79—69120
SiO_2-K_2O-CeO_2-Sb_2O_3, polychromatic glass, Sb^{4+} centre, EPR obs. 79—87317
SiO_2-Na_2O-CeO_2-Sb_2O_3, polychromatic glass, Sb^{4+} centre, EPR obs. 79—87317
Si; Sb, Czochralski growth from heavily Sb doped melt, interface morphological instability 80—2939
Si=Sb, plastic deform. and formation of dislocation loops, effect of Au atoms 79—69184
Sn:^{120}Sb, elec. qudrupole interaction, perturbed ang. distrib. method 79—99799
α-Sn:Sb, implanted, impurity-defect structs., Mossbauer expts. 80—39129
SnO_2:Cr(Sb), cassiterite, gas phase growth on seed 77—24937
SnO_2:Sb, and pure cryst., microstruct., X-ray diffr., optical and electron microscope studies 78—79619
SnO_2:Sb, film, struct. and resist., impurity addition effect 77—20469
SnO_2:Sb, prep. and material characts. for far IR detector 78—4697
SnO_2:Sb, transparent cond. film prep. by thermal decomp. of Sn salt of organic acid *(Japanese)* 77—90269
SnO_2:Sb, transparent cond. films, hydrolysis deposition, elec. and optical props. 79—43144
SnO_2:Sb,X, X=Fe,Cu,S, CVD thin film, resist. temp. coeff. 79—38198
SnO_2:Sb film, amorphous, electrotransport phenomena obs., under DC electric field 80—59840
SnO_2:Sb film, DC sputtered, substrate temp. effect on cond. 77—39971
SnO_2:Sb film, DC sputtered, correspondence between Sb content and targets 79—23847
SnO_2:Sb film, transparent cond., prep., characts., stability and struct. *(Japanese)* 78—47889
SnO_2:Sb film on glass substrates, elec. props. 80—88652
SnO_2:Sb sprayed film, growth mechanism and cryst. struct. 80—89143
SnO_2:Sb thin films DC sputtered, heat treatment effects, expt. 77—28719
SnO_2:Sb transparent conductive coatings for Cu_2S-CdS solar cells 79—61992
SnO_x:Sb,F film CVD for bistable storage CRT 77—77410
Te:Sb, 96 to 500K, cond. Hall const., hole mobility, conc., dislocation effects *(Russian)* 78—64039

antimony continued
Te:Sb, impurity spectroscopy 80—65499
Te:Sb, impurity state and impurity cond., press. effect 80—54723
Te:Sb, impurity states and impurity conduction, hydrostatic pressure 80—39521
Te:Sb, photoconductivity in strong mag. fields, doping effects, impurity levels 80—75602
Te:Sb, surface carrier effects on Hall mobility at low temp. 77—80794
TiO_2:Sb, Mossbauer effect exam. of impurities 78—31140
Zn-Sb diffusion couple, layer growth of ZnSb phase at high press., elec. meas. 80—2218
Zn-Sb diffusion couple, ZnSb phase layer growth kinetics, 240-320°C, up to 30 kbar 78—10229
ZnSe:Sb, photoconduction under Nd laser irrad., local level distrib. 77—55580
ZnTe:Sb film, elec. props. 78—76172

antimony alloys
see also antimony compounds
Babbitt grade Bk-2Sh, improvement in antifriction layer props. by impulse discharge *(Russian)* 79—1917
Babbitt-steel bimetal, exam. of structure of transition layer 79—100293
crystals, in binary or ternary alloys, shapes on solidification *(German)* 80—3020
Cu-Sb, dil., chemical etching and X-ray topography obs. of cellular struct. *(French)* 79—96249
$Mn_{1.98-x}Cr_xFe_{0.02}Sb$, Mossbauer effect exam. 78—68432
$Mn_{1-x}Cu_xSb$ films, $0 \leq X \leq 0.3$, magneto-optical props. 79—51981
rare-earth alloy, RSb, (R=Er, Ho, Dy, Tb, Nd, Gd), mag. props., hydrostatic press. depend. 77—80918
steel, alloy, Fe-Ni-Cr-Sb-C effect of Ni, Sb, on temper embrittlement 78—60813
steel, austenitic, Kh17N13M3T, activation characts. of rupture, 630-730°C, Sb and Nb microalloying effects *(Russian)* 79—5033
steel, low C Cr-Ni, temper embrittlement by antimony, Ti addition effects 77—32683
steel, martensitic, alloying element effect on coarsening behaviour of cementite particles in ferrite 80—66518
steel, Ni-Cr, temper embrittlement by Sb, Ni, Cr effects 77—36628
transition metal monoantimonides, electronic struct. determ. 77—4290
Ag-Sb, cold-worked, lattice defects, convolution relations for X-ray line breadth calcs. 78—51394
Ag-Sb, dil. alloys, single crystals, dynamic dislocation behaviour 77—4108
Ag-Sb, liquid alloy, thermoelectric power and magnetic susceptibility 77—8076
Ag-Sb, sintering and grain growth, effect of Sb solute 78—84730
Ag-Sb (1.16 wt.%), Sb effect on sintering kinetics in early stages 79—52137
Ag-Sb alloy, reflectivity, effect of electrodeposition conditions 78—13784
Ag-Sb alloy coating, electrolytes for deposition *(Bulgarian)* 80—93763
Al-Sb, ion-implanted, precipitation form. and evolution TEM obs. 79—55766
Al-Sb, laser induced surface alloy formation and Sb diffusion 80—54439
As_xSb_{1-x}, semimetal, thermopower, thermomagnetic power, 4.5 to 77K 80—107825
Au-An-Sb, and Au-Ge-Ni-Sb low resist. ohmic contacts to GaP 80—70825
Au-Sb, charge-transfer and valence-band behaviour using ^{197}Au Mossbauer and X-ray photoemission spectra 79—60695
Au-Sb, liq. alloys, ΔG^E of mixing from ht. of melting and sp. ht. of cpds. 77—4920
Au-Sb thin film interdiffusion 77—59152
AuMnSb, ferromag. Heusler alloy, mag. hyperfine fields at Au and Sb sites, Mossbauer spectra 77—32303
$AuSb_2$, core-level binding energy shifts and charge transfer 80—25268
$AuSb_2$, pyrite structure, Raman scatt., phonon frequencies 77—40235
Bi:Sb, semimetallic alloy, microwave spectroscopy 78—87908
Bi-Cd-Sb, calc. of phase equilibria using thermodynamic values from different models 78—60646
Bi-Sb, conditions for dendritic crystallisation, accompanying rapid cooling *(Russian)* 79—34020
Bi-Sb, crack appearance in diffusion zones *(Russian)* 78—76727
Bi-Sb, cryst., hopper growth 78—18564
Bi-Sb, crystallisation temp., overcooling temp. *(Russian)* 80—97472
Bi-Sb, dil., mag. field depend. electron scatt. rates, de Haas-van Alphen meas. 78—10436
Bi-Sb, dil., magnetothermal oscillation and spin splitting of electrons 78—43362
Bi-Sb, dilute, oxidation kinetics 80—25914
Bi-Sb, film, elec. resist., magnetoresist., Hall coeff., 4.2K, conc. depend., anomalous size effect *(Russian)* 77—89884
Bi-Sb, magnetic susceptibility, 4.2 to 270K, field and band parameter depend. 77—36051
Bi-Sb, magnetoplasma waves in strong mag. fields at 300 GHz 79—38116
Bi-Sb, magnetoresist. in high mag. fields *(Japanese)* 80—54720
Bi-Sb, melts, interdiffusion, long capillary method and electron probe obs. 77—89563
Bi-Sb, semiconducting, lattice dielec. const., comp. depend. 80—39516
Bi-Sb, semiconductor-semimetal transition under pressure 78—34870
Bi-Sb, semimetallic, magnetoplasma effects at 300 GHz in Voigt configuration 80—39619
Bi-Sb, semimetallic alloy, cyclotron reson. and quantum oscillations 77—28096
Bi-Sb, Shubnikov-de Haas effect and semimetal-semicond. transition in high mag. fields 80—44674
Bi-Sb, single cryst., role of complexing agents on etching characts. 80—54238
Bi-Sb, single cryst., semimetal-semicond. transition. cond. 77—1459
Bi-Sb, solid solns., thermoEMF in transverse mag. field 77—47841
Bi-Sb, solidification, predicted vol. change 77—28802
Bi-Sb, thermal EMF giant quantum oscills. *(Russian)* 80—59960
Bi-Sb, thermoelectric figure of merit, direct meas. in transverse mag. field 78—10485
Bi-Sb (0 to 6 at.%), semimetal, magnetoplasma waves at 9 to 100 GHz microwave freqs. 79—78127
Bi-Sb (1 at.%) alloy single cryst. growth solid-liq. interface study 80—107073
Bi-Sb (12 at.%), cryst. growth from melt, impurity distrib. control by electrotransfer method *(Russian)* 80—66418

antimony alloys continued
Bi-Sb (1.2-7 at.%) solid solns., microhardness of single crystals 77—28886
Bi-Sb (5-12 at.%), single cryst. cleavage plane, microhardness parameters depend. 78—35486
Bi-Sb (6 at.%) whiskers, persistent metallic behaviour, elec. resist. meas. 80—75544
Bi-Sb alloy, magnetothermoelec. quality factor of single crystals 77—51771
Bi-Sb alloy film, elec. props. *(Russian)* 79—11245
Bi-Sb alloy films, quantum size effect *(Russian)* 77—85351
Bi-Sb alloys, electron work function determ., contact pot. difference method 77—39920
Bi-Sb alloys, magnetoacoustic attenuation, tilt effect 79—91106
Bi-Sb alloys, metal-semimetal point contacts, volt-ampere characteristics *(Russian)* 80—65683
Bi-Sb alloys, thermomagnetic quality factor 77—15882
Bi-Sb film, amorphous nature, AC and DC cond. and Hall coeff. obs. 80—11114
Bi-Sb film, tunnel conductivity, proximity effect *(Russian)* 79—51726
Bi-Sb mixed cryst., zone melting crystn. parameters *(German)* 79—43140
Bi-Sb solid soln., crystallisation in capillaries *(Russian)* 78—44006
Bi-Sb solid soln., thermoelectric props., 80 to 300K *(Russian)* 78—43425
Bi-Sb-Sn, Sn and Sb partition coeffs. during crystallisation 77—48394
Bi-Sb-Te melt, Sb and Te distribution coeffs. during crystallisation *(Russian)* 80—93472
Bi-Sb-Te system, epitaxial film prep. in closed-crucible 77—52230
Bi-Sb(-As), band struct., effects of Sb and As, mag. susceptibility meas. *(Russian)* 80—65775
BiSb (>20 wt.%), electronic band struct. 80—107698
BiSb, alloys, semimetallic, camera, dispersion relations 80—59854
p-$Bi_{0.9}Sb_{0.1}$, Fermi surface anisotropy var. on press. induced transition to gapless state *(Russian)* 77—43483
$Bi_{0.91}Sb_{0.09}$, magnetoresistance anisotropy in strong magnetic field 79—82613
$Bi_{0.91}Sb_{0.09}$, thermomag. power in strong mag. field, temp. and field depend. 78—43421
$Bi_{0.924}Sb_{0.076}$, doped, optical, oscillation and galvanometric effects *(Russian)* 77—85247
$Bi_{0.925}Sb_{0.075}$, semiconductor-semimetal transition under tensile strain, Shubnikov-de Haas oscills. obs. 80—44678
$Bi_{1-x}Sb_x$ alloy films, quantum resistance oscills. at low temps., surface band distortion *(Russian)* 80—11110
$Bi_{1-x}Sb_x$, combination freq. in Shubnikov-de Haas and surface impedance oscillations *(Russian)* 78—10476
$Bi_{1-x}Sb_x$, crystalline, vibrational, spectra, second order Raman scattering 79—47455
$Bi_{1-x}Sb_x$, deformation calculations, band struct. variation, electron phase transitions due to deform. *(Russian)* 80—65137
n-$Bi_{1-x}Sb_x$, determ. carrier dispersion relation parameters 79—38107
$Bi_{1-x}Sb_x$ epitaxial layers, effect of film thickness on elec. props. *(Russian)* 79—11244
$Bi_{1-x}Sb_x$ epitaxial thin films, galvanomag. props. in semimetal and semicond. regions 79—11254
$Bi_{1-x}Sb_x$, far IR transmittance meas. *(Russian)* 77—44006
$Bi_{1-x}Sb_x$ film, evaporated, cross-sectional struct., electron microscopy and replica technique study *(German)* 78—22977
$Bi_{1-x}Sb_x$, growth by horizontal zone refining, low charge carrier conc. 77—21020
$Bi_{1-x}Sb_x$, lattice dielec. const. from helicon wave propag. 77—47756
$Bi_{1-x}Sb_x$, magnetoacoustic attenuation 80—2428
$Bi_{1-x}Sb_x$, magnetoacoustic attenuation, line shape anal. 80—2429
$Bi_{1-x}Sb_x$, magnetoresist., mag. field and ang. depend. 78—19063
$Bi_{1-x}Sb_x$, reson. Landau level transitions, magnetorefl. 77—52096
$Bi_{1-x}Sb_x$, semicond. alloy, mag. freeze-out effect, superlow temps. *(Russian)* 77—89775
$Bi_{1-x}Sb_x$, semicond. alloy, EM wave propag. in direction perpendicular to mag. field 79—60687
$Bi_{1-x}Sb_x$, semicond.-semimetal transition, temp. and press. depend. of transport props. 78—76120
$Bi_{1-x}Sb_x$ semiconducting alloy, band struct. study, Shubnikov-de Haas effect *(Russian)* 80—80181
$Bi_{1-x}Sb_x$, semimetallic, plasma effects, submm. wave expts. 77—35881
$Bi_{1-x}Sb_x$, Shubnikov-de Haas effect, Abrikosov-Falkovskii treatment of Fermi surface anisotropy *(Russian)* 78—43285
$Bi_{1-x}Sb_x$, sputtered thin films, first order Raman scatt. 79—69831
$Bi_{1-x}Sb_x$, supercond. transition temp., press. depend., 30-80 kbar 77—8223
$Bi_{1-x}Sb_x$, thin film, elec. props., composition variations *(Russian)* 79—7841
$Bi_{1-x}Sb_x$ thin films, elec. props., 4.2-300K *(Russian)* 79—24087
$Bi_{1-x}Sb_x$:Te(Sn), band struct., plasma refl. spectra and galvanomag. tensor 77—16315
$Bi_{1-x}Sb_x$:Te(Sn), dispersion law of charge carriers *(Russian)* 79—87114
$Bi_{100-x}Sb_x$, lattice dielec. const. meas. 78—10490
$Bi_{100-x}Sb_x$, chem. microhomogeneities, topographical and electron beam microanalysis obs. 79—65206
$Bi_{88}Sb_{12}$-Sn, current carrier energy spectrum *(Russian)* 78—60139
$Br_{1-x}Sb_x$, alloy wire, magnetoresistance in high longitudinal fields *(Russian)* 79—87113
Ca-Sb, phase diag. 77—52284
CaSb, resist., susceptibility and thermopower rel. to electronic struct. 78—67935
Cd-In-Sb, liq. alloy, Cd thermodynamic activities, Gibbs free mixing enthalpy *(German)* 80—45279
Cd-In-Sb, liq. alloys, thermodynamic activity of Cd between 833 and 953K *(German)* 80—45278
Cd-Sb, dil., loss of nucl. alignment of ^{115}Sb by radiation induced defects 78—43344
Cd-Sb, liq., hard-sphere struct. factors 77—51301
Cd-Sb, liq., thermoelec. power meas. 79—40591
Cd-Sb, near CdSb, Hall coeff., resistivity 79—56216
Cd-Sb alloy condensate film, phase transform. kinetics 77—15721
Cd-Sb alloys, phase diagram and melts struct., crystn. depend. on heating conditions 79—52155
Cd-Sb-Sn ternary system, phase equilib. 80—16266
$Ce_x(La_{0.76}Y_{0.24})_{1-x}Sb$, mag. phase diagrams, exchange interaction variation-thermodynamic model 79—65673

antimony alloys continued
CeSb, anisotropic mag. ordering and mag. structural transitions 79−78324
CeSb, commensurate-commensurate transitions and devil's staircase 79−78317
CeSb, ferromag., mag. excitation spectrum, inelastic neutron scatt. obs. 79−78352
CeSb, mag. phase transitions, zero applied mag. field 78−31070
CeSb, mag. transition, effect of applied mag. field 78−43590
Co-Sb, dilute ferromagnetic alloy, resistivity and magnetoresist. anisotropy 79−11106
CoSb alloys, sp. ht. and thermal expansion 77−47587
CoSb, at. struct. and mag. susceptibility 77−39561
Cr-Sb, dil., mag. phase diagram, elec. resist. and thermal expansion obs. 79−1669
$(Cr_{1-x}Fe_x)_{1+\delta}Sb$, interstitial occupancy, Cr:Fe distrib., X-ray and neutron diffr. study 79−42012
Cs-Sb, liq., metal-nonmetal transition and change in electronic and mag. props. 77−51790
Cs-Sb, liq. alloys, mag. susceptibility and electronic struct. 77−1537
Cu-Sb, cold-worked, lattice defects, convolution relations for X-ray line breadth calcs. 78−51394
Cu-Sb, dil., electron high dosage source for residual resistance specimens and irradiation expts. *(German)* 78−21274
Cu-Sb, dil., grain growth rate, 520-970°C *(Russian)* 80−29972
Cu-Sb, electron work function, contact pot. difference meas. 78−80041
Cu-Sb, growth kinetics of discontinuous precipitation, third element effects 77−36511
Cu-Sb, liq., partial interference functions, short range chem. order effects 79−7541
Cu-Sb, peculiarities in temp. behaviour of internal adsorption *(Russian)* 79−55890
Cu-Sb, thermodynamic investigation 78−39750
Cu-Sb (1 wt.%), stress removal during annealing after hydrostatic extrusion 79−83215
Cu-Sb (10-50 wt.%), thermal dilatometric anal. 79−56954
Cu-Sb (24-45 wt.%), phase transform. exam. by thermal expansion 77−63629
Cu-Sb alloy, splat-quenched, energy dispersive X-ray diffr. 78−23728
Cu-Sb melt, eutectic struct. by neutron diffr., isotopic substitution 78−47233
Cu-Sb solid soln., finely lamellar discontinuous precipitation, ternary addition effects 77−36510
Cu-Sb solid solution, dil., FCC, intergranular solid shortness mechanism *(Russian)* 79−5032
Cu-Sb system, atomic struct. and electronic props. *(Russian)* 77−20289
$Cu_{1-x}Pd_xMnSb$, mag. phase transition 80−60268
Cu_2Sb, linear muffin-tin calc. for Fermi surface 77−62802
Cu_3Sb, formed by saturation of Cu grains with Sb, electron diffraction exam. of diffusion layer *(Russian)* 79−33119
$Cu_{82.5}Sb_{17.5}$, X-ray K-absorption discontinuity, extended fine struct. 78−76556
DySb, quadrupole scatt. anisotropy, magnetically ordered material 78−64034
$Er_3Au_3Sb_4$, mag. suscept. meas., 4 to 300K 79−51742
Fe, cast, influence of Y and Sb on microhardness and lattice spacing of ferrite *(Russian)* 80−19748
Fe, cast, Mg-Sb, despheroidising composition and distribution of phases, X-ray obs. *(Russian)* 78−95732
Fe-Cr-Sb, segregation of ^{121}Sb, Mossbauer spectroscopy 79−47698
Fe-Mn-Sb, phase comp. 80−16267
Fe-Ni-C-Sb, Sb additions effect on fracture charact. of martensite *(Czech)* 77−70162
Fe-Ni-Sb, segregation of ^{121}Sb, Mossbauer spectroscopy 79−47698
Fe-Ni-Sb (4, 0.0087 at.%), surface segregation 79−96031
Fe-Ni-Sb-S, S/Sb surface site competition in segregation 80−40366
Fe-Sb, additive effect on eutectoid transformation of Fe 78−52799
Fe-Sb, dil., mag. hyperfine fields, Curie temp. and Mossbauer meas. 77−63190
Fe-Sb, dil., short range order, NMR study 80−71237
Fe-Sb, dil., size effects on mag. hyperfine fields at non-mag. impurities 78−43586
Fe-Sb, dil., spontaneous magnetoresistance anisotropy and deviations from Mattheissen's rule 79−51553
Fe-Sb, dil., XPS meas. 77−63538
Fe-Sb, magnetic transition effect on alloying element solubility *(Japanese)* 79−42256
Fe-Sb amorphous films, Mossbauer effect study 80−75896
Fe-Sb-Ni(Cr), dil., short range order, NMR study 80−71237
Fe-Sb-Ti(V)(Cr)(Mn)(Co)(Ni), dil., interactions and precip., Mossbauer study 80−39997
Fe-Sb-Ti(V)(Cr)(Mn)(Co)(Ni), interactions and segregations, Mossbauer and X-ray diffr. study 80−70415
Fe-Ti-Sb-C alloys, Sb trapping effect on temper embrittlement, ion beam study 78−92312
FeSb, dil., short-range order, neutron diffuse scatt. and spin echo NMR 80−50106
$FeSb_2$, phase structure, X-ray crystallography *(French)* 78−91305
$Fe_{1+x}Sb$, Mossbauer meas. of lattice and interstitial Fe atom mag. ordering 79−99807
$Fe_{1+x}Sb$, phase structure, X-ray crystallography *(French)* 78−91305
Ge-Sb, chemical diffusion *(Japanese)* 78−14515
Ge-Sb, eutectic alloy, exam. of morphology during solidification *(Russian)* 79−34022
Ge-Sb eutectic alloy, crystallisation in electric field *(Russian)* 77−52311
Ge-Sb liq. alloys, SRO 78−22632
Ge-Si-Sb, segregation of Si,Sb due to barometric mol. diffusion in gravitational, centrifugal fields 78−14472
Ge-Si-Sb solid soln., distrib. of components in universal furnace expt. in Soyuz-Apollo programme *(Russian)* 78−31381
Ge-Si-Sb solid soln., prod. by 'Universal Furnace' expt. Sb and Si distrib. *(Russian)* 78−23692
Ge-Si-Sb solid soln., struct. peculiarities and mech. props. under weightlessness *(Russian)* 78−23693
Ge-Sn-M, M=Cu, As, Sb, formation of Ge-based solid solns. during crystallisation 77−80625
$Ho_3Au_3Sb_4$, mag. suscept. meas., 4 to 300K 79−51742
HoSb, mag. phase diagram, quadrupolar interactions 80−65820
HoSb, quadrupole scatt. anisotropy, magnetically ordered material 78−64034

antimony alloys continued
$Ho_cY_{1-c}Sb$ system, magnetisation, elec. resist., and sp. ht. meas. 80−60213
In-Sb, binary metallic melt, deviation from the Kopp law, specific heat *(Russian)* 80−39305
In-Sb, cryst. struct. after appl. of high press., supercond. transition temp. 80−70169
In-Sb, liq., mag. susceptibility, MP to 1000°C, anomalies due to electron-ion interaction 77−20546
In-Sb, metallic soln., association 78−15373
In-Sb, thermodynamic quantity meas. by quantitative thermal anal. of heating process 78−19730
In-Sb alloys, liq., spin relax. of ^{117}Sb and ^{115}Sn 77−16216
In-Sb liquid alloy, calorimetric investigation, rel. to association equilibrium *(German)* 77−16862
In-Sb liquid alloy, mixing enthalpy, temp. depend. *(German)* 80−84298
In-Sn-Sb, liquid state, structure of eutectic alloy 78−42890
InSb-Sb, form of growth of Sb crysts., precip. temp. effects *(Russian)* 77−21144
$In_{1-x}Sb_x$, liquid, nucl. quadrupole relax. of Sb, time depend. PAD meas. 77−43899
$IrMn_{1+x}Sb$ alloys, crystal struct., and mag. props. 78−34466
La-Sb, heat of formation for various phases, 300K 79−91988
LaSb, lattice dynamics 79−37783
Li-Sb, thermodynamic props., 355-600°C 78−34634
Mn-Sb, liq., elec. resist. meas. 77−51721
$Mn_{1-x}Co_xSb$, press. effect on saturation magnetisation *(Russian)* 77−80919
$Mn_{1.88}Cr_{0.12}Sb$, antiferromag.-ferrimag. transition, neutron crit. scatt. and crossover effect 80−71023
$Mn_{1.88}Cr_{0.12}Sb$, magnon renormalisation 77−69520
$Mn_{1.88}Cr_{0.12}Sb$, thermomagnetic props., antiferromag. to ferrimag. transition 77−63194
$Mn_{2-x}Cr_xSb$, exchange-inversion interaction and acoustical magnon soft mode 77−40049
$Mn_{2-x}Cr_xSb$ film, prep. and mag. props. 78−48009
$Mn_{1-x}Cu_xSb$, ferromag., NMR exam. 77−12207
$Mn_{1-x}Cu_xSb$ film, ferromag. reson. 78−31114
$Mn_{2-x}Fe_xSb$, mag. struct. and spin flop transition, ^{57}Fe Mossbauer expts. 77−66261
$Mn_{2-x}Fe_xSb$, Mossbauer effect exam. 78−68432
$Mn_xNi_{1-x}Sb$, spin glass state and synthesis in high temp. and press. atmospheres 78−23277
MnSb, electronic state, neutron diffr. study 78−87906
MnSb, hyperfine interactions, ^{119}Sn Mossbauer obs. 77−40160
MnSb, interstitial cations, mag. and crystallographic study 79−55698
MnSb, magnetic losses, ferromagnetic resonance and antiresonance 80−100618
MnSb, resist., susceptibility and thermopower rel. to electronic struct. 78−67935
MnSb-Mn_2Sn alloy system, continuous series of solid solns., homogeneity and ferromagnetic props. 79−52159
$Mn_{1.15}Sb$, Kerr effect and TEM obs. of mag. domains 77−89974
Mn_2Sb, Bi-modified, mag. first order phase transition 79−51777
Mn_2Sb, domain and domain wall resons. in ^{55}Mn NMR spectrum 80−25219
Mn_2Sb, large anisotropy in mag. hyperfine field at ^{121}Sb, Mossbauer spectra meas. 77−73101
Mn_2Sb, spin-wave dispersion relations, exchange interactions, neutron inelastic scatt. 80−65832
$Mn_2Sb_{1-x}Bi_x$ ($0 \leq x \leq 0.175$), mag. transition, thermal expansion, thermomag. effects and lattice constant changes *(Japanese)* 79−78375
$MnSb_{1-x}Sn_x$ films, Faraday rotation, optical absorpt. coeffs. 80−97242
$MnSb_{1-x}Sn_x$, zero-field NMR investig. of domains and domain walls 77−32271
$Mn_{1+x}Sb_{1-x}Sn_x$, magnetisation and Curie temp., prep. and comp. depends. 78−64200
$Mn_{1+x}Sb_{1-x}Sn_x$, nuclear Zeeman effect, Mossbauer meas. 79−28654
$Mn_2Sb_{1-x}Sn_x$, mag. transitions, Mossbauer meas. 78−52406
$Mn_{2-x}V_xSb$, $0.08 \leq x \leq 0.25$, mag. props. modification by V 77−36071
$Na_{1-x}Sb_x$, liq., mag. susceptibility 78−14926
Nb_3Sb, 4 to 294K, magnetic susceptibility meas. 79−99675
Nb_3Sb, de Haas-van Alphen effect and Fermi surface 78−6262
Nb_3Sb, NMR of ^{93}Nb and spin-lattice relax. time at low temp. 77−85388
Nb_3Sb, NQR study, ^{93}Nb nuclear relax. 78−88073
Nb_3Sb, resist. characts. in normal state 78−51963
NbSnSb, synthesis and struct. *(French)* 79−90596
Nd-Sb, heat of formation meas. 77−90635
Ni-Sb, dil., vacancy-impurity binding enthalpy, positron annihilation 79−91525
Ni-Sb dil., impurity effects on grain boundary mobility *(Polish)* 79−96073
NiMnSb, hyperfine mag. field at Cd impurity, TDPAC study 80−39906
$Ni_{1+x}MnSb$, mag. hyperfine field on ^{111}Cd, TDPAC obs. 78−43709
Ni_2MnSb, Heusler alloy, hyperfine field at ^{111}Cd, TDPAC meas. 78−43705
NiSb, at. struct. and mag. susceptibility 77−39561
NiSb, dilute alloy, impurity-induced vacancy clustering 79−99972
NiSb, resist., susceptibility and thermopower rel. to electronic struct. 78−67935
$Ni_{0.96}Sb_{0.04}$, surface segregation, XPS and AES obs. 80−76135
Ni_5Sb_2, cryst. struct. *(German)* 78−83775
Pb-Sb, chill cast and wrought, cyclic voltammetry and electrochemical meas. of anodic activity, PbO_2 form. 78−31582
Pb-Sb, crystal struct., supercond. after subjection to high press. 78−88064
Pb-Sb, dil., US oscillations and dislocation unpinning in supercond. and normal states *(Russian)* 79−11648
Pb-Sb, dynamic destruction of supercond. 80−2529
Pb-Sb, improvement in antifriction layer props. by impulse discharge, impulse discharge treatment *(Russian)* 79−1917
Pb-Sb, influence of quench deform. on precipitation *(German)* 77−86064
Pb-Sb, phase transform. at high press., DTA, eta, beta thermodynamic stable phases *(Russian)* 79−66051
Pb-Sb, thermal analysis in non-faceted/faceted eutectic systems 80−71637
Pb-Sb (1 wt.%), highly averaged, fracture behaviour 79−8366
Pb-Sb alloy, Sb distrib. profile as function of depth in corrosion films 80−21177

antimony alloys continued
Pb-Sb battery grids, ageing behaviour obs., effects of casting and cooling 79—100517
Pb-Sb eutectic alloys, solidification in space environment 79—47671
Pb-Sb form of growth of Sb crysts., precip. temp. effects *(Russian)* 77—21144
Pb-Sb molten alloys, oxidation and drossing *(German)* 79—74313
Pb-Sb-As (1.1-1.8, ~0.01 wt.%), enhanced precip. phenomena, invest. of mechanism by elec. resist. meas. 80—104162
Pb-Sb-Sr alloys, corrosion props. by simplex-lattice planning method 77—56148
Pb-Sb-Te-Cu-Sn, influence of specimen and grain size on mech. props. *(Russian)* 77—81297
Pb-Si-Sb amorphous alloys, electrical resistometric detection of relaxation 79—60278
Pb-Sn-Sb, surface tension liquidus temp. to 550°C *(Korean)* 79—90848
$Pb_2MnSb_{0.99}Sn_{0.01}$, ^{119}Sn Mossbauer study, compositional and heat treatment effects 79—42875
PbSb foil production for TEM by electrolytic and ion beam thinning *(German, English)* 77—49812
$Pb_{1-c}Sb_c$, liquid alloys, local fluctuations and quadrupolar relaxation 80—66060
Pd-Sb film, rhombohedral phase, cryst. struct. electron diffr. determ. 80—39008
Pd-Si-Sb, amorphous, phase separation and crystallisation 79—51002
Pd-Si-Sb, mostly crystalline, rapidly quenched, mech. props. 79—61610
$Pd_2MnIn_{1-x}Sb_x$, Heusler alloy, Mossbauer effect exam., mag. coupling 79—69755
$Pd_2MnIn_{1-x}Sb_x$, Heusler alloy, Mossbauer effect exam., hyperfine interactions in ferromag. phase 79—69756
$Pd_2MnIn_{1-y}Sb$, Heusler alloy, mag. order, disorder effects 80—88723
$Pd_2MnIn_{1-y}Sb_y$, Heusler alloy, mag. order obs. 80—29528
PdMnSb, Heusler alloy, hyperfine fields of 5sp shell impurities substituting Sb, Mossbauer spectra 78—80261
PdMnSb, hyperfine field at ^{125}Te, Mossbauer expts., compared with Jena-Geldart model 78—43707
PdMnSb, Pd_2MnSb, Heusler alloys, ^{129}I mag. hyperfine struct., Mossbauer meas. 79—33580
$Pd_{1+x}MnSb$ Heusler alloys, magnetic hyperfine fields on ^{111}Cd, TDPAC and magnetisation meas. 80—93219
Pd_2MnSb and PdMnSb, Heusler alloy, hyperfine field at ^{111}Cd, TDPAC meas. 78—43705
Pd_2MnSb, Cd impurities, hyperfine field meas. 78—15074
Pd_2MnSb, ferromag. Heusler alloy, mechanical and heat treatment effects 79—78582
Pd_2MnSb, Heusler alloy, hyperfine fields of 5sp shell impurities substituting Sb, Mossbauer spectra 78—80261
Pd_2MnSb, mag. hyperfine field of ^{129}I, Mossbauer spectra 78—43706
Pd_2MnSb:^{119}Sn, ferromag., mag. hyperfine structure, Mossbauer obs. 77—32309
$Pd_{2-x}MnSb$, struct., appl. as improved neutron polariser 80—60199
$Pd_2MnSb_{1-x}Sn_x$, Mossbauer meas. of ^{119}Sn mag. hyperfine struct. 77—12258
$Pd_2MnSn_{1-x}Sb_x$, Heusler alloy, Mossbauer effect exam., hyperfine interactions in ferromag. phase 79—69756
$Pd_2MnSn_{1-x}Sb_x$, mag. order exam. 77—40036
$Pd_2MnSn_{1-x}Sb_x$, Mossbauer spectra, mag. hyperfine field 80—15868
$Pd_2MnSn_{1-y}Sb_y$-Cd, dil., Heusler alloy, hyperfine mag. field on Cd, TDPAC obs. 79—8075
PdSb, de Haas-van Alphen effect, Fermi surface 79—7773
PdSb, XPS, electronic struct. 80—7464
PdSb-Rh, dil., quadrupole interaction of ^{100}Rh 79—99520
$Pd_{20}Sb_7$, cryst. struct. determ. *(German)* 77—19905
$Pd_{75}Sb_{25}$, ordered BCC phases at high temp. 79—32948
PrSb, lattice dynamics 79—37783
PrSb, neutron scatt., press. induced antiferromag. 80—15699
Pt-Sb, amorphous sputtered film, elec. props. 78—68006
PtMnSb, Cd impurities, hyperfine field meas. 78—15074
PtMnSb, hyperfine mag. field at Cd impurity, TDPAC study 80—39906
Pt_4Sb, Ll_2 ordered alloy, positive temp. depend. on strength, phase destabilization 80—81203
$RhMn_2Sb$, mag. and cryst. props. 77—20568
Rh_2MnSb, hyperfine fields, ferromag., NMR and Mossbauer effect studies 80—71259
Sb-Au, amorphous film, elect. resist. 78—95390
Sb-Au amorphous film, quench condensed, struct. and stability 79—99459
Sb-Au amorphous films quench-condensed, resistivity and Hall effect meas. 79—99638
Sb-Bi, melting kinetics of solid soln. during high heating rates, superheating *(Russian)* 78—15358
Sb-Bi, X-ray diffr. investig. of high-press. polymorphism 77—43324
Sb-Bi (2%), medium-oriented, plastic deformation *(German)* 77—70109
Sb-Ce system, heats of form. 80—89517
Sb-Ge, unidirectionally solidified, exam. of compressive props. and struct. 78—68730
Sb-Ge (1.2 to 2.2 at.%), carrier transport, magnetoresistivity, field-dependent tensor study 80—39609
Sb-In, electronic work function, contact pot. difference meas. 77—85299
Sb-Sn, dil., de Haas-van Alphen effect, effective mass, Fermi levels 78—75982
Sb-Sn, electronic work function, contact pot. difference meas. 77—85299
Sb-Sn (0.5 to 1.0 at.%), carrier transport, magnetoresistivity, field-dependent tensor study 80—39609
Sb-Sn (8 at.%), grain boundary-migration, intergrain liq. layer effects *(Russian)* 77—15633
Sb-Sn melt, electrotransfer *(Russian)* 77—66034
Sb-Te, A1-type, superconductivity 80—29496
Sb-Te-Bi, miscibility limits, computer study 78—79773
Sb-Te(Se), liq., diamag. susceptibility, semicond./metal behaviour 78—14927
Sb-Zn, electronic work function, contact pot. difference meas. 77—85299
$SbBe_{13}$, cryst. struct. determ. 77—24291
$Sb_{1-x}Bi_x$ alloys, Shubnikov-de Haas *(Russian)* 78—23007
SbSn, ^{120}Sb elec. quadrupole interaction, temp. depend. 78—19399
Sb_2Te_3-Bi_2Te_3, low-temp. thermoelectric mats., growth of microhomogeneous crysts. 77—48337
Sb_2Tl_7, single-cryst. struct., X-ray diffr. determ. 77—65963
Se-Sb, liquid alloys, vapour phase effect on activity determ. *(German)* 79—43210

antimony alloys continued
Sn-Pb-Sb, microduplex eutectic, cavitation during superplastic flow 78—48457
Sn-Sb, A1-type, superconductivity 80—29496
Sn-Sb, small κ supercond., phase transitions higher than second order 80—88668
Sn-Sb (0.57 at.%) solid soln., yield point for cold-worked and annealed specimens *(Russian)* 78—48448
Sn-Sb (10 wt.%), decomposition of supersaturated solid soln. 80—29960
Sn-Sb (up to 0.3 at.%) whisker, supercond. crit. temp., stress depend. 77—39988
Sn-Sb alloys electrodeposition 80—25586
Sn-Sb dil. liq. alloy, electrodiffusion and electroconvection, effective diffusion coeff., apparent effective valence 78—87802
Sn-Sb molten alloys, thermodynamic study *(Korean)* 78—31383
Sn-Sb-Ag, splat cooled foils, TEM study 80—40344
SnSb film, defect density variation with deposition rate, annealing, elec. resist. meas. 77—21027
$Tb_3Au_3Sb_4$, mag. suscept. meas., 4 to 300K 79—51742
TbSc, crit. scatt. of electrons near antiferromag. transition temp. 79—69505
$Tb_cY_{1-c}Sb$, elec. resist., cryst. field and exchange interaction contribs. 80—39556
Te-Sb, liq., elec. cond. 78—84186
TiSnSb, synthesis and struct. *(French)* 79—90596
Tl-Cd-Sb, liq., Cd vapour pressure and thermodynamic functions *(Russian)* 79—51247
Tl-Sb, liq., mag. susceptibility, MP to 1000°C, anomalies due to electron-ion interaction 77—20546
$Tm_3Au_3Sb_3$, mag. suscept. meas., 4 to 300K 79—51742
$U_3Ni_3Sb_4$, and related compounds, X-ray diffr. cryst. struct. determ. 79—42009
USb, anisotropic mag. ordering and mag. structural transitions 79—78324
USb, antiferromag., neutron diffr. exam. of ordered state 77—20557
USb, crit. neutron scatt. 77—24674
USb, localised versus itinerant 5f electrons exam., reflectivity meas. 79—19905
V_3Si-Sb, cryst. struct., supercond. T_c comp. depend. 78—51494
V_3Si-Sb solid soln., supercond. T_c and paramag. susceptibility *(Russian)* 77—59348
Y-Sb compounds, heat of form. meas. 77—36783
$Y_3Au_3Sb_4$, cryst. struct., X-ray diffr. meas. 77—47378
Zn-Sb system, phase interactions and phase diagram 79—87607

antimony compounds
see also antimony alloys
α-$AgSbS_2$, X-ray diffr. study of phase transitions in quenched samples 77—15577
antimonates, $M_4{}^{II}M^{III}Sb^{V}O_8$ spinels, struct. determ., IR and Mossbauer spectra 79—91431
$Bi_{1-x}Sb_x$ narrow band gap semiconductors, galvanomagnetic, optical and photoelectric props. 80—15544
binary, with non-transition elements, at. vol. and semicond. props. 77—20089
chalcogenide glass film, M-Sb-S-I, (M=Ge, Sn, Pb, Cd, Cu), prep. and characterisation 77—12533
chemical bonding in group V and VI elements and compounds with tetradymite structure 80—15036
chlorides, methyl substituted, lone pair electrons,. ^{121}Sb Mossbauer spectroscopy study 80—39984
graphite-$SbCl_5$, intercalation compounds, development as reagents in organic synthesis 78—27444
graphite-$SbCl_5(F_5)$ intercalation compounds, elec. resist., comp. and temp. depend. *(French)* 77—62971
graphite-$SbF_5(Cl_5)$ intercalation compounds, compacts, elec. resistivity, C fluorination 80—34493
graphite-SbF_5 intercalation compounds, elec. cond. and opt. reflectance 77—62970
graphite-SbF_5 intercalation cpd., elec. cond. 77—43549
halides, mol. electronic struct., quadrupole-interaction-interaction consts., CNDO/2 calc. 77—10589
inorganic and organometallic cpds., photoelectron spectra, valence bands, ligand field broadening 77—63525
Mossbauer effect, isomer shifts, quadrupole splitting, CNDO/II calcs. 77—24766
Mossbauer effect of ^{121}Sb in mixed valence cpds. $M_2{}^{I}Sb_{0.5}M_{0.5}{}^{IV}Cl_6$, ($M^{I}=NH_4$, Rb or Cs, M^{IV}=Se, Te or Sn) 78—84506
$Pb_4Sb_4S_{11}$, synthetic, cryst. struct. by X-ray goniometry 80—6394
pentaphenylantimony cyclohexane, cryst. packing 78—9994
polyacetylene:SbF_5, elec. cond. meas. 80—60055
polyacetylene:SbF_6, metallic, band theory 80—49570
polyparaphenylene:SbF_5, metallic, absence of Pauli paramagnetism, mag. susceptibility meas. and ESR obs. 80—97060
stubnite, H_2 reduction, Sb production 79—66023
thiourea SbF_3, cryst. struct., single cryst. X-ray diffr. study, influence of secondary binding *(French)* 79—32987
trihalides, non-empirical valence electron MO calcs., ion states spin-orbit splitting 77—34544
zinckenite, chem. and structural study *(French)* 77—43181
AS_xSb_{1-x} thermomagnetic EMF, temp. and mag. flux density *(Russian)* 80—11022
Ag-Sb-S, prep. and props. of glasses in the system 77—20053
$(Ag_{x/2}Pb_{1-x}Sb_{x/2})Te$ solid solns., Hall coeff., thermoelec. power, and thermal cond., 100 to 500K 79—82614
$Ag_2S(Se)(Te)$-Sb, temp.-comp. diagram 78—44105
Ag_3SbS_3, pyrargyrite, elec. cond. rel. to impurities, melt stoichiometry deviations 77—11914
Ag_5SbS_4, electron absorption and dispersion of ultrasound velocity 80—15197
$Ag_{19}Sb_{29}Te_{52}$, single-phase, thermoelectric efficiency 80—107826
Al-Sb_2O_3-In films, negative resistance characts. 80—11103
$Al_{1-x}Sb_x$, amorphous, localised gap states, variable range hopping 77—72866
As-Ge-Se-Sb glasses, acousto-optic props. 77—27327
As-Sb-S-I system glasses, vitrification and volt-ampere characts. 77—31756
As-Se-Sb, crystallised glasses, struct. from Mossbauer spectra 80—64917
As_2S_3-Sb_2S_3, vitreous, dispersive charge transport analysis 79—95418
As_2S_3-Sb_2S_3 system glasses, long-term photocond. relax. 77—76874

antimony compounds continued
$(As_2S_3)_{0.55}(Sb_2S_3)_{0.45}$ vitreous film, dispersive charge transport, time-of-flight meas. 79—19594
$As_xSb_{1-x}SI$ mixed crystals, phonon coupling, ferroelectric phase transition, Raman study 80—108165
$As_xSb_{1-x}SI$, solid solns., ferroelec. props. 78—23409
$As_4Sb_2Se_9$ glassy semiconductors, electronic props. 80—103712
As_2Se_3-Sb_2S_3 glass, threshold and memory switching, expt. data 78—39170
As_2Se_3-Sb_2Se_3, phase relns. 77—21118
$AsTeSb_x$, chalcogenide glass, thin film crystallisation 79—7758
Au-Sb, system interactions due to heat treatment, backscattering anal. 79—91719
$Ba_3Sb_2NiO_9$, 6H, cation ordering, powder neutron diffr. obs. 78—55852
$Ba_3(Sb_4Ti_4)O_{21}$, effects of Sb substit., synthesis and cryst. chemistry 77—76379
$(Ba_xSb_{1-x})TiO_3$ 80—60514
$(Ba_xSb_{1-x})TiO_3$, ferroelectric films, dielectric and semicond. props. 79—91388
$(Bi,Sb)_2,(Te,Se)_3$, thermoelectric alloys, phase diagrams, and imperfection chemistry 80—108422
$(Bi, Sb)_2Te_3$ solid soln., semiconductor film, oxidation, electrophysical props. 80—45407
Bi-$Bi_{0.5}Sb_{1.5}Te$ system, stratified medium with artificial anisotropy, transverse cooling effect 79—28364
Bi-Sb-S-I system glasses, vitrification and volt-ampere characts. 77—31756
BiI_3-$Sb(As)I_3$, phase diags. 78—6905
$Bi_{1-x}Sb_x$, band inversion under press., Fermi surface anisotropy, galvanomag. meas. 77—51637
$Bi_{1-x}Sb_x$, EM wave propag. for rot. of mag. field from Faraday to Voigt config. 80—84419
$Bi_{1-x}Sb_x$, elec. resist., 1.8 to 77K, electron-phonon scatt. mechanism 79—15144
$Bi_{1-x}Sb_x$, far IR magnetoabsorption, band struct. study 80—50351
$Bi_{1-x}Sb_x$, galvanomag. props., energy spectrum *(Russian)* 79—56248
$Bi_{1-x}Sb_x$, non-ellipsoidal Fermi surface, cyclotron reson. meas. at 35 and 70 GHz 77—62804
$Bi_{1-x}Sb_x$, semicond., photoconductivity *(Russian)* 79—7857
$Bi_{1-x}Sb_x$, solid soln., temp. depend. of weak-field galvanomag. coeffs. *(Russian)* 80—70724
$Bi_{86}Sb_{14}$:Te, single crystal, dispersion of magnetoplasma waves *(Russian)* 80—70739
$Bi_xSb_{1-x}SI$, atomic substitution and ferroelec. phase transition 78—68464
$Bi_xSb_{1-x}SI$, low freq. Raman spectroscopy 78—15162
$(Bi_{0.25}Sb_{0.75})_2Te_3$, opt. props. of bulk and films 78—27206
$Bi_{0.5}Sb_{1.5}Te_3$ film, effect of struct. on thermal cond. 79—28257
$Bi_{0.52}Sb_{1.48}Te_3$ thermoelec. solid soln., homogeneity, effects of prep. method 78—52698
$Bi_{0.52}Sb_{1.48}Te_3$-Te, phase-equilibrium boundary, Hall coeff. meas. 78—44094
$(Bi_{1-x}Sb_x)_2Te_3$, highest valence band struct., Shubnikov-de Haas effect 78—14661
$Bi_{2-x}Sb_xTe_3$, solid soln. film on mica substrate, effect of stresses on elec. cond. 78—51859
$Bi_{88}Sb_{12}Te_{0.05}$, helicon dispersion, effect of slope of electron ellipsoids 79—28365
$Bi_xSb_{2-x}Te_3$, 2-dimens. cryst. interface props. of Bi overlayer UPS obs. 78—34881
$Bi_{2-x}Sb_xTe_{3-y}Se_y$, elec. cond. and thermoelec. props., neutral defects influence 80—60017
$Bi_{2-x}Sb_xTe_{3-y}Se_y$ solid solution, density-of-states effective mass, carrier mobility temp. depend. 80—24931
Bi_2Te_3-Bi_2Se_3-Sb_2Te_3, solid solution, single crystal, elec. cond., thermoelectric props. 80—88550
Bi_2Te_3-Sb_2Te_3, Bi:Sb=1:2, 2:1, solid soln. deviation from stoichiometric cross section 79—43221
Bi_2Te_3-Sb_2Te_3, plastically deformed by hot extrusion, diffusion meas. using micro-X-ray spectrum anal. 79—14954
Bi_2Te_3-Sb_2Te_3 film, cond., galvanomag. Seebeck and Nernst-Ettingshausen effects under press., band model 77—47907
Bi_2Te_3-Sb_2Te_3 film, residual cond. 78—52110
p-Bi_2Te_3-Sb_2Te_3 semiconducting solid solns., plastic deform. during hot extrusion 79—20143
Bi_2Te_3-Sb_2Te_3 solid soln., deviation from stoichiometric cross section 78—35362
Bi_2Te_3-Sb_2Te_3 solid solns., powders, particle shapes determ., device 78—60899
Bi_2Te_3-Sb_2Te_3:Cu, electrical cond. and thermopower, disorder effects *(German)* 77—1422
Bi_2Te_3-$SbTe_3$, ordered structure formation, heat treatment effect on thermal cond. 80—54448
BiTeI-SbTeI, solid solns., phase diagrams, photocond., elec. props. 79—38125
BiTeI-SbTeI solid solns., form., crystn., elec., thermal props. 78—44003
$(Bi_2Te_3)_{0.9}(Sb_2Te_3)_{0.5}(Sb_2Se_3)_{0.05}$ n-type alloy for thermogenerators, thermo-EMF, elec. cond. and thermoelec. efficiency factor, 300-600K 80—70735
$BrF_3.SbF_5$, NQR anal. of complex ion struct. 77—12238
$CaFeSbAs_2O_7$, stenhuggarite, cryst. struct. 77—58983
$Ca_3SbSnFe_3O_{12}$, neutron diffr. patterns, group theory approach for determ. of mag. struct. *(Russian)* 79—51749
$CdGe_{1-x}Sb_xAs_2$ system, amorphous and cryst. phases, DTA and microhardness obs. 78—22835
CeSb, mag. phase diagram for mag. field applied along ⟨111⟩ direction 79—33458
$ClF_5.xSbF_5$ and $ClF_3.xSbF_5$, NQR anal. of complex ion struct. 77—12238
$Cs_3BiSbBr_9(Cl_9)$, ^{121}Sb Mossbauer chem. shifts, optical reflectance spectra, solid state band populations 77—40162
Cs_2SbCl_6, mixed valence compound, ^{121}Sb Mossbauer spectroscopy 79—51890
$(Cu,Ag)_2Se/(Bi, Sb)_2Te_3$, P type selenide segmented element fabrication, thermoelectric props. 80—107835
Cu-Sb-S-I amorphous film formation and stimulated crystallisation, electrophysial props. *(Russian)* 78—30838
$EuSb_2S_4(Se_4)(Te_4)$ elec. cond., Hall, thermo-EMF coeffs. determ., 300-1100K 78—43386
$FeSb_xO_{4-y}$, defect struct. and mag. transition, elec. transport and Mossbauer expts. 78—59803

antimony compounds continued
Ga-In-Sb, ternary phase diagram, thermodynamic models of solidus and liquidus isotherms 79—24504
$GaAs_{1-x}Sb_x$ on GaAs, LPE growth of GaAs 79—61519
GaI_3-$SbCl_3$, total exchange of halogens, Raman spectra and phase equilibrium *(French)* 79—65874
$(GaSb)_{1-x}Ge_x$ films, single-cryst. metastable semicond., growth and phase stability 80—80115
Ge-S-Sb glasses, microgravity effect on recrystn., optical and elec. props. 80—49127
Ge-Sb-Se glass, elec. props, comp. depend. 80—70697
Ge-Sb-Se glass, physical props., purification method for Sb, Se from surface oxides 78—46735
Ge-Sb-Se system glasses, thermal capacity, 300-600K 79—65210
Ge_xSb_{1-x} amorphous film junction, I-V and C-V characts. 77—85307
$Ge_{20}Sb_{25}S_{55}$ glasses, optical props., absorption edge temp. depend. 80—2789
$GeSe_2$-As_2Se_3-Sb_2Se_3, quenched glass system, elec. cond., low temp. heat treatment effect 80—39586
$GeSe_2$-As_2Se_3-Sb_2Se_3, elec. cond. over wide range of temp. 80—88564
GeTe-Sb_2Te_3, solid solutions, cond., density of states 80—88472
GeTe-Sb_2Te_3, thermoelectric materials, physico-chemical study 78—30945
$(GeTe)_x$-$(AgSbTe_2)_{1-x}$, thermoelectric props. of monolithic and pressed samples at 300K 78—80009
In-Sb-Cd system, phase diagrams 79—87617
$In_{1-x}Ga_xAs$-$GaSb_{1-y}As_y$, new heterostruct. characts. 78—72247
$In_{2-x}Sb_xO_{3+x}$, form., struct. 77—16516
$In_2Sb_4O_9$, form., struct. 77—16516
$InSbSe_3$, cryst. prep. and props. 79—15601
$In_{1.8}Sb_{0.2}Se_3$, cryst. prep. and props. 79—15601
In_2Se_3-Sb_2Se_3 system, phase diagram 78—44090
$K_2SbNb_5O_{15}$, dielec. and pyroelec. props. 79—99841
$KrF_2.AsF_5(SbF_5)$, Mossbauer spectra, quadrupole coupling strengths, isomer shift and bonding 77—50458
$LiBa_3Sb_3Ti_5O_{21}$, insertion of Li, X-ray and neutron diffr. study *(French)* 78—91324
$(NH_4)_2Sn_{1-x}Sb_xCl_6$ (x=0.13, 0.21, 0.28, 0.33), mixed valence compound, ^{121}Sb Mossbauer spectroscopy 79—51890
$NaSbBrF_3.H_2O$, cryst. struct. *(French)* 78—18589
$NaSbClF_3.H_2O$, cryst. and mol. struct. *(French)* 77—43200
α-$NaSbS_2$, cryst. struct. and $\beta \rightarrow \alpha$ phase transform. features 80—33961
Pb-Sb, liq. alloy, Pb thermodynamic props. *(Czech)* 80—29925
PbS-Sb system alloys, phase diagram, composition depend. of microhardness and thermo-EMF 77—25028
PbS-Sb_2S_3 semicond., optical and photoelec. behaviour 80—96938
$PbSbO_2Cl$, nadorite, thermal expansion, X-ray determ. 78—18802
$(Pb_{0.66}Sb_{0.34})_6SnS_9$, garnet-like struct., synthetic, cryst. struct., X-ray diffr. study 79—19217
$(Sb,Bi)_2(Se,Te)_3$ profiled crystalline ingot continuous elongation 79—69975
Sb (III) compounds, Mossbauer spectra, direct population of solid-state bands 80—15905
Sb (III) compounds, orbital population anal. using ^{121}Sb Mossbauer data 78—21953
Sb complexes, dithiocarbamates, lone pair electrons, ^{121}Sb Mossbauer spectroscopy study 80—39984
Sb complexes, oxalate-fluoride and nitrate-fluoride cpds., NQR 77—12236
Sb complexes, $SbCl_5.L$ (L=organic radical), charge transfer and quadrupole-interaction consts. calc. 77—10590
Sb complexes, $SbCl_5.L$ (L=organic radical), charge transfer and charge distrib. calc. using NQR data 77—12243
Sb diethyldithiocarbamates, use in liquid-liquid extraction of corrosion and fission products 80—18459
Sb-Ge-Se system glasses, thermal capacity, 80 to 300K 79—42272
Sb-Ge-Se system glasses, activation energy of elec. cond. calc. 79—51568
Sb-O-Cl(Br)(I), glass-forming regions 80—88057
Sb-PbS(Te) eutectic system, crystn. 79—52190
Sb-S, saturated vap. press. 78—43116
Sb-S films, laser-beam recordings by thermal creation of holes 80—35010
Sb-S-I glasses, activation energy of crystn. 80—64920
Sb-S-I system crystals and glasses, adhesion levels, TCE spectra 77—24529
Sb-Sb_2O_3 pH electrode improvement 79—53270
Sb-Se-I, phase diagrams of various cross-sections 78—44093
Sb-Te, fused, mag. susceptibility, temp. and conc. dependence 77—36052
Sb-Te-Bi, computer study of miscibility limits, 273 to 300K 78—52781
Sb-Te(Se), liq., diamag. susceptibility, semicond./metal behaviour 78—14927
$(Sb_2\,F_4{}^{2+})[SbF_6{}^-]_2$ and $[Sb_3F_{14}{}^-]$ ion containing cpds., ^{121}Sb Mossbauer obs. of mixed oxidation state cpds. 79—28640
$Sb_{1-x}Bi_xSI$, mixed cryst., ferroelec. phase transition 79—33629
$Sb_{1-x}Bi_xSI$, SHG at microwave freqs. 79—55188
$(Sb_{1-x}Bi_x)_2Te_3$, δ phase, equilib. state, electrophysical props. 79—52178
p-$Sb_{1.48}Bi_{0.52}Te_3$, extrusion deformed, powder dispersion degree influence on thermal and elec. props. *(Russian)* 80—39366
$Sb_{1.48}Bi_{0.52}Te_3$, obtained by zone crystallisation, effect of extrusion and annealing on elec. props. 79—96038
$Sb_{1.5}Bi_{0.5}Te_3$ solid solution, electrical, thermoelectric and thermal properties, temp. influence obs. *(Slovak)* 78—30946
p-$Sb_xBi_{2-x}Te_3$ *(German)* 79—51618
$SbBr_x{}^{-y}(I_x{}^{-y})$, low freq. Raman and IR spectra, force consts. 80—55097
$SbCl_3$, bond polarisability and force constants 80—69260
$SbCl_3$ complex, with (1,3,5-triacetylbenzene), single cryst., X-ray cryst. struct. anal. 79—14761
$SbCl_3$, cryst. struct., Zeeman split fine struct. lines, FT NQR obs. 80—54982
$SbCl_3$, dynamic coeff., molecular interaction effects of media *(Russian)* 77—83601
$SbCl_3$, liquid, neutron X-ray diffraction pattern and models 80—38893
$SbCl_3$ liquid, X-ray and neutron diffraction study at 80°C 79—4230
$SbCl_3$, nuclear electric hexadecapole interactions of ^{123}Sb 79—1722
$SbCl_3$, nuclear electric hexadecapole interactions 80—65513
$SbCl_3$, quadrupole spin echo envelope EFG tensor axisymmetry in mag. field 80—20497
$SbCl_3$, X-ray struct. redeterm. 80—28970
$SbCl_3/AlCl_3$ molten mixtures, Raman spectra 80—93305
$SbCl_5$ intercalated with graphite, Raman scatt. in low stage cpds. 80—20638

antimony compounds continued
$SbCl_5$, nitrile addition compounds, mol. vibr., IR and Raman spectra *(French)* 77−23499
$SbCl_5$, phase diagram to 43 kbar 80−2144
$SbCl_5$-$NbCl_5$, melt and solid-soln. Raman spectra, $SbNbCl_{10}$ dimer *(German)* 77−4645
$SbCl_4F$-graphite intercalation cpds., prep. and props. 80−40686
$SbCl_5OPCl_3$, vibr. amplitude and normal coord. anal. *(German)* 78−66536
$SbCl_5.CD_3CN$, Raman spectra and Teller-Redlich product rule 79−69817
$SbCl_5.CH_3CN$, Raman spectra and Teller-Redlich product rule 79−69817
$SbCl_5.POCl_3$, Raman spectra, normal coordinate treatment 77−46568
$SbCl_3$naphthalene system, phonon bands in π-electron charge transfer complex 77−39644
SbF, $(f0^+, e0^-)$-X_21 transition, rot. anal. 78−74657
SbF, pot. energy curves and dissoc. energy, Hulbert-Hirschfelder calc. 80−30210
SbF_3, IR spectra of solid and gas, rel. to struct. *(French)* 78−78692
SbF_5, intercalate with graphite, optical reflectance 78−35163
SbF_5 intercalated graphite/Cu composite wires, elec. cond. 80−44687
SbF_5, intercalated with graphite, carrier density from ^{19}F NMR line shapes 80−25224
SbF_5, muon Coulomb capture ratio 78−62959
SbF_5-graphite, intercalation compound, texture 78−31355
SbF_5-graphite intercalation cpd., synthesis and elec. props. 80−70781
SbF_5+benzyl chloride, chemi-ionis. reaction, temp. depend., flow tube investig. 80−108701
SbF_6^-, produced from fast $Cs+(SbF_5)_n$ collisions, ionisation cross section energy depend. 80−81300
$^{121}SbF_6^{2-}$, radical, prep. and EPR comparison with other hexafluoride radicals 78−68381
$SbF_3.(NH_2)_2CS$ and $SbF_3.[(NH_2)_2CS]_2$, X-ray cryst. struct., IR spectrum *(French)* 78−87643
$SbF_5.OSO$, force constants, normal coordinate calculations 77−61735
$SbFe_2Si_2O_8OH$, crystal struct., space groups by RHEED 78−47297
$SbGe_xSe_y$ glasses with const. Sb content, heat capacity, thermal expansion, US vel. and elastic moduli 77−76574
SbH_3, inversion barrier, ab initio SCF calcs. 78−78615
SbI, decay branching ratios meas., transition probabilities derivation 80−95642
SbI_2, layered compound, exciton spectra, surface and stacking fault effects 80−40134
SbI_3, enthalpy, entropy of melting 78−34598
SbI_3 film, exciton peaks, temp. depend., 90-270K, and press. depend., up to 3500 atm. 77−36265
SbI_3, intermolecular bonding study using ^{129}I Mossbauer effect 78−72438
SbI_3, molten, X-ray intensity curve, short-range order 77−4034
SbI_3, photopolarisation, photoelectret state, electron-hole transitions 77−12300
SbI_3, refl. spectra of cryst., 300-800nm, and derived optical consts. 79−87456
SbI_3, valence band, UPS meas. with synchrotron radiation 79−56914
SbI_3, vapour pressure 79−60496
SbI_3-AsI_3, phase diags. 78−6905
$Sb_{0.2(0.4)}MoO_{3.1}$, synthesis, struct. and oxidation state *(French)* 80−64971
$Sb_2Mo_{10}O_{31}$, X-ray cryst. struct. determ., Patterson method *(French)* 79−99125
SbN, 3300-4000 Å, rot. and vibr. perturbations and rot. anal. *(French)* 78−37651
$SbNO_4$, ferro- and anti-ferroelec., crit. points and props. 79−38460
$SbNbO_4$, anomalous bulk photovoltage effect, Jahn-Teller mechanism 77−28218
$SbNbO_4$, anomalous photovoltaic effect and photocond. 79−38122
$SbNbO_4$, ferroelec., synthesis and hydrothermal growth 79−38731
$SbNbO_4$, ferroelec. anomalous photovoltaic effect and photocond. 78−52449
$SbNbO_4$, ferroelec. film characts. 77−48127
$SbNbO_4$, ferroelec. semiconductor, anomalously high photovoltage 77−69378
$SbNbO_4$, ferroelectric, anomalous photovoltaic effect 79−7861
$SbNbO_4$:$CoO(Fe_2O_3)(TiO_2)$, growth, pyroelectric and ferroelectric props. 79−73886
SbO, B-X system fine struct. 79−50030
SbO, dissoc. energy calcs. 77−3486
SbO^+, visible region band spectrum 79−72328
$SbO_{3/2}$-$BO_{3/2}$, glass, struct. and props. *(Japanese)* 77−27836
SbO_3-U catalyst, dynamic measurements of electrical conductivity during adsorption and catalysis 80−13096
SbO_4^{3-}, normal vib. freq. and force const. calcs. *(Russian)* 78−46318
SbO_4^{3-}, normal vibr. freqs. calc. 79−54837
Sb_2O_3, additive for activated sintering of SnO_2 77−36415
Sb_2O_3, additive in ZnO sintering 78−80497
Sb_2O_3, density of valence states, photoemission meas. 77−72808
Sb_2O_3, effect on melt viscosity of acrylonitrile-butadiene-styrene terpolymers *(German)* 78−18265
Sb_2O_3, energies of formation, solid-state electrochemical techniques 80−6527
Sb_2O_3 glass, X-ray diffr. anal. of struct. 78−87621
Sb_2O_3, NQR frequency, appl. in pulsed NQR thermometer 77−13749
Sb_2O_3, pyrochlore struct. and its relatives 79−14773
β-Sb_2O_3, Raman spectra, vibr. anal. 80−93312
β-Sb_2O_3 reduction to Sb powder, atomic H effect 80−2978
Sb_2O_3, smoke particles prep. by burning metal in Ar-O_2 gas, electron microscope obs. 77−52238
Sb_2O_3, standard free energy of formation, by EMF method with solid oxide electrolyte at low temps. *(Japanese)* 80−88338
Sb_2O_3, standard Gibbs energy of formation, meas. by electrochemical method *(Japanese)* 79−83499
Sb_2O_3, thermoelec. props., 500-1500K 80−29423
Sb_2O_3 thin film overlay, glass lightguide boundary refraction expts. 80−106639
Sb_2O_3, XPS, electronic struct. calcs. using scattered wave method 79−11502
$^{121}Sb_2O_3$ powder, NQR transverse chemical shift and quadrupole interaction strength 77−28479
Sb_2O_3-MgF_2, semitransparent wide band dielectric mirror synthesis using dispersive and absorbing materials 79−89986

antimony compounds continued
Sb_2O_3-Na_2O-B_2O_3-SiO_2 glass, elec. cond. meas., −160 to 200°C 80−20190
Sb_2O_3-Si-O, general features of reaction 79−11819
Sb_2O_3-$SiO_2(GeO_2)$-Na_2CO_3-H_2O, crystallisation 77−12605
Sb_2O_3-SnO_2 film vapour deposition in conveyor furnaces *(French)* 78−15311
$Sb_2O_3+In_2O_3$ react., complex oxide form., struct. 77−16516
α-Sb_2O_4, cryst. struct., neutron diffr. study 77−47391
β-Sb_2O_4, X-ray powder patterns 77−7695
Sb_2O_4-$NaSbO_3(KSbO_3)$-NaF, phase equilibria and crystal growth 77−70035
Sb_2O_5 hydrate, cryst. struct., P_H phase, dehydration effects 77−35540
Sb_2O_5 hydrated, preseparation stage in dehydration, phase transformation 80−35524
Sb_2O_5, single crysts., X-ray cryst. struct. full matrix least squares refinement *(German)* 79−37665
Sb_4O_6, IR and Raman spectra vibr. spectra, valence force field calc., pot. function *(French)* 78−50549
$Sb_4O_5Cl_2$, cryst. struct. refined 78−79572
$Sb_4O_5Cl_2$, single crysts., prep. and props. 80−35067
$Sb_2O_{5.n}H_2O$, crystalline, ^1H NMR study of proton transport 80−60446
$Sb_2(OH)_2(SO_4)_2.2H_2O$, X-ray cryst. struct. determ. *(French)* 79−4274
Sb_5O_7I, ferroelastic, Raman scatt. and symm. aspects of phase transition 77−8578
$2MASb_5O_7I$, polytype, crystal structure determination 78−91316
Sb_5O_7I, polytype 2MA, ferroelectric, ferroelastic, Raman scattering and symmetry anal. 79−38550
Sb_5O_7I polytypes, cryst. growth, struct., ferroelastic and ferroelec. props. 78−31309
Sb_5O_7I, polytypes 2MC and 2MA, photoferroelastic phenomena 79−95447
$Sb_8O_{11}I_2$, Raman spectra, vibr. anal. 80−93312
$Sb_5O_{12}(OH).H_2O$, prep. and cryst. struct. *(German)* 79−32975
$Sb_2O_3(S_3)$, AES and characteristic energy loss spectra, expt. and interpretation 78−27354
$Sb_2O_5.H_2O+In_2O_3$ react., complex oxide form., struct. 77−16516
$Sb_2O_5.nH_2O$ acid membranes, synthesis and characterisation 80−81027
Sb_2S_3, amorphous, density of valence states, XPS and UPS obs. 77−48308
Sb_2S_3, amorphous and crystalline thin films, optical consts. 79−91518
Sb_2S_3, amorphous layer, scattering of visible light, rel. to substrate temp. during deposition 79−65950
Sb_2S_3, anisotropic cryst., optical const. determ., reflected-light polarisation 77−43960
p-Sb_2S_3, bistable switching 79−73553
Sb_2S_3, cond. anomalies at phase transition pts. 77−43604
Sb_2S_3, crystal, domain structure 78−43828
Sb_2S_3 crystals, X-ray and DTA methods energy gap temp. dependence *(German)* 78−43119
Sb_2S_3, defect drift in elec. fields and bistable switching 80−92947
Sb_2S_3, dielec. and acoustic nonlinearity 78−15107
Sb_2S_3, elec. and mag. props., carrier transport mechanism 78−47792
Sb_2S_3, electronic struct., X-ray emission, XPS, UPS obs. 78−52638
Sb_2S_3, ferroelectric semiconductor, effect of screening by conduction electrons on phase transitions 78−84537
Sb_2S_3 film, amorphous and crystalline, optical props. 79−95867
Sb_2S_3 film, coevaporated, elec. cond. meas. 80−65726
Sb_2S_3, film, defect struct., electron microscope mode 79−28224
Sb_2S_3 film, struct., influence of laser beam 79−7761
Sb_2S_3, fundamental absorpt. edge, optical props. 79−56817
Sb_2S_3, galvanomag. props. and elec. resist., temp. depend. 78−43419
Sb_2S_3, glassy, interface with metal, photoelec. props. 79−73589
Sb_2S_3, glassy, photoconductivity dependences applied elec. field 80−107857
Sb_2S_3, hopping cond. in cryst. subjected to strong elec. fields 79−95456
Sb_2S_3, influence of temp. on NQR spectra of $^{121,123}Sb$ 78−60354
Sb_2S_3, lattice resoln. anal., of coincident-site boundaries of electron microscope images 80−33861
Sb_2S_3 layered biaxial cryst., surface phonon polaritons *(Russian)* 78−60021
Sb_2S_3 layers, sensitised photolysis, determ. of iso-opaque contours *(Russian)* 79−100418
Sb_2S_3, NQR freq. of $^{121,123}Sb$, temp. depend., phase transition 77−12228
Sb_2S_3, phase transitions and improper photoconductivity, effect of growth conditions *(German)* 78−39515
Sb_2S_3 spherolite crysts., direct lattice resolution obs. of defect struct. 80−107255
Sb_2S_3, spherulitic crysts., struct. revealed by direct resoln. of lattice by TEM 79−94982
Sb_2S_3, switching mechanism 77−15921
Sb_2S_3, thin film, dielectric props. 79−15392
Sb_2S_3 type chain crystals, ferroelec. phase transitions 79−33625
Sb_2S_3, vacuum deposited films, struct. and photoelec. props. 77−85092
Sb_2S_3, vitreous, prep. elec., opt. and struct. props. 77−76889
Sb_2S_3:Ag, sensitised photolysis and structure of latent photographic image 78−89574
Sb_2S_3-SnS, Sb_sS_3-As_2S_3, fused mixtures, resistivity 77−80815
Sb_2S_5, deep struct. changes, NQR obs., high-press. and temp. effects 80−54139
SbSBr, electronic and optical props. 78−34763
SbSBr, ferroelec. transition possibility investig. 77−73119
SbSBr glass, IR reflectivity spectra 80−71403
SbSBr, optical B_u modes of paraelectric phase, simple model 78−75747
SbSBr, single crystals, birefringence meas., ferroelec. transition obs. 80−88933
$Sb(SH_3)_3$, vibr. force fields and amplitudes, zero-point struct. 77−54551
SbSI, abrupt polarisation changes under influence of external forces 78−68459
SbSI, absorption edge, elec. field effect rel. to ferroelec. props. 80−97240
SbSI, adsorption of $O_2(H_2)$, effect on work function and spontaneous polarisation *(Russian)* 78−6211
SbSI, adsorption polarisation and depolarisation currents 77−43942
SbSI, aggregates of needle-like crystals, nonstoichiometric, ferroelectric properties *(Japanese)* 78−43821
SbSI, anomalous photovoltaic effect 79−38133
SbSI, anomalous photovoltaic effect 80−70749
SbSI, band gap photoreflectance spectra near ferroelec. transition 79−38559

antimony compounds continued
SbSI, Barkhausen effect, contrib. to repolarisation process *(Russian)* 77—32330
SbSI, birefr. and phase transitions 78—60405
SbSI, central mode, microwave freqs. 79—19852
SbSI, cryst., low temp. dielec. anomalies and domain struct. 80—40035
SbSI, cryst. and vitreous, nonlinear light absorpt., effect of temp. and phase transitions 77—75604
SbSI, cryst. struct. and thermal vibr. parameters, neutron diffr. obs. at −185, 16 and 100°C 77—43180
SbSI crystal, interchain correlations and energy spectrum, Davydov splitting 79—28309
SbSI, crystal growth from SbI_3 flux 79—66000
SbSI, crystal struct. in ferroelec. phase, displacive type transition 77—11515
SbSI, crystallisation from vapour phase, morphology 77—4726
SbSI, diffuse X-ray scatt., anisotropy in phonon dispersion relations 77—84866
SbSI, domain struct. relaxation 78—48135
SbSI, dynamic dielectric nonlinearity, in microwave band 78—35109
SbSI, electrical cond. and acceptor level shift temp. depend., para- and ferroelec. phases 77—28181
SbSI, electronic and optical props. 78—34763
SbSI, electroreflectance exam. 78—48145
SbSI, energy band struct. from modulation spectra 78—43892
SbSI, ferroelec., dielec. props. 79—38428
SbSI, ferroelec., phase transitions, birefringence meas. 78—56440
SbSI, ferroelec. phase transition and nonlinear props. 80—75988
SbSI, ferroelec. semicond., nature of low-temp. phase transition 77—69784
SbSI, ferroelec. semicond., laser-modulated reflectance near T_c 78—72552
SbSI, ferroelec. semicond., influence of internal fields on polarisation reversal process 79—38443
SbSI, ferroelec. semicond. near phase transition, anomalies of photocond. 79—42579
SbSI, ferroelec. transition, inelastic neutron scatt. 77—40189
SbSI, ferroelec. transition possibility investig. 77—73119
SbSI, ferroelec. transition critical phenomena *(Russian)* 80—7314
SbSI ferroelectric, dielectric behaviour, particle-size dependence 78—2811
SbSI, ferroelectric, anharmonic at. pot. and temp. depend. of thermal vibrs. 80—39246
SbSI, ferroelectric, dark current and spontaneous polarisation, ferro-paraelectric transitions obs. 80—60521
SbSI, ferroelectric semiconductor, polarisation switching processes, effect of surface electron states 77—90115
SbSI, ferroelectric semiconductor, effect of screening by conduction electrons on phase transitions 78—84537
SbSI, ferroelectric semicond. anomalous photovoltaic effect due to ionising radiation 80—29437
SbSI film, growth, effect of artificial nucleation centres 79—11032
SbSI, free energy function, temp. depend. and anisotropy of dielec. const., ferro- and paraelec. phases 78—64330
SbSI materials, piezoelectric props. rel. to use as electroacoustic transducers 78—52445
SbSI, max. vel. of domain boundaries in polarisation reversal, Barkhausen effect meas. 78—60411
SbSI, nonlinear sound propagation in case of polarisation switching 79—27458
SbSI, optical B_u modes of paraelectric phase, simple model 78—75747
SbSI, paraelec. phase, microwave reson. dielec. dispersion, near T_c 79—99839
SbSI, paraelectric phase, nonlinear optical props. 78—10870
SbSI, paraelectric phase, jump-like switching processes, ferroelec. surface layer 78—92038
SbSI, paraelectric-ferroelectric transition, low freq. phonon branches, neutron scatt. obs. 79—61313
SbSI, phonon echoes *(French)* 77—51461
SbSI, photoelectretic states in real time spatial light modulators, photorefractive effect 80—80676
SbSI, photoelectric current, modulated due to light intensity 79—19626
SbSI, photoinduced birefringence, effect of elec. field 77—52037
SbSI, photolum. spectra in ferroelec. phase, 600-800 nm., 14-100K 80—71468
SbSI, Raman scatt., near tricritical point 78—15159
SbSI, reversible characts. of generation of second microwave harmonic 78—39509
SbSI single crysts., nonlinear dielec. effects and microelectronic applics. 77—43944
SbSI, single- and poly-domain, complex permitt. and dielec. relax. losses 79—28699
SbSI, struct. comparison with Co_2Si, Co_2P, and $PbCl_2$ *(French)* 80—84155
SbSI, surface layer exam. 78—48119
SbSI, tricrit. point, NQR under press. 79—38469
SbSI, tricrit. point at 1.4 kbar and 235K 78—68463
SbSI, uniaxial displacive ferroelectrics, domain wall dynamics 79—73890
SbSI, vapour phase growth on seeds 78—11090
SbSI-BiSI, solid solns., phase diagrams, photocond., elec. props. 79—38125
$SbSI\text{-}GeS_2$ system glasses with and without antireflection coatings, optical props. 77—8595
$SbSI\text{-}Sb_2S_3$ system, ferroelec. phase transition temp. 79—78632
SbSI-SbSBr system, ferroelec., anharmonic effects in far IR reflectivity spectra 80—76014
$SbSI_{0.3}Br_{0.7}$, anomalous photovoltaic effect 80—70749
$SbSI_xBr_{1-x}$, T-p-x phase diagram *(Russian)* 77—16241
$(Sb_2S_3)_{0.95}(Na_2S)_{0.05}$, condensate, local states and switching effect 80—20336
Sb_2S_2O, kermesite, synthesis, controlled precipitation and crystn. 77—48332
$Sb_2(S_2O_7)_3$, X-ray powder cryst. struct. determ. *(French)* 79—55703
$Sb_2S_3(Se_3)$, ferroelec. transition possibility investig. 77—73119
$Sb_2S_3(Se_3)$, IR spectra rel. to bonding, amorphous film and cryst. 77—16410
$SbS_{1-x}Se_xI$, SHG at microwave freqs. 79—55188
$SbS_xSe_{1-x}I$ layer elec. and ferroelec. props., mech. stress effects *(Russian)* 80—50279
$SbSbO_4$, m.p. 77—84714

antimony compounds continued
SbSe, amorphous thin film high field charge transport and quasi-Fermi level location 80—70863
Sb_2Se_3 crystals, mag. and elec. props. 80—96873
Sb_2Se_3, energy gap, light absorpt., elec. cond., photocond. meas. 78—47826
Sb_2Se_3 film, struct. and photoelec. props. 77—85257
Sb_2Se_3, glassy, photoconductivity dependences applied elec. field 80—107857
Sb_2Se_3, liq. struct. anal., neutron diffr. study 78—79519
Sb_2Se_3, monostable switching effect *(Russian)* 79—33316
Sb_2Se_3, photocond., photo-EMF and photodielectric effect, expts. 80—20245
Sb_2Se_3, Raman spectra, Raman and IR-active modes 79—56776
Sb_2Se_3 single crysts., phys. prop. anomalies, 400-450K *(German)* 79—38072
Sb_2Se_3 solid, vaporization, thermodynamic props. of molecules formed 80—11943
$Sb_2Se_3\text{-}Bi_2Se_3(PbSe)(Sb)$, liq. semiconds., thermal cond. meas., resistive probe method 77—15636
$Sb_2Se_3\text{-}CdSe$ heterojunction, photoelec. props. 80—70816
$Sb_2Se_3\text{-}GeSe_2\text{-}As_2Se_3$ system glasses, vitrification and elec. cond. 79—50996
$Sb_2Se_3\text{-}Sb_2Te_3$, liquid, mixture enthalpies *(German)* 79—77770
$Sb_2Se_3\text{-}Se\text{-}SbSeI$, exam. of glass formation, IR transmission spectra 78—88452
$(Sb_2Se_3)_x\text{-}(Bi_2S_3)_{1-x}$ single crystals, elec. and photoelec. props., stoichiometry deviations influence 79—60870
$Sb_{35}Se_{65}$, polycrystalline, elec. cond. mech. 80—49705
Sb_xSe_y (x=0 to 4; y=1 to 4) molecular species formed in vaporisation of solid $SbSe_3$, thermodynamic props. 80—11943
$(Sb_2Se_3)_{0.7}(Bi_3Se_3)_{0.3}$, solid soln., prep. and elec. properties of layered crystals 80—70762
SbSeI, electronic and optical props. 78—34763
SbSeI, optical B_u modes of paraelectric phase, simple model 78—75747
SbSeI, sublimation, vapour pressure 77—11686
$Sb_xSi_yO_z$ films on Si, form. kinetics and props. 80—35358
$SbTaO_4$, ferroelec., synthesis and hydrothermal growth 79—38731
$SbTaO_4$, X-ray and ESR study of phase changes 78—72476
SbTe, reflection spectra 77—16325
Sb_2Te_3, $(Bi_{1-y}Sb_y)_2Te_3$, Raman and far infrared investigation of phonons 78—23453
Sb_2Te_3, cleavage faces, evaporation pattern determ. by decoration method in electron microscopy *(German)* 80—107626
Sb_2Te_3, crystallisation in constant electric field, thermoelectric parameters 77—44146
Sb_2Te_3 epitaxial films, growing conditions effect on elec. cond., thermo-EMF 80—39687
Sb_2Te_3 field effect, localised states and electronic transport 77—66187
Sb_2Te_3, free charge carrier mag. susceptibility, 300-600K 78—10644
Sb_2Te_3, mag. and elec. props., carrier excitation 78—43395
Sb_2Te_3, mechano-caloric energy conversion 80—10962
Sb_2Te_3, Mossbauer radiation, Rayleigh scatt., Debye-Waller factor determ., annealing effect 80—39963
Sb_2Te_3, $Sb_{1.5}Bi_{0.5}Te_3$, Te- and Se-doped cryst. growth and elec. props. 77—48334
Sb_2Te_3, semiconductor, optical props. determ. via Kramers-Kronig transform. 77—8537
Sb_2Te_3, stoichiometric, Hall effect and thermoelec. power studies 80—100470
Sb_2Te_3, thermoelectric coolers with high current pulse and finite cold junction, fast transient behaviour 80—27290
Sb_2Te_3, thermoelectric properties and phase transition, under hydrostatic pressure up to 9 GPa 80—65609
$p\text{-}Sb_2Te_3$, thermopower anisotropy, temp. depend. 77—15884
$Sb_2Te_3\text{-}Bi_2Te_3$, thermoelectric materials, physico-chemical study 78—30945
$Sb_2Te_3\text{-}Bi_2Te_3$ and $Sb_2Te_3\text{-}Sb_2Se_3$ systems, thermal cond. change during phase transitions 80—100368
$Sb_2Te_3\text{-}Bi_2Te_3$ solid solns., bladed cryst. growth, electrophysical props. 78—43387
$Sb_2Te_3\text{-}Bi_2Te_3$ solid solns., single cryst. growth and thermocouple construct. 80—104056
$Sb_2Te_3\text{-}Sb_2Se_3$, ordered structure formation, heat treatment effect on thermal cond. 80—54448
$Sb_2Te_3\text{-}Sb_2Se_3$ thin layers, struct., phase comp., and elec. cond. 80—15389
^{121}Sb, Mossbauer isomer shifts, book contrib. 79—87360
$Sc_2O_3+Sb(V)$ reaction, phase formation, structs. 77—84712
Se-Ge-Sb alloy glass, crystn. kinetics 77—20057
Se-Sb system, amorphous, electrical transport, activation energy 79—95406
Se-Te-Sb glasses, electronic transport 80—88579
$SeCl_4\text{-}SbCl_5$ systems, Raman spectra *(German)* 80—93324
$SnO_2\text{-}Sb_xS_{1-x}Sn$ structures, photovoltaic effects *(Korean)* 80—44647
$SnSe\text{-}Sb_2Se_3$ system, phase diagram, differential thermal, microstruct., X-ray phase and microstructure anal. 77—16555
$Te\text{-}(Bi_{0.1}Sb_{0.9})_2Te_3$ system eutectics, crystn. rate effect on electrophys. props. mutual solubility effect 80—60774
$Te\text{-}(Bi_xSb_{1-x})_2Te_3$ eutectic, electrophys. props., directed crystn. conditions influence and comp. depend. 80—107827
Te-Bi-Sb ternary system, phase drag. calc. 77—27980
$Te\text{-}Sb_2Te_3$ oriented eutectic, microhardness, influence of size of phases *(Russian)* 78—92322
$Te_{80}Ge_{20-x}Sb_x$, DSC studies of struct. phase transformation 80—66505
$TiO_2\text{-}NiO\text{-}Sb_2O_3$ phase equilibria 78—44098
$TiO_2\text{-}Sb_2O_3$ system, phase comp. of roasted coprecipitates 78—23651
Tl-Bi-Sb-Te system, peritectic reactions in $TlBiTe_2\text{-}TlSbTe_2$ cross section, crystn. character 80—108406
$Tl_{0.51}Sb_{0.71}{}^{III}Sb_2{}^{V}O_{6.32}$, X-ray cryst. struct. determ. *(French)* 79—69079
$(Tl_2Se)_{3x}\text{-}(Sb_2Se_3)_{1-x}$ system, phase diagram 77—16558
$Tl_2Te\text{-}Sb_2Te$ cross section of Tl-Sb-Te system, new $TlSbTe_2$ and Tl_9SbTe_6 cpds. 78—52778
$UF_6\text{-}SbF_5$, dil sol., liq.-vap. equilib. 77—62632
$UOF_4.nSbF_5$ (n=1, 2 or 3), preparation and cryst. struct. *(French)* 79—51062
$V_{2-x}Sb_xO_4$, defect struct. exam. 78—18635
$ZnO\text{-}Bi_2O_3\text{-}CoO\text{-}MnO\text{-}Sb_2O_3$ (97.5, 0.5, 0.5, 1.0 mole%), exam. of elec props. at different annealing temps. 80—3099

antimony compounds continued
- $ZnO-Bi_2O_3-Sb_2O_3-Co_2O_3-MnO_2-Cr_2O_3$, nonohmic ceramic, microstruct. exam. 78—47292
- $ZnO-Sb_2O_3-O_2$ system, cpd. forming reactions 78—52699

antineutrinos *see neutrinos*

antineutrons *see neutrons*

antinucleons *see nucleons*

antiphase boundaries
- alloys, ferromagnetic exam. of atomic ordering mech., when in mag. field *(Russian)* 79—11609
- γ-brass, displacement vector associated with inversion boundaires 78—6071
- calcic plagioclase, ordering and antiphase boundaries 79—95032
- 1,8-dichloro-9-methylanthracene, structural changes, photodimerisation and stacking fault energy 77—62548
- electron microscopy, conf., Nancy, France (May 1978) *(French)* 79—41915
- electron microscopy, multi-beam, general extinction criteria for extended defects 77—72532
- electron wave function in vicinity of planar defect 'on edge' 80—88002
- energies, investig. methods, appl. to FCC metals *(French)* 79—42080
- ferromagnetic crystal, pinning and nucleation of mag. domain walls at antiphase boundaries 80—11216
- ferromagnetic ordered structures, domain structure, effect of defects, electron microscopy 78—64214
- hard magnetic material, coercive field, planar defect influence 77—24710
- itinerant ferromagnet, effect of planar defects on electronic struct. and mag. ordering 79—99672
- kyanite, deformed, defect struct. 77—31668
- modulated struct. phenomena, survey 79—95033
- motion, microscopic diffusional theory, appl. to domain boundary coarsening 79—61563
- ordered alloys with periodic struct., decomp. invest. *(Russian)* 80—93558
- plagioclase feldspars, modulated structs., X-ray diffr. and electron microscopy obs. 79—95031
- pyroxenes, contrasting props. and behaviour 80—79813
- steel, high C, high alloy, $M_{23}C_6$ type carbides, effect of alloying elements on defect struct. and hardness 80—16481
- two-dimensional lattice, ordered phase form. by elastic stress relax. at antiphase boundaries *(Russian)* 79—14817
- Ag_3Mg, periodic antiphase boundaries, electron microscopy study *(French)* 80—59481
- Al-Cu (3.93 wt.%), planar defects within theta precipitates 77—16583
- Al_4Cu_9, rhombohedral γ-brass, direct imaging of struct. and structural defects 80—15115
- Al_8Mn_5, rhombohedral γ-brass, direct imaging of struct. and structural defects 80—15115
- Au-Mg, high resolution electron microscope and electron diffr. investigation, obs. of $Au_{15}Mg_4$ monoclinic phase 80—1968
- $Au_{11}Mn_4$, electron diffraction and microscopy obs. 78—75512
- $Au_{11}Mn_4$ ordered phase formation, electron diffr. and microscopy study 80—107418
- Au_3Mn thin films, electron diffr. study 80—92793
- Au_4Mn, fully ordered, microstruct., high resolution electron microscopy 79—1439
- Au_4Mn, high resolution dark field electron microscopy exam. of ordering 79—7615
- Au_4Zn, long period ordered alloy, selective radiation damage in electron microscopy 78—10092
- Au_4Zn, ordered alloy, electron microscopy and diffr. study of boundary structures 78—10059
- Au_4Zn, ordered alloy, long-period antiphase boundary struct., growth mechanism 79—19262
- $Au_3Zn(Cd)$, long-range ordered, periodic antiphase domain boundary struct., X-ray diffr. obs. 79—95028
- Ba ferrite compounds, microsyntactic intergrowth and cryst. defects, TEM obs. 79—10858
- $(Ba_3Nb_6Si_4O_{26})_n.Ba_3Nb_4Ti_4O_{21}$, multiple intergrowth and microdomains obs. by electron diffr. and microscopy *(French)* 78—95160
- Co-V alloy system, Co rich, low temp. phase, electron microscopy 77—84766
- CsCl type intermetallic compounds, correlation between dislocation character and operative slip system 79—10852
- CsCl-type lattice, (111) superlattice screw dislocation motion, computer simulation 80—79793
- Cu-Al alloys, α_2 phase, config. of periodic antiphase boundaries 79—95029
- Cu-Au, long-range ordered, periodic antiphase domain boundary struct., X-ray diffr. obs. 79—95028
- Cu-Au system, theory of interphase and antiphase boundaries 79—83174
- Cu-Pd, disordered, antiphase domain boundaries, high resolution electron microscopy obs. 79—95030
- Cu-Sn alloy system, long period superlattice obs. and impurity effects 80—103297
- Cu_3Au, antiphase domain growth 80—55346
- Cu_3Au, elec. resistivity, temp. depend. 79—47078
- Cu_3Au thin films, fine-grained and disordered, low temp. ordering 80—97433
- Cu_3Au-Ni, antiphase domains morphology 80—108460
- $CuFeS_2$, natural chalcopyrite, defect struct., TEM 77—62535
- Cu_2MnAl, dislocation structure, antiphase boundary energies, deformation behaviour prediction *(Russian)* 79—65085
- Cu_2MnAl, plastically deformed, domain struct., X-ray diffr. and electron microscope obs. *(Russian)* 79—20110
- Cu_2NiZn, boundary energies by effective interatomic potential methods 79—65082
- Cu_3Pd, periodic antiphase boundaries, electron microscopy study *(French)* 80—59481
- Cu_3Pt, antiphase domains morphology 80—108460
- Cu_3Sn, one-dimens. long period superstructs. with Zn and Ni additions 78—83777
- CuZn, planar faults, faint electron microscopic image contrast obs. 80—107283
- Fe-Al, antiphase boundary motion, microscopic diffusional theory, appl. to domain boundary coarsening 79—61563
- Fe-Al alloy, antiphase boundary energies 77—36460
- Fe-Al alloy, planar faults, faint electron microscopic image contrast obs. 80—107283
- Fe-Al alloys, pairwise interaction energy 77—36461

antiphase boundaries continued
- Fe-Al(16 wt.%), ordered, antiphase region obs. cooling rate effects *(French)* 77—59834
- Fe-Co-V (2 wt.%), gamma phase 77—36514
- Fe-Si-Al alloy, cryst. lattice deform. at antiphase boundaries, theoretical electron images exam. 77—11448
- Fe_3Al, ordered alloys, atomic order parameters from topology of electron-microscope diffr. contrast from antiphase boundaries, quantitative determ. 78—95016
- FeCo, planar faults, faint electron microscopic image contrast obs. 80—107283
- $Fe(Li_{0.5}Fe_{1.5-x/8}Mn_{x/8})O_4$ $0 \leq x \leq 2$ spinel system, X-ray diffr. anal. of loss of order on Cr substitution 79—73178
- Fe_2MnAl, dislocation structure, antiphase boundary energies, deformation behaviour prediction *(Russian)* 79—65085
- Fe_2MnAl, plastically deformed, domain struct., X-ray diffr. and electron microscope obs. *(Russian)* 79—20110
- Fe_3Si, ordering energy, electron micrography determ. 78—14353
- GaAs, VPE layer on Ge, antiphase domain structures 77—69193
- GaP, VPE layer on Si or Ge, antiphase domain structures 77—69193
- $Gd_2(MoO_4)_3$, ferroelec. ferroelastic, electron microscope exam., image anal. 78—15134
- α-In_2Te_3. I phase, order-disorder transform. for DO_{22} struct., thermodynamic study 80—70155
- Mg_3Cd, lattice imaging of B19 ordering transform. and interfacial struct. 77—36495
- Mn-Al alloy, domain struct., cryst. defect effects 77—69609
- Mn-Al permanent magnets, defect structure, mag. props. TEM obs. 78—91902
- $(NH_4)_2SO_4$, mechanically twinned, orthorhombic, search for antiphase boundaries 79—37715
- Nb_3Al, obs. of shear struct., electron microscopy *(Russian)* 78—6938
- $(Nb_{1-x}Ta_x)_2C$, modulated structs., periodic antiphase domains 79—94969
- Ni_3Al, cold-worked, substruct., X-ray diffr. obs. 77—59806
- Ni_3Fe, superlattice dislocations, compression induced mag. anisotropy 77—85443
- Ni_3Ga, stacking fault form. in situ obs. by stretching thin foils in electron microscope 77—62547
- Ni_3Mn, antiphase domain struct. *(Russian)* 78—39814
- Ni_3Mn, ordered at below Kurnakov temp. then deform., $a/2\langle 110\rangle$ dislocations and deform. antiphase boundaries *(French)* 77—51384
- $Pb_3(PO_4)_2$, ferroelastic phase, structure domains, electron microscope obs. 79—42078
- $Pb_3(PO_4)_2$, ferroelastic props., domain struct., electron microscopic study *(French)* 80—44216
- $Pb_3(VO_4)_2$, ferroelastic, phase transitions, boundary walls 80—107419
- Pd_3Fe foil, $L1_2$ superstructure, antiphase boundary orientation and energy 80—39112
- Ti-Al (14.4 at.%), void form. and solute segregation under Ni ion irradiation 79—42122
- TiN_x, cryst. and internal structs., electron diffr. and microscopy 77—27861
- $TiO_{0.3-0.5}$, O atom ordering, electron microscopy obs. 79—99150
- $TlBiTe_2$, epitaxial film, struct. anomalies, TEM 77—11824
- $(V_{1-x}Nb_x)_2C$, modulated structs., periodic antiphase domains 79—94969

antiphase domains
- *see also antiphase boundaries*
- antiphase boundary motion, microscopic diffusional theory, appl. to domain boundary coarsening 79—61563
- brass, γ-phase region, X-ray and electron diffr. obs. 79—61562
- γ- brass type alloys, superstructures and defect obs. 80—107284
- γ-brass type phases, inversion antiphase domains, formation and stabilisation, electron conc. effect 78—14363
- bytownite, quenched from 1723K, X-ray single cryst. struct. anal. and refinement 79—19193
- ferroelectric substances, electron microscopy investigations, review *(Japanese)* 80—71366
- omphacite, P2/n to C2/c transform. study 79—65183
- ordered alloys, long period antiphase structs. 79—95027
- plagioclase, labradorite, Al/Si distrib. in An_{66}, superstructure in An_{54} 79—94970
- pyroxenes, contrasting props. and behaviour 80—79813
- steel, high-C martensite, rel. to struct. transforms. during low temp. tempering *(Russian)* 77—59737
- Al_4Cu_9, rhombohedral γ-brass, direct imaging of struct. and structural defects 80—15115
- Al_8Mn_5, rhombohedral γ-brass, direct imaging of struct. and structural defects 80—15115
- Au-Cu-Ag dental alloy, age-hardened, struct. and morphology 78—92272
- Au-Mg alloys, long-period superstructures, electron diffr. obs. 79—94959
- Au_3Zn, R_2-phase, long period domains, transmission, scanning and optical microscopy obs. 79—38801
- Cr_5Al_8, γ-phase, microstruct., transform. strains, TEM obs. 79—11614
- α_2-Cu-Al, antiphase period and tetragonality 78—15374
- Cu-Al-Ni alloys, deformed, fine struct. of martensite *(Russian)* 78—6923
- Cu-Au off-stoichiometric alloys, long period superlattice 79—55699
- Cu-Au system, theory of interphase and antiphase boundaries 79—83174
- Cu-Ga alloy, periodic antiphases obs. *(French)* 77—4772
- Cu_3Au, antiphase domain growth, quantitative comparison between theory and expt. 79—77606
- Cu_3Au, antiphase domain growth 80—55346
- Cu_2AuPd, struct., TEM and electron diffr. meas. 78—38666
- CuAu(Pt), quenched, short-range order X-ray diffuse scatt., microdomain model anal. 79—96043
- Fe-Co alloy, atomic ordering phenomena, neutron diffr. obs. *(Russian)* 77—81254
- Fe-Co-Cr, Cr effect on struct. of ordering 78—35407
- Fe-Co-V(-Ni), annealing effect on microstruct. rel. to mag. and mech. props. 80—89267
- Fe_3Si, etching of slip produced antiphase domain boundaries 78—63769
- $Gd_2(MoO_4)_3$, electron microscopy investigs. of ferroelec. substances, review *(Japanese)* 80—71366
- $LiAlSiO_4$, β-eucryptite, heating effect on domain struct. 79—66078
- $Li_{0.5}Fe_{2.5}O_4$, antiphase domains, broadened X-ray diffr. line anal. 78—26578
- $LiNbO_3$ crystals, low temp. polarisation reversal, nucleation and development of antiparallel domains 79—61322
- β-Ni-Ti, struct. changes during annealing, TEM and selected area diffr. 79—34081

antiphase domains continued
- Ni-Zn, γ-phase region, X-ray and electron diffr. obs. 79−61562
- $Ni_3B_7O_{13}Cl$, boracite, on Cr-Cl boracite, gas phase synthesis of epitaxial layers 79−60650
- Ni_3Fe, X-ray diffraction investig. of order-disorder transform. *(Russian)* 77−70043
- Ni_4Mo, antiphase domains growth kinetics, TEM and electron diffr. *(Russian)* 77−32557
- Pd-Mn system, superstructure, electron diffr. and X-ray powder diffr. study 79−94958
- Pd-Zn, γ-phase region, X-ray and electron diffr. obs. 79−61562
- Pd_3Fe foil, $L1_2$ superstructure, antiphase boundary orientation and energy 80−39112
- Pd_3Fe, X-ray and electron microscope obs. of antiphase domains and superdislocations *(Russian)* 77−86017
- Pt complexes, chain cpds., orientational antiphase struct., X-ray scatt. determ. 80−24435
- $SrAl_2Si_2O_8$, TEM obs. of feldspar aand hexacelsian polymorphs 78−83827
- Ti_3Al-(Nb), ordering transform. and mech. props. 78−31402
- V-Mn, equiatomic, ordering kinetics and antiphase domain coarsening 80−7559
- $VD_{0.8}$, order domains, neutron diffr. 77−90348

antiprotons *see protons*

antireflection coatings
- ablative optical recording, computer modelling 80−91752
- abrasion resistance characterisation test 79−14129
- absorption coefficients meas. by laser calorimetry 78−25905
- absorption evaluation by attenuated total refl. 77−50783
- absorption of weakly absorbing thin layer 79−11481
- alkali-borosilicate glasses, antireflection film production by heat and chem. treatment 80−66677
- application technology, review of problems 78−83069
- baffle edge design using optical black coating 78−59154
- beam splitter and reflection reducing coatings on ZnSe for 3-14 μm 79−76811
- Bragg reflector statistical analysis 78−66882
- camera flare rel. to internal finish, student examination project 79−25782
- chalcogenide glass two-layer low-absorpt. antirefl. coating, for KCl laser window 78−37927
- chalcogenide glass Z 79−14063
- cold light production by high vacuum deposition of multilayer interference coatings *(German)* 80−53486
- conference on optical coatings, Washington, USA (March 1978) 79−46028
- constant-thickness film formation on axially symmetrical substrate 79−27453
- continuously varying refr. index, transmission curves 78−25947
- design method for two given wavelength coating 78−59102
- design technique 77−83948
- dielectric, on metal substrate for selective solar absorbers 79−65951
- double-layer antireflection coatings for plastic lenses, evaporation coating process 80−14491
- evaporator, tubular-type radiation-heated, ZnS film deposition 80−76191
- flat plate solar collector low cost coating 77−32705
- fusion reactor, neutral beam injecto cryogenic pumping panel chevron baffles, black coating materials, selection 80−95456
- graded-index antireflection coatings, high laser damage threshold 80−83628
- interference coating production, new ideas 79−32098
- IR coating for high energy laser reflector and window 79−45951
- IR energy-efficient interference coatings 79−23087
- IR optical scanning system, narcissus effect suppression, computer results 78−59151
- IR thin film plasma deposition processes 80−87466
- large optical component antireflection and protective coatings 79−72660
- large optical components for high-power lasers, refl. and transmission meas. 79−44927
- laser coating materials, 100 ns pulsed laser damage at 2.7 and 3.8 μm 80−33057
- laser damage resist. for pulsed CO_2 laser 79−45989
- laser damage thresholds of coatings for CO_2 laser components 79−14006
- laser focusing objectives, flare image danger reduction 79−22997
- laser induced damage on coatings immersed in liquids 77−61994
- laser optics, Shiva, system, thin film coatings technology 79−7135
- laser pulse damage rel. to index and substrate OH^- content 79−14016
- laser pulse damage resistance obs. of antireflection coated Ge:Ga 79−14020
- laser rate calorimetry analysis with coating absorption 80−33050
- laser rods, coating deposition from hydrolyzable soln. 77−58495
- laser window, mirror and reflector coatings, high power, materials selection 77−50735
- laser window coatings, ATR spectroscopy for, film absorpt. coeffs. meas. 78−37073
- laser-damage thresholds, meas. and identification 79−45988
- layer thickness calcs., thin-layer achromatic coatings 80−87468
- layered coating synthesis, optimisation formulae 78−25946
- linear programming appl. to design 78−5537
- low-loss, on window materials for DF chemical lasers 79−64262
- materials with refr. index 1.7-2.0 for optical component antirefl. coatings 79−72656
- mechanical strength of optical components, film effects 78−1318
- metal-organic derived liquid precursor coatings 80−5847
- metal-semicond. solar cells, parameter determ. method 77−763
- metallic layers, reflected wave reducement in photolithography 79−76837
- military specifications applicable to optical coatings 80−48365
- mirror coatings, selective reflectors, and antireflection coatings for non-linear optics, chemical method 80−28300
- monitoring of film deposition, error compensation 77−75721
- multilayer, dielectric reflectors, simplified description 79−89984
- multilayer, film indices and thicknesses calc. 78−33797
- multilayer, for camera objectives, practical effectiveness 78−58081
- multilayer achromatic, extended region of low reflection coeff. values 80−95982
- multilayer antireflection coatings, all-dielec. Fabry-Perot interf. filters, optimisation parameters 79−41432
- multilayer coating preformance, thin-film volume or interface absorption effect calc. 80−33130

antireflection coatings continued
- multilayer coating production with continuous thickness reoptimisation 79−76890
- multilayer coatings, high-refl. or antirefl., vol., interface absorpt. and scatt. losses 80−63915
- multilayer film, intrinsic and thermal stress modelling and interferometry 79−14059
- multilayer interference filter, design and construction 79−46052
- multilayer optical interference coatings via glow discharge polymerization techniques 78−87170
- multilayer oxide correcting coatings, u.v. transmission cutoff 77−760
- noise in optical instruments, stray light reduction, space appls. 78−59153
- optical coating adhesion characterisation pull-off tests 79−14128
- optical multiple wideband layers, expt. *(Hungarian)* 77−3645
- optical parameters, computer calcs. 77−11042
- oxide, porous transparent films as antirefl. coatings for glass surfaces, low refr. index 80−74448
- oxide layers on high-temp. alloys, for central-receiver, solar-thermal power systems 78−18071
- oxide semiconductor-on-semiconductor solar cell, low cost efficient 79−61980
- oxide single and multi-layer optical coatings, light scattering reduction and meas. 80−48381
- photographic objective colour correcting coatings 79−75631
- photosensor multilayer structure transmittance calc. 77−38008
- plasma polymerised ethane for laser window coatings 77−50737
- polymer antireflection coating of CdTe KO-6 optical ceramic components 79−27345
- polymer antireflection coatings of TlCl components 79−27346
- quartz high-transmittance antirefl. film, vacuum-etched 80−74449
- rain erosion resistant antireflective coatings for IR windows 78−83050
- rare earth fluorides, antirefl. laser window coatings at 10.6 μm 77−61963
- rare-earth fluorides, LaF_3, CeF_3 and PrF_3, new coating materials for IR laser optical components 79−65821
- reflection coefficient partial derivatives, matrix calc. *(French)* 80−89080
- removal by Al_2O_3 powder and NH_4HF_2 soln. 80−74521
- resistive wall coating's parameter determ. in short pulse accelerators 80−63418
- review of optical coatings 77−83946
- scanning acoustic microscope, effect of acoustic antireflection coating on lens surface 79−55280
- semiconductor laser, transverse modes, mirror reflectivity dependence 79−68404
- single layer gradient refr. index film, ang. refl. 78−5538
- single-layer film 2.8 μm, 3.8 μm absorpt. meas. 78−90463
- solar cell coating, high-efficiency InP homojunction cell 80−104505
- solar cell fabrication, photovoltaic process based on thick film technique 80−94016
- solar cells, inversion layer, surface passivation 80−101098
- solar collector coatings, for heating and cooling systems 78−30045
- solar collectors, chemical treatment of covers *(French)* 78−25982
- solar energy photothermal conversion, optical performance of absorber-reflector combinations 78−63168
- solar panel, low-cost, durable 79−14087
- solar photothermal non-selective and energy control films coatings 80−26157
- stabilities, refl. factor 77−83958
- stray light problems in optical systems, conf., Reston, VA., USA (Apr. 1977) 78−59112
- stray light reduction from optical components 78−59114
- synthesis by direct search method 79−10400
- testing of coated optics, reflection coeff. meas. 80−28366
- thickness monitoring during deposition 80−19114
- thickness monitoring of optical films 79−97358
- thickness monitoring with optical time-domain reflectometer 79−55254
- thin film technology, appls. in energy, optics, and electronics, review 80−78932
- three layer, design 77−50775
- three layer, thicknesses and refr. indices 78−9423
- three-layer, refractive index optimum combination 80−28306
- three-layer equivalent film design 78−66884
- tiO_2 antireflection coatings by a low temperature spray process 78−90537
- total absorbing optical coatings using black metallic mirrors 79−3767
- two-layer, error considerations in design 80−74477
- two-layer coatings close to antireflection, residual refl. 79−64301
- two-wavelength, two or three layer, design 78−25943
- unconventional structures, theory 77−75701
- vacuum UV coating technology 79−46030
- vacuum UV special application coatings, reflectance, transmission, technology 79−59788
- vinyltrimethoxy silane, plasma polymerised, abrasion resist. antirefl. coating for polycarbonate 77−42635
- wideband optical disc data recorder systems 80−102751
- window coating materials with low index, laser damage at 10.6 μm 77−61991
- X-ray screening glass antireflection surfaces 77−21601
- Al_2O_3 layer on Mo film, passivation against IR reflectance losses caused by oxidation 79−3758
- Al_2O_3 porous transparent films as antirefl. coatings for glass surfaces, low refr. index 80−74448
- Al_2O_3-MgO/ZrO_2-CeO_2/MgF_2 triple layer antirefl. coating for crown glass in visible region 78−13777
- As_2S_3, As_2Se_3, multithreshold damage meas. at HF and DF laser wavelengths 80−33058
- As_2S_3, single-layer vac. antirefl. coatings for near IR spectral region 80−33099
- As_2S_3 thin films, vacuum deposited on Ge and PbS, sealing props. and TEM 80−35097
- $As_2S_3(Se_3)$ coating defects and impurities affecting damage threshold and absorptance 79−14065
- $As_2S_3(Se_3)$ containing coatings, 10.6 μ laser damage obs. 79−14021
- As_2Se_3, IR window coating, prep. and optical props. 77−50736
- BiF_3 thin films, optical props. 79−32005
- $BiF_3(I_3)$, new coating materials for IR laser optical components 79−65821
- CaF_2 antireflection coated, 3.8 μm CW laser damage threshold obs. 80−33053
- CaF_2 trapezoid, ThF_4 and ZnSe coated, IR characterisation by internal-refl. spectra 78−71161

antireflection coatings continued
  CeO_2 coating of laser optical components, electron microscope obs. 80—43342
  CeO_2-SiO_2(MgF_2), multilayer refractory oxide interf. coatings 79—7192
  GaAs anodic oxide, refr. index meas., Sellmeier eqn. 77—12454
  GaAs homojunction solar cells, large-grained, passivation method to improve open-circuit voltage 80—94070
  GaAs laser diode, spontaneous emission reduction 80—95904
  GaAs, shallow-homojunction solar cell by MBE, conversion efficiency 80—30476
  GaAs/(GaAl)As channelled substrate narrow stripe lasers, with quarter-wavelength facet coatings 80—99746
  GaAs-oxide-metal solar cell, defect of deposition of antirefl. coating 77—20454
  Ge film black, solar selective absorber surface 79—29484
  Ge-As-Se IR transmitting glass composition, prep. and props. 80—69474
  $Ge_{30}As_{17}Te_{30}Se_{23}$-$As_2S_3$, two-layer, error considerations in design 80—74477
  $Ge_{0.45}Se_{0.55}$-As_2S_3, performance at 3.8, 5.3 and 10.6 μm 77—61964
  InAs IR filter properties, operational characts. of antireflection coatings 79—14107
  In_2O_3 films, electron beam evaporation, elec. and optical props. *(Japanese)* 80—60784
  In_2O_3:Sn films, elec. and optical props., solar energy conversion appl. 79—65945
  In_2O_3:Sn/n-Si heterojunction solar cell, fabrication and characts. 78—15314
  n-In_2O_3/p-InP heterojunction solar cell, photovolt. effects 80—12014
  In_2O_3-SnO_2, on Si, antireflection props. for photovolt. appl. 80—3513
  InP anodically grown native oxide, antirefl. coating for InGaAsP-InP photodiode 80—13137
  InSb spin-flip Raman laser external-cavity system, oscill. characts. 78—55383
  KCl window with antirefl. coating, laser damage at 10.6 μm 77—61992
  $KGaF_3$, new coating materials for IR laser optical components 79—65821
  MgF_2-Ag (Al)(Cu)(Au) film substrate tunable external-reflector retarder, computer based anal. 80—53407
  MgF_2-ZnS multilayers, high vacuum deposition for cold light mirror prod. *(German)* 80—53486
  NaF coating defects and impurities affecting damage threshold and absorptance 79—14065
  NaF, IR window coating, prep. and optical props. 77—50736
  NaF, multithreshold damage meas. at HF and DF laser wavelengths 80—33058
  Nd^{3+}:glass laser, analysis of antireflection layers 77—58340
  Nd^{3+}:YAG laser, analysis of antireflection layers 77—58340
  PbF_2, antireflection coating deposition technique, 2.87 μm laser damage threshold 80—33264
  PbF_2, laser damage resistant antirefl. coatings for 16 μm region 79—31963
  PbO-SiO_2 glass, optical coating for GaAs-$Al_{1-x}Ga_xAS$ laser 78—71113
  $Pb_{1-x}Sn_xTe$ anodic oxide film form. conditions, IR absorpt. spectra 80—11494
  SbSI-GeS_2 system glasses with and without antireflection coatings, optical props. 77—8595
  Sc_2O_3-Bi_2O_3-SiO_2, three-layer antirefl. coatings, form. and props. 77—58420
  p-Si, heavily doped contact layers on IR detectors, IR transmissivity 80—108190
  Si solar cells, proton irradiated, processing influence on elec. performance 80—94001
  Si solar cells with fire through contacts printed on anti-reflection coating 80—93993
  Si_3N_4 antireflection coating for solar cells, reactive plasma process for forming metal grid patterns 80—93990
  Si_3N_4 layer on Mo film, passivation against IR reflectance losses caused by oxidation 79—3758
  SiO, antireflection coatings for InP/CdS solar cells 78—50871
  SiO, single-layer vac. antirefl. coatings for near IR spectral region 80—33099
  SiO, vacuum deposited over absorb. coating surface of solar collector 78—5580
  SiO_2 antireflection coating effect on CW laser annealing of ion implanted Si 80—49242
  SiO_2 layer on Mo film, passivation against IR reflectance losses caused by oxidation 79—3758
  SiO_2 sputtered film performance as acoustic antireflection coating at sapphire-H_2O interface 80—106686
  SiO_2 thin films, comparison of RI and IR spectra 80—11497
  SiO_2-TiO_2 antireflection coatings, 1064 nm 150 ps laser pulse damage rel. to barrier layering and smoothness 79—14018
  SiO_2-TiO_2 antireflection coating, 1.064 μm laser damage, barrier 80—33059
  SiO_2-TiO_2 stack reflector and antireflection coating, 1064 nm 180 ps laser pulse damage 79—14017
  SnO_2 chemically sprayed antireflecting films on Si solar cells 79—72639
  SnO_2:F films, elec. and optical props., solar energy conversion appl. 79—65945
  SnO_2/n^+-pSi heterojunction solar cells, fabrication by paint-on-diffusant method 80—94048
  SrF_2 antireflection coated, 3.8 μm CW laser damage threshold obs. 80—33053
  SrF_2, IR window coating, prep. and optical props. 77—50736
  Ta_2O_5 antireflection coatings for Au-GaAs solar cells parameters determ. 77—763
  Ta_2O_5, on Si, antirefl. coating for solar cell, film-substrate interaction obs. 77—1324
  Te film and trilayer antireflection structure for optical recording 79—94329
  TiO_2, for Si solar cells by spray deposition, review 80—104511
  TiO_2, spray-on antireflection coatings for Si solar cells 80—80963
  TiO_2-SiO_2, enhanced reflectance Al mirrors 77—42636
  TiO_2-SiO_2 reactive evaporation technique for multilayer coatings 77—10994
  TiO_x antireflection coatings for solar cells, optical, struct., and compositional characts. 80—55852
  TlCl component antireflection coating 79—27346
  TlI films, polymorphic, double epitaxy and growth on KCl, X-ray and optical obs. 79—77944

antireflection coatings continued
  TlI laser window films, stoichiometry, Rutherford backscatt. study 80—59831
  TlI/KCl/TlI low absorpt. antireflection coatings for KCl surfaces 80—38078
  TlI-PbF_2 graded-index film coating technique and results 80—33265
  W solar absorbing surfaces improvement, by anodised interference coating 78—13815
  WO_3, on textured W surface, for solar absorber appl., props. 78—63157
  WO_3, on W dendritic surfaces, reflectance, geometrical study 79—91511
  ZnS, refractive index, calc. of ideal characts. for Schottky barrier solar cell coatings 80—43414
  ZnS, ZnS-CeF_3, single-layer vac. antirefl. coatings for near IR spectral region 80—33099
  ZnS-Ag-ZnS coating on glass, structure, optical props. 77—46781
  ZnS-MgF_2 mixtures, triple-layer broad band antireflection coatings 79—32011
  ZnS-MgF_2/MgF_2, homogeneous mixed dielecs. as antirefl. coatings effective at two visible wavelengths 79—76770
  ZnS-MgF_2/MgF_2 double-layer antireflection coatings, transmittance meas. 79—36967
  ZnSe laser windows, AR coated, photoacoustic chopping freq. studies using CO_2 laser 80—83629
  ZnSe laser windows, photoacoustic signal var. with chopping freq. 80—75309
  ZrO_2 for $Al_xGa_{1-x}As$ heterostructure laser, improved light-output linearity 78—17953
  ZrO_2, optical layer form. from $ZrOCl_2$ in alcoholic soln. 77—88877
  ZrO_2-SiO_2, protective antirefl. coatings, electron beam evaporation on glass 77—31143
  ZrO_2-$ZrTiO_4$, for high index layers, deposition 77—753

aperture cards *see microforms*

API gravity *see density*

apodisation *see acoustic imaging; optical images*

apparatus *see instrumentation; instruments*

apparent porosity *see porosity*

appearance potential *see ionisation potential*

appearance potential spectra
  Auger electron APS, extended fine struct. analysis 79—28863
  channelplate detector for SXAPS at primary electron currents >10 μA 79—49362
  deconvolution using cubical spline functions, stability, error propagation 80—25487
  extended fine struct. above appearance pot. thresholds, use of Fourier transforms 79—83058
  extended fine struct. anal., use of Fourier transforms 79—43066
  geometrically induced structure on SXAPS and Auger electron appearance potential spectra 79—38695
  graphite, AES/APS self-convolution inversion, FFT and digital signal processing 79—71430
  graphite, Auger electron appearance potential spectroscopy *(Japanese)* 80—50473
  inert gases, temp. effects on appearance potentials of gas phase field ions 79—19978
  layer materials, SXAPS interpret., cond. band self-convolution model, cryst. field splitting 78—23558
  metals and alloys, APS, multiple scatt. approach using muffin-tin pot. 80—25490
  rare earth metals, position of unoccupied 4f levels 80—16125
  rare-earth metals, SXAPS with sealed-off analyser tube 80—80908
  steel, low alloy, Mn determ. by AES and APS 79—48001
  steel, stainless, Type 304, surface analysis by SXAPS *(Japanese)* 77—70231
  steel, stainless 304, Auger electron appearance potential spectroscopy *(Japanese)* 80—50473
  surface analysis, spectroscopic methods, review *(Chinese)* 79—34414
  transition metal, 3d, $L_{2,3}$ soft X-ray appearance potential spectra theory 79—78791
  transition metals, 2p-shell SXAPS theory 79—87527
  transition metals, 3d, absolute $2p_{3/2}$ core binding energies and work functions 78—15253
  Ag vapour, field ion appearance potential spectroscopy, temp. effects 79—19978
  Al-O (100), extended appearance potential fine struct. anal., LEED study 80—50467
  Al(100) oxidised surface structure anal., extented appearance potential fine struct. study. 80—75411
  Ba, metallic, bremsstrahlung reson. and APS, near 3d threshold 77—69937
  Ba, oxidation, SXAPS 77—73189
  BaF_2, fluorine K absorpt. spectra using APS technique 79—99986
  Be, anisotropy, theoretical investigation by K-emission, APS, and Compton profiles 78—63970
  Ca, oxidation, SXAPS 77—73189
  Ce, metallic, bremsstrahlung reson. and APS, near 3d threshold 77—69937
  Ce, SXAPS from 0 to 1400 eV 77—4703
  Ce^+, CeI^+, CeI_2^+, CeI_3^+ formed by electron impact in CeI_3 vapour 77—23567
  CeI and CeI_2^- formed in CeI_3 vapour by electron irradiation 77—27190
  Co-Ni alloy surfaces, oxidation, APS 79—87755
  Cr, chemisorption of C, N, and O, SXAPS obs. 79—52048
  Cr, surface atom electron binding energy depend. on composition, Auger spectra, APS spectra 80—39655
  Fe, surface atom electron binding energy depend. on composition, Auger spectra, APS spectra 80—39655
  Fe-Al alloys, conduction band states, X-ray spectra obs. *(Russian)* 80—29317
  Fe-Cr, Auger electron and appearance pot. spectroscopic study of surfaces 80—11520
  Fe-Cr, surface atom electron binding energy depend. on composition, Auger spectra, APS spectra 80—39655
  FeC_2^+, electron impact appearance pot. in dissoc. of $Fe(CO)_5$ 79—34281
  $Fe(CO)_5$, electron impact appearance pots. for ion fragments, mass spectra obs. 79—34281
  Hf, isochromat spectroscopy using SXAPS equipment 79—95877
  Ho, SXAPS, N_5 and M_5 levels, anomalous structure 77—73191
  I and I_2 formed in CeI_3 vapour by electron irradiation 77—27190

appearance potential spectra continued
La, metallic, bremsstrahlung reson. and APS, near 3d threshold 77—69937
La, SXAPS from 0 to 1400 eV 77—4703
La, X-ray reson. emission, appearance pot. and charact. electron energy loss spectra 80—16126
LiF, fluorine K absorpt. spectra using APS technique 79—99986
Mo, chemisorption of C, N, and O, SXAPS obs. 79—52048
NaF, fluorine K absorpt. spectra using APS technique 79—99986
Ni (001), geometrically induced structure in SXAPS and Auger electron appearance potential spectra 79—38695
Ni, APS and band theory of magnetism 77—40303
NiTi, search for electronic phase transition, soft X-ray appearance potential spectra 79—24391
Ni(100) oxidised surface structure anal., extented appearance potential fine struct. study. 80—75411
Pd-Ag(V), H mobility and solubility, appearance pot. spectra obs. 80—55231
Rh^+, Rh^{2+}, field evaporation, field ion mass spectra and field ion appearance spectra study 80—7479
Sr, oxidation, SXAPS 77—73189
Ta, density of unoccupied electronic states, UV isochromat spectra and SXAPS 79—77977
Ti, Auger electron appearance potential spectrum, elastic and inelastic contribs. 78—35231
Ti, Auger electron appearance potential spectroscopy *(Japanese)* 80—50473
Ti, X-ray photoelectron appearance potential spectrum 79—65973
V, clean surface, nearest neighbour spacings from extended appearance pot. fine struct. 79—69329
V, extended fine struct. above 2s appearance potential edge, AEAPS spectra 78—72647
V, extended fine struct. above L-shell appearance pot. thresholds 78—92148
V, extended fine struct. above APS thresholds, effect of central atom. pot. 80—66329
V-Al alloys, conduction band states, X-ray spectra obs. *(Russian)* 80—29317
V_3Si, XPS and APS of valence band 77—20994
W, chemisorption of C, N, and O, SXAPS obs. 79—52048
YVO_4, soft X-ray APS study of empty electron states, $VO_4{}^{3-}$ cluster model 80—25488
Yb, 4f states, soft X-ray apperance pot. spectra 79—47551
Yb_2O_3, M-series soft X-ray appearance pot. spectroscopy 79—54866

appearance potential spectroscopy
AES, apparatus 80—101888
AES/APS self-convolution inversion, FFT and digital signal processing 79—71430
Auger electron appearance potential spectroscopy, core level spectroscopy *(Japanese)* 80—50473
extended appearance pot. fine struct. surface anal. 80—11512
extended fine struct. above APS thresholds, effect of central atom. pot. 80—66329
field dispersed ion analysis, comparison with conventional technique for O^+, CO^+, and $CO_2{}^+$ 78—85234
isochromat spectroscopy using SXAPS equipment 79—95877
metals, chemisorption of gases, book 79—69370
recent developments *(Japanese)* 78—78052
signal broadening in potential modulation differentiation 79—54237
soft X-ray SXAPS, noise source and sensitivity 78—49949
spectrometer, soft X-ray, with Al foil in front of photocathode *(Japanese)* 80—13193
substrate surface contamination from dark-space shielding during sputter cleaning 77—8968
surface analysis, electron-excited core level spectroscopies, book contrib. 77—63503
surface electron state characterisation by X-ray techniques 77—55868
teaching laboratory and lecture demonstrations 80—105477
$^{115}In(\gamma,\gamma')^{115m}In$, appearance energies of In complex cpds. determ. 78—8794
V_2O_5, electron beam induced decomposition, appearance pot. spectroscopy 80—85203

Appleton layer *see ionosphere*

appliances, domestic *see domestic appliances*

applied mechanics *see mechanics*

approximation theory
see also function approximation; interpolation; least squares approximations
AC signal and cell interaction *(Czech)* 78—31855
active acoustic suppression systems with finite number of couplings, approximation and stability aspects 78—18111
atmospheric saturation vapour pressure, approx. 79—70862
atmospheric thermohydrodynamic eqns., vertical derivatives approx. rel. to short-range weather forecast *(Russian)* 77—60450
Cauchy problem for Laplace's eqn., solution approximation 77—78966
charge transfer total probability in collision processes, approximations 77—34753
chemically induced spin polarisation, finite element method, stochastic-Liouville eqn. 79—64018
chemistry, method of successive approx., teaching 78—89281
convergence of exponential operators, Zassenhaus and Baker-Campbell-Housdorff formulae 78—20947
D-optimal design for quadratic regression on a hypercube 79—92921
delta-two-stream approximation in radiative flux calculations 79—96811
differential approximation method analysis of difference scheme props. 77—57172
distribution function for approx. of series of values or classes *(German)* 77—67234
education, acoustical propag. in ocean, appl. of parabolic approx. 79—25794
elasticity, pot.-type singular integral approx. algorithm 80—27132
elasticity singular integral eqns., regularisation 77—17820
EM wave scattering using successive approximation method for scattering from round dielectric cylinder *(Russian)* 80—63889
epicyclic approximation for plane galactic orbits 80—36674
experimental design, unbiased regression, practical appls. 79—97184
exponential operator approximants, many-body appl. 77—9896
field problem structure, equilibrium, eigenvalue and propagation problems *(Rumanian)* 78—45520
flow, unidirectional, unification of approxs. using stress tensor 80—27139

approximation theory continued
four term WKBJ approx., appl. to Varshni V and Lennard-Jones pot. 80—58113
frictionless elastic contact problems, approximate soln. 78—16646
generalised Pade approximation, explicit solns. 80—73623
gravity and magnetic anomalies, approx. problem *(Russian)* 78—28338
gravity field analysis, approximation of Stokes and Vening-Meinesz eqns. allowing for initial data errors 80—101459
harmonic method for anthropomorphic mechanism compensating synergy *(Slovenian)* 77—64920
heat conduction, quasilinear equations, approx. Galerkin method 80—33416
heat conduction problems, approx. soln. method 80—33415
heat exchangers, parallel and counter-flow, weighted residuals method and modal control 79—3898
inhomogeneous molecular gas radiation calc. using spectral comp. modelling 80—32697
ionospheric potential eqn. separation *(German)* 77—70916
Krylov and Bogoliubov approximation, pulse response of general nonlinear equation 79—84962
Lane-Emden functions, concise approximation formulae 77—33467
light scattering from macromolecular soln. in alternating elec. field, low angle approx. 80—84721
light scattering from spherical obstacles, validity domains of approx. methods 79—72495
linear harmonic oscillator on lattice, wave functions, energy eigenvalues, Pade approximant method 78—57817
mathematical approximations in physical systes, rules and useful appl. *(Hungarian)* 79—25783
mathematical physics students teaching 80—105474
matrix elements of $\delta(r_1)$, approx. wavefunction 80—47860
meteorological fields approx. by polynomials 79—29831
molecular dynamics, L-F approx. method, second order secular eqn. soln. 78—66458
molecule π-electron total energy, approx. topological formulae 77—38603
multipole approximations, Hilbert-Pade method, appl. to Gaussian function 80—82707
multivariate approximants with branch points, diagonal approximants 78—8228
multivariate approximants with branch points, off diagonal approximants 78—54160
multivariate approximants with branch points, practical evaluation 78—54161
Navier-Stokes equations soln. method for steady flow past cylinder 77—54956
near resonant oscillating systems, integration in slow-fluctuation approx. 80—62483
neutron point kinetics, smoothing and extrapolation method 77—65252
non-linearly coupled harmonic oscillators, asymptotic approx. 77—23792
Pade approximants, nonperturbative analytic approach in plasmas 78—20951
periodic solution of $d^2x/dt^2 = -V'(x)$, approx. value determ. for period 79—8802
planets rectangular coordinates, approximation via Chebyshev polynomials *(Russian)* 80—62033
power series, inhomogeneous differential approximants 79—92919
quasistatic approximation for atmospheric dynamics, characterisation *(German)* 80—98383
radiative transfer in nonplane geometry media, approx. and num. methods of eqns. soln. 80—33431
random-variable probability density approximation by convex function *(Russian)* 77—9865
rectangular matrix pseudoinverse using column approx., inconsistence systems of linear eqns. solns. 78—62061
relaxation distribution function, approx. methods and num. inversion of Laplace transform. 80—84720
Ritz-Galerkin approximations use in fluid dynamics 77—54955
scattering, approximate coupled equation method 80—73215
shock structure, numerical, nonlinear corrections for difference schemes in conservation form 80—36878
simple line interface calculation for treating fluid interfaces 77—58777
smeared concentration approximation, appl. to air pollution modelling 78—81381
smooth interpolation and approximation of data by anal. curve method 77—26159
steam pressure and temp. in relation to enthalpy and entropy, approximation formulae in binary polynomial form *(German)* 78—59532
stochastic approx. processes, law of iterated logarithm *(Russian)* 77—37746
stress relaxation calculations in strips, errors due to approxs. 80—23909
superfluous, meas. elimination, precision evaluation 80—90805
supersonic flow, 3D, calc. by method of characts., approx. eqns. 77—19619
temperature integral, approximative eqns., accuracy analysis 80—36834
three body problems with Coulomb interaction, adiabatic representation, two-level approx. 80—47861
time-dependent linear systems transient response, approx. anal. using orthogonal polynomials 77—37745
wave scattering, second order approx. in planar linear sheet 80—17812
weak solution and approximate methods for the transport equation 79—76049
whistler analysis, Dowden-Allcock approximation generalisation and comparison with Bernard approximation 80—51607
Wiener path integrals, approx. evaluation 80—8829

apr *see acoustic paramagnetic resonance*

APT *see problem oriented languages*

APW calculations
A15 compounds, plasma energies, tight-binding energy-band model 78—84159
A-15 compound, V_3X and Nb_3X, (X=Al, Ga, Si, Ge, Sn), electronic struct., electron-phonon interactions, and low temp. anomalies 79—60701
actinides, electronic structure and props., review 77—62813
Al (001) surface, nearly-free-electron metal, origin of surface reson. states 78—95322
angle resolved UPS and XPS disorder effects 78—15287
band structure, generalised APW method using variational expression 80—6695
crystalline thin films, band struct. calc., appl. to Cu monolayers 78—87899

APW calculations continued
- disordered system, density of states calc. using augmented space formalism, comment 80−2322
- disordered system electron energy system, calc. methods 80−75485
- films, linearized APW method for electronic band struct., appl. to Fe, Co, Ni, Cu and Al 79−69393
- halide anions, in gas, photodetachment cross-sections, OPW and APW calcs. 77−38607
- linear APW method for self-consistent calcs. 79−51467
- linearised relativistic APW method, using approx. pure spin basis functions 80−70581
- local potential problems, improved Pauli Hamiltonian 79−19499
- MAPW method, asymptotic behaviour of Fourier coeffs. 77−24510
- metal, APW dispersion relation for plasmons 77−69265
- metals, neutron mag. form factors, magnetisation densities, APW wavefunction calcs. 79−47243
- one-dimensional disordered system, average density of states, augmented space method 79−28265
- photodetachment cross-sections, OPW and APW calcs. comparison 77−38607
- rare earth intermetallic, cubic, direct coulombic contrib. of cond. electrons to cryst. elec. field 79−91005
- rare earth intermetallic, cubic direct Coulomb contrib. of cond electrons to crystalline elec. field 77−76784
- rare earth intermetallics, cubic, exchange coulombic contrib. of cond. electrons to cryst. elec. field 79−95376
- relativistic energy band calcs., linear APW method and augmented spherical wave method extensions 79−60679
- solid, cond. band calcs., use of electron atom scatt., phase shifts 77−85139
- solid, orthogonalised augmented plane wave method, appl. to ZnS 77−66105
- transition metal, model potential, generalised APW formulation 78−91579
- transition metal carbides, APW bands rel. to covalent binding 77−59245
- transition metal carbides, generalised susceptibilities, electronically driven phonon anomalies APW calcs. 79−42208
- transition metal carbides, high temp. supercond., role of electronic struct. on obs. phonon anomalies 77−24363
- transition metal carbides and borides, electronic structures calc. in conjunction with X-ray photoelectron spectroscopy *(Japanese)* 79−15074
- transition metal compounds, electronically driven lattice instabilities, role of p-d hybridisation 79−7669
- transition metal nitrides, APW bands rel. to covalent binding 77−59245
- transition metal oxides, APW bands rel. to covalent binding 77−59245
- transition metals, BCC, 3d series, numerical calc. of orbital mag. susceptibility 79−82764
- transition metals, electronic struct. and X-ray emission spectra 77−28105
- transition metals, local pseudopotential theory 78−30863
- transition metals, second series, electronic band Brillouin zone APW calc., electronic config. effects 78−51883
- XPS, angle-resolved, interpretation 78−72696
- Ag, 4d spectrum, high resolution X-ray photoelectron spectra, comparison with APW calc. 77−1784
- Ag (111) surface, photoemission, final states 78−11080
- Ag, K-edge photoabsorption spectra, linear APW calc. 78−43960
- AgH, electronic struct. and supercond., APW calc. 79−95318
- Al, CC vacancy, electron and positron densities and temp. depend. of positron lifetime 78−19001
- Al, K X-ray absorption, K-emission spectrum, band struct. using APW method 80−97380
- AlH_x, electronic struct. and electron-phonon interaction, hydrogenation effect, rel. to supercond. 80−107694
- AlP(As)(Sb), APW calc. of electronic structure and optical props. 79−99479
- Au, energy band structure, X-ray N-emission spectra, relativistic APW calcs. 80−70596
- Au, energy band structure, X-ray emission spectra, APW calc. 80−92811
- Au, photoelectron spectra, bulk and surface, rel. to band struct. 80−20770
- Be, dielectric function from APW calcs. 79−65817
- Be, eqn. of state, solid-state models, comparison 80−75332
- BeS, electronic energy bands, APW and LCAO calc. 77−20236
- BeSe, electronic energy bands, APW and LCAO calc. 77−20236
- BeTe, electronic energy bands, APW and LCAO calc. 77−20236
- CaB_6, electronic struct. APW and muffin-tin calcs. 80−29320
- Cd, band structure, density of states and Fermi surface, APW calc. 77−20232
- $CdCr_2Se_4$, energy band struct calc. by augmented plane wave method 80−103621
- CoAl, bonding, self-consistent energy bands 78−91610
- Cr, band struct. and Fermi surfce, ang. correlation of positron annihilation radiation 78−6260
- Cs, electronic transition from self consistent APW Xα calcs. 78−51884
- CsAu, band struct. and charge distrib., semicond. and metallic behaviour 77−20238
- Cu, electronic struct., linear APW method 79−51467
- Cu, positron annihilation radiation, ang. correlation, APW calc. 80−7435
- Cu, single particle lifetime 80−103612
- EuB_6, ferromag., spin-polarised energy band struct., APW calc. 80−96779
- Fe, spin dependent momentum distrib., APW calc. 78−2416
- Fe-Al, directional Compton profiles, self-consistent APW band struct. calc. 80−25476
- Fe-Al, X-ray emission spectra 80−25489
- FeAl, bonding, self-consistent energy bands 78−91610
- Fe_3Al, super-lattice, band theory 77−15758
- $Fe_3Si(Al)$, electronic structure, X-ray spectra comparison with band struct. calcs. 80−97383
- Gd pnictides, band struct., semicond.-metal trend 77−28111
- Gd, self consistent relativistic ferromag. band struct. 78−91609
- $GdCo_5$, spin polarised energy band struct., APW calc. 78−10342
- H_2, metallic, electron-phonon interaction and superconductivity, APW calcs. 78−14854
- Hf, electron structure and soft X-ray emission spectrum, RAPW calcs. 79−91536
- Hg, expanded liq., band model for electronic struct., Knight shift and electronic transport 77−89690

APW calculations continued
- I_2, FCC metallic, self-consistent APW Xα electron-band calc., up to 22000K 77−39762
- inert gases, solid, Compton profiles, APW-Xα calc. 80−80894
- Ir, energy band structure, X-ray emission spectra, APW calc. 80−92811
- La, band struct., linear APW method 79−51467
- LaAg, band calcs., rel. to mag. and electronic props. and martensitic transform. 77−8014
- $LaAl_2$, calc. of energy band-structure and Fermi surface by APW method 80−70590
- $LaAl_2$, electronic struct., APW method and local-spin-density approx. 80−65434
- LaB_6, electronic struct., APW method and local-spin-density approx. 80−65434
- LaB_6, metallic, energy band structure and Fermi surface, self-consistent APW method 77−69221
- Li, X-ray K-edge transitions, band theory 77−16426
- $Li_2Ag_{2-x}In_x$, optical props., struct., energy bands, interband transitions 78−72539
- $Li_2Cd_{2-x}In_x$, optical props., struct., energy bands, interband transitions 78−72539
- Lu, calc. of soft X-ray emission spectra by relativistic APW method 79−78792
- Mg, dielectric function from APW calcs. 79−65817
- MnP, spin polarised energy band struct., electronic specific heat, APW calcs. 80−65431
- MnSi, electronic energy band struct., self-consistent APW calc. 80−65433
- Mn_3Si, electronic structure, X-ray spectra comparison with band struct. calcs. 80−97383
- Mo, band struct. and Fermi surface angular correl. of positron annihilation radiation 78−6260
- Mo, dielec. function and energy loss function, APW band struct. calc. 77−62850
- Mo, K-edge photoabsorption spectra, linear APW calc. 78−43960
- Mo, phonon dispersion, anomalous struct., tight-binding calcs. 78−10137
- Na, X-ray edge shape, band struct. role 77−16425
- Nb, dielec. function and energy loss function, APW band struct. calc. 77−62850
- Nb, electron-phonon interaction, calc. using APW band struct. calcs. and measured phonon spectra 78−14869
- Nb, electron-phonon interaction, relativistic, APW calc. 80−92837
- Nb, electron-phonon spectral function and mass enhancement 78−26988
- Nb, electronic struct. with non-muffin-tin pot., self-consistent relativistic APW calc. 77−66108
- Nb, electronic structure, APW calcs., self-consistency and exchange effects 77−66109
- Nb, Nb-Mo alloys, phonon dispersion, anomalous struct., tight-binding calcs. 78−10137
- Nb, quasiparticle velocity, anisotropic many-body effects 79−33223
- Nb-Mo, electronic struct., thermoreflectance meas. 0.5-5.0 eV 80−45050
- $Nb_3Al(Ga)(Si)(Ge)(Sn)$, electronic struct. calcs. 79−47005
- NbC, band struct. and X-ray emission spectra, APW and Xα calc. 80−70605
- NbC, phonon anomaly rel. to Fermi surface 77−11853
- NbC, self consistent APW-Xα calc., electronic struct. 77−20237
- NbN, self consistent APW-Xα calc., electronic struct. 77−20237
- NbO_2, electronic band struct., optical props., generalised susceptibility, struct. transition 79−95328
- Nb_3Si, Nb_3Sn, Nb_3Ge, Nb_3Ga, Nb_3Al, electronic struct., electron-phonon interactions, X-ray spectra 78−91613
- Nb_3Sn, A-15 cubic phase, band calc. using APW method 79−56120
- Nb_3Sn, electronic struct., APW method 78−72066
- Nb_3Sn, normal state, Fermi surface, APW band calc. and de Haas-van Alphen oscills. 79−65369
- Ne, solid, large-gap insulator, valence excitons, integral eqn. method calc. 77−11858
- Ni (100) films, spin density by self-consistent linear APW method 80−65710
- Ni band structure, rel. to lattice const., spin polarised APW calc. 80−20073
- Ni, paramag., generalised Wannier functions to fit MAPW band struct. 79−19509
- Ni, X-ray absorption and emission K and L spectra, APW calc. 78−68579
- NiAl, bonding, self-consistent energy bands 78−91610
- NiAl, electronic struct. by cluster calc., comparison with self-consistent APW method 77−69209
- Ni_2MnSn, ferromag. Heusler alloy, electronic struct., spin polarisations, theory 80−54598
- NiSb, bandstructure and density of states calc. 80−70580
- Os, correlation effect of crystal pot., RAPW calcs. 78−6265
- Os, electronic energy band struct. 80−107697
- Pb, ab initio band struct. calcs. 80−75502
- Pb, band structure, and electron-phonon interaction, supercond. transition temp. determ. 79−19512
- Pd, electronic struct. determ. by relativistic APW method, rel. to UV spectroscopy 77−4289
- Pd, electronic structre, Compton scatt., soft X-ray emission and X-ray photoelectron spectra 79−77999
- Pd, generalised susceptibilities and phonon anomalies, band struct. calcs. 79−90953
- Pd, K-edge photoabsorption spectra, linear APW calc. 78−43960
- Pd-H(D), band struct. and supercond. props., APW calc. 79−56354
- Pd-Rh-H and Pd-Ag-H, band struct. and supercond. props., APW calc. 79−56354
- $Pd_{1-y}Ag_yH_x$, electronic struct. and supercond., APW calc. 79−95318
- $Pd_{1-y}Ag_yH_x$, superconducting transition temp., APW band struct. calcs. 78−95393
- PdH, electronic struct. and proton spin-lattice relax. calc. 78−67937
- PdH, electronic struct. and supercond., APW calc. 79−95318
- $PdH_x(D_x)$, band struct., supercond. props., APW calcs. and neutron scatt. 78−43511
- PdIn, refractive index, reflectivity and band struct., APW calcs. 80−40139
- Pd_2MnSn, ferromag. Heusler alloy, electronic struct., spin polarisations, theory 80−54598
- $Pd_{1-y}Rh_yH_x$, electronic struct. and supercond., APW calc. 79−95318
- Pt, energy band structure, X-ray emission spectra, APW calc. 80−92811
- Pt, generalised susceptibilities and phonon anomalies, band struct. calcs. 79−90953

APW calculations continued
- Pt, mag. field induced conduction electron , polarisation, magnetisation density, and neut neutron mag. form factor 78—18945
- Rh, band structure and photoemission from low index surfaces 80—24790
- Rh-Fe, dil., anti-Kondo effect, de Haas-van Alphen obs. 79—73427
- RhH, electronic struct. and supercond., APW calc. 79—95318
- SMS, band struct. and semicond. metal phase transition 80—80180
- Sc, spin susceptibility, exchange correlation enhancement 77—85167
- ScP, electronic struct., self-consistent Hedin-Lundqvist and Xα APW calcs. 80—29322
- ScP, energy band struct., exchange-correl. pot. effects, APW calcs. 80—29321
- Si, band structure selfconsistently determined with X_α potentials using MAPW method 79—33227
- Si, semi-empirical APW calc. of band structure 80—84424
- $SmCo_5$, spin polarised energy band struct., APW calc. 78—10342
- SnTe, self-consistent relativistic energy bands 80—10870
- Sr, monochalcogenides, electronic energy band struct., APW calcs. 80—65439
- Ta, electron-phonon interaction, calc. using APW band struct. calcs. and measured phonon spectra 78—14869
- Ta, electron-phonon interaction, relativistic, APW calc. 80—92837
- Ta, electronic structure, APW calcs., self-consistency and exchange effects 77—66109
- TaC, phonon anomaly rel. to Fermi surface 77—11853
- TaN, energy band struct. calc., symmetrised APW method 80—96784
- TaN_x metastable FCC, band struct. calc. 79—33231
- Th, correlation effect of crystal pot., RAPW calcs. 78—6265
- Th, electronic thermal Gruneisen parameters 80—39242
- Ti, band struct. correlation with TiC, APW calc. *(Japanese)* 78—23017
- Ti, electronic structure of omega and alpha phases, nonrelativistic APW method 79—90952
- TiC, band struct. correlation with Ti, APW calc. *(Japanese)* 78—23017
- TiC, calcs. of 2γ-ang. correlations and Compton profiles 78—39624
- TiC, electronic struct. and XPS, cluster method and band struct. 79—60710
- TiH_2, electronic density of states and tetragonal distortion, APW calc. 79—37986
- Tl, band structure and fermi surface using relativistic APW calc., optical spectra interpretation 77—20231
- UC, partially filled f bands, configurational and relativistic effect sensitivity 79—78002
- UGe_3, de Haas-van Alphen effect, band struct. calc. 78—72068
- UN, band struct., SAPW calcs. 78—26810
- US, band struct., SAPW calcs. 78—26810
- V, electron-phonon coupling constant calc. *(Russian)* 80—70624
- V, electron-phonon interaction, calc. using APW band struct. calcs. and measured phonon spectra 78—14869
- V, electronic structure, APW calcs., self-consistency and exchange effects 77—66109
- V, X-ray band spectra calcs. 79—33860
- $V_3Al(Ga)(Si)(Ge)(Sn)$ electronic struct. calcs. 79—47005
- V_3Ga, self-consistent APW band struct. calc. 78—47697
- VO, energy band spectrum, APW and Green's function method calcs. 79—7783
- $VS_2(SE_2)$ (1T), electronic struct. using nonspherical cryst. pot. 80—44498
- V_3Si, electronic struct., electron-phonon interaction and high temp. superconductivity, APW calc. 78—14871
- V_3Si, V_3Sn, V_3Ge, V_3Ga, V_3Al, electronic struct., electron-phonon interactions, X-ray spectra 78—91613
- W, semi-infinite cryst., secondary electron emission, obs. of electronic struct. 79—33871
- W(001), surface states and surface resonances, self-consistent electronic struct. 80—96960
- Xe, condensed at high press., electron-band theory and fluid theory calcs. 80—59875
- Xe, solid, zero temp. isotherm, APW calc. 79—73128
- YCo_5, spin polarised energy band struct., APW calc. 78—10342
- YS, band struct. and X-ray emission spectra, APW and Xα calc. 80—70605
- YS, electronic instability and phonon softening, APW calc. 80—29323
- YZn, self-consistent energy bands and Fermi surface 77—72814
- Z+C, band struct. correlation with Zr, APW calc. *(Japanese)* 78—23017
- Zn, band structure, density of states and Fermi surface, APW calc. 77—20232
- Zr, band struct. correlation with ZrC, APW calc. *(Japanese)* 78—23017
- Zr, electronic structure of omega and alpha phases, nonrelativistic APW method 79—90952
- Zr, K-edge photoabsorption spectra, linear APW calc. 78—43960
- ZrB_2, band struct. and XPS 77—90253
- ZrC, electronic struct. and XPS, cluster method and band struct. 79—60710

arc discharges *see arcs (electric)*

arc furnaces
- AC arc electrodes evaporation characts. of NiO, CoO, and FeO *(Russian)* 78—3051
- disordered metal ribbon production by ultrarapid quenching 80—71612
- floating-zone melting with viscous torque control 80—89140
- ignition and stabilisation *(French)* 78—47187
- metal transfer during vacuum consumable arc remelting 79—82317
- steel cathode high current free-burning arc 77—19792
- thermal plasma aspects *(German)* 78—75402
- vacuum, transition metals processing technology and appl. *(Hungarian)* 80—55318
- $MgO-ZrO_2$ ceramic sublimation at optical furnace focal spot *(Russian)* 79—95983
- Xe arc lamp imaging furnace for Y_2O_3(:Nd) floating zone growth 80—60777

arc heaters *see arc furnaces*

arc lamps
- acoustical resonances in modulated compact arc lamps 77—58907
- alkali metal vapour, source for pumping YAG:Nd^{3+} laser 80—78924
- alkali metal vapour flash lamp, absolute spectral distrib. and radiant output 78—66510
- atomic absorption spectroscopy, pulsed lamp supply, optical, elec. characts. 79—57329

arc lamps continued
- capillary-arc light source employing mixture of deuterium with neon 80—95971
- Eimac arc lamp, 300 W, spectral and noise characts. 78—32878
- Eimac Xe arc lamp, radiant power rel. to hollow cathode lamp 78—89547
- high irradiance solar simulator for thermal absorptive material evaluation 79—62063
- inert gas flash lamp, absolute spectral distrib. and radiant output 78—66510
- light and water exposure apparatus 79—15914
- metal-halogen type, nonequil. comp. developed by slow chem. reactions *(Hungarian)* 77—47288
- power source, highly regulated, for H and D lamps for UV spectrometry 79—40629
- pulsed lamps, parameter changes with different charge conditions *(Russian)* 78—83642
- pulsed short arc lamps, characteristics of controllability 78—42400
- silhouette photography, high-speed, of small biological subjects 78—44743
- start control device for ultrahigh press. short-arc lamp, current stabilisation 77—57362
- total luminous energy transfer, scatt. medium effect 77—65577
- underwater incoherent sources, spectral emission characts. 77—82043
- UV sources for curing 78—88443
- VUV light source, transfer standard, low-current AR arc with MgF_2 window 79—35856
- Ar, high-temp., vacuum UV radiation scales 77—30124
- Ar wall stabilized arc, vac. UV radiation scales 78—1309
- $DyI_3/CsI/Hg$ arc, oscillations induced by external mag. field, arc constriction 79—60205
- Fe Zeeman tuned mag. confined arc lamp, appl. to U 78—17593
- H-He arc lamp, 60-360 nm, calibration 78—87117
- Hg vertical, Hg plus I, metal halide, convection effects study 80—6299
- Hg-Ar, high-press., constant DC power supply circuit 78—12722
- Hg-Sn halide arc, molecular optical absorption obs.$_o$ 78—75457
- K vapour, as optical pump source in Nd:YAG space communications laser 79—86261
- K-Rb arc lamp development for space laser communications 78—46646
- Kr water-cooled arc lamp, anode, temp. distrib. along length, anode geometry effects 80—106994
- Li heat-pipe arc lamp as spectroscopic source 80—102787
- Na, high pressure lamp arc tube temp., Al_2O_3 sublimation 78—5532
- Na, light-induced ignition method 80—77599
- Xe, air-water cooling system, DKsSh-1000 high pressure lamp (USSR) 80—74452
- Xe arc lamp versatility 79—23036
- Xe, discharge lamp, RF excited electrodeless, atomic fluoresc. spectrometry 77—86395
- Xe lamp spectral radiation density, 400 to 1000 nm obs. 79—14072
- Xe pulsed arc lamp with adjustable plateau slope 79—68422
- Xe short-arc lamp, current modulated, arc forms and instability 80—96399

arc welding
- *see also welding equipment*
- acoustic emission method and development of equipment for monitoring crack formation during welding 80—89451
- AE monitoring of multipass submerged arc welding 77—73394
- arc constricted by radial gas flow, thermal efficiency, investigation 80—6038
- DC arc thermal characts. determ., soln. 80—37036
- dendritic solidification during welding 79—87625
- electric discharge low pressure plasma arc, energy parameters experimental study 80—75117
- electrode metal drop. free surface calc., MHD anal. *(Russian)* 78—5822
- EM forces effect on plasma flows, calc. 80—83912
- flash, for high density polyethylene tube, inspection by IR spectrometer 78—21109
- fluid flow in hemispherical container, distrib. current source-induced 78—26198
- heat flux and current density dstrib. in heat spot of arc discharge *(Russian)* 79—14625
- metal arc welds, chevron cracking, initiation and propagation 79—38981
- molten pool solidification and bead formation 80—75341
- nuclear power plant piping, inspection, by in-process acoustic-emission monitoring 77—14823
- optical fibre arc splicing unit *(German)* 80—19115
- optical fibres, practical machine for splicing in field 79—50450
- plasma appl., using surface wave microwave excitation structures 79—19059
- plasma flow effect on weld pool obs., using basic- and cellulose-coated electrodes 79—7496
- plasma jets, in welding arcs, gasdynamic characts. *(Russian)* 78—47191
- pool metal solidification kinetics in welding with electromag. stirring 80—71636
- seam US defectoscope *(Russian)* 80—43564
- shielding technique development, torches with ring nozzles operation modelling 79—7497
- single-pass butt welding methods using single electrode, productivity 80—37009
- steel, austenitic stainless, weld, ferritic-austenitic solidification mode 80—89214
- steel, brittle transition temp. comparison of arc, gas-pressure and friction-pressure welded alloy by hardness measurements *(Japanese)* 79—11691
- submerged, stainless steel, effects of flux on cold cracking resist. 77—21238
- temperature calculation, finite element anal. 78—28930
- temperature meas. and physics of welding arc 78—55771
- three-phase high performance, power source external volt-ampere characts. determ. using graphical analysis method 80—79594
- VT6 Ti alloy, diffusion welding with constrained deformation 80—81104
- welded joints in dissimilar Al alloys, fishbone testpiece axis of symmetry, residual stress investigations 80—7725
- welding arcs, gas velocity fields modelling 80—75039
- Al alloy 01420, welded joint fatigue life improvement, vacuum annealing appl. 80—7597
- Ar, of steel, resistance to cold cracking obs., C and H_2 content influence 77—21283

arc welding continued
  Ar plasma welding, compressed arc V-I characteristic obs. *(Russian)* 78—83628
  Ni-Cr alloy submerged arc weld surfacing using metal powder filler additions 79—57157
  Ti alloy VT9L, cast, welded joint mech. props., filler material and heat treatment effects 79—87671
  Ti-Al-Mo-Cr alloy weldment containing orthorhombic martensite, autotempering behaviour and alpha precip. strengthening 80—84976
  V-Zr-C-Y alloy weld metal, hardening phase precipitates examination, TEM appl. 80—7576

archaeology
  Aegean Bronze Age dating without radiocarbon 79—26202
  Al Jubail, Saudi Arabia, archaeological evidence for recent coastal uplift 79—79799
  ancient Cu alloys, epithermal neutron activation anal. method 78—8490
  ancient Japanese roofing tiles, characterisation by ^{57}Fe Mossbauer spectroscopy 79—26191
  ancient pottery, characterisation by neutron activation anal., suitable element selection 78—8484
  ancient pottery, nondestructive neutron activation anal. 78—12802
  ancient pottery, origin determ., X-ray fluorescence analysis *(German)* 77—29064
  archaeoastronomy, New Mexico site marking solstices and equinoxes 80—72794
  archaeomagnetic data compared with analytical representation of geomag. field for last 2000 years 78—73305
  archaeomagnetic field magnitude, rapid changes 79—74830
  archaeomagnetic intensity meas. using SQUID magnetometer 78—352
  artefacts, chemical analysis techniques 80—89575
  artefacts, obs. using automated PIXE-PIGME anal. system 80—61199
  artifacts as sedimentary particles in fluviatile environment 78—70239
  astroarchaeology, analysis of Stonehenge and Great Pyramid 78—32363
  Avebury, geometry and metrology of ring, new accurate survey results 77—33359
  Avebury, West Kennet Avenue, possible geometry 77—33360
  Avebury Ring, least squares fit rel. to Thom survey 78—4120
  bone, characterisation by neutron activation anal. 78—353
  bone, inclusions as source of error in radiocarbon dating 78—346
  bone dating by ESR technique 80—95209
  bristlecone pine and ancient Egypt, rel. to calibration of radiocarbon dates 78—70234
  Brogar ring, fourth lunar foresight and prehistoric mound 77—41322
  bronzes, chem. polishing and etching for metallographic exam. 78—356
  Callanish Megalithic sites, indicated declinations 78—4119
  cave sites, thermoluminescence dating of Quaternary calcite layers 79—84231
  ceramic dating by alpha-recoil tracks in mica 78—70237
  ceramic materials, thermoluminesc. dating, comparison of results 80—84791
  ceramic sculpture from Oaxaca, Mexico, authentication by thermolum. and style 78—70238
  ceramic sherds, macroporosity determ. by replica techniques 77—34065
  chert artifacts, thermolum. determ. of prehistoric heat treatment 78—24914
  clay tablets, records of barley harvest dates in ancient Mesopotamia 79—5597
  clay thermoremanent magnetisation, cooling-rate depend. 80—46174
  coin Ag concentration meas. using small neutron source 79—79332
  coins, ancient Greek, neutron activation and at. absorpt. anal. 78—8489
  coins, Septimius Severus denarii, reproducibility of X-ray fluoresc. anal. 77—34067
  Constantinian coins, neutron activation anal., using ^{252}Cf source 78—350
  dating, appl. of luminesc. of calcite under N_2 laser excitation 80—60685
  dating, scientific techniques, book 77—61172
  dating method with digital ESR 80—86542
  dating of prehistoric Great Basin petroglyphs by neutron activation anal. 78—70243
  Dead Sea-Jordan Rift, archaeological evidence for Subrecent seismic activity 77—86810
  diversity indices computation, FORTRAN program 77—33076
  Early Bronze Age pottery from Lake Vouliagmeni, neutron activation anal. 77—34063
  electron probe analysis, sampling stylus 78—70246
  ESR dating, appl. to archaeological materials from Greek Petralona cave 79—26094
  flint artefacts, ancient heat treatment identification by ESR spectroscopy 79—12831
  flint implements, provenance determ. possible appl. of SIMS 80—61197
  floating tree-ring chronology from NE.Scotland, radiocarbon meas. 78—70236
  fossil bone, age determination, nondestructive neutron activation anal. 78—15743
  fossil bones, U determ. and dating 79—52846
  gamma ray analysis of K, U and Th for dose-rate estimation in thermoluminescent dating 79—79333
  geomagnetic field record in Egyptian adobe bricks (3000-0BC) 80—104862
  geomagnetic field variation in S.E. Europe during last 8000 years 80—56351
  geomagnetism study of ceramics from Peru 80—94455
  geophysical prospecting by pseudobaseband pulse radar 78—24398
  glass, crystallisation after 1000 years storage 78—79536
  glass, X-ray fluoresc. anal., importance of sample prop. 77—34064
  glass object dating by hydration layer thickness meas. by NMR 77—74567
  Hohokam potsherds, Snaketown, Arizona, archaeomagnetic palaeointensity study 78—44769
  Inca people (Peru), evidence of astronomical knowledge *(Swedish)* 78—32640
  Indian ceramics, Hueco and Guadalupe Mountain, delayed neutron activation analysis of U content 80—85230
  Indian culture, ^{14}C dating of samples 79—40650
  inscribed jars found at Thebes, inconsistencies in comp. and provenance studies 79—26197
  Java, tektite-like material in remains 80—101365
  Jomon pattern pottery from Japanese Taishaku valley, thermoluminescent dating 79—26196
  Kerlescan megalithic store alignments, alternative geometry 77—41321
  Kilmartin Stones, lunar observatory hypothesis reassessment 79—96927

archaeology continued
  Koobi Fora Formation, Kenya, palaeomagnetic stratigraphy 77—29250
  Lake Mungo aboriginal fireplaces as geomagnetic records, dating 77—21679
  lunar megalithic site in Kintyre, survey 79—96929
  lunar megalithic sites in Britain, reconsideration 79—8854
  magnetic oxides in first American civilisation 77—60886
  malachite from patinas of ancient bronze objects, stable ^{13}C/^{12}C and ^{18}O/^{16}O ratios 79—26194
  Maya chronology and planetary conjunctions 78—36470
  Mayan and dates of planetary obs. in AD 293-1237 period 77—17392
  Mayan architectural orientations rel. to Venus rising and setting positions *(German)* 77—2352
  Mayan astronomy, depth of knowledge and archaeological evidence 80—27098
  megalithic astronomical alignments, significance tests 79—96928
  megalithic astronomical observatories, critique 77—2351
  megalithic astronomy, education 77—33759
  megalithic astronomy, statistical significance of astronomical orientations 78—36475
  megalithic lunar site a Callanish, Lewis 80—77300
  megalithic sites in Shetland, surveys 78—36474
  megalithic yars 78—24633
  Mercury silver statuette from Bonn 1896, particle induced X-ray emission analysis 80—85228
  Mesopotamia, city wall and street orientation rel. to winds 78—49074
  mineshafts, disused brick-lined, geoelectrical methods of detection 77—64451
  Minoan painted pottery pigments, XRF-XRD analysis method 80—35586
  Mossbauer effect appl., conference, Kyoto, Japan (Aug.-Sept. 78) 80—7199
  Mycenaean pottery from Megiddo, X-ray photoelectron spectroscopic analysis 79—29421
  Nahal Zin, Israel, sites, U series dating of travertine 79—34781
  Namoratunga II site in NW.Kenya, astronomical dating 80—72793
  neutron activation analysis, comparison of results from Lawrence Berkeley Lab. and Hebrew University 78—70245
  Nottingham clay tobacco pipes, chronological groups, chemical analysis 79—29422
  obsidian, from Koyukuk River, Alaska, elemental anal. by at. absorpt. spectrophotometry 77—34062
  obsidian, Mayan, source correl. for S.Belize artifacts 78—70244
  obsidian source identification by thermoluminescence 79—26195
  obsidian sources, chem. characterisation and hydration rates, W.Mexico 78—348
  palaeointensity and thermoluminescence measurements on Cretan kilns from 1300 to 2000 BC 80—36232
  pecked cross symbol in ancient Mesoamerica, possible significance 79—53954
  Peruvian whistling bottles, acoustic characts. 77—88993
  pewter, English and Scottish measures, X-ray fluoresc. anal. 78—347
  photon activation analysis of coins and art objects Au, Ag and Cu determ. 78—349
  physical methods, review 78—58104
  physics and chemistry applics., nonscience undergraduate course 77—26104
  potsherds, Melian, instrumental neutron activation anal. 78—8485
  potsherds, S.W. African, neutron activation anal. of trace elements, characterisation 78—8486
  potsherds, Turkish, neutron activation anal. 78—8487
  pottery, archaic Greek, X-ray fluoresc. 77—34068
  pottery, B and Li distrib. in glaze, appl. of (n,p) and (n,α) reactions 80—61200
  pottery, pore struct. rel. to characterisation 78—351
  pottery, sigillated, trace element archaeochem. using neutron activation anal. 78—8488
  pottery composition from Ayios Stephanos, rel. to Minoan potters on Greek mainland 78—355
  pottery manufacturing techniques, classification by X-ray anal. 78—354
  Pueblo Bonito, astronomy, architecture and adaptation 77—5463
  quartz grains, thermolum. dating, β-dose attenuation correction factors 79—75669
  quartz inclusion morphology for thermolum. dating, effect of HF etching 78—70240
  radioactive dating of ceramic samples, thermoluminescent method *(Czech)* 77—5972
  radiocarbon age determinations, procedures for comparing and combining 78—70235
  radiocarbon chronology and calibration of Late Minoan IB 79—26200
  radiocarbon dates from Akrotiri, Thera 79—26201
  radiocarbon dating discrepancies illustrated using Egyptian and Aegean samples 79—26199
  replicated diversity indices computation for random samples of specified size 77—37197
  Rhodes, discovery of Santorini (Thera) tephra from 1450 BC eruption 80—109129
  Sarawak gold artifacts, X-ray fluorescence and at. absorpt. analysis 80—85229
  sea level variations in NW Mediterranean during Roman times 77—13088
  soil bulk resistivity, meas. method 78—24381
  soil resistance meter, geological and archaeological applications *(German)* 78—57361
  soils, Mossbauer and mag. susceptibility studies of Fe oxides 77—30224
  sourcing method based on U, Th determ. in obsidian 79—2239
  stone artifacts, Japanese, trace elements, neutron activation anal., rel. to archaeological provenience 78—8492
  Stonehenge, new meas. in 1978 April survey 78—85860
  Stonehenge I and lunar apogee tracking 77—22116
  sword, 2500-yr-old, obs. using PIXE with external beam 80—61198
  Tampan Palaeolithic tools, Malaya, age from Toba Tuff K-Ar dating 79—16427
  techniques and instruments 77—197
  Terra Sigillata from La Peniche, Switzerland, chem. comp., mineralogy and porosity 79—26198
  thermoluminesc. dating, rapid-scanning interference spectrometer appl. 78—12773
  thermoluminescence, spatial distrib. determination, using image intensifier technique 80—47115
  thermoluminescence and age determination *(German)* 80—105076

- **archaeology** continued
  - thermoluminescence dating, effect of radioactivity within quartz 78—70241
  - thermoluminescence dating, error sources 78—11006
  - thermoluminescence dating, phototransfer technique 78—11005
  - thermoluminescence dating, radiation dose-rate data 80—31964
  - thermoluminescence dating, reassessment of fine grain dose-rate 77—34071
  - thermoluminescence dating, revised dose-rate data 77—34072
  - thermoluminescence dating 78—11004
  - thermoluminescence dating of ancient kiln, mag. separation of quartz 77—34070
  - thermoluminescence dating of burnt flint, appl. to lower Palaeolithic site Terra Amata 78—345
  - thermoluminescence dating of calcite and burnt flint, age relation for slices 77—34073
  - thermoluminescence dating of pottery, ^{87}Rb dose-rate contrib. 78—70242
  - thermoluminescence dating of zircon sand 79—33847
  - thermoluminescent dating of pottery by glow curve simulation method 77—5973
  - trace element analysis, pattern recognition techniques 77—40588
  - Udo Bronze Head, thermolum. dating 77—34069
  - underground cavities, geoelectric dipolar techniques appl. 79—16687
  - underground remains detection, acoustic meas. with computer data processing 79—76921
  - Unexplored Mansion, Knossos, anal. of Cu and bronze artefacts 77—34066
  - Victoria Falls, erosion rate and Batoka Gorge archaeological dates 77—2184
  - Au in thin Ag objects, quantitative analysis by γ-ray differential absorpt. 80—85227
  - ^{13}C record in tree rings, industrial CO_2 affecting ^{13}C assimilation 80—51586
  - ^{14}C dating of geological and archaeological samples 78—92993
  - ^{14}C, use in dating, review of technique 79—49922

- **architectural acoustics**
  - *see also anechoic chambers; echo; noise abatement; reverberation*
  - absorbers, dimensioning of facings for acoustically effective structural elements *(German)* 80—74600
  - absorption coefficient of wall covered with sound-absorbing cubes *(German)* 77—84081
  - acoustic coupling between rooms, meas. system using decrease in sound level method *(French)* 80—69611
  - acoustic diffuser characteristics for amateur users concert hall appl. *(Italian)* 80—91961
  - acoustic telescope appl. 80—5873
  - acoustic wave diffraction at edges of absorbent wall panels, modal analysis *(French)* 80—79060
  - Acoustical Soc. Amer. 96th meeting, Hawaii, 1978 Nov. 78—90545
  - AF vibration, transmission by building columns 80—74602
  - air-conditioning systems, acoustical characts. of certain flow-spoiling devices 77—50832
  - airborne and transmission loss anal. for single and double panel partitions 79—86293
  - aircraft jet noise reduction test facility 77—845
  - ambiophony, practical aspects and appl. in Capitol Theatre, Washington 80—96113
  - America, history of building acoustics (1920-1940) 77—45663
  - American architectural acoustics, (history to 1930) 77—45662
  - apartment blocks, noise transmission through wood joist floors, sound insulation methods 80—38178
  - audio-visual design and room acoustics for board room 79—37092
  - auditoria, 1:50 scale model investigations 80—33342
  - auditoria, eighth annual Fairey lecture 78—13859
  - auditoria, receiver sound control 77—68328
  - auditoria and studios, meas. reverberation time, digital instrum. *(Japanese)* 80—64321
  - auditoria speech amplification space and electro-acoustics study *(Dutch)* 77—68330
  - auditorium acoustics design index, S/N ratio for speech intelligibility 80—19156
  - auditorium design criteria by subjective eval. *(Japanese)* 77—31180
  - auditorium syllabic intelligibility, computer evaluation *(French)* 79—37095
  - auditoriums, effect of direct reflections 80—33345
  - auditoriums sound insulation *(Japanese)* 79—81635
  - auditory acoustic terms used in architectural acoustics, definitions *(German)* 78—18117
  - automated computer optimisation design for concert halls, quantitative criteria 80—87654
  - axisymmetric transmission system with sound absorbing wall, finite element anal. 77—88974
  - baffles in closed spaces, dependence of effectiveness on nature of closed space, economic and annoyance factors 80—67019
  - band-limited power flow into enclosures 80—58859
  - basic value definitions and commentary *(French)* 78—1513
  - Boston Symphony Hall, reverberation times in notebooks of Wallace C. Sabine 77—49545
  - broadcasting and recording studios, computer-aided method for acoustical desing 79—64402
  - Broadcasting House, SDR, Stuttgart, sound engineering planning *(German)* 78—1512
  - broadcasting studio, 'Deutsche Welle' building construction and meas. *(German)* 80—106668
  - building interaction with road traffic noise, prediction using a scale model 80—45838
  - building services design, roles of noise control and environmental engineering 79—23144
  - building sound insulation against aircraft noise, German federal regulation 79—90083
  - built-up urban environments, propag. of sound generated by point source 80—58841
  - CAD, based on digital meas. techniques *(Polish)* 78—59205
  - cavity backed panel, response to external airborne excitation 79—50511
  - Christchurch (New Zealand) Town Hall acoustical design aims and results 79—68490
  - Christchurch Town Hall, acoustical design and evaluation 79—68488
  - cinema and sound stage acoustics *(Russian)* 79—18609
  - cinemas, motion picture sound reproduction improvement methods *(Russian)* 79—10430

- **architectural acoustics** continued
  - cocktail parties, importance of ceiling and wall sound absorpt. 77—80008
  - concert hall, acoustical conditions preferred for ensemble 79—14161
  - concert hall, musical instruments directivity rel. to efficiency of acoust refl. or absorpt. *(German)* 77—829
  - concert hall acoustics, room impression as an overall concept of spaciousness and liveliness *(German)* 78—94484
  - concert hall design, lateral and ensemble reflection requirements 80—91964
  - concert hall design for orchestral balance in seats behind stage 80—91963
  - concert hall problem, coherence length and diffuse reflection formulation 80—91962
  - concert halls, auditory backward inhibition, parallelism between vision and hearing 80—14521
  - concert halls, binaural dissimilarity and optimum ceiling shapes, lateral sound diffusion 79—68489
  - concert halls, connection between subjective judgements and criteria of room acoustics *(German)* 80—102933
  - concert halls, designing for performers 79—41516
  - concert halls, electroacoustic reverberation equipment *(Czech)* 78—1514
  - concert halls, factors necessary for warm string tone 80—74603
  - concert halls, hearing impressions of loudspeaker reproductions and orchestras *(German)* 78—94485
  - concert halls, primary sound suppression *(German)* 78—75014
  - concert halls, relation of performing arts to architecture 79—94407
  - concert halls, sound reinforcement system, Nippon Budokan Hall *(Japanese)* 80—64291
  - concert halls, subjective preference tests for acoustic fields simulated by aid of computer 80—23838
  - concert halls, synthetic sound fields, effects of early multiple reflections on subjective preference judgements 79—41517
  - concert halls and auditoria, tailoring acoustic response using electro-acoustic methods 79—32137
  - concert halls and auditory backward inhibition 79—59892
  - concert-hall acoustics, multidimensional description of subjective judgement *(German)* 77—72117
  - concrete floors, structure-borne noise 77—42665
  - converted-church theatre rebuilding and acoustic treatment *(Hungarian)* 80—106667
  - corrugated surface, effective absorption coeff. 79—32119
  - courtrooms in northern England 77—50834
  - covered panels, sound insulation characteristics of panels having porous material coverings *(Japanese)* 80—33334
  - critical distance measurement of rooms from acoustic energy spectral response 79—72750
  - cuboidal spaces, computer-aided geometrical field analysis of directional props. 80—19157
  - cultural centre reconstruction, acoustic tasks and measurements *(Hungarian)* 80—106666
  - damping prediction by power flow methods of structure borne sound 78—33952
  - decay rate in rooms, formulae for spatial variance 80—38188
  - decaying sound fields and spatial variation 78—79165
  - Demey metro station, noise level increase due to echoes from passing vehicles *(French)* 80—69600
  - design criteria for concert halls 79—72756
  - design of music practice rooms, user requirements 80—74606
  - diffuse sound field around objects in a reverberant room *(Japanese)* 79—1030
  - diffuse sound reflection by max. length sequences 77—7230
  - directivity of sound radiated from large aperture in building 80—38148
  - directivity pattern of sound through an opening into diffuse sound room *(Japanese)* 77—31178
  - domestic roofing sound insulation, expt. facilities of meas. laboratory, test details 80—79058
  - domestic room acoustics, speaker positioning for optimum frequency response 77—54845
  - domestic sound insulation deficiencies and remedies 78—83175
  - door hinges and fasteners in acoustic room design 77—50836
  - double walls, influence of cavity-volume damping on air layers stiffness *(German)* 77—80016
  - double walls, sound transmission loss and cavity absorbent materials *(Japanese)* 78—79167
  - echo and reverberation generation, electronic ccts. *(German)* 79—32138
  - eigenmode analysis of the interference patterns in reverberant sound fields 80—96112
  - electronic modification of room acoustics in a concert hall 77—3702
  - enclosure, 2-dimens., stationary sound field, continuous obs. *(Japanese)* 79—32143
  - enclosure, thermoviscous dissipation at walls, normal mode theory 78—83171
  - equivalent absorpt. area of room in steady-state condition and reverberation *(German)* 80—102931
  - Exhibition Hall of Yamaha Sportland TSUMAGOI, design of auditorium with electroacoustic technology 78—13858
  - felt sound absorption rel. to airflow resistance, obs. 77—58506
  - floating for constructions, acoustic props. 77—84083
  - floors, comparison between methods for impact noise testing 79—46111
  - floors, elastic coverings, effect of thickness and hardness on impact sound insulation props. *(Japanese)* 80—79053
  - floors, problems of impact testing *(German)* 77—825
  - free field rooms for industrial applications 80—48518
  - frequency analyzer for room quality meas. for HiFi *(German)* 79—46140
  - glass panels, transmission loss and vibr. in nonreverberative conditions 77—7258
  - Gulbenkian Great Hall, Lisbon, acoustic design of auditorium 79—14162
  - Gulbenkian Great Hall, Lisbon, acoustic investigations 79—14163
  - hall, improvement of acoustics *(French)* 79—37089
  - halls, multi-purpose, sound reinforcement systems *(German)* 77—80019
  - halls, sound amplifying systems, model *(French)* 79—37090
  - hi-fi demonstration studio design *(German)* 79—94405
  - high fidelity sound, perception of sound and music 80—42014
  - history, Kircher's 'Phonurgia nova' *(German)* 78—81788
  - horizontal wall acoustic insulation methods *(Spanish)* 78—87207
  - housing, classes of acoustical comfort, measurement and control methods 79—23143
  - Hungarian developments, BEAG activities 78—46860
  - image method for simulating impulse response between two points in small room, using digital computer 79—68487

architectural acoustics continued
images sources method for sound field predictions in rooms of arbitrary shape 79—81632
impact noise in buildings, meas. equipment *(Japanese)* 77—88986
impact sound insulation, new rating system 77—11082
impulse responses in concert halls, new method using deconvolution 80—96111
insonification of halls, contrib. to study of mathematical model *(French)* 78—13857
insulating material losses and performance factors *(Spanich)* 78—55516
insulation and sound absorption testing, using pseudo-random noise generator *(Spanish)* 78—13861
insulation meas. dependence on type of loudspeaker *(German)* 78—75021
interior spaces, impulse response 80—28383
internally excited three-layer cylindrical shells, acoustic reduction 80—5874
interoffice speech privacy criteria and suspended ceiling acoustic insulation 78—83173
Joseph Haydn concert halls, room acoustics and orchestral sound *(German)* 79—18631
Karl-Marx-Stadt, great hall, small hall, sound absorption of furnishings *(German)* 77—58509
landscaped office, effect of screens on sound attenuation 78—94486
landscaped office, subjective response to sound conditioning 80—19158
large industrial hall reverberation time 78—38145
large rooms containing barriers, sound pressure level prediction 78—38144
listening room, reverberation time and reproduced sound definition *(Japanese)* 78—9499
listening room, reverberation time and reproduced sound definition 79—18606
living room loudspeaker performance problems *(German)* 79—90081
loudspeaker design for domestic appls. *(Italian)* 80—91960
loudspeaker placement, reverberation problems *(German)* 78—87204
loudspeaker radiation patterns effect on stereo imaging and clarity 79—64401
maisonettes, flanking transmission of sound, effect of woodwool shuttering in party floors 78—94487
measurements by impulsive excitation *(Japanese)* 80—64292
monosyllabic word discrimination, classroom acoustics effects 79—53160
motion picture theatres, acoustic response measurements and standards 77—19496
multidesktop distributed sound system in large room, in-depth time delay spectrometry study of early late arrivals 80—38179
multipurpose hall acoustical design and construction 79—68486
multipurpose hall with variable reverberation units and movable partition, design *(Japanese)* 79—37093
multistorey buildings, reduction of structure-borne sound levels by floors and walls *(German)* 78—94483
multivariate anal. of subjective measures for sound in rooms *(Japanese)* 77—31179
music reproduction in small rooms, theory *(Spanish)* 78—38155
music stage design 80—74605
noise, max. acceptable levels in quiet rooms *(German)* 77—68307
noise control at the design stage of buildings, mechanical services and equipment selection 79—18598
noise insulation by multiple layer walls, prediction of output probability distribution of noise level, road traffic noise 80—69593
noise level definitions and building design criteria 78—83174
noise transmission between dwellings, calculation model 80—43545
noise transmission through stiffened panels 80—102922
oblique incidence sound absorpt. characts. of materials using cross-correlation methods *(Japanese)* 78—83172
open plan offices, comparison of NIC′ and ΔdBA rating schemes for speech privacy 79—3854
open plan offices, effect of V-form ceilings 77—50835
open plan offices, noise abatement via sound absorbing partial partitions 78—18116
open plan offices, use of Articulation Index to evaluate acoustical privacy 79—32140
open plan spaces, technique for sound pulse transmission anal. 79—23151
open-plan offices, acoustical parameters 78—55520
open-plan offices, role of acoustic screening 80—87650
open-plan spaces, acoustic props. and design for school classroom 78—77653
partition airborne-sound transmission loss, effect of sound-absorptive facings 78—79166
partition and glass windows, influence of vibration damping on acoustic transmission *(French)* 77—31176
partitions, statistical energy anal. for sound insulation 79—23129
party wall and floor transmitted noise nuisance survey 78—42491
passenger compartments, modal synthesis of LF props. 77—88980
phantom sound source localisation experiments, anechoic chamber, music room *(Polish)* 77—75748
phoneme recognition with small room reverberation 79—86306
pitch change during reverberant decay 77—14854
plasterboard sound reduction indices and meas. 78—87196
power flow methods for sound transmission assessment 77—31177
radiation efficiency estimation through walls 79—81634
radio studio acoustics planning for SDR's Stuttgart Broadcasting House *(German)* 78—71243
railway passenger coaches, structure-borne noise suppression *(German)* 80—91957
ray method for acoustical treatment of halls *(French)* 80—43544
real-time room-acoustic analyzer using tone burst signal from loudspeaker *(Japanese)* 80—10087
recording studios, shortcomings of apparently improved acoustic designs 80—69601
recording studios, specification and design of Supreme Being Studios 79—64400
rectangular reverberant room, sound press. correl. coeffs. 78—18115
rectangular room, acoustics theory on basis of image methods *(Japanese)* 78—30129
rectangular room, instantaneous excitation of one-dim. sound waves *(German)* 78—87201
rectangular rooms, geometrical acoustics for predicting sound intensity and reverberation 80—23837
reduction of raod traffic noise, correct building placement, noise emitted by single source in open space 80—87647

architectural acoustics continued
regenerative sound system investigation using time-delay spectrometry 78—51006
resonator appls. to hall reverberation time modification *(Dutch)* 78—22227
reverberant enclosure, impulsive sound-level response statistics 77—84082
reverberant room, rectangular, correlation coeffs. of sound pressure 79—76914
reverberant sound absorpt. coeff. of plane porous material, theory *(Japanese)* 78—79168
reverberation chamber, space variance for rectangular modes 77—75746
reverberation in an enclosure, three dimensional computer simulation 77—75747
reverberation room, small-scale multipurpose model, design and construction 77—7259
reverberation room ANS qualification error sources and effects 77—58514
reverberation room ANS qualification for discrete frequency sound power level meas. 77—62122
reverberation room ANS qualification for wideband and discrete frequency source meas. 77—58518
reverberation room ANS qualification with microphone traverse and LF absorption 77—62123
reverberation room modifications for ANS qualification 77—58517
reverberation room qualification with computer-controlled instrumentation system 77—58516
reverberation room sound pressure level spatial averaging by microphone array and traverse 77—58515
reverberation studies, re. telephone loud speaker system 78—94488
reverberation time, absorption and impedance, theoretical model used for calcs. of a room 78—90601
reverberation time dependence on wall diffusion and room shape *(German)* 80—102932
reverberation time for two-dimens. enclosures, iterative calc. 80—102934
reverberation time measurement using Fourier transforms 80—74601
reverberation times of large spaces *(French)* 80—14504
review of international standards *(Japanese)* 80—64294
road traffic noise, effect of structure-borne tunnel vibrations on buildings 80—48492
road traffic-induced building vibration, Greater London area 80—96098
room acoustic absorption meas. using reference sound source 77—62109
room acoustics and human communications 80—96110
room acoustics and subjective sound perception, computer simulation *(Polish)* 79—7258
room acoustics correction, using Shure analyser *(German)* 80—58873
room acoustics determination, noise abatement appl. 78—75016
room having effect on plaster/wood walls open window, pressure due to sonic booms 80—69602
room impression index, definition on basin of subjective examination *(German)* 78—87202
room impulse response on speech signals 79—86294
room noise reduction, use of window cills and reveals 80—33343
room resonance, computer-aided anal. 78—87205
room resonances, absorption, effect on stereo loudspeakers freq. response *(Italian)* 78—51005
room reverberation, removal from speech signals using multimicrophone signal-processing technique 78—9501
room-acoustic directional diffusivity model *(Hungarian)* 80—106665
rooms, field anal. by finite element method *(Japanese)* 79—27465
rooms sound absorpt. meas. 77—39161
Sabine's theory rel. to ergodicity *(Japanese)* 78—9498
scattered sound field calc. of rectangular room of various proportions 80—53564
school buildings, min. acoustical requirements 80—79059
schoolroom acoustic insulation check allowing for boundary absorption *(Hungarian)* 80—106664
screen acoustic impedance evaluation, numerical method 78—13831
self-protecting buildings, acoustical performance 80—23839
shielding effect of noise barriers in open-plan offices, industrial halls 79—18610
singer and auditorium interactions 80—74604
solid-borne sound, propagation characts., field and model expts. *(Japanese)* 80—64290
sound absorption, perforated facings on porous backings, calculation of specific normal impedance 80—64281
sound absorption factor influence on reverberation time 79—81631
sound absorption factors in enclosed space *(Spanish)* 79—3856
sound absorption to improve audibility *(Spanish)* 78—18118
sound decay measurement using integrated-impulse method 79—94406
sound differences in sensory space for sound reproduction engineering *(Russian)* 78—55521
sound diffusion systems, fundamentals calc. *(Spanish)* 79—3855
sound effects transmission, uniplanar and biplanar eidophony *(German)* 80—106699
sound fields and acoustic design in rooms, review of subjective effects *(Japanese)* 80—64293
sound insulation, domestic roofing systems 80—96109
sound insulation between buildings, meas. standards 80—96108
sound insulation design and transmission field meas. 78—87206
sound isolation by glass isolating panes, influence of gas filling *(German)* 77—80017
sound isolation tests of residential buildings, correlation with subjective privacy opinions, standard sound source requirements 80—64323
sound pressure level in closed building, forecasting program *(French)* 78—13856
sound quality monitoring in cinemas, dubbing theatres 78—33961
sound reduction by barriers in rooms 80—79057
sound reproduction in cinema, automatic control *(Russian)* 80—38212
sound system design aid, HP 97 program 78—75015
sound transmission, absorption and reflection 80—64288
sound transmission at the corner of concrete plates 80—87652
sound transmission between absorbing parallel planes 80—33344
sound transmission through periodically framed parallel plates 77—50833
sound transmission through thin panel backed by rectangular cavity 80—28382
sound-absorbing wall, finite element simulation of acoustic filters *(Japanese)* 77—84032
source above rough absorbent plane, analysis of scattering 80—64289
space absorber composed of porous materials, reverberant sound absorption coeff. 78—55519
space and electro-acoustics to assist speech in halls *(Dutch)* 77—80018

architectural acoustics continued
  spatial impression of concert halls, lateral refls., musical level *(German)* 78—79164
  spherical enclosure, reverberant sound decay 78—30128
  spherical enclosure, uniformly absorbing, effect of surface roughness on reverberation time 79—14160
  sports areas, reverberation and noise levels 78—9497
  statistical models of coupled dynamical systems and the transition from weak to strong coupling 79—50500
  steady-state sound in an enclosure with diffusely reflecting boundary 79—14159
  structural noise and vibration problem solution by statistical methods 79—23126
  structure-borne and air-borne sound levels rel. to insulation of appliances in buildings *(German)* 79—94404
  structure-borne sound, procedure for meas. sensitivity of building structures to stationary excitation *(German)* 80—64287
  structure-borne sound and its transmission, measuring procedure 79—50509
  studio acoustic design using scale models 79—3857
  studios, acoustic design using scale models 79—10429
  studios, acoustic treatment using modular panels, computer calcs. of reverberation time *(Spanish)* 79—32141
  talk studios and listening rooms for BBC 79—37091
  theatrical sound effect for cine films *(Spanish)* 79—41550
  thin infinite panel, sound insulation dependence on effective loss coeff. 80—87737
  timber frame constructions, sound insulation of wood joist floors 78—87203
  traffic noise, attenuation around buildings 78—1498
  transmission function in rooms rel. to acoustic amplification systems 78—59204
  transmission loss improvement by thin plates in certain distance of building elements 80—102930
  transmission loss of a wall under random sound field *(Japanese)* 77—68329
  transmission loss of apertures, reverberent room method 78—1510
  transmission loss prediction for building elements 79—32139
  TV and motion picture stages, noise and insulation 78—79169
  TV studios, acoustically optimal room properties with regard to normal frequency spacing *(German)* 80—14522
  underground enclosures, noise distrib. prediction from free-field meas. 77—7253
  unsealed window sound insulation rel. to frame construction 79—68485
  unsymmetrical enclosures, LF resonances 79—18605
  urban built-up areas, external reverberation times 77—14846
  urban built-up environments, room acoustical model of external reverberation 80—53563
  wall systems, design for desired STC ratings 79—18608
  wall vibration, underground train systems 80—48490
  Wellington Town Hall, NZ, preliminary acoustical considerations 79—81633
  Westphalen Hall, Dortmund, equipment for intelligible and uniform sound production *(German)* 79—1029
  window sound insulation, glasses, most effective window configurations 80—87655
  wood joist floor-ceiling systems, sound-insulating efficiency upgrading 78—1515
  work rooms, acoustic characts. 79—81636
architectural CAD
  Christchurch (New Zealand) Town Hall acoustical design aims and results 79—68490
  closed building, forecasting program for determ. of noise abatement measures efficacy *(French)* 78—13856
  deflection of cables, cylindrical suspended roofs with complex loading, incremental algorithm 78—9558
  multipurpose hall acoustical design and construction 79—68486
  noise screening devices, acoustical performance of self-protecting buildings 80—23839
  studios, acoustic treatment using modular panels, computer calcs. of reverberation time *(Spanish)* 79—32141
architectural computer aided design *see architectural CAD*
architecture
  see also building; civil engineering
  aerodynamic wakes of surface-mounted cubes 79—12183
  close-range photogrammetry problems solved by analytical plotter 77—71397
  design rel. to microclimate and energy conservation 78—3916
  developing countries' architectural design for solar energy environmental control 79—57449
  education, architects, physics course description 79—25779
  glass system, layered, thermal radiative props. for solar diffuse radiation flux 79—94473
  Mayan architectural orientations rel. to Venus rising and setting positions *(German)* 77—2352
  northern solar house long-term storage systems 79—57473
  Physical Sciences Building, Washington State University 79—21499
  Pueblo Bonito, astronomy, architecture and adaptation 77—5463
  solar collector tilt, orientation, and overshadowing sensitivity rel. to Netherlands urban design 79—62073
  stress calc. in arched roof with curved longitudinal edges *(German)* 79—23217
  Taiwan velocity risk mapping for seismic resistant building design 80—31002
  thermal power stations, achievement of environmental harmony *(French)* 79—92094
arcing *see arcs (electric)*
arcing, switches *see circuit-breaking arcs*
arcs (electric)
  see also arc furnaces; arc lamps; arc welding; circuit-breaking arcs
  ablation stabilised arc theory 80—70072
  ablation stabilised arcs, theory 79—37561
  ablation-stabilised arc temp. distrib. model 78—71585
  AC, inl ongitudinal gas flow, periodic regime, exact soln. 77—27767
  AC arc, axially blown with N_2, field strength and energy balance eqn. 78—87523
  a.c. plasma jet, cross electrode type, operating characts. *(Japanese)* 77—1022
  acoustic noise 78—9890
  acoustic noise in electric arcs *(French)* 80—28865

arcs continued
  activated, duration reduction by drift field modification 77—7616
  activation as function of organic exposure and arc current for Pd and Pd/Ag electrodes 80—38778
  aerosol particles, effect on fast plasma stream form. in an elec. arc 78—51390
  air, transport coeffs. meas. 78—59709
  air, wall-stabilised arc, step and sinusoidal current change response 80—103209
  air arc discharge high-temp. transport obs. 78—71577
  air arc temp. meas. by N_2^+ integrated emission coeffs. 80—59314
  air blast arc characts., depend. on electrode position 79—23470
  air-moving arc interface, optical anal. at atm. press. 79—90482
  alkali hydride arc, laser initiated, H^- production 80—32550
  alkali metal, dense plasma, elec. and heat conds., two-probe diagnostics 80—38560
  alkali-metal hollow cathode arc, low-press. current limiting 80—6304
  alumina confined arc, ablation-induced effects 80—70073
  anode emission and heating, local plasma pot., probe meas. 77—19801
  anode initial heat flux, meas. and modelling of high-current pulsed arc 79—50903
  anode sheath in high pressure high current arc 78—67467
  anode-vapour vacuum arc with permanent hollow cathode 80—79616
  approximate model of arc in transverse aerodynamic and mag. fields 80—24285
  arc column, helical instability limits 78—71564
  arc quenching system for transient and statistical flashover, fusion reactor systems 78—75455
  arc spots, on film cathode, theory 77—39495
  arcing and surface damage in DITE Tokamak, SEM obs. 78—59611
  atmospheric, plasma electron density meas. by two-wavelengths interferometry *(Japanese)* 80—38720
  atmospheric arc initiation from erosion discharge 79—90490
  atomic processes, absolute spectral intensity meas. technique and other applications *(Croatian)* 79—10707
  automobile distributor, arc initiating processes 80—19665
  azimuthal conductivity, radial distrib. function 78—51374
  Berkeley multifilament ion source, plasma characts. 79—94807
  boundary layer cooling of atmospheric arcs, arc interruption by moving rod 78—87545
  cap-and pin-type insulators, resistance to high current arcing for 110 and 400 kV power transmission lines *(Polish)* 80—70049
  capacitor discharge, current increments, using arc channel hydrodynamic model *(Russian)* 79—82109
  cathode arc spot crater form. model 77—62414
  cathode arc spot temp., Joule heat liberation effect 78—26361
  cathode damage from 300 ns, 4.5 A arc, material comparisons 78—87579
  cathode erosion components, vac. arc, fusion temp. and charge transfer depend. 77—4010
  cathode region, easily ionised admixture effects calcs. 79—14633
  cathode region activity during transition to arc *(French)* 78—91172
  cathode spot, charact. parameters determ. *(French)* 78—14236
  cathode spot, halo and core prod. meas. 80—38829
  cathode spot current density determ. 77—62425
  cathode spot excitation, dielectric stimulator, pulsed gas discharge switch 77—19802
  cathode spot of a vacuum arc, review 80—24290
  cathode spots and erosion craters in vac. arc 80—10442
  cathode spots of the first kind, erosion rate resistivity and thermal cond. depend., explosive model 79—14630
  cathode spots on Ag, Ni, Cu, and W vac. arc discharge electrodes, model 78—91179
  channel arc, steady-state stability 78—38561
  channel bearing turbulent gas flow, arc parameters calc. 80—6298
  channel transient characts. in air under impulse voltage *(Japanese)* 78—5973
  chemically reactive arc-heated gas flow, ion saturation current fluctuation probe 78—63574
  cineholographic interferometry of evolution 77—71958
  circuit breaking air blast arc, near current zero, local elec. props., optimisation 78—87516
  coaxial plasmatron, Cu electrode degradation by arc spot, thermal shock and surface cracks 79—14629
  cold cathode arc starting, probe and high speed photography obs. 80—38832
  cold cathode low press. arc retrograde motion in strong mag. field, theory 79—27858
  cold cathode reflex arc, LF plasma instabilities *(French)* 77—62415
  column helical instability in axial mag. field, damping and RF-DC discharge 78—71595
  condensed, in hydrocarbon, cathode processes 77—35415
  conducting gas flow in high current electric arcs, calc. methods and numerical anal. 79—90478
  constant-current vacuum, ignition by plasma steam cathode spot excitation 80—75111
  constriction phenomenon due to longit. high vel. flow 78—87546
  contracted arc to crossed fields, discharge props. 77—84561
  controlled generators, spectra, rel. to quantometric meas. *(Russian)* 78—74072
  core formation, temp. profiles and elec. power input 77—24241
  cross-flow arc behaviur, theory and expt. 78—75484
  crossed-field arc discharge contraction ion source 78—86382
  CTR devices, surface effects related to voltage breakdown 77—35356
  current distribution in hollow-cathode arc discharge 78—67537
  cylindrical, radiant energy transfer, temp. profiles with boundary reflection corrections 80—79600
  cylindrical arc column, channel model 80—106995
  cylindrically symmetric arcs, radial radiative energy flux distrib. 79—14623
  DC arc, anode spot temp., buffer cpd. effect 79—48029
  DC arc, for emission spectroanal., transport mechanism 78—22464
  DC arc, selective volatilisation, direct-reading spectrometer obs. 77—73480
  DC arc, selective volatilisation of elements, in external mag. field, anal. appls. 78—68938
  DC arc, vaporization processes, thermochem. reagents effect *(German)* 79—48030
  DC arc as spectroscopic light source, mag. field effect on line intensities 78—87550

arcs continued
- DC arc in supersonic nozzle flow, appl. to gas blast circuit breaker 79—23469
- DC arc optical emission spectroscopy. appl. to C determ. 79—83527
- DC arc plasma, alterations in spectral line intensities due to external mag. fields 80—79621
- DC arc plasma, meas. of conc. ratio of component atoms *(Russian)* 77—27754
- DC C-arc for excitation temp. meas. of self-absorpt.-free FeI spectral lines 80—87965
- DC low voltage arc, anode energy balance investig. at reduced press. 80—19637
- DC melting plasmatron, low pressure characts. *(Russian)* 78—94945
- DC plasma, axial mass transport, added particle distrib. 79—86640
- DC plasma arc, for elemental anal., review 77—73478
- DC plasmatron with axially-blown arc, optimisation *(Russian)* 77—39476
- DC rotating arc as spectrochem. light source 79—52856
- DC transferred arc for refractory refining, initiation and performance characts. 78—9866
- DC vacuum arc emitted particle flux 78—75470
- DC wall stabilised, parametric excitation and amplification of Alfven waves 77—35340
- dense plasma, H_β line red shift expt. 78—67473
- dense plasma, radiative thermal cond. and elec. cond. coeffs. determ. in arc discharge 80—75033
- diagnostic of unipolar arc 79—1357
- dielectric materials spacecraft, surface discharge arc propag. and damage 80—71314
- dielectric stimulated arcs in lighting-arrestor connectors, substantial lowering of breakdown voltage 79—99013
- discharge, cathode spot high current density meas., expt. 78—9879
- discharge lamps, gas-whirl stabilized discharge, theory and calc. results *(Russian)* 80—33843
- discharge low pressure plasma arc, energy parameters experimental study 80—75117
- DITE Tokamak, arcing investigation 79—658
- double plasma arc, rotation in graphite tube 78—71599
- double plasma arc source, for powdered sample analysis in graphite tube 78—16858
- Duoplasmatron discharge resonance radiation emission model 78—67477
- duration, contact metal and organic contaminants depend. 77—31537
- dynamic characts., mathematical model 77—35409
- dynamic discharge arc driver, computer-aided circuit simulation 77—24219
- electric field strength of arc column in free turbulent jet 80—49021
- electric machines, volts-per-bar and flashover, causal mechanisms and preventive measures 80—92408
- electrical conductivity and temp. distrib. in insulating channels 79—23401
- electrode, evaporation rate from cathode spot in vac. arcs. 80—49024
- electrode geometry effects on tank conductivity arc model 78—42845
- electrode processes thermodynamic approach *(Russian)* 77—27755
- electrode vapour conc. meas. from light scatt. in air arc plasma 78—30505
- electrodynamic anomalies, ion electron mutual action, torque 77—84549
- electron density, spectroscopic meas. during arc discharge extinction *(French)* 77—80361
- electron density determ. by IR laser transmission meas. 79—7491
- electron density meas. by far IR laser beam deflection 80—59296
- electron energy spectrum, for PIG and arc type discharge plasmas, comparison *(Russian)* 77—15263
- electron field emission in arc discharge 78—1943
- electron injection into dense Hg or Ar, cathode spot simulation expt. 79—1364
- electron transport, determ. from pulsed arc meas. 77—47157
- Elenbaas Heller equation, soln. method 80—14952
- Elenbaas-Heller eqn. solution by analogy 78—71584
- Elenbaas-Heller soln., multivaluedness 77—47289
- emission spectral anal. of powdered mixtures using AC arc, optimum conditions *(Russian)* 77—16894
- emission spectrometry, current developments *(Japanese)* 78—86356
- emissive intensity distortion by transverse oscills., method of statistical regularisation *(Russian)* 77—48746
- energy balance of anode in low-pressure heavy-current discharge with hollow cathode *(Russian)* 78—51369
- enrichment by plasma centrifuge, rotational velocity meas. 78—74502
- erosion and aggregate condition near discharge, cellular structure effects *(Russian)* 79—37557
- erosion-arc duration correl. in relay contacts, atmosphere effect *(French)* 77—72518
- exploding wire, structural inhomogeneity and MHD sausage instability, arc chains, grain size and annealing 79—41904
- explosive electron emission, drop fraction of Cu cathode erosion 80—44063
- field ion emission, into arc plasma, current density eqn. 79—43108
- finite length, electrode-stabilised free arc in longit. mag. field, dynamic equilib. model 78—87551
- fireball plasma formation, transmission line model 78—59702
- flow stability, axial, cathode emission mechanism change effect 78—83638
- flow velocity meas. using laser Doppler velocimetry 77—80360
- free burning arc characteristic formulae 80—70068
- free helical arc, in mag. field, dynamic equilib. model anal. 80—19638
- free-burning arc continuous radiation rel. to electrode erosion 78—71578
- free-burning arc isothermal-channel theory 78—71587
- free-burning arcs, simple theory 80—6297
- Freeman ion source, electron trajectories 77—18722
- Freeman type ion source in low press. arc operation, discharge characteristics and beam quality 78—66006
- fusion reactor, TFTR, neutral beam source, arc current modulator design 80—102379
- gap with displacement by mag. field 78—87513
- gas blast circuit breaker model, thermal disturbance 79—60208
- gasdynamic laser, thermal nonequilibrium heating of active medium by elec. arc 80—53258
- geological materials, spectrographic thermometry and manometry using DC arc 78—16796
- glow discharge, normal, stability, rel. to transition to arc 79—10740
- glow discharge transition to arc 78—26369
- graphite, in Ar flow, meas. of anode voltage drop 80—84022

arcs continued
- graphite, unipolar arc damage in hot, dense D plasma 79—3235
- grid controlled switching element, stationary conducting state 79—77430
- grid controlled switching element, stationary conducting state, arc conditions 79—77431
- grid influence, on low-voltage Cs arc plasma in 3-electrode system 80—38844
- heat exchanges between electric arc and electrodes, dependence on electrode material and cooling conditions *(French)* 80—19655
- heat flux and current density dstrib. in heat spot of arc discharge *(Russian)* 79—14625
- heat sources of the arc cathode spot ion impact and neutralisation heating 80—38733
- heat transfer bibliography 78—63425
- heat transfer in interaction of electric arc with longitudinal gas flow 77—11189
- heat transfer to rotating water-cooled cylindrical wall *(French)* 80—28850
- helical arc column, dynamic equilibrium model 78—71593
- helical form model 80—103199
- helical in stabilising channel in mag. field 79—60206
- HF discharge mode two-valued depend. on arcing voltage, geometric reson. *(Russian)* 77—47283
- HF discharges and DC arcs in $H_2(D_2)$(inert gas), instability obs. high pressure HF discharges and DC arcs, instability obs. 80—38807
- high current, anode near-electrode layer, spot formation and sheath breakdown 80—38835
- high current, burning in channel 78—63614
- high current, vaporisation effect on roots 78—30496
- high current arc, influence of vaporisation upon roots 78—1916
- high current density arcs in narrow channels, calc. and appl. 78—55762
- high current vacuum arc, with axial mag. field, current distrib. meas. 78—87572
- high pressure, discharge, in H_2 (D_2)(inert gas), props., electrode influence, spectroscopic obs. 80—38806
- high pressure gas blast arc local thermal recovery, current zero model calcs. 78—9892
- high speed ground transportation vehicles gas-flow-controlled arcs for power collection 80—70054
- high-current, graphite cathode vaporisation, composition and temp. spectral determ. 78—14228
- high-current, low/intermediate press. arc, anode sheath and pot. drop 79—41901
- high-current, quasi-steady-state, in orifice air flow 77—68887
- high-current arc, negative anode pot. drop, existence region for ignition 77—55187
- high-current arc, positive anode pot. drop 79—41902
- high-current arc electrode vapour influence and estimation 80—70070
- high-current arc-discharge plasma chamber for CTR neutral-beam injection system 77—24105
- high-current constricted-arc anode heat balance obs. 78—71499
- high-current free burning arcs, approximate model 80—70069
- high-current free-burning arc, single-dimens. model 79—1366
- high-current free-burning arcs, magnetically-driven plasma flow model 78—71588
- high-current vacuum arc, mag. constriction effects prior to anode vapour release 77—68888
- high-energy carbon arc, radiation loss measurement 77—7613
- high-intensity, anode boundary layer, one-dimens. anal. 80—96401
- high-intesnity arc, anal. appls. *(Russian)* 78—35772
- high-speed rotating anode disc, spot motion and erosion calc. 78—71498
- hollow arc cathode, with highly ionised dense plasma, props. 79—64951
- hollow cathode, behaviour in pulse conditions *(French)* 77—24231
- hollow cathode, Cs-film coated, intermediate press. operation 80—6305
- hollow cathode, MPD arc config., 0.25-30 kA, current and pot. distribs. 78—9869
- hollow cathode, through-flow arc mode 79—27837
- hollow cathode arc, Langmuir probe meas. for discharge model 78—87533
- hollow cathode arc, plasma column parameters *(French)* 78—9885
- hollow cathode arc, theory 78—67452
- hollow cathode arc discharge, balance equations for active zone processes *(German)* 79—68963
- hollow cathode arc discharge, electron energies, excitation and ionisation speeds *(German)* 78—91170
- hollow cathode arc with fully ionized dense plasma, V-I characts. and other props. 79—14627
- hollow cathode arc with reduced gas flow, operation mode 80—38783
- hollow cathode discharge, expt. determ. of Ar and Ne metastable atom conc. *(French)* 77—31540
- hollow cathode discharge, large size, positive column expts. 77—62431
- hollow-cathode arc discharge, electron energy distrib. and ionisation velocity 78—67534
- hollow-cathode arc discharge impedance/frequency characteristic obs. 78—67536
- hollow-cathode low-pressure discharge critical current determ. 78—67538
- hook meas. in wall-stabilised arc 78—13628
- horizontal, in graphite tube, in inhomogeneous mag. field, mass spectrometric anal. 80—79620
- HV heavy-current arc gap 78—87514
- I-V characteristics of low voltage arc, theory 77—47295
- ignition of high-press. arc with emitting cathode, algorithm for soln. 77—7622
- ignition of high-press. arc with emitting cathode, algorithm soln., rel. to Cs diode 77—7623
- impulse breakdown in air gaps obs., using schlieren studies 78—87518
- impulse spark study using two-wavelength interferometry 80—86391
- inert gas, low-voltage, ionis. mechanism 79—27852
- inert gas hollow cathode arc, mol. beam sampling of metastable atoms as electron temp. probe 80—43967
- inert gas mixture, high-pressure, mixture component separation 77—19797
- inert gas rotating arc meas. in plasma centrifuge 78—75438
- inert gases, low voltage arc theory 80—38809
- insulating materials, high SiO_2 content, degradation due to SF_6 gas dissociation products formed by arc discharges 80—44005
- insulators, HV for transmission lines, power arcs occurring in networks and laboratories, comparisons 80—87983
- intense ion source discharge, delay of arc starvation saturation 78—79457
- interaction with gaseous medium, obs. and calc. 79—77447

arcs continued

- interferometric electric arc motion investigations, between closely spaced insulating walls, in air *(German)* 79—90488
- interrupted vacuum arc, deionisation, expt. 77—27760
- ion source, two-stage discharge type, operational characts. 80—47797
- ion source for fusion reactor, 1000-kVa arc power supply 80—99396
- ion source with energy selection 77—83414
- ion sources, arc-discharge-type, cathode lifetime and stability problems 80—32558
- ISX Tokamak, arcing obs. 80—33836
- joule heating in emitting sites on various nonrefractory arc cathodes 80—100106
- Knudsen arc ignition, plasma form. kinetics, spectroscopic and probe obs. 80—38808
- laminar and turbulent, longitudinal mag. field effect on characts. 78—71565
- light sources of high radiation intensity 80—19084
- liquid cathode arc, cathode sheath model, liquid K in Ar *(French)* 77—1032
- long arc simulated lightning attachment testing using 150 kW Tesla coil 80—70074
- low inductance circuit apparatus, raised frequency current inflammability *(Russian)* 79—86626
- low pressure, electrical noise in longitudinal mag. field *(Russian)* 79—10730
- low pressure, large cross section anode plasma with constricted channels, broad electron beam prod. 80—38840
- low-current vacuum arcs, cathode mechanism, erosion rate calcs. 78—75448
- low-pressure, high performance, investigation 77—35410
- luminous colour control methods in pulsed arc discharges in Ne-Hg lamps *(Japanese)* 80—103214
- LV switching-off process, phenomena *(Slovak)* 78—55761
- magnetically blown flat arc, dynamics of heavy current arcs *(German)* 78—87509
- magnetically confined arc, axial density and temp. var. 78—5966
- magnetically deflected arcs, forward and retrograde motion, cathode oxide film effects 78—87576
- magnetically rotated arc, diameter and rotation rate with superimposed gas flow, investig. 80—38769
- mathematical-physical model, elec. arc parameters, boundary value problem *(Russian)* 77—51249
- matrix effect on arc temperature and electron pressure 79—37565
- meas., natural fluctuations of voltage and emitted light correlation *(French)* 80—19654
- metal cathodes, oxidised and clean, basic erosion processes 80—103211
- metal halide arc, energy balance 79—77440
- metal halide discharges, horizontal burning, parameter meas. techniques 80—38802
- metal vaporizer with cathode spot magnetic confinement 77—77383
- metal vapour arc, cathode spot model, energy balance 78—79484
- metal vapour arc, in vacuum, axial mag. field effects 78—87573
- metal vapour arc in air, electrode damage 79—23472
- metal vapour columnar arc instability, mag. fields effect, up to 67 kA 78—9893
- metal vapour lamp, additive partial pressure determ. from self-reversed spectral line maxima 78—67476
- metal vapour-gas discharges, heavy particle distrib. 80—38782
- metal-halide arc, laser Raman scatt. determ. of local density 77—11424
- methane prod. on electrodes of electrical arcs in ultra high vacuum 77—60065
- methane pyrolysis, AC arc discharge plasma temp., electron density meas. 79—87843
- MHD accelerator, thermodynamic props., mag. field strength, Hall currents in arc region 77—65917
- MHD generator, arc switching near electrodes, elec. current oscills. 79—55569
- MHD generator, plasma interelectrode breakdown, model 79—55572
- MHD generator electrodes in arc regime of operation, math. model 79—86620
- MHD refractory materials, arc spot heat impact degradation *(Japanese)* 78—39819
- micro-arcing, in HV glow discharge, electrode surface effects 79—64955
- microarcing studies in low temp. RF-plasma 80—96407
- momentum generation in high-current arc 78—71586
- motion in narrow chamber, photography with optical waveguide and rotating mirror *(German)* 77—74542
- motion of low-press. arc in strong mag. field 78—83637
- motion of the cathode spot of a vacuum arc 80—54069
- moving arc, microcrater current and spectral fluctuations, simultaneous meas. 80—38828
- moving arc, parametric study of current density distrib. at electrodes 77—24239
- moving arc-air interface, double vortex flow, optical anal. 80—100108
- moving arc-air interface, leading edge thermal wave description 80—100109
- MPD arc, thermal analysis of conical cathode 80—24270
- multiple arc system, stability and discharge structures 79—94832
- multiple-arc system and assessment of persistence of luminosity 79—50906
- narrow slit problems, 1-diemsional 2-zone theory extended *(German)* 79—41890
- near cathode region of non-self-maintained discharge in N flux *(Russian)* 80—54056
- negative grid pulse effects, on Knudsen Cs arc discharge plasma 80—38843
- neutral beam, pulsed, arc (arc filament) power supplies, for fusion reactor 78—70637
- Nier-Bernas type ion source, factors affecting cathode performance 77—18723
- nonstationary electrical arc, expt. study of characts. *(Russian)* 78—14231
- nosetip ablation holography in 10 MW plasma arc facility 78—20621
- nozzle clogging theory 80—38791
- nozzle flow, steady state arcs 78—32664
- nozzle flow arcs, high current, scaling characts. 78—59707
- nozzle gas blast flows with arc heating 79—46502
- orifice arc, density and temp. meas. 78—1937
- origin of arcing in a Tokamak 80—92414
- oscillating arc plasma, optical characts., H_α spectral line profile *(Russian)* 77—19775

arcs continued

- oxide-coated cathodes, emitting sites, effect of Cu-oxide thickness obs. 77—55190
- partial thermodynamic equilibrium, plasma state 80—79608
- periodic processes, spectral emission characts., vidicon system investig. *(Russian)* 78—9848
- perspex confined arc, ablation-induced effects 80—70073
- plasma, electron and heavy particle temp. difference 80—38766
- plasma, influence of additive substance *(German)* 79—54196
- plasma, low-temp. diagnostics by scatt. and resonance fluorescence 78—67482
- plasma, of free jet laminar core, axial flow, strong localised disturbance effect 78—91178
- plasma, rotation speed measurement, in external magnetic field *(German)* 78—42821
- plasma, stabilised by N_2 injection through porous wall, thermodynamic nonequilib., plasma parameters 79—86629
- plasma accelerator, stationary erosion elec. arc type, with mag. cathode spot confinement, flow *(Russian)* 79—98996
- plasma arc contamination by electrode vapour 77—65924
- plasma arc heater, rotating mag. field interaction with gas stabilised discharge 78—71598
- plasma arc jet, effect of negative ion on I-V, enthalpy, cond. characts. 77—24235
- plasma column and surrounding liq. interaction, quantitative anal. under quasiisothermal conditions 80—38788
- plasma diagnostic techniques review, temp. and particle densities determ. *(French)* 80—19651
- plasma electron density, interferometric meas. 78—67479
- plasma electron density meas., high-pressure, by strioscopy and IR absorption *(French)* 80—19620
- plasma electron emitter with constricted arc discharge, characts., anode spots effects 80—70040
- plasma flame, with rectangular cross section, prod. by nozzle *(Japanese)* 78—47108
- plasma flow, velocimetry methods 80—43992
- plasma flow-cold electrode gap, electric breakdown *(Russian)* 78—34280
- plasma generator arc chamber, hydrodynamic struct. 80—1817
- plasma induced, electromotive forces 79—1356
- plasma jet, macroscopic behaviour *(Japanese)* 77—24228
- plasma jet production, fast, from vac. arc cathode spot 80—6309
- plasma magnetohydrodynamics, anal. *(Russian)* 79—32754
- plasma motion in flat and labyrinth channel, velocity calc. 79—4121
- plasma oscillations, in high current low voltage arc discharge *(Russian)* 79—55579
- plasma parameter temporal evolution recording by multi-pulse ruby laser Thomson scatt. 80—14938
- plasma parameters, probe and spectral meas. 80—24273
- plasma parameters of unipolar arc and spectral lines intensity dependence on Li additive 80—73478
- plasma processes, appl. of mag. pinch force 77—15258
- plasma smelting furnace, burning arcs 78—1944
- plasma transport functions by precision arc expts., H Balmer spectrum 80—103187
- plasma-electrode contact processes, microplasma diagnostics 80—59325
- plasmation, high-power elec. arc AC generator, phys. processes and parameters 80—19623
- plasmatron, coaxial, characteristics *(Russian)* 80—24265
- plasmatron, discharge stabilised, by gas blown through porous wall 80—75105
- plasmatron, electric arc fluctuation with vortical arc stabilisation *(Russian)* 78—30493
- plasmatron channel, spatial-temporal pulsations of arc plasma pinch 80—24210
- plasmatron gas average enthalpy, forced heat exchange calcs. *(Russian)* 80—38724
- plasmatron heater, use in apparatus for high-temp. gas flow meas. *(Russian)* 77—39368
- plasmatron melting arc in Ar and CO_2 atmosphere, performance characts., MHD calcs. *(Russian)* 80—38573
- plasmatron with interelectrode insert, characts. 80—44009
- plasmotron, DC, high-power, long-operating, coaxial elec. arc, principles 78—42832
- positive column, nonstationary arc in channel with gas discharge *(Russian)* 80—14950
- positive column of hollow cathode arc, in mag. field, discharge parameters 79—90493
- positive column of hollow cathode arc, in mag. field, model 79—90494
- positive point to plane discharge, determ. of basic quantities during glow to arc transition 79—32837
- post-arc column temp. variation obs. 78—71591
- power overdistribution to AC and DC arcs for melting metals *(Russian)* 80—54055
- pressurised field distortion spark gaps, arc voltage waveforms, electrode material effects 78—87549
- pulsed short arc lamps, characteristics of controllability 78—42400
- pumping by arc column, pressure distribution meas. *(French)* 77—27763
- quasi stationary short arc, anode spot mathematical model temp. field calcs. *(Polish)* 80—19664
- quasistationary plasma, scatt. diagnostics using periodically pulsed UV lasers 78—67481
- radial arc expansion, dynamics 79—19108
- rod/plane gap, air arc channel transient characts. under impulse voltage 78—87544
- rotating high current arc, hot wake investigation 80—1862
- self magnetic field, kink instability, plasma jets production *(Polish)* 80—19662
- selfluminous, schlieren system for time and space resolved photography 80—87471
- sheath structure at an emitting electrode 79—55606
- short pulsed arc, ion density, voltage drop, heat conduction by neutrals 77—4012
- slightly ionised inert gas plasma, hollow arc discharge in cylindrical hollow cathode, theory 80—38810
- slightly oxidated cathode *(Polish)* 80—19663
- snubber using transformer core, theory 80—59315
- spark gap resistance in arcs with semimetallic cathodes 79—23471
- spectral line intensities, discharge mode effects *(Russian)* 77—89343
- spectral line intensity, arc plasma temp. depend. 77—29079
- spectral line intensity, comp. changes effects *(Russian)* 78—75452
- spectral line intensity changes due to plasma comp. changes 79—94838

arcs continued

spectral-line shapes, in high-press. arcs, Tl+Hg, and In+Hg 79−3412
spectrochemical analysis, correlation between anal. signals, plasma parameter changes 79−52828
spectrochemical analysis of biological solns. using wall stabilised arc source 80−41343
spectrography, applic. of equidensitometry *(German)* 77−1962
spectroscopic arc source, with two rot. plasmas in graphite tube 78−40105
spectrum, correl. rels. *(Russian)* 78−70196
spiral form of arc olumn, conditions and range of existence 77−76237
stabilised, elec. field intensity meas., plate probe meas. 80−75095
stability, energy balance with charge conservation 77−11417
steady state, energy eqn. soln., boundary value problem 80−79601
steel, mild, cathode craters, oxide film thickness effects, meas. using SEM *(German)* 78−38558
steel, stainless, cathode craters, oxide film thickness effects, meas. using SEM *(German)* 78−38558
steel, stainless, unipolar arc damage in hot, dense D plasma 79−3235
steel cathode high current free-burning arc 77−19792
Steenbeck principle for arc discharges *(Chinese)* 79−64931
substance evaporation into DC arc plasma, kinetics *(Ukrainian)* 80−33780
surface, insulation as affected by immobile high-current discharge and arc resist. 79−37563
surface MHD waves in arc discharge, low freq. spectrum, instabilities *(Russian)* 77−68762
switchgear, SF$_6$-insulated metal-clad, arcing, decomposition products and pressure rise 80−100101
switchgear, SF$_6$-insulated substations, insulation design and co-ordination 80−100102
synthetic resins, arc resistance tests in various gas insulators *(Japanese)* 80−81250
tanh conductivity arc, thermal and electrical characts. 78−42846
temperature estimation from self-reversed spectral lines 80−75110
temperature meas. in cross-flow arcs 78−22559
temperature meas. using electro-optical device *(Polish)* 79−82121
thermal flux measurement, high, using calorimeter probes 80−13080
thermal ion spectrum, meas. by CW CO$_2$ laser 90° scatt. 78−67480
thermal shock fracture toughness eval. by arc discharge heating 78−72835
thermoelectric characts. in porous channel 79−32835
thin arc, stability boundary theory 80−59324
Thomson scattering with high background level of plasma scattering 80−43979
three-phase high performance, power source external volt-ampere characts. determ. using graphical analysis method 80−79594
three-phase plasma arc combustion *(Russian)* 77−55183
threshold current for glow to arc transition 77−27771
Tokamak, DITE, arcing, time-resolved meas. 80−10436
Tokamak, Diva, metal impurities origin, arcing ion sputtering, evap. 78−59691
Tokamak, electrically isolated target, formation of arcing, role of runaway electrons 80−64764
Tokamak, T-10, arc tracks, wall erosion by unipolar arcs 80−64811
Tokamak limiter, surface observation, infrared techniques 80−38693
Tokamak plasma, metal impurities due to arcing 78−42787
Tokamak wall, model of unipolar arc 79−657
tornado, contrib. of vortex-stabilised arc to energy 78−53711
transient contracted cold-cathode arc characts. in mag. field 80−24291
transition corona effect arc, cathode zone effect 78−1934
transport coefficients determ. from high press. arc meas. 77−47156
transport of atoms in arc electrode channel *(Russian)* 77−52725
triggered vacuum gap, anode spot formation, characts. 77−39485
turbulent, in channel with distributed gas flow, positive column anal. *(Russian)* 80−14949
turbulent AC arc, temp. diagnostics, radial distribs. 77−24240
turbulent flow, 20 to 200 m/s air current *(Russian)* 77−65921
two-dimensional constant property arc, extensions 77−24225
underwater arc, prebreakdown stage, energy characts. 78−5978
unipolar, axial distrib. of Tl atoms, influence of Li conc. 80−19656
vacuum, formation and development obs. using streak camera *(French)* 77−7609
vacuum, secondary electron emission by multiply charged ions 77−19791
vacuum, voltage, self-generated mag. field, current distrib. 78−30508
vacuum arc, cathode spot motion in inhomogeneous mag. field *(Russian)* 78−22593
vacuum arc, cathode vapour jet dynamics 78−5977
vacuum arc, electrode heating by cathode spot 79−55593
vacuum arc, energy dissipation in cathode 78−5970
vacuum arc, high current, novel electrode geometry 78−1933
vacuum arc, reflection of metal ions 77−35423
vacuum arc, sputtering from cathode spot region 79−82113
vacuum arc anode spot, ion currents and interaction with axial mag. fields 78−75469
vacuum arc anode spot form., threshold current time depend. 78−87515
vacuum arc at anode spot form. threshold, electron density meas. 79−55552
vacuum arc cathode, cathode spot phenomena, classification 77−24223
vacuum arc cathode plasma interaction with transverse mag. fields 78−75468
vacuum arc cathode spot dynamic models 78−75481
vacuum arc chopping current *(German)* 80−44004
vacuum arc in Cu cathode region, current parameters, theory 80−54068
vacuum arc plasma, fault current limiter mode, temp. distrib. diagnostics 78−9851
vacuum arc plasma flow in plasma-optical system *(Russian)* 80−106992
vacuum arc retrograde motion in mag. field, Hall effect study 80−6315
vacuum arcs, anode spot form., model 80−33830
vacuum arcs at high currents, anodic contraction, study *(German)* 79−73057
vacuum chamber, for arc investigations *(Polish)* 79−82120
vacuum gap following high-current arcing, dielec. recovery strength 78−9891
vacuum vibrator arc ion source, multiply-charged species rel. abundance distribs. 77−61151
variable current, element concs. during interruption, time depend. *(Russian)* 78−22597
vertical arcs stabilised by natural convection, props. 79−55589
voltage across low-current vac. arc 79−19100
voltage gradient in fully-developed turbulent air flow 78−71597

arcs continued

voltage-current characts. MHD eqns., anal. 80−38815
wall stabilised, spatially resolved electrical probe meas. 77−84516
wall stabilised arc, current step changes, conductance transient effects 78−87547
wall stabilised column in air, field intensity and current relationship 77−80380
wall-stabilised, electrical characts., effects of laminar and turbulent flows 80−1870
wall-stabilised, free recovery with imposed laminar and turbulent flows 80−59321
wall-stabilised arc, N atom Stark broadened VUV lines 78−90107
wall-stabilised arc conductivities with Cu vapour contamination 78−75458
wall-stabilized arc, in transverse magnetic field, velocity and temperature field determination 78−38569
welding arcs, gas velocity fields modelling 80−75039
wire-plane electrodes, breakdown voltage, effect of vacuum conditions 80−64798
xenon filled DC arcs, with and without focal spot, electric behaviour *(German)* 80−64800
Ag electrode, evaporation rate from cathode spot in vac. arcs. 80−49024
Al anode spot of vacuum arc 80−107006
Al, vacuum arc, excited state density from line intensities 80−96404
Al, vacuum arc, excited state density theory 80−100107
AlO, in arc, normalised temperature, localised emission, aureoles *(German)* 77−62413
Al$_2$O$_3$, anodised film, arc cathode root initiation, electron emission, UV radn. effects 78−2985
Al$_2$O$_3$, anodised film, charge storage, UV radn. effect on electron emission arc roots 78−6827
Al$_2$O$_3$, film, switching times and arc cathode emitting site lifetimes 80−59332
Ar, after-arc phenomena *(Japanese)* 77−58916
Ar arc, high-press., in longitudinal mag. field, spiral wall characts. 77−65919
Ar arc, non-LTE, electron balance, temp. and density *(French)* 78−1796
Ar arc, plasma parameters determ. by laser scatt. 79−32812
Ar arc burning, local densities meas. for metastable atoms *(French)* 77−4017
Ar arc deviation from Saha-Boltzmann equilibrium, heavy-particle effects 78−67596
Ar arc discharge atomic excitation, effect of ion conversion *(Russian)* 79−10731
Ar arc heating, high-pressure complex heat exchange expt. *(Russian)* 80−75112
Ar arc plasma, circuit-breaking, anode layer, optical diagnostics 77−80351
Ar arc plasma, decaying, temporal changes of particle densities and temps. 79−64940
Ar, arc plasma, MTE continuum emission coeff. relation for atom. press. 77−31432
Ar arc plasma, partial LTE for lower excited levels of ArI 80−79565
Ar arc plasma, temp. meas. by submillimeter diagnostic technique 80−38853
Ar arc plasmas, steady-state and decaying, mol. gas impurities 80−103177
Ar arc with hot W cathode, electron emission mechanisms 77−24224
Ar arcjet plume, freely expanding, excited state distrib. function 79−98881
Ar arcs in supersonic flow, numerical analysis 80−38776
Ar atmosphere, controlled, line intensities of metals *(Russian)* 77−56300
Ar atmospheric arc plasma deviation from LTE 78−67604
Ar, atmospheric arc-jet plasma, ζ-function evaluation, near 10^4K 77−84497
Ar, atom-atom collisions effect on thermal equilib., model 79−1360
Ar cascade arc, wall-stabilised, calibration of radiation detectors in VUV 79−80679
Ar cascade arc light emission, effect of pulsed microwave field 78−67599
Ar, cylindrically symmetric arc, atm. press., steady-state stability model 78−38561
Ar, decaying arc, electron cooling, diffusion, ionisation and recombination processes 80−33841
Ar decaying arc, numerical simulation 80−38767
Ar, decaying plasma arc, electron disappearance mechanism 80−38765
Ar full circle arc, mass flow field investig. 80−38797
Ar, HF discharge, arc type, spectral parameters 80−1873
Ar, high current, interferometric and spectroscopic study 80−59275
Ar high density plasma, highly excited atomic levels, spectral-line-blending study 80−48969
Ar, high-press., elec. cond., nonideal effects, IR continuum absorption obs. 80−38558
Ar high-pressure arc plasma, IR continuum emission obs. 78−71604
Ar high-pressure helical arc phase velocity in longitudinal mag. field 78−71594
Ar high-pressure plasma elec. conductivity obs. 78−71448
Ar, hollow cathode, in mag. field up to 2 k0e, plasma parameters 80−6306
Ar, hollow cathode arc discharge, collective scatt. meas., turbulence 80−48978
Ar I and II transition probability determ. from improved branching ratio obs. 78−66514
Ar I arc plasma, excited atom density meas., Saha-Boltzmann equilib. 80−926
Ar II arcs, transition probabilities, statistical inference 80−106357
Ar III, in pulsed arc plasma, ξ, factor determ. 79−4116
Ar ion system, collisional radiative model 78−71080
Ar laminar stream in electric arc gas heater, numerical calc. of arc parameters *(Russian)* 77−58911
Ar, low voltage arc, ionisation waves, hydrodynamical model including inelastic interaction 78−87563
Ar low voltage arc, positive column ionisation waves, hydrodynamic model 78−79481
Ar magnetic helical arc electrode, for MHD generator, visible, RF and probe diagnostics 78−9867
Ar, metastable atom density changes during arc interruption 77−51250
Ar mini-arc as spectral radiance secondary standard 77−34921
Ar neutral system collisional radiation model 78−67535

arcs continued
Ar, new cathode shape for UV spectral radiance transfer standard *(French)* 80—38082
Ar, parameters variation during extinction obs., by spectroscopy and laser interferometry *(French)* 80—19653
Ar plasma, constricted electric arc, iteration method anal. 79—90484
Ar, plasma, electron-ion recombination in extinguishing arc 78—59687
Ar plasma, viscosity determ. by stabilised elec. arc. 79—41873
Ar, plasma arc, dynamic charact., electron energy relaxation effect 80—38774
Ar, plasma arc discharge, contamination near Cu electrode *(French)* 79—77443
Ar, plasma column of hollow cathode arc, collisional radiative model of ion system 80—38749
Ar plasma diagnostic method for partial LTE 78—67606
Ar plasma MHD arcjet, recombination lasing 77—65588
Ar, radial temp. profile calc. 78—67457
Ar, radially directed, steadily rotating plasma disc form. 77—76216
Ar, stabilised electric arc, laminar plasma flow section, length and characts. 78—91177
Ar, submillimetre diagnostics, active, of Ar arc, data numerical anal. 80—48979
Ar, vacuum arc discharge, lasing action 79—18402
Ar, wall-confined, nonequilibrium effects 80—70058
Ar wall-stabilised arc electron and heavy-particle temp. variations 78—67602
Ar, wall-stabilized arcs, of medium pressures, axial pot. meas. 78—30499
Ar-air, stabilised, spectroscopic methods of temp. meas. *(Russian)* 80—38854
Ar-C arc, C I lines Stark broadening, electron density and temp. meas. 77—10634
Ar-cascade arc, spectral sensitivity of radiation detectors in VUV range, report *(German)* 78—82037
Ar-liquid K cathode arc, dense plasma prod., cathode erosion rate estimation *(French)* 80—44056
Ar-N_2 mixtures, DC arc, energy balance of electrons 78—42797
Au electrode, evaporation rate from cathode spot in vac. arcs. 80—49024
C cathode damage and vapour/thermionic arc transition obs. 78—71603
C electrode damage, and current densities 79—23468
C fibre layers on arc anodes, props. and cooling behaviour 79—52245
C, in air, electron density meas. by CO_2 laser interferometry *(Japanese)* 80—28822
C, low current for props. of graphite near sublimation temp. 79—50901
C plasma stream condensation, with RF pot., diamond-like film deposition 79—15612
C^+, vacuum arc source 79—21853
CN, in arc, normalised temperature, localised emission, aureoles *(German)* 77—62413
CN molecular bands in N_2 and air-O_2 arcs, CN origin, band identification 80—38803
CO-Ar(-N_2), high press., arc assisted elec. discharges 77—3606
CO_2, laser, TEA discharge, arc suppression 77—7056
CO_2 laser discharge, TEA, glow form. and glow-to-arc transitions, high speed camera obs. 78—25846
CO_2 laser discharges, electrode surface field and preionisation effects on spatial distrib. of arcs 78—63054
CO_2 pin-bar TEA laser, internal arcing, ultra high speed photography 78—9357
CO_2-N_2-He system, CO_2 TEA laser discharge development, high-speed-camera investigation 79—55109
CaH, in RF-excited heat pipe oven, efficient arc source 78—63162
Cd cathodes arced in vacuum, erosion structs. 80—1872
Cd electrode, evaporation rate from cathode spot in vacuum arcs 79—37566
Cl I, wall-stabilised arc, absolute transition probabilities, 5300-6850 Å 78—9105
Cl^- free-bound continuum radiation threshold broadening obs. 78—71579
Cl_2-arc, low temp., visible and IR continuum radiation 80—38784
Cr, arc, steady, vac., plasma ion mass and energy diagnostics 78—51385
Cr electrodes, arcing and breakdown meas. in vacuum 77—24238
Cs arc, low-voltage hot-cathode, plasma production and props., review 77—27766
Cs, atomic excited states population in arc 78—26368
Cs, dense plasma, elec. and radiative heat cond. evaluation 78—71452
Cs fully-ionised plasma hollow-cathode arc discharge theory 78—67533
Cs, Knudsen arc, electron beam heating and ionisation 80—75114
Cs low-temperature erosionless cathode for high current densities 79—64953
Cs plasma, elec. and radiative thermal conds., expt. data anal. method 78—42717
Cs plasma, ohmic heating, electrical conduction temp. depend. 78—71442
Cs, quenching at low Cs press. 78—5976
Cs vapour, nearly saturated, prebreakdown elec. cond. 80—48841
Cs vapour, oscill. in low voltage arc discharge growth 78—51386
Cs-Ba, high current Knudsen arc discharge, spontaneous extinction, optical diagnostics 80—44044
Cs-Ba triode arc switch, high-current, low-voltage, pulsed control 78—71551
Cu arc, fluctuating, diagnostics using spectral-image photographs *(Japanese)* 79—41896
Cu, arc, steady, vac., plasma ion mass and energy diagnostics 78—51385
Cu arc cathode with 100 nm thick oxide film, energy balance components 77—39481
Cu, cathode, oxide-coated, arc erosion rates, SEM expts. 77—55185
Cu cathode craters, oxide film thickness effects, meas. using SEM *(German)* 78—38558
Cu cathode spot, MHD generator channel conditions, temp. calc. 78—26359
Cu cathode vacuum arc, cathode spot and cell areas, meas. 80—96405
Cu cathode with oxide film, emitting site lifetimes and current densities, meas. 77—27761
Cu cathodes, erosion, vacuum to atmospheric press. arcs 78—79482
Cu cathodes arced in vacuum, erosion structs. 80—1872
Cu electrode, cryogenic, multiple anode spots during arc discharge 79—90485
Cu vacuum arc, erosion products from cathode spot region 78—75447
Cu, vapour production method, hollow cathode arc., Ar buffer gas 78—86981
Cu-N_2, effect of Cu vapour on wall stabilised arc extinguishing times 78—87548

arcs continued
CuO, sputtered pulse discharge, Cu vap. production, laser appl. *(Russian)* 77—84556
Cu_2O films arc cathode emission study 78—23583
Cu_2O, sputtered pulse discharge, Cu vap. production, laser appl. *(Russian)* 77—84556
DyI_3/CsI/Hg arc, oscillations induced by external mag. field, arc constriction 79—60205
DyI_3-Hg arc discharge plasma, spectroscopic study 80—54033
Fe, arc, steady, vac., plasma ion mass and energy diagnostics 78—51385
Fe electrode, evaporation rate from cathode spot in vacuum arcs 79—37566
Fe oxides, disperse, chemical reduction in discharges *(Russian)* 78—95915
Fe_3O_4-Cr_2O_3-Ni_2O mixture, reduction by gases heated by electric arc discharge *(Russian)* 78—15704
H, 1.06 μm laser scatt. 78—51347
H arc, electron density, interferometric determ., refr. index calc. in high press. 80—24284
H arc, laser Thomson scatt., ion temp. determ. 79—23453
H arc axial ground state population meas. 78—67598
H Balmer lines, plasma-broadening in wall-stabilised arc, low electron density 80—43891
H, contracted low-press. arc, electron energy distrib. 78—18477
H, contracted low-pressure arc, electron energy distrib. 78—18478
H evacuation at 25 m^3/sec, arc appl. 78—21144
H high power arc, standard source of continuum radiation, 53-92 nm 80—44054
H high-power arc as continuum radiation standard source, 53 to 92 nm, VUV radiometry 79—94311
H isotope separation in DC-arc plasma, mass spectrometric anal. 79—90457
H, magnetically stabilised, CO_2 laser scatt., spectrally resolved meas. 77—84504
H plasma form., in arc discharge, dissoc. excitation role 77—84398
H spark gap arc discharges, laser-triggered, electron density meas. 80—64822
H^- ion yield from duoplasmatron discharge 78—75382
H_2 arc, at. and mol. no. densities meas. by VUV spectroscopy 79—94828
H_2 arc plasma Balmer spectrum decay and two-fluid model 78—67603
H_2, dense plasma, Balmer spectrum near photorecombination threshold, press. depend. 80—38569
H_2 monoplasmatron arc plasma, electrokinetic parameters space distrib. *(Russian)* 80—53925
H_2 stabilised arc as vacuum UV radiation standard for 600 to 900 Å 78—66879
H_2-Ar arc, $H_\alpha(D_\alpha)$ Stark broadening obs. 79—36582
H_α line Stark profiles in low-density arc, exptl. discrepancies 78—67470
$H\alpha(D\alpha)$ plasma red shift meas. in Ar arc, ion dynamic depend. 80—10364
He, arc plasma Stark profile, heavy-particle temp. 79—46484
He continuum radiation, 109 to 540 nm, meas. in arc plasma *(German)* 80—106932
He continuum radiation emission obs. to near vacuum UV 78—71582
He, duoplasmatron arc, ionisation meas., line intensity ratios 80—54060
He, fast electron energy distrib. in positive column and negative glow 80—38764
He flowing discharge, glow/arc transition and cathode-zone wave structure obs. 78—75475
He, high current arc in capillary, dynamic behaviour 77—4002
He high-current pulse discharge plasma partial LTE disturbances 78—67600
He I plasma arc, spectral line profiles, $\lambda\lambda=4471$ Å and 4922 Å *(French)* 78—83625
He pulsed arc, Thomson scatt. diagnostics 80—24297
He^+, excitation in hollow cathode discharge, rel. to plasma electron density and temp. 77—7589
He-Ai-H arc plasma, nonequilib. effects, spectroscopic diagnostics 77—76191
Hg arc plasma, azimuthal RF cond. meas. by eddy current effect, expt. 77—1029
Hg, continuum radiation meas. 77—62416
Hg DC vacuum arc anchored cathode spot current density obs. 78—75467
Hg, HF discharge mode two-valued depend. on arcing voltage, geometric reson. *(Russian)* 77—47283
Hg low-pressure arc, positive column, heat flow processes 80—24135
Hg vacuum arc, vapour-cone angles of neutrals and ions emanating from cathode 77—4007
Hg vapour, optically pumped positive columm, collisional processes 78—87499
Hg, vertical high-press. arcs, convection 78—59701
Ir electrode, evaporation rate from cathode spot in vac. arcs. 80—49024
K, liquid cathode arc in AR atom., plasma prod. and parameters, cathode sheath model 77—4003
K plasma in arc and capillary devices, optical props. 80—24244
Kr arc discharge, radiative characts. computational model requirements 80—64812
Kr arc spectrum, isotope shifts in near IR lines 79—72257
Kr I lines from wall-stabilised arc measurements, transition probabilities 78—22569
Kr, plasma, high-press. arc discharge, elec. cond. 80—59181
Kr(-He) arc, wall-stabilised, atm. press. 79—46503
Mg break arc, LV, low current, electron density, temp., local thermodynamic equilib. 78—9878
MgH, in RF-excited heat pipe oven, efficient arc source 78—63162
Mo, arc, steady, vac., plasma ion mass and energy diagnostics 78—51385
Mo, arc, vac., stabilised, plasma props. 78—51384
Mo cathodes arced in vacuum, erosion structs. 80—1872
Mo, unipolar arc damage in hot, dense D plasma 79—3235
Mo-Cu cathode, spot motion and nature in UHV 80—79597
N arc, radiation transport 78—79486
N arcs, spectroscopic meas. rel. to LTE 77—76200
N, high intensity arcs, anode contraction region modeling 80—103210
N_2 arc, magnetically stabilised cross-flow, temp. and flow fields meas. 80—54054
N_2 arc, plasma parameters determ. by laser scatt. 79—32812
N_2, arc jet enthalpy meas. by fast miniature total calorimetric probe 78—67486
N_2 arc plasma, recombination with gas glow, spectroscopic diagnostics 77—7626

arcs continued

N_2 arc plasma, stabilised by gas injection, thermochem. nonequil., particle excitation, vibr. temps. 80−19634
N_2 arc vacuum UV radiation loss calc. 78−71581
N_2 high intensity arc anode region, temp., current density, flow field, numerical anal. 78−9827
N_2, laminar flow, equilib. composition deviation 80−24274
N_2 plasma jet anode root behaviour rel. to hollow-anode thermal insulation 78−71554
N_2, spectroscopic meas. w.r.t. LTE 77−19786
N_2-CO_2 mixture non-self-sustained discharge ionisation instabilities, obs. 78−71610
N_2-CO_2-H_2O gasdynamic laser mixture, electron beam diagnostics 77−83845
N_2-Cu arc plasma, transport coeffs. 80−96344
N_2-H_2 arc, bent and rot., flow mechanism 80−70047
Na arc plasma, dense, high-temp., near-reson. light scatt., collision-induced fluoresc. 77−1019
Na, high press. arc, plasma spectral change mechanism 79−82093
Na high-pressure arc, time-depend. plasma temp. meas. 77−68866
Na-Hg-Xe cylindrical high pressure arc discharge, acoustic resonance 78−67454
Nb, unipolar arc damage in hot, dense D plasma 79−3235
Ne II line Stark broadening in pulsed arc, obs. 78−67469
Ne, wall stabilised arc column in longit. mag. field, screw instability 78−87551
Ni II, oscillator strengths, near UV lines, wall-stabilized arc meas. 78−42003
Ni, unipolar arc damage in hot, dense D plasma 79−3235
NiO single crystals, growth by material transfer in DC arc, and X-ray anal. 79−52113
O^-, spectra in pure O arc plasma, 2000-9000 Å, 9000K 79−32750
Pb particles, evaporation in arc plasma, integral eqn. method calcs. 78−1942
Pd electrode, evaporation rate from cathode spot in vac. arcs. 80−49024
Rh electrode, evaporation rate from cathode spot in vac. arcs. 80−49024
SF_6, 40 kA, time-resolved temp. and radius meas. using rapid-scanning polychromator 79−50907
SF_6, arc discharge, decomposition products for SF_6 with H_2O and organic gas contaminants 79−10743
SF_6 arcs in axial flow at const. press., steady-state characts. 78−1940
SF_6 axially blown arc, current-zero behaviour, theoretical model 80−38789
SF_6, particle densities in decaying plasma 78−75442
SF_6 plasma column, in Maecker type arc, diagnostics and model *(French)* 80−19652
SF_6 temp. determ. accounting for demixing 80−70057
SF_6+H_2 mixture, equilib. composition and transport props., 300 to 15000K 77−24051
Si III, IV, Stark line broadening in pulsed arc, plasma diagnostics 78−944
Sn I, Sn II, wall-stabilised arc, absolute transition probabilities, 5300-6850 Å 78−9105
SnO_2 coated glass, surface elec. breakdown 80−25303
Ta hollow arc cathode, emission current density 78−76574
Ta, unipolar arc damage in hot, dense D plasma 79−3235
Ti, arc, steady, vac., plasma ion mass and energy diagnostics 78−51385
Ti I, oscillator strengths, hook and emission meas. 78−42002
UF_6 arc emission discharges, compared to UI plasma emission coeff. 80−64693
W cathodes arced in vacuum, erosion structs. 80−1872
W electrodes, C segregation and arc damage 80−64795
W exploding wire, peripheral arc initiation 78−87559
W, unipolar arc damage in hot, dense D plasma 79−3235
Xe, arc, wall-stabilised, dynamic analysis, radiation transport 80−44066
Xe arc discharge, radiative characts. computational model requirements 80−64812
Xe I, arc spectrum, press. shifts and broadenings in visible and near i.r. 77−440
Xe I level deviation from Boltzmann population in steady-state plasma 78−67605
Xe, plasma, high-press. arc discharge, elec. cond. 80−59181
Xe short-arc lamp, current modulated, arc forms and instability 80−96399
Zn electrode, evaporation rate from cathode spot in vacuum arcs 79−37566
Zn I, relative populations in arc, sputtering and gas phase collisions 80−934
ZrD, electrodes with externally ignited vacuum arc source of D^+ ions 80−33845

area measurement

biological planimeter for use with mechanical digital counters 78−40448
Brunauer, Emmett and Taylor surface area meas. apparatus 79−35666
Brunauer-Emmett-Teller surface areas, automatic low-cost determ. 77−55441
calorimetric determination of surface area, modified Harkins and Jura procedure 79−35667
cerebral slices from rat brain, area changes during prep. 79−25166
gas-liquid dispersion, comparison of methods for meas. of interface areas 77−63962
membrane surface area, stereological method for freeze-fracture preps. 77−64158
optical planimeter metrological characteristic test results 78−79148
pendant drops, profile area meas. 78−81943
powder, pharmaceutical, surface area determ., new instrument 77−26280
powder compacts, intermediate stage sintering, surface area reduction kinetics, anal. 78−76614
powder specific surface, X-ray determ. method 80−47012
powders, specific surface measurement, chromatographic method 77−77859
powders, surface area meas., chemical planimetry method, appl. to silicates, oxides *(German)* 79−88915
powders, surface area measurement using Knudsen diffusional flow of gas 79−40536
reservoir surface area from LANDSAT imagery 79−66834
spot size estimate in diffr. pattern of scattered field 80−95789
surface area of fine aggregate in bituminous mixtures, calc. 77−77689
surface balance, monolayer parameters meas. in radiation field 78−82092
tensile test specimens, cylindrical, area reduction determ. 79−100306

area measurement continued

tibia, human, simplified method of radiographic anal. of its cross-section, anthropometric correls. 80−89827
TV photomicrography, instrument for meas. and displaying slide mounted samples 80−195
two-phase systems, mean specific surface area, light transmission meas. *(German)* 78−89431
Al_2O_3, plasmochemical synthesis, oxidised from metals, exam. of props. 80−2984
CuO, plasmochemical synthesis, oxidised from metals, exam. of props. 80−2984
CuO powder, surface area determ. by adsorpt. of stearic acid and pyridine 80−107636
Fe ore, adsorption methods for determ. of specific surface 78−21096
Fe_2O_3, plasmochemical synthesis, oxidised from metals, exam. of props. 80−2984
Fe_2O_3 powder, heat of adsorpt. of stearic acid, surface area meas., flow microcalorimetry 78−81974
MgO, plasmochemical synthesis, oxidised from metals, exam. of props. 80−2984
MgO powder, surface area determ. by adsorpt. of stearic acid and pyridine 80−107636
NiO, plasmochemical synthesis, oxidised from metals, exam. of props. 80−2984
Pt electrodes for elec. stimulation, exposed electrode area determ. 77−86704
TiO_2, plasmochemical synthesis, oxidised from metals, exam. of props. 80−2984
ZnO, plasmochemical synthesis, oxidised from metals, exam. of props. 80−2984

argon

see also nuclei with ......
acoustic microscopy in high-pressure gases 80−43561
adiabatic compression to 25 kbar 79−86549
adsorbed dense monolayer on graphite cleavage face, phase transition 78−56034
adsorbed films on MnI_2 and PbI_2 cleavage faces, layer-like charact., neutron diffr. obs. 79−86994
adsorbed layers, two-dimensional structs., modified cell theory 80−20033
adsorbed monolayer on graphite, substrate-induced strain and orientational ordering 79−82460
adsorbed monolayers, on graphite, equilib. config. and lattice consts. 80−54524
adsorbed on Ag, curved surface physisorption, small spherical particles or pores 77−7964
adsorbed on Al, differential refl. spectroscopy, local field effect 80−80811
adsorbed on graphite, multilayer adsorbed films, mol. theory 80−80058
adsorbed on graphite, nonregistered-registered phase transition 80−39414
adsorbed on graphite, orientational epitaxy in self-consistent phonon approx. 79−95261
adsorbed on graphite, overlayer-substrate spacing, LEED determ. 80−103579
adsorption, of first layer on graphite, 55 to 62K 79−28197
adsorption, of sintered SnO_2, meas. and calcs. 77−69164
adsorption, on graphitised carbon black, surface excess isotherms, gravimetric determ. 78−51816
adsorption, on graphon, high press. and temp., gas density profile theory 78−67903
adsorption, on solid CO_2 surface, density functional theory, computer simulation 80−24735
adsorption, on Xe-plated graphite, virial coeffs. and interatomic pots. 77−9125
adsorption heat on NaCl 78−26772
adsorption heat on NaCl crystal, variation 77−85049
adsorption isotherm, determ. of porous texture of solids 79−77897
adsorption on activated C, vol. adsorption capacity 78−75933
adsorption on BN, thermodynamic values calc. from pot. parameters *(German)* 79−95268
adsorption on $CdCl_2$ cleavage face, two-dimens. condensation of second adlayer 79−99413
adsorption on Ge (111) plane, adsorpt. pot. 78−26768
adsorption on graphite, Lennard-Jones 9:3 adsorptive system, Percus-Yevick and hypernetted chain theories 80−20030
adsorption on graphite, monolayer two-dimensional phase change, calorimetric investig. 77−47669
adsorption on graphite, Monte Carlo calcs., grand canonical ensemble, long-range corrections 78−30826
adsorption on graphite, orientational ordering of incommensurate monolayers, LEED obs. 78−95233
adsorption on graphitised C black, eqns. of state predictions vs. expt. 79−69223
adsorption on metal surfaces, density functional approach 77−85061
adsorption on NaCl, energy distrib. using numerical algorithm HILDA 77−55443
adsorption on NaCl, gas-solid virial anal. 77−55444
adsorption on Pt, thermal accommodation coeffs., 300 to 1350K 80−30272
adsorption on pure and SiO_2-coated TiO_2, 77.4K, microcalorimetry obs. 80−80062
adsorption potential energies on NaBr and KBr, calc. 78−71993
aerodynamic isotope separation technique based on vel. slip in freejet expansions 80−19441
after-arc phenomena, in Ar *(Japanese)* 77−58916
afterflow stability boundaries, plasma oscillation modes in mag. field 78−38486
afterglow, electron-atom bremsstrahlung continuum, afterglow decay *(German)* 78−83626
afterglow, low press. discharge afterglow, dissoc. recombination, microwave diagnostics 78−9876
afterglow, spectra and microphotograms, dissociative recombinations 78−26365
afterglow, stationary, singly charged atomic ion obs. 80−38757
alkali metal salt solution, Ar saturated, sonoluminesc. as acoustic cavitation probe 79−60437
n-alkane+Ar mixtures, intermol. pot. using Kihara model with spherical cores 77−54591
anode sheath, crossed field low press. discharge in magnetron and Penning cell 77−11432

argon continued
aqueous soln., dil., energy and struct., pair pot. energy function, Monte Carlo calc. 80—54107
Ar_3^+, visible photoabsorpt., pot. energy surface 79—98112
$AR+Mg_2$, matrix isolated laser photoluminescence spectra, electronic absorpt., emission, vibronic and vibr. relax. 78—82744
arc, cascade, wall-stabilised, calibration of radiation detectors in VUV 79—80679
arc, cylindrically symmetric, atm. press., steady-state stability model 78—38561
arc, decaying, electron cooling, diffusion, ionisation and recombination processes 80—33841
arc, graphite, in Ar flow, meas. of anode voltage drop 80—84022
arc, $H\alpha(D_\alpha)$ plasma red shift meas., ion dynamic depend. 80—10364
arc, high current, interferometric and spectroscopic study 80—59275
arc, high-press., in longitudinal mag. field, spiral wall characts. 77—65919
arc, hollow cathode, in mag. field up to 2 k0e, plasma parameters 80—6306
arc, Lyman-α wings Stark broadening 77—27721
arc, non-LTE, electron balance, temp. and density *(French)* 78—1796
arc, plasma parameters determ. by laser scatt. 79—32812
arc, radial temp. profile calc. 78—67457
arc, radially directed, steadily rotating plasma disc form. 77—76216
arc, stabilised laminar plasma flow section, length and characts. 78—91177
arc, turbulent AC, temp. diagnostics, radial distribs. 77—24240
arc, wall-stabilized, axial pot. meas. 78—30499
arc arc plasma, temp. meas. by submillimeter diagnostic technique 80—38853
arc column, helical instability limits 78—71564
arc deviation from Saha-Boltzmann equilibrium, heavy-particle effects 78—67596
arc discharge, atom-atom collisions effect on thermal equilib., model 79—1360
arc discharge, parameters variation during extinction obs., by spectroscopy and laser interferometry *(French)* 80—19653
arc discharge atomic excitation, effect of ion conversion *(Russian)* 79—10731
arc electrode, magnetic, helical, for MHD generator, visible RF and probe diagnostics 78—9867
arc heating, high-pressure complex heat exchange expt. *(Russian)* 80—75112
arc plasma, circuit-breaking, anode layer, optical diagnostics 77—80351
arc plasma, decaying, temporal changes of particle densities and temps. 79—64940
arc plasma, electron and heavy particle temp. difference 80—38766
arc plasma, MTE continuum emission coeff. relation for atom. press. 77—31432
arc plasma, partial LTE for lower excited levels of ArI 80—79565
arc plasmas, steady-state and decaying, mol. gas impurities 80—103177
arc with hot W cathode, electron emission mechanisms 77—24224
arcs, transition probabilities, statistical inference 80—106357
arcs in supersonic flow, numerical analysis 80—38776
associative ionisation mechanisms 77—32781
atmosphere isotopic composition in pre-Cambrian, degassing from shungite 80—85749
atmospheric arc plasma deviation from LTE 78—67604
atmospheric gases condensation on cold metal surfaces, nucleation barrier 78—22838
atom, 78—78671
atom, 0-10 eV photoelectron spectra obs., new differential retarding field analyser characts. 77—41735
atom, $1s2s3p^4P_{5/2}^o$-state, relativistic effects and config. mixing 79—45640
atom, $2p_{3/2}$ subshell impact ionis., coincidence exptl. method, theory 80—1066
atom, $2p^6$ shell, oscillator strength, photoionisation cross sections, electron shell alterations determ. *(Russian)* 80—58144
atom, $3p^5$5p config. aligned in discharge, interf. signals, lifetimes and collision cross sections 78—70796
atom, 3s electron partial photoionis. cross section, branching ratios 78—29765
atom, 40 keV electron scatt. 7-200 mrad, relativistic and electron correlation effects 77—34760
atom, (e,2e) coplanar symmetry reaction, factorised distorted-wave approx., 400-1200 eV 78—55246
atom, absolute photoionis. cross sections for VUV region 77—46547
atom, and ions, two and three-electron Auger transition, with vacancies in 2p-shell 79—63972
atom, and isoelectronic sequence, E1 transitions, relativistic oscill. strengths 78—949
atom, approximate relativistic Hartree-Fock eqns., soln. using Slater-type functions 80—58168
atom, autoionising levels excited by heavy ion impact 79—13804
atom, beam-foil populations, charge state distribs., independent electron model 77—19035
atom, cascade effects on Zeeman quantum beats 79—89631
atom, CI calcs. using modified virtual orbitals 80—58163
atom, closed shell, Jastrow wave functions, var. calcs. 80—83249
atom, clustering of atoms around positron and positive ions 78—55270
atom, collision processes, photoionisation mass spectra obs. 79—31479
atom, collisional depolarisation of selectively excited 2p levels *(French)* 78—86830
atom, Compton profile, local density approx., Kohn-Sham self consistent scheme 78—94193
atom, Compton profiles using Gaussian expansion of at. orbitals 80—945
atom, correlation energies, second-order, by variational-perturbation study 80—908
atom, double ionisation by electron impact, soft X-ray emission *(Russian)* 77—34766
atom, double photoionis. cross section, calc. 77—14397
atom, elastic electron and positron scatt., optical model theory 77—19076
atom, electron and positron scattering, elastic, 100 and 500 eV, second-order eikonal approx. 78—78814
atom, electron elastic scatt., differential cross-section meas. 77—3458
atom, electron elastic scatt., phaseshift anal. of ang. distribs. 79—22833
atom, electron elastic scatt., resonance struct. 77—50532
atom, electron energy loss spectra 80—62740
atom, electron impact, elastic scatt. calcs. 78—25708
atom, electron impact, L X-ray spectrum, radiative Auger transitions 80—58227

argon continued
atom, electron impact, near threshold UV-emitting level excitation 78 -25711
atom, electron impact, struct. near $L_{2,3}$ edges 77—75083
atom, electron impact autoionisation, cross-section parametrisation 77—6932
atom, electron impact excitation, 23 to 37 eV, metastable yield 80—9739
atom, electron impact excitation, continuous spectrum radiation mechanism 79—3395
atom, electron impact excitation, electron-photon coincidence measurements for Ar excitation 80—37886
atom, electron impact excitation, extreme VUV reson. lines 77—6937
atom, electron impact excitation, L-MM, LM-M^3 Auger linewidths, L, S and J dependence 77—14588
atom, electron impact excitation, multiple-collision diffr. theory 78—82844
atom, electron impact ionis., calc. for $3s^2$ subshell 79—31700
atom, electron impact ionis., differential cross sections 78—58839
atom, electron impact ionis., L_3-shell alignment, Auger electrons ang. distrib. 78—58838
atom, electron impact ionis., single charge, inter-shell correl. 77—88567
atom, electron impact ionis. of inner shells, coincidence expt. theory 78—58837
atom, electron impact ionisation, cross section ratios 78—94326
atom, electron impact ionisation, energy resolution and ang. correl. of scatt. and ejected electrons 78—70939
atom, electron ionisation and excitation coeffs. in low E/N region 80—48090
atom, electron pulse radiolysis, 2p levels formation and decay kinetics 78—31665
atom, electron scatt., effective pot. calcs. 80—53131
atom, electron scatt., elastic, differential cross-section 79—54968
atom, electron scatt., in laser radiation field, free-free cross sections meas. 78—74762
atom, electron scatt. in intense IR field, multiphoton free-free transitions 79—81289
atom, electron scatt. in laser radiation field, free-free cross sections, reson. struct. 78—74763
atom, electron scatt. multiphoton process effects, laser-induced free-free transitions 77—79595
atom, electron scattering, elastic, at low-energy, polarised orbital calc. 78—82840
atom, electron scattering, elastic, low-energy, polarised-orbital calcs. 80—37882
atom, electron shadow scattering, cross-sections calcs. 79—59575
atom, electron total state energies, electron processes, ab initio CI investig. 77—18801
atom. electron-impact ionisation, low energy, triple-differential cross section 78—74773
atom, electron-photon coincidence obs., reson. lines, polarisation correls. 79—31697
atom, electronic binding energies, one-centre expansion method 77—6677
atom, emerging from C foil, excited ion Auger decay 77—3333
atom, ESCA spectra from 132.3 eV YMζ radiation source 77—4958
atom, excited, photoionisation for sensitive UV detect. 77—61122
atom, excited double hole state, single photon decay probability 77 34606
atom, Fermi correlation, for parallel-spin electrons in momentum space 77—10602
atom, Feshbach reson. classification, relation to ionis. pots., appl. Ne, Kr, Ar, Xe 77—54519
atom, first excited config., intermediate coupling coeff. 80—83450
atom, first order density matrix, effective core pot. valence electron UHF method 77—30786
atom, fluoresc. following slow electron impact, 380-710 nm 79—22646
atom, force constant props., 12-6 pot. model 78—13563
atom, generalised oscill. strengths, with outer shell effects, $2p^6$ subshell 78—50507
atom, heavy ion induced LMM Auger electron spectra 77—6907
atom, high resoln. pulsed electron beam time-of-flight ejected electron spectra 77—3462
atom, hydrogenlike, Lamb shift meas. by motional elec. field quenching time-of-flight expt. 80—9550
atom, impulse Compton profiles, atomic optimised pot. model 78—74618
atom, incoherent scatt. factors calc. by direct integration over impulse approx. Compton profiles 80—102475
atom, incoherent X-ray scatt., statistical atom model 78—29747
atom, independent particle pots. comparison 80—52846
atom, inner shell alignment calc. in electron impact ionisation 77—14586
atom, inner shell alignment following electron impact ionisation, distorted wave approx. calcs. 80—91682
atom, ionisation by electron impact, $2p_{3/2}$-shell alignment, Auger investig. 77—14587
atom, isoelectronic series, orbital binding energies within statistical exchange approx. 79—85895
atom, K-absorption spectrum, core electron rearrangement effect 80—47880
atom, K-MM radiative Auger transition rates, photon spectral distrib. 77—446
atom, kinetic energy functional, gradient expsn. 77—6665
atom, KLL and KLM Auger electron spectra, obs. and relativistic multiconfigurational Dirac-Fock calc. 78—50524
atom, Koopmans' ionis. pot., relax. correction 79—18308
atom, L-excitation by electron and proton impact, Auger multiplets, excitation probabilities 77—14589
atom, L-shell, X-ray emission spectra prod. by 0.3-3 keV electron impact, line intensities 79—45666
atom, L-shell internal excitation accompanying L-capture 80—95726
atom, L-shell ionisation, post-collision interaction, electron impact, energy loss meas. 77—19093
atom, lifetimes of L and LM vacancy states, X-ray emission linewidth 78—17621
atom, line strength calcs. for 6s-5p and 3d-4p transitions 77—14384
atom, M-shell photoionis., many-body interactions 79—10081
atom, magnetic hypersusceptibility *(Russian)* 77—14598
atom, metastable, electron impact excitation cross-sections calcs 78—94323
atom, metastable, excitation of $N_2(C^3\Pi_u)$, symmetry, propensity rules and alternation intensity, rot. spectrum 80—87135
atom, metastable, photoionisation rel. to laser development 78—13476

argon continued
- atom, metastable, quenching by O($2p^4$ ^3P), population and depopulation of O($3p^5P$) 80—42958
- atom, metastable $^3P_2$ deactivation in afterflow, plasma characts. 78—55769
- atom, metastable state production, microwave and DC discharges in flowing afterglows 78—46463
- atom, multiphoton ionisation, EM field gradient forces 78—66608
- atom, multiply excited, inner level X-ray emission spectra, line widths and Auger transition rates 79—36575
- atom, nonempirical calc. of X-ray K-absorpt. spectra 77—88465
- atom, ns$\rightarrow\varepsilon$p photoelectrons, spin polarisation 80—37792
- atom, optical oscillator strengths, 3p-ns and 3p-nd transitions, independ. particle model 78—86816
- atom, outer 1s, 2s and 2p electron loss cross sections by multicharged ions 78—42185
- atom, outer $p_{1/2}$ subshell photoionisation, polarised electrons, relativistic RPA calcs. 80—83331
- atom, outer shell photoionisation, relativistic RPA calcs. 80—9571
- atom, Paschen (1s) reson. state, decay mechanism and kinetics 79—27021
- atom, photoelectron angular distribution β parameters, resonance parameters 78—21886
- atom, photoelectron asymmetry parameters 80—95684
- atom, photoelectron emission, polarisation depend. on incident unpolarised VUV radiation wavelength 80—52952
- atom, photoelectron spectra, 21.2-151.4 eV and soft X-ray, ionis. cross-section 78—37683
- atom, photoelectron spectrum ang. distrib. abnormality in strong mag. field 78—50666
- atom, photoemission angular distribution, atomic pseudopotentials for soft X-ray excitations 77—23478
- atom, photoexcited LMM Auger processes, post-collision interaction 80—32682
- atom, photoionis. cross section ratio, calc. and meas. variation, energies 0 to 0.05 eV above $^2P^0_{3/2,1/2}$ thresholds 78—25492
- atom, photoionis. from excited states 79—10078
- atom, photoionisation, absolute cross-sections, exptl. meas. techniques 80—63598
- atom, photoionisation, Auger processes, decay lifetime, line shift, profile, X-ray photoelectron spectra 80—37798
- atom, photoionisation, correl. satellites and subshell cross-sections, electron spectrosc. obs. 79—31485
- atom, photoionisation, expt. techniques, processes, theory, review 77—14402
- atom, photoionisation cross sections for excited states, rel. to KrF laser 77—75110
- atom, photoionisation cross-sections, ground state inversion pot. method 78—33481
- atom, pionic, X-ray ang. distrib. meas. 77—3496
- atom, plane polarised VUV irrad., emitted photoelectron polarisation, ang. depend. 80—47952
- atom, polarisation effects in photoionisation *(Russian)* 79—3420
- atom, population inversion, intershell transitions, photoionisation, from UV irradiation *(Russian)* 78—70803
- atom, positron scatt., elastic differential cross-section 79—54939
- atom, positron scatt., positronium form. cross-section calcs. 78—9283
- atom, positron scatt., total cross sections 78—22031
- atom, positron scatt., total cross sections 79—86065
- atom, positron total scatt. cross sections 77—14573
- atom, primary ionisation by ~2 MeV relativistic electrons *(Russian)* 77—75309
- atom, props., calculation from optimised potential model 79—6895
- atom, radiative decay of collective levels, X-ray spectra *(Russian)* 77—6717
- atom, radiative level lifetime, photoionisation and photoexcitation rates, in shock tube 77—34594
- atom, Raman scatt., single particle HF approx. and RPA many-electron correlations calcs. 80—23374
- atom, Raman scatt. of light, HF approx. *(Russian)* 77—30808
- atom, reson. transition oscill. strengths, rel. to electron impact 80—27985
- atom, Rydberg states, nearly zero energy electron source 79—72433
- atom, SCF electron-gas local-spin-density model including correlation 80—9488
- atom, shake-up energies, Slater transition-state calcs. 79—89651
- atom, single-K multiple L-shell vacancy prod. in ion collisions, X-ray spectra 79—22809
- atom, spin-polarised photoelectrons by circularly polarised synchrotron radiation 80—91516
- atom, Stark shift and splitting in visible spectra 80—32659
- atom, trapping of nonreson. radiation, lifetimes of 4p and 5p levels 78—62766
- atom, two-electron one-photon transition rate 77—71772
- atom, unpolarised, spin polarisation of ejected electrons 78—78765
- atom, valence shell photoelectron spectrum, CI calcs. 79—31419
- atom, weakly ionised, energy transfer at high press. 78—58845
- atom, X-ray emission and X-ray photoelectron spectra, satellite peaks 78—66492
- atom, X-ray emission spectra, new interpretation of lines in 250+270 eV region 78—33460
- atom, X-ray scattering, anomalous, Kramers-Heisenberg dispersion calc. 79—89628
- atom, X-ray spectrum, L-spectrum meas. by soft X-ray spectrometer 78—24911
- atom+H^+, ang. and energy distrib. of ejected electrons 79—31668
- atom+H(D), ion pair formation, curve crossing model 80—87216
- atom+Li(Na)(K)(Rb), quenching cross sections of alkali n^2P states, 5-100 eV 79—76505
- atom+multicharged ion collisions, one electron capture from inner shells 80—58376
- atom beam W surface direct inelastic scatt., vel. distrib. meas. 80—66351
- atom photoionisation, double-electron, many body perturbation approach 78—17634
- atom populations in partially ionised flat plate boundary layer 77—65847
- atom-ice (solid ammonia) surface impact, 2.4 keV, secondary electron emission from $H^+(H_2O)_n$ and $H^+(NH_3)_n$ 79—15580
- atomic beam, scattered from Ag(111), time of flight meas., 79—95894
- atomic cluster formation, in rarefied nozzle flowfield 80—5639
- atomic collision-induced light scatt., spectral features 78—13493

argon continued
- atomic electron pot. scatt., 100 and 500 eV, extended Glauber approx. calcs. 77—54610
- atomic electron scatt., free-free transition meas. 77—3464
- atomic electron scattering, 20-300 eV, total cross sections 79—36778
- atomic electron scattering, elastic, 300 eV, differential cross sections, optical model 77—30990
- atomic excited states collision radiative destruction in glow discharge 79—3528
- atomic impact on W, generalised Langevin theory 77—8701
- atomic Kα X-ray satellite spectra, gas phase meas. 78—66496
- atomic line broadening by at. collisions, meas. of oscillator strength of ArI lines reson. *(French)* 78—5172
- atomic polarisabilities and shielding factors, coupled HF approx. 78—22048
- atomic polarisability, effective potential approximation method 77—88587
- atomic positron scatt., elastic, diffusion and annihilation cross sections 79—36769
- atomic reson. lines, 104.8 and 106.7 nm, polarisation, electron impact excitation 77—83739
- atomic spectra, collisional broadening and line shift 77—10641
- atomic structure, Hartree-Fock electron density, kinetic energy functional 79—26879
- atomic structure, Thomas-Fermi model with Fermi-Amaldi correction 79—81156
- atomic three-body collision-induced light scatt. spectrum moments 78—9226
- atoms, absorpt. spectra, field induced autoionisation near ionisation threshold 80—106301
- atoms, autoionising states excitation by electron impact, threshold effects 78—62923
- atoms, classical many-body collision model incorporating Heisenberg and Pauli principles 80—63511
- atoms, Compton profiles, Xalpha wavefunctions 80—106265
- atoms, electron energy loss spectra, Compton defect characterised by shift and asymmetry parameters 80—95723
- atoms, electron scatt. and ejection, electron energy loss spectra 80—58394
- atoms, free, electron bombard., subsequent X-radiation ang. distrib. 80—53144
- atoms, inner-shell level energies, absorpt. spectroscopy with synchrotron radiation 80—99583
- atoms, photoionisation, many-body atomic transition theory 77—75111
- atoms in Ne matrix, radiative and nonradiative lifetimes in excited states 80—69106
- Auger electron emission, during 3-15 keV Ar^+ bombardment of Si 77—59654
- Auger electron emission from ion-solid collision *(French)* 79—33876
- Auger spectra, using cylindrical mirror spectrometer 79—63326
- autoionising state $3s^{-1}4p\,^1P$, collision aligned, decay, triple differential cross section 78—86831
- beam source, high-flux 80—58416
- binary collision-induced light scatt., rot. Raman scatt. 80—78660
- binary collisions induced light scatt. 80—83428
- binary mixtures, separation performance of Kr and Xe by thermal diffusion column 77—42192
- biphenyl in Ne or Ar matrix, biphenyl ring torsion by vibronically resolved spectra 79—81228
- boiling point and triple point, rel. to IPTS 77—104
- breakdown in superimposed DC and HF electric fields 78—67571
- breakdown voltage and voltage-current characts. obs., up to 2400°C 78—87510
- broad beam ion source used for sputtering and etching 80—69002
- bubbles, injected into Sn, Pb and Cu melts, under laminar flow, characts. 78—38394
- bubbles in PtSi after 20 to 160 keV sputtering, TEM and backscatt. spectrometry obs. 78—64435
- cascade arc light emission, effect of pulsed microwave field 78—67599
- cascade ionisation by strong microwave field at low press. *(Russian)* 79—98854
- chloroform-Ar gaseous compressed mixture, mol. reorientation, Raman spectra 80—23422
- Clausius-Mossotti function, exam. of variation with gas density 78—52418
- Clausius-Mossotti second virial coefficient 80—79426
- cluster, FCC cluster, 40 kV electron scatt. dynamic effects 77—79721
- cluster containing tetracene molecules, excited state intramol. dynamics, laser-induced fluoresc. spectra obs. 80—78674
- cluster formation and homogeneous nucleation, comparison of expt. and theory 80—79925
- clusters, struct. and props. 80—39304
- clusters in supersonic beam, electron diffr. study 80—5655
- cold plasma generator, optical emission spectra and elec. parameters *(Ukrainian)* 78—67374
- collision induced light scatt., three- and four-body spectra 79—18260
- collision induced light scatt. spectra, pair polarisability 78—55135
- compressed gas, electron drift vel., density depend. 78—63534
- compressed gas, PVT meas. at high press. 80—98927
- condensed, electron drift, Davydov electron energy distribution function, diffusion *(Russian)* 80—80339
- condensed, luminescence decay under α- and β-particle excitation 79—38678
- condensed electron beam excited, exciton radiative lifetimes 80—6727
- condensed gas films, thermal radiation absorpt. 78—32824
- continuous optical discharge, mag. field effect 78—18479
- continuous optical discharge maintenance in applied mag. field 78—75396
- corona discharge, electron density meas. by microwave resonant cavity method 77—68881
- critical and triple pts., lattice gas model predictions 78—22818
- critical region, thermodynamic properties, correlation experimental data 78—6139
- crystal, absolute stability limit *(Russian)* 77—47373
- crystal, exciton exam. 78—51898
- crystal, laser breakdown as model of fast high-energy processes, shock wave motion 79—91541
- crystal, Monte Carlo calc. of conc. of lattice vacancies, method of overlapping distribs. 80—39077
- crystal, pure and benzene-doped, photoelectron emission, exciton states 77—44116

argon continued
- crystal, vacancy, electronic structure, Green's function theory 80—39525
- crystalline, luminesc., absorpt. spectra, free, self-localised excitons coexistence *(Russian)* 78—31231
- crystallites, self consistent phonon calc. of struct. and thermodynamic props. 77—62596
- crystals, internal energy, Monte Carlo calcs. 77—72577
- CW optical discharge in laser plasmatron mode 80—75078
- DC discharge plasma parametric instabilities near lower hybrid frequency *(Japanese)* 79—7450
- decaying arc, numerical simulation 80—38767
- degassing models of Mars 77—29700
- dense, depolarised Rayleigh scatt. 79—69851
- dense fluid, viscosity, gaussian memory function approach 80—28904
- dense gas, electron drift velocity 78—1785
- dense plasma, diagnostics of two-wavelength optical absorpt. 79—98978
- deorption, from Cu surface, production and meas. of atomically clean surface environment 80—52250
- depolarised Rayleigh scatt., mol. dynamics calcs., fluid density effects 80—24123
- desorption, on Pt (111), gas surface interactions, 3-D generalised Langevin model appl. 80—107637
- diamond:Ar, implanted, ion induced struct. changes, depth profiles, XPS 78—34554
- diffusion and solubility in PTFE 80—6561
- diffusion bonding, Ar atmosphere appl. *(Japanese)* 78—11491
- diffusion coefficient in 5A mol. sieves *(French)* 80—54508
- diffusion in liquid Fe and Ni *(Russian)* 77—55369
- diffusion in water, laser interferometric study 77—76584
- diffusion rate in Au thin layers 80—100359
- diluent in XeCl laser, performance 79—94212
- dilute gas, transport props., simple pair pot. model 80—87835
- discharge, DC, ionis. wave wavelength, electron gas state depend. 78—1918
- discharge, DC, plasma microwave propag. const. determ. by slab technique 80—53992
- discharge, DC magnetron, spectroscopic obs. 80—44010
- discharge, electrode free, appl. to plasma deposition of films *(Russian)* 80—16197
- discharge, electron swarm characts. 79—77441
- discharge, high-freq., excited atoms concentration determ., using spectral method *(German)* 80—70053
- discharge, hollow-cathode, partially ionised plasma diagnostics by electron beam scatt. 80—28824
- discharge, ion density profile, reson. laser light meas. 80—92401
- discharge, luminous channel form. meas. 79—64945
- discharge, moderate press., visible and UV radiation spectrum 77—31533
- discharge, nonequilib., atm. press., self-consistent model 78—5969
- discharge, optogalvanic and excited state photoionisation signals, space charge effects 80—14947
- discharge, plasm column of hollow cathode arc, collisional radiative model of ion system 80—38749
- discharge, plasma-treated SiO_2 surface, O_2 adsorption reactivity, EPR obs. 79—51418
- discharge, population processes of 4p levels, perturbation influence 80—38565
- discharge, positive column, axial electric field in transverse mag. field 78—55766
- discharge, pulsed, neutron species spatial distrib., laser beam diagnostics 78—38543
- discharge, pulsed, weakly ionised, neutrals effect, interferometric obs. 79—27854
- discharge, recombination coefficient meas. under diffusion-recombination conditions of plasma decay *(Russian)* 78—26324
- discharge, reson. scatt. in Ar high current low press. discharge 80—38735
- discharge, Tesla coil type, temp. diagnostics from OH A→X intensity meas. 79—64939
- discharge, two-temperature, transport eqns., transient phenomena 80—96402
- discharge, W multicavity cathode, power and V-I characts. 78—26360
- discharge HF arc type, spectral parameters 80—1873
- discharge plasma, laser diagnostics 77—19770
- discharge rotating plasma column LF oscillations 78—71481
- discharge sudden contraction, effect of gas heating 79—27859
- dispersion forces between closed shell atoms 77—88522
- drift chambers, Ar-ethylene mixtures investigation 78—25391
- dye-Ar vapour mixture, electron beam pumping 77—42535
- dynamical fluctuations in simple fluids, kinetic theory 77—7652
- electric arc gas heater, numerical calc. of arc parameters, Ar laminar stream *(Russian)* 77—58911
- electric arc with liq. K cathode, parameters, cathode sheath model 77—4003
- electric breakdown, high press. gas discharge form. 78—87567
- electric breakdown voltage, 300-2100K *(Russian)* 78—51370
- electric breakdown waves 77—31542
- electric discharge, electron energy distrib. function, Boltzmann eqn. 79—50911
- electric discharge, nonequilib. radial characts., two-temp. model 79—94833
- electric discharge, positive column and medium press., calc. 79—50912
- electric discharge structures in pure He and Ar gas 77—31541
- electrical breakdown, low-press. gap with thermionic cathode, upper and lower breakdown voltages 78—79405
- electrical discharges, electron-collisional excited-state kinetics 77—24226
- electron avalanche development, exact Boltzmann eqn. anal. 80—59318
- electron avalanches at high E/N values, Boltzmann eqn. anal. 77—35311
- electron avalanches at high E/N values, Monte Carlo simulation 77—35310
- electron back diffusion, electric field influence 78—75251
- electron drift and diffusion, Monte Carlo simulation 79—7441
- electron drift velocity, density dependence, high press., quantum mech. theory 79—1285
- electron energy deposition in Ar, Monte Carlo calcs. 80—69242
- electron energy distribution function, probe meas. in Ar afterglow 79—60195
- electron inelastic mean free path by PES 80—4822
- electron scattering, differential cross-section at 50 eV incident energy 80—22481
- electron transmission factor numerical determination 80—10350

argon continued
- electron transmission function and mean energy per ion pair, obs. 80—23566
- electron transport coeff. calc. in counting gas mixtures 79—32727
- energetic electron degradation spectra and initial yields 80—95724
- entrapment in Ni based powders, determination of content by vacuum fusion tech. 79—5193
- entropy change on melting of simple substances, thermal expansion, configurational entropy 80—59630
- EPMA of Ar in sputtered layers of Si 80—3443
- equation of state, hard core fluid with two-Yukawa tail 80—59618
- equation of state, molecules interacting via Kihara pot. with spherical core *(Spanish)* 77—31749
- equation of state, perturbed-hard-sphere, applicable to sub- and supercritical temps. 79—19350
- excimer laser, tunable vac. UV action 80—48215
- excimers and excimer lasers 80—48217
- excitation by pulsed electric discharge, luminescence obs., time resolved spectra meas. 80—102482
- excited atom+molecules reactions, electronically excited atoms and alkali metal atoms analogy 80—76490
- excited atoms, absorption spectrophotometry of fast reactions 79—52667
- field ion appearance potential spectroscopy, temp. effects 79—19978
- filament lamps, Kr-Ag-N gas mixture, thermal conduction coefficient calculational methods *(Russian)* 80—96335
- film, on Ag, Auger spectrum film thickness depend. 77—8691
- film, phase transition phenomena 77—62741
- fission fragment energy deposition kinetics, rel. to nucl. pumped laser 77—23652
- flame, Na-seeded H_2-O_2-Ar, population inversion, two-photon laser excitation 79—34307
- flash lamp, for vacuum UV spectral region 79—93236
- flow, alkali metal vap. condensation, heat and mass transfer 78—75192
- flow in vertical tube, laminar and turbulent heat transfer 78—71332
- flowing Ar spark gaps, electric breakdown study, improved method 80—64821
- fluid, dense, excess electron drift vel., hopping model 80—43838
- fluid, light scatt., 235K, statistical mech. of stationary state fluctuations 79—54035
- fluid, light scatt., collision-induced, line-shape theory and mol. dynamics 79—41921
- fluid, localised excess-electron states, quasilocalisation 80—44529
- fluid, vel. autocorrel. functions calcs. 77—58944
- fluorescent X-rays from sunlit Earth atmosphere during solar flares 77—13142
- fluoroform(-d_1)-trimethylamine-Ar(Kr), cryospectroscopic IR study of association 77—468
- fluoromethane+Ar, vibr. time depend. on equilib. and vibr. temps. *(Russian)* 79—27071
- focused ion beam designs for sputter deposition 79—89841
- formaldehyde, in Ar, 0.17-1.4 gm cm^{-3}, VUV absorpt. spectra, Rydberg excitations 77—79627
- free jet, homogeneous nucleation of clusters, noncryst. struct. *(French)* 78—79760
- free molecule flow and interdiffusion, through porous glass 79—32658
- freezing, statistical mechanical theory, appl. to Lennard-Jones fluid 78—47499
- full circle arc, mass flow field investig. 80—38797
- fusion reactor first wall protection, response to spherical blast waves 80—91245
- galactic abundance from Ar/O and Ar/Cl ratios in planetary nebulae 79—5887
- galactic centre, Ar overabundance from forbidden Ar II emission obs. 79—48922
- gas, breakdown conditions with current present before breakdown 78—42841
- gas, bulk viscosity, density depend. calcs. 77—3903
- gas, compressed, apparatus for depolarisation ratio meas. of scatt. light 80—38527
- gas, compressed, Rayleigh-Brillouin spectrum, hydrodynamic region 80—100063
- gas, compressed, Rayleigh-Buillouin spectrum, scaling 80—100062
- gas, diffusion of Na vapour, diffusion coeffs. meas. by Stefan method 79—41785
- gas, electron avalanches parallel and perpendicular to electric field, Boltzmann eqn. anal. 78—30502
- gas, electron mobility and lateral diffusion coeff. 77—35307
- gas, electron momentum transfer cross-sections, 0.4 eV 77—35308
- gas, flow through aperture into vacuum 78—9621
- gas, heated, elec. breakdown parameters 80—103202
- gas, in water, cavitation, gas supersaturation thresholds under high press. 77—16861
- gas, ionized shock wave, equilibrium zone behind shock wave *(Russian)* 77—89154
- gas, ionizing shock waves, stability, H impurities effect 78—22371
- gas, Kerr effect virial coeffs. 79—50843
- gas, laser-induced breakdown wavelength depend. meas. of threshold 79—41895
- gas, light depolaris., pair-pair correlations 78—63536
- gas, liquid, solid, refractive index, density and dielectric const. 80—66138
- gas, low-energy electron drift vel. at 293 and 90K 77—35306
- gas, metastable Hg atoms diffusion coeffs., temp. depend. 77—68731
- gas, mobilities and clustering of Li^+, Na^+ and K^+ ions 77—84389
- gas, partly ionised, viscosity calc., simplified expressions 79—18983
- gas, positron annihilation decay rates, high temp. behaviour 80—58389
- gas, proportional scintillation mechanism 79—81131
- gas, pulsed electron beam propag., self-focusing polyatomic additives effects 77—68164
- gas, Rayleigh scatt. props., nephelometer meas. 79—29865
- gas, supersonic radiation waves generated by CO_2 laser radiation 79—10593
- gas, thermal cond., 90-270K, 1 atm. press. 78—42700
- gas, thermal cond., 90-273K 80—48836
- gas, thermal cond., high temp. high press. meas. 79—68897
- gas, thermally excited density fluctuations, neutron scatt. 79—23392
- gas, third harmonic generation, bandwidth limitations in Lyman-α vicinity 79—81482
- gas, third-harmonic conversion of XeCl-laser radiation 79—89962
- gas, two body collision induced light scatt., memory function approach and mol. dynamics 78—25658
- gas, viscosity meas. at very high press. 80—59155

argon continued

- gas, weakly ionised, energetic electrons absorpt. 77—31420
- gas atoms, electron thermalization time and position distribution meas. 80—93771
- gas breakdown, for HF laser nanosecond pulse generation 79—81465
- gas breakdown by pulses from a CO_2 laser 80—6206
- gas breakdown threshold meas. using pulsed HF(DF) laser 77—11423
- gas const. meas. by acoustical interferometry 77—7492
- gas constant determ. from speed of sound meas. 78—9746
- gas discharge, ionisation waves, kinetic theory 78—22454
- gas discharge, low-pressure, energy balance and Coulomb relax. 77—43098
- gas in planar nozzle, shock-wave propag., effect of transverse mag. field 80—6094
- gas phase, 1 keV electron energy loss spectrum, Mollenstedt velocity analyser appl. 79—80721
- gas-liquid-solid equilibrium, eqn. of state 80—24563
- gaseous, positron vel. distrib. at equilib., annihilation decay rate 77—71870
- gaseous diffusion in He gas, ion mobility and longit. diffusion of Ar^+ and CH_x^+ *(French)* 79—94766
- gases, high press., laser spark, breakdown and radiation supported shock waves 79—32791
- glow discharge, cathode dark space ionisation avalanche with cold cathode *(Russian)* 80—84013
- glow discharge, cylindrical hollow cathode, ignition and breakdown expts. 78—91169
- glow discharge, gas temp. meas. by fluoresc. spectroscopy 78—18467
- glow discharge, imprisonment of reson. rad. in cold cathode region 78—59703
- glow discharge, ion flow mass-energy relations, near hollow cathode 77—84563
- glow discharge, spectral line excitation, cold cathode region 77—84552
- HCP phase obs., first order Raman scatt. 78—23454
- heat exchange, radiant plate, diametrical gas flow *(Russian)* 78—94565
- HF discharge, excited atoms and metastable state densities meas. 79—14606
- HF discharge in inert gas, optical diagnostics, bremsstrahlung 78—9871
- HF torch discharge, spectral diagnostics 79—14607
- high-frequency discharge, spectral parameters meas. *(Russian)* 79—10742
- high-pressure arc plasma, IR continuum emission obs. 78—71604
- high-pressure breakdown by Nd:glass laser radiation 78—75399
- high-pressure helical arc phase velocity in longitudinal mag. field 78—71594
- high-pressure plasma elec. conductivity obs. 78—71448
- hollow cathode, glow discharge, current balance and secondary electron emission 80—75108
- hollow cathode discharge, ion mass composition 79—68969
- hydrocarbon vapour mixtures, electron drift velocity meas. 79—41079
- ICP plasma, excitation source for flame at. fluoresc. spectrometry 80—37089
- implantation in Fe, effect on corrosion by H_2SO_4 soln. 80—71793
- implanted desorption in Ti films, reemission process 80—39453
- impurities in He quantum magnetometer, influence on signal parameters *(Russian)* 78—82010
- impurities in magnetic GdCo and GdCoMo films prepared by RF bias sputtering 77—44163
- impurity in Al foil, PIXE anal. with Ar beam 80—45609
- Incoloy 800, thin wall tubing, creep-rupture testing in steam under constant and cyclic load 79—47774
- induction plasma torch, temps. and velocities effects of cool central gas feed 78—94942
- inductively-coupled RF plasma torch, computer model 78—71559
- inner electron energy characteristics, validity of Hartree-Fock-Pauli approx. 80—42957
- interatomic potential and transport props. 77—14519
- intermolecular potential energy function determ. from thermal diffusion data 77—54590
- in interstellar grains, isotopic anomalies 78—28761
- interstellar Zr, depletion rel. to grain temps. in diffuse clouds 80—51848
- ion, energy and ang. distrib. in passing through C, Cu, Ag films 80—100292
- ion, energy-angle distrib. in C foil, test of Meyer-Klein-Wedell theory 79—49916
- ion, highly charged, prod. in electron beam superconducting ion source 77—23333
- ion, implanted in amorphous and cryst. materiaals, detection by X-ray emission anal. in TEM 78—51575
- ion+target collisions, two-electron-one-photon transitions, X-ray spectra 77—19068
- ion beam, metastable, collinear laser spectroscopy, isotope shift, fluoresc. detect. 80—37771
- ion beam divergence characteristics of two-grid accelerator systems 78—82074
- ion beams, low energy, transport through apertures, source parameter depend. 77—57422
- ion bombardment of polycryst., kinetic energy reflection 77—85869
- ion gun, for UHV microbalance, absolute meas. of sputtering yield *(Japanese)* 80—17951
- ion impact on C foil, energy loss 78—55902
- ion implantation in Fe, perturbed ang. distrib. 78—12969
- ion laser, $^{127}I_2$ stabilised, beat freq. intercomparisons at 514.5 nm 80—74338
- ion laser, appls. in research, industry and medicine *(French)* 80—83590
- ion laser, collisional radiative model and expt. 78—55338
- ion laser, CW 250 W output 79—18440
- ion laser, CW oscillation of 5062 Å line, reln. to laser Raman spectroscopy 80—1186
- ion laser, endoscopic photocoagulator for bleeding digestive lesions 78—40287
- ion laser, He, Ne, impurity effects, ignition enhancement and instability suppression 79—13948
- ion laser, high power problems 79—31944
- ion laser, mode-locked pulses, second-order intensity correls., two-quantum photoeffect 79—10332
- ion laser, multimode, photon statistics, autocorrelation 78—9358
- ion laser, resonator losses due to freq. selection using Fabry-Perot etalon *(Russian)* 77—38944
- ion laser, treatment of haemangiomas, teleangectasia, radiodermatitis and tattoos 78—35906

argon continued

- ion laser endoscopic photocoagulation in human digestive tract *(German)* 78—35915
- ion laser plasma, collision radiation model appl. *(Dutch)* 78—29934
- ion laser radiation, Faraday effect, polarisation plane negative rot. 79—98424
- ion laser therapy of skin defects *(German)* 78—35916
- ion mobilities in He gas at 82K 80—75023
- ion scattering from Cu (100), 10-35 keV 77—36348
- ion scattering on Cu crystal, 10-35 keV, diatomic models *(Russian)* 77—77337
- ion source, HF, proton yield increase, influence of various admixtures to H_2 obs. 80—57422
- ion states with two intrinsic $L_{2,3}$ vacancies, single-photon decay *(Russian)* 77—6716
- ion surface erosion of Nb 77—36342
- ion system, collisional radiative model 78—71080
- ion-laser discharges, high-power, stability limits 78—37872
- ionisation, energy dependence of $\bar{W}$ for alpha particles 79—6999
- ionisation, energy loss per ion pair for ions, 25 to 500 keV 77—35312
- ionisation, expt. results on $\bar{W}$-values for heavy particles 79—7000
- ionisation by relativistic muons, restricted energy loss 77—88355
- ionisation chamber dosimetry, Ar/propane, mixed X-ray/neutron fields 79—20682
- ionisation growth at high press., current growth obs. 80—38522
- ionised gas, high press. elec. cond. meas. 78—26233
- ionised gas behind shock wave, elec. cond. 79—10592
- ionised gas flow, quasi-steady laminar boundary layers 79—10544
- ionising boundary layer in shock-tube side-wall flow 79—60144
- ionising shocks reflection in shock tube, finite difference analysis *(Japanese)* 78—42629
- ions, electron impact ionisation, trapped ion cyclotron resonance spectroscopy 80—53140
- ions, high-energy, chromosome aberrations in aerated and hypoxic Vicia faba root meristems 78—7403
- ions, high-energy, depth-dose meas. in tissue-equivalent liq. and water 78—3614
- ions, high-energy, RBE, OER and cell cycle response 78—3558
- ions, slow, nuclear emulsion track width by photometric meas. 78—94167
- ions, spectral classification in θ-pinch plasma 79—6896
- ions for preparation of nuclear filters from polymers 78—86714
- IR lasers pumped by U fission fragments 80—28198
- isoelectronic sequence, many-body photoionization calcs. 78—17631
- isoelectronic series, Koopmans' ionis. pot., virial scaling corrections 79—45655
- isoelectronic series, negative muon capture, rel. probability meas. 77—50550
- isotope separation, plasma ion cyclotron reson. 77—10787
- isotope separation by axial flow turbomachine model 78—78500
- isotope separation by axial mol. flow turbomachine 78—17816
- isotopes prod. cross sections in natural Ca by 12-45 MeV protons 77—17310
- isotopes prod. in lunar materials by solar cosmic ray protons, rate calc. 77—17311
- isotopic compositions meas. in Allende meteorite 77—87344
- jet, supersonic, electron beam-excited, continuous VUV emission spectrum origins 79—6964
- jets, axisymmetric, turbulence mixing of gases with different densities 77—58749
- K648, halo planetary nebula, low Ar abundance meas. 80—82443
- Kerr effect in gas, statistical theory 79—50842
- laminar plasma jet, H_2 diffusion obs. 78—71557
- laser, 5145 nm wavelength stabilisers *(German)* 78—1247
- laser, 515 nm line, wavelength stabilisation for high precision length meas. 78—33766
- laser, Ar III arc discharge, CW 40 W UV output 77—54695
- laser, continuous high-power operation 351.1, 363.8 nm UV laser lines 77—38857
- laser, CW high power, design parameters *(Japanese)* 78—59019
- laser, CW UV emission, power enhancement 78—17906
- laser, discharge current control using thyristor convertor 77—14747
- laser, electron beam excited, absorpt. characts. 78—82948
- laser, freq. stabilisation at 582.49 THz using saturated absorption in $^{127}I_2$ 77—79850
- laser, He-Ar mixture, hollow cathode internal anode system, CW 78—9396
- laser, high output power in visible and near UV 78—1249
- laser, high power, for pumping CW dye laser 77—7130
- laser, high power, Ti covered BeO discharge tube 78—29962
- laser, high press. tunable 78—50755
- laser, high-power CW, resonator configs. for mode selection 79—10327
- laser, I_2 molecular beam stabilised 77—75555
- laser, intensity fluctuations obs. in emission 80—28197
- laser, internal-mirror type air-cooled discharge tube, 5 mW output power 80—38034
- laser, ionic with polarised radiation, use of three-mirror resonator 80—23712
- laser, longit. mode locking in three mirror cavity 79—55164
- laser, new IR laser transitions, 3.725 to 17.233 μm, 5.804 μm laser line identification 80—87374
- laser, pumping of CW ruby laser 78—1253
- laser, radiation spectrum and influence of Fabry-Perot plate *(Polish)* 78—78993
- laser, recombination, in expanding CO_2 laser prod. plasma 77—88698
- laser, simple high-power TEA, operating in near IR 79—94251
- laser, with system for changing working gas *(Russian)* 77—88781
- laser discharge, current modulation 77—46717
- laser discharge, spontaneous emission, at. line shapes, interferometric obs. 77—30816
- laser emission under passive mode-locking conditions, temporal structure 80—9923
- laser fusion microsphere production, low pressure gas filling 80—32441
- laser fusion target pellets, mass spectrometer determ. of AR contents 80—32442
- laser heated magnetoplasma, X-ray meas. of electron temp. 77—31493
- laser induced gas breakdown threshold at 1.06 micron 80—28594
- laser interferometer for detection of gravitational radiation 79—101076
- laser oscillation obs. in transversely initiated laser-produced plasma 77—88696
- laser power supply for discharge current and output power control 77—38912

argon continued
laser resonator, effect of axial mag. field on loss increase 79—76716
laser system, mode-locked, temporal pulse shape, streak camera meas. 77—79799
laser wavelength measurement using digital interferometer 80—37079
laser with passively locked modes, excitation of dye laser for picosecond pulse generation 80—95930
laser with wall stabilized transverse discharge 77—83849
laser-evaporated microplasma radial glow and temp. distrib. 78—67387
lasing in atomic lines obs. in excimer ArF laser 77—83858
lattice heat capacity, thermal vibrations, Lindeman parameter, lattice dynamic model *(Russian)* 80—29141
Lennard-Jones liquid, mol. dynamics studies of glass form. 80—38896
light scattering, collision induced, low density limit, mol. dynamics and memory function approach 80—43841
light scattering, collision-induced, at intermediate density, integrated intensity 80—24124
liquefied, purification for ionisation chamber appl., Li trap construction 80—47814
liquid, α-irrad., free-ion yield, geminate recomb., track model 80—24983
liquid, α-irrad., geminate recomb. of charges, hot electron thermalization length 80—20266
liquid, α-particle excited carriers, geminate recombination 78—34876
liquid, μ, ρ and T-surfaces, global behaviour, rel. to catastrophe theory 78—26226
liquid, atomic correls., three-body interactions effects calcs. 77—84618
liquid, backflow of quasiparticles in classical system 79—27614
liquid, binary non-additive particle interaction, self diffusion and at. motion, mol. dynamics method 80—59372
liquid, characteristic curves, hard- and soft-core eqns. of state 79—55861
liquid, classical, at triple pt., long-time anomalies suppression 80—24339
liquid, closed circuit for electron irrad. of LiH at 90K *(French)* 78—62214
liquid, coherent scatt. function calc. 78—42875
liquid, comparison on interaction induced light scatt. and IR absorption 80—60561
liquid, compressed, excess electron mobility theory 80—80338
liquid, compressibility, long wavelength limit of liquid struct. factor 78—67633
liquid, compressional viscosity and vibrational relaxation 80—70311
liquid, crit. exponents *(Russian)* 79—77766
liquid, critical exponent, η, X-ray scatt. 80—92660
liquid, cryogenic, elec. breakdown, time lag 80—29684
liquid, current fluctuation spectra 78—42888
liquid, depolarised scatt. lineshape correlation function theory 77—40253
liquid, depolarized Rayleigh scatt. at triple point, mol. dynamics simulation 80—60617
liquid, dielec. const. meas. by reson. method *(Russian)* 77—28511
liquid, diffusion coefficient for model potentials through mean square displacement 80—70098
liquid, drift mobility and conduction band energy of excess electrons 77—4348
liquid, drift of ionisation electrons 78—55100
liquid, drift vel. of excess electrons 80—54744
liquid, elastic modulus and stress relaxation 79—19304
liquid, elec. breakdown characts. 79—91364
liquid, electron drift vel., mol. solute effects 77—4338
liquid, electron mobility, role of shallow traps 80—34440
liquid, electron mobility/diffusion coeff. 80—44593
liquid, electrostatic free electron emission *(Russian)* 77—24933
liquid, emission coeff. of cond. electrons, depend. on elec. field intensity *(Russian)* 79—78855
liquid, empirical and anal. of computer expts. on mol. dynamics 78—21995
liquid, equation of state, square-well model calcs. 77—84883
liquid, equation of state studied using statistical theory results 80—84276
liquid, high-field carrier transport at pre-breakdown and breakdown regions 80—25305
liquid, high-field electronic conduction obs. 79—4587
liquid, intermolecular correlation effects on liquid props. determined by X-ray diffraction 77—27799
liquid, internal energy calcs. 77—28025
liquid, ionisation and scintillation, application to radiation detectors, review *(Japanese)* 78—35206
liquid, kinetic model, dynamic struct. factor 79—10768
liquid, kinetic phenomena, shear viscosity *(Russian)* 80—10694
liquid, longitudinal modes, transverse modes and vel. correls. 79—94858
liquid, magnetic field-induced temperature changes 78—57960
liquid, mobility of excess electrons, deform. pot. theory 80—24982
liquid, mode coupling theory of simple classical liquids 79—55630
liquid, modified droplet model, mean droplet interaction below T_c 80—70363
liquid, mol. dynamics calcs. 77—19857
liquid, mol. vel. correls. 77—19862
liquid, neutron incoherent scatt. functions, non-Gaussian corrections 78—42874
liquid, new description of random stacks *(French)* 78—79512
liquid, nucleate pool boiling in Ar and Ar-N_2 mixtures 79—60495
liquid, numerical anal. of density fluctuations 78—21051
liquid, numerical anal. of transverse current correl. 78—21052
liquid, O_2^- electron laser-photodetachment 79—64057
liquid, pair correlation decay rate exponent, small-angle X-ray scatt. obs. 77—76293
liquid, pair potential, Percus-Yevick and hypernetted chain approx. calcs. 77—1052
liquid, partition function, critical point, independent structure model *(Spanish)* 77—4027
liquid, perturbation theory for sound prop. vel. *(Russian)* 77—15500
liquid, principle of corresponding states for viscosity 77—84959
liquid, quasi-crystalline model, asymptotic oscills. of radial distrib. function 78—9935
liquid, quasi-crystalline structure, role of vacancies in dynamics 80—92438
liquid, radial distrib. function, quasi-crystalline model of liqs. 79—19135
liquid, Ramsauer-Townsend minimum in electron scatt. cross section 77—89821
liquid, recomb. and self-trapped exciton luminesc., free electron dynamics, excited states 80—25463
liquid, recomb. luminesc. 78—60521
liquid, reduced hard core dias. from compressibility, viscosity, and freezing data, Lindemann law 77—39521

argon continued
liquid, relative motions in molecular dynamics investigation 80—92439
liquid, scintillating target, fast neutron polarisation analyser 80—47833
liquid, scintillation decay due to α-particles and electrons 78—55099
liquid, shear viscosity coeffs., model calcs. 78—47549
liquid, shear viscosity correlation function 78—47460
liquid, shock compression temp., detonation front glow 80—43737
liquid, shock wave compression, 400 to 910 kbar 80—29101
liquid, short range order parameter 78—83712
liquid, sp. ht., hard-core eqn. of state 79—60474
liquid, specific heat determ. in tunnel theory 79—33095
liquid, struct. determ. by X-ray diffr., pair pot. calcs. 78—6003
liquid, struct. factor calc., perturbation treatment using Lennard Jones (6, 12) pot. 80—10483
liquid, sum rules and at. correlations, near triple point 77—76282
liquid, surface energy, nonadditivity contrib. 78—18874
liquid, surface properties of classical Lennard-Jones liquid *(Russian)* 79—77869
liquid, surface study, ellipticity coeff., ellipsometric method 80—84343
liquid, surface tension and density profile from expression for excess free energy 77—80681
liquid, surface tension and width, density functional theory 80—103537
liquid, surface thickness, near triple point, using surface tension data 79—99400
liquid, surface thickness near crit. point 80—34180
liquid, T_c, P_c, V_c, from eqn. of state 78—2228
liquid, transverse correlations in simple liqs., effective field approach 79—82135
liquid, transverse current correl. functions 79—77489
liquid, transverse mode, Maxwell relax. time 78—22622
liquid, triple point, depolarized Rayleigh scattering from fluids of spherical molecules 78—88319
liquid, triplet state of self-trapped exciton states, evidence of existence, luminescence meas. 78—72608
liquid, van Hove's dynamical structure factor for classical liquids 79—55631
liquid, Van Hove correlation function, convolution approximation 79—82136
liquid, variational eqn. of state and entropy 79—28070
liquid, vel. correl. function, memory function calcs. 80—49081
liquid, velocity autocorrelation from memory function, hard-sphere and square well pots. 80—28893
liquid, velocity autocorrelation function and freq. spectrum 79—27892
liquid, velocity of second meas. and thermodynamic stability *(Russian)* 79—4374
liquid, velocity-autocorrelation function from neutron scatt. 77—1058
liquid and solid, absorpt. and luminesc. spectra of self-trapped excitons 79—65893
liquid between adsorbing walls, Monte Carlo calc. of force 80—15363
liquid independent structure model, critical point, liquid-vapour equilib., second virial coeff. *(Spanish)* 77—4031
liquid ionisation chamber, increased time resolution using Ar-methane mixtures 80—27891
liquid ionisation chamber media, review of physical props. 79—41071
liquid nuclei, thermodynamic props., mol. dynamics calc. *(Russian)* 77—47325
liquid orthobaric density, 100 to 120K 79—35679
liquid-vapour interface, surface of tension near triple point, theory 80—100375
liquid-vapour interface struct., Ar like fluid in equilib., thermodynamic states 78—10259
liquid-vapour interfacial width near critical pt. 78—22931
liquid/solid interface, mol. dynamics simulation of struct. 78—26764
LMFBR, Na coolant and Ar atmos., chemical comp. 79—71893
loaded K heat pipe performance characteristics 78—89934
low pressure gases, dielectric breakdown model 78—9883
low voltage arc, ionisation waves, hydrodynamical model including inelastic interaction 78—87563
low-press. glow discharge, elec. characts. of positive column 80—100112
low-pressure gas discharges, model 79—37560
lunar ^{40}Ar gas release 77—71031
lunar dust, inert gas conc., separation methods and methods of treatment *(French)* 80—51674
magnetoplasmadynamic arcjet, recomb. lasing 80—48218
Mars, Ar content of atmosphere, Viking 1 X-ray fluorescence spectroscopy 77—13270
Mars atmosphere, ^{40}Ar origin 77—64687
mass spectroscopic chemical anal. using quadrupole mass spectrometer for fissile material accounting 80—63300
matrix for $O_3+Zn(Cd)$ matrix reactions, IR, Raman and visible spectra 80—87110
matrix isolated NO $3s\sigma(A^2\Sigma^+)$ Rydberg state 'bubbles', reson. fluoresc. obs. 77—83636
matrix-isolated high-resolution IR spectra of SF_6 and BCl_3 80—32708
melting curves, quantum corrections, effective pair pot. calcs. 77—55347
melting transitions, thermodynamic props., positional disordering energies 80—96452
mesic atom, X-ray radiation anisotropy, suppression coeffs. *(Russian)* 78—22058
metastable atom concentration; expts. determ. inside hollow cathode arc discharge *(French)* 77—31540
metastable atoms in arc burning in argon, local densities meas. *(French)* 77—4017
methane+methane (He)(Ne)(Ar), dispersion forces 78—13565
methane-Ar, liq. mixture, self-diffusion and nuclear mag. relaxation *(Russian)* 78—87799
methane-Ar liquid mixture, viscoelastic props., acoustic relax. *(Russian)* 78—75736
methanol+Ar, methoxy radical prod., UV emission spectra 80—91572
methyl cyanide-Ar mixture, thermal cond. in mag. field 80—100058
methyl iodide, in Ar, 0.25-1.38 gm cm^{-3}, VUV absorpt. spectra, Rydberg excitations 77—79627
microwave gas breakdown, ionisation pot., qualitative theory 80—43837
microwave plasma discharge, electron energy distrib. function *(Russian)* 77—11415
mini-arc as spectral radiance secondary standard 77—34921
molecular beams, nozzle-formed, energy parameter determ., time-of-flight method 79—64122
molecule, Hulburt-Hirschfelder pot. function 80—63612
momentum eigenfunctions in complex momentum plane, Hartree Fock functions 80—63517

- **argon** continued
  - monolayer, adsorbed on graphite, lattice dynamics 78—75946
  - monolayer, adsorbed on graphite, lattice spacing and isosteric heat below 50K, LEED obs. 80—34303
  - monolayer adsorbed on graphite basal planes, heat capacity 80—6636
  - monolayer coated Grafoil, sp. ht. of adsorbed submonolayer ^{4}He film 79—51379
  - monolayer on graphite, neutron diffr. study 78—34705
  - monolayers, on graphite, condensation and compression, high resolution LEED obs. 79—77906
  - multiply charged ion beam, characts. 77—18133
  - muonium formation by positive muons 79—57272
  - negative glow fast electron density rel. to discharge pressure and current 78—67528
  - nepheline syenite, dating, Rb-Sr internal isochron, ^{39}Ar-^{40}Ar plateau age methods *(French)* 78—32031
  - neutral system, complete saturation phase excited state population density 80—106284
  - neutral system collisional radiation model 78—67535
  - nonequilibrium condensation and surface tension in supersonic jet flow *(Russian)* 80—65210
  - nucleation, Ar in He carrier gas, supersonic nozzle flow 78—94871
  - nucleation, thermodymamics 78—14454
  - optical detonation threshold, press. depend., rel. to air 79—23438
  - optical gas breakdown, reduced threshold in two-freq. field 80—64819
  - pair polarisability determ. from collision induced light scatt. spectrum 79—13678
  - Penning ionisation of di/triatomic mols., electron spectra, vibr. transfer 77—14555
  - Penning mixtures, statistics of gas gain 79—45535
  - permeability and diffusion in polyvinyl fluoride and polyvinylidene fluoride, glass transition obs. 79—32919
  - permeability in hard elastic polypropylene films, extension effects 80—40412
  - permeation through Mo, monocryst. and polycryst. specimens *(Russian)* 79—60554
  - phase stability boundary, nucleus surface tension rel. to surface radius of curvature 79—60603
  - phase transition between strongly anharmonic crystal and gas 80—6510
  - photoelectron spectra, impurity lines in He resonance source 77—14787
  - physisorbed monolayer on graphite, neutron scatt. studies 80—107655
  - physisorbed on metal, polarisation due to short range interaction with substrate 80—39428
  - PK 108—76°1, 49+88°1, halo planetary nebulae, low Ar abundances meas. 80—82443
  - plasma, 14000K, continuum emission coeff., laser spark temp. meas. 77—31527
  - plasma, afterglow, pulsed discharge, acoustic oscills. in emitted radiation 77—89309
  - plasma, Ar III and IV lines, Stark broadening, Gaunt factor calcs. 77—51231
  - plasma, Ar-He mixture, ion-acoustic wave propag. 77—27670
  - plasma, arc hollow cathode, diagnostics 80—44043
  - plasma, boundary layer low-press., kinetic evolution of 3p^{5} 4s level *(French)* 77—80279
  - plasma, constricted discharge, electron density and temp. and gas temp., iterative method *(German)* 78—83627
  - plasma, constricted electric arc, iteration method anal. 79—90484
  - plasma, continuum radiation, temp. and charged particle concs. from line intensities and widths 77—68867
  - plasma, continuum radn. meas., 120 to 340 nm 77—58894
  - plasma, decaying pulsed discharge, acoustic wave density modulation 80—103143
  - plasma, dense, appl. of modified quantum defect method 80—38570
  - plasma, dense, complex refractive index 79—23397
  - plasma, dense, nondegenerate, electron transport, thermal cond. *(Russian)* 79—98865
  - plasma, dense, photoionisation absorption spectra, photorecombination radiation 78—26252
  - plasma, dense, shock-heating, calc. of equilibrium props. *(Japanese)* 80—79513
  - plasma, density meas. by Langmuir probe and microwave interferometer 80—28819
  - plasma, dynamic stabilisation of dissipative drift modes by oscillating azimuthal mag. field 78—18396
  - plasma, effects of Joule heating on plasma heat transfer 77—72412
  - plasma, electron beam excited plasma UV absorpt. by diatoms 79—68907
  - plasma, electron density, microwave refl. meas. 78—59674
  - plasma, electron distrib. function probe meas., ionis. wave irregularity effect 77—47255
  - plasma, electron temp. meas., microwave technique 78—26325
  - plasma, electron-ion pairs, correlated pairs, effect on conductivity 78—26249
  - plasma, electron-ion recombination, 300 to 500K, in discharge tube 78—59714
  - plasma, electron-ion recombination in extinguishing arc 78—59687
  - plasma, electrostatic well accumulation of multicharged ions in mag. mirror plasma by electron cyclotron reson. 79—32804
  - plasma, EM waves, parametric decay near upper hybrid freq. 78—59590
  - plasma, energetic binary collisions 79—77337
  - plasma, Gaunt factor temp. depends., from Ar II and Ca II Stark widths 78—87491
  - plasma, H impurity, equilib. state of highly ionised plasma 78—83597
  - plasma, heat transfer to sphere, appl. dimensionless rels. 77—35331
  - plasma, high current pulsed electron beam injection, oscills. excitation *(Russian)* 77—11361
  - plasma, high density, highly excited atomic levels, spectral-line-blending study 80—48969
  - plasma, high-energy, used in SpectraScan III AES system 79—96382
  - plasma, highly ionised low press., produced in pulsed discharge, characts. *(French)* 77—58901
  - plasma, hollow cathode arc discharge, collective scatt. meas., turbulence 80—48978
  - plasma, hypersonic nozzle, radiation field characts. 77—84340
  - plasma, implosion, by pulsed electron beam accelerator, 4TW, laser and X-ray obs. 80—1816
  - plasma, in electric arc, metastable atom density changes during arc interruption 77—51250
  - plasma, in gas puff Z-pinch device, formation and X-ray spectra 79—94816

- **argon** continued
  - plasma, in high-pressure. arc, elec. cond., nonideal effects, IR continuum absorption obs. 80—38558
  - plasma, in rot. steady state centrifuge, rot. rate and temp. diagnostics *(Russian)* 78—5923
  - plasma, inductively coupled, excitation transfer between plasma and impurities *(French)* 78—14211
  - plasma, inductively coupled RF, spatial distrib. of temp. and number densities of electrons, atoms and ions 77—68873
  - plasma, inelastic collisions between excited states, Chapman-Engskog procedure, electron energy distrib. 79—68902
  - plasma, interferometric study of density and electron conc. behind shock waves 78—1888
  - plasma, ion energy level populations in crossed elec. and mag. fields 78—67428
  - plasma, ion-acoustic wave-CO_2 light coherent scatt. 78—34325
  - plasma, kinetic theory calcs. of transport props. 78—14134
  - plasma, laser-induced, holographic schlieren density study 77—72503
  - plasma, laser-initiated, gasdynamic instabilities and convective flow parameters 78—22525
  - plasma, low density, shock-heated, effective collision freq. calcs., electron temp. meas. 80—75025
  - plasma, low temp. flow, interaction with intense microwave beam 80—38654
  - plasma, low-temp., low-power laser radiation scatt. diagnostics *(Russian)* 79—98975
  - plasma, microwave absorption at singularity, parametric satellite excitation obs. 77—51194
  - plasma, microwave emission spectra of low temp. plasma, electron vel. distrib. determ. 78—47167
  - plasma, microwave induced, cavity excitation source for optical emission spectrometry 77—44567
  - plasma, negative plasma potentials produced by supplemental electron emission 79—41861
  - plasma, nonseeded, nonequilibrium MHD power generation 77—24196
  - plasma, one-phase and two-phase jets, non-equilibrium in initial region *(Russian)* 77—31518
  - plasma, operating characts., numerical study 78—67309
  - plasma, optical breakdown at 10.6 μm near plasma layer boundary 79—60165
  - plasma, optical props., visible, near-IR region, using shock tube 79—55471
  - plasma, parametric excitation of backward ion cyclotron wave with a pump in the lower hybrid range 79—37490
  - plasma, photoexcitation and photoionisation ahead of strong shock wave *(French)* 77—19708
  - plasma, photon reabsorption attenuated radiation emission 80—64776
  - plasma, population density meas. in free jet expansion flow 77—27737
  - plasma, primary electron effective MFP meas. in multidipole device 77—24183
  - plasma, radiative energy loss in shock tube 77—19768
  - plasma, recombination, kinetics of stimulated atomic populations *(Russian)* 78—87436
  - plasma, reflection of high power pulsed microwave 77—31474
  - plasma, RF prod., mag. field effect on props. *(Korean)* 79—50869
  - plasma, shock compressed, radn. emission *(Russian)* 79—37554
  - plasma, shock-compressed, thermophysical and gasdynamic characts. 77—43016
  - plasma, shock-compressed optical props. 79—23426
  - plasma, shock-heated, dense, continuum radiation and optical transmittance diagnostics 80—24202
  - plasma, shock-heated, high-density, elec. cond. 80—38557
  - plasma, spectral line blending of excited at. levels 77—76038
  - plasma, stationary striations as bifurcation phenomenon 79—32767
  - plasma, submillimetre diagnostics, active, of Ar arc, data numerical anal. 80—48979
  - plasma, supersonic nonequilib. corner expansion flow, electron and particle temp. 77—89235
  - plasma, thermal equilibrium properties, estimation 78—1793
  - plasma, thermal induction, in finite cylinder, 2-dimens. analysis 77—55128
  - plasma, thermodynamic functions, composition, and elec. cond., calc. method 79—32738
  - plasma, transition probabilities, continuum emission coeffs., electron density 77—51228
  - plasma, vac. UV emission profile, temp., spectroscopic meas. 77—51229
  - plasma, viscosity determ. by stabilised elec. arc. 79—41873
  - plasma, wall stabilised arc, spectroscopic temp. and radiation standard 77—76199
  - plasma, weakly ionised, excitation rate in strong external field 77—62333
  - plasma, weakly ionised, photon echo relax. obs. in RF discharge 80—43986
  - plasma, weakly magnetised, meas. of low electronic temp. 77—68870
  - plasma, weakly-ionised, collisional drift instability 80—53977
  - plasma, Z-pinch, mag. field fast recomb. through plane pinch current sheet 80—38695
  - plasma, Z-pinch determ. by intrinsic stimulated emission 78—26311
  - plasma arc, decaying, electron disappearance mechanism 80—38765
  - plasma arc, dynamic charact., electron energy relaxation effect 80—38774
  - plasma arc, wall-confined, nonequilibrium effects 80—70058
  - plasma arc discharge, contamination near Cu electrode *(French)* 79—77443
  - plasma arcjet plume, freely expanding, excited state distrib. function 79—98881
  - plasma boundary layer electrostatic probe meas. *(Japanese)* 78—5933
  - plasma bridge neutraliser operation with 10 cm beam diameter etching source 78—74102
  - plasma continuum, emission coeff., high press. peculiarities 77—43067
  - plasma development by laser radiation absorption 78—75392
  - plasma diagnostic method for partial LTE 78—67606
  - plasma emission source for gas chromatography 79—74438
  - plasma from magnetoplasmadynamic source, of supersonic jets 77—35332
  - plasma heavy ion complex mobility in cool plasma 77—62343
  - plasma induction HF discharge in crossed fields with Cs seeding, Hall parameter 79—55465
  - plasma interaction with flat anode 78—71497
  - plasma jet, collisional line broadening, oscill. strengths of reson. lines 77—75106
  - plasma jet, electron temp. and density determ. 79—41875

argon continued
plasma jet, electrostatic probe meas. of metastable atom conc. *(French)* 79—98972
plasma jet, emission of electron-neutral atom bremsstrahlung *(French)* 78—26332
plasma jet, heat transfer and hydrodynamic struct. 79—14521
plasma jet, heat transfer to rotating water-cooled cylindrical wall *(French)* 80—28850
plasma jet, optical studies using Schlieren and shadow methods 80—59279
plasma jet, surrounded by AR, He, N_2, H_2 gases, recombinations in decaying jet 78—9753
plasma jet, turbulent, radiowave interaction and electron density fluctuation 77—989
plasma jet, under press., heavy particles temp. meas. *(French)* 78—9841
plasma jet-transferred DC arc for refractory refining, initiation and performance characts. 78—9866
plasma jets, appl. to emission spectroscopy, flame stability improvement 77—86425
plasma jets, single- and two-phase, non-equilib. in initial zones 79—82102
plasma jets, temperature distrib. by spectroscopic meas. *(Korean)* 77—80355
plasma MHD arcjet, recombination lasing 77—65588
plasma parameters, microwave scanning technique 80—64773
plasma parameters of pulsed highly ionised low press. discharge 77—62398
plasma quantometer, quantitatively coupled, for emission spectrochem. anal. *(Japanese)* 78—83624
plasma radiation obs., line and continuous spectra *(French)* 80—19619
plasma rotating, weakly ionised, diagnostics 79—82122
plasma source in TM_{010} cavity, for soln. anal. 79—48032
plasma spectroscopy, inductively coupled, development, technique and appls. 79—35839
plasma stream, at atm. press., temp. and conc. from study of electrical parameters *(Russian)* 80—53930
plasma supersonic jet, radiation in magnetoplasmadynamic source 77—35329
plasma temp. diagnostics from linewidth, inductively coupled plasma 77—43083
plasma Tokamak discharge, impurity emission spectra for diagnostics 77—11403
plasma trap for magnetic flux, loop probe meas. 79—14621
plasma welding, compressed arc V-I characteristic obs. *(Russian)* 78—83628
POPOP-Ar-N_2, electron beam pumped, intense laser emission at 381 nm 78—74898
positive column, 4S and 4P levels populations, rel. theory with recomb. 77—10766
positive column, axial elec. field in transverse mag. field 78—18472
positive column, contracted, balance equations anal. 80—6312
positive column, contracted, electron density, temp., elec. field, line emission 80—6311
positive column, dissoc. recombination coeffs. 78—26367
positive column, in transverse mag. field, plasma parameter diagnostics 79—19103
positive column, local transverse mag. field, striation freq. spectra, microwave probe 78—87562
positive column, moving striations in longitudinal homogeneous mag. field 78—67523
positive column, progressive and regressive ionisation waves *(French)* 80—43905
positron annihilation decay consts., temp., elec., and mag. field depend., computer anal. 78—78809
positron annihilation in rare gases, Doppler broadening meas., electron mom. distribs. 78—55131
potential energy functions 78—29830
precursor phenomena ahead of shock wave *(French)* 77—24087
precursor shock waves, electron density and assoc. ionisation 78—67217
preionised, CO_2 laser induced breakdown press. and pre-ionisation depend., cascade model 80—54010
pulse discharge regime, time-depend. of radiation *(Russian)* 77—84548
pulsed electrical breakdown at high temps. *(Russian)* 78—34379
pulsed plasma, elec. cond. obs. at 10 atm and 15000K 78—71449
purification, portable laboratory equipment *(Polish)* 79—12781
purification system and electronegative impurity conc. meas. instrument 80—32571
radiation induced shock tube flow nonuniformities in ionising Ar 80—43865
radiogenic Ar in phlogopite mica, press. depend. of diffusion 77—86861
Rayleigh spectrum, collision-induced, intermediate density, second freq. moment, appl. to Ar 80—24125
reaction rate consts. 78—48613
recombination luminescence in scintillation induced by alpha particles 78—50441
recombining plasma, excited levels, population kinetics 79—90376
reflected shock wave, press. anal. at Mach numbers of 10 to 35 77—15060
refractive index meas. using low temp. refractometer 77—57382
relativistic ion beam laser, continuously IR to X-ray tunable, in negative temp. state *(Chinese)* 80—87373
resonance excit. of $1s_2$ and $1s_4$ levels via He^+ 100-1000 keV impact 77—10611
resonant absorption in plasma at thermal equilib. 80—1799
RF discharge plasma, magnetically stabilised, electron temp. using optical spectroscopy *(German)* 78—63582
saturated solutions, NO_3^- effect on spectral distribution and intensity of sonoluminescence 80—76091
scintillation detectors appl. *(Czech)* 78—86727
second virial coefficients from compressibility meas., mol. pot. parameters calc. *(Spanish)* 77—47133
secondary electron energy distrib. on fast electron impact 77—34763
secondary scintillation under mag. fields, effect in gas proportional counters 80—58055
shear viscosity determination under high pressure, using capillary viscometer 78—55708
shock heated, absorpt. line broadening of Ca and Ba *(Japanese)* 80—83464
shock wave radiation, low inertia pyroprobe meas. *(Russian)* 77—31333
shock wave structure, at re-entry speeds 80—43927
shock waves, ionising, at large Mach numbers 80—6096

argon continued
shock waves in gas, temp. behind strong shock front, M=8-30 79—72910
shock waves in partially ionised gas 79—14550
shock-tube end-wall boundary layer 80—79348
single crystal, Pockel coeffs. and short-range-interaction parameters 79—73962
slightly ionised, ion density meas. with hollow probe 77—15242
slow positron annihilation and momentum transfer rates 79—22828
solar wind, inert gas abundance, 500 Myr ago from lunar dust anal. *(German)* 80—51637
solid, absorption spectra of self-trapped excitons 78—43879
solid, Brillouin scatt. intensity, elastooptical coefficients 78—10907
solid, dead layer effects in UV reflectance of excitons 78—72553
solid, density at melting and isochoric equations of state 78—83915
solid, desorption heat capacity of adsorbed ^3He 80—10735
solid, diffusion processes in plastic deform. *(Russian)* 80—92591
solid, electronic struct. of self-trapped excitons 79—19525
solid, electrostatic free electron emission *(Russian)* 77—24933
solid, energy bands, depend. on choice of exchange-correlation pot. 80—70607
solid, energy loss of 0.5 to 2 MeV ^4He ions, from backscattering meas. 79—4346
solid, enthalpy of sublimation, internal energy, determ. from vapour pressure 78—91435
solid, equilib. props., uncorrel. pairs approx. 80—84303
solid, FCC and HCP, free energy difference, from Ar-O_2 vapour press. meas. 77—11700
solid, FCC struct., temp. depend. of stability 77—35502
solid, H_2 and D_2 CoM freq. matrix shifts calc. 79—6969
solid, heat capacity, possible dimens. effect 78—75844
solid, high-temp. thermal expansion characts. 80—59680
solid, improved unsymmetrised SCF approx. for strongly anharmonic crysts. 78—75791
solid, lattice dynamics calc. using energy band theory 80—49320
solid, lattice dynamics calc. using Kihara hard core pot. 77—1193
solid, lattice parameter determ. at melting, X-ray diffr. 78—10174
solid, lattice thermal cond. analysis, low temp. 77—35768
solid, low temperature lattice thermal cond. 78—22910
solid, many-body contributions to OK binding energy 80—84135
solid, matrix absorpt. spectra and photochem. of chlorofluoro- and bromofluoromethane cations 79—96339
solid, n=1 surface excitons and LO-TO splittings of bulk excitons 79—73445
solid, NH and ND impurities, role. of rotational and translational modes in vibr. relax. 78—10132
solid, NMR study of dilute o-H_2 impurity 80—25228
solid, optical absorpt. and luminesc. spectra obs. of relaxed exciton states 77—52082
solid, phonon dispersion, many body pot. assuming variable at. polarisability, mech. props. 79—55840
solid, phonon freqs., lattice heat capacities, and Debye charact. temps. 79—10905
solid, phonon spectrum, effect of 3-body forces and anharmonicity 79—77706
solid, porous, contact heat transfer in sublimation 77—31767
solid, self consistent field calcs. of isotherms and thermodynamic props. *(Russian)* 80—10633
solid, self-trapped exciton, pseudopotential method 79—82529
solid, surface excitons 77—76892
solid, thermal eqn. of state and elastic consts., calc. *(Russian)* 78—14437
solid, thermodynamic props. under press., multiparametric pairwise and Lennard Jones potential calcs. 80—39316
solid, two-phonon Raman scatt. at low temps. 79—87433
solid, vacancy conc., X-ray study at const. vol. 80—64991
solid, vacuum UV luminesc. of N_2 molecular centres, 8K 78—10958
solid, vibr. and thermal props., effect of polarisability 78—71807
solid, vol. depend. lattice dynamics, pseudo-harmonic approach 79—99260
solid, X-ray induced point defects 80—59514
solid and gaseous, valence and inner shell excitonic band struct. 80—6735
solid and liquid, Raman spectra 78—84580
solid film, electron MFP, vacuum UV photoemission data 77—28690
solid state props., statistical thermodynamic calc. using gas phase intermol. pair pot. *(German)* 77—20083
solid-liquid transition, and mech. props., modified cell theory 79—23703
solubility and diffusion in UO_2 and UO_2-SiO_2 77—20130
solubility parameters, calc. from eqn. of state 77—11660
spark, atmospheric press., with Mg cathode, evidence for ionic toroidal post discharge environment 77—84551
spark in focused laser beam, and continuous optical discharge, numerical study 79—14632
spectral line intensities of metals in controlled argon atmospheres *(Russian)* 77—56300
spectroscopic light source carrier gas glow discharge and hollow cathode types 78—82047
sputtered atoms diffusion coeff. 79—87539
sputtering glow discharge, metastable and reson. states density meas. *(French)* 80—14955
starting gas, Hg discharge, high pressure, NaI and TlI additives, line broadening and radiative transport 80—74199
stony meteorites, light noble gases anal. compilation 78—65574
sublimation temp. determination at very low pressures, equation of state *(Croatian)* 79—28094
superheated liquid, nucleation rates 79—23741
supersonic expansion of gas, non-Maxwellian vel. distrib. function 79—98762
supersonic flow past blunt body, radn. effect on flow field and heat flux 77—47113
supersonic jet, spark line emission, 300-1000 Å 77—19793
supersonic jet, ultrasoft X-ray emission following electron excitation 77—27015
supersonic pulsed flow from conical nozzle 80—103056
supersonic radiation waves, excitation by CO_2 laser 79—90433
surface, desorption of He, appl. of simplified continuum model 78—87860
surface energy and surface tension near triple pt. 78—43218
tetrafluoro-dibromo-ethylene-Ar-Xe mixture, experimental study of stimulated emission 79—98347

argon continued
tetrazine-Ar, van der Waals bond, nonstatistical vibr. energy distrib., photochemical reaction effects 80—30255
thermal activity coeff. meas., periodic-heating method 80—42218
thermal conductivity, at constant density and pressure range *(Russian)* 77—76021
thermal conductivity, at high press. 80—103099
thermal conductivity, law of corresponding states *(Russian)* 78—87426
thermal conductivity, Lennard-Jones (12-6) pot. parameters calcs. 80—28591
thermal conductivity, near 300K, density depend., 0.8-35 MPa 78—67304
thermal conductivity coeff. meas. 1100-2200K range, differential technique 77—33989
thermal conductivity of gas and liq., eqn. verification 77—39395
thermal diffusion factors, isotopic 78—22450
thermal transpiration, theory and expt. comparison, molecular and transition flow 79—32579
thermodynamic behaviour, improved analytical representation 80—54339
thermosphere, annual var. from Aeros Nims data 80—12578
thermosphere, Ar density profiles meas. between 90 and 220 km altitude 78—77383
thermosphere, global distrib., departures from hydrostatic equilib. 78—28358
threshold photoelectron spectra by electron attachment 77—75211
tissue inert gas washout, diffusion limited obs. 79—84069
total electron impact excitation cross section, first Townsend coeffs. 77—536
total scattering cross sections for low-energy electrons 80—58417
Townsend discharge, electron energy distrib. functions 77—58912
transport props. with Lennard-Jones (12-6) pot., distance parameter 79—55437
triple point, surface tension effect on transition zone 77—35798
triple point determ. by thermal anal. *(Japanese)* 79—95123
triple point realisation, reference temperature appl. 78—73997
triple point sealed cells using stainless steel envelope 80—95099
triple point temp. determ. by calorimetry 79—12806
twin-hollow-cathode interferometer-spectrometer, discharge characts. *(German)* 78—67461
two-dimensional freezing, on differently graphitised carbon 79—77896
UHF discharge, spectral meas., Ar II lasing lines 79—99016
UHF discharge theory *(Russian)* 77—62430
in upper atmosphere, electron impact yield spectra 78—28401
US vels. and absorption coeffs., determ. of relaxation times 78—63530
UV photoion density meas. using high press. Langmuir probe 78—51340
vacancy theory of melting and condensation, cell model calcs. 77—55224
vacuum arc discharge, lasing action 79—18402
valence electron distrib., pseudopotential calcs. 80—2335
van der Waals interaction with Al I, line broadening and shifts 79—6912
vapour, opto-galvanic effect 79—98013
vapour press., entropy and enthalpy, thermodynamic consistency, two-parameter eqn. 77—80613
vapour pressure, effect of high mag. fields 78—38825
vapour-liquid interface, surface thickness determ. assuming linear density profile 79—69324
Venus atmosphere, O_2, Ar, CO abundances, error of Pioneer Venus chromatography obs. 80—105189
in Venus lower atmosphere, isotopic abundance results from Pioneer Venus 79—48720
Venus thermosphere, Ar isotope abundances upper limits 80—4281
vibrational relaxation of Cl_2, impurities, stochastic classical trajectory approach 78—79707
virial coefficient; meas. at various temps. using differential Burnett apparatus 80—22373
viscosity, meas. up to 2000K by percolation through porous medium 78—1781
viscosity under pressure, density depend. 80—1727
W-value determ. for α-particles 79—39518
wall-stabilised arc electron and heavy-particle temp. variations 78—67602
weakly ionised plasma turbulence in longitudinal mag. field 78—75338
Z-discharge, in low pressure gas, formation of current layer *(Japanese)* 79—37570
AR XI, O I like ion, solar emission lines density depend. 79—40165
AR+N^+(O^+), electron emission, double differential cross sections, Auger spectra 79—45684
AR_2^++F^-, in Ar, high press. ion-ion recomb. rate calcs. 78—31621
AR($^3P_1$)+H_2, energy transfer rate const. expts., reverse reaction effect 77—65520
Al-Al, Thomas-Fermi-Dirac model, inhomogeneity corrections 80—23308
Al+NO+Ar→AlNO+Ar, rate coeff., 600K, fluoresc. and absorption spectrum obs. 77—40521
Al+TlF, rot. excitation, M-conserving approx. 79—3546
Ar 3s, photoelectron ang. distrib., relativistic Dirac-Fock calc. 79—59411
Ar, ($^3P_2$) and ($^3P_0$) states, quenching mechanisms and rate consts. 79—13801
Ar (metastable)+dichloroethylene (dichlorobenzene), mol. ionis., collisional energy depend. 79—54950
Ar, Ar-N_2(Xe), detection gas suitability for proportional scintillation counter *(German)* 78—41901
Ar, atmospheric arc-jet plasma, ζ-function evaluation, near 10^4K 77—84497
Ar, bath gas, Br_2, long-lived $A^3\Pi(1_u)$ state, quantum-resolved dynamics of excited states 80—69178
Ar, dense gas, thermal cond. and viscosity coeffs., irreversibility and Kirkwood superposition hypothesis *(French)* 78—94881
Ar, electron radial diff. coeff. to mobility ratio 77—19666
Ar excited+bromochlorodifluoromethane, IR spectra, matrix isolation study, C-F stretching fundamentals 78—37632
Ar excited+dibromodifluoromethane, IR spectra, matrix isolation study, C-F stretching fundamentals 78—37632
Ar excited+dichlorodifluoromethane, IR spectra, matrix isolation study, C-F stretching fundamentals 78—37632
Ar I, II, fission fragment excitation of optical radiation, quenching by UF_6 77—23665
Ar I, laser line observation in Cu(Ag) hollow cathode discharges 79—68383
Ar I 3949 Å, Stark width in medium electron density plasma 79—63954
Ar I and II transition probability determ. from improved branching ratio obs. 78—66514
Ar I arc plasma, excited atom density meas., Saha-Boltzmann equilib. 80—926

argon continued
Ar I spectra, probabilities of np^{5}n′p→np^{5}n′s dipole transitons, two-config. approx. calcs. 77—71779
Ar II, (e,2e), photoelectron and conventional spectroscopies 78—90298
Ar II, beam-foil spectra, lifetimes meas. 78—42167
Ar II, lifetime meas. using photon-photon delayed coincidence 77—14389
Ar II, line-continuum interference effect in Lorentzian wings 79—18147
Ar II, lower laser levels, natural lifetime determ. 77—6724
Ar II, magnetically confined plasma, pulsating ion laser action 78—78994
Ar II, spectral line breadth due to electron impact, UV spectra 79—22661
Ar II, transition probabilities, lifetimes, intermediate coupling semiempirical calcs. 79—789
Ar II, transition probabilities and level lifetimes calc. 79—26935
Ar II laser, square current pulse discharge excitation, waveforms *(Japanese)* 77—34873
Ar III, beam-foil spectra, lifetimes meas. 78—42167
Ar III, CW laser, short wavelength multiline performance 79—926
Ar III, in pulsed arc plasma, ξ, factor determ. 79—4116
Ar III and IV, electron impact width of plasma lines, approximative semiclassical formula 80—43972
Ar IV to Ar XII, beam-foil obs. of lifetimes and oscillator strengths, spectral identifications, 400-2000 Å *(French)* 80—9555
Ar IX, Ne I like reson. and Na I-like satellite lines, relativistic HF calc., beam-foil spectra 78—94210
Ar ion laser lines, use in Raman spectrometer calibration 79—97446
Ar ions+C foils, emergent Ar-L Auger electron absolute yields 77—19061
Ar, microwave breakdown of nanosecond duration, calc. of threshold fields 78—94948
Ar, momentum density of electrons, two-gamma positron annihilation determ. 77—69211
Ar plasma, shock tube data on radiative cooling, IR laser techniques 78—79472
Ar plasma formation in crossed electric and magnetic fields, optical spectra 80—79452
Ar triple point cells, comparison 78—73996
Ar VIII, beam-foil lifetime meas. using ANDC anal. for reson. doublet 79—93964
Ar XI, excited level populations, line intensity ratios, solar corona appl. 80—32637
Ar XIII, Ar XIV in solar flares, atomic data rel. to XUV electron density diagnostics 79—88633
Ar XV, 2s2p($^3P_1^0$)→2s^2($^1S_0^e$) transition probabilities, CI calcs. 79—36544
Ar XV, wavefunctions and oscill. strengths, CI calcs. 80—23317
Ar XVI, in plasma, ion electron collisional radiative recomb. coeffs., bottleneck calc. 80—53942
Ar XVI, lithiumlike ions, excitation by electron impact 78—13606
Ar XVIII Lyman-α line Stark broadening, hot dense laser-produced plasma 77—11402
Ar$^-$, electron capture expts. to search for long lived states 79—72410
Ar$^-$, free-free radiative absorpt. coeff. calcs. 77—423
Ar$^{+,2+,3+}$, electron impact, <800 eV, multiple ionis., L-shell contribs. 80—37892
Ar$^+$, 30-cm multipole sputtering electron-bombardment ion source, design and characts. 77—87870
Ar$^+$, acceleration by intense relativistic electron beam in spatially periodic mag. field *(Russian)* 79—10255
Ar$^+$ and Ar$^+$-Kr$^+$ ion lasers, I_2 stabilized, beat frequency 80—95916
Ar$^+$, Ar^{2+}, relative confinement efficiencies in quadrupole ion storage trap 79—2869
Ar$^+$, Au(Cu) surface-grazing scatt., 1 MeV, excited-state orientation depend. on scatt. angle 77—61847
Ar$^+$ beam, deflection in two-dimensional electrostatic quadrupole field 78—5417
Ar$^+$, beam metastable fraction determ., by W surface impact, secondary electron obs. 79—28873
Ar$^+$, bombard. sputtering of ZrO_2:Y_2O_3 film, Auger and XPS spectra obs. 79—52071
Ar$^+$ bombarded Mo surface, 40 keV, excited at. emission 80—11481
Ar$^+$ bombardment induced ripple topography on amorphous Si 77—77336
Ar$^+$ bombardment of Cu (001) with adsorbed O, particle ejection, ang. depend. mechanism 80—50489
Ar$^+$ bombardment of Pt(110), O_2 adsorption, effect on reactivity 80—89099
Ar$^+$, conversion to mol. ions, three body association coeffs. determ. using drift-tube mass spectrometer 80—108699
Ar$^+$, electron impact excitation, extreme VUV reson. lines 77—6937
Ar$^+$, electron impact ionis. cross section 78—50647
Ar$^+$, in Ar, transverse diffusion coeff., reson. charge exchange effects 78—63533
Ar$^+$, in rarefied plasma stream, energy accommodation coeffs. meas. by thermoanemometric sounding 80—16722
Ar$^+$ ion laser, active mode locking study 80—91827
Ar$^+$ ion laser, plasma instability, suppression by He admixture 79—64204
Ar$^+$ ions moving through Ar gas in strong elec. field, energy spectrum 80—5679
Ar$^+$ laser 582 THz stabilisation by I_2 cell, improvements 80—102741
Ar$^+$ laser freq. stabilisation by $^{127}I_2$ absorption lines at 582 THz 78—90430
Ar$^+$ laser plasma, localised probe diagnostics 79—55113
Ar$^+$ lasers, freq. stabilisation by saturated absorption in external $^{127}I_2$ cells 79—22965
Ar$^+$, metal surface bombardment, 20-30 keV, adsorbed C^+ layer removal, in plasma 77—76103
Ar$^+$, metastable, electron impact cross section, laser fluoresc. 77—3465
Ar$^+$, mobility in Ar, spin-orbit coupling effect 78—26232
Ar$^+$ mobility in He gas at 82K 80—1733
Ar$^+$ orientation angular depend., beam-tilted foil interaction 78—5335
Ar$^+$, orientation by collision with tilted surface, appl. to zero-field level crossing 77—3452
Ar$^+$, reson. line regularities in plasma Stark widths and shifts 80—43881
Ar$^+$, scatt. on Ni crystal, light emission polaris. 78—1072
Ar$^+$, upper laser levels collisional excitation and de-excitation, rate coeffs. 79—7112
Ar^{++} ions, 4.8 MeV, bombardment of C stripper foils, shrinkage, rupture, lifetime 78—33352

argon continued
Ar^{+++}, prod. from RF sources 79–18070
Ar^{12+}, impact on highly-ionised Ne target, selective target electron capture effects 80–14202
Ar^{15+} and Ar^{16+}, beam-foil obs. of lifetimes of metastable states 80–14116
Ar^{15+}, Ar^{16+}, population of $^3P_2$ and $^4P_{5/2}$ states by cascading process 79–63966
Ar^{15+}, population of $^4P_{5/2}$ state meas. by cascading processes 78–94315
Ar$^{16,17+}$ filled glass shell, symmetric laser compression 80–64759
Ar^{16+}, radiative decay from 2^3P_2 and 2^3P_0 levels, beam-foil time of flight meas. 77–68015
Ar^{17+}, Lamb shift, elec. field quenching time of flight method 79–13674
Ar^{18+} detection, efficiency of ^{7}LiF TLD 78–53504
Ar^{2+}, beam metastable fraction determ., by W surface impact, secondary electron obs. 79–28873
Ar^{2+} dissociative recombination in Ar+N_2 early afterglow 79–34305
Ar^{2+}, levels of $2p^53p^5$ 78–74574
Ar^{2+}, mobility in parent gas 79–7439
Ar^{2+}, multiple open shell configs. calcs., modified HF method 77–50356
^{40}Ar^{+}, stopping power in Au at 50-500 eV 77–76478
Ar^{5+}, Ar^{6+}, excited state lifetimes, beam-foil meas. 77–10750
Ar^{6+} +inert gases, collisional excitation, excitation cross sections 79–98209
Ar^{6+}, static dipole quadrupole polarisabilities and shielding factors calc. using HF scheme 80–99450
Ar^{8+}, Na like ions, dielectronic recombination rate, scaling props. 80–32668
Ar^{8+}, second order correl. energy, Z depend. of irreducible-pair energies 80–91417
Ar^{i+}, (i=1, 2, 3, 4, 5), absolute electron impact ionisation cross section 80–83496
Ar^{n+}, electron impact inner-shell excitation/ionis. cross section 77–23564
Ar^{n+}, $n \leq 8$, extracted from ECR plasma ion source, charge state distrib. 80–24268
Ar^{x+}, high resolution spectroscopy of prompt and metastable decaying levels 78–33462
Ar:CS_2 (OCS), thermoluminesc. following VUV photolysis 77–52659
Ar:Eu, matrix isolated, obs. of Stokes and anti-Stokes vibrational sidebands in emission spectra 77–73164
Ar:H, solid, struct., pair pot. calcs. 78–2215
Ar:H crystalline matrix, Xα scattered wave cluster model 79–73468
Ar:H_2, nuclear spin relax. of H_2, crystal field meas. 79–51875
Ar:He, scatt. pot., He in (2^3S) state, 0.02-0.12 eV 79–54938
Ar:K seeded plasma, temperature diagnostics 78–67427
Ar:Li$^+$, interstitial interaction energy calc. 78–38692
Ar:methane, impurity rotational states, inelastic neutron scatt. study 79–51020
Ar:N_2O, O(^{1}S) photodissociative prod., photoluminesc. excitation spectra, exciton energy transfer 80–89508
Ar:N_2O(CO)(CO_2), fluoresc. and thermoluminesc. after photolysis 79–89700
Ar:NH, solid, crystal impurity librational relax., phonon assisted transitions, direct, Orbach and Raman processes 78–83887
Ar:NO_2, Raman spectra, high press., low temp. effects 78–52479
Ar:Ne, localised mode due to Ne impurity, Green function technique 77–1201
Ar:O_2 (6%) cryst., vibr. Raman spectra 80–60558
Ar:O_2(N_2), long-wave UV luminesc. *(Russian)* 78–88347
Ar:OCS, liq., dissoc. studies 80–78716
Ar:OCS, O(^{1}S) and S(^{1}S) photodissociative prod., photoluminesc. excitation spectra, exciton energy transfer 80–89508
Ar:OCS:O_2 matrix, $S+O_2 \rightarrow SO_2$ chemiluminescence reaction, SO_2 thermoluminescence 77–48647
Ar:PH_3:N_2O, photolysis, HPO and PO form., IR(UV) matrix isolation spectra 80–47985
Ar:S, plasma, atomic S lines above first ionisation limit 78–25462
Ar:S_2, absorpt. spectra, matrix-isolated in van der Waal solid 77–52139
Ar:Xe, liq. 0-1.4 g cm^{-3}, vac. UV absorpt. spectra, Wannier impurity states 77–77232
Ar:Xe film, solid, competition between electronic energy transfer and relax., photoelectron spectra 77–24929
Ar:Xe:Cl_2, photochem. XeCl prod., ESR 77–18947
Ar:Xe$^+$, 0.1-1.4 gm cm^{-3}, adiabatic electrostatic polarisation energy, calc. 77–85640
^{40}Ar:^{41}K, matrix isolation model system 78–45722
Ar/O_2 plasma treatment of SiO_2 surface, reactivity modification 78–64890
Ar-acetonitrile mixture, anomalous thermal cond. in const. elec. field 77–7505
Ar-acetylene van der Waals molecule, radiofreq. spectroscopy and Stark effect meas., equilib. struct. and props. 80–91543
Ar-air, transformer plasmatron, LF discharge, electrical and energy props. 80–103200
Ar-air arc, stabilised, spectroscopic methods of temp. meas. *(Russian)* 80–38854
Ar-Ar pot. parameters, from CO in Ar matrix, empirical evaluation 80–48057
Ar-Br_2, positive column at. state densities 80–44007
Ar-CH_4 proportional counter, light emission obs. 80–78488
Ar-CO, glow discharge, ion cluster in positive column, ion mass spectra diagnostics 80–38752
Ar-CO, pulsed non self sustained discharges, peculiarities 80–38811
Ar-CO glow discharges, positive ion spectra, ion clusters obs. 80–64807
Ar-CO_2 atmosphere melting plasmatron arc characts. *(Russian)* 80–38573
Ar-CO_2 mixture, Ar* prod. by electron excitation, transfer reaction kinetic study 80–63824
Ar-CO_2(He), natural diffusion coeffs., press. effects 78–26229
Ar-CO(-N_2), C_2 and CN form. by optical pumping, room temp. 80–16701
Ar-cascade arc, spectral sensitivity of radiation detectors in VUV range, report *(German)* 78–82037
Ar-Cs plasma, HF induction discharge, Hall effect *(Russian)* 77–43101
Ar-Cs plasma stream, electrodynamic braking with strong MHD interaction 78–9763
Ar-Cs plasmas, electron momentum transfer cross section, cyclotron reson., temp., cond., and vel. meas. 80–106930

argon continued
Ar-Cs$^+$, ion mobility and interaction pot., drift tube meas. at 300K 78–59537
Ar-Cu, Cu diffusion coeff. determ. volatile salt dissoc. in pulsed discharge 80–33721
Ar-ether(acetone)(benzene)(ethanol), conc. profile and interdiffusion coeffs. meas. 79–94763
Ar-F_2, Ar-Kr-F_2 mixtures, excimer emission bands *(Russian)* 77–71885
Ar-F_2, mixtures, low-press. excimer form. and quenching by e-beam excitation 79–50071
Ar-F_2 excimer laser, kinetics of excimer formation 80–14328
Ar-graphite system, effects of dynamic coupling 80–10771
Ar-H_2, elec. breakdown, time and space resolved spectra 78–18470
Ar-H_2, H_2 separation in thermogravitational column 80–45561
Ar-H_2 arc, $H_\alpha(D_\alpha)$ Stark broadening obs. 79–36582
Ar-H_2 plasma, thermodynamic properties 78–63542
Ar-H_2 solution, far IR spectra, density narrowing of rot. line 79–50086
Ar-H_2O mixture, thermally ionised behind shock wave, cross section for collisions of electron with H_2O 77–11309
Ar-H_2O vapour mixture, H_2O droplets nucleation rate const. 80–61131
Ar-H_2S plasma, spectroscopic study, electron density, ionis. temp. meas. 77–19764
Ar-HBr, intermol. pot. energy surfaces calcs. 80–91625
Ar-HCl, liq. density fluctuations, far IR absorpt., neutron scatt. mol. dynamics calc. 78–19461
Ar-HCl, van der Waals mol., far IR spectra 77–79611
Ar-HCl, Van der Waals mol., far IR spectrum, anisotropic intermol. force effects 78–62869
Ar-HI, low electron beam excitation rates 79–86163
Ar-He, binary diffusion coeffs., press. depend., 300 and 323K, Thorne's eqn. 80–1724
Ar-He, heat of mixing, 2-15 bar *(French)* 79–7436
Ar-He, heat of mixing, low press., theories comparison 78–26230
Ar-He, liq. soln., sound vel., perturbation theory *(Russian)* 77–47512
Ar-He glow discharge with different potential cathodes, expt. *(Russian)* 77–39484
Ar-He ion laser, population inversion radial distrib. and output characts., mag. field depend 80–19019
Ar-He mixture, mass separation during molecular beam sampling process 80–31937
Ar-He plasma, ion acoustic soliton form., mechanism 78–18457
Ar-He plasma, thermal diffusion factors, binary mixture hypothesis 79–27749
Ar-He plasma, thermal diffusion factor, 2000-4000K, binary mixture hypothesis 79–32743
Ar-He plasma, thermal diffusion of neutral species in plasma jet, 2000-4000K 79–32742
Ar-He rarefied mixture in supersonic nozzle and jet, longit. translational nonequilib. 79–27678
Ar-He(Kr)(Ne), solubility in Ar, and related functions, three-body forces 79–10776
Ar-He(Ne), thermal cond., composition dependence 78–51276
Ar-hexamethyldisiloxane, glow discharge positive column ion mass spectra identification 80–38834
Ar-Hg, gas mixture, diffusion coeffs. and electron temps. 77–62327
Ar-Hg mixture, RF discharge, frequency characts. investig. 80–38761
Ar-Hg-Cl_2, elec. discharge, electron inelastic collision props. 80–79617
Ar-I_2, low electron beam excitation rates 79–86163
Ar-Kr, gas, diffusion coeffs. meas., 350-1200K 80–14869
Ar-Kr, glory structure in total cross section, crossed supersonic atomic beam, n(x)-6 potential 80–48060
Ar-Kr, internal pot. function calcs. 79–68292
Ar-Kr, liq. mixture, excess thermodynamic props. 78–75836
Ar-Kr, mol. force const. from viscosity data, thermal cond. 78–33565
Ar-Kr, pair pot. energy functions, gas phase bulk property reproduction 77–27642
Ar-Kr, pair pot. function calcs. 78–74726
Ar-Kı, thermal cond., 90-270K, 1 atm. press. 78–42700
Ar-Kr jet, electron excited, VUV emission spectra 80–933
Ar-Kr liq. and gas. solns., collision-induced dipole moment, far IR band obs., self-diffusion coeff. 77–38627
Ar-Kr liquid mixtures, volume and shear viscosities *(Russian)* 77–84961
Ar-Kr mixture, thermal cond., 120-273K 78–83514
Ar-Kr mixtures, liq.-vap. isotope fractionation factors 78–33626
Ar-Kr white light lasers *(Russian)* 77–27303
Ar-Kr-F_2 discharge, inelastic electron collisions, energy distrib. and rate consts. 80–87980
Ar-Kr-F_2 excimer laser, kinetics of excimer formation 80–14328
Ar-Kr-F_2 mixture, electron beam pumped, spectroscopy and kinetics of 248, 414 nm bands 78–63081
Ar-Kr-F_2 mixture, nucl. induced excimer fluoresc. for I laser excitation 80–78846
Ar-Kr-F_2 nuclear pumped laser, high energy beam deposition 80–63999
Ar-Kr(Xe), mol. interactions, thermodynamic props., mol. dynamics calcs. 77–61044
Ar-Kr(Xe), UV absorption spectra, induced lines and line-shift meas. *(French)* 77–61697
Ar-Kr(Xe)(N_2), electron beam ionis., low temp. plasma prod. 80–87908
Ar-like atoms, gradient expansion of atomic kinetic energy functional 80–95530
Ar-methane, cryogenic fluid mixture, transport phenomena, shear viscosity *(Russian)* 80–29198
Ar-methane, gas diffusion of Cs atoms, by reson. ionis. spectrosc. 79–18984
Ar-methane, liq., drift vel. of excess electrons 80–54744
Ar-methane liquid mixtures, excess electrons drift vel. 77–59288
Ar-methane+Cl ions, energy straggling 78–58785
Ar-Mg plasma, near reson. charge exchange spectra *(German)* 77–31425
Ar-monochlorodifluoromethane mixture, US vels. and absorption coeffs., determ. of relaxation times 78–63530
Ar-N_2, electron-beam-excited laser lines at 337.1, 357.7, and 380.5 nm, gain conditions 79–86166
Ar-N_2, proton beam pumped, laser actqn at 3577 Å 80–9861
Ar-N_2 electron beam pumped laser characts. at 25-350°C 78–58984
Ar-N_2 gas mixture, vapour-liq. equilib. data *(German)* 77–84915
Ar-N_2 gas scintillation MWPC for high-intensity 5-10 keV X-rays 78–82575
Ar-N_2 interaction, electron gas pot. calc., Gordon-Kim model, ang. orientation depend. 78–70893

argon continued
Ar-N_2 laser, electron beam excited, gain measurements using amplified spontaneous emission 80−37986
Ar-N_2 laser, intense proton beam pumping 78−78998
Ar-N_2 laser, UV emission, 100-500K, kinetic model 77−58321
Ar-N_2 liquid soln., selective adsorption by plane homogenous surface and C atoms, mol. dynamics calc. 80−59806
Ar-N_2 mixture, adsorption on chabazite, test of eqns. for gas mixture adsorption on heterogeneous surface 78−60030
Ar-N_2 mixture, electrodeless RF discharge, discharge current harmonics obs., conc. depend. 80−44029
Ar-N_2 mixture, electron beam pumped, lasing obs. at 337, 358, 380 and 406 nm 80−102700
Ar-N_2 mixture, fission fragment energy deposition kinetics, rel. to nucl. pumped laser 77−23652
Ar-N_2 mixture, lasing at four lines 80−99713
Ar-N_2 mixtures, DC arc, energy balance of electrons 78−42797
Ar-N_2 plasma, diffusion separation N_2 dissociation 77−76036
Ar-N_2-H_2 plasma equilibrium compositions and thermodynamic props. 78−71433
Ar-N_2(CO_2), thermal diffusion factors meas. 80−10344
Ar-N_2(CO), non-self-sustained discharge instability, negative differentiated cond. *(Russian)* 80−38740
Ar-N_2(Cl_2)(F_2)(H_2O) laser, energy pathways by proton excitation 78−5459
Ar-NF_3, electron attachment coeffs. using swarm techniques 80−53915
Ar-NH_3 mixtures, viscosity under press., density depend. and mol. assoc. 80−1727
Ar-NO, thermal cond. Senftleben effect meas. 79−18985
Ar-Ne, mixture, cataphoretic segregation, spectroscopic meas. 79−79261
Ar-Ne gas, positron vel. distrib. at equilib., annihilation decay rate 77−71870
Ar-Ne mixture, thermal conductivity, 400-1500K 79−18987
Ar-Ne mixture in critical region, renormalised one-chain approx. 77−11452
Ar-Ne mixtures, thermal diffusion 80−1726
Ar-Ne(-He)(-Kr), gas mixtures, thermal cond. meas. in the range 0.5-15 MPa 80−14874
Ar-Ne(H_2), liquid solution, dielectric props., intermolecular interactions *(Russian)* 80−88904
Ar-Ne(Kr) systems, pot. parameters from binary diffusion coeffs. 78−37700
Ar-O_2, diffusion, search for Senftleben-Beenakker effect 77−15155
Ar-O_2, gas, thermal cond., mag. field effects 78−34255
Ar-O_2 liquid mixture, dielectric polarisation and permittivity *(Russian)* 77−90095
Ar-O_2 mixture, adsorption on CsI, test of eqns. for gas mixture adsorption on heterogeneous surface 78−60030
Ar-O_2 mixtures, positronium form. and quenching, orthopositronium quenching cross section determ. 80−74261
Ar-O_3 Van der Waals complex, struct. and props., RF and microwave obs. 80−32704
Ar-SF_6, condensing flow, gasdynamic and IR meas. 80−6501
Ar-SF_6, thermophysical props., second virial and diffusion coeffs., thermal diffusion factors 78−42699
Ar-SF_6, volume discharge excited by electron beam, stable region *(Russian)* 78−22589
Ar-SF_6 mixture, space discharge excited by electron beam *(Russian)* 78−83629
Ar-SF_6 mixture, space discharge excited by electron beam *(Russian)* 78−83630
Ar-SF_6(CF_4) mixtures, viscosity and diffusion coeffs. 77−89225
Ar-Ti hollow cathode afterglow, energy transfer mechanisms and excited metallic ion prod. 80−43857
Ar-Xe, liq., Zwanzig perturbation expansion convergence, free energy 77−76274
Ar-Xe, low-threshold nuclear pumped laser, generation characts. 80−19018
Ar-Xe gaseous mixtures, collision-induced microwave absorpt. 78−78680
Ar-Xe high press. transverse discharge laser using Xe IR transitions 80−63978
Ar-Xe high-press. neutral IR laser emission from Xe 79−86159
Ar-Xe IR laser pumped by electron beam stabilised discharge, lasing parameters 80−102698
Ar-Xe mixture, microwave absorption, collision-induced 79−22626
Ar-Xe-NF_3, mixture in XeF laser, discharge stabilised by short-pulse electron beam 80−14358
Ar-Xe-NF_3 mixture, fluorescence from e-beam excitation at low temp. and high press. *(French)* 78−58727
Ar-Xe-tetrachloromethane, self-sustained electrophotoionised discharge in compressed gas 80−38003
Ar-Xe-tetrachloromethane excimer discharge laser 79−13957
$Ar+{}^4He^{2+}$, ionis. cross section, Z^3 effect 78−33595
Ar+10% CH_4, Fano factor determ. from α-particle pulse height distribs. 79−76284
Ar+AR, potential well depth estimation method 79−86034
Ar+acetylene, vibr. relax. study using laser-induced fluoresc. 80−74219
Ar+Ar, isotropic intermolecular forces evaluation using semi-empirical approach 79−36726
Ar+Ar, K-X-ray excitation, 2.5-8 MeV, impact parameter depend. 78−50628
Ar+Ar, low-energy collision induced UV radiation 79−50125
Ar+Ar, optical emission spectra 77−14551
Ar+Ar, Thomas-Fermi-Dirac interaction pots. 77−75253
Ar+Ar (Kr)(Ne), elastic scatt., Monte Carlo averaging of differential cross-section data 78−21997
Ar+Ar low energy collisions, K X-ray excitation, impact parameter depend. 80−23539
Ar+Ar partially stripped ion, stopping power 80−91651
$Ar+Ar_2$, exchange and dissoc. interactions, three-body effects calcs. 77−9069
$2Ar+Ar_2{}^+=Ar+Ar_3{}^+$, equilib. consts., mass spectrometric determ. 79−100347
$Ar+Ar^-$, charge exchange, Σ oscill. and spin change 80−74247
$Ar+Ar^+$, differential cross section, pot. curve fitting, reson. electron exchanges 77−58118
$Ar+Ar^+(Ar^{2+})(Ar^{3+})$, electron stripping cross-sections meas. 80−83477
$2Ar+Ar^+(Kr^+)$, three body reaction, rate coeffs., temp. depend., 100 to 300K 80−108703
$Ar+Ar^{2+}$, charge transfer, energy defect and sealing laws 80−48083

argon continued
$Ar+Ar^{2+}(Ne^{2+})$, single electron capture excitation, photon emission, VUV spectroscopy 80−58379
$Ar+Ar^{6+}$, collisional excitation, excitation cross sections 79−98209
$Ar+Ar^{z+}(Ne^{z+})$, outer s-subshell vacancy production 79−18275
$Ar+Ar({}^3P_2)({}^3P_0)$, flowing afterglow metastable decay rates, diffusion, two- and three-body rate consts. 78−73027
$Ar+Ar(Ar^+)$ collisions, multielectron excitation energy calcs. 78−1071
Ar+Ar(He)(Ne), dispersion interaction, series coeffs., variation method 79−3518
Ar+Ar(Kr)(Xe), total cross section, glory struct. 80−23494
Ar+Ar(Kr)(Xe), total scatt. cross-sections, glory undulations 77−10732
Ar+BaCl, intermultiplet energy transfer 79−27063
$Ar+BaCl(C^2\Pi)$, collisional quenching, laser induced fluoresc. decay meas. 79−27075
Ar+BaO, in Ar flame, rot. and translational relax. by sub-Doppler optical-optical double reson. 80−95583
$Ar+Be^+$, Be II 2^2P excitation, alignment and orientation 80−91647
Ar+benzene (${}^1B_{2u}(S_1)$), rot. relax. to Boltzmann distrib. 78−86936
$Ar+Br_2$, effective vibr. pot. of Br_2 in Ar gas, Monte Carlo simulation 79−59526
$Ar+Br_2$ dissociation reaction, trajectory study by ensemble method 80−66765
Ar+BrCN(HCN), CN quartet state production, fluoresc. anal. 78−68888
$Ar+C^-(O^-)(F^-)(Cl^-)$, negative ion stripping, at. beam form. 77−6926
$Ar+C^{+*}$, charge transfer cross-sections, 0.7-2.4 keV, $C^+({}^2P)$ and $C^+({}^4P)$ 78−58806
$Ar+C^{4+}(C^{6+})$, K-shell X-ray prod. at high energy, charge state independ. 77−6905
$Ar+C^{6+}(O^{8+})$, bound- and continuum-state electron capture in gas, strong correlations 80−9730
$Ar+C^{q+}(O^{q+})$, continuum electron capture and loss, 1.6-2.8 MeV/A 78−46443
$Ar+CHF_3$, vibr. relax. times at 298K 77−525
Ar+CO, intermol. pot. energy surfaces from electron gas model, ang., distance, and vibr. depend. 79−3520
Ar+CO spin transfer reaction, CO triplet state form. *(French)* 79−34289
$Ar+CO_2$, 301_{III}-000 band, intensities, press.- and self-broadening coeffs. meas. 78−78695
$Ar+CO_2$, drift properties of tubular drift chambers in high magnetic fields 80−53917
$Ar+CO_2$, rot. inelastic wide angle scatt., differential cross sections 77−14536
$Ar+CO_2$, rot. transitions, classical trajectory calcs. 77−50501
$Ar+CO_2$, total differential scatt., IOS approx. calcs. 79−98194
$Ar+CO_2(HCl)$, press. broadening, rot. energy transfer, infinite order sudden approx. 78−22011
$Ar+CO_2(N_2)$, repulsive pot. energy surface, approx. calc. and differential scatt. expt., comparison 79−22788
Ar+Ca, quenching cross section of Ar atom for Ce reson. line 77−19021
Ar+Cl, highly charged low vel. recoil ion time of flight spectra, cross section energy depend. 80−14222
$Ar+Cl^-(Br^-)$, total electron detachment cross sections, near threshold energies 79−3555
$Ar+Cl^{4+}(I^{5+})$, 20 MeV, electron loss cross sections, pot. model data anal. 79−27082
Ar+Cs, shift, halfwidth, satellite and absorpt line in square-well pot. 80−42993
Ar+Cs, two-photon ionisation spectra, satellites, absorption line shape 78−82668
Ar+CsF, sudden, body-fixed and semiclassical approx. calcs. 78−42164
$Ar+Cu^{x+}(11\leq x\leq 22)$, 1 MeV/amu, X-ray production cross-sections 78−37714
$Ar+D_2$, state-resolved $\Delta j=2$ rot. transitions 80−63772
$Ar+D^+(O^{q+})(Si^{q+})(C^{6+})$, electron capture to continuum states, forward ejected electron spectra 79−45831
Ar+F, coupled channel study, rel. to elastic approx. 79−81255
$Ar+F_2$, vibr. relax. times, 3D semiclassical theory 78−25667
$Ar+F^-$, inner-shell ionisation, X-ray cross sections 80−58369
Ar+Fe, Fe I reson. line, collisional broadening at high temp. *(German)* 80−106298
$Ar+Fe^{4+}$, 20 MeV, gaseous targets, electron loss, charge state yields 79−54957
Ar+formaldehyde, mol. isolated Voigt line, off-peak spectral absorpt. coeff. 80−106355
Ar+H, 20-500 eV, ion pair and free electron production, integral cross sections 78−46437
Ar+H, collisional coherent excitation, meas. of Lyman α-photons 80−99552
Ar+H, electron energy loss 80−87217
Ar+H, Hα and Hβ emission cross sections 80−63782
Ar+H, low energy elastic scatt. cross section MCSCF calc., van der Waals forces 78−70897
$Ar+H_2$, 4500K dissoc. collision vibr. selectivity, Monte Carlo trajectory method 79−70307
$Ar+H_2$, 4500K shock wave expt. simulation, vibr. state changes and dissoc. 79−61850
$Ar+H_2$, atmosphere for thermal damage suppression of InP 79−100275
$Ar+H_2$, dissoc., recombination and inelastic scatt. pot. energy surface and cross section Monte Carlo calc. 77−27162
$Ar+H_2$, metastable state breakdown, temp. depend. 79−98211
$Ar+H_2$, near-reson. energy transfer, fluoresc. excitation 78−9187
$Ar+H_2$, plasma, transport coeff. calcs., 2000-25000K 77−11314
$Ar+H_2$, vibr. and rot. transfer enhancement of dissoc. cross section 77−34732
$Ar+H_2$, vibr. energy transfer rate, ab initio calcs. 78−82821
$Ar+H_2$, vibr. transition rates, thermally averaged, Monte Carlo trajectory calcs. 80−23519
$Ar+H_2{}^+$, 10 keV dissoc. charge exchange collisions 78−94319
$Ar+H_2{}^+$, endothermic charge transfer reaction, low energy crossed beam study 80−95720
$Ar+H_2{}^+$, low energy proton transfer reactions, crossed beam studies 80−108697
$Ar+H_2O+SO_2$, condensation nuclei form., ion polarity and age depend. 79−39220
$Ar+H_2O(D_2O)$, (${}^3P_{0,2}$) state quenching cross sections 78−70912
$Ar+H_2O(O_3)$, collisional energy transfer in unimol. reaction, classical trajectory calcs. 78−62882

argon continued

- $Ar+H_2(D_2)(O_2)$, thermal dissoc. of dilute mols., vibr. bias mechanism 79−61854
- $Ar+H_2(HD)(D_2)$ reson. energy transfer cross section, 1st Born approx. appraisal 77−65519
- $Ar+H_3^+$, dissoc., 400-800 keV, product charge state distrib. model 78−82838
- $Ar+H^-$, 1 to 5 keV, production cross sections for 3d,3s,4s,5s states of H 78−33603
- $Ar+H^-$, collisional electron detachment, complete ang. distrib. 78−66650
- $Ar+H^-$, differential scatt. cross-sections, time of flight spectra 78−42161
- $Ar+H^-$, electron detachment, 0.5 to 1.0 MeV 78−22021
- $Ar+H^-$, low-energy total electron detachment cross-sections, approximation 79−72405
- $Ar+H^-(He)^-$, collisional detachment cross-sections, high-energy obs. 77−3442
- $Ar+H^+$, charge transfer and ionisation cross sections 79−89766
- $Ar+H^+$, charge transfer to H(n=2), mixed parity elec.-dipole oscillations 79−31678
- $Ar+H^+$, electron capture, 4-20 keV, production of highly excited H atom 79−54963
- $Ar+H^+$, electron capture, charge-state distrib. 80−32814
- $Ar+H^+$, electron capture cross sections 78−62912
- $Ar+H^+$, H(n=4) s-d coherence, zero-field quantum beats obs. 80−32676
- $Ar+H^+$, $H\alpha$ and $H\beta$ emission cross section 80−63783
- $Ar+H^+$, importance of d-state couplings in charge transfer, ionisation 79−89760
- $Ar+H^+$, ionisation, doubly differential cross sections calcs. 80−9726
- $Ar+H^+$, ionisation, projectile energy depend., secondary electron energy distrib. 78−42211
- $Ar+H^+$, K- and L-shell electron capture, 1-15 MeV 77−54607
- $Ar+H^+$, K-electron capture, cross section scaling, high energy 79−41236
- $Ar+H^+$, K-shell ionisation cross-sections, Glauber approx. calcs. 77−46629
- $Ar+H^+$, low energy, L-shell ionisation, binding energy correction 77−54604
- $Ar+H^+$, subshell electron capture cross sections 79−89771
- $Ar+H^+$ charge exchange excitation, alignment tensor components, coincidence method 80−63795
- $Ar+H^+$ ions, K-Auger spectra, relative satellite line intensities, X-ray spectra 77−19066
- $Ar+H^+(H_2^+)$, emitted electron's energy and angular distrib. support for charge transfer to continuum theory 78−37740
- $Ar+H^+(H_2^+)\ (He^+)$, ionisation double differential cross sections 80−18913
- $Ar+H^+(H_2)^+(H_e)^+(He^{2+})$, ionisation processes viewed in forward direction 77−71866
- $Ar+H^+(He^{2+})(Li^{3+})$, inner shell electron capture cross-sections 79−76510
- Ar+HCN (001), relax. rate consts., using Cs vap. IR source 80−9696
- $Ar+HCN(H_2O)$, electron excitation of Ar* and Ar_2*, fluoresc. and dissoc. energy transfer collisions 77−14580
- Ar+HCl, classical and quantum centrifugal decoupling 77−58127
- Ar+HCl, differential cross section, quasiclassical close coupling approx. 80−63743
- Ar+HCl, inelastic scatt. exponential perturbation theories 80−74217
- Ar+HCl, infrared line shape, rotational lines, influence of collision duration 80−43110
- Ar+HCl, line broadening, short range force effects, semiclassical calcs. 79−98085
- Ar+HCl, rot. energy transfer, quasiclassical trajectory calcs. 78−42173
- Ar+HCl, rot. excitation, quasiclassical close coupling approx. 79−27068
- Ar+HCl, rotationaly inelastic collision, planar trajectory, classical centrifugal decoupling calcs. 78−58788
- Ar+HCl, spectral line shift of vibr.-rot. lines. press. shift 79−18237
- Ar+HCl(DCl) potential, asymmetric, isotope substitution effect, Legendre expansion coord. transformation 78−70894
- $Ar+HCl(H_2)$, intermol. forces, generalised electron gas-Drude model 79−98182
- Ar+HCl(HF), mol. IR line shape broadening 77−61802
- $Ar+HCl(O_2)$, shock-heated, collision induced dissoc. 79−34290
- Ar+HF, rot. relax. of high rot. levels at 1 torr press. 79−10181
- Ar+HF, state-to-state cross sections for rot. to translational energy transfer determ. 80−91644
- Ar+HF(HCl)(CO), shock heated steady state dissoc. rate consts. calc. 78−40039
- $Ar+HHe^+$, ab initio pot. energy data, SCF-LCAO calcs. 80−63530
- Ar+H(D), free electron production, integral cross-sections determ. 79−89754
- $Ar+H(H_2)$, orbiting resons., van der Waals pots., beam scatt. obs. 79−89739
- $Ar+H(H^-)$, 0.5 MeV $H(H^-)$ ionisation comparison 79−41230
- Ar+H(2S), excitation and ionisation contributions to sum-rule Born cross sections 80−99551
- Ar+H(2s), 5-25 keV, H(n=3) excitation, Balmer α emission obs. 80−53113
- Ar+H(2s), collisional de-excitation, 5-26 keV 79−59546
- Ar+He, 2^1S and 2^3S assoc. and Penning ionisation cross sections vel. depend. 79−3551
- Ar+He, Penning ionis., ejected electrons energy and ang. distrib. 79−81266
- Ar+He, Penning ionis. of Ar, He in (2^3S) state 79−41228
- $Ar+He_2(^3\Sigma)$, press. depend. reactions, rate coeffs. 78−64823
- $Ar+He^+$, (Ne^+), charge transfer reaction rate coefficient 79−91932
- $Ar+He^+(He^{2+})$, ionisation, differential cross-sections, 0.3 to 2 MeV 79−81271
- $Ar+He^+(Li^+)$, up to 70 keV, symmetric (antisymmetric) reson. charge transfer cross sections *(Korean)* 78−50636
- $Ar+He^+(2s)$, metastable ion electron capture, loss and de-excitation 77−6904
- Ar+He*, Penning ionisation, angular distrib. of electrons 79−89763
- Ar+He* Penning ionisation, semiclassical descretisation procedure 78−90275
- Ar+He*$(1s2s,{}^3S)$, coupled channel calcs. of chemi-ionisation 77−27166
- Ar+He*$(1s2s,{}^3S)$, Penning ionis., multichannel calcs. 80−53111
- $Ar+He(2^1S,2^3S)$, Van der Waals forces, one-electron model pot. calcs. 80−14094

argon continued

- $Ar+He(2^3S)$, differential cross-section meas., optical interaction pots 77−3443
- Ar+Hg, spectral line broadening of Hg in UV, interaction pot 79−26937
- Ar+highly charged ion, inner-shell charge transfer calcs. 77−50528
- Ar+Highly stripped ion, multiple-ionis. cross sections, Monte Carlo calcs. 79−64091
- Ar+isobutane+methylal, drift properties of tubular drift chambers in high magnetic fields 80−53917
- Ar+K, K 5^2P level broadening and collisional relax., quantal, semiclassical and expt. comparison 80−18903
- Ar+K, photon emission polarisation anal., coincidence studies 80−5614
- $Ar+K^+$, inelastic collisions, emission cross sections, quasimol. state interference 77−61848
- $Ar+K(Zn^+)$, 0.7-500 keV, $K(Zn^+)$ excitation, reson.-line emission and polaris. 80−18911
- Ar+Kr, $(4p^55p)$ and $(4p^55p')$ states, radiative lifetimes and two-body collisional deactivation rate consts. 80−95572
- Ar+Kr, binary diffusion coeff. pressure depend. meas. 80−43826
- Ar+Kr, elastic collision total cross-section, low energy 80−5603
- $Ar+Kr^++F^-$, three body ion-ion recombination probability, Monte Carlo simulation 80−85160
- $Ar+Kr(^3P_2)$, flowing afterglow metastable decay rates, diffusion, two- and three-body rate consts. 78−73027
- Ar+Kr(Xe), collision induced microwave absorpt. spectra 80−74216
- $Ar+Li^+$, interaction pot. of $X^1\Sigma$ state, CI calc. 79−50100
- $Ar+Li^{+1,2,3}$, K-shell ionisation depend. on projectile charge state 77−34743
- Ar+LiF, polarisation cross section, close-coupling calcs. 80−69214
- Ar+LiF, polarised rot. state-selected cross sections, anisotropic intermol. pots. 79−72398
- Ar+LiH, rot. transition cross-section, 0.8 eV 79−36742
- Ar+LiH, rotationally inelastic cross-sections, state resolved, determ. 78−13577
- Ar+Li*, Li principal series line broadening and shift, interat. pot. consts. 78−42165
- Ar+Li*(2^2P_J), collision induced fine struct. transition 80−74220
- $Ar+Li(Be^+)(Na)(Mg^+)(K)(Zn^+)$, collision-induced alignment, reson.-line emission polaris. obs. 80−18912
- $Ar+M\rightarrow Ar^++M+e^-$ or $+M^-$, $(M=O_2, NO, NO_2, N_2, CO)$, keV energies, translational spectroscopy 78−5339
- Ar+methane, CH chemiluminesc. in flowing afterglow 78−64839
- Ar+methane, enthalpy of mixing, 123 to 145K and 2.03 to 9.12 MPa 77−70330
- Ar+methane, low energy collision, close coupling and coupled states, rot. transitions 78−78784
- Ar+methane, rot. compound state resons. 80−28090
- Ar+methane compressed-liquid dielectric const., derived excess vol. 79−11377
- Ar+methane-d_4, vibr.-translational relax. 80−99537
- $Ar+Mg^+$, 3^2P differential excitation, alignment and orientation 79−86053
- Ar+N ion, $K\alpha$ X-ray satellites prod. 80−9541
- $Ar+N_2$, 0.06-0.41 eV, metastable at. electronic excitation transfer 79−64071
- $Ar+N_2$, $(A^3\Sigma_u{}^+, \nu=0,1)$ metastable state quenching rate coeffs. 78−90206
- $Ar+N_2$, bimol. and three body quenching, reson. state $^1P_1$, $^3P_1$ and excimer Ar atoms 79−3540
- $Ar+N_2$, collinear collision, vibr.-translation energy transfer, model calc. 78−66634
- $Ar+N_2$, cross sectional factorization expressions, close coupling input tested in sudden approximation 79−43571
- $Ar+N_2$, excitation of triplet states *(French)* 77−83704
- $Ar+N_2$, form-factors, l-dominant, analytical formulae 80−1052
- $Ar+N_2$, IOS opacities and integral cross sections, partial wave parameter identification effects 77−38719
- $Ar+N_2$, inelastic scatt. exponential perturbation theories 80−74217
- $Ar+N_2$, N_2 molecule, formation of $C^3\Pi_u$ and $B^3\Pi_g$ in early afterglow 79−34305
- $Ar+N_2$, polarisation in elastic scatt., close-coupling calcs. 78−25650
- $Ar+N_2$, pulsed microwave discharge, early afterglow and radiative transitions, Penning ionisation 78−9874
- $Ar+N_2$, quantual cross-sections, j,CCS and statistical j, approx. surprisal anal. 77−14513
- $Ar+N_2$, rot. and vibr. inelastic mol. collision cross section calc. 79−59542
- $Ar+N_2$, rot. excitation, classical transition probabilities calc. 77−88533
- $Ar+N_2$, rot. excitation, planar trajectory approx. calcs. using body-fixed coords. 77−75267
- $Ar+N_2$, rot. inelastic collision, orientation depend., close coupling calcs. 78−9232
- $Ar+N_2$, rot. inelastic collision cross section, centrifugally decoupled exponential distorted wave approx. 79−842
- $Ar+N_2$, rot. inelastic cross section, classical trajectory calc. surprisal anal., pot. energy surface depend. 77−14542
- $Ar+N_2$, rot. inelastic cross-section, IOS calcs., partial wave parameters 78−50616
- $Ar+N_2$, rotational cross-sections, energy depend., modified exponential model 79−50115
- $Ar+N_2$, rotational excitations, close-coupling calcs. 77−27157
- $Ar+N_2$, vibr. cross-section, exponential distorted wave and effective Hamiltonian 78−37709
- $Ar+N_2$, vibr. excitation of $N_2(C)$ and $N_2(B)$, reaction rate and branching ratio determ. 78−25662
- $Ar+N_2$ rotational excitation, differential cross sections and orientation effects, classical trajectory method 80−23523
- $Ar+N_2+POPOP$, electron beam excited, energy transfer mechanisms 80−23497
- $Ar+N_2(CO)$, intermolecular pots. from Thomas-Fermi-Dirac functional 77−19009
- $Ar+N_2(H_2)(CO_2)$, rot. energy transfer, power scaling law 79−54942
- $Ar+N_2(O_2, CO)$, molecular fluid mixtures, equilibrium props 80−64867
- $Ar+N_2(SF_6)$, 1s states deactivation 77−50398
- $Ar+N_2(SF_6)$, proton excited, time resolved VUV, UV and visible emission 77−14547
- $Ar+N_2(TlF)$, rot. excitation, body-fixed approx. 77−19015
- $Ar+N_2(TlF)$, scatt., l,-conserving sudden approx. calcs. 78−66628

argon continued
Ar+N_2(TlF), sudden approx. of Cross, computational tests, cross section factorisation, scatt. phenomena 80−58352
Ar+N^+, charge exchange, 1-3 keV, $N^+(^3P)$ and (^1D) states 79−36760
Ar+N^{2+}, electron capture, product ion energy loss spectra 79−36762
Ar+NH_3, pure rot. line, press. broadening calcs. 80−78656
Ar+NO, $^2\Pi_{3/2}$, $^2\Pi_{1/2}$ states, line broadening, mag. moment effect 79−72391
Ar+NO, angle depend. intermolecular pot., crossed beams study 80−9682
Ar+NO, NO $\gamma(0,0)$ band, oscillator strength and line broadening 80−106356
Ar+NO_2, continuum quenching in upper atmosphere 79−88520
Ar+NO^+, reaction rate consts. meas. 80−7782
Ar+$NO(X^2\pi)$, intermol. pot. surfaces, electron gas model calcs. 77−34721
Ar+Na, 3^2P differential excitation, mechanism 79−86052
Ar+Na, 3^3P-3^2D line broadening obs. 80−78684
Ar+Na, backward-wave three-pulse echo in two-level system 79−64289
Ar+Na, differential cross-section at thermal energy, Na-Ar ground state pot. 78−58769
Ar+Na, excited state, collisional depopulation cross-sections meas. 79−86057
Ar+Na, Na spectral lineshape, orientation and vel. relax. contribs., low press. region 80−5503
Ar+Na, Na two-photon transition broadened by Ar impact 79−22681
Ar+Na, non-Lorentzian spectral line shape 80−106297
Ar+Na, press. broadening coeffs. of Na 3S-4D transition 78−25481
Ar+Na, scatt. cross-section, thermal energy, interaction pot. for $Na(3^2P)$ 79−27060
Ar+Na_2, collision induced dissoc. rate, vibr. distrib. depend. 79−22791
Ar+Na_2, differential cross sections meas. for rot. energy transfer process, obs. of halos 80−91643
Ar+$Na(^3P_{1/2}) \rightarrow Na(^3P_{3/2})$+Ar, angular scatt. distrib., Doppler spectrosc. obs. 78−94309
Ar+Na(nd), l-changing Rydberg at. collisions, rel. to low-energy electron scatt. 79−50112
Ar+Ne, elastic scatt. absolute total cross section, long range interaction 78−58768
Ar+Ne, fluoresc. spectra, mol. bands, 0.1 to 6 atm., 3000-8200 Å 79−3394
Ar+Ne_2, total integral cross sections for excitation, exchange and dissoc. 80−1044
Ar+$Ne^{2+}(Ar^{2+})$, electron transfer cross-section, <100 eV 78−66654
Ar+Ne^{n+}, (n=1, 2, 3, 4), energy spectra of electrons produced 79−45822
Ar+Ne^{n+}, slow ion and electron prod., VUV radiation 78−5321
Ar+Ne*, quenching rate const. for metastable $Ne(^3P_2)$, flowing afterglow 78−46295
Ar+Ne*(He*) Penning and assoc. ionisation, correl. diagrams calcs. 77−50521
Ar+negative ion, electron-loss cross sections 80−37877
Ar+O, magnetically selected $O(^3P)$ state scatt. 80−99543
Ar+O^-, 0.2-1 keV, elastic and inelastic reduced differential cross-sections 80−32829
Ar+$O^+(^4S)(^2D)$, charge transfer reactions, cross-sections meas. 78−92462
Ar+$O^+(^4\Sigma^-)$, differential elastic cross sections, 2-20 eV, interatomic pot. 77−6885
Ar+OCS, gas, EPR of rot. transitions, T_1 press. depend. 80−9621
Ar+OCS, rot. lines, collisional broadening 79−18267
Ar+OCS, rot. spectral line shift and widths, collision induced phase shifts 77−75222
Ar+$O(^1D)$, deactivation rate consts., 110-330K 78−88628
Ar+$O(^1D)$, inelastic collisions, spin-orbit coupling 80−5605
Ar+one-electron ion, sum-rule Born cross sections, excitation and ionis. contribs. 79−22812
Ar+PCl_3 reaction PCl emission spectra 78−21938
Ar+proton, charge transfer, target K-shell electron capture, impact parameter depend. 80−102552
Ar+Rb(Cs), metal atom spectral line breadth and shift, Van der Waals pot. calc. 78−90126
Ar+S, collision-induced emission of $S(^1S)$, 232 and 425K 79−81264
Ar+S_2, fluoresc. quenching and lifetimes of S_2 78−46386
Ar+S^{15+}, K-shell vacancy sharing, interference effects 80−5606
Ar+S^{n+}, molecular K-X-ray production, projectile charge depend. 78−90188
Ar+S^{q+}, (q=6-16), K X-ray prod., charge-state depend. 80−106391
Ar+SF_6, mol. vibrational-translational energy transfer, mass spectrometric meas. 79−36739
Ar+SF_6(tetrafluoromethane), differential scatt. cross-sections, intermol. pots. calcs. 79−89742
Ar+SO_2, dissoc. rate meas. behind shock wave, laser Schlieren method 80−81296
Ar+SO_2, vibr. relax., shock tube study 80−48062
Ar+S(Cl), branching ratio dependence on projectile velocity and nuclear charge 79−31475
Ar+$Si^{n+}(Al^{n+})(Cl^{n+})(Ar^{n+})$, K-shell vacancy sharing ratio 78−42198
Ar+TiO, collision cross-section meas. 78−55202
Ar+Tl, stimulated collision-induced fluoresc. and stimulated Raman scatt., simultaneous obs. 78−13463
Ar+TlF collisions, small angle scattering, calc. cross sections 78−70915
Ar+U^{36+}, radiative charge exchange 16, 64, 256 MeV/amu 78−55234
Ar+UF_6^-, UF_6^- internal excitation 80−106386
Ar+$UO^+(UO_2^+)$, collision-induced dissoc. cross section and threshold 80−95706
Ar+Xe, lightly doped, Xe $5d(3/2)_1$ photoexcited state radiative decay and energy transfer 78−74605
Ar+Xe, relaxation processes of $Xe^*(^3P_2)$ metastable atoms 78−50624
Ar+Xe^+, $XeAr^+$ form., dissoc. energy, reaction equilib. and rate consts. 80−61071
Ar+Xe^{10+} depend. of charge transfer on ionisation pot. of atoms 79−64096
Ar+Xe^{2+}, charge transfer from ground and metastable states 79−31677
Ar+$Xe(^3P_2)$, flowing afterglow metastable decay rates, diffusion, two- and three-body rate consts. 78−73027
Ar+$Xe(F_2)$, proton excited mixtures, energy transfer processes 78−66647
Ar+Xe→Xe*, electronic energy transfer, emission spectra, electron beam excitation 77−38722
$Ar^+ + 2Ar \rightarrow Ar_2^+ + Ar$, gas phase reaction rate const. calc. 78−92457

argon continued
$Ar^+ + (N_2)(H_2)(O_2)$, charge exchange reaction rates 77−86295
Ar^++Ar, 1-10 keV, charge exchange cross section meas. 78−25697
Ar^++Ar, 1-500 keV, inelastic energy loss, ionis. phenomena, theoretical model 77−34747
Ar^++Ar, charge transfer, fine-structure transitions 80−63808
Ar^++Ar, elastic scatt. and charge exchange, differential cross section, 2.7-20 eV 78−66660
Ar^++Ar, L-shell X-ray cross sections, 0.2-1.5 MeV, fluoresc. yield 78−1068
Ar^++Ar, L-vacancy production, close collisions, 50-375 keV 77−54599
Ar^++Ar, quasi-resonant charge transfer at thermal energies 80−48082
Ar^++Ar, quasimol., Auger transition probability, internucl. distance effect *(Russian)* 77−75116
Ar^++Ar(He), 100-550 keV, 3s vacancy production 79−13809
Ar^++C, beam-foil spectra, Ar^+ ion orientation, ang. variation 78−86944
$Ar^+ + CO_2$, CO_2^+ electronically excited states prod. 77−3454
$Ar^+ + Cl^-(F^-)$ in Ar, high press. ion-ion recomb. rate calcs. 78−31621
Ar^++Cu surface, orientation and alignment prod. 78−25687
Ar^++ethylene (haloethylenes), 2-stage ion beam mass spectrometric obs. 77−9061
Ar^++H, in plasma, H line Stark broadening, role of ion dynamics simulation 80−24144
$Ar^+ + H_2$, $a^3\Sigma_g^+ \rightarrow b^3\Sigma_u^+$ continuum emission excitation 79−41200
$Ar^+ + H_2$, charge transfer kinematics 78−9242
$Ar^+ + H_2$, charge transfer reactions, excited products, Ar initially metastable 78−68879
$Ar^+ + H_2$, collinear reactions, electronic nonadiabatic transitions 78−7180
$Ar^+ + H_2O$, 50 to 250 keV, OH radical form. 78−56890
$Ar^+ + H_2O$, reaction rate consts., product distrib., ICR obs. 79−8428
$Ar^+ + H_2O$, thermal-energy charge transfer, H_2O^+ product internal and kinetic energy 80−16654
$Ar^+ + H_2(D_2)(N_2)$, small angle charge exchange, 0.5 to 1.0 keV, time of flight spectra 78−33604
$Ar^+ + H_2(N_2)(O_2)(CO)$, near-resonant charge transfer, 4-45 keV 77−27176
$Ar^+ + H_2(N_2)(O_2)(CO)(NO)$, charge transfer cross sections 77−34751
$Ar^+ + H_2(O_2)(CO_2)$, reactions in flow-drift tube, rate consts. 78−15664
$Ar^+ + H_2(v_i=0) \rightarrow ArH^+ + H$, electronic nonadiabatic transitions, two-state model calc. 78−73035
Ar^++He, integral elastic scatt., repulsive potentials derivation 80−63744
Ar^++He, $X^2\Sigma$ and $A^2\Pi$ states, CI pots. 78−74727
Ar^++Kr collisions, quasimol. Auger transitions 77−19070
Ar^++Kr(Xe), thermal energy charge transfer reaction rates, mass spectrometric obs. 78−61000
Ar^++molecule (atom), dissociative reaction rate coeffs., in high-press. afterglow 79−87837
$Ar^+ + N_2$, energy transfer, vibronic excitation, emission spectra 78−66578
Ar^++NO, reaction product ratios, 300K 80−7783
$Ar^+ + O_2$, charge transfer mech., implication of inner-shell level mixing 77−61852
$Ar^+ + O_2(N_2)(NO)(CO_2)$, reaction kinetics, mass spectrometer with selective introduction drift tube *(French)* 79−11839
$Ar^+ + O_2 \rightarrow Ar + O_2^+$, thermal energy charge transfer, energy disposal determ. 79−64099
$Ar^+ + SO_2(H_2S)$, emission spectra obs. 78−50622
$Ar^+ + Y \rightarrow Ar + Y^+$, (Y=He, Ne, Ar), keV energies, translational spectroscopy 78−5339
Ar^++fluoromethanes, thermal energy charge transfer reactions mechanism 77−63889
$Ar^{12+} + N_2(NH_3)(CO_2)$(methane)(acetylene), C and N Auger effect 77−6908
Ar^{12+}+Ne, highly charged very slow Ne recoil ions, K X-ray transition 80−91649
Ar^{2+}+Al(Sn), impact-parameter depend. of K- and L-X-rays 79−76501
Ar^{2+}+Ar, (Ne)(He), charge transfer, energy defect and sealing laws 80−48083
Ar^{2+}+Ar, radiative charge transfer coeffs. 79−7010
Ar^{2+}+Ar(Kr)(Xe), single electron capture excitation, photon emission, VUV spectroscopy 80−58379
$Ar^{2+} + Ar \rightarrow 2Ar^+$, thermal rate const. in negative glow 78−9241
Ar^{2+}+He(Ne)(Ar)(Kr), electron transfer cross-section, <100 eV 78−66654
Ar^{2+}+inert gas, low energy reactions, SIFT and drift tube obs. 80−97705
Ar^{2+}+Kr(Xe), thermal energy charge transfer reaction rates, mass spectrometric obs. 78−61000
Ar^{2+}+Na, Ar^+ form, electron capture Ar^+ excited states relative population distrib. 80−23544
Ar^{2+}+Na collision, single electron capture into Ar^+ excited states, 0.2-12 eV, emission cross section 80−48071
Ar^{2+}+Na collision, single electron capture into Ar^+ excited states, relative population distrib. 80−48072
Ar^{2+}+Ne(Ar)(Kr) single electron capture cross-section 77−88550
$Ar^{2+} + O_2(CO_2)(C_2H_2)$, reactions in flow-drift tube, rate consts. 78−15664
Ar^{3+}+He, electron transfer cross-section, <100 eV 78−66654
Ar^{5+}+Al(Si)(S)(Cl), chem. environment effect on $K\alpha$ satellites intensity 77−54527
$Ar^{6+} + H_2$ collisions, ionisation and excitation resulting from electron capture 80−78683
$Ar^{n+} + H_2$, charge transfer, collision defects and dynamics, cross section meas. 80−53099
Ar^{n+}+He, $3 \leq n \leq 8$, single and double electron transfer cross-sections 77−6924
Ar^{n+}+He, electron capture into different excited states in plasma 80−64679
Ar^{n+}+S(Ar)(Al)(Cu), K-shell vacancy sharing ratio, foil or gas target 78−42198
Ar^{q+}+H, (H_2), electron capture by heavy multicharged ions at low velocities total cross sections meas. 80−99548
$Ar^{x+} + Kr(N_2)$, (x=2-7), electron capture cross sections, 10-110 keV 77−6923
Ar^{x+}+Sn(Sb)(Xe), vacancy sharing between K and L shells in $3d\sigma$ mol. orbital 79−22807
Ar^{z+}+inert gas atom (z=1-8), radiative and non-radiative deexcitation after electron capture 79−7008

argon continued
Ar_2 $^1\Sigma_u^+$ excimer state, photoionis. cross section 78−70882
Ar_2, accurate ab initio calc. of intermol. energy 80−18899
Ar_2, Ar_3, Ar_4, short-range intermol. interaction nonadditivity, pseudopot. anal. 79−50179
Ar_2, collision-induced Raman spectrum, absolute cross sections 78−46349
Ar_2, collision-induced Raman scatt., polarisability anisotropy 78−46350
Ar_2, electron impact ionisation, relative cross-sections, mass spectrometric meas. 79−86078
Ar_2, electron-beam pumped, visible absorpt. rel. to laser development 79−59671
Ar_2, emission continua in VUV, new oscill. struct. 79−54905
Ar_2, emission spectra, VUV region 79−31543
Ar_2, excimer laser action in coaxial field emission diode, comparison with Kr_2, Xe_2 80−28201
Ar_2, excited state pot. curves, ab initio CI calc. 78−78643
Ar_2, excited state pots., fast calc. 80−9490
Ar_2, interatomic potential single parameter 80−48059
Ar_2, mean force constants and rectilinear law of mean force calcs. 78−33414
Ar_2, near IR absorpt. spectra 78−66547
Ar_2, photoelectron spectra 78−78748
Ar_2, photoionisation 77−54578
Ar_2, Raman spectra, press. broadened transitions, calc. 79−64009
Ar_2, short range interactions between two rare gas atoms 79−26888
Ar_2, VUV emission spectrum, rot. anal. 79−98119
Ar_2 van der Waals dimer, intermol. pot., SCF CI ab initio calcs. 80−106274
Ar_2, vibr. level spacings calc. from Lennard-Jones pot. 77−42369
Ar_2^+, $A^2\Sigma_{1/2u}^+ \rightarrow D^2\Sigma_{1/2g}^+$ system, theoretical absorption spectrum 80−32734
Ar_2^+, bound-free absorpt. cross section for Π and Σ states 78−5140
Ar_2^+, dimer ions, electronic struct., chem. binding 79−31376
Ar_2^+, dissoc. recomb., total rate coeff. depend. on electron temp. 78−58817
Ar_2^+, electronic states, pot. curves, with/without spin-orbit interaction 78−33443
Ar_2^+, electronic struct., pot. energy curves, spectroscopic consts. 79−18114
Ar_2^+, mobility and clustering reaction in Ar 79−10628
Ar_2^+, near UV absorption spectra, config. interaction methods 78−17680
Ar_2^+, photodissoc., pot. curves and photofragment spectra 77−88514
Ar_2^+, photodissoc. cross sections at 3.0 and 3.5 eV 78−62861
Ar_2^+, photodissoc. cross-section, 6200-8600 Å 78−78761
Ar_2^+, photodissoc. mass spectrometric obs. 77−6867
Ar_2^+, photodissociation cross sections, 3500-5400 Å 79−81243
Ar_2^+, vibr. excited, form. by assoc. ionisation, photodissoc. 79−68279
Ar_2+, weakly bound excited states, dissoc. energies 78−78748
$Ar(Ar^+)+H_2^+(H_2) \rightarrow ArH^+ + H$, electronic transitions, collinear reaction, curve crossing model, DIMZO surface 79−74373
$Ar^+(Ar^{2+})+N_2$, reaction rate consts. 78−48613
$ArF^* + Ar + Ar \rightarrow ArKrF^* + Ar$, recombination rate consts. calc. 77−75488
Ar(I), $3p^54p$ config., level lifetimes meas. 80−102490
ArI, transition probabilities calc. 80−32666
$Ar_{N-1}K^+$, ionic clusters, thermodynamic props., struct. 77−88615
$Ar^{2+}Li$, electron capture excitation, VUV spectroscopy 80−63810
ArN_2, interaction potential, modified electron gas model potential 79−72385
$Ar(^3P_{0,2})+H(^2S)$, energy transfer rate const. and mechanism 78−37727
$Ar(^3P_{0,2})+H(^2S)$, energy transfer collisions, Lyman-α emission profile obs., in microwave discharge and reaction cell 80−58359
$Ar(^3P_{0,2})+N_2$, rate consts. and $N_2(C)$:$N_2(B)$ branching ratio 78−5327
$Ar(^3P_{0,2})+XeF_2 \rightarrow XeF$ ArF mechanisms 77−30897
$Ar(^3P_{2,0})$ metastable state, collision with chlorine atoms and molecules 77−46537
$Ar(^3P_{2,0})+H_2O$ crossed mol. beams, ionisation and dissociative fluorescence, energy depend. 79−52669
$Ar(^3P_2)+F$, donor reagent, quenching, excimer form. 79−63953
$Ar(^3P_2)$ + fluorine containing molecules, quenching rate consts. 77−9072
$Ar(^3P_2)+H(^2S)$, energy transfer, Lyman-α line obs. 79−64085
$Ar(^3P_2)+N_2(C^3\Pi_u)$ excitation transfer cross section, radiative lifetimes, in N_2 laser transitions 79−27246
$Ar(^3P_{2,0})$ + F-containing mols., rate consts. for ArF^* formation 79−24731
$Ar^+(^2P_J)+H_2(D_2)$, Ar^+ two spin orbit state, reaction cross section, direct determ. 80−93748
$Ar_2(^3\Sigma_u^+)+N_2$, quenching, fast absorption spectrophotometry 79−54940
^AAr, A=36, 38, appl. for PWR gas tagging 79−59222
^AAr, A=37,39, simultaneous activity meas. 80−23270
^{36}Ar excess in Venus atmosphere, implications for Venus accretion 80−12700
^{36}Ar, liq. dynamic struct. factor, 120K, press. depend., quasi-elastic NDE-MAT 79−50981
^{36}Ar, separation, calc. of thermal diffusion cascade *(Rumanian)* 78−58862
$^{36}Ar/^{40}Ar$ in Mars atmosphere, composition at surface, Viking 1 lander preliminary analysis 77−13268
^{36}Ar-^{40}Ar, thermal diffusion column transport coefficients *(Rumanian)* 78−51274
^{38}Ar, low abundant, isotrope shift meas., time averaging using dye laser spectrometer 80−101850
^{39}Ar in meteorites, evidence for Maunder minimum in solar activity 78−57529
^{40}Ar 450 MeV/amu beam microdosimetry with wall-less proportional counters 80−26370
^{40}Ar concentrations in sialic crust and atmosphere, rel. to form. from upper mantle 79−44153
^{40}Ar, excess, in Alpine biotites, evolution from ^{40}Ar-^{39}Ar anal. 80−94521
^{40}Ar excess in lunar soils, retrapping mechanism 77−60671
^{40}Ar, mobility in metamorphic terrain, excess in biotite 80−17260
$^{40}Ar/^{36}AV$ in Devonian atmosphere, isotopic ratio from Rhynie chert 77−66917
$^{40}Ar/^{36}Ar$, atmospheric abundance ratio for use in geochronology and cosmochronology 78−28189
$^{40}Ar/^{36}Ar$ trapped in Cretaceous deep-sea basalts 79−16423
$^{40}Ar/^{38}Ar/^{36}Ar$ in Type I diamond from Arkansas 80−94493
$^{40}Ar/^{39}Ar$, in Mesozoic tholeiites from Antarctica, interpretation of discordant age spectra 77−49047

argon continued
$^{40}Ar/^{39}Ar$ age and irradiation history of Luna 24 basalts 80−82245
$^{40}Ar/^{39}Ar$ age and thermal history of Kirin H5 chondrite meteorite 80−101567
$^{40}Ar/^{39}Ar$ dating, felsic and mafic mineral separates from an Abitibi dike 80−17237
^{40}Ar-^{39}Ar dating, inert gas extraction system incorporating ultra-high vac. furnace 78−77918
^{40}Ar-^{39}Ar dating of magnetizations in Archaean Shelley Lake granite 80−30982
^{40}Ar-^{39}Ar stepheating analyses of clay concentrates in Irish orebodies 79−66684
^{40}Ar-^{39}Ar systematics, temp. and pressure effects 79−44178
$^{40}Ar^+$, excited state polarisation transfer due to optical cascades 78−9238
^{41}Ar meas., radioactive release from Institution of Nuclear Research *(Czech)* 77−6568
^{41}Ar release from TRIGA reactor, comparison of γ-ray detectors 78−57309
$Ar^* + Br_2$, producing Br, fluoresc. of Br in $Ar^* + Br_2$ lamp, Br atom conc. meas. by line absorpt. 78−46466
$Ar^* + CS_2$, Penning ionisation and dissoc. fluoresc, collisional energy depend. 78−33584
$Ar^* + Fe(CO)_5$, chemiionisation and chemiluminescence reactions, Penning ionisation and fluoresc. obs. 80−97689
Ar^* + formaldehyde thermal collisions, $CH(A^2\Delta = X^2\Pi)$ emission 77−86304
$Ar^* + H$, assoc. ionis., rovibronic struct. in electron energy spectrum 80−106380
$Ar^* + H$, collisional quenching rates 80−95548
$Ar^* + I_2$, ion-pair form. differential cross-section, 25-133 eV, metastable Ar 78−78787
$Ar^* + Kr^*$, metastables, chemi-ionis., merging beams, 0.01-10 eV 80−14198
$Ar^* + N_2$, 3371 and 3577 Å laser emission, kinetic model 78−5465
$Ar^* + N_2$, excitation transfer collision, vibronic energy partitioning 77−75264
$Ar^* + N_2$, metastable mol. form., emission spectra 77−19019
$Ar^* + N_2(H_2)(D_2)$, de-excitation processes, by pulse radiolysis optical emission obs. 77−65529
$Ar^* + N_2 \rightarrow Ar + N_2^*$, electronic to vibr. energy transfer, time depend. theory 80−23514
$Ar^* + Ne^*$, associative ionisation studied by merging-beams technique 80−91646
$Ar^* + Ne^*$, Penning ionisation studied by merging-beams technique 80−91646
$Ar^* + O_2$, ion pair form. explained by charge transfer model 80−99546
$Ar^{*+} + Kr$, flowing afterglow, energy transfer reaction and quenching rates 80−23529
Ar_2^*, electron impact ionisation cross sections in binary encounter approx. 79−68320
Ar_2^* excimer, electron-beam excited, time-resolved fluoresc. spectra 79−813
Ar_2^*, kinetic behaviour and energy transfer 79−68305
$Ar^*(^3P)+CO_2(X^1\Sigma_g^+)$, differential elastic and quenching cross-sections 78−58773
$Ar^*(^3P)+Co_2(X^1\Sigma_g^+)$, T-R and T-V energy transfer, collisional energy depend. 79−18262
$Ar^*(^3P)+Fe(CO)_5$, chemiluminesc. 78−61014
$Ar^*(3p^54p)_i + Ar(^1S_0)$, collisional population transfer rate coeffs., 300K 79−10177
$Ar^*(4p)$,(5p) states, lifetimes and two-body rate consts. meas. 78−63058
$Ar^*(4s)+H_2$, H_2 continuum emission, kinetic studies in Ar-H_2 mixture, e-beam pumped 80−43153
$Ar^*(4s^3{}_{2,0})+Kr(Xe)$, elastic and reactive scatt., ang. distribs. 77−6919
$Ar(3p^5, 4p)$ and $(3p^5, 4p')$ states, radiative lifetimes, two-body deactivation rate consts. 79−10068
$Ar(4s^3P_{2,0})+Xe(O)(Cl)$, electronic energy transfer 77−46627
atom, oscillator strengths, determ. from self-absorption of reson. radiation 79−89641
$B + He(Ne)(Ar)$, ground and excited states interaction, B spectral line breadth 77−68092
$B^{q+} + Ar(He)(H_2)$, keV electron capture cross section 80−14229
BN_3, adsorpt. of Ar, Kr and Xe 79−73395
$BaCl(C^2\Pi_{3/2}, \nu=0)+Ar$, intermultiplet energy transfer, laser induced fluoresc. obs. 78−9227
Be:Ar, ion-implanted, high resolution LMM Auger spectra 79−83066
$Br + Br + Ar$, photoinduced recombination, numerical simulation 79−16018
$Br + Br + Ar \rightleftarrows Br_2 + Ar$ recombinations rate const. calcs. 80−40685
Br_2-Ar liquid mixture, vibr. relax., 1-D mol. dynamics study 79−73079
Br_2-Ar system, mol. rot. effects on V-T energy transfer 80−14195
$Br_2 + Ar$, collision de-energisation of highly vibr. excited Br_2, mol. dynamics simulation 77−42378
$Br_2 + Ar$, ergodic deactivation, anharmonic effects on transfer rate 78−82818
$Br_2 + Ar$, vibr. excited Br_2, de-energisation in high press. Ar 77−71845
$Br_2 + Ar \rightarrow 2Br + Ar$, 3500K trajectory anal., rate const. 77−52617
CO-Ar, cryst. at 5K, absorpt. and emission spectra, exciton interpretation 79−87481
CO-Ar, liq., polarised vibr. Raman scatt. lineshapes 78−27199
CO-Ar dil. liq. solns. resonant IR third harmonic generation 77−31116
CO-Ar gasdynamic laser, output power, specific output energy and efficiency 78−46583
CO-Ar mixture non-self-sustained discharge instability obs. 78−71612
CO-Ar(-N_2), high press., arc assisted elec. discharges 77−3606
CO-N_2-Ar mixture, supersonic expansion, CO vibr. level populations, gasdynamic laser appl. *(French)* 77−23659
$CO + Ar(CO)$, rot. band, line shape, collisional broadening, impact approx. 78−42134
CO_2-Ar laser, thermally pumped, output power enhancement by Ar gas addition 78−55336
CO_2-Ar solution, diffusion near crit. point in solns. with large conc. gradients in capillary *(Russian)* 77−84958
CO_2-Ar(He), stepwise pulsed photoionisation 77−50479
CO_2-F_2-Ar mixture, vibr. relax. in shock wave, 4.3 μm radn. 78−1062
$CO_2 + Ar$, bending vibr. mode deactivation rate meas., 150 to 1500K 77−10738
$CO_2 + Ar$, broadening of $30^01_{II} \leftarrow 00^00$ band 78−86865
$CO_2 + Ar$, press. broadening, rot. energy transfer, infinite order sudden approx. 78−22011

argon continued
CO_2+Ar, rot. line width of vibr. bands 78−33552
CO_2+He(Ar), dipole and Raman line press. broadening temp. depend. 79−68265
CO_2+He(Ar), rot. relax. rates and cross sections 79−848
CS_2-Ar gas binary diffusion coeff. obs. *(Japanese)* 79−10627
CS_2+He(Ar)(N_2), perturbed rot. diffusion of CS_2, IR spectra 78−75245
$^{40}Ca(n,\alpha)^{37}Ar$, system for meas. total body Ca in man 79−25083
Cd-Ar low-pressure discharge column, energy balance obs. 78−67504
CdSe:Ar, implanted, electroreflection obs. 80−40089
Cl, in Ar and He gas, diffusion const. of atom 78−71417
Cl -Ne(Ar)(Kr)(Xe), longitudinal diffusion coeff., generalised Einstein relation 79−86552
Cl^-+Ar→Cl+Ar+e, rate const., absolute total cross section, expt. results discrepancy 77−513
Cl^-+Ar→Cl+Ar+e, rate const., expt. discrepancy 77−514
Cl^++Ar, L-shell X-ray cross sections, 0.2-1.5 MeV, fluoresc. yield 78−1068
Cl^{n+}+Ar, K X-ray cross sections, 15 and 30 MeV, impact parameter depend. 77−19032
Cl^{n+}+Ne(SiH_4)(H_2S)(HCl)(Ar), K X-ray cross section, projectile charge depend. 77−19029
Cl_2+Ar(He)(Cl_2), dissoc. in shock wave, density gradient meas. 77−83682
ClF+Ar, shock wave, vibr. relax., laser schlieren meas. 78−90267
Co-Ar film, struct., electron diffr. meas., rel. to metal-nonmetal transition 77−51626
Cr-SiO, Ar^+, implantation effects on elec. props. of film 79−11239
Cs diffusion in Ar, time-resolved meas. 77−90588
Cs-Ar, low-pressure discharge, energy balance and Coulomb relax. 77−43098
Cs-Sr(He) mixtures, photocond. at atm. press. 80−87844
Cs^+-Ar, gaseous ion transport, three-temp. theory appl., interaction pot. 80−6202
Cs+Ar, laser two-photon ionisation, collisional line broadening, atomic forces 77−83543
Cs+Ar, optical pumping, spectral line shape *(Spanish)* 79−22662
Cs+Ar^+(Kr^+)(H_n^+)(He^+)(N^+)(N_2^+)(Ne^+)(Xe^+), total charge-transfer cross-sections meas. 77−50527
Cs_2+He(Ne)(Ar)(Kr)(N_2)(CH_4), collision-induced dissoc., atom-mol.-exchange optical pumping 78−22008
CsCl(Cs_2Cl_2)+Ar(Kr)(Xe), collision-induced ion-pair form., absolute cross sections 78−73029
CsF+Ar, 87.7 meV, reorientation effects by approx. quantum methods 77−79680
CsF+Ar, elastic and rot. inelastic scatt., quantum mech. calcs. 77−14525
CsI-Hg-Ar discharge, high-press., temp. and plasma comp. determ. 79−10709
CsI+Ar, elastic and inelastic scatt. 77−58119
Cs($6^2P_{3/2}$)+He(Ne)(Ar)(Xe), collisional depolaris., nucl. spin depend., by Zeeman scanning 77−19012
Cs(8^2P)+He(Ar)(Xe), fine-struct. transition cross sections, semiclassical calcs. 77−30972
D-Ar mixture, effect of Ar admixture on plasma temp. 79−37446
D_2 lamps, influence of Ne and Ar on spectral parameters 80−86460
D_2-HCl-Ar gasdynamic lasers, gain 79−64217
D_2O+Ar, energy transfer isotope effect, rate consts. 79−8422
F ions+Ne(Ar)(Kr) and C foil and slab, K shell X-ray spectra 78−17599
F+Ne(Ar)(Kr), thermal energy interaction pots., crossed beam study 79−68288
F_2-Ar mixtures, electron attachment rate to F_2, elec. cond. meas. 79−7019
F_6S-Ar, compressibility 0 to 50°C, second virial coeffs. calcs. 77−15147
Fe:Ar, mag. hyperfine interaction, temp. depend. 78−68420
Fe-Ar low press. flow discharge, axial density profiles of sputtered cathode atoms 80−49029
GaAs:Ar^+-metal, capacitor, capacitance-voltage and current-voltage meas., assuming intermediate dielec. layer 79−56316
Ge particles, grown in Ar gas, cryst. struct. and habit, electron microscope study 79−74071
H+Ar, collisional charge production, differential scatt. calcs. 77−68107
H+Ar, collisional charge production cross-sections 77−71860
H+H^+(Arq^+)(Kr^{q+})(B^{q+})(C^{q+})(N^{q+})(O^{q+}) charge transfer and impact ionis. cross sections calcs. 77−88555
H+He(Ar), press. effects on H_α and H_β Balmer series 77−18845
H+inert gas atom, interaction pot. from electron gas model 79−31637
H+O_2+Ar, HO_2 free radical prod., rate const. calc. 80−101026
H +H_2(He)(Ar), electron detachment, Born cross sections, Pade approximants 78−17742
H^-+He(Ar), electron detachment cross sections 78−58810
H^++Ar, 5-1.5 MeV, ejected-electron energy and ang. distrib., differential cross sections 77−88547
H^++Ar, inner-shell charge transfer calcs. 77−50528
H^++He(Ar), charge exchange, differential cross sections 79−7006
H^++He(Ar) electron transfer cross sections 78−58809
H^++He(Ar)(Kr)(O_2)(H_2)(N_2), 2.2-8.2 keV, H(n=3) form., absolute cross sections 77−34755
H^++Kr(Ar) charge exchange, oscillating cross sections 77−58158
H_2 ionising collisions, ArH^+ 79−100338
H_2-Ar, bound complex form., anisotropic intermol. pot., IR spectra anal. 78−37634
H_2-Ar, liq.-vapor equilib. 83 to 141K, to 52 MPa 79−42226
H_2-Ar, relaxation rates, thermal dissociation, decomposition, master equation theory 79−74368
H_2-Ar, states velocity auto-correl. function, relax time, neutron scatt. obs. 80−58401
H_2-Ar, vibr. energy relax. 80−106384
H_2-Ar hollow cathode discharge, effect of additional gas ionisation by oscillating electrons *(Russian)* 77−31536
H_2-Ar(Kr)(Xe) mixtures, intermol forces 78−62867
H_2-N_2-Ar, two-phase flow film boiling, in vap. generator, heat transfer 78−75190
H_2-N_2(Ar) gas mixture, correl. between kinetic theory of thermal cond. and expt., 90 to 300K, 1 bar 79−81707
H_2-O_2-Ar flame, excitation profiles of Na D-doublet 77−88436
H_2+Ar, Arrhenius dissoc. activation energy, vibr. depend., trajectory calc., 4500K 78−35662

argon continued
H_2+Ar, H_2 dissoc. rates, nonequilib. vibr. populations, elec. discharge conditions 77−88535
H_2+Ar, induced IR spectrum, overlap dipole moment determ. 77−18924
o-H_2+Ar, relax. and kinetic cross sections, DWBA calc. 78−25655
H_{2n+1}^++Ar, $n\leq7$, double differential fragmentation cross section 79−89821
H_3+Ar→H_2+ArH^+, crossed beam reaction, energy distrib. 77−52626
HCN compact CW laser, output increased by He, Ar, air and O_2 buffer gases 79−10293
HCl, Ar-perturbed rot. linewidths, temp. depend. 79−45766
HCl+Ar, elastic and rot. inelastic collisions, quasiclassical and quantum mech. results 77−79679
HCl+Ar, pure rot. line shift, density depend. 77−79652
HCl+Ar, rot. linewidth calcs., using different pots. 78−66602
HCl+Ar(He), rot. excitation, classical and quantum calcs. 78−1059
HCl+Ar(He), rot. excitation, infinite order sudden approx. 78−74740
HCl+HCl(Ar), pure rot. Raman lines, press. broadening cross sections 78−74702
HCl+He(Ar), press. broadening, rot. energy transfer, infinite order sudden approx. 78−22011
HCl+Kr(Ar), pot. energy surface determ. from rot. line broadening data 79−13784
HF-Ar mixture; HF rotational relax., laser IR fluoresc. 77−83634
He/Ar and N_2/Ar ratio vars. in fault zone groundwater air bubbles for earthquake prediction 78−88803
He-Ar, Ar I TEA lasers, energy characteristics 80−63977
He-Ar, collision-induced absorption, exact line shapes 78−66512
He-Ar, corresp. states law and thermal diffusion, two-bulb meas. 77−3910
He-Ar, diffusion coeff., two-bulb meas. 77−11299
He-Ar, ion laser transitions, hollow cathode excitation 80−1184
He-Ar, spherical expansion into flooded space, separation 79−81948
He-Ar, van der Waals pot. determ. 79−10167
He-Ar gas mixture, velocity slip in free jet expansions 78−90951
He-Ar high voltage hollow cathode discharge, new Kr II CW laser lines new Ar II CW laser lines 79−13947
He-Ar hollow cathode discharge, CW laser oscill. obs. 78−5454
He-Ar hollow cathode discharge, laser generation on Ar II 4765 Å line 80−23671
He-Ar in Cu^+ hollow-cathode laser, IR output depend. on gas press. ratio 80−48223
He-Ar ion lasers, hollow cathode, CW operation and excitation mechanism 80−69363
He-Ar mixture, collision induced far IR absorption at high press. 78−5161
He-Ar mixture, mass separation with rot. plasma 79−13842
He-Ar mixture, RF discharge, mass spectroscopy, floating double probe meas. 80−84016
He-Ar mixture, thermal conductivity, 400-1500K 77−39394
He-Ar mixture, translational IR spectrum at 165K, binary and ternary absorptances 77−68042
He-Ar mixture HP collision-induced translational far IR absorption obs. 77−38628
He-Ar mixtures, thermal diffusion 80−1726
He-Ar mixtures, US vel. meas., phase separation 79−27738
He-Ar plasma, linear longit. oscill. damping and dispersion, development of turbulence 77−51185
He-Ar-H arc plasma, nonequilib. effects, spectroscopic diagnostics 77−76191
He-Ar(Kr)(Ne), thermal diffusion, conc. depend. determ. 77−11300
He-Ar(Kr)(Xe), 208 and 707K, intermol. forces, virial, diffusion, and viscosity coeffs. 77−75256
He-like ion, spectral broadening in plasma, theory 80−6223
He+Ar, interatomic pot. well depth, SPFD pot., diffusion, viscosity and second virial coeff. 80−5599
He+Ar, van der Waals pot., from crossed at.-mol. thermal beams scatt. 79−27053
He+Ar mixture, collision induced absorpt. calcs. 77−6777
He+Ar^{+Z} (Z=3 to 7), electron capture into different electron states by multiply charged ions *(Russian)* 78−17788
He+Ar+polyatomic fluorides, VUV spark emission spectra 79−3457
He+Ar(Kr), translation band spectral moments, induced dipole moments 78−55218
He+Ar(Kr)(Xe), He*(2^1S) scatt., low energy repulsion systematic struct. 78−22000
He+H_2(He)(Ar)(N_2), fast metastable at. collisional destruction cross section 78−74760
He+H_2(He)(N_2)(Ne)(Ar), 25-450 keV, metastable ion beam electron loss and deexcitation cross section 77−34745
He+Ne(Ar)(Kr)(Xe), energy transfer, time-resolved VUV spectra 77−19028
$He^{+,2+}$+Ar, 2 MeV, ejected electron spectra, 20-450 eV, 0-10° 77−34746
He^++Ar, attenuation and single electron charge exchange cross sections, 500-5000 eV 77−34752
He^++Ar, charge exchange, quasimolecule model, four-state calcs. 77−14571
He^++Ar, charge transfer cross section, kinetic energy dependence in low energy region *(Japanese)* 78−90100
He^++Ar, direct excitation and charge exchange processes 77−75279
He^++Ar, low energy charge transfer collisions, kinetic energy depend. 78−86947
He_2^++Ne(Ar)(N_2)(CO)(CO_2)(Ch_4), bimol. and termol. charge transfer reactions, rate coeffs. 77−1910
He(He_2)+Ar, metastable destruction rates 78−37728
$He_2(^3\Sigma_u)$+Ne(Ar)(N_2)(CO)(C_2)(CH_4), excitation transfer reaction rates 78−5332
^{3}He-Ar, direct nuclear pumped lasers using $^3He(n,p)^3H$ reaction 79−31863
^{3}He-Ar, nucl. lasing, population inversion mechanism 80−63980
^{3}He-Ar nuclear pumped laser, first order model, lasing action depend. on Ar conc. 79−76668
^{3}He-Ar plasma, electron temp. and density, estimation method 80−64785
^{3}He-Ar volume pumped nuclear laser survey of lasing 80−63979
^{3}He-Ar volumetric nucl. pumped laser, dominating processes and reaction physics 80−63981
He*+Ar, complex potential from elastic differential cross sections 77−23534

argon continued
He*+Ar, Penning ionisation, laser modified collisional effects in electron energy spectrum 78—90278
He*+Ar(Kr)(Xe), elastic scatt., repulsive rainbows and optical pots. 79—840
He*+D_2(Ar)(Kr) interaction pots. 77—83674
He*(^{3}S)+Ar+$\hbar\omega \rightarrow$He+Ar$^+$(^{2}P)+e^-, intense laser radiation assisted collisional ionis. 79—76497
He*(1s2s,^{3}S)+Ar, Penning ionis., discrete-continuum states coupling 79—10193
He*(2^{1}P)+Ar$\rightarrow$He+Ar$^+$+e^-, anisotropic interaction potential, impact parameter method 77—68102
He(2^{1}S)+Ar, optical interaction pots. from differential cross sections 77—30956
Hg-A positive column discharges, scaling towards display cells 77—84565
Hg-Ar, HF discharge, electron energy distrib. and atom ionisation processes 80—44048
Hg-Ar, low press. discharge positive column ionisation processes 78—75445
Hg-Ar, low-pressure discharge, energy balance and Coulomb relax. 77—43098
Hg-Ar, mixtures, prebreakdown discharges, discharge current depend. on electron mobility 79—77433
Hg-Ar, two phase flow in vertical tube, transverse mag. field, bubbles and slug flow 77—84303
Hg-Ar quench condensed system, annealing effects on elec. cond. 79—60880
Hg-He(Ar), modulated discharge, elec. and optical props. 77—7627
Hg-Xe(Kr)(Ar), fluoresc. emission, high press., electron beam excitation, laser appl. 77—34676
Hg*+Ar(Ne), 6^{3}P$_0$ and 6^{3}P$_2$ metastable states, interaction pot. parameters 77—79670
I+Ar(Xe), collision-induced $^2P_{1/2} \rightarrow {}^2P_{3/2}$ emission 77—83528
I_2+Ar, D-state lifetime and UV laser action 77—14471
I_2+Ar, mol. rot. axes, collisional alignment calcs. 77—42376
K-Ar dating of ore mineralisations in Erma River Area, Bulgaria 78—81115
K-He(Ne)(Ar)(Kr)(Xe), oscill. strengths, for induced dipole transitions, pot. energy curves 77—75100
K$^+$+Ar(Kr)(Xe), differential elastic cross-section meas. *(German)* 77—58130
KBr*+Ar, inelastic collision, classical trajectory anal., vibr. excitation effects 77—34737
KBr*+Ne(Ar)(CO)(N_2)(CO_2), information theoretic anal. 77—521
Kr-Ar, phase matched, generation of Lyman-α radiation 80—91845
Kr-Ar binary mixture, expt. determ. of temp. depend. of thermal diffusion factors *(Russian)* 79—60095
Kr-Ar gas mixture, vapour-liq. equilib. data *(German)* 77—84915
Kr-Ar mixture, shock-heated, ionisation relax. processes 77—84277
Kr+Ar*, 123.6 nm emission excitation of Kr by metastable Ar, press. depend. 78—5331
Kr*+He(Ar), vel. changing collisions studied by saturated absorpt. 78—62892
LiF+Ar, polarised rot. selected mol., high resolution differential cross section 77—27147
LiF+Ar(Kr), anisotropic system intermol. pot. determ. 77—58121
Li_2O, Ar$^+$ implantation, depth distrib. by proton backscatt. 78—51577
Li*+He(Ne)(Ar), thermal, high-Rydberg Li behaving as ion core 78—22004
N$^+$+Ar(Kr)(Ne), single electron detachment cross-sections, 35 to 140 keV 77—6909
N_2-Ar, laser high power, energy and power output *(Russian)* 77—7065
N_2-Ar, liq. mixture, isotropic Raman line shape theory 78—88298
N_2-Ar, liquid, high resolution CW CARS spectra 80—63635
N_2-Ar, visomag. diffusion flux theory 78—47087
N_2-Ar corona dishcharge, convection and mixing, atm. press., mass spectra obs. 80—1853
N_2-Ar equimolar mixture, transverse Dufour effect 80—6194
N_2-Ar laser, stimulated emission obs. at 337.1, 357.7 and 380.5 nm 78—17925
N_2-Ar liq. mixtures, coherently excited mol. vibrs., dephasing time 78—62813
N_2-Ar mixture, picosecond dephasing of coherently excited vibrations 78—22172
N_2-Ar mixture non-self-sustained discharge instability obs. 78—71612
N_2-Ar mixtures in 300-1050K range, rot. energy relaxation 78—50617
N_2-Ar plasma, coupled thermal-chem. relax., thermodynamic nonequilib. 78—34265
N_2-Ar-O_2, liq. vap. equilib. prediction using cubic eqn. of state 78—18737
N_2-Ar-O_2 system, vapour-liq. equilib. 80—54358
N_2-Ar(methane)(ethane) binary and ternary mixtures, dielec. const., excess vol. 80—7254
N_2-O_2-Ar saturated air vapour mixture, film, mixed condensation, comparison with water vapour 77—11780
N_2+Ar, binary diffusion coeff. pressure depend. meas. 80—43826
N_2+Ar, rot. relax., approx. treatments 79—76494
N_2+Ar, total differential cross section, diffr. oscills. quenching 78—66625
N_2+Ar*($^3P_{0,2}$), rot. and vibr. energy transfer, relative reaction rates 78—9233
N_2+Ar*(He*), sensitised fluoresc., vel. depend. 77—10744
NH_3-Ar mixture, thermal cond., viscosity, Senftleben-Beenakker effect 80—100054
NH_3-N_2(H_2)(Ne)(Ar)(Kr)(Xe), as R(1,1) vibr-rot. line parameters, ν_2 band, using CO_2 laser light 79—3444
NH_3+He(Ar), ammonia inversion spectrum press. broadening 78—86915
NH_3+NH_3(He)(Ar)(N_2)(O_2), ν_2 state vibr. relax., laser induced vibr. fluoresc. obs. 79—18269
N_2(N_2+Ar) pulse excited microwave discharge diagnostics at moderate press. 78—9873
NO($X^2\Pi$)+Ar(NO), lower vibr. states relax. rates meas. 77—65527
$N_2(X^1\Sigma_g^+)$+Ar($^3P_{2,0}$)$\rightarrow$Ar(^{1}S)+$N_2(C^3\Pi_u)$, sensitised fluoresc., vel. depend. 78—90204
Na-(Ne)(He)(Ar)(Kr)(Xe), oscill. strengths, for induced dipole transitions, pot. energy curves 77—75100
Na-Ar, nonlinear optical 5th order susceptibility meas., VUV harmonic generation 78—42381
Na-Ar film, metal-nonmetal transition 77—62966

argon continued
Na-Ne-Ar, low-pressure discharge, AC operated, time-resolved afterglow 77—43099
Na-Ne-Ar AC discharge, positive column 77—39487
Na-Ne-Ar discharge low-press., instability 78—9868
Na+Ar, collisional relax. by tri-level echo 78—17774
Na+Ar, fine structure transition cross-sections, emission spectra, NaAr form. 78—9085
Na+Ar, Rydberg states, collisional angular momentum mixing meas. 77—68093
Na+Ar, Rydberg transitions, excitation transfer cross-section calcs. 77—50520
Na+Ar, total elastic cross sections meas. 77—30954
Na+Ar, two-photon near-reson. light scatt. 77—30941
Na+Ar*, Penning, associative and total ionis. cross sections 77—79683
Na+Ar$\rightarrow$NaAr, quasimol. form., laser spectroscopic obs. 77—57920
Na+He(Ne)(Ar), Rydberg S and D state relax., trilevel echo effect 79—72409
Na_2+Ar, rot. level repopulation rate by laser-induced depopulation 77—65528
NaCl+Ar, dissoc.-ionis. process rates in shock tube 78—35674
Ne:Ar, electronic relax. cascades in Wannier and Frenkel type exciton states 79—33759
Ne:Ar, luminesc. in vacuum UV 79—15519
Ne-Ar, glow discharges, AC cataphoresis meas. using light spectrometry 79—60096
Ne-Ar, high press. mixture, AC discharges, one-dimensional numerical simulation 78—67451
Ne-Ar, mol. force const. from viscosity data, thermal cond. 78—33565
Ne-Ar, thermal cond., 90-273K 80—48836
Ne-Ar (0.1%) mixture, AC plasma panel, Paschen breakdown curves 77—11418
Ne-Ar (1%), 250 kV pulsed electron beam-excited, at. line rel. intensities 79—89646
Ne-Ar discharge, transient cataphoresis, time depend. 80—38753
Ne-Ar liquid mixtures, collision induced absorpt. 77—4638
Ne-Ar mixture, cataphoretic segregation, mass spectra obs. 77—52649
Ne-Ar mixtures, glazed electrode AC discharge mode transition obs. 78—67558
Ne-Ar Penning mixture, pulsating discharge, emission spectra, Ne state population 79—55594
Ne-Ar-I_2, low electron beam excitation rates 79—86163
Ne+Ar^{12+}, heavy-ion induced K-shell Auger effect 77—6908
Ne+Ar(Kr), translation band spectral moments, induced dipole moments 78—55218
Ne^{2+}+He(Ne)(Ar)(Xe)(Kr), cross sections for electron capture, 60 to 200 keV 78—46442
Ne^{Z+}+Ar, projectile charge dependence *(Dutch)* 79—50121
Ne^{z+}+He(H_2)(Ar), (z=1-4), electron capture into excited projectile states 77—75291
NeAr, detection in nozzle beam, total collision cross section determ. 77—61826
^{20}Ne/^{36}Ar ratio in chondrites, abundance pattern established in solar nebula 78—32424
O+NO+M$\rightarrow$$NO_2$+M, (M=He, Ne, Ar, Kr), 217-500K, absolute rate consts. 77—16787
O$^{4,5,6,7+}$+Ne(Ar)(Kr)(Xe), 10-30 MeV, charge exchange 77—34757
O_2-Ar system, low temp. liquid-vapour equilib. 78—83927
O_2-H_2-Ar flame, atm. press., Na(3^{2}P) lifetime obs. 79—39149
O_2-sseded Ar plasma supersonic free jet expansion flow, population density measurements *(Japanese)* 80—96351
O_2+Ar, 118750 GHz transition, press. broadening 77—75136
O_2+Ar, binary diffusion coeff. pressure depend. meas. 80—43826
O_2+Ar(O_2), collision induced UV absorpt. in Herzberg continuum, dimer form. 77—30883
O_3-Ar, photorecombination laser, shock wave triggered, waveguide mode optical gain 80—5730
O_3^-+X$\rightarrow$$O^-$+$O_2$+X, X=He, Ar, CO_2, long-lived excited (or isomeric) state of O_3^- 78—5318
OCS in Ar soln., IR spectra, solvent shifts, vibr. band assignment and anharmonic force consts. 80—9607
OH ($A^2\Sigma^+$)+H_2(N_2)(Ar), collisionally induced population change rates, laser-induced fluoresc. obs. 78—5326
OH+Ar, pure rot. collisionally pumped laser, vibr.-rot. transfer 77—42523
O(^{3}P)+n-butane(NO(M=Ar)), reaction rate constants using flash photolysis-NO_2 chemiluminesc. method 77—44458
O(^{5}S)+Ne(Ar)(Kr)(Xe), total cross sections 78—42188
Pb-Ar film, struct., electron diffr. meas., rel. to metal-nonmetal transition 77—51626
Pb-Ar films, atomic arrangements, high energy electron energy diffractogram study, Ar conc. depend. 79—99444
Rb$^+$, ionic mobility in Ar, Kr and Xe, interaction pot. determ. 79—18991
Rb-Ar, oscill. strength, for induced dipole transitions, pot. energy curve 77—75100
Rb+Ne(Ar), spin relax., van der Waals mols. form. 77—19027
Rb(6^{2}P)+He(Ar)(Xe), fine-struct. transition cross sections, semiclassical calcs. 77—30972
S+Ar, 32 MeV, $K_\alpha{}^h/K_{\alpha\alpha}$ branching ratios, S projectile charge state depend. 79—63947
S$^+$+Ar, double K-vacancy prod., X-ray X-ray coincidence and fluoresc. yields obs. 78—55230
S^{n+}+Ne(SiH_4)(H_2S)(HCl)(Ar), K X-ray cross section, projectile charge depend. 77—19029
$S_2(B^3\Sigma_u^-\ \nu=4)$+He(Ar)(Xe), collision-induced transfer rates 79—94062
SF_6-N_2-Ar mixture high-current multispark discharge switching characteristic 78—67444
SF_6-R-He(Ar) ternary mixtures, formation of inert gas fluorides in AC discharge 80—64817
SF_6Ar, multiple photon excitation, saturation and linear absorpt., pulsed optoacoustic detect. 78—42148
SeO_2+Ar, radiative lifetime and quenching rates 80—95685
Si, high-dose Ar implantation, X-ray topographic obs. of strains and damage 80—59496
Si particles, grown in Ar gas, cryst. struct. and habit, electron microscope study 79—74071
Si:Ar, amorphous, implanted and sputtered, epitaxial regrowth, influence of noble gas atoms 80—2289
Si:Ar, As, ion implanted, laser annealing, doping profiles, channelling 80—97506

argon continued
  Si:Ar, ion implantation, high fluence retention 79—23627
  Si:Ar, ion implantation damage, annealing, comparison with Si:Ne and Si:Kr 79—10867
  Si:Ar, ion implanted, amorphous, epitaxial regrowth 79—10868
  Si:Ar, ion implanted, electroreflection spectra 79—51983
  Si:Ar, ion implanted, nature of defect reverse annealing 80—88875
  Si:Ar, ion-implanted, epitaxial regrowth by laser annealing, microstruct. 80—84404
  Si:Ar, ion-implanted, high resolution LMM Auger spectra 79—83066
  n-Si:Ar, single cryst., ion implantation, positron annihilation meas. 79—15555
  Si:Ar^+, implantation effect on carrier lifetime, damage obs. by TEM 79—65493
  Sr+Ar, press. effect on Sr 4607 Å reson. line shape width, and shift 79—22653
  $Sr(^1S)$+Ar, $Sr(^1P)$ collisional excitation in nonreson. laser field, four-state model 79—10191
  Tl-Ar, Tl line shape in Ar gas, collisional redistrib. of near-reson. rad. 79—31469
  UF_6 admixture effect on N_2 and Ar excited state lifetimes 79—10281
  VO_2, thin films, doping by ions of Ar, B, P 77—84781
  Xe-Ar, 3547 to 1182 Å conversion efficiency limited by Kerr-induced dispersion 78—37940
  Xe-Ar binary mixture, expt. determ. of temp. depend. of thermal diffusion factors *(Russian)* 79—60095
  Xe-Kr-Ar mixtures, VUV continuous spectrum prod. in low volt. lamp *(Russian)* 78—75451
  Xe+Ar^{x+} multiple scatt., combined ang. and lateral spread 78—46441
  Xe+Ar(He)(Ne)(Kr), thermal cond., 800 to 2000K from Wassiljewa's expression 79—27736
  XeAr, obs. in Xe-inert gas far UV spectra, press. (temp.) depends., interaction const. 77—61698
  Zn-Ar mixture, binary diffusion coefficients, 1 atm., 720-1120K 80—1725

argon compounds
  Ar-methane (iodomethane), mol. interactions, differential scatt. cross-sections meas. 79—89732
  Ar-methyl chloride, mol. beam elec. reson. spectrosc. 80—23477
  Ar-Xe system, band formation exam. by photoelectron spectroscopy 77—66116
  $ArBF_3$, microwave spectrum and struct. 79—76420
  ArBr, B(1/2)-A(1/2) system, emission spectra 79—6934
  ArBr, emission spectrum and chemiluminesc. 80—45508
  ArBr, pot. curves, population distribs. and chemiluminesc. for B(1/2) and C(3/2) electronic states 80—45509
  ArC^+, pot. energy curves calcs. 79—45651
  $ArCO_2$, struct. determ. by mol. beam elec. reson. spectrosc. 79—64019
  ArCl, neutral and negative ion states SCF pot. energy curves 78—62745
  ArCl superfluorescent laser, discharge-pumped, laser action at 175 nm 77—38859
  ArCl*, excimer formation rate consts., B state radiative lifetimes, quenching, VUV excitation 80—55631
  ArF, 50 mJ double discharge excimer laser, spectroscopy and characts. 78—63082
  ArF, Ar_2F, electronic struct., pot. energy curves, radiative transition probability calcs. 77—57879
  ArF, Ar_2F, time depend. emission meas., Ar-Kr-F_2 laser mixture kinetics 80—32768
  ArF, covalent and ionic states, ab initio CI calcs. 78—78634
  ArF, discharge laser, operating characts. 79—22937
  ArF discharge laser, steady state amplification 80—5726
  ArF, discharge pumped multiwavelength lasers *(Chinese)* 80—102703
  ArF, double discharge laser, operating parameters, discharge characts. 77—88704
  ArF, double discharge laser, prism tuning 78—37892
  ArF, electron quenching rate consts. meas. by fluoresc. anal., laser implications 80—32969
  ArF excimer laser, electron-beam pumped, efficiency and gain 80—78844
  ArF excimer laser, providing high-power stimulated radiation in Ar and F lines 77—83858
  ArF excimer laser multiphoton ionisation mass spectra 80—81381
  ArF, excimer laser with improved beam quality 77—72007
  ArF, excimers, power superluminescence, in elec. discharge *(Russian)* 77—7621
  ArF, high efficiency laser, photolysis of OCSe producing Se 80—33032
  ArF high power lasers, const. E/N pumping 77—88711
  ArF, inert gas halide lasers, 60-ns electron beam excitation 80—74340
  ArF laser, closed cycle characts. 80—33030
  ArF laser, closed cycle flow type, operating characts. 80—43349
  ArF laser, excimer gas-discharge tunable, intense laser oscill. obs. 77—38862
  ArF, laser emission, ab initio config. interaction calcs. on electronic states 78—63083
  ArF, laser expts. on $^2\Sigma$-$^2\Sigma$ transitions 78—63080
  ArF laser pump source, tunable efficient VUV generation using stimulated Raman scatt. in H_2 80—38072
  ArF, laser spectra, absorpt. lines 80—9604
  ArF, Raman shifting of laser wavelengths 77—75539
  ArF superradiance laser excited by electric discharge 77—19236
  ArF, UV preionised transverse discharge laser, theoretical model 79—22938
  ArF, UV preionized discharge pumped laser 77—10889
  ArF^+, selected valence-electron split-shell MO calc., ground state props. 79—22585
  ArF_2, ab initio diatomics in mols. pot. surface, spin-orbit coupling 79—3519
  Ar_2F, electronic states, ab initio POL CI calcs. 78—66474
  Ar_2F excimer laser, electronic structure, pot. energy curves, radiative transition probabilities, quantum mech. calcs. 79—10284
  Ar_2F molecule low-lying electronic states 77—65491
  ArF*, Ar_2F*, kinetics of proton-excited Ar-F_2 mixtures, time-resolved and time-integrated spectra 79—36883
  ArF*, formation and quenching kinetics 77—88482
  ArF* formation from $Ar(^3P_{2\,0})$ reactions from F-containing mols. 79—24731
  ArF*, in Ar-F_2 proton-excited mixtures, production and quenching 78—94307
  ArF* laser, electron beam pumped, dominant formation and quenching processes 79—938

argon compounds continued
  Ar_2F*, in Ar-F_2 proton-excited mixtures, production and quenching 78—94307
  Ar_2F*, radiative lifetimes, quenching rate consts., emission spectra 78—46577
  ArH exciplex emission obs. in rarefied Ar-H_2 plasma jet *(French)* 80—48054
  ArH, excited states, theoretical pot. curves 80—95548
  ArH, neutral and negative ion states SCF pot. energy curves 78—62745
  ArH^+, $^1\Sigma^+$ ground state, molecular consts. calc. from pot. curves 80—9680
  ArH^+, dissociative recombination rates 77—86295
  ArH^+, transition moments, perturbation calcs. 80—102542
  $ArH^+ + H_2 \rightarrow Ar + H_3^+$, crossed beam reaction, energy distrib. 77—52626
  ArH^++He, ab initio pot. energy data, SCF-LCAO calcs. 80—63530
  ArH_2, van der Waals complexes, lifetimes calcs. 78—13564
  ArH_2, van der Waals mols., rot. predissoc. 80—63721
  ArHBr, ArHCl, and isotopic forms, rot. spectra, mol. struct., mol. consts. 80—58246
  ArHBr, bond energy, IR spectra determ. 77—58000
  ArHCl, ab initio FGO calc. 78—50467
  ArHCl, mol. interactions, differential scatt. cross-sections meas. 79—89732
  ArHCl, pot. energy surface of Van der Waals complex 78—94299
  ArHF, van der Waals complex, ab initio RHF calc., struct. 79—76339
  $Ar_nH(H^+)$, excited and ground state struct. energies and binding energy, vibr. modes, LCAO-SCF-MO calc. 79—3608
  ArHO, van der Waals complex, ab initio RHF calc., struct. 79—76339
  ArHX, (X=F,Cl,Br,I) van der Waals mols. vibr. and thermodynamic props., WKB calcs. 77—71740
  ArI_2, van der Waals mol., fluoresc. spectrum, predissoc. 78—66584
  $Ar_{N-1}K^+$ clusters, equilib. configs. and binding energies 80—48115
  ArKr, electron impact ionisation, relative cross-sections, mass spectrometric meas. 79—86078
  ArKr, intermol. pots., differential cross-sections inversion calcs. 78—66619
  ArKr, mol. interactions, differential scatt. cross-sections meas. 79—89732
  $ArKr^+$, absorpt. spectra, ab initio calc. of potential energy curves 78—74568
  ArN_2, van der Waals mols., rot. predissoc. 80—63721
  ArO, in doped inert gas matrix, photoluminesc. 79—31579
  ArO, lasing, low-lying electronic states, ab initio config. interaction calcs. 78—63084
  ArO^+, $X^4\Sigma^-$ state, pot. energy curves and correl. effects, elastic scatt. cross sections 80—23502
  ArS, photoluminesc. in rare gas matrices 80—5568
  $ArSO_3$, weakly bound complex, struct., MBER obs. 80—95701
  ArXe, continuous VUV emission spectrum 80—43066
  ArXeF*, gain meas. at 4416 Å 78—50758
  Ar.HBr(DBr), van der Waals complexes, rot. spectra and struct. 80—48055
  Ar.HCl bond energy from IR spectra 77—27061
  Ar.HCl, Van der Waals mols., SCF energies and dispersion forces 80—74279
  Ar.HF, Van der Waals mols., SCF energies and dispersion forces 80—74279
  Ar.H_2O, Van der Waals mols., SCF energies and dispersion forces 80—74279
  $KrAr^+$, quasimolecule Auger spectra 79—68269
  Xe-Ar system, band formation exam. by photoelectron spectroscopy 77—66116
arithmetic (digital) *see digital arithmetic*
armouring (cables) *see cable sheathing*
aromatic compounds *see organic compounds*
arrays (antenna) *see antenna arrays*
arsenic
    see also nuclei with ......
  3d binding energy in As, GaAs, As_2O_3, and As_2O_5, ESCA absolute energy calibr. 78—92171
  3d subshell, photoionisation partial cross-section, energy depend. meas. 80—29850
  adsorption on GaAs (110), UPS and EELS study, tight-binding calcs. 80—49496
  Aegean Sea, Cu, As and Hg conc. determ. 79—2292
  allotropic phase transition, low temperature *(Russian)* 80—54553
  amorphous, absence of photodarkening 80—103970
  amorphous, AC cond. and photo-induced states 79—87128
  amorphous, bonding coord. defects, Cayley trees appl. 79—65373
  amorphous, bonding coordination defects, Raman scatt. and IR absorption meas. 78—60498
  amorphous, bulk, sp. ht. meas., 1.8-20K 78—22866
  amorphous, bulk and sputter-deposited film, vibr. props., Raman spectra meas. 77—63411
  amorphous, cooperative charge disproportionation of defects, rel. to ESR 80—54649
  amorphous, defect controlled electronic props. 80—49658
  amorphous, defects, band gap states 80—80215
  amorphous, effect of high press. on elec. props. 77—59309
  amorphous, electron and phonon density of states calcs., comp. to XPS 78—56066
  amorphous, electron irrad.-induced paramag. centres, 77K 78—88187
  amorphous, electronic and phonon densities of states 77—8001
  amorphous, electronic struct. of defects using cluster-Bethe-lattice method 79—73471
  amorphous, electronic struct. of even-ring network model 79—23884
  amorphous, intermediate range order from polarised features of Raman spectrum 80—49113
  amorphous, localised gap states, variable range hopping 77—72866
  amorphous, low temp. thermal cond. and sp. ht. 79—28161
  amorphous, low-temp., elementary excitations, struct. 80—49577
  amorphous, neutron diffr. investig. of local order 77—35480
  amorphous, NQR for tunnelling modes and local struct. order 79—61261
  amorphous, opt. and elec. props. 77—39894
  amorphous, optical, vibr., transport and defect-related props., review 79—51935
  amorphous, optical props., lecture 78—31219
  amorphous, optically induced metastable paramag. state, optical absorpt. and ESR meas. 77—40113
  amorphous, phonon frequency distrib. 78—30723
  amorphous, phonon states 79—60464

arsenic continued
  amorphous, pulsed NQR, bonding, bond angle distrib. obs. 80—54984
  amorphous, refr. index meas. near absorpt. edge 78—2819
  amorphous, short-range order, theory and probes 80—79698
  amorphous, sp. ht. and thermal cond. at low temp. 79—65213
  amorphous, spontaneous crystallisation temp. determ. 77—27833
  amorphous, struct. models 79—37628
  amorphous, theoretical calc. of defect states 80—49657
  amorphous, thermally generated paramagnetism 79—19720
  amorphous, US attenuation and sound vel. meas., 4.2 to 300K; 80—49308
  amorphous, vibr. excitations at defect sites, IR and Raman spectra calc. 80—49329
  amorphous, vibrational excitations of defect sites 80—49332
  amorphous 80—25457
  amorphous and cryst., phonon density of states calc., comp. to IR absorpt and neutron scatt. data 78—55924
  amorphous film, interference enhanced Raman scatt. 80—50326
  amorphous semiconductor, defect states 79—87057
  amorphous solid dielectric loss meas. by submillimetric waveguide laser 79—33603
  amorphous vibr. props. calc. for models 77—84873
  Atlantic Ocean waters, As and Sb content *(Russian)* 77—60428
  atmosphere quantitative analysis of aerosols 79—12179
  atom, ($4^5S_{3/2}$) state, kinetic obs. using time resolved reson. fluoresc. 78—94211
  atom, electron impact ionisation, in RF ion source, effective cross-sections 78—22034
  atom, $K\beta/K\alpha$ rel. intensity obs. 80—32665
  atom, L-shell soft X-ray emission spectra, oscillator strengths 80—32651
  atom, $np^2(n+1)s$ excited-state config. quadrupole moments, Sternheimer shielding factor 80—37755
  atom, rel. oscill. strengths, 193.8 and 197.3 nm lines 79—791
  atom, spin magnetic moment densities, spin density functional method calcs. 77—67969
  band structure and cryst. energy, pseudopot. calc. 79—90954
  band structure on Jones zone boundary, pseudopot. calc. 80—54603
  biological material analysis, As and Hg determ. by neutron activation anal. 80—36216
  chemical bonding in group V and VI elements and compounds with tetradymite structure 80—15036
  concentration measurement in Si_3N_4 thin film by CAMECA probe *(French)* 77—86411
  continuum source, for atomic fluorescence spectrometry 78—45716
  crystal structure, pseudopot. expansion method 77—27848
  Debye-Waller factors and thermal expansion 78—43089
  depth profiles in Si-SiO_2-Si structs., ion microanal. *(Japanese)* 78—85251
  determination, in beef extract, by NAA 78—27856
  determination, in combustible municipal solid waste, by AAS 78—85229
  determination, in Si, by AES *(Japanese)* 78—91356
  determination in ores of reduced heteropoly acids, photometric method 78—61103
  determination in rocks and soils by at. absorpt. 79—88475
  determination in seaweed and related products, hydride generation system, at. absorpt. spectrophotometry 80—30294
  determination in Si by ion microanal. *(Japanese)* 78—85250
  diffusion coefficient in Ga at 720°C during LPE growth 80—54419
  diffusion in Ni, 970-1360°C *(Russian)* 80—29218
  diffusion in p-Si monocryst., Henry const., temp. depend., 1448 to 1523K 79—42399
  diffusion in Si, proton enhanced diffusion and vacancy migration 78—67747
  diffusion in Si, radn. enhanced 80—29216
  diffusion in Si from As doped oxide film, stress effect on film roughening 78—2389
  diffusion in Si from doped polycryst., conc. depend. 78—34656
  diffusion in Si melted by high power ns laser pulse 78—79789
  diffusion in SiO_2, diffusivity and masking oxide thickness 80—39350
  diffusion in SiO_2, O_2 effects 78—43180
  diffusion in solids, double, gettering of impurities 80—75383
  diffusion in steel, glass fusion treatment *(Russian)* 78—35585
  diffusion into Si, from As-doped oxide source, mechanism 77—47477
  distribution and speciation in natural waters and marine algae 78—81210
  doping of amorphous tetrahedrally bonded semicond., mechanism, gap density of states 79—19545
  dose depend. in laser annealing 78—91354
  elastic moduli, calc. from interatomic forces 79—95071
  electric field gradient, temp. and press. variation 80—93205
  electrical and thermal props. 78—14747
  electrical conductivity and density, crit. parameters, liq. and vap. phases 77—47562
  electrical resist., thermal cond. and thermopower, low temp. transport props. 80—49708
  electrical resistivity and anisotropy coeff. at press. up to 80 kbar 77—43554
  electrical resistivity meas., 50 mK-7K 79—60839
  electroplating, conditions of operation and quality of coatings, expt. *(Bulgarian)* 77—4744
  film, inelastic-elastic scatt. ratio of 80 keV electrons use for radiation damage monitoring 77—4127
  film, sputtered, density of valence states by XPS and UPS 77—24926
  film A1-type supercond. vapour-quenched transition temp., A7-type phase transition 78—52145
  Gaussian basis sets, Ga, Ge, As, Se, Br, and Kr, HF calcs. 77—38611
  n-Ge:As, photoemission, into electrolyte soln., energy diagram, Volta pots., voltage drop 77—62990
  implantation, in Si *(Japanese)* 78—38738
  implantation, laser annealing in short channel MOSFET fabrication 80—20312
  impurity in Cr-Mo-V low-alloy steel, effect on high-temp. ductility and crack growth 80—66652
  incorporation in GaAs oxide grown thermally under As_2O_3 vapour 79—77928
  interlattice displacement and second-order elastic consts. 80—34121
  ion implantation in laminar Si-SiO_2 systems struct. change investig. by MSSI *(Russian)* 80—107918
  ion prod. in 2 MV Van de Graaff 80—14031
  K shell photoelectric cross section, at 74.409 keV 79—72288
  laser annealing, optical constants, ellipsometry observation 80—34024

arsenic continued
  liquid, Anderson transition, cond., at high temp. and supercrit. press. 78—34869
  loss peaks elimination using Ga in metal-GaAs contacts 80—80370
  magnetoreflection for circularly polarised radiation 78—2840
  magnetoreflection of circularly polarised IR radiation, band struct. 77—52094
  migration capacity, effect of acid-alkaline conditions on hydrogeochem. 77—37244
  muonic Knight shift, temp. and mag. field depend. 79—91331
  neutron activation analysis, in environmental materials, reliability aspects 78—40106
  orthorhombic, pulsed NQR, bonding, bond angle distrib. obs. 80—54984
  orthorhombic and rhombohedral, comparison of electronic band struct. 78—23016
  oxide:As films, thermal stress effects on roughening 79—23813
  phonon dispersion curves, of α-phase, neutron scatt. study 79—42178
  photoemission relax. energies *(French)* 77—36357
  pseudopotential, self-consistent, band struct. 78—84141
  Raman vibr. spectra and bonding 80—11411
  rhombohedral, electronic struct. and optical props. var. with internal displacement parameter 79—60702
  rhombohedral, phonon states 79—60464
  rhombohedral, pulsed NQR, bonding, bond angle distrib. obs. 80—54984
  rhombohedral crystals, slip dislocations and slip systems 79—23617
  rhombohedral nucl. quadrupole spin-lattice relax. 79—15373
  sediment pollution by Hg and As, instrumental neutron activation and atomic abs. spectrometric anal. 80—16890
  solid state As, new phase identification 79—99315
  spectrochemical analysis, atomic absorption using vapour generation method 80—16745
  spectrophotometric determ. using haematoxylin 78—20104
  structure, pseudopotential method calcs., using untruncated pot. 78—18582
  superconductor, A1-type, critical mag. field 79—69638
  surface, freshly cleaved, vaporisation, surface morphology changes obs. 77—80612
  thermal accommodation coefficient of gaseous As_4 on As(111) surface determ. 77 1319
  thermal diffusivity by laser flash technique 78—6189
  thermopower and thermal cond. from 8K down to 0.3K 79—19610
  thin epitaxial layer surface As concentration meas. 79—95037
  troposphere, conc. determ. over marine and continental regions 79—70486
  troposphere, enrichment, sources and flux 79—70487
  vapour pressure above solution of GaAs and GaP in Sn 77—51485
  water pollution, arsenic in freshwater fish traced to fly ash leachate using neutron activation analysis 80—97827
  X-ray absorption edge, chem. shift, electron binding energy in compounds 78—62822
  X-ray K absorpt. edge, effective ionic charge and bonding schemes 80—29827
  X-ray K-absorpt. edge shifts 77—4701
  zone centre phonons and elastic consts., hydrostatic press. depend. 78—59905
  Al:As, anodic oxidation, mobility of foreign atoms 77—90494
  As $4p^3(^4S_{3/2})$, collisional quenching 78—33464
  As, $4p^3 \rightarrow 4p^25s$, transition probabilities 80—47943
  As conc. meas., column chromatography versus flameless atomic absorption spectrophotometry 80—55969
  As I, level identification and Zeeman effect obs. 80—95571
  As III, radiative lifetimes, calcs. and beam-foil spectra 77—75223
  As IV isoelectronic series, $4s4p\,^1P$ lifetimes meas. 80—42998
  a-As, second and third order elastic consts., ultrasonic velocity meas. 80—103408
  As VI, VII, spectra 100 to 300 and 500 to 1200 Å ranges 80—83307
  As XXV, 2p-4d and 2p-4s transition arrays, wavelengths and oscillator strengths 80—47933
  As^-, photodetachment cross-section meas., crossed beam expt. 77—61723
  As^+, CW laser oscill. on transitions in He-AsH_3 gas discharges 80—38004
  As^{2+}, and isoelectronic ions, excited-state energy level k-ordering, l-patterns 77—88406
  As:Ni(Ge)(S)(Se)(Te) film, amorphous, chemical modification of props. 80—49250
  As_2 , photodetachment cross section, 0.5 to 3.0 eV photon energy *(German)* 77—65518
  As_3, 3-body nonadditive interaction, nodal struct. 78—1049
  As_4, gaseous, atomisation enthalpy and enthalpy of form., mass-spectroscopic Knudsen cell method 78—80780
  AsF_6^-, bond order and Raman intensity, delta function eqn. 77—61693
  As(III) and As(V), redox stability in aq. soln. 80—61068
  As(III) + Br_2 reaction, flow coulometry, with ring-disk electrode 80—71966
  As_4O_6, high temp. Raman band contours, vibr. anal. 79—10116
  ^{A}As, A=69-72, $^4S_{3/2}$ ground state hyperfine struct. and nuclear moments 80—32853
  ^{33}As, L-shell X-ray prod. by H(He) ion bombardment 79—47548
  ^{33}As, origin of high and low freq. K-satellites in X-ray emission spectra 80—50466
  ^{75}As, slowing down of atoms/ions with KE$\leq$5 eV by inert gases 79—31650
  CdS:N, P, As, Sb, Bi photoluminescence obs. 78—10965
  CdTe:As, ion implanted, elec. props. 80—65021
  CdTe:As^{2+}, photovol. props. of p-n junction prod. by ion implantation 78—43038
  Co:As, temp. anomalies of hyperfine fields 78—23265
  Ga + As reaction temp. determ. for GaAs synthesis 77—24978
  GaN:As, implanted single cryst. film, cathodolum. 78—60523
  GaP:As, form. of $GaAs_{1-\eta}P_\eta$ by diffusion 80—54389
  Gd:^{75}As, mag. hyperfine field determ. by PAC 77—8459
  Ge:As, containing dislocation loops, dynamic scatt. of X-rays, extinction effect 78—47384
  Ge:As, D states in mag. fields, photocond. spectra, and far IR absorption spectra 79—95370
  Ge:As, D^- states investigated by long wavelength photoconductivity 78—6323
  Ge:As, donor bound exciton luminesc. and absorpt. 80—29777
  n-Ge:As, far IR absorpt. spectra 79—91469
  Ge:As, far IR transmission spectra, singlet-triplet optical transitions in ground states of donors 78—2887

arsenic continued

- n-Ge:As, heavily doped, luminesc. from electron-hole drops 77—81144
- Ge:As, implantation doping, annealing and doping profile determ. 77—19972
- Ge:As, impurity photocond. spectra under uniaxial compression 80—44656
- Ge:As, interaction of muonium with atoms 79—11373
- n-Ge:As, irradiated with fast electrons at 77K, investigation of 300K annealing stage 79—51155
- n-Ge:As, magnetothermal cond., 4.2K 80—24688
- Ge:As, many-valley semicond., donor binding energies, variational calc. 78—23041
- Ge:As, moderately heavily doped, electron-hole drops photoluminesc. 80—7417
- Ge:As, NMR, conduction electrons in impurity band, metal-nonmetal transition 79—78544
- Ge:As, phonon-bound donor resonance scatt., donor-electron radius mag. field depend. 79—77847
- Ge:As, photoconductivity oscillation with respect to applied mag. field *(Russian)* 78—80026
- Ge:As, piezospectroscopy 79—99915
- Ge:As, recomb. of donor bound excitons, luminesc. intensity decay 80—25441
- Ge:As, thermally induced defects properties obs. 77—63692
- Ge:As, uniaxially stressed, electronic Raman scatt. from valley-orbit transitions 78—15166
- n-Ge:As closely compensated, photolum. of charge carriers localised in trails of density of states 77—77294
- Ge:As thermal phonon scatt., piezo-thermal cond. 80—70482
- Ge:As(Se$^+$), energy spectra, multivalley effective mass calcs. 77—59266
- Ge:Sb, fast-neutron irradiated, shallow radiation defect levels, electronic props. 78—23049
- Ge:Sb (As), isolated D$^-$ states and D$^-$ complexes in mag. fields 80—15473
- Ge$_{1-x}$Si$_x$:Ga,As, interimpurity radiative recombination, composition depend. 79—11465
- He-As CW laser, excitation mechanism 79—3685
- In-Ge:As, Schottky barrier tunnel junction, zero bias resistance, temp. depend. 78—72258
- Ni-Si:As, implanted dopant redistrib. after silicide form., appl. to ohmic contacts 79—37729
- PbTe:As, hole conc. control, in LPE layers, plasma reflectivity and thermoelec. probe meas. 79—99640
- PbTe:As, ion implanted, magneto-optical expts. *(German)* 79—28848
- Pd-Si:As, implanted dopant redistrib. after silicide form., appl. to ohmic contacts 79—37729
- Pt-Si:As, implanted dopant redistrib. after silicide form., appl. to ohmic contacts 79—37729
- Pt-Si:As, silicide form. during laser irrad., p-n junctions and ohmic contacts 80—84397
- Se:As, amorphous, pure and doped, photoelectronic preps. in glass transition region 79—4583
- Se:As, amorphous film, dielec. activity obs. near glass transition temp. 80—75933
- Se:As, continuous crystn. kinetics 77—24382
- Se:As, trigonal, defect and impurity electron levels, surface photovoltage spectra 78—72108
- Se:As X-ray plates, electronic transport *(German)* 80—80290
- Si, As implantation profiles, calc. comparison with expt. 78—38748
- Si ion implanted, doping profile meas. by He$^+$ backscattering spectra 79—60390
- Si junction, As-diffused, ion implantation effects on leakage current 77—62555
- Si: As, ion implantation and pulsed laser annealing, supersat. alloy form. 80—54267
- Si:Ar, As, ion implanted, laser annealing, doping profiles, channelling 80—97506
- Si:As, ^{75}As implantation, scanned CW electron beam annealing 79—99225
- Si:As, 1.5 MeV H$^+$ and He$^+$ irradiations of As diffused layers 78—47447
- Si:As, amorphous, appl. of EXAFS methods for struct. determ. 79—37624
- Si:As, amorphous, field effect and thermoelectric power 79—33289
- Si:As, amorphous layers, laser induced As profile broadening 79—95045
- Si:As, and Si:As,Gd, depth of energy levels of As from impurity photocond. 79—90996
- Si:As, annealed, dopant profile parameter contactless probing by IR spectroscopy 79—77629
- Si:As, anomalous tail generation, As ion channelling 80—49246
- Si:As, appl. of high throughput 80—34029
- Si:As, As implantation damage and atom location, channelling meas. 77—59032
- Si:As, bound excitons and bound multiexciton complexes for shallow donors, luminesc. meas. 79—24363
- Si:As, CVD, doping using SiH$_4$-H$_2$-AsH$_3$ system 80—79823
- Si:As, CW CO$_2$-laser annealing, comparison with thermal annealing 80—84193
- Si:As, CW laser annealing mechanism, annealed spot size, solid phase epitaxial regrowth 79—78798
- n-Si:As, characts. of piezoresist. 77—51750
- Si:As, conc. profiles of As and recoiled O atoms after ion implantation into SiO$_2$-Si, SIMS obs. 79—51138
- Si:As, conc. profiles of ions and recoiled N after implantation through Si$_3$N$_4$ films 79—55764
- Si:As, depth profile detect. limit of 3×10^{15} atom cm^{-3} using Cs$^+$ bombardment negative SIMS 77—65988
- Si:As, depth profiling using Cs$^+$ bombardment and negative SIMS in UH vac. 79—99232
- Si:As, diffused, laser irrad., stability study 80—65547
- Si:As, diffusion model, degeneracy and partial ionisation effects 80—96693
- Si:As, diffusion of implanted As induced by laser annealing 77—89590
- Si:As, displacement effect beam energy depend., vacancy trapping 80—33996
- Si:As, donor-polarizability enhancement as the insulator-metal transition is approached from the insulating side 80—80184
- Si:As, dopant profile changes induced by laser irrad. using SIM and backscatt. meas. 79—69148
- Si:As, doping, new paint-on diffusion source 77—4118

arsenic continued

- Si:As, dual wavelength, laser ion implantation damage annealing 79—69117
- Si:As, effects of recoil-implanted O on elec. activation of As 79—99227
- Si:As, elec. activation of implanted As during low temp. anneal, Hall effect meas. 78—51571
- p-Si:As, electrochem. doping, depth profile analysis 77—72630
- Si:As, electrochemical doping 79—90684
- Si:As, electrochemical doping profiles 79—90685
- Si:As, electron induced displacement, channelling study 80—29058
- Si:As, electron irrad. induced defect levels, annealing, deep level transient spectroscopy obs. 77—59044
- Si:As, electron irradiated, majority carrier trap prod., effect of O$_2$ enhanced annealing 77—1151
- Si:As, epitaxial growth, adsorbed layer model for autodoping mech. 80—7505
- Si:As, epitaxy, lateral autodoping kinetics 78—39699
- Si:As, H, amorphous system, struct. and defects, Raman and EPR meas. 80—49103
- Si:As, heavily As-diffused, Hall mobility and resist. rel. to carrier conc. 80—107815
- Si:As, heavy-doping effects and impurity segregation during high-press. oxidation 80—65014
- Si:As, high conc. diffusion from double-layer sources 78—10075
- Si:As, high resolution study of group V impurities absorption 80—7388
- Si:As, high-dose implanted, irrad. time and subsequent heat treatment effects on laser annealing 80—29041
- Si:As, high-dose ion implanted and annealed, implant redistribution 80—107309
- Si:As, implantation damage removal by laser irrad. and its thermal stability, TEM study 79—74024
- Si:As, implantation into polycryst. Si and diffusion into Si substrate 77—59025
- Si:As, implanted, laser annealing reduction in defect conc. 77—62559
- Si:As, implanted, pulsed ruby-laser annealing, Rutherford backscatt., TEM and ion channelling study 79—86805
- Si:As, implanted, residual defects after one- and two-step annealing 78—6083
- Si:As, implanted, spatially varied activation during regrowth of amorphous layers, sheet resist. and backscatt. obs. 78—71749
- Si:As, implanted, substrate for epitaxial Si 78—6243
- Si:As, implanted, thermal diffusion of As 80—39352
- Si:As, implanted As redistrib. during annealing in oxidising ambient, carrier distrib. meas. 79—19275
- Si:As, implanted CW laser annealing, elec. props., cryst. struct. and limitations 80—39131
- Si:As, implanted through SiO$_2$ films, elec. props., defect struct. 80—54264
- Si:As, impurity diffusion from implanted layer, influence of radiation damage 77—76621
- Si:As, ion implant lattice location after pulsed ruby laser annealing 79—73204
- Si:As, ion implantation, 20-2800 keV, obs. of X-rays produced 78—14367
- Si:As, ion implantation system, high current, design of end station 80—34030
- Si:As, ion implanted, amorphous-cryst. transition induced by multiple-pulsed ruby laser 79—90555
- Si:As, ion implanted, annealing characts., elec. props. 77—19974
- Si:As, ion implanted, annealing of heavy ion cascade damage, channelling meas. 80—89255
- Si:As, ion implanted, anomaly of elec. activation by additional Ne irradiation 78—84211
- Si:As, ion implanted, anomalous diffusion of As 79—14842
- Si:As, ion implanted, beam techniques 80—24474
- Si:As, ion implanted, comparison of effects of ruby laser and electron beam annealing 79—69135
- Si:As, ion implanted, doping profile, pulsed laser annealing effects 80—88197
- Si:As, ion implanted, formation of As complexes 80—59511
- Si:As, ion implanted, glow discharge optical spectroscopy 78—22755
- Si:As, ion implanted, laser scanning apparatus for annealing 78—34526
- Si:As, ion implanted, laser annealed, lattice defects, epitaxial regrowth 80—103334
- Si:As, ion implanted, lattice location of impurities after pulsed laser annealing 80—88196
- Si:As, ion implanted, low temp. thermal annealing 80—96552
- Si:As, ion implanted, pulsed laser annealing appl. to device fabrication 79—73180
- Si:As, ion implanted, pulsed ion beam annealing 80—103395
- Si:As, ion implanted, pulsed laser annealing, partial solid-state regrowth 80—103591
- Si:As, ion implanted, recrystallisation by free running ruby laser 79—73185
- Si:As, ion implanted, redistrib. of dopants by pulsed laser annealing 79—7620
- Si:As, ion implanted, scanning-electron-beam annealing 79—60391
- Si:As, ion implanted, TEM study after laser and furnace annealing 80—70234
- Si:As, ion implanted, two-step annealing 78—18664
- Si:As, ion implanted, two-step annealing, TEM study 79—82249
- Si:As, ion implanted film, elec. prop. impurity depend. 80—24467
- Si:As, ion implanted layers in device structures, boundary effects in laser annealing 79—73188
- Si:As, ion-implanted, CO$_2$ laser annealing 79—73183
- Si:As, ion-implanted, CW IR laser annealing 80—34022
- Si:As, ion-implanted, channelling anal. of CW Ar laser annealing 79—73186
- Si:As, ion-implanted, dislocation loops and etch pits, X-ray diffr. and TEM obs. 79—42068
- Si:As, ion-implanted, impurity redistrib. during laser irrad. 80—100280
- Si:As, ion-implanted, laser annealing, channelling obs. of As cluster form. 79—69128
- Si:As, ion-implanted, laser recrystallisation by freq.-doubled Nd:YAG laser 79—77613
- Si:As, ion-implanted, scanned laser and electron beam annealing 79—73182
- Si:As, ion-implanted, thermally assisted Xe-flash annealing, Rutherford backscatt. meas. 79—10881
- Si:As, ion-implanted and post-annealed, dislocation loops, TEM obs. 77—84776

arsenic continued
Si:As, ion-implanted layers, ellipsometric anal. of laser annealing 79−73190
Si:As, ion-implanted polycrystalline films, laser annealing 79−73181
Si:As, laser annealing, channelling, optical obs., and resist. meas. 79−1444
Si:As, laser annealing of implanted layers 77−55296
Si:As, laser assisted doping for surface layers 80−19824
Si:As, laser induced diffusion and annealing processes 77−69943
Si:As, laser-doped, impurity distrib., Rutherford backscatt. and channelling anal. 80−59507
Si:As, luminescence associated with transitions from bound exciton excited states 78−23534
Si:As, MBE, ion implantation for n-type doping 80−15126
Si:As, MBE with simultaneous ion implant doping 80−66432
Si:As, mean square dynamic displacement of atoms, effect of electron-phonon interactions *(Russian)* 78−10145
Si:As, neutron damage mechs. in IR detectors 78−30668
Si:As, nonequilibrium solid solutions obtained by heavy ion implantation and laser annealing 80−92544
Si:As, Orbach spin-lattice relax. rate, uniaxial stress depend. 78−72391
Si:As, oxidation-enhanced diffusion of impurities 79−46840
Si:As, p-n junction form. by laser annealing, space charge region, effects on reverse current 80−54772
Si:As, planar and axial channelling of 800 keV As 77−19995
Si:As, polycrystalline, As segregation at grain boundaries, elec. props. meas. 80−75259
Si:As, polycrystalline, ion implanted, AES analysis 77−31690
Si:As, relation between total and electrically active As conc. produced by diffusion 79−55773
Si:As, SIMS, energy distrib. of sputtered ions 79−38706
Si:As, scanning electron beam annealing, spreading resistance, junction depth 80−75267
Si:As, segregation, TEM obs. 77−63674
Si:As, segregation and desorption kinetics for evaporation of As 79−99410
Si:As, shallow donor electrons, hyperfine interactions, reply to Onffroy's calcs. 78−51934
Si:As, shallow donor states with strong central cell perturbation theory 78−51933
Si:As, shallow junctions by high-dose implants 80−96694
Si:As, solid solubility and thermal behaviour of metastable 80−75359
Si:As, solid solubility of As determ. by ion implantation, CW laser annealing 80−6517
Si:As, temp. depend. of irradiation-induced displacement of As, backscattering meas. 78−26605
Si:As, thermal oxidation in wet ambient from 650°C to 850°C 79−61758
Si:As, time-resolved reflectivity during laser annealing 78−92086
Si:As,Sb, amorphous, damage depend. of epitaxial regrowth during annealing 78−47679
Si:As detector, high-low junction contact at low temp. 77−39925
Si:As device, anal. using SEM-AES-IMA combination with SIM spectrometer *(Japanese)* 78−85249
Si:As film, implanted, elec. cond., sheet resist. as function of ion dose and temp. 79−78235
Si:As film, polycryst. laser annealed, resistivity changes during thermal annealing 79−91163
Si:As high-dose implanted single crysts., pulsed electron-beam annealing 80−103373
Si:As implanted emitters, oxidizing drive-in ambient deleterious effect 80−2044
Si:As ion implanted, laser induced diffusion modelling 80−24672
Si:As ion implanted layers, annealing by CO_2 laser, doping profile shift 80−84965
Si:As ion implanted shallow junction 80−70228
Si:As ion implanter system, high current, architecture and control 80−31942
Si:As laser annealing, heat and mass transport model 80−92546
Si:As p-n junction diode, electron-beam annealing of ion-implantation damage 79−77622
Si:As sputter rate meas. SIMS combination with Rutherford backscatter 80−21334
Si:As thermal diffusion retardation by inert gas ion implantation 79−77616
Si:As wafers, laser annealing, Rutherford backscatt., optical, and TEM obs. 79−1445
Si:As$^+$, annealing by scanning Ar ion laser, dislocation loop density comparison 78−47438
Si:As$^+$, implanted, CW laser annealing, electron-beam induced current 80−100709
Si:As$^+$ sheet resistivity rel. to isochronal annealing and defect structures 77−76443
Si:As(Li)(P), luminesc., stress effects on donor exciton satellites 77−85786
Si:B, As, diffusion of As atoms from ion implanted layers, conc. profiles 77−43376
Si:B, As, first and second order Raman scatt. by pair modes 79−65869
Si:B,As selective area simultaneous doping 80−34015
Si:Bi, As, optical polarisation of ^{29}Si nuclei, nucl. relax. due to optical pumping 80−2665
Si:Ga, As, sequential diffusion, radiotracer obs. 78−10073
Si:Ga,P(As), sequential diffusions, comparison of interactions 77−80655
Si:Sb,As, autodoping effect of Sb-As simultaneous diffusion 77−80522
Si-Ge:As,P, heavily doped, electron scatt., Hall coeff., Seebeck coeff. and resist. meas., 4-300K 77−4379
Si-H:As alloy, amorphous film, coordination of impurities, EXAFS of data 77−84780
Si_3N_4:As film, penetration of As ions, 50 to 500 eV 77−76444
Si_3N_4-SiO_2:As, graded and stepped energy band-gap MIS struct. 80−2473
SiO_2, As-implanted, electron trapping and detrapping characts. 80−65692
SiO_2 film, on Si, As-implanted, dopant range distrib. He$^+$ backscatt. obs. 77−39611
SiO_2:As film, penetration of As ions, 50 to 500 eV 77−76444
SiO_2:As$^+$ implanted layers in MOS struct., electron trapping and detrapping characts. 80−92982
SiO_2-Na_2O-CaO:Fe(As)(Cr) glasses, optical absorpt. changes on heat treatment 78−31224

arsenic continued
SiO_2-Si:A, effects of recoil-implanted O on elec. activation of As 79−99227
SnO_2:As film, prep. and elec. cond. 80−2959
^{99m}Tc radiopharmaceuticals, As for P substitution, bone-seeking agent analogues 80−51250
Te:As, impurity spectroscopy 80−65499
Te:As, photoconductivity in strong mag. fields, doping effects, impurity levels 80−75602
ZnP_2:As, local vibrs. of impurity ions, Raman study 80−29745
ZnSe:As, defect struct., Hall effect and Zn self-diffusion meas. 79−1427
ZnSe:As, high temp. electron mobility, lattice scatt. and ionized impurity scatt. 79−91042
p-ZnSe:As, ion implantation and heat treatment 78−87700
ZnSe:Ga,As, characts. of simultaneous incorporation, by Mn^{2+} ESR and X-ray fluoresc. anal. 80−34017
ZnSe:Ga(As), edge luminesc. 80−20699
Zn_2SiO_4:As,Mn, enhanced luminesc. stimulation, 20-320K *(German)* 77−20900
ZnTe:As, binding energy of shallow acceptors from photoluminesc. excitation spectra for donor-acceptor pairs 79−95809
ZnTe:As, donor-acceptor pair excitation and recomb., photoluminesc. obs. 80−20691
ZnTe:As, electronic Raman scatt., mag. field depend. 79−73928
ZnTe:As, electronic Raman scatt. and IR absorpt. spectra of shallow acceptors 79−73978
ZnTe:As, g-values, spin temp., determ. from Raman spectra 78−43856
ZnTe:As, ion implanted, cathodoluminescence emission spectrum 80−108281
ZnTe:As, shallow-acceptor, donor, free-exciton, and bound-exciton states 80−60667

arsenic alloys
see also arsenic compounds
steel, austenitic, grain growth in 16G2S. 16G2SF, AND 09G2SF, As effect 77−70060
steel, low alloy, ferritic, As effect on grain size 77−70062
Ag-As, α-phase alloy, thermopower at low temps. 78−84196
Ag-As, thermopower at low temp., Fe impurities 79−65440
As-Pb, eutectic, temp. determ. up to 35 kbar 77−85989
As-Te, Ge-As-Te molten system, metal-semicond. transition, cond. obs. *(German)* 77−1457
As_xSb_{1-x}, semimetal, thermopower, thermomagnetic power, 4.5 to 77K 80−107825
Bi-Sb-As, band struct., effects of Sb and As, mag. susceptibility meas. *(Russian)* 80−65775
Cd-As, liq. alloys, thermodynamic props. and cpd. formation 77−1238
$CdGeAs_2$, amorphous, thermal gradient expts., recrystn. 80−55438
$CdGeAsMn_x$ glass, recrystallisation 80−44133
$(Cr, Mn)_2As$, mag. props. and struct. 78−64190
CrAs, anisotropy of compressibility 79−7648
Cu-As, dil., magnetic susceptibility, impurities effect, free electron gas model 79−91206
Cu-As, dil., magnetic susceptibility, impurities effect, Fermi surface effects 79−91207
Cu-As, dil., optical props. and electronic struct. 78−35164
Cu-As-Fe, Mossbauer effect of Fe impurities 78−31131
Eu-As system, cryst. struct. of phases formed 78−26493
$Eu_{11}As_{10}$, Eu_5As_{10}, $Eu_{3+x}As$, Eu_5As_3, Eu_4As_2O, cryst. struct. 78−18585
Eu_5As_3, cryst. struct. of high and low temp. phases 78−75626
Fe-As, dil., mag. hyperfine fields, Curie temp. and Mossbauer meas. 77−63190
Fe-As, dil., short range order, NMR study 80−71237
Fe-As, dil., XPS meas. 77−63538
Fe-As, liquid alloy, density and surface free energy *(Russian)* 78−11204
Fe-As (0.22 to 1.68 wt.%), martensitic transform., struct. features 77−36499
Fe-As melts, influence of Sn, Si, Mn and Cr additions on surface tension and density *(Russian)* 80−15337
Fe-As melts, surface tension, density, adsorption *(Russian)* 80−92757
Fe-As system, mag. props., Mossbauer study 80−88897
Fe-As-Su-Si (Cr)(Mn) melts, As and Sn distrib., Si, Cr, and Mn influence *(Russian)* 80−16274
Fe-Mn-As, crystal struct. and magnetic props. of intermetallic cmpds. with Cu_2Sb type struct. *(Japanese)* 78−59785
FeAs, dil., short-range order, neutron diffuse scatt. and spin echo NMR 80−50106
FeAs, Mossbauer spectra of paramag. and ferromag. states, helimagnetic spin ordering 80−7197
$Fe_{2.1-x}Mn_xAs$, $0 \leq x \leq 2.1$, mag. phase transitions 78−2679
Ge-Sn-M, M=Cu, As, Sb, formation of Ge-based solid solns. during crystallisation 77−80625
$Hg_{99}As$, struct. reinterpretation 78−38660
MnAs, high spin state electron config. *(Japanese)* 77−43812
$MnAs_{0.925}P_{0.075}$, low spin state electron config. *(Japanese)* 77−43813
$MnAs_{0.97}P_{0.03}$, orthorhombic, mag. anisotropy 77−43832
$Mn_{0.97}Fe_{0.03}As$, field induced ferromag. phase *(Russian)* 77−36070
$Mn_{1-x}Fe_xAs$, high-pressure phase, magnetic properties 78−52247
$Mn_{1-x}Fe_xAs$, mag. props. in ground state *(Russian)* 78−56294
$Mn_{1-x}Fe_xAs$, magnetic transition under high press., exchange striction model calcs. *(Russian)* 80−50096
$Mn_{1-x}M_xAs$, M=V, Cr, Fe, Co, mag. props., phase diags. 77−66300
Nb-Sn-As, ternary A15 phase regions, solubility 77−44215
Nb_3As, structural and supercond. props. press. effects 80−39700
Ni-As, dil., ferromagnetic, hyperfine field and relax. time obs. of impurity heavy nuclei 80−75533
Ni-As, dil., temp. depend. of hyperfine field, TDPAD meas. 78−43700
$Pb_{1-c}As_c$, liquid alloys, local fluctuations and quadrupolar relaxation 80−66060
Pd_5As, cryst. struct. and cryst. binding *(German)* 78−42958
$Tb_cY_{1-c}As$, singlet ground state systems, resistivities 77−62912
UAS, anisotropic mag. ordering and mag. structural transitions 79−78324
UAs, localised cryst. field states, neutron inelastic scatt. obs. 78−14697
U_3As_4, high-field magnetisation, field-induced phase transition near hard (100) directions 77−28413
V_4As_3, defect struct. 77−4112
Zn-As system, homogeneity range of $ZnAs_2$ and electrophys. props. 80−60833

arsenic compounds

- *see also arsenic alloys*
- arsenolite, As_2O_3, vapour mol. mass determ. using repulsion Knudsen cell 78—46464
- arsonium salts, aq. soln., ^{75}As NMR spectra depend. on alkyl chain 77—69714
- a-As_2Se_3, diffusion of Ag and Au 77—51549
- binary, with non-transition elements, at. vol. and semicond. props. 77—20089
- chalcogenides, deep levels, photoluminesc. and photocond. 80—70641
- chalcohalide glasses of Ge-As-S-I system, acousto-optical parameters 77—36199
- chemical bonding in group V and VI elements and compounds with tetradymite structure 80—15036
- claudetite, As_2O_3, vapour mol. mass determ. using repulsion Knudsen cell 78—46464
- deep struct. changes, NQR obs., high-press. and temp. effects 80—54139
- graphite-AsF_5 intercalated species, fractional ionisation and identification 80—97397
- graphite-AsF_5 intercalation compounds, de Haas-van Alphen effect, charge transfer rate 80—54595
- inorganic As in freshwater environment, stability and solubility theoretical aspects 79—16553
- pentaphenylarsenic cyclohexane, cryst. packing 78—9994
- bis-catena-poly(methylarsenic), one-dimensional homonuclear molecular systems, nature of energy gap 79—11063
- polyacetylene: AsF_5, one-dimens. spin diffusion, NMR T_1 and dynamic mol. polarisation meas. 80—44946
- polyacetylene:AsF_5, AES, XPS, UPS, and X-ray induced 80—66400
- cis-polyacetylene:AsF_5, conductivity meas., non-Ohmic effects 80—96891
- polyacetylene:AsF_5, electronic excitations, momentum depend., EELS study 80—76121
- polyacetylene:AsF_5, Hall effect meas. 80—24955
- polyacetylene:AsF_5, heavily doped, transport props., evidence for metallic state 79—87121
- polyacetylene:AsF_5, mag. susceptibility, Fermi surface density of states, semicond.-metal transition 79—95566
- polyacetylene:AsF_5, soliton doping mechanism, mag. susceptibility meas. 80—107979
- polyacetylene:AsF_5, synthesis, elec. cond., thermoelec. power 80—60016
- polyacetylene:AsF_5, thermal decomp. kinetics, elec. cond., ESCA and mass spectra 80—50830
- polyacetylene:AsF_5, thermopower and transport props. 80—65611
- polyacetylene:AsF_5, X-ray absorpt. meas. of mol. struct., orientation and charge transfer 80—25486
- polyacetylene:$AsF_5(AsF_6)$, metallic, band theory 80—49570
- trans-polyacetylene, and AsF_5 doped, EPR 79—42835
- salt toxic effect on activated sludge micro-organisms *(Chinese)* 79—24919
- silicones, fungicidal protection of optical components made of chem. unstable glass 78—59107
- temp. depend. of conductivity and photocond. at 632.8 nm *(Russian)* 80—44666
- AS_xSb_{1-x} thermomagnetic EMF, temp. and mag. flux density *(Russian)* 80—11022
- Ag-As_2S_3 sandwich structure, holographic characts., recording kinetics 78—29913
- Ag-As-S system glass, struct., props. and vibr. spectra 79—65901
- Ag-As-Se system, glass-forming 79—65001
- Ag-As-Se system glasses, soln. rate 79—43456
- Ag-As-Te glasses, elec. props. *(Russian)* 77—85211
- Ag-As-Te system, vitrification region, physiochem. props. 79—41960
- Ag_3AsS_3, proustite, elec. cond. rel. to impurities, melt stoichiometry deviations 77—11914
- Ag_3AsS_3, proustite crystals, stoichiometric composition derivation influence on phase transition 79—95715
- Ag_3AsS_3, prustite ferroelectric order model in prustite type nonlinear crystals *(Russian)* 79—65807
- $Ag_2S(Se)(Te)$-As, temp.-comp. diagram 78—44105
- Al-As_2Se_3-Al, photographic process based on electrochem. reactions *(Russian)* 79—6213
- $Al_{.20}As_{.40}Te_{.40}$, amorphous alloy, radial distribution function anal., X-ray diffr. *(Spanish)* 80—28915
- amorphous, Raman scatt. investig. of irreversible thermostruct. transform. 77—48163
- As-Ge-Se and As-Ge-Se-Sb glasses acousto-optic props. 77—27327
- As-Ge-Se based glasses, refr. index, 1-11 μm 78—39520
- As-Ge-Se system, synthesis and phys. props. of amorphous layers 77—52252
- As-Ge-Se system glasses, alkali-free, optical absorpt. 79—65883
- As-Ge-Te, chalcogenide glass, elec. cond. and dielec. const. 80—75567
- As-Ge-Te glass, dielectric meas. 79—87382
- As-O, single bond stretching force consts. and bond orders 77—26994
- As-S, amorphous, glass transition and specific heat, intermolecular bond saturation 80—15011
- As-S, amorphous film, photoinduced RI changes, heterodyne interferometry 77—3639
- As-S, glass, IR vibr. spectra, optical characts. calc. 80—40119
- As-S, glassy film optical props., photostimulated effects and hologram recording 79—27215
- As-S, melt struct., orientation birefr., viscosity, refr. index, and density 80—84713
- As-S amorphous chalcogenide thin film, transient photoinduced phenomena 80—80884
- As-S amorphous film, photo-induced optical changes, annealing effect 78—27345
- As-S chalcogenide glassy semiconductors, induced anisotropy 79—32013
- As-S film, amorphous, photo-induced dynamical changes in refr. index 79—28705
- As-S film, guided light reversible control by electron beam irrad. 78—1331
- As-S glass media, temp. control of hologram props. 78—17883
- As-S glasses, acousto-induced structural changes, optical props. 80—49122
- As-S glasses, resonance Raman scatt. 80—50325
- As-S glasses, spectral variation of SKβ emission with S content 79—8209
- As-S glassy film, photobrightening effect 80—11498
- As-S semiconducting glass film holographic recording media *(Russian)* 77—10864
- As-S system, glass forming ability and phase diagram 78—59760

arsenic compounds continued

- As-S system glasses, photostruct. transforms. under laser radiation, use in holographic recording 77—76316
- As-S-Br glasses, IR spectra 79—95780
- As-S-I system, glasses, Raman spectra, struct. 79—65857
- As-S-I system glasses, IR transmission spectra, structure-chem. comp. 79—42974
- As-S-Se glasses, solubility, photostimulated changes 80—24602
- As-S-Se-Ge semiconducting glasses, IR characts. *(Czech)* 80—25332
- As-S-Te, vitreous semiconductor, photoconductivity *(Russian)* 79—11172
- As-S-Te, vitrification, density and elec. cond. measurements 79—7645
- As-S-Tl, glass, viscosity and elastic props. 80—100180
- As-S-Tl(Te) glasses, opt. and mag. props., comp. influence 77—77225
- As-S(Se) glasses, solubility, photostimulated changes 80—24602
- As-Sb-S-I system glasses, vitrification and volt-ampere characts. 77—31756
- As-Se, amorphous, glass transition and specific heat, intermolecular bond saturation 80—15011
- As-Se, amorphous film, kinetics of photo-induced processes *(Russian)* 79—69896
- As-Se, glassy, surface phenomena, gas adsorption effects on elec. props. 79—42621
- As-Se, optical parameter optimisation for holographic recording appl. *(Russian)* 80—43299
- As-Se, relation between glass-transition temp. and optical memory-eraser temp. 80—10650
- As-Se amorphous film, density of upper valence band states, annealing effects, UPS obs. 80—29845
- As-Se amorphous film, optical props. change under high-power light pulse action 79—47534
- As-Se amorphous films, photo-induced changes in IR vibr. spectra 79—91514
- As-Se amorphous system, photocond. props. 80—88587
- As-Se amorphous system, Raman scatt. 80—88984
- As-Se and As_2S_3 films, electron-stimulated changes in optical props. and dissolution rate 80—29709
- As-Se and As-Se-Te glasses, effect of Ag electrodiffusion on volt-ampere characteristics 79—7869
- As-Se based glasses, refr. index, 1-11 μm 78—39520
- As-Se chalcogenide glass, optical const. photoinduced changes mechanism 80—7321
- As-Se films, chalcogenide vitreous semiconductors, reversible photoinduced changes in optical, physicochem. and contact props. 79—24378
- As-Se films, laser-beam recordings by thermal creation of holes 80—35010
- As-Se glass, magnetic susceptibility meas. at room temp. *(Japanese)* 79—82748
- As-Se glass film, MgF_2 coated, effectiveness for optical holographic recording *(Russian)* 77—71960
- As-Se glass film, photoinduced absorpt. changes 79—87519
- As-Se glass thin-film waveguide, for 10.6 μm range 77—50770
- As-Se glasses, elec. transport studies 80—103695
- As-Se glasses, low temp. photocond. 80—49808
- As-Se glassy film, photostimulated changes in microhardness 77—15723
- As-Se glassy system, mag. susceptibility 77—55657
- As-Se system, chalcogenide vitreous semiconductors, darkened films, thermal and optical bleaching, light transmission obs. 80—50447
- As-Se system glasses, electronic props. and localised states, review 77—62871
- As-Se system glasses, opt. absorpt. edge shift on densification 77—77250
- As-Se system glasses, point defects, positron lifetime spectra meas. 78—88380
- As-Se system glasses, structural and electronic transitions 77—76890
- As-Se system glasses, thermal expansion coeff. and free vol. at transition temp. *(Japanese)* 79—55876
- As-Se:^{197}Au, glassy, Au impurity influence, elec. cond., optical absorpt. and Mossbauer meas. 77—24558
- As-Se-Bi, semicond. chalcogenide glasses, crystallisation and electrophys. props. 78—9955
- As-Se-Cu system glass films, elec. and photoelec. props. variation with photostruct. transforms. 77—76980
- As-Se-Ge, amorphous film, relief-type hologram mode, hologram replication *(Japanese)* 78—78959
- As-Se-Ge film, master for hologram copying 78—29912
- As-Se-Ge(-S), photostructural change in Urbach tail 80—76021
- As-Se-S glasses, isothermal sintering, surface area reduction 77—8779
- As-Se-S-Ge chalcogenide glass films, appls. to passive optical waveguide components 79—37048
- As-Se-S-Ge chalcogenide amorphous film, computer-generated holograms using electron beam irrad. 80—95846
- As-Se-Sb, crystallised glasses, struct. from Mossbauer spectra 80—64917
- As-Se-Te, amorphous, electron and hole drift mobilities 80—34442
- As-Se-Te glasses, electron transport props. 78—10439
- As-Se-Te glasses, glass form., charact. temp., density, thermal expansion and dynamical viscosity, struct. model 78—26672
- As-Se-Te system glasses, AC cond. and permittivity, freq. and temp. depend. 77—76857
- As-Se-Te thin films, laser induced crystn. kinetics 77—76317
- As-Se-Tl system, chalcogenide glasses, NMR spin-lattice relax. time meas. 79—95671
- As-Se(-Ge) chalcogenide glasses, mode-guiding layer in IR microwaveguides 80—28329
- As-Se(S), glassy and crystalline, point defect exam. by positron annihilation 78—72637
- As-Se(Te)-Ge, fabrication of amorphous semicond. thin films with graded band struct. *(Japanese)* 77—55623
- As-Te, Ge-As-Te molten system, metal-semicond. transition, cond. obs. *(German)* 77—1457
- As-Te films, laser-beam recordings by thermal creation of holes 80—35010
- As-Te system glasses, DC and AC cond., thermo-EMF, 140 to 350K 79—42549
- As-Te-Cu system glasses, DC and AC cond., thermo-EMF, freq. depend., 100 to 370K 77—76827
- As-Te-Cu system glasses, elec. cond. and thermo-EMF 79—42540
- As-Te-Cu(Ag) system glasses, absorpt. coeff. and optical band gap 79—65829
- As-Te-Ga, glass, elec. cond., 190-300K *(Russian)* 80—54702
- As-Te-Ga system, glass-forming region and props. 80—25674

arsenic compounds continued

- As-Te-Ge chalcogenide films, thermally induced transformations, TEM obs. 79−94917
- As-Te-Ge system glasses, thin films, effect of S, Se, Sb, Bi, Tl on volt-ampere characts. 77−15976
- As-Te-Ge/n-Si, film on cryst., heterojunction, elec. and photovolt. props. 80−100514
- As-Te-Ge-Si, amorphous film, high-speed switching mechanism 77−8153
- As-Te-Ge-Si sandwich type amorphous films with metal electrodes, space-charge-limited switching, pre-breakdown characts. *(Japanese)* 77−69385
- As-Te-In, glass-forming, density and microhardness 80−103257
- As-Te-Si-Ge amorphous chalcogenide semiconductor, thin film interface, elec. charact. *(Korean)* 80−97014
- As-Te-metal amorphous film, switching, memory effects 80−44677
- As$_2$-Se$_3$-Bi$_x$ amorphous system, elec. and photocond. props. 79−51574
- o-As$_2$B$_{10}$H$_{10}$, ^{1}H and ^{11}B CW NMR, mol. reorientation in cryst., phase transition 77−85583
- AsBr$_3$, electron impact positive ion form., appearance energy obs. 80−53151
- AsBr$_3$, gas-phase electron diffr., mol. struct., force consts., vib. unharmonicities 77−546
- AsBr$_3$, microwave spectra, rot. consts., mol. struct. 77−3485
- AsBr$_3$, Raman scatt. spectrum, intermol. interaction and dimeric assoc. *(Russian)* 77−54562
- AsCl$_3$, 100 to 200 GHz spectra, mol. struct., harmonic force field 78−42042
- AsCl$_3$, bond polarisability and force constants 80−69260
- AsCl$_3$, electron impact positive ion form., appearance energy obs. 80−53151
- AsCl$_3$, low temp. struct. study *(French)* 79−32968
- AsCl$_3$, Raman scatt. spectrum, intermol. interaction and dimeric assoc. *(Russian)* 77−54562
- AsCl$_3$-CCl$_4$(C$_2$H$_4$Cl$_2$) mixtures, purification by selective photodissociation 77−79708
- AsD$_3$, IR spectra, vibr. relax., rot. reorientation in solid phase 78−19463
- AsD$_3$, solid and liq., vibr. relax., Raman ν_1 band, 54, 160K 78−27198
- AsF, molecular constants determ. from b$^1\Sigma$-X$^3\Sigma$ transition, nonlinear least squares procedure 79−798
- AsF, pot. energy curves and dissoc. energy, Hulbert-Hirschfelder calc. 80−30210
- AsF, UV band system, e0$^-$-X$_2$1 and f0$^+$-X$_2$1 rot. anal. 77−27083
- AsF$_3$, cryst. struct. at 193K *(French)* 80−49194
- AsF$_3$, inversion barrier, STO SCF calc. 80−63567
- AsF$_3$, millimetre rot. spectra, vibr. excited states, anharmonic force field 78−33502
- AsF$_3$, mol. geometry calcs. using centrifugal distortion const. 80−18841
- AsF$_3$ X-ray and UV photoemission spectra, Auger spectra 79−98150
- AsF$_3{}^-$, protein anion binding site NMR probe 78−48748
- AsF$_5$ doped poly(p-phenylene), highly cond. charge transfer complexes, elec. and optical props. 80−70778
- AsF$_5$ doped polyacetylene, cond. and Hall effect 79−28353
- AsF$_5$ doped polyacetylene films, photocond. and junction props. 80−70770
- AsF$_5$ doped polyacetylene, X-ray absorpt. meas., 5K to room temp. 80−71516
- AsF$_5$, doping of polyacetylene, mechanism, effect on elec. cond. and spectra 80−24473
- AsF$_5$, E′ vibr. assignments, bending modes, parameter method 77−10658
- AsF$_5$, intercalate with graphite, optical reflectance 78−35163
- AsF$_5$ intercalated in graphite, first stage, to synthesis of first stage graphite salt C$_8{}^+$AsF$_6{}^-$ 79−24738
- AsF$_5$ intercalated with graphite, Raman scatt. in low stage cpds. 80−20638
- AsF$_5$ intercalated with graphite, quantum oscillatory phenomena 80−107823
- AsF$_5$ intercalation compound with graphite, lamellar, highly two dimensional synthetic metal, room temp. elec. cond. 78−6349
- AsF$_5$ intercalation compound with graphite, metallic optical reflectance meas. 78−6683
- AsF$_5$ intercalation with graphite and benzenoid systems, EPR, NMR and X-ray diffr. obs. 80−19775
- AsF$_5$, normal coord. anal., generalised valence force field calcs. 77−58195
- AsF$_5{}^-$, form. from AsF$_6{}^-$ by radiolysis, ESR spectrum 77−16845
- AsF$_5$-graphite intercalation compounds, elec. cond. meas. with high anisotropy 78−26837
- AsF$_5$-graphite intercalation compound, high elec. cond. 78−26838
- AsF$_5$-graphite intercalation compound, resist. and magnetoresist. 79−99590
- AsF$_5$-graphite intercalation cpd., synthesis and elec. props. 80−70781
- AsF$_5$-graphite intercalation compound nature 80−103308
- AsF$_5$-intercalated graphite, mag. spin susceptibility, density of states at Fermi energy 79−7966
- AsF$_6$, mol. image reconstruction by electron holography 79−68367
- ^{75}AsF$_6{}^{2-}$, radical, prep. and EPR comparison with other hexafluoride radicals 78−68381
- AsF$_3$(AsF$_5$), electron impact positive ion form., appearance energy obs. 80−53151
- AsF$_5$.BrF$_3$ complex, F NMR 78−37658
- AsFs X-ray and UV photoemission spectra, Auger spectra 79−98150
- AsGe amorphous film, far IR absorpt. spectra, refractive index 80−80785
- AsGeS, valence electron spectrum, SRO and LRO effects 78−52639
- As$_2$Ge$_2$SeTe, semiconducting glass, elastic props., US vel. meas. 78−26628
- As$_2$Ge$_3$T$_{15}$, semiconducting glass, elastic props., US vel. meas. 78−26628
- AsGeTe, semiconducting glass, elastic props., US vel. meas. 78−26628
- As$_{10}$Ge$_{15}$Te$_{75}$, glass, cond. and switching characts. 77−32054
- As$_{10}$Ge$_{15}$Te$_{75}$:Ag glasses, elec. props. 79−91045
- As$_{25}$Ge$_{10}$Te$_{65}$, chalcogenide glasses, dielectric relaxation 80−55027
- As$_4$Ge$_{15}$Te$_{81}$, crystal-glass transition influence on local struct. 77−36163
- As$_x$Ge$_{10}$Te$_{90-x}$ glass, cond. and dielec. const. from 77 to 383K and from DC freq. to 5 MHz 79−23964
- As$_{10}$Ge$_{15}$Te$_{75}$Ag$_x$ glass, elec. and dielec. props., Ag additions effect 80−65558
- AsH$_3$, forbidden millimetre-wave transitions 78−55165
- AsH$_3$, IR spectra, vibr. relax., rot. reorientation in solid phase 78−19463
- AsH$_3$, inversion barrier calc. 78−9271
- AsH$_3$, monitoring using Fourier IR technique 79−16106

arsenic compounds continued

- AsH$_3$, plastic cryst., dipolar autocorrelation function, phonon contrib., IR absorption 78−42928
- AsH$_3$, vibr. relax. in dense media, memory functions approach 78−37722
- AsH$_3$(AsD$_3$)(AsT$_3$), harmonic force fields, equal coord. method calcs. 77−30845
- AsI$_3$, enthalpy, entropy of melting 78−34598
- AsI$_3$, mol. beam photodissoc. 78−56906
- AsI$_3$, molten, X-ray intensity curve, short-range order 77−4034
- AsI$_3$, photopolarisation, photoelectret state, electron-hole transitions 77−12300
- AsI$_3$, X-ray cryst. struct. refinement 80−64961
- As$_2$I$_4$, ^{127}I, ^{75}As NQR freqs. meas. 80−58285
- AsO, dissoc. energy calcs. 77−3486
- AsO$_2$, X-ray cryst. struct. determ. 80−39026
- AsO$_{3/2}$-BO$_{3/2}$, glass, props. and struct. *(Japanese)* 77−27836
- AsO$_4{}^{3-}$ ion in silicate glasses, Raman scatt. obs. 77−12379
- AsO$_4{}^{4-}$, in mixed crystals, EPR central peak dynamics 79−33523
- As$_2$O$_3$, amorphous, network dynamics, vibr. band splittings 79−42199
- As$_2$O$_3$, As 3d and O 1s binding energies, ESCA absolute energy calibr. 78−92171
- As$_2$O$_3$ crystalline and amorphous, EXAFS study of struct. 80−19776
- As$_2$O$_3$, cubic and glassy, phase shift calcs. for EXAFS 77−48275
- As$_2$O$_3$, cubic modification, struct. refinement *(German)* 78−30590
- As$_2$O$_3$, density of valence states, photoemission meas. 77−72808
- As$_2$O$_3$, electronic struct., X-ray emission, XPS, UPS obs., CNDO cluster calc. 78−52638
- As$_2$O$_3$, glassy, intermediate range order from polarised features of Raman spectrum 80−49113
- As$_2$O$_3$ in (K$_2$O)$_x$(SiO$_2$)$_{1-x}$ glass, Raman study of As 80−84733
- As$_2$O$_3$, multiple reactions by single electron impact 78−22037
- As$_2$O$_3$, vapour phase equilibria over GaAs 79−66181
- As$_2$O$_3$, vitreous, local struct. and vibrational spectra 80−55091
- As$_2$O$_3$, vitreous, Raman and IR spectra 79−73933
- As$_2$O$_3$, vitreous, X-ray diffr. study of struct. 80−92464
- As$_2$O$_3$-SO$_3$, polarised Raman and IR spectra, force field calc. *(French)* 78−6674
- (As$_2$O$_3$)$_n$, claudetite I, vibr. spectra, force field calc. *(French)* 78−60447
- As$_2$O$_5$, As 3d and O 1s binding energies, ESCA absolute energy calibr. 78−92171
- As$_2$O$_5$-Rb$_2$O(Rb$_2$CO$_3$) system, phase diagram, polymorphic transform. 79−83181
- As$_4$O$_6$, IR and Raman spectra vibr. spectra, valence force field calc., pot. function *(French)* 78−50549
- As$_4$O$_6$, matrix isolated, IR isotope freq. and intensity patterns 78−46338
- As$_4$O$_6$, UV photoelectron spectra, mol. orbital symm. 77−14494
- AsO$_3$H$^-$, localised near impurity in irrad. ferroelec. KH$_2$AsO$_4$, ENDOR 77−24762
- (AsO$_4$)$_2$H$_2$(UO$_2$)$_2$.8H$_2$O, point group symmetry for ferroelec., antiferroelec. and paraelect. phases 78−42983
- AsO$_2$(OH)$_2{}^-$ ion, O$_2$ exchange in water, in NaAsO$_2$ aq. solns. 78−92459
- As$_2$(S,Se,Te)$_3$ glasses, Hall mobility composition depend. 78−68042
- As$_x$(S,Se)$_{1-x}$, covalent non crystalline topology, short range order 80−15009
- AsS$_3$ barrier layer for As$_2$Se$_3$-Ag photosensitive semiconductor-metal systems *(Russian)* 80−62777
- As$_{1-x}$S$_x$ glasses, building blocks and bonds 80−54141
- As$_{2-x}$S$_{3+x}$, hydrogenated chalcogenide glasses, prep. by plasma decomposition 80−49735
- As$_2$S$_3$, amorphous, AC cond. magnitude and variation *(French)* 79−47095
- As$_2$S$_3$, amorphous, acousto-induced struct. change, Brillouin scatt. meas. 79−27928
- As$_2$S$_3$, amorphous, acousto-optical effects *(Japanese)* 79−82946
- As$_2$S$_3$, amorphous, band to band radiative recomb. 80−25435
- As$_2$S$_3$, amorphous, band-to-band luminesc., electronic band states 79−61432
- As$_2$S$_3$, amorphous, charged defect pair photolum. meas. 80−16078
- As$_2$S$_3$, amorphous, density of valence states, XPS and UPS obs. 77−48308
- As$_2$S$_3$, amorphous, elec. cond. at room temp., contact effect 77−20354
- As$_2$S$_3$, amorphous, elec. cond. mech. obs., in bulk material and evaporated thin films *(Japanese)* 80−11028
- As$_2$S$_3$, amorphous, electrodiffusion profile meas. of Ag migration 78−87822
- As$_2$S$_3$, amorphous, kinetics of photoconductivity, near fundamental absorption edge, energy gap determ. *(Russian)* 79−56263
- As$_2$S$_3$, amorphous, low temp. US meas., two-level systems role 78−30703
- As$_2$S$_3$, amorphous, luminesc. and optically detected ESR, photoinduced struct. change 80−50399
- As$_2$S$_3$, amorphous, luminescence 80−80862
- As$_2$S$_3$, amorphous, optical detection of ESR 79−38408
- As$_2$S$_3$, amorphous, photodissolution of Ag film 78−26737
- As$_2$S$_3$, amorphous, quantum efficiency and fatiguing behaviour of luminesc. processes 80−7402
- As$_2$S$_3$, amorphous, shear wave attenuation and high freq. elec. cond. 80−11027
- As$_2$S$_3$, amorphous, struct. determ. by electron diffr. 77−11485
- As$_2$S$_3$, amorphous, temp. below 1K, props., tunnelling 80−49576
- As$_2$S$_3$, amorphous, time resolved spectroscopy of valence alternation pair luminesc. 80−50400
- As$_2$S$_3$, amorphous, time resolved luminesc. 80−66288
- As$_2$S$_3$, amorphous, time-resolved photolum., spectrosc. 79−24360
- As$_2$S$_3$, amorphous, US attenuation obs. 79--46756
- As$_2$S$_3$, amorphous, ultrasonic velocity, 1.5 to 296K 79−37764
- As$_2$S$_3$, amorphous, XPS, electronic struct. calcs. using scattered wave method 79−11502
- As$_2$S$_3$, amorphous and cryst., optically induced changes, ps. spectroscopy 80−48326
- As$_2$S$_3$, amorphous film, light enhanced vaporisation, photolithographic process, photographic appls. 77−5949
- As$_2$S$_3$, amorphous film, photodissolution of Ag, struct. changes 77−11815
- As$_2$S$_3$ amorphous film, photodissolution of Ag elec. resist. meas. 77−62786
- As$_2$S$_3$, amorphous film, photooxidation, substrate depend. 78−64866

arsenic compounds continued

- As_2S_3 amorphous films, meas. of photoinduced transformations by optical waveguiding 79−43050
- As_2S_3 amorphous films, photo-induced changes in IR spectrum 79−52033
- As_2S_3, amorphous semicond., photo-induced optical and structural changes *(Japanese)* 78−47244
- As_2S_3, amorphous thin films resonant Raman scattering 78−68505
- As_2S_3 and As_2S_3-Sb_2S_3 system glasses, long-term photocond. relax. 77−76874
- As_2S_3, antireflection coating for KCl, design, prep. and performance 79−14063
- As_2S_3, antireflection coating, 100 ns pulsed laser damage at 2.7 and 3.8 μm 80−33057
- As_2S_3 antireflection coating, multithreshold damage meas. at HF and DF laser wavelengths 80−33058
- As_2S_3, chalcogenide glass, effect of press. on elastic props. 80−10590
- As_2S_3 chalcogenide glass films, photographic Ag photodoping to produce negative relief image 80−59490
- As_2S_3 coating defects and impurities affecting damage threshold and absorptance 79−14065
- As_2S_3 coatings, transmission and refraction dispersion spectra *(Russian)* 77−48264
- As_2S_3 containing coatings, 10.6 μ laser damage obs. 79−14021
- As_2S_3, cryst., vitreous or amorphous, nonlinear light absorption, temp. depend. *(Russian)* 77−48199
- As_2S_3, cryst. and glassy, two-photon spectrum at room temp. 79−24334
- As_2S_3, cryst. and vitreous, nonlinear light absorpt. 77−75605
- As_2S_3, cryst. and vitreous, struct. determ. by electron spectroscopy 79−65979
- As_2S_3 crystal, polarisation anal. of Raman spectrum 79−47461
- As_2S_3, crystal-glass transition influence on local struct. 77−36163
- As_2S_3, crystalline, two phonon vibrational spectra 78−35142
- As_2S_3, crystalline and amorphous, surface charging effects on valence band spectra in XPS 77−8725
- As_2S_3, crystalline and amorphous, inelastic neutron scatt. spectra 77−24276
- As_2S_3, crystalline and vitreous, nonlinear absorption of ruby laser radiation *(Russian)* 78−22165
- As_2S_3, crystalline struct. X-ray induced paramag. states and luminesc. 78−95520
- As_2S_3, D-centres, microscopic model *(Russian)* 79−46654
- As_2S_3, determination of stoichiometric discontinuity, using US velocity 79−5242
- As_2S_3, drift mobility, along molecular direction, 207-465K 77−43643
- As_2S_3, electron beam deposited film, photoinduced birefringence and dichroism *(Russian)* 78−2934
- As_2S_3, electron drift mobility temp. depend., transient photocond. obs. 77−66164
- As_2S_3, electron irradiated, effects on elec., photoelec. and optical props. 80−49806
- As_2S_3, electronic struct., X-ray emission, XPS, UPS obs. 78−52638
- a-As_2S_3, energy gap meas., by Faraday rotation 80−66161
- As_2S_3 evaporated film, optical props., depend. on light exposure and heat cycling 78−68572
- As_2S_3 film, amorphous, deposited at different temps., IR spectra 80−40102
- As_2S_3 film, amorphous, opt. const. changes under illumination 77−77316
- As_2S_3 film, amorphous, photo-induced dynamical changes 80−66142
- As_2S_3 film, diffr. efficiency of continuously etched gratings 78−38019
- As_2S_3 film, effect of light exposure and heat cycling 78−94417
- As_2S_3 film, evaporated, switching effects 80−96952
- As_2S_3 film, hologram recording using total-internal-refl., polarisation depend. 80−106491
- As_2S_3 film, IR absorpt. coeffs. meas. by laser calorimetry 78−25905
- As_2S_3 film, on Ag, light activated reactive diffusion of metal into chalcogenide 77−55393
- As_2S_3 film, optical recording, light scatt. enhancement due to coherence 80−97362
- As_2S_3 film, strain induced anisotropy, ellipsometer and reflector meas. 79−33856
- As_2S_3 film, vacuum deposited, selective etching characts. obs. *(Russian)* 80−3207
- As_2S_3 film on KCl, strain-induced refractivity anisotropy, 10.6 μ ellipsometric obs. 79−14064
- As_2S_3 film optical constants, wedged-film meas. 79−14066
- As_2S_3, film waveguide, acoustooptic deflection and modulation of light by stationary phase grating struct. 80−5841
- As_2S_3 film waveguide, integrated optical functional elements based on holographic gratings 77−79972
- As_2S_3 film waveguide, microgratings for guided-beam deflection, electron-beam direct-writing fabrication 80−102856
- As_2S_3 films, amorphous, structural implications from Raman spectra of As_4S_4 polymorphs 79−61385
- As_2S_3 films, kinetics of light-enhanced vaporisation rel. to photocond. 77−84919
- As_2S_3 films, use in recording phase relief holograms *(Russian)* 78−50741
- As_2S_3 focusing diffraction grating with const. spacing 79−23096
- As_2S_3 glass, at. struct. changes due to irrad., comp. variations and annealing 77−76323
- As_2S_3 glass, band gap and trap levels, determ. from elec. props. 77−4337
- As_2S_3 glass, elastic moduli, hydrostatic press. effect, US wave vel. meas. 80−34115
- As_2S_3 glass, localised paramag. states, As_4S_6, As_4S_4 units, mol. analogue models 78−60087
- As_2S_3 glass, melt-quenched, reversible photostruct. change 77−68925
- As_2S_3 glass, natural optical activity and related phenomena 79−73895
- As_2S_3 glass, natural optical activity and related phenomena 79−95727
- As_2S_3 glass, press. effect on optical props. 80−50363
- As_2S_3, glass, US attenuation, enhanced after elec. field removal 79−65145
- As_2S_3 glass fibre, elongation, force depend., deviations from linearity 80−45334
- As_2S_3 glasses, DC elec. cond. and thermo-elec. power 80−96865
- As_2S_3 glasses, quasi-eutectic structure, X-ray and IR investig. 77−15320
- As_2S_3, glassy, build-in mechanism of impurities, electronegativity influence 77−76313
- As_2S_3, glassy, deep struct. changes, NQR obs., high-press. and temp. effects 80−54139

arsenic compounds continued

- As_2S_3, glassy, diffusion, elec. transport and first group impurities effect on elec. and opt. props. 77−76623
- As_2S_3, glassy, interface with metal, photoelec. props. 79−73589
- As_2S_3, glassy, optical absorption spectra after 4.5 MeV electron bombardment *(Russian)* 77−32408
- As_2S_3, glassy, photoconductivity dependences applied elec. field 80−107857
- As_2S_3, glassy, photoinduced defects, EPR and absorpt. spectra 80−59398
- As_2S_3, glassy, photoreactive diffusion of Ag 80−19991
- As_2S_3, glassy, photosensitive etching in nonoxidising etchants 80−78813
- As_2S_3, glassy, thermally stimulated depolarisation 77−24782
- As_2S_3, glassy, X-ray induced paramag. colour centres 78−19327
- As_2S_3, glassy film, photostructural effects, NQR study 80−49549
- As_2S_3 high-resist. vitreous, photopolarisation and photoelectret effects 77−76876
- As_2S_3, IR transparent materials, forward and backward scatt. data 78−59099
- As_2S_3, inorganic resist, optical monitoring of etching 79−52412
- As_2S_3, LF inelastic light scatt. meas. 78−15181
- As_2S_3 layered crystal and amorphous analogues, XPS valence band spectra, electronic struct. 77−52218
- a-As_2S_3, luminescence with short decay time 78−2906
- As_2S_3, network dynamics, vibr. band splittings 79−42199
- As_2S_3, non-cryst., Faraday rotation, 0.7-2 μm 77−16307
- As_2S_3, optical props., electronic struct., photocond., book contrib. 77−44024
- As_2S_3, photoacoustic spectroscopy, app of expt. system for powdered samples 77−87846
- a-As_2S_3, photodesactivation, direct positive imaging 79−17544
- As_2S_3 polyethersulphone sandwich ribbon fibre for coupling high refractive index integrated optics 79−32089
- As_2S_3 radiator bonded LED's, with optical guide struct., efficient coupling to optical fibres 77−39043
- As_2S_3, rain erosion mechanisms 79−34154
- As_2S_3, relation between glass-transition temp. and optical memory-eraser temp. 80−10650
- As_2S_3, secondary electron emission, fluctuation state effect 80−40193
- As_2S_3, semiconducting glass, elastic props., US vel. meas. 78−26628
- As_2S_3 single-layer film 2.8 μm, 3.8 μm absorpt. meas. 78−90463
- As_2S_3, single-layer vac. antirefl. coatings for near IR spectral region 80−33099
- As_2S_3 structure simulation of some tellurite and chalcogenide glasses quasi-crystalline structural diffusion method *(Russian)* 80−54147
- As_2S_3 suspension dispersed in gelatin, photoinduced dichroism 79−98453
- As_2S_3, thermodynamic of evaporation 77−47568
- As_2S_3 thin film, diffr. grating production, using laser photolithographic process, image evaluation 78−42479
- As_2S_3 thin films, vacuum deposited on Ge and PbS, sealing props. and TEM 80−35097
- As_2S_3 thin films for integrated optics, photodetector elements, relief-type diffraction gratings 79−32094
- As_2S_3 thin glassy films, hole drift mobility, interaction with deep localised levels 80−11117
- a-As_2S_3, time-resolved photoluminescence study 80−89057
- As_2S_3, two photon light absorpt. dispersion, induced linear light absorpt. *(Russian)* 80−66231
- As_2S_3, two-phonon vibrational spectra, crystalline and amorphous forms, Raman and IR spectra 78−39537
- As_2S_3, vacuum deposited film, kinoform optical element prod. *(Russian)* 77−14670
- As_2S_3, vaporisation, mass spectrometric analysis 78−22843
- As_2S_3, vapour-deposited, pure and doped, hole mobility 80−49728
- As_2S_3 vapour-deposited films, valence states, thermal and photo-induced changes UPS study 80−93459
- As_2S_3 vitreous, Ag, Cu, Sn and Ge impurities infleunce on electrophys. props. 77−76826
- As_2S_3, vitreous, thermal capacity, 300 to 600K 80−103492
- As_2S_3 vitreous film, hole transport obs. 80−49727
- As_2S_3 vitreous film, photodecomp. and photostruct. changes 77−76318
- As_2S_3, vitreous local struct., elec. field gradient tensor asymmetry obs. 79−73847
- As_2S_3:Ag, AC conductivity determ. 77−66167
- As_2S_3:Ag, amorphous US props. 78−51616
- As_2S_3:Ag, glassy film, doped by photodiffusion and thermodiffusion, photocond. 80−29441
- As_2S_3:Ag, vitreous, doping influence on photolum. at 77K 77−77293
- As_2S_3:Ag film, Ag photodoping rate, localised struct. transform. effect, absorpt. meas. 77−31914
- As_2S_3:Ag glassy films, optical transmission spectra, photodoping effect 80−66317
- As_2S_3:B glass, impurity effect on photoluminesc. and optically induced EPR 79−65918
- As_2S_3:Fe glass, photolum. and ESR, Fe impurities as non-radiative recomb. centres 80−29788
- As_2S_3:Ga system chalcogenide glasses, thermophysical and struct. props. 80−15007
- As_2S_3:Te glasses, doping influence on AC conductivity, electron transport by hopping 79−78106
- As_2S_3-Ag, light sensitivity for high exposure densities *(Russian)* 79−6212
- As_2S_3-Ag, resistance meas. during form., supersensitivity *(Russian)* 77−80839
- As_2S_3-Ag interface, photodissolution kinetics of Ag in amorphous films 77−15955
- As_2S_3-Ag light sensitive material, development of non-interchangeability under continuous laser radiation *(Russian)* 80−50870
- As_2S_3-Ag photosensitive film systems, hologram recording 78−1194
- As_2S_3-Ag system, activation energy for photochem. conversion, 80-340K, radiation intensity depend. *(Russian)* 78−3356
- As_2S_3-Ag system, photosensitivity depend. on As_2S_3 thickness *(Russian)* 80−54784
- As_2S_3-Ag system, photosensitivity depend. on metallic layer thickness *(Russian)* 80−54785
- As_2S_3-Ag_2S glass, Ag diffusion, 50-120°C 78−18828
- As_2S_3-$AsBr_3$, glass, exam. of combination scatter spectra in IR 78−88315
- As_2S_3-$AsBr_3$ and As_2Se_3-$AsBr_3$ systems, phase diagrams 77−8804
- As_2S_3-CdSe heterostructure, energy bands and interface props., photoelectron spectroscopy 78−2551

arsenic compounds continued
- As_2S_3-$Ge_{30}As_{17}Te_{30}Se_{23}$, two-layer antirefl. coating, error considerations in design 80–74477
- As_2S_3-HgS, phase diag., IR spectra 77–36479
- As_2S_3-HgSe structure, anomalous photocond., relax. curves 77–55567
- As_2S_3-PbS glass, DC elec. cond. and photocond. 78–39107
- As_2S_3-PbS glasses, structural props. 79–27925
- As_2S_3-Sb_2S_3, vitreous, dispersive charge transport analysis 79–95418
- As_2S_3-Se, glass-forming system, phase diagram 77–16551
- As_2S_3-Si isotype amorphous-crystalline heterojunctions, electrophys. props. 79–24063
- As_2S_3-Tl_2S, As_2Se_3-Tl_2Se and As_2Te_3-Tl_2Te systems, vitrification and reaction characts. 77–15560
- As_2S_3-Tl_2S and As_2Se_3-Tl_2Se system glasses, comp. depend. of IR absorpt. props. 77–16292
- As_2S_3-Tl_2S glass, phase relns. and crystallisation 78–23675
- As_2S_5, amorphous, struct., vibr. and electronic spectra 80–64908
- As_2S_5, thin film optical waveguide, for acoustooptic modulators 78–83051
- As_2S_5-AsSI glasses, IR and Raman spectra, struct. rel. to comp. *(Russian)* 77–81107
- As_2S_x glass, Raman and IR spectra, struct. model 78–80330
- $As_{40}S_{60}$ glass, structure modelling by Monte Carlo method *(Russian)* 79–55672
- As_4S_3, UV photoelectron spectra, mol. orbital symm. 77–14494
- As_4S_4, effects of pressure and temp. on phonons, Raman scattering study 80–7360
- As_4S_4, electronic struct. and vertical electron affinities, INDO-type ASMO SCF calcs. 79–31402
- As_4S_4 polymorphs, Raman spectra, structural implications for As_2S_3 amorphous films 79–61385
- As_4S_4, VP and thermodynamic functions calc. 77–36470
- As_4S_4 vapour-deposited films, valence states, thermal and photo-induced changes UPS study 80–93459
- As_4S_4, vibrational spectra, effect of temp. and press. on phonons 79–37776
- $As_4S_4^-$, electronic struct. and vertical electron affinities, INDO-type ASMO SCF calcs. 79–31402
- As_xS_{1-x} glass, Raman spectra, chem. struct. *(Russian)* 78–76469
- As_xS_{100-x} amorphous film, photoinduced changes in optical props. 80–50445
- As_xS_{100-x} amorphous films, optical props. and photoinduced changes 80–60700
- As_xS_{100-x}, chalcogenide glass, hole trap levels, TSC *(Russian)* 79–91074
- As_xS_{100-x}, chalcogenide glass thin films, absorption in range of large optical densities *(Russian)* 80–11428
- As_xS_{100-x} glasses, band gap and neighbouring order *(Russian)* 79–60694
- As_xS_{100-x} glasses, Raman spectrum and structure 80–60593
- As_xS_{100-x}, localised states density near valence band edge *(Russian)* 80–103638
- As_xS_{100-x}, structural changes *(Russian)* 78–51427
- As_xS_y, bulk and vapour deposited films, comparison of struct., X-ray diffr. meas. 77–69195
- As_xS_y vapour deposited film, struct. determ., X-ray and neutron diffr. correl. functions 79–60654
- $As_{15}S_{40}Ag_{45}$ glass, photosurface deposition of metallic Ag discs 77–76650
- $(As_2S_3)_{1-x}(AsBr_3)_x$ glass, struct. interpretation of Raman spectra 79–65856
- $(As_2S_3)_x(AsI_3)_{1-x}$, glass, Raman spectra, chem. struct. *(Russian)* 78–76469
- $(As_2S_3)_{1-x}(As_2Se_3)_x$ and $(As_2Se_3)_{1-x}(As_2Te_3)_x$ pseudobinary glasses, comp. depend. of opt. props. 77–90157
- $(As_{0.4}S_{0.6})_{100-x}Cu_x$, glassy, struct. and elec. cond. study 80–59399
- $As_2S_3Ge_x$ glasses, vibr. props. and struct., IR refl. and Raman scatt. 79–78682
- $(As_2S_3)_{1-x}(GeS_2)_x$ and $As_2S_3Ge_x$ glasses, struct. and vibr. spectra 79–91440
- $(As_2S_3)_{1-x}(GeS_2)_x$, LF inelastic light scatt. meas. 78–15181
- AsSI, cryst. and vitreous, struct. determ. by electron spectroscopy 79–65979
- AsSI, crystal-glass transition influence on local struct. 77–36163
- AsSI, X-ray diffr. study in vitreous and fused states 77–7675
- $(AsSI)_x(GeS_2)_{1-x}$ glasses, Raman and long-wave IR spectra obs. of struct. 79–51964
- $(As_2S_3)_{1-x}(PbS)_x$, high field effects 79–42553
- $(As_2S_3)_{0.55}(Sb_2S_3)_{0.45}$ vitreous film, dispersive charge transport, time-of-flight meas. 79–19594
- $As_{1-x}S_x(Se_x)$, bulk-quenched glasses, opt. freq. dielec. const., chem. ordering effects 78–23472
- $As_2S_{2.66}Se_{0.34}$, X-ray photoelectron spectra, electron binding energy, effect of Ag alloying 79–11499
- $As_2S_{3-x}Se_x$, amorphous, ps. relax., optically induced absorpt. 80–48325
- $As_2S_{3-x}Se_x$, amorphous, picosecond relax. of optically induced absorption 80–97302
- $As_2S_3(Se_3)$, amorphous, network dynamics, vibr. band splittings 79–42199
- $As_2S_3(Se_3)$, dispersion curve calc. 79–7659
- $As_2S_3(Se_3)$ evaporated films, optical absorpt. and thermally induced effects 79–42989
- $As_2S_3(Se_3)$ evaporated films, struct. and thermally induced effects 79–41963
- $As_2S_3(Se_3)$, thermal conductivity, 1.5-30K *(French)* 77–39704
- $As_2S_3(Se_3)$, thermal expansion at low temperatures 78–83982
- $As_2S_3(Se_3)$, vitreous, photostimulated light absorpt. 77–77221
- AsS(Se)I films, electrophys. and opt. props. 77–51741
- $As_{40}S_{25}Se_{25}Si_{10}$ glass film, transient photoinduced absorpt. 77–40295
- $As_2S_3(Se_3)(Te_3)$ glass, electronic struct. calc. by extended Huckel theory 78–23012
- $AsS_{3.5}Te_{2.0}$ glass, gamma-irradiated, TSC meas. 77–66166
- $As_2S_{3-x}Te_x$, ternary chalcogenide glassy system, optical absorpt., mag. susceptibility and AC cond. meas. 80–55125
- As_3Sb, As_2Sb_2, $AsSb_3$, and AsSb, gaseous, atomisation enthalpy and enthalpy of form., mass-spectroscopic Knudsen cell method 78–80780
- $AsSbO_4$, X-ray cryst. struct. determ. 80–107127
- $As_2Sb_2O_6$, $AsSb_3O_6$ and As_3SbO_6, gaseous, atomisation enthalpy and enthalpy of form., mass-spectroscopic Knudsen cell method 78–80780
- $AsSbS_3$-CdSe heterostructure, energy bands and interface props., photoelectron spectroscopy 78–2551

arsenic compounds continued
- $As_{0.2}Sb_{0.8}SI$ cryst., ferroelec., soft mode Raman and IR spectroscopy 80–76016
- $As_xSb_{1-x}SI$ mixed crystals, phonon coupling, ferroelectric phase transition, Raman study 80–108165
- $As_xSb_{1-x}SI$, solid solns., ferroelec. props. 78–23409
- $As_4Sb_2Se_9$ glassy semiconductors, electronic props. 80–103712
- $As_2(Se,Te)_3$ glasses, X-ray absorption and photoelectron spectroscopy study 80–7463
- AsSe and As_2Se_3, glassy and liq. states, elec. cond. freq. depend. 77–76856
- AsSe chalcogenide glass, efficiency of optical recording and erasing, temp. depend. *(Russian)* 77–79908
- AsSe film, chalcogenide glasses band gap variation 78–90461
- AsSe film, light-induced light absorption changes 77–73181
- AsSe, molten semicond., pseudogap, elec. cond. and optical absorption meas. 77–8160
- AsSe, relaxation of photoinduced refr. index changes *(Russian)* 78–23426
- AsSe-$GeSe_2$-PbSe, glass form., struct. defects, elec. cond., assoc. *(Russian)* 80–54144
- AsSe-GeSe-PbSe, glass form., elec. cond., struct. defects, assoc. *(Russian)* 80–54145
- $AsSe_{10}$, stable thermoelectret, effects of anisotropic external perturbation *(Russian)* 77–63361
- $AsSe_{1.2}$:Fe, Fe effect on physiochem. props. of glass 80–24370
- $AsSe_x$ amorphous films, high field behaviour 79–87172
- $As_{1-x}Se_x$, ave. energy gap, optical freq. dielec. const. and refr. index 77–76739
- $As_{1-x}Se_x$ glass, refr. index comp. depend. and photo-induced variation 79–91398
- $As_{2-x}Se_{3+x}$, hydrogenated chalcogenide glasses, prep. by plasma decomposition 80–49735
- As_2Se_3, amorphous, AC cond. magnitude and variation *(French)* 79–47095
- As_2Se_3, amorphous, DC Hall effect, elec. cond. mechanism 78–23121
- As_2Se_3, amorphous, dark discharge, relaxation current meas. *(German)* 80–49760
- As_2Se_3, amorphous, defect states, exptl. study. 80–54645
- As_2Se_3, amorphous, elec. cond. at room temp., contact effect 77–20354
- As_2Se_3, amorphous, electrophotographic props., photodecomp. effect 78–49918
- As_2Se_3, amorphous, electron irrad.-induced paramag. centres, 77K 78–88187
- As_2Se_3, amorphous, electron and hole transport, charge defect model 79–15162
- As_2Se_3, amorphous, field-depend. dispersive hole transport 78–14728
- As_2Se_3, amorphous, hole emission defect states 80–49759
- As_2Se_3, amorphous, hole mobility expt., transient photocurrent shape 79–99582
- As_2Se_3, amorphous, ionicity dependence of defect reactions and negative-U states in glasses 80–88511
- As_2Se_3, amorphous, laser radiation induced struct. changes, electron microdiffr. obs. 79–10874
- As_2Se_3, amorphous, luminescence 80–80862
- As_2Se_3, amorphous, modulated photocurrent 78–10500
- As_2Se_3, amorphous, modulated photoconductivity anal. 80–44650
- As_2Se_3, amorphous, nonradiative recombination of photocarriers 80–11046
- As_2Se_3, amorphous, photoconductivity exam. 78–30953
- As_2Se_3, amorphous, photocond. and photoinduced optical absorpt. 79–82645
- As_2Se_3, amorphous, richardson-Schottky type photoinjection current from photoconductor into insulating liquid 80–15608
- As_2Se_3, amorphous, struct. determ. by electron diffr. 77–11485
- As_2Se_3, amorphous, theoretical calc. of defect states 80–49657
- As_2Se_3, amorphous, time resolved meas. of photoinduced optical absorpt. and photocond. 80–49807
- As_2Se_3, amorphous, transient hole transport props., trap controlled hopping model 77–47820
- As_2Se_3, amorphous, transient electrical transport, general and unified treatment 80–59977
- As_2Se_3, amorphous, ultrasonic velocity, 1.5 to 296K 79–37764
- As_2Se_3, amorphous AC cond. and photo-induced states 79–87128
- As_2Se_3, amorphous and single cryst., ODMR expts. 80–50230
- As_2Se_3, amorphous chalcogenides, optically broadened lattice vibration spectra 79–77712
- As_2Se_3 amorphous film, comp. ratio variation by annealing and laser irrad., ESCA meas. 79–99447
- As_2Se_3 amorphous film, pulse hologram recording 79–55091
- As_2Se_3, amorphous layers, injected charge drift and localisation *(German)* 78–91794
- As_2Se_3 amorphous layers with Al electrodes, photoelectrochem. process 77–76953
- As_2Se_3, amorphous radiative interband recombination 80–66286
- As_2Se_3 amorphous thin films, illumination-induced change in contact pot. 80–20251
- As_2Se_3, and $As_{1-x}Se_x$, amorphous, struct. models 79–37628
- As_2Se_3 and $As_2Se_3.As_2Te_3$, crystal-glass transition influence on local struct. 77–36163
- As_2Se_3, and $As_2(Se,Te)_3$ glasses, as ion-selective materials for solid-state electrochem. sensors 80–50897
- As_2Se_3 antireflection coating, multithreshold damage meas. at HF and DF laser wavelengths 80–33058
- As_2Se_3, AsSe and As_3Se_2 films, photostimulated changes in opt. and elec. props. 77–76979
- As_2Se_3 bulk glass, physical parameters anisotropy, cooling effects 77–36545
- a-As_2Se_3 chalcogenide glass, influence of thermally induced defects on transport props. 80–49766
- As_2Se_3 coating defects and impurities affecting damage threshold and absorptance 79–14065
- As_2Se_3, contact influence on AC cond. 78–76076
- As_2Se_3 containing coatings, 10.6 μ laser damage obs. 79–14021
- As_2Se_3, cryst., electroabsorption on indirect gap 80–80812
- As_2Se_3, cryst. and amorphous, optically induced absorption in band gap, picosec. dynamics 79–87439
- As_2Se_3, cryst. and vitreous, struct. determ. by electron spectroscopy 79–65979
- As_2Se_3, crystalline, electron drift mobility and DC cond., trapping model 77–47815

arsenic compounds continued
- As_2Se_3, crystalline, photocurrent spectral distribution 79—56259
- As_2Se_3, crystalline and amorphous, inelastic neutron scatt. spectra 77—24276
- As_2Se_3, D-centres, microscopic model *(Russian)* 79—46654
- As_2Se_3 disordered films in flash evap. systems, nonsteady-state behaviour of interface states 77—76952
- a-As_2Se_3, doped film, photoluminescence intensity and lineshape study 80—50448
- As_2Se_3, effect of Cu and I, investigated by Mn^{2+} EPR spectra 77—73075
- As_2Se_3, effect of impurities on paramagnetic gap states 80—24848
- As_2Se_3, electron irradiated, effects on elec., photoelec. and optical props. 80—49806
- As_2Se_3, film, amorphous, fatigue and recovery of electrophotographic props. 78—21253
- As_2Se_3, film, influence of electric field on crystallisation kinetics 78—42914
- a-As_2Se_3 film, metallic impurity effect on transport props. 80—49963
- As_2Se_3 film, strain induced anisotropy, ellipsometer and reflector meas. 79—33856
- As_2Se_3 film on CaF_2, interface and bulk absorption meas. 80—35001
- As_2Se_3 film on KCl, strain-induced refractivity anisotropy, 10.6 μ ellipsometric obs. 79—14064
- As_2Se_3, glass, density of optically induced localised paramagnetic states 78—52354
- As_2Se_3 glass, elastic moduli, hydrostatic press. effect, US wave vel. meas. 80—34115
- As_2Se_3 glass, mech. props. var. due to high press. phase change 77—76481
- As_2Se_3 glass, microwave elec. cond. and struct. 80—49793
- As_2Se_3 glass, mol. struct. model 80—100179
- As_2Se_3 glass, struct. changes, Mn^{2+} EPR expts. 78—79534
- As_2Se_3 glasses, impurity effect on photoluminesc. and optically induced EPR 79—65918
- As_2Se_3, glassy, dielectric const. determ. 78—72449
- As_2Se_3, glassy, drift mobility of holes, 20 to 120°C 79—51583
- As_2Se_3, glassy, elec. cond. meas. in high elec. field 77—4355
- As_2Se_3, glassy, IR spectra and intrinsic band assignments 77—77223
- As_2Se_3, glassy, influence of oxygen added in As_2O_3 and SeO_2 forms on phys. props. 77—76314
- As_2Se_3, glassy, optical absorption spectra after 4.5 MeV electron bombardment *(Russian)* 77—32408
- As_2Se_3, glassy, photoconductivity dependences applied elec. field 80—107857
- As_2Se_3, glassy, photostimulated changes in contact props. 78—19162
- As_2Se_3, glassy, with adsorbed $H_2O(NH_3)(NO_2)(O_2)(CO_2)(CO)$, surface cond., photocond. 78—80038
- As_2Se_3, glassy, X-ray induced paramag. colour centres 78—19327
- As_2Se_3, glassy defect electron states, tight binding calc. 80—96818
- As_2Se_3, glassy film, photostructural effects, NQR study 80—49549
- As_2Se_3 glassy films, current-voltage characts., temp. depend., SCL current 80—92902
- As_2Se_3, glassy struct. X-ray induced paramag. states and luminesc. 78—95520
- As_2Se_3, glossy, Cu, Ag and 0 impurities influence on electronic energy spectrum and mol. vibr. spectrum 77—90181
- As_2Se_3, IR window coating, prep. and optical props. 77—50736
- As_2Se_3, in evaporated layer systems, electric field forming and ageing processes 77—12021
- As_2Se_3, LF inelastic light scatt. meas. 78—15181
- As_2Se_3 layers for electrophotographic use *(German)* 80—42283
- As_2Se_3, liq., semicond.-metal transition at high temp. and press. 77—51784
- As_2Se_3, liquid, struct., investigation using neutron diffr. meas. 79—23514
- As_2Se_3, localised gap states estimated by dielec. relax. 78—35087
- As_2Se_3, lone-pair semiconductor, defect chemistry 80—25421
- As_2Se_3, modulated photocurrent, analysed for trap-limited case *(Japanese)* 80—60030
- As_2Se_3, molten chalcogenide semicond., temp. depend. of 10^{10} Hz elec. cond. 77—4388
- As_2Se_3, molten semicond., pseudogap, elec. cond. and optical absorption meas. 77—8160
- As_2Se_3, monoclinic, chem. bonds rel. to electronic and vibr. states 80—64951
- As_2Se_3, neutrality of luminescence centres 78—88356
- As_2Se_3, optical props., electronic struct., photocond., book contrib. 77—44024
- As_2Se_3, photodarkening and photostructural effects, Raman, IR and NQR studies 80—16036
- As_2Se_3, photosensitive layer, in metal-photosemiconductor-insulator multilayered struct., optical image recording 80—42286
- As_2Se_3, semiconducting glass, elastic props., US vel. meas. 78—26628
- As_2Se_3, single crysts., fine struct. of direct gap from electrorefl. spectra 80—93280
- As_2Se_3 single-layer film 2.8 μm, 3.8 μm absorpt. meas. 78—90463
- As_2Se_3, solid and liq., elec. cond. meas. 77—28185
- As_2Se_3, struct. determ. in amorphous and liq. state using EXAFS meas. 77—89366
- As_2Se_3, thermally reversible photodarkening effects obs. 80—103970
- As_2Se_3, vacuum evaporation, composition of condensates 78—44012
- As_2Se_3, vitreous, effect of gamma-radiation on solution kinetics 77—19986
- As_2Se_3, vitreous, elec. and opt. prop. changes on densification 77—11958
- As_2Se_3, vitreous, hole drift mobility, temp. and field depend. 77—76830
- As_2Se_3, vitreous, hologram recording light sensitivity spectral distrib. *(Russian)* 78—1191
- As_2Se_3, vitreous, short-range structure, neutron diffr. in high momentum transfer region 77—4045
- As_2Se_3, vitreous, thermal capacity, 300 to 600K 80—103492
- As_2Se_3 vitreous film, photodecomp. and photostruct. changes 77—76318
- As_2Se_3 vitreous films, crystn. stimulated by org. subst. and electrophotographic parameters 77—76319
- As_2Se_3:Ag, amorphous, doping effect of gap states and elec. cond., dielec. relax. and DC cond. meas. 79—47098
- As_2Se_3:Ag, amorphous, US props. 78—51616
- As_2Se_3:Ag, glassy film, doped by photodiffusion and thermodiffusion, photocond. 80—29441
- As_2Se_3:Ag amorphous, freq. depend. cond. 80—88565
- As_2Se_3:Al, glassy, energy spectrum of deep localized states, thermal dielectric relaxation 78—15088

arsenic compounds continued
- As_2Se_3:B:, devitrification kinetics, Bi impurity effects 77—35675
- As_2Se_3:Bi, annealing kinetics, cond. activation energy and density 79—73503
- As_2Se_3:Fe, glassy, mag. susceptibility investig. of doping effect 77—77024
- As_2Se_3:I, hole drift velocity enhancement by I doping 77—39883
- As_2Se_3:In, amorphous, photoluminesc. fatigue, metallic additive effect 79—61434
- As_2Se_3:Mn^{2+} film, reversible photostructural change, ESR obs. 77—32411
- a-As_2Se_3:Mn(Fe)(Ni)(Cu)(Zn)(Ga)(Tn)(Il)(Na), hole drift mobility depend. on impurity conc. 79—60846
- As_2Se_3:Pt, vitreous, effect of impurities on elec. props. 80—103699
- As_2Se_3:Tl, hole transport, photoluminesc. and photoinduced ESR 79—8183
- As_2Se_3:X (X=Cu, Ag, Tl, I, Ge), effect of doping, NMR meas. 80—11282
- As_2Se_3-Ag photosensitive semiconductor-metal systems, effect of AsS_3 barrier layer *(Russian)* 80—62777
- As_2Se_3-As_2Te_3, liquid, mixture enthalpies *(German)* 79—77770
- As_2Se_3-As_2Te_3, molten semicond., thermoelec. power and elec. cond. near metallic cond. transition 78—10486
- As_2Se_3-As_2Te_3, solid and liq., elec. cond. meas. 77—28185
- As_2Se_3-As_2Te_3, vitreous, localised states role in cond. in high elec. fields 77—76841
- As_2Se_3-As_2Te_3 glass thermoelec. power, and transport mechanism 80—2408
- As_2Se_3-As_2Te_3 glasses, crystallisation 77—43156
- a-As_2Se_3-Au contact sandwich, response to voltage step in dark and with illum. 77—69431
- As_2Se_3-Au sandwich cell, origin of dark currents 77—76920
- As_2Se_3-based glasses, crystallization, DTA investig. 78—22658
- As_2Se_3-Bi_2Se_3, semiconducting crystallized glasses, elec. conductivity mechanism 77—39843
- As_2Se_3-Cu (10-20%) film, glassy, darkening kinetics, and hologram diffr. efficiency 77—62027
- As_2Se_3-Ge glassy thin films, flash photoresponse 80—107863
- As_2Se_3-$GeSe_2$ glass, bulk and impurity IR absorpt. 80—71455
- As_2Se_3-$GeSe_x$-$SnSe_x$ (x=1,2), exam. of Sn valency and physical props. 79—4753
- As_2Se_3-HgSe double-layer system detector for temp. meas. 79—88952
- As_2Se_3-InI_3, glass system, IR spectra 78—64365
- a-As_2Se_3-metal system, time-resolved dark injection 79—91139
- As_2Se_3-Sb_2S_3 glass, threshold and memory switching, expt. data 78—39170
- As_2Se_3-Sb_2Se_3, phase relns. 77—21118
- As_2Se_3-Sb_2Se_3-$GeSe_2$ system glasses, vitrification and elec. cond. 79—50996
- As_2Se_3-Si amorphous-cryst. heterojunction, energy band diagram construction 77—55602
- As_2Se_3-$SnSe_2$-$GeSe_2$ system glasses, vitrification and elec. cond. 79—50997
- As_2Se_3-Ti_2Se (Tl_2Se_2) (Tl), glass, hot pressed, temp. dependence of optical absorption edge 78—88328
- As_2Se_3+Cu, amorphous, diffusion, electrodiffusion profile determ., migrating impurities charge determ. 78—6185
- As_3Se, vitreous, optical transparency, photostimulated changes *(Russian)* 79—65941
- As_3Se_2 amorphous film, photocond., TSC, light-induced changes 80—49810
- As_3Se_2 chalcogenide semicond. film, thermoptical transitions with photostructural transformations *(Russian)* 80—16016
- As_3Se_2, electron irradiated, effects on elec., photoelec. and optical props. 80—49806
- As_3Se_3:Cu, glassy, broadening of electrodiffusion profiles at high elec. fields 79—55939
- As_4Se_4, electronic struct. and vertical electron affinities, INDO-type ASMO SCF calcs. 79—31402
- $As_4Se_4^-$, electronic struct. and vertical electron affinities, INDO-type ASMO SCF calcs. 79—31402
- $As_{50}Se_{50}$ and $As_{20}Se_{80}$ semicond. glasses, densified, photoluminesc., inelastic deform. effect 80—66293
- $As_{60}Se_{40}$, amorphous films, spectral characts. of photodarkening 78—76494
- As_7Se_3 amorphous films, thermal relax. processes determ. by optical props. 77—15716
- As_xSe_{100-x}, chalcogenide glass, TSC *(Russian)* 79—91074
- As_xSe_{100-x} glasses, temp. depend. of mag. susceptibility and EPR 77—63073
- As_xSe_{100-x}, localised states density near valence band edge *(Russian)* 80—103638
- As_xSe_{100-x}:Mn^{2+}, $0 \leq x \leq 70$, EPR, composition depend. and struct. 77—24736
- $As_2Se_3Ag_x$, amorphous, optical absorpt. coeff. and DC cond. 80—54699
- $As_2Se_3Ag_x$ glassy semicond. film, prep. by photodiffusion of Ag, negative photocond. 80—92934
- $(As_2Se_3)_{1-x}(As_2Te_3)_x$ amorphous films, changes in optical props. under elec. fields and optical excitation 79—61455
- $AsSe_{1.5}Bi_{0.05}$ glasses, soln. rate in alkali solns. 80—16531
- $As_{10}Se_{67.5}Ge_{22.5}$, film as master for PVC copied holograms 77—23632
- As_4Se_5Ge, glass, light irrad. induced changes in optical and elec. props. *(Japanese)* 78—68031
- As_4Se_5Ge glass, struct. changes, Mn^{2+} EPR expts. 78—79534
- $As_4Se_5Ge_1$, amorphous chalcogenides, optically broadened lattice vibration spectra 79—77712
- $As_2Se_3Hg_x$, semicond. glassy system, struct. 77—35489
- AsSeI, cryst. and vitreous, struct. determ. by electron spectroscopy 79—65979
- AsSeI, crystal-glass transition influence on local struct. 77—36163
- AsSeI, X-ray diffr. study in vitreous and fused states 77—7675
- $AsSeI_{0.1}$, glassy, photostimulated changes in contact props. 78—19162
- $AsSeI_x$, glasses, cond. and photocond. 80—20253
- $As_2(Se_{1-x}S_x)_3$, crystal growth and at. struct. 79—60289
- $As_{40}Se_{50-x}S_xGe_{10}$ film strip-loaded waveguide formed in graded-index $LiNbO_3$ planar waveguide 78—74965
- $AsSe_{1.5}Sn_x$ glasses, crystallisation, Mossbauer obs. 77—47557
- $(AsSe)_{1-x}Te_x$ glasses, thermal props. and viscosity, temp. and conc. depend. 77—76324
- $AsSe_{1.1}Te_{0.2}$:Fe, Fe effect on physiochem. props. of glass 80—24370
- $AsSe_{1.5-x}Te_x$ glasses, physical props. 78—68028

arsenic compounds continued
As_2SeTe_2, between Al and Sb electrodes, rectifying effects 80−75654
As_2SeTe_2, field effect, localised states and electronic transport 77−66187
$As_2(Se_{1-x}Te_x)_3$ semiconducting glasses, solid and liquid, thermal cond. 80−6574
$As_2(Se_{1-x}Te_x)_3$, thermal cond. of solid solution and melt 78−67874
$As_2(Se_{1-x}Te_x)_3$, thermal cond., temp. and press. depend. 79−82396
$As_2Se_{1.5}Te_{1.5}$, thermally reversible photodarkening effects obs. 80−103970
As_2Se_2Te, electrical conductivity at strong elec. fields and high hydrostatic press. *(Czech)* 77−24560
As_2Se_2Te, field effect, localised states and electronic transport 77−66187
$As_2Se_xTe_{3-x}$ chalcogenide glasses, cond. meas., field strength and temp. depend. 78−84225
$As_{40}Se_xTe_{60-x}$ amorphous system, resistivity press. depend. 79−82592
$As_{60}Se_xTe_{40-x}$ glasses, crystallisation 77−35488
$As(SiH_3)_3$, vibr. force fields and amplitudes, zero-point struct. 77−54551
As_2Te_3, amorphous, AC conductivity, temp. depend. 78−72153
As_2Te_3, amorphous, defect and impurity states, hopping cond. obs. 80−54650
As_2Te_3, amorphous, localised gap states, hopping cond. and chem. bonding 78−23052
As_2Te_3, amorphous, press.-induced semicond.-metal and supercond. transitions 77−43671
As_2Te_3, amorphous, struct. determ. by electron diffr. 77−11485
As_2Te_3 and As_2Te_3Ge, amorphous, AC cond. at low temps. 80−80269
As_2Te_3 and $As_4Te_3Se_3$, amorphous, localised gap states, variable range hopping, susceptibility and EPR 77−72866
As_2Te_3, $As_4Te_5I_2$, $TlAsTe_2$, local struct. changes on crystal-glass transition, Mossbauer spectra 77−36157
As_2Te_3, chalcogenide glass film, charge screening length 79−23974
As_2Te_3, cryst. and vitreous, struct. determ. by electron spectroscopy 79−65979
As_2Te_3, crystal-glass transition influence on local struct. 77−36163
As_2Te_3, D-centres, microscopic model *(Russian)* 79−46654
As_2Te_3, field effect, localised states and electronic transport 77−66187
As_2Te_3, glassy, field depend. elec. cond. and localised states role 77−76829
As_2Te_3, liq., neutron diffraction study 79−77485
As_2Te_3, molten semicond., thermoelec. power and elec. cond. near metallic cond. transition 78−10486
As_2Te_3, phase transitions and elec. cond. 78−10440
As_2Te_3, solid and liq., elec. cond. meas. 77−28185
As_2Te_3, vitreous, thermal capacity, 300 to 600K 80−103492
As_2Te_3-GaAs, amorphous-monocrystalline heterojunctions, space charge limited conduction 78−64099
As_2Te_3-Tl_2Te system, phase diagram 77−16559
$As_2Te_3+Tl_x$, glassy system, composition depend. of activation energy, thermopower meas. 78−64052
$As_{25}Te_{75}$, and $As_{45}Te_{55}$, vitreous, local struct., elec. field gradient tensor asymmetry obs. 79−73847
$As_{50}Te_{50}$, amorphous films, metal and semicond. contacts, threshold switching, IR emission 80−49831
$As_{50}Te_{50}$, amorphous semicond., elec. props. after heavy-ion irrad. *(French)* 77−72639
$As_{50}Te_{50}$ amorphous switches, light emission charact. 79−78139
$As_{50}Te_{50}$ glass, thermal cond., 100-500K, and sp. ht., 373-600K 77−20138
As_xTe_{100-x}, glassy system, composition depend. of activation energy, thermopower meas. 78−64052
As_xTe_{100-x}:Mn^{2+}, $40 \leq x \leq 70$, EPR, composition depend. and struct. 77−24736
$AsTeCu_x$ ($0 \leq x \leq 0.4$) glass, effect of Cu on elec. cond. and thermoelectricity, 100 to 370K 78−87978
$AsTeE_x$, E=S, Se, Sb, Bi, annealing effects on elec. cond. of films 77−43594
$As_{10}Te_{75}Ge_{15}$, dielec. props. 77−63355
$(As_2Te_3)_{1-x}Ge_x$, amorphous, AC cond. magnitude and variation *(French)* 79−47095
$As_{45}Te_{40}Ge_{15}$, amorphous, elec. cond. at room temp., contact effect 77−20354
$As_xTe_{90-x}Ge_{10}$, $As_{35}Te_{55}Ge_{10-x}Si_x$ glasses, elec. and optical props., comp. depend. 77−24555
$As_{35}Te_{28}Ge_{16}S_{21}$, chalcogenide semiconductor study of electric properties *(French)* 80−29414
$As_{0.3}Te_{0.48}Ge_{0.1}Si_{0.12}$, amorphous film, transient switching processes 78−84232
$As_4Te_5Ge(Si)$ glass, struct. changes, Mn^{2+} EPR expts. 78−79534
$As_4Te_5I_2$, cryst. and vitreous, struct. determ. by electron spectroscopy 79−65979
$As_4Te_5I_2$, crystal-glass transition influence on local struct. 77−36163
$As_{50}Te_{45}I_5$, glass, semicond., elec. switching, high press. effects 78−72212
$As_xTe_xS_xSe_{100-3x}$ glasses, IR absorpt. spectra 77−12378
$AsTeS_x(Se_x)(Sb_x)(Bi_x)$, chalcogenide glass, thin film crystallisation 79−7758
$As_2Te_{3-x}Se_x$, amorphous and cryst. phases, ^{125}Te Mossbauer expts. 78−88232
$As_xTe_xSe_{100-2x}$, x=2.5 and 5.0, chalcogenide glasses, IR absorpt. spectra 77−24842
$As_{30}Te_{48}Si_{12}Ge_{10}$, chalcogenide glass film, charge screening length 79−23974
$As2S_3$ amorphous chalcogenide film inorganic photoresists, holographic resolution evaluation 79−76629
Au-As, system interactions due to heat treatment, backscattering anal. 79−91719
Au-As_2Se_3 contact, model of charge injection 78−68088
BiI_3-AsI_3, phase diags. 78−6905
C_8AsF_5 intercalation compound, NMR and static mag. susceptibility meas. 78−88214
Cd-As system, phase diagram, $CdAs_4$ struct. 79−74138
Cd-As-S chalcogenide glass system, prod. and acoustooptic props. *(Russian)* 78−63158
$Cd_{23}Ge_{12}As_{65}$, amorphous, threshold switching, expt. 80−49830
$CdGe(P_xAs_{1-x})_2$, glass, static current-voltage characteristics *(Russian)* 77−15925
$CdSeTl_x$-$As_2Se_3Tl_x$ thin layer system, capacitance and I-V characts., charge transport mechanism 77−76985
Cu-As-Se glasses, recording and erasure by laser beam *(Russian)* 78−71170
$Cu_x(As_{0\,4}Se_{0\,6})_{1.x}$, amorphous, ^{77}Se NMR, comp. depend. 78−76329

arsenic compounds continued
$Cu_{10}As_{31}Se_{38}O_{21}$, chalcogenide glass, exam. of electron mechanism of photo induced changes 78−87998
Fe-As, phase equilib. diagram *(German)* 80−16280
$Ga_2As_{49}Te_{49}$ glassy film, nonlinear current voltage characts., Poole-Frenkel effect 80−7007
Ge-As, p-T-x diagram 77−11669
Ge-As, supersaturated solid soln., dislocation form. during thermocyclic treatment *(Russian)* 80−3057
Ge-As-Se, amorphous film, condensation formation and struct. props. *(Russian)* 78−38629
Ge-As-Se, and Se-As glasses, for IR appl., prod. using H_2 distillation 77−32551
Ge-As-Se films, light irrad., heat treatment rel. to optical props. *(Russian)* 79−4858
Ge-As-Se glass, appl. to 8 to 12 μm thermal imaging system 78−25935
Ge-As-Se glasses, elastic moduli, US vel. and reson. freq. meas. 78−23756
Ge-As-Se system glasses, thermal capacity, 300-600K 79−65210
Ge-As-Te, thin chalcogenide glass film, high-field switching effects 77−32052
Ge-As-Te glass, between metal electrodes, contact props. determ. 79−7908
Ge-As-Te glass, thermoelec. power and DC cond., temp. depend. 77−62955
Ge-As-Te system, glasses, magnetochemical exam. 78−88092
Ge-Te-As glass, local struct., ^{119}Sn Mossbauer obs. 79−41968
Ge-Te-As-In quaternary compounds, elec. resist. of thin sheets, Mott's theory *(Spanish)* 77−69320
Ge-Te-As-In quaternary compounds, elec. props., Hall effect *(Spanish)* 77−69344
Ge-Te-As-In quaternary compounds, thin sheets elec. props., thermoelec. power *(Spanish)* 77−69358
$Ge_xAs_xS_xSe_{100-3x}$ and $Ge_xTe_xS_xSe_{100-3x}$ glasses, IR absorpt. spectra 77−12378
$Ge_{33}As_{27}S_{15}Te_{25}$, chalcogenide thin films, coupled carrier theory test, high field conditions 80−100466
$Ge_{33}As_{27}S_{15}Te_{25}$ glass, switching, microstructural changes 79−65523
$Ge_{10}As_xTe_{90-x}$ glass, thermal cond., 100-500K, and sp. ht., 373-600K 77−20138
$Ge_{15}As_4Te_8$, film, influence of elec. field on crystallisation kinetics 78−42914
$Ge_{15}As_4Te_{81}$ glassy film, nonlinear current voltage characts., Poole-Frenkel effect 80−7007
$Ge_{10}As_{40}Te_{40}I_{10}$, chalcogenide glass film, switching delay time 78−26926
$Ge_{30}As_{17}Te_{30}Se_{23}$, antireflection coating for KCl, design, prep. and performance 79−14063
$Ge_{30}As_{17}Te_{30}Se_{23}$-$As_2S_3$, two-layer antirefl. coating, error considerations in design 80−74477
$Ge_xAs_xTe_xSe_{100.3x}$, glassy, IR absorpt. spectra 78−23448
$GeSe_2$-As_2Se_3-Sb_2Se_3, quenched glass system, elec. cond., low temp. heat treatment effect 80−39586
$GeSe_2$-As_2Se_3-Sb_2Se_3, elec. cond. over wide range of temp. 80−88564
$GeSe_2$-$SnSe_2$-As_2Se_3, GeSe-SnSe-As_2Se_3, Mossbauer investigation 77−20052
$Ge_{0.45}Se_{0.55}$-As_2S_3, antirefl. coating, performance at 3.8, 5.3 and 10.6 μm 77−61964
$(Ge_{0.32}Se_{0.32}Te_{0.32}As_{0.4})_{100-x}Ni_x$, ESR, rel. to elec. cond. 80−7155
$Ge_{10}Si_{12}As_{30}Te_{48}$, monostable chalcogenide glass threshold switch, temp. meas. *(German)* 77−4412
$Ge_7Si_9As_{39}Te_{35}Ga_{10}$, chalcogenide thin films, coupled carrier theory test, high field conditions 80−100466
GeTe-As_2Te_3 system, phase diagram, eutectic comp., thermographic and X-ray anal. *(Russian)* 77−63646
$Ge_{13.3}Te_{61.7}As_{19}$ film, amorphous, characts. of optical switching 78−18031
$Ge_{15}Te_{81}As_4$, influence of O_2 on phase separation of chalcogenide glasses 77−47354
H_3AsO_4, polarisable acid-acid and acid-water hydrogen bonds 79−76423
H_3AsO_4, reduction with aqu. SO_2 77−4901
$H(UO_2AsO_4)4H_2O$, H motion, PMR obs. 78−80239
Hg-As-S chalcogenide glass system, prod. and acoustooptic props. *(Russian)* 78−63158
Hg-As-S modulating glasses, optical parameters and struct. *(Russian)* 78−63159
Hg-As-S-I system, glasses, optical and acousto-optical props. 78−83053
Hg_3AsF_6, one dimensional conductor *(Japanese)* 79−73499
$Hg_{3-\delta}AsF_6$, Fermi-surface of incommensurate Hg-chain compounds 79−56115
$Hg_{3-\delta}AsF_6$, quasi one-dimensional, anomalous magnetoresistance 80−24884
In-As system, p-T-x diagram 77−8801
In-As-Se-I system, glass form. obs. 77−77466
$In_{1\,9}As_{0.1}Se_3$, growth by chem. vap. transport, characterisation as photoelectrode 78−43994
$KAsO_3$-K_3AsO_4, phase diag. 78−23681
K_2CO_3-SiO_2-As_2O_3, laser Raman spectrosc. study of ions in quenched reaction mixtures 80−25357
KH_2PO_4:AsO_4^{4-}, ferroelec., low freq. fluctuations, isotope effects, EPR, ENDOR and ESCA expts. 77−73118
KH_2PO_4:AsO_4^{4-}, ESR, paraelectric phase, proton dynamics 77−81011
$KrF_2.AsF_5(SbF_5)$, Mossbauer spectra, quadrupole coupling strengths, isomer shift and bonding 77−50458
$(MnTe)_{1-x}$-$(As_2Te_3)_x$ solid solns., thermoelec. props. 79−42567
$(NH_4)_3AsO_4.3H_2O$, cryst. struct. 78−18600
$(NH_4)_4H_6(As_6V_4O_{13}).4H_2O$, cryst. struct. determ. by X-ray diffr. *(French)* 79−69076
$NH_4H_2PO_4$:AsO_4^{4-}, antiferroelec., low freq. fluctuations, isotope effects, EPR, ENDOR and ESCA expts. 77−73118
Na_2O-B_2O_3-SiO_2-$As_2O_3(As_2O_5)$ glasses, DC and AC resist., bipolaronic hopping cond. 80−88558
$O_2^+AsF_6^-$, thermal decomposition, Raman spectra study, free radical mechanism 80−55652
$(P,As)_2O_7^{4-}$, vibr. calc. by method of normal coordinates 78−22796
Pb-Se-As-Ge, phase separation in melt centrifugal quenching 80−25701
PbS-As_2S_3 glass, elastic props. temp. depend. 78−71780
$S_4N_4.AsF_5$, molecular adduct cyclotetra(azathiene), X-ray cryst. struct. determ. 80−54180
SbI_3-AsI_3, phase diags. 78−6905
Sb_2O_3, electronic struct., X-ray emission, XPS, UPS obs., CNDO cluster calc. 78−52638

arsenic compounds continued
Sb_2S_3-As_2S_3, fused mixtures, resistivity 77—80815
Se-As, amorphous, dipolar activity at glass transition temp., AC method 77—66454
Se-As, photoelectronic behaviour, in glass transition region 80—60045
Se-As 36.4 at % amorphous alloy, heat treatment effect on acoustic props. 79—86843
Se-As film, evaporated, thickness, substrate temp. effects 79—15610
Se-As_2Se_3 system glasses, vibr. spectra and partial vols. of components 79—42973
Se-As-Ge, glass alloy system, annealed light irradiated, photoinduced absorption change, random network model 79—59773
Se-Ge-As, chalcogenide glass, self-diffusion, investigation using radioactive tracers 79—23770
Se-Te-As-Ge glasses, absorpt. spectra, diffuse reflectivity loss correction 79—82995
Se-Te-As-Ge glasses, elec. transport 79—60833
$Se_{12}Te_{49}As_{29}Ge_{10}$ semiconductor amorphous films, field effect, trapping 80—84472
Si-$As_2Se_3Ge_4$ heterojunction, elec. props. 78—6434
Si-As-Te glass, thermoelec. power and DC cond., temp. depend. 77—62955
Si-As-Te glasses, crystallisation kinetics under influence of water vapour 78—59762
$Si_{12}Ge_{10}As_{30}Te_{48}$, amorphous, energy controlled switching obs. *(Japanese)* 78—34867
$Si_{12}Ge_{10}As_{30}Te_{48}$, chalcogenide glasses, direct obs. of switching filaments 77—24595
$Si_{12}Ge_{10}As_{30}Te_{48}$, chalcogenide glass threshold switches, turn-on state maintenance *(Russian)* 77—85271
$Si_{12}Ge_{10}As_{30}Te_{48}$, chalcogenide glass film, switching delay time 78—26926
$Si_{12}Ge_{10}As_{30}Te_{48}$ chalcogenide glass threshold switch conductivity in high ohmic state *(Russian)* 78—43502
$Si_{12}Ge_{10}As_{30}Te_{48}$ chalcogenide glass, switching in thin layers with semicond. electrodes 79—4586
$Si_{12}Ge_{10}As_{30}Te_{48}$, conducting filaments and switching phenomena 79—87134
$Si_{12}Ge_{10}As_{30}Te_{48}$, dark cond. and thermoelec. power, thermal activation energies interpret. 78—23123
$Si_{12}Ge_{10}As_{30}Te_{48}$, energy-controlled switching obs. 77—35973
$Si_{12}Ge_{10}As_{30}Te_{48}$ glass, thermally stimulated depolarization current meas. *(Japanese)* 78—34875
$Si_{12}Ge_{10}As_{30}Te_{48}$ glass, nonlinear I-V characts. 79—99557
$Si_{12}Ge_{10}As_{30}Te_{48}$ surface, heat treatment and electron bombard. effects. SEM obs., rel. to switching filament form. 77—47700
$Si_{12}Ge_{10}As_{30}Te_{48}$, vitreous, localised states role in cond. in high elec. fields 77—76841
$SiO_2B_2O_3$-K_2O-Al_2O_3-As_2O_3 glass fibres containing metallic granules, tensile strength, Young's modulus, DC conductivity 80—30023
$Si_{12}Te_{48}As_{30}Ge_{10}$ amorphous film, high-field transient conduction 78—43500
$Si_{12}Te_{48}As_{30}Ge_{10}$, amorphous film, elec. cond. mechanisms, temp. depend. *(Japanese)* 78—80078
$Si_{12}Te_{48}As_{30}Ge_{10}$ amorphous film, current-voltage characts. 79—87104
$Si_{12}Te_{48}As_{30}Ge_{10}$ film, temp.-depend. of non-ohmic current and switching characts. 77—8158
$Si_{12}Te_{48}As_{30}Ge_{10}$ film, amorphous, transient cond. characts. in preswitching regime 77—32055
$Si_{12}Te_{48}As_{30}Ge_{10}$ film, amorphous, Poole-Frenkel cond. for centres with screened Coulomb pot. 78—19044
$Si_{12}Te_{48}As_{30}Ge_{10}$-Au, Schottky barrier props. 79—7897
$Si_{10}Te_{40}As_{30}P_{20}$, amorphous films, optically assisted mono-stable switching 77—11968
$SnF_2.AsF_5$, cryst. struct., X-ray diffr. 77—19921
SnSe-$GeSe_2$-As_2Se_3 glasses, vitrification region and elec. cond. 80—15008
Te-As-Ge, RF sputtering, temp. and bias effects on comp. 77—40367
Te-Ge-As-Si amoprhous film, voltage controlled negative resistance type characts. 79—69614
$Te_{40}As_{35}Ge_7S_{18}$ film, threshold switching in relax. oscill. mode 77—69389
$Te_{40}As_{35}Ge_7Si_{18}$, amorphous, threshold switching, expt. 80—49830
$Te_{40}As_{35}Ge_7Si_{18}$ with pyrolytic graphite electrodes, threshold switching characts. 77—24593
$Te_{48}As_{18}Ge_6Si_{28}$ amorphous film, I-V curve, memory switching 79—69615
a-TeAsSiGe film with Mo contacts, AC performance *(German)* 77—63012
$Te_{39}As_{36}Si_{17}Ge_7P_1$ amorphous film, electroluminescence from on state 79—8188
$Te_{0.81}Ge_{0.15}As_{0.04}$, amorphous and cryst., sp. ht., 1-20K 78—22864
$Te_{81}Ge_{15}As_4$, Hall effect in electrically switched memory state 80—2403
$TlAsSe_2$, diamag., thermal expansion rel. to temp. at cryst.-melt transition 78—34954
Tl_3AsSe noncollinear acousto-optic tunable filter, operation at 10 μm 79—41434
Tl_3AsSe_3, refractive index, thermal expansion temp. depend. 80—97223
Tl_2Se-As_2Se_3-SnSe system alloys, covalent component of chem. bond effect in vitrification processes, Mossbauer obs. 77—36156
Tl_2Se-As_2Te_3 and Tl_2Te-As_2Te_3, vitreous, photo-EMF kinetics 77—76877
$Tl_2SeAs_2Te_3$, amorphous semicond., nuclear spin-lattice relaxation by localised electronic states, modification by spin diffusion 78—52372
$Tl_2SeAs_2Te_3$, glassy and liq. states, elec. cond. freq. depnd. 77—76856
$Tl_2SeAs_2Te_3$, molten chalcogenide semicond., temp. depend. of 10^{10} Hz elec. cond. 77—4388
$TlSe.As_2Se_3$, $Tl_2Se.As_2Se_3$, γ-irrad. effects on mech. props. 77—80567
$Tl_2Se.As_2Te_3$, vitreous, thermal switching process in high electric fields 80—2432
$Tl_2Te.As_2Te_3$, vitreous, temp. depend. of cond. and thermopower, electron energy spectrum 77—76831
V_2O_5-As_2O_3-RO, R = Ba, Ca, Pb, semicond. glass, electronic props. 80—88557
Zn-As-S chalcogenide glass system, prod. and acoustooptic props. *(Russian)* 78—63158
Zn-As-Te system, phase diagram, As_2Te_3-ZnTe cross section investig. 77—36473

art
Ambrosian picture gallery, Milan, Settala astrolabe collection *(Italian)* 79—35132

art continued
cinematography film production, use of different computer techniques 80—77887
colour, primaries as used in physics and art, for teaching 79—35464
course, sound and light in the arts 77—22340
display hologram, 3D coloured images reconstruction 79—81387
educational courses, physics, for non-science students, rel. to history and arts 77—71165
graphic arts imaging material and laser source cost tradeoffs 80—14383
holography, artistic appls., using 3-dimens. recording and Lippman photography 79—55089
Istra wall paintings in Yugoslavia, X-ray identification of pigments 77—16876
laser line art optical processor, optimal enhancement filter 79—59648
laser-compatible materials for graphic arts 80—13180
oil paintings, neutron activation anal., for teachers 78—81761
thermal imaging system design for graphic arts, laser scanning unit 80—14487
Ag diffusion transfer systems, graphic arts appl. 80—37106
articulation (speech) *see speech*
artificial hearts *see artificial organs*
artificial intelligence
see also adaptive systems; automata theory; biocybernetics; brain models; heuristic programming; learning systems; neural nets; self-adjusting systems
cardiac dynamic imagery, gross and segmental motion anal. 79—70632
cardiac image description and analysis, interactive knowledge-based systems approach 78—81031
chemical inference, automatic rule formation in mass spectroscopy, meta-DENDRAL 77—18775
heat transfer, problem solver, system design outline 80—99916
information processing and origin of pure geometry 77—44624
IR spectra, computer-assisted interpretation, pattern recognition and artificial intelligence methods 78—15732
IR spectral interpretation 78—300
microscopes, recent and near-future advances 80—98166
NMR spectra, computer-aided interpretation using artificial intelligence system 80—62701
nuclear reactor, point-model, heuristic approach to reinforcement learning control 78—46144
optical coding method, scene analysis 78—82924
artificial kidneys *see artificial organs*
artificial limbs
above knee prostheses, normal knee control in level walking using hydraulic simulator system 77—48955
above knee prosthesis, feasibility of active control scheme 78—81081
above knee prosthetic knee control finite sensor state anal. 77—40935
above-knee prosthesis, myoelectric control system development 78—53575
above-knee prosthesis, polycentric knee-ankle mechanism 79—48379
above-knee prosthesis simulator system in eval. of proposed damping torque control schemes 77—44854
adaptive control system for a complete hand/arm prosthesis 80—109059
afferent nerve stimulation in below-elbow amputees 78—57125
amputee-appliance system, lower extremity, functional status analysis and evaluation, integrated approach 77—13032
arm, decentralised control hierarchical approach 77—40924
arm, externally pneumatic powered controlled, features 77—90961
arm, hydraulically actuated, performance criterion 77—48951
arm, hydraulically powered, with seven degrees of freedom 78—40404
arm, lower, multifunctional, control signal generation using EMG signal processing 80—8219
arm, supplemental sensory feedback for below elbow amputee 77—40931
arm prosthesis, gas-press. actuated fingertip mechanism *(Japanese)* 77—66872
arms, muscle- and externally-powered, comparative frequency of use *(German)* 79—12030
below-knee amputees with patellar-tendon-bearing prosthesis, load carrying 77—60301
biomechanics of below-knee amputees, pylon transducer signal variability anal. 79—74715
computer controlled techniques 78—15923
connector, flexible, reduced skin stresses achievement 80—76863
control, method for relating skeletal joint torques to EMG signals 77—48953
control device design for severe motor impairment patients 78—96114
control signals and transducers for the control of upper extremities in plegic patients, computer controlled experiment *(Slovak)* 80—109061
coupled arm for feeding, kinematic anal. 78—3682
electrocutaneous tracking, evaluation of sensory feedback codes 79—25004
EMG digital processor design and performance 79—96712
femoral stress and strain calc., finite element method *(German)* 79—2089
foot, vulcanised rubber, for lower limb amputees 79—74791
function discrimination performance using EMG parameter identification 80—8220
hand, myoelectrically controlled, with sense of touch 79—12035
hand, myoelectrically operated with dynamic control, practical trial *(German)* 79—12029
hand, myoelectrically operated with dynamic control *(German)* 79—8571
hand motion in grasping, mechanical model 79—57694
hand pinch force, sensory-feedback system compatible with myoelectric control 80—41324
hand prostheses, ideas on sensory feedback 80—51295
hand prosthesis, computer simulation and electromyograph controlled aid development *(Spanish)* 78—15924
hand prosthesis myoelectric aid *(Spanish)* 79—84011
hand with sensory feedback, production 80—36191
hip disarticulation amputee locomotion 78—44696
knee, adjustable pneumatic swing-phase control 79—74792
knee, mobility, stability and stress 79—12032
knee simulator requirements and prototype trials *(German)* 79—8578
knee-ankle mechanism, polycentric, for above-knee prostheses 80—94413
knee-torque controller, electrohydraulic, for prosthesis simulator 78—11779
leg, EMG operated controller for locking/unlocking of knee joint 78—7545
leg, EMG operated prosthesis controller 77—48954
leg, force-line visualisation system 80—17200

artificial limbs continued
leg controlled by 6800 microprocessor *(French)* 79—100792
lower limb prosthetics, present and future 80—56287
manipulator, computer controlled, for use as remotely controlled arm 78—81083
microcomputer-aided arm prosthesis using myoelectric pattern recognition 78—53576
microcomputer-controlled, motion analysis using goniometers 80—51138
multifunctional arms development 77—25594
multifunctional prosthetic hand portable control system 78—57127
myoelectric control of an artificial hand, sequential movement, tropical climate 80—41323
myoelectric processor and human operator dynamic error performance 79—96714
myoelectric processor sampling rate selection 79—96713
myofeedback prosthesis with sense of touch, operating experience 80—36190
myopotential controlled elec. operated hand with sensory feedback 79—57815
optoelectronic two-component spirit-level for whole-arm prostheses *(German)* 79—8572
phantom hand sensations elicited by afferent nerve stimulation, discrimination in below-elbow amputees 80—97892
power source development 78—15917
power supply requirements for disabled, survey 78—15929
sensory feedback code comparison using electrocutaneous tracking 78—69255
sensory feedback for artificial limbs 79—84012
sensory feedback system, stimulation freq. discriminability 78—44714
shoulder disarticulation, bilateral, prosthetic principles 79—74793
tracking task evaluation by display system using data compression methods 77—86697
two-leg, Duckling type, hydraulically powered dummy rider control system 78—57124
uCL hydraulic arm dynamics 79—100791
upper extremity prosthesis online control based on EMG signal identification using microprocessor hardware 79—2166
upper limb prostheses multifunctional control via EMG signal identification 78—3683
upper-limb prostheses multifunctional control microprocessor system, myoelectric signal identification method 78—88766
upper-limb prosthesis neuroelec. control 78—44704
voice command of a six-degree-of-freedom manipulator, robotic arm appl. 80—12313

artificial organs
see also prosthetics
bioengineering, international conf., Cape Town, S.Africa (April 1977) 79—20695
biomedical engineering textbook for undergraduates 80—8750
blood cell damage in extracorporeal circulation, haemorheological effects of mech. factors 79—62280
blood cell-vessel wall interaction, fluid dynamic aspects 80—97998
blood circulation assistance and replacement devices *(German)* 78—53564
blood circulation system electrical control *(Spanish)* 78—3680
blood damage by artificial part-hearts and pumps, dwell minimisation model *(German)* 79—16345
blood intermittent pump with linear motor drive *(German)* 79—5401
blood manifold hydrodynamics and thrombotic problems 79—79588
blood membrane oxygenator effectiveness 79—48365
blood oxygenation, extracorporeal, in treatment of acute pulmonary failure 78—7539
blood oxygenation, membrane oxygenator design with curved tubes wound in woven patterns 79—84020
blood oxygenation in complex coiled silicone rubber tubes 77—60304
blood oxygenation simulation in stirred membrane cell 78—40421
blood oxygenation using coiled tubes 78—40422
blood oxygenator, biocompatibility of continuously generated and collapsed blood-fluorocarbon interface 77—48944
blood oxygenator, convective-diffusion model 78—44711
blood oxygenator, membrane flat-plate type, CO_2 transfer 79—25154
blood oxygenator, membrane type 79—84023
blood oxygenator, rotating disc design 78—44710
blood oxygenator, stationary membrane type, O_2 and CO_2 diffusion process 77—78046
blood oxygenator design, data on diffusion of O_2 and CO_2 through blood flowing in channel 77—60303
blood oxygenators, progress and problems 78—36064
blood platelet adhesion obs. in flow chamber 79—79589
blood pump, biventricular, brushless DC motor powered, development and in vivo evaluation 79—53285
blood pump, pulsatile, in vitro eval. of erythrocyte bulk lysis 77—44840
blood pump fabrication for durability 79—84026
blood pump regulation with pressure controlled servo-drive *(German)* 79—84003
blood pumps, leaflet valve manufacturing technique *(German)* 79—84002
blood purification methods and portable kidney machines *(German)* 79—5405
blood transfusion filters, comparison of methods for microaggregate removal evaluation 80—46097
blood ultrafilter design analysis 77—64152
blood unsteady flow model, rel. to extracorporeal dialysis and oxygenatory system design 80—16998
bubble oxygenator, O_2 transfer controlling factors 78—53568
cardiotomy circuit, factors affecting haemolysis 78—36073
circulation system with gas enrichment using membrane oxygenators, mass spectrometer inlet system study *(German)* 78—73294
circulatory regulation by artificial heart *(Japanese)* 77—36971
dialyser, development of a portable system 79—44055
dialyser membrane, steady nonionic countergradient transport by coupled diffusion 80—16718
dialyser performance improvement by osmotic flow induction 77—48946
dialysis and simultaneous diafiltration for blood purification *(German)* 78—31967
dialysis at home, tap-water purification *(German)* 79—2160
dialysis efficiency prediction using convective field theory 77—48945
dialysis equipment elec. hazards and safety 79—84010
dialysis systems, recirculating, assessment of mathematical theory and appl. *(German)* 79—39601

artificial organs continued
dialysis therapy, single compartment model appl. to urea and creatinine kinetics 78—48931
dialysis without circulating dialysate, approach to portable artificial kidney 77—48949
ear, IEC, proposal for audiometric zero 79—12039
ear, IEC 318, reference equivalent threshold sound pressure level 79—88091
ear model and freq. response of external ear *(Chinese)* 80—56063
electronic eye for blind people, implementation through the optical nerve *(Croatian)* 80—109060
endocrine pancreas, blood glucose monitoring technique 78—36062
exchange unit, effect of flow channel thickness on surface-induced blood damage 79—39439
extracorporeal blood oxygenator safety and efficacy, review 78—77153
extracorporeal circulation, blood filter evaluation 78—69250
extracorporeal oxygenation, blood trauma, conf., Stolberg, Germany (Nov. 1978) 80—94922
extracorporeal processing devices, review, book contrib. 80—12308
eye, vision model using optical engineering theory concepts 79—96555
haemodialyser, Casson fluids flow in non-circular ducts 79—20563
haemodialyser, lumped-parameter model, simulation of artificial kidney-patient system 80—56281
haemodialyser membranes, permeability of Cuprophane and polyacrylonitrile *(Japanese)* 77—66873
haemodialysers, hollow fibre type, haemofiltration and thrombus formation effects 78—3672
haemodialysis, effect on evoked pots. and EEG freq. 78—61160
haemodialysis, ethylene-vinyl alcohol copolymer membranes, prep. conditions and props. *(Japanese)* 80—12299
haemodialysis, fracture phenomena, of bovine, swine 78—92746
haemodialysis, use of reinforced expanded PTFE grafts 80—8211
haemodialysis and haemoperfusion, joint system, evaluation of novel sorbent systems 78—7542
haemodialysis by extra corporeal ultrafiltration method, parameter estimation of vascular bed 79—84015
haemodialysis cellulosic films and hollow fibres, diffusive and hydraulic permeabilities 78—28128
haemodialysis membranes, for disposable dialysers, comparison of cuprophane and cellophane 77—78049
haemodialysis membranes, permeability and rejection coeffs. 80—26207
haemodialysis membranes prepared from acrylonitrile-methylacrylate-acrylamide latexes graft copolymerised onto PVA *(Japanese)* 80—12297
haemodialysis rel. to EEG, spectral anal., Hjorth's descriptors, blood variables and psychological data 78—31968
haemodialysis single needle design and tests 78—48936
haemodialysis treatment model for metabolic waste conc. dynamics and cerebrospinal fluid pressure 77—60305
haemodialysis ultrafiltration, transient characts. governing eqn. 78—36075
haemodialysis with hollow fibre membranes, flow maldistribution effect on performance 80—26248
haemofiltration control system *(German)* 79—5403
haemofiltration experiments and application limits *(German)* 79—5402
haemofiltration treatment, chronically intermittent, principles and results *(German)* 79—5404
haemoperfusion, large agarose beads, prep., props. and appls. 79—16349
haemoperfusion devices, comparative studies, press. drop and flow uniformity tests 80—35929
haemoperfusion through fixed-bed adsorber 78—31976
heart, ^{238}Pu power units 77—78052
heart, antithrombotic polymeric materials 78—36052
heart, appl. to US echography to performance studies 78—44728
heart, atrial charact. estimation using analogue simulation 77—44846
heart, automatic control system 77—44841
heart, bench test technique 79—48366
heart, circulatory physiology appl., meas. of resistance to venous return in calves 77—52941
heart, computer simulation 79—70709
heart, control software and haemodynamics system analysis 79—84018
heart, control system, anal. of effectiveness of algorithm using aortic blood press. as regulated parameter 80—3864
heart, driven by automatic driving system 78—7541
heart, elec. powered totally implantable total artificial heart 78—40434
heart, electronic pressure control with fast variable aperture valve *(French)* 77—40928
heart, heparinised elastomer antithrombogenicity and mech. props. *(Japanese)* 80—12296
heart, impelling pump, energy source 77—78043
heart, implantable, definition of technological problems 77—44839
heart, left ventricular work requirements to exercise before and after artificial heart implantation 77—44847
heart, microcomputer based automatic controls 80—67289
heart, miniature Stirling engine power source, long-life, test results 79—53287
heart, miniaturised Stirling heat engine for power source 80—35724
heart, non-invasive determ. of instantaneous cardiac output and dynamic performance 77—44845
heart, nuclear powered, thermal oscill. pump design 78—20317
heart, nuclear powered, using modified Stirling engine *(Croatian)* 78—44695
heart, pneumatically actuated echographic anal., air chamber inlet design 77—48943
heart, pneumatically driven, cardiac output meas. 78—44729
heart, pump development 77—25599
heart, recent advances in total artificial heart 78—36065
heart, rigid-vane system development 79—84025
heart, role of valves in organ performance 80—21575
heart, simulation of fluid dynamics *(Japanese)* 79—43954
heart, Stirling heat engine for blood pumps 80—35720
heart, stroke vol. and cardiac output meas. by echographic technique 80—41319
heart, system for continuously monitoring pumping diaphragms 77—44844
heart, thermal convertor component, R&D 78—20318
heart, total artificial system 79—84016
heart, total artificial system and left ventricular assist device 79—84017
heart, transfer function governing ventricular ejection in assisted circulation 80—104817
heart, using fluorosiloxane rubber 77—78048

artificial organs continued
heart and assisted circulation apparatus, hydrodynamic test bench rigs 79—48372
heart and mock circulatory system, math. model 78—81080
heart blood heat exchangers with radioisotopic power supplies 80—85532
heart blood pump ventricle, mech. driven, visual study of flow field 77—56539
heart designs compared 79—48367
heart experiments with animals, data acquisition and monitoring system *(German)* 79—8582
heart operation and monitoring system *(German)* 79—8583
heart power supply and control, implantable hydraulic modules 78—31978
heart prostheses pumping, effect on mech. props. of vascular walls 78—40429
heart test system, simulation of artificial ventricle and mock circulatory system 77—52933
heart valve element, artificial, visual representation of flow *(Russian)* 77—32926
heart-lung machine, automatic controller of venous press. and venous outflow 77—78053
heart-lung machine blood flow line gas bubble US detector 77—77954
heart-lung machine two-circuit thermocontrol device 79—48374
hearts, pneumatic powered, telemetric monitoring system, in calves 77—90956
hollow fibre dialyser, mass transfer 80—66873
implantable electronic pancreas and blood glucose monitor 78—88767
implantable middle ear, development prospects *(Japanese)* 80—81775
insulin/glucose transfer regulation for diabetics, user programmable system *(French)* 79—39614
Japanese research *(Japanese)* 80—12303
kidney, automatic extrasomatic dialysis system 80—98177
kidney, blood filtration efficiency of Nuclepore Membrane Filter obs., in dog, with pore-size 0.6 μ 79—44051
kidney, dialysate recycle by electrochem. degradation of waste metabolites 78—40411
kidney, effects of blood and dialysing soln. flow rates on efficiency 78—36053
kidney, electrochem. removal of urea, basis for a regenerative dialysis system 80—26417
kidney, evaluation using systems anal. 78—36074
kidney, extracorporeal blood correcting unit 78—7535
kidney, filtration-adsorption type, filtrate treatment system 80—51293
kidney, mobile apparatus for uremic patients 79—84022
kidney, monitoring instrumentation for wearable artificial kidney 77—64154
kidney, problem of removing urea from ultrafiltrate *(German)* 80—21574
kidney, regenerated cellulose-activated charcoal membrane adsorpt. characts. *(Japanese)* 80—12298
kidney, single-needle dialysis, factors affecting blood flow 78—31972
kidney, staged tortuous microcapillary system, haemodialysis and ultrafiltration 77—37107
kidney, tubular haemodialyser anal., ultrafiltration and dialysate concentration effects 78—7544
kidney, ultrafilter adsorber, parametric design analysis 78—40410
kidney, ultrafilter-adsorber system in interaction with uraemic patient model 78—48937
kidney construction for solution mixing, heating and degassing *(German)* 79—2161
kidney dialysis exchange model reliability tests *(German)* 79—2165
kidney microporous membrane plasma filtration efficiency 78—48926
larynx, electronic, Polish developed, design and operation 80—46098
left ventricle, auto-regulating, with 4 operational modes, evaluation in dogs 77—48942
left ventricle, pneumatically regulated, in-vitro/in-vivo performance 78—3681
left ventricular assist device design and performance 79—96708
liver, blood filtration efficiency of Nuclepore Membrane Filter obs., in dog, with pore-size 0.6 μ 79—44051
liver assist, improved haemoperfusion sorbents and plasma filtration system 78—48939
liver support, detoxifying enzymes bound to artificial carriers, extracorporeal application 79—25160
liver support, protein-bound metabolite adsorbent equilibrium props. 79—20709
liver support, protein-bound substance removal kinetics 79—20710
liver support, using affinity chromatography systems 78—7538
lung, computer-assisted PaO_2 management during veno-arterial bypass and mech. ventilation 77—44838
lung, membrane oxygenator, fluid vortices and mass transfer 77—52919
lung, membrane type, for extracorporeal circulation 77—78051
lung, oscillating helix membrane design employing O_2 perfused inner capillaries 78—44712
lung tissue simulation, O_2 exchange in silicon rubber capillaries 79—44060
lungs, membrane design and application 77—25601
membrane oxygenator using dimethylpolysiloxane rubber reinforced film 79—48373
membranes, DECHEMA symposium, Tutzing, Germany, (Mar. 1978) 80—62373
middle ear, and problems with hearing aids 79—84009
neonatal pulmonary assist membrane oxygenator 79—25159
oxygenator, bubble, blood damage test standardisation *(German)* 79—2158
oxygenator, capillary membrane, semiautomatic fabrication 79—20711
oxygenator, coiled tube membrane, unsteady viscous flow in curved elastic tube 79—92281
oxygenator, membrane envelope type, capacity improvement *(German)* 79—2157
oxygenator efficiency prediction using convective field theory 77—48945
oxygenator gas transfer performance test standardisation *(German)* 79—2159
oxygenator membrane blood compatibility, correl. of IR spectroscopy with platelet morphology 79—53279
oxygenator using microchannel membrane, transport and flow phenomena 78—69253
oxygenator/haemodialyser combined system, development and feasibility study 79—84024
pancreas programmed control technology *(German)* 79—16346
plasma filtration, stagnant 77—48948

artificial organs continued
plasma filtration through microporous membranes 77—48947
platelet stimulation under influence of high shear stresses in tube flow 80—97996
platelet transport between blood and artificial filtering surfaces 78—40423
poly(vinyl alcohol)-based membranes for haemodialysis *(Japanese)* 78—96115
polyurethane artificial ventricle construction with seamless interior *(German)* 79—8581
quality health care and cost containment, conf., Washington, USA (Mar.-Apr. 1978) 79—39333
red blood cell mechanical disruption 80—98001
renal dialysis membrane leak detector 77—60294
renal support using microorganisms 77—48950
review, terminology, physical form 77—78042
sensory substitution systems—current status and future trends *(Japanese)* 80—36195
silicone rubber biomaterial, filler free, radiation chemical and physical evaluation 79—39608
sorbent haemoperfusion systems, characterisation of solute removal 78—44689
ventricle, all-pneumatic system, cardiovascular dynamics simulation 78—81082
ventricle, pneumatically driven, sac-type, dynamic model 78—15925
ventricle, sac-type, in mock circulation, mathematical model and digital simulation 78—11780
ventricles with atrial chamber for assisted circulation 80—3862
viscoelastic properties dynamic evaluation for use in cardiac prosthetics 78—40405

artificial satellites
76-115-B, tumbling cylindrical Earth satellite, rot. axis location using visual obs. 79—80201
1966-51C orbit anal., upper atm. zonal wind speeds determ. 77—56786
1967-92A, tidal perturbations 78—61307
1970-34 A satellite, HF transionospheric long range propag. obs. at Florence 78—36396
1973-101A orbit, upper atmosphere wind determ. 78—73560
1975 launchings *(French)* 77—29624
acquired image geometric distortion correction 79—74588
advanced European communication satellites, Be support structures 78—7079
AE-C, low-energy electrons obs. in S polar cusp during 1977, September 21 geomag. storm 79—35076
aerospace photovoltaic generators, symposium, Noordwijk (1978) 79—96449
aerospace systems and electronics, IEEE conference, Washington D.C., USA, 26-29 Sept (1976) 77—5420
aircraft satellite data link, for meteorological reconnaissance data transmission 78—96299
Alouette ionospheric satellites parametric generation of oscills. during EM sounding 77—60510
altimetry, algorithm for subsatellite point position vector length determ. 79—29869
altimetry, appl. to ocean geoid spectrum determ. 80—3904
altitude control by two-stage force gyroscopes *(Russian)* 79—30458
Amsat-Oscar 7 subhorizon ratio signals beacon, above F2 layer, 30 MHz 77—70937
analytical orbiter theory based on Lie transform 77—17340
analytical satellite theory in extended phase space 80—67524
analytical theory of motion 80—46373
Anik 1 data collection development program, environmental data 79—39867
anomalistic period, solar radiation press. effects 80—77255
Apollo spacecraft and subsatellites, lunar gravity determs. 77—60653
applications and benefits of US and USSR space programmes 77—87227
Applications Explorers, Heat Capacity Mapping Mission 79—5640
Ariabata, first Indian satellite, preliminary data 77—53390
Ariel 1, orbit at 29:2 reson., geopot. 29th order harmonics determ. 77—56572
Ariel 4, diurnal var. of ELF and VLF noise at invariant latit. of Sanae 77—87181
Ariel 4 (1971-109A), defenitive orbit 78—73604
artificial satellite orbital inclination changes due to resonance 77—17334
Aryabhata, design, analysis and testing of structure 79—84634
Aryabhata, India's first satellite, technology and scientific expts. 79—58218
Aryabhata, Indian scientific satellite, magnetic testing 78—40793
Aryabhata, orbit computations 79—84655
Aryabhata, spin decay calc. 80—21900
Aryabhata, statistical analysis of weight and cost parameters 79—84635
Astronomical Netherlands Satellite, orbit prediction 79—21139
astronomical observatory, Ariel 5 X-ray astronomy, Cos-B γ-ray astronomy satellites 80—90317
Atmosphere Explorer B, remote sensing of middle atmospheric aerosol 80—109269
Atmosphere Explorer C, simultaneous obs. of field-aligned currents and plasma drift vels. 80—72681
Atmosphere Explorer C (AE-C) satellite, near-wake struct. parametric investigation 79—53647
Atmosphere Explorer-D, comparison of self-contamination expts. and scatt. return flux calcs. 78—40722
atmosphere temperature sounding data, impact on weather forecasts 80—77028
atmospheric drag effects in orbit determ. upper atm. density models comparison 80—17428
atmospheric drag perturbations 77—17342
Atmospheric Explorer, low perigee aerodynamic heating during orbital flight 77—45290
ATS 1 pictures for cirrus ouflow divergence determ. 77—53239
ATS 6/Geos 3, satellite to satellite range-rate obs. for 5° mean gravity anomalies recovery 80—41366
ATS-1, geostationary satellite, mag. field records appl. to plasma condensations diagnostics 79—58189
ATS-5 location by L-band trilateration 77—9652
ATS-6, attenuation meas. of copolar and cross-polar signals at 30 GHz *(French)* 78—49064
ATS-6, ionospheric scintillations assoc. with features of equatorial ionosphere 80—77191

artificial satellites continued
ATS-6, substorm-assoc. energetic ions injections obs. in and near synchronous altitude 79—35075
ATS-6 30 GHz propag. meas. during heavy thunderstorms 77—64377
ATS-6 radio beacon experiment, ground refls. effects 77—53144
ATS-6 radio beacon results of ionosphere and plasmasphere, review 80—56677
ATS-6 satellite 20 GHz carrier, attenuation and depolarisation meas. *(French)* 78—49063
ATS-6 satellite radio beacon, meas. at Ootacamund, India rel. to electron density 79—48611
attitude and orbit control systems, conference, Noordwijk (1977) 78—65480
attitude control, gravitational, satellite dynamics 77—25905
attitude control, inertially fixed pitch stabilisation by solar radiation press. 80—101523
attitude determ., meas. errors 79—88561
attitude determ. of uncontrolled satellite, correlated meas. error effect 78—16262
attitude stability under aerodynamic torque, total stability anal. 77—56805
AUOS-MAGIK satellite, instruments and measurements *(German)* 79—88562
AUREOLE 2 satellite, numerical study of the RF mass spectrom. 79—2470
autonomous navigation problems, shoreline information 78—53732
bearing and power transfer assembly development status 79—96462
Bhaskara, flux-gate magnetometer flight performance 80—72746
Bhaskara, India's X-ray satellite 79—70943
Bhaskara, remote sensing with satellite microwave radiometer, geophysical data 80—56638
British space prospects 79—84644
broadcasting satellites, use in education in developing countries 80—4485
broadcasting satellites for Europe, associated European Space Agency programme 80—12638
cable-connected satellites in Earth orbit, mag. force effect on motion 79—44347
Cactus accelerometer, in-orbit performance on D5B satellite 78—61698
Canadian government research, role and development in communications 80—43481
Castor, Cactus accelerometer payload *(French)* 79—75505
CASTOR, in-orbit electrification of proof mass of CACTUS high sensitivity accelerometer *(French)* 77—64589
Castor satellite, Cactus accelerometer flight results synthesis for accels. below 10^{-9}g 80—77251
CETI from Earth satellite orbit 80—4275
CETI transmitter/receiver in Earth orbit 78—61758
charge neutralisation, electron emitter neutralisation *(Japanese)* 80—94673
charging at geosynchronous orbit during eclipse 79—16792
charging by magnetospheric plasmas, effects, counter measures 77—22035
charging phenomena, positive ion beam system development for charge ejection 79—12379
China 2 rocket (1971-18B), orbit determ. and geophysical interpretations 80—4231
circular orbit satellites, approximate soln. of Euler-Lambert problem 77—53410
Clairaut eqn., connection to satellite geodesy and Jupiter 78—11795
climatology satellite, SEOCS, design 79—29965
clock synchronization using Symphonie satellite 80—68184
close-Earth satellite perturbations due to radiation pressure of reflected sunlight from Earth 77—91411
coasting satellite trajectory, first-order effects of Earth's oblateness 77—60582
collision avoidance method, 2 counter orbiting polar satellites, relativity mission appl. 77—45296
collision frequency, debris belt creation 78—89035
combination turning manoeuvre of orbital plane with constraints on motion 77—64592
communication satellite, medium-capacity, single carrier per channel system 77—60573
communication satellites, history 77—64602
communication satellites, orbital perturbation and stationkeeping, literature survey 78—89039
communication systems in developing countries, fundings 77—64604
communications satellite system measurements 78—61712
comparison of classical analytic theories for the motion of artificial satellites 80—8515
comsat revolution, historical review 77—87239
conference on satellite Doppler tracking and geodetic appl., London, England (Oct. 1978) 80—77264
conical precession stability of symmetrical rigid body *(Russian)* 78—4091
coordinates determ. from nonsynchronous data 78—7870
Copernicus, UV spectroscopy 78—16310
COS-B, ESA extraterrestrial gamma radiation obs. project *(German)* 79—21151
COS-B, instrument description *(Danish)* 80—82544
COS-B satellite obs., appl. of X-γ synchronisation to non-parametric anal. of NP 0532 pulsar 78—73729
Cosmic Background Explorer, instrumentation 80—61988
cosmic gamma-ray astronomy, use of artificial satellites 79—53727
cosmic rays, shielded by geomagnetic field, cutoff probability 80—12626
Cosmos 248 (1968-90A), orbit analysis and gravity odd zonal harmonics 78—81100
Cosmos 462, orbit. rel. to air density vars. from January 1972 to April 1975 near 200 km 78—57377
Cosmos 731, gamma-telescope expt. 77—53258
Cosmos 782, American biological expts., results 78—85818
Cosmos 929, atmospheric re-entry 1978 February 78—85819
Cosmos 954, estimating fallout on Great Slave Lake 79—85830
Cosmos 954 crash in Canada, air pollution, obs. of lichens 80—55960
Cosmos 954 debris, airborne gamma-ray spectrometer detection 78—85784
Cosmos series, applications, review 78—69650
counter-orbiting drag-free satellites in Earth polar orbit, general relativity test and geodetic meas. 77—22047
counter-orbiting polar satellites, Earth tide information 77—2083
critical inclination problem with small eccentricity 80—67525
data applications to marine activities 78—36439

artificial satellites continued
decay and re-entry date prediction for highly eccentric satellite 77—25931
design for optimal continuous coverage 78—73603
despinning with continuous axial thrust, Geos-1 dynamic experiment 80—61982
differential photoelectric charging of nonconducting surfaces in space 79—25439
digital data, radiometric correction and equalisation 79—74587
disc in rarefied plasma flow, external mag. field effect on wake electrostatic field struct. 79—10648
distance meas. by laser 77—9673
Dive and Ascent Satellite, programme for lower ionosphere research 80—77252
DMSP visible imagery, causes of anomalous grey shades 80—77111
DMSP-F2, cusplike electron precip. regions obs. during 1977, September 19 to 21 event 79—35056
Doppler satellite obs. for polar motion determ. 77—44887
Doppler tracking and polar motion determ., MEDOC 80—101445
drag perturbations of near-circular satellite orbits in oblate diurnal atm. 77—25915
drag-free satellite, anal. modelling of orbital motion *(French)* 77—73936
dual-spin satellite magnetic attitude control system, geomag. field effects 78—65484
dual-spin satellites, nutational motion damping *(Russian)* 77—60570
Earth's resources and environment obs., satellite meas. capabilities 79—5654
Earth albedo contribution to satellite solar array perf. 78—40798
Earth artificial satellites motion, relativistic effects 79—2465
Earth gravity field meas., satellite systems comparison 79—53298
Earth obs. systems, planning, design and control 79—58220
Earth observation, periodic coverage pattern quantisation and symmetry 77—78444
Earth observation from space, review 79—34983
Earth Observation satellite programmes 77—29631
Earth Radiation Budget Satellite, climate appls. 80—109283
Earth resource satellite attitude meas. and control requirements 78—65482
Earth resources data, satellite on-board processing 78—61626
Earth resources survey satellite, on-board radiometric preprocessing for multispectral linear arrays 80—56693
Earth satellite, near-circ. orbit dispersion 79—44349
Earth scene dynamics, satellite-borne mosaic sensor performance 80—90321
Earth surface obs. satellite remote sensor/attitude control system interface 78—65481
Earth surface obs. satellites and remote sensor/attitude control interface 78—45182
Earth survey, orbit determination 79—25442
at Earth-Moon libration points, search for natural or artificial objects 80—98647
Earth-resources satellite using optical preprocessor 80—67430
Earthnet, monitoring Earth's environment 78—88921
eccentric orbit motion analysis, von Zeipel perturbation method 77—45295
eccentricity oscills., compensation with stabilizer 78—69643
eccentricity var. of satellite-gyrostat in nearly circular orbit 78—16280
educational expts. using satellite telecommunications 77—60861
effective isotropic radiated power meas., error anal. using calibrated radio star 78—93070
Einstein X-ray observatory, HEAO-2, results to date 80—56692
electric charge build up in sunlight, model of photosheath 80—90316
electric field structure in disturbed zone behind cylinder streamlined by rarefied plasma 79—53623
electronic units development, within INTERCOSMOS programme *(Spanish)* 77—91401
electrostatic charge buildup on ATS 6 and 1976-059A 80—72744
electrostatic field, struct. in wake of body in rarefied plasma flow 77—91402
electrostatic shielding from cosmic radiation, Cosmos 605 meas. 77—29622
ELF antenna, ferrite rod, for Magion satellite for 0.1 to 16 kHz freq. range *(Czech)* 80—85775
elliptical orbits, determ. from parameters of apparent motion 77—53403
elliptical orbits, eccentricity probability characts. 77—64599
energy conversion, Conf., San Diego, CA, USA (Aug 1978) 79—48038
energy storage, Ni-H_2 battery appl. 80—81430
environmental data collection with Geostationary Operational Environmental Satellite 79—29977
ephemerides representations, Chebyshev approximation, satellite navigation 80—61993
equations of motion, numerical integration methods *(Japanese)* 78—85837
equations of motion in nonsingular variables 77—60581
equatorial satellite in J_2-field, periodic solns. *(French)* 78—45205
ESRO IV, solar array orbital performance data assessment 78—40797
ESRO-4, equatorial ionosphere plasma density bubbles obs. 80—4194
ETS-II, radiowave propag. expt. facility *(Japanese)* 79—2471
ETS-II satellite, 1.7 GHz, 11.5 GHz, 34.5 GHz wave propag. rel. to rain precipitation strength *(Japanese)* 78—85669
European potential climatological satellite missions 79—70886
European remote sensing satellite programme benefit identification and quantification methodology 78—32231
European Space Agency activities *(German)* 80—8516
European Space Agency programmes, developmental or operational status 80—72742
European Space Agency remote sensing programme activities and plans 79—70885
European Space Agency satellite, programmes and projects 79—12377
European space technology developments, Swiss role *(German)* 80—4234
EXOS-A, fifth scientific satellite 'KYOKKO' *(Japanese)* 80—101525
EXOS-B, magnetospheric research satellite, instrumentation 79—48649
EXOS-B, sixth scientific satellite JIKIKEN *(Japanese)* 80—101526
EXOS-B (JIKIKEN), obs. and comparative study of VLF emissions and high energy electron flux *(Japanese)* 80—94652
EXOSAT, lunar occultations optimisation for point-like X-ray sources positions determ. 79—92652
Explorer, launch procedure, appl. to thunderstorm analysis *(Italian)* 77—81988

artificial satellites continued
- Explorer 35, magnetometers data errors and lunar induction studies 79—96932
- Explorer I, United States first satellite, launched in 1958, achievements 78—85817
- external surfaces, conductive materials for grounding 78—45187
- flexibility experiment design, control/flexible structure interaction 77—70970
- flexible damped satellites, Liapunov stability anal., comparative study 79—37148
- Fourier spectroscopy methods and problems *(German)* 80—36477
- Fourier spectroscopy problems, mechanical disturbance effects on optical elements *(German)* 80—36478
- fragmentation in orbit 78—53858
- French satellites, research applications *(French)* 80—82170
- French space programme, review 79—101045
- future applications, reliability and cost considerations *(Italian)* 80—109334
- gamma-ray astronomy prospects 80—21889
- gamma-ray telescope artificial satellite, axis orientation determ. 78—53787
- GEDS in wrong orbit, effects and counteraction 78—16271
- geodesy, accuracy of satellite-derived geopotential models 79—25183
- geodesy, determ. of gravity anomalies at Earth topographic surface by cosmic methods 80—56337
- geodesy, Doppler satellite positioning in Canada, review 77—44883
- geodesy, generalisation of Laplace expansion to Earth's surface 77—60337
- geodesy, geometrical and dynamic methods, development *(Polish)* 78—88780
- geodesy, Great Britain triangulation geocentric positioning via satellite Doppler techniques 79—29695
- geodesy, satellite to satellite tracking for geoid improvement in local areas 79—62423
- geodesy and geophysics appls., review 77—64183
- geodesy techniques *(German)* 77—64190
- geodesy using satellites, review *(German)* 77—44905
- geodetic meas. methods and geophysical appl., review 79—66835
- geodetic networks connection problems, stiffening problem, error anal. 80—81799
- geodetic satellites, appl. to adjustment of N American horizontal datum 77—2079
- geodetic satellites, appl. to realisation of ocean dynamics four-dimensional reference system 78—77176
- geodetic satellites, basic mechanical principles of gravimeters and gravity gradiometers *(German)* 80—101461
- geodetic satellites, longitude-averaged meridional profile of Earth pear-shaped section 80—94450
- geodetic satellites, ocean tides mapping computer simulation 79—39880
- geodetic satellites, refinement of short arc satellite altimetry model 77—60336
- geodetic satellites, role of orbit determ. in altimeter data anal. 78—77177
- geodetic satellites, trends and prospects for crustal movement meas. 79—29738
- geodetic satellites, twin probes method 79—25443
- geodynamic monitoring and earthquake research, radiointerferometry appl. 80—31151
- geodynamic research techniques using satellites 80—109282
- geomagnetic field meas. from near-Earth orbit, review of obs. 80—56347
- geomagnetic substorm charging simulation 79—96886
- geopotential appls. of $\beta/2$ orbital reson. of artificial satellites 79—53296
- GEOS, booms/mechanisms for equipment protection against interference 78—4073
- GEOS, Earth's magnetosphere dynamics response study mission 78—4072
- GEOS, Europe's first geosynchronous scientific satellite 77—37495
- GEOS, IUE and METEORSAT Earth Station antennas, design, characts. *(German)* 77—56764
- GEOS, IUF, and METEOSAT ground stations, weather obs., Earth exploration *(German)* 77—56763
- GEOS, technical features 78—4071
- Geos 1 and 2 satellites, keV plasma expt., magnetospheric electrons and ions distrib. 80—41695
- Geos 3, altimeter data anal. in Tasman and Coral seas 80—3903
- Geos 3, altimeter data appl. to sea surface topography obs. 80—3908
- Geos 3, altimeter data for determ. of geoid of Kerguelen Islands area 80—3900
- Geos 3, altimeter data on coincident orbits rel. to ocean transients 80—72535
- Geos 3, altimeter data rel. to Earth gravity model improvement (GEM 9 and 10) 80—3909
- Geos 3, altimeter data rel. to geoid heights along Hawaiian-Emperor seamount chain 80—3899
- Geos 3, altimetric geoid comparison with gravimetric geoid 80—3898
- Geos 3, calibration and evaluation of STDN S-band stations, using Doppler and laser ranging data 80—4228
- Geos 3, geodetic base line estimation using single passes of laser data 80—3910
- Geos 3, orbit determ. expt. 80—4226
- Geos 3, radar altimeter data rel. to large-scale Gulf Stream frontal study 79—5488
- Geos 3, satellite-satellite tracking data appl. to geocentric gravit. const. (GM) determ. 80—3911
- Geos 3 altimeter data, appl. to geoid undulation and anomaly estimation 77—64178
- Geos 3 altimeter data, processing for recovery of geoid undulations and gravity anomalies 80—3896
- Geos 3 altimetry, appl. to ocean gravity anomalies and geoid determ. 80—3905
- Geos 3 altimetry data, appl. to ocean geoid investigation 80—3906
- Geos 3 orbit determination expt., results of Geos 3/ATS 6 satellite-to-satellite tracking 80—4225
- Geos 3 project, review 80—4224
- Geos 3 satellite, altimeter data rel. to oceanic geoid and tides determ. in NW.Atlantic Ocean 80—3901
- Geos 3 satellite, altimetry data for ocean geoid estimation near Blake Escarpment 80—3902
- Geos 3 tracking systems, intercomparison 80—4227
- GEOS booms and mechanisms 78—85825
- GEOS electron beam experiment S 329 78—93075
- Geos I, natural magnetospheric emissions identification 78—53774

artificial satellites continued
- Geos mission, launch malfunction, experimental program procedure 77—70979
- GEOS orbital characts. *(German)* 77—82105
- Geos satellite, first six months' obs. 78—61705
- GEOS-1, keV plasma expt. early results 79—35068
- GEOS-1, magnetosphere electron density and temp. meas. by mutual impedance expt. 79—35071
- GEOS-1, magnetosphere plasma density and temp. multi-expt. determ. 79—35074
- GEOS-1, magnetosphere plasma resons. on-line tracking for electron density small-scale struct. 79—35073
- GEOS-1, magnetosphere thermal/suprathermal plasmas obs. by S-302 expt. 79—35070
- GEOS-1, mass spectrometer obs. of magnetospheric ion comp. dynamics 79—35069
- GEOS-1, obs. of substorm-assoc. particle flux vars. (L=6 to 8) 79—35067
- GEOS-1, relaxation sounder meas. of magnetosphere plasma density 79—35072
- GEOS-1, substorm-assoc. energetic ions injections obs. in and near synchronous altitude 79—35075
- GEOS-1 and magnetosphere physics advances (conference, Innsbruck, Austria, 1978) 79—35066
- GEOS-1 mission, review 79—29971
- GEOS-1 wave experiment 79—25444
- GEOS-3 proposed mission to far geomagnetic tail 80—82163
- GEOS-III obs., SFB 78 contrib. in 1975-6 period *(German)* 77—70591
- geostationary, libration points rel. to position of Earth's mass centre 79—21156
- geostationary, methods for numerical integration of eqns. of motion 78—69659
- geostationary, plasmapause sounding feasibility 78—93043
- geostationary, semi-passive attitude control and trajectory stabilisation 77—41282
- geostationary, station-keeping activator subsystem reliability 78—4074
- geostationary, use in determ. of geocentre position var. 80—82083
- geostationary meteorological, role played in Global Weather Expt. 80—77256
- geostationary satellite, orbit determ. by single ground station tracking 80—109329
- geostationary satellite investigation of gravitational Doppler effect 80—109351
- geostationary satellite orbit, relationship between arc and min. angle of elevation from Earth's surface area 77—13223
- geostationary satellite signals, mid-latit. ionospheric scintillation at 137 MHz 79—25388
- geostationary satellite VHF Faraday rotation mea. for ionospheric electron content 78—61599
- geostationary satellites, appl. to incident solar radiation of Earth surface estimation 80—82006
- geostationary satellites, optical observations 79—84627
- geostationary satellites, severe scintillation of VHF and GHz waves during mag. storm 80—109302
- geostationary weather satellites, global network *(German)* 78—24389
- geosynchronous, ATS programme progress 78—81515
- Geosynchronous Earth Orbitors operational meteorological satellite for regional remote imaging 79—5727
- geosynchronous satellite orbit determination using VLBI and computer program *(Japanese)* 80—21925
- geosynchronous satellite plane-mirror solar concentrators 79—96474
- geosynchronous satellites, libration centre shift 79—84649
- geosynchronous spacecraft potential, photoelectron flux var. effects 79—80087
- Global Positioning System, computationally efficient modelling for long-term prediction of orbits 79—80198
- Global Positioning System (GPS) satellites, geodetic system using radio interferometric Earth surveying 79—100804
- Global Weather Expt., roles played by METEOSAT and TIROS-N 80—26714
- gravitational acceleration recurrent calc. 77—56818
- gravitational stabilization system, optimum parameters 77—41280
- gravitational theory of Fujii, test by spaceship orbiting Mars 78—4550
- gravitationally oriented elastic satellite, spatial oscills. and stability of relative equilib. 78—4068
- gravity anomaly probing by satellite-to-satellite tracking 77—56768
- gravity observations, appl. to inverse isostatic problem global soln. 80—3893
- gravity oriented, with thermally flexed appendages, librational dynamics 78—7868
- gravity stabilized axisymm. satellite, solar radiation press. induced coupled librations 80—21888
- Grazing-Incidence Solar Telescope facility 79—70956
- ground-to-satellite power transfer by laser beam 79—62724
- gyrodampers in passive attitude control system 78—96379
- GYROLITE, derivation of stability criterion 79—92649
- gyrostatic satellite in circular orbit, regular precessions 79—93082
- gyrostatic satellite in Kepler orbit, rot. motions 80—86080
- halo orbiter mission design, scientific satellite appl. 77—73920
- HEAO 2 satellite (Einstein Observatory), successful launch 79—44333
- HEAO B, scheduled launch and observing opportunities 78—69647
- HEAO mission 79—5730
- HEAO programme outline 77—78595
- HEAO-1, successful launch report 77—82102
- HEAO-1 for X-ray astronomy 79—62722
- HEAO-1 spacecraft, pointed obs. of selected sources 78—7856
- HEAO-2, Einstein X-ray Observatory, hardware, instruments performance characts. 79—70941
- HEAO-2, X-ray pictures from space 79—92892
- HEAO-2, X-ray telescope description, obs. and sources 80—12643
- HEAO-A, scanning modulation collimator instrument 77—71003
- HEAO-A 79—25445
- HEAO-B, high-energy astrophysical satellite lab., X-ray observ. facilities *(Dutch)* 80—61986
- HEAO-B, orbiting X-ray telescope, Si:Li spectrometer 77—5460
- HEAO-B satellite, sensitivity rel. to deep X-ray surveys predictions and strategies 78—96567
- HEAO-B X-ray Observatory 79—25446
- HEAO-B X-ray telescope orbiting observatory, aspect system providing absolute referencing to celestial sphere 78—40791
- HEOS-2 meas. of magnetospheric charged particles 78—61671

artificial satellites continued
- Hermes, geostationary communications satellite, Canadian design 78—93068
- Hermes, joint Canadian-American satellite, radiotelescope linking for VLBI 77—70977
- Hermes communications satellite, real-time very-long-baseline interferometry 78—24469
- high altitude Earth satellite, elimination of short and intermediate period terms 77—17339
- high altitude Earth satellite orbit, doubly averaged effect of Moon and Sun 77—17335
- High Energy Astronomy Observatory (HEAO) programme 79—44368
- Hills method appl. to orbit construction *(Russian)* 79—40067
- HIPPARCOS, astrometric obs. from space *(Polish)* 80—67519
- Hipparcos, European astrometric satellite, prospects 79—96880
- HIPPARCOS, global astrometry by space techniques 80—109369
- Hipparcos, meas. of stellar distances *(French)* 80—94688
- Hipparcos astrometric satellite project and space telescope astrometric program, review *(French)* 80—46365
- Hipparcos satellite, proposed space-astrometry mission 80—82164
- image data processing in Geostationary Meteorological Satellite System *(Japanese)* 79—92627
- image sensing and multiplexing system tradeoffs 77—60498
- inclination, gravity effect, first order theory error determ. 80—17475
- India's domestic satellite, positioning agreement and interference problems 77—82099
- Infrared Astronomical Satellite, features and performance 80—61989
- Infrared Astronomical Satellite telescope 77—49298
- initial orbit determ., multiple obs. using angles and angular rates 80—56694
- initial orbit determ. using angles and angular rates of movement 78—53795
- INTASAT, ionospheric plasma obs., data analysis *(Spanish)* 78—16270
- INTELSAT IV, in-orbit liquid slosh tests, anal. 78—81516
- Intelsat V, solar array design and development 79—48135
- Intercosmos-10, Langmuir probe expts. results *(German)* 79—2469
- Interkosmos 10, inclination var. analysis 80—41693
- Interkosmos 7, photometry of eclipses observed in situ 77—91408
- Interkosmos 9 and 10 orbital inclination changes at 14/1 resonance 78—20342
- Interkosmos program and Magion satellite project 80—98535
- Interkosmos-Kopernik 500 in ionosphere plasma, Debye screening and electron conc. nonuniformity 78—69563
- Internation UV explorer, inclined elliptical geosynchronous orbit mission design implications 78—4104
- International Magnetospheric Study, Satellite Situation Center 77—53197
- International Sun-Earth Explorer, three-spacecraft programme for magnetosphere study 78—28485
- International Sun-Earth Explorer (ISEE) mission, review 80—90320
- International Sun-Earth Explorer B minimum-model project 78—61702
- International Sun-Earth Explorer mission 78—12069
- International Sun-Earth Explorer mission 78—61701
- international time synchronisation, precision tracking package TEMPUS, NAVSTAR satellite network appl. 80—22332
- International Ultraviolet Explorer, orbiting telescope, 1978 observations *(French)* 80—8540
- International Ultraviolet Explorer, results after one year 79—96915
- International Ultraviolet Explorer, spacecraft, instrumentation and program *(Italian)* 78—32320
- International Ultraviolet Explorer (IUE), in-flight performance 78—96383
- International Ultraviolet Explorer (IUE), new era in UV astronomy 79—48671
- International Ultraviolet Explorer (IUE), spacecraft and instrumentation 78—96382
- International Ultraviolet Explorer (IUE) second European conference (Tubingen, Germany, 1980 March 26 to 28) 80—82584
- International Ultraviolet Explorer geosynchronous orbit 78—89060
- International UV Explorer, obs. of sample targets 78—32315
- International UV Explorer (IUE), image processing 79—80234
- ion beam injection into magnetosphere, from solar power satellite engine 80—82149
- ionosphere, electron density profiles determ. from transionospheric sounding data 78—28371
- ionosphere, simulation of satellite flight using synthesised plasmas *(French)* 78—16269
- ionosphere, struct. of electrostatic field in wake of spherical satellite 77—60509
- ionosphere satellite wake, assessment ion current distrib. 80—101527
- ionosphere satellites, MF wave propag. expts. using Z-mode pulses 79—53646
- ionosphere satellites, waveguide propag. expts. at MF, general results 78—69604
- ionosphere satellites, whistler-mode pulse propag. expts. at medium freqs. 78—69605
- ionosphere sounding, satellite gyroharmonic reson. obs. interpretation 79—48614
- Ionosphere Sounding Satellite, data analysis of topside sounding mission *(Japanese)* 79—16750
- Ionosphere Sounding Satellite, operation planning and data analysis ground support system *(Japanese)* 79—16799
- Ionosphere sounding satellite control, automated system 77—60572
- ionosphere-satellite interaction, ion density in wake of O^+ plasma 80—82136
- ionospheric plasma probe measurements, commutable source of ref. voltages 80—31192
- Ionospheric Sounding Satellite, automated control system *(Japanese)* 77—78607
- Ionospheric Sounding Satellite, command system *(Japanese)* 77—78609
- Ionospheric Sounding Satellite, summary of control centre *(Japanese)* 77—78606
- Ionospheric Sounding Satellite, telemetry receiving system *(Japanese)* 77—78610
- Ionospheric Sounding Satellite control, data recording and anal. system *(Japanese)* 77—78611
- Ionospheric Sounding Satellite control, tracking system *(Japanese)* 77—78608
- IR Astronomical Satellite (IRAS), ground operations and data processing 79—80193
- IR Astronomical Satellite (IRAS), on board computer, design 79—80191

artificial satellites continued
- IR Astronomical Satellite (IRAS), on board computer software 79—80192
- IR astronomical satellite telescope and detector arrays 78—45226
- IR detector cooling by multimission solid cryogen cooler 80—86423
- IR Doppler wind-sensing system, atmospheric effects 79—96828
- IR sensor systems, interfering space radiation background 77—22011
- IR sky simulation 79—29975
- IR telescopes, control of contamination due to cryogenic cooling 80—31209
- ISEE 1 and 2, electron density expt. 78—85803
- ISEE 1 and 2, medium energy particles expt. 78—85811
- ISEE 1 and 2 fluxgate magnetometers 78—85804
- ISEE spacecraft, experimental investigations and instruments, review 78—85785
- ISEE spacecraft instrumentation for solar and interplanetary electron meas. 78—85786
- ISEE-1, electron spectrometer expt. 78—85809
- ISEE-1, solar wind expt. 78—85800
- ISEE-1 and -2, quadrispherical LEPEDEAS for plasma meas. 78—85801
- ISEE-1 and -2, results of meas. on magnetosphere 79—29935
- ISEE-1 and ISEE-2, fast plasma expt. 78—85800
- ISEE-1 and ISEE-2, plasma wave investigation 78—85802
- ISEE-1 and ISEE-C, nuclear and ionic charge distrib. particle expts. 78—85790
- ISEE-1 spacecraft, quasi-static and low-freq. elec. fields meas. via spherical double probes 78—85808
- ISEE-2 results from EGD plasma expt. 79—58211
- ISEE-A, DC and low-freq. elec. field meas. instrumentation 78—85807
- ISEE-A, plasma comp. expt. 78—85810
- ISEE-A and -B, energetic particle fluxes in magnetosphere and interplanetary space, expt. 78—85799
- ISEE-A spacecraft, Stanford University VLF wave injection expt. receiver 78—85806
- ISEE-B project, Sun-Earth Explorer *(German)* 78—81526
- ISEE-B satellite, EGD positive ion expt. 78—85805
- ISEE-C cosmic ray electrons and nuclei expt. 78—85792
- ISEE-C cosmic ray isotope spectrometer 78—85797
- ISEE-C low energy proton expt. 78—85791
- ISEE-C medium energy cosmic ray expt. 78—85798
- ISEE-C multidetector cosmic ray telescope expt. 78—85789
- ISEE-C plasma wave expt. 78—85794
- ISEE-C solar wind ion comp. expt. 78—85793
- ISEE-C solar wind plasma expt. 78—85788
- ISEE-C three-dimens. radio mapping expt. 78—85796
- ISEE-C vector He magnetometer 78—85795
- ISEE-C X-ray spectrometer expt. 78—85787
- Isis ionospheric satellites, parametric generation of oscills. during EM sounding 77—60510
- isotope-powered satellite design for Shuttle launches 78—61709
- isotopic heat source of multihundred watt design 77—42194
- isotopic power source, health physics aspects 77—46414
- IUE, first year of obs., conference, London, England (1979 April 4 to 6) 80—51960
- IUE, search for stellar coronae 80—4233
- IUE preliminary results, workshop, Udine, Italy (1978 October 12) *(Italian)* 80—86033
- IUE ultraviolet telescope, initial results *(French)* 79—84639
- Japanese, Ume-2, ionosphere-sounding *(Japanese)* 79—88564
- Japanese space projects *(Japanese)* 77—87237
- Japanese weather satellite, on board equipment, geostationary orbit 78—4076
- Japanese weather satellite, purpose and instrumentation 78—49290
- Jikiken, obs. of mini-substorm and long-period Pi 2 event, (1978 December 11) *(Japanese)* 80—94653
- JIKIKEN (EXOS-B), plasmapause and propag. waves meas. using stimulated plasma wave results *(Japanese)* 80—94650
- JIKIKEN (EXOS-B), stimulated plasma wave expts. in magnetosphere *(Japanese)* 80—94649
- JIKIKEN (EXOS-B), terrestrial and planetary radio and plasma waves obs. *(Japanese)* 80—94675
- JIKIKEN (EXOS-B), terrestrial kilometric radiation obs. *(Japanese)* 80—94648
- JIKIKEN (EXOS-B), VLF Doppler shift meas. *(Japanese)* 80—94651
- JIKIKEN (EXOS-B) scientific satellite, magnetosphere obs. *(Japanese)* 80—94674
- JIKIKEN satellite, electron beam emission for magnetosphere beam-plasma interaction expt. *(Japanese)* 80—94655
- JIKIKEN scientific satellite, magnetosphere charged particle fluxes *(Japanese)* 80—94654
- Jupiter orbiter, periodic orbits in restricted six-body problem 77—13216
- non-Keplerian orbit, Keplerian representation 80—90324
- Keplerian tritangential orbit analysis 77—5421
- Kiku-2 (ETS-II), MM wave propag. expts., satellite-to-Earth link 79—79909
- Kosmos 426 obs. of outer radiation belt dynamics during 1971, December 17 magnetic storm 77—33281
- Kosmos 484, constant electric field strength vector meas. problems 78—16245
- Kosmos 782 biosatellite, HZE particle radiation studies 79—16778
- Kosmos 954 descent and radioactivity surveillance in Switzerland *(German)* 78—77119
- KYOKKO (EXOS-A), ionospheric and auroral research satellite, instrumentation 79—48648
- Lageos, Earth's rotation and Earth's crust movement meas. by employing laser tracking technique 77—41206
- Lageos, semimajor axis secular decrease, atmospheric drag 80—94628
- Lageos for crustal movement meas. 78—65441
- LAGEOS high-mobility ranging station, geodesy appl. 79—79723
- LAGEOS orbit, long-term evolution 80—94676
- Lagrange configurations in space system dynamics 78—73606
- Landsat, data acquisition and processing *(Italian)* 78—4070
- Landsat, digital image rectification system 77—56734
- Landsat, forest and range inventory of S.E.Texas counties by administrative boundaries 77—56748
- Landsat, multidate lake quality monitoring, data extraction program 80—17299
- LANDSAT, proposed parameters 78—7858
- Landsat, satellite-aided evaluation of population exposure to air pollution 79—92116
- LANDSAT, surface albedo changes monitoring 78—32104

artificial satellites continued
LANDSAT 77—56812
Landsat 2 cloud imagery rel. to future meteorological obs. systems 78—40626
LANDSAT agricultural monitoring program to monitor corn in Iowa 77—78495
LANDSAT and SEASAT oceanographic data acquisition 79—12309
Landsat D wideband communications system 80—101529
LANDSAT data anal. for geological structure research *(Italian)* 80—109281
LANDSAT data applications 77—82060
LANDSAT Data Collection Platform for surface hydrography 77—49174
LANDSAT geoexploration, digital mosaicking and lineament enhancement *(Japanese)* 80—82169
Landsat imagery, use in land system classification of Jordan 79—2388
LANDSAT imagery and synthetic aperture radar combination 79—5650
LANDSAT imagery photoprints, pulp mill stack plume meas., air pollution appl. 78—88905
LANDSAT images, processing method for geological faults and other linear features detect. 80—77177
Landsat images of Earth, processing by digital techniques 77—25784
Landsat MSS points location on maps, methods and accuracy 79—2389
Landsat multispectral scanner for mapping and land-use classification 79—35017
LANDSAT pictures, interactive digital image processing system, DIBIAS 77—82062
LANDSAT remote sensing of hailstorm damage to vegetation *(Italian)* 77-81986
LANDSAT satellite images; low-cost enhancement of multispectral data 78—20559
Landsat satellite observations of Earth 79—84280
Landsat satellite programme for remote sensing of the Earth *(French)* 79—40058
LANDSAT snow mapping data 77—82061
Landsat-D systems, design and implementation progress 80—77259
Large Infrared Telescope on Spacelab 78—12070
large structures, construction in space 80—98533
laser ranging, corrections for atm. reflectivity 77—75663
laser ranging, future developments 77—64483
laser ranging, scintillation statistics 77—88900
laser ranging for upper atmosphere wind determ. 77—64485
laser ranging system, Space Borne Event Timer, meas. of Earth movement along San Andreas fault 80—61984
laser tracking, current status and future prospects of technology 79—66906
laser tracking data, ray tracing evaluation of refraction errors 79—8588
LASSO experiment on Spiro-2 spacecraft laser synchronisation from stationary orbit 80—82211
Lense-Thirring effect and satellite relativistic nodal precession meas., covariance anal. 78—126
LES 8/9 mission, safety programme concerning radioisotope thermoelectric generator 77—46412
LES 8/9 spacecraft, integration of multihundred watt isotopic generators 77—46413
LF radio sounding of plasmapause by geostationary satellite 78—69648
location by tone-code trilateration 77—9653
loci of nongravitational foci, apsides of set of paths analysis 78—7867
Low Earth Orbitors operational meteorological satellite for global remote imaging 79—5727
low-altitude, appl. of altitude control techniques 79—25441
low-eccentricity Earth satellite at critical inclination, orbital motion 79—12388
low-orbiting, tracking errors estimation 80—36470
Luna 10, 12, 14, 19 and 22 data and model of lunar gravitational field 78—45249
lunar satellites, long term Keplerian rates rel. to gravity field 77—87291
lunar satellites, orbital elements rel. to gravity field mass point model 77—87289
lunar satellites, orbits and gravity field harmonic anal. 77—87290
luni-solar perturbations in extended phase space representation of Vinti problem 79—35101
lunisolar perturbations of near-circular orbits 77—49278
Magion, design and construction 80—98536
Magion satellite, ELF ferrite rod antenna for 0.1 to 16 kHz freq. range *(Czech)* 80—85775
magnetic damper, asymptotic theory *(Russian)* 79—30496
magnetic damping of rotation, shielding effects 78—69646
magnetic field effects, exponential damping 78—69645
magnetosphere contamination at geosynchronous orbit 80—72701
magnetosphere reasearch, Ariel 3, 4, Geos, ISEE satellites 80—90317
magnetosphere satellites, appl. to plasmapause displacements recording 77—22034
magnetosphere satellites, connected with International Magnetosphere Research programme *(Russian)* 80—17467
manned satellites, study of Earth by astronauts *(Russian)* 78—40795
Mapsat (Automated Mapping Satellite System), proposed parameters 80—17468
material charging in space environment 80—109327
mesoscale satellite system design 79—58224
Meteor 25, USSR, IR spectrometer measurements and control, atmosphere surveillance appl. *(German)* 78—32321
Meteor satellite, IR spectrometer bolometer amplifier *(German)* 78—28484
meteorological, communication systems for weather sensitive economic activities 80—46244
meteorological, future and present *(Japanese)* 77—87109
meteorological, SMS-1, SMS-2, GMS-1, METEOSAT systems *(Polish)* 79—58219
meteorological, visible and IR instrumentation 77—22041
meteorological NOAA, data A/D conversion for digital image processing *(Japanese)* 78—7711
meteorological obs. future role 79—79965
meteorological satellite imagery, appl. to numerical forecasting model initial conditions assessment 80—31084
meteorological satellite NOAA, digital signal processing techniques *(Japanese)* 78—24424
meteorological satellites, appls. in weather modification programmes 78—96259
meteorological satellites, operation and appls. 79—29967
meteorological satellites and ocean storm forecasting appl. 78—69423

artificial satellites continued
meteorological satellites development, new trends 79—29964
Meteosat, electrostatic discharge phenomena obs. 80—17463
METEOSAT, Europe's first weather satellite 78—53785
Meteosat, geostationary meteorological satellite, brief particulars *(French)* 80—17469
Meteosat, in-orbit performance, results, meteorological appl. 78—88875
Meteosat, ocean surface temperature measurements, derivation from Meteosat image data 80—76985
Meteosat, role in meteorological services 78—45196
Meteosat, role in meteorology 78—36219
Meteosat, weather and communications satellite 79—16790
Meteosat, weather forecast appl., Europe *(Swedish)* 77—56769
Meteosat 78—93072
METEOSAT 1 weather satellite pictures, amateur facsimile reception *(German)* 80—81982
METEOSAT appls., conf., Rome, Italy (Mar. 1978) 78—96384
Meteosat data collecting platform *(Danish)* 80—12637
Meteosat for weather data collection, single cabinet telecommunication equipment 78—36419
Meteosat image processing 78—36297
Meteosat imaging payload, functional aspects 78—36424
Meteosat in-orbit calibration, appl. to lunar thermal props. obs. 80—17511
Meteosat launch operations 78—36425
Meteosat programme organisation and management 78—36422
METEOSAT project, interactive image system 80—109330
METEOSAT project overview *(Italian)* 80—109331
Meteosat remote sensing equipment for atm. general circulation obs. 80—94595
METEOSAT role in global observing system *(German)* 78—36437
Meteosat spacecraft, elec./mech. configurations 78—36423
METEOSAT synchronisation and image channel system *(Italian)* 77—82110
Meteosat system, missions and performances 78—36421
Meteosat system, organizational aspects *(French)* 79—29969
Meteosat water vapour channel, new insight into troposphere 79—25292
Meteosat-1, research uses of early data, review 80—77257
Meteosat-I, observational history *(French)* 80—8513
Meteostat, wind deviation from cloud motion 80—109244
microchannel X-ray image convertors *(French)* 78—24436
microwave power transmission for Earth use, environmental aspects 79—52896
Miranda (X4) satellite, Earth radiance obs., IR expt. design and performance 80—72745
mirrors, large orbiting structures reflecting sunlight to Earth, appl. to lighting, agriculture, and power generation 80—45632
mission analysis mathematical background, orbit selection and mission constraints 78—40790
modular solar collector development for large solar generators 79—96467
molecular wake shields of various shapes for vacuum expts. 79—88966
Molniya 1, radiation doses meas. in magnetosphere 79—8774
motion, error evaluation, averaging method for canonical eqns. *(French)* 77—67028
motion, error evaluation, averaging method for canonical eqns. *(French)* 77—67029
motion, numerical integration of near-parabolic orbits 77—25925
motion, of satellite in reson. with second-degree sectorial harmonic 78—24452
motion, recurrence relations for inclination functions 77—22054
motion about oblate spheroid, Vinti problem, extended phase space formulation 78—53801
motion around a source whose luminosity changes 79—12394
motion around spheroidal planet *(Russian)* 77—73939
motion in coordinates, theory for arbitrary intermediate orbit case 79—62720
motion in gravitational and mag. dipole fields *(Russian)* 80—36487
motion in oblate atmosphere, orbitally stable multistep methods 78—85834
motion in vicinity of triangular libration points 78—12488
motion of stationary satellite, arbitrary integration constants in approx. analytical theory *(Russian)* 78—32331
motion prediction by extrapolation methods *(Russian)* 78—49299
MS-T3, TANSEI-3 test satellite *(Japanese)* 80—101524
multi-mission spacecraft, modular satellite 77—73931
multispectral analysis by NOAA and METEOR satellites 77—82009
multispectral scanner, high resolution, for Earth obs., optical design 80—82174
NASA astrophysics activity 79—5729
natural resource determ. from weather satellite TV images 77—70876
navigation and position location, conf., San Diego, CA, USA, Nov. (1978) 79—25374
navigation systems, ionospheric and plasmaspheric effects 77—82100
Navigation Technology Satellite-2, Ni-H_2 battery appl., first-year operating experiences 79—48107
navigational, GaAlAs solar cells appls. for power systems 80—35694
NAVSTAR, satellite Global Positioning System 79—101042
NAVSTAR, satellite navigation system 78—61711
NAVSTAR Global Positioning System, sea trials results 80—12645
NAVSTAR Global Positioning System satellite clock, H maser design 78—58969
NAVSTAR Global Positioning System satellites Doppler meas., geodetic solns. accuracy 79—100803
NAVSTAR satellites appl. to Earth surveying, miniature radio interferometer terminals 79—100805
NAVSTAR system plans 77—70978
Navy navigation satellite system TRANSIT, on-board computer 79—29978
near circular Earth satellite orbits, element perturbation 79—21165
near-Earth satellite, perturbations due to sunlight diffusely reflected from Earth 78—24444
near-Earth satellite laser ranging for geocentric gravitational constant determ. 79—34724
Nimbus 1 rocket (1964-52B), 15th-order resonance effects 78—65168
Nimbus 5, cloud altitude measurements 79—88444
Nimbus 5, evapotranspiration sensing using IR radiometer, evaluation *(French)* 77—17156
Nimbus 5, microwave meas. of oceanic precip. seasonal freqs. 77—60455
Nimbus 5 weather satellite, IR radiation meas. rel. to temp. field spatial. anal. 78—20488
NIMBUS 6, extraterrestrial solar irradiance meas. 77—25766

artificial satellites continued
- Nimbus 6, SCAMS liq. water data over NE.Pacific Ocean, rel. to United States west coast rainfall 80—82005
- Nimbus 6 clear radiance soundings rel. to TIROS/N processing system 79—58228
- Nimbus G, LIMS expt., stratospheric HNO_3 channel spectral meas. 77—87054
- Nimbus instrumentation description, for remote sensing of stratosphere 80—26713
- Nimbus IV, IRIS and BUV total O_3 meas. comparison with ground based meas. 78—81291
- Nimbus-5, atmospheric temp. fields deviation from radiosonde data over winter Antarctic 78—32138
- NIMBUS-6, microwave remote sensing over W.Australia 80—98485
- Nimbus-6 Earth radiation budget expt. 77—41106
- NIMBUS-7, global atmosphere pollution monitor 79—21149
- Nimbus-7 satellite remote sensing equipment 79—25437
- Nimbus-G, multichannel scanning microwave radiometer 77—29625
- NOAA 4 obs. of 1975 eruption of Tolbachik volcano 77—33032
- NOAA 5, atmospheric picture anal. 79—8713
- nodal period, direct solar radiation pressure effects 77—70987
- non-stationary gravitational problem *(Russian)* 78—32328
- NTS-2, solar cells radiation damage obs., GaAs and Si 79—48134
- NTS-2 satellite Cs frequency standard stability estimates 79—54110
- nuclear explosions EMP, system generated by photoelectron emission current, anal. 78—21772
- oblate planet orbiter, optimal low-thrust takeoff from orbit 77—60580
- observations, reduction method using selected reference stars *(Polish)* 78—36441
- ocean-related imagery, appls. programme 79—5681
- oceanography remote satellite, USA proposal for 1986 launch 80—105088
- Ogo 4, VLF signals reception, numerical study using waveguide concepts 80—90282
- onboard feature classification by CCD analogue signal processing 77—70980
- operational environmental satellite system, next phase planning, USA 79—5728
- optimal trajectory-meas. program and meas. error effects 77—53409
- optimum launching trajectory of an Earth satellite *(Chinese)* 79—40056
- optimum low-thrust multiple rendezvous between inclined orbits 78—4086
- orbit, influence of tidal forces rel. to Love number determ. 77—91410
- orbit, time regularisation of Adams-Moulton-Cowell algorithm, geodesy appls. 78—45208
- orbit analysis, rel. to upper atmosphere zonal winds 77—13143
- orbit analysis for upper atm. zonal wind determ. 77—56785
- orbit and attitude manoeuvres for spin stabilised satellites, semianal. soln. 77—17338
- orbit computation, appl. of Urabe's method to Moon and artificial satellite cases 80—17477
- orbit contraction due to atmospheric drag, analytic theory 80—17474
- orbit data, M_2 ocean tide parameters and Moon's meas. longit. decel. determ. 80—31048
- orbit design for geomagnetic tail mission 79—92647
- orbit determ. by astromeas. optimisation 78—16279
- orbit determ. by combined photographic and laser obs. *(Russian)* 77—73971
- orbit determ. from two posns. and radial vel. 80—8521
- orbit determ. method from observational results 79—84654
- orbit determ. of geostationary satellites using VLBI 80—4238
- orbit determ. using probe satellite relative motion 77—33316
- orbit determ. using range meas. *(Italian)* 78—24439
- orbit determination, Green's functions appl. 80—61992
- orbit determination accuracies, satellite to satellite tracking 79—25451
- orbit injection autonomous system 78—65485
- orbit perturbations, M_2 ocean tide parameters determ. 77—33093
- orbit perturbations, semi-analytical method 80—8522
- orbit perturbations due to Earth, ocean and atmospheric tides 77—87243
- orbit sections determ. where instruments are under critical illumination 78—49288
- orbit stability in restricted three-body problem 79—21162
- orbital antenna farm, concept 80—8514
- orbital data processing algorithm *(Russian)* 80—46401
- orbital element improvement using photographic or laser obs. *(Russian)* 80—46364
- orbital elements and station coords. determ. by least-squares collocation *(Russian)* 78—49296
- orbital lifetimes, prediction methods 78—73605
- orbital motion, flexible appendage effects 78—77456
- orbital motion in resonance with second-degree sectorial harmonic, comments 79—66910
- orbital perturbations by direct solar radiation press., general expansion of perturbing function 77—78605
- orbital perturbations due to Earth radiation, new albedo model 79—21020
- orbital plane rotation, gradient method for optimal control 78—69638
- orbital power satellites, features *(Portuguese)* 79—70452
- orbital speed, in Kepler ellipse, theory 77—70984
- Orbital Test Satellite, system design rel. to communications 77—64603
- Orbital Test Satellite solar array design and testing 79—96470
- orbital theory, appls. of Pfaff's equations of motion 79—12386
- orbital vars. *(French)* 79—58240
- orbiter around large satellite of giant planet, perturbations due to primary planet oblateness 77—17343
- orbiting mirrors, solar illumination after dark appl. 78—33816
- orbits, resonance effects of geopotential, simple layer model 79—16364
- orbits, second species periodic solns. with one near-Moon passage 78—45207
- orbits, short periodic drag perturbations 80—67522
- orbits, third and fourth-order perturbations rel. to flattening of planet 80—67529
- orbits, tidal perturbations rel. to Love number and phase lag 77—64187
- orbits and general relativity, motion in Schwarzchild metric 77—64622
- orbits with resonance lunisolar perturbations, dependent on inclination 80—90326
- orientation, optimal parameters of passive systems 77—41279
- orientation determ. of unstabilized slightly perturbed satellite 78—69642
- orientation determ. of unstabilized weakly perturbed satellite 79—8809
- orientation stability of double spin satellite 77—53398

artificial satellites continued
- oscillating orbit utilisation, determ. by apparent motion *(Russian)* 80—26717
- OSO-8, high-energy celestial X-ray instrument 78—28522
- OSO-8, LPSP expt. instrumentation, laboratory calibration and pre-launch performance 77—64649
- OSO-8, LPSP instrument in-flight performance and preliminary results 78—49317
- OTS payload performance, in-orbit RF meas. 80—82167
- P78-1 satellite, high resolution γ-ray spect. 80—58019
- Pageos 1, orbital effects of direct solar and Earth albedo radiation pressure 79—88566
- PALAPA, Indonesian domestic telecommunications satellite 77—64601
- particle pitch angle measurement from satellites using telescopes with multiple view directions 78—24425
- passive ground-based electro-optical detection of artificial Earth satellites 79—62717
- periapsis passage for bitangential turn of path by given angle, anal. 79—44340
- periodic and quasi-periodic orbits, theory 77—13214
- periodic motions of axisymmetric satellite in elliptical orbit 78—96378
- periodic oscillations in plane of elliptical orbit 79—8810
- periodic satellite coverage pattern generation computer graphic system 77—37496
- perturbations of close-Earth orbit due to lunar inequalities 78—53786
- Phase 3A satellite, Ariane three-stage launcher, AMSAT Oscar 9 designation following ejection 80—98534
- photogrammetry, dynamical constraints 78—15943
- photographic tracking, astronomical method *(Chinese)* 80—77254
- planar oscillations of satellite equipped with two gyroscopes 79—62714
- planetary orbiters, tracking for planets gravit. spectra determ. 80—41744
- planetary zero angle approx. of orientation *(Russian)* 79—12381
- plasma sheaths of satellite and spherical probe, static and dynamic behaviour, simulation 77—25907
- Polar Orbiting Lunar Observatory (POLO), appl. to lunar volatile emissions detect. 79—44385
- polar satellite motion and short-wavelength gravity vars. 80—98216
- power satellite solar array blanket interface problems 79—96466
- power satellite solar cell array conception and efficiency analysis 79—96464
- power station satellite, ionospheric heating by radio waves 78—77403
- power systems evolution, solar photovoltaic and solar thermal concepts 79—52891
- power transmitting, induced ionospheric thermal instability 77—25826
- Powersats, economic assessment 77—91404
- preliminary orbit determination, method having no co-planar singularity 77—60578
- Prognoz satellites, meas. of absorbed radiation from 1972 Aug. 4 solar flare 77—29614
- Prognoz satellites, solar wind studies 77—64596
- Proton 4, orbit determ., 31st order geopot. coeff. and atm. rot. rate calc. 77—64632
- radar systems development, appl. 78—81525
- radial and cross track errors analysis 77—45297
- radiation dose meas. by Molniya satellites, 1965-71 period 78—96350
- radionavigation onboard orbit determ., algorithm 79—25450
- range measurements, formula for refr. effects computation 78—73609
- real-time multispectral feature classification by analogue CCD 78—24438
- recording satellites and instrumentation, 1976-8 launchings *(German)* 80—36471
- relativistic Doppler shift in satellite tracking 80—46951
- remote sensing, geophysical applications, data acquisition *(Swedish)* 77—67001
- remote sensing and ranging systems from space, conf., Rome, Italy (March 1980) 80—105432
- remote sensing appls. for 1980s 78—69494
- remote sensing of global phenomena by automatic satellites 77—64457
- remote sensing of natural resources *(Japanese)* 78—16211
- remote sensing satellites, error in atmospheric temp. profiles due to aerosol particles effects 80—98449
- remote sensing satellites, introductory review 77—2286
- remote sensing technology, Canadian advances 78—16170
- rendezvous trajectories determ., autonomous system 77—53392
- reorientation of satellite-gyrostat, optimal attitude control 80—61980
- resonance due to solar radiation pressure 79—25456
- resonant inclination variations of ten satellites, 30th order gravity harmonics determ. 79—84071
- retroreflector arrays, method of calculating transfer functions 80--5778
- rocket and satellite space obs. (1966-76) *(Japanese)* 78—28481
- S3-1, atm. winds and aerodynamic lift effects on orbit inclination 77—53262
- S-band reception for meteorological satellite, monopulse aerials *(German)* 79—92628
- Salyut 4 cosmic X-radiation obs. 77—91665
- Salyut-4, equipment for measuring X-ray emission from extraterrestrial sources 78—28521
- Salyut-5, piloted satellite, visual obs. of environment from space *(Russian)* 78—40796
- Salyut-6, photographic investigation of ionospheric D- and F-regions *(French)* 79—40059
- SAS-3, general description 77—2324
- SAS-3, power and thermal subsystems 77—2325
- SAS-3 delayed command system 77—2327
- SAS-3 X-ray astronomical satellite, attitude control system using gyro 77--2326
- SAS-3 X-ray astronomical satellite, programmable format telemetry system 77—2328
- SAS-3 X-ray observatory 77—2329
- satellite, geodesy, appl. to GRIM 2 gravit. pot. model determ. and evaluation *(French)* 79—8587
- Satellite Power Station microwave health and ecology programme 79—70443
- satellite solar cell power plant, operating experience 80—94055
- satellite VHF/UHF communications, effect of ionospheric scintillation 77—41264
- satellite-to-satellite statistical orbit determ. error analysis 78—65486
- scientific instrument development problems and solns. 77—82111
- search systems, night sky model 77—73923
- Seasat, altimeter sensor file algorithms 80—94680
- Seasat, Gulf of Alaska expt., comparison data set winds 80—94570

artificial satellites continued
Seasat, microwave instrums., history 80—94678
SEASAT, ocean wave and wind obs., appls. to offshore oil, gas and mining industries 79—80044
Seasat, performance evaluation 80—94677
Seasat, radar altimeter, initial performance assessment 80—94679
SEASAT, radar altimeter resolution capability estimates 80—72645
Seasat, scanning multichannel microwave radiometer, antenna pattern corrections 80—94683
Seasat, scanning multichannel microwave radiometer, calibration algorithm development 80—94682
Seasat, scanning multichannel microwave radiometer, description and performance 80—94681
Seasat, scatterometer evaluation 80—94684
Seasat, scatterometer scattering coeff. algorithm 80—94685
Seasat, synthetic aperture radar system 80—94686
SEASAT, synthetic aperture radar system and appls. 80—12572
Seasat, visible and IR radiometer 80—94687
SEASAT A and spaceborne oceanography 79—66907
SEASAT program, Canadian participation 78—20535
SEASAT synthetic aperture microwave-imaging radar expt., overview 80—46267
Seasat-1, first ocean observation satellite, appl. to marine research from outer space *(German)* 79—74979
Seasat-A, data processing and distrib. 78—45005
Seasat-A, experimental oceanographic satellite 78—77455
SEASAT-A, for oceanographic research 79—84496
Seasat-A, ocean waves detect. and direction meas. via microwave radars 79—5685
SEASAT-A, orbit analysis 79—80199
SEASAT-A, remote sensing, synthetic aperture radar appl., technology trends 79—5655
SEASAT-A, satellite scatterometer data regional integration, validation and appl. 79—5680
SeaSat-A, scatterometer for ocean surface wind speed meas. 77—29626
SeaSat-A multichannel scanning microwave radiometer 77—29625
SEASAT-A satellite intersystem interference minimisation 78—49294
SEASAT-A satellite microwave scatterometer for wind sensing 77—5417
SEASAT-A satellite ocean surface truth expts. 77—5419
SEASAT-A satellite project 77—5414
SEASAT-A satellite radar altimeter spaceborne microcomputer 79—75073
SEASAT-A satellite scanning multichannel microwave radiometer 77—5416
SEASAT-A satellite synthetic aperture radar 77—5418
second order perturbation computation *(Chinese)* 79—80207
second order perturbation soln. *(Chinese)* 80—77270
shallow resonant orbits, appl. for gravit. harmonics determ. 78—40805
Shuttle Orbiter re-entry, remote IR imagery and tracking 80—82171
simulation of the infrared astronomical satellite (IRAS) telescope system 79—29976
SIRIO, evaluation of performance of subsystems *(Italian)* 80—4236
SIRIO satellite dynamics and control in geostationary orbit *(Italian)* 77—82108
Sirio-2 programme for meteorological data distribution and laser synchronisation from synchronous orbit 80—31193
sky survey project EXUV 10-1000 Å waveband, proposed mission 80—82165
Skylab, spacecraft-produced neutron fluxes meas. 78—28486
Skylab 1 (1973-27A), orbital vars. rel. to upper atmosphere density derivation 80—21867
Skylab 1 rocket, 1973-27B, orbit determ. and anal., geopotential resonance 80—67515
Skylab conical multispectral scanner IR data statistics 80—90223
Skynet, system-generated EM pulse response, spontaneous discharges, electron charging effect 79—25432
Skynet, system-generated EM pulse testing with exploding-wire photon 79—25433
SMS, geostationary satellite, soil thermal inertia and humidity cartography over Africa 80—76980
SMS images during GATE, wind field determ. accuracy 77—53147
Sneg-3, for solar radiation obs. *(Russian)* 78—16268
Sneg-3, gamma-ray telescope, Franco-Soviet cooperation in gamma-ray astronomy *(Russian)* 78—40844
solar battery panel mounting, optimal ang. determ. 79—39291
solar battery power increase using solar radiation reflected from Earth 77—33318
solar cell calibration using high-altitude balloon *(Japanese)* 78—61700
solar cell panel monitoring by ground station telemetry 79—62003
solar cells, for satellite solar power systems, developments and future trends 80—45694
Solar Maximum Mission Satellite, for Solar Maximum Year project 80—90404
Solar Maximum Mission satellite, hard X-ray imaging spectrometer control 79—80194
Solar Mesosphere Explorer mission description (1981-2), O_3 and related chemistry 80—105096
Solar Mesosphere Explorer optical-mechanical systems engineering 79—58230
solar occultation sounding of middle atm. 80—105079
solar power, design nomogram 79—70433
solar power, electronic systems 79—92065
solar power, Europe base-load electricity supply appl. 79—39288
solar power, thermal analysis 79—48094
solar power conversion, photovoltaic, 10 GWe plant construction and installation 79—52895
solar power conversion for Earth-based utility appl., 5 GW, using GaAlAs cells 79—52892
solar power satellite, construction in space, fabrication methods, materials, tools 80—21377
solar power satellite, technical considerations 79—34425
solar power satellite, theoretical anal. of nonlinear interaction between strong microwaves and ionosphere *(Japanese)* 80—94634
solar power satellite design and system engineering issues 79—96465
solar power satellites, alternate favourable option 80—16791
solar power satellites, economic, political, and environmental problems 80—45633
solar power satellites, effect of transmissions on radio-astronomical research 80—61291
Solar Power Satellites, energy anal. 80—50937
artificial satellites continued
solar power satellites, interference with space communications systems 80—45634
solar power satellites, output power variations, evaluation 79—29455
solar power satellites, solar energy conversion methods developments, general aspects *(French)* 79—100494
solar power satellites microwave power transmission system rectennas, Yagi-Uda receiving elements design, characteristics and economics 80—66938
solar power satellites technical considerations 80—72014
solar power satellites using microwave link, developments 79—24891
solar power station, multi-gigawatt, in space, progress review in field since 1979 *(German)* 80—81424
solar power station, review 79—8984
solar power stations, preliminary cost benefit anal. 77—87231
solar power stations and solar energy monitors 80—50982
solar power stations in Earth orbit, survey 80—21376
solar radiation perturbation of ecliptic plane orbit 78—4088
solar radiation pressure induced orbital perturbation analysis 78—89041
solar radiation resistance improvement 77—39015
solar-power station spherical solar collectors, enhanced power generation 80—12009
solid-state imaging for meteorology and astronomy 77—39074
Solrad 11 satellites, preliminary results from gamma-ray burst detection 77—57108
Soviet meteorological satellite development review 78—16266
Soyuz 22, Earth exploration from satellite, Raduga expt. *(German)* 77—56765
Soyuz 9, determ. of height of Earth optical horizon 77—53186
Soyuz spacecraft, modelling of boundary layer flow by reactive streams of controlling motors of Apollo spacecraft *(Russian)* 77—82098
space communications appl. of Nd:YAG laser 78—28483
space research growth, India's participation 77—13203
Space Shuttle, flight schedule and Spacelab 2 mission 78—85816
space shuttle, space telescope planned astronomical studies 79—21183
Space Shuttle Orbiter, elec. charging calcs. 77—25860
Space Shuttle Orbiter wideband PCM tape recorder 77—64614
space shuttle-tethered balloon subsatellite, current collection by long wire 77—25859
space shuttle-tethered balloon subsatellite for ionospheric plasma studies and power generation 77—25912
space solar electric power plants 79—39281
Space Solar Power Laboratory, atmospheric modification by 22.2 GHz water vapour line beam 78—49171
space station, scheme for automatic rendezvous with unmanned (or manned vehicle) 80—77249
space stations for large orbiting energy systems, NASA philosophy 77—78602
space stations for the international future, review 78—32322
space technology and scientific satellites, conf., Rome, Italy (Mar. 1977) 77—82107
Space Telescope, scientific instruments 80—61987
space-manufactured satellite power systems, costs anal. using lunar materials 80—97767
spacecraft heat rejection improvements using thermoelectric devices 80—108810
spacecraft-artificial satellite closest approach times calc. 79—62713
Spacelab, effects of probe-created plasma disturbances on low-energy ionospheric meas. 78—77458
Spacelab, high rate data handling in space and on ground, multiplexing system 79—21138
Spacelab and artificial satellites appls., conf., Rome, Italy (Mar. 1978) 78—96384
Spacelab as orbiting atmospheric laboratory 77—21941
Spacelab atmospheric trace contaminant meas. and identification 79—70387
Spacelab lidar for atmospheric topside sounding 77—21942
Spacelab passive atm. sounders, attitude control and stabilisation 78—65483
Spacelab project, zero gravity physics review 77—29619
spatial oscills. of gravit. oriented elastic satellite, nonlinear resonances 78—69644
spherical motion of satellite with varying mass geometry in Newtonian gravitational field *(Russian)* 78—16282
spheroidal satellite, orbital perturbations due to direct solar radiation press. 80—4219
spin-stabilised satellite, nutation damping *(Russian)* 77—64626
spin-stabilised satellites, effect of orbital eccentricity and nodal regression on gyroscopic motion 78—45206
spin-stabilised spacecraft, optimal aerodynamic attitude controlZ 80—77250
spinning notion, optimal nutation damping by flywheel 77—53396
spinning symmetric satellite, in planar periodic orbit, attitude stability 80—4220
SPOT, experimental Earth observation system, features *(French)* 77—82097
Sputnik 1, effects on advance of astronomy 78—36471
sputnik Meteor series, TV communication system *(Russian)* 77—64612
stabiliser system with 2-stage suspension, dynamics *(Russian)* 79—32222
stability, aerodynamic effects *(French)* 79—21159
stability limits for satellite motion 79—21163
stability of cylindrical precession of elliptic orbit *(Russian)* 77—42729
stability of plane periodic motion of satellite in circular orbit *(Russian)* 78—16281
stabilization system optimal parameters allowing for atm. resistance 79—62715
stabilizer system, rate-optimal parameters 78—69641
Starlette satellite, precision orbit computation 78—65478
stationary satellites of Earth, Moon and Mars, coordinates of gravit. fields stationary points 78—53805
step-stare spaceborne optical system smear compensation by focal plane manipulation 80—82172
stratospheric O_3 monitoring, satellite benefit assessment 77—78613
streaming instabilities in satellite plasma sheaths, elec. equilib., one-dimens. particle simulation 77—22036
subsatellites launched from Spacelab, for atm., magnetospheric and plasma physics research 77—21944
symmetric gyroscope motion, differential eqns. stabilisation procedure including perturbing torques 80—4244

artificial satellites continued
- Symphonie geostationary satellite, time transfer link for atomic clock synchronisation 80—47038
- synchronous Earth, DSCS II, attitude changes due to solar torque, analytical model 77—45285
- synchronous telecommunication and research satellites *(German)* 78—20610
- synthetic aperture radar imaging in geosynchronous orbit 78—65442
- table top pulsed solar simulator, design and construction, for testing solar cell arrays powering artificial satellites 80—45696
- TAIYO *(Japanese)* 79—25431
- Taiyo (1975-014A), attitude determ. system *(Japanese)* 77—17319
- telecommand transmission, Yagi antenna 77—45286
- telecommunication, solar cell arrays appl., rigid, fold-out array prototype development 79—48137
- temperature control using In_2O_3 or In_2O_3-SnO_2 thin films 79—80187
- test phase optimisation *(French)* 80—17464
- tethered satellite systems, orbital perturbation investigation 78—96381
- Thematic Mapper of Landsat-D, optical component design 80—77260
- third-order soln. of satellite motion 78—16285
- three-dimensional periodic orbits around Moon and planets 78—20627
- time transfer experiment using Nova satellite time signals 80—47036
- TIROS satellite program of meteorological research 80—109328
- Tiros-N, meteorological monitoring satellite 79—29973
- TIROS-N, meteorological satellite, early operational temp. soundings evaluation 80—77133
- TIROS-N, polar-orbiting meteorological satellite, operational vertical sounder 80—77132
- TIROS-N High Resolution Infrared Radiation Sounder 79—58227
- TIROS-N microwave sounder unit for global temp. distribution meas. 80—90265
- TIROS-N weather satellite, detection circuits and sync pulses for picture facsimile machine 79—53577
- tracking, data relay satellite system, NASA, exp. data transmission appl. 79—21131
- tracking station geocentric coordinate determination, short arc station coordinate method 77—44902
- trajectories, appl. to oceanic tide semidiurnal wave and Moon secular accel. calc. *(French)* 79—8634
- trajectory estimation, real time, of lowest flying Earth satellite by square root filter *(Japanese)* 80—4235
- Transit satellites, precise time recovery 80—47037
- TRANSIT satellites' contribution to navigation and geodesy 78—57161
- transition of Keplerian elements to apparent motion *(Russian)* 78—32330
- tropical observing system, role of geostationary satellites 79—92651
- tumbling cylindrical Earth satellite, rot. axis location using visual obs., theory 79—80200
- TV broadcasting satellite, appl. to accurate time dissemination 77—60334
- TV broadcasting satellite, use for precise real-time signal dissemination 80—47033
- two-position orbit-determination problems 79—88573
- UK-6 satellite, computer command system 79—25440
- undirected Earth satellite, estimate of attitude precision 77—64593
- US Navy navigation satellites, mean elements for 1974-6 period 79—48642
- USA space science missions and satellites 77—29630
- visibility calc., explicit method *(Japanese)* 77—82104
- VLBI using geostationary satellite link 79—29968
- Voyagers 1, 2, interplanetary probes, projected itineraries *(French)* 77—70976
- weather, Russian, amateur reception signals 77—56808
- weather forecasting appl., technology development (1960 to 1979) *(Dutch)* 80—12559
- weather forecasting impact of meteorological satellites 78—7861
- weather forecasting systems, local short-period forecasts 80—94558
- weather picture transmission, NOAA satellites 77—60458
- weather satellite, detection of 300 Hz pulses 78—36420
- weather-satellite picture facsimile machine, constructional details 77—21870
- worldwide maritime satellite system 77—64600
- X-ray astronomy satellites and missions 79—8793
- X-ray satellite availability for obs. of burst sources 79—40297
- Cs beam clock development for satellites 78—57910
- Cs beam frequency standard design for satellites 78—57911
- H maser, operating development model 79—54105
- Ni-Cd battery system design for tracking and data relay satellite system 80—30460

asbestos
- aerosol electron microscopy and analysis *(French)* 77—37461
- aerosol spectrometer using two-pulse Fraunhofer holography, fibrous particle motion anal. 80—58476
- airborne, X-ray diffr. anal., calibration standards 78—69517
- asbestos-reinforced friction materials, wear and thermal processes 80—40559
- chemical analysis, elemental intensity ratio variation used to identify fibres 80—3462
- chrysotile, adsorpt. of organic micropollutants, XPS and gas solid elution chromatography exam. 78—80790
- chrysotile, crushed, temp.-induced changes in struct. 77—24305
- chrysotile, cryst. struct. rel. to milling, X-ray diffr. 77—55278
- chrysotile, fibres, texture rel. to mech. props. 77—81300
- chrysotile, thermal expansion coefficients, reinforcement of phenol formaldehyde resin and effects 79—55908
- chrysotile asbestos, photoacoustic spectrum using CW HF laser 80—7980
- chrysotile determ. in rainwater 78—44895
- chrysotile fibres, aggregation to form pseudocrystals 77—76310
- composites with rubber, classification 80—7484
- crocidolite, adsorpt. of organic micropollutants, XPS and gas solid elution chromatography exam. 78—80790
- crocidolite fibre fine structure rel. to pulmonary tissue immunoresponse 79—74824
- dehydroxylation, PMR investigation 80—21269
- dusts in environment, health hazards 77—87068
- fibre, collection efficiency of nuclepore filters 78—57351
- fibre, identification techniques 77—60018
- fibre counting by automatic image analysis 80—73538
- fibre identification, selected area electron diffr. patterns in analytical TEM, optimum procedure using tilted specimens 78—24009

asbestos continued
- fibre reinforced cement, strength and fracture props. 80—108533
- fibre reinforced cement strength and fracture properties 79—100241
- fibre suspension, drag reduction in turbulent flow 79—68786
- fibres, optical diameter, appl. of four-parameter distrib. model 78—85213
- fibres, particulate analysis, aspects of specimen prep. and a limitations of precision by SEM and TEM 79—17574
- fibres concentration meas., in air and liquid, analytical methods review 80—72120
- fibres identification, electron microscope techniques comparison 78—66012
- fibrous amphiboles, hydrothermal crystn. from talcs in NaOH soln. 80—20810
- fluor-analogous, of natural asbestos, synthesis by unidirectional crystn. 80—2941
- health hazards 77—86732
- industrial atmosphere submicroscopic asbestos fibre evaluation 79—74585
- insulation, evaluation by polarised light microscopy 80—95134
- mining area river pollution meas. by proton-induced X-ray emission 79—100556
- moisture content in asbestos-cement pipes, nondestructive neutron-radiation testing 79—75539
- paragenesis, health hazards of fibres 77—81876
- particulate concs. in Thetford Mines area of Quebec 77—37394
- piezoelectricity, rel. to asbestosis and model of carcinogenesis 77—78075
- pollution, rel. to use of quarried serpentine rock 77—91261
- polyorganosiloxane-asbestos composites, high-temp. transitions 79—38802
- PVC, asbestos reinforced, CIR/Palram process preparation, mechanical and thermal properties measurements 79—66106
- silicate mineral, identification and asbestiform varieties, election optical and X-ray techniques 80—8446
- surface coating constituent mat., adsorpt. of Cs^+ 78—23843
- suspension of asbestos fibres, heat transfer and friction coeffs. for tubular flow 78—22405
- Tremolite, fibrous, high temp. phases, transformations, DTA 79—77742
- Fe loss from asbestos fibres in pulmonary tissue, obs. 79—74825
- Fe-P-Cu-SiO_2-$FeAl_3$-asbestos composite, thermal and elec. conds., temp. and composition depends. 77—66609

asdic *see sonar*

aspherical lenses
- *see also aberrations*
- air bearing and diamond machine design for optics 80—1365
- aplanatic optical system containing two aspheric surfaces, design 79—81500
- axisymmetric lens figuring, wear pattern prediction 77—27398
- bi-aspherical objective lens for Philips video long play system 79—46026
- Bragg diffraction imaging, aspect ratio restoration by holographic lenses 79—46122
- computationally directed axisymmetric aspheric figuring 79—23105
- conference, optical production technology advances, London, England (Jan. 1977) 78—50954
- continuous zoom forward-looking IR optical system design and implementation 79—23046
- for coronograph *(Japanese)* 78—89063
- cylindrical lens surface generation, grinding and polishing machinery design 80—79023
- cylindrical mirror and lens optical figure characterisation with conventional interferometer 80—78944
- design and manufacturing techniques advancement 80—5813
- design and testing for laser systems, assets and liabilities 78—46753
- design principles 78—50888
- diamond turning at large optical manufacturer, aspheric surface generation 79—23101
- diamond turning of optics, past, present and future 79—23100
- EKTRAMAX camera lens design and performance 80—77894
- finishing, low scatter, of aspheric optics, polishing of f/2 paraboloids 79—59855
- forward-looking IR system improvement by aspheric elements 79—23048
- forward-looking IR type optical system design programs 79—23047
- Fresnel lens design, construction and performance as solar concentrator 79—62121
- Fresnel lens film prep. by electron beam irradiated mould polymerisation 79—98515
- Fresnel lens optical design and utilisation, advantages and limitations 80—78936
- Fresnel zone plate support UV window as lens and monochromator 80—1326
- geodesic, perfect, general sol. for integrated optics 80—10049
- geodesic diffraction limited lens for integrated optic cct. 80—1357
- geodesic lens, axially symmetric, geometrical theory 80—33238
- geodesic lens, diffraction-limited, in polyurethane waveguide struct. 78—94453
- geodesic lens design for integrated optics signal processing 80—33247
- geodesic lenses for integrated optical circuits, signal spectral analysis appl. 79—27437
- grating acoustic scanner for underwater imaging and NDT 79—57198
- grinding concave and convex faces 77—65645
- high aperture lens, for laser plasma compression expt. 79—14076
- hyperboloid lens manufacturing technique 80—96039
- image defects of optical system, aspherical effect *(German)* 78—9332
- IR aspherical lens and surface evaluation 77—39019
- IR material and lens evaluation interferometer 77—39121
- IR optical components, diamond turning fabrication 78—5590
- laser focusing lens design for nucl. fusion 77—18706
- Luneberg lens for laser diode coupling to graded-index fibre *(German)* 78—33875
- manufacturing and testing techniques development, use of computer *(Italian)* 80—48467
- multiplexer/demultiplexer, low-loss, using interf. filters and rod lenses 80—58728
- night vision goggles, military low-cost, design and development 80—78990
- non-coaxial aspherical IR optical system, automatic design *(Chinese)* 80—5810
- one-dimensional Fourier hologram line data recording scheme *(Russian)* 79—22912
- optical characterisation for IR diamond-turned aspherical elements 80—1373
- optical fibre rod lens connector design and applications 80—53473

- **aspherical lenses** continued
  - optical system aspherical area shape predeterm. method *(German)* 80—28294
  - optimised spheric and aspheric optical systems for thermal IR 79—86244
  - optometer, refractive error correction optical system with continuously variable spherocylindrical power 79—62385
  - plastic lenses, aspherical-surface, for large screen TV, optical design and evaluation 80—78937
  - plastic optical component specification 80—48362
  - plastic optical components and systems 78—25967
  - plastic optics, components 79—32010
  - polishing of aspherical surfaces with ring polisher 79—41465
  - polishing technique with equal polishing rate distrib. 80—58818
  - precision manufacture with programmed microelectronic control 80—1368
  - primary characteristics of aspheric surfaces, analysis using Delano diagram *(German)* 78—90381
  - production costs, instrumental and photographic applications 80—28308
  - production of aspherical surfaces, review 77—7224
  - production of aspherical surfaces by mechanical means 78—50964
  - profile gauging using bootstrap data interpretation technique 79—59786
  - quality assurance of aspheric surfaces 78—50962
  - refracting objectives for 8 to 13 μm 80—86421
  - refractive null corrector design for testing aspheric surfaces 77—19377
  - replicated and plastic optics, conf., San Diego, USA (Aug. 1977) 78—66961
  - replication of refracting optics 78—50963
  - rod lens analysis and application to optical fibre communications 80—87549
  - rotational symmetric aspheric in compensated interferometers, computer-generated-holography testing 80—33128
  - rotationally symm. surface generation, computer control 77—27395
  - scanning gauge for surface form meas., spherical and aspherical 79—32100
  - Schmidt corrector plate replication, testing and performance calc. 78—66967
  - Schmidt corrector plate replication 78—66966
  - Selfoc conically graded medium, aberration anal. 80—1142
  - SHIVA laser optical component manufacture and testing 79—22980
  - side band Ronchi test, hologram appl. 78—33798
  - single-mode optical fibre coupling techniques using microscopic lenses 80—53462
  - solar thermal collector, line-focus Fresnel lens and secondary concentrator 79—62112
  - spheroidal geodesic lenses for integrated optical processing, design 77—27385
  - steep aspheric surface measurement, holographic comparison test 78—42402
  - stigmatic, for ruby or He-Ne laser, CAD *(Czech)* 78—55427
  - surface diamond turning machine development 80—1372
  - surface profile testing by goniometer 79—76895
  - surface testing, interferometer optical system modification 79—7236
  - testing, in-line and carrier freq. holograms, comparison 80—87349
  - testing in reflected light using blazed synthetic holograms 80—91881
  - testing of aspherical wavefront by shearing interferometer 77—31144
  - testing using interferometer with computer generated holograms 77—42632
  - variable-focus objectives, use of aspherical surfaces 80—33124
  - virtual image display using Fresnel lenses 80—1295
  - wave aberrations caused by misalignments of aspherics, and their elimination 80—33127
  - $LiNbO_3$, diamond-turned aspheric geodesic waveguide lenses 80—58804
  - $LiNbO_3$ geodesic lens fabrication by single-point diamond turning 80—33239
- **assemblers (program)** *see program assemblers*
- **assembling**
  - fusion reactor, ASDEX, assembly and commissioning, review 80—102334
  - fusion reactor, PDX, assembly, description 80—99308
  - fusion reactor, TFTR, assembly 80—102335
  - fusion reactor, TFTR, gas injection assembly 80—99342
  - injection laser mounting in single heat cycle 78—82982
  - IR scanning system modular design, assembly and alignment 80—78989
  - objective lenses, high performance, development trends *(German)* 78—71182
  - optical fibre ribbon-splicing injection-moulded connector with Si chip insert 78—1412
  - Vishnya rack adaptation to other instrument system chassis 80—31731
- **assembly lines** *see assembling*
- **assembly methods** *see assembling*
- **assembly programs** *see program assemblers*
- **association**
  - *see also association of liquids; associative ionisation*
  - $A+A_n \rightleftarrows A_{n+1}{}^*$, cluster dynamics, classical trajectory study 80—3316
  - acetaldehyde, carbonyl addition, model transition states, vibr. anal. 80—71898
  - acetic acid, protonated complexes, IR and Raman spectra *(French)* 78—78691
  - acetic acid dimer, gas phase, H-bonded complex struct. from elec. dipole moment obs. 78—74791
  - acetone vapour, mol. assoc., monomer-dimer equilib., thermal cond. meas., MO calcs. 79—52647
  - anthracene, ultrathin films on fused quartz and sapphire 80—59812
  - anthracene and dianthracene, phase equilib. in photocondensation *(Russian)* 79—7561
  - bis(9-anthryloxy)polyoxaalkanes,, intramolecular excimer form. and photodimerisation, kinetic anal., rate constants determ. 80—66800
  - atomic radiative binding in slow collisions into molecules in a laser field *(Russian)* 80—93753
  - 9-aza-bicyclo (3,3,1)nonan-3-one-9-oxyl, dimerisation, ESR, NO radical pair exchange 78—19330
  - benzene, bromination on zeolite adsorption complex, Raman spectroscopic anal. 80—16670
  - benzene+$Si^+(SiH^+)(SiH_3{}^+)(SiD_3{}^+)$, energy-rich collision complex form. 77—9068
  - 2-benzyl-5-benzylidenecyclopentanone, and substituted form, topochem. single-cryst.-to-single-cryst. photodimerisation 80—66819
  - biological functions of LF phonons *(Chinese)* 78—24024
  - biopolymers, assoc.-dissoc. phenomena, review 79—11884
  - biopolymers, electro-optical changes, chem. and rotational contribs. 80—85352
- **association** continued
  - bisphenol A-phthallic anhydride epoxy resin, diglycidyl ether, Rayleigh scatt., Brillouin and IR spectra 80—66211
  - t-butyl alcohol, mixtures, assoc., thermodynamic study using 2-constant model 80—66789
  - carboxylic acid dimer, Fermi reson. 79—31501
  - carboxylic acid systems, H(D) complexes and dimers, ν_{CO} IR band intensities 80—63715
  - carboxylic acids+urea, γ-irradiated reactions under high pressure *(Japanese)* 79—52707
  - cartilage proteoglycan, association with hyaluronic acid, elec. birefringence obs. 80—85332
  - chloroaluminium phthalocyanine, sublimed layer, IR absorption, vibr. assignments 78—55174
  - chloroform-d, intermol. assoc. with solvent mols., Raman spectra 80—63636
  - chlorophyll-a (b), dimerisation, fluoresc. and ODMR study 80—18876
  - choline salts, hydration, NMR spin-lattice relax. obs. 79—87830
  - cluster ions, formation and reactions, SIFT study, review 80—58435
  - clusters, small, formation, struct. and props. 80—58437
  - clusters in imperfect vapour, eqn. of state 77—31413
  - clusters in imperfect vapour, nucleation theory 77—35289
  - cobalt, phthalocyanine, sublimed film, absorption spectra and association 78—48174
  - collagen, polarisation, contribution of permanent and induced dipole moments, elec. birefringence 80—85351
  - colloidal photochromic dyes, quasi-crystals produced in applied electric field 80—85225
  - complex molecules, synthesis in interstellar clouds 79—92826
  - copper phthalocyanine, sublimed film, absorption spectra and association 78—48174
  - cosmic dust condensation onset, role of association reactions 80—26931
  - 4-cyano-4′-octylbiphenyl, dielec. props., 1 Hz-1 GHz, in smectic, nematic and liq. phases *(French)* 77—40168
  - decanoic acid, associated vapours, homogeneous nucleation 80—96638
  - dense interstellar clouds, radiative association reactions 80—82441
  - desorption kinetics with precursor intermediates 78—87876
  - diatomic molecules, form. and dissoc. in interstellar medium 80—23471
  - 1,5-dichloroanthracene, photodimerisation, orientational defects, lattice energy 78—80724
  - diffusion controlled reaction, passage time approach 80—71903
  - dimer triplet state line shape, small excitons, appl. to phenazine, naphthalene, tetrachlorobenzene 80—48041
  - dimers, dissociating, in nonisothermal ideal gas phase, stationary state anal. 78—76848
  - dimers of Group IIA, low-lying states binding energy, local spin density functional formalism calcs. 79—97994
  - dimethyl ether.HCl, gas-phase Raman spectra, profile of stretching vibr. 79—45728
  - dimethyl sulphoxide, form. of $(CH_3SOCH_3)_2H^+$ and $CH_3.CH_3SOCH_3{}^+$ in ICR mass spectrometry, proton affinity 78—3319
  - dimethylamine proton-bound dimers, form. in ion-mol. assoc. reactions, rates analysis 77—60054
  - dimethylketene, thermal dimerisation mechanism, CNDO/2-INDO calcs. *(German)* 79—54771
  - N,N-dimethylmethanesulphonamide+phenol (chlorophenol), assoc., PMR 78—23941
  - disperse systems, powdered Pt electrode 79—11830
  - double molecules, with weak reson. bond, quasilinear *(Russian)* 78—74640
  - ethanol vapour, isothermal Joule-Thomson coefficient, equation of state 80—24119
  - ettringite, expansion by H_2O adsorption, exam. 78—64806
  - ferrofluids, agglomeration, review 80—61162
  - ferrofluids, exptl. obs. of agglomeration in presence of mag. field *(French)* 78—92514
  - fluids with assoc. mols., van der Waals type eqn. of state 77—967
  - fluorescein dye, halogen substituted, in dimethyl sulphoxide, spectral evidence for anion-counterion association 80—71909
  - fluorescein dye(-Yb^{3+}), triplet state energy transfer, fluoresc. quenching obs. 79—54897
  - fluoroanthene in micelles soln., fluoresc., halide ion induced quenching and enhancement 80—95672
  - formate ion, hydration, ab initio LCMO calcs. 79—59342
  - formic acid, dimerisation energy, ab initio calcs., distortion energy effects 79—10022
  - formic acid dimer, gas phase, H-bonded complex struct. from elec. dipole moment obs. 78—74791
  - formic acid-water polymers, gas phase, H-bonded complex struct. from elec. dipole moment obs. 78—74791
  - gas mixture, self sustained volume photoionisation discharge existence conditions 80—79610
  - gas phase self-association theory 79—29347
  - graphite intercalation by HNO_3, chemistry 79—43564
  - graphite-$FeCl_3$ intercalation compound form., effect of added O, Cl, and water vapour *(German)* 79—52634
  - graphite-Na-N-H intercalation compounds *(French)* 79—52633
  - graphite-$TiCl_4$ intercalation compound 80—40675
  - graphite-$TlCl_3$ intercalation *(German)* 79—43562
  - graphitised viscose fibre, fluorination, change in struct. 80—88039
  - Hamaker functions, calc. from coagulation data, influence of Stern layers 78—48698
  - heavy particle shock-radiational recombination, chemiluminesc., kinetics, reversed predissoc. 77—1924
  - heptanoic acid, associated vapours, homogeneous nucleation 80—96638
  - histones, H2a and H4, aggregation ionic strength effect *(Russian)* 80—55697
  - hydracids, monatomic matrix-trapped, assoc. forms, struct. and spectral response, intermol. pot. calcs. 79—93996
  - hydrophobic interaction, solubility and solvent struct. changes 78—83705
  - II-VI semiconductors, thin epitaxial layer, direct synthesis *(German)* 80—104070
  - in Kr matrix, isolation and aggregation 78—45723
  - indoles, in glassy hydrocarbons, complexation vs. aggregation, absorption and fluoresc. obs. 79—98132
  - inert gas dimer formation, free-jet expansions, rate coeffs. 77—66745
  - inert gas dimers, Gordon-Kim intermol. force model 79—45781
  - inert gas Van der Waals dimers, electron impact ionis. 80—58400
  - inert gases, doubly charged ions, association reactions 79—91946
  - interstellar chemistry, long-chain hydrocarbons, formation mechanism 80—46653

association continued
- ion+molecule, radiative and ternary association 80-30227
- ion+molecule, slow reactions, carbonyl addition rate consts. rel. to struct. 80-30232
- ion+molecule, slow reactions, three body assoc., rate consts. rel. to struct. 80-30232
- ion+molecule, temp. depend., rate coeffs. calc. 80-16661
- ion+molecule association density of quantum states and temp. depend. of rate coeff. 80-101015
- ion $(H_2O)_n+H_2O \rightleftharpoons ion(H_2O)_{n+1}$, standard free energies of reaction 79-34348
- ion-molecule association rate calc. 80-81282
- ion-molecule association reacts., gas phase, statistical phase space theory approach 80-50839
- ionic crystals, evaluation of association parameters of quadrupoles 77-43365
- laser-controlled unimolecular and bimolecular processes, field-depend. rate const. 80-11906
- laser-induced chemical processes, optical selection of reagent orientation 80-11914
- lithium oligopentadienyl and complexes, IR spectra *(Russian)* 80-71424
- maleimide, monomer, valence force field in Ar matrix at 20K, self-assoc. *(French)* 79-81165
- malic acid+formamide, γ-irradiated reactions under high pressure *(Japanese)* 79-52707
- matrix isolation vibr. spectroscopy, complex form. studies 78-62952
- membrane surfaces, antibody association kinetics with spin-label haptens 80-66787
- mesic atom and molecule production, photoassociation, induced, in field of strong EM wave *(Russian)* 80-1091
- metallic dimers, formation enthalpy 79-74411
- methane, high density fluid, LF Raman spectra, dimer formation 77-46566
- methanol, gas thermal conductivity, H-bonds, tetramer form. 77-34776
- methanol, gaseous and dil. soln. in nonpolar solvent, lattice models, association, consts. 79-82141
- methanol dimer, intermol. function from ab initio calcs. 80-32629
- methanol vapour, isothermal Joule-Thomson coefficient, equation of state 80-24119
- methanol-$d_3(d_1)$ in freon 11, self-associated, OH frequency temp. depend. 80-37809
- methyl(-d_3) ions, association reactions, isotopic exchanges, SIFT study, review 80-58435
- methyl cation+$H_2(N_2)(O_2)(CO)(CO_2)$, ternary assoc. reaction, rate coeffs., 100-300K 79-61845
- methyl ion+$H_2O(He)$ ternary association reaction in energy range 0.04-0.1 eV 80-71896
- methylamine, proton-bound dimers, form. in ion-mol. assoc. reactions, rates analysis 77-60054
- molecular dynamic study of polymer form., trimers tetramers and pentamers 78-5313
- molecular self-assoc. and complex form. in soln., IR and Raman spectra, book contrib. 78-21931
- myoglobin+CO, recombination, kinetics meas. using minicomputer 78-7200
- myoglobins, Fe-, Co-substituted, O_2 binding, comparisons, thermodynamic investig. 80-67030
- myristic acid, associated vapours, homogeneous nucleation 80-96638
- N-allyloxymethyl-poly(ε-caprolactam), electron crosslinkable, electron and photosensitivity *(Japanese)* 79-91951
- N-substituted amides, liquid, acoustic spectroscopy method for H-bond studies 79-96303
- nitrosofluorene-lipid adducts, mutagenicity, ESR spectra investig. 80-91583
- NO, adsorbed on Ir(111), flash desorption spectra, identification of recombined mols. 79-86996
- nonisothermal ideal gas mixture, stationary state, inert and dissoc.-assoc. components 77-60042
- nylon 6, influence of monomer and water diluents on mech. relax. 79-4993
- peroxymethyl radical+peroxymethyl radical, reaction kinetics, H_2O vap. depend 79-61844
- pheophytin-a (b), dimerisation, fluoresc. and ODMR study 80-18876
- phthalocyanine, sublimed film, absorption spectra and association 78-48174
- plasma, ion+mol., interstellar species form. radiative assoc., reaction types 80-31348
- poly-γ-benzyl-L-glutamate, synthetic polypeptide, nonlinear dielectric effect in nonpolar medium 80-84682
- polyimide, influence of monomer and water diluents on mech. relax. 79-4993
- polymer gelation theory *(Chinese)* 79-74379
- polymethine-cyanine molecular aggregate, band struct. 80-53174
- polysiloxane dizwitterionomers, morphology, ionic aggregation 80-49130
- polystyrene photophysical behaviour, solvent effect obs. *(Spanish)* 79-57267
- preassociation, laser induced, in presence of natural predissociation 78-85174
- propionic acid, homogeneous nucleation in associated vapour 79-10933
- protein supramolecular structures, calorimetric and van't Hoff enthalpies of assembly comparison 77-90717
- pyrene-naphthalene complex radical cation, in γ-irrad. glass, visible spectrum obs. 78-44385
- radiative preassociation, in presence of natural predissociation 78-85174
- rare earth nickelates, form conditions and props. 80-21270
- rare earth niobates, pyrochlore structure, synthesis and props., 79-11533
- recombination, in steady supersonic flow, in devices for laser isotope separation 79-31717
- red blood cell aggregation detect. during blood flow by US 79-84068
- retinal Schiff-base, photochem. step of vision, H-bonds, intermol. associations 78-31812
- rhodamine $6G_2$ molecules in solution, photoluminescence study, fluorescence decay time 80-80832
- rhodamine 6G, aggregation, modulation Stark spectrosc. obs. 79-27030
- rhodamine 6G, associated, in polyvinyl alcohol film and soln., emission, room temp. 79-54896
- rhodamine 6G, delayed fluoresc. of simple associates in polar and nonpolar solvent mixtures *(Russian)* 78-48185
- salt solutions, in liquid alkali metals, phase equilib. and chemistry 78-73040

association continued
- semiconductors, multiply doped, donor-acceptor complexes and interactions, physicochem. nature 80-15472
- serum albumin, bovine, 2 types of soluble complexes with polyelectrolytes 79-92120
- shock-wave-initiated photorecombination kinetics and lower mode waveguide amplification *(Russian)* 79-96313
- sulphonyl compounds, H-bonding by methyl groups, Raman spectra obs. 79-24320
- supersaturated gas condensation kinetic model, cluster nucleation assoc. and dissoc. 78-85151
- suspensions, appl. of Gibbs-Thomson eqns. to particles of dissociative and associative substances 77-4944
- TCNE, K salt, in nematic liq. crystal solvent, ion pairing, EPR spectra 78-73020
- s-tetracyanobenzene+p-xylene, photoassoc., exciplex form., excitation energy and isotope depend., vibr. effects 80-55634
- tetraphenylsilane, crystn. from chem. transport reaction 80-104439
- tri(trifluoromethyl) germanium halides, gas, liq. and solid, IR and Raman spectra, normal coord. anal. 79-72316
- two-atom system, with weakly bound electron, s-term passing through continuum parabolic boundary 79-72392
- urea+acrylic acid (acrylamide), γ-irradiated reactions under high pressure *(Japanese)* 79-52707
- vanadyl phthalocyanine, sublimed layer, IR absorption, vibr. assignments 78-55174
- vapour with different degrees of polymerization, mass spectra, line overlap coeff. calc. 79-96392
- vinylidene+H_2, addition reaction, MINDO/3 study 80-108705
- water, vap., dimerization, from thermal cond. meas., 373K 78-44359
- water association, in superheated vap., equilib. consts., H bond vibr. 77-66750
- water vapour polymers, in atmosphere, rel. to absorpt. in IR window 77-45145
- xanthine, planar autoassoc. energy 80-53086
- zero range Fermi method, appl. to assoc. detachment processes 80-63798
- $2NO_2 \rightleftharpoons N_2O_4$, multiple stationary states, hysteresis 77-9074
- $3CaO.Al_2O_3$, hydration retardation by $CaSO_4$ 79-61856
- Ag aggregates, matrix isolation spectra 78-46476
- Ag, in Kr matrix, isolation and aggregation 78-45723
- $Ag_2S+Ln_2S_3$, powdered mixtures, reaction rate, production of ionic semiconductors 80-93741
- Al oxides and hydroxides, electro-erosional prep. *(Russian)* 80-81297
- Al powder with N, in low-temp. plasma 80-16257
- AlI_3, UV absorbance, dimer-monomer dissoc. equilib., vap. press. of solid 78-13511
- Ar and Ar-NH_3 mixtures, viscosity under press., density depend. and mol. assoc. 80-1727
- Ar^+, conversion to mol. ions, three body association coeffs. determ. using drift-tube mass spectrometer 80-108699
- $2Ar+Ar^+(Kr^+)$, three body reaction, rate coeffs., temp. depend., 100 to 300K 80-108703
- $Ar+Xe^+$, $XeAr^+$ form., dissoc. energy, reaction equilib. and rate consts. 80-61071
- Ar_2^+, mobility and clustering reaction in Ar 79-10628
- ArF^*, Ar_2F^*, kinetics of proton-excited Ar-F_2 mixtures, time-resolved and time-integrated spectra 79-36883
- BaO, association with $N_2O_4 \rightleftharpoons 2NO_2 \rightleftharpoons 2NO+O_2$ system, 350-650K *(Russian)* 79-20363
- $Ba_2UO_2(HPO_3)_2$, synthesis and comp. 80-35516
- $BeAl_2O_4$, chrysoberyl, kinetics and mechanism of formation, in presence of V_2O_5 79-11535
- Br_2 recombination in supersonic expansion in nozzle *(Russian)* 78-1757
- C fibre layered compounds with alkali metals, prep. 80-20809
- C^+, association reactions, isotopic exchange, SIFT study, review 80-58435
- C^++H radiative association, implications of CH^+ predissociated levels obs. 80-37838
- $C_{12}Cl$ and $C_{16}Cl$ intercalation compounds, form. and struct. *(French)* 80-40674
- CF_2 dimerisation reaction, UHF and MINDO/2′ calcs. 77-12793
- CH_2, dimerisation reaction, UHF and MINDO/2′ calcs. 77-12793
- CH_2^+, radiative association, rate const. rel. to interstellar clouds 77-45512
- CHF dimerisation reaction, UHF and MINDO/2′ calcs. 77-12793
- $CO+O+M \rightarrow CO_2+M$, time-resolved and flame-band emissions in shock tube expts. 77-36729
- CO_2, liq. and gas, state of aggregation effect on 1-4 μm absorpt. bands intensities 79-27042
- CS_2^+, and $(CS_2)_2^+$, photoionis. in supersonic mol. beam 79-98165
- $CaCeAl_3O_7$, melilite struct., prep. and props. 80-93524
- $CdFe_2O_4$, ferrite, synthesis 77-16523
- Cl_2 partially dissociated, recomb. reaction freezing in supersonic nozzle, chemiluminescence *(Russian)* 77-52644
- Co^{2+} complex, ammoniated zeolite, oxygenated product form., electronic spectrosc. obs. 80-991
- Cs-H_2 vapour, resonant character of laser induced formation of particles 80-89481
- Cs^++Cs, mol. ion form. rate, from mobility meas. 79-34299
- Cs_2, laser-excited fluoresc. in Cs-Xe mixture, pumping, level scheme 78-86909
- Cu-Ni sulphidised alloys, Ru and Os behaviour during carbonylation *(Russian)* 80-40584
- Cu_2, in supersonic free jet expansion, laser induced excitation spectrum obs. 80-14151
- $Cu_2S+Ln_2S_3$, powdered mixtures, reaction rate, production of ionic semiconductors 80-93741
- DCN, self-assoc. in matrices, IR vibr. spectra of multimers 78-86858
- D_2O, vapour, mol. association entropy and enthalpy, thermal cond. meas. 80-7777
- $EuCl_3$-$NaPO_3$-H_2O system, Eu polyphosphates form. at 0°C 80-35515
- F atoms, recombination const. meas. 77-36749
- $FeCl_3$, solns. and hydrated melts, complexes form., X-ray diffr. obs. 80-24342
- GaAs {100} surface, interaction kinetics of As_2 and Ga 77-60115
- $GdCl_3(s)+1.5L_2Cl_6(g)=GdL_3Cl_{12}(g)$, (L=Al,Fe), entrainment, quenching, and chem. transport, rel. to appl. for GdIG CVD 80-24750
- Ge-GeO_2 mixtures, gasification kinetics and GeO form. mechanism *(Russian)* 80-21273

association continued
- H bonding molecules, self assoc., intermolecular interactions, matrix isolation vibr. spectra obs. Raman and IR spectra 80−52995
- $H+Cl^- \to HCl+e$, associative reaction, product vibr. state distrib. 80−66794
- H+H, interstellar, H_2 form. on grain surfaces 79−21367
- $H+H^+$, vibr. excited H_2^+ form. by stimulated radiative association 79−100346
- $H+N^{3+}$, charge exchange, assoc. reaction, rel. to interstellar gas 80−7763
- $H+OH \to H_2+h\nu$, radiative association reaction for mol. synthesis in interstellar clouds 80−90509
- $(H_2)_2$, $(D_2)_2$, $(HD)_2$ and H_2-D_2, Van der Waals complexes, mol. symmetry 80−42963
- HBr, and DBr, in monatomic matrices, near IR spectra and aggregate structs. 79−89667
- HBr, far IR Ar matrix isolated spectra, 4.2K, press. and conc. effects 78−62801
- HCN, self-assoc. in matrices, IR vibr. spectra of multimers 78−86858
- HCl, and DCl, in monatomic matrices, near IR spectra and aggregate structs. 79−89667
- HCl, far IR Ar matrix isolated spectra, 4.2K, press. and conc. effects 78−62801
- HF oligomers, Gibbs free energies, gas. equilib., ab initio calc. 79−20456
- $(HNO_3)_2$, gas phase, H-bonded complex struct. from elec. dipole moment obs. 78−74791
- HO_2+HO_2, gas phase reaction mechanism, FT IR spectrosc. obs. 80−85163
- H_2O, vapour, mol. association entropy and enthalpy, thermal cond. meas. 80−7777
- $H_3O^+(H_2O)_n$, ion clustering, diffusion, flowing afterglow obs. 77−12799
- $H_2O.H_2O$ and $H_2O.Ne$, excited, first order interaction energy, ab initio calc. 80−32598
- $H_3O^+.nH_2O$ cluster ions, stability, assoc. and dissoc. 77−60055
- $H_3S^+.H_2O$ cluster ions, stability, assoc. and dissoc. 77−60055
- $H_3S^+.nH_2S$ cluster ions, stability, assoc. and dissoc. 77−60055
- He^+, conversion to mol. ions, three body association coeffs. determ. using drift-tube mass spectrometer 80−108699
- He^+, electron scatt., reson. state assoc., incomplete spectrum of Hamiltonian matrix 80−99568
- $2He+He^+(Ne^+)$, three body reaction, rate coeffs., temp. depend., 100 to 300K 80−108703
- ^4He, threshold condition for forming atomic trimer 80−63741
- Hf solvent extraction and complex formation with tridentate organophosphorus compounds 78−76853
- Hg+Hg*, combination into ungerade dimer states 80−55633
- Hg_2 excimers, photoassoc., spectroscopy and kinetic processes of high-lying vibronic states, laser applics. 80−9649
- Hg_2, photoassoc., $0_u^+ \to 0_g^+$ fluoresc., Condon internal diffraction 78−78747
- Hg_2, photoassociated, collision-induced predissoc. with Hg 79−31626
- $Hg(6^3P_0)$+t-butylamine, attachment mechanism, kinetics, dimer emission, luminesc. spectra 77−73442
- I_2-aromatic complexes, photodissociation, I-aromatic complex in soln. formation ps laser studies 80−40711
- ICl selective photoaddition to acetylene, isotope enrichment, influence of press., buffer and wavelength 80−11927
- $InX(X_2)(X_3)$, $InAlX_4$, X=Cl,Br, Raman spectra, up to 1200K 80−48003
- $K_2(A^1\Sigma_u^+)$, form. by K(4P) ats. in K discharge 80−44013
- KCl-CsCl solid soln., SIMS, clustering distance critical to metal dimer form. 79−72379
- KF, KCl and KI, monomers and dimers, Ar matrix-isolated, IR spectra, vibr. assignments and calcs. 79−45718
- K_2O-Ga_2O_3-P_2O_5-H_2O, reactions, 150-500°C 80−35514
- $K_2UO_2(HPO_3)_2$, synthesis and comp. 80−35516
- KrF*, Kr_2F*, kinetics of proton-excited KrF_2 mixtures, time-resolved and time-integrated spectra 79−36883
- LaB_6-Cu, form. by wetting of LaB_6 with Cu 80−100813
- LaN, form. conditions 80−101019
- $LaNiO_3$, form. conditions and props. 80−21270
- Li^+, mobility and clustering in Ar gas 77−84389
- Li-graphite intercalation compounds, prep. from Na-Li melts *(French)* 80−2970
- Li_n, at. cluster with H_2O mol. attached, MO study 79−76541
- LiF, aggregation, microcryst. form., IR spectra obs. 78−46331
- $MgCO_3^0$, in solution, ion-pair relaxation rel. to acoustic absorpt. 79−74914
- MoF_5, prep., melting temp., vapour density, press., enthalpy of fusion, meas., assoc. 78−38813
- MoF_5, vapour, thermodynamic props. calc. 78−38826
- N, assoc. on metal catalyst surface, chemical energy accommodation, flow reactor obs. 79−24816
- N_2+Fe (atomic), interaction mechanism via clusters 77−25263
- $N_2^+ + N_2$, three-body ion-neutral assoc. reactions, saturation 79−39134
- $N_2^+ + N_2 + He \to N_4^+ + He$, ternary assoc., selected ion flow tube obs. 79−39128
- NH_3, assoc. mols., struct. and dynamics, atom-atom pots., gas, solid and liq., props. 80−23487
- NH_3 proton-bound dimers, form. in ion-mol. assoc. reactions, rates analysis 77−60054
- NH_3+SO_3, donor-acceptor adduct form., ab initio calcs. 78−82612
- $(NH_3)_3$, open-chain and cyclic structs. 80−45480
- $(NH_4)_2UO_2(HPO_3)_2$, synthesis and comp. 80−35516
- NO, on Pt, Ni, Ru, associative desorption from adlayers of interacting O and N particles 80−54512
- $(NO)_2$, heat of form., UV spectrum temp. depend. 78−64872
- NO_2-N_2O_4 gaseous system, self-association theory 79−29347
- Na vapour, assoc. ionis. by CW dye laser and applics. *(Japanese)* 80−5515
- Na^--solvated electron, reversible capture by 1,1-diphenylethylene, equilib., kinetics 78−7177
- Na_2, mol. spectroscopy by photodeflection in supersonic nozzle beam 79−54995
- Na_2+He(Ne)(Ar), collision induced dissoc. rate, vibr. distrib. depend. 79−22791
- Na_x, matrix-isolated, formed in supersonic nozzle beam, 400-800 nm absorption and mass spectra obs. 79−76439
- NaK dimer formed in supersonic beam, laser-induced emission 80−9636
- Nd_2O_3-HfO_2 system, phase relationships 80−35169

association continued
- Ne^+, conversion to mol. ions, three body association coeffs. determ. using drift-tube mass spectrometer 80−108699
- O+O, atomic recomb. rel. to O_2 metastable emission bands 79−64015
- O+O, radiative assoc. in upper atmosphere rel. to nightglow near IR continuum 77−78551
- O_2, reson. cross-sections, predissoc. and preassoc., isotope effects 78−58750
- O_2-N_2, O_4 and O_2N_2 form., influence on N_2-induced O_2 absorption in Herzberg continuum 78−87429
- $O_2+Ar(O_2)$, collision induced UV absorpt. in Herzberg continuum, dimer form. 77−30883
- $O_2^+ + O_2$, three-body ion-neutral assoc. reactions, saturation 79−39134
- $(O_2)_2$ formation, rot.-vibr. symmetry correlation, building-up principle from mol. fragments 78−76849
- OD, reson. cross-sections, predissoc. and preassoc., isotope effects 78−58750
- OH, reson. cross-sections, predissoc. and preassoc., isotope effects 78−58750
- PCl_5-$TiCl_4$, gas, melt, and solid, dimer-monomer conversion, Raman spectra obs. *(German)* 79−70320
- PN, matrix IR spectra, aggregation to P_3N_3 77−83599
- $Pb(Zr,Ti)O_3$, synthesis from cryochem. mixtures, chem. reacts. in sublimation drying 79−11538
- RbF, RbCl and RbI, monomers and dimers, Ar matrix-isolated, IR spectra, vibr. assignments and calcs. 79−45718
- SF_6-Ar, condensing flow, gasdynamic and IR meas. 80−6501
- Si_3N_4, finely dispersed, high-temp. synthesis 80−55331
- SiS, matrix IR spectra, aggregation to Si_2S_2 77−83599
- SmN, form. conditions 80−101019
- Sr^+, hydration, gas phase clustering mass spectra, thermodynamics, bonding 77−16814
- Sr_2 dimer, photoassoc., photoluminesc., collisional dissoc. 80−58303
- TaC and Ta_2C, self-propag. high-temp. synthesis 80−60815
- $TiCl_4$-graphite intercalation compound 80−40675
- $TiCl_4$.trimethylaluminium+ethylene, Zeigler-Natta reaction mechanism, restricted Hartree-Fock calcs. 77−73441
- TiS_3 synthesis 80−35141
- $TlBr_3$-graphite intercalation *(German)* 79−43563
- XeF_6, monomeric charact., electron ionisation mass spectra 77−75322
- Zn+P reaction mechanism and kinetics, effect of Ag and Mn impurities 77−21416
- ZnSb, orientated crystn. conditions during reaction diffusion *(Russian)* 80−70558
- Zr solvent extraction and complex formation with tridentate organophosphorus compounds 78−76853
- ZrB_2-Nb, reactions between components 80−100812
- ZrS_3 synthesis 80−35142

association factor (liquids) *see association of liquids*

association of gases *see association*

association of liquids
- *see also colloids*
- acetic acid-carbon tetrachloride, US absorption, coupled dimerisation cyclisation reaction *(French)* 79−42148
- acetic acid-H_2O, assoc. liq., struct. props., static and dynamic phys. props. meas. 79−70316
- acetic acid-pyridine, H-bonding, proton transfer, isolated system, solvent effect, MO calc. 80−55629
- acetone-chloroform (-iodomethane) (-CS_2), liq. mixture, excess Gruneisen parameter, intermol. interaction 78−67635
- acetone-toluene-tetrachloromethane, mol. interaction and thermodynamic props. 80−71935
- acetonitrile binary liq. mixtures, excess thermodynamic functions, complex formation 79−52736
- acetonitrile-toluene-benzene, mol. interaction and thermodynamic props. 80−71935
- acetylenic compound, 1,5-hexadiyne, hydrogen bonding effects on Raman line $\nu(\equiv C\text{-}H)$ *(French)* 77−75167
- acoustic relaxation time in associated liqs., correl. with dielectric relaxation time 78−9925
- acridine, methanol soln., edge excitation red shift, excited state proton association 79−18228
- acridine orange in ethanol, soln., excited single state lifetimes, aggregates, visible luminesc. spectra, conc. depend. 80−55172
- albumin, human serum, assoc. solns., excited state deactivation, flash photolysis obs. 79−54895
- alcohol, dielec. const., hindered mol. rot. influence 78−43767
- alcohol binary mixtures, nonlinear dielec. effects, shift in assoc. equilib. 77−73108
- alcohol-active soln., assoc. soln. thermodynamics, H^E, V^E curves 78−31671
- alcohol-inert compounds mixtures, thermodynamic props. *(German)* 79−52748
- alcohol-inert soln., assoc. soln. thermodynamics, enthalpy, Gibbs free energy 78−31670
- alcohol-solvent, associated, excess free energy and enthalpy of mixing 78−31680
- alcohol-unassociated active component liquid mixtures, associated soln. theory, thermodynamic parameters 80−7836
- alcohols, assoc. liq., viscous props. 80−2186
- alcohols, self-association in binary mixtures, 2-const. model, vap. press. meas. *(German)* 78−18532
- alcohols in organic solvents, H_2O absorption 80−66788
- aliphatic alcohols in carbon tetrachloride, association processes, NMR spectroscopy 77−16792
- alkali iodides in acetone, press. effects on Walden products, ion-solvent interactions 80−3398
- alkaline earth halides, solns. in methanol, conductance data anal., assoc. consts. 78−71875
- alloy melts, association, effect on thermodynamic behaviour *(German)* 78−20050
- amide group in soln., interactions, IR. Raman spectral investigs., peptide, protein struct., review 78−90330
- amines, self-association in binary mixtures, 2-const. model, vap. press. meas. *(German)* 78−18532
- anisole, in cyclohexane-ethanol mixtures, UV spectra, solvent effect 79−22770
- anthracene anion radicals, enthalpy of disproportionation, calorimetric determ. technique 79−96296

association of liquids continued
benzene, in Br_2-carbon tetrachloride soln., complex form., IR spectra 78−70828
benzene-2,5-dibromothiophene, self-association, proton mag. relax. 77−28471
benzene-ethylene dichloride (-CCl_4), liq. mixture, excess Gruneisen parameter, intermol. interaction 78−67635
benzene-p-dioxan, mixtures, mol. reorientation and assoc., depolarised Raman scatt. obs. 80−7341
binary alloy melts, assoc., liquidus curve calcs. *(German)* 79−20352
binary liq. mixture, chain assoc., excess Gibbs free energy 77−16860
binary mixture, inert solvent and self-associating component, Wilson consts. 79−82351
binary system forming simple association complexes, liq. diffusivities prediction 80−34216
t-butanol and -d_1, deuteration effect on self-assoc., dielectric polaris meas. 79−28672
t-butanol-acetone-cyclohexane, complexation, thermodynamic parameters *(Russian)* 78−76905
t-butyl alcohol, self-assoc., linear and nonlinear dielec. effects obs. 80−60484
3-butyn-1-ol, vibr. spectra, assignments, rot. isomerism 80−58257
carbon tetrachloride-benzene, liq. mixture, excess Gruneisen parameter, intermol. interaction 78−67635
cellulose trinitrate, in soln., gel-like aggregate form. rel. to configuration 77−31036
chloroform-acetone, liq. mixture, excess Gruneisen parameter, intermol. interaction 78−67635
chloroform-ethanol solns., light scatt. spectra, conc. fluctuations, assoc. complex form. 77−40254
chloroform-hexamethylphosphoramide complex, mol. motion and assoc., PMR obs. *(French)* 78−72429
chloroform-methanol mixtures, thermodynamic props. 79−87865
chloroform-p-dioxan and chloroform-benzene mixtures, mol. reorientation and assoc., depolarised Raman scatt. obs. 80−7341
chlorophyll a and b, assoc. solns., excited state deactivation, flash photolysis obs. 79−54895
chlorophyll a-water interaction, NMR obs. in CCl_4 and trichloromethane 79−34501
cholesterol, in carbon tetrachloride, self-assoc., IR absorbance 79−47920
cholinesterase-acetylcholine soln., anion-cation site interactions, solvent effects on aggregate stability 80−61070
cyanine dye sensitisers, J-aggregates, meso substituents effect on mol. assoc. 77−70320
cyclodextrins, diffusion in aq. polymer solns., complex form. 78−91460
dielec. props. calc. 77−81045
dielectric relaxation time in associated liqs., correl. with acoustic relaxation time 78−9925
dilute solution, associated, lattice model, chem. equilib. laws 79−82139
dioxan(-oxalic acid)(-benzoic acid), solns., compressibility, internal press., US vol., H-bonding 79−82272
dioxan-$H_2{}^{16}O(H_2{}^{18}O)(D_2{}^{16}O)$, solns., FP determ., equilib. method 77−20048
dioxan-methanol system, US vel., compressibility, complex form. 79−82283
disperse systems, coagulation, slow, turbulent 78−53259
electrolyte solutions, thermodynamics, transport props., semi-phenomenological approach including short range forces 80−3353
eosin, in glycerine-water mixture, excitation and emission peaks, concentration shifts 78−33540
eosine^{2-}, in dimethylsulphoxide, transition metal ionic associations, fluoresc. quenching 77−73163
ethanol, assoc. in dil. soln., dielec. obs., dipole moment meas. 78−83714
ethanol, solns., local struct. equilib., light scatt. and IR spectra obs. 78−84564
ethanol-carbon tetrachloride, binary soln. with mol. assoc., interdiffusion anal. 79−55912
ethyl p-methoxybenzilidene aminocinnamate, dimer, mesogenic, intermol. interactions 79−46564
ethylene dichloride-benzene, liq. mixture, excess Gruneisen parameter, intermol. interaction 78−67635
ethylenediamine-H_2O mixtures, inhibition of Ps form. by NO_3^- ions 78−95988
fluoradene, absorpt. and fluoresc. in solvents, excimer form., aggregation 77−79625
fluoroform(-d_1)-trimethylamine-Ar(Kr), cryospectroscopic IR study of association 77−468
formic acid, liq., microdynamic behaviour, struct., nucl. spin-lattice relax. 77−76270
glycerol, highly viscous state, static and dynamic Kerr effect obs. 80−60545
glycerol, reorientation in associated liqs. 79−77481
hole theory, appl. to US absorpt. in associated liqs. 78−10124
ion-selective electrodes, liq. membrane, free and supported, ion transport, bulk elec. props. 79−83534
ionic equilibria in water and mol. dynamics of pure liqs. using high-press. Raman spectroscopy 79−24301
Lennard-Jones liquid mixtures, equimolar, mol. dynamics, struct. and thermodynamic props. 78−18517
liquid-liquid phase equilibria, theory, chem. models 78−18781
macromolecular solns., associating, sedimentation equilib. distrib. anal. 77−14628
macromolecular solution, dil., assoc. influence on reduced viscosity 79−90518
metal ethoxide ethanol system, thermodynamic anal. of ion-ion association, conductance meas. 79−29386
methanol, dil. soln. in nonpolar solvent, lattice models, association consts. 79−82141
methanol-carbon tetrachloride, binary soln. with mol. assoc., interdiffusion anal. 79−55912
methanol-d_1, H-bonded in soln., ν_s(OD) band 79−18183
methanol-water, assoc. mixture, rot. barrier solvent effect, CNDO/2 calc. 78−29861
methyl propionate−$H_2O(Ba^{2+})$ mixtures, in DMSO, acetonitrile solns. IR, assoc., solvent, catalytic effects *(French)* 79−87827
micellar solutions, fluoresc. quenching rel. to aggregation numbers 79−34364
micelles, surfactant, H_2O penetration, hydration 80−45572
molecular hyperpolarisability in mixtures, SHG 77−552
molecular orientation, cooperative, rel. to OH proton chem. shift 78−1974

association of liquids continued
2(4)-monooxopyrimidines, gaseous, matrix, soln., tautomeric equilib., IR and UV absorpt. spectra 80−58256
naphthalene TCNE π-π three mol. complexes, absorpt. spectra, assoc. consts., extinction coeffs. *(German)* 77−35465
naphthalene-TCNE π-π three mol. complexes, UV-visible spectra assoc. const., extinction coeff. determ. *(German)* 77−35464
nitroxide free radicals, neutral, EPR spectra, localised solvent-radical adducts 79−96290
1-octanol, dielec. consts., solvent struct., effect of H bonding solutes, chain length 77−48674
1-octanol-H-bonding solute system, chain assoc., dipole correl. theory, dielec. const. anal 77−48675
1-octanol-nonhydroxylic solvent complexes, H bonding, assoc. consts., elec. dipole moments, dielec. consts. 77−48672
p-n-pentyl-p′-cyanobiphenyl, nematic liq. cryst., Raman depolaris. ratios, order parameters 79−28733
phenetole, in cyclohexane-ethanol mixtures, UV spectra, solvent effect 79−22770
phenol, in cyclohexane ethanol mixtures, UV absorption, solvent effects 79−22767
phenol(-d_1)-dioxan(-acetonitrile), in carbon tetrachloride ($CDCl_3$) solns., H-bonds vibr. relax. bands anal. 78−84560
phenol-chloromethane, US absorpt., phenol cyclic assoc. 77−15501
phenol-cyclohexane (-ether), UV spectra, solvent effects, matrix rank anal., species determ. 79−22768
phenol-cyclohexane US absorpt., phenol cyclic assoc. 77−15501
phenol-organic solvent mixtures, UV spectra, solvent effects 79−22769
phenols, substituted, in cyclohexane-ethanol mixtures, UV spectra, solvent effect 79−22770
pheophytin a and b, assoc. solns., excited state deactivation, flash photolysis obs. 79−54895
pigment associations, conc. effects, luminesc., absorpt. spectra and dichroism obs. 80−1007
pivalic acid(-d_1, d_9), liq. and soln., Raman assignments, CH_3 rot. barrier, dimerisation 79−26991
pivalic anhydride, liq. and soln., Raman assignments, CH_3 rot. barrier, dimerisation 79−26991
PMMA, stereoregular, assoc. 79−11793
PMMA, stereoregular, assoc. in dilute soln., PMR obs. 78−76321
PMMA, syndiotactic, solns. in toluene, NMR obs. of struct. and dynamics of associates 80−75867
PMMA isotactic, syndiotactic stereocomplex formation in soln., composition, struct. 79−66292
poly-γ-benzyl-L-glutamate-dichloroethane in conc. soln., mol. assoc., electro-opt. investig. 78−1973
polyethylene oxide aqueous solns., spectroscopic obs. of structural variability WRT turbulent resistance reduction 77−7356
polymer, synthetic, solns., assoc., quantitative evaluation, review 79−10773
polymer solutions, order, conf., Midland, USA, (Aug 1973) 79−10769
polypeptide in conc. soln., mol. assoc., electro-opt. investig. 78−1973
polyphenyl melts, viscosity near freezing pt., association 79−51292
polyproline, optical activity rel. to ordered aggregation 79−11899
polywater, discovery, production and appls. 78−30529
n-propanol mixtures, US vel. depend. on association compounds 79−60436
PVC in DMF, THF solns., mol. wt., aggregation, light scatt. investig. *(Polish)* 77−28587
pyridine N-oxide, in benzene, dipolar assoc. investig. 80−107035
quasilattice theory, complexation, thermodynamic parameters calcs., spectroscopic appls. *(Russian)* 78−76905
radial correlations, comparison of Monte Carlo and Ewald mol. dynamics calc. methods 80−14984
radiationless energy transport in ion pairs in assoc. soln. 79−56835
Raman spectra of liq. phase weak H-bonds, short range order and anharmonicity effects 78−64357
reaction field theory modification for solvent polarities 79−91913
rhodamine 6G, associated, in polyvinyl alcohol film and soln., emission, room temp. 79−54896
rhodamine 6G, electronic spectra, intermol. interactions effect *(Russian)* 77−48237
rhodamine 6G, in glycerine-water solns., anti-Stokes fluoresc., conc. quenching 79−24349
rhodamine 6G, solns., delayed fluoresc. of simple associates 79−56847
rhodamine B, in glycerine-water mixtures mol. agglomeration effect on fluoresc. polaris. spectrum 78−25595
rhodamine dyes, methanol-water solns., triplet state EPR spectra, aggregation, mol. orientation 77−48031
sodium cholate-decanol, soln., aggregate form., comp. and dynamics 80−45575
solution, characteristic sums method in stat. theory 80−10480
solutions, H bonding and anomalous saturation 78−52426
solvation, classical mean space charge model 78−76841
symmetrical electrolytes, conductance-concentration function calcs. 77−21392
tetracene anion radicals, enthalpy of disproportionation, calorimetric determ. technique 79−96296
tetramethylammonium chloride solns., aq. and methanolic, Raman spectra 79−28750
toluene, in benzene soln., mol. motion, correl. functions 80−96431
urea, aqueous solutions, mol. associations, X-ray diffr. meas. 77−76290
vanadium hexacarbonyl, EPR in frozen glasses, optical spectra in soln., solid, assoc., bonding 77−6807
vinyl polymers, precip. from solns., temp. determ. *(German)* 80−85208
water, and ionic dissoc. products, polarisation model 78−91216
water, IR spectrum, influence of Cu^{2+} ions 78−72501
water aggregates, dimer and octomers, dipole moments, polaris. model calcs. 79−77482
water-carbon tetrachloride soln., fundamental H_2O IR spectrum, liq. struct. 80--23419
water-formic acid (acetic acid)(propionic acid)(n-butyric acid), PMR relax. obs., mol. assoc. 79−33553
water-HF(HBr)(HCl) complex, in supersat. soln., Raman spectra assignments 78−70840
CO_2, liq. and gas, state of aggregation effect on 1-4 μm absorpt. bands intensities 79−27042
CaO-SiO_2-MnO molten mixtures, struct. and phys. props. *(French)* 80−24635
Co complexes, nitropentaammine and hexaammine Co(III) complexes, ion assoc. in aq. soln., conductance meas. *(Japanese)* 78−40059

association of liquids continued
- $Cu(ClO_4)_2$ in ethylene glycol solns., US absorpt., relaxation rel. to temp. 77−31727
- $Cu(NO_3)_2$, in ethylene glycol solns., US absorpt., relaxation rel. to temp. 77−31727
- D_2O, assoc. liq., viscous props. 80−2186
- D_2O, US excess absorption and compressional viscosity, temp. depend., hole theory 77−4157
- D_2SO_4, pure, IR and Raman spectra in liq. state, assignments and cryst. spectra comparison *(French)* 79−33699
- $FeCl_3$, nonaq. solns., solvent-solute interactions, Mossbauer investig. of equilib. consts. 79−1729
- $Fe(NO_3)_3$, aq. soln., Fe (III) hydration shells, X-ray diffr. 79−29337
- H-bonded species, in soln., vibr. relax. model 78−84559
- HCl in DMSO-H_2O soln., ion assoc., US absorpt. obs. 79−23513
- HNO_3-H_2O, liq. and glass, mol. assoc., ion pairs, Raman obs. 79−28749
- H_2O, and aq. solns., IR spectral investigations of assoc. 79−65847
- H_2O, assoc. liq., viscous props. 80−2186
- H_2SO_4, pure, IR and Raman spectra in liq. state, assignments and cryst. spectra comparison *(French)* 79−33699
- Hg, thermophys. props. rel. to clustering in liqs. 77−1065
- In-As, melt, mutual diffusion of components 80−88345
- In-Sb liquid alloy, calorimetric investigation, rel. to association equilibrium *(German)* 77−16862
- Kr-NO, thermodynamics, monomer-dimer assoc. of NO, vap. press. meas. 79−90798
- Li, thermophys. props. rel. to clustering in liqs. 77−1065
- Li^+-amide, assoc. in aq. soln., potentiometric obs. 77−29005
- LiCNS, ether solns., dimer struct. and force consts., IR and Raman spectra 79−72442
- Mg-Sn, melt, assoc., liquidus curve calcs. *(German)* 79−20352
- $Mg(NO_3)_2$, aq. soln., ionic coordination by X-ray diffr. 79−29338
- Na, thermophys. props. rel. to clustering in liqs. 77−1065
- Pb, thermophys. props. rel. to clustering in liqs. 77−1065
- SCN^-, associated with metallic cations in aq. soln., press. effect, Raman spectra *(French)* 78−80333
- $Sc_2(SO_4)_3+Al_2(SO_4)_3$ aq. solns., complex form. reacts., kinetics, US relax. investig. 79−1942
- $ZrCl_4$, cryst., melt, gas, Raman spectra interpretation *(German)* 79−28753

associative ionisation
- accelerated atom+O_2, chemiionisation, crossed beam obs. 77−9085
- associative ionisation, merging beams experiment 80−63789
- atom+atom collision, Penning and assoc. ionisation, complex. pot. and electron spectrum 78−94310
- atom+metastable atom collisions, ionis. processes 78−62907
- chemiluminescent, reaction mechanisms 77−32781
- collisional ionisation, Penning and associative ionisation produced by laser field 80−63802
- collisional ionisation in intense laser field, quasimol. state reson., quantum mechanical anal. 78−33589
- diatomic systems, mol. orbital correl. diagrams calcs. 77−50521
- electronic and at. collisions, conference, Kyoto, Japan (Aug.-Sept. 1979) 80−62394
- excited atoms, merging-beams experiments 80−63789
- ice, electron-irrad., cluster-ion prod., lattice and fragmentation energies 77−4911
- self-contained discharge, mechanism of short form. time at high press. 78−1922
- Ar, collision processes, photoionisation mass spectra obs. 79−31479
- Ar, precursor shock waves, electron density and assoc. ionisation 78−67217
- Ar^+, conversion to mol. ions, three body association coeffs. determ. using drift-tube mass spectrometer 80−108699
- $Ar+He^*(1s2s,{}^3S)$, coupled channel calcs. of chemi-ionisation 77−27166
- $Ar_2{}^+$, vibr. excited, form. by assoc. ionisation, photodissoc. 79−68279
- Ar^*+H, assoc. ionis., rovibronic struct. in electron energy spectrum 80−106380
- Ca+Rydberg Ca**, collision cross sections, $Ca_2{}^+$ pot. energy calcs. 79−27055
- Cs arc, low-voltage hot-cathode, plasma production and props., review 77−27766
- Cs+Cs, nP, dD excited states, assoc. ionisation, state and thermal energy depend. *(Russian)* 79−5153
- Cs(nP)+Cs(6S), assoc. ionisation, threshold energy, $Cs_2{}^+$ dissoc. energy 78−58804
- $D+He(2^1S)(2^3S)$, associative and Penning ionisation, autoionisation, calcs. 78−25674
- $H+H^-$ collisions, assoc. detachment process theory 79−44351
- $H+He(2^1S)(2^3S)$, associative and Penning ionisation, autoionisation, calcs. 78−25674
- $H^++H^-\rightarrow H_2{}^*\rightarrow H_2{}^++e$, 0.001 to 3 eV assoc. ionisation cross-sections meas. 79−3512
- H_2, solid, electron-irrad., cluster-ion prod., lattice and fragmentation energies 77−4911
- He, excitation in $n=4$ levels after laser pumping 77−3324
- He^+, conversion to mol. ions, three body association coeffs. determ. using drift-tube mass spectrometer 80−108699
- He+Ar(Kr)(Xe), 2^1S and 2^3S assoc. and Penning ionisation cross sections vel. depend. 79−3551
- He+He, (2^3S) and (2^1S) metastable states, direct and assoc. ionisation rate consts. in afterglow, electron energy spectra 79−13812
- He+He, metastable atoms, collisional ionisation cross-sections 78−70911
- He_2 high press. afterglows, reviews 80−64823
- He^*+D, Penning and assoc. ionis. with metastable He, 0.01 to 10 eV beams 79−27074
- $He^*+H(H_2)(Ar)$, metastable state, ionis. processes 78−62907
- $He^*(1s2s,{}^3S)+Ar$, Penning ionis., discrete-continuum states coupling 79−10193
- $He(2^3S,2^1S)+H$, Penning ions. 79−64089
- $He(2^3S)+H(D)$, Penning and assoc. ionis. cross sections, vel. depend. 79−22815
- $He(3^3S)(3^3P)(3^3D)+He(1^1S)$, deactivation rate, 300-600K, time-resolved spectra 77−19037
- $Hg(6^3P_0)+Hg(6^3P_1)\rightarrow Hg_2{}^++e$, plasma formation by strong Hg line irrad., mechanism 78−83585
- K, associative ionis. from resonance levels 77−30978
- K, photosensitised assoc. ionisation, excited from reson. levels 77−83710
- K^*+molecule, assoc. ionisation, mass spectra *(Russian)* 77−42393

associative ionisation continued
- Kr^*+Ar^*, metastables, chemi-ionis,, merging beams. 0.01-10 eV 80−14198
- ${}^6Li^*+{}^7Li^*$, laser-induced Penning and associative ionis., ${}^{13}Li_2{}^+$ enrichment 78−58796
- $N+O({}^3P)$, endoergic assoc. ionisation, merged beam obs. 79−100348
- N_2, collisional destruction of singlet He I states in low press. glow discharge 80−49030
- N_2, glow discharge, ionis. mechanism 78−13613
- $N({}^2D)+O$, associative ionisation 80−4161
- NH_3, cluster-ion prod. in electron-irrad. solid, lattice, and fragmentation energies 77−4911
- $(NH_3)_nH^+$, $n=1$-9, detected in photoionisation of supersonic mol. beam mass spectra, H-bonding 79−74356
- Na beam, resonance fluorescence 79−98215
- Na, ionisation and energy pooling in laser-excited vapour 79−795
- Na, photosensitised assoc. ionisation, excited from reson. levels 77−83710
- $Na+Ar^*$, Penning, associative and total ionis. cross sections 77−79683
- Na+Na, crossed-beam collision, laser-induced Penning and assoc. ionisation, struct. obs. 80−83476
- Ne^+, conversion to mol. ions, three body association coeffs. determ. using drift-tube mass spectrometer 80−108699
- $Ne_2{}^+$ formation and destruction in Townsend discharges 80−38747
- Ne^*+Ar, associative ionisation studied by merging-beams technique 80−91646
- Ne^*+H, assoc. ionis., rovibronic struct. in electron energy spectrum 80−106380
- Ne^*+Kr, Penning and associative ionisation 77−6910
- Ne^*+Xe, chemiionis. in metastable state collisions 79−68306
- $O_3+U(Th)$, assoc. ionis. cross sections, in crossed beams, mass spectra obs. 78−94317
- Rb, 6^2D excited levels, assoc. ionisation efficiency 77−10747
- Rb, radiatively excited states, ionis. rate coeffs. in two atom collisions 80−43160
- $U+O_2$, assoc. ionisation, electron energy distrib. 78−35656
- Xe precursors, associative ionisation and photoionisation, relative contrib., electron density prediction 80−43858

associative storage *see content-addressable storage*

astatine
- *see also nuclei with ......*
- At^-, in KNO_3 soln., ion vel., carrier free 79−34318
- ${}^{211}At$ protein labelling technique using an acylation reaction 80−36130

astatine compounds
- $AtO_3{}^-$, in KNO_3 soln., ion vel., carrier free 79−34318
- $AtO_4{}^-$, in KNO_3 soln., ion vel., carrier free 79−34318

asteroids
- 13 Egeria, occultation of SAO 92603, photoelectric obs. rel. to minor planet possible satellite 80−46460
- 1932 HA (Apollo), ephemerides for 1930, 1941, 1964 and (1966) 80−105193
- 1936 CA (Adonis), 1977 tentative rediscovery, elements and ephemeris 77−29703
- 1936 CA (Adonis), elements and ephemerides, perihelion uncertainty 77−9692
- 1936 CA (Adonis), ephemerides for 1943 and (1984) 80−105193
- 1936 CA (Adonis), precise positions and magnitudes (1977 February 24 to March 22) 77−37552
- 1936 CA (Adonis), recovery confirmed and improved elements 77−25970
- 1947 XC=1979 XA, positions, UBV photometry and ephemeris continuation 80−31233
- 1947 XC=1979 XA, precise positions, orbital elements and ephemeris 80−31238
- 1950 LA (1980), ephemeris (1977 March-1978 April) 77−29704
- 1960 UA, orbital elements, ephemeris for 1977 May 17-1978 Feb. 21 period 77−45346
- 1960 UA, precise posns. for 1977 July and Aug. of Amor-type object 78−28570
- 1960 UA, recovery on 1977, June 16 77−60709
- 1963 UA, 1976 July 23 precise position 77−82151
- 1963 UA, precise positions (1976, November-1977, January) 77−29705
- 1963 UA, precise positions for 1976 June 26, 27 77−22132
- 1963 WA, precise positions (1976, October-1977, January) 77−53459
- 1972 RA, Amor-type object, precise positions for 1979 Aug., approx. position for 1979 Sept. 79−92691
- 1973 NA, precise position (1973, August 1) 77−9694
- 1974, review of Institute of Theoretical Astronomy (USSR) activities *(Russian)* 78−49368
- 1974OT, astrometric obs. 78−89107
- 1974OU, astrometric obs. 78−89107
- 1975 YA, ephemeris for 1978 July-1979 May period 78−69733
- 1975 YA, orbital elements and ephemeris for 1977, Aug. to Oct. 77−67059
- 1975 YA, precise positions and photographic magnitude (1976, June-July) 77−5486
- 1975 YA, precise positions for 1976 June 25 77−22132
- 1976 AA, Apollo asteroid, Earth's neighbour in space *(Danish)* 77−60706
- 1976 AA, diameter and albedo, radiometric obs. 77−82145
- 1976 AA, discovery review 77−78712
- 1976 AA, orbit determ. and evolution 77−82143
- 1976 AA, photometric obs. at 0.56 and 2.2 μ 77−82144
- 1976 AA, position, elements and ephemeris (1977 Dec.-1978 Apr.) 78−12138
- 1976 AA, precise position (1976, December 27) 77−37553
- 1976 AA, precise position for 1977 Dec. 16 78−73673
- 1976 AA, precise positions 1976, June-Dec., ephemeris for 1977, Jan.-Apr. 77−17418
- 1976 AA, precise positions 1977, Mar. and Apr. 77−60710
- 1976 AA, precise positions and ephemeris extension (1977, Apr.-Dec.) 77 29706
- 1976 AA and 1973 EC, manned and unmanned round-trip mission requirements 77−82101
- 1976 August obs. at ESO La Silla with GPO plus three discoveries *(French)* 78−45260
- 1976 UA, improved orbital elements 77−17420
- 1976 UA, precise positions, 1976, Nov. 77−17417
- 1976 UA, precise positions 1976, Oct. 77−2365
- 1976 UA, precise positions 1976, Oct. 77−9696

asteroids continued

- 1976 UA, precise positions (1976, October and November) 77—33392
- 1976 UA, precise positions and photographic magnitude (1976 October) 77—5487
- 1976 UA, precise positions for 1976 October-November period 77—9693
- 1976 WA, precise positions, ephemeris for 1977, Jan.-May 77—17419
- 1976 WA, precise positions 1976, Nov. and ephemeris for 1976/77 Dec.-Jan. 77—13278
- 1976 WA, precise positions 1976 Nov. and Dec. 77—9697
- 1976 WA, precise positions (1976, December) 77—37551
- 1976 WA, precise positions (1976, May and November) 77—53458
- 1976 WA (Object Schuster), positions, elements and ephemeris (1976 Dec.-1977 Jan.) 77—9695
- 1977 BA, approx. posn., improved elements and ephemeris (1979 Mch.-Apr.) 79—34904
- 1977 HA, astrometric obs. 78—89107
- 1977 HA, discovery, positions, elements and ephemeris (April-May) 77—45344
- 1977 HA, improved elements and ephemeris (1977, May-July) 77—49325
- 1977 HA, precise positions (1977, April) 77—53457
- 1977 HA, precise positions (1977 April-May) and improved elements 77—82153
- 1977 HA, precise positions for 1977 Apr. 22 77—45345
- 1977 HA, recovery, posns. and ephemeris (1979 June-July) 79—70986
- 1977 HB, discovery of fast-moving asteroidal object, positions 77—41348
- 1977 HB, improved orbital elements, ephemeris for 1978 Jan.-July 78—20719
- 1977 HB, positions, elements and ephemeris (1977, May-August) 77—49327
- 1977 HB, precise position for 1978 Apr. 10 78—73673
- 1977 HB, precise positions 1977, May 77—53461
- 1977 HB, precise positions 1977 June 77—87310
- 1977 HB, precise positions (1977, May 21) 77—67060
- 1977 HB, precise positions and possible ephemerides (1977, April-May) 77—56869
- 1977 HB, recovery, precise positions for 1978 May 9-10 78—53862
- 1977 OA, discovery, 1977 July 18-19 positions 78—77518
- 1977 RA, positions, elements and ephemeris for Amor-type object 77—82152
- 1977 RA, positions, improved elements, and ephemeris 78—4137
- 1977 RA, precise positions, (1977 September 23 to December 8) 78—53860
- 1977 RA, precise positions, orbital elements and ephemeris, rot. period estimate 77—87309
- 1977 RA, precise positions 1977 Sept. 77—91466
- 1977 RA, precise positions (1977 Oct. 16) 78—20715
- 1977 RA, precise posns. for 1977 October of Amor-type object 78—28570
- 1977 UB, mini planet between Saturn and Uranus 78—20721
- 1977 UB, posn. in 1895 and improved orbital elements 78—20713
- 1977 UB, precise positions, 1977, Nov. 78—7915
- 1977 UB, precise positions for 1977 Nov. 13-18 period 78—12139
- 1977 UB, precise prediscovery positions 78—20716
- 1977 UB, prediscovery positions, improved elements, orbital stability 78—12140
- 1977 UB, prediscovery positions and ephemeris continuation 78—16331
- 1977 UB (Chiron), accurate orbit, nature and status 78—53863
- 1977 UB (Chiron), discovery, orbital elements 78—45264
- 1977 UB (Chiron), origin, theory 78—40863
- 1977 UB (Chiron), past and future orbit calc. 79—35171
- 1977 UB (Chiron), precise positions 1945 Apr. 16 and 1978 Jan. 9-10 78—49372
- 1977 UB (Chiron) astrometric obs. 78—89107
- 1977 UB (slow-moving Object Kowal), precise positions 1977 Nov. 9-10 78—7911
- 1977 VA, ephemeris (1977 November 23 to 1978 February 21) 78—7914
- 1977 VA, precise positions, 1977, Nov. 78—20717
- 1977 VA, precise positions, photoelec. obs., 1977 Nov. 78—12144
- 1977 VA, precise positions 1977 Dec. 78—49371
- 1977 VA, precise positions (1977 November 9 and 10) 78—7912
- 1977 VA, precise posns. for 1977 November of Amor-type object 78—28570
- 1977 VA (Object Helin-Shoemaker), discovery position 78—7908
- 1977 VA (Object Helin-Shoemaker), positions elements and ephemeris 78—7909
- 1977 VB, discovery positions 78—7910
- 1977 VB, Phocaea-type Mars-crosser, ephemeris (1977 November 13 to December 13) 78—7913
- 1977 YA, asteroid designation for former Comet Lovas (1977t) 78—36485
- 1978 (18) 1, discovery of possible satellite of Melpomene 79—16870
- 1978 (18) 1, secondary extinction event obs. during occultation of SAO 114159 by 18 Melpomene 80—56749
- 1978 (532) 1, discovery of possible satellite of Herculina 78—69734
- 1978 CA, position, elements, ephemeris and B magnitude law 78—40860
- 1978 CA, positions 1978 Feb. 17-Mar. 8, photometric obs. 78—36487
- 1978 CA, precise positions, orbital elements, ephemeris 78—73672
- 1978 CA, precise positions 1978 March, ephemeris for 1978 Apr.-July 78—40862
- 1978 CA, precise positions (1978, March 7 to 12) 78—57486
- 1978 CA (Object Schuster), positions, elements and ephemeris (1978 Feb.-March) 78—36483
- 1978 CA and DA, photoelectric obs. of rotation periods 79—101106
- 1978 CA and DA, UBV photometry, rotation periods, albedos and diameters 78—36489
- 1978 CA and DA, UBV photometry 78—36486
- 1978 DA, discovery, positions, elements, ephemeris and magnitude law 78—36484
- 1978 DA, ephemeris continuation for 1978 July-September period 78—61784
- 1978 DA, position, elements, ephemeris and B magnitude law 78—40861
- 1978 DA, positions 1978 March 1-8, photometric obs. 78—36488
- 1978 DA, precise position for 1978 Apr. 9 78—73673
- 1978 DA, precise positions (1978, March 4 to 12) 78—57487
- 1978 DA, precise positions (1978 March 8 to 15) 78—45262
- 1978 PA, discovery positions for probable Amor-type object 78—81579
- 1978 PA, semiaccurate positions, (1978 August 14 and 15) 78—81580
- 1978 RA=1975 TB, ephemeris continuation and B magnitude law 78—89106

asteroids continued

- 1978 RA, fast-moving asteroidal object approximate positions and photometry 78—85887
- 1978 RA (=1975 TB), precise positions, orbital elements and ephemeris 78—93141
- 1978 SB, fast-moving object, discovery positions and magnitudes 78—93142
- 1978 SB, positions, orbital elements and ephemeris 78—93143
- 1978 SB, positions and UBV photometry 78—96422
- 1978 SB, precise positions for 1978 Oct., orbital elements, ephemeris for 1978 Oct.-Dec. 78—96423
- 1979 (65) 1, discovery of possible satellite of Cybele 80—31237
- 1979 BA, fast-moving object, discovery, precise positions, orbital elements and ephemeris 79—35177
- 1979 ephemerides fo minor planets 79—12422
- 1979 QA, fast-moving asteroidal object, discovery and precise positions (1979 August 22 to 23) 79—92692
- 1979 QB, Amor-type object, precise positions, orbital elements and ephemeris 79—92693
- 1979 QB, precise posns., elements and ephemeris (1979 Aug.-Nov.) 79—101108
- 1979 VA, discovery of fast-moving object 80—12703
- 1979 VA, ephemeris, 1979 Feb. 11th until March 2nd 80—31240
- 1979 VA, not Alinda-type asteroid, ephemeris (1980 January 2 to February 11) 80—31232
- 1979 VA, precise positions, orbital elements and ephemeris 80—26776
- 1979 VA, precise posns., and rotation period from UBV photometry 80—17534
- 1979 VA, precise posns., elements and ephemeris (1979 Nov.-1980 Jan.) 80—26777
- 1979 XA, fast-moving asteroidal object in Aries, discovery 80—26771
- 1979 XA, precise posns. (1979 Dec. 15 and 19) 80—31235
- 1979 XA (=1947 XC), discovery, precise positions, orbital elements and ephemeris 80—26774
- 1979 XB, precise positions, orbital elements and ephemeris 80—46458
- 1979 XB, very fast-moving asteroidal object in Eridanus-Fornax, discovery and positions 80—26772
- 1979 YA, discovery and approx. posn. (1979 December 16) 80—26775
- 1979 YA, nonexistence and cancellation of designation 80—77320
- 1979 YA, posn. for 1979 Dec. 20 and comet-like appearance 80—31234
- 1980 AA, discovery of fast-moving object in Gemini 80—41756
- 1980 AA, extension ephemeris (1980 Feb.-May) 80—41758
- 1980 AA, position Jan 20-22 1980 and ephemeris until Feb. 21st 80—31239
- 1980 AA, precise positions, 1980 January 16, orbital elements and ephereris 80—36556
- 1980 AA, rot. period observed photometrically 80—36558
- 1980 LB, improved orbital elements rel to 2:1 Jupiter librator hypothesis 80—94744
- 1980 LB, precise posns., orbital elements and ephemeris (1980 June-July) 80—82259
- 1980 PA, fast-moving asteroidal object, discovery and semi-accurate positions (1980 August 6 to 7) 80—94745
- 1980 PA, positions, improved orbital elements and ephemeris 80—98597
- 1980 PA, posns., elements and ephemeris (1980 August) 80—94746
- 1980 PA, precise posns., improved elements and ephemeris (1980 Sept.-Oct.) 80—101548
- 1980 QA, fast-moving asteroidal object in Capricornus, discovery and positions (1980 August 16 to 18) 80—98598
- 19791 BA, precise positions, orbital elements and ephemeris 79—40121
- absolute magnitudes for numbered asteroids 79—21219
- accretion model of planet formation rel. to minor planet size 78—12137
- 2101 Adonis, orbital problem soln. 80—72842
- Adonis (1936 CA), precise positions (1977, February 26) 77—49326
- 887 Alinda, duration of stay in Kirkwood gap (1:3) *(Russian)* 80—36559
- 887 Alinda, light curves and rotation period for Amor object 79—44401
- Amor objects, mining, to provide raw materials for space manufacture 77—91467
- 29 Amphitrite, photoelectric lightcurve and synodic rotation period 78—45259
- 270 Anahita, photoelectric photometry during 1975-77 period 78—61783
- 1943 Anteros, spacecraft rendezvous potential target, request for photometry and spectrophotometry 80—90356
- 129 Antigone, photoelectric photometry and synodic rot. period 77—45343
- 1862 Apollo, close approach and ephemeris (1980 Nov.-Dec.) 80—109389
- Apollo objects, mining, to provide raw materials for space manufacture 77—91467
- Apollo objects, total number and chance rediscoveries 78—89105
- Apollo objects 79—75137
- Apollo-Amor objects, steady state distrib. of orbits 79—40118
- 387 Aquitania, rotation period near 24 hours, problems 79—21220
- 387 Aquitania, slow spinning asteroid with rot. period of nearly one day, photometric evidence 80—17529
- 197 Arete, possibility of astrometric obs. for determining mass of 4 Vesta 77—2364
- asteroid 1947 XC(=1979 XA), ephemeris, 1980, 11th Feb.-1st May 80—36557
- 5 Astraea, photometric obs., pole orientation, rot. period 78—40858
- astrometric 1978 positions from ESO GPO obs. 80—72841
- astrometric observations, least squares soln. of ill-conditioned systems 80—26747
- astrometry, equatorial coords. for 19 objects in 1972-4 period *(French)* 78—81577
- astrometry, FK4 equinox corrections from meridian obs. 80—8519
- astrometry (1975-1978), Uppsala southern station obs. 80—85883
- astrometry for 74 objects in 1977, Swedish obs. 80—62065
- astrometry in 1978 April, ESO obs. 80—85882
- astrometry of four objects found during Jupiter satellite study 79—75139
- 63 Ausonia, BV photometric obs., light curve, rot. period 77—82150
- belt depletion by gravit. forces, numerical calc. of orbits 79—35173
- belt existence beyond Neptune, cosmogony *(Russian)* 80—82237
- 776 Berbericia, rotation period near 24 hours, problems 79—21220
- 776 Berbericia, slow spinning asteroid with rot. period of nearly one day, photometric evidence 80—17529
- 1580 Betulia, Amor asteroid, photographic lightcurve 77—91465
- 1580 Betulia, broadband visual and 10.6 μ photometry 79—2511
- 1580 Betulia, radar obs. and radius of Amor-type object 80—36544
- 1580 Betulia, UBV photometry and polarimetry 79—2512

asteroids continued
binary systems, detect. and form., occultation and light curve anal. 80—77322
bombardment by planetesimals scattered from Jupiter zone 78—53859
952 Caia, rot. period and light curve from photoelectric obs. 80—46454
1245 Calvinia, photographic photometry, light curves, magnitudes 79—12418
carbonaceous chondrites parent bodies, form. 80—36580
carbonaceous objects, capture by photoatmospheric drag rel. to Mars' satellites 79—40110
558 Carmen, photoelectric light curves, synodic rot. periods, amplitudes of var. 79—53752
186 Celuta, slowly spinning asteroid, photometry rel. to rot. period and comp. type 78—61782
Ceres, Belgian obs. and computed orbital elements *(French)* 77—71049
Ceres, carbonaceous chondrite mineralogies remote spectroscopic identification from IR obs. 79—96946
Ceres, diameter, interferometric meas. *(Russian)* 80—67634
Ceres, evidence for water of hydration 78—32386
Ceres, far IR obs., temp. determ. 79—12431
Ceres, meridian obs. (1974 to 1977) 78—69660
Ceres, new reduction and collection of meridian obs. 77—13277
Ceres, occultations of stars during 1979/1980 apparition, predictions 79—62785
Ceres, prograde rotation 78—16329
Ceres, radar obs. at 12.6 cm wavelength, surface roughness 80—36545
Ceres and Vesta, densities and bulk comp. 77—22131
313 Chaldaea, photoelectric photometry during 1975-77 period 78—61783
chemical analysis by neutron-gamma techniques 79—53728
1125 China, long period motion calc. 77—13276
2060 Chiron, orbital history and evolution 80—36543
chondrites and C1 carbonaceous chondrites origin, rel. to solar gases in meteorites 79—71008
close approaches to Earth, list of events 78—73621
close encounters with Jupiter, mass distrib. throughout Solar System implications 80—77329
close-approaches to Earth, Amor and Apollo groups 78—61785
collision processes, orbital depend. 78—12136
Comet Lovas (1977t), asteroid-like appearance and orbit 78—28582
comets origin from former asteroidal planet 79—16888
commensurabilities in solar system 80—109418
conference (Tucson, March 1979) 80—31406
conference on celestial mechanics and positional astronomy, Washington, DC, USA (Nov.-Dec. 1978) 80—90605
corrections to FK4 zero points from minor planet obs. *(Russian)* 80—82228
cosmogony of asteroidal belt 77—13275
Crimean obs. (1963-76) *(Russian)* 80—46456
65 Cybele, occultation of AGK3+19°599, 1979 October 17, obs. 80—31237
65 Cybele, occultation of AGK+19°0599, 1979 October 18, obs. using photoelectric photometer *(Chinese)* 80—105172
41 Daphne, photoelectric photometry and synodic rot. period 77—45343
349 Dembowska, IR spectral obs., candidate for meteorite parent bodies 80—98595
349 Dembowska, rot. period and phase curve 79—35174
development from comets, Monte Carlo orbit evolution simulations 80—82261
337 Devosa, unusual object with triple extrema in photoelectric light curve, rot. period 79—40116
diameters and albedos 77—56870
78 Diana, occultation of SAO 75392, 1980 September 4, predicted central path revision 80—101547
differentiation, petrography and chemistry of igneous lithic clasts from mesosiderites and howardites 80—72890
Djermaia (H) chondritic breccia parent body, asteroid regolith preirradiation history 80—36579
200 Dynamene, photoelec. light curve, rot. period, low spin rate object 78—32383
dynamic processes on Earth, extraterrestrial causes, rel. to extinction of life 78—92820
dynamical families, correl. with spectral classes 77—91464
dynamics and evolution, review 80—82260
E-type, rel. to origin of enstatite achondrites 78—32384
early history, coalescence prevention by Jupiter 79—5774
eccentricities, origin in nebular resonances 80—46449
eclipsing binary asteroids, lightcurve analysis of 171 Ophelia 80—36549
element abundance analysis, space mission goals 80—36474
354 Eleonora, rot. period and phase curve 79—35174
59 Elpis, photoelectric lightcurves and rotation period 78—69729
182 Elsa, photoelec. light curve and rot. period 80—56750
EM heating of minor planets in early solar system 80—36555
283 Emma, light curves and rot. period 79—16868
ephemerides, orbits computation using Chebychev polynomials *(French)* 80—61997
433 Eros, astrometric obs. during 1975 opposition 78—57485
433 Eros, Belgian obs. and computed orbital elements *(French)* 77—71049
433 Eros, brightness changes during major oposition 77—67061
433 Eros, photographic obs. at 1975 opposition 78—49373
433 Eros, rotation axis motion *(Chinese)* 77—67058
433 Eros, shape and spin axis orientation determ. by photometric method *(Russian)* 80—8581
433 Eros, thermal props. from radiometric and refl. light obs. 80—31231
eucrite parent asteroid, bulk composition, planetary evolution bearing 80—56786
eucrite parent body, size from melt/solid segregation numerical treatment 79—40144
45 Eugenia, photoelectric light curves, synodic rot. periods, amplitudes of var. 79—53752
45 Eugenia, rot. period and photoelec. light curve determ. 80—72846
247 Eukrate, UBV photometry, light curve and rot. period 80—21942
185 Eunike, photoelectric lightcurve and probable synodic rotation period 78—45259
15 Eunomia, close approaches to SAO stars, prediction accuracy 79—30003
15 Eunomia, occultation of ζ Cancri on 1978 January 19, further predictions 78—20714
15 Eunomia, occultation of SAO 97745, visibility track 78—12081
52 Europa, photometry and rot. period 78—12133

asteroids continued
164 Eva, rotation period from photoelectric obs. 77—60707
families, concs. in proper elements space statistics and mapping 78—96420
families, obs. evidence for common origins 77—91468
family detection by new criterion, orbital data 80—82256
Farmington meteorite last parent body, as undiscovered Apollo asteroid *(Russian)* 79—101124
37 Fides, photoelectric photometry during 1975-77 period 78—61783
Flora family origin 80—36548
19 Fortuna, prograde rotation 78—16329
Fourier transform spectroscopy appl. to remote identification of solids in solar system 77—87273
fragmentation in asteroid belt, process types 80—36552
fragmentation in orbit 78—53858
148 Gallia, positions (1977 September-December) 79—88618
148 Gallia, UBV photoelectric lightcurves and rotation period 79—101105
gravitational heating of interior during form. process 80—36529
6 Hebe, dimensions as result of occultation obs. 79—92694
6 Hebe, occultation of γ Ceti, 1977, Mar. 77—33407
6 Hebe, occultation of γ Ceti AB on 1977 March 5, predictions 77—29702
6 Hebe, phase functions 77—64689
6 Hebe, size from 1977 March 5 γ Ceti A occultation obs. 78—53856
108 Hecuba, motion in restricted three-body problem, nonlinear oscills. *(German)* 78—57488
Hecuba family resonance asteroids intermediate orbit, three fixed centres generalized problem internal variant 79—84726
Hecuba-type, evolution of orbits *(Russian)* 77—49328
624 Hektor, light curve indicating elongated shape 80—98600
624 Hektor, nature of Trojan object 79—35176
624 Hektor, possible dumbbell shape and slow collisions 79—62787
103 Hera, photoelectric light curves, synodic rot. periods, amplitudes of var. 79—53752
532 Herculina, occultation of SAO 120774, discovery of 1978 (532) 1 possible satellite 78—69734
532 Herculina, photoelectric light curves, synodic rot. periods, amplitudes of var. 79—53752
532 Herculina, satellite detect from occultation obs. 80—67629
532 Herculina satellite, age and lifetime 79—40122
121 Hermione, photoelectric lightcurve too smooth for rotation period determ. 78—45259
69 Hesperia, close to zero phase on 1977 Sept. 28, obs. requested 77—78713
944 Hidalgo, UBV obs. of rotation and CN band not in spectra 77—5485
Hilda group, resonant orbital motion of Palomar-Leiden Survey objects 77—9690
howardite parent body, layered crust model 80—36554
hyper-periods and Kirkwood Gaps 80—105153
hypothetical observations giving equinox and equator determ. 80—94742
1566 Icarus, ephemeris for 1977, July-Sept. 77—64690
impacts at high velocities, catastrophic destruction mechanism 80—82257
improved orbits for ten objects rel. to quality of observations *(Russian)* 78—49369
173 Ino, photometric vars., light curves and rot. period 79—16869
704 Interamnia, occultation of SAO 206553 on 1978 April 28, details 78—16332
704 Intermnia, positions (1977 February-April) 79—88618
internal structures, model of accretional histories 80—36553
85 Io, definitive orbit from obs., (1865-1977) 80—4284
IR (JHK) photometry, of meteorites and asteroids 79—2531
IR reflectance spectra, obs. rel. to search for water of hydration 80—77318
7 Iris, photometry rel. to rot. and pole orientation 77—74004
42 Isis, photoelectric light curves, synodic rot. periods, amplitudes of var. 79—53752
3 Iuno, positions (1977 March-August) 79—88618
Juno, meridian obs. (1974 to 1977) 78—69660
Juno, occultation of AGK3 +0°1022, obs. 80—26773
Juno, occultation of AGK3 +0°1022 re-analyzed 80—41757
22 Kalliope, light curves, phase function, pole and dimensions 78—53857
22 Kalliope, pole coordinates from photoelectric photometry 80—31230
Kirkwood, gaps, origin 79—16867
Kirkwood gap 1:3, width *(Russian)* 80—36559
Kirkwood gaps, kinematic theory 77—60712
Kirkwood gaps, spectral anal. 77—60711
Kirkwood Gaps and stability of conservative periodic systems 78—65544
216 Kleopatra, photoelectric photometry during 1975-77 period 78—61783
216 Kleopatra, photometry rel. to comp., diameter, elongated shape and possible stellar occultations 80—94743
97 Klotho, photoelectric photometry during 1975-77 period 78—61783
39 Laetitia, positions (1977 April-August) 79—88618
393 Lampetia, long rotation period from photoelectric lightcurve 79—40120
68 Leto, rot. period and photoelec. lightcurves determ. 80—98594
light curve survey of 9 objects during 1977 oppositions 79—53753
light curve survey of faint objects 80—4283
lightcurves, simulation by rot. of three-axes ellipsoid model 78—61781
599 Luisa, photoelectric light curve 78—16328
M-type, composition from optical polarimetry 79—40119
magnitudes and phase relations, compilation 79—88617
main belt objects, precise posns. in 1975-6 period 78—77515
main-belt asteroids, positions 78—12135
mass content and mass distrib. 77—74005
mean motion resonant with Jupiter, short-periodic perturbations 78—53803
56 Melete, photoelectric light curves, synodic rot. periods, amplitudes of var. 79—53752
18 Melpomene, occultation of SAO 114159; discovery of 1978 (18) 1 possible satellite 79—16870
18 Melpomene, occultation of SAO 114159, photoelectric obs. 79—12420
18 Melpomene, occultation of SAO 114159, secondary extinction event obs. rel. to 1978 (18) 1, possible satellite 80—56749
18 Melpomene, occultation of SAO 114159 on 1978 Dec. 11, revision obs. 79—12423
18 Melpomene, positions (1977 March-August) 79—88618
18 Melpomene, rot. period from photoelec. obs. 80—82258
meteorite parent bodies, orbits, perihelia distrib. *(Russian)* 77—49345

asteroids continued
meteorite parent body, impact melting rel. to origin of Fe meteorites of groups IAB and IIICD 80—109404
9 Metis, pole coordinates from photoelectric photometry 80—31230
9 Metis, UBV photometry, light curve and rot. period 80—21942
9 Metis occultation of SAO 80950, Guianan obs. 80—31236
mining prospects 78—61786
Minor Planet Center, history and future 80—94712
Minor Planet Circular 5333-5390, precise posns., elements, ephemerides, new nos. and names 80—77325
Minor Planet Circulars, precise posns., elements, new nos. and names 80—31241
Minor Planet Circulars 4391-4424, precise posns., elements, ephemerides, new nos. and names 78—81578
minor planet circulars 4425-4482, precise posns., elements, ephemerides, new nos. and names 78—85886
Minor Planet Circulars 4483-4520, precise posns., elements, new nos. and ephemerides 78—93140
minor planet circulars 4521-4548, precise posns., elements, ephemerides, new nos. and names 79—2514
minor planet circulars 4549-4582, precise posns., elements, ephemerides, new nos. and names 79—12421
Minor Planet Circulars 4583-4622, precise posns., elements, ephemerides and new nos. 79—16871
Minor Planet Circulars 4623-4648, precise posns., elements, ephemerides and names 79—25538
Minor Planet Circulars 4649-4688, precise posns., elements, ephemerides identifications and new nos. 79—35178
Minor Planet Circulars 4689-4722, precise posns., and orbital elements 79—53754
Minor Planet Circulars 4723-4746, precise posns., elements, ephemerides, new nos. and names 79—66953
Minor Planet Circulars 4747-4788, precise posns., elements, ephemerides, new nos. and names 79—75136
Minor planet circulars 4789-4844, precise posns., elements, ephemerides, new nos. and names 79—84729
Minor Planet Circulars 4845-4936, precise posns. elements, ephemerides and new nos. 79—101107
Minor Planet Circulars 4937-5016, precise posns., elements, ephemerides, new nos. and names 80—8580
Minor planet circulars 5017-5066, precise posns., elements, ephemerides, new nos. and names 80—17533
Minor Planet Circulars 5137-5188, precise posns., elements, ephemerides, new nos. and names 80—46459
Minor Planet Circulars 5189-5248, precise posns., elements, ephemerides, new nos. and names 80—67631
Minor Planet Circulars 5249-5286, precise posns., elements, ephemerides, new nos. and names 80—67632
Minor Planet Circulars 5287-5332 precise posns; elements, ephemerides, new nos. and names 80—67633
Minor Planet Circulars 5391-5422, precise posns., elements, ephemerides, new nos. and names 80—85884
Minor Planet Circulars 5423-5454, precise posns., elements, ephemerides, new nos. and names 80—98599
minor planet satellite observations, reliability 80—46460
minor planets, 1978, April, astrometric positions determ., ESO GPO obs. 80—77319
missing planet origin rejected 78—69732
multiple flyby mission feasibility study 80—36473
51 Nemausa, astrometric posns. for coord. system error reduction 80—72849
128 Nemesis, long rotation period from photoelectric lightcurve 79—40120
128 Nemesis, photoelectric light curve 78—16328
287 Nephthys, photoelectric photometry and rot. period 79—84727
1206 Numerowia, improved elements of lost object 78—7906
44 Nysa, pole coordinates from photoelectric photometry 80—31230
Object Kowal, positions, indeterminate orbit, elements and ephemeris 78—7907
object Kowal, slow-moving asteroid discovery and positions 78—4136
object Schuster, approx. positions, 1976, Nov. 77—5489
Object Schuster, discovery and positions for fast-moving Apollo-type object 78—32385
object Schuster, fast moving asteroid, discovery obs. 77—5488
Object Sebok, fast-moving asteroidal object, discovery and positions 77—17416
observations and theories, review 78—20720
171 Ophelia, binary asteroid evidence from light curve 80—4287
171 Ophelia, lightcurve analysis, possible eclipsing binary asteroid 80—36549
opposition effect, similarity among asteroids 80—62064
orbit determ. for some unnumbered Purple Mountain Observatory minor planets 80—72848
orbit determination method by filter technique *(French)* 79—101050
orbit determination using Chebyshev's approx. *(French)* 80—94720
orbit-orbit resonances between asteroids and planets 78—4093
orbital characteristics, explanation based on restricted three-body problem 79—8874
orbital elements, probability distribs. 80—46461
orbital elements from Munich meridian obs. (1941-61) *(German)* 80—77306
orbital evolution near 1:3 Kirkwood gap 80—36541
orbital perturbations, regular proximities concept and approximate perturbation methods 80—72843
orbital resonance in dissipative medium rel. to asteroids and Saturn's rings 78—28491
orbital resonances in solar system, review 77—25998
orbits, chem. comp. and origin *(Swedish)* 77—71048
orbits, invariant relation in elliptic restricted three body problem 79—88616
orbits and FK4 equator and equinox corrections 78—69727
orbits determination, method for study of error propag. 77—25914
orbits identification, ephemerides calc. *(Chinese)* 78—69731
orbits in vicinity of 1:3 commensurability with Jupiter, evolution, model calcs. results *(Russian)* 80—36486
origin, effect of planetesimals sweeping asteroid belt *(Chinese)* 80—8579
origin, initial rotation periods and relative formation times *(Chinese)* 80—105182
osculating elements reduction to proper elements for entire solar system 80—21897
outer belt objects, distrib. and motion 80—36540

asteroids continued
palaeoglaciation due to solar radiation reduction *(French)* 79—34857
49 Pales, binary asteroid evidence from light curve 80—4287
49 Pales, photoelectric photometry and rotation period 79—44402
Pallas, 1978 May 29 occultation of SAO 85009, diameter determ. 79—44400
Pallas, ang. diameter from speckle interferometric meas. 79—35172
Pallas, carbonaceous chondrite mineralogies remote spectroscopic identification from IR obs. 79—96946
Pallas, meridian obs. (1974 to 1977) 78—69660
Pallas, new reduction and collection of meridian obs. 77—13277
Pallas, occultation of SAO 120836, 1973 February 6, reliability of obs. 80—46460
Pallas, occultation of SAO 85009, 1978 May 29, corrected prediction, photoelec. obs. 78—57430
Pallas, occultation of SAO 85009 on 1978, May 29, revised position 78—12080
Pallas, occultation of SAO 85009 on 1978 May 29, prediction 78—53861
Pallas, occultation of SAO 99401 on 1977, July 8 77—53460
Pallas, prograde rotation 78—16329
2 Pallos, position (1977 March-April) 79—88618
Palomar planet-crossing asteroid survey, 1973-1978 period 80—36539
55 Pandora, photometric vars., light curves and rot. period 79—16869
471 Papagena, photoelectric photometry during 1975-77 period 78—61783
471 Papagena, rotational period and photoelectric lightcurve *(German)* 78—4134
471 Papagena, rotational period and photoelectric lightcurve 78—4135
11 Parthenope, positions (1977 April-August) 79—88618
peculiar direct motions, loops made by objects in strange orbits 80—109346
118 Peitho, rot. period and light curve from photoelectric obs. 80—46454
554 Peraga, photoelectric photometry and rot. period 79—84727
Phobos, probably captured asteroid *(Norwegian)* 78—36478
photoelectric observations by high school teachers 77—45347
photoelectric photometry during 1975-77 period 78—61783
photoelectric photometry of seven asteroids, rot. periods 79—35175
photographic astrometry at Observatoria Nacional do Brasil (Sept. 1977) 79—70985
photographic photometry during 1977 and 1978, light curves and rot. periods 80—72844
photographic photometry of 110 main-belt asteroids 78—40859
photometry in 0.56-2.2 μ range for 30 objects 78—69725
physical properties, results from photometric obs. *(Polish)* 78—16330
planetary atmospheres interactions, rel. to 1908 Tunguska event 78—49378
planetary orbits perturbations by asteroid belt, analytical method 79—75082
in planetary science conference (Boston, MA, 28 October 1977) 79—53740
planetesimal population, equilib. vels. 80—31219
planetoids in early solar system, ^{26}Al as heat source 78—65511
polarimetric, radiometric and spectrophotometric obs., review *(Polish)* 78—36490
polarimetry of particulate surfaces 78—58011
308 Polyxo, photoelectric lightcurves and rotation period 80—46455
32 Pomona, photoelectric photometry, composite light curve and synodic period of rot. 77—9691
population in circumterrestrial space 78—73599
position determination in April 1979, data reduction *(French)* 80—72845
position obs. at Sydney Observatory during 1975 77—53462
positional catalogue from photoelectric meridian obs. 77—91453
positional photographs reduction by method of dependences 80—4237
positions in 1978, visible obs. 80—67630
positions in August 1977 from Observatorio Nacional, Rio de Janeiro *(French)* 80—94740
positions meas. at ESO-La Silla during 1978 April 79—58293
positions of minor planets, (1977) 79—40117
positions of minor planets from Torino Observatory (1977-1979) 80—94739
positions of selected minor planets (August 1975 to May 1976) 78—12134
precise astrographic positions for 1958-1967 period 79—62786
precise positions, obs. at Sydney Observatory during (1976) 78—69735
precise positions for 18 objects meas. at Torino 78—69730
precise positions for 35 objects 79—8873
precise positions for nine selected objects in 1976-7 period 78—77514
precise positions of 25 objects 79—58292
790 Pretoria, C-type asteroid, light vars. obs. and rot. period 80—21941
primordial metamorphism via elec. induction in T Tauri-like solar wind 78—69728
prograde rotation of Ceres, Pallas, Vesta, Fortuna 78—16329
196 Prokne, photoelectric photometry and rot. period 79—84727
26 Proserpina, photoelectric photometry and rot. period 79—84727
16 Psyche, occultation of SAO 159250 on 1978 Feb. 25, details 78—16332
16 Psyche, opposition effect and surface structure *(Russian)* 80—67635
1915 Quetzalcoatl, duration of stay in Kirkwood gap (1:3) *(Russian)* 80—36559
radar detectability, opportunities for 1977-87 period 77—82149
radii, absolute mags., and discovery distribs. 80—109390
radiometric diameters and geometric albedos from 10 and 20 μ photometry 77—53456
radiometry and surface properties of Apollo, Amor, and Aten asteroids 79—75135
regolith props. rel. to lunar phase relation 80—36551
regoliths 80—17530
relative observations, use in accuracy improvement of fundamental system of star position and motion 80—94692
resonance in the restricted problem of three bodies with short period perturbations in elliptic case 79—25455
resonant asteroids motion, theory based on quasi-periodic solns. of restricted three-body problem *(Russian)* 79—48727
review of present knowledge 79—88619
rotation rates, collisional evolution theory 80—17532
rotation rates, pole positions and shapes 80—17531
S-type, spin rate 78—77516
80 Sappho, photoelectric photometry during 1975-77 period 78—61783
Saratov obs. (1974 April-Oct.) *(Russian)* 80—46457
satellite detect. from occultation obs. 80—67629

asteroids continued
satellites, occulting of stars 80—94741
satellites of minor planets, discovery from occultations of stars 80—4286
secular orbital vars., seminumerical calc. method 80—51686
shape after collisions with meteoroids, theoretical anal. 80—77321
shape determination, photometric method *(Russian)* 80—8581
shape distrib. from high-vel. impacts, laboratory expts. 78—45263
shapes and gravitational moments of tidally and rot. distorted objects 79—53757
140 Siwa, C-type asteroid, light vars. obs. 80—21941
size and albedo determ., radiometric method 77—82148
sizes and albedos, review 77—60708
solar wind sputtering rate 80—85835
spin axis orientation determination, photometric method *(Russian)* 80—8581
structure of asteroid belt 78—69737
563 Suleika, rot. period and photoelec. lightcurves determ. 80—98594
Sun-Jupiter-asteroid circular and elliptic problem comparison at commensurabilities 77—56819
surface albedo and colour contracts 80—36547
surface grooves, prediction 80—36550
surface materials mineralogical characts. from reflectance spectra 78—69736
surface studies from Earthbound obs., technique 80—77324
survey for high-inclination minor planets 79—75156
87 Sylvia, UBV photometry, light curve and rot. period 80—21942
taxonomy, five-class system 79—2510
terminator configuration, rel. to dust electrostatic transport and surface denudation 79—35157
terrestrial cratering, plate tectonics and evolution of life 78—96421
thermal evolution, calc. 79—2501
17 Thetis, opposition effect and surface material, UBV photometry *(Russian)* 79—58294
88 Thisbe, photoelectric light curves and rotation 80—17528
88 Thisbe, photoelectric photometry and rotation period 79—44402
three body averaged plane restricted problem, first integrals, computer calc. *(Russian)* 77—56820
three-body problem, elliptic, Jacobian integral development *(German)* 79—92655
three-body problem, long-periodic solns. *(Russian)* 78—49370
115 Thyra, astrometry and orbit improvement *(German)* 80—85881
topocentric positions for 11 objects (Sept. 1977-Oct. 1978) *(German)* 80—46453
topographic changes on airless bodies, meteorite impact and ejecta deposition 78—65523
1685 Toro, orbital resonances with Earth and Venus 79—2513
TRIAD computer file, Tucson revised index of asteroid data 78—45261
Trojan, perihelion motion 79—84725
Trojan, three-dimens. motion 79—5773
Trojan asteroids, asymptotic soln. of plane elliptic restricted three body problem 77—60587
Trojan asteroids, comp. 80—56751
Trojan asteroids, long-period effects in motion and problems of 1/1 resonance 80—41755
Trojan asteroids, orbital theory 79—12419
Trojan asteroids, radii and albedo 77—33399
Trojan asteroids, restricted three body problem 77—74003
Trojan asteroids and fictitious objects at 1/1 resonance, long-period effects 78—85830
Trojan group, discovery of new members, orbital elements and ephemerides 80—72847
Trojans, elliptic restricted three-body problem, invariant relation 78—69726
Trojans, long-periodic solution in restricted three body problems 77—17337
Trojans, origin 80—36542
Trojans with large orbital inclination, dynamics 80—77323
truncation of asteroid belt, theory of tidal torques on infrequently colliding particle discs in binary systems 80—98596
UBV photometry, shapes and rot. characts. 77—5484
UBV photometry of 145 faint objects 78—69724
UBV photometry of small and distant asteroids 77—82147
92 Undina, photoelectric photometry and rotation period 79—44402
unidentified objects found during search for short-period comets 78—85907
612 Veronika, identifications and ephemeris (1979 Sept.-1980 Feb.) 80—4285
Vesta, ang. diameter from speckle interferometric meas. 79—35172
Vesta, ang. diameter from speckle interferometry 78—20712
Vesta, diameter, interferometric meas. *(Russian)* 80—67634
Vesta, IR spectral obs., candidate for meteorite parent bodies 80—98595
Vesta, meridian obs. (1974 to 1977) 78—69660
4 Vesta, parent body of eucrites, evidence from rare earth elements 78—20766
Vesta, possible eucrite parent body, implications of Moore County quench temp. 78—96444
4 Vesta, predictions for 1980 January 24 lunar occultation 79—84728
Vesta, prograde rotation 78—16329
Vesta, spectral refl. meas., pyroxene absorpt. band 77—82146
Vesta, UBV photometry and lightcurve 80—36546
Vesta as basaltic achondrite parent body, evidence from rare earth element abundance patterns 80—36581
Fe meteorite origin in asteroid belt, thermodynamic model evidence 80—36577
Fe meteorites parent bodies, interpretation of age distribs. from cosmic ray produced nuclides 79—30015

astigmatism *see aberrations*

astrobiology *see extraterrestrial life*

astrometry
1309—216, probable BL Lacertae object with absorpt. red shift 1.49, precise position 80—67856
1936 CA (Adonis), 1977 tentative rediscovery, elements and ephemeris 77—29703
1936 CA (Adonis), precise positions and magnitudes (1977 February 24 to March 22) 77—37552
1947 XC=1979 XA, positions, UBV photometry and ephemeris continuation 80—31233
1947 XC=1979 XA, precise positions, 1979 December 18 to 1980 January 5 80—31238
1963 UA, 1976 July 23 precise position 77—82151

astrometry continued
1963 UA, precise positions (1976, November-1977, January) 77—29705
1963 UA, precise positions for 1976 June 26, 27 77—22132
1963 WA, precise positions (1976, October-1977, January) 77—53459
1972 RA, Amor-type object, precise positions for 1979 Aug., approx. position for 1979 Sept. 79—92691
1973 NA, precise position (1973, August 1) 77—9694
1974OT, astrometric obs. 78—89107
1974OU, astrometric obs. 78—89107
1975 YA, precise positions and photographic magnitude (1976, June-July) 77—5486
1975 YA, precise positions for 1976 June 25 77—22132
1976 AA, position, elements and ephemeris (1977 Dec.-1978 Apr.) 78—12138
1976 AA, precise position (1976, December 27) 77—37553
1976 AA, precise position for 1977 Dec. 16 78—73673
1976 AA, precise positions 1976, June-Dec., ephemeris for 1977, Jan.-Apr. 77—17418
1976 AA, precise positions and ephemeris extension (1977, Apr.-Dec.) 77—29706
1976 UA, precise positions, 1976, Nov. 77—17417
1976 UA, precise positions 1976, Oct. 77—2365
1976 UA, precise positions 1976, Oct. 77—9696
1976 UA, precise positions (1976, October and November) 77—33392
1976 UA, precise positions and photographic magnitude (1976 October) 77—5487
1976 UA, precise positions for 1976 October-November period 77—9693
1976 WA, precise positions, ephemeris for 1977, Jan.-May 77—17419
1976 WA, precise positions 1976, Nov. and ephemeris for 1976/77 Dec.-Jan. 77—13278
1976 WA, precise positions 1976 Nov. and Dec. 77—9697
1976 WA, precise positions (1976, December) 77—37551
1976 WA, precise positions (1976, May and November) 77—53458
1976 WA (Object Schuster), positions, elements and ephemeris (1976 Dec.-1977 Jan.) 77—9695
1977 HA, astrometric obs. 78—89107
1977 HA, discovery, positions, elements and ephemeris (April-May) 77—45344
1977 HA, precise positions (1977, April) 77—53457
1977 HA, precise positions (1977 April-May) and improved elements 77—82153
1977 HA, precise positions for 1977 Apr. 22 77—45345
1977 HA, recovery, posns. and ephemeris (1979 June-July) 79—70986
1977 HB, precise position for 1978 Apr. 10 78—73673
1977 HB, precise positions (1977, May 18) 77—49327
1977 HB, precise positions (1977, May 21) 77—67060
1977 HB, precise positions and possible ephemerides (1977, April-May) 77—56869
1977 HB, recovery, precise positions for 1978 May 9-10 78—53862
1977 HB asteroid, precise positions 1977 June 77—87310
1977 OA, discovery, 1977 July 18-19 positions 78—77518
1977 RA, positions, elements and ephemeris for Amor-type object 77—82152
1977 RA, positions, improved elements, and ephemeris 78—4137
1977 RA, precise positions, (1977 September 23 to December 8) 78—53860
1977 RA, precise positions, orbital elements and ephemeris 77—87309
1977 RA, precise positions 1977 Sept. 77—91466
1977 RA, precise positions (1977 Oct. 16) 78—20715
1977 UB, posn. in 1895 and improved orbital elements 78—20713
1977 UB, precise positions, 1977, Nov. 78—7915
1977 UB, precise positions for 1977 Nov. 13-18 period 78—12139
1977 UB, precise prediscovery positions 78—20716
1977 UB, prediscovery positions, improved elements, orbital stability 78—12140
1977 UB, prediscovery positions and ephemeris continuation 78—16331
1977 UB (Chiron), precise positions 1945 Apr. 16 and 1978 Jan. 9-10 78—49372
1977 UB (Chiron) astrometric obs. 78—89107
1977 UB (slow-moving Object Kowal), precise positions 1977 Nov. 9-10 78—7911
1977 VA, precise positions, 1977, Nov. 78—20717
1977 VA, precise positions, photoelec. obs., 1977 Nov. 78—12144
1977 VA, precise positions 1977 Dec. 78—49371
1977 VA, precise positions (1977 November 9 and 10) 78—7912
1977 VA (Object Helin-Shoemaker), positions elements and ephemeris 78—7909
1978 CA, position, elements, ephemeris and B magnitude law 78—40860
1978 CA, precise positions 1978 March, ephemeris for 1978 Apr.-July 78—40862
1978 CA, precise positions (1978, March 7 to 12) 78—57486
1978 CA, precise positions for 1978 Mar. 78—73672
1978 CA (Object Schuster), positions, elements and ephemeris (1978 Feb.-March) 78—36483
1978 DA, discovery, positions, elements, ephemeris and magnitude law 78—36484
1978 DA, position, elements, ephemeris and B magnitude law 78—40861
1978 DA, precise position for 1978 Apr. 9 78—73673
1978 DA, precise positions (1978, March 4 to 12) 78—57487
1978 DA, precise positions (1978 March 8 to 15) 78—45262
1978 P 1, speckle obs. rel. to orbital radius and system mass and density 80—109394
1978 RA (=1975 TB), precise positions, (1978 September 10 to 12) 78—93141
1978 SB, precise positions, (1978 October 6 to 11) 78—93143
1978 SB, precise positions for 1978 Oct., orbital elements, ephemeris for 1978 Oct.-Dec. 78—96423
1979 BA, fast-moving object, discovery and precise positions, (1979 January 23 to 31) 79—35177
1979 BA, precise positions, (1979, February 28 and March 4) 79—40121
1979 QA, fast-moving asteroidal object, discovery and precise positions (1979 August 22 to 23) 79—92692
1979 QB, Amor-type object, precise positions (1979 August 22 to 23) 79—92693
1979 QB, precise posns., elements and ephemeris (1979 Aug.-Nov.) 79—101108
1979 VA, precise positions, (1979 November 15 to 16) 80—26776
1979 VA, precise posns., and rotation period from UBV photometry 80—17534
1979 VA, precise posns., elements and ephemeris (1979 Nov.-1980 Jan.) 80—26777

astrometry continued
1979 XA, precise posns. (1979 Dec. 15 and 19) 80—31235
1979 XA (=1947 XC), discovery and precise positions (1979 December 13 to 15) 80—26774
1979 XB, precise positions, (1979 December 11 to 15) 80—46458
1980 AA, precise positions, 1980 January 16, orbital elements and ephereris 80—36556
1980 LB, precise posns., orbital elements and ephemeris (1980 June-July) 80—82259
1980 PA, positions, 1980 August 8 to 17, improved orbital elements and ephemeris 80—98597
1980 PA, precise posns., improved elements and ephemeris (1980 Sept.-Oct.) 80—101548
1980 S 10, precise positions, 1980 March 15 to 16, and relation to Dione 80—85893
1980 S 1, 3, 6, 25, new Saturnian satellites, positional obs., (1980 March 9 to 14) 80—94749
absolute declinations observation by micrometric method, lateral refr. elimination *(Russian)* 79—96890
absolute star positions, determ. by Sanders-Raimond method 77—53404
Adonis (1936 CA), precise positions (1977, February 26) 77—49326
ADS 1538=Σ 168≐BDS 1015, orbit of visual double *(French)* 78—8056
ADS 7251, photographic obs. in 1962-73 period, orbital motion *(Russian)* 78—28726
ADS 8887, photographically unresolved visual binary, parallax and orbit 78—57593
ADS 9537 (BV Draconis and BW Draconis), ang. separation and position angle 79—35296
AFCRL Sky Survey sources, accurate photometric positions 77—45603
AGK2, error corrections and new reductions *(French)* 77—64616
AGK2-AGK3 solutions, comparison by separate plates and overlapping *(French)* 77—64615
AGK3 stars, proper motion system in polar region *(Russian)* 80—12647
AGK3R declinations improvement using Toepfer meridian circle obs. *(Russian)* 78—28645
Allegheny Observatory parallax program, astrometric constants for 47 stars 78—53923
Allegheny parallax program, stars in region of 91 and 92 Tauri, Lalande 20111, 18 Bootis and HD 187399 77—74037
Amalthea, 1976-8 absolute astrometric posns. 79—62789
Amor-type asteroids 1960 UA, 1977 RA, and 1977 VA, precise posns. for 1977 period 78—28570
AO 0235+164, BL Lacertae object, radio position and struct. of halo 78—4386
α Aquilae (Altair), 1941-77 astrometric obs. 79—12470
197 Arete, possibility of astrometric obs. for determining mass of 4 Vesta 77—2364
Ariel 1524-61 optical counterpart, identification and position 77—45611
asteroid, 1980 AA, position Jan 20-22 1980 and ephemeris until Feb. 21st 80—31239
asteroid position determination in April 1979, data reduction *(French)* 80—72845
asteroid positions in 1978, visible obs. 80—67630
asteroids, 1976 August obs. at ESO La Silla with GPO plus three discoveries *(French)* 78—45260
asteroids, four objects found during Jupiter satellite study 79—75139
asteroids, from ESO GPO obs. 80—72841
asteroids, improved orbits for ten objects rel. to quality of observations *(Russian)* 78—49369
asteroids, main-belt, positions 78—12135
asteroids, Munich meridian obs. (1941-61), orbital elements determ. *(German)* 80—77306
asteroids, orbit determ. for some unnumbered Purple Mountain Observatory objects 80—72848
asteroids, photographic astrometry at Observatoria Nacional do Brasil (Sept. 1977) 79—70985
asteroids, position obs. at Sydney Observatory during 1975 77—53462
asteroids, positions meas. at ESO-La Silla during 1978 April 79—58293
asteroids, precise 1977 posns. for 7 objects, Sydney obs. 79—88618
asteroids, precise astrographic positions for 1958-1967 period 79—62786
asteroids, precise positions, (1977) 79—40117
asteroids, precise positions (August 1975 to May 1976) 78—12134
asteroids, precise positions for 18 objects meas. at Torino 78—69730
asteroids, precise positions for 35 objects 79—8873
asteroids, precise positions for nine selected objects in 1976-7 period 78—77514
asteroids, precise positions of 25 objects 79—58292
asteroids, precise posns. for 74 objects in 1977, Swedish obs. 80—62065
asteroids, precise posns. in 1975-6 period for 30 main belt objects 78—77515
asteroids, Saratov obs. (1974 April-Oct.) *(Russian)* 80—46457
asteroids, Trojan group, discovery of new members, orbital elements and ephemerides 80—72847
asteroids (1975-1978), Uppsala southern station obs. 80—85883
asteroids in 1978 April, ESO obs. 80—85882
astrographic plates, reduction model 79—44334
astrolabes concurrent obs., 1966-1975 period, Universal Time determ. *(Russian)* 78—73617
astronomical azimuth determ., accuracy, geodetic networks orientation control appl. 78—92774
astronomical refraction, general theory *(Russian)* 78—89045
ε Aurigae, eclipsing binary, astrometric study from Sproul 61-cm refractor plates 78—89219
ε Aurigae, eclipsing binary, distance from astrometric obs. 79—53859
α Aurigae (Capella), orbital motion determ. using phase effect detect. at CERGA stellar interferometer *(French)* 80—36508
automatic astrometric and photometric system appl. *(Russian)* 78—24467
automatic astrometric instrument for use on lunar surface 77—17372
azimuth alterations, influence on absolute right ascension calcs. *(Russian)* 79—35134
Barnard's star 1916-1976, sexagintennial report 77—45432
Basle catalogue of 1906 blue objects at high galactic latitudes 78—32360
BD +11° 4571=ADS 15010, subdwarf binary, history of astrometric obs. 79—62874
binary stars, meas. via speckle interferometry 77—71011
binary stars, obs. by speckle interferometry 80—90477
binary stars, speckle interferometry with 1 m telescope 78—69831
binary stars, visual, speckle interferometric meas. 77—78820
binary stars, visual obs. 79—35303

astrometry continued
binary stars ang. separation meas. by speckle interferometry 79—40215
binary stars orbital solutions, derivation for unseen companions 78—93313
binary stars unresolved by speckle interferometry, epochs of obs., (1975-77) 78—73735
binary systems, speckle interferometric obs. with Haute-Provence 1.93 m telescope 80—90475
Bordeaux Observatory, equatorial coords. for asteroids, planets and Moon in 1972-4 period *(French)* 78—81577
Bradfield (1979c), precise positions for 1979 Jun.-Jul., parabolic orbital elements 79—84746
bright nearby stars, astrometric anals. from Sproul 61 cm refractor plates 80—61991
Brorfelde transit circle, diameter corrections 80—105164
4C 03.59, BL Lacertae object, radio position and struct. of halo 78—4386
CC 1299 (BD+27°4120), unresolved astrometric binary, orbital anal., mass and parallax 80—109464
3C 345 and NRAO 512, relative position to submilliarcsecond accuracy via VLBI 80—22097
4C radio galaxies, positions, structs. and optical identifications 79—71137
Cagliari VZT obs. of polar latitude variations *(Italian)* 79—21153
α Canis Majoris, relative positions of components of visual binary 77—82274
α Canis Majoris (Sirius), astrometric study rel. to distance and components masses 79—5858
β Capricorni, triple star, fundamental parameters from occultation astrometry and spectroscopy 79—40216
celestial mechanics and astrometry, book 79—12384
celestial navigation, with stereographic projection 77—60866
celestial photography with wide-angle astrographs, for astrometric catalogue *(Russian)* 78—40800
celestial pole, exact definition 79—53703
VV Cephei, eclipsing binary, astrometric obs. at Sproul Observatory 78—4290
VV Cephei, eclipsing binary, distance from astrometric obs. 79—53859
Cepheids, ultrashort period, classification from photometric and astrometric data 80—62135
Ceres, Belgian obs. and computed orbital elements *(French)* 77—71049
Ceres, new reduction and collection of meridian obs. 77—13277
Ceres, occultations of stars during 1979/1980 apparition, predictions 79—62785
γ Ceti AB, occultation by 6 Hebe on 1977 March 5, predictions 77—29702
charge injection device as stellar tracking sensor 80—85861
Charon (1978 P 1), posns. in 1980 April rel. to probable occultation 80—67651
Charon (1978 P 1), satellite of Pluto, positions and dynamical parameters 80—62069
Ci 182354, astrometric anal. of unseen companion from 61 cm Sproul refractor plates 78—16459
CL4 optical counterpart, accurate position 79—17116
CL 4, radio source, optical counterpart detect. and position 79—71138
CL 4, radio source, optical identification and optical position 79—21453
clock stars, R.A. correction, Melbourne obs. reduction *(Russian)* 79—92653
CC Comae, W Ursae Majoris star, proper motion 77—74099
Comet, Bradfield (1979l), precise positions (1979 December 28 to 30) 80—31255
Comet Bowell (1980b), discovery posns., elements and ephemeris 80—51695
Comet Bowell (1980b), precise positions, elements and ephemeris (1980 March-July) 80—62075
Comet Bowell (1980b), precise posn. and orbital evolution 80—56770
Comet Bradfield (1974 III), precise positions 80—46494
Comet Bradfield (1974 III), precise positions 1974 April 7-May 12 period 77—91473
Comet Bradfield (1975p), precise positions for 1976 Jan. 31-Feb. 1 77—17446
Comet Bradfield (1976a), precise position for 1976, Mar. 77—2371
Comet Bradfield (1976d), precise positions 1976 Mar. 27, 28 77—22140
Comet Bradfield (1978c), positions, elements and ephemeris 78—32401
Comet Bradfield (1978c), positions, improved elements and ephemeris 78—36514
Comet Bradfield (1978c), positions, magnitudes and UBV photometry 78—36521
Comet Bradfield (1978c), positions and appearance (1978 February) 78—32405
Comet Bradfield (1978c), positions and visual magnitude estimates 78—40873
Comet Bradfield (1978c), precise position 1978 March 12 78—40879
Comet Bradfield (1978c), precise positions, 1978 (February 15 to March 12) 78—65551
Comet Bradfield (1978c), precise positions 1978 Feb.-Mar., total visual magnitude estimates 78—45288
Comet Bradfield (1978c), precise positions and magnitudes (1978 Feb.) 78—32404
Comet Bradfield (1978c), precise psoitions, (1978 February 28 to March 8) 78—40875
Comet Bradfield (1978o), precise position for 1978 Oct. 18 78—96439
Comet Bradfield (1978o), precise positions for 1978 Oct. 78—96433
Comet Bradfield (1979c), precise position for 1979 August 18 79—84751
Comet Bradfield (1979c), precise positions for 1979 Aug. 79—88624
Comet Bradfield (1979c), precise positions for 1979 Jun.-Jul. 79—80271
Comet Bradfield (1979c), precise posns., elements and ephemeris (1979 June-July) 79—75159
Comet Bradfield (1979c), precise posns. (1979 June 25) 79—70999
Comet Bradfield (1979l), obs. of precise position in 1980, 8th to 22nd Jan. 80—36572
Comet Bradfield (1979l), posns., elements and ephemeris (1980 Jan. 5-26) 80—31256
Comet Bradfield (1979l), precise props., orbital element and ephemeris (1979 Dec.-1980 Feb.) 80—26813
Comet Cernis-Petrauska (1980k), antitail, precise posns., parabolic elements and ephemeris 80—105206
Comet Cernis-Petrauskas (1980k), positions, 1980 August 2 to 16, orhital elements and ephemeris 80—98614
Comet Cernis-Petrauskas (1980k), precise position, (1980 August 17) 80—101556

- **astrometry** continued
  - comet discovery, 1977 July 18-19 positions 78—77518
  - Comet Fujikawa (1978n), precise position, (1978, October 10) 78—93166
  - Comet Fujikawa (1978n), precise position for 1978 Oct. 11 78—96434
  - Comet Fujikawa (1978n), precise positions, (1978, October 11 to 16) 79—5779
  - Comet Fujikawa (1978n), precise positions, (1978, October 13 to 14) 78—93168
  - Comet Giclas (1978k), precise positions, (1978 September 10 to 12) 78—89122
  - Comet Haneda-Campos (1978j), precise positions for 1978 Sept. 78—85913
  - Comet Harlan (1976g), precise positions 1976, Jun.-Oct. 77—5506
  - Comet Harlan (1976g), precise positions 1976 Jul. 19, Sept. 18, Oct. 24 77—22139
  - Comet Helin (1977e), positions, appearance parabolic elements and ephemeris 77—49335
  - Comet Helin (1977e), precise positions, elements and ephemeris (April-May 1977) 77—45364
  - Comet Helin (1977e), precise positions 1977 April-May 77—64700
  - Comet Helin (1977e), precise positions (1977, May) 77—49338
  - Comet Helin (1977e), precise positions (1977 April 18-29) 78—7935
  - Comet Helin (1977e), precise positions for 1977 April 18-22 period 77—41360
  - Comet Kobayashi-Berger-Milon (1975 IX), precise positions 80—46494
  - Comet Kobayashi-Berger-Milon (1975 IX), precise positions 1975 Aug. 4-14 period 77—91473
  - Comet Kobayashi-Berger-Milon (1975h), positions 77—13287
  - Comet Kohler (1977 XIV), precise positions for 1977 Sept.-Dec. from photographic obs. 80—4302
  - Comet Kohler (1977m), positions, elements, ephemeris and magnitude estimates 77—91484
  - Comet Kohler (1977m), positions, spectral emissions and magnitudes 78—7924
  - Comet Kohler (1977m), precise positions, (1977 October 4 to 1978 April 8) 78—73680
  - Comet Kohler (1977m), precise positions, (1977 October 5 to 19) 80—105203
  - Comet Kohler (1977m), precise positions, magnitudes, elements and ephemeris 77—87328
  - Comet Kohler (1977m), precise positions 1977 Oct. and 1978 Jan. 78—45286
  - Comet Kohler (1977m), precise positions 1977 Sept.-1978 Jan., total visual magnitude estimate 78—36518
  - Comet Kohler (1977m), precise positions (1977 Oct.-Nov.) 78—16355
  - Comet Kohler (1977m), precise positions (1977 September-October) 78—4155
  - Comet Kohler (1977m), precise positions and total magnitudes 1977, Sept. 77—87335
  - Comet Kohler (1977m), precise positions for 1977, Oct. to Dec. 78—20751
  - Comet Kohler (1977m), precise positions for 1977 Oct.-Dec. period 78—28590
  - Comet Kohler (1977m), precise positions for 1977 Oct.-Nov., total visual magnitude estimates 78—20743
  - Comet Kohler (1977m), precise positions for 1977 Sept. 7-18 period 77—87334
  - Comet Kohler (1977m), precise positions for 1977 Sept.-Dec., total visual magnitude estimates 78—20753
  - Comet Kohler (1977m), precise posns. for 1977 October-1978 March period 78—61806
  - Comet Kohler (1977m) precise positions (1977 October 13 to November 10) 78—7937
  - Comet Kohoutek (1973 XII), precise position determ. 80—46494
  - comet Kowal (1977f), precise positions 1977, May and orbital elements 77—53481
  - Comet Kowal (1977f), precise positions and possible ephemerides (1977, April-May) 77—53476
  - Comet Kowal (1979a), precise positions, (1979 February 1) 79—35195
  - Comet Kowal (1979a), precise positions 1979 Jan., orbital elements, ephemeris 79—25549
  - Comet Kowal (1979h), precise positions for 1979 Jul. 79—88625
  - Comet Lovas (1974c), precise positions, 1976, Aug.-Oct 77—5501
  - Comet Lovas (1974c), precise positions 1976, July 26-Sept. 18 77—17435
  - Comet Lovas (1974c), precise positions 1976, Oct.-Nov. and orbital elements 77—22145
  - Comet Lovas (1975 VIII), precise positions and ephemeris for (1977 May 17 to December 23) 77—37578
  - Comet Lovas (1975 VIII), precise posns. (1977 Aug. and Sept.) 78—12159
  - Comet Lovas (1976 XII), precise posn. (1978 February 4) 78—49386
  - Comet Lovas (1976k), precise position 1976, Dec. 77—33421
  - Comet Lovas (1976k), precise position 1977 Jan. 20 77—64701
  - Comet Lovas (1976k), precise positions 1976, Dec., ephemeris for 1977, Jan.-Jun. 77—17442
  - Comet Lovas (1976k), precise positions 1976, Nov. 77—5505
  - Comet Lovas (1976k), precise positions 1976, Nov. and Dec. and improved elements 77—9709
  - Comet Lovas (1976k), precise positions 1976, Nov. and Dec. and improved elements 77—17434
  - Comet Lovas (1976k), precise positions 1976 Dec. 26-30 77—22141
  - comet Lovas (1976k), precise positions 1976/77 and ephemeris for 1978 Mar.-Jun. 78—24491
  - Comet Lovas (1976k), precise positions (1976 November 23) 77—9708
  - Comet Lovas (1976k), precise positions (1977, January) 77—29726
  - Comet Lovas (1976k), precise positons for 1977 Feb. 11, 19 and Mar. 14 77—53480
  - Comet Lovas (1977c), precise position, improved elements and ephemeris 77—82174
  - Comet Lovas (1977c), precise position (1977, March 12) 77—33417
  - Comet Lovas (1977c), precise positions, orbital elements and ephemeris 77—41358
  - Comet Lovas (1977c), precise positions, parabolic elements, ephemeris correction 77—33416
  - Comet Lovas (1977c), precise positions (1977, March-April) 77—49337
  - Comet Lovas (1977c), precise positions and corrected ephemeris 77—33415
  - Comet Lovas (1977c), precise positions for 1977 Feb. 28 and Mar. 19 77—37577

- **astrometry** continued
  - Comet Machholz (1978l), precise positions, total visual magnitude estimates, 1978 Sept. 78—89130
  - Comet Machholz (1978l), precise positions 1978 Sept.-Oct., magnitudes 78—93163
  - Comet Meier (1978 XXI), position from 1979 April 21 to 30, meas. and reduction *(French)* 80—72884
  - Comet Meier (1978f), positions, elements, ephemeris, magnitudes and spectrum 78—53881
  - Comet Meier (1978f), posns., elements, ephemeris and magnitudes 78—61801
  - Comet Meier (1978f), precise position, orbital elements, ephemeris and magnitude law 79—5781
  - Comet Meier (1978f), precise position, total visual magnitude estimate, 1978 Nov. 79—5789
  - Comet Meier (1978f), precise positions, 1978, April 30 to (May 8) 78—53884
  - Comet Meier (1978f), precise positions, (1978, May 2 to June 9) 78—69751
  - comet Meier (1978f), precise positions and magnitude estimates (1978 May-June) 78—69748
  - Comet Meier (1978f), precise positions for 1978 Apr.-May, total visual magnitude estimates 78—57505
  - Comet Meier (1978f), precise positions meas. at ESO, La Silla, in (April 1979) 80—105204
  - Comet Meier (1978f), precise posn. and visual mag. estimate (1978 Nov.) 79—5784
  - Comet Meier (1978f), precise posns. (1978 May-July) 78—77520
  - Comet Meier (1978f), precise posns. and total visual mag. estimates (1978 Apr.-May) 78—57504
  - Comet Meier (1979i), precise positions (1979 September 22 to 28) 80—4306
  - Comet Meier (1979i), precise posns., orbital elements, ephemeris and magnitudes (1979 Sep.-Oct.) 79—101118
  - Comet Meir (1978f), precise positions 1978 Apr. 78—49387
  - Comet Mori-Sato-Fujikawa (1975 XII), precise positions 1975, May and June 77—53483
  - Comet Mori-Sato-Fujikawa (1975j), positions, 1975 Dec. 4-10 period 77—74012
  - Comet Mori-Sato-Fujikawa (1975j), precise position (1976, October) 77—29728
  - Comet Mori-Sato-Fujikawa (1975j), precise positions 1976, Mar.-Sept. 77—17438
  - Comet Russell (1979d), precise posns., elements and ephemeris (1979 June-July) 79—71002
  - Comet Russell (1980l), precise positions, 1980 September 6 to 8, and ephemeris 80—101559
  - Comet Sanguin (1977p), precise positions for 1977 October 78—4151
  - Comet Schuster (1975 II), precise positions, 1977, February 12 to 25, and orbital elements 77—37579
  - Comet Schuster (1975 II), precise positions 1977 Feb. and May 77—71065
  - Comet Schuster (1975 II), precise positions 1978 Jan. 78—40880
  - Comet Schuster (1975 II), precise posns. (1977 June) 78—12158
  - Comet Schuster (1976c), precise position and tail obs. (1977, January) 77—29727
  - Comet Schuster (1976c), precise positions 1976 July 28 77—17437
  - Comet Schuster (1976c), precise positions for 1976 Mar. 25 and Jun.2 77—22147
  - Comet Seargent (1978m), precise positions, (1978, October 2 to 4) 78—93164
  - Comet Seargent (1978m), precise positions (1978, October 6) 78—96432
  - Comet Seargent (1978m), precise positions for 1978 Oct. 78—96436
  - Comet Seargent (1978m), precise positions for 1978 Oct. 78—96438
  - Comet Torres (1979e), precise position, 1979 July 31, and ephemeris 79—84749
  - Comet Torres (1979e), precise positions, (1979 July 3) 79—75161
  - Comet Torres (1979e), precise positions for 1979 Jun.-Jul. 79—84747
  - Comet Torres (1979e), precise posns., elements and ephemeris (1979 June-Aug.) 79—75160
  - Comet Torres (1980e), precise posns., elements and ephemeris (1980 June-July) 80—85900
  - Comet Tritton (1978d), positions, elliptical elements, ephemeris and magnitude law 78—36522
  - Comet Tsuchinshan (1977q), 1977 November 8 precise positions and appearance 78—4154
  - Comet Tsuchinshan (1977q), positions, elements, and ephemeris 78—16350
  - Comet Tsuchinshan (1977q), precise positions, elements and ephemeris 78—16353
  - Comet Tsuchinshan (1977q), precise positions (1977 December) 78—28584
  - Comet Tsuchinshan (1977q), precise positions (1978, January 3) 78—45284
  - Comet Tsuchinshan (1977q), precise positions for 1977 Nov.-Dec. 78—20746
  - Comet Tsuchinshan (1977q), precise posns. (1977 Nov.-1978 Jan.) 78—61804
  - Comet van den Bergh (1974 XII), precise position (1976, October 31) 77—29729
  - Comet West (1975n), nucleus A precise positions, nuclei B and D separations and position angles 77—53478
  - Comet West (1975n), positions from photographic obs. 77—33411
  - Comet West (1975n), precise positions 1976 Apr. 1 and Jun. 2, orbital elements 77—17447
  - Comet West (1975n), precise positions of nuclei, 1976 May and September 77—9707
  - Comet West (1976 VI), precise positions 80—46494
  - Comet West (1978a), positions, parabolic elements and ephemeris 78—28583
  - Comet West (1978a), positions and ephemeris extension (1978 Jan.-July) 78—36516
  - Comet West (1978a), precise positions 1978 Jan., Mar. 78—49383
  - Comet West (1978a), precise positions for 1978 Jan.-May 78—61799
  - Comet West (1978a), precise posns. (1978 February-March) 78—40872
  - Comet West (1978a), precise prediscovery positions, hyperbolic elements 78—40878
  - Comet West (1978a), semiaccurate positions 1978, Jan. 78—24492
  - Comets Kowal, two probable objects, discovery posns. and ephemerides 79—96973
  - compact radiosources positions from VLBI obs. 78—81698

astrometry continued
composite spectrum stars susceptible to lunar occultation, identification list of 68 stars 80—26908
conference on celestial mechanics and positional astronomy, Washington, DC, USA (Nov.-Dec. 1978) 80—90605
coordinate measurements using phase and fringe freq., tropospheric limitations 79—44375
Crab pulsar, proper motion 77—82269
CTC right ascensions, synthetic catalogue for Chinese time service *(Chinese)* 78—28540
V1500 Cygni, accurate position and praenova search 77—2440
$31=o^2$ Cygni, astrometric studies 78—69779
61 Cygni, detect. of three invisible companions to visual binary star 78—28730
β Cygni, visual obs. of brighter component close companion 80—8663
Cygnus A compact radiosource, astrometric obs. 77—74152
daily latitude variations anal. 80—21891
Danjon astrolabe, instrumental const. *(French)* 79—75101
data reduction, least-squares adjustment with probabilistic constraints 78—32352
daytime astrometric observations, correction for anomalous refr. and personal errors 78—24441
declination improvement inc. flexure determs. *(Russian)* 79—92654
declination obs. of circumpolar stars with meridean circle *(Japanese)* 78—89044
declinations, differential determ. from obs. with vertical circle *(Russian)* 79—96888
Deimos, photographic positional obs. with Ukrainian Academy 400 mm astrography *(Russian)* 79—44395
78 Diana, astrometric obs. rel. to central path of occultation of SAO 75392, (1980 September 4) 80—101547
differential astrometry and method of arcs *(Russian)* 79—80205
diffuse moving object, discovery and precise positions for (July 1, 1976) 77—33423
digital image centring algorithm for astrometric positioning 78—69696
diurnal latitude vars. spectra based on obs. at Gor'kii 79—35100
dMe-stars, multiplicity 79—44544
double star measures at Lick Observatory, Mount Hamilton, California 78—85979
double stars, micrometer obs. 78—57582
double stars, new discoveries at Nice, 15th series *(French)* 79—35304
double stars, Nice obs. of 267 objects *(French)* 79—44531
double stars, obs. using phase-grating stellar interferometer *(Russian)* 79—101070
double stars, obs. with Herstmonceux 28-inch refractor, (1963-1970) 80—41863
double stars, photographic measures 78—57581
double stars, position angles and separation, Venezuelan obs. *(French)* 80—77450
double stars, rectilinear trajectories calc., appl. to L 5094, effects of erroneous positions *(French)* 78—20857
double stars, separation and position angle obs. 80—98691
double stars discovered at Nice, 14th series *(French)* 77—78654
Earth daily free nutation parameters, determ. technique 78—96126
Einstein effect (gravitational deflection of light), obs. at solar eclipse (1981 July 31) *(Russian)* 80—51651
Einstein gravitational light deflection in astrometry 77—17359
emulsion shifts and astrometric accuracy of the photographic plate 77—71006
equatorial coordinates derivation from astronomical photographs, Palomar Sky Survey appl. 78—32324
equatorial stars declinations, obs. programme of Pulkovo Observatory expedition to Equator *(Russian)* 79—96892
equinox, position and motion during 250 yrs. 77—73935
433 Eros, astrometric obs. during 1975 opposition 78—57485
433 Eros, Belgian obs. and computed orbital elements *(French)* 77—71049
15 Eunomia, close approaches to SAO stars, prediction accuracy 79—30003
extra-solar planetary systems, detection by Space Telescope 80—109356
extragalactic radio sources from NRAO-Bonn 5 GHz survey, positions of optical candidates 77—78880
extragalactic radiosources, optical identification, astrometry using Palomar Sky Survey prints 77—87274
extrasolar planetary systems, dynamical instability and detection 80—82429
fitting procedures for stellar positions on Schmidt photographs 80—72783
Fk4, corrections based on photographic posns. of Venus 79—8851
FK4, corrections to zero points from minor planet obs. *(Russian)* 80—82228
FK4, equinox and equator improvement *(Russian)* 79—58277
FK4 catalogue, right ascension and declination corrections from meridian obs. *(Russian)* 77—71016
FK4 equator and equinox corrections from asteroid orbits 78—69727
FK4 equinox corrections from minor planet meridian obs. 80—8519
FK4 star coord. improvements using Ni2 astrolabe obs. *(German)* 80—26719
FK4 stars general catalogue of astrolabe obs. (1958-75) *(French)* 78—36468
FK4 supplementary stars, right ascensions obs., definitive results 80—17473
FK5, equinox and equator of new fundamental reference coord. system 80—109341
FKSZ stars, differential catalogue of RA in 20-90° zone, Pulkovo obs. *(Russian)* 78—28644
FKSZ stars, meridian circle obs. at Kiev University Observatory, (1972 to 1975) *(Russian)* 79—44336
fundamental astrometry rel. to celestial mechanics and radioastronomy *(German)* 78—45200
fundamental bright southern stars, $\Delta\alpha_\delta \cos\delta$ corrections *(Russian)* 77—56817
fundamental coordinate system, rot. 79—62727
fundamental star catalogue system, improvement via relative determs. of celestial bodies coordinates 78—53797
fundamental system of star position and motion, accuracy improvement using asteroid obs. 80—94692
G139-29, perturb. from rectilinear motion, astrometric red dwarf binary system with subluminous component 79—8910
galactic clusters, membership probabilities, photographic meas. of relative proper motions of stars 80—51817

astrometry continued
galactic clusters in Cassiopeia, stellar photometry and proper motions obs. *(Russian)* 79—97042
galactic inertial-coordinate frame rel. to celestial reference, for starship navigation 78 -49346
S.Galactic Pole, astrometry of B<14 stars, UK Schmidt results 79—66929
galactic/equatorial coordinate systems, interconversion 79—88569
Galilean satellites, 1976-8 relative posns. 79—62789
Galilean satellites, astrometric obs. in (1977) 79—48728
Galilean satellites, mutual phenomena during 1979, obs. 79—80266
Galilean satellites, photometric eclipses anal. rel. to theory of motion 78—53864
general catalogue of 1139 stars obs. with astrolabes, 1957-75 period, FK4 stars position corrections *(French)* 78—32359
geodetic astronomy and astrometry, international colloquium (Dresden, Germany, 1978) *(German)* 80—36223
Gor'kii latitude observations, half-year nutation wave terms errors 79—62728
Greenwich Obs. Time and Latitude Service, Time Report (April-June, 1977) 78—69661
Greenwich Obs. Time and Latitude Service, Time Report (January-March 1978) 79—25453
Greenwich Obs. Time and Latitude Service, Time Report (January to March 1979) 80—72749
Greenwich Obs. Time and Latitude Service, Time Report (July-September 1977) 78—73619
Greenwich Obs. Time and Latitude Service, Time Report (July-September 1978) 79—62729
Greenwich Obs. Time and Latitude Service, Time Report (October to December, 1977) 78—89046
Greenwich Obs. Time and Latitude Service Time Report (April-June 1979) 80—72750
Greenwich Obs. Time and Latitude Service Time Report (October-December 1978) 79—101053
GX 339—4, variable X-ray source identification with faint blue object 79—40294
gyro. instruments, precession-correction monitoring, expt. planning 79 -71422
gyroinstruments testing under operating conditions using system with astrocorrections 79—71413
h 3556, triple star, binary orbit and masses and third component relative motion 79—88701
H-H 28, H-H 29, large proper motion Herbig-Haro objects, astrometric obs. 79—71022
halfsecond levels, investigations using atuomatic comparator *(Russian)* 78—40675
HD 165590, high eccentricity visual binary, periastron time, radial vel. vars. 78—45363
HD 87892, visual binary nucleus of NGC 3132, separation and position angle 78—20859
Herbig-Haro object 1 exciting star, precise position and nature 80—17633
Hipparcos, European astrometric satellite, prospects 79—96880
HIPPARCOS, global astrometry by space techniques 80—109369
Hipparcos, meas. of stellar distances *(French)* 80—94688
Hipparcos astrometric satellite project and space telescope astrometric program, review *(French)* 80—46365
Hipparcos satellite, proposed space-astrometry mission 80—82164
Hyades, convergent point method for kinematic parallaxes determ. 77—91596
image analysis system, software and astrometric appl. 78—53834
instrument index mark optimum brightness calc. 79—53720
85 Io, astrometric obs., 1865-1977, and definitive orbit 80—4284
Jupiter, astrometric obs. of faint satellites during 1975-6 opposition 79—75139
Jupiter, Galilean satellites, 1975-6 astrometric obs. 80—4288
Jupiter's satellites, precise positions during 1973 77—17421
Jupiter and Galilean satellites, astrometric position determ. 80—77327
Jupiter and Galilean satellites, image photometric anal. technique *(French)* 80—85880
Jupiter and Galilean satellites, position determ. (1977) *(French)* 80—77326
Jupiter and Galilean satellites, positions obtained in 1978 at ESO-La Silla *(French)* 80—21943
Jupiter faint satellites, astrometric obs. during 1976 to 1977 opposition 80—26778
Jupiter faint satellites (VI-XIII), astrometric obs., (1974 to 1977) 78—89107
Jupiter inner satellites, mutual phenomena in 1979, ephemerides and astrometric aspects 78—53866
KUV09313+4052, variable UV excess object, discovery, position and photometry 80—62159
laser range measurements, atmospheric correction determ. *(Russian)* 80—12674
latitude variation, computation for national ephemerids calc. 78—88776
latitude vars. and diurnal polar motion *(Russian)* 80—51641
Leda (Jupiter XIII), precise positions for 1976 Nov. 2 and Dec. 13 77—22135
Lick proper motions referred to galaxies, precession and galactic rot. determ. 78—65487
long-baseline interferometer for astrometry 77—37506
lunar occultations, obs. at Sydney Observatory during (1974-1976) 78—69658
lunar occultations during 1943-74, anal., rel. to Brown's theory, FK4 right ascension system and Watt's charts corrections 79—48696
lunar position computation algorithm 79—25452
RR Lyrae stars, absolute proper motions for 64 stars *(Chinese)* 79—80319
M13, globular cluster, astrometric membership probabilities from old proper motions 79—88708
M13, globular cluster, new stellar proper motions and membership probabilities 79—75252
M1-78, emission nebula, optical position and 15.4 GHz struct. 78—41025
major planets, positions determ. with Odessa meridian circle, (1974 to 1975) *(Russian)* 79—44394
Mars, astrolabe obs. from Paris Observatory (winter 1977-78) *(French)* 79—70982
Mars, ephemerides and position, 1975 to 1976, additional information *(French)* 79—44392

astrometry continued
Mars, obs. with Algiers astrolabe (winter 1973) *(French)* 78−61775
Mars, obs. with Danjon astrolabe of San Fernando Observatory *(French)* 78−57483
Mars, photographic position meas. *(Russian)* 78−93137
Mars, photographic positional obs. with Ukrainian Academy 400 mm astrograph *(Russian)* 79−44395
Mars, photographic positions in 1973 and 1974, Pulkovo normal astrograph obs. *(Russian)* 78−28567
Mars, photographic zenith tube obs. during 1975 and 1978 oppositions 79−40109
Mars, position and ephemerides (1975-1976) *(French)* 78−45252
Mars, position obs. with Paris astrolabe (1975 to 1976) *(French)* 78−61776
Mars, positional photographic obs. with Pulkovo double short-focus astrograph, (1973 to 1974) *(Russian)* 79−96944
Mars, positions, with Danjon astrolabe at San Fernando Observatory (Jan. to Feb. 1978) *(French)* 80−94736
Mars, positions (1975-6), Paris Astrolabe obs., corrections *(French)* 79−44393
Mars, positions and ephemeris corrections from Paris astrolabe obs. *(French)* 79−101103
Mars, rot. period determ. from transits of albedo stations across central meridian (1659 to 1971) 80−98588
Mars, satellites, positional photographic obs. during 1973 October at Pulkovo *(Russian)* 78−28568
Martian satellites, history of discovery and positional obs. (1877 to 1977) 78−89101
Me, globular cluster, stellar proper motions, membership and cluster internal motions 80−8665
18 Melpomene, occultation of SAO 114159 on 1978 Dec. 11, revision obs. 79−12423
Merate Observatory, time and latit. results of astrolabe obs. (1977) 79−40061
Mercury, right ascension determ. from radio obs. *(Russian)* 79−21213
meridian circles pivot errors, new determ. method 78−53822
meridian instrument pivot irregularities meas. method 80−94718
meridian meas. of Zhang Sui and first astronomical geodetic survey in China *(Chinese)* 77−64911
meridian passages of stars obs. at Dresden Univ., microclimatic effects *(Russian)* 78−73612
Minor Planet Circular 5333-5390, precise posns. for asteroids and eight comets 80−77325
Minor Planet Circulars, precise posns. for asteroids and eight comets 80−31241
Minor Planet Circulars 4391-4424, precise posns. for asteroids and 15 comets 78−81578
minor planet circulars 4425-4482, precise posns. for asteroids and eight comets 78−85886
Minor Planet Circulars 4483-4520, precise posns. for asteroids and 13 comets 78−93140
minor planet circulars 4521-4548, precise posns. for asteroids and 16 comets 79−2514
minor planet circulars 4549-4582, precise posns. for asteroids and five comets 79−12421
Minor Planet Circulars 4583-4622, precise posns. for asteroids and 14 comets 79−16871
Minor Planet Circulars 4623-4648, precise posns. for asteroids and three comets 79−25538
Minor Planet Circulars 4649-4688, precise posns. for asteroids and 11 comets 79−35178
Minor Planet Circulars 4689-4722, precise posns. for asteroids and 23 comets 79−53754
Minor Planet Circulars 4723-4746, precise posns. for asteroids and 14 comets 79−66953
Minor Planet Circulars 4747-4788, precise posns. for ateroids and five comets 79−75136
Minor planet circulars 4789-4844, precise posns. for asteroids and 14 comets 79−84729
Minor Planet Circulars 4845-4936, precise posns. for asteroids and ten comets 79−101107
Minor Planet Circulars 4937-5016, precise posns. for asteroids and 16 comets 80−8580
Minor planet circulars 5017-5066, precise posns. for asteroids and 11 comets 80−17533
Minor Planet Circulars 5137-5188, precise posns. for asteroids and seven comets 80−46459
Minor Planet Circulars 5189-5248, precise posns. for asteroids and 13 comets 80−67631
Minor Planet Circulars 5249-5286, precise posns. for asteroids and six comets 80−67632
Minor Planet Circulars 5287-5332, precise posns. for asteroids and eight comets 80−67633
Minor Planet Circulars 5391-5422, precise posns. for asteroids and eight comets 80−85884
Minor Planet Circulars 5423-5454, precise posns. for asteroids and seven comets 80−98599
minor planets, 1978, April, astrometric positions determ., ESO GPO obs. 80−77319
minor planets, hypothetical observations giving equinox and equator determ. 80−94742
minor planets, meridian obs. (1974 to 1977) 78−69660
minor planets, positions from Torino Observatory (1977-1979) 80−94739
minor planets, positions in August 1977 from Observatorio Nacional, Rio de Janeiro *(French)* 80−94740
minor planets, precise positions obs. at Sydney Observatory during (1976) 78−69735
minor planets observations, least squares soln. of ill-conditioned systems 80−26747
Miranda (Uranus V), appulse to BD−14°3996 on 1977, March 10, predictions 77−2369
Moon, ALSEP-quasar differential very long baseline interferometry technique 78−45245
Moon, crater/stars superimposed photography using automatic device, lunar coords. meas. *(Russian)* 79−92675
Moon, Kazan heliometric obs. (1895-1958), new reduction *(Russian)* 79−92688
Moon, positional photographic obs. at Pulkovo with long-focus horizontal telescope *(Russian)* 78−28533
Moon, topocentric aberration, reduction method for astrometric obs. 78−4081

astrometry continued
Moon, Watts datum centre determ. rel. to lunar centre of mass 77−71020
multi-frequency radio interferometry, effect of noise on coordinate accuracy *(Russian)* 77−78644
multiple stars, parallaxes and proper motions, Sproul 61 cm refractor astrometric meas. 77−9768
multiple stars, visual obs. 79−35303
MXB 1659-29, burst source identification with faint blue object 79−40294
narrow field optical astrometry, atmospheric turbulence limitations 80−109340
nearby stars, search for unseen and sub-stellar companions 79−30092
nearby stars, space astrometry 80−67518
nearby stars, trigonometric parallaxes published (1969-1978) 80−36513
51 Nemausa, astrometric posns. for coord. system error reduction 80−72849
NGC 6494 (M23), open star cluster, membership from astrometry with PDS microdensitometer 80−98697
NGC 7027, planetary nebula, position meas. with small Schmidt telescope 78−73749
Nova Cygni 1978, discovery report and precise position 78−85962
Nova Cygni 1978, spectrum, precise position and photometry 78−89211
nova in Sagittarius, discovery of probable declining nova (1978 March) 80−4376
Nova Ophiuchi 1976, precise position 77−2444
Nova Sagittae 1977, precise position, photographic and visual magnitudes 77−17602
Nova Sagittarii 1977, position and visual magnitude estimates 77−33519
Nova Sagittarii 1978, precise position, visual magnitude estimates 1978 Apr. 78−49458
Nova Serpentis 1978, precise position, spectra, visual magnitude estimates 78−36596
Nova Vulpeculae 1979, posn., magnitudes, spectrum and photometry 79−48818
Nova Vulpeculae 1979, precise position and spectroscopic obs. 79−48820
novae, astrometric posns. and identifications for old classical and recurrent objects 79−21315
O-type stars, positional catalogue on mag. tape, third edition 77−2348
Object Kowal, positions, indeterminate orbit, elements and ephemeris 78−7907
object Kowal, slow-moving asteroid discovery and positions 78−4136
objectivisation of observations with circumzenithal, using photoelec. device *(Russian)* 78−73654
observations from space-borne platform *(Polish)* 80−67519
Ohio radio sources, optical identification using radio and optical positions meas. by Texas interferometers 78−28808
optical sensor array systems for astronomic longitude determ. 77−82023
χ^1 Orionis, new solar-type astrometric binary, parallax and orbital elements 78−73740
overlapping plate method 80−36479
overlapping plates, block adjustment *(German)* 78−45237
Pallas, new reduction and collection of meridian obs. 77−13277
Palomar Schmidt plates, astrometric reduction, least squares prediction appl. 79−40082
Palomar Sky Survey plates, microdensitometer meas., photometric parameters and positions of images 78−24440
Palomer Schmidt plates, astrometric accuracy 78−57455
parallax and proper motion meas. for seven stars 80−62109
parallax techniques, discussion 79−88568
parallaxes, need for space-borne and ground-based obs. 79−66992
parallaxes and Astrometric Satellite 79−30051
parallaxes of objects at cosmological distances, meas. via radiointerferometric techniques 78−53796
Paris astrolabe observations, time and latitude (1976) *(French)* 77−78078
Paris astrolabe time and latitude obs. for 1977-8 period *(French)* 79−101051
Period Comet Brooks 2 (1980f), recovery, positions and perihelion passage correction 80−85899
Periodic Comet Arend-Rigaux (1977k), position and tail obs. (1978 March 5) 78−40874
Periodic Comet Arend-Rigaux (1977k), positions, appearance and spectrum 78−12157
Periodic Comet Arend-Rigaux (1977k), precise positions 1977 Aug. 77−91477
Periodic Comet Arend-Rigaux (1977k), precise positions 1977 Oct.-1978 Jan., total visual magnitude estimates 78−36517
Periodic Comet Arend-Rigaux (1977k), precise positions for 1977 Nov.-Dec. 78−20745
Periodic Comet Arend-Rigaux (1977k), precise positions for 1977 Oct.-1978 Mar. 78−65548
Periodic Comet Ashbrook-Jackson (1977g), 1978 April precise posns. from ESO La Silla *(French)* 79−101117
Periodic Comet Ashbrook-Jackson (1977g), precise position (1977 Oct. 13) 78−20749
Periodic Comet Ashbrook-Jackson (1977g), precise position for 1978 Apr. 5 78−53887
Periodic Comet Ashbrook-Jackson (1977g), precise positions (1977 May and Sept.) 77−91485
Periodic Comet Ashbrook-Jackson (1977g), recovery, appearance and positions 77−49334
Periodic Comet Ashbrook-Jackson (1978 XIV), precise posns. (1978 April) *(French)* 80−41767
Periodic Comet Chernykh, precise positions and magnitudes (1977 Sept.-Oct.) 78−7926
Periodic Comet Chernykh (1977l), precise positions, improved elements and magnitudes 78−7932
Periodic Comet Chernykh (1977l), precise positions 1977, Sept. 77−91475
Periodic Comet Chernykh (1977l), precise positions 1977, Sept. and Oct., ephemeris to 1978 Apr. 78−7941
Periodic Comet Chernykh (1977l), precise positions 1977 Aug.-1978 Mar. 78−53886
Periodic Comet Chernykh (1977l), precise positions 1977 Dec.-1978 Jan. 78−49379
Periodic Comet Chernykh (1977l), precise positions 1977 Sept.-Dec. 78−24490
Periodic Comet Chernykh (1977l), precise positions (1977 November 17 to 1978 January 8) 78−32400

astrometry continued
Periodic Comet Chernykh (1977l), precise positions and definitive orbit at first apparition (1977 to 1978) 80—62079
Periodic Comet Chernykh (1977l), precise positions and ephemeris for 1977 Aug.-Oct. 77—82170
Periodic Comet Chernykh (1977l), precise positions and visual magnitudes 1977, Aug. and Sept. 77—87330
Periodic Comet Chernykh (1977l), precise positions for 1977 September 77—82173
Periodic Comet Chernykh (1977l), precise positions for 1977 Sept. 6-19 period 77—87333
Periodic Comet Chernykh (1977l), precise positions for 1977 Oct.-Dec., total visual magnitude estimates 78—20755
Periodic Comet Chernykh (1977l), precise positions for 1977 Sept. 79—25546
Periodic Comet Chernykh (1977l), precise posns., improved elements and ephemeris 78—69747
Periodic Comet Chernykh (1977l), precise posns. (1977 Sept.-Nov.) 78—16351
Periodic Comet d'Arrest (1976e), precise positions, 1976, Aug.-Nov. 77—5503
Periodic Comet d'Arrest (1976e), precise positions 1976, July-Oct. 77—17441
Periodic Comet d'Arrest (1976e), precise positions 1976 Aug. 14-23 period *(French)* 77—91474
Periodic Comet d'Arrest (1976e), precise positions (1976, July-August) 77—37571
Periodic Comet d'Arrest (1976e), precise positions and antitail 77—37580
Periodic Comet d'Arrest (1976e), precise positions for 1976 Oct. 15, Nov. 14, Dec. 23 77—22151
Periodic Comet d'Arrest (1976e) precise positions 1976 Jun.-Aug. and total visual magnitudes 77—2372
Periodic Comet Daniel (1979b), recovery on 1979 Feb. 2, precise position, ephemeris 79—30013
Periodic Comet Denning-Fujikawa (1978n), precise positions, (1978, October 28 and November 2) 79—5780
Periodic Comet Encke, precise positions, 1977, Aug. to Oct. 78—7942
Periodic Comet Encke, precise positions, 1977, Sept. 77—91476
Periodic Comet Encke, precise posn. for 1980 Oct. 8 and perihelion passage correction 80—109398
Periodic Comet Encke, semiaccurate position, CN production rate and ephemeris correction 77—67070
Periodic Comet Faye (1976i), precise position 1976 Nov. 23 77—22150
Periodic Comet Faye (1976i), precise position for 1977 Feb. 19 77—82166
Periodic Comet Faye (1976i), precise positions (1976, September-1977, January) 77—45362
Periodic Comet Faye (1976i) precise positions 1976, Jul.-Oct. 77—13289
Periodic Comet Gehrels 3 (1975o), 1976, Oct.-Dec. precise positions 77—25982
Periodic Comet Gehrels 3 (1975o), precise positions, (1977 November 18 to 1978 March 5) 78—40876
Periodic Comet Gehrels 3 (1975o), precise positions 77—60726
Periodic Comet Gehrels 3 (1975o), precise positions for 1978 Feb.-Mar. 78—73677
Periodic Comet Gehrels 3 (1975o), precise posns. for 1978 March-April period 78—49385
Periodic Comet Giclas (1978k), precise position, (1978, September 14) 78—85916
Periodic Comet Giclas (1978k), precise positions 1978 Sept., elliptical elements, ephemeris 78—93162
Periodic Comet Griff-Skjellerup (1977b), precise positions 1977 Jan. 21-26 77—22143
Periodic Comet Grigg-Skjellerup (1977b), precise positions, magnitudes and coma diameters (1977, March-April) 77—49339
Periodic Comet Grigg-Skjellerup (1977b), precise positions 1977 April 22 and May 20 77—60729
Periodic Comet Grigg-Skjellerup (1977b), precise positions 1977, Apr.-May and meteor activity 77—71064
Periodic Comet Grigg-Skjellerup (1977b), precise positions (1977 Jan.-Aug.) 78—7928
Periodic Comet Grigg-Skjellerup (1977b), precise positions and ephemeris, 1977, Mar.-Apr. 77—33414
Periodic Comet Grigg-Skjellerup (1977b), precise positions and appearance (1977, April) 77—45360
Periodic Comet Gunn, position, osculating elements and ephemeris for 1977/8 77—33420
Periodic Comet Gunn, precise positions, 1976, Jul.-Oct. 77—17432
Periodic Comet Gunn, precise positions, Aug., Sept. and Oct. 78—12155
Periodic Comet Gunn, precise positions for 1977 Oct. and Dec. 78—69750
Periodic Comet Haneda-Campos, precise positions, (1978 August 11 to September 5) 78—89121
Periodic Comet Haneda-Campos (1978j), precise position for 1978 Sept. 29 78—93167
Periodic Comet Haneda-Campos (1978j), precise positions, (1978 September 2 and September 8) 78—89124
Periodic Comet Haneda-Campos (1978j), precise positions 1978 Aug.-Sept., ephemeris for 1978 Sept.Oct. 78—89131
Periodic Comet Haneda-Campos (1978j), precise positions (1978, September 6 and 8) 78—85914
Periodic Comet Haneda-Campos (1978j), precise positions (1978, August 10 to September 12) 78—89127
Periodic Comet Harrington (1980m), recovery and precise positions (1980 September 4 to 9) 80—101558
Periodic Comet Holmes, recovery and precise position (1979 July 20) 79—80272
Periodic Comet Klemola (1976j), precise positions 1976, Aug. and Sept. 77—2370
Periodic Comet Klemola (1976j), precise positions 1976, Oct. 77—17431
Periodic Comet Klemola (1976j), precise positions for 1976 Sept. 16-19 77—17445
Periodic Comet Kojima (1977r), precise positions 1977 Dec.-1978 Jan. 78—36519
Periodic Comet Kojima (1977r), precise positions (1977 Dec. 5, 20) 78—20748
Periodic Comet Kojima (1977r), precise positions for 1978 Jan. and Mar. 78—65549
Periodic Comet Kojima (1977r), recovery posns. and earlier obs. 78—20739

astrometry continued
Periodic Comet Kopff (1976b), precise positions 1977 June, July, Sept. 77—91478
Periodic Comet Kopff (1976b), precise posns. (1977 June-Oct.) 78—16356
Periodic Comet Kopff (1976b), precise posns. (1977 Oct. and Dec.) 78—28587
Periodic Comet Kowal 2 (1979a), precise positions, (1979, February 1 to 28) 79—40140
Periodic Comet Kowal 2 (1979a), precise positions (1979, March 1 to 28) 79—48739
Periodic Comet Kowal (1977f), precise position for 1977 June 13 77—82164
Periodic Comet precise positions, 1977, Jul. 77—71061
Periodic Comet Reinmuth 2 (1980n), recovery posns. and appearance (1980 Sept.) 80—101560
Periodic Comet Russell (1979d), precise posns. (1979 June-July) and improved elements 79—84748
Periodic Comet Sanguin (1977p), positions, improved elements and ephemeris 78—16352
Periodic Comet Sanguin (1977p), precise positions 1977, Oct. to Dec. 78—20752
Periodic Comet Sanguin (1977p), precise positions (1977 October 11 and 19) 78—7936
Periodic Comet Sanguin (1977p), precise posns. (1977 Nov.-1978 Jan.) 78—73685
Periodic Comet Sanguin (1977p), prediscovery position, elliptical elements, and ephemeris 78—4153
Periodic Comet Schuster, (1977o), positions, orbital elements and ephemeris 77—91481
Periodic Comet Schuster (1977o), precise positions, 1977 October 16 and (1978 January 2) 78—65550
Periodic Comet Schuster (1977o), precise positions 1977, Nov. 78—12156
Periodic Comet Schuster (1977o), precise positions (1977, October 9-17) 77—91483
Periodic Comet Schuster (1977o), precise positions (1977 September) 78—7933
Periodic Comet Schuster (1977o), precise positions and ephemeris for 1977/78, Dec. to May 78—7940
Periodic Comet Schuster (1977o), precise positions for 1977 Sept.-Dec. 78—20754
Periodic Comet Schuster (1977o), precise posns. (1977 Dec.-1978 Jan.) 78—36524
Periodic Comet Schuster (1977o), precise posns. (1977 Nov. and Dec.) 78—20741
Periodic Comet Schwassmann-Wachmann 1, precise positions, 1978 January 1 to 16, and outburst date 78—32399
Periodic Comet Schwassmann-Wachmann 1, precise positions, (1978 February 27 to March 12) 78—49381
Periodic Comet Schwassmann-Wachmann 1, precise positions 1976, Oct. and magnitudes for Dec. 77—17439
Periodic Comet Schwassmann-Wachmann 1, precise positions 1976 Oct. 30-Dec. 27, visual magnitudes 77—22138
Periodic Comet Schwassmann-Wachmann 1, precise positions 1977 Dec.-1978 Feb., total visual magnitude estimates 78—36520
Periodic Comet Schwassmann-Wachmann 1, precise positions (1976, Sept.-Nov.) 77—29725
Periodic Comet Schwassmann-Wachmann 1, precise positions and magnitudes (1976 Oct.-Nov.) 77—5498
Periodic Comet Schwassmann-Wachmann 1, precise positions and magnitudes 1976/77 Nov.-Feb. 77—37574
Periodic Comet Schwassmann-Wachmann 1, precise posns. (1977 Dec.-1978 March) 78—69746
Periodic Comet Schwassmann-Wachmann 1, precise posns. (1977 March and Aug.) 78—16354
Periodic Comet Schwassmann-Wachmann 1, precise posns. and magnitudes (1977-8) 78—28585
Periodic Comet Schwassmann-Wachmann 2 (1979k), recovery posns. and ephemeris 80—26811
Periodic Comet Schwassmann-Wachmann 3 (1979), discovery report and precise positions 79—88622
Periodic Comet Schwassmann-Wachmann 3 (1979g), precise position for 1979 August 19 79—84750
Periodic Comet Schwassmann-Wachmann 3 (1979g), precise position (1979 August 22) 79—92719
Periodic Comet Schwassmann-Wachmann 3 (1979g), precise positions (1979 August 19 to 22) 79—92720
Periodic Comet Smirnova-Chernykh (1975e), precise position 1976 June 4 77—33426
Periodic Comet Smirnova-Chernykh (1975e), precise positions (1976, May-June) 77—37572
Periodic Comet Taylor (1916 I = 1977a), precise positions, orbital elements, ephemeris 77—22142
Periodic Comet Taylor (1977a), precise and prerecovery positions 77—45363
Periodic Comet Taylor (1977a), precise position 1977, Jan. 77—22144
Periodic Comet Taylor (1977a), precise positions (1977, February-March) 77—49340
Periodic Comet Taylor (1977a), precise positions (1977, March-April) 77—64702
Periodic Comet Taylor (1977a), precise positions and prediscovery obs. (1976 Nov.-1977 Feb.) 77—33419
Periodic Comet Taylor (1977a), precise positions for 1977 Jan. 14 77—22146
Periodic Comet Tempel 1 (1977i), precise position 1977, June 77—71062
Periodic Comet Tempel 2 (1977d), precise position 1977, April 77—71063
Periodic Comet Tempel 2 (1977d), recovery obs. (1977, March 27) 77—37576
Periodic Comet Tritton (1978d), precise positions 1978 March 78—40877
Periodic Comet Tsuchinshan 1 (1978e), precise position (1978 March 8) 78—45285
Periodic Comet Tsuchinshan 1 (1978e), recovery, precise position 1978 Feb. 4 78—36526
Periodic Comet Tuttle (1980h), recovery and precise position (1980 July 14) 80—85901
Periodic Comet Van Biesbroeck (1977s), precise positions 1977 Dec. and 1978 Mar. 78—45289

astrometry continued
Periodic Comet Van Biesbroeck (1977s), precise posns. (1978 April-May) 78—73686
Periodic Comet Van Biesbroeck (1977s), precise posns. (1978 Jan.-May) 78—61802
Periodic Comet Whipple (1977h), precise positions 1977, Jul. and Aug. 78—24487
Periodic Comet Wild 2, (1978b), precise positions, (1978 February 8 to April 12) 78—53885
Periodic Comet Wild 2 (1978b), discovery and precise posns. (1978 January) 78—28586
Periodic Comet Wild 2 (1978b), positions, appearance and magnitudes (1978 Jan.-Mch.) 78—36530
Periodic Comet Wild 2 (1978b), positions, elements, ephemeris and magnitude estimates 78—36515
Periodic Comet Wild 2 (1978b), positions, elements and ephemeris 78—28589
Periodic Comet Wild 2 (1978b), precise positions 1978 Feb.-Mar., total visual magnitude estimates 78—45287
Periodic Comet Wild 2 (1978b), precise positions (1978 Feb.-Apr.) 78—53880
Periodic Comet Wild 2 (1978b), precise positions (1978 January 27) 78—32398
Periodic Comet Wild 2 (1978b), precise positions for 1978 Jan.-Feb. 78—32402
Periodic Comet Wild 2 (1978b), precise positions for 1978 Mar.-May 78—73676
Periodic Comet Wild 2 (1978b), precise posns. (1978 February-April) 78—73681
Periodic Comet Wild 2 (1978b), precise posns. and magnitudes (1978 Jan.-May) 78—61803
Periodic Comet Wild 3 (1980d), discovery posns., orbital elements and ephemeris (1980 April-June) 80—67657
Periodic Comet Wild 3 (1980d), precise positions, (1980 May 9 to 17) 80—72885
Periodic Comet Wolf-Harrington (1977j), Japanese recovery positions 77—71067
Periodic Comet Wolf-Harrington (1977j), precise position 1978 Jan. 3 78—36528
Periodic Comet Wolf-Harrington (1977j), precise positions (1977, July-August) 78—7931
γ Persei cluster, stellar membership determ. by proper motion meas. 80—56890
phase photoelectric device for time service transit instrument *(Russian)* 78—73632
phase photoelectric device on Dresden Univ. transit instrument, obs. results *(Russian)* 78—73634
photoelectric astrolabe type II, accuracy, time and latit. obs. *(Chinese)* 77—22063
photoelectric device for stellar transit times recording *(Russian)* 78—73635
photoelectric device with high time resolution, obs. results *(Russian)* 78—73633
photoelectric method of recording stellar transit times *(Russian)* 78—73652
photoelectric obs. of star transits *(Czech)* 80—41729
photoelectric star positions, chromatic refr. correction tables *(Russian)* 79—96889
photoelectric transit instrument results *(Russian)* 78—73613
photographic astrometry, techniques using PDS microdensitometer 78—16306
photographic astrometry against bright daylight sky, theory and appl. 79—8797
photographic star positions obtained with wide-angle astrographs, astroclimatic influences on precision *(Russian)* 80—72748
photographic vertical circle plates, reduction using semi-automatic measuring machine *(Russian)* 79—96920
photographic zenith telescope, PZT 1, stellar position obs. at Ondrejov Observatory 77—67035
photographic zenith telescope, PZT 2, for time and latitude service 77—67036
photographic zenith tube, Chinese design and operational characts. *(Chinese)* 78—28514
Photographic Zenith Tube at Tokyo Astron. Observatory, observational errors anal. 80—98547
photographic zenith tube obs., building design effect 80—85856
photographic zenith tube obs. for time and latit. determ., meas. errors estimation 77—56816
photographic zenith tube plates, new reduction method 78—73656
photography against stellar background, iterative trajectory search algorithm *(Russian)* 77—17376
planetary geodesy role, meas. methods *(German)* 77—17332
planetary nebulae, optical positions rel. to radio identification improvements 77—5551
planetary nebulae in M31 (Andromeda galaxy), astrometric catalogue 79—40087
planetary observations, phase reduction formulae *(Russian)* 79—96891
planetary position determ., Mars, Jupiter, Saturn, Jovian satellites *(French)* 80—72809
planetary positions calc. using programmable pocket calculator *(Norwegian)* 78—69700
planetary systems, search strategies 80—46615
planets, Danjon obs. *(French)* 80—94715
planets, meridian obs. (1974 to 1977) 78—69660
planets, Munich meridian obs. (1941-61), orbital elements determ. *(German)* 80—77306
planets, obs. with Danjon astrolabe 77—64651
planets, phase corrections to position obs. 79—8861
planets, position meas., photographic image expansion estimation *(Russian)* 77—71007
planets, reduction of astrometric obs. using ecliptic zone plates *(Russian)* 80—46400
planets and natural satellites position meas. 78—81573
plate reduction study of stellar photographs taken with a TV camera *(French)* 77—17330
Pleiades central field, stellar proper motions rel. to cluster internal motions 79—88711
Pluto, accurate posns. (1975 May-1978 May) 79—70993
Pluto, geocentric positions for the 1974-8 period 80—46478
Pluto (1973 to 1979) 80—85894

astrometry continued
polar regions, appl. of overlapping plates method for stellar positions catalogue *(Russian)* 78—40801
positional astronomy and astro-navigation computing, new approach using pocket calculator, book 79—12383
positional astronomy and definition of ephemeris pole 78—93078
positional catalogue for faint stars from AGK3 78—16311
positional photographs reduction by method of dependences 80—4237
precession, lunisolar, determ. via obs. of extragalactic radiosources 77—5129
precession quantities based on IAU (1976) system of astronomical consts. 77—60577
precision comparator, Zeiss PK-1, accuracy, appls. *(German)* 79—97359
precision comparator, Zeiss PK-1, astrometric plate meas. appl. *(German)* 79—97360
prismatic astrolabe, improved drive and instrumental characts. *(Russian)* 78—89066
probable comet on Palomar Sky Survey prints, 1954 Feb. 11 position 79—80270
proper motion programmes, importance of star coords. determ. *(Russian)* 78—12079
proper motion star catalogues, comparison, systematic errors *(Russian)* 78—93126
PSR 1913+16, binary pulsar, companion star, possible optical obs. and position 79—84823
PSR 1913+16, optical candidate, astrometry and high-speed photometry 80—101609
Pu 60, R.A. corrections for clock (equatorial) stars *(Russian)* 78—28643
Pulkovo large transit instrument in S.Hemisphere, systematic collimation errors *(Russian)* 79—92673
pulsars, periods, positions and proper motion determ. from pulse arrival times, UHF, obs. 80—77431
PZT stars, mean posns. and proper motions for 304 stars, obs. at Ondrejov 80—82175
QSOs, optically selected, accurate positions 79—9022
quasars, from $\delta<-45°$ zone, accurate positions 77—87566
radio astrometry, review 77—25952
radio astrometry using interferometers *(Danish)* 77—22087
radio astronomy, arc meas. procedure optimisation using radiointerferometer *(Russian)* 79—101082
radio interferometric differential meas. of coordinates, influence of troposphere 80—67581
radio source near YY Herculis, precise position 79—35274
radio sources, extragalactic, 5 GHz maps and nearby optical objects positions 78—12391
radio sources, optical identifications using accurate radio and optical positions 77—37660
radio sources, optical positions 77—78881
radio sources, position coincidence optical identifications using Texas Interferometer radio positions 79—88753
radio sources, positions meas. by radio-link interferometer 77—5452
radio sources, precise optical positions in FK 4 system, pilot programme results 78—65709
radio sources, precise positions measured on 35 km baseline 78—16551
radio stars, positions for extragalactic reference frame 78—16278
radioastrometry, Z *(French)* 80—46411
radiosource positions, astrometric catalogues 80—105180
radiosources, flat spectrum, optical identification of complete sample 79—5911
radiosources, galaxies and quasars, optical counterparts, astrometry 80—90551
radiosources, positions, reference catalogue 80—105176
radiosources, rotating, VLBI response freq. technique *(Russian)* 77—22093
radiosources, tropospheric limitations on meas. accuracy *(Russian)* 77—22092
radiosources using differential VLBI, accuracy estimation *(Russian)* 77—22091
reduction of 19th century obs. of Uranus and Neptune positions, method comparison 80—94691
reduction of photographs and calibration of wide-angle cameras *(Russian)* 78—28532
reference frame for positional astronomy, appl. of lunar laser ranging 77—64618
relativistic celestial mechanics, astron. meas. and coord. systems 80—36481
relativistic deflection of light, effect on meas. of Gorky latitude *(Russian)* 78—40462
right ascension determ. with Sukharev horizontal meridian circle *(Russian)* 78—28646
right ascensions, uniform whole-sky system *(Russian)* 78—4082
Rst 4036, red-dwarf binary star, orbital period and total mass 80—12780
S-type stars, secular parallax and mean absolute magnitude 78—81623
San Juan astrolabe obs., catalogue 77—13253
Santiago astrolabe, time, latit. and radius obs. (1968 to 1971) 78—12077
Santiago astrolabe observations from 1972 to 1976, results 80—46363
satellite, observations, reduction method using selected reference stars *(Polish)* 78—36441
Saturn, 1966 ring plane passage time and rings thickness 79—66959
Saturn, 1978 opposition astrometric obs. of satellites 79—75149
Saturn, astrolabe obe. at Paris (1971-6) *(French)* 78—85896
Saturn, astrometric results from 1974 lunar occultations of satellites 78—36506
Saturn, obs. with Algiers Observatory Danjon astrolabe (1969 to 1974) *(French)* 78—61794
Saturn, obs. with CERGA Observatory Danjon astrolabe, (1974 to 1976) *(French)* 78—61793
Saturn, obs. with Paris astrolabe (1975-1976) *(French)* 78—89115
Saturn, possible offset from ephemeris position discovered by aperture synthesis study 79—96963
Saturn, satellites, astrometric obs. from McCormick Observatory (1977) 80—105200
saturn, satellites 1966 S 2 and 1980 S 15-18, separations 80—67645
Saturn, satellites I to IX from McDonald Observatory (1975-1976) 80—105199
Saturn, time of Earth 1966 passage through ring plane 79—35186
Saturn's satellites, precise positions during 1973 77—17421
Saturn and its satellites, positional photographic obs. at Pulkovo, (1971 to 1974) *(Russian)* 79—96965

astrometry continued

- Saturn innermost satellites, separations and times of elongation, (1980 February 29 to March 18) 80—56762
- Saturn satellites, 1966 December and 1980 March positions for five objects 80—94750
- Saturn satellites mutual phenomena in 1979-1980, ephemerides and astrometric aspects 78—53868
- β Scorpii, multiple star, lunar occultation astrometry 78—57583
- U Scorpii, probable identification of recurrent nova at minimum 78—45343
- VY Sculptoris, novalike variable, precise position 80—101597
- selenodetic reference network construction, choice of coordinate system *(Russian)* 80—72797
- Shanghai astrolabe and diurnal latitude and longitude var. *(Chinese)* 77—67025
- sky photographs, star position meas. error reduction by Gaussian freq. distribution curves *(German)* 77—17384
- sky photography programme with wide-angle astrographs, for stellar positions and proper motions *(Russian)* 80—72747
- SMC stars, Herschel catalogue rel. to CPD 79—44337
- SMC X-2, colours, spectral type and position of optical candidate 78—12421
- SMC X-3, colours, spectral type and position of optical candidate 78—12421
- SN 1572 (Tycho's supernova), small dia. radio source discovery and precise position 80—98680
- SN 1979C in M100 (NGC 4321), precise position 80—85962
- SN 1979c in NGC 4321 (M100), radio position 80—82402
- solar apparent instantaneous diam., atmospheric limits on astrometric precision 77—74021
- solar obs. with CERGA astrolabe *(French)* 77—45380
- southern visual double stars, meas. at Cerro Tololo Observatory 78—8057
- space and ground based astrometry, prospects 78—12083
- space astrometry, general principles 78—12082
- Space Telescope appls. 80—105175
- Space Telescope astrometry from CCD images 80—109370
- space-borne interferometers, astrometry and planetary detection 80—109357
- spherical projections in teaching position-finding 77—41437
- SS 433, discrepancy between optical and radio positions 80—31303
- SS 433, photometric and astrometric obs. 79—84801
- SS 433, radio and optical positions 79—88661
- SS 433, radio and optical positions coincidence 80—56840
- star catalogue coord. system orientation errors, effect on planetary ephemerides *(Russian)* 80—51640
- star catalogue data presentation in galactic coordinates 77—78657
- star declination determ. using vertical circle near equator *(Russian)* 79—92681
- star pair latitude obs. anal., mean pole position calc. 80—21892
- star positions, comprehensive general catalogue construction 80—105178
- star positions, statistical approach to Brosche's model for catalogue comparisons 78—81559
- star positions obtained by block adjustment, accuracy 78—20623
- star positions obtained from overlapping plates, accuracy of average 78—20622
- stars, absolute declinations system construction for entire sky using high-latit. obs 80—67520
- stars, absolute RA determ. precision rel. to geographic latitude *(Russian)* 78—28647
- stars, absolute right ascensions catalogue deduction for whole sky from high latit. obs. *(Russian)* 79—16801
- stars, CASF 3 astrolabe catalogue of San Fernando *(French)* 77—78653
- stars, lunar occultations photoelectric obs. at Dominion Astrophysical Observatory (DAO) 79—75198
- stars, mean places within 1° of 1978.0 NCP 77—82281
- stars, parallax and proper motion anals. of Sproul long-interval plate series 79—71015
- stars in vicinity of PSR 1913+16 binary pulsar, astrometry and photometry 78—93219
- stars of southern sky, reference photographic catalogue introduction *(Russian)* 80—72789
- stars right ascensions, determ. via horizontal meridian circle 77—53405
- stars trigonometric parallaxes, determ. by Yerkes Observatory 40 inch refractor 78—89168
- stars with planetary systems, photoelectric detection equipment 80—56882
- Stein 2051, orbital motion, evidence for triple system 78—4289
- stellar aberration and Doppler shift rel. to barycentric motion of Earth 80—8520
- stellar aberration and the Kepler problem hodograph, teaching 78—24622
- stellar absolute right ascension meas. *(Russian)* 79—12382
- stellar azimuth determ. method *(Russian)* 77—60579
- stellar distance meas. by parallax method, undergraduate expt. 77—60871
- stellar perturbation analysis 79—44379
- stellar position, magnitude and colour index meas. from astronomical photographs, automated technique 79—21194
- stellar position determ. on Schmidt plate, standard coord. and Stevenson's method 80—82176
- stellar proper motion, radial vel. and parallaxes, perspective secular motion 77—91524
- stellar right ascensions obs. with large transit instrument, accuracy of absolute chain method of equalisation *(Russian)* 79—96887
- stellar transit times recording and errors *(Russian)* 78—73653
- stellar trigonometric parallaxes, appl. to luminosity systems calibration 80—4343
- stellar trigonometric parallaxes, freq. distribs. and systematic effects 80—94785
- stellar trigonometric parallaxes, systematic differences 77—78776
- student laboratory demonstration, distance measurement with a spectrometer 79—62969
- Sun, positions in 1976, CERGA astrolabe obs. *(French)* 78—69760
- Sun annular eclipse, 1976, April 29, photographic obs. for ephemeris time correction determ. *(German)* 79—44335
- supernova in MCG -4-32-23, precise position, photographic magnitude 78—57568
- supernova in NGC 1411, spectral obs. and precise position 77—82266
- systematic errors elimination in obs. with transit instrument *(Russian)* 78—73615

astrometry continued

- systematic errors in astrometric obs., spectral anal. of obs. series *(Russian)* 78—73614
- 45, 97 and 102=ι Tauri, astrometric studies 78—69779
- telescope tube flexure, determ. via autocollimation method *(Russian)* 78—40818
- 115 Thyra, orbit improvement *(German)* 80—85881
- time and latitude, astrolabe obs. at Merate Observatory for (1976) 78—12078
- time observations, scientific problems and organization *(Russian)* 78—73616
- time service, data acquisition and real time processing system *(Italian)* 80—8549
- Tokyo Astronomical Obs., Time and Latitude Bulletins (Apr.-June 1978) 79—101052
- Tokyo Astronomical Obs., Time and Latitude Bulletins (April/June 1979) 80—72752
- Tokyo Astronomical Obs., Time and Latitude Bulletins (Jan-Mch. 1978) 80—17476
- Tokyo Astronomical Obs., Time and Latitude Bulletins (Jul-Sep 1979) 80—82177
- Tokyo Astronomical Obs., Time and Latitude Bulletins (July-September 1977) 78—73618
- Tokyo Astronomical Obs., Time and Latitude Bulletins (July-Sept. 1978) 80—4239
- Tokyo Astronomical Obs., Time and Latitude Bulletins (Oct.-Dec. 1978) 79—84646
- Tokyo Astronomical Obs., Time and Latitude Bulletins (October-December 1977) 79—5736
- Tokyo Astronomical Observatory Time and Latitude Service, Bulletin (January to March 1979) 80—72751
- Tokyo meridian circle obs., true external errors, from SAO 158687 occultation by Uranus 78—28487
- topocentric positions for 11 asteroids and two comets (Sept. 1977-Oct. 1978) *(German)* 80—46453
- transatlantic long base line interferometry at 10680 MHz 79—48390
- transit circles, design, discussion of main parameters *(French)* 79—62744
- transit instrument automation *(Russian)* 78—73636
- Trapezium type multiple systems, relative proper motions *(Russian)* 78—93314
- trigonometric parallaxes, external error estimation 77—67087
- trigonometric parallaxes, internal and external errors 77—91523
- trigonometric parallaxes, proper motions, magnitudes and colours for 44 stars 79—35235
- trigonometric parallaxes, systematic errors 77—74042
- trigonometric parallaxes for southern hemisphere stars 78—69780
- trigonometric parallaxes of 14 stars 79—5808
- 3U 0042+32, variable mid-latitude X-ray source, accurate position 77—78897
- Universal Time observations, short period terms anal. *(Chinese)* 79—8589
- unresolved visual binaries, suspected, reexamination 78—40993
- Uranus, astrolabe obs. during 1977 at Santiago, Chile 79—58298
- Uranus, astrometric obs. with Danjon Astrolabe of Santiago during 1975 and (1976) 78—12151
- Uranus and SAO 158687 position meas. rel. to 1977 Mar. 10 occultation 77—22044
- Uranus occultation of SAO 158687 on 1977, March 10, predictions 77—29717
- Uranus satellites, astrometric obs. 80—67654
- Ursa Major group, new members 79—84830
- α and β Ursae Minoris, astrometric obs. (1953-61) for Pulkovo large transit instrument orientation parameters determ. *(Russian)* 79—96910
- UV excess object, variable, discovery and precise position 79—40280
- Valinhos astrolabe obs. (April 1974-December 1977) *(French)* 79—70944
- van Maanen's star, astrometric study of Sproul plate series, radial vel., gravit. redshift 78—40936
- variable emission-line star in core of M15, spectrum, photometry and position 79—5840
- Venus, astrometric radar meas. in 1977, results 80—17522
- Venus, photographic position meas. *(Russian)* 78—93121
- Venus, photographic position meas. *(Russian)* 78—93135
- Venus, positional observations at UKrainian Main Astronomical Observatory, (1972) *(Russian)* 79—44390
- Venus, positions, photographic obs. (1967-72) from Nikolaev *(Russian)* 79—92689
- vertical circle meas. of stars, aberration of light rel. to spectral type *(German)* 78—73702
- vidicon appl. to low intensities meas., with Si-intensified target *(German)* 80—98545
- visual binaries, orbital elements and masses for 18 pairs 80—62180
- visual binaries, radial velocities for objects with astrometric orbits 79—67057
- visual binaries with variable components, orbital elements, visible obs. *(Russian)* 80—77455
- visual binary stars, astrometric obs. rel. to gravit. const. var. *(Russian)* 79—44537
- visual binary stars, measurements and orbital elements 80—46607
- visual binary stars, parallaxes, mass ratios and masses for six pairs 77—64795
- visual binary stars, southern, new obs., orbits and masses 78—96502
- visual double stars, ang. separation and position angles, photographic obs. 78—40997
- visual double stars, astrometric meas. at Nice *(French)* 78—89224
- visual double stars, meas. at Las Campanas Observatory, Chile 78—8058
- visual double stars, micrometer obs., (1975 to 1977) 78—89218
- visual double stars, photographic meas. of position angles and separations 80—26909
- visual double stars, photographic measures 79—17024
- visual double stars, photographic obs., ang. separations and position angles 78—20860
- visual double stars, southern, measures 79—21360
- visual double stars measured at Las Campanas Observatory, Chile 78—85978
- VLBI applications *(Russian)* 78—32357
- VLBI appls. *(Japanese)* 80—21930
- VLBI using geostationary satellite link 79—29968
- W3(OH), interstellar OH maser components absolute positions from VLBI synthesis obs. 80—105368

astrometry continued
- W851, high-velocity star, parallax and tangential vel. 77—49387
- Wolf 1062, astrometric anal. of unseen companion from 61 cm Sproul refractor plates 78—16459
- Wolf 1062, red dwarf, astrometric perturbation 77—49439
- Wolf 922, nearby red dwarf, evidence for low-mass unseen companion 80—51809
- X-ray sources near galactic centre, positions meas. by Ariel-5 RMC expt. 78—4407
- zenith telescope, use as astrolabe for time and latitude meas. 80—98550
- ZTL-180 zenith telescope, micrometer screw turn from declination arc. obs. *(Russian)* 78—89067
- ZTL-180 zenith telescope, objective distortion determ. from visual obs. of star pairs *(Russian)* 78—89068
- 1228, nearby red dwarf, evidence for low-mass unseen companion 80—51809
- 20,986, new unresolved astrometric binary 78—57594
- H_2O maser sources in W3, accurate positions 78—4332

astronautics *see space research*

astronomical catalogues
- *see also astrometry*
- 2-micron objects in N Monoceros region, survey 80—8555
- 5 GHz galactic plane sources, catalogue 80—4269
- 2A catalogue and supplementary results from Ariel 5 sky survey 79—58276
- 2A catalogue of X-ray sources, review 78—73659
- A- and F-type stars in Selected Areas, photoelectric uvbyβ photometry 78—16412
- Abastumani, catalogue of Bright Galaxies, spiral galaxy orientation anisotropy 77—17678
- Abell and Shane-Wirtanen catalogues, cross-correl. anal. 78—4118
- Abell galaxy clusters catalogue, cluster props. distortion by inclusion of spurious clusters 80—101643
- absorption-line objects 78—86036
- AFCRL IR sources, optical, IR and radio studies 78—4393
- AFCRL Survey, subcatalogue of brightest sources 77—87283
- AFCRL/AFGL sources obs., AFGL catalogue evaluation 78—28846
- AGK2, error corrections and new reductions *(French)* 77—64616
- AGK2-AGK3 solutions, comparison by separate plates and overlapping *(French)* 77—64615
- AGK3 declinations, random errors determ. by Sanders-Raimond method 77—53404
- AGK3 stars, proper motions rel. to determ. of precession and galactic rot. 77—45402
- AGK3R declinations improvement using Toepfer meridian circle obs. *(Russian)* 78—28645
- Am-type stars with known spectral types, second catalogue 80—36514
- Arecibo 2380 MHz survey of bright galaxies 78—57470
- Ariel V catalogue of X-ray sources and source counts at high galactic latitude 78—49565
- B-type stars, catalogue of photometric data rel. to surface mag. fields 80—85873
- Basle catalogue of 1906 blue objects at high galactic latitudes 78—32360
- bibliographic star index, information retrieval system *(Japanese)* 79—101086
- bibliography of catalogues published in 1951-1975 period 78—20658
- Bologna survey at 408 MHz, statistical analysis 78—28816
- bright galaxies, integrated magnitude and colours in UBV system, second catalogue 79—12509
- bright nebulosities in opaque dust clouds 77—64668
- bright stars, fourth edition consideration 77—78667
- Bruce telescope photographic plates, computer readable mag. disc catalogue 79—88605
- 5C2 survey revised distances of optical objects from radiosources 78—57472
- 5C9 survey of radiosources, 214 objects 78—16312
- 5 C 1 to 5 survey areas sources, 1421 MHz obs. 79—84864
- 5C 6 survey of 292 radiosources 78—24471
- 5C 7 survey of 271 radiosources 78—24471
- 4C radiosources between declinations 20° and 40°, samples 80—73057
- 4C radiosources clustering, statistical analysis 79—5761
- 4C radiosources clustering 78—96556
- 6C survey at 151 MHz, prospects 78—28813
- RS Canum Venaticorum systems, candidate list for southern HD stars 80—4395
- CASF 3, astrolabe catalogue of San Fernando *(French)* 77—78653
- cD galaxies, in poor clusters 77—22111
- clusters of galaxies, catalogue inhomogeneity, cluster props. distortion, statistical anal. method 80—67888
- Coma Cluster galaxies, photometric catalogue 78—12381
- cometary nebulae, list of 79 new objects found on Palomar Sky Survey prints *(Russian)* 77—60630
- cometary orbits, third edition 79—40092
- comets, ancient and naked-eye objects (2314 BC-AD 1970) 80—105181
- comets, obs. in Greek and Roman sources before 410 AD 78—77658
- compact galaxies diameters and magnitudes, study of galaxy catalogues *(Russian)* 78—49514
- compact galaxies in neighbourhood of Abell 193, list of 140 objects 79—88736
- compact galaxies on UK Schmidt plates 78—81687
- compact groups of compact galaxies, eighth list, 32 objects *(Russian)* 78—93125
- compact groups of compact galaxies, ninth list 79—88751
- compact groups of compact galaxies, seventh list *(Russian)* 77—22110
- compact groups of compact galaxies, tenth list 80—26991
- compact radiosources in galactic centre, data for 74 objects 79—21430
- conference on star catalogues, Washington, DC, USA (Nov.-Dec. 1978) 80—90605
- cool stars in near IR, spectrophotometry and Cassiopeia 79—88658
- 3CR and 4C catalogues quasars comparative study 77—67136
- 3CR identifications 78—28825
- 3Cr radio sources in directions of Zwicky clusters of galaxies, statistical investigation 78—4378
- CTC right ascensions, synthetic catalogue for Chinese time service *(Chinese)* 78—28540
- Culgoora-3 list of 2045 radiosources, obs. at 160 MHz 78—20655
- Curtis-Schmidt thin prism survey for extragalactic emission line objects, Univ. of Michigan list I 77—71012
- dark dust clouds in southern hemisphere, props. and formaldehyde obs. 77—13434

astronomical catalogues continued
- dark nebulae in M31, catalogue 80—72787
- decametric survey of discrete northern sources, catalogue of 329 objects, 10-20° declinations 78—57471
- decametric survey of discrete northern sources, spectra of 266 sources in 10-1400 MHz range 78—57664
- diffuse objects and planetary nebula in galactic centre direction *(French)* 79—21434
- double stars, Webb Society handbook 80—8744
- double stars discovered at Nice, 14th series *(French)* 77—78654
- dwarf stars, M-type, in South Galactic Pole direction, catalogue of 282 objects 79—5762
- eclipsing binaries, Princeton-Pennsylvania-Florida card catalogue 77—78666
- emission line galaxies and quasars, classification system and list of 116 objects 77—22308
- emission regions in M33, catalogue 80—46416
- Equatorial Infrared Catalogue development from satellite data 79—101091
- Equatorial Infrared Catalogue No.2 astronomical source distrib. 80—90346
- equatorial IR catalogue (EIC), 2.7 μ high-precision sky survey results 78—81560
- ESO-(B)-survey, characteristics curves from stellar image diameters *(German)* 79—70966
- ESO-B and SRC-J sky surveys, limiting magnitude 78—69706
- ESO/Uppsala galaxies, second catalogue 78—77497
- ESO/Uppsala survey of ESO(B) Atlas of southern sky, fifth list containing 2395 objects 78—20653
- ESO/Uppsala survey of ESO(b) Atlas of southern sky, fourth list, 2920 objects 77—26059
- ESO/Uppsala survey of ESO (B) Atlas of S. sky, pt.VII 80—56722
- ESO/Uppsala survey of ESO (B) Atlas of southern sky, sixth list containing 3162 objects 79—8850
- extended radiosources, catalogue of 77 objects, 408 MHz obs. 77—26078
- extragalactic emission line objects, third list from Curtis Schmidt thin prism survey 78—28538
- extragalactic emission-line objects, second list from Curtis Schmidt thin prism survey 78—28537
- extragalactic emission-line objects, Univ. of Michigan List IV 78—77494
- extragalactic objects, statistical anal. 80—94875
- extragalactic objects catalogues statistical anal., QSOs and Lick galaxy counts correl. 79—25700
- extragalactic radiosources, index of catalogues 77—60629
- faint blue stars in high galactic latits., search of PSS fields near South Galactic Pole 80—46415
- faint blue stars near North Galactic Pole 77—49314
- faint star clusters in LMC, survey, visible obs. 80—73011
- faint stars from AGK3, positional catalogue 78—16311
- FK4, $\Delta\alpha_\delta \cos \delta$ corrections *(Russian)* 77—56817
- Fk4, corrections based on photographic posns. of Venus 79—8851
- FK4, corrections to zero points from minor planet obs. *(Russian)* 80—82228
- FK4, equinox and equator improvement *(Russian)* 79—58277
- FK4, right ascension and declination corrections from meridian obs. *(Russian)* 77—71016
- FK4 catalogue stars, declinations systematic errors determ. from vertical circle obs. *(Russian)* 79—96888
- FK4 equator and equinox corrections from asteroid orbits 78—69727
- FK4 equinox corrections from minor planet meridian obs. 80—8519
- FK4 star coord. improvements using Ni2 astrolabe obs. *(German)* 80—26719
- FK4 stars general catalogue of astrolabe obs. (1958-75) *(French)* 78—36468
- FK4 supplementary stars, right ascensions obs., definitive results 80—17473
- FK4 system rel. to calibration of radio positions 77—71014
- FK4 systematic errors *(French)* 77—87282
- FK5, equinox and equator of new fundamental reference coord. system 80—109341
- FK5 fundamental astrometry rel. to celestial mechanics and radioastronomy *(German)* 78—45200
- FKSZ stars, differential catalogue of RA in 20-90° zone, Pulkovo obs. *(Russian)* 78—28644
- flare stars, catalogue of 68 objects in solar neighbourhood 77—53431
- flare stars in Pleiades, photometric obs. and numbering *(Russian)* 77—91536
- fluorescent molecular lines originating in or around stellar objects 77—23514
- fundamental star catalogue system, improvement via relative determs. of celestial bodies coordinates 78—53797
- G- and K-type giants in short period binaries 77—87394
- galactic bright nuclei, survey of 448 galaxies 78—32569
- galactic clusters observed in three colours, catalogue and distances 79—40089
- galactic disc emission at 4 cm wavelength, large-scale and small-scale cloud structs. 78—28795
- galactic globular clusters, UBV colour-magnitude diagrams, catalogue bibliography 78—24531
- galactic non-stellar objects, data centre proposal 77—78905
- galactic plane radio survey at 4.875 GHz, list of 1186 sources 79—21431
- galaxies, compact and bright-nucleus, in S.hemisphere, spectroscopic survey 80—94725
- galaxies, correlation function, computer simulation *(Russian)* 80—36729
- galaxies, four-point correlation function for Lick and Zwicky catalogues 78—45413
- galaxies, multiply observed, revised standard total magnitudes and colours catalogue 78—8116
- galaxies, optically bright, radio survey at 1400 MHz, 248 radiosources detect. 77—60627
- galaxies, survey of irregular and late-type southern objects, classifications 77—91618
- galaxies, with UV continuum, tenth list *(Russian)* 77—91445
- galaxies and clusters of galaxies in SMC direction 78—96410
- galaxies from ESO/Uppsala list, first catalogue of spectroscopic obs. 77—22113
- galaxies in Abell 2255, red shifts 79—40276
- galaxies in ZwCl 1710.4+6401 cluster, data for 396 objects *(Russian)* 77—87555
- galaxies near galactic plane between $l=245°$ and 255° 77—2346

astronomical catalogues continued
galaxies of Ames, Reiz and Zwicky catalogues, magnitudes reduction to standard B_T system 79—92852
galaxies with UV continuum, eighth list *(Russian)* 77—22109
galaxies with UV continuum, eleventh list *(Russian)* 78—28767
galaxies with UV continuum, ninth list *(Russian)* 77—49464
galaxies with UV continuum, twelfth list 80—67585
galaxies with UV excess, list of 136 new objects 80—26968
galaxies with UV excess, second list 80—67584
galaxies within 10 Mpc 80—51670
galaxy catalogues, statistical anal. 80—46417
galaxy distribution, statistical anal. of galaxy catalogues 80—26987
galaxy groups, catalogue of 103 systems 77—17385
galaxy morphological types in rich clusters 80—85872
galaxy redshift catalogue rel. to local mean mass density and galaxy clustering 78—45436
gamma-ray bursts, galactic origin and chronological catalogue 77—37672
gamma-ray sources, COS B catalogue and identifications 78—73775
gaseous nebulae, Webb Society handbook 80—8743
GB2 sky survey at 1400 MHz, differential radiosource counts 78—54063
general catalogue for southern stars, proper motions in α, corrections *(Russian)* 79—92685
general catalogue of 1139 stars obs. with astrolabes, 1957-75 period, FK4 stars position corrections *(French)* 78—32359
globular clusters in M31, list of 355 objects 78—32568
Green Bank second survey of extragalactic radiosources of 1400 MHz, catalogue of 2022 sources 79—62761
Green Bank surveys at 1400 MHz 78—28543
Hauck-Mermilliod catalogue of early type star four colour data, astrophysical parameter determ. 80—72951
HD catalogue and E.C. Pickering, American astrophysics, history 78—86102
Herbig-Haro objects, new, list 79—5763
Herbig-Haro objects in southern dark clouds, objective prism survey 78—28536
HIA sources, near quasar PKS 2344+09, obs. 77—37659
image processing/facilities, catalogue 78—45239
interacting galaxies, atlas of 1500 objects, galaxy fragmentation theory 77—41320
interacting galaxies, catalogue of nonequilibrium systems near bright galaxies 78—36682
International Latitude Service obs., errors 77—45324
interstellar dark globular filaments, catalogue 80—26756
interstellar diffuse bands, catalogue of meas. 77—64666
interstellar low mass clouds in solar vicinity, photometric survey results 80—36512
IR astronomical survey data processing techniques 78—81553
IR bright stars in region of galactic centre, catalogue and photometry 80—77299
IR sources, in compact H II region G45.5+0.1 78—4396
IR sources in Cygnus X region 80—82538
IRC catalogue, reddest stars at 2 μ 79—62841
Jupiter, disturbances and dislocations (1857-1975) 80—72867
late-type stars, intermediate-band photometry, catalogue 78—81558
late-type stars, revised MK spectral types for G, K, and M stars 80—82226
late-type stars with OH, H_2O or SiO maser emission 79—70965
Lick catalogue of galaxies, new reduction 77—71013
LMC, catalogue of radical vels. 79—101089
LMC OB and supergiant stars, deep objective prism survey catalogue 79—40090
LMC radiosources at 3.4 cm catalogue and spectral indices 78—65695
LMC stars, catalogue and photoelectric UBV photometry *(German)* 80—21932
LMC supergiant stars, comments on catalogue of Stock et al. *(French)* 78—53941
luminous stars in Milky Way, supergiants and O-type stars catalogue 79—40183
lunar crater arcs, catalogue and distribs. 77—41333
lunar crater dimensions catalogue from Apollo data 77—37527
lunar occultations of stars (1943 to 1971), catalogues 79—88606
lunar transient phenomena, catalogue of observations, 1178-1977 period 79—21208
Luyten proper motion catalogues, nearby star suspects selection using Luyten's magnitude estimates 80—82353
β Lyrae primary and secondary, catalogue of absorption lines *(Russian)* 78—28725
RR Lyrae stars, bibliographical catalogue at Strasbourg Stellar Data Center 78—16431
RR Lyrae stars in LMC, list of 76 objects 77—91549
M31, Hα survey, catalogue of 981 H II regions 78—40840
Magellanic Clouds, lists of planetary nebulae 79—58405
Magellanic Clouds stars, five-channel photometric obs. 78—16398
Mars, conjunctions with ε Cancri in Praesepe (1950-2000 period) 77—91460
MC2(3) radio sources, optical positions from Palomar Sky Survey 80—31375
MC2 and MC3, radio spectra and optical identification of sources 77—33670
Mercury, transits in 1677-1973 period, collected obs. of internal contacts 77—25964
meteorite craters on Earth, form., props. and catalogue 78—96411
meteors, 19 obs. with TV apparatus 77—67047
Mira variables, discovery of 123 new stars in Palomar 10 globular cluster region 78—40837
MIT/OSO 7 catalogue of X-ray sources, intensities, spectra, long-term vars. 79—80243
Molonglo Deep Sky Survey, 373 radiosources in declination zone −20° 77—56840
Molonglo Deep Sky Survey, source counts 77—56842
Molonglo deep sky surveys 77—33358
Molonglo radio source surveys at 408 MHz 78—28541
Molonglo radiosource catalogues MC2 and MC3, optical identifications, 11^h28^m to 17^h00^m right ascensions 78—20900
Mononglo Deep Sky survey, 95 radiosources in declination zone −62° 77—56841
Moon transient phenomena observations, fourth list (1821 to 1978) 80—62038
Morphological Catalog of Galaxies, discovery, apparent distrib. and props. of compact galaxies 78—28792

astronomical catalogues continued
Morphological Catalogue of Galaxies, distrib. homogeneity *(Russian)* 79—8849
Morphological Catalogue of Galaxies, occurrence of various galaxy types 80—17662
nearby star data published 1969-1978, catalogue 80—36513
nearby stars brighter than tenth mag. 80—56825
nearby stars catalogue, third edition requirements 77—78660
NGC 188, old open cluster, photographic photometry 77—53430
NGC 3247, RGU photometry of open cluster, catalogue of 129 stars *(German)* 77—82290
NGC 5617, open cluster, photoelec. and photographic photometry of member stars 79—17032
NGC 5662, open cluster, photoelec. and photographic photometry of member stars 79—17032
NGC 6397, metal-poor globular cluster, BV photometry of 399 stars 77—82292
NGC 6656, metal-poor globular cluster, BV photometry of 374 stars 77—82291
non-stellar objects, master list 77—78668
NRAO-Bonn 5 GHz radio source survey, optical identifications of extragalactic sources 77—78880
O-type stars, catalogue on mag. tape, third edition 77—2348
OB stars, in Vela region, list of 166 objects 77—87280
Ohio Sky Survey and other radio surveys, review 77—45325
open clusters, transit tables for star numbering, magnetic tape 79—44573
optical quasars, radio and optical obs. of 91 objects, redshifts, luminosity function 78—49552
Orion OB 1 association, photometric study and observational catalogue 77—82128
OTL radio sources, position and struct. determ. from 327 MHz lunar occultation obs. 80—73061
OTL radio sources, position and struct. determ. from 327 MHz obs. 80—73060
OTL radiosources, position and struct. determ. from 327 MHz lunar occultation obs. 80—73062
paired galaxies, classification into groups differing in phys. and kinematic props. 79—21443
pairs and triplets of galaxy clusters, list of 68 pairs and 21 triplets 79—35408
parallax stars in Herstmonceux programme, second list 78—77498
parallax stars with MK spectral classifications 80—56721
Parkes 2700 MHz survey, catalogue for Declinations −4° to −15°, Right Ascensions 10^h to 15^h 79—75121
Parkes 2700 MHz survey, optical identifications 77—49489
Parkes 2700 MHz survey, part twelve 77—49315
Parkes 2700 MHz survey, source counts and distrib. 78—28544
Parkes 2700 MHz survey of radiosources, 13th part, 404 objects 78—20656
Parkes 2700 MHz survey of radiosources, 13th part, optical identifications 78—20901
periodic comets, major semi-axis less than 30 AU 80—72791
Perth 70 catalogue, determ. of meridian circle pivot errors 78—53822
PG quasars, bright optical objects, radio emission at 2.7 and 8.1 GHz 78—45424
Phobos, crater catalogue 78—28566
photographic four-colour sky atlas 78—24472
photographic plates taken by 105 cm Schmidt telescope *(Japanese)* 79—101090
photometric sequences, second supplement considerations 77—78664
planetary nebulae, bibliographical index for period (1965 to 1976) 78—12106
planetary nebulae, catalogue of new and misclassified objects 80—109378
planetary nebulae, southern, red-sensitive objective-prism survey list of suspected objects 78—77496
planetary nebulae, Webb Society handbook 80—8743
planetary nebulae detected since 1966 78—16495
planetary nebulae in M31 (Andromeda galaxy), astrometric catalogue 79—40087
planetary nebulae in southern hemisphere, new discoveries 77—64667
planets and asteroids, positional catalogue from photoelectric meridian obs. 77—91453
proper motion star catalogues, comparison, systematic errors *(Russian)* 78—93126
proper motion stars, catalogue of stars with $m_V<15$, annual motion >1″ 79—58275
Ptolemy's star catalogue in Syntaxis, position meas. method 80—67586
Pu 60, R.A. corrections for clock (equatorial) stars *(Russian)* 78—28643
pulsars, obs. data for 147 known objects 77—9763
QSO spectra, catalogue of absorpt. line lists for 108 objects 78—53840
QSOs, catalogue of 403 objects 77—26080
QSOs and BL Lacertae objects, revised optical catalogue 80—105177
QSOs in Tololo deep survey, apparent red shift cut-off unreal 79—12539
QSOs of small and intermediate emission redshift, absorpt. lines homogeneous survey results 80—31218
quasar-galaxy associations, ang. separations 77—60846
quasars, optical catalogue 77—49492
radio continuum sources near galaxies, catalogue and obs. at 11 cm 80—94872
radio galaxies, optical catalogue 80—21931
radio sources, extragalactic, confusion-limited survey at 4.755 GHz, source list and areal distribs. 80—98577
radio sources, linear polarisation catalogue 80—51671
radio sources in NGC 7331/Stephan's Quintet area, obs. at 1421 MHz 78—12392
radio sources in North Polar Spur region, 1420 MHz obs. and catalogue 80—22100
radio sources observed during continuum interferometric obs. of interstellar dark clouds, catalogue 80—98699
radiosource positions, reference catalogue derivation 80—105176
radiosources, astrometric catalogues 80—105180
radiosources, catalogue of 347 sources obs. at 610 MHz, source parameters, identifications 78—40838
radiosources, in fields of five unidentified high latit. X-ray sources, list of 249 objects 77—87281
radiosources, S4 5 GHz survey between +35° and +70° declination 78—69893
radiosources, search for clustering in 5C surveys 77—60839
radiosources, search for clustering in Parkes and Bologna catalogues 77—60838

astronomical catalogues continued
- radiosources, small diameter, 23 objects in field of CTA1 SNR 79−62890
- radiosources in Coma cluster, Westerbork survey at 610 MHz 77−60628
- radiosources isotropy in B2 catalogue 78−73766
- radiosources near North Celestial Pole, 1421 MHz survey 77−45590
- radiosources near North Celestial Pole, deep survey at 4.85 GHz 79−12536
- RC1 galaxies, nuclei, lenses, rings diameters for 532 galaxies 80−90525
- red and nebulous objects in dark clouds, survey, catalogue of 150 objects 80−56904
- red degenerates, eleventh list 79−25596
- red stars survey in 30 Doradus region of LMC, list of 298 stars 79−48794
- revised 3C catalogue, study of confusion and resolution 78−12105
- revised 3C catalogue of radiosources, optical identifications and spectroscopy 77−22114
- rich clusters of galaxies, study of 1889 clusters from Abell's catalogue 77−87556
- ring galaxies near rich clusters, catalogue 77−33629
- Royal Astronomical Society, catalogue of archives and manuscripts 78−69705
- RSO 1 catalogue cross correl. with IRC, AFGL and EIC catalogues 80−77511
- S-type stars in Southern Milky Way, objective prism survey and BVI photometry 78−61754
- SAO proper motions *(French)* 79−30089
- Sculptor dwarf galaxy, photoelectric sequence and preliminary colour-magnitude diagram 77−53429
- Seyfert galaxies, survey of 80 objects based on large-scale image-tube plates 77−45323
- Shane-Wirtanen galaxies, two- and three-point correl. functions 78−8132
- SIMS, C and SC stars, new discoveries on southern, red-sensitive objective-prism plates 80−36511
- sky survey at 8085 MHz of 0.181 steradians, 64 sources, identifications, spectral indices 78−40836
- SKYMAP: a new catalogue of stellar data 79−35151
- small-scale radio struct. in Sharpless H II regions at 4.995 GHz, high-resolution catalogue 78−61755
- SMC, atlas of variable stars, clusters, emission regions and supergiant stars, book 79−44619
- SMC probable members and foreground stars, additional tests 79−40091
- SMC stars, Herschel catalogue rel. to CPD 79−44337
- SMC wing, photoelectric UBV sequence 78−69874
- SNR candidates in nearby galaxies 80−62037
- solar activity centres during descending branch of 20th cycle, catalogue and peculiarities *(Russian)* 79−96926
- solar diatomic molecular lines in 7100-7600 Å range, table 78−77495
- solar neighbourhood C and M-type stars 79−16946
- solar proton flares in 1942-76 period 78−20811
- solar radiobursts 1966-76 having characts. predictive of proton activity 77−49356
- solar type IV bursts, catalogue preparation *(Italian)* 78−96459
- southern compact and bright nucleus galaxies 77−74136
- southern compact and bright-nucleus galaxies, spectroscopic survey 79−84683
- southern dark dust clouds, centres coordinates, areas and opacity classes 77−56844
- southern groups and clusters of galaxies, catalogue 78−28539
- Southern Peculiar Galaxies and Associations, preliminary results 77−82129
- southern rich clusters of galaxies, finding list for 474 clusters 78−24470
- southern sky, reference photographic catalogue introduction *(Russian)* 80−72789
- spectrophotometric survey of stars along Milky Way in Perseus 78−45403
- spectroscopic binaries, seventh catalogue, statistical analysis 80−82422
- spectroscopic binaries, thirteenth complementary catalogue *(French)* 77−22112
- spectroscopic binary orbits, catalogue improvements 77−78665
- spectroscopic binary systems orbital elements, seventh catalogue 79−16843
- standard stars for uvby photoelectric photometry south of +10°, photometry 77−2347
- star catalogue coord. system orientation errors, effect on planetary ephemerides *(Russian)* 80−51640
- star catalogue zero points, pseudoperturbations method *(Russian)* 77−73975
- star catalogues, appl. to far UV interstellar radiation field prediction 77−64739
- star catalogues zero points and orientation angles of coord. axes *(Russian)* 77−71015
- star clusters in M33, list of 58 candidates 79−9002
- star clusters in SMC, identifications and coordinates 78−89086
- star data presentation in galactic coordinates 77−78657
- star identification using coded numbering system for open clusters 77−78829
- star positions, comprehensive general catalogue construction 80−105178
- star positions, general catalogue compilation, material evaluation 80−109375
- star positions, statistical approach to Brosche's model for catalogue comparisons 78−81559
- stars, absolute right ascensions catalogue deduction for whole sky from high latit. obs. *(Russian)* 79−16801
- stars, catalogue of photometric parameters meas. in Geneva Observatory system 77−73974
- stars, first astrolabe catalogue of San Juan 77−13253
- stars, general magnitude eqn. between FK4 and southern catalogues 80−67705
- stars, linear polarisation catalogue 77−13255
- stars, MK spectral classifications, third general catalogue 77−78671
- stars, trigonometric parallax catalogue considerations 77−78776
- stars, UV fluxes, S2/68 obs. of 31215 objects 79−8852
- stars in field centred at $\alpha=2^h17^m.9$, $\delta=+58°59'$, BV magnitudes and spectral classes *(Russian)* 78−40841
- stars in open clusters, mag. tape catalogue of HD, HDE and DM identifications 77−13254
- stars near South Galactic Pole, UBV photometry of 51 stars 78−4216
- stars observed with Bordeaux tracking photoelectric meridian micrometer 77−37509
- stars with Ca II H and K emission lines *(Polish)* 80−82227
- stellar absolute proper motion compiled catalogue, composition method *(Russian)* 80−51747
- stellar data, conf. (Strasbourg, France, 19-21 Aug. 1976) 77−78828
- stellar data in machine-readable catalogues, critical evaluation 77−78830
- stellar designation ambiguities, improvement proposals, IAU list 77−78661
- stellar designation organization using bibliography-type data base 77−78658
- stellar far UV spectra at 0.2 Å resolution, catalogue of Copernicus obs. 77−56843
- stellar H_2O masers, catalogue of 82 objects 79−8909
- stellar identifications, CDS data base 77−78659
- stellar occultations by Neptune, predictions for 1978-80 period, list of 26 stars 78−40868
- stellar photometric catalogue, meas. in Geneva seven colour system 77−13252
- stellar photometric catalogues: present and future 80−105179
- stellar photometry, catalogue of homogeneous data in UBV photoelectric system 78−96409
- stellar relative radial vels. for 500 stars near southern open clusters *(German)* 80−94724
- stellar spectra, Texas Univ. UV catalogue 77−78662
- stellar spectral energy distribution for 50 stars, 3200-7550 Å region *(Russian)* 78−65620
- stellar spectrophotometric data, energy distrib. in Hayes-Latham calibration 80−72790
- stellar spectrophotometric scans 77−5520
- stellar UBV photoelectric photometry, general catalogue on mag. tape 77−78656
- Stockholm Southern Milky Way Survey, uniform edition on mag. tape 77−78655
- Strasbourg Stellar Data Centre 77−91447
- sunspot observations, 466 BC to AD 1638, catalogue and historical review *(Norwegian)* 79−75312
- sunspot pretelescopic records from Orient, catalogue, 28 BC-AD 1604, activity excursions 79−66975
- sunspots, photoheliographic results and general catalogue, (1968 to 1971) 79−2487
- supergiant stars in LMC, spectral types and magnitudes, catalogue of 1882 objects 78−32361
- supergiant stars in the SMC 78−16411
- supernova remnants, galactic, new catalogue corrected for distance from galactic plane 79−75120
- supernova remnants, galactic, systematic search for optical nebulosity 79−29998
- supernova remnants in M33, catalogue 80−41734
- Tautenburg catalogues of blue objects, real number of suspected quasistellar objects (QSO) 79−80365
- Tokyo PZT star catalogue, third improvement 77−91446
- Tr 22, open cluster, photoelec. and photographic photometry of member stars 79−17032
- Trapezium-type multiple systems, catalogue of 87 systems with O- and B-type primaries *(Russian)* 78−61753
- trigonometric parallaxes, proper motions, magnitudes and colours for 44 stars 79−35235
- UBV photoelectric standards in SA 1-115, final catalogue 80−41733
- UBVRGI photometric measurements of 1297 stars, catalogue on mag. tape 78−40839
- UBVRIJKLMNH photoelectric photometric catalogue on mag. tape 79−16842
- Uppsala Catalogue of galaxies, systematic errors rel. to galaxies position angle distrib. *(Russian)* 78−41049
- US Naval Observatory data associated with stellar parallax determ. 80−72788
- US Naval Observatory data files 77−78670
- UTR-2 survey, sources in $0°<\delta<+10°$ range 79−97091
- UTRAO 335-380 MHz survey, interim report 78−28815
- UV Celescope Catalogue, comparison with IRC, common objects identification 77−9676
- uvbyβ photoelectric photometric catalogue 80−62036
- variable stars, General Catalogue and international cooperation 77−78663
- variable stars in Sculptor dwarf spheroidal galaxy, catalogue, of 602 stars 79−58431
- VBLUW photoelectric photometric catalogue on mag. tape 80−36515
- Vilnius photometric catalogue of stars on mag. tape, description 80−98578
- visual double star catalogues 77−78669
- 18W catalogue of radiosources in Abell 2197 and 2199, Westerbork survey at 610 MHz 80−67883
- 29, 30 and 31W catalogues, Virgo cluster galaxies 80−98721
- 17W list from 610 to 1415 MHz obs. of Abell 1367 cluster of galaxies 79−35401
- 28 W sources and catalogue in NGC 7000 IC 5070 H II region complex 80−105308
- 20W sources in Hercules supercluster 79−44625
- 22W sources in Perseus cluster, WSRT 610 MHz obs. 79−75283
- Westerbork 1415 MHz survey of background radiosources, optical identifications 77−64867
- Westerbork 610 MHz sources counts and spectral index distrib. 79−44630
- Westerbork radiosource surveys at 610 and 1415 MHz 78−28542
- Westerbork Synthesis Radio Telescope, 6 cm sources survey data 79−88604
- Wolf-Rayet stars in LMC, new discoveries, positions, spectra and magnitudes 80−46569
- Wroclaw FKSZ catalogue reduction to FK4 system *(Polish)* 77−64669
- X-ray sources, catalogue of 517 objects 80−56720
- X-ray sources, fourth Uhuru catalogue 79−40088
- X-ray sources at high galactic latit. $(|b|>10°)$, Ariel V (SSI) catalogue 78−32362
- young galaxies in catalogues of quasars and radiosources 78−28799
- ZB flare stars and nebular variables in Ophiuchus-Scorpius region *(Chinese)* 78−28702
- Zwicky catalogue magnitude scale, comparison with Holmberg and de Vaucouleurs galactic magnitudes 77−22309
- Zwicky catalogue selection effects and intercluster dust tests 79−9012
- Zwicky galaxy clusters and 3CR radio sources, statistical investigation of positional coincidences 78−4378
- C stars, catalogue of 302 stars in LMC 78−20654

astronomical catalogues continued
- C stars in Cygnus, new discoveries catalogue 80—46551
- Fe/H abundance determ., catalogue for 515 stars 77—29815
- Fe/H abundance in 628 stars 80—98579
- Fe/H determ. catalogue for stellar atmospheres, comments 77—29806
- H I 21 cm absorption towards extragalactic radiosources, catalogues of 819 sources 78—57638
- H II regions near OH 43.79-0.13 and OH 48.61+0.02, compact continuum sources catalogue 78—36669
- Hα emission objects in Coalsack direction, finding list 77—22115
- Hα emission stars in Milky Way, catalogue of new discoveries 77—64665
- Hα emission stars in southern dark clouds, objective prism survey 78—28536
- He rich stars, intermediate and extreme, spectral atlas in 3700 to 4600 Å range 80—94806
- OH large-scale sky survey at 1612 MHz 78—32358
- SiO maser stars, list of 49 objects 78—32467

astronomical ephemerides
- 1932 HA (Apollo), ephemerides for 1930, 1941, 1964 and (1966) 80—105193
- 1936 CA (Adonis), 1977 tentative rediscovery, elements and ephemeris 77—29703
- 1936 CA (Adonis), elements and ephemerides, perihelion uncertainty 77—9692
- 1936 CA (Adonis), ephemerides for 1943 and (1984) 80—105193
- 1947 XC=1979 XA, orbital elements and ephemeris, 1980 January 7 to 22 80—31238
- 1947 XC=1979 XA, positions, UBV photometry and ephemeris continuation 80—31233
- 1950 LA (1980), ephemeris (1977 March-1978 April) 77—29704
- 1960 UA, orbital elements, ephemeris for 1977 May 17-1978 Feb. 21 period 77—45346
- 1966 S 2, Saturnian satellite, ephemeris 80—56762
- 1975 YA, ephemeris for 1978 July-1979 May period 78—69733
- 1975 YA, orbital elements and ephemeris for 1977, Aug. to Oct. 77—67059
- 1976 AA, position, elements and ephemeris (1977 Dec.-1978 Apr.) 78—12138
- 1976 AA, precise positions 1976, June-Dec., ephemeris for 1977, Jan.-Apr. 77—17418
- 1976 AA, precise positions and ephemeris extension (1977, Apr.-Dec.) 77—29706
- 1976 WA, precise positions, ephemeris for 1977, Jan.-May 77—17419
- 1976 WA, precise positions 1976, Nov. and ephemeris for 1976/77 Dec.-Jan. 77—13278
- 1976 WA (Object Schuster), positions, elements and ephemeris (1976 Dec.-1977 Jan.) 77—9695
- 1977, BAA handbook 77—2350
- 1977, observer's handbook of Royal Astronomical Society of Canada 79—8796
- 1977 BA, approx. posn., improved elements and ephemeris (1979 Mch.-Apr.) 79—34904
- 1977 HA, discovery, positions, elements and ephemeris (April-May) 77—45344
- 1977 HA, improved elements and ephemeris (1977, May-July) 77—49325
- 1977 HA, recovery, posns. and ephemeris (1979 June-July) 79—70986
- 1977 HB, improved orbital elements, ephemeris for 1978 Jan.-July 78—20719
- 1977 HB, positions, elements and ephemeris (1977, May-August) 77—49327
- 1977 HB, precise positions and possible ephemerides (1977, April-May) 77—56869
- 1977 RA, ephemeris for 1977 Sept.-Dec. 77—87309
- 1977 RA, positions, elements and ephemeris for Amor-type object 77—82152
- 1977 RA, positions, improved elements, and ephemeris 78—4137
- 1977 UB, prediscovery positions and ephemeris continuation 78—16331
- 1977 VA, ephemeris (1977 November 23 to 1978 February 21) 78—7914
- 1977 VA (Object Helin-Shoemaker), positions elements and ephemeris 78—7909
- 1977 VB, Phocaea-type Mars-crosser, ephemeris (1977 November 13 to December 13) 78—7913
- 1978, Belgian Astronomical Society edition *(French)* 78—40802
- 1978 British Astronomical Association Handbook 77—73937
- 1978 CA, ephemeris for 1978 Jul.-Oct. 78—73672
- 1978 CA, position, elements, ephemeris and B magnitude law 78—40860
- 1978 CA, precise positions 1978 March, ephemeris for 1978 Apr.-July 78—40862
- 1978 CA (Object Schuster), positions, elements and ephemeris (1978 Feb.-March) 78—36483
- 1978 DA, discovery, positions, elements, ephemeris and magnitude law 78—36484
- 1978 DA, ephemeris continuation for 1978 July-September period 78—61784
- 1978 DA, position, elements, ephemeris and B magnitude law 78—40861
- 1978 RA=1975 TB, ephemeris continuation and B magnitude law 78—89106
- 1978 RA (=1975 TB), ephemeris (1978 September 13 to October 3) 78—93141
- 1978 SB, orbital elements and ephemeris, (1978 September 9 to October 29) 78—93143
- 1978 SB, precise positions for 1978 Oct., orbital elements, ephemeris for 1978 Oct.-Dec. 78—96423
- 1979, general ephemerides *(French)* 79—40062
- 1979 BA, fast-moving object, discovery and ephemeris, (1979, February 16 to March 28) 79—35177
- 1979 BA, orbital elements and ephemeris, (1979, March 18 to June 16) 79—40121
- 1979 QB, Amor-type object, orbital elements and ephemeris (1979 August 25 to October 4) 79—92693
- 1979 QB, precise posns., elements and ephemeris (1979 Aug.-Nov.) 79—101108
- 1979 VA, not Alinda-type asteroid, ephemeris (1980 January 2 to February 11) 80—31232
- 1979 VA, orbital elements and ephemeris (1979 October 24 to December 23) 80—26776

astronomical ephemerides continued
- 1979 VA, precise posns., elements and ephemeris (1979 Nov.-1980 Jan.) 80—26777
- 1979 XA (=1947 XC), orbital elements and ephemeris (1979 December 13 to 28) 80—26774
- 1979 XB, orbital elements and ephemeris, (1979 November 23 to December 23) 80—46458
- 1980, British Astronomical Association Handbook 79—96893
- 1980, general ephemerides for Belgium *(French)* 80—77267
- 1980 AA, extension ephemeris (1980 Feb.-May) 80—41758
- 1980 AA, orbital elements and ephereris (1980 January 14 to 30) 80—36556
- 1980 LB, precise posns., orbital elements and ephemeris (1980 June-July) 80—82259
- 1980 PA, positions, improved orbital elements and ephemeris, (1980 August 25 to September 30) 80—98597
- 1980 PA, posns., elements and ephemeris (1980 August) 80—94746
- 1980 PA, precise posns., improved elements and ephemeris (1980 Sept.-Oct.) 80—101548
- 1980 S.Africa handbook 80—27046
- ADS 11871 (β 648), visual binary star, orbital elements and ephemeris 80—51805
- aids for calculator programming, book review 80—8764
- RT Andromedae, eclipsing binary, three-colour photoelectric obs. and improved ephemeris 80—22043
- 1862 Apollo, close approach and ephemeris (1980 Nov.-Dec.) 80—109389
- Apollo asteroids, chance rediscoveries rel. to reliable ephemerides 78—89105
- V342 Aquilae, eclipsing binary, orbital period changes and eclipses ephemeris 80—67791
- asteroid, 1980 AA, position Jan 20-22 1980 and ephemeris until Feb. 21st 80—31239
- asteroid 1947 XC(=1979 XA), ephemeris, 1980, 11th Feb.-1st May 80—36557
- asteroid 1979 VA, ephemeris, 1979 Feb. 11th until March 2nd 80—31240
- asteroid orbits identification, ephemerides calc. *(Chinese)* 78—69731
- asteroids, Trojan group, discovery of new members, orbital elements and ephemerides 80—72847
- asteroids in 1974; review of Institute of Theoretical Astronomy (USSR) activities. *(Russian)* 78—49368
- British Astronomical Association Handbook 78—85828
- l Carinae, Cepheid variable, Fourier anal. of light var. and ephemeris 80—90442
- Chebyshev approximations, satellite navigation 80—61993
- Comet Bowell (1980b), discovery posns., elements and ephemeris 80—51695
- Comet Bowell (1980b), precise positions, elements and ephemeris (1980 March-July) 80—62075
- Comet Bradfield, parabolic elements and ephemeris, 1978 July 31 to (1979 January 7) 78—65551
- Comet Bradfield (1978c), improved orbital elements and ephemeris (1978 March 18 to April 22) 78—40875
- Comet Bradfield (1978c), positions, elements and ephemeris 78—32401
- Comet Bradfield (1978c), positions, improved elements and ephemeris 78—36514
- Comet Bradfield (1978o), parabolic orbital elements, ephemeris for 1978 Oct.-Nov. 78—96433
- Comet Bradfield (1978o), parabolic orbital elements and ephemeris, (1978 October 29 to 1979 January 27) 79—2524
- Comet Bradfield (1979 l), parabolic orbital elements and ephemeris (1979 December 25 to 1980 January 14) 80—26812
- Comet Bradfield (1979c), ephemeris (1979 October 4 to December 23) 79—92721
- Comet Bradfield (1979c), parabolic elements, ephemeris for 1979 Sept.-Oct 79—88624
- Comet Bradfield (1979c), precise posns., elements and ephemeris (1979 June-July) 79—75159
- Comet Bradfield (1979c) parabolic orbital elements ephemeris, for 1979 Aug.-Sept. 79—80271
- Comet Bradfield (1979l), ephemeris and IR mags. (1980 Jan.-May) 80—41769
- Comet Bradfield (1979l), extension ephemeris (1980 Jan.-Mar.) 80—31257
- Comet Bradfield (1979l), posns., elements and ephemeris (1980 Jan. 5-26) 80—31256
- Comet Bradfield (1979l), precise props., orbital element and ephemeris (1979 Dec.-1980 Feb.) 80—26813
- Comet Cernis-Petrauska (1980k), antitail, precise posns., parabolic elements and ephemeris 80—105206
- Comet Cernis-Petrauskas (1980k), orbital elements and ephemeris (1980 August 4 to September 28) 80—98614
- Comet Fujikawa (1978n), orbital elements and ephemeris (1978, October 9 to December 8) 78—93168
- Comet Giclas (1978k), elliptical orbit ephemeris, (1978, September 9 to October 19) 78—89122
- Comet Haneda-Campos (1978j), orbital elements, ephemeris for 1978 Sep. 78—85913
- Comet Harlan (1976g), elliptical orbital elements and ephemeris for 1977 Apr. 7-Oct. 24 77—22148
- Comet Helin (1977e), ephemeris for 1977 Jul.-Nov. 77—64700
- Comet Helin (1977e), positions, appearance parabolic elements and ephemeris 77—49335
- Comet Helin (1977e), precise positions, elements and ephemeris (April-May 1977) 77—45364
- Comet Kohler (1977m), elliptical elements, ephemeris for 1978 Jun.-Dec. 78—45286
- Comet Kohler (1977m), ephemeris (1977 December 3 to 1978 June 1) 78—7937
- Comet Kohler (1977m), orbital elements ephemeris for 1977 Oct.-Dec. 77—87334
- Comet Kohler (1977m), positions, elements, ephemeris and magnitude estimates 77—91484
- Comet Kohler (1977m), precise positions, magnitudes, elements and ephemeris 77—87328
- Comet Kowal (1977f), ephemeris for 1977 May 17-July 16 77—53479
- Comet Kowal (1977f), precise positions and possible ephemerides (1977, April-May) 77—53476
- Comet Kowal (1979a), ephemeris, (1979, February 16 to March 28) 79—35195

astronomical ephemerides continued
Comet Kowal (1979a), ephemeris for 1979 Jan.-March 79—25549
Comet Kowal (1979h), ephemerides for parabolic and elliptical orbits (1979 May-Oct.) 79—96972
Comet Kowal (1979h), parabolic elements, ephemeris for 1979 Aug.-Sept. 79—88625
Comet Lovas (1975 VIII), precise positions and ephemeris for (1977 May 17 to December 23) 77—37578
Comet Lovas (1976k), ephemeris for 1977 Aug.-1978 Mar. 77—64701
Comet Lovas (1976k), precise positions 1976, Dec., ephemeris for 1977, Jan.-Jun. 77—17442
Comet Lovas (1976k), precise positions 1976, Nov. and ephemeris for 1976/77 Nov.-Feb. 77—17433
comet Lovas (1976k), precise positions 1976/77 and ephemeris for 1978 Mar.-Jun. 78—24491
Comet Lovas (1977c), precise position, improved elements and ephemeris 77—82174
Comet Lovas (1977c), precise positions, orbital elements and ephemeris 77—41358
Comet Lovas (1977c), precise positions, parabolic elements, ephemeris correction 77—33416
Comet Lovas (1977c), precise positions and corrected ephemeris 77—33415
Comet Lovas (1977t), tentative positions for 1978 Jan.-Feb. period 78—28582
Comet Machholz (1978l), ephemeris for 1978 Nov.-1979 Feb. 79—5785
Comet Machholz (1978l), parabolic orbital elements, ephemeris for 1978 Oct.-Nov. 78—93163
Comet Machholz (1978l), total visual mags. and ephemeris continuation 78—93159
Comet Macholz (1978l), orbital elements and ephemeris (1978, September 19 to October 9) 78—89126
Comet Meier (1978f), ephemeris for 1978 Nov.-1979 May period 79—5789
Comet Meier (1978f), orbital elements and ephemeris, (1978 May 12 to July 11) 78—53884
Comet Meier (1978f), positions, elements, ephemeris, magnitudes and spectrum 78—53881
Comet Meier (1978f), posns., elements, ephemeris and magnitudes 78—61801
Comet Meier (1978f), precise position, orbital elements, ephemeris and magnitude law 79—5781
Comet Meier (1979i), ephemeris (1979 October 14 to December 3) 80—4306
Comet Meier (1979i), ephemeris continuation (1979 December 3 to January 2) 80—26815
Comet Meier (1979i), non-parabolic orbit, ephemeris with elliptical elements (1980 January 2 to March 22) 80—31259
Comet Meier (1979i), precise posns., orbital elements, ephemeris and magnitudes (1979 Sep.-Oct.) 79—101118
Comet Mori-Sato-Fujikawa (1975j), ephemeris for 1977 Feb. 6-Aug. 5 77—17443
Comet Russell (1979d), ephemeris continuation (1979 July 6 to November 3) 79—80273
Comet Russell (1979d), precise posns., elements and ephemeris (1979 June-July) 79—71002
Comet Russell (1980l), discovery posns. and ephemeris (1980 September) 80—101557
Comet Russell (1980l), ephemeris (1980 Sept.-Dec.) 80—105207
Comet Russell (1980l), parabolic orbital elements and ephemeris, (1980 September 12 to October 2) 80—101559
Comet Sanguin (1977p), positions, elements and ephemeris 77—91486
Comet Schuster (1975 II), ephemeris for 1978 Apr.-1979 Mar. 78—40880
Comet Schuster (1976c), ephemeris for 1977 Feb. 6-1978 Apr. 22 period 77—17437
Comet Seargent (1978m), continuation ephemeris for 1978 Nov.-Dec. period 79—5782
Comet Seargent (1978m), ephemeris extension and magnitude estimate 79—44416
Comet Seargent (1978m), parabolic orbital elements, ephemeris for 1978 Oct.-Nov. 78—96436
Comet Seargent (1978m), parabolic orbital elements and ephemeris, (1978, September 29 to October 29) 78—93164
Comet Torres (1979e), parabolic orbital elements and ephemeris, (1979 July 26 to November 23) 79—84749
Comet Torres (1979e), precise posns., elements and ephemeris (1979 June-Aug.) 79—75160
Comet Torres (1980e), precise posns., elements and ephemeris (1980 June-July) 80—85900
Comet Tritton (1978d), positions, elliptical elements, ephemeris and magnitude law 78—36522
Comet Tsuchinshan (1977 X), osculating orbital elements, hyperbolic orbit determ. *(Chinese)* 79—80269
Comet Tsuchinshan (1977q), improved parabolic elements and ephemeris (1978, May 12 to December 18) 78—45284
Comet Tsuchinshan (1977q), positions, elements, and ephemeris 78—16350
Comet Tsuchinshan (1977q), precise positions, elements and ephemeris 78—16353
Comet van Biesbroeck, orbital elements and ephemeris for 1977 Feb.-Aug. 77—9710
Comet West (1978a), ephemeris, (1978, June 11 to September 9) 78—61807
Comet West (1978a), positions, parabolic elements and ephemeris 78—28583
Comet West (1978a), positions and ephemeris extension (1978 Jan.-July) 78—36516
comets, brightness prediction 79—75164
comets, minor planet circulars 4521-4548 ephemerides for four objects 79—2514
Comets Kowal, two probable objects, discovery posns. and ephemerides 79—96973
P/Daniel, predicted orbital elements 78—53883
Draconid meteor shower, prediction for (1979 October 9) 79—92728
Earth-Moon distance, extreme values for 1970-1979 period 77—37498
Eckert's lunar ephemeris, numerical evaluation 79—75124
elliptic orbit determ. by applying least squares method to observation residues *(French)* 78—40799
Galilean satellites, improved ephemerides for Voyager mission 80—62066
handbook for Southern Africa (1978) 78—32626

astronomical ephemerides continued
HD 153919 (3U 1700-37), X-ray binary, five-colour photometry and ephemeris 77—29877
HR 1099, optical ephemeris and radio flux vars. obs. 78—36641
EZ Hydrae, eclipsing binary, photometric obs. and primary min. ephemeris 78—73737
Iapetus, eclipse by Saturn's ring shadows, predictions 77—91472
1566 Icarus, ephemeris for 1977, July-Sept. 77—64690
Jupiter, triple shadow phenomena caused by Galilean satellites (AD 1900-2100) ephemerides 80—67641
Jupiter's Galilean satellites, ephemeris using Samson's theory *(French)* 78—16334
Jupiter inner satellites, mutual phenomena in 1979, ephemerides 78—53866
Kepler and ephemerides of the early seventeenth century 78—77659
SW Lacertae, W Ursae Majoris star, photoelectric obs. and updated ephemeris 80—62196
LDS 720-BC, visual binary with flare star, orbit calc. 77—13391
Leda (Jupiter XIII), continuation ephemeris (1978 Sept.-1979 May) 78—69739
Leda (Jupiter XIII), ephemeris for 1977/78, Aug.-Apr. 77—82156
Leda (Jupiter XIII), orbit and ephemeris for 1974-2000 period 79—8875
lunar ephemeris, Earth oblateness effects, corrections 77—22043
β Lyrae, orbital period variability and ephemeris (1971 to 1990) 80—72997
major planets, motion and coordinates, 1950 to 2150, from numerical study 79—92657
Mars, brightness temp. predictions, 1975 December to 1978 October 77—9683
Mars, ephemerides and position, 1975 to 1976, additional information *(French)* 79—44392
Mars, physical ephemeris from Viking landers radio tracking data 78—20685
Mars, position meas. and comparison with ephemerides (1975-1976) *(French)* 78—45252
Mars, positions and ephemeris corrections from Paris astrolabe obs. *(French)* 79—101103
Mars, rot. period determ. and albedo markings longits. in N.A.3 ephemeris system 80—98588
Minor Planet Circular 5333-5390, ephemerides for 92 asteroids 80—77325
Minor Planet Circulars, ephemerides for nine asteroids 80—31241
Minor Planet Circulars 4391-4424, ephemerides for five asteroids 78—81578
minor planet circulars 4425-4482, ephemerides for seven asteroids and four comets 78—85886
Minor Planet Circulars 4483-4520, ephemerides for 45 asteroids 78—93140
minor planet circulars 4521-4548, ephemerides for 11 asteroids 79—2514
minor planet circulars 4549-4582, ephemerides for five asteroids 79—12421
Minor Planet Circulars 4583-4622, ephemerides for 25 asteroids and four comets 79—16871
Minor Planet Circulars 4623-4648, ephemerides for nine asteroids 79—25538
Minor Planet Circulars 4649-4688, ephemerides for 41 asteroids and eight comets 79—35178
Minor Planet Circulars 4723-4746, ephemerides for nine asteroids 79—66953
Minor Planet Circulars 4747-4788, ephemerides for eight asteroids 79—75136
Minor planet circulars 4789-4844, ephemerides for 32 asteroids and two periodic comets 79—84729
Minor Planet Circulars 4845-4936, ephemerides for seven asteroids 79—101107
Minor Planet Circulars 4937-5016, ephemerides for eight asteroids 80—8580
Minor planet circulars 5017-5066, ephemerides for 68 asteroids 80—17533
Minor Planet Circulars 5137-5188, ephemerides for 13 asteroids 80—46459
Minor Planet Circulars 5189-5248, ephemerides for 60 asteroids and six comets 80—67631
Minor Planet Circulars 5249-5286, ephemerides for four asteroids 80—67632
Minor Planet Circulars 5287-5332, ephemerides for 11 asteroids and ten comets 80—67633
Minor Planet Circulars 5391-5422, ephemerides for nine asteroids and three comets 80—85884
Minor Planet Circulars 5423-5454, ephemerides for seven asteroids 80—98599
minor planets, 1979 ephemerides 79—12422
minor planets ephemerides, orbits computation using Chebychev polynomials *(French)* 80—61997
AU Monocerotis, eclipsing binary, ephemerides for overlapping photometric phenomena 80—77448
Moon, improvements to lunar motion theory using laser ranging results 80—21933
Moon, introductory review of ephemerides for laser ranging 77—64617
Moon, laser ranging ephemerides and reduction of observations 77 -56815
Moon, occultations during 1943-74, anal., rel. to Brown's theory, FK4 right ascension system and Watt's charts corrections 79—48696
Moon, orbital theory rel. to lunar laser ranging 77—64676
Moon, solar terms, corrections 80—12684
national ephemerides, latit. var. calc. 78—88776
navigational almanacs for small computers, calculators 79—62726
Neptune, ephemeris, 1612 December 28 to 1613 January 30 rel. to obs. by Galileo 80—105485
Neptune II (Nereid), ephemeris, (1978 May 12 to September 19) 78—53873
Nereid, ephemeris continuation (1977, May-October) 77—49330
Nereid (Neptune II), ephemeris (1979 May-Sept.) 79—53770
Nereid (Neptune II), ephemeris (1980 March 2 to September 8) 80—46481
Object Kowal, positions, indeterminate orbit, elements and ephemeris 78—7907
observational predictions, for Sun, Moon, constellations and planets, 1977, September to October *(French)* 77—87241
occultations by rings of Uranus, 1977-1980, predictions 78—16343
Pallas, occultation of SAO 85009 on 1978 May 29, prediction 78—53861

astronomical ephemerides continued
MW Pavonis, eclipsing binary star, UBV light vars., orbital elements and linear ephemeris 77—49429
DY Pegasi, dwarf Cepheid, revised ephemeris, period decrease 79—67040
Periodic Comet Arend-Rigaux, orbital elements, ephemeris for 1977 Apr. 7-Dec. 3 77—25986
Periodic Comet Arend-Rigaux (1977k), recovery and ephemeris continuation 77—74013
Periodic Comet Ashbrook-Jackson, ephemeris for 1977, Feb.-Oct. 77—17440
Periodic Comet Ashbrook-Jackson (1977g), ephemeris for 1978 Mar.-1979 Mar. 78—24486
Periodic Comet Chernykh (1977l), orbital elements, ephemeris for 1977 Sept.-Dec. 77—87333
Periodic Comet Chernykh (1977l), precise positions 1977, Sept. and Oct., ephemeris to 1978 Apr. 78—7941
Periodic Comet Chernykh (1977l), precise positions and ephemeris for 1977 Aug.-Oct. 77—82170
Periodic Comet Chernykh (1977l), precise posns., improved elements and ephemeris 78—69747
Periodic Comet Clark (1973 V), orbital elements, ephemeris for 1978 Feb.-Sept. 78—20744
Periodic Comet Comas Sola, ephemeris for 1977/78 Jul. to Feb. 77—53482
Periodic Comet Comas Sola (1977n), ephemeris for 1978 July-1979 June period 78—69749
Periodic Comet Daniel (1979b), ephemeris for 1979 Feb.-Apr. 79—30013
Periodic Comet Denning-Fujikawa (1978n), ephemeris, (1978 November 8 to 1979, January 27) 79—5780
Periodic Comet Encke, ephemeris, (1978 June 1 to November 8) 78—49380
Periodic Comet Encke, ephemeris (1980 Oct.-Dec.) 80—105209
Periodic Comet Encke, ephemeris and total magnitude predictions 77—49336
Periodic Comet Encke, semiaccurate position, CN production rate and ephemeris correction 77—67070
Periodic Comet Faye (1976i), ephemeris for 1977 Oct. 4-1978 June 1 period 77—82166
Periodic Comet Forbes (1980a), recovery obs. and corrected ephemeris 80—46490
Periodic Comet Gehrels 3 (1975o), orbital elements, ephemeris for 1977 Oct. 4-1978 Aug. 20 period 77—82165
Periodic Comet Giacobini-Zinner, ephemeris for 1978 April-November period 78—28588
Periodic Comet Giclas (1978k), elliptical elements, ephemeris for 1978 Oct.-Dec. 78—93162
Periodic Comet Grigg-Skjellerup, ephemeris for close Earth approach in 1977 April 77—13286
Periodic Comet Grigg-Skjellerup (1977b), precise positions and ephemeris, 1977, Mar.-Apr. 77—33414
Periodic Comet Gunn, ephemeris continuation for 1978 July-1979 April period 78—61805
Periodic Comet Gunn, position, osculating elements and ephemeris for 1977/8 77—33420
Periodic Comet Halley, orbit parameters and ephemeris, 1759-2024 period 80—62076
Periodic Comet Halley, orbital motion and viewing conditions for 1986 apparition 77—74011
Periodic Comet Haneda-Campos, ephemeris (1978, September 19 to November 18) 78—89121
Periodic Comet Haneda-Campos (1978j), ephemeris for 1978 Oct.-Dec. 78—93167
Periodic Comet Haneda-Campos (1978j), precise positions 1978 Aug.-Sept., ephemeris for 1978 Sept.Oct. 78—89131
Periodic Comet Holmes, elements and ephemeris for 1978 Apr.-1979 Jan. period 78—36525
Periodic Comet Jackson-Neujmin, ephemeris for 1978 June 21-1979 January 7 period 78—53878
Periodic Comet Jackson-Neujmin (1978q), recovery, and ephemeris for 1978 Nov.-1979 Feb. period 79—12435
Periodic Comet Johnson (1976h), continued ephemeris (1977, May-December) 77—45361
Periodic Comet Kojima (1970 XII), ephemeris for 1977/78 Aug.-July 77—71066
Periodic Comet Kopff (1976b), ephemeris for 1977 Feb. 6-1978 Jan. 12 period 77—13290
Periodic Comet Kowal 2 (1979a), elliptical elements and ephemeris, (1979, March 28 to June 16) 79—40140
Periodic Comet Kowal 2 (1979a), improved orbital elements and ephemeris (1979, May 7 to July 6) 79—48739
Periodic Comet Kowal (1977f), ephemeris for 1977 Jun.-Oct. 77—64699
Periodic Comet Kowal (1977f) ephemeris continuation (1978 Jan-Aug) 78—12160
Periodic Comet Olbers, orbit parameters and ephemeris, 1759-2024 period 80—62076
Periodic Comet Pons-Winnecke (1976f), continued ephemeris (1977 Apr.-Nov.) 77—37575
Periodic Comet Sanguin (1977p), positions, improved elements and ephemeris 78—16352
Periodic Comet Sanguin (1977p), prediscovery position, elliptical elements, and ephemeris 78—4153
Periodic Comet Schuster, (1977o), positions, orbital elements and ephemeris 77—91481
Periodic Comet Schuster (1977o), precise positions and ephemeris for 1977/78, Dec. to May 78—7940
Periodic Comet Schwassmann-Wachmann 1, 1978-9 ephemeris 78—77521
Periodic Comet Schwassmann-Wachmann 1, ephemeris for 1977 Aug. 5-1978 April 12 period 77—60727
Periodic Comet Schwassmann-Wachmann 2 (1979k), recovery posns. and ephemeris 80—26811
Periodic Comet Schwassmann-Wachmann 3 (1979g), orbital elements and ephemeris (1979 September 14 to December 23) 79—92720
Periodic Comet Schwassmann-Wachmann 3 orbital elements, ephemeris for 1979 Aug- Sept. 79—84750
Periodic Comet Shajn-Schaldach, ephemeris for 1978 June-1979 March period 78—53879
Periodic Comet Smirnova-Chernykh (1975 VII), ephemeris for 1978, Feb.-Dec. 78—20750
Periodic Comet Smirnova-Chernykh (1975e), ephemeris for 1977, Jan.-Nov. 77—5504

astronomical ephemerides continued
Periodic Comet Stephan-Oterma (1980g), recovery positions, elements and emphemeris 80—82307
Periodic Comet Taylor (1976 I = 1977a), ephemeris for 1976 Nov. 18-1977 June 26 period 77—22142
Periodic Comet Tempel 1, ephemeris for 1977, Jan.-Jul. 77—17430
Periodic Comet Tempel 1 (1977i), ephemeris for 1978 Feb.-Nov. 78—20742
Periodic Comet Tempel 2, 1976 December-1977 September ephemeris 77—5499
Periodic Comet Tempel 2 (1977d), ephemeris (1978 June 1 to 1979 February 16) 78—49382
Periodic Comet Tritton (1978d), positions, elements and ephemeris 78—36531
Periodic Comet Tsuchinshan 1, ephemeris for 1977 Oct.-1978 July period 77—82167
Periodic Comet Tsuchinshan 2, ephemeris for 1977 Nov.-1978 Apr. period 77—91480
Periodic Comet Tuttle (1980h), ephemeris (1980 Oct.-1981 Feb.) 80—105208
Periodic Comet Tuttle-Giacobini-Kresak, 1978-9 ephemeris 78—73684
Periodic Comet Van Biesbroeck, ephemeris continuation (1977 Nov.-1975 Nov.) 77—91479
Periodic Comet Whipple, ephemeris for 1977 Apr. 7-1978 Feb. 1 77—22149
Periodic Comet Whipple (1977h), ephemeris, (1978 June 21 to 1979 April 17) 78—53882
Periodic Comet Wild 2 (1978b), ephemeris for 1978 Jul.-Sept. 78—73676
Periodic Comet Wild 2 (1978b), positions, elements, ephemeris and magnitude estimates 78—36515
Periodic Comet Wild 2 (1978b), positions, elements and ephemeris 78—28589
Periodic Comet Wild 3 (1980d), discovery posns., orbital elements and ephemeris (1980 April-June) 80—67657
Periodic Comet Wild 3 (1980d), improved orbital elements and ephemeris (1980 May 31 to August 9) 80—72885
Periodic Comet Wolf-Harrington, ephemeris for 1977 June 6-1978 June 1 period 77—53477
Periodic Comets Tsuchinshan 1 and 2, orbital elements, ephemerides for 1977-79 *(Chinese)* 77—22137
planetary ephemerides construction, rectangular coordinates approximation by Chebyshev polynomials *(Russian)* 80—62033
planetary ephemeris, direct computation method *(French)* 78—7862
planetary satellites, ephemerides representation by Chebyshev polynomials *(Russian)* 79—16800
planetary terms in lunar ephemeris 79—84645
planets, effect of star catalogue coord. system orientation errors *(Russian)* 80—51640
Pluto, 1978 P 1, discovery of possible satellite, ephemeris 78—69744
Pluto, 1978 P 1, possible satellite, orbit and eclipses ephemeris 78—93152
Pluto, no occultation of star on 1980 April, 6 ephemeris 80—62070
Pluto, opposition on 1979 April 8, satellite confirmation opportunity 79—44409
Saturn ring disappearances (1600 to 2100) 80—72876
Saturn ring system, ephemeris for Earth ring plane crossing (1979 October 27) 79—101115
Saturn satellites mutual phenomena in 1979-1980, ephemerides 78—53868
RY Scuti, eclipsing binary, ephemeris and UBV obs. 80—94832
solar eclipses in 1977 predictions and circumstances 77—56895
solar position, formulae *(German)* 80—77367
solar position computation procedure 79—5734
solar total eclipse, 1979, February 26, ephemeris 78—85928
Southern Africa, 1977 astronomical handbook 77—25954
SS 433, IR light curves from BVIJHK photometry, period and ephemeris 80—8642
stars occulted by rings of Uranus, 1977-1980, colours and magnitudes 78—16277
4 U 1538—52, eclipsing X-ray source, corrections to ephemeris and revised period 79—25760
Uranus occultation of SAO 158687 on 1977, March 10, predictions 77—29717
US Naval Observatory data files 77—78670
612 Veronika, identifications and ephemeris (1979 Sept.-1980 Feb.) 80—4285
visual binary stars, orbital elements and ephemerides 80—46607
visual double stars, rectilinear trajectories calc. *(French)* 79—17023
BW Vulpeculae, V photometry, light curve, quadratic ephemeris 80—26881
X-ray sources occultations by Moon, first and last dates (1980 to 1985) 80—77513

astronomical instruments
see also astronomical observations; astronomical techniques; astronomical telescopes; radiotelescopes
Abbe comparator, improved, for mag. stars meas. 77—67043
AC contactless machine of double supply, props. *(Russian)* 77—17375
acousto-optical high-resolution radiospectrometer, mm wave astronomy appls. 78—4109
acousto-optical radio spectrograph for spectral integration 78—69694
acousto-optical solar radio spectrograph 78—73631
acousto-optical spectrum analyser *(Russian)* 77—29652
active coded aperture for direction meas. of high energy γ-rays 80—62022
Advanced X-ray Astrophysics Facility, results obtained 80—109366
airborne 33 GHz radiometer system for 3K background anisotropy mapping 78—61735
airborne far IR Fabry-Perot astronomical spectrometer 80—109371
airborne far IR Fabry-Perot spectrometer for astronomical fine structure lines 80—62026
airborne IR observations, methods and instruments 78—69688
airbrush, for planetary mapping from photographic obs. 78—53833
altazimuth and equatorial telescope mountings, home made, construction method 78—40830
amplitude interferometer, white light, 180 degree rot. shear astronomical appl. 78—77977
analogue system for fast light curve registration, lunar occultations appl 79 53725

astronomical instruments continued
annular scanning photometer, detect. of optical halo around spiral galaxy (NGC 4565) 78—12364
Apollo lunar surface science stations shutdown 78—57425
Apollo Telescope Mount and solar instruments of Skylab, overview 77—60593
Apollo Telescope Mount television monitors, obs. and recording of instantaneous images 77—60605
Ariel 5 Bragg spectrometer, calibration data 77—5441
Aryabhata satellite, technology and scientific expts. 79—58218
Aryabhata satellite payload for detection of energetic solar neutrons and gamma rays 79—84636
Ascoris photometer, description and use 80—4256
aspheric grating for EUV astronomy 78—57451
aspheric objective for a coronagraph *(Japanese)* 78—89063
aspherical diffraction gratings produced by dioptric elasticity method 77—73962
astrographs, wide angle, sky photography programme *(Russian)* 80—72747
astrographs, wide-angle, astroclimatic influences on precision of photographic star positions *(Russian)* 80—72748
astrolabe instrumental errors and transversal scale, work of Levi ben Gerson 78—21
astrolabes, Settala collection in Ambrosian picture gallery, Milan *(Italian)* 79—35132
astrometric instrument index mark optimum brightness calc. 79—53720
astronomical TV system, appl. to study of meteor bright line spectra 78—61817
Atkinson sundial at Indiana University 79—84678
Australian Astronomical Society, conf. Melbourne, Australia (May-June '77) 78—69655
automated isophotometer for large photographic plates *(Japanese)* 78—89069
automated spectrum scanner, 3000-11000 Å region 79—53724
automated system for detect. of cosmic radio bursts at VHF and UHF 78—77489
automatic astrometric instrument for use on lunar surface 77—17372
automatic CCD measuring machine for star images *(Japanese)* 80—82212
automatic device for lunar crater/stars superimposed photography *(Russian)* 79—92675
automatic microdensitometer, astron. plates meas. 79—80230
automatic sun sighting system, for incident solar radiation meas. *(Italian)* 77—22062
automation system, for solar spectrometric research on-line processing *(Russian)* 80—12659
balloon borne interference spectrometers operation and appl. to solar UV obs. *(Japanese)* 78—57442
balloon-borne equipment, data communications 79—16793
balloon-borne experiment, for obs. of diffuse cosmic X-radiation above 20 keV 78—54096
balloon-borne probes in stratosphere, atm. and astron. research 77—37435
Balloon-borne UV Stellar Spectrograph, first obs. results 79—70955
Balloon-borne UV Stellar Spectrograph, instrumentation and obs. 79—70954
balloons, transatlantic, self-ballasting, for astronomical research 80—21917
bandpass interference filters for 1-3 mm window 80—109368
Bent Crystal Spectrometer for solar X-ray spectroscopy 79—25489
Berkeley stellar spectrometer and EUV Explorer, Wolter-Schwarzschild optics 80—82197
bifilar sundial, theory 78—93119
birefringent filter improvements, field of view effects 80—14428
birefringent filters, transmission expression derivation 79—18522
blink comparator, semi-automated, for large photographic plates *(Japanese)* 78—89081
blink microscope, exam. of new microscope at Lyon Observatory *(French)* 78—61742
bolometer, composite, for submm. wavelengths 78—65964
Bragg X-ray analyser crystal polarimeters, calibration 77—64664
broad-band multifunctional recording system for radioastronomical interferometer *(Russian)* 77—29650
Brorfelde transit circle, diameter corrections 80—105164
BUSS, echelle and SEC-vidicon for balloon-borne UV spectroscopy 79—25482
C-CD camera, appl. to Einstein X-ray Observatory fields RI photometry 80—62315
C-CD camera, description performance and calibration 80—73499
C-CD camera on Galileo Jupiter Orbiter Mission 80—85859
C-CD imaging systems, large area, for deep space photography 77—57426
C-CD Si detectors for space astronomical appl., UV sensitization 79—84668
camera, wide-field filter 78—49335
camera lens, focal length determ. *(Spanish)* 77—64663
capacity type detector for low vel. dust meas. during cometary fly-by mission 78—93113
Cassegrain echelle spectrograph 79—62749
Cassegrain echelle spectrograph at Mt. John Observatory, New Zealand 78—69689
Cassegrain scanning system for IR images 80—82204
Castle Frederick, eighteenth-century Nova Scotia observatory, history 78—40843
catadioptric lens system, possible appl. for satellite and astronomical photography *(German)* 79—76793
cavity pyrheliometer, total solar optical irradiance meas. 79—35130
CCD spectrometer for 500 to 900 nm range 80—82207
CERGA stellar interferometer, phase effect detect. and appl. to orbit of α Aurigae (Capella) *(French)* 80—36508
charge coupled devices, cosmic ray background model 80—51669
charge injection device as stellar tracking sensor 80—85861
charge injection devices for astronomy 77—41317
charged particles in space, meas. instruments review *(Russian)* 77—17368
Cherenkov atmospheric detectors for gamma-ray astronomy, sensitivity 77—3232
chopper for deep space IR interferometer/spectrometer 78—81545
chopping photometer, for stellar obs. in northern light zone *(Norwegian)* 78—69699
chopping photometer to eliminate auroral sky background 80—72776

astronomical instruments continued
chronometric system using punched tape for star transit obs. *(Russian)* 78—4110
circumsolar radiation meas. appl. 77—25767
coherent speckle interferometry system, for stars cold satellites searching *(Russian)* 80—12672
cold camera, description 80—72779
cold camera, for astronomical cooled emulsion photography 80—56714
collimators, for astronomical soft X-ray meas. 77—5436
coma-free two-mirror systems, astronomical appls. *(Russian)* 77—64641
comet discovering machine hoax, hydrocarbon bond detection 80—13
compact echelle spectrograph 77—87271
compact solar camera, student project 80—67975
computer controlled narrow band optical filters for solar astronomy *(Russian)* 78—16292
computerized differential photometer for Geneva seven colour system 79—48682
concave grating, meridional focal curves of Seya-Namioka mounting *(Russian)* 77—64658
concentric spectrograph using holographic grating 78—32896
conference, Tucson, Arizona (29 January to 1 February 1979) 79—75108
conference on nuclear power systems, Washington, USA (1978) 79—41045
conic reflectors, meridional caustics 77—72044
CORAVEL, Cassegrain spectrophotometer for stellar radial vel. determ. 80—82210
coronal photometer, automatic, 5303 Å emission line photoelectric meas. 79—12454
correlator back-end for Culgoora radioheliograph, advantages and disadvantages 80—85865
Cosmic Background Explorer, satellite instrumentation 80—61988
cosmic ray spectrometer, for study of 6 to 50 MeV electrons 78—45235
cosmic ray telescopes composed of Si solid state detectors, neutral particle background 78—28472
cosmic-ray stations global network, appl. as spectrographic instrument set 79—12404
COSMOS measuring machine 77—64652
coude camera for image tube work 77—22080
Coude spectrograph for 2.6 m Shajn Telescope *(Russian)* 77—64644
cryostat using ^{3}He for space appls. 77—22077
curved crystal X-ray spectrometer, for HEAO-B satellite 78—49331
Danjon astrolabe, appl. to obs. of planets 77—64651
Danjon astrolabe, instrumental const. *(French)* 79—75101
Danjon astrolabe, planetary obs. *(French)* 80—94715
Danjon astrolabe, temp. effects on focal plane position *(Russian)* 78—4112
data acquisition system for lunar occultations obs., microprocessor control 77—49311
design of reflective and catadioptric systems 79—86242
differential photometer, 6800 microprocessor control, astronomical appl. *(French)* 79—58253
diffraction grating, transmission efficiencies on EUV and soft X-rays 77—60621
diffraction mountings, conical and classical, for XUV gratings 79—3780
digital electronic integrator, for radioastronomical obs. processing *(Russian)* 78—57465
digital instrument for astronomical meas. recording *(Polish)* 79—88598
digital microdensitometer, for automatic photographic wavelength meas. 77—64655
digital register for elec. photometer *(Russian)* 78—93117
digital system for image processing *(Italian)* 80—98558
discrete photoelectric tracking system of variable precision *(Russian)* 78—57458
dispersion-removing radiometer, obs. tests on PSR 1913+16 binary pulsar 79—35142
Dollfus stellar polarimeter, modification for linear polarization meas. 79—53723
double astrograph photometric system, investigation of colour eqns. *(Russian)* 80—72771
double-station camera, for meteors trajectories and orbits determ. 77—74014
doublet system resolution, random speckle structure model and expt. *(Russian)* 79—7082
drift chamber detector, performance figures, γ-ray astronomy appl. 79—48674
drift chamber detector for high resolution gamma-ray astronomy 77—9660
EAS detectors, pulse profiles studies 79—25421
echelle Czerny-Turner spectrometer, 5 m, instrumental functions 78—8449
echelle spectrograph, high-resolution, for far UV and visible astronomy, design and performance 80—26744
echelle spectrograph, moderate resolution, wide band 77—33351
echelle spectrograph for high-resolution stellar spectra 78—96396
electrically erasable and programmable read only memory writer *(Japanese)* 79—101072
electrographic image detectors, development, and applications in UV astronomy and scientific research 80—43465
electrographic instrumentation for ultraviolet imaging and spectrography 80—46399
electronic camera for Geneva seven-colour photometry *(French)* 79—84682
electronic detectors to enhance optical information from telescopes, image intensifiers and CCDs *(French)* 80—67569
electronic metronome for astrophotography 80—67572
electronographic camera, development and use 77—56829
electronographic camera, polarisation maps of nebulae 77—57081
equatorial sub-mounting, rocking type, in Hill-Poncet heated observatory 79—70953
equatorial table mounting, semi-kinematic, for short-focus telescopes and cameras 79—70958
equivalent concentric systems *(Russian)* 77—64659
European USSR bolide network, photographic determ. of bolides topocentric coordinates 78—61818
EUV instrumentation 79—25484
EUV spectrograph, Skylab Apollo Telescope Mount expt. S082B 77—60598
EUV spectrograph with single toroidal grating, stigmatic performance 80—36498

astronomical instruments continued
- EUV spectroheliographic, in Apollo Telescope Mount experiment S082A 77—60597
- EUV spectroheliometer on Apollo Telescope Mount 77—60594
- EUV spectroheliometer on Skylab Apollo Telescope Mount, photometric calibration 77—60595
- EUV spectrometer, reliability anal. technique appl. 80—85864
- external occulting disc as radially-graded neutral density filter, for solar coronal obs. during eclipses 79—80233
- Fabry ten-colour photometer on Skylab for gegenschein and zodiacal light obs. 77—60610
- Fabry-Perot etalon, optically contacted, stability to cosmic radiation 80—98544
- Fabry-Perot etalons as high-resolution IR interferometers 77—45888
- Fabry-Perot imaging device TAURUS for radial velocity field maps 80—82205
- Fabry-Perot interferometer and solar obs. 79—44378
- Fabry-Perot interferometers, description 80—4261
- Fabry-Perot scanning interferometer with piezoelec. spacers, appl. to solar UV spectrum 80—12678
- Fabry-Perot spectrometer for solar vel. field meas. 80—90333
- Fabry-Perot versalite multimode instrument for nebulae obs. 77—33350
- Faint Object Camera calibration 79—25479
- Faint Object Camera on Space Telescope 79—25478
- Faint Object Spectrograph for Space Telescope 79—25483
- far IR calibration source for balloon-borne telescopes 80—62027
- far IR interference filters 77—22592
- far IR polarimeter for balloon astronomy 79—35094
- far UV source, 1150-3100 Å, for spectrometer calibration 77—41696
- far UV spectrograph with microchannel plate detector,for rocket-borne astronomy 77—22086
- FAUST, far UV camera on Spacelab 79—25476
- Fehrenback prism for stellar radial vel. meas. 79—84681
- Fick Observatory rasdial velocity spectrometer 78—12098
- field correctors, for telescopes at better observing sites 80—4257
- filter, birefringent alternate partial polariser, design 77—7188
- fluxgate magnetometer on Pioneer Venus Orbiter, design and operation 80—67496
- focal coronograph detection of new Saturn ring *(French)* 80—72772
- focal grating photometer for magnitude difference determ. of double stars 80—67567
- focal plane IR detector arrays for planetary missions 80—85862
- focal reducer using Fresnel lens, appl. to stellar photometry 80—67568
- focal-reducer system, for slitless fieldspectroscopy 80—36504
- FOCAS, faint object classification and analysis system, galaxy counts 80—105350
- focusing Fe line crystal spectrometer for Spacelab 79—25500
- foil mirror, with automatic phase correction, construction *(German)* 77—88883
- four-channel photon-counting spectrophotometer, for stellar Ca II H and K flux meas. 78—73646
- Fourier interferometer for IR line emission obs. of molecular clouds *(Italian)* 79—48679
- frequency-agile phase lock system for mm wave klystron suitable for radioastronomy 77—5446
- Fulton's orrery, 19th century instrument to demonstrate planetary system motions 78—69695
- Gamma Ray Experiment on Solar Maximum Mission, spectrometer 80—51657
- Gamma Ray Observatory instrums. and operations 80—109365
- gamma-ray burst detectors, critical comparison 77—64648
- gamma-ray detectors, angular resolution 80—8539
- gamma-ray detectors, counters and telescopes *(Polish)* 78—96394
- gamma-ray instrumentation, for low and medium energy ranges 79—25492
- gamma-ray spectrometer with various shaped scintillators, for gamma-ray spatial pattern anal. 79—16831
- gamma-ray spectrometers with cooled Ge sensors on P78-1 satellite 80—58019
- gas analysis equipment, on automatic interplanetary stations (Venera-4, 5, 6 and 8) 78—28520
- gas scintillation counter for spectral line studies in X-ray astronomy 77—13247
- gas scintillation counter X-ray spectrometer performance figures astronomy appl. 79—48673
- gas scintillation proportional counter, burst length discrimination system 78—21824
- gas scintillation proportional counter, large-area focusing, for X-ray astronomy 79—25494
- gas scintillation proportional counter for first Spacelab mission 79—25488
- gas scintillation proportional counter for X-ray astronomy 77—71004
- gas scintillation proportional counter of large area for X-ray astronomy 79—80222
- gas scintillation proportional large area counter, X-ray astronomy appl. 79—45556
- gas-scintillation proportional counters, high resolution, for X-ray astronomy, developments 77—54439
- gradiometer systems for lunar gravity meas. 80—94730
- graphic processor for pseudo-colour images representation *(Italian)* 80—98562
- grating spectrographs, anamorphic magnification and appl. 79—66927
- grating spectrographs, physical principles *(German)* 77—56830
- grating spectrometer, liquid He cooled, for far IR astronomical obs. 79—66925
- grating spectrometers and spectrographs, design method 80—62742
- gratings for UV space instrumentation, comprehensive analysis 79—8839
- gravitational radiation detectors, implications of extension to noise theory for RF SQUIDs 77—87685
- gravitational wave astronomy, introductory review 77—67368
- gravitational wave detectors, appls. to astronomy 79—92664
- gravitational-wave antenna, small, cryogenic, meas. at 1.5K 79—21646
- gravitational-wave resonant antennas, optimum filtering and sensitivity 80—8545
- Hadamard transform IR imaging device 77—13240
- halfsecond levels, investigations using atuomatic comparator *(Russian)* 78—40675
- Hard X-Ray Burst Spectrometer on Solar Maximum Mission 80—51658
- hard X-ray camera for study of gamma ray burst sources 79—25502
- hard X-ray experiment for long-duration balloon flights 79—25493
- hard X-ray imaging collimator 77—5437

astronomical instruments continued
- hard X-ray imaging instrument, for solar and cosmic sources 78—49332
- Hard X-ray Imaging Spectrometer on Solar Maximum Mission 80—51659
- Harriot, Thomas, 1560-1621, biography, astronomical instruments and obs. 79—35512
- Hartmann method for studying astronomical optics 77—25949
- HEAO 1 scanning modulation collimator, X-ray source positions meas. 78—93459
- HEAO 2 satellite (Einstein Observatory), successful launch 79—44333
- HEAO-1, successful launch report 77—82102
- HEAO-1 Cosmic X-ray experiment (A-2) 79—58248
- HEAO-2, Einstein X-ray Observatory, hardware, instruments performance characts. 79—70941
- HEAO-B satellite, sensitivity rel. to deep X-ray surveys predictions and strategies 78—96567
- HEAO-B X-ray Observatory 79—25446
- heliostat, polar axis alignment methods 79—70957
- heterodyne gravitational wave detector, sensitivity 77—41298
- High Altitude Observatory Coronagraph/Polarimeter on the Solar Maximum Mission 80—51662
- high detective quantum efficiency image detectors, review 77—71010
- high pressure gas scintillation spectrometers for X-ray astronomy 80—105166
- high resolution imaging X-ray detector, for astronomical meas. 78—49333
- high resolution UV solar spectroscopy, instruments and obs. 78—45313
- high speed photometer of Asiago Observatory 79—25505
- high-energy celestial X-ray instrument on OSO-8 78—28522
- highly polarised objects detection device *(Japanese)* 80—82209
- History of Sciences Collections, Royal Swedish Academy of Sciences, catalogue 78—81789
- holographic grating, calc., for very wide field camera *(French)* 78—81547
- horizontal meridian circle, appl. to determ. of stellar right ascensions 77—53405
- horizontal spectrograph for solar mag. and vel. field meas. 77—17366
- HSFA solar research system, description 80—4251
- Hvar Observatory, instrumentation and reduction techniques for photoelectric photometry 77—78643
- hypersensitised astronomical plates, detective quantum efficiency gains and speed 77—64660
- IKA-65 UV stellar photometric equipment on Cosmos 215 satellite *(Russian)* 77—64642
- image convertor camera for use with universal astrograting spectrograph 77—67037
- image convertor-intensifier detector for interference spectroscopy in balloon UV 80—56707
- image intensifier tube with self-scanned photodiode array, photoelectron counting 77—18090
- image intensifier with fibre optic plates *(Russian)* 79—40079
- image isocon, appl. in astrophysical obs. *(Russian)* 80—12671
- image sensors, electronic, for ground-based astronomy 79—35135
- image sensors for spaceborne astronomy 77—87268
- image tube with fibre optics, cooling effect 78—96401
- image-intensifier spectrograph, description and use 78—73647
- image-tube systems, effects of phosphor decay on time-modulated meas. 79—88602
- imaging detector for hard X-rays/soft γ-rays 79—58250
- imaging gas scintillation counter for X-ray astronomy 80—98551
- imaging photon detectors 80—86405
- imaging system, real-time, for solar coronal X-ray obs. from sounding rockets 80—41725
- imaging system using intensity triple correlator 78—74846
- impaact mass spectrometer for chemical analysis on comet fly-by mission 78—93112
- IMPATT source, frequency-stabilised, 115 GHz 80—67573
- Infrared Astronomical Satellite, features and performance 80—61989
- integrating vidicon systems at Cerro Tololo 79—66924
- integrating wide-field IR photometer for globular clusters study 80—62029
- intensified CCD test results 77—41318
- intensity microphotometer with step-drives, for negatives transparency conversion *(Russian)* 78—57457
- interactive system for computer reduction and display of two-dimensional data 79—58257
- interference filter for submillimetre astronomy 80—48393
- interference filters, defects in transmission profiles 78—25952
- interference filters, nebulae observations, urban light pollution 79—88599
- interferometer, IR spatial, design and operation 78—45232
- interferometer, long-baseline amplitude, pupil space design 78—53832
- interferometer, Michelson far IR 78—93118
- interferometer, triple, Fabry-Perot, for solar spectroscopy, instrumental profile 78—40817
- interferometer, wide-angle Mach-Zehnder, for Na D-emission photography 77—60617
- interferometer-grating spectrograph for high resolution spectroscopy in middle UV 78—77490
- Internation UV explorer, inclined elliptical geosynchronous orbit mission design implications 78—4104
- International Sun Earth Explorer 1, electron spectrometer expt. 78—85809
- International Sun-Earth Explorer 1, solar wind expt. 78—85800
- International Sun-Earth Explorer 1 and 2, fast plasma expt. 78—85800
- International Sun-Earth Explorer 1 and 2, plasma wave investigation 78—85802
- International Sun-Earth Explorer A, DC and low-freq. elec. field meas. instrumentation 78—85807
- International Sun-Earth Explorer A, plasma comp. expt. 78—85810
- International Sun-Earth Explorer B, EGD positive ion expt. 78—85805
- International Sun-Earth Explorer spacecraft, expts. and instruments 78—85785
- International Sun-Earth Explorer spacecraft instrumentation for solar and interplanetary electron meas. 78—85786
- International Sun-Earth Explorer-1, quasi-static and low-freq. elec. fields meas. 78—85808
- International Sun-Earth Explorers, electron density expt. 78—85803
- International Sun-Earth Explorers 1 and 2, fluxgate magnetometers 78—85804
- International Sun-Earth Explorers 1 and 2, medium energy particles expt. 78—85811

astronomical instruments continued
International Ultraviolet Explorer, spacecraft, instrumentation and program *(Italian)* 78—32320
International Ultraviolet Explorer (IUE) instrumentation, in-flight performance 78—96383
International Ultraviolet Explorer (IUE) spacecraft, instrumentation 78—96382
interplanetary plasma wave expt. on International Sun-Earth Explorer C spacecraft 78—85794
IR and sub-MM spectroscopy, conf., Bonn, Germany (Mar. 1977) 78—12778
IR and submillimetre astronomy, book *(Russian)* 80—72773
IR astronomical satellite telescope and detector arrays 78—45226
IR detector, low-temp. modulated calibration method, space appls. 77—79152
IR detector performance, operating characts. of thermal and photon detectors 78—45231
IR detectors, for Sunyaev-Zel'dovich effect obs. in millimetric region 79—25765
IR detectors, trends in low-temp. thermal and photon detectors *(Russian)* 80—72778
IR Fabry-Perot interferometer for astrophysics 80—8672
IR Fourier spectrometer, lamellar grating type, for balloon-borne telescope 78—16294
IR Fourier transform spectrometers 78—16309
IR heat trap field optics, compact lens-mirror system 78—55422
IR instrumentation on NASA airborne observatories 78—45224
IR interferometer, 11 μm heterodyne system *(French)* 80—46397
IR Michelson interferometer on Voyager 80—77290
for IR obs. from space platforms, cryogenic design problems 78—16298
IR photometer for stellar obs. 78—69795
IR photometer with vibrating dichroic filter, southern stars obs. 77—26017
IR pinhole photometer for solar intensity obs. in 1.5-2.4 μm range 79—101069
IR radiometer on Pioneer Venus orbiter 80—36469
IR sensors, long-wave, for astronomical obs., ground calibration 79—5749
IR sensors and assoc. signal processing, performance evaluation 77—49313
IR space sensors, low-background large-aperture, meas. facility for evaluation 79—21125
IR space sensors, low-background large-aperture, meas. facility for evaluation 79—21126
IR spatial interferometer, space-borne, exposure time 79—35131
IR spectrometers at U.C. Berkeley, current status 78—16293
IR system for radiating source meas., calibration and spectral props. 77—49300
IR upconvertor for astronomical imaging 78—7883
IR-array spectrometer 7-25 μ astronomy 77—22081
iris photometer for large photographic plates *(Japanese)* 78—89070
ITS-4 IR telescope-spectrometer on Salyut 4 station 77—78635
ITT FW-130 photomultiplier, linearity test 79—58255
ITT FW-130 photomultiplier, nonlinearities 78—85852
Jai Singh observatories and 'instruments' in N.India 80—17490
Jodrell Bank 1024 channel digital autocorrelation spectrometer 77—73970
Joyce-Loebl microdensitometer, computer control for objective-prism spectra meas. 80—105173
King's Observatory at Richmond, history 77—67033
Kodak spectroscopic plates type 103a long term storage in dry N 77—71391
LAMAR X-ray facility for high sensitivity obs. 79—25497
lamellar-grating interferometer, balloon-borne, appl. to solar brightness temp. meas. 78—85921
large imaging CCD array development and test results 77—41316
laser experiments on Spacelab missions, for atmospheric meas. 78—53793
laser ranging equipment, computer system *(Japanese)* 78—89080
laser ranging equipment, photoelectric circuit *(Japanese)* 78—89075
laser ranging equipment, range gate *(Japanese)* 78—89076
laser ranging equipment, range meas. system *(Japanese)* 78—89074
laser ranging equipment, system controller *(Japanese)* 78—89079
laser ranging equipment, telescope drive *(Japanese)* 78—89078
laser ranging equipment, timing system *(Japanese)* 78—89077
laser ranging systems, space appl. 79—40081
LEAM response to electrostatically charged lunar dust 79—58259
Leicester solar coronal Bragg spectrometer, wavelength calibration and resolution 77—5442
light collector for near IR, for stellar spectroscopy 77—73960
linear astrolabe using Gall's stereographic projection 78—36463
linear digicon detector, appl. to speckle interferometry 77—78648
long-baseline interferometer for astrometry 77—37506
low level light detectors 78—28525
low light level device applications, conference, Reston, USA (1976) 77—39091
low-background astronomical integrated IR detector array development 80—85860
low-noise photon counting system using photosil detector 77—45890
low-temperature narrow-bandpass interference filter construction 79—32049
LPSP instrument on OSO-8, in-flight performance and preliminary results 78—49317
lunar magnetometers, data errors and EM induction studies 79—96932
Lyman α camera, for high resolution solar Lyman α filtergrams 80—82323
Lyot depolarizer in quasimonochromatic light 79—62747
magneto-optical filter, for solar vel. fields meas. 79—25507
magnetograph, for weak solar mag. field meas. 77—71085
magnetometer, ring core, for mag. meas. in interplanetary space during Halley-Venus mission *(Japanese)* 80—94672
magnetometer for Pioneer Venus Orbiter spacecraft 77—87229
mass spectrometer, space-borne, in-flight calibration device 78—93115
mass spectrometer-molecular beam expt. for planetary atmosphere investigation 78—49327
McMullan 4 cm electronographic camera, appl. to high-dispersion stellar spectroscopy 78—73644
mechanical displays, early astronomical visual aids 78—36787
membrane mirrors for image compensation system, performance and manufacture 77—42587

astronomical instruments continued
meniscus-concave mirror systems, misaligning effects *(Russian)* 77—53426
meridian circles pivot errors, new determ. method 78—53822
meridian instrument pivot irregularities meas. method 80—94718
metallic mesh interference filters, low temp. narrowbandpass 80—14430
meteor radar system, Illinois University, description and results 77—41205
Michelson Fourier transform spectrophotometer for stellar obs. 78—81550
Michelson Fourier transform stellar spectrometer 80—98552
Michelson interferometer, high spectral resolution, for Isaac Newton Telescope 78—4105
Michelson interferometer, sequential analysis of fringes, scanning rate influence 78—77976
Michelson interferometer for airborne IR obs. of interstellar media 77—73966
Michelson interferometer for airborne IR obs. of interstellar media 77—73967
Michelson interferometer for balloon-borne IR spectroscopy 80—51654
Michelson stellar interferometer, reconstituting nonstationary optical pattern from 2-photon correls. *(Russian)* 77—82125
Michelson stellar interferometer, seeing effects removal 77—29659
microchannel plate, X-ray quantum efficiency 78—45768
micrometeoroid detector film, penetration expts. 80—77292
microphotometer, with rebuilding struct., for registration of spectra in terms of intensities *(Russian)* 77—13244
mirrors, large scale lightweight, replication 78—66963
mirrors for space use, light-weight replicated optics 78—66965
mm radioheliograph, design *(Chinese)* 80—12661
modulating anticollimator for low and medium energy gamma-ray telescope *(Russian)* 79—16832
modulation collimator, X-ray imaging device 79—25510
modulation radiometer, two-channel, simultaneous meas. in 6 and 8 mm wave ranges *(Russian)* 77—29647
monitor photometer for Dodaira 91 cm telescope *(Japanese)* 79—101071
monochromatic imaging using filters, slitless (multislit) spectrograph, and interferometers, appl. to Io Na cloud 79—8840
MOSFET preamplifier, liquid He-coooled, for use with astronomical bolometer 77—61123
Mount Wilson magnetograph, ang. resolution effects on solar mag. field studies 77—22082
Mount Wilson solar magnetograph, computer-operated image scanning and data system 77—22073
MSP-4 multispectral projector, description and use 80—4255
multi-anode microchannel array detector tube, effects of 1 MeV gamma-rays 79—71582
multi-anode microchannel arrays for detector systems 79—25480
multi-channel subtractive double pass spectrograph, solar filament obs. 78—12189
multichannel analogue detector system, for stars and planetary nebulae spectroscopic obs. 78—36461
MWPC, for cosmic drift X-ray imaging 79—41063
MWPC, high press., for X-ray astronomy 79—5748
Mylar beam splitter efficiency in far IR interferometer 78—55434
nebular filters 79—62746
nocturnal, simple construction method 77—67034
nuclear emulsion type BA-2, pulsed electric field effect on cosmic ray detection 79—26829
objective prism for UK 1.2 m Schmidt telescope 77—45311
objective-prism spectrograph, for UV stellar spectral obs. from Skylab 77—60609
observatory clock, crystal-controlled, with computer-readable output, design 80—26746
observatory scanning spectrophotometer *(French)* 78—20638
Ondrejov meteor radar, antenna radiation pattern 77—78634
Ondrejov Observatory, instrumentation 77—17361
optical beam-splitter of variable ratio 79—40078
optical instrument measuring mark parameters rel. to stellar visibility 78—61736
optical instrumentation, advances and appl. to planetary nebulae studies 80—109522
optical multi-element detectors, characts. 78—53830
optical multichannel analyser of Sao Paulo University, astronomical obs. 80—26743
optical noise reduction, space appls. 78—59153
optical polarimeter, detector array and polarising optics 78—57453
optical stellar interferometer, imaging using aperture synthesis 79—58244
optical surface shaping automation methods 79—84675
optical surface shaping process automation 80—105169
OSO-8, LPSP expt. instrumentation, laboratory calibration and pre-launch performance 77—64649
OSO-8 Univ. of Colorado UV spectrometer expt., optical design 78—49326
palette design for lunar radial vel. determ. from parallax and phase 77—67038
Palomer Schmidt plates, astrometric accuracy 78—57455
parametric amplifiers for radioastronomy at 18 and 1.35 cm wavelengths, characts. *(Russian)* 77—9658
Paris observatory, collection of astronomical instruments 79—84929
patrol balloon, long duration flight *(Japanese)* 79—80218
pattern recognition in digitalised images *(Italian)* 80—98554
PDS microdensitometer, appl. to stellar photographic photometry 79—88600
PDS microdensitometer, astrometric meas. technique and appl. to membership of cluster (NGC 6494) 80—98697
PDS microdensitometer, astrometric techniques 78—16306
periodic slot collimator, for accurate gamma ray burst source location 77—64647
phase photoelectric device for time service transit instrument *(Russian)* 78—73632
phase photoelectric device on Dresden Univ. transit instrument, obs. results *(Russian)* 78—73634
phase-tracking stellar interferometer, first fringe meas. 80—82215
phoswich-type scintillation detector system for X-ray astronomy 78—49328
photodiode array, self-scanned, for high dispersion astronomical spectrophotometry 78—45230
photodiode array spectrometer for David Dunlap Obs. 78—12097
photodiode detectors, thermal background subtraction 80—90342

astronomical instruments continued
photoelectric astrolabe type II, accuracy, time and latit. obs. *(Chinese)* 77—22063
photoelectric detection equipment for astrometric detection of planetary systems 80—56882
photoelectric device for circle reading recording meas. *(Russian)* 78—20644
photoelectric device for objectivisation of obs. with circumzenithal *(Russian)* 78—73654
photoelectric device for stellar transit times recording *(Russian)* 78—73635
photoelectric device with high time resolution, obs. results *(Russian)* 78—73633
photoelectric image acquisition system at Trieste Observatory *(Italian)* 79—58256
photoelectric lunar scanner 80—46396
photoelectric magnetograph, new type with electro-optic deflector 77—22074
photoelectric meridian instrum., performance characts., sensitivity *(German)* 77—17374
photoelectric occultation observing, techniques and apparatus 78—4117
photoelectric photometer, appl. to occultations obs. *(Chinese)* 80—105172
photoelectric photometer, multifunction, system design 77—73949
photoelectric photometry system at Trieste, data acquisition and processing software *(Italian)* 79—58258
photoelectric photometry system at Trieste, real time data acquisition and processing *(Italian)* 79—62757
photoelectric photometry system at Trieste, real time spectral analysis *(Italian)* 79—62756
photoelectric spectrophotometer, accurate absolute calibration in wide spectral region 79—96919
photographic astrolabe at Turku observatory, description 80—36499
photographic plate scanner, description 80—72780
photographic zenith tube, Chinese design and operational characts. *(Chinese)* 78—28514
Photographic Zenith Tube at Tokyo Astron. Observatory, observational errors anal. 80—98547
photographic zenith tube obs., automatic control using minicomputer *(Japanese)* 79—101083
photometer, classroom demonstration with artificial star 77—74180
photometer, EUV, obs. of He in interplanetary space 77—45309
photometer, far IR, for Kuiper Airborne Observatory 79—66926
photometer, LED field stop boundary and reticle illumination control circuit 80—37070
photometer, sub-mm, for ESO 3.6 m telescope 78—16296
photometer, sub-mm, opt. components 78—16297
photometer, twin-beam multiband computer-controlled, URSULA 78—49334
photometer, using Si diodes as light detectors 78—20651
photometer, with repetitive filter cycle and sky background compensation 80—62025
photometer calibration for extended astronomical sources 77—9669
photometer for night natural illumination measurement in 0.4 to 1.2 μm spectral region 78—57367
photometer for rapid stellar light variation, microprocessor controlled *(Spanish)* 80—82222
photometers, thermal stability rel. to Balmer-index photometry 78—96404
photometric devices, nonlinearity meas. 79—71505
photometric system, two-colour, for near IR, instrumentation 79—62759
photometric twin reflector, test results on Ap stars *(German)* 77—17365
photomultiplier, cosmic ray induced noise from Cherenkov radiation 77—33308
photomultipliers for weak light flux recording in pulsed mode 77—13242
photon counter for remote stellar objects monitoring, TV type, minicomputer-controlled *(Russian)* 80—31212
photon counting magnetograph and polarimeter for stellar circular polarisation meas. *(Russian)* 78—65500
photon-counting multichannel spectrometer 77—22079
Pioneer Venus, Orbiter and Multiprobe spacecraft instrumentation 80—67491
Pioneer Venus Bus and Orbiter, Bennett ion mass spectrometers 80—67499
Pioneer Venus Bus neutral gas mass spectrometer 80—67513
Pioneer Venus entry probes, atmosphere structure instruments 80—67562
Pioneer Venus large probe neutral mass spectrometer for measurement of composition and abundance of atmospheric gases 79—88563
Pioneer Venus Orbiter, electron temp. probe 80—67500
Pioneer Venus Orbiter, radar mapper design and operation 80—67495
Pioneer Venus Orbiter cloud photopolarimeter 78—57429
Pioneer Venus Orbiter Gamma Burst Detector 80—67505
Pioneer Venus Orbiter radiometer (VORTEX) 80—67504
Pioneer Venus Orbiter UV spectrometer, design and operation 80—67503
Pioneer Venus small probes net flux radiometer experiment 80—67512
Pioneer Venus Solar Flux Radiometer 80—82198
Pioneer Venus Sounder and small probes nephelometer instrument 80—67511
Pioneer Venus Sounder Probe gas chromatograph 80—67507
Pioneer Venus Sounder Probe IR radiometer 80—67509
Pioneer Venus Sounder Probe neutral gas mass spectrometer 80—67506
Pioneer Venus Sounder Probe Particle Size Spectrometer 80—67510
Pioneer Venus Sounder Probe Solar Flux Radiometer 80—67508
Pioneer-Venus large probe infrared radiometer optical system 78—81543
Pioneer-Venus large probe IR radiometer optical system 78—61715
plane analemmic dials 79—16834
plane grating as polar heliostat for solar chromosphere and prominence obs. during eclipse 79—84674
planetarium, gear mechanisms to reproduce planetary movement 80—4258
planetarium, mobile equipment for Alberta, Canada 79—58508
planetary lander, biological and soil chemical testing system 77—45284
planetary lander camera, quasi-microscope for improved resolution 77—91426
planetary radiometers for space probes 77—49299
planetary spectrograph 77—73954
plasma analyser experiment on Pioneer Venus Orbiter 80—67498
plasma wave instrument on Pioneer Venus Orbiter, design and performance 80—67497
polarimeter, attached to multi-channel spectrophotometer *(Japanese)* 78—89072
polarimeter, elliptical, for astronomy and atm. sciences 78—61745
polarimeter, near IR, for solar corona emission line obs. 78—61740
polarimeter, near IR, of Hatfield Polytechnic Observatory, design 79—2482
polarimeter, spectrum scanning Stokes, for solar research 78—61741
polarimeters, linear, stellar photometric appl. for interstellar grain size meas. 80—12792
polychromator, Astro 7, UV, for zodiacal light obs., absolute radiometric calibration 78—49336
position sensitive detectors in X-ray astronomy 79—25496
preamplifier, low-noise, for photoconductive IR detectors 77—61124
precision comparator, Zeiss PK-1, accuracy, appls. *(German)* 79—97359
precision comparator, Zeiss PK-1, astrometric plate meas. appl. *(German)* 79—97360
principles and practice of astronomy, book 78—32629
prismatic astrolabe, improved drive and instrumental characts. *(Russian)* 78—89066
Prognoz satellites, instrumentation for solar wind studies 77—64596
proportional, low-background counter for X-ray astronomy 78—29705
proportional control autoguidance system using photosil detector 77—49296
proportional counter, spherical, with isotropic sensitivity, for soft γ-radiation 78—61732
proton spectrometer for directional distrib. meas. in space 79—58252
prototype Nb gravitational radiation antenna, microwave parametric accelerometers 79—44841
Pulkovo meridian circle, horizontal axis posn., unloading mechanism effects *(Russian)* 78—28516
pulse counting photometer modified for occultation obs. 80—72921
pyranometer for total hourly horizontal solar radiation data, USA 77—25765
quasi-microscope concept for planetary missions, stereo pictures 78—81546
Radcliffe Cassegrain d-camera, vel. system 78—73645
radial velocity spectrometer, on McDonald Observatory 2.1 m telescope 80—51667
radial-velocity spectrometer with compound masks, for long-period variables obs. 79—88684
radio mapping expt. in International Sun-Earth Explorer C spacecraft 78—85796
radio spectrograph, appl. to interplanetary scintillation spectra obs. 80—72741
radioheliograph phase error meas. and correction 77—87269
radiometer, wide-band, for short millimetre range wavelengths, based on superconducting point contact 79—62750
radiometer with InSb detector, radioastronomical appl. in 0.2-5 mm wavelength range 77—13241
reflecting all-sky cameras, design 79—40074
resonance absorption spectrometer for monitoring profile of solar He I 58.4 nm line 80—62019
resonant electromechanical modulators, appl. as choppers and scanners 78—53831
retarding potential analyzer for Pioneer-Venus Orbiter Mission 79—58251
Reticon spectrophotometer at Asiago Observatory, data anal. procedure *(Italian)* 80—98565
Reticon spectrophotometer at Cima Ekar Observatory, first obs. 79—58254
RETICON spectrophotometer at Cima Ekar Observatory *(Italian)* 79—21190
retroreflector, temp. stability testing under space conditions 77—62078
ring sundial, imitation old scientific instrument, identification by neutron activation anal. 78—8491
rocket borne imaging detector and grating spectrograph far UV spectrophotometry 80—62014
rocket borne resonant absorption spectrometer and photometer for geocoronal and interplanetary He obs. 80—4155
rotation collimators, positively constrained imagery 77—9665
rotational shearing interferometer, 180° shear increased optical efficiency 80—47095
Royal Observatory, Greenwich, 1675-1975, conf., Greenwich, England (July 1975) 77—29646
SAS-3 X-ray observatory 77—2329
satellite solid-state imaging for meteorology and astronomy 77—39074
satellite-borne instrument development problems and solns. 77—82111
scanning Fabry-Perot interferometer, for high-resolution meas. of solar spectral lines 80—77298
scanning Fabry-Perot interferometer for balloon-borne astrophysical obs. 79—35092
scanning Fabry-Perot interferometer for far IR balloon astronomy 79—35093
scanning microphotometer with on-line reduction of Schmidt plate data 78—7884
Schmidt camera, direct, quasi-telecentric and telecentric combinations of interference filters 78—57441
scintillation proportional counter, built in K getter 78—29707
scintillation proportional large area gas counter for X-ray astronomy 78—49321
scintillation proportional large area gas counter for X-ray astronomy 78—49322
scintillator material activation during spaceflight, data for assessment 77—23382
screw photoelectric measuring machine for circle reading photographs *(Russian)* 78—24463
sealed position sensitive hard X-ray detector having large drift region for all sky camera with high angular resolution 79—48675
SEC Vidicon photometer, appl. to photometry of ω Centauri main sequence 80—90491
secondary electron conduction image tube, WX-32193, features 79—35137
secondary electron conduction vidicon digiral TV camera for stellar obs. 78—54457
semi-automatic measuring machine for plates taken with photographic vertical circle, errors *(Russian)* 79—96920
sensitometer for photographic photometry *(French)* 77—13246
Shuttle/Spacelab program rel. to solar flare buildup studies 77—17498
sidereal digital clock 78—36464
sidereal time source, electronic convertor for mean to sidereal time 79—84677

astronomical instruments continued
- Signe II MP, satellite expt. for study of solar and cosmic X-ray and γ-ray bursts 80—41696
- single photon X-ray detection with a CDD image sensor 79—35836
- SIT vidicon detector system, for Palomar 1.5 metre telescope 79—92674
- Skylab Apollo Telescope Mount XUV spectrograph, thin Al filters fabrication 77—60602
- Skylab colour TV as primary data recording system 77—60569
- Skylab S-056 instrument, solar X-ray photographs anal. and interpretation 78—4179
- slow scan SEC vidicon system coupled to telescope 77—25945
- soft X-ray imaging experiments with CCD 79—35138
- soft X-ray polychromator for Solar Maximum Mission 80—51660
- solar, used for solar spectra exam. during eclipse 80—8614
- solar double-pass monochromator, with digital device for obs. and spectrum processing automation *(Russian)* 80—72777
- solar filter using metallized polyester film 80—51666
- solar graticules, descriptions and appl. 78—16299
- solar interference spectrograph 80—109362
- solar luxmeter, calibration 77—9661
- solar magnetograph calibration programme *(Russian)* 78—65499
- solar magnetometer at Kodaikanal Observatory, design and performance 78—61743
- Solar Maximum Mission UV polarimeter design, operation and calibration 79—80225
- solar neutrino detectors, absorpt. cross section rel. to neutrino problem 80—17566
- solar neutrino radiochemical detectors, internal contamination backgrounds 79—16827
- solar neutrino spectroscopy at low energies, In loaded liq. scintillator 78—73639
- solar neutrinos detectors, cosmic ray neutrinos ^{37}Ar prod. rate estimate 79—16837
- solar polarimeter, for UV light polarisation meas. at limb 78—45302
- solar radio bursts, recording instrumentation and data reduction *(Italian)* 78—96458
- solar radiospectrographs complex for frequency range 100-1000 MHz *(Russian)* 77—29648
- solar simulator calibration photometer 79—26103
- solar spectrometer, reson. scatt., apparatus and instrumental errors 78—96393
- solar spectrum projection system at Flandrau Planetarium, Tucson 77—91433
- Solar Thermal Test Facility, description appl. to stellar astronomy 80—77301
- solar ultraviolet Doppler camera 79—25485
- solar visual and photographic survey instrument *(Chinese)* 80—77291
- solar wind spectrometer, ion frequencies and velocities *(German)* 80—51636
- solar X-ray imaging techniques, past and future, review 79—25495
- solar X-ray photometer, rocket-borne, construction details *(Polish)* 79—58247
- solar X-ray photometer on Prognoz satellites, description and meas. method 80—17462
- solar X-ray spectrograph, cylindrical-crystal, design and characteristics 79—29990
- solar XUV, grazing incidence spectrograph on Skylab 77—60601
- solid state detector for spectra obs. of binary stars 80—109469
- space astronomy, new instrumentation, conference (Tel Aviv, 7-18 June 1977) 79—25473
- space borne optical systems, meteorite damage 77—90445
- space experiments for Solar Maximum Year, review 80—90404
- space optics, conference Huntsville, Alabama (1979 May 22 to 24) 80—62385
- space optics, imaging X-ray optics workshop, Huntsville, Alabama (1979 May 22 to 24) 80—62384
- Space shuttle, X-ray astronomical instrums. and expts. 80—109363
- Space Telescope, scientific instruments 80—61987
- space telescopes, optical systems *(Russian)* 77—17367
- Spacelab, payload data path from user input (on-board) to user ouput (laboratory) 79—21137
- Spacelab facility for X-ray source spectroscopy and polarimetry 78—32314
- Spacelab Instrument Pointing Subsystem 79—25447
- ‘Spacemaster’ planetarium, Halle, E.Germany, description and operation 80—4259
- spark-chamber, wide-gap chamber for gamma-ray astronomy, Soviet-French design 78—17503
- speckle camera, Kitt Peak National Obs., design, double star meas. 79—62745
- speckle interferometer, subsystems and S/N ratio 77—41678
- speckle interferometer construction, review 77—71369
- Spectracon image tubes, operation and results in stellar spectroscopy 77—5451
- spectral analyser, acousto-optical, at RATAN-600 radio telescope, first test *(Russian)* 80—51668
- spectral comparator, for automatic meas. of small line shifts 77—82123
- spectral energy standard, for stellar absolute spectrophotometry *(Russian)* 79—44372
- spectral image analysis device, Chromotron 80—83683
- spectrograph, with holographic and ruled diffr. gratings 78—40831
- spectrograph balloon-borne UV, for stellar obs. 78—49318
- spectrograph with echelle-type grating, advantages *(Polish)* 80—26745
- spectrograph-photometer, four-channel, on Danish 50 cm reflector at ESO, photometric system stability 77—60622
- spectrographic camera shorter than Schmidt 77—73951
- spectrometer, bent crystal, for solar X-ray spectroscopy 78—7881
- spectrometer, Fabry-Perot, piezoelectric scanning nonlinearities 79—6183
- spectrometer, high resolution Fabry-Perot, for IR astronomy 79—53722
- spectrometer, mm-wave, intensity calibration error evaluation 78—53821
- spectrometer, multiplexing, S/N ratio in high background 78—49339
- spectrometer, Si diode vidicon, IR capability for solar research 77—9657
- spectrometer for 100 MeV-100 GeV cosmic ray electrons study 80—8503
- spectrometer for near IR stellar spectra obs., automatic system *(Russian)* 80—51664
- spectrometer for prime focus of parabolic mirror, new design *(Chinese)* 79—80226
- spectrometers, secondary spectrum of thin three-lens optical systems *(Russian)* 78—57456
- spectrophotometer, double-pass, with digital registration, spectrum registration precision *(Russian)* 79—96917

astronomical instruments continued
- spectrophotometer, for short term variability obs. in stellar spectra 78—73643
- spectrophotometer using intensifier Si vidicon 78—32356
- spectropolarimetry with an intensifier-dissector-scanner 80—109367
- spectrum analyser, 32-channel filtering type *(Russian)* 77—29653
- spectrum analyser, real-time, with on-line definition of confidence levels 77—73959
- spectrum expander for multichannel filter spectromers 79—35790
- spectrum microphotometer connection to PDP 11 digital processor for photographic plate meas. *(Italian)* 80—8550
- spectrum scanning Stokes polarimeter for solar work 80—51663
- spherical lamellar grating interferometer for airborne far IR astronomy 77—25942
- star magnitude simulator, IC device 78—81742
- star simulator design 78—85814
- star tracker, utilising solid state image sensor *(Japanese)* 79—80227
- stellar electrophotometer, 50 MHz passband amplifier for photomultiplier 77—74434
- stellar interferometer with incoherent signal accumulation, sensitivity 77—25946
- stellar phase-grating interferometer, appl. to double-star obs. *(Russian)* 79—101070
- stellar sensor assembly, solar simulation for testing off-axis light attenuation 78—61714
- stellar simulator, continuous action radiolum. emitter as reference source 77—10993
- stellar spectrograph for large azimuthal telescope 77—91431
- stellar spectrograph with electron optical convertor for large azimuthal telescope 77—91432
- stellar spectrography with crossed dispersion 78—49337
- Steward Observatory speckle camera 80—4254
- stigmatic EUV spectroheliometer for photometry of dynamic phenomena 78—53825
- Stuttgart Planetarium 78—16304
- sundial, latitude-independent, theory and construction 78—81549
- sundial at National Maritime Museum, Greenwich 79—40080
- superheterodyne mm wave spectrometers, intensity calibration 77—33353
- superheterodyne receiver of solar emission obs. at 220 GHz *(Italian)* 77—49292
- television system, appl. to Perseid meteors obs. 80—4309
- television system, narrow band, appl. as balloon-borne solar telescope view-finder *(Japanese)* 79—80228
- television systems, photon counting and analogue, with digital real time image processing 78—96402
- Terskol Peak telescope and electrophotometer, apparatus function and atmosphere monochromatic extinction coeffs. *(Russian)* 79—44246
- theorica orbium of Hieronymus Vulparius 77—37705
- thermoluminescence measurement apparatus, lunar samples and meteorites appl. 77—13803
- time of flight directional coincidence telescope for gamma ray telescopes 77—390
- Tokyo meridian circle obs., true external errors, from SAO 158687 occultation by Uranus 78—28487
- toroidal diffraction grating, spectral image at point at spectrometer entrance slit *(Russian)* 78—57452
- toroidal mirror fabrication for soft X-ray imaging 78—41384
- transit circle, automatic photoelec. recording 77—91435
- transit circle photoelec. recording, grating inclination effect 77—91436
- transit instrument automation *(Russian)* 78—73636
- transmission grating efficiencies for wavelengths between 5.4 Å and 44.8 Å 79—40077
- transmission grating efficiencies in 50 to 250 Å range 79—98466
- transmission grating fabrication, photochemical replication for space astronomy 80—14490
- TV detector, for stellar radial vels. determ. using cross-correl. techniques 78—16305
- TV imaging tubes, utilisation *(French)* 78—40829
- TV monitor on Skylab Apollo Telescope Mount, for solar EUV image obs. 77—60600
- two-channel recording system for punched tape *(Russian)* 77—29651
- two-dimensional buffer store based on a multichannel amplitude analyzer for neutrino detect. 79—26838
- two-star photoelectric photometer at Wise Observatory, performance assessment 78—73657
- Tycho Brahe's instruments, errors 78—32642
- UBV photoelectric photometer for amateur use 78—65502
- UBV photometer, double head, for simultaneous fast photometry 80—72775
- ultralow light level imaging by intensified CCD 77—41287
- Ultraviolet Spectrometer and Polarimeter on Solar Maximum Mission 80—51661
- universal stellar photometer *(German)* 77—17379
- UTEX, integrated UV and X-ray astronomy facility on Spacelab 79—25475
- UV channel photographic photometer, for stellar obs. from Skylab 77—60608
- UV detector, self-scanned anode array, for Mariner Jupiter/Saturn spectrometer 77—78632
- UV detectors, response of InGaAsP photocathodes 77—57387
- UV optics, high intensity solar irrad. testing 77—5431
- UV reflecting mirrors, coatings, for satellite instrumentation *(French)* 77—67022
- UV spectrometer, microchannel plate life tests 77—61117
- UV spectrometer in airglow expt. on Mariner 10 spacecraft 77—64611
- UV spectrometer on Mariner 10, Mercury occultation expt. 77—67023
- UV spectrometers, on OSO-8, computer-controlled, mission operations 80—41723
- UV stellar spectrograph BUSS, optical system, appls. *(Dutch)* 78—7880
- UV stellar spectroscopy, spaceborne instrumentation 79—25518
- vacuum UV monochro-collimator *(Japanese)* 77—73957
- vacuum-cold camera, appl. to astronomical near IR photography 80—90341
- variable iris photometer as automation example *(French)* 79—62748
- variable star simulator 77—22357
- vector He magnetometer on International Sun-Earth Explorer C spacecraft 78—85795
- Venera 9 and 10 construction, instrumentation and preliminary results 77—41339
- Venezuela, new observatory near Merida, review 78—49316

astronomical instruments continued
Venus Orbital Imaging Radar (VOIR), stereo side-looking radar accuracy anal. 80—56646
vertical circle, appl. to differential determ. of declinations *(Russian)* 79—96888
Viking 1 and 2 expeditions, scientific results *(Hungarian)* 78—73666
Viking IR thermal mapper, design 78—57440
Viking Lander camera, optical system and design 78—53794
Viking Lander camera, stray light control 78—61713
Viking lander cameras, calibration and performance 78—20639
Viking Lander seismometer 78—16274
Viking Mars lander camera, spectral refl. curves determ. 78—32886
Viking orbiters, scientific missions and instrumentation 78—20612
Viking spacecraft, Mars atm. struct. expt., techniques, instruments and accuracy 77—13205
Viking visual imaging subsystem, inflight performance 78—36417
VNG-derived frequency reference, adapting for astronomy 79—35139
voltage-frequency convertor for astronomical photometry 78—45233
Voyager Cosmic Ray Experiment, telescopes, electron energy meas., pulse height analysers 79—48643
Voyager IR spectroscopy and radiometry experiments 78—24428
Voyager magnetic field experiment 78—24431
Voyager missions to outer planets, instrumentation 78—49289
Voyager photopolarimeter experiment 78—20616
Voyager planetary probes for outer planets, review 78—24435
Voyager radio science experiment 78—24430
Voyager UV spectrometer experiment 78—24429
wavelength calibration device for large dispersion spectrographs 80—41728
wedge-sensitometer for photographic photometry *(Japanese)* 79—44373
wide field UV cameras, Marseille Obs. *(Italian)* 78—32346
wide-angle astrographs, celestial photography for astrometric catalogue *(Russian)* 78—40800
Wollaston prism as convergent light beam splitter 79—14092
X-ray, polarimeter, for solar and extrasolar obs. 78—57454
X-ray and γ-ray spectrometers on Prognoz satellites 79—21127
X-ray and gamma-ray remote sensing spectrometers, data analysis system for planetary mission appl. 79—12411
X-ray astronomy balloon, microprocessor-controlled payload 79—62716
X-ray astronomy gas scintillation spectrometer, performance characts. 80—56709
X-ray camera, wide field for astronomy, design, sensitivity and performance 80—85863
X-ray collimators, testing via parallel X-ray beam generation technique 78—28526
X-ray crystal spectrometer, new type 77—5443
X-ray detector, large area MWPC, high-background rejection 78—93108
X-ray detector on Ariel 5 satellite, design and performance 78—53826
X-ray diffraction grating, spectroscopy appl. 77—10155
X-ray focusing gas scintillation proportional counters 77—83461
X-ray graphite cryst. spectrometer on OSO-8 satellite 77—13238
X-ray imaging scintillation detectors, design 79—25511
X-ray imaging spectrometer polychromator, solar obs. from Space Shuttle 80—17495
X-ray mirror objectives, testing 78—85850
X-ray modulation collimators, design and construction 77—5434
X-ray multigrid collimators, design and fabrication 77—5435
X-ray optical systems, construction and appls. 79—17582
X-ray polarimeter, mosaic graphite, on OSO-8 satellite, design, preliminary results 79—25490
X-ray polarimeter, Thomson-scatt., satellite-borne, for solar obs. 79—25491
X-ray proportional spectrom. for Viking Lander 78—40792
X-ray spectrometer expt. on International Sun-Earth Explorer C spacecraft 78—85787
X-ray spectrometer for rocket-borne, solar obs., biaxial optical guider *(Polish)* 78—61744
X-ray spectrometer on Kosmos 428 satellite, for hard X-ray sources obs. 77—64640
X-ray spectrometer-telescope system for solar corona studies 80—105168
X-ray spectroscopy, solar and cosmic, instrumentation 77—13243
X-ray transmission gratings, aberrations, testing 79—25508
X-ray transmission gratings, expt. and theoretical props. 79—25509
X-ray transmission gratings for 7-304 Å operation, efficiency and resolution 80—82195
XUV spectrographs in Apollo Telescope Mount, optical contamination prevention 77—60603
XUV spectroheliometer on SMM 79—25487
Zeeman analyzer system on McDonald 2.7 m telescope's coude spectrograph 80—62021
ZKP2 planetarium at Suhl, E.Germany, description and use 80—4260
Ar laser interferometer for detection of gravitational radiation 79—101076
Au coated surface, reflectivity in soft X-ray range 78—45221
CdTe spectrometers for hard X-ray astronomy 77—13206
CsI crystals, in scintillation counters, nonstatistical counting rates due to phosphoresc. 78—95597
Cs_2Te photocathode middle UV low light level imaging devices 77—41319
Ge spectrometers, cooled, for X-ray and gamma-ray astronomy 77—5438
Ge:Be photoconductive detectors for obs. from space platform, 30-55 micron 79—5754
Ge:Ga photoconductive detectors for obs. from space platform, 50-120 micron 79—5754
Ge(Li) balloon borne spectrom. for obs. of neutron star cyclotron line emissions 80—41721
Ge(Li) spectrometer, high resolution, appl. to galactic gamma-ray lines obs. *(Japanese)* 79—80353
H absorption-cell spectrophotometer for Lyman α radiation, on Mars 4-7 space probes 78—28519
InSb IR detectors, integrating premaplifier 80—90337
Si digital Sun sensor electrical and optical props. *(Japanese)* 78—32313
Si vidicon, performance at low signal levels, astronomical spectroscopy appl. 77—22085
Si:As photoconductive detector for IR astronomy, responsivity and system noise 80—51665
Si:Li detector system for X-ray astronomy rocket expt. 77—5439
Si:Li spectrometer, appl. to X-ray astronomical spectroscopy 77—5460
Si(Li) thin window detectors for NASA ISEE-C cosmic ray telescope 78—40819

astronomical instruments continued
Xe filled gas scintillation proportional counter in space environment, background radiation rejection efficiency 78—21819
Xe gas proportional counter for astronomical hard X-rays detect., risetime discrimination appl. *(Japanese)* 79—80219

astronomical observations
see also gamma-ray astronomical observations; infrared astronomical observations; radioastronomical observations; ultraviolet astronomical observations; visible astronomical observations; X-ray astronomical observations
1610—771, radio QSO with steep optical spectrum, obs. 80—94887
2A 0526—328 optical counterpart, identification and spectrum 80—22118
AFCRL IR sources, optical, IR and radio studies 78—4393
ζ Andromedae, spectroscopic binary, photometric and spectroscopic obs. *(Russian)* 78—57588
Anglo-Australian Telescope, observational results 77—91434
AO 0235+164, BL Lacertae object, photometric obs. of optical outburst 80—56924
AO 0235+164, BL Lacertae object, UBVI photographic magnitude obs. during flare 79—25724
R Aquarii, UV, visible and 85 GHz continuum obs. 80—85946
η Aquilae, Cepheid variable, absolute energy distrib. in radiation spectrum *(Russian)* 80—72974
UX Arietis, co-ordinated UV, optical and radio obs. of RS Canum Venaticorum binary 79—16963
asteroids, polarimetric, radiometric and spectrophotometric obs., review *(Polish)* 78—36490
asteroids, surface albedo and colour contracts 80—36547
asteroids 1978 CA and DA, UBV photometry, rotation periods, albedos and diameters 78—36489
atmospheric extinction data, optical depths for observatory sites 77—49162
atmospheric extinction data, seasonal var. 77—53185
atmospheric extinction data, time trend and internal errors 77—49161
ε Aurigae, photometry during 1955-57 eclipse rel. to wavelength-depend. fluctuations 80—62190
KR Aurigae, X-ray source nearby, X-ray, IR and visible obs. 80—67742
B2 1225+31, high-redshift QSO, abundances in z=1.7941 absorpt. line system 80—12826
BD+61° 1211 (2A 1052+606), RS Canum Venaticorum binary star, spectroscopic obs. 80—36663
Be-stars, IUE obs. 80—82383
bipolar nebula, new, in Centaurus, discovery, photometry and spectral type 79—84837
bipolar nebulae, study of general phenomenon 78—41026
bright galaxies, UBVRI photoelectric photometry 78—32578
3C 120, Seyfert galaxy, IUE and visual spectrophotometry 79—92856
4C 39.11, N galaxy, radio and optical obs. 78—16553
XX Camelopardalis, R Coronae Borealis star, photometry in optical and IR ranges 80—101601
RS Cancri, late-type variable star, spectral energy distrib. and spectral types *(Russian)* 78—40958
α Canis Majoris (Sirius), optical image improvement via real-time phase correction system 77—22084
γ Cassiopeiae, Be star, rapid linear polarisation variability *(Russian)* 80—77417
γ Cassiopeiae, polarisation obs. rel. to circumstellar envelope model 78—40952
UV Cassiopeiae, R Coronae Borealis star, photometry in optical and IR ranges 80—101601
CD-38°245, metal-deficient halo red giant, spectrum, photometry and Ca/H ratio 78—69797
U Cephei, excess light obs. rel. to accretion discs 80—82412
U Cephei, mass transfer from light vars. outside primary eclipse, obs. and anal. 78—36636
UV Ceti, anomalous flare activity obs. 78—89202
Circinus galaxy, optical and radio obs. 77—41409
Circinus X-1, changes in optical, IR and radio emission 80—67910
Comet Bradfield (1979l), photographic obs. and spectra 80—51693
comets in 1973, review of observations, discoveries and recoveries 78—73683
comets in 1974, review of observations, discoveries and recoveries 78—73682
compact groups of compact galaxies, seventh list *(Russian)* 77—22110
cool stars, narrow-band polarisation effects 78—16427
cosmic ray anomalous ^{4}He component, solar latit. and radial depend. 79—35080
cosmic ray electrons, high energy primary spectrum obs. by emulsion chamber *(Japanese)* 79—80153
cosmic ray flux, altitude depend., polar orbiting satellite obs. 80—46353
cosmic ray intensity diurnal variation, two approaches to study 79—29953
cosmic ray intensity variations of interplanetary, magnetospheric and atmospheric origins, Sayan spectrograph data 79—84606
cosmic ray large air showers, Cherenkov radiation image reconstruction 79—25420
cosmic ray nuclei from 3000 MeV to 50 GeV per nucleon, charge comp. and energy spectra 78—93059
cosmic rays, abundances of elements in $26\leq Z\leq 30$ interval 79—40044
cosmic rays, short-term fluctuations obs. 80—67483
cosmic rays, studies using gas Cherenkov counter with ionisation spectrometer 80—94662
cosmic rays new particles, balloon meas. *(Japanese)* 79—80112
cosmic-ray components in atmosphere, altitude depend. rel. to environmental radiation meas. *(Japanese)* 79—80144
SU Cygni, classical Cepheid and spectroscopic binary, UBVRI photometry 79—62852
CH Cygni, linear polarisation vars. rel. to circumstellar dust grains form. 78—69808
V1016 Cygni, new spectroscopic obs., simultaneous presence of increasing excitation and cool features 80—26874
V1016 Cygni, photometric and spectroscopic obs. rel. to proto-planetary nebula mass ejection 78—85947
CH Cygni, symbiotic star, spectroscopic obs. during 1977 to 1978 outburst 79—75211
V645 Cygni (AFGL 2789), spectroscopic and photometric obs. 80—73066
V1500 Cygni (Nova 1975), spectrum and heavy element abundances 79—21295

astronomical observations continued
V1500 Cygni (Nova 1975), thirteen-colour photometry and anal. of short period variability 79—92788
Cygnus OB2 association, wavelength depend. of polarisation and interstellar birefringence 77—33577
Cygnus X region, mapping and physical parameters of H II regions 77—9783
Cygnus X-1, optical and X-ray evidence for 78/39-day period 78—89274
Cygnus X-2, X-ray and optical obs., (1973 to 1977) 79—30148
data reduction problem, pattern recognition appl. 80—8554
Deimos, 100 years since discovery, review of studies 78—73670
HR Delphini (Nova 1967), simultaneous X-ray, UV and optical obs. 80—109440
dose rate and flux density estimations by TLD method 79—58208
EAS, detectors pulse profiles studies 79—25421
education, radius vector determ. from two position obs. 77—33760
elementary particle physics, information from astronomical observations 80—51935
RX Eridani, RR Lyrae variable, radial vels., light curve and radius 77—2436
faint UBVRI standard stars, photometric obs. 80—51813
Fairall-9 (ESO 113-IG 45), extreme Seyfert galaxy, IR and visible photometry 79—25720
fireball networks, review of 12 years of operation 77—33427
flare stars in Pleiades, new discoveries *(Russian)* 77—13366
Fourier transforms of data sampled at unequal observational intervals 78—69697
G 307.1+1.2, G 309.7+1.7, low-latit. radio galaxies, optical and radio obs. 79—12535
galactic cosmic ray intensity out to 18 AU, Pioneer 10 and 11 obs. 80—90297
galactic cosmic rays, Fe nuclei isotopic comp. 80—72729
galactic cosmic rays, Ne, Mg and Si isotopes high resolution meas. 80—51631
galactic cosmic rays, Ne isotopes abundances 79—101036
galactic neutrino sources, expt. neutrino astronomy, test of stellar evolution theories 77—70964
galactic particle radiation, satellite obs. *(Danish)* 78—69631
galaxies with UV continuum, eighth list *(Russian)* 77—22109
Galilean satellites, eclipse spectrophotometry 79—96949
GD 428, extreme dwarf Cepheid, photometry and spectrum 77—78798
U Geminorum, dwarf nova, spectrophotometric parallax 79—67012
globular clusters, six-colour photometry rel. to interstellar reddening and metal abundances 77—13407
globular clusters in Galaxy, Fornax and M31, integrated colours and metallicity 78—16469
gravitational radiation, Munich-Frascati expt., final negative results 79—8830
gravitational waves, meas. at 1.5K with small cryogenic antenna 79—21646
H 2155—304 optical candidate, spectrophotometric obs. 79—25761
Hartung-Boothroyd Observatory, 25-inch training telescope for Cornell Univ. 78—7882
HD 01891, subdwarf, photometry and spectrum rel. to UV excess and metal abundance 80—17574
HD 10783, Ap star, spectrophotometric obs. 80—98663
HD 175305, red horizontal branch star in general field, spectroscopic and photometric anal. 79—40189
HD 219150, F0 V star with remarkable UV excess, optical and UV photometry and spectrum 80—90429
HD 45677, peculiar Be-star, 0.12-12.6 μm obs. 80—72957
HDE 226868 (Cygnus X-1), anomalous light curve during X-ray increase of 1975 April-May 78—28850
OP Herculis, late-type variable star, spectral energy distrib. and spectral types *(Russian)* 78—40958
AM Herculis (3U 1809+50), X-ray eclipsing binary, multicolour photometry 77—78887
DQ Herculis (Nova 1934), high time resolution spectrophotometry 80—22017
HR 1099, co-ordinated UV, optical and radio obs. of RS Canum Venaticorum binary 79—16963
HR 1614 group of metal-overabundant stars, late-type stars intermediate-band photometry 78—53935
Hyades, late-type stars intermediate-band photometry 80—31289
Hydra I (Abell 1060) galaxies, UBV photoelectric photometry 80—51887
image processing/facilities, catalogue 78—45239
interplanetary magnetic field, large-scale struct. between 1 and 0.3 AU during Helios 1 primary mission 79—29962
interplanetary magnetic field between 0.3 and 1 AU, Helios 1 and 2 obs. 80—21887
interplanetary magnetic field structures between 0.3 and 1 a.u., two-spacecraft obs. comparison 79—25429
interplanetary shock wave, He$^+$ obs. in driver gas 80—72735
interplanterary magnetic fields and flows between 1 and 0.3 AU during Helois 1 primary mission 79—29963
interstellar polarisation of reddened stars, obs. of four deviating stars rel. to grain size 80—12792
IR stars, review of observational data *(Russian)* 77—49377
Jupiter, electron propag. out of solar equatorial plane, Pioneer 11 obs. 79—40123
Jupiter, haze layers, Voyager 1 obs. from UV to IR 79—92714
Jupiter, ion fluxes out to 1200 R_J, Voyager 1 and 2 obs. 80—94667
Jupiter, magnetosphere, high β plasma in dynamic current sheet 79—16872
Jupiter, magnetosphere, low-energy charged particle environment, Voyager 1 first look 80—26797
Jupiter, magnetosphere, tailward directed ion beam, Voyager-2 obs. 80—72854
Jupiter, magnetosphere low energy plasma, Voyager obs. 80—72855
Jupiter, phase effect for disc features brightness coeff. 80—98602
Jupiter, Voyager I results, diverse features 79—84738
Jupiter's ring, Pioneer 11 obs. 79—88620
Jupiter and satellites, Voyager I encounter, general description of 80—12642
Jupiter and satellites from Voyagers 1 and 2, general results 80—17542
Jupiter as source of electrons observed at Earth orbit 80—90357
Jupiter magnetic field studies by Voyager 1, preliminary results 80—26793
Jupiter magnetosphere, electrostatic waves obs. 80—72865

astronomical observations continued
Jupiter magnetosphere, kilometric radiation spatial and temporal studies 80—77328
Jupiter magnetosphere, Voyager 1 obs. of energetic ions and electrons 80—26798
Jupiter magnetosphere, Voyager 1 plasma wave obs. 80—26795
Jupiter magnetosphere disturbed by Ganymede, Voyager-2 obs. 80—72856
Jupiter magnetosphere plasma observations, Voyager 1 initial results 80—26794
King's College Observatory, Nova Scotia, and Joseph Everett 79—34
EV Lacertae, flare star, polarimetric and photometric obs. *(Russian)* 77—13368
BL Lacertae objects, spectral flux distribs. from 0.36 to 3.5 micrometers 77—45537
late-type main-sequence stars near Sun, intermediate-band photometry 78—53934
LP 790-29 mag. degenerate with heavily blanketed energy distrib., obs. 79—5815
LTT 2437, most metal-deficient subdwarf, spectrum, photometry and Ca/H ratio 78—69797
luminous variable stars in M31 and M33, spectra and photometry 78—28686
lunar magnetic fields, magnetometer data errors and EM induction studies 79—96932
α Lyrae, absolute energy distrib. from 3295 Å to 9040 Å 78—20828
XY Lyrae, late-type variable star, spectral energy distrib. and spectral types *(Russian)* 78—40958
M17, dusty H II region, stellar optical polarisation meas. 78—45379
M31, interstellar polarization, wavelength depend. 79—92835
M32, absolute spectrophotometry rel. to galaxy spectral synthesis and age 80—67842
M51 system, photometric study 79—30125
M67, main-sequence stars differential blanketing rel. to Hyades and Coma 78—57597
M82, polarimetry of irregular galaxy 77—17692
M83, UBVR surface photometry of bright southern spiral galaxy 79—44598
M87 halo globular clusters, metallicity meas. 78—89244
Mare Serenitatis, elec. cond. anomaly detect. by Lunokhod 2 and Apollo 16 magnetometers 80—56730
Markarian 231, Seyfert galaxy, spectra, photometry and electronograph 77—45558
Markarian 295, 296, 297, spectroscopic and 21 cm line investigations 79—44608
Markarian 296, clumpy irregular galaxy, spectroscopic and 21 cm line investigations 79—44608
Markarian 3, 231, Seyfert galaxies, optical polarisation obs. 80—90533
Markarian 79, Seyfert galaxy, IUE and visual spectrophotometry 79—92856
Mars, integral photometry 78—61780
Mars, magnetic field, measurements of Mars 2, 3 and 5 spacecraft 80—36538
Mars, magnetic minerals, obs. by Viking extended mission 80—72830
Mars, thermal and albedo mapping during Viking primary mission 78—20683
Mars atmosphere, water vapour vertical distrib. 79—84713
Mercury, optical obs. interpretation rel. to surface material props. 78—12130
Mercury magnetosphere and mag. field, Mariner 10 obs. and theory 80—36530
meteor trails, ionised, initial radius, height and time depend. investigation 79—58301
meteoritic material, meas. from spacecraft near Earth and in interplanetary space 77—53486
meteors, observation methods in Poland, review *(Polish)* 78—61750
Michigan 239, peculiar extragalactic or extreme halo emission-line star, obs. 80—4380
micrometeroids of inner solar system, Helios 1 obs. 80—77355
minor planets, hypothetical observations giving equinox and equator determ. 80—94742
Molonglo southern radio sources, optical spectra 78—96555
Monterey Institute for Research in Astronomy, planned observatory, Chews Ridge, California 79—88593
Moon, mag. anomalies detected by Apollo subsatellite 80—36525
Moon, optical obs. interpretation rel. to surface material props. 78—12130
Moon, radar expts. on automatic lunar stations 77—53438
Moscow meridian circle pavilion, error correction for daytime astrometric obs. 78—24441
Mt. Zao, Japan, decametric radio reception system 80—51656
multiple stars, discovery and observation 79—44541
multispectral scanning sensor system digital simulation 79—29997
NGC 2110, X-ray/radiogalaxy, elliptical morphology questioned 79—21426
NGC 2423, 2482, Hyades-like clusters, late-type stars intermediate-band photometry 80—31289
NGC 2768, galaxy, optical and IR photometric study 78—36683
NGC 2915, southern galaxy, optical and H I obs. 77—67126
NGC 3115, galaxy, optical and IR photometric study 78—36683
NGC 3227, 3516, Seyfert galaxies, optical polarisation obs. 80—90533
NGC 3293, open cluster, UBVRI photometry and relation to OB complex in Carina 80—90490
NGC 5195 (M51 comparison), struct. obs. using negatives superposition method *(Russian)* 77—13251
NGC 5367, young open cluster, relation to X-ray source (Ariel 1353-40) 77—82294
NGC 5383, barred spiral galaxy, vel. field 78—24549
NGC 6052, possible collision of two late type spiral galaxies, observational evidence 80—8681
NGC 6250, young southern cluster, extinction law and high R-values in dust clouds 78—16490
NGC 6624 (3U 1820-30), globular cluster, optical, IR and X-ray obs. 77—45498
Nova, Sagittarri 1977, UBV photoelec. obs. (1977, March-April) 77—53607
Nova Cygni 1978, spectrum, precise position and photometry 78—89211
Nova Persei 1974 (V400 Persei), light curve and spectral evolution 78—73715
Nova Scuti 1975 (V373 Scuti), light curve and spectral evolution 78—73715

astronomical observations continued
NP 0532, Crab pulser, gravitational radiation obs., energy flux upper limit 80−36655
Orion cluster, pre-main-sequence stars masses and age spread 77−13339
X Persei (3U 0352+30), UBVRI photometry 78−8049
X Persei (4U 0352+30), Be star, photoelectric photometry rel. to 6-year periodicity 80−109446
PG 1413+01, white dwarf-red dwarf eclipsing binary, photometry and spectral types 79−8944
PHL 1070, quasar spectrum and redshift of surrounding halo 78−28771
PHL 938, quasar, continuum spectrum reddening due to dust 78−96561
Phobos, 100 years since discovery, review of studies 78−73670
photon rest mass upper limits from astrophysical data 77−34200
Pic du Midi Observatory, history 80−72770
PKS 1144−379 BL Lacertae object, radio, IR and optical obs. 80−4451
PKS 2126−15, bright quasi-stellar object with neutral colour and redshift of (3.27) 78−93450
PKS 2155-304 (H2155−304), newly discovered BL Lacertae object, optical and X-ray props. 80−36702
planetary nebulae, photometry and spectra of (Abell 30 and 78) 77−91602
primary cosmic ray N and O, isotopic comp. with consequences for source models 79−84609
Pulkovo, history and connection with Struve family 78−24632
Pulkovo, short history 78−81538
VV Puppis, circular polarimetry in active state and evidence for two accreting poles 79−48854
PZT reduction procedures *(Japanese)* 77−73972
QSOs, high-redshift emission-line spectra and emitting regions props. 79−21458
QSOs from Molonglo Deep Survey, optical spectra 80−94884
QSOs lying in spiral arms of NGC 1073, spectrophotometric obs. and redshifts 80−22110
quasars, faint red 3C QSO candidates spectrophotometry and red shifts 80−67897
quasars, slitless spectroscopy of large redshift objects 78−96562
quasars and related objects, morphology, electronographic obs. *(French)* 79−88759
quasars in southern hemisphere, spectra and redshifts 77−67137
Quebec astronomical observatory, new 1.6 m reflecting telescope 79−88592
red variable stars of medium amplitude, UBVRI obs. 77−82224
reduction of 19th century obs. of Uranus and Neptune positions, method comparison 80−94691
RMB 56 (1216+141), compact blueshifted galaxy, radio and optical obs. 78−16527
Roberts 22, bipolar nebula with OH emission, visual, radio and IR obs. 80−94859
FG Sagittae, anomalous planetary nebula, spectrophotometry and UBV photometry (1968 to 1977) 79−88687
HM Sagittae, eruptive BQ forbidden line star, obs. 78−20835
HM Sagittae, new spectroscopic obs., simultaneous presence of increasing excitation and cool features 80−26874
HM Sagittae, variable emission object, spectrophotometry 80−17599
SAO 015338, possible RS Canum Venaticorum star and counterpart of 2A 1052+606, spectrum 80−22118
Saturn, atmosphere upper layers props. from polarimetry photometry and spectrophotometry *(Russian)* 78−40867
Saturn, phase effect for disc centre brightness coeff. 80−98602
V861 Scorpii (HD 152667), eclipsing binary, identification with X-ray source (OAO 1653−40) 78−69838
V818 Scorpii (Scorpius X-1), UV, visible, IR and X-ray obs. 80−82541
Sculptor dwarf spheroidal galaxy, abundance vars. on giant branch rel. to ω Centauri anomaly 79−5904
RT Serpentis (Nova 1909), spectrum in 1964, 1975 and (1978) 80−46566
Seyfert galaxies, photometry and thermal emission vars. 80−67865
Skibotn Observatory, in northern light zone, stellar obs. with chopping photometer *(Norwegian)* 78−69699
SN 1979c in M100, coordinated obs. (1979 April-June) 80−101604
solar cosmic rays, anomalous flux anisotropy, 1973 September probe meas. 77−33300
solar cosmic rays, obs. of events with high relative ^{3}He abundances during 1976 November to December 80−61972
solar eclipse, 1968 September 22, coordinated optical, radio, geomag. and ionospheric obs. *(Chinese)* 77−22154
solar ephemeral active regions during solar minimum 80−31279
solar flare, 1973, September 5, pre-onset morphology 79−40169
solar flare electron events, Oct. 1972 to Dec. 1974 obs. 80−56796
solar flare energetic particle events from same active region, p/α enhancement 79−40151
solar flares, accelerated Ne nuclei, IMP 8 obs. 79−92740
solar flares, C-poor events, IMP 8 ULET sensor meas. 79−92739
solar flares, studies using optical, X-ray and radio data 78−89156
solar heavy-ion-rich particle events, ^{3}He/^{4}He ratios energy depend. and temporal evolution, ^{3}He/^{4}He in heavy-ion-rich solar energetic particle events, energy depend. and temporal evolution 80−90299
solar large-scale magnetic fields spatial distrib. rel. to interplanetary mag. field 79−84772
solar limb flare of 1972, August 11, optical, radio and X-ray obs. 77−37587
solar limb spicules, time evolution study of spectra 77−2387
solar photospheric poloidal and toroidal mag. field components near solar min. 79−66978
solar proton region development in 1973, September 7 flare 77−37588
solar spectrum, 300 to 900 nm, Fe I lines interpretation using precise oscillator strengths 79−40155
solar wind, evolving streams and shocks beyond 1 AU, Pioneer 10 and 11 obs. 78−49283
solar wind, Helios 1 obs. of latitudinal extent of high-speed stream 78−57419
solar wind, obs. of flows associated with hot heavy ions 80−51635
solar wind, proton temp. heliocentric gradient from Pioneer 10 obs. 79−40052
solar wind, studies from Prognoz satellites 77−64596
solar wind, upstream particle events close to bow shock and 200 R_E upstream 80−77247
solar wind alpha particle component, results of Prognoz satellite meas. 77−53385
solar wind electrons epithermal dumbbell distrib. Prognoz 7 obs. following shock wave 80−109321

astronomical observations continued
solar wind flow observed by satellites, 0.6 to 1.6 AU 80−90303
solar wind ion acoustic waves, high-resolution spectrograms 79−96878
Southern Milky Way stars, photometry, extinction curves, and R values 77−13443
southern standard stars, monochromatic flux from 3200 Å to 8800 Å 80−51742
spectral hyperfine structure, spectral anal. efficiency enhancement 79−66930
SS 433, photometric and astrometric obs. 79−84801
star transit, external medium effect on accuracy of time meas. 77−87746
stars, solar-type, thirteen-colour photometry 77−22230
stars with intrinsic polarisation, obs. and statistical anal. *(Russian)* 77−13346
stellar photometry, secondary standards spectrophotometric obs. rel. to Ap stars HD 10783 and CU Virginis 80−98663
stellar spectrophotometry, Moscow and Alma-Ata data comparison with multicolour photometric systems 80−101590
STIP Intervals I and II, significant solar-terrestrial events 78−49420
subdwarf stars thirteen-colour photometric obs., sensitivity of indices and evolutionary effects 79−92767
Sun, derived thirteen-colour photometry 77−22230
Sun, luminosity variation (solar const.), direct obs. from rockets 80−90386
Sun, metallicity meas., chromospheric activity effects 79−53784
Sun, supergranules, magnetograph obs. of velocities 77−53555
sunspot magnetic fields spiral config. 77−82192
sunspots, characts. of penumbral bright grains displacement 77−22177
supernova remnant, extragalactic, in NGC 4449, spectrophotometry 80−56895
symbiotic star candidates in LMC, optical spectroscopy and IR photometry 80−62139
ζ Tauri, Be star, rapid linear polarisation variability *(Russian)* 80−77417
SU Tauri, R Coronae Borealis star, photometry in optical and IR ranges 80−101601
V711 Tauri (HR 1099), 1977-1978 photometry before radio outburst 79−21337
RR Telescopii, nova-like variable, spectrophotometry 77−45460
time obs., data smoothing method *(Japanese)* 77−73973
Toyokawa Observatory, Solar Radio Data Acquisition and Communication System (SORDACS) 79−101074
Trapezium-like objects, visual and IR photometric obs. 79−92805
47 Tucanae stars, N anomaly anal. 79−48867
two-micron sources in N Monoceros region, broad-band photometry and objective prism spectra 80−8555
3U 0042+32 and 1728−16, optical counterparts 77−74163
4U 0115+63, transient X-ray source, optical and X-ray obs. 78−32605
4U 0241+62, identification with QSO or Seyfert nuclei-like object 78−16572
Ulugh Beg observatory, meridian instrument axis azimuth rel. to continental blocks rot. 78−53613
Ursa Minor dwarf spheroidal galaxy, abundance vars. on giant branch rel. to ω Centauri anomaly 79−5904
US Naval Observatory data files 77−78670
UV excess objects, ubvi photometry 80−46698
variable stars unpublished observations, IAU archives and 1978-79 data 79−88688
Vela star cloud, large scale photometric survey 80−90482
Venus, atmosphere composition and structure, Pioneer results 80−46230
Venus, atmosphere thermal contrast from Pioneer probe data 80−46229
Venus, bow shock observations, 4th Dec. 1978 80−41747
Venus, dayside ion comp. dynamic effects, Pioneer obs. of ionsphere 79−48703
Venus, dayside ion composition, Pioneer meas. of ionosphere 79−48702
Venus, disk, linear polarization, wavelength dependence 79−66942
Venus, electron obs. and ion flows, Pioneer orbiter plasma analyzer expt. 80−46448
Venus, electron temp. and densities, Pioneer Orbiter meas. of ionosphere 79−48705
Venus, ionospheric diurnal ion comp. vars., Pioneer orbital meas. 80−46440
Venus, magnetic field, nightside Pioneer magnetometer obs. 80−46447
Venus, Pioneer meas. of physical props. up to 200 km altitude *(French)* 80−46421
Venus, Pioneer orbiter cloud photopolarimeter investigation 79−48713
Venus, Pioneer Venus magnetic field meas. on dayside ionosphere 79−48700
Venus, plasma electron obs. in wake 78−77510
Venus, plasma waves, solar wind interaction, Pioneer electric field meas. 79−48701
Venus, radar and spectroscopic observations, measurements by spacecraft 79−92690
Venus, thermal structure and major ion comp. of ionosphere, Venus Orbiter retarding potential analyzer obs. 79−48704
Venus, thermosphere, comp. meas., temp. profile and homopause altitude 79−48707
Venus, upper atmosphere neutral composition, Pioneer quadrupole mass spectrometer obs. 79−48708
Venus atmosphere structure up to 110 km, Pioneer Venus entry probes preliminary results 79−48715
Venus bow shock, Pioneer magnetometer obs. 80−36535
Venus clouds, particle size distrib. meas. 79−48717
Venus clouds, Pioneer Venus nephelometer expt. preliminary results 79−48716
Venus dust ring, evidence from Venera 9, 10 obs. 79−75131
Venus ionosphere composition, meas. by ion mass spectrometers on Pioneer Venus Bus and Orbiter 80−67499
Venus lower atmosphere composition, anal. by gas chromatography 79−48721
Venus lower atmosphere composition, preliminary results from Pioneer Venus 79−48720
Venus magnetic tail field structure, role of unipolar induction effects 80−62060
Venus plasma environment, study via plasma analyser expt. on Pioneer Venus Orbiter 80−67498
Venus surface, preliminary analysis of images from Venera-9 and -10 77−17395
Venus thermosphere, Ar isotope abundances upper limits 80−4281
Venus upper atmosphere, N detect. 80−77310

astronomical observations continued
109 Virginis, absolute energy distrib. from 3295 Å to 9040 Å 78−20828
CU Virginis (HD 124224), Ap star, spectrophotometric obs. 80−98663
SV Vulpeculae, Cepheid, period change meas. rel. to evolution 79−92777
W3, dusty H II region, stellar optical polarisation meas. 78−45379
water vapour comparison for IR observatory sites 78−11973
weak G-band stars, photometry and spectra 77−49386
X-ray novae, spectroscopic obs. in 3800-10900 Å range 77−87577
zodiacal light, colour and polarization from UV to near IR, rocket-borne obs. 79−48737
Ba stars, spectroscopic, radial vel. and photometric obs. 78−12226
Hα emission line star near Gum nebula, UBVRI photometry and variability 78−32449

astronomical observatories
American observatories, visits 77−37502
N.American observatories, VLBI meas. rel. to intra-plate crustal deformation 80−51379
Arecibo Observatory, ionospheric props. meas. without rockets 78−81488
Arecibo Observatory, radiotelescope and instrumentation description 80−4249
Argentine National Observatory and Charles Dillon Perrine 77−37702
Asiago Observatory, high speed photometer 79−25505
bad seeing conditions avoidance within telescope domes 79−70960
Bologna survey at 408 MHz, statistical analysis 78−28816
Boyden Observatory, 152 cm reflector, history 80−12665
building design effect on photographic zenith tube obs. 80−85856
Byurakan Observatory, 1975 visit report 77−33342
Canadian camera network and Innisfree meteorite recovery and orbit determ. 78−65563
Canary Islands, site selection by JOSO for solar observatory 78−65497
Castle Frederick, eighteenth-century Nova Scotia observatory, history 78−40843
Cerro Tololo, integrating vidicon systems 79−66924
Cloudcroft Observatory 80−77289
dome seeing rel. to dome heat sources, theory 80−12657
ESO formation and use of Danish telscopes in Chile *(Danish)* 77−53425
European Southern Observatory, role in Southern Sky Survey 80−12658
Germany, 1976 annual report of astron. institutes *(German)* 78−32341
Goethe Link, new control room and instrumental improvements 79−62743
Gornergrat, TIRGO project *(Italian)* 79−48678
Green Bank surveys at 1400 MHz 78−28543
Herstmonceux parallax programme, second list of meas. stars 78−77498
Hill-Poncet heated observatory, with rocking-type equatorial submounting 79−70953
IR instrumentation on NASA airborne observatories 78−45224
IR sites, water vapour data 79−21181
Iraq National Astronomical Observatory, siting and features 80−4248
Jai Singh observatories and 'instruments' in N.India 80−17490
Kanzelhohe solar observatory, sunspot obs. *(German)* 80−98631
Karl-Schwarzschild Observatory Tautenberg, effect on night sky of light pollution over Jena 80−51533
King's Observatory at Richmond, history 77−67033
Kitt Peak National Observatory, probability of clear daytime skies 80−12512
Kitt Peak National Observatory telescopes, cost effectiveness in terms of publications and citations 80−90334
Kitt Peak Observatory, seeing meas. 80−61899
Kottamia Observatory site, seasonal atm. extinction due to aerosol 80−46253
Kuiper Airborne Observatory, far IR photometer 79−66926
La Palma, Canary Islands 80−21916
Lick Observatory, life of Edward S. Holden and California-Wisconsin astron. connection 79−75310
Louisbourg Observatory and the Marquis de Charbert (1724-1805) 80−68010
Lyon, new blink microscope *(French)* 78−61742
Mauna Kea Observatory, 0.65 to 2.50 μm atmospheric extinction meas. 80−12546
megalithic yars 78−24633
Meudon solar tower, coelostat pointing method 80−90338
Minor Planet Center, history and future 80−94712
mirror temperature effects on telescope seeing, compensation method 79−70961
Molonglo radio source surveys at 408 MHz 78−28541
Mont Megantic, new observatory in Canada *(French)* 79−80215
Monterey Institute for Research in Astronomy, 36-inch telescope 78−16315
Mt. Hopkins multiple mirror telescope 78−93109
Mt. Hopkins Observatory, Multiple Mirror Telescope and ground-based astronomy, conference, Arizona (1979 May 9) 80−62386
National Radio Astronomy Observatory, W.Virginia 79−80216
night sky zenithal brightness monitoring, light pollution rel. to astronomical observations 78−49141
Northern Cross Observatory, new receivers for radiotelescope *(Italian)* 79−2478
observatories in Queensland, Australia 77−2337
Observatorio Astronomico Nacional, Baja California, climatological and meteorological characts. 78−20635
Ondrejov Observatory, Czechoslovakia *(Norwegian)* 80−82193
Paris observatory, collection of astronomical instruments 79−84929
Paris Observatory, history 80−77288
Potsdam Observatory, long-term latitude determs. rel. to principal components var. 78−57158
public viewing observations, USA and Chile 79−21182
Pulkovo Observatory, equatorial stars declinations obs. programme *(Russian)* 79−96892
Rao Observatory in Sweden, history and current research *(Swedish)* 78−28513
review of recent developments 78−16307
Royal Greenwich Observatory, Isaac Newton Telescope, telescope equipment guide 78−12099
Royal Observatory, Greenwich, 1675-1975, conf., Greenwich, England (July 1975) 77−29646
Sacramento Peak Observatory, night sky brightness conditions 80−12545
Sacramento Peak Observatory night sky conditions, cloud cover, seeing and precipitable water 80−51653

astronomical observatories continued
satellites Ariel 5, Cos-B, X-ray and γ-ray astronomy respectively 80−90317
Skibotn, N.Norway, min. precip. H_2O in atmosphere, rel. to IR astron. obs. 79−92572
Skibotn Observatory, in northern light zone, stellar photometric obs. *(Norwegian)* 78−69698
Smithsonian Astrophsyical Observatory, H maser improvements 78−58971
Smithsonian Astrophysical Observatory, solar const. program (1902-1962) 80−36606
Smithsonian Astrophysical Observatory, VLG-11 H maser performance evaluation 79−55098
solar optical observatory testing sites in China, atm. temp. vars. in surface layer *(Chinese)* 78−69680
South African Astronomical Observatory, user guide to telescope facilities 78−73628
Southern Africa, astronomical archives in observatory libraries 78−36473
southern hemisphere observatories, cooperative obs. programmes feasibility 78−69681
Strasbourg Stellar Data Centre 77−91447
Tokyo Astronomical Observatory, Photographic Zenith Tube observationa errors anal. 80−98547
Torun Observatory 127 MHz solar data since 1958, survey *(Polish)* 78−36549
Toyokawa Observatory, λ 8-cm radioheliograph sensitivity and phase stability improvement project 79−101066
Turku observatory, new photographic astrolabe 80−36499
UTRAO 335-380 MHz survey, interim report 78−28815
Venezuela, new observatory near Merida, review 78−49316
Vridslosemagle, Denmark *(Danish)* 80−8765
Westerbork radiosource surveys at 610 and 1415 MHz 78−28542
Wise Observatory, photoelectric UBV photometry performance assessment 78−73657
Wolf's astronomical observatory in Gdansk, Poland, in 18th century *(Polish)* 79−88591
Wroclaw Observatory, new telescope *(Polish)* 79−88594

astronomical spectra
see also atmospheric spectra; stellar spectra
1-100 MeV gamma-ray background, spectrum rel. to cosmological cosmic rays and light elements prod. 78−12436
3K blackbody cosmic background radiation meas. 77−41422
49+88.1°, halo planetary nebula, photoionisation models for line emission spectrum rel. to chemical abundances 80−109507
108−76.1°, halo planetary nebula, photoionisation models for line emission spectrum rel. to chemical abundances 80−109507
108-76°1, new halo planetary nebula, chemical abundances 77−45510
0241+62, nearby quasar, radio spectrum 79−25752
0254−334/2, high-redshift QSO without Lyman α emission or absorpt., spectroscopic obs. 79−92886
0957+561 A, B, twin QSOs, spectroscopic obs. with multiple-mirror telescope 80−12827
0957+561A, B, double quasar, unusual IR spectral energy distrib. 80−73065
1008−3814, southern ring galaxy in Vela, struct. and spectrum 79−58413
1309−216, probable BL Lacertae object with absorpt. red shift 1.49, optical spectrum 80−67856
1331+170, quasi-stellar object, 21 cm absorpt. detect. at $Z\approx1.8$ 79−75292
1401−33, radio structure and spectrum 77−29942
1610−771, radio QSO with steep optical spectrum, obs. 80−94887
γ195+5, γ-ray source, X-ray emission obs. and photon number spectrum 79−97101
γ195+5, high-energy spectrum, SAS-2 obs. 77−33688
γ-ray sources, possible X-ray counterparts spectra rel. to identifications 78−54092
A0035, large southern ring galaxy, spectra and struct. 77−45559
2 A 1102+384 (Markarian 421=B2 1101+38), soft X-ray flux discovery 79−25721
2A 1102+384 (Markarian 421) BL Lacertae object, low-energy X-ray spectrum 78−54083
2A 1251−290, high-latit. X-ray source, X-ray spectrum and variability 78−32611
2A 1348+700, 1415+255, 1410−029, Seyfert galaxies, X-ray spectra and variability 78−32611
A non 0945−30, intermediate luminosity X-ray galaxy, X-ray and optical spectra 79−2578
Abell 1060 galaxy cluster, X-ray spectrum obs. by (HEAO A-2) 80−82518
Abell 1367 galaxy cluster, obs. rel. to galaxies redshift-magnitude bands and evolution 78−54033
Abell 2142, spectroscopic obs. of X-ray cluster (40 1556+27) 79−48940
Abell 2256, X-ray cluster of galaxies, radio emission spectral indices 80−36726
Abell 2634 galaxy cluster, spectroscopic study and radial vels. 77−64857
Abell 399/Abell 401, X-ray binary galaxy cluster, radial vels. and mass 80−90546
Abell 401 cluster of galaxies, vel. dispersion meas. 77−26072
Abell 754 cluster of galaxies (3U 0901-09), radio source spectrum 77−26089
Abell cluster radio sources, spectra and optical identification, SHF obs. 80−98729
Abell clusters of galaxies extended radio emission, Westerbork obs. and spectral indices 80−36727
absorption line profile of isothermal atmos., under general freq. redistrib. function 77−37500
absorption spectra of QSOs and BL Lacertae objects, origin 79−5894
absorption spectra of QSOs and BL Lacertae objects 78−86036
AFCRL Sky Survey objects, 2-14 μ spectrophotometry 77−22331
AFGL 437, optical and IR obs., young star cluster embedded in nebulosity 78−4394
AFGL IR sources, mol. line obs. 80−51856
AL0827+24, quasar, absorpt. lines in optical spectrum 78−4390
Anon 0050+72.8, peculiar emission line galaxy 77−91627
anticorrelated spectral var. in black hole candidate and other X-ray sources 77−53709
AO 0235+164, BL Lacertae object, radio study of $z=0.524$ absorpt. system 78−65680

astronomical spectra continued
AO 0235+164, nature of nebulosity assoc. with BL Lacertae object 78—28778
AO 0235+164, nonthermal emission spectral break development 77—57092
Arakelian galaxies, emission line spectra 77—74138
Arakelyan 120, Seyfert galaxy, spectrophotometry 79—62913
Ariel 0620—00, transient source, X-ray spectra obs. with Bragg crystal spectrometer 79—12542
asteroid surface materials mineralogical characts. from reflectance spectra 78—69736
asteroids, IR reflectance spectra obs. and search for water of hydration 80—77318
asteroids, spectral classes correl. with dynamical families 77—91464
atomic level population of plasma, Jeffries' level population ratios and Seaton's cascade matrix 80—52934
atomic line identification lists bibliography, August 1978 supplement 79—54787
automated reduction by microcomputer based system 80—77296
B2 1225+31, high-luminosity quasar, H emission line intensity ratios 79—25748
B2 1225+31, high-redshift QSO, abundances in $z=1.7941$ absorpt. line system 80—12826
B2 1225+31, spectrum of bright quasar 78—93447
B2 1502+28, head-tail galaxy in Abell 2022, Westerbork obs. of spectral index and polarisation distrib. 80—36727
B2 quasars, radio spectral props. 79—44632
B 0844+31, extended radio galaxy, spectral index distrib. from multifreq. obs. 80—56963
B 35, bright rimmed molecular cloud, CH obs. 80—62238
background gravitational radiation spectra in early state of the Universe *(Russian)* 80—36745
background radiation spectrum, cosmological significance of obs. *(Italian)* 79—48972
background radiation spectrum meas. in near-mm region 80—62327
Balmer discontinuity strengths, interstellar absorption effects 78—89238
Barnard Loop, $H\beta$ obs. 79—80346
BD+30°3639, IR spectrum of planetary nebula 77—22297
BD+30° 3639, S III 18.7 μ fine-struct. forbidden line obs. in planetary nebula 77—37637
Becklin's star, in Orion, 4 to 8 micron spectrum 77—29903
Becklin-Neugebauer object, Brackett-alpha emission obs. 78—36657
Becklin-Neugebauer object, CO band emission detect. 79—101184
Becklin-Neugebauer source in Orion, 3.3 to 5.5 microns spectrum 80—12796
Becklin-Neugebauer source in Orion, high resolution 1.5 to 5 micron spectroscopy 78—93368
bipolar nebula, new, in Centaurus, discovery, photometry and spectral type 79—84837
bipolar nebulae, photometry and spectra rel. to evolutionary status 78—41026
black hole, massive, radiation spectrum of gas debris from tidally disrupted star 80—90467
black holes, accreting, gamma rays emission spectrum 78—32504
black holes, supermassive, unsaturated Compton accretion discs models for hard X-ray spectra 80—22033
blending effects 78—62851
blue compact Zwicky galaxies, spectroscopic survey 79—58417
Bok globules, search for H I 21 cm emission 77—29904
bright galaxy nuclei, optical and radio survey, sample selection and obs. 80—73039
bright quasars discovery program, preliminary results 77—17715
bright sporadic meteor, spectrum obtained with Wampler scanner 78—57508
broad line regions, luminosity and radio emission in active nuclei and quasars 80—105340
5C1 radiosources, optical identification by photographic photometry and spectra 80—77503
3C273, spectroscopic obs. and redshift of associated galaxy 78—77606
5C3 sources, optical idents., spectroscopic results 80—46689
3C 111, radio galaxy, 1.38 cm obs. and instantaneous radio spectrum of nuclear source *(Russian)* 80—109558
3C 111, spectrum and redshift of luminous N-type galaxy 77—33666
3C 120, radio galaxy, vars. in optical spectrum *(Russian)* 80—90540
3C 120, Seyfert galaxy, IUE and visual spectrophotometry 79—92856
3C 120, Seyfert galaxy, spectrophotometric obs. of assoc. nebulosity 80—67890
3C 132, 3C 192, radio galaxies, radio spectra of bridge components 77—91658
3C 147, 3C 286, quasars, spectral indices from VLBI obs. at 329 MHz 80—67898
3C 178, H I absorption within radiogalaxy 79—5910
3C 232, quasar, Ca II absorpt. lines due to galaxy (NGC 3067) 78—36719
4C 25.05, H_2 lines identification in spectrum of quasar *(Russian)* 78—69905
3C 264, radio galaxy, radio struct. and spectra 77—5582
3 C 273, H I spectral line intensities *(Russian)* 79—88763
3C 273, IUE obs. of quasar spectrum 79—71149
3C 273, quasar, detailed UV obs. with IUE 80—94886
3C 273, quasar, UV emission line spectrum 77—87567
3C 273, UV spectrum, 1200-1700 Å, cosmological implications 78—45425
3C 273, X-ray spectrum, 2-60 keV 80—12824
3C 273, X-ray variability, spectrum and position 79—62929
3C 286, quasar, optical absorpt. lines detect., redshift 80—4454
3C 286, quasar, radio absorpt. line obs. and appl. to cosmological deceleration mea. 78—20902
3C 310, 326, relaxed double radio sources, radio lobes spectra from fine scale struct. model 80—51891
3C 310, extended radio galaxy, spectral index distrib. from multifreq. obs. 80—51890
3C 326, very large radio galaxy, multifreq. obs. 78—28810
3C 33, 98, 184.1 and 218, rotation axes 80—26997
3C 33, emission-line vels. rel. to rot. axis of assoc. optical galaxy 78—4355
3C 33, optical line emission rel. to physical conditions in compact head 80—51892
3C 343.1, distant radio galaxy, spectroscopy and photometry, redshift 78—8123

astronomical spectra continued
3C 345, 418, 371, compact radio sources, secondary components spectral indices 80—4450
3C 345, optical spectrum variability 80—8709
3C 390.3, obs. of radio galaxy with International UV Explorer 79—67101
4C 39.04, powerful giant radio galaxy, spectral index from multifreq. obs. 80—17682
4C 39.11, N galaxy, radio and optical obs. and red shift 78—16553
3C 391, supernova remnant, spectral index from 1.4 and 10.7 GHz obs. 80—4417
3C 405 (Cygnus A), 1.38 cm obs. and instantaneous radio spectrum of nuclear source *(Russian)* 80—109558
3C 48, emission-line spectrum of quasar 79—71147
3C 48, quasar, spectrum and model of assoc. nebulosity 77—13487
4C 55.27, quasar, redshift and spectrum 77—45596
3C 58, spectra of faint knots in SNR 78—93375
3C 98, 3C 178, 3C 192, 3C 327, narrow-line radio galaxies, optical spectra 77—33664
4C sources with steep radio spectra, Westerbork obs. 79—35414
CA 0340—538 (3U 0328—523), southern cluster of galaxies, vel. dispersion and global parameters 78—36705
Callisto, identification of water frost 78—4141
Callisto, IR emission spectra 80—82264
Canes Venatici I galaxy group, neutral H obs. of NGC 4136, 4144, 4190, IC 4182 and (DDO 133) 79—84853
Canis Major R1 and OB1 associations, Fabry-Perot obs. of assoc. expanding gas shells 78—93336
Carafe group of galaxies, spectroscopic and photographic obs. of peculiar galaxies 79—35387
Cassiopeia A, absolute radio spectrum 78—8090
Cassiopeia A, OH and formaldehyde absorpt. obs. 78—45381
Cassiopeia A, radio spectrum evolution 79—30104
Cassiopeia A, SNR, X-ray spectrum, line emission obs. 80—26961
Cassiopeia A, spectral intensity variations *(Russian)* 77—91661
Cassiopeia A, supernova remnant, explanation of secular flattening of radio spectrum 80—101637
Cassiopeia A, supernova remnant, flux density meas. and radio spectrum flattening 77—45531
Cassiopeia A, supernova remnant, search for X-ray line emission 78—57607
Cassiopeia A, young SNR, radio spectral index evolution according to observational data 79—75256
Cassiopeia A supernova remnant, forbidden lines strengths rel. to abundance inhomogeneities 80—12797
cD galaxies in poor clusters, photometry, spectra and redshifts 79—48907
cD galaxies in poor clusters, radial vel. meas. 79—8994
cD galaxy in Abell 2029, envelope spectra rel. to dynamics and struct. 79—92850
cD galaxy in Abell 401, spectral obs. of halo 78—32584
Centaurus A, nuclear gamma-ray lines, origin in relativistic plasma 80—41890
Centaurus A (NGC 5128), 1.38 cm obs. and instantaneous radio spectrum of nuclear source *(Russian)* 80—109558
Centaurus cluster, Fe XXV and Fe XXVI line emission obs. in X-ray spectrum 77—45580
Centaurus galaxy cluster, X-ray spectrum obs. by (HEAO A-2) 80—82518
β Cephei stars, line profile variables, Si III 456.7 nm line modelling 80—85951
Cepheus IV star formation region, continuum and recomb. lines, SHF obs. 80—90501
Cepheus OB3 association molecular cloud, mol. obs. rel. to star form. 80—12798
Ceres, carbonaceous chondrite mineralogies remote spectroscopic identification from IR obs. 79—96946
Ceres, evidence for water of hydration 78—32386
CG 135+1, gamma ray source, spectrum obs. 20 keV-25 MeV 80—105398
CG sources, 100 MeV, very high energy gamma-ray emission search 79—40293
Circinus galaxy, H I 21 cm line obs. 77—33652
CL 4, H I emission-absorption meas. at 1420 MHz 79—62922
Cloud 2, mol. cloud, detect. of HC_5N (cyanodiacetylene) and HC_7N (cyanohexatriyne), SHF obs. 80—101627
clusters galaxies, redshift determ. using Image Dissector Scanner, visible spectra 80—90544
clusters of galaxies, H I broad band emission search 80—46667
clusters of galaxies, intracluster relativistic electrons hard X-ray spectra and gas heating 79—25735
clusters of galaxies, OSO 8 X-ray spectra discussion 79—25734
clusters of galaxies, radio spectrum slope rel. to intracluster gas heating and X-ray emission 78—57655
clusters of galaxies, X-ray source structure and spectra 79—58448
clusters of galaxies, X-ray spectra 78—12387
clusters of galaxies, X-ray spectra and relationship to other cluster props. 80—22093
clusters of galaxies, X-ray spectra and temps. rel. to other cluster props. 77—91668
clusters of galaxies, X-ray spectra in 2-20 keV range, OSO 8 obs. 79—5908
clusters of galaxies, X-rays energy spectra 77—13472
Cn 3-1, planetary nebula, emission line obs. 77—33621
collapsing molecular clouds, self-reversed CO profiles 77—33581
colliding gas clouds system, struct. and spectrum and relationship to QSOs 78—28836
Coma galaxy cluster, low energy X-ray absorpt. obs. 78—86025
Coma/A1367 supercluster of galaxies and environment 78—65700
GQ Comae Berenicis, QS0 or N galaxy, spectrophotometry obs. 80—77488
comet, artificial, solar radiation interaction and gas and dust emission 79—16887
Comet Arend-Roland (1957 III), visible and UV spectra anal. *(Chinese)* 80—12709
Comet Bennett (1970 II), CN (0-0) band brightness profile obs. rel. to CN prod. 80—82303
Comet Bennett (1970 II), emission features, coma comp. 79—16884
Comet Bennett (1970 II), O(^1D) and H_2O^+ brightness profiles 79—35192
Comet Bradfield (1978c), emissions from head 79—96971

astronomical spectra continued
Comet Bradfield (1978c), search for mm wave emission from HCN, CO and methyl cyanide 79—75157
Comet Bradfield (1978c), spectroscopic obs. 78—40879
Comet Bradfield (1979l), photographic obs. and spectra 80—51693
Comet Bradfield (1979l), spectra and visual obs. (1980 Jan.-Feb.) 80—41768
Comet Bradfield (1979l), spectroscopic and photographic obs. in near IR 80—105205
Comet Bradfield (1979l), UV spectrum, UE obs. 80—90371
comet debris (meteors) spectra studies video techniques appl. 79—80241
Comet Kobayashi-Berger-Milon (1975 IX), Lyman-α obs. 80—4301
Comet Kobayashi-Berger-Milon (1975h), visual spectroscopic obs. 77—33424
Comet Kohler (1977m), OH 1667 MHz line absorption detection 78—4152
Comet Kohler (1977m), positions, spectral emissions and magnitudes 78—7924
Comet Kohoutek (1973 XII), analysis of IR continuum 79—62792
Comet Kohoutek (1973 XII), C and O spectra and prod. rates 77—49331
Comet Kohoutek (1973 XII), CN and C_2 spectrophotometry 78—20738
Comet Kohoutek (1973 XII), CN violet (0,0) spectra 80—82308
Comet Kohoutek (1973 XII), Mariner 10 UV obs. of Lyman-α line 79—96970
Comet Kohoutek (1973 XII), spectrum interpretation by means of Franck-Condon factors, Rydberg-Klein-Rees method calc. *(French)* 77—17428
Comet Kohoutek (1973 XII), visible spectra, band intensity var., electrospectrophotometer meas. 80—8588
Comet Kohoutek (1973XII), Swann band profiles 78—85909
Comet Meier (1978f), positions, elements, ephemeris, magnitudes and spectrum 78—53881
Comet Meier (1978f), precise positions 1978 Apr., spectroscopic obs. 78—49387
Comet Mrkos (1957 V), CN (0,0) vibr. band anal. 78—20734
Comet Seargent (1978m), UV spectral obs. by IUE 78—96436
Comet Seargent (1978m), UV spectrum 79—44413
Comet Tago-Sato-Kosaka (1969 IX), H and OH emission rel. to prod. rates 78—28580
comet tail spectrum, $^{13}C^{16}O^+$ (2,0) band rot. anal. 80—74157
Comet West (1975n), search for CH RF emission 78—20735
Comet West (1975n), spectrographic obs. 77—29730
Comet West (1976 VI), CN (0-0) band brightness profile obs. rel. to CN prod. 80—82303
comet West (1976 VI), emission bands and continuum flux heliocentric depend. 80—36575
Comet West (1976 VI), IR obs., results 78—81591
Comet West (1976 VI), spectrophotometry, emission bands and lines obs. 80—56768
Comet West (1976 VI), spectrophotometry after perihelion passage, emission features vars. 78—57503
Comet West (1976 VI) ionosphere CO^+ brightness profile 80—85896
cometary coma, IR continuum rel. to dust grains props. 78—7923
cometary nebula near NGC 7023, brightening and spectra 77—74118
comets, brightness var. in molecular emission bands 78—81590
comets, C_2 synthetic spectra calcs. 78—28579
comets, CN abundance from radiance of violet CN spectral bands 78—16348
comets, CO and CO^+ bands intensities reson. fluoresc. calc. 79—35191
comets, molecular Λ-doublets transitions induced by collisions with ions 80—14132
comets, neutral species brightness profiles, average random walk model for mol. photodissociation 80—77351
comets, possible detect. of newly created CN radicals 78—61798
compact and interacting southern galaxies with emission line spectra 78—41048
compact galaxies, spectroscopic and photometric obs. 78—77603
compact galaxies on UK Schmidt plates 78—81687
compact H II regions, IR spectral indices, large-beam obs. 78—16488
compact H II regions assoc. with OH masers, $^{12}CO/^{13}CO$ intensity ratios rel. to cloud densities 77—57078
compact H II regions in areas of DR 21, W75N and K3-50, IR line obs., extinction determ. 80—12788
compact H II regions near Type I OH maser sources, radio spectra 78—8094
compact IR sources, dust shell models 77—29948
compact nebulae, very-low-excitation, in Magellanic Clouds, spectra 78—32556
compact radiosource at galactic centre 79—21422
compact thermal sources, linear polarisation spectrum appl. to mag. fields determ. *(Russian)* 80—90344
compact X-ray sources, Comptonisation of Fe X-ray spectral features 78—20908
Compton effect and resonance scattering in astrophysical spectra 79—58242
Compton scattering at nonzero particle fluxes, radiation and relativistic electrons spectra 79—8825
Comptonization of X-rays by low-temperature electrons, rel. to X-ray sources spectra 79—35108
cosmic background radiation, isotropy and Planck spectrum rel. to generalised cosmological principle, in Newtonian and relativistic theories *(Polish)* 80—27025
cosmic background radiation spectrum, early energy release distortion in Rayleigh-Jeans region 80—73077
cosmic dust grains, observed IR props. 80—26943
cosmic gamma burst, possible obs. at radio freqs. 77—9819
cosmic gamma rays of galactic disc, contrib. of non-thermal electron bremsstrahlung 78—24414
cosmic glack body radiation meas. using low temp. optical techniques, 2-40 cm^{-1} 79—71161
cosmic microwave background, spectral lines of prestellar origin *(Russian)* 78—77628
cosmic microwave background, Sunyaev-Zel'dovich effect in millimetric region 79—25765
cosmic microwave background, temp. diminution distrib. by Coma cluster X-ray source 79—92896
cosmic microwave background spectrum, distortion by intercluster medium 80—4426
cosmic microwave background spectrum, distortion by pregalactic dust 80—67916

astronomical spectra continued
cosmic radio background 77—17723
cosmic radiosources, Compton effect and relativistic electrons spectra in plasma turbulent reactor *(Russian)* 77—19760
cosmic X-ray bursts, OGO-5 satellite obs. 77—13492
cosmological microwave black body radiation spectrum, implications for Population III stars 80—67915
3CR, radio galaxies, spectrophotometry spectral energy distrib. 79—21413
3CR radio galaxies, optical spectra 79—71124
3CR radio galaxies, redshifts, strong emission line spectra 77—33666
3 Cr radio sources, spectral index breaks 79—67108
Crab Nebula, emission line spectrum 80—22068
Crab Nebula, emission-line spectra of condensations 79—35327
Crab Nebula, gamma-ray spectrum, SAS-2 obs. 77—33688
Crab Nebula, hard X-ray spectrum 79—62891
Crab Nebula, high energy X-ray spectrum, OSO-8 obs. 78—12315
Crab Nebula, low-energy gamma-ray obs. 77—29894
Crab Nebula, millimetre and submillimetre meas. rel. to power law spectrum 79—75267
Crab Nebula, optical spectrum rel. to baryon star magnetosphere *(Russian)* 77—91555
Crab Nebula, photoelectric spectrophotometry of filaments, abundances 78—41006
Crab Nebula, possible line feature at 73 keV, intensity and width 79—92829
Crab Nebula, radial distrib. of radio spectrum, occultation obs. 78—12339
Crab Nebula, radio emission features spectra 79—75257
Crab Nebula, relativistic particles injection rel. to synchrotron spectrum 78—36678
Crab Nebula, search for thermal X-ray line emission 78—8095
Crab Nebula, spectral index at decametre wavelengths from lunar occultation obs. 80—62248
Crab Nebula, spectrograms of filaments, faint forbidden lines 78—45388
Crab Nebula, X-ray line emission, balloon-borne obs. 80—41884
Crab Nebula filaments, shock waves hydrodynamics effects on spectra 78—85997
Crab Nebula outskirts, remarkable spectra and element abundances 78—36662
CRL 2688 (Egg Nebula), 8000-11000 Å spectrum 77—41400
CTB 80, peculiar supernova remnant, central radio source optical and H I obs. 80—56896
Cygnus A, emission line vels. rel. to rot. axis of assoc. optical galaxy 78—4355
Cygnus Loop, 25 MHz struct. and radio spectrum 78—54027
Cygnus Loop, far UV emission line spectrum, C depletion in interstellar medium 79—21398
Cygnus Loop, fast shock wave detection, optical spectra 80—82467
Cygnus Loop, forbidden Fe XIV emission radial distrib. 78—32545
Cygnus Loop, high-rel. gas Hα emission origin 80—41873
Cygnus Loop, radial distrib. of Fe X and XIV forbidden line emission 80—51828
Cygnus Loop, search for O VII X-ray line emission 78—93379
Cygnus Loop, SNR, abundances and filament shock vel., UV obs. 80—94848
Cygnus Loop, SNR, soft X-ray spectra emission line features obs. 80—94849
Cygnus Loop, supernova remnant, spectra of filaments and high vel. gas *(Russian)* 78—41028
Cygnus Loop, supernova remnant, UV spectral obs. of bright filament 78—45387
Cygnus Loop, supernova remnant, X-ray spectra var. with position 80—82472
Cygnus Loop, Voyager 2 UV spectrometer obs. 79—92816
Cygnus X radio source, radio and optical spectra and identification of components 78—28809
Cygnus X-1, accretion disk round black hole, temp. var., X-ray obs. 80—109561
Cygnus X-1, hard X-ray intensity and spectrum short term changes 77—9814
Cygnus X-1, hard X-ray spectrum 79—71156
Cygnus X-1, hard X-ray spectrum during 1975 November transition 77—2496
Cygnus X-1, high-energy X-ray spectra, 0S0-8 obs. 79—71151
Cygnus X-1, temporal and spectral var., X-ray rocket obs. 78—8163
Cygnus X-2, spectroscopic obs., orbital period, spectral-type var., X-ray heating 79—9036
Cygnus X-2, spectroscopic obs. *(Russian)* 77—26092
Cygnus X-3, observational constraints, on models 78—16567
Cygnus X-3, X-ray Fe line emission meas. with Bragg crystal spectrometer 79—12544
DA 240, radio galaxy, jet, high-vel. gas obs. 78—28773
dark clouds, formaldehyde obs., 5 GHz survey 80—73028
dark clouds, H I 21 cm line obs. 79—21393
dark dust clouds in southern hemisphere, formaldehyde absorpt. line profiles 77—13434
decametric survey of discrete northern sources, spectra of 266 sources in 10-1400 MHz range 78—57664
Deimos, spectral evidence for carbonaceous chondrite surface comp. 80—41754
diatomic astrophysical molecules, review of spectroscopic information in visible and UV regions 77—88459
dielectronic recombination spectra, appls. in astronomy 80—46391
diffuse cosmic far UV background, rocket obs. 80—46708
diffuse cosmic UV background, spectrum 80—17696
diffuse gamma radiation, SAS-2 obs. 78—8169
diffuse gamma-ray emission from active galaxies 80—12806
diffuse interstellar absorpt. bands origin, Ti depletion, accretion onto oxide grains 79—53879
diffuse interstellar bands, rel. to optical behaviour of grains with reson. impurities 77—53660
diffuse interstellar features at 6379 and 6614 A, high resolution profiles 78—4314
diffuse interstellar line at 6284 Å, obs. and relation to interstellar reddening 80—51843
diffuse interstellar lines, identification 77—87518
diffuse interstellar lines 79—21401
diffuse nebulae, formaldehyde and H110α recomb. lines obs. towards bright rims 77—87510

astronomical spectra continued

- diffuse nebulae, low-excitation, spectra rel. to effective temps. of exciting stars 77−13427
- diffuse soft X-ray background, three-band obs. rel. to thermal emission models 77−45604
- diffuse soft X-ray sources, search for spectral lines 77−5440
- diffuse soft X-rays from H I deficient region in Hercules, O VII emission line obs. 79−25759
- diffuse X-ray background spectrum, 20 keV spectral index change determ. 78−69916
- dimethyl ether, review of microwave spectrum, tabulated data 80−51965
- Doppler broadening parameters and Doppler shifts, meas. without spectrograph 78−20646
- 30 Doradus direction, unique interstellar Ca II K-line profile obs. 80−51850
- 30 Doradus nebula, emission line spectrum rel. to chemical comp. and density struct. 80−62226
- 30 Doradus nebula, in LMC, interstellar Ca II and Na I obs. 80−46643
- double radio sources in directions of rich galaxy clusters, spectral indices and polarisation 78−57662
- DR21(OH) obs. of $J=1\rightarrow0$ emission from $H^{15}NC$ 77−82299
- DR 21 OH, relationships of N_2H^+, HCO^+, HCN and CN 77−33587
- dwarf galaxies in Nilson's Uppsala General Catalogue, H I 21 cm line survey 79−92846
- echelle spectroscopy, applications 77−25951
- electron scattering in strong mag. field effects on radiation spectrum 79−92662
- elliptical galaxies, internal dynamics 79−53902
- elliptical galaxies, late M giants population synthesis rel. to colours and spectra, comp. effects 78−57626
- elliptical galaxies, rot. meas. rel. to oblate models 78−16529
- ELSPEC/2, interactive procedure for spectrogram processing *(Italian)* 80−98566
- emission line asymmetry in QSOs and Seyfert galaxies 79−101214
- emission line galaxies, spatial distrib. rel. to clusters, visible spectra obs. 80−73046
- emission line galaxies and quasars, classification system and list of 116 objects 77−22308
- emission line object, spectral obs., possible planetary nebula 77−49451
- emission line redshift, and true redshift differences 77−64853
- emission line spectra, automatic reduction 80−77294
- emission nebulae with strong S II forbidden lines in LMC 77−29891
- emission-line, galaxies and active radio-emitting nuclei, red and IR spectral obs. *(French)* 79−48815
- emission-line galaxies, phys. conditions in nuclei *(Russian)* 79−80359
- Enceladus, IR photometry rel. to presence of water frost 78−12146
- equivalent widths meas. criterion 79−35141
- 433 Eros radiometric and refl. light obs. rel. to thermal props. 80−31231
- ESA/NASA ASSESS II Mission, far IR spectroscopy *(Italian)* 79−48687
- ESO 012-G21, Seyfert 1 galaxy, spectrum, redshift, UBV photometry and X-ray identification 80−8695
- ESO 012-G21, type I Seyfert galaxy, Ariel V X-ray spectra 80−90539
- ESO 103-G35, Seyfert galaxy and possible X-ray source 79−88741
- ESO 103-G35, type I Seyfert, optical counterpart of H 1834−653 X-ray source 78−96547
- ESO 113-IG45, galaxy and/or quasar, spectrum, photometry and struct. 78−28782
- ESO 113-IG 45, interacting galaxy, Type 1 Seyfert spiral with bright central quasar 78−8126
- ESO 113-IG 45 (=Fairall 9), Seyfert galaxy, spectroscopic and multiaperture photometric obs. 80−31362
- ESO 140-G43 (Fairall-51), new southern Seyfert 1 galaxy, spectrum and red shift 78−54044
- ESO 263-PN 02, spectroscopic obs. of southern planetary nebula 80−101626
- ESO/Uppsala galaxies, spectroscopic and photometric obs., second catalogue 78−77497
- ethane, intensity of $^RQ_0$ branch in ν_9 fundamental 77−6856
- ethane, long path photoelec. absorpt. spectra 4200-10600 Å, appl. to Uranus 77−83592
- EUV spectrum of hot, optically-thin interstellar plasma 78−81665
- extended emission line source radial vel. maps, TAURUS imaging device 80−82205
- extragalactic background between 0.5 and 400 MHz 77−74166
- extragalactic compact X-ray sources, synchrotron self-Compton model rel. to spectra 77−29961
- extragalactic emission line objects, third list from Curtis Schmidt thin prism survey 78−28538
- extragalactic emission-line objects, second list from Curtis Schmidt thin prism survey 78−28537
- extragalactic H II regions, spectra anal. and models 80−73024
- extragalactic IR background radiation, meas. technique 80−17496
- extragalactic IR sources, synchrotron radiation model 80−31387
- extragalactic objects, millimetre wavelength energy distribs. 78−36720
- extragalactic objects UV spectra, International Ultraviolet Explorer (IUE) obs. 78−96540
- extragalactic powerful radiosources, compact and extended components spectra 77−41415
- extragalactic sources with strong mm components, simultaneous radio obs. 80−73055
- faint blue objects in field of open cluster M67, spectroscopic obs. 77−22329
- faint light detection and spectrometry, book 77−25950
- faint quasars, spectroscopy and props. of CTIO 4 metre survey 78−32592
- Fairall 9 and Fairall 51, spectrophotometry, Seyfert 1 class galaxies 79−17076
- far IR background at high galactic latitudes 77−53712
- far IR spectra, airborne interferometry 77−25942
- filaments surrounding RR Pictoris (Nova 1925), spectrophotometry, abundances, ionization 79−40194
- fluorescent molecular lines originating in or around stellar objects, catalogue 77−23514
- forbidden lines in quasars and active galaxies, theory 78−93408
- formaldehyde, ^{18}O isotope, 4389 MHz obs. 79−44591
- formaldehyde, in ρ Ophiuchi dark cloud complex, lifetimes and 6 cm line intensities 78−8080
- formaldehyde, interstellar, 5 GHz absorpt. spectra obs. in directions towards galactic centre regions 79−84855

astronomical spectra continued

- formaldehyde in giant molecular clouds, H_2 densities and $^{12}C/^{13}C$ ratio 80−51837
- formaldehyde near Cone nebulae and NGC 2264 IR source, kinematics and distrib. 80−4418
- Fourcade-Figueroa galaxy near NGC 5128, struct., spectrum and red shift 78−73758
- Fourier analysis of spectral line profiles 77−22105
- G0.7-0.0 (Sagittarius B2), continuum and recomb. line spectra, He abundance 78−45380
- G127.1+0.5, compact flat-spectrum radio source as supernova stellar remnant 78−16555
- G286.8−0.5, nonthermal radiosource in front of Carina Nebula, SNR 79−35355
- G287.8−0.5, possible supernova remnant in Carina *(Italian)* 79−53924
- G292.0+1.8, abundance anomalies, radial vels., possible Crab-like SNR 80−46628
- G292.0+1.8, supernova remnant, optical identification and spectrum 79−84839
- G292.0+1.8, young supernova remnant, high vel. material obs. 80−22064
- G326.3−1.8, G348.5+0.1, G348.7+0.3, unusual supernova remnants, radio obs. 79−84841
- G333.6−0.2, compact H II region, S III 18.7 μ fine-struct. forbidden line obs. 77−37637
- G333.6−0.2, G298.2−0.3, southern compact H II regions, IR emission lines obs. 78−96522
- G333.6−0.2, Ne II 12.81 μm forbidden line obs. at high resolution 80−85983
- G333.6−0.2, powerful H II region, 2 μm line emission detect. 78−54017
- G339.2−0.4, radio recombination line obs. of low-excitation H II region 80−46650
- G339.2−0.4, supernova remnant or planetary nebula, radio and optical obs. 80−22104
- G45.1+0.1, 8-13 μm spectrophotometry of compact H II region 78−65672
- G46.8−0.3, galactic supernova remnant, H I emission and absorpt. features rel. to distance 79−84833
- G48.6+0.0, galactic H II region, direction, H I, OH and H_2CO absorpt. line meas. 78−85996
- G65.2+5.7, soft X-ray spectrum and structure of SNR 79−71093
- G74.9+1.2, H I absorpt. rel. to distance of supernova remnant and nearby point source 77−64864
- G 0.7−0.0 (Sagittarius B2), interpretation of radio recomb. line emission 77−17651
- G 21.5−0.9 supernova remnant resembling Crab Nebula radio spectrum 77−5553
- galactic γ-ray emission from inverse Compton scatt. 77−73911
- galactic centre, 2.2 μm spectroscopy 78−36686
- galactic centre, 4 to 8 micron spectrum 79−48922
- galactic centre, forbidden O III 88 μm line emission obs. 78−49503
- galactic centre, formamide ^{13}C isotope detect. 79−25680
- galactic centre, gamma-ray lines rel. to high energy particle fluxes 80−36713
- Galactic Centre, H recomb. lines obs. at decimetric wavelengths 77−82310
- galactic centre, Ne II 12.8 micron emission obs. 78−32572
- galactic centre, OH absorpt. struct. determ. using regularisation method 80−17505
- galactic centre, positron annihilation gamma radiation spectrum 79−44309
- galactic centre, Prognoz-6 obs. of X-ray fluxes and energy spectra *(Russian)* 80−109562
- galactic centre, radio recomb. lines obs. rel. to extended thermal emission ionising agent 79−97059
- galactic centre direction, low-freq. radio recomb. lines studies 78−32589
- galactic centre point source, 1.4-2.7 μ spectrum 77−5569
- Galactic Centre region, 252α recomb. line emission 77−45587
- galactic coronae, ionisation struct. and absorpt. line spectra 77−13448
- galactic diffuse soft X-ray emission, distrib. and energy spectrum 78−28853
- galactic disc, bremsstrahlung gamma radiation emissivity and local interstellar electron spectrum 79−25417
- galactic dust clouds, far IR emission rel. to translational anisotropy of cosmic microwave background 77−33706
- galactic dust globules, microwave spectral lines obs. 78−57609
- galactic gamma radiation, 0.03-4.1 MeV energy spectrum, Kosmos 461 meas. 77−67144
- galactic gamma-ray lines, balloon obs. with high resolution Ge(Li) spectrometer *(Japanese)* 79−80353
- galactic gamma-ray spectra, rel. to cosmic ray electrons flux and cosmic ray gradients 78−40784
- galactic H I absorption, obs. of struct. on small ang. scales 80−22051
- galactic H I spectra analysis 79−44605
- galactic H II regions, O III 51.8 μm forbidden emission line obs. 79−25685
- galactic interstellar extinction law, effect of varying 2200 Å feature 78−85990
- Galactic IR obs. at 2.4 μ wavelength by balloon *(Japanese)* 78−61924
- galactic LF background radiation, spectra and absorpt. 77−33707
- galactic masers, role of plasma effects in generating high-vel. and symmetric spectral features 80−31378
- galactic non-thermal radio radiation from polar regions, spectra 80−22082
- galactic nonthermal radio spectrum, rel. to cosmic ray electrons spectrum and gamma-rays prod. 80−62257
- galactic nuclei, bright line emission, contrib. of H II regions and shock waves 80−109552
- galactic nuclei, stellar population synthesis 78−36688
- galactic nucleus, H110α recomb. line emission vels. 78−69885
- galactic OH absorption in direction of extragalactic radiosources, survey 77−64822
- galactic plane, fine resolution gamma-ray spectrum, Ge spectrometer obs. 77−53701
- galactic radio emission, spectrum rel. to cosmic ray electrons confinememt 77−73910
- galactic radio emission, spectrum rel. to interstellar gas hydrostatic equilib. 77−29919
- galactic radio emission rel. to cosmic ray electron spectra 77−29610
- galactic radio spectrum, influence of primordial black holes 80−62179

astronomical spectra continued

- galactic synchrotron radiation, distrib. from cosmic ray electrons propag. diffusion model 79−53679
- galaxies, absorption features radial gradients rel. to metallicity 79−40254
- galaxies, active nuclei, physical props. from emission-line spectra 78−57650
- galaxies, bright nuclei activity, emission line sources and radio sources 80−98709
- galaxies, compact and bright-nucleus, in S.hemisphere, spectroscopic survey 80−94725
- galaxies, distance determ. from H I line profiles 77−29920
- galaxies, distance scale from IR magnitude/H I vel.-width relation 80−82480
- galaxies, Doppler shifts distrib. for relativistic gas 78−65492
- galaxies, early-type, H I obs. 78−45401
- galaxies, elliptical, vel. dispersions rel. to mass to light ratios 80−98707
- galaxies, elliptical and S0, absorpt.-line strengths 80−4430
- galaxies, extended optical-rotation curves for spirals 79−97083
- galaxies, H I profiles appl. to mass determ. 80−56937
- galaxies, IR magnitude/H I vel. width relation rel. to distance scale and Universe expansion rate outside Local Supercluster 80−105325
- galaxies, large, H I mapping survey and line profiles 80−94870
- galaxies, late-type H I obs. rel. to integral props. derivation 78−86015
- galaxies, Markarian and Seyfert types, search for CO emission 80−26975
- galaxies, nearby, H I profiles obs. 80−41895
- galaxies, nearby, interstellar CO survey 80−62276
- galaxies, optical and UV spectra of active nuclei 79−97094
- galaxies, radial vels. distortion by night sky spectrum 77−41406
- galaxies, radial vels. for 42 southern objects 80−41902
- galaxies, radio recombination line obs. 79−101193
- galaxies, radio recombination line studies of nearby objects 78−93397
- galaxies, radio spectral indices rel. to mean surface brightness *(Russian)* 77−91615
- galaxies, redshifts, vel. dispersions and line strengths meas. 77−29916
- galaxies, small, accurate 21 cm H I spectra 79−35382
- galaxies, southern, strong emission line spectra, characts. 79−21432
- galaxies, southern, with broad emission lines 78−20891
- galaxies, southern peculiar objects and pairs, spectra and radial vels. 78−45411
- galaxies, spectral inversion technique for stellar population synthesis 80−90339
- galaxies, spectrophotometric gradients *(Russian)* 79−92861
- galaxies, spectroscopy and photometry rel. to evolution of faint objects 80−105353
- galaxies, X-ray spectrum and variability of active objects 79−58420
- galaxies active and normal nuclei, radio spectra compared with quasars 78−57646
- galaxies active nuclei, continuous optical spectra 78−57644
- galaxies active nuclei, contrib. of irradiated stars mass loss to broad line emission regions 80−56949
- galaxies active nuclei, emission line spectra rel. to ionised gas and dust 79−88730
- galaxies active nuclei, extreme nonthermal radiation physics rel. to spectral parameters 80−90531
- galaxies active nuclei, H emission-line spectra 78−96557
- galaxies active nuclei, role of inelastic collisions 77−45599
- galaxies active nuclei, [O III] and [Ne III] spectra rel. to narrow line region physical conditions 80−31364
- galaxies assoc. with QSOs, spectroscopic search 80−105355
- galaxies from ESO/Uppsala list, first catalogue of spectroscopic obs. 77−22113
- galaxies in Abell 2255, red shifts 79−40276
- galaxies in clusters, spectral var. in brightest objects 78−41030
- galaxies in rich clusters, redshifts 80−85872
- galaxies nuclei, spectra and vel. dispersions 77−57083
- galaxies of high surface brightness, spectra, redshifts absolute magnitudes *(Russian)* 77−49467
- galaxies of high surface brightness, spectral obs. *(Russian)* 77−49466
- galaxies primordial protoclusters, search for H I emission at Z=3.33 and (4.92) 78−41066
- galaxies with active nuclei, spectroscopic and photometric obs. 77−37650
- galaxies with emission lines and IR excesses, 8000-11000 Å spectra 77−67124
- galaxies with emission-line spectra, review 77−64855
- galaxies with UV continuum, emission lines obs. *(Russian)* 77−22109
- galaxies with UV continuum, spectra 80−67585
- galaxies with UV continuum, tenth list, emission lines obs. *(Russian)* 77−91445
- galaxies with UV excess, morphological descriptions and spectra 80−67584
- galaxies with UV excess, spectra and morphology of 58 objects 80−26968
- galaxies with UV excess and double and multiple nuclei, spectral study 80−67848
- galaxies young massive halos, spectral energy distribs. at large redshifts 77−78866
- galaxy cluster, soft X-ray spectra, constraints on models for Coma Berenices and Perseus clusters 78−36702
- galaxy clusters, X-ray line spectroscopy 78−36701
- galaxy clusters, X-ray rel. to optical cluster props. 80−26996
- Galaxy gamma-ray emission, fluxes determ. from cosmic ray electron spectrum 80−62257
- galaxy group in Cetus with redshift discrepancy 78−36708
- galaxy groups, radial vel. meas., membership, mass/light ratios and distances 77−33660
- galaxy groups and clusters, southern, redshift data 79−84861
- galaxy nuclei, stellar population models 77−2467
- galaxy nuclei, stellar populations and H II regions, spectral anal. 80−98708
- galaxy pairs containing one Markarian and one normal galaxy, morphology and spectra 78−96535
- galaxy pairs with Markarian components, spectroscopy *(Russian)* 77−37648
- galaxy redshifts survey, data reduction techniques 80−22074
- Galilean satellites, near IR spectra rel. to surface composition 79−35180
- Galilean satellites, water ice existence, IR spectral reflectance obs. 80−82263
- gamma ray spectroscopy 80−67582
- gamma rays, medium energy, from galactic centre region, obs. 79−9030

astronomical spectra continued

- gamma rays from galactic disc, obs. between $-45° < l^{II} < 45°$ in 80 keV to 8 MeV energy range 80−82540
- gamma-ray burst, distance and spectrum of 1972 April 27 event 80−67903
- gamma-ray burst production near rapidly rotating accreting black holes 77−49422
- gamma-ray burst source on 1976 August 16, balloon-borne obs., energy spectrum 78−54078
- gamma-ray bursts, 0.2 to 2 MeV spectra from Solrad 11 detectors 77−57108
- gamma-ray diffuse radiation, MeV excess in energy spectrum 78−73777
- gamma-ray line astronomy, review 79−44641
- gamma-ray lines, appls., window to Universe 78−45241
- gamma-ray lines in 10 keV-100 MeV range, book 77−37673
- gamma-ray source in Taurus region, 1-10 MeV spectrum in 1971 August 77−45605
- gamma-ray spectra of Centaurus A, 3C 273 and NGC 4151, Penrose powered black holes model 80−56925
- gamma-ray spectroscopy 80−31271
- gaseous nebulae, Fe abundances from forbidden Fe III and Fe VI lines intensities 78−53806
- gaseous nebulae, intensity ratios of Brackett to Balmer H lines 77−74121
- gaseous nebulae, riddle of spectra, history 80−8676
- GB2 1400 MHz survey, radio spectra of flat-spectrum sources 79−44628
- giant molecular cloud near M17, structure and extent from CO 115 GHz obs. 79−71084
- giant molecular clouds, turbulent cores, CS obs. 80−51822
- giant planets, IR spectra rel. to atmospheric thermal structs. 79−84735
- GL 2636, star form. region in Cygnus-X, IR obs. 80−105302
- glaaxies, far IR (30-300 μm) emission 80−51861
- gravitational bremsstrahlung freq. spectrum, post-Newtonian theory 78−40811
- gravitational waves, cosmological, spectrum rel. to temp. fluctuations in primordial background radiation 78−65728
- gravitational waves, energy spectra from trajectories plunging into nonrotating black hole 80−4246
- GX 17+2 (3U 1813-14), correlated X-ray intensity and spectral slope vars. 78−41081
- GX 17+2 (3U 1813-14), optical spectroscopic search 77−2485
- GX 301−2, spectra and pulse period vars. 77−2486
- H 1538−32, extended soft X-ray source and possible old supernova remnant, energy spectrum 80−51912
- H 2155−304, highly luminous BL Lacertae object, spectral obs. 80−4459
- H 2155−304, optical counterpart position and spectrum 78−93478
- H 2156−304, possible new BL Lacertae object, soft X-ray energy spectrum 79−92891
- H I regions, 42 cm absorpt. search rel. to protons mag. monopole struct. limits 79−53717
- Haro 15, spectrophotometry and morphology of galaxy with UV excess *(Russian)* 78−93387
- HB 3, supernova remnant, H thermal bremsstrahlung model for soft X-ray spectrum 80−56915
- HB 9, soft X-ray emission obs. from old SNR 80−36697
- HD 44179 (Red Rectangle), obs. and interpretation of IR spectrum 77−78859
- He 2-111, planetary nebulae, giant halo with very high vels. discovery 79−25691
- He II 304 Å line redshifted to 1450 Å in far UV background 80−41893
- Heiles 2, interstellar dark dust cloud, HC$_5$N and HC$_7$N obs. 78−54023
- Heiles 2 interstellar dark cloud, NH$_3$ hyperfine struct. 77−78852
- Heiles Cloud 2, obs. of H I self absorpt. 77−29901
- Helix Nebula, abundance anomalies in planetary nebula 78−86001
- Herbig-Haro objects, radio obs. and nearby compact H II regions 80−51756
- Hercules X-1, 64 keV line feature in X-ray spectrum 77−78895
- Hercules X-1, high-energy X-ray spectrum 78−93473
- Hercules X-1, pulse phase spectroscopy, 6-60 keV 79−84870
- Hercules X-1, X-ray spectra, Fe line fluoresc. from subrelativistic shell 78−4405
- AM Herculis, OSO-8 X-ray obs., 2-250 keV energy range 79−71075
- 944 Hidalgo, UBV obs. of rotation and CN band not in spectra 77−5485
- high positive velocity H I clouds, 21 cm line profiles 77−13442
- high velocity clouds, line profiles and vels. rel. to intergalactic interpretation 77−41399
- high velocity H I clouds, fine struct. and 21 cm line widths 77−29898
- high-velocity H I clouds, map and vel. dispersions 80−26923
- hot optically thin plasma, soft X-ray spectrum, interstellar medium appl. 78−34275
- hyperfine structure, spectral anal. efficiency enhancement 79−66930
- Iapetus, dark and light faces refl. spectra 80−26800
- IC 10, irregular galaxy, H I envelope complex line profiles 79−67094
- IC 1318, giant H II region, large-scale line splitting discovery 78−96521
- IC 1795, HF C I recomb. line emission obs. 78−28748
- IC 1795 (W3), N II forbidden line unusual profiles over giant H II region 80−46645
- IC 2149, planetary nebula, near IR emission line fluxes 77−17669
- IC 2149, planetary nebula, two-photon emission of H in UV spectrum 77−22301
- IC 342, H$_2$O maser emission detect. 78−45417
- IC 342, Scd galaxy, H I radial vel. field and large-scale struct. 80−67857
- IC 342 companion galaxy, H I line obs. 80−36712
- IC 3568, planetary nebula, spectrum rel. to struct. and internal extinction 80−31338
- IC 418, IR spectra, heated dust emission, atomic emission lines 80−46629
- IC 418, near-IR obs. of planetary nebula 80−4421
- IC 418, planetary nebula, UV spectra and C abundance 80−67832
- IC 4329A, Seyfert galaxy, photographic photometry and optical spectrum 80−36706
- IC 4329A, spectrophotometry of extreme Seyfert, possible quasar 79−101190
- IC 443, supernova remnant, detect. of gas at 10^{6}K 79−53875
- IC 443, supernova remnant, Hα inteferometric obs. of fast filaments and high vel. gas 79−75258
- IC 443, supernova remnant, high-rel. gas Hα emission origin 80−41873

astronomical spectra continued
IC 4593, planetary nebula, emission line obs. 77—33621
IC 4593, planetary nebula, near IR emission line fluxes 77—17669
IC 4997, compact planetary nebula, rapid emission-line vars. origin 79—92838
IC 4997, O III 4363 Å forbidden line/$H\gamma$ intensity ratio vars. 78—86003
IC 4997, O III 4363 Å/$H\gamma$ ratio reversal in spectrograms of planetary nebula 79—92821
IC 4997, [O III] 4363 Å line intensity in variable planetary nebula 78—8100
instantaneous spectra determ. by inversion technique 80—82218
interacting galaxies, physical characts. *(Russian)* 77—57097
interference spectroscopy, Fourier decomposition technique appl. 77—49784
International UV Explorer satellite, obs. of sample targets 78—32315
interplanetary H, Lyman α radiation meas. with absorpt. cell spectrophotometer 78—28519
interplanetary H I, Lα emission profiles reanal. rel. to local interstellar gas temp. and vel. 80—105141
interplanetary He, dynamical effects in 584 Å reson. scatt. 80—8509
interplanetary magnetic field fluctuations, freq. spectra rel. to mean field direction 78—85905
interplanetary scintillations, radiosource size influence 79—25545
interplanetary scintillations spectra, influence of source sizes, obs. 80—46361
interstellar, gamma-ray energy spectra in 0.02-12.27 MeV range 77—2501
interstellar, SO, millimetre wave emission obs. 78—24535
interstellar *(Russian)* 80—36698
interstellar 10 and 20 μm absorpt. bands, comparison with Nogoya meteorite IR spectrum. 79—48741
interstellar 10 micrometer absorpt. band, comparison with phyllosilicates laboratory spectra 79—80344
interstellar 2175 Å band, rel. to elemental depletions in interstellar medium 78—36654
interstellar 2175 Å feature, strength rel. to C depletion 80—17638
interstellar 2200Å band, prod. by organic mols. in interstellar dust 77—57074
interstellar 2200 Å absorption band, detect. in meteoritic inclusions spectra 77—25987
interstellar ^{13}CO emission distrib. in galactic plane, rel. to giant mol. clouds distrib. in Galaxy 79—101183
interstellar λ4430 band, obs. in Carina Nebula, NGC 3603 and VI Cygni 78—32555
interstellar absorption band at 10 μ, curves of growth for terrestrial and meteoritic olivine particles 77—78846
interstellar absorption bands in O, B and A stars, polarized intensities 79—8915
interstellar absorption lines, fine struct. levels population ratios 79—35351
interstellar C II, line emission rel. to Cl chemistry and H ionisation 79—40245
interstellar C II region, narrow radio recomb. lines prod. around X-ray source 79—8972
interstellar C in mol. clouds, 492 GHz line detection 80—90508
interstellar C IV and Si IV column densities 80—73018
interstellar cloud towards gamma Arae, model from stellar spectra anal. 80—105312
interstellar clouds, cyanoacetylene and cyanodiacetylene obs. 80—46634
interstellar clouds, H_2 and C I absorpt. rel. to UV radiation field *(Russian)* 80—73026
interstellar clouds, non-linear relationships between N(Ca II), N(K I) and N(H) 79—92832
interstellar clouds, spectral line widths rel. to vel. fields 79—12398
interstellar CO^+, HCN^+, HNC^+, and CN^+ ions, radio search 78—24534
interstellar cyanodiacetylene, detect. of J=9 to 8 transition 77—91603
interstellar cyanodiacetylene (HC_5N), J=2-1 transition detect. 79—25692
interstellar cyanodiacetylene (HC_5N) $J=4\rightarrow3$ transition 80—22054
interstellar dark clouds, evidence for CO isotopic fractionation 80—46638
interstellar dark clouds with assoc. young stellar objects, radio obs. of mol. lines 79—58390
interstellar dark globules, IR surface brightness and emergent spectra 78—53999
interstellar dense cloud complexes, H I lines Zeeman splitting rel. to mag. fields determ. 79—5757
interstellar dense clouds, CO self-absorpt. towards embedded stars 77—53670
interstellar diatomic oxide grains, IR absorption features 78—49509
interstellar diffuse absorption bands, origin, transition metal ions in oxide grains 79—30101
interstellar diffuse absorption bands, origin in zero phonon lines in MgO and CaO 77—57073
interstellar diffuse bands, catalogue of meas. 77—64666
interstellar diffuse bands, origin in irradiated cosmic dust 77—13432
interstellar diffuse clouds, OH and HD column densities rel. to temps. determ. 78—93385
interstellar DNC detection, difficulties of chemical equilibrium hypothesis for D enrichment 77—82298
interstellar dust, IR and UV spectra of mixed oxide grains material 80—26934
interstellar dust grains, temp. fluctuations effects on far IR emission spectrum 80—26938
interstellar dust spectra, comparison with artificially condensed silicate dusts spectra 80—26940
interstellar ethylene oxide, possible detect. in Kleinmann-Low IR nebula 77—53662
interstellar excited H, decametric range radio lines search *(Russian)* 80—12822
interstellar extinction, 2200 Å extinction hump prod. by porous graphite grains 80—62228
interstellar extinction at UV wavelengths, role of biochemical chromophores 80—26945
interstellar extinction curve, comparison with visible and UV extinction of silicate, C and SiC smokes 80—82180
interstellar extinction feature at 220 nm and diffuse 443 nm band, ANS obs. 80—62244
interstellar faint optical emission lines, limits on temp. and ionization state of emitting gas 77—37634

astronomical spectra continued
interstellar formaldehyde, absorpt. spectra in four small dust clouds 77—5558
interstellar formaldehyde excitation, effects of microwave background radiation observed spectrum 80—36681
interstellar gas, local, in southern sky, single 21 cm component study 79—84834
interstellar gas, UV absorption line obs. of vel. distrib. 78—89235
interstellar gas properties from spectral line surveys 79—5879
interstellar grain composition constraints from 10 μm data 80—82471
interstellar grain mantle molecules, middle IR fluoresc. and absorpt. spectra 79—88716
interstellar grains, IR spectra compared to IR extinction of irradiated and amorphous olivine 79—53873
interstellar grains surface activity, adsorbed mol. ions rel. to diffuse spectral bands 77—26040
interstellar H_2, rot. transitions rel. to hot gases cooling 79—12505
interstellar H_2, vibrationally excited, search for 8150 Å emission line 78—93346
interstellar H_2O maser emission, new sources detect. 80—62298
interstellar H_2O masers in H II regions, time vars. obs. 79—88725
interstellar H_2O masers in NGC 6334, positions and spectra rel. to star form. 80—73025
interstellar H I survey from Lyman α absorption meas. towards 100 stars 78—93357
interstellar HCN, 3.5 mm line obs. rel. to isotopic abundance vars. 77—53657
interstellar HCN, absorpt. lines obs. towards Cassiopeia A 80—101624
interstellar HCN, DCN, rot. excitation by electrons 77—22292
interstellar HCO^+, shock enhancement of abundance in supernova remnant (IC 443) 80—82464
interstellar He, 584 Å obs. rel. to local density, correction 79—92834
interstellar high velocity cloud near ζ Orionis, density, temp. and comp. 77—22291
interstellar high-velocity gas clouds, abundance vars. 77—26039
interstellar ice, 45μm signature possible identification in Orion 79—17068
interstellar ionisation fronts, narrow radio recomb. lines emission 77—29940
interstellar IR spectra rel. to mol. form. in grain mantles, laboratory analogue expts. 80—26944
interstellar lines towards 15(=S) Monocerotis, UV obs. 80—90494
interstellar matter, hot component information from np^4 ions 80—83305
interstellar medium, 3.3 to 3.4 μm absorpt. and organic grains upper limit 79—21397
interstellar medium, far IR fine structure line obs. 80—62253
interstellar medium, radio emission obs. and temp. spectrum 77—17724
interstellar medium, role of H I Lyman-α 1216 Å flux 77—2459
interstellar medium Lyman α emission, line profile, temp. and polarisation from geocoronal absorpt. 77—67120
interstellar methanol in Orion A, two new transitions obs. 79—25667
interstellar methyl alcohol, obs. 79—25666
interstellar mol. cloud complex assoc. with bright rim near VY Canis Majoris, CO spectra 78—24536
interstellar molecular cloud near RCW 36, H_2CO and OH obs. 78—69862
interstellar molecular cloud struct. from 2 cm formaldehyde and 2.6 mm CO lines 79—80341
interstellar molecular clouds, 3.1 μm absorpt. attributed to amorphous H_2O ice 80—26956
interstellar molecular clouds, CO(J=2-1) emission obs. 79—92827
interstellar molecular clouds, CO rot. transitions obs. 77—33612
interstellar molecular clouds, detect. of new transitions of H, OCS and CH_2O, search for F 77—60808
interstellar molecular clouds, line profiles rel. to radiation transport and kinematics 78—93347
interstellar molecular clouds, microturbulence, systematic motions and spectral line form. 77—33586
interstellar molecular clouds, props. from molecular lines 77—57079
interstellar molecular line intensities, appl. to kinetic temp. and density determ. 79—97056
interstellar molecular transitions, rest freqs. 80—62218
interstellar molecules, Λ-doublets transitions induced by collisions with ions 80—14132
interstellar molecules, matrix isolation spectra, review 78—46340
interstellar molecules, RF emission spectra obs. towards ζ Ophiuchi 80—26958
interstellar molecules, vibr. excited, in grain mantles, IR emission lines 78—36670
interstellar molecules in grain mantles, IR absorpt. line interpretation 80—90504
interstellar NH_3, nonmetastable levels obs. 79—25665
interstellar NH_3 absorpt. in Sagittarius B2 direction 79—35341
interstellar O edge detectability and possible interp. 77—60811
interstellar O VI, spectroscopic tracer for hot interstellar gas, Copernicus obs. 78—16505
interstellar O VI absorption, rel. to 0.1-2.0 keV soft X-rays diffuse background 78—16581
interstellar OH, $^{16}OH/^{18}OH$ abundance ratio obs. in three H II regions 78—54024
interstellar OH main line maser pumping mechanism 80—67824
interstellar radio recomb. line emission, galactic plane obs. 77—13433
interstellar radio recombination lines, atomic b_n factors at low temps. 80—36696
interstellar radio spectrum lines, review 77—71138
interstellar resonance absorptions, polarisation reversals by small grains 79—2564
interstellar S_2, upper limits on abundance in mol. clouds 78—28738
interstellar Sc II in ζ Ophiuchi spectrum, abundance upper limit 80—82445
interstellar silicate absorption bands rel. to IR laboratory spectra of protosilicate particles 80—56907
interstellar southern molecular clouds, $^{12}C/^{13}C$ abundance ratio derived from H_2CO obs. 79—84838
interstellar submillimetric lines, possible detect. via laser heterodyne techniques 79—44377
interstellar thioformaldehyde (H_2CS), 3 GHz absorpt. transition obs. 80—67837
interstellar UV absorption lines due to ionized gas round galactic X-ray sources 77—13439

astronomical spectra continued
interstellar UV absorption lines in HR 1099 direction, Copernicus obs. 78—93358
intersteller CH, radio obs. 78—28751
intestellar medium, 2200 Å band rel. to heating by photoelectrons from O ions 78—36666
Io, absorpt. bands in near IR spectrum 79—5776
Io, evidence of SO_2 from UV obs. 80—36561
Io, implications of Na and K salts spectral refl. changes and luminesc. during proton bombardment 79—96950
IO, IR reflectance spectrum, absorption features 79—92706
Io, IR spectrum and intense transient brightening near 5 micrometres 79—101113
Io, Na I D_2 emission line profiles, var. with orbital phase angle and mag. latit. 78—4139
Io, Na I D-line emission synoptic obs. 77—13281
Io, Na spectrum and emission region morphology 77—49329
Io, periodic variations obs. in Na and K clouds 78—4138
Io, reflectance spectrum, evidence for sublimates and adsorbates 79—92707
Io, spectroscopic obs. rel. to colour changes and brightening upon eclipse reappearance 77—91469
Io, spectrum, S-containing mixtures and surface albedo 79—40127
Io, surface composition, comparison of observed and lab. reflectance spectra 77—60716
Io, UV spectrum rel. to global SO_2 abundance upper limit 80—77332
Io, visible spectrum, search for new features 79—35185
Io Na cloud, obs. rel. to Jupiter magnetosphere thermal electron density 79—40133
Io Na D-line emission, comparison of observed and theoretical line profiles 78—93145
Io plasma torus, radiative cooling and spectra 80—72850
Io plasma torus props. from Voyager EUV data 80—82262
IR heterodyne spectroscopy 78—85859
IR molecular line emission from grain surfaces in dense interstellar clouds 78—61905
IR source, obscured, in NGC 2264, spectrophotometric anal. and model 79—21370
IR source assoc. with Sh 2-149, spectral type and luminosity class 78—73772
IR sources, 10 μm silicate absorpt. band equivalent widths and dust temps. 78—57614
IR sources, 3 μm absorpt. identification with water ice questioned 78—49499
IR sources, effect of multiple grain components on radiation transfer and 10 micron silicate feature 78—36659
IR sources, extragalactic, spectra rel. to metagalactic IR flux 77—29964
IR sources, galactic, 3 μ spectral feature identification 80—62227
IR sources, galactic, IR fluxes calcs. for polysaccharide grain model 78—54008
IR sources, obs. of [O III] 88.35 microns and [O I] 63.2 microns for IR fine struct. lines 80—12794
IR sources, polysaccharides and related hydrocarbons identification 78—28763
IR sources, unidentified emission features, possible mechanism 80—82452
IR sources, unidentified spectral features review 80—26936
IR sources assoc. with double-lobed refl. nebulae, far IR continua 78—54009
IR spectroscopy, future objectives *(Italian)* 79—48686
IRC+10216, butadiynyl $N=12\rightarrow11$ doublet study 80—51829
JR features, laboratory simulation 80—26728
Jupiter, 5-8 μm spectrophotometry 77—29711
Jupiter, absorpt. bands in refl. sunlight rel. to atmospheric comp. and cloud struct. 80—56758
Jupiter, absorption band profiles and reflectivities during 1976 opposition 79—40124
Jupiter, atm. acetylene abundance 78—16337
Jupiter, atm. H_2 content from spectral line equivalent width *(Russian)* 78—12143
Jupiter, atmos. comp., IR spectral obs., 800-1000 cm^{-1} 78—16336
Jupiter, atmosphere, $^{12}CH_4(^{13}CH_4)$ ν_4 band, line parameters, 7.7 micron transmission 78—85894
Jupiter, atmosphere, $^{74}GeH_4$ transition moment for ν_3 79—72363
Jupiter, atmosphere, equatorial belt, spectrophotometry in 0.6-1.1 μm range 79—96960
Jupiter, atmosphere constituents, comparison with Saturn, visible spectra obs. *(French)* 80—101550
Jupiter, atmospheric CO obs. at 5 μm, airborne spectroscopic obs. 78—36491
Jupiter, C/H, $^{12}CH_4/^{13}CH_4$ ratios determ. from near-IR spectra 77—9698
Jupiter, C/H and D/H ratios from 8-9 μm IR spectrum 80—67638
Jupiter, CO IR spectrum and abundance 78—49374
Jupiter, D abundance from visible and IR spectrum 78—45265
Jupiter, D/H and C/H ratios from methane-d_1 spectrum 78—28572
Jupiter, decametric radio emission, dynamic spectra *(Japanese)* 79—8877
Jupiter, evidence for telluric value of $^{12}C/^{13}C$ atmospheric ratio 78—20723
Jupiter, far IR spectral obs. 77—29681
Jupiter, far IR spectrum, depend. on atm. vertical thermal struct. 77—60713
Jupiter, far IR spectrum showing NH_3 rotational bands 78—85891
Jupiter, far UV (1200-1900 Å) spectrum, rocket-borne multichannel spectrometer obs. 77—25974
Jupiter, GeH_4, ν_3 and 2 ν_3 bands, high resolution IR spectra 78—37636
Jupiter, H_2 quadrupole lines in spectrum 79—70990
Jupiter, H quadrupole absorption, spatial and temporal variations 77—37561
Jupiter, high spectral resolution obs. around 80 μm 78—45267
Jupiter, high spectral resolution obs. between 30 and 50 μm 80—46462
Jupiter, high-resolution IR spectra in 10.2-13.4 μm range 79—96947
Jupiter, IR and visible spectrum, C/H ratio 79—48729
Jupiter, L-bursts in decametric radio spectra 78—96424
Jupiter, Lyman α albedo, Copernicus UV obs. 80—94747
Jupiter, Lyman α emission var. with solar cycle 80—41759
Jupiter, Lyman alpha emission obs. rel. to auroral hot spots 78—16333
Jupiter, mean temp. struct. from far IR spectral obs. 80—17540
Jupiter, methane absorpt. interpretation 77—29707

astronomical spectra continued
Jupiter, methane and NH_3 bands, longitudinal variability, visible obs. 80—82270
Jupiter, methane and NH_3 bands spectropolarimetry, 6800-8200 Å 79—66955
Jupiter, methane band photometry, absolute reflectivity, centre-to-limb vars. 79—53759
Jupiter, methane line profiles near 1.1 μ as probe of cloud struct. and C/H ratio 80—62067
Jupiter, microwave spectrum of atmosphere 78—85889
Jupiter, near IR spectral albedo 80—31242
Jupiter, NH_3 abundance from 2 μ spectrum 79—35182
Jupiter, NH_3 abundance from visible obs. 80—82269
Jupiter, NH_3 spectral line meas. using 10μm superheterodyne receiver 78—16335
Jupiter, NH_3 vertical density profiles from IR and radioelectric emissivity data 80—82267
Jupiter, O^+ forbidden emission detect. in inner magnetosphere 80—51687
Jupiter, PH_3 absorpt. in 5 μm window 80—31243
Jupiter, S II forbidden line emission from thermal plasma 78—93146
Jupiter, S II forbidden line emission nebula studies 80—67636
Jupiter, S II forbidden line emission round planet, distrib. and intensity 80—85885
Jupiter, S II torus, longitudinal asymmetry visible spectra 80—82271
Jupiter, spectral emission of upper atm., Galatry profile 77—78642
Jupiter, spectrophotometric and polarimetric obs. *(Russian)* 77—71050
Jupiter, spectrophotometry in 0.6 to 1.1 μ region, Jovian atmosphere optical parameters latit. vars. 80—46468
Jupiter, spectrophotometry in far IR 78—85890
Jupiter, spectrum between 10 and 13 μ, Jovian $^{15}N/^{14}N$ ratio estimate 79—8876
Jupiter, thermal profiles and NH_3 distribs. from IR spectral meas. 79—40126
Jupiter, thermal radiation spectrum between 12 and 24 μ 77—17425
Jupiter, thermal structure from IR spectral meas., filtered iterative inversion method 78—7918
Jupiter, Voyager 1 EUV obs. 80—26792
Jupiter, Voyager 1 planetary radio astronomy obs. 80—26796
Jupiter, whistler mode noise spectrum in inner magnetosphere 78—89112
Jupiter and satellites, IR obs. from (Voyager 1) 80—26790
Jupiter atmosphere, GeH_4 abundance from IR spectrum anal. 78—61791
Jupiter atmosphere, trace constituents upper limits from 5 μm spectrum anal. 78—61790
Jupiter clouds spectropolarimetry, lines equivalent widths information content 80—31215
Jupiter decametre radio emission, dynamic spectrum modulation lines origin 80—67643
Jupiter decametric emission dynamic spectrum, nonlinear phase bunching effects 77—2366
Jupiter decametric radio bursts, polarisation patterns in dynamic spectra 77—5490
Jupiter decametric radio emission, S-bursts dynamic spectra 78—20722
Jupiter disc features spectral reflectivity, phase effect 80—98602
Jupiter H_2 2-O quadrupole spectrum in atm. 77—45351
Jupiter magnetosphere, S II obs. rel. to S plasma discontinuities 80—4291
Jupiter S-bursts, 32 MHz spectra and drift rates 78—36498
Jupiter spectrum, obs. from 1500 to 2000 Å with IUE 80—56752
Jupiter tropical and temperate belts, 0.6 to 1.1 μm spectrophotometry, brightness distrib. and atmosphere optical parameters 79—92715
K3-50, compact H II region, 2 to 4 micron spectrophotometry 77—13422
K3-50, H and He lines in obscured luminous H II region 80—51830
K3-50, ionized gas, IR and optical spectrophotometric meas. of compact H II region 79—53870
K648, halo planetary nebula, Ar III line obs. and low Ar abundance meas. 80—82443
K648, halo planetary nebula, spectrophotometry and element abundances 78—41011
K 648, halo planetary nebula, photoionisation models for line emission spectrum rel. to chemical abundances 80—109507
Kepler's SN 1604 remnant, spectrum 80—85982
Kepler's supernova remnant, X-ray obs. from Einstein Observatory 80—82465
Kerr black hole, low freq. EM and gravit. radiation spectra from infalling particle 80—62176
Kirchoff's laws of spectral analysis, computer laboratory exercises 78—73790
Kleinmann-Low nebula, nature of broad molecular line emission 77—5556
Kleinmann-Low nebula, optically thin CO emission 78—4315
Kleinmann-Low nebula, spectrum from 29 to 125 microns 77—33680
Kobayashi-Berger-Milon (1975IX), Swann band profiles 78—85909
L134 N interstellar dark cloud, NH_3 hyperfine struct. 77—78852
L1544, L1521B, interstellar clouds in Taurus, HC_5N detect. 80—26957
L1641 and Orion Nebula, submillimetre emission obs. 80—36685
BL Lacertae, spectrum and redshift 77—26055
BL Lacertae objects, absence of redshifted C IV absorpt. lines rel. to distances 80—62267
BL Lacertae objects, constraints on X-ray spectrum flattening from high-energy obs. 80—31353
BL Lacertae objects, radio structure and spectral index, reviews 80—46672
BL Lacertae objects, spectral flux distribs. from 0.36 to 3.5 micrometers 77—45537
BL Lacertae-type objects absorption spectra, effects of intervening galaxies 78—16561
Leonid meteors, spectral analysis 79—16890
AP Librae, BL Lacertae object, emission line obs. in (1976) 77—29932
lifetime meas. astronomical applications, beam-foil method 77—41313
line broadening by electron scatt., calc. methods *(Russian)* 77—17347
line broadening by photon interaction with new field and red shifts 79—48663
line formation, asymptotics of partial redistrib. in non-LTE radiative transfer 80—62008
line shifts, variational study *(French)* 79—75093
LkHα 101, IR spectra of emission line object, preplanetary disc obs. 78—16423
LMC, Apollo 17 far UV spectra 77—13461
LMC, dynamics of giant interstellar shells from line profiles 80—46674

astronomical spectra continued
LMC, interstellar 4428 Å feature 79−35335
LMC OB associations, Apollo 16 for UV spectra 77−33634
LMC X-2, spectrogram confirms optical counterpart 79−21463
luminous obscured galaxy assoc. with G127.11+0.54, optical spectroscopy and photometry 80−31371
lunar mare grounds relative spectral reflectivity 80−12695
Lupus Loop, X-ray spatial extent and spectrum of SNR 80−82457
Lyman α sky background, Copernicus high-resolution obs. 77−29963
M101, extended H I envelope spectrum and vel. field 79−62904
M101, spectra of H II regions, comp. gradient across spiral galaxy 78−65683
M101 companion galaxies, H I spectra and integral props. 78−49532
inner M101 galaxy group, H I spectra rel. to galaxies total masses 80−67885
M15, globular cluster, core, $H\alpha$ and continuum obs. 79−17031
M16, O III 5007 Å forbidden line profiles from core of H II region 79−8976
M17 (Omega Nebula), O III 51.8 μm forbidden emission line obs. 79−25685
M17 SW, obscured IR point source spectroscopic anal. 79−48878
M1-67 possible H II region, internal motions 79−92841
M1-76, possible forbidden line BQ star rather than planetary nebula 79−84847
M1-92, bipolar nebula, OH emission obs. 78−41016
M31, H I emission in SW region 80−51873
M31, high-resolution H I obs., spectra and major axis rel. plots 78−41057
M31, inner nuclear regions, spectral features and dwarf content 78−86005
M31, line intensity distrib., contour maps, vel. profiles, 21 cm HI line survey 80−73038
M31, M32 nuclei, luminosity-sensitive spectral features obs. 78−49431
M31, reddening of 22 H II regions 79−71082
M31, vel. dispersions in nucleus and bulge 77−26049
M31 and M32, IUE spectra of nuclei 79−71117
M31 and M32, Na I 8190 Å absorption feature equivalent widths 80−51862
M31 and M81 nuclei, UV continua, spectrophotometry obs. from ANS satellite 80−77478
M32, absolute spectrophotometry rel. to galaxy spectral synthesis and age 80−67842
M32-1, planetary nebula in M32, spectrophotometry and filter photometry 79−25664
M32-1, planetary nebula in M32, spectroscopic evidence that M32 is in front of (M31) 78−93394
M33, 4850 MHz radiocontinuum emission and radio spectral index 78−28783
M33, detect. of H_2O maser emission 77−29926
M33, ionisation of interarm medium 77−67131
M33 H I tail, obs. rel. to adjacent high-vel. H I cloud 80−12815
M4-18, emission line spectra of peculiar planetary nebula 79−84846
M4-18, spectroscopic obs. of compact planetary nebula 80−67829
M51, high resolution obs. at 21 and 49 cm and spectral index 77−29921
M51, radio spectral index distrib. 78−8119
M81, spectrum and kinematics of gas in nuclear disc 77−9795
M82, $H125\alpha$ recomb. line, SHF obs. 80−82486
M82, H 102α radio recomb. line detect. 77−49476
M82, nature of radio recomb. lines in extragalactic sources 78−45418
M82, Ne II 12.8 micron emission obs. and galactic dynamics 79−17082
M82, nuclear source nature from IR obs. 80−82485
M82, stimulated recomb. line emission obs. 77−41408
M82 as exploding radiogalaxy, image tube spectrogram evidence 78−69880
M82 nucleus, λ6 cm formaldehyde absorpt. detect. 79−17088
M82 nucleus, Brackett-line obs. 79−25704
M82 nucleus, compact radio source size-spectrum relationship from VLBI obs. 80−22078
M83, H II regions spectral characts. and chemical abundances 80−56927
M87, high-resolution X-ray spectroscopy, O VIII emission line detect. 80−26977
M87, interstellar gas vel. dispersion rel. to presence of large central mass 80−94873
M87, spectroscopic obs. of galaxy nucleus 79−92858
M87, spectrum rel. to vel. dispersion and central mass concentration 78−49529
M87, UV spectrum, IUE obs. 80−82502
M87 (NGC 4486), vel. dispersion from a population model 80−77490
M87 halo, Compton-scattered X-ray spectrum calc. from radio emission Faraday rot. 80−67844
M87 jet knots, polarisation, spectroscopic and radio props. 80−12817
M87/Virgo cluster X-ray source spectrum, 1.1 keV Fe line emission discovery 79−25758
M8, radio recomb. line obs. at 5 and 10 GHz 79−84832
M8, spectra of IR sources, evidence for silicate absorpt. 77−64817
M8 (Lagoon Nebula), far IR obs. 80−4413
M 1-2, planetary nebula, emission line obs. 77−33621
M 33, H_2O maser emission detect. 78−45417
M 81, CO emission upper limits 78−36693
Maffei 2, CO emission obs. 78−16530
Magellanic Cloud supernova remnants, forbidden O II spectra rel. to optical emission from shocks 79−92831
Magellanic Clouds, UV brightness maps and UV spectra 80−85994
magnetic null line tables for elements of astrophys. interest 77−70998
major planets, effects of Raman scatt. in atmospheres 78−28571
Markarian 132, spectrum and redshift systems 78−89248
Markarian 205, spectrum and redshift of nearby condensation rel. to distance 79−97058
Markarian 231, IR emission obs. 77−5570
Markarian 231, Seyfert galaxy, spectra, photometry and electronograph 77−45558
Markarian 231, Seyfert galaxy, substructure with UV excess, UV and visible obs. 80−82512
Markarian 296, clumpy irregular galaxy, spectroscopic and 21 cm line investigations 79−44608
Markarian 298 (=IC 1182-4) central condensations, spectral energy distribs. *(Russian)* 78−57641
Markarian 325, irregular galaxy, emission clumps observational props. 80−67869

astronomical spectra continued
Markarian 335, Seyfert galaxy, spectroscopic investigation *(Russian)* 79−101204
Markarian 348, Seyfert galaxy, spectrophotometry 79−88735
Markarian 359, peculiar emission line spectrum 79−17075
Markarian 374, Seyfert galaxy, spectra of double nucleus components 78−69882
Markarian 3, 231, Seyfert galaxies, optical emission lines polarisation 80−90533
Markarian 3, class 2 Seyfert galaxy, visible spectra obs. 80−85999
Markarian 421, BL Lacertae object, X-ray spectrum index vars. 79−48921
Markarian 421, X-ray spectrum change in BL Lacertae-type object 79−101196
Markarian 464, type I Seyfert galaxy, Ariel V X-ray spectra 80−90539
Markarian 501, UV and X-ray obs. of BL Lacertae-type object 80−36717
Markarian 59 , supergiant H II region in SBm galaxy NGC 4861 spectrum and struct. 80−98705
Markarian 668 (=OQ 208), Seyfert, $H83\alpha$ and $H99\alpha$ radio recomb. lines detect. 80−94864
Markarian 79, analysis of spectra of type 1 Seyfert 79−71103
Markarian 79, Seyfert galaxy, IUE and visual spectrophotometry 79−92856
Markarian galaxies, 3.2 mm and IR continuum obs. 77−22317
Markarian galaxies, emission line intensities depend. on colour index *(Russian)* 77−17672
Markarian galaxies, radio continuum obs. at 1410, 2380 and 5000 MHz 80−46668
Markarian galaxies, radio spectra 77−37647
Markarian galaxies, spectroscopic obs. *(Russian)* 77−49465
Markarian galaxies with broad emission lines, spectroscopic obs. *(Russian)* 77−45567
Markarian II, 180 and 421, spectra of stellar population 78−54047
Markaryan 372, $H\beta$ profile of Seyfert galaxy 80−26972
Markovian 297, IUE UV spectra of clumpy irregular galaxy 80−26981
Mars, atm. O_3 vertical distrib., Mariner 9 UV spectral obs. 79−66952
Mars, CO_2 IR heterodyne spectroscopy 77−41344
Mars, CO 15 GHz microwave line detect. 77−74000
Mars, disc IR spectra compared with terrestrial analogues optical props. 78−85879
Mars, far IR spectral obs. 77−29681
Mars, N_2 UV dayglow prediction 77−53452
Mars, near IR spectral reflectance, surface comp. determ. 79−21216
Mars, reflectance spectroscopy rel. to surface comp. 80−72834
Mars, surface struct. from optical and IR refl. spectrum and thermal props. 77−29690
Mars, UV spectra and photometry by TD1A and OAO-2 satellites 77−91459
Mars atmosphere, absorpt. spectrum rel. to thermal radiative transfer numerical modelling 80−8574
Mars atmosphere thermal IR properties, dust and ice clouds detect. from Viking IRTM spectral meas. 79−84712
Mars surface, Viking lander sites spectral reflectance and colours 78−85881
Mars upper atmosphere, H Lyman α radiation meas. with absorpt. cell spectrophotometer 78−28519
Martian atmosphere, W.W. Campbell's spectroscopic study 77−71047
massive black holes, X-ray spectrum from disc accretion 78−40985
MC2 and MC3 sources, radio spectra and optical identification 77−33670
MC5 1307+121, BL Lacertae object, radio spectrum shape, VHF and SHF obs. 80−67866
MCG−6-30-15, type 1 Seyfert galaxy, X-ray and optical obs. 80−82479
MCG 8-11-11, Seyfert galaxy inside error box of 2A0551+466, optical spectra 77−74130
MCG -5-23-16, spectroscopic obs. of possible X-ray source 78−45404
MCS 141, 232, 275, quasars, spectra interpretation, visible obs. 80−90562
metagalactic nuclei, ultrahigh-energy, spectrum calc. 77−53342
meteor, fast sporadic spectrum 78−93170
meteor bright line spectra, study via astronomical TV system 78−61817
meteor trails televised spectra, photometry 78−20764
meteors, N_2^+ 4278 Å bands in spectra, quantitative anal. 78−45290
meteors, O I 5577 Å emission, vel. dependence 78−20758
meteors, spectral line excitation in faint trains 79−35197
meteors photographic spectra, identification of air radiation 77−29733
meteors television spectra, prod. and study 77−67076
methane, 4350-10600 Å bands, intensity profile, vibr. assignments, rel. to major planets spectra 78−42084
methane, absorption and press. coeffs., 4500-10500 Å, band model calcs., astronomy appls. 77−83593
methane, liquid, laboratory optical absorpt. spectra rel. to detectability on outer planets 80−93278
methane(-H_2), long path photoelec. absorpt. spectra 4200-10600 Å, appl. to Uranus 77−83592
methane 6819 Å line interpretation rel. to inhomogeneous scattering models for Uranus and Neptune 78−53871
methyl formate, microwave spectra, rot. consts., moments and struct., radio astronomy appl., review 80−17637
microwave background, interaction with crosmic ray protons, Hubble radius 77−87211
microwave background, spectrum distortions 80−62334
microwave background longward of 3 mm, spectral distortions 80−62326
microwave background polarization transport in anisotropic universes 78−8174
microwave background radiation, influence of observed spectrum on interstellar formaldehyde excitation 80−36681
microwave background radiation, temp. and spectrum rel. to universe origin 79−25770
microwave background radiation spectrum, effect of interstellar dust and molecules *(Russian)* 80−8719
microwave background radiation spectrum, statistical anal. of data 78−86039
microwave background rel. to cosmic dust density limit 77−17653
microwave background spectrum, survey of results 78−28864
microwave background spectrum 80−105406
microwave background spectrum distortion by dust 80−27022
Milky Way, H radio recomb. lines obs. at 8.87 GHz near (l=333°) 80−22102

astronomical spectra continued
MIT/OSO 7 catalogue of X-ray sources, intensities, spectra, long-term vars. 79−80243
mm emission from extragalactic objects, luminosities, spectra, microwave background contrib. 77−17677
mm radio spectra, baseline ripple reduction by quasi-optical phase modulation 80−56710
mm wavelength spectral lines detectability from planetary atms. 79−5769
molecular spectra, predicted radioastronomical freqs. accuracy, determ. from OH spectrum 79−48666
Molonglo catalogue sources selected at 408 MHz, radio spectra 77−5583
Molonglo southern radio sources, optical spectra 78−96555
Monoceros R2, IR obs. of CO line 79−25654
Monoceros R2 cloud, near IR and mol. obs. of rot. collapsing cloud 77−78840
Moon, far UV spectrum and albedo, Apollo 17 meas. 77−37513
Moon, microwave spectrum, effect of subsurface inhomogeneities 77−82133
MR 2251−178, X-ray QSO, spectrophotometric obs. 79−17122
MSH 11-54 (H1122−59), supernova remnant, X-ray spectrum 80−82463
MSH 14−63, probable remnant of A.D. 185 supernova, X-ray spectrum 78−45427
MWC 349, IR spectra of emission line object, preplanetary disc obs. 78−16423
N132 D, SNR in LMC, rapidly moving material, visible and UV solns. 80−82449
N132D, supernova remnant in LMC similar to Cassiopeia A, photographic and spectroscopic study 78−93345
N51D, giant filamentary shell in LMC, nature and dynamics 80−105343
N70, giant filamentary shell in LMC, line profiles rel. to dynamics 80−90511
N-type galaxies, optical spectra 79−40258
NAB 0137−01, spectrophotometry of possible X-ray quasar 77−13490
near IR mapping spectrometer design and testing for Galileo Jupiter Orbiter 80−90336
nebulae, dusty, lines surface brightnesses in non on-the-spot (OTS) models 78−85995
nebulae, emission lines due to interstellar dust in visible spectra 79−53874
nebulae, emission-line spectrum from a slab of hydrogen at moderate to high densities 80−72759
nebulae, forbidden O III lines as quantitative indicators of central stars temps. 78−41015
nebulae, He^+ radio recombination lines, stimulated emission 78−8092
nebulae, N and O line intensities rel. to abundances 78−8093
nebulae, photoelectric spectrophotometry of compact objects 78−89236
nebulae, UV radiative pumping of N^+ fine structure levels 79−53871
nebular complexes, radio spectra of thermal and nonthermal components 77−57101
Neptune, 5-20 micron obs. 78−32393
Neptune, evidence for optically thin high-altitude cloud form. 77−53469
Neptune, IR refl. spectrum, evidence for weather 77−53468
Neptune, IR spectrum from 0.8 to 2.5 microns 80−21946
Neptune, methane 6825 Å band obs. 77−78715
Neptune, methane and ethane emission detect. 78−16344
Neptune, rot. period from spectral line tilts 78−20726
Neptune, UV albedo wavelength var. 80−82295
Neptune reflected spectrum, effects of seeing rel. to rot. period determ. 80−46479
Neptune rotation period, correction, photometric and spectroscopic results comparison 80−82301
neutrinos spectra, role of neutral currents and neutrino Comptonisation in high-temp. nuclear matter 80−21905
NGC 1023 galaxy group, H I obs. and possible intergalactic H I cloud discovery 80−67886
NGC 1052, elliptical galaxy, electron density and N II/$H\alpha$ line intensity ratio in nucleus 77−33642
NGC 1052, elliptical galaxy, H I 21 cm spectrum and rot. 78−69873
NGC 1055, 681, 4594, galaxies, optical spectra rel. to rot. curves and mass distribs. *(Russian)* 80−90541
NGC 1068, Seyfert galaxy, 2-2.5 μm spectrum, H_2 detect. 78−57636
NGC 1068, Seyfert galaxy, forbidden O III lines high-resolution profile 80−46665
NGC 1068, Seyfert galaxy, nucleus, radiation spectrum rel. to H_2 existence and form. 80−12816
NGC 1068, Seyfert galaxy, radiative transfer in dust rel. to spectral flux distrib. 77−29914
NGC 1068, Seyfert galaxy, silicate emission feature from IR photometry 78−54035
NGC 1068, type 2 Seyfert, recombination spectrum and reddening 80−90519
NGC 1275, ionization and excitation mechanisms in surrounding filaments 79−71107
NGC 1275, photometric and spectrum vars. 80−22075
NGC 1275, Seyfert galaxy, emission line variability and nucleus conditions 77−37649
NGC 1275, Seyfert galaxy, nucleus, emission line intensities rel. to gas and radio source structs. *(Russian)* 79−48936
NGC 1275, Seyfert galaxy, spectroscopic obs. *(Russian)* 77−17670
NGC 1275, Seyfert galaxy, vars. of emission line spectrum and conditions in nucleus envelope 77−17688
NGC 1275, spectroscopic and photometric obs. 77−33630
NGC 1275 as BL Lacertae object, evidence from spectrum 78−45406
NGC 1275 as pair of interacting galaxies, spectra and structure 80−26969
NGC 128, S0 galaxy, spectra and rot. curve 77−33631
NGC 1365 and 1386, optical spectrophotometry of emission-line galaxies 80−51867
NGC 1499 (California Nebula) ionisation front, CO obs. and vel. struct. 78−24537
NGC 1566, Sbc galaxy, spectrophotometry of nucleus and nine H II regions 80−51824
NGC 1851, 6624, globular cluster, abundance gradients spectroscopic investigation 80−82437
NGC 2023, reflection nebula, far IR study 80−51831
NGC 2024, H II region, recomb. line obs. of nearby partially ionised medium 77−57077

astronomical spectra continued
NGC 2024, HF C I recomb. line emission obs. 78−28748
NGC 2024 (Orion B) nebula, CO J=2 to 1 line obs. 80−8673
NGC 2110, Seyfert 2 X-ray galaxy, optical studies 80−22071
NGC 2264, N II forbidden line unusual profiles over giant H II region 80−46645
NGC 2366 H II region visible and radio obs. 80−77475
NGC 2467, H II regions complex, $H\alpha$ spectrum and internal motions 77−22304
NGC 2536, spiral galaxy, radial vars. of emission line ratios 80−82497
NGC 253, Ne II 12.8 μm emission and galactic dynamics 79−92844
NGC 253, nuclear source nature from IR obs. 80−82485
NGC 253, Sc-type galaxy, two-micron spectrophotometry 80−4442
NGC 253, spiral galaxy, spectrum rel. to nuclear gas outflow and stellar population 78−28776
NGC 2623, interacting galaxy, H I absorpt. and emission obs. 79−17087
NGC 2715, 5033, 5055, rot. curves and orientation parameters 79−12517
NGC 2742, spiral galaxy, rot. and mass. *(French)* 78−89255
NGC 2776, rotation and mass from image-tube spectra of Sc galaxy *(French)* 79−101199
NGC 281, H II region, CO and H_2O spectra 78−28740
NGC 281, H II region, CO and H_2O spectra rel. to shock-induced star form. 79−25688
NGC 2903, spiral galaxy, nucleus identification and visual energy distrib. 80−62273
NGC 2915, southern galaxy, spectrum and red shift 77−67126
NGC 2974, 4105, 5846, elliptical galaxies, H I contents and line widths 79−62906
NGC 2997, late-type galaxy, spectrum, rot. and mass 79−21409
NGC 3115, galaxy, line strengths rel. to optical and IR photometry 78−36683
NGC 3115, S0 galaxy, rotation and mass of inner 5 kiloparsecs 80−105326
NGC 315, NGC 6251, very large radio galaxies, 11.1 cm obs. rel. to spectral index vars. 78−86014
NGC 3227, 3516, Seyfert galaxies, optical emission lines polarisation 80−90533
NGC 3227, Seyfert galaxy, photoelectric and spectroscopic study and comparison with galaxy chain (VV 150) 80−98724
NGC 3242, 7009, 6210, high excitation planetary nebulae, high dispersion EUV obs. 80−77466
NGC 3242, UV emission lines, Copernicus obs. of planetary nebula 79−12501
NGC 3256, peculiar galaxy, kinematics from emission lines meas. 78−96537
NGC 3372, H II region, forbidden O III emission obs. rel. to η Carinae location 80−4383
NGC 3379, elliptical galaxy, spectroscopic obs. rel. to rot. and vel. dispersion 78−49529
NGC 3448, optical and H I 21 cm line obs., peculiar nucleus 78−36696
NGC 3516, SBO type Seyfert galaxy, extended nebulosity, UV and visible obs. 80−82487
NGC 3516, Seyfert galaxy, charge transfer reactions rel. to low excitation forbidden line 80−56701
NGC 3516 Seyfert galaxy, optical spectrum 77−26052
NGC 3556, edge-on galaxy, multi-freq. radio continuum study, spectral index distrib. 79−44607
NGC 3620, southern emission-line galaxy at low galactic latitude 78−86022
NGC 3686 galaxy quartet, spectra and rot. curves rel. to mass distribs. and group stability 80−62297
NGC 4088, rotation curve and mass of spiral galaxy *(French)* 78−36698
NGC 4151, Seyfert galaxy, for UV line profiles 80−22083
NGC 4151, Seyfert galaxy, gamma-ray emission, Compton scatt. model 80−98711
NGC 4151, Seyfert galaxy, low energy gamma-ray obs. 78−12368
NGC 4151, Seyfert galaxy, low-energy γ-ray spectrum 80−31370
NGC 4151, Seyfert galaxy, nuclear region far UV spectrum 78−32573
NGC 4151, Seyfert galaxy, UV spectrum 77−13468
NGC 4151, Seyfert galaxy, X-ray spectrum, Uhuru obs. 78−12411
NGC 4151, UV photometry and extended spectrum of Seyfert galaxy 78−89249
NGC 4151 (4U 1206+39), Seyfert galaxy, hard X-ray spectrum 78−49537
NGC 4214, barred Im galaxy in Canes Venatici I group, H I obs. 79−92862
NGC 4235, Seyfert galaxy, spectrum and radial. vel. 78−49536
NGC 4248, galaxy, H I spectrum and radial vel. 78−4358
NGC 4378, anaemic Sa galaxy, spectrum, photometry and extended rot. curve 79−8990
NGC 4473, flattened elliptical galaxy, spectroscopic obs., dynamics 78−57631
NGC 4485/90 interacting galaxies, radio continuum and H I obs. 80−62274
NGC 4593, Seyfert galaxy, spectrophotometry 80−51878
NGC 4631, edge-on spiral galaxy, radio continuum halo obs. 77−26054
NGC 4636, elliptical galaxy, H I line profile and large-scale distrib. 78−45400
NGC 4762, S0 galaxy, rot. curve from Ca II absorpt. lines 78−28774
NGC 488, Sb galaxy, rotation curve from emission line spectra 80−62266
NGC 4945, galaxy, water vapour emission obs. 78−93427
NGC 4945, late-type spiral galaxy, spectrum rel. to excited gas kinematics 80−109547
NGC 4945, spiral galaxy, H I absorpt. obs. 77−33651
NGC 5128, H I, OH and formaldehyde absorpt. line obs. in lenticular galaxy 77−33649
NGC 5128 (Centaurus A), formaldehyde absorpt. obs. at 14 GHz 80−17657
NGC 5128 (Centaurus A), high-resolution spectroscopy and tubelike model of dust band 80−56945
NGC 5128 (Centaurus A), struct. and evolution from photographic and spectroscopic obs. 80−4429
NGC 5128 (lentaurus A), image tube spectrograms 80−41892
NGC 5195, M51 companion galaxy, spectrum rel. to rot. and relative mass 77−22306
NGC 520, Irr II galaxy, new photographic and spectroscopic obs. 80−41889

astronomical spectra continued
NGC 5236, spiral galaxy peculiar nucleus continuum and reddening 80−73031
NGC 5236 (M83), Sc galaxy, CO emission distrib. and vels. 78−65689
NGC 5291, massive gas-rich peculiar lenticular galaxy in IC 4329 cluster 79−71127
NGC 5383, barred spiral galaxy, optical and H I spectra rel. to vel. field 78−24549
NGC 5506, X-ray Seyfert, spectra 78−93411
NGC 5728, barred spiral, vels. and mass distrib., visible spectra obs. 80−94863
NGC 5907, rotation and mass of edge-on galaxy from spectra *(French)* 78−77595
NGC 604, 5471, giant extragalactic H II regions, IUE UV spectra 80−77467
NGC 604, H II region in M 33, Hα line profile width rel. to core-halo struct. 80−85984
NGC 6052, possible collision of two late type spiral galaxies, observational evidence 80−8681
NGC 6210, 6543, 6572, planetary nebulae, spectroscopic obs. using multi-channel analogue detector system 78−36461
NGC 6210, planetary nebula, near IR emission line fluxes 77−17669
NGC 6217, spectra of galactic nucleus *(Russian)* 79−92869
NGC 6221 and NGC 7213, optical spectrophotometry of X-ray galaxies 79−35377
NGC 6240, unusual radio galaxy, radio and optical spectra 80−4440
NGC 6251, very large radio galaxy with exceptional jet, radio spectral index 78−12394
NGC 6302, emission nebula, forbidden Ne V 3426 Å wings rel. to energetic stellar wind 80−67835
NGC 6302, line profiles from ionised and neutral gas in peculiar nebula 78−12341
NGC 6302 chem. composition of planetary nebula 78−96525
NGC 6334, CO spectra and detailed struct. in mol. cloud complex 78−4324
NGC 6334, relationships of N_2H^+, HCO^+, HCN and CN 77−33587
NGC 6357A, O III 51.8 μm forbidden emission line obs. 79−25685
NGC 650/1, planetary nebula, emission line profiles and internal kinematics 80−17639
NGC 6543, planetary nebula, emission line obs. 77−33621
NGC 6572, 6891, 7662, near IR spectrophotometry of planetary nebulae 78−8105
NGC 6572, IR spectra, heated dust emission, atomic emission lines 80−46629
NGC 660, barred spiral galaxy, spectra and kinematics 77−5566
NGC 6720, O III 5007 Å forbidden line obs., vel. structure of planetary nebula 78−61909
NGC 6720 (Ring Nebula), strong forbidden N II emission and element abundances 77−26035
NGC 6745, peculiar ring-like galaxy, struct. *(Russian)* 79−25732
NGC 6822, galaxy, CO emission upper limits 78−36693
NGC 6853, planetary nebula, spectroscopic obs., element abundances 77−53667
NGC 6853 (Dumb-bell Nebula), emission line profiles rel. to neutral and inoised gas motions 78−24539
NGC 6853 (Dumbbell Nebula), ionization and abundances 78−45390
NGC 6888, around Wolf-Rayet star HD 192163, IUE obs. of absorpt. by hot gas 79−53896
NGC 6888, circumstellar nebula, spectroscopic investigations 77−57076
NGC 6888, emission nebula, forbidden N II/Hα ratio 79−8964
NGC 6888, filamentary nebula, optical spectra calc. 80−105304
NGC 6888, ring nebulae around Wolf-Rayer star HD 192163, spectra of filaments and smooth gas *(Russian)* 80−90515
NGC 6946, galaxy, radio continuum spectrum of nonthermal disc 77−41407
NGC 6946, spiral galaxy, N overabundance in nucleus *(French)* 78−89257
NGC 7000 (North America Nebula), rocket UV imagery 80−82440
NGC 7000/IC 5070 (North American/Pelican) nebular complex, Hα/[N II] ratios and obscuration 78−36667
NGC 7009, spectral comparisons of ring and ansae 79−71101
NGC 7027, 16-38 μ spectral obs. and dust model of planetary nebula 78−93354
NGC 7027, IR spectrum of planetary nebula 77−22297
NGC 7027, planetary nebula, 0.9-2.7 μ spectrum 77−2461
NGC 7027, planetary nebula, 3.3 microns unidentified feature, high resolution spectra 80−82466
NGC 7027, planetary nebula, anal. of low excitation emission lines 77−64823
NGC 7027, planetary nebula, C abundance 77−87526
NGC 7027, planetary nebula, charge transfer reaction rate rel. to forbidden Ne II 12.8 μ emission 80−56701
NGC 7027, planetary nebula, effect of dust on [O II] emission 80−8667
NGC 7027, planetary nebula, far IR obs. 77−22288
NGC 7027, planetary nebula, forbidden Mn V transitions identification 78−50496
NGC 7027, planetary nebula, H_2 emission spatial distrib. obs. 80−98698
NGC 7027, planetary nebula, He I 2.0 μm line strength rel. to He I 584 Å transfer problem 80−67550
NGC 7027, planetary nebula, ionization struct. and comp. 78−28745
NGC 7027, planetary nebula, line intensity ratios rel. to density gradient 77−87513
NGC 7027, planetary nebula, radio recomb. line obs. 77−9780
NGC 7027, planetary nebula, struct. from electronographic obs. 80−12789
NGC 7027, planetary nebula, UV emission line spectrum rel. to interstellar reddening, IUE obs. 78−96524
NGC 7027, planetary nebula, UV spectrum rel. to physical conditions and CNO elements abundances 80−82459
NGC 7027, planetary nebula 4 to 8 micron spectrum 78−12333
NGC 7027, planetary neubla, near IR obs. 78−73748
NGC 7027, S III 18.7 μ fine-struct. forbidden line obs. 77−37637
NGC 7027, S IV and Ne II IR emission line obs. of planetary nebula 79−21400
NGC 7027 and NGC 7293, spectral obs. of planetary nebulae *(Russian)* 78−61897
NGC 7213, S0 galaxy with Seyfert nucleus, spectra and direct obs. 78−86024
NGC 7293, Helix Nebula, O III 5007 Å forbidden line splitting 79−25694

astronomical spectra continued
NGC 7293 (Helix Nebula), planetary, obs. of [O I] λ6300 vel. field 78−12340
NGC 741, 1316, 7626, radio galaxies, optical spectra and dynamics 80−94871
NGC 7469, Seyfert galaxy, spectrum 77−57089
NGC 7538 (IRS 1+2), compact H II region, 2 to 4 micron spectrophotometry 77−13422
NGC 7538 and Sherpless 159, H II region/mol. cloud complex, H I aperture synthesis obs. 80−90510
NGC 7541, rotation curve and mass distrib. in spiral galaxy *(Russian)* 80−94874
NGC 7582, narrow emission line X-ray emitting nucleus, UV spectra 80−101640
NGC 7635, Bubble Nebula, line intensities 77−33605
NGC 7662, Ne IV forbidden $^2D \rightarrow {}^4S$ lines obs. in UV spectrum of planetary nebula 79−48896
NGC 7662, planetary nebula, photoionisation model with charge transfer reactions rel. to emission-line spectrum 80−62233
NGC 7662, planetary nebula, rocket UV spectrum and models 78−28746
NGC 7793, late-type galaxy, ionized gas phys. conditions and mass-luminosity distrib. 80−26967
NGC 7822, NGC 281, bright rimmed mol. clouds, CH obs. 80−62238
NGC 7822 (W1) optical studies of kinematics rel. to supernova remnant struct. 78−54028
NGC 7822 (W 1), supernova remnant, radio spectrum 78−4383
NGC 891, edge-on disc galaxy, radio continuum spectral index distrib. 78−28786
NGC 925, barred spiral galaxy, high-resolution H I spectra and vels. 80−105329
NGC 931, interacting Seyfert galaxy, struct. and spectra 79−25716
NGC 935-IC 1801, close pair of spiral galaxies, rot. curves and mass distribs. 77−45556
NHC 2768, galaxy, line strengths rel. to optical and IR photometry 78−36683
NHC 4594 (Sombrero Galaxy), H II regions and ionised interarm gas detect. 78−36685
nightglow continuum between 0.8 and 1.1 μ, Soviet obs. 78−81483
non-uniform gas at high z, spectral appearance 79−92898
nonlinear inverse Compton radiation spectrum, deepest descents method 78−85840
North Polar Spur, SNR, soft X-ray spectra emission line features obs. 80−94849
OAO 1653−40, pulsating hard X-ray source spectrum and position 79−67118
objective-prism spectra meas., computer control of Joyce-Loebl microdensitometer 80−105173
OH 205.1−14.1, unusual OH maser, left circularly polarised 1667 MHz line obs. during flare 80−98734
OH 471, OX 057, quasars, millimetre wave spectra and variability *(Russian)* 80−90559
Omega Nebula (M17, W38, NGC 6618), S III, O III, N III, IR obs. 80−90495
Omega Nebula (M17), O I 63 μm forbidden emission line obs. 79−25684
Ooty occultation extragalactic sources radio spectrum obs. in SHF 80−105371
ζ Ophiuchi cloud, Copernicus UV obs. of interstellar C_2 78−41022
ρ Ophiuchi dark cloud, ^{13}CO self absorpt., EHF obs. 80−90500
ρ Ophiuchi dark cloud, atomic and mol. obs. 78−41013
ρ Ophiuchi dark cloud, C II and S II recomb. line spectra 78−49500
optical counterparts of 5C radiosources and blue objects, spectrographic obs. 79−101212
optical quasars, radio and optical obs., redshifts, luminosity function 78−49552
OQ 172, H_2 lines identification in spectrum of quasar *(Russian)* 78−69905
OQ 172, quasar, H_2 lines in absorpt. spectrum 80−36734
OQ 208, red shift difference between broad and narrow emission lines 79−67100
OQ 208 (Markarian 668), radio spectrum 79−12531
Orion, Nebula 77−5557
Orion A, 22 GHz water line giant outburst 80−8703
Orion A, confirmation of H_2O 22 GHz line outburst 80−8704
Orion A, H66α radio recomb. line obs. rel. to electron temp. distrib. 77−87558
Orion A, methanol 84.5 GHz and 96.7 GHz lines obs. 80−62245
Orion A, probable detect. of methylamine-d_1 77−33610
Orion A, relationships of N_2 H^+, HCO^+, HCN and CN 77−33587
Orion B (NGC 2024), recomb. line obs. 77−29895
Orion methanol masers, interferometric and multitransitional study 80−67891
Orion Molecular Cloud, H_2 2.1 μm emission line vel. profiles 79−71094
Orion Molecular Cloud, H_2 quadrupole line reddening determ. 79−71095
Orion Molecular Cloud, HCN, HNC and HCO^+ J=3-2 lines detect. 79−25669
Orion Molecular Cloud, NH_3 emission obs. 80−36687
Orion Molecular Cloud, NH_3 spectrum and new dynamical model 78−93373
Orion Molecular Cloud 2, relationships of N_2H^+, HCO^+, HCN and CN 77−33587
Orion nebula, C and Mg abundances from UV spectrum 80−41882
Orion Nebula, C I IR forbidden emission lines obs. 78−85987
Orion Nebula, C recomb. line mapping 78−20866
Orion Nebula, chem. comp. from emission line obs. 77−49456
Orion Nebula, Fabry-Perot high-resolution O I 8446 Å mapping 79−35344
Orion Nebula, fine-struct. lines obs. and elemental abundances 80−4410
Orion Nebula, forbidden Cl II and forbidden Fe II near IR high resolution mapping 80−62217
Orion Nebula, H_2 2.121 μ emission line vel. and width meas. 79−17061
Orion Nebula, H_2 emission from shock-heated region in molecular medium 78−4321
Orion Nebula, IUE obs. of UV continuous spectrum 80−90499
Orion Nebula, lamellar grating obs. in 100-500 μm region 78−28743
Orion Nebula, macroscopic motions from atomic line vels. 80−62243
Orion Nebula, near IR Fourier spectroscopy 77−57071
Orion Nebula, near IR Fourier spectroscopy of weak lines 79−35328
Orion Nebula, O I 63 μm forbidden emission line obs. 79−25684

astronomical spectra continued
Orion Nebula, O III 51.8 μm forbidden emission line obs. 79−25685
Orion Nebula, physical conditions from optical and radio lines obs. 77−45524
Orion Nebula, S III 9096 Å forbidden line, Fabry-Perot obs., abundance determ. 78−96515
Orion Nebula, S III emission at 534.37 cm^{-1} 77−73966
Orion Nebula, spherical model, emission spectrum 77−53666
Orion Nebula, submillimetre emission obs. 80−36685
Orion Nebula (NGC 1976), long-slit spectroscopy in rocket UV 80−105297
Orion Nebula molecular cloud, anomalous var. of $N_2H^+/HCO^+/SO_2$ rel. to ion-molecule reactions 77−26034
Orion Nebula peripheral regions, spectrum obs. rel. to element depletion and ionisation 80−36686
Orion Nebulae, IR studies of ionization front 79−75261
Orion region, radiocontinuum emission struct. and spectral index distrib. 78−49549
Orion triple emission nebula, Fabry-Perot radial vels. 77−13430
outer planets spectra rel. to abundance ratios determ. method, appl. to Jupiter 79−84734
P0735+178, variable quasi-stellar source, high-freq. IR spectral cutoff 78−16528
P-K 164+31°1, spectroscopic obs., identification of planetary nebula 77−74123
Pallas, carbonaceous chondrite mineralogies remote spectroscopic identification from IR obs. 79−96946
particle falling into Kerr black hole, high-freq gravit. and EM spectra 78−16452
peculiar and interacting galaxies in southern sky, emission line obs. of 37 objects *(Russian)* 78−49511
peculiar extragalactic objects, spectral indices from multiaperature UBV photometry 78−28772
peculiar galaxy system in Hydra 79−58433
Periodic Comet Arend-Rigaux (1977k), positions, appearance and spectrum 78−12157
Periodic Comet Ashbrook-Jackson (1977g), spectroscopic obs. 78−96437
Periodic Comet Giclas (1978k), spectroscopic obs. 78−96437
Periodic Comet Schwassmann-Wachmann 1, objective prism spectrograms and new outburst 79−53774
Periodic comet Schwassmann-Wachmann 1 (1974 II), outburst and CO^+ detect. spectrophotometric obs. 80−72881
Periodic Comet Tempel 2, optical spectrophotometry at 3 AU distance, albedo, nucleus radius 80−26814
X Persei, X-ray spectra, binary model 79−25757
Perseus galaxy cluster, low energy X-ray absorpt. obs. 78−86025
Perseus galaxy cluster, obs. rel. to galaxies redshift-magnitude bands and evolution 78−54033
Perseus OB2 association molecular cloud, mol. obs. rel. to star form. 80−12798
PG 0026+129, $L\alpha/H\beta/P\alpha$ ratio following IUE UV obs. of quasar 79−12537
PG 1115+08, triple QSO, spectroscopic obs. and gravit. lens model 80−86012
PHL 1070, quasar spectrum and redshift of surrounding halo 78−28771
PHL 1092, narrow line quasar, discovery of extreme Fe II emission 80−77508
PHL 5200, quasar, relevance of 4C −05.93 source 79−88760
PHL 938, quasar, continuum spectrum reddening due to dust 78−96561
PHL 957, quasar, H_2 and CO absorpt. lines obs. *(Russian)* 79−101216
PHL 957, quasar, upper limits on Lyman α halo 80−51907
photoelectric stellar radial velocity spectrometry, use of echelle grating *(French)* 77−91438
Pictor A, powerful radio galaxy, photographic and spectrophotometric obs. 77−49481
Pioneer 10 and 11 radio signals, spectral broadening by ionospheres of Jupiter and Saturn 80−109391
PK 108−76°1, 49+88°1, halo planetary nebulae, Ar III line obs. and low Ar abundances meas. 80−82443
PK 181+1.1, new weak planetary nebula near galactic anticentre, spectrum and radial rel. 79−17049
PK 60−7°1, nebula around FG Sagittae, spectrophotometric study 79−40240
PK 6-2°1, southern planetary nebula, N and He overabundance 77−78849
PKS 0237−23, absorpt. spectrum obs., absorpt. lines origin 78−41074
PKS 0237−23, absorption redshift of QSO 79−35417
PKS 0237−23, Lymanα/Hα intensity ratio from IR obs. of quasar 78−41078
PKS 0521−36, BL Lacertae object, optical spectrum and redshift 79−84854
PKS 0528−250, abundances in absorbing material towards QSO 79−40288
PKS 0528−250, neutral stellar object with no emission and rich absorption 78−49551
PKS 0537−286, high-z QSO with extreme Lyman continuum cutoff 79−12538
PKS 0548−322, BL Lacertae object, X-ray spectrum 80−17654
PKS 0735+178, BL Lacertae object, spectrum, multiple components in $z=0.424$ absorpt. system 79−25707
PKS 0735+178, flat radio spectrum, 0.3-90 GHz obs. of BL Lacertae object 80−94880
PKS 0735+178, flat spectrum radio source struct. 78−16549
PKS 0736+01, optical spectrum variability 80−8709
PKS 1144−379 BL Lacertae object, optical and IR photometry and optical spectrum 80−4451
PKS 1157+014, spectral obs., of QSO with no Lα emission 80−31384
PKS 1158+007, redshift from QSO spectrum 79−58440
PKS 1345+12, radio galaxy, optical spectrum 78−4341
PKS 2126−158, absorption spectrum, high resolution study 79−53928
PKS 2126−15, bright quasi-stellar object with neutral colour and redshift of (3.27) 78−93450
PKS 2155−304, BL Lacertae object, spectral slope from far UV obs. 80−82509
PKS 2155-304, BL Lacertae object, no evidence for redshifted forbidden O III emission 80−73035
PKS 2155-304 (H2155−304), newly discovered BL Lacertae object, optical polarisation, spectrum and variability 80−36702
PKS 2322-12, narrow-line radio galaxy, optical spectrum 77−33664
planetary atmospheres, absorpt. bands depths rel. to two-layer model parameters determ. 78−24480

astronomical spectra continued
planetary atmospheres, temperature depend. of possible S_8 IR bands 77−29709
planetary corona, collisional model for spectral line profiles 78−77508
planetary nebula, faint new object discovered near NGC 6401 globular cluster 77−49461
planetary nebula IC 418, search for absorpt. in CO fourth positive system 80−46647
planetary nebula in irregular galaxy NGC 6822, spectrophotometry and He, N, O and Ne abundances 80−41867
planetary nebula obs. in red globular cluster NGC 1852 in LMC 77−17668
planetary nebulae, 10 micron props. obs. 79−48879
planetary nebulae, 8 to 13 micron spectrophotometry 80−22057
planetary nebulae, absolute flux densities for emission lines in 6000-11000 Å range rel. to physical parameters 80−51857
planetary nebulae, abundances from weak diagnostic spectral lines 80−109531
planetary nebulae, bipolar, emission line isophotes *(Russian)* 77−13447
planetary nebulae, C IV 1550 Å lines fluxes meas. and C abundances 79−17051
planetary nebulae, central stars temps. determ. from O III/O II line ratios 79−2565
planetary nebulae, emission line fluxes in truncated composite shell models 79−25677
planetary nebulae, emission line intensities for small ang. size moderate excitation nebulae 79−21407
planetary nebulae, emission mechanisms and spectral features 79−67080
planetary nebulae, emission-line fluxes rel. to O/H ratios and Galaxy O enrichment 80−105328
planetary nebulae, EUV spectra of young objects 79−35336
planetary nebulae, forbidden-line ratios rel. to electron density evolutionary changes 77−78861
planetary nebulae, geometry effects on H Lyman α form. 78−20871
planetary nebulae, H β fluxes rel. to distances determined from ionised mass/radius relation 80−101625
planetary nebulae, H and He II spectra rel. to central stars temps. and evolution 80−67724
planetary nebulae, He II Ly α photons absorpt. rel. to forbidden lines intensities 80−67833
planetary nebulae, interpretation of UV spectra 80−109524
planetary nebulae, ionisation models rel. to spectra 80−109529
planetary nebulae, IR emission lines in 12 faint objects *(French)* 78−12337
planetary nebulae, IR line and continuum spectra 80−109525
planetary nebulae, line intensity ratios evolution 77−64820
planetary nebulae, low excitation, of small ang. size, spectral studies 80−17646
planetary nebulae, low-excitation, spectra rel. to effective temps. of exciting stars 77−13427
planetary nebulae, moderately bright, spectroscopic study 79−84835
planetary nebulae, molecular abundances and IR spectra 78−53998
planetary nebulae, OH emission search 79−48787
planetary nebulae, photoelectric spectrophotometry of emission lines, abundances 78−81677
planetary nebulae, radial vel. meas. rel. to kinematics 80−46633
planetary nebulae, radio continuum spectra and electron temps. 78−41027
planetary nebulae, radio recomb. lines and mol. emission lines obs. 80−109526
planetary nebulae, S abundance from IR and visible line meas. 80−82444
planetary nebulae, S abundance in 20 galactic objects, spectrophotometry 78−45375
planetary nebulae, spectra at visible, radio and IR wavelengths *(Italian)* 77−91604
planetary nebulae, spectrophotometry, emission line intensities, physical conditions 78−36651
planetary nebulae, spectrophotometry and chemical abundances 78−36663
planetary nebulae, theoretical models, low to medium excitation objects 80−67817
planetary nebulae, theory of physical processes rel. to spectra 80−109527
planetary nebulae, UV continuum and line spectrum obs. and theory 80−109523
planetary nebulae, UV spectra 79−92843
planetary nebulae central stars, interpretation of UV continuum radiation 80−109524
planetary nebulae in galactic centre field, spectra and classification 80−8674
planetary nebulae in Magellanic Clouds, spectra rel. to excitation classes and comps. 80−109519
planetary nebulae in Magellanic Clouds 79−58405
planetary nebulae of overall field and galactic centre, spectra and physical characts. 78−54029
planetary nebulae optical spectra, effects of inhomogeneous struct. 80−109522
planetary nebulae spectra, effects of He shell flashes in nuclei 80−73021
planetary nebulae spectra correction for interstellar absorpt., typical spectrum derivation 77−53677
planetary nebulae UV emission line spectra, excitation mechanisms *(Italian)* 78−32550
planetary satellites of outer solar system, IR photometry and identification of new class 78−12146
planets, absorption line var. across disk for inhomogeneous atm. 80−8569
planets, anisotropic scatt. effects 77−2357
planets, far IR and submillimetre obs. 77−71037
plasma, high temp., thermal bremsstrahlung radiation and spectral emission rate 80−94697
plasma clouds, comptonisation of X-rays, radiation spectra 80−85850
plasma turbulent sources, radiation distrib. functions calc. 77−70990
Pluto, 1.5 to 2.5 μm spectrum obs. 80−56765
Pluto, image tube spectra, 6800-9000 Å, search for possible atm., methane upper limit 79−16880
Pluto, surface composition, IR photometry 79−53768
PN 108-76°1, halo planetary nebula, spectrophotometry and element abundances 78−41011
PN 173+3.1, planetary nebula near galactic anticentre, coords., radial vel. and orbit 80−105309

astronomical spectra continued
PN 49+88°1, halo planetary nebula, spectrophotometry and element abundances 78−41011
polysaccharides, evidence in IR astronomical spectra 77−78857
primaeval galaxies, model emission spectra 80−46655
primaeval radiation, polarisation and spectrum in anisotropic universes 80−82552
primordial microwave radiation, recomb. lines calc. 78−54097
propyne, microwave spectra and mol. consts., rot. anal. 79−76411
pulsar radio signals spectra and microstruct., relativistic electron beam model 78−65639
pulsars, gamma-ray spectra 79−30083
pulsars, low latitude, H I absorption in spectra, interstellar electron density determ. 79−92792
pulsars, radio emission spectra, 17-1420 MHz 79−62863
pulsars, spectra and flux densities in 61-1420 MHz range for 9 objects 79−12487
Puppis, A Fe X and XIV forbidden line emission 79−44580
Puppis A, Fe XIV coronal line and filamentary emission 79−84843
Puppis A, O VIII 18.97 Å resonance line emission detect. 77−45535
Puppis A, optical spectral obs. of filaments *(Italian)* 79−53883
Puppis A, X-ray and Fe XIV 5303 Å emission 80−26962
Puppis A supernova remnant, X-ray spectra var. with position 80−82472
Puppis A supernova remnant, X-ray spectrum and struct. 78−20876
Q0002−422 and 0453−423, QSO absorption spectra, high resolution study 79−62925
Q0353−383, QSO abundance anomalies, UV and visible spectral obs. 80−82532
Q0453−423, quasar, absorption line spectrum 78−8144
Q2227.6−3928, highest redshift quasar from Tololo deep survey 78−12403
Q2228.1−4033, high redshift quasar from Tololo deep survey 78−12403
Q 0002−422, QSO with $z_{abs} \ll z_{em}$ 78−16565
Q 0932+501, bright quasar with broad absorption features 80−46697
Q 0957+561, double quasar, red shift of galaxy component of spectrum 80−27005
Q 1246−057, absorpt. line spectrum, presence of outflowing material 78−93453
Q 2204−408, IUE UV spectrum of high redshift radio-quiet quasar 79−35424
Q 2240.9-3702, Q 2238.9-4115, optically selected QSOs with broad-lined absorpt. systems spectra 80−4456
QSO 0242+622, spectrum and luminosity of low redshift object 78−93451
QSO 0957+561, double quasar, visible spectrophotometry, gravitational lens interpretation 80−82533
QSO 0957+561 AB, double quasar, IR spectrum confirms gravitational lens 80−77510
QSO 1756+237, absorbing regions, physical conditions from visible obs. 79−71146
QSO absolute spectral energy distrib. in $0.3-10\ \mu$ range 79−62926
QSO absorbing regions, extended Lyman α emission obs. 79−44631
QSO absorption line spectra for six high-redshift objects 78−93449
QSO absorption line systems, radiation-driven outflow models 78−57687
QSO absorption lines and intergalactic clouds 80−62311
QSO absorption spectra origin 80−105387
QSO candidates, spectroscopic obs., indentifications 80−31385
QSO emission lines, hard X-ray effects 80−26974
QSO line spectra, influence of radiative field spectral shape 80−41909
QSO line spectra, review 77−26081
QSO pairs, spectroscopic obs. 77−5587
QSO redshift $(1+z_i)/(1+z_j)$ distrib. 78−65715
QSO resonance lines as luminosity calibrators 80−105388
QSO spectra, catalogue of absorpt. line lists for 108 objects 78−53840
QSOs, absorpt. from clouds in emission-line regions 80−62308
QSOs, absorpt. line redshift distrib. 80−90563
QSOs, absorption lines shortward of Lα emission, redshifts, origin in moving H I clouds 79−9025
QSOs, absorption systems in high redshift objects 78−28843
QSOs, accretion disc model rel. to optical continuous spectrum 77−64872
QSOs, Cherenkov line radiation, emission line spectra *(Chinese)* 79−80366
QSOs, emission-line spectra and redshift distrib. 78−57677
QSOs, high-redshift, Image Dissector Scanner (IDS) spectrometry and redshifts 80−22111
QSOs, high-redshift emission-line spectra and emitting regions props. 79−21458
QSOs, line shape analysis, of absorption spectra 78−36718
QSOs, Lyman α/Hβ intensity ratio 77−45600
QSOs, new type, identified through IR meas. 80−8708
QSOs, physics of absorpt. line regions 78−57680
QSOs, profiles and redshifts of broad lines 78−16566
QSOs, redshift doublets in absorpt. spectra, model 77−22325
QSOs, redshifted clouds, 21 cm line studies 80−105389
QSOs, relativistic jets and continuum emission 80−51898
QSOs and Seyfert galaxies, He I lines in spectra 78−36717
QSOs from Molonglo Deep Survey, optical spectra 80−94884
QSOs lying in spiral arms of NGC 1073, spectrophotometric obs. and redshifts 80−22110
QSOs of small and intermediate emission redshift, absorpt. lines homogeneous survey results 80−31218
QSOs UV emission lines, photoionization model analysis 79−71148
quasar, absorption spectra and Wu states, plasma-laser star model 79−48950
quasar, strong emission line, with redshift $z=0.189$, spectrum and photometry 80−8710
quasar 0933+733, redshift determ. from low dispersion objective prism plates 79−2485
quasar absorption line systems, lack of dust 77−49493
quasar absorption lines, origin 78−57684
quasar absorption lines, rel. to galactic coronae and intracluster medium origin 80−31355
quasar absorption lines due to intervening interacting galaxies 77−17714
quasar emission lines, review 80−27009
quasar near companion galaxy NGC 5296, spectrum and redshift 77−13489
quasar plasma-laser star model, O VI and He II emission lines 77−45597
quasar redshift determ. from low dispersion objective prism plates 79−2485

astronomical spectra continued
quasar spectra, theory of H line emission from dense plasmas 80−51900
quasars, absorpt. line spectra and redshift systems 77−13488
quasars, absorpt. line systems, wind driven shell model 79−21461
quasars, absorpt. lines statistics and line-locking 78−57681
quasars, absorpt. systems assoc. with image doubling 80−22112
quasars, absorption line spectra, accidental redshift system estimation 78−16562
quasars, absorption spectra, effects of intervening galaxies 78−16561
quasars, accretion discs thermal emission as source of optical continuum 78−54075
quasars, broad lines rel. to gas cloud containment by particle flux 79−8820
quasars, Cherenkov line radiation, QSO emission-like spectra *(Chinese)* 80−105378
quasars, collision strengths of UV emission lines 77−82318
quasars, Comptonised spectrum, Monte Carlo simulation 80−90566
quasars, continuous and emission-line spectra and relationship with Seyfert galaxies 79−2571
quasars, CTIO Curtis Schmidt survey −40° zone, discoveries and spectrophotometry 80−73064
quasars, distance determ. to absorbing clouds 79−35421
quasars, Doppler shifts distrib. for relativistic gas 78−65492
quasars, emission line clouds, radiation pressure-driven Rayleigh-Taylor instability 79−35419
quasars, emission line redshift distrib. gaps, trend analysis 78−45423
quasars, emission spectra, photoionisation anal. 78−16560
quasars, emission spectra and radio struct. relations 79−40290
quasars, faint red 3C QSO candidates spectrophotometry and red shifts 80−67897
quasars, Fe II emission profiles interpretation 77−9791
quasars, H absorpt. lines rel. to intergalactic medium struct. 77−67129
quasars, H emission-line spectra 78−96557
quasars, H I Lyman α/Balmer β intensity ratio interpretation 79−35418
quasars, H line and continuum emission calcs. 80−27003
quasars, high-redshifts, optical or radio selection rel. to emission line spectra 77−53696
quasars, intrinsic spectra rel. to reddening 79−67113
quasars, IR energy distribs. obs. 78−57645
quasars, IR spectra, H I line ratios 80−105391
quasars, large-red shift, spectra, implications of neutrino rest mass for H I obs. problem *(Russian)* 80−105414
quasars, line identifications, red shifted UV lines or violet shifted IR lines 80−8707
quasars, low redshift X-ray selected, visible spectra and UDVR photometry 80−105397
quasars, Lyman α absorpt. line distrib., intergalactic origin 80−67899
quasars, Mg II 2798 Å and Hβ emission, line profiles 80−12807
quasars, Mg II and Fe II lines excitation 80−67896
quasars, narrow line absorpt. systems, form. model 80−82535
quasars, O VI 1035 A emission and Lyman β 77−2483
quasars, optical and near UV spectrum synthesis 77−60843
quasars, optical and UV spectra 79−97094
quasars, optical surveys, electronographically recorded low-dispersion slitless spectra 78−57467
quasars, origin of absorpt. lines 77−33679
quasars, permitted Fe II lines form. and low excitation region parameters 80−62278
quasars, props. of $Z_{abs} > Z_{em}$ systems rel. to origins of QSO absorpt. line systems 78−57682
quasars, radio recombination line obs. 79−101193
quasars, role of inelastic collisions 77−45599
quasars, selection effect in absorption line redshifts 79−92885
quasars, Si II spectrum calc. 77−60844
quasars, slitless spectroscopy of large redshift objects 78−96562
quasars, spectra obtained with low-dispersion Fehrenbach prism computer simulation 78−57468
quasars, spectral characts. of three high redshift objects 80−4455
quasars, spectral line profiles interpretation *(Russian)* 79−101203
quasars, spectral props. of 85 objects from spectrophotometry 80−51897
quasars, statistical tests for line-locking evidence 77−33675
quasars, systematic surveys with slitless spectrum technique 80−105384
quasars, with $2.5 \leqslant Z < 3.1$, emission line spectra 77−9806
quasars, X-ray properties from Einstein Observatory obs. 80−27004
quasars, X-ray spectral indices rel. to contrib. to X-ray background 80−82551
quasars, [O III] and [Ne III] spectra rel. to narrow line region physical conditions 80−31364
quasars 0957+561 A, B, twin quasistellar objects or gravit. lens theories 79−67114
quasars absorption line features of Fe II and Mg II 78−16559
quasars absorption line problem, optically selected high-redshift objects spectrophotometry 79−25746
quasars absorption line redshifts, limits to past variability of proton/electron mass ratio 77−61338
quasars absorption line spectra, implications of disc galaxies sizes in Virgo and Hercules clusters 79−75269
quasars absorption lines, line-locking hypothesis, intervening galaxies absorpt. and $z=1.95$ peak in redshifts 78−57685
quasars absorption lines and galaxy Faraday rotation *(Russian)* 79−40273
quasars absorption redshifts, evidence for large-scale uniformity of physical laws 80−73079
quasars and related objects, contrib. of stellar debris clouds to spectra 78−32597
quasars from Parkes survey, high resolution obs., spectra 79−75295
quasars in CTIO 4 m survey, visible and UV spectrophotometry 80−86009
quasars in region of NGC 1629 companion galaxy, spectra and redshifts 80−56965
quasars in southern hemisphere, spectra and redshifts 77−67137
quasars near peculiar pair of galaxies NGC 7714−7715, spectra and redshifts 78−28835
quasars of 3CR and 4C catalogues, comparative study of struct. and radio spectra 77−67136
quasars of high redshift, search for 21 cm absorpt. 80−4453
quasars of Michigan-Tololo survey, spectrophotometry 80−22105
quasars PG 0026+129 and 3C 273, optical and IR spectrophotometry 79 17123
quasars relative luminosities determ. from emission line strengths 78−61931

astronomical spectra continued
- quasars spectra, absorpt. effects due to intergalactic pyrolitic graphite whiskers 80−94866
- quasars with absorption redshifts greater than emission redshifts, spectroscopic study 77−45595
- quasars with high redshift, discovery and spectroscopic obs. 77−45594
- quasars with optical absorption spectra, radio polarization 78−12405
- quasi-stellar objects, 1400 Å emission feature rest wavelength and identification 80−12825
- quasi-stellar objects, absorpt. lines in spectra 78−57679
- quasi-stellar objects, H emission line ratios implications 80−56968
- quasi-stellar objects, low-redshift, spectra, absorpt. lines obs. 79−21459
- quasi-stellar objects, luminosity indicators in emission-line spectra 77−57103
- quasi-stellar objects, radio spectra rel. to shot-noise interpretation of light curves 77−37666
- quasi-stellar objects, spectra and element abundance ratios 78−20903
- quasi-stellar radio sources from 4C and Parkes catalogues, spectra and photometry 78−65714
- radiation redistrib., diffuses reflection effects 78−53819
- radiation sources spectral shapes, influence on local ionisation equilib., thermal equilib. and radiative accel. 80−41909
- radiative transfer, Cauchy problem for Milne integral eqn. with Pincherle-Goursat kernel 77−2513
- radio and Seyfert galaxies, optical spectra 77−17686
- radio galaxies, broad-line Mg II 2798 Å and $H\beta$ emission, line profiles 80−12807
- radio galaxies, narrow-lined, spectrophotometry 78−93391
- radio galaxies, optical emission-line spectra 78−57643
- radio galaxies, optical spectra, morphological classification rel. to spectroscopic classification 78−41038
- radio galaxies, search for H I clouds 78−12316
- radio galaxies components, radio continuum spectra rel. to fly away velocities *(Russian)* 80−62306
- radio galaxies with radio jets, optical spectra of nuclei 79−84859
- radio quiet quasistellar objects, obs. at 3.3 mm wavelength 78−81703
- radio recombination lines, high-n, Zeeman splitting 80−58210
- radio source near refl. nebula NGC 7023, non-thermal spectrum 79−17048
- radio sources, compact, extragalactic, interpretation of spectra 80−62299
- radio sources, compact in bright galaxies, ang. sizes and spectral indices from VLBI 79−48943
- radio sources, complex, in Abell clusters, 2.7 GHz maps and spectral index vars. 79−92881
- radio sources, discrete, flux densities and spectra meas. at centimetre wavelengths 77−37664
- radio sources, extended, extragalactic, relation between radio luminosity and spectrum 80−51894
- radio sources, extragalactic, spectral polarisation and polarisation index 79−53920
- radio sources, form. of universal and diffusion regions of relativistic electrons non-linear spectra 80−109555
- radio sources, galactic, OH radio lines absorpt. obs. 78−54068
- radio sources, obs. by Jodrell Bank 1024 channel digital autocorrelation spectrometer 77−73970
- radio sources, peculiar, in Abell 1367 galaxy cluster, Westerbork obs. and spectral indices 79−2574
- radio sources, southern, extragalactic, of large ang. extent, emission spectrum vars. 80−17683
- radio sources, spectral index distribs. rel. to source counts freq. depend. 78−96554
- radio sources, superluminal, spectrum shape from mag. dipole model 80−56959
- radio sources, variable, with flat spectra, identified with supernovae stellar remnants 79−17117
- radio sources, weak, low freq. scintillation obs. and spectral index distrib. 79−53921
- radio sources from Molonglo Deep Survey, radio and optical spectra 78−69900
- radio sources from NRAO-MPIfR 6 cm surveys, 21 cm flux densities and spectral indices 79−88754
- radio sources in 3 C 27 area, spectra from 2695 MHz continuum obs. 80−46688
- radio sources in clusters of galaxies, spectra and morphology 78−12398
- radio sources in clusters of galaxy, spectral index correl. with cluster class 78−12397
- radio sources of 5C 1 to 5 survey areas, 1421 MHz obs. and mean spectral indices 79−84864
- radio spectra of nonuniform synchrotron sources with internal absorpt. 77−5580
- radio spectroscopy *(Japanese)* 80−62031
- radioastronomical equipment, techniques and observations, review *(German)* 77−56827
- radiofrequency recombination lines, computation of b_n factors 77−64832
- radiogalaxies, faint southern objects, identification and spectrophotometry 80−56935
- radiogalaxies, optical spectroscopy and redshifts for 18 objects 80−56966
- radiogalaxies, spectrophotometry of three objects 78−54066
- radiogalaxies from B2 Catalogue, optical identification, radio positions and redshifts 80−86005
- radiosource at galactic nucleus, radio spectrum 77−5572
- radiosources, compact, particle accel. rel. to spectrum vars. 77−13479
- radiosources, coordinated photometric and spectroscopic observations of strong extragalactic 90 GHz sources 78−93440
- radiosources, extragalactic, hard X-ray emission rel. to radio and optical spectra 77−29939
- radiosources, extragalactic with strong millimetre-wave emission, high and low freq. radio spectra 78−16548
- radiosources, isotropy of spatial densities, source counts and spectral index distribs. 77−45584
- radiosources, optical identifications, spectrophotometric obs. 79−92879
- radiosources, spectroscopic identification of three southern PKS sources 79−25744
- radiosources, spectroscopic obs. in 3200-5700 Å range of 34 program objects 78−86032
- radiosources in 10°-20° declination strip, freq. spectra in 10-180 MHz range 78−28814
- radiosources nonlinear spectra, rel. to relativistic electrons accel. in plasma turbulent reactors 79−8824
- radiosources with flat or inverted spectra, optical and radio props. 78−81697

astronomical spectra continued
- RCW 107 (NGC 6164/5), ionisation struct. of southern H II region 77−45526
- Red Rectangle, refl. nebula assoc. with HD 44179, spectrum interpretation 77−49462
- Red Rectangle (HD 44179), precessing jets model rel. to broad $H\alpha$ emission 80−4422
- redistribution of scattered radiation by collisions in nonimpact region of spectral line profile 79−35109
- reduction techniques in X-ray astronomy 79−96924
- relic radiation spectrum and Universe thermal history 78−20921
- relict radiation spectrum distortion by 21 cm absorpt. line *(Russian)* 78−4422
- resonance line scattering in absorbing medium, scaling laws 80−98538
- resonant X-ray lines, freq. redistrib. and radiation diffusion, Voigt profile, thermalisation length *(Russian)* 79−5747
- ring galaxy, physical characts. *(Russian)* 77−57097
- RMB 56 (1216+141), compact blueshifted galaxy, photometry and spectrum 78−16527
- Roberts 22, bipolar nebula with OH emission, visual, radio and IR obs. 80−94859
- Rosette Nebula (NGC 2237/2246), radio recomb. line and continuum obs. rel. to physical parameters 80−4414
- S0 galaxies, radio continuum and H I obs. 77−87549
- S104, 609 MHz aperture synthesis obs. of H II region 78−57618
- S106, H II region, radio obs. of assoc. mol. cloud, CO, HCO^+ HCN, OH and formaldehyde lines 78−61906
- S106 IR, S235 B, obscured IR point sources, 2 μm spectroscopic anal. 80−12795
- S140 IR, far IR spectrum 78−93372
- S252 (NGC 2175), H II region, mol. line obs. of star-forming complex 80−4411
- S255, molecular cloud, molecular line, radio continuum and IR data 78−8087
- Sa type spiral galaxies, redshifted 21 cm line profiles, radio obs. 80−73041
- HM Sagittae, near-IR spectrographic obs. of young planetary nebulae 80−94810
- HM Sagittae, planetary nebula excited by Wolf-Rayet star, spectrum 78−54003
- HM Sagittae, possible proto-planetary, nebula, emission line widths 78−45389
- FG Sagittae, spectrum of assoc. nebula 78−49498
- Sagittarius A, H recomb. lines obs. at decimetric wavelengths 77−82310
- Sagittarius A, Sagittarius B2, probable detect. of methylamine-d_1 77−33610
- Sagittarius A-west, IR obs. of Ne II forbidden line emission 78−36680
- Sagittarius B2, far IR spectrum obs. 78−8073
- Sagittarius B2, He recombination line obs. interpretation 80−62300
- Sagittarius B2, methanol 84.5 GHz and 96.7 GHz lines obs. 80−62245
- Sagittarius B2, mol. cloud, detect. of HC_5N (cyanodiacetylene) and HC_7N (cyanohexatriyne), SHF obs. 80−101627
- Sagittarius B2, recomb. lines obs. rel. to He abundance problem 78−49496
- Sagittarius B2 molecular clouds, intensity ratios of ^{13}C isotopes of cyanoacetylene 77−29900
- Saturn, atm. H_2 content from spectral line equivalent width *(Russian)* 78−12143
- Saturn, atmosphere constituents, comparison with Jupiter, visible spectra obs. *(French)* 80−101550
- Saturn, atmosphere upper layers props. from polarimetry photometry and spectrophotometry *(Russian)* 78−40867
- Saturn, atmospheric seasonal phenomena from $3\nu_3$ methane band obs. 80−26803
- Saturn, deuterated methane obs. in 5 μm spectrum 79−25543
- Saturn, echelle spectrogram 78−96426
- Saturn, evidence for telluric value of $^{12}C/^{13}C$ atmospheric ratio 78−20723
- Saturn, far IR spectral obs. of planetary disc and rings 78−16341
- Saturn, far IR spectrum, PH_3 and NH_3 absorpt. lines 78−12147
- Saturn, H_2 2-O quadrupole spectrum in atm. 77−45351
- Saturn, H_2 quadrupole lines in spectrum 79−70990
- Saturn, HD detect. at 6063.88 Å, D/H abundance ratio calc. 78−57495
- Saturn, near IR spectral albedo 80−31242
- Saturn, NH_3 abundance from visible obs. 80−82269
- Saturn, origin of Lyman-alpha emission from rings vicinity 79−12430
- Saturn, PH_3 abundance, IR obs. 80−82278
- Saturn, spectrophotometry in far IR 78−85890
- Saturn, UV spectra and photometry by TD1A and OAO-2 satellites 77−91459
- Saturn atmosphere, acetylene detect. using IUE satellite 79−48731
- Saturn D-ring methane 890 nm band obs. 79−44407
- Saturn disc centre spectral reflectivity, phase effect 80−98602
- Saturn far UV spectrum, rocket obs. 78−53867
- SC 0627−544, Fe XXV and Fe XXVI emission lines in X-ray spectrum 79−48941
- Sc galaxies, nuclear regions stellar content 77−9793
- Sc galaxies, rot. props. from major axis visible spectra obs. 80−90517
- SchuWe-3, spectroscopic obs. of southern planetary nebula 80−101626
- Schwarzschild black hole, absorpt. and emission spectra, computational methods, cross sections 79−2558
- α Scorpii (Antares) nebula, spectrum 78−41014
- Scorpius X-1, extended X-ray obs. with Bragg crystal spectrometer 79−12543
- Scorpius X-1, Salyut-4 X-ray spectrometry *(Russian)* 77−26091
- Serpens X-1, Ariel 5 obs. and models of spectrum and time var. 78−81707
- Seyfert 1 galaxies, emission line intensities rel. to colour index 80−26971
- Seyfert 1 galaxies, forbidden line emission suppression 79−35358
- Seyfert 1 galaxies, H I Balmer lines correl. with disk struct. 80−82503
- Seyfert 1 galaxies, O I 8446 Å emission excitation mechanism, visible and IR obs. 80−85991
- Seyfert 1 galaxies, theory of asymm. broad H I emission lines 79−71108
- Seyfert 1 galaxies and QSOs, Fe II permitted emission, excitation mechanism 79−21412
- Seyfert 1 galaxy 1224+04, discovery from spectrophotometry obs. 80−77488
- Seyfert 1 X-ray emitting galaxies, HEAO 1 spectra 80−51860
- Seyfert 2 galaxies, spectrophotometry 78−93391
- Seyfert 2 X-ray galaxies, nucleus spectra and photometry obs. 80−98712

astronomical spectra continued
- Seyfert and related galaxies, 1415 MHz survey and radio spectra 77—9800
- Seyfert galaxies, broad H lines prod. by suprathermal protons passing through neutral gas *(Russian)* 78—57642
- Seyfert galaxies, class 1, theoretical and obs. anal. of He I triplet lines in spectra 78—49519
- Seyfert galaxies, continuous and emission-line spectra and relationship with quasars 79—2571
- Seyfert galaxies, emission lines, hard X-ray effects 80—26974
- Seyfert galaxies, exploratory obs. of gas near nuclei 79—48906
- Seyfert galaxies, Fe II emission profiles interpretation 77—9791
- Seyfert galaxies, Fe XI 7892 Å forbidden line emission 78—49520
- Seyfert galaxies, H I spectra and distrib. survey 79—8988
- Seyfert galaxies, IR emission obs. 79—17083
- Seyfert galaxies, IR energy distribs. obs. 78—57645
- Seyfert galaxies, Mg II 2798 Å and $H\beta$ emission, line profiles 80—12807
- Seyfert galaxies, Mg II and Fe II lines excitation 80—67896
- Seyfert galaxies, nearby, $H\beta$ line width correl. with morphology 80—82478
- Seyfert galaxies, obs. at 1.3 and 2.8 cm wavelength, spectra 78—69866
- Seyfert galaxies, optical emission-line spectra 78—57643
- Seyfert galaxies, profiles and redshifts of broad lines 78—16566
- Seyfert galaxies, radio spectra and luminosities 78—49535
- Seyfert galaxies, spectral line profiles interpretation *(Russian)* 79—101203
- Seyfert galaxies, type 1, dust heating rel. to IR spectra 78—12357
- Seyfert galaxies, type 1, nuclei props., UV emission, colour index *(French)* 79—48923
- Seyfert galaxies, type 1, permitted Fe II lines form. and low excitation region parameters 80—62278
- Seyfert galaxies and quasars, charge exchange model for broad emission line prod. 77—53681
- Seyfert galaxies from lists of Markarian galaxies, spectroscopic obs. *(Russian)* 79—80360
- Seyfert galaxies from Zwicky lists, spectrophotometry 79—75274
- Seyfert galaxies spectra, theory of H line emission from dense plasmas 80—51900
- Seyfert galaxy nuclei, absolute spectrophotometry 79—12508
- Seyfert galaxy nuclei, spectroscopic obs. 77—9792
- Seyferts and quasars, broad line emission from black hole accretion disc 77—60819
- Seyferts in 12th list of galaxies with UV continuum *(Russian)* 80—17659
- Sh 2-158 (NGC 7538), bright high excitation galactic nebula, morphology, excitation and kinematics 79—40241
- Shahbazian 1 group of galaxies, spectroscopic obs. rel. to dynamics 80—67878
- Sharpless 106 IR sources, 8-13 micron spectrophotometry 80—105305
- Sharpless 159 and NGC 7538, H II region/mol. cloud complex, H I aperture synthesis obs. 80—90510
- Sharpless 176, large nearby planetary nebula, radius and distance determ. 77—87503
- Sharpless 88A-B and 106, compact H II regions, optical obs. 79—8969
- Sharpless H II regions, radio line and continuum spectra 77—87509
- silicates, emission and extinction in 4-14 μ range 79—44581
- Simkin effect and Hg I 4047 Å night sky contamination effect on galaxy redshift determ. 78—41032
- SN 1006 optical remnant, peculiar spectrum obs. 79—21371
- SN 1006 remnant, X-ray spectrum 80—82457
- SNR radio shells, spectral index distrib. 80—77462
- SNR X-ray spectra, two component appearance 80—82475
- SNRs, coronal line emission obs. and shock-heated plasma temp. determ. 78—65676
- SNRs in Magellanic Clouds 77—91613
- soft X-ray background 78—16582
- soft X-ray diffuse background flux, southern galactic hemisphere 78—8170
- soft X-rays diffuse background, 0.1-2.0 keV spectrum rel. to origins 78—16581
- solar system objects, International Ultraviolet Explorer (IUE) obs. 78—93133
- solar wind, low freq. continuum from ISEE 3, thermal electrostatic noise, LF obs. 80—101519
- solar wind ion acoustic waves, high-resolution spectrograms 79—96878
- Southern Coalsack, CO emission spectrum 77—29902
- southern compact and bright-nucleus galaxies, spectroscopic survey 79—84683
- southern peculiar galaxies and galaxy pairs, morphologies, spectra and redshifts 78—32579
- southern planetary nebulae identifications 77—22302
- southern radiosources, redshift meas. 77—26075
- Space Telescope, prospects for spectroscopic and direct work 78—57444
- spectroscopy role in basic plasma props. meas. 77—58900
- spectroscopy role in present-day astronomy 77—60623
- spherically symmetric radially moving clouds, spectral line shapes 78—20865
- spiral galaxies, comp. gradients rel. to density wave theory 77—2468
- spiral galaxies, interpretation of line intensity gradients across discs 77—13459
- spiral galaxies nuclei, spectra and stellar population 80—56926
- spiral galaxies with unusual radio morphology, radio continuum obs. 77—60822
- star formation regions, IR spectroscopy of assoc. lineless objects 79—44586
- starlight, integrated, synthetic spectrum between 3000 and 10000 Å, calc. method and results 80—46536
- steep spectrum radiosources, spectral index dependent props. 80—36730
- stellar stmospheres, spherical transonic flow, reson. line radiative transfer 80—94698
- Stephenson's planetary nebula, optical, near IR and radio obs., position 79—67086
- Stephenson-Sanduleak 433, Thomson scatt. lines in spectrum, relativistic gas motions 80—22019
- supernova in NGC 1411, spectral obs. and precise position 77—82266
- supernova remnant, extragalactic, in NGC 4449, spectrophotometry 80—56895
- supernova remnant candidates, spectroscopic survey in 6000-6800 Å region 77—60815
- supernova remnant candidates in M33 central region, forbidden S II emission 79—21402

astronomical spectra continued
- supernova remnant optical emission spectra, effect of shock wave intermediate zone radiative cooling 80—109517
- supernova remnant with broad optical emission lines near NGC 4449 irregular galaxy 79—17057
- supernova remnants, coronal lines, RGO spectrograms *(Italian)* 79—53892
- supernova remnants, far UV spectrophotometry and astrophysical interpretation 80—90498
- supernova remnants, Fe X and XIV forbidden line emission 79—44580
- supernova remnants, $H\alpha$/N II forbidden line ratio, evidence for grain destruction 77—45520
- supernova remnants, H abundance rel. to H deficiency in Type I supernovae 78—53969
- supernova remnants, low surface brightness, optical and radio obs. 79—88717
- supernova remnants, optical emission from shock waves 77—64816
- supernova remnants, optical spectra rel. to surface brightness-diam. correl. 77—29899
- supernova remnants, radio spectra rel. to physical parameters and interstellar absorpt. 77—13431
- supernova remnants, S II lines intensity ratio rel. to density and energy 78—20868
- supernova remnants, young, thermal X-rays theoretical spectra 78—73751
- supernova remnants in Large Magellanic Cloud, high-resolution mapping in coronal [Fe XIV] emission 79—97051
- supernova remnants in M33, catalogue and spectroscopic survey 80—41734
- supernova remnants in M33, forbidden S II emission obs. rel. to optical identification 79—62894
- supernova remnants in M33, spectra, element abundances 79—35354
- symposium (Victoria, Canada, 20-22 October, 1976) 77—78645
- synchrotron radiation, radio and electron components, effect of interstellar mag. field inhomogeneities 80—85849
- Sz 80, southern emission-line galaxy at low galactic latitude 78—86022
- T Tauri nebula, ionisation and emission line spectrum calc. 80—67820
- Taurus dark cloud, mol. spectra rel. to gas temps. and motion 77—78851
- Taurus HL-1, small H I velocity bridge, 21 cm obs. 78—28755
- Taurus Molecular Cloud 2 (TMC-2), HC_5N and NH_3 obs. 80—26957
- Tautenburg objective prism survey objects, high-resolution spectra and redshifts 80—4436
- Titan, IR spectrum from 0.8 to 2.5 microns 80—21946
- Titan, Kuiper bands detect. in spectrum 78—85898
- Titan, search for H_2 (3,0) S1 line in spectrum 78—4143
- Titan, visible and near IR spectrum of methane in atmosphere 80—46471
- TMC2, interstellar dark dust clouds, HC_5N and HC_7N obs. 78—54023
- Tololo emission line galaxies, size, morphology and spectroscopy, visible obs. 80—73044
- Tololo emission-line galaxies, nature from photometric and spectroscopic obs. 78—49531
- Tololo quasars, follow up visible spectroscopy for five candidates 79—17125
- transient astronomical phenomena, video detection and analysis techniques 79—80239
- transrelativistic plasmas, effect of photon pair prod. on radiation spectrum 78—20632
- Triton, image tube spectra, 6800-9000 Å, search for possible atm., methane upper limit 79—16880
- Triton, satellite with atmosphere, IR spectrum obs. 80—21945
- Trojan asteroids, albedo and reflection spectra rel. to comp. 80—56751
- Tycho's supernova remnant, filaments spectrum 78—73747
- Tycho SNR spectrum, model of optical emission from fast shock wave 80—46631
- Tycho supernova remnant, radio struct. and spectral index distrib. 80—56919
- Tycho supernova remnant, Type I SNR, elemental abundances from X-ray spectrum 80—46635
- Tycho supernova remnant, X-ray line emission obs. 80—46636
- 3U 1207+39 (NGC 4151), Seyfert galaxy, high-energy X-ray obs. 77—45610
- 3U 1915—05, X-ray burst source discovery 78—8155
- 4U 1916—79, high-latit. X-ray source, X-ray spectrum and variability 78—32611
- 3U 1957+40 (Cygnus A region), X-ray spectrum 77—53700
- ultralow dispersion spectroscopy ultralow dispersion spectroscopy of stars and galaxies 79—53733
- ultrasoft X-ray background spectrum, obs. in S galactic hemisphere 77—45615
- Uranus, 5-20 micron obs. 78—32393
- Uranus, albedo and spectral features from IR obs. 80—82299
- Uranus, disc profiles, narrow waveband, 6000-8500 Å region 79—66960
- Uranus, disk structure in 7300 methane band 80—17544
- Uranus, H_2 quadrupole lines detect. in spectrum 78—93149
- Uranus, HD detect. at 6063.88 Å, D/H abundance ratio calc. 78—57495
- Uranus, HD line obs. and atmospheric D/H ratio 78—57497
- Uranus, IR spectrum from 0.8 to 2.5 microns 80—21946
- Uranus, limb brightening within methane 7300 Å band 78—85902
- Uranus, methane 6825 Å band obs. 77—78715
- Uranus, methane absorpt. band in spectrum 78—45275
- Uranus, rot. period, modified spectroscopic technique 78—16345
- Uranus, rot. period from spectral line tilts 78—20726
- Uranus, rot. period meas. 78—7920
- Uranus, rot. period spectroscopic determ. 80—51691
- Uranus, rotation velocity determ. 78—36508
- Uranus, unsuccessful search for ethane emission 78—16344
- Uranus, UV albedo wavelength var. 80—82295
- Uranus occultation of SAO158687, obs. possibilities in methane bands 77—29719
- Uranus reflected spectrum, effects of seeing rel. to period determ. 80—46479
- Uranus visible and near IR spectrum, appl. of methane band-model parameters 80—98609
- UTR-2 survey, spectra of sources in 10-1400 MHz range 79—97092
- UV galaxies, double nuclei, visible spectra obs. *(Russian)* 80—77495
- variable compact object discovery in Perseus, bright blue N-galaxy, photometry and spectrum 79—12524
- variable radiosources, spectra, RATAN-600 radiotelescope obs. *(Russian)* 78—61927
- Vela SNR, IUE UV spectrum 80—101635

astronomical spectra continued
  Vela X supernova remnant, radio polarisation and spectral index distribs. 80—56909
  Vela X-1, X-ray spectrum obs. by OSO 8 78—49555
  Venus, cloud and temp. struct., from 12-20 μm spectrum 79—66946
  Venus, cloud properties from airborne obs. of near-IR reflectivity spectrum 78—53850
  Venus, CO_2 7883 Å band, high-dispersion spectroscopic obs. near superior conjunction 78—53851
  Venus, CO_2 8689 Å band high-dispersion spectroscopy near superior conjunction 79—75129
  Venus, CO_2 band spectroscopic obs. at 7820 Å 77—37540
  Venus, CO_2 IR absorpt. bands, 3900-10000 cm^{-1}, assignment 78—7896
  Venus, CO_2 line Doppler shift rel. to retrograde winds possible periodic vars. 79—25530
  Venus, CO_2 nighttime luminescence, Venera 9 and 10 spectroscopic obs. 77—78701
  Venus, CS_2 as candidate for 3150 Å band 79—40108
  Venus, emission spectrum, 17-38 μm, aqueous H_2SO_4 droplets in CO_2 atm. 78—40855
  Venus, far IR spectral obs. 77—29681
  Venus, H Lyman α emission rel. to exosphere temp. day-to-night var. 79—35164
  Venus, high spectral resolution ground-based obs. in 450 to 1250 cm^{-1} region 77—91456
  Venus, interpretation of weak spectral absorpt. lines 78—24481
  Venus, IR bands rel. to H_2SO_4 aerosol medium optical props. 78—65526
  Venus, IR spectrometer obs. on Venera 9 and 10 spacecraft 77—78698
  Venus, night airglow excitation, O_2 Herzberg II bands 77—41340
  Venus, nighttime luminescence, CO molecule identification 77—78702
  Venus, NO nightglow bands 80—46428
  Venus, O_2, $^1\Delta g \rightarrow {}^3\Sigma g^-$ band, prod. mechanisms 80—82251
  Venus, $O_2(^1\Delta)$ airglow and nightglow emission 80—17515
  Venus, SO_2 detect. in UV spectrum 79—62781
  Venus, spectral line profiles and phase curves for Rayleigh scatt. 77—29684
  Venus, UV nightglow, IUE obs. 79—62782
  Venus, winds, spectroscopic obs., techniques and data reduction 79—75130
  Venus atmosphere, absorpt. spectrum rel. to thermal radiative transfer numerical modelling 80—8574
  Venus atmosphere, information from equivalent widths in spectropolarimetry 79—70976
  Venus atmosphere, solar raldiation spectra comp. rel. to Venera 9 and 10 illumination meas. 79—88612
  Venus clouds, UV absorbers identification 78—20665
  Venus clouds spectropolarimetry, lines equivalent widths information content 80—31215
  Venus dayglow spectrum, 1250 to 1430 Å, Pioneer Venus obs. 80—77311
  Venus dust ring, scattering spectrum obs. by (Venera 9, 10) 79—75131
  Venus nightglow spectrum, $O_2(C^3\Delta_u$ to $a^1\Delta_g)$ 79—16856
  Venus UV reflectance spectrum, SO_2 detect. by IUE 79—101101
  Venus UV spectroscopy, initial results from Pioneer Venus orbiter 79—48711
  Vesta, spectral refl. meas., pyroxene absorpt. band 77—82146
  vinyl cyanide, microwave spectra data tables 79—59445
  Virgo, Perseus and Coma clusters, X-ray obs., spectral evidence for hot evolved gas 77—17695
  Virgo A (M87), radio components, spectral indices from 1.3 cm obs. 78—49550
  Virgo cluster spiral galaxies, H I deficiency from 21 cm obs. 80—62277
  Virgo cluster X-ray source, power-law spectrum rel. to two-source struct. 78—54090
  Virgo galaxy cluster, low energy X-ray absorpt. obs. 78—86025
  Voyager 2 radio signals, ang. and spectral broadening during coronal occultation, 1979 August 80—51639
  VRO 42.05.01, Hα inteferometric obs. of fast filaments and high vel. gas 79—75258
  VV 126, multicomponent interacting galaxies, visible spectroscopy obs. *(Russian)* 80—77494
  VV 150, galaxy chain, photoelectric and spectroscopic study 80—98724
  VV 493 (UGC 07910), unusual extragalactic object, morphology and spectrum rel. to probable nature 80—98718
  VV 5-32-63/64 in Abell 1775, supermassive double galaxy theory questioned 80—8693
  VV 794 H II regions, photographic and spectral obs. *(Russian)* 80—77493
  VV 8, galaxy, spectrum rel. to rot., mass and surface brightness obs. *(Russian)* 79—48937
  W33, recomb. lines as evidence for cool H II region with mass flow 78—49501
  W33 A, 4.5-8 μm spectrum 79—101181
  W35, W43, H II regions, low-freq. radio recomb. lines studies 78—32589
  W3, IR spectra and IR emission maps from 4.9 μm to 20 μm 78—49495
  W3(OH), high vel. water maser features obs. 80—31339
  W3 compact sources, 8 to 13 micron spectrophotometry, silicate absorpt. spectra 77—57070
  W3 H II region, CO, CS and HCN obs. LF obs. 80—82446
  W48, H II region, H 85α recomb. lines obs. 78—28762
  W48, OH emission and absorption, spatial distrib. in H II region *(Russian)* 80—36733
  W49 A, struct. deduced from mol. and recomb. line obs. 77—33665
  W49 region, CH radio emission spectra 77—87511
  W49A, high sensitivity Hnα radio recomb. line obs. 80—26998
  W49A, W51A, compact H II regions, H109α recomb. line, aperture synthesis obs. 80—105314
  W50, supernova remnant, N II emission enhancement and distance rel. to assoc. with (SS 433) 79—92783
  W50, supernova remnant, optical filaments spectra rel. to SS 433 mass loss rates and lifetime 80—12804
  W50, supernova remnant, optical nebulosity discovery from Hα and forbidden S II obs. 79—88723
  W50, supernova remnant, optical spectrum 80—90557
  W50, supernova remnant, spectrum of optical nebulosity 80—51851
  W51, detect. of impact broadening of recomb. line 78—28741
  W51, O III 51.8 μm forbidden emission line obs. 79—25685
  W51, probable detect. of methylamine-d_1 77—33610
  W51, W49, airborne for IR spectroscopic obs. rel. to dust cloud model 80—36684

astronomical spectra continued
  W51 (IRS 2), compact H II region, 2 to 4 micron spectrophotometry 77—13422
  W51 (IRS 2), H and He lines in obscured luminous H II region 80—51830
  W51-IRS 2 and W49 NW, compact H II regions, IR spectra obs. 80—90497
  W 3, H II region, recomb. line obs. of nearby partially ionised medium 77—57077
  W 51 region, possible detect. of Na I 17 cm hyperfine emission 78—8139
  X-radiation diffuse background above 20 keV, spectrum from balloon obs. 78—54096
  X-ray and gamma-ray lines, prod. by nonthermal ions 78—36725
  X-ray binary systems, K-fluorescence lines in spectra 78—93456
  X-ray burst, spectral evolution 77—29958
  X-ray bursters, spectroscopic study of optical counterparts 80—46699
  X-ray bursts spectra, effects of thermal limit for spherical accretion 78—45430
  X-ray clusters of galaxies, radial vel. dispersions 80—8696
  X-ray diffuse background, spectrum from 3 to 50 keV 80—41916
  X-ray emission from optically thin plasmas, abundance effects on continuum spectrum 78—53814
  X-ray emission lines, obs. by HEAO-2 satellite 79—92892
  X-ray emission spectrum, multiple Compton scatts. effect, Monte Carlo calcs. 78—96389
  X-ray heated medium phase transfer, optical spectral line emission bursts *(Russian)* 80—77286
  X-ray line emission from clusters of galaxies, numerical models 78—8149
  X-ray pulsars, cyclotron line formation in accretion column 80—67901
  X-ray source in Orion Nebula (M42), X-ray spectrum from Astronomical Netherlands Satellite 78—28852
  X-ray sources, 0.2 to 10 keV spectra obs. from on board (Salyut 4) 77—91665
  weak X-ray sources, ANS meas. 80—46701
  X-ray sources, ANS obs. of intensity and spectral vars. 79—17127
  X-ray sources, Compton scattering effects, thermal bremsstrahlung spectra 79—84869
  X-ray sources, Comptonization and radiation spectra, Monte Carlo calc. *(Russian)* 79—80372
  X-ray sources, emission mechanisms, detection techniques 77—22061
  X-ray sources, non-thermal, spectral props. constraints rel. to X-ray background synthesis 80—27021
  X-ray sources, optical spectrum of high temp. gas, emission line formation *(Russian)* 80—36740
  X-ray sources, spectra determ. via high-energy instrument on OSO-8 78—28522
  X-ray sources, time-dependent Comptonisation and X-ray reverberations rel. to fluctuations spectral evolution 80—86013
  X-ray sources in galactic centre and Cygnus region, spectral characts. 78—54079
  X-ray sources similar to Scorpius X-1, flux and spectrum vars. 77—13498
  X-ray sources spectroscopic obs., review *(German)* 77—60854
  X-ray spectra, direct deconvolution method 80—85867
  X-ray spectra, limitations, comments and reply 77—56824
  X-ray spectra, use of a priori information in derivation of temp. structs. 78—20778
  X-ray spectra, usefulness 77—56823
  X-ray spectra restoration 79—25515
  X-ray spectral lines profile evolution due to Comptonisation, Monte Carlo computations 79—66916
  X-ray spectral observations, value 77—5455
  X-ray spectroscopy, solar and cosmic, symposium, Holmburg, England (May 1975) 77—5433
  young supernova remnants, radio spectral index evolution according to observational data 79—75256
  Zeeman components with hyperfine structure, line strengths and splittings 78—77482
  zodiacal light, search at 1550 Å, and 1550 to 4200 Å spectrum 79—16882
  zodiacal light, UV spectroscopy at 20° elongation 78—20728
  zodiacal light Fraunhofer lines Doppler shift, interplanetary dust dynamics 78—45278
  zodiacal light IR radiance model and meas. 78—81588
  zodiacal light spectrum, Doppler shifts meas. 78—85904
  Zw 1400+0949 cluster (NGC 5416 group), 21 cm obs. 80—22090
  I Zw 1727+5015, redshift and spectra of BL Lacertae-type object 78—41044
  I Zw 1, analysis of spectra of type 1 Seyfert galaxy 79—71103
  III Zw 2, quasar, spectrophotometry of assoc. galaxies and nebulosity, redshifts 79—21460
  II Zw 40, 70, 71, CO emission upper limits 78—36693
  II Zw 40, dwarf galaxy, line and continuum radio spectra 79—8992
  VII Zw 421 and II Zw 67, spectrophotometry of S0 galaxies 80—51866
  I Zw 92, III Zw 77, compact galaxies with broad emission lines, spectra 78—73760
  Zwicky compact galaxies, spectroscopic survey 79—17074
  Ar I 3949 Å, Stark width in medium electron density plasma 79—63954
  C abundance in Orion Nebula and IC 418 from visible and UEI obs. 80—82451
  C II regions assoc. with reflection nebulae, recombination line spectra 78—69857
  C III spectral lines, IUE obs. of optically thin emission regions 79—71089
  C_2 absorption bands in stellar spectra, 876 nm obs. 80—12805
  C_2, calc. of bands strengths of Swann bands 77—61810
  C_2 in comets, Swan/Phillips band ratio, statistical equilib. 79—96969
  CH in diffuse interstellar medium, optical and radio obs. 78—93356
  CH, interstellar, radio obs. towards various galactic objects 77—87512
  CH, interstellar, rot. levels struct., excitation mechanisms 78—21908
  C_4H (butadiynyl) radical, detect. towards (IRC+10216) 78—93374
  CO emission from late-type galaxies 78—89250
  CO, fourth positive system in 1115-4759 Å range 77—49291
  CO, in galactic reflection nebulae, emission lines obs. 77—53658
  CO, interstellar, distrib. around (l=30°, b=0°) 80—41868
  CO, interstellar, obs. in young cluster (IC 5146) 79—48881
  CO interstellar emission intensity rel. to H I absorption column density 79—35319
  CO J=1-0 and 2-1 obs. of Lynds 1551 dark interstellar cloud 80—105318

astronomical spectra continued

- CO line profiles for dark molecular clouds 79—5877
- CO line radiation transfer in collapsing dark cloud, Monte Carlo method appl. 79—44357
- CO, microwave spectral line profiles, rotation effects in CRL 437 peculiar IR source 78—45426
- CO vel. features in OMC rel. to shock fronts and expansion of Orion H II region 80—41880
- CO$^+$ in Periodic Comet Schwassmann-Wachmann 1 near minimum brightness 80—82305
- ^{12}C^{16}O emission, unsuccessful search at 2.6 mm wavelength of globular clusters 78—41000
- ^{13}CH, predicted Λ-doubling spectrum 77—30857
- ^{13}CO in external galaxies, ^{12}CO/^{13}CO intensity ratios 80—4416
- CaO, J=4-3 106 GHz undetected transition in stars and molecular clouds 79—71090
- Cr I, discrepancies between theoretical and experimental oscillator strengths 77—83539
- Cr I excited levels, lifetime meas., oscill. strengths 77—71777
- Fe I 3719.94 Å line broadening by He, line width and shift meas., lab. expt. 77—73942
- Fe II permitted emission in Seyfert 1 galaxies and QSOs, obs. 79—35361
- Fe II permitted lines in spectra of type 1 Seyferts and quasars 79—44602
- Fe II UV lines in QSOs, spectrophotometry obs. 80—73063
- Fe III in astronomical sources, multiplet table 80—41732
- Fe VI, forbidden emission under nebular conditions 79—8970
- FeH, wavelengths and line intensities for visible and near IR bands, astronomical appls. 77—10680
- H, Balmer spectrum at line merging region, statistically extended recomb. continuum and line dissolution 77—27006
- H I, galactic, high angular resolution emission spectra, self absorpt. and other characts. 79—35350
- H I, galactic subsystem, 21 cm line profile rel. to galactic rot. curve *(Russian)* 80—36724
- H I, hot, interstellar, between Sun and Earth, solar Lyman α absorpt. 80—31185
- H I 21 cm line radial vel. contour maps 80—17626
- H I absorption at intermediate galactic latit., aperture synthesis obs. 79—12503
- H I absorption from CL 4, compact radiosource 79—48944
- H I absorption in galactic centre direction 80—77465
- H I absorption in QSO spectra, search for absorption by clusters of galaxies 78—93448
- H I and Mg II absorpt. lines obs. in QSOs and BL Lacertae objects 78—28838
- H I at high galactic latitudes, time variable 21 cm line profiles correction 80—51844
- H I in field of elliptical galaxy NGC 1052, 21 cm emission mapping and line profiles 80—98719
- H I Lα/Hα ratio for flares, quasars and prominences 78—61826
- H I Lyman α formation in expanding spherical nebulae with dust 79—8975
- H I Lyman α line formation in expanding spherical planetary nebula 79—30110
- H I Lyman α profile in interplanetary space 80—8586
- H I near Orion Nebula, obs. of absorpt. line vels. and 21 cm emission distrib. 80—105322
- H I profiles classification system for dwarf galaxies, discrete redshift and asymm. 78—49517
- H I regions, 21 cm spectra rel. to galactic shocks 78—54042
- H I regions, comparison of 21 cm obs. with UV and optical absorpt. line meas. 78—24532
- H I regions, galactic, emission absorpt. obs. from Arecibo 78—57610
- H I regions, high latit., search for OH 18 cm absorpt. line spectra 80—67841
- H I regions, transition probabilities and absolute oscillator strengths for C I, O I and N I absorpt. 77—49448
- H I regions and assoc. H II regions, H and C radio recomb. lines obs. 77—17659
- H I regions towards extragalactic radio sources, 21 cm emission, and absorpt. obs. 80—94854
- H I survey, contour maps, 21 cm obs. 80—85986
- H I within 10° of galactic centre direction, 21 cm emission line profiles 77—78853
- H II Brackett α line survey of compact IR sources 79—62882
- H II compact regions, theoretical spectra *(Russian)* 78—4337
- H II condensation in NGC 2175, spectrum and vels. 78—20883
- H II regions, ^{12}C^{16}O and ^{12}C^{18}O $J=2\rightarrow1$ transitions obs. 80—73022
- H II regions, chemical comp. of galactic and extragalactic regions 78—93359
- H II regions, compact, IR obs. in 3.4 to 33 microns range 77—22287
- H II regions, compact, in galaxy NGC 6822, near spectroscopic discoveries 80—51854
- H II regions, effects of dust on radio and optical spectra 77—33588
- H II regions, electron temps. determ. from radio recomb. line obs. at 22 GHz 79—35334
- H II regions, forbidden O III 88 μm line emission obs. 78—49503
- H II regions, galactic, forbidden S III 18-71 micron emission obs. 79—97046
- H II regions, giant, extragalactic, vel. dispersions from Hα line widths 79—44606
- H II regions, H I absorption profiles towards 11 galactic sources 79—12499
- H II regions, H137β/109α intensity ratio interpretation 80—31344
- H II regions, H166α recomb. line obs. at 1425 MHz 80—90512
- H II regions, high-excitation, effects of inhomogeneities on spectra 78—54007
- H II regions, line intensity data compilation 79—88721
- H II regions, multiple-component, radio recomb. lines press. broadening 80—4419
- H II regions, radio recombination line obs. of C and H from 10 areas 78—93360
- H II regions, search for Zeeman effect in RF recomb. lines 77—60809
- H II regions, spectrophotometry from 4 to 8 μ of compact regions 79—35321
- H II regions, weak emission lines spectrophotometry using image tube *(French)* 79—88601
- H II regions, weak shocks props. rel. to line strengths 78—93348

astronomical spectra continued

- H II regions emission line spectra, influence of star, gas density and chemical comp. 78—61911
- H II regions forbidden line emission spectrum, effects of motion of hot exciting star 77—78845
- H II regions in barred spiral galaxies NGC 1313, 5236 and 7552 visible obs. 80—82510
- H II regions in Magellanic Clouds, model nebulae anal. rel. to chemical comp. determ. 80—22085
- H II regions in NGC 5128, picture processing anal. and spectra 79—53907
- H II regions in Perseus arm, spectrophotometry and reassessment of galactic abundance gradients 80—22055
- H II regions in southern galaxies NGC 300 and 1365, spectra and comp. 80—4441
- H II regions near nucleus of spiral galaxy NGC 3310, absolute and relative line intensities 80—62235
- H II regions radio emission spectra, consequences of improper analytic methods 78—54000
- H-like ions, departure coeffs. from thermodynamic equilib., rel. to radiosources recomb. lines 79—76369
- H$_2$ 2.1 μm line detected in IC 443 SNR 80—17630
- H$_2$ 2.12 μ emission from Orion Nebula, temporal vars. possibility 80—17631
- H$_2$ (4,0) and (3,0) S(1) lines, absorption strengths 79—16852
- H$_2$, interstellar, reson. fluoresc. with Lyman α 79—8821
- H$_2$, interstellar, search for 2.1 μ emission in southern hemisphere IR sources 80—22059
- H$_2$ S(2) 12.28 μm rotational line in Orion Molecular Cloud 80—41881
- HC$_9$N, detect. in interstellar space 78—93370
- HCl in diffuse interstellar clouds, abundance and chem. models 80—91570
- HD 4-0 and 5-0 bands, absorption strengths in outer planet atmospheres 80—43059
- HNC, millimetre spectrum, rot. consts., force consts., U90.7 interstellar line, struct. parameters 77—57989
- HN^{13}C and HNC, hyperfine structure in dark interstellar clouds 79—101182
- H$_2$O 22 GHz maser emission from W3(OH), 49N and 51, spatial distrib. 78—93355
- H$_2$O, interstellar, 183 GHz line emission obs. 80—41869
- H$_2$O, interstellar maser lines very-high-velocity satellite features generation by stimulated Raman scatt. 78—73746
- H$_2$O maser emission from NGC 4945 galaxy 79—40271
- H$_2$O maser in H II region complex RCW 48-49, spectrum 77—57102
- H$_2$O maser source in Orion A, radio flux density and line width during outburst *(Russian)* 80—105320
- H$_2$O maser source near NGC 2071, discovery and spectrum 78—73768
- H$_2$O maser sources in different stages of evolution, new VLBI maps 80—26954
- H$_2$O maser sources near Herbig-Haro objects 7-11, 22 GHz obs. 80—73019
- H$_2$O masers, interstellar, high-resolution spectroscopic obs. 77—74154
- H$_2$O masers assoc. with newly formed OB stars, spectra and positions 78—12390
- H$_2$O masers located near Herbig-Haro objects, discoveries 79—21369
- H$_2$O sources spectra, autocorrel. anal. 78—65713
- H$_2$O$^+$, electronic spectrum, predicted IR and microwave lines, comet tail bands 77—473
- H$_2$O$^+$, interstellar, unsuccessful search and abundance upper limit 78—69860
- Hα emission objects in Coalsack direction, finding list 77—22115
- Hα emission stars, pre-main sequence evolution 80—56827
- Hα(Dα) plasma red shift meas. in Ar arc, ion dynamic depend. 80—10364
- He, forbidden radio lines, 2^{3}P state fine struct. 77—23447
- He H$^+$, formation and destruction in gaseous nebulae, assoc. IR emission line spectrum 79—44589
- He I, rate coeff. for 2^{3}S$\rightarrow$2^{3}P transition electron impact excitation 79—48664
- He I 584 Å in quasars and gaseous nebulae, line transfer problem and line strength 80—67550
- He II recombination lines, calc. intensities in UV 78—94212
- Hnα radio recombination lines, profile in static ion field 77—78629
- Hnβ radio lines profiles in static ion field 79—62740
- Io, Na I, Ca I, Fe I, and Mg I emission lines in spectrum 79—21223
- ^{7}Li and ^{7}Be gamma ray lines from $\alpha\alpha$ reactions 77—87248
- Mg complex, bis-pyridal-Mg-tetrabenz-porphyrin, disagreement with diffuse interstellar bands 80—56905
- Mg II, interstellar column density towards nearby stars 78—41023
- Mg II 2934 Å emission in QSOs, possible identification 78—41073
- MgH, $A^2\pi-X^2\Sigma^+$ system, dissoc. energy 77—10686
- N I interstellar absorption in γ Cassiopeiae direction, UV obs. 80—51823
- N II 6584 Å forbidden line profiles of giant H II regions 79—67081
- N V, hot interstellar gas diagnostic, IUE obs. 80—101634
- N$_2$D$^+$, interstellar, radio emission spectra detect. 78—16492
- NGC 1499, H II region nebula parameters determ. from decametre wavelength obs. *(Ukrainian)* 79—40243
- NH$^+$, interstellar radioastronomical freq. prediction at 13625 MHz 78—24544
- NH$_3$ emission and absorption at 23 GHz toward radiosource W3(OH) 78—36714
- NH$_3$, interstellar, obs. in mol. cloud near (S106) 79—84840
- NH$_3$, interstellar, spectra in southern radio sources 78—69863
- NH$_3$, interstellar emission line in Orion, 23 GHz obs. 79—30109
- NH$_3$, non-metastable absorption at 23.1 GHz, first obs. towards W3 (OH) 78—65677
- NO$^+$, interstellar transitions in mm and IR wavelengths 80—56906
- NO$^+$, R$_e$-function of A-X system, rel. to astrophysical meas. 78—13554
- Ne V forbidden lines, collision strengths for electron impact excitation, astrophys. appl. 79—50138
- O, absolute fluoresc. production cross section, 1304 angstrom, from CO(CO$_2$) UV photodissoc. 80—32652
- O I 5577 Å forbidden line in meteor trains, emission mechanism 78—49395
- O I 7990 Å and 11287 Å branching ratios, astron. appl. 79—41134
- O II, relative intensities and lifetimes in nebulae, conventional radiation theory 80—109513
- O II and S II forbidden lines as determinant of reddening and electron density 79—30114

astronomical spectra continued
O III 51.8 μ forbidden emission line obs. of Orion Nebula 78—65510
O VI absorption in interstellar cloud surfaces 79—97049
O_2 dayglow and O_3 abundance latit. var. on Mars 79—53750
OH 18 cm emission sources, fluxes and circular polarisation (1965-1972) 77—13441
OH 1.6 GHz maser emission from W3(OH), 49 N and 51, spatial distrib. 78—93355
OH 26.5+0.6, IR spectrum, polysaccharide grain model 78—12342
OH and H_2O masers, radial vel. struct. 77—33617
OH astronomical maser sources OH 231.8+4.2, CY Canis Majoris, M1—92, UHF obs. 80—90550
OH emission obs. of Lynds 134 dark nebula 80—22062
OH excited states, satellite lines anomalies 77—42315
OH, interstellar, new main line maser obs. with probable Zeeman pattern 80—56908
OH, interstellar, radio obs. towards ζ Ophiuchi and evidence for interstellar shock 79—97052
OH maser clouds, line spectra rel. to saturation 77—91657
OH maser emission from W3 (OH), Zeeman effect 78—93377
OH maser sources, IR lines optical thicknesses effects on inversion 80—17681
OH maser sources near galactic centre, systematic search at 1612 MHz 79—35415
OH masers, type I, positions, polarisation, nearby H_2O masers, radio and IR props. 79—25671
OH masers in Orion Nebula, evidence for Zeeman splitting 78—16493
OH, nonthermal main lines in interstellar dust clouds and OH abundance 80—36683
OH, radical, microwave spectra, search possibilities 79—26972
OH radicals, microwave spectra data tables 78—50542
OH radio emission sources, type IIc, in W33, obs. *(Russian)* 80—62247
OH sources, 1720 MHz transition survey, comparisons with 1612, 1665, and 1667 MHz obs. 77—45586
OH weak masers detect. in H_2O masers direction 77—33618
S II, fine-structure transitions by electron impact 78—65493
S II forbidden line emission from SNRs in M33 galaxy 78—36665
Si lines as spectral diagnostics for astrophysical plasmas, effect of charge transfer 80—41717
SiH^+, oscillator strengths and dissoc. energy determ. from time resolved precision spectroscopy 80—58272
SiO maser in Orion-KL nebula, VLBI obs. at 43 GHz 79—92836
SiS, and isotopes, microwave spectra and consts., review 77—23493

astronomical spectroscopy *see astronomical spectra; spectroscopy*

astronomical techniques
see also astrometry; radioastronomical techniques
6″ reflecting telescope construction, assembly 77—87266
76-115-B, tumbling cylindrical Earth satellite, rot. axis location using visual obs. 79—80201
abundance determ. in sequences of old open star clusters 77—29888
abundance determ. methods for novae in nebular stage 77—87279
abundance determ. using reddening-independent stellar characts. 79—5898
active aperture imaging for direction meas. of high energy γ-rays 80—62022
active optics imagery, postprocessing 77—29654
adaptive optics, rubber mirrors to compensate for atm. aberrations, book contrib. 79—35150
adaptive optics for imaging, wideband real time atm. compensation 77—45320
adaptive optics systems, bandwidth specification 77—46799
airborne IR observations, methods and instruments 78—69688
AKAIHOSHI flexible real time software system for radio astronomy obs. 80—82214
amplification of optical stellar images by atm. turbulence 80—72782
analemma construction using year-long solar images on photograph 80—12649
analysis of UK Schmidt trigonometric parallaxes and proper motions 79—66929
angular diam. determ. from IR photometry, appl. to Arcturus 77—64760
Ap and Am stars, numerical taxonomy 80—22015
Ap stars, line identifications, new wavelength lists 79—16967
Ap stars, recognition in Vilnius photometric system 78—65635
aperture synthesis using very long baseline interferometry 80—46414
artificial satellites electrostatic shielding from cosmic radiation, Cosmos 605 meas. 77—29622
asteroid families, clustering technique for concs. anal. in proper elements space 78—96420
asteroid family detection by new criterion, orbital data 80—82256
asteroid surface studies from Earthbound obs., technique 80—77324
asteroids, carbonaceous chondrite mineralogies remote spectroscopic identification from IR obs. 79—96946
asteroids orbital perturbations, analytical integration using regular proximities concept 80—72843
asteroids shape and spin axis orientation determination, photometric method *(Russian)* 80—8581
asteroids sizes and albedos, radiometric and polarimetric determs. 77—60708
astrometric and photometric system appl., automatic *(Russian)* 78—24467
astrometric plate reduction, least squares prediction appl. 79—40082
astrometric reduction of photographs and calibration of wide-angle cameras *(Russian)* 78—28532
astrometric reduction of planetary obs. using ecliptic zone plates *(Russian)* 80—46400
astrometric search for unseen stellar and sub-stellar companions to nearby stars and the possibility of their detection 79—30092
astrometric telescopes flexure, determ. via autocollimation method *(Russian)* 78—40818
astrometry, appl. of celestial photography with wide-angle astrographs *(Russian)* 78—40800
astrometry, astroclimatic influences on precision of photographic star positions obtained with wide-angle astrographs *(Russian)* 80—72748
astrometry, chromatic refr. correction tables for photoelectric stellar positions *(Russian)* 79—96889
astrometry, daytime obs., correction for anomalous refr. and personal errors 78—24441
astrometry, declinations differential determ. from obs. with vertical circle *(Russian)* 79—96888

astronomical techniques continued
astrometry, lateral refr. elimination from absolute declinations observed by micrometric method *(Russian)* 79—96890
astrometry, obs. of planets with Danjon astrolabe 77—64651
astrometry, overlapping plates method appl. to stellar positions catalogue for polar regions *(Russian)* 78—40801
astrometry, PDS microdensitometer meas. appl. to NGC 6494 (M23) cluster membership determ. 80—98697
astrometry, photographic vertical circle plates reduction using semi-automatic measuring machine *(Russian)* 79—96920
astrometry, photography against stellar background, iterative trajectory search algorithm *(Russian)* 77—17376
astrometry, reference photographic catalogue of southern sky *(Russian)* 80—72789
astrometry, rot. of fundamental coordinate system 79—62727
astrometry, sky photography programme with wide-angle astrographs *(Russian)* 80—72747
astrometry, space and ground-based, prospects 78—12083
astrometry, stellar absolute declinations system construction for entire sky using high-latit. obs 80—67520
astrometry and planetary detection using space-borne interferometers 80—109357
astrometry using Paloma Schmidt plates, accuracy 78—57455
astrometry with small Schmidt telescope, NGC 7027 position meas. 78—73749
astronometry, absolute star positions determ. by Sanders-Raimond method 77—53404
astrophotography, exptl. summer course 77—64902
astrophotography, isoplanicity meas., speckle holography 80—56717
atmosphere modulation transfer function, estimation via coherence interferometer *(Russian)* 79—16715
atmosphere refraction calc., theory for three-dimensional model 80—46260
atmosphere surface layer optical inhomogeneities, investigation via acoustic method 80—67434
atmospheric dispersion minimisation, correctors for compensated imaging 77—46695
atmospheric extinction reduction, anal. of Rufener's method 77—22083
atmospheric turbulence effect on seeing, mean vertical profile meas. 77—29379
Australian Astronomical Society, conf. Melbourne, Australia (May-June '77) 78—69655
auto-correlation method for supergiant semi-period of variation determ. 78—61854
automated faint galaxy counts and galactic evolution 80—105350
automated plate reduction techniques for globular clusters struct. determ. 77—41394
automatic photographic wavelength meas. with digital microdensitometer 77—64655
automatic reduction of low dispersion objective prism stellar spectra *(Italian)* 80—98567
automatic reduction of nebular emission line spectra 80—77294
autoregressive technique, appl. to astronomy and geodynamics *(Chinese)* 80—85869
averaging method for secular behaviour of dynamical systems 78—77469
B-type stars, luminosity and effective temp. determ. 80—17582
B-type stars detect. in interstellar clouds, use of interstellar molecules distrib. *(Russian)* 80—105321
background subtraction problem in panoramic photometry *(Italian)* 80—98570
bad seeing conditions avoidance within telescope domes 79—70960
balloon and satellite obs. of gamma-ray lines, appls. 78—45241
balloon-borne probes in stratosphere, atm. and astron. research 77—37435
balloons, Japanese 1966 to 1975 activities *(Japanese)* 77—82016
Balmer-index photometry, quantitative anal. of influencing factors 78—96404
barycentric radial velocities, computation with classical perturbation theories 77—45291
Be stars, emission shell diameter meas. possibility by lunar occultation method 80—56839
Be-stars, binary detection methods 77—56997
beam-foil spectroscopy, appl. to oscill. strengths meas. 79—50168
beam-foil spectroscopy appl. to solar UV spectrum 77—41314
binary star light and velocity curves simultaneous solution, eccentric orbit generalisation 80—36664
binary star orbital elements calc. using Fourier transform of eqns. 77—56832
binary star orbital inclination, polarimetric determ. for five systems 78—45358
binary star orbits solution, Fourier transform method 80—26899
binary stars, reflection effects evaluation, generalised approach 79—25631
binary stars, speckle interferometry appl. 77—71011
binary stars, stellar wind and gas streams obs. using multichannel spectropolarimetry 80—109471
binary stars in open clusters, freq. estimation from colour-magnitude diagrams 77—49441
binary stars minimum projected distance calc., recursive method for eccentric orbits 80—26904
binary stars orbital solutions, derivation for unseen companions 78—93313
close binary systems, radial vel. curves anal. 80—94829
black hole explosions, theory of optical and radio detect. 77—53622
black hole explosions detection, search for powerful radio bursts 77—37613
black holes, detect. via gravit. mirror effect *(Russian)* 78—40987
bolides topocentric coordinates determination, use of photography 78—61818
Bragg mode analyser potassium acid phthalate, Bragg refl. coeff. obs. 80—95204
Buoyant Venus Station placed by inflated balloon entry 78—4058
RS Canum Venaticorum systems, detect. technique using X-ray emission 79—21345
Cassegrain telescopes, automatic design of corrector systems *(Chinese)* 77—22088
celestial mechanics, 2101 Adonis problem soln. by recurrent power series integration 80—72842
celestial mechanics, analytical method for determ. of perturbations of orbital motion 78—24455

astronomical techniques continued
celestial mechanics, applied modern mathematical techniques *(German)* 78—45211
celestial mechanics, common derivation of averaging method and two-timescale method 78—85835
celestial mechanics, Fourier series fast evaluation 80—56711
celestial mechanics, orbitally stable multistep methods 78—85834
celestial mechanics, regularised numerical method based on Taylor-Steffensen power series *(Russian)* 78—49300
Cepheid binary detection from U-V curve obs. 80—98667
Cepheid variables, distance determ. method 77—45467
Cepheid variables, phase shift technique for determining incidence of duplicity 80—90453
Cepheid variables, radii determ. via method of max. likelihood 77—45459
Cepheids, reddenings from mean UBV colours 79—71056
Cherenkov radiation from large air showers, image reconstruction 79—25420
chondritic meteorites chemical anal. scheme, appl. to Cocklebiddy 79—2483
circumstellar dust envelopes, calc. of eclipse light curves and fringe visibilities 79—35234
classical Cepheids distances, check on phase shifts determined by ang. dia. method 78—16439
classification criteria for stars and star clusters, statistics from co-occurrence matrix *(Italian)* 80—98574
close binary stars, obs. by H I α and β line photometry 80—109470
close binary systems, polarimetric determ. of revolution directions and spatial orientations 79—35309
close binary systems, radial vel. curves anal. 80—90470
clusters of galaxies assoc. with QSOs, detection using radio source morphology 78—93434
CMT$_1$T$_2$ photometric system, southern standard stars 77—37507
coelostat pointing method 80—90338
colour astrophotography, slide and print developing 79—29996
comet motion, data processing for comparison of obs. and theory 77—41307
cometary equations of motion, recurrent power series integration 80—72882
cometary nuclei, brightness meas. technique 79—84745
comets, direct investigation by space probes 77—37494
comets motion, correction for nongravitational effects, comparison of methods 78—61811
compact galaxy detect. method *(Russian)* 77—49302
compact radio sources, mapping from VLBI data 78—89266
compensated imaging of celestial objects, atm. dispersion effects 77—42501
computer aided calibration technique for EUV instruments 80—85839
computer solutions for studying solar mag. fields and Skylab X-ray obs. correls. 77—82198
convolution of cometary brightness profiles by circular diaphragms 79—12433
cool DA white dwarf and subdwarf discrimination by spectroscopy and photometry 78—7999
cool stars, effective temps; ang. dias. and reddening determ. from 1 to 5 μm flux curves 79—44458
cooled emulsion photography for amateurs, astronomical appls. 80—56714
coordinate measurements using phase and fringe freq., tropospheric limitations 79—44375
CORAVEL, Cassegrain spectrophotometer for stellar radial vel. determ. 80—82210
coronal plasma diagnostics with broad-band X-ray imaging systems, physical parameter method 78—49414
coronograph, external occulting disc, scattered light reduction 78—36455
correlation analysis, appl. to galaxies deep samples large scale distrib. 79—67104
cosmic distance measurement using Cepheid variables 79—84920
cosmic dust condensation processes investigation, expt. techniques 80—26940
cosmic ray detection methods for energies $>10^{20}$ eV 80—82157
cosmic ray electrons, detect. by synchrotron radiation in geomag. and interstellar mag. fields 78—57412
cosmic ray intensity diurnal variation, two approaches to study 79—29953
cosmic ray variations, investigation via spectrographic method with inclined muon telescopes 78—45167
cosmic ray wide atmospheric shower development, cascade curves restoration *(Russian)* 80—36463
cosmic-plasma diagnostics 79—90469
cosmic-ray air showers, acoustic detect. 79—66901
cosmochronology, implications of Allende meteorite isotopic anomalies 80—4462
cosmological constant and data reduction 80—41923
cosmological deceleration parameter, direct meas. via 3C 286 radio absorpt. line 78—20902
cosmological density parameter, determ. from redshifts of complete sample of galaxies 77—29965
cosmological proper motion-redshift relation, determ. using superluminal radio sources 80—22095
cosmology, evolution free test for non-zero cosmological const. 80—4465
COSMOS machine for automatic photographic plate image meas. 80—77293
COSMOS measuring machine 77—64652
cosmothermometry, appl. of Ti^{3+}/Ti^{4+} ratios in Allende meteorite 79—12437
Cousins VRI photometric system, temp. and absolute flux calibration, appls. 80—26750
Crab Nebula X-ray spectrum, interstellar absorpt. features meas. via Si:Li detector 77—5439
crater size-freq. data presentation and analysis, standard techniques 79—44387
cross correl. detection of rapid stellar var. using two telescopes 77—82127
dark nebulae, visual extinctions determ. via star counts 78—57612
data acquisition and processing at Italian observatories *(Italian)* 79—62751
data acquisition and real time processing system for time service *(Italian)* 80—8549
data compilation and acquisition techniques at telescope 77—78649
data processing in IR astronomy 79—101087

astronomical techniques continued
data reduction for Saturn ring obs. 80—4294
data reduction methods, least-squares polynomial fitting technique 80—12682
deconvolution by maximum entropy, appl. to M87 jet optical photograph 80—62032
deconvolution method and appl. to lunar occultations 80—105174
deconvolution techniques applied to astronomical images 80—46407
deep galaxy samples correlation anal., techniques and appl. to two-colour sample 78—41056
degenerate star candidates, identification via UBV photometry 80—12763
Delaunay-Hill averaging method in limited circular three-body problem, error estimation *(Russian)* 80—8530
Delaunay-Zeipel transformation, use in reson. props. of celestial mechanics 80—46378
densitometers standardized density scale for photographic photometry *(Japanese)* 79—101075
design method for field corrector for parabolic reflector, design method *(Chinese)* 80—85857
detection of stellar systems by lunar occultations 79—44542
diffuse cosmic X-ray component separation in balloon borne meas. 78—28862
digital image centring algorithm for astrometric positioning 78—69696
digital image processing, local filtering methods *(French)* 80—46406
digital image processing applications, conference, San Diego (1977) 78—81528
digital image processing of simulated turbulence and noise degraded lunar images 77—45321
digital image processing techniques for planetary program and Earth resources information 78—96408
digital processing techniques applied to astronomical images 77—60626
digitized image presentation and evaluation, software package 79—58267
digitized stellar spectrogram processing using microdensitometer, ELSPEC/1 procedure *(Italian)* 79—62758
distance determ., Baade's method for pulsating stars 80—73082
distance determination, method for extragalactic objects with active nuclei *(Russian)* 80—51880
Doppler broadening parameters and Doppler shifts, meas. without spectrograph 78—20646
double star observations, phase-grating stellar interferometer *(Russian)* 79—101070
double stars, rectilinear trajectories calc., appl. to L 5094, effects of erroneous positions *(French)* 78—20857
dust complexes in spiral galaxies, optical anal. method, visible obs. 80—101638
dynamical astronomy numerical simulation, new Runge-Kutta algorithms 79—12387
early-type stars photospheric expansion, meas. via. Fourier anal. technique 78—93224
Earth daily free nutation parameters, determ. technique 78—96126
Earth satellite, tumbling, cylindrical, rot. axis location using visual obs., theory 79—80200
echelle spectrograms reduction, single procedure 80—56713
eclipsing binaries light curve analysis, new techniques and appl. to V444 Cygni 80—82417
eclipsing binaries light curves anal. by automated Fourier techniques, appl. to SX Aurigae 79—92798
eclipsing binaries orbits, appl. of Kalman filter to light curves 77—5546
eclipsing binaries photometric peculiarities anal., appl. to AU Monocerotis 80—77448
eclipsing binary light curve analysis, Fourier techniques 79—58261
eclipsing binary light curves anal., linearised limb-darkening coefficients 78—49480
eclipsing binary light loss analysis, Fourier techniques 79—58262
eclipsing binary solutions, coeffs. of approx. polynomials 77—17380
eclipsing binary star light curve anal. in freq. domain by automatized Fourier technique 80—22039
eclipsing binary stars, anal. of proximity and eclipse effects on light curves 77—53635
eclipsing binary stars, light curve analysis by Fourier techniques 80—72993
eclipsing binary stars, light curve analysis by Fourier techniques 80—72994
eclipsing binary stars, light curves Fourier anal. 77—9769
eclipsing binary stars, soln. of light curve by Kopal's iterative process 79—35310
eclipsing binary systems with disclike envelopes, light curve interpretation, appl. to HZ Herculis 78—65658
eclipsing variable stars, Fourier anal. of light curves, photometric perturbations for total and transit eclipses 78—12291
eclipsing variable stars, Fourier anal. of light curves 77—49428
eclipsing variable stars, Fourier anal. of light curves 78—93311
eclipsing variable stars, Fourier analysis of light curves, error anal. in freq. domain 80—31214
eclipsing variable stars, light curves Fourier analysis, appls. to eccentric orbits 79—25630
eclipsing variable stars Fourier anal., $B_{n,m}{}^q$ integrals explicit expression 79—35298
eclipsing variable stars with extended atmospheres, Fourier anal. of light curves 80—46604
eclipsing variables, Fourier anal. of light curves, geometric elements soln. 79—25634
eclipsing variables, Fourier anal. of light curves, photometric perturbs. 78—96507
eclipsing variables, Fourier anal. of light curves, photometric perturbs. for partial eclipses 79—25635
eclipsing variables, Fourier anal. of light curves 78—20854
eclipsing variables, Fourier anal. of light curves 79—25632
eclipsing variables, Fourier anal. of light curves 79—25633
eclipsing variables, Fourier anal. of light curves 79—30088
eclipsing variables, Fourier analysis of light curves 79—8946
eclipsing variables, Fourier analysis of light curves 79—8945
eclipsing variables, light curve Fourier analysis, eclipse parameters, geometrical determinacy 78—96503
eclipsing variables, light curves linear analysis, fractional light loss anal. 80—82416
Eggen's moving groups, high-dispersion analysis check 77—29838
Einstein effect observation at solar eclipse, 1981 July 31, scale correction determ. method *(Russian)* 80—51651
electron-positron pair track analysis in multilayer gamma-ray telescope 80—63469

astronomical techniques continued
electronographic imaging polarimetry of reflection nebulae 80—26964
electronographic photometry, calibration of UK 1.2 m Schmidt plates 79—88703
electronographic photometry, narrow-band high spatial resolution, appls. *(French)* 80—46408
electronographic recording of low-dispersion slitless spectra, quasar appl. 78—57467
electronography, developments for astronomical research 77—91440
elemental abundances, empirical determ. method tested on H II regions 78—61908
elliptical galaxies, ang. size determ., 2-D Fourier transform technique 79—35373
elliptical galaxies isophotes structure, meas. procedures 78—41058
elliptical galaxy rotation curve determ. 80—46675
ELSPEC/2, interactive procedure for spectrogram processing *(Italian)* 80—98566
EM sounding of Moon using surface magnetometer meas. 78—65518
energy method in stellar stability problem 79—35239
equidensitometric determ. of angular diameters of compact galaxies 78—16308
equidensitometry, photographic, astronomical appl. 77—56833
RX Eridani, RR Lyrae variable, radius determ., van Hoof method 77—2436
EUV spectra and solar atmosphere plasma diagnostics 79—30050
EUV spectroscopic method for electron density determ. in stellar atms. 79—16836
exospheres of Moon and Mercury, Monte Carlo simulation methods 80—67588
exospheres of Moon and Mercury, Monte Carlo simulation methods 80—67589
exploding black holes, search using atm. Cherenkov method 78—49473
external occulting disc as radially-graded neutral density filter, for solar coronal obs. during eclipses 79—80233
extragalactic distance determ., using UBV data and light curve models for Type II supernovae 79—62856
extragalactic distance scale, rel. to Hyades Cluster distance 78—8121
extragalactic distance scale, tertiary distance indicators 79—25708
extragalactic distance scale calibration, appl. to distance of giant spiral galaxy (M 101) 80—67852
extragalactic IR background radiation, meas. technique 80—17496
extragalactic object reddening determ. method 78—54039
extrasolar planet detect. using speckle interferometry 77—41309
extrasolar planets, direct imaging with space telescope during stationary occultations 78—85858
extrasolar planets detection, imaging theory 77—29882
extraterrestrial civilisations signals search, simulation approach 80—62039
extreme subdwarf stars, metal abundances from mol. band strengths, theoretical approach 78—93221
faint and low-contrast objects observations, image isocon appl. *(Russian)* 80—12671
faint light detection and spectrometry, book 77—25950
faint stars, spectral-type standards for objective prism plates 80—46539
fast transient phenomena, physical mechanisms affecting observations *(Italian)* 78—93105
fitting procedures for stellar positions on Schmidt photographs 80—72783
FK4, equinox and equator improvement *(Russian)* 79—58277
focal grating photometer obs. of southern visual star magnitude differences 80—67785
Fourier analysis of data with closely spaced frequencies, erroneous results 78—89298
Fourier analysis of eclipsing binary light changes 79—75247
Fourier analysis of eclipsing binary light curves, series expansions 79—75248
Fourier analysis of eclipsing variable light curves for partial phases 79—21350
Fourier analysis of light curves of eclipsing binaries for transit eclipses 78—96506
Fourier analysis of spectral line profiles 77—22105
Fourier analysis of the light curves of W Uma-type stars 79—21349
Fourier deconvolution of electronographic images 79—75112
Fourier method for stellar rot. vel. determ. using stellar spectrum *(Russian)* 79—80240
Fourier transform IR spectroscopy appl., conf., Columbia, USA (June 1977) 78—58067
Fourier transform spectrometry, appl. to stellar spectral energy distribs. and classification 77—82215
Fourier transform spectroscopy, airborne IR obs. 78—61747
Fourier transform spectroscopy appl. to remote identification of solids in solar system 77—87273
Fourier transformation of data sampled at unequal intervals 78—69697
Fourier transforms appl. to contrast profile method of vector mag. field meas. 78—53839
Fourier transforms of data sampled in unequally spaced segments 79—35140
frequency analysis of low-amplitude δ Scuti stars 79—35276
frequency analysis of low-amplitude δ Scuti stars 79—35275
Fresnel zone plate imaging, of solar active regions 78—49342
fringe visibility intensities, uniquely related to brightness distribs. 79—8842
fundamental quasimonochromatic stellar photoelectric photometry, accuracy *(Russian)* 78—65505
fundamental star catalogue system, improvement via relative determs. of celestial bodies coordinates 78—53797
G and K dwarf stars, flares detect. via Hβ emission line obs. 77—45456
galactic cluster membership probabilities, photographic meas. of relative proper motions of stars 80—51817
galactic nuclei, variable, photometric techniques, finding charts and comparison stars 78—81691
galactic reddening determ. 79—5875
galactic/equatorial coordinate systems, interconversion 79—88569
galaxies, spiral, rot. direction determ. by means of edge-on systems *(Russian)* 80—36722
galaxies, surface photometry, computerized analysis method 78—12100
galaxies ages, determ. from N/O ratio 79—25728
galaxies angular diameter counts, determ. of selection criteria for deep Schmidt plates 77—91623
galaxies distance scale, determ. from IR magnitude/H I vel. width rel. to expansion rate outside Local Supercluster 80—105325
galaxies distances determination, appl. of H II regions rel. dispersions 80—31360
galaxies distances determination, new method 77—29920
galaxies distribution in clusters, determ. via maximum likelihood method 80—56954
galaxies H I spectra, line calibration using small galaxies obs. 79—35382
galaxies high-order clusters, detect. techniques 78—12386
galaxies mean mass density estimation 77—49486
galaxies nuclei, vel. dispersions meas. using composite stellar spectra 77—57083
galaxies optical redshifts determ., Fourier transform filtering and cross correl. techniques 80—56936
galaxies photometry, seeing effects on elliptical galaxies cores light distrib. 80—12814
galaxies space distribution determination, statistical anal. of galaxy catalogues 80—46417
galaxies stellar population synthesis, spectral inversion technique 80—90339
galaxy and quasar observational magnitude cutoff bias elimination 80—56940
galaxy clustering models discrimination, n-point galaxy correl. functions applicability test 80—8699
galaxy clusters, mass density and gravitational potential estimation 79—12529
galaxy covariance function shape determ. at small scales 80—82506
galaxy groups classification technique, appl. to nearby groups quantitative membership probabilities 79—62919
Galaxy local structure, determ. from stellar kinematics *(Russian)* 78—77608
galaxy mass determination from binary galaxies, anal. of Turner's (1976) sample 80—67849
galaxy mass distrib. models, regularization method *(Russian)* 79—12507
galaxy masses, determ. from H I total profile widths 80—56937
galaxy models, numerical orbit computation algorithms comparison 79—12497
galaxy photography, image picture processing system for colour 77—49303
galaxy photometry, reduction to B_T system of Ames, Reiz and Zwicky catalogues of Virgo cluster area 79—58411
galaxy surface photometry, numerical mapping by interactive procedure *(Italian)* 80—98572
Galilean satellites, edge-finding technique for dias. determ. from Pioneer data 78—85893
gamma rays in 10^{11}-10^{14} eV range using atmospheric Cherenkov technique 79—25422
gamma-ray bursts, search with coincident balloon flights 77—49506
gamma-ray spatial pattern anal. via spectrometer with various shaped scintillators 79—16831
gamma-ray telescope artificial satellite, axis orientation determ. 78—53787
gamma-ray telescope on satellite, axis orientation determ. 79—2479
Geminid meteor stream, orbital period from quantitative simplicity index 78—53889
giant planets atmospheres, radiative transfer eqn. inversion for thermal struct. determ. 79—84735
global astrometry by space techniques, HIPPARCOS 80—109369
globular clusters, age and chemical comp. determ., review *(Polish)* 78—61751
globular clusters, parametric approach to slope of giant branch 77—53649
globular star cluster age and distance determ. method 80—82435
grating scanner meas. of stellar energy distrib., polarization effects 78—32355
gravitational experiments, search for relativistic effects on Earth artificial satellites motion 79—2465
gravitational radiation, seismometer detection possibility 80—86196
gravitational radiation detection, Ar laser interferometer appl. 79—101076
gravitational wave astronomy, introductory review 77—67368
gravitational waves detection, proposed search for correl. with neutrino bursts 78—77567
grid photography, appl. to NGC 4565 halo photometry 80—62261
ground-based astronomy, future, conference, Arizona (1979 May 9) 80—62386
Hadamard techniques in optics and their relationship to other multiplexing schemes 79—80242
hard X-ray detection, risetime discrimination appl. to pressurised Xe gas proportional counter *(Japanese)* 79—80219
Helios zodiacal light expt., data processing and evaluation 79—80235
heterodyne detection, optical IR tuning, wavefront distortions effect *(French)* 79—62755
hierarchical clustering techniques, appl. to NGC 1023 galaxy group membership 80—82521
high detective quantum efficiency image detectors, review 77—71010
high resolution UV solar spectroscopy, review 78—45313
high-energy neutrino astronomy, as probe of galactic nuclei 80—4432
high-resolution astronomical imaging, results 80—82225
high-resolution stellar vidicon spectrophotometry, appl. to α Bootis Ca II K-line 77—22213
high-speed digital image processing 78—12680
holographic emulsions for stellar spectra recording by interferometric method 78—73651
holography, twin-image, chromatic lens system, astron. appls. 80—87346
Hubble constant, determ. from H II region dias. 80—41887
Hubble constant determination, Type I supernovae appl. 79—40304
hypersensitisation of photographic emulsion *(Swedish)* 78—85853
hypersensitised astronomical plates, detective quantum efficiency gains and speed 77—64660
image anal. system 78—7886
image analysis, general system software and appls. 78—53834
image coding in near IR, multiplex technique 77—53428
image data processing system, Skylab X-ray solar obs. appl. 77—60619
image enhancement of solar corona photographs 79—16841
image photometric analysis for astrometry, appl. to Jupiter and Galilean satellites *(French)* 80—85880
image processing, atmospheric turbulence effects, interferometer data technique 80—12679
image processing, digital system *(Italian)* 80—98558
image processing at Trieste Observatory *(Italian)* 79—58270
image processing by digital filtering *(Italian)* 80—98573

astronomical techniques continued
- image processing digital techniques 78—81555
- image processing of galaxy photographs 77—9664
- image processing technique appls. to scanned radiometer data of stellar sources 77—49312
- image processing techniques 78—87022
- image reconstruction, from incomplete and noisy data 78—53837
- image reconstruction, iterative computer method 80—102634
- image reconstruction, turbulence degraded by spectral ratio meas. 78—9334
- image reconstruction from divergent ray, 3D 79—98299
- image reconstruction performance of image-plane sharpness criteria 78—93123
- image restoration appls., conf., Bordeaux, France (Mar. 1979) 80—41935
- image restoration by regularisation method, appls. *(Italian)* 78—93124
- image restoration using flexible mirror telescope 77—45319
- image restoration with max. entropy, entropy expression 78—42283
- image restoring with maximum entropy, Poisson sources and backgrounds 78—66769
- image sharpening telescope, atm. distortion compensation 77—49294
- image synthesis, computer simulation, for strip telescope 77—29660
- imagery multiple analysis at JPL's Image Processing Laboratory 80—82219
- images, bidimensional Fourier filtering *(Italian)* 79—58269
- images coherent optical processing, expts. *(Russian)* 80—12675
- images digital display, interactive program *(Italian)* 80—98559
- images iterative reconstruction, non-negativity constraint 79—101081
- images optimal classification into stars or galaxies, Bayesian approach 80—21920
- imaging in the presence of random wave aberrations 79—76607
- imaging of extrasolar planetary systems 80—82426
- imaging through randomly fluctuating media, speckle interferometry appl. 77—13248
- imaging through turbulence with telescope array, speckle interferometry 77—5458
- information processing methodologies, conference, Trieste, Italy (1979 February 23 to 24) *(Italian)* 80—94917
- information processing of astronomical negatives, using thick-film holograms 79—48690
- information treatment methods, meeting (Trieste, 1977 Nov. 24-25) *(Italian)* 79—58265
- information treatment methods, meeting (Trieste, 1977 Nov. 24-25) *(Italian)* 80—8548
- infrared heterodyne spectroscopy in astronomy 78—85859
- initial orbit determ. using angles and angular rates of movement of artificial satellites 78—53795
- instrumental stray radiance meas. in Skylab coronagraph 77—60607
- integral evaluation for Fourier analysis of eclipsing binary light curves 78—45236
- integrated IR photometry and wide field techniques for globular clusters 80—67574
- interference spectrograph, solar spectrum 78—24866
- interference spectroscopy, Fourier decomposition technique appl. 77—49784
- interference-phase method of mag. field meas. in solar atm. *(Russian)* 78—65509
- interference-phase method of ray vel. meas. in solar atm. *(Russian)* 78—65508
- interferometric observing efficiency of arrays of large aperture telescopes 79—80238
- interferometry, high-resolution techniques, atm. degradation effects, book contrib. 77—33357
- interferometry, optical intensity and speckle techniques, review *(German)* 77—56835
- intermediate-band photometry of late-type stars, calibration, standards 77—22104
- International UV Explorer (IUE), image processing 79—80234
- interplanetary dust, density and phase function determ. 80—109324
- interplanetary low energy charged particle measurements, Compton-Getting effect complications 78—49269
- interplanetary magnetic field meas., appl. of Borok B-index of geomag. pulsations 77—29589
- interplanetary magnetic sector structure, mapping via comet plasma tail disconnections 78—93155
- interplanetary particle sampling 78—57459
- interplanetary plasma, multifreq. interrogation with coherent response dispersion interferometer 77—22038
- interplanetary plasma meas. by modulation method, amplifiers sensitivity increase 79—92676
- interplanetary scintillation, appl. for solar wind probing 78—45178
- interplanetary shocks identification, by computer on board HELIOS-1 and (HELIOS-2) 79—92679
- interplanetary space research, use of comets as probes 77—25983
- interstellar clouds electron abundances determ., new method 80—41866
- interstellar diffuse clouds temperatures, determ. from HD and OH column densities 78—93385
- interstellar electron density determ. from decorrel. bandwidth of pulsar scintillation 77—78850
- interstellar magnetic fields, determ. in dense cloud complexes via Zeeman splitting obs. 79—5757
- interstellar medium, kinetic temp. and density determ. from mol. line intensities 79—97056
- interstellar medium, temp. and density determ. from fine struct. levels population ratios 79—35351
- interstellar molecules, unobservable by radioastronomy, indirect obs. possibility 78—4307
- interstellar reddening law and dust content determ. in nearby extragalactic systems, new method *(German)* 80—67850
- interstellar scintillation analysis, second-order moment eqn. analytic soln. 80—26726
- interstellar scintillation method for quasar and galaxy superfine radiostructure *(Russian)* 80—77297
- interstellar shock waves, vel. determ. from high vel. H I absorpt. features 79—48891
- interstellar shocks molecular diagnostics, chemical theory 80—56899
- interstellar submillimetric lines, possible detect. via laser heterodyne techniques 79—44377
- inverse multiple scatt., approx. models, limb darkening and phase curves 79—44388
- inversion technique for determ. of instantaneous spectra 80—82218
- ionized medium, technique for rot. freq. meas. 80—41730

astronomical techniques continued
- IR and mm wave techniques, for Cosmic Background Explorer Satellite 78—49344
- IR astronomy, appl. to galactic dust obs. *(French)* 78—12352
- IR detection techniques, for low background satellite expts. 78—49343
- IR flux method for stellar temps. and diameter determ. 80—62030
- IR heterodyne detect. of stars, atm. turbulence effects, corrections *(French)* 80—46409
- IR image production, high resolution, use of totally computer controlled telescope 80—72785
- IR laser heterodyne spectroscopy for trace gases remote detect. in planetary atms. 78—61606
- IR measurements at liquid He temperatures *(German)* 79—5760
- IR multiple freq. sounding of anomalous clouds in Jupiter's atmosphere 79—2515
- IR observation technique 78—61738
- far IR observations, via liquid He cooled grating spectrometer 79—66925
- IR photographs, processing techniques for revealing faint objects *(Russian)* 77—13250
- near IR photography, with vacuum-cold camera 80—90341
- IR photometry, atmospheric extinction meas. above Mauna Kea 80—12546
- IR radiation absorption calc. method for Venus atmosphere 77—53446
- IR sky survey by Air Force Geophysics Laboratory, extended source extraction 79—101088
- IR speckle images of α Orionis, two-dimens. obs. *(French)* 80—46553
- IR speckle interferometry, appl. to accreting young stars ang. dimensions determ. 79—44482
- IR speckle interferometry, principle, performance and appl. to NML Cygni 80—31216
- IR stellar speckle interferometry, modulation transfer function and evidence for log-normal statistic 79—101079
- IR television imaging appls. 79—92678
- IR upconversion for astronomy 80—46412
- IR upconversion to visible, as detect. method 78—45240
- iris diaphragm photometry, nonuniform background correction 80—12680
- isoplanatic patch measurement using phase-correcting telescope, turbulent air height determ. 79—53732
- iterative nonlinear pulsation theory, extension to double mode case for Cepheids 80—82369
- J-integrals assoc. with close eclipsing binary stars, numerical evaluation 77—9668
- J-integrals assoc. with close eclipsing binary stars, recursion formulae 77—9666
- Jovian centre location in Voyager image transformation 80—101534
- Jupiter clouds spectropolarimetry, lines equivalent widths information content 80—31215
- Jupiter magnetosphere, diffusion coefficients determ. from Io observed effects 78—32388
- Jurkevich period search method, appl. to southern δ Scuti stars AI, WZ and XX Sculptoris 80—90452
- K-type giant stars, reddening determ. from David Dunlap Observatory (DDO) photometry 78—4222
- Kodak IIIaJ hypersensitized plates, low intensity reciprocity failure elimination 77—9667
- Kopal's iteration method for close binary light curves, convergence problem *(Chinese)* 79—62872
- L-group chondrites, shock classification from incipient melting 79—88629
- large azimuthal telescope, primary mirror testing by interferometry 77—73952
- large azimuthal telescope, primary mirror testing by isophotometric recording 77—73953
- laser lunar ranging, scientific progress, 1969-77 period 78—36476
- laser mass spectrometry, for element anal. of extraterrestrial samples 79—16717
- laser range measurements, atmospheric correction determ. *(Russian)* 80—12674
- laser range-differencing, Earth pole posn. and rotation determ. 80—101312
- late-type stars, luminosities and distances from Ca II H and K wing emission lines 77—78766
- late-type stars intermediate-band photometry, calibration of indices 78—49424
- late-type stars photometry, photoelectric MgH + Mgb index meas. 80—12753
- latitude meas. for continental movements and rotation determ. *(French)* 78—40529
- latitude measurement, effect of relativistic deflection of light *(Russian)* 78—40462
- latitude variation, computation for national ephemerids calc. 78—88776
- least squares method, generalisation 80—62028
- least-squares adjustment with probabilistic constraints, astronomical appls. 78—32352
- Lick reduced galaxy counts, smoothing method 80—41897
- lidar temperature profiling of planetary atmsopheres 77—33352
- life in planetary soils, chemical-biological search possibilities 79—40176
- light curve analysis for eclipsing binary stars appl. to V444 Cygni 80—109374
- light source displacement vel. meas. for improving telescope photoguide system *(Russian)* 77—41306
- line profile calc. for close systems with mass transfer 80—41860
- line profile computation methods for stellar envelopes 80—85868
- local non-polar terms determ. by Okuda's method, discussion *(Chinese)* 80—85842
- long-focus photographic astrometry, appl. to Barnard's star (1916-1976) 77—45432
- low light ground based astronomy, review and history 77—29657
- low-temperature star automatic recognition by two-channel IR systems 79—75118
- luminosity calibrations from trigonometric parallaxes, practical improvement method 79—40083
- luminosity function determination method from preselected random samples, appl. to quasars 80—94719
- lunar and satellite laser ranging, future developments 77—64483
- lunar core samples, technique for thermal cond. meas. 80—72781
- lunar crater image edge determ. 80—98581
- lunar crater/stars superimposed photography using automatic device *(Russian)* 79—92675
- lunar features, absolute heights from photographs, computer processing technique *(Russian)* 80—109380

- **astronomical techniques** continued
  - lunar fines, radiation tracks etching by adsorbed water, effect of annealing temp. 77—60632
  - lunar fines determination of ancient mag. field 80—36526
  - lunar gravity field, long-term Keplerian rate method 77—87291
  - lunar laser ranging, polishing and Foucault test of receiving telescope mirror *(Japanese)* 78—89065
  - lunar laser ranging, reference frame for positional astronomy 77—64618
  - lunar laser-ranging, review 77—5459
  - lunar limb automatic meas. with Nice Obs. microdensitometer *(French)* 80—12692
  - lunar mapping, conf., Lagonissi, Greece (May 1978) 80—12688
  - lunar mapping, from Schmidt's 1878 map to Apollo photography 80—12689
  - lunar mapping program of United States and Apollo project 80—12690
  - lunar microseismic background, observing possibilities 78—16319
  - lunar minerals trace element nondestructive anal. using proton microprobe 78—64911
  - lunar occultation obs. using TV camera *(French)* 79—58263
  - lunar occultation technique appl., limiting ang. resolution calc. 77—87272
  - lunar occultations of stars, new technique for photoelec. obs. of dark limb reappearances 78—4115
  - lunar occultations scans, object shape retrieval from new algorithm 80—105149
  - lunar photography for amateur astronomers 78—45238
  - lunar pyroxenes thermal history, indications from cation distrib. and exsolution 78—45246
  - lunar regolith, secondary electron emission characts. determ. method 80—12687
  - lunar rock magnetism, palaeointensity method and lunar sample 10017135 application 80—36527
  - lunar seismograms, use of surface reflections 78—65504
  - lunar seismology, data processing methods of Apollo program 80—51676
  - lunar soils, volatile trace elements determ. by RNAA 79—44276
  - lunar surface chemical composition from albedo and colour index 77—87296
  - lunar surface gravimetric surveying process optimization 79—8846
  - lunar surface magnetisation determ. from orbital surveys 77—37531
  - lunar surface mapping from side looking orbital radar images 77—37520
  - lunar surface rock comp. remote sensing, regolithic radioactivity in Mare Crisium 80—62045
  - lunar synthetic-aperture mapping from Earth-orbiting telescope 79—75119
  - lunar volatile emissions, detect. techniques 79—44385
  - β Lyrae, eclipsing binary, intrinsic and interstellar polarisation separation by Hα, Hβ lines obs. 77—41390
  - RR Lyrae stars, van Hoof's variation appl. to radii determ. by Baade's method 77—53613
  - M-type supergiants, photoelectric two-dimensional spectral classification 78—53936
  - magnetic fields, dual magnetometer method extension for use on dual spinning spacecraft 78—77459
  - magnetic fields detection in late-type dwarf stars, line profiles Fourier deconvolution method 80—72949
  - magnetic fields of compact thermal sources, determ. via linear polarisation spectrum *(Russian)* 80—90344
  - magnetic measurement in interplanetary space during Halley-Venus mission, Planet-A project *(Japanese)* 80—94672
  - Mariner 10 images of Venus and Mercury, digital processing 77—78647
  - Mars, Viking biology gas exchange expt., life indicators 77—37549
  - Mars, Viking labelled release expt., radiorespirometry 77—37548
  - Mars, Viking pyrolytic release expt., C assimilation meas. 77—41346
  - Mars surface topography, photometric study method 79—25537
  - mass determinations, tracking data processing *(Russian)* 78—49297
  - masses of giant molecular cloud complexes, estimation method 79—5888
  - massive meteoroids, mass distrib. determ. from occurrence of brilliant fireballs 77—45366
  - maximum entropy method of period determ., accuracy 80—56712
  - maximum entropy spectral anal., confidence limits 80—22284
  - maximum entropy spectral analysis, model data anal. situation study 79—8843
  - maximum-entropy image processing in gamma-ray astronomy 79—48684
  - mean latitude non-polar var., techniques anal. *(Chinese)* 80—85841
  - megalithic astronomical alignments, significance tests 79—96928
  - meridian circles pivot errors, new determ. method 78—53822
  - meridian instrument pivot irregularities meas. method 80—94718
  - meridional flow calc. method for slowly rotating stars 77—56880
  - metal abundance determ. in late-type stars, new method 79—12405
  - metal abundance determ. using CORAVEL radial vel. scanner for dwarf stars 80—94791
  - metallicity determ. for K-type giants, problems 79—44474
  - meteor bright line spectra, study via astronomical TV system 78—61817
  - meteor counts, statistical analysis method 80—8594
  - meteor data from visual obs., rigorous method of normalization and analysis 79—88627
  - meteor observation, effective field of view for line sources 78—36535
  - meteor observation 78—57509
  - meteor observations, telescope performance 78—49319
  - meteor shower radiant precise determ. by means of many photographs *(Japanese)* 79—101085
  - meteor stream radiant determ. from single station obs. 78—20647
  - meteor stream radiant distrib. using spherical harmonic analysis 78—20648
  - meteor streams, statistical simulation of radar obs., algorithm 78—20763
  - meteor tracks, initial radius measurement, simultaneous radar observations, three wavelengths *(Russian)* 77—22108
  - meteor trails televised spectra, photometry 78—20764
  - meteoric material structure, determ. via fireball end heights 77—29732
  - meteorite etching with Cl$_2$, for group IA and IIA irons 80—36593
  - meteorite thermoluminescence as measure of irrad. history, validity of method 80—36584
  - meteorites, diamond-containing, polished thin section preparation technique 78—65566
  - meteorites, velocity meas. by radar technique *(Spanish)* 79—5759
  - meteorites orbits and Earth residence times, determ. from thermoluminesc. 80—31262
  - meteoroid orbits determination, accuracy of meteorite dropping fireballs radiants 79—71006
  - meteors, observation methods in Poland, review *(Polish)* 78—61750

- **astronomical techniques** continued
  - meteors, real luminosity function determ. from apparent luminosity function, least squares method 79—80231
  - meteors, simultaneous visible and radar obs. technique 80—77354
  - meteors, television photographs photometry 78—96441
  - meteors, trajectories and orbits determ. via NASA-NMSU double-station camera 77—74014
  - meteors television spectra, prod. and study 77—67076
  - methane, liquid, detectability on outer plaets, laboratory optical absorpt. spectra 80—93278
  - Michelson stellar interferometer, reconstituting nonstationary optical pattern from 2-photon correls. *(Russian)* 77—82125
  - micrometeoroid detection, acoustic method reliability 79—80232
  - microparticle studies by space-borne instrumentation 78—57460
  - microwave spectroscopy, appl. to interstellar molecules, in book 80—51973
  - minor planet orbit determ. using Chebyshev's approx. *(French)* 80—94720
  - minor planets observations, least squares soln. of ill-conditioned systems 80—26747
  - mirror grinding and polishing for 6″ reflector 77—56826
  - mirror temperature effects on telescope seeing, compensation method 79—70961
  - MK spectral classification from uvbyβ photometry, general case 80—82216
  - Monte Carlo model, N-body, for galaxy correl. functions evolution 80—62292
  - Moon, moment of inertia determ. improvement, proposed strategy 78—24477
  - Moon, orbital gamma-ray data rel. to large-scale lunar problems 78—12123
  - Moon EM sounding, variable induced mag. field calc. 77—82135
  - moving object imagery using large aperture telescope arrays 80—53225
  - multicolour photometric systems, early-type stars synthetic UBV colours and temp. scale 79—16933
  - multicolour stellar photometric systems, investigation of UBV, RGU and uvby systems 78—28528
  - multicolour stellar photometric systems, transforms. between UBV and RGU systems 78—28529
  - multidimensional power spectral anal., new method, radioastron. appl. 77—17378
  - multigradation image decomposition by iso-image technique 77—56834
  - multiple beam technique for overcoming atmospheric limitations to single-dish observations of extended radio sources 79—75113
  - multiple star discovery techniques and spectroscopic meas. 79—44540
  - near IR interferometry, high spatial resolution methods, speckle and aperture synthesis *(French)* 80—46405
  - nearby star suspects selection from Luyten proper motion catalogues, use of Luyten's magnitude estimates 80—82353
  - nebulae central stars, temps. determ. from forbidden O III lines 78—41015
  - neutrino astronomy, high energy, possible point sources 79—2484
  - neutrino bursts detection, proposed search for correl. with gravit. waves 78—77567
  - neutrinos, ultrahigh energy, prod., fluxes and detect. techniques 78—49264
  - neutron stars, surface temp., density and mag. field determ. from thermal radiation 80—56869
  - novae, spectrophotometric estimate of electron density in rapidly rot. accretion discs 79—16968
  - numerical image manipulation and display, Skylab EUV solar obs. appl. 77—60618
  - numerical integration of stellar orbits 79—21361
  - objective prism radial velocities, of NGC 3114 open cluster *(French)* 79—48868
  - objective prism spectroscopy, limiting magnitudes on IIIa-J emulsion 80—46551
  - objective-prism spectroscopy, appl. to new compact H II regions discovery in (NGC 6822) 80—51854
  - occultations photometry, photoelectric photometer appl. *(Chinese)* 80—105172
  - one-dimensional stellar and solar speckle interferometry 77—64662
  - opacity sampling technique for early B-star LTE model atm. 80—90414
  - open clusters membership determ., maximum-likelihood method for proper motions 78—16471
  - optical data processing methods for solar granulation spectral analysis 80—101570
  - optical interferometry of solar phenomena 79—44378
  - optical interferometry with two telescopes *(French)* 80—46403
  - optical lunar occultation meas., statistically rigorous reduction 78—73650
  - optical post-processing of imagery from active phase compensation devices 77—42502
  - optical surface control, Hartmann method, use of splines 79—35149
  - optical techniques, old and modern *(Italian)* 77—56839
  - optical testing of Schmidt camera aspheric corrector, simple null test 80—91940
  - optical wavefront distortion compensation in real time 77—17219
  - optimal curve fitting procedure appl. to classical Cepheids light curves 77—78795
  - option systems design, algorithm *(Chinese)* 80—8544
  - orbit computation, semi-analytical method *(Chinese)* 79—8798
  - orbit determination, four-obs. method having no co-planar singularity 77—60578
  - orbit determination for cosmic object, Green's functions appl. 80—61992
  - orbit determination method by filter technique for asteroids and satellites *(French)* 79—101050
  - orbital gamma-ray spectroscopy, geochemical mapping of Moon 77—25953
  - Orwo ZU 2 plate with improved props., astron. appl. *(German)* 78—89571
  - out-of-ecliptic space research, by Sun polar-orbiting probe 77—87228
  - panoramic photometry reduction, search algorithms 78—32354
  - parameter estimation, via appl. of likelihood ratio 79—44374
  - parameter estimation in X-ray astronomy using max. likelihood 79—62752
  - patrol balloon *(Japanese)* 77—82018
  - peculiar stars, anal. of ionised Fe emission in low-resolution spectra 77—13364
  - period computation for δ Scuti stars *(French)* 78—85949
  - period-finding technique, Fortran IV computer program 79—21195
  - periodic source absolute timing, limiting standard deviation 77—45314

astronomical techniques continued
personal equation determ. method 78−89443
photodiode detectors, thermal background subtraction 80−90342
photoelectric obs. of star transits *(Czech)* 80−41729
photoelectric occultation observing, techniques and apparatus 78−4117
photoelectric photometry, reduction of obs. to standard system *(Russian)* 77−64657
photoelectric photometry, UBV obs. method and reduction 80−72784
photoelectric photometry, zero point drift 79−53735
photoelectric photometry at Hvar Observatory, instrumentation, colour systems and extinction 77−78643
photoelectric photometry at Wise Observatory, performance assessment 78−73657
photoelectric scanning of globular clusters *(Italian)* 78−93343
photoelectric spectrophotometer, accurate absolute calibration in wide spectral region 79−96919
photoelectric stellar radial velocity meas. with echelle spectrometer 77−56836
photoelectric stellar radial velocity meas. with echelle spectrometer 77−56837
photoelectric stellar radial velocity spectrometry, use of echelle grating *(French)* 77−91438
photoelectrical photometry at Trieste, real time data acquisition and processing *(Italian)* 79−62757
photogram optimal filtering technique *(Italian)* 79−58268
photographic amplification of faint astronomical images 79−16839
photographic detection at large telescopes, optimisation 78−24468
photographic image expansion estimation, for planetary position meas. *(Russian)* 77−71007
photographic limiting magnitudes, determ. method for large telescope *(Russian)* 78−28531
photographic method optimisation in astronomical obs. *(Russian)* 79−35144
photographic negatives superposition method, appl. to galaxy NGC 5195 (M51 comparison) *(Russian)* 77−13251
photographic patrol station network for bright meteors 77−87278
photographic photometry, reduction algorithm 78−32528
photographic photometry for clusters of galaxies *(German)* 80−46681
photographic photometry of bright galaxies, Numerical Mapping Technique *(Italian)* 77−91443
photographic plate background fitting, interactive procedure *(Italian)* 80−98571
photographic plate calibration, new computerised method, galaxy photometry appl. 79−92677
photographic plates, hypersensitisation by forming gas baking and $AgNO_3$ bathing *(Japanese)* 79−101084
photographic plates, meas. via automatic microdensitometer 79−80230
photographic position meas. of Venus *(Russian)* 78−93121
photographic post-development image intensification by autoradiography, technique, astron. appls. 80−26752
photographic solar aureole meas., validity of aerosol single scatt. 77−5448
photographic stellar spectra recording 79−16956
photographic zenith tube plates, new reduction method 78−73656
photography, controlling contrast by special development techniques 77−67046
photography, gain of quality by plates superposition 79−75114
photography, hypersensitisation, review 78−32348
photography, hypersensitisation, state of the art review 77−2344
photography, hypersensitisation, testing of emulsions for threshold imagery 78−32351
photography, limiting magnitudes on IIIa-J emulsion 80−46551
photography, of solar faculae and sunspots with balloon-borne 10 cm telescope *(Japanese)* 79−80292
photography, Skylab environmental effects on film 77−60620
photography, unsharp masking technique 79−88603
photography and emulsion hypersensitization techniques 77−33356
photometric analysis of solar flares onset phase 77−82212
Photometric Data Systems (PDS) photometry of open cluster NGC 2420, error anal. 78−57600
photometry, appl. of single repetitive filter cycle photometer with sky background compensation 80−62025
photometry, appl. of SIT vidicon detector system for Palomar 1.5 metre telescope 79−92674
photometry, choice of photomultipliers 77−13242
photometry, data collection with aid of microcomputer *(Czech)* 80−67570
photometry, investigation of double astrograph system *(Russian)* 80−72771
photometry, props. of Walraven VBLUW system 77−17377
photometry of atmospheric IR emission, statistical props. of sky noise *(French)* 78−53731
photometry of compact galaxies near M3 and M92 with two telescopes, selection and statistics 80−77485
photometry of rich clusters of galaxies 78−89264
photometry of white dwarf stars, calibration 78−85938
photometry using twin refractor 77−17382
photometry with SEC TV camera at Loiano telescope 79−58272
photon counting, dead time correction for bright star photometry 77−22106
photon position determination using microchannel plates, X-ray imaging for HEAO-B 79−45555
photosphere total velocity field, determ. using weak absorpt. lines *(Russian)* 78−40894
physical systems instabilities, variational principles for complex eigenvalues 79−21527
picture processing, appl. to Venus cloud layer struct. determ. from Venera 9 televised pictures 80−67604
picture processing analysis, appl. to NGC 5128 (Centaurus A) optical struct. 79−53907
planet thermal radiation intensity field modelling; principles 80−62056
planetary, nebulae observation 77−87514
planetary atmosphere, remote sensor, high resolution Fourier transform spectropolarimetry 78−57469
planetary atmosphere investigation by mass spectrometer-molecular beam expt. 78−49327
planetary atmosphere single-scatt. albedo determ., theory for Rayleigh-scatt. atmosphere with true absorpt. 80−94704
planetary atmosphere studies by occultations, wavelength depend. of turbulence effects on refr. angles 79−48697

astronomical techniques continued
planetary atmospheres, eqn. of transfer for optical depths >100, soln. method 78−96414
planetary atmospheres, light scatt. process meas. via laser beam *(Russian)* 79−44365
planetary atmospheres, remote sounding, new inversion method 80−12677
planetary atmospheres, two-layer model parameters determ. from obs. of absorpt. bands 78−24480
planetary atmospheric composition, mass spectrometry 80−8518
planetary diameter meas. by occultation obs., teaching expt. 78−12457
planetary electrically conducting fluid core location from external mag. obs. 78−32248
planetary ephemeris, direct computation method *(French)* 78−7862
planetary geodetic control using natural satellite imaging 79−70959
planetary mapping by airbrush technique 78−53833
planetary nebulae, distances determ. through nebular ionised mass/nebula radius relation 80−101625
planetary nebulae, spatial structure investigation by mathematical modelling *(Russian)* 79−101188
planetary nebulae central star, far UV flux determ. from nebula ionisation state 80−72945
planetary nebulae central stars, temps. determ. from nebulae ionic abundance ratios 79−2565
planetary nebulae distance scale, meas. techniques 80−109521
planetary orbits computation using Chebychev polynomials, appl. to minor planets *(French)* 80−61997
planetary positions calc. using programmable pocket calculator *(Norwegian)* 78−69700
planetary reflectance meas. in thermal emission region, thermal component removal 80−17497
planetary surface elemental anal. via orbital gamma-ray spectroscopy 79−12412
planetary surface temp. determ. using simplified model 79−84695
planetary surfaces brightness characts. calc. method 79−62754
planetary systems, search strategies 80−46615
planets, nonsolar, detect. via spinning IR interferometer 78−85977
outer planets atmospheres, abundance ratios determ. method, appl. to Jupiter 79−84734
planets gravitational spectra, determ. from planetary orbiters tracking 80−41744
planets rectangular coordinates, approximation via Chebyshev polynomials *(Russian)* 80−62033
planets surface shape determ. from limb photographs by spacecraft 79−8845
plasma diagnostics, dielectronic recomb. spectra appl. 80−46391
plasma electron temp. and density diagnosis 79−5793
plasma local optical obs. *(French)* 77−15244
plasma X-ray diagnostics 80−59282
plate analysis, interactive imaging technique appls. 79−58266
plate processing, two-dimensional digital filtering techniques 79−16835
point summation technique, appl. to faint X-ray sources detect. near COS-B γ-ray positions 78−54093
polar axis misalignment determ. for equatorial instruments 78−69685
polarimetric method for nature of cataclysmic binary stars (CBS), critique and appl. to (Cygnus X-1) 80−109486
polarimetry, new automatic technique for galaxy obs. 77−17692
polarimetry of atmosphereless solar system bodies 78−58011
polarimetry with Norikura Observatory coronagraph *(Japanese)* 80−82223
positional astronomy and astro-navigation computing, new approach using pocket calculator, book 79−12383
post-detection compensation for atm. distortion of faint scene images 77−45322
power spectrum analysis, nested variance technique, space physics, appl. in FORTRAN 77−87275
principal component analysis, appl. to solar flares soft X-ray flux 80−41781
principles and practice of astronomy, book 78−32629
projection blink comparison, appl. to nova searching 79−12407
proton flux from solar flares, determ. from ^{3}He in lunar rocks 80−98576
protostar, rotating, fragmentation, comparison of two three-dimensional computer codes 80−26850
pseudo-colour images representation, graphic processor appl. *(Italian)* 80−98562
pulsating star period determ. methods, comparison 80−41835
PZT obs. reduction procedures *(Japanese)* 77−73972
quasars, absolute magnitude-volume diagrams construction and cosmological appls. *(French)* 80−8705
quasars, luminosity function and density vars. determ. from Hubble diagram statistics 79−97093
quasars, magnitude estimation from Palomar Sky Survey prints 80−36510
radar observations of meteorites Moon and planets *(Spanish)* 79−5759
radial support methods for large telescope mirrors 77−49293
radial vel. determ., survey of different methods 80−73006
radial-velocity standard stars, list of 200 stars 80−26849
radiative transfer, adding algorithm for Markov chain formalism 80−21902
radiative transfer, exponential integrals Λ-transform determ. 79−35114
radiative transfer, resonance scattering with absorpt. or differential expansion, Monte Carlo calcs. 80−21901
radiative transfer eqn., filtered iterative inversion method 78−7918
radiative transfer inversion problems, Backus-Gilbert formalism 78−89054
radiative transfer Wiener-Hopf technique, appl. for new representation of X- and Y-eqns. 79−53710
radical vel. meas. using telluric A-band on ojective prism spectra *(Japanese)* 78−89083
radio interferometry, amateur radio telescope design 78−85849
radio occultation technique for planetary atmospheres profiles, statistical and computational uncertainties 79−96938
radio occultations, dual-freq., of Veneras 9 and 10, rel. to Venus daytime ionosphere profiles 79−96939
radio sources, ang. struct. investigation via lunar occultations, resolving power 78−65712
radio sources cosmological evolution, free-form anal. method 78−41070
radio telescopes, tiltable, design and improvement 77−45313
radiometric method for asteroids size and albedo determ. 77−82148
radiometry in quasi-isotropic atmosphere 80−90345

astronomical techniques continued
radiosource angular struct. determ., lunar occultation technique 77—13249
radiosources, method for distance determ. 80—109559
radiosources cosmological evolution, free-form analysis, self-consistent luminosity function 80—46716
Raman effect for probing outer planets 77—87277
range measurements to moon, subnanosecond laser 77—82126
Rayleigh atmosphere single-scatt. albedo, determ. from polarisation meas. 79—35117
real time atmospheric compensation, active optical imaging 77—49307
real time image restoration through Walsh filtering 77—27264
red giant mean initial mass from visual binary data 78—49429
reddening determ. method in uvby photometric system 78—73655
reduction of 19th century obs. of Uranus and Neptune positions, method comparison 80—94691
refracting telescope chromatic curve determ., spectrographic technique 77—5432
refraction angles accuracy obtained by statistical orthogonal expansion of refr. index *(Russian)* 77—70829
relativistic electron spectra, inference from meas. of inverse Compton radiation 80—90339
reliability analysis appl. to EUV spectrometer 80—85864
review of recent developments 78—16307
RI photometry with CCD camera, appl. to Einstein X-ray Observatory fields 80—62315
rotating body observation using high-resolution spectroscopy, appl. to Sun 78—96403
rotation collimators, positively constrained imagery 77—9665
satellite, observations, reduction method using selected reference stars *(Polish)* 78—36441
satellite dynamics, appl. of higher-order stroboscopic method 79—66913
satellite mass estimation from multiple Viking Orbiter encounters 77—56831
satellite motion prediction by extrapolation methods *(Russian)* 78—49299
satellite orbit determ. by astromeas. optimisation 78—16279
satellite orbital elements and station coords. determ. by least-squares collocation *(Russian)* 78—49296
satellite orbital lifetimes, prediction methods 78—73605
satellite photographic tracking, astronomical method *(Chinese)* 80—77254
Saturn ring thickness measurement, ephemeris for Earth ring plane crossing (1979 October 27) 79—101115
Schwarzschild black holes, discovery via focusing gravit. mirror effect 80—46602
second order perturbation theory for inner planets *(French)* 80—72801
seeing effects removal from iris photometry of nonstellar object 77—74139
seeing effects removal in Michelson stellar interferometer 77—29659
selenodesic work in France 80—12693
selenodetic reference network construction, choice of coordinate system *(Russian)* 80—72797
selenographic coords. determ. of ALSEPs using RATAN-600 equipment *(Russian)* 79—25517
self consistent FORTRAN subroutines for Earth motion determ. 80—85845
Shuttle/Spacelab program rel. to solar flare buildup studies 77—17498
size limit, for uniformly pulsating EM radiation sources 79—84656
sky background estimation on starfield plate 80—67577
sky photographs, star position meas. error reduction by Gaussian freq. distribution curves *(German)* 77—17384
Skylab photographic X-ray images, analysis 78—49341
slitless fieldspectroscopy, focal-reducer system appl. 80—36504
slitless spectroscopy for quasars 80—86009
slitless spectrum technique for quasar systematic surveys 80—105384
smoothing of observational data 77—73969
SNR hydrodynamical evolution, analytical methods 79—5885
solar 5 min. oscills., spectral lines use as temp. indicator 77—37585
solar atmosphere velocity field, estimation by measuring solar spectrum integral characts. 80—46530
solar chromosphere active regions, bidimensional spectroscopy obs. with birefringent filter *(Italian)* 80—98568
solar chromosphere flares, initial phase parameters determ. method 80—62104
solar constant determ. methods 80—77376
solar corona, density determ. from Fe IX lines 79—44429
solar corona, polar temps. determ. via heavy ions abundances in solar wind 77—37591
solar corona and comet details enhancement, digital image processing 79—25516
solar corona and comet digital image enhancement 78—81556
solar coronal plasma density, determ. from reson. lines fine struct. components 80—101581
solar coronal temperature, determ. from spectrum of electron scatt. continuum 77—22169
solar cosmic ray proton spectra, determ. methods 78—28459
solar EUV output measurement, techniques and appl. to aeronomy 78—57535
solar features, lifetime determ. 77—2385
solar flare energy disposition by non-thermal electrons, indirect determ. 79—25581
solar flare proton energy spectra slope prediction using radio burst data 79—53683
solar flare protons, identification from accompanying EM emission 79—12443
solar flare protons, near-Earth parameters determ. from radio bursts 78—45165
solar flares, electron beam diagnostic 80—26827
solar flares, EUV radiation, detect. using ionosphere sudden freq. deviations (SFD) 80—8484
solar flares, Fe XXV dielectronic satellite line spectra as measure of non-thermal electron energy distribs. 80—21911
solar flares, radio brightness distrib. processing in one-dimensional synthesis *(Italian)* 80—98628
solar flares, XUV electron density diagnostics 79—88633
solar flares spectral diagnostics for turbulent elec. fields 77—17493
solar flux distribution determ., photoelectric spectrophotometry and Sun B—V and U—B colours 79—66970
solar force-free constant α mag. fields, determ. from magnetograph data 79—12445

astronomical techniques continued
solar granulation, digital enhancement of balloon-borne imagery rel. to photometric props. 78—7956
solar granulation mean vertical vel. determ., spectrograms correction function 80—62094
solar Hα photography 78—40833
solar interior neutrino spectroscopy, proposed long-term programme 80—17566
solar limb local radial velocities, Doppler shift meas. 77—17537
solar mag. field intensity determ. for nonspot mag. regions 78—96452
solar magnetic field above flocculus, determ. from radio obs. 80—98635
solar magnetic field meas. review 78—81607
solar magnetic field neutral line, Stanford obs. compared with Hα synoptic charts 78—28612
solar magnetic fields, meas. from saturated and blended lines via Fourier transform techniques 77—22165
solar magnetic fields determination, multi-dimensional non-LTE polarised radiation transfer in mag. fluxtubes 78—69673
solar magnetic fields measurement, effects of ang. resolution 77—22082
solar neutrino detection, new expts. proposal 80—31181
solar neutrino experiments, appl. to cosmological hypothesis testing 79—16918
solar neutrinos, proposed Earth flux determ. by mass spectrometry of ^{205}Pb in Tl minerals 77—5447
solar neutrinos measurement, cosmic ray neutrinos ^{37}Ar prod. rate estimate 79—16837
solar non-force-free magnetic fields, determ. from plasma props. 79—92733
solar observation, atmospheric thermal perturbations detect. via transparency meas. *(French)* 77—53532
solar photosphere, vel. gradients retrieval from line asymmetries, linearised approach 80—62093
solar photosphere 'microturbulent' vel., determ. from Fraunhofer lines equivalent widths *(Russian)* 80—12719
solar photosphere microturbulent vels. and damping const. determ., errors *(Russian)* 80—72899
solar photospheric faculae, contrasts at solar disc centre using filigree pictures 78—12181
solar plasmas density determination, N III and O IV intersystem multiplets appl. 80—31264
solar proton events, forecasting quality improvement *(Chinese)* 77—22158
solar proton flares, quantitative identification from characts. of microwave radio bursts at 9 GHz 80—4323
solar radiation measurement, techniques and instrumentation, survey 77—5348
solar radio emission polarisation in 1.9-3.5 cm wavelength region, obs. method *(Russian)* 78—65587
solar research, by Kitt Peak National Observatory 60 cm vacuum telescope *(Norwegian)* 77—60613
solar rotation meas. using nonradial p-mode oscills. 79—29994
solar seeing, determ. from arrival angle statistics, comparison with microthermal meas. 80—26740
solar speckle interferometry calibration, atm.-lens MTF changes 79—2370
solar spectra, line profiles, rough reconstruction from series of narrow-band filtergrams *(Italian)* 80—98564
solar spectra, small line shifts meas. via automatic comparator 77—82123
solar spectral lines, high-resolution meas. using scanning Fabry-Perot interferometer 80—77298
solar spectrometric research, automation system for on-line signal processing *(Russian)* 80—12659
solar spectroscopy, instrumental profile of triple Fabry-Perot interferometer 78—40817
solar system exploration, appl. to planetary atmospheres and solar nebula theory *(Czech)* 78—32374
solar type IV radio events, FFT anal. rel. to pulsating structs. 78—96455
solar UV radiation meas. using ferrioxalate actinometer 80—41731
solar UV spectroscopy, OSO-8 LPSP instrument in-flight performance and results 78—49317
solar vector magnetic fields, determ. from Stokes profiles 78—28611
solar wind MHD discontinuities, identification method 80—109322
solar wind parameter measurement using charged-particle spectrometer, instability of analyzing voltages 80—67565
solar wind speed near Sun, determ. from interplanetary mag. field 77—17318
solar wind velocity meas. with spacecraft phase scintillations 77—41310
solar wind VLF signals, preprocessing on spacecraft 77—64609
solar X-ray images, quantitative interpretation by filter ratio anal. 79—40085
solar X-ray imaging techniques, past and future, review 79—25495
solar X-ray photographs, anal. and interpretation 78—4179
solar X-ray photographs anal. and interpretation, filter ratio method 79—40086
space astrometry, general principles 78—12082
space astronomy, planned studies from space shuttle telescope 79—21183
space plasmas, new concept for EM and electrostatic waves detect. 77—9549
Space Telescope pointing control fine guidance subsystem design 80—82201
space-time experiments, potential of an orbiting interferometer 79—35624
spacecraft location determ. on planetary surface from Sun's azimuth meas. 78—49287
spacecraft orbital plane, autonomous determ. via landmarks on central planet surface 77—64595
spacecraft position determination on planetary surface, optimal navigation meas. 77—29621
spacecraft trajectory meas. errors, motion parameters estimation 77—29633
spacecraft trajectory meas. process optimisation, visibility limitations 77—29632
speckel interferometry with multiple mirror telescopes, laboratory expts. 79—80237
speckle, interferometric measurements of binary stars 79—71065
speckle holography measurements of stars ζ Cancri and ADS 3358 78—93120
speckle image reconstruction of solar features 77—33354
speckle imaging, photon by photon, diffr. limited performance for large telescopes 79—53729

astronomical techniques continued
speckle imaging for diffr. limited image recovery 77−45318
speckle interferogram masking, holography and phase flipping 80−109373
speckle interferometer on 2.5m Isaac Newton telescope 77−22102
speckle interferometric meas. of ang. diameters of asteroids Vesta and Pallas 79−35172
speckle interferometric obs. of solar photospheric granulation *(French)* 80−46523
speckle interferometry, ang. diameter of asteroid Vesta 78−20712
speckle interferometry, appl. to binary stars obs. 80−90477
speckle interferometry, appl. to Hyades spectroscopic binary 51 Tauri 77−29876
speckle interferometry, appl. to image reconstruction of α Orionis 77−22222
speckle interferometry, atm. nonisoplanicity meas. using double stars 78−65387
speckle interferometry, atmosphere turbulence effect ang. depend 79−101080
speckle interferometry, binary stars obs. with 1 m telescope 78−69831
speckle interferometry, defocusing effects 78−40834
speckle interferometry, effects of spectral bandwidths and exposure times 78−69701
speckle interferometry, focused radiation scintillations freq. correl. 79−94153
speckle interferometry, fringe visibility recovery from recorded images quantised to two levels 78−12104
speckle interferometry, image reconstruction by speckle masking 77−49308
speckle interferometry, image reconstruction of single stars 78−32350
speckle interferometry, image restoration by least squares method 79−25514
speckle interferometry, meas. of astronomical objects, simulated multiple mirror telescopes 80−56716
speckle interferometry, meas. of binary stars 78−85973
speckle interferometry, meas. of visual binary stars 77−78820
speckle interferometry, obs. of binary stars with Huate-Provence 1.93 m telescope 80−90475
speckle interferometry, obs. using linear digicon detector 77−78648
speckle interferometry, one-dimensional, appl. to solar granulation 78−45299
speckle interferometry, online digital autocorrelator 78−81548
speckle interferometry, stellar image recovery, photon noise limitations 77−49309
speckle interferometry, two-point, astron. appls. and disadvantages *(Russian)* 79−16840
speckle interferometry, wideband, true imaging of astronomical objects 80−53226
speckle interferometry appls. *(French)* 80−46404
speckle interferometry bandwidth extension using simple optical system 79−26114
speckle interferometry for looking at star surfaces 77−9675
speckle interferometry for stellar diameters and close binary star separation meas. *(Russian)* 78−40922
speckle interferometry image processing technique requiring no reference point 80−98556
speckle interferometry in astronomical image reconstruction 77−37508
speckle interferometry lens-atm. MTF meas. 77−22103
speckle interferometry meas. of Pluto diameter 80−41763
speckle interferometry of binary stars, computer simulations in photon-counting mode 78−53836
speckle interferometry S/N ratio, photon counting autocorrelation mode at low light levels 79−76613
speckle interferometry with severely aberrated telescopes 78−12103
speckle patterns, image retrieval 77−22100
speckle patterns, interference, point spread functions 77−22101
spectra reduction by microcomputer based system 80−77296
spectral anal. analytical method for solar flare impulsive hard X-ray burst *(Chinese)* 80−85919
spectral line equivalent widths meas. criterion 79−35141
spectral line formation in axisymmetric moving envelopes, numerical method and appl. to YY Orionis stars 80−41813
spectral line polarisation meas. in solar VUV spectra, technique and data reduction 80−67691
spectral line profile correction for instrumental influence, numerical methods 79−35148
spectral line profile measurements, accuracy 80−26751
spectral reduction technique in X-ray astronomy 79−96924
spectral synthesis in mag. field appl. to sunspot umbra 77−17459
spectral wavelength shift determ. method, appl. to C_2 molecule in solar spectrum 78−49340
spectrogram calibration by multiple exposure 77−22107
spectrogram calibration using Lyot filter element 78−36466
spectrometer, Fabry-Perot, piezoelectric scanning nonlinearities 79−6183
spectrophotometric data processing by large scale interactive one dimens. array processing system 80−82220
spectrophotometric identification of late type binaries in open clusters 79−44548
spectrophotometry, image tube, of weak emission lines, precision *(French)* 79−88601
spectrophotometry of low-luminosity stars with Carnegie image tube 78−57466
spectrophotometry using intensifier Si vidicon 78−32356
spectrophotometry with TV-type detectors 77−78646
spectroscopic binaries, precession period determ. from spectroscopic data 79−67062
spectroscopic binary member of visual double, mass determ. method *(French)* 79−44549
spectroscopic binary stars, massive, Fourier transform anal. rel. to low eccentricity orbits detect. 79−67060
spectroscopic binary stars orbits, test of circularity 78−93321
spectroscopic binary stars photographic anal., influence of Schwarzschild effect on orbital and system elements *(German)* 80−8653
spectroscopic method and solar corona rotation investigation 77−53551
spectroscopic observations of stars and planetary nebular, via multichannel analogue detector system 78−36461
spectroscopy, appl. of grating spectrographs anamorphic magnification 79−66927
spectroscopy, appl. of SIT vidicon detector system for Palomar 1.5 metre telescope 79−92674

astronomical techniques continued
spectroscopy, high-resolution Michelson interferometer for Isaac Newton Telescope 78−4105
spectroscopy, review 79−12408
spectroscopy, submm. line, detector-telescope systems 77−49305
spectroscopy role in basic plasma props. meas. 77−58900
spectroscopy role in present-day astronomy 77−60623
spectroscopy with holographic and ruled diffr. gratings 78−40831
spectrum registration using double-pass spectrophotometer with digital registration, precision *(Russian)* 79−96917
spiral galaxies distance determ., spectroscopic method 80−56926
spiral galaxies surface photometry, computerised data reduction system, (appl. to NGC 157) 79−40264
standard candle location, giant elliptical galaxy selection 80−105353
star cluster composition determ. method using evolved members 77−29889
star cluster high resolution imaging by speckle interferometry, simulation 78−77492
star colours, refr. corrections for atmospheric spectral transmission changes 78−28535
star counts, indicator of galaxy struct. and quasar evolution 80−82507
star escape from isolated clusters, numerical methods *(Polish)* 80−26922
star images on Palomar Sky Survey prints, magnitude-diameter relations 77−49310
star mass meas. using gravit. starlight deflection in close visual doubles *(French)* 79−62753
star simulator lightguide test instrument and method 79−27422
stars, abundance determ. by photometric and spectroscopic methods 77−29807
stars, very high resolution obs. using central bright spot in planetary occultation 77−67053
stars cold satellites searching via speckle interferometry, coherent optical system appl. *(Russian)* 80−12672
stars space densities derivation, new method 80−85932
statistical methods for star field and config. anal. 80−82224
stellar Δa-photometry, appl. to meas. of 5200 Å feature in Ap stars 80−67734
stellar absolute luminosity calibration using binary stars, relevance and consistency 80−62111
stellar absolute magnitude determ. methods 78−96405
stellar absolute magnitudes determination, comparison between Geneva photometric boxes and MK spectral types 80−77385
stellar absolute spectrophotometry, spectral energy standard *(Russian)* 79−44372
stellar absolute spectrophotometry and UBV photometry, comparison of results 78−96476
stellar angular diameters and effective temperatures determination, IR flux method appl. 79−92682
stellar angular diameters by lunar occultations, appl. to 11 late-type stars 77−74048
stellar atmosphere laser line emission detection 77−41312
stellar atmospheres, turbulent elements sizes determ. from weak lines macro and microturbulence 79−53803
stellar atmospheres, vel. gradients determ. from spectral lines differential Doppler shifts 78−57538
stellar BCD classification for different chemical constitution 77−29811
stellar broadband linear polarimetry, zero polarisation standards list 79−40187
stellar BVRI photometry, secondary standards 79−70962
stellar Ca II H and K emission, flux meas. by four-channel photon-counting spectrophotometer 78−73646
stellar characteristics, appl. of 0.2 Å resolution far UV spectra catalogue 77−56843
stellar classification dispersion spectra synthesis from atmos. theory and high-dispersion spectra 77−29804
stellar clusters, appls. to cosmic distance measurement 78−57599
stellar clusters, membership probabilities interpretation 78−28736
stellar convection parameters, meas. technique 79−21273
stellar diameters from photoelec. obs. of lunar occultations 78−7866
stellar disc brightness distrib. determ, from photoelec. obs. of lunar occultations 79−35146
stellar distances, max. likelihood technique appl. to variables 80−51746
stellar distances, max. likelihood technique tests 80−51745
stellar distances, parallax and relative magnitude, laboratory model for students 78−16610
stellar flare data reduction and interpretation, interactive method *(Italian)* 80−8552
stellar gravity and effective temp. determ. by automatic procedure 80−98557
stellar high-dispersion spectroscopy, appl. of McMullan 4 cm electronographic camera 78−73644
stellar holographic interferometric technique, mutual coherence function 78−53838
stellar image real-time atm. compensation by active wavefront control 78−45242
stellar image sharpening, real-time phase correction 79−12410
stellar image spatial freq. modulation, atm. correlation scale meas. 78−40661
stellar images, atmospherically degraded, restoration using complex spectral ratios 79−29854
stellar interferometry, first fringe meas. 80−82215
stellar interferometry, high ang. resolution obs., review 77−33355
stellar interferometry, long baseline, S/N ratio 80−26749
stellar interferometry, phase effect detect. and appl. to orbit of α Aurigae (Capella) *(French)* 80−36508
stellar interferometry of star cluster with prominent variable 79−84680
stellar light curve analysis, by automated Fourier techniques 79−17020
stellar luminosity systems calibration, trigonometric parallaxes appl. 80−4343
stellar magnetic field meas. using circular polarization analyzer on 6 m telescope *(Russian)* 78−40923
stellar magnetic fields, vector-operator algebra technique for stationary states determ. 78−73698
stellar magnetic fields measurement techniques 80−82213
stellar magnitude, colour index and position meas. from astronomical photographs, automated technique 79−21194
stellar MK spectral classification from photometric obs., appl. to uvbyβ photometry with assumed luminosity class 80−67700
stellar models, tidally distorted, small oscills., Roche coordinates appl., second-order terms effect 79−44462

astronomical techniques continued
stellar motion and vel. from previous surveys 80—82395
stellar near IR photometry, effects of atmospheric extinction 80—51539
stellar occultation TV scanning, image freq. limitation *(French)* 79—58264
stellar occultations by Earth, spacecraft obs., tropopause height determ. 77—2280
stellar open clusters, age determ. methods *(Italian)* 80—90489
stellar open clusters, metal abundance determ. from H-R diagrams 77—49370
stellar optical images, improvement via real-time phase correction system, appl. to Sirius 77—22084
stellar perturbation analysis 79—44379
stellar photoelectric photometry, efficiency as function of image quality 80—62034
stellar photoelectric photometry, fundamental problems *(Russian)* 77—64656
stellar photographic photometry, PDS microdensitometer technique 79—88600
stellar photometry, absolute calibration of spectral energy distrib. of 16 stars in 3500 to 7500 Å region 80—67710
stellar photometry, appl. of focal reducer using Fresnel lens 80—67568
stellar photometry, catalogue of parameters of stars measured in Geneva Observatory system 77—73974
stellar photometry, extinction oscills. caused by atmospheric disturbances 80—56606
stellar photometry, photographic, digitalised image processing, reduction procedures *(Italian)* 80—98569
stellar photometry, response functions in red and near IR 80—56715
stellar photometry, two colour system for near IR 79—62759
stellar photometry, UBVR sequences around globular clusters (NGC 5946, 6440 and 6624) 79—88702
stellar photometry anal., vector space methods and appls. to O stars and interstellar reddening 78—49338
stellar photometry in auroral zone, UBV obs. at geographic latit. 69°22′ north 79—44376
stellar polarisation meas., data reduction method 80—26748
stellar pulsations, period determination using phase dispersion minimisation 79—5756
stellar radial vel. determ. methods 78—96406
stellar radial velocities, determ. from perspective secular changes in proper motion 77—91524
stellar radial velocities, meas. via HF absorpt. cell 80—12681
stellar radial velocities, Radcliffe Cassegrain d-camera vel. system 78—73645
stellar radial velocities determ. via cross-correl. techniques and TV detector, appl. to (NGC 6327) 78—16305
stellar radial velocities meas., via McDonald Observatory 2.1 m radial rel. spectrometer 80—51667
stellar radial velocity meas., standard wavelengths and vels. for twelve stars 77—17547
stellar radial velocity measurement with objective prism 79—84681
stellar radiation atmospheric extinction, allowance for IR absorpt. by H_2O mols. *(Russian)* 78—40832
stellar right ascensions obs. with large transit instrument, accuracy of absolute chain method of equalisation *(Russian)* 79—96887
stellar rotation in lower main-sequence stars, spectral lines Fourier anal. appl. 80—51767
stellar rotational velocities, determ. via appl. of Bessel transform 77—49369
stellar secondary spectrophotometric standards, obs. in 5840-10800 Å range 79—29995
stellar simultaneous UBV photometry, by fast double head photometer 80—72775
stellar space density derivation methods, systematic comparison 78—61917
stellar spatial distrib. in globular star clusters, recovery method *(Russian)* 80—94722
stellar speckle interferometer data for astronomical object reconstruction, iterative method 80—106475
stellar speckle interferometry, atmospheric effects, laboratory simulation 79—53730
stellar speckle interferometry, lens-atmosphere modulation transfer function meas. 79—101078
stellar speckle interferometry, phase var. estimation 77—45317
stellar speckle interferometry, S/N ratio 78—12102
stellar speckle interferometry, two aperture pupil plane 79—35145
stellar speckle interferometry, wave correlation scale meas. 78—65388
stellar speckle interferometry and holography, isoplanicity and temporal correl. meas. *(German)* 79—75116
stellar speckle interferometry data processing method 79—12409
stellar speckle interferometry in near IR 79—53734
stellar spectra, atomic line profile calc. method *(Russian)* 79—92684
stellar spectra, line equivalent width errors due to photon statistics, calc. formalism 80—8625
stellar spectra, MK classification of metal-poor late-type stars 80—4340
stellar spectra, photographic equivalent widths calibration against solar photoelectric equivalent widths, feasibility 78—73658
stellar spectra, quantification technique 77—29791
stellar spectra, recalibration of quantitative three-dimensional classification for F8-K1 stars 77—78768
stellar spectra interferometry, spatial power spectrum estimation 79—76608
stellar spectra simulation using optical filters, G- and F-type stars 77—37505
stellar spectral analysis, Fe lines equivalent widths in cool standard stars 77—78771
stellar spectral classification, errors detect. by cluster anal. 78—20819
stellar spectral classification, rel. to use of H-R diagram as astronomical tool 78—81619
stellar spectral classification calibration using TV multichannel system 77—67091
stellar spectral classification from interesting Stromgren indices, appl. to bright southern stars 79—88645
stellar spectral line analysis, effect of waves 79—44465
stellar spectral synthesis, appl. to broad flux depressions of Ap stars and comparison with spectrophotometry 80—67735
stellar spectrograms, relative Zeeman and Doppler shifts determ. via statistical approach 78—36467
stellar spectrograms smoothing by Whittaker method *(Russian)* 77—71008

astronomical techniques continued
stellar spectrophotometric standards calibration against α Lyrae 79—62760
stellar spectrophotometry, accuracy anal. 79—21193
stellar spectrophotometry, Moscow and Alma-Ata data comparison with multicolour photometric systems 80—101590
stellar spectrophotometry, multivariate anal. 77—78772
stellar spectroscopy, appl. of linear filtering theory to line profiles *(Italian)* 80—90340
stellar spectroscopy, optical classification of low luminosity M-type dwarfs 79—58339
stellar structure theory, appl. of Clairaut coordinates to vibr. stability of distorted stars 80—90408
stellar trigonometric parallaxes, internal and external errors 77—91523
stellar trigonometric parallaxes, statistical use 77—45315
stellar two-dimensional spectral classes, accuracy of derivation from DDO photometry 78—16395
stellar UBV photometry, influence of Balmer discontinuity on reductions 77—74046
stellar uvbyβ photometric system, absolute luminosity calibrations check by means of small trigonometric parallaxes 78—57463
stellar uvby Hβ photometric system, empirical calibration for B-type stars 78—32454
stereophotogrammetry of Mars surface 78—77493
stochastic image restoration procedure 77—10858
Stokes parameters meas. 77—17381
stone meteorite, laboratory simulation of impact *(Russian)* 77—91489
strip photometry of diffuse objects, globular clusters multicolor obs. 78—89229
Strømgren four colour indices, grid for calc. of log g and effective temp. 80—36507
submillimetre astronomy, sky emission and absorpt. noise reduction 77—41308
submillimetre waves and applications, conference, Guildford, England (1978) 79—31916
submillimetric multicolour photometry and calibration 79—35143
Sun, millimetre wave brightness temp. determ. rel. to new Moon 77—22171
Sun, photosphere temp., luminosity vars. and global oscills. from C I 5380 Å line obs. 77—53487
Sun, use of MHD pulses as diagnostic technique 80—109405
sunspot mag. flux tubes, method for magnetostatic equilib. solns. 80—98637
sunspot positions determination, use of solar graticules 78—16299
superconducting superheated granules as X-ray and γ-ray imaging detectors 79—25504
supergiant stars, atmospheric struct. from freq. depend. diam. 77—56924
supernova remnants, element abundances and shock conditions determ. from optical emission 77—64816
supernovae, soft X-ray flux prediction method 79—71060
superposition of epochs, statistical method, anal. and appl. 80—4267
SURF storage ring calibrations for NASA stratosphere and climate programs 80—94721
surface photometry of barred spiral galaxies, computerised digital reduction method 78—81690
synchronous photometry of periodical optical sources, optimum meas. time estimation 77—73965
synthetic spectra calc. method for hot stars with circumstellar clouds 80—77382
synthetic topographic contour mapping of Mars 78—45253
synthetic-aperture radar on satellites, digital processing techniques 80—61914
taxonomy, appl. to Virgo galaxy cluster area morphological study *(French)* 79—35400
telescope, orbiting, celestial object sighting accuracy anal. 78—4057
telescope optics testing by Hartmann method, estimation of reliability of results 80—67564
telescope polar axis alignment, methods 79—70957
television-electronics study of faint astronomical objects, review 80—82208
terrestrial longit. determ., without time, from obs. of lunar altitude 78—85836
test for superclustering, 2 D nearest neighbours test, appl. to Abell galactic clusters 80—41905
time histogram method for weak X-ray source variability anal. 78—20652
time obs., data smoothing method *(Japanese)* 77—73973
time-modulated measurements with image-tube systems, effects of phosphor decay 79—88602
timing method for astrophotography 80—67572
transformation-elimination technique for soln. of perturbed Hamiltonian systems 79—44346
transient astronomical phenomena, video detection and analysis techniques 79—80239
transit times, calc. using new photographic astrolabe at Turku observatory 80—36499
turbulence-degraded image compensation, computer simulation techniques 77—60625
turbulent cosmic plasma, vel. field determ. via EM waves polarisation angle variance 77—17358
turbulent-degraded image reconstruction using nonredundant aperture arrays 78—93122
TV apparatus for meteor spectra photography 77—67047
TV cameras for planetary observations 80—31197
UBV stellar photometry from N.Norway during auroral activity, technique and results 79—40084
UK 1.2-m Schmidt telescope alignment and pointing accuracy, optimum setting determ. technique 80—4252
ultralow dispersion spectroscopy ultralow dispersion spectroscopy of stars and galaxies 79—53733
universal time measurement, results from lunar laser ranging 78—85854
unstable systems, absolute and convective instabilities discrimination method 80—98539
W Ursae Majoris binary stars, synthetic light curves calc., appl. to V566 Ophiuchi 77—74097
UV and visible astronomy from space 78—61704
UV astrophysical studies from space vehicles 79—25519
UV measurement, accurate techniques 80—47103
UV spectrophotometry absolute calibration, 1750-3350 Å region 79—70963
uvbyβ photometric system, appl. to stellar temps. determ. 77—64740

astronomical techniques continued
vacuum UV Cherenkov source as radiation standard *(Russian)* 78–63164
variable star period determination method *(French)* 78–36465
variable star radius determ. by Wesselink method, appl. to nonradially oscill. star 79–48824
VBLUW photometry of stars in Magellanic Clouds and Milky Way, photometric system characts. 78–16398
Venus, Mariner 10 UV images normalisation 77–56850
Venus, wind speed meas. by anemometers on Venera-9 and Venera-10 probes 77–37542
Venus clouds spectropolarimetry, lines equivalent widths information content 80–31215
Venus internal structure, computation from terrestrial seismic data 77–87298
Venus rock density, method, equipment and results of Venera 10 meas. 78–28564
video stereophotogrammetry, interactive computerised, for Mars Viking 1975 Lander data 78–81557
video techniques, appl. to comet debris (meteors) studies 79–80241
Viking 1975 Mars lander interactive computerized video stereophotogrammetry 78–20650
Viking 1 and 2 expeditions, scientific results *(Hungarian)* 78–73666
Viking Lander tracking contributions to Mars mapping 80–12702
Viking Orbiter and Lander stereo image processing 78–81554
Viking Orbiter rectified photography, planimetric Martian triangulation 77–87276
Viking spacecraft, Mars atm. struct. expt., techniques, instruments and accuracy 77–13205
visual binary star orbit, computation method for any eccentricity *(French)* 78–85974
VLBI, appl. to relative proper motion of radioemitting QSO pair 1038+528 A,D 80–51902
Voigt lines, random array, curve-of-growth function 78–89055
Washington Photometric System, props. and standard stars 80–31213
wave tilt sounding of multilayered structures on planetary surfaces 80–61926
wavefront correction in real time for atm. distortion, Bragg diffr. by acoustic wave 77–42500
wavelength calibration of low dispersion objective prism plates, quasar redshift determ. 79–2485
weighted-filter imaging technique appl. to lunar surface chem. 78–12124
white dwarf planetary companions, detection by direct photometry from space telescope 79–71076
white dwarfs magnetic fields measurement, anal. of atomic spectra in intense mag. fields 80–105160
Wolf sunspot number forecasting, appl. of freq. anal. 80–56797
Wolf-Rayet stars, faint, photometry by u′ubvv′ system 79–40200
Wollaston prism as convergent light beam splitter 79–14092
X-ray and gamma-ray diffuse background meas. using nondirectional detectors 77–73968
X-ray astronomy, lunar occultations optimisation for point-like sources positions determ. 79–92652
X-ray astronomy, point source imaging via automodulation collimator telescope *(Russian)* 80–62018
X-ray astronomy, point-like sources lunar occultations data anal. 79–88567
X-ray astronomy, technique for Cygnus X-1 flux variability characts. determ. *(Russian)* 80–51921
X-ray burst detection by atmospheric fluorescence in near UV 77–9663
X-ray detection of cosmological objects 80–62323
X-ray image processing techniques for Ariel 5 rot. modulation collimator 79–80236
X-ray imaging, conf., Reston, USA (Apr. 1977) 78–45762
X-ray photometry from Prognoz satellites 80–17462
X-ray source position determ., parameter estimation method 78–61748
X-ray sources, binarity detect. via Doppler effect *(Russian)* 78–77623
X-ray sources, two-dimensional image synthesis via modulation collimators 77–5434
X-ray sources spectra, meas. in rapidly varying sources 77–5443
X-ray spectra, use of a priori information in derivation of temp. structs. 78–20778
X-ray spectra deconvolution 80–85867
X-ray spectra restoration 79–25515
X-ray spectroscopy, transmission grating behind grazing incidence telescope 77–64654
X-rays diffuse component, separation method using growth curves 79–25512
Zeeman line profile, mag. field determ. by radiative transfer method 80–82221
zodiacal light brightness integral inversion, three-dimensional eqn. 79–75155
zodiacal light UV observation from D2B-Aura satellite, extraneous light evaluation 79–58299
Zwiers graphical method for visual binary stars orbital elements, appl. to ADS 11871 (β 648) 80–51805
C stars, C and N isotope ratios from spectral analysis 79–30057
H II regions density fluctuatons, statistical approach 80–77468
H II regions radio emission analysis, consequences of improper analytic methods 78–54000
H II regions weak shocks, isothermal Mach number determ. from line ratios 78–93348
H II regions' exciting stars mean temp. determ. method 80–73024
Hα interferometric obs. of supernova remnants IC 443 and VRO 42.05.01, high vel. gas discovery 79–75258
Hα photometry through narrow-band interference filter 77–56838
Hγ equivalent width computation method for objective-prism astrograph, for SMC stars 78–57462
Li, Be, B, isoelectronic sequences, ionization equilib. balance, solar and stellar atms. appl. 79–36587
N III lines for solar diagnostics 79–30031
Si lines as spectral diagnostics for astrophysical plasmas, effect of charge transfer 80–41717
ZnS:^{90}Sr, continuously acting luminous solid for photoelec. meas. over 300-800 nm range 79–3757

astronomical telescopes
see also radiotelescopes
1.25 m ZTEh telescope of P.K. Shternberg State Astron. Inst., image quality and sidereal drive accuracy 77–78638
6″ reflector construction, assembly of telescope 77–87266

astronomical telescopes continued
25 m equivalent aperture, optical and IR, design concepts 80–82203
32.5 cm IR airborne telescope 78–28523
60 cm reflector, at Kagoshima rocket launching centre *(Japanese)* 78–32344
60 cm reflector with high speed photometer *(Japanese)* 78–32345
74-inch at Sutherland, S.Africa 78–49323
80 cm X-ray telescope, facilities and observational possibilities *(German)* 80–109358
105 cm Schmidt at Kiso Station of Tokyo Astronomical Observatory 77–91425
ABP-2 telescope, star trail image vibrations rel. to temp. fluctuations *(Russian)* 78–20636
adaptive optics dither systems for space telescopes 77–49301
altazimuth and equatorial telescope mountings, home made, construction method 78–40830
altazimuth mounted, primary mirror deflection and stress anal. 80–58659
altazimuth-mounted computer-controlled, zenithal blind spot 78–53823
Anglo-Australian 3.9 m telescope, computer-controlled slewing, setting and tracking 77–17371
Anglo-Australian Telescope, survey 77–91434
Apollo Telescope Mount and solar instruments of Skylab, overview 77–60593
Apollo-Soyuz Test Project EUV telescope, 584 Å sensitivity rel. to local interstellar He density 79–92834
Aryabhata satellite X-ray astronomical telescopes and electronics system 79–84638
aspheric surfaces, two axis, design 79–86245
astrographic cameras, value to the amateur 77–17364
astrometric telescopes flexure, determ. via autocollimation method *(Russian)* 78–40818
autoguider, photoelectric control component *(German)* 78–73649
autoguiders and acquisition systems for optical telescopes 80–82206
autoguiders for optical telescopes 79–75109
automatic Ritchey-Chretien telescope at Abastuman Observatory *(Russian)* 77–87270
azimuth alterations, influence on absolute right ascension calcs. *(Russian)* 79–35134
AZT-24, design formulas for construction elements 79–35133
bad seeing conditions avoidance within telescope domes 79–70960
Baker-Schmidt flat-field telescope, reflecting corrector plate, design theory 78–36454
balloon-borne 102 cm, for far IR obs. of celestial sources 78–45227
balloon-borne 102 cm telescope and Palermo four-colour far IR *(Italian)* 79–48688
balloon-borne 10 cm telescope, appl. to solar faculae and sunspots direct photography *(Japanese)* 79–80292
balloon-borne IR telescope for absolute surface photometry of night sky 78–36453
balloon-borne slow-scan TV camera performance test *(Japanese)* 80–12635
balloon-borne solar telescope viewfinder, narrowband TV system appl. *(Japanese)* 78–24464
Bamberg zenith telescope, Talcott photoelectric micrometer for latitude obs. *(Russian)* 78–4113
beam expander telescope design utilizing fast spherical primaries 79–66921
bimorph piezoelectric flexible mirror constructed from glass plates and Pb(Zr,Ti)O$_3$ ceramic 79–59787
blank fabrication for large azimuthal telescope primary mirror, work program 78–16302
Boyden Observatory 152 cm reflector, history 80–12665
British large IR telescope on Mauna Kea, construction 78–69686
Bruce telescope, photographic plates computer readable mag. disc catalogue 79–88605
Byurakan Observatory, 1975 visit report 77–33342
Byurakan Observatory 2.6 m telescope dedication 77–37504
calibration, visible nd IR source, VISIR 80–36506
Calver mirror remounted at Wollongong Univ. 77–91428
Cambridge Schmidt telescope, Quadrant Photosil Autoguider 77–60612
Canada-France-Hawaii reflector, design and construction 77–64646
Canada-France-Hawaii telescope, before-focus optical design 79–101062
Canada-France-Hawaii Telescope, general features 77–60614
Cassegrain, automatic design of corrector systems *(Chinese)* 77–22088
Cassegrain adjustments *(Japanese)* 77–73955
Cassegrain telescope, corrector lens system using wide field doublet *(Japanese)* 77–91427
Cassegrain telescope, wide-field, design 77–2338
Cassegrain telescope design and tolerancing optimisation 80–82199
Cassegrain telescopes, focal-reducer system for slitless fieldspectroscopy 80–36504
Cassegrainian 40 cm reflector, qualitative and quantitative examination *(Japanese)* 79–44366
catadioptric system with gradient index corrector plate 78–12096
catoptric Schmidt telescope correcting mirrors, aspherisation by elastic relax. *(French)* 80–62015
chromatic curve determ., spectrographic technique 77–5432
coded mask X-ray telescope for rocket appls., optimum design 77–13239
coelostat, star pointing, Meudon solar tower 80–90338
comet telescope, timing system *(Japanese)* 78–89071
compound catadioptric telescopes with all spherical surfaces, design 78–69682
compound eyepiece development, late 17th century 77–37704
Compton telescope, appl. of Anger camera principle, for gamma-ray astronomy 79–80223
control, computer appls. 78–4111
Cornell 25-inch training telescope 78–7882
cosmic ray scintillation supertelescope, computation of meteorological coeffs. 77–13202
cosmic ray telescope, solid state, detection system for heavy ions, element and isotope separation 80–67563
cost-scaling laws applicable to very large optical telescopes and radiotelescopes 80–41722
Coude spectrograph of 188 cm reflector, integrating exposure meter *(Japanese)* 77–73961
CTIO 4 m telescope, grating spectrograph anamorphic magnification and appl. 79–66927
design and construction technology 80–31211
design of reflective and catadioptric systems 79–86242
development and history, review *(Italian)* 77–56839

astronomical telescopes continued
diffraction figure calc. by Fourier transform. *(French)* 79—48672
digital processing techniques applied to astronomical images 77—60626
direct imaging with space telescope during stationary occultations for extrasolar planet detection 78—85858
Dodaira Station 91 cm. telescope clock system *(Japanese)* 77—73964
domeless solar telescope, design 77—78640
double astrograph photometric system, investigation of colour eqns. *(Russian)* 80—72771
double Compton gamma-ray telescope, background sensitivity to atmospheric neutrons 78—53827
double scatter telescope for medium energy gamma ray astronomy from a satellite 79—48676
double telescope system for cross correl. detection of rapid stellar var. 77—82127
drift chamber telescope for gamma-ray astronomy 79—21185
drive, controlled 300 Hz freq. supply 78—61746
drive, of laser ranging equipment *(Japanese)* 78—89078
Einstein X-ray observatory, HEAO-2, results to date 80—56692
ESO 3.6 m telescope, first photographs 77—45308
ESO 3.6 m telescope operational *(Danish)* 78—4101
ESO formation and use of Danish telscopes in Chile *(Danish)* 77—53425
EUV telescope, high performance, design 79—58245
extinction coefficient meas. from distant contrast, using astronomical telephotometer 78—61730
Faint Object Spectrograph for Space Telescope 79—25483
Faint Object Telescope for far UV spectrophotometry of galaxies and quasars 79—25481
far IR 41 inch balloon telescope with composite bolometers 78—45228
far IR astronomy, detectors and sources, review 80—56726
far IR focal plane array, test facility 79—5755
far IR telescopes, balloon-borne, calibration source 80—62027
FAUST instruments, high focal ratio telescope for UV imagery 80—41724
field correction for 188 cm reflector *(Japanese)* 77—73958
field corrector for parabolic reflector, design method *(Chinese)* 80—85857
field corrector for paraboloid, small-field single lens 77—33344
field correctors, for telescopes at better observing sites 80—4257
flexible mirror, for active image restoration 77—45319
focused radiation scintillations, freq. correl. by speckle interferometry 79—94153
focusing mechanism, semi-kinematical design 79—96918
focusing testers, anal. of optical and construction parameters 78—83070
four-mirror unobscured anastigmatic telescope, with all-spherical surfaces 78—57439
frame-type mount, anal. of static loading effects 78—28518
fused silica fibre link to spectrograph, operation and prospects 79—53721
gamma-ray, large scale telescopes for high resolution obs. 78—93114
gamma-ray Compton telescope, high ang. resolution, 0.3-10.0 MeV directivity *(Portuguese)* 78—85847
gamma-ray telescope, high-energy use of drift chambers 80—41726
gamma-ray telescope, large area, coordinate-sensitive time-of-flight scintillation system 79—84676
gamma-ray telescope, large sensitivity, energy and angular resolution 80—62016
gamma-ray telescope, low and medium energy, modulating anticollimator *(Russian)* 79—16832
gamma-ray telescope, spark chamber, scintillation counter time-of-flight system 80—62017
gamma-ray telescope artificial satellite, axis orientation determ. 78—53787
gamma-ray telescope on satellite, axis orientation determ. 79—2479
gamma-ray telescope spark chamber, e^+e^- track analysis 80—63469
gearless telescopic drive, transference from elec. motor to polar axis 80—67571
GEODSS, optical moving target indication, multi-minicomputer network 77—5445
giant mirrors, telescope design for 1990s, conf. report and review 80—105170
glass discs, thermal-optical distortions, rel. to solar obs. using 50 cm lens 79—72640
grazing incidence telescopes, design, fabrication and performance, for EUV obs. 78—49329
Grazing-Incidence Solar Telescope facility 79—70956
Gregorian reflector, renovation of 18th century instrument 78—61734
grid telescope for imaging hard X-rays 79—25501
Grubb 102 mm. refractor, renovation and remounting 77—33343
guidance of large telescopes, atmospheric dispersion effects *(Russian)* 78—24372
Hadamard transform X-ray telescope, characts. *(Japanese)* 80—94714
Hadamard transform X-ray telescope 78—53828
Hadamard transform X-ray telescope *(Japanese)* 79—84672
Hadamard X-ray spectrometer with wide field-of-view 78—53829
hard X-ray imaging instruments, solar obs. from Space Shuttle 80—17495
hard X-ray telescope, balloon borne, background noise calc. 77—5427
Hartmann test at Okayama *(Japanese)* 77—73956
HEAO B, scheduled launch and X-ray telescope observing opportunities 78—69647
HEAO-1, successful launch report 77—82102
HEAO-2, X-ray telescope description, obs. and sources 80—12643
HEAO-B, focal plane crystal X-ray spectrom. 78—40825
HEAO-B, imaging proportional X-ray counter 78—40823
HEAO-B, orbiting X-ray telescope, Si:Li spectrometer 77—5460
HEAO-B, solid state X-ray spectrom. 78—40824
HEAO-B monitor proportional counter instrument 78—40822
HEAO-B X-ray Observatory 79—25446
HEAO-B X-ray spectrometer, high voltage power module and charge amplifier design 78—40826
HEAO-B X-ray telescope, focal plane transport assembly controls 79—48677
HEAO-B X-ray telescope, gas control system 78—40827
HEAO-B X-ray telescope, high resolution imaging instrument 78—40821
HEAO-B X-ray telescope, mirror design, fabrication and expected performance 78—49330
HEAO-B X-ray telescope, observing program 78—57443
HEAO-B X-ray telescope 78—40820
Herschel's 20 ft. telescope, discovery of original copperplate engraving 77—2340

astronomical telescopes continued
high resolution X-ray optics, for astronomical and laboratory sources 78—45766
high-performance telescope aspheric mirror test error budget 80—48386
Hipparcos, European astrometric satellite, prospects 79—96880
HIPPARCOS, global astrometry by space techniques 80—109369
IAC 80 cm telescope, image quality, alignment tolerances 77—82122
image contrast of diffraction-limited telescopes for circular incoherent sources of uniform radiance 80—82194
image sharpening telescope, atm. distortion compensation 77—49294
image sharpening telescope, observatory results 77—49295
imaging double Compton telescope for balloon obs. of MeV gamma radiation 79—25503
imaging soft X-ray telescope for Spacelab 79—25498
imaging system with obscured pupils, OTF and point spread function 78—25809
imaging through turbulence with telescope array, speckle interferometry 77—5458
Infrared Astronomical Satellite telescope 77—49298
interferometric observing efficiency of arrays of large aperture telescopes 79—80238
International Ultraviolet Explorer, results after one year 79—96915
IR, cryogenically cooled sensors, calibration in space, AFGL expts. 79—5753
IR, current developments review 78—61737
IR, NASA 3-m telescope on Mauna Kea 78—96398
IR, on Space Shuttle, contaminant environment effect 77—91398
IR, Spacelab telescope facility 77—45283
IR, UK 3.8-m telescope on Mauna Kea 78—96397
IR and sub-MM spectroscopy, conf., Bonn, Germany (Mar. 1977) 78—12778
IR Astronomical Satellite Telescope, focal plane design 79—5750
IR astronomical satellite telescope and detector arrays 78—45226
IR detection techniques, for low background satellite expts. 78—49343
IR flux collector on Tenerife 78—69684
IR instrumentation of Calar Alto telescopes 78—16295
IR sky survey telescope, wide field photography 80—105167
Irenee du Pont 2.5 m telescope at Las Campanas, first tests 78—4107
Isaac Newton Telescope, high-resolution Michelson interferometer 78—4105
Isaac Newton Telescope, telescope equipment guide 78—12099
isoplanatic patch measurement using phase-correcting telescope, turbulent air height determ. 79—53732
ITS-4 IR telescope-spectrometer on Salyut 4 station 77—78635
IUE satellite, observing experience 80—36476
IUE ultraviolet telescope, initial results *(French)* 79—84639
Keplerian, magnifying power meas. method 79—18497
Kitt Peak National Observatory, 60 cm vacuum telescope *(Norwegian)* 77—60613
Kitt Peak National Observatory telescopes, cost effectiveness in terms of publications and citations 80—90334
KSC 60 cm reflector, data recording system *(Japanese)* 80—94717
large altazimuth telescope, design and construction 78—16303
large aperture IR optical system, design 77—2339
large azimuth telescope, hydrostatic bearings 80—12668
large azimuth telescope, load relief system of primary mirror 80—12667
Large Azimuth Telescope penetrative power determ. 79—48681
Large Azimuth Telescope primary mirror blank testing 79—50367
Large Azimuthal Telescope, 6 m, test results using Hartmann method with stars 79—8838
large azimuthal telescope, axes coords. determ. system 77—60615
large azimuthal telescope, glass for 6 m primary mirror 77—62025
large azimuthal telescope, initial design 78—32347
large azimuthal telescope, large aperture spectrograph with electron optical convertor 77—91432
large azimuthal telescope, primary mirror, glass blank annealing 77—72101
large azimuthal telescope, primary mirror testing 78—30099
large azimuthal telescope, primary mirror testing by interferometry 77—73952
large azimuthal telescope, primary mirror testing by isophotometric recording 77—73953
large azimuthal telescope, primary mirror testing in observatory 78—20642
large azimuthal telescope, primary stellar spectrograph 77—91431
large azimuthal telescope, search and guide system 78—57446
large azimuthal telescope complex, automated control system 78—73641
large azimuthal telescope major system design 78—73640
large azimuthal telescope mirror, shop tests using modified Hartmann method 78—87173
Large Azimuthal Telescope mirror blank fabrication facilities 79—14123
large azimuthal telescope primary mirror, blank grinding and polishing 78—90541
Large Azimuthal Telescope primary mirror, glass blank quality 79—29991
large azimuthal telescope primary mirror, Hartmann test 77—91430
Large Azimuthal Telescope program control system 79—16829
Large Infrared Telescope on Spacelab 78—12070
large mirror telescopes of world, review 77—33349
large mirrors, radial support methods 77—49293
large precision mirrors, possibilities of mass reduction 78—79100
Large Space Telescope, optimal manoeuvring and fine pointing control with annular momentum storage device 77—22078
Large Space Telescope mirror figure control, adaptive optical techniques 77—22076
Large Space Telescope optimal fine pointing control using Annular Momentum Control Device 77—73934
large transit instrument, accuracy of absolute chain method of equalising star right ascensions obs. *(Russian)* 79—96887
large transit instrument pivots, radius var. and figure changes *(Russian)* 78—24462
lens compensators for testing concave mirrors of astron. telescopes, design 80—28305
Lick, Kitt Peak and Hale reflectors, scales and distortion coeffs. for prime-focus correctors 77—22071
lifting system, hydraulic, for domeless solar telescope *(Japanese)* 79—96914
light source displacement velocity meas. method *(Russian)* 77—41306
Lixiscope, X-ray and gamma-ray telescope system 80—62020
Loiano telescope, photometry with SEC TV camera 79—58272

astronomical telescopes continued
long wavelength IR, ang. response meas., off-axis rejection performance 78−61739
long-focus horizontal telescope for positional photographic obs. of Moon *(Russian)* 78−28533
lunar laser ranging telescope, Earth/Moon motion study appl. 78−93106
McDonald Observatory 2.1 m telescope, radial velocity spectrometer 80−51667
meridian instrument pivot irregularities meas. method 80−94718
metal mirrors, Al, Ni and Au surfaces, EUV reflection efficiencies 79−14073
metals for mirror substrates, manufacturing processes, review 78−5542
meteor observations, telescope performance 78−49319
Michelson stellar interferometer for binary star obs. 79−44370
mirror, point spread function energy distrib. rel. to surface deform. 77−58422
mirror, primary, of large azimuthal telescope, testing by Hartmann method 78−20641
mirror design, economical construction of large lightweight glass mirrors *(French)* 77−17370
mirror for 6 inch reflector, figuring 77−64639
mirror grinding and polishing for 6″ reflector 77−56826
mirror of lunar laser ranging receiving telescope, polishing and Foucault test *(Japanese)* 78−89065
mirror reflection coefficient checking against control samples 79−75106
mirror surface testing of 6m LAT mirror, Hartmann method under shop conditions 78−90540
mirror suspended on belt, deforms. during horizontal control 80−17494
mirror temperature effects on telescope seeing, compensation method 79−70961
mirror testing, portable visible-IR reflectometer 77−62033
mirror testing using autocollimation method with multiple pendulum mirrors 80−102792
mirror type, thermal deformation characts. of graphite/epoxy, testing 77−78636
mirrors, low-cost temp.-compensated cell 77−17369
mirrors, zonal Foucault test, diffr. effects 77−72099
MISO low energy γ-ray telescope 79−25472
monochromators of concave grating mounting for space telescopes, VUV region 78−73629
Monterey Institute for Research in Astronomy, planned observatory, Chews Ridge, California, 36″ telescope 79−88593
mountings for 6″ reflector 78−4102
moving object imagery using large aperture telescope arrays 80−53225
Mt. Hopkins multiple mirror telescope 78−93109
multidetector cosmic ray telescope expt. on International Sun-Earth Explorer C spacecraft 78−85789
multilayer wide-gap spark chamber for a gamma telescope 79−76267
Multiple Mirror Telescope, brief description and early discoveries 80−12669
multiple mirror telescope, design, review 78−69687
multiple mirror telescope, design *(Norwegian)* 79−40072
Multiple Mirror Telescope, Smithsonian Astrophys. Obs., design and construction rel. to previous instruments 78−49325
Multiple Mirror Telescope and ground-based astronomy, conference, Arizona (1979 May 9) 80−62386
Multiple Mirror Telescope guide alignment system 79−75107
multiple-mirror telescope systems, astronomical appls. 80−94713
Multipurpose Utility Pointing and Stabilisation System *(Italian)* 77−82114
Nanjing lightweight 4 m telescope design and construction 80−105162
NASA 91 cm aircraft-borne telescope for IR astronomy 77−22075
Newton's telescope, review of design for teachers 78−8187
Newtonian reflector with rocking-type equatorial mounting, in Hill-Poncet heated observatory 79−70953
next generation designs, rotating shoe mounting *(Norwegian)* 78−69683
next-generation telescope concepts 80−12666
nonfocusing collimating telescope, IR to XUV range 77−25943
objective, 3-mirror design, optical scheme 78−55431
observatories siting, nighttime darkness duration, depend. on latit. 77−25632
optical, 3.9 m, Anglo-Australian, with highly automated operation 78−16291
optical interferometry with two telescopes *(French)* 80−46403
optical multichannel analyser of Sao Paulo University, astronomical obs. 80−26743
optical surface control, Hartmann method, use of splines 79−35149
optical table 10 m telescope 80−105163
optics, computer modelling 79−8836
optics, quick Hartmann method 79−8837
optics testing by Hartmann method, estimation of reliability of results 80−67564
optimised spheric and aspheric optical systems for thermal IR 79−86244
orbiting, IR detector cryogenic cooling requirements 78−96400
orbiting star-tracking telescope, celestial object sighting accuracy anal. 78−4057
orbiting telescope, appl. to detect. of extrasolar planets 77−29882
Palomar 1.5 metre telescope, SIT vidicon detector system 79−92674
Palomar Hale telescope, first 30 years 80−72774
parabolic reflector, coma corrector for off-axis guiding 80−82196
particle telescopes with multiple view directions for pitch angle meas. from satellites 78−24425
Perspex for astronomical telescope lens and mirror manufacture 78−36458
photoelectric automatic control system for large azimuthal telescope 78−16301
photoelectric meridian instrum., performance characts., sensitivity *(German)* 77−17374
photographic detection optimisation at large telescopes 78−24468
photographic limiting magnitudes, determ. method for large telescope *(Russian)* 78−28531
photographic zenith telescope, PZT 1, stellar position obs. at Ondrejov Observatory 77−67035
photographic zenith telescope, PZT 2, for time and latitude service 77−67036
photographic zenith tube, Chinese design and operational characts. *(Chinese)* 78−28514
photometer, sub-mm, for ESO 3.6 m telescope 78−16296
pointing and stabilisation by fine control of secondary mirror 77−82124
polar axis alignment, methods 79−70957
polar axis misalignment determ. for equatorial instruments 78−69685

astronomical telescopes continued
Pulkovo large transit instrument, orientation parameters determ. from 1953 to 1961 obs. *(Russian)* 79−96910
Pulkovo large transit instrument in S.Hemisphere, systematic collimation errors *(Russian)* 79−92673
Pulkovo meridian circle, horizontal axis posn., unloading mechanism effects *(Russian)* 78−28516
Quebec astronomical observatory, new 1.6 m reflecting telescope 79−88592
Radcliffe Cassegrain telescope, d-camera vel. system 78−73645
reflecting, with concave and flat mirrors *(Hungarian)* 78−32841
reflecting optical system, seventh order design 80−48378
reflecting telescope, 6m diam. (USSR) 77−33348
reflecting telescope design, appl. of plate diagram 79−94321
reflective Schmidt anastigmat telescopes, elasticity method 77−29649
reflector technology, Third Earl of Rosse expts. 78−18
reflectors, Cassegrain-type, with zero expansion material mirrors, temp. *(Russian)* 79−96912
resolution, physical and geometrical optics explanation *(Spanish)* 79−40075
resolution in turbulent atmosphere, diffraction limit *(Russian)* 77−25948
review of optical telescopes 77−33348
review of recent developments 78−16307
RGO 30-inch coude, appl. of McMullen 4 cm electronographic camera to high-dispersion spectroscopy 78−73644
Ritchey Chretien telescope, microprocessor control system *(German)* 79−53726
Ritchey-Chretien-Coude 2 m reflecting telescope in Bulgaria, description 80−4250
rocket-borne cryogenically cooled IR system technology 78−45225
S056 X-ray telescope expt. on Skylab Apollo Telescope Mount 77−60596
Salyut 6 submm. telescope with InSb receiver 80−67566
Salyut-4 orbiting solar telescope, design, obs. results 78−53783
satellite IR, control of contamination due to cryogenic cooling 80−31209
satellite-borne instrument development problems and solns. 77−82111
Schmidt 105 cm, Hartmann test *(Japanese)* 78−89073
Schmidt 105 cm, polar axis setting *(Japanese)* 78−89064
Schmidt achromatic corrector plates for near IR, spherical aberration elimination 78−28515
Schmidt achromatic correctors, off-axis aberration 78−45223
Schmidt all-reflecting telescopes, resolution *(French)* 79−75102
Schmidt camera, simple null test for aspheric corrector plate 80−91940
Schmidt correction plates, aspherical surfaces, testing 78−20643
Schmidt folded telescope for deep photographic survey from Spacelab 79−25474
Schmidt telescope, 105 cm, pointing anal. *(Japanese)* 79−101068
Schmidt telescope, 105 cm, software *(Japanese)* 79−101067
Schmidt telescope, astrometry appl., NGC 7027 position meas. 78−73749
Schmidt telescope, wide vignetting free field *(Japanese)* 78−20640
Schmidt telescope at Campo Imperatore, automatic control using PDP 11 processor *(Italian)* 80−8541
Schmidt telescopes, achromatic condition *(Japanese)* 78−89062
Schmidt-Cassegrain, for atm. refractive turbulence profiles meas. 77−5331
Schmidt-Cassegrain system, optical figuring 79−46025
secondary mirror centering of Tirgo telescope 80−101533
secondary mirror flexure, elasticity theory *(French)* 77−14789
sectional mirror, optoelectronic control system 78−20645
seeing, wavelength depend., atm. inhomogeneity effects 78−92979
Shajn 2.6 m telescope, Coude spectrography *(Russian)* 77−64644
Shajn 2.6 m telescope design *(Russian)* 77−64643
shearing interferometer as filter for scattered light reduction 77−25941
short-focus telescopes, semi-kinematic equatorial table 79−70958
Shuttle IR Telescope Facility, detector performance conditions 79−5752
Shuttle IR Telescope Facility, focal plane design 79−5750
Shuttle IR telescope facility 77−49297
Shuttle/Spacelab, platform for cooled IR astronomical telescope 77−73921
simulated multiple mirror telescopes, speckle interferometry, meas. of astronomical objects 80−56716
simultaneous optical and X-ray imaging telescope 77−82121
Sir John Herschel 20 feet reflector, description 79−88788
sky noise at focus, photometry of atmospheric IR emission, statistical props. *(French)* 78−53731
sky noise correl. for IR telescope focal plane *(French)* 78−53725
small-aperture wide-field, for optical IR sky survey appl. 79−21198
Sneg-3, gamma-ray telescope, Franco-Soviet cooperation in gamma-ray astronomy *(Russian)* 78−40844
solar horizontal telescope, instrument polarisation study 80−17492
solar limb motion, expt. verification of atm. turbulence inertial model 79−5614
solar prominences, filter type telescope for amateurs 79−84670
solar stratospheric station, automatic, construction, selection of variant *(Russian)* 79−96913
solar telescope, balloon-borne, narrow band TV system appl. as viewfinder *(Japanese)* 79−80228
solar telescope, correl. between angle of arrival fluctuations at entrance pupil 78−7879
solar telescope, nearby turbulence deduced from arrival angle statistics compared with microthermal meas. 80−26740
solar telescope at Stanford University, mean solar mag. field obs. 78−20800
South African Astronomical Observatory, user guide to telescope facilities 78−73628
Soviet 6 m diam. optical and RATAN 600 radio telescopes *(German)* 77−78639
Soviet 6 metre reflector, review *(Norwegian)* 78−36456
space, low-cost, pointing control system 77−5430
space, telescope, double roll-out solar array appl. 79−52939
space telescope, 2.4 m, to be put into orbit by Space Shuttle *(Danish)* 77−71002
Space Telescope, adaptation to Space Shuttle capabilities 80−109364
Space Telescope, design and projected performance 80−105165
space telescope, design features 78−45229
Space Telescope, history 79−84928
Space Telescope, image sensors performance, planning 79−35136
Space Telescope, NASA plans *(German)* 79−16828
Space Telescope, prospects for spectroscopic and direct work 78−57444

astronomical telescopes continued
- Space Telescope, reviews 77—17363
- Space Telescope, scientific instruments 80—61987
- Space Telescope 79—25477
- Space Telescope astrometry from CCD images 80—109370
- Space Telescope astrometry project 80—105175
- Space Telescope detection of extra-solar planetary systems 80—109356
- Space Telescope in orbit above Earth's atmosphere, potential 79—88595
- space telescope on space shuttle planned astronomical studies 79—21183
- Space Telescope optical design and performance control 79—80224
- Space Telescope pointing control fine guidance subsystem design 80—82201
- Space Telescope solar array requirements and design 79—96885
- Space Telescope spectrograph Digicons 80—85858
- space telescope-observatory 2.4 m, instrumentation and appl. *(French)* 80—17493
- space telescopes, optical systems *(Russian)* 77—17367
- speckel interferometry with multiple mirror telescopes, laboratory expts. 79—80237
- speckle imaging, photon by photon, diffr. limited performance for large telescopes 79—53729
- speckle interferometer on 2.5m Isaac Newton telescope 77—22102
- speckle interferometry with severely aberrated telescopes 78—12103
- speckle patterns, image retrieval 77—22100
- spectrometer for prime focus of parabolic mirror, new design *(Chinese)* 79—80226
- standing wave and pellicle, proposed design for very large space telescopes 79—92672
- star seeker using semidisc light-flux modulator, accuracy anal. 78—73648
- steerable dish of mirror units, next generation telescope *(Norwegian)* 78—85846
- stellar image sharpening, real-time phase correction 79—12410
- stellar speckle interferometer, lens-atmosphere modulation transfer function meas. 79—101078
- stray radiation, expt. meas. and computer analysis 78—61752
- strip telescope, image synthesis, computer simulation 77—29660
- submillimetre detector-telescope systems, for spectroscopy 77—49305
- surface configuration control by conc. loads applic., mirrors case 79—94317
- surface configuration control of nonuniformly heated shells, actuators effectiveness for mirrors 79—94318
- synthetic aperture objectives, use of toroidal elements 77—75650
- three mirror anastigmatic telescope design 77—87265
- TIRGO project *(Italian)* 79—48678
- transit circles, design, discussion of main parameters *(French)* 79—62744
- transmission grating, facet-type, aberrations for cosmic X-ray and XUV spectroscopy 78—85851
- triple-prism beam deflection compensation 79—75105
- turbulence-degraded image a posteriori restoration using multiframe imagery 77—60469
- turbulence-degraded image compensation, computer simulation techniques 77—60625
- two telescope interferometer, 1 arc-millisecond resolution, telescopes 25 cm diameter *(French)* 77—91439
- two-mirror anastigmatic telescopes, designs 77—60611
- two-mirror corrector, well baffled, for parabolic telescope mirror 77—62030
- two-mirror grazing incidence telescopes with one conical surface 79—84673
- two-mirror system with zero spherical aberration *(Russian)* 77—64645
- two-mirror telescopes, image quality estimation and utilisation in cosmic astronomy *(Russian)* 79—96911
- UK 1.2 m Schmidt telescope plates, electronographic calibration 79—88703
- UK 1.2-m Schmidt telescope, alignment, pointing accuracy and field rot. 80—4252
- UK 3.8 m IR telescope, description 78—16300
- UK 3.8 m IR telescope in Hawaii, features 79—75103
- UK 48-inch Schmidt, progress report 77—91429
- UK Schmidt Telescope, obs. 79—48680
- upper atmosphere, background effects in scintillation telescopes 78—85823
- UV high-resolution optical telescope design 80—90335
- UV telescope, onboard International Ultraviolet Explorer, orbiting telescope *(French)* 80—8540
- Venezuela, new observatory near Merida, review 78—49316
- very large optical telescope array, linked with fused SiO$_2$ fibres 78—32342
- vidicon appl. to low intensities meas., with Si-intensified target *(German)* 80—98545
- visits to American observatories 77—37502
- weak object image distorted by atm. effect, restoration possibility *(Russian)* 78—32349
- Wolter type I telescope for rocket appl., X-ray optical props. 79—25499
- Wolter-Schwarzschild optics for Berkeley stellar spectrometer and EUV Explorer 80—82197
- Wroclaw Observatory, new telescope *(Polish)* 79—88594
- Wynne telescope with FAUST, far UV camera on Spacelab 79—25476
- Wyoming Infrared Telescope (Jelm Mountain), IR universe exploration 78—85848
- X-ray, actively shielded 78—81540
- X-ray, large scale telescopes for high resolution obs. 78—93114
- X-ray, mirror, on Salyut-4, gas-filled proportional photon counter 78—86746
- X-ray imaging, conf., Reston, USA (Apr. 1977) 78—45762
- X-ray multiple-grid telescopes, diffr. effects 79—44367
- X-ray optics, surface roughness meas., by X-ray scattering and differential interference contrast microscopy 79—30410
- X-ray SO56 telescope, energy throughput variation with off-axis angle 77—60592
- X-ray spectrometer-telescope system for solar corona studies 80—105168
- X-ray spectroscopy, transmission grating behind grazing incidence telescope 77—64654
- X-ray telescope, balloon-borne, for Crab Nebula imaging *(Japanese)* 79—80220
- X-ray telescope, HEAO-2 Observatory, protective design considerations, system reliability 80—61983
- X-ray telescope, new design using automodulation collimator *(Russian)* 80—62018

astronomical telescopes continued
- X-ray telescope, space-borne, pulse shape analysers investigation for phoswich detectors 80—36501
- X-ray telescope on Skylab, S-054 expt., for solar obs. 77—60616
- X-ray telescopes, appl. of lobster eye optical configuration 80—17491
- X-ray telescopes, design of optimum coded masks 79—66923
- X-ray Wolter I type, paraboloid-hyperboloid combination, imaging props. 77—45310
- X-ray XUV telescope/white light coronagraph expt., quadratic A/D converter 80—62024
- XUV solar telescope and white light coronagraph, CCD camera systems and support electronics 80—62023
- Zelenchuk 6 m. azimuthal telescope, construction and operation *(Russian)* 77—25944
- zenith telescope, use as astrolabe for time and latitude meas. 80—98550
- ZTL-180 zenith telescope, micrometer screw turn from declination arc. obs. *(Russian)* 78—89067
- ZTL-180 zenith telescope, objective distortion determ. from visual obs. of star pairs *(Russian)* 78—89068
- Hα telescopes on Skylab, high resolution solar obs. 77—60604
- SiO$_2$ lightweight 370 mm mirror fabrication and testing 78—57447

astronomy *see astronomy and astrophysics*

astronomy and astrophysics
- *see also astronomical catalogues; astronomical instruments; astronomical observations; astronomical observatories; astronomical spectra; clusters of galaxies; cosmology; extraterrestrial life; galaxies; gamma-ray astronomy; infrared astronomy; intergalactic matter; interplanetary matter; interstellar magnetic fields; occultations; radioastronomy; solar system; stars; ultraviolet astronomy; X-ray astronomy*
- 1977, BAA handbook 77—2350
- Abel integral eqn. inversion in astrophysical problems 80—26732
- acceleration of particles in astrophysical conditions 78—81537
- aether drag and radiation press. in dispersive medium 79—35124
- Alfven wave accelerated particles, distrib. function self-similar soln. 80—56702
- Alfven waves, finite amplitude circularly polarised, instability 78—28502
- Ambartsumian's proto-matter hadronic nature from ang. momentum-mass relation 80—77528
- American Astron. Soc., 149th meeting (Honolulu, 16-19 January 1976) 77—41289
- American Astronomical Soc., 153rd meeting (Mexico City, 7-10 Jan. 1979) 79—62763
- American Astronomical Soc. 154th meeting (Massachusetts, USA, June 1979) 80—17506
- American Astronomical Society, 150th meeting (Atlanta, Ga., 12-15 June, 1977) 77—78615
- American Astronomical Society, 152nd meeting, Madison, Wisconsin (June 1978) 78—96385
- ancient astronomical records from the Orient 77—45326
- anisotropic explosion of rotating, self-gravitating uniform spheroids, astrophysical appls. 79—8822
- Ann Arbor school of astronomers, foundation, 1852-63 80—86062
- annihilation model of quasi-stellar objects 80—22109
- annual review, 14th volume 77—25956
- annual review, 17th volume 80—12646
- annual review, 18th volume 79—5733
- annual review (volume 15) 78—24473
- anti-matter, possible role in high energy astrophysics 80—94705
- archaeoastronomy, Namoratunga II site in NW.Kenya, astronomical dating 80—72793
- archaeoastronomy, New Mexico site marking solstices and equinoxes 80—72794
- archive collections, in Southern Africa 78—36473
- Aryabhata, 5th century Indian astronomer and mathematician, life and works 78—65741
- Asian-South Pacific regional meeting in astronomy, Wellington, New Zealand (1978 December 5 to 8) 80—77538
- association reactions, rel. to cosmic dust condensation onset 80—26931
- astroarchaeology, analysis of Stonehenge and Great Pyramid 78—32363
- astroarchaeology, Avebury, geometry and metrology of ring, new accurate survey results 77—33359
- astroarchaeology, Avebury, West Kennet Avenue, possible geometry 77—33360
- astroarchaeology at Broger ring, fourth lunar foresight and prehistoric mound 77—41322
- astroarchaeology at Kerlescan megalithic stone alignments, alternative geometry 77—41321
- astrology in undergraduate astronomy courses 78—61991
- astronomer, Sir James Hopwood Jeans (1877-1946), biographical review 78—32635
- Astronomical Soc. of Pacific, Park City summer meeting (1978 June 21-23) 79—21201
- Astronomical Society of India, fifth meeting, Nainital, India (1979 November 6 to 9) 80—101658
- astronomy liberal studies course 79—71171
- astrophotometric scale definition by N.R. Pogson 77—49306
- astrophysical obs. by space vehicles (1966-76) *(Japanese)* 78—24417
- atmosphere light propagation, problems and trends 79—100947
- atmosphere refraction calc., theory for three-dimensional model 80—46260
- atmosphere seeing, effects on elliptical galaxies cores light distrib. 80—12814
- atmospheric refraction, general theory *(Russian)* 78—89045
- atom motion in very strong mag. fields, mass anisotropy effect *(Russian)* 80—67557
- atomic autionisation, astronomically oriented bibliography 78—32340
- atomic b$_n$ factors at low temperatures, appl. to interstellar C II regions 80—36696
- atomic collision, coherence and correlation, book 80—90615
- atomic excited levels, mean lifetimes in C, N and O 77—46528
- atomic line identification lists bibliography, August 1978 supplement 79—54787
- Australian Astronomical Soc. 10th annual meeting, Sydney, Australia (May 1976) 77—33325
- Australian Astronomical Society, conf. Melbourne, Australia (May-June '77) 78—69655
- Avebury Ring, least squares fit rel. to Thom survey 78—4120
- axions, astrophys. constraints on axion mass and number of quark flavours 79—36009

astronomy and astrophysics continued
axions, very low mass, astrophysical bounds and stellar-energy loss 80—109353
axions and Higgs particles, astrophysical mass bounds 79—5745
axisymmetric accretion, energy considerations 77—33335
axisymmetric accretion near compact objects, theory 77—33334
Ball, Sir Robert Stawell, Victorian astronomer and mathematician 79—88783
balloon and rocket programs, conf. Bournemouth, England (1980, Aug.) 80—105433
balloons, transatlantic, self-ballasting, for astronomical research 80—21917
beta strength function, half life and delays, nuclear- and astro-physics consequences 80—102149
beta strength function structures, nuclear- and astro-physics consequences 80—99152
Bibliographia Kepleriana. Supplements and continuation 1975-1978 78—77657
bimetric gravitation theory, existence of incompressible matter 77—33329
Bondi accretion, linear stability problem 79—44359
book, discovering astronomy 79—8855
Brahe, Tycho, instruments and observational techniques *(Swedish)* 77—57139
British Astronomical Association Handbook (1978) 78—85828
British optical astronomy, advances 78—69844
Callanish Megalithic sites, indicated declinations 78—4119
Cambridge Encyclopaedia of Astronomy 78—45199
catalogue of Universe, illustrated book 79—101093
celestial chaos related to Earth's climatic and biological catastrophes 79—53509
celestial masers physics, review 79—21455
charge transfer reactions, appl. to photoionisation model of planetary nebula (NGC 7662) 80—62233
charge transfer reactions, empirical rate coeffs. status and astrophysical appls. 80—56701
charged particles drifts in mag. field with arbitrary spatial var. 80—46382
China, research activities reflected in Acta Astronomica Sinica 78—7888
Christmas star, possible explanations 78—32364
civilisation and astronomy in time of Aryabhata I, 5th century AD 78—89289
coherent curvature radiation 80—56704
collective radio-emission from plasmas 80—46392
comets, computer generated pictures 80—17549
communication with civilisation around other stars 78—16314
Compton scattering, induced, in electron gas, relax. effects, manifestation in astrophys. obs. *(Russian)* 77—27231
Compton scattering by unmagnetised electrons in ambient mag. field, vacuum polarisation effects 80—86631
concise encyclopaedia of astronomy 78—32627
condensed matter in huge magnetic fields, astrophysical problems 80—82187
conference, general congress, Societe Francaise de Physique, Toulouse, France (June 1979) 80—77536
conference, New Delhi, India (Jan. 1979) 80—94912
conference, trends in physics, York, England (Sep. 1978) 80—31416
conference of American Astronomical Society, proceedings of 155th meeting, San Francisco (Jan. 1980) 80—73091
constellation concept and projective classical group 80—62869
convection, turbulent, in Boussinesq fluids, viscosity, conductivity and power spectra 80—98543
convection in meteorology, aspects relevant to astrophysics 78—88898
cosmic betatron model, general relativistic induction accelerator 77—37793
cosmic dust condensation processes investigation, expt. techniques 80—26940
cosmic plasma properties from magnetospheric research, use in astrophys. 78—93051
cosmic rays, research programme at Blackett Lab., Imperial College, review 79—66890
cosmic systems charge polarisation, appl. to stars and universe 79—48771
cosmology, sources luminosity evolution from scale parameter for Friedmann models 80—77527
Coulomb excitation functions, numerical calc. of limiting props. 79—9604
crater size-freq. data presentation and analysis, standard techniques 79—44387
Cretaceous-Tertiary extinctions, possible terrestrial and extra-terrestrial causes 78—31999
current-carrying beams 78—49313
current-carrying plasma, discontinuous transitions 78—9754
Dahlgren, amateur astronomer, reminiscences *(Swedish)* 78—36469
darkness, nocturnal, variation of duration with latit. 77—25632
data centres, survey from questionnaire replies 77—78675
data distrib. 77—78673
data files, critical examination 77—78832
data growth, anal. 79—21202
Davis Planetarium, Maryland Academy of Sciences, Baltimore 77—2343
Dedekind ellipsoids, deformed figures in post-Newtonian approximation to general relativity 78—32734
deformable medium, rotational dynamics 78—20631
dense matter in laser driven fusion, laboratory expts. 80—75077
dense matter physics, conference, Paris, France (1979 September 17 to 21) 80—73094
dense plasmas and nuclear reactions, astrophysical appls. 80—77281
dense plasmas transport coefficients, kinetic theory 80—77280
diacetylene, obs. of ν_4 band near 3 microns 80—47977
dictionary of astronomy, book 80—22151
Doppler shift, distrib. for relativistic gas 78—65492
dust diffusion through gas in force field, theory 78—18366
Dynamical Astron. Division of Am. Astron. Soc. meeting/Stanford, CA, 28 Feb.-2 Mar. 1979 80—36762
dynamical astronomy, stability theory 79—92656
dynamical system with increasing number of degrees of freedom, Kolmogorov entropy 79—80562
dynamo polarity reversals rel. to geodynamo 80—51645
dynamo problem, hydromag.-intertial-gravity waves propag. in mag.-vel. shear 79—55422
Earthlike planets, prevalence in Universe 80—41735
education, 'Olbers' paradox', history and resolution 77—33758
education, by radio programmes 77—67157

astronomy and astrophysics continued
education, Ken Mattingly Planetarium 79—84921
education, megalithic astronomy 77—33759
education, nonscience majors, innovative course based on mass-radius diagram of states of matter 78—62002
education, nonscience majors, professionally oriented astronomy laboratory course 80—51981
education, test item file construction and use 78—86054
education, Titius-Bode law, Piagetian learning cycle for astronomy study unit 80—51985
education, university courses and career prospects 78—69931
education, university science course for talented high-school students 78—89282
education, use of line-of-sight transparency 79—35508
education at Florida's Brevard Community College 79—12557
education in astronomy, review of Canadian activities 77—45626
education in India 79—62947
education in US schools, reasons for decline 79—84882
educational courses, new approaches 79—3
Einstein's contribution to cosmology 80—77530
electric currents in cosmic plasmas 78—12094
electromagnetic vacuum, isotropy, testing 77—87254
electromagnetism, conducting sphere, rot. in mag. field relativistic, co-rot. frame 79—53714
electron beams, counter-streaming in stationary background, longitudinal mode instability 78—26273
electron burst relaxation in fluctuating plasma, formal dynamical model 78—83579
electron gas interacting with radiation in mag. field, relaxation 80—17489
EM ion waves in cold relativistic plasmas, astrophys. appl. 80—21910
EM mode coupling in inhomogeneous magnetised plasma, normal incidence case 77—84435
EM response of electron gas and vacuum in strong mag. field 77—13641
EM space isotropy, possible expt. check 77—13228
EM waves, polarisation transfer eqn. in inhomogeneous magnetised plasma 77—84436
Ephemeris time, relativity and uniform time in astronomy 77—53402
Evans, Thomas Simpson, 1777-1818, mathematician and astronomer 78—89287
evolving systems instability, elastic stability theory and catastrophe theory approaches 78—44442
experimental nuclear astrophysics, review 79—25471
experimental nuclear astrophysics, review book contrib. 79—22161
extragalactic distance scale, rel. to Hyades Cluster distance 78—8121
extrasolar planetary systems, direct imaging 80—82426
extraterrestrial laser signals detect. likelihood, instrumentation 80—4276
Ferraro's theorem, validity in non-flat space time 80—4247
FK5, equinox and equator of new fundamental reference coord. system 80—109341
flicker noises, stochastic prop. 78—57473
fluid dynamics, boundary conditions imposed by stratified fluid 79—55404
fluid layer with rot. and mag. field, cell sizes at thermal convection onset 77—54991
fluid theory, universality in short range struct. in simple classical fluids 80—75141
formulae for programmable calculators, book 79—88571
Fraunhofer, Joseph, contributions to astronomy *(German)* 77—57142
Fredericton, New Brunswick, astronomy in mid-19th century 77—25955
frontiers of astrophysics, book 77—33341
fundamental system of star position and motion, accuracy improvement using asteroid obs. 80—94692
Galileo, first telescopic obs. of Moon (December 1609) 77—29978
gamma-ray astronomy and neutral pion production *(Polish)* 77—70999
gamma-ray astrophysics, new look at universe 79—80373
gas flow, isothermal accretion, stability 78—49303
Gauss, C.F. Contrib. to astronomy 78—19
general relativity, astronomical tests 80—36934
gravitating fermions, thermodynamic functions 79—80552
gravitating fermions, thermodynamic potentials 79—80551
gravitational collapse, finite-particle scheme for three-dimens. gas dynamics 78—67218
gravitational radiation, collapsed objects and exact solns., Einstein Centenary Summer School, Perth, Australia, 1979 January 80—105434
gravitational wave astronomy 79—92664
gravity, general scalar-tensor theory with constant G 78—21041
Gray, Stephen (1666-1736) 80—77601
Great Debate of galactic astronomy, actual proceedings 77—29979
great year in Greek, Persian and Hindu astronomy 78—81790
ground-based astronomy, future, conference, Arizona (1979 May 9) 80—62386
group IV homologous ions, oscillator strength trends 80—42991
H-R diagram, IAU Symposium 80 review 78—96511
H-R diagram, use as astronomical tool, review of IAU Symposium (No.80) 78—81619
handbook for Southern Africa (1978) 78—32626
handbook for Southern Africa (1979) 79—30164
Harriot, Thomas, 1560-1621, biography, astronomical instruments and obs. 79—35512
heavy Majorana particles, cosmological and astrophysical implications 80—90331
heavy stable neutral lepton, astrophysical consequences of existence 78—93091
hebdomadal calendar, theory *(Danish)* 78—36440
Henry Norris Russell, and Hertzsprung-Russell (H-R) diagram 78—69957
High Energy Astronomy Observatory (HEAO) programme 79—44368
High Energy Astronomy Observatory Program, mission 79—5730
high energy astrophysics, handbook 80—73113
high energy physics, conf., Schladming, Austria (Feb.-Mar., 1977) 78—8494
high energy research, AAS meeting (Honolulu, 20 Jan. 1977) 77—91419
high-energy neutrino astronomy, as probe of galactic nuclei 80—4432
high-energy nuclear reactions, comparison of methods for cross sections calc. 78—28505
highlights of astronomy, IAU conference, Grenoble, France (August 1976) 78—16316
historical astronomical events and Gospel records rel. to Christ's birth date 78—93127

astronomy and astrophysics continued
historical astronomy, Latin terminology relating to aurorae, comets, meteors and novae 80—62437
history, effects of defence science on advance of astronomy 78—36471
Holden, Edward S., founder of Astronomical Society of Pacific, California-Wisconsin astron. connection 79—75310
Hopi Indians astronomy, social and theological aspects 78—36472
hot astrophysical bodies, mass ejection, energy conversion process 77—68800
hydrodynamic turbulence in weak large scale mag. field, effective mag. viscosity 77—33340
hydrodynamics, absolute and convective instabilities distinction and appl. to interstellar medium 80—98539
hydrodynamics, Rayleigh-Taylor instability of self-similar spherical expansion 79—8823
hydromagnetic free convection flow in Stokes problem, for porous vertical limiting surface with const. suction 80—90328
hydromagnetic surface waves, props. and astrophysical appls. 79—25462
hydromagnetic thermal convection instability, effect of suspended particles 79—53709
IAU Commission 4 Working Groups, numerical values of consts. in Joint Report 78—40845
IAU reports from Commissions for 1976 (Part 1), book 77—5464
IAU reports from Commissions for 1976 (Part 2), book 77—5465
IAU reports from Commissions for 1976 (Part 3), book 77—5466
Inca people (Peru), evidence of astronomical knowledge *(Swedish)* 78—32640
Indian epicyclic astronomy, history and chronology of treatises 80—62448
inhomogeneous stars, adiabatic pulsations, deviations from linear wave motion 77—71001
International Astronomical Union 1976 system of constants *(Russian)* 78—73611
interstellar communication, binary stars use as time markers 79—101092
interstellar radiolink, using Sun as gravitational lens antenna 80—62040
interstellar ramjet acceleration runway 79—101047
interstellar space, disequilib. condensation environments as frontier in thermodynamics 80—26942
inverse Compton radiation sources, inference of relativistic electron spectra 80—90339
ion-atom collisions, projectile charge dependence *(Dutch)* 79—50121
ionic mixtures, phase separation 80—77279
ions, proton excitation approximations, erratum and extension 79—35118
isothermal self-similar blast waves, one-dimensional flow and its stability 78—45214
isothermal self-similar blast waves, two-dimensional flow and its stability 78—49307
Israel Physical Society 1980 annual meeting, Rehovot, Israel (April 1980) 80—94909
Italian Astronomical Soc., 20th meeting (Frascati, 7-10 Oct. 1976) *(Italian)* 79—21199
Italian Astronomical Soc., 20th meeting (Frascati, 7-10 Oct. 1976) *(Italian)* 79—80247
Italian Astronomical Soc., 21st. meeting (Bologna, 20-23 Oct. 1977) *(Italian)* 79—21200
IUE, first year of obs., conference, London, England (1979 April 4 to 6) 80—51960
Jacobi's virial eqn. soln. for celestial bodies 79—8832
James Veitch, 1771-1838, history and astronomy 77—29977
Jeans, Sir James Hopwood (1877-1946) 79—35
Johann Georg Soldner (1776-1834), forgotten bicentenary 78—81787
Johannes Hevelius (1611-1687) 77—26120
Kepler, rejection of solid celestial spheres 80—36830
Kepler and Galileo, correspondence during late 16th and early 17th centuries 78—20934
Kepler and Mars, construction and rejection of first oval orbit 78—62027
Kilmartin Stones, lunar observatory hypothesis reassessment 79—96927
Kukarkin, Boris Vasil'yevich (1909-77), Russian astronomer *(Russian)* 80—101701
Lambert, Johann Heinrich, 1728-1777, biography *(German)* 79—17174
Langmuir waves, turbulent bremsstrahlung process 80—62009
Laplace, P.S., chronology and citations of early work, 1770-1773 period 78—93505
line sources, elec. and mag., interaction with moving magnetoplasma slab, EM radiation 80—67537
lunar megalithic site in Kintyre, survey 79—96929
lunar megalithic sites in Britain, reconsideration 79—8854
Lyapunov, M.V. (1820-68), work as third Kazan astronomer (1840-55) *(Russian)* 79—88789
magnetic buoyancy in rotating gas, effect of fine electrical and thermal conductivities 78—57436
magnetic dynamo α-effect, determ. for slow and fast rot. 79—40069
magnetic field mirroring, classical surface of section determ. 77—13231
magnetic fields, generation at high mag. Reynolds number 78—36448
magnetic fields $>10^{20}$ gauss, existence in astrophysical systems 78—4094
magnetic oblique rotator, EM field prod., exact vacuum soln. 80—58442
magneto-ionic rays, propag. in shearing plasma 79—84659
magnetogasdynamic spherical shock waves, propag. in exponential medium 79—84664
Marquis de Charbert (1724-1805), biography and link with Louisbourg Observatory 80—68010
matter at high temperatures, comp. and adiabatic index 79—44354
Maxwell's equations, photon rest mass as cosmic test 77—45708
Maya chronology and planetary conjunctions 78—36470
Mayan and dates of planetary obs. in AD 293-1237 period 77—17392
Mayan architectural orientations rel. to Venus rising and setting positions *(German)* 77—2352
Mayan astronomy, depth of knowledge and archaeological evidence 80—27098
Mayan astronomy, Venus studies 79—88782
megalithic astronomical alignments, significance tests 79—96928
megalithic astronomy, statistical significance of astronomical orientations 78—36475
megalithic lunar site a Callanish, Lewis 80—77300
megalithic observatories, critique 77—2351
megalithic sites in Shetland, surveys 78—36474
Mesoamerican calendrical systems chronology reconstruction 78—81782
methane, ν_4 fundamental band strength, line-intensity meas. 79—22700
methanol-d_1, (CH_2DOH), microwave torsional-rot. spectrum, rel. to interstellar search 80—99498
methanol-d_1, laboratory freqs. of $J=2\text{-}1$, a-type transitions 80—63624

astronomy and astrophysics continued
MHD, monograph 78—40816
MHD, root mean square mag. field on turbulent diffusion 78—36449
MHD induction, simplest physical model of generator 78—71548
MHD kinks in nonresistive plasma, astrophys. appl. 79—27763
MHD oscillatory flow past impulsively started porous limiting surface, variable suction 79—86518
Miksa Hell, Hungarian astronomer, historical note *(Danish)* 80—8766
Milne integral equation with Pincherle-Goursat kernel, Cauchy problem 77—2513
Minor Planet Center, history and future 80—94712
modified Saha equation at high press. thermodynamic inconsistency 78—36450
Monterey Institute for Research in Astronomy, self-sufficiency 78—16315
Moon surface features nomenclature, reason for name Aristarchus for brightest crater 79—49004
morphological method in astrophysical research 79—71216
multicharged ion thermal charge exchange reaction, rel. to astrophysics 80—63815
multiply-ionized species, thermal energies, in astrophysical plasmas 78—33596
N.American astronomy, seventeenth century 78—28907
NASA astrophysics activity 79—5729
near-Sun objects, twilight visibility function 77—5321
nearly collisionless spherical accretion, theory 78—12090
negative specific heat paradox, theory and appls. 78—9557
neutrino and photon emission from blackbody, thermodynamic laws 80—105451
neutrino astronomy, review *(Russian)* 80—13344
neutrino astrophysics, review, book contrib. 80—72769
neutrino processes, reaction rates 78—45215
neutrino-free β-decay theory, new aspects 79—13254
Newcomb, Simon, American astronomer, 1835-1909, life and works 78—93504
Newton and mutual gravitation of fixed stars 78—20
non-thermal emission mechanisms 79—48667
nonlinear astrophysical dynamos, multiple period dynamo wave oscills. and solar cycle modulations 79—16813
nonlinear astrophysical dynamos, solar cycle as nonlinear oscill. of general mag. field 78—40889
nonlinear interaction between monochromatic wave and particles in gravitating system *(Russian)* 77—82285
nonlinear magnetic dynamos, bifurcation of steady dynamos from oscillating dynamos 78—49306
nuclear, detonation waves, initiation and propagation conditions 79—93834
nuclear and differentiated abundance patterns 77—9656
nuclear astrophysics, introduction to form. and evolution of matter in Universe, book 80—105447
nuclear astrophysics, recent developments 78—4100
nuclear partition functions 79—21167
nuclear synthesis, cluster aspects 79—5744
observational accuracy and theory in ancient and mediaeval astronomy 77—37703
observational astronomy, contrib. of Tobias Mayer 80—62438
observational astronomy teaching, report on symposium 79—71208
observer's handbook of Royal Astronomical Society of Canada, (1979) 79—8796
observers handbook of Royal Astronomical Society of Canada 80—22152
optical spectral line emission bursts in X-ray heated medium *(Russian)* 80—77286
orbit determination, Gibbs' formulae 77—45292
origin of the elements, review 79—97118
oscillatory flow past infinite porous vertical limiting surface with constant suction, free convection effects 79—92751
Pacific Astron. Society meeting (Rohnert Park, California, 26-30 June 1979) 80—22137
particle acceleration mechanisms, AIP conf. (La Jolla, CA, 1979 Jan.) 80—27026
particle acceleration near singular line of mag. field, energy spectrum *(Russian)* 80—90332
particles accelerated by Alfven waves, distrib. function self-similar solns. 79—32757
Pauli's exclusion principle for strong interactions in hadrons, nuclei, and astrophysics 80—37206
pecked cross symbol in ancient Mesoamerica as orientational device or calendar 79—53954
Perry, Rev. Stephen J. (1833-89), Jesuit priest, astronomer and teacher 80—46781
phoenix of nature, fire and evolutionary cosmology in Wright and Kant 79—5764
photoabsorption cross sections for positive atomic ions with $Z\leq30$ 80—26727
photon helicity detection for matter/antimatter star discrimination 78—12092
physical systems instabilities, variational principles for complex eigenvalues 79—21527
planetarium design, model from Mesquite Schools, near Dallas 78—81777
planetarium run by students in Durham, New Hampshire 78—65503
planetary nebulae, advances in theory of physical processes 80—109527
planetary nebulae, atomic and molecular data for heavy particle processes 80—109528
planetary nebulae, observations and theory, IAU Symposium 76, Ithaca, New York, USA (1977 June 6 to 10) 80—105435
planetary science, conference (Boston, MA, 28 October 1977) 79—53740
planets, Universe, and cosmic evolution 77—32971
plasma, Fe-H mixture, confined atom-, and Debye Huckel-, Thomas-Fermi-Dirac models 77—24053
plasma, Fresnel drag in transversely moving dispersive media 79—96902
plasma, interaction of knowledge from magnetospheric, astrophysical and lab. plasmas 80—59166
plasma, mag. field line reconnection via clouds-in-cells model 77—84490
plasma, relativistic modes of tearing instability in background plasma 80—62012
plasma, rotating, effect of suspended particles on gravit. instability 80—109347
plasma, self-gravitating, isotropic pressure, gravit. instability 80—72763
plasma, self-gravitating, with finite ion gyroviscosity, rotating layer instability 80—56706

astronomy and astrophysics continued
plasma, stability of anisotropic jet 77—17353
plasma, turbulent, anomalous EM wave electron radiation 80—43889
plasma astrophysics, nonthermal processes in diffuse magnetised plasmas, wave physics, book 80—105446
plasma astrophysics 79—16820
plasma discontinuities, shocks and neutral layers 79—60106
plasma magnetoparametric instabilities, appl. to Crab nebula 79—8829
plasma nonlinear magnetoacoustic waves, damping, simulation 78—79423
plasma physics conduction mode var. and inertial conductivity 77—84407
plasma physics in astronomy *(Russian)* 78—89057
plasma second harmonic emission, head-on approximation 79—41803
plasma trans-relativistic shock relations, numerical solns. 80—31202
plasma turbulence and nonlinear waves 79—60142
plasmas, di-electronic recombination *(French)* 80—82188
plasmas, electron impact excitation coeff. for highly ionised ions 77—7510
polarised radiation, from point source orbiting Schwarzschild black hole 77—67109
polarised radiation, transfer through rarefied magnetoactive plasma 79—92669
polytrope of index three, parameters 79—62819
positronium decay, in strong mag. fields, 10^{12} Gauss 79—88578
precession change, revision of IAU System of Astronomical Constants 77—17331
precession matrix based on IAU (1976) system of astronomical constants 79—48653
principles and practice of astronomy, book 78—32629
pseudoscalar bosons rule in astrophysics *(French)* 79—44361
Ptolemy (2nd century astronomer), reassessment 79—67131
Pueblo Bonito, astronomy, architecture and adaptation 77—5463
Quetelet, A.L.J., life and spread of science in Belgium during 19th century *(French)* 78—65742
radiation diffusion in two gas clouds *(Russian)* 77—41297
radiative transfer, comoving-frame transfer eqn. soln. in spherically symmetric relativistic flows 80—82181
Regiomontan, Johannes, astronomer, life and work *(German)* 77—53726
Regiomontanus, Johannes, 15th century astronomer, life and works 78—20929
relativistic astrophysics, Einstein's theory *(German)* 79—80213
relativistic astrophysics, meaningless questions, philosophy 77—13515
relativistic astrophysics, pulsars, supernovae, and X-ray sources *(German)* 79—101060
research worldwide growth, 1967-75 period 77—66884
review of recent developments 78—16307
right ascensions, uniform whole-sky system *(Russian)* 78—4082
Romer, Ole, determ. of hesitation (velocity) of light *(Danish)* 77—57140
rotating fluids, convective modes and convective stability 79—16818
Royal Astronomical Society, catalogue of archives and manuscripts 78—69705
Royal Astronomical Society, manuscript archives 78—32636
s-process studies, exact soln. for unbranched network 78—28649
scintillation theory, mathematical anal. of physically thin screen 78—28501
scintillations in astrophysics, analytic soln. of second-order moment eqn. 80—26726
seeing, meas. at Kitt Peak 80—61899
selections from 1977 Comments on Modern Physics, book 79—30181
self-gravitating gas-particle suspension, magneto-gravitational instability, with conduction 79—29989
self-gravitating rotating masses, book contrib., review 80—21915
self-similarity and ang. momenta of astronomical systems, basic rule in astronomy 80—36490
SETI at 18 cm, high sensitivity search 80—82229
shock waves, cylindrical relativistic propag. in presence of mag. field 79—53708
shock waves, in relativistic MHD 78—9770
shock waves, plane, relativistic, propag. 79—53707
shock waves, plane, relativistic, propag. in slowly moving medium 80—62005
shock waves, post-collisional propag. and amplification *(Russian)* 79—44360
SI units 77—78672
signal detection, statistical considerations 80—17500
singularities in general relativity theory 79—35591
sky charts for amateur astronomers 79—62762
Smiley, Charles Hugh (1903-77), solar eclipse authority, biography 78—62024
Smyth, Charles Piazzi (1819-1909) at Cape of Good Hope 80—68011
sociology of innovation in modern astronomy 78—12108
solar and solar-terrestrial physics, illustrated glossary 78—57537
solar astrophysics, extension to stellar and galactic astrophysics 77—9736
solar neutrino astrophysics, review 79—16917
solar observations, site testing with balloon borne radiosondes 77—29645
space age progress *(Spanish)* 79—62719
space astronomy, NASA prospects 78—69654
space exploration and astronomical research, first 20 years *(Russian)* 78—16267
space optics, conference Huntsville, Alabama (1979 May 22 to 24) 80—62385
Space Shuttle, payload specialist experience of astronomer 77—64588
Space Shuttle, prospects for astronomers in space 77—56806
spacecraft data processing and analysis 77—78650
Spacelab 2 mission, astrophysical payload summary 78—85816
spectral line formation depth in mag. field, theory *(Chinese)* 80—105159
spherical astronomy, conversions between galactic and equatorial coordinate systems 79—88569
spin-flip and normal synchrotron radiation from rot. charge in mag. plasma 80—28153
spin-orbit resonance, mathematical aspects 79—12389
star fields and configurations, anal. by statistical methods 80—82224
Star of Bethlehem, identifications rel. to Nativity chronology 79—67136
Star of Bethlehem, possible nova in 5 BC 78—32365
starfield, appearance from relativistic spaceship, nonexistence of 'starbow' 79—62955
Stark broadening, trends in homologous ions series 80—105157
stars and star systems, conference, Uppsala, Sweden (1978 August 7 to 12) 80—51959
steady disc accretion by stars, ang. momentum transfer 78—65609

astronomy and astrophysics continued
stellar data, conf. (Strasbourg, France, 19-21 Aug. 1976) 77—78828
stellar data base standards, management and security 77—82282
stellar systems, two component Emden sphere theory 80—22045
Stephen Gray, astronomer (1666-1736) 80—22182
stochastic phenomena 80—105161
Stokes problem, effects of free convection on oscillatory flow past infinite porous vertical limiting surface 80—109348
Stokes problem, for infinite vertical plate with const. heat flux 80—79108
Stonehenge, new meas. in 1978 April survey 78—85860
Stonehenge I and lunar apogee tracking 77—22116
strong EM waves in collisionless homogeneous plasma, waveform, polarisation and nonlinear effects 78—53809
strongly coupled classical plasmas in laser fusion and astrophysics, review 79—10634
structure of the universe, book 78—32628
Struves of Pulkovo, family of astronomers 78—24632
student projects in American 1977 science fairs 77—87617
sundial, latitude-independent, theory and construction 78—81549
sunrise, sunset and eqn. of time 77—33326
superdense celestial bodies, pionisation effects *(Russian)* 79—96907
superdense celestial bodies, theory 80—67773
synchrotron sources, boundary effects and circular polarisation 79—48668
synchrotron-transient radiation of charged particle in plasma with random inhomogeneities, spectrum 78—45213
tachyons interaction with gravity, rel. to cosmology and black holes 79—25839
teaching, demonstrational appliances *(Hungarian)* 78—36772
teaching, spherical projections in position finding 77—41437
The Universe, book 77—26102
theoretical physics and astrophysics, book 79—44363
thermal-convective instability of partially ionized plasma, radiative transfer, medium porosity and collisional effects 80—67538
thermonuclear reaction rates, thick target meas. 80—73108
thioformyl ion, theoretical study rel. to interstellar mols. 78—37553
Thomson scattering in strong mag. field, vacuum polarisation effects 80—86632
time-resolved molecular spectroscopy, astrophys. appls. 80—21913
transrelativistic plasmas, photon pair prod. 78—20632
tribo-induced discharge luminesc. 80—25471
turbulent cosmic plasmas, EM waves depolarisation rel. to vel. field determ. 77—17358
Universum, Swedish astronomical information project *(Swedish)* 78—86048
unstable modes of an equilibrium, number calc. 80—36493
Voigt functions, partial derivatives 78—89052
Voigt functions analysis, appl. to astrophys. spectral line profiles and neutron cross sections 80—22879
warm nuclei, Thomas-Fermi model rel. to stellar collapse 80—51648
wave propagation, gravit. instability, rot. and streaming effects 79—37293
wave propagation and evolution in self-gravit. medium *(Chinese)* 79—80211
weak interactions in astrophysics and cosmology 77—25934
Weinberg-Salam model and extensions, ν EM form factors and mag. moments, neutral currents, astrophysics applics. *(German)* 80—62904
white holes, optical appearance 79—21323
Zeeman splitting of high-n recomb. lines, theory 80—58210
zodiacal constellations and solar movement *(French)* 77—70981
$\gamma \rightarrow \nu\bar{\nu}$ in strong mag. field, absorpt. coeff. and energy loss rate 77—22728
(p,xn) reactions, cross-sections and astrophysical appls. 78—28504
pp reaction, exchange current corrections π and ρ exchange 80—26733
B-like ions, highly ionised, up to Fe XXII, Breit-Pauli approximation 78—53810
Be isoelectronic sequence, mag. quadrupole transitions probabilities 78—37592
CH^+, electron impact excitation, rot. transitions 79—41244
CNO isotope importance in astrophysics 77—87263
CNO isotopes in astrophysics, conf. Grenoble, France, 1976, Aug. 77—87262
Co I, excited level lifetime meas. 78—5178
Cr II lines, A_{mn} transition probabilities 80—14099
D origin, obs. and interpretations 77—71160
Fe I, excited levels measured lifetimes compared with calcs. from oscillator strengths 79—36586
Fe I, precision oscillator strengths from levels $a^5F_{1\text{-}5}$ and $a^5D_{0\text{-}4}$, comparison 79—36584
Fe I transition from levels $a^5F_{1\text{-}5}$, relative oscillator strengths precision meas. 79—36585
Fc I transitions from levels $a^5D_{0\text{-}4}$, relative oscillator strengths precision meas. 79—36583
Fe VI, forbidden emission under nebular conditions 79—8970
$Fe^{11+}+H^+$, collisional excitation cross-sections for ground configuration 78—33582
H, longit. excited states in intense mag. fields, rel. to pulsars 80—91469
H plasma, consequences of electron energy distrib. departure from Maxwellian 77—80274
H plasma, departures of electron energy distrib. from Maxwellian, electron kinetic eqn. 77—80266
H^-+H collisions, assoc. detachment process theory 79—44351
H_2, (4,0) S(1) quadrupole line intensity and pressure shift 78—90178
$H_2{}^+$, mol. props. in intense mag. fields 79—81169
H_{22} quadrupole vibration-rotation transition probabilities 78—25512
$HSiO^+$, $HOSi^+$, theoretical study rel. to interstellar mols. 78—37541
He like ions Z=12-19, $1s^2\ {}^1S_0\text{-}1s3p\,{}^1P_1$ lines satellites obs. in laser 79—22640
He-like ions, level populations and line intensities for stationary plasmas 78—53811
He-like ions, line intensities results 78—89051
HeH^+, electron impact excitation, rot. transitions 79—41244
${}^6Li(p,{}^3He)$, 0.1-3.0 MeV, absolute differential and total cross sections, astrophysical S-factor 80—27642
Mg I isoelectronic sequence, intercombination line oscillator strengths 80—23360
Mg isoelectronic sequence, mag. quadrupole transitions probabilities 78—37592
Mg XI resonance lines, dielectronic satellite lines atomic parameters calcs. 80—78567

astronomy and astrophysics continued
^{25}Mg(p,γ) reaction, relative yields of ^{26}Al^{g} and ^{26}Al^{m} 79—101058
Mn abundance meas. by sun model 80—91501
N IV, dipole lengths, dipole vels. and transition probabilities 79—35113
N IX to Ni XII, wavelengths of transitions between lower configurations 80—99474
O, absolute fluoresc. production cross section, 1304 angstrom, from CO(CO_2) UV photodissoc. 80—32652
O III, optical oscillator strengths for astrophysically interesting lines 80—32660
O III, prod. through Auger effect 78—20633
O V, O VI, dipole lengths, dipole vels. and transition probabilities 79—35113
PtH(D), pot. energy curves, r-centroids, Franck Condon factors, rot. depend. 80—28082
YO, $A^2\Pi-X^2\Sigma^+$ and $B^2\Sigma^+-X^2\Sigma^+$ systems, Fourier transform spectroscopy anal. 79—22718
ZrO, singlet-triplet separation meas. 80—78623
ZrO spectrum, new $^3\Pi$-$^3\Delta$ system identification 80—23414
ZrO$^+$ spectrum, $^2\Pi$-$^2\Sigma$ system identification 80—23413

astronomy computing
see also computerised instrumentation
8550 MHz sky survey, appl. of computer data processing techniques 77—17708
Adams-Moulton-Cowell multistep integrator for satellite orbit, time regularisation 78—45208
aids for calculator programming, book review 80—8764
AKAIHOSHI flexible real time software system for radio astronomy obs. 80—82214
amateur calculations using programmable pocket calculators, manual *(French)* 79—92683
artificial satellites, orbital data processing algorithm *(Russian)* 80—46401
artificial satellites, orbital element improvement using photographic or laser obs. *(Russian)* 80—46364
artificial satellites second order perturbation computation *(Chinese)* 79—80207
asteroid orbits identification, ephemerides calc. *(Chinese)* 78—69731
astrometry, photography against stellar background, iterative trajectory search algorithm *(Russian)* 77—17376
astronomical plates meas. via automatic microdensitometer, data compression filters 79—80230
astronomy, integral evaluation for Fourier analysis of eclipsing binary light curves 78—45236
automated plate reduction techniques for globular clusters struct. determ. 77—41394
automatic reduction of low dispersion objective prism stellar spectra *(Italian)* 80—98567
blink comparator, semi-automated, for large photographic plates *(Japanese)* 78—89081
Bruce telescope photographic plates, computer readable mag. disc catalogue 79—88605
Cassegrain telescopes, automatic design of corrector systems *(Chinese)* 77—22088
CDCA-Nice software package, implementation in Italian institutes implementation in Italian institutes *(Italian)* 80—98561
celestial mechanics, computer simulations of self focusing particle streams 79—53704
celestial mechanics, diurnal motion of Sun seen from Mercury, computer aided soln., teaching aspects 78—61969
celestial mechanics, Fourier series fast evaluation 80—56711
chronometric system using punched tape for star transit obs. *(Russian)* 78—4110
colliding particles in gravitational field, numerical simulations 79—16802
comet motion, data processing for comparison of obs. and theory 77—41307
cosmic ray variation spectrograph, data reliability ensurance 79—84610
COSMOS plate-measuring machine, design and software 77—64652
data acquisition and processing, Rome Observatory *(Italian)* 80—8551
data acquisition and processing at Italian observatories *(Italian)* 79—62751
data analysis, procedure for Asiago Reticon spectrophotometer *(Italian)* 80—98565
data centres, digital recording and image processing 77—78676
data centres, future role 77—78677
data centres, survey from questionnaire replies 77—78675
data compilation and acquisition techniques at telescope 77—78649
data coordination, general aspects 77—78678
data distrib. 77—78673
data files, critical examination 77—78832
data reduction methods, least-squares polynomial fitting technique 80—12682
digital image centring algorithm for astrometric positioning 78—69696
digitised images, anal. via interactive data processing system (CIPS) *(Italian)* 80—98560
digitized images, structural pattern recognition *(Italian)* 80—98554
Easter date determ. for any year, program for HP 29C 80—77268
eclipsing binaries light curve analysis, new techniques and appl. to V444 Cygni 80—82417
eclipsing binary light curves soln. using LIGHT computer program 80—77454
eclipsing variables, light curves linear analysis, fractional light loss anal. 80—82416
elliptic orbit determ. by applying least squares method to observation residues *(French)* 78—40799
ELSPEC/2, interactive procedure for spectrogram processing *(Italian)* 80—98566
EUV instruments, computer aided calibration technique 80—85839
formulae for programmable calculators, book 79—88571
galactic non-stellar objects, data centre proposal 77—78905
galactic radiation, distributed, linear polarization obs. results processing optimal algorithm selection *(Russian)* 77—91441
galactic/equatorial coordinate systems, interconversion 79—88569
galaxies, angular momentum redistrib. by spiral waves 79—53909
galaxies, correlation function, computer simulation of catalogue *(Russian)* 80—36729
galaxies, flat disc, retrograde stars effect on global bar-forming mode 79—21411
galaxies, surface photometry, computerized analysis method 78—12100
galaxy evolution, three-dimens. computer simulation 78—81551

astronomy computing continued
galaxy photographs, image processing techniques 77—9664
galaxy redshifts survey, data reduction techniques 80—22074
galaxy surface photometry, numerical mapping by interactive procedure *(Italian)* 80—98572
Galilean satellites motion theory 77—45352
Ganymede image restoration by maximum entropy method 77—60624
graphic routines for interactive Tektronix video unit and Printronix printer *(Italian)* 80—8553
gravitational parameter inaccuracy consequences computation, for orbits in Earth's gravitational field 78—40460
handbook for pocket calculators 80—8745
image analysis, general system software and appls. 78—53834
image processing, digital system *(Italian)* 80—98558
image processing at Trieste Observatory *(Italian)* 79—58270
image processing of simulated turbulence and noise degraded lunar images 77—45321
image processing/facilities, catalogue 78—45239
image reconstruction, from incomplete and noisy data 78—53837
image reconstruction formulae, computer implementation 80—52179
image reconstruction from projections, book 80—51961
image reconstruction from projections 80—52178
images digital display, interactive program *(Italian)* 80—98559
images optimal classification into stars or galaxies, Bayesian approach 80—21920
information processing methodologies, conference, Trieste, Italy (1979 February 23 to 24) *(Italian)* 80—94917
information treatment methods, meeting (Trieste, 1977 Nov. 24-25) *(Italian)* 79—58265
information treatment methods, meeting (Trieste, 1977 Nov. 24-25) *(Italian)* 80—8548
integrating vidicon systems at Cerro Tololo, data acquisition and reduction software 79—66924
interactive system for computer reduction and display of two-dimensional data 79—58257
IR Astronomical Satellite (IRAS), on board computer software 79—80192
IR astronomical survey data processing techniques 78—81553
IR photographs, processing techniques for revealing faint objects *(Russian)* 77—13250
Japan, astronomical data systems group 77—78674
Jovian centre location in Voyager image transformation 80—101534
Julian Day-calendar date conversion algorithm *(French)* 78—12107
Kepler's equation for elliptic orbits, soln. using general algorithm 80—21898
Keplerian systems, computer simulations 80—26720
Kirchoff's laws of spectral analysis, computer laboratory exercises 78—73790
large cosmic ray showers, computer simulation using models of hadronic collisions 78—57415
large scale interactive one dimens. array processing system, spectrophotometric appl. 80—82220
laser ranging equipment, computer system *(Japanese)* 78—89080
LISP programming language appl. *(Polish)* 78—61749
lunar crater image edge determ. 80—98581
lunar data, logical searching, FORTRAN program incorporating Boolean search capabilities 79—2491
lunar features, absolute heights from photographs, computer processing technique *(Russian)* 80—109380
lunar position computation algorithm 79—25452
lunar seismograms, use of surface reflections 78—65504
lunar surface elemental composition, analytical determ. from Apollo X-ray and γ-ray spectrometer data 79—2495
lunar theory of Hill and Brown, POLYPAK appl. 80—46370
Mariner 10 images of Venus and Mercury, digital processing 77—78647
Mars, Viking orbiter images IPL processing 78—20679
meteor streams, statistical simulation of radar obs., algorithm 78—20763
Mimas and Tethys, orbital theory including perturbs. 80—36568
minor planets ephemerides, orbits computation using Chebychev polynomials *(French)* 80—61997
minor planets observations, least squares soln. of ill-conditioned systems 80—26747
MK spectral classification from uvbyβ photometry, general case 80—82216
Mount Wilson solar magnetograph, computer-operated image scanning and data system 77—22073
multidimensional power spectral anal., new method, radioastron. appl. 77—17378
N-body computer simulations in expanding Universe 79—97114
navigational almanacs for small computers, calculators 79—62726
NGC 5195 (M51 comparison), appl. of negatives superposition method, processing of obs. *(Russian)* 77—13251
non-LTE radiative transfer, multi-dimensional, computer program 77—22057
Northern Cross radiotelescope, data acquisition system *(Italian)* 77—5426
numerical image manipulation and display, Skylab EUV solar obs. appl. 77—60618
optical astronomy, appls. 78—4111
optical surface control, Hartmann method, use of splines 79—35149
optics, computer modelling 79—8836
orbit computation in galaxy models, algorithms 80—67797
orbital elements, nonlinear least squares minimisation 77—33761
orbital motion on an interactive-graphics terminal, teaching appl. 80—73152
overlapping plates, block adjustment and star positions *(German)* 78—45237
period-finding technique, Fortran IV computer program 79—21195
photoelectric photometry at Trieste, data acquisition and processing software *(Italian)* 79—58258
photoelectric photometry at Trieste, real time data acquisition and processing *(Italian)* 79—62757
photoelectric photometry at Trieste, real time spectral analysis *(Italian)* 79—62756
photographic plate calibration, new computerised method, galaxy photometry appl. 79—92677
photographic plate digitalised image, object detect. using FINDER program *(Italian)* 80—98575
photographic zenith tube plates, new reduction method 78—73656
photometer data evaluation, photoelectric high speed *(Japanese)* 78—32345

astronomy computing continued
photometry, data collection with aid of microcomputer *(Czech)* 80−67570
photon flare centre determ., online optoelectronic convertor *(Russian)* 79−75111
planetary, solar and lunar positions, low-precision formulae 80−61990
planetary and satellite systems evolution 80−77308
planetary ephemeris, direct computation method *(French)* 78−7862
planetary system evolution, simulations 80−94733
planets around multiple stars, computer simulations 79−2559
planets rectangular coordinates, approximation via Chebyshev polynomials *(Russian)* 80−62033
plate analysis interactive imaging technique appls. 79−58266
positional astronomy and astro-navigation computing, new approach using pocket calculator, book 79−12383
positional photographs reduction by method of dependences 80−4237
programs for high-school expts. 78−86094
protostar, rotating, fragmentation, comparison of two three-dimensional computer codes 80−26850
pseudo-colour images representation, graphic processor appl. *(Italian)* 80−98562
Pulkovo Observatory, stellar data and computing facilities 77−78631
radiative transfer exponential integrals, Λ-transform determ. 79−35114
radio astronomy, arc meas. procedure optimisation using radiointerferometer *(Russian)* 79−101082
radio astronomy, direct transform hardware processing of rot. synthesis data 78−85856
radio astronomy, direct transform hardware processing of rot. synthesis data 78−85857
radio astronomy, interference-excising correlator 79−75110
radio sources Faraday rotation measures, computation method 80−4263
radioastronomical data recording and processing, real-time, multichannel system *(Russian)* 78−65507
radioastronomical interferometric obs., data storage requirements 77−78651
radioastronomical systems and radioastronomical information processing methods *(Russian)* 77−22097
radioastronomy image reconstruction 80−56718
radioheliograph phase error meas. and correction 77−87269
radiometer instability influence on meas. results, reduction by computer *(Russian)* 78−65506
radiosources, two-dimensional max. entropy reconstruction of radio brightness 78−28534
radiotelescope antenna array performance, simulation of super-synthesis telescope 80−98548
radiotelescope RT-22 spectrometry, data reduction and analysis *(Russian)* 77−9674
satellite orbital lifetimes, prediction methods 78−73605
scanning microphotometer with on-line reduction of Schmidt plate data 78−7884
self consistent FORTRAN subroutines for Earth motion determ. 80−85845
software package for the presentation and evaluation of digitized images 79−58267
solar corona, global-scale 3-D reconstruction 80−56719
solar flares, principal component anal. in soft X-ray flux 80−41781
solar nebula, nebula, primitive, interaction with giant gaseous protoplanets, computer anal. 80−56727
solar position computation procedure 79−5734
solar radio bursts, recording instrumentation and data reduction *(Italian)* 78−96458
Solar Radio Data Acquisition and Communication System (SORDACS) of Toyokawa Observatory 79−101074
solar spectrometric research, automation system for on-line signal processing *(Russian)* 80−12659
spacecraft data processing and analysis 77−78650
speckle patterns, image retrieval, computer simulation 77−22100
spectra automated reduction by micromputer based system 80−77296
spectra obtained with low-dispersion Fehrenbach prism, computer simulation 78−57468
spiral galaxies surface photometry, computerised data reduction system, (appl. to NGC 157) 79−40264
stellar bibliographic file for automatic information retrieval 77−78833
stellar classification dispersion spectra synthesis from atmos. theory and high-dispersion spectra 77−29804
stellar data, conf. (Strasbourg, France, 19-21 Aug. 1976) 77−78828
stellar data base, retrieval techniques and graphics display 77−78652
stellar data base standards, management and security 77−82282
stellar data in machine-readable catalogues, critical evaluation 77−78830
stellar designation organization using bibliography-type data base 77−78658
stellar identifications, CDS data base 77−78659
stellar magnitude, colour index and position meas. from astronomical photographs, automated technique 79−21194
stellar observational data, surface distribs. on celestial sphere 77−2423
stellar photoelectric photometry at Hvar Observatory, data reduction and computing routine 77−78643
stellar photometric data, critical evaluation 77−78831
stellar spectrogram processing using microdensitometer, ELSPEC/1 procedure *(Italian)* 79−62758
strip telescope, image synthesis, computer simulation 77−29660
sunspot cycle normalisation according to period, algorithm *(Russian)* 79−75117
teaching aids in schools 80−73126
telescope stray radiation, expt. meas. and computer analysis 78−61752
telescope system features and operation, 3.9 m, Anglo-Australian 78−16291
three body averaged plane restricted problem, first integrals, computer calc. *(Russian)* 77−56820
time service, data acquisition and real time processing system *(Italian)* 80−8549
universe model, computer simulation of galaxy distrib . in Lick catalogue 78−81718
US Naval Observatory data files 77−78670
Viking 1975 Mars lander interactive computerized video stereophotogrammetry 78−20650
Westerbork Synthesis Radio Telescope, standardized data formats 77−78641
X-ray source counts, spectral anal. rel. to binarity detect. via Doppler effect *(Russian)* 78−77623

astronomy computing continued
X-ray source position determ., parameter estimation method 78−61748
H_2O sources spectra, autocorrel. anal. 78−65713

astrophysics computing
see also computerised instrumentation
acoustic waves in solar atmosphere, efficiency of one-dimens. hydrodynamic codes 78−57520
asymmetric rigid body problem, arbitrarily torqued, variation of parameters approach 78−93528
atmospheric showers, γ-ray initiated, computer simulations, Cherenkov radiation, geomag. field effects 77−49254
Be stars, emission line profiles from envelopes, elliptical gaseous ring model 80−4373
Be stars, emission line profiles from envelopes, theoretical profiles 80−4374
coronal emission line strengths 77−64715
cosmic ray anisotropy, COS approx. appl. to expt. data, computer simulation 77−5457
cosmic ray data selection and preprocessing in realistic error evaluation 77−53337
directional charged particle flux meas. in space, digital onboard processor appl. 77−64610
eclipsing binary star light curve anal. in freq. domain by automatized Fourier technique 80−22039
ellipsoidal potentials of polynomial distributions of matter, rotating stars appl. 80−46532
flare stars, model chromospheres, Balmer-line profiles 80−46558
galaxy collisions, deformation caused by tides, computer simulation *(French)* 80−56952
galaxy evolution, appl. of parallel computers in University research 79−54114
general relativistic stellar evolution code 79−58317
gravitating, 3-dimens. system of colliding masses, numerical simulation 77−9654
gravitational collapse to neutron stars and black holes, computer generation of spherical spacetimes 80−46385
integrals of motion for hamiltonian of coupled harmonic oscillators, calculation program 79−58239
ionospheric disturbance forecasting through solar radiation measurements from NRL SOLRAD satellites 79−58134
M31, H I sheets ejected by M32, multiple disk radial vels. computer simulation 78−16523
massive stars presupernova evolution 79−16930
maximum entropy spectral analysis, model data anal. situation study 79−8843
meteorite impact and ejecta deposition on airless planetary bodies, topographic effects 78−65523
Mie scattering by sphere, numerical methods 79−50225
multispectral scanning sensor system digital simulation 79−29997
Newtonian spheroid, homologous oscill., gravit. radiation, appl. to stars 80−46533
objective prism spectra of stars, computer classification *(German)* 77−49304
optical depth, integral of Voigt function 79−25468
planetary positions calc. using programmable pocket calculator *(Norwegian)* 78−69700
plasma and astrophysics computing conference 77−29639
plasma diffusion rates, automatic computation, stellar interiors appl. 78−57434
Poisson's eqn. numerical soln. for flattened centrally condensed objects, stellar models 79−35110
polytropic star, equilib. poloidal mag. field, finite difference-finite expansion method, Fortran program 77−13322
power series expansions by computer 79−84679
power spectrum analysis, nested variance technique, space physics, appl. in FORTRAN 77−87275
protostellar cloud, rotating isothermal axisymm. collapse 79−62737
protostellar clouds evolution, three dimens. dynamics 79−16929
radiative transfer, adding algorithm for Markov chain formalism 80−21902
radiofrequency recombination lines, computation of b_n factors 77−64832
self-consistent smoothing program 77−13596
solar activity, coronal index, for 1971-76 period 80−4322
speckle interferometry of binary stars, computer simulations in photon-counting mode 78−53836
spectral line equivalent widths meas. criterion 79−35141
spectroscopic data, real-time acquisition and preprocessing via RETIC interactive package *(Italian)* 80−98553
stellar atmosphere, expanding, radiative transfer by Feautrier method 79−25593
stellar bar, dynamics, computer model 79−30093
stellar flare data reduction and interpretation, interactive method *(Italian)* 80−8552
stellar speckle interferometry data processing method 79−12409
swirling particle fluids, computer studies, evolution of planetary-type bodies 79−35121
thermonuclear react. rates, computation with STEEP code 78−18375
tidally distorted stars, form factor method for struct. determ. 80−21991
W Ursae Majoris stars, atm. parameters of A-type systems 80−36672
Viking experiment, computer image processing, basic techniques 77−91403
GeH_4, IR spectra, Jovian atm. absorpt. profile, computer simulation 78−81584

asynchronous electric machines *see asynchronous machines*

asynchronous generators
60 m diameter wind turbine generator, appl. 80−61262
accelerometer, induction generator type transient characts. and Law-Novotny expression development *(Japanese)* 79−88921
variable speed wind power generator, control strategy for 3-phase output *(French)* 80−76591
wave power generation, from randomly varying input 79−48081
windpower development programme in Sweden, appl. 80−61237

asynchronous machines
see also asynchronous generators; induction motors; slip (asynchronous machines)
EM noise reduction, method *(Hungarian)* 77−14841
helical induction machine, laminar flow in channel, boundary effects *(Russian)* 77−47105
induction machine, duct local flow charact. at large EM interaction parameter *(Russian)* 78−5818

asynchronous machines continued
induction pump, linear, cylindrical EM field distrib. *(Russian)* 78−5820
induction stirring of semicontinuously cast ingots *(Russian)* 78−6915
MHD coaxial induction machine travelling mag. field, laminar flow *(Russian)* 78−5815
MHD flow of liquid metal plane layer, industrial furnace appl. *(Russian)* 78−5817
MHD pump, performance indices channel geometry *(Russian)* 78−5821
precison measuring table with hollow rotor asynchronous motor, digital control system 80−105607
slotted boundary machine field soln., conformal transformation and integral methods 79−41272

asynchronous motors *see induction motors*

atmosphere, solar *see solar atmosphere*

atmosphere, terrestrial *see terrestrial atmosphere*

atmosphere, upper *see upper atmosphere*

atmospheric acoustics
absorption by air in 10-100 kHz range, NPL report 77−7239
absorption processes, 10 to 10^5 Hz 80−53531
acoustic-gravity wave propag. in diffusively separated atmosphere 79−74933
acoustic-gravity waves generated by horizontally-moving sources *(Russian)* 80−21795
acoustical-gravity waves in plane waveguide, interaction and self-action *(Russian)* 78−36221
aeroacoustics, book contrib. 77−50807
aerodynamically generated sound, mathematical formalisation of Lighthill's theory 77−62245
aerosol particles, sonic agglomeration 77−29411
aerosol systems in acoustic field, exptl. study 80−89529
air-water fogs, audible sound propag. 78−1473
aircraft noise, excess attenuation of high freq. 78−33939
aircraft noise propag., review 80−64258
aircraft wake vortices, acoustic refr. scatt. appl. in tracking system 77−46840
arbitrary continuously stratified environments, propagated, reflected and transmitted acoustic waves 78−13829
atmosphere, gravity waves generation by HF acoustic waves, Cherenkov radiation *(Russian)* 77−17265
auroral electrojet, gravity waves and infrasound generation, Joule heating and Lorentz force 79−66866
auroral electrojet as infrasonic wave source *(Japanese)* 80−17434
auroral infrasonic wave emission, multiplicity of wave forms 77−29534
auroral infrasonic wave emissions, temporal and spatial changes rel. to polar substorms 79−100996
auroral infrasonic wave emissions on night of low geomag. disturbance 77−25811
backscatter in GATE, effect of wind shear and moisture fluctuations 80−85709
bands of noise, influence of atmospheric absorption on propag. 79−98524
boundary layer, acoustic backscatter, beamwidth effects 79−70859
boundary layer, quantitative bistatic acoustic sounding 78−49176
boundary layer, simultaneous horizontal and vertical sounding obs. 80−61846
boundary layer eddy correl. using sonic anemometer 80−56637
boundary layer gravity waves, acoustic sounding obs. 80−61847
brontides, summary 80−12523
clouds and fog, sound attenuation obs. 77−34981
Concorde sonic boom, long distance focusing 78−83160
Concorde sonic booms as probe of atm. temp.-wind parameters 77−91323
correlation of the phase and amplitude fluctuations between direct and ground-reflected sound 80−96067
detonations, sound ranging in atmosphere, anal. problems 79−94393
diffraction by screen above locally reacting, infinitely large plane 78−79158
discontinuous solns. of differential eqns. using generalized differentiation 78−33940
Doppler acoustic sounding of lower atm., convective plumes detect. *(French)* 78−40603
Doppler sounding of falling snow 79−53467
Doppler vel. extraction from echoes, zero-crossing technique 79−53542
ducted acoustic wave generation by terminator 78−49191
echo sounding, Doppler shift extraction by adaptive linear-prediction filtering 77−64453
echosonde antenna radiation patterns, effects of phase-front distribs. 77−39123
echosonde antennas performance, simulation rel. to influence of echo carrier freq. and antenna dimensions 78−1474
echosonde signals, excess attenuation 80−83694
explosion waves, atmospheric attenuation 77−31155
explosion waves, vibrational relaxation effects on atmos. attenuation and rise times 79−7244
finite amplitude distortion of intense sinusoidal pressure waves 80−33273
fireball, over Japan 1977 May 10, sonic boom recorded on seismographs *(Japanese)* 79−66962
fluid dynamic equations, acoustic energy conservation, vibrational relaxation effects 78−90566
forecasts production, method using digital computer 79−79960
frequency shift of wave train due to absorpt. 80−64255
gas dynamics with relaxation effects, acoustic waves, nonequilibrium atmosphere effects, review 78−79390
gravity-acoustic waves, dispersive eqns. obtained by kinetic eqn. method *(Russian)* 78−85620
HF sound absorption, meas. 78−1475
high frequency atmospheric acoustic sounders 79−84489
infrasonic bow wave from travelling auroral arc 78−12040
infrasonic pulses detect. from thunderclouds 77−29362
infrasonic signals from thunder 79−70846
infrasound, asymmetry in generation by travelling aurora 77−87152
infrasound, detect. by homing pigeons 77−29156
infrasound, natural, ten years obs. and appl. to lower thermosphere investigation 79−21089
infrasound, refr. by upper atmosphere winds 77−33229
infrasound generated by Concorde used to monitor stratospheric winds 80−51492
infrasound generated by ocean waves, propag. in atmos. 79−74960
infrasound in ionosphere, HF Doppler obs., due to earthquake-generated oceanic Rayleigh waves, group vel. dispersion curve determ. 79−70756

atmospheric acoustics continued
infrasound observations of circulation vars. during stratospheric warmings 79−2339
infrasound originating near mountainous regions in Colorado 79−20946
infrasound waves, in the Earth's atmosphere *(Russian)* 78−32143
infrasound waves recording methods and computer anal. *(Russian)* 78−65407
ionosphere, acoustic waves generation by LF radiowaves 78−69581
ionosphere, propag. of acoustic gravity waves, explosion excitation *(French)* 78−12042
ionosphere, sound propagation, weakly ionised quasihydrodynamics approx. *(Russian)* 77−82079
ionosphere sound generation, theory 80−41604
lower atmosphere, acoustic-gravity waves generation by ionosphere press. oscills. 78−77296
lower thermosphere, heating by acoustic waves dissipation 77−53266
mesoscale phenomenon, acoustic sounder obs., comments and reply 77−64385
meteor acoustic gravity wave generation *(Russian)* 77−91340
meteorological appl. of acoustic radar *(Spanish)* 78−88944
minimized sonic boom waveforms, subjective loudness 79−16221
monostatic sounding, pattern recognition studies 78−65416
mountain-assoc. infrasound, source mechanism 77−78324
N-wave sonic booms, subjective loudness tests 79−16220
noise attenuation over an absorbing terrain, theoretical models comparison, aircraft noise appl. 79−18572
noise propagation, review 77−84065
nonlinear absorption of sound, rel. to atmosphere acoustic and radio acoustic exploration *(Russian)* 80−94567
nonuniform wind, error in Rayleigh's theory of sound refraction 79−72743
outdoor process plant design, atm. noise attenuation calc. 79−70497
plane sound waves in air, finite-amplitude saturation 78−1465
powerful radio waves sound excitation, heating effect investigation *(Russian)* 77−78554
propagation in an inversion and reflection at the ground relevance of underwater acoustics 77−14835
propagation in fluctuating media 77−53073
propagation in nonhomogeneous ducts, acoustic energy flux 79−7243
propagation over hard ground for distances under 200 ft, exp. study, community noise appl. 79−18600
pulse-modulated intense wave propag., low freq. component nonlinear generation *(Russian)* 79−98522
radio-acoustic sounders for remote sensing of lower atmosphere *(Japanese)* 78−16209
radioacoustical sounding, expression for scatt. signal freq. spectra *(Russian)* 80−94612
radioacoustical sounding by continuous radiation method *(Russian)* 78−88927
radiowave scattering from acoustic atmospheric formations 79−92579
ranging with sound source and rangers at different levels *(German)* 77−54824
reflection and refraction, analytical solns. of wave eqn. 80−53530
reflection from the ground, theoretical model 79−18573
refraction effects in echo sounding multilayer model appl. 77−84041
resonances in sound scattering from water droplets in air 80−33306
review of recent advances 78−73493
scattering from locally homogeneous turbulence 78−87177
scattering of EM waves by acoustical formations of atmosphere in field of moving point source of sound 78−32210
shear layer scatt. of acoustic wave, linearised theory with causality 77−42643
shock formation in unsteady flow 79−37351
sodar, appl. for acoustic detection in lower atmosphere *(French)* 80−8435
sodar, sounding technique appl. to siting studies 78−81467
sodar and aircraft simultaneous meas. of turbulence 79−20923
sodar meas., improved quantitative display techniques 78−77332
sodar network meas. of mixing depth and stability regional patterns 79−100965
sodar obs. of tropospheric thermal struct. at Delhi 78−32151
sonic boom propag. in thermosphere 80−33305
sonic booms during launch and reentry of Space Shuttle, environmental effects 78−85681
sonic booms focusing conditions 77−50804
sonic booms from Concorde aircraft flight, atm. struct. information 79−66742
sonic-boom press. signature distortion by high-speed jets 78−79156
sound attenuation, air-to-ground propag., effects of temp., humidity gradients 79−1019
sound attenuation, through interaction with internal gravity waves *(Russian)* 77−3693
sound attenuation by turbulence 77−7238
sound attenuation by wide barriers, acoustical scale model study 78−1499
sound level decay from steady source in built-up area 77−72109
sound propagation, over ground layer with large refr. index 77−50805
sound propagation in atmosphere, historical review 78−15
sounder for lower atm. remote probing 77−17243
sounding, appl. to boundary layer obs. from top of steep mountain 80−98409
sounding, records obtained for Christchurch, boundary layer study 80−26638
sounding and meas. of diffusion in freely convective boundary layer 79−34966
sounding at Calgary, boundary layer struct. 78−24376
sounding of lower atmosphere using 79−74972
sounding of radiation fog 78−69419
sounding with balloonborne instrument, scatt. structs. vertical profile 78−57353
stratosphere and ionosphere, LF waves relax. absorpt. *(Russian)* 78−65356
surface layer, acoustic method for optical inhomogeneities fluctuations 80−67434
temperature struct. parameter determ. from acoustic sounding and direct meas 77−33125
temperature structure parameter profiles meas. by acoustic sounder 79−21049
thunder, appl. to lightning study *(Russian)* 80−56532
thunder propag., status of current research 80−87618
tornado over Delhi, of 1978 March 17, sodar obs. 80−109188

atmospheric acoustics continued
- troposphere sounder, metric radiowave-acoustic sounder 80—46276
- turbojet noise suppression investigations using hydrodynamic press. meas. and cross-correlation techniques 78—79157
- turbulence effects on interference near hard boundary 78—83159
- turbulence effects on interference of sound waves above finite impedance boundary 79—41493
- turbulence in boundary layer, sounder return interpretation 77—37417
- typhoons, detection and appl. of associated acoustic waves *(Chinese)* 79—34996
- vertical propagation of powerful sound beam in inhomogeneous atm. *(Russian)* 77—64375
- VLF wind-generated noise produced by turbulent pressure fluctuations in atmosphere near ocean surface 80—19137
- wave interaction with ocean surface waves, model *(Russian)* 80—12402
- weak shocks, short-wave asymptotics 77—37763
- wind determination by acoustic radar *(Chinese)* 80—46290
- wind vertical velocity, acoustic Doppler power spectra comparison with direct meas. 79—57999

atmospheric boundary layer
- Aberdeenshire, mesoclimate of Upper Don Basin 80—61889
- acoustic backscatter, beamwidth effects 79—70859
- acoustic sounder observations, from top of steep mountain 80—98409
- acoustic sounding obs., simultaneously in horizontal and vertical directions 80—61846
- acoustic wave interaction with ocean surface waves, model *(Russian)* 80—12402
- adiabatic boundary layer height vars., simulation in wind tunnel 78—7691
- advection, local analytical model *(French)* 79—84404
- advection dominated flows, finite element anal., book contrib. 79—34934
- aerodynamic drag of sea surface, role of high freq. gravity waves 80—26536
- aerodynamic roughness as function of wind direction over asymm. surface elements 78—92890
- aerosol inhomogeneities struct. and dynamics in ground layer, light scatt. 77—81955
- aerosol meas. at Algarve coast, Portugal 79—58062
- aerosol optical attenuation statistics, spring and autumn 79—84484
- air flow above sea surface, eddies transfer rate investigation *(Russian)* 79—16578
- air flow over irregular surface, three dimens. finite difference model, terrain following coord. transform 77—60452
- air modification due to step change in surface temp. 77—78294
- air pollution effects on planetary boundary layer, numerical model 77—41143
- air-sea heat and moisture exchange during stormy weather 77—78375
- air-sea heat exchange, optical meas. methods 77—49184
- air-sea interaction, stratification effect on evaporation *(French)* 80—31085
- air-sea interaction buoy performance 79—70894
- air-sea interaction model 79—79969
- air-sea interface, CO_2 flux meas., eddy correl. method 79—25303
- air-sea interface, gas transfer 77—91154
- air-sea interface, heat and momentum flux in const. flux layer, from temp. meas. 78—44899
- air-sea interface, heat transfer coeffs. meas. 200 km from land 80—72552
- air-sea interface, latent and sensible heat flux calc., AMTEX-74 77—91224
- air-sea interface, momentum flux determ., wind-wave interaction method 77—33130
- airborne contamination, deposition-resuspension process effect, simulation 80—16860
- airflow above waves, numerical simulation *(Russian)* 80—4076
- airflow over irregular terrain, numerical study 77—86969
- airflow transformation over nonuniformly heated underlying surface 80—82031
- Ampere glacier (Kergueler Is.) *(French)* 77—56666
- anisotropic homogeneous turbulence statistical description 79—79917
- Antofagasta, N.Chile, boundary layer dynamics in arid desert 80—56512
- Arabian Sea, ISMEX-1973 data 80—56534
- Arctic leads, atmos. boundary layer turbulence spectra obs. 80—56588
- Arctic leads, turbulent heat flux 80—56513
- assessment of proposed similarity theories 77—33126
- tropical Atlantic surface atm. and oceanic circulation patterns assoc. with Subsaharan weather anomalies 79—5587
- atmosphere-soil system, turbulent heat and mass transfer, simple predictive model 78—24331
- auto-oscillation solns. of barotropic boundary layer problem *(Russian)* 77—49106
- available potential energy over uneven topography, theory 80—51514
- balloon meas. in boundary layer, wind vel. determ. *(German)* 79—84421
- balloon obs. of local air currents 77—91307
- baroclinic atmosphere, two layer model, Helmholtz term effect 79—79986
- baroclinic model for vertical temp. and moisture stratification in baroclinic boundary layer 79—53502
- baroclinic planetary boundary layer above sea, parameterisation *(Russian)* 79—16576
- baroclinic spatially growing waves finite amplitude dynamics on f-plane 79—79985
- baroclinic wave development *(Russian)* 77—33140
- baroclinicity effects on Lagrange trajectories of diffusing particles 77—66949
- baroclinicity-cum-stratification effect on Lagrange characts. 79—66765
- barotropic Ekman layer over urban terrain 77—70733
- barotropic flow crossing mountain barrier, dynamic initialisation 77—21855
- biogeochemical cycles, role of atmosphere 79—79427
- Birmingham, England, heat island synoptic climatology (1965-74) 80—85740
- body force effect on turbulent transport near surface 78—26116
- breeze circulation along complex coastline 80—36364
- bulk model, for wind and pot. temp. 80—77030
- bulk transfer velocity to and from natural and artificial surfaces 79—25302
- buoyancy effects in a wind tunnel simulation of the atmospheric boundary layer 79—68687

atmospheric boundary layer continued
- buoyancy effects in entraining turbulent boundary layers: a second-order closure study 80—21815
- buoyant plume in stably stratified boundary layer, max. ground conc. 80—72573
- buoyant plumes behaviour on release at ground level, lab. wind tunnel obs. 80—30624
- Calgary, air quality affected by Chinooks, acoustic sounding expt. 80—16876
- canopy flow, higher order closure model 78—44944
- canopy index values for various canopy densities 79—53420
- canopy resistances for partially wet canopies 78—44904
- Cape Canaveral sea breezes, elliptical clockwise diurnal oscill. 79—100921
- centripetal heat island circulations, St. Louis, USA 79—66753
- characteristics and simulation, review of current simulation techniques, recommendations for new technique 80—51469
- circularly polarised inertial wave vectors 77—3829
- circulation, quasigeostrophic model, mountain barrier effects 77—66974
- circulation in desert regions, variable surface albedo effects 77—49123
- classification of pollutants and pathways in atmosphere 79—70489
- clear air wind perturbs., dual Doppler radar obs. 79—53462
- clear radiance estimates from truncated observations 79—80025
- climates, book 79—8682
- cloud and fog, formation conditions in frontal zone, theory 80—41532
- cloud condensation nuclei flux, continental surface meas. 79—53443
- cloud depth relation between Pasquill stability and Kazanski-Monin stability 80—17304
- coastal internal boundary layer characts. during onshore flows 80—41479
- coherent structures effect on on temp. struct. functions 77—64361
- cold easterly circulations over Canadian Western Plains, mesoscale model 77—78295
- cold-air advective conditions, lake moderating effects on surface temps. 79—25299
- conference (Smolenice, Czechoslovakia, 1974 February 18-21) 78—88873
- convection, Doppler acoustic sounders and balloon meas. *(French)* 79—66763
- convection development over inhomogeneous heated surface *(Russian)* 77—29365
- convection in boundary layer, lidar obs. 78—65366
- convection in thin layer above water surface *(Russian)* 77—45073
- convective, temperature-humidity covariance budget 78—73430
- convective boundary layer, boundary layer, appl. of mixed-layer similarity scaling to observed dispersion from ground-level source 80—105021
- convective boundary layer, turbulence struct. of upper region 80—56576
- convective boundary layer slab model, study using Air-Mass Transformation Expt. data 79—57995
- convective disturbance thermodynamic struct. 80—81978
- convective layer, max. ground level conc. 80—41474
- convective layer over sea, turbulence meas. by instrumented aircraft 79—12214
- convective matching layer 78—81310
- convective velocity scale estimation for diffusion appls. 79—79914
- coronae effects on elec. fields beneath thunderstorms 79—79978
- coupled ocean-atmosphere expt., ocean response, rel. to climate 80—12430
- cumulus capped planetary boundary layer, numerical model *(French)* 80—94574
- cyclone waves and front development, surface friction effects 77—86966
- daytime urban moisture field struct. 79—57998
- Denver air quality, effects of meteorological and climatological factors 79—84350
- depth and vertical wind profile 77—9462
- diabatic baroclinic, parametrisation for circulation modelling *(Russian)* 78—88882
- diabatic heating profile, rel. to preferred mode of Ekman conditional instability of second kind (CISK) 80—72617
- diffusion experiments in unstable conditions over inhomogeneous terrain 79—58059
- diffusion flux close to surface, mol. sublayer effect 80—4068
- diffusion from ground-level source in turbulent boundary layer, Lagrangian statistical anal. 80—12517
- diffusion in freely convective boundary layer, meas. by acoustic sounding 79—34966
- diffusion parameters on local scale, determ. by no-lift balloons 79—70853
- diffusion props. over urban site, anal. using radioactive tracers, effect of air masses 79—84347
- diffusion props. over urban site, anal. using radioactive tracers, effect of meteorological variables 79—84348
- dispersion from elevated point source 79—12245
- dispersion from elevated source in convective layer 79—12246
- dispersion in turbulent shear flow, theory 79—88393
- dispersion of gases into atmosphere from volatile liq. evaporation, diffusion model *(Dutch)* 79—79425
- dissipation modelling under forced convection conditions 78—92900
- diurnal var. of Rn and mixing height for USA Gulf Coast 80—101404
- diurnal wind var., diffusion eqn., theory 79—48540
- double diffusive convection during 1975 hurricane Eloise 77—70738
- drag coefficent vars. for air flow above water waves 79—44232
- dry deposition of peroxyacetylnitrate and O_3 to natural surfaces 77—45139
- dry season in steppe of S.W.Africa *(German)* 79—34923
- dry thermals forecasting for gliding 78—49103
- dust transport in Maricopa County, Arizona 79—70824
- dynamic structure in urban areas, numerical simulation 79—66741
- dynamics, IR radiation effects 79—39815
- dynamics of stable boundary layers and nocturnal jets 80—41491
- eddy and turbulent diffusion at 0-65 km altitude, model simulation 79—84438
- eddy convection vel. 78—92894
- eddy correl. using sonic anemometer 80—56637
- eddy exchange coeffs. in numerical models 77—73791
- eddy flux meas. over ocean, related transfer coeffs. 78—81265
- eddy flux measurement of various quantities corrected for density fluctuations 80—72576
- eddy flux measurements above pine forest 77—17198
- eddy flux measuremnts using instrumented powered glider 80—51509
- eddy viscosity coeff. var. 77—70737
- Ekman, universal functions in drag and heat transfer laws *(Russian)* 77—91216

atmospheric boundary layer continued
- electrode effect, obs. at mountain station 79—25307
- EM waves refraction, expt. investigation 80—36400
- energy budget over grasslands, eddy correl. sampling techniques 77—78446
- energy budgets of turbulent vel. components and vel.-press. gradient interactions 79—58026
- energy characts. of urban-rural surfaces in greater St. Louis area 78—61484
- entrainment process, laboratory expts. reinterpretation for stratified fluid 80—51405
- equations soln. using sensitivity analysis 77—54957
- equatorial region circulation, boundary layer zonal wind soln. 79—29821
- escarpment wind profile 79—12217
- evaporation fog, growth and disappearance during cold air mass transformation 80—56585
- evaporation fogs formation theory and prediction 78—61522
- evolution and nocturnal inversion dispersal 79—25295
- evolution and nocturnal inversion dispersal 79—25296
- fair weather electric charge transfer by convection in unstable mixed layer 79—58037
- finite amplitude Kelvin-Helmholtz billows, evolution 78—81293
- flow above gentle topography, model 77—91199
- flow of stratified fluid over obstacle *(Russian)* 78—24291
- flow over hills, stratification effects 78—53707
- flow over isolated hill of moderate slope 80—12515
- flow over topography, Cartesian model 78—92904
- flow over two-dimensional obstruction, description by parabolic partial differential equations *(Italian)* 79—20956
- flow over water during stable conditions, Eulerian and Lagrangian time scales 79—25300
- flow over wavy boundary, water waves 77—73792
- flux calculation methods, relative errors 79—79953
- fluxes determ. over natural grassland, aerodynamic method 78—73480
- fog and haze microphysics, visual range obs., and particle size distrib. 80—109195
- forced turbulent plumes, rise times 79—100932
- forecasting of average air temp., underlying ocean surface influence 79—29827
- forest evapotranspiration determined using Bow ratio and eddy correl. meas. 80—31103
- forested land evaporation, Priestley-Taylor eqn. 80—31102
- formaldehyde, in marine air and rainwater, wet season obs. 80—85703
- formation and evolution of radiative fog and stratus cloud *(Russian)* 77—49104
- free convection along nonisothermal vertical flat plate, soln. technique 77—58682
- free convection structure in surface layer 77—37294
- friction and orography rel. to energy conversions during weak monsoon 77—56711
- friction vel. and temp. scale from temp. and wind vel. profiles 78—81268
- frictional and orographic effects on precip. in coastal areas 77—60442
- gamma radiation field of seawater and atm. surface layer rel. to cosmic ray neutrons *(Russian)* 79—39746
- GATE aircraft measurements, their value 80—82071
- geostrophic balance of horizontally periodic motions 79—39824
- geostrophic drag and heat transfer relations 77—78298
- geostrophic flow over shallow topography 80—90120
- geostrophic large-scale drag coefficient estimation 78—61488
- gravity wave generation and breaking over ocean 80—26571
- gravity wave-critical level encounter, calc. 80—26583
- gravity waves generated by shear layers 77—2195
- gravity waves observed by acoustic sounding 80—61847
- ground level gravity waves occurrence in SE.Australia, microbarographs obs. 78—73439
- ground level wind departure from geostrophic wind, effects of orography, stability and baroclinity *(German)* 79—66771
- ground surface roughness change, affecting air flow characts. 80—51501
- ground surface temperature and moisture content, prediction with inclusion of vegetation layer 78—73373
- ground surface temperature prediction, force-restore method investigation 80—98469
- ground-based inversion frequencies determined from surface climatological data 80—41475
- ground-based inversions, expt. data and boundary-layer models 79—66748
- heat and humidity exchange laws, model approach 77—66948
- heat and momentum transfers under strong stability 79—16584
- heat and pulse transport *(Dutch)* 78—3890
- heat flux. max., relation to wind speed 80—17345
- heat fluxes, latent and sensible, from lakes, prediction from surface water temps. 80—72562
- heat transfer bulk characts. in unstable baroclinic boundary layer 79—79911
- heat transfer with ocean, reef effects, AMTEX 1975 obs. 80—26567
- heated air, ascending bubbles, interaction with ambient cold air 79—84362
- height and circulation prod. in sea breeze model 79—53438
- height diurnal var. 77—60446
- heterogeneous surface of large aerodynamic roughness, transfer characts. 78—73487
- hill affecting airflow, overspeed effect 80—72577
- hill affecting turbulent diffusion from point source in stratified flow 80—56505
- hill crest, obs. of wind speed, shear and turbulence 80—85722
- horizontal coherence decay near large mesoscale variations in topography 79—58025
- horizontal roll vortices, two dimens. numerical obs. 80—101409
- horizontal trajectory computation based on surface geostrophic wind 77—37284
- horizontal wind profiles about block building 77—73789
- hourly mixing depths, estimation from historical meteorological data 80—51482
- humidity characts. rel. to atm. total H_2O vapour content 79—39836
- humidity diurnal variation over continents, absorpt. in hygroscopic soil layer 79—29825
- hurricane boundary layer response to sea surface temp. changes, model 79—53439
- hurricane sea surface wind speed, L-band radar backscatt. obs. 80—56561

atmospheric boundary layer continued
- Indian Ocean, sea levels in western equatorial region rel. to tides, meteorology and ocean circulation 80—4018
- Indian Ocean, surface temp. rel. to Indian summer monsoon intensity 80—90121
- inertial and frictional effects on flow over topography 77—45106
- instability of boundary layer with Rossby number similarity, inflection point and convective instability 79—66757
- interaction of boundary layer with free atmos. *(Russian)* 80—77037
- internal boundary layer development, dynamics, slab model 77—91198
- internal boundary layer development and fumigation 77—81956
- internal gravity waves generated by penetrative convection 77—2196
- internal gravity waves generation and breaking over ocean 78—44901
- internal gravity waves in time-varying stratification 78—3864
- inversion descent in mountain valleys, air pollution implications 79—62550
- irradiance, seminumerical method accounting for atmos. H_2O *(Spanish)* 80—36373
- isentropic and sigma coord. hybrid numerical model 80—12485
- isentropic coordinate models, boundary problems soln. 77—29372
- jet drops from bubbles bursting in seawater, ejection height rel. to organic material 79—39727
- jet stream struct. over Arabian Sea and Indian Peninsula, MONEX-73 obs. 77—53122
- jetlike wind at 100-600 m altitude over open coast, mesoscale nocturnal phenomena 80—81971
- Joint Air-Sea Interaction (JASIN) Experiment 1978, general review 80—4113
- katabatic wind observations 80—56587
- kinetic energy balance of large-scale motion over British Isles 80—56578
- Kolmogorov-von Karman relationship generalisation 77—78299
- kurtosis of velocity field, prediction method 80—23990
- Lagrange characts. of turbulent diffusion 77—33131
- Lagrange diffusion in planetary boundary layer 77—56667
- Lake Michigan, cold water modifying boundary layer struct. 80—72571
- lake moderating effect on downwind temp. and humidity, model simulation 79—88400
- layer under stable conditions, aircraft obs. 77—37295
- lee waves generated by isolated islands, three-dimens. patterns, satellite obs. 79—44230
- light scattering variability over N.Atlantic rel. to humidity and aerosol 80—82052
- lipid composition of marine aerosols, sea surface microlayer and subsurface water 80—17297
- liquid phase mass transfer coeffs. at natural air-water interfaces 79—20922
- local circulation in Rome area, surface obs. 78—81264
- local mesoscale circulation over Venice due to mountain-sea interaction 79—88401
- log-linear profile relationship over rough terrain during stable conditions 77—60444
- longitudinal wind vel. component meas. 77—78369
- low latitudes, meridional struct. *(Russian)* 77—73802
- low vortex over S.E. Chinghai-Tibetan Plateau, annulus expt. simulation *(Chinese)* 77—70787
- low-level air circulation over Arabian Sea during summer monsoon balloon obs. 77—17192
- low-level air flow in central valley, Maui, Hawaii 79—20929
- Magnus effect in saltation, lab. expt. 77—70764
- marginally unstable interfacial gravity waves *(French)* 78—92888
- marine, aerosol optical thickness, satellite radiance measurements 80—17326
- marine, diurnal temp. cycle in boundary layer 78—20434
- marine, microwave radiometric sensing of atmospheric structure 78—57272
- marine, optical refractive index fluctuations, statistical props. 79—62580
- marine, ranked interaction with ocean on sub-semidiurnal time scales *(Russian)* 78—77260
- marine aerosols influx into atmosphere, influence of coastal-zone physicogeographic conditions 79—29818
- marine atmosphere, elec. field short-period fluctuations 79—39816
- marine atmosphere, surface layer stability rel. to oceanic whitecaps and sea state 80—72554
- marine atmosphere diurnal kinetic photochemistry 79—48549
- marine boundary layer, turbulence effects on laser propag. 77—45156
- marine boundary layer, turbulence struct. obs. 80—56575
- marine boundary layer along California coast, instability rel. to marine fog and fog-stratus systems 80—77060
- marine layer, optical beam propag., analytical model 80—8329
- marine layer, shipboard use of low-level atmospheric thermograph in fog and stratus investigation 80—105073
- marine layer at San Diego, California, depth and moisture content rel. to cool season precip. forecasts in Arizona 80—101395
- marine stratocumulus convection, governing eqns. and horizontally homogeneous solns. 80—56542
- marine stratocumulus convection, horizontally inhomogeneous solns. 80—56543
- marine surface layer, air-sea exchange of heat and water, model 80—61809
- marine surface layer, temperature ramp struct. 79—66760
- marine surface layer turbulence structure, humidity and temp. spectra study, N.Pacific 80—21798
- maritime boundary layer model for fog prediction 77—78293
- maritime model for fog prediction 77—78293
- mass consistent model for wind fields over complex terrain 78—92906
- mean and turbulent structures, 24 hour evolution, modelling 79—58024
- mean maximum mixing heights across coastal zone, operational forecasting model 79—84357
- mean velocity and temperature profile calculation *(Russian)* 80—8415
- mechanical effect of urban area on convective precip. 78—81338
- mechanical resist. law over tropical ocean 77—45066
- mesoscale flow over complex terrain 78—49101
- mesoscale pollution transport, quantitative evaluation 79—70825
- meteorological episodes increasing air pollution in Belgium 78—81374
- methane conc. from IR absorpt. meas. *(Russian)* 77—29366
- methane concentration in surface air layer from IR absorpt. meas. *(Russian)* 77—29366
- methane content of atmospheric surface layer and vertical air column, synchronised meas. *(Russian)* 79—88407
- micrometeorological characteristics, during 1976 hot spells 79—79961

atmospheric boundary layer continued
micrometeorological temperature profile from optical data inversion 79—80034
microscale temp. and vel. spectra 78—16109
mixed layer, growth in turbulent stably stratified fluid 79—55358
mixed-layer model with penetrative convection, critical evaluation 80—51483
mm wave radar, measurements of effective sea reflectivity and attenuation due to rain at 81 GHz 79—80001
model, two-dimens., appl. to Nanticoke region, Lake Erie north shore 79—66750
modified flow propag. downstream from surface roughness change 77—17200
Mohliner Feld (east of Basle), topoclimate investigations *(German)* 80—61890
moist, finite element model, eqns. 79—5585
moist, finite element model, soln. method 79—5586
moist convection, effect of vertical moisture distrib. *(French)* 80—56567
moisture struct. with higher order turbulence closure model 77—78310
molecular resistance, during diffusion, universal function determ. 80—26573
molecular temperature boundary layer above sea, dynamics 79—66756
momentum, heat and moisture fluxes from struct. parameters 79—53435
momentum boundary layer in numerical weather prediction model 80—51451
Monin-Obukhov similarity functions, from closure model 80—81972
monsoon airstream at 12 metres height, temp. fluctuations 80—61845
motion simulations, wind tunnel characts. review *(Italian)* 80—4156
mountain barrier baroclinity effect on wind direction, Alaskan arctic coast 80—90118
mountain drag meas. 79—53452
mountain in airflow, 2-D numerical simulation *(Russian)* 80—81986
mountain ridges effect on frontal waves development, numerical simulation *(Russian)* 78—53701
mountain waves and severe downslope windstorms, theory 80—56551
mountainous terrain, atmosphere turbulent kinetic energy budgets 80—105022
multi-level model suitable for mesoscale dynamic models 77—29383
natural cycle of gases *(German)* 79—53404
Navier-Stokes eqns. soln. 78—92956
near water atmospheric layer, mean wind vel. meas. 77—9461
neutrally stable atmospheric layer, mass and energy transport 79—74927
neutrally stratified planetary boundary layer flow over gentle topography 78—3851
nighttime boundary layer, vertical struct. obs. 80—61848
nighttime turbulence, wind and temp. obs. compared with model calcs. 80—85707
nocturnal, height determ. 78—73450
nocturnal evolution, high-order model *(French)* 79—84397
nocturnal surface inversion height prediction 80—41520
non-neutral surface, parameterisation 80—17316
non-neutral surface, theoretical parameterisation study 80—17315
nonlinear small-scale sea-air interaction parameterisation, effects of ice cover *(Russian)* 77—53068
nonstationary advective layer, resistance law hypothesis 77—60441
numerical calc. method for meteorological variable fields 78—7733
numerical method for stratified shear flows over long obstacle, numerical method 77—33157
numerical modelling, turbulence 79—84396
numerical modelling 78—44900
ocean, diurnal temp. cycle in boundary layer 78—20434
ocean, Lagrangian wind and current vectors very close to short-fetch windswept sea surface 80—72553
ocean atmosphere interaction, mean wind speeds and turbulence at coastal site and offshore location 80—98406
ocean bottom, flow of stratified fluid over obstacle *(Russian)* 78—24291
ocean cold film calc. from diurnal temp. vars. 79—20855
ocean interaction, sea waves influence on wind profile 78—92895
ocean interaction parametrisation for storm conditions, atm. circulation models appl. *(Russian)* 78—65359
ocean interactions along North American west coast, 1965-69 period, preliminary anal. 78—61508
ocean interface, energy transfers at high wind speeds, effect of spray 78—85574
ocean interface, wind vel. profiles and drift current along wind-generated wave profile *(Russian)* 78—61429
ocean interfacial conditions, influence on bulk evaporation coeffs., isotopic method determ. 78—85576
ocean surface mixed layer, energy and momentum transfer by wind 78—44856
ocean-atmosphere boundary layer, heat transfer meas. using radio thermal microwave systems 79—84546
ocean-atmosphere heat balance over northern hemisphere, annual cycle 77—41040
ocean-atmosphere heat exchange influenced by surface waves *(Russian)* 80—56479
ocean-atmosphere heat leak effects of passage of tropical cyclone *(Russian)* 77—53069
ocean-atmosphere momentum, heat and H_2O vapour fluxes, meas. methods 78—32213
ocean-atmosphere sensible heat flux in extratropical synoptic-scale systems 77—78223
oceanic boundary layer, effect on pack ice drift, model 80—26528
oceanic eddy formation in Somali Current, wind effects 80—26523
oceanic planetary boundary layer, wind driven current, temp. profile, model 80—26526
optical inhomogeneities, investigation via acoustic method 80—67434
optical scintillometer, large-aperture, fine calibration, optical estimate of turbulence inner scale 79—21026
orography, influence on atmospheric movement with Coriolis force included *(Russian)* 80—94565
oscillating, stratified boundary layer, driven by surface temp. variation 80—51515
over ocean, long waves effects on wind boundary layer 77—45005
Oviedo, Spain, global solar radiation and air temp. *(Spanish)* 80—36377
tropical Pacific, coupled air-sea model 79—16581
parameterisation of convective and nonconvective planetary boundary layers, for use in numerical models 80—82009
parameterisation of surface layer and active soil layer *(Russian)* 78—44924
parameterization technique 79—29830

atmospheric boundary layer continued
parameters of boundary layer determined solely from vel. profile 80—81970
parametrisation, turbulence covariances 77—70758
particle cloud, dispersion in boundary layer, theory 80—61842
particle sources over Australia 79—20907
particulate deposition, eddy correl. meas. 78—3930
passive contaminant vertical dispersion in surfac layer 79—62547
penetrative convection at top of growing boundary layer 80—12521
planetary, equations soln. using sensitivity analysis 77—54957
planetary, similarity theory appl. to Lagrange diffusion characteristics 77—56667
planetary boundary layer, above ocean, stratification parameter 80—82037
planetary boundary layer barotropic model, geostrophic balance 78—7738
planetary boundary layer processes, incorporation into numerical forecasting models 80—17312
planetary boundary layer similarity profile by turbulence closure model 80—72574
planetary waves, feedback with stochastically driven ice sheet, model 80—77025
plume dispersion from ground level sources, simulation 79—12231
plume dispersion near large buildings, simulation in wind tunnel, flow field 77—70724
plume dispersion near large buildings, simulation in wind tunnel, concentration field 77—70725
plume nonturbulent dispersion in complex terrain 77—45054
plume spread in calm environment, for negative buoyancy case 80—55952
point heat source, natural convection in rotating environment 79—10445
pollutant dispersal from point source, Ekman-type model 80—105039
pollutant dispersion from elevated source 80—85312
pollutant dispersion in stratified layer, numerical simulations 79—12251
pollutant dispersion over highways, wind and temp. study of turbulence 80—12038
pollutant field from multiple sources *(Russian)* 78—69443
pollutant transport, stack and inversion height effects, model 80—16865
pollutant transport and turbulent dispersion over rugged mountainous terrain 79—84349
pollutants deposition velocities over water 79—8683
pollutants deposition vels., determ., limitations 78—44903
pollutants dispersion, model for continuous shoreline fumigation 79—100914
pollutants dispersion in flow over shoreline of large water body, model 79—100913
pollutants vertical dispersion in neutral surface layer, Markov Chain simulations 79—88399
polluted, radiation model 77—49168
polluted boundary layer, radiation model 77—49168
polluted urban planetary boundary layer, radiative transfer 78—7708
pollution dispersion from point source 80—81973
pollution dispersion from tall stack, into shore line environment 80—97832
prediction of atmospheric flows on nested grids 79—44240
pressure distribution variations in geostrophic wind 80—17348
pressure fluctuations, ground effects 78—61498
probe support, upwind turbulance study 80—12506
psychrometry, appl. of portable differential system 80—105072
pumping effects on synoptic-scale flow 77—5288
quantitative bistatic acoustic sounding 78—49176
quasigeostrophic flow, horizontal boundary conditions and stability 79—53446
quasigeostrophic stratified atm. stationary flow past obstacles 79—100928
radiation balance above forest and grassland 77—17196
radiation balance over salt marsh 78—61481
radiation balance over water surface 79—20889
radiative and actual nocturnal cooling rates over grass and snow 79—79947
radiative cooling rate and flux, theory 80—85711
radiative flux divergence effect on entrainment of saturated convective boundary layer 79—79979
radio refr. index struct. parameter height distrib. with lower boundary spatial transition 78—73491
radio refractive index structure in transitional boundary layer 78—57268
radio waves beyond horizon propag. in offshore ducting environments 77—41132
radio-acoustic sounder operating at metre radiowavelengths 80—46276
radiowave propagation, refr. index derivation for ultrashort waves 80—36380
rain, mixing with near-surface water 79—53371
rainfall interception by forests, analytical model, evaporation 79—79966
rainfall modification by topographical vars. 79—100888
Raman lidar humidity sounding 79—66809
random field fluctuations of near-water atm. layer and upper ocean layer, linear filtration errors 80—12425
rapid morning boundary-layer transition, case study from Haswell, Colorado, expt. 80—81996
refractive index in atmospheric boundary layer, structural charact. vertical profiles *(Russian)* 80—94597
remote forcing of Somali Current, cross-equatorial inertial jets model 79—88357
resistance law over wavy surface 77—91202
Rossby number similarity, turbulent diffusion 78—92896
roughness length and zero-plane displacement, wind and temp. profiles 78—24329
salt spray contamination of atm. temp. sensors over ocean 78—69489
scatter channel for ELOS optical communications system, scattering from marine aerosols 79—29862
sea breeze, numerical results, truncation errors 79—10447
sea breeze over gulf or lake, numerical model 77—49115
sea breeze processes, Alaskan Beaufort Sea Coast 80—41485
sea salt quantitative meas. over N.Atlantic 79—16624
sea surface layer temperature gradient, depend. on wind stress and total heat flux 77—60378
sea surface stress measurements 79—66701
sea-air CO_2 flux meas., eddy correl. method 78—32191
sea-air heat and moisture exchange, zonally averaged model *(Russian)* 77—17161
sea-air interface fluxes of sensible heat and moisture, parameterization 77—41041

atmospheric boundary layer continued
second-order closure modelling of diffusion 77—78300
sensible heat advection, local and regional components 79—20942
sensible heat flux time and height variability 77—78296
sensible heat flux time and height variability in surface layer 77—78296
separation effects in Ekman layer flow over ridges 79—79971
shallow lake heat balance, simple model, Lake Chad appl. 79—66716
shear flow instability, Kelvin-Helmholtz and reson. overreflection modes, vortex pairing interactions 80—90129
shoreline escarpment affecting boundary layer turbulence, wind profile etc. 80—109243
shortwave and longwave radiative flux, mid-ocean obs. 80—12547
similarity functions for H_2O vapour in unstable layer 79—25293
similarity parameters from first-order closure and data 78—92893
similarity theory *(Polish)* 77—25753
similarity theory for baroclinic planetary boundary layer *(Russian)* 78—11962
similarity theory for stratified boundary layers, use in Soviet work *(Russian)* 78—16174
similarity theory for turbulence and convection *(Polish)* 77—25753
small-scale wind vars. over water surface, computation model 78—61480
smoke plumes in surface layer, cross section diffusion *(Russian)* 80—104532
snow cover energy budget, energy flux meas. 78—92859
snow surface, model of planetary boundary layer 80—41477
snow surface and wind interaction 79—84356
SO_2 max. surface conc. from moderate-sized power plant rel. to power plant load 79—83659
sodar echoes at Miyakojima Is., AMTEX 77—21843
soil erosion, wind tunnel simulation, effects on fine dust production 79—20834
soil gas fluxes determination, chamber methods numerical evaluation 79—16700
soil-atmosphere boundary, heat and moisture transport 80—77023
solar eclipse affecting heat and radiation budget above pine forest *(German)* 80—46226
sounding system for meas. of wind speed and direction, and temp. *(German)* 80—94616
source disturbances simulating orographic effects, upstream boundary values *(German)* 78—65375
source height dependence of lateral and vertical dispersion characts. 79—70823
spatial temp. derivatives in surface layer 80—56514
spectral analysis of parameters over vegetated surface in sensible heat advection conditions 80—17343
spectral scale of wind fluctuations 78—20481
spectral struct. of radiation attenuation, statistical characts. *(Russian)* 78—24371
spray in surface layer, lab. and oceanic results 79—70844
stability, baroclinicity and scale-height ratio effects on drag laws 78—73429
stability, rel. to atmospheric variables spectra deduced from ground-based radiometry 79—92567
stably stratified, resonant parallel shear instability 77—2200
stably stratified planetary boundary layer, model study 79—34909
stationary mesoscale fields, method of calc. from remotely sensed data 80—85734
steady barotropic nocturnal layer, evolution and structure 80—56511
steady-state characts. of temp. inversions capping well-mixed layer 78—61483
steam fog in Fenlands, obs. after heavy rain, (1979 May 1) 80—98431
steppe meteorology, boundary layer universal profiles in rainy season *(German)* 79—84420
stratified, conc. profile, admixture-underlying surface interaction effect 80—31089
stratified, tensor diffusivity of inert trace constituent 77—56675
stratified, turbulent diffusion from stationary linear source 77—56668
stratified boundary layer, tensor diffusivity of inert trace constituent 77—56675
stratified flow over object upstream influence, theory 80—56527
stratified inlet, anal. of wind influence on surface layer 77—41051
stratified inlet, obs. of wind influence on surface layer 77—41050
stratified surface boundary layer, turbulent diffusion from stationary linear source 77—56668
stratified tensor diffusivity of inert trace constituent 77—56675
stratified water surface layers, unsteady energy transfer 77—41092
stratocumulus-capped planetary boundary layer, entrainment rate *(French)* 79—53489
streamwise turbulence vertical coherence inside and above model plant canopy 79—25297
structure and development over SE.England, aircraft and balloon meas. 80—12516
structure during light wind, water vapour IR absorpt. meas. 77—91197
structure evolution over oceanic and continental sites *(French)* 79—25294
structure of axisymm. vortex, lower boundary condition effect 79—25298
subcloud layer over land, temp. and humidity struct. 77—91200
subsurface energy storage influence on seasonal temp. vars. 77—49122
subtidal sea level fluctuations, rel. to atm. forcing, North Carolina coast 79—16498
sunrise effect on elec. pot. near ground, origin in upper atmos. 80—61866
surface air temperature over N.America, solar cycle signal 79—58042
surface and soil temperature anals. in humid tropics, case study from Sierra Leone 80—109242
surface based remote sensors, coding technique for boundary layer echoes 80—17400
surface boundary conditions arising from particulate plume dispersion 79—79944
surface contamination, air conc. and horizontal fluxes estimation 79—5599
surface flow above gentle topography, model 77—91199
surface flow over equatorial oceans, dynamics and climatology, 1911-70 period 79—58061
surface fluxes, scheme for computation from mean flow obs. 80—77031
surface fluxes and mean profiles of vel. temp. and conc. downwind of roughness change 78—20484
surface friction influence on neutrally stratified mean and shear air flows 77—70790
surface layer, air density correction to eddy flux meas. 79—66761

atmospheric boundary layer continued
surface layer, airflow over nonhomogeneous surfaces with discontinuities in roughness and temp., two dimens. model *(Italian)* 79—84454
surface layer, horizontal turbulent heat flux 79—66740
surface layer, organised motion features 80—72602
surface layer, small ion number density time fluctuations 78—7730
surface layer, spectra of temp. derivatives 79—66759
surface layer, visible and IR attenuation statistical characts. *(Russian)* 80—4104
surface layer as part of overlying convective layer 79—92576
surface layer flux parameters determ. in absence of temp. profile 79—66752
surface layer height *(Russian)* 77—73807
surface layer height diurnal var. 77—60446
surface layer over Poona, temp. field 79—48544
surface layer press. perturbs. due to ocean swell waves *(Russian)* 78—65362
surface layer profile-gradient function integral 78—16115
surface layer structure parameters, turbulence props. 80—51510
surface layer turbulence response to partial solar eclipse 79—70843
surface layer turbulent flows 79—39838
surface layer turbulent vel. components characts. under convective conditions 79—66754
surface ocean current response to wind, quadratic and linear laws 80—26529
surface roughness change effects, wind tunnel study 79—53416
surface roughness change effects 78—77306
surface temperature, determ. of diurnal var. in mountainous terrain 80—82011
surface wind rel. to topography 77—60440
surface wind speed over drifting pack ice, determ. using surface weather charts 80—41476
surface wind strength estimation methods 79—88392
synoptic scale flow, influence of boundary layer pumping 77—5288
synoptic scale processes effects on equatorial surface air layer meteorological variables 77—70689
temp. inversion determ. via ground-based long-range sounding in O_2 5 mm absorpt. band *(Russian)* 78—11963
temperature and humidity correl. above warm wet surface 78—85646
temperature fluctuation study 77—37293
temperature fluctuations, heat flux and struct. functions meas. with acoustic Doppler sodar 80—105023
temperature forecasting for nighttime, short-range model 80—109200
temperature inversion, characts. of stable nighttime layer 80—41533
temperature profile, microwave radiometer, for indirect determ. 79—25369
temperature profile determ., ground-based microwave radiometry *(German)* 80—82097
temperature profile from inferior mirage obs., simple soln. 79—80035
temperature ramps in surface layer 79—88434
temperature skewness budget in convective boundary layer, implications for turbulence modelling 80—21816
temperature structure coeff. detect. by acoustic radar 80—98386
temperature structure function parameter obs. over ocean 79—79918
temperature variance profile parameterisation in convective boundary layer *(French)* 80—56518
temperature vertical profile determ. by ground-based microwave radiometry 79—79915
temporal boundary layer and multitime scales of motion in rot. atm. *(Chinese)* 79—84447
terrestrial surface features effects, instrumented aircraft meas. 79—39808
tethersonde system for remote meas. of wind and temp. 79—80038
thermal eddy diffusivity modelling at canopy height 78—24330
thermal stability diurnal and seasonal var. at Poona, rel. to pollution 77—53130
thermal structure at Cardington from acoustic sounding 77—53153
thermally forced planetary waves 79—34910
thermally forced Rossby and gravity waves, frictional effects 77—78384
thermodynamic structure, trade-wind, theoretical formulation and sensitivity tests 79—88432
thermodynamic structure of trade-wind boundary layer, applications of model 79—88433
three-dimens. model rel. to expt. data 78—73428
topographic influence on surface wind 78—81266
topographic perturbations of zonal flow, rel. to multiple flow equilibria and blocking 80—56536
trace constituents transfer past air-sea interface 79—62544
trajectories changed by nocturnal jet *(German)* 79—66769
trajectories from balloon obs. 77—91307
transfer of mass and heat between ground and atmosphere *(French)* 79—84403
transport and diffusion in near wake regions of surface-mounted cubes 79—12183
trigger for squall line form. boundary layer forcing and temp. gradient, model 80—8396
tropical, circulation over Arabian Sea during summer monsoon, flow field anal. 79—44231
tropical air-sea interaction at large scale, numerical study 80—56549
tropical atmosphere, Taifun-75 data from equatorial Pacific area, typhoons 79—58052
tropical atmosphere, thermally driven motion, influence of stable stratification 77—2201
tropical boundary layer over ocean, turbulence closure model for BOMEX data 80—56583
tropical cyclone, model of ocean-atmos. boundary layer interaction 80—109231
tropical cyclones, features of boundary and surface layers 79—58053
tropical oceans, marine boundary layer 79—88460
tundra surface roughness vars. with season rel. to turbulent mixing and heat flux 77—87016
turbidity meas. on Hulunbeier grassland and dust transport study *(Chinese)* 79—84485
turbidity of Barcelona's air, anal. of 1971-7 obs. *(Spanish)* 80—36375
turbidity rel. to statistical characts. of radiation attenuation spectral struct. *(Russian)* 78—44997
turbulence, book contrib. 77—60459
turbulence, dynamic modelling *(Russian)* 77—13097
turbulence, effects on light beam, optical parameter determ. model *(Russian)* 80—12481
turbulence, inertial range bispectrum 79—92571
turbulence above pine forest 80—26569

atmospheric boundary layer continued
turbulence and vertical currents, feedbacks *(Russian)* 80—51457
turbulence and waves in planetary boundary layer, Doppler radar obs. 80—90184
turbulence and wind coherence meas. 77—91201
turbulence as function of height and stability 79—58074
turbulence characteristics 79—16628
turbulence characteristics *(French)* 79—66749
turbulence coeff. vertical profile 80—85733
turbulence evolution in nocturnal boundary layer 80—51462
turbulence in presence of cumulus cloud *(French)* 79—84412
turbulence in surface and planetary layers at unstable stratification *(Russian)* 79—34900
turbulence kinetic energy budget in convective conditions 79—79975
turbulence microstructure, meas. with hot and cold wires 80—24109
turbulence over land and water, simultaneous meas. 79—53421
turbulence spectra in stable conditions 77—73786
turbulence structure in temp. inversions and convective fields, Doppler sodar obs. 79—66762
turbulence structure over water in high wind 80—12502
turbulence under conditions of sensible heat advection 80—41516
turbulent advection, scalar spectrum model 79—32474
turbulent air-water mass transfer under varied stratification conditions 79—84389
turbulent and radiative transport interaction in development of fog and low-level stratus 78—81313
turbulent boundary layer, finite-element numerical modelling 80—77061
turbulent diffusion, Lagrangian scheme, algorithm and applications *(French)* 79—84401
turbulent diffusion of pollutants 77—41113
turbulent energy dissipation rate in unstably stratified boundary layer *(Russian)* 77—64372
turbulent flow over very rough random surface 79—53422
turbulent fluxes, H_2O vapour fluctuations influence 79—79916
turbulent heat and moisture fluxes, field study, S.England 78—20477
turbulent kinetic energy downward transport over plant canopies 79—25301
turbulent layer development above sea during generation of surface waves *(Russian)* 79—16476
turbulent mass transfer, plume dispersion *(French)* 80—61850
turbulent mixing, rel. to use of passive antenna system as cond. meas. device 80—85762
turbulent moment calculations for application to air pollution transport 79—84354
turbulent penetrative-convection planforms, laboratory obs. 79—48550
turbulent recirculating flow over rectangular depression, meas. and predictions 79—66751
turbulent stratified flow, vel. profile *(Russian)* 79—10601
turbulent transport, buoyancy effect 78—32192
turbulent transport 77—17131
two-layer model of Ekman 80—36387
typhoon Tess wake vertical struct. in upper layer of Pacific Ocean 80—26538
unstable, turbulence energy modulation by longit. rolls 77—2202
unstable surface layer, geometric similarity for temp. field 77—33127
unstable surface layer over land, flux and turbulence meas. 77—66962
unstably stratified, turbulent energy disspation rate *(Russian)* 77—64372
upper air meteorological data rel. to regional evapotranspiration determ. 77—91171
Uppsala urban meteorology project 79—53419
urban atmosphere, numerical simulation of mixing depths 80—105024
urban atmosphere, radiative effects of elevated pollutant layers on temp. struct. and pollutant dispersion 80—97841
urban environment, cold air drainage effects on temp. fields, case study of topographical influence on climate 80—94555
urban environment, meteorological obs. 79—25312
urban heat island, Rome, obs. during summer season 80—85717
urban heat island, St. Louis, theoretical study, parameter vars. 79—79943
urban layer, numerical simulation of air flow over flat terrain 79—48554
urban microclimate of Alma-Ata, significant factors 80—101418
urban valley micrometeorology of N.Saskatchwan river valley 80—61843
urban-rural canopy analysis, surface heat flux/temp. model 79—20945
urban-scale wind fields, three-dimensional, construction, objective anal. technique 80—101407
vegetation canopy influencing turbulent heat and mass transfer, theory 80—26570
vegetation interaction, simplified one-dimens. theory 78—61479
vegetation-atmosphere interaction, one-dimens. model 77—37291
velocity struct. functions and energy dissipation rates, acoustic Doppler meas. 77—66966
vertical circulation during anomalous periods of sea surface temp. over equatorial Pacific Ocean 80—12528
vertical currents induced by orography and turbulence 78—96278
vertical diffusion from sources near ground 79—62548
vertical eddy flux representation for weather forecast model 80—61844
vertical frictional motions on varying scales *(Russian)* 80—105027
vertical Gill anemometer meas. 80—56618
vertical heat flux in convective boundary layer 78—20487
vertical motion in stratified ground layer under coniferous forest canopy *(Russian)* 78—96266
vertical stability, meas. method using ^{222}Rn release *(French)* 80—56617
vertical struct. of refr. index for ultrashort radio waves at subfreezing temps. 78—16128
vertical velocity calc. at upper boundary of unsteady planetary boundary layer *(Russian)* 79—100900
vertical velocity fluctuations, meas. using sailplane variometer 79—88480
vertical velocity of air, temperature *(French)* 79—88447
viscous oscill. rot. flow 77—3804
visibility rel. to surface wind at Gutersloh, Germany, smoke pollution effects 79—29853
vortex flow, turbulent modelling, predictor-corrector multiple iteration 77—91237
water aerosol, evaporation during transport through atmosphere *(Russian)* 79—88408
waterspout in association with large cumulus congestus 80—41473
weather conditions for long gliding flights over England 79—58048
weather forecasting numerical model, parameterisation of boundary layer 80—72572
wind, fast gusts occurrence freq. inside corn canopy 79—100917

atmospheric boundary layer continued
wind and isotropic turbulence lateral coherence 80—72575
wind and temp. profile prediction model, for diabatic layer 80—77032
wind direction fluctuation statistics and lateral dispersion 80—56577
wind direction fluctuations characts. in surface layer 79—79913
wind dispersion ellipticity over ocean surface, N. Atlantic example 78—61528
wind drag coefficients for marine regime, shipboard evaluations 79—5494
wind energy transfer to near-inertial ocean waves, calc. 80—4017
wind erosion threshold velocities, tests with portable wind tunnel 79—70826
wind field temporal and spatial scales over N.Pacific and N.Atlantic Oceans 79—79942
wind flow over water, determ. from phase speeds of upwind and downwind travelling short gravity waves 80—98332
wind in planetary boundary layer, 3-D field obs. width radar 80—90183
wind in rough time terrain, derivation of mass-consistent flow field from wind obs. 80—105013
wind interaction with dry snow and bare ice surface 80—109181
wind meas. in clear air by microwave radar 77—13136
wind obs. and anal. over nonuniform terrain 77—17195
wind over surface obstructions, numerical soln. 77—33173
wind over very rough surface, momentum transfer 80—51511
wind profile, semi-empirical model of evolution *(French)* 79—84399
wind profile curvature of surface layer, rel. to Richardson number 80—81974
wind profile meas. using acoustic Doppler sounder 78—65413
wind profile power-law exponent var. as function of surface roughness and stability 79—88387
wind resistance above hilly terrain, universal functions in resist. law 77—25732
wind shear hazard in boundary layer, radar detection feasibility 80—90256
wind shear measurement, using pulsed Doppler laser 80—67415
wind shears and inversions *(German)* 78—81336
wind speed and direction prediction, statistical analysis of ground wind vector 80—17347
wind speed and temp. profiles over melting glacier, log-linear model fitting 79—79912
wind speed and water content, microwave remote sensing from Earth orbit 80—41573
wind speed anomaly in surface layer in Po Valley 80—17313
wind speed frequency distrib. near surface 79—79946
wind structure near city centre 79—66758
wind surface stress estimation, mathematics of vel. scaling parameter 80—61849
wind turbines spacing in arrays rel. to boundary layer struct. 77—73797
wind velocity gust factors, analytical expression and wind tunnel simulation 80—31107
wind vertical profile fine structure over sea in near-shore zone 77—60445
wind vertical velocity, acoustic Doppler power spectra comparison with direct meas. 79—57999
windmill array effects 80—3485
winds, topographic influence on freq. distrib. method 80—17346
C global cycle, kinetic models stability anal. *(German)* 79—53414
CO, dispersion at ground level rel. to nocturnal inversion 79—92563
CO_2 flux meas., eddy correl. method 79—25303
CO_2, meas., fast response sensor design, for eddy correl. flux meas. 79—5622
H_2 composition of marine air of N.Atlantic 80—77057
H_2 conc. in near-surface air and dissolved in seawater, tropical N.Atlantic 79—39729
^{85}Kr, latitudinal distrib. in atm. surface layer over ocean *(Russian)* 79—39813
N_2O, conc. diurnal variability in surface air 79—84369
N_2O cycle, sources and sinks 79—70871
O_3 and other gases diurnal conc. cycle and destruction at ground 79—79972
O_3 nocturnal maxima, vertical mixing of remnant daytime boundary layer 79—5547
O_3, stratospheric determ. at ground level using $^7Be/O_3$ ratios 79—58011
O_3 surface conc. affected by sea breeze, Wallops Island, Viginia 80—51473
O_3 variations in Auckland, comparison between city and urban regions 80—17350
O_3 vertical distrib. 77—49102
OH conc. meas. by monitoring CO oxidation 79—58012
^{222}Rn, ^{210}Pb, ^{7}Be and fission products conc. in South Pole atm. 79—84382
^{222}Rn, and decay products, vertical distrib., time-dependent calc. 79—84383
^{222}Rn conc. over intertropical convergence zone of Atlantic 80—26648
S compounds, reduced, emission from open oceans 79—70805
S compounds conc. in remote continental and oceanic areas 79—20983
S, estimated dry deposition vels. over E United States and surrounding regions 80—56507
SO_2 at ground level, air pollutant dispersal, Forth Valley, Scotland 80—81497
SO_2, dry deposition, field meas. with stirred chamber 79—88021

atmospheric chemistry
see also atmospheric composition
acid precipitation in W. United States, pH value obs. 80—89695
acidity of NW.Africa snowfields, 1977-79 obs. 80—98370
aeronomical models, diurnal averaging 78—49186
aerosol off W.African coast, Na, Cl and Br composition evolution 80—77053
aerosol particle formation in presence of existing aerosol 80—81962
aerosol particles, physical-chemical transformation processes, thermal-optical anal. *(Russian)* 80—12482
aerosols direct formation by reaction of NH_3 and SO_2 77—29377
air pollution removal mechanisms and processes *(Dutch)* 77—70824
ancient atmosphere, fate of OH and O_2 origin 80—77116
anthracene, photooxidation on atmospheric particulate matter 80—61487
artificial radionuclides, chemistries rel. to depositional history in Ross Ice Shelf, Antarctica 79—88027
N Atlantic marine aerosol, chemical relationships 77—53136
atmospheric rate chemistry calculations, algorithmic approach 77—13095
aurora, $N(^2D)$ emission and ion chemistry, satellite obs. 80—72673
aurora, type-B, obs. and interpretation of spectra and rapid time vars. 79 40001

atmospheric chemistry continued
AURORA machine studies of air chem., cond. and boundary layer 78−32144
auroral O, O_2 and N_2 emissions, rocket meas. rel. to chemistry and energy transfer 78−57380
auroral $O(^1S)$ production sources determ. from rocket and satellite meas. 80−26662
auroral substorms, morphology of N and NO 79−48607
ball lightning, chem. mechanism model 78−28287
chemical-diffusive model for troposphere and stratosphere 77−21873
chemiluminescent reaction, of ozone and olefins, in stratospheric ozonometer *(French)* 79−48574
chlorinated hydrocarbons in ambient air, washout effect and diurnal var. 78−28305
chlorofluorocarbons, photodecomposition under simulated tropospheric conditions *(German)* 79−53408
chlorofluorocarbons, stratospheric photodissoc., residence times 78−53703
chlorofluorocarbons and ozone depletion in the lower atmosphere 79−53498
chlorofluoromethane effects on stratospheric O_3 *(German)* 79−20959
chlorofluoromethane negative ion products, in 0-10 eV near-monoenergetic electron impact 79−41245
chlorofluoromethane photolysis in stratosphere, effect on O_3 conc. 80−109197
chlorofluoromethanes, $CHFCl_2$ and CHF_2Cl, diffusion and chem. reaction 77−70804
chloroflurometháne + $O(^1D)$, stratospheric chem. reactions 79−53499
clean air chemistry at 55°N, compared with polluted air reactions 80−98382
composition perturbations and temp. feedback, climatic effects 80−41525
conference, Konstanz, Germany (May 1978) 79−53403
conservation of species equation with chemical terms, soln., numerical methods 78−36265
coupling between neutral and ionized atmosphere, NATO conf. proceedings (Spatind, Norway, 1977 April 12-22) 80−27036
cyclohexane-NO_2-air mixtures, photochem. particulate form. 78−11529
D- and E-region, metallic species, chemistry, problems 79−35035
D-region, charged species relax. to photochem. equilib. within displaced air parcels 79−75030
D-region, Cl^- formation and destruction 78−12049
D-region, ion composition models, unified reaction scheme 79−5704
D-region, NO^+ cluster ion formation, temp. control 80−61931
D-region, positive ion chemical scheme for electron density profile 79−40007
D-region, recent advances 79−8751
D-region, water cluster ions formation rel. to mesospheric temp. 77−21842
D-region cluster ion formation, implications of laboratory determs. of NO^+ reaction rates 77−53308
D-region ion chemistry, rel. to winter anomaly in ionospheric absorpt. 78−20577
D-region ion chemistry during intense radiowave heating 80−61952
D-region $NO_2{}^-$ ion chemistry 77−75236
data uncertainty rel. to environmental decisions 80−104535
daylight or diurnally averaged photolytic rate coeffs. 79−53458
dichlorodifluoromethane, rate const. for reaction with OH and tropospheric lifetime 77−64366
dichlorodifluoromethane, total ionis. and electron attachment cross sections by electron impact 79−59586
dichlorodifluoromethane, UV photodissoc. cross-section, 223 and 296K 79−52729
diethylhydroxylamine 79−52982
dimethyl sulphide, biologically prod., contrib. to global S cycle 77−70786
dimethyl sulphide+$O(^3P)$, fast flow reson. fluoresc. obs. of absolute rate consts. 80−61077
dimethyl-N-nitrosamine in urban air, concs. and chemistry 78−81378
dispersion of chemically reacting plume 79−34453
dispersion with chemical reaction 78−16085
diurnal variations of O_3 and other pollutants in urban area 79−74568
E-region, NO var. with solar activity 78−49207
earthquake lights, proposed for study by chemiluminesc. NO air pollution apparatus 80−61906
electron loss mechanism, D-region, normal and anomalous winter absorption 79−88537
ethylperoxy radical+NO_2, reaction rate const. meas. 80−21262
F_1-layer, mid-latitude, mean diurnal var. of O^+, NO^+, $O_2{}^+$ and $N_2{}^+$ ions 79−96856
F_2-layer, chem. depletion of O^+ by H_2O and CO_2 injection 80−12610
F-region, Atmosphere Explorer photochemistry rel. to airglow obs. 80−98496
F-region, $N(^2D)$ chemistry from airglow and atm. comp. meas. 78−16241
F-region, polar cap and auroral zone, math. model 78−65458
F-region, winter anomaly causes 80−85793
fires, O_2 conc. profile from convection-diffusion, coupling model 77−7481
fluorocarbon mixing and photolysis, eddy diffusion, tropospheric lifetime 79−62551
fluorocarbon-O_3 theory, one-dimens. modelling of atm. 79−70831
fluorocarbon-ozone theory, atm. modelling, diurnal steady state calc. 79−88390
fluorocarbons, lifetime determ. methods 79−20920
formaldehyde, chem. of stratosphere, UV absorpt. spectra implications 80−109209
formaldehyde, in troposphere and stratosphere, meas. by high resolution IR absorpt. spectroscopy 79−84371
formaldehyde, photodecomposition in tropospheric clean air *(German)* 79−53405
formaldehyde+Br, reactions, rate consts. by EPR 80−93736
formaldehyde+ClO radical, expt. showing no reactivity, stratospheric implications 80−90119
formaldehyde+F reactions, rate consts. by EPR 80−93736
formaldehyde in air, photodecomposition, CO and H_2 quantum yields 79−66311
Fourier transform IR spectroscopy, use in atm. chem. 80−55743
free radical recombination reaction kinetics 79−53410
freons, tropospheric photodissoc. rates from solar 1950-2150 Å radiation ground level meas. 79−2345

atmospheric chemistry continued
gaeous and particulate pollutants transport, interconversion and removal, model, urban plume appl. 78−44984
gas dynamics with relaxation effects, acoustic waves, nonequilibrium atmosphere effects, review 78−79390
gas sources, biomass burning 80−26586
haloalkyl peroxynitrate, form., FTIR obs., rel. to stratospheric chem. 79−34283
halocarbon and N_2O destruction by siliceous land surfaces 79−12168
halocarbon lifetimes and conc. distrib. using two-dimens. tropospheric model 79−12180
halocarbons, decomp. by natural tropospheric ions 77−21889
halocarbons, hydrocarbons and SF_6, global distrib., sources and sinks, rel. to 0_3 depletion 80−4088
halocarbons, SF_6 and N_2O concs., rel. to tropospheric OH conc. 77−45069
halomethanes, electron impact dissoc., tropospheric lifetimes *(German)* 79−50141
heterogeneous reactions, role of H_2SO_4 aerosols as tropospheric sinks 80−72612
Hubbard Brook Experimental Forest, H ion input and precipitation pH 77−37337
human influence 79−12206
hydrocarbon+N oxide mixtures in air, photochemistry 79−53427
ion+molecule, rate consts., in situ ion comp. meas. 80−31154
ion and neutral chemistry, implications for radio communication and environmental hazards 77−17267
ion composition and ionisation rates 80−61885
ionosphere, atomic ions reaction to rapid changes in large-scale elec. fields 77−91350
ionosphere, calc. and obs. structure, AE-C satellite and incoherent scatter radar obs. 78−49203
ionosphere, chemistry and transport processes, numerical modelling 78−49202
ionosphere, D and F region ionisation rel. to mesosphere NO concs. 79−8651
ionosphere, equatorial, modelling of H_2 gas release effects 79−16741
ionosphere, heating by solar radiation in Schumann-Runge continuum and by chem. reactions 79−62653
ionosphere, lower, ion prod., density and comp. during auroral absorpt. event 80−36443
ionosphere, lower, NO height distribution from rocket ion comp. results 80−26674
ionosphere, lower, photodetachment as source of reflecting layer below classical D-region 80−98508
ionosphere, midlatitude, dynamical model for 100-1000 km altitude range 78−53768
ionosphere holes and spread-F, ion chemistry and transport 78−88982
ionosphere O_2 electron impact vibr. excitation, direct and stepwise, rate coeffs. 80−5630
ionospheric F_1-layer, implications of dynamical effect for dissoc. recomb. rate 79−12340
IR-absorbing molecules, collisional cross-sections, temp. depend. 79−96787
kinetic photochemistry downwind over water from urban areas 78−28278
kinetics, laboratory studies 79−53409
laser spectroscopy relevant to stratospheric photochemistry 78−88951
Livermore Regional Air Quality model, appl. in San Francisco Bay area 78−92966
Livermore Regional Air Quality model, concept and development 78−92965
lunar regolith particles in Earth's atmosphere, variation in chemical composition in surface layers *(Ukrainian)* 80−12685
marine atmosphere diurnal kinetic photochemistry 79−48549
marine fogs, characts. of air mass histories, Nova Scotia, 1975 August 79−70847
mesopause, $[NO^+.H_2O]/[NO^+]$ ratio rel. to temp. 79−96849
mesopause at high latitude, positive ion composition and chemistry 80−46224
mesopause region, ion-clustering during winter anomaly, temp. and NO density vars. effect 79−21087
mesopause water cluster ions, rocket borne expt. 80−17429
mesosphere, cluster ion chemistry for Na and Na^+ layers 79−74934
mesosphere, diurnal and seasonal variations of O, H and N components 77−9586
mesosphere, ion bunching model 78−73424
mesosphere, Na atoms distrib. and Na I 5893 Å nightglow obs. 78−88961
mesosphere diffusion-photochemical model, turbulent diffusion coeff. seasonal vars. 79−53424
mesosphere $O_2{}^+$ chemistry rel. to O conc. inference from positive ion comp. data 80−8405
meteor wakes, ion-molecule reactions rel. to red afterglow 78−36536
methane, atmospheric circulation, destruction through photochemical oxidation *(German)* 79−84424
methane+$O_2{}^+$, reaction rate const. kinetic energy depend., 300K, 0.125-0.450 torr 78−76850
methane+$O^+{}_4(O_2{}^+)$, products, rate consts., rel. to stratosphere 77−9040
methanol (dimethyl ether)+Cl, absolute rate consts., 200-500K, stratospheric chem. appl. 79−66271
methylchloroform, vapour phase, UV absorpt. spectrum, photodissoc., stratospheric appls. 79−81208
methylhydroperoxide, UV absorpt. spectra of vap. 80−69159
middle atmosphere, chemical response to changes in UV solar flux 77−33167
middle atmosphere, effects of energetic particle precip. on O_3 catalytic removal 80−109213
middle atmosphere, minor constituents, chemistry and transport, conf., Seattle, USA (Aug. 1977) 79−84428
middle atmosphere processes revealed by satellite observations 80−21803
molecular photodissociation rates calc. including mol. scatt. and refl. 79−53512
monomethylamine, dilute mixtures, decomposition, shock tube studies, IR emission obs. 79−96301
multiple scattering effect on photodissociation 78−85692
natural cycle of gases *(German)* 79−53404
negative ion photodissoc. and photodetachment 80−69199
negative ions, photodissoc. and photodetachment 78−66609
nightglow, 557.7 nm line and Herzberg bands excitation 79−75008

atmospheric chemistry continued
nitrate conc. in aerosols, SO_2 photochem. effects 77−49103
nonmethane hydrocarbons, photochemical effects 78−49090
organic aerosols, natural, of terrestrial origin, photochemical form. 80−36381
oxidant and precursors, anal. in Los Angeles Reactive Pollutant Program (LARPP) (operation 33) 80−61479
ozonosphere, chemical-kinetic criteria of effect of substances of natural and anthropogenic origin *(Russian)* 78−53699
ozonosphere, chlorofluoromethane induced O_3 depletion 80−51477
ozonosphere, photochemical-dynamical model rel. to maintenance of zonal mean O_3 distrib. in N.Hemisphere 80−109220
ozonosphere, radiative-photochemical model for temp. coupling effects on O_3 depletion 78−57246
ozonosphere reactions affected by CO_2 stratosphere cooling 80−36369
particulate matter emitted by Mount Etna volcano, heavy metal chem. 78−61491
peroxynitrates, UV absorpt., spectra, photodissoc. lifetime meas. 80−83386
peroxynitric acid form. in photochem. smog in urban atm. 77−63885
perturbed atmosphere, photochemical radiative convective model for thermal struct. and relaxation rates 80−8408
photoabsorption and photionisation, UV region meas. 78−42087
photochemical aerosol formation, primary pollutants effects *(Japanese)* 78−57305
photochemical air pollution, initiation by HONO (nitrous acid) in urban air 80−76677
photochemical air pollution in NE.United States 79−83677
photochemical air pollution potential form. in United Kingdom, numerical estimation method. form. in United Kingdom 80−76682
photochemical and condensational var. of submicron aerosol particles *(Russian)* 78−40611
photochemical and kinetic data 80−4096
photochemical data and kinetics of gas phase chemical reaction in atmosphere 80−101671
photochemical O_3 formation in Sydney airshed 79−62553
photochemical oxidants occurrence at high latits. 79−74567
photochemical pollutants day of weak vars. in St. Louis, USA 79−20988
photochemical pollutants from N oxides 78−36271
photochemical pollution during summer 1976 in Greater London 79−16648
photochemical reactivities of gaseous hydrocarbon mixtures 78−61533
photochemical smog, fresh emissions, admixing effects 79−12237
photochemical smog, transferred contaminant air pollution model *(Japanese)* 78−32217
photochemical smog formation, solar spectral distrib. effects 79−52983
photochemical tropospheric O_3 transport, effect on pollution at rural site 80−61481
photochemistry, stratosphere and mesosphere O_2 and O_3 photodissoc. through solar UV radiation absorpt. 80−109248
photochemistry and dynamics of the ozone layer 79−5590
photodissociation rate affected by Rayleigh scatt. 80−61921
photolysis, flash, in time and frequency domains, chemical behaviour obs. 79−39874
photolytic reactions and tropospheric UV flux calcs. 80−12465
photooxidation reactions, rates, reactivity and mechanism for organic compounds reaction with OH radicals 80−72104
photosmog inhibitors, O atom reaction rate constants 79−12185
photostationary state assumption in NO, NO_2, O_3 system 79−88391
plume chemistry studies at Alberta power plant 79−74565
pollutants chemistry, chloro-hydrocarbons interactions laboratory simulation *(French)* 80−7976
pollution, photochemical numerical model 80−40943
pollution long range transport rel. to acid rain, chem. aspects 78−81391
positive ions, photodissoc., 5300 to 6700 Å, mass spectroscopic obs. 78−16095
positive ions, photodissociation, 3500-8600 Å 79−24763
prebiotic model atmospheres, far UV irradiation effects 78−40668
precipitation chemistry determ., calibration of collection procedures 77−37447
rainwater chemistry and multiple H ion donor systems, obs. in Minnesota 77−37335
reaction rates and photochemical data 78−77312
reactions, IR Fourier transform spectroscopic obs. 79−66785
reactive N in unpolluted troposphere, stratospheric source 80−94561
recent advances, review 79−12204
redox regulation of atmospheric O and its consequences 78−16122
review 78−81317
second-order reactions, in turbulent fluid, model, appl. to atm. plumes 79−20350
second-order reactions, in turbulent fluid, model, formulation and validation 79−20349
space shuttle reentry, unsteady nonequilib. chemically reactive flow, parallel computation 78−47065
spontaneous radiation of ‘fresh air’ *(Russian)* 77−87035
stratosphere, at. Cl and ClO radical in situ obs., rel. to O_3 depletion 78−36241
stratosphere, atomic and diatomic radicals, meas. 80−17307
stratosphere, atomic processes, O_3 formation and destruction, book contrib. 77−37339
stratosphere, chem. of meteor trail metal ions 80−72580
stratosphere, chemistry of ozone depletion 77−91256
stratosphere, Cl-ClO-Cl cycle, possible roles of ClO*, $ClNO_3$ and HOCl 77−17185
stratosphere, ClO remote meas. from IT solar spectrum obs. 79−58005
stratosphere, $ClONO_2+O(^3P)$, rate consts. 77−77796
stratosphere, CO_2-O_3 coupling in Cl free atm., photochemical-radiative column model 80−85723
stratosphere, concise chem. model 78−85634
stratosphere, effect of increased N fixation 78−28288
stratosphere, effects on chemistry of ethane and acetylene from vertical profiles 80−4073
stratosphere, fluorocarbon hazard to O_3 layer, assessment 79−79963
stratosphere, gas composition, comparison of one-, two- and three-dimens. models 79−70870
stratosphere, highly excited metastable O_3 rel. to photochemistry and heat balance 79−44225
stratosphere, HO_2NO_2 chemistry and abundance 78−20467
stratosphere, intense ionisation events, effects on NO_2, O_3 and climate, rel. to life extinction 78−96273

atmospheric chemistry continued
stratosphere, interaction of Cl and Cl_2 with H_2SO_4 and water, surface reactions at low temps. 79−79288
stratosphere, laser photochemistry of O_3 and distant spectroscopy *(Russian)* 78−28314
stratosphere, minor constituent chemistry, volcanic eruption effects 79−84437
stratosphere, model, Monte Carlo anal. of imprecisions due to reaction rates 78−85635
stratosphere, model, temp. feedback effect on O_3 conc. 78−28277
stratosphere, multiple solns. 79−58008
stratosphere, N_x^+, O_x^+ and NO^+ reactions with various mols., reaction rate coeffs. and product distribs. 78−81305
stratosphere, NO and ClO at twilight rel. to interpretation of conc. meas. via solar occultation 80−85756
stratosphere, NO photolysis rel. to NO_y mixing ratios 77−29399
stratosphere, $NOHSO_4$ and $NOHS_2O_7$ identification in aerosols, rel. to N oxides pollutants removal 79−39795
stratosphere, O_3 destruction by fluorocarbons 77−9459
stratosphere, O_3 diurnal var. and scattering rel. to Cl concs. 78−7710
stratosphere, O_3 heterogeneous decomposition, lab. study 79−70850
stratosphere, O_3 natural depletion mechanism, radiation belt energetic electron precip. 77−41134
stratosphere, O_3 reduction by NO_x injection, effects of water vapour changes 78−73444
stratosphere, O_3 response to nuclear bomb tests 77−81966
stratosphere, photochemical model, input sensitivity study 79−84434
stratosphere, photochemistry, orbital simulator using superpress. balloon 79−29966
stratosphere, photochemistry interpretations 79−74943
stratosphere, positive ion chemistry of formaldehyde and methanol 78−57251
stratosphere, SO_2, oxidation role for HSO_3 layer, reaction rate consts. 78−32202
stratosphere, trace species vars. during solar eclipse, theoretical study 79−58013
stratosphere, volcanic plume contributing sulphur and halogen to atmos. 80−51474
stratosphere aerosol, modification by supersonic transport and space shuttle operations, climatic implications 80−98408
stratosphere and mesosphere, transport and chemical processes 77−25761
stratosphere F chemistry, comparison between theory and meas. 79−16568
stratosphere natural structure rel. to chlorofluoromethanes effect on O_3 layer 79−84436
stratosphere O_3-CO_2 coupling, photochemical radiative column model with Cl chemistry 80−85724
stratosphere photochemical-radiative damping and instability, numerical results 78−81286
stratosphere photochemistry model, O_3 calcs. uncertainty 79−16567
stratosphere S budget, CS_2 and COS oxidation effects 79−84423
stratosphere sulphate aerosol layer, physical and chemical processes models and simulation 80−109212
stratospheric photochemistry, computer simulation 79−21481
stratospheric photochemistry and kinetics, modelling 79−53495
sulphate aerosols, form. rel. to diurnal var. at rural sites in E.United States 80−30621
tetrachloromethane, UV photodissoc., mechanism and quantum yield 79−52723
thermosphere, chemistry rel. to polar airglow mag. ordering 78−57378
thermosphere, disturbed, N_2 anharmonic mols. vibr. relaxation rel. to NO conc. 79−12322
thermosphere, diurnal and seasonal variations of O, H and N components 77−9586
thermosphere, gravity wave activity effects on photochem. and comp. 80−41583
thermosphere, ion photochemistry from Atmosphere Explorer C meas. 78−32261
thermosphere, ionic reactions rate coeffs., AE satellite meas. 79−48594
thermosphere, lower, diffusion-photochemical model, turbulent diffusion coeff. seasonal vars. 79−53424
thermosphere, lower, NO^+ daytime chemistry rel. to ionisation rate 77−33230
thermosphere, lower, one-dimensional diffusion-photochemical model for O and O_2 distrib. simulation 80−4159
thermosphere and ionosphere, chemical processes 80−17431
thermosphere and mesosphere, average daily closed model 77−17264
thermosphere satellites, gas-surface reactions impact on N mass spectrometric meas. 79−66849
trace gas transport and photochemistry rel. to greenhouse effect *(Russian)* 80−81989
trichloroethane$+OH\rightarrow H_2O+CH_2CCl_3$, rate const. and tropospheric chem. 80−16658
trichlorofluoromethane, rate const. for reaction with OH and tropospheric lifetime 77−64366
trichlorofluoromethane, UV photodissoc. cross-section, 223 and 296K 79−52729
trichlorofluoromethane reaction rate with atmospheric-like ions 77−70723
trihalonitromethanes, mol. dissoc. lifetime in atmosphere 79−22720
trihalonitrosomethanes, mol. dissoc. lifetime in atmosphere 79−22720
troposphere, effects on chemistry of ethane and acetylene from vertical profiles 80−4073
troposphere, evidence for significant in situ photochemical O_3 source 80−72619
troposphere, halocarbon decomp. by natural ionisation 77−33139
troposphere, methane variations, transport and photochemistry 77−53138
troposphere, negative ions evolution times 79−70829
troposphere, NO_2 vertical column abundance, optical absorpt. meas. 78−85632
troposphere, NO_x concentrations, predicted CO-OH-CH_4 perturb., sensitivity 79−58043
troposphere, NO emission effects on O_3 and OH 77−86992
troposphere, nonurban, conf., Hollywood, Florida (Nov. 1976) 78−32174
troposphere, nonurban, oxidation of NH_3, H_2S and methane 78−32183
troposphere, O_3 budget, one-dimens. photochem. model 78−32180
troposphere, O_3 distrib. and origin 78−85663
troposphere, O_3 form. and long-range transport 78−61514
troposphere, O_3 photochemical prod. and influence on climate 80−36365
troposphere, O_3 photochemistry 77−81968

atmospheric chemistry continued
- troposphere, O_3 transport and photochemistry 77—53137
- troposphere, photochemical mechanisms, computational methods 78—49084
- troposphere, SO_4^{2-} aerosols chem. props. 78—96254
- troposphere, solar UV flux meas., $O(^1D)$ photoprod. rate determ. 79—12197
- troposphere, trace gases and free radicals, two-dimens. model 78—32214
- troposphere, urban photochemistry, computer simulation 78—49085
- troposphere chemistry, implications of NO meas. in equatorial Pacific region 79—100893
- lower troposphere modelling, chemical kinetic data needs, conference, Reston, Virginia (1978 May 15 to 17) 80—62383
- upper atmosphere, effect of chemical reactions on neutral gas diffusion model 79—66846
- upper atmosphere, exothermic ion-molecule reactions, review 78—33563
- upper atmosphere, ion and neutral densities rel. to $N_2^+ + O$ reaction rate coeff. 77—53288
- upper atmosphere, odd N prod. by meteoroids 79—2404
- upper atmosphere at nighttime, 400-450 km altitude, anal. of Ogo 6 data 80—90267
- upper atmosphere H chemistry, role of H-implanted interplanetary dust grains 78—65445
- urban kinetic chemical calculations with altered source conditions 79—16560
- urban photochemical product concs., effects of entrained species 79—92566
- urban photochemistry, O group anal. and O_3 prod., theory 78—48626
- urban troposphere, photochemistry, kinetic study 77—45058
- urban-suburban air pollutant transport, chemical and physical transformations 77—37399
- Van der Waals molecules comp. of lower atmos. 80—85699
- water vapour photolysis in primitive prebiological atmosphere 78—73514
- Al hydration, in vap. phase, rel. to upper atmosphere chemiluminesc. 79—29362
- Br chemistry of stratosphere, and O_3 depletion 80—98391
- $BrONO_2$, stratospheric photolysis, UV and IR spectra 78—53227
- C global cycle, kinetic models stability anal. *(German)* 79—53414
- $CCl_2FO_2 + NO(NO_2)$, reaction, photolysis obs. 79—74931
- $CCl_2FO_2NO_2$, thermal dissoc., rel. to photodissoc. and stratospheric Cl budget 79—74931
- $CCl_3O_2NO_2$, thermal decomposition, form. and lifetime in stratosphere 79—57256
- CH^+, form. in upper atmosphere following trimethylaluminium high altitude release 79—48591
- $CH_3O_2 + NO$, rate const., flash photolysis and kinetic spectroscopy 79—70305
- CO, air quality criteria using a COHb model 80—16864
- CO, anthropogenic emissions, implications for atm. $CO\text{-}OH\text{-}CH_4$ cycle 77—49160
- CO production by lightning 79—70836
- CO production in electric discharge 79—96786
- CO, tropospheric latitude distrib., model involving production and transport 80—41483
- CO_2 in lower thermosphere, chemistry rel. to concs. 78—96336
- CO_2 increase effects on stratospheric O_3, photochem. and radiative transfer model 78—65370
- $CO_2\text{-}HCO_3^-\text{-}CO_3^{2-}$ system through geologic time 78—73515
- $C0_2$ solution in ocean surface waters, role of homogeneous buffer factor 80—21783
- Cl effects on O_3 layer, zonally averaged two-dimens. model 79—84435
- $Cl + C_2H_2$, reaction kinetics, stratospheric implication 78—31618
- Cl+formaldehyde, rate const., 200-500K 79—39133
- Cl+formaldehyde$\rightarrow HCl + HCO$, stratospheric O_3 decreased sensitivity to Cl perturbations 79—12190
- $Cl + HNO(H_2O_2)(HO_2)$, rate consts., stratospheric appl. 78—85125
- $Cl + HO_2$ react. rate const. determ. at 298K *(French)* 78—64817
- Cl+methane, reaction rate const., stratospheric modelling appl. 79—20345
- $Cl + NO + N_2 \rightarrow NOCl + N_2$, rate const. temp. depend. 78—76828
- $Cl + O_3 \rightarrow ClO + O_2$, rate consts. meas. 77—60059
- $Cl + SO_2$, rate const. rel. to stratospheric Cl chemistry and Venus atm. 79—84353
- $ClCO_3NO_2$, synthesis by UV irrad. of Cl_2, NO_2, CO in air, decomp. kinetics 78—76880
- ClO, predissociation cross sections and rate consts. 77—70763
- $ClO + NO_2 \rightarrow ClNO_3$, reaction rate consts., stratospheric appl. 77—78306
- $ClO + NO_2 \rightarrow ClONO_2$, fall-off curves, N inclusion effects 77—63910
- $ClO + O(NO) \rightarrow Cl + O_2(NO_2)$ rate consts. meas. 77—60059
- $ClO + O \rightarrow Cl + O_2$, rate consts. calc. 220-1000K 79—79233
- $ClO^- + NO(NO_2)(SO_2)(CO_2)$, rate consts. at 300K 78—76829
- $ClO_2\text{-}O_3$ mixtures, photolysis quantum yields, atmos. chem. 79—52724
- ClO_x, reaction rate consts., atmospheric gas phase reactions, review 77—81390
- ClONO, near UV absorpt. spectrum, rel. to atm. chem. 77—30881
- $ClONO_2$, chem. degradation in stratosphere 77—33134
- $ClONO_2$, in stratosphere, mechanism of UV photolysis at 302.5 nm 78—20031
- $ClONO_2$, photolysis products, very-low press. meas. 79—29376
- $ClONO_2$, relative abundance among stratospheric Cl compounds 77—33155
- $ClONO_2$, solar photodissoc. rates, current levels in stratosphere 79—53496
- $ClONO_2$, stratospheric distrib. at sunset, balloon borne IR solar spectra obs. 80—41487
- $ClONO_2 + OH$, reaction kinetics, stratospheric conditions 77—86303
- $ClONO_2 + O(^3P)$, fast flow reaction, rate const. 77—12777
- $ClONO_2 + O(^3P)$, photolytic gas phase kinetics at 245K 79—52719
- ClOO, stratospheric chem., formation and loss reactions 78—16138
- ClOO+NO, reaction in stratosphere 79—34889
- $ClO.O_2$ in stratosphere, possible existence and chemistry 80—77066
- $Cl(^2P) + ClONO_2$, reactive channels, stratospheric altitudes 77—60038
- $Cl(^2P)$+methane, absolute rate and temp. depend. 78—80731
- ^{38}Cl and ^{39}Cl in lower stratosphere, chemical form 78—44913
- Cs_2, precursor for atm. COS 79—53490
- $H + O_3 \rightarrow HO_2 + O(^3P)$, reson. fluoresc. obs. 79—70317
- $H^+ + N_2$ collision, binary encounter calcs. of proton energy deposition 78—74746
- H_2 sources and sinks, anthropogenic activity influence 77—64394
- $HBr + OH \rightarrow H_2O + Br$, absolute rate const., 249-416K 79—70303

atmospheric chemistry continued
- HCl production mechanism, in cloud, chemical model with trace gases 77—37325
- $HCl + O^-(O_2^-)(NO_2^-)(CO_3^-)(CO_4^-)$, rate consts. at 300K 78—76829
- $HCl + O(OH)$, reaction rate const. temp. depend., stratospheric implications 78—31616
- HNO_2, air pollution obs. in W.Europe 80—72106
- $HNO_2 + O_3$ reaction kinetics under stratospheric conditions 78—11499
- HNO_3 and H_2O_2, photodissociation, solar radiation effects in atmosphere 79—58045
- HNO_3/NO_2 conc. ratio in daytime stratosphere 78—73460
- HO fluorescence detection, interference suppression by sampling method 80—8431
- HO_2 radical, atmospheric reactions studied by laser mag. reson. spectroscopy 80—12511
- $HO_2 + ClO$, reaction product distrib. 80—72586
- $HO_2 + HO \rightarrow H_2O + O_2$, rate coeff. meas. by laser mag. reson., atm. chem. appl. 77—52614
- $HO_2 + NO$, reaction kinetics meas. 78—31624
- $HO_2 + NO$ reaction rate constant effects on O_3 perturbations, model of stratosphere 78—73474
- $HO_2 + NO \rightarrow OH + NO_2$, kinetics temp. depend. 80—3313
- $HO_2 + O_3 \rightarrow OH + 2O_2$, rate coeff., effects on stratospheric O_3 78—96275
- $HO_2 + O \rightarrow HO + O_2$, rate coeff. meas. by laser mag. reson., atm. chem. appl. 77—52614
- H_2O near mesopause, dissoc. during auroras rel. to ionosphere winter absorpt. anomaly 79—58152
- H_2O_2, UV absorpt. cross sections and photodissoc. coeffs. 78—42086
- HOCl, HOOCl, stratospheric chem., formation and loss reactions 78—16138
- HOCl, photodissoc. cross-sections rel. to prospects as atmospheric Cl reservoir 79—12207
- HOCl, UV spectrum, stratospheric lifetime rel. to photodissoc. 79—36661
- $H_3O^+(H_2O)_n$, photodissoc. meas. and calc., rel. to atmospheric stability 79—86017
- HO_2NO_2 significance in atmospheric NO_x chemistry 78—11971
- HO_2NO_2, stratospheric, UV and IR absorpt. cross sections rel. to photodissoc. loss 79—13733
- HO_2NO_2, thermal decay kinetics 79—5135
- $HO_2NO_2 + N_2 \rightleftarrows HO_2 + NO_2 + N_2$ react., kinetics, RRKM theory appl. 78—73032
- H_2S in troposphere, photochem. production reactions 80—90112
- H_2SO_4, aerosols form., expt. and theory 78—96256
- H_2SO_4 vapour pressure rel. to gas-particle conversion 80—94560
- $H_2SO_4 + O,(N),(OH)$, collisional reaction probabilities 80—90168
- Li^+ diffusion and ion-neutral interactions, laser sounding obs. *(French)* 80—82115
- N fixation by lightning 80—90147
- N fixation in instantaneous linear discharges, variable energy input effect 79—20952
- N fixation in lightning channels, theory 80—90148
- N fixation in prebiotic atmosphere 79—58096
- N oxides, tropospheric photochemistry 78—44914
- N oxides produced by thermonuclear explosions, effect on O_3 79—84345
- N production in upper atmos., model of far UV dayglow 80—90271
- N^+ photochemistry in thermosphere 79—96847
- N^+ sources and sinks in thermosphere 79—96848
- $N^+ + H_2$, electron capture and ion-loss cross-section, 2.4-24.3 keV 80—58373
- $N^+ + O_2$, electron capture and ion-loss cross-section, 2.4-24.3 keV 80—58373
- N_2 chemistry, history *(German)* 79—53415
- N_2 dissociation by electron impact and EUV photoabsorpt., rel. to aurora and airglow 78—58847
- N_2 in aurorae, vibrational distrib. 79—80068
- N_2^+, dissociative recombination in ionosphere, rate cont. 80—17435
- N_2^+, electron impact dissociative recomb. coeffs. inferred from Atmosphere Explorer meas., objections 78—86957
- N_2^+ upper atmos. photochem. rel. to solar cycle phase 80—85783
- $N_2^+ + O_2$, electron capture and ion loss cross-section, 2.4-24.3 keV 80—58373
- $N_2^+ + O \rightarrow NO^+ + N$, aeronomical determ. of rate coeff. 79—75000
- $N(^2D) + O$, associative ionisation 80—4161
- $N(^2D) + O_2$, chemiexcited NO form., 90-180K IR obs. 78—90163
- $N(^2D) + O_2$ as source of $O(^1D)$ atoms in aurorae 79—35028
- $NH_2 + NO_2$, reaction rate const. meas. 80—7772
- $NH_2 + O_3$, reaction rate const., rel. to atmospheric processes 80—85155
- NH_3 in troposphere, vertical distrib. by photochem. model 80—85701
- $NH_3 \rightarrow NH_4^+$ conversion, in atmosphere, pseudo first-order reaction rate const. 80—94132
- NH_4^+, mutual neutralisation, with simple and clustered positive (negative) ions 78—44372
- NH_4Cl, gas $^1A_1$ ground state, pot. surface 80—32626
- $NH_4NO_3 \rightleftharpoons NH_3 + HNO_3$ equilib. in atmosphere 79—88389
- NO density variations in E-region, theory, ion-neutral chem. constraints 79—75027
- NO, γ and δ bands auroral emission, from radiative recomb. of N and O 77—91343
- NO, in upper atmosphere, excitation of auroral 2150 Å emission 77—9594
- NO oxidation to NO_2 in power plant chimney plume 79—12178
- NO, photodissoc. in mesosphere and stratosphere, theory 80—41580
- NO predissociation in mesosphere and stratosphere, photochemistry 80—21802
- NO, production by lightning, shock and channel heating methods 80—72581
- NO, stratospheric and mesospheric photodissoc. rate, calc. 80—51498
- NO, stratospheric growth before sunrise by photolysis 77—29356
- NO^+ recombination in mid-latitude trough and polar ionization hole 80—12575
- $NO/NO_2/O_3$, photostationary state relationship rel. to monitors intercalibration 78—69529
- $NO + N\ ^4(S)$ state reaction rate, discharge flow and photolysis reson. fluoresc. method 79—5142
- $NO + S^+ \rightarrow NO^+ + S + 1.1$ eV, rate consts. kinetic energy depend., drift tube meas. 80—7778
- NO_2 and NO_3, photodissociation, solar radiation effects in atmosphere 79—58045
- NO_2 nighttime concs., hydrocarbon reductions, potential effects, outdoor smog chamber expts. 77—70720

atmospheric chemistry continued
NO_2 photodissociation rate constant depend. on altitude 78—11949
NO_2, stratospheric composition during major warming, 1979 obs. 80—51476
$NO_2^+ + O \rightarrow NO^+ + O_2$, rate constant rel. to atm. ion chem. 77—41245
NO_3 in polluted troposphere, spectroscopic detect. and possible sinks 80—77036
NO_3 in troposphere, obs. of content in mountain air 80—72582
NO_3^-, $NO_3^-.H_2O$, NO_2^-, $NO_2^-.H_2O$, and peroxy isomers, photodissoc. and photodetachment 3500-8250 Å 80—35554
NO_x and airborne particles interactions 78—81342
NO_x production in lightning 77—56677
NO_x removal rate in urban atmosphere 80—56524
NO_x^--HNO_x-H_2O clusters, gas phase, thermodynamic quantities, mass spectra obs. 80—50875
N_2O, atm. life cycle, ground surface sink mechanism 77—66971
N_2O, atmospheric life cycle rel. to O_3 reductions 78—16140
N_2O cycle, sources and sinks 79—70871
N_2O, decomposition over particulate matter 79—16014
N_2O from fertilisers and O_3 content of stratosphere, latitudinal effects 80—36370
N_2O, instantaneous global photochemical reaction rates 80—17335
N_2O production in electric discharge 79—96786
N_2O sources and sinks, O_3 reduction due to industrial fixed N fertilizers 77—78383
N_2O, sources and sinks, review 77—37374
N_2O^+, pot. energy hypersurface characts. calc. in $O^+ + N_2 \rightarrow N + NO^+$ react. 78—60996
$N_2O_5 + O$, rate const., 220K, 300K, discharge-flow method 78—44352
$NO^+.H_2O + O \rightarrow NO_2^+ + H_2O$, rate constant rel. to atm. ion chem. 77—41245
$N(^2P)$ in auroral arc, excitation and collisional deactivation processes 80—72658
Na catalytic cycle, origin for luminosity of meteor trains, lifetimes 80—12711
Na excitation and abundance in nightglow 80—98497
Na I, twilight and nightglow D-line profiles rel. to excitation process 78—36353
Na^+ and Na layers, meteor ablation-cluster ion theory 79—58138
$Na + O_3 \rightarrow NaO^* + O_2$, in upper atm., rel. to Na I nightglow intensity vars. 79—70905
O I 6300 Å airglow rel. to O atoms creation and destruction 79—8735
O quenching coeff. by molecular collision, optical meas. 79—2419
O remote sensing in mesosphere and lower thermosphere, two-photon lidar technique 79—39869
O^+ reactions with N_2, O_2, and NO, nonthermal rate coeffs. in ionosphere 78—57375
O^+ to NO^+ conversion in dayside auroral oval, rel. to rocket-borne VLF and ELF waves meas. 80—98504
O^{++} in thermosphere, photochemistry 77—45226
O^{2+} collisions with O_2 and N_2, reaction rates 79—16726
O^{2+} reactions with atoms or molecules of ionospheric importance, lab. meas. 80—26004
$O + NO + M$, rate const., 217-500K 79—52626
$O^+ + N_2$, charge exchange collision, rate coeff. and ionosphere implications 80—87224
$O^+ + N_2$, reaction rate coeff. in ionosphere 77—87167
$O^+ + N_2(O_2)$, excited ion reactions, charge transfer coeffs. at thermal energy 80—95721
$O^+ + N_2(O_2)$, reaction rates, 300-900K 79—8434
$O^+ + O_2$, charge exchange collision, rate coeff. and ionosphere implications 80—87224
O_2, IR nightglow bands excitation mechanism, reaction rate consts. 78—65448
O_2 levels in prebiological atmosphere, photochem. model 79—84486
O_2, photodissoc. and spectral absorpt. in stratosphere and mesosphere 80—51497
O_2^+ dissociative recombination in auroral region 80—41581
$O_2^+ + N \rightarrow NO^+ + O$, rate constant rel. to atm. ion chem. 77—41245
O_3 and airborne particles interactions 78—81342
O_3 and related chemistry in mesosphere, Solar Mesosphere Explorer mission description (1981-2) 80—105096
O_3, Chapman mechanism, appl. of sensitivity analysis, numerical Green's function procedure 79—100334
O_3 column, increase rel. to NO_x emission from SST and subsonic aircraft 78—11979
O_3 column density effect on radiative-photochemical relaxation 79—16592
O_3 conc. and vars. in clean remote atm. 79—62554
O_3 conc. in troposphere and stratosphere effects of NO_x emissions of high-altitude aircraft 78—32176
O_3 content evolution, one-dimensional coupled chemistry-flow model 80—98400
O_3 depletion by chlorofluoromethanes, two-dimens. time-depend. model 78—24341
O_3 depletion by chlorofluoromethanes, contradiction of theory 78—49099
O_3 depletion chemistry 79—70872
O_3 depletion theories, rel. to atm. nuclear tests 79—70848
O_3 destruction, ion cycle importance 78—53697
O_3 electronically excited state, role in stratospheric chemistry and nightglow 78—20472
O_3 formation and control strategy options for Sydney, precursor distrib. 80—16859
O_3 formation dynamics in cities 80—31112
O_3, global distribution, effects of pollutants, book contrib. 77—29429
O_3 in lower atmosphere, transport processes 80—109196
O_3 in stratosphere, CO_2 conc. increase effects 78—57250
O_3, in stratosphere, seasonal composition variation at high-latitude 80—77051
O_3, instantaneous global balance including observed NO_2 80—109211
O_3 layer, changes in chemical balance 78—92933
O_3 layer, depletion and chemistry 80—104534
O_3 layer, photochemical-diffusive model, chlorocarbon industry impact 78—40648
O_3 layer, photochemistry rel. to possible O_3 reductions and Earth surface UV radiation 80—94577
O_3 layer depletion by chlorofluorocarbons, calc. using two-dimensional model 80—109221
O_3, photochemical, nocturnal depletion at rural site 79—57527
O_3, photochemical model evolution and variability over geological time 79—96788

atmospheric chemistry continued
O_3 photochemical production, W.Europe, rel. to meteorology 77—78292
O_3 photodissoc., annual var. of effects of diffuse solar radiation 80—109210
O_3 photodissoc., $O(^1S)$ yield at 1700-2000 Å 80—97714
O_3 photolysis, $O(^1D)$ quantum yields as function of temp. (230-320K) and wavelength (295-320 nm) 78—56903
O_3 photolysis, primary products electronic and vibr. state distrib. 80—50865
O_3 photolysis by sunlight, rate constants at ground level 80—61836
O_3, production transport and distribution, numerical simulations with global general circulation model 80—56544
O_3 profiles and chemical loss rates in tropical stratosphere, BUV meas. 78—49091
O_3 reduction due to industrial fixed N fertilizers 77—78383
O_3, stratospheric, simultaneous effects of CO_2 and chlorofluoromethanes on column density 79—74940
O_3, UV photodissoc. rate, expt. and theory 80—40722
O_3-precursor relationships in Sydney airshed 79—34880
O_3 + cis-2-butene + formaldehyde → propylene ozonide, gas phase reaction mechanism 77—33132
$O_3 + OH \rightarrow HO_2 + O_2$, reaction rate const., 238-357K 79—47902
$O^+(^2D)$ in thermosphere, quenching by electrons 80—94630
$O^+(^2D)$ quenching by O in thermosphere, Atmospheric Explorer data 78—28355
$O(^1D)$, chemical reactions of stratospheric importance, temp. depend. 79—53494
$O(^1D)$ formation by O_3 photolysis, tropospheric meas. 78—73536
$O(^1D)$ formed by $N(^2D) + O_2$ reaction in thermosphere, 6300 Å dayglow implications 80—90270
$O(^1D)$ quantum yield from O_3 photolysis 79—53492
$O(^1D)$, quantum yields from O_3 photolysis as function of temp. (230-320K) and wavelength (295-320 nm) 78—56903
$O^+(^2D) + N_2$, charge exchange rate coefficient, effect of N_2^+ recomb. on aeronomic determ. 78—88954
$O^+(^2D) + N_2$, thermal rate coeff., products and branching ratios 80—82117
$O^+(^2D) + N_2$ charge exchange, rate coeff. temp. depend. 80—77179
$O(^1D) + H_2O$, rate coeff., atm. OH prod. 79—58009
$O(^1D) + H_2(HCl)(NH_3)(N_2O)$(methane), rate consts., temp. depend. 78—27747
OH conc. meas. in boundary layer by monitoring CO oxidation 79—58012
OH Meinel bands, in airglow, rot. temp., radiative lifetime 78—61643
OH Meinel bands intensity distrib. in airglow, OH^* quenching mechanisms 78—65447
OH, NO, NO^+, inverted populations due to moving bodies and ejected gas, upper atm. 78—32265
OH, radical, atmospheric reactivity with organic compounds 79—61860
OH radical chemistry in troposphere and stratosphere, rel. to OH calculated densities, uncertainties 79—53426
OH radical in upper atmosphere, meas. using lidar from Space Shuttle 80—51590
OH, vibr. energy distrib., atm. chem. modification 77—25735
OH, vibrationally excited states, time and altitude vars. 80—41589
$OH + ClO(Cl_2)(Cl_2O)$, rate const. at 298K, rel. to stratospheric O_3 depletion 79—87831
OH + dimethyl sulphide, flash photolysis reson. fluoresc. rate consts. determ., pollution aspects 78—95913
OH + gaseous S compounds, lower atmos. chem. 80—61870
$OH + HO_2 \rightarrow H_2O + O_2$, rate const. meas. *(German)* 79—52629
OH + halocarbons rate consts., appl. to tropospheric degradation 79—52622
$OH + OCS(CS_2)$, flash photolysis reson. fluoresc. rate consts. determ., global S cycle 78—95914
$OH + RH \rightarrow H_2O + R$, radical substitution reaction 80—81321
$OH + CO(N_2O)$, rate consts. 77—16781
$O(^3P)$ atoms, translationally hot, form. and energy distrib. function 80—21811
$O(^3P)$ + mercaptans, reaction rate consts., O_2 effect 79—52630
$O(^3P) + NO + HCl$, rate const. 79—52627
$O(^1S)$, auroral production and loss processes, artificial auroral expt. Precede meas. 79—66855
$O(^1S)$ production in lower thermosphere, comparison of Chapman and Barth mechanisms 77—33235
$O(^1S)$ production indirect mechanism in aurora 79—48597
$O(^1S)$ source in aurora, energy transfer from excited N_2 and O_2 79—48598
$O_2(^1\Sigma)$ airglow, gravity waves interaction theory 79—29918
$^{18}O^{16}O$, photodissociation as source of atmospheric O_3 80—94559
$O^{+*} + N_2(O_2)$, metastable ion reactions, rate consts. and ion mobility at 300K 80—95722
$O(2^1D_2) + N_2(O_2)(N_2O)(CO_2)(H_2O)$(methane), collisional deactivation meas., 295K, rel. to atmospheric processes 80—16663
$O_2^+.O_2$, reactions with CO_2, O_3 and methane rel. to stratospheric ion chemistry 79—2343
$O_2^+.O_3$, reactions with H_2O and methane rel. to stratospheric ion chemistry 79—2343
$O_2(b^1\Sigma_g^+)$ quenching by $O(^3P)$ and O_3, rate coeffs. 79—70309
S, and trace metal content of nonurban and marine aerosols, PIXE anal. 77—49136
S budget of eastern N.America, anthropogenic and natural contribs. 80—97834
S budget over Europe, residence times 79—70475
S chemistry in E-region 79—96854
S chemistry of lower atmosphere, reactions with OH 80—61870
S compounds, homogeneous chemistry 78—49119
S compounds, reduced, emission from open oceans 79—70805
S compounds homogeneous oxidation in atmosphere 78—96258
S compounds transform. and removal, time-dependent diffusion model 79—20972
S compounds wet removal from atmosphere 79—2363
S cycle study, atmospheric pollution modelling appl. 78—92902
S, linear eight-box model for tropospheric global cycle 80—56506
$S^+ + NO \rightarrow NO^+ + S + 1.1$ eV, rate consts. kinetic energy depend., drift tube meas. 80—7778
SO and SO_2 deposition and transformation rates during transport over Atlantic Ocean, comment 77—66975
SO_2, adsorption and oxidation on atmospheric particles 78—96287
SO_2, aerosol-catalysed oxidation, expt. under atm. conditions 79—1941

atmospheric chemistry continued
SO_2, atmospheric removal rate meas. using ^{38}S tracer *(German)* 79—53411
SO_2, atmospheric transport and conversion to sulphates 79—16654
SO_2 conversion in smoke plumes *(Dutch)* 77—70825
SO_2 conversion to SO_4^{2-}, meas. during manned balloon flight 79—83658
SO_2 diffusion-coupled oxidation 78—65371
SO_2, dispersion and wet deposition from power plant plume 80—16861
SO_2, heterogeneous conversion to SO_4^{2-}, rel. to urban air pollution 78—80789
SO_2, homogeneous oxidation mechanism in troposphere 78—96257
SO_2 low core, equilibria between air and water 78—16137
SO_2, NH_3 and CO_2 reversible washout and acid rain prod. 79—83657
SO_2, oxidation, precursor effects, rel. to air pollution 79—1960
SO_2, oxidation by O_2 and O_3 in aq. soln., kinetics, rel. to atm. rate processes 79—20905
SO_2 oxidation by O_3 in cloud droplets, HSO_3^- aerosols form. 78—44894
SO_2 oxidation chemiluminesc., appl. to atm. chem. *(German)* 79—52670
SO_2 oxidation in clouds and rain, O_2, O_3 and H_2O_2 role 79—84351
SO_2, oxidation in moist atm., aerosol growth kinetics 78—96255
SO_2 oxidation in stored rainwater samples, rel. to Mn content 79—84352
SO_2, oxidation on surface of fly ash particles under low relative humidity conditions 79—62160
SO_2 oxidation to SO_4 in urban atmosphere 80—81964
SO_2 oxidation to sulphate in troposphere, model predictions 80—81963
SO_2, oxidation via OH radical, rel. to atm. fate of HSO_x radicals 79—62559
SO_2, photochem. oxidation 79—70873
SO_2, photooxidation, aerosol evolution, rel. to air pollution 78—81392
SO_2 pollution long-distance transport, numerical model 79—44238
SO_2 reaction with O_3 in water rel. to atmospheric oxidation 78—16083
SO_2, reversible washout by rain, improved model 79—2364
SO_2, sources in CS_2 and COS oxidation 80—4085
SO_2 to sulphate conversion processes 77—37389
SO_2, vertical distrib., influence of clouds and rain, one-dimens. model 79—20982
$SO_2+H_2O+O_2(N_2)(Ar)$, condensation nuclei form., ion polarity and age depend. 79—39220
SO_4^{2-} aerosol form., CO effect, smog chamber expt. 79—74925
SO_4^{2-}, maritime atm. aerosols, sources over N.Atlantic Ocean 79—20904
SO_4^{2-} production in rain and raindrops in polluted atm. 79—88388
$^{35}SO_2$ interaction with atmospheric particulates 77—41137
^{38}S in SO_2 and SO_2 oxidation rate meas. 77—73814
T 80—41588

atmospheric composition
see also atmospheric chemistry; atmospheric structure
absorption spectrum in 583-605 nm region by intracavity laser spectroscopy 79—53517
acetylene, ambient concs. and ratios to other hydrocarbons 79—12182
acetylene, tropospheric and lower stratospheric vertical profiles 80—4073
acid precipitation at Ithaca, New York, comp. and air masses origin 79—16655
acid precipitation in central Texas, chemical comp. 77—37329
acid sulphate in aerosol, detection from S/N ratio 80—61494
aearosol global distribution, 162-238 millibar altitude 80—56591
aeronomical models, diurnal averaging 78—49186
aerosol, absolute element concs., PIXE and AAS, comparison 78—85237
aerosol, ambient sulphate particles size discrimination and chemical comp. by diffusion sampling 78—69528
aerosol, chem. components depend. on air mass and meteorology *(German)* 79—53412
aerosol, coagulation and condensation, dynamic behaviour 77—25312
aerosol, individual microparticles identification via micro-Raman spectrometer 78—68970
aerosol, large particles in convective storm environment 80—41512
aerosol, Nigeria during dry dusty season 80—81960
aerosol, particle conc., meteorological factors effect 80—4060
aerosol, particle size distrib. statistical characters. rel. to light attenuation coeffs. *(Russian)* 78—53702
aerosol, particle size distribs. evolution via Brownian coagulation, num. simulation 80—41513
aerosol, produced by α-particles, evolution of <0.02 micron particles *(French)* 79—43640
aerosol, Pt metals analysis by neutron activation 78—3989
aerosol, seasonal vars. in vertical profiles in lower troposphere *(Russian)* 78—16092
aerosol, size fractionated, comp. in Charleston, W.Virginia 80—89687
aerosol, S.Pole, chem. comp. determ. by instrumental neutron activation analysis 78—3988
aerosol, stratospheric, in S hemisphere, meas. by impactor and in situ single-particle detect. 78—73437
aerosol, use of lidars, laser rangefinders 80—51580
aerosol above Black Sea, spectral transmission and sky brightness obs. *(Russian)* 80—94603
aerosol air composition at Barrow, Alaska, wind direction depend. 80—85704
aerosol Al composition after rocket launch 80—81503
aerosol climatology in Europe, Project OPAQUE 79—66784
aerosol comp. rel. to K/Na ratios in dew drops 77—91190
aerosol conc. meas. by lidar 78—85693
aerosol conc. statistics for N. tropical Atlantic region 78—32188
aerosol concentration, Antarctica, seasonal and frontal vars. 79—70855
aerosol content from ERST (LANDSAT), obs., comment 78—28282
aerosol effects on diffuse and direct solar radiation at Earth's surface 77—37406
aerosol in Florida, time series anal. 80—89688
aerosol mass loadings evaluation from multispectral extinction data 79—12221
aerosol meas. at Algarve coast, Portugal 79—58062
aerosol measurement problems 79—66839
aerosol measurements, visual range and relative humidity relationship 77—56728
aerosol microstructure, lower stratosphere, sounding with multifreq. lidar 80—56645
aerosol of Sudan Gezira airstream, chem. composition and pH 80—51518
aerosol off W.African coast, Na, Cl and Br composition evolution 80—77053

atmospheric composition continued
aerosol particles, physical-chemical transformation processes, thermal-optical anal. *(Russian)* 80—12482
aerosol particles and trace gases meas. in St. Louis area 79—16600
aerosol particles characterisation by Raman spectroscopy 77—49188
aerosol particles water uptake and equilib. sizes at high relative humidities 78—61516
aerosol pollution, urban, chemistry rel. to cloud modification effects 80—56571
aerosol properties at S.Pole, 1978 obs. 80—41484
aerosol samples, simulated, Be content by proton scatt. anal. 79—5217
aerosol samples, trace substance concs. rel. to sources identification and relative importance estimation 80—72105
aerosol sampling by in situ and standard methods 79—66840
aerosol size and comp. at Mauna Loa Obs., Hawaii 77—78333
aerosol solid particles, diffusive evaporation, laser spectrochemical analysis 79—92040
aerosol sources identification in St. Louis area using factor anal. 79—12200
aerosol species optical consts. rel. to radiation balance determ. 77—17163
aerosol vertical distribution, meas. by Skylab photographic coronagraph 77—60568
aerosols, charged, occurrence before earthquakes 79—16407
aerosols, chem. comp. of particles with diameters $>1\ \mu m$ over Tasmania 77—87014
aerosols, chemical characterisation, progress and problems 78—68969
aerosols, chemical components of particles in lower troposphere above central Europe 77—29354
aerosols, erroneous elemental mass-size functions from high vol. impactor 79—20997
aerosols, from Jungfraujoch, Switzerland, chem. comp. 77—45056
aerosols, granulometric spectrum, in slightly polluted marine atm. 78—44893
aerosols, Hg, As and Br quantitative analysis 79—12179
aerosols, humidity effects on gravit. settling and Brownian diffusion 78—32203
aerosols, instrumental anal. of light element comp. 78—69516
aerosols, IR spectrometry theory and appl. to spectroscopic effects of atmospheric constituents 80—101428
aerosols, mean bulk densities of dry samples 78—32204
aerosols, physical characts. 78—69430
aerosols, remote anal. by differential scatter lidar system 78—69524
aerosols, remote sensing using laser radar techniques 79—66841
aerosols, size distrib. meas. with particle Doppler shift spectrometer 78—69515
aerosols, size distrib. of water-soluble and insoluble particles 78—36218
aerosols, sulphate and nitrate assay via ion chromatography anal. 78—68974
aerosols, trace element conc. over Lake Michigan 80—81968
aerosols, urban, in Nagoya area, Si and Al concs. for atmospheric soil particles characterisation 80—26581
aerosols, X-ray fluorescence anal. *(Spanish)* 77—87045
aerosols and ice nuclei, elemental comp. 78—3882
aerosols direct formation by reaction of NH_3 and SO_2 77—29377
aerosols from Mount Agung eruption as test of global climatic perturbation 78—69440
aerosols from urban and desert regions in Israel 80—41503
aerosols in Kashmir region, study of chemical components 80—94594
aerosols in marine air near Europe, 632 nm light absorpt. obs. 80—90136
aerosols in urban atmosphere, distrib. rel. to mixing depths numerical simulation 80—105024
aerosols in W.Africa, brush fires influence *(French)* 79—34883
aerosols of Antarctica, orgins and props. 80—90197
aerosols over tropical N.Atlantic Ocean, water-soluble K, Ca and Mg contents 80—72598
air pollution emission, transmission and immission, fundamentals *(Dutch)* 77—70820
air pollution planning techniques for new city 77—70818
air pollution removal mechanisms and processes *(Dutch)* 77—70824
air pollution water vapour effect, damp air and plumes *(Dutch)* 77—70823
air quality evaluation, daily profiles method *(French)* 78—92969
aircraft ambient and cabin air O_3 conc. simultaneous determ. 80—90198
aldehydes in air, gas chromatography 79—12284
n-alkane pollutants, N.Atlantic gas and particle concs. in troposphere 80—7969
alkyl Pb and Se compounds, detect. via gas chromatograph-microwave plasma detector 78—68975
alkylbenzene concentration study in New South Wales 77—70817
ammonium sulphate vapour pressures, nucleation of new particles in atmosphere 79—81708
ancient atmosphere, fate of OH and O_2 origin 80—77116
Ankara atmosphere aerosol, trace elements and size distribs. determ. by thermal neutron activation anal. 78—81377
Antarctic aerosols particle anal., comp. 80—77091
Antarctica, surface O_3 meas., annual variations 77—9465
anthracene, photooxidation on atmospheric particulate matter 80—61487
Arctic aerosol and snow compositional differences 79—88377
Arctic haze bands, probable Asian desert origin 77—78349
artificial satellites future role in meteorological obs. 79—79965
N Atlantic marine aerosol, chemical relationships 77—53136
atoms and radicals in situ reson. fluoresc. meas. in upper atmosphere 79—53600
aurora modelling, time-depend. study 80—72672
aurora primary ions, above diffuse midnight aurora 80—41595
auroral arc, ionic struct. meas. 77—2292
auroral E-region, ion comp. and NO profile 77—41258
auroral ion composition and energy spectrum vars. 77—64509
auroral NO densities, horizontal winds effects 80—26656
auroral origin of medium scale gravity waves in neutral composition and temperature 79—74998
background aerosol comp. on Chacaltaya Mtn., Bolivia 77—91188
Barcelona, SO_2 stability and conc. *(Spanish)* 77—87042
Belgium, SO_2 and smoke daily concs. from 1968, Jan. to 1973, Mar. *(Flemish, French)* 77—82003
bipolar ionic atmosphere, equilib. charge distrib. on aerosols 79—70830
boundary layer, baroclinicity effects on Lagrange trajectories of diffusing particles 77—66949
boundary layer, stratified, conc. profile, admixture-underlying surface interaction effect 80—31089

atmospheric composition continued
boundary layer fluxes determ. over natural grassland, aerodynamic method 78—73480
Brazil, precipitable water, distrib. maps 80—77075
caffeine in New York City air 77—91191
carbon tetrafluoride, atmospheric content, sources and residence time 80—61879
carbon tetrafluoride, atmospheric content meas. 79—34927
carbonaceous pollutants, $^{14}C/^{12}C$ ratios rel. to origins and residence times 78—69445
chemical composition of precipitation, Trinidad, West Indies, meteorological parameters effects 79—79945
chemical-diffusive model for troposphere and stratosphere 77—21873
chlorinated hydrocarbons in ambient air, washout effect and diurnal var. 78—28305
chlorofluorocarbon residence times in stratosphere, two-dimens. model 80—45834
chlorofluorocarbons 11 and 12, observability of possible atmospheric removal processes 77—25773
chlorofluoromethanes, $CHFCl_2$ and CHF_2Cl, diffusion and chem. reaction 77—70804
chlorofluoromethanes CCl_2F_2 and CCl_3F in Wuppertal-Dusseldorf region, ground level meas. 78—73478
chlorofluoromethanes in stratosphere, vertical distrib. 78—73476
chlorofluoromethanes in upper troposphere and lower stratosphere, vertical distrib. 78—73477
cirrus clouds, remote sensing of thickness and composition from satellites 77—64461
cloud condensation nuclei, obs. over N.Atlantic 80—77074
cloud condensation nuclei from paper mill, calc. effects on rainfall 78—11970
cloud condensation nuclei from paper mill, measured effects on clouds 78—7721
cloud condensation nuclei in urban environment, comp. effects on cloud microphysical model 80—82004
cloud condensation nuclei on USA Atlantic seaboard 77—5310
CO from arctic surfaces during spring thaw 80—41511
coal smoke particles, atmospheric natural radioactivity *(Rumanian)* 78—53723
coastal atmosphere, H_2SO_4 aerosol, form. of particulates 80—90113
condensation nuclei, counter with inherent size resolution capability 78—81470
condensation nuclei conc. over Mediterranean Sea 77—45057
condensation nuclei conc. records, 1965-77, SW.Germany *(German)* 79—84422
condensation nuclei vertical profiles 79—79956
Copenhagen area urban aerosols on heavy loaded membrane filters, PIXE anal. 77—49138
corpuscular radiation flux variations in daytime midlatit. mesosphere 77—29538
D-region, equatorial, ionisation processes and ion comps. review 78—36362
D-region, ion composition at midlatitude in quiet conditions, model 80—109307
D-region, ion composition models, unified reaction scheme 79—5704
D-region, negative ions effect on Thomson scatt. in presence of electron heating 79—16739
D-region, NO density enhancement on winter anomalous day at S. Uist 80—82130
D-region, NO prod. rel. to winds and electron densities time vars. correl. 79—25389
D-region, obs. and chem., recent advances 79—8751
D-region, positive ion chemical scheme for $H^+.(H_2O)_n$ abundance profile 79—40007
D-region, positive ion comp. diurnal vars. during storm after-effect 78—65451
D-region, quiet daytime, H_2O cluster positive ions prod. 77—45242
D-region, transport conditions var. and winter anomaly 79—66864
D-region, water cluster ions formation rel. to mesospheric temp. 77—21842
D-region cluster ion formation, implications of laboratory determs. of NO^+ reaction rates 77—53308
D-region ion composition, ionisation and profiles 77—49226
D-region irregularities, comp. effects on partial refls. 78—81495
D-region NO_2^- ion chemistry 77—75236
D-region over Sardinia (40°N), positive ion relative comp. during winter anomaly 80—21871
D-region winter anomaly, recent advances 80—17437
daytime D-region, ion and neutral comps. during polar cap absorpt. 77—37481
Devonian atmosphere, isotopic ratio of Ar in Rhynie chert 77—66917
dichlorodifluoromethane, rate const. for reaction with OH and tropospheric lifetime 77—64366
dichlorofluoromethane pollution, conc. obs. in background troposphere air 80—97843
differential absorption lidar, complementarity of UV and IR systems for atmospheric species meas. 80—72634
differential-absorption lidar technique for remote meas. of atm. gases 78—61603
dimethyl sulphide, biologically prod., contrib. to global S cycle 77 ·70786
dimethyl-N-nitrosamine, assessment is urban air 78—81378
Dobson O_3 spectrophotometer calcs., generalized treatment of particulate scatt. 79—12267
dust, imaginary refr. index rel. to particle size 78—7763
dust, neutron activation anal. 77—70718
dust, planetary radiation balance, climatological consequences 78—36242
dust aerosols, activation analysis experience at Karlsruhe Nuclear Research Center 78—3941
dust deposition in N.Nigeria, Harmattan dust (1978-79) 80—94578
dust fallout in Kuwait, summer 1978 obs. 80—81966
dust in stratosphere, of interplanetary origin, optical absorpt. spectra 80—101554
dust loading index, 1923-54, pyrheliometric and circumsolar sky radiation obs. 80—46240
E_s-layer meteor ions rel. to occurrence 77—25837
E_s-layers, mid-latitude, ion comp. rel. to electron temp. gradients 78—28397
E-region, electron conc. profiles during sunrise and sunset 79—88526
E-region, midlatit. nighttime model including metallic ions 77—45249
E-region, NO var. with solar activity 78—49207

atmospheric composition continued
E-region, O_2 conc. seasonal vars. rel. to winter anomaly 79—53613
E-region, O density rel. to O I green line airglow, obs. during Winter Anomaly Campaign (1975/76) 78—45075
E-region nighttime neutral conc. vars. meas., expt. method 77—45200
early balloon borne obs. 78—16617
electrochemical concentration cell ozonesonde, performance characts. 79—21039
elemental abundances of S, K and P in aerosols from S.American rain forests 79—100910
elemental conc. and particle size distribs. in background aerosol 77—49139
energy deposition in a gaseous mixture 79—25380
SE.England, 1976 summer O_3 concs. 77—91240
N.W. England, coastal site, ambient air quality determ. 80—89690
enhanced CO_2 greenhouse effect, compensation for reduced solar luminosity on early Earth 79—39865
environmental protection *(Japanese)* 78—16152
ethane, tropospheric and lower stratospheric vertical profiles 80—4073
W.Europe, ion production obs., 50-120 km altitude, 1975/6 winter anomaly 80—36439
W.Europe, mesosphere and lower thermosphere trace constituents, 1975/6 winter anomaly 80—36433
W.Europe, neutral atmosphere composition 1975/6 winter anomaly 80 —36432
European Community, information exchange concerning pollution by S compounds and suspended particulates 80—7979
evolution, computer simulation, composition and surface temp. 78—28263
evolution over last 4.5 billion years, computer simulation 77—64396
exobase, local perturbations of H density distrib. inferred from Lyman α airglow meas. 78—24400
exosphere, dayside sub-solar H bulge 77—21957
exosphere, global comp. and temp. during quiet times 77—33227
exosphere, H atoms vel. distrib. from OGO-5 meas. of Lyman α emission 78—61642
exosphere, H global density distrib. vars., escape fluxes 78—93023
exosphere, H latitude vars., rel. to polar wind, heating and charge exchange processes 78—93024
exosphere, N_2 and O densities under active solar conditions 77—33234
F_1-layer, ion comp. and temp. profiles from incoherent scatter radar studies 80—72654
F_1-layer, mid-latitude, mean diurnal var. of O^+, NO^+, O_2^+ and N_2^+ ions 79—96856
F_1-layer at nighttime, ion composition near mag. equator 80—72683
F_2 layer seasonal anomaly rel. to composition changes 77—33252
F_2-layer, night-time, over Arecibo, light ion comp. seasonal mean struct. 80—31163
F-region, bottomside, mol. ion densities rel. to airglow anal. 80—98496
F-region, electron conc. profiles during sunrise and sunset 79—88526
F-region, high latit., Fe^+ ions distrib. 79—16736
F-region, midlatit., parameters diurnal behaviour in summer 79—84570
F-region, midlatitude, neutral comp. vars. rel. to quiet time electron density depressions 78—36385
F-region, $N(^2D)$ chemistry from airglow and atm. comp. meas. 78—16241
F-region, N atoms and O ions in dynamic model 80—72693
F-region, neutral atmosphere comp. changes rel. to O I 6300 Å airglow 78—36354
filter media suitable for air pollutant analysis (HNO_3, nitrates and acidity) 80—104541
fires, O_2 conc. profile from convection-diffusion, coupling model 77—7481
fluorocarbon mixing and photolysis, tropospheric mixing ratios 79—12181
fluorocarbon-11, estimated future atmos. concs. for various tropospheric removal rates 77—21892
fluorocarbons, global distrib. 79—53407
fluorocarbons, lifetime determ. methods 79—20920
fluorocarbons conc. meas., model validation 77—45138
formaldehyde, air over N.Germany coast, obs. 80—26584
formaldehyde, concs. in rain water and on atmospheric aerosol 78—57243
formaldehyde, in marine air and rainwater, wet season obs. 80—85703
formaldehyde, in troposphere and stratosphere, meas. by high resolution IR absorpt. spectroscopy 79—84371
formaldehyde, meas. in atm. by ground based IR absorpt. obs. *(French)* 79—66764
fossil fuel use consequences, CO_2 concentration increase 80—12041
Fourier far IR spectroscopy from Spacelab 77—21949
Fourier transform IR absorpt. spectroscopy, airborne, for atm. comp. meas. 78—61604
free radical meas. by matrix isolation and EPR 78—73535
free radicals, meas. by matrix isolation EPR 78—46374
Freon 21, evidence for presence in atmosphere 79—62565
gas absorption lines, half width and intensity, lidar remote probing technique *(Russian)* 80—21844
gas phase inorganic ion clusters 80—77068
gaseous halogens in the atmosphere during 1975 77—56681
gaseous hydrocarbons, removal from atmosphere with allophane adsorber *(Japanese)* 77—78412
gases emitted by Volcano Mihara, meas. using automatic recording instrument, comparison with tremors 77—66899
gases emitted by Volcano Mihara meas. using automatic recording instrument, comparison with tremors 77—66899
gases identification and conc. meas. from spectral absorpt. patterns, anal. methods 77—87059
gases identification and conc. meas. from spectral absorpt. patterns, system appls. and design 77—87060
general study of upper atm. *(Chinese)* 79—75039
geocoronal H conc. models, $H\alpha$ emission rates and solar Lyman β flux 77—25808
greenhouse effects of some atmospheric constitutents 79—70882
Greenland, summer aerosols and trace gases 80—72609
N.Greenland summer tropospheric aerosol, ground level meas. and elemental anal. 78—85645
ground level abundances of N_2O, CO_2, CO and H_2O, simultaneous determ. 78—11969
Haicheng, China, anomalous meteorological phenomena obs. before 1975 Feb. 4 earthquake *(Chinese)* 78—24224
halocarbon meas. in Alaska troposphere and lower stratosphere 77—70719
halocarbons, decomp. by natural tropospheric ions 77—21889

atmospheric composition continued
- halocarbons, global budget analysis 79—34881
- halocarbons, identification and meas. in troposphere and lower stratosphere 78—32186
- halocarbons, SF_6 and N_2O concs., rel. to tropospheric OH conc. 77—45069
- halofluorocarbons, background levels in situ quantification 78—69530
- halogenated compounds, meas. in air over Europe 77—37351
- heavy metals, Belgian network meas. 77—70833
- high aerosol layers, influence on atmospheric and oceanic temp. determ. by remote sounding *(Russian)* 78—81430
- historical atm. comp. and climate from gas parameters meas. on Greenland ice cores 79—8681
- Hubbard Brook Experimental Forest, H ion input and precipitation pH 77—37337
- hydrocarbons, concs. over Pacific 78—73468
- hydrofluorocarbon monitoring using telluric absorption line *(German)* 78—49133
- hydrometeors, pH detailed struct. 79—92111
- ice nuclei, bacterial sources 77—5292
- ice nuclei, terrestrial and marine biogenic sources 77—5291
- ice nuclei from snowfall induced by power plant plume, comp. 78—81284
- Iceland, Hg natural conc. 77—64244
- inert gas composition, Earth's origin from solar nebula 80—61785
- inorganic clusters, gas phase 80—58436
- ion and neutral chemistry, implications for radio communication and environmental hazards 77—17267
- ion and neutral density determ. by mass spectrometers, mass discrimination under spacecraft conditions 80—4230
- ion comp. and episodic var. rel. to arctic snowfield contamination 77—91159
- ion concentration, elec. cond. and vertical elec. field intensity meas., 0-85 km altitude 77—29359
- ion concentration, elec. parameters and space charge density correls. 77—13104
- ion depletion in AE-C satellite wake, electron temp. and relative ion comp. influence 79—62667
- ionic composition of rain during sixteen convective showers 79—58003
- ionic stability of precipitation samples 79—70828
- ionosphere, AEROS and TAIYO satellite results 80—46340
- ionosphere, analytic partial derivatives for incoherent scatter data least-squares fitting 78—73581
- ionosphere, atomic ions reaction to rapid changes in large-scale elec. fields 77—91350
- ionosphere, atomic processes, book contrib. 77—37482
- ionosphere, calc. and obs. structure, AE-C satellite and incoherent scatter radar obs. 78—49203
- ionosphere, comp. vars. due to solar EUV flux changes, calcs. 79—44293
- ionosphere, components concs. rel. to multiple-layer model of small-scale dynamo 79—53612
- ionosphere, disturbed, above 100 km, ion comp. rel. to electron kinetics 77—64512
- ionosphere, electron conc. and collision freq., rocket meas. 79—80074
- ionosphere, electron conc. var. with height, improved model 78—49214
- ionosphere, electron content quasiperiodic fluctuations during 1976 April 29 partial solar eclipse 78—24407
- ionosphere, electron density and recomb. coeff. profiles calc. rel. to absorpt. and rocket meas. 78—69559
- ionosphere, electron density in South Atlantic Anomaly region 80—12611
- ionosphere, electron density models, review 79—48617
- ionosphere, electron density profile analyses of ionograms, model starting heights 79—66869
- ionosphere, electron prod. and loss rates, satellite meas. 79—35047
- ionosphere, equatorial Mg^+ ion distrib. from Mg II 2800 Å airglow obs. 80—26673
- ionosphere, evolution of comp. 77—2300
- ionosphere, H^+ distribution in equatorial anomaly, empirical model 79—8768
- ionosphere, high-latit., energy spectra and origin of 1 to 500 eV electrons 77—29568
- ionosphere, high-latitude, elec. fields rel. to ions vertical distrib. 78—28370
- ionosphere, ionic conc., satellite eas. appl. to low altitude incoherent scatt. interpretations 77—78568
- ionosphere, lower, electron density space-time vars. 77—17282
- ionosphere, lower, electron distrib. function and ion concs., Boltzmann-Fokker-Planck theory 77—78564
- ionosphere, lower, ion prod., density and comp. during auroral absorpt. event 80—36443
- ionosphere, lower, NO height distribution from rocket ion comp. results 80—26674
- ionosphere, lower, O conc. determ. by fluoresc. technique 80—36434
- ionosphere, lower NO densities rel. to radiowave absorpt. meas. 78—81492
- ionosphere, metallic ions of meteor origin effect in VHF forward scattering, contribution to sporadic-E formation 80—67461
- ionosphere, midlatitude, dynamical model for 100-1000 km altitude range 78—53768
- ionosphere, nighttime field aligned O^+ and H^+ fluxes in mid-latit. mag. field tube 77—33273
- ionosphere, $O_2+N^+(N_3^+)$, drift tube mass spectra, rate coeffs., prod. distrib. 77—77746
- ionosphere, $O^+/(NO^+ + O_2^+)$ ratio in dayside auroral oval rel. to rocket-borne VLF and ELF waves meas. 80—98504
- ionosphere, O^+/n_e relative densities at 170 km for specific heliogeophysical conditions 79—12332
- ionosphere, photoelec. distrib. determ. from plasma line intensity meas. 77—41259
- ionosphere, relative ion comp. model at midlatits. 79—21094
- ionosphere, semiannual variations of n(O), 120-500 km heights 77—49214
- ionosphere, subtrough O^+ density gradients assoc. with small-scale irregularity structs. 78—40753
- ionosphere, time-depend. auroral model with comp. meas. 80—12609
- ionosphere, topside, O^+ to H^+ transitions level height rel. to very low dispersion whistlers 79—44301
- ionosphere, total electron content and F-region electron density distrib. near mag. equator 79—75028
- ionosphere, total electron content diurnal and seasonal trends, obs. at Waltair 78—69596

atmospheric composition continued
- ionosphere, total electron content from group delay meas. at Ootacamund 79—101006
- ionosphere, total electron content meas. at Gauhati, using ATS-6 140 MHz transmissions 78—69598
- ionosphere, total electron content meas. during 1976 Oct. 23 solar eclipse over Australia, rel. to induced gravity waves 78—49210
- ionosphere, total electron content numerical model, corrections for satellite tracking systems 78—69587
- ionosphere, total electron content obs. at Kurukshetra, suing ATS-6 140 MHz transmissions 78—69597
- ionosphere, total electron content over Indian subcontinent, electrojet effects 77—64523
- ionosphere, total electron content over mag. equator rel. to solar cycle during 1964-69 period 79—53636
- ionosphere, two-ion plasma comp. rel. to whistlers group vel. 78—87452
- ionosphere and plasmasphere at midlatitude, computer model 80—105120
- ionosphere equatorial bubbles, ion comp. changes from topside sounder obs. 79—16737
- ionosphere holes and spread-F, ion chemistry and transport 78—88982
- ionosphere modification by release of highly reactive molecules, diffusion aspects 77—21988
- ions, large and positive, hourly variation of source intensity, Ovieda *(Spanish)* 80—51449
- IR atmospheric remote sensing, theoretical problems 79—80052
- IR cooling rate in standard atmosphere, influence of CO_2, O_3 and water vapour contents 80—26609
- IR laser heterodyne spectroscopy for trace gases remote detect. 78—61606
- Lake Michigan dry deposition loading by airborne particulate matter 77—29410
- laser absorption spectroscopy for point monitoring of gases ambient concs. using tunable lasers 78—61607
- laser analysis, from orbiting satellite 77—9571
- laser beam detection of atmos. constituents, review *(French)* 79—34952
- Leningrad, air pollution forecasts *(Russian)* 77—53181
- lidar techniques for atm. struct. and comp. obs., proposed Spacelab program 78—61602
- lidar theory and methods for composition meas. *(Japanese)* 78—16206
- Liege industrial region, five year record of atmospheric fall-out 78—81375
- Limb Infrared Monitor of Stratosphere (LIMS) radiometer, design and performance, expt. goals 78—61601
- Livermore Regional Air Quality model, appl. in San Francisco Bay area 78—92966
- Livermore Regional Air Quality model, concept and development 78—92965
- lower atmosphere, energetic O atoms distrib. functions 77—41127
- lower ionosphere ionis. struct. and composition, winter anomaly conditions 80—36442
- lower thermosphere, compositional modelling taking account of airglow tidal variation 80—109288
- lunar regolith particles in Earth's atmosphere, variation in chemical composition in surface layers *(Ukrainian)* 80—12685
- magnetic particle fallout recorded in recent ombrotrophic peat sections 78—61519
- magnetosheath bursts of predominantly medium nuclei, Imp 8 obs. (1974 February 16) 79—29937
- magnetosphere, contamination by spacecraft at geosynchronous orbit 80—72701
- magnetosphere, lower, ion comp. from Intercosmos-10 Langmuir probe expts. *(German)* 79—2469
- magnetosphere, outer, discovery of He^{2+} and O^{2+} ions of terrestrial origin 78—32295
- magnetosphere, plasma comp. expt. on International Sun-Earth Explorer A 78—85810
- magnetosphere, polar, plasma comp. from electrostatic H^+ cyclotron waves obs. 78—45154
- magnetosphere, ring current O^+ ions rel. to hiss generation by magnetosonic waves 77—82085
- magnetosphere ion composition during mag. storm, high-altitude region 80—82144
- magnetosphere ion composition dynamics, GEOS mass spectrometer obs. 79—35069
- magnetosphere noble gas precipitation, gas of solar and terrestrial origin, Skylab foil obs. 80—41653
- magnetotail, O^+ obs. 77—33284
- magnetotail lobe plasma, double-peaked ion spectra as evidence for massive ions 78—32299
- S. central Maine, precipitation composition rel. to local source 77—37331
- marine aerosol, Bermuda, alkali and alkaline earth chemistry 77—70727
- marine aerosol alkali and alkaline earth metal chemistry 77—70726
- marine aerosols, organic and inorganic Cl gas concs. and particulate Cl size distrib. 78—32187
- marine aerosols influx into atmosphere, influence of coastal-zone physicogeographic conditions 79—29818
- marine atmosphere, extreme E. Pacific Ocean Aitken nuclei concs. 77—37305
- marine atmosphere, lightly polluted, dark smokes and acid pollution study 78—81376
- marine atmosphere, mineral and sea salt aerosol concs. 79—58039
- marine atmosphere, ocean as source or sink of reactive trace gases 78—3894
- marine atmosphere, SO_2 meas. at concs. lower than ppb 78—81340
- marine atmosphere, trace elements in size separated aerosols 79—20989
- marine atmosphere, trace metal concs. 79—44199
- marine atmosphere particulate matter, organic C conc. and particle size distrib. 78—32139
- marine atmosphere particulate Na and Cl vertical distrib. 77—37304
- mass spectrometer beam system, stratospheric comp. meas. appls. 78—7808
- mass spectrometry for in situ meas. 80—17388
- mesopause, lidar meas. of Na conc. and neutral temp. 78—61613
- mesopause, $[NO^+.H_2O]/[NO^+]$ ratio rel. to temp. 79—96849
- mesopause at high latitude, positive ion composition and chemistry 80—46224
- mesopause region, ion-clustering during winter anomaly, temp. and NO density vars. effect 79—21087
- mesopause water cluster ions, rocket borne expt. 80—17429

atmospheric composition continued
mesosphere, comp. changes due to Earth encounter with interstellar cloud, climatic effects 78−57292
mesosphere, diurnal and seasonal variations of O, H and N components 77−9586
mesosphere, H_2O rocketborne obs. in auroral zone 78−7688
mesosphere, H_2O vapour amount rel. to particle sizes in noctilucent clouds 78−57248
mesosphere, ion bunches form. and concs. 78−73424
mesosphere, ion mobility and elec. cond. height var. 77−21837
mesosphere, IR nonthermal emissions from O_3, Spacelab obs. 77−21906
mesosphere, lower, O_3 abundance from backscattered solar radiances 78−69414
mesosphere, major characts., processes and dynamics 77−25734
mesosphere, midlatit., NO vertical density profiles 77−87012
mesosphere, minor constituents distrib. in thermal interface 78−3891
mesosphere, Na atoms distrib. and Na I 5893 Å nightglow obs. 78−88961
mesosphere, Na layer at 23°S, nocturnal and seasonal vars. 79−74932
mesosphere, O_2 densities meas. from atmospheric absorpt. of solar Lyman α radiation 77−87010
mesosphere, O_2 density profiles from solar H Lyman-α radiation extinction meas. 78−44947
mesosphere, O_3 concs. meas. from 1.27 μm O_2 airglow at middle latit. 80−72606
mesosphere, O_3 increase from obs. of shadow on D-region in ionosphere VLF guide 79−58161
mesosphere, O_3 meas. from ground-based millimetre wave obs. 77−29381
mesosphere, O_3 meas. from ground-based mm wave obs., comment 78−11967
mesosphere, O conc. inferred from positive ion comp. data 80−8405
mesosphere, O-H atmospheric model rel. to OH emission problem 77−60503
mesosphere, O-H model rel. to OH nightglow emission intensity 77−29529
mesosphere, positive and negative ions conc. meas. via payload B III instrument package 78−45194
mesosphere, seasonal and latitudinal variations in temp. and composition 77−45207
mesosphere and lower thermosphere, O_2 and O distrib., effect of magnetospheric elec. fields 79−66850
mesosphere at Thumba from in situ UV absorpt. photometry obs. 80−105051
mesosphere CC Na layer, seasonal var. at low latits. 79−79964
mesosphere NO concentration, geomag. control from simultaneous D and F regions ionisation meas. 79−8651
metal-containing particles, release into atm. from vegetation 77−41135
meteoritic material in upper atmosphere, meas. from spacecraft 77−53486
methane, atmospheric content meas. in N and S hemispheres *(Russian)* 77−13103
methane, conc. over ocean, var. with latit. 78−81372
methane, stratosphere content at mid-latitude, simultaneous N and S hemisphere obs. 80−77052
methane, troposphere vertical profile, eastern USA in winter 80−77035
methane, tropospheric abundance and flux from Earth surface *(Russian)* 78−36223
methane$+O^+{}_4(O_2{}^+)$, products, rate consts., rel. to stratosphere 77−9040
methane atmospheric sources and sinks 78−73472
methane concentration in surface air layer from IR absorpt. meas. *(Russian)* 77−29366
methane content of atmospheric surface layer and vertical air column, synchronised meas. *(Russian)* 79−88407
methane flux from wetlands areas rel. to mean air temp. 77−78382
methane gas plumes, tracking via atmospheric acoustic sounder 80−55968
methane in stratosphere at several latitudes in 0-35 km altitudes 79−34894
methyl chloride conc. profile up to 32 km. altitude 80−36368
microwave absorpt. coeffs. of atmospheric pollutants and constituents 77−64378
microwave spectroscopic imagery of Earth from Nimbus 6 satellite 78−12026
middle atmosphere, chemical response to changes in UV solar flux 77−33167
middle atmosphere, minor constituents, chemistry and transport, conf., Seattle, USA (Aug. 1977) 79−84428
middle atmosphere, plasma and neutral gas comp. and struct. anal. via mass spectrometer probe 78−45191
middle atmosphere chemical comp., importance of energetic particle precip. 80−109213
middle atmosphere in situ meas. 80−17339
middle atmosphere processes revealed by satellite observations 80−21803
minor constituents concentration profiles, Spacelab obs. 77−21967
minor constituents detection using tunable spin flip Raman laser, review 80−55762
minor constituents transport between troposphere and stratosphere 80−105034
minor gases in middle atm., optical meas. 79−84480
minor species in stratosphere and lower mesosphere, meas. using cryogenic-spectrometer on Space Shuttle 79−58232
minor species meteorological control of lower stratosphere 79−12171
molecular complexes presence and role in residual absorpt., light scatt. obs. 80−56607
monoterpene hydrocarbons in rural atmospheres, gas chromatography/mass spectrometric anal. 80−17336
negative ions evolution, computer simulation *(French)* 77−21869
neutral and ionized atmosphere in 60-150 km altitude range, problems 77−21961
neutral atm. disturbances, reaction of midlatit. ionosphere 77−25805
neutral atmosphere, O_2 seasonal vars. rel. to E-region ionisation 79−12331
neutral composition, magnetic storm circulation significance 77−49206
neutral composition variations at F-region heights, meas. from incoherent scatt. and nightglow obs. *(Portuguese)* 80−41584
neutral upper atmosphere, components density vars. semi-empirical models 79−21085
neutrons, high-energy, flux and energy spectrum meas. at balloon altitudes 77−21836

atmospheric composition continued
NH_3, spectral line meas. using 10μm superheterodyne receiver 78−16335
nitrate conc. in aerosols, SO_2 photochem. effects 77−49103
nitrate determ. using HNO_3 collection on NaCl impregnated filters 80−81509
nitrates, gaseous, concentrations, investigations in urban and rural area 80−94123
nitrates, gaseous and particulate, conc. meas. 77−45137
nitrates over Ontario, weather pattern rel. to suspended particle composition 80−17365
nitrogenous trace gases, preliminary ^{15}N studies 78−73470
noctilucent cloud particles, sunlight scattering rel. to characts. 78−11945
noctilucent cloud region, ion comp. 77−87011
non-methane hydrocarbons, monitoring via photoionisation 78−73549
O_3 distrib. vars. rel. to urban heat island circulation in St. Louis 80−51488
organic aerosols, natural, of terrestrial origin, review 80−36381
organic compounds+OH, reaction rate consts., photochem. air pollution 78−7171
organic compounds in aerosol samples 78−73463
organic compounds photooxidation, rates, reactivity and mechanism for reaction with OH radicals 80−72104
organic constituents of particulate matter, total conc. estimate 77−37289
organic pollutants, determ. via gas chromatography after cryogenic sampling 78−81468
organochlorine residues in rainwater 78−73495
oxidant and precursors, anal. in Los Angeles Reactive Pollutant Program (LARPP) (operation 33) 80−61479
ozonograms, Oct.-Dec. 1978, Uccle, Belgium *(French, Flemish)* 80−21797
Pacific marine aerosol, continental component identification by combined neutron activation and SEM with X-ray anal. 78−3990
palaeoatmosphere, O_3 conc. effect on surface temp. 79−96807
palaeoatmosphere O_2 content, since Lower Carboniferous, fossil charcoal evidence 80−51542
palaeoatmosphere O_3 content rel. to biological evolution 77−78425
particle size distribution, observed variation over 49 day period 77−25321
particulate element conc. over USA 80−76679
particulate material, trace elements analysis by nucl. activation techniques 78−3991
particulate matter, props. inferred from lidar and solar radiometer obs. and aircraft meas. 78−61501
particulate matter emitted by Mount Etna volcano, heavy metal chem. 78−61491
particulate nitrate, pollution of S.Ontario, Canada, rel. to weather 80−76678
particulate nitrate in marine air of equatorial Pacific 80−85702
particulate size distrib. and refr. index, new lidar-radiometer method 80−77153
particulates, chemical characterisation via light scatt. method 78−69533
particulates and gaseous pollutants measurement, anal. and calibration techniques 78−69531
particulates in Cameroon air, Yaounde, urban and rural *(French)* 80−61478
particulates in Montana air, element composition, background study 80−77034
peroxyacetyl nitrate, absorpt. by grass, soil and water surfaces 77−45139
peroxyacetyl nitrate (PAN), dosage in photochemical smog, depend. on latit. 77−2227
peroxynitrates, UV absorpt., spectra, photodissoc. lifetime meas. 80−83386
peroxynitric acid form. in photochem. smog in urban atm. 77−63885
perturbations in comp. and temp. feedback, climatic effects 80−41525
perturbed atmosphere, O_3 and CO_2 rel. to thermal struct. and relaxation rates 80−8408
pesticide, DDT translocation by resuspension over Pacific N.W. forests 77−29422
Phanerozoic O budget, S isotope variations in marine sulphate evaporites 77−73810
photochemical smog, gas-to-particle conversion, organic aerosol growth rates 77−73826
photochemical smog enhancement by N,N′-diethylhydroxylamine in polluted ambient air 77−91262
plasma convection, high-latit., and ionospheric depletion, effect of displaced geomag. and geographic poles 80−26680
plasmasphere, electron temp. and conc. at 3000 km altitude, ISIS-1 meas. 79−101004
plasmasphere, mid-latit., He ions behaviour 80−41630
plasmasphere composition and density, equilib. model 79−66860
plume diffusion at Rancho Seco Generating Station, LIDAR obs. 78−11991
plumes subject to dry deposition, concs. prediction 78−28307
pollutant annual average concentration around single source, rapid estimation technique 78−81382
pollutant conc. statistical parameters determ. from truncated data sets 77−37414
pollutant concentrations freq. distrib. 77−37352
pollutant concentrations in urban atmosphere, radiation effects of elevated pollutant layers 80−97841
pollutant ground-level concentration, field meas. of benefits of increased stack height 80−76676
pollutants, atmospheric turbulent transport Monte Carlo simulation and comparison with exptl. data 79−53479
pollutants, concentrations from analytical diffusion model for long distance transport 80−94125
pollutants concentration fields determ., comparison of interpolation methods for sparse data 80−51575
pollutants in urban atmosphere, prediction of long-term mean and mean square concs. 77−2226
pollutants vertical diffusion, study using airborne gas-chromatography and numerical modelling 78−69435
pollutent, Gaussian plume model parameters for ground-level and elevated sources 80−82010
pollution, monitoring by tunable dual-line CO_2 laser 78−3977
pollution tolerance levels and norms, threshold values establishment *(Dutch)* 78−49129
positive ion concentration, in urban centre, meas. method *(Spanish)* 80−4059
positive ion concentration below 90 km altitude, rocket meas. 77−29539
precipitation, D-^{18}O relationship global climatic interpretation 80−17331

atmospheric composition continued
  precipitation, trace constituents chemical anal. in global baseline samples 79—16566
  precipitation chemical composition around Tokyo, 1967-68 obs. *(Japanese)* 78—49120
  precipitation chemistry determ., calibration of collection procedures 77—37447
  precipitation comp., pH and amount of rainfall in Michigan 77—37332
  primitive ionosphere O content rel. to thermal struct. 78—40754
  proton-induced X-ray emission and proton elastic scatt., atmospheric particles anal. 77—70399
  protonosphere, electron conc. inhomogeneities meas. by whistler method 77—67011
  protonosphere, electron content meas. from American and European sectors 78—45151
  pyrheliometric ratioing for apparent atm. transmission determ., rel. to atm. comp. 79—96809
  radiating molecules, in upper atm., rot. relax., IR emission and vibr.-rot. transitions calcs. 77—65462
  radiation belts, energetic O ions charge states theory 78—77427
  rainfall in Trinidad conc. determ. 80—82045
  relative aerosol content determ. from ERTS obs. 77—37303
  remote measurements of emitted thermal radiation, comp. estimation 77—45202
  remote monitoring using discretely-tunable IR gas lasers and heterodyne detect. techniques 78—61605
  remote sensing of cloudy atmospheres by microwave radiometry *(Chinese)* 80—51549
  retrospective analysis of air samples in UK for 1957 to 1974 period 78—3942
  ring current, energetic neutral particles as source of low-latit. E-region ionisation 78—77415
  ring current composition change from equatorial aurora obs. 78—36401
  ring current ion composition at L>4, Prognoz-7 obs. 80—98517
  rocket exhaust effluents from space shuttle model, meas. using electrets 79—53548
  Sahara dust mass, satellite radiance meas. 77—9456
  sea salt quantitative meas. over N.Atlantic 79—16624
  secondary nucleon spectra, 10^2-10^4 GeV, 2-component model *(Russian)* 78—41612
  secondary pollutants, photochemical form. from hydrocarbon+N oxide mixtures 79—53427
  smoke and SO_2 long-term mean conc. in England and Wales country areas 77—37360
  snow in Kashmir region, study of chemical components 80—94594
  SO_2 air pollution levels modelling and forecasting, statistical approach 78—81398
  South Pole, particulate trace elements, conc. and size distrib. 79—79937
  Spacelab lidar, for atm. props. meas. 77—21943
  spectral radiometric meas. of constituent vertical profiles 77—70883
  spectroradiometric measurement of temp. and gaseous composition profiles 77—9568
  St. Augustine volcano, Alaska, search for atmospheric ice nuclei production 77—13110
  St. Augustine volcano eruptions, airborne meas. and obs. 77—49053
  St. Louis aerosol, variation of elemental composition with particle size 77—49137
  stratosphere, acidic Cl vapour, midlatit. seasonal meas. 78—32142
  stratosphere, aeronomy rel. to Cretaceous-Tertiary extinctions 78—32215
  stratosphere, aerosol and gaseous constituents from spacecraft solar extinction data, inversion retrieval 79—74961
  stratosphere, aerosol conc. at Mildura, Australia following 1974 Fuego eruption in Guatemala 77—5276
  stratosphere, aerosol layer, climatic effects, review 78—81331
  stratosphere, aerosol meas., southern hemisphere, time vars., rel. to 1974-75 volcanic eruptions 79—48551
  stratosphere, aerosols latit. vars. 79—58040
  stratosphere, Aitken nuclei meas. with aircraft-borne instrument 77—64399
  stratosphere, Aitken particles, nature and sources 77—87050
  stratosphere, at. and mol. fluoresc. as species monitor, review 77—9472
  stratosphere, at. Cl and ClO radical in situ obs., rel. to O_3 depletion 78—36241
  stratosphere, atmospheric constituents mass spectrometric obs. *(Japanese)* 79—79920
  stratosphere, atomic and diatomic radicals, meas. 80—17307
  stratosphere, atomic processes, O_3 formation and destruction, book contrib. 77—37339
  stratosphere, balloon obs. of particle layer injected by aircraft at 23 km 78—81283
  stratosphere, chemical studies using Concorde aircraft, air sampling equipment 79—80058
  stratosphere, chemistry of ozone depletion 77—91256
  stratosphere, chlorofluoromethanes and N_2O latitudinal profiles 78—44989
  stratosphere, Cl-ClO-Cl cycle, possible roles of ClO*, $ClNO_3$ and HOCl 77—17185
  stratosphere, ClO remote meas. from IT solar spectrum obs. 79—58005
  stratosphere, $ClONO_2+O(^3P)$, rate consts. 77—77796
  stratosphere, $ClONO_2$ upper limits from balloon borne IR meas. 77—70743
  stratosphere, CO_2-O_3 coupling in Cl free atm., photochemical-radiative column model 80—85723
  stratosphere, COS detect. 79—58014
  stratosphere, daytime, HNO_3/NO_2 conc. ratio 78—73460
  stratosphere, dichlorodifluoromethane and N_2O conc. meas., mixing ratios 78—81281
  stratosphere, dust meas., (1970-1977) 78—73445
  stratosphere, effect of increased N fixation 78—28288
  stratosphere, emission spectrum, balloon-borne far IR Michelson interferometer meas. 79—39870
  stratosphere, F mass mixing ratio, direct meas. 77—53106
  stratosphere, gas composition, comparison of one-, two- and three-dimens. models 79—70870
  stratosphere, gas concentrations from limb sounding radiometry, inversion algorithm 80—82000
  stratosphere, global time vars. of aerosol burden and source considerations 77—25739
  stratosphere, H_2O vapour distrib., temporal and spatial vars. 77—45112
  stratosphere, H_2O vapour meas. using UV fluoresc. hygrometer *(French)* 78—65401

atmospheric composition continued
  stratosphere, halocarbons and N_2O height profile meas. at several latits. 80—72601
  stratosphere, halogen compounds global monitoring by satellite borne spectrometer 77—45162
  stratosphere, HCl and HF volume mixing ratios simultaneous meas. 80—72587
  stratosphere, HCl mixing ratio profile, radiometric meas. 77—25745
  stratosphere, HF acid, presence confirmed by solar spectrum obs. *(French)* 77—53105
  stratosphere, HO_2NO_2 abundance 78—20467
  stratosphere, intense ionisation events, effects on NO_2, O_3 and climate, rel. to life extinction 78—96273
  stratosphere, latitude-dependent O_3 depletion due to supersonic transports, model predictions 77—45051
  stratosphere, lower, H_2O and O_3 conc., far IR spectroscopy, quantitative anal. 79—39790
  stratosphere, lower, H_2O vapour latit. distrib., aircraft meas. 78—32173
  stratosphere, lower, NO and O_3 concs. geographical vars. 78—73438
  stratosphere, lower, simultaneous balloon meas. of elec. cond. and aerosols 77—73813
  stratosphere, mass spectrometric meas. of negative ions 78—96274
  stratosphere, methane meas. and predictions 79—84432
  stratosphere, minor constituent chemistry, volcanic eruption effects 79—84437
  stratosphere, minor constituent meas. 77—21874
  stratosphere, minor gases determ. using occultation technique *(Russian)* 79—25342
  stratosphere, model, temp. feedback effect on O_3 conc. 78—28277
  stratosphere, multi-ion complexes, implications for aerosols and trace gases 80—61872
  stratosphere, N_2O_5 abundance upper limit 77—5299
  stratosphere, N_2O conc. in northern hemisphere during 1975, July 77—78304
  stratosphere, N_2O vertical distrib., from balloon meas. of solar spectra 78—61493
  stratosphere, NO_2 and HNO_3 conc., simultaneous meas. *(French)* 78—16107
  stratosphere, NO and HNO_3 obs. in N.hemisphere for three seasons 78—81288
  stratosphere, NO photolysis rel. to NO_y mixing ratios 77—29399
  stratosphere, numerical model of effect of N oxides on O_3 77—53269
  stratosphere, O_3, conc. obs. by XeCl excimer laser radar 79—16681
  stratosphere, O_3, effect of CH_4, HCl and ClO 77—87032
  stratosphere, O_3, effects of agriculture 78—16123
  stratosphere, O_3 and aerosol monitoring using orbiting photodetectors 77—78445
  stratosphere, O_3 and Aitken nuclei conc. correl. over Americas 77—49141
  stratosphere, O_3 and temps., satellite obs. for 1970-71 period 77—9466
  stratosphere, O_3 and tracer particles creation and destruction, probability distribs. 78—20496
  stratosphere, O_3 conc. meas. at sunrise and sunset *(French)* 79—48535
  stratosphere, O_3 depletion, ClO influence 77—75052
  stratosphere, O_3 destruction by fluorocarbons 77—9459
  stratosphere, O_3 destruction by NO_x catalysis, comment 77—73812
  stratosphere, O_3 distrib. and circulation in meridional plane *(French)* 77—49100
  stratosphere, O_3 global distrib. Ogo obs. 77—73809
  stratosphere, O_3 meas. with ozonometer using chemiluminescent reaction of ozone and olefins *(French)* 79—48574
  stratosphere, O_3 natural depletion mechanism, radiation belt energetic electron precip. 77—41134
  stratosphere, O_3 perturbation by N fertilisers, independent variables anal. 77—53134
  stratosphere, O_3 reduction assoc. with 1972 August 4 solar proton event 78—7732
  stratosphere, O_3 reduction by natural NO_x and man-made pollution, model 77—60461
  stratosphere, O_3 reduction due to pollution, system-theoretic model 77—73848
  stratosphere, O_3 response to nuclear bomb tests 77—81966
  stratosphere, O_3 total content vars. correl. with ionospheric f_0F_2 vars. 78—45098
  stratosphere, O_3 vertical profile determ. by lidar sounding from ground 78—11972
  stratosphere, pollution meas. using balloon-borne grab-sampling system 77—29504
  stratosphere, positive ion comp., balloon-borne mass spectrometric meas. 78—32194
  stratosphere, positive ion density meas. by rocket-borne Gerdien condenser, 23-39.5 km altitude 79—84378
  stratosphere, positive ions, mass spectrometric meas. 77—49133
  stratosphere, post-Fuego aerosol layer, lidar meas., radiative and thermal implications 77—56679
  stratosphere, response to solar eclipse, sunrise and sunset 79—100907
  stratosphere, SO_4^{2-} concs. at high altitudes 78—20468
  stratosphere, temp. and O_3 vars. (1958 to 1977) 80—109222
  stratosphere, thermal response to 0_3 fluctuations 79—39797
  stratosphere, thermal struct. and trace constituents, effects of solar UV variability 78—61492
  stratosphere, thermal structure and total O_3 obs., Nimbus 4 Iris expt. 77—21839
  stratosphere, trace constituents, in situ meas. 79—8676
  stratosphere, trace constituents, laser heterodyne spectroscopy 80—109257
  stratosphere, trace constituents correlated seasonal and climatic vars. 79—84433
  stratosphere, trace gas concs. during 1976 in N.Hemisphere 80—67016
  stratosphere, trace gas concs. meas. using Michelson interferometer 80—17408
  stratosphere, trace gases, temporal and latitudinal vars. 78—40619
  stratosphere, trace species vars. during solar eclipse, theoretical study 79—58013
  stratosphere aerosol, determ. of characteristic parameters *(French)* 80—8387
  stratosphere aerosol, laser radar meas. *(Japanese)* 80—21810
  stratosphere aerosol at 34°S, change in nature 78—28286
  stratosphere aerosol content var., rel. to atm. transparency and direct solar radiation 80—82035

atmospheric composition continued
  stratosphere aerosol event, 1974-1975, balloon obs. of time development 77—45084
  stratosphere aerosol layer, Earth zonal radiation balance perturbation 80—56602
  stratosphere aerosol layer, simulated lidar return from one-dimensional model 79—44247
  stratosphere and mesosphere, microwave limb sounding 77—21940
  stratosphere and mesosphere, transport and chemical processes 77—25761
  stratosphere and troposphere, H_2, CO, N_2O, methane, chlorofluoromethanes, vertical profiles meas. 79—84384
  stratosphere minor constituents, concs., chemiluminescence in situ instrums. and techniques 80—16886
  stratosphere NO_2, global behaviour 80—17334
  stratosphere NO_2 and O_3 variations during solar eclipse 80—105017
  stratosphere NO_2 determination, observational method and behaviour at mid.-latit. 80—17414
  stratosphere NO and ClO meas. via solar occultation, influence of concs. vars. at twilight 80—85756
  stratosphere O_3 density perturbations, photochemical-radiative damping rel. to instability 78—81286
  stratosphere O_3 depletion prediction, effect of temp. coupling 78—57246
  stratosphere O_3 depletion thermal effects at 85°N latit., airborne particles influence 78—81279
  stratosphere O_3 reduction estimates, effects of water vapour changes 78—73444
  stratosphere odd N mixing ratio 77—70744
  stratosphere particles, detect. of ^{4}He rel. to extraterrestrial origin 77—56878
  stratosphere positive ions, comp. meas. 78—88877
  stratosphere sulphate aerosol, kinetics of growth by condensation in homogeneous medium *(Russian)* 80—94566
  stratosphere sulphate aerosol layer, processes, models, obs. and simulations 80—109212
  stratosphere sulphur and halogen cpds. orginating in volcanic plume 80—51474
  stratosphere water vapour, meas. via balloon-borne IR instrument 79—8718
  stratospheric aerosol particles, collection and analysis techniques 80—17306
  stratospheric O_3 density meas. using lidar, feasibility 77—60493
  stratospheric tracers, use of cosmogenic isotopes 77—41237
  sulphate aerosol, individual submicron particles detect. technique 78—69527
  sulphate aerosols, diurnal var. at rural sites in E.United States 80—30621
  sulphate concentration, Southwestern Desert of US, X-ray emission anal. 80—8378
  sulphate removal by precipitation 79—53472
  surface aerosols in Cape Verde Is., physical and chemical props. 78—85640
  surface layer aerosols variability, spectral transmittance method *(Russian)* 78—69448
  Teheran atmosphere, Pb conc. 79—21011
  terpenes, conc. meas. in Adirondack Mountains pine forest 78—32185
  tetraalkyllead, natural source 79—2367
  tetrafluoromethane, v_3 vibr.-rot. band identification in balloon-borne IR solar spectra 79—100894
  thermal power station environment, airborne elec. and microphys. obs. 77—37354
  thermosphere, annual He, N, O, N_2 and Ar vars. from Aeros Nims data 80—12578
  thermosphere, Ar global distrib., departures from hydrostatic equilib. 78—28358
  thermosphere, auroral energy deposition and neutral comp. changes, simultaneous satellite obs. 77—53264
  thermosphere, circulation and comp., effects of magnetospheric elec. field and currents 80—17446
  thermosphere, comp. changes during mag. storms, spherical asymm. 77—64501
  thermosphere, comp. changes inferred from twilight $O^+(^2P)$ airglow emission 79—62635
  thermosphere, comp. effects in acoustic gravity waves 77—21959
  thermosphere, comp. vars. rel. to temps. determined from incoherent scatter and global models 80—8467
  thermosphere, comparison of calc. and meas. O_2 densities 78—28357
  thermosphere, comparison of meas. and inferred temps. from AEROS-B 77—21958
  thermosphere, composition and temp., longitude/UT vap., global model 79—53591
  thermosphere, daytime, O_2 density indirect determ. from AE-C satellite meas. 78—12032
  thermosphere, disturbed, Ar, N_2, O and He densities, global model from Esro 4 meas. 77—37468
  thermosphere, disturbed, NO conc. rel. to anharmonic N_2 mols. vibr. relaxation 79—12322
  thermosphere, diurnal and seasonal variations of O, H and N components 77—9586
  thermosphere, diurnal vars. in temp., comp. and winds 77—87141
  thermosphere, double photoionization and doubly charged ions 79—84559
  thermosphere, eddy diffusion vars. and assoc. transport processes 77—33226
  thermosphere, electric field momentum coupling characts. 78—88958
  thermosphere, electron density and ion comp. meas., X-ray and EUV solar flux estimation 77—87145
  thermosphere, electron temp. and density relationship in daytime at solar minimum, model 78—61638
  thermosphere, empirical model of temp. and composition 80—77183
  thermosphere, Esro 4 meas. rel. to upper atmosphere heating by solar wind energy 77—37471
  thermosphere, global comp. and temp. during quiet times 77—33227
  thermosphere, global comp. and temp. empirical models during quiet times compared with ESRO 4 data 79—8732
  thermosphere, global model based on mass spectrometer and incoherent scatt. data, N_2 density and temp. 77—70897
  thermosphere, global model based on mass spectrometer and incoherent scatt. data, composition 77—70898
  thermosphere, global semiempirical models 79—66852
  thermosphere, ion photochemistry from Atmosphere Explorer C meas. 78—32261

atmospheric composition continued
  thermosphere, longitudinal comp. vap. in geomagnetically quiet conditions 79—75001
  thermosphere, lower, CO_2 concs. meas. 78—96336
  thermosphere, lower, O and O_2 density meas. by mass spectrometer technique 78—57348
  thermosphere, lower, O and O_2 distrib. 80—4159
  thermosphere, lower minor components concs. rel. to turbulent diffusion coeff. seasonal vars. 79—53424
  thermosphere, middle, ion comp. and temp. profiles from incoherent scatter radar studies 80—72654
  thermosphere, midlatit. models seasonal vars. at solar max. and low geomag. activity 78—57376
  thermosphere, model based on satellite drag data 78—69555
  thermosphere, N_2, Ar densities response to major geomag. storm 77—9582
  thermosphere, N and NO conc. depend. on solar activity 80—77178
  thermosphere, N densities at high altitudes 79—16729
  thermosphere, N density, global empirical model 77—33232
  thermosphere, N number density meas., 180-450 km altitude 77—87143
  thermosphere, Ne density in situ meas. by AE-C satellite 77—21956
  thermosphere, neutral comp. meas. between 90 and 220 km by rocket-borne mass spectrometer 78—77383
  thermosphere, neutral comp. vars. 77—87142
  thermosphere, neutral composition intercomparison of satellite obs. 77—53261
  thermosphere, NO daytime conc. 79—2408
  thermosphere, O_2 concs. and absorpt. cross sections from EUV occultation profiles 78—28356
  thermosphere, O concs. rel. to low-latit. NmF2 annual and semiannual periodicities 77—53306
  thermosphere, O concs. rel. to nighttime F_2-layer height 79—8745
  thermosphere, O global distrib., dynamical effects 79—74996
  thermosphere, photoelectron daytime energy distrib. meas. by AE-E satellite 78—88953
  thermosphere, semiannual variations of n(O), 120-500 km heights 77—49214
  thermosphere, temp., density and comp., new models 77—64502
  thermosphere, tidal dynamics model with O-N_2 diffusion effects 80—101465
  thermosphere, tidal vars. 78—96334
  thermosphere, transport processes in diurnal tide, satellite meas. 78—88959
  thermosphere and mesosphere, average daily closed model 77—17264
  thermosphere constituents, density vars. rel. to eddy diffusion coeff. global models determ. 79—21086
  thermosphere N and NO, diurnal variability 77—78549
  thermosphere neutral composition, momentum source signatures 78—77380
  thermosphere $O(^1D)$ content, role of $N(^2D)+O_2$ reaction 80—90270
  thermosphere O and O_2 densities, photochemical deviations from diffusive equilib. 77—37470
  thermosphere seasonal and latitudinal variations in temp. and composition 77—45207
  thermosphere storms, comp. vars. and related ionospheric effects 77—9583
  thunderstorm production of O_3 and N oxides 77—37300
  topside ionosphere, comp., temps. and electron loss coeff. over Arecibo 78—36386
  topside ionosphere, ion composition changes during 13 Sept. 1967 storm 78—16232
  topside ionosphere ion comp. from VLF hiss obs. near plasmapause *(Japanese)* 77—21999
  topside ionosphere model, O^+ and H^+ continuity and momentum eqns. 80—51603
  topside magnetospheric cleft ionosphere, ion and electron densities and temps. 77—29571
  trace constituents, LIDAR teledetect. and meas. for pollution control *(French)* 80—7992
  trace constituents by IR spectra, altitude distrib. technique 79—34985
  trace constituents during May 1976 over continental United States 78—16084
  trace constituents in Indian west coast SW monsoon aerosols and rain 80—81967
  trace element concentrations in Valencia region under typical meteorological conditions *(Spanish)* 78—44992
  trace elements, 1976 survey in UK 78—32212
  trace elements, long range transport 79—58044
  trace elements in UK, 1978 survey 80—90208
  trace elements in United Kingdom atmosphere, 1975 survey results 77—25759
  trace gas concentration determ. by Spacelab passive sounding expt. 77—21950
  trace gas sampling, chemical absorption filter techniques 80—17305
  trace gas sinks in Sahara 79—34888
  trace gas transport and photochemistry rel. to greenhouse effect *(Russian)* 80—81989
  trace gases and pollutants, data compilation on mag. tape 78—44995
  trace gases at Sepik River coast, Papua New Guinea 78—85642
  trace gases vertical conc. from solar radiation absorpt. spectra *(Russian)* 78—69442
  trace metals, global cycles, anthropogenic impact 80—3547
  trace metals and sulphates, record in Greenland Ice Sheet core 78—7667
  trace metals concentrations, meas. in Antarctic snows (1914 to 1974) 79—34867
  trace species, multiple scattering effect on concs. 78—85692
  trichlorofluoromethane, rate const. for reaction with OH and tropospheric lifetime 77—64366
  trichlorofluoromethane, tropospheric lifetime 79—53497
  trichlorofluoromethane reaction rate with atmospheric-like ions 77—70723
  tropopause, ^{7}Be, ^{137}Cs and shortlived fission product concs. *(German)* 77—29408
  tropopause, sulphate and nitrate mixing ratios obs. 80—61835
  troposphere, ^{3}H in water vapour, rel. to reactor release detect. 78—11988
  troposphere, aerosol monitoring using Spacelab lidar system 77—21876
  troposphere, composition, natural and effects of pollution 78—28262
  troposphere, H_2O vapour large-scale irregularities, effects on radioastronomical seeing 78—24339
  troposphere, halocarbon decomp. by natural ionisation 77—33139
  troposphere, Hg conc. determ. *(German)* 79—53406

atmospheric composition continued
troposphere, HNO_3 vapour and particulate NO_3 global meas. 78—88904
troposphere, interhemispheric gradients of CF_2Cl_2, $CFCl_3$, CCl_4 and N_2O 78—81289
troposphere, mean temp. rel. to sea surface temps. and volcanic aerosols 77—33168
troposphere, mesoscale anal. of O_3 meas. in Boston metropolitan area 78—32178
troposphere, methane and ethane conc. meas. in nonurban area 78—32184
troposphere, methane conc. meas., geographical and altitude distrib. *(Russian)* 77—60449
troposphere, methane variations, transport and photochemistry 77—53138
troposphere, methyl chloroform as indicator of OH radical abundance 77—49134
troposphere, N_2O continuous meas. 78—81318
troposphere, negative ions evolution times 79—70829
troposphere, NO_2 vertical column abundance, optical absorpt. meas. 78—85632
troposphere, NO emission effects on O_3 and OH 77—86992
troposphere, nonurban, conf., Hollywood, Florida (Nov. 1976) 78—32174
troposphere, O_3 background mean. conc., balloon obs. 78—32189
troposphere, O_3 budget, one-dimens. photochem. model 78—32180
troposphere, O_3 conc. and vars. in clean remote atm. 79—62554
troposphere, O_3 distrib., evidence for higher background values, comment 79—39801
troposphere, O_3 distrib. and origin 78—85663
troposphere, O_3 distribs. meas. with airborne laser absorpt. spectrometer 79—2344
troposphere, O_3 meas. in rural areas 78—32179
troposphere, O_3 mixing ratio meas. rel. to stratospheric-tropospheric exchange at polar latits. in summer 80—72599
troposphere, O_3 photochemical prod. and influence on climate 80—36365
troposphere, O_3 photochemistry 77—81968
troposphere, O_3 transport and photochemistry 77—53137
troposphere, O_3 variations along meridional band 78—32190
troposphere, OH concs. rel. to CH_4, CO, H_2 and CH_3CCl_3 budgets 77—86991
troposphere, particle size distrib. skewness and mode radius relationships 77—45121
troposphere, reduced S, H_2S role 78—49123
troposphere, Sahara dust cont. over N.Atlantic from air cond. meas. 78—92897
troposphere, trace gases and free radicals, two-dimens. model 78—32214
troposphere aerosols having soil-derived component, commonalities in measured size distribs. 77—60454
troposphere and stratosphere, H_2 mixing ratio vertical profiles 78—32181
lower troposphere modelling, chemical kinetic data needs, conference, Reston, Virginia (1978 May 15 to 17) 80—62383
troposphere OH radical concentration, determ. method using atmospheric ^{14}CO meas. *(German)* 80—8419
troposphere over equatorial N.Atlantic Ocean, dust conc. rel. to Sahelian drought 77—78356
turbidity of Barcelona's air, anal. of 1971-7 obs. *(Spanish)* 80—36375
turbidity rel. to atmospheric contamination, helicopter soundings *(Spanish)* 77—9499
turbulent diffusion, of particles in air, analytical numerical method 78—32257
UK, trace elements survey, 1977 results 79—20960
ultrafine particles and ions, form. from trace gases 77—25742
upper atm. parameters daily vars. at midlatits., reference system 77—29521
upper atmosphere, comparison of satellite self-contamination expts. and scatt. return flux calcs. 78—40722
upper atmosphere, constituents detection, using submillimetre wave heterodyne radiometry 78—49183
upper atmosphere, dynamical properties 79—75005
upper atmosphere, general review 79—39997
upper atmosphere, H_2O prod. from H-implanted interplanetary dust grains 78—65445
upper atmosphere, ion and neutral densities rel. to $N_2^+ + O$ reaction rate coeff. 77—53288
upper atmosphere, mag. storm effects on comp. and tropical UV airglow 77—45214
upper atmosphere, N content temporal vars. 77—60501
upper atmosphere, N density from dayglow far UV N and N_2 emissions 78—28361
upper atmosphere, neutral and ion densities response to mag. storm, OGO 6 obs. 77—9588
upper atmosphere, neutral comp., rel. to F_2-layer hemispherical differences 78—69603
upper atmosphere, neutral comp. vars. rel. to negative ionospheric storms numerical simulation 79—25393
upper atmosphere, neutral particles conc. rel. to ionosphere slow MHD waves speed 78—45093
upper atmosphere, neutral waves determ. from AE satellite meas. 79—58139
upper atmosphere, nightglow near IR continuum rel. to comp. 77—78551
upper atmosphere, O_2 and O_3 concs. from $O_2(^1\Delta_g)$ airglow height profile meas. 78—45077
upper atmosphere, O_3 and Cl densities from OAO 3 stellar occultation meas. 77—9580
upper atmosphere, $O(^3P)$ concs. rel. to 557.7 nm line and Herzberg bands excitation 79—75008
upper atmosphere, O and N density meas. by Apollo-Soyuz UV spectroscopy 77—33228
upper atmosphere, O concs. rel. to F-region electron density parameters 77—91346
upper atmosphere, odd N prod. by meteoroids 79—2404
upper atmosphere, secondary proton fluxes above 500 MeV at 200-300 km 77—64497
upper atmosphere, semiannual density vars. form. mechanism 77—25807
upper atmosphere, UV extinction meas. of O_2 density 79—2406
upper atmosphere, water vapour rel. to winter radio absorpt. and Na nightglow 77—33239
upper atmosphere H distribution and daily density vars. 77—29522
upper atmosphere He distrib., dynamical model 77—70896
upper atmosphere He dynamics, use of Jacchia (1977) empirical model 78—77381

atmospheric composition continued
upper atmosphere N_2/O ratio, seasonal vars. of negative storm effects 77—53289
upper atmosphere neutral composition, cryo mass spectrometer meas. in winter anomaly campaign 78—45192
upper atmosphere research applics., of quadrupole mass spectrometer, book contrib. 77—25911
upper atmospheric constituents, absolute high-resolution far IR meas. 77—41249
urban aerosols, Boston area, multivariate anal. for element sources identification 77—37357
urban air, total suspended matter estimation, comparison of three methods 77—37416
urban air pollution, area-source model 77—37358
urban area, photochemical pollutants, atmospheric parameters effect 77—17212
urban atmosphere, thin layer brown haze form. 77—56685
urban atmospheres, modelling of temp. and pollutant conc. distribs. 77—45143
urban plume particulates collected on Anderson 8-stage impactor stages, chemical anal. 78—69433
urban pollutants inorganic nonmetallic species, precipitation scavenging by convective storm systems 80—12039
urban troposphere, photochemistry, kinetic study 77—45058
urban ultragiant aerosol particles conc. meas., St. Louis, Missouri, USA 77—49159
urban-suburban air pollutant transport, chemical and physical transformations 77—37399
UV spectrophotometric obs. of upper atm. from Spacelab 77—21964
Van der Waals molecules comp. of lower atmos. 80—85699
vehicle generated air pollutants, correl. study 79—21012
Vizcaya, Spain, B, Mg, Cr, Mn, Fe, Co, Ni, Pb, Ga, Ge and Si conc. in atm. and rainwater *(Spanish)* 78—57264
Vizcaya, Spain, Na, Mg, Cr, Al, Ti, Cu, Ag, Zn, Co and Ni content in sedimentable powders *(Spanish)* 78—57265
volatile elements enrichment by volcanic activity, Augustine volcano example 79—39796
volatile organic compounds determ. in city air, gas chromatography techniques 78—12003
volatiles, comparison with Mars, rel. to meteoritic source 78—36482
volcanic activity, continual degassing of Earth, rel. to atm. comp. 79—70775
volcanic dust, apparent periodicity in dust veil index 79—92514
volcanoes airborne particle and gas emissions, meas. 79—2203
Washington, D.C., chemical element balances and pollution sources 79—12174
water droplets, sources and effects of surface organic monolayers 78—69412
water drops, quasi-steady approximation for evaporation and condensation 77—21854
water drops collision efficiency in atmosphere 77—29378
water vapour, Raman lidear meas., daytime atmosphere 80—85718
water vapour comparison for IR observatory sites 78—11973
water vapour conc. rel. to microwave frequency atmospheric transparency, 3-13 cm^{-1}, meas. 80—12476
water vapour concs. above mesopause 77—73898
water vapour contamination of Lyman-α ion chambers 79—8731
water vapour of extraterrestrial origin, possible role in Sun-weather relationships 78—69416
water vapour polymers, rel. to absorpt. in IR window 77—45145
water vapour variations, baseline results from Smithsonian obs. 78—32197
water vapour vertical profile in stratosphere *(French)* 80—77033
AgI, atmospheric ice forming props., impurities and surface state effects *(French)* 78—20459
Ar isotopes in ancient atmos., shungite Ar degassing 80—85749
^{40}Ar concentrations in sialic crust and atmosphere, rel. to form. from upper mantle 79—44153
^{7}Be aerosols content increase over Pacific Ocean during strong jet stream 77—78373
^{7}Be as a tracer for helio-geophysical phenomena 80—98525
^{7}Be, cosmic-ray-produced, mean tropospheric residence time at north temperate latits. 78—85633
^{7}Be, distrib. within high-press. systems in E.United States 80—4072
Br/Pb ratios in atmospheric particulate matter over Perth, W.Australia, 1971-6 var. 79—34455
C cycle, global modelling perturbations 80—31114
C in suspended particulates, meas. technique 80—76686
C, non-methane organic, in global troposphere 78—73462
C particles in aerosol, obs. of Denver Brown Cloud 80—81961
CH^+ in upper atmospher, obs. following trimethylaluminium high altitude release 79—48591
CO abundance, geographical, seasonal and secular vars. *(Russian)* 78—53700
CO, abundance determ. by analysing solar spectra 78—85643
CO abundance meas. method *(Russian)* 79—25343
CO, air pollution in Sheffield, conc. var. 80—16863
CO, anthropogenic emissions, implications for atm. CO-OH-CH_4 cycle 77—49160
CO, atmospheric content meas. in N and S hemispheres *(Russian)* 77—13103
CO, condensation nuclei and O_3, meas. on aircraft flight 79—58010
CO, content observed on circumpolar airliner flight 80—51475
CO distribution, comments on appl. of one-dimensional mixing models 77—45086
CO, global prod. rate from methane surface flux meas. *(Russian)* 78—36223
CO, global production by plants 77—86993
CO in troposphere, interhemispheric transport study 80—31106
CO mixing ratio in mesosphere from ground-based microwave meas. 79—58036
CO near highways, line source dispersion models, comparison 79—12247
CO, pollution from road traffic, street level conc. 80—81500
CO, production from oxidation of vegetation hydrocarbon emissions 78—88881
CO, stratosphere content at mid-latitude, simultaneous N and S hemisphere obs. 80—77052
CO, troposphere vertical profile, eastern USA in winter 80—77035
CO, tropospheric latitude distrib., model involving production and transport 80—41483

atmospheric composition continued
CO_2, accumulation in atmosphere, effect on climate and harvests 80−40940
CO_2 affected by biomass burning 80−97838
CO_2, air composition at Barrow, Alaska, wind direction depend. 80−85704
CO_2 and N_2 vibrational temps. at 40 to 140 km altitude 77−70762
CO_2 and stratospheric O_3, two-dimens. model calc. 79−62564
CO_2, anthropogenic, possible influence on atmospheric temp. 80−51486
CO_2, atmos. var. at Mauna Loa Obs., Hawaii during 1964-71 period 77−37365
CO_2, atmos. var. at S.Pole in 1957-71 period 77−37366
CO_2, atmospheric content, climatological consequences *(Dutch)* 80−98411
CO_2 baseline monitoring station network, intercalibration 77−64491
CO_2, biosphere as source and/or sink 79−88030
CO_2 climate and society, IIASA conf. (Laxenburg, Austria, 1978 February 21-24) 79−8679
CO_2, climatic effects of increasing content 79−88029
CO_2 conc., effects of different future energy strategies, rel. to global climate 79−83640
CO_2 conc. increase problem, radiative-convective model 77−66977
CO_2, conc. increases rel. to ^{13}C vars. in N.hemisphere trees during last 150 years 80−17363
CO_2 conc. meas., comparability 78−20495
CO_2, conc. meas. at Baring Head, New Zealand 79−100931
CO_2, conc. vars., cycles and trends 79−84381
CO_2 concentration doubling, climatological significance 80−101426
CO_2 concentrations, meas. via solar occulatation sounding using narrow-band radiometers 80−98452
CO_2 concs. over native grassland in Saskatchewan 77−45120
CO_2, content, climate sensitivity study with global climate mathematical model 80−31117
CO_2 content, continuous automatic monitoring by coulometric method 79−53537
CO_2 content, impact on snow and water surfaces cooling 79−92569
CO_2 content, response to deep-sea injections of fossil-fuel CO_2 80−31090
CO_2 content of atmosphere, role of C storage by forests and oceans 78−53718
CO_2 content of polar ice, 20000 yr BP 80−61891
CO_2 content rel. to temp. changes since 1665, statistical study 79−8680
CO_2 correl. with Pacific sea surface temp. 77−29307
CO_2 cycle, effects of soil organic C 79−58063
CO_2, decrease during 1963-69 period 79−84380
CO_2 diurnal and seasonal vars. in air over Tehran 77−37396
CO_2 effect on global radiative heat balance model 78−3863
CO_2 effects on long-term global sea surface temp. vars. 78−73398
CO_2 emissions reduction approach *(German)* 78−49121
CO_2, form. from fossil fuel combustion in atm., effect on climate 79−2359
CO_2, fossil fuel generated, models for ocean uptake 79−88031
CO_2 from fossil fuel burning and global C budget 80−77080
CO_2, future atm. level prediction using atm. and ocean models 78−61549
CO_2, global problem of increasing levels 79−88032
CO_2 greenhouse effect, surface temp. calc. 80−26587
CO_2, impact on climate 80−31118
CO_2 in atmosphere, significance of deforestation 79−74572
CO_2 in urban atmosphere, dependencies and trends 80−16870
CO_2 increase and global warming, atmospheric temp. and precipitation changes 80−36389
CO_2 increase effects, radiation energy balance and temp. 80−12498
CO_2 increase effects on stratospheric O_3, photochem. and radiative transfer model 78−65370
CO_2 increase from fossil fuel burning, greenhouse effect, threat to W.Antarctic ice sheet 78−28296
CO_2 increase in ocean water masses, direct obs. 79−34854
CO_2 increase rel. to future climate, coupled atm.-ocean model 79−58082
CO_2 increase rel. to Mesozoic greenhouse and climatic warming 79−20963
CO_2, increasing concs. effect on heating rates 80−17376
CO_2 induced atmospheric temp. rise, Arctic sea ice decay 80−61802
CO_2 input from burning wood 78−81368
CO_2, land biota changes rel. to C cycle 77−70785
CO_2, meas., fast response sensor design, for eddy correl. flux meas. 79−5622
CO_2 meas. at Hauna Loa Obs. 1974-76 period 78−7685
CO_2 problem, increase from fossil fuel combustion 79−16623
CO_2, recent trends of $^{13}C/^{12}C$ ratio, rel. to tree ring studies 79−25311
CO_2 record at Mauna Loa Observatory, short-term disturbances 78−88879
CO_2 rel. to C reservoir changes 78−57278
CO_2, source functions and future CO_2 burden 78−24368
CO_2, stratosphere content at mid-latitude, simultaneous N and S hemisphere obs. 80−77052
CO_2, uncertainties associated with effect on global climate 79−88028
CO_2, wood vs. fossil fuel as source 77−53162
CO_2-climate problem developments 78−20460
CO_3^-, thermally relaxed, photodetachment cross-section and solar detachment rate determ. 77−58094
$COCl_2$ (phosgene) in ambient air of California 77−13119
CS_2, COS, oxidation as SO_2 sources 80−4085
$^{13}C/^{12}C$ from tree ring ^{13}C records, interpretation problems 79−62573
$^{13}C/^{12}C$ in atmosphere CO_2, vars. in last 22 yrs. 80−104530
$^{13}C/^{12}C$ ratio variations in Pinus longaeva (bristlecone pine) cellulose during the last millennium 79−44217
^{14}C content, measurement from tree rings, effects of ^{14}C radial flow 78−28346
^{14}C, cosmogenic, diffusion distrib. in dynamic reservoir 80−101510
^{14}C meas. on submerged forest floating chronologies, rel. to atm. ^{14}C vars. 79−48563
^{14}C natural var., Suess effect determ. accuracy 79−96801
^{14}C production in Tunguska cometary impact 77−78720
^{14}C temporal fluctuations 79−5591
^{14}C variability due to variable Sun 80−85730
$^{14}C/^{13}C/^{12}C$ vars., Bermuda coral 200 yr. record 79−16570
^{14}CO measurement, method for tropospheric OH radical conc. determ. *(German)* 80−8419
Cd, Pb, Mn in particle size fractionated aerosols, flameless atomic absorpt. determs. 78−69434

atmospheric composition continued
Cl particulate distrib. in Houston-Galveston area 79−12252
$Cl+methane \rightarrow HCl+CH_3$, absolute reaction rate, flash photolysis-reson. fluoresc. obs. 77−56222
$Cl+O_3 \rightarrow ClO+O_2$, rate consts. meas. 77−60059
$^{38}Cl+ethane$ (methane)(vinyl bromide), rate consts., stratospheric temps., radiotracer meas. 77−48632
Cl_2-O_3 system photochemistry rel. to stratospheric composition 77−16849
ClO, aircraft search for 3 mm emission in stratosphere 80−41510
ClO composition of stratosphere, balloon borne in situ reson. fluoresc. obs. 80−90167
ClO, fundamental vibr.-rot. spectrum, rel. to remote sensing 77−42317
ClO, predissociation cross sections and rate consts. 77−70763
ClO radical, IR vibr.-rot. spectra, background data for atm. meas. 78−58679
ClO, UV absorpt., lab. spectra rel. to atmos. identifications 77−34653
$ClO+NO_2 \rightarrow ClNO_3$, reaction rate consts., stratospheric appl. 77−78306
$ClO+NO_2 \rightarrow ClONO_2$, fall-off curves, N inclusion effects 77−63910
$ClO+O(NO) \rightarrow Cl+O_2(NO_2)$ rate consts. meas. 77−60059
ClO_x, reaction rate consts., atmospheric gas phase reactions, review 77−81390
ClONO, near UV absorpt. spectrum, rel. to atm. chem. 77−30881
$ClONO_2$, chem. degradation in stratosphere 77−33134
$ClONO_2$, form., photolysis in stratosphere, photochem. absorpt. cross sections, UV spectra 77−33154
$ClONO_2$, relative abundance among stratospheric Cl compounds 77−33155
$ClONO_2$, solar photodissoc. rates, current levels in stratosphere 79−53496
$ClONO_2$, stratospheric distrib. at sunset, balloon borne IR solar spectra obs. 80−41487
$ClONO_2+OH$, reaction kinetics, stratospheric conditions 77−86303
$ClONO_2+O(^3P)$, fast flow reaction, rate const. 77−12777
$Cl(^2P)+ClONO_2$, reactive channels, stratospheric altitudes 77−60038
$Cl(^2P_{3/2})+O_3(H_2O_2)$(methane) reaction kinetics, temp. depend., reson. fluoresc. obs. 77−4903
^{60}Co, gamma radioactive source, buildup factor determination for meas. in air *(Rumanian)* 78−49132
^{137}Co, gamma radioactive source, buildup factor determination for meas. in air *(Rumanian)* 78−49132
Cs_2, precursor for atm. COS 79−53490
Cu, meas. in aerosol particles produced by ocean 79−58050
Fe aerosol source determ. by gamma-ray spectroscopy 77−41235
H, energetic, from radiation belts, rel. to interplanetary H origin 77−9645
H in mesosphere and thermosphere, UV dayglow Lyman α and β obs. 80−109290
H^+ in E United States precip., concs. behaviour 78−92962
H^+, O^+, conc. in upper atm., Aureole 2 satellite mass spectrometer obs. 78−53766
H_2 and O_2 densities near 100 km altitude, from UV stellar occultation obs. 77−9579
H_2, composition of marine air and surface water in N.Atlantic 80−77057
H_2 in troposphere, latitudinal and vertical distrib. 78−49089
H_2, production from oxidation of vegetation hydrocarbon emissions 78−88881
H_2 residence time from interhemispheric HT transport meas. 78−32182
H_2 sources and sinks, anthropogenic activity influence 77−64394
H_3BO_3 evaporation from seawater, major source of atm. B 79−2293
HCl, atmospheric measurements using ground based IR spectroscopy *(French)* 80−81975
HCl production mechanism, in cloud, chemical model with trace gases 77−37325
HCl, stratosphere content at mid-latitude, simultaneous N and S hemisphere obs. 80−77052
HCl, vertical distrib. in stratosphere 78−20470
HF, atmospheric measurements using ground based IR spectroscopy *(French)* 80−81975
HF meas. in upper stratosphere 77−45070
HF, stratosphere content at mid-latitude, simultaneous N and S hemisphere obs. 80−77052
HF/HCl, ratio in 14-38 km region of stratosphere 78−20469
HNO_2, obs. of lower atmos. pollution in W.Europe 80−72106
HNO_3, IR spectra rel. to abundance in stratosphere 80−12464
HNO_3 in marine air of equatorial Pacific 80−85702
HNO_3, stratospheric composition, in situ obs. 80−105077
HO, average tropospheric concs. in northern and southern hemispheres 78−32140
HO fluorescence detection, interference suppression by sampling method 80−8431
HO_2 and HOCl, struct., vibr. freqs., IR intensities, ab initio calcs. 79−98007
HO_2 radical, atmospheric reactions studied by laser mag. reson. spectroscopy 80−12511
$HO_2+HO \rightarrow H_2O+O_2$, rate coeff. meas. by laser mag. reson., atm. chem. appl. 77−52614
$HO_2+O \rightarrow HO+O_2$, rate coeff. meas. by laser mag. reson., atm. chem. appl. 77−52614
H_2O, abundance determ. by analysing solar spectra 78−85643
H_2O dimer, conc. in H_2O vapour of different temps. and vapour press. *(Chinese)* 80−109237
H_2O dimer, meteorological implications 80−8418
H_2O in stratosphere, maintenance of extreme aridity 80−105028
H_2O in stratosphere, mixing ratio profiles from IR solar spectra obs. 80−105015
H_2O isotopic sampling apparatus for troposphere *(French)* 80−94614
H_2O, liquid and vapour, remote sensing with Nimbus 5 microwave spectrometer 77−49129
H_2O mixing ratio, in-situ obs. using NOAA UV fluoresc. instrument 80−90137
H_2O, stratosphere content at mid-latitude, simultaneous N and S hemisphere obs. 80−77052
H_2O, stratospheric composition, in situ obs. 80−105077
H_2O, vapour, condensation in presence of H_2SO_4 and HNO_3 pollutants 78−81343
H_2O vapour, laser sounding by reson. method *(Russian)* 77−33185
H_2O vapour conc. meas. by laser absorpt. techniques 78−61595
H_2O vapour meas. in mesosphere from ground-based microwave obs. 77−33161

atmospheric composition continued

- H_2O vapour mixing ratio and influence on tropopause over India 77—53123
- H_2O vapour-phase complexes, rel. to anomalous submm. atm. spectra 78—16156
- H_2O vertical distrib. in stratosphere, UV fluorescence meas. 79—34891
- H_2O-CO_2, IR radiation transfer, CO_2 build-up effects on climate 79—80028
- H_2O_2 vapour, UV absorpt. cross sections, photodissoc. rate 78—32222
- HOCl abundance in stratosphere 79—84427
- HOCl as inert atmospheric Cl reservoir, prospects 79—12207
- HONO (nitrous acid), obs. in urban atmosphere by differential optical absorpt. 80—76677
- HO_2NO, unimol. dissoc., rate consts., temp. depend., atmospheric implications 78—7175
- HO_2NO_2, gas phase, in stratosphere, UV and IR absorpt. cross sections 79—13733
- H_2S contrib. to atmospheric S cycle 78—73473
- H_2S in N. equatorial Atlantic rel. to global S cycle 79—12165
- H_2S in troposphere, photochem. production reactions 80—90112
- H_2SO_4 aerosol, filter sampling of air, possible artifacts 80—82079
- H_2SO_4, aerosols heterogeneous reactions and role as tropospheric sinks 80—72612
- H_2SO_4 gas phase meas. in stratosphere 80—36366
- H_2SO_4 secondary aerosol form. in urban atmosphere 77—33137
- H_2SO_4-H_2O droplets, equilib. size and comp., quick estimation method 79—66767
- H_2SO_4-H_2O solution aerosol particles nucleation in stratosphere 77—56678
- HT and HTO, stratospheric vertical transport of water 77—9463
- HT, HTO, concs. rel. to water vertical transport in stratosphere 79—2347
- HTO, atmospheric condensation-evaporation model 77—29326
- He^+ in thermosphere, Atmosphere Explorer-C abundances rel. to solar EUV flux 79—16919
- $^3He/^4He$ ratio in atm. He, mass spectrometric meas. 77—9447
- Hg, average future content of air in European Economic Community 79—8687
- Hg in S.New England coastal rain 80—41508
- ^{131}I, gamma radioactive source, buildup factor determination for meas. in air *(Rumanian)* 78—49132
- K-rich aerosol emission by tropical forest *(French)* 79—100551
- ^{85}Kr conc. 80—93756
- ^{85}Kr, separation technique, preliminary results *(German)* 78—16222
- N and NO in lower thermosphere polar regions under auroral perturbs. 77—73897
- N compounds exchange between ocean-atmosphere-continent system 78—3794
- N, in equatorial thermosphere, seasonal and diurnal variation 80—85782
- N in upper thermosphere, impact of gas-surface reactions on mass spectrometric meas. 79—66849
- N oxides, release by burning of fossil fuels, rel. to acidity of rain and snow 80—26590
- N oxides and ammonia, atmospheric cycles 79—48562
- N production in upper atmos., model of far UV dayglow 80—90271
- N_2 in thermosphere, seasonal-latitudinal tidal struct. and mass density 80—101467
- N_2 in upper atmos., vibr. level distrib., theory 80—41576
- N_2, thermosphere composition, temp. and turbulence, 1967-75 obs. 80—51588
- N_2^+ 4278 Å emission and electron flux comparison in auroral zone 77—87151
- N_2/O disturbances in upper atmosphere, seasonal vars. in latit. struct. 78—32264
- NH_3 budget contribs., aircraft meas. 78—73469
- NH_3 content of Southern Ocean air 80—61871
- NH_3 determination, method 80—56614
- NH_3 fluxes into free atmosphere over W.Germany evaluation 80—94132
- NH_3 from undisturbed land 77—81967
- NH_3, gas complex analysis method, resonance absorption with pulsed laser light *(Japanese)* 80—36421
- NH_3 gas conc. and acid sulphate aerosols existence 77—81998
- NH_3 in troposphere, vertical distrib. by photochem. model 80—85701
- NH_3 microdetermination by ring oven technique 77—45164
- NH_3, ν_2 vibr.-rot. band identification in ground level solar spectra 78—81287
- NH_3, troposphere vertical profile, daily and seasonal variation 80—85700
- NH_4^+, NO_3^-, in rain water collected at Julich, Germany, N isotope comp. 78—57284
- $(NH_4)_2SO_4$ aerosol production under elevated temp. inversion in Cleveland Country, model 78—81397
- $(NH_4)_2SO_4$, aqueous solns. and cryst., optical consts. meas. rel. to atm. aerosol props. 77—52034
- NO abundance meas. in equatorial upper atm. 77—78547
- NO airglow, 2150 Å (1,0) γ-band intensity meas. with polarising NO photometer 78—45076
- NO and NO_2 mixing ratio profiles of stratosphere from IR sunset spectra 80—94563
- NO, conc. in auroral arc from ionic struct. meas. 77—2292
- NO, concs. in aurora 77—2291
- NO densities in upper atmosphere, rel. to global ionospheric absorpt. meas. on board ships 80—98500
- NO density, high-altitude rocket meas. 78—45068
- NO density in lower E-region, diurnal and seasonal effects at low latits. 78—88976
- NO, density profile from airglow obs., 72-120 km altitude 80—105094
- NO density variations in E-region, theory, ion-neutral chem. constraints 79—75027
- NO, gamma band emission rate factor, rel. to upper atm. comp. determ. 77—54572
- NO, gas complex analysis method, resonance absorption with pulsed laser light *(Japanese)* 80—36421
- NO global morphology in lower E-region 78—88975
- NO, high frequency discharge 79—82105
- NO, in high-latit. lower thermosphere 77—37467
- NO in lower thermosphere, joint meas. by rocket borne UV photometer and mass spectrometer 78—40723
- NO in middle atmosphere, role of eddy diffusion in mesosphere and lower thermosphere 80—109198
- NO, in upper atmosphere, excitation of auroral 2150 Å emission 77—9594

atmospheric composition continued

- NO, latitudinal gradient in thermosphere 79—100991
- NO meas. to 45 km altitude using balloon-borne chemiluminesc. detector 77—29397
- NO mixing ratios near stratopause, chemiluminescent meas. 79—34893
- NO, NO_2, O_3 conc. meas. at ground level at unpolluted maritime site 78—3951
- NO production by lightning discharges 77→17189
- NO, production by lightning, shock and channel heating methods 80—72581
- NO, stratospheric growth before sunrise by photolysis 77—29356
- NO, surface mixing ratios meas. in equatorial Pacific region 79—100893
- NO, thermosphere UV spectral absorpt. and density profile 80—85781
- NO, time-depend. profile rel. to temporal vars. in HF ionospheric absorpt. 77—53305
- NO, troposphere content, 0-7 km altitude over clean and polluted areas 80—51478
- NO^+ cluster ion formation in D-region, temp. control by ion obs. 80—61931
- NO^+, in ionosphere, form. by $N(^2D)+O$ associative ionisation 80—4161
- $NO/NO_2/O_3$ contents measurement, monitors intercalibration 78—69529
- $NO+O_3 \rightarrow NO_2+O_2$, rate const., 203-361K, fast flow method 77—33143
- $NO^+ + 2N_2 \rightleftharpoons NO^+.N_2 + N_2$, rate const., enthalpy and bond strength 77—16809
- NO_2, air over N.Germany coast, obs. 80—26584
- NO_2, atmospheric abundance meas. using solar absorpt. method *(Japanese)* 80—94556
- NO_2, atmospheric content optical determ. *(Russian)* 77—81962
- NO_2, atmospheric content from aircraft-borne spectrophotometry *(Russian)* 79—34903
- NO_2 concs. in dwellings with gas or electric stoves 78—16086
- NO_2 continuum, quenching by Ar, CO_2 and NH_3 79—88520
- NO_2, determ. from solar and lunar spectra in visible region obs. from ground *(French)* 79—53511
- NO_2, in stratosphere at latitude 45°S at midsummer, ground based meas. 79—96784
- NO_2 in stratosphere during Antarctic winter 79—34892
- NO_2 in stratosphere mixing ratio profiles from IR solar spectra obs. 80—105015
- NO_2, minor atm. components, visible absorpt. spectra, temp. depend. *(French)* 80—36355
- NO_2 nighttime concs., hydrocarbon reductions, potential effects, outdoor smog chamber expts. 77—70720
- NO_2, stratospheric, ground based obs. 80—85697
- NO_2, stratospheric composition during major warming, 1979 obs. 80—51476
- NO_2, stratospheric vertical distrib. at night, NO_3 layer effect *(French)* 77—66947
- NO_2, tangent ray meas. technique, effect of NO_2 conc. vars. at twilight 78—32141
- NO_2 total content, var. during solar eclipse, diurnal var. in tropics *(French)* 77—2208
- NO_2 total content meas. by absorption spectroscopy *(Japanese)* 80—12469
- NO_2, transport into stratosphere, prod. in thunderstorms 80—8376
- NO_2 vertical profile, balloon obs. in stratosphere *(Japanese)* 80—31086
- $NO_2^+ + O \rightarrow NO^+ + O_2$, rate constant rel. to atm. ion chem. 77—41245
- NO_3, detect. in polluted troposphere by differential optical absorpt. 80—77036
- NO_3 in nighttime stratosphere, composition change following sunset 80—31097
- NO_3 in troposphere, obs. of content in mountain air 80—72582
- NO_3 particles size distrib. and chem. comp., Nagoya, area, Japan 78—11980
- NO_3, stratospheric, obs. 78—88880
- NO_3^- in E United States precip., concs. behaviour 78—92962
- NO_x, air pollution in Sheffield, conc. var. 80—16863
- NO_x production in lightning 77—56677
- N_2O, abundance determ. by analysing solar spectra 78—85643
- N_2O abundance meas. over USSR *(Russian)* 78—96265
- N_2O altitude profiles at five latitudes in stratosphere and troposphere 77—78318
- N_2O, atm. life cycle, ground surface sink mechanism 77—66971
- N_2O, atmos. warming due to N_2O release from fertiliser 80—94579
- N_2O, atmospheric fluxes from N_2O supersaturated surface waters 78—57223
- N_2O, conc. diurnal variability in surface air 79—84369
- N_2O, conc. meas. using electron capture-gas chromatography technique 77—9531
- N_2O cycle, sources and sinks 79—70871
- N_2O, distrib., mixing ratio 78—32175
- N_2O emission from soils during nitrification of fertiliser 78—57313
- N_2O from soil treated with nitrogenous fertilisers 78—61419
- N_2O, global and regional meas. 78—73471
- N_2O, global atmos. composition and residence time 80—51519
- N_2O, greenhouse effect and climatic implications 77—9460
- N_2O in mid-latitudes of S.hemisphere 79—100908
- N_2O in N.American troposphere and stratosphere 79—79430
- N_2O, meas. in marine air over tropical E.Pacific Ocean 80—94542
- N_2O measurements, laboratory intercalibration 78—81277
- N_2O mixing ratio meas. and residence time 78—49088
- N_2O, potential of soil as natural sink 77—21772
- N_2O, prod. by coal and fuel oil combustion 77—21890
- N_2O, rates of evolution from N fertilised soil 79—16656
- N_2O, soil gas fluxes determ. by chamber methods, numerical evaluation 79—16700
- N_2O, sources, sinks and vars. meas. 78—85631
- N_2O sources and sinks, O_3 reduction due to industrial fixed N fertilizers 77—78383
- N_2O, sources and sinks, review 77—37374
- N_2O, stratosphere content at mid-latitude, simultaneous N and S hemisphere obs. 80—77052
- N_2O, three-dimens. distrib. and variability, numerical simulation three-dimens. distrib. and variability, numerical simulation 79—58006
- N_2O, trichlorofluoromethane and dichlorodifluoromethane conc. meas. in stratosphere 78—32171
- N_2O, vertical profiles rel. to instantaneous global photochemical reaction rates 80—17335
- $NO^+.H_2O+O \rightarrow NO_2^+ + H_2O$, rate constant rel. to atm. ion chem. 77—41245
- $N(^2P)$, auroral arc conc. and altitude distrib. 80—72658

atmospheric composition continued
$^{15}N/^{14}N$ ratio rel. to solar nebula differentiation 80—36519
Na abundance from nightglow obs. of Na I D doublet 80—98497
Na and minor constituents, meteoric origin 79—70835
Na density correl. to nightglow emissions of Na, OH and O 80—41585
Na enhancement and nightglow, space lidar obs. 80—101466
Na in upper atmosphere, absorpt. studies of daytime abundance 77—87140
Na, K, mesospheric abundances, simultaneous nighttime lidar meas. 78—36239
Na layer, laser sounding and interp. in terms of global atmospheric parameters 78—20570
Na layer, mesosphere, meas. by efficient forced oscillator dye laser 80—41563
Na layer in 80-105 km height range, lidar obs. of horizontal var. 78—36347
Na layer in mesosphere, extra-terrestrial source, evidence 79—12191
Na^+ and Na layers, meteor ablation-cluster ion theory 79—58138
NaCl-gas reactions, atmospheric, in situ TEM studies 80—104544
$NaOH_2^+(H_2O)_n(NaOH)_m$ cluster in stratosphere 79—34895
^{24}Na, gamma radioactive source, buildup factor determination for meas. in air *(Rumanian)* 78—49132
No_2 concentrations in stratospheric, experimental investigation *(Russian)* 77—49109
O and N density determ. by optical reson. absorpt.-reson. fluoresc. techniques 77—21951
O and N_2 densities in upper atm., OSO-7 meas. 77—21960
O and O_2 distrib. in lower thermosphere assuming tidal effects, one dimens. nonstationary diffusion-photochemical model 80—4160
O atoms in exposure, polar corona atom distrib. 80—82120
O conc. at 400 km altitude, incoherent scatter obs., model construction *(French)* 78—12030
O content of lower thermosphere, 100-160 km, new spectral method 80—41578
O deficit in Earth atmosphere, consequences *(German)* 77—70799
O I 5577 Å nightglow obs., evidence for vertical transport latit. var. near mesopause 79—70903
$O\ I(^3P)$ in lower thermosphere, nighttime conc. obs., using new rocket borne instrument 80—105066
O in thermosphere, seasonal-latitudinal tidal struct. and mass density 80—101467
O in upper atmos., atom density rel. to airglow green line *(Chinese)* 80—90269
O, O_3 abundances, effects of nearby supernova 80—94584
O profile of mesosphere and lower thermosphere 80—72660
O remote sensing in mesosphere and lower thermosphere, two-photon lidar technique 79—39869
O^+ and H^+ daily vars. at mid-latitudes at sunspot max. 79—58167
O^{++} in thermosphere, photochemistry 77—45226
$O^+ + N_2$, reaction rate coeff. in ionosphere 77—87167
O_2 and O semi-annual and annual vars. in upper atm. 79—53589
O_2 and O_3 early history 79—84487
O_2 column density and spectrally integrated transmittance in O_2 Schumann-Runge bands, 76-102 km altitude 79—70902
O_2 column density at 70-120 km altitude and UV absorpt. cross section 77—53263
O_2 density, 110-170 km altitude, using 1450 Å photometer 77—87144
O_2 density in thermosphere, solar flux var. 80—72659
O_2 density profile in upper atmosphere rel. to O_2 atmospheric and OH Meinel bands in nightglow *(Japanese)* 80—94631
O_2 density seasonal vars. near 100 km altitude 78—12034
O_2, Dobson total content meas., aerosol effects 80—12463
O_2 in early Precambrian atmosphere, photodissociation rather than photosynthesis 78—81409
O_2 in Precambrian atmosphere, elements in sedimentary rocks 77—5272
O_2 levels in prebiological atmosphere, photochem. model 79—84486
O_2 thermal and wind-induced var., AE-D thermospheric meas. 79—53592
O_2^+, NO^+, cones, correl. with meteor head echo heights 78—36537
O_2^+ recombination rate in ionosphere 77—25830
$O_2 + Ar(O_2)$, collision induced UV absorpt. in Herzberg continuum, dimer form. 77—30883
$O_2^+ + N \rightarrow NO^+ + O$, rate constant rel. to atm. ion chem. 77—41245
O_3, absorpt. by grass, soil and water surfaces 77—45139
O_3, aerosols and H_2O vapour effects on turbidity 77—78420
O_3 affected by sea breeze, Wallops Island, Virginia 80—51473
O_3 affecting ground-level oxidant concs. at Santa Rosa 78—16112
O_3, air composition at Barrow, Alaska, wind direction depend. 80—85704
O_3, air over N.Germany coast, obs. 80—26584
O_3 and mass transport, stratosphere to troposphere, Project Dustorm, tropopause folding 78—32177
O_3 and other gases diurnal conc. cycle and destruction at ground 79—79972
O_3 and related chemistry in mesosphere, Solar Mesosphere Explorer mission description (1981-2) 80—105096
O_3, atmospheric content from aircraft-borne spectrophotometry *(Russian)* 79—34903
O_3 budget, zonal mean circulation model and linearized photochem. 77—70780
O_3 calibration reference instrument calibration 78—73524
O_3, chemical analysis by acoustic emission following laser irradiation *(Russian)* 77—21451
O_3 column density effect on radiative-photochemical relaxation 79—16592
O_3 column increase, subsonic and SST NO_x emission 78—11979
O_3, columnar meas. by aircraft-borne UV spectrophotometer 78—73522
O_3 conc., fast oscills. in 3140 and 3690 Å obs. 77—53161
O_3 conc. affected by hydrocarbon emission from car factory 80—76674
O_3 conc. and distrib. from absorption spectrum in UHF region *(Russian)* 79—100897
O_3, conc. at ground-level, Oslo, Norway, summer 1977 obs. 80—81965
O_3 conc. in troposphere and stratosphere effects of NO_x emissions of high-altitude aircraft 78—32176
O_3 conc. in troposphere rel. to general weather situation 80—101397
O_3 conc. meas. at high latit. during twilight 77—41128
O_3, conc. meas. by differential absorpt. CO_2 laser radar 79—96829
O_3, conc. rel. to visibility reduction in Midwest 78—61507
O_3 concentrations meas., UV photometric standards interagency comparison 79—35000
O_3 concs., seasonal vars., Umkehr and Nimbus 4 BUV obs. of stratosphere 79—100911

atmospheric composition continued
O_3 concs. and meteorology in 1975 in Tel-Aviv 79—12172
O_3 concs. over Australia, review 80—109223
O_3 content, evolution 80—98400
O_3 content, meas. by Dobson spectrophotometer in Seychelles 77—17250
O_3 content, natural fluctuations 79—29819
O_3 content in tropics, during March-April 1976 stratospheric warming 80—12494
O_3 content rel. to solar UV vars. 80—26607
O_3, daytime and nighttime distrib., ground-based mm wavelength obs. 78—57256
O_3, daytime layer, photographic obs. from Skylab 77—60505
O_3, densities in stratosphere and mesosphere rel. to radiative equilib. temps. 78—81280
O_3 depletion, supersonic gas sampling error 77—33193
O_3 depletion, uncertainty in calcs. from stratospheric photochemistry model 79—16567
O_3 depletion by chlorofluoromethanes, contradiction of theory 78—49099
O_3 depletion by chlorofluoromethane, theory 80—51477
O_3 depletion in stratosphere, space-time distrib. and UV radiation changes at Earth surface 80—94577
O_3, depletion resulting from nitrogen oxides pollution *(Russian)* 78—16154
O_3 depletion theories, rel. to atm. nuclear tests 79—70848
O_3, determ. by Chappuis-band absorpt. 80—77063
O_3 distribution in winter polar low region 77—78371
O_3, Dobson meas. of total content, aerosol extinction effects 79—84431
O_3, dosage in photochemical smog, depend. on latit. 77—2227
O_3 during summer rel. to winter rain in San Francisco Bay Area 79—12224
O_3 elevated levels from natural sources 79—62552
O_3 enhancement by jet stream *(Russian)* 80—94568
O_3 estimates from Dobson direct Sun meas., atm. temp. variations and scatt. effects 77—45049
O_3 estimation for solar radiation models 79—70875
O_3, evolution and variability over geological time 79—96788
O_3 fluxes, from zonal mean circulation model of atmosphere *(Russian)* 78—36224
O_3 formation and control strategy options for Sydney, precursor distrib. 80—16859
O_3, global distribution, effects of pollutants, book contrib. 77—29429
O_3, global monthly vars. correl. with solar activity 78—85664
O_3, global vertical distrib. 78—73475
O_3, ground level conc., rel. to regional transport of pollutants 78—44990
O_3, ground level monitoring apparatus, chemiluminescence reaction with ethylene 78—96310
O_3, high conc. in rural surface layer correl. with high press. systems 78—24325
O_3, high resolution spectroscopy of ν_3 band, rel. to atm. O_3 monitoring 79—63993
O_3, IR heterodyne absorpt. spectrum 77—91267
O_3, IR heterodyne spectroscopy 77—45160
O_3, in lower atmos., Uccle, Belgium, April-June 1979 obs. *(French, Flemish)* 80—98385
O_3, in lower atmos. Jan.-March 1979, obs. over Uccle, Belgium *(French, Flemish)* 80—94571
O_3 in lower mesosphere, number density profile obs. 80—41579
O_3 in lower stratosphere, Nimbus 4 remote sensing method 80—77154
O_3 in mesosphere and stratosphere, obs. by satellite IR limb scanning method 80—105086
O_3 in stratosphere, CO_2 conc. increase effects 78—57250
O_3 in stratosphere, depleted by chem. reactions involving bromine 80—98391
O_3 in stratosphere, implications of OH + trichloroethane reactions 80—16657
O_3 in stratosphere, perturbing influences, 1955-75 catalogue 80—41502
O_3, in stratosphere, seasonal composition variation at high-latitude 80—77051
O_3 in stratosphere, two-dimens. model *(French)* 78—49104
O_3 in stratosphere and troposphere, vertical distrib. during polar front passage 80—94582
O_3 in troposphere, differential absorption lidar appl. 80—12554
O_3 in troposphere, evidence for significant in situ photochemical source 80—72619
O_3 in troposphere, implications of stratosphere vertical flux 80—101402
O_3 in troposphere, meridional distrib. and seasonal vars. 77—60453
O_3 in urban air at night, Jerusalem and Tel-Aviv 80—89689
O_3, instantaneous global balance including observed NO_2 80—109211
O_3 layer, changes in chemical balance 78—92933
O_3 layer, depletion and chemistry 80—104534
O_3 layer, depletion by nearby supernova explosion 78—32499
O_3 layer, fluorocarbon hazard assessment 79—79963
O_3 layer depletion by chlorofluorocarbons, calc. using two-dimensional model 80—109221
O_3 layer depletion by supersonic flight, rel. effects of latitude and altitude 77—64360
O_3 line parameter data, 10 μm and 4.8 μm regions 80—61895
O_3, long-term vars. global distrib. during 1957-75 period 79—84429
O_3, maintenance of zonal mean distrib. in N.Hemisphere 80—109220
O_3 meas. during Aladdin 74 program above Wallops Island 78—57247
O_3 meas. in troposphere using microprocessor controlled lidar 79—58137
O_3 meas. over snow surfaces 79—12281
O_3 meridional migration *(Russian)* 77—73816
O_3 monitoring with airborne laser absorpt. spectrometer 77—91303
O_3 monitoring with IR heterodyne radiometer 78—16216
O_3, near surface meas. at Hohenpeissenberg, historical review *(German)* 78—65369
O_3, nighttime conc. from OH nightglow obs. 79—5698
O_3, nighttime concentration (15-68 km), Nimbus 6 obs. comparison with OAO-3 obs. 80—105016
O_3, nighttime equatorial density determ. from UV stellar occultation obs. 77—53259
O_3 nocturnal maxima, vertical mixing of remnant daytime boundary layer 79—5547
O_3 obs. and atm. physics research at Belsk, Poland *(Polish)* 77—21825
O_3, obs. of meridional flux by transient eddies in 0 to 30 km height range 80—109224
O_3 observations, 1976 July-September period *(French, Flemish)* 77 70752
O_3 observations, 1976 October-December period *(French, Flemish)* 77—70753

atmospheric composition continued
O_3 observations for 1978 January 4 to March 31 period *(French, Flemish)* 79—5561
O_3 over Uccle, Belgium, 1977 July-Sept. obs. *(French, Flemish)* 78—40618
O_3 over Uccle, Belgium, 1978 April-June obs. 79—53429
O_3 overabundances over Pacific Ocean during Gametag, August 1977, stratospheric source 80—72600
O_3 photochemical production, W.Europe, rel. to meteorology 77—78292
O_3, possible role in ice form. in clouds *(Russian)* 77—29367
O_3, pot. energy surface analytical function, atmospheric reactions 78—7174
O_3 problem, reassessment of stratospheric models 79—5553
O_3, production transport and distribution, numerical simulations with global general circulation model 80—56544
O_3 profile, determ. from outgoing thermal radiation 78—92945
O_3 profile, from photodissoc. wave obs. 78—79407
O_3 profiles rel. to solar mag. activity 78—65373
O_3 reduction due to industrial fixed N fertilizers 77—78383
O_3, reduction effects on sunburn dosage 77—37285
O_3, remote meas. in IR absorpt. bands, information content estimation *(Russian)* 78—88883
O_3 seasonal var. from rocket-borne UV obs. in upper stratosphere and mesosphere 77—29402
O_3 sounding correction procedures and implications 78—20486
O_3 soundings at Uccle, Belgium, 1976, April, May, June *(French)* 77—64407
O_3, sources and transport in NE. United States 79—92110
O_3 sources in NE.USA, air pollution assessment 80—41482
O_3 stability and depletion scares 77—70722
O_3, stratosphere and troposphere composition observed on circumpolar flight 80—51475
O_3, stratosphere content at mid-latitude, simultaneous N and S hemisphere obs. 80—77052
O_3, stratospheric, perturbation by N fertilisers, independent variables anal. 78—73505
O_3, stratospheric, simultaneous effects of CO_2 and chlorofluoromethanes on column density 79—74940
O_3 stratospheric 10 μ absorption line obs. with IR heterodyne spectrometer 78—61494
O_3, stratospheric determ. at ground level using $^7Be/O_3$ ratios 79—58011
O_3 stratospheric layer, laser-radar obs. using excimer lasers 80—17410
O_3 surface concentration forecasts for polluted areas, Model Output Statistics appl. 80—12035
O_3 total, seasonal and interannual vars., Nimbus 4 BUV expt. 80—41506
O_3 total, spectrophotometric determ. using interference filters 78—16180
O_3 total accuracy of filter instrument, bandwidth effect 78—16181
O_3, total amount and vertical distrib. periodic vars. 77—78336
O_3 total amount at Belsk, Poland, harmonic anal. 78—92883
O_3, total content, backscatter UV and ground-based meas. comparison 79—84430
O_3 total content, comparison of simultaneous IRIS, BUV and ground based meas. 78—81291
O_3 total content, determ. using satellite meas. 80—77027
O_3 total content, Dobson spectrophotometer meas. errors 80—72644
O_3 total content, monthly averages correls. with solar activity vars. 79—16571
O_3, total content 1964-75, season and latitude depend. 80—41534
O_3, total content and mixing ratios obs., (1976 January 5 to March 31) *(French, Flemish)* 77—33174
O_3 total content determ. by UV spectroradiometry 79—53401
O_3 total content determ. from total optical depth spectral var., solar radiometer meas. 77—53235
O_3 total content determ. using remote spectroscopy 78—65437
O_3 total content determination, large particle light scatt. coeffs. approximation 80—82091
O_3, total content estimation from UV radiance meas., aerosol effects 79—8662
O_3 total content in atmos. rel. to solar activity 80—41488
O_3, total content meas., evaluation of electrochem. conc. cell sonde 79—70860
O_3, total content meas. using four-filter photometer 78—61597
O_3, total content meas. using Dobson spectrophotometer 80—72643
O_3 total content trends, from daily Dobson data 78—92915
O_3 total content vars. rel. to general circulation 79—44233
O_3 total field, statistical anal. *(French)* 79—84358
O_3, total value determ., particulate scattering approx. 77—21864
O_3 tranpsort mechanisms, general circulation model 80—109196
O_3 trends rel. to lower stratosphere circulation over Australia 77—21866
O_3, tropospheric, long-range transport 78—61514
O_3, twilight obs. from Atmosphere Explorer 5 78—28261
O_3, UV absorption bands, new vib. quantum no. assignments, based on isotope effect 79—94008
O_3, Uccle, Belgium, 1973, Jul.-Sept. *(French, Flemish)* 77—17204
O_3, Uccle, Belgium, 1973, Jul.-Sept. *(French, Flemish)* 77—17205
O_3, Uccle, Belgium 1977, Jan.-Mar. 77—86998
O_3, Umkehr vertical profile errors caused by presence of stratospheric aerosols 79—70849
O_3 variations in Auckland, comparison between city and urban regions 80—17350
O_3, variations rel. to general atmospheric circulation over Middle East in summer *(Russian)* 77—53156
O_3 vars. correl. with cloudiness vars. rel. to UV radiation protection 78—73456
O_3 vars. from Gasp meas. in troposphere 79—100905
O_3 vars. rel. to 11-yr. solar cycle 79—12189
O_3, vertical and horizontal distrib. covering Kanagawa Prefecture, Japan, meas. *(Japanese)* 77—70768
O_3 vertical and horizontal fluxes at tropopause, GASP data 78—7720
O_3 vertical distrib., shortened version of Umkehr ob. method 80—8430
O_3 vertical distrib. in boundary layer 77—49102
O_3 vertical distrib. in upper stratosphere, satellite and surface-based obs. 78—40620
O_3, vertical distrib. meas. (1977, April 1 to June 29) *(French, Flemish)* 78—11966
O_3 vertical distrib. over Aspendale, Australia, climatology 78—20475
O_3, vertical profile calc. from umkehr obs. 78—81328
O_3 vertical profile correl. with thermodynamic parameters *(Russian)* 77—73804
O_3, vertical profile rel. to UV backscattering 78—7762
O_3 worldwide total conc. trends 77—33138

atmospheric composition continued
O_3+cis-2-butene+formaldehyde$\rightarrow$propylene ozonide, gas phase reaction mechanism 77—33132
OCS, atmospheric concs. in S.W. and E.United States 78—20466
OCS, sources rel. to contrib. to stratospheric aerosols and climate 80—41524
OCS, stratosphere content, solar spectra meas. by 12 km attitude aircraft 80—41486
$O^+(^2D)$ in thermosphere, quenching by electrons 80—94630
$O(^1D)$ in thermosphere, role of $N(^2D)+O_2$ reaction 80—90270
OH and trace gases, laser induced fluorescence system for aircraft appl. 80—36425
OH column densities in stratosphere from far IR rotational lines 80—36367
OH, conc. meas. by laser fluoresc., O_3 dissoc. interference 77—49110
OH conc. meas. in boundary layer by monitoring CO oxidation 79—58012
OH in troposphere, implications of OH+trichloroethane reactions 80—16657
OH, laser absorption spectrum, scanning technique, appl. to atmospheric monitoring 78—17664
OH radical calculated densities in troposphere and stratosphere, uncertainties 79—53426
OH radical in upper atmosphere, meas. using lidar from Space Shuttle 80—51590
OH, submicron airglow bands correl. studies during Spacelab simulation 79 -25381
OH, vibr. energy distrib., atm. chem. modification 77—25735
OH+methane+M, absolute rate consts., 296K, flash-photolysis reson. absorpt. technique 77—86290
$O^+(^2P)$ ionisation freq. determ. using satellite airglow and neutral comp. data 77—5384
$O(^1S)$, auroral production and loss processes, artificial auroral expt. Precede meas. 79—66855
$O(^1S)$ production in lower thermosphere, comparison of Chapman and Barth mechanisms 77—33235
^{18}O concentration in Amazon Basin water, evidence for recycling 80—81955
$^{18}O/^{16}O$ ratio in precipitation over KFA Julich, (1974-1978) *(German)* 79 12227
$^{18}O/^{16}O$ ratio in precipitation, correl. with temp. and altitude 80—77067
$^{18}O^{16}O$, photodissociation as source of atmospheric O_3 80—94559
$O(2^1D_2)+N_2(O_2)(N_2O)(CO_2)(H_2O)$(methane), collisional deactivation meas., 295K, rel. to atmospheric processes 80—16663
$O(2^3P,2^1D)+N_2O(CO_2)$, diabatic correlations 77—25256
Oz, Belgian obs. (1977 Oct.-Dec.) *(French, Flemish)* 78—92903
P, atmosphere contrib. to aquatic system 79—100545
Pb, concs. in bulk precipitation in Denmark rel. to atmospheric long range transport 80—94131
Pb, contamination, rel. to traffic density *(German)* 79—70470
^{210}Pb fluxes, determ. from soil profiles 79—2346
$^{210}Po/^{210}Pb$ modification by volcanic emissions 80—41507
^{226}Ra background levels in lower troposphere from coal burning 77—37361
Rn and Rn decay products, disequilibrium ratio in the atmosphere *(Spanish)* 80—31083
Rn concentrations, influence of meteorological parameters *(Spanish)* 79—92562
Rn concentrations, statistical analysis of stability indexes *(Spanish)* 79—92561
Rn, diurnal var. in boundary layer, for USA Gulf Coast 80—101404
Rn, evolution in neutral atmospheres *(Spanish)* 80—4058
Rn, induced radioactivity increase rel. to geomag. perturbations biotropicity 79—96621
Rn series disequilib. in S.California coastal air 78—49087
Rn, use in determination of vertical stability of lower atmosphere, influence of air flow on Rn content *(Spanish)* 79—92560
^{222}Rn, and its descendants, radioactivity in low atmosphere, pollution-dust dynamics *(Rumanian)* 80—12524
^{222}Rn, automatic counter for continual unattended operation 78—73539
^{222}Rn continuous meas. for air-sea gas exchange field determ. 78—73534
^{222}Rn evasion rates in Atlantic and Pacific, Geosecs determ. 79—79875
S aerosol, of S. American troposphere 80—67401
S and trace elements in aerosols from South American continent, conc. relationships 78—57245
S, and trace metal content of nonurban and marine aerosols, PIXE anal. 77—49136
S budget in stratosphere, CS_2 and COS oxidation effects 79—84423
S budget of eastern N.America, anthropogenic and natural contribs. 80—97834
S burdens in troposphere 80—56506
S, compact X-ray fluoresc. analyser 78—68971
S compounds, homogeneous chemistry 78—49119
S compounds, meso-scale transport obs. in rurual East Midlands, England 80—94124
S, estimated dry deposition vels. over E United States and surrounding regions 80—56507
S, natural and anthropogenic emissions in Central Europe, calc. from atm. meas. 77—73827
S oxide pollutants, SURE/MAP3S obs. comparison with regional model predictions 80—81501
S pollutants in atm., conf., Dubrovnik, Yugoslavia (Sep. 1977) 78—96281
S pollutants in atm., conf., Dubrovnik, Yugoslavia (Sept. 1977) 79—20965
S, release by burning of fossil fuels, rel. to acidity of rain and snow 80—26590
S uptake by forest and farmland, dry deposition 79—74939
SF_6 and tracer gases, electron capture detection method 77—25785
SO and SO_2 deposition and transformation rates during transport over Atlantic Ocean, comment 77—66975
SO_2 and smoke pollution in Belgium (1973-4) *(French, Flemish)* 77—41147
SO_2 and sulphates, residence times under non-steady-state conditions 80—77092
SO_2 at ground level, air pollutant dispersal, Forth Valley, Scotland 80—81497
SO_2, city concs., box model and acoustic sounder anal. 80—7982
SO_2 conc., urban built-up area, Japan 79—21006
SO_2 conc. decrease near Rotterdam rel. to meteorological parameters during 1961-74 winters 77—37359

atmospheric composition continued
SO_2 conc. determ. using HBr laser *(Russian)* 78—69484
SO_2 conc. downwind of coal fired power station, Montana, USA 80—108821
SO_2 conc. in Milan urban atmosphere in winter *(Italian)* 78—53721
SO_2 concentration for Rijnmond, Netherlands, comparison with Gaussian plume model obs. 80—85314
SO_2 concentrations, maximum, and averaging time, in industrialised area of Bilbao (Spain) 80—51020
SO_2 conversion in smoke plumes *(Dutch)* 77—70825
SO_2 detect. in stratosphere, analytical technique 77—5314
SO_2 from sour gas plants in Alberta 77—37372
SO_2, gas complex analysis method, resonance absorption with pulsed laser light *(Japanese)* 80—36421
SO_2 levels in Sarnia area, Ontario, modelling 77—37368
SO_2 mass spectrometric obs. in stratosphere 77—33200
SO_2, minor atm. components, near UV absorpt. spectra, temp. depend. *(French)* 80—36355
SO_2, movement in atmosphere *(Dutch)* 80—97844
SO_2 over E. United States, regional residence time 79—16651
SO_2 oxidation chemiluminesc., appl. to atm. chem. *(German)* 79—52670
SO_2, pollution zones definition and assessment 78—81383
SO_2 small automatic monitoring network, practical experiences 78—81462
SO_2, sources in CS_2 and COS oxidation 80—4085
SO_2 to sulphate conversion processes 77—37389
SO_4 aerosol, geographical extent in Midwestern and Southern USA 77—49145
SO_4^{2-} aerosol layer, form. and evolution model for stratosphere and troposphere 80—21801
SO_4^{2-} aerosols, ambient, laser-Raman monitoring 78—69532
SO_4^{2-}, airborne particles, size meas. and chem. comp. by diffusion sampling 78—45007
SO_4^{2-} in E United States precip., concs. behaviour 78—92962
^{38}S in SO_2 and SO_2 oxidation rate meas. 77—73814
V, transport from urban to remote marine areas 77—37355
^{133}Xe, separation technique, preliminary results *(German)* 78—16222
atmospheric density *see atmospheric pressure and density*
atmospheric disturbances *see atmospheric movements; thunderstorms*
atmospheric duct *see atmospheric electromagnetic wave propagation*
atmospheric dynamics *see atmospheric movements*
atmospheric electricity
see also atmospheric electromagnetic wave propagation; atmospheric ionisation; atmospherics; aurora; electrojets; ionosphere; lightning; thunderstorms
active auroral arc, electric fields, energetic particles and suprathermal electrons obs. 77—70912
aerosol, effects of elec. fields and charges on collisions with cloud drops and rain 77—25748
aerosol, scavenging of particles by cloud drops and small rain drops, elec. field effect 80—82001
aerosol particles, motion due to inertia, Brownian diffusion, phoretic and elec. forces 79—53460
aerosol particles scavenging by clouds and raindrops, elec. charge effect 79—53459
aerosol plume detection theory and meas. 80—7984
aerosols, charged, occurrence before earthquakes 79—16407
aerosols, limitation on electrical measures 78—69431
air diffuse discharge, gasdynamic effects 78—81294
air-Earth current density latit. var., aircraft meas. 77—53141
American Meteorological Soc. Conf. (Issaquah, Wash., 1978 July-Aug.) 79—5551
asymmetric ring current coupling with eastward electrojet 78—7823
aurora, current systems rel. to infrasonic wave emissions and polar substorms 79—100996
aurora, structured field-aligned current system 77—33243
aurora irregularities, overnight north-south movements obs. at 42 MHz 80—67449
AURORA machine studies of air chem., cond. and boundary layer 78—32144
aurora rays and arcs, field-aligned elec. fields and currents 80—41593
aurorae and field-aligned currents, satellite obs. 80—12593
auroral arc, energy source for electron accel. and field-aligned currents 77—9593
auroral arc during quiet conditions, electrostatic model 80—72669
auroral arc electric fields, radar obs. 80—72692
auroral arcs, Birkeland currents and polar cap elec. fields rel. to arcs global form. 80—67446
auroral arcs, radar obs. of elec. fields and currents 78—28396
auroral arcs array, magnetosphere/ionosphere pot. difference rel. to electron accel. 78—36357
auroral Birkeland current, determ. from plasma line meas. at Chatanika 80—98507
auroral Birkeland current systems, anomalous resistivity effects 77—9591
auroral currents and potentials, generation by magnetosphere correction elec. field divergence 80—67453
auroral effect on fair weather electric field 79—44285
auroral elec. field, non-neutral field-aligned current sheet, theory 80—77196
auroral electric field, description based on plasma interaction with geomag. field 80—46342
auroral electric field, model 79—53608
auroral electric field obs., comparative rocket obs. 80—85789
auroral electric fields, comparison of F-region plasma drifts and E-region irregularity drifts 77—33262
auroral electric fields, implications of extreme thinness of pulsating auroral structs. 80—72667
auroral electrojet region, elec. fields and mag. effects of solar flares 78—69576
auroral field lines, region of intense plasma elec. field turbulence 77—45228
auroral forms, observed characts. rel. to elec. fields 79—8738
auroral ionosphere, electric field and conductivity meas. during substorms 79—80073
auroral ionosphere, electric fields and conductivity in quiet periods 77—53280
auroral ionosphere, heating by elec. fields 77—21973
auroral ionosphere, large parallel elec. fields obs. 77—9595
auroral ionosphere field-aligned currents and collisional ion cyclotron waves 77—29574

atmospheric electricity continued
auroral oval, dayside, elec. fields meas. 80—98501
auroral oval, dayside, elec. fields rel. to neutral wind profiles between 115 and 175 km altitude 80—98494
auroral oval, dayside, evidence for parallel elec. field particle accel. 80—98503
auroral oval, dayside, field-aligned currents rel. to radio aurora and energetic particles 78—88966
auroral oval, dayside, ULF elec. field fluctuations obs. 80—98505
auroral particle distrib. rel. to mag. field perturbations assoc. with field-aligned currents 80—41596
auroral particles injection region, electrodynamic processes and compensation currents 78—45095
auroral phenomena, role of mag. mirroring in magnetosphere-ionosphere current system 78—20572
auroral radio backscatter at 42 MHz, amplitude rel. to Doppler shift 80—61955
auroral region, self-consistent particle and parallel electrostatic field distrib. 78—45120
auroral regions, electric fields from ion and electron distribs. 77—87155
auroral substorm absorption events, at low auroral latits., apparent equatorward propag. 79—8769
auroral substorm expansion phase, ionospheric currents and elec. field vars. assoc. with absorpt. spikes 79—35039
auroral zone, elec. currents induction in Alaska pipeline 79—39645
auroral zone, elec. fields rel. to field-aligned suprathermal electron fluxes below 270 km 77—33278
auroral zone, electrodynamic struct. of evening sector 80—72691
auroral zone, quasiperiodic elec. fields and assoc. electron precip., models 78—88977
auroral zone current system, fluctuations rel. to geomag. pulsations 77—87188
auroral zone currents, obs. in morning sector pass 80—98510
auroral zone electric currents, ground-based obs. using two-dimensional magnetometer array 80—90245
auroral zone electric fields, conductivities and currents, latitudinal distrib. 78—77399
auroral zone electric fields at 1 R_E altitude 78—57397
bay phenomena, theory of equivalent current systems including ground induction 80—41610
beam-plasma discharge, near Zarnitsa-2 rocket, parameter estimation *(Russian)* 78—26357
Birkeland currents, high altitude obs. 78—36397
Birkeland currents, ionospheric, rel. to geomag. disturbance theory *(Norwegian)* 80—31158
Birkeland currents, primary sources 80—31176
Birkeland currents, TRIAD satellite obs. 79—16755
Birkeland currents and auroral structure 80—77209
bow shock, current-driven instabilities in laminar perpendicular shock 78—77430
breakdown and corona characts. under AC voltage for rod to plane air gaps *(Japanese)* 79—84416
breakdown voltage of air, effect of sand particle pollution 78—81363
cathodic protection using lightning conductors connected with diodes, for metals and concrete reinforcements 79—52418
charge separation, rel. to secondary ice crystal prod. 80—81998
charge separation laboratory meas., associated with secondary ice crystal production, thunderstorm electrification exam. 80—72623
charged particles precip. by parallel elec. field, model 78—65459
charged thin ice plates, spherical aerosol particle scavenging efficiency 78—44934
cloud droplets, effect of electric charges and fields on collision freq. 80—8401
cloud drops collision efficiency, elec. charges and vertical external elec. field effects 77—25738
cloud electric fields measuring instruments 77—41226
cloud electrification in axisymmetric time-dependent model 79—16594
cloud growth and precipitation development, refined charge distrib. in stochastic elec. model 77—29374
cloud physics rel. to atm. electricity, review 79—70842
clouds, electrical and microphysical meas. in maritime and urban environments 79—12173
clouds, electrical charges fate in evaporating droplets 79—48559
coherent anomalous resistivity, in region of electrostatic shocks 80—4189
conduction current, direct meas. 78—85637
conductivity, rel. to small ions recomb. and attachment to aerosol particles 79—39817
conductivity meas. in lower stratosphere over Poona 77—70750
conductivity meas. rel. to pollution determ. 77—91233
conductivity of atmosphere and lower ionosphere, effects on Schumann reson. freqs. and ELF attenuation 80—31099
conductivity of atmosphere and lower ionosphere, profiles evaluation from expt. Schumann reson. data 80—36360
corona, positive, onset in atmospheric air, expt. 80—36354
corona discharge, insect swarm, as unidentified flying object 79—96728
corona discharges in atmospheric air under AC voltage, observation *(Japanese)* 79—84417
corona point discharge current magnitude 78—44935
coronae effects on elec. fields beneath thunderstorms 79—79978
cumulonimbus clouds, elec. field strength and raindrop spectra, study from mobile ground station 78—92943
cumulus clouds, elec. and microphys. meas. before and after seeding 77—56686
current system, steady state, for high-latit. mag. activity, comprehensive model 79—92636
daily mag. variations meas. in Alaska, atmos. current system 80—85590
dayside magnetopause, electric field topology 78—57398
dayside polar cusp, ionospheric and field-aligned currents relationship 79—35058
dayside south polar cusp, field-aligned currents rel. to interplanetary mag. field 79—35059
DC source in continuously var. conductivity, electric and magnetic fields 77—49140
diffuse aurora, elec. field meas. 77—82077
DP-2 current system, rel. to pulses in interplanetary mag. field B_z-component 78—73583
drop collision coalescence in presence of elec. field, simulation expts. 80—51516
drop electrification by evaporation or vapour condensation *(French)* 78—61511
droplet collision efficiency enhanced by elec. field 80—61863

atmospheric electricity continued
dry and moist air, primary ionisation coeffs., secondary ionisation coeffs. for water surface 78—65376
E_s-layer formation, unified theory, neutral wind and elec. field effects 79—5710
E_s-layer ionisation at high latitude, quiet and disturbed conditions 80—61941
E- and F-regions, nighttime Hall and Pedersen cond. comparison 77—41260
E-region, cross polar cap horizontal currents rel. to mag. disturbances and elec. fields 78—77405
E-region, cross-polar cap horizontal currents rel. to mag. disturbances and measured elec. fields 77—45230
E-region, equatorial, dynamics rel. to currents and elec. fields vars. 78—36369
E-region, nighttime electric fields and conductivity rel. to magnetosphere-ionosphere-atmosphere coupling 79—35034
E-region, unstable polar cap, rocket-borne wave, field and plasma obs. 77—21978
E-region, winds and elec. fields meas. over Malvern 78—49206
E-region distortion effect of Sq current 77—45237
E-region low latitude dynamoc current system, seasonal vars. near solar max. 80—8479
E-region luni-solar currents, electron density distortion meas. using group and phase height meas. 80—109299
E-region overhead horizontal current at high latits., discrepancy with mag. D-component vars. 79—75037
E-region Pedersen current, effects on Perkins spread-F instability 78—40755
Earth's negative charge, supply mechanism 80—61758
earthquake lights, proposed for study by chemiluminesc. NO air pollution apparatus 80—61906
EAS, small atm. elec. field variations 77—60558
EAS and radiowaves produced from secondary electrons in geoelectric field, 10 kHz-10 MHz 79—21118
electric field, rapid vars. connected with EAS 79—66739
electric fields time and amplitude props. near lightning in VLF, LF and HF bands 77—78352
electrode effect in strong turbulent mixing limit, analysis 78—40622
electrodynamics of an arc, auroral vector electric field and particle comparisons 77—70907
electrojet model involving field-aligned currents 77—9600
electrostatic fields generated by ionospheric dynamo region, penetration into lower atm. *(Russian)* 77—9606
electrostatic force between charged aerosol particles and charged water drops 77—25749
electrostatic V-shocks in auroral plasma, approximate equipotentials 80—21870
Elk Mountain, Wyoming, electrification expts. 79—16595
environmental electromagnetic simulator 77—73894
equatorial E-region, current density rel. to solar cycle var. of horizontal drifts 78—36390
equatorial ionosphere elec. fields rel. to geomag. vars. during mag. storms 77—78578
external transverse elec. field effects on whistlers polarization 78—28427
F_2-layer, global distrib. of electron density rel. to elec. fields in closed magnetosphere 77—64514
F_2-layer, low-latit., elec. vector rel. to vertical motions during mag. storms 77—37479
F_2-layer, night-time, over Arecibo, elec. fields seasonal mean struct. 80—31163
F_2-layer, polar substorm elec. field and ionisation vertical drift 79—53618
F-region, ambient elec. field rel. to gradient drift instability high-altitude limit 78—88984
F-region, convective elec. field rel. to electron density and ion vel. during isolated substorm 78—65452
F-region, current convective instability, rel. to localised nighttime auroral zone scintillation enhancements 80—98506
F-region, elec. field induced drifts, incoherent scatt. radar obs. 77—29576
F-region, equatorial, solar cycle effects on elec. fields 78—28405
F-region, horizontal elec. fields rel. to equatorial spread-F seasonal and solar cycle vars. in American zone 80—109298
F-region, large-amplitude oscillating field appl. to equatorial spread-F control 78—69602
F-region, low latit. elec. field irregularities rel. to spread-F and plasma irregularities 77—53290
F-region, polar cap and auroral zone, math. model 78—65458
F-region, poleward-directed elec. fields at subauroral latits. 78—88970
F-region at night time, negative correl. of wind to elec. field 80—41603
F-region auroral elec. fields and convection obs. over $60^\circ \leq \Lambda \leq 75^\circ$, Millstone Hill results 80—67454
F-region convective electric field determ. from rocket meas. of thermal ion spectra 78—57386
F-region horizontal elec. field reversal assoc. with spread-F in equatorial ionograms 78—69560
F-region ion drifts, radar obs. 80—51573
F-region Joule heating events, zonal winds estimation via incoherent scatter technique 78—36344
F-region overhead horizontal current at high latits., discrepancy with mag. D-component vars. 79—75037
fair weather condition concept in atm. elec. 78—61517
fair weather electric charge transfer by convection in unstable mixed layer 79—58037
field aligned current above auroral arc, e^- and H^+ precipitation obs. 80—77215
field aligned current distribution, from S_q^p obs. in Alaska 80—85813
field aligned currents carried by suprathermal electrons, relation with auroral arc 78—28362
field disturbances, prior to earthquakes, appearance time rel. to earthquake energy 77—13061
field growth in finite cloud, comments and reply 77—78327
field structure in disturbed zone behind cylinder streamlined by rarefied plasma 79—53623
field-aligned current closure and Joule heating near Harang discontinuity 80—72682
field-aligned currents and ionospheric electric fields 77—53282
Florida lightning return stroke electric fields, 200 km propagation 77—25754
Florida thunderstorms, electric fields 78—40621

atmospheric electricity continued
gamma-ray pulse from nuclear explosion disturbing field 79—70852
geomagnetic solar-flare effect and ionospheric induction 79—53632
geomagnetic variations and equivalent current systems, UT and diurnal variation 80—51330
geomagnetic variations in N. polar cap region, rel. to interplanetary field 80—41644
global atmospheric electricity, quasi-static model for lower atmosphere 79—96799
global diurnal variations over continents 80—82039
global electric circuit model for long-period, micropulsations 80—41646
global fields and currents, origin and structure *(German)* 78—32196
Harang discontinuity, elec. current continuity 78—49220
Harang discontinuity electric field, auroral radar and rocket double-probe obs. 78—88971
high-energy particle prod. and nonstationary convection 77—53312
high-latitude ionosphere, currents prod. by vars. of asymmetric ring current 77—21971
ice clouds, elec. field changes rel. to ice particles rapid orientation and alignment changes 80—17330
ice particles, electric charge meas. by negative-feedback electrometer 79—70895
industrial chimney stack plumes, large elec. fields 78—44987
industrial stack plumes, elec. fields 77—5315
interplanetary elec. field penetration of magnetosphere, balloon meas. 78—57408
inverted V event, scale of elec. field along mag. field, satellite obs. 80—41662
ion concentration, elec. cond. and vertical elec. field intensity meas., 0-85 km altitude 77—29359
ion mobility spectrum, trace gases effect 77—25742
ionosphere, 3-dimens. current model rel. to quiet time vertical magnetic field component over India · 78—61326
ionosphere, anomalous equatorial elec. fields assoc. with northward turning of interplanetary mag. field 79—70914
ionosphere, anomalous resistivity, review 77—64528
ionosphere, atomic ions reaction to rapid changes in large-scale elec. fields 77—91350
ionosphere, auroral breakup and westward current flow 80—51593
ionosphere, auroral electron flux obs. 80—67466
ionosphere, Chatanika incoherent scatter radar obs. of field-aligned currents 78—57387
ionosphere, cleft currents determined from magnetic and electric fields 79—35036
ionosphere, collision frequencies, recomb. coeffs., rel. to resistivity of semiconductors and metals 79—8742
ionosphere, cond. and electron density of reflecting layer below classical D-region 80—98508
ionosphere, conductivity and drifts 78—36366
ionosphere, conductivity differences during quiet periods rel. to weak global mag. disturbances 79—53660
ionosphere, conductivity rel. to geomag. pulsations damping 78—49218
ionosphere, conductivity rel. to Pi 2 pulsations attenuation 78—45101
ionosphere, convection elec. field influence on thermal proton outflow 77—45243
ionosphere, coupling of mid-latit. spread-F between conjugate stations 77—53304
ionosphere, current and wind systems, influence of magnetospheric convection 77—5386
ionosphere, current and wind systems generation by motion of plasmasphere material 77—13161
ionosphere, current collection by long wire in near-Earth orbit 79—25438
ionosphere, day-night conductivity gradient effect on polar cap convective flow 78—45121
ionosphere, daytime winter midlatit., zonal elec. field effects 78—28379
ionosphere, DC elec. fields and ion-neutral collisions rel. to ion vel. distrib. 77—29565
ionosphere, differences between regions of upflowing and outflowing current 79—100999
ionosphere, dynamo currents from EMFs at different latitudes 77—64524
ionosphere, dynamo electrostatic fields rel. to lunar perturbations in columnar electron content 77—29570
ionosphere, dynamo theory for low latit. geomag. daily var. 78—36098
ionosphere, eastward elec. field rel. to equatorial anomaly form in E.Asia and India 80—109301
ionosphere, effect of elec. fields and vertical neutral-gas drifts on total electron content 78—45089
ionosphere, effect of finite conductivities on axisymmetric toroidal Alfven wave resons. 79—75035
ionosphere, elec. cond., field-aligned currents and electrojets 77—21974
ionosphere, elec. cond. and field in vicinity of aurora 77—9592
ionosphere, elec. currents in late evening plasma flow reversal 80—26675
ionosphere, elec. field, balloon meas., SAMBO-1 expt. 79—66738
ionosphere, elec. field configuration rel. to Ps 6 mag. disturbances seasonal and diurnal var. 80—67477
ionosphere, elec. field from aurora azimuth-scan radar Doppler data 77—41266
ionosphere, elec. field oscills. meas. near auroral arc, assoc. with MHD wave 78—65457
ionosphere, elec. field rel. to electron density depletion prod. by ionospheric modification expt. 77—33263
ionosphere, elec. field rel. to southward midnight surge in F-region wind 77—33233
ionosphere, elec. field wavelike fluctuations obs. at Ft. Churchill, Canada 77—21982
ionosphere, elec. fields and conds. response to August 1972 mag. storms 77—25858
ionosphere, elec. fields during positive mag. disturbances of 1972 February 24 and 1970 (November 21) 77—21970
ionosphere, elec. fields induced by ion drag and substorms 80—77199
ionosphere, elec. fields prod. by polar field-aligned currents 78—65455
ionosphere, elec. fields rel. to transverse motion of atomic and mol. ions 77—13155
ionosphere, elec. pot. rel. to solar mag. sector struct., obs. over solar cycle 77—33271
ionosphere, electric currents and fields due to field-aligned auroral currents 78—96339
ionosphere, electric field at high latitudes, ULF oscills. 79—75025
ionosphere, electric fields and currents in quiet periods, simulation 80—12600

atmospheric electricity continued
  ionosphere, electric fields and currents in substorms, simulation 80—12601
  ionosphere, electric fields of magnetospheric origin, simulation 79—62655
  ionosphere, electrodynamic lifting and electron content during storm positive phase 77—37480
  ionosphere, electron concentration profile, vert. struct. 80—61936
  ionosphere, electrons collision freq. and transport props. 79—80079
  ionosphere, electrostatic field struct. in wake of body in rarefied plasma flow 77—91402
  ionosphere, electrostatic fields theory 78—36387
  ionosphere, electrostatic waves obs. in unstable polar cap 79—29927
  ionosphere, EM induction, thin two-dimens. anisotropic conducting model *(German)* 77—70917
  ionosphere, equatorial, elec. field and electrojet changes correlated with interplanetary mag. field 78—85766
  ionosphere, equatorial, elec. fields generated by gravity wave winds 77—53283
  ionosphere, equatorial, electric field meas. 77—87177
  ionosphere, equatorial, meridional currents detect. 78—85767
  ionosphere, equatorial convection field rel. to mid-latit. trough location, Ariel 4 obs. 78—85765
  ionosphere, equatorial elec. fields during mag. disturbances, interplanetary mag. field effect 80—26676
  ionosphere, equatorial elec. fields during mag. disturbances, auroral and equatorial meas. 80—31160
  ionosphere, equivalent currents to explain daily geomag. variations, 1978 obs. 80—41374
  ionosphere, field aligned currents driven by ionospheric dynamo 77—87178
  ionosphere, field-aligned currents and auroral electrojets rel. to nightside auroras distrib. 78—32267
  ionosphere, field-aligned currents in morning sector rel. to auroral electrojet 77—29573
  ionosphere, field-aligned high-latit. current sources and induced elec. fields 80—26669
  ionosphere, general photoelectron current meas. technique 80—12636
  ionosphere, global distrib. of elec. fields and currents produced by magnetosphere field-aligned currents 80—109303
  ionosphere, global scale electrodynamic coupling of auroral and equatorial dynamo regions 79—44297
  ionosphere, global scale electrodynamic coupling of high-latit. and low-latit. regions 80—77194
  ionosphere, Harang discontinuity and substorm injection boundary relation 78—20576
  ionosphere, high latit. electric field turbulence, polarization determ. from satellite data 80—26679
  ionosphere, high-altitude auroral zone, electron temp. enhanced by electron current 80—85803
  ionosphere, high-latit., elec. cond. determ. from auroral electrons 79—12334
  ionosphere, high-latit., elec. field and currents 79—80075
  ionosphere, high-latit., field-aligned current sources 80—72674
  ionosphere, high-latitude, elec. fields rel. to ions vertical distrib. 78—28370
  ionosphere, inhomogeneous cond. rel. to Alfven waves boundary condition 79—53611
  ionosphere, ion current and space pot. in wake of Atmosphere Explorer C (AE-C) satellite 79—53647
  ionosphere, ion cyclotron wave spectrum generated by Ba injection 79—53648
  ionosphere, large-scale elec. field rel. to geomag. activity and terrestrial kilometric radiation 77—87159
  ionosphere, latitudinal struct. of elec. fields and particle precip. on (November 21, 1975) 77—87160
  ionosphere, lunar semi-diurnal elec. field rel. to total electron content lunar var. 79—21100
  ionosphere, lunar tides contrib. to elec. current system 78—77382
  ionosphere, midlatitude obs. of ALADDIN rocket 80—101488
  ionosphere, molecular ions conc. reaction to large-scale elec. field vars. 79—62654
  ionosphere, nighttime equatorial, polarisation elec. field rel. to Rayleigh-Taylor instabilities 79—96855
  ionosphere, Pc 5 geomag. pulsation elec. fields meas. from Stare auroral radar obs. 79—96862
  ionosphere, perpendicular electric fields rel. to He$^+$ outflow 78—49221
  ionosphere, polar, current systems computation 78—45090
  ionosphere, polar cap elec. fields from Tordo 1 polar cusp Ba plasma injection expt. 78—77402
  ionosphere, polar elec. fields transmission to Equator 78—65456
  ionosphere, polar region, elec. field distrib. from crochet type mag. disturbances 78—40733
  ionosphere, polar three-dimens. current system reconstruction from ground-based geomag. meas. 78—45103
  ionosphere, polarisation elec. field prod. by solar tides 78—36391
  ionosphere, polarisation electric field vert. distrib. in topside 80—61935
  ionosphere, potential eqn. separation *(German)* 77—70916
  ionosphere, quiet nighttime, elec. fields rel. to calculated and measured decay rates 78—81493
  ionosphere, radio aurora, 398 MHz echoes, depend. on electron density and elec. field 79—66854
  ionosphere, response to mag. storm sudden commencements and Pc 5 event 77—33264
  ionosphere, reversal of horiz. elec. field assoc. with VHF scintillation 80—101489
  ionosphere, simulation of elec. fields of magnetospheric origin 80—4177
  ionosphere, simultaneous obs. of field-aligned currents and plasma drift vels. by Atmosphere Explorer C 80—72681
  ionosphere, striations assoc. with Ba clouds, electrostatic pot. calcs. 77—9607
  ionosphere, strong radio waves elec. field rel. to self-focusing instability near caustic 78—45107
  ionosphere, struct. of electrostatic field in wake of spherical satellite 77—60509
  ionosphere, tensor conductivity 77—13172
  ionosphere, topside, electrical props. of plasma bubbles near dawn terminator 79—101016
  ionosphere, transitional electrodynamic processes rel. to geomag. disturbances 77—60515
  ionosphere, two-layer current model for geomag. crochet 79—44300

atmospheric electricity continued
  ionosphere, uniform, transient response to geomag. storm sudden commencement rel. to preliminary reverse impulse 80—8477
  ionosphere, zonal and meridional elec. fields effects in evening sector 78—69571
  ionosphere, zonal electrostatic potential 78—36393
  ionosphere and magnetosphere, adiabatic potential transitions properties in polar regions 79—5713
  ionosphere and magnetosphere, current distribution quantitative modelling 78—88988
  ionosphere auroral acceleration regions, energetic particle meas., rel. to elec. fields 79—53644
  ionosphere current systems, rel. to press. oscills. and atmosphere acoustic-gravity waves 78—77296
  ionosphere currents, night-time induced effects on geomag. regular daily var. 77—9627
  ionosphere currents, obs. by S-310-5 rocket *(Japanese)* 80—94635
  ionosphere disturbance dynamo, caused by thermospheric wind 80—82134
  ionosphere during auroral substorm expansion, riometer absorpt. of spikes obs. 80—85799
  ionosphere dynamo, contrib. to O$_1$ tidal component of geomag. lunar daily var. at Alibag 80—56355
  ionosphere electric currents during 23 October 1976 solar eclipse, mag. obs. in Australia 78—81498
  ionosphere electric field spreading, two-dimensional and three-dimensional mapping comparison 79—66861
  ionosphere electric fields generated during magnetosphere substorms, determ. from Doppler sounding 80—4169
  ionosphere electrostatic field structure in wake of disc, external mag. field effect 79—10648
  ionosphere field-aligned currents at subauroral latitude, assoc. with convection elec. fields 80—90278
  ionosphere fine structure at low latitude from impedance obs. at 406 kHz 80—67468
  ionosphere high-latitude electrostatic turbulence, polarisation, freq. and wavelengths 78—88981
  ionosphere hot electron layer, electron heating near Sq focus anomaly 80—51599
  ionosphere inhomogeneity formation, influence of elec. field temporal variation 80—105105
  ionosphere moving current systems, EM induction in Earth 79—16370
  ionosphere plasma conductivity, kinetic theory 79—53609
  ionosphere plasma conductivity, limits of applicability of formulae of mean free path theory 77—60512
  ionosphere polar cap, elec. fields rel. to slant-E condition and plasma flow entry region position 80—67472
  ionosphere polar electric field, horizontal transmission to equator 80—8478
  ionosphere transverse electrical conductivity 77—49227
  ionosphere waveguide, effect of weak disturbance of permittivity on ray trajectories 80—61966
  ionosphere-magnetosphere, field-aligned current rel. to 100-500 kHz noise and auroral arcs 79—66859
  ionosphere-magnetosphere, high-latit., average parallel elec. field from perpendicular elec. field vars. below 8000 km 80—72706
  ionosphere-magnetosphere electrodynamic interaction, during 1960, April 1, disturbance 78—28372
  ionosphere-magnetosphere small-scale dynamo, multiple layer model 79—53612
  ionosphere-magnetosphere system, induced elec. fields, review 80—94647
  ionospheric current, of polar cap and sunlit cleft, obs. and theory 80—41615
  ionospheric current determ. from surface geomagnetic obs. *(Japanese)* 78—24406
  ionospheric currents, EM induction at S.American geomagnetic equator 79—75021
  ionospheric currents, mutual interaction between E- and D-regions during solar flare 77—45236
  ionospheric dynamo calculations with semidiurnal winds 77—91366
  ionospheric effects of magnetospheric substorms at night 79—62656
  ionospheric electric fields, incoherent scatter radar studies 77—22001
  ionospheric field-aligned currents role in mag. disturbances generation 80—41631
  ionsophere, polar-equatorial coupling during mangetically active periods 78—93029
  Joule dissipation of elec. currents during equatorial spread-F events 78—45127
  K-field changes, VLF spectral characts. rel. to lightning 77—2217
  lightning, elec. field changes rel. to optical radiation obs. from above and below clouds 80—85698
  lightning, generation of strong RF radiation, elec. field pulse obs. 80—98401
  lightning intracloud discharges, elec. dipole axis inclination determ. 78—73440
  lightning stepped leaders, electric field production 77—37301
  lightning strokes to Earth per km^2 per year, CIGRE count (since 1962) *(German)* 78—40606
  lower atmosphere, ion conc., elec. parameters and space charge density correls. 77—13104
  magnetic field aligned pot. diff. meas. from photoelectron energy spectra 78—7825
  magnetic storm main phase ring current, origin by inward displacement of preexisting particles 80—72708
  magnetic storm sudden commencement amplitudes, equatorial enhancement, elec. field effect 77—78575
  magnetopause, MHD flow, elec. field generation 78—40760
  magnetopause, tangential component obs. 79—70930
  magnetopause form and electric field in continuum medium model 79—75041
  magnetosphere, anomalous resist. in geomag. tail region 79—12353
  magnetosphere, assoc. elec. field, mag. field and electron precip. fluctuations 78—81507
  magnetosphere, auroral electrons accel. by MHD surface waves 77—9621
  magnetosphere, Birkeland current sheets in dayside polar region 80—90289
  magnetosphere, Birkeland currents and limits to double-adiabatic approximation for hot collisionless plasma 78—75262
  magnetosphere, Birkeland currents at high-latitude, suprathermal electron contrib. 80—90290

atmospheric electricity continued
magnetosphere, constant electric field strength vector meas. problems 78—16245
magnetosphere, contrib. to regular geomag. daily var. 77—9627
magnetosphere, convection and field-aligned currents during weak global mag. disturbances 79—53660
magnetosphere, convection elec. field model based on Explorer 45 obs. 79—12350
magnetosphere, current fields at magnetopause and in radiation zone 79—53658
magnetosphere, current instability on short wave drift oscills., nonlinear theory *(Russian)* 80—53981
magnetosphere, current interruption in collisionless plasma by non-linear electrostatic waves 79—75052
magnetosphere, dawn-dusk elec. field from substorm electrons obs. 77—33292
magnetosphere, double layers and electrostatic shocks review 80—36460
magnetosphere, effects of solar wind EM field 78—28419
magnetosphere, elec. and mag. fields at high latits. 78—12057
magnetosphere, elec. currents over auroral arc 77—33296
magnetosphere, elec. field, plasma density and temp., field-aligned currents, S3-3 satellite obs. 80—26699
magnetosphere, elec. field around rot. mag. dipole 78—45141
magnetosphere, elec. field assoc. with Pc 4 compressional pulsation obs. from geostationary orbit 79—80094
magnetosphere, elec. field effect on charged particle drift in Mead and Mead-Williams geomag. field 79—84592
magnetosphere, elec. field induced instability 77—70942
magnetosphere, elec. field on disturbed days, at mid-latitude 80—77230
magnetosphere, elec. fields and currents influence on thermospheric circulation and comp. 80—17446
magnetosphere, elec. fields effect on O_2 and O distrib. in mesosphere and thermosphere 79—66850
magnetosphere, elec. fields generated by fast charged particle drift, cold plasma polarization drift effect 77—17298
magnetosphere, elec. fields parallel to mag. field, remote sensing expt. 78—40776
magnetosphere, elec. fields parallel to mag. lines, studied by electron injection expts. 80—72702
magnetosphere, elec. fields rel. to plasma two-dimensional inertial turbulence 78—36399
magnetosphere, electric field sources and streams *(German)* 78—28453
magnetosphere, electric fields absence rel. to particle entry 80—41669
magnetosphere, electric fields from phase and group path meas. of VLF whistlers 78—49234
magnetosphere, electrostatic field struct. in wake of body in rarefied plasma flow 77—91402
magnetosphere, electrostatic shocks, double layers and anomalous resistivity 78—45152
magnetosphere, electrostatic shocks as source of discrete auroral arcs 78—45153
magnetosphere, energy flow and current systems closure, rel. to upstream solar wind parameters 78—57400
magnetosphere, equatorial elec. field during storm, obs. of whistlers 80—85817
magnetosphere, equivalent current systems during substorm and auroral activity development 78—28435
magnetosphere, field-aligned currents, OGO 5 and Triad satellite obs. 77—33279
magnetosphere, field-aligned selfconsistent elec. field 78—69615
magnetosphere, fluctuating elec. fields rel. to counterstreaming electron beams over auroral zone 80—67474
magnetosphere, GEOS-1 meas. of electric and magnetic wave fields and cold plasma parameters 79—48620
magnetosphere, high-latit. convection field, parallel elec. fields and inverted-V precip. events 77—33297
magnetosphere, inductive electric fields calcs. 79—80093
magnetosphere, kilometric radiation elec. fields meas. by JIKIKEN (EXOS-B) satellite *(Japanese)* 80—94648
magnetosphere, large transient elec. fields obs. 78—28440
magnetosphere, large-scale elec. field, from VLF chorus dynamic spectrum 79—8775
magnetosphere, large-scale elec. fields 77—87208
magnetosphere, large-scale electric field from VLF burst freq. drift rate 79—92639
magnetosphere, macroscopic elec. fields 78—49238
magnetosphere, macroscopic electric fields 78—69609
magnetosphere, mag. field-aligned pot. drops due to electrostatic ion cyclotron turbulence 78—45155
magnetosphere, mag. mirroring of charged particles, cause of parallel elec. fields 77—25868
magnetosphere, mag. storm elec. fields meas. by GEOS-1 keV plasma expt. 79—35068
magnetosphere, magnetic-field-aligned elec. fields generation mechanisms 80—77233
magnetosphere, nightside, transient dusk to dawn elec. field origin 79—96863
magnetosphere, paired electrostatic shocks in polar regions, satellite obs. 77—29601
magnetosphere, parallel elec. field effect on whistler mode instability 80—26700
magnetosphere, parallel elec. fields signature in collisionless plasma 77—53323
magnetosphere, polar, electrostatic H^+ cyclotron waves near one Earth radius altitude 78—45154
magnetosphere, polar caps elec. fields distrib. in two-sheet configuration 78—45140
magnetosphere, potential and inductive elec. fields during auroras 80—21878
magnetosphere, quasistatic elec. fields meas. between 3-7 R_E 79—29942
magnetosphere, reverse polarity field-aligned currents at high latit. 77—53322
magnetosphere, signature of parallel electric fields in collisionless plasma 78—77439
magnetosphere, substorm-assoc. particle-flux vars. due to drift in geoelectric field 79—35067
magnetosphere, transverse electrical conductivity 77—49227
magnetosphere, turbulent generation of electrostatic fields 78—28439
magnetosphere, turbulent plasma conductivity anisotropy and effects 77—13182

atmospheric electricity continued
magnetosphere, two-snake current system model for Pi3 long-period irregular mag. pulsations 78—45164
magnetosphere and ionosphere, elec. and mag. fields, rel. to coupling 79—66870
magnetosphere and ionosphere, elec. field power spectra, double probe meas., Doppler shift effects 80—26634
magnetosphere and ionosphere, mag. field aligned elec. fields 77—9618
magnetosphere boundary layer, field-aligned currents theory 80—67473
magnetosphere boundary layer, model involving interaction with ionosphere 80—85808
magnetosphere convection elec. field, effect on neutral upper atmosphere dynamics 77—29525
magnetosphere convection electric field, divergence rel. to auroral currents and elec. pots. and precip. generation 80—67453
magnetosphere current systems, N.polar cap mag. variations associated with interplanetary field 80—41645
magnetosphere currents, density evaluation from results of scalar geomag. field meas. 77—13186
magnetosphere dayside cups, DC elec. fields and thermal electrons densities and temps. 77—78574
magnetosphere dayside cusp, field-aligned currents obs. 77—29591
magnetosphere elec. field obs. used to locate LF radiation source at 2.5 R_E 80—41656
magnetosphere electric convection field, model 78—89004
magnetosphere electric field, boundary condition for Alfven waves at ionosphere 79—53611
magnetosphere electric field, influence on thermosphere N.Polar Cap winds 80—67445
magnetosphere electric field model used to predict ionosphere plasma convection at high latitude 80—41612
magnetosphere electric fields and convection, role of particle precip. 79—25400
magnetosphere equatorial electric field at $L=2.3$, power density 80—82146
magnetosphere field-aligned electric currents, global distrib. of induced ionospheric fields and currents 80—109303
magnetosphere high-latitude electrostatic turbulence, polarisation, freq. and wavelengths 78—88981
magnetosphere longitudinal currents, dynamic processes in turbulence development 80—67469
magnetosphere midlatitude convection elec. fields, rel. to ring current development 78—57395
magnetosphere open model, current sheets rel. to plasma populations 80—90295
magnetosphere parallel electric field, signature in ion and electron distribs. in vel. space 78—89005
magnetosphere plasma sheet, plasma flows during substorms rel. to field-aligned elec. field 78—96357
magnetosphere polar cap, elec. field and convection after interplanetary mag. field becomes northward 80—94658
magnetosphere ring currents rel. to D_{st} variations of mag. storms 80—41643
magnetosphere substorm and simultaneous thunderstorm, elec. fields, electron precip. and VLF radiation 80—67392
magnetosphere tail, explosive tearing mode reconnection and cross-tail EMFs 78—88992
magnetosphere tail plasma sheet, convection elec. field rel. to electron transport 79—25408
magnetosphere-ionosphere, empirical models of high-latit. elec. fields 77—45255
magnetosphere-ionosphere current loops during polar magnetic substorm 79—8776
magnetosphere-ionosphere current system, generating Pi ULF waves 80—85819
magnetosphere-ionosphere electrical coupling, two-dimens. model 80—61938
magnetosphere-solar wind interaction, Chapman-Ferraro image method graphs correction 80—12620
magnetospheric and ionospheric currents, induced magnetic var. 77—70594
magnetospheric plasma convection, numerical simulation 79—62679
magnetospheric substorms, assoc. three-dimens. current system modelling 77—56793
magnetospheric substorms, energetic particle accel., lab. and space expts. 77—5400
magnetotail, current system rel. to energy transfer in magnetosphere substorm 79—12343
magnetotail, distant, lower-hybrid-drift wave turbulence 79—25399
magnetotail, large-scale elec. field rel. to magnetosphere convection and polar ionosphere 80—4176
magnetotail, localised induced elec. field 77—53329
magnetotail, lower-hybrid-drift instability and mag. field line reconnection 77—45254
magnetotail, particle accel. by induced substorm electric field 77—73909
magnetotail, substorm assoc. current changes 79—12347
magnetotail, transient elec. field evidence from energetic proton and electron anisotropies 77—53318
magnetotail field-aligned currents, self-consistent theory in three dimensions 77—33286
magnetotail magnetic current sheets, effect of press. anisotropy on equilib. struct. 79—12354
magnetotelluric apparent resistivity, effect of localised source 80—72429
magnetotelluric investigations at Ronde, effects of atmospheric discharges and ionosphere elec. currents *(Danish)* 80—8250
magnetotelluric methods, use of geomag. depth sounding below surface magnetometer array 80—98486
marine atmosphere, elec. field short-period fluctuations 79—39816
measurement of elec. cond. and small ion mobility, pollution aspects 78—92931
measurement with multielectrode ion mobility spectrometer construction 80—31145
measurements with spherical mesh detectors 80—8436
mesosphere, elec. field strength max. meas., 30-90 km altitude range 77—29358
mesosphere, ion mobility and elec. cond. height var. 77—21837
mesosphere, Joule heating at high-latitude 80—41500
mesosphere, positive and negative ions cond. meas. via payload B III instrument package 78—45194
micropulsations near plasmapause, elec. field obs. 80—85814

atmospheric electricity continued
microwave signals cross-polarisation rel. to atm. elec. field strength 77—49132
midlatitude electric fields at ionospheric heights, magnetospheric effect 79—2433
monsoon clouds, aircraft meas. of elec. parameters 78—7792
mountain station, electrode effect obs. 79—25307
near-Earth plasma, elec. fields penetration along geomag. force lines, electrostatic approach applicability 80—4178
parachute-deployed payload for elec. field meas. below 80 km 77—64376
particles of aluminosilicate, charge state depend. on thermal history 80—97840
passive antenna system, comparative study for use as elec. cond. meas. device 80—85762
passive probe for free atmosphere electric field meas. 79—8710
Pc5 pulsation theory, consequences of ionosphere Hall current 80—105129
Pc5 pulsation theory, consequences of N. and S. hemispheres ionosphere electricity 80—109316
Pc5 pulsations, model of magnetosphere and ionosphere elec. and mag. fields 80—77234
Pc 5 micropulsation resonance region, elec. fields meas. by dual auroral radar system 78—65454
plasma sheet, electrostatic shock waves assoc. with auroral electron precip., model 77—9616
plasma sheet, magnetised plasma slow convection rel. to mag. field aligned currents 80—109312
plasmapause electric field variation from pulsation-pearl method, effect of substorm phases 77—25848
plasmasphere, corotation electric field 77—25841
plasmasphere, dynamo electric field aligned currents theory 78—81499
plasmasphere, heavy ions convection and magnetospheric circulation 77—64533
plasmasphere, large scale elec. fields and currents, related geomag. vars., review 80—105121
plasmasphere, nightside, substorm elec. fields detect. by whistler obs. 79—40009
plasmasphere, outer, elec. currents and fields rel. to whistler ducts form. 78—57407
point discharge current, effect of meteorological factors 79—88409
point discharge current for fog forecasting 77—70748
point discharge current meas. during different types of rainfall 79—84379
point discharge currents during solar eclipses 78—16094
point discharge from ground surface objects, annual charge change per km^2 80—77077
point-discharge currents, meas. via portable instrument using junction FETs 79—39972
polar cap and low latitude bays during substorms, ionospheric current systems 77—17300
polar cap electric field, simplified model 78—12046
polar cap ionosphere, elec. field orientation and field aligned currents 80—41616
polar caps, elec. field resulting from geomag. and interplanetary mag. fields reconnection 77—22007
polar cusp, field-aligned currents, convection elec. fields and ULF-ELF waves 79—75043
polar cusp, low altitude, correlated elec. field and low-energy electron meas. 78—40770
polar cusp, Pedersen cond. from impulsive penetration of filamentary plasma elements 77—78581
polar F-region, elec. fields, drifts and winds 77—33274
polar ionosphere, neutral winds and ion drifts 77—87173
polar magnetic substorm development, ionosphere-magnetosphere current loops model 77—91368
poleward-directed electric fields, near ionospheric projection of plasmapause 78—20574
pollution, electrical climate relationship 77—73837
potential gradient, slow vars. and short-period pulsations of magnetospheric origin 79—12188
potential gradient diurnal var. at southern hemisphere continental site 77—21841
potential gradient over N.Dakota, seasonal changes and diurnal var. 77—49142
potential gradient sunrise effect 77—45089
potential of rocket and electron beam injection expts. *(Russian)* 78—93069
precipitation particle alignment by electrostatic fields, radar obs. 77—9464
premidnight convection topology, auroral vector electric field and particle comparisons 77—70906
protonosphere-ionosphere thermal plasma flow, convection elec. field effects 79—62672
radial electric fields from air polarisation due to Compton electrons excited by γ-quanta pulse 80—21805
radiation fields, of multiple return stroke lightning 78—3885
radio aurora (diffuse), rel. to field-aligned currents and particle precipitation 80—105119
raindrop charge and assoc. electric field for different rain types 78—44933
riming electrification as a charge generation mechanism in thunderstorms 79—34917
ring current, growth rel. to interplanetary quantity ε 79—75057
ring current, particle boundary motions rel. to proton flux obs. by Geostationary Meteorological Satellite (GMS) 79—75056
ring current, quiet-time, obs. concerning relationship to ionosphere electron temps. at trough latits. 79—101015
ring current, storm-time, D_{st} contrib. to aurora equatorward shift 79—75013
ring current behaviour during mag. storm 80—82144
ring current composition change from equatorial aurora obs. 78—36401
ring current during quiet field variability, mid-latitude 80—72714
ring current dynamics, role of proton-cyclotron instabilities in non-uniform loss-cone plasma 80—90286
ring current proton interaction with electron cyclotron emissions 77—25853
ring current unstable waves, role of charge exchange 77—49225
rotational electric field of auroral origin 78—45102
S_q current system, sharp displacements of focus 77—60529
S_q variation, magnetosphere or ionosphere dynamo? 80—109090
S_q variation currents, day to day variability over Europe 79—44299

atmospheric electricity continued
S_q variations field, magnetically conjugate structs. variability 79—58191
S_q-field, seasonal and latit. vars. deduced via natural nonorthogonal functions method 78—36359
Schumann resonances, elec. vertical component obs. by stratosphere balloon 79—44221
small ion conc., influence of smoke, SO_2 and wind speed 78—3896
small ion number density time fluctuations in surface layer 78—7730
solar corpuscular radiation effects 79—79982
solar modulation of atmospheric electrification, possible implications for Sun-weather relationship 78—57261
space charge generated by surf, meas. 78—36235
space simulation plasma chamber, elec. field meas. with double probes, atm. appl. 79—64909
spectral analysis of elec. field near ground 78—11950
sporadic-E layer, equatorial formation, electric fields and neutral winds effect 78—12045
spruce budworm visible glow as UFO explanation 79—16361
Sq at low latitude, hourly study of secondary effect 80—56362
Sq current system during International Geophysical Year 77—45219
Sq currents, appl. to equatorial F-region motions deduction 78—96344
Sq currents of N. and S. hemispheres affecting equator mag. variations 80—76904
Sq vars. at low latitudes during magnetic storms 79—25402
stable auroral red arc, 4th Aug. 1972, obs. during ring current growth 80—51594
static charges accumulatiion and limitation, discharging to earth *(Italian)* 80—43226
static electrification, by electrolytic process 80—72624
static electrification hazard, review 78—28283
storm clouds, observed by elec. field sensor *(French)* 80—85712
storm-time ring current ions of ionospheric origin 78—28430
stratosphere, elec. field, balloon meas., SAMBO-1 expt. 79—66738
stratosphere, electric field in mag. storm negative phase, 1975 March 20-21, balloon obs. 79—79921
stratosphere, electric fields and currents at Syowa Station, horizontal component 77—87021
stratosphere, electrical parameters and aerosols, meas. *(Japanese)* 80—31087
stratosphere, ion mobility and conductivity, comparison balloon and rocket obs. 80—72605
stratosphere, lower, simultaneous balloon meas. of elec. cond. and aerosols 77—73813
stratosphere, solar flare modification of elec. fields, direct evidence 79—48553
stratosphere, vertical elec. fields and currents meas. at Syowa Station, Antarctica 77—53142
substorm associated field-aligned currents large-scale characts. 78—45156
substorm current systems, rel. to dayside aurora and mag. field merging 79—96852
substorm electric fields in plasmasphere, model based on whistler data 80—41661
substorm variation field modeling, current system anal. 80—105130
substorms, comprehensive model current system for high-latit. mag. activity 79—92640
sunrise effect on elec. pot. near ground, origin in upper atmos. 80—61866
supply current, solar modulation 80—17329
temperature inversion, vertical elec. field strength and ionic cond. meas. 78—20478
thermal power station environment, airborne elec. and microphys. obs. 77—37354
thermosphere, auroral energy input rel. to electrodynamics and neutral and ion drifts 78—65446
thermosphere, electric field momentum coupling characts. 78—88958
thermosphere, lower, electric current and atmospheric motion, symposium, Seattle, Washington, 1977 August to September 80—62371
thundercloud, positive streamer velocities meas., in quasi-uniform electric fields 80—72625
thundercloud elec. field meas. by balloon-borne coronasonde 78—61577
thundercloud electrification by precip. mechanism in presence of ion generation, model 79—84388
thunderclouds, corona charging of frozen precip. 77—5295
thunderclouds, effect of elec. forces on charge separation caused by combined precip. and convection 80—17333
thunderclouds, elec. field inclination effect on inductive charging mechanism 77—78315
thunderclouds, electrification rel. to sudden increases in shower intensity 78—20491
thunderstorm, charge generation and time-depend. elec. field 80—72595
thunderstorm, electric field and wind profile, balloon meas. 78—85636
thunderstorm charge build up, charging mechanisms 78—81320
thunderstorm charge separation, ice particle surface pot. obs. 80—51495
thunderstorm charging by polarization-induction mechanism 78—32166
thunderstorm electric charge separation, model 80—77076
thunderstorm electric fields, 10-year study of Minneapolis area 78—57253
thunderstorm electrification, airborne expts. 77—66970
thunderstorm electrification, field expt. 80—72622
thunderstorms, contribs. of cloud and precip. particles to elec. cond. and air relaxation time 80—17332
thunderstorms, elec. field growth, field struct. and charge distrib. 77—70777
thunderstorms, elec. fields, precip. elements charge and size, airborne obs. 78—73485
thunderstorms, max. elec. field intensities meas. over water 77—33160
thunderstorms, microwave radiometric detect. of corona from chaff 78—16106
thunderstorms, nontropical, initiation by solar activity 78—49096
thunderstorms, vertical potential gradient profile under point discharge current and wind 77—53117
thunderstorms near Langmuir Laboratory, airborne and ground based studies 80—85725
topside ionosphere, anomalous resistivity of auroral plasma 77—5389
tornado, contrib. of vortex-stabilised arc to energy 78—53711
tornadoes, Huntsville, AL, luminous electrical phenomena 77—45060
transmission lines, high voltage, depend. of coronal discharge power loss on instantaneous rainfall rate 80—98471
ULF elec. fields and particle precip. in aurora, rocket meas. 78—96337
ULF electric and magnetic fields due to lightning 78—7731

atmospheric electricity continued
upper atmosphere electrical coupling to lower atmos., quasi-static model 80—61865
vertical component, obs. in Arctic Ocean at North Pole-22 drifting station *(Russian)* 79—48537
vertical component pulsations correl. with mag. components during Pc 1 event 78—61687
vertical currents connected with ionospheric Pedersen currents, ground magnetic effect 77—29579
vertical electric component of Pc 3-4 pulsations, effect of doubling period 77—41270
vertical intensity component meas. 77—91209
warm cloud electricity, shallow axisymmetric cloud model 80—81999
water droplet collision and coalescence for small Reynolds numbers, electric force effects 77—78326
water drops, impaction and electrical effects on collisions with spherical particles 78—28272
winter thunderstorms, anomalous, of Hokuriku coast, lightning polarity and charge struct. 78—73443
zonal electrostatic potential distrib. at ionospheric heights 78—7824

atmospheric electromagnetic wave propagation
see also atmospheric light propagation; ionospheric electromagnetic wave propagation; magnetospheric electromagnetic wave propagation; tropospheric electromagnetic wave propagation
35 GHz wave attenuation along slant path by rain *(Japanese)* 78—85671
aerosol scattering, spectral-zonal functions *(Russian)* 80—21824
aerosols, role in attenuation of 10.6 μm radiation *(Russian)* 78—45000
aerospace propagation environment operational modelling conf., Ottawa, Canada, 1978, April 79—53651
amplitude spectra in absorption region at 60 GHz 78—44920
amplitude spectrum rel. to fluctuation frequency in absorption region 77—21878
Amsat-Oscar 7 subhorizon ratio signals beacon, above F2 layer, 30 MHz 77—70937
antenna elevation patterns computation, piecewise homogeneous ground models appl. 79—66774
Arctic summertime stratus clouds, solar radiation pyranometric meas. 78—32165
astronomical site testing with balloon borne radiosondes, turbulence meas. 77—29645
atmosphere, radiation modulation of aerosol state by moving clouds *(Russian)* 78—88916
atmosphere, surface radiative flux, clear and cloudy conditions, parametrisation accuracy 78—77325
atmospherics noise variation with sunspot number during 1600-2000 hours at Delhi 78—49083
ATS-6 radio beacon experiment, ground refls. effects 77—53144
ATS-6 satellite radio beacon, meas. at Ootacamund, India rel. to electron density 79—48611
attenuation at 230 GHz, meas. 78—73425
attenuation meas., satellite Earth path, in the freq., bands 20 and 30 GHz 78—7822
attenuation meas. using radiometer, satellite link system *(Czech)* 78—36351
attenuation measurement at 22.75 GHz, broadcasting appl. *(German)* 78—20465
aurora, radio emissions in 2.5-6 MHz range 79—70906
auroral hiss emissions, assoc. with region of intense plasma wave turbulence 77—45228
auroral kilometric radiation, ISIS 1 obs. at source 79—84558
auroral O I (989 Å) and O I (1027 Å) emissions, radiation transfer theory 78—28367
auroral radio absorption, spike events 80—12589
auroral radioscattering anisotropy, from 42 MHz polarisation investig. 77—21968
backscattered pulse shape, small-angle multiple scatt. in random media 80—77079
bandwidth limitations in turbulent atmosphere using coherency and differential amplitude spectra *(French)* 78—49070
Bremmer, H., contrib. to radiowave propag. 79—62984
circumglobal signals in Atlantic equatorial zone *(Russian)* 78—69585
classical radiowave propagation criteria, attenuation 80—67390
clear air radar echo mechanisms 80—90181
cloud effects on global middle UV radiation meas. at ground 78—92882
cloud liquid H_2O obs. from 28 GHz satellite signal absorpt. 80—94623
cloudy atmosphere, scatt. and line absorpt. of radiation, interaction, analytical calc. method 79—100940
conference, IR and MM waves and appls., Miami Beach, USA (Dec. 1979) 80—57009
decametric radiowaves emitted by dipole, propag. problem 78—69399
dielectric spheroids, backscatter matrix 78—66716
direct solar radiation spectral distrib. 79—12268
dispersion, appl. in multi-wavelength distance measuring instrument 77—29484
Doppler radar probing of clear atmosphere 79—66811
Earth-ionosphere cavity, resonance phenomena *(Russian)* 77—73801
Earth-ionosphere cavity, Schumann resonance problem, convergence of zonal harmonic series 79—2348
Earth-ionosphere waveguide, geomag. disturbances propag. 77—17157
Earth-ionosphere waveguide, mode conversion coeffs. for VLF propag. below stratified anisotropic ionosphere 77—53143
Earth-ionosphere waveguide, program to compute EM fields in irreg. spheroidal model 80—94638
Earth-ionosphere waveguide, VLF propag., multimode nature effects on correlation factors *(Russian)* 77—70745
Earth-ionosphere waveguide channel parameters, influence of geomagnetic activity and statistical props. of VLF signals 79—88452
Earth-ionosphere waveguide model, inverse propag. problem soln. 79—58154
Earth-ionosphere waveguide parameter determ. by VLF transitional route meas. 77—91234
Earth-ionosphere waveguide propag., rel. to geomag. storm sudden commencement preliminary reverse impulse 80—8477
Earth-satellite paths, 11.5 GHz, annual and annual-worst-month statistics of fading 78—57238
Earth-space communication links, path diversity performance 78—69424
Earth-space radio propagation path, ice particles orientation and alignment rapid changes obs. 80—17330
effects on remote sensing 77—56732

atmospheric electromagnetic wave propagation continued
EHF propag. in air, atmospheric medium characterization and modelling 79—53504
EHF propag. in clear air, modelling 79—58075
ELF coherent radiation, search at Crab pulsar freq., upper limit 79—16728
ELF field strength meas. in Connecticut in 1975, summary 79—48557
ELF propagation in Earth-ionosphere transmission line, rel. to ionospheric profiles 78—36234
ELF propagation in Earth-ionosphere waveguide 80—41634
ELF sferics in polar region during solar proton event, June 1968 Antarctic obs. 80—90291
ELF waves in Earth-ionosphere cavity, field eqn. for inhomogeneous ionosphere 80—61950
EM mode coupling in inhomogeneous magnetised plasma, normal incidence case 77—84435
ETS-II, radiowave propag. expt. facility *(Japanese)* 79—2471
ETS-II satellite, 1.7 GHz, 11.5 GHz, 34.5 GHz wave propag. rel. to rain precipitation strength *(Japanese)* 78—85669
evaporation ducts, polarisation depend. of transient signals 78—57269
field intensity and propagation mode of JJY signal at Okinawa *(Japanese)* 77—81980
geomagnetic atoms effects, variation during low solar activity *(Japanese)* 79—40032
global daily radiation estimation for any surface 79—39805
ground reflectances, atmospheric effects in space meas. 80—17373
ground screening factor evaluation to protect systems from interference *(French)* 78—49071
ground wave propagation, ground-air interface of smooth hills and depressions 78—24352
ground wave propagation of Loran-C signal, theoretical review 80—94580
ground-wave atmospherics, lightning generation, statistical simulation 78—44967
guiding of radio waves using ducting refr. gradients, review 79—84374
hail, equivalent reflectivity factor rel. to vertical fluxes of mass, kinetic energy 79—84393
hail, radar detection technique, quasilinear discriminant function 80—21861
HF radio meteor echoes duration rel. to dense trains deionisation 79—5697
HF wave propagation with lateral deflection from great circle arc, investigation 78—45096
hydromagnetic wave rotation between magnetosphere and ground 80—61969
hydrometeors, extinction and scattering in 0.25-15 μm range 79—53501
incoherent energy and coherent time of depolarised microwaves, interferometric analysers 78—96277
incoherent scatter results for co-ordinated special intervals at St. Santin (France) 79—2416
India, solar radiation meas. and atm. transmission at high altitude stations 78—32152
insolation estimation over ocean, clear and cloudy skies 77—87023
interaction with magnetospheric plasma oscills. *(Russian)* 78—4036
ionosphere polar electric field, horizontal transmission to equator 80—8478
IR attenuation, 8-13 μm, by H_2O vapour *(Russian)* 78—88915
IR irradiance, anal. of GATE aircraft radiation instrumentation 78—32134
IR laser beam transmission, coagulation-sedimentation effects 80—36393
IR lidar, atmospheric refractive effects at 10.6 μm wavelength 80—36392
IR radiation transfer, statistical model 78—26024
irradiance meas. from aircraft, computer simulation 77—70830
ITCZ, 13.9 GHz radar altimeter obs. of total attenuation 77—29355
kilometric radiation, theory 79—70900
LF absorption events during meteor showers, rel. to meteoric constituents ionization 78—40736
LF band, noise field and skywave propag. 79—5708
LF radio navigation signal affected by variable meteor ionis. 80—82309
LF/VLF propag. below nonuniform isotropic ionosphere 79—44224
long-delay echoes, 28 MHz amateur band obs. 80—90277
lower atmosphere remotely sensed by two satellites, radio illumination method 80—51550
magnetosphere, HF and VLF propag. between mag. conjugate pts. on Earth surface 80—41639
magnetosphere ELF emissions, atmospheric propag. rel. to obs. at Moshiri, Japan 78—24413
mesosphere, high-resolution VHF radar refl. rel. to turbulence structs. obs. 79—100895
mesosphere, LF radio wave absorpt. temp., seasonal variation 79—48602
mesosphere, LF radio wave absorpt. variations, press. and temp. depend. 79—44282
mesosphere, major characts., processes and dynamics 77—25734
mesosphere, partial refl. method for neutral wind vels. determ. 77—87019
mesosphere, VHF radar scatt. and vertical vels. meas. at temp. latits. 79—16572
mesosphere, VLF absorpt. seasonal variations, geopot. field 79—66766
mesosphere incoherent scatter spectrum, ion component meas. in 60 to 90 km region over Arecibo 79—16569
mesosphere VHF radar signal scattering, tropical latitude 80—90193
MeV gamma radiation, theoretical zenith angle distrib. at high balloon altitudes 77—45208
microwave absorpt. coeffs. of atmospheric pollutants and constituents 77—64378
microwave absorption coefficient and refractive index, optimal orthogonal functions 80—36379
microwave Earth-space link rain cell attenuation 80—94586
microwave measurement of absolute values of H_2O vapour absorpt. 79—66773
microwave propag. in 1 to 300 GHz band, computer model for atmospheric propag. conditions 79—53505
microwave propagation, rel. to pollutant gases monitoring from space using passive sensing techniques 80—76690
microwave radiation transfer, Nimbus 6 scanning spectrometer data parameterisation for atmosphere liq. water content 79—58047
microwave radiometry from satellites 77—70882
microwave refr. and absorpt. coeffs., optimal orthogonal expansion props. 80-98414

atmospheric electromagnetic wave propagation continued
- microwave satellite paths, crosspolarisation phase due to ice crysts. 78—7684
- microwave scatt. and depolarization by spheroidal raindrops 77—9480
- microwave scattering by melting hailstone 79—64179
- micrwwave remote sensing of wind and water content, from Earth orbit 80—41573
- middle atmosphere, 50 MHz radiowave depolarisation on backscattering 80—85729
- middle atmosphere, radar obs. at UHF and VHF, review of obs. 80—90180
- Mie scattering improved algorithms 80—78771
- millimetre wave transmission, spectral distrib. obs. by wide-band radiometer 79—62750
- millimetric and submillimetric atmospheric scintillation theory 80—61884
- mm wave attenuation in rain 78—96280
- MM wave propag. in 100-1000 GHz range 79—92578
- MM wave radiometry conducted at Appleton Laboratory 80—67442
- MM wave radiometry for atmospheric sounding 79—84551
- MM wave systems, atmospheric attenuation factors 80—67405
- MM waves, propag. expts. using Kiku-2 satellite-to-Earth link 79—79909
- MM-wave, Earth's sphericity and radiowave refraction influence on atmospheric radio emission 80—56589
- modelling, orientation of solar collectors, appl. 77—81965
- monochromatic radiation in cloudy media *(Russian)* 78—32145
- multidimensional radiative transfer 77—64638
- Nimbus 6 high-resolution IR sounder channels, upwelling radiance sensitivity to clouds 78—32227
- nonlinear self-distortion in magnetoplasma 79—40031
- nonspherical extinction and absorption efficiencies 79—7074
- nonstandard atmosphere, arrival angle and echo delay meas. 77—64397
- one-hop path, field intensity vertical pattern 79—58156
- optical beam propag. of partially coherent source in turbulent atmosphere 80—12533
- optically thick, radiative transfer eqn., direct soln. 77—41170
- planetary atmosphere HF radio occultation meas., phase screen concept 80—56735
- planetary atmospheres, complex geometric optics of radiowave propag. under superrefraction *(Russian)* 78—49353
- plasmapause, spectra peculiarities of VLF emission 77—25852
- plasmapause afternoon sector, simultaneous ULF and strong riometer absorption events 77—25849
- polar electric fields, transmission to Equator 78—65456
- polarisation state of waves, applied to ULF magnetic waves 80—56525
- power line radiation, propag. rel. to magnetospheric VLF wave activity Sunday decreases 79—66883
- problems connected with special source structs., review 80—87272
- propagation problems connected with infinitesimal point source, review 80—90194
- pulse propagation, scatt. and diffusion in scatterers and turbulence 79—66775
- radar, returns digitisation for storm depth-area relations determ. 77—91249
- radar meteor A/D filter characts. *(Italian)* 79—80032
- radar meteor echo rates, correl. with zonal winds at 95 km altitude 80—56775
- radar propag. through turbulence, scintillation detection using monopole techniques 78—85717
- radar propagation refractivity measurements, Bass Strait, Australia 77—49131
- radar reflectivity gradients 77—91229
- radar return from radar-acoustic sounding system, refractive turbulence effect 79—39821
- radar scatter from waves of short-period, 13-25 km altitude 80—90192
- radar signal scatt. from turbulent air, VHF and UHF 80—85728
- radiances in absorpt. bands, calc. methods including multiple scatt. 78—61554
- radiation detection in turbulent atmosphere, photodetector current fluctuation statistics *(Russian)* 79—92591
- radiation fields, of multiple return stroke lightning 78—3885
- radiative flux calcs., delta-two-stream approx. 79—96811
- radiative flux calcs. for asymm. phase functions, delta-M method 78—32338
- radiative transfer, doubling initialization, interaction of ang. and initial-layer error 77—70996
- radiative transfer, doubling initialization and ang. discretization errors 77—70997
- radiative transfer, fixed cloud-top temp. and fixed cloud-top altitude approximations for temp. profile 80—72616
- radiative transfer, inverse problems method in transport and filter theory 79—29920
- radio aurora, spatially ordered structure, spaced radar obs. 78—73561
- radio beacon signals from ATS-6 satellite, ground refl. effects on polarization 78—40612
- radio emission of the atmosphere in the 5-13 cm^{-1} band 80—61878
- radio interferometric meas., atm. turbulence effects *(French)* 80—46402
- radio meteor rates observed with meteor wind radar during non-shower period 79—84753
- radio meteor wind meas. over Atlanta 79—2411
- radio noise statistical models for reception in VLF band 80—72611
- radio propagation in natural waveguides, survey 77—78328
- radio refractive index variations over Arabian Sea during MONEX 1973 77—2281
- radio refractivity gradient analysis over S.E.Asia 77—91244
- radioacoustical sounding, expression for scatt. signal freq. spectra *(Russian)* 80—94612
- radiometeorological characteristics, statistical structure *(Russian)* 79—84376
- radiowave, ground wave attenuation function for a spherical Earth with arbitrary surface impedance 80—94585
- radiowave backscatter from vegetation, water cloud model 78—57274
- radiowave generation, by auroral electron beams, mechanism *(Russian)* 78—40724
- radiowave propag., rel to mass distrib. by latitude 80—90115
- radiowave propag. at 30 GHz during heavy thunderstorms, ATS-6 meas. 77—64377
- radiowave propag. through turbulent atmosphere, phase difference and derivative fluctuations 78—92951
- radiowave propagation, disturbance effects and their predictability 79—58171

atmospheric electromagnetic wave propagation continued
- radiowave propagation, numerical approximations of Sommerfeld integral for fast convergence 78—66727
- radiowave propagation, refr. index derivation for ultrashort waves 80—36380
- radiowave propagation problems, soln. using parabolic equations and transformation operators method 79—36816
- radiowave propagation studied by FM-CW radar 80—90186
- radiowave refraction corrections for exponential atmosphere, real-time computational method 80—98432
- radiowave scattered by 1-D power law phase screen 80—77220
- radiowave scattering from acoustic atmospheric formations 79—92579
- radiowave scattering from meteoric ionisation, theory 77—87337
- radiowave scattering theory appl. to radio meteor obs. 79—5696
- radiowave wind obs. of waves during 1976 over Saskatoon 79—79935
- radiowaves, delay fluctuations with scale sizes >1 km, obs. with radio interferometer array 79—8675
- radiowaves, propagation aspects in planning of radiocommunication services 80—12613
- radiowaves, refr. index struct. parameter from refractivity and amplitude scintillation meas. at 36 GHz 78—81316
- radiowaves, statistical distrib. and max. critical value for refractivity gradient variation 80—12522
- radiowaves in isotropic inhomogeneous atmosphere with refractive index arbitrary profile, mode theory anal. *(Japanese)* 78—44968
- radiowaves in magnetised plasma, modulation instability saturation *(Russian)* 77—47203
- radiowaves produced from secondary electrons in geoelectric field, 10 kHz-10 MHz during EAS 79—21118
- rain attenuation and depolarization of Earth-satellite transmissions at freq. greater than 10 GHz *(French)* 78—53689
- rain-scatter interference between satellite, terrestrial communications systems *(Japanese)* 79—16612
- random EM wave field in magnetoplasma, anal. of six component meas. 79—27782
- random media, wave propag. and weak scatt. 78—66722
- refraction of MM-wave radio noise from cosmic sources near horizon, meas. 80—21813
- refractive index, effect on line length changes resolution by EM distance meas. ratio method 80—4143
- refractive index microstructure and scintillation fading meas. in tropical region 79—16629
- refractivity and temp.-humidity cospectrum 79—39819
- remote probing for wind and struct. const., line-of-sight method 80—36426
- remote sensing, atmosphere, temp. and emittance effects on data 77—78393
- remote sensing and telecommunication, book 80—36431
- remote sensing of atmosphere, land and sea props. 78—93015
- satellite effective isotropic radio power meas., error anal. using calibrated radio star 78—93070
- satellite links at 20 and 30 GHz, crosspolar phase variations on satellite-Earth path, meas. 77—81957
- satellite-Earth path from SIRIO 1 experimental satellite, propag. meas. in circular polarisation 79—84334
- scattering by turbid medium, role of spatial inhomogeneities *(Russian)* 78—7765
- scattering by turbulent flows in wake of artificial satellites 79—8730
- scattering in presence of background slab, algorithm for profile reconstruction 80—94644
- scattering on acoustical formations of atmosphere in field of moving point source of sound 78—32210
- Schumann resonance in ionosphere-Earth waveguide, line splitting detection, chirp-z transform 78—3861
- Schumann resonances, balloon meas. *(Japanese)* 79—79919
- Schumann resonances, elec. vertical component obs. by stratosphere balloon 79—44221
- Schumann resonances, expt. data appl. to atmosphere and lower ionosphere elec. cond. profiles evaluation 80—36360
- Schumann resonances and elec. cond. of atmosphere and lower ionosphere, reson. freqs, and ELF attenuation 80—31099
- Schumann resonances in Earth-ionosphere cavity, book 80—86050
- SIRIO satellite link 11.6 GHz attenuation, meas. and estimated from sky noise temp. 79—84341
- SIRIO-1 satellite link, analysis of oblique propag. measurements made at Gometz-la-Ville Earth station *(French)* 80—56504
- sky-wave mixed-path loss computation, piecewise homogeneous ground models appl. 79—66774
- skywave field strength prediction, North America, new method 77—73904
- soft particles scattering, Mie series appl. 79—36824
- solar constant, effects of sunspots and faculae 78—4163
- solar diffuse and direct radiation at Earth's surface, aerosol effects 77—37406
- solar flare X-rays, atmosphere reflected fluxes rel. to flare spectrum beyond 200 keV 80—51710
- solar radiation, absorpt. by NO_2 causing stratospheric heating 77—17199
- solar radiation absorpt. by O_2 and O_3, heating rate parameterization, 15-120 km altitude 79—39798
- solar radiation absorpt. spectra, atm. trace gases vertical conc. *(Russian)* 78—69442
- solar radiation absorption, cloud and aerosol effects on heating rate 78—57319
- solar radiation absorption, effects of gases, aerosols and clouds 77—37407
- solar radiation absorption, radiation balance 77—33183
- solar radiation absorption by stratospheric aerosols from Agung volcano eruption 77—87072
- solar radiation budget in cloudy atm., modified two-stream approx. 79—58090
- solar radiation diffusive reflection by plane parallel planetary atmosphere 77—5471
- solar radiation distribution in cloudy atmosphere 78—3955
- solar radiation input in tropical ocean regions, influence of clouds 78—3956
- solar radiation intraregional vars. in E United States 79—39804
- solar radiation obs. and predicted values in urban area 78—57317
- solar radiation reaching Earth's surface directly, turbid ideal Rayleigh atm. 78—36274
- solar radiation transmission, Monte Carlo simulation *(Russian)* 79—12265

atmospheric electromagnetic wave propagation continued
solar radition absorption in stratosphere by O_2-O_2 and O_2-N_2 dimers 78–9167
solar UV radiation penetration, sunburn dosage spatial and temporal vars. 77–37285
solar X-rays, lower thermosphere attenuation meas. by rocket-borne proportional counters 78–45072
spectral bidirection refl. props. meas., at 0.52 μm, for savannah, bog, pasture, and coniferous forest vegetation 78–40649
spectral distribution of global and diffuse solar radiation 79–44229
stratosphere, LF radio wave absorpt. variations, press. and temp. depend. 79–44282
stratosphere, N_2O UV absorpt. spectrum at stratospheric temps. 78–28260
stratosphere, radar signal refl. and scatt. from refr. index structs. 80–90182
stratosphere and mesosphere, review 78–49105
stratosphere and mesosphere, UHF radar echoes, for wind and turbulence obs. 77–33135
stratosphere turbulence near tropopause, review of radar obs. 80–90179
submillimetre sky emission and absorpt., freq. spectrum of fluctuations 77–41308
submillimetre spectrum meas. with high resolution Fourier spectroscopy 77–87133
surface and interface aspects, Conf. Istanbul, Turkey (Oct. 1976) 78–22075
surface layer aerosols variability, spectral transmittance method *(Russian)* 78–69448
sweeper activity in the HF and VHF bands, relation to magnetospheric phenomena 77–56689
synthetic IR transmittance spectra, 15 and 4.3 μm CO_2 bands 78–28316
thermal radiation, influence of large hailstones on spectral depend. in 0.86 to 17 cm range *(Russian)* 78–36222
thermosphere, diurnal tide excited by EUV and UV solar radiation absorpt. 77–53260
thermosphere, incoherent scatter meas. of props. 79–53597
thunderstorm location by single station techniques, improved method, radiowave propag. effects 80–67438
transfer functions, space-variant, for inhomogeneous scatt. media characterisation 78–71012
transmission functions, analytical determ. in LOWTRAN code 79–58095
transmittance of inhomogeneous atm., interpolation method for rapid calc. *(Russian)* 79–29850
tropical atmosphere, influence of stratospheric aerosols on solar and long-wave radiative fluxes 77–25743
tropopause, VHF radar partial specular refl. rel. to detect. 80–8411
troposphere and stratosphere sounding by pulsed VHF radar 80–51566
turbulence, Doppler radar clean-air echo, intensity 80–90190
turbulent media, beam propag., comments 77–41125
two-layer model appl. to calibration of astronomical mm. obs. 78–53691
UHF diffuse radar aurora, rapid scan Doppler vel. maps 78–77388
UHF meas. of atm. O_3 absorpt. spectrum, O_3 conc. and distrib. determ. *(Russian)* 79–100897
unified wave propagation theory, tenuous random medium 78–4491
upper atmosphere, incoherent scattering, physical processes *(Portuguese)* 79–2417
upper atmospheree, O I 6300 Å nightglow profiles meas. by incoherent scatt. radar *(Portuguese)* 80–41591
Urbana Meteor Radar observations during GRMWSP/CTOP periods 79–2412
URSI Commission F, First Open Symposium (La Baule, France, 1977 April 28-May 6) 78–57321
UV and integrated solar radiation received, influence of cloud layers 79–70883
UV backscatter expt., airborne, for O_3 distrib. determ., error anal. 78–92985
UV extinction meas. of O_2 density 79–2406
UV solar radiation effects on upper atmosphere, review of Saha's work 79–53599
UV solar radiation intensity meas. by chem. actinometer 77–45163
vegetation reflectivity, effect on atmospheric radiance and polarisation 78–40650
VHF coherent radar sounding, wind and refractivity turbulence struct. 78–28281
VHF radar obs. of stratosphere, specular reflection 79–39822
VLF, anisotropic 3-layer model *(German)* 78–36358
VLF, signal variations spectral anal. in Earth-ionosphere waveguide *(Russian)* 77–78305
VLF hiss emissions, simultaneous obs. at Brorfelde, Chambon-la-Foret and Moshiri 78–81509
VLF hiss propag. characts. obs. at low latit. ground stations 78–69561
VLF navaid signals used for synoptic windfinding, 10-14 kHz 80–17309
VLF signals, numerical study of satellite reception using waveguide concepts 80–90282
VLF spectral characteristics of K-field changes, expt. 77–2217
water droplet aerosol interaction with EM radiation, temp. field and refractive index distrib. model 78–3899
wavy water surface thermal radioemission obs. at 3.5 and 14.5 MHz *(Russian)* 78–61425
weather radar calibration, correl. with rain gauge data *(Japanese)* 78–85670
weather radar for mm wave propag. expt. *(Japanese)* 78–16208
whistlers, effect of Earth-ionosphere waveguide propag. on polarisation and arrival angles 79–100924
X-band, dielectric constant of dust, effect of moisture content 80–72578
Zenneck surface wave, excitation by vertical aperture 79–39820
ν sea, cosmological, EM wave propagation, torsionic background 80–77283
^{60}Co skyshine, continuous γ-spectra unfolding 79–81118
H_2O 1.35 cm absorption resonance, atmospheric radio emission features 80–46228
H_2O vapour laser 118.6 μm radiation absorption by H_2O vapour, temp. and press. effects meas. 78–75255
O_2 induced absorption band effects on transmission in 6 μm region *(Russian)* 78–69446
O_2 photoabsorption cross section near Lα line, temp. depend. 77–64499

atmospheric electron precipitation
see also aurora; radiation belts
0.005 to 0.5 Hz precipitation pulsations and concurrent mag. field pulsations, obs. 77–53307
AEROS and TAIYO satellite results 80–46340
artificial aurora, conjugate to a Hawaiian launched electron accelerator 80–82124
aurora, low-energy electron precip. rel. to F-layer scintillations 77–87158
aurora, precipitation spikes rel. to small scale absorpt. events assoc. with substorms 77–56791
aurora, pulsating, electrons charact. energy from optical spectra 78–88969
aurora, pulsating, precipitating electrons flux modulation 78–73562
aurora, time-depend. model, effects on ionospheric and atm. props. 78–4021
aurora, ULF elec. fields and particle precip., rocket meas. 78–96337
aurora and high-energy auroral electrons, simultaneous meas., discussion of differences 77–53271
aurora in F-region, assoc. with magnetospheric cusp 80–90273
aurora location rel. to position of eastward electrojet and energetic electrons trapping boundary 77–25822
auroral absorption event, energetic particle precip. in lower ionosphere rel. to ion prod., density and comp. 80–36443
auroral activity in midnight sector, electrojet and precip. particle characts. 78–12039
auroral arc, relation with field aligned currents carried by suprathermal electrons 78–28362
auroral arcs, precip. primary electrons and bremsstrahlung X-rays, satellite correlated obs. 79–35029
auroral arcs array, electron accel. models 78–36357
auroral brightness fluctuations at mid-latitudes 77–87150
auroral bulge expansion features during substorms 80–41597
auroral diffuse forms, 10 eV to 25 keV electrons energy spectra 77–29536
auroral elec. field, non-neutral field-aligned current sheet, theory 80–77196
auroral electric field, description based on plasma interaction with geomag. field 80–46342
auroral electron accel. by electrostatic double layers, discrete auroral forms prod. 77–25809
auroral electron beam, electrostatic noise generation 78–85759
auroral electron current sheet, rel. to elec. field model 79–53608
auroral electron diffuse surge zone, equatorial boundary model 78–69610
auroral electron flux, rel. to field aligned elec. pot. difference 80–72684
auroral electron modulation at 2.2 Hz, geomagnetic equatorial origin 80–94632
auroral electron precipitation regions, generation by magnetosphere convection elec. field divergence 80–67453
auroral electron spectrum, rocket meas. correl. with photometric obs. 78–32266
auroral electron transport and energy degradation 80–77219
auroral electron vel. distrib. function, 25 eV to 15 keV 78–45085
auroral electrons, accel. by MHD surface waves rel. to arc form. 77–9621
auroral electrons, accel. rel. to 100 to 500 kHz noise and field-aligned current 79–66859
auroral electrons, bounce periods rel. to latitude effect in pulsating patches periodicity 80–31155
auroral electrons, flux meas. and auroral emission calcs., comparison with obs. 77–9592
auroral electrons, heating of auroral ionosphere 77–21973
auroral electrons, high resolution energy spectra, 1976 Mar. 26 mag. storm onset 77–33257
auroral electrons, implications of extreme thinness of pulsating auroral structs. 80–72667
auroral electrons, large-scale longit. intrusions 77–64510
auroral electrons, magnetosphere plasma two-dimensional inertial turbulence rel. to auroral curls and folds 78–36399
auroral electrons, mechanisms for discrete aurora 79–8737
auroral electrons, pitch angle and energy distrib., ESRO 4 satellite obs. 79–29921
auroral electrons, precip. mechanisms from X-ray illuminating regions obs. in Canada 80–31156
auroral electrons, precip. rel. to discrete and diffuse auroras, Isis 2 satellite and aircraft obs. 77–29532
auroral electrons, precip. rel. to E_s-layer props. at Sodankyla, Finland 77–87183
auroral electrons, precip. rel. to elec. fields and currents assoc. with auroral arcs 78–28396
auroral electrons, precip. rel. to NO densities in lower thermosphere 77–37467
auroral electrons, precip. rel. to pulsating aurora induction by Ba vapour releases 77–49211
auroral electrons, pulsations harmonic anal. 79–8736
auroral electrons, spatial distrib. rel. to high-latit. ionosphere cond. 79–12334
auroral electrons, spectrum rel. to thermal plasma enhancements in topside ionosphere 77–9617
auroral electrons, structured field-aligned current system 77–33243
auroral electrons acceleration, role of turbulent generation of electrostatic fields in magnetosphere 78–28439
auroral electrons acceleration by electrostatic V-shocks, approximate equipotentials 80–21870
auroral electrons acceleration mechanisms 80–77210
auroral electrons energy distrib., incoherent scatter radar and photometric meas. comparison 78–77390
auroral electrons precip., electrostatic shock waves model 77–9616
auroral events, electron spectra meas. 20 eV to 18 keV 79–62642
auroral forms, magnetic field aligned electric fields rel. to downward electron energy fluxes 79–53606
auroral forms relationship with high latit. particle precip. 80–77189
auroral hiss, nearly reson. whistler amplified Cherenkov radiation, limitations 80–101482
auroral intensity and electron flux, in situ rocket meas. 79–39998
auroral kilometric radiation, ISIS 1 obs. at source 79–84558
auroral kilometric radiation coherent generation by nonlinear beatings between electrostatic waves 80–26691
auroral kilometric radiation correl. with inverted-V electron precip. 80–26692

atmospheric electron precipitation continued
auroral low energy electrons, energy dissipation 77—45217
auroral luminosity rel. to geomag. field changes 80—77187
auroral oral size diurnal var. assoc. with geomag. pole precession 80—26661
auroral oval, dayside, electron precip. rel. to rocket-borne VLF and ELF waves meas. 80—98504
auroral oval size, effect on mag. substorm occurrence probability 78—32298
auroral particle distrib., parallel electric field acceleration 80—12602
auroral particle dumping into ionosphere and magnetotail structure 80—109313
auroral particle precipitation, rel. to turbulence at 500 mb level 80—77218
auroral patches and deteched arcs, equatorward of auroral oval, Isis 2 obs. of particle precip. 79—70911
auroral patches caused by energetic particle precip. near plasmapause 77—33241
auroral phenomena, role of mag. mirroring 78—20572
auroral precipitation stimulated by Cs doped explosion 80—17436
auroral radio absorption obs. by riometers rel. to 10-80 keV electron precip. at geosynchronous orbit 79—48606
auroral region, self-consistent particle and parallel electrostatic field distrib. 78—45120
auroral secondary electrons spectrum at low altitudes, collisionless effects 79—40008
auroral spectrum vars. at latit. of polar cleft 79—25384
auroral substorm, expansive phase, rocket obs. 78—45115
auroral substorms, morphology of N and NO 79—48607
auroral westward travelling surges and low-energy electron precip. obs. 78—45084
auroral X-ray bremsstrahlung rel. to VLF emissions 78—45106
auroral zone, Kosmos 721 obs. of relativistic electrons 80—8492
auroral zone, quasiperiodic elec. fields and assoc. electron precip., models 78—88977
auroral zone electrons, effects of transit times on power spectra of X-ray microbursts 77—78556
auroral zone energetic electron precipitation and Pc 3 pulsations 80—8493
auroral zone microburst precipitation phenomena 80—77208
auroral zone precipitation and convection reversal, satellite obs. 80—101479
BDI position and plasmapause position during Feb. 1972 mag. storm 80—56666
bremsstrahlung produced by precipitating electrons, theoretical characts. 79—66862
bremsstrahlung X-rays from relativistic electron precipitation 79—75014
conjugate photoelectrons influx rel. to predawn 630 nm airglow, direct meas. 78—49196
coordinated rocket and satellite obs., Atmosphere Explorer C 77—70908
cusp region of magnetosphere, rel. to interplanetary mag. field 80—90288
cusp region on dayside, field line topography, precipitation implications 80—85822
cusplike electron precipitation regions during 1977, September 19 to 21 event, DMSP-F2 obs. 79—35056
D-region, midlatit. localized nighttime disturbances rel. to ELF propag. 77—21989
D-region, midlatit. winter electron density vars. 77—60532
daily variations, rocket meas. 78—69575
dayside auroral precipitation, relevance to substorm current systems and dayside merging 79—96852
diffuse aurora equatorward boundary, electron precipitiation interpretation 80—72668
diffuse aurora with assoc. electron precipitation, electron origin in plasma sheet 80—41614
diffuse auroral precipitation mechanisms 79—12327
diffuse auroral zone, form. and dynamics of polar edge of ionospheric trough 79—8743
discrete auroral arcs, prod. by electrostatic shocks 78—45153
duroral zone ionospheric modification, incoherent scatter radar obs. 77—82083
dynamics and auroral morphology, photometric data interpretation 80—82141
electrodynamics of an arc, auroral vector electric field and particle comparisons 77—70907
electron and proton precipitation, during auroral and geomag. substorm activity development 78—28435
electrostatic noise damping by warm auroral electrons 80—41668
energetic electron belt form. and decay during 1974 July 4-6 mag. storm. 78—69617
energetic particles injection into magnetosphere, evolution of energy spectra and pitch angle distrib. 78—45148
energetic particles precipitation during baylike disturbance of mid-latit. D-region, radio obs. 79—12333
energy degradation in N_2, spatial yield spectra, microplume model 79—98235
energy selective precipitation of inner zone electrons 79—2428
energy spectra from rocket flight through dayside auroral oval 78—20578
equatorial ionosphere, electron production by energetic particle precipitation 77—33255
equatorward boundary, Isis 1 and 2 obs. rel. to instantaneous nightside auroral oval 78—32289
evening diffuse aurora and conjugate electron fluxes near magnetospheric equator 79—101008
Feyerverk experiment, electron precip. induced by electron injection 77—13160
field aligned current above auroral arc, e^- and H^+ precipitation obs. 80—77215
field-aligned suprathermal electron fluxes below 270 km in auroral zone 77—33278
geostationary orbit, strong electron pitch angle diffusion obs. 79—58194
harmonic instabilities in electron plasma 78—77424
high energy radiation belt electrons, contrib. of geomag. pulsations interaction to precip. 78—28422
impact cross-sections of atmospheric gases 78—28398
impact on atmospheric gases, yield spectra 78—28401
inner magnetosphere penetrated by energetic particles during storms 80—72716
inner radiation belt electron precipitation, meas. 80—67452

atmospheric electron precipitation continued
inner zone electrons induced precip., obs. 78—88996
intensity modulation in auroral zone and coincident Pi 2 77—60539
inverse loss cone electrons, temp. anisotropy quasi-linear relaxation due to interaction with electrostatic waves *(Russian)* 80—109314
inverted V event, electron flux fluctuations, Nov. 5 1975 obs. 80—41618
inverted-V event characteristics 79—75019
inverted-V precipitation events, assoc. intense plasma wave turbulence 77—45228
inverted-V precipitation events and parallel electric fields, rel. to high-latit. convection field 77—33297
ionosphere, auroral electron flux obs. 80—67466
ionosphere, bremsstrahlung X-ray flux depend. on electron energy spectrum 78—40744
ionosphere, channel lower hybrid resonance excitation by superthermal particle streams *(Russian)* 78—4025
ionosphere, conjugate photoelec. fluxes obs. on AE-C satellite 77—45224
ionosphere, electron flux vars. induced by HF waves *(Portuguese)* 80—41592
ionosphere, electron precip. rel. to radio waves winter absorpt. anomaly at middle latits. 80—67459
ionosphere, ELF transmission anomalies and energetic particle precip. 78—93040
ionosphere, energetic electron efflux, caused by plasma jet injection from rocket *(Russian)* 79—5701
ionosphere, fluxes during positive mag. disturbances of 1972 February 24 and 1970 (November 21) 77—21970
ionosphere, high-altitude auroral zone, electron temp. enhanced by electron current 80—85803
ionosphere, high-energy electron flux during 1971 December 16 magnetic storm 78—69564
ionosphere, high-latitude, energy spectra of 1 to 500 eV electrons, Atmosphere Explorer C obs. 77—29568
ionosphere, ionization due to low energy solar and magnetospheric particles 79—53625
ionosphere, latitudinal struct. of elec. fields and particle precip. on (November 21, 1975) 77—87160
ionosphere, particle flux instability and geomag. pulsations generation 77—49232
ionosphere, suprathermal electron fluxes meas. during Western European Winteranomaly Campaign 78—45125
ionosphere, topside, transient response to precip. 77—78566
ionosphere, unusual mid-latitude disturbance of corpuscular origin 78—28374
ionosphere energetic electron fluxes, mid-latit. modulation theory 79—12335
ionosphere energetic electrons, incoherent Cerenkov process as source of low-latit. VLF emissions 79—75036
ionosphere turbulent polar cusp, temps. and low-energy particles and Kelvin-Helmholtz instability 78—96343
IPDP pulsation polarisation, correl. with particle precipitation 80—51612
low energy electrons, precip. rel. to ionosphere electron content asymmetry 79—21097
low-energy electrons in S polar cusp, AE-C obs. during 1977, September 21 geomag. storm 79—35076
magnetic field aligned pot. diff. meas. from photoelectron energy spectra 78—7825
magnetic storm, 1971 December 16, energetic electron precip. and VLF phase disturbances at midlatit. 77—53284
magnetosphere, assoc. elec. field, mag. field and electron precip. fluctuations 78—81507
magnetosphere, electron enhancements assoc. with VLF emissions 77—33285
magnetosphere, electrons injection rel. to ELF emissions during substorm activity 77—53328
magnetosphere, energetic particle precipitation, Kosmos 484 polar meas. 80—8491
magnetosphere, multi-harmonic electron cyclotron instabilities 78—87442
magnetosphere, particle precip. caused by monochromatic VLF signals 77—49238
magnetosphere, particle precip. caused by single injected whistler-mode wave 77—56797
magnetosphere, role of precip. in convection 79—25400
magnetosphere, VLF transmission induced slot electron precip. 78—32296
magnetosphere conjugate electron precipitation, high time resolution riometer and X-ray meas. 80—41666
magnetosphere dayside cusp region, electron precip. and spectra 79—12352
magnetosphere electron precipitation, obs. during simultaneous substorm and thunderstorm 80—67392
magnetosphere energetic electrons, nonlinear pitch angle scatt. by coherent VLF waves 78—89011
magnetospheric electrons energy dispersion with progressive precip. 77—53293
magnetospheric energetic electron environment model revision 78—61681
microburst precipitation at L~4 77—33260
mid-latitude charged particle precipitation, optical evidence 79—44291
middle latitudes precipitation, maintenance of nocturnal D-region by energetic electrons 77—25856
midnight trapping boundary, energetic particles pitch angle distribs. 78—28445
modulation by geomag. pulsations 77—49236
modulation of precipitating electrons and VLF emissions, anal. from Interkosmos 5 data 77—64511
nightside auroras, electron precip. rel. to field-aligned currents and auroral electrojets 78—32267
nighttime global zones of energetic particle precipitation 80—61947
onset latitude of precip. of electrons responsible for auroral absorpt. 77—91357
optical auroral arcs and low-energy electron precip., DMSP 32 obs., comment 77—60507
optical emission excited by electron ejection from rocket 80—51592
outer radiation belt dynamics during strong mag. storm 79—62678
outer zone electrons, evidence for very weak pitch angle diffusion 78—28399
parallel electric field effects on precip., model 78—65459
Pc 1 pulsation polarisation, correl. with particle precipitation 80—51612
Pc 4-5, obs. showing ULF mag. fields affect precipitation 80—82147
pitch angle diffusion, instabilities rel. to pulsating aurora 3 Hz modulation 79—25391

atmospheric electron precipitation continued
- pitch-angle diffusion with asymmetric loss cones, rel. to precip. longit. depend. 77—13162
- plasma sheet precipitation, correl. with terrestrial kilometric radiation struct. 77—25873
- plasmapause, correlated electron precipitation and magnetic IPDP events 78—28388
- plasmapause, electron precip. caused by unducted VLF energy from tropical lightning 77—21980
- plasmasphere, electron precip. and LF noise emissions during mag. storm. 79—80069
- plasmasphere origin, dimensions and particle precip. 78—69584
- plasmasphere quiet time electron precip., effects of localised sources 77—87157
- polar auroras and electron precip. 79—29932
- polar cap, intense keV electron fluxes during poststorm quieting 77—25835
- polar cap, intense uniform low-energy electron precip., interplanetary origin 77—70910
- polar cap, precip. dawn-dusk gradient rel. to interplanetary mag. field 78—28408
- polar cap aurora, proton-induced, secondary electron flux 79—53605
- polar cap precipitation during 1971 December 14 to 21 event, rel. to 6300 Å emission pattern 79—75012
- polar cusp, precip. geographical distrib. rel. to airglow mag. ordering 78—57378
- postmidnight precipitation time structure and stable trapping limit 79—101013
- premidnight convection topology, auroral vector electric field and particle comparisons 77—70906
- pulsating auorora, obs. of precipitating electrons 80—85794
- pulsating aurorae electrons, evidence for limiting flux 80—72666
- pulsating auroras electrons, evidence for noncollisional thermalisation 79—96851
- pulsating precipitation, self-modulated VLF wave-electron interactions in outer radiation belt 80—41658
- pulsations, spectral characts., Intercosmos 5 data 77—70938
- pulsations with long period at 75° magnetic latitude 78—28433
- quiet dayside cusp, AE-C and -D low-energy particle obs. 78—28390
- radiation belt electrons, struct. of atmospheric loss cone 77—33294
- radiation belt electrons, struct. of loss cone 78—40774
- radiation belts, effects of man-made VLF waves 78—45150
- radiation belts electrons, influence of power-line harmonic radiation 79—80098
- radiaton belt energetic electron loss, natural depletion mechanism for stratospheric O_3 77—41134
- radio aurora (diffuse), rel. to field-aligned currents and particle precipitation 80—105119
- rapid auroral fluctuations, obs., classification 80—77186
- relativistic electron precip. spikes at midlatits. 77—29599
- relativistic electron precipitation and resonance with ion cyclotron waves 79—8758
- relativistic electron precipitation events, assoc. with magnetospheric substorm activity 77—25827
- Sanae, Antarctica, precip. event on (1974 November 14) 77—87182
- SAR arc event, soft electron flux as excitation source 80—77217
- short-term intensity pulsations of precipitating and quasitrapped electrons 77—25854
- simultaneous particle precipitation and auroral emission obs. by Isis 2 77—70905
- slot region, time persistence of electron precip. features 78—28395
- soft electrons, effects on distrib. of vibr. energy of N_2 77—33261
- South Atlantic Anomaly spatial shift 78—28449
- sporadic events in local dusk sector of auroral zone, X-emission obs. 80—101480
- substorm associated precipitation, hydromagnetic wave modulated 80—105113
- substorm expansion, intense electron and proton fluxes poleward of trapping boundary 77—87164
- substorm growth phase effects, Scandinavian obs. 78—96352
- substorms, satellite obs. of impulsive bremsstrahlung X-ray events, electron precip. 79—2438
- sudden commencement absorption events at S. pole, rel. to lower cleft boundary latit. 78—77437
- thermosphere, dynamics at high latits., magnetospheric convection effects 79—8733
- thermosphere, ionisation and dissoc. due to electron precip., N and NO density calc. 77—73897
- thin field-aligned beam, stability in plasma 77—76124
- topside ionosphere, electron precip. obs. in magnetospheric cleft 77—29571
- trapping region, quasiperiodic electron density pulsations, satellite detection 80—4198
- trough region auroral patches and detached arcs characts., Isis 2 obs. 79—70910
- VLF subionospheric propag., whistler-induced anomalies 80—26668
- whistler wave interaction with electron rel. to precipitation 80—46349
- widespread electron precipitation morphology, from X-ray bremsstrahlung obs. 80—77205
- X-ray aurorae prod. by energetic electrons precip., imaging from Spacelab 78—61608
- X-rays from low latitude nighttime atmosphere, HEAO-1 obs. 79—44283
- X-rays from magnetospheric electrons, rocket-borne, astronomy affected 78—61640
- N_2 gas, electron energy degradation, Monte Carlo study 80—69969

atmospheric energetics *see atmospheric movements*

atmospheric humidity
- *see also hygrometers*
- 100 GHz to 1 THz atmospheric emission and absorption meas. 79—34980
- absolute humidity, correl. with atmospheric absorpt. at 460 μ 78—96295
- absorption by HDO depleted water vapour, meas. 3.5 to 4 μm 77—87075
- aerosol formation, vapour condensation of various humidities, size spectra model *(Russian)* 80—12483
- aerosol light scattering, obs. of polarisation and intensity 80—51541
- aerosol particle conc. variation with relative humidity *(Russian)* 78—32146
- aerosol particles water uptake and equilib. sizes at high relative humidities 78—61516

atmospheric humidity continued
- aerosols, atoms and ions attachment rate, nuclei conc. and humidity effects 79—62555
- aerosols, humidity effects on gravit. settling and Brownian diffusion 78—32203
- aerosols, in moist atmosphere, equilib, sizes and size spectra *(Russian)* 79—12194
- aerosols, relative humidity and light scatt. of homogeneous two-layer particles *(Russian)* 77—82007
- W.Africa, mean tropospheric conditions for 11-year period, climatological features 77—2221
- air-sea heat and moisture exchange during stormy weather 77—78375
- aircraft meteorograph, design, appls., accuracy *(Chinese)* 80—17387
- Arabian Sea, moisture distrib. and H_2O vapour flux during S.W. monsoon 77—53111
- artificial clouds form. possibilities and methods 79—29823
- astronomical IR sites, water vapour data 79—21181
- atmosphere ocean interfacial conditions, influence on bulk evaporation coeffs., isotopic method determ. 78—85576
- Bahrain, discomfort index based on wet-bulb temps. 79—20964
- Baltic Sea region, humidity meas. rel. to atmospheric heat and moisture balance 77—87057
- baroclinic model for vertical temp. and moisture stratification in baroclinic boundary layer 79—53502
- Belgium, weather in 1975, review 77—25747
- Belgium, weather in 1977 79—58049
- Bihar and neighbouring areas, atmospheric water balance 77—56709
- boundary layer, eddy flux meas. corrected for density fluctuations 80—72576
- boundary layer, eddy flux meas. made by powered glider 80—51509
- boundary layer, heat and humidity exchange laws, model approach 77—66948
- boundary layer, moisture struct. with higher order turbulence closure model 77—78310
- boundary layer, momentum, heat and moisture fluxes from struct. parameters 79—53435
- boundary layer, over sea, momentum, heat and H_2O vapour fluxes, meas. methods 78—32213
- boundary layer, Raman lidar humidity sounding 79—66809
- boundary layer, temp. and humidity correl. above warm wet surface 78—85646
- boundary layer, turbidity rel. to spectral struct. of radiation attenuation *(Russian)* 78—44997
- boundary layer fluxes determ. over natural grassland, aerodynamic method 78—73480
- boundary layer humidity characts. rel. to atm. total H_2O vapour content 79—39836
- boundary layer structure during light wind, water vapour IR absorpt. meas. 77—91197
- Brazil, precipitable water, distrib. maps 80—77075
- capacitive dew-point sensor 78—81421
- circulation associated with cold front, moist case 79—2334
- cirrus clouds, falling ice particles survival distance in subsaturated air 77—33151
- cirrus clouds, ice content determ. from radiative props. in NOAA 4 VTPR channels 79—39853
- cloud clearing by laser beams, liq. water content fluctuations in clearance zone *(Russian)* 78—44999
- cloud temperature and humidity changes and overcloud inversion 80—77083
- cloudy atmosphere integral humidity determ., by remote sensing method *(Russian)* 79—5635
- cloudy atmosphere moisture content determ., long-range, by thermal radioemission meas. *(Russian)* 79—5637
- coastal zone, indicators of long-term var. of hydrometeorologic elements *(Russian)* 78—77258
- convective boundary layer, temperature-humidity covariance budget 78—73430
- convective systems, life cycles, GATE data 79—53440
- daytime urban moisture field struct. 79—57998
- dew meter, β-absorpt. type, appl. to meas. on soil and plant surfaces 78—24803
- dew monitoring network for SE.United States 79—66818
- diurnal variation, harmonic anal. *(Rumanian)* 79—21009
- diurnal variation over continents, absorpt. in hygroscopic soil layer 79—29825
- droplet growth rel. to condensation coeff. *(Russian)* 79—34901
- electrical and electronic equipment operating climatic conditions in Rumania, classification *(Rumanian)* 79—44242
- enthalpy meas. by LiCl humidity sensors 80—90858
- equatorial region, air and moisture transport during S.W. monsoon, MONEX-73 obs. 77—53112
- W.Europe, IR attenuation meas. of water vapour content 78—53698
- evaporation calc. using measured wind, temp. and humidity profiles 77—17194
- evapotranspiration, actual/potential relationship 80—41465
- evapotranspiration meas., Bowen ratio precision 77—33122
- evapotranspiration of continents real land surface, Penman concept calcs. *(German)* 80—98368
- Fenlands, temp. and humidity meas. rel. to steam fog form. criterion 80—98431
- flashover characteristics of air gaps dependence obs., w.r.t. Indian standards 78—22585
- fluctuations, as cause of errors in sea salt contaminated temp. sensors 80—82095
- forests, Ge diodes for temp. and humidity profile meas. 77—64463
- free atmosphere, temp. and humidity effects on theoretical and exptl. long-wave IR radiation fluxes *(Russian)* 80—94598
- frost, snow, heat transfer, cond., radiation and water vapour diffusion model 78—94563
- frost point meas. systematic error using Meteorological Office Mk3 hygrometer 78—73538
- gaseous hydrocarbon removal, with allophane adsorbers *(Japanese)* 77—78412
- global January and July climate, numerical simulation with two-layer circulation model 77—56722
- global palaeohumidity, determ. from precip. D-^{18}O relationship 80—17331
- greenhouse effect of water vapour, influence of CO_2 rel. to atmospheric temp. 80—51486

atmospheric humidity continued

- heat and mass atmospheric transfer from nuclear power station spray cooling 78−94078
- high altitude obs. of atmospheric water vapour, using airborne millimeter-wave radiometer, multi-channel, dual frequency 79−80061
- hydrologic cycle, climatic sensitivity, numerical model 79−8654
- hydroscopic particle humidification process, electrooptic scatt. meas. 80−77107
- ice crystals, props. rel. to atmospheric halos 79−2373
- ice platelets, IR radiation attenuation 80−66141
- India, moisture flux across west coast and rainfall during SW monsoon 77−70783
- India, summer monsoon, water vapour transport and vergence patterns 78−7727
- integral transparency, spectral transparency and humidity relationships 77−78423
- intertropical convergence zone struct. over GATE area 78−57283
- ionosphere, meas. by self-contained tethered balloon sounding system 78−28343
- IR aerosol extinction, 3 to 5 and 8 to 15 μm spectral regions, relative humidity effects 79−62581
- IR astronomical sites in high-mountain regions, astronomical-climatic conditions evaluation 79−62566
- IR attenuation by H_2O vapour, hygrometer meas. 79−34943
- IR continuous absorption by water vapour, calc. *(Russian)* 78−96293
- IR cooling rate in standard atmosphere, influence of water vapour content 80−26609
- IR fluctuation hygrometer, design, calibration, field trial results 78−77368
- IR transmission rel. to precipitable H_2O at Gornergrat Obs., Switzerland 79−34941
- lake moderating effect on downwind temp. and humidity, model simulation 79−88400
- laser beam attenuation, H_2O continuum, meteorological factors 77−2242
- lidar scattering and relative humidity 80−77113
- liquid water content, determ. from Nimbus 6 scanning microwave spectrometer data parameterisation 79−58047
- London storm, August 1975, humidity meas. and urban effects on precip. 78−81339
- marine boundary layer, humidity fluctuations affecting light scatt. 80−82052
- marine boundary layer, optical refractive index fluctuations, statistical props. 79−62580
- marine layer at San Diego, California, depth and moisture content rel. to cool season precip. forecasts in Arizona 80−101395
- marine stratocumulus convection boundary layer humidity and temp. in horizontally inhomogeneous solns. 80−56543
- marine surface layer turbulence structure, humidity and temp. spectra study, N.Pacific 80−21798
- measurement, from effects on IR and microwave propag., optimization of conditions from effects on IR and microwave propag., optimization of conditions *(Russian)* 79−34898
- measurement data 1971-75, river water pollution study appl. *(Japanese)* 79−70874
- measurements with standard hygrometer *(German)* 78−16194
- mesopause, H_2O dissoc. during auroras rel. to ionosphere winter absorpt. anomaly 79−58152
- mesoscale temp. and moisture fields from satellite IR radiance meas. 78−7717
- microwave radio links, data meas. over 10 years rel. to radiowave propag. 78−3857
- microwave radiometry for precipitable water vap. and liq., dual-channel method 80−51564
- microwave refraction coeff. rel. to humidity 78−69398
- minimum precipitable H_2O above Skibotn, N.Norway, rel. to IR astron. obs. 79−92572
- moist available energy, numerical procedure 80−46241
- moist penetrative convection and incipient cloud form. 79−66755
- moisture and heat flux in stratified boundary layer 77−21867
- moisture budget and cumulus friction in tropical wave-CISK 79−16580
- moisture content determ. of cloudless atmosphere, microwave radiation meas. 80−94624
- moisture fluctuations, effect on acoustic backscatter in GATE 80−85709
- moisture flux and turbulence meas. in unstable moisture layer over land 77−66962
- moisture processes in quasi-geostrophic model 78−7696
- monolayer desorption kinetics at air-water interface, humidity effects 79−52770
- monsoon, moisture eqn. development rel. to digital simulation of evaporation phase 77−56712
- nonconvective condensation, parameterization scheme, cloud water content prediction 79−12215
- objective statistical analysis using remote sounding data 78−61524
- ocean surface layer rel. to atmospheric temp. and humidity *(Russian)* 80−17282
- Orange Lake, Florida, humidity fluctuations rel. to lake latent and sensible heat fluxes prediction 80−72562
- outdoor process plant design, atm. noise attenuation calc. 79−70497
- NE.Pacific Ocean, clouds liq. water data rel. to United States west coast rainfall 80−82005
- tropical Pacific Ocean, humidity effects on satellite-determined sea-surface temps. 80−31044
- point discharge current, effect of humidity 79−88409
- precipitable water, computation from upper air data 79−34886
- precipitable water vapour determ. from surface meteorology and IR hygrometer meas. *(Italian)* 79−48587
- precipitable water vapour in atm. with temp. inversion 77−78330
- precipitable water vapour variations, baseline results from Smithsonian obs. 78−32197
- psychrometer for relative humidity of air meas., modification *(French)* 77−78451
- psychrometer non-constant, gamma 77−29389
- psychrometry, appl. of portable differential system 80−105072
- radar meas., passive, integral humidity and clouds drop phase characts. determ. 79−74991
- radiation fog, water vapour meas. and relationship to dew 78−73446
- radiometric measurements precision from GATE-74 data *(Russian)* 77−29368
- radiowave attenuation at 225 GHz meas., correlation with surface water vapour density 78−85624
- radiowave refractivity and temp.-humidity cospectrum 79−39819

atmospheric humidity continued

- rain, effect of humidity on evaporation of large water drops falling at terminal vel. 80−56541
- relative humidity and visual range relationship from aerosol meas. 77−56728
- relative humidity rel. to cloud coverage and condensation in wave model 79−34911
- relative humidity rel. to opacity index *(Spanish)* 79−29856
- remote measurement of water density and size distribs., using laser radar 77−91299
- remote sensing, passive microwave profiling technique 80−21856
- remote sensing, water vapour content retrieval from scanning multichannel microwave radiometer obs. 80−90261
- remote sensing by satellite, thermal radiation obs. 80−85660
- remote sensing by satellite microwave sounding, anomalous profiles, errors *(Russian)* 77−17266
- remote sensing from Earth orbit using microwave technique 80−41573
- Rome, effect of urban heat island on humidity during summer season 80−85717
- Sacramento Peak Observatory night sky conditions, cloud cover, seeing and precipitable water 80−51653
- saturated water vapour pressure standardization 80−26596
- saturation vapour pressure, approx. 79−70862
- sea and land breeze obs. over Goa, India 78−32155
- sea surface moisture-flux parametrisation 77−73788
- sea-air heat and moisture exchange, zonally averaged model *(Russian)* 77−17161
- sea-air interface fluxes of sensible heat and moisture, parameterization 77−41041
- smoke aerosol microstruct. and refr. index, optical determ., inversion method 80−36399
- sound attenuation, air-to-ground propag., effects of temp., humidity gradients 79−1019
- South Pole, water vap. content, rel. to IR astronomical obs. 77−81954
- Southern Hemisphere, moisture conditions and precipitation efficiency 80−98424
- spectral analysis over vegetated surface in sensible heat advection conditions 80−17343
- St. Louis downwind plume, thermodynamic props. and aerosol patterns 79−16603
- steppe meteorology, boundary layer universal profiles in rainy season *(German)* 79−84420
- stratification, effect on conditions for free convection *(Russian)* 79−10562
- stratified atmosphere, nonadiabatic heat dynamics with mass exchange and water phase transitions 79−58004
- stratocumulus clouds, IR absorption and liquid water content 77−21858
- stratosphere, H_2O mixing ratio determ. using NOAA UV fluoresc. instrument 80−90137
- stratosphere, H_2O vapour distrib., temporal and spatial vars. 77−45112
- stratosphere, H_2O vapour meas. using UV fluoresc. hygrometer *(French)* 78−65401
- stratosphere, H_2O vapour mixing ratio, Australia, 1973-76 period 78−49116
- stratosphere, lower, aircraft meas. of humidity, S.England, 1972-76 period 78−73488
- stratosphere, lower, frost-point hygrometer for horizontal soundings 79−21048
- stratosphere, lower, H_2O vapour latit. distrib., aircraft meas. 78−32173
- stratosphere, lower, obs. of unusually high humidity 79−79980
- stratosphere, temperature/O_3/water vapour trends in N. temperate latitudes 79−53474
- stratosphere, thunderstorms as micrometeorological sink for H_2O 79−84385
- stratosphere, water transport rel. to sulphate aerosol growth by condensation *(Russian)* 80−94566
- stratosphere, water vapour burden areal distrib. and jet stream 77−5275
- stratosphere, water vapour mixing ratio from solar brightness temp. balloon-borne obs. 78−85921
- stratosphere, water vertical transport rel. to atmosphere HT and HTO 79−2347
- stratosphere water vapour, meas. via balloon-borne IR instrument 79−8718
- stratosphere water vapour budget, contrib. of extratropical severe storms 77−87029
- stratosphere water vapour changes, effects on O_3 reduction estimates 78−73444
- stratospheric composition, in situ obs. of H_2O 80−105077
- stratospheric H_2O, maintenance of extreme aridity, review 80−105028
- stratospheric water vapour 0.94 μ absorption cross-section obs. *(Japanese)* 80−17427
- subcloud layer over land, temp. and humidity struct. 77−91200
- supersonic jet noise spectrum, effect of humidity on discrete component 78−9493
- surface humidity rel. to precipitable water vap., India 78−81273
- surface layer, accuracy of moments of vel., temp. and humidity vars. 78−92891
- surface layer structure parameters, turbulence props. 80−51510
- surface temp.-humidity feedback in vertical-column energy balance models 77−66959
- thermal diffusion cloud chambers, aspect ratio. rel. to supersaturation distrib. 80−56631
- thermocouple psychrometry, effect of and correction for different wet and dry bulb response 80−98472
- thermodynamics of moist air 78−85673
- total precipitable water effects on atmospheric transmission, Smithsonian Astrophysical Observatory meas. 80−17374
- transport of water vapour in atmosphere, rel. to water balance of S.America 79−29820
- tree growth rel. to transpirational flow and air humidity *(Russian)* 78−65066
- tropical cloud clusters, temp., moisture and precipitation 77−29406
- troposphere, temp. and moisture conditions rel. to radiothermal radiation at waveguide propag. *(Russian)* 79−88406
- troposphere, total column moisture content meas. by TIROS-N operational vertical sounder 80−77132
- troposphere humidity, new insight with Meteosat water vapour channel 79−25292
- troposphere moisture, temp., IR soundings anal. by statistical struct. and correl functions 80−8398
- tropospheric dynamics, Nimbus 4 THIR obs. at 6.7 microns 77−17164

atmospheric humidity continued
tropospheric studies, microbarographs, sodar, FM-CW radar, review 77—91332
Tsumeb, S.W.Africa, boundary layer profiles for dry season in steppe *(German)* 79—34923
two-balance direct method of mixing ratio determ. 77—73866
Typhoon June (1975), water vapour and clouds liq. water meas. by scanning microwave spectrometer 78—73436
upper air meteorological data, rel. to regional evpotranspiration determ. 77—91171
upper atmosphere, H_2O prod. from H-implanted interplanetary dust grains 78—65445
vapour conc. rel. to microwave frequency atmospheric transparency, 3-13 cm^{-1}, meas. 80—12476
vertical moisture profile estimation from satellite IR radiance meas. 78—45021
water aerosol, evaporation during transport through atmosphere *(Russian)* 79—88408
water content and turbidity in Thailand, calc. 79—5580
water drops evaporation and condensation, quasi-steady approximation 77—21854
water heat transport, rel. to ocean temperature-salinity curve 80—72534
water metastable states, phase diagram *(Russian)* 78—95129
water vapour, in situ meas. with new moisture sensor 79—74930
water vapour, influence on atmospheric scintillation at millimetre and submillimetre wavebands 80—61884
water vapour, radiometric and rawinsonde profiling, comparison 79—84392
water vapour content, rel. to diurnal var. of underwater irradiances on horizontal surfaces 80—72549
water vapour diffusion, rel. to sensible and latent heat fluxes influence on four-day forecast 79—96805
water vapour IR continuum absorpt., appl. of aerosol IR spectrometry theory 80—101428
water vapour of extraterrestrial origin, possible role in Sun-weather relationships 78—69416
water vapour polymers, rel. to absorpt. in IR window 77—45145
water vapour profile, meas. from atmosphere brightness temps. in H_2O 1.35 cm resonance region *(Russian)* 78—81403
wet bulb potential temperature charts, meteorological use 77—91232
wet bulb temperature and precipitable water calc. 77—53114
wet bulb temperature distrib. over India 77—53115
AgI surface, adsorption of water, effective pair pot. model 80—100394
H_2O dimer, props., influence on tropic meteorology 79—2349
H_2O vapour continuum absorpt., 4.5-5.0 μm 80—36395
H_2O vapour fluctuations influence on turbulent fluxes 79—79916
He-Ne lasers, propag. studies *(Italian)* 77—91331
$Li_5Al(Ga)O_4$, ionic cond. depend. on moisture, potential humidity sensors 79—65248
NaCl-gas reactions, atmospheric, in situ TEM studies 80—104544
Rn decay products, influence of elec. charge and humidity on diffusion coeff. 80—6192
SO_4^{2-} aerosol particles size depend. on relative humidity 79—20906

atmospheric ionisation
see also atmospheric radioactivity; ionosphere
S.Atlantic geomagnetic anomaly, ionization rates during total eclipse 80—12608
Auger electrons and photoelectrons in ionosphere and plasmasphere fluxes and spectra 78—45094
Auger electrons in upper atmosphere, fluxes and spectra 78—28376
aurora, ionisation calc. from electron flux meas., comparison with obs. 77—9592
aurora, ionisation rel. to high-latit. convection field and parallel elec. fields 77—33297
aurora, N(^{2}D) emission and ion chemistry, satellite obs. 80—72673
aurora, pulsations of electron and ion intensity 80—61934
aurora, travelling arcs, ionisation rel. to electrojets and asymmetry in infrasound generation 77—87152
aurora modelling, time-depend. study 80—72672
auroral arc, ionic struct. meas. 77—2292
auroral D-region, enhanced ionisation and strong partial refls. during absorpt. event 78—36388
auroral E-region, form. by proton precip. 78—45088
auroral electrojet, ionisation function rel. to nonpotential waves 77—49212
auroral F-region ionosphere form. role. of neutral winds and particle precip. 79—44296
bipolar ionic atmosphere, equilib. charge distrib. on aerosols 79—70830
charge transport, rel. to ion chamber response to particulate matter 78—88933
climatic parameter *(German)* 77—73905
concentration, study *(French)* 78—16125
cosmic ray ion-pair production rate above 18 km altitude, parametrisation 78—65469
cosmic ray ionisation, hysteresis, fluctuations and barometric and ionospheric effects 79—84604
critical ionization vel., Spacelab expt. 79—44289
D- and F-regions, geomag. control and possible coupling mechanism 77—9598
D-region, charged species relax. to photochem. equilib. within displaced air parcels 79—75030
D-region, effects from cosmic X-ray sources 79—35048
D-region, electron detachment and loss coeff. at S. Uist 80—82130
D-region, enhanced electron conc. at mid-latitude, positive-ion model 80—105115
D-region, equatorial, ionisation processes and ion comps. review 78—36362
D-region, ion composition at midlatitude in quiet conditions, model 80—109307
D-region, ionisation enhancements rel. to radio waves winter absorpt. anomaly at middle latits. 80—67459
D-region, mid-latit., ionisation due to energetic particles precip. during baylike disturbance 79—12333
D-region, midlatit. winter electron density vars. 77—60532
D-region, negative ions, Thomson scatt. detect. using Arecibo radar 79—62665
D-region, nocturnal mid-latitude, maintenance by energetic electrons precip. 77—25856
D-region, positive ion chemical scheme for electron density and comp. 79—40007

atmospheric ionisation continued
D-region, quiet daytime, H_2O cluster positive ions prod. 77—45242
D-region, relaxation after sudden cut-off of ionisation source 77—33254
D-region, solar X-ray control of ionisation 80—77198
D-region, time vars. in winds and electron densities at Sastakoon, Canada 79—25389
D-region, water cluster ions, mass spectrometer results analysis 78—61659
D-region, water cluster ions formation rel. to mesospheric temp. 77—21842
D-region electron density during W.Europe 1975/6 winter anomaly 80—36440
D-region ion composition, ionisation and profiles 77—49226
D-region ionisation prod. by solar 1-8Å X-rays rel. to VLF phase deviations 77—87170
D-region ionisation transient compressional response 77—53295
D-region of ionosphere VLF guide over Atlantic Ocean, obs. of mesosphere O_3 shadow 79—58161
D-region over Sardinia (40°N), positive and negative ion densities during winter anomaly 80—21871
deionisation processes and meteoroid properties, rel. to radio echo characteristics 80—17550
diffuse auroral zone, form. and dynamics of polar edge of ionospheric trough 79—8743
disturbed ionosphere above 100 km, approx. method for electron kinetics calc. 77—64512
dry and moist air, primary ionisation coeffs., secondary ionisation coeffs. for water surface 78—65376
E_s-layer, creation, effect of variable meteor particle sizes 80—105108
E_s-layer, ionisation irregularities rel. to Langmuir wave propag. and enhanced plasma line 79—29928
E_s-layer, mid-latit., effect of strong radio waves on form. 77—60514
E_s-layer ionisation at high latitude, quiet and disturbed conditions 80—61941
E_s-layer occurrence at temperate latits., small and large wind shears effects 77—29556
E_s-layer peak occurrences latit. var. during half solar cycle 77—29562
E_s-layer phenomena in Brazilian geomag. anomaly, rel. to regular particle ionisation source 77—78558
E-layer, auroral, seasonal vars. 79—8746
E-region, anomalous ionisation at high latits., ground based sounding obs. 77—60523
E-region, blanketing layer type ionisation irregularities, growth and decay 80—101477
E-region, correl. with solar flares X-ray and UV radiation 77—25815
E-region, electron prod. rate from solar X-rays intensity meas. 78—45072
E-region, ion production function from meteor particles 79—12336
E-region, ionization by solar UV and X-rays 77—17278
E-region, low-latitude, ionisation by energetic ring current particles 78—77415
E-region, midlatit. nighttime model including metallic ions 77—45249
E-region, nighttime ionisation rate rel. to night sky emission *(Russian)* 77—45223
E-region, nighttime ionization during meteor showers 77—29560
E-region, winter anomaly as result of upper atmosphere seasonal vars. 79—53613
E-region ionisation effect of neutral atmosphere seasonal vars. 79—12331
E-region ionisation vars. and mag. disturbances in polar region 77—13151
EAS, small atm. elec. field variations 77—60558
electron impact on atmosphere gases, cross-sections 78—28398
electron impact on atmospheric gases, yield spectra 78—28401
electron loss mechanism, D-region, normal and anomalous winter absorption 79—88537
energetic ions of ionospheric origin in magnetosphere 79—66874
energetic neutral atom precipitation, optical emission, ionization and energy deposition 79—75047
equatorial anomaly, counter electrojet assoc. changes, upward drifts reversal 80—109292
equatorial ionosphere, electron production by energetic particle precipitation 77—33255
equatorial ionosphere, phase scintillation of 40 MHz signals rel. to ionisation irregularities 79—44303
W.Europe, ion production obs., 50-120 km altitude, 1975/6 winter anomaly 80—36439
F_1-layer, mid-latitude, mean diurnal var. of O^+, NO^+, O_2^+ and N_2^+ ions 79—96856
F_1-layer at nighttime, ion composition near mag. equator 80—72683
F_2-layer, night-time, over Arecibo, ionisation downward flux seasonal mean struct. 80—31163
F_2-layer, parameters at high latitude during quiet conditions 80—105106
F_2-layer, seasonal difference in ionisation and height due to neutrals 80—61951
F_2-layer ionisation through a solar cycle, (1958-69), SW radiocommunication appl. 80—41626
F_2-layer nighttime ionisation latit. depend., var. in solar activity cycle 79—53617
F_2-layer noon ionization seasonal var. at dip-conjugate places 77—33259
F-region, diffusion-recomb. parameters 77—13156
F-region, diffusion-recomb. parameters 77—53300
F-region, equatorial ionisation density irregularities rel. to HF and VHF spread-F echoes 78—85764
F-region, equinoxial asymmetry due to ionizing agency outside solar system 77—29559
F-region, geomag. activity effects on h_mF_2 80—8480
F-region, interhemispheric ion transport induced by neutral zonal winds 80—98509
F-region, ion convection and midlatit. ionisation trough form. 79—2429
F-region, ionisation enhancements rel. to localised nighttime auroral zone scintillation enhancements 80—98506
F-region, ionisation rel. to O I 6300 Å airglow 78—36354
F-region, low latit. elec. field irregularities rel. to spread-F and plasma irregularities 77—53290
F-region, mechanism for anomalously enhanced ionisation 78—45108
F-region, mid-latitude, ionisation gradients rel. to spread-F activity occurrence 78—36389
F-region, N atoms and O ions in dynamic model 80—72693
F-region, polar cap and auroral zone, math. model 78—65458
F-region, winter anomaly causes 80—85793

atmospheric ionisation continued

- F-region, winter high-latitude, 300 km altitude, AE-C thermal plasma obs. 79—16740
- F-region electron density max., harmonic analysis and periodicities 78—57383
- F-region peak electron density, diurnal and solar cycle variation 80—61949
- F-region polarisation field, nighttime maintenance of equatorial ionisation 80—4192
- gas phase inorganic ion clusters 80—77068
- HV laboratory ion density due to repetitive impulse generation 78—65913
- ion+molecule reactions, atmospheric ion chemistry 80—61885
- ion formation, nonstationary effects of gravity waves in lower ionosphere 78—73567
- ion-ion recombination rates 77—66972
- ionic deprivation, biological effects *(French)* 78—3947
- ionisation, quiet nighttime, calculated and measured decay rates comparison 78—81493
- ionosphere, artificial spread-F generation by parametric instability 77—45247
- ionosphere, bubbles in equatorial spread F, nonlinear evolution 80—85801
- ionosphere, calc. technique for ground and satellite obs. 80—90275
- ionosphere, comparison between calculated and measured photoelectron fluxes from Atmosphere Explorer C and E 78—28400
- ionosphere, cond. functions during solar flare rel. to model for geomag. crochet 79—44300
- ionosphere, daytime positive storm effects at middle latits., prod. by travelling atmospheric disturbances 79—25394
- ionosphere, effective recombination coeffs. for quiet conditions and solar flare occurrence 80—12595
- ionosphere, electron concentration variations rate use 80—12598
- ionosphere, electron density and recomb. coeff. profiles calc. rel. to absorpt. and rocket meas. 78—69559
- ionosphere, electron distrib. rel. to electron production and heating 80—41605
- ionosphere, electron gas effective energy reception per created ion electron pair 80—67463
- ionosphere, electrons collision freq. and transport props. 79—80079
- ionosphere, equatorial, modelling of H_2 gas release effects 79—16741
- ionosphere, equatorial Mg^+ ion distrib. from Mg II 2800 Å airglow obs. 80—26673
- ionosphere, general photoelectron current meas. technique 80—12636
- ionosphere, high-latitude, formation, role of elec. fields 78—28370
- ionosphere, ion formation at high latits. during mag. quiet periods 78—69582
- ionosphere, ion prod. at high latit. by auroral electrons and short-wave solar radiation 77—60518
- ionosphere, ionisation density fluctuations rel. to SHF refr. scatt. and scintillations 79—48615
- ionosphere, ionisation irregularity drift motion from spaced fading and scintillation obs. 80—82133
- ionosphere, ionisation profiles rel. to ELF propag. in Earth-ionosphere transmission line 78—36234
- ionosphere, ionisation waves reson. coupling with acoustic gravity waves in mag. field 77—25832
- ionosphere, ionization due to low energy solar and magnetospheric particles 79—53625
- ionosphere, ionization due to low level meteors, contrib. to LF propag., radio and optical obs. system 79—84514
- ionosphere, lower, effects of solar flares Fe XXV 1.87 Å line emission 78—65588
- ionosphere, lower, ion prod., density and comp. during auroral absorpt. event 80—36443
- ionosphere, lower, ionisation correl. with interplanetary mag. field sector struct. 80—4167
- ionosphere, lower, ionisation enhancement rel. to long-distance mid-latit. VLF transmission disturbance 80—8485
- ionosphere, lower, ionisation model for reflecting layer below classical D-region 80—98508
- ionosphere, meteor trail ionization effects on radio propag. 79—101001
- ionosphere, midlatit., effective recomb. coeff., model 79—62652
- ionosphere, midlatit. disturbances caused by high energy particles 77—60517
- ionosphere, midlatitude, dynamical model for 100-1000 km altitude range 78—53768
- ionosphere, midlatitude, mathematical model of photoelectron fluxes 77—67009
- ionosphere, molecular ions conc. reaction to large-scale elec. field vars. 79—62654
- ionosphere, O^+ and H^+ equal ionisation level, during max. of solar activity 80—90280
- ionosphere, photoionisation by solar flares X-ray and EUV emission 77—5515
- ionosphere, plasma cloud striations, study of outer scale size 80—90279
- ionosphere, plasma density changes rel. to radio waves self-action, nonstationary theory *(Russian)* 79—48604
- ionosphere, plasma heating by photoelectrons from ionization by solar UV radiation 79—53622
- ionosphere, primary ion-electron prod. rates change with solar EUV flux 80—72675
- ionosphere, rel. to quiet Sun EUV and soft X-ray fluxes 77—13307
- ionosphere, topside, trough morphology, occurrence freq. and diurnal, seasonal and altitude vars. 79—53645
- ionosphere, total electron content fluctuations rel. to scintillation of VHF and GHz waves 80—109302
- ionosphere, total electron density nighttime behaviour 78—69570
- ionosphere, vertical ionisation gradient max. identification from ionogram trace derivatives 77—60522
- ionosphere, winter, thermal electrons energy distrib. obs. by S-310-5 rocket *(Japanese)* 80—94636
- ionosphere balance equation, theoretical model 78—28369
- ionosphere D and F regions, simultaneous ionisation meas. rel. to mesosphere NO concs. 79—8651
- ionosphere D and F-regions, effect of geomag. storms 80—101474
- ionosphere electron density during winter anomaly, 70-100 km 80—36441
- ionosphere equatorial anomaly, dissimilar forms in E.Asia and India 80—109301
- ionosphere equatorial bubbles, topside sounder obs. 79—16737

atmospheric ionisation continued

- ionosphere F_1-layer, dynamical effect obs. 79—12340
- ionosphere ionization var. caused by powerful radiowaves in lower region *(Russian)* 78—32273
- ionosphere negative storms, plasma density vars. simulation using neutral comp. data 79—25393
- ionosphere photoelectrons, Coulomb-collision induced trapping by geomag. field 79—8739
- ionosphere plasma line enhanced by HF radiowave heating 80—82140
- ionosphere total electron content, storm-time changes at nearby mid-latit. locations 80—31164
- ionosphere upward flowing energetic ions, latit., diurnal and altitudinal distribs. 78—49199
- ionosphere-state interaction, ion density in wake of O^+ plasma 80—82136
- ionospheric records over Shanghai, March 1953 to June 1955, effective coefficient of recombination *(Chinese)* 80—77192
- IR brightness obs. 80—94629
- latitudinal variation of auroral ionization, radar meas. 77—5385
- lightning, ionisation vel. in transmission line model 77—33156
- low latitude interlayer ionisation variations during max. and min. solar activity *(Russian)* 77—73902
- lower atmosphere, ion conc., elec. parameters and space charge density correls. 77—13104
- lower ionosphere ionis. struct. and composition, winter anomaly conditions 80—36442
- magnetosphere, doubly charged ions comp. and origin from GEOS mass spectrometer obs. 79—35069
- magnetosphere, ion flux oscillations of ultralow frequency, particle obs. 80—41657
- magnetosphere, ionisation ducts of detect. via JIKIKEN (EXOS-B) satellite VLF Doppler shift meas. *(Japanese)* 80—94651
- magnetosphere plasma, hot ion component rel. to electron component, obs. and implications 79—80106
- measurement by automated environmental monitoring system 80—81513
- mesopause, ionisation rel. to LF radio waves signal vars. over sunspot cycle 77—78560
- mesopause, $[NO^+.H_2O]/[NO^+]$ ratio rel. to temp. 79—96849
- mesosphere, cluster ion chemistry for Na and Na^+ layers 79—74934
- mesosphere, equatorial, effect of galactic X-ray source 78—36233
- mesosphere, ion bunching model 78—73424
- mesosphere, ion comp. in noctilucent cloud region 77—87011
- mesosphere, ion mobility and elec. cond. height var. 77—21837
- mesosphere, ion prod. by energetic charged particles precip. during winter anomaly 78—45001
- mesosphere, major characts., processes and dynamics 77—25734
- mesosphere, meas. of ion component of incoherent scatter spectrum in 60 to 90 km region 79—16569
- mesosphere, positive and negative ions cond., conc. and mobility meas. via payload B III instruments 78—45194
- mesosphere and stratosphere ion mobility and concentration, and conductivity, 10-70 km altitude 80—36358
- meteor collisional ionisation, thermalisation 78—36346
- meteor ionisation trails, characts. 77—71069
- meteor rate seasonal var., atmos. ionisation effect on LF radio navigational signals 80—82309
- meteor trail, maximum ionization height detect. method 80—8487
- meteor trail diffusion, radio refl. determination 80—46329
- meteor trails, causes of fluctuations in effective linear electron density 78—73687
- meteor trails, influence of recomb. on under-dense radio-meteor data 79—80279
- meteor trails, ionised, initial radius, height and time depend. investigation 79—58301
- meteor trains, ionisation rel. to radar echo drift deceleration 78—36538
- meteor trains deionisation rel. to HF radio echoes duration 79—5697
- meteor trial, diffusion of weakly ionised plasma filament forming angle with mag. field 79—53610
- meteor wakes, excitation of ionic lines and mol. bands 79—29919
- meteoric ionisation column, radiowave scatt. 77—87337
- meteoric ionization rel. to LF radiowave absorpt. events 79—48608
- meteors, ionization curve length and vaporization altitude var. with speed 79—21232
- meteors ionisation columns, initial radii meas. 80—94762
- moist air, ion content and IR absorption 80—41493
- mountain station, electrode effect obs. 79—25307
- negative ion hydration in stratosphere and lower ionosphere 79—100909
- negative ion photodissoc. and photodetachment 80—69199
- negative ions evolution, computer simulation *(French)* 77—21869
- negative superionisation, biological effects, investigation *(French)* 78—3946
- night-time E-region, mid-latit., ionisation by charged particle precip. 79—44291
- nighttime E-region valley, ionisation layers obs. above Arecibo 77—29569
- nighttime ionization by energetic particles, 120-200 km altitude 79—62666
- NmF2, low latit. features of annual and semiannual periodicities in America and India 77—53306
- Oviedo, Spain, hourly ion concs. *(Spanish)* 80—51449
- palaeoionosphere, evolution 77—2300
- photoionisation and photoabsorption cross sections of He, O, N_2 and O_2 for aeronomic calcs., data tables 80—41599
- photoionization peaks, photoelectron flux in ionosphere 79—16738
- plasma bubbles in nighttime equator region, field-aligned characts. 80—109308
- plasma sheet, ion populations rel. to electrostatic shock waves and electron precip. 77—9616
- plasmasphere, mid-latit., He ions behaviour 80—41630
- plasmasphere, mid-latitude, nighttime electron content, geophysical disturbance effects, 1974 August to November 80—94642
- plasmasphere total electron content, ATS-6 radio beacon obs. over Europe and USA 80—77201
- plumes from power stations, ionisation effects 78—88909
- polar D-region aeronomy 77—53311
- polar F_2-layer, winds and drifts rel. to nighttime maintenance 77—33274
- pollution, electrical climate relationship 77—73837
- positive corona discharge time lag obs. 79—27849
- positive ion concentration, in urban centre, meas. method *(Spanish)* 80—4059
- radial electric fields from air polarisation due to Compton electrons excited by γ-quanta pulse 80—21805

atmospheric ionisation continued
  radiation belts, energetic O ions charge states theory 78–77427
  radio aurora (diffuse), rel. to field-aligned currents and particle precipitation 80–105119
  radio phase path corrections for very long baseline interferometry, atmospheric modelling techniques 77–78637
  SITEC disturbances (1966-1977), rel. to solar flare occurrence 80–90276
  small ion spectrum, meas. of atmospheric electricity 77–91233
  small ions, recomb. rates and attachment to aerosol particles 79–39817
  snowfield contamination in arctic, ion comp. and episodic var. 77–91159
  solar flare protons effects, stratospheric elec. fields modification 79–48553
  sporadic meteors, ionisation height meas., VHF obs. 80–82312
  sporadic-E ionization and H aurorae 79–62659
  spread-F bubbles, nonlinear Rayleigh-Taylor mode theory in two dimensions 78–88986
  spread-F intensity, at Halley Bay high latitude station, India 79–75034
  static charges accumulatiion and limitation, discharging to earth *(Italian)* 80–43226
  stratosphere, energetic radiation belt electron precip. natural depletion mechanism for O_3 77–41134
  stratosphere, intense ionisation events, effects on NO_2, O_3 and climate, rel. to life extinction 78–96273
  stratosphere, ion conc., comparison of rocket and balloon results 80–72605
  stratosphere, mass spectrometric meas. of negative ions 78–96274
  stratosphere, multi-ion complexes, implications for aerosols and trace gases 80–61872
  stratosphere, positive ion chemistry of formaldehyde and methanol 78–57251
  stratosphere, positive ion density meas. by rocket-borne Gerdien condenser, 23-39.5 km altitude 79–84378
  stratosphere positive ions, comp. meas. 78–88877
  summertime atmospheric ion obs. by travelling coaxial counters 79–25310
  summertime obs. in Hyogo Prefecture, Japan 80–31109
  thermosphere, double photoionization and doubly charged ions 79–84559
  thermosphere, ion photochemistry from Atmosphere Explorer C meas. 78–32261
  thermosphere, ion-drag effects 80–17432
  thermosphere, lower, NO^+ daytime chemistry rel. to ionisation rate 77–33230
  thermosphere and ionosphere, chemical processes 80–17431
  thermosphere ionisation and variable solar UV flux, 1974-9 obs. 80–17430
  thundercloud electrification by precip. mechanism in presence of ion generation, model 79–84388
  topside ionosphere, ion composition changes during 13 Sept. 1967 storm 78–16232
  trichlorofluoromethane reaction rate with atmospheric-like ions 77–70723
  troposphere, halocarbon decomp. by natural ionisation 77–33139
  troposphere, halocarbon decomp. by natural ions 77–21889
  troposphere, negative ions evolution times 79–70829
  upper atmosphere, ionisation due to X-ray pulse, Auger electrons form. 78–53767
  upper atmosphere, photoelectron spectra allowing for Auger effect 78–69557
  UV solar radiation effects on upper atmosphere, review of Saha's work 79–53599
  virtual height-freq. curves, nocturnal, reduction method using ionisation models *(Chinese)* 80–105099
  whistler ducts in outer plasmasphere, form. 78–57407
  β-active aerosol particles, stationary charge distribution 79–92581
  H^+ midlatitude trough location from Oreol 2 data 80–8473
  $H^+(H_2O)_c$ ion-induced water clusters, mass spectra, IR continuum absorpt. 80–87257
  H_2O cluster ions at cold mesosphere, rocket borne expt. 80–17429
  He^+ escape fluxes from polar ionospheres, calcs. 79–35037
  He^+ in thermosphere, Atmosphere Explorer-C abundances rel. to solar EUV flux 79–16919
  Li^+ diffusion and ion-neutral interactions, laser sounding obs. *(French)* 80–82115
  Mg^+, photochemistry and vertical distrib. 77–21954
  N^+ photochemistry in thermosphere 79–96847
  N^+ sources and sinks in thermosphere 79–96848
  N_2 in upper atmosphere, spatial yield spectra, microplume model for electron energy degradation 79–98235
  $N(^2D)+O$, associative ionisation 80–4161
  NO density variations in E-region, theory, ion-neutral chem. constraints 79–75027
  Na^+ and Na layers, meteor ablation-cluster ion theory 79–58138
  $NaOH_2{}^+(H_2O)_n(NaOH)_m$ cluster in stratosphere 79–34895
  O, low-energy electrons integral scatt. cross section 78–69556
  O, photoionisation rate rel. to O II 7319-7330 Å dayglow 77–37475
  O, UV photoionisation cross-section calc., 304 and 584 Å 80–43015
  O^+ and H^+ daily vars. at mid-latitudes at sunspot max. 79–58167
  O^{++} in thermosphere, photochemistry 77–45226
  O^{2+} ions in disturbed ionosphere 79–62647
  $O_2{}^-$, in ionosphere, effects on EM wave propag. 79–8762
  $O_2{}^+$, NO^+, cones, correl. with meteor head echo heights 78–36537
  $O^+(^2D)$ in thermosphere, quenching by electrons 80–94630
  $O^+(^2D)$ metastable ions, charge exchange with O_2 in thermosphere 79–58141
  $O^+(^2P)$, ionisation freq. vars. during solar cycle 21 from airglow meas. 80–77195
  SO^- in E-region 79–96854

atmospheric light propagation
  8 to 12 μ IR emission attenuation obs. *(Russian)* 78–61556
  850 nm window, appl. in aspect sensor for small geophysical vehicles 77–45279
  absorbing gas, transmittance model for slant paths 77–64427
  absorbing gases with variable mixing ratios, transmittance model 77–23616
  absorption, effects on auroral brightness obs. from satellites 80–12538
  absorption at 460 μ, determ. 78–96295
  absorption by particulates, remote sensing determ., theory 79–88438
  absorption coefficient for line with Voigt profile *(Russian)* 77–64429

atmospheric light propagation continued
  absorption in 8-12 μm transparency window, effects of fine aerosol particles *(Russian)* 78–16159
  actual light scattering coefficient as meas. in haze and fog 79–80013
  adaptive correction by high-power-laser phase-conjugation array 80–33005
  adaptive optics, atmospheric compensation, book contrib. 79–31972
  adaptive optics, book 79–31921
  adaptive optics for imaging, wideband real time atm. compensation 77–45320
  adaptive optics in astronomy, rubber mirrors to compensate for atm. aberrations, book contrib. 79–35150
  adaptive optics in high energy laser systems, book contrib. 79–31971
  adaptive phased array expt. with independent laser sources, compensation for atm. effects 78–42367
  aerosol, H_2O-droplet, CO_2 laser beam clearing process, transmission function ratios 78–88919
  aerosol, laser beam propag., UV, visible and IR regions *(Russian)* 78–28313
  aerosol, soil derived, extinction between 0.55 and 10.6 μm 77–91264
  aerosol, thermal clearing by laser radiation *(Russian)* 78–28312
  aerosol absorption of visible light, spectrophone meas. 78–4000
  aerosol angular scatt., in situ photometric obs. over New Mexico (June 1974) 77–9492
  aerosol atmosphere, MTF and PSF calcs. rel. to space-meteorological photography, multiple scatt. effect 79–66792
  aerosol attenuation, influence on atmospheric and oceanic temp. determ. by remote sounding *(Russian)* 78–81430
  aerosol concentration deduction from 1.06 μm lidar meas. 79–25323
  aerosol constituents, absorpt. coeff. rel. to imaginary refr. index 79–74956
  aerosol content determ. from photometric obs. of stars 78–92976
  aerosol droplet size and conc., simple transmittance meas. 77–9511
  aerosol effects on polarisation of scatt. light from point source *(Russian)* 80–4106
  aerosol extinction at 500 nm in urban and rural air at Milwaukee, USA 79–100946
  aerosol extinction coeff. from outgoing solar radiation meas. in O_2 0.76 μm band *(Russian)* 79–8690
  aerosol inhomogeneities struct. and dynamics in ground layer, light scatt. 77–81955
  aerosol inhomogeneity expt. meas. 78–77304
  aerosol layer at 3 km causing sky brightness fluctuations in daytime *(French)* 80–81959
  aerosol layer depth remote meas. by microwave-modulated laser *(Russian)* 78–57338
  aerosol light scattering, obs. of polarisation and intensity 80–51541
  aerosol light scattering turbidity and visibility obs. 80–105047
  aerosol mass from Lidar concentration-solar radiometer expt. 80–90171
  aerosol medium bleached zone, probe radiation propag., intensity and phase fluctuations 80–67411
  aerosol microstructure, lower stratosphere, sounding with multifreq. lidar 80–56645
  aerosol optical attenuation statistics, spring and autumn 79–84484
  aerosol optical extinction coefficients, practical upper limits 79–72486
  aerosol particle characterisation with electrooptical nephelometry 80–77106
  aerosol particle size evaluation, response function optimisation of light scatt. instruments 79–50214
  aerosol pollution above urban site, monitoring by Lidar meas. *(French)* 77–25780
  aerosol scattering altitude depend., soln. by Monte Carlo methods *(Russian)* 77–60465
  aerosol scattering indicatrices under clear sky conditions in 0.55 to 2.4 μ spectral region, determ. *(Russian)* 80–94600
  aerosol single scattering rel. to photographic solar aureole meas. 77–5448
  aerosol size distribution retrieval, simulated aureole data inversion in presence of multiple scatt. 79–74957
  aerosol turbidity characteristics, determ. from spectral actinometric obs. 78–92986
  aerosols, differential scatt. coeff. to mass conc. ratio, spectronephelometer, cascade impactor obs. 80–72628
  aerosols, in situ meas. of absorpt. coeff./extinction coeff. ratio 80–90217
  aerosols, relative humidity and light scatt. of homogeneous two-layer particles *(Russian)* 77–82007
  aerosols, UV light absorpt. *(Russian)* 78–16160
  aerosols microphysical parameters from complex optical meas. *(Russian)* 77–13123
  aerospace propagation environment operational modelling conf., Ottawa, Canada, 1978, April 79–53651
  airborne meas. of atmospheric extinction and irradiating fluxes in Germany and the Netherlands 79–53523
  albedo, spherical effect of forward and backward scatt., finite plane-parallel atm. 79–92592
  Ambartsumyan's function for a cloudless atmosphere in the case of isotropic scattering *(Russian)* 79–39850
  amplitude modulated laser beam prog. in random inhomogeneous medium, phase fluctuation anal. 78–87017
  amplitude phase distortions correction of wave propag. in turbulent atm., efficiency 79–27178
  angular multiple scattering data, math. inversion 79–89847
  anisotropic scattering by ice crystals in artificial cloud *(Russian)* 78–40658
  anomalous diffraction approx. solns. for particle size remote sensing 80–17386
  anomalous refraction, effects on daytime astrometric obs. 78–24441
  apodisation filters, atm. turbulence effects on central irradiance in Fraunhofer diffr. by slit apertures 78–25796
  aqueous aerosol cloud containing medium, light beam propag., thermal self-interaction 80–91750
  aqueous polydisperse aerosol, bleaching by high intensity beam 77–58394
  astrometry, astroclimatic influences on precision of photographic star positions obtained with wide-angle astrographs *(Russian)* 80–72748
  astrometry, chromatic refr. correction tables for photoelectric stellar positions *(Russian)* 79–96889
  astronomical high-resolution techniques, atm. degradation effects, book contrib. 77–33357
  astronomical image degradation, contrib. of lower atmospheric layers, use of photodiode array 79–21019

atmospheric light propagation continued
- astronomical refraction, general theory *(Russian)* 78–89045
- astronomical refraction calc., theory for three-dimensional model of atmosphere 80–46260
- astronomical seeing, effects on reflected spectra of Uranus and Neptune 80–46479
- astronomical seeing, influence of spatial resolution on Ca$^+$ K-line width and shift in solar prominence 80–77364
- astronomical seeing, stellar optical image improvement via real-time phase correction system 77–22084
- astronomical sites testing, solar seeing and stellar scintillation meas. 77–29645
- atmosphere, turbidity meas. across Los Angeles Basin 78–92982
- attenuation and turbulence simulation in pulsed laser Doppler velocimeter system 78–73513
- attenuation at 6328 Å rel. to optical communication, statistical meas. 77–45144
- attenuation by aerosols in absorpt. bands of moistened particles *(Russian)* 78–65384
- attenuation by surface layer, spectral structure *(Russian)* 78–36277
- attenuation coefficient determ. by horizon line broadening *(Russian)* 77–60478
- attenuation coefficients, rel. to aerosol particle size distrib. statistical characts. *(Russian)* 78–53702
- attenuation exponents in visible and near IR up to 30 km, experimental profiles *(Russian)* 78–61558
- attenuation of HF/CO$_2$ laser beam by water vapour 80–61905
- aureole around UV source at finite distance 78–77320
- aureole radiance field about point source in scatt.-absorbing medium 78–77319
- backscattering amplification during large intensity fluctuations 80–18994
- band radiation pyrometry for error reduction in transmission coeff. calc. of IR radiation energy depend. on atmospheric props. *(German)* 80–105649
- beacon/tracker system simulation turbulent atmospheric propag. 79–53525
- beam broadening in randomly inhomogeneous cloudy aerosol medium *(Russian)* 78–58911
- beam volume scattering coefficient inadequacy 77–27251
- binary optical communication system, atm. scintillation effects 77–71943
- blue Moon phenomenon, due to light scatt. and mixed plate interference 77–2244
- boundary layer, birefringence under wind speed gradient shear 78–69453
- boundary layer, form. and evolution of radiative fog and stratus cloud *(Russian)* 77–49104
- boundary layer above ocean waves, scaling laws for optically relevant turbulent parameter C_T^2 78–85677
- boundary layer structure during light wind, water vapour IR absorpt. meas. 77–91197
- boundary layer temperature profile from inferior mirage obs., simple soln. 79–80035
- brightening of disperse media, role of laser fluctuations 79–41405
- circumsolar radiation, single and multiple scatt. contribs. 79–25325
- cirrus clouds backscatter and extinction coeffs. from laser radar obs. 77–60456
- cloud, multiple scatt. and depolarisation obs. using lidar 78–36292
- cloud, vertical laser beam heating causing convection *(Russian)* 80–56529
- cloud droplet spectrometry using light scatt. technique 77–41219
- cloud hole-boring by high-intensity laser beams, theory 78–28319
- cloud multiple radiation scatt., stochastic approximation 79–80012
- cloud reflectance with laser beam illumination, multiple scatt. contrib. 78–85686
- cloud rotational Raman and double scatt., lidar meas. 78–77318
- clouds, droplets volume extinction coeffs. at visible and IR wavelengths 77–25750
- clouds, light pulse reflection, height meas. *(Russian)* 80–82056
- clouds, mathematical model of radiative transfer 80–90215
- clouds, optically thick medium, asymptotic radiance and polarisation 77–21776
- clouds, radiant energy density calc. and photon equiv. trajectories *(Russian)* 77–45149
- clouds, satellite IR nephanalyses 77–41122
- clouds, scatt. intensity phase angle depend. rel. to contrast bow obs. 79–80029
- clouds, thick, light pulse propag., pulse width expression for scatt. slab 80–82059
- cloudy atmosphere, IR radiation flux approximation 79–39854
- coherence of light beam through optically dense turbid layer 78–55300
- coherent light beam, atm. propag. fluctuations, quantum phenomena 77–608
- coherent light source angular coordinates, meas. using received wave phase front 78–46526
- coherent optical adaptive Modal Wavefront Control System 77–19295
- collimated laser beam propag., corner-cube reflector and plane mirror comparison in folded-path and direct transmission 78–85697
- collimated laser beam propag. in turbulent atm., phase fluctuations spectrum 78–78914
- colour of ocean, Monte Carlo model including atm. and ocean scatt., absorpt. 78–61421
- colour structure of atmosphere, vertical profile obs. by astronauts *(Russian)* 78–40795
- communication line operating under photon counting conditions, adaptation to turbulence 80–9930
- communication links 77–83980
- conference, Washington, USA (March 1978) 79–66794
- contrast reduction of broadband optical signals 78–69455
- correlation scale measurement, spatial freq. modulation of stellar images 78–40661
- crystalline clouds, artificial, light scatt. matrices *(Russian)* 77–5317
- cumulus clouds, downward scatt. solar radiation 78–3876
- cumulus clouds, scattered and total solar radiation fluxes *(Russian)* 77–41169
- daylight, spectral distrib., 280-2800 nm, Australia 78–69452
- daytime r_0 evaluation from vertical microthermal meas. 78–3953
- degradation of electrooptical system performance 79–34940
- differential absorption lidar system sensitivity with heterodyne reception 79–27310

atmospheric light propagation continued
- diffraction limited image from obs. through irregular atmosphere *(Ukrainian)* 80–9814
- diffuse reflection and transmission of light, soln. for three-term phase function *(Russian)* 77–13260
- diffuse reflection by semi-infinite atmosphere *(Russian)* 77–82008
- diffuse solar radiation below overcast sky, ang. distrib. 80–85719
- diffuse solar radiation field in cloud layer *(Russian)* 79–29851
- diffusion equation derived from space-time transport equation 80–78772
- diffusively evaporating water aerosol 77–728
- directional fluctuation law of laser beam propagation *(Chinese)* 79–96824
- directional scattering coeffs. in droplet and crystal clouds, meas. *(Russian)* 78–96292
- discrete PPM signal reception accuracy *(Russian)* 79–94171
- dispersion effects on compensated imaging, phase distortion due to turbulence 77–42501
- dispersion minimisation, correctors for compensated imaging 77–46695
- dispersive particle sizes, from scattering and polarization meas. *(Russian)* 79–34950
- distant light visibility calc., colour and flash time corrections 79–83781
- drops of water, ice or mixed phase, backscatt. at 633 nm 77–64426
- dust, soil derived atmospheric, IR spectra, Christiansen effect, Rayleigh limit 80–105046
- dye laser, high energy pulsed, for atm. sounding 79–39868
- dynamic turbulence corrections for wavefront distortions 77–42487
- Earth surface UV radiation regime, effects of stratosphere pollution 78–16153
- Earth-space-Earth retroreflector link, scintillation statistics 78–11996
- EAS, associated prod. of radiopulses and optical Cherenkov radiation 77–60559
- EAS, correl. between optical Cherenkov pulses and radiopulses anal. 77–60560
- electro-optical system performance atm. degradation 79–66805
- emergent radiation, computation method for region ranging from UV to IR 77–87069
- extended source in turbulence, asymptotic parameters, scintillation scales 77–606
- extinction, 0.65 to 2.50 μm above Mauna Kea, obs. 80–12546
- extinction, monochromatic coeffs. determ. from spectrophotometric obs. of Terskol Peak *(Russian)* 79–44246
- extinction, rel. to fog and clouds liq. water content 78–81404
- extinction and absorpt., effects of particulate complex refr. index and size distribs. 79–29849
- extinction and absorption coeffs. of fog and clouds, organic aerosol effects 78–73465
- extinction and scattering efficiencies for spherical particles 77–78421
- extinction at 10.6 μm CO$_2$ laser wavelength, from meteorological records 79–39848
- extinction coefficient meas. from distant contrast, using astronomical telephotometer 78–61730
- extinction in 3.98-4.07 μm wavelength region 79–96808
- extinction of sunlight in mountainous regions 80–90202
- far IR laser radiation absorption, theory and expt. 77–41250
- finite optical beam in extremely strong turbulence, variance, covariance of irradiance 78–63008
- fluctuating signal, detector threshold and saturation effects on statistics 79–31803
- fog, droplets volume extinction coeffs. at visible and IR wavelengths 77–25750
- fog, IR extinction and absorption, linear relation to water content 80–56603
- fog, spectral transmission data, IR propag. and performance modelling 80–90218
- fog hole boring with pulsed high-energy lasers 79–16662
- Freons, IR absorpt. band intensities meas. in atm. window region 77–30871
- Gaussian beam self-focusing in supersonic gas flow, thermal self-action effect 79–76768
- geocorona, Lyman β and Balmer α emissions meas. rel. to optically thick model 77–37476
- Global Solar Radiation Index, vars. at Kew 77–17217
- ground-to-satellite power transfer by laser beam 79–62724
- halos, forms and relation to ice crystals 79–2373
- haze, radiative transfer model rel. to anomalous gray shades in DMSP visible imagery 80–77111
- haze and fog, visible and near IR attenuation 77–45153
- haze and fog vertical struct., effects on visible and IR extinction 79–58086
- haze microstruct. and refr. index from scatt. light polarisation characts. *(Russian)* 79–29852
- haze scattering by arbitrary shape nonuniform particles 77–7003
- hazes, brightness and polarisation phase functions rel. to particle size distrib. formation *(Russian)* 78–44998
- heterodyne array, joint signal probability distrib., clear air turbulent atm. 79–66804
- heterodyne optical radar S/N ratio in atmospheric turbulence 80–106558
- heterodyne receiver array for light propag. through turbulent atm. 79–64183
- heterodyne receiver arrays in turbulent atm., joint signal current probability distrib. 79–81368
- high power laser propag., thermal blooming review 78–30035
- horizontal imaging, spectral characts. of image quality 77–91265
- Huygens-Kirchhoff method, phase approx. for light reflection in turbulent atmosphere 80–28160
- hydrometeor backscattering cross sections, meas. at 6328 Å 78–49135
- hydrometeors, extinction and scattering in 0.25-15 μm range 79–53501
- hydroscopic particle humidification process, electrooptic scatt. meas. 80–77107
- ice, hexagonal crystals, solar radiation scatt. 79–94150
- ice clouds, visible and LR optical props. from lidar and radiometer meas. 80–82060
- ice crystal scattering and absorpt. 78–25795
- ice crystals, light scatt. expts. *(Russian)* 80–94601
- image degradation, linear invariant restoration 77–42503
- image degradation, post-processing from active phase compensation devices 77–42502
- image degradation due to refractive irregularities in clear turbulent atm. 77–42485
- image distortion for faint scenes, post-detection compensation 77–45322

atmospheric light propagation continued

image formation, optical and IR, turbulence effects, astron. appl. *(French)* 80—46257
image phase conjugate laser adaptive control, isoplanatic effect simulation 77—19294
image processing of simulated turbulence and noise degraded lunar images 77—45321
image reconstruction performance of image-plane sharpness criteria 78—93123
image resolution through atmospheric turbulence 79—36855
image resolution through turbulence over ocean, optical transfer function 78—85695
image restoration, astrophys. appls., conf., Bordeaux, France (Mar. 1979) 80—41935
image transmission, two-dimens., through randomly inhomogeneous medium, using Jamin interferometer 78—50706
images aberrated by turbulence, undersampling errors in moments meas. 80—1137
imaging and optical communication through atmospheric turbulence, book contrib. 79—34960
imaging in the presence of random wave aberrations 79—76607
imaging through atmosphere, conference, Reston, Va., USA (Mar. 1976) 77—42484
imaging through turbulence with telescope array, speckle interferometry 77—5458
imaging through turbulent atm., spatial freq. resolution of rot. shearing interferometer 78—69450
inclined-plane insolation computation, hourly and daily methods compared 79—83572
incoherent, absorption and scattering, effects on optical/optronical systems 78—92987
India, solar radiation meas. and atm. transmission at high altitude stations 78—32152
integral transparency, spectral transparency and humidity relationships 77—78423
intense light in gaseous medium with solid microfilling, theoretical analysis *(Russian)* 78—25797
intensity fluctuations, frozen turbulence hypothesis expt. *(Russian)* 78—61557
intensity fluctuations, statistical props. of sum of partially correlated complex variables 77—79754
intensity fluctuations and fourth-order coherence function in random media 80—78774
intensity fluctuations of atm. degraded beam at focus of large lens 77—64425
intensity fluctuations of optical carrier, turbulent atm. influence *(German)* 79—89861
intensity in horizontally-inhomogeneous scattering layer *(Russian)* 78—36278
interference fringe visibility and spacing, atmospheric turbulence effects 80—51572
interference pattern fluctuation statistics in turbulent atmospheric layer 78—53727
inverse greenhouse effect prod. by cometary impact, rel. to ice ages and ecological catastrophes 78—53714
inverse multiple scatt., approx. models, limb darkening and phase curves 79—44388
IR absorption by stratospheric HCl, radiometric meas. 77—25745
IR absorption meas. for surface methane conc. determ. *(Russian)* 77—29366
IR aerosol extinction, 3 to 5 and 8 to 15 μm spectral regions, relative humidity effects 79—62581
IR attenuation by H_2O vapour, hygrometer meas. 79—34943
IR broadband transmission rel. to meteorological events 80—85744
i.r. CO laser beam absorpt. by water vapour, optoacoustic meas. 77—2241
IR Doppler wind-sensing system, spaceborne, atmospheric effects 79—96828
IR extinction meas. using lidar, with CO_2 laser radiation 78—40655
IR extinction rel. to aerosols mass conc. 79—84473
IR extinction spectra of liquid droplet smokes and fogs 77—78416
IR image nonlinear conversion allowing for turbulent atm. influence 80—23751
IR imaging system performance in degraded atmospheres 77—19445
IR integral transmission function of clouds *(Russian)* 77—60466
IR laser beam transmission 77—70873
IR laser energy absorpt. by atm. dust, spectrophone meas. 77—9513
IR laser propag. 79—53521
IR long-wave (8 to 13 μm) radiation in free atmosphere, comparison of theoretical and experiment fluxes *(Russian)* 80—94598
IR propag. over long atm. paths, instrumentation 79—39875
IR radiation, attenuation by ice platelets 80—66141
IR radiation brightness at crossing of sea horizon *(Russian)* 77—29438
IR radiation extinction coeffs. for haze and fog droplet polydispersions 77—9496
IR radiation progag. aerosol. effects rel. to error in satellite retrieved temp. profiles 80—98449
IR spectral transmission meas., laser-calibrated, high-resolution 77—91266
IR spectral transmissivity, temp. depend., CO_2 and H_2O bands below 10 μm *(Russian)* 80—12542
IR transmission, rel. to relative importance of surface reflected and emitted flux densities 79—92542
IR transmission at Mauna Kea, determ. from obs. of H Paschen α in P Cygni and other OB-type stars 80—62156
IR transmission spectra, high resolution field meas. and computer code calc. 79—66798
IR transmission through turbid atmosphere *(Russian)* 79—34947
IR transmissivities, rel. to cooling rate in standard atmosphere 80—26609
IR transmissivities for H_2O vapour, CO_2 and O_3 78—11998
IR transmittance and radiance meas. and calc. 77—64431
IR transparency window, 10-13 μ, H_2O and aerosol effects in winter and summer *(Russian)* 80—105048
IR wavelengths extinction by aerosols in coastal fog 78—81400
IR window, absorpt. due to water vapour polymers 77—45145
irradiance enhanced variance from target glint 80—5691
irradiance fluctuations of beam waves, probability distrib. in weakly turbulent atm. 77—13125
irregular particle scattering, meas. results versus Mie theory 78—58918

atmospheric light propagation continued

isoplanatic degradation of tilt correction and short-term imaging systems 80—53219
isoplanation measurement using speckle interferometry 78—65385
isoplanatism and turbulence of the upper atmosphere 79—96810
isoplanatism varieties for imaging through turbulence 77—42499
kinetic cooling of CO_2 laser beam 77—62018
large particles scattering coefficients, approximation for total O_3 determ. 80—82091
large transparent sphere effective extinction efficiencies using weakly collimated light 79—72487
laser, high-energy, simplified aberrated lens model 78—69454
laser absolute transmission in 3.5 to 4 μm window, long-path high-resolution field meas. 78—28317
laser absorption method for H_2O vapour conc. meas. 78—61595
laser absorption spectrometer, long path length, effect of scintillation and multiwavelength coherence 78—40653
laser application to atmospheric environmental research *(German)* 80—97849
laser atmospheric studies, review 79—66789
laser backscattering from dense water-droplet clouds 79—53513
laser beam, atmospheric correction to celestial bodies range meas. *(Russian)* 80—12674
laser beam, atmospherically degraded, higher-order propag. statistics, recording process effect 79—14004
laser beam, atmospherically degraded, log-normally distributed intensity fluctuations 79—50228
laser beam, chopped, signal distortion due to beam pointing error 78—37937
laser beam, detection effects on statistics of intensity fluctuations 79—16672
laser beam, freq. spectrum of random displacements meas. *(Russian)* 79—96813
laser beam, integrals evaln. 77—79879
laser beam, intensity fluctuations in snowfall *(Russian)* 80—94602
laser beam, liquid water content and temp. fluctuations in cloud clearance zone *(Russian)* 78—44999
laser beam, monochromatic, absorption and scattering problems 78—92988
laser beam, multiple scatt. by radiational and advective fogs 79—100950
laser beam, phase compensated, propag. through atm. turbulence 78—83012
laser beam, repetitively pulsed, target intensity enhancement, thermal blooming 77—65604
laser beam, scatt. coeff. as function of visibility and wavelength, empirical formula 79—34944
laser beam, thermal blooming, mirror deform. for phase compensation 80—8423
laser beam, thermal blooming reduction vice phase correction, experimental demonstration 79—98449
laser beam, thermal self-action over path in medium moving at variable vel., expt. and numerical simulation 79—32003
laser beam amplitude fluctuation statistics in turbulent atmosphere 80—106458
laser beam arrival angle fluctuations meas. apparatus using telescope 80—109258
laser beam attenuation by snowfall, characts. 80—26611
laser beam broadening and depolarization in dense water-droplet fogs 78—92981
laser beam displacements, due to turbulence invest. using Karman spectrum *(Russian)* 78—20511
laser beam expt., Earth-Skylab path 79—100945
laser beam hygroscopic aerosol interaction 77—79888
laser beam in turbulent atm. 77—38975
laser beam in turbulent atmosphere, wave parameter fluctuations 77—38805
laser beam in turbulent medium, short-term average irradiance profile 77—7098
laser beam intensity fluctuations, averaging effect saturation with distance, expt. *(Russian)* 78—46512
laser beam intensity fluctuations during precipitation *(Russian)* 77—29432
laser beam intensity fluctuations in medium with Kolmogorov turbulence, distrib. function *(Russian)* 78—71034
laser beam intensity fluctuations in turbulent atm. over water surface *(Russian)* 78—69449
laser beam intensity profile distortions in turbulent media, theory 78—22162
laser beam line spread instrumentation for propag. meas. 78—83013
laser beam line spread instrumentation for propag. meas. 78—83015
laser beam nonlinear propag. through fog, thermal blooming 77—91268
laser beam off-axis propag. in low visibility weather conditions, non-small-angle scatt. 80—102621
laser beam phase aberration correction via stimulated Brillouin scatt. 78—37944
laser beam propag. in evap. liq. drop medium, wind refr. 77—5322
laser beam propag. through turbulence, long- and short-term Strehl ratios 79—62577
laser beam propag. through turbulent atm., statistical anal. *(Italian)* 77—45796
laser beam propagation in atmosphere, book 79—34955
laser beam propagation in particulate media, radiative transfer eqn. soln. 79—50222
laser beam propagation in turbulent atm., spectral expansion soln. method 79—18350
laser beam propagation through atmospheric turbulence 80—41550
laser beam propagation through snowfall, characts. 79—74958
laser beam propagation through turbulent atmosphere, interferometric evaluation of imaging characts. 77—88643
laser beam scintillation, in turbulent atmosphere 79—80018
laser beam scintillation beyond turbulent atm., numerical calc. 77—7005
laser beam spatial coherence, turbulent distortions 77—79756
laser beam spread, turbulence induced, isoline approach 77—72016
laser beam thermal blooming, enhanced focal plane irradiance 77—7096
laser beam time-depend. propag., thermal blooming in stagnation zone 77—75588
laser beam transmission, coagulation-sedimentation effects 80—36393
laser beam transmission at 10.6 μm, analytic model of bleaching 78—85688
laser beam transversing particulate multiple scatt. medium, radiance prod. 78—9325

atmospheric light propagation continued

- laser beam turbulence compensating tracking system, lead angle effects 78—33763
- laser beam vertical propagation through troposphere 79—39851
- laser beam wandering in turbulent atm., error probability in binary signal reception 79—10337
- laser beam wandering in turbulent atm., fluctuation power probability density distrib. 79—10336
- laser beam wave case and remote sensing, book contrib. 79—34959
- laser beam-exploded aerosol, light focusing and defocusing 80—8426
- laser beams, coaxial beams technique for increasing range of visibility of laser beacons in fog 80—101434
- laser beams, thermal self-action on heterogeneous atmospheric paths *(Russian)* 78—28311
- laser blue-green pulsed propagation through fog 79—39846
- laser cloud location, microstructure of scatt. particles *(Russian)* 77—73850
- laser communication line, error probability 77—14731
- laser experiment in low visibility atm. 77—88829
- laser experiment in low visibility atmosphere 78—46703
- laser irradiation intensity fluctuations, influence of transmitting aperture diffr. size and turbulence 79—45906
- laser light nonlinear transmission in fog 80—1256
- laser light propag. through turbulence, K distribs. 79--80023
- laser link confidence level, error probability deterioration causes 77—38977
- laser measurement of refr. index struct. parameter, altitude depend. 77—37316
- laser monitoring, book 77—25799
- laser propagation enhancement of CO_2 line due to offline centre tuning 79—84472
- laser propagation in turbulent atm., detector nonlinearity effects on statistics of fluctuating signal 78—55301
- laser propagation statistics in Montreal area, rel. to optical communication 80—4099
- laser pulse attenuation, reson. absorption by water vap. *(Russian)* 78—49138
- laser pulse interaction with aerosol particles 77—7097
- laser radiation field, four-point coherence function meas. in turbulent atm. 80—23623
- laser radiation intensity fluctuation in fine-droplet water aerosol at 630 nm 80—4109
- laser radiation intensity fluctuations reflected from turbulent atm. 77—50621
- laser radiation nonlinear propagation in corundum particle aerosol 79—23033
- laser radiation of CO_2 and HeNe sources, meteorological parameters effects 79—58093
- laser radiation propagating though artificial mist, intensity fluctuations *(Russian)* 78—37806
- laser radiation scattered by atmosphere, photocount distrib. 80—9921
- laser radiation strong intensity fluctuations, similarity relations and expt. verification, book contrib. 79—34958
- laser ranging system, effects of random path fluctuations 77—7094
- laser sounding of atmospheric H_2O vapour by reson. method *(Russian)* 77—33185
- laser technology for atm. science, conf., San Diego, USA (Aug. 77) 78—85748
- laser transmission, anomalous effects during August, 1976 at Farnborough, England 79—39862
- laser transmission in far IR 77—19237
- laser transmission meas. at 10.6 μm 78—92977
- laser-radiation-intensity fluctuations in rainfall, statistical characts. 80—101433
- lateral refraction, elimination from astrometric absolute declinations observed by micrometric method *(Russian)* 79—96890
- lens MTF changes, solar speckle interferometry calibration 79—2370
- lidar, incoherent backscatter heterodyne, antenna parameters 79—72613
- lidar, mobile system tests on cloud and natural aerosol 77—53248
- lidar, multiple scatt. from turbid atm., Monte Carlo anal. 77—25779
- lidar, on Spacelab, for atm. properties meas. 77—21943
- lidar, simultaneous nighttime meas. of Na and K abundances 78—36239
- lidar, stratospheric aerosols meas. during winter (1973) 77—33159
- lidar, stratospheric differential absorpt. meas. rel. to O_3 vertical profile 78—11972
- lidar antenna aerosol vol. optical field scatt., laser atmospheric sounding 77—88641
- lidar backscatter from horizontal ice crystal plates 78—92984
- lidar beam, two-wavelength obs. of stratosphere aerosol 77—41120
- lidar differential absorpt. *(French)* 80—41554
- lidar equation analysis for scatt. and fluoresc. targets 77—58370
- lidar equation for inhomogeneous atm., double-scatt. approx. 79—29855
- lidar equation for inhomogeneous atmos. *(Russian)* 80—82054
- lidar for atm. meas. 77—37436
- lidar investigation of inhomogeneous atmosphere optical parameters *(Dutch)* 79—80026
- lidar measurements of post-Fuego stratospheric aerosol layer 77—56679
- lidar observations of altostratus mixed-phase cloud 77—91220
- lidar observations of smoke and dust clouds at 0.7 and 10.6 μm wavelengths 78—69459
- lidar polarisation meas. for cloud phase discrimination 78—96269
- lidar probing of fogs and clouds, double scatt. approx. 78—73512
- lidar return, simulated, from one-dimensional stratospheric aerosol model 79 44247
- Lidar return from fogs, effect of non-uniform extinction coeff. on double scatt. contrib. 79—100952
- lidar return signal geometrical compression, atm. remote sensing appl. 78—57329
- lidar returns, interpretation problems with single-wavelength transmissometers 79—21054
- lidar returns from clouds, double scatt. contrib. 79—5615
- lidar returns from fog, doubly scatt. radiation contrib. 78—77326
- lidar scattering, four-component polarisation meas. 78—44996
- lidar scattering and relative humidity 80—77113
- lidar scattering from clouds at 347, 694 nm, polarisation props. 78—85689
- lidar sounding, nondispersive gas analyser appl. *(Russian)* 77—60477
- lidar sounding of atmosphere, optical system parameters effect 80—33065
- lidar system, geometrical optics anal., atmospheric backscatt. 78—37936

atmospheric light propagation continued

- liquid-drop aerosol, laser beam distortion in illumination channels *(Russian)* 77—14727
- long-path high-resolution transmission meas., comparison with LOWTRAN 3B predictions 78—92972
- long-path light absorption cell meas., automation, optical alignment 79—17491
- Lorentzian coefficient approx. for efficient transmittance profile calc. 78—61552
- marine boundary layer, humidity fluctuations affecting light scatt. 80—82052
- marine boundary layer, optical beam propag., analytical model 80—8329
- marine boundary layer, turbulence effects on laser propag. 77—45156
- marine boundary layer refractive effects in IR 79—96763
- marine propag. conditions for electro-optical systems, weather to propag. data conversion 79—58094
- maritime aerosol near Europe, albedo and 632.8 nm absorpt. 80—90136
- maritime air, aerosol distribs., IR scatt. coeffs. 77—45050
- Mauna Kea, atmospheric absorpt. between 4 and 30 cm^{-1} 78—3888
- measurement aggregate for statistical characts. analysis, by sounding with laser 80—36412
- measurement using CO_2 laser radar 80—90225
- mesosphere, solar H Lyman-α radiation meas. rel. to O_2 density, press. and temp. profiles 78—44947
- micrometeorological temperature profile from optical data inversion 79—80034
- middle atmosphere, solar occultation expt. rel. to aerosol remote sensing 80—109269
- middle atmosphere, solar UV radiation absorpt. rel. to numerical model of zonal mean circulation 80—109218
- Mie calculations for different aerosols, use of average complex refr. index 78—57314
- mirages, stratified medium light ray trajectories, educational aspects 78—69940
- modal wavefront compensative system performance, finite bandwidth effect 79—81361
- modulated laser beam propag., acoustic pulse generation, thermal defocusing 79—92597
- modulated wave propag. in turbulent atm., correlation functions and freq. spectrum 79—34954
- modulation phase fluctuation dispersion in turbulent atmosphere *(Russian)* 79—98277
- modulation transfer function, rel. to IR speckle interferometry 80—31216
- moist air, ion content and IR absorption 80—41493
- molecular absorption, Lowtran 3B model 78—85690
- molecular complexes presence and role in residual absorpt., light scatt. obs. 80—56607
- molecular scattering and reflection, inclusion in calcs. of photon fluxes and photodissoc. rates 79—53512
- molecule embedded in dielectric sphere, fluoresc. and Raman scatt. 79—76435
- monochromatic atmospheric transmission determination, laser heterodyne spectrometry 80—72653
- mountain and desert atmospheric MTF comparison 80—82063
- multiple atmospheric parameter meas. laser radar system 78—4009
- multiple pulse detection in atmospheric turbulence 78—92974
- multiple pulse thermal blooming, phase compensation 77—50732
- multiple scattered radiation problems, plane-parallel model appls. *(Russian)* 78—36275
- multiple scattering, Hovenier's exit function eqn., numerical props. 80—62054
- multiple scattering, theory for dispersive media with spherical particles *(Russian)* 80—94599
- multiple scattering in atmosphere with rough surface, azimuth-independent case 78—12085
- multispectral extinction data, analytic inversion in anomalous diffr. approx. 78—87016
- multispectral extinction data, analytical inversion formulae compared 80—18992
- narrow field optical astrometry, atmospheric turbulence limitations 80—109340
- near IR extinction spectrum, calcs. 80—51539
- nephelometer visual range estimates, contrast brightness theory, operational theory 80—8424
- noctilucent clouds, circularly polarised light detect. 79—48568
- nonisoplanatic effects, speckle interferometry meas. using double stars 78—65387
- nonspherical particle scattering, polydisperse scatt. matrix *(Russian)* 80—12543
- nonspherical particles size distrib. from scatt. meas., Mie theory 78—58909
- ocean surface with waves, radiance distrib. over surface, glitter and sky contrib. 77—21902
- optical communication link, laser beam size 80—33064
- optical extinction by aerosols in 0.5-14 μ wavelength range 78—57318
- optical glory, theory, physical effects 77—60468
- optical parameters determ. by aerial photography at sunset 80—90219
- optical phase and scintillation, observation and prediction comparisons 79—53524
- optical propagation, problems and trends 79—100947
- optical propagation through strong turbulence 79—66802
- optical scintillometer, large-aperture, fine calibration, optical estimate of turbulence inner scale 79—21026
- optics, scatt. by mols. and particles, book 77—5323
- OTF degradation meas. by TV system 79—92590
- OTF separation in turbulent medium 77—42498
- outgoing thermal radiation, meas. rel. to O_3 profile determ. 78—92945
- over-the-horizon optical propagation in a maritime environment 80—41547
- partial tracking optical heterodyne receiver arrays, operating in turbulent atm. 79—41345
- partially coherent beam intensity fluctuation calc. in turbulent atmosphere 80—78775
- partially coherent light propagating through atm. turbulence, intensity fluctuations 79—58087
- partially coherent radiation, extended Rayleigh-Sommerfeld integral method results 78—65386
- partially coherent source in turbulent atmosphere 80—9806
- particle light absorpt. index, using diffuse light radiometer 80—51465
- particle size distribs. remote sensing, Rayleigh-Gans-Born approx 79—27174

atmospheric light propagation continued
particle size spectrometry, use of low power gas lasers 77—78485
particulates, light scatt. method for chemical characterisation 78—69533
permittivity gradient effect on laser beam propagation 77—83814
phase adaptation by nonlinear techniques, optical propag. distortion compensation, book contrib. 79—31973
phase correlation scale effects rel. to atmospheric imaging characts., theory 80—94604
phase expansion coefficients spatial correlation, propag. through atm. turbulence 79—80021
phase fluctuations of optical wave in turbulent atm., elementary derivation 77—42486
photoabsorption cross sections of He, O, N_2 and O_2 for aeronomic calcs., data tables 80—41599
photodissociation fluxes, tropospheric and stratospheric, Mie scatt. contrib. improved model 80—77103
photoelectron counting distributions of laser light signal through turbulent atm. *(Japanese)* 77—50711
photon transport problems, modified Monte Carlo procedure 78—61560
plane waves in strongly turbulent media, two-frequency mutual coherence function 77—21907
polarised laser light, angular depolarisation and multiple scattering by water/ice clouds 80—41549
polarised laser light, angular scattering by water/ice clouds 80—41548
polarised light transfer problem in presence of absorpt., soln. 80—67561
polarization and scattering 79—96814
pollutant particulate volume conc. determ. by atmospheric Mie scatt. method *(Korean)* 80—45835
polydisperse particulate systems, light extinction 78—33667
polydispersion, forward scatt. corrections for optical extinction meas. 79—7075
polydispersion, moments determ. of size distrib. function in scatt. 79—18347
polydispersion scattering, size distrib. function determ. 77—10834
polydispersive cloudy medium, containing water droplets, brightening by intense monochromatic radiation 78—9407
power detected by receiver, narrowly collimated beam backscattered by reflector in turbulent atm. 80—32918
propagation problems, conf., Oslo, Norway (May 1978) 78—93044
pulse broadening in multiple-scatt. media, closed form expression 78—42277
pulse diffusion in densely distributed scatterers 79—3632
pulsed beam wave propag. through turbulence, cloud, rain, fog 78—12000
pyrheliometric ratioing for apparent atm. transmission determ. 79—96809
radiation attenuation in atmospheric surface layer, statistical characts. of spectral struct. *(Russian)* 78—24371
radiation field in semi-infinite medium with internal radiation sources *(Russian)* 77—29437
radiative transfer, atmospheric effects on remote sensing and laser propag., conference, San Diego, California (1979 August 29 to 30) 80—62376
radiative transfer, non-LTE, in CO_2 15 μm band *(Russian)* 78—36341
radiative transfer, soln. of equation for Rayleigh's phase function by principle of invariance 79—84660
radiative transfer, theory for remote sensing of layered random media 80—36413
radiative transfer eqn., appl. to satellite remote sensing of phytoplankton 80—77105
radiative transfer in scatt. absorbing plane-parallel media, approximate method 78—37805
radiative transfer multiple nonstationary scatt. with curved surfaces 77—29641
radiative transfer theory, six-beam model 77—17924
radiative transfer through fog, 2D numerical soln. algorithm 78—71032
random medium, correl. and struct. functions for arbitrary optical beams 78—66756
randomly inhomogeneous medium, spatially limited light beam displacement 78—5421
ranging laser atmospheric transmissometer with retroreflector 77—21905
Rayleigh optical depth, appl. to solar radiation problems 77—91269
Rayleigh scattering, luminance and colour temperature of clear sky *(Japanese)* 79—92594
Rayleigh scattering, optical thickness values 80—90216
real time atmospheric compensation, active optical imaging 77—49307
reflection, climatic effects of albedo sudden change 79—44241
reflection by clouds, path length difference and wavelength correl. *(Russian)* 78—69447
reflection in turbulent atm., fluctuations of wave beam field 79—66793
reflection optical radiation echo signal temporal broadening by atmospheric turbulence, anal. 79—8693
refraction, interactive computer graphics applied to visual image transmission 79—8689
refraction, student demonstration using var. density sugar soln. 77—57134
refraction angles accuracy obtained by statistical orthogonal expansion of refr. index *(Russian)* 77—70829
refraction between synchronous satellites *(Russian)* 80—21821
refraction determination by automatic obs. of meteorological elements *(Japanese)* 80—82110
refraction in atmospheric boundary layers 80—36400
refraction over lakes, rel. to image distortion and lake monsters 80—46259
refractive index in atmospheric boundary layer, structural charact. vertical profiles *(Russian)* 80—94597
refractive index structure const., height depend. 80—36397
refractive index structure parameter meas. by optical scintillator 78—65411
refractive index temp. struct. parameter estimation over ocean 77—41033
refractive index turbulence vertical profile, stellar scintillation meas. 77—45126
refractive scattering, weak, model system 79—89849
refractivity corrections to satellite laser ranging 77—75663
remote imaging of Earth surface with nonuniform albedo, contrast reduction due to haze 80—101431
remote probing for wind and struct. const., line-of-sight method 80—36426
remote sensing by aerosol lidar backscatter *(Dutch)* 80—4110
remote sensing by laser beam *(Chinese)* 80—46292
remote sensing of particle size distribs., analytical inversions 78—73508
remote sensing of particle size distribs., analytical inversions 78—73509

atmospheric light propagation continued
RI fluctuation spectrum in region of convection above heated surface *(Russian)* 77—9497
Rustavi, USSR, coordinated radiation and meteorology study, CENEX-72 77—78413
Saharan aerosols, complex refractive index between 300 and 700 nm 77—81970
satellite laser ranging, effect of horizontal refractivity gradients 77—25910
satellite laser ranging, scintillation statistics 77—88900
satellite laser tracking data, horizontal refractivity gradient correction 77—91276
satellite laser tracking data, ray tracing evaluation of refraction errors 79—8588
satellite solar occultation sounding of the middle atmosphere 80—105079
scatering corrections for atm. aerosol extinction measurements 80—98445
scatter channel for ELOS optical communications system, scattering from marine aerosols 79—29862
scattered light intensity and polarisation degree in model atm., mol. anisotropy effect 80—77104
scattering, adjacency effects on imaging 79—100939
scattering, by optically thin spherically symmetric atmosphere rel. to brightness at zenith near terminator 80—109382
scattering by artificial ice crystals *(Russian)* 77—29436
scattering by model atmosphere, spherical harmonics and iterative methods 77—66986
scattering by tenuous particles, generalisation of Rayleigh-Gans-Rocard approach 77—7006
scattering coeff., Barrow, Alaska 77—29386
scattering coeff. and scatt. directivity coeff. in 0-165° angle range, statistical relations *(Russian)* 77—29433
scattering directivity coeff. between 0.5 and 170 degrees 77—5319
scattering from large dielec. spheres, lidar signal analysis from rainfall 78—66754
scattering from naturally occurring aerosols, rel. to particle size statistics, 3.8 μ meas. 78—49136
scattering indicatrix for large optical depth *(Russian)* 77—29440
scattering layer with extended scattering indicatrix, radiative transfer eqn. *(Russian)* 78—40660
scattering matrices, Mueller, for nonspherical particles 78—90366
scattering measurement extension into UV using integrating nephelometer 79—74955
scattering medium, stratified, narrow beam propagation theory 80—106455
scattering of middle UV radiation from an internal source, Monte Carlo model 79—12263
scattering of partially coherent radiation by surface, atm. turbulence influence 78—58915
scattering of solar radiation refl. from ocean surface *(Russian)* 77—29435
scattering rel. to size distrib. determ. of spheroids *(Russian)* 78—36279
scintillation, conditional fading statistics 78—66757
scintillation, in optical lunar occultation meas., statistically rigorous reduction 78—73650
scintillation, phenomenological model 77—9491
scintillation effect, optical pulse detection 77—7004
scintillation of astronomical bodies, determ. of stratosphere density inhomogeneity struct., Salyut obs. *(Russian)* 80—109186
scintillation spectral covariance, 1.6 km path, 0.488 and 10.6 μm 77—607
scintillations in weak turbulence, source temporal coherence effects 79—50223
scintillations of focused radiation, freq. correl. by speckle interferometry 79—94153
scintillometer, finite aperture, for profiling wind and refr. index struct. parameter 79—25331
sea spray and coastal aerosol effects on transmission 79—39861
seasonal extinction due to aerosol at Kottamia Observatory site 80—46253
seeing for astronomical telescope, wavelength depend., atm. inhomogeneity effects 78—92979
semi-empirical theory 80—90220
short-exposure imaging through turbulence, wavefront distortion 79—41336
signal current probability distrib., optical heterodyne receivers in turbulent atm., theory 78—78916
signal current probability distrib., optical heterodyne receivers in turbulent atm., expt. 78—78917
signal discrete reception in turbulent atm. 78—73511
single-scatter radiation, temporal characts. 79—59634
size spectra from inversion of optical scatt. and spectral extinction 79—62578
slant path propag. characts. *(French)* 78—96294
smoke aerosol microstruct. and refr. index, optical determ., inversion method 80—36399
solar 1950-2150 Å radiation, ground level meas. using NH_3 actinometry 79—2345
solar aureole contribution to pyrheliometer meas. 77—2284
solar Lyman α radiation, atmospheric absorpt. rel. to O_2 densities 77—87010
solar Lyman-α extinction, meas. during European Winter Anomaly Campaign (1975-76) 78—45001
solar radiation, atmospheric propag. rel. to solar power systems 77—73798
solar radiation, extinction 77—78546
solar radiation, NO_2 absorpt. meas. rel. to atmospheric content *(Russian)* 77—81962
solar radiation, propag. rel. to direct beam solar irradiance and illuminance 80—90174
solar radiation atmospheric attenuation, effect of O_3 and H_2O vapour content and atmos. turbidity 80—93855
solar radiation geometric Brownian distribution, implications for economical solar heating system 79—83571
solar radiation reflected from Earth, brightness field, atm. transmission function calc. *(Russian)* 80—4105
solar radiation scatt. from gradient particulate atm., background noise in optical communication 79—62576
solar radiation scattering, cloud dimensions and orientation effects 77—33188
solar radiation UV limit at Earth surface, photon counting monochromator meas. 78—49134

atmospheric light propagation continued

- solar radiometry correction for diffuse atmospheric scatt. 79—80015
- solar telescope, arrival angle statistics rel. to nearby turbulence deduction 80—26740
- solar UV radiation, absorpt. in mesosphere and stratosphere 80—109248
- solar UV transmission calc. down to 28.7 altitude 79—62575
- soot particle absorpt. of near IR *(Russian)* 80—82055
- space-limited optical propag. in turbulent atm., phase approx. of Huygens-Kirchhoff method 79—92595
- spatial filtering function for collimated laser beam amplitude fluctuations in turbulent atm. 80—9810
- speckle interferometry, atmosphere turbulence effect ang. depend 79—101080
- speckle interferometry, bandwidths, exposure times, effects on MTF 78—69701
- speckle propagation statistics through turbulent atm., log-amplitude covariance function effect 80—82058
- speckle propagation through turbulence 78—66758
- speckle propagation through turbulent atmosphere research progress 79—66803
- spectra of random shifts analysis, in turbulent atmosphere 79—74942
- spectral absorption of solar radiation by Denver Brown Cloud 78—16158
- spectral structure of radiation attenuation, depend. on atmospheric surface layer turbidity *(Russian)* 78—44997
- spectral transfer function influence on remote meas. of surface albedo *(Russian)* 77—60464
- spectral transmittance profiles calc. method 78—85696
- spectral transmittance sensitivity to line and meteorological parameters 80—26610
- spectral transparency in 400-700 cm^{-1} range *(Russian)* 77—13121
- spherical wave propagation, effect of turbulence 80—82066
- stellar extinction. oscills. caused by disturbances in Earth atmosphere 80—56606
- stellar images, atmospherically degraded, restoration using complex spectral ratios 79—29854
- stellar photoelectric photometry at Hvar Observatory, colour systems and extinction meas. 77—78643
- stellar photometry, atmospheric extinction effects in Walraven VBLUW system 77—17377
- stellar radiation, allowance for IR absorpt. by atmospheric H_2O mols. *(Russian)* 78—40832
- stellar speckle pattern statistics, photon counting techniques 79—25324
- stratiform clouds, structure and optical props. *(Russian)* 78—16088
- stratosphere, aerosol and gaseous constituents from spacecraft solar extinction data, inversion retrieval 79—74961
- stratosphere, laser photochemistry of O_3 and distant spectroscopy *(Russian)* 78—28314
- stratosphere, NO_2 light extinction rel. to Cretaceous-Tertiary extinctions 78—32215
- stratosphere, scatt. profiles rel. to dust meas., (1970-1977) 78—73445
- stratosphere, simulated radiances for ClO and NO concs. determ. via solar occultation meas. 80—85756
- stratosphere aerosol, multifrequency lidar sounding rel. to microstruct. *(Russian)* 77—64374
- stratosphere aerosol, radiation transport model rel. to climatic effects of aerosol layer modification 80—98408
- stratus cloud, in Arctic regions, radiation trapping rel. to layering 77—5290
- strong fluctuations of light intensity, numerical calculation of spatial correlation function 80—18995
- submillimetre radiation, propag. in tropical cloud clusters, Cosmos 669 obs. *(Russian)* 77—49165
- submillimetric laser wave propagation, range and resolution 77—41242
- sunlight, spectral struct. of radiation field refl. by ocean-atmosphere system *(Russian)* 77—33086
- sunlight diffuse reflection, radiation press. perturbations of near-Earth satellite 78—24444
- sunlight reflection by clouds, fast azimuthally dependent model 80—51532
- sunlight scattering, Rayleigh and Mie theory 80—56605
- sunlight transmission through uniform waterdrop atmosphere study 78—36244
- sunlight transmission vars., sunspots influence rel. to weather 77—91238
- sunset obs. from Apollo-Soyuz, light refr. study from space *(Russian)* 78—65383
- surface layer, visible and IR attenuation statistical characts. *(Russian)* 80—4104
- surface layer aerosols variability, spectral transmittance method *(Russian)* 78—69448
- surface layer optical inhomogeneities, investigation via acoustic method 80—67434
- surface layer turbulence, effects on light beam, optical parameter determ. model *(Russian)* 80—12481
- Tanggula region, global and net radiation *(Chinese)* 79—92568
- temperature effect on 15 μm region transmission function, thermal remote sounding appl. 78—77327
- temperature fluctuations, modified spectrum rel. to optical propag. 78—92980
- temperature turbulence meas. and theory, AMOS site in Hawaii 79—53503
- terrestrial optical links at 10.6 μm, optimum design 79—84455
- thermal blooming, continuum-lens model 80—78918
- thermal blooming, theoretical aspects of compensation 78—32226
- thermal blooming cell design for adaptive optics evaluation 80—33096
- thermal blooming compensation, equivalent thin lens model 78—87108
- thermal blooming effect on laser beam propag. with on-axis null 77—27323
- thermal blooming in atmosphere, book contrib. 79—34961
- thermal defocusing of light beams, phase conjugation compensation method 80—64123
- thermosphere, O_2 concs. and absorpt. cross sections from EUV occultation profiles 78—28356
- time correlation of gravity centre displacements, in lowest layer, effect of winds *(Russian)* 78—20510
- transfer through horizontally non-uniform scattering cloud layer *(Russian)* 79—25326
- transmission, 1923 to 1957, from Smithsonian Astrophysical Observatory pyrheliometric meas. 80—17374
- transmission and scatt. phase function, 1.9-2.3 microns, aircraft meas. *(Russian)* 77—29434

atmospheric light propagation continued

- transmission at Mauna Loa, volcanically related secular trends 79—62585
- transmission functions, analytical determ. in LOWTRAN code 79—58095
- transmission measurement and prediction, 4.0 to 5.3 μm, CO_2, N_2 continuum absorpt. contribs. 79—92589
- transmission modelling and prediction scheme 79—53519
- transmittance, algorithm accuracies 80—101429
- transmittance, profile depend., line parameter vars. 78—77322
- transmittance and radiance, high-resolution HITRAN and data compilation 79—66795
- transmittance and radiance, moderate-resolution, LOWTRAN code 79—66796
- transmittance functions generated by numerical methods, trace gas appls. 80—98455
- transmittance model for variable-mixing-ratio absorbent gases 79—80011
- transmittance of inhomogeneous atm., interpolation method for rapid calc. *(Russian)* 79—29850
- transparency, meas. on Maidanak mountain during autumn and winter (1977 to 1978) *(Russian)* 80—72627
- transparency from ground actinometric meas. 79—39859
- transparency in high-mountain regions, astronomical-climatic conditions evaluation for IR astron. obs. 79—62566
- transparency meas., computer prediction, modelling *(Italian)* 77—91333
- troposphere, aerosol monitoring using Spacelab lidar system 77—21876
- troposphere, O_3 effects on Earth-atmosphere system radiative energy budget and climate 80—36365
- troposphere and stratosphere anisotropic multiple scatt. effects on solar radiation 79—80016
- turbid atmosphere, multiple scatt. effects on refl. light pulses 77—29442
- turbid atmosphere, transparency characts. calc. 78—81407
- turbid atmospheres, path length distrib. of scattered photons 77—45147
- turbidity, meas. via polarisation of UV light of daytime sky 78—20517
- turbidity, water vapour, O_3 and aerosol effects 77—78420
- turbidity at Athens Observatory, solar radiation meas. 78—7768
- turbidity caused by air pollutants, assessment 79—100941
- turbidity effects on classification of remotely sensed Earth surface features 78—16204
- turbidity index, skylight at South Pole station, Antarctica, polarising radiometer meas. 78—57320
- turbidity parameters from pyrheliometric meas. over India 77—78424
- turbidity rel. to circumsolar radiation intensity 77—37405
- turbulence, laboratory-generated, simulating atm. turbulence effects on optical propag. 80—9803
- turbulence, laser beam propag. Huygens-Kirchhoff method 78—32228
- turbulence, mean vertical profile, rel. to astronomical seeing 77—29379
- turbulence, optical path fluctuations, calibration of distributed temp. sensor 77—2688
- turbulence, phase distortion compensation efficiency 78—1177
- turbulence, phase distortions, correction via nonlinear optical techniques 77—88855
- turbulence, RMS phase var. estimation 77—45317
- turbulence and aerosol effects on optical coherence 80—82064
- turbulence and intermittency, Kolmogoroff's theory, laser beam propag. expt. 79—7368
- turbulence chamber for optical transmission expt., characterisation by thermal method 79—25330
- turbulence degradation compensation by nonlinear optical mixing 77—42558
- turbulence degraded beam quality, improvements with tilt-correcting aperture 77—42481
- turbulence effect on optical goniometer accuracy 78—55461
- turbulence effect on vertical optical path, phase coherence function meas. 77—45155
- turbulence effects on IR and near-millimetric-wave propagation 80—61902
- turbulence effects on optical imaging 79—66806
- turbulence effects on optical imaging systems performance 79—66799
- turbulence effects on target irrad. by laser beam 77—58254
- turbulence inertial model, expt. verification from solar limb motion 79—5614
- turbulence measurement by remote sensors, optical propag. parameters 77—45125
- turbulence phase distortion, modal compensation 78—69451
- turbulence problems, probability distrib. of sum of N complex random variables 77—50617
- turbulence profile and parameters, expt. data 79—66801
- turbulence scale from light fluctuation meas. *(Russian)* 77—17162
- turbulence sensor using atm. optical dispersion 77—45204
- turbulence structure function along laser propag. path, angular spectrum meas. 77—53133
- turbulence-induced wave-front errors, power spectra, optical and IR propag. 79—66800
- turbulence-induced wavefront tilt error tracking with shared apertures 77—19459
- turbulence-structure parameter meas. using space-limited laser beam 80—46285
- turbulent air influence 79—76593
- turbulent atmosphere, beam props. of partially coherent curved beam waves 80—95798
- turbulent atmosphere, displacement spectra of light beam gravity centres *(Russian)* 79—3631
- turbulent atmosphere, four-point field coherence function 79—98279
- turbulent atmosphere, light intensity two-freq. fluctuations correl. 79—98280
- turbulent atmosphere, optical DPSK system performance 78—42293
- turbulent atmosphere, optical mixing effects 77—34839
- turbulent atmosphere, space struct. of light strong intensity fluctuations 79—98278
- turbulent atmosphere, speckle propag. statistics 77—19170
- turbulent atmosphere, time depend. geometrical optics 77—605
- turbulent atmospheres, optimum processing of light fields, synthesis of algorithms 78—71047
- turbulent irradiance probability distrib. in saturation regime 79—76588
- turbulent medium, classical theory of wave propag. book contrib. 79—34956
- turbulent medium, light intensity fluctuations at focus *(Russian)* 78—46511
- turbulent medium, linear propagation of radiation, coherence length evaluation 80—48150

atmospheric light propagation continued
- turbulent medium, modern theories, book contrib. 79−34957
- turbulent medium, phase fluctuations 78−33668
- turbulent-degraded image reconstruction using nonredundant aperture arrays 78−93122
- ultrashort light pulse, propag. in region of absorpt. line *(Russian)* 77−47141
- upper atmosphere, light propag. rel. to solar irradiation flux between 120 and 400 nm 78−57536
- upper atmosphere, O I 1304 Å nadir intensity/column prod. rate rel. to airglow 77−45213
- urban-rural solar radiation and atm. turbidity, meas. in Los Angeles basin 79−80024
- UV, intensity of direct and scattered radiation at large air masses *(Russian)* 77−49166
- UV backscattering rel. to vertical O$_3$ profile 78−7762
- UV communication based on molecular and aerosol scattering in atmosphere 79−3736
- UV diffuse-direct ratios meas. with compact double monochromator 78−49144
- UV propagation and optical communications range 77−79770
- UV spectral distribution under clear day conditions 77−41171
- Uzhgorod, atmospheric transparency meas. *(Russian)* 78−40656
- vertical path modulation transfer function meas. 79−84478
- vertically nonuniform stratocumulus water clouds, radiation transfer 77−45146
- visibility at Fort Hood, Texas, correl. with solar insolation 78−24333
- visibility at ground level, two meas. methods 80−82078
- visibility definition weaknesses in atm. expts. 79−8688
- visibility in turbid media with coloured illumination 79−72489
- visibility range of objects in horizontal direction, atm. haze effect 78−16161
- visibility reduction by sulphates in photochemical smog 77−21904
- visual range monitors, optical transmissometers 80−13122
- Voigt profile, fast calculational algorithm, line-by-line transmittance 78−7767
- water droplets, small, weakly absorbing, motion in bounded laser beam 79−12269
- water droplets size distrib. in mist, vol. extinction coeff. at visible and IR wavelengths 77−37287
- water vapour, attenuation of 10.6 μm radiation, role of (H$_2$O)$_2$ dimers 78−13741
- water vapour, IR attenuation meas. in W.Europe 78−53698
- water vapour, IR continuum absorpt. calc. *(Russian)* 78−96293
- water vapour, pressure broadened absorpt. in 10 μm region, O$_2$ addition effects 78−92975
- water vapour absorption, LOWTRAN 3B predictions 79−44245
- water vapour absorption in 8 to 13 μm spectral region for different atmospheric conditions 79−39855
- water vapour absorption of CO$_2$ laser beam, optoacoustic detector meas. 77−9512
- water vapour continuum, 10.6 μm laser beam attenuation, meteorological factors 77−2242
- water vapour continuum absorption, 3.5 to 4.0 μm region 78−92973
- water vapour continuum IR absorpt. near 1200 cm^{-1}, temp. depend. 78−85687
- water vapour-N$_2$, absorption at CO$_2$ laser frequencies 79−50011
- wave correlation scale meas. with stellar speckle interferometry 78−65388
- wave fluctuations in turbulent atmosphere 80−48157
- wave front mutual coherence function corrected by zonal adaptive optics 79−72490
- wavefront correction in real time for atm. distortion, Bragg diffr. by acoustic wave 77−42500
- wavefront distortion compensation in real time 77−17219
- wavefront random deform. due to turbulence near ground, statistical anal. *(French)* 77−87074
- wavefront random deformations, due to turbulence, correl. function estimation *(French)* 78−36280
- wavelength selection for transhorizon optical communication 79−7088
- weak object image distorted by atm. effect, restoration possibility *(Russian)* 78−32349
- wind velocity lidar meas. by spatial filtering 79−29901
- Wise Observatory, extinction coeffs. for photoelectric UBV photometry 78−73657
- zenith observation, contrast reduction due to atm. extinction, calc. 79−84479
- C particulate, airborne, photacoustic and absorption spectrum using tunable dye laser 80−4102
- C sphere aerosol, black smoke opacity, calc. variation with particle size and refr. index 79−72488
- CO$_2$ laser, radiation absorpt. by propane and propane-N$_2$ gas mixture, atm. simulation 77−58366
- CO$_2$ laser, two-freq. differential absorpt. rel. to pollutants detect. *(French)* 80−7991
- CO$_2$ laser Doppler system atmospheric attenuation 77−75601
- CO$_2$ laser radiation influence on liquid drop cloud medium, dissipation 79−39858
- CO$_2$ laser radiation reson. absorpt., atm. NH$_3$ conc. determ. on long path 79−29904
- CO$_2$, transmission functions for 15 μm band, calc. and expt. *(Russian)* 77−64428
- H Lyman α reson. emission, obs. during 1973 June 30 solar eclipse 79−8901
- HF chemical laser radn. attenuation in 2.7-3.3 μm region 79−58088
- H$_2$O vapour continuum absorpt., 4.5-5.0 μm 80−36395
- HO$_2$NO$_2$, gas phase, in stratosphere, UV and IR absorpt. cross sections 79−13733
- H$_2$SO$_4$ aerosol, extinction, absorpt., backscattering and mass content relations 80−101403
- He-Ne laser, atmospheric extinction meas. 78−40654
- He-Ne laser transmitter/receiver to measure optical parameters of turbulent atmosphere 80−98450
- He-Ne lasers, atmospheric condition meas., humidity *(Italian)* 77−91331
- N$_2$, collision-induced absorpt., temp. depend., rel. to atm. far IR transmission 79−62584
- O$_2$, Schumann-Runge bands, atmospheric absorpt. model 79−96823
- O$_2$, UV absorpt. into $^3\Pi_u$ state, calc., atmos. opacity 80−12582
- O$_2$+Ar(O$_2$), collision induced UV absorpt. in Herzberg continuum, dimer form. 77−30883
- O$_3$ absorption coefficients for backscatter UV expt. 80−46254
- O$_3$, mesospheric, obs. of shadow on D-region in ionosphere VLF guide over Atlantic Ocean 79−58161
- O$_3$ total content determ. from total optical depth spectral var., solar radiometer meas. 77−53235
- OH fluorescence lidar instrument for stratospheric temp. and press. determ. 79−80033

atmospheric measuring apparatus
see also air pollution detection and control; ionospheric measuring apparatus; meteorological instruments
- 10 cm radar, for cloud-to-ground lightning cross section meas. 77−2279
- 100 GHz to 1 THz atmospheric emission and absorption meas. 79−34980
- accelerator, impulsive, investigation under cosmic conditions 77−53399
- acoustic Doppler sodar, appl. to atmospheric temp. fluctuations heat flux and struct. functions meas. 80−105023
- acoustic Doppler sounder for wind profile meas. in boundary layer 78−65413
- acoustic echo sounder, design from loudspeaker elements 78−87226
- acoustic echo sounder array for surface layer vorticity meas. 78−7810
- acoustic FM-CW radar for atmospheric sound 79−74972
- acoustic instrument, for atmosphere surface layer optical inhomogeneities investigation 80−67434
- acoustic sounder, appl. to methane gas plumes tracking 80−55968
- acoustic sounder, balloonborne, design and construction 78−57353
- acoustic sounder, design, wind velocity meas. appl., review 79−53528
- acoustic sounder, phase sensitive, phase shift correl. with temp. profile 78−49170
- acoustic sounder, records obtained for Christchurch, boundary layer study 80−26638
- acoustic sounder, temp. struct. parameter profiles meas. 79−21049
- acoustic sounder for lower atm. remote probing 77−17243
- actinometric radiosondes comparison during GATE-74 period 79−29906
- adiabatic condensation nuclei counter, growth of polydisperse aerosol 79−79306
- aerosol automatic mass conc. meas. techniques 77−64459
- aerosol dispersed comp. analyser, small-size instrument design 77−17257
- aerosol particle counter and size analysers with automatic correction 80−41574
- aerosol S content, continuous flame photometric detection system 80−81508
- aerosol sampler using two Nuclepore filters 77−91278
- air pollutant analysis and control instrumentation and organisation *(French)* 78−20549
- air pollutant sensing 77−37458
- air pollution, Dutch national monitoring system, focal and reference point 78−69465
- air pollution automatic analysis, spectrosc. methods *(Spanish)* 80−81516
- air pollution fall our measurement techniques and apparatus *(Dutch)* 77−25774
- air sampling equipment, for stratosphere chemical studies using Concorde aircraft 79−80058
- air-sea interaction buoy performance 79−70894
- airborne laser scanner, modulation techniques 80−5770
- airborne lidar system for geophysical and atmospheric expts. *(Italian)* 80−109277
- airborne millimeter-wave radiometer, multi-channel, dual frequency, high altitude obs. of atmospheric water vapour 79−80061
- aircraft-borne instruments for meas. monsoon clouds elec. parameters 78−7792
- airglow observatories intercalibration with AE-C satellite 77−41210
- Aitken counter, portable photo-recording, for small atm. aerosols detect. 78−57355
- all-sky camera for airglow and aurora studies 77−70903
- altazimuth sky scanner optical system, polarization characts. 80−77123
- anemometers, hot wire, comparison of dynamic and static calibrations for vel. perturbation meas. 77−19644
- antenna for dual-wavelength radiometry at 21 and 32 GHz 80−26628
- Aryabhata satellite, technology and scientific expts. 79−58218
- Aryabhata satellite aeronomy expt. 79−84637
- Atmosat balloon for tropospheric research, flight history and appls. 78−7775
- Atmospheric Cloud Physics Laboratory on Shuttle/Spacelab, droplets optical motion control appl. 80−12634
- Atmospheric Cloud Physics Laboratory simulation, vorticity transport eqn. solns. 80−94690
- aurora, weakly luminous artificial events, optical equipment 79−21075
- automated environmental monitoring system for pollution studies 80−81513
- automatic ^{222}Rn counter for continual unattended operation 78−73539
- automatic coulometric analyser for continuous monitoring of CO$_2$ content 79−53537
- automatic light scattering cloud condensation nucleus counter 78−3980
- automatic nulling radiometer for the 3-4-mm band 80−18016
- automatic weather stations, use in United Kingdom observational network 79−80047
- Balloon Altitude Mosaic Measurements Program 78−81455
- balloon borne mass spectrometer, liquid He cryopump and opening device 78−77370
- balloon-borne ion sampling package 78−69497
- balloon-borne IR telescope for absolute surface photometry of night sky 78−36453
- balloon-borne probes in stratosphere, atm. and astron. research 77−37435
- balloon-borne stratosphere grab-sampling system for air pollution meas. 77−29504
- BASORA secondary radar, sounding ballon tracking appl. 80−17357
- boundary layer meas. system for wind and temp. obs. *(German)* 80−94616
- ceilometer using low-power laser radar 78−24390
- chemical actinometer for UV solar radiation intensity meas. 77−45163
- chlorinated hydrocarbon, dry aerial deposition rate, meas. techniques 80−81506
- cine and television high-resolution obs. of noctilucent clouds 79−39891
- cine camera, time-lapse mechanism design, clouds and lightning photography appl. 78−85747
- cloud base recorder, Mk3, potential accuracy limitations 78−45024

atmospheric measuring apparatus continued
  cloud chamber, thermal diffusion, continuous flow parallel plate type, analysis w.r.t. atm. water droplet growth 80—36416
  cloud chamber with continuous flow diffusion, improved design 77—2277
  cloud condensation nuclei counters using diffusion chambers 77—41224
  cloud condensation nucleus spectrometer, new design 80—85765
  cloud condensation nucleus spectrometer, with horizontal thermal gradient 80—77158
  cloud electric fields measuring instruments 77—41226
  cloud granulometers, Knollenberg ASSP-100 performance *(French)* 77—53244
  cloud liquid water content measuring devices 77—41223
  cloud nucleus counter, dual-range performance 79—53543
  coastal aerosol sampling instruments, Californian workshop 78—7681
  COCHISE, cryogenic apparatus for IR excitation studies 80—95166
  coherent polarization-diversity radar techniques in meteorology 79—58111
  condensation nuclei, balloonborne meas. using condensation nuclei counter 77—64460
  condensation nuclei counter with inherent size resolution capability 78—81470
  condensation nuclei counters, calibration and intercomparison 79—83684
  condensation nuclei counters, counting efficiency 78—36293
  condensation nuclei counters, efficiency improvement for particle detection 80—7983
  contrast telephotometer, multiwavelength, instrument design, data interpretation 79—66842
  coronasonde, balloon-borne, for thundercloud elec. field meas. 78—61577
  correlation spectrometer, computer assisted, for remote sensing of air pollution 78—4002
  Correlation Spectrometer Remote Sensor, baseline drift minimisation 78—16167
  cryo mass spectrometer, for upper atmosphere neutral comp. meas. during winter anomaly 78—45192
  cryogenic etalon-spectrometer on Space Shuttle 79—58232
  cryostat using ^{3}He for space appls. 77—22077
  DC pressure summator, theoretical operation, tests and appls. 78—12005
  dew monitoring network for SE.United States 79—66818
  differential absorption lidar, complementarity of UV and IR systems for atmospheric species meas. 80—72634
  differential absorption lidar at 724 nm water vapour line 80—17384
  differential absorption lidar system sensitivity with heterodyne reception 79—27310
  differential absorption lidar systems for atm. gases remote meas. 78—69525
  diffraction and stray fields measurement, angular and amplitude characteristics *(Russian)* 80—67433
  digital image system for atmospheric research 79—39873
  digital instrument, for radio refr. index meas. 78—86321
  digital raingauge recording system 77—70862
  directional dust gauges, collection efficiency 77—37415
  directional dust gauges collection efficiency, comments and reply 77—70843
  distributed temperature sensor of optical path fluctuations, calibration 77—2688
  Dobson instrument, optical stop and focusing faults 80—101454
  Dobson O_3 spectrophotometer, automation *(Dutch)* 77—70867
  Dobson O_3 spectrophotometer, installation in Seychelles 77—17250
  Dobson spectrophotometer, for total O_3 content 80—72643
  Dobson spectrophotometer for O_3 determ., aerosol attenuation effect 77—45186
  Dobson spectrophotometer meas. errors in O_3 total content determ. 80—72644
  Doppler light detection and ranging systems for turbulence meas. 78—73554
  double Compton gamma-ray telescope, background sensitivity to atmospheric neutrons 78—53827
  droplet spectra in fogs, new meas. instrument 77—53219
  dual-Doppler radar, coverage area as function of meas. accuracy and spatial resolution 80—82093
  dust, airborne, respirable fraction, performance characts. of samplers matched to them 78—53438
  dust sampler, CIP type, for personal use 78—81469
  dye laser differential lidar for atm. SO_2 and NO_2 conc. meas. 78—32250
  Earth Observation satellite programmes 77—29631
  echosonde, excess attenuation of signals 80—83694
  echosonde (acoustic-radar) antennas, echo carrier freqs. and antenna dimensions rel. to performance 78—1474
  echosonde antenna, effects of phase-front distribs. on radiation patterns 77—39123
  echosonde applications, review 78—73493
  echosonde interferometer for atmospheric research 78—57347
  electrets, use in measuring rocket exhaust effluents from space shuttle model 79—53548
  electric field measuring device, for max. intensity meas. over water during thunderstorms 77—33160
  electrical aerosol analyzer for number and mass conc. meas. 80—108753
  electrochemical concentration cell ozonesonde, performance characts. 79—21039
  electrographic instrumentation for ultraviolet imaging and spectrography 80—46399
  electron analysers on ATS 6 and 1976-059A satellites, charge buildup study 80—72744
  electron capture detector, const. current, with modulated freq. *(Japanese)* 80—55764
  electron registration instrument in MeV range 79—5645
  electron spectrometers for the study of artificially injected particles during the ARAKS experiments 79—21143
  electronic chopper for UV source for cloud extinction meas. 78—79087
  electronic detector for conducting particles and fibrils 79—62164
  electrostatic mobility analyser, variable freq., for aerosol charge distrib. meas. 78—77945
  ELF/VLF goniometer receiver, remote, unmanned, in Antarctica, UHF telemetry link 80—21854
  environmental aerosol sampler, particle size depend. of collection efficiency 78—12002
  EXOS-B, magnetospheric research satellite, instrumentation 79—48649
  Fabry-Perot interferometer, multiple-zone aperture design for airglow temp. 80—82075
  Fabry-Perot pressure-scanned interferometer for nightglow meas. 77—9510

atmospheric measuring apparatus continued
  Fabry-Perot spectrometer for airglow studies, with large aperture and high resolution 80—67424
  Fabry-Perot-interferometer imaging system for thermospheric temp. and wind meas. 80—101441
  far IR polarising interferometer, emission meas. from aircraft 78—7766
  field meas. Fourier transform spectrometer 80—86470
  filter instrument total O_3 accuracy, bandwidth effect 78—16181
  filter-tilting type nightglow photometer 77—73889
  flash counter and interval recorder 78—88928
  flash holography investigation of atmospheric aerosols 78—16217
  Fourier interferometric spectrometer system 79—34979
  Fourier transform spectrometer for atmospheric trace molecules spectroscopy, optical design 80—82099
  French incoherent scatter facility, gravity waves detect. in lower atmosphere 78—81478
  French meteor radar facility 79—2386
  Funk net pyrradiometers for shipboard net radiation meas. 79—21055
  gamma telescope of Kosmos-461 satellite 79—97480
  gas chromatograph-microwave plasma detector, appl. to atmospheric alkyl Pb and Se compounds detect. 78—68975
  gas conc. cells for S oxides and S-bearing pollutants sensing 77—70842
  GATE aircraft radiation instrumentation, anal., IR irradiance meas. 78—32134
  Geos 1 and 2 satellites, keV plasma expt., magnetospheric electrons and ions distrib. 80—41695
  GEOS-1 keV plasma expt., early results 79—35068
  GEOS-1 wave experiment 79—25444
  grille spectrometer for first spacelab payload *(French)* 79—80202
  HF radioemission during ARAKS expt., ground-based equipment 79—21078
  high acidity analysers, comparative tests near industrial installations in Fos-Etang de Berre region 78—81464
  high frequency atmospheric acoustic sounders 79—84489
  holocamera for particulate studies 79—22919
  horizontal wind meas., airborne system automatic calibration *(French)* 78—24386
  hot wire anemometers used for turbulence meas. in marine environment, freq. response 77—33214
  IAS triangulation camera for artificial clouds altitude determ. *(French)* 77—33192
  ice crystal collectors, spherical aerosol particle scavenging efficiency 78—44934
  ice nucleation, study of different modes 79—48530
  ice nucleus counters 77—41225
  ice particle counting in mixed-phase clouds by optical techniques 77—41221
  Illinois climate centre, review 80—77118
  imaging devices for cloud particle shape meas. 77—41222
  impactor design for aerosol meas. 77—29448
  impactor-replicator for laboratory cloud comp. analysis 79—53544
  insolation meas., Si-cell based sunstation system 79—5582
  interference spectrometer, selective modulation, far IR, design and appl. to atmospheric absorpt. meas. 80—57397
  interferometer, balloon-borne far IR Michelson, for stratospheric emission spectrum obs. 79—39870
  interferometer, for atmospheric modulation transfer function estimation *(Russian)* 79—16715
  interferometer, rot. shearing, for imaging through turbulent atm., spatial freq. resolution 78—69450
  interferometer for modulation transfer function meas. 80—41567
  International Sun Earth Explorer 1, electron spectrometer expt. 78—85809
  International Sun-Earth Explorer 1 and 2, fast plasma expt. 78—85800
  International Sun-Earth Explorer 1 and 2, plasma wave investigation 78—85802
  International Sun-Earth Explorer (ISEE) mission, payload instruments 80—90320
  International Sun-Earth Explorer A, DC and low-freq. elec. field meas. instrumentation 78—85807
  International Sun-Earth Explorer A, plasma comp. expt. 78—85810
  International Sun-Earth Explorer A, Stanford University VLF wave injection expt. receiver 78—85806
  International Sun-Earth Explorer B, EGD positive ion expt. 78—85805
  International Sun-Earth Explorer-1, quasi-static and low-freq. elec. fields meas. 78—85808
  International Sun-Earth Explorers, electron density expt. 78—85803
  International Sun-Earth Explorers 1 and 2, fluxgate magnetometers 78—85804
  International Sun-Earth Explorers 1 and 2, medium energy particles expt. 78—85811
  International Sun-Earth Explorers 1 and 2, quadrispherical LEPEDEAS for plasma meas. 78—85801
  ion analyzers for DC electric field and ion temp. meas. 79—21147
  ion detectors with spherical meshes 80—8436
  ion mass spectrometer, satellite-borne, 0-16 keV energy range, magnetosphere appl. 77—13207
  ion mobility spectrometer, multielectrode, for atm. elec. meas. 80—31145
  IR heterodyne radiometer for temp. profiling 77—49200
  IR hygrometer, meas. of attenuation by atm. H_2O vapour 79—34943
  IR instrumentation in ambient air monitoring, overview 77—49194
  IR multidetector spectrometer for atm. temp. sounding 79—25365
  IR optical system input diffr. effects and use of spatial apodisation 78—79113
  IR propag. over long atm. paths, instrumentation 79—39875
  IR radiometer, balloon-borne, for stratosphere water vapour meas. 79—8718
  IR radiometer, passbands for clear-air-turbulence detect. 78—96318
  IR radiometer calibration, for atm. temp. remote sounding 77—41174
  IR spectrometer, atmosphere surveillance from Meteor 25 satellite *(German)* 78—32321
  IR spectrometer performance testing using CO line parameters 77—91275
  IR spectroradiometer, ground-based, for vertical temp. profile meas. *(Japanese)* 77—29499
  IR spectroscopy instrumentation, stratospheric research, design study 80—17391
  IR system for radiating source meas. 77—70891
  IR system performance in airborne environment 78—82039
  isokinetic sampler for particle flux determ. 77—91279

atmospheric measuring apparatus continued
JROE II LIDAR, technical and constructional details, communication system *(Italian)* 78—3957
laboratory discharge lamp source for O_2 atmospheric bands and 0 I 5577 Å and 6300 Å lines 80—4148
Langmuir probe expts. on Intercosmos-10 satellite, results *(German)* 79—2469
laser absorption spectrometer, for point monitoring of gases ambient concs. 78—61607
laser anemometer, time-of-flight, for velocity meas. in atm. 78—69469
laser application to atmospheric environmental research *(German)* 80—97849
laser beam, multiple scatt. by radiational and advective fogs 79—100950
laser beam arrival angle fluctuations meas. apparatus using telescope 80—109258
laser Doppler velocimeter, accuracy, turbulence effects 79—55433
laser experiments on Spacelab missions, for atmospheric meas. 78—53793
laser induced fluorescence system for OH and trace gas meas. 80—36425
laser interferometer, active, digital, features 77—67492
laser photoelectric spectrometer for large condensation nuclei meas. *(Russian)* 78—65408
laser polar nephelometer for stratospheric aerosol particle meas. 80—17389
laser radar system, steerable 78—53746
laser radar system at University of West Indies 77—13134
laser radar system for atm. parameters monitoring, water droplet remote meas. 77—91299
laser scattering system for marine aerosol meas. 78—36316
laser transmissometer, long-path, for visibility meas., field testing 78—85751
laser velocimeter, differential Doppler system, transverse vel. meas. at remote point 77—65816
lasers for long path monitoring of ambient gases 79—16682
lidar, airborne, multidisciplinary, planned operation 78—36335
lidar, airborne continuous long-distance system, flight tests *(German)* 78—36338
lidar, alternate-pulse wavelength switching of dye laser 78—25890
Lidar, appl. to monitoring of air pollution above urban site *(French)* 77—25780
lidar, laser rangefinder, characteristics of atmospheric aerosols 80—51580
lidar assembly, appl. to plume struct. and trajectories meas. 79—58016
lidar for atmospheric multiple backscatt. and depolarisation obs. 78—36292
lidar observations of atmosphere at Kingston, Jamaica 78—36284
lidar Raman spectroscopy of atmosphere *(Russian)* 78—24387
Lidar return from fogs, effect of non-uniform extinction coeff. on double scatt. contrib. 79—100952
lidar system, heavy, for environmental protection control, containerisation 78—36336
lidar system, two-freq. downward looking, for atm. monitoring 78—69523
lidar systems, two- and three-freq., for aerosol meas. 78—36334
lidar theory and methods for composition meas. *(Japanese)* 78—16206
light radiometer for downward diffuse light flux 80—51465
lightning counter, multichannel, with digital display 80—51570
lightning peak current meas. and recording device results *(Japanese)* 80—46288
lightning stroke current measurement, automatic observation system *(Japanese)* 77—29506
Limb Infrared Monitor of Stratosphere, radiometer spatial frequency response 79—101048
Limb Infrared Monitor of Stratosphere (LIMS) radiometer, design and performance, expt. goals 78—61601
liquid water content measuring device 79—88489
low-level atmospheric thermograph, shipboard use in fog and stratus investigations 80—105073
low-speed anemometer, with const. temp. thermistor *(French)* 77—21922
Lyman-α ion chambers, water vapour contamination 79—8731
magnetometer, ring-core type, for space vehicles, geomag. fluctuations high-sensitivity obs. *(Japanese)* 80—94671
magnetosphere proportional counter, with thin mica windows, for low-energy particles 80—109260
marine air temp. sensor error analysis 77—78437
mass spectrometer, quadrupole, on 'Vertical-7' geophysical rocket 80—31935
mass spectrometer, rocket-borne, for NO meas. in lower thermosphere, comparison with UV photometer meas. 78—40723
mass spectrometer beam system, stratospheric comp. meas. appls. 78—7808
mass spectrometer meas. technique for O and O_2 in lower thermosphere 78—57348
mass spectrometer probe, for middle atmosphere plasma and neutral gas comp. and struct. anal. 78—45191
mass spectrometer with sputter ion pump for stratospheric comp. meas. 77—33200
mass spectrometers for in situ meas. 80—17388
MATEC (matched tandem etalon camera), appl. to auroral obs. 80—101442
membrane filter inefficiencies for particulate collection under low loading conditions 77—70721
meridian scanning photometer for airglow and aurora studies 77—70903
meteor radar system, Illinois University, description and results 77—41205
meteor wind radar, semiautomatic display and photographic recording system 79—8712
meteorological radar in Switzerland *(German)* 80—17358
Meteosat, geostationary meteorological satellite, brief particulars *(French)* 80—17469
Meteosat water vapour channel, near insight into troposphere 79—25292
Michelson interferometer, cryogenic, rocket-borne, for EXCEDE II expt. 80—95133
Michelson interferometer, use as selective filter for stratospheric trace gas concs. meas. 80—17408
Michelson interferometer on Canberra aircraft for stratospheric studies 77—87132
Michelson-Fourier transform spectrometer for night airglow visible spectra 80—36424
micro-Raman spectrometer, for individual aerosol microparticles identification 78—68970
microbarographs, sodar, FM-CW radar, review, tropospheric studies 77—91332

atmospheric measuring apparatus continued
micrometeorological measurement principles, book 77—9559
microprocessor controlled lidar for tropospheric O_3 meas. 79—58137
microprocessor-controlled 64-cell pulsed optical receiver for crosswind sensing 77—18096
microwave radiation monitor 77—26401
microwave radio refractometer, expendable, lightweight, construction and performance 79—8708
microwave radiometer, for indirect determ. of atmospheric boundary layer temp. profile 79—25369
microwave radiometers, for atmos. temp. profile meas. *(Chinese)* 79—80188
MM wave radar system for remotely sensing atmospheric pressure from satellite 80—67443
mobile lidar system, for smokestack emission meas. 77—53248
modulation radiometer, portable instrum. for SHF atmospheric sounding *(Russian)* 78—49159
moisture sensor for in situ meas. of stratospheric and tropospheric water vapour 79—74930
monochromator, compact double, for diffuse-direct UV ratios meas. 78—49144
monochromator, photon counting, solar radiation UV limit meas. at Earth surface 78—49134
monochromator, vacuum UV 6 m, photoabsorpt. obs. in atm. gases 78—37969
multifrequency lidar, appl. to stratosphere aerosol microstruct. sounding *(Russian)* 77—64374
multiple atmospheric parameter meas. laser radar system 78—4009
multislit spectrometer for the night airglow observation 78—73542
Mylar bags, aluminised, for aerosol storage, submicron aerosol losses 79—58114
narrow beam spectral radiometer for 4-14.5 μm atm. radiance meas. 78—61596
negative-feedback charge-sensitive electrometer, for atm. ice particles elec. charge meas. 79—70895
nephelometer, backward hemispheric integrating, accuracy 77—45189
nephelometer, integrating, ang. truncation error in fog droplet size range 77—70861
nephelometer, integrating, atm. light scatt. meas. extension into UV 79—74955
nephelometer, meas. of Rayleigh scatt. props. of aerosols and gases 79—29865
nephelometer, polar, aerosol scatt. obs. over New Mexico (June 1974) 77—9492
nephelometer visual range estimates, contrast brightness theory, operational theory 80—8424
neutral mass spectrometers, fly-through mode theory 79—58274
Nimbus instrumentation description, for remote sensing of stratosphere 80—26713
Nimbus-7 satellite remote sensing equipment 79—25437
Nolan-Pollak condensation nucl. counter, droplet growth rate, supersaturation 77—60480
nuclepore filters, amosite fibres collection efficiency 78—81341
Nuclepore filters, anomalous filtration of solid particles 79—12283
O_3 meas. by CW CO_2 lasers, using long path differential absorption 78—32256
objective sensor placement for sampling regional turbidity 79—5626
odour analyser, automatic, for atmospheric sulphide anal. *(Japanese)* 80—50924
OPEN program for investigation of origins of plasma in Earth's neighborhood 80—109318
operational vertical sounder, on TIROS-N polar-orbiting meteorological satellite 80—77132
optical array probes evaluation for cloud particle size distrib. meas. 77—41220
optical baffling system, high rejection, terrestrial meas. of performance 78—7802
optical ice particle counter, for ice particle/water droplet discrimination 79—100973
optical observation systems for the ARAKS experiment 79—21073
optical particle counters, field comparison 79—12279
optical radar, logarithmic fast-response photodetector for atm. sounding, photometric properties 80—51585
optical radar ceilometer measures cloud base height using laser beam 77—29441
optical scintillometer, finite aperture, for profiling wind and refr. index struct. parameter 79—25331
optical scintillometer, saturation-resistant, for refr. index struct. parameter meas. 78—65411
optoacoustic cell with improved performance for NO detect. 77—66987
optoacoustic detector, water vapour absorpt. meas. of CO_2 laser beam 77—9512
optoelectronic Kvant classifier for aerosol dispersion anal. 78—12739
PAG-5 air and marine proton magnetometer *(Russian)* 77—60489
particle camera, aircraft-borne, for in situ photography of cloud particles 78—85750
particulate chem. composition, use of laser induced mass spectrosc. instrument 80—97848
particulate sampler, size selective, modification and operation 78—36294
passive antenna system, comparative study for use as elec. cond. meas. device 80—85762
passive probe for free atmosphere electric field meas. 79—8710
passive remote crosswind sensor 78—7773
payload B III, instrument package for meas. of cond., conc. and mobility of mesosphere positive and negative ions 78—45194
Pc 1 geomagnetic pulsation sources, location using ULF goniometer techniques *(French)* 79—70890
photodiode detector, for rocket-borne photometry of near IR airglow 77—13128
photoelectric aerosol counter, use of laser light sources *(Russian)* 79—100969
photoelectric aerosol detection system 80—51578
photoelectric condensation nucleus counter with digital recording 80—8448
photoelectric detector for daytime lightning 78—57336
photoelectric particle counter for stratospheric aerosol particle meas. 80—17389
photoelectric scanning spectrometer for vacuum UV molecular photoabsorpt. cross-section meas. 80—37096
photoelectric spectrometer giving integrated parameters in real time *(French)* 78—53730

atmospheric measuring apparatus continued

- photoionisation mass spectrometer, balloon-borne for stratospheric gas meas. 78—85732
- photometer, 2972 Å, for rocket studies of aurora 79—25334
- photometer, four-filter, for total atm. O_3 meas. 78—61597
- photometer, high resolution, for daytime Li releases obs., winter anomaly project appl. 78—45023
- photometer for Li release tracking, upper atm. daytime neutral winds obs. 79—39871
- photometer for night natural illumination measurement in 0.4 to 1.2 μm spectral region 78—57367
- Photozavr modulation photometer for artificial aurorae/airglow 79—21076
- plasma front-end electroreactive accelerators, appl. to study of Earth magnetosphere 77—53400
- polarimeter, elliptical, for astronomy and atm. sciences 78—61745
- polarising NO photometer, for meas. of NO 2150 Å (1,0) γ-band intensity 78—45076
- polarising radiometer, data reduction technique 77—78472
- polarization scanner for radiation monitoring from geosynchronous satellite 79—58222
- pollution analyser using Harwell 6000 series electronics 79—5649
- pollution in Paris streets, survey network 78—81463
- pollution instrumentation, evidence of electronic malpractice 77—37453
- pollution monitoring, centralised supervision system in Fos-Etang de Berre region 78—81410
- pollution remote sensing from space 78—61621
- Portable Automated Mesonet, design, performance and operation, for meteorology 77—78426
- portable instrument for point-discharge currents meas. using junction FETs 79—39972
- portable multipass cell, for aerosols scattering and extinction coeff. simultaneous meas. 79—62588
- pressure measuring instruments, for density determ. between 50 and 120 km 78—45193
- pressure modulator radiometer, balloon-borne, appl. to stratosphere HCl meas. 77—25745
- pressure modulator radiometer for atm. gas emission meas. 78—81457
- psychrometer for relative humidity of air meas., modification *(French)* 77—78451
- pulse compression radar, appl. to strong wind shear obs. 78—32193
- pyranometer, solar radiation incident on slopes of different orientations meas. appl. 77—53164
- pyrgeometer performance improvement 77—70860
- pyrheliometers, solar aureole contribution to radiation meas. 77—2284
- pyrheliometers of the UK Meteorological Office, and radiation reference scales 80—109206
- quasioptical superheterodyne radiometer for upper atmosphere 77—41241
- radar meteor monitoring, A/D filter characts. *(Italian)* 79—80032
- radar polarimeter, for study of air flows in clouds 77—91243
- radars calibration with raindrop disdrometers, field expt. 77—91311
- radiation instrument calibration, for radiant flux meas. of arbitrary source 77—34022
- radio, acoustic and radio-acoustic sounders *(Japanese)* 78—16209
- radio meteor wind facility at Christchurch, New Zealand 79—2387
- radio receivers, oxide-barrier-tunnel junctions, low-noise 115 GHz mixing 79—51722
- radiometer, airborne dual-channel IR heterodyne, for atm. meas. 78—57369
- radiometer, directional, for longwave radiation meas. at ground 78—73537
- radiometer, high sensitivity heterodyne, using diode laser, spectroscopy of ethylene 77—91300
- radiometer, remote sensing, four band mm-wave radiometer design 78—96324
- radiometer for IR emission meas. of atm. and targets 78—4681
- radiometers, general theory for wideband receivers *(Russian)* 77—21926
- radiometers for rain attenuation measurements at X, K bands communication appl. 80—68254
- radiometric instrument high-rejection optical baffling system 77—70888
- radiosonde system, 403 MHz, for boundary layer study 78—85723
- radiosonde temperature sensing systematic anomalies, obs. evidence 79—70864
- radiosondes, temp. data over winter Antarctic deviation from Nimbus-5 temp. fields 78—32138
- radiotheodolite windfinding system of USA National Weather Service 80—17379
- Raman lidar humidity sounding of atm. boundary layer 79—66809
- ranging laser atmospheric transmissometer with retroreflector 77—21905
- real time whistler analyzer 77—87119
- remote automatic station on radio link for wind and temp. monitoring 78—85726
- remote sensors for temp. turbulence and optical propag. parameters 77—45125
- RF mass spectrometer, numerical study of the AUREOLE 2 satellite spectrom. 79—2470
- rime, meas. of quantity, using fog-gauge 80—56654
- rocket, monoaxial controlled solar pointer for atmospheric occultation meas. *(Japanese)* 78—32312
- rocket borne resonant absorption spectrometer and photometer for geocoronal and interplanetary He obs. 80—4155
- rocket-borne cryogenically cooled field-widened interferometer for the 2 to 8 μm spectral region 80—95163
- rocketborne IR spectrometer 78—81460
- sailplane variometer, calibration and use to meas. vertical atm. vel. fluctuations 79—88480
- Salyut 6 submm. telescope with InSb receiver 80—67566
- satellite cloud picture recorder for reception of APT pictures 78—81434
- satellite-borne IR scanning radiometer obs. of stratosphere, optimum field view and spacing 78—16201
- satellite-borne lidar for global wind meas., computer simulation 79—58231
- scanning interferometric multiplex photometer, airglow appls. 78—62216
- scanning laer velocimeter appl. to remote Doppler meas. of intensity fluctuations 77—791
- scanning microwave spectrometer (SCAMS) on Nimbus 6 synoptic scale studies 78—16114
- scanning spectrometer, programmable, appl. to weak airglow emissions meas. 80—8469
- sea area surveillance using side looking airborne radar system *(Dutch)* 80—12560

atmospheric measuring apparatus continued

- selective modulation radiometer for gaseous pollutant remote sensing *(French)* 78—20550
- sensible heat-flux detector 77—73863
- sequential sampler for automatic gas tracer studies 79—83686
- SERBE, low-energy (1-16 keV) electron spectrometer 79—21145
- shock tube, aqueous fog form. 80—19531
- short-range altimeter, use of NS LX1600A press. transducer 78—28344
- single particle correlated time of flight velocimeter, wind speed meas. 78—32251
- six channel radiometer for spectral investigations *(Russian)* 77—29468
- sky background brightness meas., 4500-10600 Å *(Chinese)* 80—12540
- sky brightness and polarisation, using photomultiplier, for teachers 78—81768
- smoke detector, ionisation type, model for response 78—88933
- snow, crystal conc. in air near ground, automatic meter 77—53242
- snowfall by dual-gauge and Wyoming shield systems 80—61928
- solar aureole radiometer for aerosol studies 77—53240
- Solar Mesosphere Explorer optical-mechanical systems engineering 79—58230
- solar radiation and wind power measuring instrument design 79—57404
- solar radiation monitoring system 77—52839
- sondes, meteorological meas. rel. to weather changes and air pollution *(French)* 80—17359
- space environment device on Japanese weather satellite, for solar particle activity monitoring 78—49290
- Space Experiments with Particle Accelerators (SEPAC), program for first Spacelab mission 79—48650
- space instrumentation for atmospheric obs. IEEE Region V annual conf. (El Paso, 3-5 April 1979) 79—58221
- Spacelab image intensifying TV camera for airglow and meteor obs. 77—21966
- Spacelab lidar, atm. expts. and methods 77—21948
- Spacelab lidar, for atm. props. meas. 77—21943
- Spacelab lidar for atmospheric topside sounding 77—21942
- Spacelab passive atm. sounders, attitude control and stabilisation 78—65483
- Spacelab passive atmospheric sounders 77—82113
- Spacelab passive sounder packages for atm. research 77—21945
- Spacelab passive sounding expt. for trace gas conc. determ. 77—21950
- speckle interferometer, subsystems and S/N ratio 77—41678
- spectrograph, fisheye field 79—8698
- spectrometer, diode laser correlation, low SO_2 conc. meas. 77—91301
- spectrometer, Fabry-Perot, signal noise limitations in data retrieval, winds, temp. and emission rate 78—93763
- spectrometer, intracavity Nd:glass laser, with dispersive resonator 77—74530
- spectrometer, laser heterodyne four-channel, monochromatic atm. transmission determ. 80—72653
- spectrometer, PbSe diode laser, for air pollution monitoring and mineral prospecting 77—82044
- spectrophone measurement of visible light absorpt. by aerosols 78—4000
- spectrophotometer for airglow and aurora studies 77—70903
- spectroradiometer for whole sky coverage *(French)* 77—53243
- spectroradiometers, for atm. meas. 77—9568
- spin scan camera system, on geostationary satellite, for global weather monitoring 78—61600
- STARE: a new radar auroral backscatter experiment in northern Scandinavia 79—39977
- static omnidirectional pressure probe 77—53238
- stratosphere extensible balloons, buoyancy control expts. 77—87113
- stratospheric balloon trajectory analysis for long-term missions *(Italian)* 77—82055
- stratospheric balloons flight behaviour 77—13138
- stratospheric ozonometer, using chemiluminescent reaction of ozone and olefins *(French)* 79—48574
- stratospheric tethered balloon system, feasibility study *(Italian)* 79—44251
- stratospheric water vapour 0.94 μ absorption cross-section obs. *(Japanese)* 80—17427
- submillimetric laser wave propagation, range and resolution 77—41242
- subsatellites launched from Spacelab, for atm., magnetospheric and plasma physics research 77—21944
- superpressure balloons for airflow circulation obs. over Arabian Sea during summer monsoon 77—17192
- supersonic sampling probe, errors in O_3 depletion studies 77—33193
- surface pressure measured using microwave signals transmitted from orbiting satellite 80—94581
- telephotometer for aerosol scattering function determ. 80—105055
- temperature sensors, aircraft borne, wetting in cloud rel. to entrainment overestimates 79—53483
- temperature sensors, humidity effects and sea salt contamination 80—82095
- temperature sensors, salt spray induced humidity sensitivity 78—69489
- temperature sounding, filter for CO_2 ν_2 band 77—10998
- testing instrums., standardisation and determ. of dynamic errors 79—8714
- tethered balloon sounding system, instruments and results 78—28343
- tethersonde system for remote meas. of wind and temp. 79—80038
- thermal diffusion cloud chambers, aspect ratio. rel. to supersaturation distrib. 80—56631
- thermocouple psychrometers, effect of and correction for different wet and dry bulb response 80—98472
- thin-walled sampling tube for aerosols 77—37460
- TIROS N microwave sounder unit, blackbody calibration 78—93016
- TIROS-N High Resolution Infrared Radiation Sounder 79—58227
- TIROS-N microwave sounder unit for global temp. distribution meas. 80—90265
- tracking receiver direction finder for whistler mode signals, initial results 78—77429
- transmission meas. using IR lasers, Fourier transform spectroscopy, gas-filter correl. techniques 77—70873
- transmissometer/radiometer for electro-optical sensor evaluation 77—70884
- transmittance meter, absolute filter device 80—51584
- tropical constant-level balloon system 80—17395
- tunable diode laser instruments, appl. advanced meas. and anal. 77—75600
- turbulence chamber for optical transmission expt., characterisation by thermal method 79—25330

atmospheric measuring apparatus continued
turbulence meas. instrumentation, on aircraft, for boundary layer obs. 79—12214
turbulence measurement, computerised instrumentation system 77—56761
turbulence sensor using atm. optical dispersion 77—45204
TV camera, intensified, for monochromatic obs. of all-sky auroral images 77—73859
two channel rocket photometer, for O I 5577 Å nightglow meas. 78—45078
two-scatter-plate low-speckle-noise integrator for atmospheric laser beam transmission meas. 80—90252
two-wavelength double-pulse tunable dye laser for differential absorption lidar 77—21939
USSR Hydrometeorological Service, automation of data collection and processing 79—34994
UV fluorescence hygrometer, stratospheric M_2O vapour meas. *(French)* 78—65401
UV fluorescence water vapour instrum. for stratospheric aircraft 80—82100
UV photometer, rocket-borne, for NO meas. in lower thermosphere, comparison with mass spectrometer meas. 78—40723
UV photometer for atmospheric ozone monitors calibration 78—77960
UV photometric standards for atmospheric O_3 concs. meas., interagency comparison 79—35000
UV radiation detection, space appls. 77—70881
UV spectrophotometer, aircraft-borne, for columnar atm. O_3 meas. 78—73522
velocimeter based on CO_2 laser for long-range anemometry 78—36333
vertical air velocity, airborne meas. system 80—77159
VHF radar, high power equipment *(German)* 80—46294
VIDIAZ disdrometer for raindrop terminal vel. determ. *(French)* 79—88448
visibility meter design, visibility concepts 77—87803
visible IR spin-scan radiometer, fibre optics 78—59160
VLF wave measurement at ground station, antenna pickup for vertical elec. field 80—105063
water vapour meas. in stratosphere by photodissociation with $L\alpha$ 78—77369
weather radar calibration, correl. with rain gauge data *(Japanese)* 78—85670
Whatman GF/A filter, collection efficiency for ^{222}Rn short lived decay products in air 78—20526
whistler analyser, semiautomated, using spectrum analyser and programmable tracking filter 79—74975
whistler occurrence rate and dispersion real-time analyser 77—87129
whistlers polarisation and arrival direction meas. at low latit., equipment and methods 77—45240
wide-angle electron detector 79—21144
wind vel. meas. system, computerised 77—56742
X-ray fluorescence S analyser, for particulate effluent meas. 78—68971
Zeeman photometer for Na I dayglow meas. 78—69558
CO, CO_2 lasers, appl. to atmospheric pollutants selective quantitative meas. 78—69526
CO_2 laser radar used to measure average atmospheric temp. 80—90225
CO_2 sensor, fast response, for eddy correl. flux meas. 79—5622
CO_2 tunable dual-line laser for atmospheric spectroscopy and pollution monitoring 78—3977
Ge diodes for temp. and humidity profile meas. over forests 77—64463
H_2O isotopic sampling apparatus for troposphere *(French)* 80—94614
H_2SO_4 aerosol, filter sampling of air, possible artifacts 80—82079
InGaAsP LED sources, for near-IR absorpt. meas. 80—77135
NH_3, gas conc. meas. using ring oven technique 80—81507
$NO/NO_2/O_3$ monitors, intercalibration 78—69529
NO_2, cyclic chemiluminescent monitoring device, NO conc. effects 77—49177
NO_2 fluorescence monitor with flashlamp pumping atm. tests 77—64443
NaCl aerosol generators, for cloud droplets nucleation expts. 80—82003
Nd:YAG laser as source for airborne lidar system for atmospheric expts. *(Italian)* 80—109278
O I(^{3}P) in lower thermosphere, nighttime conc. obs., using new rocket borne instrument 80—105066
O_3 calibration reference instrument calibration 78—73524
O_3, ground level monitoring apparatus, chemiluminescence reaction with ethylene 78—96310
O_3 monitoring, satellite benefit assessment 77—78613
O_3 monitoring with IR heterodyne radiometer 78—16216
^{222}Rn daughter prods. meas. using diffusion sampler 80—81510
SO_2 rural background pollution meas. network 77—37465
SO_2 small automatic monitoring network, practical experiences 78—81462

atmospheric measuring instruments *see atmospheric measuring apparatus*

atmospheric motion *see atmospheric movements*

atmospheric movements
see also atmospheric turbulence; wind
accelerating flow horizontal divergence, turning vorticity eqn. anal. 80—77013
acoustic and optical study, lower atmosphere *(Italian)* 77—91327
acoustic wave interaction with ocean surface waves, model *(Russian)* 80—12402
acoustic-gravity wave propag. in diffusively separated atmosphere 79—74933
acoustic-gravity waves, diffr. around spherical Earth 78—4016
acoustic-gravity waves, relaxational dissipation 78—4018
acoustic-gravity waves, theoretical props. 77—33270
acoustical-gravity waves in plane waveguide, interaction and self-action *(Russian)* 78—36221
acoustogravity waves generation mechanism 79—66776
adaptation processes in rot. atmospheric motion *(Chinese)* 80—67387
adaptive optics aberration coefficient estimation 77—19179
adiabatic invariants in N.Hemisphere *(Russian)* 78—36225
admixtures, atmospheric diffusion in calm conditions 80—40935
advection, local analytical model *(French)* 79—84404
advection eqn., anal. of local second moment conserving quasi-Lagrangian scheme 79—72871
advection equation soln., using second-order moments with and without width correction 78—85655
advection in flux formulations for variable grid models, appl. to atm. models 77—29380

atmospheric movements continued
advection-diffusion model, for real-time forecasting of air pollution episodes in Venetian region 80—77096
aerodynamic roughness length for complex terrain 79—53475
aerosol dry deposition, filtration model rel. to trace metal deposition from atmosphere 78—73441
aerosol inhomogeneities struct. and dynamics in ground layer, light scatt. 77—81955
aerosol movement in lake-land breeze circulation, pollution study 80—31101
African easterly jet, stability analysis 78—28274
African intertropical aerojet, eastern inertial perturbations *(French)* 78—61512
E.African jet, dynamics, July mean conditions simulation 80—77045
E.African jet dynamics, transients 80—77046
E.African low-level jet stream, five-day oscill. 78—53705
African wave disturbances, convection role, linear primitive eqn. model 80—77043
African waves generation 77—37299
ageostrophic motion forcing, semi-geostrophic eqns., isentropic coord. model 78—69405
air flow above sea surface, eddies transfer rate investigation *(Russian)* 79—16578
air flows in clouds, radar study 77—91243
Air Mass transformation Experiment (AMTEX), preliminary results 77—53196
air masses producing acid precipitation at Ithaca, New York, origin and trajectories 79—16655
air motion meas. from aircraft 77—70858
air pollutants long distant transport, analytical diffusion model 80—94125
air pollution density distrib., flow pattern in Tanabe area, Japan, numerical anal. *(Japanese)* 78—96289
air quality protection, role of tall stack 78—24362
air-sea interactions influencing large-scale circulation, math. modeling 80—41535
airflow, diffusion and momentum flux patterns in high mountain valley 79—5544
airflow over irregular terrain, numerical study 77—86969
airflow over mountainous terrain, numerical simulation 80—51450
airflow over snowpack, two-dimens. turbulent diffusion model 77—78277
airflow transformation over nonuniformly heated underlying surface 80—82031
airglow structures within intertropical arc, movements over Kenya 78—36352
airmasses over Asia in winter *(Japanese)* 79—66768
Alfven wave at ATS 6, soln. with finite ionospheric conductivity 79—12346
Alfven wave resonances, toroidal, in ionosphere/magnetosphere, finite ionosphere conds. effects 79—75035
AMTEX 75, structure of mixed layer and inversion layer, mesoscale cellular convections 79—88416
angular momentum advection by axisymmetric motions 77—87039
angular momentum fluctuations and day length changes 80—85715
annual circulation cycle, hydrodynamical model *(Russian)* 80—51455
Antofagasta, N.Chile, boundary layer dynamics in arid desert 80—56512
aperiodic trajectories and stationary points in three-component spectral model of atmospheric flow 77—5287
Arabian Sea, atm. circulation feedback with sea cooling 80—104979
Arakawa-Schubert convective parameterization scheme appl. 79—16587
Arctic Basin, air movement rel. to summertime stratus form. and persistence 77—5290
ash cloud trajectory, Mt. St. Augustine 1976 eruption 77—2234
Asia, change in sign of relation between sunspots and press., rainfall and monsoons 77—45123
S.Asia, monsoon circulation, role of mountains 77—49121
Asian monsoon effects on ang. momentum and kinetic energy balances in tropics 78—40630
Asian summer monsoon, hemispheric simulation 78—40629
Asian summer monsoon, simulation by general circulation models 78—40637
asymmetric jets, instability 80—56537
E.Atlantic International Convergence Zone, synoptic-scale wave disturbances 79—88431
N.Atlantic Ocean, September-October 1976, jet stream rel. to British wet spell 77—45124
atmosphere, stratified surface layer, turbulence and diffusion, basic Lagrange characts. 78—81270
atmosphere, surface tides, New Zealand 78—85665
aurora irregularities, overnight north-south movements obs. at 42 MHz 80—67449
aurora-generated gravity waves dynamic effects on midlatit. ionosphere 80—17438
auroral arcs, electrostatic turbulence and plasma transverse Kelvin-Helmholtz instability 77—53287
auroral convection over $60° \leq \Lambda \leq 75°$: Millstone Hill incoherent scatter obs. 80—67454
auroral E-region, proton and electron drift trajectories rel. to form. 78—45088
auroral electrojets, movements during high-latit. substorms 80—109315
auroral electron current sheet, rel. to elec. field model 79—53608
auroral forms, observed characts. rel. to shear processes and elec. fields 79—8738
auroral infrasonic waves and the auroral electrojet 79—35023
auroral ionosphere, comparison of F-region plasma drifts and E-region irregularity drifts 77—33262
auroral oval, evening sector, dynamics from DMSP photographs 79—96853
auroral particles, adiabatic movement in magnetosphere neutral sheet field 78—28421
auroral plasma, current flow rel. to electrostatic V-shocks approximate equipotentials 80—21870
auroral zone convection observation, radar scatt. method 80—51573
auroral zone E-region, atmospheric motions deduced from spaced receiver obs. 77—87172
available potential energy budget eqns., limited region, time depend. of reference press. 78—20497
axially asymmetric flow model, topography and diabatic heating 79—88435
Baffin Island, circumpolar vortex vars. rel. to Holocene palaeo-winds and palynology 78—57262

atmospheric movements continued
- baroclinic atmosphere, two dimensional, dynamics *(Russian)* 80—94564
- baroclinic atmosphere, two layer model, Helmholtz term effect 79—79986
- baroclinic eddies, convective and absolute instabilities 78—44918
- baroclinic equatorial motions, mathematical analysis 78—49098
- baroclinic fluid, rapidly rotating, sine-Gordon eqn. model 80—46820
- baroclinic instabilities in deep fluid model 77—49113
- baroclinic instabilities of deep fluid 78—79307
- baroclinic instability, finite amplitude model, supercriticality 77—17166
- baroclinic instability, model with realistic tropopause 77—78307
- baroclinic instability, numerical modelling *(Russian)* 78—44922
- baroclinic instability, wavelength of max. growth rate, comment 78—32170
- baroclinic instability, wavelength of max. growth rate 78—32169
- baroclinic instability and sensible heat exchange rel. to blocking ridge development 77—56680
- baroclinic instability and transient eddies in middle latitudes 80—41489
- baroclinic instability at long wavelengths on β-plane 77—66953
- baroclinic instability development *(Russian)* 78—65357
- baroclinic instability in summer circulation 77—45111
- baroclinic instability in three-layer fluid 78—16099
- baroclinic instability of short-wavelength two-layer Eady model 80—72593
- baroclinic instability of zonal flow, modified quasi-geostrophic eqns. 80—56574
- baroclinic instability on sphere, normal modes of primitive and quasi-geostrophic eqns. 77—5286
- baroclinic instability on sphere, two layer models 78—49108
- baroclinic models, growth rate and vertical propag. of initial error 79—16620
- baroclinic nonlinear waves life cycles 79—2332
- baroclinic planetary boundary layer above sea, heat and moisture fluxes parameterisation *(Russian)* 79—16576
- baroclinic planetary boundary layer perturbation functions from similarity theory *(Russian)* 78—11962
- baroclinic shear flow, forced waves, evolution near instability threshhold 80—8393
- baroclinic spatially growing waves finite amplitude dynamics on f-plane 79—79985
- baroclinic ultralong waves stability on midlatit. beta-plane 78—73484
- baroclinic unstable wave field modulation 77—33144
- baroclinic unstable wave vertical scale, rel. to eddy heat flux parameterisation 79—5563
- baroclinic waves, amplitude vacillation theory, numerical solns. 78—16101
- baroclinic waves, amplitude vacillation theory 77—29382
- baroclinic waves, influence of planetary boundary layer on development *(Russian)* 77—33140
- baroclinic waves, influence of static stability and wind shear time changes 80—109226
- baroclinic waves, unstable, downstream and upstream development 80—56540
- baroclinic waves (unstable), finite-amplitude dynamics 80—72592
- baroclinic waves growth rates and phase speeds, multilevel models 79—58022
- baroclinic waves of finite amplitude, four-layer models 80—98387
- baroclinic zonal flow, stability of stationary Rossby wave 79—39794
- baroclinically unstable modes, of two-layer model on sphere 77—2192
- barotropic and baroclinic instability in tropics, model study 79—58023
- barotropic atmosphere eqns., boundary problem soln. *(Russian)* 77—45072
- barotropic boundary layer problem, auto-oscillation solns. *(Russian)* 77—49106
- barotropic flow crossing mountain barrier, dynamic initialisation 77—21855
- barotropic instability in zonally varying easterly jet 79—53441
- barotropic instability of zonal flow over Indian subcontinent 78—7700
- barotropic Rossby wave drag due to isolated shallow topography 77—78323
- barotropic systems, low order, with forcing and dissipation, steady states and stability props. 80—72614
- barotropic waves, large amplitude, interaction with ambient shear flow, critical modes 77—80175
- barotropic waves, resonance and energy variation 79—84445
- bi-Gaussian atmos. diffusion model, influence of turbulence typing scheme for environmental anal. of nuclear power 80—3554
- billows, gravity and geostrophic waves, exact solns. 79—34908
- blocking anticyclones, further remarks 79—20958
- blocking anticyclones, prediction possibilities, comments 78—44974
- blocking anticyclones, rel. to cold spells and heat waves in British Isles 79—80006
- blocking highs dynamics 79—58020
- blocking problem, role of wavegroup vel. 78—3892
- blocking stability in barotropic channel flow 79—96785
- boundary layer, advection dominated flows, finite element anal., book contrib. 79—34934
- boundary layer, body force effect on turbulent transport near surface 78—26116
- boundary layer, height and circulation prod. in sea breeze model 79—53438
- boundary layer, internal gravity waves in time-varying stratification 78—3864
- boundary layer, microscale temp. and vel. spectra 78—16109
- boundary layer, momentum, heat and moisture fluxes from struct. parameters 79—53435
- boundary layer, similarity theory for turbulence and convection *(Polish)* 77—25753
- boundary layer dynamics, IR radiation effects 79—39815
- boundary layer gravity waves, acoustic sounding obs. 80—61847
- boundary layer heat and pulse transport *(Dutch)* 78—3890
- boundary layer mixing, evaluation of simple model with penetrative convection 80—51483
- boundary layer model with variable eddy viscosity coeff. 77—9482
- boundary layer parameterization technique 79—29830
- boundary layer turbulence and vertical currents, feedbacks *(Russian)* 80—51457
- boundary layers, convective and nonconvective, parameterisation for use in numerical models 80—82009
- boundary layers, numerical modelling 78—44900

atmospheric movements continued
- NE Brazil, large scale circulation rel. to extreme drought and floods 77—45134
- British Isles, kinetic energy balance of large-scale motion 80—56578
- bubbles seen in topside soundings of spread F, characts. 80—85800
- buoyancy driven mixed layers modelling 77—33150
- buoyant axisymmetric plume in atmospheric inversions, entrainment characts. 77—82004
- buoyant plume rise in atm. inversions 77—41114
- California, synoptic circulation rel. to late Quaternary climate and existence of Ice Age refugium 78—57293
- Cape Verde Islands, hurricane form., general circulation from Meteosat 80—105042
- cellular convection and assoc. cloud patterns 78—36249
- Chandler tides, comments and reply 79—88424
- Chandler tides calc. 78—69413
- chemical tracer expts. on precip. systems, review 78—24324
- NE.China, persistently low summer temp., causative circulation pattern *(Chinese)* 80—109235
- circulation, by two-level quasi-geostrophic model 80—56546
- circulation, hyperbolic partial differential equatns. numerical solution 80—21864
- circulation, large-scale phenomena in forced barotropic model 77—86980
- circulation, linear theory of response to sea surface temp. anomalies 77—78308
- circulation, MHD effects in electrolytes as model *(Russian)* 78—40610
- circulation, nonlinear axially symm., in nearly inviscid atm. 80—109190
- circulation, quasigeostrophic model, mountain barrier effects 77—66974
- circulation, rel. to 500 mb geopotential height in N.Hemisphere, climatological spectral anal. 77—5311
- circulation above mountains in central Asia, orographic effects *(Russian)* 79—34899
- circulation and pollution analysis using hydrodynamic models *(Italian)* 79—100892
- circulation associated with cold front, moist case 79—2334
- circulation associated with dry frontal system 78—28270
- circulation at high latitudes over S.Atlantic and S.W.Indian oceans 77—91204
- circulation change during 1976/77 winter 77—78391
- circulation changes correl. with solar and interplanetary mag. sector struct. 80—17340
- circulation characts. forecasting rel. to autumn low temp. over Yangtze basin 80—12531
- circulation correl. between Tibetan Plateau and low latitude areas *(Chinese)* 79—74937
- circulation driven by diurnal heating in Po Valley 80—85716
- circulation flow patterns, laboratory simulation of abrupt changes, catastrophe theory appl. 78—40721
- circulation in desert regions, variable surface albedo effects 77—49123
- circulation index rel. to solar activity 80—104853
- circulation model, 12-component, energetics *(Russian)* 79—84375
- circulation model study of stratospheric radiative-dynamic coupling 77—86965
- circulation models, general 79—84418
- circulation over Antarctica, seasonal vars. 77—21829
- circulation over oceans in equatorial latits., numerical calc. 78—92949
- circulation rel. to arctic sea ice extent 80—41501
- circulation rel. to inflow to Clutha Lakes 78—11926
- circulation type over N.Atlantic, effect on Gulf Stream channel line oscills. 78—92841
- circulation types, correl. with temp. and precip. fluctuations for Europe and N.America 78—92958
- cirrus outflow divergence determ. using ATS 1 pictures 77—53239
- climatic fluctuations in 1870-1969 period, statistical study of likely causes 78—7751
- cloud, vertical laser beam heating causing convection *(Russian)* 80—56529
- cloud dynamics rel. to hail form., axisymmetric model 77—5294
- cloud motion estimates, aircraft verification expt. 78—16113
- cloud updraughts, microphysical model sensitivity to urban environment 80—82004
- clouds influence on atm. dynamics *(Russian)* 79—8653
- coastally trapped waves 77—91242
- cold easterly circulations over Canadian Western Plains, mesoscale boundary layer model 77—78295
- cold front, obs. of 3-D circulation, precipitation and wave motions 80—90142
- cold front of midlatitude cyclone, air flow assoc. with mesoscale rain bands 80—109192
- cold front passage in Southern Hemisphere near equator 77—53102
- Complex Atmospheric Energetics Experiment (CAENEX), results and prospects 78—3904
- contaminant movement, Galerkin finite element method 80—74902
- convecion assoc. with pyrocumulus cloud over North Canterbury, New Zealand, anal. 80—109240
- convection, energy considerations, two dimensional model *(French)* 79—84409
- convection, fixed cloud-top temp. and fixed cloud-top altitude approximations for temp. profile 80—72616
- convection, Lorenz system, 14-D generalization 78—75131
- convection, moist plume from a cooling tower *(French)* 79—84400
- convection, obs. of smoke plume assoc. with intense local fire 77—49148
- convection and mesoscale motions during Phase III of GATE 80—90153
- convection caused by rejected waste energy 79—12169
- convection currents in axisymmetric cyclone 80—77084
- convection dynamics equations, non-Archimedean approach 80—77048
- convection in boundary layer, Doppler acoustic sounders and balloon meas. *(French)* 79—66763
- convection in boundary layer, lidar obs. 78—65366
- convection in cloudy atmos., axisymm. numerical model 80—26600
- convection in extratropical cyclone, enhancement after separation from polar front *(French)* 80—56517
- convection in general circulation, efficiency and vel. estimation via laboratory models *(Russian)* 77—81961
- convection in meteorology, aspects relevant to astrophysics 78—88898
- convection in thin layer above water surface *(Russian)* 77—45073
- convection in tropics 79—88461
- convection meas. of heat flux and struct. functions of temp. fluctuations with acoustic Doppler sodar 80—105023
- convection parameterization for large scale numerical forecasts at midlatitudes 77—86967

atmospheric movements continued
convection plume over fire in polytropic atmosphere *(Russian)* 78—96262
convection with cloud formation and development, numerical model *(Russian)* 80—81987
convective flow inside rotating annulus, influence of geometry *(Russian)* 77—91212
convective flow of incompressible stratified fluid, Euler-Poisson eqns. *(Russian)* 77—31300
convective instability, Brunt-Vaissala frequency *(French)* 80—77058
convective mesoscale wave disturbance during GATE investigated by spectral methods 80—101398
convective motion perturbed stochastically, model 80—92146
convective motions in air flow that changes direction and vel. with height 77—78368
convective planetary boundary layer, eddy diffusivities from numerical model 78—85667
convective plumes in lower atmosphere, detect. by Doppler acoustic sounding *(French)* 78—40603
convective precipitation, mechanical effect of urban area 78—81338
convective velocity scale estimation for diffusion appls. 79—79914
convective/mesoscale interaction mechanism 78—28268
cooling tower plume rise and visible plume length, prediction and obs. 77—45053
Coriolis force field, influence on fluid motion within ellipsoidal cavity *(Russian)* 78—81296
coupled ocean-atmosphere expt., ocean response, rel. to climate 80—12430
critical levels in a vertically rotating compressible atmosphere 80—6073
cumulonimbus, atmospheric dynamics problems 77—25729
cumulonimbus anvils, protrusion into stratosphere, lifting of tropopause *(French)* 77—29357
cumulonimbus convection, numerical modelling 79—84414
cumulonimbus convection, theoretical modelling 79—84405
cumulus cloud convection, perturbation pressure and density model 80—17325
cumulus convection in shear flow—three-dimensional numerical experiments 79—34915
cumulus scale motion assumptions, effect on cloud mass and heat flux 80—90155
cumulus updraft and downdraft rel. to GATE A/B-scale motion systems 78—16097
cumulus updraft var. and water content 78—16105
currents in presence of isolated obstacle *(French)* 80—53806
cusp region of magnetosphere, ion convection rel. to interplanetary mag. field 80—90288
cyclone-anticylcone couplets, quasi-Lagrangian kinetic energy budgets 77—66958
cyclones, rotary flow, simplified model 77—37283
cyclonic and anticyclonic conditions, wind and temp. field var. *(Russian)* 77—29394
D-region, horizontal drift obs., mean and periodic components at 35°S near Adelaide 77—9613
D-region drift, by spaced fading obs. 80—41627
dayside magnetopause, ISEE obs. of flux transfer events 79—44306
daytime r_0 evaluation from vertical microthermal meas. 78—3953
DC pressure summator, theoretical operation, tests and appls. 78—12005
density inversion, Taylor instability 77—9476
depression life-cycle as function of latitude, rel. to meridional transport 80—51508
Devon Island, NWT, Canada, air movements rel. to snow $\delta^{18}O$ vars. 80—4050
diffuse energy depositions, rise of fluid elements 77—91241
diffusion, pseudospectral soln. 78—32172
diffusion, sensitivity anal. of partial differential eqns. 79—49178
diffusion, steady state 3-D model, numerical anal. *(Japanese)* 79—79984
diffusion, steady state model, effect of terrain 79—92582
diffusion, tracking elec. charged air by ground level elec. field meas. 77—78450
diffusion class rel. to wind shear up to 700 m *(German)* 78—44954
diffusion coefficient and height relation from radar meteor echoes 78—49187
diffusion coefficients and criterion determ. *(German)* 80—94576
diffusion coefficients deduced from closing times of helicopter-produced clearings in fog 79—39810
diffusion flux close to surface, mol. sublayer effect 80—4068
diffusion from small island and undisturbed ocean site 78—85647
diffusion in canyon with rough mountainous terrain, comments 77—45096
diffusion model for use with directional samplers 79—62549
diffusion parameters estimation, use of routine meteorological data 78—85649
diffusion parameters from balloon obs. *(Italian)* 79—21067
diffusion parameters on local scale, determ. by no-lift balloons 79—70853
diffusion plume model, estimation of model parameters *(Japanese)* 79—79983
diffusion problems soln., pseudo-spectral and orthogonal collocation method 79—12170
diffusion props. over urban site, anal. using radioactive tracers, effect of air masses 79—84347
diffusion props. over urban site, anal. using radioactive tracers, effect of meteorological variables 79—84348
diffusion spreading of weak inhomogeneities in ionospheric according to electrostatic approx. 80—4187
dispersion expts. in Sydney region using SF_6 as tracer 80—67389
dispersion from ground-level source, appl. of mixed-layer similarity scaling 80—105021
dispersion in turbulent shear flow, theory 79—88393
dispersion models incorporating fast reversible chem. reactions 77—73784
disturbances propagation in tropical zone 77—78376
diurnal oscills. in upper atmos., energy flux propag. 77—37473
diurnal tide meas., 80-100 km altitude, Arecibo radar obs. 77—2290
divergence and vorticity from observed winds over India during monsoon 78—7695
Doppler mean vel. estimates, ambiguity removal 78—3983
Doppler vel. extraction from acoustic echoes, zero-crossing technique 79—53542
double diffusive convection in boundary layer during 1975 hurricane Eloise 77—70738

atmospheric movements continued
dry and moist cellular convection, stable wave lengths in 2-dimens. model *(Russian)* 77—21848
dry convection, thermals, structure 78—44910
dust diffusion through gas in force field, theory 78—18366
dust transport in Maricopa County, Arizona 79—70824
dusty buoyant thermal with vortex ring 79—48561
dynamic meteorology fundamentals, book contrib. *(French)* 77—87052
dynamic model of low atmos., low-order spectral difference type 80—98415
dynamic model of the mesosphere and lower thermosphere 79—48592
dynamical eqns. for atmosphere of an aspherical Earth *(Russian)* 77—73805
dynamical meteorology, trough-ridge systems as slantwise convection 79—79993
dynamical/statistical initialization, evaluation for operational forecasting 77—86970
dynamical/statistical initialization for numerical weather prediction 77—41118
dynamics in quasistatic approximation, characterisation of approximation *(German)* 80—98383
dynamics of stationary ultra-long waves in middle latitudes 77—87037
E_3-layer clouds over Japan, drift vectors from sky-wave backscatter obs. 79—44298
E_s-layer, h-type, at Uppsala, downward movements rel. to origin 78—81497
E_s-layer, Langmuir wave propag. and enhanced plasma line 79—29928
E_s-layer, temperate latit., duration and movement from skywave backscatter obs. 78—85761
E-region, equatorial, dynamics 78—36369
E-region, solar tides, electrodynamic effects, equatorial electrojet 77—9611
E-region, travelling planetary scale waves 77—9612
E-region drift above Ibadan 79—5711
E-region drift speeds, magnetic activity effects 79—88541
E-region gravity waves, obs. of Es 80—72657
E-region horizontal drifts, search for solar cycle var. at Ibadan 78—36390
E-region plasma waves, radiofreq. cosmic noise absorpt. 80—82139
E-region small amplitude short period waves from radio reflection virtual height meas. 77—73906
E-region solar tides, electrodynamic effects, Sq current system 77—9610
E-region valley, nighttime ion drift vel. from ionisation layers obs. 77—29569
Eady wave evolution in basic flows, frontogenesis 79—88426
Earth's negative charge, supply mechanism 80—61758
easterly waves and tropical storm formation, development 78—7703
easterly waves over W.Africa and Atlantic 79—88459
eddies, large-scale, parameterization problem 77—78385
eddies and linear baroclinic waves similarities 77—33149
eddy diffusion, models for mesosphere and lower thermosphere 80—109198
eddy fluxes of conserved quantities by small-amplitude waves 80—61858
eddy formation over California coastal waters 77—70732
eddy heat fluxes and temp. variances in baroclinic waves, weakly nonlinear theory 80—8390
eddy momentum fluxes within maize canopy 77—91203
eddy transports, large-scale, linear parameterisation 80—17361
eddy viscosity in truncated and averaged hydrodynamical eqns. 78—44936
Ekman boundary layer, suspended particles effect 78—24349
Ekman boundary layer pumping and topography interaction in stratified atm. 78—73486
Ekman boundary layer universal functions in drag and heat transfer laws *(Russian)* 77—91216
Ekman conditional instability of second kind (CISK), preferred mode 80—72617
electrojet induced press. and vel. fluctuations 80—82118
electrojet influenced by lunar tide, semimonthly variation 80—61937
electrojet strength, rel. to ionospheric drift variability above Tiruchirapalli 80—82129
elliptically rotating liquid, generation of vortical perturbations as atm. model *(Russian)* 77—49146
emissions over urban area sources, transport 79—12184
energetic particle movement and distrib. rel. to Pc 1 generation 78—61680
energy dispersion in barotropic atm. 78—20473
energy-balanced discrete models of atmospheric process dynamics 79—39828
England, airmass anal. rel. to early warm spell (1977 March 2) 79—79994
S.England 1968, September 14-16, mesoscale and small scale motions during outstanding rainfall event 77—45122
entraining convection at upper limit of convection 80—26568
entrainment, overestimates from aircraft temp. sensors in cloud 79—53483
entrainment coeff. of convective air in hail-producing clouds *(French)* 77—53151
entrainment into cumulus clouds, peculiarities of mechanism *(Russian)* 78—24334
equation of motion for small aerosol in a continuum 78—3895
equatorial anomaly, counter electrojet assoc. changes, upward drift reversal obs. 80—109297
equatorial electrojet, irregularity drift vels. observed by close-spaced antenna technique and Doppler radar 78—36365
equatorial F-region, drift measurement of Ba cloud, spaced receiver technique 80—72678
equatorial gravity waves, generation and props. 78—36232
equatorial planetary waves, Eliassen-Palm relation and mean zonal accel. 77—49111
equatorial planetary waves in horizontal and vertical shear 77—49112
equatorial region, air and moisture transport during S.W. monsoon, MONEX-73 obs. 77—53112
equatorial spread-F, high freq. drift waves with wavelengths below ion gyroradius 78—88973
equatorial stationary zonal circulation, numerical calcs. 80—85732
equatorial stratopause, planetary wave disturbances 79—5557
equatorial stratospheric westerlies rel. to Indian monsoon 77—29370
equatorial transient planetary waves, expts. with GFDL general circulation model 79—79927

atmospheric movements continued
- equatorial travelling ionospheric disturbances, assoc. with penetrative cumulus convection 78−36361
- equatorial vortices over South China Sea and Malaysia during winter monsoon 78−40633
- equatorial wave mean-flow interaction, role of latitudinal shear 80−51461
- equatorial wave model for cumulus parametrization and wave-CISK hypothesis testing 77−45080
- equatorial wave resonant interaction, nonlinear dynamics 80−56550
- equatorial waves, effects of latitudinal shear, applications to atmosphere 79−88413
- equatorial waves, effects of latitudinal shear, theory and methods 79−88412
- equatorial waves, nonlinear interactions 77−66961
- equatorial waves, zonal boundary effects 78−85586
- equatorial waves in cloud vel. field over Pacific 80−67395
- equatorial waves in upper stratosphere and mesosphere, rel. to zonal wind semiannual oscill. 79−5575
- equivalent zonal model, adiabatic motion invariants appl. *(Russian)* 77−29363
- Eulerian and Lagrangian mean meridional circulations during stratosphere warming 80−21799
- Europe, long range transport of air pollution 77−37412
- NW Europe, polar air outbreak, subsynoptic disturbance case study 80−101408
- exchange stabilities principle *(French)* 78−88871
- exosphere, collisionless, satellite atoms depletion by radiation press. 79−96933
- exosphere, non-Maxwellian effects assoc. with H and He thermal escape 79−80264
- exosphere, satellite particle theory 79−101097
- extratropical circulation, effects on typhoons 78−3908
- F_2-layer, low-latit., vertical motions during prolonged and isolated mag. storms 77−37479
- F_2-layer, night-time, over Arecibo, ion drift vel. seasonal mean struct. 80−31163
- F_2-layer, vertical drift assoc. with polar substorm 79−53618
- F_2-layer field-aligned and field-perpendicular vels. theory 78−85760
- F_2-layer of mid-latit. ionosphere, internal gravity waves day and night effects 79−58150
- F-layer, ion convection at high-latitude, nighttime 80−85797
- F-region, artificially-injected gases dispersal in night-time atm. 78−65460
- F-region, convection and scintillation rel. to aurora 77−87158
- F-region, convection vortices rel. to neutral wind southward midnight surge 77−33233
- F-region, elec. field induced drifts, incoherent scatt. radar obs. 77−29576
- F-region, equatorial, irregularity patches origin and motion 78−77404
- F-region, equatorial, motions deduction from Sq currents 78−96344
- F-region, equatorial spread-F, 3-metre irregularities due to plasma instability 80−41624
- F-region, high latit, Fe^+ distrib. rel. to upward plasma transport 79−16736
- F-region, high latit., gravity waves obs. using fixed freq. sounding 79−25390
- F-region, incoherent scatter radar meas. of electron density and ion vel. during isolated substorm 78−65452
- F-region, interhemispheric ion transport induced by neutral zonal winds 80−98509
- F-region, neutral zonal winds rel. to interhemispheric ion transport 80−98509
- F-region, nonstationary nighttime disturbances produced by internal gravity waves 78−73565
- F-region, plasma ambipolar diffusion eqn. in gravit. field 77−78562
- F-region, post sunset rise rel. to equatorial spread-F seasonal and solar cycle vars. in American zone 80−109298
- F-region, travelling disturbances, frequency of occurrence over Waltair, India 79−40011
- F-region, upward drifts reversal, evidence from equatorial anomaly counter-electrojet assoc. changes 80−109292
- F-region, wavelike vars. in path of totality of 1976 October 23 solar eclipse 79−66865
- F-region dynamics in equatorial region 78−36376
- F-region electron content and atmospheric gravity waves at high magnetic dip station 77−53277
- F-region equatorial ionisation motions from Sq current distrib. 77−21981
- F-region equatorial vertical drifts depend. on season and solar cycle 80−31159
- F-region gravity wave effects, obs. of TID at nighttime 80−77206
- F-region ion drift rel. to anomalously enhanced ionisation during winter 78−45108
- F-region nighttime dynamics from airglow features mapping 78−88980
- F-region plasma cloud, intermediate wavelength E×B gradient drift instability 80−105114
- F-region polarisation field, nighttime maintenance of equatorial ionisation 80−4192
- F-region small amplitude short period waves from radio reflection virtual height meas. 77−73906
- finite-amplitude baroclinic waves, friction and β effects 78−44927
- five-day wave, rel. to coherence of ionospheric absorpt. and 30 mb temp. 77−33275
- flow, kinetic energy three power law kinematic props. 80−77087
- flow around hollow, math. model, natural quarry ventilation appl. *(Russian)* 78−65358
- flow over irregular surface, three dimens. finite difference model, terrain following coord. transform 77−60452
- flow over north Urals assuming stable stratosphere *(Russian)* 78−53712
- flow over two-dimensional obstruction, steady-state, description by parabolic partial differential equations *(Italian)* 79−20956
- flow pattern forecasts, impact of synoptic observing and analysis systems 77−45061
- flow patterns from pollutant dispersion near highways, gas tracer release study 80−7972
- fluid dynamics, specialist symposium, (Munich, 6 to 9 September 1977) 79−57951
- fluid dynamics conference, Aug. 1978, Strasbourg, France 80−36764
- forced equiv.-barotropic flow, stationary heating effect 77−86983
- forced Rossby waves on a zonal shear flow, model 80−77072

atmospheric movements continued
- forced standing wave instability in viscous stratified fluid, stratosphere quasibiennial oscill. simulation 79−55396
- forward air flow effect on evolution of convection 80−90116
- four-day forecast, influnece of sensible and latent heat fluxes over land 79−96805
- free atmospheric convection, rigorous formulation using matched asymptotic expansions *(French)* 77−65740
- free convection structure in surface layer 77−37294
- freely convecting atmosphere over water surface, oscills. natural freq. *(Russian)* 78−11964
- frictional effects in strongly divergent flows 79−53434
- front formation over central Europe, internal processes 80−81979
- front position, precise determination from temp. and press. field data 80−98426
- frontal instability, semigeostrophic eqns. appls. 77−45077
- frontal passage, VHF radar obs. of enhanced humidity layers descent 79−53482
- frontal waves development, numerical simulation accounting for mountain ridges effect *(Russian)* 78−53701
- frontogenesis, 3-dim. study using stream axis coords. 77−87001
- frontogenesis, Hoskins-Bretherton model and surface frontal zone anal. 80−94572
- frontogenesis, warm rel. to cold surfaces 78−49086
- frontogenesis caused by cumulonimbus convection 77−21845
- fronts, numerical investigation of motion employing two-layer model *(Russian)* 77−53109
- fronts and depressions at middle latitudes, mesoscale struct. 80−26604
- fronts dynamics, numerical modelling *(Russian)* 77−64370
- gaeous and particulate pollutants transport, interconversion and removal, model, urban plume appl. 78−44984
- gas clouds released at satellite orbital velocity, dynamics expts. 80−14748
- gas dynamics with relaxation effects, acoustic waves, nonequilibrium atmosphere effects, review 78−79390
- gas releases, collisionless-diffusive flow transition in upper atmosphere 80−12577
- gaseous pollutants mesoscale transport, math. modelling 78−44986
- GATE C-scale triangle, mass and energy budgets rel. to weather 79−16583
- Gaussian plume model parameters determ. from diffusion-convection eqn. integration 78−81399
- general circulation, anal. of rocket soundings on Kerguelen Island (February-May, 1973) 78−20489
- general circulation, effects of Earth rot. rate vars. rel. to climate 80−4097
- general circulation, eqns. of kinetic and available pot. energy evolution in wave-number freq. space 80−109227
- general circulation, fluid energetics theory for dynamical meteorology 79−66780
- general circulation, glacial interglacial fluctuations rel. to lake levels since 30000 yr BP 80−51447
- general circulation, hemispheric model 80−81976
- general circulation, hydrodynamical zonal model, development, climatology data comparison *(Russian)* 80−12479
- general circulation, interannual var. from northern hemisphere upper winds 77−25740
- general circulation, many-year fluctuation rel. to Earth annual polar motion many-year var. *(Chinese)* 80−104848
- general circulation, models with lower boundary condition and energy consistency 80−56547
- general circulation, NCAR model response to mid-latitude ocean surface temp. changes 78−16098
- general circulation, polar motion excitation function power spectral anal. *(Chinese)* 80−104849
- general circulation, prediction rel. to long-range weather forecasting 80−109184
- general circulation, simulation, global spectral model 79−53447
- general circulation, struct. using six-component spectral model *(Russian)* 77−29364
- general circulation, surface temp. changes, cloud amount effects 79−88467
- general circulation, twelve-component model *(Russian)* 78−96263
- general circulation above 100 km, empirical model 78−73558
- general circulation at altitudes >100 km, empirical model 78−61664
- general circulation at mid-latitude, fluctuations seen in rawinsonde data 80−81980
- general circulation by GLAS model, cumulus friction and Jan. Hadly circulation 80−72588
- general circulation efficiency, theory 77−73808
- general circulation from Meteosat obs. 80−94595
- general circulation in N.hemisphere, features assoc. with poor summers in British Isles 80−109241
- general circulation model, angular momentum and heat balance effects *(Russian)* 80−51456
- general circulation model, clear air turbulence effect 77−86968
- general circulation model, climatic characts. response to solar radiation vars. 78−36260
- general circulation model, Earth rot. increased or decreased 5 times 80−56545
- general circulation model, extended range prediction expt. 77−86963
- general circulation model, involving estimation of nonlinear energy transfer spectra 80−98389
- general circulation model, response time rel. to ocean surface temp. change 80−98422
- general circulation model, sensitivity to chlorofluoromethane induced IR cooling 80−90122
- general circulation model, space-time spectral anal. of midlatit. disturbance 77−66951
- general circulation model (NCAR), response to sea surface temp. change 80−98390
- general circulation model energetics with variable Coriolis parameter *(Russian)* 80−21791
- general circulation model of atm. without clouds 78−49110
- general circulation model response to N.Pacific sea surface temp. anomalies 79−53431
- general circulation model with variable Coriolis parameter *(Russian)* 79−100896
- general circulation models, stability and extremal props. *(Russian)* 78−53716

atmospheric movements continued
general circulation models, statistical considerations in climatic expt. evaluation 78—16141
general circulation of 2-dimens. turbulent flow on β-plane 77—78317
general circulation of midlatitude troposphere, NCAR and GFDL models 80—61856
general circulation of N.hemisphere in winter, horiz. transport by transient eddies 80—72589
general circulation rel. to atmospheric tides and planetary waves *(French)* 77—21962
general circulation rel. to total O_3 vars. 79—44233
general circulation response to addition of waste heat 80—89694
general circulation types, selection from objective computer classification of composite charts 78—3906
geopotential height fluctuations, geographic variation of vertical struct. 80—90132
geostrophic 1000 mb back trajectories rel. to Pb concs. at Quillayute, Washington 77—29421
geostrophic adjustment in rot. fluid 77—66952
geostrophic adjustment on the spherical Earth, theory 77—45064
geostrophic adjustment theory, large-scale motion of atmosphere, adaptation, turning and equilibration 80—67404
geostrophic flow past walled crater in rotating fluid 77—45068
geostrophic large-scale drag coefficient estimation 78—61488
SW.Germany, Mediterranean warm air advection rel. to heavy rainfall (1978 May 22 to 24) *(German)* 80—61869
global barotropic primitive eqns. with Hough harmonic expansions 79—79925
global circulation, weather and climate and technological implications 77—45101
global circulation anomalous changes rel. to Earth Rot. vel. irregular vars. 78—32000
global energy budget, annual cycle of available pot. energy, variability 79—20909
global flows, lab. modelling, review *(Russian)* 77—81958
global general circulation, 4th order model 78—11952
global general circulation model, rel. to O_3 prod., transport and distrib. numerical simulation 80—56544
global general circulation model *(Russian)* 80—12478
global general circulation model for ice-age climate simulation 77—33176
global January and July climate, numerical simulation with two-layer circulation model 77—56722
global models with subgrid-scale vertical transport parameterization 78—20461
global problems of fluid dynamics 78—96173
global scale transport processes in atm. *(Dutch)* 78—3889
global seasonal circulation, evidence fo seesaw behaviour rel. to quasi-cycles in meterology 80—109239
global vorticity budget over tropics and subtropics at 200 mb during northern summer 78—40640
global-scale 4-5 day-period wave motion 77—41116
gravity and buoyancy waves rel. to stellar extinction oscills. 80—56606
gravity oscills. in shallow water model, dynamics rel. to normal mode initialization 77—86984
gravity wave critical level flow, viscous stabilization 77—45074
gravity wave generation and breaking over ocean 80—26571
gravity wave induced Brunt-Vaisala oscillations 79—53603
gravity wave production during 1976, October 23 solar eclipse, predictions 77—17181
gravity wave production during 1976 October 23 Australian total solar eclipse 79—92558
gravity wave propagation, 'potential' well treatment 80—67396
gravity wave sources, review 80—26572
gravity wave-critical level encounter, calc. 80—26583
gravity wave-critical level interaction, nonlinear model 79—1205
gravity wave-critical level interaction 79—88427
gravity wave-meanflow interaction, indication in upper atmosphere radar obs. 78—81282
gravity waves, effect on ionosphere causing VLF anomalies 80—82127
gravity waves, energy production and dissipation in thermosphere 79—74997
gravity waves, energy transfer in atmosphere with discontinuous parameter, theoretical treatment 77—37309
gravity waves, ground level, in SE.Australia, microbarographs obs. 78—73439
gravity waves, interpretation for Mitra drift near travelling ionospheric disturbances 80—82128
gravity waves, nonlinear interaction with mean flow 79—53463
gravity waves, ray tracing, tornadic storms and hurricanes warning system 78—73448
gravity waves and LF oscillations, tropical lower atmos., theory 80—12496
gravity waves and thermospheric winds *(French)* 77—53256
gravity waves and travelling ionospheric disturbances (TIDs), Hooke perturbation formula testing 79—40005
gravity waves assoc. with 1976 January 13 tornadic storms 80—41515
gravity waves from auroral electrojet, Joule heating and Lorentz force effects 78—28393
gravity waves generated by shear layers 77—2195
gravity waves generated during solar eclipse, obs. 78—88887
gravity waves generated in region of solar terminator, role in E_s-layers form. 79—12337
gravity waves generation by HF acoustic waves, Cherenkov radiation *(Russian)* 77—17265
gravity waves in inhomogeneous atmosphere, wave-field calc. 77—17186
gravity waves in ionosphere, radar obs. of electron density 80—77182
gravity waves in lower thermosphere over S. Australia 78—36348
gravity waves in thermosphere, source in tropospheric jet stream *(French)* 78—69554
gravity waves in troposphere, generated by shear flow instability 80—31098
gravity waves in upper atmosphere, obs. via $O_2(^1\Sigma)$ airglow, theory 79—29918
gravity waves in upper atmosphere, possible effect on Loran-C 100 kHz signals 80—109304
gravity waves propag. through critical layer 80—51591
gravity-acoustic waves, dispersive eqns. obtained by kinetic eqn. method *(Russian)* 78—85620
gravity-inertia oscillations in nonlinear flows, suppression 78—11955

atmospheric movements continued
ground layer, stratified, under coniferous forest canopy, vertical air motions *(Russian)* 78—96266
ground level trajectory of diffusing cloud, wind vector turning effect 79—12232
growing baroclinic waves, released latent heat effects 77—29371
hailstorm airflow and hail growth rel. to hail suppression 77—21856
heat heat transport, rel. to ocean temperature-salinity curve 80—72534
heat transfer from spheres in naturally turbulent outdoor environment 77—42701
heat transport parameterization in midlatits., large-scale stationary waves and Ferrel cell 79—16618
heated fluid annulus with semicond. walls, temp. gradients, lab. expt. 77—65744
heated stack effluents in disturbed flows, wind tunnel modelling 79—92564
Hebei Plain, summer drought and flood rel. to atm. circulation seasonal var. 80—90203
N.Hemisphere, 1975, circulation rel. to exceptional European weather 77—25756
S Hemisphere, 200 mbar flow determ. from satellite data 77—33158
N.hemisphere, climatic aspects of zonal flow vars. (1950-1975) 77—70803
N.Hemisphere transient motions, RMS 1000 and 500 mb geopotential height 80—90163
N. hemisphere winter circulation, general circulation model, comparison with obs. 80—109189
hemispheric flow patterns, spectral representation 78—7694
high-latitude ionospheric dynamics, Doppler method studies 78—73569
horizontal scales of motion in free convectional GATE obs. 78—85653
horizontally heated rotating fluid, spatial oscillations 77—55004
hurricanes, inertia-buoyancy waves 78—7705
hurricanes, interaction between symmetric mean vortex and shearing steering current rel. to spiral bands excitation 80—56538
hydrocarbons, assoc. with airborne particles, dispersion and transport 79—20990
hydrodynamic forecasting problem, coupling-moment atmospheric turbulence characts. 78—7734
hydrodynamic weather prediction 77—70801
hydrodynamic-type system, existence of anomalous modes, rel. to weather patterns *(Russian)* 78—65361
hydrodynamics, vertical eqn. of motion and wind eqns. 78—69428
hydrostatic mountain waves, steepening 78—28271
hydrostatic mountain waves, terrain shape effects for stratified fluid 80—21804
hydrostatic mountain waves numerical simulation 78—73432
incompressible fluid motions approx. within ellipsoid *(Russian)* 78—7689
India, westerly upper air troughs rel. to western disturbances development 80—90173
Indian Ocean, equatorial currents during NE.monsoon 79—2270
W.Indian Ocean, METEOSAT obs. of low-level airflow 79—44222
Indian sub-continent summer monsoon, trans-equatorial air flow rel. to 1899 drought 77—56705
Indian summer monsoon rel. to tropospheric flow patterns over southern hemisphere 78—81334
inertial and frictional effects on flow over topography 77—45106
initial vorticity field in short-range numerical weather forecasting, effect of subjective enhancement 80—82008
intense tropical convective system, mesoscale motion contrib. to convective fluxes 80—90156
interhemisphere transphere in troposphere, CO content study 80—31106
interlatitudinal angular momentum exchange 79—39834
intermittent gaseous release from nuclear plant, probability distrib. of atm. dispersion factor 78—11994
internal boundary layer development, dynamics, slab model 77—91198
internal boundary layer development and fumigation 77—81956
internal gravity wave modulation and stability 77—37231
internal gravity wave packet modulation, reson. with mean motion 78—5761
internal gravity waves, generation by movement of solar terminator, rel. to ionospheric electron densities 77—91348
internal gravity waves and upper atmosphere emissions 80—105093
internal gravity waves generated by penetrative convection 77—2196
internal gravity waves generation and breaking over ocean 78—44901
internal gravity waves in accelerating shear flow 79—32628
internal gravity waves meas. in meteor zone 77—25806
internal gravity waves momentum flux and orographic scatt. 79—8663
internal gravity waves nature obs. from OH emission 77—41246
internal solitary waves, obs. 79—8656
internal waves, hydrodynamic instability *(Russian)* 80—61852
internal waves excited by travelling forcing effects, compressibility influence 78—61495
intertropical convergence zone, air circulation 78—92948
intertropical convergence zone, Indian Ocean basin cloud clusters seasonal migration 79—29822
inviscid flow on sphere, statistical mech. 80—90152
ionisation irregularity drift motion from spaced fading and scintillation obs. 80—82133
ionisphere, plasma drifts above Saint-Santin on quiet days, seasonal vars. 79—101011
ionosphere, auroral disturbances movements rel. to infrasonic wave emissions and polar substorms 79—100996
ionosphere, bubbles in equatorial region, obs. by radiowave propag. 80—41621
ionosphere, bubbles in equatorial spread F, nonlinear evolution 80—85801
ionosphere, charge carriers transport model rel. to balance eqn. 78—28369
ionosphere, chemistry and transport processes, numerical modelling 78—49202
ionosphere, comparison between calculated and measured photoelectron fluxes from Atmosphere Explorer C and E 78—28400
ionosphere, conductivity and drifts 78—36366
ionosphere, conjugate photoelectrons meas. rel. to predawn 630 nm airglow 78—49196
ionosphere, daytime drift obs., tests of electrodynamic consistency 77—70934
ionosphere, diffusion and heat flow eqns. with large temp. differences between interacting species 79—66857

atmospheric movements continued
- ionosphere, disturbance caused by magnetosphere substorm, location and development study 80—4185
- ionosphere, disturbances during 1976 December 8 substorm 80—4201
- ionosphere, effect of elec. fields and vertical neutral-gas drifts on total electron content 78—45089
- ionosphere, effect of ion-neutral collisions on ion vel. distrib. 77—29565
- ionosphere, elec. fields and plasma convection in dayside auroral oval 80—98501
- ionosphere, electrodynamic drifts during 1972 August 4-5 storm 77—33269
- ionosphere, electrodynamic lifting and electron content during storm positive phase 77—37480
- ionosphere, equatorial, gravity waves rel. to total electron content fluctuations 78—36360
- ionosphere, equatorial, plasma bubbles motion in nighttime F-region 77—87156
- ionosphere, equatorial, zero and maximal vel. contours rel. to mid-latit. absorpt. 80—12597
- ionosphere, equatorial daytime topside, plasma temps. and ion dynamics 79—84584
- ionosphere, equatorial irregularity belt movement during magnetic storm 78—40757
- ionosphere, equatorial spread-F irregularities drifting patches rel. to spatial reson. mechanism 79—21095
- ionosphere, generation of small-scale inhomogeneities by internal gravity waves 78—45100
- ionosphere, global scale electrodynamic coupling of high-latit. and low-latit. regions 80—77194
- ionosphere, gradient drift instability, Ba cloud release study 80—85802
- ionosphere, gravity waves due to total solar eclipse, detect. by radio technique 77—91364
- ionosphere, gravity waves rel. to radio waves phase path changes 79—35043
- ionosphere, He^+ ion outflow 78—49221
- ionosphere, HF Doppler observations at Chubu Inst. Tech. (Japan) *(Japanese)* 80—31165
- ionosphere, high-latit., ion velocity distribs. 79—101018
- ionosphere, induced plasma drifts determ. using numerical simulation 77—53268
- ionosphere, ion cyclotron wave spectrum generated by Ba injection 79—53648
- ionosphere, ion vels. in four-component plasma 77—13154
- ionosphere, ion vels. latitudinal struct. on November 21, 1975, Chatanika obs. 77—87160
- ionosphere, ionisation waves reson. coupling with acoustic gravity waves in mag. field 77—25832
- ionosphere, low latitude, total electron content nighttime enhancements motion 80—72677
- ionosphere, lunar tides rel. to monthly mean lunar daily geomag. vars. in Japan (1958-1973) 79—96739
- ionosphere, mid-latitude F_2-layer, ion and neutral gas vel. oscills. rel. to lunar tide 78—61656
- ionosphere, nighttime field aligned O^+ and H^+ fluxes in mid-latit. mag. field tube 77—33273
- ionosphere, obs. of gravity waves assoc. with Hurricane Eloise 79—66872
- ionosphere, obstacle waves, steady-state soln. 77—49215
- ionosphere, plasma convection at high latitudes, model rel. to incoherent scatter obs. 80—72687
- ionosphere, plasma density depletions motion in artificially created equatorial spread-F 78—88972
- ionosphere, plasma drifts rel. to lunar perturbations in columnar electron content 77—29570
- ionosphere, polar, dynamics and interrelations with magnetosphere convection struct. 80—4176
- ionosphere, polar, motions rel. to airglow mag. ordering 78—57378
- ionosphere, polar, plasma drift meas., at Ny Alesund, Spitsbergen 77—45245
- ionosphere, polar cap connection during Tordo 1 polar cusp Ba plasma injection expt. 78—77402
- ionosphere, prompt striation of Ba cloud due to plasma instability 80—72685
- ionosphere, propag. of acoustic gravity waves, explosion excitation *(French)* 78—12042
- ionosphere, quiet nighttime thermal plasma fluxes rel. to calculated and measured decay rates 78—81493
- ionosphere, rapid subauroral ion drifts obs. by Atmosphere Explorer C 80—4188
- ionosphere, Rayleigh-Taylor instability of equatorial region, linear theory 80—41619
- ionosphere, rocket-borne meas. of ion convection in dayside aurora 78—77391
- ionosphere, S. hemisphere gravity wave obs. using total electron content technique 79—21096
- ionosphere, semidiurnal tide rel. to E_s-layer props. at Sodankyla, Finland 77—87183
- ionosphere, simultaneous obs. of field-aligned currents and plasma drift vels. by Atmosphere Explorer C 80—72681
- ionosphere, slow MHD waves theory 78—45093
- ionosphere, solar tides and electrodynamic effects, polarisation elec. field 78—36391
- ionosphere, solitary drift waves excitation and propag. *(Russian)* 77—70915
- ionosphere, sporadic-E and F_2 layers, disturbances, electron density fluctuation origin 80—101475
- ionosphere, stationary and non stationary conditions, semi empirical models 80—4181
- ionosphere, striations assoc. with Ba clouds, particle densities and fluxes 77—9607
- ionosphere, topside, large scale wave-like struct. at low and middle latits. 77—21985
- ionosphere, topside, movements of plasma bubbles near dawn terminator 79—101016
- ionosphere, topside, relative flow of H^+ and O^+ ions at midlatit. 78—4031
- ionosphere, topside, transient response to precip. 77—78566
- ionosphere, transitional electrodynamic processes rel. to geomag. disturbances 77—60515
- ionosphere, travelling (wave) disturbances of absorpt. near 100 km height 79 25392
- ionosphere, travelling disturbances, directional filtering 79—62661

atmospheric movements continued
- ionosphere, travelling disturbances, electron density spectra 78—77398
- ionosphere, travelling disturbances, possible correl. with jet stream activity 78—69601
- ionosphere, travelling disturbances characts. over Thumba 78—69590
- ionosphere, travelling disturbances determ. by Faraday rot. modulation 79—21101
- ionosphere, upward surge, during August 1972, mag. storm 77—25858
- ionosphere, vertical $E\times B$ plasma drift vel. rel. to forbidden O I 6300 Å emission at mag. equator 80—36435
- ionosphere, wave meas. via satellite-borne cross-power spectrum analysers 80—94621
- ionosphere accel. mechanism, satellite obs. 77—21975
- ionosphere and plasmasphere at midlatitude, computer model 80—105120
- ionosphere auroral zone precipitation and convection reversal, satellite obs. 80—101479
- ionosphere disturbances, day-night terminator temperature gradient study 80—4186
- ionosphere drift parameters determined by full correl. anal., effect of filtering 78—65450
- ionosphere drifts, simultaneous obs. by different techniques low and mid-latits. 77—53303
- ionosphere E-region, drift meas. at Ahmedabad (1970-75) 78—40727
- ionosphere F_1-layer, dynamical effect obs. 79—12340
- ionosphere F-region, equatorial stratified irregularities movement, time and magnetic dependence 80—8470
- ionosphere F-region, gravity waves, obs. during tornado outbreak (1974, April 3) 78—85753
- ionosphere height rises, relationship with polar mag. substorms and spread-F occurrence 78—81494
- ionosphere holes and spread-F, ion chemistry and transport 78—88982
- ionosphere main valley, dynamics and electron temp. behaviour from satellite meas. 80—4170
- ionosphere moving current systems, EM induction in Earth 79—16370
- ionosphere multispecies flows, transport eqns. mathematical struct. 78—47084
- ionosphere partial reflection drifts, comparison with winds determined by rocket techniques 77—87019
- ionosphere photoelectrons flux, low-altitude plasma line anisotropy theory 78—77414
- ionosphere plasma, lower hybrid drift instabilities, electron collisional effects 80—101484
- ionosphere plasma, positive ions interdiffusion rel. to cond. 79—53609
- ionosphere plasma clouds, deform. and striation, multilevel model with recomb. chemistry 77—25834
- ionosphere plasma clouds, late time striation spectra 77—25836
- ionosphere plasma convection at high latitude, using magnetosphere elec. field model 80—41612
- ionosphere plasma instability, driven by auroral electron distrib. secondary peak 80—82135
- ionosphere plasma stream propag., controlled expt. with rocket-borne plasma gun 78—57424
- ionosphere propagation of Pc 1 pulsation signals 80—51604
- ionosphere radio drift meas. simulation and analysis of correlation methods 78—45033
- ionosphere transverse motions of atomic and mol. ions, generation by elec. fields 77 13155
- ionosphere travelling disturbance, vel. meas. by auroral zone incoherent scatter radar 79—48610
- ionosphere travelling disturbances, wave-normal depression and disturbance amplitude height depend. 79—40006
- ionosphere upward flowing energetic ions, latit., diurnal and altitudinal distribs. 78—49199
- ionosphere waves in D- and F-regions, temporal vars. 80—8483
- ionosphere-magnetosphere small-scale dynamo, multiple layer model 79 53612
- ionosphere-protonosphere interaction, dynamic model 77—45220
- ionospheric, lower, layer structs. response to gravity waves 78—81290
- ionospheric disturbances due to gravity waves generated by 1973 June 30 solar eclipse 77—21993
- ionospheric drift meas. geomagnetic storm effects of mesopause wind 79—35025
- ionospheric drifts, review 78—36364
- isentropic and sigma coord. hybrid numerical model 80—12485
- isentropic coordinate models, boundary problems soln. 77—29372
- ITCZ, 13.9 GHz radar altimeter obs. of total attenuation 77—29355
- jet, horizontal five-layer, instability 78—79348
- jet flow baroclinic instability in frontogenesis 80—61855
- jet instability, severe storm formation 79—88415
- jet stream, fronts and wave disturbances compared with Gulf Stream 79—2268
- jet stream, influence on evolution of environmental radioactive pollution *(Spanish)* 79—100549
- jet stream, medium scale gravity waves generation and vertical energy flux into thermosphere 78—81479
- jet stream as source of medium scale thermospheric gravity waves, exptl. study 79—21088
- jet stream over Pacific Ocean, ^7Be aerosols content increase in surface layer 77—78373
- jet stream structure over Arabian Sea and Indian Peninsula, MONEX-73 obs. 77—53122
- jet streams, low level SW over S.China April to June *(Chinese)* 79—66744
- jet streams, rel. to satellite-derived radiance gradient 80—98447
- K-stability index, rel. to thunderstorms and severe local storms automated 12 to 36 hour probability forecasts 80—77062
- Kelvin wave, role in westerly phase of semiannual zonal wind oscillation 79—88429
- Kelvin waves in mesosphere and stratosphere, struct. and behaviour from Nimbus 5 IR meas. 80—8394
- Kelvin-Helmholtz billows, finite amplitude, evolution 78—81293
- Kelvin-Helmholtz instability, jet stream generated, radar obs. and model 80—90165
- Kelvin-Helmholtz instability waves and breaking gravity-waves 79—81847
- Kelvin-Helmholtz wave, large amplitude, struct. determ. from altocumulus billows 80—72621
- Kelvin-Helmholtz waves, aircraft obs. of life cycle in low level inversion 79 53417
- Kelvin-Helmholtz waves under subtropical jetstream 79—66781

atmospheric movements continued
kinematic models of dry convective boundary layer rel. to dual-Doppler radar wind obs. 77–37292
kinetic energy budget of cyclone form. 78–16127
kinetic energy of divergent and nondivergent flow 77–37318
kinetic energy spectra in mid-latitudes 78–7707
Labadie Power Plant plume, lidar obs. of particulate density distrib. and behavior 80–55956
Lagrangian convection, application to simulation of cooling tower buoyant plume *(French)* 79–88450
Lagrangian conveection model, representation of isolated thermals *(French)* 79–88449
Lagrangian-mean flow, exact theory of nonlinear waves 79–37331
Lamb waves generated by 1975 May 11 solar eclipse, magnitude upper limit 77–29376
Lamb waves originating in nongeostrophic disturbances, a case study 77–45085
Laplace's tidal eqn. asymptotic eigensolns. 77–33166
large scale flow, quasisteady primitive equations with associated upper boundary conditions 79–62563
large scale flow, two-dimensional turbulent flow anal. 78–69395
large-scale hydrodynamic system simulation programs 77–21799
large-scale moving wave maintenance and nonlinear interactions 77–66960
large-scale travelling Rossby waves 80–94588
lee wave and cirrostratus formation, satellite photograph 79–84462
lee wave clouds, S.W. airflow over Bank's Peninsula, New Zealand 80–85739
lee waves generated by isolated islands, three-dimens. patterns, satellite obs. 79–44230
line convection, radar obs., high resolution colour display 78–88894
linear and jet profiles of lower atmos., baroclinic instability 80–90126
linear balance eqn., spectral form 77–64398
linear lee waves reson. characts. in three-layer atm. 79–44228
linearly stratified fluid, gravitational collapse of mixed region 80–33653
Livermore Regional Air Quality model, concept and development 78–92965
local circulation in Rome area, surface obs. 78–81264
local mesoscale circulation over Venice due to mountain-sea interaction 79–88401
London storm, August 1975, urban effects on airflow and precip. 78–81339
long distance transport of pollutants rel. to dry deposition in initial phase 79–83667
long period oscillations, homogeneous vertical struct. problem soln. 80–90125
long range pollutant transport, Lagrange model 80–61851
long waves in inviscid compressible isothermal atmosphere 79–29811
long waves in polar-plane approx. to Earth's spherical geometry 80–105019
long-range circulation var. in northern summer stratosphere *(German)* 77–56694
long-range travel of airborne material with dry deposition 77–49101
low vortex over S.E. Chinghai-Tibetan Plateau, annulus expt. simulation *(Chinese)* 77–70787
low-level jet, struct. investigations *(German)* 78–69422
lower atmosphere, general circulation and surface press. vars. during high and low geomag. activity 78–36245
lower atmosphere, movements rel. to atmosphere total O_3 content natural fluctuations 79–29819
lower atmosphere instability in different seasons, correl. with solar corpuscular activity 80–61881
lower atmosphere vertical stability determ. from Rn concs., influence of meteorological parameters *(Spanish)* 79–92562
lower atmosphere vertical stability determ. from Rn content, stability indexes statistical anal. *(Spanish)* 79–92561
lower thermosphere, compositional modelling taking account of airglow tidal variation 80–109288
lower thermosphere gravity wave obs., 5-90 minute period 80–61930
lunar O_1 tide, detect. in geomag. lunar daily var. at Alibag and contamination by M_2 component 80–56355
lunar semidiurnal oceanic and atmospheric tides, interfacial effects 79–100871
lunar tide, solar modulation anal. 80–94593
magnetic tail, plasma flow pulsations obs. 78–77436
magnetoatmospheric waves, max. growth rates of instabilities 77–53573
magnetopause, compressible field reconnection model and plasma boundary layer flow 77–37485
magnetopause, energetic particle obs. and boundary motion 80–41650
magnetopause at dawn, plasma flow obs. by Voyager 1 80–41655
magnetopause Kelvin-Helmholtz instability, effect of finite ion Larmor radius 79–80096
magnetopause surface fluctuations, Voyager 1 obs. 80–51613
magnetosheath, dawnside, H^+ and He^{++} bulk flows 80–4204
magnetosheath, dayside, plasma flow rel. to press. anisotropy and mirror instability 77–37483
magnetosheath, plasma flow states rel. to energetic plasma ions 79–21106
magnetosphere, adiabatic plasma convection in tail plasma sheet 79–25408
magnetosphere, Alfven and compressional waves coupling 78–89001
magnetosphere, anomalous resist. in geomag. tail region 79–12353
magnetosphere, auroral electrons drift rel. to large-scale longit. intrusions 77–64510
magnetosphere, connection elec. fields rel. to global distrib. of electron density in F_2-layer 77–64514
magnetosphere, convection and empirical models of high-latit. elec. fields 77–45255
magnetosphere, convection and field-aligned currents during weak global mag. disturbances 79–53660
magnetosphere, convection intensification, effect on mid-latitude ionosphere 80–105122
magnetosphere, current interruption in collisionless plasma by non-linear electrostatic waves 79–75052
magnetosphere, day cusp dynamics tracking via long-period geomag. pulsations obs. 79–53656
magnetosphere, drift boundary approxs. in simple convection models 80–26693
magnetosphere, dynamics of protons trapped in geomag. field 79–16756
magnetosphere, electrostatic shocks, double layers and anomalous resistivity 78–45152

atmospheric movements continued
magnetosphere, electrostatic shocks as source of discrete auroral arcs 78–45153
magnetosphere, electrostatic waves rel. to electron density small scale struct. 79–35073
magnetosphere, equatorward-moving absorpt. during auroral absorpt. substorm onset 78–96362
magnetosphere, flow patterns rel. to poleward-directed elec. fields near ionospheric projection of plasmapause 78–20574
magnetosphere, heavy ion circulation 77–64533
magnetosphere, high-energy electron drift echoes at geostationary orbit 78–61678
magnetosphere, high-latit. convection field, parallel elec. fields and inverted-V precip. events 77–33297
magnetosphere, low energy electrons and protons motion 78–36407
magnetosphere, low-energy plasma sunward flow obs. at synchronous orbit 78–77435
magnetosphere, lunar and solar tidal effects 77–87184
magnetosphere, particle streaming obs. by GEOS-1 keV plasma expt. 79–35068
magnetosphere, particles pitch angle diffusion by bounce reson. 78–36408
magnetosphere, pitch angle dispersion of drifting energetic protons at synchronous orbit 78–77428
magnetosphere, plasma accel. by large transient elec. fields 78–28440
magnetosphere, plasma accel. caused by shocks resulting from mag. reconnection 80–51618
magnetosphere, plasma convection dynamics rel. to macroscopic elec. fields 78–49238
magnetosphere, plasma convection rel. to model current system for high-latit. mag. activity 79–92636
magnetosphere, plasma convection system 80–41651
magnetosphere, plasma drift vel. vars. prod. by Pc 5 waves, Ogo 5 obs. 77–87190
magnetosphere, plasma dynamics in mag. field laboratory simulation 79–16757
magnetosphere, plasma flow and populations in simple open model 80–90295
magnetosphere, plasma mantle dynamics rel. to plasma sheet form. 79–40022
magnetosphere, plasma mantle flow rel. to plasma sheet thinning during substorms 80–72705
magnetosphere, plasma oscills. interaction with EM waves propagating along magnetic field lines *(Russian)* 78–4036
magnetosphere, plasma stability during storm conditions 80–82150
magnetosphere, polar, electrostatic H^+ cyclotron waves near one Earth radius altitude 78–45154
magnetosphere, polar cap convection after interplanetary mag. field becomes northward 80–94658
magnetosphere, polar cap convection rel. to boundary mag. fields, laboratory simulation 78–57396
magnetosphere, polar cap plasma flow entry region longit. position 80–67472
magnetosphere, solar wind induced convection rel. to plasmapause struct. 77–53285
magnetosphere, solar wind plasma injection at dayside cusp 78–40775
magnetosphere, substorm-associated trapped particle outer boundary motion at synchronous orbit 77–29586
magnetosphere, transport coeffs. for plasma with quasicollisions 78–71440
magnetosphere, transport of dissipating photoelectrons 78–69611
magnetosphere, variability of plasma sheet dynamics assoc. with substorms 80–98518
magnetosphere boundary layer, plasma flow rel. to field-aligned currents 80–67473
magnetosphere boundary layer at low-latitude, fluid mech. model 80–85808
magnetosphere convection, development of stratified precip. struct. 78–28377
magnetosphere convection, one-dimensional gasdynamical model 78–81508
magnetosphere convection, role of particle precip. 79–25400
magnetosphere convection, variability of S_q vars. field magnetically conjugate structs. 79–58191
magnetosphere convection affecting ionosphere electron density disturbance spatial struct. 80–41606
magnetosphere convection and auroral arcs, pattern correl. 80–17433
magnetosphere convection causing auroral latitude, assoc. with convection elec. ionosphere field-aligned currents 80–90278
magnetosphere convection electric field, divergence rel. to auroral currents and elec. pots. and precip. generation 80–67453
magnetosphere convection role of hot plasma 78–32297
magnetosphere convection vel. fields, dynamics and interrelations with polar ionosphere struct. 80–4176
magnetosphere dayside cleft, convection direction rel. to mag. field perturbations 79–40023
magnetosphere dayside cusp region, plasma flow props. 79–12352
magnetosphere dynamics during auroral electrojet events, from energetic electron intensity changes at synchronous orbit 79–66882
magnetosphere dynamics rel. to equatorial ionosphere, effects of polar-equatorial elec. coupling 78–93029
magnetosphere electric convection field, model 78–89004
magnetosphere frontside boundary layer, plasma flow and reconnection problem 78–89010
magnetosphere hydromagnetic wave rotation between magnetosphere and ground 80–61969
magnetosphere midlatitude convection elec. fields, rel. to ring current development 78–57395
magnetosphere particles drift, tracking from GEOS-1 plasma density meas. 79–35072
magnetosphere plasma convection, assoc. with type Pi pulsations at high latitude 80–77226
magnetosphere plasma convection, rel. to elec. current system over auroral arc 77–33296
magnetosphere plasma sheet, particle dynamics 79–66879
magnetosphere plasma sheet, plasma flows rel. to discrete auroras occurrence and lifetimes 80–67447
magnetosphere polar cleft, position and motion rel. to F-lacunae distrib. and occurrence freq. 80–4193
magnetosphere polar cusp, convection patterns rel. to dayside magnetopause mag. merging 79–66884

atmospheric movements continued
magnetosphere polar cusp, movements from dayside aurora rel. to substorm currents and dayside merging 79—96852
magnetosphere ring current plasma injection, correl. with solar wind parameters 78—96363
magnetosphere source movements assoc. with IPDP pulsations 79—25404
magnetosphere time dependent ring current, inductive elec. fields 79—80093
magnetosphere trapped particles, self-consistent diffusion on bounce-drift reson. with geomag. pulsations 79—58188
magnetospheric boundary layer, hydromagnetic waves driven by vel. shear 80—105133
magnetotail, energetic particle pitch angle data rel. to tail configuration near midnight 78—96354
magnetotail, mag. merging obs. and form. of plasma sheet 77—87189
magnetotail, O^+ fluxes in streaming plasmas 77—33284
magnetotail, plasma flow obs. during substorm rel. to mag. merging 77—17301
magnetotail, plasma flows, fireballs and boundary layers 77—29588
magnetotail magnetic current sheets, effect of press. anisotropy on equilib. struct. 79—12354
marine aerosols influx into atmosphere, influence of coastal-zone physicogeographic conditions 79—29818
marine atmosphere, surface layer stability rel. to oceanic whitecaps and sea state 80—72554
marine boundary layer along California coast, instability rel. to marine fog and fog-stratus systems 80—77060
marine layer at San Diego, California, vertical motion field rel. to cool season precip. forecasts in Arizona 80—101395
marine stratocumulus convection, governing eqns. and horizontally homogeneous solns. 80—56542
marine stratocumulus convection, horizontally inhomogeneous solns. 80—56543
mass distrib. by latitude, seasonal changes 80—90115
mass motions, mean meridional, stratosphere and mesosphere 79—88419
mass transfer, three dimensional numerical model *(French)* 79—84398
mass vertical transport across temp. inversion 77—87015
mean flow dynamic forcing by Reynolds' stresses 79—53448
mean meridional circulations of stratosphere and mesosphere, monthly mean planetary wave fluxes 80—109219
mean zonal circulation in meteor zone above France and Sweden 79—75003
mean zonal flows accel. by planetary waves 80—105033
meridional circulation, effect on baroclinic instability of winter zonal flow 79—88421
meridional motions, estimation of intensity *(Russian)* 77—53154
meridional movement, simulation studies for oceanic anomalies, atm.-ocean link 80—8316
mesometeorological stationary problem of flow around obstacle 78—81271
mesoscale cellular convection during AMTEX 75, kinematic analysis 77—78322
mesoscale cellular convection over E. China Sea, buoy and satellite obs. 78—3850
mesoscale cellular convection rel. to seagull flight behaviour 78—81269
mesoscale convective system, momentum budget and temporal evolution 77—70757
mesoscale convective systems, inertial instability 80—90131
mesoscale dispersion expts., trajectory-diffusion modelling 80—61837
mesoscale divergence of horizontal vel. field and press. gradient force, rel. to momentum transport 78—11954
mesoscale flow over complex terrain during Eastern Tennessee Trajectory Expt. (ETTEX) 78—49101
mesoscale flow patterns in northern Israel, subjective anal. 80—12503
mesoscale pollution transport, quantitative evaluation 79—70825
mesoscale transport and air quality in remote location 80—40938
mesosphere, acoustic-gravity waves propagation 78—44912
mesosphere, circulation rel. to mesosphere clouds and thermosphere semi-annual temp. vars. 78—45061
mesosphere, equatorial circulation indices seasonal vars. at Thumba 78—85630
mesosphere, extensions of Leovy's linear circulation model 78—32201
mesosphere, gravity waves component in partial refl. drift obs. 80—81993
mesosphere, long-period waves at 60 to 90 km altitude 80—77056
mesosphere, major characts., processes and dynamics 77—25734
mesosphere, planetary waves in winter, Nimbus 6 PMR preliminary results 77—87040
mesosphere, Southern hemisphere, wind speed quasi 2-day wave obs. 80—109207
mesosphere, tides and gravity waves at mid and low latits. 78—36231
mesosphere, winds and waves over Jicamarca, 1974 May 23-24 VHF radar obs. 80—12497
mesosphere, winter, partial reflection drift obs. 77—64393
mesosphere dynamics, obs. by incoherent radar scatt. 80—90117
mesosphere internal gravity waves, propag. range *(Russian)* 79—16575
mesosphere positive and negative ions mobility meas. via payload B III instrument package 78—45194
mesosphere vertical velocities, first VHF radar meas. at temperate latits. 79—16572
meteor region, winter motions meas. in S. hemisphere 80—109287
meteor trails, effect of thermal on measured drift speed 77—21955
meteor trial, diffusion of weakly ionised plasma filament forming angle with mag. field 79—53610
meteor zone, seasonal variations of solar and lunar tides 77—87134
methane, atmospheric circulation, destruction through photochemical oxidation *(German)* 79—84424
MHD planetary waves propag. on beta plane through mag. and vel. shear 77—60457
MHD wave propagation, in presence of rot. and variable mag. field 79—40024
MHD waves, as cause of simultaneous ionospheric and geomag. oscills. 77—9615
MHD waves, long-period, synchronous obs. on ATS-6 satellite and at Earth surface 79—12345
MHD waves in upper atmosphere, absorpt. rel. to neutral atmosphere heating 79—53588
microclimatic and mesoclimatic stability indices, statistical relation, rel. to pollutants diffusion *(Spanish)* 78—44964
middle atmosphere, interaction between radiatively damped planetary wave and zonally averaged circulation 80—109217
middle atmosphere dynamics, review 80—17338

atmospheric movements continued
middle atmosphere processes revealed by satellite observations 80—21803
Middle East, general circulation in summer rel. to change in O_3 *(Russian)* 77—53156
midlatitude synoptic scale disturbances, energy sources 78—32162
minor atmosphere constituents transport between troposphere and stratosphere implications for pollutant transport 80—105034
mixed fluid, nonlinear internal wave formation from gravitational collapse 80—33619
mixed layer diffusion, use of Taylor's translation hypothesis 77—17193
mixing during pollution incident, acoustic and temp. meas. 79—12234
moist circulation maintenance and available energy 78—57281
moist convection, effect of vertical moisture distrib. *(French)* 80—56567
moist convection, six-component spectral model 80—61859
moist convection over heated island, two-scale model 80—41492
moisture processes in quasi-geostrophic model 78—7696
momentum boundary layer in numerical weather prediction model 80—51451
momentum exchange, global maps *(German)* 78—44955
momentum flux by standing eddies 78—81314
momentum flux-angle distrib. from propeller anemometer meas. 77—17190
momentum horizontal transport, cumulus-scale, in monsoon depression over India 78—44961
momentum transport by tilted troughs, kinematics 77—53131
momentum transports in simple baroclinic flows, spherical geometry effect 77—17197
monsoon, model of large scale seasonal struct. 80—98393
monsoon, vertical vels. rel. to droughts in quasi-geostrophic diabatic four level model 77—56713
monsoon circulation and rainfall S.Asia 78—44958
monsoon circulation dynamics 79—5559
monsoon circulation over Bay of Bengal, 1976, winter to spring 80—82038
monsoon depression, vorticity budget and vertical vel. distrib. 77—78321
monsoon depression September, 1976, at Masirah, Oman, movements 79—8669
monsoon depressions, life history, struct. and movements 78—44963
monsoon disturbances over India, quasi-geostrophic model 80—98394
monsoon driving mechanisms, model of seasonal struct. 80—98392
monsoonal quasistationary ultralong waves, real data numerical prediction over global tropical belt 78—40631
mountain barrier waves on planetary scale, model 80—46239
mountain lee waves, calcs. *(German)* 77—33163
mountain lee waves, satellite photos and aircraft meas. 77—37319
mountain lee waves, three-layer model *(German)* 77—5304
mountain wave drag, influence of Earth's rotation 79—88440
mountain waves, effect of non-uniform shear 80—90127
mountain waves of finite amplitude evolution and stability 78—44929
multimodal Doppler spectra in terms of sub-beam scale motions 77—29385
multiple flow equilibria, rel. to blocking 80—56536
NCAR general circulation model, appl. to regional climatic effects of large-scale thermal pollution 79—53478
near-stack reactor effluent dispersion studies, SF_6 tracer technique 78—11992
neutral atmosphere layer structures, density response to gravity waves 78—81290
neutral gas diffusion in nonuniform chemically reactive atmosphere, three-dimensional time depend. modelling 79—66846
neutral thermosphere dynamic behaviour, effects of turbopause height and exospheric temp. vars. 79—21085
neutrally stable Eady wave stability 79—53449
neutrally stratified planetary boundary layer flow over gentle topography 78—3851
neutron transport in upper atmosphere, Monte Carlo calcs. 80—8468
nightglow emissions revealing downward propag. waves 80—41585
nocturnal jets over Great Plains, dynamics of stable boundary layers 80—41491
non-frictional equations of motion validity in high troposphere *(Flemish)* 77—17184
non-linear small-scale sea-air interaction parameterisation, effects of ice cover *(Russian)* 77—53068
nonBoussinesq forced plumes 79—57997
nongeostrophic baroclinic instability problem 78—7702
nonlinear quasi-geostrophic eqn., props. of thermally-forced and unforced flows 77—2191
nonlinear Rossby wave critical level development in barotropic zonal flow 77—49114
nonlinear Rossby wave critical level evolution, viscosity effects 79—58021
nonlinear stationary waves in atmosphere, theory *(Russian)* 78—16089
normal mode initialisation technique, variational nonlinear, atm. gravity waves appl. 79—5584
normal mode linear initialisation on sphere 80—77042
northern atmosphere in summer and winter, vertical eddy momentum transport 78—57249
northern hemisphere circulation, quasibiennial oscill. and southern oscill. effects 77—78386
northern hemisphere circulation anomalies and seasonal weather forecasts 77—2237
numerical dynamic model atmosphere on a spherical Earth, used in forecasting 80—101416
numerical model *(French)* 80—21814
numerical models of dynamic processes, time integration step *(Russian)* 79—16573
numerical simulation models, optimal numerical filters fitted for noise damping 78—92997
ocean boundary layer meas. distortion caused by rolling ship 78—3805
ocean dynamic response to atm. disturbances 77—13084
ocean tide caused by meteorological conditions, energy transfer calc. *(Russian)* 80—76988
ocean-atmosphere interaction parametrisation for storm conditions, atm. circulation models appl. *(Russian)* 78—65359
ocean-atmosphere system, interannual variability 79—2330
omega equation, rederivation, appl. to synoptic situations 78—49106
one-dimensional models, critical comment and appl. to CO 77—45086
optical properties of moving atmosphere, simulation by rotating phase plate 80—79021
orographic disturbances over N Urals, lee wave clouds form. *(Russian)* 77—60448

atmospheric movements continued
orographic flow over Rocky and Andes Mountains, analytical model appl. 80—17318
orographically scattered gravity waves, momentum and energy exchanges 77—67057
orography, influence on atmospheric movement with Coriolis force included *(Russian)* 80—94565
orography influence, linearized eqns. anal. 80—8395
oscillation model of atm. action centres, vortices interactions *(Russian)* 80—4075
outer radiation belt dynamics during 1971, December 17 storm, Kosmos 426 obs. 77—33281
ozonosphere, photochemical-dynamical model rel. to maintenance of zonal mean O_3 distrib. in N.Hemisphere 80—109220
Pacific and E.Asia, average vertical circulation in winter 80—90199
NW.Pacific Ocean, low-freq. propagating disturbances rel. to press. and sea level vars. 80—101415
W.Pacific subtropical high, summer, form. and struct. simulation *(Chinese)* 80—109233
palaeo-atmosphere, coupled chemistry-flow model for O_3 content evolution 80—98400
particulate material, meteorological transport to South Polar Plateau 80—51481
particulate thermal coagulation and downstream transport from urban area source, math. model 78—44985
Pasquill stability classification for coastal site 79—16610
passive contaminant vertical dispersion in surfac layer 79—62547
Pc 5 micropulsation resonance region, drift vels. meas. by dual auroral radar system 78—65454
penetrative convection model, appls. to atmopshere, ocean and laboratory expts. *(Russian)* 78—24335
perturbations, laminar and turbulent, from photodissoc. wave obs. 78—79407
photochemical smog dynamics and control strategies *(Japanese)* 78—32220
physics of atmospheres, book 79—62568
plane periodic flow, post-critical regime construction *(Russian)* 78—34109
plane waves, group vel. in inhomogeneous media *(Russian)* 78—5755
planetary boundary layer, waves obs. by radar in clear air conditions 80—90184
planetary boundary layer barotropic model, geostrophic balance 78—7738
planetary jet stream inner structure, hydrodynamical model *(Russian)* 77—64371
planetary long waves, effect on cyclogenesis regions, quasi-geostrophic model 80—8392
planetary scale monsoon, mechanisms affecting structure and evolution 78—40639
planetary scale monsoons, theoretical problems 78—44956
planetary standing waves in northern hemisphere in July, model 78—61487
planetary wave causing sudden stratospheric warming, model 80—90150
planetary wave forcing, quasigeostrophic theory 78—73482
planetary wave secondary circulation, vertical air exchange implication 80—72584
planetary wave vertical penetration into lower ionosphere 79—58142
planetary waves, amplitude and phase below 60 km altitude *(Russian)* 78—36226
planetary waves, effect on eddy momentum and heat fluxes 80—85720
planetary waves, feedback with stochastically driven ice sheet, model 80—77025
planetary waves, rel. to stratosphere zonal winds correl. with 27-day solar rot. 78—88878
planetary waves, stratosphere-ionosphere-magnetosphere coupling at mid-latitudes, 1969-74, southern hemisphere 77—9471
planetary waves, upward propag. rel. to ionospheric equatorial anomaly in E.Asia and India 80—109301
planetary waves, vertical propag. rel. to lower ionosphere VLF transmission disturbances 80—8485
planetary waves, zonal mean states baroclinic instability 80—90124
planetary waves and zonal flows instability, two-layer model on sphere 79—44226
planetary waves at 20-80 km altitude rel. to ionospheric absorpt. winter anomaly 80—36359
planetary waves blocking mid latitude westerly winds 80—105036
planetary waves in mesosphere struct.-correction 80—8403
planetary waves in stratosphere global propag. in spherical atmos. 80—90139
planetary-scale waves, vertical energy flux, obs. results 77—2193
plasma convection, high-latit., and ionospheric depletion, effect of displaced geomag. and geographic poles 80—26680
plasma convection in polar regions, model calcs. 80—82151
plasma drift in radial direction at nighttime, and coupling to ionosphere 80—77239
plasma dynamics, vertical displacement during substorms 80—4184
plasma sheet, magnetised plasma slow convection theory 80—109312
plasma sheet, plasma flows and mag. field vectors during substorms 78—96357
plasma sheet, thinning model rel. to Earthward plasma flow 77—78579
plasma sheet oscillations, magnetospheric substorms effect 77—17296
plasmapause, drift wave analysis 78—61650
plasmapause, drift waves 78—40748
plasmapause, surface waves rel. to topside ionosphere ELF emission pulsations and geomag. SPP 79—58157
plasmasphere, corotation electric field 77—25841
plasmasphere, dynamo electric field aligned currents theory 78—81499
plasmasphere, geophysical disturbances effect on ionisation downward flow and nighttime electron content 80—94642
plume diffusion at Rancho Seco Generating Station, LIDAR obs. 78—11991
plume diffusion over hilly terrain, validity of Gaussian model 80—3552
plume dispersion near large buildings, simulation in wind tunnel, flow field 77—70724
plume dispersion near large buildings, simulation in wind tunnel, concentration field 77—70725
plume nonturbulent dispersion in complex terrain 77—45054
plume rise at large distances from multiple-source region 78—85683
plume structure and trajectories, lidar meas. 79—58016
plume trajectories, comparison of observations and model predictions 77—87062
plumes, dry deposition rel. to concs. prediction 78—28307

atmospheric movements continued
point explosion in arbitrary atmosphere with radiative heat transfer 78—53708
polar air outbreaks, cyclone-anticyclone couplet construction, vorticity budget computation 80—8391
polar low as extratropical CISK disturbance 80—51502
pollutant concs., deposition vs. transport effects in industrial area 79—12243
pollutant dispersal from point source into boundary layer, Ekman-type model 80—105039
pollutant dispersion, following instantaneous release, eddy diffusion model 77—87067
pollutant dispersion during calm wind situations, analytical modelling 78—81385
pollutant dispersion in urban atmosphere, radiative effects of elevated pollutant layers 80—97841
pollutant long range transport in Europe 77—37371
pollutant transport, short- and medium-range material balance 77—37373
pollutant transport and deposition from point source, analytical model 77—70805
pollutant transport and diffusion, puff-on-cell model 78—85682
pollutant transport and struct., in lower troposphere 80—85319
pollutant transport and turbulent dispersion over rugged mountainous terrain 79—84349
pollutants, dispersion models applicable to environmental problems 79—100552
pollutants, Gaussian diffusion-deposition model for elevated point sources 77—49156
pollutants diffusion, field meas. of benefits of increased stack height 80—76676
pollutants diffusion transport, variational imbedding calc. method 77—73785
pollutants dispersal, three-dimens. particle-in-cell method, comparison to regional tracer studies 78—92967
pollutants dispersion, completely Lagrangian random-walk model 78—81380
pollutants dispersion, model for continuous shoreline fumigation 79—100914
pollutants dispersion and transport within coastal regions, tracer study of power plant emissions 79—62545
pollutants dispersion and transport within coastal regions, tracer study of industrial emissions 79—62546
pollutants dispersion in flow over shoreline of large water body, model 79—100913
pollutants long-range transport, meteorological aspects 79—20969
pollutants long-range transport, meteorology 79—20966
pollutants long-range transport, OECD study assessment 79—20967
pollutants long-range transport, SO_2, SO_4 and Aitken nuclei airborne meas. over Denmark 78—3950
pollutants long-range transport modelling, OECD study 79—20970
pollutants regional transport rel. to ground-leYel O_3 conc. 78—44990
pollutants transport, objective anal. technique for three-dimensional urban-scale wind fields construction 80—101407
pollutants transport across North Sea and English Channel 78—24357
pollutants turbulent diffusion in Ekman boundary layer 77—73783
pollutent, Gaussian plume model parameters for ground-level and elevated sources 80—82010
pollution, diffusion-deposition-resuspension problem, formulation and soln. 77—2229
pollution, long-distance transportation model incorporating washout and dry deposition components 77—2228
pollution dispersal, Gaussian moment-conservation diffusion model 80—85317
pollution dispersion, modelling by smeared conc. approximation 78—81381
pollution dispersion from elevated source in convective boundary layer 80—85312
pollution long-range transport modeling review 80—108823
pollution pseudospectral dispersion model, inter grid sources representation 79—12259
pollution transport, air quality models development for limited wind fetch 80—104533
pollution transport, monitoring via Atmosat balloon for tropospheric research 78—7775
pollution transport in Upper Silesian Industrial District, deposition and washout 78—92960
pollution transport near buildings, wind tunnel expts. 78—11984
potential stability, determ. using wet-bulb pot. temp. charts 77—91232
potential vorticity, conservation by finite difference eqns. in generalised vertical coordinates 80—26576
potential vorticity, meridional fluxes *(Russian)* 77—81960
prediction of atmospheric flows on nested grids 79—44240
pressure waves in neutral atmosphere and auroral pulsations 80—12588
probability density function of simplified flows, temporal behaviour 78—7701
proton flow, induced, in collapsing post-sunset ionosphere and protonosphere 78—49222
protonosphere, plasma flux rel. to positive ionospheric storms worldwide distrib. 79—44290
protonosphere to ionosphere diffusion flows, rel. to F_2-layer nighttime ionisation latit. depend. 79—53617
protons of inner radiation belt, radial diffusion rel. to energy and pitch angle distrib. 80—67471
quadratic friction effect in multi-storeyed nonlinear systems *(Russian)* 77—91213
quasi-geostrophic eqn., bifurcation and nonlinear soln. stability 78—57242
quasi-geostrophic equation, stationary solns. with nonlinear boundary conditions 79—48529
quasi-geostrophic flow, bifurcation and catastrophe 79—88430
quasi-geostrophic flow over anisotropic mountain 80—61860
quasi-geostrophic flow over mountains 80—90128
quasi-geostrophic flow over topography in bounded basin 77—37306
quasi-stationary wave maintenance mechanism in quasi-geostrophic model 80—90140
quasigeostrophic approximation, large scale flow, Ekman layer effects 79—2355
quasigeostrophic flow, horizontal boundary conditions and stability 79—53446
quasigeostrophic models, horizontal boundary condition 79—5576

atmospheric movements continued
quasigeostrophic stratified atm. stationary flow past obstacles 79—100928
radiating instabilities and resonant overreflection 79—53433
radiation balance, sensitivity to cloud changes, zonal model 77—78419
radiation belts, ELF turbulence rel. to energetic electrons precip. and nocturnal D-region ionisation 77—25856
radiation belts, particles radial diffusion from geomagnetic field fluctuations at synchronous orbit 78—96359
radiation belts electron dynamics, influence of power-line harmonic radiation 79—80098
radiation belts electrons diffusion, effects of man-made VLF waves 78—45150
radioactive gaseous effluents, AEOLUS code for dispersion during normal, sea-breeze, and accident conditions 78—11993
radioactivity dispersion, population dose calc. 78—85381
rain, representation in three dimensional convection model *(French)* 79—84413
rapidly rotating flows in geophysical fluid dynamics 77—45102
realistic models, computation of waves, instabilities and eddy transport 80—90164
remote intensity fluctuation meas. by optical Doppler radar 77—791
remote sensing by VHF radar expts. 78—88938
resistance law over wavy surface 77—91202
resonantly interacting baroclinic waves, dynamics 77—56670
resonantly interacting baroclinic waves, spectral energetics 79—88422
response to external forcing, pattern detection, S/N problem 79—88464
reversed shear flow, baroclinic instability 78—44952
Rossby gravity wave propagation in latitudinally sheared zonal flows 78—16124
Rossby neutral mode, secular stability 80—81983
Rossby nonlinear waves, stochastic closure 77—89133
Rossby small amplitude wave stability in channel 77—56684
Rossby solitary waves, theory 78—1678
Rossby wave, critical layer evolution 78—79329
Rossby wave, theory of ultra-long waves *(Chinese)* 80—46232
Rossby wave critical level development 77—33153
Rossby wave flow, finite-amplitude stability 79—16579
Rossby wave packet, vertical propag. in dissipative medium *(German)* 78—36220
Rossby waves, large amplitude 79—62567
Rossby waves, long period oscills., book contrib. 78—61435
Rossby waves, stability *(Russian)* 78—44923
Rossby-Haurwitz waves, rel. to sunspots influence on weather 77—91238
rotating atmospheres, nonlinear interaction of motion and rot. adaptation process 80—17355
rotating fluid, vortices formation near reson. for elastoid-inertia waves 80—12473
rotating fluids, Rossby and Kelvin waves, open boundary conditions 80—61810
rotating stratified fluid, internal and inertial waves 78—67245
rotating stratified fluid, parallel shear flow, baroclinic and barotropic instability 80—98328
rotation rate of upper atmosphere from Cosmos 408 rocket orbit 78—73559
rotational vel. of upper atmosphere from Interkosmos 10 inclination var. analysis 80—41693
rotor streaming, assoc, with severe low level turbulence near Cross Fell, England 79—79962
Sahel rainfall 1975-6, D, T and ^{18}O evidence and regional winds *(French)* 80—21809
Sahel region, general and regional circulation effects on climate *(French)* 79—20962
sea breeze numerical model, heat convection parameterization 79—12223
sea surface temp. response to atm. forcing, N.Atlantic 78—73399
secondary flows in lee of porous shelterbelts 78—3852
semiannual oscillation in tropical middle atmosphere, review of observational evidence 80—109216
semidiurnal pressure variation over equatorial Atlantic, TROPEX-74 data 80—41536
separation effects in Ekman layer flow over ridges 79—79971
shallow water equations, soln., partly-implicit time-differencing scheme 79—20910
shear flow simulation in wind tunnel, industrial aerodynamics appl. 77—55110
shear flow/topography interaction, in homogeneous rot. fluid 79—55354
shear instabilities in presence of jump in Brunt-Vaisala freq. 79—53451
shear instability in airflow near ground 77—87004
shearing instability mechanism model, effect of horizontal differencing 80—26578
shock waves propagation, influence of aqueous fog 80—19531
short internal waves, nonlinear instability *(Russian)* 77—49107
S.Sicily coast, passage of fronts rel. to 'Marrubbio' phenomenon 77—53062
similarity theory, use in Soviet work on geophysical fluid dynamics *(Russian)* 78—16174
solar atmospheric tide in Barcelona, study for 1968-70 period *(Spanish)* 77—9479
solar semidiurnal tide influenced by zonal wind, theory 80—61853
solar semidiurnal tide influenced by zonal wind, theory 80—61854
solitary Rossby waves, variational principle 80—56539
solitary Rossby waves in two-layer system, theory 80—17293
solitary Rossby waves in zonal shear flows, interactions 79—7379
Somali jet, numerical simulation 77—45078
source disturbances simulating orographic effects, upstream boundary values *(German)* 78—65375
Southern Oscillation, spatial and temporal var. 77—21862
Spacelab lidar, for atm. props. meas. 77—21943
spectral energetics, determ. via numerical filtering anal. 80—26577
spectral evolution of strongly interacting waves 79—77144
spectral kinetic energetics, diagnostic study 77—41117
spectrum analysis of motions 79—20957
spherical movements of viscous incompressible fluids, meteorological model 79—16598
spiral bands in linear model of cyclonic vortex 77—25736
sporadic-E auroral zone, short and long term movement 78—16235
sporadic-E wavelike oscills. due to atm. gravity waves 79—101002
spread F bubble drift velocity, radar obs. 80—51598
squall line at midlatitude, thermodynamic and kinematic struct. obs. 80—109191

atmospheric movements continued
St. Louis urban plume, O_3 and aerosols, form. and transport of secondary pollutants 77—5316
stable air flow over complex region, linear model 79—53466
stably stratified flow over shallow topography, compressibility effects 78—44928
stack plumes, flow rel. to necessary height of stack close to building 77—2225
stationary perturbations, statistical-dynamical model 79—2333
stationary planetary waves, propag. in longit.-depend. basic wind flow *(German)* 80—56526
stationary planetary waves and zonal wind, southern hemisphere 78—28276
stationary planetary waves in winter, structure calc. 78—16100
steady axially symm. motions, linearised calcs. for instability and climate studies 77—70755
steady axially symm. motions, nonlinear calcs. for instability and climate studies 77—70756
steady state two-dimens. transport over area source, nonequilib. theory, pollutant dispersion 79—79924
storm splitting and simulation of right- and left-moving storms 79—16591
strain-dependent eddy viscosity, spectral characts. 78—44937
stratified and rotating fluids, review of selected aspects 77—68660
stratified flow past three-dimens. obstacles 78—71383
stratified fluid, flow over obstacle *(Russian)* 78—24291
stratified rotating fluid, vortex created by mass transfer 80—12401
stratified shear flows over long obstacle, numerical method 77—33157
stratocumulus-topped mixed layer, entrainment rate 77—21859
stratosphere, annual and semi-annual waves obs. using Nimbus 5 selective chopper radiometer data 78—81315
stratosphere, circulation change dates determ. from limited-area data 79—58054
stratosphere, circulation in circumpolar vortex, model 80—77082
stratosphere, circulation response to solar activity oscills. 77—45118
stratosphere, energy dissipation within intermittent clear air turbulence patches 77—56676
stratosphere, gas composition, comparison of one-, two- and three-dimens. models 79—70870
stratosphere, global quasi-horizontal transport rel. to NO_2 behaviour at mid-latit. 80—17414
stratosphere, global scale waves with zonal wave number zero 78—61515
stratosphere, inertial waves, obs. 79—12216
stratosphere, interaction of O_3 with circulation over Australia, review 80—109223
stratosphere, internal waves interaction with mean flow, rel. to quasi-biennial oscill. 78—69404
stratosphere, Lagrangian motion of air parcels 80—109215
stratosphere, lower, circulation appl. in five-day average air temp. forecasting technique 79—29817
stratosphere, lower, trajectory slopes, countergradient heat fluxes and mixing by waves 79—2340
stratosphere, mean flow vacillations, role of wave transience and dissipation 79—5577
stratosphere, meridional shear and spherical geometry effects on long waves 79—12212
stratosphere, movements rel. to NO_2 global behaviour 80—17334
stratosphere, O_3 distrib. and circulation in meridional plane *(French)* 77—49100
stratosphere, potential vorticity and transport 77—87009
stratosphere, seasonal and interhemispheric vars. in circulation 77—49118
stratosphere, southern hemisphere, spring transformation from cyclonic to anticyclonic circulation 80—98420
stratosphere, southern hemisphere, winter 1973, from satellite obs. 77—5282
stratosphere, sudden warming forced by mountain 80—72583
stratosphere, travelling planetary waves 80—105030
stratosphere, tropical O_3 spatial variations, influence of meridional transport and planetary waves 78—20463
stratosphere, vertical eddy diffusion profile from N_2O profiles and instantaneous global photochemical reaction rates 80—17335
stratosphere, water vapour burden areal distrib. and jet stream 77—5275
stratosphere, water vertical transport rel. to atmosphere HT and HTO 79—2347
stratosphere, wave spectra resembling turbulence rel. to turbulent transport estimates 79—79981
stratosphere, wave-mean flow interaction rel. to sudden warmings, numerical model 77—5297
stratosphere, zonal mean Arctic flow reversal during January-February 1979 warming event 80—4074
stratosphere and mesosphere, review 78—49105
stratosphere and mesosphere, transport and chemical processes 77—25761
stratosphere and troposphere waves of short-period, radar obs. 80—90192
stratosphere circulation, meas. via solar occultation sounding using narrowband radiometers 80—98452
stratosphere circulation and total O_3 trends over Australia 77—21866
stratosphere intrusions, ^7Be distrib. within high-press. systems in E.United States 80—4072
stratosphere long waves, comparison of thermal struct. in N. and S. Hemispheres 77—5296
stratosphere O_3 net vertical flux, implication for troposphere O_3 budget 80—101402
stratosphere photochemical-radiative damping and instability, numerical results 78—81286
stratosphere temperature wave propagation, polar region in winter 80—72597
stratosphere transport, one-dimensional parametrisation using ^{95}Zr data from Chinese thermonuclear explosions 79—2342
stratosphere warmings, thermal and kinetic interactions with troposphere 80—105031
stratosphere water vapour budget, contrib. of extratropical severe storms 77—87029
stratosphere wave motion, balloon obs. using data storage system on balloon 80—46263
stratosphere-mesosphere, circulation rel. to wind regime of lower thermosphere 78—4019
stratosphere-troposphere exchange at polar latits. in summer, from O_3 concs. meas. 80—72599
stratospheric H_2O, maintenance of extreme aridity 80—105028

atmospheric movements continued
subpolar atmospheric circulation 80—51530
subsynoptic vortex flow models, radial boundary conditions rel. to dust devils 77—87041
suction vortex formation, surface roughness effects, simulation 78—7704
sulphate aerosols, vertical mixing rel. to diuranl var. at rural sites in E.United States 80—30621
sulphate concs. in New YOrk State, summertime trajectory analysis 79—34882
sulphates in Canadian air, long-range transport 79—16561
summer average vertical circulation over E.Asia and Pacific regions 80—12525
summer circulation in N.Hemisphere in low and high years of spring wheat yields in Kazakhstan 77—70795
summer large scale convective system over Tsinghai-Tibetan plateau, annulus simulation meas. 79—16616
summer monsoon circulation, Indian Ocean surface temp. anomaly patterns effect 78—40634
summer monsoon circulation aspects 80—8413
Sun-weather relation, energetics study 78—81285
supergradient flows, divergence and pressure patterns 77—45076
surface flow in statistical climate model, parameterization of large-scale momentum fluxes 77—45104
surface flow over equatorial oceans, dynamics and climatology, 1911-70 period 79—58061
surface fluxes and mean profiles of vel., temp. and conc. downwind of surface roughness change 78—20484
surface friction influence on neutrally stratified mean and shear air flows 77—70790
surface layer, accuracy of moments of vel., temp. and humidity vars. 78—92891
surface layer, airflow over nonhomogeneous surfaces with discontinuities in roughness and temp., two dimens. model *(Italian)* 79—84454
surface layer, organised motion features 80—72602
surface layer vorticity meas. using acoustic echo sounder array 78—7810
surface pressure waves, 10 to 20-day westward propag. mode rel. to breaks in monsoons 80—94592
Sydney thunderstorms of 10 November 1976, movements 79—79995
symmetric instability of stratified geostrophic flow 80—98425
synoptic scale flow, influence of boundary layer pumping 77—5288
synoptic-scale vertical motion calcs. in Atmospheric Variability Experiment (AVE) IV 77—21831
temporal boundary layer and multitime scales of motion in rot. atm. *(Chinese)* 79—84447
thermal convection in rotating fluid subject to horizontal temp. gradient, baroclinic waves 77—84251
thermal perturbations, influence on solar images quality *(French)* 77—53532
thermal wave effect on circulation 80—8388
thermally driven flow in beta-plane channel, regime diagrams 80—56552
thermally driven vortices, numerical model, dust-devil dynamics appl. 77—17191
thermally forced planetary waves, assoc. boundary layers 79—34910
thermally forced Rossby and gravity waves, frictional effects 77—78384
thermals models, scales of motion rel. to self-similarity soln. 80—109228
thermoconvective instabilities of confined fluids, review 80—38399
thermosphere, circulation and comp., effects of magnetospheric elec. field and currents 80—17446
thermosphere, circulation response to mag. storm. 77—9588
thermosphere, circulation systems, northern hemisphere, 80-100 km altitude 78—81481
thermosphere, dissipation and diffusion effects on gravity waves propag. 77—13141
thermosphere, diurnal tide excited by EUV and UV solar radiation absorpt. 77—53260
thermosphere, diurnal tide seasonal-latitudinal struct. 78—77377
thermosphere, dynamic processes from optical meas. of emissions 78—36342
thermosphere, dynamics at high latits., magnetospheric convection effects 79—8733
thermosphere, dynamics calcs., Navier-Stokes eqns. validity 80—26659
thermosphere, equatorial, wave propag. rel. to density perturbations during geomag. atom *(French)* 79—96846
thermosphere, Fabry-Perot spectrometer obs. of dynamics 80—12573
thermosphere, global circulation vars. rel. to midlatit. F-region quiet time depressions 78—36385
thermosphere, gravity wave activity effects on photochem. and comp. 80—41583
thermosphere, gravity wave generation, propag. and dissipation 79—2405
thermosphere, gravity wave spectra propag. 79—66848
thermosphere, internal gravity waves, rel. to tropospheric weather systems 77—91339
thermosphere, ion-drag effects 80—17432
thermosphere, large-scale waves, obs. during mag. storms 79—35021
thermosphere, lower, dynamics, incoherent scatt. radar technique appl. 79—8734
thermosphere, lower, electric current and atmospheric motion, symposium, Seattle, Washington, 1977 August to September 80—62371
thermosphere, lower, gravity waves detect. by French incoherent scatter facility 78—81478
thermosphere, lower, vertical motions rel. to O and O_2 distrib. simulation 80—4159
thermosphere, macroturbulent scales estimation around 100 km altitude 78—61635
thermosphere, meridional circulation and temp. latit. var. calc. for solstice conditions 77—56783
thermosphere, middle, incoherent scatter radar studies rel. to energy and mass transport 80—72654
thermosphere, momentum sources signatures in neutral comp. 78—77380
thermosphere, neutral winds above Millstone Hill, 1970 to 1971, rel. to global circulation 79—39996
thermosphere, quiet, dynamics, review 80—21866
thermosphere, seasonal-latitudinal tidal struct. 80—101467
thermosphere, tidal and planetary wave propag. 77—87147
thermosphere, tidal dynamics model with O-N_2 diffusion effects 80—101465
thermosphere, tides, simultaneous incoherent scatt. obs. 77—87135
thermosphere, transport processes in diurnal tide, satellite meas. 78—88959
thermosphere, turbopause altitude vars. during night 77—78548

atmospheric movements continued
thermosphere, wave-induced diffusion effects on acoustic-gravity waves 78—61637
thermosphere, wave-like winds during August 4-5 ionospheric storm 77—33269
thermosphere and mesosphere, average daily closed model 77—17264
thermosphere circulation, seasonal and solar cycle variation 80—56661
thermosphere gravity waves, minor species relative phase and amplitude response 79—58140
thermosphere heating during magnetic storm, dynamic energy transport from high to low latits. 80—26657
thermosphere neutral and ion drifts, effect of auroral energy input 78—65446
thermosphere neutral waves, direct meas. 77—9581
thermosphere structure and dynamics rel. to tides and diffusion waves 79—35026
thermosphere tides, semidiurnal and terdiurnal 80—82119
thermosphere waves, review 77—45211
thermosphere zonal mean circulation, seasonal and solar cycle vars. 78—32262
thunderclouds, effect of elec. forces on charge separation caused by combined precip. and convection 80—17333
TID phenomena in F-region, influences of thermosphere winds 80—109305
tidal, gravity and planetary waves during 1976 over Saskatoon 79—79935
tidal energy distrib. with altitude, wind field influence *(Russian)* 78—69402
tide, solar semidiurnal, obs. of surface press. oscill. 80—77054
tide (solar semidiurnal), zonal motion and meridional temp. gradient effects 80—98399
tides, anal. methods 77—87079
tides, generated by differential heating between land and sea 78—65374
tides, quasi-fortnightly rhythm, space-time characts. *(Russian)* 78—7726
tides, review 77—86957
tides, theoretical work since 1970, review 80—94589
tides, thermal exciting energy, numerical anal. 79—70833
tides at meteor altitudes, CTOP radar obs. 80—77181
tides caused by Moon, data filtering method 80—46223
tides effects on artificial satellite orbits 77—87243
topographic Rossby waves, mean flow generation 79—96800
topographic wave clouds in central and northern Urals, characts. 80—101413
topside, transport eqns. for low speed thermal proton flows 79—44304
topside ionosphere, H^+ and O^+ ion transport obs. 80—61940
topside ionosphere, polar wind in mag. quiet conditions 80—72713
topside magnetospheric cleft ionosphere, H^+ polar wind flows obs. 77—29571
tornado funnel formation, simulation expt. 77—21853
tornado-like vortex dynamics, calculations 79—86440
tornado-like vortices, lab. simulation 77—55003
tornadoes, multiple vortex phenomenon, inertial instability 79—53454
tornadoes, numerical simulation of lab. vortex expts. 78—69411
trace elements, long range transport 79—58044
trace gas transport and photochemistry rel. to greenhouse effect *(Russian)* 80—81989
trace gases, transport by planetary waves 79—88411
tracer simulation using a global general circulation model: results from a midlatitude instantaneous source experiment 79—34907
trajectories, discrete model concepts appl. 80—85706
transfer model possibilities and criticisms 77—37382
transfer of mass and heat between ground and atmosphere *(French)* 79—84403
transient inertio-gravity waves, induced mean motion 80—105029
transport modelling and climate stability 78—28294
travelling disturbances, as explanation for daytime positive storm effects at middle latits. 79—25394
travelling ionospheric disturbance, 1F_D propag. obs. *(French)* 78—12043
travelling ionospheric disturbances, effect on statistical characts. refl. signals 78—45092
travelling ionospheric disturbances, in F1 region, phase path technique obs. 80—36436
travelling ionospheric disturbances, rel. to thermosphere storms 77—9583
travelling ionospheric disturbances, spectral comp. meas. 77—25824
travelling ionospheric disturbances, Tromsoe-Valensole propag. *(French)* 78—12041
travelling ionospheric disturbances, wave model and appl. to equatorial ionosphere 78—36232
travelling ionospheric disturbances and group delay var. at oblique incidence 78—45132
travelling ionospheric disturbances rel. to triangular enhancements of HF signal strength 78—16236
travelling planetary waves 79—58017
trichlorofluoromethane, transport processes indicator in urban atmosphere 78—36264
N tropical atmosphere, mean thermodynamic instability 77—25751
tropical atmosphere, phase-lagged wave conditional instability of second kind 80—12513
tropical belt, local vortex propag., numerical expts. *(Russian)* 77—21847
tropical boundary layer, air circulation over Arabian Sea during summer monsoon, balloon obs. 77—17192
tropical boundary layer, circulation over Arabian Sea during summer monsoon, flow field anal. 79—44231
tropical boundary layer, thermally driven motion, influence of stable stratification 77—2201
tropical circulation, hurricane formation and structure 79—88462
tropical circulation, role of horizontal friction forces *(Russian)* 78—65360
tropical circulation modes and climate anomalies 79—88468
tropical cloud clusters, wind and dynamic fields 77—29405
tropical convection in anvil clouds, hydrometeor precipitation, melting and evaporation 80—17323
tropical cyclone model vortex motion with and without current 78—28266
tropical cyclone motion 77—53146
tropical cyclone rainband microstructure 79—100927
tropical cyclones, convective fluxes 78—28267
tropical easterly waves over Pacific during sea surface temp. anomaly periods 77—78309
tropical forcing in general circulation models 77—21860
tropical large scale disturbances instability theory 77—5302

- **atmospheric movements** continued
  - tropical meteorology, review 77−64365
  - tropical regions, simulation of air flow during ice age 78−16144
  - tropical stratopause, 2-day oscill. of meridional wind 80−56557
  - tropical stratospheric waves 79−92585
  - tropical transient planetary waves in general circulation model, seasonal var. 80−90151
  - tropical troposphere, Fourier component eigenvalue anal. of CISK-induced disturbances 77−2199
  - tropical wave-CISK with a moisture budget and cumulus friction 79−16580
  - tropical waves 79−74945
  - Tropical Wind, Energy Conversion and Reference Level Experiment (TWERLE), results 78−40605
  - tropics, convection and conditional instability 80−26594
  - troposphere, buoyancy waves, Doppler radar obs. and theoretical model 79−84367
  - troposphere, circulation charge rel. to solar wind proton boundary transits 79−53491
  - troposphere, circulation intensity assoc. with solar mag. sector boundary transits 79−74936
  - troposphere, dynamical motion, spectral representation of primitive eqns. 77−78314
  - troposphere, eddy transport of sensible heat and momentum, time spectral anal. 78−92899
  - troposphere, gravity waves nature and role 79−92575
  - troposphere, growth and decay of large-scale waves in tropics during northern summer 79−88428
  - troposphere, internal gravity waves generated by jet streams 77−25737
  - troposphere, intrusive density flows, soliton source 80−12499
  - troposphere, jet stream, source of thermospheric gravity waves *(French)* 78−69554
  - troposphere, large-scale flow patterns rel. to weak monsoon over Kerala 77−56706
  - troposphere, lee waves, models, limiting cases *(Russian)* 80−12480
  - troposphere, Lee waves classical theory, asymptotic approx., upper boundary condition role 80−12472
  - troposphere, meridional and zonal cells rel. to drought forecasting in Indian subcontinent 77−56710
  - troposphere, methane flux from Earth surface *(Russian)* 78−36223
  - troposphere, middle, organised vertical vels. and correl. with clouds 78−92939
  - troposphere, midlatit., large-scale fluctuations zonal propag. 77−2194
  - troposphere, N.Hemisphere wintertime disturbance, transient disturbance 80−51459
  - troposphere, planetary waves of N.Hemisphere, space time anal. 80−51468
  - troposphere, press. instability connected with solar activity 79−92580
  - troposphere, radar obs. of vel. and irregularities, spaced antenna VHF method 80−90185
  - troposphere, relative diffusion observations 77−78337
  - troposphere, spherical model, zero-gravity, thermo/hydrodynamic characts. 78−24351
  - troposphere, standing planetary waves induced by Sun, comment, statistics reanal. 79−74935
  - troposphere, stationary waves, vorticity and heat balance calcs. 80−51460
  - troposphere, steady perturbations, two-level primitive eqn. model 77−25755
  - troposphere, stratospheric air intrusion rel. to ^{7}Be var. 80−98525
  - troposphere, Sun-induced large-amplitude standing planetary waves 78−36236
  - troposphere, synoptic and mesoscale movements rel. to Kansas City flash flood (1977, September 12) 79−25291
  - troposphere, thermal balance in low latits. in zonal circulation model 79−25316
  - troposphere, viscous internal gravity waves and low freq. oscills. in tropics 77−87003
  - troposphere, water balance over Bihar and neighbouring areas 77−56709
  - troposphere circulation in equatorial latits., contrib. to theory 79−29821
  - troposphere circulation patterns, affected by stratosphere wind spring reversal date 80−82021
  - troposphere circulation patterns, influenced by stratosphere winter strength 80−82021
  - troposphere dynamical indices, lack of response to solar mag. sector crossings 78−57244
  - troposphere gravity waves, effect on condensation initiation and growth 80−90159
  - troposphere planetary pressure waves, transient coupling with D-region short wave absorpt. vars. 77−33162
  - troposphere planetary waves, theory of nonlinear interaction 80−36385
  - tropospheric circulation, solar cycle influences 79−34919
  - tropospheric circulation in N.Pacific rel. to sea surface temp. anomaly gradient 80−85674
  - tropospheric dynamics, Nimbus 4 THIR obs. at 6.7 microns 77−17164
  - tropospheric mean zonal velocities determ. by detection of radioactive clouds *(Spanish)* 77−73782
  - tropospheric studies, microbarographs, sodar, FM-CW radar, review 77−91332
  - tropospheric-stratospheric polar vortex breakdown 1977 January 77−53107
  - Tsinghai-Tibetan high movement, annulus simulation, summer flow pattern forecast of high troposphere 78−32211
  - turbidity meas., air pollution and solar radiation interaction obs. 77−37314
  - turbulence, semiempirical theory rel. to vertical heat flux determ. 78−3907
  - turbulent atmospheric transport, Monte Carlo simulation and comparison with exptl. data 79−53479
  - turbulent recirculating flow over rectangular depression, meas. and predictions 79−66751
  - turbulent vertical exchange in surface layer, nonlocal parameterization 78−3902
  - two layer shear flow, radiation field and baroclinic eddy development in β-plane 79−81897
  - typhoons, transform in northern latits. 78−92947
  - ultralong waves, β-effect influence on baroclinic instability *(Chinese)* 80−4062
  - ultralong waves forced on cyclone scale, numerical expt. 80−61857
  - uniform potential vorticity flow, wave interactions and turbulence theory 79−8655

- **atmospheric movements** continued
  - uniform potential vorticity flow, wave interactions model 79−12196
  - United Kingdom, 1975-6 drought, atmospheric circulation 77−70770
  - unstable surface layer, horizontal vel. spectra 78−73427
  - unstably stratified, turbulent energy disspation rate *(Russian)* 77−64372
  - upper air circulation rel. to rainfall over Sahel 77−87038
  - upper atmosphere, coupled time-dependent diffusion eqns., numerical method using self-diffusion coeff. 80−109285
  - upper atmosphere, daytime Li releases obs. via high resolution photometer 78−45023
  - upper atmosphere, dynamical properties 79−75005
  - upper atmosphere, dynamics from seasonal and long-term airglow vars. 77−33237
  - upper atmosphere, general review 79−39997
  - upper atmosphere, ion drag effects on winds in N.Polar Cap thermosphere 80−67445
  - upper atmosphere, irregular motions from radiometric meas. *(Russian)* 78−96333
  - upper atmosphere, mag. storm effects on movements and tropical UV airglow 77−45214
  - upper atmosphere, meridional transport during winter anomaly, results of meteor obs. from Sheffield 78−45070
  - upper atmosphere, neutral waves determ. from AE satellite meas. 79−58139
  - upper atmosphere, OH emission, waves and winds, 80-100 km altitude 78−93025
  - upper atmosphere, rot. rate and density, obs. of satellite orbit 80−85785
  - upper atmosphere, rot. rate determ. from China 2 rocket (1971-18B) orbit 80−4231
  - upper atmosphere, travelling quasi 2-day wave in meteor region 78−81480
  - upper atmosphere, wavelike perturbations vertical propag. rel. to OH, Na D-line and O I 5577 Å nightglow 79−80067
  - upper atmosphere Ba$^+$ clouds, BaO flow rel. to clouds struct. 77−25833
  - upper atmosphere He dynamics, use of Jacchia (1977) empirical model 78−77381
  - upper atmosphere hydrodynamical accelerator, numerical modelling *(Russian)* 78−16225
  - upper atmosphere mean flow, rate of energy transfer from internal waves *(Russian)* 77−13101
  - upper atmosphere perturbations due to mountain ridge air flow *(Russian)* 80−105018
  - upper atmosphere wave structure, obs. by Illinois University meteor radar 77−41205
  - upper atmosphere winds at 95 km altitude, meteor obs. at 45°N 80−46330
  - upper westerly waves, interaction with intertropical convergence zone rel. to Zambian weather during rainy season 80−90175
  - upward sensible heat flux by synoptic-scale transients, observational study 80−94591
  - urban areas, atm. stability classification schemes 77−49127
  - urban atmosphere, numerical simulation of mixing depths 80−105024
  - urban environment, cold air drainage effects on temp. fields, case study of topographical influence on climate 80−94555
  - urban heat island, St. Louis, theoretical study, parameter vars. 79−79943
  - urban heat island convergence in calm periods, St. Louis USA 80−90169
  - urban mixed layer, persistent horizontal rolls revealed by dual-Doppler radar 79−12203
  - urban mixing layer, mesoscale perturbs. on airflow 79−16602
  - urban planetary boundary layer, pollution effects on thermal struct. and dispersion 78−11986
  - urban temp. field dynamics in Calgary area 77−17168
  - useful potential energies rel. to geomagnetic disturbances 77−70791
  - vacillations coupling 79−79926
  - vacillations in general circulation model, large-scale energy cycle 79−53430
  - vertical air motions and radar reflectivity/rainfall rate relation 77−45098
  - vertical air velocity, airborne meas. system 80−77159
  - vertical circulation during anomalous periods of sea surface temp. over equatorial Pacific Ocean 80−12528
  - vertical diffusion, study using airborne gas-chromatography and numerical modelling 78−69435
  - vertical diffusion from ground-level source, Lagrangian similarity modelling 80−51480
  - vertical diffusion from meteorological tower meas. 80−61838
  - vertical diffusion from sources near ground 79−62548
  - vertical diffusion parameters meas. using smoke plume data *(Russian)* 78−36227
  - vertical inhomogeneous currents predictability *(Russian)* 79−29809
  - vertical mass diffusion coeff., Rn tracer determ. *(Spanish)* 77−70717
  - vertical motion, parachute dropsonde appl. 78−16185
  - vertical oscills. of constant volume balloons 79−53545
  - vertical sounder radiances rel. to midlatit. 300 mb flow patterns 78−92983
  - vertical stability near ground, meas. method using ^{222}Rn release *(French)* 80−56617
  - vertical vel. fields from paired tetroon flights, comparison of vertical motions 78−16111
  - vertical vel. variations in soln. of complete atmospheric eqns. by decomposition method *(Russian)* 77−73806
  - vertical velocity calc. at upper boundary of unsteady planetary boundary layer *(Russian)* 79−100900
  - N.Vietnam, cold intrusions forecasting 3 to 7 days in advance via discrimination anal. 78−3910
  - viscosity spatial inhomogeneity and dynamic effects in upper atm. 79−53590
  - viscous flow of stably stratified fluid over barrier 77−75961
  - vortex cloud street during AMTEX 75 79−79988
  - vortex systems stochastisation, configurational temp. range in which quasiperiodicity is absent *(Russian)* 79−77132
  - vortices in rotating stratified fluids, theory 79−39814
  - vorticity, conservation as criterion for evaluation of barotropic schemes *(Russian)* 77−64369
  - vorticity and divergence, appl. to dynamical meteorology 79−12226
  - vorticity and divergence in dynamic meteorology 78−88893
  - vorticity and vertical motions over E.Asia, AMTEX 75 78−20492
  - vorticity area index, correl. with solar plages 78−73459

atmospheric movements continued
vorticity area index at 500 mb, geomagnetic disturbance effects 80—61873
vorticity budget of easterly wave rel. to cumulus convective transport 77—56671
vorticity equation, large-scale, representation of cumulus cloud effects 79—88436
vorticity index rel. to geomag. field vars. and solar activity, spectral anal. 77—5308
vorticity response to IMF sector boundary crossing, at 500 mb level 80—109199
wake and dispersion models for EBR-II building complex 77—91186
Walker circulation, heat balance 78—16096
warm frontal clouds in midlatitude cyclones, air motion and precipitation 80—109193
water aerosol, transport through atmosphere and evaporation *(Russian)* 79—88408
water heat transport, rel. to ocean temperature-salinity curve 80—72534
water pollutants atmospheric transport, new direction in hydrometeorology 78—96240
water vapour transport in atmosphere, rel. to water balance of S.America 79—29820
water vapour transport to Antarctica, factors controlling fallen snow O isotopic comp. 78—36237
wave amplitude vacillation in baroclinic flow, model 78—69407
wave disturbances 78—32209
wave disturbances of temp. and geopotential height 80—51452
wave effects on brightness oscillations of daytime sky 78—81406
wave generation and frontal collapse 78—77300
wave generation by terminator 78—49191
wave interactions, explosive, reson., in three-layer fluid flow 79—64680
wave interactions in stratified media *(Russian)* 77—11231
wave model, cloud coverage rel. to humidity and condensation 79—34911
wave motions and daily neon winds, 52-110 km altitude, at midlatits. 79—5565
wave motions in tropical spectral expt. 78—3893
wave motions in zonal model of narrow equatorial belt 78—16134
wave noninteraction with zonally av. flow and energy, heat and momentum fluxes 77—45075
wave overreflection and baroclinic instability 80—90141
wave overreflection and shear instability 79—53450
wave propagation, linear and non-linear *(French)* 77—56683
wave propagation in distorted background flows, spectral series convergence 77—29375
wave system nonlinearities, forced packet-scale motions 79—2331
wave-CISK model for convective mesosystems 77—45081
wave/mean flow interaction, introduction to generalised Lagrangian-mean distribution 80—109214
wavenumber-frequency anal. of 500 mb geopotential at 50°N 79—5578
waves, adaptive spectral anal. *(Russian)* 77—29475
waves, radiative damping 78—32163
waves, relaxational dissipation, basic formulation 78—4017
waves, viscous diffusion, heat loss damping mechanism 80—56516
waves and jet stream growth and decay, linear and nonlinear contribs. 78—57280
waves in equatorial stratosphere, effect on SW monsoon 79—8664
waves in lower atm. rel. to wind vel. fluctuations in 95-100 km altitude region *(Russian)* 77—29523
waves in lower stratosphere, radar meas. 78—44917
waves in lower stratosphere, radar meas. 78—81292
waves in Mediterranean area, zonal harmonic anal. 77—78380
waves in OH emission layer and F_2-layer, comparison 78—45065
waves in upper troposphere (tropical), dynamical anal. 80—98388
waves of long- and synoptic-scale, growth and decay in mid-troposphere 79—39793
waves on axisymm. mean flows in compressible atms., generalised Eliassen-Palm and Charney-Drazin theorems 78—81306
waves rel. to dynamics of mesosphere and lower thermosphere 79—53464
weak monsoon, atmospheric circulation and energy conversions 77—56711
weather modification due to waste heat release from large dry cooling towers 79—84471
westerly jetstream, effects on summer weather and climate 80—72620
western boundary currents and detached shear layers in rot. liq. 80—81984
wet plume rise from cooling towers in strong winds 77—33182
wind tunnel characts. review *(Italian)* 80—4156
winds in meteor region, periodic fluctuations of recurrent nature 80—90266
winter orographic storms, precipitation-forced circulations 79—34912
wintertime circulation in N.Hemisphere, observational study 78—7706
zonal and meridional circulation in N. Hemisphere middle latitudes 77—49130
zonal and meridional circulation indices rel. to winter sensible heat poleward flux 77—17188
zonal and meridional large scale flow over British Isles 80—56579
zonal atmospheric circulation model, numerical expts. *(Russian)* 78—81295
zonal climate models, inclusion of meridional motion and large eddies 80—90138
zonal flows and planetary waves in multi-level models on sphere, baroclinic instability 80—90123
zonal flows generation by interacting Rossby waves 78—3911
zonal mean circulation of middle atmosphere, numerical model 80—109218
zonally averaged circulation, 15-125 km altitude region 79—5564
zonally averaged circulation response to stratospheric O_3 reductions 79—53461
CO, tropospheric latitude distrib., model involving production and transport 80—41483
^{14}C, cosmogenic, diffusion distrib. in dynamic reservoir 80—101510
F_2-layer, plasma ambipolar diffusion and vertical drift at low latitude 80—101472
H, escape rate due to charge exchange with hot plasmaspheric ions 77—37469
H thermal escape, influence of thermosphere 63 μm radiation field 79—80066
H^+ field-aligned downward vels. at mid-latitudes 79—40015
H^+, transport behaviour rel. to concs. in E United States precip. 78—92962
H_2O dimer, props., influence on tropic meteorology 79—2349

atmospheric movements continued
Hg dispersion, expt. meas. 79—92565
Li^+ diffusion and ion-neutral interactions, laser sounding of upper atmosphere *(French)* 80—82115
NH_3 fluxes into free atmosphere over W.Germany evaluation 80—94132
NO_2, transport into stratosphere, prod. in thunderstorms 80—8376
NO_3^-, transport behaviour rel. to concs. in E United States precip. 78—92962
Na layer wave-like structure, lidar obs. 78—88955
O and O_2 distrib. in lower thermosphere assuming tidal effects, one dimens. nonstationary diffusion-photochemical model 80—4160
O^{2+}, ionosphere and plasmasphere prod. and upward transport to magnetosphere 79—35069
O_3 and mass transport, stratosphere to troposphere, Project Dustorm, tropopause folding 78—32177
O_3 budget, zonal mean circulation model and linearized photochem. 77—70780
O_3 fluxes, from zonal mean circulation model of atmosphere *(Russian)* 78—36224
O_3 layer, photochemistry and dynamics 79—5590
O_3 layer, role of dynamic and radiative processes in O_3 depletion by chlorofluorocarbons 80—109221
O_3 layer, transport rel. to chemistry and depletion 80—104534
O_3 long-range transport across mid-W. and E. United States 78—16147
O_3 meridional migration *(Russian)* 77—73816
O_3, obs. of meridional flux by transient eddies in 0 to 30 km height range 80—109224
O_3, of stratospheric origin, measured over Pacific Ocean, source and large-scale wave transport 80—72600
O_3, sources and transport in NE. United States 79—92110
O_3, stratospheric-tropospheric injection rel. to meridional distrib. and seasonal vars. 77—60453
O_3 tranpsort mechanisms, general circulation model 80—109196
O_3 transport by stratospheric planetary waves, mechanistic model 80—8402
O_3 transport in St. Louis area 79—16650
O_3, tropospheric, long-range transport 78—61514
OCS, troposphere to stratosphere transport as source of stratospheric S 78—20466
Pb, atmospheric long range transport to Denmark 80—94131
S airborne transport over N.Atlantic 78—20507
S balance and washout by precip. in industrial atm. *(Russian)* 79—100898
S compounds, meso-scale transport obs. in rurual East Midlands, England 80—94124
S compounds long term region patterns in Europe 79—20973
S pollutants, long-range transmission, simulation, two-dimens. pseudospectral dispersion model 78—57306
S pollutants dispersion over western Europe 79—70490
S, transfer rates in linear eight-box model for global S cycle 80—56506
SO_2, atmospheric transport and conversion to sulphates 79—16654
SO_2, dispersion and wet deposition from power plant plume 80—16861
SO_2, movement in atmosphere *(Dutch)* 80—97844
SO_2 plume detect. 400 km from source 78—24361
SO_2 pollution, mesoscale transport over English Midlands 78—44983
SO_2 pollution long-distance transport, numerical model 79—44238
SO_2 transport model for United States 77—37370
SO_4^{2-}, transport behaviour rel. to concs. in E United States precip. 78—92962
V pollution transport from urban to remote marine areas 77—37355

atmospheric noise *see atmospherics*

atmospheric optics
see also airglow; atmospheric light propagation; sky brightness; sunlight; twilight
46° halo and its arcs, prod. by hexagonal ice crystals 80—82065
absorption, far IR, appl. of selective modulation interference spectrometer 80—57397
active optics imagery, postprocessing 77—29654
active wavefront compensation device image degradation and postprocessing 77—58283
aerosol, particle size, opt. and geom. determs. *(German)* 77—91259
aerosol, soil derived, extinction between 0.55 and 10.6 μm 77—91264
aerosol, solar radiation absorpt., visual photometric meas. technique 80—85750
aerosol above Black Sea, spectral transmission and sky brightness obs. *(Russian)* 80—94603
aerosol absorption coeff. rel. to measurable bulk props. 77—45154
aerosol climatology in Europe, Project OPAQUE 79—66784
aerosol extinction in 0.2-40 μm wavelength range, meteorological affects 80—17371
aerosol light scattering, obs. of polarisation and intensity 80—51541
aerosol light scattering turbidity and visibility obs. 80—105047
aerosol particle growth and size distrib., humidity effects, effects on visibility 77—25321
aerosol particles, optical props. from light scatt. 78—11995
aerosol scattering of IR radiation, atmos. heating and cooling rates 80—72630
aerosol size distribs. from inversion of spectral optical depth meas. 79—80020
aerosols, coastal meas. by 1.06 μm Mie lidar scatt. 80—98403
aerosols, Mie optical cross-sections calcs., sensitivity to size distribs. sampling errors 77—2243
aerosols, polydisperse, Rayleigh-Gans approx. appl. to light scatt. 79—44249
aerosols from urban and desert regions in Israel 80—41503
aerosols with Junge size distrib., IR extinction 80—51537
air pollution, smoke plumes visual effects, computer simulation 79—66429
albedo change due to aerosol 80—56604
anisotropic reflection properties of vegetated surfaces 77—82010
anomalous refraction rel. to aerological data *(Japanese)* 77—73855
Antarctica, geodetic and meteorological meas. of refraction 77—87073
anthelic arcs, comments on appearance 80—105050
anthelion, anthelic arcs and pillar origin 79—96821
anthelion, form. theory, light refl. in ice crysts. in cirrus clouds 79—62583
arcs assoc. with halos of unusual radii 79—96818
astronomical extinction data, optical depths for observatory sites 77—49162
astronomical extinction data, seasonal var. 77—53185

atmospheric optics continued
astronomical extinction data, time trend and internal errors 77—49161
astronomical observatories, dome seeing theory 80—12657
astronomical seeing, effects on elliptical galaxies cores light distrib. 80—12814
astronomical seeing, meas. at Kitt Peak 80—61899
aureole phase function interp., logarithmic derivative method *(Russian)* 77—45148
backscattered fraction in two-stream approxs. 77—45150
backscattered pulse shape, small-angle multiple scatt. in random media 80—77079
balloon optical sounding inverse problem, ranking of model components 77—9533
Bhavnagar solar radiation, atm. turbidity and sunshine obs. 79—58072
Bombay Airport, visibility diurnal var. 77—53187
circumhorizontal arc, obs. in central Texas, USA 79—39847
circumhorizontal arc observed over Austin, Texas 78—77324
circumzenithal arc and plate ice crystal oscills. 79—96822
clear sky radiance, standard distribs. 77—87076
cloud, solar radiation absorpt., vertical and horiz. distrib. 80—72596
cloud contrast bow, obs. from high flying aircraft 79—80029
cloud extinction coefficient, estimation from multiwavelength lidar backscatter meas. 80—98446
cloud layer IR radiative transfer 80—72629
cloud/fog extinction coefficients, spectral correls., theory 79—96812
clouds, distortion of satellite imagery, removal by filtering 77—56744
clouds, optical props., similarity criteria *(Russian)* 80—85745
clouds, reflected brightness, effects of cloud size and cloud particles, comments and reply 79—88425
concentric solar halo display, 1974 April 14 77—2245
conference, Washington, USA (March 1978) 79—66794
contrast attenuation factors calc., for remote sensing, using atmospheric models 80—4135
daylight from north sky at Nagaoka, Japan, principal component anal., spectral distribs. *(Japanese)* 77—64433
Denver Brown Cloud, obs. of C particles in aerosol 80—81961
differential extinction, effect on Doppler meas. of solar oscills. 79—101131
diffraction image intensity in turbulent atm., Huygens-Kirchhoff principle calcs. 80—63926
diffusion effect, const. transmission function estimation 80—4100
direct solar radiation rel. to cloudiness and solar altitude 79—58073
dispersion effects on guidance of large telescopes *(Russian)* 78—24372
DMSP visible imagery, causes of anomalous grey shades 80—77111
dust, imaginary refr. index rel. to particle size 78—7763
dust haze of African Harmattan wind, 1962-1973 visibility obs. 80—61900
dust loading of atmos., 1923-54, pyrheliometric and circumsolar sky radiation obs. 80—46240
Earth optical horizon, height determ. from (Soyuz 9) 77—53186
education, mirage, ray theory anal. 77—87605
effects of marine environment METEOR project 79—8695
electro-optical sensors use, prediction of atmospheric effects 79—53522
extended-line-of-sight optical communication approaches 77—19187
extinction, effect on electrophotometric obs. 79—96825
extinction, no effects on 160-min. solar oscillation obs. 80—105216
extinction coefficients for multimodal particle size distrib. 78—24370
extinction coefficients in uvby system, at European Southern Obs., Cerro La Silla, Chile 77—82006
extinction variations for UBV photometry, transformations 80—67408
fog, IR extinction and absorption, linear relation to water content 80—56603
fog and haze, visibility range obs. 80—109195
fog visibility, advection fog formed from aerosol particles 80—21808
fogs, warm, haze droplets effects on visibility in natural and treated fogs 79—100951
glory, diffr. model 80—82053
glory, formation and Airy-type diffraction by water droplets 77—53191
ground slope, diffuse solar irradiance for cloudless sky 80—51505
halo displays, meteorological conditions 78—36282
halo phenomena, deviation produced by anisotropic prisms 80—63916
haloes, rings and arcs 79—66788
halos, forms and relation to ice crystals 79—2373
halos, ice crystal sizes 79—96798
Harmattan dust rel. to visibility 80—94578
haze, light scattering, statistical model *(Russian)* 79—34946
haze and aerosol characts. from daytime sky meas. *(Russian)* 78—36276
haziness factor in image contrast of aerial landscape photographs *(Russian)* 77—37449
heterodyne lidar systems, signal-to noise ratio in presence of atmospheric turbulence 79—100949
heterodyne receivers for atmospheric optical communications 80—58663
homogeneous fogs, lidar returns, doubly scattered radiation effects 79—53516
horizontal plane diffuse insolation from clear sky 79—83575
ice crystal halo form., geometry 79—100942
ice crystals, light scatt. expts. *(Russian)* 80—94601
image degradation due to daytime turbulence, arrival angle meas. 80—41551
image sharpening telescope, atm. distortion compensation 77—49294
imaging of Earth surface, haze and nonuniform albedo affecting image contrast 80—101431
imperfect Rayleigh scattering in semi-infinite atmosphere, transport eqn. soln. 79—75094
instabilities, bibliographic index for Soviet 1945-75 literature *(Russian)* 79—74959
IR radiative cooling rate due to H_2O vapour bands, calc. 80—90161
IR stellar speckle interferometry, modulation transfer function and evidence for log-normal statistic 79—101079
IR transmittance spectrum, 2.8 to 14 μm 80—85743
IR transparency over Antarctica in 8-13 μm region, 1977-8 obs. *(Russian)* 80—21823
IR transparency window, 10-13 μm, H_2O and aerosol effects in winter and summer *(Russian)* 80—105048
iridescence in aircraft contrail 79—96797
irradiance-transmittance solar spectrum, in photovoltaic efficiency calc. 80—26137
laser beam attenuation at mountain altitudes by fog and clouds *(Russian)* 79—48566
laser beam detection of atmos. constituents, review *(French)* 79—34952

atmospheric optics continued
level surveying, atoms. refr. correction *(Russian)* 80—77127
lidar, expected returns from tornado clouds 77—21901
lidar equation for inhomogeneous atmos. *(Russian)* 80—82054
lidar measurement problems in hazy visibility conditions 77—9572
lidar method for half width and intensity of gas absorption lines *(Russian)* 80—21844
lidar scattering from snow and ice crystals in atmosphere, polarization characts. 77—64430
lidar visibility measurements, atmosphere extinction coeff. extraction accuracy 78—24369
Lidar visibility measurements, using Raman/aerosol ratio method 79—100953
light flash excited by γ-quantum pulse without direct visibility of source 78—69457
light scattering, by optically thin spherically symmetric atmosphere rel. to brightness at zenith near terminator 80—109382
longwave emission from sky for all meteorological conditions 80—56609
low light and thermal imaging systems, atmospheric effects 79—39860
Lowitz arcs, computer simulation of spinning hexagonal ice plate 79—96820
luminance field spatial structure 78—49140
lunar halos, geometrical optics of formation 77—45634
marine boundary layer, optical refractive index fluctuations, statistical props. 79—62580
maritime coastal haze, optical properties *(Russian)* 79—25327
mean twilight at zenith and scatt. coeff. height var., statistical anal. *(Russian)* 79—16666
mesosphere, light scatt. coeff. correl. to atmos. stratification *(Russian)* 80—105049
meteorological physics, recent developments, review 79—25313
mirage occurrence conditions, ray tracing theory 78—77323
mirages, form., wave eqn. calcs. 77—33749
mirages, stratified medium light ray trajectories, educational aspects 78—69940
modulation transfer function, estimation via coherence interferometer *(Russian)* 79—16715
modulation transfer function meas. with interferometer 80—41567
Monte Carlo methods, book 80—77115
moving atmosphere simulation by rotating phase plate 80—79021
Mt. Majdanak (1976 June-July), atmospheric extinction and night sky brightness *(Russian)* 79—39856
multiple scattering effect on photodissociation 78—85692
natural illumination of Earth's surface in European USSR 77—78422
new formula relating atmospheric optical parameters *(Russian)* 78—11999
night sky model for artificial satellite search systems 77—73923
nonphotographic optical sensors 77—56774
Novaya Zemlya effect, arctic mirage 79—80022
observable horizon, theory, refraction, clouds and haze effects *(Russian)* 80—4107
opacity rel. to relative humidity *(Spanish)* 79—29856
optical depth determ. by measurements of meteorological range 79—84474
optical depth of Saharan dust, NOAA 3 VHRR reflected radiance meas. 78—65390
optical mass of real atmosphere, wavelength depend. *(Russian)* 77—2239
outgoing IR radiation, in CO_2 absorpt. bands *(Russian)* 80—77109
parhelia, brilliant display 1977 January 22, obs. at Toronto, Ontario, Canada 78—85694
parhelia, intensity contour maps 77—45152
parhelic circle, polarization model of halo phenomena 79—96819
Parry arcs, computer simulation of hexagonal prism ice crystals 77—53190
particle light absorpt. index, using diffuse light radiometer 80—51465
particle optical constants and disperse aerosol comp., phase scattering function *(Russian)* 80—61898
particle size determ. using spectra attenuation data considering light dispersion *(Russian)* 79—34981
particle size distrib. determ. by spectral phase functions 77—5281
particulate size distrib. and refr. index, new lidar-radiometer method 80—77153
phase correlation scale effects rel. to atmospheric imaging characts., theory 80—94604
photochemical haze over Greater London 78—36281
photogrammetry, atmos. refr. compensation 80—56339
point spread seeing function, effect on Jupiter line profile obs. 78—3952
polarisation state, aerosol and Rayleigh scatt. 77—49171
polarized halos and double refraction 78—36283
pollution affecting solar radiation incident on St. Louis, USA 80—109247
radiance, polarisation and ellipticity of multiply scatt. solar radiation 77—9457
radiation balance, zonally averaged model, improvements 78—61559
radiative transfer eqn., soln. using Elsasser scheme 80—77112
radiometric imaging from space, atmosphere effects problems 80—98323
rain parameters meas. by optical scintillation 77—82015
rainbow, anomalous arc due to refl. image of Sun from water surface 80—77114
rainbow, physics, historical review 77—73854
rainbow, theory 79—96817
rainbow and glory, complex angular momentum theory appl. 79—96815
rainbow formation in pendant drops, angular scattering 79—96816
rainbow polarisation rel. to droplet size and scatt. angle 79—80017
Raman scattering spectrum 79—92596
random image displacements at telescope focus in turbulent atm. *(Russian)* 78—20509
Rayleigh atmosphere, scattering light estimation, up to fourth order *(Japanese)* 77—13124
Rayleigh scattering in lower atmos. affecting photodissoc. rates 80—61921
real time image restoration through Walsh filtering 77—27264
reflected light from Earth's surface in Rayleigh atmosphere, estimation *(Japanese)* 78—40663
refraction zenith displacements rel. to nonpolar latitude vars. *(Russian)* 78—20637
refractive index profiles, upper and lower atm. contribs. 77—87070
refractive index pulse spectrum from optical meas. *(Russian)* 77—29439
refractive turbulence profiles, meas. by spatial filtering of scintillation 77—5331

atmospheric optics continued
remote sensing, evaluation of atmospheric effect on aerospace information 80—4101
remotely sensed space data, atmospheric effects 79—58092
Sacramento Peak Observatory night sky conditions, cloud cover, seeing and precipitable water 80—51653
scattering by mols. and particles, book 77—5323
scattering from inhomogeneous particles, geometrical optics, glory ray and rainbow 77—29430
scintillation, optical and IR waves, simulation 77—82005
scintillation effect on capacity of polarisation and amplitude modulated links 77—75428
scintillation intensity in turbulent boundary layer, influence of refr. index structural charact. *(Russian)* 80—94597
scintillation of astronomical bodies, determ. of stratosphere density inhomogeneity struct., Salyut obs. *(Russian)* 80—109186
seeing at Chinese solar observatory testing sites *(Chinese)* 77—67032
semi-empirical theory 80—90220
shadow bands during solar eclipses 80—17372
slant meteorological visibility, definition, determ. and appl. 79—100954
smoke pollution index system for rapid source-strength determ. 77—29450
soil-derived atmospheric dusts, particle absorption contributions to mass extinction coefficients 80—61896
solar apparent diameter fluctuations due to Earth's atmosphere turbulence 77—74026
solar aureole almucantar radiance meas., comparison between photographic and photoelec. methods 78—77321
solar halo complex 79—100943
solar halo complexes 77—91272
solar halo phenomena due to reflection by ice crystals *(Norwegian)* 79—84475
solar images quality, influence of atmospheric thermal disturbances *(French)* 77—53532
solar radiation availability rel. to atmospheric turbidity 79—58071
soot particle absorpt. of near IR *(Russian)* 80—82055
spectral transmission changes, refr. corrections for star colours 78—28535
stellar, speckle patterns and plane scintillation, statistics 79—100948
stellar images, amplification by turbulent atm. 80—72782
stellar speckle interferometry, lens-atmosphere modulation transfer function meas. 79—101078
stochastic problems, soln. by Monte Carlo methods *(Russian)* 77—60465
stratified media, solns. of refraction and extinction integrals 77—27247
stratocumulus producing anticoronae, microphys. characts. *(French)* 79—53488
stratosphere, aerosol layer visible and IR optical props. influence on global climate 77—2240
stratosphere, aerosol optical thickness meas. at Adelaide (35°S) 79—44248
stratosphere, aerosol particles, optical props., instrumentation and techniques for meas. 80—17389
stratosphere, light scatt. particles obs. on circumpolar flight 80—51475
stratosphere aerosol content, preliminary results of SAGE and SAM II satellite monitoring 80—82082
stratosphere aerosol detection, ground based techniques, laser usage 80—17390
submillimetre spectrum meas. with high resolution Fourier spectroscopy 77—87133
submillimetre waves and applications, conference, Guildford, England (1978) 79—31916
Sun, atmospheric effects on setting and rising 77—91271
sunphotometer aperture effects on atmospheric turbidity meas. 79—84483
sunpillar formation, theory of light scatt. off cloud ice crysts. 80—85747
telemetry, automation of information input and processing 77—78429
telescope resolution in turbulent atmosphere, diffraction limit *(Russian)* 77—25948
thermal sounding, adaptation of optical model *(Russian)* 78—7764
trace constituents by IR spectra, altitude distrib. technique 79—34985
transparency channel form. by photodissoc. wave 78—79407
transparency effects on radial vel. meas. of solar pulsations 79—101130
tropopause height from spacecraft obs. of atm. refr. of starlight 77—2280
troposphere, light scatt. particles obs. on circumpolar flight 80—51475
troposphere, refr. index variance and its height distrib. in different air masses 77—41133
turbidity, solar noon at Edmonton, in Canada 79—29858
turbidity from Campbell-Stokes sunshine recorder traces 78—88912
turbidity monitored by satellite, obs. of reflected sunlight 80—51471
turbidity of Barcelona's air, anal. of 1971-7 obs. *(Spanish)* 80—36375
turbidity over Canada 79—53515
turbidity rel. to atmospheric contamination, helicopter soundings *(Spanish)* 77—9499
turbidity vars., Sahara dust particle effects 80—51536
turbulence, effect on apparent instantaneous solar diam. 77—74021
turbulence characteristics meas. under convective conditions, optical methods *(Russian)* 79—16577
turbulence effect on sunspot fine struct. image form. 80—77108
turbulence-degraded image a posteriori restoration using multiframe imagery 77—60469
turbulence-degraded image compensation, computer simulation techniques 77—60625
turbulent atmosphere, light propag. rel. to use of multiple-mirror telescope systems in astronomy 80—94713
twilight in Sun's meridian, single- and multiple-scattered light dependencies, on air dispersion factor *(Russian)* 79—5612
twilight observations, Monte Carlo simulation *(Russian)* 77—33186
twilight visibility function of near-Sun astronomical objects 77—5321
twinkling of stars 78—53726
UFO sightings explained by refr. of light, Novaya Zemlya effect 80—77110
urban atmosphere, thin layer brown haze form. 77—56685
urban visibility degradation, multivariate statistical anal. 79—62579
UV solar radiation photometric obs. with Sun near horizon *(Russian)* 79—8691
vertical optical struct. determ. from angular depend. of IR radiation *(Russian)* 78—32223
vertical path modulation transfer function meas. 79—84478
visibility, contrib. of particulate pollution 77—73852

atmospheric optics continued
visibility, correct spectral weighting 79—21017
visibility, CW lidar meas. 78—40651
visibility, definition, confirmation using marine optics data 80—23633
visibility, form. and transport of O_3 and aerosols in St. Louis urban plume 77—5316
visibility and aerosol extinction determ. by multiwavelength contrast telephotometry 79—66842
visibility at Bombay Airport during 1974-75 and 1975-76 winters 79—21018
visibility at ground level, two meas. methods 80—82078
visibility meas. by modulated CW lidar, comment 77—64440
visibility meas. by modulated CW lidar, reply to comment 77—64441
visibility meas. using long-path laser transmissometer 78—85751
visibility meter design, visibility concepts 77—87803
visibility probed with lidar 80—31141
visibility reduction by aerosols, linear system theory of visual acuity appl. 78—11997
visibility reduction due to pollution at Bombay Airport during monsoon season 78—32225
visibility reduction rel. to O_3 conc. in Midwest 78—61507
visibility rel. to airborne soil particles mass conc. 77—73849
visibility rel. to surface wind at Gutersloh, Germany, smoke pollution effects 79—29853
visibility statistics rectification 79—5610
visibility temporal vars. beside motorway, England 79—39852
visibility trends, appl. of ridit anal. 80—82051
visibility var. over SW.United States, historical database of pollution effects 80—21424
visibility-reducing aerosols in Los Angeles air basin 78—16157
vision systems, active and passive, 0.35-14 μm *(German)* 77—9500
visual observations from space 80—21825
visual range and relative humidity relationship from aerosol meas. 77—56728
VUV solar scatt. radiance, aurora and nightglow, satellite obs. 80—90272
water droplet, IR emissivity 80—36394
water vapour, Raman lidear meas., daytime atmosphere 80—85718
water vapour refractive index meas. from 0.3 to 1.5 THz 77—82596
wind remote measurements, individual particle scatt. and single-burst digital correl. 79—100980
C aerosol visibility vs. particle size distrib. 78—88911
H_2O vapour causing IR and visible non-selective absorpt. 80—56608
H_2O, weak spectral absorpt. of vap., visible and near IR 80—82062
NO, absorpt. characts. of γ-O band, rel. to atm. meas. 78—57316
NO_2 optical depths rel. to atmospheric turbidity studies 77—17216
SO_2 optical depth meas., mask correlation spectrophotometry 77—82066

atmospheric pollution *see air pollution*

atmospheric precipitation
see also atmospheric electron precipitation; atmospheric proton precipitation; ice; rain; snow
15 GHz propagation losses on long-range air-to-ground transmission 77—17218
35 GHz short-range pulse radar, effects of precipitation *(German)* 77—49147
abundant precipitations on the Hohenpeissenberg (1979-1975) *(German)* 77—81977
acid precipitation, development of regulatory programs in USA 77—73842
acid precipitation, effect on forest soils 77—73771
acid precipitation, effect on soil acidification 77—73775
acid precipitation, effect on soil chemical processes 77—73773
acid precipitation, effects on humid temperate zone soils 77—73772
acid precipitation, effects on soil pH and base saturation 77—73774
acid precipitation, soil Al leaching response effects on high-elevation watersheds in NE.United States 80—12442
acid precipitation and acidification of Canadian lakes, effects on fish populations 77—37259
acid precipitation and forest ecosystem, symposium (Columbus, Ohio, 1975, May 12-15) 77—37322
acid precipitation at Ithaca, New York, origin of air masses 79—16655
acid precipitation effects, Norwegian SNSF-project on forest and fish 77—37411
acid precipitation effects on aquatic ecosystems, review 77—37257
acid precipitation effects on freshwater ecosystems in Norway 77—37258
acid precipitation in central Texas, chemical comp. 77—37329
acid precipitation in N.E. United States, H ion speciation 77—37336
acid precipitation in N.E. United States 77—37328
acid precipitation in Norway 77—37371
acid precipitation in W. United States, pH value obs. 80—89695
acid precipitation meas., interpretation and review 77—37323
acid precipitation meas. in Norway 77—37324
acid rain, Pittsburgh (Pennsylvania) area 80—94129
acid rain and cation leaching in Douglas fir ecosysgem 77—78392
acidity measurement, error anal. applied to indirect methods 80—72108
acidity of open and intercepted precipitation in Alberta forests 77—73844
acoustic particle agglomeration due to hydrodynamic collision between monodisperse aerosols 80—26191
acoustic particle agglomeration of aerosols under standing-wave condition 80—30627
aerosol, precip. processes rel. to background aerosol props. at S.Pole 80—41484
aerosol particle precipitation on evaporating droplet in turbulent gas flow 80—7870
aerosol particle precipitation on fixed evaporating droplet 80—7869
aerosol particle size distribs. evolution via Brownian coagulation, num. simulation 80—41513
aerosol washout, direct obs. of particles attached to falling snow crysts. 80—17362
airmasses over Asia in winter *(Japanese)* 79—66768
alignment of particles by electrostatic fields, radar obs. 77—9464
N.America, precip. vars. since 1602, reconstruction from tree rings 80—51528
N.America, Quaternary temps. and precip. for NW. coast region 80—98438
S.America, water balance rel. to water vapour transport in atmosphere 79—29820
American Southwest, evidence for cold, dry full-glacial climate 78—57296

atmospheric precipitation continued
angular scattering of water drops and ice particles [electromagnetic interference], electromagnetic interference at freq. above 10 GHz appl. 80—109183
annual precipitation series, stochastic anal. rel. to effects of urbanisation 80—98407
annual totals rel. meridional interactions with surface pressure 77—2214
Antarctica, ice crystals precip. rel. to particulate material transport to South Polar Plateau 80—51481
N.Atlantic, precipitation maps 80—51523
attentuation and cross polarisation meas. at 20 GHz, ATS-6 satellite and radar system 79—20912
attenuation studies from meas. of ATS-6 20/30 GHz beacon signals 79—20911
aurora, dayside, rocket-borne meas. of particle precip. and ion convection 78—77391
aurora primary ions, above diffuse midnight aurora 80—41595
auroral oval, dayside, evidence for parallel elec. field particle accel. 80—98503
auroral particle fluxes during substorm, rel. to magnetosphere global fine structural forms. development 79—58190
auroral particle instantaneous energy deposition, determ. from optical emissions 78—81491
auroral particles, electrodynamic processes in injection region 78—45095
auroral particles, precip. rel. to auroral forms observed characts. 79—8738
auroral particles, precip. rel. to N I (^2D) 5200 Å emission 79—21090
auroral particles, source regions rel. to dayside auroral morphology at 6300 Å, 5577 Å and 3914 Å 80—85786
auroral particles, stratified precip. struct. development during magnetospheric convection 78—28377
auroral particles precipitation, influence of ring current and plasma sheet drift instabilities 79—12351
auroral zone, joule and particle heating 77—45218
Badlands, moisture budget vars. rel. to mass movement and piping in slope development 80—41468
Baltic Sea region, evaporation-precipitation during IHP 78—44865
Belgium, annual maximum intensity distribs. *(French)* 77—64392
Belgium, weather in 1977 79—58049
Brazil, precipitable water, distrib. maps 80—77075
Brazilian geomagnetic anomaly, regular particle ionisation source rel. to E_s-layer phenomena 77—78558
Britain, water balance, 50000 yr BP to present day 80—72566
British Isles, 1975-76 drought 77—17201
Canada, acid precipitation rel. to S and N oxide emissions 77—37338
NW.Canada, palaeoclimate in late glacial times 78—20500
Canadian Middle North, surface heat and water budgets 77—29409
Caspian Sea, atmospheric contrib. to biogenous elements balance 80—31073
Central Europe, large-scale precip. field components extraction for forecasting purposes 78—92940
chain-dependent process, daily precip. amounts calc. 78—7712
charged particles precipitation, parallel elec. field signature in vel. space distribs. 78—89005
chemical composition around Tokyo, 1967-68 obs. *(Japanese)* 78—49120
chemical composition of precipitation, Trinidad, West Indies, meteorological parameters effects 79—79945
chemical tracer expts. on precip. systems, review 78—24324
climate fluctuations, relation of moistening to thermal regime 78—92937
cloud chamber, thermal diffusion, continuous flow parallel plate type, analysis w.r.t. atm. water droplet growth 80—36416
cloud droplet growth studies, optical motion control appl. to Atmospheric Cloud Physics Laboratory 80—12634
cloud microphysics, precip. initiation in updraughts, seeding 79—20924
cloud seeding, studies of AgI ice-forming activity, verification of theory 80—101406
cloud seeding, Wolf Creek Pass, USA, re-anal. of 1960 expts. 80—31100
cloud seeding criteria, winter orographic clouds 79—84391
cloud seeding experiment, comparison of night-time and day-time seeding 79—88441
coastal areas, frictional and orographic effects on precip. 77—60442
collection procedures, calibration for precipitation chemistry determ. 77—37447
Colorado Rockies, affects of Climax and Wolf Creek Pass cloud seeding expts. 80—82094
convective precipitation, mechanical effect of urban area 78—81338
convective shallow cloud model, precip. mechanisms 78—81311
N.E. Cororado, hailfall rel. to convective motion 80—31104
correlation with annual streamflow record 80—81950
cumulus congestus clouds, NE Colorado, graupel particles characts. 78—81312
cyclonic storm, rainbands, precip. cores and generating cells 78—81307
cyclonic storms, mesoscale and microscale organization and struct. of clouds and precip. 79—74946
daily precip. amounts, modelling with Markov-I chain 80—101401
daily precipitation occurrence process, Markov chain modelling 78—61464
daily precipitation stochastic models, estimation of Fourier coeffs. to describe parameters seasonal vars. 79—53481
deserts, positive feedback through precipitation 77—21863
dew, relationship to radiation fog 78—73446
dew formation on cooled glass surface, surface resist. changes 77—11777
Doppler radar data analysis 80—41564
dryness line localisation on all continents *(German)* 77—17179
duration at Hohenpeissenberg Meteorological Observatory *(German)* 77—56693
dust deposition in N.Nigeria, Harmattan dust (1978-79) 80—94578
Earth's negative charge, supply mechanism 80—61758
eastward electrojet and field-aligned current flow at dusk meridian 79—80076
El Tatio geothermal field, N.Chile, meteoric and thermal waters isotopic comp. 79—16525
electrojet boundary definitions using energetic electron spectra and magnetometer data 79—75026
EM wave multiple scatt. effects from stochastic medium 78—44941
energetic neutral atom precipitation, optical emission, ionization and energy deposition 79—75047
energetic particle precip., contrib. to middle atmosphere chemical comp. 80—109213
Europe, exceptional weather in (1975) 77—25756

atmospheric precipitation continued
F-region, midlatitude wind source, energetic neutral atom precipitation 79—70913
Fergana Valley, heavy precip. forecasting 78—92946
five-day forecasting using successive graphical regression *(Russian)* 77—29492
flash floods, American National Weather Service (NWS) warning and disaster preparedness program 79—25289
fog, quantitative meas. of precipitation onto surfaces 80—56654
forecasting 0-6 hours ahead, radar and satellite imagery, FRONTIERS plan 80—12509
forecasting hail, thunderstorms, and showers, book 77—73821
forecasting in Arizona, rel. to marine layer depth and moisture content at San Diego, California 80—101395
forecasting precipitation, evaluation of real time operation 79—88443
forecasting quantitative precipitation, prediction formula using Spanish data *(Spanish)* 80—36374
forecasting skill, daily precipitation and temp. 1966-78, Boston, USA 80—56509
forecasts using a single radiosonde 79—88397
formation in rolled stratocumulus *(French)* 77—9473
France, meteorological events at the end of the 14th century and the beginning of the 15th *(French)* 77—86960
frontal precipitation forecasting, contrib. of weather radar network, case study 77—56692
fronts and depressions at middle latitudes, mesoscale struct. 80—26604
frozen precipitation, corona charging 77—5295
frozen precipitation forecasting, regression estimation of event probabilities method *(German)* 79—66770
gauge undercatch, meas. precipitation adjustment 77—45095
generating cell of precipitation trail with wind shear *(French)* 77—53152
Germany, 1851-1975 precipitation changes *(German)* 77—33164
global January and July climate, numerical simulation with two-layer circulation model 77—56722
global warming due to CO_2 increase, temp. and precipitation changes 80—36389
Gran's plot, acid-base titration 79—79432
graupel, freely falling, wind tunnel study of hydrodynamic behaviour 78—49113
graupel development, numerical simulation 79—5573
graupel formation and growth, wind tunnel investigation 80—17324
Great Lakes, precip. rel. to W. Lake Michigan shoreline erosion 79—5542
Gulf of Alaska, coastal circulation, precipitation and runoff effects 80—36312
N.Gulf of Alaska, precip. rel. to coastal flow meas. by drogued drift buoys 80—51431
hail, cloud identification and suppression, lightning obs. *(Chinese)* 77—66968
hail, correl. with O_3 conc. *(Russian)* 77—29367
hail, crop damage, effect of wind and shelter by trees 77—45097
hail, Doppler radar spectra at vertical incidence 78—65368
hail, dual wavelength Doppler radar obs. at vertical incidence 79—79952
hail, during thunderstorm of 1976 June 27 at Heatree, Devon, England 78—57288
hail, equivalent reflectivity factor rel. to vertical fluxes of mass, kinetic energy 79—84393
hail, form. in axisymmetric cloud model 77—5294
hail, N.America, time and space scales 78—3877
hail, radar detection technique, quasilinear discriminant function 80—21861
hail, radio emission characts. in cm waves 79—96802
hail, review of meas. instruments 77—33196
hail, sampling errors in parameter meas. 78—28279
hail and crop damage, wind effects and hailcube meas. 77—17173
hail cell detection, for cloud seeding criteria, radar method 80—90170
hail development during cumulus cloud seeding by ice particles *(Russian)* 77—81959
hail falls and storms in Oklahoma, characts. 80—12504
hail growth and airflow in supercell hailstorms, rel. to hail suppression 77—21856
hail growth in supercell cloud, theory 80—98419
hail growth simulation, fresh and annealed accretions struct. 79—58034
hail growth simulation, rotation and mixed clouds effects 79—58033
hail identification by radar, ice samples backscatter matrix 79—58046
hail nuclei determ. in clouds by radar and radiometric combined meas. *(Russian)* 79—12195
hail probability rel. to radar echo heights, South African Highveld 79—20925
hail producing clouds, N.E.Colorado, observed and computed microstruct. 78—7716
hail reports rel. to 45 dBZ contour level 77—56688
hail size sorting in three-dimens. updraught, rel. to hail suppression 79—20926
hail suppression, crop protection, involvement of society 79—8677
hail suppression, current status 77—64363
hail suppression experiment, value assessment 78—7713
hail suppression expts., improvements 77—91218
hail suppression paradox, stratification approach to statistical expt. 77—37312
hail suppression seeding, Ag analysis 78—65367
hail suppression seeding, crop response anal., Nelspruit project, South Africa 78—57257
hail volume model extrapolation from surface meas. 77—21871
hail-prevention operations, cost effectiveness estimation methods anal. 78—93013
hailfalls kinetic energy, 10 cm radar and hailpad meas. 79—79951
hailfalls kinetic energy, hailstone spectra anal. 78—92924
hailpads calibration 78—93001
hailstone, melting, microwave scatt. 79—64179
hailstone formation, growth and suppression programs *(German)* 80—46243
hailstone formation within cloud, microphys. recycling 80—90146
hailstone growth, mixing processes effect on competition 79—79934
hailstone growth studies, wind tunnel expts. and thin sectioning 80—90160
hailstone nuclei formation, role of giant aerosols *(Russian)* 80—56530
hailstone samples, Project DUSTORM, microprobe anal., element abundances 78—73453
hailstone size determ. from dents in cold-rolled Al sheet 79—39890

atmospheric precipitation continued

- hailstone trajectories determ. from crystallography, D content and radar backscatt. 78—61614
- hailstones, foreign material obs. and derivation 78—96260
- hailstones, free-fall kinematics near ground 80—12519
- hailstones, from storms in Transvaal, 1972 November 29, D content determ. 78—20483
- hailstones, influence on spectral depend. of thermal radiation in 0.86 to 17 cm range *(Russian)* 78—36222
- hailstones, isotopic, crystal and air bubble struct. 77—87008
- hailstones, oblate, aerodynamics 78—20485
- hailstones, size distribution spectra *(German)* 80—56593
- hailstones, water-insoluble particle studies 80—41496
- hailstones diameters rel. to entrainment rate in hail clouds *(French)* 77 53151
- hailstorm, finger radar echoes, form. mechanism *(Chinese)* 80—109234
- hailstorm damage to vegetation, LANDSAT remote sensing epxt. *(Italian)* 77—81986
- hailstorms, Switzerland, time-resolved hailstone size distrib. and radar struct. 78—49109
- hailstorms in Transvaal, 1972 November 29, radar obs. 78—20482
- hailstorms variability on South African plateau 78—92911
- hailstripes, aerial photographs of crop damage patterns 78—3848
- Hebei Plain, summer drought and flood rel. to atm. circulation seasonal var. 80—90203
- heterogeneous nucleation of artificially modified ice *(Russian)* 77—29395
- high-latitude winter precipitation, rel. to rapid ice-sheet growth and last glaciation 80—51530
- Hubbard Brook Experimental Forest, H ion input and precipitation pH 77—37337
- Hudson Valley, USA, periodicity of July Palmer Drought Severity index, tree rings 80—26606
- central Hungary, precipitation amounts, steelworks effects 79—20943
- Hurst phenomenon, evidence for nonstationarity from precipitation records 77—29348
- hydrometeor backscattering cross sections, meas. at 6328 Å 78—49135
- hydrometeor melting and evaporation from anvil clouds of deep tropical convection 80—17323
- hydrometeorological data for US, autocorrelation characts. 77—66939
- hydrometeorological fields objective analysis, probabilistic models *(Russian)* 77—56697
- hydrometeorological time series, spectral analysis for United States 77 64341
- hydrometeors, pH detailed struct. 79—92111
- ice, bacterial sources of nuclei 77—5292
- ice, cryst. growth from vap., diffusion eqn., theory 80—12489
- ice, terrestrial and marine sources of biogenic nuclei 77—5291
- ice accretions, crystal structure rel. to hailstones 78—85668
- ice layers, evaporation effects at base, theory and radar obs. 77—78312
- Indian region, rain and snow correl. with tree growth rel.to tree-ring anal. appl. in palaeoclimatology 80—90212
- ion precipitation events in morning auroral oval, evidence for solar wind ion injections 80—98502
- ionic stability of precipitation samples 79—70828
- ionosphere, energetic particle meas. within structs. responsible for auroral accel. processes 79—53644
- ionosphere, particle precip. during geomag. disturbances assoc. with VLF waves midlatit. phase anomalies 80—56671
- isotope geochemistry rel. to climatic change, 230000 to 100000 BP, speleothem results 79—2234
- Jerusalem, evaluation of spectral density of precip. vars. *(Russian)* 77—5337
- Jerusalem, seasonal precip. temporal fluctuations 80—72618
- Kennedy Space Center, unusual lightning flash 79—20953
- Kenya high-frequency hail area, clouds microstruct. 79—53484
- La Porte (Indiana) precipitation anomaly reexamined 78—49076
- La Porte anomaly, hydrological reanalysis 80—46206
- La Porte precipitation anomaly, relocation effects 78—49077
- land-lake precip. relationships, using Lake Michigan data 78—44942
- laser beam propagation, intensity fluctuations during precip. *(Russian)* 77—29432
- lidar observations of high plains thunderstorm precipitation 78—32167
- liquid water content, determ. from Nimbus 6 scanning microwave spectrometer data parameterisation 79—58047
- London, urban effects in severe storm in August (1975) 78—81339
- magnetosphere dayside cusp, particle fluxes rel. to thermal electron densities and temps. 77—78574
- magnetosphere ions at high-altitude, particle origin during mag. storm 80—82144
- magnetosphere noble gas precipitation, gas of solar and terrestrial origin, Skylab foil obs. 80—41653
- S. central Maine, precipitation composition rel. to local source 77 37331
- management, Project Skywater, environmental impact 77—91192
- mapping with airborne synthetic aperture imaging radar 77—87106
- maritime tropical and continental mid-latitude precipitation lines 77—45093
- maximum rate rel. to mesoscale parameters 79—53469
- mesoscale precipitation forecasting over mountainous terrain 77—49143
- mesosphere, energetic charged particle precip. meas. during European Winter Anomaly Campaign (1975-76) 78—45001
- meteoric precipitation rel. to D/H ratio in speleothem fluid inclusions 79—44201
- meteorological physics, recent developments, review 79—25313
- Michigan, precipitation chemical comp. 77—37332
- microphysics, book 78—88896
- microwave cross-polarization due to precipitation in atmosphere *(French)* 78—53674
- microwave ground-based radiometer, regional precipitation meas. *(Chinese)* 79—84547
- microwave radiometry for precipitable water vap. and liq., dual-channel method 80—51564
- microwave signal attenuation by rain cell, Earth-satellite link 80—94586
- Middle Europe, 1708-54 precipitation record for Zurich *(German)* 78—85661
- mountain meas. accuracy, raingauge corrections 80—26597
- natural organic aerosols, role in condensation and precip. 80—36381
- S New Mexico, Holocene soils props. in semiarid region rel. to precip. 77—78184
- non-spherical hydrometeors scattering properties *(French)* 78—53676

atmospheric precipitation continued

- E. North America, acid precipitation, 1920 onwards 77—37334
- numerical prediction, methods and results 78—69393
- nutrient content and acidity over Iowa 77—37330
- oceanic precipitation, seasonal freqs. from Nimbus 5 microwave data 77—60455
- optical wind and precipitation sensors *(Japanese)* 78—16207
- organic micropollutants in precipitation in Norway 78—36262
- orographic cloud seeding during Utah winter 80—41514
- orographic precipitation distrib., simulation for hydrologic analysis 77—53087
- N.Pacific, precipitation maps 80—51523
- palaeoclimatology, precip. rel. to lake-level fluctuations since 30000 yr BP 80—51447
- palaeohydrology, continental record of environmental conditions at 18000 yr BP 80—51529
- parameter meas. method using radar reflectivity and optical extinction *(French)* 78—53729
- Parana river basin, atmospheric moisture inflow and outflow rel. to water balance *(Russian)* 77—53090
- particle precipitation, energetic, nighttime global zones 80—61947
- particle precipitation, role in auroral F-region ionosphere form. 79—44296
- particle precipitation during near-steady state conditions, comparison with aurora and ionosphere parameters 79—40000
- particles, size distrib. in frontal clouds 79—88437
- particles pitch angle diffusion by bounce reson., theory 78—36408
- particulate conc. changes during precipitation, field studies 79—12167
- periods of no precipitation rel. to streamflow fluctuations 77—64406
- peroxyacetyl nitrate, absorpt. by grass, soil and water surfaces 77—45139
- persistence, runs and recurrence characts. of precip. 78—3865
- pine forest wet canopy evap. meas. 78—61460
- pitch angle diffusion eqn. of trapped particles in presence of loss. cone, finite difference integration 79—70931
- plasma sheet convection rel. to diffuse auroral precipitation 79—88544
- pluvia activity, increase following Earth albedo sudden change 79—44241
- polar cap absorption event, August 1972, auroral diagnostics of particle precip. 77—29567
- pollution, diffusion-deposition-resuspension problem, formulation and soln. 77—2229
- pollution, washout and dry deposition components in long-distance transportation model 77—2228
- pollution from coal-fired power plants, effects on cloud and precip. processes 79—20933
- precipitable water determ. using vapour pressure data 78—7739
- precipitable water in total solar radiation determ. 77—56687
- precipitable water vapour determ. from surface meteorology and IR hygrometer meas. *(Italian)* 79—48587
- precipitation over ocean, quantity rel. to precipitation freq. 80—31105
- precipitation probability forecasts, nonparametric technique based on pattern recognition algorithm 78—44946
- NE Queensland, last interglacial-glacial cycle, dry land precipitation sequence 78—40598
- radar derived statistics on precip. patterns struct. 78—57260
- radar detection of area precipitation *(German)* 80—46227
- radar measurement of clouds and precipitation, correl. and spectral anal. 80—12529
- radar obs., time-domain computation of mean and variance of Doppler spectra 79—100972
- radar observation method, vertically pointing X- and K_a-band technique 80—46273
- radar observation of hydrometeors 80—46219
- radar observation of precipitating clouds, RONSARD system 80—51568
- radar observation of rain cell, automatic detection and tracking 80—51544
- radar polarisation techniques for precip. props. determ. 80—61925
- radar reflection from clouds and clutter target, broad-band noise technique 80—51454
- rain and drizzle, scavenging effect on cloud condensation nuclei, meas. by horizontal thermal gradient spectrometer 80—77158
- Ralston Creek hourly precipitation model 79—16542
- regional climatic effects of large-scale thermal pollution, simulation with NCAR general circulation model 79—53478
- rime, meas. of quantity, using fog-gauge 80—56654
- rime deposits as indicators of wind direction 80—98428
- riming process, laboratory expts. 80—105037
- Saint John, New Brunswick, air quality and precipitation meas. 77—37369
- sampling and chemical anal. of precip. for mass balance studies 79—84329
- scavenging and dry removal of particles and gases 77—73845
- scavenging of SO_2 in Sheffield industrial area 77—29424
- scavenging rates of background aerosol 78—85648
- seeding, hygroscopic, in cumulus clouds, a model 79—88442
- sequential precipitation sampler, design and operation 77—70844
- Skagit Cloud Seeding Project, Washington, effects on river annual runoff 79—79949
- small-particle precipitation, response of optical array precip. probe 80—51577
- snow, accuracy of water equivalent meas. with standard densitometer 79—29796
- snow, estimated water equivalents and melting characts. in river drainage basins 78—96249
- snow on Devon Island ice cap, NWT, Canada $\delta^{18}O$ 80—4050
- Sognefjord, Norway, local climates and growth climates, precipitation 77—21846
- Southern Hemisphere, moisture conditions and precipitation efficiency 80—98424
- Spain, orographic precipitation, Laplacian of altitude *(Spanish)* 77—87043
- Standard Light Antarctic Precipitation (SLAP), stable isotopes meas. standard 78—32246
- storm depth-area relations, from digitised radar returns 77—91249
- storm precipitation estimated with dual-wavelength radar 80—46220
- storms, principal component anal., hail index *(French)* 78—96267
- stratiform ice clouds, precip. development, aircraft and Doppler radar meas. 77—70761
- stratocumulus cloud, finestructure of precipitation and temperature 79—88418
- sulphate, dry deposition on snow surface 77—2231
- sulphate removal 79—53472

atmospheric precipitation continued
surface humidity rel. to precipitable water vap., India 78−81273
surface precipitation, results of simultaneous meas. with 3.2 cm and 5.4 cm weather radar *(German)* 77−82038
Swiss randomized hail suppression expt., design of Grossversuch IV 79−84542
temporal fluctuations, averaging for continents Europe and N.America 78−92958
terminal vel. adjustment for cloud and precipitation drops 78−16103
Texas High Plains, precipitation climatology 78−92959
thunderclouds, effect of elec. forces on charge separation caused by combined precip. and convection 80−17333
thunderstorms, contribs. of cloud and precip. particles to elec. cond. and air relaxation time 80−17332
thunderstorms, elec. fields, precip. elements charge and size, airborne obs. 78−73485
thunderstorms location of flashes to ground rel. to precipitation 77−45087
thunderstrom observed by radar, depolarisation rel. to precipitation 80−51453
tornado activity rel. to precipitation, assessment 80−61882
tornadogenesis, precipitation and rotating wind, comments and reply 77−66963
trace constituents in global baseline precip. samples, chemical anal. 79−16566
trace element analysis by neutron activation analysis 77−41154
Tromso, Norway, intensive precip., 1965-73 period *(German)* 79−16609
tropical cyclone rainband microstructure 79−100927
tropical regions, precip. as palaeoclimatic indicator rel. to climatic ice core records appl. 80−8345
tropical regions, precip. rel. to generation of large-scale disturbances 77−5302
Ukraine, statistics of spatial distrib. of precip. on Experimental meteorological test range 80−101414
N.E.United States, acid precipitation, pH and acidity 77−53184
NE.United States, filtering and intervention anal. 80−8359
N.E.United States, precipitation patterns, 1941-70 period 80−31116
E United States precipitation, SO_4^{2-}, NO_3^- and H^+ concs. behaviour 78−92962
urban bulk precipitation and streamflow quality relationships 79−88382
urban effects on precipitation, metropolitan Detroit-Windsor example 78−92917
USA, temp. and precipitation rel. to sunspot numbers 80−17328
USSR, air temp. and precipitation var., five-year changes 78−16130
volcanic ash particles, influence of shape on atmospheric settling vel. 79−84364
warm frontal region, wind and precipitation struct., Doppler radar study 80−81995
water, supercooled, probability of ice nuclei form. 78−3909
water table var. on Gdansk coast rel. to precipitation *(Polish)* 79−25281
water vapour absorption of mm- and sub-mm-waves, calc. 77−49144
water vapour refractive index meas. from 0.3 to 1.5 THz 77−82596
weather modification single area expts., confidence limits for seeding effect 79−79948
weather modification technology, statistical approach, review 78−53706
winter orographic storms, precipitation-forced circulations 79−34912
AgI particles in seeded storms, detection 78−3884
AgI surface, adsorption of water, effective pair pot. model 80−100394
D/H ratios in meteoric water over N.America (9500-22000 BP), climatic implications 77−60462
H atoms of keV energy in equatorial region, Monte-Carlo calc. 80−51596
^3H, conc. in atmospheric precip., rivers, and seas, USSR 79−74560
$^{15}N/^{14}N$ ratios in gaseous NH_3, NO_2 and NO_3^- in aerosols and precip. 78−44896
O_3, absorpt. by grass, soil and water surfaces 77−45139
$^{18}O/^{16}O$ ratio, correl. with temp. and altitude 80−77067
$^{18}O/^{16}O$ ratio in precipitation over KFA Julich, (1974-1978) *(German)* 79−12227
Pb, dry deposition on snow surface 77−2231
Pb dry deposition onto snow surface 77−37288
Pb in rain water and dustfall, meas. in Denmark rel. to atmospheric long range transport 80−94131
^{222}Rn concentration in tunnel air, atmospheric press. and precipitation effects *(Japanese)* 80−97845
S balance and washout by precip. in industrial atm. *(Russian)* 79−100898
S compounds wet removal from atmosphere 79−2363
S dry deposition onto snow surface 77−37288
S, estimated dry deposition vels. over E United States and surrounding regions 80−56507
S isotopic comp. in atm. precip. around Sudbury, Ontario 78−81361
S isotopic composition in precipitation within Great Lakes Basin 79−16625
SO_2 and SO_4^{2-}, dry and wet removal from atmosphere 79−2361
SO_2 concentration in Norwegian air rel. to sulphates in precipitation 77−37385
SO_2 effect on precipitation and soil S content and acidity in Alberta 77−73843
SO_2 low core, equilibria between air and water 78−16137
SO_4^{2-} conc. in precip. 79−100915

atmospheric pressure *see atmospheric pressure and density*

atmospheric pressure and density
30 mb level and long-range circulation var. in northern summer stratosphere *(German)* 77−56694
50 mb geopotentials from SIRS soundings and analyzed charts 77−78345
500 mb geopotential height in N.Hemisphere, climatological spectral study 77−5311
500 mb height, anal. error development, (1946 to 1969) 80−72615
500 mb height evaluation from Nimbus-6 soundings 78−53695
500 mbar level periodicity, Sun- weather effect, coincident turbulent processes 79−44219
Adriatic Sea, meteorology contrib. to high tides prediction 77−86906
AEROS and TAIYO satellite results 80−46340
W.Africa, mean tropospheric conditions for 11-year period, climatological features 77−2221
Africa, southern east coast rainfall rel. to southern oscill. and subtropical high press. belt 80−12518

atmospheric pressure and density continued
air density at 300 km altitude from China 2 rocket orbit anal. 77−91341
air density variations at 435 km altitude from Skylab 1 orbital elements 79−5694
air-sea interaction model 79−79969
aircraft meteorograph, design, appls., accuracy *(Chinese)* 80−17387
airmasses over Asia in winter *(Japanese)* 79−66768
Alaska north coast, long range sea ice forecasting from press. systems obs. 77−2174
N.America, sea-level press. 80−51528
annual variations in density 79−53423
anomalous local atm. press. correl. with secular gravity vars., USSR *(Russian)* 78−53612
Arctic Basin, ice movements, external factors 80−26541
Asia, change in sign of relation between sunspots and press., rainfall and monsoons 77−45123
Assam valley, low press. area intensification into mesoscale depression 77−53125
N.Atlantic, near sea level pressure, solar influence 77−87033
S.Atlantic Ocean, high press. area rel. to high waves in Benguela Current 80−51434
Atlantic Ocean, meteorological parameters changes and interaction with different-scale processes *(Russian)* 77−60447
N.Atlantic Ocean, sea level press. fields rel. to Gulf Stream channel line oscills. 78−92841
N.Atlantic weather forecasting, multiday, for press. field 80−98417
atmosphere, surface tides, New Zealand 78−85665
atmospheric oscillations and Ruchhardt's experiment, theory, for teachers 79−71198
aurora, O densities rel. to O, O_2 and N_2 emission meas. 78−57380
auroral electrojet, plasma density fluctuations rel. to nonpotential waves 77−49212
auroral infrasonic wave emission, multiplicity of wave forms 77−29534
auroral infrasonic wave emissions on night of low geomag. disturbance 77−25811
auroral oval, dayside, press. gradient rel. to neutral wind profiles between 115 and 175 km altitude 80−98494
available potential energy budget eqns., limited region, time depend. of reference press. 78−20497
available potential energy in atm. in press coords. *(Russian)* 80−109187
Azores high, northward extension rel. to summer weather in SE.England in 54 BC 77−49149
ballistic density determ. from satellite radiance obs., direct method 78−16186
balloon rise rate calcs. for constant lapse-rate layer 77−64387
Baltic Sea region, press. meas. rel. to atmospheric heat and moisture balance 77−87057
baric depressions formation near Alps 77−49099
baroclinic equatorial motions, linear differential eqn. 78−49098
baroclinic instability, finite amplitude model, supercriticality 77−17166
baroclinic instability and transient eddies in middle latitudes 80−41489
baroclinic instability in reversed shear flow 78−44952
baroclinic instability max., wavelength, quasigeostrophic model 78−44926
barometric distribution, elementary kinetic derivation 77−62323
barometric effect in low level counting in the proportional counter 78−33374
barometric pressure, effects on cosmic rays 79−84604
barometric pressure vars. influence on gravity 77−44894
Bay of Bengal and Arabian Sea, cyclones and depressions during 1975 78−32148
Beaufort Sea, mesoscale press. distrib. 80−101366
Belgium, continental anticyclonic conditions rel. to air pollution increases 78−81374
biennial cycle in extratropical latitudes 78−16131
blocking anticyclones, rel. to cold spells and heat waves in British Isles 79−80006
blocking problem, role of wavegroup vel. 78−3892
boundary layer, baroclinicity effects on Lagrange trajectories of diffusing particles 77−66949
boundary layer, press. fluctuations, ground effects 78−61498
boundary layer near water surface, diurnal characts., equatorial region, GATE meas. 78−61527
Brussels-Uccle region, press. records 1833 to 1952 period *(French)* 80−82028
Budapest, evaluation of spectral density of press. vars. *(Russian)* 77−5337
charged particle drag on Lageos, semimajor axis secular decrease 80−94628
coastal zone, indicators of long-term var. of hydrometeorologic elements *(Russian)* 78−77258
cold fronts, resonance generation of ocean surface waves *(Russian)* 77−29309
contour heights at 30 mbar level in stratosphere for 1957-65 period 78−24350
convection dynamics equations, non-Archimedean approach 80−77048
cumulus cloud convection, perturbation pressure and density model 80−17325
cyclogenesis in lee of Alps 78−77305
cyclones, causing Earth surface deform. 77−53018
cyclones, pressure drop reduction using deswirler 79−12176
cyclonic systems in SW monsoon period moving towards lower latits. 79−96796
D-region, neutral density meas. via payload B I rocket-borne expt. package 78−45190
D-region plasma density measurement, rocket borne expt. 78−45126
daytime D-region, electron and ion densities during polar cap absorpt. 77−37481
density function and gravit. pot., influence on Earth gravity field 79−57841
density inversion, Taylor instability 77−9476
distribution variations in geostrophic wind pressure distrib. vars. 80−17348
diurnal variation, harmonic anal. *(Rumanian)* 79−21009
dynamical meteorology, trough-ridge systems as slantwise convection 79−79993
E-region, O density rel. to O I green line airglow, obs. during Winter Anomaly Campaign (1975/76) 78−45075
E-region, plasma densities rel. to cross-polar cap horizontal currents 77−45230

atmospheric pressure and density continued

- Earth shape deformed by seasonal atmos. press. variations 80—21609
- easterly perturbation intensification under westerly trough influence, India, 1975 Feb. 79—48548
- education, gas pressure gauge for student expt., mol. weight determ. by law of atm. 79—25795
- S.England, 1977 January 25 rapid pressure var. 78—44972
- equatorial quasi-biennial oscill. strength rel. to max. temp. at Oxford 77—81975
- equatorial trough zone occurrence and struct. in Venezuela 79—79974
- W.Europe, mesosphere and lower thermosphere temp. and density, 1975/6 winter anomaly 80—36357
- exobase, H density and temp. from Lyman alpha absorpt. and polarisation meas. 77—29526
- exobase, local perturbations of H density distrib. inferred from Lyman α airglow meas. 78—24400
- exosphere, geomagnetic density and temp. effect propag. 79—48593
- exosphere, global temps. and densities under active solar conditions 77—33234
- exosphere, satellite particles theory rel. to density profiles 79—101097
- extratropical cyclone, enhancement after separation from polar front *(French)* 80—56517
- F-region, electron density irregularities rel. to pulse spreading and unresolved spread-F 77—78557
- F-region, incoherent scatter radar meas. of electron density and ion vel. during isolated substorm 78—65452
- flying snow caused by pressure drop in front of avalanches *(Japanese)* 77—87025
- flying snow in front of avalanches, expansion flow out conditions *(Japanese)* 77—87026
- flying snow in front of avalanches, snow cover descent *(Japanese)* 77—87027
- forecast model with 10 levels, lower boundary condition 80—51494
- forecasting of daily pressure by statistical method 80—56528
- forecasting of sea-level press. with allowance for surface press. tendency 80—85738
- free air press. estimation from radio sonde data 79—88508
- frontal instability, semigeostrophic eqns. appls. 77—45077
- frontogenesis, warm rel. to cold surfaces 78—49086
- geomagnetic tail, plasma press. anisotropy rel. to B_y field distrib. 79—80091
- geopotential along 50°N on 500 mb level 80—101399
- geopotential effects of geomag. vars. 80—4067
- geopotential field of 10 mbar surface and geomag. disturbance fields characts. 77—13055
- geostrophic correlation of initial geopot. and wind fields *(Russian)* 79—100899
- global January and July climate, numerical simulation with two-layer circulation model 77—56722
- global scale transport processes *(Dutch)* 78—3889
- gravity waves, ground level, in SE.Australia, microbarographs obs. 78—73439
- gravity waves generated during solar eclipse, obs. 78—88887
- NE. Gulf of Alaska, development of synoptic climatology 80—98405
- S Hemisphere, 200 mbar flow from satellite geopotential height data 77—33158
- N.hemisphere, climatic apsects of pressure vars. (1950-1975) 77—70803
- N.hemisphere, press. distrib. assoc. with poor summers in British Isles 80—109241
- high pressure systems, correl. with high O_3 conc. in rural surface layer 78—24325
- hurricane Camille, wind speed and direction, ocean wave height and barometric press. meas. 78—36254
- Hurricane Gladys (1975), subcloud layer energy transformations 80—77089
- India, westerly upper air troughs rel. to western disturbances development 80—90173
- Indian sea areas, 1976 cyclonic storms and depressions 80—56533
- Indian sub-continent summer monsoon, press. distrib. rel. to causes of 1899 drought 77—56705
- infrasound, asymmetry in generation by travelling aurora 77—87152
- ion and neutral density determ. by mass spectrometers, mass discrimination under spacecraft conditions 80—4230
- ionosphere, atomic ions reaction to rapid changes in large-scale elec. fields 77—91350
- ionosphere, density vars. due to solar EUV flux changes, calcs. 79—44293
- ionosphere, electron density vars. during 1972 August 4-5 storm 77—33269
- ionosphere, electron temp. and density fluctuations meas. by Aeros-B, global distrib. 79—58160
- ionosphere, equatorial, plasma density bubbles obs. by (ESRO-4) 80—4194
- ionosphere, evolution of comp. and density profiles with increasing O content 77—2300
- ionosphere, ion density meas. rel. to lower hybrid reson. freq. obs. and calcs. 78—28416
- ionosphere, lower, ion prod., density and comp. during auroral absorpt. event 80—36443
- ionosphere, lower, rocket meas. of electron density from VLF waves propag. characts. 78—49219
- ionosphere, meas. by self-contained tethered balloon sounding system 78—28343
- ionosphere, O^+/n_e relative densities at 170 km for specific heliogeophysical conditions 79—12332
- ionosphere, plasma bubbles spatial relationship with 1 m equatorial spread-F irregularities 80—67457
- ionosphere, plasma density changes rel. to radio waves self-action, nonstationary theory *(Russian)* 79—48604
- ionosphere, press. oscills. transfer to neutral atmosphere during substorms 79—58158
- ionosphere, principal ions relative densities at midlatits. 79—21094
- ionosphere, props. meas. at Arecibo Observatory 78—81488
- ionosphere, small-scale irregularity structs. assoc. with subtrough density gradients, Ogo 6 obs. 78—40753
- ionosphere, striations assoc. with Ba clouds, particle densities and fluxes 77—9607
- ionosphere, topside, transient response to precip. 77—78566
- ionosphere D- and E-regions, electron densities, diurnal, seasonal and solar cycle vars. 77—33267

atmospheric pressure and density continued

- ionosphere E-region, latit., geomag. storms effect on electron density 79—44294
- ionosphere electron density in S hemisphere middle latits., Universal Time effect model 79—25396
- ionosphere modification, plasma densities in artificially created equatorial spread-F 78—88972
- ionosphere negative storms, plasma density vars. simulation using neutral comp. data 79—25393
- ionosphere pressure oscillations, generation of atmospheric acoustic-gravity waves 78—77296
- ionosphere total electron content, nighttime enhancements at low latits. 80—72677
- ionosphere total electron content at Sagamore Hill, solar cycle var. 78—81496
- ionospheric, lower, layer structs. response to gravity waves 78—81290
- Japan, Niigata prefecture, mean daily temp. rel. to pressure in winter *(Japanese)* 79—96803
- Lake Superior, coastal upwelling/downwelling cycles 78—44889
- Lamb waves generated by 1975 May 11 solar eclipse, magnitude upper limit 77—29376
- Lamb waves originating in nongeostrophic disturbances, press. vars. obs. 77—45085
- lidar observations of atmosphere at Kingston, Jamaica 78—36284
- lower thermosphere, thermobaric field rel. to dynamical processes *(Russian)* 78—24401
- lunar tide, solar modulation anal. 80—94593
- magnetosheath, dayside, plasma press. anisotropy and mirror instability 77—37483
- magnetosheath, plasma depletion obs. at dayside magnetopause 79—66876
- magnetosphere, elec. field, plasma density and temp., field-aligned currents, S3-3 satellite obs. 80—26699
- magnetosphere, electron density and temp. meas. by GEOS-1 mutual impedance expt. 79—35071
- magnetosphere, electron density gradients rel. to HF signals propag. mechanism 80—4196
- magnetosphere, press. gradients and convection, role of hot plasma 78—32297
- magnetosphere, thermal electron densities and temps. in dayside cusp region 77—78574
- magnetosphere cold plasma densities, comparison of ULF and VLF meas. 78—28436
- magnetosphere electron density, small scale struct. from plasma resons. on-line tracking 79—35073
- magnetosphere irregularities, formation and evolution by mag. flux tubes interchange 80—21876
- magnetosphere low-energy plasma at synchronous orbit, temp. and density 78—77435
- magnetosphere plasma density, GEOS-1 relaxation sounder meas. 79—35072
- magnetosphere plasma density and temperature, GEOS-1 multi-expt. determ. 79—35074
- magnetosphere plasma sheet, plasma flows during substorms rel. to field-aligned press. gradient 78—96357
- magnetosphere tail plasma sheet, press. anisotropy due to adiabatic plasma convection 79—25408
- magnetotail, O^+ and H^+ densities 77—33284
- magnetotail, press. anisotropy effect on mag. current sheets equilib. struct. 79—12354
- marine atmosphere, baric disturbances ocean stationary surface and internal waves generation *(Russian)* 78—77252
- marine equatorial atmosphere, surface press. rel. to general circulation features 78—92949
- mass distrib. by latitude, anal. 80—90115
- mean daily pressure over Mediterranean, power spectrum anal. 78—3913
- mesopause, ion-neutral collision freqs. and mean temps., Arecibo radar meas. 78—88957
- mesoscale divergence of horizontal vel. field and press. gradient force, rel. to momentum transport 78—11954
- mesoscale structure of line convection at surface cold fronts 80—12514
- mesoscale trade wind field, role of advective acceleration 77—70793
- mesosphere, Arctic, vertical temp. and density patterns anal. as gravity waves 79—16622
- mesosphere, ion bunches form. and concs. 78—73424
- mesosphere, LF radio wave absorpt. variations, press. and temp. depend. 79—44282
- mesosphere, O_2 density and press. profiles from solar H Lyman-α radiation extinction meas. 78—44947
- mesosphere, O_3 density meas. from ground-based millimetre wave obs. 77—29381
- mesosphere and lower thermosphere, profiles based on obs. of Lyman-α extinction 80—77180
- mesosphere and stratosphere structure from noctilucent cloud presence 80—8412
- meteorological conditions by radiothermal sounding at 5 mm *(Russian)* 80—77038
- meteorological index, effect of interplanetary magnetic field 77—86994
- meteorological wave separation method for Earth tide obs. *(Russian)* 78—4014
- microseisms in lakes, longitudinal waves, origin from atm. press. variations *(Italian)* 77—81798
- middle atmosphere, plasma and neutral gas comp. and density meas. by mass spectrometer probe 78—45191
- Middle East, summer anticyclone circulation rel. to change in O_3 *(Russian)* 77—53156
- monsoon depression, composite structure 77—45117
- monsoon depressions, life history, struct. and movements 78—44963
- monsoon depressions and tropical cyclones, movement prediction 77—17167
- monsoon depressions in Bay of Bengal, freq. of first occurrence, 10-day epochs, 1891-1970 period 78—81303
- monsoon system oscillations, spectral anal. of obs. records 77—33148
- monthly sunshine percentage rel. to 700 mb height field 78—3867
- mountain drag meas. 79—53452
- mountains affecting geopotential, Coriolis force variability 80—26602
- moving pressure disturbance energy generation in ocean *(Russian)* 77—33087
- Navier-Stokes type eqns. for determ. wind vel. from press. field 77—78374

atmospheric pressure and density continued

neutral atmosphere, press. oscills. transfer from ionosphere during substorms 79−58158
neutral atmosphere layer structures, density response to gravity waves 78−81290
neutral upper atmosphere, components density vars. semi-empirical models 79−21085
neutral upper atmosphere, density, temp. and winds 79−75006
neutral upper atmosphere, magnetospheric convection effects on global density field 77−29525
northern hemisphere circulation anomalies and seasonal weather forecasts 77−2237
Norway Station/Sanae (Antarctica), surface temp. and sea-level press. 78−81324
numerical weather forecasting, long-range, filtering method 79−84446
ocean baroclinic Rossby waves generation by meteorological forces 77−86916
ocean internal wave generation by advecting atmospheric fields 77−53066
ocean pressure cell, topographic Rossby waves generation and kinetic energy on continental shelf 80−51425
ocean surface wind and pressure fields during TROPEX-72 near Equator 77−37320
ocean-atmosphere interactions along North American west coast, 1965-69 period, preliminary anal. 78−61508
oscillation model of atm. action centres, vortices interactions *(Russian)* 80−4075
ozone number density from STRATCOM VII-A meas. 79−58079
W.Pacific high long-term fluctuation, tropical ocean effects *(Chinese)* 78−16117
NW.Pacific Ocean, relation between atmospheric press. and sea level 80−101415
W.Pacific subtropical high, summer, form. and struct. simulation *(Chinese)* 80−109233
periodic pressure disturbances, ocean internal gravity wave generation *(Russian)* 79−100853
physics field course, for school pupils 77−87612
plasma sheet, press. anisotropies meas. 78−89009
plasmapause location and H^+ density decreases, correl. 78−81500
plasmasphere, ion and electron densities rel. to charge exchange and H escape rate 77−37469
plasmasphere composition and density, equilib. model 79−66860
polar low as extratropical CISK disturbance 80−51502
polar lows, numerical model, shallow baroclinic waves struct. 77−70775
polar thermosphere, pressure gradients rel. to F-region drifts and winds 77−33274
pollutant aerosols, mass density function multimodality 77−70807
pressure, long-period fluctuations, statistical analysis *(Russian)* 78−81298
pressure effects of water level in wells tapping deep unconfined aquifers 80−81953
pressure field during geomagnetic disturbances, geographical dependence of solar-atmospheric connections 79−25315
pressure field Fourier expansion, rel. to intensity of atmosphere meridional motions *(Russian)* 77−53154
pressure fluctuations, influence on Earth surface tidal tilts *(Russian)* 78−88790
pressure force and large-scale moving wave maintenance 77−66960
pressure gradient force and advection scheme for forecasting with topography 77−86977
pressure jump detector array, gust front detect. at Dulles Airport 78−32234
pressure perturbations in deep convection, expt. study 79−53457
pressure sensing by solar occultation using wideband CO_2 absorption 79−80037
pressure waves in neutral atmosphere and auroral pulsations 80−12588
probe for static pressure sensing in 2D flow, wind effect on buildings 79−71403
protonosphere, plasma densities meas. rel. to quiet night ionosphere decay rates 78−81493
psychometric constant γ, pressure depend. 77−53149
remotely sensed pressure, satellite-borne MM wave radar system 80−67443
scale heights and radio meteor echo data 79−84560
sea level, bottom pressure and geostrophic adjustment 77−37215
sea level nonperiodic vars. of synoptic freq. on tidal sea shelf *(Russian)* 78−65320
sea level pressure anomalies predictability over N.Pacific Ocean 78−92905
sea surface, press. drifting buoy, development 79−5661
seasonal forecasts based on pressure anomaly rules, accuracy 78−7744
semidiurnal pressure variation over equatorial Atlantic, TROPEX-74 data 80−41536
semidiurnal pressure wave seasonal var. above Atlantic Ocean, Polygon-70 region 77−64390
Siberian anticyclone, intensity rel. to annual motions of Earth rot. and excitation poles *(Russian)* 78−40461
solar activity effects, surface press. maps during geomag. disturbances 77−78359
Southern Oscillation, spatial and temporal var. 77−21862
stability evaluation of statistical couplings, meteorology appl. 77−74204
static omnidirectional pressure probe 77−53238
steering level rel. to precipitation line orientation 77−45093
stratosphere, 10 mbar geopot. height vars. rel. to solar activity 79−29824
stratosphere, 200 mb geopotential heights rel. to annual and semi-annual waves 78−81315
stratosphere, cosmic ray and pressure oscills., balloon obs. *(Japanese)* 80−31182
stratosphere, density vars. during northern hemisphere winter 77−78372
stratosphere, LF radio wave absorpt. variations, press. and temp. depend. 79−44282
stratosphere, lower, power spectral anal. of meteorological data 78−40616
stratosphere, southern hemisphere, temp. and press. field spring transformation anal. 80−98420
stratosphere, temp. and press. determ. from OH fluoresc. lidar instrument 79−80033
stratosphere, temp. and press. profiles meas. via solar occultation sounding using narrowband radiometers 80−98452

atmospheric pressure and density continued

stratosphere circulation at 10 mb, response to solar activity oscills. 77−45118
stratosphere density inhomogeneity struct. determ. from Salyut obs. of astronomical scintillation *(Russian)* 80−109186
stratosphere density oscills. rel. to gamma-ray quasi-periodic intensity variations *(Russian)* 80−90177
stratosphere O_3 density perturbations, photochemical-radiative damping rel. to instability 78−81286
student demonstration of atom. press. using beer can 80−31460
student experiment for atm. press. meas. with syringe 77−57122
subarctic frontal zone position rel. to typhoon trajectories seasonal activity over NW.Pacific 78−61526
subsoil behaviour in Potsdam rel. to storms and atmospheric pressure *(German)* 79−62425
summer monsoons over Africa and India, comparison 78−32149
supergradient flows, divergence and pressure patterns 77−45076
surface atmospheric pressure field, vars. in periods of high and low geomag. activity 78−36245
surface high pressure and rainfall, meridional interactions 77−2214
surface layer, air density correction to eddy flux meas. 79−66761
surface layer press. perturbs. due to ocean swell waves *(Russian)* 78−65362
surface pressure, fluctuations rel. to internal gravity waves and tropospheric wind *(Russian)* 77−33141
surface pressure, remote meas. by multicolour laser ranging system 80−8429
surface pressure, vars. rel. to Earth rot. multiyear vars. excitation 79−96734
surface pressure anomalies rel. to sea surface temp. anomalies 78−49034
surface pressure changes, effect on tiltmeter and gravity obs. *(Russian)* 78−48957
surface pressure field, lower atmosphere instability correl. with solar corpuscular activity 80−61881
surface pressure fields, forecasting via baroclinic model with horizontal discretisation 77−45065
surface pressure measured using microwave signals transmitted from orbiting satellite 80−94581
surface pressure waves, 10 to 20-day westward propag. mode rel. to breaks in monsoons 80−94592
surface wind of Arizona cool season, correl. to press. gradients 80−98379
synoptic object localisation, long-period tidal fluctuations *(Russian)* 78−81321
thermosphere, circulation systems, northern hemisphere, 80-100 km altitude 78−81481
thermosphere, density correl with charged particle precip. through magnetospheric cleft 77−87146
thermosphere, density meas. rel. to neutral waves 77−9581
thermosphere, density variations from AE-C accelerometer meas. 77−64500
thermosphere, disturbed, Ar, N_2, O and He densities, global model from Esro 4 meas. 77−37468
thermosphere, diurnal variability of N and NO densities 77−78549
thermosphere, diurnal vars. in temp., comp. and winds 77−87141
thermosphere, global model based on mass spectrometer and incoherent scatt. data, N_2 density and temp. 77−70897
thermosphere, ion photochemistry and density profiles from Atmosphere Explorer C meas. 78−32261
thermosphere, local time var. of density, altitude depend. 78−61636
thermosphere, mass density, O and N_2 composition, seasonal-latitudinal tidal struct. 80−101467
thermosphere, minor species relative phase and amplitude response to gravity waves 79−58140
thermosphere, model based on satellite drag data 78−69555
thermosphere, N_2, Ar densities response to major geomag. storm 77−9582
thermosphere, neutral comp. and density profiles between 90 and 220 km 78−77383
thermosphere, neutral densities and winds above Millstone Hill, mathematical model and results 79−39995
thermosphere, nighttime, press. pattern rel. to neutral atmosphere parameters var. *(Portuguese)* 80−41584
thermosphere, temp., density and comp., new models 77−64502
thermosphere, tidal var. in total mass density from AE-E Mesa expt. 79−53593
thermosphere constituents, density vars. rel. to eddy diffusion coeff. global models determ. 79−21086
thermosphere density enhancement and perturbations form. during geomag. storm, obs. in equatorial zone *(French)* 79−96846
thermosphere O and O_2 densities, photochemical deviations from diffusive equilib. 77−37470
thunderstorm density currents, wind shear obs. 77−13109
thunderstorm gust front detection, sensitive pressure-jump sensor design 78−57357
tide, solar semidiurnal, obs. of surface press. oscill. 80−77054
topside magnetospheric cleft ionosphere, ion and electron densities and temps. 77−29571
tropical circulation, role of horizontal friction forces *(Russian)* 78−65360
tropical cyclone nested grid model, noise control 78−11957
tropical cyclones in Bay of Bengal and Arabian Sea, max. wind speed calc. 77−53124
tropical E.Atlantic, press. and wind fields from TROPEX data 80−82040
Tropical Wind, Energy Conversion and Reference Level Experiment (TWERLE), results 78−40605
troposphere, geopotential response to tropical forcing 77−21860
troposphere, lower, solar flare effects on temp. and press. 78−40615
troposphere, press. instability connected with solar activity 79−92580
troposphere, pressure and temp. meas. by lidar differential absorpt., influence of laser emission spectral width *(French)* 80−41554
troposphere, pressure correl. with interplanetary mag. field struct. and solar wind 80−56515
troposphere, sensor for constant-level balloon expt., boundary layer to 100 mbar level 79−21047
troposphere, Sun-induced large-amplitude standing planetary waves 78−36236
troposphere, temperature-pressure profile meas. by microwave remote sensing *(Chinese)* 80−4116

atmospheric pressure and density continued
- troposphere, upper air pressure field anal. using surface-derived data 78-61523
- troposphere, wind-height data for tropical cyclone recurvature forecast 77-64380
- troposphere 500 mbar level, vars. rel. to sunspots influence on weather 77-91238
- troposphere and lower stratosphere, time spectra of press. fluctuations 77-78367
- troposphere over ocean areas, geopotential height data supplementary method 80-26647
- troposphere planetary pressure waves, transient coupling with D-region short wave absorpt. vars. 77-33162
- Tsinghai-Tibetan high movement, annulus simulation, summer flow pattern forecast of high troposphere 78-32211
- typhoon and hurricane areas, distrib. models of press. and wind over sea surface 79-62570
- typhoons structure over Soviet Far East during transformation of decay 77-78378
- United States, synoptic weather situations assoc. with major wildland fires 78-61499
- unusual weather frequency variability over last century 78-73479
- upper atm. density models rel. to drag on artificial satellites 80-17428
- upper atm. parameters daily vars. at midlatits., reference system 77-29521
- upper atmosphere, background gas press. rel. to He dynamics, use of Jacchia (1977) empirical model 78-77381
- upper atmosphere, density depend. of bright meteors ionisation columns initial radii 80-94762
- upper atmosphere, density distrib. from Cactus accelerometer flight result on Castor satellite 80-77251
- upper atmosphere, density fluctuations rel. to meteor trails linear electron density 78-73687
- upper atmosphere, density models rel. to extinction of solar radiation 77-78546
- upper atmosphere, density rel. to meteor trails initial radius height and time depend. 79-58301
- upper atmosphere, density scale height determ. from China 2 rocket (1971-18B) orbit 80-4231
- upper atmosphere, density vars. from January 1972 to April 1975 near 200 km 78-57377
- upper atmosphere, energy balance, importance of IR radiation 79-8729
- upper atmosphere, ion and neutral densities rel. to $N_2^+ + O$ reaction rate coeff. 77-53288
- upper atmosphere, N density from dayglow far UV N and N_2 emissions 78-28361
- upper atmosphere, neutral and ion densities response to mag. storm, OGO 6 obs. 77-9588
- upper atmosphere, O_3 and Cl densities from OAO 3 stellar occultation meas. 77-9580
- upper atmosphere, pitot press. meas. for density determ. between 50 and 120 km 78-45193
- upper atmosphere, rot. rate and density, obs. of satellite orbit 80-85785
- upper atmosphere, semiannual density vars. form. mechanism 77-25807
- upper atmosphere density, accuracy of nonspherical model from satellite drag obs. 77-29520
- upper atmosphere density derivation from near-circular satellite orbits, effect of temp. diurnal var. 80-21867
- upper atmosphere density var. and meteor rates correl. with solar activity 77-53485
- upper atmosphere H distribution and daily density vars. 77-29522
- water precipitable water determ. for vapour pressure data 78-7739
- wave disturbances of temp. and geopotential height 80-51452
- weather forecasting for central Asia, for short-term press. field 80-98416
- westerly trough unusual SE. movement over India, 1974 December 78-32161
- western depression over N. India, mean model 77-53113
- western disturbance intensification moving from central Iran to NW India 78-81302
- Western Pacific subtropical high in summer, exptl. simulation *(Chinese)* 79-84415
- winter measurements, correl. between mean daily temp. and atmos. press. *(Japanese)* 79-66777
- CO_2, number densities in lower thermosphere 78-96336
- H density distrib. at exobase near solar minimum 78-45067
- He^+ outflow from ionosphere, press., density and temp. profiles 78-49221
- NO, density in high-latit. lower thermosphere during aurora 77-37467
- O, upper atmos. atom density, rel. to airglow intensity *(Chinese)* 80-90269
- O_2 A band differential absorpt. lidar meas., for pressure height and vertical temp. profiles 79-39904
- O_2 density in thermosphere, solar flux var. 80-72659
- O_3, partial press. and mixing ratios obs., (1976 January 5 to March 31) *(French, Flemish)* 77-33174
- $O(^3P)$ concentrations in lower thermosphere, rel. to $O(^1S)$ prod. mechanisms 77-33235
- ^{222}Rn concentration in tunnel air, atmospheric press. and precipitation effects *(Japanese)* 80-97845

atmospheric propagation *see atmospheric electromagnetic wave propagation*

atmospheric proton precipitation
- *see also aurora; radiation belts*
- 440 keV proton precipitation at middle latitudes during the recovery phase of magnetic storms 78-20579
- AEROS and TAIYO satellite results 80-46340
- S.Atlantic anomaly region, aeronomic and geophysical indicators anal. 79-58187
- aurora, ULF elec. fields and particle precip., rocket meas. 78-96337
- aurora in F-region, assoc. with magnetospheric cusp 80-90273
- auroral E-region, form. by proton precip. 78-45088
- auroral oval, dayside, energetic protons rel. to radio aurora and field-aligned currents 78-88966
- auroral particle precipitation, rel. to turbulence at 500 mb level 80-77218
- auroral proton bursts struct. during mag. quiet times and substorms 77-29531
- auroral protons, as source of atmospheric water vapour, role in Sun-weather relationships 78-69416

atmospheric proton precipitation continued
- auroral protons, energy rel. to N_2^+ 1 NG emissions anomalous vibr. distrib. 80-67448
- auroral protons, precip. rel. to auroral E-layer seasonal vars. 79-8746
- auroral protons energy and pitch angle spectra vars. in upper atm. 79-75032
- auroral protons origin at dayside oval 77-9597
- auroral zone, electrostatic ion-cyclotron instability during quiet times 77-33256
- auroral zone, protons energy spectra and pitch angle distrib. 77-9596
- auroral zone precipitation and convection reversal, satellite obs. 80-101479
- cusp region of magnetosphere, rel. to interplanetary mag. field 80-90288
- cusp region on dayside, field line topography, precipitation implications 80-85822
- D-region, heating by high energy protons 77-82078
- diffuse auroral precipitation mechanisms 79-12327
- dynamics and auroral morphology, photometric data interpretation 80-82141
- E-region, nighttime occurrence rel. to protons precip. and night sky emission *(Russian)* 77-45223
- electron and proton precipitation, during auroral and geomag. substorm activity development 78-28435
- energetic particles injection into magnetosphere, evolution of energy spectra and pitch angle distrib. 78-45148
- energetic solar protons, auroral zone precip. assoc. with storm sudden commencements 77-82081
- energy deposition in N_2, binary encounter calcs. 78-74746
- equatorial ionosphere, electron production by energetic particle precipitation 77-33255
- field aligned current above auroral arc, e^- and H^+ precipitation obs. 80-77215
- inner magnetosphere penetrated by energetic particles during storms 80-72716
- ionosphere, channel lower hybrid resonance excitation by superthermal particle streams *(Russian)* 78-4025
- ionosphere, energy release from precipitation 78-32268
- ionosphere, low energy particles equatorial ring in 400-1100 km altitude range 77-49213
- ionosphere, nighttime field aligned O^+ and H^+ fluxes in mid-latit. mag. field tube 77-33273
- ionosphere turbulent polar cusp, temps. and low-energy particles and Kelvin-Helmholtz instability 78-96343
- IPDP field fluctuations and proton precipitation, simultaneous obs. 80-77238
- IPDP pulsation polarisation, correl. with particle precipitation 80-51612
- keV energy protons in equatorial region, Monte-Carlo calc. 80-51596
- low altitude meas. during 1976 March 26-27 geomagnetic storm 79-53667
- magnetosphere, energetic particle precipitation, Kosmos 484 polar meas. 80-8491
- magnetosphere, precip. due to proton-cyclotron instabilities in non-uniform loss-cone plasma 80-90286
- magnetotail protons, influence of bounce effects in Pc 4,5 geomag. pulsations generation 80-4197
- mesosphere, Joule heating at high-latitude 80-41500
- midnight trapping boundary, energetic particles pitch angle distribs. 78-28445
- nighttime global zones of energetic particle precipitation 80-61947
- outer zone proton precipitation during magnetic storms, Intercosmos 5 obs. 77-25855
- Pc 1 pulsation polarisation, correl. with particle precipitation 80-51612
- pitch angle distribs. of solar protons, magnetosheath distortion 78-40768
- pitch-angle diffusion with asymmetric loss cones, rel. to precip. longit. depend. 77-13162
- polar atmosphere, penetration by monoenergetic and unidirectional proton beams 77-29528
- polar cap aurora, proton-induced, N_2 bands intensities 78-77389
- polar D-region aeronomy 77-53311
- quiet dayside cusp, AE-C and -D low-energy particle obs. 78-28390
- radio aurora (diffuse), rel. to field-aligned currents and particle precipitation 80-105119
- ring current proton precipitation, energy depend. 77-78565
- solar proton injections and polar cap absorpt. events, recording using ULF meas. 79-53620
- South Atlantic Anomaly spatial shift 78-28449
- stable auroral red arc formation, proton obs. supporting ion cyclotron wave heating theory 78-49197
- substorm expansion, intense electron and proton fluxes poleward of trapping boundary 77-87164
- substorms, latit. morphology of >100 keV protons precip. 79-80080
- thermosphere, dynamics at high latits., magnetospheric convection effects 79-8733
- X-ray K-shell emission at satellite altitude 78-61641

atmospheric radiation
- *see also aurora*
- 100 to 500 kHz noise, rel. to auroral arcs and field aligned currents and auroral electrons accel. 79-66859
- Aberdeenshire, mesoclimate of Upper Don Basin 80-61889
- absorption line parameters compilation, AFCRL, accuracy in 10 μm atm. window 77-9494
- absorption line profile of isothermal atmos., under general freq. redistrib. function 77-37500
- absorption of solar, diffuse and reflected visible radiation *(Russian)* 78-96291
- absorption rel. to solar EUV spectrum and cycle 21 development 79-75174
- aerosol particles influence on warming of urban and rural atm. 79-16671
- aerosol temp. and energy exchange in Earth's atmosphere 77-45082
- aerosol-scattered radiation, effect on O_3 photodissociation 79-2371
- aircraft irradiance meas., computer simulation 77-70830
- albedo of ground and index of absorption of atmospheric particulates, theory 79-88438
- American Meteorological Soc., third conf. (Davis, California, 1978 June 28-30) 79-5611
- Antarctica, winter, Nimbus-5 radiance data temp. field deviation from radiosonde data 78-32138

atmospheric radiation continued
  area skyshine from radioactive waste, gamma-ray backscatt. photon spectra 80—31119
  artificial satellites future role in meteorological obs. 79—79965
  aurorae, optical emission height profiles of medium intensity 79—40002
  auroral arcs, precip. primary electrons and bremsstrahlung X-rays, satellite correlated obs. 79—35029
  auroral electron beam, electrostatic noise generation 78 -85759
  auroral hiss, nearly reson. whistler amplified Cherenkov radiation, limitations 80—101482
  auroral location, visual and radio emission 80—82122
  auroral O I 6300 Å emission production efficiency by energetic electrons 80—72671
  auroral X-ray bremsstrahlung rel. to VLF emissions 78—45106
  auroral X-rays, balloon obs. in Canada rel. to X-ray illuminating regions determ. 80—31156
  Austria, global radiation climate, 13 years records *(German)* 77—64412
  azimuth dependent terms of radiation intensity in deep layers of semiinfinite medium *(Russian)* 77—73851
  balance of radiation over water surface 79—20889
  bidirectional reflectance and transmission for space appl. 77—56809
  boundary layer, IR radiation effects on dynamics 79—39815
  boundary layer, radiation balance over salt marsh 78—61481
  boundary layer, turbulent and radiative transport interaction in development of fog and low-level stratus 78—81313
  bremsstrahlung produced by precipitating electrons, theoretical characts. 79—66862
  bremsttrahlung X-rays from relativistic electron precipitation 79—75014
  brightness temperatures in H_2O 1.35 cm reson. region, vars. *(Russian)* 78—81403
  Cherenkov radiation in large cosmic ray showers, computer simulation using hadronic collision models 78—57415
  chlorofluoromethane IR radiation, effect on zonal atmospheric temp. 79—80019
  cirrostratus clouds, IR emissivity meas. by remote sounding 80—82061
  cirrus, radiative transfer model for IR region 80—98397
  cirrus cloud, IR reflectance of cloud base 80—98397
  cirrus clouds, IR emissivity calc. from lidar and radiometer meas. 80—82060
  cirrus clouds, radiative props. in NOAA 4 VTPR channels rel. to satellite exploration 79—39853
  clear atmosphere, radiative transport and thermal turbulence *(French)* 80—82018
  clear radiance estimates from truncated observations 79—80025
  clear radiance soundings from Nimbus 6 rel. to TIROS-N processing system 79—58228
  clear sky conditions, solar radiation and illumination simultaneous meas. 80—81985
  climate, energy balance models, global and one dimens., stability comparison 80—94596
  climate model, zero-dimens., with ice-albedo and greenhouse feedback, catastrophes and resilience 79—80007
  climatology of global solar radiation in California and an interpolation technique based on orthogonal functions 80—67402
  cloud, solar radiation absorpt., vertical and horiz. distrib. 80—72596
  cloud cover influence on atmos. top radiation budget 80—98398
  cloud temp. fluctuation meas. by IR radiometry, feasibility study 80—56636
  cloud-free atmosphere long wave cooling rate determ. method *(German)* 77—64474
  clouds, internal radiation field, cloud blackness determ. technique 79—58089
  clouds, IR emissivity in 10.5 to 12 μ band *(Russian)* 77—49167
  clouds, radiation rel. to diurnal var. of underwater irradiances on horizontal surfaces 80—72549
  clouds, radiative properties parameterisation 80—56601
  cloudy atmosphere, IR radiation flux approximation 79—39854
  cloudy atmosphere, radiative transfer model, solar radiation and cloud struct. 79—21016
  clounds, stratiform, modelling and effect on radiation balance *(French)* 80—82017
  colour structure of atmosphere, vertical profile obs. by astronauts *(Russian)* 78—40795
  Complex Atmospheric Energetics Experiment (CAENEX), interaction of radiation and dynamics 78—3904
  cosmic ray induced neutron background sources 78—40781
  cosmic rays, atmospheric nuclear cascade characts. calc. for Pamir expt. 79—80157
  cosmic rays, height depend. of gamma-quantum families of 10 to 100 TeV energy 79—80159
  cosmic-ray components in atmosphere, altitude depend. rel. to environmental radiation meas. *(Japanese)* 79—80144
  cyclotron soliton theory of Earth's kilometric radiation 80—94657
  daily scattered radiation totals variability over European USSR 79—29861
  daily solar total irrad. fluctuations, temporal statistical anal. *(French)* 80—61292
  damping of temp. waves in finite non-grey atmosphere *(Russian)* 80—81990
  daylight, broadband filter radiometry error anal. 77—53163
  daylight, spectral distrib., 280-2800 nm, Australia 78—69452
  diffuse and beam, average, hours of bright sunshine correlations 80—40841
  diffuse atmosphere, diurnal evolution of stratocumulus cloud *(French)* 79—84402
  diffuse cosmic and atmospheric MeV γ-rays, balloon obs. 78—4048
  diffuse radiation, models with aerosols and common absorbing gases, data sets 79—44235
  diffuse solar radiation, anisotropy 79—88398
  diffuse solar radiation below overcast sky, ang. distrib. 80—85719
  diffuse solar radiation effects on O_3 photodissoc., annual var. 80—109210
  direct solar energy, Markov chain simulation with one minute binning *(French)* 80—61293
  direct solar irradiance, indirect meas. 80—45644
  direct solar radiation and diffuse radiation calcs. from synoptic weather obs. *(German)* 79—34925
  direct solar radiation and global radiation for 69 places in West Germany, solar power appls. *(German)* 79—70837
  direct solar radiation spectral distrib. 79—12268
  direct solar transmittance for clear sky, model 79—74948

atmospheric radiation continued
  Dirmhirn global radiation recorder rel. to Campbell-Stokes sunshine recorder *(German)* 78—44953
  divergence budget estimates from cloud data, GATE 80—17319
  dust loading of atmos., 1923-54, pyrheliometric and circumsolar sky radiation obs. 80—46240
  earth radiation budget: simulation of fluxes and accelerometric measurements *(French)* 79—84482
  Earth radiation budget, accelerometer direct meas. *(French)* 80—46287
  Earth radiation budget rel. to climate, effects of atmospheric OCS and stratospheric aerosols 80—41524
  Earth Radiation Budget Satellite, climate appls. 80—109283
  Earth surface thermal radiation, calc. for randomly inhomogeneous stratified media *(Russian)* 78—96312
  Earth surface thermal radiation effects of doubling of atmospheric CO_2 conc. and climatological signficance 80—101426
  Earth zonal radiation balance, perturbation by stratospheric aerosol layer 80—56602
  Earth-atmosphere radiative heating effects, NOAA radiometer meas. 80—8425
  earthquake lights, proposed for study by chemiluminesc. NO air pollution apparatus 80—61906
  EAS radio emission, field strength at 44, 60 and 80 MHz 80—8505
  EAS radio pulses, correlation at 60 and 80 MHz 80—8504
  ELF coherent radiation, search at Crab pulsar freq., upper limit 79—16728
  ELF emission, ionospheric generation and spatial distrib. 80—4174
  ELF emissions, magnetospheric, obs. Moshiri, Japan 78—24413
  Elsasser formulation and downward IR fluxes, comments on discussion 77—56729
  EM radiation from lightning 79—58038
  emergent radiation, computation method for region ranging from UV to IR 77—87069
  energetic ions and EM radiation in auroral regions 78—81490
  energetic neutral atom precipitation, optical emission, ionization and energy deposition 79—75047
  energy balance and temp. in surface-troposphere system, CO_2 increase effects 80—12498
  energy balance determ. methods *(French)* 77—33208
  energy balance model, climate sensitivity to radiation flux calcs. 80—8421
  EUV dayglow, obs. by He gas absorpt. cell 79—12326
  excess radiation flux at heights of 200-300 km meas. 77—53278
  exosphere, H atoms vel. distrib. from OGO-5 meas. of Lyman α emission 78—61642
  exosphere, UV extinction meas. by OSO-8 French expt. 77—21963
  finite plane parallel atmos., polarisation studies, F_N method 79—40070
  Fourier far IR spectroscopy from Spacelab 77—21949
  gamma radiation, north-south anisotropy at balloon altitudes 77—29608
  gamma-quanta flux in upper atm., short-period pulsations *(Russian)* 77—9638
  gamma-rays, spectra and angular distrib. 0.3 to 10 MeV 77—49205
  GATE radiation subprogram, aircraft studies 78—81408
  geocorona scattered $L\alpha$ enhancement during 1972 August solar flares 77 78582
  global and diffuse solar radiation meas. at Genoa *(Italian)* 79—100886
  global and net radiation distribution over Greece 80—21382
  global solar radiation at Lyon and at Macon, France, for (1978) *(French)* 80—55812
  global solar radiation computation from sky cover obs. 77—25758
  global solar radiation est. and prediction by stepwise multiple regression anal. for Greece (1961 to 1975) 80—61880
  global spectral distrib. determ. using rapid spectral radiometer for solar cell appls. 80—61369
  global surface irradiance, effect of aerosol props. and surface reflectivity 80—76611
  greenhouse effect, component contrib. 80—101544
  greenhouse effects rel. to trace gas perturbations 77—53179
  ground albedo and absorpt. by atmos. particulate, determ. using diffuse light radiometer 80—51465
  ground slope, diffuse solar irradiance for cloudless sky 80—51505
  heat budget and albedo determ. using balloon-borne pyranometers 79—58135
  high-energy radiation near lightning strokes 80—36361
  hiss associated with active auroral arcs, sounding rocket obs. 80—98512
  horizontal, monthly average daily, diffuse and total, in Canada, correlation 79—70876
  horizontal, monthly average hourly diffuse and total, in Canada, correlation 79—70877
  horizontal surface solar irradiance prediction models compared 80—36384
  hourly global radiation sequences, stochastic simulation 80—36382
  hourly solar radiation amounts in Thailand, statistical distrib. 78—96271
  insolation absorption and thermal excitation of atmospheric tides 79—34890
  insolation meas., Si-cell based sunstation system 79—5582
  insolation measurements at Las Vegas, in United States 78—69427
  insolation modelling, review of solar radiation resource assessments 80—35640
  ionosphere, auroral, ELF radio signals generation by LF and MF transmissions nonlinear demodulation 80—94639
  ionosphere, electron beam injection into plasma causing HF emission 80—56670
  ionosphere, obs. of concurrent 0.005 to 0.5 Hz precip. pulsations and mag. field pulsations 77—53307
  ionosphere, rocket-borne VLF and ELF waves meas. in dayside auroral oval 80—98504
  ionosphere lower hybrid reson. freq., obs. and calcs. from ion density meas. 78—28416
  ionosphere VLF emission, mid-latit. modulation theory 79—12335
  Iowa, urban/rural radiances, seasonal and wavelength dependence 77—64384
  IR, evaluation of flux over Atlantic Ocean *(Portuguese)* 79—2372
  IR absorption by CO_2 at large optical thicknesses, mechanisms *(Russian)* 78—40659
  IR and microwave radiances meas. from TIROS-N processing for temp. sounding 80—77133
  IR anomalous absorption, temp. dependence 79—34951
  IR attenuation through low atmosphere *(Italian)* 79—48567
  IR brightness obs. 80—94629
  IR cooling rate, in standard atmosphere 80—26609

atmospheric radiation continued
- IR emission, effects on IR propagation and system performance modelling in fog 80—90218
- IR emission, Lambertian, of spherical surface, radiation press. on satellite *(French)* 78—81529
- IR emission, sky noise correl. for IR telescope focal plane *(French)* 78—53725
- IR emission, statistical props. of sky noise *(French)* 78—53731
- IR emission meas. using radiometer 78—4681
- IR emission meas. using versatile sensitive radiometer 77—70887
- IR emission obs. at balloon altitudes 79—16669
- IR emission of upper atm., obs. with Meteor satellite 79—62632
- IR emissions in auroral regions, origin 77—33247
- IR enhancements assoc. with bright auroral breakup, 1.5-5.3 μm 78—12036
- IR high-resolution emission spectra in two passbands 77—25782
- IR long-wave (8 to 13 μm) radiation in free atmosphere, comparison of theoretical and experiment fluxes *(Russian)* 80—94598
- IR properties relevant to building envelope heat losses 80—58895
- IR radiance, meas. and calc. 77—64431
- IR radiance (15 μm), aerosol particle effects rel. to error in satellite retrieved temp. profiles 80—98449
- IR radiance fluctuations, spectra deduced from ground-based IR radiometry 79—92567
- IR radiance meas., 4-14.5 μm range, by narrow beam spectral radiometer 78—61596
- IR radiation budget, outgoing IR flux and albedo obs., diurnal variation 80—51538
- IR radiation flux in upper atmosphere, meas. in 4 to 6 μm spectral range 80—61929
- IR radiation intensity, satellite meas. appl. to atmosphere total O_3 content determ. 80—77027
- IR radiation plane layer of mol. gas, Earth temp. calc. as function of atmospheric CO_2 conc. 77—35021
- IR radiation transfer in inhomogeneous atmos., transmission function 77—91270
- IR radiative energy exchange in troposphere from six-layer general circulation model 80—101432
- IR radiative transfer, absorpt. in partial cloud cover model 80—12544
- IR radiative transfer in cloud layer 80—72629
- IR radiative transfer in cloudy sky, theoretical scheme 80—51540
- IR radiative transfer model, comparison of obs. and calcs. 79—2369
- IR sky temp. computation and surface temp. comparison 79—34953
- IR solar radiance reflected from the rough sea surface *(Russian)* 79—84477
- IR spectral transmissivity, temp. depend., CO_2 and H_2O bands below 10 μm *(Russian)* 80—12542
- IR system for radiating source meas. 77—70891
- irradiance, seminumerical method accounting for atmos. H_2O *(Spanish)* 80—36373
- irradiance at Table Mountain, California 1926-1977, meas. 79—29816
- isotropically scattering semi-infinite medium, diffusely reflected radiation intensity *(Russian)* 79—34948
- Israel, estimation of solar radiation and ambient temps. 80—76607
- Israel's coastal plain (1967 to 1976), temp. and global radiation meas. 79—80003
- kilometric radiation, rel. to ionosphere large scale elec. field 77—87159
- kilometric radiation, source localization and polarization determination using LF satellite radioastronomy *(French)* 79—70940
- kilometric radiation, theory 79—70900
- kilometric radiation from auroral zone, coherent nonlinear theory 80—101495
- kilometric radiation from auroral zone, propagation direction 80—101497
- kilometric radiation generation, inner magnetosphere auroral zone 80—105128
- kilometric radiation polarization, Voyager 1 and 2 direct meas. 79—12373
- km radiation, satellite obs. of spectral props. 77—82084
- km wavelength radn. generation by cyclotron solitary waves *(Russian)* 78—40764
- Lake Erie terrestrial radiation in 1952-1968 period 77—29343
- Lake Victoria, incident global solar radiation, 1970-1974 obs. 80—81940
- LF radiation source located at 2.5 R_E, satellite elec. field data 80—41656
- lightning, effect of pulse interval statistics on radiation spectrum 77—53135
- lightning, RF radiation generation, elec. field var. obs. 80—98401
- lightning, simultaneous obs. of optical radiations from above and below clouds 80—85698
- lightning radio emission, Maxwell's eqns. soln. 77—29403
- lightning return streamer, EM radiation 79—8652
- Lisbon solar radiation climate, direct, diffuse and global intensities 80—36383
- local γ-ray source obs. by Cosmos 731 77—53258
- long-wave radiation meas., comparison of actinometric radiosondes during GATE-74 period 79—29906
- longwave emission from sky for all meteorological conditions 80—56609
- longwave radiation calc., analytical and empirical formulae 79—53518
- longwave radiation from cloudless skies, comparison of meas. and calc. 79—44250
- longwave radiation incident upon inclined surfaces 80—16785
- low-frequency emission pulsations in topside ionosphere, spectra rel. to surface geomag. SPP spectra 79—58157
- lower thermosphere O, Na, OH, O_2 emissions, vars. rel. to thermal tides 77—78550
- luminance field spatial structure 78—49140
- luminous efficacy of daylight at Tokyo *(Japanese)* 80—72631
- Lyman α emission in antisolar direction on Earth's night side 77—87138
- Lyman α geocoronal emission effect on rocket meas. of proton fluxes 77—53273
- magnetic noise of low-freq., generated on auroral field lines 80—101494
- magnetopause, plasma wave turbulence obs. 80—51610
- magnetosphere, elec. field in VLF to HF range, EXOS-B obs. 80—67478
- magnetosphere, H^+ cyclotron waves and upstreaming ions 80—51620
- magnetosphere, hectometric and kilometric emission in August 1972, effect on solar emission obs. 77—25994
- magnetosphere, quasi-periodic ELF-VLF emissions assoc. with Pc 3-4 mag. pulsations, geomag. conjugacy 80—67475
- magnetosphere, RF emission in electron beam-plasma and beam-beam interactions 78—45137

atmospheric radiation continued
- magnetosphere, source regions of fine struct. in whistlers, auroral hiss and ELF hiss 77—87203
- magnetosphere, spatial struct. of terrestrial kilometric radiation 77—25873
- magnetosphere, ULF activity in Pc 3-4 range correl. with interplanetary mag. field radial orientation 78—28434
- magnetosphere, wave emissions prod. by JIKIKEN electron beam-plasma interaction expt. *(Japanese)* 80—94655
- magnetosphere chorus and hiss observed by GEOS, automatic recognition using coherence function 79—44307
- magnetosphere coherent VLF waves, nonlinear pitch angle scatt. of energetic electrons 78—89011
- magnetosphere ELF chorus, substorm dependences of two types 78—28437
- magnetosphere ELF emissions during substorm activity periods, local time var. 77—53328
- magnetosphere mid-latitude hiss, quiet band prod. by VLF transmitter signals 77—64534
- magnetosphere natural emissions, Geos I identification 78—53774
- magnetosphere VLF wave activity, Sunday decreases 79—66883
- magnetosphere-cusp interface, EM and electrostatic emissions during substorms 79—66880
- magnetospheric VLF emissions, modulation temporal-spectral anal. from Interkosmos data 77—64511
- measurement of irradiation above thermal collector critical levels for 10-min and 1-hr integrals 80—16789
- mesosphere, IR nonthermal emissions from O_3, Spacelab obs. 77—21906
- mesosphere, OH emission rel. to thermospheric semi-annual temp. vars. 78—45061
- mesosphere, temp. waves of annual and semiannual period, radiometer obs. 80—51500
- mesosphere at Thumba from in situ UV absorpt. photometry obs. 80—105051
- meteor wakes, red afterglow origin 78—36536
- meteorite fireball, deduction of props. from behav. in atoms 80—82311
- methane, IR radiation flux 78—71268
- methane and N_2O greenhouse effects, climate model 80—90211
- MeV gamma radiation, theoretical zenith angle distrib. at high balloon altitudes 77—45208
- microwave radiometry, remote temp. sensing 80—46293
- microwave radiometry for precipitable water vap. and liq., dual-channel method 80—51564
- microwave radiometry for temp. retrieval, climate in variational scheme 80—56649
- microwave radiometry from satellites 77—70882
- microwaves, Nimbus 6 scanning spectrometer data parameterisation for atmosphere liq. water content 79—58047
- middle atmosphere, IR cooling rel. to numerical model of zonal mean circulation 80—109218
- millimetre wave radiation, obs. by wide-band radiometer based on superconducting point contact 79—62750
- MM wave radiometry conducted at Appleton Laboratory 80—67442
- mode coupling of Z-mode waves as source of terrestrial kilometric radiation 77—29537
- moisture content determ. of cloudless atmosphere, microwave radiation meas. 80—94624
- monthly mean solar radiation calc. using daily time intervals 80—17353
- natural sky radiance and smoke stack radiance spectral characts. meas. and modelling, 3.8-5.5 μm region 79—66797
- near IR solar radiation, direct and scattered fluxes *(Russian)* 78—81299
- net radiation meas. from shipboard Funk net pyrradiometers 79—21055
- nightside auroral km radiation origin and polarization 78—45161
- ocean surface absorption of short-wave radiation and albedo *(Russian)* 77—60415
- ocean surface effective radiation calc. *(Russian)* 78—16040
- ocean surface radiation budget calc. methods, evlauation *(Russian)* 77—29494
- ocean surface radiation budget calc. methods compared *(Russian)* 77—29495
- oceanic precipitation, Nimbus 5 microwave meas. rel. to seasonal freqs. 77—60455
- optical phenomena, review including airglow and aurora 77—70831
- optical-acoustical method for radiative heat flux divergence meas. *(Russian)* 78—7789
- outgoing IR radiation, in CO_2 absorpt. bands *(Russian)* 80—77109
- outgoing longwave radiation estimation from meteorological variables in numerical models 78—49192
- outgoing spectral radiation, Nimbus 5 selective chopper radiometer meas., vertical temp. profiles 80—12520
- outgoing thermal radiation, meas. rel. to O_3 profile determ. 78—92945
- Oviedo, Spain, global solar radiation and air temp. *(Spanish)* 80—36377
- penetrating radiation composition, Cosmos 721 obs. 77—53279
- Peru, two-parameter statistical model of daily irradiation *(French)* 79—29812
- photodissociation of NO_2, NO_3, HNO_3 and H_2O_2, solar radiation effects 79—58045
- Planck blackbody radiation function integration 77—45059
- plane parallel atmospheres, radiative transfer eqn. soln. 80—67409
- planes tilted facing equator, solar radiation charts 79—66779
- planetary radiation budget, Nimbus 6 meas., first 18 months 80—12493
- planetary wave in middle atmosphere, radiative damping rel. to interaction with zonally averaged circulation 80—109217
- plasmapause, 1-30 Hz waves generation by reson. electron instability 78—49235
- plasmasphere, wave-particle interactions, ELF-HF obs. from EXOS-B 80—67467
- polarization scanner for monitoring from geosynchronous satellite 79—58222
- pollutant layers, elevated, radiative effects on urban atmosphere temp. struct. and pollutant dispersion 80—97841
- pollutant layers, radiative effects 78—65382
- pollution, radiative effect, latitudinally depend. radiation calcs. with clouds 79—34942
- positron annihilation line at 511 keV in upper atmosphere 80—41582
- precipitation flux climatology of free atmosphere 77—78397
- profiles in extended water clouds, obs. 79—79931
- profiles in extended water clouds, parameterization schemes 79—79930
- profiles in extended water clouds, theory 79—79929
- pyrgeometer performance improvement 77—70860
- Quebec, hourly radiation values for horizontal surface 80—17354

atmospheric radiation continued
- radiactive transfer in solar, IR and microwave spectral range, modelling 79—53520
- radiation balance, heat balance, heat and cold sources, E.Asia 80—12548
- radiation balance meas. as instrument design problem 77—41173
- radiation balance of ocean-atmosphere system *(Russian)* 77—78200
- radiation budget expt., Nimbus-6 obs. 77—41106
- radiation intercepted by a tilted surface, estimation of daily, clear sky, spatial distrib. 80—81423
- radiative balance, meas. by Cactus accelerometer on Castor satellite *(French)* 78—81530
- radiative equilib. temp. change due to stratospheric aerosol pollution 77—45092
- radiative flux transfer, delta-Eddington approx. for absorbing-scattering atmosphere 77—45151
- radiative forcing of atmosphere, sensitivity to variable cloud and moisture 80—56553
- radiative heating, rel. to global general circulation model and O_3 prod., transport and distrib. 80—56544
- radiative processes and thermal structure 80—82016
- radiative transfer, nonisothermal inhomogeneous layers, exiting monochromatic intensity 79—37139
- radiative transfer, variational and discrete ordinate calc. methods 77—53188
- radiative transfer eqn., soln. using Elsasser scheme 80—77112
- radiative transfer eqn. for scattering layer with extended scattering indicatrix *(Russian)* 78—40660
- radiative transfer in atmosphere-ocean system, matrix operator approach 80—8330
- radiative-convective model for CO_2 conc. increase problem 77—66977
- radio emission, aircraft meas., temp. height profile determ. *(Russian)* 79—16574
- radio emission fluctuations at 0.8 and 1.35 cm, aircraft obs. over USSR *(Russian)* 78—32229
- radio emission fluctuations of cloudy atmosphere at mm wavelengths *(Russian)* 77—21833
- radio emission of cloudy atmosphere, expt. characts. of fluctuation 80—67399
- radio emission of the atmosphere in the 5-13 cm^{-1} band 80—61878
- radiometer, directional, for longwave radiation meas. at ground 78—73537
- radiometric measurement for height temp. profile determ. *(Russian)* 77—64498
- radiometric sounding data and operational numerical weather prediction 78—53696
- radiometry methods (Soc. Photo-Optical Instrum. Engrs., Proc. vol.91, San Diego, 26-27 Aug. 1976) 77—70880
- radiometry programme at Cagliari *(Italian)* 79—100958
- radiowave generation, by auroral electron beams, mechanism *(Russian)* 78—40724
- rainfall measurement, combined usage of radar and radiometry techniques *(Chinese)* 80—109272
- rainfall over land, microwave radiometry by Nimbus 6 ESMR 80—56635
- remotely sensed Earth imagery, atmospheric blurring removal 79—88517
- Saharan dust affecting radiative transfer rates, model 80—90149
- satellite IR radiance meas., moisture vertical profile estimation 78—45021
- satellite radiance meas., temp. retrievals, empirical method 77—70859
- satellite-derived radiance gradient, rel. to upper tropospheric/lower stratospheric winds 80—98447
- scattering effects for high-rejection optical baffling system 78—7802
- Schumann resonances, balloon meas. *(Japanese)* 79—79919
- sea ice, energy exchange in central Arctic 78—85584
- sea surface radiobrightness temp. from satellite sounding *(Russian)* 77—60412
- shortwave and longwave radiative flux, mid-ocean obs. 80—12547
- shortwave spectral characts. over desert, calc. from CAENEX-70 data 79—100956
- sky brightness at zenith near terminator, light scatt. theory for optically thin atmosphere 80—109382
- solar, atmospheric attenuation, effect of O_3 and H_2O vapour content and atmos. turbidity 80—93855
- solar, daily irradiation, ARIMA modelling with constant and seasonal parameters 80—55821
- solar, mesoscale mapping of available solar energy at the Earth's surface by use of satellites 80—72613
- solar, monthly average radiation estimates for shaded vertical receivers 80—35646
- solar and terrestrial radiation dependent on the amount and type of cloud 80—67403
- solar anisotropic diffuse insolation, calc. of instantaneous flux on tilted surfaces 80—101412
- solar declination and the length of the solar day 80—45648
- solar diffuse irradiance measurement using shadowband, corrections 80—101410
- solar direct irradiance at the ground, parametric modelling 80—101411
- solar eclipse affecting radiation and heat budget above pine forest *(German)* 80—46226
- solar energy estimations, isotropic distribution approximation 79—66778
- solar energy flux prediction in polluted urban areas 80—30394
- solar energy utilisation, global and sky radiation estimates for Austria 80—93861
- solar energy utilisation, prediction of hourly diffuse solar radiation from measured hourly global radiation on a horizontal surface 80—93864
- solar flare X-rays, atmosphere reflected fluxes rel. to flare spectrum beyond 200 keV 80—51710
- solar flux var. rel. to climate 77—21872
- solar insolation, in India, daily total and diffuse, estimation from weather data 79—100926
- solar insolation meas. using CdS photoresistor 80—31092
- solar intensity obs., global insolation on horizontal and tilted surfaces 78—81275
- solar irradiance, model for determining the spectral quality of daylight on a horizontal surface at any geographical location 80—93856
- solar irradiance on horizontal surface, estimation of totals from UK average meteorological data 80—81422
- solar loading on fixed, tracking surfaces, solar energy availability investig. 80—40838
- solar radiation, monthly mean calcs. on vertical and inclined surfaces 80—45746

atmospheric radiation continued
- solar radiation characts. and intensity calc. 80—45649
- solar radiation from cloudy skies, Cole's model extension 79—74947
- solar radiation incident on St. Louis, Missouri, USA, urban-neural differences 80—109247
- solar radiation levels on tilted surfaces, computer model validification 80—35641
- solar radiation measurement, reference scales 80—109206
- solar radiation models, atmospheric ozone estimation 79—70875
- solar radiation statistics, linear spatial interpolation 80—93859
- solar UV radiation, absorpt. in mesosphere and stratosphere 80—109248
- soot particle absorpt. of near IR *(Russian)* 80—82055
- spectral extinction by atmosphere, meas. 0.3 to 10 µm 80—8427
- spectral global and diffuse radiation and atm. aerosols, pyranometer meas. errors 79—21050
- spectral irradiance in middle UV and visible at Durban, S.Africa 79—12264
- spontaneous radiation of 'fresh air' *(Russian)* 77—87035
- St. Louis metropolitan area, net radiation budget 79—12266
- stratocumulus clouds, IR absorption and liquid water content 77—21858
- stratocumulus water clouds, radiation transfer and IR flux and radiance 77—45146
- stratosphere, aerosol optical props. and size distrib. effects on heating rates 79—12222
- stratosphere, gamma-ray quasi-periodic intensity variations *(Russian)* 80—90177
- stratosphere, radiance variation seen by horizon sensors 79—100957
- stratosphere, radiative-dynamic coupling, 3-dimens. circulation model 77—86965
- stratosphere, radiometric obs. using superpress. balloon 80—85763
- stratosphere, simulated radiances for ClO and NO concs. determ. via solar occultation meas. 80—85756
- stratosphere, temperatures and geostrophic winds during 1973-74, Nimbus 5 radiance meas. 79—79976
- stratosphere, upper, radiative damping, obs. evidence 79—84368
- stratus clouds, shortwave radiative effects of unactivated aerosol particles 77—64382
- subauroral red arc event caused by kinetic Alfven waves 78—93026
- submillimetre outgoing radiation obs. in broad spectral bands *(Russian)* 78—65443
- submillimetre radiation from tropical cloud clusters, Cosmos 669 obs. *(Russian)* 77—49165
- submillimetre sky emission and absorpt., freq. spectrum of fluctuations 77—41308
- submillimetre waves and applications, conference, Guildford, England (1978) 79—31916
- summer radiation budget rel. to Asian monsoon 78—40664
- sunlight scattering, Rayleigh and Mie theory 80—56605
- surface and atmospheric radiation balance from satellite data 80—101396
- surface radiation from normal and dusty oceanic atmosphere *(Russian)* 77—60409
- surface radiative flux, clear and cloudy conditions, parametrisation accuracy 78—77325
- temperature vertical profile, from satellite data, information retrieval 78—3959
- terrestrial solar spectral irradiance distrib. variations, sensitivity of solar transmittance, reflectance and absorptance 80—82739
- Thailand radiation climate, calcs. from routine meteorological data 79—29814
- thermal, fluctuations, influence on radiotelescope sensitivity, expt. *(Russian)* 77—21832
- thermal microwave emission from two-layer medium, theory 77—49170
- thermal microwave radiances from hydrometeor clouds 78—85638
- thermal radiation, ground based obs. of temp. distrib. *(Chinese)* 80—82041
- thermal radiation, influence of large hailstones on spectral depend. in 0.86 to 17 cm range *(Russian)* 78—36222
- thermal radiation, particulate pollution effects rel. to climatology 78—85678
- thermal radiation, rel. to Earth global heat balance annual var. 78—73300
- thermal radiation fluxes calc. for cloudy atm. *(Russian)* 80—4103
- thermal radiation observations from satellites, moisture content characts. 80—85660
- thermosphere, 63 µm radiation field and influence on H temp. 79—80066
- thermosphere, dynamic processes from optical meas. of emissions 78—36342
- thermosphere, nighttime, energy balance 79—35022
- thermosphere, NO radiative cooling 80—72656
- thunderstorm VHF emission, rel. to three-dimens. motion 80—46218
- thunderstorms, microwave radiometric detect. of corona from chaff 78—16106
- Tokyo, downward radiation obs. during winter nights 80—41478
- topside magnetospheric cleft ionosphere 6300 and 5577 Å emissions meas. 77—29571
- total radiation intensity, universal formula using climatological data 80—31108
- total solar radiation, cooling tower plume effects, obs. 79—12177
- total solar radiation at Earth's surface using satellite measurements 80—4147
- total solar radiation determ. using obs. and estimated precipitable water 77—56687
- transfer of mass and heat between ground and atmosphere *(French)* 79—84403
- transfer of solar radiation under fractional cloud cover, two-stream approx. 80—51534
- transmissivity rel. to atmospheric path length 77—56730
- transmittance and radiance, high-resolution HITRAN and data compilation 79—66795
- transmittance and radiance, moderate-resolution, LOWTRAN code 79—66796
- tropical region, heat budget estimate of ocean and atmosphere 80—104968
- tropics, total atmospheric emissivities 79—29859
- tropopause height estimation from nonlinear functions of satellite meas. spectral radiance 77—78335
- troposphere, IR fluxes meas. by radiometric soundings, parametric law derivation *(French)* 79—25358

atmospheric radiation continued
troposphere, IR radiation, cloud height, thickness and overlap effects 78—57252
troposphere, radiative cooling rate and flux, theory 80—85711
troposphere, thermal balance in low latits. in zonal circulation model 79—25316
troposphere, UV flux calcs. and photolysis rates 80—12465
troposphere radiative divergence in GATE, results 80—17320
troposphere radiative energy balance, affected by stratospheric O_3 content 80—51466
troposphere radiothermal radiation, waveguide propag. *(Russian)* 79—88406
tropospheric aerosols, effect on surface and surface-atmosphere radiation budgets 80—17375
turbidity monitored by satellite, obs. of reflected sunlight 80—51471
Typhoon June (1975), obs. by scanning microwave spectrometer 78—73436
United States, solar climates 80—76612
upper atmosphere, energy balance, importance of IR radiation 79—8729
upper atmosphere, IR emission at high latitudes from Meteor satellite, radiometer obs. 80—72655
upper atmosphere, IR radiation, model 78—12035
upper atmosphere, IR radiation from mol. vibr.-rot. transitions 79—5695
urban atmosphere, roof level, long wave radiative flux divergence and nocturnal cooling 77—33123
urban atmosphere, urban canyon, long wave radiative flux divergence and radiative cooling 77—33124
UV albedo obs., by TAIYO satellite *(Japanese)* 79—44281
UV irradiation of filtered air, particle production expts. 78—24336
UV polarisation characteristics using Monte Carlo methods *(Russian)* 78—32224
UV radiation detection, space appls. for remote sensing 77—70881
UV radiation sources modelling, upper atmosphere appl. 80—1288
vacuum UV background, meas. 80—90221
Van der Waals mols. in lower atmos., IR emission and absorpt. 80—85699
variable-path Lyman α hygrometer, operating characts. 77—33194
vegetation reflectivity, effect on atmospheric radiance and polarisation 78—40650
visible range spectrometric investigation from Salyut 4 80—51638
VLF emission modulation freq. shift relative to geomagnetic pulsation freq. 80—77229
VLF radiation during simultaneous magnetospheric substorm and thunderstorm, rel. to elec. fields and electron precip. 80—67392
VLF wave events at $L=4$ correl. to optical emission 80—101468
VLF wave measurement at ground station, antenna pickup for vertical elec. field 80—105063
VLF waves, magnetospheric, obs. and comparison with high energy electron flux by EXOS-B satellite *(Japanese)* 80—94652
VLF waves triggered by natural whistlers 80—98521
VUV solar scatt. radiance, aurora and nightglow, satellite obs. 80—90272
whistler precursor emissions and whistlers, ducted propagation 80—85809
X-ray bremsstrahlung from widespread electron precipitation 80—77205
X-ray K-shell emission at satellite altitude from proton precipitation 78—61641
X-ray microbursts in auroral zones, power spectra rel. to primary electron transit times 77—78556
X-ray pulsations with long period at 75° magnetic latitude 78—28433
X-rays, bremsstrahlung, produced by magnetosphere conjugate electron precip., high time resolution meas. 80—41666
X-rays, separation from primary diffuse X-ray component using growth curves 79—25512
X-rays from electron precipitation, obs. at Sanae (1974 November 14) 77—87182
X-rays from electron precipitation events in local dusk sector 80—101480
X-rays from low latitude nighttime atmosphere, HEAO-1 obs. 79—44283
X-rays from magnetospheric electrons, rocket-borne astronomy affected 78—61640
γ-ray flux above 40 MeV in upper atmosphere 77—53257
Ar fluorescent X-rays from sunlit Earth atmosphere during solar flares 77—13142
CO_2 15 μ band radiant energy inflow in disturbed LTE *(Russian)* 78—40657
CO_2 15 μm band radiation, weather satellite meas. rel. to temp. field spatial anal. 78—20488
H, geocoronal Lyman α rel. to local perturbations of H density distrib. near exobase 78—24400
H_2O 1.35 cm absorption resonance, atmospheric radio emission features 80—46228
H_2O vapour band, IR radiative cooling rate, calc. 80—90161
H_2O vapour meas. in mesosphere from ground-based microwave obs. 77—33161
H_2O, weak spectral absorpt. of vap., visible and near IR 80—82062
N_2 3371 Å dayglow emission, excitation by photoelectron impact 77—33236
N_2^+ 427-8 nm emission, obs. rel. to mid-latit. charged particle precip. 79—44291
N_2O, IR emissivity and band-model parameters, 200-500K 77—83591
O I 1304 Å, nadir intensity/column prod. rate ratio rel. to airglow studies 77—45213
O I 5577 Å, Na and OH nightglow emissions var. during stratospheric warmings 77—53270
O I 5577 Å forbidden line and O_2 7620 Å band auroral excitation 78—88964
O I 6300 Å, enhanced emission regions prod. by Plateville ionospheric modification expt. 77—33263
O I 6300 Å emission, nighttime vertical distrib. models 79—53602
O I 6300 Å forbidden line high resolution obs. in dayglow 77—41252
O II forbidden line emission, 7320-7330 Å, intensity ratio and centre wavelengths 79—44284
O_2 5 mm absorption band, appl. of ground-based radiometry for temp. inversion detect. *(Russian)* 78—11963
O_3, 9.6 μm band radiance calc., excitation processes 78—36350
O_3 conc., fast oscills. in 3140 and 3690 Å obs. 77—53161
O_3 layer, role of dynamic and radiative processes in O_3 depletion by chlorofluorocarbons 80—109221
OH emission as recorder of internal gravity waves near mesopause 78—12031
OH near IR emissions, Spacelab image intensifying TV obs. 77—21966

atmospheric radioactivity
see also fallout
aerosol, laminar flow in cylindrical tube, conc. distrib. of free and attached Rn and Tn decay products 79—29412
aerosol particles from nuclear explosion, rel. to thundercloud electrification 79—84388
aerosols, atoms and ions attachment rate, nuclei conc. and humidity effects 79—62555
airborne radioactivity meas. in HFEF/N 80—18687
Antarctica, radioactive pollution of near-surface air *(Russian)* 77—29393
artificial radioactivity migration in environment, survey of models 79—96487
Australia, east coast, radioactivity seasonal and latit. vars. 77—64400
biosphere, radioactive contamination, influencing factors, 1962-76, Hungary *(Hungarian)* 78—92711
boundary layer, natural radioactivity continuous meas. method *(Flemish)* 78—61612
BWR power plant stack effluent inert gas nuclide monitor 79—3255
cloud dose data file fast correction for changes in dispersion parameters 78—80969
collective dose commitments from the release of radioactive nuclides to the atmosphere 80—3556
cosmogenic radioisotope flux onto Earth's surface and atm., magnitude and time var. 78—61634
Cosmos 954 crash in Canada, air pollution, obs. of lichens 80—55960
Czechoslovak Rez Nuclear Research Institute airborne radioactive release monitoring 78—89991
diffusion, steady state 3-D model, numerical anal. *(Japanese)* 79—79984
diffusion of pollutants after hypothetical accidents at nuclear plants *(German)* 77—64421
diffusion plume model, estimation of model parameters *(Japanese)* 79—79983
dispersion, population dose calc. 78—85381
diurnal variation, harmonic anal. *(Rumanian)* 79—21009
dose calculations of deposited activity and cloud activity 80—3551
dust, long-lived beta-activity, freq. distrib. anal. 77—73835
dust captured by wind from Earth's surface, radioactive fallout *(Russian)* 80—16869
environmental γ radiation, variation during rainfall *(Japanese)* 78—36240
environmental pollution evolution, influence of jet stream *(Spanish)* 79—100549
environmental radiation dose assessment of a growing nuclear industry 80—3553
environmental radioactive releases from nuclear installations, computer simulation of effects 80—3550
ERDA nuclear plants, radiation levels in environmental vicinity 78—9002
fallout in air and rain, results to end of (1978) 79—79997
fission products, removal rate seasonal vars. 80—55957
fission products, washout by rain *(Spanish)* 79—92399
fly ash, from coal power plants, radioactivity 79—62161
gamma radioactive source measurement, in dynamic condition, error sources *(Rumanian)* 78—46243
gamma-ray flux measurement, NaI(Tl) scintillation counter *(Japanese)* 77—71732
gamma-rays, spectra and angular distrib. 0.3 to 10 MeV 77—49205
gamma-rays from extended sources, energy distrib. calc., rel. to remote spectroscopy 78—61586
gas monitoring by silicone oil absorbent scintillation counter 80—12044
gaseous release monitoring and γ spectrometric analysis *(French)* 79—3259
gross beta radioactivity data, applicability of Weibull distrib. function 77—2230
inner radiation belt, max. radiation dose following 1962 STARFISH explosion 78—69612
Kyoto University reactor, airborne radioactivity from primary coolant 80—22959
LWR core meltdown, activity release and aerosol characts. 78—82469
maximum radiation exposure calc. around German nuclear plants 80—856
meteorological information system for response to nuclear power station accidental release of radioactivity 80—16888
midwest USA, ^{85}Kr concs. 77—73834
mountain station, soil emanations rel. to atmospheric electrode effect 79—25307
natural, pollution with coal smoke particles *(Rumanian)* 78—53723
natural radiation exposure, New Zealand, soil survey and air doses for ^{226}Ra and ^{232}Th daughters and ^{40}K 78—88747
neutron skyshine from nucl. facilities *(Japanese)* 79—18054
nuclear plant emission, radiation exposure calc. *(German)* 78—82531
nuclear power plant vent-air monitoring by nuclide-specific detection system 79—3249
nuclear power reactor fission product release, dispersal 77—14250
nuclear power station effluent discharge, absorbed doses *(Spanish)* 78—8998
nuclear power station stack effluents, radiation monitoring 78—46179
nuclear power stations, radioactive emissions, heat emissions, other environmental effects 79—22491
nuclear reactor accident dispersion model, direction depend. probability limits consistent with NRC practice 78—17372
nuclear tests, maximum credible concentrations 79—83948
Ontario Hydro nuclear power plant stack effluent monitoring 79—3254
organ-specific radiological impact of airborne effluents from model PWR and FBR reprocessing plants 80—3825
Pasquill's index importance in natural atmospheric radioactivity studies *(Spanish)* 77—87044
plume diffusion at Rancho Seco Generating Station, LIDAR obs. 78—11991
pollution control at Nuclear Research Institute *(Czech)* 78—88906
power plant effluents, AEOLUS code for dispersion during normal, sea-breeze, and accident conditions 78—11993
power stations, radiological impact from model coal-fired power plants and from nuclear systems 80—3557
radiation levels of naturally occurring radioactive sources 78—9001
radioactive fallout water deactivation using sorption props. of clinoptilolite, vermiculite, bentonite 79—43995
radioactive releases from nuclear installations, eval. of accidental atmos. discharges 79—39529
radioelement transfer in marine aerosols *(French)* 78—24338

atmospheric radioactivity continued
- radionuclide airborne release assessment, determ. of atm. stability categories 78−73504
- radionuclide and chemical pollutants, pulmonary effects *(French)* 80−8102
- radionuclide concentration determ. in ground level air 79−24927
- radionuclide influences on ice formation in clouds 79−48530
- radionuclide release assessment, importance of vars. in deposition vel. 78−80979
- radionuclides in N.European air due to Chinese nucl. explosions 80−108826
- reactor near-stack dose calc., diffusion model applicability 78−94147
- reactor waste air plumes, diffusion in atmosphere 77−53183
- release from nuclear facility, dose calcs. using on-site meteorological data 77−40798
- release to atmosphere, calc. of consequences with TIRION-4 code 79−29494
- risk anal. of high-level waste management systems in Germany 78−50272
- Rn series disequilib. in S. California coastal air 79−58041
- short-lived radionuclides of unknown origin in Sweden (1976) 78−32219
- skyshine dose due to gamma-rays from nucl. power plant *(Japanese)* 79−29917
- stack effleunt monitor in-place testing 79−3257
- stack release radioactivity monitoring with digital processing 79−3253
- stratosphere, residence times from β activity of Antarctic and Greenland snows 79−79421
- Switzerland, radioactivity surveillance and descent of Kosmos 954 *(German)* 78−77119
- troposphere, tritiated water vapour natural fluctuation rel. to environmental radiation surveillance 77−88287
- tropospheric mean zonal velocities determ. by detection of radioactive clouds *(Spanish)* 77−73782
- turbulent atmospheric transport, Monte Carlo simulation, radioactive pollution appl. 78−61550
- West German LWR power plant stack monitoring, legal and technical aspects 78−89988
- West German nuclear plant airborne radioactive effluent monitoring 78−89990
- West German nuclear power plant airborne radioactive release control 79−13549
- β-active aerosol particles, stationary charge distribution 79−92581
- ^{7}Be bearing aerosols mean residence time in troposphere 77−87018
- ^{7}Be, cosmic-ray-produced, mean tropospheric residence time at north temperate latits. 78−85633
- ^{14}C concentration in Earth's atmosphere, corrections with astrophysical and geophysical phenomena 78−61477
- ^{14}C concentration in Earth's atm. with variations of geomag. field, spectral anal. 78−61478
- ^{14}C formation by solar flare particles 78−92886
- ^{14}C produced in advanced FBR fuels, potential radiation doses 77−40799
- ^{14}C production in Tunguska cometary impact 77−78720
- ^{14}C released to atmosphere as CO_2, population dosimetry 78−35958
- ^{14}C variations rel. to 11-year solar cycle 78−92885
- $^{14}CO_2$ meas. in Karlsruhe Reprocessing Plant exhaust air 79−3231
- ^{60}Co, gamma radioactive source, buildup factor determination for meas. in air *(Rumanian)* 78−49132
- ^{60}Co skyshine, continuous γ-spectra unfolding 79−81118
- ^{137}Co, gamma radioactive source, buildup factor determination for meas. in air *(Rumanian)* 78−49132
- ^{137}Cs, time variation of low concentrations in rain water 79−43994
- fission products, ^{222}Rn and cloud nuclei particles in N.Atlantic air 80−77074
- HTO data, applicability of Weibull distrib. function 77−2230
- ^{3}H, environmental levels, detection with liquid scintillation spectrometers 77−9489
- ^{3}H formation by solar flare particles 78−92886
- I, $A=123$ to 135, derived air concs. annual limits 78−31909
- ^{131}I air concentrations, comparison of calculated and meas. values 77−34477
- ^{131}I, airborne conc. at Swierk nuclear research centre 1975-1977 80−7978
- ^{131}I and methyl iodide sampling, filter materials selection 79−83673
- ^{131}I, gamma radioactive source, buildup factor determination for meas. in air *(Rumanian)* 78−49132
- ^{131}I in nuclear power plant gaseous discharge, cumulative meas. *(Russian)* 79−3224
- $^{131}I_2$, $CH_3{}^{131}I$, airborne, diffusion coeffs. 79−2142
- Kr activity meas. using ^{85}Kr 77−78454
- ^{85}Kr conc. 80−93756
- ^{85}Kr concentration in atmosphere over USSR (1971-1975) 78−37453
- ^{85}Kr, latitudinal distrib. in atm. surface layer over ocean *(Russian)* 79−39813
- ^{85}Kr, radioactive pollution in atmos., Warsaw 1975 to 1977, meas. methods 79−34458
- ^{24}Na, gamma radioactive source, buildup factor determination for meas. in air *(Rumanian)* 78−49132
- ^{210}Pb conc. or climatic changes at South Pole 78−7748
- ^{210}Pb fluxes, determ. from soil profiles 79−2346
- ^{210}Pb, time variation of low concentrations in rain water 79−43994
- Pu, air concs. near Rocky Flats, $^{239+240}$Pu 78−16150
- Pu laboratory stack monitoring, computerised system 79−3256
- ^{239}Pu data, applicability of Weibull distrib. function 77−2230
- Ra A (^{218}Po) adsorption to monodispersed aerosol 80−32535
- Ra daughters in air, meas. by gamma spectrometry 80−30628
- Rn, aerosol particle size distrib. in uranium mine *(French)* 78−32195
- Rn and Rn decay products, disequilibrium ratio in the atmosphere *(Spanish)* 80−31083
- Rn concentrations, statistical analysis of stability indexes *(Spanish)* 79−92561
- Rn daughter concentrations in air of dwellings in Great Britain 78−77118
- Rn daughter sampling, relative filter efficiencies 77−56725
- Rn daughter's radioactivity levels over Arabian Sea, air mass mixing ratio 77−91227
- Rn daughters in air, conc. meas. by α-spectrom. 78−32218
- Rn decay products, appl. to atmos. diffusion props. anal. 79−84347
- Rn decay products, appl. to atmos. diffusion props. anal. 79−84348
- Rn emanation, seasonal vars. rel. to subterrestrial fluid convection 77−37246

atmospheric radioactivity continued
- Rn, emanation on San Andreas fault 78−32022
- Rn, evolution in neutral atmospheres *(Spanish)* 80−4058
- Rn, induced radioactivity increase rel. to geomag. perturbations biotropicity 79−96621
- Rn short lived daughters, atmospheric conc. estimation by least squares anal. 78−7728
- Rn, short lived daughters, detection method *(Chinese)* 80−42889
- Rn, use in determination of vertical stability of lower atmosphere, influence of air flow on Rn content *(Spanish)* 79−92560
- ^{222}Rn, ^{210}Pb, ^{7}Be and fission products conc. in South Pole atm. 79−84382
- ^{222}Rn, and decay products, vertical distrib., time-dependent calc. 79−84383
- ^{222}Rn, and its descendants, radioactivity in low atmosphere, pollution-dust dynamics *(Rumanian)* 80−12524
- ^{222}Rn conc. over intertropical convergence zone of Atlantic 80−26648
- ^{222}Rn content in air, diffusion in lower atm., U deposits prospecting appl. *(Spanish)* 77−78303
- ^{222}Rn daughter conc., meas. sensitivity computer optimisation 78−49126
- ^{222}Rn daughter prods. meas. using diffusion sampler 80−81510
- ^{222}Rn emanation from uraniferous materials, influence of variability on prospecting 79−62498
- ^{222}Rn evasion rates in Atlantic and Pacific, Geosecs determ. 79−79875
- ^{222}Rn exhalation meas., soil and meteorological effects *(Spanish)* 80−31082
- ^{222}Rn, in calcite caves at Akiyoshi Karst Plateau, meas. and calc. *(Japanese)* 79−83671
- ^{222}Rn low conc. meas. in air, α-scintillation method 78−92970
- ^{222}Rn meas. during marine fog off Nova Scotia 78−40624
- ^{222}Rn, props. and behaviour of short lived daughter nuclides in the atmos. *(Japanese)* 80−72339
- ^{222}Rn, release to atm. due to UK coal combustion, annual rate of release determ. 80−17143
- ^{222}Rn short lived decay products in air, collection efficiency of Whatman GF/A filter 78−20526
- ^{38}S in SO_2 and SO_2 oxidation rate meas. 77−73814
- ^{90}Sr, time variation of low concentrations in rain water 79−43994
- Th(B) conc., appl. to atmos. diffusion props. anal. 79−84347
- Th(B) conc., appl. to atmos. diffusion props. anal. 79−84348
- ^{238}U decay products, optical detect. system 77−87104
- ^{133}Xe, plume from Three Mile Island nucl. reactor 80−89696

atmospheric spectra
- *see also atmospheric optics*
- 2.2 μm window, plane-parallel model appls. to multiple scattered radiation problems *(Russian)* 78−36275
- 100 GHz to 1 THz atmospheric emission and absorption meas. 79−34980
- absorption at 460 μ, determ. 78−96295
- absorption continuum in the near IR near 1 μm 80−61894
- absorption line parameters, AFGL, compilation update 79−21013
- absorption line parameters compilation, AFCRL, accuracy in 10 μm atm. window 77−9494
- absorption line parameters compilation, AFCRL, updating 77−9495
- absorption lines of atmospheric gases, determination of parameters *(Russian)* 79−84507
- absorption lines recorded by intracavity Nd:glass laser spectrometer 77−74530
- absorption near 2400 cm^{-1} 78−11968
- absorption of solar, diffuse and reflected visible radiation *(Russian)* 78−96291
- absorption spectra of air and components at 1.06 μm 79−66791
- absorption spectrum in 583-605 nm region by intracavity laser spectroscopy 79−53517
- aeronomical reference spectrum for solar UV below 2000 Å 79−25379
- aerosol above Black Sea, spectral transmission and sky brightness obs. *(Russian)* 80−94603
- aerosol IR spectrometry, theory and appl. to spectroscopic effect of atmospheric constituents 80−101428
- aerosol mass loadings evaluation from multispectral extinction data 79−12221
- aerosol particles characterisation by Raman spectroscopy 77−49188
- aerosol scattering indicatrices under clear sky conditions in 0.55 to 2.4 μ spectral region, determ. *(Russian)* 80−94600
- aerosol solid particles, diffusive evaporation, laser spectrochemical analysis 79−92040
- AFCRL atm. absorpt. line parameters in 2900-3000 cm^{-1} atm. window 80−36396
- air pollution remote sensing, use of computer-assisted correl. spectrometer 78−4002
- air radiation in photographic meteor spectra 77−29733
- airglow, F-region, anal. of consistency of ground-based obs. with satellite results 80−98496
- airglow and aurora, visible spectrum, detection and study 77−70903
- airglow emissions, semi-annual vars. 78−28360
- airglow spectrometer, Fabry-Perot instrument for daytime use 80−77156
- airglow studies using large-aperture, high-resolution Fabry-Perot spectrometer 80−67424
- airglow weak emissions, meas. with programmable scanning spectrometer 80−8469
- area skyshine from radioactive waste, gamma-ray backscatt. photon spectra 80−31119
- at twilight 79−92596
- atmosphere, spectral transmissivity, rel. to direct beam solar irradiance and illuminance 80−90174
- atmospherics spectrum, effects of return stroke lightning current and vel. 79−25306
- attenuation by surface layer, spectral structure *(Russian)* 78−36277
- Auger processes and photoelectron spectra formation 79−2403
- aurora, 2150 Å spectral feature, contrib. from N II lines 78−61645
- aurora, artificial, ground-based optical meas. during Excede 2 test 78−89038
- aurora, artificial, $N_2{}^+$ and O I emission rel. to O(^{1}S) prod. and loss processes 79−66855
- aurora, artificial, time-depend. spectrum in Precede expt. 78−89037
- aurora, correl. of ground-based and topside photometry with electron spectra meas. 78−32266
- aurora, equatorial, EUV Apollo-Soyuz obs. of mag. quiet conditions 80−12591
- aurora, EUV spectrum obs. in 750-1230 Å region 77−33242

atmospheric spectra continued

- aurora, near IR spectrum obs. 77—53272
- aurora, pulsating, 5577 Å/4278 Å column emission ratio rel. to particle characts. 78—88969
- aurora, quantitative spectroscopy, 8800 to 11400 Å 77—13144
- aurora, rocket meas. and anal. of O_2, N_2 and O emissions 78—57380
- aurora, type-B, obs. and interpretation of spectra and rapid time vars. 79—40001
- aurora, UV spectrum, 2000-2800 Å region 79—70908
- aurora, UV spectrum between 2100 Å and 2300 Å 78—88963
- aurora initiated by electron injection from rocket, optically observed from ground 80—41559
- auroral bremsstrahlung X-ray flux comp. 77—60508
- auroral electron beam, electrostatic noise power flux spectra 78—85759
- auroral emissions, photometry rel. to precipitating electrons energy distrib. 78—77390
- auroral N_2, N_2^+ bands, airborne spectroscopic studies 77—29533
- auroral O I (989 Å) and O I (1027 Å) emissions 78—28367
- auroral secondary electrons spectrum at low altitudes, collisionless effects 79—40008
- auroral spectrum observations, appl. of matched tandem etalon camera (MATEC) 80—101442
- auroral spectrum vars. at latit. of polar cleft 79—25384
- auroral UV spectrum, 1200-3200 Å, OGO-4 obs. 77—9594
- boundary layer turbulence spectra in stable conditions 77—73786
- cirrus clouds, radiative props. in NOAA 4 VTPR channels rel. to satellite exploration 79—39853
- cloud droplet spectrometry using light scatt. technique 77—41219
- clouds, particle size distrib. from spaceborne line spectrum imagery, theory 79—5613
- clouds, spectral radiative props. parameterisation 80—56601
- cosmic ray electrons in stratosphere, spectrum above 3 GeV 77—53374
- dayglow spectrum, far UV N and N_2 emissions 78—28361
- daylight, model for determining spectral quality on horizontal surface at any location 80—93856
- dichlorodifluoromethane, diode laser spectra near 10.8 μm, air-broadening effects 78—61555
- dichlorodifluoromethane spectral parameters for atm. sensing 79—84481
- difluorodichloromethane, spectral data evaluation for atm. sensing 79—62582
- direct visible spectra and aerosol optical depths at urban and rural locations during summer 1975 at Milwaukee, meas. 79—29857
- dispersion correlation spectroscopy, mask optimisation procedures 77—73857
- Dobson O_3 spectrophotometer calcs., generalized treatment of particulate scatt. 79—12267
- Doppler spectra of current-driven plasma instabilities in electrojets 79—58163
- dust, soil derived atmospheric, IR spectra, Christiansen effect, Rayleigh limit 80—105046
- electron spectra in Earth's radiation belts during mag. storms 77—53314
- electron spectra in magnetosphere dayside cusp region, hard spectrum population 79—12352
- electrons, 1 to 500 eV, in high-latit. ionosphere, characteristic energy spectra 77—29568
- emission obs. by Fourier transform IR spectrometer *(Japanese)* 80—12541
- emission spectra, 5-40 cm^{-1}, high resolution meas. from aircraft 78—7766
- ethylene, high resolution spectroscopy with diode laser heterodyne system 77—91300
- ethylene dibromide, photoabsorption spectra 190-300 nm 79—50038
- EUV dayglow, spectra, atomic and ionic emissions, 530-1240 Å 79—70904
- F-region convective electric field determ. from rocket meas. of thermal ion spectra 78—57386
- far IR atmospheric emission and absorption spectrum calc. program 79—35020
- far IR emission spectra calcs. 78—92978
- fluorotrichloromethane, spectral data evaluation for atm. sensing 79—62582
- fog, spectral transmission data, IR propag. and performance modelling 80—90218
- formaldehyde, Doppler-limited spectra of C-H stretching fundamentals 78—70831
- formaldehyde, in troposphere and stratosphere, meas. by high resolution IR absorpt. spectroscopy 79—84371
- formaldehyde, meas. in atm. by ground based IR absorpt. obs. *(French)* 79—66764
- formaldehyde, mol., UV absorpt. cross-section, and stratosphere chem. 80—109209
- Fourier far IR spectroscopy from Spacelab 77—21949
- Fourier transform method for inhomogeneous atmosphere transmittance calc. 80—12555
- Fourier transform spectroscopy from South Pole 80—98448
- Freon IR mass absorption coefficients, 3 to 15 μm 79—76422
- Freon-12, absorpt. coeffs. for CO_2 laser radiation, press. and temp. depend. 78—55170
- Freons, IR absorpt. band intensities meas. in atm. window region 77—30871
- Galatry profile convolved with Fabry-Perot instrument function 77—78642
- gamma rays, medium energy, spectrum meas. 79—9030
- gamma-ray spectra from double Compton gamma-ray telescope, background sensitivity to atmospheric neutrons 78—53827
- gamma-rays, hard intensity radiation pulsations in the atmosphere *(Russian)* 80—17454
- gas absorption lines, half width and intensity, lidar remote probing technique *(Russian)* 80—21844
- gases identification and conc. meas. from spectral absorpt. patterns, anal. methods 77—87059
- gases identification and conc. meas. from spectral absorpt. patterns, system appls. and design 77—87060
- geocorona, collisional model for spectral line profiles 78—77508
- geocoronal Lyman α Doppler line profiles 80—12579
- geomagnetic pulsations observed on ATS-6 satellite and at Earth surface, spectral-temporal characts. 79—12345
- global and diffuse radiation and atm. aerosols, pyranometer meas. errors 79—21050
- ground level abundances of N_2O, CO_2, CO and H_2O, simultaneous determ. 78—11969

atmospheric spectra continued

- ground level air spectra at 9, 92 and 993 m path lengths 77—73823
- hail, Doppler radar spectra at vertical incidence 78—65368
- hydrazine, rocket fuel in ambient air, CO_2 laser absorption spectra and photoacoustic detection 80—104540
- hydrofluorocarbon monitoring using telluric absorption line *(German)* 78—49133
- interplanetary dust in stratosphere, visible absorpt. spectra 80—101554
- ionosphere, auroral, field-normal plasma-line scatt. detect. expt. 78—73580
- ionosphere, circumrocket glow spectral obs. in Zarnitsa.2 electron injection expt. *(Russian)* 80—12596
- ionosphere, ion cyclotron wave spectrum generated by Ba injection 79—53648
- ionosphere, predawn, conjugate photoelectrons, rocket obs. 79—29931
- ionosphere, travelling disturbances, electron density spectra 78—77398
- ionosphere, UV fluoresc. at 391.4 nm excited by electron beam 80—77214
- ionosphere artificial irregularity spectra disturbed by SW transmission *(Russian)* 78—32275
- ionosphere incoherent ion backscatter spectrum, stimulated Brillouin scatt. detect. 78—77412
- ionosphere plasma line, low-altitude anisotropy theory 78—77414
- ionosphere plasma line, meas. at Chatanika with high-speed correlator and filter bank 80—98507
- IR absorption spectra in 8-14 μm region, water cluster interpretation 79—98081
- IR cooling calcs., simple strategies for inclusion of Voigt effects 79—94768
- IR emission meas. using radiometer 78—4681
- IR emission spectrum and vibr.-rot. transitions of molecules in upper atmosphere 77—65462
- IR emissions, auroral enhancement 80—12586
- IR emissions in auroral regions, origin 77—33247
- IR heterodyne spectroscopy, stratospheric sounding 79—100971
- IR high resolution spectra, ground based obs. 77—41167
- IR high resolution spectra, numerical simulation 77—41166
- IR high-resolution emission spectra in two passbands 77—25782
- IR mosaic background obs. from balloon altitude expt. 80—90222
- IR nightglow continuum near 8500 Å, intensity meas. 78—49195
- IR optoacoustic spectroscopy of atmospheric gases 77—41243
- IR radiance meas., 4-14.5 μm range, by narrow beam spectral radiometer 78—61596
- IR radiative energy exchange through strong lines wings 80—101432
- IR scanning radiometer data interpretation 79—30541
- IR spectra of soil-derived atmospheric dusts, Christiansen effect 80—26608
- IR spectral band transmittance, modelling, Prony's method 78—70202
- IR spectral radiance through atm. path, hot source 77—9493
- IR spectral transmission meas., laser-calibrated, high-resolution 77—91266
- IR transmission spectra, high resolution field meas. and computer code calc. 79—66798
- IR window, absorpt. due to water vapour polymers 77—45145
- IR-absorbing molecules, collisional cross-sections, temp. depend. 79—96787
- irradiance in middle UV and visible at Durban, S.Africa 79—12264
- kinetic energy spectra in mid-latitudes 78—7707
- Lidar Raman/aerosol signal ratio, obs. for visibility meas. 79—100953
- lightning, atmospherics spectra rel. to transmission line model 77—33156
- Lorentz function convolution with spectral line data, accelerated convolution algorithm 79—81239
- Lowtran molecular absorption empirical transmission function analysis 79—76400
- Lyman α geocoronal emission effect on rocket meas. of proton fluxes 77—53273
- Lyman-α absorber in winter thermosphere, satellite occultation meas. 78—36349
- magnetopause, energetic electron spectrum meas. from Prognoz 3 80—72697
- magnetosphere, signal freq. offset during nonlinear amplification of 6.6 kHz transmission 78—40771
- magnetosphere dayside cleft region, photometric obs. at 6300 Å 80—41586
- magnetosphere electron distrib. function and electrostatic emissions 80—17445
- magnetosphere kilometric radiation, emission spectrum fine struct. from JIKIKEN (EXOS-B) satellite obs. *(Japanese)* 80—94648
- magnetosphere mid-latitude hiss, quiet band prod. by VLF transmitter signals 77—64534
- magnetosphere noise spectrum, influence of CW whistler injection 77—82087
- magnetotail lobe plasma, double-peaked ion spectra as evidence for massive ions 78—32299
- mesosphere at Thumba from in situ UV absorpt. photometry obs. 80—105051
- mesosphere incoherent scatter spectrum, ion component meas. in 60 to 90 km region over Arecibo 79—16569
- mesosphere solar Lyman α radiation absorpt. rel. to O_2 densities 77—87010
- meteor bright line spectra, study via astronomical TV system 78—61817
- meteor train, long-lived, IR brightness obs. 80—94629
- meteor wakes, excitation of ionic lines and mol. bands 79—29919
- meteors, O I 5577 Å emission, vel. dependence 78—20758
- methane, absorpt. spectra meas. rel. to abundance in vertical air column *(Russian)* 79—88407
- methane content, spectrometric meas. in N and S hemispheres *(Russian)* 77—13103
- methyl bromide, photoabsorption spectra 190-300 nm 79—50038
- methylchloroform, vapour phase, UV absorpt. spectrum, photodissoc., stratospheric appls. 79—81208
- methylhydroperoxide, UV absorpt. spectra of vap. 80—69159
- microwave frequency atmospheric transparency, 3-13 cm^{-1}, meas. rel. to water vapour conc. 80—12476
- microwave limb sounding for composition and temp. determ. 77—21940
- minor constituents detection using tunable spin flip Raman laser, review 80—55762
- molecular absorption over Antarctica in 8-13 μm region, 1977-8 obs. *(Russian)* 80—21823
- molecular transmission in surface atmosphere *(Russian)* 79—34949
- motions, spectrum analysis in dynamic meteorology 79—20957

atmospheric spectra continued
multispectral analysis by NOAA and METEOR satellites 77–82009
natural sky radiance and smoke stack radiance spectral characts. meas. and modelling, 3.8-5.5 μm region 79–66797
near IR extinction spectrum, calcs. 80–51539
night airglow visible spectrum, obs. using field compensated interference spectrometer 80–36424
night sky spectrum, distortion of galaxies radial vels. meas. 77–41406
nightglow, 557.7 nm line and Herzberg bands excitation 79–75008
nightglow, IR emission meas. (0.9-2.3 μm) using interferometer-spectrometer 80–12583
nightglow, OH, Na D-line and O I 5577 Å emissions correl. 79–80067
nightglow, rocket meas. of O_2 atmospheric system and OH Meinel bands *(Japanese)* 80–94631
noctilucent clouds, spectral brightness in visible and near IR *(Russian)* 77–13098
O I, 6300 Å airglow enhancements by high powered HF radiowaves *(Portuguese)* 80–41592
O I nocturnal 6300 Å luminesc., profiles from incoherent scatt. radar and photometry *(Portuguese)* 80–41591
optical measurements of minor gases in middle atm. 79–84480
optical phenomena, review including airglow and aurora 77–70831
Optical Society of America meeting on atmospheric spectroscopy (Keystone, CO, USA, 30 Aug.-1 Sept. 1978) 80–8731
outgoing thermal radiation, O_3 9.6 μm absorpt. band rel. to density profile 78–92945
Pc 4,5 geomagnetic pulsations, bounce effects influence on spectral characts. 80–4197
peroxynitrates, UV absorpt., spectra, photodissoc. lifetime meas. 80–83386
photoabsorption spectra of trihalonitrosomethane and trihalonitromethanes 79–22720
photoelectron energy spectra in upper atmosphere 78–49190
photon, spectra of gamma rays backscattered by infinite air (skyshine) 80–101436
plasmasphere, wave-particle interactions, ELF-HF obs. from EXOS-B 80–67467
polar airglow, N, N_2 emission obs. rel.to mag. ordering 78–57378
polar cap keV electrons during poststorm quieting, intensities and spectra 77–25835
pollutant gases microwave spectra, monitoring from space using passive sensing techniques 80–76690
pollutants remote sensing by satellite, correl. spectroscopy techniques 77–64456
pollution, urban, spectral meas. of direct and scatt. solar radiation 78–3949
pressure sensing by solar occultation using wideband CO_2 absorption 79–80037
pressure-scanning millimetric-wave dispersion spectrometer expt. 80–61904
proton spectrum and spatial distrib. in Earth's radiation belts 77–53313
radar echoes, type 1, from equatorial electrojet, with double-peaked Doppler spectra 80–67458
radiation attenuation spectral struct., depend. on atmospheric surface layer turbidity *(Russian)* 78–44997
radiometric meas. of constituent vertical profiles 77–70883
radiowave bandwidth limitations in turbulent atmosphere using coherency and differential amplitude spectra *(French)* 78–49070
rain drop spectra and fine structure on different time bases *(French)* 78–53681
rainbow polarisation rel. to droplet size and scatt. angle 79–80017
raindrop spectra, evolution in warm-based convective storms 79–88417
Raman scattering analytical techniques using tunable lasers 78–61134
sea level muon spectrum, Bugaev model 77–82094
SF_6 IR mass absorption coefficients, 3 to 15 μm 79–76422
shortwave spectral characts. over desert, calc. from CAENEX-70 data 79–100956
silver clouds, visible spectroscopic investig. from Salyut-4 orbit 80–82014
Skylab conical multispectral scanner IR data statistics 80–90223
solar radiation, global and diffuse, spectral distrib. 79–44229
solar radiation absorpt. spectra, atm. trace gases vertical conc. *(Russian)* 78–69442
solar radiation at Earth's surface, spectral distribution model 78–69456
Spacelab launch conditions for absorption spectroscopy *(French)* 79–8791
spectrally integrated transmittance in O_2 Schumann-Runge bands and O_2 column density, 76-102 km altitude 79–70902
spectrophotometry using compact spectrometer 79–2396
spectroradiometric measurement of temp. and gaseous composition profiles 77–9568
spectroradiometry of daylight at sea level in Durban. 79–100955
strain-dependent eddy viscosity, spectral characts. 78–44937
stratosphere, emission spectrum, balloon-borne far IR Michelson interferometer meas. 79–39870
stratosphere, fluorocarbon contamination of HNO_3 channel spectral meas. 77–87054
stratosphere, halogen compounds global monitoring by satellite borne spectrometer 77–45162
stratosphere, HCl and HF near IR absorpt. spectra and volume mixing ratios meas. 80–72587
stratosphere, HCl mixing ratio profile, radiometric meas. 77–25745
stratosphere, HNO_3 concs. in N.hemisphere from 11.2 μm band radiance 78–81288
stratosphere, IR spectra and N_2O_5 abundance upper limit 77–5299
stratosphere, laser spectroscopy relevant to photochem. 78–88951
stratosphere, lower, H_2O and O_3 conc., far IR spectroscopy, quantitative anal. 79–39790
stratosphere, lower, high resolution IR spectra, airborne obs. 100 to 140 cm^{-1} 77–49164
stratosphere, NO_2, concs. from solar absorpt. spectroscopy *(Russian)* 77–49109
stratosphere, solar radiation absorption, in O_2 Herzberg continuum, influence of O_4 and O_2N_2 dimers 78–87429
stratosphere, spectral lineshape calc. for emission model 79–62586
stratosphere, trace constituents, laser heterodyne spectroscopy 80–109257
stratosphere, trace constituents correlated seasonal and climatic vars. 79–84433
stratosphere, trace gases detection *(German)* 79–53003

atmospheric spectra continued
stratosphere NO_2 and H_2O, mixing ratio profiles from IR solar spectra obs. 80–105015
stratosphere trace molecule Fourier transform spectrometer optical design 80–82099
stratospheric far IR emission, balloon-borne obs. 79–34896
stratospheric gas monitoring, two-photon spectroscopy, Doppler-free technique 77–9514
stratospheric water vapour 0.94 μ absorption cross-section obs. *(Japanese)* 80–17427
submillimeter anomalous spectra 78–16156
submillimetre spectrum meas. with high resolution Fourier spectroscopy 77–87133
submillimetre wave spectroscopy, review 78–7796
submillimetric wave atmospheric spectroscopy, review 77–41240
submillimetric-wave interferometric spectrometry 79–34979
sunlight, spectral actinometric obs. for atmospheric aerosol turbidity characts. determ. 78–92986
sunlight, spectral struct. of radiation field refl. by ocean-atmosphere system *(Russian)* 77–33086
superthermal electron spectra in auroral E-layer, rel. to plasma lines meas. 79–25386
surface layer, statistical characts. of radiation attenuation spectral struct. *(Russian)* 78–24371
synthetic IR transmittance spectra, 15 and 4.3 μm CO_2 bands 78–28316
temperature sounding by high precision satellite,. spectral band passes 77–41175
temperature sounding with partially scanned interferograms 77–41176
terpenes, IR absorption bands of α- and β-pinenes above forests 80–12539
tetrafluoromethane, v_3 vibr.-rot. band identification in balloon-borne IR solar spectra 79–100894
thermal radiation, influence of large hailstones on spectral depend. in 0.86 to 17 cm range *(Russian)* 78–36222
thermosphere, Fabry-Perot spectrometer obs. of dynamics 80–12573
thermosphere, O I 63 μm emission spectrometric meas. 78–81474
thermosphere, photoelectron energy spectra, rocket born meas. in 2-100 eV range 78–77379
Toronto, city light pollution and night sky spectra 79–16668
trace constituents by IR spectra, altitude distrib. technique 79–34985
trace gases and pollutants, data compilation on mag. tape 78–44995
transmission meas. using IR lasers and Fourier spectroscopy 77–70885
transmittance and radiance, high-resolution HITRAN and data compilation 79–66795
transmittance and radiance, moderate-resolution, LOWTRAN code 79–66796
transmittance profiles calc. method 78–85696
transparency spectrum, meas. on Maidanak mountain during autumn and winter (1977 to 1978) *(Russian)* 80–72627
trichlorofluoromethane, 8-12 μm band model calcs. 80–43112
trichlorofluoromethane, 8-12 μm bands intensities, temp. depend. 80–43048
troposphere, IR transmittance in region of NH_3 927 cm^{-1} absorpt. 80–85700
turbulence in lower bundary layer, influence of built-up area on spectral energy distrib. *(Russian)* 78–44925
turbulence spectra and thermal plumes in boundary layer 77–73793
twilight spectrum, new diffuse emission bands obs. 80–72662
upper atmosphere, O and N density meas. by Apollo-Soyuz UV spectroscopy 77–33228
upper atmospheric constituents, absolute high-resolution far IR meas. 77–41249
UV dayglow, mesosphere and thermosphere H distrib. from Lyman α and β obs. 80–109290
UV extinction meas. of O_2 density 79–2406
UV spectrophotometric obs. of upper atm. from Spacelab 77–21964
UVB spectral irradiance monitoring at 9°, 39° and 71°N 79–58070
vacuum UV background, meas. 80–90221
Van der Waals mols. in lower atmos., IR emission and absorpt. 80–85699
VHF double-peaked spectra at negative Doppler shifts in the morning sector of radio aurora 79–40014
Voigt profile, fast calculational algorithm, line-by-line transmittance 78–7767
water cluster interpretation of IR water vapour continuum, comments 79–12262
water droplets, volume extinction coeffs. at visible and IR wavelengths 77–25750
water vapour, 1 to 8 μm absorpt. 78–81402
water vapour, absorpt. at 7.1 cm^{-1}, temp. depend. 78–82722
water vapour, absorption near 4250 cm^{-1} 78–82729
water vapour, HDO depleted, continuum absorpt. meas. 3.5 to 4 μm 77–87075
water vapour, IR absorpt. spectrum, contrib. by molecular clusters 80–9598
water vapour, IR continuum absorpt. calc. *(Russian)* 78–96293
water vapour, precipitable water amounts meas. using integrated absorption in 1.38μm 80–4108
water vapour, pressure broadened absorpt. in 10 μm region, O_2 addition effects 78–92975
water vapour, Raman lidear meas., daytime atmosphere 80--85718
water vapour, spectral transmission at wavelengths 0.7 to 1 μm 78–85685
water vapour absorption in 8 to 13 μm spectral region for different atmospheric conditions 79–39855
water vapour absorption line profile, N_2 induced broadening 78–20516
water vapour band absorption, remote sensing 78–65389
water vapour channel, atmospheric transmission function, cloudless radiances 80–46256
water vapour continuum absorption, 3.5 to 4.0 μm region 78–92973
water vapour continuum absorption (3.5 to 4 μ) temp. dependence obs. 80–61903
water vapour continuum IR absorpt. near 1200 cm^{-1}, temp. depend. 78–85687
water vapour in troposphere under stable anticyclonal conditions, CO_2 laser radiation absorpt 78–20515
water vapour submillimetric-wave absorption obs. with photoacoustic cell 80–61901
water vapour variations, baseline results from Smithsonian obs. 78–32197

atmospheric spectra continued
weak absorption lines, detect. by Nd:glass and dye laser system 78—89561
whistlers, partly ducted, over Europe, spectrographic traces and morphology 78—65463
whistlers, spectral-temporal anal. by digital methods 80—4175
wind spectral kinetic energetics, diagnostic study 77—41117
X-ray bremsstrahlung produced by precipitating electrons, energy spectra 79—66862
X-ray microbursts in auroral zones, power spectra rel. to primary electron transient times 77—78556
0 I, 63 μm emission as cooling mechanism in thermosphere and ionosphere 79—16732
0 I 5577 Å in thermosphere and mesosphere, seasonal and long-term vars. and dynamics 77—33237
Al hydration, in vap. phase, rel. to upper atmosphere chemiluminesc. 79—29362
Ar fluorescent X-rays from sunlit Earth atmosphere during solar flares 77—13142
CH^+ in upper atmospher, obs. following trimethylaluminium high altitude release 79—48591
CO content, spectrometric meas. in N and S hemispheres *(Russian)* 77—13103
CO, ground level abundance, simultaneous determ. of CO_2, N_2O and H_2O 78—11969
CO, solar radiation absorpt. spectra rel. to atmospheric abundance *(Russian)* 78—53700
CO_2 15 μ band radiant energy inflow in disturbed LTE *(Russian)* 78—40657
CO_2 15 μm band, effect of CO_2 conc. on radiative transfer and atmospheric heating rates 80—17376
CO_2 15 μm band, non-LTE radiative transfer in Earth atmosphere *(Russian)* 78—36341
CO_2 15 μm band radiation, weather satellite meas. rel. to temp. field spatial anal. 78—20488
CO_2, $1\pi_g{}^3\ 2\pi_\mu{}^1$ config., ab initio eqn. of motion excitation energies 77—50376
CO_2, 4.3 μ absorption spectrum appl. to atm. temp. sounding 78—16166
CO_2 4.3 μm band absorption, solar occultation sounding for temp. and press. profiles meas. 80—98452
CO_2, absorpt. and emission over mean long optical paths 77—49163
CO_2 absorption at 2.7 μ in atmosphere at large optical thicknesses, mechanisms *(Russian)* 78—40659
CO_2 continuum absorpt. contrib. to atm. transmission, 4.0 to 5.3 μm 79—92589
CO_2, ground level abundance, simultaneous determ. of CO, N_2O and H_2O 78—11969
CO_2, IR absorpt. in regions of weak absorpt., lab. meas. rel. to atm. windows 79—64005
CO_2, IR absorpt. spectrum, line parameters, spectral transmittance function *(Russian)* 77—57998
CO_2, IR energy levels and line intensities 78—85691
CO_2, in troposphere under stable anticyclonal conditions, CO_2 laser radiation absorpt. 78—20515
CO_2 line freqs. in 4.3 μ region 78—88910
CO_2 line width effect on 15 μm emission 77—21903
CO_2, plume emission-absorpt., band model appl. 80—43047
CO_2, reson. absorpt. of CO_2 laser radiation 78—20514
CO_2, SCF vertical spectrum for valence, mixed character and Rydberg states 77—50375
CO_2, transmission functions for 15 μm band, calc. and expt. *(Russian)* 77—64428
$CO_2+CO_2(N_2)$, IR spectral absorpt. induced by press. in atmos. *(Russian)* 80—56600
ClO, aircraft search for 3 mm emission in stratosphere 80—41510
ClO radical, IR vibr.-rot. spectra, background data for atm. meas. 78—58679
$ClONO_2$, high resolution IR absorptivity 77—33184
$ClONO_2$, stratospheric distrib. at sunset, balloon borne IR solar spectra obs. 80—41487
FNO_2, UV photoabsorption spectrum 79—10123
H, geocoronal Lyman β and Balmer α emissions meas. during Apollo 16 mission 77—37476
HCl, atmospheric measurements using ground based IR spectroscopy *(French)* 80—81975
HCl, in stratosphere, vertical distrib. meas. from IR absorpt. spectra 78—20470
HF, atmospheric measurements using ground based IR spectroscopy *(French)* 80—81975
HF chemical laser radn. attenuation in 2.7-3.3 μm region 79—58088
HF/HCl, stratospheric abundance ratio in 14-38 km from IR spectra 78—20469
$H^+(H_2O)_c$ ion-induced water clusters, mass spectra, IR continuum absorpt. 80—87257
HNO_3, high resolution spectral meas. of 5.9 μm band using tunable diode laser 80—32707
HNO_3 IR spectra, 865.5-871.0 and 884.5-887.0 cm^{-1} regions, equiv. width meas., atm. spectrum appl. *(French)* 80—87114
HNO_3, IR spectra rel. to abundance in stratosphere 80—12464
HNO_3, spectral linewidth, broadened in air, O_2 and N_2 at 200 and 300K 78—46399
HNO_3 vapour line parameters meas. by CO laser transmittance 79—26976
HO fluorescence detection, interference suppression by sampling method 80—8431
HO_2 and HOCl, struct., vibr. freqs., IR intensities, ab initio calcs. 79—98007
H_2O 79—63992
H_2O 1.35 cm resonance region, atmospheric brightness temp. vars. *(Russian)* 78—81403
H_2O absorption bands at 1.4 and 1.9 μm, extinction meas. above Mauna Kea 80—12546
H_2O absorption lines at ruby laser wavelengths, saturation effect 80—4098
H_2O dimer, continuum absorpt. spectra in 8-13 μm range *(Chinese)* 80—109237
H_2O, dimer config., vib.-rot. band intensities, rel. to 8-13 μm atmospheric extinction 80—9610
H_2O, ground level abundance, simultaneous determ. of CO, CO_2 and H_2O 78—11969

atmospheric spectra continued
H_2O, IR absorpt. in regions of weak absorpt., lab. meas. rel. to atm. windows 79—64005
H_2O, IR continuum absorpt. due to librational mode of dimer 78—66542
H_2O mesospheric vapour line at 22.2351 GHz, hyperfine structure 79—8666
H_2O molecules IR absorption, allowance for effect on stellar radiation *(Russian)* 78—40832
H_2O, narrowing of collision shape of mol. absorpt. line in powerful laser field 79—29860
H_2O, residual IR absorption obs. during solar brightness temp. balloon-borne meas. 78—85921
H_2O vapour absorpt. coeff. at HF laser wavelengths 79—80010
H_2O vapour absorpt. in 10-12 μm atm. window 78—20513
H_2O vapour band, IR radiative cooling rate, calc. 80—90161
H_2O vapour causing IR and visible non-selective absorpt. 80—56608
H_2O vapour meas. in mesosphere from ground-based microwave obs. 77—33161
H_2O, weak spectral absorpt. of vap., visible and near IR 80—82062
H_2O-CO_2, IR radiation transfer 79—80028
H_2O_2 vapour, UV absorpt. cross sections, photodissoc. rate 78—32222
HONO (nitrous acid), obs. in urban atmosphere by differential optical absorpt. 80—76677
HO_2NO_2, in stratosphere, abundance rel. to detect. of IR spectrum 78—20467
H_2SO_4, dissociation and absorpt. consts., ultrahigh resolution obs. of 8.2, 11.3 μm bands 78—70825
H_20 vapour continuum absorpt., 4.5-5.0 μm 80—36395
He I 584 Å dayglow emission and exospheric He seasonal-latitudinal var. 79—75007
He I 584 Å dayglow meas., contrib. of O II 537 and 581 Å lines 77—41253
Li I 6708 Å twilight emission enhancement following rocket release 77—53255
MgO, wavelengths and relative intensities of IR bands 79—2407
N I 1.04 μm forbidden multiplet relative intensity, auroral forms mean height indicator 79—70909
N I 5200 Å forbidden line nightglow, ground-based meas. contamination by OH emissions 78—4020
N I (^{2}D) 5200 Å emission, prod. in auroral zone 79—21090
N_2 3371 Å dayglow emission, excitation by photoelectron impact 77—33236
N_2 bands in proton-induced poalr cap aurora, intensities 78—77389
N_2, collision-induced absorpt., temp. depend., rel. to atm. far IR transmission 79—62584
N_2 continuum absorpt. contrib. to atm. transmission, 4.0 to 5.3 μm 79—92589
N_2 dayglow intensity from photoelectron impact 80—46331
N_2 in upper atmos., vibr. level distrib., theory 80—41576
N_2, spatial yield spectra for electron energy degradation 79—100992
N_2 Vegard Kaplan bands in bright auroral displays, ground-based photometry 77—33245
$N_2{}^+$ 1 NG emissions from proton aurora, anomalous vibr. distrib. 80—67448
$N_2{}^+$ 3914 Å, auroral emission rel. to instantaneous particle energy deposition rate 78—81491
$N_2{}^+$ 3914 Å emission in dayside cleft aurora 77—2294
$N_2{}^+$ 427-8 nm emission, obs. rel. to mid-latit. charged particle precip. 79—44291
$N_2{}^+$ 4278 Å auroral emission, calc. from electron flux meas., comparison with obs. 77—9592
$N_2{}^+$ 4278 Å band nightglow intensity meas. at Arecibo 77—64504
$N_2{}^+$ 4278 Å intensity v. film density in DMSP data calibration 80—8443
$N_2{}^+$, auroral Meinel band excitation rel. to pulsating structs. extreme thinness 80—72667
$N_2{}^+$ first negative (0-1) band temp. height profile in auroral arc 78—40725
$N_2{}^{2+}$, auroral ionosphere spectral emission process 80—41577
$N_2+CO_2(O_2)(N_2)$, IR spectral absorpt. induced by press. in atmos. *(Russian)* 80—56600
$N_2{}^+(A^2\Pi_u$-$X^2\Sigma_g{}^+)$ system in aurora, vibr. development and quenching effects 78—88967
$N_2(B^3\Pi_g$-$A^3\Sigma_u{}^+)$ system in aurora, vibr. development and quenching effects 78—88967
NH, IR emission studied using Fourier spectroscopy 80—95628
NH_3, ν_2 vibr.-rot. band identification in ground level solar spectra 78—81287
NH_3, photoacoustic spectroscopy at 9 μm, 10 μm $^{12}C^{16}O_2$ laser wavelengths 79—21014
NH_3 remote atmospheric sensing by multiphoton sequential photodissociative excitation 79—48199
NO 5.3 μm emission, effect of thermosphere N_2 anharmonic mols. vibr. relaxation 79—12322
NO, absorpt. characts. of γ-0 band 79—39845
NO abundance meas. in equatorial upper atm. 77—78547
NO airglow, 2150 Å (1,0) γ-band intensity meas. with polarising NO photometer 78—45076
NO airglow, UV emission rel. to zodiacal light spectroscopy at 20° elongation 78—20728
NO and NO_2 mixing ratio profiles of stratosphere from IR sunset spectra 80—94563
NO chemiluminescent emission at 2.9 μm wavelength, auroral enhancement 80—12586
NO, far IR spectral lines and absorptance calcs. 77—46564
NO, gamma band emission rate factor, rel. to upper atm. comp. determ. 77—54572
NO, γ (1,0) band auroral emission at 2150 Å probably N_2 feature 78—45083
NO, high frequency discharge 79—82105
NO, reson. absorpt. meas. with CO laser, spectroscopic data for pollution monitoring 77—37350
NO, Salyut 4 IR spectral obs. in upper atmosphere mid-latitudes 78—16223
NO, self-N_2- and O_2-broadened linewidths 5.4 micron band, quadrupole moment 77—30930
NO, stratospheric growth before sunrise by photolysis 77—29356
NO, thermosphere UV spectral absorpt. and density profile 80--85781
NO, υ=0,1 states, spectroscopic data calc. 78—86851
NO_2, absolute integrated intensity for 3.44 μm band 77—3418

atmospheric spectra continued
NO_2, absorpt. spectrum rel. to atmospheric content meas. *(Russian)* 77−81962
NO_2, atmospheric abundance meas. using solar absorpt. method *(Japanese)* 80−94556
NO_2, conc. determ. from solar and lunar spectra in visible region obs. from ground *(French)* 79−53511
NO_2, continuum emission in aurora 79−2422
NO_2, in stratosphere, spectroscopic determ. and behaviour at mid-latit. 80−17414
NO_2, minor atm. components, visible absorpt. spectra, temp. depend. *(French)* 80−36355
NO_2, remote sensing of air pollution using optical multichannel analyser 79−79439
NO_2 total content meas. by absorption spectroscopy *(Japanese)* 80−12469
NO_2, total content var. during solar eclipse, visible spectrophotometric meas. *(French)* 77−2208
NO_3, absorpt. spectrum nighttime obs. 78−88880
NO_3, detect. in polluted troposphere by differential optical absorpt. 80−77036
N_2O, ground level abundance, simultaneous determ. of CO_2, CO and H_2O 78−11969
N_2O_5 gaseous, integrated band intensity data, stratospheric detection implications 80−58250
NOBr, photoabsorption spectra 190-300 nm 79−50038
$N(^2P)$ in aurora, UV spectra of metastable atom 80−77185
$N(^2P)$ in auroral arc, excitation and collisional deactivation processes 80−72658
Na I airglow in thermosphere and mesosphere, seasonal and long-term vars. and dynamics 77−33237
Na I D doublet in nightglow, Na excitation and abundance 80−98497
Na I D_2-line at 5890 Å, laser obs. of ground-state hyperfine structure 80−931
Na I D-line, nightglow spectra correl. to atmos. Na density 80−41585
Na I D-lines, twilight and nightglow line profiles, interferometric studies 78−36353
Na I nightglow intensity vars. rel. to Na photochem. 79−70905
Na in upper atmosphere, absorpt. studies of daytime abundance 77−87140
Na winter nightglow, correl. with radio absorpt. 77−33239
NaD, nightglow spectral intensity changes, correl. with O_2 spectra 80−61932
O 2.53 mm line, Zeeman splitting rel. to geomagnetic field vars. 80−77124
O, 557.7 nm spectral emission mechanism at 100 km altitude 80−61933
O, airglow intensity of green line rel. to atom density *(Chinese)* 80−90269
O content of lower thermosphere, 100-160 km, new spectral method 80−41578
O I, 5577 Å and 6300 Å intensity ratio, rel. to auroral particle spectrum characteristic energy 77−29532
O I, 5577 Å emission, plasma column dynamic and reaction processes in meteor wakes 77−82176
O I, nightglow spectra correl. to atmos. Na density 80−41585
O I, red line luminesc. amplification by radiowave anomalous absorpt. *(Russian)* 79−29925
O I 1304, 1356 Å tropical airglow, mag. storm effects 77−45214
O I 1304 Å, nadir intensity/column prod. rate ratio rel. to airglow studies 77−45213
O I 5577 and 6300 Å emissions in dayside cleft aurora 77−2294
O I 5577 Å, night sky emission rel. to occurrence of nighttime E-region *(Russian)* 77−45223
O I 5577 Å airglow wave vars. and meteor zone wind speed 79−62637
O I 5577 Å and 6300 Å, laboratory discharge lamp source for lines of known width 80−4148
O I 5577 Å and 6300 Å forbidden emissions during aurora, line profile vars. 78−45081
O I 5577 Å auroral emission, calc. from electron flux meas., comparison with obs. 77−9592
O I 5577 Å forbidden line rel. to O_2 and OH band spectra 78−61639
O I 5577 Å line depend. on E_s-layer 77−67006
O I 5577 Å line nightglow, intensity var., related to solar tides *(Russian)* 80−12585
O I 5577 Å lower thermosphere emissions, vars. rel. to thermal tides 77 78550
O I 5577 Å nightglow, meas. via two-channel rocket photometer 78−45078
O I 557.7 nm forbidden line emission structure in airglow 79−35027
O I 557.7 nm nightglow in central polar cap 77−33238
O I 630 nm airglow profile, daytime thermospheric temps., wind vels. and emission intensities 79−58144
O I 630 nm nightglow line profiles, thermospheric temps. and winds 79−58143
O I 6300 Å airglow, interferometer meas. rel. to global model of exospheric temp. 77−53265
O I 6300 Å airglow, relationship to ionospheric F-region parameters 78−36354
O I 6300 Å airglow spectrum, appl. to exosphere global temps. determ. 77−33234
O I 6300 Å emission in twilight airglow, thermospheric temp. depend. 77−45215
O I 6300 Å forbidden emission at mag. equator, rel. to vertical E×B plasma drift vel. 80−36435
O I 6300 Å forbidden line high resolution obs. in dayglow 77−41252
O I 6300 Å forbidden line nightglow, ground-based meas. contamination by OH emissions 78−4020
O I 6300 Å in type A aurora rays, emission intensification 80−4163
O I 6300 Å line, ground meas. for exospheric temp. determ. 77−67003
O I 6300 Å line correl. with electron content in nighttime F-region 77−67007
O I 6300 Å line meas. of $O(^1D)$ quenching coeff. by molecular collision, optical meas. 79−2419
O I 6300 Å mid-latitude nightglow fluctuations rel. to F-region 78−49194
O I 6300 Å nightglow, Doppler shifts rel. to thermosphere midlatit. winds at 105°W and 79°W 79−16727
O I 6300 Å nightglow, line profiles and Doppler shifts rel. to thermospheric winds and temps. 78−32263
O I 6300 Å nightglow, obs. rel. to neutral comp. vars. at F-region heights *(Portuguese)* 80−41584

atmospheric spectra continued
O I 6300 Å pre-dawn emission and super-thermal ions from conjugate points 77−9589
O I 6300 Å red emission, first obs. in Guinea 79−58146
O I 7774 Å multiplet obs. of nightglow over Arecibo during magnetic storm 80−72663
O I 7990 Å branching ratio, lab. study, rel. to airglow and auroral emissions 79−775
O I airglow and aurora, 3s′ $^3D^0$ and 3d $^3D^0$ levels excitation and radiative decay 79−80064
O I and N I forbidden lines emission in nightglow, historical review 79−5699
O I auroral emissions, ground-based photometric meas. 78−77387
O I EUV and far UV emissions obs. in tropical ionosphere 77−2297
O I forbidden line nightglow intensity var. 77−73899
O I green line (5577 Å) in nightglow 79−48596
O I green line airglow, obs. during Winter Anomaly Campaign (1957/76) 78−45075
O I UV nightglow obs. at midlatit. 78−81482
O II 7319-7330 Å dayglow, meas. and theory 77−37475
O II 7320-7330 Å emissions meas. at twilight 78−88962
O II forbidden line emission, 7320-7330 Å, intensity ratio and centre wavelengths 79−44284
O, spectral line shape in upper atm. following dissociative excitation 80−105097
O^+ airglow, UV emission rel. to zodiacal light spectroscopy at 20° elongation 78−20728
O_2 0.762 μ band absorption coeff. *(Russian)* 78−28315
O_2 1.27 μ A-band intensity in lower atmosphere *(Japanese)* 78−61486
O_2 1.27 μm airglow, middle latit. meas. rel. to mesospheric O_3 concs. 80−72606
O_2 1.27 μm airglow emission, zenith angle dependence 77−45216
O_2 1.27μ emission, auroral enhancement 78−81485
O_2 5 mm absorption band, appl. of ground-based radiometry for temp. inversion detect. *(Russian)* 78−11963
O_2, 60 GHz absorpt. spectra for lower atmos. temp. 80−77172
O_2 7594 Å A-band on objective prism spectra of stars, radical vel. meas. appl. *(Japanese)* 78−89083
O_2 7619 Å band in aurora, rocket obs. 77−25813
O_2 $(^1\Delta_g)$ auroral emission, vibr. excitation process 80−82125
O_2, $(0,1)b^1\Sigma_g{}^+ - X^3\Sigma_g$ band, integral absorption coeff. 78−20512
O_2 (0-0) atmospheric band, laboratory discharge lamp source 80−4148
O_2 (0-1) band at 8645 Å, nightglow intensity var. 77−73899
O_2, (0-1) spectral emission band in upper atmos. 80−61933
O_2, $(b^1\Sigma_g{}^+ - X^3\Sigma_g\ )$ system in auroras, vibr. development 77−2293
O_2 A band differential absorpt. lidar meas., using ruby lidar and stimulated Raman scatt. 79−39904
O_2 A-band in nightglow 79−48596
O_2, absorpt. 177.5 to 178.3 nm, appl. of vac. UV 6 m monochromator 78−37969
O_2 absorption of solar Lyman-α in mesosphere and lower thermosphere 80−77180
O_2, $b'\Sigma_g{}^+ - X^3\Sigma_g{}^-$ electronic transition, absorpt. coeffs. and transition moments 80−43061
O_2 bands, lidar temp. profiling 80−21827
O_2, electric quadrupole transitions detection in A band 80−85746
O_2 emission from atom recomb. 79−31576
O_2, IR nightglow bands excitation mechanism, reaction rate consts. 78−65448
O_2 induced absorption band effects on transmission in 6 μm region *(Russian)* 78−69446
O_2, mag. dipole transitions, line positions and strengths from stratospheric emission spectra 80−78604
O_2 microwave spectrum, expt. v. theory 77−37298
O_2, nightglow spectral intensity changes correl. with NaD spectra 80−61932
O_2, OH, NO_2, NO emissions, Spacelab obs. 77−21967
O_2, Schumann-Runge bands, predissoc. linewidths and oscill. strengths, vibr. level depend. 79−45735
O_2, Schumann-Runge bands, atmospheric absorpt. model 79−96823
O_2, thermosphere concs. and absorpt. cross sections from EUV occultation profiles 78−28356
O_2 UV absorpt. cross section and column density at 70-120 km altitude 77−53263
O_2, UV absorpt. in stratosphere and mesosphere 80−51497
O_2, UV absorpt. into $^3\Pi_u$ state, calc., atmos. opacity 80−12582
O_2, UV bands rel. to solar UV radiation absorpt. in stratosphere and mesosphere 80−109248
$O_2{}^+$, 1NG bands spectral synthesis, for auroral obs. anal. 77−2296
$O_2{}^{2+}$, auroral ionosphere spectral emission process 80−41577
$O_2+O_2(N_2)$, IR spectral absorpt. induced by press. in atmos. *(Russian)* 80−56600
O_3, 9.6 μm band radiance calc., excitation processes 78−36350
O_3, Chappuis-band absorpt. rel. to conc. determ. 80−77063
O_3, columnar meas. by aircraft-borne UV spectrophotometer 78−73522
O_3 conc. and distrib. from absorption spectrum in UHF region *(Russian)* 79−100897
O_3, daytime and nighttime distrib., ground-based mm wavelength obs. 78−57256
O_3 estimates from Dobson direct Sun meas., atm. temp. variations and scatt. effects 77−45049
O_3, high resolution spectroscopy of ν_3 band, rel. to atm. O_3 monitoring 79−63993
O_3, IR absorption rel. to atmosphere total O^3 content determ. using satellite meas. 80−77027
O_3, IR heterodyne absorpt. spectrum 77−91267
O_3, IR heterodyne spectroscopy 77−45160
O_3 in lower mesosphere, number density profile obs. 80−41579
O_3, in mesosphere, ground-based 110.8 GHz line obs. 77−29381
O_3 line parameter data, 10 μm and 4.8 μm regions 80−61895
O_3 monitoring with airborne laser absorpt. spectrometer 77−91303
O_3, remote meas. in IR absorpt. bands, information content estimation *(Russian)* 78−88883
O_3 spectrum for atmosphere total O_3 determ., large particle scatt. coeffs. approximation 80−82091
O_3, stratospheric, spectroscopy with CO_2 waveguide laser 77−13117
O_3 stratospheric 10 μ absorption line obs. with IR heterodyne spectrometer 78 -61494
O_3 stratospheric layer, laser-radar obs. using excimer lasers 80−17410
O_3, UV absorption bands, new vib. quantum no. assignments, based on isotope effect 79−94008

atmospheric spectra continued
O_3, UV bands rel. to solar UV radiation absorpt. in stratosphere and mesosphere 80—109248
OCS, stratosphere content, solar spectra meas. by 12 km attitude aircraft 80—41486
O^1D 6300 Å photoelectron induced predawn enhancement, altitude profiles 77—17290
$O_2(^1\Delta_g)$ airglow, emission height profile meas. during winter anomaly event 78—45077
OH (6-2) and (8-3) nightglow bands, rotational temps. and intensities 79—58147
OH (8, 3), nightglow spectra correl. to atmos. Na density 80—41585
OH (8-3) Meinel band in nightglow 79—48596
OH airglow, spectrum rel. to atmosphere warming at 90 km during 1976-77 winter *(Russian)* 79—88518
OH emission, 5-1 band rot. temps. rel. to waves in emission layer and F_2-layer 78—45065
OH emission, spectrometric thermometry rel. to internal gravity waves in upper atmosphere *(Russian)* 78—16224
OH emission as recorder of internal gravity waves near mesopause 78—12031
OH emissive layer, waves, near IR photographic studies 80—51545
OH far IR rotational lines in stratosphere, column densities 80—36367
OH Meinel bands, in airglow, rot. temp., radiative lifetime 78—61643
OH Meinel bands intensity distrib. in airglow, OH* quenching mechanisms 78—65447
OH Meinel bands intensity var. in nightglow at Poona, rel. to O_3 conc. 79—5698
OH near IR emissions, Spacelab image intensifying TV obs. 77—21966
OH nightglow, photometric obs. to find mesosphere neutral temp. 80—82121
OH nightglow emission, intensity meas. during 1969 NASA airborne auroral expedition 77—29529
OH radical, in Earth's atmosphere, pure rot. lines 79—92593
OH, submicron airglow bands correl. studies during Spacelab simulation 79—25381
$OH(A^2\Sigma^+)+N_2(O_2)(H_2O)$(air), quenching rates and fluoresc. efficiency, rel. to atmosphere 80—14199
$OH(X^2\pi)$ nightglow emissions, theory and meas. in (9-3) band 78—88960
OH(8-3) 7274 Å band rel. to O_2 and forbidden O I spectra 78—61639
OI, F-region neutral temp. by 630 nm spectra, during spread-F activity 80—41587
$O^+(^2P)$ airglow, meas. rel. to ionisation freq. vars. during solar cycle 21 80—77195
$O(^1S)$ airglow, lab. prod. rate coeff. meas. 79—53604
O_2(0-1) 8645 Å band rel. to OH and forbidden O I spectra 78—61639
$^{18}O^{16}O$, Schumann-Runge bands transmission rel. to photodissoc. and O_3 prod. 80—94559
SO_2, 4 μm $\nu_1+\nu_3$ band, Doppler-limited and atmospheric spectra 77—27064
SO_2, absorption spectrum, meas. using frequency doubled pulsed dye laser 80—87144
SO_2, absorption spectrum, meas. using frequency doubled CW dye laser 80—87145
SO_2, conc. determ. for coal-burning power plant stack, Fourier spectrometry appl. 77—49196
SO_2 IR absorption spectra *(Russian)* 79—25328
SO_2, long-path automatic monitoring using diode laser system 79—29892
SO_2, low conc. meas. using diode laser correlation spectrometer 77—91301
SO_2, minor atm. components, near UV absorpt. spectra, temp. depend. *(French)* 80—36355
SO_2 transmittance over IR spectral bands, model 80—51535
$SOCl_2$, photoabsorption spectra, 190-300 nm 79—50038
SO_2Cl_2, photoabsorption spectra, 190-300 nm 79—50038

atmospheric structure
see also atmospheric composition
50 mb geopotentials from SIRS soundings and analyzed charts 77—78345
500 mb height, anal. error development, (1946 to 1969) 80—72615
acoustic remote sensing, review 78—73493
adiabatic boundary layer height vars., simulation in wind tunnel 78—7691
adiabatic invariants in N.Hemisphere *(Russian)* 78—36225
aerosol inhomogeneities struct. and dynamics in ground layer, light scatt. 77—81955
aerosol steady-state coagulation eqns. and particle size spectrum model *(Russian)* 77—41115
Aleutian anticyclone, development during January-February 1979 stratospheric warming event 80—4074
altitude dependence of refr. index struct. parameter, laser meas. 77—37316
altocumulus billows, example of large amplitude Kelvin-Helmholtz wave 80—72621
annual zonally averaged climatic model with diffuse cloudiness feedback 77—29416
Antarctica and equatorial India, atm. struct. during southern summer 77—53121
atmosphere optics, gas and aerosol struct. rel. to light scatt., book 77—5323
aurora, dayside morphology from large scale obs. at 6300 Å, 5577 Å and 3914 Å 80—85786
aurora pulsating structures, implications of extreme vertical thinness 80—72667
auroral arc, ionic struct. meas. 77—2292
auroral arc structure, numerical simulations 79—53607
auroral E-region fine structure obs. in substorm 80—36452
auroral infrasonic wave emissions, repeated pulse group rel. to atmospheric struct. 77—25811
auroral oval, obs. of high-latit. mag. substorms 80—109315
auroral oval size, effect on mag. substorm occurrence probability 78—32298
auroral zone, nighttime scintillation localised enhancements struct. 80—98506
auroral zone, postmidnight electron precipitation time structure and stable trapping limit 79—101013
baroclinic boundary layer structure 78—81326
baroclinic instability on sphere, normal modes of primitive and quasi-geostrophic eqns. 77—5286

atmospheric structure continued
baroclinic model using high accuracy horizontal discretisation 77—45065
baroclinic planetary boundary layer, similarity theory *(Russian)* 78—11962
baroclinically unstable modes, of two-layer model on sphere 77—2192
barotropic 3-dimens. instability in upper stratosphere 80—41498
barotropic atmosphere eqns., boundary problem soln. *(Russian)* 77—45072
barotropic systems, low order, with forcing and dissipation, steady states and stability props. 80—72614
boundary layer, acoustic sounder obs. from top of steep mountain 80—98409
boundary layer, assessment of proposed similarity theories 77—33126
boundary layer, during light wind, water vapour IR absorpt. meas. 77—91197
boundary layer, height and circulation prod. in sea breeze model 79—53438
boundary layer, mean and turbulent structures, 24 hour evolution, modelling 79—58024
boundary layer, momentum, heat and moisture fluxes from struct. parameters 79—53435
boundary layer, nonstationary, under influence of strong wind, engineering model *(Russian)* 77—5280
boundary layer, similarity theory *(Polish)* 77—25753
boundary layer, steady barotropic nocturnal evolution and structure 80—56511
boundary layer, surface roughness change effects 78—77306
boundary layer, turbulence structure in temp. inversions and convective fields, Doppler sodar obs. 79—66762
boundary layer at low latitudes, meridional struct. *(Russian)* 77—73802
boundary layer depth and vertical wind profile 77—9462
boundary layer echoes from surface based remote sensors, coding technique 80—17400
boundary layer evolution and nocturnal inversion dispersal 79—25296
boundary layer evolution and nocturnal inversion dispersal 79—25295
boundary layer probing by acoustic sounder 77—17243
boundary layer structure and development over SE.England, aircraft and balloon meas. 80—12516
boundary layer structure evolution over oceanic and continental sites *(French)* 79—25294
boundary layer structure from records obtained for Christchurch acoustic sounding technique 80—26638
boundary layer structure of axisymm. vortex, lower boundary condition effect 79—25298
boundary layer thermal structure at Cardington from acoustic sounding 77—53153
boundary layer turbulence, boundary layer, appl. of mixed-layer similarity scaling to observed dispersion from ground-level source 80—105021
boundary layers, numerical modelling 78—44900
bow shock, orientation and shape in three dimensions 79—101030
cloud field over Transcaucasia, statistical struct. 78—92942
cloud microstructure numerical models, condensation process parametrisation *(Russian)* 78—16091
clouds, microstruct. in Kenya high-frequency hail area 79—53484
clouds influence on atm. dynamics *(Russian)* 79—8653
convective boundary layer slab model, study using Air-Mass Transformation Expt. data 79—57995
critical levels in a vertically rotating compressible atmosphere 80—6073
cusplike electron precipitation regions during 1977, September 19 to 21 event, DMSP-F2 obs. 79—35056
D-region, ion structure and winter anomaly 79—62660
D-region, southern hemisphere, radio wave scatt. rel. to irregularities struct. 78—36363
D-region winter anomaly, Western European study campaign (1975/76) 78—45122
dayside aurora, particles and ion convection meas. rel. to ionosphere struct. 78—77391
diffuse auroral zone, form. and dynamics of polar edge of ionospheric trough 79—8743
downdraught caused by nimbostratus rainfall evaporation, numerical anal. 80—8400
dry convection, thermals, structure 78—44910
dynamic features sizes, effects of Earth rot. rate vars. rel. to climate 80—4097
dynamic tropopause, isentropic anals. rel. to polar stratosphere-troposphere exchange in summer 80—72599
E_3-layer over Japan, cloud struct., movement, diurnal and seasonal vars. 79—44298
E_s-layer, ionisation irregularities rel. to Langmuir wave propag. and enhanced plasma line 79—29928
E_s-layer, temperate zone, maps of $f_0E_s>7$ MHz 78—73579
E_s-layer, temperature latit., skywave backscatter studies 78—85761
E_s-layer of auroral ionosphere, large-scale inhomogeneities 80—4171
E_s-layer studies and latit. regluarities *(Russian)* 79—8749
E-region height variations, influence of lunar tides 78—77382
E-region tilts, results from reflected radio waves arrival direction 79—25387
equatorial electrojet, irregularity drift vels. observed by close-spaced antenna technique and Doppler radar 78—36365
equatorial electrojet longitudinal differences, radar studies review 78—36371
equatorial electrojet models, comparison 78—36372
equatorial ionosphere holes and spread-F, ion chemistry and transport 78—88982
European Grosswetterlagen, temporal vars. and possible causes 79—58081
exosphere, dayside sub-solar H bulge 77—21957
F_2-layer, hmF_2, NmF_2, high-latit. behaviour along noon-midnight meridian under quiet conditions 79—40004
F_2-layer, mid-latit., internal gravity waves day and night effects on h_mF_2 79—58150
F_2-layer, night-time, over Arecibo, seasonal mean struct. 80—31163
F_2-layer, peak electron densities in main trough region, empirical model 78—28417
F_2-layer, temp. and thickness from vertical sounding and incoherent scatt. 77—45221
F_2-layer nighttime ionisation latit. depend., var. in solar activity cycle 79—53617
F-layer height and equatorial spread-F 79—88535
F-region, electron density trough form. during isolated substorm, incoherent scatter radar meas. 78—65452

atmospheric structure continued
F-region, equatorial, irregularity patches localised origin 78—77404
F-region, equatorial, topside and bottomside, review of struct. 78—36373
F-region, equatorial ionisation density irregularities rel. to HF and VHF spread-F echoes 78—85764
F-region, geomag. activity effects on h_mF_2 80—8480
F-region, high latit., Fe^+ ions distrib. 79—16736
F-region, hmF2 meas. at low. latit. mag. conjugate regions rel. to neutral winds determ. 78—81477
F-region, irregularities and scintillation rel. to aurora 77—87158
F-region, nightside, distortion prod. by plasmasphere substorm elec. fields 79—40009
F-region, nighttime equatorial, coexistence of km and m scale irregularities, radar and scintillation obs. 79—2427
F-region, nocturnal, heights over Arecibo, band struct. 79—66863
F-region, plasma ambipolar diffusion in gravit. field rel. to Chapman layer struct. 77—78562
F-region, travelling ionospheric disturbances by gravity waves due to tornado outbreak 78—85753
F-region irregularities in situ meas. by OGO-6 correl. with scintillation meas. 77—21977
F-region irregularity model, reconciliation with sunspot cycle vars. in spread-F occurrence 77—41262
F-region striated Ba clouds, electron density struct. meas. 78—88974
F-region vars. rel. to thermospheric diurnal tide seasonal-latitudinal struct. 78—77377
free convection structure in surface layer 77—37294
fronts and depressions at middle latitudes, mesoscale struct. 80—26604
fronts and ocean currents in tropical Pacific 80—41509
general study of upper atm. *(Chinese)* 79—75039
Harang discontinuity, elec. current continuity 78—49220
Harang discontinuity, electric field meas. by auroral radar and rocket double-probes 78—88971
homopause height, vars. rel. to global model of disturbed thermosphere 77—37468
hurricanes, spiral bands excitation by interaction between symmetric mean vortex and shearing steering current 80—56538
inclinations of atmospheric layers, determ. from sounding data *(Russian)* 80—72569
inhomogeneous troposphere model, microwave ducting anal. 79—39818
intertropical convergence zone, air circulation 78—92948
intertropical convergence zone, Indian Ocean basin cloud clusters, features 79—29822
intertropical convergence zone, interaction with upper westerly waves rel. to Zambian weather during rainy season 80—90175
intertropical convergence zone struct. over GATE area 78—57283
inversion descent in mountain valleys, air pollution implications 79—62550
inversion height in urban atmosphere, determ. from numerical simulation of mixing depths 80—105024
inversions, time dependent behaviour in different climatic regions 79—20908
inverted atmosphere, Taylor instability 77—9476
ion-exosphere, rot. effects on plasma distrib. 77—2301
ionosphere, analytic partial derivatives for incoherent scatter data least-squares fitting 78—73581
ionosphere, auroral zone, irregularities, simultaneous rocket probe, scintillation and incoherent scatter radar obs. 80--94640
ionosphere, bottomside, mid-latitude trough discovery 80—109300
ionosphere, calc. and obs. structure, AE-C satellite and incoherent scatter radar obs. 78—49203
ionosphere, cond. struct. rel. to elec. field two-dimensional and three-dimensional mapping 79—66861
ionosphere, D and F region ionisation rel. to mesosphere NO concs. 79—8651
ionosphere, daytime slab thickness depend. on geomag. activity 77—21992
ionosphere, disturbances and nonlinear effects during partial radio wave refls. 77—60516
ionosphere, dynamics of equatorial irregularity patch form., motion and decay 80—67456
ionosphere, elec. cond. spatial inhomogeneity rel. to simulation of elec. fields of magnetospheric origin 80—4177
ionosphere, electron concentration variations rate use 80—12598
ionosphere, electron density daily vars. at 100-200 km at middle latits. 77—64515
ionosphere, electron density obs. at 1000 km during calm and disturbed conditions 77—64513
ionosphere, electron density profile analyses of ionograms, model starting heights 79—66869
ionosphere, ELF emission spatial distrib. 80—4174
ionosphere, energetic particle meas. within structs. responsible for auroral accel. processes 79—53644
ionosphere, equatorial, EM state rel. to interplanetary mag. field vars. 78—77413
ionosphere, equatorial, features assoc. with radio scintillations 80—77191
ionosphere, equatorial, plamsa density bubbles obs. by (ESRO-4) 80—4194
ionosphere, equatorial, plasma bubbles and irregularities in nighttime F-region 77—87156
ionosphere, equatorial irregularity experiment (Equion) 77—33266
ionosphere, equatorial spread-F irregularities drifting patches rel. to spatial reson. mechanism 79—21095
ionosphere, evidence for reflecting layer below classical D-region 80—98508
ionosphere, F-lacunae geographical distrib. and simultaneity of occurrence 80—4193
ionosphere, from satellite radio beacon signals 78—12050
ionosphere, generation of small-scale inhomogeneities by internal gravity waves 78—45100
ionosphere, Harang discontinuity latit. struct. on November 21, 1975, Chatanika obs. 77—87160
ionosphere, heterogeneous structure of low-latitude region 78—96338
ionosphere, high-latit., morphology rel. to aurora and particle precip. 79—40000
ionosphere, high-latitude, elec. fields rel. to ions vertical distrib. 78—28370
ionosphere, horizontal struct. of scintillation-producing irregularities in southern mid-latits. 79—12339
ionosphere, in situ irregularity spectra rel. to scintillation calcs. 78—28415

atmospheric structure continued
ionosphere, ionisation density fluctuations rel. to SHF refr. scatt. and scintillations 79—48615
ionosphere, irregular struct. in field of strong obliquely incident radio-wave 79—62648
ionosphere, irregularities at mag. equator rel. to long-term 1.5 GHz amplitude scintillation meas. 80—85792
ionosphere, localised changes rel. to VLF nighttime propagation anomalies 78—28414
ionosphere, lower, electron density disturbances during Soyuz-Apollo expts. 78—45110
ionosphere, mid-latitude sporadic-E layer, irregular structure from incoherent scatter radar obs. 78—96342
ionosphere, model effects on thermospheric calcs. 78—36345
ionosphere, parameters rel. to radiowave magnetoionic components lateral deviations during vertical sounding 79—8747
ionosphere, plasma bubbles spatial relationship with 1 m equatorial spread-F irregularities 80—67457
ionosphere, polar, structure, dynamics and interrelations with magnetosphere convection struct. 80—4176
ionosphere, polar region struct. rel. to magnetospheric convection behind plasmapause 78—40731
ionosphere, random and induced inhomogeneities rel. to scatt. of strong radio waves 77—91345
ionosphere, random inhomogeneities rel. to diffusion of limited radio beam 77—91349
ionosphere, scale lengths of mid-latit. spread-F rel. to coupling between conjugate stations 77—53304
ionosphere, small-scale irregularity structs. assoc. with subtrough density gradients, Ogo 6 obs. 78—40753
ionosphere, spread-F and E_s-layers struct. rel. to quasiperiodic scintillations morphology 77—91361
ionosphere, topside, O^+ to H^+ transitions level height rel. to very low dispersion whistlers 79—44301
ionosphere, topside, trough morphology, occurrence freq. and diurnal, seasonal and altitude vars. 79—53645
ionosphere, upper, small-scale stratification, influence of strong radio wave with amplitude modulation 79—12330
ionosphere balance equation, theoretical model 78—28369
ionosphere baselevel trough, struct. 78—28402
ionosphere currents, obs. by S-310-5 rocket *(Japanese)* 80—94635
ionosphere discrete and homogeneously structured irregularities, radio waves diffr. 79—48612
ionosphere electron content in S.Atlantic geomag. anomaly region, east-west asymmetry 79—21097
ionosphere electron density equatorial anomaly, dissimilar forms in E.Asia and India 80—109301
ionosphere electron density in S hemisphere middle latits., Universal Time effect model 79—25396
ionosphere electron density trough, Intercosmos-10 Langmuir probe expts. results *(German)* 79—2469
ionosphere equatorial bubbles, model computations of assoc. radio wave scintillation 80—94641
ionosphere equatorial bubbles, topside sounder obs. 79—16737
ionosphere F-region, equatorial stratified irregularities movement, time and magnetic dependence 80—8470
ionosphere fine structure at low latitude from impedance obs. at 406 kHz 80—67468
ionosphere height rises, relationship with polar mag. substorms and spread-F occurrence 78—81494
ionosphere irregularities, mid-latit., geometry from geostationary satellite signals scintillation 79—25388
ionosphere main valley, dynamics and electron temp. behaviour from satellite meas. 80—4170
ionosphere mid-latitude trough, low energy plasma obs. during major mag. storm 78—88987
ionosphere mid-latitude trough, scintillation of extraterrestrial radio noise sources signals 78—73574
ionosphere mid-latitude trough location, noon and midnight obs. by Ariel 4 78—85765
ionosphere plasma clouds, deform. and striation, multilevel model with recomb. chemistry 77—25834
ionosphere plasma clouds, late time striation spectra 77—25836
ionosphere regular absorption, differences in daily vars. and annual pattern in N.hemisphere 78—45091
ionosphere travelling disturbances, wave-normal depression and disturbance amplitude height depend. 79—40006
ionosphere trough region, detached auroral arcs obs. 78—88965
ionosphere turbulent polar cusp, temps. and low-energy particles and Kelvin-Helmholtz instability 78—96343
ionospheric, lower, layer structs. response to gravity waves 78—81290
ionospheric valley, electron-density inhomogeneities rel. to internal gravity waves 77—91348
layer structures, density response to gravity waves 78—81290
layer thickness determ. from Nimbus E microwave spectrometry and radiosonde obs. 77—29384
lidar techniques for atm. struct. and comp. obs., proposed Spacelab program 78—61602
low level turbulence near Cross Fell, England, turbulent element size 79—79962
low-level jet, struct. investigations *(German)* 78—69422
lower atm., thermal struct., sodar obs. at Delhi, India 79—53428
lower atmosphere, anal. of rocket soundings on Kerguelen Island (February-May, 1973) 78—20489
magnetopause, three-dimensional shape 79—101029
magnetopause structure from Ogo 5 obs., classical reconnection model 79—58195
magnetosphere, cusp geometry rel. to dayside magnetopause mag. merging 79—66884
magnetosphere, energetic electrons distrib. in geomag. field 77—22006
magnetosphere, field-aligned electron irregularities rel. to partly ducted whistlers propag. 78—65463
magnetosphere, global fine structural forms. development during substorms 79—58190
magnetosphere, high-latit., plasmapause and polar cap boundary and parallel elec. field below 8000 km 80—72706
magnetosphere, high-latit., struct. of solar proton fluxes in April (1972) 77—64532
magnetosphere, low-energy plasma obs. at synchronous orbit 78—77435
magnetosphere, open model plasma populations 80—90295

atmospheric structure continued
magnetosphere, plasma condensations diagnostics from mag. field records on geostationary satellite 79—58189
magnetosphere, structure and stability properties 78—77440
magnetosphere, whistler duct struct. and formation 80—94659
magnetosphere dayside cleft, mag. field perturbations rel. to interplanetary mag. field 79—40023
magnetosphere dayside cusp region, plasma props. 79—12352
magnetosphere electron density, small scale struct. from plasma resons. on-line tracking 79—35073
magnetosphere irregularities, formation and evolution by mag. flux tubes interchange 80—21876
magnetosphere low altitude polar cusp, correlated elec. field and low-energy electron meas. 78—40770
magnetosphere morning sector, auroral electron discontinuity location meas. by Molniya-1 satellite 79—8778
magnetosphere physics, review 79—12356
magnetosphere plasma sheet, form. resulting from plasma mantle dynamics 79—40022
magnetosphere regions, thermal/suprathermal plasmas obs. by GEOS-1 S-302 expt. 79—35070
magnetosphere S polar cusp, low energy electrons obs. by AE-C during 1977, September 21 geomag. storm 79—35076
magnetosphere three-parameter two-dimensional model, configurations with least energy 77—91370
magnetotail configuration near midnight during quiet and weakly disturbed periods, mag. field modelling 78—96354
Manabe-Wetherald radiative convective model, fixed cloud-top temp. and fixed cloud-top altitude approximations 80—72616
marine atmosphere, ranked interaction with ocean on sub-semidiurnal scales *(Russian)* 78—77260
marine boundary layer, microwave radiometric sensing 78—57272
marine layer at San Diego, California, depth and moisture content rel. to cool season precip. forecasts in Arizona 80—101395
mass distrib. by latitude, anal. 80—90115
mesophere and stratosphere, related to noctilucent cloud presence 80—8412
mesosphere, equatorial, struct., waves and winds from multiheight radar obs. 78—36230
mesosphere, Na layer at 23°S, nocturnal and seasonal vars. 79—74932
mesosphere, Southern Hemisphere, quasi 2-day wave vertical and horizontal struct. 80—109207
mesosphere, structures diurnal vars. in different seasons, VHF radar meas. 79—84370
mesosphere at Thumba from in situ UV absorpt. photometry obs. 80—105051
mesosphere turbulence structures, high-resolution VHF radar obs. 79—100895
meteor zone, statistical modelling from Geminid shower radar obs. 78—61816
methane gas plumes, equivalent temp. struct. parameter rel. to tracking via acoustic sounder 80—55968
middle atmosphere, plasma and neutral gas comp. and struct. anal. via mass spectrometer probe 78—45191
middle atmosphere (mesosphere) 80—98412
middle atmosphere winter anomaly, ionospheric absorpt. meas. (1975/76) 78—45124
mixed layer, growth in turbulent stably stratified fluid 79—55358
mixed layer depth model based on turbulent energetics 77—5284
mixed layer growth, penetrative convection in stratified fluid 78—44908
mixed-layer model with penetrative convection, critical evaluation 80—51483
mixing layer height rel. to temp. inversions over Bombay 77—53119
molecular temperature boundary layer above sea, dynamics 79—66756
monsoon depression, composite structure 77—45117
multilayer model, electrodynamic state, horiz. mag. field component influence *(Russian)* 78—73556
neutrally stable atmospheric layer, mass and energy transport 79—74927
nightside auroral oval, instantaneous, from electron precip. equatorward boundary obs. 78—32289
nocturnal boundary layer, height determ. 78—73450
nocturnal surface inversion height prediction 80—41520
nongeostrophic baroclinic instability problem 78—7702
nonlinear stationary waves in atmosphere, theory *(Russian)* 78—16089
ocean-atmosphere interactions along North American west coast, 1965-69 period, preliminary anal. 78—61508
palaeoionosphere, evolution 77—2300
palaeomagnetosphere, third type of planetary magnetosphere during polarity reversals and geomag. excursions 78—61683
perturbed atmosphere thermal struct. and relaxation rates, photochemical radiative convective model 80—8408
physics of atmospheres, book 79—62568
planetary jet stream inner structure, hydrodynamical model *(Russian)* 77 64371
plasma sheet, cause of thinning during magnetospheric substorms 80—72705
plasmapause, drift waves 78—40748
plasmapause, position obs. by (Explorer 45) 77—53285
plasmasphere, horiz. inhomogeneities, whistler obs. 80—4168
plasmasphere, outlying struct. from whistler obs. 77—2304
plasmasphere, thermal struct. and plasmapause positions 79—12329
plasmasphere, whistler duct positions 77—53301
plasmasphere composition and density, equilib. model 79—66860
plasmasphere structure from whistler records at Belsk, Poland 78—20581
plume structure and trajectories, lidar meas. 79—58016
pollutant trapping by local circulation, obs. 77—37397
primitive ionosphere, thermal struct. 78—40754
protonosphere, electron content meas. from American and European sectors 78—45151
protons, high-energy, precipitation zone, substorm morphology 79—80080
pulsating auroras, vertical extent rel. to precipitating electrons noncollisional thermalisation 79—96851
inner radiation belt trapping zone boundary, electron flux boundaries displacement during substorms 80—67470
radiation belts, effects of man-made VLF waves 78—45150
radiation belts outer boundary variations, Kosmos 426 data 78—69614
rain, fine structure meas. *(French)* 78—53680
rain drop spectra and fine structure on different time bases *(French)* 78—53681
refractive index in atmospheric boundary layer, structural charact. vertical profiles *(Russian)* 80—94597

atmospheric structure continued
refractive index structure parameter, determ. from refractivity and amplitude scintillation meas. at 36 GHz 78—81316
ring current, particle boundary motions rel. to proton flux obs. by Geostationary Meteorological Satellite (GMS) 79—75056
solar terminator, effect of slope on atmospheric disturbance prod. 77—91208
solar terminator, gravity waves generation rel. to E_s-layers form. 79—12337
sonic booms from Concorde aircraft flight, atm. struct. information 79—66742
Spacelab lidar, for atm. props. meas. 77—21943
spread F structure, radar obs. 77—29566
spread-F bubbles, nonlinear Rayleigh-Taylor mode theory in two dimensions 78—88986
squall line, formation from boundary layer forcing and temp. gradient, model 80—8396
stability index measurement by natural radioactive tracers *(Spanish)* 80—51448
statically stable zones, simultaneous tethered balloon and monostatic acoustic sounder records comparison 78—73451
stationary planetary waves in winter, structure calc. 78—16100
steppe meteorology, boundary layer universal profiles in rainy season *(German)* 79—84420
stratification effect on evaporation, air-sea interaction *(French)* 80—31085
stratified aerosol layers meas. by searchlight probing technique 78—92892
stratiform clouds, structure *(Russian)* 78—16088
stratopause, double, thermal struct. features over Thumba 79—100901
stratosphere, quasi-biennial oscills. in temp. and O_3 conc. (1958 to 1977) 80—109222
stratosphere, southern hemisphere, winter 1973, from satellite obs. 77—5282
stratosphere, thermal structure and total O_3 obs., Nimbus 4 Iris expt. 77—21839
stratosphere, zonal mean winds vars. rel. to planetary wave props. and links with troposphere 80—109225
stratosphere aerosol, microstruct. from sounding by multifrequency lidar *(Russian)* 77—64374
stratosphere density inhomogeneity struct. determ. from Salyut obs. of astronomical scintillation *(Russian)* 80—109186
subauroral ionosphere, persistent scintillation enhancement obs. rel. to irregularities struct. 78—20573
subauroral ionosphere, rapid ion drifts obs. by Atmosphere Explorer C 80—4188
subcloud layer structure and interaction with shallow cumulus layer 77—45079
subsynoptic scale vorticity perturbations, influence on short-range numerical weather forecast 80—82008
surface layer, organised temp. struct. as signature of organised motion 80—72602
surface layer, structural turbulence coeff. depend. on height *(Russian)* 78—69400
surface layer above snow *(Russian)* 78—96264
surface layer height *(Russian)* 77—73807
surface layer height diurnal var. 77—60446
surface layer parameterisation, influence of active soil layer *(Russian)* 78—44924
temperature field over tropical Atlantic statistical struct. and objective anal. *(Russian)* 77—64373
temperature fluctuations, heat flux and struct. functions meas. with acoustic Doppler sodar 80—105023
temperature inversion, determ. via ground-based long-range sounding in O_2 5 mm absorpt. band *(Russian)* 78—11963
temperature regime, numerical model *(Russian)* 77—64368
terrestrial near-space environment, review 77—67002
thermal plumes detect. by acoustic echo sounder 78—57259
thermal structure, effects of nearby supernova 80—94584
thermosphere, lower, thin shear turbulent layers induced by tides and gravity waves non-linear interaction 78—65444
thermosphere, mid-latitude, lower, winds and dynamic regime longit. effect 79—53587
thermosphere, polar airglow mag. ordering 78—57378
thermosphere, tidal struct. at equinox 78—81476
thermosphere and mesosphere, average daily closed model 77—17264
thermosphere structure and dynamics rel. to tides and diffusion waves 79—35026
thermosphere-exosphere transition layer, structure, temps., H escape 79—66845
Thumba, India, temp., circulation and struct. 77—78362
thundercloud structure and interactions in subcloud region 77—45094
tidal oscills. rel. to horizontal winds and temp. structure 78—20457
tidal structures in joint presence of friction and rot., f-plane approximation 79—66847
travelling ionospheric disturbances and gravity waves, obs. at S. hemisphere mid-latit. station 79—21096
tropical atmosphere, large-scale features 79—92584
tropical atmosphere, struct. and energy fluxes 77—2203
tropical cloud cluster, struct. and evolution 80—12488
tropical middle atmosphere, observational evidence of semiannual oscillation 80—109216
tropopause, detect. by partial specular refl. with VHF radar 80—8411
tropopause, height vars. rel. to atmosphere total O_3 content natural fluctuations 79—29819
tropopause height estimation from nonlinear functions of satellite meas. spectral radiance 77—78335
tropopause height from spacecraft obs. of atm. refr. of starlight 77—2280
tropopause height over India, influence of tropospheric H_2O vapour mixing ratio 77—53123
tropopause height rel to sunspot activity 80—77090
troposphere, ducting environments rel. to radio waves beyond horizon propag. 77—41132
troposphere, obs. of smoke plume assoc. with intense local fire 77—49148
troposphere, refr. index struct. parameter height distrib. with lower boundary spatial transition 78—73491
troposphere, refr. index variance and its height distrib. in different air masses 77—41133
troposphere, refractive struct. using Rake probing 77—91231

atmospheric structure continued
- troposphere, stratified layers rel. to VHF radar partial refl. from clear atmosphere 78—81278
- troposphere, subcloud layer over land, temp. and humidity struct. 77—91200
- troposphere, synoptic and mesoscale struct. rel. to Kansas City flash flood (1977, September 12) 79—25291
- troposphere, transhorizon radiowave propag. rel. to remote sensing and atmospheric structure 78—44921
- troposphere, vertical structure from ground-based IR radiometry 78—57273
- troposphere over Bay of Bengal, during Aug. 1977 active and break monsoon 80—56570
- troposphere synoptic features in satellite picture, anal. 79—8713
- troposphere thermal structure, acoustic sounding technique appl. to siting studies 78—81467
- troposphere velocities and irregularities, VHF radar studies using spaced antenna techniques 79—16701
- troposphere vertical structure during frontal passage, VHF radar obs. 79—53482
- troposphere vertical thermal structure, variables spectra deduced from ground-based radiometry 79—92567
- turbopause eddy diffusion coefficient, semi-theoretical global based on satellite data 79—21086
- turbopause height variations, appl. to neutral atmosphere semi-empirical models 79—21085
- turbulent flow in two and three dimensions, microstructures rel. to numerical weather prediction 78—69395
- turbulent interface layers, theory 78—71323
- two-layer atmosphere, orographic perturbations *(Russian)* 78—16136
- typhoons, transform in northern latits. 78—92947
- unstably stratified atmosphere, axial characts. of turbulent convective plume *(Russian)* 77—49108
- upper atm. parameters daily vars. at midlatits., reference system 77—29521
- upper atmosphere, general review 79—39997
- upper atmosphere, numerical modelling of zone of instability and hydrodynamic accelerator *(Russian)* 78—16225
- upper atmosphere, O I 6300 Å nighttime emission vertical distrib. models 79—53602
- upper atmosphere disturbances, seasonal vars. in latit. struct. 78—32264
- urban atmosphere, radiative effects of elevated pollutant layers on temp. struct. and pollutant dispersion 80—97841
- vertical structure, general props. 78—4128
- whistler ducts, formation theory 78—57407
- Ba$^+$ clouds in upper atmosphere, striation struct. due to presence of BaO flow 77—25833
- Na layer wave-like structure, lidar obs. 78—88955
- O and O_2 distrib. in lower thermosphere assuming tidal effects, one dimens. nonstationary diffusion-photochemical model 80—4160
- OH airglow layer (90 km), atmosphere warming during 1976-77 winter *(Russian)* 79—88518

atmospheric techniques
- *see also air pollution detection and control; geophysical equipment; ionospheric measuring apparatus; ionospheric techniques; meteorological instruments*
- 500 mb height measurement, anal. error development, (1946 to 1969) 80—72615
- absorption lines of atmospheric gases, determination of parameters *(Russian)* 79—84507
- absorption of shortwave radiation by plant cover, calc. procedures 78—16219
- acoustic and optical methods for lower atmosphere dynamics study *(Italian)* 77—91327
- acoustic and radio acoustic exploration, effects of sound nonlinear absorpt. *(Russian)* 80—94567
- acoustic Doppler and angle of arrival wind detect., comparison with direct meas. 79—39884
- acoustic Doppler meas. of boundary layer turbulent vel. and energy dissipation rates 77—66966
- acoustic echo sounding, Doppler shift extraction by adaptive linear-prediction filtering 77—64453
- acoustic forecasts production, method using digital computer 79—79960
- acoustic probing, appls. of external noise spectrum model 80—58858
- acoustic remote sensing, review 78—73493
- acoustic remote sensing using modified microwave dish-antenna 79—72770
- acoustic sounding, appl. to boundary layer obs. from top of steep mountain 80—98409
- acoustic sounding, influence of varying system parameters 77—70863
- acoustic sounding, records obtained for Christchurch, boundary layer study 80—26638
- acoustic sounding of atmosphere, pattern recognition studies 78—65416
- acoustic sounding of boundary layer at Calgary 78—24376
- acoustic sounding technique, appls. to siting studies 78—81467
- actinometric method for tropospheric meas. of $O(^1D)$ formation by O_3 photolysis 78—73536
- active microwave sensing *(Japanese)* 78—16213
- adaptive optics, compensation for atm. effects 78—42296
- adaptive optics, real-time atm. compensation, using lateral shear heterodyne interferometer 80—77843
- adaptive spectral analysis of surface and internal waves *(Russian)* 77—29475
- aerial landscape photography, haziness factor in image contrast *(Russian)* 77—37449
- aerological sounding, appl. to atmospheric layers inclinations determ. *(Russian)* 80—72569
- aerosol, ambient sulphate particles size discrimination and chemical comp. by diffusion sampling 78—69528
- aerosol, individual microparticles identification via micro-Raman spectrometer 78—68970
- aerosol, middle atmospheric, remote sensing techniques 80—109269
- aerosol, stratospheric, conc. and sizes, meas. via impactor and in situ single-particle detect. 78—73437
- aerosol absorption meas. in situ using reson. CW laser spectrophone 77—73860
- aerosol charge distribution, determ. via variable freq. electrostatic mobility analyser 78—77945
- aerosol containing acid sulphate, detection using S/N ratio 80—61494
- aerosol content determ. from photometric obs. of stars 78—92976

atmospheric techniques continued
- aerosol droplet size and conc., simple transmittance meas. 77—9511
- aerosol IR spectrometry, theory and appl. to spectroscopic effect of atmospheric constituents 80—101428
- aerosol layer depth remote meas. by microwave-modulated laser *(Russian)* 78—57338
- aerosol layer detect., solar occultation technique using Skylab coronagraph 77—9540
- aerosol mass conc., meas. by lidar-solar radiometry expt. 80—90171
- aerosol mass conc. meas. by Nd:glass lidar, ASSESS II Spacelab mission simulation *(German)* 78—69649
- aerosol measurement, particle deposition in sampling lines 78—81472
- aerosol measurement problems 79—66839
- aerosol measurements with calibrated two- and three-freq. lidars 78—36334
- aerosol number and mass conc. meas. 80—108753
- aerosol particle concentration over Chicago, comparison of methods 80—7981
- aerosol particles sizing, influence of chemical struct. 78—81471
- aerosol samples, X-ray diffraction compound analysis 77—49176
- aerosol sampling by in situ and standard methods 79—66840
- aerosol scattering function determ. with telephotometer 80—105055
- aerosol size distrib. approx. determ. method 77—45188
- aerosol size distribution determ., optical attenuation meas. *(Chinese)* 80—72570
- aerosol turbidity characteristics, determ. from spectral actinometric obs. 78—92986
- aerosol vertical distribution, meas. by Skylab photographic coronagraph 77—60568
- aerosols, chemical characterisation, progress and problems 78—68969
- aerosols, detection and meas. of 10^{-4} to 10^{-1} μm particles *(French)* 80—7985
- aerosols, pyrotechnically produced, use as atmospheric tracers 77—41236
- aerosols, single particle dia. and aerodynamic relaxation time anal. 77—80205
- air collection and analysis techniques, troposphere and stratosphere 80—26566
- air flows in clouds, radar study 77—91243
- air monitoring techniques, esp. long path optical meas. *(Italian)* 77—91329
- air pollutant deposition research using rain gauges *(Dutch)* 78—81367
- air pollution, evaluation of Co_3O_4 catalysts for oxidation of organic compounds 77—37353
- air pollution analysis, automated X-ray fluorescence technique *(French)* 77—41234
- air pollution automatic analysis, spectrosc. methods *(Spanish)* 80—81516
- air pollution conc. statistical parameters determ. from truncated data set 77—37414
- air pollution detection by X-ray fluoresc. anal. of environmental samples, book 77—41217
- air pollution episodes in Venetian region, real-time forecasting via advection-diffusion model 80—77096
- air pollution episodes in Venetian region, real-time forecasting via Kalman predictor 80—82046
- air pollution monitoring, active and passive systems 77—70889
- air pollution remote meas. using chem. laser lidar system 77—21910
- air quality evaluation, daily profiles method *(French)* 78—92969
- air quality models development for limited wind fetch, method 80—104533
- air temperature, five-day average, forecasting, combined technique improvement 79—29817
- air-truth lidar polarisation studies of orographic clouds 78—73454
- airborne continuously recording ice nucleus counters, data anal. technique 77—78447
- airborne gas-chromatography, appl. to atmosphere vertical diffusion meas. 78—69435
- airborne particulates sources identification and relative importance estimation, regression model 80—72105
- aircraft ambient and cabin air O_3 conc. simultaneous determ. 80—90198
- aircraft EM environment meas. near thunderstorm cells 78—49180
- aircraft measurement of air motion 77—70858
- aircraft-to-satellite data relay system 80—17380
- airglow spectrometer, Fabry-Perot instrument for daytime use 80—77156
- all-sky photography and radiometric methods, diffuse solar radiation, anisotropy 79—88398
- anemometer and lidar meas. of wind vel., comparison 79—39885
- areal rainfall amount assessment, two techniques compared 79—62612
- Arecibo radar meas. of tropical winds 79—100975
- artificial clouds form. possibilities and methods 79—29823
- artificial satellite laser ranging for upper atmosphere wind determ. 77—64485
- astronomical refraction calc., theory for three-dimensional model of atmosphere 80—46260
- atmosphere dust, eval. using nuclear methods *(French)* 80—7993
- atmosphere pollution by S compounds and suspended particulates in European Community, information exchange 80—7979
- atmosphere pollution dust dynamics, study via ^{222}Rn descendants radioactivity meas. *(Rumanian)* 80—12524
- atmosphere temperature profile, IR remote sounding, error anal. and data acquisition *(Chinese)* 80—109273
- atmosphere turbidity monitored by satellite, obs. of reflected sunlight 80—51471
- Atmospheric Cloud Physics Laboratory on Shuttle/Spacelab, droplets optical motion control appl. 80—12634
- atmospheric temperature sounding from CO_2 4.3 μm absorption spectrum 78—16166
- atomic and molecular fluoresc. as stratospheric species monitor 77—9472
- atoms and radicals in situ reson. fluoresc. meas. in upper atmosphere 79—53600
- auroral brightness obs. inversion 80—12538
- auroral spectrum observations, appl. of matched tandem etalon camera (MATEC) 80—101442
- auroral zone convection observation, radar scatt. method 80—51573
- automated weather service rocket sounding system, information theory effectiveness rating 79—58057
- automatic coulometric analyser for continuous monitoring of CO_2 content 79—53537
- automatic observation of meteorological elements for atm. refr. determ. *(Japanese)* 80—82110
- available potential energy in press. coords. *(Russian)* 80—109187

atmospheric techniques continued
ballistic density determ. from satellite radiance obs., direct method 78—16186
balloon altitude mosaic measurements programme, IR mosaic background meas. 80—90222
balloon and rocket programs, conf. Bournemouth, England (1980, Aug.) 80—105433
balloon appl., hot-air, mile-long 79—48583
balloon data storage, prior to transmission to ground via satellite 80—46263
balloon obs. of nightglow, intensity distribution *(Japanese)* 77—82076
balloon obs. of nightglow over sky, intensity distribution *(Japanese)* 77—82075
balloon optical sounding inverse problem, ranking of model components 77—9533
balloon tethering system, for very low altitude meteorological obs. 80—36430
balloon two-dimensional sounding method for stratospheric shallow layer 78—3985
balloon-borne chemiluminescent meas. of stratospheric NO to 45 km altitude 77—29397
balloon-borne probes in stratosphere, atm. and astron. research 77—37435
balloons, Japanese 1966 to 1975 activities *(Japanese)* 77—82016
band-pass filtering of European air temp. series, correls. and phases 80—26579
beam-swinging expt. on troposcatter link, Doppler crosswind relations 77—5303
bistatic acoustic sounding of boundary layer 78—49176
Bouleyev-Marchuk eqn. soln. methods *(Russian)* 79—100967
boundary layer, eddy flux meas. corrected for density fluctuations 80—72576
boundary layer, eddy flux meas. made by powered glider 80—51509
boundary layer, horizontal trajectory computation based on surface geostrophic wind 77—37284
boundary layer, hourly mixing depths estimation from historical meteorological data 80—51482
boundary layer echoes from surface based remote sensors, coding technique 80—17400
boundary layer meas. system for wind and temp. obs. *(German)* 80—94616
boundary layer parameter determ. using vertical Gill anemometer 80—56618
boundary layer temp. profile determ. from ground-based 60 GHz radiometry *(German)* 80—82097
boundary layer temperature profile from inferior mirage obs., simple soln. 79—80035
boundary layer trajectories from balloon obs. 77—91307
boundary layer turbulence characts. determ. method 78—7815
boundary layer turbulence meas., acoustic sounder return interpretation 77—37417
boundary layer tuurbulence, meas. of microstruct. with hot and cold wires 80—24109
boundary layers, convective and nonconvective, parameterisation for use in numerical models 80—82009
buoy for data acquisition, using Meteostat data transmission *(German)* 80—90224
chamber methods for soil gas fluxes determ., numerical evaluation 79—16700
chemical tracer expts. on precip. systems, review 78—24324
chemiluminescence, in situ instruments and techniques, stratospheric minor constituents conc. 80—16886
cirrus clouds, remote sensing of thickness and composition from satellites 77—64461
cirrus clouds satellite exploration, radiative props. in NOAA 4 VTPR channels 79—39853
cirrus outflow divergence determ. using ATS 1 pictures 77—53239
clear air turbulence detect. by IR obs. of water vapour 77—73890
climate data archiving and quality control by computer 80—61907
climate from tree ring width interpretation, South Africa Widdringtonia cedarbergensis anal. 80—98439
climate prediction, problems 79—92570
climatic change, computer modelling 79—92587
climatological power spectra computation technique 77—91305
climatology, hydrology, atmospheric research and meteorology from space, conference, Ajaccio, Corsica (1979 November 12 to 16) 80—62397
climatology, information from ^{18}O/^{16}O in cellulose, lignin and whole wood from tree rings 78—24355
climatology, usefulness of satellite-determined sea-surface temps. in tropical Pacific 80—31044
cloud altitude measurements 79—88444
cloud analysis via space-derived pictures, appl. of photographic equidensity curve method *(Russian)* 77—53155
cloud and precipitation particles observed by radar, X- and K_a-band 80—46273
cloud classification techniques, comparative study 78—7809
cloud clearing by laser beams, liq. water content and temp. fluctuations *(Russian)* 78—44999
cloud condensation nucleus spectrometer, new design 80—85765
cloud cover, forecasting from middle troposphere organised vertical vels. 78—92939
cloud cover, photography via Japanese weather satellite 78—49290
cloud droplet size meas., comparison of electrostatic disdrometer with impactor slides 77—2278
cloud droplet spectrometry using light scatt. technique 77—41219
cloud entrainment determ. via temp. meas., aircraft temp. sensors wetting effects 79—53483
cloud extinction coefficient, estimation from multiwavelength lidar backscatter meas. 80—98446
cloud extinction meas. using electronic chopper for UV source 78—79087
cloud height meas. using light pulse reflection *(Russian)* 80—82056
cloud hole-boring by high-intensity laser beams, theory 78—28319
cloud identification against snow background, aircraft obs. *(Russian)* 77—29392
cloud liquid content measurement, ground based microwave instrument 80—94623
cloud microwave radiation emission meas. 80—17351
cloud motion estimation, Fourier phase difference technique 79—21046
cloud motion winds from ATS 6 images comparison with coinciding SMS 1 winds 79—79954

atmospheric techniques continued
cloud motions, automatic tracking system using weather satellite picture sequences 78—45022
cloud particle composition analysis using continuous impactor-replicator 79—53544
cloud photogrammetry from aircraft nose camera movies 79—53547
cloud seeding, anal. of Florida Area Cumulus Expt. (FACE) rainfall results, natural variability effects 80—82002
cloud seeding, Climax and Wolf Creek Pass expts. 80—82094
cloud seeding, expt. in Tasmania 80—51485
cloud seeding, Florida Area Cumulus Experiment, rainfall results, 1970-75 77—45113
cloud seeding, num. simulation technique 79—84519
cloud seeding, studies of AgI ice-forming activity, verification of theory 80—101406
cloud seeding devices, AgI nuclei formation efficiency 80—41552
cloud seeding experiments, statistics appl. 80—8438
cloud seeding method for lightning triggering 78—3880
cloud seeding studies application of lidar remote sensing 80—109203
cloud study chamber, study of ice nucleation by aerosol particles 80—61864
cloud temp. fluctuation meas. by IR radiometry, feasibility study 80—56636
cloud top height meas. using satellite imagery stereographic pairs 78—45017
cloud top heights determ. from satellite remote temp. sounding instruments 77—17256
cloud type and amount, objective nephanalysis 79—53541
cloud vortices, pressure from satellite obs. 80—26592
cloud winds over oceans, satellite technique verified by aircraft obs. 80—85764
cloud-free atmosphere long wave cooling rate determ. method *(German)* 77—64474
clouds, satellite IR nephanalyses 77—41122
clouds and atm. phenomena, integrated automatic processing of obs. data 79—29907
clouds numerical models, methods of parametrisation of condensation process *(Russian)* 78—16091
cloudy atmosphere, scatt. and line absorpt. of radiation, interaction, analytical calc. method 79—100940
cloudy atmosphere moisture content determ., long-range, by thermal radioemission meas. *(Russian)* 79—5637
cloudy atmosphere remote sensing, integral humidity, integral moisture, temperature and height of drop cloud phase determ. *(Russian)* 79—5635
cloudy atmospheric parameter determination using microwave radiometric method 80—67435
combination technique for weather forecasts, optimally and economically *(Russian)* 80—21792
computer graphics analysis of atm. refr., visual image transmission 79—8689
Concorde sonic booms as probe of atm. temp.-wind parameters 77—91323
condensation eqn. soln. method for droplet growth 78—7795
condensation nuclei, balloonborne meas. 77—64460
conduction current meas., direct method, new instrumentation 78—85637
conjugate equations use in calc. meteorological fields, inclusion of a priori information *(Russian)* 80—4136
convection in general circulation, efficiency and vel. estimation via laboratory models *(Russian)* 77—81961
correlation and spectral analysis, appl. to hydrometeorologic elements in coastal zone *(Russian)* 78—77258
coupled vector systems of nonlinear parabolic partial differential eqns., soln., geophys. appl. 77—41468
cross-wind velocity meas., interference fringe visibility and spacing, atmospheric turbulence effects 80—51572
crosswind profiles, remote sensing using correlation slope method 80—31131
cryogenic spectrometry for airglow and aurora studies 77—70886
cumulonimbus clouds, elec. field strength and raindrop spectra, study from mobile ground station 78—92943
cumulus cloud seeding technique, preliminary tests 78—57352
CW lidar meas. of atmospheric visibility 78—40651
cyclone centre location using kinematical determinant 80—56535
cyclones, pressure drop reduction using deswirler 79—12176
daily precipitation stochastic models, estimation of Fourier coeffs. to describe parameters seasonal vars. 79—53481
daily temperatures, statistical forecasting using short records of previous temps. 79—58015
data analysis using interactive satellite video display systems 79—58229
data assimilation with one-level primitive eqn. spectral model 77—2274
data collection and processing system at Leningrad TV tower 78—4004
data processing of M-100 meteorological rocket system 77—53233
derivatives computation from equally spaced data, rainfall rate determ. 77—49125
differential-absorption lidar technique for remote meas. of atm. gases 78—61603
diffusion in freely convective boundary layer, meas. by acoustic sounding 79—34966
diffusion parameters from balloon obs. *(Italian)* 79—21067
diffusion problems soln., pseudo-spectral and orthogonal collocation method 79—12170
dimensional analysis and power laws limitations 79—25333
direct solar radiation and diffuse radiation calcs. from synoptic weather obs. *(German)* 79—34925
dispersion correlation spectroscopy, mask optimisation procedures 77—73857
Dobson total O_3 meas., aerosol effect 80—12463
Doppler acoustic sounding of lower atm., convective plumes detect. *(French)* 78—40603
Doppler mean vel. estimates, ambiguity removal 78—3983
Doppler radar data analysis 80—41564
Doppler radar meas. of wind in extratropical cyclones, colour display system 78—61594
Doppler radar obs. of gust front evolution and tornado genesis 77—91219
Doppler radar probing of clear atmosphere 79—66811
Doppler vel. extraction from acoustic echoes, zero-crossing technique 79—53542
double theodolite measurements, control of inherent uncertainties 80—77160

- **atmospheric techniques** continued
  - drop size distribution airborne meas. for drops >60 μm diameter 78−45008
  - dry ice appls. to on-top seeding of convective clouds 78−73531
  - dust deposition rates on snow, satellite remote sensing of snow albedo 80−17385
  - dustfall, short term, from dust generating industry, meas. and effect on residential development 78−81386
  - dye laser, high energy pulsed, for atm. sounding 79−39868
  - dynamics and auroral morphology, photometric data interpretation 80−82141
  - earth radiation budget: simulation of fluxes and accelerometric measurements *(French)* 79−84482
  - Earth resources satellite picture web grammar model applic. 77−37466
  - Earth surface temperature in mountainous terrain, diurnal var. prediction and errors 80−82011
  - earthquake lights, proposed for study by chemiluminesc. NO air pollution apparatus 80−61906
  - edge detection for meteorological data 79−100989
  - EHF clear air refractivity calc. procedure 78−57266
  - electric field double probe meas., Doppler shift effects on power spectra 80−26634
  - electrical aerosol plume detection, theory and meas. 80−7984
  - electrical conductivity measurement by passive antenna system, comparative study 80−85762
  - electrical conductivity of atmosphere and lower ionosphere, profiles evaluation from expt. Schumann reson. data 80−36360
  - electrically charged air tracking, for atm. diffusion meas., by ground level elec. field meas. 77−78450
  - electro-optic and holographic meas. techniques for atmospheric sciences, review 78−49184
  - electron beam injection, beam-plasma discharge at low press. and mag. field strengths 78−42769
  - electron capture-gas chromatography for N_2O conc. meas. 77−9531
  - electron echoes, from conjugate regions of magnetosphere, distrib., Araks expt. *(Russian)* 79−40019
  - electron microscopy of raindrops, particulate conc. determ. 77−81971
  - electron pitch angle distrib. determ. using Molniya 1 omnidirectional detectors 80−8437
  - electrostatic charges meas. and localisation, neutralised during lightning flashes 80−77097
  - elemental analysis at sub parts per trillion concs., via SONRES 78−81465
  - energy balance determ. methods *(French)* 77−33208
  - energy budget over grasslands, eddy correl. sampling technique 77−78446
  - environmental samples, proton induced X-ray anal. method appl. 77−63990
  - EUV and visual obs. from Spacelab 77−22201
  - evapotranspiration remote sensing Nimbus 5 satellite IR radiometer, evaluation *(French)* 77−17156
  - Excede 2 test, artificial auroral expt., ground-based optical meas. 78−89038
  - exosphere, temp. determ. by ground meas. of ionosphere and O I 6300 Å line 77−67003
  - extinction coefficient meas. from distant contrast, using astronomical telephotometer 78−61730
  - F-region neutral winds, determ. from ionosonde meas. of hmF2 at low latit. mag. conjugate regions 78−81477
  - F-region zonal winds, estimation during Joule heating using incoherent scatter techniques 78−36344
  - FGGE observing system, data system tests 80−56610
  - filter media suitable for air pollutant analysis (HNO_3, nitrates and acidity) 80−104541
  - finite difference equations in generalised vertical coordinates, appl. to pot. vorticity conservation 80−26576
  - finite difference schemes for initial value problems, derivation technique 77−86986
  - flameless atomic absorption spectroscopy, appl. to Cd, Pb and Mn determ. in size fractionated aerosols 78−69434
  - flash holography investigation of atmospheric aerosols 78−16217
  - fluoride concentration meas. methods *(Dutch)* 77−82002
  - fluorocarbon, detect. using computer simulated IR solar spectra 77−53217
  - fluorocarbons, lifetime determ. methods 79−20920
  - flux estimation techniques for unstable surface layer over land 77−66962
  - fog, quantitative meas. of precipitation onto surfaces 80−56654
  - fog, supercooled, dispersal using compressed air 77−49185
  - fog, warm, modern thermo-kinetic dispersal system for commercial airports 80−51576
  - fog clearance, haze droplets effects on visibility in natural and treated fogs 79−100951
  - fog clearing by laser beam, thermal self-defocusing effect 77−64432
  - fog meas. on motorways 79−16608
  - foil impactor impressions of water and ice particles, interpretation, rel. to hail research 78−57356
  - forecasting nocturnal temperature, short-range model 80−109200
  - forecasting of thunderstorms and severe local storms, automated 12 to 36 hour probability forecasts 80−77062
  - forest evapotranspiration determined using Bow ratio and eddy correl. meas. 80−31103
  - four-day forecast, influnece of sensible and latent heat fluxes over land 79−96805
  - Fourier far IR spectroscopy from Spacelab 77−21949
  - Fourier transform IR absorpt. spectroscopy, airborne, for atm. comp. meas. 78−61604
  - Fourier transform method for inhomogeneous atmosphere transmittance calc. 80−12555
  - Fourier transform spectroscopy, Doppler-limited high-accuracy, 10^6 samples 78−58068
  - Fourier transform spectroscopy appl., far IR 78−58069
  - free air press. estimation from radio sonde data 79−88508
  - free radical meas. by matrix isolation and EPR 78−73535
  - frontal precipitation forecasting, contrib. of weather radar network, case study 77−56692
  - gamma radioactive source measurement, in dynamic condition, error sources *(Rumanian)* 78−46243
  - gamma-ray flux measurement, NaI(Tl) scintillation counter *(Japanese)* 77−71732
  - gas chromatography for volatile organic compounds determ. in city air 78−12003

- **atmospheric techniques** continued
  - gas complex analysis method, resonance absorption with pulsed laser light *(Japanese)* 80−36421
  - gas filter spectroscopy for stratospheric halogen compound monitoring 77−45162
  - gas remote meas. using discretely tunable IR lasers 77−91298
  - gaseous atmospheric pollutants, teledetect. *(French)* 80−7988
  - gaseous hydrocarbon removal, with allophane adsorbers *(Japanese)* 77−78412
  - gaseous impurities continuous automatic meas. *(Dutch)* 77−82000
  - gases abundance determ. by analysing solar spectra 78−85643
  - gases identification and conc. meas. from spectral absorpt. patterns, anal. methods 77−87059
  - gases identification and conc. meas. from spectral absorpt. patterns, system appls. and design 77−87060
  - GATE aircraft measurements, their value 80−82071
  - GATE ship surface meas. systems, anal. or drift 80−82070
  - generalized inverse theory application and spectral expansion method for temperature profile retrieval 80−17412
  - geomagnetic field meas. from near-Earth orbit, review of obs. 80−56347
  - geomagnetic field variations, remote sensing at mesospheric heights 80−77124
  - geomagnetic pulsations, detect. using solenoid with ferrite core 78−24384
  - geopotential height data over ocean areas, supplementary method 80−26647
  - gravity waves in upper atmosphere, obs. via $O_2(^1\Sigma)$ airglow, theory 79−29918
  - ground albedo and absorpt. by atmos. particulate, determ. using diffuse light radiometer 80−51465
  - ground surface temperature prediction, force-restore method investigation 80−98469
  - ground wave attenuation function, computation methods 80−94585
  - ground-based inversion decay, analysis by direct and indirect meas. methods *(German)* 77−37310
  - gusts, local forecasting method *(German)* 78−85727
  - hail, radar detection technique, quasilinear discriminant function 80−21861
  - hail cell detection, for cloud seeding criteria, radar method 80−90170
  - hail identification by radar, ice samples backscatter matrix 79−58046
  - hail suppression expts., improvements 77−91218
  - hail-prevention operations, cost effectiveness estimation methods anal. 78−93013
  - hailpad calibration for Italian hail damage documentation 77−29488
  - hailstone kinetic energy meas. inc. wind effects using hailcube 77−17173
  - hailstone size determ. from dents in cold-rolled Al sheet 79−39890
  - hailstone thin sectioning technique, for growth study 80−90160
  - hailstone trajectories determ. from crystallography, D content and radar backscatt. 78−61614
  - halofluorocarbons background levels, in situ quantification technique 78−69530
  - hazes, information provision on particle size distrib. of brightness and polarisation phase functions *(Russian)* 78−44998
  - heat budget and albedo determ. using balloon-borne pyranometers 79−58135
  - heat transfer meas. in boundary layer, radio thermal microwave systems appl. 79−84546
  - heavy precipitation of Fergana Valley, short-term forecasting 78−92946
  - high acidity measurement, comparative tests near industrial installations in Fos-Etang de Berre region 78−81464
  - high-altitude wind measurement, radiowave drifts technique 80−31137
  - holographic droplet image analysis by TV camera and table calculator via IEC-Bus 78−36337
  - horizontal turbulent diffusion coeffs. in stratified baroclinic boundary layer, determ. method 78−32135
  - humidity 80−85660
  - humidity of cloudy atmosphere and clouds drop phase characts. meas., by means of passive radar 79−74991
  - humidity profile, passive microwave profiling technique 80−21856
  - hurricane dection by Doppler radar for coast of U.S.A. 80−67414
  - hurricane-intensity extratropical storms, satellite forecasting, comments and reply 77−17249
  - hydrocarbon concentrations, measuring methods *(Dutch)* 78−36300
  - hydrocarbons, volatile, detect. and meas. techniques, review 77−64492
  - hydrometeor size and shape determ. using radar differential reflectivity and differential phase shift 78−57270
  - hydrometeorological fields objective analysis, probabilistic models *(Russian)* 77−56697
  - hydrometeorological information, optimum conversion to digital form 79−29903
  - hydrometeorological large scale processes, spectral density, evaluation *(Russian)* 77−5337
  - hydrometeors in clouds, size, conc. and struct. meas. with impactor and replicating devices 77−41218
  - ice crystal continuous replicator for laboratory cloud chambers 77−78448
  - ice crystal growth on membrane filter, vapour depletion, chamber parameters effects 79−70858
  - ice crystal habit discrimination using optical backscatt. depolarization technique 77−91309
  - ice nucleation at -1°C using bacteria 77−53221
  - ice nuclei conc. meas., filtration theory appl. 79−39887
  - ice nucleus concentration meas. with static vapour diffusion chamber 77−91308
  - ice particle counting in mixed-phase clouds by optical techniques 77−41221
  - ice particle types in melting layer vicinity, determ. from Doppler radar meas. 77−78338
  - incoherent scatter radar on Spacelab, for field-aligned currents meas. 77−21946
  - incoherent scatter radar sounding, appl. to daytime middle thermosphere 80−72654
  - incoherent scatter radar technique appl. to lower thermospheric dynamics 79−8734
  - incoherent scatter radar techniques, appl. to O I 6300 Å nightglow profiles meas. *(Portuguese)* 80−41591
  - infrasound waves recording methods and computer anal. *(Russian)* 78−65407
  - initialization methods for gravity wave generation in two-layer linearized model 77−86971

atmospheric techniques continued

- instruments and objectives for Atmospheric, Magnetospheric and Plasmas in Space (AMPS) study 77—25802
- interferogram radiance measurement techniques for sounding, temp. profile 80—17413
- internal gravity waves near mesopause rel. to OH emission, recording method 78—12031
- interpolation methods for sparse data, comparison and appl. to wind and conc. fields 80—51575
- ion chromatographic anal. of air pollution samples, appls. 80—30625
- ion chromatography, new analytical technique for sulphate and nitrate assay in ambient aerosols 78—68974
- ionosphere and magnetosphere elec. fields and currents from artificial Ba clouds obs. 77—35194
- IR atmospheric remote sensing, theoretical problems 79—80052
- IR attenuation by H_2O vapour, hygrometer meas. 79—34943
- IR emission, statistical props. of sky noise at telescope focus *(French)* 78—53731
- IR fluxes meas. by radiometric soundings, parametric law derivation *(French)* 79—25358
- IR heterodyne spectroscopy, appl. to O_3 77—45160
- IR heterodyne spectroscopy, stratospheric sounding 79—100971
- IR laser heterodyne spectroscopy for trace gases remote detect. 78—61606
- IR laser technique for SO_2 conc. determ. *(Russian)* 78—69484
- IR optoacoustic spectroscopy of atmospheric gases 77—41243
- IR remote sounding of atmosphere with multiple cloud formations 77—78319
- IR remote sounding of cloudy atmosphere, CO_2 radiance data 77—78320
- IR scanning radiometer data interpretation 79—30541
- isentropic objective analyses, theory and appl. to meteorology *(Polish)* 80—51546
- iterative methods for treating multiple radiowave scattering 79—8709
- Lagrangian similarity modelling, of vertical diffusion from ground-level source 80—51480
- large scale electric fields, modelling from F_2-layer global electron density distrib. 77—64514
- laser absorption method for H_2O vapour conc. meas. 78—61595
- laser absorption spectroscopy, airborne, troposphere O_3 distribs. meas. 79—2344
- laser absorption spectroscopy for point monitoring of gases ambient concs. using tunable lasers 78—61607
- laser absorption techniques for air pollution 77—9570
- laser analysis, from orbiting satellite 77—9571
- laser atmospheric studies, review 79—66789
- laser beam detection of atmos. constituents, review *(French)* 79—34952
- laser beam study of crystalline clouds, light scatt. matrices *(Russian)* 77—5317
- laser Doppler anemometry, instrumentation, appls., explanation using Moire patterns 77—7490
- laser fluorescence meas. of OH conc., O_3 dissoc. interference 77—49110
- laser heterodyne spectroscopy for stratospheric trace constituents meas. 80—109257
- laser PROBE technique, density profile meas. of specific constituent 78—28320
- laser remote sensing methods *(Japanese)* 78—45019
- laser single-beam transverse velocity meas. 78—53747
- laser technology for atm. science, conf., San Diego, USA (Aug. 77) 78—85748
- laser velocimetry techniques using CO_2 laser 78—61623
- laser-radar observations of stratospheric O_3, excimer laser appls. 80—17410
- lasers in air pollution detection, review 77—9569
- LF radio sounding of plasmapause by geostationary satellite 78—69648
- lidar, airborne, multidisciplinary, planned operation 78—36335
- lidar, airborne continuous long-distance system, flight tests *(German)* 78—36338
- lidar, differential absorpt., from Space Shuttle, for atm. trace constituents meas. 78—45179
- lidar, laser rangefinder, characteristics of atmospheric aerosols 80—51580
- lidar, meas. of effective stake height of smoke plumes *(German)* 77—9490
- lidar, multifreq., lower-stratospheric aerosol microstruct. sounding 80—56645
- lidar, simultaneous nighttime meas. of Na and K abundances 78—36239
- lidar and solar radiometer obs. compared with aircraft meas. of particulate props. 78—61501
- lidar equation for inhomogeneous atmos. *(Russian)* 80—82054
- lidar for atm. meas. 77—37436
- lidar for stratospheric O_3 density meas., feasibility 77—60493
- lidar investigation of inhomogeneous atmosphere optical parameters *(Dutch)* 79—80026
- lidar measurement of Na conc. and neutral temp. at mesopause level 78—61613
- lidar measurement of stratospheric aerosol size distrib., 0.6943 and 1.06 μm obs. 77—41120
- lidar measurement of temp. profiles, rot. Raman and elastic scatt. 77—9515
- lidar measurement problems in hazy visibility conditions 77—9572
- lidar method for half width and intensity of gas absorption lines *(Russian)* 80—21844
- lidar observation of smoke and dust clouds, at 0.7 μm, 10.6 μm 78—49181
- lidar observations of altostratus mixed-phase cloud 77—91220
- lidar observations of atmosphere at Kingston, Jamaica 78—36284
- lidar observations of high plains thunderstorm precipitation 78—32167
- lidar observations of Labadie Power Plant plume, particulate density and behaviour obs. 80—55956
- LIDAR observations of plume diffusion at Rancho Seco Generating Station 78—11991
- lidar observationsof aerosol props. 79—66841
- lidar polarisation meas. for cloud phase discrimination 78—96269
- lidar probing of fogs and clouds, double scatt. approx. 78—73512
- lidar Raman spectroscopy of atmosphere *(Russian)* 78—24387
- lidar return signal geometrical compression, atm. remote sensing appl. 78—57329
- lidar returns depolarization, scatt. from virga and source cloud 77—49169
- lidar sounding, nondispersive gas analyser appl. *(Russian)* 77—60477
- lidar sounding of atmosphere, optical system parameters effect 80—33065

atmospheric techniques continued

- lidar techniques for atm. struct. and comp. obs., proposed Spacelab program 78—61602
- LIDAR teledetection and measurement of minority atmospheric constituents for pollution control *(French)* 80—7992
- lidar temp. profiling in O_2 bands 80—21827
- lidar velocimeter detect. of atm. aerosol flow 77—13127
- Lidar visibility measurements, using Raman/aerosol ratio method 79—100953
- light propagation, emergent radiation computation method for UV to IR region 77—87069
- lightning, direction finding at close range, VHF method 80—98481
- lightning, intracloud discharges inclination from mag. fields meas. 78—73440
- lightning current wave forms, deduction from radiated EM fields, Maxwell eqns. exact soln. appl. 78—73442
- lightning direction finding, by mag. method 80—77078
- lightning ground-flash multiple-stroke discriminator cct. 78—81446
- lightning return stroke rise speed meas. method *(French)* 80—51493
- lightning source directions, 34 MHz interferometry 79—79939
- lightning stroke current meas. using optical fibre cable and optoelectronic conversion, rocket launched 78—92930
- lightning stroke obs., at isolated high tower *(Japanese)* 78—40641
- lightning study using thunder meas., thunder duration rel. to strike pt. *(Russian)* 80—56532
- liquid drop cloud medium dissipation by CO_2 laser radiation 79—39858
- liquid water content, determ. from Nimbus 6 scanning microwave spectrometer data parameterisation 79—58047
- long-range weather forecasting, appls. of quasi-cycles in meterology 80—109239
- long-range weather forecasting, art and science 80—109184
- lower atmosphere remotely sensed by two satellites, radio illumination method 80—51550
- lower atmosphere vertical stability determ. from Rn concs., influence of meteorological parameters *(Spanish)* 79—92562
- lower atmosphere vertical stability determ. from Rn content, influence of wind regime *(Spanish)* 79—92560
- lower atmosphere vertical stability determ. from Rn content, stability indexes statistical anal. *(Spanish)* 79—92561
- magnetopause obs., techniques and results 78—61668
- magnetosphere, constant electric field strength vector meas. problems 78—16245
- magnetosphere, day cusp dynamics tracking via long-period geomag. pulsations obs. 79—53656
- magnetosphere, elec. fields parallel to mag. lines, studied by electron injection expts. 80—72702
- magnetosphere, electron temp. estimation via VLF waves propagating in directions near reson. cone 77—82086
- magnetosphere, high-latit., Echo 4 electron beam expt. and artificial auroral streaks obs. 78—89036
- magnetosphere, local electron density and mag. field meas. via JIKIKEN (EXOS-B) satellite stimulated plasma wave expts. *(Japanese)* 80—94649
- magnetosphere, measuring technique using in situ excitation of plasma resonances *(French)* 78—20529
- magnetosphere, nonstationary processes study via incoherent response method, phase fluctuations effects 78—45184
- magnetosphere, quiet band prod. by VLF transmitter signals 77—64534
- magnetosphere, ULF waves anal. techniques using spectral matrix 77—13137
- magnetosphere chorus and hiss observed by GEOS, automatic recognition using coherence function 79—44307
- magnetosphere cold plasma densities, comparison of ULF and VLF meas. 78—28436
- magnetosphere cold plasma diagnostics using satellite meas. of VLF signals from ground transmitters 77—49183
- magnetosphere electron density, small scale struct. from plasma resons. on-line tracking 79—35073
- magnetosphere experiments, appl. of EM ion cyclotron instability enhancement by cold plasma 77—33287
- magnetosphere magnetic fields, dual magnetometer method extension for use on dual spinning spacecraft 78—77459
- magnetosphere plasma, new concept for EM and electrostatic waves detect. 77—9549
- magnetosphere plasma diagnostics, use of trigger VLF emission 78—45149
- magnetosphere relaxation sounding by GEOS-1, plasma density results 79—35072
- magnetosphere sounding, beam-plasma interaction expt. by JIKIKEN satellite *(Japanese)* 80—94655
- magnetosphere substorms, onset identification via Pi 2 mag. pulsation 77—9626
- magnetosphere VLF wave injection experiment, receiver on International Sun-Earth Explorer A 78—85806
- magnetospheric detached plasma formations, investigation by noncoherent response method *(Russian)* 77—29584
- magnetotail, Alfven wave generation via proton accelerator 78—73582
- magnetotelluric methods, methods to study crust cond. beneath magnetometer array, review 80—98486
- marine atmosphere, microwave radiometry appls. 78—81415
- marine wind velocity, remote sensing using oceanic whitecaps 80—72554
- Markov chain modelling of weather data 77—49124
- mask correlation spectrophotometry, long horizontal path appls. 79—12277
- mass spectrometric measurement of thermospheric wind 78—28359
- mass spectrometric obs. of SO_2 in stratosphere 77—33200
- mass spectrometry, for atmos. composition 80—8518
- mass spectrometry for in situ meas. 80—17388
- mass-mean temperature determ. from cosmic ray intensity vars., Sayan spectrograph data 79—84606
- mathematical analysis of meteorology data 80—56521
- matrix isolation EPR for free radicals meas. 78—46374
- meridional motions, estimation of intensity *(Russian)* 77—53154
- mesosphere, equatorial wind meas. techniques 78—36229
- mesosphere, neutral wind vels. meas. via partial refl. technique 77—87019
- mesosphere neutral winds, incoherent scatter spectrum meas. in 60 to 90 km region 79—16569
- meteor trail, maximum ionization height detect. method 80—8487
- meteoradiolocator echo signals, optical spectral processing *(Russian)* 79—100968

atmospheric techniques continued
meteorological conditions, press. and geopot. by 5 mm radiothermal sounding *(Russian)* 80—77038
meteorological conditions forecasting procedures for aviation, development and improvement 78—92950
meteorological data analysis, interpretation of asynchronous data 80—109271
meteorological data sets, form. from first GARP Global Experiment (FGGE) obs. 80—101437
meteorological element field adaptation, variational method *(Russian)* 77—29491
meteorological field analysis and forecasting pattern-recogniton theory methods appl. 80—98421
meteorological observations from space and the FGGE 80—36403
meteorological physics, recent developments, review 79—25313
meteorological radar equipment signals processing, interpretation device *(Russian)* 80—67432
meteorological radar network optimal positions, multiple-Doppler system 80—31140
meteorological radar system synthesis, economical aspects 79—62543
meteorological satellite images, interpolation methods, analysis 79—58136
meteorological satellite visible and IR image data, computer processing 79—29864
meteorological time-averaged data, variance by simple approx. 80—31139
meteorology, aspects of satellite anal. at Central Forecasting Office 77—41123
meteorology, forecasting of cold intrusions into N.Vietnam via discrimination anal. 78—3910
meteorology, forecasting of summer weather in England 79—84425
meteorology, objective computer classification of composite charts 78—3906
meteorology inverse problems, estimation theory appls. 79—35018
meteorology radar, airborne pulse Doppler method 80—85757
METEOSAT project overview *(Italian)* 80—109331
methane gas plumes, tracking via atmospheric acoustic sounder 80—55968
microclimatic modification by small water droplet evaporation 77—17248
micrometeorological measurement principles, book 77—9559
micrometeorological temperature profile from optical data inversion 79—80034
microwave attenuation through rain, correl. with predicted values using radar 77—5279
microwave link rain attenuation, year and worst-month rain rate distrib. estimation method 79—5648
microwave radiation from clouds meas. by Nimbus 6 for rainfall distrib. determ. 78—3981
microwave radiometry from satellites 77—70882
microwave remote sensing, radiative transfer eqns. 80—21855
microwave sensing from satellites, appl. to meteorological meas. over W.Australia 80—98485
microwave sensors in satellites appl., passive and active 79—80060
microwave spectroscopic imagery of Earth from Nimbus 6 satellite 78—12026
minor constituents detection using tunable spin flip Raman laser, review 80—55762
mixing ratio determ., two-balance direct method 77—73866
MM and subMM wave appl. in 100-1000 GHz range 80—17962
mm wave attenuation and bistatic scatter simultaneous meas. tech. 77—9554
MM wave radiometry for atmospheric sounding 79—84551
modelling and prediction of climatic var. 77—21882
modification by space borne microwave beam at water vapour absorption line, 22.2 GHz 78—49171
modulation transfer function, estimation via coherence interferometer *(Russian)* 79—16715
moisture content determ. of cloudless atmosphere, microwave radiation meas. 80—94624
moisture profile estimation from satellite IR radiance meas. 78—45021
monitoring techniques for neutral atmosphere *(Japanese)* 78—16126
motion simulations, wind tunnel characts. review *(Italian)* 80—4156
moving atmosphere, optical simulation by rotating phase plate 80—79021
MST radar, VHF pulsed Doppler method 80—46277
multiple scattered radiation in Earth atmosphere, plane-parallel model appls. *(Russian)* 78—36275
multispectral obs. of pollutants, near UV imaging system 77—70892
natural orthogonal components of meteorological fields calc. *(Russian)* 80—4137
natural radioactivity continuous meas. method in surface layer *(Flemish)* 78—61612
negative DC corona study in atmospheric air using Schlieren and interferometric techniques 80—49023
nephelometry, electrooptical, characterisation of nonspherical atm. aerosol particles 80—77106
nested grid for 3-dimens. 3-level model of tropical cyclone 78—28342
neutrino detection, high-energy, using acoustic pulse from hadron shower *(Russian)* 77—38580
nitrate detection in aerosol particles using nitron 79—12280
non-methane hydrocarbons, monitoring via photoionisation 78—73549
normal mode initialisation technique, variational nonlinear, atm. gravity waves appl. 79—5584
normal mode linear initialisation method 80—77042
northern hemisphere annual temperature approximation, simple method 78—81345
nuclear fission aerosol products, bioindication using needles of common pine tree 79—100550
numerical filtering analysis, appl. to atmos. spectral energetics determ. 80—26577
numerical weather forecasting, determ. of boundary layer orography and turbulence-induced vertical currents 78—96278
numerical weather prediction, modified forward- backward scheme for two-grid-interval noise 80—26575
occultation technique for stratosphere minor gases determ. *(Russian)* 79—25342
ocean interface investigations using stable and radioactive isotopes *(Russian)* 77—60486
ocean surface wind and waves, radar meas. techniques 78—81418
ocean-atmosphere momentum, heat and H_2O vapour fluxes, meas. methods 78—32213
oceanic precipitation, meas. by satellite microwave obs. 77—60455
odour intensity measurement techniques *(Dutch)* 77—25775

atmospheric techniques continued
oil polluted sea surface, atmosphere-ocean system apparent contrast 79—25265
optical attenuation coeff. determ. by horizon line broadening *(Russian)* 77—60478
optical depth determ. by measurements of meteorological range 79—84474
optical detection of ^{238}U decay products 77—87104
optical measurement of turbulence, refr. index pulse spectrum *(Russian)* 77—29439
optical methods for thermal exchange meas. above warm water surface 77—49184
optical properties of turbulent atmosphere, determ. via He-Ne laser transmiter/receiver 80—98450
optical remote sensing of turbulence, comparison with simultaneous thermal meas. 79—34965
optical resonance absorption-resonance fluorescence techniques for O and N density determ. 77—21951
optical signals propagation, measurement aggregate for statistical characts. analysis 80—36412
optical-acoustical method for radiative heat flux divergence meas. *(Russian)* 78—7789
optimal raingauge densities and accumulation times, decision making precedure 77—29485
optimal sampling and anal. method 78—73530
optimum difference schemes, synthesis on sphere 78—93011
optoacoustic measurement of i.r. CO laser beam absorpt. by water vapour 77—2241
organic pollutants, determ. via gas chromatography after cryogenic sampling 78—81468
organochlorine residues in rainwater, extraction method 78—73495
outdoor velocimetry with CO_2 lasers 77—91296
overdetermined windfinding systems, error anal. 80—17399
palaeoclimates evaluation in Middle East, appl. of monthly temps./rainfall relation 80—31091
palaeoclimatology, appl. of global climatic interpretation of precip. D-^{18}O relationship 80—17331
palaeoclimatology, Quaternary temps. and precipitation determ. from pollen factors 80—98438
palaeoclimatology, role of tree-ring anal. in Indian region from preliminary survey 80—90212
panoramic lightning recorder, operational use for aviation weather support 77—78482
parachute-deployed payload for elec. field meas. below 80 km 77—64376
parallel electric field, signature in ion and electron distribs. in vel. space 78—89005
particle acid content determ. method 77—37448
particle elastic scattering analysis, appl. to C, N and O determ. in size fractionated urban aerosols 78—81466
particle size determ. using spectra attenuation data *(Russian)* 79—34981
particle size distribution meas. using electronic cascade impaction 80—72652
particle size spectrometry, use of low power gas lasers 77—78485
particle sizing, 0.05 to 5.0 μm, using laser instrument 78—61624
particulate detection, solar occultation technique, horizon radiance inversion 77—9539
particulate size distrib. and refr. index, new lidar-radiometer method 80—77153
particulates, chemical characterisation via light scatt. method 78—69533
particulates and gaseous pollutants measurement, anal. and calibration techniques 78—69531
Pc 1, short-term prediction of pulsation occurrences 80—109317
Pc micropulsations, polarization states, detection 79—74966
photochemical air pollution potential form. in United Kingdom, numerical estimation method. form. in United Kingdom 80—76682
photochemistry, mol. scatt. and refl. inclusion in photon fluxes and photodissoc. rates calcs. 79—53512
photogrammetry of waves in OH emissive layer 80—51545
photolysis, flash, in time and frequency domains, chemical behaviour obs. 79—39874
photometric systems, comparison at observatories in Arecibo and Stara Zagora 79—48575
photometric technique for aersol absorption meas. 80—85750
photon transport problems, modified Monte Carlo procedure 78—61560
physics field course, for school pupils 77—87612
PIXE analysis of atmospheric aerosols 79—53004
PIXE analysis of atmospheric gases, cryogenic conc. technique 79—53005
plasmapause sounding from geostationary satellite, feasibility 78—93043
plate reduction study of stellar photographs rel. to thermospheric release expt. *(French)* 77—17330
plume model for diffusion, parameters estimation *(Japanese)* 79—79983
point-discharge currents, meas. via portable instrument using junction FETs 79—39972
Poisson's type eqn., reliability of iterative solns. 79—96837
pollutant annual average concentration around single source, rapid estimation technique 78—81382
pollutant detection, quantitatively analysing spectroscopy by continuously scanned tunable dye laser 77—78486
pollutant gases, monitoring from space using passive microwave techniques 80—76690
pollutant measurement techniques, for H_2SO_4 and particulate strong acidity 80—104542
pollutants, selective quantitative meas. using CO and CO_2 lasers 78—69526
pollutants dispersion, completely Lagrangian random-walk model 78—81380
pollutants emission control, He tracers appl. *(French)* 80—7987
pollutants monitoring from municipal wastewater plants 79—80050
pollutants origin and residence times determination, ^{14}C appl. 78—69445
pollutants teledetection, by CO_2 laser two-freq. differential absorpt. meas. *(French)* 80—7991
pollution, continuous point sources, effects prediction *(Dutch)* 78—61545
pollution, factor of safety calc. method 80—94140
pollution by S compounds and suspended particulates in European Community, detect. techniques and information exchange 80—7979
pollution cartography, teledetect. data acquisition and anal. *(French)* 80—7989
pollution detection, development of const. current electron capture detector with modulated freq. *(Japanese)* 80—55764

atmospheric techniques continued

- pollution dispersion, modelling by smeared conc. approximation 78—81381
- pollution effects indicators, provisional map 78—81387
- pollution meas. using tunable lasers 77—60499
- pollution remote sensing from space 78—61621
- pollution spatial distrib., objective interpolation formulae 78—65412
- positive ion concentration, in urban centre, meas. method *(Spanish)* 80—4059
- Precede, artificial auroral expt., summarised results 78—89037
- precip. time struct., daily precip. amounts modelling with Markov-I chain 80—101401
- precipitable water vapour and liquid, by dual-channel microwave radiometry 80—51564
- precipitable water vapour determ. from surface meteorology and IR hygrometer meas. *(Italian)* 79—48587
- precipitating clouds observed by RONSARD radars 80—51568
- precipitation, depth-area relations from digitised radar returns 77—91249
- precipitation acidity measurement, error anal. applied to indirect methods 80—72108
- precipitation cell detection and tracking by radar, automatic detection and tracking 80—51544
- precipitation chemistry determ., calibration of collection procedures 77—37447
- precipitation collection and chemical anal. 78—57368
- precipitation five-day forecasting using successive graphical regression *(Russian)* 77—29492
- precipitation forecasting 0-6 hours ahead, radar and satellite imagery, FRONTIERS plan 80—12509
- precipitation forecasting in Arizona, rel. to marine layer depth and moisture content at San Diego, California 80—101395
- precipitation mapping with airborne synthetic aperture imaging radar 77—87106
- precipitation over Central Europe, large-scale field components extraction for forecasting purposes 78—92940
- precipitation parameter meas. method using radar reflectivity and optical extinction *(French)* 78—53729
- precipitation properties using radar polarisation techniques 80—61925
- pressure measurement with syringe, student expt. 77—57122
- pressure sensing by solar occultation using wideband CO_2 absorption 79—80037
- progressive and retrogressive waves coherence and space-time power spectra partition 77—91306
- propeller anemometer and thermistor meas., meas. interpretation *(French)* 79—16708
- proton activation analysis for determ. of F_2 pollution from brick kiln 78—20504
- pseudospectral method for pollutant dispersion eqn. numerical integration 77—56727
- psychrometry, appl. of portable differential system 80—105072
- pulse Doppler radar obs. of severe thunderstorms 78—85651
- pulse Doppler radar probing of tornadoes 78—20558
- pyrheliometric ratioing for apparent atm. transmission determ. 79—96809
- quasistatic approximation for atmospheric dynamics, characterisation *(German)* 80—98383
- radar and radiometric combined meas. for hail nuclei determ. in clouds *(Russian)* 79—12195
- radar applications in Polish meteorological service 78—92992
- radar appls. in meteorology and atmospheric behaviour research, review 78—77371
- radar determination of winds at sea 80—26644
- radar echoes from distributed targets, averaging of time, angle and range 80—109264
- radar for observing middle and upper atmosphere, Yaggi antenna array design 80—90255
- radar meas. of upper atmosphere 80—72661
- radar measurement of snowfall, accuracy assessment 79—12316
- radar meteorology, time-domain computation of mean and variance of Doppler spectra 79—100972
- radar obs., high resolution colour display of line convection 78—88894
- radar observation of lower atmos., MST radar at Poker Flat, Alaska 80—90254
- radar precipitation maps as lightning indicators 78—85652
- radar propag. through turbulence, scintillation detection using monopulse techniques 78—85717
- radar signal processing, for SOUSY-VHF-radar, using preprocessor 80—85774
- radar signal recording on video machine, for coherent Doppler radar 80—46275
- radar signals refl. from mesosphere, VHF signal detection 80—46274
- radar studies of strato- and mesospheres, review 80—90180
- radar techniques for middle atmos. dynamic struct. 80—105078
- Radar-Acoustic Sounding Systems, range limitation due to atmospheric refractive turbulence 77—41195
- radiation detection in turbulent atmosphere, photodetector current fluctuation statistics *(Russian)* 79—92591
- radiative divergence budget estimates from cloud data GATE 80—17319
- radiative flux calcs., delta-two-stream approx. 79—96811
- radiative transfer eqn. inversion, Chahine relaxation method extension 78—7794
- radiative transfer eqn. soln. methods for model atmosphere light scattering 77—66986
- radiative transfer modelling techniques extension using Bayes' rule 77—78443
- radio meteor method for upper atm. internal gravity waves meas. 77—25806
- radio meteor wind data, anal. using finite element approximation 78—81475
- radio meteorology in Switzerland *(French)* 79—25319
- radio propag. methods, quasi-single freq. Doppler-Faraday technique 80—77128
- radio refractive index measurement, digital instrument appl. 78—86321
- radio-acoustic sounding methods for tropospheric temp. meas. 78—53728
- radio-acoustical sounding, theory *(Russian)* 77—41199
- radioacoustical sounding, expression for scatt. signal freq. spectra *(Russian)* 80—94612
- radioacoustical sounding by continuous radiation method *(Russian)* 78—88927
- radioactive tracer method for meas. SO_2 deposition to pine forest 78—20508

atmospheric techniques continued

- radiometric monitoring method for dust in gaseous effluents *(German)* 77—29452
- radiometry, ground-based, atmospheric variables spectra deduction 79—92567
- radiometry and spectroscopy from aircraft 77—70890
- radiometry methods (Soc. Photo-Optical Instrum. Engrs., Proc. vol.91, San Diego, 26-27 Aug. 1976) 77—70880
- radiometry of stratosphere, use of superpress. balloon 80—85763
- rain attenuation, radiometric determ. at millimetre wavelengths, multiple-scatt. effects metric determ. at millimetre wavelengths, multiple-scatt. effect 80—90260
- rain estimation, using geostationary satellite data from extratropical region 80—90244
- rain induced attenuation and cross-polarization calcs., two new methods *(French)* 78—53677
- rain intensity distribution, conversion to shorter or longer integration times 78—61520
- rain measurement and forecasting in UK using radar as part of integrated system, progress and plans 80—98490
- rain measurement by dual-polarisation radar, drop size and fall rate 80—72650
- rain observed by radar, differential refl. method 80—46221
- rain parameter diagram, methods and appls. 78—57349
- rain parameters, meas. by optical scintillation, correl. method simulation 78—36290
- rain parameters meas. by optical scintillation 77—82015
- rain-rates, estimates for attenuating radar 78—73540
- rainfall, convective, meas. over small areas using high-density raingauges and radar 80—77157
- rainfall estimation by satellite borne microwave radiometry 80—105085
- rainfall instantaneous rate, meas. technique and influence on high-voltage transmission lines 80—98471
- rainfall meas. by microwave attenuation in 1-3 cm band 78—65414
- rainfall measurement, combined usage of radar and radiometry techniques *(Chinese)* 80—109272
- rainfall measurement by radar, methods and interpretation of data 80—81969
- rainfall on convective days, analysed with respect to radar obs. atmos. parameters 80—109205
- rainfall over land, microwave radiometry by Nimbus 6 ESMR 80—56635
- rainfall prediction over United States west coast, appl. of Nimbus 6 liq. water data over NE.Pacific Ocean 80—82005
- rainfall rate mapping over oceans by satellite 78—3982
- rainfall rate meas. from weighing raingauge records 77—49126
- Raman lidar humidity sounding of atm. boundary layer 79—66809
- Raman lidar meas. of atm. temp. profiles 79—100974
- Raman scattering analytical techniques using tunable lasers 78—61134
- Raman spectroscopy for aerosol particles characterisation 77—49188
- Rayleigh scattering effect determ. method 80—61921
- refractive index meas., microwaves non-conventional appl. survey *(Italian)* 80—13093
- remote meas. of tropospheric pollution from aircraft 77—49195
- remote measurements of emitted thermal radiation, atm. temp. and comp. estimation 77—45202
- remote monitoring using discretely-tunable IR gas lasers and heterodyne detect. techniques 78—61605
- remote sensing, by TIROS-N operational vertical sounder 80—77132
- remote sensing, contrast attenuation factors calc., using atmospheric models 80—4135
- remote sensing, determination of ground albedo and index of absorption of atmospheric particulates 79—88438
- remote sensing, parameters retrieval from scanning multichannel microwave radiometer obs. 80—90261
- remote sensing *(Japanese)* 78—16205
- remote sensing and profiling of lower atmosphere using radiowaves, ground-based 80—56628
- remote sensing by aerosol lidar backscatter *(Dutch)* 80—4110
- remote sensing by laser beam *(Chinese)* 80—46292
- remote sensing by VHF radar expts. 78—88938
- remote sensing of atmosphere, land and sea props. 78—93015
- remote sensing of cloudy atmospheres by microwave radiometry *(Chinese)* 80—51549
- remote sensing of particle size distribs., analytical inversions 78—73508
- remote sensing of particle size distribs., analytical inversions 78—73509
- remote sensing of pollutants by satellite, correl. spectroscopy techniques 77—64456
- remote sounding, new inversion method 80—12677
- remote sounding of high clouds, visible and LR optical props. from lidar and radiometer meas. 80—82060
- remote spectroscopy for total O_3 content determ. 78—65437
- remotely sensed Earth images, atmospheric effects on classification 79—58091
- rime, meas. of quantity, using fog-gauge 80—56654
- ring oven technique, NH_3 microdeterm., air pollution appl. 77—45164
- RONSARD radar, calibration techniques 80—46278
- sampling method for pollution detection using separated deposition 77—82031
- satellite auroral photometry, Earth albedo effects 77—56737
- satellite effective isotropic radio power meas., error anal. using calibrated radio star 78—93070
- satellite image gridding, line scan method 80—61915
- satellite picture, synoptic features anal. 79—8713
- satellite radiance meas., temp. retrievals, empirical method 77—70859
- satellite remote sensing, temp. profiles error due to aerosol particles effects 80—98449
- satellite solar occultation sounding of the middle atmosphere 80—105079
- satellite sounding radiometer obs., interpretation using eigenvectors of covariance matrices 77—5341
- satellite temp. determ. in troposphere, sensitivity due to water vapour estimates 78—3874
- satellite-borne monitoring of atmospheric and surface characteristics, tropospheric propagation of microwaves 78—24353
- satellites appl., European Space Agency activities *(German)* 80—8516
- saturation vapour pressure computation, polynomial approx. 77—64462
- sea surface and atmosphere radio brightness temp. meas. from satellite *(Russian)* 77—60407
- sea-surface wind, meas. by radar backscatter at 13.9 GHz from Skylab 77—91304

atmospheric techniques continued

- sea-surface wind stress determination using SEASAT-A microwave scatterometer, algorithm 79—39883
- searchlight probing technique for stratified aerosol layers meas. 78—92892
- severe storm warning using Doppler radar 78—49148
- severe-storm identification, multimoment Doppler display 77—56756
- shadow mapping to study rain attenuation on satellite microwave links 77—29505
- shearing instability mechanism model, effect of horizontal differencing 80—26578
- SHF signal attenuation by rain, monitored by radar 80—51567
- shipboard automated information processing system, for hydrometeorological data 80—41553
- shipboard sounding system for GWE 80—17394
- short-range numerical weather forecasting, effect of subjectively enhancing initial vorticity field 80—82008
- simulation of electromagnetic environment 77—73894
- simultaneous tethered balloon and monostatic acoustic sounder records of statically stable zones 78—73451
- sky background brightness meas., 4500-10600 Å *(Chinese)* 80—12540
- sky-wave mixed-path loss computation, piecewise homogeneous ground models appl. 79—66774
- smoke pollution index system for rapid source-strength determ. 77—29450
- smoke/dust cloud temporal analysis algorithm 80—98484
- snowfall systems induced by Lake Ontario, objective forecast method 80—51484
- sodar, appl. for acoustic detection in lower atmosphere *(French)* 80—8435
- sodar application in aviation 80—31132
- sodar meas., improved quantitative display techniques 78—77332
- sodar network meas. of mixing depth and stability regional patterns 79—100965
- sodar obs. of lower atm. thermal struct. at Delhi, India 79—53428
- sodar obs. of tropospheric thermal struct. at Delhi 78—32151
- soil particles in Nagoya area, characterisation via urban aerosol Si and Al concs. 80—26581
- solar 1950-2150 Å radiation, ground level meas. using NH_3 actinometry 79—2345
- solar absorption spectrum method, appl. to atmospheric NO_2 abundance meas. *(Japanese)* 80—94556
- solar aureole almucantar radiance meas., comparison between photographic and photoelec. methods 78—77321
- solar aureole rel. atm. aerosol props., photogrammetry 78—57315
- solar irradiance outside atmosphere, Bouguer method for ozonometer determ. *(Russian)* 80—61918
- solar occultation sounding, appl. to press. and temp. profiles meas. 80—98452
- solar radiation determ. using obs. and estimated precipitable water 77—56687
- solar radiation measurement, reference scales 80—109206
- solar radiation measurement, techniques and instrumentation, survey 77—5348
- soot particle conc. meas. by near IR extinction coeff. *(Russian)* 80—82055
- sounding techniques in IR and microwave regions, recent progress 80—82096
- Spacelab image intensifying TV obs. of airglow and meteors 77—21966
- Spacelab Langmuir probe for plasma instability obs. in equatorial spread-F 77—21947
- Spacelab lidar, atm. expts. and methods 77—21948
- Spacelab lidar, for atm. props. meas. 77—21943
- Spacelab lidar system for tropospheric aerosol monitoring 77—21876
- Spacelab passive sounder packages for atm. research 77—21945
- Spacelab passive sounding expt. for trace gas conc. determ. 77—21950
- spatial filtering of scintillation, for refractive turbulence profiles meas. 77—5331
- speckle interferometry, atm. nonisoplanicity meas. using double stars 78—65387
- speckle interferometry for atm. isoplanatism meas. 78—65385
- spectral multiplication, props. as viewed in physical space, meteorological appls. 80—94607
- spectral radiometric meas. of constituent vertical profiles 77—70883
- spectral transmittance method, for surface layer aerosols variability meas. *(Russian)* 78—69448
- spectrophone measurement of IR laser absorpt. by atm. dust 77—9513
- spectrophone measurements of solar radiation absorpt. by aerosol 79—80027
- spectrophotometric determ. of total O_3 using interference filters 78—16180
- spectroscopy, IR heterodyne, of atm. O_3 77—91267
- statistical analysis of ground wind vector, speed and direction prediction 80—17347
- stellar occultation meas. by stratospheric balloon, ceiling altitude var. compensation *(French)* 78—11947
- stellar speckle interferometry, wave correlation scale meas. 78—65388
- stochastic analysis, appl. to annual rainfall data affected by urbanisation 80—98407
- storm intensity at sea, microwave remote monitoring of sea foam 80—41528
- storm motion in three dimensions, detection by conventional weather radar 78—57360
- storm precipitation estimated with dual-wavelength radar 80—46220
- storm spotting, National Weather Service's training programme 80—8382
- stratosphere, aerosol and gaseous constituents from spacecraft solar extinction data, inversion retrieval 79—74961
- stratosphere, H_2O mixing ratio determ. using NOAA UV fluoresc. instrument 80—90137
- stratosphere, laser spectroscopy relevant to photochem. 78—88951
- stratosphere, O_3 and aerosol monitoring using orbiting photodetectors 77—78445
- stratosphere, O_3 vertical profile determ. by lidar sounding from ground 78—11972
- stratosphere, trace constituents, in situ meas. 79—8676
- stratosphere, turbulence from IR astronomy data 80—12475
- stratosphere aerosol, laser radar meas. *(Japanese)* 80—21810
- stratosphere aerosol, satellite monitoring systems, SAM II and SAGE 80—82082

atmospheric techniques continued

- stratosphere aerosol detection, ground based techniques, laser usage 80—17390
- stratosphere and mesosphere temp. and O_3, satellite IR limb scanning method 80—105086
- stratosphere data compatibility used in meteorological analysis, empirical study 80—17308
- stratosphere NO_2 determination, observational method and behaviour at mid.-latit. 80—17414
- stratosphere NO and ClO meas. via solar occultation, influence of concs. vars. at twilight 80—85756
- stratosphere trace gases, meas. via positive ions comp. meas. 78—88877
- stratosphere transport, one-dimensional parametrisation using ^{95}Zr data from Chinese thermonuclear explosions 79—2342
- stratosphere turbulence struct., using 430 MHz Arecibo radar 80—90258
- stratospheric aerosol particles, collection and analysis techniques 80—17306
- stratospheric composition, IR meas. radiometer, H_2O vapour profile 79—8718
- stratospheric composition investigation using gas expansion and mass spectrometer beam system 80—31934
- stratospheric gas monitoring, two-photon spectroscopy, Doppler-free technique 77—9514
- stratospheric O_3 layer obs. by XeCl excimer laser radar 79—16681
- stratospheric tracers, use of cosmogenic isotopes 77—41237
- stratospheric water vapour 0.94 μ absorption cross-section obs. *(Japanese)* 80—17427
- submillimetre spectrum meas. with high resolution Fourier spectroscopy 77—87133
- submillimetre wave heterodyne radiometry, for upper atm. comp. meas. 78—49183
- submillimetre wave spectroscopy, review 78—7796
- submillimetric wave atmospheric spectroscopy 77—41240
- subsatellites launched from Spacelab, for atm., magnetospheric and plasma physics research 77—21944
- sulphate aerosol, individual submicron particles detect. technique 78—69527
- superpressure balloon sounding of meso- and microscale phenomena 79—66815
- supersonic expansion method of ice nuclei generation for weather modification 77—29487
- SURF storage ring calibrations for NASA stratosphere and climate programs 80—94721
- surface layer optical inhomogeneities, investigation via acoustic method 80—67434
- surface layer temperature extremes, probability determ. method 78—45020
- surface pressure, remote meas. by multicolour laser ranging system 80—8429
- surface wind speed over drifting pack ice, determ. using surface weather charts 80—41476
- Swiss randomized hail suppression expt., design of Grossversuch IV 79—84542
- synoptic climatology development for NE.Gulf of Alaska, automated correl. technique appl. 80—98405
- synoptic windfinding using Omega VLF navaid, atmos. radiowave propag. 80—17309
- synoptic windfinding using radiotheodolite system, of USA National Weather Service 80—17379
- synoptic windfinding using tropical constant-level balloon system 80—17395
- telemetry, automation of information input and processing 77—78429
- TEM, in situ meas. of aerosol-gas interaction 80—104544
- temp. by microwave radiometry, climate in variational scheme 80—56649
- temperature, five-day average low and high temp. anomalies forecasting procedure 78—92938
- temperature and humidity meas. methods *(French)* 79—12318
- temperature corrections for Menaka-II meteorological rocket payload 79—5558
- temperature determination by remote sounding, aerosol attenuation effects on accuracy *(Russian)* 78—81430
- temperature field, spatial anal. from weather satellite meas. 78—20488
- temperature fluctuations, heat flux and struct. functions meas. with acoustic Doppler sodar 80—105023
- temperature inversion, determ. via ground-based long-range sounding in O_2 5 mm absorpt. band *(Russian)* 78—11963
- temperature meas., by IR method from Earth satellite *(French)* 77—9550
- temperature meas. by surface to orbit gas laser, absorpt. of vibr.-rot. band 78—12015
- temperature measurement, remote sensing by microwave radiometry 80—46293
- temperature measurement in fog and stratus, shipboard use of low-level atmospheric thermograph 80—105073
- temperature profiles, methods of retrieval from IR satellite meas. 77—87111
- temperature rel. to geographic latit., correl. charts construction by graphical method 79—29905
- temperature sounding by high precision satellite, spectral band passes 77—41175
- temperature sounding from TIROS-N, early operational soundings evaluation 80—77133
- temperature sounding with partially scanned interferograms 77—41176
- temperature vertical profile, from satellite data, information retrieval 78—3959
- temperatures correction for non-climatic trends 80—51524
- thermal analysis for in situ detection of aerosol pollutants 77—37364
- thermal balance meas. by radiation pressure on satellite microaccelerometer 79—2380
- thermal neutron activation analysis, appl. to Ankara aerosol trace elements and size distribs. 78—81377
- thermal oscill. for nocturnal min. temp. prediction *(Spanish)* 77—9478
- thermal remote sounding, temp. effect on 15 μm region transmission function 78—77327
- thermal sensing from Earth orbit, spatial temp. and geopot. fields 80 36429
- thermal wind-field disturbances in sea coastal zone, statistical forecasting of frequency 80—36371
- thermocouple psychrometry, effect of and correction for different wet and dry bulb response 80—98472

atmospheric techniques continued
thermosphere, mathematical model for neutral winds deduction, uncertainties results 79—39995
thermosphere, Na clouds as indicators of turbopause altitude 77—78548
thermosphere, props. determ. from ionospheric obs. using numerical simulation 77—53268
thermosphere at. O content, spectral method for 100-160 km altitude 80—41578
thermosphere N mass spectrometric meas., gas-surface reactions impact 79—66849
thermosphere temperature and wind measurement Fabry-Perot-interferometer imaging system appl. 80—101441
thunderstorm and lightning observations from Space Shuttle 79—58078
thunderstorm distance determination, calcs. and examples *(German)* 78—40680
thunderstorm location by single station techniques, improved method, radiowave propag. effects 80—67438
thunderstorms, corona generation using chaff, microwave radiometric detect. 78—16106
thunderstorms, severe, forecasting and effects on society 79—5560
thunderstrom observed by radar, depolarisation rel. to precipitation 80—51453
tides caused by Moon, data filtering method 80—46223
tornadic storm research, implications for dual-Doppler radar spacing of effective coverage area anal. 80—82093
toxic gases, IR anal., solvent extraction technique 77—73479
trace constituents by IR spectra, altitude distrib. technique 79—34985
trace gas analysis of stratosphere, based on in situ ion composition obs. 80—105077
trace gas sampling, chemical absorption filter techniques 80—17305
trace gases vertical conc. from solar radiation absorpt. spectra *(Russian)* 78—69442
transmission meas. using IR lasers and Fourier spectroscopy 77—70885
transmittance functions, generation by numerical methods 80—98455
triggering lightning by pulsed laser 80—72626
triple-Doppler radar obs. of convective storm 79—39886
TROPEX-74, USSR meteorology expedition, consistency of shipboard meas. with 'Meteor' buoy 80—36402
tropical cyclone intensity measurement from tropospheric aircraft 80—67416
tropical cyclones, photometric method for estimating cloud cover from satellite data 78—4007
tropical open-ocean rainfall estimation from satellite obs. 77—29486
tropical palaeoclimatology, appl. of climatic ice core records from Quelccaya Ice Cap 80—8345
tropopause detection, by partial specular refl. with VHF radar 80—8411
tropopause height estimation from nonlinear functions of satellite meas. spectral radiance 77—78335
tropopause height from spacecraft obs. of atm. refr. of starlight 77—2280
troposphere, pressure and temp. meas. by lidar differential absorpt., influence of laser emission spectral width *(French)* 80—41554
troposphere, radar obs. during clear air conditions, review 80—90178
troposphere, radar obs. of vel. and irregularities, spaced antenna VHF method 80—90185
troposphere and stratosphere sounding by pulsed VHF radar 80—51566
troposphere OH radical concentration, determ. method using atmospheric ^{14}CO meas. *(German)* 80—8419
troposphere research, appls. and flight history of Atmosat balloon 78—7775
troposphere sounder, metric radiowave-acoustic sounder 80—46276
troposphere velocities and irregularities, VHF radar studies using spaced antenna techniques 79—16701
tropospheric waveguide, numerical comparison of ray method and normal wave method 80—21858
turbidity, meas. via polarisation of UV light of daytime sky 78—20517
turbulence around solar telescope, deduction from arrival angle statistics compared with microthermal meas. 80—26740
turbulence breakdown coefficient determ., influence of data treatment technique *(Russian)* 78—7690
turbulence characteristics meas. under convective conditions, optical and meteorological methods *(Russian)* 79—16577
turbulence estimation using range statistics 77—17169
turbulence parameters from Doppler radar clear-air echo intensity 80—90190
turbulence-structure parameter meas. using space-limited laser beam 80—46285
turbulent boundary layer, finite-element numerical modelling 80—77061
turbulent diffusion, of particles in air, analytical numerical method 78—32257
typhoons, detection and appl. of associated acoustic waves *(Chinese)* 79—34996
UK climatology network, significance of spatial variability of daily temps. and sunshine 78—3887
ULF wave generation by peninsular loop currents 80—90247
upper atmos., 391.4 nm light excited by electron beam from sounding rocket 80—77214
upper atmos. temp. and wind, meas. with Fabry-Perot airglow spectrometer 80—77156
upper atmosphere, diffusion coeff. and initial radius from overdense meteor trails 77—13140
upper atmosphere, electron beam injection into neutral gas, laboratory study 80—54004
upper atmosphere, statistical modelling from Geminid meteor shower radar obs. 78—61816
upper atmosphere composition, comparison of satellite self-contamination expts. and scatt. return flux calcs. 78—40722
upper atmosphere daytime Li releases, obs. via high resolution photometer 78—45023
upper atmosphere daytime winds, meas. by trace constituents sounding rocket campaign 78—45071
upper atmosphere density derivation from near-circular satellite orbits, effect of temp. diurnal var. 80—21867
upper atmosphere research applics., of quadrupole mass spectrometer, book contrib. 77—25911
upper atmosphere wind and temperature meas., laboratory discharge lamp source appl. 80—4148
upper atmosphere wind velocities, determ. from atomic and mol. ions vel. meas. 77—13155
urban aerosols, Boston area, multivariate anal. for element sources identification 77—37357

atmospheric techniques continued
urban air, total suspended matter estimation, comparison of three methods 77—37416
urban air pollution, theoretical methods, basic concepts 79—83669
urban plume particulates collected on Anderson 8-stage impactor stages, chemical anal. 78—69433
UV radiation detection, space appls. 77—70881
UV spectrophotometric obs. of upper atm. from Spacelab 77—21964
vertical cross-section analysis based on cylindrical projection 79—84549
vertical path modulation transfer function, meas., photographic techniques 79—84478
vertical stability near ground, meas. method using ^{222}Rn release *(French)* 80—56617
VHF direction finder studies of lightning 79—20928
VHF radar measurement, obs. of frontal passage 79—53482
VHF technique for space-time mapping of lightning discharge processes 78—85721
visibility at ground level, two meas. methods 80—82078
visibility meas. by modulated CW lidar, comment 77—64440
visibility meas. by modulated CW lidar, reply to comment 77—64441
visibility probed with lidar 80—31141
VLF radiometeorology for thunderstorm location *(German)* 77—17254
Voigt profile, fast calculational algorithm, line-by-line transmittance 78—7767
vorticity budget computation from cyclone-anticyclone couplet construction, polar air outbreaks 80—8391
warm fog dispersed with electrostatically charged bubbles 78—20546
warm fog dissipation by electrically enhanced coalescence, charged drop seeding 78—7714
water droplet conc. and size determ. from cloud liquid water content and extinction meas. 80—51579
water droplets in mists, clouds, size, density distrib. meas., laser remote sensing technique *(Japanese)* 78—49175
water vapour and liquid monitoring using radiometry at 21 and 32 GHz 80—26628
water vapour dielectric constant, rotational part, engineering method of calc. 78—40717
water vapour profile, meas. from atmosphere brightness temps. in H_2O 1.35 cm resonance region *(Russian)* 78—81403
wave component identification on airglow charts, multiple-point method 78—73526
weak absorption lines, detect. by Nd:glass and dye laser system 78—89561
weather charts transmission by facsimile for military appls. 80—90206
weather event forecasting at two locations, joint probability estimation 79—53480
weather forecasting, analysis method *(Chinese)* 80—46238
weather forecasting, assessment of model initial conditions using satellite imagery 80—31084
weather forecasting, conditional probabilities prediction method *(Chinese)* 80—109238
weather forecasting, expected results from First GARP Global Experiment 80—12550
weather forecasting, satellite technology development, (1960 to 1979) *(Dutch)* 80—12559
weather forecasting, stochastic dynamic prediction appl. to real data 77—56669
weather forecasting games at American Universities, survey 80—98770
weather forecasting nonlinear evolutionary problems, finite element methods appl. 80—21865
weather forecasting processing of radar and satellite imagery data 80—109252
weather forecasting via oceanographic buoys, electronics and telemetry evolution 79—5659
weather forecasts, impact of satellite temp. sounding data 80—77028
weather identification by laser forward scatt., feasibility study 79—70893
weather maps, structural description of contour maps 80—101419
weather modification, covariance anal. technique based on bivariate lognormal distrib. 77—70767
weather modification, prospects and problems, book 80—36790
weather modification and droughts in India, review 77—56715
weather modification experiments, appl. of monthly rainfall spatial correls. 80—51479
weather modification programmes, meteorological satellites appls. 78—96259
weather radar, Doppler, estimation of echo spectral moment 80—51563
weather radar, signal anal. *(French)* 80—36418
weather radar echo, receiver bandwidth effect on refl. and Doppler vel. estimates 79—53549
weather satellite data, complex demodulation 78—49177
weather surveillance near airports using Doppler radar 80—46272
weather-forecasting, statistical model 78—92941
whistler analysis, Dowden-Allcock approximation generalisation and comparison with Bernard approximation 80—51607
whistler dispersion, automatic meas. by phase locked loop discriminator *(Japanese)* 77—91312
whistler extrapolation, comparison of systematic errors in different methods 77—53334
whistler extrapolation via linear-Q anal. and extrapolation factor, systematic errors 77—53333
whistler inversion, spectral expansion technique 80—8495
whistler mode signals direction finding, initial results from tracking receiver system 78—77429
whistlers, automatic observation 78—89014
whistlers, nature, types and observations, review 80—36458
wind boxplot, graphic display of speed and direction data 77—91310
wind determ. by airborne Doppler radar bias error 78—3879
wind determination by acoustic radar *(Chinese)* 80—46290
wind direction meas. by vane, graphic recording and averaging 80—82098
wind field in frontal system, determ. from single-Doppler radar 79—21057
wind fields, mesoscale, satellite-derived, covariance anals. 80—82013
wind fields, urban-scale, three-dimensional, construction 80—101407
wind in lower atmos., clear air Doppler radar methods, vertical component 80—72642
wind in rough time terrain, derivation of mass-consistent flow field from wind obs. 80—105013
wind local climate, determ. using trees as indicators 80—82007
wind meas. from orbit using lidar system 80—4114

atmospheric techniques continued
- wind meas. in severe storms using airborne pulsed Doppler lidar system 79−66812
- wind meas. technique for WTG siting 80−48830
- wind measurement (absynoptic scale) using dual Doppler radar and vel. azimuth display 80−109263
- wind measurement by radar, technique for strato- and troposphere 80−90257
- wind measurements, using OMEGA radiosonde, error estimation 79−29916
- wind measurements by radar in Arctic troposphere and stratosphere 78−49172
- wind measurements in clear air by microwave radar 77−13136
- wind monitoring using Concorde-generated infrasound in stratosphere 80−51492
- wind pattern determ. from rime deposits 80−98428
- wind profile in subcloud layer of thunderstorm from lightning photographs 77−87013
- wind profile radar obs., tropo-stratosphere, Poker Flat MST radar 80−72579
- wind profiles, comparison of Doppler radar and rawinsonde balloons meas. 78−44916
- wind remote measurements, individual particle scatt. and single-burst digital correl. 79−100980
- wind shear detection radar, for airport use 80−51565
- wind shear hazard in boundary layer, radar detection feasibility 80−90256
- wind shear measurement, using pulsed Doppler laser 80−67415
- wind speed and direction prediction, empirical eigenvector method *(German)* 79−34924
- wind speed and direction prediction using empirical eigenvector method *(German)* 77−87030
- wind speed and water content, microwave remote sensing from Earth orbit 80−41573
- wind speed freq. distrib. determ. for lowest 200 m 79−21052
- wind speed freq. distrib. using monthly average and fastest mile data 77−78331
- wind speed remote meas., single particle correlation by laser backscatt. 77−91302
- wind speed remote meas., single-particle correl. techniques, aerosol condition, meas. rate 79−62609
- wind speeds, probabilities calc. from parameters of truncated distrib. curve *(Russian)* 77−53157
- wind transverse vel., remote meas. using laser Doppler velocimeter 80−4115
- wind tunnel investigation into graupel formation and growth 80−17324
- wind tunnel testing of flue gas dispersion 79−12282
- wind vel. determ. from laser intensity fluctuation meas. *(Russian)* 78−36302
- wind velocity, remote meas. using video equipment for pollution monitoring *(French)* 80−7990
- wind velocity and direction meas. by laser sounding, correl. method *(Russian)* 77−29474
- wind velocity estimation via optical signal processing 77−41107
- wind velocity lidar meas. by spatial filtering 79−29901
- wind velocity spectra, determ. from cup anemometer meas. *(Russian)* 77−13102
- windfinding, NCAR aircraft dropwindsonde system 80−17393
- windfinding, rocket sounding methods, since World War II 80−17398
- windfinding, satellite imagery of cloud drift 80−17397
- windfinding technique, Loran and VLF navaids used with radiosondes 80−17392
- winds, ground level freq. distrib. calc. method 80−17346
- winds and turbulence continuous meas. using VHF Doppler radar, preliminary results 80−8444
- winds in upper troposphere/lower stratosphere, determ. from satellite-derived radiance gradient 80−98447
- wing and struct. const., MM wave and optical line-of-sight probing 80−36426
- X-ray aurorae prod. by energetic electrons precip., imaging from Spacelab 78−61608
- Zephyr radar system for meteorological measurements 80−90228
- zonal atmospheric circulation model, numerical expts. *(Russian)* 78−81295
- C in suspended particulates, meas. technique 80−76686
- CO abundance meas. method *(Russian)* 79−25343
- CO_2 baseline monitoring station network, intercalibration 77−64491
- CO_2 palaeoconcentrations meas., implications of ^{13}C vars. in tree rings during last 150 years 80−17363
- CO_2 record in polar ice, CO_2 extraction method 80−61891
- ^{14}C content, measurement from tree rings, effects of ^{14}C radial flow 78−28346
- ^{14}CO measurement, method for tropospheric OH radical conc. determ. *(German)* 80−8419
- ClO composition of stratosphere, balloon borne reson. fluoresc. method 80−90167
- F, stack sampling apparatus for the collection of gaseous and particulate pollutants *(French)* 80−7986
- Fe aerosol source determ. by gamma-ray spectroscopy 77−41235
- Fe conc. and sources determ. by Mossbauer technique 79−79442
- HCl, atmospheric measurements using ground based IR spectroscopy *(French)* 80−81975
- HCl gas in ambient air, detection using coated piezoelec. quartz cryst. 78−92532
- HF, atmospheric measurements using ground based IR spectroscopy *(French)* 80−81975
- HO fluorescence detection, interference suppression by sampling method 80−8431
- H_2O vapour and cloud liquid determ. by dual freq. ground-based microwave radiometry 78−93007
- H_2S in air, preconc., determ. by flame photometric detection 78−92535
- H_2SO_4 aerosol, filter sampling of air, possible artifacts 80−82079
- H_2SO_4 aerosol particle size measured by impaction method 80−31134
- He-cooled LWIR spectrometer for exo-atmospheric airglow measurement, calibration 79−97450
- Hg determ. in troposphere *(German)* 79−53406
- Kr activity meas. using ^{85}Kr 77−78454
- ^{85}Kr, separation technique, preliminary results *(German)* 78−16222
- Li, release in upper atm. for daytime neutral winds obs., photometer detect. 79−39871

atmospheric techniques continued
- N_2, rot. temp. meas., rocketborne electron beam fluoresc. meas., reflected mol. effects 77−29519
- NH_3 determination, method 80−56614
- NH_3, gas conc. meas. using ring oven technique 80−81507
- NO, absorpt. characts. of γ-O band, rel. to atm. meas. 78−57316
- NO, optical detection in air, gamma band fluoresc. *(German)* 77−60494
- $NO/NO_2/O_3$ contents measurement, monitors intercalibration 78−69529
- O I airglow emission rate, midlatitude maximum characts. obs. 79−84561
- O remote sensing in mesosphere and lower thermosphere, two-photon lidar technique 79−39869
- O_2 A band differential absorpt. lidar meas., using ruby lidar and stimulated Raman scatt. 79−39904
- O_3, chemical analysis by acoustic emission following laser irradiation *(Russian)* 77−21451
- O_3 conc. and distrib. from absorption spectrum in UHF region *(Russian)* 79−100897
- O_3, conc. meas. by differential absorpt. CO_2 laser radar 79−96829
- O_3, determ. by Chappuis-band absorpt. 80−77063
- O_3 in lower stratosphere, Nimbus 4 remote sensing method 80−77154
- O_3 meas. over snow surfaces 79−12281
- O_3, nighttime equatorial density determ. from UV stellar occultation obs. 77−53259
- O_3 profile, determ. from outgoing thermal radiation 78−92945
- O_3 total content, comparison of simultaneous IRIS, BUV and ground based meas. 78−81291
- O_3 total content, determ. using satellite meas. 80−77027
- O_3 total content, Dobson spectrophotometer meas. errors 80−72644
- O_3 total content determ. by UV spectroradiometry 79−53401
- O_3 total content determ. from total optical depth spectral var., solar radiometer meas. 77−53235
- O_3 total content determination, large particle light scatt. coeffs. approximation 80−82091
- O_3, total content meas. using Dobson spectrophotometer 80−72643
- O_3 vertical distrib., shortened version of Umkehr ob. method 80−8430
- OH fluorescence lidar instrument for stratospheric temp. and press. determ. 79−80033
- OH monitoring using CW tunable laser 78−17664
- Pb micro fall-out, furnace atomic absorption spectrometry appl. 78−49125
- Rn daughters as atmospheric tracers *(Spanish)* 77−9553
- ^{222}Rn continuous meas. for air-sea gas exchange field determ. 78−73534
- S compounds detection, via automatic odour analyser *(Japanese)* 80−50924
- S pollution, meas. via compact X-ray fluoresc. analyser 78−68971
- SF_6 and tracer gases, electron capture detection method 77−25785
- SF_6 tracer technique for near-stack reactor effluent dispersion studies 78−11992
- SO_2 conc. meas. using box model and acoustic sounder anal. 80−7982
- SO_2 density prediction for Tokyo, adaptive transformation network method 79−5609
- SO_2 detect. in stratosphere, analytical technique 77−5314
- SO_2, long-term monitoring method using permeation sampling, development 80−26189
- SO_2, meas. in marine atmosphere at concs. lower than ppb 78−81340
- SO_2, norm determ., technical meas. aspects *(Dutch)* 78−49131
- SO_2, optoacoustic detect. in air-pollution control below parts per billion level 78−41355
- SO_4^{2-} aerosols, ambient, laser-Raman monitoring 78−69532
- V pollution, low level meas. 77−41239
- ^{133}Xe, separation technique, preliminary results *(German)* 78−16222

atmospheric temperature
- *see also atmospheric thermodynamics*
- 500 mb temperatures, rel. to cloud top temps. and Climax and Wolf Creek Pass cloud seeding expts. 80−82094
- Aberdeenshire, mesoclimate of Upper Don Basin 80−61889
- acoustic sounder, phase sensitive, phase shift correl. with temp. profile 78−49170
- acoustic sounder returns comparison with direct meas. 77−33125
- acoustic sounding of boundary layer at Calgary 78−24376
- adiabatic invariants in N.Hemisphere *(Russian)* 78−36225
- aerosol IR radiation scattering, calc. of heating and cooling rates 80−72630
- aerosol particles influence on warming of urban and rural atm. 79−16671
- aerosol temp. and energy exchange in Earth's atmosphere 77−45082
- aerosols from Mount Agung eruption as test of global climatic perturbation 78−69440
- W.Africa, criterion for locating subtropical high, rel. to Sahelian drought 78−7718
- W.Africa, mean tropospheric conditions for 11-year period, climatological features 77−2221
- air min. and grass temps. rel. to streamflow fluctuations in no precipitation periods 77−64406
- air modification due to step change in surface temp. 77−78294
- air pollution survey vehicle measurements *(Dutch)* 78−81365
- air warming and cooling rates, urban and rural sites 79−88454
- air-sea interface, heat and momentum flux in const. flux layer, from temp. meas. 78−44899
- aircraft meteorograph, design, appls., accuracy *(Chinese)* 80−17387
- airglow temp. measurement, with new interferometer aperture design 80−82075
- Alaska, climate reconstruction from modern climate-tree ring relations 80−101425
- altitude gradient for N.Pennines in Great Britain, airflow model 80−4094
- N America, late Pleistocene palaeoclimates inferred from speleothems stable isotope studies 78−57297
- N.America, Quaternary temps. and precip. for NW. coast region 80−98438
- N.America, seasonal temp. vars. since 1602, reconstruction from tree rings 80−51528
- American Southwest, evidence for cold, dry full-glacial climate 78−57296
- ancient Mesopotamia, barley harvest dates rel. to temp. 79−5597
- annual and semiannual oscills. in northern hemisphere 79−48545
- annual mean temperature, information from $^{18}O/^{16}O$ in cellulose, lignin and whole wood from tree rings 78−24355

atmospheric temperature continued
annual zonally averaged global climatic model with diffuse cloudiness feedback 77—87056
anomaly over European USSR, monthly forecasting 79—39830
Antarctic snow surface dust contamination, climatonomical modelling of temp. response 78—24354
Antarctica, 30000 yr isotope climatic record from ice core 79—92586
Antarctica, temp. as determinant of polar desert pond dynamic chemical equilib. 80—12441
Antarctica, winter, Nimbus-5 atmospheric temp. fields deviation from radiosonde data 78—32138
Antarctica and equatorial India, atm. struct. during southern summer 77—53121
artificial satellites future role in meteorological obs. 79—79965
tropical Atlantic air temp. field statistical struct. and objective anal. *(Russian)* 77—64373
Atlantic Ocean, meteorological parameters changes and interaction with different-scale processes *(Russian)* 77—60447
N.Atlantic region, temp. trend 1970-77 period, warming *(German)* 79—16640
Atlantic tropical ocean temp. anomaly, atmospheric response 77—17187
aurora, SAR arc event, 1978 Sept. 25/26 event 80—12594
auroral arc, N_2^+ first negative (0-1) band temp. height profile 78—40725
auroral E-region, electron temp. rel. to plasma line meas. 79—25386
auroral origin of medium scale gravity waves in neutral composition and temperature 79—74998
Australian region forecasts using Nimbus 6 temp. sounding 79—5550
available potential energy concept 79—12218
bad seeing conditions avoidance within telescope domes 79—70960
Bahrain, discomfort index based on wet-bulb temps. 79—20964
Baikal-Amur region, climatic regionalization of estimated winter temps. 79—39842
Baltic Sea region, temp. meas. rel. to atmospheric heat and moisture balance 77—87057
baroclinic boundary layer structure 78—81326
baroclinic instability, critical temp. gradient, eddies, climate model 79—5562
baroclinic model for vertical temp. and moisture stratification in baroclinic boundary layer 79—53502
baroclinic unstable wave vertical scale, rel. to eddy heat flux parameterisation 79—5563
baroclinity over India in winter, rel. to western disturbances and jet streams 79—20914
Beaufort Sea, winds and surface temps. rel. to August ice cover vars. 80—101366
Belgium, 1952-71 air temps. 77—70800
Belgium, near-ground temps. rel. to air pollution increases 78—81374
Belgium, weather in 1975, review 77—25747
Belgium, weather in 1977 79—58049
Benguela Current, air temp. anomalies rel. to high waves region 80—51434
Bergen, Norway, annual av. temp. and climatic vars. *(Norwegian)* 79—39840
Birmingham, England, heat island synoptic climatology (1965-74) 80—85740
Bombay Airport, urbanisation and industrial development effects on air temp. 77—53167
boundary layer, effect of coherent structures on temp. struct. function 77—64361
boundary layer, energy characts. of urban-rural surfaces in greater St. Louis area 78—61484
boundary layer, friction vel. and temp. scale from temp. and wind vel. profiles 78—81268
boundary layer, log-linear profile relationship over rough terrain during stable conditions 77—60444
boundary layer, microscale temp. and vel. spectra 78—16109
boundary layer, momentum, heat and moisture fluxes from struct. parameters 79—53435
boundary layer, normalization of second order moments of vertical air velocity and temperature *(French)* 79—88447
boundary layer, roughness length and zero-plane displacement, wind and temp. profiles 78—24329
boundary layer, sodar echoes at Miyakojima Is., AMTEX 77—21843
boundary layer, stably stratified, temp. vars. rel. to turbulence and internal waves spectra *(Russian)* 78—81297
boundary layer, steady-state characts. of inversions capping well-mixed layer 78—61483
boundary layer, temp. and humidity correl. above warm wet surface 78—85646
boundary layer, temp. dimensionless structural charact. rel. to refr. index profiles *(Russian)* 80—94597
boundary layer, temperature inversion, characts. of stable nighttime layer 80—41533
boundary layer, temperature structure coeff. detect. by acoustic radar 80—98386
boundary layer, terrestrial surface features effects, instrumented aircraft meas. 79—39808
boundary layer, thermal plumes and turbulence spectra 77—73793
boundary layer, turbulence structure in temp. inversions and convective fields, Doppler sodar obs. 79—66762
boundary layer, unstably stratified, temp. profiles rel. to turbulent energy dissipation *(Russian)* 77—64372
boundary layer, vertical temp. profile determ. by ground-based microwave radiometry 79—79915
boundary layer, wind shears and inversions *(German)* 78—81336
boundary layer evolution and nocturnal inversion dispersal 79—25296
boundary layer evolution and nocturnal inversion dispersal 79—25295
boundary layer fluxes determ. over natural grassland, aerodynamic method 78—73480
boundary layer heat and pulse transport *(Dutch)* 78—3890
boundary layer measurement system, for wind and temp. struct. *(German)* 80—94616
boundary layer model, two-dimens., appl. to Nanticoke region, Lake Erie north shore 79—66750
boundary layer near water surface, diurnal characts., equatorial region, GATE meas. 78—61527
boundary layer of marine atmosphere, diurnal temp. cycle 78—20434
boundary layer probing by acoustic sounder 77—17243
boundary layer structure evolution over oceanic and continental sites *(French)* 79—25294

atmospheric temperature continued
boundary layer temp. fluctuation study 77—37293
boundary layer temp. fluctuations of cloud-laden airstream 80—61845
boundary layer temp. profile, microwave radiometer, for indirect determ. 79—25369
boundary layer temp. profile determ. from ground-based 60 GHz radiometry *(German)* 80—82097
boundary layer temperature profile from inferior mirage obs., simple soln. 79—80035
boundary layer thermal structure at Cardington from acoustic sounding 77—53153
boundary layers, convective and nonconvective, parameterisation for use in numerical models 80—82009
Bowen ratio and surface temp. over sea surface 77—60400
brightness temperatures in H_2O 1.35 cm reson. region, vars. *(Russian)* 78—81403
lowland Britain, wind chill anal. 79—66782
British Isles, 1976 June 23-July 8 heat wave 78—20471
British Isles, cold spells and heat waves prod. by blocking anticyclones 79—80006
British Isles, freezing level during rainfall 77—29391
British Isles, October weather recent trends 77—17210
British spring weather, survey (1950 to 1979) 80—98427
British winters (1659 to 1979), study of temp. correl. with precipitation 80—98444
Budapest and Jerusalem, evaluation of spectral density of temp. vars. *(Russian)* 77—5337
Budyko-Sellers climate models, variational formulation from temp. field 80—8420
buoyant axisymmetric plume in atmospheric inversions, entrainment characts. 77—82004
Calgary, Alberta, temp. fields variability 79—5545
California coast, marine fog and fog-stratus systems rel. to marine boundary layer inversion development 80—77060
NW.Canada, palaeoclimate in late glacial times 78—20500
canonical correl. method study 80—26593
catalogues of rainfall and temp. anomalies, 1891-1975, for European USSR, N.Kazakhstan, and W.Siberia 79—39826
centripetal heat island circulations, St. Louis, USA 79—66753
China, agricultural growing season vars. in historical time *(Chinese)* 80—109246
N China, human climates 79—84468
NE.China, persistently low summer temp., causative circulation pattern *(Chinese)* 80—109235
chlorofluoromethanes effect on atm. surface temp. 79—70832
circular anomaly, Knoxville, Tenn. 77—53104
circulation characts. forecasting rel. to autumn low temp. over Yangtze basin 80—12531
climate model including aerosol effects 80—77102
climate modelling using radiative-convective models 79—74954
climate of central England, 1660-1977, air temp. variability 80—98437
climatic change, long-term, prod. by fossil fuel usage, proposed space obs. 79—29844
climatic consequences of solar energy utilisation *(French)* 77—73822
climatic effects of sunspots and volcanic dust, statistical evidence from long-term temp. records 78—69439
climatic models of Budyko-type, nonlinear albedo-temp. coupling effects 77—45129
climatic temperature changes since 1665, statistical study of causative factors 79—8680
cloud clearing by laser beams, temp. fluctuations in clearance zone *(Russian)* 78—44999
cloud temp. fluctuation meas. by IR radiometry, feasibility study 80—56636
cloud temperature and humidity changes and overcloud inversion 80—77083
cloud temperature meas. rel. to entrainment, aircraft temp. sensors wetting effects 79—53483
cloudiness as climatic feedback mechanism, effects of cloud amounts on surface temp. changes 79—88467
clouds influence on atm. dynamics *(Russian)* 79—8653
coastal internal boundary layer characts. during onshore flows 80—41479
coastal zone, indicators of long-term var. of hydrometeorologic elements *(Russian)* 78—77258
coastal zone, sea level air temp. correlations 79—12122
cold front passage in Southern Hemisphere near equator 77—53102
cold-air advective conditions, lake moderating effects on surface temps. 79—25299
Cologne, heat-electric power station effects *(German)* 79—20999
composition perturbations and temp. feedback, climatic effects 80—41525
Concorde sonic booms as probe of atm. temp.-wind parameters 77—91323
Coningsby, Lincolnshire, temp. rise assoc. with snow rollers form. (1979 January 2) 80—72568
constant lapse-rate layer, balloon rise rate calcs. 77—64387
convection in thin layer above water surface *(Russian)* 77—45073
convective boundary layer, temp. skewness budget and implications for turbulence modelling 80—21816
convective boundary layer, temperature-humidity covariance budget 78—73430
convective cloud activity, urban induced influences 77—78341
convective systems, life cycles, GATE data 79—53440
D-region, electron and neutral gas temps. 77—82078
D-region, neutral temp. meas. via payload B I rocket-borne expt. package 78—45190
D-region, temp. control of NO^+ cluster ion formation 80—61931
D-region, temp. rel. to $H^+.(H_2O)_n$ abundance profile 79—40007
D-region, temps. rel. to cluster ion form. by NO^+ reactions 77—53308
daily maximum and minimum temperatures and sunshine, spatial variability over uniform terrain 78—3887
daily maximum and minimum temps., time of observation vars. and apparent climatic change 77—81993
daily maximum on mountain slope, time series anal. 78—73457
daily temperatures, Modena, Italy anthropogenic climate change evidence 80—41542
daily temperatures, statistical forecasting using short records of previous temps. 79—58015
De Bilt, Netherlands, 1634-1977 average winter temps. 79—74949
dendrochronology, Japanese cedar record of air temp. 77—21880
Denton County, Texas, temp. data Fourier transform anal., cyclic behaviour 77—33179

atmospheric temperature continued
E.Derbyshire, local temp. var. 77—64404
deserts, negative feedback through temp. 77—21863
dew point data, simultaneous eqns. soln. method for noise variance spectra estimation 78—57354
dew point rel. to global solar radiation, phase delay calc. *(Spanish)* 77—9477
distribution from ground based obs. of thermal radiation *(Chinese)* 80—82041
diurnal surface temp. range sensitivity to changes in physical parameters 78—3875
diurnal variation, harmonic anal. *(Rumanian)* 79—21009
diurnal variations in surface layer *(Russian)* 77—13100
Drake Passage, temp. changes rel. to Antarctic polar frontal zone variability during summer (1976-1977) 78—85579
droplet growth and initial dew point temp. accuracy in cloud chamber on space shuttle 78—96268
dry penetrative convection 78—92889
dry thermals forecasting for gliding 78—49103
E_s-layers, mid-latitude, electron temp. gradients obs. 78—28397
E-region, electron temp. compared to neutral temp., 100-120 km altitude 80—77211
E-region, temps. and collision freq. in polar regions, incoherent scatter meas. 80—72688
early spring warm spells, case study for (1977 March 2) 79—79994
Earth surface temperature, climatological significance of doubling of atmospheric CO_2 conc. 80—101426
Earth surface temperatures, implications of stratospheric aerosol modification by supersonic transports and space shuttle 80—98408
Earth-atmosphere radiative heating effects on climate, NOAA radiometer meas. 80—8425
earthquake prediction, rel. to temp., rainfall and soil tilt 77—91058
eddy heat fluxes and temp. variances in baroclinic waves, weakly nonlinear theory 80—8390
eddy momentum flux convergence rel. to potential temperature 80—41490
eddy temp. variances in weakly nonlinear theory 79—79928
effect on ABP-2 astronomical telescope, star trail image vibrations *(Russian)* 78—20636
effect on soil drying 80—8373
effect on underground temp. var. with depth and time 79—5463
electrical and electronic equipment operating climatic conditions in Rumania, classification *(Rumanian)* 79—44242
electron temperature profiles, satellite meas. up to 800 km altitude in late afternoon sector 79—70917
energy consumption effects on climate 79—29848
energy use and climatic changes 79—29846
S.England, 1968, September 14-16, surface temp. rel. to outstanding rainfall event 77—45122
England, hot spell of 1976 June-July 77—17203
central England, monthly mean temps. for quintile distrib. 77—29418
England, spectral anal. of temp. data for 1659-1973 period 77—17208
England's climate since 1830, increased October temp. 80—56599
central England temp. rel. to N.Atlantic climatic change 77—78402
enhanced CO_2 greenhouse effect, compensation for reduced solar luminosity on early Earth 79—39865
equatorial topside ionosphere, ion temp. troughs and interhemispheric plasma transport 78—96340
equilibrium temperature gradient in atmosphere at incomplete automodelity 80—41480
W.Europe, atmos. temp. 20-110 km altitude, 1975/6 winter anomaly 80—36356
Europe, exceptional weather in (1975) 77—25756
W.Europe, mesosphere and lower thermosphere temp. and density, 1975/6 winter anomaly 80—36357
European air temperature band-pass filtered series, correls. and phases 80—26579
European air temperature change patterns 78—92957
evaporation calc. using measured wind, temp. and humidity profiles 77—17194
exobase, H density and temp. from Lyman alpha absorpt. and polarisation meas. 77—29526
exosphere, determ. by ground meas. of ionosphere and O I 6300 Å line 77—67003
exosphere, diurnal temp. var. effect on densities derived from near-circular satellite orbits 80—21867
exosphere, electron temp. meas., night time, 2500 km altitude 79—16730
exosphere, from incoherent scatt. radar and satellite meas. 77—33224
exosphere, geomagnetic density and temp. effect propag. 79—48593
exosphere, global comp. and temp. during quiet times 77—33227
exosphere, global model based on meas. from Fabry-Perot interferometer on OGO-6 satellite 77—53265
exosphere, global model using optical and incoherent scatter meas. 78—36343
exosphere, global temps. and densities under active solar conditions 77—33234
exosphere, H non-Maxwellian cooling assoc. with thermal escape 79—80264
exosphere, representation by sum of series in Legendre polynomials 78—45063
exosphere, temp. determ. using OSO-8 meas. of H absorption 77—21963
exosphere, temp. rel. to Hα airglow semi-annual vars. 78—28360
exosphere, temp. rel. to heating by solar wind energy 77—37471
exosphere, temp. vars. appl. to neutral atmosphere semi-empirical models 79—21085
exosphere neutral temperature observations 80—56661
exosphere temperature and thermosphere neutral winds above Millstone Hill, mathematical model 79—39995
exosphere temperatures at high latits., geomag. activity effects 80—109286
exospheric, models seasonal vars. at solar max. and low geomag. activity 78—57376
F_1-layer, ion comp. and temp. profiles from incoherent scatter radar studies 80—72654
F_2-layer, night-time, over Arecibo, ion and electron temps. seasonal mean struct. 80—31163
F_2-layer, temp. and thickness from vertical sounding and incoherent scatt. 77—45221
F-region, electron density and ion temp. profiles rel. to airglow ground-based obs. anal. 80—98496
F-region, electron heat cond. importance in energy balance 78—61649

atmospheric temperature continued
F-region, electron temp. model, Aeros-A data compared to radar obs. 80—67465
F-region, electron temperatures, theory and obs. 79—48618
F-region, energetic electrons spectra meas. by Hadamard energy spectrometer *(Japanese)* 80—94637
F-region, global electron temp. distrib. model, 300-700 km altitude 80—67464
F-region, neutral temp. and zonal wind computed bounds during Joule heating 79—21084
F-region, neutral temp. and zonal winds estimation during Joule heating 78—36344
F-region, neutral temp. rel. to diffusion-recomb. parameters 77—13156
F-region, solar activity rel. to temp. and electron density 80—46337
F-region, temps. at Malvern and S. Santin 77—91360
F-region, winter anomaly causes 80—85793
F-region neutral temp., during equatorial spread-F, OI spectra 80—41587
F-region temp., satellite meas. rel. to incoherent scatter radar results 79—2435
Fenlands, temp. and humidity meas. rel. to steam fog form. criterion 80—98431
fires, temp. profile from convection-diffusion coupling model 77—7481
five-day average air-temp. forecasting, combined technique improvement 79—29817
five-day average low and high temp. anomalies, forecasting procedure 78—92938
fluctuations, heat flux and struct. functions meas. with acoustic Doppler sodar 80—105023
fluctuations, struct. functions 78—30274
fluctuations in stable boundary layer 77—73786
flux used to determine oceanic temp. flux 80—104986
flux-profile relationships for wind vel. and temp. 77—70735
forecasting, short-term via statistical model, method and accuracy 78—92941
forecasting max. and min. temp., use of probabilities 80—82020
forecasting nocturnal temperature, short-rnage model 80—109200
forecasting of average air temp., underlying ocean surface influence 79—29827
forecasting of diurnal average air temp. in N.Vietnam 78—3903
forecasting of sharp temp. drops in Ararat Valley using circulation indices 79—25317
forecasting skill, daily precipitation and temp. 1966-78, Boston, USA 80—56509
forecasts, case for an operational programme 80—17311
forests, Ge diodes for temp. and humidity profile meas. 77—64463
free atmosphere, temp. and humidity effects on theoretical and exptl. long-wave IR radiation fluxes *(Russian)* 80—94598
Fresnel zone and diffraction fields anal. near boresight of acoustic radar antennas 80—64318
frontal passage, VHF radar obs. of temp. vars. at frontal surface 79—53482
frontogenesis, warm rel. to cold surfaces 78—49086
fronts and depressions at middle latitudes, mesoscale struct. 80—26604
frost point meas. systematic error using Meteorological Office Mk3 hygrometer 78—73538
frost prone areas, Niagara fruit belt, defined by thermal imagery 79—25314
funnel cloud observed from Glastonbury, assoc. with cold trough 79—66783
geographic latit. rel. to temp., correl. charts construction by graphical method 79—29905
global January and July climate, numerical simulation with two-layer circulation model 77—56722
global surface temp. increase rel. to CO_2 conc. increase 77—66977
global synoptic meas. using cryogenic etalon-spectrometer on Space Shuttle 79—58232
global temp. distrib. from TIROS-N microwave sounder unit meas. 80—90265
global temperature distribution, rel. to Earth heat balance annual var. 78—73300
global warming due to CO_2 increase, temp. and precipitation changes 80—36389
global warming in N.Hemisphere, analysis and future var. 78—7736
gradient over snow surface, effects on Pb and sulphate deposition vels. 77—2231
gradients and clear-air turbulence probability 77—49128
grassland surface temperature rel. to air temperature in summertime 77—78396
great frost of January 1776 77—56721
Great Lakes, ice formation, freeze-up, breakup predictions 77—45038
greenhouse effects of some atmospheric constitutents 79—70882
Greenland Sea area, climatic normals 80—77100
ground based radiometric measurement, lower troposphere 77—91330
ground layer, stratified, under coniferous forest canopy, temp. distrib. *(Russian)* 78—96266
ground surface temperature prediction, force-restore method investigation 80—98469
ground-based inversion decay, analysis by direct and indirect meas. methods *(German)* 77—37310
ground-based inversion frequencies determined from surface climatological data 80—41475
ground-based inversions, expt. data and boundary-layer models 79—66748
Haicheng, China, anomalous meteorological phenomena obs. before 1975 Feb. 4 earthquake *(Chinese)* 78—24224
halocarbon depletion of O_3 layer, climate effects 80—98436
harmonic perturbations, radiative damping 78—32163
heat wave and cold wave days in Indian subcontinent 78—7699
heating due to 9.6 μm O_3 band in inhomogeneous atm. 78—88918
heating effect of Mount Jolmo Lungma on atmosphere from April to July *(Chinese)* 80—8406
heating rate parameterization, 15-120 km altitude, due to O_2 and O_3 absorpt. of solar radiation 79—39798
heavy rain, anal. by potential pseudoequivalent temp. field *(Chinese)* 79—48532
heavy rain, dynamical anal., potential pseudoequivalent temp. condition conservation *(Chinese)* 79—48533
height profile determ. by aircraft meas. of outgoing radio emission *(Russian)* 79—16574

atmospheric temperature continued
height temperature profile determ. from radiometric meas. of atmospheric radiation *(Russian)* 77—64498
N.hemisphere, climatic aspects of surface temp. vars. (1950-1975) 77—70803
N.hemisphere, sea surface temps. assoc. with poor summers in British Isles 80—109241
N.Hemisphere surface temp. anomalies, correl. with sunspot struct. vars. 80—31272
hemispheric mean surface temp., non-equilib. model, comments and reply 78—44938
hemispheric mean surface temp., nonequilib. model, pollution effects 77—49150
hemispheric mean temp. response to stratospheric dust 77—29419
HF radio acoustic sounder, atm. wind and temp. remote meas. 78—32235
historic climate correl. with wheat prices and wages 78—81346
hourly temperatures generation, stochastic model 78—61502
Hudson Valley, New York, tree ring-drought relationships 78—28299
hydrologic cycle, climatic sensitivity, numerical model 79—8654
ice albedo feedback with temp., one dimens. radiative convective climate model 80—109245
incoherent scatter results for co-ordinated special intervals at St. Santin (France) 79—2416
Indian region, temp. correl. with tree growth rel.to tree-ring anal. appl. in palaeoclimatology 80—90212
Indiana, correction for non-climatic trends in divisional and state mean temps. 80—51524
internal gravity waves nature obs. from OH emission 77—41246
intertropical convergence zone struct. over GATE area 78—57283
inversion, determ. via ground-based long-range sounding in O_2 5 mm absorpt. band *(Russian)* 78—11963
inversion, thermodynamics of gravitating fermions 79—57994
inversion persistence at Long Kesh, Northern Ireland 79—79996
inversion region, vertical elec. field strength and ionic cond. meas. 78—20478
inversions, time dependent behaviour in different climatic regions 79—20908
inversions height and mixing layer height over Bombay 77—53119
ion depletion in AE-C satellite wake, electron temp. and relative ion comp. influence 79—62667
ion temp., International Reference Ionosphere 1978 rel. to Vertical'-6 rocket meas. 80—90285
ion temp., Vertical-6 rocket flight results 80—90268
ion temp. estimation with ion trap data from rockets and satellites 78—16237
ion temp. meas. using ion analyzers 79—21147
ionosphere, analytic partial derivatives for incoherent scatter data least-squares fitting 78—73581
ionosphere, calc. and obs. structure, AE-C satellite and incoherent scatter radar obs. 78—49203
ionosphere, D-region electron temp., investigation by cross modulation tech. *(Russian)* 78—24404
ionosphere, effect of ion-neutral collisions on ion vel. distrib. 77—29565
ionosphere, effect of recomb. processes and plasma nonisothermability on thermal parametric instability 80—61967
ionosphere, electron and ion temps., ground-based incoherent scatt. and AE-C satellite meas. 77—29575
ionosphere, electron densities and temps. from Intercosmos-10 Langmuir probe expts. *(German)* 79—2469
ionosphere, electron density and temp. rel. to primary ion-electron prod. rates changes 80—72675
ionosphere, electron temp. and density fluctuations meas. by Aeros-B, global distrib. 79—58160
ionosphere, electron temp. changes rel. to radio waves self-action, nonstationary theory *(Russian)* 79—48604
ionosphere, electron temp. distrib., approx. expressions using vertical rockets data 80—12599
ionosphere, electron temp. in near wake of Atmosphere Explorer C (AE-C) satellite 79—53647
ionosphere, electron temp. meas. by HF probe method 79—92632
ionosphere, electron temp. meas. from satellite gyroharmonic reson. obs. 79—48614
ionosphere, electron temp. profiles during Western European Winteranomaly Campaign 78—45125
ionosphere, electron temp. var. with solar activity satellite meas. 80—26678
ionosphere, electron-ion conc. and electron temp., Vertikal' 4 rocket meas. 79—84566
ionosphere, equatorial daytime topside, plasma temps. and ion dynamics 79—84584
ionosphere, F-region temp. meas. by satellite and incoherent scatter radar 78—36394
ionosphere, heating by solar radiation in Schumann-Runge continuum and by chem. reactions 79—62653
ionosphere, heating during aurora 77—21973
ionosphere, heating effects of conjugate photoelectrons 79—62670
ionosphere, high-altitude auroral zone, electron temp. enhanced by electron current 80—85803
ionosphere, ion temp. troughs in equatorial topside region, OGO-6 obs. 77—64526
ionosphere, lower, warming by planetary waves rel. to VLF transmission winter anomaly 80—8485
ionosphere, meas. by self-contained tethered balloon sounding system 78—28343
ionosphere, mid-latit. N_2^+ 427.8 nm temp. rel. to emission height and origin 79—44291
ionosphere, nighttime, $O(^1D)$ contrib. to heating 79—44288
ionosphere, nonlinear stationary temp. domains 79—35052
ionosphere, plasma thermal response to electron and ion heat sources 77—45239
ionosphere, props. meas. at Arecibo Observatory 78—81488
ionosphere, storm time auroral, anomalous transport coeffs. effect on thermal struct. 79—16743
ionosphere, temp. and electron density relaxation rel. to radiowave interaction nonstationary processes *(Russian)* 78—93028
ionosphere, temp. vars. due to solar EUV flux changes, calcs. 79—44293
ionosphere, topside, electron temp. models for low and medium solar activity conditions 80—67460
ionosphere, topside, transient response to precip. 77—78566

atmospheric temperature continued
ionosphere, topside, turbulent transport and heating of auroral plasma 79—35054
ionosphere, winter, thermal electrons energy distrib. obs. by S-310-5 rocket *(Japanese)* 80—94636
ionosphere and plasmasphere at midlatitude, computer model 80—105120
ionosphere and protonosphere, electron temp. profile over S.Atlantic geomag. anomaly *(Japanese)* 78—28368
ionosphere disturbances, day-night terminator temperature gradient study 80—4186
ionosphere electron temp., calc. technique for ground and satellite obs. 80—90275
ionosphere electron temperatures, effect of HF-induced plasma instabilities 78—40756
ionosphere electron temperatures at trough latits., obs. concerning relationship to quiet-time ring current 79—101015
ionosphere EM wave absorpt. rel. to wind and temp. struct., winter 1975/6 obs. 80—36438
ionosphere heat nonlinearity, meas., by partial reflection method *(Russian)* 78—24379
ionosphere heating by radio waves, predictions for Arecibo and satellite power station 78—77403
ionosphere main valley, satellite meas. of electron temp. and behavioural characts. 80—4170
ionosphere NO^+ daytime chemistry, depend. on electron temp. 77—33230
ionosphere plasma, electron densities and temps. during major mag. storm 78—88987
ionosphere turbulent polar cusp, temps. and low-energy particles and Kelvin-Helmholtz instability 78—96343
ionosphere unstable polar cap, electron density and temp. rel. to electrostatic waves 79—29927
IR anomalous absorption, temp. dependence 79—34951
IR atmospheric remote sensing, theoretical problems 79—80052
IR cooling during stratospheric warming of 1971 Jan. 77—87020
IR cooling rates for 2-dim. thermal perturbation in nonuniform atmosphere 77—87000
IR radiation plane layer of mol. gas, Earth temp. calc. as function of atmospheric CO_2 conc. 77—35021
IR remote sounding, error anal. and data acquisition *(Chinese)* 80—109273
IR sky temp. computation and surface temp. comparison 79—34953
Iraq, frost phenomena and damage 77—73795
Israel's coastal plain (1967 to 1976), temp. and global radiation meas. 79—80003
Japan, Niigata prefecture, mean daily temp. rel. to pressure in winter *(Japanese)* 79—96803
Joule dissipation of elec. currents during equatorial spread-F events 78—45127
Kew, monthly mean temp. and rainfall in August 1973-July 1976 period 77—73820
lake moderating effect on downwind temp. and humidity, model simulation 79—88400
lakes, surface temp. inversion rel. to atmospheric refr. and lake monsters 80—46259
land and sea surface temp. fields, seasonal vars., NOAA 5 satellite IR obs. 78—85676
lapse rate, control of inherent uncertainties in double theodolite meas. 80—77160
lapse rate depiction for clear-air convection 77—53145
lapse rate in troposphere and climatic sensitivity, two-level atmospheric model 79—80004
lapse rate regimes and parameterisation 80—12486
laser beam attenuation, H_2O continuum, meteorological factors 77—2242
latitudinal variations, comparison with minimum entropy exchange models *(Russian)* 78—53716
lidar measurement of temp. profiles, rot. Raman and elastic scatt. 77—9515
lidar temp. profiling in O_2 bands 80—21827
Limb Infrared Monitor of Stratosphere (LIMS) radiometer, design and performance, expt. goals 78—61601
line thermal numerical model, initial conditions influence 78—92932
Little Ice Age, N.Hemisphere average temp. obs. rel. to model calcs. 80—82050
Little Ice Age, palaeotemps. from high altitude tree growth in S. Norway 77—5312
local weather prediction, hydrodynamic methods 78—61521
London, 1976 June-July heat island 77—91248
London storm, August 1975, urban heat island effects on precip. 78—81339
lower atm., thermal struct., sodar obs. at Delhi, India 79—53428
lower atmosphere, O_3, temp. and wind obs. for 1978 January 4 to March 31 period *(French, Flemish)* 79—5561
lower atmosphere, temp. and O_3 obs. (1976 January 5 to March 31) *(French, Flemish)* 77—33174
lower atmosphere, temp. and O_3 vertical distrib. meas. (1977, April 1 to June 29) *(French, Flemish)* 78—11966
lower atmosphere, temp. corrections for Menaka-II meteorological rocket payload 79—5558
lower ionosphere, heating by radio waves rel. to nonlinear focusing 77—60511
lower thermosphere, thermobaric field rel. to dynamical processes *(Russian)* 78—24401
macroscale local eddy flux of heat rel. to mean horizontal temp. gradient 77—45108
Madrid, temp. in 1871-1975 period, Fourier series *(Spanish)* 77—9486
magnetosheath, dawnside, H^+ and He^{++} temp. anisotropies 80—4204
magnetosphere, dayside plasma trough obs., at geosynchronous orbit 80—51611
magnetosphere, electron density and temp. meas. by GEOS-1 mutual impedance expt. 79—35071
magnetosphere, electron temp. estimation via VLF waves propagating in directions near reson. cone 77—82086
magnetosphere, lower, electron densities and temps. from Intercosmos-10 Langmuir probe expts. *(German)* 79—2469
magnetosphere, polar, electron and ion temps. from electrostatic H^+ cyclotron waves obs. 78—45154
magnetosphere, thermal electron densities and temps. in dayside cusp region 77—78574
magnetosphere, thermal/suprathermal plasmas obs. by GEOS-1 S-302 expt. 79—35070

atmospheric temperature continued
magnetosphere low-energy plasma at synchronous orbit, temp. and density 78−77435
magnetosphere plasma, hot ion component rel. to electron component, obs. and implications 79−80106
magnetosphere plasma density and temperature, GEOS-1 multi-expt. determ. 79−35074
magnetosphere-ionosphere, electron- and ion temps. from time-depend. heat eqns. numeric 80−21875
magnetosphere-ionosphere, temp. profile rel. to irregularities form. by mag. flux tubes interchange 80−21876
maize canopy, turbulent transport 77−33129
major anomalies forecasting using parametric linear discriminant anal. 79−58056
Manabe-Wetherald radiative convective model, fixed cloud-top temp. and fixed cloud-top altitude approximations 80−72616
marine air temp. sensor error analysis 77−78437
marine atmosphere, temp. annual var. rel. to ocean temp. var. model 78−20433
marine boundary layer, optical refractive index fluctuations, statistical props. 79−62580
marine layer, temp. profiles meas. in fog and stratus using low-level atmospheric thermograph 80−105073
marine stratocumulus convection boundary layer humidity and temp. in horizontally inhomogeneous solns. 80−56543
marine surface layer, temperature ramp struct. 79−66760
marine surface layer turbulence structure, humidity and temp. spectra study, N.Pacific 80−21798
mass consistent atmospheric flux model (MASCON) for complex terrain regions 78−92964
mass-mean temperature rel. to cosmic ray intensity vars., Sayan spectrograph data 79−84606
maximum temp. forecast for cloudy or overcast days *(German)* 77−37311
mean monthly temp., year-to-year var., statistical characts. *(Russian)* 77−21849
mean temperature of thickness layers along 50°N 80−101399
mean-mass temp. vars. determ. from cosmic ray intensity data 77−91387
measurement, by IR method from Earth satellite *(French)* 77−9550
measurement by automated environmental monitoring system 80−81513
measurement by surface to orbit gas laser, absorpt. of vibr.-rot. band 78−12015
measurement data 1971-75, river water pollution study appl. *(Japanese)* 79−70874
mesopause, ion-neutral collision freqs. and mean temps., Arecibo radar meas. 78−88957
mesopause, lidar meas. of Na conc. and neutral temp. 78−61613
mesopause, positive ion composition and chem. at high altitude 80−46224
mesopause, radiative cooling 80−26660
mesopause region, ion-clustering during winter anomaly, temp. and NO density vars. effect 79−21087
mesopause temperature, determ. from $[NO^+.H_2O]/[NO^+]$ ratios 79−96849
mesophere, heating effects of gravity waves induced by Earth's diurnal rotation 78−40613
mesoscale temp. and moisture fields from satellite IR radiance meas. 78−7717
mesosphere, Arctic, vertical temp. and density patterns anal. as gravity waves 79−16622
mesosphere, day-night depend. of geomag. activity effects on temp. 77−21835
mesosphere, LF radio wave absorpt. temp., seasonal variation 79−48602
mesosphere, LF radio wave absorpt. variations, press. and temp. depend. 79−44282
mesosphere, major characts., processes and dynamics 77−25734
mesosphere, minor constituents distrib. in thermal interface 78−3891
mesosphere, OH nightglow emission obs. 80−82121
mesosphere, pot. temp. field rel. to eddy diffusion models 80−109198
mesosphere, seasonal and latitudinal variations in temp. and composition 77−45207
mesosphere, temp. during D-region winter anomaly over Sardinia (40°N) 80−21871
mesosphere, temp. profile rel. to O_2 Schumann-Runge bands absorpt. model 79−96823
mesosphere, temp. profiles from solar H Lyman-α radiation extinction meas. 78−44947
mesosphere, temp. rel. to water cluster ions form. in D-region 77−21842
mesosphere, temp. vars. rel. to solar mag. sector struct. 79−34905
mesosphere, temp. waves of annual and semiannual period, radiometer obs. 80−51500
mesosphere, temps. during winter anomaly from Lyman-α extinction meas. 78−45001
mesosphere and lower thermosphere, profiles based on obs. of Lyman-α extinction 80−77180
mesosphere and stratosphere, obs. by satellite IR limb scanning method 80−105086
mesosphere periodic temp. and wind fluctuations 77−78361
Mesozoic greenhouse and climatic warming 79−20963
meteor collisional ionisation, thermalisation 78−36346
methane gas plumes, equivalent temp. struct. parameter rel. to tracking via acoustic sounder 80−55968
microclimatic effects on stellar obs. with photoelec. transit instrument *(Russian)* 78−73612
micrometeorological temperature profile from optical data inversion 79−80034
microwave radiometry, remote temp. sensing 80−46293
microwave radiometry for temp. retrieval, climate in variational scheme 80−56649
microwave spectroscopic imagery of Earth from Nimbus 6 satellite 78−12026
middle atmosphere, plasma and neutral gas comp. and temp. meas. by mass spectrometer probe 78−45191
middle atmosphere, temps. calc. from numerical model of zonal mean circulation 80−109218
middle atmosphere (mesosphere) 80−98412
middle atmosphere processes revealed by satellite observations 80−21803
Middle East, monthly temps./rainfall relation appl. to palaeoclimates evaluation 80−31091
Middle Europe temp. averages in last 200 years *(German)* 77−2222

atmospheric temperature continued
Mohliner Feld (east of Basle), cold air distrib. rel. to topoclimate *(German)* 80−61890
molecular boundary layer struct. over sea *(German)* 77−86989
monitoring by remote automatic station on radio link 78−85726
monsoon rainfall rel. to summer solar radiation and temperature 78−32154
monthly mean anomalies, mathematical treatment and forecasting *(German)* 79−62557
monthly means over central England 78−73497
morning and evening temp. differences of cloud tops over tropical continents and oceans 79−12219
Moscow meridian circle pavilion, temp. regime rel. to daytime astrometric obs. 78−24441
Mount Kenya, vertical temp. struct. rel. to condensation nuclei concs. 80−82012
Munster, minimum ground temperatures, var. *(German)* 80−4083
Neogene explosive volcanicity, temperature and glaciation 80−26481
Netherlands, winter temps. rel. to solar cycle 79−5596
neutral atm. disturbances, reaction of midlatit. ionosphere 77−25805
neutral gas temperature at the F1-Fs transition region over Delhi during low scalar activity 79−88519
neutral upper atmosphere, density, temp. and winds 79−75006
neutral upper atmosphere, magnetospheric convection effects on global temp. field 77−29525
New York State, ambient temp. decrease rel. to local snowfall trends in four cities 80−105044
New Zealand, temp. record, historical data and agricultural implications of climatic var. 80−61886
New Zealand, temps. and short-term climate change during last millennium 79−62574
nightglow, internal gravity wave effects on temps. 78−45066
NOAA spacecraft high resolution imagery data 77−78389
noctilucent cloud aerosol particles, temp. profiles *(Russian)* 78−16093
nocturnal increases in surface temp. at Bombay Airport 78−32156
nocturnal min. temp. prediction using thermal oscill. *(Spanish)* 77−9478
non-neutral surface boundary layer, parameterisation 80−17316
northern hemisphere, stratosphere, av. temp. for 1957-65 period 78−24350
northern hemisphere, temp. trend to year 2000, prediction 79−16646
Northern Hemisphere, temp. var. in 1881-1975 period 78−7737
northern hemisphere annual temperature approximation, simple method 78−81345
Northern Hemisphere temp. changes rel. to dust from major volcanic eruptions 78−36258
Northern Hemisphere temperature, 1579-1880, reconstruction 80−12535
Norway Station/Sanae (Antarctica), surface temp. and sea-level press. 78−81324
numerical model of atmospheric temp. regime *(Russian)* 77−64368
numerical weather forecasting, long-range, filtering method 79−84446
ocean near-surface layer, heat exchange in small-scale sea-air interaction 78−3810
ocean surface layer rel. to atmospheric temp. and humidity *(Russian)* 80−17282
ocean-atmosphere system, interannual variability 79−2330
oceanic rainfall estimates, temp. correction 79−12220
optical systems affected by temperature turbulence meas. and theory, AMOS site in Hawaii 79−53503
Orange Lake, Florida, temp. fluctuations rel. to lake latent and sensible heat fluxes prediction 80−72562
Oviedo, Spain, global solar radiation and air temp. *(Spanish)* 80−36377
Oxford, cold winters (1767-8, 1776 and 1814) 80−51520
Oxford max. temp. anomaly rel. to quasi-biennial oscill. strength in equatorial stratosphere 77−81975
ozonosphere, temp. coupling effect on O_3 depletion prediction 78−57246
palaeoatmospheric surface temperature, effect of O_3 conc. 79−96807
palaeoclimatology, continental record of environmental conditions at 18000 yr BP 80−51529
palaeoclimatology, overview, and European air temp. trends *(German)* 79−16639
palaeotemperature, O isotopes of mid-Wisconsin limestone cave deposits 80−82069
palaeotemperature, parallel changes in species diversity, Lower Miocene, meas. by O isotope anal. 79−39866
palaeotemperature series from last 700000 years, statistical study 79−5598
palaeotemperatures, 230000 to 100000 BP, results from speleothems stable isotope geochemistry 79−2234
perturbed atmosphere thermal struct. and relaxation rates, photochemical radiative convective model 80−8408
plasmasphere, electron temp. and conc. at 3000 km altitude, ISIS-1 meas. 79−101004
plasmasphere, ion and electron temps. rel. to charge exchange and H escape rate 77−37469
plasmasphere, temp. anisotropy in energetic electron distrib. function 78−4035
plasmasphere, thermal struct. and plasmapause positions 79−12329
point discharge current, effect of temperature 79−88409
polar thermosphere, neutral temp. during solar cycle 79−53595
power spectrum of temp. fluctuations, rel. to optical propag. 78−92980
Prairies, temp. trends and cycles 77−56724
precipitation, $^{18}O/^{16}O$ ratio correl. with temp. and altitude 80−77067
primitive atmosphere temp. history with reducing greenhouse effect 77−87031
primitive ionosphere, thermal struct. 78−40754
probability forecasts, nonexistence of ordinal relationships between measures of accuracy and value 78−61503
profile, interferogram radiance meas. techniques for sounding 80−17413
profile retrieval, generalized inverse theory appl. and spectral expansion method 80−17412
profile retrieval with passive microwave sounder using Kalman-Bucy filters 79−21053
profiles from Nimbus-6 soundings 78−53695
profiling using IR heterodyne radiometer 77−49200
psychrometry, appl. of portable differential system 80−105072
pyrocumulus cloud over North Canterbury, New Zealand, air temp. due to heating by surface fires 80−109240
radiational damping of temp. waves in finite non-grey atmosphere *(Russian)* 80−81990
radiative cooling by use of inverse greenhouse effect 79−25329

atmospheric temperature continued
  radiative eqn. rel. to remote sensing of thermal struct. 77−9498
  radiative equilib. temp. change due to stratospheric aerosol pollution 77−45092
  radiative equilibrium temperatures in stratosphere and mesosphere, stellar occultation and BUV O_3 data 78−81280
  radiative forcing of atmosphere, sensitivity to variable cloud and moisture 80−56553
  radiometric and rawinsonde profiling, comparison 79−84392
  radiosonde temperature sensing systematic anomalies, obs. evidence 79−70864
  radiowave refractivity and temp.-humidity cospectrum 79−39819
  rapid morning boundary-layer transition, case study from Haswell, Colorado, expt. 80−81996
  recording instrument, long-term *(Japanese)* 77−82035
  refractive index temp. struct. parameter estimation over ocean 77−41033
  remote air pollution meas. expts., estimation of surface temp. 79−70854
  remote IR satellite temp. profile retrieval 79−48586
  remote measurements of emitted thermal radiation, temp. estimation 77−45202
  remote sensing, by TIROS-N operational vertical sounder 80−77132
  remote sensing by satellite microwave sounding, anomalous profiles, errors *(Russian)* 77−17266
  remote sensing of cloudy atmospheres by microwave radiometry *(Chinese)* 80−51549
  remote sensing of temp. profile, microwave radiometry characts. *(Chinese)* 79−80188
  remote sounding, IR radiometer calibration 77−41174
  remote sounding, temp. effect on 15 μm region transmission function 78−77327
  remote temperature sounding from CO_2 4.3 μm absorption spectrum 78−16166
  remote thermal sensing of atmos. from Earth orbit, spatial temp. and geopot. fields 80−36429
  Rome, effect of urban heat island on air temp. during summer season 80−85717
  Sapporo, Hokkaido, urban-rural temp. differences during night *(Japanese)* 80−36362
  satellite determ. of temp. profile *(Hungarian)* 79−44218
  satellite radiance meas., temp. retrievals, empirical method 77−70859
  satellite radiance obs., direct method of ballistic density determ. 78−16186
  satellite temperature sounding data, impact on weather forecasts 80−77028
  satellite-retreived temperature profiles, error due to aerosol particles effects 80−98449
  sea and land breeze obs. over Goa, India 78−32155
  sea surface and atmosphere radio brightness temp. meas. from satellite *(Russian)* 77−60407
  sea surface radiobrightness temp. from satellite sounding *(Russian)* 77−60412
  sea surface temp. anomalies rel. to general circulation prediction 77−86963
  seasonal temperature variations, subsurface energy storage influence 77−49122
  Shetland weather during 1975 77−56718
  solar activity-weather relationship, study of temp. and rainfall at Oxford 78−85674
  sound attenuation, air-to-ground propag., effects of temp., humidity gradients 79−1019
  sounding by high precision satellite, spectral band passes 77−41175
  sounding from TIROS-N, early operational soundings evaluation 80−77133
  sounding with partially scanned interferograms 77−41176
  spatial analysis of temp. field from weather satellite meas. 78−20488
  spectra determ. from propeller anemometer and thermistor meas. *(French)* 79−16708
  spectral analysis over vegetated surface in sensible heat advection conditions 80−17343
  spectral transfer of turbulent energy and temp. variance 78−61489
  spectroradiometric measurement of temp. and gaseous composition profiles 77−9568
  squall line, formation from boundary layer forcing and temp. gradient, model 80−8396
  St. Louis downwind plume, thermodynamic props. and aerosol patterns 79−16603
  stability category determ. for airborne radionuclide release assessment 78−73504
  statistical struct. characts. of temp. field 77−78363
  stochastic climate models, appl. to zonally averaged energy models 78−20502
  stratocumulus cloud, finestructure of precipitation and temperature 79−88418
  stratopause, double, thermal struct. features over Thumba 79−100901
  stratosphere, 30 mb temp., coherence with ionospheric absorpt., five-day wave 77−33275
  stratosphere, aerosol optical props. and size distrib. effects on heating rates 79−12222
  stratosphere, annual and semi-annual waves obs. using Nimbus 5 selective chopper radiometer data 78−81315
  stratosphere, correl. with ionospheric f-min at southern midlatitudes 77−9469
  stratosphere, correl. with mesospheric electron densities and drifts 77−9470
  stratosphere, diurnal variation of wind and temp. in equatorial region 80−82022
  stratosphere, eddy kinetic energy budget for winters with and without warmings 77−37297
  stratosphere, LF radio wave absorpt. variations, press. and temp. depend. 79−44282
  stratosphere, lower, power spectral anal. of meteorological data 78−40616
  stratosphere, lower, temperature vars. rel. to atmosphere total O_3 content natural fluctuations 79−29819
  stratosphere, model, temp. feedback effect on O_3 conc. 78−28277
  stratosphere, nightglow intensity fluctuations during warmings 80−4162
  stratosphere, O_3 and temps., satellite obs. for 1970-71 period 77−9466
  stratosphere, O_3 behaviour and thermal structure during S. Hemisphere spring 80−105014
  stratosphere, periodic temp. and wind fluctuations 77−78361

atmospheric temperature continued
  stratosphere, planetary-scale temp. waves seasonal var., Nimbus 5 obs. 77−21868
  stratosphere, recent temp. trends 79−29845
  stratosphere, seasonal climate, numerical simulation, zonal temp. and wind 79−5566
  stratosphere, southern hemisphere, temp. and press. field spring transformation anal. 80−98420
  stratosphere, sudden warming forced by mountain 80−72583
  stratosphere, summertime temps. during solar cycle 20 (1965-77) 79−79936
  stratosphere, temp. and O_3 vars. (1958 to 1977) 80−109222
  stratosphere, temp. and press. determ. from OH fluoresc. lidar instrument 79−80033
  stratosphere, temp. and press. profiles meas. via solar occultation sounding using narrowband radiometers 80−98452
  stratosphere, temp. fluctuations, latitudinal-wavenumber power spectra 80−41499
  stratosphere, temp. profile vars. rel. to effect of water vapour changes on O_3 reduction 78−73444
  stratosphere, temp. trends and O_3 conc. rel. to 11-yr. solar cycle 79−84443
  stratosphere, temperature/O_3/water vapour trends in N. temperate latitudes 79−53474
  stratosphere, temperatures and geostrophic winds during 1973-74, Nimbus 5 radiance meas. 79−79976
  stratosphere, thermal response to 0_3 fluctuations 79−39797
  stratosphere, thermal struct. and trace constituents, effects of solar UV variability 78−61492
  stratosphere, thermal structure and total O_3 obs., Nimbus 4 Iris expt. 77−21839
  stratosphere, ultralong temp. waves during 1973 austral winter 78−92901
  stratosphere, upper, radiative damping, obs. evidence 79−84368
  stratosphere, vars. during total solar eclipse 80−105017
  stratosphere, warming of 1976-77, temp. and wind fields 77−56699
  stratosphere, winter temps. rel. to NO_2 global behaviour 80−17334
  stratosphere and mesosphere, microwave limb sounding 77−21940
  stratosphere and mesosphere, wind and temp. diurnal and semidiurnal oscills., rocket meas. 79−5556
  stratosphere cooling by CO_2, effect on O_3 content 80−36369
  stratosphere sudden warming, caused by planetary wave secondary circulation 80−72584
  stratosphere sudden warmings, wave-mean flow interactions numerical model 77−5297
  stratosphere temperature wave propagation, polar region in winter 80−72597
  stratosphere temperatures, no correl. with seasonal var. of equatorial ionosphere radio waves absorpt. 78−85762
  stratosphere warming, Eulerian and Lagrangian mean meridional circulations 80−21799
  stratosphere warming event of January-February 1979, tropospheric-stratospheric interaction 80−4074
  stratosphere warmings, influence on lower thermosphere natural infrasound refl. 79−21089
  stratosphere winter warmings, ionospheric characts. vars. 77−29550
  stratosphere-mesosphere, winter-warmings rel. to wind regime of lower thermosphere 78−4019
  stratospheric balloon trajectory analysis for long-term missions *(Italian)* 77−82055
  stratospheric sudden warming, 1973 January-February, energetics and dynamics 79−79973
  stratospheric sudden warming, planetary-scale forcing of USA Jan. 77 weather 78−57279
  stratospheric warming, 1976-77, dynamical development 79−79968
  stratospheric warmings, O I 5577 Å, Na and OH nightglow emissions var. 77−53270
  stratospheric warmings, obs. and theory 79−74944
  stratospheric warmings, rel. to wind field disturbances at 90-100 km altitude *(German)* 77−70894
  structure parameter profiles meas. by acoustic sounder 79−21049
  subcloud layer over land, temp. and humidity struct. 77−91200
  summer max. temp. recorded in Glaisher stand and Stevenson screen 77−81976
  summer monsoon over S. Asia, break and active phases 78−3912
  surface air temperature over N.America, solar cycle signal 79−58042
  surface and soil temperature anals. in humid tropics, case study from Sierra Leone 80−109242
  surface and upper air temperature data, appl. to hourly mixing depths estimation 80−51482
  surface boundary layer, hot-wire meas. on S.W. Kansas, Denmark, expt. 77−9458
  surface fluxes and mean profiles of vel., temp. and conc. downwind of surface roughness change 78−20484
  surface layer, accuracy of moments of vel., temp. and humidity vars. 78−92891
  surface layer, air density correction to eddy flux meas. 79−66761
  surface layer, calc. of mean velocity and temp. profiles *(Russian)* 80−8415
  surface layer, spatial temp. derivatives 80−56514
  surface layer, spectra of temp. derivatives 79−66759
  surface layer, temp. traces and features of organised motion 80−72602
  surface layer flux parameters determ. in absence of temp. profile 79−66752
  surface layer over ocean, temperature structure function parameter obs. 79−79918
  surface layer over Poona, temp. field 79−48544
  surface layer temp. ramps 79−88434
  surface layer temp. vars. at solar optical observatory testing sites in China *(Chinese)* 78−69680
  surface layer temperature, fluctuations investigation via acoustic method 80−67434
  surface layer turbulence response to partial solar eclipse 79−70843
  surface temp. trend in N. Hemisphere, 1969-73 extension 77−21883
  surface temp.-humidity feedback in vertical-column energy balance models 77−66959
  surface temperature, determ. of diurnal var. in mountainous terrain 80−82011
  surface temperature, influence of CO_2 effect on atmospheric heating rates 80−17376

atmospheric temperature continued
surface temperature changes nonlinear response in climate model, ice-albedo, lapse-rate and cloud-top feedbacks 78—69438
surface temperature climate, differences between seasonal and mean annual energy balance model calcs. 80—56595
surface temperature extremes, probability determ. method 78—45020
surface var. and compensation in soil moisture remote sensing 77—17247
surface-troposphere system, radiation energy balance and temp., CO_2 increase effects 80—12498
Tbilisi, air temp. rel. to solar activity (1848-1970) 80—26595
temperature in range —20° to 45°, 253-318K, resistance thermometer 80—46291
temporal fluctuations, averaging for continents Europe and N.America 78—92958
terrestrial thermal balance, influence of human activity *(French)* 79—74553
tethersonde system for remote meas. of wind and temp. 79—80038
Thailand tropical atmospheric radiation and sky temp. calc. 79—58084
thermal effects of stratosphere O_3 depletion at 85°N latit., airborne particles influence 78—81279
thermal history, CO_2 content rel. to thermodynamic balance 79—29847
thermal plumes detect. by acoustic echo sounder 78—57259
thermal pollution, large-scale, regional climatic effects simulation with NCAR general circulation model 79—53478
thermal pollution from fuel and energy consumption, effects on weather and climate 78—61539
thermal structure, effects of nearby supernova 80—94584
thermistor, microbead, as atm. temp. sensor, response between 0-80 km altitude 77—53234
thermosphere, auroral heating rel. to midlatit. F-region quiet time depressions 78—36385
thermosphere, auroral particle and Joule heating, global effects on undisturbed days 78—45069
thermosphere, comparison of meas. and inferred temps. from AEROS-B 77—21958
thermosphere, composition and temp., longitude/UT vap., global model 79—53591
thermosphere, differential operator and integro-differential eqn. *(Chinese)* 80—56660
thermosphere, disturbed, global model from Esro 4 gas analyser meas. 77—37468
thermosphere, diurnal and semidiurnal components, solar cycle variability 79—75002
thermosphere, diurnal vars. in temp., comp. and winds 77—87141
thermosphere, eddy diffusion vars. and assoc. transport processes 77—33226
thermosphere, electric field momentum coupling characts. 78—88958
thermosphere, electrodynamic and particle heating in disturbed polar regions 77—33231
thermosphere, electron temp. and density relationship in daytime at solar minimum, model 78—61638
thermosphere, empirical model of temp. and composition 80—77183
thermosphere, equatorial, midnight temp. max. 79—84555
thermosphere, from O I 5577 Å nightglow line profiles, long-term vars. 77—9584
thermosphere, global comp. and temp. during quiet times 77—33227
thermosphere, global comp. and temp. empirical models during quiet times compared with ESRO 4 data 79—8732
thermosphere, global model based on mass spectrometer and incoherent scatt. data, N_2 density and temp. 77—70897
thermosphere, global semiempirical models 79—66852
thermosphere, gravity wave activity effects on photochem. and comp. 80—41583
thermosphere, large-scale waves, obs. during mag. storms 79—35021
thermosphere, lower, gravity waves detect. by French incoherent scatter facility 78—81478
thermosphere, lower, pot. temp. field rel. to eddy diffusion models 80—109198
thermosphere, lower, thermal tides rel. to nightglow emissions vars 77—78550
thermosphere, meridional circulation and temp. latit. var. calc. for solstice conditions 77—56783
thermosphere, middle, ion comp. and temp. profiles from incoherent scatter radar studies 80—72654
thermosphere, midlatitude F-region winds and temps. during 1976 March 26 magnetic storm 79—53594
thermosphere, model based on satellite drag data 78—69555
thermosphere, neutral gas temperature, in situ meas. by Atmosphere Explorer 80—12576
thermosphere, nighttime, energy balance 79—35022
thermosphere, nighttime meas. during mag. storms 77—9585
thermosphere, NO radiative cooling 80—72656
thermosphere, seasonal and solar cycle vars. of temp. and zonal mean circulation 78—32262
thermosphere, semi-annual temp. vars. rel. to atmospheric circulation and mesopsheric clouds 78—45061
thermosphere, temp., density and comp., new models 77—64502
thermosphere, temp.-depend. model of odd N species 78—16226
thermosphere, temperature depend. of O I 6300 Å emission in twilight airglow 77—45215
thermosphere, temps., wind vels. and emission intensities from O I 630 nm airglow 79—58144
thermosphere, temps. and winds from O I 630 nm line profiles in nightglow 79—58143
thermosphere, tidal struct. at equinox, temp. and vel. fields predictions 78—81476
thermosphere, tides and midnight temp. anomaly 79—84556
thermosphere, transport processes in diurnal tide, satellite meas. 78—88959
thermosphere, winds and temps. determ. from ionospheric obs. using numerical simulation 77—53268
thermosphere and exosphere, neutral temperature and winds, geomag. disturbances effects 80—26658
thermosphere H temperature, influence of 63 μm radiation field 79—80066
thermosphere heating during magnetic storm, dynamic energy transport from high to low latits. 80—26657
thermosphere nighttime winds and temps., monthly vars. during solar min. 78—32263
thermosphere seasonal and latitudinal variations in temp. and composition 77—45207

atmospheric temperature continued
thermosphere storms, temp. vars. and related ionospheric effects 77—9583
thermosphere temperature, N_2 content and turbulence, 95-150 km altitude 80—51588
thermosphere temperature and wind measurement Fabry-Perot-interferometer imaging system appl. 80—101441
thermosphere temperatures over Malvern, incoherent scatter data comparison with two global thermospheric models 80—8467
thermosphere-exosphere transition layer, structure, temps., H escape 79—66845
thermosphere-exosphere transition region, reduced H temp. 77—33225
Thumba, India, temp., circulation and struct. 77—78362
tidal oscills. rel. to horizontal winds and temp. structure 78—20457
tide in temperature of stratosphere due to Moon, NIMBUS 5 obs. 80—101405
tides, thermal exciting energy, numerical anal. 79—70833
time derivative, rel. to atmospheric thermal perturbations and solar image quality *(French)* 77—53532
time variability of wind and temp. vertical profiles, uncorrelated standing waves *(Russian)* 77—91215
Tokyo, winter temps., spectral anal. of data for 1443-1970 period 77—45128
topside ionosphere, comp., temps. and electron loss coeff. over Arecibo 78—36386
topside magnetospheric cleft ionosphere, ion and electron densities and temps. 77—29571
tropical cloud clusters, temp., moisture and precipitation 77—29406
tropical cyclone, intensity inferred from troposphere temp. 80—67416
tropical iridescent cloud occurrence rel. to tropopause temp. 78—85675
tropical middle atmosphere, observational evidence of semiannual oscillation 80—109216
tropical regions, temp. and climate during ice age, simulation 78—16144
Tropical Wind, Energy Conversion and Reference Level Experiment (TWERLE), results 78—40605
tropopause height estimation from nonlinear functions of satellite meas. spectral radiance 77—78335
troposphere, equatorial, response to heat sources 79—29832
troposphere, lapse rate effect on pilot balloon ascent rate, further comments 77—17175
troposphere, lapse rate parameterization in terms of surface temp. 77—86999
troposphere, lower, solar flare effects on temp. and press. 78—40615
troposphere, mean temp. rel. to sea surface temps. and volcanic aerosols 77—33168
troposphere, pressure and temp. meas. by lidar differential absorpt., influence of laser emission spectral width *(French)* 80—41554
troposphere, sensitivity in satellite determ. due to water vapour estimate errors 78—3874
troposphere, sodar obs. of thermal struct. at Delhi 78—32151
troposphere, solar radiation and temp. fluctuations rel. to stratospheric aerosol vars. 78—81327
troposphere, temp. and moisture conditions rel. to radiothermal radiation at waveguide propag. *(Russian)* 79—88406
troposphere, temp. anomalies, conjugate functions appl. in anal. and forecasting 79—39829
troposphere, temp. lapse rate effects on pilot balloons ascent rates 77—2204
troposphere, temp. lapse rate rel. to refr. effects on satellite range meas. 78—73609
troposphere, temp. meas. by radio-acoustic sounding methods 78—53728
troposphere, temp. meas. rel. to climatological effects of particulate pollution 78—85678
troposphere, temp. profiles from ground-based angular microwave meas. 80—51551
troposphere, temp. profiles meas. using Raman lidar 79—100974
troposphere, temperature-pressure profile meas. by microwave remote sensing *(Chinese)* 80—4116
troposphere, virtual temperature rel. to height of isobaric surface *(French)* 80—21806
troposphere and lower stratosphere, cirrus clouds influence on IR cooling rate 78—73455
troposphere energy balance, diurnal variation 80—56548
troposphere moisture, temp., IR soundings anal. by statistical struct. and correl functions 80—8398
troposphere sounder, metric radiowaveacoustic sounder 80—46276
troposphere temperature fluctuations, spectra deduced from ground-based radiometry 79—92567
troposphere temperatures and winds, evidence for solar cycle signal 80—72604
troposphere thermal structure, acoustic sounding technique appl. to siting studies 78—81467
troposphere/stratosphere, temp. rel. to radiance gradient and jet streams 80—98447
tropospheric dynamics, Nimbus 4 THIR obs. at 6.7 microns 77—17164
tropospheric-stratospheric polar vortex breakdown 1977 January 77—53107
Tsumeb, S.W.Africa, boundary layer profiles for dry season in steppe *(German)* 79—34923
turbulence chamber for optical transmission expt., characterisation by thermal method 79—25330
turbulence measurement by remote sensors, optical propag. parameters 77—45125
turbulence spectrum with temp. gradient 77—2198
Typhoon June (1975), temp. distrib. meas. by scanning microwave spectrometer 78—73436
United Kingdom, first cold snap of autumn mean date, 1871-1920 period 77—9484
United States, 1896-1975 interannual temp. variability 80—61888
W.United States, climatic regionalization 77—29417
unstable atmospheric surface layer, geometric similarity for temp. field 77—33127
unusual weather frequency variability over last century 78—73479
upper atm. parameters daily vars. at midlatits., reference system 77—29521
upper atmos. temp. meas. with Fabry-Perot airglow spectrometer 80—77156
upper atmosphere, dynamical properties 79—75005
upper atmosphere, energy balance, importance of IR radiation 79—8729
upper atmosphere, general review 79—39997

atmospheric temperature continued
upper atmosphere, ion and neutral temps. rel. to $N_2^+ + O$ reaction rate coeff. 77—53288
upper atmosphere, neutral waves determ. from AE satellite meas. 79—58139
upper atmosphere, pitot press. meas. for temp. determ. 78—45193
upper atmosphere, temp. and wind distrib. between 100 and 120 km altitudes *(Russian)* 77—29527
upper atmosphere, temp. meas. rel. to internal gravity waves *(Russian)* 78—16224
upper atmosphere, temp. stratification rel. to acoustic-gravity waves diffr. around spherical Earth 78—4016
upper atmosphere, temp. vars. from twilight and nightglow Na I D-line vars. 78—36353
upper atmosphere, warming at OH airglow heights (90 km) during 1976-77 winter *(Russian)* 79—88518
upper atmosphere at nighttime, 400-450 km altitude, anal. of Ogo 6 data 80—90267
upper atmosphere wind and temperature meas., laboratory discharge lamp source appl. 80—4148
urban atmosphere, numerical simulation of mixing depths 80—105024
urban atmosphere, radiative effects of elevated pollutant layers on temp. struct. and pollutant dispersion 80—97841
urban atmosphere, roof level, long wave radiative flux divergence and nocturnal cooling 77—33123
urban atmosphere, urban canyon, long wave radiative flux divergence and radiative cooling 77—33124
urban atmospheres, modelling of temp. and pollutant conc. distribs. 77—45143
urban environment, cold air drainage effects on temp. fields, case study of topographical influence on climate 80—94555
urban heat island in subtropical environment rel. to city size 77—33170
urban mixing layer, mesoscale perturbs. on airflow 79—16602
urban planetary boundary layer, pollution effects on thermal struct. and dispersion 78—11986
urban temp. field dynamics in Calgary area 77—17168
urban temperature field, dynamics, comments 78—7722
urban-rural canopy analysis, surface heat flux/temp. model 79—20945
USA, temp. and precipitation rel. to sunspot numbers 80—17328
USSR, air temp. and precipitation var., five-year changes 78—16130
variability, secular changes 80—21820
variability of wind and temp. fields in cyclonic and anticyclonic conditions *(Russian)* 77—29394
variance spectrum in inertial and dissipation range of isotropic turbulence 78—61490
vertical profile, from satellite data, information retrieval 78—3959
vertical profiles, methods of retrieval from IR satellite meas. 77—87111
vertical profiles from STRATCOM VII-A meas. 79—58079
vertical sounder radiances rel. to midlatit. 300 mb flow patterns 78—92983
vertical temp. profile estimation, system identification method 77—91342
vertical temp. profiles, meas. using ground based IR spectroradiometer *(Japanese)* 77—29499
vertical temp. profiles, microwave remote sensing meas. *(Chinese)* 79—84452
vertical temp. profiles from microwave radiometers 79—58226
vertical temperature profiles, determ. by remote sounding, influence of aerosol attenuation *(Russian)* 78—81430
vertical temperature profiles, from Nimbus 5 selective chopper radiometer data 80—12520
volcanic eruption, dust causing temp. drop at Earth surface 80—85726
water droplet aerosol interaction with EM radiation, temp. field and refractive index distrib. model 78—3899
wave disturbances of temp. and geopotential height 80—51452
wave-wave interactions in vel. and temp. fields, kinetic and available pot. energy evolution 80—109227
weather satellite data, complex demodulation 78—49177
western hemisphere, rocketsonde-derived temperature vars. 79—58018
wet bulb potential temperature charts, meteorological use 77—91232
wet bulb temperature and precipitable water calc. 77—53114
wet bulb temperature distrib. over India 77—53115
wind speed and temp. profiles over melting glacier, log-linear model fitting 79—79912
winter heat island formation over Milan city *(Italian)* 78—53709
winter measurements, correl. between mean daily temp. and atmos. press. *(Japanese)* 79—66777
winter season temperature outlooks by objective methods 78—85641
winter temp. in central England, time series, running means appl. 78—65378
winter temperatures in central England and Newfoundland, 1870 to 1970, anal. 79—80009
wire sensor temperature probes, frequency response meas. by internal and acoustic heating 80—31123
zonal, effect of chlorofluoromethane IR radiation 79—80019
zonally averaged climate model 78—81347
CO_2 and N_2 vibrational temps. at 40 to 140 km altitude 77—70762
CO_2, anthropogenic, possible influence on atmospheric temp. 80—51486
CO_2 effect on global radiative heat balance model 78—3863
CO_2 greenhouse effect, surface temp. calc. 80—26587
CO_2 increase from fossil fuel burning, greenhouse effect, threat to W.Antarctic ice sheet 78—28296
CO_2 increase rel. to future climate, coupled atm.-ocean model 79—58082
CO_2 laser radar used to measure average atmospheric temp. 80—90225
CO_2 model run in tandem with climate model, 1800-2100 AD 80—98381
CO_2-induced atmospheric temp. rise, Arctic sea ice decay 80—61802
H^+ temp. in high-latitude topside ionosphere, diffusion-thermal heat flow effects 78—49217
He^+ outflow from ionosphere, press., density and temp. profiles 78—49221
N_2, rot. temp. meas., rocketborne electron beam fluoresc. meas., reflected mol. effects 77—29519
$(NH_4)_2SO_4$ aerosol production under elevated temp. inversion in Cleveland Country, model 78—81397
N_2O pollution causing atmos. warming, interaction with O_3 80—94579
Na layer temp. from laser obs. of Na I D_2-line 80—931
O_2 A band differential absorpt. lidar meas., for pressure height and vertical temp. profiles 79—39904
O_2 microwave absorpt. at 60 GHz 80—77172
O_3 heating, induced antisymmetric tidal modes at equinox 79—35024
OH (6-2) and (8-3) nightglow bands, rotational temps. and intensities 79—58147

atmospheric temperature continued
OH emission, 5-1 band rot. temps. rel. to waves in emission layer and F_2-layer 78—45065
OH, nightglow emissions, equilib. nature of rot. temp. 77—64508
OH nightglow rotational temp., correl. with Na D-line and **O I** 5577 Å emissions 79—80067
$O_2(^1\Sigma)$ airglow, temp. as gravity waves diagnostic 79—29918

atmospheric thermodynamics
see also atmospheric temperature
adiabatic invariants, conservation as criterion for evaluation of barotropic schemes *(Russian)* 77—64369
aerosol particles, motion due to inertia, Brownian diffusion, phoretic and elec. forces 79—53460
aerosol scattering of IR radiation, atmos. heating and cooling rates 80—72630
aerosol-induced heating effects on convective boundary layer 78—69409
Air Mass transformation Experiment (AMTEX), preliminary results 77—53196
air-sea heat and moisture exchange during stormy weather 77—78375
air-sea heat flux during AMTEX 75 mesoscale cellular convection 77—78322
air-sea interface, gas transfer 77—91154
air-sea interface, heat and momentum flux in const. flux layer, from temp. meas. 78—44899
air-sea interface, latent and sensible heat flux calc., AMTEX-74 77—91224
air-sea sensible and latent heat transfer coeffs., meas. 200 km from land 80—72552
air-water interface, energy transfers at high wind speeds, effect of spray 78—85574
airflow turbulent kinetic energy, budgets in mountainous terrain 80—105022
Ampere Glacier, Kerguelen Is., heat balance in ablation area 77—64335
AMTEX 75, structure of mixed layer and inversion layer, mesoscale cellular convections 79—88416
annual zonally averaged climatic model with diffuse cloudiness feedback 77—29416
Arabian Sea, wind stress, sensible and latent heat fluxes, ISMEX-73 data 78—85627
Arctic Basin, thermodynamics rel. to summertime stratus form. and persistence 77—5290
Arctic leads, atmos. boundary layer turbulence spectra obs. 80—56588
Arctic leads, turbulent heat flux 80—56513
N.Atlantic, sea-air large-scale interaction, thermodynamics 78—3786
Atlantic tropical ocean temp. anomaly, atmospheric response 77—17187
atmosphere, exchange stabilities principle *(French)* 78—88871
auroral particle instantaneous energy deposition, determ. from optical emissions 78—81491
available potential energy budget eqns., limited region, time depend. of reference press. 78—20497
available potential energy budget eqns., limited-area 79—53453
available potential energy concept 79—12218
available potential energy in atm. in press coords. *(Russian)* 80—109187
available potential energy over uneven topography, theory 80—51514
Baltic Sea, atmospheric heat balance, seasonal var. 77—91235
Baltic Sea region, atmospheric heat and moisture balance from aerological climatology 77—87057
baroclinic atmosphere, two dimensional, zonal flows convective instability *(Russian)* 80—94564
baroclinic atmosphere, two layer model, Helmholtz term effect 79—79986
baroclinic boundary layer structure 78—81326
boundary layer, bulk model for wind and pot. temp. 80—77030
boundary layer, buoyantly interactive with entrainment, similarity theory 77—49116
boundary layer, diabatic baroclinic, parametrisation for circulation modelling *(Russian)* 78—88882
boundary layer, energy characts. of urban-rural surfaces in greater St. Louis area 78—61484
boundary layer, geostrophic drag and heat transfer relations 77—78298
boundary layer, heat and humidity exchange laws, model approach 77—66948
boundary layer, height and circulation prod. in sea breeze model 79—53438
boundary layer, heterogeneous surface of large aerodynamic roughness, transfer characts. 78—73487
boundary layer, kinetic energy flow between large and mesoscale perturbations *(Russian)* 77—49106
boundary layer, lakes latent and sensible heat fluxes prediction from surface water temps. 80—72562
boundary layer, mol. resistance during diffusion, universal function determ. 80—26573
boundary layer, over sea, momentum, heat and H_2O vapour fluxes, meas. methods 78—32213
boundary layer, quantitative bistatic acoustic sounding 78—49176
boundary layer, Reynolds shear stress and heat flux fluctuations over rough surface 78—44902
boundary layer, steady-state characts. of inversions capping well-mixed layer 78—61483
boundary layer, terrestrial surface features effects, instrumented aircraft meas. 79—39808
boundary layer, thermal eddy diffusivity modelling at canopy height 78—24330
boundary layer, three-dimens. model rel. to expt. data 78—73428
boundary layer, turbulence characteristics *(French)* 79—66749
boundary layer, unstable, turbulence energy modulation by longit. rolls 77—2202
boundary layer, unstably stratified, turbulent energy disspation rate *(Russian)* 77—64372
boundary layer above warm water surface, thermal exchange, optical meas. methods 77—49184
boundary layer during convective disturbance, thermodynamics 80—81978
boundary layer evolution and nocturnal inversion dispersal 79—25296
boundary layer evolution and nocturnal inversion dispersal 79—25295
boundary layer heat and pulse transport *(Dutch)* 78—3890
boundary layer structure and development over SE.England, aircraft and balloon meas. 80—12516
boundary layers, convective and nonconvective, parameterisation for use in numerical models 80—82009

atmospheric thermodynamics continued
boundary layers, numerical modelling 78—44900
Bowen's ratio determ. in equatorial Atlantic region 78—81330
Bowen ratio and surface temp. over sea surface 77—60400
bulk transfer velocity to and from natural and artificial surfaces 79—25302
buoyancy driven mixed layers modelling 77—33150
buoyant clouds, lateral interaction, numerical simulation 77—2197
buoyant plume rise in atm. inversions 77—41114
Canadian Middle North, surface heat and water budgets 77—29409
centripetal heat island circulations, St. Louis, USA 79—66753
circulation, forced by heating, transient mass flow adjustment 79—53455
circulation in desert regions, variable surface albedo effects 77—49123
circulation model, 12-component, energetics *(Russian)* 79—84375
cirrus, radiative transfer model for IR region 80—98397
cirrus clouds, falling ice particles survival distance in subsaturated air 77—33151
climate and thermodynamic systems of max. dissipation 79—70881
climatic change, atm. feedback mechanisms with zonal climatology 77—33175
climatic models, stability and extremal props. *(Russian)* 78—53716
closure conditions in Lilley-type inversion models 79—5589
cloud detrainment effects on properties of cumulus populations 77—70760
cloud IR radiative cooling rate, theory 80—56565
cloud layer cooling by IR radiative transfer 80—72629
cloud source thermodynamics rel. to snow crystalline forms *(Rumanian)* 77—33169
clouds influence on atm. dynamics *(Russian)* 79—8653
coastal zone, local thermal wind-field disturbances freq. statistical forecasting 80—36371
Complex Atmospheric Energetics Experiment (CAENEX), results and prospects 78—3904
composition perturbations and temp. feedback, climatic effects 80—41525
condensation of water, thermodynamics of nucleation on charged centres 79—20955
convecting columns interaction over linear heat sources, wind effect *(Russian)* 78—55637
convection, energy considerations, two dimensional model *(French)* 79—84409
convection, gravitational, with compressibility 79—58051
convection, moist plume from a cooling tower *(French)* 79—84400
convection caused by rejected waste energy 79—12169
convection development over inhomogeneous heated surface *(Russian)* 77—29365
convection initiation and development in temperate latits. 78—20480
convection parametrisation, conditional instability of second kind hypothesis appl. 78—61530
convection parametrization for 10-level atm. model 77—70782
convective boundary layer, temperature-humidity covariance budget 78—73430
convective boundary layer, vertical heat flux 78—20487
convective boundary layer turbulence struct. 77—49117
convective breaking localisation in perturbed stratified atm. 77—70716
convective clouds, one-dimensional models *(Polish)* 80—12466
convective clouds and rain showers form. over Indian Ocean 78—7735
convective flow of incompressible stratified fluid, Euler-Poisson eqns. *(Russian)* 77—31300
convective instability and thermodynamic parameters of tropical atm., GATE obs. 79—39827
convective instability in rotating gas, tornado model 79—27642
convective plumes in lower atmosphere, detect. by Doppler acoustic sounding *(French)* 78—40603
convective scale precipitation downdraughts in cumulus and synoptic scale interactions 77—33145
convective velocity scale estimation for diffusion appls. 79—79914
convective vortex model, unsteady two-cell similarity soln. 79—16626
convective-radiative equilibrium, numerical soln. 78—32164
convectively mixed layer, flux ratio relation to energy ratio 78—49107
cooling tower plume rise and visible plume length, prediction and obs. 77—45053
coupled ocean-atmosphere expt., ocean response, rel. to climate 80—12430
cumulonimbus convection, theoretical modelling 79—84405
cumulus cloud life cycle effects on heat and moisture budget 77—56672
cumulus cloud transient ensemble, large-scale interactions 77—66954
cumulus convection initiation mechanisms and development 78—69410
cumulus transports in tropical wave composite during GATE 79—2336
cyclone at temperature latitude, water vap. and energy budget 80—85731
cyclone-anticylcone couplets, quasi-Lagrangian kinetic energy budgets 77—66958
daily average solar heating or photolysis, exponential approx. 77—5285
desert region, surface albedo and vertical vel. relations 78—11953
diabatic heating and topography, axially asymmetric flow model 79—88435
diabatic heating climatology of zonal atm. 79—53432
diabatic heating profile, rel. to preferred mode of Ekman conditional instability of second kind (CISK) 80—72617
difference equations, generalized vertical coordinate, total energy conservation 79—84363
diurnal heating in Po Valley, dynamic circulation 80—85716
dry penetrative convection 78—92889
dry thermals forecasting for gliding 78—49103
dynamical meteorology topics, atmospheric energetics 79—66780
Earth encounter with interstellar cloud, effects on terrestrial heat budget 78—57292
Earth radiation budget data collection and interpretation model 77—37497
Earth surface vertical heat fluxes, N.hemisphere distribs. computed by bulk method 79—96804
eddies and linear baroclinic waves similarities 77—33149
eddy available potential energy, large-scale, growth and decay 79—58058
eddy flux measurements above pine forest 77—17198
eddy fluxes of conserved quantities by small-amplitude waves 80—61858
eddy heat flux and temp. variances in weakly nonlinear theory 79—79928
eddy heat fluxes and temp. variances in baroclinic waves, weakly nonlinear theory 80—8390
eddy momentum flux convergence rel. to vorticity and temp. 80—41490
eddy transports, large-scale, linear parameterisation 80—17361

atmospheric thermodynamics continued
Ekman boundary layer universal functions in drag and heat transfer laws *(Russian)* 77—91216
energetics in dynamical meteorology 79—58064
energetics of entrainment across density interface 77—5283
energy and enstrophy nonlinear cascades in two-dimens. spectral index 79—16619
energy balance climate model response to parameter changes *(Russian)* 79—100938
energy balance climate models tests 80—77098
energy balance climatic models, differences between seasonal and mean annual model calcs. 80—56595
energy balance model, climate sensitivity to radiation flux calcs. 80—8421
energy budget of equatorial atmosphere, meridional heat transfer *(Russian)* 80—81988
energy budget over grasslands, eddy correl. sampling technique 77—78446
energy budgets, Priestley-Taylor large scale evaporation, comments and reply 77—45039
energy budgets of turbulent vel. components and vel.-press. gradient interactions 79—58026
energy fluxes propagated by diurnal oscills. in upper atmos. 77—37473
energy parameters, hemispheric-scale, vacillation during winter season 77—53132
energy parameters, non-random fluctuations 77—86982
energy transfer in tropical subcloud layer, aircraft meas. during GATE 79—79989
energy transfer to ionosphere from lower atmosphere 78—28381
energy-balance climate models, ice-albedo feedback effects 78—7749
energy-balanced discrete models of atmospheric process dynamics 79—39828
England, hot spell of 1976 June-July 77—17203
equatorial mesosphere and stratosphere, vertical vel. determ. from Diurnal Experiment 80—77047
equatorial trough zone, heat balance 80—81977
equatorial trough zone occurrence and struct. in Venezuela 79—79974
equilibrium temperature gradient in atmosphere at incomplete automodelity 80—41480
equivalent zonal model, adiabatic motion invariants appl. *(Russian)* 77—29363
evaporating downdraught model comparison with obs. behind squall lines 78—92913
evaporation calc. using measured wind, temp. and humidity profiles 77—17194
evaporation from land surfaces, diurnal vars. 79—57987
evaporation from natural surfaces, Penman's eqn. modification 77—70781
evapotranspiration of continents real land surface, Penman concept calcs. *(German)* 80—98368
evapotranspiration remote sensing Nimbus 5 satellite IR radiometer, evaluation *(French)* 77—17156
F_2-region, nighttime thermal balance at mid-latitudes 79—84583
F-region Joule heating, zonal wind computed bounds 79—21084
feedback in ocean-atmosphere coupled model 80—12500
flow over irregular surface, three dimens. finite difference model, terrain following coord. transform 77—60452
freely connecting atmosphere over water surface, oscills. natural freq. *(Russian)* 78—11964
freezing nuclei sources, large aerosol particle conc. 80—41512
general circulation, eqns. of kinetic and available pot. energy evolution in wave-number freq. space 80—109227
general circulation, struct. using six-component spectral model *(Russian)* 77—29364
general circulation efficiency, theory 77—73808
general circulation model, angular momentum and heat balance effects *(Russian)* 80—51456
general circulation model with variable Coriolis parameter *(Russian)* 79—100896
geopotential values retrieved by objective anal. methods 80—36386
glaciers-ocean-atmosphere global system, numerical modelling 79—84469
global climate, steady-state format 79—44244
global energy balance, environmental fluctuation effects 80—4084
global energy budget, annual cycle of available pot. energy, variability 79—20909
global energy budget, wave disturbances of temp. and geopotential height 80—51452
global general circulation model for ice-age climate simulation 77—33176
global heat balance, annual var. 78—73300
global heat budget for tropical Atlantic and E. Pacific 77—86935
global January and July climate, numerical simulation with two-layer circulation model 77—56722
global roughness length distrib. rel. to energy dissipation on ground *(German)* 77—64388
global scale transport processes *(Dutch)* 78—3889
global weather model, thermodynamic, with turbulent transport *(Spanish)* 80—36372
greenhouse effect, component contrib. 80—101544
greenhouse effects of methane and N_2O, climate model 80—90211
heat advection over Caspian Sea 77—78213
heat and moisture flux in stratified boundary layer 77—21867
heat budget and albedo determ. using balloon-borne pyranometers 79—58135
heat exchange between atmosphere and land surface, force-restore method for ground surface temp. prediction 80—98469
heat exchange investigation with general circulation model energetics *(Russian)* 80—21791
heat flux and turbulence meas. in unstable surface layer over land 77—66962
heat flux in stable boundary layer, rel. to wind speed 80—17345
heat fluxes, sensible and latent, over land, influence on four-day forecast 79—96805
heat fluxes, zonal and meridional var. long planetary wave induced 80—85720
heat heat transport, rel. to ocean temperature-salinity curve 80—72534
heat release, effect on atm. general circulation and climate 80—89694
heat transfer, characts. of nonstationary processes 80—41481
heat transfer bulk characts. in unstable baroclinic boundary layer 79—79911

atmospheric thermodynamics continued
heat transfer causing density effects in CO_2 or water flux, corrections 80—85721
heat transfer from cooling ponds, atm. effects, numerical model study 80—8380
heat transport parameterization in midlatits., large-scale stationary waves and Ferrel cell 79—16618
heat transport parameterization in midlatits., large-scale transient eddies 79—16617
heated air mass in stratified atm., vortex ring form. 79—84365
heating rates, effect of CO_2 80—17376
high-latitude heat input, reduction rel. to rapid ice-sheet growth and last glaciation initiation 80—51530
housing estate heat supply methods comparison *(Hungarian)* 79—2366
Hurricane Gladys (1975), subcloud layer energy transformations 80—77089
hydrologic cycle, climatic sensitivity, numerical model 79—8654
hydrostatic stability, influence on wind drag coeffs. for marine regime 79—5494
Indian summer monsoon meteorology 79—74938
interaction with ocean, expt. study North Pacific, NORPAX 77—56649
internal boundary layer development, dynamics, slab model 77—91198
internal waves, rate of energy transfer to upper atmosphere mean flow *(Russian)* 77—13101
inversions, time dependent behaviour in different climatic regions 79—20908
ionosphere, cooling by 0 I, 63 μm emission, meas. 79—16732
ionosphere, diffusion and heat flow eqns. with large temp. differences between interacting species 79—66857
ionosphere, elect. heating and cooling rates discrepancy, Atmosphere Explorer-C meas. 77—29564
ionosphere, electrons collision freq. and transport props. 79—80079
ionosphere, equatorial, energy release from precipitating proton flux 78—32268
ionosphere, midlatitude, dynamical model for 100-1000 km altitude range 78—53768
ionosphere, press. oscills. transfer to neutral atmosphere during substorms 79—58158
ionosphere, topside, protonospheric heat flux rel. to electron temp. models 80—67460
ionosphere auroral zone, ion heating by electrostatic ion cyclotron waves 80—72686
ionospheric electron heat budget 77—53276
IR cooling, chlorofluoromethane induced, effect on general circulation model 80—90122
IR cooling rate, in standard atmosphere 80—26609
IR fluxes in stratiform model clouds 79—84361
IR radiative cooling rate due to H_2O vapour bands, calc. 80—90161
IR radiative transfer in cloudy sky, theoretical scheme 80—51540
Irish Sea, backing of W. and N.W. winds rel. to differential heating 78—24340
isentropic coordinate models, boundary problems soln. 77—29372
isentropic objective analyses, theory and appl. to meteorology *(Polish)* 80—51546
island wind shadows, stable thermal stratification 77—45062
Italy, vorticity generation and energy budget, 1961-65 period 78—81350
Kelvin-Helholtz billows, finite amplitude, evolution and energy budget 78—81293
kinetic energy budget of cyclone form. 78—16127
kinetic energy maintenance in tropical disturbances over E.Atlantic, GATE data 78—77307
land-breeze sea-breeze circulation asymmetry, comments 77—70784
lapse rate depiction for clear-air convection 77—53145
lapse rate regimes and parameterisation 80—12486
linear model atmosphere thermodynamic props. 77—53097
local severe storms in summer, anal. and forecasting method *(Chinese)* 79—84450
lower thermosphere, heating by acoustic waves dissipation 77—53266
macroscale local eddy flux of heat rel. to mean horizontal temp. gradient 77—45108
magnetosphere, significance of plasma flow pulsations in mag. tail 78—77436
magnetosphere energetics, comparison with Jovian magnetosphere 79—58201
magnetosphere open model, current sheets rel. to plasma populations 80—90295
magnetosphere substorm, energy transfer 79—12343
magnetosphere three-parameter two-dimensional model, configurations with least energy 77—91370
magnetosphere time-dependent heat energy eqns., numerical soln. 80—21875
Manabe-Wetherald radiative convective model, fixed cloud-top temp. and fixed cloud-top altitude approximations 80—72616
marine stratocumulus convection, governing eqns. and horizontally homogeneous solns. 80—56542
marine stratocumulus convection, horizontally inhomogeneous solns. 80—56543
mean maximum mixing heights across coastal zone, operational forecasting model 79—84357
mean meridional circulations of stratosphere and mesosphere, monthly mean planetary wave fluxes 80—109219
mean zonal wind in upper troposphere, determ. with allowance for turbulent heat fluxes *(German)* 78—32137
W.Mediterranean, energy budget *(Spanish)* 78—88846
mesopause, radiative cooling 80—26660
mesopause heat budget 78—28258
mesoscale convective system, momentum budget and temporal evolution 77—70757
mesoscale divergence of horizontal vel. field and press. gradient force, rel. to momentum transport 78—11954
mesoscale downdraughts, assoc. with cool ocean surface waters, GATE results 78—69365
mesosphere, extensions of Leovy's linear circulation model 78—32201
mesosphere, Joule heating at high-latitude 80—41500
middle atmosphere (mesosphere) 80—98412
middle atmosphere processes revealed by satellite observations 80—21803
midlatitude synoptic scale disturbances, energy sources 78—32162
mixed layer depth model based on turbulent energetics 77—5284
mixed-layer model with penetrative convection, critical evaluation 80—51483

atmospheric thermodynamics continued
moist adiabatic ascent in NE Colorado cumulus congestus clouds 79—53456
moist air behaviour 78—85673
moist available energy, numerical procedure 80—46241
moist boundary layer, finite element model, eqns. 79—5585
moist boundary layer, finite element model, soln. method 79—5586
moist penetrative convection and incipient cloud form. 79—66755
moisture processes in quasi-geostrophic model 78—7696
molecular temperature boundary layer above sea, dynamics 79—66756
monsoon, quasi-geostrophic diabatic four level model rel. to droughts diagnostics 77—56713
monsoon circulation dynamics 79—5559
monsoon in winter over warm ocean current, heat and moisture budgets 80—72590
monsoon over Indian region, energy anal. by baroclinic model 80—77073
monsoon system oscillations, spectral anal. of obs. records 77—33148
neutrally stable atmospheric layer, mass and energy transport 79—74927
nocturnal increases in surface temp. at Bombay Airport 78—32156
non-linear small-scale sea-air interaction parameterisation, effects of ice cover *(Russian)* 77—53068
nuclear power station spray cooling, heat and mass atmospheric transfer 78—94078
ocean surface, heat flow conditioned by wind pulsations *(Russian)* 77—60414
ocean surface layer thermal struct. and atmospheric heat exchange *(Russian)* 77—73751
ocean-atmosphere coupled model, tropical sea surface temp. anomaly effect 80—12418
ocean-atmosphere heat balance over northern hemisphere, annual cycle 77—41040
ocean-atmosphere heat exchange, model rel. to study of climate 78—20433
ocean-atmosphere heat leak, effects of passage of tropical cyclone *(Russian)* 77—53069
ocean-atmosphere interaction parametrisation for storm conditions, atm. circulation models appl. *(Russian)* 78—65359
ocean-atmosphere interface, coupled energy transfer, turbulent and radiative 79—2290
ocean/atmosphere ranked interaction on sub-semidiurnal time scales *(Russian)* 78—77260
oceanic heat flux, effect on wintertime of W.Europe 80—26542
N.Pacific, South China Sea and Indonesian Seas, regional energetics during winter 78—44960
W.Pacific subtropical high, summer, form. and struct. simulation *(Chinese)* 80—109233
parameterisation on non-neutral surface boundary layer, theory 80—17315
penetrative convection, AMTEX obs. 79—58028
penetrative convection linear stability 77—33146
perturbed atmosphere thermal struct. and relaxation rates, photochemical radiative convective model 80—8408
physics of atmospheres, book 79—62568
planetary long waves, effect on cyclogenesis regions, quasi-geostrophic model 80—8392
planetary scale monsoon, mechanisms affecting structure and evolution 78—40639
planetary scale monsoons, theoretical problems 78—44956
planetary scale vertical eddy flux of heat and linear momentum 77—86972
planetary standing waves in northern hemisphere in July, model 78—61487
planetary wave in middle atmosphere, radiative damping rel. to interaction with zonally averaged circulation 80—109217
plasmasphere, Coulomb collision-induced photoelectron trapping by geomag. field 79—8739
point explosion in arbitrary atmosphere with radiative heat transfer 78—53708
point heat source, natural convection in rotating environment 79—10445
polar surface energy budget, stratospheric warming effect 77—66957
potential temperature, first-order jump model, convectively mixed layer 80—12487
potential vorticity, conservation by finite difference eqns. in generalised vertical coordinates 80—26576
power-plant heat rejection, regional climatic effects 77—25768
precipitation flux climatology of free atmosphere 77—78397
pressure perturbations in deep convection, expt. study 79—53457
protonosphere, Gliddon's model of heat cond. 78—32294
radiation balance, heat balance, heat and cold sources, E.Asia 80—12548
radiation balance, sensitivity to cloud changes, zonal model 77—78419
radiation balance above forest and grassland 77—17196
radiation problems, thermal struct. 80—82016
radiative and actual nocturnal cooling rates over grass and snow 79—79947
radiative forcing of atmosphere, sensitivity to variable cloud and moisture 80—56553
radiative heat exchange in tropics *(Russian)* 79—84476
radiative heating, rel. to global general circulation model and O_3 prod., transport and distrib. 80—56544
radiative heating model from GATE multispectral scanning radiometer expt. 77—91221
radiative transfer eqn., soln. using Elsasser scheme 80—77112
released latent heat effects on growing baroclinic waves 77—29371
ring current, growth rel. to interplanetary quantity ε 79—75057
river to atmosphere heat and mass transfer data 78—96253
river/atmosphere time dependent, single dimensional heat exchange, analysis *(Bulgarian)* 78—57221
Rossby wave packet, vertical propag. in dissipative medium *(German)* 78—36220
Saharan dust affecting radiative transfer rates, model 80—90149
sea-air heat and moisture exchange, zonally averaged model *(Russian)* 77—17161
sea-air heat exchange, rel. to poleward heat flux by ocean gyre 80—85668
sea-air interface fluxes of sensible heat and moisture, parameterization 77—41041
sea-air small-scale interaction, heat exchange estimates 78—3810
sea-atmosphere heat-transfer expts. *(Russian)* 78—81206
seasonal temperature variations, subsurface energy storage influence 77—49122
sensible heat advection, local and regional components 79—20942

atmospheric thermodynamics continued

- sensible heat flux determ. from propeller anemometer and thermistor meas. *(French)* 79—16708
- sensible heat flux from ocean to atm. in extratropical synoptic-scale systems 77—78223
- sensible heat poleward flux during winter rel. to zonal and meridional circulation indices 77—17188
- sensible heat-flux detector 77—73863
- snow cover energy budget, energy flux meas. 78—92859
- solar eclipse affecting heat and radiation budget above pine forest *(German)* 80—46226
- Southern Hemisphere, oceans and atmosphere mean annual poleward energy transports 80—51406
- spectral energetics, determ. via numerical filtering anal. 80—26577
- spectral transfer of turbulent energy and temp. variance 78—61489
- squall line at midlatitude, thermodynamic and kinematic struct. obs. 80—109191
- St. Louis downwind plume, thermodynamic props. and aerosol patterns 79—16603
- stationary perturbations, statistical-dynamical model 79—2333
- steady axially symm. motions, linearised calcs. for instability and climate studies 77—70755
- steady axially symm. motions, nonlinear calcs. for instability and climate studies 77—70756
- steady convection, two-dimens., in const. vertical shear, dynamical struct. 79—12209
- steam fog in Fenlands, temp. and humidity meas. rel. to fog form. criterion 80—98431
- storms, principal component anal., hail index *(French)* 78—96267
- stratified atmosphere, nonadiabatic heat dynamics with mass exchange and water phase transitions 79—58004
- stratiform clouds, convective motions 79—53486
- stratiform clouds, structure and thermodynamics *(Russian)* 78—16088
- stratocumulus-capped planetary boundary layer, entrainment rate *(French)* 79—53489
- stratosphere, dynamical climatology during late winter 1973 in southern hemisphere 77—25769
- stratosphere, eddy kinetic energy budget for winters with and without warmings 77—37297
- stratosphere, highly excited metastable O_3 rel. to photochemistry and heat balance 79—44225
- stratosphere, lower, trajectory slopes, countergradient heat fluxes and mixing by waves 79—2340
- stratosphere, seasonal and interhemispheric vars. in circulation 77—49118
- stratosphere, seasonal climate, numerical simulation, energetics 79—5567
- stratosphere, sudden warming forced by mountain 80—72583
- stratosphere, thermal relaxation rate 79—79940
- stratosphere, vacillation cycles, quasigeostrophic β-plane channel model 77—49119
- stratosphere, winter warmings in N.Hemisphere 80—26591
- stratosphere, zonal mean winds vars. rel. to planetary wave props. and links with troposphere 80—109225
- stratosphere and mesosphere, review 78—49105
- stratosphere long waves, comparison of thermal struct. in N. and S. Hemispheres 77—5296
- stratosphere O_3 depletion thermal effects at 85°N latit., radiative-convective model 78—81279
- stratosphere photochemical-radiative damping and instability, numerical results 78—81286
- stratosphere warming event of January-February 1979, tropospheric-stratospheric interaction 80—4074
- stratosphere warmings, thermal and kinetic interactions with troposphere 80—105031
- stratosphere-mesosphere, O_3 densities rel. to radiative equilib. temps. 78—81280
- stratospheric sudden warming, 1973 January-February, energetics and dynamics 79—79973
- stratospheric warming, 1976-77, dynamical development 79—79968
- stratospheric warmings, obs. and theory 79—74944
- subsynoptic-scale energy transformations in severe storm situations 77—56673
- sudden stratospheric warming initiated by planetary wave, model 80—90150
- summer monsoon over S. Asia, break and active phases 78—3912
- Sun-weather relation, energetics study 78—81285
- Sun-weather relation, vorticity area index to interplanetary mag. sector struct. 80—46222
- surface boundary layer as part of overlying convective layer 79—92576
- surface evaporation rate parameterization for numerical modelling 77—91222
- surface layer, drag coeff. rel. to intermittent convection 78—44898
- surface layer, horizontal turbulent heat flux 79—66740
- surface layer, sensible heat flux time and height variability 77—78296
- surface layer, turbulent heat and mass transfer, simple predictive model 78—24331
- surface layer during 1976 hot spells, energy budget micrometeorological characts. 79—79961
- surface layer over Poona, temp. field 79—48544
- surface layer vorticity meas. using acoustic echo sounder array 78—7810
- synoptic fields, local energetic contribs. to numerical predictions 77—86973
- temperature fluctuations, heat flux and struct. functions meas. with acoustic Doppler sodar 80—105023
- temperature inversion, thermodynamics of gravitating fermions 79—57994
- temperature perturbations, radiative damping 78—32163
- temperature skewness budget in convective boundary layer, implications for turbulence modelling 80—21816
- temperature variance spectrum in inertial and dissipation range of isotropic turbulence 78—61490
- temperature wave generator for diurnal temp. wave propag. simulation 78—85735
- temporal boundary layer and multitime scales of motion in rot. atm. *(Chinese)* 79—84447
- terrestrial thermal balance, influence of human activity *(French)* 79—74553
- thermal balance meas. by radiation pressure on satellite microaccelerometer 79—2380
- • thermal history, CO_2 content rel. to thermodynamic balance 79—29847

atmospheric thermodynamics continued

- thermal mixing layer development over water and heated land, lab simulation 78—73449
- thermal pollution, large-scale, regional climatic effects simulation with NCAR general circulation model 79—53478
- thermal pollution from fuel and energy consumption, effects on weather and climate 78—61539
- thermal sensing from Earth orbit, spatial temp. and geopot. fields 80—36429
- thermally driven vortices, numerical model, dust-devil dynamics appl. 77—17191
- thermals models, scales of motion rel. to self-similarity soln. 80—109228
- thermohydrodynamic equations, vertical derivatives approx. rel. to short-range weather forecast *(Russian)* 77—60450
- thermosphere, cooling by 0 I, 63 μm emission meas. 79—16732
- thermosphere, dynamics at high latits., magnetospheric convection effects 79—8733
- thermosphere, dynamics calcs., Navier-Stokes eqns. validity 80—26659
- thermosphere, eddy diffusion vars. and assoc. transport processes 77—33226
- thermosphere, effect of auroral energy input on neutral and ion drifts 78—65446
- thermosphere, effect of turbulence on thermal conditions 79—88610
- thermosphere, energy sources for diurnal var. in temp., comp. and winds 77—87141
- thermosphere, heating by solar UV, efficiency at mid-latitude 80—85780
- thermosphere, lower, gravity waves detect. and vertical energy flux 78—81478
- thermosphere, midlatitude, neutral wind enhancement by geomag. heating due to polar substorms 80—31153
- thermosphere, neutral winds seasonal vars., 1970 to 1971, rel. to high-latit. heating 79—39996
- thermosphere, nighttime, energy balance 79—35022
- thermosphere, NO radiative cooling 80—72656
- thermosphere, response to heating during mag. storm 77—9582
- thermosphere, thermodynamic balance at middle latitudes *(French)* 78—12029
- thermosphere, vertical energy flux from medium scale gravity waves generated by jet stream 78—81479
- thermosphere and mesosphere, average daily closed model 77—17264
- thermosphere zonal mean circulation, seasonal and solar cycle vars. 78—32262
- thermotidal exciting function for water vapour absorption of solar radiation 78—28310
- tide (solar semidiurnal), zonal motion and meridional temp. gradient effects 80—98399
- tides, generated by differential heating between land and sea 78—65374
- topside ionosphere, electron heating rates during medium solar activity 77—70919
- topside ionosphere at high latitudes, diffusion-thermal heat flow effects 78—49217
- topside of nocturnal equatorial ionosphere, diffusion-thermal effects 78—40751
- trade-wind boundary layer, applications of model 79—88433
- trade-wind boundary layer, theoretical formulation and sensitivity tests 79—88432
- transfer of mass and heat between ground and atmosphere *(French)* 79—84403
- transient eddy statistics of northern hemisphere winter circulation 79—58027
- transport processes, effects of Earth rot. rate vars. rel. to climate 80—4097
- N tropical atmosphere, mean thermodynamic instability 77—25751
- tropical atmosphere, phase-lagged wave conditional instability of second kind 80—12513
- tropical atmosphere, struct. and energy fluxes 77—2203
- tropical atmosphere, Taifun-75 data from equatorial Pacific area, typhoons 79—58052
- tropical coastal region, lower troposphere features during rainfall 78—81332
- tropical cumuli, props. and bulk thermodynamic effects 79—8657
- tropical depression, synoptic scale kinetic energy source, cumulus cloud convection 80—77088
- tropical region, heat budget estimate of ocean and atmosphere 80—104968
- tropical troposphere, Fourier component eigenvalue anal. of CISK-induced disturbances 77—2199
- troposphere, eddy transport of sensible heat and momentum, time spectral anal. 78—92899
- troposphere, equatorial, response to heat sources 79—29832
- troposphere, growth and decay of large-scale waves in tropics during northern summer 79—88428
- troposphere, radiative cooling rate and flux, theory 80—85711
- troposphere, spherical model, zero-gravity, thermo/hydrodynamic characts. 78—24351
- troposphere, stationary waves, vorticity and heat balance calcs. 80—51460
- troposphere, thermal balance in low latits. in zonal circulation model 79—25316
- troposphere, virtual temperature rel. to height of isobaric surface *(French)* 80—21806
- troposphere energy balance, diurnal variation 80—56548
- troposphere jet stream-frontal system, pot. vorticity, role of turbulence 80—77044
- troposphere radiative energy balance, affected by stratospheric O_3 content 80—51466
- tropospheric aerosols, effect on surface and surface-atmosphere radiation budgets 80—17375
- turbulence, two-layer quasi-geostrophic, baroclinic energy transport and conversion 78—81186
- turbulence kinetic energy budget in convective conditions 79—79975
- turbulent boundary layer, penetrative convection regime, entrainment rate *(Russian)* 78—69401
- turbulent exchange coefficients for sensible heat and H_2O vapour under advection conditions 78—92907
- turbulent fluxes, H_2O vapour fluctuations influence 79—79916
- turbulent fluxes of heat and moisture, field study, S.England 78—20477
- turbulent mixing and heat flux over tundra rel. to surface roughness 77—87016
- turbulent viscosity rel. to turbulent thermal conductivity *(Russian)* 80—21796

atmospheric thermodynamics continued
two-level primitive eqn. atm. model for climatic sensitivity expts. 78—81348
typhoons structure over Soviet Far East during transformation of decay 77—78378
typhoons transformation, effects of thermodynamics and extratropical circulation 78—3908
upper atmosphere, effects of magnetospheric convection 77—29525
upper atmosphere, energy deposition during mag. storm rel. to comp. vars. and dynamics 77—9588
upper atmosphere, field-aligned auroral currents energy input 78—96339
upper atmosphere, heating by solar wind energy 77—37471
upper atmosphere, MHD waves absorpt. as heating source 79—53588
upper atmosphere, non-LTE radiative transfer in CO_2 15 μm band rel. to radiative heating *(Russian)* 78—36341
upper troposphere, horizontal momentum transfer by mesoscale turbulence *(Russian)* 78—16090
upward sensible heat flux by synoptic-scale transients, observational study 80—94591
urban atmospheres, modelling of temp. and pollutant conc. distribs. 77—45143
urban canyon, energy balance 77—64379
urban heat island, Rome, obs. during summer season 80—85717
urban heat island, St. Louis, theoretical study, parameter vars. 79—79943
urban heat island circulation and O_3 vars. in st. Louis 80—51488
urban heat island convergence in calm periods, St. Louis USA 80—90169
urbanisation and pollutant effects on thermal struct. in various climatic regimes 78—61500
vacillations in general circulation model, large-scale energy cycle 79—53430
vegetation-atmosphere interaction, simplified one-dimens. theory 78—61479
vertical eddy heat flux in northern atm. 77—33133
vertical energy flux in planetary-scale waves, obs. results 77—2193
vertical heat flux, determ. on basis of semiempirical turbulence theory 78—3907
vertical-column energy balance models, feedback effects 77—66959
vorticity and vertical motions over E.Asia, AMTEX 75 78—20492
vorticity budget of easterly wave rel. to cumulus convective transport 77—56671
Walker circulation, heat balance 78—16096
warm core cyclone over North Sea, conditional instability *(German)* 78—16118
waste heat release from nuclear power plant, convective cloud model appl. 79—34452
wave noninteraction with zonally av. flow and energy, heat and momentum fluxes 77—45075
waves, viscous diffusion, heat loss damping mechanism 80—56516
weak monsoon, atmospheric energy conversions 77—56711
weather forecasting, atmospheric prediction models, computing and numerical methods 80—77095
zonal mean circulation of middle atmosphere, numerical model 80—109218
zonally averaged climate model 78—81347
O_3 vertical profile correl. with thermodynamic parameters *(Russian)* 77—73804

atmospheric turbulence
200 mbar eddy flow in S Hemisphere, determ. from satellite data 77—33158
acoustic interference effects above finite impedance boundary 79—41493
adiabatic boundary layer height vars., simulation in wind tunnel 78—7691
advection, turbulent, scalar spectrum model 79—32474
aerosol jet, turbulent, normalised radial conc. profiles meas. using laser-Doppler anemometer 77—84311
air diffuse discharge, gasdynamic effects 78—81294
aircraft generated turbulence obs. by FM-CW radar 80—90186
aircraft response, math. modelling 78—81274
airflow, diffusion and momentum flux patterns in high mountain valley 79—5544
airflow above waves, numerical simulation *(Russian)* 80—4076
airflow over snowpack, two-dimens. turbulent diffusion model 77—78277
amplification of optical stellar images 80—72782
amplitude phase distortions correction of wave propag. in turbulent atm., efficiency 79—27178
amplitude scintillation meas. on mm. microwave links 78—85623
AMS symposium (Reno, Nevada, 15-18 January 1979) 79—66745
anisotropic homogeneous turbulence statistical description 79—79917
Arctic leads, atmos. boundary layer turbulence spectra obs. 80—56588
Arctic leads, turbulent heat flux 80—56513
astronomical image degradation, contrib. of lower atmospheric layers, use of photodiode array 79—21019
astronomical image form. under poor seeing conditions, speckle interferometry appl. 77—13248
astronomical image processing, atmospheric turbulence effects, interferometer data technique 80—12679
astronomical sites, turbulence meas. with balloon borne radiosondes 77—29645
attenuation and turbulence simulation in pulsed laser Doppler velocimeter system 78—73513
aurora rays and arcs, field-aligned elec. fields and currents 80—41593
auroral arcs, electrostatic turbulence and plasma transverse Kelvin-Helmholtz instability 77—53287
auroral arcs electrostatic turbulence, appl. of transverse Kelvin-Helmholtz instability 77—53287
auroral oval, dayside, low-amplitude turbulence rel. to ULF elec. field fluctuations obs. 80—98505
auroral particle precipitation, rel. to turbulence at 500 mb level 80—77218
balance eqns. in unstable boundary layer 77—73787
baroclinic boundary layer structure 78—81326
baroclinic instability, wave overreflection mechanism 80—90141
baroclinic instability and turbulence rel. to circulation in atmosphere of Jupiter 79—40132
baroclinic instability of short-wavelength two-layer Eady model 80—72593
billows, splitting into two layers 79—79991
boundary layer, acoustic backscatter, beamwidth effects 79—70859

atmospheric turbulence continued
boundary layer, acoustic sounding at Calgary 78—24376
boundary layer, auto-oscillation solns. of barotropic problem *(Russian)* 77—49106
boundary layer, birefringence under wind speed gradient shear 78—69453
boundary layer, book contrib. 77—60459
boundary layer, characts. 79—16628
boundary layer, clear air wind perturbs., dual Doppler radar obs. 79—53462
boundary layer, diffusion modelling, Gaussian plume and spectral solns. 78—24328
boundary layer, dissipation effects on parallel shear instability near ground 78—69406
boundary layer, dissipation modelling under forced convection conditions 78—92900
boundary layer, dynamic structure in urban areas, numerical simulation 79—66741
boundary layer, eddy convection vel. 78—92894
boundary layer, eddy flux meas. made by powered glider 80—51509
boundary layer, horizontal roll vortices, two dimens. numerical obs. 80—101409
boundary layer, hourly mixing depths estimation from historical meteorological data 80—51482
boundary layer, Lagrange characts. of turbulent diffusion 77—33131
boundary layer, lateral coherence of isotropic turbulence and wind 80—72575
boundary layer, lower, influence of built-up area on turbulence *(Russian)* 78—44925
boundary layer, mean and turbulent structures, 24 hour evolution, modelling 79—58024
boundary layer, model scale factor in wind tunnel simulations 78—28285
boundary layer, mol. resistance during diffusion, universal function determ. 80—26573
boundary layer, momentum, heat and moisture fluxes from struct. parameters 79—53435
boundary layer, multi-component linear digital simulation 78—61513
boundary layer, numerical modelling 79—84396
boundary layer, quantitative bistatic acoustic sounding 78—49176
boundary layer, review of current simulation techniques, recommendations for new technique 80—51469
boundary layer, Reynolds shear stress and heat flux fluctuations over rough surface 78—44902
boundary layer, similarity theory for turbulence and convection *(Polish)* 77—25753
boundary layer, stably stratified, turbulence and internal waves spectra *(Russian)* 78—81297
boundary layer, stratified, conc. profile, admixture-underlying surface interaction effect 80—31089
boundary layer, three vel. component modelling 78—28252
boundary layer, three-dimens. model rel. to expt. data 78—73428
boundary layer, turbulence characteristics *(French)* 79—66749
boundary layer, turbulence coeff. vertical profile 80—85733
boundary layer, turbulence rel. to refr. index structural charact. *(Russian)* 80—94597
boundary layer, turbulence structure in temp. inversions and convective fields, Doppler sodar obs. 79—66762
boundary layer, turbulent and radiative transport interaction in development of fog and low-level stratus 78—81313
boundary layer, turbulent diffusion of pollutants 77—41113
boundary layer, turbulent penetrative-convection planforms, laboratory obs. 79—48550
boundary layer, turbulent transport, buoyancy effect 78—32192
boundary layer, unstable, turbulence energy modulation by longit. rolls 77—2202
boundary layer, vertical currents induced by orography and turbulence 78—96278
boundary layer, vertical eddy flux representation 80—61844
boundary layer, vertical frictional motions on varying scales *(Russian)* 80—105027
boundary layer, wind speed and turbulence characts. near ground over escarpments 78—44897
boundary layer, with Rossby number similarity, turbulent diffusion 78—92896
boundary layer above ocean waves, scaling laws for optically relevant turbulent parameter C_T^2 78—85677
boundary layer and wind coherence meas. 77—91201
boundary layer at nighttime, case study comparison with model calcs. 80—85707
boundary layer at nighttime, vertical struct. obs. 80—61848
boundary layer development above sea during generation of surface waves *(Russian)* 79—16476
boundary layer during convective disturbance, thermodynamics 80—81978
boundary layer eddy correl. using sonic anemometer 80—56637
boundary layer evolution at nighttime 80—51462
boundary layer flow over water during stable conditions, Eulerian and Lagrangian time scales 79—25300
boundary layer over sea, turbulence struct. obs. 80—56575
boundary layer parameterization technique 79—29830
boundary layer turbulence, boundary layer, appl. of mixed-layer similarity scaling to observed dispersion from ground-level source 80—105021
boundary layer turbulence, dynamic modelling *(Russian)* 77—13097
boundary layer turbulence, finite-element numerical modelling 80—77061
boundary layer turbulence, inertial range bispectrum 79—92571
boundary layer turbulence and air-sea interactions 78—92953
boundary layer turbulence and vertical currents, feedbacks *(Russian)* 80—51457
boundary layer turbulence as function of height and stability 79—58074
boundary layer turbulent flows 79—39838
boundary layer turbulent fluxes modelling in stable conditions 78—61482
boundary layer turbulent transport 77—17131
boundary layer tuurbulence, meas. of microstruct. with hot and cold wires 80—24109
boundary layers, numerical modelling 78—44900
Bowen's ratio determ. in equatorial Atlantic region 78—81330
bulk transfer velocity to and from natural and artificial surfaces 79—25302
buoyancy effects in entraining turbulent boundary layers: a second-order closure study 80—21815

atmospheric turbulence continued

- buoyant plume in stably stratified boundary layer, max. ground conc. 80—72573
- buoyant plumes behaviour on release at ground level, lab. wind tunnel obs. 80—30624
- canopy flow, higher order closure model 78—44944
- characteristics near neutral stability 77—29369
- chemical reactions, second-order, in turbulent fluid, model, appl. to atm. plumes 79—20350
- chemical reactions, second-order, in turbulent fluid, model, formulation and validation 79—20349
- clear air turbulence and in cumulus clouds, vertical gust vels. and normal gravity vars. 79—48543
- clear air turbulence detect. by IR obs. of water vapour 77—73890
- clear air turbulence effect on general circulation model of atmosphere 77—86968
- clear air turbulence over S.Asia 78—7692
- clear atmosphere, radiative transport and thermal turbulence *(French)* 80—82018
- clear-air turbulence, 1976 turbulence Survey 79—100922
- clear-air turbulence probability and temp. gradients 77—49128
- clear-air-turbulence detection, IR radiometer passbands 78—96318
- closure conditions in Lilley-type inversion models 79—5589
- cloud, eddy viscosity parameterisation in two-dimens. model 80—85708
- cloud development in turbulent atm., drop spectrum evolution 78—81325
- cloud drop collision in turbulent environment 80—56555
- cloud droplet size evolution and small-scale turbulence 80—56554
- cloud droplets collisional problem 77—5293
- cloud model, trade wind cumuli, turbulence parameterization 78—44931
- cloud vortices, pressure from satellite obs. 80—26592
- clouds, Canadian cumulus, turbulent characts. 77—64383
- clouds, droplet condensation growth, hygroscopicity and surface tension effects *(Russian)* 77—33142
- clouds, hygroscopicity and surface tension effects on droplet condensation growth *(Russian)* 77—33142
- clouds, relation between Pasquill stability and Kazanski-Monin stability 80—17304
- clouds, turbulence rel. to drops stochastic coagulation kinetic eqn. 78—92944
- clouds, water droplet coalescence 77—45114
- coastal internal boundary layer characts. during onshore flows 80—41479
- collimated laser beam propag., corner-cube reflector and plane mirror comparison in folded-path and direct transmission 78—85697
- convection, energy considerations, two dimensional model rel. to turbulence formation *(French)* 79—84409
- convection in nondiffusional approx. *(Russian)* 77—73803
- convective boundary layer, turbulence struct. of upper region 80—56576
- convective boundary layer over sea, turbulence meas. by instrumented aircraft 79—12214
- convective mixed-layer entrainment, for realistic capping inversion layer 80—12487
- convective plume in unstably stratified atmosphere, theory *(Russian)* 77—49108
- convective turbulence characteristics, investigation *(Russian)* 79—16577
- cooling tower plumes, interaction with atm., numerical model simulation *(French)* 80—94126
- Coriolis force, linear spectral study *(French)* 79—84408
- correlation of the phase and amplitude fluctuations between direct and ground-reflected sound 80—96067
- correlation scale measurement, spatial freq. modulation of stellar images 78—40661
- cumulus, droplet distrib. broadened by turbulence 80—56582
- cumulus cloud in tropical boundary layer *(French)* 79—84412
- cumulus clouds, peculiarities of turbulent air entrainment *(Russian)* 78—24334
- cumulus convection, vorticity horizontal transport parameterisation 80—90158
- current convective instability in auroral F-region 80—72680
- D-region, auroral, strong turbulence layer rel. to partial refls. during absorpt. event 78—36388
- D-region, turbulent motions meas. via payload B I rocket-borne expt. package 78—45190
- decaying vortex core, boundary layer dynamics 79—55394
- degradation of electrooptical system performance 79—34940
- detection by IR obs. of water vapour 77—73890
- Diablo Canyon, range statistics as estimators 77—17169
- diffraction image intensity in turbulent atm., Huygens-Kirchhoff principle calcs. 80—63926
- diffusion, gradient transfer theorem generalisation, plume dispersion spectral diffusivity model 80—12037
- diffusion, gradient transfer theorem generalisation 80—12036
- diffusion, Lagrangian scheme, algorithm and applications *(French)* 79—84401
- diffusion, simple exponential function as Lagrangian vel. correl. function simple exponential function as Lagrangian vel. correl. function 79—58001
- diffusion, Sutton's formula criticised *(French)* 79—44223
- diffusion above and within forest, SO_2 pollution appl. 77—45055
- diffusion experiments in unstable conditions over inhomogeneous terrain 79—58059
- diffusion from ground-level source in turbulent boundary layer, Lagrangian statistical anal. 80—12517
- diffusion in cloudless summer atmosphere, radar study 77—91228
- diffusion in surface layer 77—66950
- diffusion parameters estimation, use of routine meteorological data 78—85649
- dispersion concentration valves, system for wind tunnel meas. 79—5191
- dispersion in turbulent shear flow, theory 79—88393
- distorted wavefront compensation, optimal estimates 77—42487
- Doppler light detection and ranging systems for turbulence meas. 78—73554
- downslope severe windstorm and aircraft turbulence event induced by mountain wave 78—73431
- dynamics, Fourier transform ambiguity 77—5300
- eddies, transfer rate in air flow above sea surface *(Russian)* 79—16578
- eddies, transient, in 0 to 30 km height range, O_3 flux obs. 80—109224
- eddy and turbulent diffusion at 0-65 km altitude, model simulation 79—84438
- eddy diffusion, explicit scale-depend. coeffs. 78—67191
- eddy diffusion, models for mesosphere and lower thermosphere 80—109198

atmospheric turbulence continued

- eddy flux measurements over ocean, related transfer coeffs. 78—81265
- eddy fluxes, large-scale, parametric study 79—53436
- eddy fluxes, zonal and meridional var., long planetary wave induced 80—85720
- eddy fluxes of conserved quantities by small-amplitude waves 80—61858
- eddy momentum flux in asymmetric jets, instability theory 80—56537
- eddy properties, large-scale, parametric study, zonal scale 79—53437
- eddy viscosity in two and three dimensions 77—5289
- eddy-viscosity model constructed by homogenization *(French)* 79—84407
- eddy-viscosity turbulence in anelastic flow 79—88414
- effect on three-axis thermal anemometers, eddy correlation flux meas. 80—17401
- effect on vertical optical path, phase coherence function meas. 77—45155
- effects in cyclotron resonance of monochromatic whistlers 79—16759
- effects on central irradiance in Fraunhofer diffr. by slit apertures with apodisation filters 78—25796
- effects on IR and near-millimetric-wave propagation 80—61902
- effects on radar return from radar-acoustic sounding system 79—39821
- electro-optical system image evaluation, subjective effects of electronic and turbulent noise 78—65023
- electro-optical system performance atm. degradation 79—66805
- electrode effect in strong turbulent mixing limit, analysis 78—40622
- electrojet, equatorial, type II irregularities, nonlinear theory 80—61958
- electrojet induced press. and vel. fluctuations 80—82118
- electrostatic ion cyclotron turbulence, rel. to coherent anomalous resist. assoc. with electrostatic shocks 80—4189
- electrostatic turbulence, spectral energies 78—77433
- EM pulse propagation in turbulent atmosphere, forward-scatt. theory 79—66775
- EM pulsed beam wave propag. 78—12000
- EM waves scattering by turbulent flows in wake of artificial satellites 79—8730
- energy and enstrophy nonlinear cascades in two-dimens. spectral index 79—16619
- energy budget parameterisation at top of daytime boundary layer 77—56674
- energy budgets of turbulent vel. components and vel.-press. gradient interactions 79—58026
- energy dissipation, statistical props. 78—81267
- energy dissipation rate in unstably stratified boundary layer *(Russian)* 77—64372
- energy-balanced discrete models of atmospheric process dynamics 79—39828
- enstrophy transfer in two-dimens. turbulence, subgrid scale modelling 79—16586
- entrainment 77—78344
- entrainment as a cause 77—78344
- equatorial electrojet, radar obs. of two dimens. turbulence, nighttime type 1 waves 79—35038
- equilibrium temperature gradient in atmosphere at incomplete automodelity 80—41480
- exchange coefficients for sensible heat and H_2O vapour under advection conditions 78—92907
- F-region, collisional Rayleigh-Taylor instability in equatorial spread F 80—82138
- F-region, equatorial turbulence spectrum rel. to HF and VHF spread-F echoes 78—85764
- fair weather electric charge transfer by convection in unstable mixed layer 79—58037
- finite optical beam in extremely strong turbulence, variance, covariance of irradiance 78—63008
- flow in simulated plant canopy 77—60443
- flow over isolated hill of moderate slope 80—12515
- flow over very rough random surface 79—53422
- flow over wavy boundary, water waves 77—73792
- flows, nonlinear perturbation development and predictability problem *(Russian)* 77—62238
- flux of CO_2 or water, correction for density effects 80—85721
- forced plume characteristics 78—18286
- forced turbulent plumes, rise times 79—100932
- free convection, characts., lab. visualisation expt. 79—18888
- frequency response of cold-wire thermometers used for atmospheric turbulence meas. in marine environment 80—56650
- frozen turbulence, thermal structs. spectra deduced from ground-based radiometry 79—92567
- GATE sub-cloud layer, eddy fluxes and spectra 80—105035
- general circulation model, clear air turbulence effect 77—86968
- general circulation of 2-dimens. turbulent flow on β-plane 77—78317
- general circulation of N.hemisphere in winter, horiz. transport by transient eddies 80—72589
- geometric objects with fractional dimension, book contrib. 77—87640
- geostrophic balance of horizontally periodic motions 79—39824
- geostrophic turbulence, book contrib., review 80—19336
- global weather model, thermodynamic, with turbulent transport *(Spanish)* 80—36372
- ground surface roughness change, affecting air flow characts. 80—51501
- heat and moisture fluxes, field study, S.England 78—20477
- heat transfer from spheres in naturally turbulent outdoor environment 77—42701
- heat transport parameterization in midlatits., large-scale transient eddies 79—16617
- heat turbulence effect on sunspot fine struct. image form. 80—77108
- heated air mass in stratified atm., vortex ring form. 79—84365
- heterodyne optical radar S/N ratio in atmospheric turbulence 80—106558
- heterodyne receivers for atmospheric optical communications 80—58663
- hill affecting airflow, in boundary layer, overspeed effect 80—72577
- hill affecting turbulent diffusion from point source in stratified flow 80—56505
- hill crest, obs. of wind speed, shear and turbulence 80—85722
- horizontal coherence decay near large mesoscale variations in topography 79—58025
- horizontal eddy diffusivity in cumuli, measurement by radar method *(Russian)* 79—88404
- hot-wire linearised anemometer with bridge circuit, characts. 77—55118
- Hurricane Gladys (1975), subcloud layer energy transformations 80—77089
- hydrodynamic turbulent processes, MHD effects in electrolytes as model *(Russian)* 78—40610

atmospheric turbulence continued
image degradation due to daytime turbulence, arrival angle meas. 80—41551
image formation, optical and IR, turbulence effects, astron. appl. *(French)* 80—46257
image reconstruction, turbulence-degraded, using nonredundant aperture arrays 78—93122
image resolution through atmospheric turbulence 79—36855
image resolution through turbulence over ocean, optical transfer function 78—85695
image restoration, astrophys. appls., conf., Bordeaux, France (Mar. 1979) 80—41935
imaging and optical communication through atmospheric turbulence, book contrib. 79—34960
imaging in the presence of random wave aberrations 79—76607
imaging through turbulent atm., spatial freq. resolution of rot. shearing interferometer 78—69450
IMF sector boundary crossing affecting 500 mb level atmos. of southern hemisphere 80—109199
induced laser beam spread, isoline approach 77—72016
inertial model, expt. verification from solar limb motion 79—5614
inhomogeneous turbid atmosphere and IR fluxes in stratiform model clouds 79—84361
instability of boundary layer with Rossby number similarity, inflection point and convective instability 79—66757
intensity at Diablo Canyon, range statistics as estimators 77—17169
interference fringe visibility and spacing, atmospheric turbulence effects 80—51572
interference pattern fluctuation statistics in turbulent atmospheric layer 78—53727
ionization inhomogeneities advected neutral gas motions, geomag. field effects 80—26677
ionosphere, auroral, turbulence rel. to irregularities obs. via rocket probe, scintillation and incoherent scatter radar 80—94640
ionosphere, auroral inhomogeneities revealed by VLF propag. 80—105107
ionosphere, bubbles in equatorial spread F, nonlinear evolution 80—85801
ionosphere, high latit. electric field turbulence, polarization determ. from satellite data 80—26679
ionosphere, partially ionised plasma, strong turbulence 80—79499
ionosphere, topside, turbulent transport and heating of auroral plasma 79—35054
ionosphere auroral zone, ion heating by electrostatic ion cyclotron waves 80—72686
ionosphere high-latitude electrostatic turbulence, polarisation, freq. and wavelengths 78—88981
ionosphere inhomogeneity formation, influence of elec. field temporal variation 80—105105
ionosphere turbulent polar cusp, temps. and low-energy particles and Kelvin-Helmholtz instability 78—96343
IR airborne astronomy, fluctuating sky emission meas. and interpretation 78—81552
IR heterodyne detect. of stars, atm. turbulence effects, corrections *(French)* 80—46409
IR image nonlinear conversion allowing for turbulent atm. influence 80—23751
IR noise caused by turbulent flows, IR detector obs. 79—31799
irradiance fluctuations of beam waves, probability distrib. 77—13125
irradiance probability distrib. in saturation regime 79—76588
isoplanatic degradation of tilt correction and short-term imaging systems 80—53219
isoplanatic patch measurement using phase-correcting telescope, turbulent air height determ. 79—53732
isoplanatism and turbulence of the upper atmosphere 79—96810
Kelvin-Helmholtz instability, jet stream generated, radar obs. and model 80—90165
kinetic energy budget in convective conditions 79—79975
kinetic energy maintenance in tropical disturbances over E.Atlantic, GATE data 78—77307
Kolmogoroff's theory of turbulence and intermittency, laser beam propag. expt. 79—7368
Lagrangian conveection model, representation of isolated thermals *(French)* 79—88449
Lagrangian scheme of turbulent diffusion *(French)* 79—53487
Lake Ontario atmosphere turbulence, vel. and scalar statistics 77—33128
laser absorption spectrometer, long path length, effect of scintillation and multiwavelength coherence 78—40653
laser beam, atmospherically degraded, log-normally distributed intensity fluctuations 79—50228
laser beam, phase compensated, propag. through atm. turbulence 78—83012
laser beam amplitude fluctuation statistics in turbulent atmosphere 80—106458
laser beam arrival angle fluctuations meas. apparatus using telescope 80—109258
laser beam intensity fluctuations, averaging effect saturation with distance, expt. *(Russian)* 78—46512
laser beam intensity fluctuations in medium with Kolmogorov turbulence, distrib. function *(Russian)* 78—71034
laser beam intensity fluctuations in turbulent atm. over water surface *(Russian)* 78—69449
laser beam intensity profile distortions in turbulent media, theory 78—22162
laser beam propag., long- and short-term Strehl ratios 79—62577
laser beam propag., monochromatic, problems 78—92988
laser beam propag., random displacement invest. using Karman spectrum *(Russian)* 78—20511
laser beam propag. Huygens-Kirchhoff method 78—32228
laser beam propagation, detection effects on statistics of intensity fluctuations 79—16672
laser beam propagation, thermal self-action *(Russian)* 78—28311
laser beam propagation in atmosphere, book 79—34955
laser beam propagation in turbulent atm., spectral expansion soln. method 79—18350
laser beam propagation through turbulent atmosphere, interferometric evaluation of imaging characts. 77—88643
laser beam scintillation, in turbulent atmosphere 79—80018
laser beam short-term average irradiance profile 77—7098
laser beam turbulence compensating tracking system, lead angle effects 78—33763

atmospheric turbulence continued
laser beam wandering in turbulent atm., error probability in binary signal reception 79—10337
laser beam wandering in turbulent atm., fluctuation power probability density distrib. 79—10336
laser Doppler anemometer measurement, effect of finite-size probe vol. 77—24036
laser irradiation intensity fluctuations, influence of transmitting aperture diffr. size and turbulence 79—45906
laser light propag. through turbulence, K distribs. 79—80023
laser propagation, high-energy, simplified aberrated lens model 78—69454
laser propagation in turbulent atm., detector nonlinearity effects on statistics of fluctuating signal 78—55301
laser radiation field, four-point coherence function meas. in turbulent atm. 80—23623
laser radiation strong intensity fluctuations, similarity relations and expt. verification, book contrib. 79—34958
lateral diffusion parameters vars. 79—20931
light beam coherence through optically dense turbid layer 78—55300
light beam gravity centre displacements, time correlation, in the lowest layers *(Russian)* 78—20510
light beam gravity centres displacement spectra *(Russian)* 79—3631
light beam propagation, spectra of random shifts analysis 79—74942
light fields optimum processing, synthesis of algorithms 78—71047
light intensity in turbulent medium, two-freq. fluctuations correl. 79—98280
light intensity strong fluctuations, spatial correlation functions, numerical calculation 80—18995
light propagation, space struct. of strong intensity fluctuations 79—98278
light propagation, turbulence and aerosol models 79—100947
light reflection, Huygens-Kirchhoff method, phase approx. 80—28160
light spherical wave propagation, effect of turbulence 80—82066
light wave fluctuations in turbulent atmosphere 80—48157
linear propagation of radiation, coherence length evaluation 80—48150
longitudinal spectral coherence, displacement and freq. dependence 80—17314
longitudinal turbulence and mean wind speed, comparison at coastal site and offshore location 80—98406
low level turbulence, severe, occurrence near Cross Fell, England 79—79962
lower atm., simultaneous meas. using sodar and aircraft 79—20923
lower atmosphere turbulence modelling, implications of temp. skewness budget 80—21816
lower thermosphere, compositional modelling taking account of airglow tidal variation 80—109288
macroturbulence rel. to zonal circulation model, numerical expts. *(Russian)* 78—81295
magnetopause, plasma wave turbulence obs. 80—51610
magnetosheath, electrostatic turbulence meas. 79—66881
magnetosheath, MHD turbulence rel. to form. time of isotropic particle vel. distrib. 78—28420
magnetosheath, turbulence rel. to solar wind ion injections in morning auroral oval 80—98502
magnetosphere, electrostatic ion cyclotron turbulence rel. to mag. field-aligned pot. drops 78—45155
magnetosphere, evidence for plasma two-dimensional inertial turbulence 78—36399
magnetosphere, turbulence generation by proton-cyclotron instabilities in non-uniform loss-cone plasma 80—90286
magnetosphere, turbulence rel. to electrostatic shocks, double layers and anomalous resistivity 78—45152
magnetosphere, turbulent generation of electrostatic fields 78—28439
magnetosphere and ionosphere, elec. field power spectra, double probe meas., Doppler shift effects 80—26634
magnetosphere high-latitude electrostatic turbulence, polarisation, freq. and wavelengths 78—88981
magnetosphere longitudinal currents, dynamic processes in turbulence development 80—67469
magnetosphere plasma sheet, variability of turbulent dynamics 80—98518
magnetotail, distant, lower-hybrid-drift wave turbulence 79—25399
maize canopy, turbulent transport 77—33129
marine boundary layer, optical refractive index fluctuations, statistical props. 79—62580
marine boundary layer, turbulence effects on laser propag. 77—45156
marine stratocumulus convection, turbulent fluxes in horizontally inhomogeneous solns. 80—56543
marine surface layer turbulence structure, humidity and temp. spectra study, N.Pacific 80—21798
marine turbulent boundary layers, disturbance by wind waves, dynamical eqns. *(Russian)* 78—44840
mass diffusion from point source in turbulent shear layer 78—92968
mass transfer in boundary layer, plume dispersion *(French)* 80—61850
mean flow dynamic forcing by Reynolds' stresses 79—53448
mean vertical profile, rel. to astronomical seeing 77—29379
measurement, computerised instrumentation system 77—56761
measurement, continuous, using VHF Doppler radar, preliminary results 80—8444
measurement by echosonde, phase front distribs. rel. to antenna radiation 77—39123
measurement by remote sensors, optical propag. parameters 77—45125
measurement in marine environment, freq. response of hot wires 77—33214
measurement in marine environment freq. response of hot wires 77—33214
measurement via low-speed anemometer with const. temp. thermistor *(French)* 77—21922
measurement with propeller vane devices, dynamic props. 80—31138
meridional fluxes of pot. vorticity *(Russian)* 77—81960
mesometeorological stationary problem of flow around obstacle 78—81271
mesoscale, $k^{-5/3}$ law inertial range to two-dimens. turbulence 80—72594
mesoscale turbulence in upper troposphere, experimental studies *(Russian)* 78—16090
mesosphere, characts. from D-region partial refl. method 78—49215
mesosphere, equatorial, gravity waves rel. to radar obs. of turbulence over Jicamarca 78—36230
mesosphere, turbulent diffusion coeff. seasonal vars. 79—53424
mesosphere turbulence structures, high-resolution VHF radar obs. 79—100895
mesosphere turbulent structure, spectral range *(Chinese)* 80—105092

atmospheric turbulence continued
- mesosphere vertical velocities, first VHF radar meas. at temperate latits. 79−16572
- middle atmosphere, minor constituents, chemistry and transport, conf., Seattle, USA (Aug. 1977) 79−84428
- middle atmosphere, VHF radar obs. 80−105032
- middle atmosphere (mesosphere), eddy energy dissipation rel. to energetics and thermal struct. 80−98412
- middle atmosphere dynamics, review 80−17338
- mixing, rel. to use of passive antenna system as cond. meas. device 80−85762
- mixing depth and stability regional patterns, sodar network meas. 79−100965
- modal wavefront compensative system performance, finite bandwidth effect 79−81361
- models, medium and small scale *(French)* 79−84406
- models of atmospheric random vortices 78−28265
- modulated wave propag. in turbulent atm., correlation functions and freq. spectrum 79−34954
- moist boundary layer, finite element model, eqns. 79−5585
- moist boundary layer, finite element model, soln. method 79−5586
- momentum and heat flux profile relations above tall vegetation 78−49115
- momentum transfer during abrupt laminar-turbulent transition in boundary layer 78−65365
- mountain and desert atmospheric MTF comparison 80−82063
- mountainous terrain, atmosphere turbulent kinetic energy budgets 80−105022
- multiple pulse detection in atmospheric turbulence 78−92974
- narrow field optical astrometry, atmospheric turbulence limitations 80−109340
- neutral wind profile following surface roughness change, calc. 78−73483
- nocturnal increases in surface temp. at Bombay Airport 78−32156
- non-neutral surface boundary layer, parameterisation 80−17316
- nonlinear small-scale sea-air interaction parameterisation, effects of ice cover *(Russian)* 77−53068
- optical and IR propag., power spectra of turbulence-induced wave-front errors 79−66800
- optical beam propagation for partially coherent source in turbulent atmosphere 80−9806
- optical carrier intensity fluctuations, measured at receiver *(German)* 79−89861
- optical coherence, atm. effects 80−82064
- optical communication line operating under photon counting conditions, adaptation to turbulence 80−9930
- optical DPSK system performance 78−42293
- optical effects, rel. to use of multiple-mirror telescope systems in astronomy 80−94713
- optical goniometer accuracy effect of atm. turbulence 78−55461
- optical heterodyne array, joint signal probability distrib., clear air turbulent atm. 79−66804
- optical heterodyne receiver array for light propag. through turbulent atm. 79−64183
- optical heterodyne receiver arrays, partial tracking, operating in turbulent atm. 79−41345
- optical heterodyne receiver arrays in turbulent atm., joint signal current probability distrib. 79−81368
- optical heterodyne receivers in turbulent atm., signal current probability distrib., theory 78−78916
- optical heterodyne receivers in turbulent atm., signal current probability distrib., expt. 78−78917
- optical imaging, turbulence effects 79−66806
- optical imaging systems performance, turbulence effect 79−66799
- optical intensity fluctuations, frozen turbulence hypothesis expt. *(Russian)* 78−61557
- optical modulation phase fluctuation dispersion in turbulent atmosphere *(Russian)* 79−98277
- optical path fluctuations, calibration of distributed temp. sensor 77−2688
- optical phase and scintillation, observation and prediction comparisons 79−53524
- optical propag. through turbulent atmosphere, He-Ne laser transmitter/receiver 80−98450
- optical propagation, expt. turbulence profile and parameters 79−66801
- optical propagation, laboratory-generated turbulence simulating atmosphere 80−9803
- optical propagation through strong turbulence 79−66802
- optical propagation through turbulent air 79−76593
- optical remote sensing, comparison with simultaneous thermal meas. 79−34965
- optical scintillometer, large-aperture, fine calibration, optical estimate of turbulence inner scale 79−21026
- optical signal discrete reception in turbulent atm. 78−73511
- optical systems affected by temperature turbulence meas. and theory, AMOS site in Hawaii 79−53503
- optical transmission expt. using atm. turbulence chamber, characterisation by thermal method 79−25330
- optical wave propagation in turbulent medium, modern theories, book contrib. 79−34957
- OTF degradation meas. by TV system 79−92590
- overwater dissipation and drag coefficients for marine regime, shipboard evaluations 79−5494
- ozonosphere, eddy transport rel. to maintenance of zonal mean O_3 distrib. in N.Hemisphere 80−109220
- parameterisation on non-neutral surface boundary layer, theory 80−17315
- partially coherent beam intensity fluctuation calc. 80−78775
- partially coherent curved beam waves in turbulent atm., beam props. 80−95798
- partially coherent light propagating through atm. turbulence, intensity fluctuations 79−58087
- partially coherent radiation propag., extended Rayleigh-Sommerfeld integral method results 78−65386
- particle cloud, dispersion in boundary layer, theory 80−61842
- Pasquill stability classification for coastal site 79−16610
- penetrative convection, AMTEX obs. 79−58028
- penetrative convection at top of growing boundary layer 80−12521
- phase adaptation by nonlinear techniques, optical propag. distortion compensation, book contrib. 79−31973
- phase distortion, modal compensation 78−69451
- phase expansion coefficients spatial correlation, propag. through atm. turbulence 79−80021

atmospheric turbulence continued
- photoelectron counting distributions of laser light signal through turbulent atm. *(Japanese)* 77−50711
- pine forest affecting boundary layer, turbulence and heat transfer 80−26569
- plane wave scattering in inhomogeneous turbulence 79−39857
- planetary boundary layer, Doppler radar obs. in clear air conditions 80−90184
- planetary boundary layer, nocturnal evolution *(French)* 79−84397
- planetary boundary layer, tapped with cumulus, numerical model *(French)* 80−94574
- planetary boundary layer processes, incorporation into numerical forecasting models 80−17312
- planetary boundary layer similarity profile by turbulence closure model 80−72574
- plume monitoring, airborne sampling system 79−21027
- plumes in laminar cross flow, entrainment 77−24006
- pollutant dispersion in horizontally-homogeneous boundary layer 78−36263
- pollutant turbulent diffusion 77−91228
- pollutant turbulent diffusion model, K-theory 80−89697
- pollutants concentration equation, wind speed averaging 78−57307
- pollutants dispersion, completely Lagrangian random-walk model 78−81380
- pollutants dispersion from area sources in convective turbulence, model 78−28303
- pollutants dispersion in flow over shoreline of large water body, model 79−100913
- pollutants dispersion over highways, wind and temp. study 80−12038
- pollutants turbulent diffusion in Ekman boundary layer 77−73783
- pollutants turbulent transport, Monte Carlo simulation and comparison with exptl. data 79−53479
- pollutants vertical dispersion in neutral surface layer, Markov Chain simulations 79−88399
- pollution distrib., aerodynamic aspects, test results and numerical solution *(German)* 79−8686
- pollution fumigation, lab. simulation 77−78390
- pollution release into turbulent atm., exposure freq. distrib. from multiple cloud sources 78−57255
- pollution transport, Monte Carlo simulation, radioactive particles appl. 78−61550
- power detected by receiver, narrowly collimated beam backscattered by reflector in turbulent atm. 80−32918
- probe support, upwind turbulance study 80−12506
- puff combustion *(Japanese)* 80−12470
- puff pollutant dispersion model with wind shear and dynamic plume rise 79−57996
- radar detection of turbulence parameters, from clear-air echo intensity 80−90190
- radar propag. through turbulence, scintillation detection using monopulse techniques 78−85717
- radar signal scatt. from turbulent air, VHF and UHF 80−85728
- radiation detection in turbulent atmosphere, photodetector current fluctuation statistics *(Russian)* 79−92591
- radiative and actual nocturnal cooling rates over grass and snow 79−79947
- radiative flux divergence effect on entrainment of saturated convective boundary layer 79−79979
- radio interferometric meas., atm. turbulence effects *(French)* 80−46402
- radiowave bandwidth limitations in turbulent atmosphere using coherency and differential amplitude spectra *(French)* 78−49070
- radiowave propag. through turbulent atmosphere, phase difference and derivative fluctuations 78−92951
- radiowave propagation, ionospheric turbulent layer, phase and frequency spectra, after nuclear explosion 78−24405
- rain, difference between atmospheric and laboratory fallspeeds due to turbulence *(French)* 79−88448
- random field fluctuations of near-water atm. layer and upper ocean layer, linear filtration errors 80−12425
- random image displacements at telescope focus in turbulent atm. *(Russian)* 78−20509
- rapid morning boundary-layer transition, case study from Haswell, Colorado, expt. 80−81996
- recirculating flow over rectangular depression, meas. and predictions 79−66751
- reflected laser radiation intensity fluctuations 77−50621
- reflection in turbulent atm., fluctuations of wave beam field 79−66793
- reflection optical radiation echo signal temporal broadening by atmospheric turbulence, anal. 79−8693
- refractive index profiles, upper and lower atm. contribs. 77−87070
- refractive index structure const., height depend. 80−36397
- refractive index variance and its height distrib. in different air masses 77−41133
- refractive scattering, weak, model system 79−89849
- refractive turbulence effect on Radar-Acoustic Sounding Systems, range limitations 77−41195
- refractive turbulence profiles, meas. by spatial filtering of scintillation 77−5331
- remote sensing, laser beam wave case, book contrib. 79−34959
- Reynolds stresses for nonisotropic turbulence *(Russian)* 77−58648
- Rock of Gibraltar, wind-tunnel simulation at 1:5000 scale, compared to meteorological meas. 78−28284
- rotating atmospheres, nonlinear interaction of motion and rot. adaptation process 80−17355
- rotating fluid, vortices formation near reson. for elastoid-inertia waves 80−12473
- scale from light fluctuation meas. *(Russian)* 77−17162
- scattering of partially coherent radiation by surface, atm. turbulence influence 78−58915
- scintillation, conditional fading statistics 78−66757
- scintillation, optical and IR waves, simulation 77−82005
- scintillation statistics for satellite laser ranging 77−88900
- seeing for astronomical telescope, wavelength depend., atm. inhomogeneity effects 78−92979
- sensible heat advection conditions 80−41516
- sensor using atm. dispersion 77−45204
- sensor using atm. optical dispersion 77−45204
- shear flow instability, Kelvin-Helmholtz and reson. overreflection modes, vortex pairing interactions 80−90129
- shearing layers, dominant eddy scale, growth, limiting thickness 77−87022

atmospheric turbulence continued
shearing layers, growth, limiting thickness, dominant eddy scale 78—92955
shoreline escarpment affecting boundary layer turbulence, wind profile etc. 80—109243
short-exposure imaging through turbulence, wavefront distortion 79—41336
signal-to noise ratio in presence of atmospheric turbulence 79—100949
simulation in Oxford University wind tunnel 78—22443
simultaneous measurements of turbulence over land and water 79—53421
small-scale struct., airborne hot-film meas. during GATE 77—29373
smoke plumes in surface layer, cross section diffusion *(Russian)* 80—104532
snowfall, turbulence rel. to laser beam intensity fluctuations *(Russian)* 80—94602
solar apparent diam. fluctuations 77—74021
solar apparent diam. fluctuations 77—74026
solar mag. sector rel. to tornadoes and similar phenomena, 1955-77 period 80—77094
solar telescope, nearby turbulence deduced from arrival angle statistics compared with microthermal meas. 80—26740
Somali jet, planetary boundary layer model 80—72591
sound attenuation 77—7238
sound attenuation by turbulence 77—7238
space-limited laser beam meas. of turbulence-struct. parameter 80—46285
space-limited optical propag. in turbulent atm., phase approx. of Huygens-Kirchhoff method 79—92595
spatial filtering function for collimated laser beam amplitude fluctuations in turbulent atm. 80—9810
speckle interferometry, atmosphere turbulence effect ang. depend 79—101080
speckle interferometry of stars, S/N ratio 78—12102
speckle propagation statistics through turbulent atm., log-amplitude covariance function effect 80—82058
speckle propagation through turbulence 78—66758
speckle propagation through turbulent atmosphere research progress 79—66803
spectra above vegetated surface, sensible heat advection conditions 80—17343
spectra in stable conditions 77—73786
spectral evolution of strongly interacting waves 79—77144
spectral inequalities in two-dimens. turbulence *(Russian)* 78—69403
spectral theory of stratified turbulent shear flow, interactions between motion fields 80—90114
spectral transfer of turbulent energy and temp. variance 78—61489
spectrum with temp. gradient 77—2198
spread F bubble drift velocity, radar obs. 80—51598
spread-F plasma bubbles in equatorial topside region 80—72694
St. Louis downwind plume, thermodynamic props. and aerosol patterns 79—16603
stability class determ. on 481 m tower in Oklahoma 79—58000
stability classification schemes applied to non-homogeneous terrain coastal region 80—8379
stably stratified atmosphere, turbulence rel. to mixed layer growth 79—55358
stably stratified shear flow, turbulence theory in buoyancy subrange 79—5568
statistical characts. from optical meas. *(Russian)* 77—29439
stellar speckle interferometry, atmospheric effects, laboratory simulation 79—53730
stellar speckle pattern statistics, photon counting techniques 79—25324
storm-time characteristics near top of spruce forest 80—17349
stratified, turbulent diffusion from stationary linear source 77—56668
stratified atmosphere, disturbances generated by horizontally-moving sources *(Russian)* 80—21795
stratified baroclinic boundary layer, method for determ. coeffs of horizontal turbulent diffusion 78—32135
stratified boundary layer, vel. profile *(Russian)* 79—10601
stratified shear flow, weakly nonlinear stability theory 78—18331
stratified surface layer, turbulence and diffusion, basic Lagrange characts. 78—81270
stratified turbid medium, small-angle approx. soln. of radiative transfer eqn. *(Russian)* 80—82057
stratocumulus-capped planetary boundary layer, entrainment rate *(French)* 79—53489
stratosphere, energy dissipation within intermittent clear air turbulence patches 77—56676
stratosphere, turbulence and mean flow study by tracer balloons 79—8661
stratosphere, turbulence from IR astronomy data 80—12475
stratosphere, turbulent layer struct., 2380 MHz radar obs. 80—90191
stratosphere and lower mesosphere, horizontal eddy diffusivity in northern hemisphere 79—84439
stratosphere and mesosphere, UHF radar echoes, for wind and turbulence obs. 77—33135
stratosphere turbulence near tropopause, review of radar obs. 80—90179
stratosphere turbulence struct., using 430 MHz Arecibo radar 80—90258
stratosphere turbulent transport estimates, implications of wave spectra resembling turbulence 79—79981
streamwise turbulence vertical coherence inside and above model plant canopy 79—25297
structural characts., meas. using spatially limited laser beam 80—98413
structure function along laser propag. path, angular spectrum meas. 77—53133
structure over water in high wind 80—12502
Sun- weather effects, coincident turbulent processes 79—44219
surface and planetary layers at unstable stratification, vertical profiles *(Russian)* 79—34900
surface boundary layer as part of overlying convective layer 79—92576
surface layer, air density correction to eddy flux meas. 79—66761
surface layer, airflow over nonhomogeneous surfaces with discontinuities in roughness and temp., two dimens. model *(Italian)* 79—84454
surface layer, calc. of mean velocity and temp. profiles *(Russian)* 80—8415
surface layer, discrete turbulent gust concept 78—44907
surface layer, drag coeff. rel. to intermittent convection 78—44898
surface layer, effects on light beam, optical parameter determ. model *(Russian)* 80—12481
surface layer, horizontal turbulent heat flux 79—66740

atmospheric turbulence continued
surface layer, structural turbulence coeff. depend. on height *(Russian)* 78—69400
surface layer, turbulent heat and mass transfer, simple predictive model 78—24331
surface layer, turbulent moment calculations for application to air pollution transport 79—84354
surface layer and marine bottom layer, turbulence spectra similarity scaling 78—44860
surface layer flux parameters determ. in absence of temp. profile 79—66752
surface layer over paddy field, turbulent kinetic energy, vertical transport 78—44906
surface layer over plant canopies, kinetic energy downward transport 79—25301
surface layer over Poona, temp. field 79—48544
surface layer parametrisation, turbulence covariances 77—70758
surface layer structure parameters, turbulence props. 80—51510
surface layer turbulence response to partial solar eclipse 79—70843
surface layer turbulent vel. components characts. under convective conditions 79—66754
surface shear flow, turbulent bursts 77—11178
symmetric instability of stratified geostrophic flow 80—98425
target irrad. by laser beam 77—58254
Taylor's hypothesis and high-frequency turbulence spectra 77—87005
temperature field structure, new formula *(Chinese)* 80—109236
temperature fluctuations, modified spectrum rel. to optical propag. 78—92980
temperature fluctuations, struct. functions 78—30274
temperature gradients and clear-air turbulence probability 77—49128
temperature ramps in surface layer 79—88434
temperature structure parameter profiles meas. by acoustic sounder 79—21049
temperature variance spectrum in inertial and dissipation range of isotropic turbulence 78—61490
thermal defocusing of light beams, phase conjugation compensation method 80—64123
thermocline, turbulent viscosity rel. to turbulent thermal conductivity *(Russian)* 80—21796
thermosphere, 95-150 km altitude, 1967-75 obs. 80—51588
thermosphere, effect of turbulence on thermal conditions 79—88610
thermosphere, lower, thin shear turbulent layers induced by tides and gravity waves non-linear interaction 78—65444
thermosphere, lower, turbulent diffusion coeff. seasonal vars. 79—53424
thermosphere, lower, turbulent mixing rel. to O and O_2 distrib. simulation 80—4159
thermosphere, macroturbulent scales estimation around 100 km altitude 78—61635
thermosphere, turbulent motions caused by temp. fluctuations, critical review of Boussinesq approx. *(German)* 77—45206
thermosphere, vertical winds and turbulence from Ba cloud release over Thumba 78—49188
thermosphere turbulent structure, spectral range *(Chinese)* 80—105092
topographic, two-dimens. turbulence, statistical theory 78—44930
transient eddy statistics of northern hemisphere winter circulation 79—58027
tropical cyclone model vortex motion with and without current 78—28266
troposphere, cat's eye turbulence at 4.4 km altitude, VHF radar obs. 80—51566
troposphere, entraining convection at upper limit of convection 80—26568
troposphere, momentum flux maintenance by transient eddies 78—73435
troposphere, radiosonde meas. and spectral anal. of LOS fading 80—56568
troposphere, refractivity turbulence struct. const., Sunset Radar obs. comparison with theoretical model 79—8673
troposphere, sodar obs. of thermal struct. at Delhi 78—32151
troposphere, stationary waves, vorticity and heat balance calcs. 80—51460
troposphere, storm turbulence zones prediction at 400 and 300 mb levels 77—70789
troposphere, turbulence effects on meas. accuracy in radioastronometry *(Russian)* 77—22092
troposphere, turbulence rel. to refr. index variance in different air masses 77—41133
troposphere, turbulence scale rel. to scatter transmission path loss 79—48556
troposphere, VHF radar signals turbulence scatt. from clear atmosphere 78—81278
troposphere, wind field turbulence rel. to near-surface internal gravity waves *(Russian)* 77—33141
troposphere turbulence, influence on radio-interferometric differential meas. of astronomical coordinates 80—67581
troposphere turbulence effect on pot. vorticity in jet stream-frontal systems 80—77044
troposphere winds, radar obs. made at Kwajalein Atoll, equatorial Pacific 80—90188
tropospheric long-distance propag., multiple scatt. effect 80—109229
tropospheric studies, microbarographs, sodar, FM-CW radar, review 77—91332
trough-ridge systems as slantwise convection 79—84456
turbopause eddy diffusion coefficient, semi-theoretical global models based on satellite data 79—21086
turbulence, book 78—90839
turbulence breakdown coefficient determ., influence of data treatment technique *(Russian)* 78—7690
turbulent boundary layer, penetrative convection regime, entrainment rate *(Russian)* 78—69401
turbulent diffusion, of particles in air, analytical numerical method 78—32257
turbulent interface layers, theory 78—71323
twinkling of stars 78—53726
two and three dimensional turbulent flow, vorticity anal. rel. to numerical weather prediction 78—69395
two-dimensional, above topography, enstrophy 77—7372
two-dimensional turbulence on the surface of a sphere 78—73447
two-layer quasi-geostrophic turbulence, simple special case 78—81186
typhoon characteristics over South China Sea 79—25309
uniform potential vorticity flow, wave interactions and turbulence theory 79—8655

atmospheric turbulence continued
unstable surface layer, horizontal vel. spectra 78—73427
unstable surface layer over land, flux and turbulence meas. 77—66962
unstably stratified, turbulent energy disspation rate *(Russian)* 77—64372
upper atmosphere, irregular motions from radiometric meas. *(Russian)* 78—96333
upper atmosphere, turbulent diffusion coeff. determ. from meteor trail photographs 78—45073
urban atmosphere, local mixing and turbulence effects on CO_2 concs. 80—16870
urban environment, meteorological obs. 79—25312
urban planetary boundary layer, pollution effects on thermal struct. and dispersion 78—11986
vegetation canopy influencing turbulent heat and mass transfer, theory 80—26570
velocity components in surface layer under convective conditions 77—78297
vertical diffusion parameters meas. using smoke plume data *(Russian)* 78—36227
vertical inhomogeneous currents predictability *(Russian)* 79—29809
vertical profile, rel. to astronomical seeing 77—29379
vertical profile of refr. index turbulence, stellar scintillation meas. 77—45126
vertical turbulent diffusion in a stably stratified fluid 79—16585
vertical velocity fluctuations, meas. using sailplane variometer 79—88480
vortex boundary layer flow, turbulent modelling, predictor-corrector multiple iteration 77—91237
wave front mutual coherence function corrected by zonal adaptive optics 79—72490
wave induced eddy transport, computation in realistic atm. model 80—90164
wave propagating in turbulent medium, four-point field coherence function 79—98279
wave propagation in turbulent medium, classical theory, book contrib. 79—34956
wavefront random deform., statistical anal. *(French)* 77—87074
wavefront random deformations, due to turbulence, correl. function estimation *(French)* 78—36280
wavelike eddies in zonal flows with shear props., cyclone model perturbation anal. 80—81994
whirlwind, ring-shaped, onset caused by rising air in stratified atmosphere *(Russian)* 78—77298
wind flow around tall buildings 78—36256
wind generator design, atmospheric turbulence structural influences 80—61247
wind obs. in clear air using FM-CW Doppler radar 78—57271
wind profile meas. disturbance by slim mast 77—73790
wind simulation, wind tunnel expts., turbulent boundary layers on rough surfaces, simple roughness elements 80—69774
wind velocity gust factors, analytical approach 78—88897
CO_2 IR laser velocimetry, processing techniques and applications 80—87831
H_2O vapour fluctuations influence on turbulent fluxes 79—79916

atmospheric wind *see wind*

atmospherics
see also atmospheric electromagnetic wave propagation; whistlers
100 to 500 kHz noise, rel. to auroral arcs and field aligned currents and auroral electrons accel. 79—66859
absorption by pine trees, swept freq. meas. 79—50494
aquatic system, precip. rel. to atmospheric P contrib. 79—100545
E.Asia, atmospheric noise source contour maps 77—91245
auroral hiss at $L \simeq 4$ on the ground 77—70931
auroral oval, dayside, rocket-borne VLF and ELF waves meas. 80—98504
auroral radiation, theory of generation 79—75051
auto and cross-correlation analysis techniques on-board spacecraft *(French)* 79—70925
chorus generation, critical electron pitch angle anisotropy 77—2308
chorus generation by energetic electrons during substorms, theory 78—96356
chorus VLF and ELF emission, plasmapause origin model 80—41608
counting circuit, uses two ICs 77—29360
cyclotron soliton theory of Earth's kilometric radiation 80—94657
diffraction and stray fields measurement, angular and amplitude characteristics *(Russian)* 80—67433
discrete VLF line radiation within transmitter-induced amplification bands, satellite obs. 78—96360
EAS radio emission, field strength at 44, 60 and 80 MHz 80—8505
EAS radio pulses, correlation at 60 and 80 MHz 80—8504
electrostatic noise damping by warm auroral electrons 80—41668
ELF and VLF noise, diurnal var. observed on low-altitude satellite at latit. of Sanae 77—87181
ELF emission, ionospheric generation and spatial distrib. 80—4174
ELF hiss, rel. to time persistence of electron precip. features in slot region 78—28395
ELF radio signals is auroral ionosphere, generation by LF and MF transmissions nonlinear demodulation 80—94639
ELF sferics in polar region during solar proton event, June 1968 Antarctic obs. 80—90291
ELF waves assoc. with equatorial spread-F, satellite obs. 79—35051
ELF/VLF ground-based obs. at high latits. during GEOS-1 and ISEE-1 and -2 passes 79—29949
equatorial hiss in topside ionosphere, obs. 80—61939
ground wave atmospherics generated by lightning return strokes, initial peaks, model 80—61876
HF and VHF radiation produced by intracloud lightning discharges, temporal struct. 80—17337
HF band, statistical characts. of signal and atmospheric noise mixture 78—57276
hiss, auroral and ELF, source regions of fine struct. 77—87203
ionosphere, natural radio noise, Bernstein mode, excited by solar electron streams 79—62646
ionosphere low-latitude VLF emissions, prod. by incoherent Cerenkov process 79—75036
ionosphere lower hybrid reson. freq., obs. and calcs. from ion density meas. 78—28416
ionosphere VLF emission, mid-latit. modulation theory 79—12335
kilometric radiation characts., initial results from JIKIKEN (EXOS-B) satellite obs. *(Japanese)* 80—94648

atmospherics continued
LF hiss, wide band obs. at Frobisher Bay 77—70930
lightning, 2200 MHz atmospherics, rel. to optical radiation obs. from above and below clouds 80—85698
lightning, effect of pulse interval statistics on radiation spectrum 77—53135
lightning, return stroke current and vel 79—25306
lightning, VLF spectral characts. of K-field changes, expt. 77—2217
lightning return stroke generation of ground-wave atmospherics, statistical simulation 78—44967
low-frequency emission pulsations in topside ionosphere, spectra rel. to surface geomag. SPP spectra 79—58157
magnetosphere, determ. of mode of propag. electrostatic and radio waves using stimulated plasma wave results *(Japanese)* 80—94650
magnetosphere, elec. field in VLF to HF range, EXOS-B obs. 80—67478
magnetosphere, electrostatic emissions and cold plasma densities 80—26696
magnetosphere, quasi-periodic ELF-VLF emissions assoc. with Pc 3-4 mag. pulsations, geomag. conjugacy 80—67475
magnetosphere, radio and plasma waves obs. during JIKIKEN (EXOS-B) satellite initial phase *(Japanese)* 80—94675
magnetosphere, RF emission in electron beam-plasma and beam-beam interactions 78—45137
magnetosphere, VLF plasma waves obs. and comparison with high energy electron flux by EXOS-B satellite *(Japanese)* 80—94652
magnetosphere, wave emissions prod. by JIKIKEN electron beam-plasma interaction expt. *(Japanese)* 80—94655
magnetosphere chorus, occurrence patterns and normalised freq. 77—9625
magnetosphere chorus and hiss observed by GEOS, automatic recognition using coherence function 79—44307
magnetosphere ELF chorus, substorm dependences of two types 78—28437
magnetosphere ELF hiss, generation beyond plasmapause by magnetosonic waves 77—82085
magnetosphere hiss emissions, VLF transmitter-induced quiet bands quantitative interpretation 79—66878
magnetosphere natural emissions, Geos I identification 78—53774
magnetosphere VLF wave activity, Sunday decreases 79—66883
magnetosphere-cusp interface, EM and electrostatic emissions during substorms 79—66880
magnetospheric ELF chorus, OGO 5 search coil magnetometer data anal. 77—25887
magnetospheric noise, influence of CW whistler injection 77—82087
multicomponent time-varying signals, unambiguous determ. of fine structures *(French)* 79—70921
noise field in VLF band, observation time limits *(Spanish)* 79—16758
noise variation with sunspot number during 1600-2000 hours at Delhi 78—49083
partially coherent radiation by charged particle beams in ionosphere 78—28407
plasmapause, 1-30 Hz waves generation by reson. electron instability 78—49235
plasmasphere, electron precip. and LF noise emissions during mag. storm. 79—80069
plasmasphere, wave-particle interactions, ELF-HF obs. from EXOS-B 80—67467
plasmasphere hiss, effects on radiation belts struct. compared with man-made VLF waves 78—45150
plasmaspheric ELF hiss, origin, importance of wave propag. and plasmapause 80—26672
polar cusp, field-aligned currents, convection elec. fields and ULF-ELF waves 79—75043
premonsoon thunderstorms, integrated field intensity of atmospherics, Calcutta 79—39792
pulsating gas flow, aeroacoustic charact. eval. method 79—46141
radiation field, rel. to transmission line model for lightning with general vels. 77—33156
radio noise field strengths prediction for Indian subcontinent 79—84578
radio noise statistical models for reception in VLF band 80—72611
radio noise vars. at Ping-Cheng, Taiwan 77—45246
radiometric measurement at 30 GHz, ATS-6 satellite link appl. *(Dutch)* 78—7742
Schumann resonances, balloon meas. *(Japanese)* 79—79919
Schumann resonances, expt. data appl. to atmosphere and lower ionosphere elec. cond. profiles evaluation 80—36360
Schumann resonances and elec. cond. of atmosphere and lower ionosphere, reson. freqs, and ELF attenuation 80—31099
Schumann resonances in Earth-ionosphere cavity, book 80—86050
SEA rel. to X-ray radiation and active areas, statistical study *(French)* 78—20788
simultaneous obs. made in Japan and Thailand propag. study 80—98520
sources location, via triangulation direction finding network 79—100981
sporadic pulse sources, lower boundary for ang. dimens. *(Russian)* 78—24411
sweepers modulation struct. in HF and VHF bands 79—5707
thunderstorm distance determination, calcs. and examples *(German)* 78—40680
thunderstorms at sea rel. to VLF atmospherics, nighttime effect 80—26585
thunderstorms in Asia, anal. of errors of location 80—101421
tropical regions, atm. noise data 80—61875
tweek atmospherics propag. mechanism 78—49213
UHF emissions from lightning discharge considered as plasma 78—61497
ULF or VLF emissions, apparent and real fine struct. 80—26697
V_d ratio specification atmospheric noise models 77—81992
VHF direction finder studies of lightning 79—20928
VLF, spectral parameters random scatt. 78—49095
VLF, studies over Calcutta 79—88550
VLF anomalies, rel. to rainy days over Calcutta 80—82127
VLF atmospheric disturbance flux, intra-group structure 80—56683
VLF chorus, cause of apparent longit. variation, OGo 3 obs. 80—72720
VLF chorus, evidence for excitation by electrical power transmission lines 77—78572
VLF chorus dynamic spectrum, estimation of large-scale elec. field of magnetosphere 79—8775
VLF chorus events dynamic spectrum 79—8770
VLF emissions during mag. storms, Ariel 3 and ground-based obs. 77—56794
VLF emissions during mag. storms, ring current electrons intensity enhancements 79—2444

atmospherics continued
- VLF emissions rel. to auroral X-ray bremmstrahlung 78—45106
- VLF hiss, convective beam amplification 79—40029
- VLF hiss emissions, simultaneous obs. at Brorfelde, Chambon-la-Foret and Moshiri 78—81509
- VLF hiss from auroral zone, direction find method and obs. 80—85777
- VLF hiss in plasma penetrated by electron beam 78—26293
- VLF hiss propag. characts. obs. at low latit. ground stations 78—69561
- VLF meas. at San Miguel, Argentina, rel. to thunderstorms 79—39799
- VLF noise event observed at Sakushima (1978 September 29) 79—101031
- VLF noise generation by electron beams in polar magnetosphere 78—4039
- VLF noise intensity, modulation by hydromagnetic oscills. 78—45139
- VLF noise storms rel. to magnetospheric ring current 77—91376
- VLF quasiperiodic emissions interaction with micropulsations, model 78—61682
- VLF radiation during simultaneous magnetospheric substorm and thunderstorm, rel. to elec. fields and electron precip. 80—67392
- VLF sferics from Union City, Oklahoma tornadic storm 78—85639
- VLF signals, time-varying, determination of wave normal directions *(French)* 79—70927
- VLF waves obs. by GEOS-1 79—29943
- VLF/ELF noise, amplitude-probability distribution model 78—32288
- whistler extrapolation, sferic identification rel. to systematic errors in linear-Q anal. 77—53333

atom-atom collisions
includes reactive collisions
- 2pπ orbital transitions Auger study *(Russian)* 80—91639
- 2s and 2p electrons removal, impact parameter dependence 77—65531
- absorption, collision-induced, at. electronic transitions 78—33594
- absorption spectrum oscill. struct. due to quasimol. states 79—64093
- alkali+inert gas collisions in laser beam, transition probability 79—50120
- alkali atom+alkali atom, laser-induced ionis. collisions 78—5333
- alkali atom+inert gas, three-body interaction, secondary satellites of alkali line 77—83683
- alkali atom+inert gas atom, $^2P_{1/2}$ state depolaris., mag. field effect 78—33590
- (alkali atom)$^+$+(halogen atom)$^-$, recombination 78—7192
- alkali metal, nonresonant excitation of fluoresc. *(Russian)* 77—10633
- alkali metal, photon absorpt. cross-section and quasimol. transitions *(Russian)* 77—75285
- alkali metal, resonance levels relax., hyperfine struct. effect 77—38725
- alkali metal+inert gas, adiabatic pots. 79—81254
- alkali metal+inert gas, role of different interactions in intramultiplet relax. at nonresonant interactions 77—6902
- alkali metal +He(s^{3}S), Penning ionisation by slow collisions 77—50512
- alkali metal atom+inert gas, collisional broadening and shifts, semiempirical pots. calcs. 77—10727
- alkali metal atom+inert gas atom, hyperfine transition spectral line shift, quantum corrections 78—82655
- alkali metal atomic collisions, dimer intramultiplet mixing 80—1059
- alkali metal atoms, Zeeman coherences relaxation in ground state by spin-exchange and sudden collisions 77—50402
- alkali metal mag. reson. spectrum, rapid spin exchange effects 78—25460
- alkali metal vapour, optically pumped, longit. relax. in hyperfine states 77—57908
- alkali metal-He quantum magnetometer 80—17965
- alkali-rare gas atom systems, electronic collisionally induced transition dipole moments 79—98195
- anisotropic collisions, spectral line breadth and shift, polarisation depend. 78—46305
- associative and Penning ionisation, autoionisation, calcs. 78—25674
- atom, Schumann region absorpt. spectrum, oscill. strengths, line profiles, collisional and autoionis. broadening 77—18818
- atom+metastable atom collisions, ionis. processes 78—62907
- atom pair recombination, on solid surface, dynamics pot. calcs. 78—7197
- atomic hyperfine transitions in buffer gas, quantum theory *(Russian)* 78—21881
- atomic radiative binding in slow collisions into molecules in a laser field *(Russian)* 80—93753
- atomic to molecular ion conversion, rate constant calc. 78—64835
- binary collision, energy transfer and ionisation cross-section calcs. 77—50522
- body-fixed theory, two-system collision, arbitrary ang. momenta 78—25642
- catalysis, heterogeneous recombination, Smith-Linnett theory, H_2 appl. 77—48634
- charge exchange, quantum mechanical and impact parameter capture amplitude 80—87226
- coalescing atoms, X-ray continua 77—530
- colliding atoms, two-photon ionisation 78—13482
- collision anisotropy and spectral line impact contour *(Russian)* 80—52942
- collision systems $\alpha(Z_1+Z_2)\gtrsim 1$, quasimolecular 1 sσ orbital, excitation and spectroscopy 80—87199
- collisional intense-field fluoresc., Zeeman degeneracy effects 80—99477
- collisional ionisation, Penning and associative ionisation produced by laser field 80—63802
- complex atom*+inert gas atom, model pot. curves, including CI 78—42154
- conference, electronic and atomic collisions, Paris (July 1977) 78—58758
- cross section depend. on at. orientation and direction of relative motion *(Russian)* 79—98213
- degenerate atomic level perturbation by neutral particles 79—792
- diatom dissociation and recombination mechanisms, bound complex and triple collision mechanisms 80—23478
- diatomic molecules, variable screening model 78—74587
- diatomic transition operators, numerical calcs., variable phase and amplitude calcs. 78—25653
- differential and total scatt. cross sections using spectroscopic line shape anal. 79—36735
- diffraction and angular momentum effects, semiclassical atomic scattering theory 79—89734
- direct scattering theory for neutral and charged ats. 80—23483
- discrete-continuum electronic states coupling, appl. to He+Ar 79—10193
- electronegativity equalisation in atom-atom reactions 79—66272
- electronic energy transfer, in excited atom collisions, review, book contrib. 77—40543

atom-atom collisions continued
- electronic state transitions, two-level collision system calcs. 78—62893
- energy transfer, reaction dynamics and collisional ionisation, review 80—63801
- exciplex gas lasers, pumping by barrier tunnelling 78—17908
- excitation transfer, with small reson. defect, mag. field effects 77—3449
- excitation transfer in slow collisions between identical particles *(Russian)* 78—78799
- excited atom+excited atom collision semiquantal calcs. 79—81270
- excited atom ionisation due to collisions in their own gas *(Russian)* 80—91654
- fine-structure transition probability, semiclassical multichannel scatt. matrix 80—37854
- flame, rate constants for $A+X \rightleftarrows A^+ + X^-$ and $AX+M \rightleftarrows A^+ + X^- + M$ (A=metal, X=halogen, M=flame species) 79—34310
- foreign gas broadening, translational heat-bath model, variational methods 78—9124
- form factors and cross sections for $nl \rightarrow n'l'$ direct collisional transitions 79—31636
- gas laser, atomic constants and collision cross sections determ. by level crossing 78—50763
- gas laser, output power profile collision induced asymmetry, simplified model 80—87366
- gases, two-body collision induced light scatt., memory function approach and mol. dynamics 78—25658
- graphite, tritium effects, first wall controlled thermonuclear reactor conditions, simulation 79—647
- ground state atoms+excited atoms, anisotropic collision rate 79—76488
- halogen atom (^{2}P)+inert gas atom (^{1}S), coupled channel study, rel. to elastic approx. 79—81255
- He, Rydberg, series transitions, opto-galvanic spectroscopy 79—54779
- heavy collision systems, vacancy prod. in strongly bound quasimol. states, impact parameter depend. 78—22003
- heavy ion collisions, possible electron compression waves 77—23536
- heavy ion collisions, rotational transitions, effect of spin-orbit coupling 78—13573
- heavy particle collisions, electron spectroscopy 77—42397
- heavy particles, impact-parameter treatment, differential scattering amplitude 78—37711
- high Rydberg atom+neutron atom (molecule), collisional quenching, theory 79—86051
- high-energy, review 77—27150
- hot-atom collisional energy density function, stochastic calc. 79—29342
- hydrogenic atom, Coulomb excitation, by heavy projectile, nucl. screening effect 78—17777
- inelastic, Penning and assoc. ionisation, complex. pot. and electron spectrum 78—94310
- inert gas, at. excited states in discharge, Hanle effect 79—76394
- inert gas, metastable atoms, scatt. 78—62906
- inert gas+alkali metal, collision studies of quasi-one-electron systems 80—63750
- inert gas atom+high-Rydberg atom, thermal collision, l-changing cross section calc. 80—14190
- inert gas collisional perturbation of 6^3D_1, 6^1D_2 Hg levels 80—74223
- inert gas liquid mixtures, collision induced absorpt. 77—4638
- inert gas metastable state collisions, intermediate energies 78—62904
- inert gas mixture, collision induced microwave absorpt. spectra 80—74216
- inert gases, collision induced polarisabilities, perturbation treatment 78—86778
- inner shell excitation, impact parameter dependence 77—19047
- intense laser irradiation effects, ang. momentum approx. 79—94058
- interacting atoms, retarded energy shift and pair polarisability, field theoretical perturbation theory 80—102560
- ion pair forming collisions, dynamics 78—66661
- ion-ion collisions, crossed beam expts. 78—58843
- ionisation collisions, improved impulse approx. 78—74754
- ionising collision, with excitation and deexcitation of atom, impulse approx. 79—59548
- isotope separation, atomic collisions, influence on resonant excitation selectivity 79—27098
- laser, high-intensity, multimode, dynamics theory 79—41363
- laser excitation mechanisms for atomic and ionic lasers, book contrib. 80—106512
- laser induced collision processes, numerical analysis 78—17748
- laser induced Penning ionisation two step optical collisional perturbation sequence 80—63778
- laser radiation field effects, ang. momentum anal., quantum mech. theory 78—74733
- laser radiation field effects, quantum mechanical close coupled expansion 77—50485
- laser-induced collisional energy transfer, level crossing expansion 80—83461
- laser-induced collisions with energy conservation by photons 77—60098
- laser-induced inelastic collisions, theory 77—14552
- laser-induced radiative collisions, review 79—10196
- light scattering, collision-induced and multiple, by simple fluids 80—53919
- long range interaction, polarisation of emitted light 78—62902
- long-range interaction, effect of strong e.m. fields *(Russian)* 77—10734
- Lorentz gas, two-dimens., collision-induced absorption, simulation 78—46424
- low energy, ionisation cross sections, diffusion eqn. calcs. 77—54605
- measurements of reaction rate consts., reliability criterion 79—8423
- mol. target internal motion 80—78697
- molecular approach, radial couplings between approx. wavefunctions 77—38713
- molecular orbital K X-ray anisotropy peaks, Z-depend. 77—58043
- molecular theory of atomic collisions, electron translational effect 77—88528
- molecular-orbital X-rays yield 78—13587
- momentum transfer phase factors, mol. integral evaluation with travelling GTO basis set 79—22778
- multi-crossed-beam method, differential cross-section meas. 79—45797
- multiphoton laser assisted excitation transfer, grazing collisions, Heisenberg eqn. of motion 77—57953
- multiplet mixing collisions, effect on near resonant light scatt. 79—6908
- multistate mol. treatment, impact parameter approx., differential cross sections from transition amplitudes 77—61820
- N-atom system, superradiance and energy transfer 77—3558
- near-resonant processes, excitation transfer cross sections 77—3446

atom-atom collisions continued
neutral+high Rydberg atom, thermal collisions, review 80−63756
neutral atom collisions, hyperfine component broadening and shift of spectral lines 80−74136
nonadiabatic collision, threshold region, tunnelling effects 77−6901
nonadiabatic collisions, Franck-Condon approach for electronic state quenching 78−66640
nonadiabatic coupling integrals evaluation 78−1041
nonadiabatic transitions, with pseudocrossing of a group of terms 77−65522
nondegenerate optical transitions of excited atom in buffer gas, line shape kinetic theory 80−42997
nonresonant collisions in intense mag. field, van der Waals pot. 77−3440
nonresonant excitation transfer, Doppler profiles, donor levels *(French)* 77−30824
nuclear motion, quantum-mech. and classical treatment, book contrib. 78−74736
O+O, $O_2(c^1\Sigma_u^-, C^3\Delta_u, A^3\Sigma_u^+)$ emission from at. recomb. 79−31576
off-shell t-matrix elements, first rank separable approximations, invalidity 78−1051
one electron excited atom ionisation collisions at high energy, improved impulse approx. 79−94072
one-atom detection in individual ionisation tracks, heavy ion stopping in buffer gas 78−70802
optical excitation, centrifugal barrier effect on nonadiabatic transitions probability 79−64095
optical excitation to state of quasibound motion *(Russian)* 78−58784
optical processes in close atomic collisions 79−13790
optically pumped vapour, transverse relaxation *(Polish)* 78−55229
oscillator strength sums, dynamic polarisabilities, one-term approximations 79−22782
outershell excitation, diabatic mol. orbitals 78−62901
P-S state atomic collisions, quantum mechanical treatment, decoupling approx. 80−99542
P-state collisions, quantum mechanical treatment, angular momentum coupling 80−99541
Penning collision processes, review *(Japanese)* 79−64092
Penning ionis., radiative, photoionis. cross section depend. of continuum radiation 77−19034
Penning ionisation and excitation transfer, unified treatment 78−25672
perturbed stationary-state method limitations for slow collisions 77−3433
photon-scattered atom coincidence expts., appl. of position sensitive particle detect. techniques 80−53112
polarised excited atom, freq. depend. polarisation of emitted radiation 77−61705
positronium+N_2 (inert gas), fine struct. interval, collisional density shifts 77−34788
potential well depth estimation method 79−86034
quasiclassical theory, transition between spatially degenerate levels 80−43150
quasimolecule form., adiabatic satellites of at. lines 77−50513
quasimolecules, electron spectra on autoionisation *(Russian)* 77−79690
quasimolecules, intermediate, relax. times 78−42170
radiative atom collisions involving excitation transfer with small reson. defects *(Russian)* 80−53101
radiative collision-induced photoionisation 78−62858
radiative collisions, laser-induced energy transfer 77−46626
radiative collisions and two-photon transitions 77−46552
radiative electron transitions *(Russian)* 79−98212
radiative interatomic collisions in bichromatic field *(Russian)* 80−14224
recombination reactions, energy transfer mechanisms studied using trajectory calcs. and Monte Carlo method 80−66785
relaxation processes, at. vel. effect on spectral line breadth 79−49985
resonance broadening in strong light field *(Russian)* 77−27149
resonance energies, complex, diverging wave functions, least squares bivariational method 78−17741
resonance scatt., enhanced isotope separation 77−61825
resonance spectral broadening in high density gas, many body shielding 77−79579
resonant collisions in intense mag. field *(French)* 77−527
resonant impurity gas, translational nonequilibrium in resonance optical field *(Russian)* 80−106865
resonant ionisation spectroscopy, chem.-physics appls. 80−68259
resonant light field effect on interaction *(Russian)* 79−54936
Rydberg atom+atom, l-changing collision, rel. to low-energy electron scatt. 79−50112
Rydberg atom+atom (photon), separation of Rydberg electron and ion core 80−63754
Rydberg atom+atom collision, depopulation, ionisation 78−62908
Rydberg atom+ground state atom, slow collision, excitation and deexcitation processes 80−23508
Rydberg atom+inert gas atom, ang. momentum mixing 79−10175
Rydberg atom+Rydberg atom, ionisation cross sections 79−81267
Rydberg atom+Rydberg atom, ionisation cross-section calcs. 79−31664
semiclassical theory for near adiabatic photon assisted mol. collisions 79−5141
sensitised fluorescence, inverse problem 79−98020
single-electron loss, total Born-approx. cross-sections atoms up to Fe 77−83714
slow atomic particle collisions, quasiresonant processes 79−41216
slow collision, electron detachment, energy spectrum and isotope effects *(Russian)* 77−30984
slow collisions, electron translational effect, diagonalisation calcs. 77−3441
spectral line broadening by foreign gas, translational heat bath model, T-approx. 78−9125
spectral line broadening theory, use of multipole expansions 78−74611
spectral line collision damping consts. rel. to stellar atmospheres 77−42279
spectral line collisional broadening 77−88426
spin exchange cross section between unlike atoms, laser technique 78−33637
stellar atmospheres, atomic line broadening by neutral H 79−92665
stimulated collision-induced fluoresc. 78−86811
stripping cross sections, binary encounter approx. theory 78−50618
superheavy and intermediate atomic collision systems, UNILAC expts. 80−63751
three-atom collision, mol. form., eikonal approx. calcs. 77−14531
three-atom collision dynamics, diatomics-in-mol. calcs. 77−34719
total cross section, explicit bounds by geometric method 80−43130

atom-atom collisions continued
transition probability between two electronic states, curve crossing 77−3445
triple collision, mol. formation, Morse oscill. calcs., dissoc. cross sections *(Russian)* 77−32786
turning point problems, uniform JWKB amplitudes and phases 80−53081
two photon ionisation, radiative collision effect 80−106388
two-level system, saturated lineshape, collisional and radiative damping effects 77−58124
two-photon absorpt., collisionally perturbed, reson. profile and strengths, degeneracy and Doppler shift 78−55156
two-photon spectroscopy, Doppler-free *(Dutch)* 79−50167
unified atom limit, adiabatic approx. for transitions between $l=2$ states 79−22781
X-ray spectra, mol., collision dynamic effects 77−19045
$Z_1+Z_2>120$, 1sσ excitation probability, scaling law, expt. confirmation 80−58365
Zeeman coherence in saturated absorpt., velocity changing collisions study 77−46527
Zeeman resonance lineshapes, motional narrowing, analytical results 77−46524
Zeeman resonance lineshapes, motional narrowing, expt. 77−46525
$\mu d+d$ elastic scatt. cross section for muonic d 79−89811
$(\mu p)+{}^ZX\rightarrow(\mu^ZX)+p$ muon transfer, probe for study of $(\mu p)_{2S}$ system 77−27209
Ar, $3p^55p$ config. aligned in discharge, interf. signals, lifetimes and collision cross sections 78−70796
Ar $(^3P_{2,0})$+Cl, rate constants for specific product channels 77−46537
Ar atomic excited states collision radiative destruction in glow discharge 79−3528
Ar, autoionising levels excited by heavy ion impact 79−13804
Ar, collision induced light scatt., three- and four-body spectra 79−18260
Ar, collision-induced light scatt., spectral features 78−13493
Ar, collisional depolarisation of selectively excited 2p levels *(French)* 78−86830
Ar gas, two body collision induced light scatt., memory function approach and mol. dynamics 78−25658
Ar line broadening by at. collisions, meas. of oscillator strength of ArI lines reson. *(French)* 78−5172
Ar, pair polarisability determ. from collision induced light scatt. spectrum 79−13678
Ar, production of Ar_2*, kinetic behaviour and energy transfer 79−68305
Ar, spectral line collisional broadening and line shift 77−10641
Ar, three-body collision-induced light scatt. spectrum moments 78−9226
Ar-Kr liq. and gas. solns., collision-induced dipole moment, far IR band obs., self-diffusion coeff. 77−38627
Ar+Ar, K-X-ray excitation, 2.5-8 MeV, impact parameter depend. 78−50628
Ar+Ar, low-energy collision induced UV radiation 79−50125
Ar+Ar, multielectron excitation energy calcs. 78−1071
Ar+Ar, optical emission spectra 77−14551
Ar+Ar, stopping power 80−91651
$Ar+Ar(^3P_2)(^3P_0)$, flowing afterglow metastable decay rates, diffusion, two- and three-body rate consts. 78−73027
Ar+Ar(Kr)(Xe), total scatt. cross-sections, glory undulations 77−10732
Ar+Ca, quenching cross section of Ar atom for Ce reson. line 77−19021
Ar+He* Penning ionisation, semiclassical descretisation procedure 78−90275
Ar+He*(1s2s,^{3}S), coupled channel calcs. of chemi-ionisation 77−27166
Ar+He*(1s2s,^{3}S), Penning ionis., multichannel calcs. 80−53111
Ar+Kr, $(4p^55p)$ and $(4p^55p')$ states, radiative lifetimes and two-body collisional deactivation rate consts. 80−95572
$Ar+Kr(^3P_2)$, flowing afterglow metastable decay rates, diffusion, two- and three-body rate consts. 78−73027
Ar+Xe, lightly doped, Xe $5d(3/2)_1$ photoexcited state radiative decay and energy transfer 78−74605
Ar+Xe, relaxation processes of $Xe^*(^3P_2)$ metastable atoms 78−50624
$Ar+Xe(^3P_2)$, flowing afterglow metastable decay rates, diffusion, two- and three-body rate consts. 78−73027
$Ar+Xe(F_2)$, proton excited mixtures, energy transfer processes 78−66647
Ar+Xe→Xe*, electronic energy transfer, emission spectra, electron beam excitation 77−38722
ArN_2, interaction potential, modified electron gas model potential 79−72385
$Ar(^3P_{0,2})+H(^2S)$, energy transfer rate const. and mechanism 78−37727
$Ar(^3P_2)+H(^2S)$, energy transfer, Lyman-α line obs. 79−64085
Ar*+H, assoc. ionis., rovibronic struct. in electron energy spectrum 80−106380
Ar*+H, collisional quenching rates 80−95548
$Ar^*(3p^54p)_i+Ar(^1S_0)$, collisional population transfer rate coeffs., 300K 79−10177
$Ar^*(4s^3{}_{2,0})+Kr(Xe)$, elastic and reactive scatt., ang. distribs. 77−6919
$Ar(3p^5, 4p)$ and $(3p^5, 4p')$ states, radiative lifetimes, two-body deactivation rate consts. 79−10068
$Ar(4s^3P_{2,0})+Xe(O)(Cl)$, electronic energy transfer 77−46627
$Au+{}^3He(^4He)$ L-subshell ionisation, Coulomb deflection effects 78−22020
$Au+H^+$, L-subshell ionisation cross-sections, X-ray meas. 77−46520
Au+Xe,4.7 MeV. u^{-1}, meas. of shape and absolute value of 1sσ excitation probability 79−13816
B+Ar(Kr)(Xe), B emission line broadening in glow discharge lamp 77−3304
B+He (methane), B atom K-shell binding energy by Auger spectra 78−50525
B+He (methane), collisional excitation, prompt decay line energy, projectile Auger spectrosc. 79−85941
B+He(Ne)(Ar), ground and excited states interaction, B spectral line breadth 77−68092
B+Xe(Kr), reson. radn. quenching 77−30820
Ba, Hanle effect in reson. line density depend. 77−23473
Ba in shock heated Ar, absorpt. line broadening obs. *(Japanese)* 80−83464
Ba, time-resolved saturated absorption expt., collisions effects 78−29758
Ba+Ba, atomic pair absorpt. obs. with white-light source 79−63944
Ba+Ba(Tl), laser induced collisional and radiative energy transfer 80−53108
Ba+Kr, collision induced dipole transition, elec. quadrupole transition, oscillator strengths 79−41128

atom-atom collisions continued
- Ba+Tl, atomic pair absorpt. obs. with white-light source 79—63944
- Ba+Tl, dipole-quadrupole radiative collisional fluoresc. 80—83315
- Ba+Tl, radiative collisional fluoresc. obs. from thermally excited atoms 80—102480
- Ba+Xe, spectral line contour meas. determ. of potentials 78—25477
- Ba*+Ba*, radiative collisional fluoresc. at sum freq. 79—18261
- Be+Be, polarisability and London coeff., ab initio variation perturbation calc. 79—13635
- Be+He (methane), Be atom K-shell binding energy by Auger spectra 78—50525
- Be+He (methane), collisional excitation, prompt decay line energy, projectile Auger spectrosc. 79—85941
- Be+Mg, polarisability and London coeff., ab initio variation perturbation calc. 79—13635
- Bi, $6p^3(^2D_{3/2}{}^0)$ and $6p^3(^2D_{5/2}{}^0)$, collisional deactivation 77—61702
- Bi, metastable states collisional quenching, temp. depend. 77—88526
- Bi+N, BiN form., IR matrix spectra, comparison with group V nitrenes 80—18853
- Br, recomb., in presence of inert gas atoms and mols. 80—45496
- Br+Br+Ar, photoinduced recombination, numerical simulation 79—16018
- Br+target atom, 12-60 MeV, K-vacancy cross sections, target depend. 77—19026
- C, fine struct. excitation by H impacts 77—42384
- C+C, K-shell excitation, Auger electron spectrosc. obs. 80—9714
- C+He (methane), C atom K-shell binding energy by Auger spectra 78—50525
- C+He (methane), collisional excitation, prompt decay line energy, projectile Auger spectrosc. 79—85941
- C+N(O), K-shell excitation, Auger electron spectrosc. obs. 80—9715
- Ca in shock heated Ar, absorpt. line broadening obs. *(Japanese)* 80—83464
- Ca-Ca symmetric collisions, molecular-K-X-ray anisotropy spectra, discrete struct. 77—14560
- Ca+Ca(Mg)(inert gas), metastable ^{3}P-state, quenching reactions, fluoresc. meas. 80—102477
- Ca+He, nonstatistical excitation of mag. substates of $^1P_1$ level 78—42194
- Ca+He(Ne), press. broadening, line shifts 78—5290
- Ca+inert gas, $^1P_1$-$^3P_1$ excitation transfer 80—102559
- Ca+inert gas, collision-induced dipole transitions, absorpt. study 80—37865
- Ca+inert gas, collision-induced dipole transitions assoc. with high-lying states 80—37866
- Ca+Rydberg Ca**, collision cross sections, $Ca_2{}^+$ pot. energy calcs. 79—27055
- Ca+Sr, laser-induced collisions, large cross sections meas. 79—64075
- Ca+Sr, laser-induced inelastic collision, fluoresc. obs. 77—54603
- Ca+Xe, collision-induced dipole transition due to long range interaction, absorpt. obs. 80—63779
- Ca*+He(Ne), model pot. curves, including CI 78—42154
- Ca(4p ^3P_J)+Ba, collisional deactivation and optical lifetime 80—48070
- Cd, 6^3P_1 level, relax. of alignment and population 78—70795
- Cd, broadening of 5^1P_1 level 80—83479
- ^{114}Cd λ326.1 nm reson. line, self-broadened, temp. depend. of parameters 79—63964
- Cd+Cs, excitation energy transfer in sensitized fluoresc. 79—98210
- Cd+He, Penning ionisation cross section of target atom, for He(2^3S_1) 80—63777
- Cd+inert gas, (ns nd)$^1D_2$ states, Hanle effect, alignment destruction *(French)* 78—5324
- Cd+inert gas, transitions between excited Cd states 78—17773
- Cd+K(+N_2), optical excitation, rate consts., collisional energy transfer kinetics 80—32801
- ^{114}Cd+He, collisional effects on 326.1 nm line rel. to temp. and conc. 78—5336
- Cl atoms, photorecombination, rate constants determ., identification of spectral distribution of recombinative emission intensity 80—85195
- Cl, recomb., in presence of inert gas atoms and mols. 80—45496
- Cl+Cl, radiative recomb., behind incident shock wave front *(Russian)* 77—65525
- Cl+Cl collisions, impact parameter dependence of emitted noncharacteristic rad. 77—14563
- Cl+inert gas, $3p^5(^2P_{1/2})$ state quenching 78—42192
- Cr, gas-phase, plasma, sputtering and beam-foil excitations 80—32820
- Cs, 6s-9p doublet, Xe perturbations, simultaneous additive effect on multiple satellite lines 79—76389
- Cs, assoc. inoisation, in low press. discharge, 6P and 5D states effects 77—75284
- Cs, assoc. ionisation, in low press. discharge, upper and intermediate states effects 77—75283
- Cs, collisions between excited atoms, highly excited states excitation 78—17771
- Cs, HFS of first doublet, He, Ne and Ar press. effects 77—38638
- Cs inert gas, pot. energy curves, collision induced oscillator strengths 79—22659
- Cs principal series lines, self-broadening 77—46541
- Cs, quadrupole lines, oscillator strengths, broadening 77—18846
- Cs, Rydberg states collisional ionis. 79—64097
- Cs, self-broadening of Doppler-free two-photon lines 79—41135
- Cs, transverse, relax. in strong reson. RF field 78—5323
- Cs+Ar, laser two-photon ionisation, collisional line broadening, atomic forces 77—83543
- Cs+Ar, two-photon ionisation spectra, satellites, absorption line shape 78—82668
- Cs+Ar(Kr)(Xe), spectral line breadth and shift, Van der Waals pot. calc. 78—90126
- Cs+Cs, Rydberg states collisional disalignment determ. by fluoresc. quantum beat damping 79—13789
- Cs+Cs, spin destruction, obs. 80—63781
- Cs+Cs*, collisional and radiative relax. as eigenvalue problem 78—29827
- Cs+Cs→Cs_2, inelastic light scatt. processes and mol. fluoresc. *(Russian)* 77—61787
- Cs+F(Cl), quasiclassical charge transfer cross section, rel. vel. depend. 77—19073
- Cs+He, interaction pot. and oscill. strength 80—91645
- $Cs+He^m(2^3S)\rightarrow Cs^++He+e$, reaction rate const., meas. in afterglow plasma 79—82116

atom-atom collisions continued
- Cs+He(Ne)(Ar), optical pumping, spectral line shape *(Spanish)* 79—22662
- Cs+inert gas, hyperfine struct., broadening and shift calcs. 77—58153
- Cs+inert gas, three body interaction, fluoresc. spectra principal series lines and secondary satellites 80—83313
- Cs+insert gas, $5d^2D_{5/2}$ level excitation by laser photon absorpt. 77—3438
- Cs+Xe, collision-induced 6s-ns transitions in absorpt. spectrum 78—9101
- Cs+Xe, Cs emission line profile, satellites in square well pot. approx. 78—46303
- Cs+Xe, Cs spectral line profile and absorpt. transitions 80—47944
- Cs+Xe, effect on Cs $^2P_{1/2}$ and $^2P_{3/2}$ levels lifetimes 77—3307
- Cs+Xe (neopentane), Cs line shape broadening, satellite data inversion, interaction pot. 78—74608
- ^{133}Cs, time-resolved fluoresc. spectra, collisional perturbation of Rydberg states 77—83529
- $Cs^*(6D_{3/2})+Cs(6S_{1/2})$, preferential excitation transfer from laser populated state 78—37732
- $Cs(6^2P_{3/2})$+He(Ne)(Ar)(Xe), collisional depolaris., nucl. spin depend., by Zeeman scanning 77—19012
- $Cs(8^2P)$+He(Ar)(Xe), fine-struct. transition cross sections, semiclassical calcs. 77—30972
- $Cs(n^2D_J)+Cs(6^2S_{1/2})$ collisions, inelastic cross sections 78—74753
- Cs(nP)+Cs(6S), assoc. ionisation, threshold energy, $Cs_2{}^+$ dissoc. energy 78—58804
- Cu+Cu collisions, Kα X-ray energy shifts, target thickness depend. 80—83311
- Cu+Ni foil target, 50-65.5 MeV, K-vacancy production, impact parameter depend. 79—54958
- D+alkaline earth, D^- ion production, multiple charge-transfer collisions 79—89776
- D+Ar(Kr)(Xe), ion pair formation, curve crossing model 80—87216
- $D+M\rightarrow D^-+M^+$ (M=alkali metal atom), ion-pair form. 78—58779
- Eu, excitation transfer cross section, luminesc. meas. *(Russian)* 77—61706
- Eu+Sr, absorptive collisional energy transfer, laser induced excitation spectra 80—63584
- Eu+Sr, laser induced collisional energy transfer profile, high resolution study 80—83471
- $Eu^*+Sr+h\omega\rightarrow Eu+Sr^{**}$, photon assisted collisional energy transfer 78—90285
- F+F, homogeneous recombination, room temp. rate consts. 77—32766
- F+Ne(Ar)(Kr), thermal energy interaction pots., crossed beam study 79—68288
- F+Xe, differential scatt. cross sections, crossed beam study, interaction pot. 79—3517
- F+Xe, enhanced quenching in intense KrF laser light, computer modelling 78—55232
- $F+Xe(H)^+(H_2)$, $(^2P_{3/2})$ state quenching, Franck-Condon approach 78—66640
- $F(^2P_{1/2})+H^+(Xe)$, nonadiabatic collision processes, electronic degrees of freedom, classical model 79—64062
- Fe+Ar, Fe I reson. line, collisional broadening at high temp. *(German)* 80—106298
- Fe+Fe symmetric collisions, molecular-K-X-ray anisotropy spectra, discrete struct. 77—14560
- Fe+H in solar atmosphere, Fe I lines press. shifts rel. to limb shift 78—89150
- Fe+H in type 1 Seyfert galaxies and quasars, collisional ionisation rel. to permitted Fe II lines 80—62278
- Fe^{26+}+H, electron removal by collision 79—76508
- Ga+inert gas atom, diffuse series head lines, hyperfine components, broadening calcs. 80—32632
- Ge+Ge, quasimolecular K X-ray anisotropy and ang. distrib. 78—1073
- H (D)+Cs, 40 keV, prod. of polarised H^- or D^- ions, low emittance 78—55078
- H beam, charge transfer cross sections in gases and vapours, 10 eV to 10 keV, graphs and tables 80—32824
- H, gaseous, high-resolution mag. reson. study, 1 to 1.3K 80—95560
- H:He, 15 to 150 keV ionising collision, electron ang. and energy distrib. 80—53121
- H+ adsorbed H, W(001) surface, pot. model 77—10726
- H+alkali metal atom, interaction potentials 80—63736
- H+Ar, 0.5 MeV H(H^-) ionisation comparison 79—41230
- H+Ar, collisional charge production, differential scatt. calcs. 77—68107
- H+Ar, collisional charge production cross-sections 77—71860
- H+Ar, Hα and Hβ emission cross sections 80—63782
- H+Ar(Kr)(Xe), ion pair formation, curve crossing model 80—87216
- H+atom (ion), ionis. by one or two electron at. particles, Born approx. 79—54960
- H+atom collisions, appl. to line broadening in stellar spectra 77—13237
- H+atom(ion)(electron), general excitation cross section theory 80—37869
- H+C, surface chemical reaction of thermal at. H 78—20071
- H+Cs, fast atom collisions, charge exchange, equilib. fractions calcs. 78—33601
- H+Cs(Rb)(K)(Na), single-electron capture total cross sections 80—91656
- H+D, close coupling calc., resonant spin-flip process, Ramsauer-Townsend effects 80—99547
- H+D, excitation transfer, spectral line broadening and shift 77—46531
- H+D, excitation transfer, thermal energy, dipole-dipole interaction 79—31666
- H+D, near-resonant excitation transfer cross sections 77—3446
- H+H, 1s-2s excitation of fast H atoms 79—89764
- H+H, atom-atom pots., Hilbert Schmidt expansion, transition operators 78—66621
- H+H, cross-section for excitation of high-lying levels, quasiclassical approx. *(Russian)* 77—79676
- H+H, diatomic transition operators, numerical calcs., variable phase and amplitude calcs. 78—25653
- H+H, electron loss cross section, four-body trajectory calcs. 80—99566
- H+H, excitation transfer, thermal energy, dipole-dipole interaction 79—31666
- H+H, excited atom ionisation collision, excitation transfer effect 79—81272
- H+H, excited states, ionisation collision cross-section energy depend., semiquantal theory 78—42160
- H+H, recombination, orbiting reson. theory, rate consts. meas. 77—83681

atom-atom collisions continued
H+H, spin-exchange and freq. shift cross sections at low temps. 80−83452
H+H, two body multipole-multipole Pade approximants, second order dispersion energy 80−28081
H+H collisions in laser field, excitation, charge exchange and ionis. *(Russian)* 79−94078
H+H interaction, second order dispersion energy, Borel integral investigation 80−74218
H+H*, electron loss cross section, four-body trajectory calcs. 80−99566
H+H(^{4}He$^+$), electron transfer calc., electron ionization calc., Monte Carlo method, 79−72387
H+H(Mu), electron spin exchange cross-sections 80−9685
H+H(inert gas), negative ion form. 77−30988
H+He, H Balmer-α fine struct. lines, anomalous shifts, in He-H_2 DC discharge 79−45677
H+He, H Balmer-α fine-struct. line shift and broadening 80−37783
H+He, H hyperfine press. shift, MCSCF-variational procedure 77−6735
H+He, H hyperfine shift, exchange perturbation theory 77−6736
H+He, long and intermediate range interaction, model pot. calc. 79−22789
H+He (2^3S), pot. energy surfaces and autoionisation lifetimes calcs. 77−34740
H+He(Ar), collisional coherent excitation, meas. of Lyman α-photons 80−99552
H+He(Ar), press. effects on H_α and H_β Balmer series 77−18845
H+He(Xe), simultaneous ionisation investig. 80−32815
H+He(2^1S)(2^3S), associative and Penning ionisation, autoionisation, calcs. 78−25674
H+Hg, differential cross sections, orbiting contribution 79−41221
H+Li(Li_2), superthermal collisions, photon and positive ion prod. 78−78788
H+N, stripping cross-sections, binary encounter approx. theory 78−50618
H+Ne(Ar), electron energy loss 80−87217
H+Ne(Ar)(Kr)(Xe), free electron production, integral cross-sections determ. 79−89754
H+Ne(Ar)(Kr)(Xe), orbiting resons., van der Waals pots., beam scatt. obs. 79−89739
H+Ne(Ar)(Kr)(Xe)(O_2), 20-500 eV, ion pair and free electron production, integral cross sections 78−46437
H+O collisions in thermosphere, rel. to 63 μm radiation field and H temp. 79−80066
H+positronium→H^++positronium$^-$, low energy, field theoretic approach 77−10790
H+T, excitation transfer, thermal energy, dipole-dipole interaction 79−31666
H+Xe, electron-loss cross section struct., 0.05-4 MeV 78−9236
H^0+Cs collisions, H^- production cross sections 80−78698
H^++Ar, charge exchange excitation, alignment tensor components, coincidence method 80−63795
H^++He^+, charge transfer and ionis. cross sections, coincidence meas. 78−50634
H^++He^+, He^{2+} form. by charge exchange and ionis., cross sections 77−83708
H^++He^+, ionis. and charge transfer cross sections 78−42186
H^++He^+, ionisation and charge transfer using intersecting beams 77−68104
H(D)+Ar, differential collision cross sections, diffraction oscills., data anal. 79−22783
H(^{2}S)+Ar($^3P_{0,2}$), energy transfer collisions, Lyman-α emission profile obs., in microwave discharge and reaction cell 80−58359
H*+H(Li), resonant ionisation, cross section and ionisation probability 80−63785
H(1^2S)+H_2 (inert gas), electron capture, electron loss and deexcitation cross sections meas. 78−22025
H(1^2S)+He(2^1S), Penning ionisation, semiclassical and Born total cross-sections 78−33586
H(1s) and (2s), electron loss in passing through inert gases 79−13805
H(2S)+inert gas, collisional quenching, mass spectral obs. 78−25685
H(2S)+Kr(Ne)(Xe)(H_2), metastable atom total quenching 77−46628
H(2^2S)+H_2(inert gas), electron capture, electron loss and deexcitation cross sections meas. 78−22025
H(2s)+H_2(He)(Ne)(Ar)(Kr), collisional de-excitation, 5-26 keV 79−59546
H(2s)+He(Ne)(Ar)(Kr), 5-25 keV, H(n=3) excitation, Balmer α emission obs. 80−53113
He (1^1S) and (2^3S), electron loss in passing through inert gases 79−13805
He, depolarising collision cross sections, quantum beat obs. 80−87203
He, electron and neutral collisions, Rydberg level transitions 79−45821
He, excitation in n=4 levels after laser pumping 77−3324
He, excited, optically-allowed, long-range interaction pots. with electrons, protons and atoms 77−14520
He flow discharge, intermediate press., positive column conc. of ions and metastables 80−44017
He glow discharge, n=3 sublevel quenching and energy transfer, laser perturbation method 80−44060
He I+He, excitation energy transfer 77−50514
He in transient plasma, excitation transfer between excited states 78−70914
He, light scattering spectra of gas, collision-induced scatt. 79−18137
He, long-lived states population decay 79−54954
He-Ar mixture, collision induced far IR absorption at high press. 78−5161
He-Ar mixture HP collision-induced translational far IR absorption obs. 77−38628
He+2I→I_2+He, energy transfer mechanisms studied using trajectory calcs. and Monte Carlo method 80−66785
He+Ar, interatomic pot. well depth, SPFD pot., diffusion, viscosity and second virial coeff. 80−5599
He+Ar, van der Waals pot., from crossed at.-mol. thermal beams scatt. 79−27053
He+Ar mixture, collision induced absorpt. calcs. 77−6777
He+Ar(Kr), translation band spectral moments, induced dipole moments 78−55218
He+Ar(Kr)(Xe), 2^1S and 2^3S assoc. and Penning ionisation cross sections vel. depend. 79−3551
He+Ar(Kr)(Xe), He*(2^1S) scatt., low energy repulsion systematic struct. 78−22000

atom-atom collisions continued
He+Ar(N_2)(NO)(O_2)(N_2O)(CO_2), Penning ionisation of target mol., for He(2^3S) 79−41228
He+atom, He upper states, excitation energy transfer mechanisms 80−28102
He+atom (ion), ionis. by one or two electron at. particles, Born approx. 79−54960
He+Cs(Rb), interatomic pots., hyperfine shifts, diffusion coeffs., perturbation exchange theory 79−41220
He+H, 2^1S and 2^3S states excitation 77−42412
He+H, associative and Penning ionis. cross-sections, pot. energy curve study 79−87836
He+H, excitation cross-section, Born-Ochkur approx. calcs. 77−19088
He+H, stripping cross-section, 0.3 to 3 keV 78−78807
He+H_2(He)(Ar)(N_2), fast metastable at. collisional destruction cross section 78−74760
He+He, (Ne), (Ar), optical emission spectra 77−14551
He+He, (2^3S) and (2^1S) metastable states, direct and assoc. ionisation rate consts. in afterglow, electron energy spectra 79−13812
He+He, He^- decay cross section oscills. *(Russian)* 77−19038
He+He, interatomic force calcs., zeroth-order exchange energy for optimised atomic basis set 80−43131
He+He, ionisation mechanism, theory 77−14550
He+He, low-energy interactions with phenomenological pots. 77−34714
He+He, metastable atoms, collisional ionisation cross-sections 78−70911
He+He, Rydberg states ang. momentum transfer, singlet-triplet anticrossing 77−88543
He+He, weak intermol. interactions, intramol. correl. effects, perturbation anal. 79−86038
He+He (2^1S, 2^3S), differential cross sections, rel. to He_2 excimer long range pots. 79−81167
He+He(Ne)(Ar)(Li)(Na), metastable and ground state electron loss cross section 80−53117
He+Hg, metastable He, collision rate consts. in pulsed discharge afterflow 78−50627
He+Ne, 2^1s_0-level excitation, rate const., temp. depend. 80−87218
He+Ne, afterglow, metastable state energy transfer, spectra 80−43167
He+Ne, NE transitions, 1.52 μm and 633 nm, mode crossing resonance shape 79−18163
He+Ne, Ne disalignment collision cross sections of $2p_4$, $2s_2$ levels, mode crossing determ. 79−18162
He+Ne, scatt., orbiting reson. total cross-sections 78−5320
He+Ne collisions, MO calcs. for excitation processes 78−25676
He+Ne pot., differential cross section, quantum mechanical inversion 78−70896
He+Ne(Ar)(Kr)(Xe), energy transfer, time-resolved VUV spectra 77−19028
He+Ne→HeNe, detection in nozzle beam, total collision cross section determ. 77−61826
He+Rb, spin exchange collision, polarisation transfer, NMR of He 78−33453
He+Xe, electron-loss cross section struct., 0.05-4 MeV 78−9236
He^++He(Ne), model pot. for law energy scatt. 78−66642
He^++Pb, at. beam and surface interaction, scatt. ion yield oscills. 78−55221
He^{2+}+He^+, ionis. and charge transfer cross sections 78−42186
He(He_2)+Ar, metastable destruction rates 78−37728
He($^1S_0$)+Na(Li) radiative Penning ionis., photoionis. cross section depend. of continuum radiation 77−19034
^{3}He-^{3}He interatomic potls., nonlocality, Brueckner calcs. 77−26593
^{3}He-^{4}He isotope mixtures, mag. resonance line widths of 2^3S_1 states, metastability exchange cross sections *(Russian)* 77−10614
^{3}He+^{3}He, collision cross-sections, Ramsauer-Townsend effect 77−6892
^{3}He+^{4}He, metastability exchange, coherency transfer *(Russian)* 78−13594
^{3}He+^{4}He, metastability exchange cross-sections, coherent transfer in 2^3S_1-state 79−89743
^{4}He +X, (X=Nb through to Gd), X-ray production, 0.6 to 2.4 MeV 78−13586
^{4}He+^{4}He, collision cross-sections, Ramsauer-Townsend effect 77−6892
He*, collisional transfer rates between excited levels 79−22793
He*+Ar, Penning ionisation, angular distrib. of electrons 79−89763
He*+D, Penning and assoc. ionis. with metastable He, 0.01 to 10 eV beams 79−27074
He*+H(H_2)(Ar), metastable state, ionis. processes 78−62907
He*+He, (*=excitation or charge), differential scatt. inversion procedure, symmetric exchange, classical, semiclassical theory 79−13802
He*+He, collisional ionisation, cross-section meas. 77−46631
He*+He, collisional ionisation, He_2 $^1\Sigma_g{}^+$ state pot. curve calcs. 77−46632
He*+He, excitation exchange and collisional relax. 80−69226
He*+He, inelastic collision, 1-5 keV, autoionising states 78−13581
He*+Ne, (3^1S, 3^3S, 3^1P, 3^3P) de-excitation cross section temp. depend., time resolved spectra 80−28100
He*+Ne*→He+Ne^++e, Penning ionisation, merging beams obs. 78−33585
He*(^{3}S)+Ar+$\hbar\omega$→He+Ar^+(^{2}P)+e^-, intense laser radiation assisted collisional ionis. 79−76497
He*(2^1P)+Ar→He+Ar^++e^-, anisotropic interaction potential, impact parameter method 77−68102
He*(2^1S)+Ne, elastic and reactive scatt., ang. distribs. 77−6919
He*(2^3S)+F, Penning ionisation and excitation transfer, unified treatment 78−25672
He(2^1S, 2^3S)+Ne(e^-), transition probs., pots. 80−58371
He(2^3S, 2^1S)+Ba(Y)(Ce), Penning process. double ionisation 77−3439
He(2^3S,2^1S)+H, Penning ions. 79−64089
He(2^3S), bi- and ter-mol. deexcitation reaction rate coeffs. meas. in afterglow 79−36748
He(2^3S) collisions, elastic scatt., Penning ionisation, polarisations *(Russian)* 78−70922
He($2^{1,3}$S)+H, autoionising system, Siegert eigenvalues, variational calcs. 79−50106
He(2^1S)+Ar, optical interaction pots. from differential cross sections 77−30956
He(2^1S)+He, long-range excimer pot. determ., high resolution at. beam expt. 77−42371
He(2^3S)+Ar, differential cross-section meas., optical interaction pots. 77−3443
He(2^3S)+H(D), Penning and assoc. ionis. cross sections, vel. depend. 79−22815

atom-atom collisions continued
He(2^3S)+Ne(Ar)(N_2)(CO)(CO_2)(CH_4), high press. afterglow, bi- and termolecular de-excitation rates 77–27168
He($2s^1$S,2^3S)+Ne(Ar)(Kr)(Xe), Van der Waals forces, one-electron model pot. calcs. 80–14094
He($2s^3S_1$)+Sr, alignment of ions in Penning collisions, polarised emission obs. 80–23533
He(3^3S)(3^3P)(3^3D)+He(1^1S), deactivation rate, 300-600K, time-resolved spectra 77–19037
He(5^3D)+He, collisional quenching probability, 2-250 mtorr 78–25679
Hg, 6^3P_0 and 6^3P_1 states, relax. effects. 78–5272
Hg, lifetimes and cross sections of depolaris. collisions of laser working levels 79–76387
Hg, odd isotopes, Lande factor of 6^3P_0 metastable level *(French)* 78–5162
Hg+Ar, spectral line broadening of Hg in UV, interaction pot. 79–26937
Hg+Cd, quantum beats under transfer of orientation 79–98206
Hg+Cs(K)(Na)(Rb), scatt. cross-sections, pseudopot. calcs. 78–9225
Hg+H^+, L-subshell ionisation cross-sections, X-ray meas. 77–46520
Hg+H(H_2), resonance scatt., HgH potential determ. 77–61830
Hg+He, laser excitation of Hg $6s6d6^3D_1$ level, transition probabilities and collisional excitation transfer 78–55146
Hg+He, metastable ccts., in afterglow, $Hg^+(7^2P_{1/2})$ excitation rate const. *(Russian)* 78–29848
Hg+He(Xe), collisionally induced coherence, orientation and alignment, transfer among 6s6d levels 78–74747
Hg+Hg, depolarising collisions in positive column of discharge 78–83639
Hg+Hg*, combination into ungerade dimer states 80–55633
Hg+inert gas, 1849 Å absorption line broadening and shift *(French)* 77–30825
Hg+inert gas interaction potential *(French)* 78–25647
Hg+Na(K)(Rb), 15-1400 eV, electronic excitation, integral cross sections 80–43159
Hg+Ne(Ar), metastable state quenching cross section 77–68731
Hg+Tl, excitation energy transfer, excitation rate consts. 80–37772
Hg+Tl, Tl sensitised fluorescence 78–70778
Hg+Tl vap., sensitised fluoresc. 77–88423
Hg+Zn(Cd), sensitized fluoresc., orientation and alignment transfers *(French)* 79–13808
Hg*+Ar(Ne), 6^3P_0 and 6^3P_2 metastable states, interaction pot. parameters 77–79670
Hg(6^3P_0)+Hg(6^3P_1)$\rightarrow Hg_2^+$+e, plasma formation by strong Hg line irrad., mechanism 78–83585
Hg(6^3P_0)+Hg(6^3P_2), line excitation and population decay in afterglow 80–74242
Hg(6^3P_0)+Na, energy transfer, rate consts. *(Russian)* 79–54952
Hg(6^3P_1)+Hg(6^1S_0), collisional excitation transfer in high mag. fields, fluoresc. obs. 80–9689
Hg($6^3P_{2,0}$)+inert gas, diffusion in low-current discharge 78–63618
Hg(6^3P_2)+Cd(5^1S_0), spectral width of Cd(5^3P_1) line *(French)* 77–50397
Hg(6^3P_2)+Hg, aligned metastable ats., longitudinal and transverse relax. times, simultaneous meas. 78–13585
I, collision-induced $5^2P_{1/2}$-$5^2P_{3/2}$ radiative transition 79–31461
I, recombination in inert gas buffer, computer simulation, rate const., press. depend. 77–25261
I+Ar, press. induced freq. shifts in I photodissociation laser 78–37875
I+Ar(Xe), collision-induced $^2P_{1/2}\rightarrow{}^2P_{3/2}$ emission 77–83528
I+Fe, Fe K-α X-ray emission, high-resolution meas. 80–37871
I+I±I_2, termolecular chemiluminesc. reaction, rate const. for interaction with n-C_3F_7I 79–96291
I+target atom, 15-80 MeV, K-vacancy cross sections, target depend. 77–19026
I+Z (total $Z\geq 100$) adiabatic collision, inner shell X-ray prod., vacancy prod. 79–31675
I_2, recomb. shock heating in unsteady Ar expansion, vibr. relax. effect 77–16794
In+inert gas atom, diffuse series head lines, hyperfine components, broadening calcs. 80–32632
K, 5^2P to 4^2S resonance line, rare gas perturbations, broadening, shift and dipolaris. 78–9126
K atom, formation of electronically excited molecules by photorecomb. of 4P and 4S states *(Russian)* 79–3531
K discharge plasma, K_2 excited mols. form. by K(4P) collisions 80–44013
K, resonance lines broadening and shift by noble gases 79–10070
K+Ar, photon emission polarisation anal., coincidence studies 80–5614
K+Cl$\rightleftharpoons K^+ + Cl^-$, chemi-ionis. and recomb. cross sections 78–33583
K+F(Cl), quasiclassical charge transfer cross section, rel. vel. depend. 77–19073
K+H, covalent and ionic states interaction, config. mixing 78–50613
K+He, 4^2P state $j_1m_1\rightarrow j_2m_2$ Zeeman transition, total cross section energy depend. 80–83475
K+He, 93 eV, excitation of K atom, photon-scatt.-atom coincidence study 78–82829
K+He, fine struct. transitions, energy depend. crossed beam determ. 79–86035
K+He, photon emission polarisation anal., coincidence studies 80–5614
K+He(Ar)(Ne)(Xe), K 5^2P level broadening and collisional relax., quantal, semiclassical and expt. comparison 80–18903
K+He(Ne)(Ar), 0.7-80 keV, K excitation, reson.-line emission and polaris. 80–18911
K+Hg, electronic excitation, integral cross-section, 50-1500 eV 78–62888
K+I chemi-ionisation, integral cross section calc. for two state model 79–18282
K+I chemiionis. differential cross-section calc. for two-state model 79–18283
K+inert gas, quenching cross sections of alkali n^2P states, 5-100 eV 79–76505
K+inert gas atom, resonance levels relax. 77–83684
K+K(Na), excitation in slow collisions 78–70918
K+Kr, differential cross-section meas. by multi-crossed-beam method 79–45797
K+Ne, photon emission polarisation anal., coincidence studies 80–5614
K+Xe, photon emission polarisation anal., coincidence studies 80–5614
K(4^2P)+He(Ne)(Ar)(Kr)(Xe), collisional excitation, differential cross-sections 78–66643

atom-atom collisions continued
K(4p)+He, fine struct. transitions, vel. depend., interatomic pots. 77–42388
Kr plasma, of positive column, at. alignment, radiative lifetimes, collision cross sections 79–4203
Kr, three-body collision-induced light scatt. spectrum moments 78–9226
^{86}Kr, discharge, metastability-exchange cross section 80–99464
^{86}Kr-^{78}Kr, discharge, metastability-exchange cross section 80–99464
Kr+^{75}As, slowing down of atoms/ions with KE≤5 eV by inert gases 79–31650
Kr+Ar*, 123.6 nm emission excitation of Kr by metastable Ar, press. depend. 78–5331
Kr+Ar(Kr)(Xe), total scatt. cross-sections, glory undulations 77–10732
Kr+K, photon emission polarisation anal., coincidence studies 80–5614
Kr+Kr, low-energy collision induced UV radiation 79–50125
Kr+Kr, metastable ats. in afterglow 77–427
Kr+Kr, VUV fluoresc. under monochromatic excitation 78–9237
Kr+Kr(Xe), X-ray prod. cross sections for Kr L-shell vacancies 79–10190
Kr+Rb, spin exchange collison, polarisation transfer, NMR of Kr 78–33453
Kr+target atom, 200-330 MeV, K-vacancy cross sections, target depend. 77–19026
Kr+Ti, 200 MeV, collision, quasimol. bremsstrahlung, semiclassical calcs. 77–88530
Kr+Xe, excitation transferred populations, absorpt. profile analysis 78–74748
Kr+Xe, nonresonant excitation transfer, Doppler profiles, donor levels *(French)* 77–30824
^{83}Kr, nucl. mag. relax. meas. in gas 80–43072
Kr*+Ar*, metastables, chemi-ionis,, merging beams. 0.01-10 eV 80–14198
Kr*+He, $^3P_2$ metastable state, disorientation cross-sections 77–71853
Kr*+He(Ar), vel. changing collisions studied by saturated absorpt. 78–62892
Kr*+Kr, $^3P_2$ state, metastability-exchange and depolarisation, press. broadening of mag. reson. curves 77–71853
Kr_2*, VUV time resolved spectra, formation and decay kinetics 79–31544
Li, wings of resonance lines perturbed by inert gases, intensities 78–37596
Li+He, direct excitation of Li I (nl) levels in keV collisions 78–90280
Li+He, gas-phase collisions, intermediate and high velocities, excitation 80–32822
Li+He, $P_{1/2\text{-}3/2}$, fine-structure transition probability, semiclassical multichannel scatt. matrix 80–37854
Li+He, press. broadening, line shifts 78–5290
Li+He (methane), collisional excitation, prompt decay line energy, projectile Auger spectrosc. 79–85941
Li+He(Ne), 2s$\rightarrow$2p excitation cross sections, model pot. calcs. 77–58152
Li+He(Ne), excitation cross sections, Li I resonance line emission and polarisation 77–61846
Li+He(Ne), inelastic collisions, Baylis-Gombas pseudopot. appl. 77–58151
Li+inert gas, Doppler and collisional broadening, correls. 77–14530
Li+inert gas, fluoresc. reson. line broadening 77–6734
Li+inert gas, quenching cross sections of alkali n^2P states, 5-100 eV 79–76505
Li+inert gas atom, low energy, excitation, emission cross sections and polarisation fractions 80–37867
Li+Li*(H*), resonant ionisation, cross section and ionisation probability 80–63785
Li+Ne, autoionising Ne levels excited in 5-10 keV collisions 78–22017
^{6}Li*+^{7}Li*, laser-induced Penning and associative ionis., $^{13}Li_2^+$ enrichment 78–58796
Li*+He(Ne)(Ar), thermal, high-Rydberg Li behaving as ion core 78–22004
Li*(2^2P_J)+He(Ne)(Ar)(Kr)(Xe), collision induced fine struct. transition rate coefficients determ. 80–74220
Li(2^2S), electron loss in passing through inert gases 79–13805
M+atom, 1 keV to 1 MeV binary encounter stopping cross sections, straggling and screening 78–17754
Mg I, $3^1P_1^0$ level reson. broadening and lifetime 77–57916
Mg, reson. line, Hanle effect, density depend. 79–6917
Mg+H, Mg I lines broadening and shift by van der Waals interaction 77–3303
Mg+Mg, polarisability and London coeff., ab initio variation perturbation calc. 79–13635
Mg+Xe(Ar)(Ne)(He)(Kr), collisional broadening of 285.2 nm line 77–79580
$Mg^+ + H^+$, Mg^{2+} form. by charge exchange and ionis., cross sections 77–83709
Mg(^{3}P)+K(Ca), energy transfer and excimer form. in flowing afterglow 77–60049
Mg*+He(Ne), model pot. curves, including CI 78–42154
Mn-He laser, stimulated emission mechanism, energy characts. 77–3571
N+N, K-shell excitation, Auger electron spectrosc. obs. 80–9714
N+N$\rightarrow N_2$, recombinational afterglow spectra, 10-300K 78–44355
N+Ne, electron excitation, multi-state impact parameter approx. 78–42200
N+O, endoergic chemiionisation, semiclassical theory 79–98208
N+O(^{3}P), endoergic assoc. ionisation, merged beam obs. 79–100348
N+O(C), K-shell excitation, Auger electron spectrosc. obs. 80–9715
N(^{4}S) recombination rate in Lewis-Rayleigh afterglow 79–68968
Na 4D level, relax. by inert gas collisions, expt. 79–68307
Na 4D level, relax. by inert gas collisions, theory 79–68308
Na, energy transfer with 3P-excited atoms, fluoresc. spectrum 78–66498
Na, f-states collisional ang. momentum mixing by inert gas 78–58780
Na, resonant collisions in laser beam 78–78782
Na, wings of resonance lines perturbed by inert gases, intensities 78–37596
Na+Ar, collisional relax. by tri-level echo 78–17774
Na+Ar, excited state photon echo relax. 78–37606
Na+Ar, fine structure transition cross-sections, emission spectra, NaAr form. 78–9085
Na+Ar, two-photon near-reson. light scatt. 77–30941
Na+Ar*, Penning, associative and total ionis. cross sections 77–79683
Na+Ar$\rightarrow$NaAr, quasimol. form., laser spectroscopic obs. 77–57920
Na+Cl$\rightleftharpoons Na^+ + Cl^-$, chemi-ionis. and recomb. cross sections 78–33583

atom-atom collisions continued
- Na+F(Cl), quasiclassical charge transfer cross section, rel. vel. depend. 77−19073
- Na+H, covalent and ionic states interaction, config. mixing 78−50613
- Na+H(Ne)(Kr) vel.-changing collisions, effect on 2 photon and stepwise absorpt. line shape 80−87221
- Na+He, collisional freq. redistrib. of scatt. laser light 77−30815
- Na+He, Na ($3S_{1/2}$-$3P_{1/2}$) photon echo, collision vel. changes and dissimilar electronic states superposition 80−32803
- Na+He (Ne), two-photon optical free induction decay meas. by broadband excitation in unidirectional beams 79−76489
- Na+He(Ar), collision broadening and shift of 3S-4D and 3S-5S lines 79−3406
- Na+He(Ar)(Ne), press. broadening coeffs. of Na 3S-4D transition 78−25481
- Na+He(Ar)(Xe), excited state, collisional depopulation cross-sections meas. 79−86057
- Na+He(Ne), 3s→3p excitation cross sections, model pot. calcs. 77−58152
- Na+He(Ne), excitation cross sections, Na I resonance line emission and polarisation 77−61846
- Na+He(Ne), Rydberg states, cross sections for collisional ang. momentum transfer 79−6997
- Na+He(Ne)(Ar), 3^2P differential excitation, mechanism 79−86052
- Na+He(Ne)(Ar), Rydberg states, collisional angular momentum mixing meas. 77−68093
- Na+He(Ne)(Ar), Rydberg S and D state relax., trilevel echo effect 79−72409
- Na+He(Ne)(Ar), Rydberg transitions, excitation transfer cross-section calcs. 77−50520
- Na+Hg, collision processes, laser excitation, fluoresc. 79−94059
- Na+inert gas, $4D_{3/2}$ and $4D_{5/2}$ levels relax. 78−50526
- Na+inert gas, collisional redistrib., two-photon absorpt. with near-reson. intermediate state 80−23505
- Na+inert gas, fine struct. state changing cross-sections, crossed beam determ. 77−50496
- Na+inert gas, non-Lorentzian spectral line shape 80−106297
- Na+inert gas, Rydberg states, collisional ang. momentum mixing theory 77−10748
- Na+inert gas, Rydberg states transitions, broadening cross-sections meas. 80−69110
- Na+inert gas atom, 4^2D fine struct. transition 79−850
- Na+inert gas atom collisions, optical emission cross section, reson. lines 78−13584
- Na+inert gases, 3S-4D and 3S-5S two-photon line broadening and shift 77−75105
- Na+Kr collisions in laser beam, transition probability 79−50120
- Na+Kr(Xe), excimer bands, multiperturber interactions 78−66497
- Na+Kr(Xe), reson. line broadening, press. depend. 78−66596
- Na+Na, crossed-beam collision, laser-induced Penning and assoc. ionisation, struct. obs. 80−83476
- Na+Na, electronic-field pot. curves determ. for large interatomic distances, excitation cross sections calc. 80−95704
- Na+Na, excited atoms, coupling terms, asymptotic pot., excitation energy transfer 80−23530
- Na+Na, excited atoms, electronic energy transfer, doublets obs. 77−3448
- Na+Na, mol. form. by excited-unexcited atom collision, emission band 4160 to 4570 Å 77−88422
- Na+Na* resonant collisions mechanisms, excitation transfer in strong mag. fields between Zeeman sublevels 77−83712
- Na+Ne, autoionising Ne levels excited in 5-10 keV collisions 78−22017
- Na+Ne, differential cross section at thermal energy, expt. and theoretical results comparison 80−37851
- Na+Ne, electron excitation, multi-state impact parameter approx. 78−42200
- Na+Ne, interaction model potential calcs. 79−86036
- Na+Ne, Na(3p) excitation 80−1056
- Na+Ne, Na(3s→3p) excitation, impact parameter depend. 78−58794
- Na+Ne(Ar)(Kr)(Xe)(N_2)(CO_2), fine struct. changing collisions, vel. depend. 79−22803
- Na+Ne(Ar)(Xe), 3^3P-3^2D line broadening obs. 80−78684
- Na+Ne(CO), 13d-13f transition, collisional dephasing, Ramsey method investig. 79−54791
- Na+Xe, nonreson. two-photon absorpt., 4s excited states and pot. energy curves, close coupled eqns. 80−48068
- Na+Xe+$\hbar\omega$, collisions in presence of nonresonant lasers 80−99567
- Na_2, form., collision-produced diffuse violet emission band obs. 79−27026
- Na(^2P)+Hg, differential cross section, orbiting backward peak, obs. 79−76482
- Na($^3P_{1/2}$)+Ar→Na($^3P_{3/2}$)+Ar, angular scatt. distrib., Doppler spectrosc. obs. 78−94309
- Na($^2P_{3/2}$)+Hg, differential scatt. cross sections 78−66644
- Na($^2P_{3/2}$)+Hg, laser excited atoms, differential cross sections 78−62905
- Na(3^2P_J)+Na($3^2S_{1/2}$), collisional excitation transfer, pot. symm. rules and cond. function 80−9690
- Na($3S_{1/2}$, $3P_{1/2}$) + He, total cross section, stimulated photon echo obs. 79−76503
- Na($3S_{1/2}$,$3P_{1/2}$)+He, total cross section, stimulated photon echo obs. 79−76503
- Nb+Nb, selected MO X-ray coincidence with separated at. K X-rays 80−43148
- Ne, 2p levels prod. by dissoc. recomb. in afterglow, recomb. coeffs., level population 80−43855
- Ne, $2p_1$ level relax. and populations of $1s_2$ and $1s_4$ in afterglow 78−9111
- Ne, $2p^5 3s^3P_0$ state, optical pumping, g-factor, metastability exchange cross section 80−947
- Ne 6328 Å laser transition, homogeneous saturation due to collisions, weak collision model 78−78995
- Ne, collisional transfer coeffs. between 2p levels, in afterglow, laser excitation obs. 80−43856
- Ne, in magnetised positive column fluoresc. obs., 4s and 3d levels props. 77−68006
- Ne, thermalisation of level populations 78−66649
- Ne-Ar liquid mixtures, collision induced absorpt. 77−4638
- Ne-Kr mixture, collision-induced microwave absorpt. 77−88411
- Ne+^{3}He(^{4}He), $2p_4$ state alignment destroying cross sections 79−89757
- Ne+Ar(Kr), translation band spectral moments, induced dipole moments 78−55218

atom-atom collisions continued
- Ne+Ar→NeAr, detection in nozzle beam, total collision cross section determ. 77−61826
- Ne+He, 2p-levels, excitation obs. 80−9712
- Ne+He, population transfer between Ne 2p levels *(French)* 77−30975
- Ne+He$^+$, He(3^1P) level excitation, total emission cross section, fast oscills. obs. 80−58362
- Ne+heavy inert gas, small clusters, beam cluster intensity and collision cross section 77−38711
- Ne+Kr slow collisions, four-state treatment of K-L vacancy sharing 79−45793
- Ne+Na, inelastic scatt. differential cross-section calcs. 77−10730
- Ne+Ne, (He) low pressure broadening and shift of Ne line, Lennard-Jones pot. 80−102554
- Ne+Ne, distorted frozen-orbital method for diabatic mol. orbitals 78−41936
- Ne+Ne, exchange-repulsion energy, many-orbital cluster expansion 80−18896
- Ne+Ne, excitation transfer between 2p levels 78−22006
- Ne+Ne, excitation transfer, coupling coeffs., temp. depend., fluoresc. meas. 78−58620
- Ne+Ne collisions, simultaneous emission of two photons 78−70917
- Ne+Ne(Ar), optical emission spectra 77−14551
- Ne+Ne(He), 7d′ states, isotope shift, press. shift, press. broadening, two-photon spectra obs. 78−55155
- Ne+Ne(He), population transfer from 2p levels *(French)* 79−851
- Ne+Ne(Ne$^+$)(Ne^{2+}), 2s vacancy prod. 78−50623
- Ne+Rb, spin exchange collision, polarisation transfer, NMR of Ne 78−33453
- Ne_2, collision induced Raman spectra and diatom polarisability 80−63647
- Ne($^3P_{0,2}$)+Ne, differential cross sections 80−58370
- Ne* 5882 Å line, Doppler free spectra, press. broadening and shifts, saturation spectroscopy 80−78565
- Ne*+H, assoc. ionis., rovibronic struct. in electron energy spectrum 80−106380
- Ne*+Kr, Penning and associative ionisation 77−6910
- Ne*+Ne, close coupling calc. 78−66652
- Ne*+Ne, metastability exchange by optical pumping *(French)* 77−61845
- Ne*+Xe, chemiionis. in metastable state collisions 79−68306
- Ne($2p^5 3p$)states, radiative lifetimes, collisional deactivation rate consts. 80−69107
- Ni+H$^+$(^{4}He^{2+})(O)(Li), K-shell ionis., impact parameter depend. 77−83707
- Ni+Ni, 39 MeV, X-ray emission spectra, nonLorentzian shape of atomic line tail 78−21872
- Ni+Ni interaction, ab initio HF and CI calcs. 79−59535
- Ni+Ni symmetric collisions, molecular-K-X-ray anisotropy spectra, discrete struct. 77−14560
- ^{58}Ni+p, K-shell X-ray photon proton coincidences, nucl. time delay 79−18281
- O (^1D), collisional quenching by inert gas atoms 78−66648
- O, fine struct. excitation by H impact 77−42384
- O I 5577 Å meteoric forbidden line collisional quenching 77−17448
- O+Ar(Kr)(Xe), magnetically selected O(^3P) state scatt. 80−99543
- O+C(N), K-shell excitation, Auger electron spectrosc. obs. 80−9715
- O+O, K-shell excitation, Auger electron spectrosc. obs. 80−9714
- O+O→O_2, chemiluminesc. matrix reaction, diffusion controlled, 8-20K 78−61013
- ^{17}O+^{16}O, fractionation by chemical equilib. 80−89513
- ^{18}O+^{16}O, fractionation by chemical equilib. 80−89513
- O^{2+}+inert gas, electron transfer meas., 60-200 keV 80−83480
- O(^1D)+Ar(Kr)(Xe), inelastic collisions, spin-orbit coupling 80−5605
- O(^5S)+inert gas, de-excitation cross sections 80−53118
- O(^5S)+Ne(Ar)(Kr)(Xe), total cross sections 78−42188
- O(Se)(S)+inert gas, ^1S-^1D collision-induced transitions 78−33588
- Pb+buffer gas, $^3P_1{}^0 \rightarrow {}^3P_0{}^0$ transition cross section 80−1058
- Pb+Cm, 1sσ excitation probability, scaling law, breakdown at very small internuclear distances 80−58365
- Pb+Pb quasimolecules ab initio calc. of K X-ray spectra 78−21941
- Pb+target atom, 90-110 MeV, K-vacancy cross sections, target depend. 77−19026
- ^{208}Pb+Ag(Au), 5.8 MeV/amu, Pb K-shell excitation probability 78−5338
- Pt+H$^+$, L-subshell ionisation cross-sections, X-ray meas. 77−46520
- Rb, $5^2P_{1/2} \rightarrow 5^2S_{1/2}$ resonance line perturbed by inert gases, depolaris., broadening and shift 78−21880
- Rb in Xe, collision-induced dipole transitions, absorpt. meas. 80−95718
- Rb, laser saturation spectra, collision broadened line struct. *(Russian)* 79−45678
- Rb, quenching cross sections, highly excited states 79−89761
- Rb, radiatively excited states, ionis. rate coeffs. in two atom collisions 80−43160
- Rb, Zeeman resonance lineshapes, motional narrowing 77−46525
- Rb-rare gas collisions with He, Kr, Xe, disorientation cross-section temp. depend. 77−23546
- Rb+^{131}Xer, spin-exchange cross section, ^{131}Xe nucl. spin relax. obs. 80−37868
- Rb+Ar(Kr)(Xe), spectral line breadth and shift, Van der Waals pot. calc. 78−90126
- Rb+atom, Rb Rydberg states, collisional ionisation, rate consts. 80−32817
- Rb+H, single-electron capture total cross sections 80−91656
- Rb+He, quasielastic and inelastic collisions in S and D Rydberg states 80−83462
- Rb+inert gas, hyperfine struct., broadening and shift calcs. 77−58153
- Rb+inert gas, quenching cross sections of alkali n^2P states, 5-100 eV 79−76505
- Rb+Na, spin exchange cross section 78−33637
- Rb+Ne(Ar), spin relax., van der Waals mols. form. 77−19027
- Rb+Rb, ^2P states, near IR spectra, collision induced features 77−10637
- Rb+Rb, radiatively excited states, chemi-ionisation, ionisation rate consts. determ. 80−58363
- Rb+Rb**, freq. shift, line broadening, phase interference effects, Doppler free two photon spectra 80−58200
- Rb+Rb→Rb_2, inelastic light scatt. processes and mol. fluoresc. *(Russian)* 77−61787
- Rb+Xe, interatomic spectrum, theoret. and exptl. obs. 78−9112
- ^{87}Rb+Kr, D_1 line broadening and shift 77−38640

atom-atom collisions continued
- Rb*+He(Xe), thermal, 5p $^2P_{1/2}$ state depolarisation cross-sections 77−71852
- Rb*+Xe+Xe, mol. form., eikonal approx. calcs. 77−14531
- Rb(6^2P)+He(Ar)(Xe), fine-struct. transition cross sections, semiclassical calcs. 77−30972
- Rb(nP)+Rb(inert gas), collisional depopulation Rydberg P state 77−75281
- Rb(nS, $nD_{3/2}$)+Rb(ground state), collisional quenching cross sections 80−43146
- S+Ar, 32 MeV, $K_\alpha{}^h/K_{\alpha\alpha}$ branching ratios, S projectile charge state depend. 79−63947
- S+He(Ar)(N_2)(H_2)(Kr)(Xe), collision-induced emission of S(^{1}S), 232 and 425K 79−81264
- S+inert gas (N_2)(H_2), rare gas sulphide S(^{1}S) emissions 78−82828
- S+S$\rightarrow S_2$, chemiluminesc. matrix reaction, diffusion controlled, 8-20K 78−61013
- S(^{3}P)+N(^{4}S), NS($B^2\Pi$) form. kinetics, chemilum. obs. 79−39151
- Se($^3P_1$)+inert gas, gas phase flash photolytic deexcitation obs., 1000K *(Russian)* 78−50626
- Si $3p^2$($^1D_2$) state collisional quenching 79−22806
- Si+H_2(O_2)(He)($SiCl_4$), $3p^2$($^1D_2$) state behaviour, at. absorpt. spectra 78−29846
- Si*+He, collisional quenching, reson. line absorpt. expt. 78−46297
- Sr, associative ionisation of laser-excited Rydberg states, mass spectrometry obs. 78−94303
- Sr, near reson. laser beam Rayleigh scatt., collisional redistrib. and saturation 77−57938
- Sr+Ca, laser-induced dipole-quadrupole collision 79−98207
- Sr+Ca(Ca^+), laser induced collisional and radiative energy transfer 80−53108
- Sr+D, 2.7 to 31 keV, D^- equilib. charge-state fractions 78−17750
- Sr+He, $^1P_1$ level lifetime, Hanle measurement 80−23365
- Sr+He, nonstatistical excitation of mag. substates of $^1P_1$ level 78−42194
- Sr+inert gas, $^1P_1$-$^3P_1$ excitation transfer 80−102559
- Sr(^{1}S)+Ar, Sr(^{1}P) collisional excitation in nonreson. laser field, four-state model 79−10191
- Sr($5p^1P^0$)+Ca($4s^2\ ^1S$), laser-induced inelastic collisions, theory 77−14552
- Te($^3P_1$)+inert gas, gas phase flash photolytic deexcitation obs., 1000K *(Russian)* 78−50626
- Tl, effect of intrinsic vapour pressure on shape of 258 nm line 77−46539
- Tl, hyperfine struct. optical pumping, O-O transition perturbation 80−949
- Tl, metastable atoms quenching, diffusion and decay in buffer gases 79−54953
- Tl, sensitised fluoresc. in Hg-Tl vap., Doppler broadening 77−3314
- Tl+Ar, stimulated collision-induced fluoresc. and stimulated Raman scatt., simultaneous obs. 78−13463
- Tl+Ba, radiative collisional fluoresc. obs. from thermally excited atoms 80−102480
- Tl+Cs, Tl $6^2P_{3/2}$-state relax., NMR obs. 80−95653
- Tl+inert gas, $6^2P_{1/2}$-$7^2S_{1/2}$ and $6^2P_{3/2}$-$7^2S_{1/2}$ line broadening 77−50475
- Tl+inert gas atom, diffuse series head lines, hyperfine components, broadening calcs. 80−32632
- Tl+Xe, broadening of Tl 377.5 nm line 77−71781
- Tl($^7S_{1/2}$)+inert gas, long-range interaction, spectral line shifts and broadening 79−10174
- U+Pb, K-vacancy form., rot. coupling effect in quasimol. L-shell 78−25692
- U+U, K-shell ionis., classical relativistic trajectory method appl., 1, 10 GeV/n 80−43129
- U+U, superheavy quasimolecule, direct Coulomb formation of 1sσ vacancies 77−3450
- Xe, 3.51 μm broadening due to velocity-changing collisions 78−37597
- Xe, 3.51 μm line press. broadening 77−14390
- Xe, in gas discharge, collisional excitation, radiation lifetimes, macroscopic alignment obs. 80−33734
- Xe, lifetimes and cross sections of laser levels, Hanle effect 77−75480
- Xe, three-body collision-induced light scatt. spectrum moments 78−9226
- Xe+ inert gas, Xe three level system, collisional transfers, disalignment cross section 80−53098
- Xe+^{75}As, slowing down of atoms/ions with KE$\leq$5 eV by inert gases 79−31650
- Xe+Bi, Bi Kα X-ray lines, Doppler broadening 78−62759
- Xe+F, collision in laser field, ang. momentum anal., quantum mech. theory 78−74733
- Xe+He, saturated absorpt. of 3.51 μm line, vel. changing collisions by line width 78−86819
- Xe+Ne, quenching of excited Xe*($^3P_2$, $^3P_1$, $^1P_1$) states 80−63578
- Xe+Pb, 4.6 MeV/amu, 1 sσ vacancy production, impact parameter depend. 79−72393
- Xe+Rb, spin exchange collision, polarisation transfer, NMR of Xe 78−33453
- Xe+target atom, 326-470 MeV, K-vacancy cross sections, target depend. 77−19026
- Xe+Xe, near threshold collision, UV emission 79−54799
- Xe+Xe, VUV fluoresc. under monochromatic excitation 78−9237
- Xe+Xe(6s′(1/2)), (6p(1/2)), energy transfer, rate coeffs. 78−33573
- XeF_2(C) state lifetime, quenching rate consts., photolysis in inert gas atmospheres 80−66816
- ^{136}Xe+Au(Pb)(Bi)(Th), 625 MeV, probability of forming 1sσ vacancies 78−25681
- Xe*+Xe, $^3P_2$ state, metastability-exchange and depolarisation, press. broadening of mag. reson. curves 77−71853
- Zn, gas-phase, plasma, sputtering and beam-foil 80−32820
- Zn I, relative populations in arc, sputtering and gas phase collisions 80−934
- Zn, self-broadened 3075.9 Å line, temp. effects 77−3318
- Zn+inert gas, (ns nd)$^1D_2$ states, Hanle effect, alignment destruction *(French)* 78−5324
- Zn^++He(Ne)(Ar), 1-500 keV, Zn^+ excitation, reson.-line emission and polaris. 80−18911
- Zn(4^3P_2)+Zn(4^1S_0)$\rightarrow$Zn($4^3P_{0,1}$)+Zn(4^1S_0), metastable Zn depopulation, diffusion coeff. determ. 77−23542

atom-ion collisions
includes reactive collisions
see also charge exchange
- 2s-2p excitation probabilities, semiclassical Coulomb approx. calcs. 79−86058
- A^{Z+}+atom, electron capture cross section into arbitrary principal shell, approximation scheme 79−18287
- alkali atom+H^+ charge exchange, eikonal approx. 80−32830
- alkali ion+alkali atom, differential scatt. cross sections 77−28999
- alkali ion+alkali atom, differential scatt. meas. 78−62903
- alkali ion+inert gas, interaction pots., gaseous ion mobilities 77−54584
- alkali metal atom+ion coupling energy, internuclear separation depend. 77−14523
- alkaline earth atom+inert gas ion, double ionisation, cross-section and defect energy *(Russian)* 77−83703
- anisotropic collisions, direct meas. method 80−23498
- Ar^++Cu surface orientation and alignment prod. 78−25687
- asymmetric, polarisation and binding of inner-shell electrons, recoil in close encounters 80−18915
- atom, K_α/K_β X-ray intensity ratio, depend upon energy of incident proton 80−47934
- atom+charged particle, autoionisation state decay 80−9565
- atom+H^+, innershell ionisation 78−62930
- atom+H^+, ionising central collisions and nucl. excitation 80−43164
- atom+H^+, K-shell ionis., plane wave Born approx. model 77−34748
- atom+H^+(He^{2+}), excitation functions rel. to ionisation *(French)* 79−31669
- atom+ion collisions, electron capture, quasi-molecular binding corrections 78−90287
- atom+light ion, dipole transitions in K-shell ionisation 78−90281
- atom+multicharged ion, exchange interaction energy *(Russian)* 80−1047
- atom+multiply charged ion, charge exchange 78−58813
- atom+multiply charged ion, slow collisions, MO calcs. 80−23504
- atom+negative ion, term parameters, electron spectra and scatt. cross sections 77−27148
- atoms and highly charged ions, charge exchange 78−62913
- Auger electrons in mol. ion+solid (gas) targets 79−45814
- Auger spectra, high-resolution 77−83558
- autoionising transitions excited in atom+ion (electron) collisions 77−42390
- Ba^++inert gas, ($^2P_{3/2}$) states relax. cross sections 78−13595
- bare ion+hydrogenic ion, forward electron capture, third Born approx. calcs. 78−58782
- Bates distortion approx., impact-parameter formulation 78−17739
- CA(s)+$B^{++}\rightarrow A^+ + B^+$(p), charge exchange, at term pseudointersection, level degeneracy effect 79−27084
- chamber 1.5 m diameter for experiments *(Japanese)* 77−54625
- channelled ions, atomic collisions in crystal lattices, resonant coherent excitation 80−15170
- charge exchange, symmetric, below 1 keV, cross sections calcs. 77−532
- charge transfer, new integral eqn. calc. method 79−45832
- charge transfer between target inner shells, projectile K shells 79−89778
- charged particle excitation processes 77−71862
- closed shell atom+ion interaction, electron gas model, polarisation inclusion 78−37699
- collision spectroscopy, book 79−27065
- collision system, pot. curves at low collision energies, beam studies 80−61088
- Coloumb excitation of atoms by fast protons, proton energy loss depend. on impact parameters *(Russian)* 80−53123
- conference, electronic and atomic collisions, Paris (July 1977) 78−58758
- continuum electron capture and loss in ion-gas and ion-solid collisions, cusp spectroscopy of forward peak 80−14201
- continuum photon emission, radiative electron capture, mol. orbital emission 77−42401
- coulomb deflection in ion-atom collisions 79−94074
- Coulomb ionisation of inner shell electrons, screening effects 78−74749
- Coulomb ionisation of K-shell electrons in heavy ion collisions, DWBA calcs. 78−37731
- Coulombic ionisation of inner shells 78−62898
- coupled state equation 79−50109
- diabatic molecular orbitals for inner-shell excitation 78−62897
- diatomic molecules, variable screening model 78−74587
- direct scattering theory for neutral and charged ats. 80−23483
- drift tube studies, buffer gas mixture choice, for ion-neutral reactions 79−57232
- drift tube technique in ion-neutral collisions, cross sections determ. 80−63748
- elastic scattering, inversion problem, quasi-potential method 80−37850
- electron angular and energy distrib., first Born approx. 80−53116
- electron capture, at. expansion method 79−45833
- electron capture, non relativistic theory and Coulomb pot. anal. 80−32804
- electron capture from inner shells by fully stripped ions 77−54607
- electron capture into arbitrary principal shells of energetic projectile ions 79−89777
- electron capture processes in ion-atom collisions, review 78−70930
- electron detachment in atom-negative ion collisions, linear approx. in generalised zero-range pot. model *(Russian)* 79−94076
- electron ejection from fast ions, low electron velocity, anisotropy effect 80−37856
- electron excit., variational method 77−23547
- electron loss cross section, asymptotic form 79−13807
- electron rearrangement in K X-ray spectra due to heavy ion bombardment 77−85846
- electron spin coupling in rot. frame, X-ray emission 79−36724
- electron transfer collisions time independ. quantum theory with nonorthogonal basis and R-matrix propag. 79−89769
- electronic and at. collisions, conf., Kyoto, Japan (Aug.-Sept. 1979) 80−57011
- electronic and at. collisions, conference, Kyoto, Japan (Aug.-Sept. 1979) 80−62394
- electronic stopping power of ions, (ions C-Xe; targets H-Xe) 80−12859
- emission electron angular and energy distribution 80−87222
- exchange matrix elements with momentum transfer, impact-parameter formulation 79−31648
- excitation in energetic ion-atom collisions accompanied by electron emission, book contrib. 78−74756
- F ions recoiling in gases, hyperfine interactions 78−74735

atom-ion collisions continued
fast heavy ion + atom, and solid targets, ionis. and excitation states 78−70927
fast heavy particle collisions, radiative ionisation 77−14562
fast ion + atom, energetic electron emission as charge transfer process, Born approx. 80−53126
fast numerical calcs. 80−43161
flame, mutual ion neutralisation 80−35537
fully ionised heavy ions, scaling of electron capture in light gas targets, low MeV energies 79−64102
gas-phase and ion-surface collisions, optical emission 80−32821
H^+ + Mg collisions double electron capture 78−58777
halogens, surface ionisation, on LaB_6, using ion source 78−60538
heavy atom + $^4He^{2+}$ 2-5 MeV, inner shell ionisation cross section 79−45825
heavy atoms, α-particle impact K-shell ionisation, 40 to 110 MeV 78−17752
heavy ion + at. collisions using GSI linear accelerator, X-ray production, appls. 77−19041
heavy ion + atom, 1sσ MO excitation probability and binding energy, X-ray coincidence 78−94316
heavy ion + atom, 3dπ-2pπ radial coupling, symm. and near symm. collisions 77−71857
heavy ion + atom, double K-shell vacancy sharing 79−45809
heavy ion + atom, K-vacancy production, universal scaling law 79−22811
heavy ion + atom, outer shell electron emission, differential cross sections 79−45817
heavy ion + atom, radiative electron capture, target thickness depend. 78−58778
heavy ion + atom (molecule), multiple electron loss cross sections meas. 79−45818
heavy ion + atom collisions, accelerators and X-ray emission spectra *(Norwegian)* 78−22013
heavy ion + atom collisions, K X-ray transition energies, two electron-one photon mechanism 77−18828
heavy ion + atom collisions, mol. M-X-rays, self-consistent relativistic HF-Slater many electron correl. diagrams 77−14567
heavy ion + atom collisions, quasimol. X-ray line tails 77−14564
heavy ion + atom collisions, small impact parameters, K-vacancy prod., molecular theory 80−69229
heavy ion + C coil collisions, electron emission, energy distribs., solid state effects 77−19062
heavy ion bombardment, swift, X-ray prod. *(Japanese)* 77−23540
heavy ion collision, K-shell vacancy sharing, variation-perturbation mol. model 79−31665
heavy ion collisions, 3dσ mol. orbital ionisation 78−94311
heavy ion collisions, Doppler shift of continuum X-rays from quasimols. 79−22808
heavy ion collisions, electronic states in rot. two-centre Coulomb systems 77−14561
heavy ion collisions, quasimol. KX-ray spectra, Doppler shift 77−19044
heavy ion collisions, radiative electron capture, line profiles 77−14565
heavy ion interactions with gases, measurement apparatus 79−31741
heavy ion quasimol. collisions, electron pair prod., vacuum polaris. shakeoff 77−30945
heavy ion reactions, dynamical properties, field overview 80−18327
heavy ion small impact parameter collisions, dynamic screening model 77−50525
heavy ion-atom collisions, cross sections for electron production 79−89767
heavy ion-atom collisions, inner shell ionis. X-ray emission and Auger spectra obs., appls. *(Japanese)* 78−9240
heavy ions, critical two-centre distance, HFS relativistic calc. 79−22801
heavy ions in gases, charge state distribs. 78−5334
heavy ions moving in solids, vacancy config. determ. 77−69019
heavy ions passing through C foils and gases, charge-state distrib. 78−42191
heavy ions passing through gas or solid target, electron capture effect on X-ray emission 77−27169
heavy particles, impact-parameter treatment, differential scattering amplitude 78−37711
heavy particles, stopping in gases, $\bar{W}$-values expt. results 79−7000
heavy-ion collision, azimuth angle depend. of quasimolecular anisotropy 79−68298
heavy-ion collision, quasimolecular L X-rays, relativistic self-consistent correlation diagram 78−5247
heavy-ion collisions, 3dσ mol. orbital, ionisation probability 80−23538
heavy-ion collisions, charge transfer, target K-shell electron capture, impact parameter depend. 80−102552
heavy-ion collisions, electron slip effects on quasimolecular X-ray emission 77−19040
heavy-ion collisions, intermediate L-K mol. orbital radn. spectral distrib. 77−50511
heavy-ion collisions, K-vacancy production, 1sσ excitation of transient mol. orbital 77−83718
heavy-ion collisions, K-vacancy production, 2 pσ mol. orbital, single and multiple collisions 77−83717
heavy-ion collisions, nuclear charge movement induced, X-ray transitions 77−50510
heavy-ion collisions, $Z \geq 35$ projectiles, 12 to 470 MeV, K-vacancy cross sections 77−19026
heavy-ion collisions at high-energies, positron prod. 77−27137
high-Rydberg atom + gaseous target technique, thermal energy 78−22004
high-Rydberg state high-impact-velocity forward charge transfer as classical process 79−22824
high-Z atom + H(He)(O)(F)(Cl) ions, 1sσ vacancy prod., relativistic and Coulomb deflection effects 78−58801
highly charged atom + ion, slow collisions, one-electron capture 78−58776
highly excited states, decay spectra 80−63780
highly ionised ion + atom (molecule), many-electron transitions in violent encounter 78−90274
hyperfine perturbation of ions recoiling in gas, Scherer-Blume theory 77−46617
impact ionisation, inner shell alignment calcs. 80−83473
impact parameter method, excitation and electron capture cross sections 78−33591
inelastic transitions between close at. levels, cross sections, rate coeffs. 77−3467

atom-ion collisions continued
inert gas, field ionis. and proton capture, critical energy deficits 78−82853
inert gas, metastable composition of inert gas beam from ion-neutral reaction 77−29008
inert gas + F , hyperfine interactions of recoiling fast ions 77−18469
inert gas + O^{n+}, (n = 4 to 7) small impact parameter collisions, dynamic screening model 77−50525
inert gas + S^{n+} (n = 5 to 9), small impact parameter collisions, charge exchanging processes, electron promotion 80−14227
inert gas atom + alkali ion, collision studies of quasi-one-electron systems 80−63750
inert gas atom + H^+, outer S-shell ionisation cross-sections calcs. *(French)* 78−42212
inert gas atom + highly stripped ion, multiple-ionis. cross sections, Monte Carlo calcs. 79−64091
inert gas atom + ion, electron capture cross section, 200-4000 eV 79−76512
inert gas atom + $Ne^{2+}(Ar^{2+})(Kr^{2+})(Xe^{2+})$, low energy reactions, SIFT and drift tube obs. 80−97705
inert gas atom + H^+, electron capture, charge-state distrib. 80−32814
inert gas hollow cathode arc, mol. beam sampling of metastable atoms as electron temp. probe 80−43967
inert gas ion + atom electron transfer collisions, cross section meas. 79−5143
inert gas ion-atom collisons, momentum transfer rate consts., energy depend., polarisation pots. 77−75260
inert gas ions, $X^+(^2P_{1/2})$, conversion into dimer ions 78−70903
inert gases, ionis. in energy range 200-4000 eV 77−27174
inert gases + Ar^{6+}, collisional excitation, excitation cross sections 79−98209
inner atomic shell ionisation, binary collision model, low vel. 80−5612
inner shell electron excitation by heavy ion collisions 80−37873
inner shell excitation, impact parameter dependence 77−19047
inner shell excitation 80−63749
inner shell excitation processes in heavy ion-atom collisions, review 80−37874
inner shell ionisation by electron, positron and proton impact 77−19090
inner shell ionisation by heavy charged particles, semiclassical approx. 77−14559
inner shell ionisation by nuclei, impact parameter dependence 77−23557
inner shell two-electron one-photon transition probabilities 77−14557
inner shell vacancy formation 78−70926
inner-shell collisionally-induced excitation spectra, single electron description failure 79−45815
inner-shell excitation cross sections, scaling props. 77−19048
inner-shell excitation in heavy ion collisions, variational method 79−31428
inner-shell ionisation, binary collision model, electron momentum distrib. 79−54962
inner-shell ionisation, by proton impact, at. pot. calcs., Ramsauer effect 77−10745
inner-shell ionisation, heavy charged particles, review 78−42181
inner-shell ionisation of quasimolecular system, perturbation theory 79−31667
innershell ionisation, proton and electron impact equivalence at high vel. 77−14556
interference structure, He^- + He optical emission interpretation 79−45816
intermediate energy, close coupled and Glauber eikonal theory 78−25643
intermediate energy, electron capture cross-section calcs. 78−42206
interstellar molecules synthesis, laboratory studies of ion-atom reactions 80−67812
ion + atom collisions, ionis., charge transfer, model 77−75278
ion + ion, Coulomb-Born and unitarised Coulomb-Born cross-sections 78−82815
ion + neutral atom, reactant internal energy, rate constants, drift tube 80−30231
ion accelerator applications, outside nuclear physics *(Polish)* 79−40641
ion beam pumped X-ray laser, progress report 79−45920
ion excitation cross section calc., effective Feynman diagram approach 80−23531
ion excited state lifetimes meas. using orientation transfer in Penning collisions *(French)* 78−50621
ion kinetics in high-pressure laser plasmas 80−64002
ion motion, in RF quadrupole field, collision effects 77−75261
ion-induced electron distributions, experimental resolution and background effects 79−36749
ion-metal atom processes, charge exchange cross sections, calcs. and computer program 78−55236
ion-neutral atom, in foil, inner-shell processes, oscill. X-ray spectra excitation 77−54565
ion-Rydberg atom collision cross sections, classical trajectory Monte Carlo calcs. 80−43174
ionisation, post collision interactions in at. excitation processes 78−58803
ionisation or excitation, binary encounter approx. 79−22804
ions, proton excitation approximations, erratum and extension 79−35118
ions, supermultiplet lines excited by beam surface interaction 78−13459
K- and L-shell ionis. by protons, plane-wave Born cross sections 80−12858
K-L and L-K vacancy sharing in highly asymmetric collisions 79−45812
K-shell atomic ionisation by heavy particle, electronic relativistic effects, Dirac wavefunctions, semiclassical effects 78−78792
K-shell Coulomb ionisation, scaling parameter, relativistic correction 79−72407
K-shell double ionis., K$\alpha\alpha$ and K$\alpha\beta$ obs. 77−57918
K-shell excitation absolute cross section, $0 < Z < 11$, 40-600 keV 79−41231
K-shell hole, multiple hole production, charge transfer and antisymmetry 80−43168
K-shell hole production by light ions, hydrogenic and Hartree-Fock model of target 77−83715
K-shell ionis., X-ray prod. cross section for incident H^+, ^4He and ^{14}N ions 78−70923
K-shell ionis. by charged particle impact, electronic relativistic effects 80−28099
K-shell ionisation, by heavy ion impact, Magnus (sudden) approx. 77−68106
K-shell ionisation, light ion-induced, Coulomb deflection effects 77−71855

atom-ion collisions continued
K-shell ionisation, refinement to simple ionisation theories 77−75275
K-shell ionisation, X-ray or Auger-electron prod. by ion impact, cross section tables 79−54947
K-shell ionisation by Coulomb excitation, plane-wave Born-approx. 79−18272
K-shell ionisation by H^+, electronic final states description 77−38723
K-shell ionisation by heavy particles, theoretical cross-sections and expts. 80−48076
K-shell ionisation by protons, semiclassical approx. 77−19039
K-shell ionisation probability by protons, $E_p=100$ keV-2 MeV, impact parameter depend. *(Japanese)* 78−86945
K-shell ionization in heavy-ion collisions, book contrib. 78−82834
K-shell vacancy prod., impact parameter depend. 79−13803
K-vacancy production, heavy ion collisions, K-L level matching 78−42196
K-vacancy production by relativistic H^+ or e^- 79−50126
K-vacancy sharing probabilities 77−27146
kinematic dipole model for the anisotropy of quasimolecular X-rays 79−13814
KK-vacancy sharing, X-ray emission 78−42190
L_I-shell ionisation, high-energy impact, relativistic plane-wave Born approx. 79−54970
L-shell Coulomb ionisation, electronic relativistic effects 77−42391
l-shell Coulomb ionization by heavy charged particles 79−94073
L-shell ionisation by heavy charged particles, binding energy correction 77−54604
L-shell X-rays of elements $Z=35$ to 56, Coster-Konig threshold effects 77−18831
L-vacancy production, near symmetric heavy ion collisions 79−89768
lanthanide atom$+H^+$, L-subshell ionisation cross-section, 150-400 keV 79−45665
laser excitation mechanisms for atomic and ionic lasers, book contrib. 80−106512
light ion+heavy atom, inner-shell ionisation, adiabatic effects 80−99561
long-range interaction, anal. Born-Oppenheimer pot. energy function calcs. 78−1048
low energy, ionisation, total cross-section meas. 77−54606
low energy, ionisation cross sections, diffusion eqn. calcs. 77−54605
M-subshell direct Coulomb ionisation, X-ray emission, PWBA calcs. 79−45664
M-subshell ionisation cross section, by H^+ impact, binary encounter approx. 78−62890
many-electron stripping in heavy ion collisions 77−75277
molecular beam or atomic beam as target for ion-atom collision studies 78−70971
molecular orbital X-ray emission, from primary exciting collision 77−50449
molecular orbital X-rays, scaling law derivation 79−18284
molecular orbital X-rays from atomic and molecular impact on solid targets 79−36750
molecular X-rays from heavy-ion collisions, superheavy quasi-molecule spectroscopy 80−23509
multielectron collisions, charge transfer at intermediate energy, atomic model 80−91652
multielectron target+multiply charged ion, electron capture, review 80−63812
multiple electron transfer to highly charged ions, scaling of cross sections 77−83711
multiple ionisation by fast nuclei, cross sections calc. 77−23558
multiple scattering in molecular gases, target at.+energetic ion spatial correlation influence 79−27062
multiply charged collision systems, slightly asymm., curve crossings, constraints, MO theory 78−74734
multiply charged ion+atom, autoionisation, electron and photon emission 80−63813
multiply charged ion+one-electron target, electron capture, review 80−63811
negative ion+atom, electron detachment, zero range Fermi approach 80−63798
negative ion+neutral atom, autoionisation states investigation by Rydberg series broadening and displacement *(German)* 79−85938
negative ions, at. and mol. collisions electron detachment for energies near threshold 80−63797
neutral atom$+H^+$ calculation of certain second Born integrals 79−59578
nonadiabatic couplings for ionizing transitions and the determination of switching functions 79−22813
nonadiabatic transitions between decaying states *(Russian)* 77−10754
nuclear motion, quantum-mech. and classical treatment, book contrib. 78−74736
nucleus+hydrogenic atom electron capture, ultrarelativistic limit relativistic corrections 80−14230
one electron charge transfer and capture, partial and total cross sections 78−70931
one-electron ion+He(N)(Ar), sum-rule Born cross sections, excitation and ionis. contribs. 79−22812
perturbed stationary state, improved approach 78−90282
PIXE, single photon emission in double K-shell ionisation 77−71864
plasma containing multiply charged ions, two-electron capture processes 80−43854
positron formation by heavy ion collision, calibration energy transfer for Coulombionisation 79−76506
projectile charge dependence *(Dutch)* 79−50121
quantum scattering theory, R-matrix propagation methods in inelastic and reactive collisions 79−59534
quasi molecular description, diabatic correl. diagrams 79−3525
quasiatoms formed in heavy-ion collisions, high energy electron emission spectra 79−3554
quasiclassical theory, transition between spatially degenerate levels 80−43150
quasimolecular formation in heavy ion collisions, X-ray radiation *(Russian)* 78−33568
quasimolecules, superheavy, M-like X-ray transitions 79−6951
radiative charge exchange, high energy 78−55234
radiative collision-induced photoionisation 78−62858
radiative electron capture, photon ang. distrib., retardation effects 79−41234
rainbows, interference, and diffr. effects *(Dutch)* 79−50110
repulsive potential reconstruction from ion mobility in gas data 80−23486

atom-ion collisions continued
rotationally induced atomic excitation, quasimolecular orbital rot. coupling, uniform Airy approx. 78−25644
Rydberg atom+ion, collision theory 78−62909
Rydberg atoms, cross sections, theory 77−58172
Rydberg state atom+ion, electron capture, asymptotically high impact vel. 79−54965
screening, relativistic effects in variable-screening model 77−14516
semiclassical approx., atomic excitation 77−58149
semiclassical approx. for inelastic collision 79−6989
single-electron loss, total Born-approx. cross-sections atoms up to Fe 77−83714
sloping boundary of continuum, term entry, Born method calcs. 79−89744
slow collision, electron detachment *(Russian)* 77−30985
slow collision, K-shell ionisation, variational calcs. 78−42162
slow collisions, K-shell excitation, impact parameter depend. 79−72388
slow collisions, K-shell excitation of relativistic atoms 80−48073
slow ion+atom collisions, coherent excitation and decay of autoionising states 79−45789
slowly colliding asymmetric systems, equivalence of Born and adiabatic approxs. 80−18894
strong field QED in atomic phys., Dirac eqn., autoionisation model, QFT 77−54495
structure and collisions of ions and atoms, book 78−74554
superheavy, positron form. 78−62873
superheavy elements, proton-induced K- and L-shell ionis. cross sections, comparison with actinide fission prod. X-rays 77−50581
superheavy ion-atom collisions, quasiats., K-vacancy form., positron emission 80−63753
superheavy quasimolecules, Bang Hansteen scaling rule, $K\alpha_1$ line anal. 79−10126
superheavy quasimolecules, inner-shell ionisation, scaling behaviour 78−25691
superheavy quasimolecules, inner-shell vacancy formation, coupled channel anal. 80−48116
symmetric, two-electron excitation, scaling rule for 2-electron and 2-hole systems 79−81265
third-row elements, at. K-shell X-ray prod. by $^{14}N^+$ bombardment 80−91482
total cross section, explicit bounds by geometric method 80−43130
transition between highly excited levels, cross section *(Russian)* 78−13593
two k-shell vacancy systems, one-electron and two-electron one-photon transitions 78−58775
two-electron rearrangement X-ray transitions, theory 77−38633
vacancy sharing process, Nikitin two-state model 80−9684
variable screening model appl. for slow collisions 77−42387
variational method for polarisation and energy loss, time depend. 79−59536
very heavy ion-atom collisions, inner shell electron binding energies 80−43169
wake-bound electron contrib. to convoy electron vel. distrib., effect of ionic field 80−60729
X-ray cross-sections, plane wave Born approx. 77−68094
X-ray emission, in low vel. collision, ang. distrib., MO calc. 79−54803
X-ray emission, mol., produced in heavy ion+at. collisions, anisotropy 77−19046
X-ray emission, noncharacteristic, in heavy ion+at. collisions, by direct (Coulomb) ionisation 77−19045
X-ray emission, noncharacteristic, MO, radiative electron capture X-rays 77−19043
X-ray polarisation 79−45810
x-ray production in heavy ion-atom collisions, book contrib. 78−74757
X-ray spectra excited by high-energy ions 79−49976
X-ray transitions, K_α/K_β ratio 80−27972
X-ray transitions for F and O ions moving in Ne, Ar, Kr gases and C foils and slabs 77−69020
X-ray transitions in heavy ion collisions 80−43170
$A^+ + 2A \rightarrow A_2^+ + A$, gas phase reaction rate const. calc. 78−92457
$AR+N^+(O^+)$, electron emission, double differential cross sections, Auger spectra 79−45684
Ag, K-shell ionis., X-ray prod. cross section for incident H^+, ^4He and ^{14}N ions 78−70923
Ag+Ag symmetric collisions, MO-2pσ radiation anisotropy, quasimolecular nature 78−70924
$Ag+H^+$, 1 MeV, K-shell ionisation probability, ang. depend. 77−71859
$Ag+H^+$, characteristic X-ray emission polaris. *(Russian)* 79−59394
$Ag+H^+$, excited X-ray polarisation, Born approx. calcs. *(Russian)* 80−78566
$Ag+H^+$, K-shell ionisation, 7-15 MeV, relativistic effects 78−82830
$Ag+H^+$, K-shell ionisation cross-section determ. 80−48077
$Ag+H^+$, L-shell ionisation at large scatt. angles 78−90283
$Ag+H^+$, X-ray emission, optical transition radn. 78−58618
$Ag+H^+(He^+)$, K-shell X-ray prod. cross sections 78−5337
$Ag+H^+(O^{5+})$, L-shell X-ray prod. cross-section determ. 77−6913
$Ag+I^+$, impact parameter depend. of K X-rays 78−94308
$Ag^{+14}N^{n+}$, 7-35 MeV, K-shell X-ray production cross sections 77−75090
Al, ion beam bombardment, $(1s^{-1}2p^{-1})^1P_1$ state nonstatistical population, X-ray spectrum 78−62894
Al, K-shell hole production by light ions, hydrogenic and Hartree-Fock model of target 77−83715
Al+Al, (Cl)(F), molecular K X-ray transitions, mol. radiative electron capture effect 78−58802
$Al+H^+$, K-shell ionis., impact parameter depend., 90-200 keV 78−17775
$Al+H^+$, K-shell ionisation 0.5 to 40 MeV, meas. and PWBA-BEA calcs. 80−78699
$Al+H^+(^3He)$ ion collisions, K-shell ionisation cross sections 77−23555
Al+H(D)(He)(Li) ions, K-shell ionis., universal cross sections 78−62895
$Al+He^+$, X-ray spectra, two-electron one-photon transition in solid target, 2 MeV 78−94209
$Al+He^+(H^+)$, 1.9 MeV, $K\alpha$ X-ray polaris. and line strengths 77−30983
Al+He(C)(O)(Ne), K-shell ionising collisions, average L-shell ionisation probability, K_α spectra 79−72408
Al+heavy ion, X-ray spectra, one-photon two-electron rearrangements 77−6712

atom-ion collisions continued
- $Al+N^{4+}$, $K\alpha$ and $K\beta$ X-ray spectra for 84 MeV incident energy 77-50517
- $Al+N^{n+}(O^{n+})(F^{n+})$, X-ray prod. and electron transfer cross-section 79-45790
- $Al^{n+}+S(Ar)(Al)(Cu)$, K-shell vacancy sharing ratio, foil or gas target 78-42198
- Ar, autoionising levels excited by heavy ion impact 79-13804
- Ar, energy dependence of $\bar{W}$ for alpha particles 79-6999
- Ar, He^+ 100-1000 keV impact excit. $1s_2$ and $1s_4$ reson. states 77-10611
- Ar, heavy ion induced LMM Auger electron spectra 77-6907
- Ar ion+target collisions, two-electron-one-photon transitions, X-ray spectra 77-19068
- Ar, outer 1s, 2s and 2p electron loss cross sections by multicharged ions 78-42185
- Ar, single-K multiple L-shell vacancy prod. in ion collisions, X-ray spectra 79-22809
- Ar, stationary afterglow obs. of singly charged atomic ions, three-body rate coeffs. 80-38757
- Ar-Ti hollow cathode afterglow, energy transfer mechanisms and excited metallic ion prod. 80-43857
- $Ar+{}^4He^{2+}$, ionis. cross section, Z^3 effect 78-33595
- Ar+Ar low energy collisions, K X-ray excitation, impact parameter depend. 80-23539
- Ar+Ar partially stripped ion, stopping power 80-91651
- $2Ar+Ar_2{}^+=Ar+Ar_3{}^+$, equilib. consts., mass spectrometric determ. 79-100347
- $Ar+Ar^+$, charge exchange, Σ oscill. and spin change 80-74247
- $Ar+Ar^+$, differential cross section, pot. curve fitting, reson. electron exchanges 77-58118
- $Ar+Ar^+$, multielectron excitation energy calcs. 78-1071
- $Ar+Ar^+(Ar^{2+})(Ar^{3+})$, electron stripping cross-sections meas. 80-83477
- $2Ar+Ar^+(Kr^+)$, three body reaction, rate coeffs., temp. depend., 100 to 300K 80-108703
- $Ar+Ar^{2+}$, charge transfer, energy defect and sealing laws 80-48083
- $Ar+Ar^{z+}(Ne^{z+})$, outer s-subshell vacancy production 79-18275
- $Ar+C^{2+}(O^{4+})(Si^{n+})$, n=10,11,12, intense low energy autoionisation lines 79-31674
- $Ar+C^{4+}(C^{6+})$, K-shell X-ray prod. at high energy, charge state independ. 77-6905
- $Ar+C^{6+}(O^{8+})$, bound- and continuum-state electron capture in gas, strong correlations 80-9730
- $Ar+Cu^{x+}(11\leq x\leq 22)$, 1 MeV/amu, X-ray production cross-sections 78-37714
- $Ar+F^-$, inner-shell ionisation, X-ray cross sections 80-58369
- Ar+H collisions, L Auger multiplet excitation 77-14589
- $Ar+H_2{}^+$ endothermic charge transfer reaction, low energy crossed beam study 80-95720
- $Ar+H^-$, collisional electron detachment, complete ang. distrib. 78-66650
- $Ar+H^-$, low-energy total electron detachment cross-sections, approximation 79-72405
- $Ar+H^+$, ang. and energy distrib. of ejected electrons 79-31668
- $Ar+H^+$, charge transfer and ionisation cross sections 79-89766
- $Ar+H^+$, importance of d-state couplings in charge transfer, ionisation 79-89760
- $Ar+H^+$, ionisation, doubly differential cross sections calcs. 80-9726
- $Ar+H^+$, low energy, L-shell ionisation, binding energy correction 77-54604
- $Ar+H^+$, subshell electron capture cross sections 79-89771
- $Ar+H^+$ ions, K-Auger spectra, relative satellite line intensities, X-ray spectra 77-19066
- $Ar+H^+(H_2{}^+)(He^+)$, ionisation double differential cross sections 80-18913
- $Ar+HHe^+$, ab initio pot. energy data, SCF-LCAO calcs. 80-63530
- $Ar+He^+(He^{2+})$, ionisation, differential cross-sections, 0.3 to 2 MeV 79-81271
- $Ar+K^+$, inelastic collisions, emission cross sections, quasimol. state interference 77-61848
- $Ar+Li^{+1,2,3}$, K-shell ionisation depend. on projectile charge state 77-34743
- Ar+multicharged ion collisions, one electron capture from inner shells 80-58376
- Ar+N ion, $K\alpha$ X-ray satellites prod. 80-9541
- $Ar+NO^+$, reaction product ratios, 300K 80-7783
- $Ar+NO^+$, reaction rate consts. meas. 80-7782
- Ar+negative ion, electron-loss cross sections 80-37877
- Ar+proton, charge transfer, target K-shell electron capture, impact parameter depend. 80-102552
- $Ar+Xe^+$, $XeAr^+$ form., dissoc. energy, reaction equilib. and rate consts. 80-61071
- Ar^++Ar, 1-10 keV, charge exchange cross section meas. 78-25697
- Ar^++Ar, 1-500 keV, inelastic energy loss, ionis. phenomena, theoretical model 77-34747
- Ar^++Ar, charge transfer, fine-structure transitions 80-63808
- Ar^++Ar, L-shell X-ray cross sections, 0.2-1.5 MeV, fluoresc. yield 78-1068
- Ar^++Ar, L-vacancy production, close collisions, 50-375 keV 77-54599
- Ar^++Ar, quasi-resonant charge transfer at thermal energies 80-48082
- Ar^++Ar, quasimol., Auger transition probability, internucl. distance effect *(Russian)* 77-75116
- $Ar^++Ar(He)$, 100-550 keV, 3s vacancy production 79-13809
- Ar^++H_2, $a^3\Sigma_g{}^+\rightarrow b^3\Sigma_u{}^+$ continuum emission excitation 79-41200
- Ar^++He, integral elastic scatt., repulsive potentials derivation 80-63744
- Ar^++molecule (atom), dissociative reaction rate coeffs., in high-press. afterglow 79-87837
- $Ar^{2+}+Ar(Kr)(Xe)$, single electron capture excitation, photon emission, VUV spectroscopy 80-58379
- $Ar^{2+}+Na$ collision, single electron capture into Ar^+ excited states, 0.2-12 eV, emission cross section 80-48071
- $Ar^{2+}+Na$ collision, single electron capture into Ar^+ excited states, relative population distrib. 80-48072
- $Ar^{5+}+Al(Si)(S)(Cl)$, chem. environment effect on $K\alpha$ satellites intensity 77-54527
- $Ar^{n+}+He$, $3\leq n\leq 8$, single and double electron transfer cross-sections 77-6924
- $Ar^{n+}+S(Ar)(Al)(Cu)$, K-shell vacancy sharing ratio, foil or gas target 78-42198
- $Ar^{x+}+Kr(N_2)$, (x=2-7), electron capture cross sections, 10-110 keV 77-6923

atom-ion collisions continued
- $Ar^{x+}+Sn(Sb)(Xe)$, vacancy sharing between K and L shells in $3d\sigma$ mol. orbital 79-22807
- Au, ion impact, L-subshell ionis. cross-section ratios 77-6920
- Au, X-ray production cross sections for protons, fluoresc. obs. 80-102476
- $Au+{}^4He^{2+}$, L-shell ionis. probability, X-ray prod. 79-18276
- $Au+Au^{x+}(Br^{x+})(Cl^{x+})$, differential single-scatt. cross sections at MeV energies 78-33570
- $Au+H^+$, atomic K-shell ionis., X-ray emission 79-18280
- $Au+H^+$, K-shell ionisation, 7-15 MeV, relativistic effects 78-82830
- $Au+H^+$, L-subshell X-ray prod., cross-section meas. 77-46575
- $Au+H^+$, relativistic K-shell ionisation cross-section meas. 78-33593
- $Au+H^+$ ionisation, induced L-shell alignment 80-32813
- $Au+H^+(D^+)$, L-subshell vacancy production, Coulomb deflection effects 80-9711
- $Au+H^+(He^{2+})$, L-subshell ionisation with high vel. positive ions 79-50122
- $Au+He^{2+}$, high energy ionis. probability, semiclassical approx. with relativistic Hartree-Fock function 79-6998
- Au+I, 25 MeV I, average ionisation probability of Au meas. 77-68005
- Au+I, noncharacteristic X-ray emission, self-consistent relativistic many-electron correl. diagram 77-19023
- Au+light and heavy ions, L-shell X-ray production and subshell ionisation cross sections meas. 80-91637
- Au^++X, $X=H$, H_2, He, C, N, O, cross-section, closure-Born approx. 78-66630
- B, K-shell ionis., double and single, cross section meas. by ion bombardment 78-50629
- B, X-ray spectra, chemical bonding and multiple ionis. effects 78-50630
- $B+C^{2+}(N^{2+})(O^{2+})$, K Auger electron spectra 79-89758
- B+C(N)(O) ions, 10-40 MeV, soft X-ray spectra 77-75089
- $B+H^+(He^+)$, double K-shell ionis., projectile Z depend. 78-25680
- $B^{3+}+H$, charge transfer cross sections, ab initio potential energy curves 78-37741
- $B^{5+}+He(C)(Ne)$, K-shell charge transfer cross sections, Bates-Born formalisms 79-45834
- $B^{q+}+Ar(He)(H_2)$, keV electron capture cross section 80-14229
- ${}_5{}^{10}B^{n+}+Cu$ to Rb, 4-38 MeV, K-shell ionis., X-ray obs. 79-59549
- Ba^+ + inert gas atom, spectral line polarisation 79-13811
- Ba^++Ba, $6p^2P$ level lifetimes, depolaris. cross-sections, Hanle effect obs. 79-26943
- Ba^++inert gas atom collision, polarisation of emitted radiation, quasimol. interf. effect *(Russian)* 77-46633
- Ba^++Kr, quasimolecular states interference, degree of polaris. oscill. *(Russian)* 77-6917
- Be isoelectronic series, atom$+H^+$, low-lying ^3P term excitation, cross-sections and rate consts. 79-94069
- Be, K-shell ionis., double and single, cross section meas. by ion bombardment 78-50629
- Be, X-ray spectra, chemical bonding and multiple ionis. effects 78-50630
- $Be+H^+(He^+)$, double K-shell ionis., projectile Z depend. 78-25680
- $Be^++H_2(He)(Ne)$(methane), Be Auger spectra 77-57951
- Be^++He, autoionising core-excited Be II states, alignment prod. 80-14204
- $Be^++He(Ne)$, charge transfer and excitation, differential cross sections, 2-5 keV 79-36764
- $Be^++He(Ne)$, ns-np excitation, alignment and orientation, impact, parameter theory 80-91648
- $Be^++He(Ne)(Ar)$, Be II 2^2P excitation, alignment and orientation 80-91647
- Be^++Ne, 180 degree phase jumps for Be^+(2s-2p) excitation amplitudes, coherence obs. 80-63793
- Be^++Ne, $2s\rightarrow 2p$ excitation probability for Be^+, coherence parameters 79-54955
- Bi, ion impact, L-subshell ionis. cross-section ratios 77-6920
- Bi+Xe, 1.13 GeV, deep inelastic nuclear reaction, electronic $1s\sigma$ vacancy prod., compound nucleus 80-27662
- ${}^{209}Bi+{}^{209}Bi$ collisions, 1 GeV, mol. orbital X-rays 79-49978
- Br, 12-60 MeV, ion-atom collision, K-vacancy prod., mol.-orbital model 77-68095
- Br, ion collisions, 12-60 MeV, K-vacancy production, multiple and single collisions in mol. orbital excitation 77-83717
- Br ion+target collisions, K-X-ray yields, $1s\sigma$ excitation 77-19051
- Br, ion+target collisions, X-ray yields, K-L level matching 77-19052
- Br ions+target collisions, K-X-ray yields, K-vacancy sharing 77-23548
- Br K-X-ray yields, $2p\sigma$ excitation 77-23549
- Br+Br, symmetric collisions, MO-$2p\sigma$ radiation anisotropy, quasimolecular nature 78-70924
- Br^-+He, electron detachment, SCF calcs., $BrHe^-$ and BrHe pots. 80-23503
- $Br^-+He(Ne)(Ar)(Kr)$, total electron detachment cross sections, near threshold energies 79-3555
- Br^-+K, differential cross-section, small angle scatt. 79-98186
- $Br^{25+}+Br^{25+}$. correlation diagrams, inner-shell vacancy prod., characteristic X-rays 77-83503
- C, cross sections of interactions of protons 77-50538
- C+C(N)(O) ions, 10-40 MeV, soft X-ray spectra 77-75089
- C+C(N)(O) ions, 4 to 40 MeV, beam-foil K-shell X-ray prod. cross sections 78-33461
- $C+H^+$, absolute C K X-ray production cross sections, 18-26 MeV 77-83719
- $C+H^+$, K-shell ionis., impact parameter depend., 90-200 keV 78-17775
- $C+H^+$ collision, electron capture cross section 80-63804
- $C+H^+(H_2{}^+)$, vel. distrib. of convoy electrons, anal. 78-33600
- $C+H^+(He^+)$, K-shell ionisation, impact parameter depend. 78-62891
- $C+H^+(He^{2+})$, K-shell Auger electrons ang. distrib. 79-89756
- C+proton, charge transfer, target K-shell electron capture, impact parameter depend. 80-102552
- C^++H, fine struct. excitation cross section 77-38724
- C^++H radiative association, implications of CH^+ predissociated levels obs. 80-37838
- $C^++H(H_2)$, 0.1-13 keV electron capture cross-sections meas. 79-36761
- C^++Ne, energy loss collision spectrosc. 79-86037
- $C^{2+}+H(H_2)$, electron capture cross-sections, 0.5-14 keV 78-42205
- $C^{3+}+Al(Si)(S)(Cl)$, chem. environment effect on $K\alpha$ satellites intensity 77-54527
- $C^{4+}+H$, charge transfer cross sections, ab initio potential energy curves 78-37741

atom-ion collisions continued
$C^{6+}+Ar$, electron capture to continuum states, forward ejected electron spectra 79—45831
$C^{6+}+H$, low velocity charge transfer, two-state approximation calcs. 78—42207
$C^{q+}+Ar$, continuum electron capture and loss, 1.6-2.8 MeV/A 78—46443
$C^{q+}+Ar$, continuum electron capture, projectile vel. and Z depend. 78—55222
$C^{q+}+H(H_2)$, q=1-4, single electron capture cross sections 78—55233
$C^{x+}+He$, electron capture, K X-ray emission ang. distrib. 77—57919
$CO_2^{+}(CO_2^{2+})$+atom(mol.), dissoc. and charge transfer 77—65532
$^{12}C+X$, X=Ti-Pb, atomic K-vacancy production 77—23543
Ca, X-ray production by protons by 0.5 to 2.0 MeV energy 78—66646
$Ca+{}^{41}Ca$, transverse decoupling of hyperfine interactions in free atoms 77—18468
$Ca+Ca^{+}$, collision cross sections, Ca_2^{+} pot. energy calcs. 79—27055
$Ca+H^{+}$, K X-ray production, 0.2-0.5 MeV, ionis. cross-section 79—31459
$Ca+NH_4^{+}(CH_3NH_3^{+})(PH_4^{+})$, proton transfer reaction cross sections, 1-6 eV 78—20003
Ca^{+}+ inert gas atom, spectral line polarisation 79—13811
Ca^{+}+inert gas atom collision, polarisation of emitted radiation, quasimol. interf. effect *(Russian)* 77—46633
$Ca^{+}(4s\ ^2S_{1/2})+Sr(5s^2\ ^1S_0)$, laser induced charge transfer to excited electronic state 79—81274
Cd II+He, relax. consts. for depolarising collisions 77—19239
$Cd+H^{+}(^2H^{+})(He^{2+})$, inner-shell ionisation, Coulomb repulsion effects 80—48075
$Cd+H^{+}(He^{2+})$, L- and M-shell Auger electrons 79—27076
$Cd+He^{+}(He_2^{+})$, Cd^{+} excited state prod. by Penning and charge exchange reactions 77—15252
$Cd+He^{+}(He_2^{+})$ collisions, slow, Cd II excitation 77—83701
$Cd+Na^{+}$, $Cd(5^3P_1)$ and (5^1P_1) and mag. sublevels, excitation cross-sections 80—9710
$^{106}Cd+H^{+}$, simultaneous nucl. and K-shell excitation, ^{107}In lifetime meas. 80—63130
Cl ion+target collisions, two-electron-one-photon transitions, X-ray spectra 77—19068
Cl ions+Ar-methane, (isobutane), energy straggling 78—58785
Cl+Al, molecular K X-ray transitions, mol. radiative electron capture effect 78—58802
Cl+He(C)(O)(Ne), K-shell ionising collisions, average L-shell ionisation probability, K_α spectra 79—72408
$Cl^{-}+Ar \rightarrow Cl+Ar+e$, rate const., absolute total cross section, expt. results discrepancy 77—513
$Cl^{-}+Ar \rightarrow Cl+Ar+e$, rate const., expt. discrepancy 77—514
Cl +He(Ne)(Ar)(Kr), total electron detachment cross sections, near threshold energies 79—3555
Cl^{-}+inert gas atom, electron detachment and inelastic processes 78—42208
$Cl^{-}+Na(K)$, differential cross-section, small angle scatt. 79—98186
$Cl^{+}+Ar$, L-shell X-ray cross sections, 0.2-1.5 MeV, fluoresc. yield 78—1068
$Cl^{+}+He(Ne)(Ar)$, highly charged low vel. recoil ion time of flight spectra, cross section energy depend. 80—14222
$Cl^{13+}+Ne$, Li-like Ne X-ray and Auger line intensities and populations 77—10625
$Cl^{4+}+Xe(Ar)$, 20 MeV, electron loss cross sections, pot. model data anal. 79—27082
$Cl^{5+}+Ca(Sc)(Ti)$ thick targets, 30 MeV, near symmetry collisions, double-K-vacancy sharing 79—3391
$Cl^{n+}+Ar$, K X-ray cross sections, 15 and 30 MeV, impact parameter depend. 77—19032
$Cl^{n+}+Cl(Ar)$, branching ratio dependence on projectile velocity and nuclear charge 79—31475
$Cl^{n+}+Cu$, effect on projectile charact. X-rays and REC of target thickness 79—45662
$Cl^{n+}+Ne(SiH_4)(H_2S)(HCl)(Ar)$, K X-ray cross section, projectile charge depend. 77—19029
$Cl^{n+}+S(Ar)(Al)(Cu)$, K-shell vacancy sharing ratio, foil or gas target 78—42198
$Cl^{n+}+Ti(Ni)$, 35 MeV, K-shell vacancy sharing, impact parameter depend., X-ray obs. 77—71858
$Cl^{q+}+Cu$, K X-ray production and radiative electron capture, fluoresc. yield determ. 80—99553
$Cl^{x+}+Cl(Ti)(Ni)$, K-shell ionization probability in energetic nearly symmetric heavy-ion collisions, 35 MeV 79—27078
$Cl^{x+}+Sn(Sb)(Xe)$, vacancy sharing between K and L shells in 3dσ mol. orbital 79—22807
$Cl^{x+}+X$, (X=atom with Z=11-22), K-shell ionis. cross sections 78—13596
$^{35}Cl^{4+}$+atom (molecule), multiple electron loss cross sections meas. 79—45818
Co, X-ray spectra, chemical bonding and multiple ionis. effects 78—50630
$Co+H^{+}$, K-shell ionisation cross-sections calcs. 80—43165
Cr, gas-phase, plasma, sputtering and beam-foil excitations 80—32820
Cr, X-ray production by protons by 0.5 to 2.0 MeV energy 78—66646
Cr, X-ray spectra, chemical bonding and multiple ionis. effects 78—50630
$Cr+H^{+}$, K X-ray production, 0.2-0.5 MeV, ionis. cross-section 79—31459
$Cr+H^{+}$ ion collisions, K-shell ionisation cross sections 77—23556
$Cr+N^{4+}$, Kα and Kβ X-ray spectra for 84 MeV incident energy 77—50517
$Cs+He^{+}$, spin dependent charge transfer in low-energy collisions 77—75293
$Cs^{+}+Ar(Kr)(Xe)$, elastic beam scatt., repulsive pots. 79—98184
$Cs^{+}+Cs$, mol. ion form. rate, from mobility meas. 79—34299
$Cs^{+}+X$, X=H, H_2, He, C, N, O, cross-section, closure-Born approx. 78—66630
Cu, K-shell ionis., X-ray prod. cross section for incident H^{+}, ^4He and ^{14}N ions 78—70923
Cu, large angle K-shell ionisation probabilities, projectile charge and mass depend. 78—74750
$Cu+C^{n+}$, radiative electron capture, target electron momentum distrib. 78—1075
$Cu+Cl^{q+}$, X-ray cross sections, projectile fluoresc. yields 78—74751
$Cu+H^{+}$, atomic K-shell ionis., X-ray emission 79—18280
$Cu+H^{+}$, Cu K-shell ionis., probability ang. depend. 77—14553
$Cu+H^{+}$, K-shell ionis., Coulomb deflection effects, 0.5-2 MeV 78—17779
$Cu+H^{+}$, K-shell ionisation cross-sections calcs. 80—43165
$Cu+H^{+}$, K-shell ionisation cross-section determ. 80—48077
$Cu+H^{+}$, K-shell ionisation 0.5 to 40 MeV, meas. and PWBA-BEA calcs. 80—78699
$Cu+H^{+}$, X-ray emission, optical transition radn. 78—58618
$Cu+H^{+}(He^{+})$, K-shell X-ray prod. cross sections 78—5337
$Cu+X^{n+}$, X=F, Al, Si, S, K X-ray production, target thickness depend. 77—75280
$Cu^{q+}+Kr$, K-vacancy production, impact parameter depend. 79—72390
$D+D_2^{+}(CO_2^{+})(CO^{+})(N_2^{+})(HCN^{+})$, reaction, ion cyclotron reson. mass spectrometric obs. 79—64098
$D+H^{+}(D^{+})(He^{+})(Ne^{+})(Ar^{+})(Kr^{+})$, reson. charge charge transfer from photoexcited donor state 79—22820
$D^{+}+Ar$, electron capture to continuum states, forward ejected electron spectra 79—45831
D^{+}+atoms (Z=27 to 34), K shell ionisation, nuclear Coulomb effect 80—91650
$D^{+}+D$, thermal energy collisions, quantum mech. calcs. 80—23507
$D_2^{+}+N \rightarrow ND^{+}+D$, product kinetic energy distrib. obs. 77—46619
D_3^{+} +inert gas, ion decay, 1-40 eV *(Russian)* 78—90286
$D_3^{+}+Cs$, electron capture to D_3^{-} and D_3^{0} repulsive states 79—59563
$D^{0}(D^{+})+Cs$, D^{-} formation, ang. distrib., total cross sections 77—529
$Dy+H^{+}$ ionisation, induced L-shell alignment 80—32813
Eu^{+} metastable states in discharge plasma, anomalously high speed deexcitation, modulation of induced radiation obs. 80—44014
$Eu+H^{+}$, atomic K-shell ionis., X-ray emission 79—18280
F ion+solid target collisions, K-shell ionisation, X-ray emission cross sections 77—19069
F ions+Ne(Ar)(Kr) and C foil and slab, K shell X-ray spectra 78—17599
F^{7+}, $1s2p\,^3P_1$ collisional quenching, perturbation theoretic calc. 77—54602
F+Al, molecular K X-ray transitions, mol. radiative electron capture effect 78—58802
$F+C^{2+}(N^{2+})(O^{2+})$, K Auger electron spectra 79—89758
F+Co(Fe) recoil, transient mag. field 78—29838
$F+N^{4+}$, bonding effect on Kα satellite struct. 79—59392
$F+Xe(H)^{+}(H_2)$, $(^2P_{3/2})$ state quenching, Franck-Condon approach 78—66640
F^{-}+atom (Z=10-57), K-shell ionisation, X-ray prod. in transition region, collision symmetry effects 80—43163
$F^{-}+Na(K)$, differential cross-section, small angle scatt. 79—98186
$F^{6+}+He$, 10 to 40 MeV, F^{6+} K-vacancy production, role of excitation 80—37859
$F^{7+,8+}+H_2(He)$, 20-56 MeV, F K X-ray cross sections, inner shell Coulomb excitation 77—19025
$F^{8+}+He$, X-ray prod. cross sections resulting from electron capture and electron excitation of F^{8+} ions 79—3557
F^{n+}+Ag foil, 10-40 MeV, Ag L-shell X-ray production 77—71856
$F^{q+}+He$, (q=1-9), X-ray prod. by electron excitation, ionisation and capture 79—76379
$F^{q+}+Ne$, MO X-ray prod. obs. 79—45663
$F^{q+}+Ne$, radiative electron capture X-ray profiles from fast collisions, calcs. 79—49975
$F^{q+}+Ti(V)(Cr)(Fe)(Co)$, target and projectile cross-sections, X-ray prod. yields 79—81269
$F^{x+}+He$, electron capture, K X-ray emission ang. distrib. 77—57919
$F(^2P_{1/2})+H^{+}(Xe)$, nonadiabatic collision processes, electronic degrees of freedom, classical model 79—64062
$^{19}F+Z$, Z=22 to 57, 2 to 28 MeV, prod. of target atom K-shell X-rays 79—18285
Fe group elements, singly ionised, charge transfer, rel. to laser action 80—74246
Fe II+H in type 1 Seyfert galaxies and quasars, collisional excitation rel. to permitted Fe II lines 80—62278
Fe ion+Fe(Ni) collisions, X-ray spectra, two-electron transitions 77—19050
Fe, X-ray production by protons by 0.5 to 2.0 MeV energy 78—66646
Fe, X-ray spectra, chemical bonding and multiple ionis. effects 78—50630
Fe+Fe, symmetric collisions, MO-2pσ radiation anisotropy, quasimolecular nature 78—70924
$Fe+H^{+}$, K X-ray production, 0.2-0.5 MeV, ionis. cross-section 79—31459
$Fe+H^{+}$, K-shell ionisation calcs. 80—23534
$Fe+H^{+}$, K-shell ionisation cross-section determ. 80—48077
$Fe+H^{+}$ ion collisions, K-shell ionisation cross sections 77—23556
$Fe+N^{4+}$, Kα and Kβ X-ray spectra for 84 MeV incident energy 77—50517
Fe+Ni, two electron one-photon X-ray transitions, Dirac-Fock calcs. 78—17600
$Fe^{4+}+N_2(Ar)(Kr)(Xe)(SF_6)$, 20 MeV, gaseous targets, electron loss, charge state yields 79—54957
Fe^{n+}+atom(molecule), multiple electron loss cross sections meas. 79—45818
$Fe^{n+}+H(H_2)$, 50-1200 keV amu^{-1}, impact ionis. and electron capture cross-sections 78—42204
$Gd+H^{+}$, K-shell ionisation, 7-15 MeV, relativistic effects 78—82830
$Ge+{}^{14}N^{n+}$, 7-35 MeV, K-shell X-ray production cross sections 77—75090
Ge+Ge, symmetric collisions, MO-2pσ radiation anisotropy, quasimolecular nature 78—70924
$Ge+H^{+}$, K-shell ionisation cross-sections calcs. 80—43165
H, collisional ionisation by fast low-charge-state ions 79—86056
H, Coulomb ionisation, Glauber scatt. amplitude, integral representation 77—6915
H, cross sections of interactions of protons 77—50538
H, excitation by charged particles, differential cross-section, quasiclassical approx. *(Russian)* 77—79676
H, excited state electron and ion quantum scatt. cross sections, dipole approx. *(Russian)* 79—6996
H, highly excited atom, H^{+} and e collision processes, transitions between degenerate states at low energies 77—79685
H, highly excited atom, H^{+} and e collision processes, Glauber approx. and n-changing transitions 77—79686
H, Stark broadening by ion impact on moving emitter, Doppler H shift, theory 80—47940
H , electron loss in passing through inert gases 79—13805

atom-ion collisions continued

- $H^+ + X$, ($X = Nb$ through to Gd), X-ray production, 0.6 to 2.4 MeV 78−13586
- H^+ and H^- beams, charge transfer cross sections in gases and vapours, 10 eV to 10 keV, graphs and tables 80−32824
- H^+, calc. of mobility in He, 10 to 700K 78−66629
- H^+ induced ionisation cross-sections, thick target technique 78−37726
- H-like ion + H charge stripping processes 77−19072
- H-like ion + H^+, 1s-2s excitation probabilities, low energy, Coulomb-Born approx. 80−37870
- H-like ions + heavy particle, bound state effect on ionisation cross sections 78−25682
- H + charged particle, Glauber approx. scatt. amplitudes 80−14191
- $H + {}^{16}O$, hyperfine interactions of highly stripped ions recoiling into H 77−22932
- H + atom (ion), ionis. by one or two electron at. particles, Born approx. 79−54960
- H + atom(ion)(electron), general excitation cross section theory 80−37869
- $H + B^{4+}(C^{5+})(O^{7+})$, excitation distrib. following electron capture 79−36763
- $H + B^{n+}(C^{n+})$, one electron capture and loss 80−18921
- $H + C^{6+}$, collisional electron removal, cross-sections, mechanisms 78−25683
- $H + C^{6+}(He^{2+})$, ionis. cross sections 79−22805
- $H + Cl^- \rightarrow HCl + e$, associative reaction, product vibr. state distrib. 80−66794
- H + completely stripped positive ions, electron capture 77−23559
- $H + H_2^+(HeH^+)(CO_2^+)$, reaction, ion cyclotron reson. mass spectrometric obs. 79−64098
- $H + H^-$, electron loss by 1-300 keV H^- ions 80−37857
- $H + H^-$ collisions, assoc. detachment process theory 79−44351
- $H + H^- \rightarrow H + H + e$, electron detachment from H^- 80−37855
- $H + H^+$, 1s→2s excitation at intermediate energy, close coupled and Glauber eikonal theory 78−25643
- $H + H^+$, 50-200 keV, excitation and ionis., U-matrix method calcs. 78−17778
- $H + H^+$, charge exchange and differential scatt., theoretical calcs. 77−10729
- $H + H^+$, charge exchange probability 79−98216
- $H + H^+$, classical 3 body collision, cross section, energy transfer, computer calcs. 78−17783
- $H + H^+$, coupled state calc., charge transfer and direct ionis. 79−22810
- $H + H^+$, cross section for production of metastable H(2S) state 78−13588
- $H + H^+$, differential energy loss cross-sections 77−46630
- $H + H^+$, electron capture, H(2s) cross section meas. 79−72386
- $H + H^+$, electron capture in 3s level, distortion approx. 80−37876
- $H + H^+$, energy transfer and ionisation cross-section calcs 77−50522
- $H + H^+$, excitation, differential cross-section 79−59547
- $H + H^+$, excitation, distorted wave and coupled-channel calcs. 80−9713
- $H + H^+$, excitation, pseudostate expansions and second Born approx. 79−45796
- $H + H^+$, excitation and charge transfer to 2s(2p) states, 49-125 keV 80−18910
- $H + H^+$, excitation ang. differential cross section, 25, 50 and 100 keV incident 78−66651
- $H + H^+$, excited atom collisions, transitions between degenerate states 77−30976
- $H + H^+$, fast proton total electron capture cross section, fixed scattered approx. 79−22819
- $H + H^+$, H excitation, angular differential cross sections 80−63784
- $H + H^+$, H(2p) production in slow collisions, peak struct. 80−1057
- $H + H^+$, ionis. modified second Born approx. 77−88546
- $H + H^+$, low energy, optimised translation factors 80−18813
- $H + H^+$, nuclear repulsion, contrib. to charge transfer 80−18922
- $H + H^+$, quantum theory of ionisation in fast collisions 79−3553
- $H + H^+$, resonant charge exchange in planetary coronas rel. to spectral line profiles 78−77508
- $H + H^+$, resonant charge transfer in presence of lower field 79−64072
- $H + H^+$,(He^{2+}), excitation, asymptotic cross-sections calcs. 79−18279
- $H + H^+$ close capture collision spectroscopy, impact parameter perturbed stationary states 78−22002
- $H + H^+$ collision, eikonal approximation, reson. charge exchange ang. distrib. and atom refl. *(Russian)* 77−34759
- $H + H^+$ coupling energy, internuclear separation depend. 77−14523
- $H + H^+$ low energy, quantum theory, integrated cross sections, phase shifts 77−30957
- $H + H^+(Arq^+)(Kr^{q+})(B^{q+})(C^{q+})(N^{q+})(O^{q+})$ charge transfer and impact ionis. cross sections calcs. 77−88555
- $H + H^{2+}$, electron capture in 3s level, distortion approx. 80−37876
- $H + He^+$, excitation of H to n=2 state, cross-section calc. 79−41229
- $H + He^{2+}$, charge transfer cross sections, molecular bases calcs. 79−98217
- $H + He^{2+}$, electron transfer, plane-wave factor, mol. state treatment 80−63807
- H + heavy charged ion, total electron capture cross section charge depend. oscill. behaviour 78−66656
- H + heavy ion (highly stripped), electron loss, charge state depend. 78−70921
- H + highly stripped ions, energy gap and couplings at pseudocrossings 79−3526
- H + highly stripped ions, S-matrix construction 79−3527
- H + hydrogenic ion, one electron excited atom ionisation collisions at high energy, improved impulse approx. 79−94072
- H + ion, charge exchange and ionis. cross sections *(Russian)* 79−50130
- $H + Li^{3+}(Be^{4+})(B^{5+})(C^{6+})$, charge transfer cross sections, distorted wave Born approx. 79−72415
- $H + Ne^{10+}(Si^{14+})(Ca^{20+})$, charge transfer, total and partial cross-sections calcs. 80−23542
- $H + O^{8+}$, electron removal, charge transfer and impact ionisation cross-section 79−76504
- $H + O^{n+}(N^{n+})(C^{n+})(B^{n+})$, charge transfer cross sections, oscillatory behaviour in low-energy collisions 80−63806
- H + positive ion collisions, producing H atoms in arbitrary p-state, charge transfer 79−64074
- H + proton, high-Rydberg state high-impact-velocity forward charge transfer as classical process 79−22824
- $H + Xe^{n+}(Ar^{q+})(Fe^{q+})$, electron capture by heavy multicharged ions at low velocities total cross sections meas. 80−99548

atom-ion collisions continued

- $H + Zn^{2+}(Cd^{2+})(B^{2+})(Mg^{2+})(C^{6+})$, electron capture by slow ions, pseudo-crossing 80−43176
- $H^- + Ar$, 0.5 MeV H(H) ionisation comparison 79−41230
- $H^- + Ar$, electron detachment, 0.5 to 1.0 MeV 78−22021
- $H^- + Ar(H_2)(He)(N_2)(Ne)$, collisional detachment cross-sections, high-energy obs. 77−3442
- H^- + atom, electron loss high energy cross sections 78−13597
- $H^- + H^+ \rightarrow H(1S) + H$, level degeneracy effect on charge exchange at term pseudointersection 79−27084
- $H^- + H(He)$, electron detachment cross sections 78−90265
- $H^- + H(He)$, electron detachment in adiabatic regime, mechanisms 80−63800
- $H^- + H(He)$, electron-loss cross-section, double closure calcs. 77−50518
- $H^- + He$, electron detachment, theoretical obs. 80−63799
- $H^- + He$, electron detachment collision 80−23536
- $H^- + He(Ar)$, electron detachment cross sections 78−58810
- $H^- + He(Ne)(Ar)$, differential scatt. cross-sections, time of flight spectra 78−42161
- H^- + inert gas, negative ion detachment cross section determ. 80−63796
- $H^- + N_2$ (inert gas), charge transfer, ejected electron spectra 79−45828
- $H^0 + N^{3+}$, electron loss cross section 80−63805
- $H^+ + Ag(Zr)(Fe)(Cu)(Ti)$, K-shell ionisation cross-section, 85 to 790 keV 80−106390
- H^+ + alkali metal, charge exchange, eikonal approx. calcs. 80−78703
- $H^+ + Ar$, 5-1.5 MeV, ejected-electron energy and ang. distrib., differential cross sections 77−88547
- $H^+ + Ar$, Hα and Hβ emission cross section 80−63783
- H^+ + atom, electron capture, two-state atomic expansion 78−62912
- H^+ + atom, inner shell ionis., coincidence exptl. method, theory 80−1066
- H^+ + atom, inner shell ionisation, electronic relativistic effects 77−23552
- H^+ + atom, ionis. cross section, realistic vel. distrib. for target electron 78−46439
- H^+ + atom, K-shell ionis. cross section for atoms, modified binary encounter model 78−46440
- H^+ + atom, K-shell ionisation, semiclassical approx., projectile trajectory dependence 77−23551
- H^+ + atoms (Z=27 to 34), K shell ionisation, nuclear Coulomb effect 80−91650
- $H^+ + Au(Bi)(u)$, L X-ray production cross sections, 0.3-1.8 MeV, expt. rel. to PWBA prediction 80−53115
- $H^+ + C(N)(O)(Ne)(Ar)$, electron capture cross sections 78−62912
- $H^+ + Cs$, electron capture, H metastable fraction of n=2 population 77−30988
- $H^+ + Cs(Rb)(K)(Na)$, single-electron capture total cross sections 80−91656
- $H^+ + Cs(6s)$, elastic scatt., pot. determ. from differential cross-sections meas. 78−78778
- $H^+ + Cs \rightarrow H^- + Cs^{2+}$, proton conversion, 0.2 to 6.0 keV *(Russian)* 77−1920
- $H^+ + H$, 1-7 keV, H(2s) form. and Lyman-α polarisation 80−14221
- $H^+ + H$, 15-200 keV, excitation and charge transfer cross sections, Sturmian expansion 77−19024
- $H^+ + H$, 1s charge exchange amplitudes, impact parameter calcs. 77−534
- $H^+ + H$, capture cross sections, Faddeev anal. 77−27178
- $H^+ + H$, charge transfer, variationally consistent approximation scheme 79 22825
- $H^+ + H$, charge transfer collisions, angular distribution 78−13599
- $H^+ + H$, charge transfer cross section calc., up to 100 keV 78−55235
- $H^+ + H$, excitation and electron capture, impact parameter calc. 78−33591
- $H^+ + H$, gas-phase collisions, intermediate and high velocities, excitation 80−32822
- $H^+ + H$, inelastic collision, time depend. Schrodinger eqn. for electron motion 79−89774
- $H^+ + H$, ionisation and electron capture to continuum 80−58366
- $H^+ + H$, vibr. excited H_2^+ form. by stimulated radiative association 79−100346
- $H^+ + H$ high energy collision, excitation multipole moments, classical trajectory approx. 80−106389
- $H^+ + H(He)(Ar)$, K-electron capture, cross section scaling, high energy 79−41236
- $H^+ + H(1s)$, radiative charge exchange, 1-50 MeV 78−55234
- $H^+ + H(1s) \rightarrow H(1s) + H^+$, electron capture at relativistic energies, scatt. amplitude 80−1061
- $H^+ + He$, 25-1000 keV, $1^1S \rightarrow n^1S$ excitation cross sections, Glauber approx. calc. 79−54959
- $H^+ + He$, double electron capture, close-coupling approx. calcs. 77−71868
- $H^+ + He$, electron capture total cross sections 78−5322
- $H^+ + He$, excitation, ang. differential cross-sections for 25, 50 and 100 keV protons 78−82832
- $H^+ + He^+$, fast collision, ionisation and charge transfer, cross section meas. 78−25698
- $H^+ + He^+$, ground-state electron capture cross-sections, Coulomb-Born calcs. 78−42166
- $H^+ + He(Ar)$, emitted electron's energy and angular distrib. support for charge transfer to continuum theory 78−37740
- $H^+ + He(Ar)$ electron transfer cross sections 78−58809
- $H^+ + He(Ar)(C)$, ionisation processes viewed in forward direction 77−71866
- $H^+ + He(C)(Ne)$, K-shell charge transfer cross sections, Bates-Born formalisms 79−45834
- $H^+ + He(Ne,Ar)$, charge transfer into continuum 79−89765
- $H^+ + He(Ne)(Ar)$, ionisation, projectile energy depend., secondary electron energy distrib. 78−42211
- $H^+ + He(Ne)(Ar)$, K-shell ionisation cross-sections, Glauber approx. calcs. 77−46629
- $H^+ + He(Ne)(Ar)(Kr)$, charge exchange, 80 to 1500 eV, total cross sections 77−61854
- $H^+ + Kr$, mol. orbit approach, spin-orbit interaction, adiabatic pot. and projected valence band treatments 77−533
- $H^+ + Li$, charge exchange, eikonal approx. calcs. 80−78703
- $H^+ + Li^+$, charge transfer and ionisation, total cross sections for production of Li^{2+} determ. 80−91657
- H^+ + methane, (Ne), (Ar), inner shell electron capture cross-sections 79−76510
- H^+ + multielectron atom, fast collision, electron capture, differential cross section calcs. 78−94318

atom-ion collisions continued
$H^+ + N^+(O^{2+})(Ne^{4+})(Na^{5+})(Mg^{6+})$, ^3P_J fine structure transitions 80−37864
$H^+ + Na(K)$, excited state form. by inelastic processes, energy partitioning 78−82833
$H^+ + Na(Mg)(Al)(Si)(Ti)$, K-shell ionisation cross sections for 15-65 keV protons 78−90284
$H^+ + S(K)(Ni)(Cu)(Ga)(Br)(Ag)(Cs)(W)$, 4 MeV beam-foil X-ray production cross-section 79−7003
$H^+ + U(Ni)(Au)(Sn)$, 4.88 GeV, K-vacancy production cross sections 77−19036
H_2 formation, reaction rates and chemical kinetics 79−17070
$H_2^+ + Ar$, low energy proton transfer reactions, crossed beam studies 80−108697
$H_2^+ + CO_2$, charge transfer, energy transfer, product ion excitation and fluoresc. 77−75288
$H_2^+ + He(Ar)$, emitted electron's energy and angular distrib. support for charge transfer to continuum theory 78−37740
$H_2^+ + He(Ar)(C)$, ionisation processes viewed in forward direction 77−71866
$H_2^+ + He \rightarrow H + HeH^+$, endoergic exchange, DWBA calcs. 77−9055
$H_2^+ + He \rightarrow H + HeH^+$, product ion ang. distrib., quantum mech. impulse approx. calcs. 79−24727
$H_2^+ + Kr$, collisional dissoc., 6 to 60 keV *(German)* 77−10733
$H_{2n+1}^+ + Ar$, $n \leq 7$, double differential fragmentation cross section 79−89821
$H_3^+ + Kr$, collisional dissoc., 6 to 60 keV *(German)* 77−10733
H_n^+, $(n=1,2,3)$, impact on metal surfaces, excited H form. 78−42199
$H_x^+ + Al$, $x=1,2,3$, relative K X-ray yields 77−75282
HD^+, radiative recombination rates 78−37708
HD^+ scattering states, elastic and charge transfer cross sections 78−9221
$H^-(D^-) + He$, collisionally induced electron detachment, 0.5 MeV, target effect 80−37858
$H_2^+(H_3^+) + He$, Hadamard mass spectroscopy, mass spectra 79−30601
$H_2^+(HeH^+) + C$ thin solid target, 50-300 keV, collisional at. physics using mol. projectiles 79−45813
^AH, $A=1,2,3$, $\bar{p}$ radiative atomic recombination, antiprotonic atoms 80−83527
$H(1s) + p \rightarrow p + H(1s)$, 15-200 keV, ang. distrib., differential cross sections calc. 78−82839
$H(2S) + He(N)(Ar)$, excitation and ionisation contributions to sum-rule Born cross sections 80−99551
$H(2s)$ + energetic projectile ion, charge exchange, cross-sections calcs. 79−59554
$H = H^+$ collisions, $H(2s)$, $H(2p)$ production, 1-7 KeV, differential, total cross sections 80−32818
He, collisional ionisation by fast low-charge-state ions 79−86056
He, excited, optically-allowed, long-range interaction pots. with electrons, protons and atoms 77−14520
He, Glauber scatt. amplitude, numerical method in Lommel function 79−22795
He I, heavy ion impact excitation, alignment relax. of nonresonant levels *(French)* 77−61842
He I, heavy ion impact excitation, relax. of 3 ^1P level *(French)* 77−61843
He I, heavy ion impact excitation, orientation by anisotropic relax. of 4 ^1D level *(French)* 77−61844
He ions $+ Ti(Fe)(Cu)$, K-shell ionisation cross-section, 85 to 790 keV 80−106390
He, outer 1s, 2s and 2p electron loss cross sections by multicharged ions 78−42185
He^-, electron loss in passing through inert gases 79−13805
He-like target + fast projectile, electron capture cross-sections 80−69231
$He + {}^{16}O$, hyperfine interactions of highly stripped ions recoiling into He 77−22932
$He + Ar^{+Z}$ $(Z=3$ to $7)$, electron capture into different electron states by multiply charged ions *(Russian)* 78−17788
$He + Ar^{2+}$, charge transfer, energy defect and sealing laws 80−48083
$He + ArH^+$, ab initio pot. energy data, SCF-LCAO calcs. 80−63530
He + atom (ion), ionis. by one or two electron at. particles, Born approx. 79−54960
$He + B(C)(N)(O)(F)$ bare nuclei, electron capture to excited states, X-ray cross-sections 77−71814
$He + Be^+(Mg^+)$ high energy, excitation cross sections, impact radiation polaris., models comparison 78−1069
$He + Br^-(Cl^-)(I^-)(Sb^-)$, term parameters, electron spectra-scatt. cross sections 77−27148
$He + e^-(H^+)$(pion), specific primary excitation by fast accelerator particles 80−23559
$He + H_2^+$, collinear trajectories, pattern recognition 80−45481
$He + H_2^+$, collisional dissoc., expt. and quasiclassical trajectory calcs., eV region 78−42201
$He + H_2^+$, endothermic reactive and vibr. inelastic collisions, pot. well effects 79−8430
$He + H_2^+$, form of selected vibr. state H_2^+ beam at high press. by electron impact 77−65547
$He + H_2^+(H^+)(H_3^+)$, interaction pots. from ion mobility data 77−14518
$He + H_2^+ \rightarrow HeH^+ + H$, diatomics-in-mols. and spline fitted ab initio surface, vibr. effects 78−20010
$He + H_2^+ \rightarrow HeH^+ + H$, vibr. state distrib. prod. by H_2 vibr. autoionisation cross-section depend. 77−48628
$He + H_3^+$, 100 to 500 eV, dissociation of H_3^+ 77−42383
$He + H^-$, low-energy total electron detachment cross-sections, approximation 79−72405
$He + H^+$, 25-3000 keV, electron-capture, continuum distorted wave approx., correl. energy 77−83727
$He + H^+$, 293 keV, electron capture differential cross sections 77−88552
$He + H^+$, ang. and energy distrib. of ejected electrons 79−31668
$He + H^+$, collisional excitation, 2nd order pots. method calcs. 78−13608
$He + H^+$, determ. of He excited state populations by two-photon reson. ionisation spectroscopy 78−82707
$He + H^+$, differential scatt., 1-12 eV, high resolution beam meas. 80−58348
$He + H^-$, double He ionis., polarised electron vel. distrib. effect 80−53109
$He + H^-$, double ionis. of He, binary-encounter theory 78−1066
$He + H^+$, elastic scatt. and 2^1s and 2^4p excitation cross-sections 79−36747
$He + H^+$, electron capture cross sections, electron correlations 77−34758

atom-ion collisions continued
$He + H^+$, electron capture into ground and 2s states, cross sections 77−27177
$He + H^+$, electron ejection, energy and ang. distrib. calcs. 77−6914
$He + H^+$, electron ejection differential cross sections 77−46625
$He + H^+$, excitation process *(Japanese)* 78−42193
$He + H^+({}^4He^{2+})$, $1^1S \rightarrow 4^1S$ excitation cross-section calcs., 10 to 5000 keV 78−25689
$He + H^+(H_2^+)(H_3^+)(He^+)$ collisions, polarisation degree of prominent He lines 78−70916
$He + H^+(He^{2+})(N^{x+})$, multiply ionised ats. prod. 80−28098
He + He ion, He I fluoresc. excitation, mag. field depend. *(German)* 77−27037
$He + He^+$, 0.7-2 MeV, charge-changing collisions, electron capture 80−58372
$He + He^+$, 2 and 3 keV, one and two electron excitations in He, quantal treatment 78−37730
$He + He^+$, (Ne)(Li), gas-phase collisions, intermediate and high velocities, excitation 80−32822
$He + He^+$, autoionising transitions interference 77−42390
$He + He^+$, cross-section oscills., 5 to 40 keV 79−45785
$He + He^+$, double collision spectroscopy 80−58378
$He + He^+$, excitation cross-section calcs. 78−90273
$He + He^+$, He I excitation, zero-field quantum beats 78−961
$He + He^+$, low energy collisions, excitation of 2 ^1S, 2 ^1P and 3 ^1P, 3 ^3P levels 80−58342
$He + He^+$, resonant charge transfer cross sections, 2 to 100 eV 78−66655
$He + He^+$, triplet excitation cross-section, Ochkur-Rudge approx. calcs. 80−28101
$He + He^+$ interactions, electronic forces 79−22790
$2He + He^+(Ne^+)$, three body reaction, rate coeffs., temp. depend., 100 to 300K 80−108703
$He + He^+(Ne)$, tensor polarisabilities of 1snd ^1D level, fluoresc. depolarisation obs. 80−69099
$He + He^{2+}$, single and double electron capture, high vels., independent electron approx. calc. 80−18923
$He + Li^+$, 2 to 5 keV, ejected electron profile variation with impact angle 78−37729
$He + Li^+$, Li excitation mechanisms, Auger and autoionisation spectra, collisional excitation 77−19042
$He + Li^+$ autoionisation, electron spectra 80−91653
$He + Li^+(C^+)(N^+)(Ne^+)(Na^+)(Mg^+)$, slow collision, ionis. obs. 79−10194
$He + Li^+(Mg^+)(Mg^{2+})(Na^+)(Ne^+)$, relative level excitation, orbital ang. momentum quantum number depend. 78−25688
$He + Mg^+(Ne^+)$, charge exchange, Rydberg state excitations 77−58159
He + multiply charged ions, electron capture and impact-ionis. cross sections, Monte Carlo calcs. 79−27083
$He + N_2^+$, $(A^2\Pi_u)$ Meinel band deactivation cross sections above thermal energies 78−66635
$He + N_2^+$, vibronic excitation, curve-crossing trajectories 80−23520
$He + Ne^+$, impact excitation, cascade-fluorescence spectroscopy, level-crossing techniques 80−23357
$He + Ne^{n+}$ $(n=1,2,3,4)$, excitations, emission cross-sections 77−57914
He + negative ion, electron-loss cross sections 80−37877
$He^- + Ar(H_2)(He)(N_2)(Ne)$, collisional detachment cross-sections, high-energy obs. 77−3442
$He^{+,2+} + Ar$, 2 MeV, ejected electron spectra, 20-450 eV, 0-10° 77−34746
He^+ + alkali metal atom, ionisation cross sections, binary encounter approx. with HF electron vel. distrib. 78−55225
$He^+ + Ar$, charge exchange, quasimolecule model, four-state calcs. 77−14571
$He^+ + Ar$, direct excitation and charge exchange processes 77−75279
$He^+ + Ar(H_2)(He)(Kr)(N_2)(O_2)$, metastable ion electron capture, loss and de-excitation 77−6904
He^+ + atom, metastable state deexcitation, 2S- and 2P-state mixing and Penning ionisation 77−42394
$He^+ + Ca(Ba)$, 2-1000 eV, spontaneous ionis. mechanisms 79−64090
$He^+ + H$, 4-343 keV, change transfer process, cross section meas. 78−25696
$He^+ + H$, unpolarised and spin-change collision, low energy 78−86943
$He^+ + He$, 1-10 keV, charge exchange cross section meas. 78−25697
$He^+ + He$, 150 eV, one-electron excitations, quantal treatment 77−71854
$He^+ + He$, 2^1P level, direct and charge-exchange excitation, 150-1000 keV 78−70913
$He^+ + He$, 2^3S and 2^1S excitations, differential cross sections 77−3444
$He^+ + He$, autoionisation electrons and scatt. ions, ang. correl. determ. 80−63792
$He^+ + He$, autoionising state excitation, ion-electron coincidence, electron azimuthal depend. 78−37734
$He^+ + He$, charge transfer, appl. of atom-photon coincidence meas. 79−45829
$He^+ + He$, electron loss cross section 79−27080
$He^+ + He$, He_2^+ mol. collision complex, pot. energy curve spectrum 77−19008
$He^+ + He$, $He^+(2s)$ destruction, $He^+(2s/2p)$ form. 77−30977
$He^+ + He$, $He(2^3S)$ formation, elastic and resonance charge exchange perturbations 77−42386
$He^+ + He$, high-energy collisions, experimental device for study of elastic and inelastic diffusion *(French)* 78−22053
$He^+ + He$, multicurve-crossing problem, numerical test of semiclassical approx. 78−13590
$He^+ + He$, scattered ion-autoionisation electron ang. correl. determ. 80−9725
$He^+ + He$ 35 keV collisions, He I 1s3d levels, cascade-free lifetime meas. 78−58607
$He^+ + He(2p^2\ {}^1D)$, collisionally excited, autoionisation electron ang. distrib., interference struct. 80−32819
$He^+ + Hg_0 \rightarrow He_0 + (Hg^+)^* + \Delta E$, cross sections, rate consts. 78−17785
He^+ + inert gas, binary encounter calc., cross section calc. 79−72413
He^+ + inert gas, collisional quenching cross sections, two-state theory calcs. 80−69217
$He^+ + Mg(Zn)$, inelastic collisions, 2-800 eV, excited state form. 78−94312
$He^+ + Na(K)$, excited state form. by inelastic processes, energy partitioning 78−82833
$He^+ + Na(K)$ single-electron capture cross-sections 78−37737
$He^+ + Na(K)(Cs)$, 5-100 keV, electron capture form. of fast metastable He 78−74760

atom-ion collisions continued
- He^+ + Ne, 10-150 keV, Rydberg-state total cross section, oscillatory behaviour 77–83716
- He^+ + Ne, $2s^02p^6$-$2s^12p^5$ radiative transition in Ne III, UV spectra 79–6900
- He^+ + Ne(Ar), attenuation and single electron charge exchange cross sections, 500-5000 eV 77–34752
- He^+ + Pb, at. beam and surface interaction, scatt. ion yield oscills. 78–55221
- He^+ + Xe, internal energy distrib. at 100 eV 80–99564
- He^+ + Xe charge transfer, optical emission cross sections 77–61853
- He^{2+} + Al(Si)(S)(Cl), chem. environment effect on Kα satellites intensity 77–54527
- He^{2+} + atom, 10 MeV, binary encounter stopping cross sections, straggling and screening 78–17754
- He^{2+} + C foil collisions, electron emission, energy distribs., solid state effects 77–19062
- He^{2+} + H, 4-343 keV, charge transfer process, cross section meas. 78–25696
- He^{2+} + H, mol. treatment, cross sections and charge exchange probabilities 77–58128
- He^{2+} + He, 2 MeV, non-occurrence of Fadeev interference struct. in 245 eV electron spectrum peak 77–58155
- He^{2+} + He, diatom. quasimolecule form., shielded-orbital model 79–10165
- He^{2+} + He, He^+ form. in various electron states *(Russian)* 78–58815
- He^{2+} + He, K-electron capture, cross section scaling, high energy 79–41236
- He^{2+} + He, thermal energy collisions, quantum mech. calcs. 80–23507
- He^{2+} + He, two-electron excitation of quasimol. states 79–18274
- He^{2+} + He(Ne), electron capture collisions, spin conservation 78–82837
- He^{2+} + He($1s^2$), differential and total cross-sections 80–23506
- He^{2+} + Li, electron capture, ionis. cross section, low-vel. He^+(3l) production, X-ray production 79–22822
- He^{2+} + Li collisions, soft X-ray emission obs. 80–83591
- He^{2+} + methane, (Ne), (Ar), inner shell electron capture cross-sections 79–76510
- $He_2{}^+$, dissociation by Ne to form Ne^+ 79–45635
- $He_2{}^+$ + Mg(Zn), inelastic collisions, 2-800 eV, excited state form. 78–94312
- HeH^+, collisional formation, SCF calcs. 77–6893
- HeH^+, radiative recombination rates 78–37708
- He^{2+}(H^+) + X, (X = Nb to Gd), K-shell X-ray prod. cross-sections 77–71865
- $^4HeH^+$ + He, 1 keV, collision-induced dissoc., ro-vibr. assignments, proton spectra obs. 79–3556
- He_2H^+, ground state pot. energy surface for form. by collinear collision, DIM calcs. 79–97996
- He^+(He^{2+}) + He(Ar)(C), ionisation processes viewed in forward direction 77–71866
- HeI + Na^+, anisotropic collisions, direct meas. method 80–23498
- He(Ne,Ar,Kr) + Ne^{n+}, (n = 1, 2, 3, 4), energy spectra of electrons produced 79–45822
- $HeNe^+$, collisional form., excitation, pot. energy curves calcs. 77–6697
- $^3He^{2+}$ + He, many-electron systems OEDM orbitals 80–48081
- $^4He^+$ + $^3He^{2+}$, charge exchange, cross section meas. 80 32827
- $^4He^+$ + H, 35-1000 keV, electron loss cross-section 78–22018
- $^4He^+$ + H, electron transfer calc., electron ionization calc., Monte Carlo method, 79–72387
- $^4He^+$ + He, electron vel. distrib., nonexistence of wake bound states 78–13571
- He(1^1S) + H^+, He(n^1P) excitation cross sections computation 79–94070
- He^+(1s) + H^{2+} symmetric resonance charge transfer 80–32826
- He^+(1s) + H(1s), excitation and ionis. processes 78–42189
- Hg + H^+, L-subshell X-ray prod., cross-section meas. 77–46575
- Hg + He^{2+}, autoionisation, 5-20 eV, electron and ion ang. distrib. 78–78795
- Hg + Xe^{x+}, single and multiple collisions, charact. and quasimolecular X-rays 77–83713
- Hg(6^3P_1) + Li^+(Na^+)(K^+), excitation, optical polarisation fractions and mag. sublevels obs. 78–50619
- H(n = 2) excitation by ion impact, precision doubly differential cross section meas. 79–45811
- Ho + H^+, relativistic K-shell ionisation cross-section meas. 78–33593
- Ho + H^+($^3He^+$), X-ray intensity ratios, projectile energy depend. 80–23535
- H^+(relativistic) + atom, K-shell ionis., double differential and total cross sections 78–42182
- H^+(spin polarised) + atom, inner-shell ionis., subsequent radiation ang. distrib. 80–53114
- I, 15-80 MeV, ion-atom collision, K-vacancy prod., mol.-orbital model 77–68095
- I, ion collisions, 15-80 MeV, K-vacancy production, multiple and single collisions in mol. orbital excitation 77–83717
- I ion + target collisions, K-X-ray yields, 1sσ excitation 77–19051
- I ion + target collisions, K-X-ray yields, K-vacancy sharing 77–23548
- I ion + target collisions, K-X-ray yields, 2pσ excitation 77–23549
- I ion + target collisions, X-ray yields, K-L level matching 77–19052
- I + Au, slow collision, M MO radiation anisotropy 79–72269
- I^- + Ne, electron detachment collision, 1-3 keV, differential cross-section 79–72403
- I^+ + $_Z$A, Z ≥ 47, inner shell X-ray prod., vacancy configurations and cross sections 79–13815
- I^{10+} + In, double K-shell vacancies obs., K_α hypersatellite transitions, shift, shared double vacancies 79–72268
- I^{25+} + Te^{24+}, I^{43+} + Au^{69+}, I^{25+} + Au^{51+}, correlation diagrams, inner-shell vacancy prod., characteristic X-rays 77–83503
- I^{5+} + Xe(Ar), 20 MeV, electron loss cross sections, pot. model data anal. 79–27082
- $^{127}I^{5+}$ + atom (molecule), multiple electron loss cross sections meas. 79–45818
- In + H^+, inner-shell ionisation, Coulomb repulsion effects 80–48075
- In + He^+, chem. effects on oscillatory cross sections in low energy scatt. 77–6889
- K + K^+ collisions, charge exchange cross section 80–58374
- K + M^+, M = alkali ion, K resonance doublet excitation cross sections 77–27167
- K^+ + Ar(Kr)(Xe), differential elastic cross-section meas. *(German)* 77–58130
- K^+ + inert gas atom potential, determ. from total cross section meas. 77–68091

atom-ion collisions continued
- K^+ + Na, differential scatt. cross section, electronic excitation via. rot coupling in NaK^+ 78–13579
- Kr, 202-330 MeV, ion-atom collision, K-vacancy prod., mol.-orbital model 77–68095
- Kr, heavy ion induced MNN Auger electron spectra 77–6907
- Kr, ion collisions, 200-330 MeV, K-vacancy production, multiple and single collisions in mol. orbital excitation 77–83717
- Kr, ion + target collisions, K-X-ray yields, 1sσ excitation 77–19051
- Kr ion + target collisions, X-ray yields, K-L level matching 77–19052
- Kr ion + target collisions, K-X-ray yields, 2pσ excitation 77–23549
- Kr plasma, of positive column, at. alignment, radiative lifetimes, collision cross sections 79–4203
- Kr, stationary afterglow obs. of singly charged atomic ions, three-body rate coeffs. 80–38757
- Kr + $^{75}As^{n+}$, slowing down of atoms/ions with KE ≤ 5 eV by inert gases 79–31650
- Kr + Ar^+(Kr^+) collisions, quasimol. Auger transitions 77–19070
- Kr + C^+(H^+)(N^+)(O^+)(S^+), charge exchange cross-sections *(German)* 77–10753
- Kr + Cu^{q+}, (16 ≤ q ≤ 23), 1.4 MeV/amu, X-ray emission, charge state dependence 78–37713
- Kr + F^+, inner-shell ionisation, X-ray cross sections 80–58369
- Kr + $H_3{}^+$, 100 to 500 eV, dissociation of $H_3{}^+$ 77–42383
- Kr + H^+(He^{x+}), energy loss straggling, ion energies of 50-500 keV per nucleon 77–46620
- Kr + $Kr_3{}^+$ quasimolecule $Kr_2{}^+$, Auger transitions obs. by electron-scattered-ion coincidence method 80–74243
- Kr^+ + Kr, quasi-resonant charge transfer at thermal energies 80–48082
- Kr^{24+} + Ge, K X-ray prod., impact parameter depend. 78–58800
- Kr^{n+} + Ta(W)(Pt)(Au)(Pb)(Bi)(Th)(U), K-L level matching, X-ray obs. 79–63948
- ^{84}Kr ions + target collisions, K-X-ray yields, K-vacancy sharing 77–23548
- La, ionisation cross sections for L_1 and L_2 subshells by 250-500 keV protons *(Russian)* 77–6918
- Li ions, 65 to 500 keV, stopping power and straggling in H_2, He, CO_2, N_2, O_2, Ne, Ar, Kr, and Xe 79–3529
- Li + doubly charged ions, electron capture excitation, theoretical predictions in fusion plasma 80–63810
- Li + H^+, Li core excitation cross section, correlation and reorganisation effect 80–87215
- Li + H^+($H_2{}^+$)(He^+)(He^{2+})($He_2{}^+$), excited state form. obs. 80–9686
- Li + H^+(He^+) ions, Li excitation mechanisms, Auger and autoionisation spectra 77–19042
- Li + He(Ne)(benzene), relative level excitation, orbital ang. momentum quantum number depend. 78–25688
- Li + inert gas collisions, electron loss cross-section meas. *(French)* 78–86941
- Li^+ + He, 10-50 keV, mol. promotion, many-electron aspects 79–50124
- Li^+ + He, < 5 keV, autoionised electron spectra 80–32823
- Li^+ + He, excitation, optical emission line shapes 80–18820
- Li^+ + He, quasimol. study of collisions in 0.3-50 keV range 77–88529
- Li^+ + He collisions, K-shell vacancy sharing, ab initio LCAO-SCF, CI calcs. 77–19054
- Li^+ + He collisions, Li-K shell excitation, autoionisation spectra meas., total cross sections 77–19053
- Li^+ + K, differential scatt. cross section, electronic excitation via. rot. coupling in LiK^+ 78–13579
- Li^+ + K, rot. coupling, Fraunhofer diffraction effects 77–65526
- Li^+ + Li(Na)(Cd), electron capture cross sections 10-60 keV 80–48084
- Li^+ + Na, direct and charge exchange scatt., differential scatt. cross-sections meas. 78–42158
- Li^+ + Ne, autoionising Ne levels excited in 5-10 keV collisions 78–22017
- Li^+ + Ne, low energy, ionisation, total cross-section meas. 77 54606
- Li^+ + Ne collisions, vel. dependence of Ne 2s and 2p, vacancy production, electron spectroscopy 80–58344
- Li^+ + X, X = H, H_2, He, C, N, O, cross-section, closure-Born approx. 78–66630
- Li^{q+} + H(H_2), (q = 1-3), electron capture and loss cross sections 78–42187
- Li^{3+} + He(C)(Ne), K-shell charge transfer cross sections, Bates-Born formalisms 79–45834
- Li^{3+} + methane, (Ne), (Ar), inner shell electron capture cross-sections 79–76510
- $Li_1{}^+$, potential energy curves, exchange and ion-multipole interactions, vibrational energy levels 79–98175
- Li* + He(Ne)(Ar), thermal, high-Rydberg Li behaving as ion core 78–22004
- Mg isoelectronic series, atom + H^+, low-lying ^3P term excitation, cross-sections and rate consts. 79–94069
- Mg-H^+ $2p_{3/2}$ vacancy alignment electron capture role 80–83465
- Mg + C^-(O^-), electron detachment cross-sections, 20-150 keV 78–25690
- Mg + H^+, electron capture and impact ionisation cross sections, CI calc. 80–23343
- Mg + H^+(He^+), inner-shell ionisation, target atom ionic alignment, Born approx. 78–78789
- Mg + H^+(He^+) and electron impact ionis., Auger study of collisionally induced alignment 78–90279
- Mg + heavy ion, X-ray spectra, one-photon two-electron rearrangements 77–6712
- Mg^+ + alkali metal, effective charge exchange cross section, 20 to 1000 eV 77–42398
- Mg^+ + H, Mg II lines broadening and shift by van der Waals interaction 77–3303
- Mg^+ + He,(Ne)(Ar), 3^2P differential excitation, alignment and orientation 79–86053
- Mg^+ + He(Ne), ns-np excitation, alignment and orientation, impact, parameter theory 80–91648
- Mg^+ + Na(K)(Rb)(Cs), charge exchange and excitation processes 78–17772
- Mn, X-ray spectra, chemical bonding and multiple ionis. effects 78–50630
- Mn + H^+, K X-ray production, 0.2-0.5 MeV, ionis. cross-section 79–31459
- Mn + H^+ ion collisions, K-shell ionisation cross sections 77–23556
- Mo + Nb, K-shell vacancy prod., impact parameter depend 80–14225
- N, cross sections of interactions of protons 77–50538

atom-ion collisions continued
N, outer 1s, 2s and 2p electron loss cross sections by multicharged ions 78-42185
$N+H^+(He^{2+})$, K-shell Auger electrons ang. distrib. 79-89756
$N^++Ar(Kr)(Ne)$, single electron detachment cross-sections, 35 to 140 keV 77-6909
N^++elements Ca to Zn, X-ray production cross section, $K\beta/K\alpha$ ratio, 0.5-2.5 MeV/amu 77-54526
$N^++H(H_2)$, 0.1-13 keV electron capture cross-sections meas. 79-36761
N^++inert gas, electron capture (loss) by metastable (ground-state) ions, 2-30 keV 78-25695
N^++N, 35-200 keV, K MO X-rays, production mechanism, spectral distrib. 78-42183
N^++N_2, X-ray emission ang. distrib., MO calc. 79-54803
$N^{2+}+He(Ne)(Ar)$, electron capture, product ion energy loss spectra 79-36762
N^{2+}+inert gas target, 60-200 keV single electron capture 80-43172
$N^{q+}+H$,(q=1 to 7), electron capture and impact ionisation cross sections 77-75290
$N^{q+}+H(H_2)$, q=1-5, single electron capture cross sections 78-55233
$N^{x+}+He$, electron capture, K X-ray emission ang. distrib. 77-57919
$N_2{}^++H^+$, fluoresc. efficiency, 3914 Å band of $N_2{}^+$ (1N), 100 eV-10 MeV 78-74697
$N_2{}^++O \rightarrow NO^++N$, aeronomical determ. of rate coeff. 79-75000
$NH_4{}^+$, mutual neutralisation, with simple and clustered positive (negative) ions 78-44372
$N^+(^5S)$+inert gas, de-excitation cross section, 2-30 keV 78-25695
$Na+Ar^+$, Ar^+ form, electron capture, Ar^+ excited states relative population distrib. 80-23544
$Na+H^+$, $2p^53s^{22}P_{3/2}$ state alignment, collisionally induced, impact parameter calc. 80-83474
$Na+H^+$, charge transfer cross section and equilibrium fractions, 1-25 keV 80-5616
$Na+H^+$, configuration interaction potentials and rainbow angle scatt. cross section 80-37745
$Na+H^+$ collisions, L-Auger electron emission, autoionising states, line broadening effects 77-14568
$Na+H^+(He^+)$, Na $2p^53s^2\,{}^2P_{3/2}$ state alignment by 5-30 keV excitation 80-14200
$Na+He^+$, 25-90 keV, fast beam form., $He(2^3S)$ population 79-31740
$Na+He^+$, crossed beams, l-changing collisions, n-depend. 80-58345
Na^++Hg, low-energy collision, quantum mech. phase interference and optical polarisation 77-42385
Na^++K, differential scatt. cross section, electronic excitation via. rot. coupling in NaK^+ 78-13579
Na^++Li, direct and charge exchange scatt., differential scatt. cross-sections meas. 78-42158
Na^++Ne, autoionising Ne levels excited in 5-10 keV collisions 78-22017
Na^++Ne, nonadiabatic transitions, effective ionisation cross-section calcs. 79-10195
Na^++Ne, quasimolecular states, coherent population *(Russian)* 77-10718
Na^++Ne collisions, Na KK vacancy prod. 78-17781
$Na^++Ti(Ni)(Zn)(Fe)$, 0.2-3.0 MeV, united-at. limits, mol.-orbital continua 77-19030
Nb+Kr, excitation of $1s\sigma$ and $2p\sigma$ quasimolecular radiation 78-78801
Nb+Nb symmetric collisions, MO-$2p\sigma$ radiation anisotropy, quasimolecular nature 78-70924
Ne, 100 keV region ion collisions, quasimol. effects, population of Ne I to Ne IV levels 80-14205
Ne, He^+ 100-1000 keV impact excit. $1s_2$ and $1s_4$ reson. states 77-10611
Ne, highly-ionised, heavy ion impact, selective electron capture effects 80-14202
Ne III, ion impact excited, branching ratio method for quantum efficiency determ. of UV spectrometer 79-22848
Ne IV, ion impact excited, branching ratio method for quantum efficiency determ. of UV spectrometer 79-22848
Ne, one-electron and two-electron one-photon transitions 78-58775
Ne, outer 1s, 2s and 2p electron loss cross sections by multicharged ions 78-42185
Ne^{9+} high ionisation-excitation states and mass dependent symmetric collision interactions 77-83720
Ne-highly ionised heavy ion impact, L-shell excit. 78-1074
Ne-N_2, charge transfer kinetics, weak H^+ beam effects 78-9243
Ne^{n+}-Ne, K-shell vacancy prod. cross section, X-ray and Auger electron prod. fluoresc. yield 78-13582
$Ne+{}^4He^{2+}$, optical transition excitation function and cross sections 80-63787
$Ne+Ar^{12+}$, heavy-ion induced K-shell Auger effect 77-6908
$Ne+Ar^{12+}(Xe^{24+})(Pb^{40+})$, X-ray transitions 78-66641
$Ne+Ar^{2+}$, charge transfer, energy defect and sealing laws 80-48083
$Ne+Be^+(Mg^+)$, high energy, excitation cross section, impact radiation polaris., models comparison 78-1069
$Ne+C^{N+}(N^{n+})(O^{n+})$, charge exchange contribution to K-vacancy production 80-102553
$Ne+Cl^{12+}(S^{14+})$ soft X-ray emitting slow multiply charged ion prod., recoil ion spectroscopy 77-50516
$Ne+Cl^{7+}$, many-electron stripping 77-75277
$Ne+e^-(H^+)$(pion), specific primary excitation by fast accelerator particles 80-23559
$Ne+H_2{}^+$, form. of selected vibr. state $H_2{}^+$ beam at high press. by electron impact 77-65547
$Ne+H_2{}^+ \rightarrow NeH^++H$, vibr. state distrib. prod. by H_2 vibr. autoionisation cross section depend. 77-48628
$Ne+H^-(D^-)$, electron detachment, dynamical phenomenon 80-106305
$Ne+H^+$, ang. and energy distrib. of ejected electrons 79-31668
$Ne+H^+$, K-shell capture cross-section 78-33602
$Ne+H^+$ 80-18916
$Ne+H^+(H_2{}^+)(He^+)$, $Ne(2p^53s, 2p^53p)$ excitation 80-43185
$Ne+H^+(He^+)$, K-shell ionisation, AES meas. 77-10749
$Ne+H^+(He^+)(Ne^+)$, multiple ionisation of Ne 2s and 2p electrons 80-18918
$Ne+H^+(He^{2+})$, K-shell Auger electrons ang. distrib. 79-89756
$Ne+H^+(He^{2+})(N^{x+})$, multiply ionised ats. prod. 80-28098
$Ne+He^+$, inelastic scattering data inversion, interaction function recovery 79-89741
$Ne+He^+(Li^+)(Mg^+)(Na^+)(Ne^+)$, autoionising level excitation, electron spectra 77-14554

atom-ion collisions continued
$Ne+He^+(Ne^+)$, coherent excitation and decay of autoionising states 79-45789
$Ne+He^+ \rightarrow HeI+Ne^+$, $HeI3^3P$ polarisation 79-13813
$Ne+He^{x+}$, energy loss straggling, ion energies of 50-500 keV per nucleon 77-46620
Ne+heavy ion, highly charged very slow Ne recoil ions, K X-ray transition 80-91649
Ne+ion, 100 keV, excited Ne 2s vacancy singlet/triplet population ratio, ion Z depend. 78-37733
$Ne+Li^{+1,2,3}$, K-shell ionisation depend. on projectile charge state 77-34743
$Ne+Mg^{2+}$ collisions, 2p-3p excitation, optical spectroscopy investig. 77-19064
$Ne+Ne^+$, 2s vacancy prod., coupling state calcs. in mol. basis 79-13806
$Ne+Ne^+$, coulomb deflection in ion-atom collisions, K-shell excitation 79-94074
$Ne+Ne^+$ collisions, satellite struct. of 2s-subshell ionisation of Ne 77-19065
$Ne+Ne^{m+}(N^{n+})$, K-shell vacancy prod. cross-section, charge state depend. 78-17751
$Ne+Ne(Ne^+)(Ne^{2+})$, 2s vacancy prod. 78-50623
Ne+proton, charge transfer, target K-shell electron capture, impact parameter depend. 80-102552
$Ne^-+Na^+(K^+)(Li^+)$, electron gas model pots. and collision integrals *(French)* 78-42169
Ne^++Ar integral elastic scatt., repulsive potentials derivation 80-63744
Ne^++Ba, 2-1000 eV, spontaneous ionis. mechanisms 79-64090
Ne^++He, 10-150 keV, Rydberg-state total cross section, oscillatory behaviour 77-83716
Ne^++He, multiple ionisation of Ne 2s and 2p electrons 80-18918
Ne^++Kr, low vel. collision, enhanced K-L vacancy sharing ratios, X-ray prod. cross section 78-78790
Ne^++Ne, (He^+), gas-phase collisions, intermediate and high velocities, excitation 80-32822
Ne^++Ne, quasi-resonant charge transfer at thermal energies 80-48082
Ne^++Ne, reson. transitions, direct and charge-exchange excitation 77-19020
Ne^++O, K-shell excitation cross sections, variable screening model 77-42387
$Ne^{2+}+Ar\ (Kr)(Xe)$, single electron capture excitation, photon emission, VUV spectroscopy 80-58379
$Ne^{2+}+Xe$, electron capture collisions, 15 to 50 keV, excitation 80-102566
$Ne^{3+}+Al(Si)(S)(Cl)$, chem. environment effect on $K\alpha$ satellites intensity 77-54527
$Ne^{n+}+Ar(He)$, slow ion and electron prod., VUV radiation 78-5321
$Ne^{n+}+He(Ne,Ar,Kr)$, (n=1, 2, 3, 4), energy spectra of electrons produced 79-45822
$Ne^{n+}+Ne$ collisions, n=1 to 4, K-X-ray production, projectile charge state dependence 77-14570
$Ne^{Z+}+Ar$, projectile charge dependence *(Dutch)* 79-50121
Ne^{z+}+inert gas atom (z=1-4), radiative and non-radiative deexcitation after electron capture 79-7008
$Ne^{z+}+Ne(Ar)$, outer s-subshell vacancy production 79-18275
$Ne_2{}^+$+atom (molecule), bimolecular and termolecular reaction rate coeffs. 80-81308
$Ne_2{}^++He$, pot. energy surface, reaction cross sections, ab initio calcs. 80-11881
Ni ion+Ni(Fe) collisions, X-ray spectra, two-electron transitions 77-19050
Ni K-shell hole production by light ions, hydrogenic and Hartree-Fock model of target 77-83715
$Ni+H^+$, K-shell ionisation calcs. 80-23534
$Ni+H^+$, K-shell ionisation cross-sections calcs. 80-43165
$Ni+H^+({}^4He^{2+})(O)(Li)$, K-shell ionis., impact parameter depend. 77-83707
Ni+H(D)(He)(Li)(C)(O)(F) ions, K-shell ionis., universal cross sections 78-62895
Ni+Mn(Pb), inner shell vacancy prod., impact parameter depend. 77-6906
$Ni+N^{4+}$, $K\alpha$ and $K\beta$ X-ray spectra for 84 MeV incident energy 77-50517
Ni+Ni, 12-90 MeV, molecular orbital K X-rays ang. distrib. 79-10125
$Ni+Ni^+$, with nuclear sticking, molecular orbital and compounds nucleus X-ray emission 80-1048
$Ni+Ni^{x+}$, K X-rays, two-electron-one-photon excitation 78-13589
Ni+Ni(Nb), Doppler shift of continuum X-rays from quasimols. 79-22808
${}_{28}{}^{58}Ni^{n+}+{}_{25}Mn({}_{50}Sn)({}_{82}Pb)$, 45, 94, and 138 MeV Ni inner shell vacancy production, impact parameter depend. 79-41130
O, cross sections of interactions of protons 77-50538
O ion, A=16, 18,+atom collisions, K-X-ray production 77-23554
O ion+inert gas, small impact parameter scatt., charge distrib. 77-30989
O, K-shell ionis., double and single, cross section meas. by ion bombardment 78-50629
O^{2+} reactions with atoms or molecules of ionospheric importance, lab. meas. 80-26004
$O+CO_2{}^+$, in Mars thermosphere, effects of energetically produced $O_2{}^+$ on ion temps. 79-96945
$O+H^+(He^+)$, double K-shell ionis., projectile Z depend. 78-25680
$O+H^+(He^{2+})$, K-shell Auger electrons ang. distrib. 79-89756
$O+N_2{}^+(O^+)(O^{2+})$, rate coeffs. in thermosphere, AE satellite meas. 79-48594
$O^-+Ne(Ar)(Kr)$, 0.2-1 keV, elastic and inelastic reduced differential cross-sections 80-32829
O^++Al, Al K-vacancy cross sections, 0.15 to 91 MeV, recoil effects and mechanisms 77-19033
$O^++H(H_2)$, 0.1-13 keV electron capture cross-sections meas. 79-36761
O^++inert gas, potential energy curves from elastic scatt. cross sections 80-23502
O^++Ne, pot. energy curves, nonadiabatic coupling matrix elements 80-53110
$O^{2+}+Al(Si)(S)(Cl)$, chem. environment effect on $K\alpha$ satellites intensity 77-54527
$O^{8+}+H(1s)(He(1s^2))$, electron capture into n,l excited states 80-23543
$O^{q+}+Ar$, continuum electron capture and loss, 1.6-2.8 MeV/A 78-46443

atom-ion collisions continued
O^{q+}+Ar, continuum electron capture, projectile vel. and Z depend. 78−55222
O^{q+}+H(H_2), q=1-5, single electron capture cross sections 78−55233
O^{q+}+He, charge exchange measurements using double-tandem accelerator-decelerator source of low-energy highly-stripped O ions 80−81317
O^{q+}+He(Ar)(Ne), electron capture to continuum states, forward ejected electron spectra 79−45831
O^{x+}+He, electron capture, K X-ray emission ang. distrib. 77−57919
OH^-+inert gas, collision-induced dissociation 78−29834
O^{7+}(O^{8+})+He, p-state alignment, X-ray emission polaris. obs. 79−50123
$^{16}O^{8+}$+Au K-shell ionis., δ-ray emission 77−79557
$^{16}O^{x+}$+Al, energy-loss straggling, charge exchange effects 78−58799
Pb, 90-110 MeV, ion-atom collision, K-vacancy prod., mol.-orbital method 77−68095
Pb, ion collisions 90-110 MeV, K-vacancy production, multiple and single collisions in mol. orbital excitation 77−83717
Pb, K-shell ionis. probability, 25- 40-and 74-MeV α particles 77−528
Pb, X-ray production cross sections for protons, fluoresc. obs. 80−102476
Pb+H^+, K-shell ionisation, 7-15 MeV, relativistic effects 78−82830
Pb+H^+ (L_α, L_β, L_γ) X-ray emission probability, impact parameter dependence 77−23553
Pb+H^+(D^+), L-subshell vacancy production, Coulomb deflection effects 80−9711
Pb+Pb K-MO spectrum, impact parameter depend. 80−5613
Pb+Pb^+, δ-electrons from K- and L-shell ionisation in adiabatic collisions 80−23541
Pb+Pb^+, inner-shell ionisation of quasimolecular system, perturbation theory 79−31667
Pb^++Z ($42 \leq Z \leq 92$), 1sσ MO excitation probability and binding energy, X-ray coincidence 78−94316
^{82}Pb+H^+, L-subshell ionisation probabilities, impact parameter depend. 77−30981
^{208}Pb, 1.4 to 5.9 MeV/u, K-shell ionisation cross-section meas. 79−31671
^{208}Pb+^{208}Pb collisions, 1 GeV, mol. orbital X-rays 79−49978
Pd, ionisation cross sections for L_1 and L_2 subshells by 250-500 keV protons *(Russian)* 77−6918
Pd+H^+(O^{5+}), L-shell X-ray prod. cross-section 77−6913
Pt+H^+, L-subshell X-ray prod., cross-section meas. 77−46575
Pt+H^+(He^{2+}), L-subshell ionisation with high vel. positive ions 79−50122
Rb+$^{14}N^{n+}$, 7-35 MeV, K-shell X-ray production cross sections 77−75090
Rb+H^+, atomic K-shell ionis., X-ray emission 79−18280
Rb+H^+, single-electron capture total cross sections 80−91656
Rb+H^+($^2H^+$), inner-shell ionisation, Coulomb repulsion effects 80−48075
Rb+He^+, 3-20 keV, fractional yield of He^- ions 77−1919
Rb+He^+→Rb^++He^0, charge exchange cross section, 1-36 keV 77−1919
Rb+Rb^+, total resonant charge transfer cross section determ. using model pot. simulation 79−64073
Rb^++Ar(Kr)(Xe), elastic beam scatt., repulsive pots. 79−98184
S ion+target collisions, two-electron-one-photon transitions, X-ray spectra 77−19068
S to Br, $O^{2+,3+,4+,5+}$ induced K-shell ionis., 7 to 24 MeV X-ray production cross section 77−61850
S+F^-, inner-shell ionisation, X-ray cross sections 80−58369
S+X, (X=atom with Z=11-22), K-shell ionis. cross sections 78−13596
S^++Ar, double K-vacancy prod., X-ray X-ray coincidence and fluoresc. yields obs. 78−55230
S^{15+}+Ar, K-shell vacancy sharing, interference effects 80−5606
S^{n+}+Ar, molecular K-X-ray production, projectile charge depend. 78−90188
S^{n+}+Cl(Ar), branching ratio dependence on projectile velocity and nuclear charge 79−31475
S^{n+}+inert gas, electron promotion effects for small impact parameter 79−18278
S^{n+}+Ne(SiH_4)(H_2S)(HCl)(Ar), K X-ray cross section, projectile charge depend. 77−19029
S^{q+}+O_2(Ar)(He), (q=8-19), K X-ray prod., charge-state depend. 80−106391
SF_6^-+He, decomposition, SF_5^- form. 78−29833
Sb, ionisation cross sections for L_1 and L_2 subshells by 250-500 keV protons *(Russian)* 77−6918
Sc, X-ray production by protons by 0.5 to 2.0 MeV energy 78−66646
Sc+H^+, K X-ray production, 0.2-0.5 MeV, ionis. cross-section 79−31459
Se+H^+, K-shell ionisation cross-sections calcs. 80−43165
Se+H^+, K-shell ionisation cross-section determ. 80−48077
Si, K-shell ionis., X-ray prod. cross section for incident H^+, ^{4}He and ^{14}N ions 78−70923
Si, two electron one photon transitions, Kαα X-rays 77−30813
Si+Co(Fe) recoil, transient mag. field 78−29838
Si+F^-, inner-shell ionisation, X-ray cross sections 80−58369
Si+F^{q+}, q=3-9, Si K-shell ionis., electron transfer cross sections, solid targets 79−10192
Si+H^+(^{3}He) ion collisions, K-shell ionisation cross sections 77−23555
Si+He^4, X-ray spectra, two-electron one-photon transition in solid target, 2 MeV 78−94209
Si+He(C)(O)(Ne), K-shell ionising collisions, average L-shell ionisation probability, K_α spectra 79−72408
Si+heavy ion, X-ray spectra, one-photon two electron rearrangements 77−6712
Si+$Li^{+1,2,3}$, K-shell ionisation depend. on projectile charge state 77−34743
Si^{12+}+He, K X-rays for population in $^3S_1$ metastable state, Si^{12+} from C, Au foils 78−17776
Si^{n+}+S(Ar)(Al)(Cu), K-shell vacancy sharing ratio, foil or gas target 78−42198
Si^{q+}+Ar, electron capture to continuum states, forward ejected electron spectra 79−45831
Si^{q+}+He, q=2-11, K-shell fluoresc. yields, charge-state depend. 78−55231
Sm+H^+($^3He^+$), X-ray intensity ratios, projectile energy depend. 80−23535
Sn+H^+(O^{5+}), L-shell X-ray prod. cross-section determ. 77−6913
Sr+Ca^+, laser induced charge transfer 80−53108

atom-ion collisions continued
Sr+D^+, 2.7 to 31 keV, D^- equilib. charge-state fractions 78−17750
Sr+H^+($^2H^+$), inner-shell ionisation, Coulomb repulsion effects 80−48075
Sr^++ inert gas atom, spectral line polarisation 79−13811
Sr^++inert gas atom collision, polarisation of emitted radiation, quasimol. interf. effect *(Russian)* 77−46633
Ta, ion impact, L-subshell ionis. cross-section ratios 77−6920
Ta+H^+, K-shell ionisation, 7-15 MeV, relativistic effects 78−82830
Ta+H^+(He^{2+}), L-subshell ionisation with high vel. positive ions 79−50122
Tb^{3+}+O_3(SO_5^{2-})(SO_2), in H_2SO_4 soln., electrochemiluminesc. emitters quenching by electrolysis products 79−1794
Th+H^+, K-shell ionisation, 7-15 MeV, relativistic effects 78−82830
Th+H^+(D^+), L-subshell vacancy production, Coulomb deflection effects 80−9711
Ti, K-shell hole production by light ions, hydrogenic and Hartree-Fock model of target 77−83715
Ti, X-ray production by protons by 0.5 to 2.0 MeV energy 78−66646
Ti+H^+, K X-ray production, 0.2-0.5 MeV, ionis. cross-section 79−31459
Ti+H^+, K-shell ionisation calcs. 80−23534
Ti+H^+, K-shell ionisation cross-section determ. 80−48077
Ti+H^+ ion collisions, K-shell ionisation cross sections 77−23556
Ti+He^{2+}(C^{4+})(O^{5+})(N^{4+})(N^{5+}), ratio of single K-shell ionisation cross section to double K-shell ionisation cross section 80−53119
Ti+N^{4+}, Kα and Kβ X-ray spectra for 84 MeV incident energy 77−50517
Ti+S ion, KL^n X-ray satellites, intensity distrib., photoabsorpt. effects 78−78657
Ti^{2+}+H(H_2), electron capture cross-sections, 0.5-14 keV 78−42205
Ti^{q+}+O_2(Ar)(He), (q=8-19), K X-ray prod., charge-state depend. 80−106391
U, ion impact, L-subshell ionis. cross-section ratios 77−6920
U+H^+, relativistic K-shell ionisation cross-section meas. 78−33593
U+H^+(D^+), L-subshell vacancy production, Coulomb deflection effects 80−9711
U+H^+(He^+), 2-18 MeV, L-subshell ionis. cross section, projectile energy depend. 77−19031
U^++U^+, critical two-centre distance, HFS relativistic calc. 79−22801
U^{36+}+N(Ne)(Ar)(Kr), radiative charge exchange, 16, 64, 256 MeV/amu 78−55234
UO^++Ar, collision-induced dissoc. cross section and threshold 80−95706
UO_2^++Ar, collision-induced dissoc. cross section and threshold 80−95706
$^{238}U^{n+}$+Z, Z=6 to 92, 3.6 to 5.9 MeV/amu K-vacancy prod. 79−31672
V, X-ray production by protons by 0.5 to 2.0 MeV energy 78−66646
V+H^+, K X-ray production, 0.2-0.5 MeV, ionis. cross-section 79−31459
V+H^+ ion collisions, K_α satellite intensity meas. 77−23550
V+H^+ ion collisions, K-shell ionisation cross sections 77−23556
W, N-shell ionisation by proton impact 78−78800
W+H^+, inner-shell ionisation, Coulomb repulsion effects 80−48075
Xe, 326-470 MeV, ion collisions, K-vacancy production, multiple and single collisions in mol. orbital excitation 77−83717
Xe, 326-470 MeV, ion-atom collision, K-vacancy prod., mol.-orbital method 77−68095
Xe ion+Hg vapour collisions, quasimol. M-radiation 77−14566
Xe^{2+}, energy level radiative lifetimes using 1-5 MeV ions 80−47947
Xe+$^4He^{2+}$, optical transition excitation function and cross sections 80−63787
Xe+$^{75}As^{n+}$, slowing down of atoms/ions with KE≤5 eV by inert gases 79−31650
Xe+Ar^{x+} multiple scatt., combined ang. and lateral spread 78−46441
Xe+Cu^{q+}, ($16 \leq q \leq 23$), 1.4 MeV/amu, X-ray emission, charge state dependence 78−37713
Xe+H^+, M-subshell ionisation cross section, binary encounter approx. 78−62890
Xe+H^+ ionisation, induced L-shell alignment 80−32813
Xe+ion ($1 \leq Z_1 \leq 90$), 2.5-400 keV, 1-6°, effective interat. pots. 80−23492
Xe+Xe^+, 0.3-1.2 MeV, multiple N- and M-shell excitation, inelastic energy loss meas. 79−852
Xe+Xe^+, differential cross section, pot. curve fitting reson. electron exchange 77−58118
Xe^++Ag, quasimolecular L and Ag L X-ray excitation thresholds, electron correl., calc. and expt. 78−78793
Xe^++Xe, quasi-resonant charge transfer at thermal energies 80−48082
Xe^++Xe, XeI reson. line excitation 80−87220
Xe^++Xe collisions, Auger electron ionisation, inelastic energy loss meas., multiple inner shell excitation 77−19055
Xe^{10+}+He(Ne)(Ar)(Kr)(Xe)(Cd)(Na)(Cs), depend. of charge transfer on ionisation pot. 79−64096
Xe^{31+}+Ne, 200 MeV collision, Auger emission 77−57952
^{132}Xe, 1.4 to 5.9 MeV/u, K-shell ionisation cross-section meas. 79−31671
^{136}Xe ion+target collisions, K-X-ray yields, 1sσ excitation 77−19051
^{136}Xe ion+target collisions, X-ray yields, K-L level matching 77−19052
^{136}Xe ion+target collisions, K-X-ray yields, K-vacancy sharing 77−23548
^{136}Xe ion+target collisions, K-X-ray yields, 2pσ excitation 77−23549
Y+$^{14}N^{n+}$, 7-35 MeV, K-shell X-ray production cross sections 77−75090
YB^++inert gas, ($^2P_{3/2}$) states relax. cross sections 78−13595
Yb+H^+, K-shell ionisation, 7-15 MeV, relativistic effects 78−82830
Yb+Yb^+, with nuclear sticking, molecular orbital and compounds nucleus X-ray emission 80−1048
Zn, gas-phase, plasma, sputtering and beam-foil 80−32820
Zn+H^+, K-shell ionisation calcs. 80−23534
Zn+H^+, K-shell ionisation cross-sections calcs. 80−43165
Zn+H^+(He^{2+}), L- and M-shell Auger electrons 79−27076
Zr+$^{14}N^{n+}$, 7-35 MeV, K-shell X-ray production cross sections 77−75090
Zr+H^+, K-shell ionisation cross-section determ. 80−48077
Zr+H^+($^2H^+$), inner-shell ionisation, Coulomb repulsion effects 80−48075

atom-molecule collisions
see also atom-molecule reactions; molecular rotational-vibrational energy transfer
A+BC($^1\Sigma$), structured collision, quantum mech. theory 77−88527
acetylene+inert gas, vibr. relax. study using laser-induced fluoresc. 80−74219
alkali+molecule, apparatus for energy, angle and mass anal. of products 78−70970
alkali atom+hexafluoride molecule, collisional ionisation 78−55226
alkali atom+methane derivative, collisional ionisation, nitromethane, perfluoromethyl bromide (iodide) electron affinities 78−66639
alkali atom dimer polarisation transfer, atom-molecule-exchange reaction 78−13574
alkali halide+inert gas, inelastic scatt., short-lived complex form. 79−13796
alkali metal+N_2, temp. depend. of vibr. relax. time 77−34725
anisotropic interaction pot., influence on transport cross sections, appl. to He-alkali dimer 80−9677
anisotropic molecule-atom interactions, glory scatt. calc. in sudden approx. 78−25654
anisotropic potentials, rainbow scatt. 77−82407
atom+diatom, anisotropic interaction pot., total cross-section calcs. 78−29835
atom+diatom, body-fixed formulation for close-coupling calc. 78−78768
atom+diatom, classical inelastic collinear system, energy transfer calcs., anal. method 78−21998
atom+diatom, collinear, vibr. energy transfer, stochastic theory, nonmarkovian effects 79−81262
atom+diatom, collinear collision with exponential repulsive interaction, generalised distorted wave calcs. 78−9060
atom+diatom, collision induced dissoc., multiple scatt. theory 78−21999
atom+diatom, collision-induced dissoc., quantum mech. probabilities, close coupling calcs. 77−75259
atom+diatom, collision-induced dissoc., quantum mech. probability calcs. 78−25657
atom+diatom, degeneracy averaged scatt. cross-section calcs. 79−89735
atom+diatom, energy correction of infinite order sudden approx., improved phase shift approach 80−95710
atom+diatom, energy transfer, reaction dynamics, review 80−63801
atom+diatom, energy transfer, vibronic excitation, emission spectra 78−66578
atom+diatom, inelastic cross-sections, rot. quantum number, energy scaling 77−83692
atom+diatom, long-lived trajectories near reactivity band boundary 78−29836
atom+diatom, reactive scatt. theory using DWBA 77−70296
atom+diatom, rot. and vibr. excitation, S-matrix element calcs. 78−17763
atom+diatom, rot. inelastic cross sections, ang. and rot. energy moments 79−81261
atom+diatom, rot. inelastic scatt., mag. transitions, time reversal symm. 80−48066
atom+diatom, rot. infinite-order sudden-approximation, low energy appls. 78−1052
atom+diatom, scatt., l_z-conserving sudden approx. calcs. 78−66628
atom+diatom, stochastic one-dimens. model 78−42159
atom+diatom, T-matrix element approx., j_z-CCS calcs. 77−19003
atom+diatom, vibr.-translational energy transfer, mol. rot. effects calcs. 77−34736
atom+diatom, vibr.-translational energy transfer, self-consistent and stochastic treatment 77−83693
atom+diatom collinear collision, refined Born approx. 78−74724
atom+diatom collision, energy sudden, centrifugal sudden and IOS approx. calcs. 80−23499
atom+diatom collisions, reorientation cross section calc., distorted wave and Bernstein Kramers approx. 79−843
atom+diatom collisions, vibr. to electronic energy transfer, semiclassical decoupling scheme 80−95714
atom+diatom inelastic scattering, exponential gap law 77−10737
atom+diatom scattering eqns., generalised phase shift, semiclassical series soln. 80−43142
atom+diatomic molecule, collinear collision, light absorption 79−76486
atom+diatomic molecule, coupled states, P-helicity, and effective pot. methods comparison 77−30944
atom+diatomic molecule, restricted 2-D Morse oscillator model, semiclassical calcs. for mol. dissoc. 80−74222
atom+linear molecule, rot. excitation, classical and quantum calcs. 78−1059
atom+molecule, electronic to vibrational/rotational/translational energy transfer, crossed beam expt. 79−89750
atom+rigid rotor, differential scatt. cross-section, quantum mech. inversion, IOS approx. calcs. 79−89736
atom+rigid rotor collision, sudden rot. approx. 77−30966
atom+symmetric top, rot. excitation, IOS approx. calcs. 79−45801
atom+symmetric top, rot. inelastic collisions, physical anal. 79−6991
atom+triatom collisional energy transfer, ergodicity in mol. vibr., Henon-Heiles pot. 80−18906
atom+vibrator, stochastic theory, master or Fokker-Planck eqn. numerical solns. 77−30965
atom-diatom collinear collision, first order nonlinear matrix differential eqn. 80−37853
atom-diatom collinear reaction, potential classical transition collinear state theory 79−98191
atom-diatom kinetic cross section, ES, CS and IOS approx. with translational-internal coupling, viscomag. effect 80−63764
atomic ionisation, polar mol. rot. effect 77−83702
body-fixed coordinates collision theory, asymptotic scatt. matrix solns., appl to $H+H_2$ 79−64070
classical theory of collisional entropy production 79−10162
classical trajectory calcs., empirical testing of nonrandom integration method 78−50607
collinear atom-diatom inelastic scatt., Green functions method 78−25660
collisional relax. of highly excited states, laser-induced fluoresc. obs. 80−58205
CS approximation, total angular momentum labeled, inadequacies 79−22777
cyanoacetylene+He, collisional excitation of interstellar molecule 78−81664
degenerate atomic level perturbation by neutral particles 79−792
diatom+atom, rot. transitions, mols. in Π state 78−82825

atom-molecule collisions continued
diatom+atom (electron) scatt., vibr.-rot. excitation, generalised field theory method 77−23537
diatom dissociation and recombination mechanisms, bound complex and triple collision mechanisms 80−23478
diatomic transition operators, numerical calcs., variable phase and amplitude calcs. 78−25653
differential and total scatt. cross sections using spectroscopic line shape anal. 79−36735
differential cross section, classical perturbation scatt. theory 78−5319
dissociation, collision-induced, Morse oscill. model 78−37710
electron contact, model system *(Dutch)* 79−50111
electronic energy transfer, in excited atom collisions, review, book contrib. 77−40543
energy transfer, vibr. and rot. excited states, field theory 77−14533
foreign gas broadening, translational heat-bath model, variational methods 78−9124
high Rydberg atom+neutron atom (molecule), collisional quenching, theory 79−86051
high-Rydberg atom+polar molecule, state-changing collisions 80−9727
induced IR spectra, overlap dipole moment determ. 77−18924
inelastic molecular collisions appl. of non-interger Bessel uniform approx. 79−36733
inert gas+H_2**, ionising or deactivating collisions 79−100338
inert gas dimer+atom, IOSA calc. for total integral cross sections for excitation, exchange and dissoc. 80−1044
inert gas ion+oxides, energy loss spectra 78−58798
infrared line shape, rotational lines, influence of collision duration 80−43110
intermolecular potential, rot. energy transfer, sensitivity anal. 80−63762
internal degrees of freedom collisional excitation, statistical model 79−45803
ion+dipole scatt., differential cross section, classical perturbation scatt. theory 78−5319
ion pair forming collisions, dynamics 78−66661
IR induced vibr. transition, Schrodinger eqn. distorted wave calc. 77−23538
Lorentz gas, two-dimens., collision-induced absorption, simulation 78−46424
methane+Ar, rot. compound state resons. 80−28090
methane+monatomic collisions, photoacoustic study of vibr. relaxation *(French)* 77−30969
molecular basis sets as energy approaches excitation threshold 78−78783
molecular orbital X-rays from atomic and molecular impact on solid targets 79−36750
molecular scattering amplitude, j_z=conserving approx., space- and body-fixed formulation 78−21987
momentum transfer rate consts. meas. by ion cyclotron resonance 77−86287
Morse oscillator+atom, collinear collision, T-V energy transfer, de-excitation process 78−90268
Morse oscillator+atom, collinear collision, T-V energy transfer, excitation and dissociation processes 78−90269
Morse oscillator collinear collision, inelastic vibr. energy transfer, mol. continuum influence 80−106383
Morse oscillator collinear collision induced dissoc., vibr. enhancement, quasiclassical trajectory study 80−28089
multiply charged collision systems, slightly asymm., curve crossings, constraints, MO theory 78−74734
naphthylamines, excited state pK_a* values, proton-induced fluorescence quenching 78−21958
non-reactive heavy particle collision calculations, review 79−59541
nonadiabatic collisions, Franck-Condon approach for electronic state quenching 78−66640
one-electron atom+methane, collisional energy transfer by octupole coupling 78−62881
orbital angular momentum quantum numbers in definite parity j_z CCS approx. 77−14511
Penning collision processes, review *(Japanese)* 79−64092
Penning ionisation processes investig. by electron spectroscopy 80−58364
polar molecule+high Rydberg atom, l-changing collision 79−10185
polyatomic molecule+atom, many body approach 79−31645
positronium+N_2 (inert gas), fine struct. interval, collisional density shifts 77−34788
potential scattering, refined Born approx. 80−77
quantal cross-sections, j_zCCS and statistical j_z approx. surprisal anal. 77−14513
quantal many-body approach to atom-polyatom collisions 77−30943
quantum scattering theory, R-matrix propagation methods in inelastic and reactive collisions 79−59534
quasielastic atom ejection by high energy atom impact *(Russian)* 78−37712
reactivity band boundaries, trapped trajectories, theory 78−29836
rotational energy transfer in collisions between orbitally non-degenerate open-shell systems 79−50118
rotational excitation cross sections, use of rot. and orbitally adiabatic basis functions 79−59543
rotational inelastic scattering, effect of interaction pot. 79−59533
rotational rainbow maxima: a time dependent study 80−58353
rotational transitions, classical cross sections, sudden approx. calcs. 79−89751
rotationally inelastic, classical scattering from an anisotropic rigid shell potential of rotation symmetry 80−18907
rotationally inelastic collisions, tensorial factorisation 80−28096
rotationally inelastic scatt., coupled eqns. for single initial state, variation-iteration method 79−68301
Rydberg atom+molecule, reaction channels, expt. vs. theory 80−63755
semiclassical collision theory, non-integer Bessel uniform approx. 79−36730
spectral line broadening, approx. trajectories calc. 78−46413
spectral line broadening, semiclassical straight line vs. curved trajectories 79−45765
spectral line broadening by foreign gas, translational heat bath model, T-approx. 78−9125
sudden approx., differential cross sections 78−13570
tetrafluoromethane+He gas mixture, collision induced for IR translational spectra 80−83353
theory, book 79−72394
toluene+OH(D), vibrational and rotational energy effect 80−76497
1,3,5-trimethylbenzene+OH(D), rotational and vibrational energy effect 80−76497

atom-molecule collisions continued
unitary approx. for inelastic collisions 78−13569
vibration-rotation transitions, optical potential approach 78−62885
vibrationally inelastic collision, rot. energy sudden approx. 79−68303
wavefunction, total ang. momentum body frame radial, coupled states and infinite order approxs. 78−25641
Ar, ($^3P_2$) and ($^3P_0$) states, quenching mechanisms and rate consts. 79−13801
Ar+BaO, in Ar flame, rot. and translational relax. by sub-Doppler optical-optical double reson. 80−95583
Ar+Br_2 collisions, dissociation reaction, trajectory study by ensemble method 80−66765
Ar+CO_2, rot. inelastic wide angle scatt., differential cross sections 77−14536
Ar+CO_2, total differential scatt., IOS approx. calcs. 79−98194
Ar+CO_2(N_2), repulsive pot. energy surface, approx. calc. and differential scatt. expt., comparison 79−22788
Ar+H_2, metastable state breakdown, temp. depend. 79−98211
Ar+H_2, vibr. transition rates, thermally averaged, Monte Carlo trajectory calcs. 80−23519
Ar+H_2O(D_2O), ($^3P_{0,2}$) state quenching cross sections 78−70912
Ar+HCl, differential cross section, quasiclassical close coupling approx. 80−63743
Ar+HCl, inelastic scatt. exponential perturbation theories 80−74217
Ar+HCl, line broadening, short range force effects, semiclassical calcs. 79−98085
Ar+HCl, rotationaly inelastic collision, planar trajectory, classical centrifugal decoupling calcs. 78−58788
Ar+HCl(H_2), intermol. forces, generalised electron gas-Drude model 79−98182
Ar+HF, state-to-state cross sections for rot. to translational energy transfer determ. 80−91644
$Ar+M \rightarrow Ar^+ + M + e^-$ or $+M^-$, ($M=O_2$, NO, NO_2, N_2, CO), keV energies, translational spectroscopy 78−5339
Ar+methane, low energy collision, close coupling and coupled states, rot. transitions 78−78784
Ar+methane-d_4, vibr.-translational relax. 80−99537
Ar+N_2, ($A^3\Sigma_u^+$, $\nu=0,1$) metastable state quenching rate coeffs. 78−90206
Ar+N_2, bimol. and three body quenching, reson. state $^1P_1$, $^3P_1$ and excimer Ar atoms 79−3540
Ar+N_2, collinear collision, vibr.-translation energy transfer, model calc. 78−66634
Ar+N_2, cross sectional factorization expressions, close coupling input tested in sudden approximation 79−43571
Ar+N_2, excitation of $N_2(C^3\Pi_u)$, symmetry, propensity rules and alternation intensity, rot. spectrum 80−87135
Ar+N_2, inelastic scatt. exponential perturbation theories 80−74217
Ar+N_2, quantual cross-sections, j_zCCS and statistical j_z approx. surprisal anal. 77−14513
Ar+N_2, rot. excitation, planar trajectory approx. calcs. using body-fixed coords. 77−75267
Ar+N_2, rot. inelastic collision cross section, centrifugally decoupled exponential distorted wave approx. 79−842
Ar+N_2, rotational excitations, close-coupling calcs. 77−27157
Ar+N_2 rotational excitation, differential cross sections and orientation effects, classical trajectory method 80−23523
Ar+N_2(CO), intermolecular pots. from Thomas-Fermi-Dirac functional 77−19009
Ar+N_2(TlF), scatt., l_z-conserving sudden approx. calcs. 78−66628
Ar+NO($X^2\pi$), intermol. pot. surfaces, electron gas model calcs. 77−34721
Ar+Na_2, differential cross sections meas. for rot. energy transfer process, obs. of halos 80−91643
Ar+SF_6(tetrafluoromethane), differential scatt. cross-sections, intermol. pots. calcs. 79−89742
Ar+TiO, collision cross-section meas. 78−55202
Ar+TlF collisions, small angle scattering, calc. cross sections 78−70915
Ar+Xe(F_2), proton excited mixtures, energy transfer processes 78−66647
Ar($^3P_{0,2}$)+N_2, rate consts. and N_2(C):N_2(B) branching ratio 78−5327
Ar($^3P_{2,0}$)+H_2O, energy depend. of ionisation and dissociative fluorescence in crossed mol. beams 79−52669
Ar($^3P_2$)+fluorine containing molecules, quenching rate consts. 77−9072
Ar($^3P_2$)+$N_2(C^3\Pi_u)$ excitation transfer cross section, radiative lifetimes, in N_2 laser, transitions 79−27246
Ar*+Fe$(CO)_5$, chemiionisation and chemiluminescence reactions, Penning ionisation and fluoresc. obs. 80−97689
Ar*+I_2, ion-pair form. differential cross-section, 25-133 eV, metastable Ar 78−78787
Ar*+N_2, 3371 and 3577 Å laser emission, kinetic model 78−5465
Ar*+N_2, excitation transfer collision, vibronic energy partitioning 77−75264
Ar*+N_2(H_2)(D_2), de-excitation processes, by pulse radiolysis optical emission obs. 77−65529
$Ar^* + N_2 \rightarrow Ar + N_2^*$, electronic to vibr. energy transfer, time depend. theory 80−23514
Ar*+O_2, ion pair form. explained by charge transfer model 80−99546
Ar_2^*+Kr(Xe), kinetic behaviour and energy transfer 79−68305
Ar*(^3P)+$CO_2(X^1\Sigma_g^+)$, differential elastic and quenching cross-sections 78−58773
Ar*(4s)+H_2, H_2 continuum emission, kinetic studies in Ar-H_2 mixture, e-beam pumped 80−43153
B+He (methane), B atom K-shell binding energy by Auger spectra 78−50525
B+He (methane), collisional excitation, prompt decay line energy, projectile Auger spectrosc. 79−85941
BN, X-ray spectra, chemical bonding and multiple ionis. effects 78−50630
Ba+CO, radiation quenching of metastable Ba (5d ^1D) in gas 79−85932
Ba+D_2, radiation quenching of metastable Ba (5d ^1D) in gas 79−85932
Ba+H_2, radiation quenching of metastable Ba (5d ^1D) in gas 79−85932
Ba+HBr, laser induced fluoresc. study at different collision energies 80−91632
Ba+HCl, laser induced fluoresc. study at different collision energies 80−91632
Ba+HF, product rot. and vibr. distributions and reaction cross sections depend. on reagent translational energy 80−93745
Ba+N_2, radiation quenching of metastable Ba (5d ^1D) in gas 79−85932
BaCl+Ar(He)(N_2), intermultiplet energy transfer 79−27063

atom-molecule collisions continued
BaCl($C^2\Pi$)+He(Ar)(N_2), collisional quenching, laser induced fluoresc decay meas. 79−27075
Be+He (methane), Be atom K-shell binding energy by Auger spectra 78−50525
Be+He (methane), collisional excitation, prompt decay line energy, projectile Auger spectrosc. 79−85941
BeO, X-ray spectra, chemical bonding and multiple ionis. effects 78−50630
Bi, metastable states collisional quenching, temp. depend. 77−88526
Bi+NF, near-resonant electronic energy transfer, surface-hopping model 79−86030
Br+CO_2(HCl), quenching of $4^2P_{1/2}$ state, vib. excitation, temp. depend. 78−58792
Br+H_2, proximity induced electric dipole moment effect in laser field 80−83456
Br+O_2(NO), quencher paramagnetism, deactivation rate const., spin-orbit relax. study 80−21263
Br_2+Ar, collision de-energisation of highly vibr. excited Br_2, mol. dynamics simulation 77−42378
Br_2+Ar, ergodic deactivation, anharmonic effects on transfer rate 78−82818
Br_2+K, nonreactive differential scatt., 0-10 eV, scatt. angle 78−42156
Br*+I_2(Br_2)(Cl_2)(IBr)(ICl)(BrCl), deactivation rates of Br*($^2P_{1/2}$), collision complex form model 78−42179
Br($4^2P_{1/2}$)+$^{12}CO_2$($^{13}CO_2$), electronic-vibr. energy transfer, temp. depend. meas. 79−10136
Br($4^2P_{1/2}$)+CO_2(COS)(CS_2), electronic to vibrational energy transfer rates 78−29839
Br($4^2P_{1/2}$)+H_2(HD)(D_2), electronic-vibr. energy transfer, fluoresc. meas. 79−72347
Br($4^2P_{1/2}$)+HCl, electronic to vibr. and rot. energy transfer from flash photolysis of HCl-Br_2-Ar 80−48069
Br($4^2P_{1/2}$)+N_2O, electronic-vibr. energy transfer obs. 78−55220
C+He (methane), C atom K-shell binding energy by Auger spectra 78−50525
C+He (methane), collisional excitation, prompt decay line energy, projectile Auger spectrosc. 79−85941
C^++H_2, fine struct. transition excitation 77−42389
CN($B^2\Sigma$)+N(C)(O) collisions, in CO-N_2-Ar mixtures, shock wave induced, cross section *(Russian)* 78−74638
CO+He, collisional excitation of interstellar molecule 78−81664
CO+K, atom electronic excitation, vibr. to electronic energy transfer, seeded mol. beam studies 80−47919
CO+Kr($^3P_1$)($^1P_1$) $A^1\Pi$-$X^1\Sigma^+$ and $b^3\Sigma^+$-$a^3\Pi$ sensitised fluorescence, isotope effects 78−82761
CO_2-He-Cs glow discharge, quenching cross section of resonant Cs(6P) state by CO_2 mols. 80−43860
CO_2+Ar(N_2), 301_{III}-000 band, intensities, press.- and self-broadening coeffs. meas. 78−78695
CO_2+He, rot. inelastic collision, ab initio SCF, electron gas and pot. energy surfaces 80−83468
CO_2+He(Ar), dipole and Raman line press. broadening temp. depend. 79−68265
CO_2+Ne, intermol. pot. in repulsive short-range region, ab initio 80−69204
CO($\nu=1$)+He, vibr. relax., collinear and 3D rate consts., temp. depend. 77−38717
CO($\nu=1$)+He, vibr. relax., collinear and 3D rate consts., temp. depend. 77−38718
CS_2+Ar*, Penning ionisation and dissoc. fluoresc, collisional energy depend. 78−33584
C(2^1S_0)+H_2(O_2)(ethylene) 80−74241
Ca*+Cl_2, collision and reaction cross section meas. 79−59537
Cd+alkane hydrocarbon, $^3P_{0,1,2}$ state distrib., E to V,R transfer 80−28088
Cd+molecule collisions efficient cross-sections determ. 80−58338
Cd+N_2, $A^3\Sigma_u^+$ state, vibr. excitation 80−1054
Cd+N_2, vap., creation of inverse population of atomic Cd 6^3S and 5^3P_2 levels 80−58219
Cd($^1P_1$) excited state quenching by mols., cross sections, chem., phys. exit channels 79−779
Cd($^1P_1$)+N_2(alkanes), laser excitation, absolute quenching cross sections and branching ratios 79−49979
Cd(5^3P_1)+POPOP, vap., electronic energy transfer, laser appl. 77−30980
Cl_2+Ar(He)(Cl_2), dissoc. in shock wave, density gradient meas. 77−83682
ClF+Ar, shock wave, vibr. relax., laser schlieren meas. 78−90267
Cl($3p^5$($^2P_{1/2}$))+carbon tetrachloride (Cl_2)(He), VUV metastable state quenching, absolute rate const. 77−79641
Cs+Cs_2, nuclear spin polarisation exchange collisions, optical pumping method obs. 77−16797
Cs+D_2O, ion-pair form., energy, angle and mass anal. of products 78−70970
Cs+I_2, ion-pair formation, energy transfer and differential scatt. 77−75272
Cs+methyl cyanide, collisional ionisation obs. 80−95716
Cs+O_2, collisional ionisation, energy spectra of forward and backward directed positive and negative ions 80−87200
Cs+O_2, mol. target internal motion 80−78697
Cs+TCNQ, TCNQ-form., electron affinity, compound states 77−65530
Cs+UF_6, ionisation reactions, absolute cross sections 80−99565
Cs+UF_6(WF_6), collisional ionisation, crossed beam obs. 79−68299
Cs+Xe (neopentane), Cs line shape broadening, satellite data inversion, interaction pot. 78−74608
Cs_2+He(Ne)(Ar), exchange collisions, optical pumping method obs. 77−16797
Cs_2+He(Ne)(Ar)(Kr)(N_2)(CH_4), collision-induced dissoc., atom-mol.-exchange optical pumping 78−22008
CsCl(Cs_2Cl_2)+Ar(Kr)(Xe), collision-induced ion-pair form., absolute cross sections 78−73029
CsF+Ne, (Ar)(Kr)(Xe), sudden, body-fixed and semiclassical approx. calcs. 78−42164
CsXe+Xe, time resolved fluoresc. decay and collisional transition rates 77−27111
Cs*+N_2, excited states quenching 78−5330
Cu+N_2, preferential energy transfer from N_2 to specific Cu energy levels 80−43152
D+H_2, pot. surface, isotropic part determ. 79−36729

atom-molecule collisions continued
$D+N_2$, fast collision, electron scatt. resons., ionisation, deexcitation 79−81268
D_3^+ +inert gas, ion decay, 1-40 eV *(Russian)* 78−90286
$D^{**}+N_2$ fast collisions, impulse approx. 80−106281
$F\ (^2P_{1/2})+H_2$, quenching, classical path calcs. 79−22800
$F+H_2$, collision in intense laser field, formalism for mag. dipole interaction 79−98190
$F+H_2$, electronic-rot. energy transfer, for $F(^2P)$ 79−36740
$F+H_2$, electronic-rot. energy transfer, partial cross-section interweaving 79−59538
$F+H_2$, electronic-to-rotational energy transfer 77−3431
$F+H_2$ nonadiabatic effects, scatt. theory, coupled-channel calcs. 78−22010
$F+H_2+\hbar\omega$, reactive scatt. and inelastic collision in laser field, semiclassical calc. 79−47948
$F+Xe(H)^+(H_2)$, $(^2P_{3/2})$ state quenching, Franck-Condon approach 78−66640
^{18}F+hexafluoropropylene nonequilibrium effects in moderated nuclear recoil experiments 80−89509
^{18}F+methane, nonequilibrium effects in moderated nuclear recoil experiments 80−89509
F^*+H_2, quenching of excited state, semiclassical studies, comparison between reactive and nonreactive processes 80−106375
$F^*(^2P_{1/2})+H_2$, appl. of classical model for electronic degrees of freedom 79−98192
$Fe^{n+}+H(H_2)$, 50-1200 keV amu^{-1}, impact ionis. and electron capture cross-sections 78−42204
$H+Br_2(Cl_2)$, nonreactive scatt., long range anisotropic pot. determ. 78−66626
$H+Br_2(HBr)$, H* prod., IR chemiluminesc. meas. 79−100336
$H+C^{3+}(N^{3+})$, charge exchange collisions, quantal calcs. 79−94079
H+CO, total different collision cross section meas., interstellar gas clouds appl. 79−45786
$H+Cl_2$, stochastic-collision complex model theory 80−108696
$H+D_2$, collinear motion, energy transfer and dissociation, collision dynamics 80−99563
$H+D_2$, pot. curve, thermal energy absolute integral cross-sections meas. 80−53096
$H+H_2$, 1s-2s excitation of fast H atoms 79−89764
$H+H_2$, ang. momentum decoupling approx., quantum mech. reactive and nonreactive scatt. 77−12780
$H+H_2$, anisotropic interaction pot., total cross-section calcs. 78−29835
$H+H_2$, atom-atom pots., Hilbert Schmidt expansion, transition operators 78−66621
$H+H_2$, barrier penetration theory in more than one dimension *(Russian)* 77−33879
$H+H_2$, cross sectional factorization expressions, close coupling input tested in sudden approximation 79−43571
$H+H_2$, elastic differential cross section high resolution meas. 78−50610
$H+H_2$, excited states quenching in glow discharge 79−7001
$H+H_2$, interstellar collisions rel. to hot gases cooling by H_2 79−12505
$H+H_2$, reactions and collisions in IR laser field, collision-induced absorpt. spectra 80−76499
$H+H_2$, rot. excitation 79−89746
$H+H_2$ excited states relax. in glow discharge *(French)* 79−849
$H+H_2(\nu_i=1)$, exchange reaction, integral and differential cross sections determ. 80−85153
$H+H_2 \rightarrow H+H+H$, two path dissoc. 78−62875
H+HF, low barrier quantum model, vibr. deactivation 80−69216
H+ICl, three dimens. collision, exponentiating trajectories and statistical behaviour 80−5595
$H+Li(Li_2)$, superthermal collisions, photon and positive ion prod. 78−78788
H+methane, abstraction and exchange reaction, barrier height calc. using POL-CI wave functions 80−81304
H+methane, differential collision cross sections, diffraction oscills., data anal. 79−22783
$H+N_2$, excitation of $H\alpha$ and $L\alpha$ emissions, rel. to aurora 79−68309
$H+NH_2$, spin exchange effects, rot. energy transfer, absolute rate coeff. 79−50119
$H+NH_2$ rot. energy transfer in vibronic levels, absolute transfer rates 80−9701
$H+O_2$, excitation of $H\alpha$ and $L\alpha$ emissions, rel. to aurora 79−68309
$H+O_2(N_2)$, collisional coherent excitation, meas. of Lyman α-photons 80−99552
$H+O_3$, reaction mechanism studied using photoionisation mass spectrometer, form. of $O_2(a'\Delta g)$ 80−85168
$H^-+N_2 \rightarrow N_2^-+H$, vibr. autodetaching states, excitation and decay 78−33620
$H^++O_2(N_2)(Ne)$, K-shell capture cross-section, Auger effect 78−33602
$H^++p\text{-}H_2$, angular momentum and cross sections, sudden centrifugal pot. calcs. 78−42157
$H_{2\text{-}41}^++He$, 200-850 eV, attentuation and fragmentation 78−62968
H_2+ He (metastable), Penning ionisation *(French)* 80−1060
$p\text{-}H_2+{}^4He$, vibr. relax., 50-2000K, coupled channel, coupled states and effective pot. methods comparison 79−6995
H_2+Ar, induced IR spectrum, overlap dipole moment determ. 77−18924
H_2+Ar, near-reson. energy transfer, fluoresc. excitation 78−9187
$o\text{-}H_2+Ar$, relax. and kinetic cross sections, DWBA calc. 78−25655
$H_2+Ar(Kr)(Xe)$, orbiting resons., van der Waals pots., beam scatt. obs. 79−89739
H_2+atom, quasielastic H atom ejection *(Russian)* 78−37712
H_2+atom (ion), ionis. by one or two electron at. particles, Born approx. 79−54960
H_2+C^+, C^+ fine-struct. excitation, interstellar cloud cooling 78−25675
H_2+H, diatomic operator, separable approx., variational approach 78−42150
H_2+H, exponential gap relation, rot. inelasticity 80−78693
(H_2+H^+, H_2^++H) collinear system, electronically nonadiabatic effects 78−1063
H_2+HCD, vibr. excitation cross-sections, rot. averaging calcs. 78−9231
H_2+He, exponential gap relation, rot. inelasticity 80−78693
$o\text{-}H_2+He$, relax. and kinetic cross sections, DWBA calc. 78−25655
H_2+He, vibr. relax. cross section 80−99494
H_2+He potential surfaces, SCF and MRD-CI calcs. 79−10172
H_2+He^*, Penning ionisation, singlet interaction pot. anomalous struct. 77−75274
$H_2+He(Ar)$, intermol. forces, generalised electron gas-Drude model 79−98182

atom-molecule collisions continued
$H_2+He(2^3S_1)$, isotope effects, 77 to 300K 79−36752
$H_2+He(2^3S_1)$ mol. ionis., optical atom orientation method *(Russian)* 78−13591
$H_2+He(2^3S)$, pot. energy surfaces and autoionisation lifetimes calcs. 77−34740
H_2+heavy inert gas, small clusters, beam cluster intensity and collision cross section 77−38711
H_2+inert gas, cross section meas. with state selected beams 78−62910
H_2+inert gas, intermol. pot. anisotropy determ. from total collision cross sections, expt. 78−21988
H_2+inert gas, intermol. pot. anisotropy determ. from total collision cross sections, theory 78−21989
H_2+Kr, differential cross-sections, diffraction undulations, anisotropic pot. calcs. 78−9223
H_2+Li, exponential gap relation, rot. inelasticity 80−78693
$HBr+He(2^3S)$, Penning ionis. electron spectra, 584å photoelectron spectra 77−79687
HCl+Ar, pure rot. line shift, density depend. 77−79652
HCl+Ar, rot. excitation, quasiclassical close coupling approx. 79−27068
HCl+Ar, rot. linewidth calcs., using different pots. 78−66602
HCl+Ar(Xe), infrared line shape, rotational lines, influence of collision duration 80−43110
HCl+Cl(Br)(H), vibr. relaxation and reaction rates determ. 80−108698
HCl+HCl(Ar), pure rot. Raman lines, press. broadening cross sections 78−74702
HCl+He, mag. transitions, initial-l labelled CS approx. computations 79−3552
$HCl+He(2^3S)$, Penning ionis. electron spectra, 584å photoelectron spectra 77−79687
HCl+iert gas, weak collisions, HCl spectral line broadening of IR spectra 80−74161
HD-inert gas mixtures, $R_1(J)$ and $P_1(J)$ absorpt. spectra, positive intercollisional interference 79−54843
HD-Kr, $R_1(1)$ absorpt. spectra, positive intercollisional interference 79−54843
HD+Ne, j=0 to 1 scatt. differential cross section, interaction pot. anisotropy 77−42382
$HF+He(2^3S)$, Penning ionis. electron spectra, 584å photoelectron spectra 77−79687
$HF+I^*(5^2P_{1/2})$, electronic-vibr. energy transfer fluoresc. decay meas. 77−71846
$H_2^+(HeH^+)+C$ thin solid target, 50-300 keV, collisional at. physics using mol. projectiles 79−45813
$HI+He(2^3S)$, Penning ionis. electron spectra, 584å photoelectron spectra 77−79687
H_2O+atom, quasielastic H atom ejection *(Russian)* 78−37712
$H_2O+H(n=3)$, $O(3p^3P)$, radiation quenching in pulse radiolytically excited water vap. 79−89738
H_2O+He, collisional excitation of interstellar molecules, rate consts. 80−67816
H_2O+positive ion, inelastic scatt., 4-6 eV energy loss region 78−90277
$H(1^2S)+H_2$ (inert gas), electron capture, electron loss and deexcitation cross sections meas. 78−22025
$H(2S)+H_2(N_2)(NH_3)$(acetone)(methanol), collisional quenching, mass spectral obs. 78−25685
$H(2^2S)+H_2$(inert gas), electron capture, electron loss and deexcitation cross sections meas. 78−22025
$H(2s)+H_2$, 5-25 keV, $H(n=3)$ excitation, Balmer α emission obs. 80−53113
$H(2s)+H_2(He)(Ne)(Ar)(Kr)$, collisional de-excitation, 5-26 keV 79−59546
$H(2s)+N_2$, 5-25 keV, $H(n=3)$ excitation, Balmer α emission obs. 80−53113
$He\ (2^3S_1)+H_2$, ionis., interaction pot. at thermal energies *(Russian)* 79−94077
He, excited state formation from He_2^+ in afterglow, theory 79−22802
He flow discharge, intermediate press., positive column conc. of ions and metastables 80−44017
$He\text{-}CO_2$ atomic C nuclear pumped laser collision processes, output delay 80−38002
He-LiH, rot. inelastic collisions, ab initio pot. energy surface calcs. 80−87208
$He+Ar(N_2)(NO)(O_2)(N_2O)(CO_2)$, Penning ionisation of target mol., for $He(2^3S)$ 79−41228
He+CO, nuclear mag. shielding consts., interaction geometry depend., chemical shift, gauge invariant method 78−62866
He+CO, polarised mol., differential scatt. cross-sections calcs. 79−89733
He+CO, rot. inelastic scatt., coupled eqns. for single initial state, variation-iteration method 79−68301
He+CO, unitary approx. for inelastic collisions 78−13569
$He+CO_2$, anisotropic intermol. pot. for differential scatt. cross-section 79−13788
$He+CO_2$, collinear atom-triatom transition probabilities for anharmonic triatom pots., quantum mech. calcs. 80−83455
$He+CO_2$, repulsive pot. energy surface, approx. calc. and differential scatt. expt., comparison 79−22788
$He+CO_2$, translational-vibrational energy transfer, quantum dynamical study 80−63746
He+CO(HCl)(HCN)(HD), press. broadening cross-section, ang. momentum approx. calcs. 77−34696
$He+CO(N_2)$, differential scatt. 0 to 5×10^{-2} rad. detector angle, 800 eV He *(Russian)* 77−79674
He+CS, Penning ionisation, $CS^+(B^2\Sigma^+ \rightarrow A^2\Pi_i)$ fluoresc., flowing afterglow 80−14197
$He+CS_2$, metastable atoms, energy transfer processes 80−83466
$He+H_2$, adiabatic distorted-wave infinite order sudden approx. 80−99558
$He+H_2$, anisotropic interaction pot., total cross-section calcs. 78−29835
$He+H_2$, averaged definite parity j_zCCS approx. calcs. 77−34710
$He+H_2$, collinear collision, first order nonlinear matrix differential eqn. 80−37853
$He+H_2$, collision dynamics, generalised Langevin eqn. approach 78−70900
$He+H_2$, collision induced dipole IR spectra, ab initio SCF LCAO calc. 79−89737
$He+H_2$, collision-induced dipole, ab initio VB calc. 78−94202
$He+H_2$, collisional dissoc., quasiclassical trajectory calcs. 78−42172
$He+H_2$, final quantum state assignment, improved quasiclassical histogram method 78−66617

atom-molecule collisions continued
He+H_2, formation of polarised H-atoms in ionising collisions *(Russian)* 79−7002
He+H_2, inelastic scatt., vibr. effects, classical mech. calcs. 77−34735
He+H_2, inelastic scatt., vibr. adiabatic basis functions calcs. 80−102551
He+H_2, inelastic scatt. exponential perturbation theories 80−74217
He+H_2, mag. transitions, close coupling calcs. in uncoupled space frame 78−17769
He+H_2, mol. energy transfer by quasiclassical trajectory methods, vibr. relax. and dissoc., rot. effect 80−99557
He+H_2, orbital angular momentum quantum numbers in definite parity j_z CCS approx. 77−14511
He+H_2, pot. energy surface, analytical expressions from constrained optimisation 77−6698
He+H_2, rot. excitation, 0.403-1.900 eV total energy, classical trajectory method 77−30962
He+H_2, rot. excitation, effective pot. and classical trajectory calcs. 77−88539
He+H_2, simultaneous rot. and vibr. transitions, cross-sections calc. 77−68098
He+H_2, stochastic theory, master or Fokker Planck eqn. numerical solns. 77−30965
He+H_2, sudden rot. approx., rot. and vibr. cross sections 77−30966
He+H_2, T-matrix element approx., j_z-CCS calcs. 77−19003
He+H_2, vibr. inelastic integral cross-sections, transitions to $\nu=2$ level 80−99559
He+H_2, vibrationally inelastic collision, rot. energy sudden approx. 79−68303
He+$H_2O(D_2O)$, chemi-ionisation and secondary ion reactions, $^{3,1}S$ He metastables 77−40531
He+$H_2(D_2)(T_2)$, vibr.-rot. transitions, optical potential approach 78−62885
He+H_2(He)(Ar)(N_2), fast metastable at. collisional destruction cross section 78−74760
He+$H_2(N_2)$, metastable and ground state electron loss cross section 80−53117
He+$H_2(\mu H)$, interaction pots. and rot. scatt. calcs. 80−43158
He+HCN, HCN excited vibr. state, T_2 meas. 80−102498
He+HCN, translational-vibrational energy transfer, quantum dynamical study 80−63746
He+HCl, state-selected collision cross-sections calcs. 78−22001
He+HCl(CO), energy sudden approx., beam scatt. meas. mol. anisotropy effects 78−78802
He+HCl(HF)(DCl)(DF), slow collisions, rot. excitation cross-sections, quantum mech. calcs. 77−12795
He+HF(DF)(HCl)(DCl), cross sectional factorization expressions, close coupling input tested in sudden approximation 79−43571
He+hydrocarbon scattering at high velocities, short-range pots. determ. 77−27142
He+hydrocarbon scattering at high velocities, short-range pot. determ. 77−27143
He+I_2, energy transfer, centrifugal sudden approx., classical infinite order sudden approx. 80−27933
He+I_2*, sudden rot. approx., rot. and vibr. cross sections 77−30966
He+I_2*, sudden rot. total rot. inelastic cross section 77−30967
He+I*, low energy collisions, energy redistrib. 80−63765
He+LiH, rot. inelastic collisions, dynamics 80−87209
He+LiH, rot. inelastic collisions, state-to-state cross sections determ. 80−87210
He+methane, ^1H and ^{13}C mag. shielding, intermol. effects 78−37571
He+N_2, intermolecular pots. from Thomas-Fermi-Dirac functional 77−19009
He+N_2, rot. inelastic scatt., appl. of sudden approx. 80−95705
He+$N_2(O_2)$, He(2^3S) quenching reactions 78−22014
He+$N_2(O_2)$(CO)(NO), anisotropic intermol. pots., crossed beam expts. 79−31639
He+NF_3 collisional quenching rates for F atomic laser 79−81410
He+NH_3(formaldehyde), rot. excitation, IOS approx. calcs. 79−45801
He+NO, multiphoton ionisation spectra in supersonic expansion, laser entranced collisional effects 80−83459
He+Na_2, optically pumped state to state differential cross sections for rot. transitions, rainbow phenomena 80−5609
He+Na_2, rot. excitation, rainbow oscills., coupled states and IOS approx. calcs. 80−23518
He+Na_2, rotational inelastic scatt., uniform semiclassical sudden approx. 80−99544
He+NaK collisions studied using circularly polarised laser fluorescence, molecular reorientation obs. 80−69215
He+OCS, emission spectra in He afterglow 80−87139
He+OCS, translational-vibrational energy transfer, quantum dynamical study 80−63746
He^++CS_2, dissoc. charge-transfer, $CS^+(B^2\Sigma^+-A^2\Pi_i)$ emission prod., Morse pot. Franck-Condon factors calc., vibr. anal. 80−99539
He^++OCS, dissoc. charge-transfer, $CS^+(B^2\Sigma^+-A^2\Pi_i)$ emission prod., Morse pot. Franck-Condon factors calc., vibr. anal. 80−99539
He_2H^+, ground state pot. energy surface for form. by collinear collision, DIM calcs. 79−97996
He(He_2)+Ar, metastable destruction rates 78−37728
$He_2(^3\Sigma_u)$+Ne(Ar)(N_2)(CO)(C_2)(CH_4), excitation transfer reaction rates 78−5332
^{4}He+H_2, inelastic collision, R-matrix study 80−87204
He*+H(H_2)(Ar), metastable state, ionis. processes 78−62907
He*+N_2, Penning ionisation, ejected electron spectra obs. 80−48074
He*(2^3S), (2^1S)+O_2, ion pair form., ion beam neutralisation reionisation spectroscopy 80−53120
He(2^3S), bi- and ter-mol. deexcitation reaction rate coeffs. meas. in afterglow 79−36748
He(2^3S)+molecule collisions, exit channels rate consts. 79−13800
He(2^3S)+Ne(Ar)(N_2)(CO)(CO_2)(CH_4), high press. afterglow, bi- and termolecular de-excitation rates 77−27168
He(2^3S and 2^1S)+$H_2(D_2)$, Penning, rearrangement and total ionis. cross sections, vel. depend. 79−22816
Hg 6^3P_1 collisional transfer rate between m-sublevels mag. field depend. 80−32802
Hg+Cl_2+$\hbar\omega$→HgCl*+Cl, laser-induced harpooning reactions 80−83458
Hg+N_2, inelastic collision, 6^3D_1 population transfer to other 6s6d Hg levels, fluoresc. obs. 78−78791
Hg_2, photoassociated, collision-induced predissoc. with Hg 79−31626
HgBr+$O_2(N_2)(H_2)$(He)(Ne)(Ar)(Kr)(Xe), vibr. relax., rate coeffs., fluoresc. obs. 80−63697

atom-molecule collisions continued
Hg($^3P_0$)+N_2 fluorescence decay following pulsed laser excitation 77−30817
Hg($^1P_1$)+CO, Hg($^3P_1$) production mechanisms 78−29847
Hg*+NH_3, UV emission at low press., pulsed excitation, relax. meas. 77−79570
Hg(6^3P_1)(6^3P_0)+CO(NO), electronic-vibr. energy transfer collision, IR obs. 79−45716
$H_2(j=0)$+F($^2P_{1/2}$) quenching, quantum mech. study, ortho-para mixing role 79 76485
I+HCl, quenching of I($5^2P_{1/2}$), temp. depend., time resolved at. absorpt. spectrophotometry 80−32655
I+methane $^-d_0(^-d_3),(^-d_4)$, excited atoms, quenching, isotope effects, time resolved reson. fluoresc. 80−32656
I+O_2, chemical generation of population inversion between spin-orbit states of I 78−17767
I+O_2, near-resonant electronic energy transfer, surface-hopping model 79−86030
I_2+Ar, mol. rot. axes, collisional alignment calcs. 77−42376
I_2+Ar(Ne)(tetrafluoromethane), D-state lifetime and UV laser action 77−14471
I($^2P_{1/2}$)+n-iodopropane (iodoethane), quenching rate coeff., in UV photolysis of n-iodopropane (iodoethane) 79−11799
I*+$H_2O(D_2O)$(HDO), $5^2P_{1/2}$ electronic to vibr. energy transfer, quenching and time resolved IR fluoresc. 79−3537
I_2*+He(Ne), energy depend. of collision induced intramolecular energy transfer 80−83470
I*($5^2P_{1/2}$)+HF(HCl)(HBr)(HI), collisional quenching rate consts. meas. 77−3299
I($5^2P_{1/2}$)+benzene-d_0(-d_6), fluoresc. quenching, spin-orbit interaction, isotope effect obs. 78−62763
I($5^2P_{1/2}$)+Br_2, deactivation kinetics, time-resolved spectrosc. obs. 78−95916
I($5^2P_{1/2}$)+$H_2O(D_2O)$(HX)(DX), collisional quenching, isotope effects 77−34583
I($5^2P_{1/2}$)+HCl(HBr)(NO), electronic-vibrational energy transfer, fluoresc. obs. 78−66579
I($5p^2P_{1/2}$)+I_2, metastable relax., rate const. 77−19022
K discharge plasma, K_2 excited mols. form. by K(4P) collisions 80−44013
K+alkyl halide potentially reactive collisions, electronic excitation 80−74239
K+alkyl iodide, collisional electronic excitation, time-of-flight obs. 79−86049
K+Br, harpooning mechanism interactions, semiclassical optical model 79−89755
K+Br_2, inelastic scatt., total cross-sections, trajectory surface hopping calcs. 78−46420
K+CO, rotational inelastic scatt., uniform semiclassical sudden approx. 80−99544
K+D_2O→OD^-+K^++D, 100-200 eV, $D_2O^-(^2A_1)$, state 78−17770
K+H_2S(DS), collisional ionisation, positive and negative ion energy spectra obs. 80−63775
K+halogenated methane, negative ion form., electron affinities, bond dissoc. energies 78−82827
K+I_2, ion-pair formation, energy transfer and differential scatt. 77−75272
K+I_2(IBr)(Br_2)(ICl)(Cl_2), ion-pair form., bond stretching effect on cross sections 78−1064
K+methyl cyanide, collisional ionisation obs. 80−95716
K+N_2 collision, electronic excitation and energy transfer, time of flight spectra 80−43151
K+N_2(CO), anisotropy of the repulsive intermolecular potential from rotationally inelastic scattering 79−41226
K+$N_2(H_2)(O_2)$, excited atom quenching, semi-empirical model 78−1065
K+NaCl, three dimens. collision, exponentiating trajectories and statistical behaviour 80−5595
K+NaK reactive collisions studied using circularly polarised laser fluorescence 80−69215
K+O_2, collisional ionisation, energy spectra of forward and backward directed positive and negative ions 80−87200
K+O_2 mol. target internal motion 80−78697
K+UF_6, ionisation reactions, absolute cross sections 80−99565
KBr*+Ar, inelastic collision, classical trajectory anal., vibr. excitation effects 77−34737
K(4^2S)+CO→K(4^2P)+CO, differential cross section meas. by atom-photon coincidence techniques 79−31673
K(4^2S)+N_2→K(4^2P)+N_2, differential cross section meas. by atom-photon coincidence techniques 79−31673
Kr+CO_2, collision dynamics, generalised Langevin eqn. approach 78−70900
Kr+CO_2, collisional energy transfer, anharmonicity effects 80−28097
Kr+CO_2 80−83455
Kr+CO_2(001), deactivation pathways, quantal close-coupling calcs. 78−58787
Kr+carbon tetrachloride, differential elastic scatt. cross-section 79−45784
Kr+$H_2O(D_2O)$, ($^3P_{0,2}$) state quenching cross sections 78−70912
Kr+$H_2S^+(CS_2{}^+)(CH_3I^+)(CF_3I^+)$, collision induced molecular ion dissociation, mass spectra *(Russian)* 77−88549
KrF*+Ar, three-body quenching and broad-band emission at 415 nm 77−75486
KrF*+Ar(Kr)+Ar(Kr)→Ar(Kr)KrF*+Ar(Kr) recombination rate consts. calc. 77−75488
Kr($^3P_2$), quenching mechanisms and rate consts. 79−13801
Kr($^3P_2$)+fluorine containing molecules, quenching rate consts., KrF* formation branching ratios 77−9072
Kr**+HCl rot. effect on collisional ionis. 77−83702
Li ions, 65 to 500 keV, stopping power and straggling in H_2, He, CO_2, N_2, O_2, Ne, Ar, Kr, and Xe 79−3529
Li seeded in acetylene-air flame, optoacoustic pulses, energy transfer from laser excited atoms 78−25490
Li+H_2, inelastic collision, ab initio pot. energy surface 79−10055
Li+He (methane), collisional excitation, prompt decay line energy, projectile Auger spectrosc. 79−85941
Li+$N_2(H_2)(O_2)$, excited atom quenching, semi-empirical model 78−1065
Li^++CO, differential cross-sections, ab initio CI vibrotor pot. energy surface calcs. 78−46421
Li^++CO(N_2), differential cross-sections, classical trajectory calcs. 78−29841

atom-molecule collisions continued

- $Li^{+}+H_2$, dissoc., multiple scatt. theory 78−21999
- $Li^{1+}+H(H_2)$, (q=1-3), electron capture and loss cross sections 78−42187
- Li_2+inert gas, collision induced transition rate consts., two-laser spectrosc. 80−9629
- LiF+Ar, polarisation cross section, close-coupling calcs. 80−69214
- LiF+Ar, polarised rot. selected mol., high resolution differential cross section 77−27147
- LiF+inert gas atom, interaction anisotropy, Van der Waals forces 79−6985
- LiH+Ar, rotationally inelastic cross-sections, state resolved, determ. 78−13577
- LiH+He, rot. inelastic collisions, rigid shell models 80−99545
- $Li^{*}+H_2(N_2)$, thermal, high-Rydberg Li behaving as ion core 78−22004
- $Li^{*}(2^2P_J)+H_2(D_2)$, collision induced quenching and fine struct. transition rate coefficients meas. 80−74221
- $Li(2p)+H_2(N_2)$, Li(2p) excitation, alignment and orientation obs. 80−63794
- $Mg^{*}+Cl_2$, collision and reaction cross section meas. 79−59537
- $N^{+}+N_2$, 35-200 keV, X-ray spectrum, rel. to $N^{+}+N$ mechanism 78−42183
- $N^{n+}+N_2(O_2)(Ne)$(methane), K-shell vacancy prod. cross-section, charge state depend. 78−17751
- N_2^{+} $(B^2\Sigma_u^{+})$ state in Ne-N_2 mixture, excitation kinetics 78−9239
- N_2+Ar, 0.06-0.41 eV, metastable at. electronic excitation transfer 79−64071
- N_2+Ar, total differential cross section, diffr. oscills. quenching 78−66625
- N_2+Ar, triplet state excitation *(French)* 77−83704
- $N_2+Ar^{*}(He^{*})$, sensitised fluoresc., vel. depend. 77−10744
- N_2+Ar(Xe), $A^3\Sigma_u^{+}$ state energy pooling in flowing afterglow, Herman IR system 80−83503
- N_2+H, stripping cross-section, 0.3 to 3 keV 78−78807
- N_2+H^{+}, excitation process, N_2 and N_2^{+} light emission *(Japanese)* 78−25678
- $N_2+He(2^{1,3}S,2^{1,3}P)$, Penning ionis., N_2^{+}, $B^2\Sigma_u^{+}$ state effective cross sections 77−79688
- N_2+heavy inert gas, small clusters, beam cluster intensity and collision cross section 77−38711
- N_2+K (Na), atom electronic excitation, vibr. to electronic energy transfer, seeded mol. beam studies 80−47919
- N_2^{+}+He, N_2^{+} selectively excited, collisional deactivation 80−83338
- $NF(a^1\Delta)$+Bi, near-reson. electronic energy transfer, rate const. and cross-section meas. 79−18273
- NH_3+He, interaction potentials, ghost orbital SCF and Gordon-Kim calcs. 79−94057
- NH_3+He(Ar), ammonia inversion spectrum press. broadening 78−86915
- NH_3+He(Ar), inversion spectrum press. broadening, linewidths calcs. 80−95599
- NH_3+He(Ne)(Ar)(Kr), pure rot. line, press. broadening calcs. 80−78656
- NH_3+Hg, photosensitisation, NH_3 fluoresc. 78−90198
- NO, fundamental intensity and linewidth of IR absorpt. spectra, press. broadening 78−25530
- NO+heavy inert gas, small clusters, beam cluster intensity and collision cross section 77−38711
- NO+inert gas, cross section meas. with state selected beams 78−62910
- $NO+N_2(Ar)$, $^2\Pi_{3/2}$, $^2\Pi_{1/2}$ states, line broadening, mag. moment effect 79−72391
- $NO+Na(3p^2P_{3/2})$, electronic energy quenching dynamics, crossed beam expt. 80−9683
- NO+Ne(AR)(Kr)(Xe), angle depend. intermolecular pot., crossed beams study 80−9682
- $NO+Ne(Ar)(N_2)(H_2)(CO)$, $E^2\Sigma^{+}$ and $B'^2\Delta$ states fluoresc. collisional deactivation 79−6965
- NO+O, vibr. relaxation of NO, laser induced IR fluoresc. study 80−9626
- N_2O+He, in afterglow, N_2O^{+} optical emission obs. 79−68251
- N_2O+inert gas ion, mol. ionis., emission obs. 79−31707
- $N_2(X^1\Sigma_g^{+})+Ar(^3P_{2,0})\rightarrow Ar(^1S)+N_2(C^3\Pi_u)$, sensitised fluoresc., vel. depend. 78−90204
- Na I reson. line broadening by collisions with dipolar mols. 80−941
- Na in flames, laser-induced fluoresc. temp. meas. 80−11893
- Na seeded in acetylene-air flame, optoacoustic pulses, energy transfer from laser excited atoms 78−25490
- $Na+CO(NO)(CO_2)(C_2H_2)(CH_4)$, total cross sections 79−27064
- $Na+H_2$, electronic to vibr. energy transfer, close coupling calcs. 79−98203
- $Na+I_2$, ion-pair formation, energy transfer and differential scatt. 77−75272
- Na+methyl iodide, anisotropic interactions from double rainbow struct., interaction pot. meas. 80−99540
- Na+molecule, likelihood of vibr. or electronic excitation, model 79−76496
- $Na+N_2$, collisional deactivation of Na excited states, time resolved fluoresc. 78−42197
- $Na+N_2$, higher Na s and manifold states deactivation cross sections 79−10176
- $Na+N_2$, Na excitation in non-equilib. conditions behind shock wave 77−23539
- $Na+N_2$, rot. excitation and fine struct.-changing collisions 78−42176
- $Na+N_2(H_2)(O_2)$, excited atom quenching, semi-empirical model 78−1065
- $Na+Ne(Ar)(Kr)(Xe)(N_2)(CO_2)$, fine struct. changing collisions, vel. depend. 79−22803
- Na+Ne(CO), 13d-13f transition, collisional dephasing, Ramsey method investig. 79−54791
- $Na+SiCl_4(C(CH_3)_4)(Si(CH_3)_4)(Sn(CH_3)_4)$, rainbow scatt. at thermal energy, anisotropic pot. 78−29837
- Na+t-butyl bromide, anisotropic interactions from double rainbow struct., interaction pot. meas. 80−99540
- Na+t-butyl chloride, anisotropic interactions from double rainbow struct., interaction pot. meas. 80−99540
- Na+t-butyl iodide, anisotropic interactions from double rainbow struct., interaction pot. meas. 80−99540
- Na_2+Ar, rot. level repopulation rate by laser-induced depopulation 77−65528
- Na_2+He, rotationally inelastic scatt., state-to-state differential cross sections 80−74234

atom-molecule collisions continued

- Na_2+Xe rate const., energy corrected scaling laws 80−69225
- $Na^{*}+N_2$, differential quenching cross-section, polarisation effects 77−27019
- Na_2^{*}, fluoresc. red continuum emission, atom-mol. energy transfer 80−43086
- $Na_2^{*}(A\Sigma)+He(H_2)(N_2)$(methane), rot. energy transfer, power law scaling 79−98204
- $Na^{*}(3^2P)+H_2(D_2)(O_2)(N_2)(CO)(CO_2)(N_2O)(C_2H_4)$, electronic to vibr.-rot. energy transfer, differential cross sections 77−38715
- $Na(3^2P)+O_2(SO_2)$, near-threshold ionis. of Na^{*} 77−88544
- $Na(n^2D)+N_2(CO)$, collisional l-mixing, highly excited states, fluoresc. obs. 77−83686
- $Ne+CO_2$, energy transfer, anharmonic coupling terms, semiclassical calcs. 80−37861
- $Ne+CO_2$, energy transfer rate consts., semiclassical method 80−91640
- $Ne+CS_2$, metastable atoms, energy transfer processes 80−83466
- $Ne+D_2$, anisotropic inversion pot., rot. inelastic cross sections 80−78696
- $Ne+D_2$, anisotropic potentials, direct inversion methods calcs. 80−69090
- $Ne+D_2$, energy-loss scaling in 0.5-3.5 keV 80−63768
- $Ne+H_2$, metastable state breakdown, temp. depend. 79−98211
- $Ne+H_2O(D_2O)$, chemi-ionisation and secondary ion reactions, $^3P_{2,0}$ Ne metastables 77−40531
- Ne+HD, j=0 to 1 rot. excitation, differential cross sections, time of flight obs. 80−48104
- $Ne+SF_6(N_2)$, metastable state de-excitation, rate consts., radiolysis obs. 80−40709
- Ne_2+Ar, total integral cross sections for excitation, exchange and dissoc. 80−1044
- Ne_2+Kr total integral cross sections for excitation, exchange and dissoc. 80−1044
- $Ne^{*}+Fe(CO)_5$, chemiionisation and chemiluminescence reactions, Penning ionisation and fluoresc. obs. 80−97689
- $Ne^{*}+H_2O$, pot. energy surfaces, MO and CI calcs., Penning ionisation electron spectra 80−106376
- O I 5577 Å meteoric forbidden line collisional quenching 77−17448
- $O+N_2$, excitation and deactivation at above-thermal energies 80−43171
- $O+N_2$, intermolecular pots. from Thomas-Fermi-Dirac functional 77−19009
- $O+N_2$, quenching of $O(^1D)$ state, at 300K, semiclassical study 79−45823
- $O+N_2(^1\Sigma_g^{+})$, energy transfer, classical trajectory model *(Spanish)* 79−89745
- $O+O_2$, quenching of $O(^1S)$ state, rate coeff. 80−41581
- O_2+Ar, 118750 GHz transition, press. broadening 77−75136
- O_2+He, 118750 GHz transition, press. broadening 77−75136
- O_2+heavy inert gas, small clusters, beam cluster intensity and collision cross section 77−38711
- O_2+Na(K)(Cs), negative ion pair form., total cross sections 79−3550
- O_3+inert gas, rot. energy transfer, centrifugal sudden approx. 80−27933
- $O(^1D)+O_2\rightarrow O(^3P)+O_2(b^1\Sigma_g^{+})$, energy transfer during O_2 photodissoc. 79−11810
- $O(^1D_2)+N_2O$, chemical-ionisation mass spectrometry branching ratio measurements in N_2O/He mixtures 79−47905
- $O_2(^1\Delta_g)+I(^2P_{3/2})$, possible electronic transition chem. laser 78−63116
- OH-CH rotationally inelastic collisions, maser action 79−94068
- OH+Ar, pure rot. collisionally pumped laser, vibr.-rot. transfer 77−42523
- $O(^3P)$+dimethyl disulphide, absolute reaction rate const. determ. 80−89472
- $O(^1S)+CO_2(H_2O)(NO)(N_2O)$, product channels 78−46422
- $O(^1S)+O_2$, collisional interaction products, reson. fluoresc. obs. 78−46423
- $O(^5S)+O_2\rightarrow O(^3S)+O_2$, reson. radiation 80−53122
- $O(2^1D_2)$, prod. by O_3 photolysis, collisional deactivation 79−20384
- $O(2^1D_2)+N_2(O_2)(N_2O)(CO_2)(H_2O)$(methane), collisional deactivation meas., 295K, rel. to atmospheric processes 80−16663
- $O(2^3P,2^1D)+N_2O(CO_2)$, diabatic correlations 77−25256
- $O_2(b^1\Sigma_g^{+})$ quenching by $O(^3P)$ and O_3, rate coeffs. 79−70309
- PH+He, collisional deactivation of $PH(b^1\Sigma^{+})$, time resolved quenching 79−54948
- Pb+buffer gas, $^3P_1{}^0\rightarrow{}^3P_0{}^0$ transition cross section 80−1058
- Rb+methane (and deuterates), $5^2P_{1/2}\rightleftarrows 5^2P_{3/2}$ excitation transfer, isotope effects, temp. depend. 80−91630
- $Rb+N_2$, spin relax. rate 77−19027
- S+inert gas $(N_2)(H_2)$, rare gas sulphide $S(^1S)$ emissions 78−82828
- $SF_6+H^{+}\rightarrow SF_6^{+}+e^{-}+H^{+}$, 0.3-1.8 MeV, electron energy and ang. distrib. 78−22015
- SO_2+He, Penning ionis. due to $He(2^3S)$, SO_2^{+} fluoresc. 79−13758
- SeO_2+Ar, radiative lifetime and quenching rates 80−95685
- Se^{*}+OCSe, radiation quenching rates 79−86050
- Si $3p^2(^1D_2)$ state collisional quenching 79−22806
- $Si+H_2(O_2)(He)(SiCl_4)$, $3p^2(^1D_2)$ state behaviour, at. absorpt. spectra 78−29846
- $Si^{*}+He(H_2)(N_2)(O_2)(Cl_2)(CO)(NO)(C_2H_2)(C_2H_4)$, collisional quenching, reson. line absorpt. expt. 78−46297
- $Si(3p^2(^1S_0))+He(SiCl_4)(O_2)(N_2O)$, attenuation of reson. radiation, time-resolved kinetic obs. 78−5329
- Sr+HF, endothermic reaction, comparison of effectiveness of vibr. and translational excitation 80−93746
- $Sr+N_2$, $A^3\Sigma_u^{+}$ state, vibr. excitation 80−1054
- $Sr^{*}+Cl_2$, collision and reaction cross section meas. 79−59537
- $TeF_6+H^{+}\rightarrow TeF_6^{+}+e^{-}+H^{+}$, 0.3-1.8 MeV, electron energy and ang. distrib. 78−22015
- $Tl+CO_2$, relax. of $6^2P_{3/2}$ and $7^2S_{1/2}$ states 79−64094
- $Tl+N_2$, Hg sensitised fluoresc., quenching 79−22643
- TlF+Kr(Xe), collision-induced ion-pair formation 78−17749
- Tl_2F_2+Kr(Xe), collision-induced ion-pair formation 78−17749
- U+molecule, collisional relax. of highly excited states, laser-induced fluoresc. obs. 80−58205
- $U(f^3ds^2)$+molecule, collisional relax. of $^5K_5{}^0$ and $^5L_7{}^0$ states, laser-induced fluoresc. obs. 80−52925
- Xe, high Rydberg state, ionis. by collision with organic mols. 78−50620
- Xe, ionisation of high Rydberg states by collision with molecules 77−88545
- $Xe+CO(N_2)$, ^{129}Xe chem. shielding, second virial coeff. 78−66563
- $Xe+Cl_2$, classical trajectory calcs., energy threshold for collision induced dissoc. determ., 80−95709
- $Xe+H_2$ 79−98211
- $Xe+NH_3(H_2S)(SO_2)(HCl)$, ionis. cross sections calc. 77−68103

atom-molecule collisions continued
$Xe+Na_2^*$, rot. energy transfer, level-to-level dynamics, laser fluoresc. obs. 79−64029
$Xe+Na_2^*$, rot. energy transfer, vel. depend. 80−95715
$XeCl$+inert gas atom, ground state destruction, quenching rate consts. meas. 80−63758
$XeF+He(Ne)(Xe)$, radiative lifetime and collisional quenching kinetics 78−94289
$XeF_2(C)$ state lifetime, quenching rate consts., photolysis in inert gas atmospheres 80−66816
XeF^*+F_2+Xe, temp. dependent quenching rate constants 80−63701
$XeF^*+He(Xe)(NF_3)(F_2)$, quenching rates for XeF in (B) state 78−58730
XeO^* production through collisional electronic energy transfer from two-photon excited Xe atoms 78−62775
$Xe(^3P_2)$, quenching mechanisms and rate consts. 79−13801
$Xe(^3P_2)$+fluorine containing molecules, quenching rate consts., XeF^* formation branching ratios 77−9072
$Xe_2(-Kr,He)$, time-resolved excitation spectra, 1500 Å region, fluoresc. lifetime 77−75195
^{129}Xe+nonspherical molecule, interaction pots., effect on mag. shielding, NMR meas. 77−71816
$Xe(nf)+NH_3$, at. Rydberg state further excitation by rot. transfer, field ionis. obs. 78−58795
$Xe(nf)+SF_6$, l-changing collisions obs. 80−91633
Xe(nf Rydberg state)+NH_3, n- and l-changing and ionising collisions 80−58360
Zn, excited states, collisional quenching cross sections and exit channels, fluoresc, quenching obs. 80−18919
$Zn+N_2$, $A^3\Sigma_u^+$ state, vibr. excitation 80−1054

atom-molecule reactions
see also atom-molecule collisions
$A+BC\rightarrow AB+C$, reactive collision model for use in kinetic theory 78−35665
$A+BC\leftrightarrows AB+C$, dilute gas phase, mass and momentum transport model 78−35666
$AB+M\rightarrow A+B+M$, nonequilibrium gas at low press., dissociative instability, role of vibr. energy 80−74227
accelerated atom+O_2, chemiionisation, crossed beam obs. 77−9085
alkali atom+halogen mol., ion pair form., trajectory model 77−16800
alkali metal+HX (X=F,Cl,Br,I), reaction, semiempirical pot. surfaces calcs. 79−74362
alkali metal+N_2, thermal ionis. rate coeff. 77−30982
alkali metal atoms+molecules reaction, electronically excited atoms and alkali metal atoms analogy 80−76490
1-alkynes+$O(^3P)$, CO prod., vibr. population distrib., rate consts., laser reson. absorpt. technique 80−40676
allene+$O(^3P)$, absolute rate consts. meas., 297-439K 78−7196
atom+diatom, collinear exchange reaction rates and probabilities, threshold behaviour 78−27738
atom+diatom, collinear quantum mech. reactive scatt., hyperspherical coords. 80−108694
atom+diatom, collinear trajectories, pattern recognition appls. 80−45481
atom+diatom, long-lived trajectories near reactivity band boundary 78−29836
atom+diatom, microcanonical reaction probability, classical transition state theory 80−50842
atom+diatom, planar reaction, cross section calcs., vibr. and rot. convergences 77−21376
atom+diatom, planar reaction, Schrodinger eqn., expansion as partial differential eqns. 77−21375
atom+diatom, prior statistical distribs., collinear reactions, theory review 78−35670
atom+diatom, reaction products ang. distribs., Franck-Condon theory 79−87835
atom+diatom, reactive scatt. theory using DWBA 77−70296
atom+diatom, three dimens. reaction, Schrodinger eqn. soln. for Porter-Karplus pot. energy surface 77−21378
atom+diatom, three dimens. reaction, theory 77−21377
atom+diatom, transition states, trapped trajectories and classical bound states in continuum 78−88630
atom+diatom collinear collisions, exponentiating trajectories and statistical behaviour, variational eqns. 78−27742
atom+diatom reaction, endoergic, vibr. energy consumption 77−52621
atom+diatom reactions, semiclassical tunnelling probabilities, trajectory calc. 80−71886
atom+diatom reactive collision, three dimens., exact classical formulation in natural coords. 80−50835
atom+diatom reactive scatt., DWBA transition amplitude kernel 80−81310
atom+diatom scattering, field theoretic calcs. 77−50484
atom+diatomic molecule, exchange reaction, 3-dimens., natural coord. calcs. 80−26010
atom+polyatom systems, rotation-vibration symmetry correlation 80−61074
atom-diatom collision, vibrationally inelastic scattering by quantum mechanical calculations 77−46624
averaged definite parity j_z approx. with Clebsch-Gordan weights 77−58111
benzene+$O(^3P)$, phenol radical prod., crossed mol. beam investig. 80−71902
benzene+$O(^3P)$, reaction product identification by mass spectrometer 78−7185
benzene-d+$O(^3P)$, phenol radical prod., crossed mol. beam investig. 80−71902
1,3-butadiene, absolute rate consts. meas., 297-439K 78−7196
chemi-ionisation reactions of Ca, Sr, Ba, and Yb with halogens and interhalogens 77−32791
chemical radiative collisions *(Russian)* 78−23942
chemiluminescence, beam-gas, kinetics of metastable excited state products 77−56231
chemiluminescence, single collision, kinetics temp. depend., expt. 77−63915
chemiluminescence, single collision, kinetics temp. depend., theory 77−63914
collinear reactive scattering, coupled eqns., soln., R-matrix calcs. 77−16812
collinear reactive scattering, generalised hyperbolic coords. 79−74363

atom-molecule reactions continued
complex formation in collinear collision, trajectory study using pot. surface 79−87821
computational atomic and molecular physics, conf., Nottingham, England, (Sept. 1978) 79−59567
crossed-beam meas. of reactive scatt. using short lived radioactivity 77−4969
cyclopropane+inert gas, reactant decomp., rot.-vibr. energy transfer, relax. analytic soln. 80−55650
diatom+atom, cross section, translational excitation features, dynamical model 80−16655
diatomic molecule, dissoc. and recombination involving two states interacting via at. species, soln. 77−23535
diatomic molecule, dissoc. and recombination involving two states interacting via at. species, model 77−27145
direct reaction sequential impulse model 77−16808
dissociation cross section, recomb. rate coeffs. *(Russian)* 77−32786
dye-inert gas vapour mixture, electron beam pumping 77−42535
dynamics, translational energy effects, reviews 80−76489
electron transfer reactions, semiempirical pot. energy surfaces calcs. 78−73022
ethyl isocyanide, thermal isomerisation in presence of at. gases, vibr.-translational energy transfer 78−23924
ethylene, adsorption on Ni, Pd and Pt films, reactivity with adsorbed H, surface pot. meas. 79−86995
ethylene+F, dynamics, stochastic reduction for reactions with complex form. 78−3315
ethylene+$H\rightarrow C_2H_5^*$, rate const., 198-320K, high press. 78−48618
ethylene+$H\rightleftharpoons$ethyl radical, pot. energy surface, analytic function 79−11779
excited atoms+molecules reactions, electronically excited atoms and alkali metal atoms analogy 80−76490
exothermic triatomic exchange reactions, prod. energy distrib., statistical dynamic model 78−92455
exothermic trihalogen Borne-Bunker reaction, long lived intermediates, comment 78−92464
exothermic trihalogen Borne-Bunker reaction, long lived intermediates, reply 78−92465
F+dichloromethane, reaction products, modulated mol. beam mass spectrosc. obs. 80−97742
final state energy distributions for exoergic reactions 79−5131
finite element methods for reactive scattering 78−92453
flame, rate constants for $A+X\rightleftarrows A^++X^-$ and $AX+M\rightleftarrows A^++X^-+M$ (A=metal, X=halogen, M=flame species) 79−34310
fluoromethane+Br, isotope selective photobromination, using c.w. CO_2 laser irrad. in excess inert gas 78−76843
fluoromethane+D(H)(O), reactions, selective vibr. excitation effects 78−35643
formaldehyde+Br reactions, rate consts. by EPR 80−93736
formaldehyde+Cl, rate const. 78−85136
formaldehyde+F reactions, rate consts. by EPR 80−93736
formaldehyde+O, absolute rate consts., discharge flow and flash photolysis reson. fluoresc. meas. 80−55648
Franck-Condon factors in model for stripping reactions 77−28990
Franck-Condon factors in reactive collision dynamics, general theory and applic. 77−36741
Franck-Condon factors in reactive collision dynamics, vibr.-rot. distribs. in atom-diatom reactions 77−36742
halogen atoms produced in IR photodissoc., hydrogen halides form., IR chemiluminesc. 77−63932
$^4He+H_2(\nu=0,j=0)\rightarrow {}^4He+H_2(\nu'=1,j')$, fully converged sudden rotation total integral cross sections 77−58135
heavy atom+$H_2(HD)(D_2)$, intramultiplet transitions 77−54597
hot atom+mol. reaction, steady state vel. distrib., Boltzmann eqn. with BGK elastic collision model 80−66856
impulsive triatomic reaction, vibr. state distrib., impulsive energy release model 78−92456
inert gas, metastable composition of inert gas beam from ion-neutral reaction 77−29008
inert gas+diatom, dissoc. of HCl, HF and O_2, rot. energy depend. 79−100341
inert gas+diatomic (triatomic) mol., Penning ionis. process from electron spectroscopy 77−14555
inert gas+H_2^{**}, ionising or deactivating collisions 79−100338
inert gas atom, total cross section anal. method, mol. quadrupole moment determ. 77−50495
inert gas atom+halogen mol., halide form., relax. and quenching 80−81314
inert gas atom+halogen molecule, chem. radiative collisions *(Russian)* 78−23942
inert gas dimer+atom, IOSA calc. for total integral cross sections for excitation, exchange and dissoc. 80−1044
inert gas metastable atom+$HgBr_2$, dissoc. excitation 80−63774
interstellar chemistry, long-chain hydrocarbons, formation mechanism 80−46653
interstellar dense molecular clouds, chem. evolution 78−28749
iodomethane+K, mol. rearrangement, optical pot. calcs. 77−81399
iodomethane+Rb reaction cross section, translational energy depend. min. 77−66753
ion pair form., vibr. energy depend. 79−34287
ionic reaction products, laser induced fluoresc. detect. and characterisation 79−1978
ionosphere modification by release of highly reactive molecules, diffusion aspects 77−21988
IR laser isotope separation appls. 79−64113
ketene+H, reaction rate consts., lab. meas., rel. to interstellar cloud processes 79−74359
large mol. reaction with intermediate complex, vibr., translational distrib., pot. hypersurface calc. 77−52612
large mol. reaction with intermediate complex, vibr. distrib., R-matrix, hybrid quantum statistical mechanics 77−52611
measurements of reaction rate consts., reliability criterion 79−8423
metal halide (oxide) dissociation energies, calc. from chemiluminesc. reactions, temp. depend. rate const. correction 77−40524
metastable reaction products, laser induced fluoresc. detect. and characterisation 79−1978
methane+Cl, rate const., discharge flow-reson. fluoresc. meas. 78−7178
methane+$H(HO)(O)(O_2)$, H abstraction, rate consts. calcs. 78−95921
methanol+Ar(Kr) methoxy radical prod., UV emission spectra 80−91572

atom-molecule reactions continued
methanol (dimethyl ether)+Cl, absolute rate consts., 200-500K, stratospheric chem. appl. 79−66271
methyl bromide+$K \rightarrow KBr+CH_3$, yields, crossed mol. beam study 79−34293
methyl bromide+$Rb \rightarrow RbBr+CH_3$, yields, crossed mol. beam study 79−34293
methyl iodide+alkali metal reaction cross section energy depend. 77−28991
methyl iodide+K(Rb), reaction cross sections 78−40043
methyl isocyanide, thermal isomerisation in presence of at. gases, vibr.-translational energy transfer 78−23924
molecular bond energies from time-of-flight chemiluminesc. 78−40051
monothioformate anion, protonation site, ab initio SCF calc. 79−47894
perhalo-compounds, labelled, high yields from ^{18}F and ^{38}Cl reactions with CCl_xF_{4-x} and C_3F_6 80−109025
product state distrib., laser photolysis-laser induced fluoresc. determ. 79−83446
quantum reactive scatt. theory, 3-dimens. 80−55637
rate measurement, laser photolysis IR fluoresc. method 80−16676
rates, classical and near classical, for dissoc. and exchange 79−11778
reaction rate constants 79−100350
reactive molecular collision calculations, review 79−61851
reactivity band boundaries, trapped trajectories, theory 78−29836
reactivity band origin 77−32774
reactivity bands, collinear SSMK surface calcs. on X+HX 77−36738
reversible chemical reactions involving H atoms, formation rates and lifetimes of intermediate complexes 79−15956
rotated Morse curve-spline pot. function 78−80729
rotationally inelastic collision, rot. alignment calcs., quantum formulation 77−61834
semiclassical theory for near adiabatic photon assisted mol. collisions 79−5141
statistical models characterisation, prior distribs., appl. to at.-diat. exchanges 77−66744
tetrafluoroethylene+O, triplet difluoromethane spectra, phosphoresc. and triplet-triplet annihilation 78−53196
tetramethyldioxetane, collisional dissoc. by supersonic Xe beam, chemiluminesc. 78−40029
theory, book 79−72394
thermal rate constants, quasiclassical trajectory calcs., detailed balance 79−87822
three-dimensional electronic nonadiabatic reactive collision theory, electronuclear basis 78−3321
toluene+$O(^3P)$, reaction product identification by mass spectrometer 78−7185
toluene+OH(D), vibrational and rotational energy effect 80−76497
transition state theory, absolute rate theory and variational formulations, Porter Karplus pot. surface 80−16642
trifluoroiodomethane+O, I atom abstraction by O, mol. beam study 78−48638
trimethylbenzene+$O(^3P)$, reaction product identification by mass spectrometer 78−7185
1,3,5-trimethylbenzene+OH(D), rotational and vibrational energy effect 80−76497
vibr.-translational energy transfer 78−23924
vibrational-translational energy transfer, forced harmonic oscill. model 79−59540
vibrationally excited molecule-atom reactions, rel. to high power lasers 79−5155
vinyl methyl ether+$O(^3P)$, absolute rate consts. meas., 297-439K 78−7196
$XY+Z \rightarrow X+YZ$, three-body Coulomb interaction, adiabatic representation 79−31640
$Al+CO_2 \rightarrow AlO+CO$, HTFFR kinetics obs., 300 to 1900C 77−90596
$Al+NO+Ar \rightarrow AlNO+Ar$, rate coeff., 600K, fluoresc. and absorption spectrum obs. 77−40521
$Al+O_2 \rightarrow AlO+O$, product. rot., vibr. translational energy, AlO fluoresc. 78−23928
$Al+O_3(N_2O)$, AlO chemilum. obs., perturbations and vibr. population anomalies, mechanisms 77−63917
$Al+O_3 \rightarrow AlO+O_2$, chemiluminesc., $A^2\pi$-$X^2\Sigma^+$ transition obs. 78−31639
$Al+SO_2$, high temp. fast flow reactor obs. of kinetics 80−30226
AlF+O, matrix reaction, OAlF IR spectrum *(German)* 79−11785
AlN+Ni(Co)(Fe), reactions at sintering temps. 79−74377
Ar excited+bromochlorodifluoromethane, IR spectra, matrix isolation study, C-F stretching fundamentals 78−37632
Ar excited+dibromodifluoromethane, IR spectra, matrix isolation study, C-F stretching fundamentals 78−37632
Ar excited+dichlorodifluoromethane, IR spectra, matrix isolation study, C-F stretching fundamentals 78−37632
$Ar+Ar_2$, exchange and dissoc. interactions, three-body effects calcs. 77−9069
Ar+BrCN(HCN), CN quartet state production, fluoresc. anal. 78−68888
Ar+CO spin transfer reaction, CO triplet state form. *(French)* 79−34289
$Ar+CO_2$, rot. transitions, classical trajectory calcs. 77−50501
$Ar+H_2$, 4500K dissoc. collision vibr. selectivity, Monte Carlo trajectory method 79−70307
$Ar+H_2$, dissoc., recombination and inelastic scatt. pot. energy surface and cross section Monte Carlo calc. 77−27162
$Ar+HCN(H_2O)$, electron excitation of Ar^* and Ar_2^*, fluoresc. and dissoc. energy transfer collisions 77−14580
Ar+HCl, classical and quantum centrifugal decoupling 77−58127
$Ar+He_2(^3\Sigma)$, press. depend. reactions, rate coeffs. 78−64823
Ar+methane, CH chemiluminesc. in flowing afterglow 78−64839
$Ar+NO^+$, reaction product ratios, 300K 80−7783
Ar+OCS, rot. spectral line shift and widths, collision induced phase shifts 77−75222
$Ar+PCl_3$ reaction PCl emission spectra 78−21938
$Ar+SO_2$, dissoc. rate meas. behind shock wave, laser Schlieren method 80−81296
ArF^*, in Ar-F_2 proton-excited mixtures, production and quenching 78−94307
Ar_2F^*, in Ar-F_2 proton-excited mixtures, production and quenching 78−94307
$Ar(^3P_{2,0})+Cl_2$, Cl(4s) production 77−46537
$Ar(^3P_{2,0})+H_2O$, energy depend. of ionisation and dissociative fluorescence in crossed mol. beams 79−52669
$Ar(^3P_2)+F$, donor reagent, quenching, excimer form. 79−63953

atom-molecule reactions continued
$Ar^+(^2P_J)+H_2(D_2)$, Ar^+ two spin orbit state, reaction cross section, direct determ. 80−93748
Ar^*+Br_2, producing Br, fluoresc. of Br in Ar^*+Br_2 lamp, Br atom conc. meas. by line absorpt. 78−46466
Ar^*+CO_2, CO^* prod., use in laser systems 80−63824
$Ar^*+Fe(CO)_5$, chemiionisation and chemiluminescence reactions, Penning ionisation and fluoresc. obs. 80−97689
Ar^*+formaldehyde thermal collisions, $CH(A^2\Delta = X^2\Pi)$ emission 77−86304
Ar^*+HBr, product energy distrib. 80−45509
B+CsF(RbF)(KF)(NaF), gas phase chemiluminescence reaction 77−29013
$B+N_2O$, chemiluminesc. reaction, vibr. state distribs. 79−20354
$B+O_2$, chemiluminesc. reaction, vibr. state distribs. 79−20354
$B+O_2(NO_2)(N_2O)(O_3)(ClO_2)$, chemiluminesc. metal oxide formation 80−35509
$B+O_2(SO_2)(CO_2)(N_2O)$, gas phase rate consts., 300K, at. absorption obs. 79−83445
$Ba+Br_2(I_2) \rightarrow BaBr(BaI)+Br(I)$, time-of-flight chemiluminesc., mol. bond energies determ. 78−40051
$Ba+CCl_4 \rightarrow BaCl_2+CCl_2(\bar{A})$, chemiluminesc. spectrum and ang. distrib. obs. 79−15962
$Ba+CH_3I(CF_3I)$, product translational distrib., crossed beam reaction 78−31629
$Ba+CO_2(O_2)$, crossed beam kinetics, BaO recoil velocity spectra 80−76500
$Ba+CO(CO_2)$, flame spectra, 500-1150 nm mechanism 77−48646
$Ba+Cl_2$, 10^{-5} torr, dynamics, chemiluminesc. ang. depend., radiative lifetime 77−40539
$Ba+Cl_2 \rightarrow BaCl^+ + Cl^-$, chemi-ionis. reaction, mol. beam obs. 80−104434
Ba+HBr, laser induced fluoresc. study at different collision energies 80−91632
Ba+HCl, beam-gas reaction, multiphoton ionisation, product identification 78−23946
Ba+HCl, laser induced fluoresc. study at different collision energies 80−91632
Ba+HF, product rot. and vibr. distributions and reaction cross sections depend. on reagent translational energy 80−93745
$Ba+HF \rightarrow BaF+H$, dual mol. beam excitation difference spectroscopy, state-to-state vibr. resolved dynamics 80−89474
$Ba+N_2O$, crossed mol. beams, BaO recoil vel. spectra 78−7184
$Ba+N_2O$, intracavity dye laser spectroscopy 77−86293
$Ba+N_2O$, reaction, electronic branching, statistical and dynamical influences 78−92451
$Ba+N_2O \rightarrow BaO+N_2$, chemiluminesc., ang. distrib. 78−44361
$Ba+N_2O \rightarrow BaO^*+N_2$, model electronically nonadiabatic reaction, large quantum effects 77−4897
$Ba+O_2$, $Ba+N_2O$, BaO formation, vibr. pop. distribs. of ground state 77−34731
$Ba+O_2$ flame, chemilum. from three-body recombination reactions 77−77759
$Ba+S_2Cl_2 \rightarrow S_2^*+BaCl_2$, rearrangement reaction, crossed-beam chemiluminesc. 77−29009
$Ba+SO_2 \rightarrow BaO+SO$, reaction kinetics, BaO recoil velocity spectra 79−74361
$Ba+SO_2 \rightarrow BaO+SO$ reaction, laser-induced fluoresc. obs., vibronic distrib. of BaO, collisional energy depend. 80−11917
Ba+trifluoromethyl iodide, BaI vibr. states bimodal distrib. 78−27743
$Ba(^1S,^3D)+$ halogenated methanes, laser induced fluorescence 79−66270
$Be+FH \rightarrow BeF+H$, collinear, pot. energy surface study 79−11782
$Be(2^3P)$+methane, reaction, ab initio MO calcs. 79−8431
$Bi(6^4S_{3/2})$+acetylene(ethylene), absolute rate consts., time-resolved reson. fluoresc. meas. 78−27731
$Br+Br_2$, atom-exchange, rate and activation energy, trajectory model and pot. energy surface 78−64811
$Br+F_2$, reaction kinetics, mass spectroscopic obs. 77−77743
$Br+H_2$, laser field interacting with collision dynamics, model system 78−62876
$Br+H_2$, laser radiation field effects, quantum mechanical close coupled expansion 77−50485
$Br+H_2O_2$, rate constant upper limit 80−30216
Br+HCl(DCl), relax. rates, vibr. photochem. 79−66290
$Br+HCl(\nu')$, $Br+DCl(\nu')$, reaction and relax., classical trajectory calcs. 77−48625
$Br+HI \rightarrow HBr+I$, thermal rate const., 220-400K, H/D isotope effect 79−47906
Br+NOBr, primary and secondary photochemistry, vibrationally excited NO, IR fluoresc. obs. 80−48030
$Br+NO \rightarrow Br+NO_2$, reaction rate const., mass spectrometric determ. 79−34288
$Br+O_3 \rightarrow BrO+O_2$, rate consts., mass spectrometric obs. 77−63897
$Br+O_3 \rightarrow BrO+O_2$, reaction rate constant, 200-360K 78−73024
Br+OClO, reaction rate consts., mass spectrometry meas. 78−3316
$Br_2+Ar \rightarrow 2Br+Ar$, 3500K trajectory anal., rate const. 77−52617
Br_2+H reaction Br prod., matrix isolated ESR 80−106336
$Br_2+H(d) \rightarrow HBr(DBr)+Br$, reactive cross-section, collision energy depend. obs. 79−11784
$BrO+O \rightarrow Br+O_2$, reaction rate constant, 200-360K 78−73024
$C+N_2$ reaction, CNN radical prod., matrix isolation study 78−86880
$C+N_2O \rightarrow CN+NO$, chemiluminesc., CN $(A^2\Pi_i)$ vibr. distrib. 79−39152
$C+PbO \rightarrow CO+Pb$, chemiluminesc. from gas phase reaction 79−8426
CH+O reaction, absolute rate const. 80−97690
$CN+O \rightarrow CO+N$, flash photolysis, absorption spectrosc. obs. 79−66289
CO+Ar, shock heated steady state dissoc. rate consts. calc. 78−40039
CO+Ni, complex form. in NiCa-Y zeolite, EPR, UV obs. 77−63949
CO+O on Rh surface, Langmuir-Henshelwood reaction 79−47965
CO_2+He, rot. transition classical integral cross section, surprisal predictions 77−54594
CO_2+inert gas, reactant decomp., rot.-vibr. energy transfer, relax. analytic soln. 80−55650
$C(^3P)+O_2(^3\Sigma_g^-) \rightarrow CO(^3\Sigma^+)+O(^1D)$, pot. energy surface, vibr. population inversion, classical dynamics 77−52630
$CS+O \rightarrow CO+S$, rate const. temp. depend., ESR-mass spectrometer obs. 78−20013
$CS+O \rightarrow CO+S$, $S+O_2 \rightarrow SO+O$ chain reaction in CO chem. laser 80−23678
CS_2+O, reactive scatt. in supersonic at. beam 79−36753
Ca+HF(DF), beam reaction, vibr. excitation 78−68877

atom-molecule reactions continued
$Ca+N_2O+CO$, intracavity dye laser spectroscopy 77−86293
$Ca+NaCl$, crossed beam reaction, collision complex lifetime internal state depend. fluoresc. 77−56217
$Ca+O_2$ reaction, chemiluminesc. absolute cross sections, photon yields and CaO dissoc. energy 80−97697
$Ca+O_2(CO_2)$, CaO form., product states obs. 78−92450
$Ca+O_2(CO_2)(N_2O)$, reaction, electronic branching, statistical and dynamical influences 78−92451
$Ca+S_2Cl_2 \rightarrow S_2{}^*+CaCl_2$, rearrangement reaction, crossed-beam chemiluminesc. 77−29009
Ca^+NO^-, $Ca^+NO_2{}^-$ in solid Ar, IR spectra at 15K 77−57996
$^{44}Ca+O_2(O_3)$, reaction products identification by IR spectra in N_2 matrix 78−9151
Ca^*+Cl_2, collision and reaction cross section meas. 79−59537
$Ca^*+Cl_2(HCl)$, luminesc. reactive collisions 77−16816
Ca^*+HCl, reaction performed under high resolution, luminescence obs. 80−95662
$Ca(4s4p\,^3P)+N_2O$, absolute chemiluminesc. cross-section and photon yield 78−53208
$Cd+H_2 \rightarrow CdH+H$, product initial rot. state distrib., pump and probe laser obs. 80−85158
$Cd+N_2$, (ns nd)$^1D_2$ states, Hanle effect, alignment destruction *(French)* 78−5324
$Cd+O_3$, matrix reactions, IR, Raman and visible spectra in Ar and N_2 matrices 80−87110
$Cd(^1P_1)+NO(X^2\Pi) \rightarrow NO(A^2\Sigma^+, \nu=0)$, electronic energy transfer react., collisional fluoresc. quenching 77−14548
$Cd(^3P_J)(^1P_1)+H_2(HD)(D_2)$ reacts., CdH(CdD) yields, quenching cross sections 79−1948
$Cl+Br_2 \rightarrow BrCl+Br$, crossed mol. beam, translational energy depend. 78−25693
$Cl+C_2H_2$, reaction kinetics, stratospheric implication 78−31618
$Cl+D_2 \rightarrow DCl+Cl$, LEPS pot. energy surface, rate consts., isotope effect, quasiclassical trajectory calc. 78−56887
$Cl+DI \rightarrow DCl+I$, thermal rate const., 220-400K, H/D isotope effect 79−47906
Cl+fluoromethane, photochlorination electron and oscill. energy 80−81320
Cl+formaldehyde, photolysis, Fourier transform IR studies, metastable species detection 80−81293
Cl+formaldehyde, rate const., 200-500K 79−39133
$Cl+H_2$, absolute reaction rate consts., 200-500K 78−15655
$Cl+H_2$, atom transfer reactions, reaction rate computing, trajectory calcs. 79−74371
$Cl+H_2$, reaction rate constants, Monte Carlo quasi-classical trajectory calculations 79−74366
$Cl+H_2O_2$, absolute rate const., 265-400K 78−15652
$Cl+H_2S \rightarrow HCl+HS$, laser-initiated chain reactions, rate consts., product energy distrib. 78−85144
Cl+HBr, rotated Morse curve-spline pot. function 78−80729
Cl+HD, reactions, branching ratio, energy partitioning and ang. distrib. 79−70312
Cl+HI, chem. laser, energy distrib., spectrosc. obs. 78−71096
$Cl+HI \rightarrow HCl+I$, Monte Carlo quasiclassical trajectory anal., product distribs. 77−16783
$Cl+HNO(H_2O_2)(HO_2)$, rate consts., stratospheric appl. 78−85125
Cl+H(D)I, exothermic triatomic exchange reactions, prod. energy distrib., statistical dynamic model 78−92455
$Cl+K_2 \rightarrow KCl+K^*$, chemiluminesc., electronic emission intensity 78−35689
Cl+methane, reaction rate const., stratospheric modelling appl. 79−20345
$Cl+\text{methane} \rightarrow HCl+CH_3$, absolute reaction rate, flash photolysis-reson. fluoresc. obs. 77−56222
$Cl+NH_3$, reaction rate consts., flash photolysis-reson. fluoresc. obs. 78−3327
$Cl+NO_2$, ClONO prod., FT IR obs. 79−8427
$Cl+NO_2$, matrix reactions, IR absorpt. obs. 78−15667
Cl+NOCl, primary and secondary photochemistry, vibrationally excited NO, IR fluoresc. obs. 80−48030
$Cl+NO+N_2 \rightarrow NOCl+N_2$, rate const. temp. depend. 78−76828
$Cl+O_2F.+O_2$ react., $ClF^*(B^3\pi_0+)$ prod., B-X emission spectrum 79−57216
$Cl+O_3 \rightarrow ClO+O_2$, rate consts. meas. 77−60059
$Cl+SO_2$, rate const. rel. to stratospheric Cl chemistry and Venus atm. 79−84353
$Cl+T_2$, atom transfer reaction in gas phase, reaction rate computing, tunnelling corrections 79−79237
Cl+vinyl bromide-d_3 reaction, IR chemiluminesc. 80−102506
^{38}Cl+ethane (methane)(vinyl bromide), rate consts., stratospheric temps., radiotracer meas. 77−48632
$Cl_2+Ar(He)(Cl_2)$, dissoc. in shock wave, density gradient meas. 77−83682
$Cl_2+Ca(4s4p\,^3P) \rightarrow CaCl+Cl$, chemiluminescent reaction, state-to-state cross-section, beam-gas expt. 80−45510
Cl_2+F, reaction kinetics, pot. energy surface and Franck-Condon integrals 79−61855
Cl_2+H, Faddeev equations and Franck-Condon models for chemical reactions 80−35507
$Cl_2+H(D)$, uni- and bimodal product energy distribs. 79−57207
Cl_2+muonium (H)(D), pot. energy surfaces, inversion calcs. 80−93734
Cl_2+O, reactive scatt. in supersonic at. beam 79−36754
$ClO+O(NO) \rightarrow Cl+O_2(NO_2)$ rate consts. meas. 77−60059
$ClO+O \rightarrow Cl+O_2$, rate consts. calc. 220-1000K 79−79233
$ClONO_2+O(^3P)$, fast flow reaction, rate const. 77−12777
$ClONO_2+O(^3P)$, photolytic gas phase kinetics at 245K 79−52719
$ClONO_2+O(^3P)$, rate consts., flash photolysis-reson. fluoresc. obs. 77−77796
$Cl(^2P)+CH_4 \rightarrow CH_3+HCl$, reaction rate const., laser flash photolysis-resonance fluoresc. kinetic study 80−45485
$Cl(^2P)+ClONO_2$, rate consts., flash photolysis resonance fluoresc. meas. 77−60038
$Cl(^2P)$+methane, absolute rate and temp. depend. 78−80731
$Cl'+HCl \rightarrow Cl'H+Cl$, barrier height, PNO-CEPA calculation 77−16795
$^{38}cl+H_2(D_2)$ reactions, characterisation, effect of ethylene-I_2 scavenger 78−73071
$Cs+(AuF_5)_n$, prod. of $AuF_5{}^-$, ionisation cross section energy depend. 80−81300
$Cs+(SbF_5)_n \rightarrow Cs^++SbF_6{}^-+SbF_4+(SbF_5)_{n-2}$, ionisation cross section energy depend. 80−81300

atom-molecule reactions continued
$Cs+CO_2$, in CO_2-Cs-He discharge, reaction rate meas. by IR absorption, press. depend. 78−44367
$Cs+Cl_2$, transient species, matrix isolation spectra 78−48635
$Cs+F_2$, electronic excited states, chemiluminesc. in flame, spectra 77−52643
$Cs+H_2O(D_2O)$, ionising collisions in crossed-beam systems 78−48641
$Cs+I_2$, ionising collision, trajectory surface hopping calc. 77−50509
$Cs+O_2$, reaction kinetics, time-resolved meas. 77−90588
$Cs+UF_6$, ion pair form. and atom abstraction reactions 79−1946
$Cs+UF_6(WF_6)(MoF_6)(TeF_6)(SeF_6)$, crossed beams, reaction cross section 77−77740
Cs^++benzyl chloride, beam reactions for 5.8 eV collision energy, mechanism 80−66777
$CsCl(Cs_2Cl_2)+Ar(Kr)(Xe)$, collision-induced ion-pair form., absolute cross sections 78−73029
CsI+Ar(He), elastic and inelastic scatt. 77−58119
$Cu+Cl_2(Br_2)(I_2)$, beam-gas chemiluminesc. reactions 80−85151
$Cu+F_2$, chemiluminesc. reactions, mol. beam study 80−97702
$Cu+F_2(NF_3)(SF_6)$, photon yields, chemi- and photo-luminesc. 79−5157
Cu+oxidant, chemiluminescence spectra and photon yields, population inversion 79−79255
$D+Cl_2$, collinear reaction rate consts., quantum and semiclassical calcs. 77−12782
$D+Cl_2$, reaction probabilities, information theoretic anal. 77−16799
$D+D_2$, collinear reaction, transmission coeff. isotope depend., statistical theory, invariance 77−36748
$D+D_2(\nu)$, vibr. relax. in at. exchange reactions, classical trajectory calcs. 77−44467
$D+F_2$, DF initial vibr. energy distrib., IR chemiluminesc. obs. 80−45497
$D+F_2(Cl_2)$, exothermic triatomic exchange reactions, prod. energy distrib., statistical dynamic model 78−92455
$D+F_2 \rightarrow DF+F$, exchange reaction, quasiclassical dynamics calcs. 79−91942
D+FD(H), low barrier quantum model, vibr. deactivation 80−69216
$D+H_2$ reaction, transition state theory calculations, kinetic isotope effect explanation 80−66784
$D+H_2$ rearrangement collision, vibr. excitation effects 80−71910
D+HCl(HBr), elastic scatt., van der Waals pot. meas. 77−58120
D+HCl(HBr)(HI), abstraction and exchange reactions 78−73025
$D+HCl \rightarrow HD+Cl$ or DCl+H, branching ratios determ. 78−40046
D+HX(H=Cl,I), HX dissociative ionisation, H^+ signal origin, mol. beam obs. 80−66778
D+PTFE, DF* prod., Fourier transform IR spectroscopy 80−87105
$D+T_2$, H-exchange studied by crossed molecular beam experiments 80−93747
D_2+D, atom transfer reaction in gas phase, reaction rate computing, tunnelling corrections 79−79237
D_2+F, reaction kinetics, pot. energy surface and Franck-Condon integrals 79−61855
D_2+Y, high temp. equilib. meas. 80−66780
$D_2{}^++N \rightarrow ND^++D$, product kinetic energy distrib. obs. 77−46619
$D_2{}^++O(^3P) \rightarrow OD^++D$, reaction dynamics, cross-section at. quadrupole moment effects 78−3324
DF+H, reaction rate, DF fluoresc., shock tube obs. 77−12784
D_2O+Ar, energy transfer isotope effect, rate consts. 79−8422
$Eu+O_2$, reaction cross-section, energy depend. 77−9054
$F+CH_3I(CF_3I)$, IF product internal rot.-vibr. distribs., fluoresc. obs. 80−48078
F+CO in Ar matrix, vibr. and electronic spectra, valence force potential determ., mol. photodissoc. obs. 80−85170
F+carbonyl compounds, HF IR chemiluminesc., vibr. and rot. energy disposal 77−86318
$F+\text{chlorobenzene} \rightarrow \text{fluorobenzene}+Cl$, statistical theory, phase space theory 79−74369
$F+D_2$, reaction rate constants, modified collision theory expression, comparison with exact expression 79−74370
F+DX, (X=I, Br, Cl), H abstraction, absolute reaction rate, H/D isotope effect 78−80721
F+ethylene, intermediate complex reaction, vibr., translational distrib., pot. hypersurface calc. 77−52612
F+ethylene (benzene) derivatives, deuterated, IR chemiluminesc. 80−102506
F+formic acid (formaldehyde), microscopic reaction dynamics, branching ratio, IR chemiluminesc. 78−73021
$F+H_2$, 3-dimens. electronic nonadiabatic reactive collision theory, electronuclear basis 78−3321
$F+H_2$, collinear quasiclassical trajectory study 78−80718
$F+H_2$, collinear trajectories, reaction dynamics calcs. 79−70311
$F+H_2$, Franck-Condon factors in reactive collision dynamics 77−36741
$F+H_2$, Franck-Condon factors in reactive collisions dynamics, vibr.-rot. distribs. 77−36742
$F+H_2$, hot-atom reactions, Boltzmann eqn. for hot-atom relax. 79−100423
$F+H_2$, in pulsed HF chem. laser evolution, irreversible thermodynamic anal. 79−31887
$F+H_2$, quenching, rot. energy transfer, quantum mech. calcs. 77−50499
$F+H_2$, reaction probabilities, information theoretic anal. 77−16799
$F+H_2$, reaction quantum dynamics, reson. model, transition state props. 79−11781
$F+H_2$, reaction rate constants, Monte Carlo quasi-classical trajectory calculations 79−74366
$F+H_2$, reaction rate constants, modified collision theory expression, comparison with exact expression 79−74370
$F+H_2$, reactive collision, semiclassical dynamics on multiple electronic surfaces, 3-dimens. calcs. 78−27746
$F+H_2$, reactivity, multiple electronic surface effects 77−21363
$F+H_2$, reactivity-selectivity, bounds derivation 80−66763
$F+H_2$, transition states, trapped trajectories and classical bound states in continuum 78−88630
$F+H_2$, two electronic pot. energy surfaces, collinear quantum calcs. 80−16646
$F+H_2$ rotated Morse curve-spline pot. function 78−80729
$F+H_2+\hbar\omega$, reactive scatt. and inelastic collision in laser field, semiclassical calc. 79−47948
$F+H_2(Cl_2)(HCl)$(methane), delay and decay times of stimulated emission 78−3317
$F+H_2(D_2)$, absolute rate coeffs. at 295-765K 80−81303
$F+H_2(D_2)$, absolute reaction rate coeffs., time resolved IR emission meas. 79−68258

atom-molecule reactions continued
$F+H_2(D_2)$, rate consts., temp. depend. 80−81302
$F+H_2 \rightarrow FH+H$, collinear probability, quantum calc. using pot. energy surface 78−64829
$F+H_2 \rightarrow FH+H$, vibr.-rot. energy distrib. of HF, DWBA calc. 78−80722
$F+H_2 \rightarrow HF+H$, DWBA transition amplitude kernel 80−81310
$F+H_2 \rightarrow HF+H$, reson. struct., quantum scatt. calc. 79−61847
$F+HBr(HI) \rightarrow HF+Br(I)$, electronic and vibr. energy transfer 77−63899
$F+HCl(DCl) \rightarrow HF(DF)+Cl$, dynamical props., pot. energy hypersurface computer anal. 77−77735
$F+HCl(HBr)(DBr)(HI)$, H abstraction reactions, temp. depend., laser photolysis IR fluoresc. obs. 80−93744
$F+HCl \rightarrow HF+Cl$, time resolved vibr. chemiluminesc. and rate consts. 80−61069
$F+HD \rightarrow FD+H$, multiple scatt. theory, knockout-pickup mech. 79−66265
$F+HD \rightarrow HF+D(DF+H)$, branching ratios, information theory test by classical trajectory calcs. 78−64822
$F+HI$, ${}^2P_{1/2}$-state excited I form. 78−23923
$F+HX$, ($X=I$, Br, Cl), H abstraction, absolute reaction rate, H/D isotope effect 78−80721
F+hydrocarbon (substituted methane)(inorganic hydride), HF IR chemiluminesc., H abstraction rel. rate consts. 77−86319
$F+I_2 \rightarrow IF+I$, energy partitioning, vibr. populations and rot. temp., population inversion 80−50832
F+iodobistrifluoromethylphosphine, reaction mechanism and kinetics, ESR 77−86294
F+methane, reaction in Ar matrix, IR spectra obs. 79−96293
$F+O_2$, quantum reactive scatt. theory, 3-dimens. 80−55637
$F+O_2+M \rightarrow FO_2+M$, flash photolysis IR chemiluminesc., rate const. 78−3311
$F+O_3$ reaction, $FO(X^2\Pi_i)$ radical VUV photoelectron spectra 80−104455
$F+T_2 \rightarrow TF+T$, rate meas. using TF-molecule chemical laser 77−86291
$F_2+H(D)(T)(Mu)$, impulsive triatomic reaction, vibr. state distrib., impulsive energy release model 78−92456
$F_2+Mg(Ca)(Sr)(Ba)$, crossed beam chemilum., kinetics and mechanisms 80−21264
$F_2+TeH_2(TeD_2)$, TeF radical form., chemiluminescence obs. 80−43058
$F_2+X \rightarrow XF+F$ ($X=Mu$, H, D, T), exoergic reaction, calcs. 79−61851
$F_2+X \rightarrow XF+F$ ($X=Mu,H,D,T$), isotope effects, quantum mech. and information theoretic calcs. 78−44360
${}^{18}F+H_2$, hot-atom reaction, nonequilib. vel. distrib. and reaction rate calcs. 77−63942
${}^{18}F+H_2$, nuclear recoil reaction, steady state hot atom kinetic theory calc., rate coeffs. 78−35712
$Fe+O_2$, cyclic complex form., matrix isolated IR spectra assignments 77−88449
$Fe(CO)_5$, gas phase collisions, negative ion form., struct. 77−6945
$Fe(CO)_5+Ar^*({}^3P)$, chemiluminesc. 78−61014
$Fe(CO)_5$+inert gas, dissoc. energy transfer, chemiluminesc. 80−55647
$F_2(\nu=0)+Mu \rightarrow MuF(\nu' \leq 3)+F$, ($Mu=$muonium), quantum mech. calcs. 77−21366
GaF+O matrix reaction, OGaF IR spectrum 79−11787
$Ge+N_2O$, chemiluminesc. reaction, HTFFR kinetics study 80−76496
$Ge+O_2(NO)(N_2O)$, reaction rate consts. at 350K 78−53186
$Ge({}^3P_0)+N_2O$, reaction rate const. meas., in flowing afterglow 77−77731
H+acetaldehyde, absolute reaction rate consts., 298-500K 77−16788
$H+Br_2 \rightarrow HBr+Br$, HBr ang. momentum alignment, scatt. ang. depend. 78−3323
$H+Br_2 \rightarrow HBr+Br$, pot. energy surface, ab initio generalised valence bond calc. 78−73026
$H+BrF(IF) \rightarrow HF+Br(I)$, reaction product energy distrib. 80−30219
H+bromotrifluoromethane, reaction rate consts., flash photolysis-reson. fluoresc. obs. 78−3327
$H+CF_4(SF_6)$ scattering, obs. of resonance maximum 77−58126
$H+CH_2$, IR matrix isolation spectra 80−97706
$H+CH_4 \rightarrow H_2+CH_3$, transition state, UHF method in INDO approx, 79−43578
$H+CN(NC)(NSi)$, bimolecular exchange reactions, dynamical-statistical method calcs. 80−104435
$H+Cl_2$, collinear nonreactive collision, classical trajectory eqns. calcs. 77−57233
$H+Cl_2$, collinear reaction rate consts., quantum and semiclassical calcs. 77−12782
$H+Cl_2$, collinear reaction, quantal transition probabilities from classical trajectories 77−32773
$H+Cl_2$, Franck-Condon factors for reactive collision processes 77−36741
$H+Cl_2$, Franck-Condon factors in reactive collision dynamics, vib.-rot. distribs. 77−36742
$H+Cl_2$, impulsive triatomic reaction, vibr. state distrib., impulsive energy release model 78−92456
$H+Cl_2$, stochastic-collision complex model theory 80−108696
$H+Cl_2(H_2)$, activation energy and trajectory calcs., temp. and isotope effects 78−76835
$H+Cl_2(SCl_2)(S_2Cl_2)(SOCl_2)(SO_2Cl_2)$, energy disposal, HCl IR chemiluminesc. obs. 78−92484
$H+Cl_2$(organic molecule), rate const., discharge flow-reson. fluoresc. meas. 78−7178
$H+Cl_2 \rightarrow HCl+Cl$, quantum mech. reaction coords., point transformation calcs. 77−36730
$H+Cl_2 \rightarrow HCl+Cl$, rate consts. meas., Lymaπ-α fluoresc. technique 77−16780
$H+ClBr \rightarrow HCl+Br(HBr+Cl)$, product energy distrib., rate const., IR chemilum. obs. 77−81391
$H+ClF$, IR chemilum., energy disposal and branching ratios 80−26017
$H+ClO_2 \rightarrow OH+ClO$, primary energy disposal, laser-induced fluoresc. 79−24726
$H+D_2$ reaction, transition state theory calculations, kinetic isotope effect explanation 80−66784
$H+DCl \rightarrow HD+Cl$ or $HCl+D$, branching ratios determ. 78−40046
H+ethane, chemical reaction, 357-544K 78−7198
H+ethylene episulfide→HS+ethylene, absolute rate parameters, flash photolysis reson. fluoresc. 78−3312
$H+F_2$, vibr. prod. distrib., Einstein coeffs. 78−92448
$H+F_2(Cl_2)$, exothermic triatomic exchange reactions, prod. energy distrib., statistical dynamic model 78−92455

atom-molecule reactions continued
$H+F_2(Cl_2)$, reaction probability, information theoretic anal. 77−16799
$H+F_2 \rightarrow HF+F$, 3-dimens. vibrot. reaction probabilities from collinear results, information theoretic synthesis 79−74354
$H+F_2 \rightarrow HF+F$, exchange reaction, quasiclassical dynamics calcs. 79−91942
$H+F_2 \rightarrow HF+F$, vibr. adiabatic and static distorted wave Born approx. calcs. 80−7768
$H+FH(FD)$, low barrier quantum model, vibr. deactivation 80−69216
H+formaldehyde, reaction, absolute rate coeffs., 250-500K 79−100349
$H+H_2$, 3-dimens. exchange reaction, surprisal theory, quantum dynamics 79−15964
$H+H_2$, ang. momentum decoupling approx., quantum mech. reactive and nonreactive scatt. 77−12780
$H+H_2$, CI calc. of three dimens. pot. energy surface 78−56882
$H+H_2$, collinear, collision-induced dissoc., quantum mech. probabilities calcs. 79−20359
$H+H_2$, collinear, quantum mech. reactive scatt., exchange kernels calcs. 78−68880
$H+H_2$, collinear classical dynamics, chemically accurate pot. energy surface 77−48620
$H+H_2$, collinear exchange reaction, quantum dynamics, surprisal theory 79−6988
$H+H_2$, collinear exchange reaction, unified statistical model 79−34295
$H+H_2$, collinear quantum mech. reactive scatt., hyperspherical coords. 80−108694
$H+H_2$, collinear reaction, isotope depend. transmission coeff., transition state theory 77−36747
$H+H_2$, collinear reaction, transmission coeff. isotope depend., statistical theory, invariance 77−36748
$H+H_2$, collinear reaction, Delves radial coord. S-matrix propag. calcs. 80−108695
$H+H_2$, collinear reactive scatt., Magnus approx. 77−16801
$H+H_2$, collinear reactive scattering, coupled eqns., soln., R-matrix calcs. 77−16812
$H+H_2$, exchange reaction, three-dimens., dynamical S matrix method 79−91930
$H+H_2$, Franck-Condon factors in reactive collision dynamics, vibr.-rot. distribs. 77−36742
$H+H_2$, H_3 dynamics, on accurate H_3 pot. surface 79−5139
$H+H_2$, integral total reactive cross section, infinite order sudden approx. 80−30214
$H+H_2$, least squares fit to ab initio pot. energy function 78−56883
$H+H_2$, planar reaction, cross section calcs., vibr. and rot. convergences 77−21376
$H+H_2$, planar reaction, Schrodinger eqn., expansion as partial differential eqns. 77−21375
$H+H_2$, reaction, quasi-classical trajectory calcs. using new pot. energy surface 80−7767
$H+H_2$, reaction probability, max. entropy derivation, statistical theories 80−66781
$H+H_2$, reaction rate constants, modified collision theory expression, comparison with exact expression 79−74370
$H+H_2$, reactions and collisions in IR laser field, collision-induced absorpt. spectra 80−76499
$H+H_2$, reactive scatt., sudden approx. calcs. 78−68878
$H+H_2$, rot. cross-section, linear surprisal plots, theory 77−50498
$H+H_2$, scatt. wave function modal struct. and global behaviour 80−81307
$H+H_2$, sudden rot. reactive scatt., 3-dimens., approx. quantum mech. calcs. 80−76498
$H+H_2$, three dimens. reaction, theory 77−21377
$H+H_2$, three dimens. reaction, Porter-Karplus pot. energy surface, rot. distribs., rate consts. 77−21378
$H+H_2$, transition states, trapped trajectories and classical bound states in continuum 78−88630
$H+H_2(Cl_2)$, reactivity-selectivity, bounds derivation 80−66763
$H+H_2(D_2)(T_2)$ reactions, accurate pot. energy surface, isotope effects, quasiclassical trajectory study 80−97698
$H+H_2(HD)(D_2)$, exchange reaction rate consts. meas., vibr. effects 79−5134
$H+H_2(O_2)$, quantum reactive scatt. theory, 3-dimens. 80−55637
$H+H_2(0,0) \rightarrow H+H_2$, quasiclassical cross sections, pot. surfaces comparison 79−74364
$H+H_2(\nu_i=1)$, exchange reaction, integral and differential cross sections determ. 80−85153
$H+H_2(\nu=1, j=0)$ exchange reaction, 0.9-1.1 eV, sudden rot. calcs. 79−79230
$H+H_2(\nu=1) \rightarrow H_2+H$, exchange reaction, classical trajectory method, vibr. excitation, partial rate consts. 78−60993
$H+H_2(\nu)$, vibr. relax. in at. exchange reactions, classical trajectory calcs. 77−44467
$H+H_2 \rightarrow H_2+H$, classical three-body problem. calcs., effective reaction cross section *(Russian)* 79−39144
$H+H_2 \rightarrow H_2+H$, IR laser induced reaction 78−80761
$H+H_2 \rightarrow H_2+H$, tunnelling path for reaction 78−11514
$H+H_2 \rightarrow H_2+H$ three dimens. chem. reaction, distorted-wave calcs. 80−81294
$H+HCO \rightarrow H_2+CO$, classical trajectory study 80−93750
$H+HCl$, barriers for abstraction and exchange reactions 77−48629
$H+HCl$, semi-empirical pot. energy surfaces calc. by diatomics-in-molecules method 80−95556
$H+HR \rightarrow H_2+R$, ($HR=$hydrocarbon), tunnelling reaction, classical S-matrix calc. 77−29007
$H+ICl \rightarrow HCl+I$, IR chemiluminesc., product energy distrib. 78−23926
$H+ICl \rightarrow HCl+I$, product energy distrib., rate const., IR chemilum. obs. 77−81391
$H+Li_2$, collinear reactions, SCF correl. diagram for Li_2H form. 77−70292
H+LiF, laser-induced nonadiabatic collision process, classical model 80−97701
H+methane, abstraction and exchange reactions, energy barriers, UHF-CI calcs. 78−11512
H+methane, abstraction and exchange reaction, barrier height calc. using POL-CI wave functions 80−81304
$H+N_2$, nitrogen fixation, semiempirical INDO study 80−16898
$H+N_2O \rightarrow N_2+OH$, rate const., 2000-2850K, combustion of $H_2/N_2O/CO/Ar$ 78−85162
$H+N_2(O_2)$, charge prod. cross sections and differential scatt. calcs. 78−94313

atom-molecule reactions continued

- $H+N^{3+}$, charge exchange, assoc. reaction, rel. to interstellar gas 80−7763
- $H+NH_2 \rightarrow NH_3$ react., force, density anal. 78−60997
- $H+NO_2$, population inversion of Λ doublets in microwave spectrum of $OH(^2\Pi_{3/2}, v=1)$ 80−974
- $H+NO_2 \rightarrow NO+OH$, hydroxyl group internal state distrib., laser-induced fluoresc. crossed mol. beams 77−4905
- $H+NO_2 \rightarrow NO+OH$, rate consts. from at. reson. fluoresc. 77−48618
- $H+NO_2 \rightarrow OH+NO$, energy disposal, information theory appl. 78−15658
- $H+NO_2 \rightarrow OH+NO$, $H+NOCl \rightarrow HCl+NO$, rate meas. by Lyman-α fluoresc. 77−21353
- $H+NO_2 \rightarrow OH+NO$, laser induced fluorescence for OH, $^2\pi$ to $^2\Sigma$ region, preferential population of Λ doublets 78−31620
- $H+NO_2 \rightarrow OH+NO$, primary energy disposal, laser-induced fluoresc. 79−24726
- $H+NO_2 \rightarrow OH+NO$, vel. and angular distrib., Fourier transform Doppler spectrosc. obs. 79−80692
- $H+O_2$, singlet state O_2 form., reaction mechanism, mass spectrometric obs. 78−53204
- $H+O_2+Ar$, HO_2 free radical prod., rate const. calc. 80−101026
- $H+O_2 \rightarrow OH+O$, combustion, quasiclassical trajectory calcs. 78−53201
- $H+O_2 \rightarrow OH+O$, kinetic study, pot. energy surface of HO_2, MO theory 79−74353
- $H+O_3$, absolute reaction rate const., 219-360K 78−80734
- $H+O_3$, reaction mechanism studied using photoionisation mass spectrometer, form. of $O_2(a'\Delta g)$ 80−85168
- $H+O_3 \rightarrow HO_2+O(^3P)$, reson. fluoresc. obs. 79−70317
- $H+O_3 \rightarrow HO_2+O(^3P)$, yields 80−71900
- $H+O_3 \rightarrow O_2+OH$, rate consts. from at. reson. fluoresc. 77−48618
- $H+OCS \rightarrow HS+CO$, absolute rate parameters, flash photolysis reson. fluoresc. 78−3312
- $H+PH_3$, abstraction rate consts., 209-495K, time-resolved fluoresc. 77−16807
- $H+T_2$, H-exchange studied by crossed molecular beam experiments 80−93747
- H^++H_2, rotated Morse curve-spline pot. function 78−80729
- H_2, chemiionisation by $He(2^3S)$ and $He(2^1S)$, pot. surfaces, autoionisation widths, cross sections 77−36739
- H_2 collinear reactions, transition state theory generalisations 80−26002
- H_2 collinear reactions, transition state theory generalisations 80−26003
- $H_{2\text{-}41}{}^++He$, 200-850 eV, attentuation and fragmentation 78−62968
- H_2+alkali metal, exchange reactions and rot. transfer effects on transfer coeffs. 77−66749
- H_2+Ar, 4500K shock wave expt. simulation, vibr. state changes and dissoc. 79−61850
- H_2+Ar, Arrhenius dissoc. activation energy, vibr. depend., trajectory calc., 4500K 78−35662
- $H_2+C(O)(N)$, pot. surfaces, HF calc. 80−16669
- $H_2+Cl(Br)(I)(F)$, gas phase H-atom transfer reactions, struct.-reactivity correl., pot. energy surfaces 80−104433
- $H_2+Cl(H)(F)(I)$, atom transfer reactions, reaction rate computing, trajectory calcs. 79−74371
- $H_2+D(O)(Cl)(Br)$, relax. and chem. reaction, time resolved IR fluoresc. and mass spectrometry obs. 80−69177
- $H_2+D \rightarrow HD+H$, three dimens. ab initio pot. energy surface 80−55646
- H_2+F, in pulsed HF chem. laser, kinetic modelling, rot. nonequilib. 79−36888
- H_2+F, reaction kinetics, pot. energy surface and Franck-Condon integrals 79−61855
- $H_2+F(H)$, collinear reactive scattering, coupled eqns., soln., R-matrix calcs. 77−16812
- $H_2+F(I)$, collinear trajcctories, pattern recognition 80−45481
- $H_2+F \rightarrow HG+H$, 3-dimens. vibrot. reaction probabilities from collinear results, information theoretic synthesis 79−74354
- H_2+H, reactive scatt., 3-dimensional quantum mechanical calcs. 77−30802
- $H_2+H(Cl)$, atom transfer reaction in gas phase, reaction rate computing, tunnelling corrections 79−79237
- $H_2+H(D)(T)$ reactions, accurate pot. energy surface, isotope effects, quasiclassical trajectory study 80−97698
- $H_2+H(F)$, minimum energy reaction path, reference coord. approach 78−40025
- $H_2+H(F)(Cl)$, collision induced IR laser absorpt., rate enhancement, theory 79−66275
- $H_2+H(I)$, activation energy and trajectory calcs., temp. and isotope effects 78−76835
- $H_2+H(2S)$, metastable atom total quenching 77−46628
- $H_2+H(2s) \rightarrow H_3{}^++e^-$, fluoresc. of H_2 photodissociating near threshold 78−21983
- $H_2+He(2^3S)$, Penning ionisation, quantum mech. scatt. calcs. rigid rotor approx. 77−34741
- $H_2+I \rightarrow HI+H$, collinear reaction, reson. effects, quantum mech. calcs. 77−52625
- $H_2+I \rightarrow H+HI$, quasiclassical tragectory vs. quantum calcs., vibr. state depend., kinetics 78−80733
- $H_2+O \rightarrow OH+H$, vibr. energy effects, classical trajectory calcs. 77−63904
- H_2+Y, high temp. equilib. meas. 80−66780
- $H_2{}^++He$, vibr. energy effects on kinetics, phase space model 78−11508
- $H_2{}^++He \rightarrow H+HeH^+$, product ion ang. distrib., quantum mech. impulse approx. calcs. 79−24727
- $H_2{}^++He \rightarrow H+HeH^+$, reaction dynamics, vibr. state channels, beam expt., trajectory calcs. 77−77739
- $H_2{}^++He \rightarrow H+HeH^+$, total cross sections, quasiclassical trajectory results compared with mol. beam data 77−60051
- $H_2{}^++Ne$, vibr. energy effects on kinetics, phase space model 78−11508
- H_3, form. and dissoc., kinetics, historical review, book contrib. 77−40527
- $H_3+Ar \rightarrow H_2+ArH^+$, crossed beam reaction, energy distrib. 77−52626
- $HBr+Cl \rightarrow HCl+I$, rate const. temp. depend., laser-initiated reaction 78−23929
- HBr^*+I, reaction rate, vibr. excitation effect, isotope enrichment 77−90581
- $HCl+Ar$, shock heated steady state dissoc. rate consts. calc. 78−40039
- $HCl+Ar$, shock-heated, collision induced dissoc. 79−34290
- $HCl+Ca(4s3d\,^1D) \rightarrow CaCl+H$, chemiluminescent reaction, state-to-state cross-section, beam-gas expt. 80−45510
- $HCl+Cl(Br)(H)$, vibr. relaxation and reaction rates determ. 80−108698
- $HCl+D(O)(Cl)(Br)$, relax. and chem. reaction, time resolved IR fluoresc. and mass spectrometry obs. 80−69177

atom-molecule reactions continued

- HCl+inert gas, dissoc. induced by collision, rot. energy depend. 79−100341
- $HCl+K$, ion pair form. reaction, energy loss spectra meas. 79−61849
- $HCl+K$, mol. beam reaction, rot. state depend. 79−74365
- $HCl+O(OH)$, reaction rate const. temp. depend., stratospheric implications 78−31616
- $HCl+O(2^1D_2) \rightarrow OH+Cl$, correl. diagram 77−16798
- $HCl(\nu=1,2)+O(^3P_g)$, reaction and deactivation, laser-induced fluoresc. obs. 78−35669
- $HCl(\nu=1)+H(D)(Cl)(Br)$ reactions, selective vibr. excitation effects, kinetics *(German)* 77−21364
- $H(D)+X_2$, $(X=F,Cl,Br,I)$, exoergic collinear reactions, impulsive energy release model 77−90591
- $HF+Ar$, shock heated steady state dissoc. rate consts. calc. 78−40039
- $HF+D$, vibr. threshold energies, reagent energy effects 78−85145
- $HF+H' \rightarrow H+H'F$, transition state geometry, SCF CI calcs. 78−20009
- $HF+H(D)$, kinetic isotope effect and temp. depend. 78−53202
- HF+inert gas, dissoc. induced by collision, rot. energy depend. 79−100341
- $HF+T$ hot atoms, energy loss 78−15691
- $HI+Cl \rightarrow HCl+I$, rate const. temp. depend., laser-initiated reaction 78−23929
- HN_3+F, production of $NF^*(a^1\Delta$ and $b^1\Sigma^+)$ 79−11770
- HN_3+F, strong interactions in gas-phase reactions, arrested relax. IR chemilum. obs. 80−7773
- HO_2+Cl react. rate const. determ. at 298K *(French)* 78−64817
- $HO_2+O \rightarrow HO+O_2$, rate coeff. meas. by laser mag. reson., atm. chem. appl. 77−52614
- $H'+BrH \rightarrow H'Br+H$, collinear reaction, barrier height, PNO-CEPA cals. 78−3328
- H^*+chloroform-$d_1 \rightarrow HD+CCl_3$, hot atom reaction, threshold energy meas. 78−44356
- $H(ads)+H_2O(ads) \rightarrow OH(ads)+H_2(g)$, H_2 formation mechanism 80−6628
- $He\text{-}H_2$, thermal dissociation, vibrational relaxation at high temps., ab initio calcs. 79−74367
- $He\text{-}H_2{}^+$, classical trajectories, on 3D cardinal spline fitted surfaces 77−90584
- $He+CO(HCl)$, effective pot. and coupled states approx., differential and gas kinetic cross sections 77−61827
- $He+H_2$, close coupling calcs., averaged definite parity j_z approx. with Clebsch-Gordan weights 77−58111
- $He+H_2{}^+$, collisional dissoc., expt. and quasiclassical trajectory calcs., eV region 78−42201
- $He+H_2{}^+$, endothermic reactive and vibr. inelastic collisions, pot. well effects 79−8430
- $He+H_2{}^+$, reactive and dissociative scatt., crossed-beam and trajectory obs. 78−64833
- $He+H_2{}^+ \rightarrow HeH^++H$, diatomics-in-mols. and spline fitted ab initio surface, vibr. effects 78−20010
- $He+H_2{}^+ \rightarrow HeH^++H$, spline-fitted ab initio surface, quantum mech. scatt. calcs. 77−63898
- $He+H_2{}^+ \rightarrow HeH^++H$, vibr. state distrib. prod. by H_2 vibr. autoionisation cross-section depend. 77−48628
- $He+N_2(CO)(CO_2)(N_2O)$, collisionally excited neutral and ionic emission, flowing afterglow 77−51248
- $He+NH_3$, rot. excitation rate consts., semiclassical method 79−3538
- $He+OCS$, emission spectra in He afterglow 80−87139
- $He+OCS$, rot. spectral line shift and widths, collision induced phase shifts 77−75222
- He+water (cyanomethane), afterglow, excitation and quenching reactions, optical pumping 78−35690
- He^++SO_2, dissoc. charge transfer reaction, SO^+ $(A^2\Pi\text{-}X^2\Pi_r)$ emission 80−95659
- $^4He^++H_2$, 35-1000 keV, electron loss cross-section 78−22018
- $He^*{}_2$ inert gas, optical absorpt. spectra and kinetic behaviour 80−95635
- $He(2^3S)+H_2O(H_2S)$, energy transfer processes, reaction products, UV and visible obs. in flowing afterglow 78−85138
- $He(2^3S$ and $2^1S)+H_2(D_2)$, Penning, rearrangement and total ionis. cross sections, vel. depend. 79−22816
- $He_2(2^3\Sigma_u{}^+)+He_2(Ne)$, reaction rate consts. meas. in afterglow 78−7173
- $Hg+2NH_3 \rightarrow HgNH_3+NH_3$, photosensitised, $HgNH_3$ complex lifetime 78−53193
- $Hg+Cl_2+\hbar\omega \rightarrow HgCl^*+Cl$, laser-induced harpooning reactions 80−83458
- $Hg+Cl_2 \rightarrow (HgCl_2)_n$, surface catalysed reaction 79−100430
- $Hg+H_2(HD)(D_2)$, intramultiplet transitions 77−54597
- Hg+halomethane, $^3P_1$-state total quenching 80−52927
- $Hg+I_2$ reaction, adiabatic pot. energy surface 78−15666
- $Hg+I_2 \rightarrow HgI+I$, endoergic reaction, prod. ang. distrib. 78−15665
- $Hg+N_2$, $6(^3P_0) \rightarrow 6(^3P_1)$ excitation, double modulation obs. 79−27072
- $Hg+NH_3$, excited UV luminesc., low press., $HgNH_3{}^*$ form. 77−21388
- $HgBr_2$+inert gas metastables, dissociative excitation, HgBr emission intensity 80−40687
- $Hg(^3P_0)+Br_2 \rightarrow HgBr(B)+Br$, crossed mol. beam chemiluminesc., cross section 78−31622
- $Ho+N_2O \rightarrow HoO^*+N_2$ chemiluminesc. reaction, cross-section 78−76847
- $I\ (5^2P_{1/2})+HBr$, reactive and inelastic channels rate, temp. depend., AAS obs. 78−35657
- I excited atom $(5^2P_{1/2})$ quenching by mols. with C-I bonds 79−64076
- $I+H_2(HD)(D_2)$, intramultiplet transitions 77−54597
- $I+I_2$, quenching rate const. of I metastable atoms by I_2 78 −13691
- $I_2+Na(K)(Cs)$, ion-pair form. cross section, 15-120 eV, mol. props. depend. 77−28996
- $I_2+Na(K)(Cs)$, ion-pair form., differential cross sections, I_2 internal energy effects 77−61840
- $I(^2P_{1/2})$ energy transfer and reactive collisions, laser pumping possibility 79−949
- $I^*+I_2(Br_2)(Cl_2)(IBr)(ICl)(BrCl)$, collisional deactivation and reaction rate consts., obs. 78−80738
- $I^*(^2P_{1/2})+Br_2 \rightarrow IBr+Br^*(^2P_{1/2})$, rate const., chemiluminesc. obs. 77−40520
- $I(5^2P_{1/2})+Br_2$, deactivation kinetics, time-resolved spectrosc. obs. 78−95916
- $I(5^2P_{1/2})+Br_2$, deactivation kinetics, $Br(4^2P_{1/2})$ prod., time-resolved spectrosc. obs. 78−95917
- $I(5^2P_{1/2})+HBr(DBr)$(methane)(propane), collisional deactivation, rate consts. meas. 77−86300
- $K+Br$, harpooning mechanism interactions, semiclassical optical model 79−89755

atom-molecule reactions continued
- $K+Br_2$, inelastic scatt., total cross-sections, trajectory surface hopping calcs. 78−46420
- $K+Br_2$ (Cl_2), electron transfer crossed beam reaction, energy and ang. differential cross section 79−20358
- $K+Br_2(BrI)(I_2)$, stripping reactions at hyperthermal energies 77−16815
- $K+CH_3I(CF_3I)$, product translational distrib., crossed beam reaction 78−31629
- $K+Cl_2 \rightarrow K^+(Cl+Cl^-)$, 5.5−14.0 eV, energy loss, spectrum maxima, mechanism 77−75286
- $K+CsF$ collision complex, reactive decay branching ratio, rot. energy effect 77−66752
- $K+CsF(RbF)$, complex form., decay. branching fraction and cross-sections, translational energy depend. 77−21374
- $K+H_2O(D_2O)$, ionising collisions in crossed-beam systems 78−48641
- $K+HBr$, product energy distrib. 80−45509
- $K+HCl$, ion pair form., energy loss spectra 79−34286
- $K+HgBr_2$, laser irrad., HgBr form., chemiluminescence 80−55658
- $K+I_2$, ionising collision, trajectory surface hopping calc. 77−50509
- $K+NO_2$, charge transfer reactions, energy and ang. differential cross-sections meas. 80−53125
- $K+NO_2$, ion pair form. reaction, energy loss spectra obs. 79−91921
- $K+NaK$ reactive collisions studied using circularly polarised laser fluorescence 80−69215
- $K+O_2 \rightarrow K^+ + O_2^-$, electron transfer kinematics 77−6903
- $K+SF_6$, ion-pair form. reaction, energy loss spectra 80−55630
- K+trifluoroiodomethane→KI+trifluoromethane, molecular beam reactive scattering, angular distribution study 79−98198
- $K+UF_6(WF_6)(MoF_6)(TeF_6)(SeF_6)$, crossed beams, reaction cross section 77−77740
- $K_2+Cl(Br) \rightarrow KCl(KBr)+K^*$ product electronic state distrib., chemilumineesc. 77−40529
- K^*+molecule, assoc. ionisation, mass spectra *(Russian)* 77−42393
- $Kr+F_2$, KrF form., relax. and quenching 80−81314
- $KrF+He(Ne)(Xe)(NF_3)$, quenching rate consts. meas. 79−24718
- $KrF^*+Ar(Kr)+Ar(Kr)$, recomb. rate consts., 300 to 800K, appl. to KrF^* laser efficiency 79−45930
- KrF^*+inert gas, three body collision rate consts., trimer form. rates 80−50831
- $Kr(^3P_1)+H_2O$, decomposition, $OH(A^2\Sigma^+)$ internal energy distrib. 79−10183
- $Kr(^3P_2)+F$ donor reagent, quenching, excimer form. 79−63953
- $Kr(^3P_2)+F_2(NF_3)(CF_3OF)$, KrF^* bound-free oscill. emission spectra calc. 80−7799
- $Kr^*(Kr^+)+NF_3$, rate consts., electron attachment coeffs., flowing afterglow 78−13578
- $La+H_2O(D_2O)$(alcohols), O atom abstraction, product internal state distrib., fluoresc. study 78−48643
- $La+OCS \rightarrow LaS$, chemiluminesc. vibr. analysis of $C^2\Pi \rightarrow X^2\Sigma^+$, $D_0{}^0$ determ. 77−48645
- $Li+CH_3I(CCl_4)(CH_3NO_2)$, mol. beam kinetics 77−28978
- $Li+Cl_2$ (SF_6) (dichlorofluoromethane) *(German)* 78−92485
- $Li+Cl_2(Br_2)$, ion pair form., double differential cross sections, 8-30 eV 78−11507
- $Li+Cl_2(Br_2)(ICl)$, product mag. deflection slotted disc velocity analysis 77−16806
- $Li+F_2(Cl_2)(NO_2)$, $4^2S_{1/2}$ excited atom crossed beam collisional ionisation 79−64087
- $Li+H_2O \rightleftharpoons LiOH+H$, equilib. consts., ab initio SCF and CEPA calcs. 78−3361
- $Li+HF \rightarrow LiF+H$, pot. energy surface, SCF and CI calcs. 80−71904
- $Li+Li_2 \rightleftarrows Li_3$, rovibronic symmetry correlation 78−92461
- $Li+LiH$, collinear reactions, SCF correl. diagram for Li_2H 77−70292
- $Li+SnCl_4(PCl_3)(SF_6)$, product mag. deflection slotted disc vel. anal. mol. beam kinetics 77−25250
- $LiF+Ar(Kr)$, anisotropic system intermol. pot. determ. 77−58121
- $LiH+H \rightarrow Li+H_2$, linear LiH_2 pot. energy surface, MCSCF functions optimisation 77−67960
- $^7Li+H_2$, electron capture collisions, 0.2 to 3 keV 77−6925
- $Mg\text{-}In+H_2 \rightarrow MgH_2$, kinetics, catalytic effect of In 78−76851
- $Mg+N_2O(O_2)$(acetylene), $(^3P_1)$metastable atom afterglow quenching rate consts. 77−6720
- $Mg+O_3$, matrix reaction, IR spectra, isotope shifts and blue matrix shift 78−80736
- Mg^*+Cl_2, collision and reaction cross section meas. 79−59537
- Mg^*+Cl_2 crossed beams, chemical reaction, metastable Mg as new light source of forbidden lines 78−90112
- $Mg^*+Cl_2 \rightarrow MgCl^*+Cl$, chemiluminesc. studies 78−40030
- MoF_6+alkali atom(dimer), ionis. reactions, electron affinity 77−81398
- $Mu+F_2 \rightarrow MuF+F$, exchange reaction, quasiclassical dynamics calcs. 79−91942
- N, at. recombination, Smith side tube method obs. 78−68881
- N+alkene (1,3-butadiene)(acetylene), reaction rate consts., pulse radiolysis obs. 80−35508
- $N+BrCn(CH_4)(C_2H_2)(CCl_4)(CH_2Cl_2)(CHCl_3)$, CN quartet state production, fluoresc. anal. 78−68888
- $N+H_2SO_4$, atmosphere chemistry, collisional reaction probabilities 80−90168
- $N+N_2O$, $NO(B^2\Pi_r)$ form., quenching 79−64038
- $N+NO$, $^4(S)$ state reaction rate, discharge flow and photolysis reson. fluoresc. method 79−5142
- $N+O_2{}^+$, rate constant rel. to atm. ion chem. 77−41245
- $N+OH$, direct rate meas. 80−30217
- N+organic molecule, rate const., discharge flow-reson. fluoresc. meas. 78−7178
- $N+S_2Cl_2$, $NS(B^2\Pi)$ form. kinetics, chemilum. obs. 79−39151
- $N_2{}^+ +O$, in ionosphere, rate coeff. determ. 77−53288
- $N(^2D)+O_2$, chemiexcited NO form., 90-180K IR obs. 78−90163
- N_2H_4+H on Titan, gas phase reaction el. to N_2 atmosphere evolution 79−30005
- $NH_3(ND_3)+Hg$, photosensitised luminesc., phase shift anal. 79−15966
- $NO+Ni$, complex form. in NiCa-Y zeolite, EPR, UV obs. 77−63949
- $NO+O$, in Ar matrix, chemiluminesc. 78−35688
- $NO+O$, O_3 effect, chemiluminesc., absolute rate const. 80−45507
- NO^++atmospheric gases, thermal energy reaction rates 78−92443
- $NO^+ +X \rightarrow NO+X$ $(X=Cl, Br, I)$, rate const. determ. in flames 78−48633
- $NO_2+N \rightarrow N_2O+O$, crossed beam study, produce ang. distrib. 79−34311
- N_2O+inert gas, reactant decomp., rot.-vibr. energy transfer, relax. analytic soln. 80−55650

atom-molecule reactions continued
- $N(^4S)+O_2(^3\Sigma_g{}^-) \rightarrow NO(^3\pi_u)+O(^3P)$ doublet surface minimum energy path calcs. 78−7194
- $N(^4S)+O_3$, rate const. at 298K, upper limit determ. 79−74360
- Na^+-solvated electron, reversible capture by 1,1-diphenylethylene, equilib., kinetics 78−7177
- $Na+CO$ velocity-changing collisions, stimulated photon echo obs. 79−81258
- $Na+HX(J;\upsilon) \rightarrow NaX+H$, $(X=F,Cl)$, reaction rate, rot. excitation depend. 78−64818
- $Na+I_2$, ionising collision, trajectory surface hopping calc. 77−50509
- $Na+N_2$, collision broadening and shift of 3S-4D and 3S-5S lines 79−3406
- $Na+N_2O$, Na chemiluminesc., excitation mechanism, appl. chem. laser 77−63916
- $Na+Na_2$, reaction probability, energy transfer 77−28998
- $NaCl+Ar$, dissoc.-ionis. process rates in shock tube 78−35674
- $Ne+H_2{}^+ \rightarrow NeH^+ +H$, vibr. state distrib. prod. by H_2 vibr. autoionisation cross section depend. 77−48628
- $Ne+He_2{}^+ \rightarrow He$+products, surface-hopping trajectory calc. 79−52637
- $Ne+HeH^+$, collinear reaction, pot. energy surface SCF-LCAO-MO and DIM calc. 78−92467
- Ne_2+Ar, total integral cross sections for excitation, exchange and dissoc. 80−1044
- Ne_2+Kr total integral cross sections for excitation, exchange and dissoc. 80−1044
- NeH_2, collision-induced dissociation, Monte Carlo quasiclassical trajectory calcs. 79−74357
- $Ne^*+Fe(CO)_5$, chemiionisation and chemiluminescence reactions, Penning ionisation and fluoresc. obs. 80−97689
- $Ni(CO)_4$, gas phase collisions, negative ion form., struct. 77−6945
- $Ni(Co)_4$+inert gas, dissoc. energy transfer, chemiluminesc. 80−55647
- O+acetaldehyde(propylene), rate const., discharge flow-reson. fluoresc. meas. 78−7178
- O+acetylene reaction, kinetics, flash photolysis-reson. fluoresc. meas. 77−73439
- $O+CS_2 \rightarrow CS+SO$, vibrational distribution of CS, laser-induced fluorescence meas. 80−71895
- $O+CS_2 \rightarrow OCS+S$, branching ratio meas. 79−52656
- O+chloroethylene reaction, kinetics, flash photolysis-reson. fluoresc. meas. 77−73439
- $O+Cl_2O$, reaction rate const. 79−20344
- $O+Cl_2(CS_2)$, reactive scatt. of beams, vel. distribs. 77−73443
- $O+Cl_2(CS_2)$, reactive scatt., O atoms seeded in Ne supersonic nozzle beam 78−48637
- O+dimethylamine, reactive routes, identification 79−39129
- O+ethylene, (OCS), reaction dynamics, IR laser excitation effects 79−66288
- O+ethylene, OH chemiluminesc., mechanism, rate const., mathematical model calcs. 78−48655
- O+formaldehyde, reaction, absolute rate coeffs., 250-500K 79−100349
- $O+H_2$, classical trajectory calcs., ab initio surface, singlet state, rate consts. 80−66786
- $O+H_2$, pot. energy surfaces and reaction rates, ab initio calcs. 80−63531
- $O+H_2$, trajectory calcs., fitted ab initio pot. energy surface 79−74358
- $O+H_2O$(methane/halomethane), direct reaction in flow system 80−3333
- $O+H_2O \rightarrow OH+OH$, energy partitioning 80−101009
- $O+H_2S$, ^3P-state, absolute reaction rate, flash photolysis reson. fluoresc. obs. 79−66283
- $O+H_2S$, matrix reactions, IR spectra of products, chemiluminesc. 77−60057
- $O+H_2SO_4$, atmosphere chemistry, collisional reaction probabilities 80−90168
- $O+H_2 \rightarrow OH+H$, rot. energy distrib. of $OH(X^2\Pi,\nu=0)$ 79−87829
- $O+HCl$, vibr. excited, laser enhanced reaction rate, OH vibr. distrib. obs. 78−95912
- $O+HI$, HOI formation, matrix reaction, IR spectra, isotope shifts and band assignments 78−80737
- $O+I_2(CS_2)(OCS)$, crossed-beam investigation of translational energy 79−5145
- O+methane, photochem. reaction, high temp., rate coeff. meas. 80−16699
- $O+N_2O_5$, rate const., 220K, 300K, discharge-flow method 78−44352
- $O+NO$ binary reaction, crossed beams, NO_2 chemiluminesc. 78−64843
- $O+NO_2{}^+(NO^+.H_2O)$, rate constant rel. to atm. ion chem. 77−41245
- $O+NO+M$, rate const., 217-500K 79−52626
- $O+NO+M \rightarrow NO_2+M$, $(M=He, Ne, Ar, Kr)$, 217-500K, absolute rate consts. 77−16787
- $O+NaO$, nightglow, excitation and abundance of Na 80−98497
- O+nitroethane (nitromethane), H atom abstraction in discharge flow system 78−35671
- $O+O_2 \rightarrow O_3$, Hartley band during formation, metastable states, vibr. excitation and relax. 80−55632
- $O+O_3$, laser-induced photolysis of ozone reactions 80−11928
- $O+O_3$ reaction, vibr. enhancement 80−30215
- $O+OH$, direct rate meas. 80−30217
- O+saturated hydrocarbon, chem. reaction dynamics. OH prod. investig. 80−101016
- O+saturated hydrocarbon, reaction dynamics, model pot. surfaces, quasi-classical trajectory calcs. 80−97696
- O+saturated hydrocarbon→OH+alkyl radical, reaction dynamics, mol. beam-laser induced fluoresc. obs. 80−97695
- O+trifluoroiodomethane, vel. distrib. 80−26011
- $O^+ +H_2$, linear approach, pot. energy surface for H_2O^+ 80−47922
- O_2, IR nightglow bands excitation mechanism, reaction rate consts. 78−65448
- O_2+Ar, shock-heated, collision induced dissoc. 79−34290
- $O_2+Be(Mg)(Ca)(Sr)(Ba)$, reaction kinetics in diffusion flame 77−90579
- O_2+H, 20-500 eV, ion pair and free electron production, integral cross sections 78−46437
- O_2+inert gas, dissoc. induced by collision, rot. energy depend. 79 100341
- O_2+inert gas, reactant decomp., rot.-vibr. energy transfer, relax. analytic soln. 80−55650
- $O_2+La(Y)(Sc)$, crossed beam chemiluminescence reaction, spectral simulation, hyperthermal energy meas. 78−80732
- $O_2+N(^2D)$ as source of $O(^1D)$ atoms in aurorae 79−35028
- O_2+Ni, complex form. in NiCa-Y zeolite, EPR, UV obs. 77−63949
- $O_2{}^+$+atmospheric gases, thermal energy reaction rates 78−92443
- $O_3+O(^1D)$, UV photolysis, $O(^3P)$ prod., rate consts. determ. 80−55636

atom-molecule reactions continued
- O_3+U(Th), assoc. ionis. cross sections, in crossed beams, mass spectra obs. 78–94317
- OCS+Si(Ge), SiS and GeS multiple collision chemiluminesc., intercombination systems 80–45505
- $O(^1D)$+CO, deactivation rate consts. temp. depend., 113-333K 78–88629
- $O(^1D)+H_2O$, rate coeff., atm. OH prod. 79–58009
- $O(^1D)+H_2(HCl)(NH_3)(N_2O)$(methane), rate consts., temp. depend. 78–27747
- $O(^1D)$+haloalkanes, deactivation reactions, absolute rate consts. determ. 79–11783
- $O(^1D)+N_2$, electronic quenching resons., collinear collision, quantum mech. calcs. 77–60050
- $O(^1D)+O_2(N_2)(CO_2)(O_3)(H_2O)$, 100-350K, reaction rate consts. 77–21355
- $O(^1D)$+Xe(Kr)(Ar), deactivation rate consts., 110-330K 78–88628
- $O(^1D_2)+NH_3\rightarrow OH(v,N)+NH_2$, bimodal OH rot. distrib. obs. and energy disposal 80–76501
- OH^-+inert gas, collision-induced dissociation 78–29834
- OH_n, ab initio LCAO SCF calcs. of ionisation pot., electron, proton, H and hydride affinities 77–88387
- $O(^3P,^1D)+H_2(^1\Sigma_g^+)\rightarrow H_2O$, potential energy surfaces, extended basis first-order CI study 80–7776
- $O(^3P)$+1-butyne (2-butyne), CO pro dynamics, mechanisms 78–11510
- $O(^3P)$+2-methyl-2-butene, reaction rate consts. meas. 78–61001
- $O(^3P)$+amines, rate consts. temp. depend., 298-440K 78–48616
- $O(^3P)$+benzene (toluene), absolute reaction rate consts., 299-440K 79–70304
- $O(^3P)+C_3O_2\rightarrow 3CO$, reaction dynamics and monoxide vibr. distrib., laser reson. absorpt. method 78–68882
- $O(^3P)+CH_3CN(CF_3CN)$, reaction mechanisms and kinetics 77–36728
- $O(^3P)+CHF\rightarrow HF+CO$, product vibr. energy distrib. 79–61853
- $O(^3P)+CN(\nu)$ react., prod. energy distribs. meas., CO vibr. level population *(German)* 78–76833
- $O(^3P)+CO(X^1\Sigma^+)$, vibr. deactivation and atom exchange, rate. consts., Monte Carlo anal. 77–48627
- $O(^3P)+CS_2\rightarrow CS+SO$, reaction rate enhancement, triat. mol. symmetric vs. asymmetric stretch excitation 79–91927
- $O(^3P)$+dimethyl disulphide, absolute reaction rate const. determ. 80–89472
- $O(^3P)$+dimethyl sulphide, fast flow reson. fluoresc. obs. of absolute rate consts. 80–61077
- $O(^3P)+H_2$, reaction rate constants, Monte Carlo quasi-classical trajectory calculations 79–74366
- $O(^3P)+H_2\rightarrow OH+H$, potential energy surface, theory 80–45492
- $O(^3P)$+HCl(HBr)(HI), rate consts. temp. depend. 79–52627
- $O(^3P)$+mercaptans, reaction rate consts., O_2 effect 79–52630
- $O(^3P)$+methane, barrier height and transition state geometry, POL-CI calc., H abstraction reaction 80–66782
- $O(^3P)$+n-butane (NO(M=Ar)), reaction rate constants using flash photolysis-NO_2 chemiluminesc, method 77–44458
- $O(^3P)+O_3^{\dagger}$, bimolecular reaction rate coeff. reactant vibr. excitation depend., reson. fluoresc. obs. 78–76837
- $O(^3P)$+tetrafluoroethylene, time-resolved absorpt. spectra, triplet CF_2 formation 77–44472
- $O(^3P)$+vinyl halides, reaction rate consts. 298-442K flash photolysis obs. 78–7195
- $O(^1S)+N_2O$, quenching rate const. determ. 77–10626
- O^*+H_2S, chemiluminesc. matrix reaction, diffusion controlled, 8-20K, $O(^3P)$ 78–61013
- $O^*+H_2\rightarrow OH^*+H$, rate const. and vibr. energy distrib. in OH^*, for $O(^3P)$ 78–60998
- $O(2^1D_2)+Cl_2$, reaction kinetics, vac. UV at. spectra 77–21365
- $O(2^1D_2)+N_2(O_2)(N_2O)(CO_2)(H_2O)$(methane), collisional deactivation meas., 295K, rel. to atmospheric processes 80–16663
- $Pb+F_2$, chemiluminesc. spectrum of PbF 79–24742
- $Pb+H_2(HD)(D_2)$, intramultiplet transitions 77–54597
- $Pb+N_2O\rightarrow PbO+N_2$, chemiluminesc. reaction, vel. depend. 78–27762
- $Pb+O_3$ reactions, chemiluminesc. 79–52673
- $Rb_2+Br\rightarrow RbBr+Rb^*$, product electronic state distrib., chemiluminesc. 77–40529
- RbF+K collision complex, rot. energy effect on branching fraction for reactive decay 78–73023
- $S+CS_2(OCS)(CH_4)$, electronically excited atom, reson. fluoresc. 80–99476
- $S+O_2\rightarrow SO_2$, chemiluminesc. matrix reaction, diffusion controlled, 8-20K 78–61013
- $S+OCS\rightarrow S_2+CO$, reaction kinetics of $S(3^1D_2)$ reactions 79–79274
- $S^++NO\rightarrow NO^++S+1.1$ eV, rate consts. kinetic energy depend., drift tube meas. 80–7778
- $S^++O_2\rightarrow SO^++O+0.26$ eV, rate consts. kinetic energy depend., drift tube meas. 80–7778
- S_2Cl_2+alkali metal, matrix reaction, examination by laser excitation 79–5148
- S_2Cl_2+alkali metal, matrix reaction, S_2Cl absorpt. spectrum 79–5149
- SF_6+Ca(Sr), F_5S-F bond energy bounds from chemiluminesc. obs. 79–86081
- SF_6+Rydberg atom, reaction channels, expt. vs. theory 80–63755
- $SO_2+O(^3P)$, vibr. excited, collision induced intramol. deactivation 78–25670
- $SO_3+Ar\rightarrow SO_2+O+Ar$, rate const. of spin forbidden dissoc. in shock wave 79–57214
- $Sb(5^4S_{3/2})+NO(O_2)$, rate consts., time-resolved reson. fluoresc. meas. 78–27732
- $Sc+H_2O(D_2O)$(alcohols), O atom abstraction, product internal state distrib., fluoresc. study 78–48643
- $Sc+NO_2$, chemiluminesc., nonequilib. product distrib. 80–101014
- $Sc+O_2(NO)(SO_2)$, nascent product state distribs., laser fluoresc. detect. 78–7187
- $Sc+O_2\rightarrow ScO+O$, chemiluminescence, $A^2\Delta X^2\Sigma^+$ transition 77–1927
- $Se+O\rightarrow SeO$, chemiluminescent reaction, $B^3\Sigma\rightarrow X^3\Sigma$ band emission 79–79254
- $Si+F_2$, chemilum., at. absorption, and laser-induced fluoresc. obs. 80–3315
- $Si+F_2$, fast flow reactor, second order rate coeff. determ. 78–80723
- $Si+N_2O$, flame chemiluminesc., SiO emission, $A^1\Pi$, $b^3\Pi$ and $a^3\Sigma$ states 77–77767
- $Si+O_2(NO)(N_2O)$, reaction rate consts. at 350K 78–53186
- $Sm+N_2O$, mol. beam chemiluminescence, cross section energy depend. 77–32792

atom-molecule reactions continued
- Sn, oxidation kinetics, in high-temp. fast flow reactor, chemiluminesc. titration meas. 77–48623
- $Sn+CH_3I(n\text{-}C_3H_7I)(CCl_4)$, crossed beam mol. kinetics, SnI and SnCl recoil vel. spectra 79–1947
- $Sn+Cl_2(Br_2)$, reactive scatt., ang. distrib. and time-of-flight spectra 78–64842
- $Sn+N_2O$, chemiluminesc., high temp. fast flow reactor kinetics obs. 78–88636
- $Sn+N_2O\rightarrow SnO(a^3\Sigma)+N_2$, chemiluminesc. high temp. fast flow reactor obs. 80–45493
- $Sn+O_2$, crossed mol. beam kinetics, SnO time of flight recoil vel. spectra 78–68883
- $Sn+O_2(NO_2)$, chemiluminescence and photon yields 77–29012
- $Sn[5p^2(^3P_0)]$, kinetic studies of ground state atoms, by resonance line absorpt. 78–85128
- Sr+HF, endothermic reaction, comparison of effectiveness of vibr. and translational excitation 80–93746
- Sr+HF(DF), beam reaction, vibr. excitation 78–68877
- $Sr+HF\rightarrow SrF+H$, product state distrib., reagent orientation and rot. effect 79–20361
- $Sr+N_2O+CO$, intracavity dye laser spectroscopy 77–86293
- $Sr+S_2Cl_2\rightarrow S_2^*+SrCl_2$, rearrangement reaction, crossed-beam chemiluminesc. 77–29009
- $Sr(^1S,^3P)$+ halogenated methanes, laser induced fluorescence 79–66270
- Sr^*+Cl_2, collision and reaction cross section meas. 79–59537
- $Sr^*+Cl_2\rightarrow SrCl^*+Cl$, chemiluminesc. studies 78–40030
- Sr^*+HCl, reaction performed under high resolution, luminescence obs. 80–95662
- $Sr^*+N_2O\rightarrow SrO^*+N_2$, visible chemiluminescence, absolute cross section and photon yields 78–92463
- $Sr^*(^3P_1)$+HCl(HF), laser-excited atom reaction, energy deposition 78–85134
- $T+F_2\rightarrow TF+F$, exchange reaction, quasiclassical dynamics calcs. 79–91942
- T+fluoroform, 4.5 to 6.0 eV, substitution reactions 78–85146
- $T+H_2O$, energetic reactions, hard sphere excitation functions 79–1963
- T+HD, variational transition field theory and unified statistical model 80–97700
- T+HD hot atom exchange reactions, trajectory calcs. 80–26037
- $T+HT\rightarrow TH+T$, collinear reactivity bands 78–85143
- T_2+Y, high temp. equilib. meas. 80–66780
- $Te+H_2(HD)(D_2)$, intramultiplet transitions 77–54597
- $Te(^3P_1)+Te_2$, gas phase flash photolytic deexcitation obs., 1000K *(Russian)* 78–50626
- tetrafluoromethane+C react. in ionising radiation of nuclear reactor 77–63934
- $Ti(^5F)+N_2O(O_2)(NO_2)$, chemiluminesc., TiO dissoc. mechanisms, confirmation of $D°_0$(TiO) 77–40534
- $Tl+H_2(HD)(D_2)$, intramultiplet transitions 77–54597
- $U+NO_2$, UN reaction product identification in Ar matrix, vibr. energy distrib. 77–9066
- $U+O_2$, assoc. ionisation, electron energy distrib. 78–35656
- $U+O_2$, laser excited atoms, chemical reactions 77–90594
- UF_6, laser chemistry 80–69198
- UF_6+alkali atom(dimer), ionis. reactions, electron affinity 77–81398
- UO^++Ar, collision-induced dissoc. cross section and threshold 80–95706
- UO_2^++Ar, collision-induced dissoc. cross section and threshold 80–95706
- WF_6+alkali atom(dimer), ionis. reactions, electron affinity 77–81398
- WF_6+Na(K) electron transfer, WF_6^- form., dissoc. energies, electron affinity 77–19071
- $X+F_2\rightarrow XF+F$ (X=Mu, H, D, T), quasiclassical smooth sampling study of threshold behaviour 79–61852
- $Xe+Br_2\rightarrow XeBr^*+Br$, rot. polaris. in chemiluminesc. 79–8432
- $Xe+Br(CCl_4)$, excitation functions and rotational polarisation, chemiluminesc., crossed beam study 80–76491
- $Xe+Cl_2(F_2)$, XeCl(XeF) form., relax. and quenching 80–81314
- $Xe+F_2$, transient species, matrix isolation spectra 78–48635
- XeF+Ne(Ar), lifetime and collisional quenching meas., XeF_2 photolysis 78–33545
- XeF_2+Ar(Kr)(Xe) metastable atoms$\rightarrow XeF^*$, mechanisms 77–30897
- XeF^*+inert gas, three body collision rate consts., trimer form. rates 80–50831
- $Xe(^3P_{0,2})+Br_2\rightarrow Xe^*+Br$, excitation function 78–40028
- $Xe(^3P_2)$+F donor reagent, quenching, excimer form. 79–63953
- $Xe(6s,^3P_2)+Cl_2(PCl_3)(CCl_4)(COCl_2)$, vibr. energy disposal from XCl^* spectrum 79–100345
- $Xe(6s,^3P_2)$+RCl, reactive quenching, XCl^* emission spectrum obs. 79–100344
- $Y+H_2O(\ D_2O)$(alcohols), O atom abstraction, product internal state distrib., fluoresc. study 78–48643
- $Y+O_2(NO)(SO_2)$, nascent product state distribs., laser fluoresc. detect. 78–7187
- $Y+O_2\rightarrow YO+O$, $A^2\Delta\text{-}X^2\Sigma^+$ transition 77–1927
- $Yb+O_2\rightarrow YbO+O$, crossed mol. beam expt. 77–44468
- $Zn+N_2$, (ns nd)$^1D_2$ states, Hanle effect, alignment destruction *(French)* 78–5324
- $Zn+O_3$ matrix reactions, IR, Raman and visible spectra in Ar and N_2 matrices 80–87110
- $Zn(g)+H_2O(g)=ZnO(s)+H_2(g)$, standard Gibbs free energy of reaction 79–11815

atom probe field ion microscopy
- alloys, relationship between results of analysis and structure of sample *(French)* 80–55732
- atoms, direct obs., application to ultra-fine processing *(Japanese)* 79–7532
- central-force interatomic pot. construction from whisker deform. data, crystal defect stress investigation 79–56103
- continuous phase transforms. obs. 78–35621
- differentially pumped low energy ion beam system 80–310
- dilute alloys, time of flight atom-probe FIM exam. of surface segregation 79–19437
- energy-focused atom probe design and performance 78–85276
- evaporation pulse generator 78–78041
- field ion microscopy, developments 79–67445
- field ionisation and field desorption mass spectrometry, review *(Japanese)* 79–66384

atom probe field ion microscopy continued

- hyperboloidal sample model, time of flight determ. by atom probe *(French)* 77—16469
- imaging atom probe for surface studies 78—14555
- imaging atom probe mass spectroscopy, appl. to surface struct. anal. 79—23818
- magnetic sector atom-probe FIM with retarding potential analyser 79—12895
- magnetic-sector atom-probe field ion microscopy *(Japanese)* 79—75660
- metal oxide surface layer, TOF atom probe anal. 78—64766
- metallic film characterisation technique, APFIM, time-of-flight spectroscopy 80—75138
- metallurgical applications *(Dutch)* 80—96425
- metals, individual atomic events on surfaces, quantitative examination 80—75409
- metals, radiation damage, FIM and atom probe FIM expts., review 78—35623
- metals and alloys, refractory, surface investigation by FIM and atom probe *(German)* 79—55623
- metals and alloys, segregation studies by imaging atom probe microscopy 80—66911
- metals and alloys, trace element detection by atom probe microanalysis 80—66910
- Nimonic 80A, rapidly solidified, struct. and initial precipitation, field-ion and TEM study 79—78982
- phase transformation studies, appl. 80—3000
- plasma-wall interactions in Princeton Large Torus Tokamak, appl. of high-field surface and techniques 79—68942
- pulsed laser atom-probe FIM, development and appls. 80—66402
- single time-gated channel plate 78—21276
- solid-solid interface chemistry, characterisation, theory 80—75448
- specimen exchange device for ultra-high vacuum use 79—67437
- specimen field corrosion caused by polymer gaskets 80—57425
- steel, atom probe microanalytical expts., review 78—35622
- steel, austenitic stainless, MC precipitate comp., APFIM study 80—104161
- steel, C martensitic, tempering induced decomposition and segregation, atom probe study 80—3112
- steel, Cr-Mo (2.8, 1.6 wt.%), atom probe anal. of bainitic phase boundaries 80—71990
- steel, pearlitic atom probe microanal., computer controlled 77—66781
- steel, stainless, 410 type, surface segregation using atom-probe FIM 79—77883
- surface analysis and grain boundary segregation using high-resolution instrument 80—37134
- time of flight atom probe, quantitative microanal., metallurgical appl. 80—86498
- time-of-flight atom probe for studying impurity atom or alloying element interaction with defects 78—45754
- time-of-flight microscope, computer-controlled, for metal defects study 77—82645
- Al alloy, FIM and microanalysis, developments 80—100155
- Cr surface reactive, field ion microscope and atom probe obs. 79—29410
- Cr_2O_3-Cr black, solar collector coating, microstruct., FIM and SEM obs. 80—26166
- Fe-Al, atom-probe field ion microscopy obs. *(French)* 78—86389
- Fe-Ti (0.15 wt.%), Ti distrib., segregation, FIM anal. 80—84200
- Ga, (3×3) superstructure on W(011) and Mo(011), FIM obs. 79—99425
- Ga, field ion microscopy using mag.-sector atom probe, ionisation characts. 79—43106
- Ga ion source, high intensity, emission characts. 80—80950
- Ga, liquid, field ionisation, surface temp. and elec. field depend. 79—78849
- GaAs, time of flight atom-probe mass spectra 78—92584
- Ge, amorphous, pure and H doped, voids, atom probe FIM 80—49107
- Ir, field depend. of spectral line energy of He-H_2 adsorbate 79—78853
- LaB_6, time of flight atom-probe FIM study 80—6652
- Mo, atomic structure of grain boundaries 79—33003
- Mo, field depend. of spectral line energy of He-H_2 adsorbate 79—78853
- Mo tips, film coated characterisation by atom probe FIM, atomic clusters, voids 80—33863
- Mo-Re-C (0.3, 0.2 at.%) time-of-flight atom-probe expts. 80—55741
- Mo-Ti (1 wt.%), fast neutron irradiated, direct obs. of solute segregation to voids 79—78971
- Ni solar collector coating, microstruct., FIM and SEM obs. 80—26166
- Ni-Al, spinodal decomposition, atom probe field ion microscopy study 80—3028
- Ni-Cr-Co superalloy, combined TEM, FIM, atom probe microanalysis of precipitates and carbide phase comp. 80—100844
- Ni-Cu, surface segregation using atom-probe FIM 79—77883
- Ni-Cu, surface segregation, computerised atom-probe FIM study 80—75412
- Ni-Nb amorphous alloy, transformation to crystalline state, ion emission microscope study *(Russian)* 79—82158
- Pt-Au, surface segregation using atom-probe FIM 79—77883
- Pt-Au, surface segregation, comp. depth profiles meas. using atom-probe field ion microscope 80—100380
- Re, field depend. of spectral line energy of He-H_2 adsorbate 79—78853
- Ru surface, clean, oxidation, atom probe anal. of oxide films 79—47797
- Si, chemisorption of H_2, atom-probe FIM obs. 78—71968
- Si, photoillumination effect on field ion microscopy 79—78850
- Si whisker, (111) oriented, FIM and atom-probe FIM obs. 80—10473
- β-SiC whisker, atom-probe FIM expts. 78—35275
- W, adsorption of benzene, isothermal ramped field desorption technique 79—82450
- W, atom-probe field ion microscopy obs. *(French)* 78—86389
- W, field depend. of spectral line energy of He-H_2 adsorbate 79—78853
- W, gas-surface interaction in atom-probe FIM 77—40336
- W, ion implantation, $^4He^+$ range profile and ^{4}He diffusivity meas. 79—33022
- W wire, AKS-doped, second phase particle obs. by TEM, SEM and atom probe microanalysis 80—108457
- W-Mo, refractory, surface investigation by FIM and atom probe *(German)* 79—55623
- W-Th, atomic structure of grain boundaries 79—33003
- W-Zr field emitter, time-of-flight atom-probe study 80—80949

atom-surface impact

see also sputtering

- adsorbed layers, gas atom scattering, hard sphere theory *(Russian)* 79—38704
- adsorption, selective, correlation of intensity features with at.-surface pot. Fourier components 79—15013
- AES, energy referencing from charging samples by implanted inert gas spectra 80—40196
- alkali halide, band struct. of selectively adsorbed atoms 79—28399
- anisotropic potentials, rainbow scatt. 77—82407
- anthracene surface, Ar impact, Penning ionisation electron spectra and photoelectron spectra 80—66352
- atomic beam diffraction from solid surfaces, struct. studies 80—65349
- atomic beam spectrometer using a LiF analyzer crystal, for surface studies in UHV 78—71651
- atomic chain model, correlation effects *(Japanese)* 80—50501
- beam scattering, semiempirical determ. of atom-surface interaction 78—72676
- biological specimen surface struct. determ. 78—53584
- Bound state vibrational spectrum of the 3-9 atom-surface interaction 78—14615
- capture of gas atoms on solid surface, non-one-dimens. interaction effects 80—60726
- classical scattering, cutoffs and shadows 78—80448
- classical scattering, rainbow peaks, energy depend. 79—43085
- conference, atomic collisions in solids, Hamilton, Canada (Aug. 1979) 80—62375
- cooling by metal snow, origin of effect and elimination 78—71494
- coordinate representation sudden approx., system depend. and independ. dynamical factors 79—78803
- coronene, metastable inert gas atom impact, surface electron emission energy distrib. 78—43970
- corrugated wall model, GR method 77—63520
- crystal surface diffraction of partially coherent beams 80—40205
- damage cascades, stochastic theory of particle transport 80—54291
- Debye-Waller factor from atom-surface scatt. 78—92164
- Debye-Waller factor rel. to He at. scatt. 77—63516
- diffraction, perturbation theory calcs. 77—85862
- diffraction by cryst. surfaces, reson. effects 77—35447
- diffraction of atoms by crystal surface, quantum theory approach 80—42104
- diffractive scatt., specular intensity near bound-state reson. 80—80928
- eikonal model modification for gas-surface interaction *(Russian)* 79—33883
- elastic collision with crystal, shell effects 80—89106
- elastic scattering, effective potential theory 79—43084
- elastic scattering, high-energy approx., appl. to He/LiF and Ne/W 79—65965
- elastic scattering, iterative integration scheme using Green function 77—48294
- electron tunnelling in external electric field, atomic resonant ionis. 77—52208
- energy accommodation coefficient, two-phonon contribs., DWBA calcs. 79—95893
- energy exchange, in thermal energy scatt., impulsive models 80—20744
- energy transfer, gas-surface scatt. in laser field 79—69941
- energy transfer and sticking coeff., classical and quantum treatments 80—40209
- excited atom sputtering, cascade and quasi-thermal processes 78—35239
- exospheres of Moon and Mercury, Monte Carlo simulation of regolith interaction 80—67588
- extinction theorem in atom-surface scatt. 78—88393
- gas-metal interactions, scatt. dynamics 80—92787
- gas-phase and ion-surface collisions, optical emission 80—32821
- gas-solid energy transfer, isotropic Debye model 77—16443
- gas-surface energy accommodation, hard-cube model anal. 80—50888
- gas-surface energy accommodation coefficients, model calc., multiple collisions and trapping 77—85870
- gas-surface potential calc., double rainbow scatt. appl. 78—80443
- gas/solid surface collisions, vel. depend. of ang. distribs., interaction pot. effect 79—11491
- graphite, ^{4}He interaction and scatt. 80—60732
- graphite, He scattering, bound state reson. and inelastic effects 79—28876
- graphite, interaction and band struct. effects for He derived from scatt. data 78—92162
- graphite, tritium effects, first wall controlled thermonuclear reactor conditions, simulation 79—647
- graphite (0001), ^{4}He selective adsorption, level crossings 80—71556
- graphite (0001), inelasticity in He scatt. 80—76127
- graphite (0001) surface, He atom scatt., bound state reson., interaction pot., band struct. effects 80—29840
- graphite (0001) surface, He atom scatt., gas-surface pot. 78—48267
- graphite surface, ^{4}He low-energy scatt., inelastic effects 80—100738
- graphite surface interaction with He atom 80—34316
- hard corrugated surface, atom scatt., threshold and Lennard-Jones reson., and elastic lifetime 78—39647
- hard corrugated surface, one phonon scatt. of atoms 79—47577
- hard corrugated surface incorporating stationary pot. well, interaction pot. model for atom scatt. 79—91555
- hard corrugated surface with attractive pot., elastic atom scatt. appl. to He-Cu(117) system 79—69944
- heat sources of the arc cathode spot ion impact and neutralisation heating 80—38733
- inelastic, multiphonon theory, tetradic scatt. formalism 79—56905
- inelastic particle reflection by Rayleigh waves 79—74022
- inelastic scatt., generalized Langevin eqn., time domain kernels 78—23568
- inelastic scatt., quantum theory, eikonal approx. 80—50499
- inelastic scatt. in impulse approx., model 78—11054
- inelastic scattering, average energy loss and energy distrib. 80—29841
- inert gas atom-solid surface beam-scatt. spectroscopy in eV range, nucl. channel, formal theory 79—78820
- ionisation, kinetic energy of ions 77—10751
- Langevin theory, generalised, dynamical solid models 77—8700
- Langevin theory, generalised, numerical simulation 77—8701
- lattice dynamics effect on scatt. 80—2909
- light atom-solid surface scatt., diffractive and inelastic, unified model 79—87553
- low energy atom scattering, appl. of soln. to Schrodinger eqn. for scatt. from hard corrugated wall 79—40404

atom-surface impact continued
  Mercury, surface interaction with exospheric atmosphere 78—49351
  metal, low energy atom scatt., theory 78—39648
  metal surface, atom scatt. at long range 78—13572
  metal surface, interaction with He metastable atoms 79—91558
  metal vapour production by sputtering in hollow-cathode discharge 80—1868
  metals, atomic and mol. beam scatt., review 80—40203
  mixed quantum model for gas-solid energy transfer 78—35235
  model surface, classical scatt. of atoms 79—28877
  monatomic solids, redefined scatt. cross sections 80—70274
  Moon, surface interaction with exospheric atmosphere 78—49351
  multiple hits in atom-surface diffraction 78—80449
  naphthacene, metastable inert gas atom impact, surface electron emission energy distrib. 78—43970
  neutral atom elastic and inelastic scatt. by corrugated hard wall 79—46899
  neutral atom scattering, long range, from solid cylinders, quantum theory 80—71549
  neutrals, keV, energy determ. method 80—89100
  one-electron resonant processes in presence of surface sub-monolayer 80—93445
  optical emission from low-energy particle-surface collisions 77—36300
  organic luminophores, luminesc. under action of atomic H *(Russian)* 79—8177
  perylene, metastable inert gas atom impact, surface electron emission energy distrib. 78—43970
  physisorption of atoms, dynamical and geometrical effects 80—70531
  plasma cooling by metal snow, expt. evidence 78—71495
  quantum rainbow, corrugated wall model 77—12478
  quantum theory, Debye-Waller factor 80—7459
  quantum theory, exact solns. and evaluation of approximations 77—1780
  rainbow effects and energy exchange, calc. 80—84825
  rainbow structure, energy spectra, surface temp. influence, in-plane scatt., 2- and 3-dimens. 79—38699
  rare gas inelastic scattering from metal surfaces, generalised Langevin theory 77—85872
  reflection and sticking coeffs., short range forces, low energy limit 80—40208
  resonant scattering of atoms from solid surfaces, atomic band struct. effects 77—85871
  response functions for cryst. and surfaces, appl. to surface scatt. 78—72669
  scattering, coupled channel calcs., symmetry appls. 78—92156
  scattering, quantum theory 78—27357
  scattering by surface and bulk phonons 77—73209
  scattering from corrugated hard wall, boundary conditions 79—74040
  scattering from cryst. surfaces in quantum regime, review 78—35244
  scattering from surface with regular one-dimens. roughness elements 78—92166
  scattering of atoms and mols. by solid surfaces, review 78—31291
  scattering of neutral atoms by exponential corrugated pot. 80—25512
  scattering phenomena, hard corrugated wall pot., diffracted peak intensities 79—61486
  scattering potential, hard corrugated wall model, Fourier components 79—61485
  scattering theory, undergraduate course 77—60863
  scattering theory, use of Debye-Waller type factor 77—73204
  selective adsorption phenomena, elastic theory 79—100012
  semiclassical treatment, and its appl. to He+LiF(001) 77—20977
  simulation by classical stochastic propagator model 77—32482
  sinusoidal hard wall, at. scatt., approx. and quantum calcs. 77—16444
  solid surface, mol. dynamic processes interaction with laser radiation 80—71943
  Space Shuttle, expts. on mol. and atomic beam interactions with surfaces 78—35243
  sputtered atoms, energy distribution, ion mass and target temp. effects 80—66361
  stationary sinusoidal hard wall, rigorous theory in (n+1) dimens. 77—36331
  stationary sinusoidal hard wall surface with one-dimens. periodicity 78—92161
  steel, stainless, type AISI 321, surface damage and mech. changes after H atom irrad. 80—39182
  sudden approximation, appl. to atom-surface scatt. 80—20745
  sudden approximation accuracy, coupled channel calcs. for scatt. 79—4873
  sudden decoupling approximations, for atom-surface scatt. 78—64437
  threshold and Lennard-Jones reson. and elastic lifetimes, corrugated wall and attractive well surface model 78—15275
  Ag (111) plane, specular refl. of He beams, Debye-Waller factor and surface Debye temp. 79—47580
  Ag, (111) surface, He impact, energy transfer isotropic Debye model 77—16443
  Ag (111) surface phonon dispersion, He atom scatt. meas. 80—75426
  Ag, Ne scatt. from (111) surface, double rainbow scatt. distrib. 78—80443
  Ag, of He, generalised Langevin theory 77—8700
  Ag surface, Ne scatt., rainbow effects and energy exchange, calc. 80—84825
  Ag surface, scatt. of He, Debye-Waller factors, expt. 80—60736
  Ag(111) surface, diffr. of He 78—39651
  Ag(111) surface, time of flight meas., of scattered Ar beams 79—95894
  Ar-ice (solid NH_3) impact, 2.4 keV, secondary electron emission from $H^+(H_2O)_n$ and $H^+(NH_3)_n$ 79—15580
  Au, adatom beam scatt. expts. on NaCl and KBr (100) surfaces 79—77924
  Au, reflection and penetration of 25 eV to 10 keV He, T and H atoms 77 - 59657
  C foil, impact of H, H abundance in emitted beam 78—35236
  CO adsorbed on Pd surface, Penning ionisation by metastable He beam, theory 80—60735
  Cu (001), inelastic scatt. of He atoms, 20K 79—8222
  Cu (001) surface, scatt. of He and Ne atoms at 20K 78—80451
  Cu, (100) surface, elastic scatt. of He 79—95892
  Cu (117) stepped surface, diffraction of He, 70 to 773K 80—35031
  Cu, blistering by He atoms, (10-20 keV), exam. of skin structure, thickness, He distribution and swelling 79—60412
  Cu, reflection and penetration of 25 eV to 10 keV He, T and H atoms 77 - 59657

atom-surface impact continued
  Cu, scattering of low energy He ions and atoms, elastic and inelastic effects 77—8708
  Cu surface, (100) coherent elastic scatt. of He, Ne, thermal attenuation 80—89105
  Cu surface, conditions for total refl. of low-energy atoms 79—19958
  Cu surface, secondary charge emission coeffs., low energy H^0 flux meas. 80—25509
  Cu, thermal displacement of surface atoms, elastic backscatt. of He atomic beam *(French)* 77—4709
  Cu-Be-O surface, $O(^5S)$ impact, secondary electron yield 78—58797
  D, adsorbed on graphite (0001), vibr. spectrum, at. beam scatt. obs. 80—92779
  Ge, film, elec. props., prep. by DC sputtering *(Japanese)* 79—78237
  Ge single cryst., atomic H interaction highly efficient electron accommodation *(Russian)* 79—78818
  Ge surface, Ar atoms scatt., energy accommodation coeffs. 77—90230
  H, adsorbed on graphite (0001), vibr. spectrum, at. beam scatt. obs. 80—92779
  H, in H_2 oscillator, unexcited transition freq. determ. 79—2749
  He atom-surface scattering pot., surface electron density depend. 80—104027
  ^{4}He, superfluid, ^{4}He atom scatt., quantum interference 79—99382
  K, Na, superthermal neutral beams impact on W surface, stimulated chemical reaction 77—9123
  KCl (001), water covered cold surface, H atom diffr. 77—66565
  Li, laser excited beam, Ta and Re surface ionis., quantum yield 79—87540
  LiF, ^{4}He scatt., selective adsorption induced intensity maxima 78—72667
  LiF, 63 meV He atom scatt., single Rayleigh phonon interaction 78—80447
  LiF (001), elastic and inelastic scatt. of He and Ne, selective adsorption 77—66564
  LiF (001), H and D beam scatt., specular bound state reson. struct. 79—52069
  LiF (001), He elastic scatt., hard corrugated surface model, GR Method 77—85863
  LiF (001), He scatt., corrugated wall model, GR method 77—63520
  LiF (001), He scatt., hard corrugated surface model, calc. methods 77—16447
  LiF (001), He scatt., sudden approximation accuracy, coupled channel calcs. 79—4873
  LiF (001), multiple Debye-Waller effects at selective adsorption in atom-surface scattering 80—76126
  LiF (001), scatt. of He(Ne), sudden decoupling approxs. 78—64437
  LiF (001), scatt. of Ne, coupled channel calcs., symmetry appls. 78—92156
  LiF (001), surface phonon obs. in He atom inelastic scatt. 80—80927
  LiF, (001) surface, diffractive scatt. of H atoms, 78K 80—76124
  LiF, (001) surface, He and Ne inelastic resonant scatt. assisted by phonons 77—73201
  LiF, He at. beam scatt., Lennard-Jones resons. and rel. displacements 77—1773
  LiF, He scatt., bound state reson. calc. 77—1779
  LiF, selective adsorption of ^{3}He and ^{4}He, atomic beam scatt. meas., binding energies 78—63935
  LiF surface, He atom inelastic scatt., phonon coupling 80—71554
  LiF type surface, He scatt., selective adsorption intensities, attractive corrugated wall model 79—28874
  LiF+He, bound state reson. data anal. 78—39644
  LiF(Cl)(Br) film, electron emission under metastable He and Ne atom impact 80—20747
  LiF(001), ethanol-covered, atomic H scatt. 77—31905
  LiF(001), He scattering, semiclassical treatment 77—20977
  MgO (001), atomic H scatt. 77—31905
  MgO, (001) surface, extremal scatt. of $H_2(HD)(D_2)$ 79—95891
  Mo [110], metastable He impact, secondary electron spectra 78—95642
  Mo, adsorption of CO, O_2, metastable He de-excitation spectroscopy and UPS study 80—34314
  Mo, refl. of metastable He atoms, O_2 adsorption effects 79—11493
  Mo surface, clean and gas covered, He* impact, deexcitation, pot. energy transfer mechanism 80—60743
  Mo surface, H^- production by low energy H atom bombardment 79—100006
  Mo surface, metastable He atom beam contamination by fast neutral atoms, effect on secondary emission 80—55253
  Na laser oriented atoms, refl. by non-disorienting surfaces, optical activity detect. 80—55252
  NaF, ^{4}He scattering, selective adsorption effects on diffr. beam intensity 77—12480
  NaF (001), H and D beam scatt., specular bound state reson. struct. 79—52069
  NaF, He atom scatt., Debye Waller effects 79—8218
  NaF, He atomic beam refl., selective adsorpt. transitions, band-struct. effects 77—11781
  NaF, selective adsorption of ^{3}He and ^{4}He, atomic beam scatt. meas., binding energies 78—63935
  NaF(Cl) film, electron emission under metastable He and Ne atom impact 80—20747
  Nb, blistering by He atoms, (10-20 keV), exam. of skin structure, thickness, He distribution and swelling 79—60412
  Nb, reflection and penetration of 25 eV to 10 keV He, T and H atoms 77—59657
  Ne atoms, surface investigations via beam spectrometery 77—28670
  Ni (100), clean and chalcogen-covered, electron ejection by metastable He atom impact 79—8217
  Ni (100) surface, electron spectra from He metastable beam impact 77—36334
  Ni (110), adsorbed H, adatom configuration, He diffr. study 80—103569
  Ni (110), clean and H saturated, structural investig. by He diffraction 79—86984
  Ni surface, Cs and K coated, survival probabilities of emerging H^- ions 80—45187
  Ni surface, mech. for reflection of protons at kilovolt energies 79—8215
  NiO (001), diffr. of monoenergetic He atoms 79—61487
  Pb, at. beam, interaction with low-temp. glass condensation surface 78—19626
  Pb, atomic beam impinging on mica and SiO in vac. deposition, thermal accommodation 79—77960
  Pd (111) surface, clean and CO covered, metastable He impact, electron emission, energy and ang. distrib. 80—60744

atom-surface impact continued
- Pt (997), terrace bending obs. from He beam scatt. 80–40202
- Pt, of Ar, gas surface interactions, 3-D generalised Langevin model appl. 80–107637
- Pt, of Xe, gas surface interactions, 3-D generalised Langevin model appl. 80–107637
- Pt surface, mean residence time and ionisation efficiency meas. of K 77–85874
- Pt(111) plane and stepped surfaces, H_2 interaction, bond breaking activity, model pot. 80–108744
- Pt(111), Xe direct inelastic scatt. with trapping-desorption scatt., vel. and ang. distribs. 80–16140
- Re surface, long range and temp.-depend. interaction with alkali metal atom, theory 80–59802
- Si (100) reconstructed surface struct. study using thermal energy He diffr. 80–60731
- Si (100) surface, diffr. of He atoms obs. 78–52609
- Si (111) 7×7, He at. beam diffr. obs. 79–33165
- SiO_2 film on Si substrate, Na transport caused by ion and atom impact 80–6682
- Ta, energy distrib. of secondary electrons during relax. of metastable inert gas atoms *(Russian)* 77–85861
- TaS_2(1T), surface CDW, obs. by atomic beam diffr. 80–39195
- W (110), ionisation of hyperthermal Na atoms, temp. depend. 80–50504
- W (110), Ne scatt., sudden approximation accuracy, coupled channel calcs. 79–4873
- W (110), scatt. of He(Ne), sudden decoupling approxs. 78–64437
- W (110), scatt. of Ne, coupled channel calcs., symmetry appls. 78–92156
- W (110), trapping probabilities and desorption kinetics of alkali atoms 77–62754
- W (112), He atom scatt., theory for stationary sinusoidal hard wall surface wall one-dimens. periodicity 78–92161
- W (112), He scattering theoretical interpretation of data 78–35241
- W, Ar beam direct inelastic scatt., vel. distrib. meas. 80–66351
- W, K atom beam impact, mean residence time of K^+ and ionisation efficiency 77–73208
- W, K atom beam impact on gas-covered surface, K^+ ion current peculiar decay 79–74045
- W, of Ar and Ne, generalised Langevin theory 77–8701
- W, polycryst., bombardment with Na and K ions, neutral component of scatt. 78–11047
- W, sorption of Ne and He, tangential momentum accommodation coeff. meas. by acoustic vel. and absorpt. obs. 80–66867
- W surface, clean and CO covered, He metastable atom bombard., secondary electron emission 79–47581
- W surface, Cs coated, survival probabilities of emerging H^- ions 80–45187
- W, thermal accommodation of He, two-phonon contribs., DWBA calcs. 79–95893
- W, trapping and desorption of alkali atoms on clean and O_2 covered (110) surface 77–11786
- WC_x, (3×5) struct. on W (110) surface, at. beam diffr. and scatt., surface characteris. 79–78819
- W(110) surface, trapping of K and Na atoms, trajectory calcs. 77–48295
- ZnS:Mn-H atom systems, surface physiochem. changes, radical recombination luminesc. investig. 79–56863

atomic absorption spectroscopy
- absolute atomic conc. determ. 77–36844
- acetylene flame, Na and MgO concs. meas., saturation vs. absorption spectroscopy 79–29425
- acetylene-N_2O flame, chem. equilib. rel. to AAS 77–4957
- advances and problems 79–39240
- aerosol, monodisperse, quantitative analysis using IR differential absorpt. analysis 79–24931
- aerosol sampling, revealed chemical heterogeneity 80–55970
- aerosols, urban, characterisation 77–41157
- AES trace analysis non-thermal excitation, comparison with AAS 80–30312
- air pollution, particulate matter, heavy metal analysis 77–41151
- air-acetylene flame, multichannel apparatus detect. limits using atomic absorpt. spectra 80–76586
- alkaline earth elements, determ., buffer action of La and Sr, mechanism *(Russian)* 79–29441
- analogue-digital convertor taking into account nonselective absorption 79–57331
- analysis instrumentation in clinical enzymology 78–88675
- analytical physico-chem. methods, characts. *(French)* 79–48033
- atmospheric aerosol, absolute element concs., PIXE and AAS, comparison 78–85237
- atmospheric constituents, spectral absorption patterns, detect. and estimation, anal. methods 77–87059
- atmospheric pollutants, quantitatively analysing spectroscopy by continuously scanned tunable dye laser 77–78486
- atomic absorption spectrophotometer, AAS 1N 78–37084
- atomic absorption spectrophotometer, two-channel, microcomputer-based, appls. 78–56926
- atomic absorption spectroscopy, transient signal recording, time const. control method 79–52855
- atomic spectrometry, using vidicon tube detectors, sensitivity 77–41695
- atomic vapour excitation temperature in graphite furnace AAS 78–7298
- atomisation, electrothermal and flame methods, for use in clinical and biochemical analysis 79–96398
- atomisation, in graphite ballast furnace, reliability improvement *(Russian)* 78–85279
- atomisation in graphite furnace with ballast 79–96389
- atomisation under pressure in graphite furnace AAS 78–11600
- automated atomic absorption spectrophotometer, operation and specifications *(Russian)* 78–27865
- automated trace analysis using injection method 79–34382
- automatic sampler, for flame at. absorption 78–65974
- background correction, design considerations 78–45719
- background correction, Zeeman effect based methods 78–27831
- background interference and measurement *(German)* 77–21454
- background light losses in complex alloy, metal anal. 77–12838
- background-corrected, factors affecting accuracy 77–36819
- bauxites, analysis, comparison of atomic absorpt., X-ray fluoresc. and other classical methods 80–89551
- bibliography, (July-Dec. 1977) 78–53276

atomic absorption spectroscopy continued
- bibliography, January-June 1978 78–95969
- bibliography, July-Dec. 1977 78–3403
- bibliography (Jan.-June 1979) 80–31441
- bibliography (July-Dec. 1978) 79–87888
- biological samples, background reduction using direction atomisation 79–74795
- biological samples, Be determ., flameless atomic absorption spectrometry *(Japanese)* 80–26428
- botanic reference materials, candidate standards, homogeneity testing, anal. methods 78–11594
- brine sulphate anal. by atomic absorpt. 80–89556
- burner system for atomic absorpt. spectrophotometers 80–73468
- calibration algorithm for improved accuracy 79–39233
- calibration curves, initial slope, expt. conditions effect *(German)* 77–16891
- calibration curves, theory *(Russian)* 77–21460
- capacitor dielectric fluid test and anal., quality assurance 78–80272
- cathode lamps for atomic absorpt. spectrometry, method of modifying used lamps 80–90898
- cathode preparation, electroplating method 79–43655
- cement, atomic absorption spectrometric determ. of Cu, Mn, Pb and Cr by direct atomisation *(Japanese)* 79–70413
- cement raw-material mix, main component determ. by atom absorption spectrophotometry 80–45615
- coins, ancient Greek, neutron activation and at. absorpt. anal. 78–8489
- combustible municipal solid waste, Sb and As determ. by AAS 78–85229
- complex matrices, mol. absorpt. spectra in premixed flames 79–92021
- continuous spectrum light source, for at. absorpt. anal. *(Russian)* 77–61136
- continuum source, selective spectral line modulation method 77–44520
- continuum source method, charact. conc. meas. 77–67501
- continuum source spectrometry with analogue data treatment for multielement analysis 78–3392
- data processing, using microcomputer 79–52794
- detector, for chromatographic systems, review 77–60138
- detector for gel chromatography, Mg-P_3 complexes determ. 79–87890
- development in USSR, 1965-1975, science metrics investig. 78–61104
- direct atomisation, in graphite furnace AAS, drift compensating digital peak leader appls. 78–68939
- discharge lamp, hollow cathode type, discharge excitation characts. obs. 80–42260
- discrete chemistry, new approach to water analysis 78–88674
- double-beam spectrometer for very low absorption coeffs. measurement 77–13801
- double-beam spectrophotometer operation and applications *(Russian)* 78–27864
- droplets produced by pneumatic nebulisers, size meas. method 80–71992
- electrodeless discharge lamps, pulsed RF excited, for at. absorpt. and at. fluoresc. spectrosc. 79–21816
- electrothermal atomisation, for absolute at. absorpt. anal. methods 78–85260
- electrothermal graphite braid atomiser use 79–34377
- equipment design, for anal. appls. *(Russian)* 77–70378
- equipment prototypes and capacity requirements *(Norwegian)* 77–56298
- filament in furnace atomisation 79–79322
- flame, improvements in methods for trace element analysis 79–16066
- flame, literature interpolation as possible source of error 77–70366
- flame, low temp., determ. of W, V, Mo, B, Al and Ca 80–30307
- flame, with discrete nebulization, automatically triggered digital integrator 80–35610
- flame atom trap for increased sensitivity 77–9148
- flame atomic absorption spectrometer, multielement, time multiplex multiple slit type 79–40617
- flame emission, atomic absorption, and atomic fluorescence spectrometry, review of literature 1975-1977 78–85224
- flame spectrometry, theoretical model 77–36803
- flame spectrometry interfs., elimination and control, theoretical anal. 80–81395
- flame spectroscopy, absorpt. and emission, analogue data processing system 77–36804
- flame spectroscopy, droplet size distrib., impact beads, mixer paddle and oxidant effects 80–93810
- flameless, improvements in cold vapour Hg and graphite rod atomisation methods 77–21442
- flameless, spectrometer modification for background correction 78–11581
- flameless AAS, anal. response shape and position 78–92545
- flameless atomisation systems, sensitivity enhancement by rigid W collar 78–35770
- flameless atomisers, diffusion process anal. 79–87925
- flames, temp., OH conc., spectrosc. determ. 77–32853
- fluid-analytical spectrophotometers *(Russian)* 78–27863
- flux-grown magnetic garnets, comp. anal. by AAS 78–92585
- furnace AAS, ultimate detection limit barrier 78–35761
- furnace at. absorpt. anal., computer-assisted, turnkey data system, natural water anal. appl. 77–77829
- furnace-flame atomiser, decrease in absorption changing from H-air to C-containing flame *(Russian)* 77–29082
- furnace-flame method, graphite boat, operational experience *(Russian)* 77–29080
- gas mixture, reacting, atom conc. reson. absorb. meas., microwave discharge lamp calibration 79–92032
- geological materials, multielement trace anal., solvent extraction-flame AAS method 78–7259
- glacier regelation ice chem. comp., indication of press. melting 78–61447
- glass 79–61919
- glow discharge, cathodic sputtering atomisation for AAS 78–44415
- graphite disc atomiser, for flameless atomic absorption spectrophotometer, exam. 78–54463
- graphite furnace, atom loss mechanism 78–3389
- graphite furnace, between-sample cleaning 79–87889
- graphite furnace, electrothermal atomisation 79–24852
- graphite furnace, mechanism of atom formation 77–21431
- graphite furnace AAS, atomisation from a platform 78–32877
- graphite furnace anal., autosampling system, timing circuit for baseline absorbance monitoring 77–73482

atomic absorption spectroscopy continued
  graphite furnace analysis, matrix interferences reduction with L'vov Platform, Pb analysis 79—92020
  graphite furnace atomic absorpt. spectrometry heated by capacitive discharge, determ. of elements 80—66892
  graphite furnace atomic absorption spectrometry, heating rates effects 79—39224
  graphite furnace atomisation and measurement 78—31715
  graphite furnace peak shape study using computer 80—21331
  graphite furnace-flame atomic absorption technique, for thermoanalytical investigs. 79—100477
  graphite thermal atomiser, sample vapour supply and removal rates meas. 78—29164
  graphite tubes, for at. absorpt. spectroscopy, pyrolytic coating method optimisation 78—76940
  Hadamard transform spectroscopy with computation and superposition procedure for multielement analysis 77—70376
  hadronic atoms, absorptive line shape 77—83767
  hair, biopsy material for trace elements in human body 79—83955
  high-intesnity arc, anal. appls. *(Russian)* 78—35772
  high-purity substances, analysis methods 79—39241
  high-purity water prep. system using disposable purification elements 77—52688
  high-solids samples, graphite furnace AAS, background correction 78—27834
  hollow cathode tubes noise levels for at. absorpt. spectroscopy, pulsed *(Russian)* 77—71385
  human tissue, Se determ. by thermal neutron activation analysis and atomic absorpt. spectrometry 79—88218
  hydrodesulphurisation catalysts, Co, Mo and Ni determ. by at absorpt. spectroscopy 77—9145
  illuminating system for double beam at. absorpt. spectrometer *(Russian)* 77—87850
  inductively coupled plasma and atomic absorption spectroscopy combined 80—104478
  inert gas mixture, collision induced light absorpt., density effects 77—42258
  interference by lithium salt mol. absorption in C tube atomiser, and flames *(Japanese)* 79—48018
  interference by potassium salt mol. absorption in C tube atomiser and flames *(Japanese)* 79—48019
  interference effects, in furnace AAS 78—48704
  internal standards, for anal. of samples atomised by sputtering 78—7251
  internal standards for sample introduction reproducibility 77—90666
  intracavity spectroscopy, spectrometer based on continuous jet dye laser 79—52831
  IR correlation process analyser, non-dispersive instrument 77—82628
  laser absorption polarising spectrometer, for meas. of small absorpt. coeffs. *(Russian)* 78—29175
  laser induced atomisation in graphite furnace 77—44566
  laser intracavity absorption for organics, analytical potential 79—34386
  laser microspectral analyser, LMA 10, combined atomic absorption and emission 79—79344
  laser-vaporised solid samples, AAS anal. 78—7252
  laterites, Venezuelan, analysis, comparison of atomic absorpt., X-ray fluoresc. and other classical methods 80—89551
  light source, Hg linewidth meas. *(Russian)* 78—4708
  line and total absorpt. comparison 80—11991
  matrix effects, in graphite furnace technique, furnace conditions effects 78—85230
  matrix effects on elemental sensitivity in graphite furnace AAS 77—90667
  metal layers, thin, atomic absorption analysis with laser atomisation 80—30308
  metal speciation applications 77—90665
  metal vaporisation, optical spectral methods of vapour press. meas., review 79—66381
  metallurgical analysis *(French)* 79—5241
  metals, atomic laser spectrosc. using cathode sputtering method 79—87917
  metals, determ. in water and organic materials, flameless atomic absorpt. spectrometry with wire loop atomiser 80—45586
  metals and alloys, thermodynamic props., evaporation, optical spectral method appls., review *(Russian)* 78—75822
  metals determ. in air particulates, graphite furnace method appl. 80—94134
  microcomputer based, 2-channel spectrometer 79—24864
  microcomputer control and data reduction, dual-channel double-beam spectrophotometer 78—35762
  microsampling nebulizer technique for premixed flame atomic spectrometry 79—34380
  modified Voigt function, speed dependent, for at. absorpt. spectrosc. 78—35765
  molar surface enamel, rat, Ca content determ. using AAS 1 spectrophotometer 80—56303
  multichannel apparatus for material analysis using atomic spectra 80—76586
  multicomponent deposition processes, monitoring and controlling techniques, review 78—11113
  multielement flameless atomic absorption spectrometer, multiple slit, time multiplex, design and performance 79—12859
  near IR absorption analysis, differential compensation method 78—80819
  noble metals anal. review 78—85264
  noise meas. in atomic absorpt. flame spectrometry, single and double beam instrum. comparison 80—76584
  non-spectral interference using graphite mini-tube furnaces 79—48028
  nonatomic absorpt. allowance for using opposite heat fluxes, Hg determ. appl. *(Russian)* 77—36853
  nonferrous metals, determination of harmful impurities 77—90673
  nonflame atomiser, programmed unit for at. absorpt. anal. 78—54462
  nonflame sample atomisation, thyristor thermostabiliser use 79—96388
  nonselective interferences 79—87900
  nuclear condensers coolant contamination control 77—373
  obsidian, from Koyukuk River, Alaska, elemental anal. 77—34062
  optimal signal recording, under pulse atomising conditions *(Russian)* 78—3436
  peak height and area measurement methods 77—40596
  photometric determination and control of solution components, automatic method 79—79350
  plasma, inductively coupled, atomisation cell, appls. 77—12839
  plasma atom conc. method *(Russian)* 77—56305

atomic absorption spectroscopy continued
  plasma emission spectroscopy, background reduction method using flame atomic absorpt. 79—16069
  plasma jet light source, intensity distribs., OH band rot. temp. 77—44555
  plasma source, inductively coupled, analyte excitation temp. and electron density distribs. 77—40592
  powdered samples blown into arc discharge, improvement of accuracy of spectral anal. *(Russian)* 77—32851
  powders, trace element determ. *(Russian)* 77—66783
  programmable multielement atomic absorption system 78—80803
  pulse aspiration sampling system, for flame AAS of small sample vols. 78—27838
  pulsed dye laser double beam spectrometer, instrumental noise sources 78—88662
  pulsed hollow cathode lamp, transient emission characts. in microsecond region for atomic absorption spectrophotometry *(Japanese)* 77—70365
  pulsed hollow cathode lamp characteristics 78—67530
  pulsed lamp supply, optical, elec. characts. 79—57329
  pulsed light sources, circuitry and characts. *(Russian)* 78—46740
  pulsed Nd laser, use in atomic absorpt. spectroscopy for direct anal. of metallic and nonmetallic solids 80—76582
  quartz, synthetic single crystal, impurity content 77—11583
  radio-frequency excited pulsed hollow-cathode lamp, absorpt. and emission characteristics 80—89550
  rainwater, multielement anal. 78—69512
  rare earth elements, and monoxides flame absorption spectra, dye laser amplified absorption method 77—29075
  rare earth oxides, Cu and Fe impurities at. absorpt. determ. 79—87905
  recorder timer control, pen overload protection systems, at. absorpt. appl. 77—73481
  refractory elements, atomisation and flame conditions for anal. *(Russian)* 79—29442
  refractory metal refining, at. absorpt. spectroscopy for continuous process control *(Russian)* 77—56302
  relative atomic transition probabilities of Na, Sc, Ti, Cr, Fe, Co and Ni 79—89642
  resonance monochromator detector with continuum source 79—83540
  review of advances in past 25 years 79—34381
  sample flow control, in flame AAS 78—11577
  sample introduction, high solids aerosol, for flame at. absorpt. 78—3396
  sampling system Auto 200^{TM}, adjustable read delay device 77—32846
  seawater trace element meas. *(French)* 77—41238
  sediment pollution by Hg and As, instrumental neutron activation and atomic abs. spectrometric anal. 80—16890
  selective spectral line modulation AAS 78—89546
  selectivity evaluation 80—89561
  self-scanned photodiode array spectrometer, for flame at. absorpt. meas. 78—70191
  separation and concentration techniques 79—87887
  sequential testing, screening method for detecting interferences in routine analysis 79—57340
  single-beam absorption-emission flame spectrophotometer design *(Russian)* 78—27866
  solid sample, method for anal. in flames 80—35614
  spectral absorption patterns, detect. and estimation, system appls. and design 77—87060
  spectral lamps, LSP type, construction and operating conditions *(Russian)* 79—50364
  spectral line recording in presence of intense background, techniques, appls. *(Russian)* 77—40613
  spectrometer control by microcomputer system 77—1958
  spectrometer with continuum source, wavelength modulated monochromator for spectral interference correction 77—77825
  spectrophotometer, dual wavelength, using pulsed hollow cathode lamp 77—40593
  spectrophotometer using Zeeman effect and polarisation characts. 77—90651
  spectrophotometric methods applied to pharmaceutical analysis 79—96397
  standard addition method, evaluation and optimisation 79—16058
  steel, low alloy, at. absorpt. anal. using electrically dispersed sample 79—74459
  steel sheet, surface anal. by ion etching and atomic absorpt. spectroscopy *(German)* 80—81377
  stream water, inorganic pollutant analysis 77—41102
  super high frequency discharge as atomiser *(Russian)* 77—86426
  Teflon sampling manifold for use with small injections 79—34383
  thyristor thermostabiliser for at. absorpt., spectroscopy with non-flame atomisation, power supply *(Russian)* 78—76977
  time and spatially resolved at. absorpt. anal. 80—40760
  trace elements, determ. in complex alloy chips using graphite furnace at. absorpt. 77—40582
  trace metal adsorption causing errors, prevention by competitive complexation 79—43651
  trace metal analysis in water, accuracy in AAS and AES using graphite furnace 78—69510
  transient signal recording, time const. control method 79—52855
  transition metal, determination in estuarine and sea water by at. absorpt. spectra 79—74557
  transitions, a-parameter and optical collisional cross-sections calcs. 77—83518
  tricresyl phosphate in gasoline, P determ. by at. absorpt. spectrometry 78—31729
  tubes design with hollow cathode, for Mo, Fe, and Si analysis *(Bulgarian)* 80—85232
  two-wave and dispersionless spectrophotometric systems *(Russian)* 78—27862
  UHF plasma use as atomiser 79—92027
  UV and visible spectra of solids using integrating sphere 80—61188
  vaporization and atomization of large particles in an acetylene/air flame 79—74445
  vidicon-echelle spectrometer with random access, design and eval. for multielement determs. in atomic absorpt. spectrometery 77—90652
  water, natural, trace metals, energy dispersive X-ray fluoresc., at absorpt. anals., comparison 77—60175
  water pollution by metals monitoring, instrument survey 79—74580
  water vapour, spectrochem. anal., effect on HF torch discharge *(Japanese)* 77—44554
  wavelength modulation spectrometry, computer modelling 77—63974
  X-ray fluorescence and at. absorpt. analysis 80—85229

atomic absorption spectroscopy continued
- Zeeman, appls. 80—76567
- Zeeman atomic absorption spectrosc. anal. curve shapes 80—22437
- Zeeman effect, using capacitively coupled RF spectral sources 77—61135
- Zeeman effect appls. 80—85245
- Zeeman effect appls. to atomic absorpt. spectrophotometer, development of spectral-line sources 80—76583
- Zeeman effect atomic absorpt. spectroscopy *(Japanese)* 80—35600
- Zeeman effect method, calibration curves 77—32866
- Zeeman effect method, mag. field strength determ. 77—63997
- Zeeman effect system, by Hitachi, Japan 77—53877
- Zeeman modulated, quantitative sensitivity *(Japanese)* 78—20124
- Zeeman modulated technique, appls., detect. limits 79—24876
- Zeeman modulation technique, line interferences 79—24877
- Zeeman spectroscopy, theory 79—43677
- Zeeman-modulated sources, RF-excited hollow-cathode lamps 78—85275
- Zeeman-modulated spectrometers with HF field modulation 79—57341
- Ag, development of standard specimen 77—90680
- Ag layers, thickness determ. by laser microprobe and flame atomic absorpt. 80—27355
- Al alloys, time and spatially resolved at. absorpt. anal. 80—40760
- Al, use of low temp. flame 80—30307
- As and other trace elements analysis, using vapour generation method 80—16745
- As conc. meas., column chromatography versus flameless atomic absorption spectrophotometry 80—55969
- As determination in rocks and soils by at. absorpt. 79—88475
- As determination in seaweed and related products, hydride generation system, at. absorpt. spectrometry 80—30294
- Au, determ. in rocks, minerals by at. absorpt. spectrometry 77—29067
- Au layers, thickness determ. by laser microprobe and flame atomic absorpt. 80—27355
- B, isotopic analysis, by AAS, using Ne-filled discharge lamp source 78—20097
- B, use of low temp. flame 80—30307
- $B+O_2(SO_2)(CO_2)(N_2O)$, gas phase rate consts., 300K, at. absorption obs. 79—83445
- Ba, determ. in seawater, matrix effects in graphite furnace AAS 78—85230
- BaO, determ. in glass, at. absorpt. method *(Polish)* 79—24872
- Be determ. in biological materials, flameless atomic absorption spectrometry *(Japanese)* 80—26428
- C atomizers, problems associated with atomization 79—34386
- Ca, determ. in lake sediments, by atomic absorption spectroscopy 78—95970
- Ca, use of low temp. flame 80—30307
- CaO, determ. in glass, at. absorpt. method *(Polish)* 79—24872
- Cd, determ. 78—27834
- Cd determ. in drinking water by graphite furnace at absorpt. anal. 80—55733
- Cd determ. in whole blood by atomic absorpt. spectroscopy 79—44071
- Cd, determ. using modified flameless at. absorpt. spectrophotometer 78—82044
- Cd, determination, in plant material, by atomic absorpt. spectroscopy 77—9143
- Cd I, absorpt. spectra, line and total absorpt. comparison 80—11991
- $Cd_xHg_{1-x}Te$, flameless atomic absorpt. anal. using interactive computer processing 79—66380
- Co alloys, determination of Ni and Co by flameless atomic absorption spectrophotometry 77—90674
- Co base heat resistant alloy, determ. of sub-ppm levels of Ag by graphite furnace atomic absorption spectrometry 78—48730
- Co, determ. using hollow sintered cathode spectral lamp *(Rumanian)* 79—17509
- Co-base heat resistant alloy, Bi and Pb trace quantity determ. with heated graphite atomizer 78—15749
- Cr, atomic absorption anal., internal standards for samples atomised by sputtering 78—7251
- Cr in urine, determ. by electrothermal atomic absorpt. spectrophotometry 80—61175
- Cu alloys, time and spatially resolved at. absorpt. anal. 80—40760
- Cu, atomic absorption anal., internal standards for samples atomised by sputtering 78—7251
- Cu, determ. 78—27834
- Cu, determ. in $Cu(NO_3)_2$ soln., by flameless at. absorpt. 77—40596
- Cu determination in serum/tissue specimens using flameless atomic absorption spectroscopy, effects of sample prep. and matrix 80—98200
- Cu, determination of Ni and Co by flameless atomic absorption spectrophotometry 77—90674
- Cu impurity in rare earth oxides, determ. 79—87905
- Cu, in powder rock samples, determ. using graphite capsule flame atomiser *(Russian)* 78—85278
- Cu-Fe-Mn-Ni-Pb-Zn copper based alloys optimisation of atomic absorption analysis 77—56274
- $CuInS_2$ films, RF sputtered, growth and props. 80—80124
- ErD_2 thin film, degradation during film processing, investigation 80—101047
- ErT_2, film, surface oxide form. and interfacial metal loss, AAS, XES 78—31733
- $F_2+SiH_4(SiD_4)(Si)$, chemilum., at. absorption, and laser-induced fluoresc. obs. 80—3315
- Fe, atomic absorption anal., internal standards for samples, atomised by sputtering 78—7251
- Fe determ. in blood serum using AAS 1 at. absorpt. spectrophotometer 77—48706
- Fe, determ. in Venezuelan laterites, interference-free at. absorpt. method 78—31728
- Fe, dterm. using hollow sintered cathode spectral lamp *(Rumanian)* 79—17509
- Fe impurity in rare earth oxides, determ. 79—87905
- Fe in seawater, graphite furnace atomic absorption spectroscopy determ. 80—40768
- Fe, purification, recrystn. temp. and elec. resistivity *(Japanese)* 80—100780
- Fe-Cu (75 ppm), internal oxidation, local struct. determ. by EXAFS 80—25916
- Fe-Ni electrodeposit, sectional analyses and impurities *(Japanese)* 80—21350
- GaAs, trace element conc. meas. by Zeeman atomic absorpt. spectroscopy 80—29046

atomic absorption spectroscopy continued
- $Ge(3^3P_0)+O_2(Cl_2)(COS)(N_2O)(NO_2)(NO+Ar)$ oxidation reacts., gas phase, kinetics 78—92468
- H , Rydberg consts., saturated absorpt., spectroscopy meas. 80—105604
- H and D, UV lamp, microwave discharge, Lyman-α line shapes 79—80698
- Hg, background absorpt. calc. *(Russian)* 79—52860
- Hg, determ., in fresh and saline waters, automated UV digestion-AAS method 78—44414
- Hg, determ. in drinking water, surface water and sewage effluent 79—92103
- Hg, determ. in water samples, error anal. 78—69519
- Hg determination by cold vapour at. absorpt. spectroscopy, effect of sorption on sensitivity 79—52829
- Hg resonance line, 253.7 nm for atomic absorpt. meas. 80—78556
- $I(5^2P_{1/2})+HBr$, reactive and inelastic channels rate, temp. depend., AAS obs. 78—35657
- I, stable conc. meas. using ^{139}Ce, absorpt.-edge transmission technique, biomedical appl. 80—56194
- K-Cs solution, activity and saturated vapour press. of Cs, reson. line absorpt. obs. 77—51509
- $Li,Na/PO_3,F$ and $Li,K/PO_3,F$ systems, low melting-point comps. for electrodeposition appl. 79—43662
- Li, at. emission obs. using modified graphite furnace at. absorpt. spectrometer 78—31727
- Li_2C_2, heat of formation, at. absorpt. spectrometric determ. *(Russian)* 78—15699
- $Mg+O_2 \rightleftharpoons MgO+O$, shock-tube study of evap. and oxidation kinetics 80—16651
- MgO, determ. in glass, at. absorpt. method *(Polish)* 79—24872
- Mn, determ. by AAS, interference effects related to atomisation methods 79—83521
- Mn, determination, in gasoline, by AAS using N_2O-H_2 flame, calibration methods 78—15729
- Mn in seawater, graphite furnace atomic absorption spectroscopy determ. 80—40768
- Mo, determination of Ni and Co by flameless atomic absorption spectrophotometry 77—90674
- Mo, use of low temp. flame 80—30307
- Na, detection limit, using CW dye laser spectroscopy *(Japanese)* 78—44435
- Na, flame absorption and fluorescence, laser saturation broadening 78—88661
- Na intracavity atomic beam, detect. by dye laser spectral narrowing 79—55159
- Na, quantitative detect. of atomic absorpt. by intracavity dye laser quenching 77—36817
- Na_2O-CaO glass, atomic absorption spectroscopy 79—43656
- Ni, atomic absorption anal., internal standards for samples atomised by sputtering 78—7251
- Ni base heat resistant alloy, determ. of sub-ppm levels of Ag by graphite furnace atomic absorption spectrometry 78—48730
- Ni, determ. in serum, matrix effects in graphite furnace AAS 78—85230
- Ni, determ. using hollow sintered cathode spectral lamp *(Rumanian)* 79—17509
- Ni, determination, in heavy crude oil, by at. absorpt. spectroscopy 77—52681
- Ni layers, thickness determ. by laser microprobe and flame atomic absorpt. 80—27355
- Ni-base heat resistant alloy, Bi and Pb trace quantity determ. with heated graphite atomizer 78—15749
- Ni-Co film, anal. of main component by atomic absorpt. spectrophotometry 77—70381
- Ni-Fe film, anal. of main component by atomic absorpt. spectrophotometry 77—70381
- Ni-Fe-Co(Mo) films, anal. of main component by atomic absorpt. spectrophotometry 77—70381
- NiZn ferrites, comp., X-ray diffr. and saturation magnetisation obs. 78—18617
- O_3, laser-induced photolysis, reactions of $O(^3P)$, $O(^1D)$ and $O_2(^1\Delta)$ 80—11928
- OCSe, quantum yields for Se, $^1S_0$, $^1D_2$, and $^3P_{0,1,2}$ atoms determ. in photolysis, lifetime and quenching rate meas. 80—97741
- P, determ. in organic media, using at. absorption with graphite atomiser, sample prep. 78—31729
- Pb alloys, time and spatially resolved at. absorpt. anal. 80—40760
- Pb, determ. 78—27834
- Pb, determ. in steel wire, AAS determ. 78—68939
- Pb determination in Earth materials by at. absorpt. 79—88035
- Pb, in powder rock samples, determ. using graphite capsule flame atomiser *(Russian)* 78—85278
- Pb micro fall-out novel appl. 78—49125
- Pb traces in human blood plasma, atomic absorpt. anal., nonspecific absorpt. correction using Zeeman effect 80—76881
- SO_4^{2-}, in natural water, determ. by at. absorpt. spectroscopy 77—40595
- Se, determ., matrix effects in graphite furnace AAS 78—85230
- SeH_2, atomisation in cool H_2-O_2 flame burning in quartz tube atomiser 80—76581
- Si:P, determ. of P content in high-purity Si using meas. of Mo in 12-molybdophosphoric acid by NAA and AAS 80—15148
- SiO_2 bricks, quartz estimation using IR spectra 78—48718
- SiO_2-B_2O_3-Na_2O-K_2O system glass, phase separated, loss of oxides during acid leaching, atomic absorpt. anal. 79—11716
- SnI, line absorpt. method use for SVP meas. of Sn 80—55747
- $Sn(4^3P_0)+O_2(Cl_2)(COS)(N_2O)(NO_2)(NO+Ar)$ oxidation reacts., gas phase, kinetics 78—92468
- Ta foil lining of graphite furnace, at. spectrosc. 78—74078
- Ta treated, graphite atomiser tubes, for high temp. AAS 78—73093
- Te I, UV line rel. oscill. strengths and unexcited atom conc., AAS meas. *(Russian)* 78—31749
- U, in water, determ. by AAS after ion exchange preconcentration 78—85231
- V, use of low temp. flame 80—30307
- W, at. absorpt. anal. using electrically dispersed sample 79—74459
- W filaments as electrothermal atomisers 78—27860
- W filaments as electrothermal atomisers, choice of solvent, gases and nebuliser assembly 78—44432
- W filaments as electrothermal atomisers, design of atomiser and power supply 78—44433
- W filaments on electrothermal atomiser, atomic absorption spectrophotometry appl. 78—86346

atomic absorption spectroscopy continued
W, use of low temp. flame 80–30307
Zn, determ. in acetone, by AAS being W filament electrothermal atomiser 78–86346
Zn I, absorpt. spectra, line and total absorpt. comparison 80–11991
Zn, in Cu alloys, determ. by at. absorpt. spectroscopy *(Russian)* 78–23998
Zn in seawater, graphite furnace atomic absorption spectroscopy deter. 80–40768

atomic beam electric resonance
phase modulation *(Chinese)* 80–37801
weak neutral electron-nucleon interaction, atomic-beam reson. expt., feasibility 77–88602
^{161,163}Dy, hyperfine struct. and hyperfine anomaly for fine transitions, high resolution meas. 77–88416
H^- resonances in electric field 80–63607

atomic beam magnetic resonance
atomic and laser spectroscopy, book 77–79554
laser-RF double reson. spectroscopy of nucl. quadrupole moments, ^{55}Mn and ^{50}V appls. 80–57682
at Middle East Technical University, Turkey 78–16824
on-line hyperfine struct. meas. in short lived nuclides 78–25379
semi-classical equations of motion, soln. by transform. to rot. co-ordinate frames 79–35586
time resolved ESR, time profile meas. and anal. 77–5878
Ag beam mag. resonance apparatus as freq. standard, features 78–89458
Ag-beam mag. resonance apparatus as freq. standard, features 79–21712
As, neutron-deficient isotopes, nuclear spin meas. by at. beam mag. resonance 77–18386
^{70}As, hyperfine struct. investig. using at. beam mag. reson. 77–22933
^{135,137}Ba, HFS of metastable 6s5d configs. 79–49971
Ba, atomic beam and resonance spectroscopy 80–58180
Ba, hyperfine structure of metastable states, atomic-beam mag. reson. with laser detection exam. 77–79558
Ba I, isotope shifts, hyperfine struct., neutron deficient nuclei, laser resonance fluorescence study 79–72436
^{43}Ca, atomic beam and resonance spectroscopy 80–58180
^{43}Ca, nucl. quadrupole moment, HFS in at. beam mag. reson. 79–63940
He fine structure interval 2^3P_0-2^3P_2, optical microwave atomic beam mag. resonance meas. 80–102585
^{3}He+^{4}He, metastability exchange cross-sections, coherent transfer in 2^3S_1-state 79–89743
^{4}He, electronic g_J-value of 2^3S_1 state, by atomic beam mag. reson. method 77–23446
^{179}Hf, hyperfine struct. in ground multiplet ^{3}F and nucl. quadrupole moments of ^{177}Hf and ^{179}Hf 77–83520
Ir, A=191, 193, hyperfine struct. of low lying fine struct. levels, hyperfine anomaly, electronic g-factor 78–66214
^{55}Mn, metastable states, hyperfine struct., laser RF double reson. study 79–72260
O($^5S_2$) metastable state g_J factor, TOF at. beam mag. reson. obs., rel. to He(^{3}S) 79–3593
Ru, A=99, 101, hyperfine struct. and nucl. moments determ. 77–26575
Tl atomic beam tubes, freq. pulling effect with mag. double reson. 80–37802
Tl, ground-state hyperfine struct. tensor polarisability 77–6708
^{47}V spin values and level scheme recalc. 78–78256
^{48}V spin values by atomic beam mag. resonance method 78–78256
^{50}V quadrupole moment and atomic ground state hyperfine intervals, laser spectroscopic determ. 79–89234
W, at. beam mag. reson., for HFS and contact interaction 79–68207
^{91}Zr, hyperfine struct. and nucl. elec. quadrupole moment. at. beam mag. reson. meas. 78–55133

atomic beams
see also atom-molecule reactions; atom-surface impact; atomic beam electric resonance; atomic beam magnetic resonance; particle velocity analysis; plasma-beam interactions
alkali beam source, three-stage oven design 77–42443
atomic frequency standard, improved system construction 78–45599
beam-foil spectroscopy, improved light collection from fast at. beams 77–75337
chemi-ionisation reactions of Ca, Sr, Ba, and Yb with halogens and interhalogens 77–32791
chemiluminescence, beam-gas, kinetics of metastable excited state products 77–56231
cluster beam, nozzle flow formation and detection, high energy beam 80–5638
coaxial atomic and light beams, simultaneous self-focusing and self channelling *(Russian)* 80–28292
coaxial electron and atomic beams sequential multiple scatterings, random walk approach 80–99574
deceleration and monochromatisation laser radiation press. 80–102491
deflection, by reson. standing EM wave 79–26959
elastic scattering, laboratory differential cross section data anal. via Monte Carlo averaging 78–21997
emission in uniaxial cryst., arbitrary beam-optical axis angle, energy spectrum 77–57923
excited atoms, merging-beams experiments 80–63789
excited state processes, collision rates obs. using single at. or mol. beam 78–13567
fast, collisional laser spectroscopy 78–37078
fast atomic beam, optical reson. detect. by at. fluoresc. 80–102479
focusing by reson. radiation press., quantum fluctuations influence 80–58217
focusing with laser beam, Na beam and dipole forces 79–7066
halogens, supersonic atomic and mol. nozzle beam source 77–31028
He, Rydberg, series transitions, opto-galvanic spectroscopy 79–54779
high resolution spectroscopy of fast beams 78–89557
high-flux beam source for He, Ne and Ar metastable atoms 80–58416
high-temperature beam source, employing radiant heating 78–330
inert gas, metastable composition of inert gas beam from ion-neutral reaction 77–29008
intense neutral beam, species composition meas. method 80–308
isotope separation, at. and mol. beams in nonuniform mag. and laser fields *(Russian)* 77–6960
laser fluorescent detection of single atoms *(Russian)* 78–1108
laser spectroscopy, high-resolution *(Dutch)* 79–50166

atomic beams continued
laser spectroscopy using atomic and molecular beams *(Japanese)* 79–35841
laser-excited atoms deflection by elec. field, isotope separation appl. 78–955
laser-surface impact, on metal surface, atom vel. distrib. 80–5637
magnetic resonance system for on-line hyperfine struct. meas. in short lived nuclides 78–25379
in magnetically confined afterglow, technique for ion+atom cross sections determ. 77–34750
maser with beam of inflying atoms, spectral line broadening mechanism 80–106503
metastable atoms, improve accuracy measurement atomic fine structure constant, electromagnetic units appl. 77–68105
microwave power relative changes meas., appl. to H Lamb shift meas. 77–75336
microwave-atomic beam resonance interactions, standing wave effects 78–41985
momentum distrib. modification by travelling wave reson. light field 79–72280
Na atomic beam focusing and defocusing using reson. radiation press. 80–47143
negative ion stripping, at. beam form. 77–6926
neutral beam armour for Doublet III vacuum vessel 80–95462
neutral beam dynamics, paraxial approximation, single particle motion across magnetic fields 78–29890
neutral beam injecto cryogenic pumping panel chevron baffles, black coating materials, selection 80–95456
neutral beam injector for Doublet III, material vacuum props. 80–95457
neutral beam injector vacuum system transient simulation anal. 80–95453
neutral beam injectors, fast, for TFR 77–76140
neutral beam injectors, multi-aperture extraction systems 80–42301
neutral particle beam, controlled energy distrib., prod. method 78–78038
neutral-beam divergence due to imperfect magnetic shielding 78–78489
nuclear spin meas. of short lived isotopes of Cs, Au, Rb 77–22882
number fluctuation effect on intensity correlations in resonance fluorescence, photon antibunching 78–50499
optical nutation and free precession, laser-atomic beam reson. fluoresc. 77–18837
polarised atomic H beam intensities, effect of dissociator nozzle cooling 78–16895
population inversion, anomalous resonance-radiation press. 80–52946
Princeton Cyclotron data acquisition system 80–102415
proton beam position monitor, based on detection of wall currents 79–58675
quantum state selected atomic and molecular beams production, developments in techniques 80–63871
Ramsey separated oscillatory field method, two-freq. excitation 78–36974
recirculating atomic beam oven 78–41374
refractive elements, magnetic resonance studies, nuclear spin and hyperfine structure meas. 79–776
resonance fluorescence, multiat. and transit-time effects on photon-correlation meas. 78–86812
saturated absorption optical Ramsey fringes 79–54204
separation by light press. in isotope-separation setup 80–52943
single atom photon burst detection in high resolution laser fluoresc. spectroscopy with atomic beam 79–72446
spectroscopy, two-freq. separated oscillating fields technique 79–21715
spin transition, nonadiabatic, in time-depend. mag. field 80–9576
supersonic beam production using microwave discharge source 79–80720
supersonic jet beam, seeded with CsF, (LiF), vibr. relax. 78–37716
surface analysis, atomic beam scatt., SIMS, and vibr. spectra, book contrib. 79–42357
surface reactions, possible expts. on Space Shuttle 78–35243
target for ion-atom collision studies 78–70971
tube with laser pump, interaction eqns. *(Russian)* 78–74801
two frequency separated oscill. fields method for beam interrogation 78–89596
vapour absorption cells and beam generating ovens for synchrotron radiation spectroscopy 78–66688
velocity, intensity and particle density, mass spectrometer determination 79–67428
velocity regulation and meas., using Doppler tuned photon-atom interaction 77–19110
Ar, clusters in supersonic beam, electron diffr. study 80–5655
Ba (5d6p)$^3D_3$ state, lifetime meas. by dye laser spectrosc. 80–78577
Ba$^+$, optical pumping and saturable absorpt. of fast ion beam superimposed on continuous laser beam *(French)* 78–5179
Ba+HCl, beam-gas reaction, multiphoton ionisation, product identification 78–23946
BaI resonance transitions, hyperfine struct. and isotope shifts, atomic beam laser spectroscopy 80–102141
Ca, time-of-flight spectrum using pulsed tunable laser fluoresc. detect. 77–49804
Cs atomic beam frequency standard performance and environmental effects 77–37858
Cs atomic beam tube operation at HFS level transition in absence of Zeeman splitting 77–82482
Cs atomic beam tube velocity distributions 77–37856
Cs atomic clock using laser optical pumping of Cs beam 80–101785
Cs atoms, pulsed high-density source 78–17825
Cs beam clock development for satellites 78–57910
Cs beam frequency standards, quadrupole and hexapole magnet combination 77–5813
Cs beam frequency standard errors due to excitation asymmetries 77–5816
Cs beam frequency standard design for satellites 78–57911
Cs beam frequency standard drift and noise performance rel. to velocity distributions 78–57912
Cs, beam tube frequency standard design and construction 79–54103
Cs dual atomic beam tube performance 77–37857
Cs freq. standard, angular distribution of atomic flux diffusing from rectangular channels 77–87744
Cs, hyperfine optical pumping, appls. 77–75108
Cs, optical pumping and detection of 0-0 transition 79–18158
Cs, pulsed high-density source, comments 80–37123
^{A}Cs, A=133, 137-139, hyperfine struct., isotope shifts, nuclear moments and radii, laser spectroscopy 79–10071
D, polarised beam source, Crypol 2 79–63324

atomic beams continued
- D^-, neutral beam production for plasma injection heating research 77−76118
- H, $2^2S_{1/2}$ state F=1 hyperfine component, Majorana transitions, LZS model 77−57959
- H, arc-heated high-intensity source 77−3493
- H atomic frequency standard and maser development by NASA 77−37861
- H, beam, $2^2S_{1/2}$ metastabld ats., nonadiabatic transition in mag. field 78−55157
- H beam, 3 to 15 keV, system using voltage pulse generator 79−18315
- H, beam prod. at. 90 to 500 eV from surface plasma source 80−38729
- H beam production in maser dissociator, performance characts. 78−87034
- H, charge transfer cross sections in gases and vapours, 10 eV to 10 keV, graphs and tables 80−32824
- H, cooled microwave discharge source 78−5373
- H, D, polarised atoms, cryogenic source 78−5079
- H, flux meas., detect. efficiency of resist. strip mag. electron multiplier particle-counting system 77−10552
- H, for atomic clock, prod. in H_2 dissociator, AES obs. of glass envelope degradation 77−61876
- H, highly excited, CW source using Doppler-tuned IR radiation 77−27204
- H isotopes, transition radiation from neutral beams, beam foil ionization 79−18299
- H, low temp., direct determ. of temp. and density 80−14875
- H, metastable 2s state, detector suitable for time-of-flight studies 77−3492
- H, microwave discharge source, extended cavity design 79−67427
- H, optical diagnostics of high-power neutral beam 79−17556
- H polarised beam, possible use as bombardment target 77−34495
- H, polarised beam source, Crypol 2 79−63324
- H, spin-aligned proposed production method 79−55003
- H^0, γ-ray yield curves from $^{27}Al(p,\gamma)$ 79−3530
- H^+ beam, control using laser radiation 79−27112
- $H^+ + H^-$, merged beams, double charge transfer cross section 79−22818
- H_α and H_β spectral profiles from neutral beams and plasmas in high mag. fields 80−83999
- ^2H, 120 keV multi-megawatt neutral beam source 77−83357
- He beam, fast, formed by 25-90 keV He^+ beam neutralisation, 2^3S population 79−31740
- He beam, highly expanded free jet, quantum and intermol. pot. effects 77−61823
- He beam charge fraction, emerging from solid 80−9716
- He, high-flux fast neutral beam source 78−54507
- He, high-intensity metastable atoms beam with good vel. resolution 77−14609
- He metastable beam, form. by alkali metal vap. charge exchange, composition 79−89775
- He, metastable beam source for surface spectroscopy 77−36334
- He, produced from nozzle flow, with high speed ratios, theory 80−5636
- He, skimmed from freejet zone of silence, speed ratios above 300 80−5635
- ^4He, velocity regulation and meas., using Doppler tuned photon-atom interaction 77−19110
- I, highly stable optical freq. standard 79−35685
- K atom clusters, cluster beam Stern-Gerlach mag. deflection 78−54504
- K atomic beam form. by charge transfer for ion-pair form. expts. 79−59555
- Kr, partially metastable, composition, charge exchange 79−85914
- Li, spin-polarisation by dual-freq. optical pumping 80−43003
- Li/Li_2 supersonic nozzle beam characts. by spectroscopic techniques 78−55255
- N, associative ionisation, merging beams experiment 80−63789
- Na atoms cooling by resonant laser radiation *(Russian)* 80−74155
- Na beam, associative ionisation, resonance fluoresence 79−98215
- Na beam, velocity spectrum determ. from Doppler shifted fluoresc. meas. 77−3210
- Na beam deflection by reson. standing wave radiation 79−98056
- Na beam deflection by reson. standing wave radiation 80−52945
- Na, low-consumption source with recycling oven 78−5376
- Na neutral atom beam, focusing and defocusing forces, radiation press. from CW dye laser 80−52944
- ^ANa, A=21-31, hyperfine struct., mag. moments and isotope shifts, laser spectroscopy 79−10072
- Ne beam, highly expanded free jet, quantum and intermol. pot. effects 77−61823
- Ne, beam spectrometer for surface investigations 77−28670
- O, cooled microwave discharge source 78−5373
- $O+Cl_2$, reactive scatt. in supersonic at. beam 79−36754
- $O+Cs_2$, reactive scatt. in supersonic at. beam 79−36753
- O_2 supersonic nozzle beam source development 80−58016
- $O(^1D)$ metastable beam form. in O^-+inert gas scatt. 80−32829
- ^{201}Pb, nuclear spin, metastable atomic states, hyperfine struct. meas. 78−25110
- ^{203}Pb, nuclear spin, metastable atomic states, hyperfine struct. meas. 78−25110
- Rb, high lying Rydberg states, atomic beam laser spectra 79−94101
- SmI, laser atomic beam spectroscopy, isotope shifts, hyperfine struct., transitions 80−102468
- Tm I, hyperfine struct., high resolution spectrosc. meas. 80−87238

atomic clocks
- *see also frequency measurement; time measurement*
- 1 metre primary Cs clocks, design and performance 80−98894
- 31st Annual Frequency Control Symposium, Atlantic City (1977) 78−57905
- absolute motion, detection from atomic timekeeping data 80−13045
- accelerating atomic clock synchronisation by radiowave propag., one-way Doppler effects 80−13044
- atomic frequency standard, optically pumped, buffer gas mixture optimisation 77−37859
- beam interrogation in Ramsey cavity, two freq. separated oscillating fields technique 78−89596
- Cs atomic-beam resonator, fractional freq. stabilities, time, freq. and physical measurement 79−26038
- Cs primary clock stand CS1, uncertainty eval. 80−98895
- design principles and characteristics of freq. and time standards, radiation effects 77−22533
- electronic-based timing systems, time standards 79−85129

atomic clocks continued
- frequency control 32nd Annual Symposium, Atlantic City (1978) 79−54100
- frequency standard prediction error analysis 78−57906
- frequency standards, transfer of freq. stability to quartz-crystal resonator 80−17927
- frequency standards using divergent beams, stability limits 79−26037
- fundamental time references, Cs clock assembly description *(German)* 80−52170
- GDR atomic time scale 80−98892
- gravitational shift of Earth, meas. by atomic-time-scale comparison 77−33925
- International Atomic Time, role of primary standards 78−89459
- International Atomic Time fluctuations, autoregressive integrated moving average model 77−57297
- International time and freq. comparison using Loran-C radio waves *(Japanese)* 78−81951
- ion-storage microwave and optical frequency standards 79−54101
- long-term frequency variations heuristic model 77−37854
- Majorana effect on atomic frequency standards 80−98897
- maser oscillator, thermal noise effect meas. on amplitude of oscillation 80−98898
- metrological Cs frequency standard MTs-1, description 77−79063
- noise in standard frequency sources 80−98899
- NTS-2 satellite Cs frequency standard stability estimates 79−54110
- phase and frequency instabilities in precision frequency sources, characterisation and mathematical models 79−2750
- principles, synchronisation, relativity theory *(Hungarian)* 77−67277
- quantum clocks, time meas., teaching 80−90632
- quantum freq. standards, output signal sidebands/resonator detuning effects on accuracy 77−87743
- quantum frequency store and Cs atomic transition frequency comparison system 77−79064
- quantum mechanically treated atomic clock in curved space time 78−54271
- Rb atomic resonator, fractional freq. stabilities, time, freq. and physical measurement 79−26038
- reference frequency stability transfer to quartz crystal oscillator 79−54108
- regulating unit, synchronisation with atomic clock, TN DCF-77 *(German)* 77−74374
- relativity experiments with clocks 80−46950
- remote synchronisation using injection laser diodes 77−82493
- Rydberg atom microwave and far IR spectroscopy 80−63564
- saturated absorption optical Ramsey fringes 79−54204
- standard time/freq. service in East Germany *(German)* 78−93658
- standards development at Shanghai Observatory, China 80−105617
- standards of time and length 77−13734
- Symphonie geostationary satellite, time transfer link for atomic clock synchronisation 80−47038
- synchronisation, VLBI obs. 78−29092
- synchronised technique, SIRIO satellite signals experiment *(Italian)* 79−2751
- time and frequency, conf., Helsinki, Finland (Aug. 1978) 80−46728
- time measurement, errors, accuracy of watches and clocks, time standard 80−90821
- time scale instability, contrib. of computation algorithm 80−98890
- time scale realisation models and predictions 78−57907
- time-freq. secondary standard comparison 77−87737
- unbiased clock variance calc. in uncalibrated atomic scale algorithms 80−105620
- US Naval Observatory clock time scale 78−89460
- USA Naval Observatory clock time scales, algorithm 79−21716
- USSR and E.German time scale comparison by transportable atomic clocks and TV signals 77−79067
- USSR State Standard of time and frequency 77−79062
- USSR state time and frequency standards *(Russian)* 78−161
- Ag beam mag. resonance apparatus as freq. standard, features 78−89458
- Ag-beam mag. resonance apparatus as freq. standard, features 79−21712
- CS beam freq. standard, new dipole beam optic 80−98896
- Cs atomic beam frequency standard performance and environmental effects 77−37858
- Cs atomic beam tube operation at HFS level transition in absence of Zeeman splitting 77−82482
- Cs atomic beam tube velocity distributions 77−37856
- Cs atomic clock using laser optical pumping of Cs beam 80−101785
- Cs atomic time standard data combination 77−5814
- Cs beam atomic freq. standards, Millman effect on freq. shift 78−32797
- Cs beam clock development for satellites 78−57910
- Cs beam clock meas. in test of general relativity, potential blue shift expt. 79−12704
- Cs beam deflection system for time and freq. primary standard 78−89453
- Cs beam freq. standard research at PTB, beam optics, Majorana transitions 79−21709
- Cs beam freq. standards, freq. offset due to spectral impurities 78−89455
- Cs beam freq. standards, freq. offset due to spectral impurities 79−21710
- Cs beam frequency standard, Millman effect origin and expt. determination 77−5810
- Cs beam frequency standards, quadrupole and hexapole magnet combination 77−5813
- Cs beam frequency standard errors due to excitation asymmetries 77−5816
- Cs beam oscillator, ambient temp. effects at Tokyo Astronomical Observatory 77−13245
- Cs beam standard, Ramsey cavity and beam optics design, expt. 78−89456
- Cs beam standard at Radio Research Lab., Japan 79−21714
- Cs beam time/freq. standard, future prospects 77−74371
- Cs, beam tube frequency standard design and construction 79−54103
- Cs clock, laser synchronisation between observatories of Paris and San Fernando *(French)* 78−89461
- Cs controlled digital clocks for high precision time meas. *(German)* 78−77871
- Cs dual atomic beam tube performance 77−37857
- Cs, environmental effects on rate in astronomical observatories 79−16833

atomic clocks continued
Cs, experiments to reduce cavity phase shift errors in the Cs beam tube 80−98893
Cs, for receiver-controlled frequency references 79−6099
Cs freq. standard, angular distribution of atomic flux diffusing from rectangular channels 77−87744
Cs freq. standard, error due to second order Doppler shift 77−87745
Cs frequency standard, construction of improved system (NRLM-II) 78−45599
Cs long beam primary clock, accuracy, reliability 78−89454
Cs optically pumped frequency standard stability limitations 79−54104
Cs, primary, time standards and scales generation 78−41283
Cs primary freq. standard, mag. shielding case for screening terrestrial mag. field *(Japanese)* 77−22582
Cs, primary frequency standard, developments at PTB 77−17942
Cs primary standard, TAI freq. estimation 77−17952
Cs primary standard operation limitations 77−5812
Cs, primary standard operation, limitations 77−17951
CsV, long-beam primary standard, continuous operation, concept 79−21711
CsV, performance and operation 77−107
CsV primary clock performance of NRC 77−74370
^{133}Cs, freq. standard, optimum conditions for population inversion for 0-0 transition 80−78824
H, collision-dependent frequency shift 80−98871
H frequency standard and maser development by NASA 77−37861
H frequency standard undisturbed transition evaluation 77−79066
H generator, freq. shift due to atomic collisions with storage flask walls 78−77870
H maser, field-operable design improvements 79−55099
H maser, frequency changes due to nonuniform magnetic field 80−99687
H maser, time-dependent freq. shift obs. 78−89457
H maser autotuning system analysis 79−55101
H maser design for NAVSTAR Global Positioning System satellite clock 78−58969
H maser failure mode identification 77−37862
H maser microwave resonator, miniature design 79−55097
H masers, with automatically tuned resonators 80−95859
H passive frequency standard 77−37860
H passive maser frequency standard 79−55100
H spacecraft maser, operating development model 79−54105
H time and frequency standards with redundancy 77−79065
H VLG-11 maser, performance evaluation 79−55098
H-maser, synchronization using very-long-baseline interferometry 79−88920
H_2 dissociator envelope degradation, AES characterisation rel. to appl. in atomic clock 77−61876
H_2 maser, time-dependent freq. shifts obs. 79−21713
H_2 maser freq. standard using dual modulation 80−98900
H_2 maser wall shift and unperturbated hyperfine freq. of ground state of H_2 atom 80−98901
$^{199}Hg^+$ trapped ion frequency standard 78−57914
Rb controlled digital clocks for high precision time meas. *(German)* 78−77871
Rb, optically pumped at. beam clock, theory 77−34866
Rb, portable clock for transcontinental and intercontinental time comparison 78−57908
Rb portable clock transcontinental/intercontinental comparison 78−54345
Rb time standards, study review *(French)* 79−174
Rb^{87} frequency standard 80−98902
^{85}Rb, unperturbed hyperfine transition freq. meas. 77−17954
^{87}Rb passive frequency standards, line inhomogeneity effects 79−54106
^{87}Rb resonant frequency change, due to spectral profile of pumping light 78−45590

atomic clusters
$A+A_n \rightleftarrows A_{n+1}^*$, cluster dynamics, classical trajectory study 80−3316
Ag clusters, latent image particles, electronic effects 80−82840
BCC clusters, electronic props., cluster size effects, theory 79−94949
binary microcluster, struct. and thermodynamics, Monte Carlo simulation 79−7736
Born-Green-Yvon eqn., two-dimensional, with anisotropic interac. 78−79882
cluster beam, nozzle flow formation and detection, high energy beam 80−5638
cluster superlattices in Na-type X zeolite matrix, N and S type volt-ampere characts. *(Russian)* 80−70665
crystalline surface, diffusion of atomic clusters, stochastic model 77−28077
density functional calculations 80−44699
density functional calculations for atoms, molecules and clusters 80−47850
density in classical monotonic dilute system, generalised physical model 79−98257
diamond, five-atom clusters, unrestricted Hartree-Fock calcs. 77−11866
electron density, bulk and surface atoms, from ab initio model calcs. 79−4590
energy, total, diatomics-in-mol., LMTO calc. pot. curve, Lanczos eigenvalue method 78−9291
formation, by ion bombardment of single cryst. surface 78−92157
free energy, Becker-Doring and Lothe-Pound theory 78−22063
free energy, of crystalline microcluster, microscopic capillarity approx. 80−5654
free jet, homogeneous nucleation of clusters, noncryst. struct. *(French)* 78−79760
homomorphic cluster CPA analyticity 78−82872
homomorphic cluster CPA for off-diagonal randomness 78−82873
inert gas small clusters, three body interaction effects on thermodynamic props., comparison bulk props. 80−28128
inert gas trimers and tetramers, ground state energies, pairwise Morse pot., few-body methods 79−72378
lattice distortions, influence on stability *(German)* 78−30584
matrix isolation spectra 78−46287
melting transition characts., small aggregates, random walk Monte Carlo calc 77−75355
metal, electronic spectrum fluctuations, appl. to Ni and Ti 79−19501
metal atom cluster compounds, bonding calc. using d-orbital overlap model, SCF-Xα-SW calc. 80−102595
metal atom cluster compounds 79−3607

atomic clusters continued
metal cluster ion energy spread from molten metal, charge exchange 80−37922
metal surface chemisorption theory, electron localisation, surface interactions 80−84376
metallic, 2 to 500 atoms, nucleation, mass spectra 80−102596
metals, individual atomic events on surfaces, quantitative examination 80−75409
MS potential from a set of overlapping densities 80−52850
muffin-tin potential and SW Xα SCF calcs. for core levels *(German)* 78−82874
N^2 problem in CI calcs. 77−23437
nozzle flowfield, cluster form., reservoir temp. scaling 80−5639
potential energy surfaces, main group elements 78−46477
rare gas, small clusters, structure thermodynamic properties 80−88341
STEM, at. resolution, adsorpt. and diffusion of heavy atoms on light element substrates 77−24484
structural stability of isolated small particles, atomistic studies 79−77957
transition metal chalcogenides, diffuse intensity contours, electron diffraction patterns 79−23504
unified theory of atoms and atomic aggregates, self consistent theory 80−102418
Van der Waals cluster, gas phase, vibr. predissoc., rel. to matrix isolated O_2 multiphonon vibr. relax. 80−18861
zeolite-S layers, high-temp. activated dipole moments in S clusters *(Russian)* 80−20575
zeolite-Y, continaing Ag atoms, ions and clusters, optical absorption spectra 79−36569
Ag cluster 78−33646
Ag, cluster and microcrystal, matrix isolated, optical absorpt. spectra, photolysis and plasmon absorpt. 79−89820
Ag clusters, charge distrib., density of states, CNDO calcs. 78−70995
Ag, in Kr matrix, isolation and aggregation 78−45723
Ag-Au clusters, latent image particles, electronic effects 80−82840
Ag-S clusters, latent image particles, electronic effects 80−82840
Ag_n, ($n<10$), uv-visible absorpt. spectra in Kr matrices 79−13858
AgBr emulsion, latent image speck size, characteristic curve anal. 79−34338
Al_4Cu_9, rhombohedral γ-brass, direct imaging of struct. and structural defects 80−15115
Ar, cluster formation and homogeneous nucleation, comparison of expt. and theory 80−79925
Ar, clustering of atoms around positron and positive ions 78−55270
Ar, clusters in supersonic beam, electron diffr. study 80−5655
Ar, FCC cluster, 40 kV electron scatt. dynamic effects 77−79721
Ar_2, Ar_3, Ar_4, short-range intermol. interaction nonadditivity, pseudopot. anal. 79−50179
$Ar_nH(H^+)$, excited and ground state struct. energies and binding energy, vibr. modes, LCAO-SCF-MO calc. 79−3608
$Ar_{N-1}K^+$ clusters, equilib. configs. and binding energies 80−48115
$Ar_{N-1}K^+$, ionic clusters, thermodynamic props., struct. 77−88615
Au, FCC cluster, 40 kV electron scatt. dynamic effects 77−79721
Au, on W support film, computer simulation of phase contrast 80−100150
Au-Fe alloys, magnetism and atomic clustering 80−103810
Be, chemisorption of H_2, ab initio calcs. 80−3404
Be cluster, multibody expansions, convergence 80−23594
Be_3, Be_4, Be_5, atomic clusters, nonadditive interactions, SCF energy anal. 78−25765
Be_4 (Be_4), atomic clusters, electronic struct., LCAO-MO-SCF and HF calcs. 80−63880
C, film, image contrast rel. to inelastic scattering 80−100154
C^+, association reactions, isotopic exchange, SIFT study, review 80−58435
C_n aggregates in equilib. C vapour, MINDO/2 calc., isomerism 78−29873
Cr-Fe (6.5 wt.%), atomic clustering and mag. defects, mag. moments 80−60246
$Cr_pC_n^+$, $p=1$ to 4, CrC_n^-, clusters, electronic props., mass spectra obs. *(French)* 79−45877
$Cs_{11}O_3$, ionic clusters in alkali metal suboxide cryst., struct., vibr. freqs., Raman spectra 79−37772
Cu, at. cluster, EXAFS study of bond length and binding energy 79−81317
Cu, atomic clusters, struct. and electronic props., Mulliken-Walsh diagrams, extended Huckel procedure 78−46479
Cu, cluster and bulk, struct. and electronic props. 78−95592
Cu, metal cluster, optical spectroscopy, atom to bulk 78−95591
Cu_n, cluster formation, by ion bombardment of single cryst. surface 78−92157
Cu(100), N chemisorption, bonding, MO theory 77−76659
$Fe_pC_n^+$, $p=1$ to 4, clusters, electronic props., mass spectra obs. *(French)* 79−45877
Ge, matrix isolated cluster, optical absorpt. 80−16045
$(GeSe_2)_x(As_2Se_3)_{1-x}$, vibr. excitations of large atomic clusters, Raman and depolarisation spectra 77−20856
H atoms, chemisorbed on cluster, indirect interactions, Grimley-Pisani model and tight-binding calc. 80−65370
H, chemisorbed on Ni (111), order-disorder transition, cluster-variation method 80−15372
H-like clusters, DIM pot. energy hypersurfaces, stationary points 78−25763
$H_{(2-4)}^+$ + He, 200-850 eV, attentuation and fragmentation 78−62968
H_{2n+1}^+ + Ar, $n\le7$, double differential fragmentation cross section 79−89821
H_n ($n=5$ to 13), ion-induced dipole clusters, binding energies and geometries 79−41261
H_n^+ ($n=3,5,7,9,11$), stability, struct., ab initio MO calcs. 78−74810
$H_n^+ + N_2$, ($n=2$ to 27), 250-900 eV collisions, fragmentation 77−88525
He, clustering of atoms around positron and positive ions 78−55270
He, microscopic gas-liquid like phase transition around positron 77−43322
He, positron induced droplet form. in gas 77−68148
$^3He_2{}^4He$, ground state binding energy, Faddeev-UPE method 79−72377
$^3He_3$, ground state binding energy, Faddeev-UPE method 79−72377
^{3}He-^{4}He few atom mixed mols., binding energy, size, particle distrib. 80−32864
^{3}He(^{4}He) clusters, metastable electronic states, electron impact excitation, time of flight spectra 80−106411

atomic clusters continued
^{4}He ground state binding energy, near threshold behaviour in 2 and 3 dimens. 80—91716
^{4}He trimer and tetramer, binding energy, appl. of ATMS 78—94349
$^{4}\mathrm{He}_2{}^{3}\mathrm{He}$, ground state binding energy, Faddeev-UPE method 79—72377
$^{4}\mathrm{He}_4$, tetramer bound state binding energy, pot. model 80—63883
$\mathrm{H}_n{}^{+}$(n=7, 9, 11, 13), geometry optimisation, ab initio SCF calcs 80—53180
K atom clusters, cluster beam Stern-Gerlach mag. deflection 78—54504
K_2, beam, multiphoton ionisation mass selective laser spectroscopy, vibronic, gyrovibronic states, clusters 78—21985
Li, cluster and microcrystal, matrix isolated, optical absorpt. spectra, photolysis and plasmon absorpt. 79—89820
Li clusters, DIM pot. energy hypersurfaces, stationary points 78—25763
Li_{2n}, (n=1, 2, 3), stable cluster configs., ionisation pots., binding energies, vibr. freqs., al initio SCF and CEPA calcs. 80—14265
Li_3, multibody and stability considerations, small clusters 78—90333
Li_n, at. cluster with H_2O mol. attached, MO study 79—76541
Li_n, equilibrium struct., effect of p-functions *(German)* 79—89823
Li_n, n=8,9,13,34,35, equilib. struct. *(German)* 78—29874
Li_n, studied by quadrupole mass analyser 77—71900
Mg cluster, multibody expansions, convergence 80—23594
$\mathrm{Mg}_4(\mathrm{Mg}_4{}^{-})$, atomic clusters, electronic struct., LCAO-MO-SCF and HF calcs. 80—63880
Mo-Be solid solutions, superconducting transition, temp. changing peculiarity due to press. *(Russian)* 80—70878
$\mathrm{Mo}_6\mathrm{Cl}_{14}{}^{2-}$, cluster ground state electronic struct. SCF Xα SW calc. 79—3607
Na, cluster and microcrystal, matrix isolated, optical absorpt. spectra, photolysis and plasmon absorpt. 79—89820
Na clusters, electronic relaxation energies in $\mathrm{KL}_{2,3}\mathrm{L}_{2,3}$ Auger transitions, SCF-Xα-SW calcs. 78—90334
Na particle, consisting of ats., metallic Na, model, electronic levels 78—50673
Na_2, beam, multiphoton ionisation mass selective laser spectroscopy, vibronic, gyrovibronic states, clusters 78—21985
Na_3, EPR spectrum, Ar matrix, bonding models 77—14462
Na_3, electronic struct., pot. energy surface, ab initio CI study 78—70996
Na_n ($n \leq 8$), equilibrium geometries and ionization energies calcs. 80—1099
NaA neolyte, Hg cluster transition to paramagnetic state due to mag. field *(Russian)* 80—60183
Ne, clustering of atoms around positron and positive ions 78—55270
Ne, metastable electronic states, electron impact excitation, time of flight spectra 80—106411
Ni (001) surface, electronic struct. of ordered S overlayers 80—84835
Ni, at. cluster, EXAFS study of bond length and binding energy 79—81317
Ni_n clusters, Ar matrix, UV-visible spectra, pot. energy curves 77 65552
O, chemisorbed on Al (100), photoemission ang. depend., MO cluster model calc. 78—76576
Pb microclusters, mol. beam electron diffr., amorphous struct. 78—66703
α-PdH_x, local mode intensity var. with conc., temp., direction and annealing 77—11653
Pt(111) stepped surface, high freq. vibr. modes, cluster recursion method calcs. 80—6615
$\mathrm{Rb}_9\mathrm{O}_2$, ionic clusters in alkali metal suboxide cryst., struct., vibr. freqs., Raman spectra 79—37772
Re_2, adsorbed on W (211) surface, dissoc., thermodynamics 78—87861
$\mathrm{Re}_3\mathrm{Br}_9$, electronic struct. and photoelectron spectra 80—69287
ReCl_9, electronic struct. and photoelectron spectra 80—69287
$\mathrm{Re}_3\mathrm{Cl}_{12}{}^{3-}$, cluster ground state electronic struct. SCF Xα SW calc. 79—3607
$(\mathrm{Re}_3\mathrm{Cl}_{12})^{3-}$, electronic struct. and photoelectron spectra 80—69287
$\mathrm{Re}_3\mathrm{Cl}_9$, cluster ground state electronic struct. SCF Xα SW calc. 79—3607
S_n, properties of small aggregates rel. to metallic character of Te_n 78—86985
SF_6, pure and H_2 mixture photolysis, S atom nucleation particulate formation 78—76836
Se_n, properties of small aggregates rel. to metallic character of Te_n 78—86985
Si, matrix isolated cluster, otpical absorpt. extended Huckel calcs., electron energy levels 80—16045
Si, vapour species rel. to amorphous film deposition 78—14641
SiGe, matrix isolated cluster, optical absorpt. 80—16045
TaSe_2, 1T and 2H superstruct., cryst. struct. using X-ray diffr. 80—39044
TaSe_2, 4Hb polytype, CWD induced atomic shifts 80—39045
TaSe_2 (4Hb), atomic displacements in CDW induced superstructure 80—10536
Te_n, small aggregate, metallic character 78—86985
U, mol. beam bombardment, aggregate form. *(French)* 79—74047

atomic collision processes *see atomic inelastic collisions; elastic scattering of atoms and molecules*

atomic electric moment
alkali metal, dynamic polarisability, variational calcs. with mode pot. *(Russian)* 78—902
alkali metal, oscillator strengths, nonlocal Simons pot. anal. 80—32795
Ca, A=40,42,43,44,46,48, laser spectroscopy, isotope shifts obs. 77 14392
coherent transients, spherical tensor treatment 79—26940
dynamic multipole polarisability 80—74252
elementary particle properties from atomic phys. expts., elec. dipole moment meas. 77—34578
f^{n} systems, electron correl. effects on elec. dipole transition probabilities 80—23316
identical atoms, dispersion intermolecular pot. anomaly prod. by intense radiation field 80—58336
inert gas mixture, collision induced microwave absorpt. spectra 80—74216
inert gas mixture, collision-induced absorption, exact line shapes, appl. to He-Ar 78—66512
inert gases, mixtures, dipole moments, IR absorpt. spectra obs. 80—28903
many-electron calc. 77—57884
muonium, quadrupole moment *(Russian)* 78—31143
neutral atom collisions, hyperfine component broadening and shift of spectral lines 80—74136

atomic electric moment continued
pressure broadening, adiabatic theory, low density approxs. 79—22628
spectral line collisional broadening, classical and quantum theories, radiator motion effect 78—86822
spectroscopy quantum chem. teaching, fluctuating elec. dipoles, light absorpt. 78—73802
Ar,K inner-shell level energies, absorpt. spectroscopy with synchrotron radiation 80—99583
As, $\mathrm{np}^2(\mathrm{n}+1)\mathrm{s}$ excited-state config. quadrupole moments, Sternheimer shielding factor 80—37755
Be, many-electron calc. 77—57884
Bi, Faraday effect and magnetic circular dichroism 80—83399
^{43}Ca, atomic beam and resonance spectroscopy 80—58180
Cs, $7^2\mathrm{P}_{3/2}$ sublevels, hyperfine struct., multiphoton elec. dipole transitions anal. 80—32692
Cs^{+} dipole and quadrupole polarisability fine struct. intervals and g-factor interval 80—91477
Cu isoelectronic series, dipole polarisability, numerical Coulomb approx. 80—43199
Eu+Sr, laser induced collisional energy transfer profile, high resolution study 80—83471
H atoms, energy levels and bound-bound transitions in strong mag. field 80—58134
$\mathrm{H}^{+}+\mathrm{H}$ high energy collision, excitation multipole moments, classical trajectory approx. 80—106389
He, isoelectronic sequence, E1 and E2 oscillator strengths, MCHF calcs. 80—106292
^{165}Ho, pionic atom, quadrupole hyperfine interactions, nucl. moment 78—37772
$\mathrm{In}(^2\mathrm{P}_{3/2})$, at. quadrupole shielding factor 79—10222
Kr, K inner-shell level energies, absorpt. spectroscopy with synchrotron radiation 80—99583
Li isoelectronic series, dipole polarisability, numerical Coulomb approx. 80—43199
Li^{-}, core-excited bound states 80—91468
^{71}Lu, $\mathrm{L}_2\mathrm{M}_3$ electric quadrupole transition detect., L X-ray spectrum 77—3294
N IV, dipole lengths, dipole vels. and transition probabilities 79—35113
N, $\mathrm{np}^2(\mathrm{n}+1)\mathrm{s}$ excited-state config. quadrupole moments, Sternheimer shielding factor 80—37755
Na isoelectronic series, dipole polarisability, numerical Coulomb approx. 80—43199
Na vapour, superradiance, quantum beat spectra 80—106311
Ne, electron impact K-shell excitation, EELS 80—106396
Ne, reson. four-photon parametric mixing conditioned by multipole relax. rates difference 79—89959
O V, O VI, dipole lengths, dipole vels. and transition probabilities 79—35113
P, $\mathrm{np}^2(\mathrm{n}+1)\mathrm{s}$ excited-state config. quadrupole moments, Sternheimer shielding factor 80—37755
Sb, $\mathrm{np}^2(\mathrm{n}+1)\mathrm{s}$ excited-state config. quadrupole moments, Sternheimer shielding factor 80—37755
TC I, HFS from spectra, mag.-dipole and electric-quadrupole hyperfine consts. 77—68002
^{181}Ta, pionic atom, quadrupole hyperfine interactions, nucl. moment 78—37772
U I, hyperfine struct. meas. of high-lying levels, mag. dipole and elec. quadrupole consts. 79—54796
Xe, $\mathrm{L}_1,\mathrm{L}_2,\mathrm{L}_3$ inner-shell level energies, absorpt. spectroscopy with synchrotron radiation 80—99583
^{91}Zr, hyperfine struct. and nucl. elec. quadrupole moment. at. beam mag. reson. meas. 78—55133

atomic electron configuration interactions *see atomic electron correlations*

atomic electron correlations
1s hole states of 3- and 4-electron systems, generalised Brillouin theorem-multiconfig. method 77—23443
3d-shell, pair correl. energies calcs. 79—31417
($\hbar\omega$,2e) reactions, Green's function method and correlated electron motion 77—88431
absorption bands, vibronic intensification obs., floating-orbital method 80—63619
acetone, absorption bands, vibronic intensification obs., floating-orbital method 80—63619
alkali metal, fine-struct. of excited nd and nf states, at. core effect 78—58606
alkali metal atoms, ground state correl., photoelectron spectra, multiconfig. Hartree-Fock calcs. 77—50471
alkali metal atoms and anions, electron affinity, model pot. SCF and CI calcs. 77—38609
alkaline earth atom, correl. lines, Rydberg excitations and ionisation pots. 77—6705
alkaline earth atoms, multiphoton spectra of high Rydberg states 77—68022
antisymmetrization wave function by method of group functions 77—3278
ATOM programme package for atomic calculations 79—10010
atomic collision, coherence and correlation, book 80—90615
atomic electron screening and correlations, effects on internal conversion coeffs. 80—18237
atomic spectra and radiative transitions, book 80—22159
atoms on semi-infinite linear chain, chemisorption theory and superoperator formalism 80—93800
Auger decay theory at. orbital non-orthogonality, Wentzel Ansatz 77—18871
Auger transitions, three-electron, in ats. with two inner-shell vacancies 77—19049
autoionisation, two electron resonances, electron correlation effects 79—89648
beta decay, K-shell internal ionisation, excitation, K-shakeoff probabilities 77—18889
Bethe-Goldstone time-depend. first-order theory, short range correl., transition moments 78—25449
book, atomic data handbook 77—23398
Breit interaction between electrons, calc. angular coeffs., computer program 80—18779
Brillouin theorem, proof 80—91415
C III, excited states, transaction oscill. states and wavefunctions 79—59367
closed shells, fast CI method calcs. 78—90090

atomic electron correlations continued
closed-subshell atom, correl. lines, Rydberg excitations and ionisation pots. 77—6705
cluster expansion, electron correlations, SAC and SAC CI calcs. 80—18802
cluster expansion electron correlations, SAC and SAC CI theories 80—18801
coherence and correlation in atomic collisions, book 80—90615
complete active space method, comparison of super C I and Newton Raphson scheme 80—47904
complex atom* + inert gas atom, model pot. curves, including CI 78—42154
Compton profiles, two-electron theory 79—86012
computational atomic and molecular physics, conf., Nottingham, England, (Sept. 1978) 79—59567
configuration interaction, iterative variational method calcs. 78—55127
configuration interaction, perturbation theory, partial transformation 78—37562
configuration interactions, appl. of unitary group methods 80—27958
correlation coefficient and electron correlation 80—78552
correlation energy, Gaussian geminal basis set calcs. 77—57885
correlation energy, many-body Rayleigh-Schrodinger perturbation theory calcs., exclusion principle violation 80—52890
correlation energy calculation, from CHF method 78—90087
coupled cluster approach, open (closed) shell systems 80—47842
coupled HF-perturbation theory of atomic and mol. props., correl. corrections 80—106269
deep levels, energies and wave functions, correl. corrections *(Russian)* 77—14364
density functional calculations for atoms, molecules and clusters 80—47850
direct CI method generalisation, graphical unitary group approach 80—47900
elecronic excitation properties, RPA-CI calcs. using hypervirial relations as constraints 79—76413
electron correlation energy, approx. 4th-order perturbation theory 79—6876
electron impact excited line radiation, polarisation, long-range electron correls. effects 80—91683
electron ionisation, coincidence meas. 77—42420
electron scatt. and photoionis., correlation effects 78—58842
electron scattering, many-electron correlations 77—42409
electron-electron interactions, radiative effects, canonical transformation calcs. 77—3275
electronic wavefunctions, Schrodinger eqn. variational form, generalised k-particle Brillouin conditions 79—81146
eqn. of motion-Green's function and config. interaction methods comparison, appls. 80—47841
equations of motion Green's function methods, higher order terms, ionisation pots. 80—52891
equations of motion Green's function methods, higher order terms, ionisation pots., CI comparison 80—52892
exchange and correlation, density function formalism 77—14367
excitation energies calc., using renormalised Green's function method *(Japanese)* 80—83295
excitation energy, validity of excited minus ground state calcs. using HF/pair correlation 77—38620
excited state structure, electron correl., var. collapse theory 79—6890
expectation values, correlation effects 79—6821
f^n systems, electron correl. effects on elec. dipole transition probabilities 80—23316
Fermi correlation, for parallel-spin electrons in momentum space 77—10602
few electron atoms, compact and accurate integral-transform wave functions 77—75066
Feynman diagrammatic technique 77—26981
first row atoms, static quadrupole and mixed dipole-octupole polarisabilities 79—22857
first row atoms and multiply excited states, SO(4) theory for electron correlation 79—22608
first-row atoms, ground states, using CI wavefunctions 78—74583
four-electron ions, excited states, one-electron approximation calcs. 79—10049
Gaussian geminal basis set optimisation, with crude SCF reference state 77—57885
geometry of electron pair correlation, Lie algebra 78—29754
ground state atoms, Van der Waals coeffs., polarisabilities and oscill. strengths calcs. 79—93913
ground state correlation energies, Green's function calcs. 77—75061
Hartree-Fock calcs., exchange pot. simplification 77—75054
heavy elements, electron config. rel. to chem. behaviour *(German)* 78—29727
heliumlike atoms, ground state energy via correl. wave function calc. of Li^+ and Be^{++} 77—23439
high Rydberg states with long range correl., single photon double excitation amplitudes 79—72251
inelastic collisions, diabatic correl. diagrams 77—14517
inert gas atom, correl. lines, Rydberg excitations and ionisation pots. 77—6705
inert gas atom, two-photon excitations, interelectron correlation 80—957
inert gas isoelectronic sequences, positive ion p-subhsell photoionisation cross-sections calcs. 77—50374
inert gases, inner-shell optical photon excitation, Auger, autoionisation, photoionisation processes 77—18867
inert gases, photoabsorption to bound state and photoabsorption to continuum state (ionisation), comparison, HF calcs. 80—47910
inert gases, photoionisation cross-sections, multiconfig. Hartree-Fock calcs. 77—50373
inner shell generalised oscill. strengths, with outer shell effects 78—50507
inner shell ionisation in electron capture decay 77—18882
integral equation numerical soln. in pair approx. 78—90065
interaction energy, direct calc. with CI wavefunctions 78—66477
intermediate-coupling eigenfunctions for f^6d and f^8d configs. 78—62732
interorbital pair correl. energies and absolute overlap integrals, 1s and 2s HF orbitals 77—46501
ion-atom collisions, two-electron rearrangement X-ray transitions, theory 77—38633
ions, two vacancies in K shell, 2 electron 1 photon, and hypersatellite transition probabilities 78—46294

atomic electron correlations continued
K-LL Auger spectra in intermediate-coupling scheme with CI, relativistic Dirac Hartree Slater calc. 80—52958
K-LL Auger spectrum, relativistic calc. 77—18872
K-shell Auger rates, level widths and fluoresc. yields, relativistic Dirac Hartree Slater calc. 80—52957
KLL Auger transition energies, relativistic multiconfig. calcs. 77—18873
light atoms (up to Ni), contact term, use of local spin density functional method 80—58158
local-density theory of multiplet structure 80—18776
m-scheme configuration interaction calcs., interaction integrals 79—45645
many body perturbation calculations and coupled electron pair models 79—59363
many body perturbation expansion, fourth order linked diagrams for quadruply-excited states 79—59364
many electron atomic Hamiltonians spectral props., method of configuration interaction 79—59368
many electron correl. problem, unitary group approach via spin algebra graphical methods 80—47902
many-body perturbation theory with radially restricted basis functions 80—78526
many-electron atoms, energy eigenvalues and eigenfunctions, CI method 77—50370
many-electron autoionisation states, transition probability and autoionisation rate, perturbation theory Z-expansion 80—52863
MC SCF theory, generalised Brillouin theorem and generalised forces 77—14366
MC-SCF theory, modified one-electron Hamiltonian, iteration convergence 79—6871
MC-SCF theory, orthonormality-constrained orbital optimisations 78—86766
MCSCF method improvement 80—52857
metal vapours, at. inner-shell optical photon excitations, Auger, autoionisation, photoionisation processes 77—18867
minicomputer open ended configuration interaction program, BERKELEY 78—37563
modified bielectronic potential method, for correl. energy calcs. 79—59365
modified virtual orbitals, for config. interaction calc. 80—58163
moment calcs., many-electron approach 77—57884
MRD-CI method for electronic wavefunctions 78—46278
multicentre multielectron system, wave function construction 78—893
multiconfiguration Hartree Fock method, appl. to at. energy levels and transition probabilities calcs. 80—23318
multiconfiguration Hartree-Fock procedures, 2nd and approx. 2nd. order, convergency 80—47901
multiplet ratios for photoionisation and electron attachment, shell model, LS coupling and correl. 78—17636
multiplet struct. obtained from HF, statistical exchange and local spin density approx. 80—32619
n-electron atoms, compactness proof for infinite systems of linear equations 79—72247
negative ions, electronic structure, stabilisation calcs. using big mol. Gaussian SCF/CI program 79—18121
negative ions of second and third period, electron affinity 77—3279
non-closed shell many-electron-theory at. charge wavefunctions, Be through Ne and Si 77—57849
nonhydrogenic atoms, radial transition integrals, Coulomb approx. calcs. 79—45625
np^6 subshells, interaction effect on ang. distribs. 79—10076
nuclear charge dependence, calc. using optimised one-electron wave functions 77—34538
open shell atom, effective electron-electron interaction, many-body perturbation theory, C appl. 80—47843
open shell atoms, LS-coupling, RPA with exchange 77—30838
open shell orbital theory with electron correl., wavefunction cluster expansion 79—13647
open shell systems, coupled cluster approach 78—58595
orbit-orbit interaction, new tensor expansion, matrix and graphical forms 80—14064
orbital functional theory for exchange and correl., local spin density approx., self interaction correction 79—76347
pair theory and reduced Green's functions 79—54774
perturbed Rydberg series, quantum defect and CI theories 80—23300
photoabsorption and slow electron scatt. processes 77—42299
photoelectron spectra, satellite struct., electron correl. using initial-state-CI 77—18980
photoemission, many-electron theory, in electron spectroscopy book 78—17714
photoionisation, ion alignment, many electron correl. effect 78—74622
photoionisation, relativistic RPA calcs. 77—61719
photoionisation cross sections, electron correl., reson. struct., relax, effects many body perturbation calcs. 80—47852
photoionisation cross-section, intershell interactions 79—26948
polarisability, of first row atoms and ions, multiconfig. approach 77—42435
polarization Green's function with multiconfiguration self-consistent-field reference states 80—37724
Politzer-Parr partitioning, electron correl., isoelectronic, isonuclear, spin and excitation aspects 80—78522
pseudo pot. model Hamiltonian, spin-orbit splitting, intercombination and relativistic orbital reorganisation 78—25424
pseudopotential calcs. of correlation energies 77—30788
radial correlation incorporation methods 77—42247
rare earth metal ions, 3d and 4f energy level parametrisation, Slater parameters and correl. corrections 80—87041
relativistic, orbit-orbit interaction, core and open-shell electrons 77—67989
relativistic average of config. wavefunctions, applicability to at. and ionic intermediate coupling props. 78—17574
s-electron binding energy regularities in $l^N S^M$ configs. 78—62731
satellite peaks, relationship between X-ray emission and X-ray photoelectron spectra 78—66492
scaling and Pade approximants, rel. to perturbation series higher-order terms 80—5487
scaling parameter, due to Wilson, evaluation with variational-perturbation results 80—5486
SCF basis sets of moderate size, efficient methods 78—58593
SCF electron-gas local-spin-density model including correlation, appl. to He through Ar 80—9488

atomic electron correlations continued
second row atoms, statistical correlation energies 78—78637
second-order calculations, scaling 79—31359
second-row atoms, static dipole polarisabilities, finite perturbation calcs. 77—6690
singly excited states, oscillator strengths, ab initio calcs. 80—920
singly ionised atom, excited state struct., electron correl., oscill. strengths, theory 79—6889
small systems, accuracy limits 80—47905
spectral props. of many electron atomic Hamiltonians, appl. to 2-electron atoms 79—63922
spin density functional formalism 79—18122
spin-adapted coupled cluster many-electron theory 77—75065
spin-coupled particle-hole excitation, general matrix element formulas 80—69086
spin-density gradient expansion for kinetic energy of electron gas, variational calc. 79—93917
strongly driven atoms, by laser field two-time correlation functions from quantum regression theorem 78—42017
structure, multiconfiguration optimised central pot. method calcs. 80—9515
superheavy elements E116 and E114, theoretical chem. 77—32824
superoperator resolvent, alternative inner projections 79—31412
ten-electron systems, correl. energy, fourth order diagrammatic, many body Rayleigh Schrodinger perturbation theory. 80—63556
theory, inverse matrix diagonal and off diagonal elements, self energy perturbation theory 78—82607
transition metal, 3-d, density functional theory 78—58578
transition metal, many-config. approx. in X-ray and electronic spectra interpret. 80—32615
transition metal atoms, neutral and ion val. states, electron correlation, ab initio effective val. Hamiltonian calc. 80—99449
transition metal ions, 3d and 4f energy level parametrisation, Slater parameters and correl. corrections 80—87041
transition metals, 1st period, at. correlation energies, perturbation calc. 79—36508
transition metals, third row, by vertical anal. 78—41964
two electron atoms, three-body problem 80—83286
two-body correls., variational approach 80—91455
two-electron atom, dipole approx. for electron-electron interaction, autoionisation widths *(Russian)* 77—61691
two-electron atom, energy eigenvalues and eigenfunctions, CI method 77—50371
two-electron atom, exchange and correlation pots., density functional theory, He appl. 80—52848
two-electron atom, momentum distrib. and Compton profiles, Fourier integral calcs. 77—3276
two-electron atom in spherical box, CI calcs., appl. to He, Li$^+$, and Be^{2+} 79—97984
two-electron atomic system, relativistic calc. of level widths 79—3376
two-electron atomic systems, correl. energy calcs. 79—36543
two-electron atoms, correl. energy, modified bielectronic potential method calcs. 79—59365
two-electron ats. and ions, low lying S states, pairwise correlated generalised VB method 77—65427
two-electron systems below N=2 threshold, widths and config. mixing 79—18129
unitary group approach, matrix element evaluation 79—31411
unitary group generators and permutations, CI matrix elements, algebraic method 80—37725
unitary group generators and permutations, CI matrix elements, graphical method 80—37726
unitary group irreducible representation subduction coeffs. 80—37723
unlinked cluster corrections for configuration interaction calculations 79—3368
valence correlation energies, contributions of triply- and quadruply excited states determ. using perturbation theory 80—78545
valence electrons local-density theory of exchange and correlation energies 80—52854
virtual orbitals for rapid convergence, perturbational method 79—85906
X-ray spectra, configurational interaction effects in region of 4f and 3d shell build up 77—27012
zeroth approximation, formally exact perturbation theory, transition energies calc. 77—42259
$e^+e^-e^-$, two-electron at., three-body problem, binding energy 79—3372
Al I, perturbed HFS, interconfiguration interaction calc. 80—9523
Ar, 1s2s3p^{4}P$_{5/2}$^{o}-state, relativistic effects and config. mixing 79—45640
Ar, 40 keV electron scatt. 7-200 mrad, relativistic and electron correlation effects 77—34760
Ar, and isoelectronic sequence, E1 transitions, relativistic oscill. strengths 78—949
Ar, CI calcs. using modified virtual orbitals 80—58163
Ar, Compton profile, local density approx., Kohn-Sham self consistent scheme 78—94193
Ar, electron impact ionis., single charge, inter-shell correl. 77—88567
Ar, electron impact ionis., calc. for 3s^2 subshell 79—31700
Ar, Fermi correlation, for parallel-spin electrons in momentum space 77—10602
Ar, KLL and KLM Auger electron spectra, obs. and relativistic multiconfigurational Dirac-Fock calc. 78—50524
Ar, M-shell photoionis., many-body interactions 79—10081
Ar, outer shell photoelectron spectrum, correl. satellites 78—78671
Ar, Raman scatt., single particle HF approx. and RPA many-electron correlations calcs. 80—23374
Ar, total state energies, L-, M-electron processes, ab initio CI investig. 77—18801
Ar, free-free radiative absorpt. coeff. calcs. 77—423
Ar^{2+}, levels of 2p^{5}3p^5 78—74574
Ar^{2+}, multiple open shell configs. calcs., modified HF method 77—50356
^{37}Ar, M/L capture ratio, multiconfig. Hartree-Fock calc. atomic electron correlations 78—62510
B, 1st order Compton profiles, momentum distribs., correlation effects 77—88429
B, atomic correlation energies, perturbations and near degeneracy 79—3371
B II, oscill. strengths for 2s^2, 2p^2, 2s3s(^{1}S)-2s2p(^{1}P) transitions 77—46533
B isoelectronic series, dipole oscill. strengths, multiconfigurational Hartree-Fock calcs. 77—83540
Ba, 4d^{10} subshell photoionisation cross section, electron shell rearrangement 77—14400

atomic electron correlations continued
Ba, Auger spectra, strong correl. in 4d-spectrum 78—50522
Ba, diamagnetic Zeeman effect, 20-40 kG, induced config. mixing 78—17608
Ba, electron scatt. cross sections, close coupling calc. with CI 80—43180
Ba, even-parity J=2 spectra, multichannel quantum-defect anal. 79—31445
Ba II, 5p excitation, relativistic anal., multiconfig. Dirac-Fock calcs. 80—69240
Ba, photoelectron spectra, strong many electron effects from core levels 77—18862
Be, and isoelectronic sequence, correlated and HF electron density differences 78—46275
Be, atom, ground state, accurate CI wavefunction 77—42245
Be, atomic correlation energies, perturbations and near degeneracy 79—3371
Be, atomic polarisability, correlation corrections finite field method 77—71889
Be, Auger transitions, fluoresc. yield calcs., correl. effects 77—18869
Be, correl. contribs. to dipole polarisability, coupled HF-perturbation theory 80—106269
Be, correl. energy, Gaussian geminal basis set calcs. 77—57885
Be, correl. energy, modified bielectronic potential method calcs. 79—59365
Be, correlation energies, Hartree-Fock Hamiltonian 78—41965
Be, Fermi correlation, for parallel-spin electrons in momentum space 77—10602
Be, ground state, CI and many-body perturbation theory 79—68198
Be, ground state energy determ., Galerkin-Petrov method 79—769
Be, ground state reduced first order density matrix CI calc., mag. shielding const. and diamagnetic susceptibility 79—6872
Be, HF polarisability, second order correlation correction 78—25429
Be ions, isoelectronic series, correlation energy and size, empirical relationship 77—79546
Be, isoelectronic sequence, transition probabilities, relativistic effects calcs. 77—27028
Be, isoelectronic sequence, relativistic transition probability calcs. 77—54533
Be isoelectronic sequence, mag. quadrupole transitions, multiconfig. HF calcs. 78—33420
Be, isoelectronic series, Coulomb holes and correl. coeffs. 77—88398
Be isoelectronic series, transitions involving 2s3l^{3}L states, oscill. strengths 77—3308
Be, multiconfig. HF procedure, 2nd- and approx. 2nd-order, convergency 79—93907
Be, multiconfig. Hartree-Fock calcs. convergency 80—47901
Be, one-particle ionis. energy, correlated wavefunction 79—45639
Be, oscillator strengths, generalised RPA with exchange calcs. 79—98030
Be, pair excitation correl. numerical coupled cluster method 80—47906
Be, second order correlation energies, variational-perturbation method, radial basis saturation errors 79—97985
Be, self-consistent electron pairs with higher order effects 78—46276
Be sequence, 2s3p ^{3}P$_1$-2s^2 ^{1}S$_0$ intercombination line transition probabilities 80—18823
Be sequence, (Z=4 to 10, 14), $^3P_1 \rightarrow {}^1S_0$ intercombination line, CI calc., Breit interaction 78—78641
Be, total nonrelativistic ground state energy, CI STO calc. 77—18800
Be^{2+}, elastic form factors, correlated two-electron-core pots., closed form expressions 79—68195
Be-like ions, 2s2p($^3P_1^0$)$\rightarrow$2s^2($^1S_0^e$) transition probabilities, CI calcs. 79—36544
Be-like ions, electron impact excitation, config. mixing 77—58175
Be-like system, numerical many-body perturbation calcs. using multiconfig. model space 80—47907
Be+Be(Li) 78—5310
^{7}Be, L/K capture ratio, multiconfig. Hartree-Fock calc., atomic electron correlations 78—62510
Bi, electron config. mixing and parity nonconservation 78—13439
Br, ESCA, lifetime broadening, CI resonances 77—18853
C, 1st order Compton profiles, momentum distribs., correlation effects 77—88429
C atom, ^{3}P state, valence shell correl. energy, IEPA-PNO method 77—10597
C, atomic correlation energies, perturbations and near degeneracy 79—3371
C, correlated and HF electron density difference 78—46275
C I isoelectronic sequence, forbidden transitions calc. 79—31444
C, photoionisation cross section, CI calcs. 79—98050
C, structure, multiconfiguration optimised central pot. method calcs. 80—9515
^{13}C III, 1s^{2}2s3p ^{3}P^0 state,, HFS, beamfoil expt., CI and Hartree-Fock calcs. 77—75276
Ca, forbidden transitions, radiative lifetimes, MCSCF and CI calcs., time of flight spectra for metastable state 80—91498
Ca I excitation series, potential barrier effects, single configuration HFC 80—78558
Ca*+He(Ne), model pot. curves, including CI 78—42154
Cd, ground state correl., photoelectron spectra, multiconfig. Hartree-Fock calcs. 77—50471
Cd, photoionisation cross section, many-body perturbation theory, dipole length and vel. calc. 78—78674
Cl I, photoionisation cross section, calc. by many-body perturbation theory 78—62771
Cl, photoionis. cross sections, RPA with exchange method generalisation 79—10077
Cl, photoionisation cross section and reson. theory, many body perturbation theory, 3p and 3s subshells 80—69114
^{35}Cl XVI, n=2, Lamb shift, fine struct. 79—13675
Cr II to VI, struct. and transition probabilities, ab initio calc. using Thomas-Fermi central pot. 79—3360
Cr XVIII, XIX, spectral energy levels, relativistic corrections, config. superposition method 80—32616
Cs, 4d^{10} subshell photoionisation cross section, electron shell rearrangement 77—14400
Cs, He IIα 5p ^{1} photoelectron spectrum, config. interaction effects 80—5510
Cu III, calc. of configurations, CI effects 77—42228
Cu, L and M Auger spectra, CI effects, anomalies 78—33488
Cu$^+$, Hartree-Fock calcs., exchange pot. simplification 77—75054
Cu$^+$, reson. transition, effect of correl. in 3d^n core, HF calcs. 80—47911

atomic electron correlations continued
Eu, hyperfine interaction calc., relativistic many-body approach 77—46504
Eu I, isotope shift meas., level classification in $4f^6 5d6s^2$ and $4f^7 5d6p$ configs. 77—30831
F, 1st order Compton profiles, momentum distribs., correlation effects 77—88429
Fe, Auger transitions, two-electron-one-photon radiative rate calc. 77—18869
Fe, fine struct. levels fitting, config. interaction effect, spin-orbit and electrostatic interaction parameters 80—69248
Fe, group ions, configuration interaction method for hyperfine contact interaction 77—3274
Fe group ions, pair excitations in refinement of d^N-shell calc., multiconfig. approx. 77—42248
Fe III to VI, struct. and transition probabilities, ab initio calc. using Thomas-Fermi central pot. 79—3360
Fe X (XI), energy levels and oscill. strengths, Slater radial integrals 77—79583
Fe XII and XIII, energy levels and oscillator strengths for XUV transitions 78—46277
Fe XIX, XXI, spectral energy levels, relativistic corrections, config. superposition method 80—32616
Fe XXI, relativistic energy levels, Dirac-Fock multiconfig. calc., triplet state fine struct. and Lamb shift 80—23315
Fe XXII, allowed transition CI wave functions, oscill. strengths and transition probabilities 80—32664
Fe XXII, intercomb. transitions, oscill. strengths, transition probs., rel. to solar spectra 80—52935
Fe-group spectra, superposition configurations in semiempirical calc. 78—920
^{57}Fe, configuration interaction, SL-dependent, effect on hyperfine structure 80—37749
Gd I and II spectra, 3930 to 4140 Å, isotope shift meas. 77—61713
Gd^{3+}, hyperfine interactions, relativistic CI using many-body calcs. 78—78638
H^-, $(2p^2)^3P$-state, CI series convergence 80—27955
H^-, and isoelectronic sequence, correlated and HF electron density differences 78—46275
H^-, bound states in mag. field, binding anal., variational calcs. 80—42940
H^-, combined CI and Hylleraas calc. for lowest ^1S and ^1P states 77—38617
H^-, elastic form factors, correlated two-electron-core pots., closed form expressions 79—68195
H^-, electron correl. effects, ang. and radial, in momentum space 77—88399
H^-, electronic structure, stabilisation calcs. using big mol. Gaussian SCF/CI program 79—18121
H^-, ground state electron correlation visualisation 79—3367
H^-, H^{2-}, bound states calc. 79—13646
H^-, photodetachment cross sections, one and two electrons, multichannel J-matrix calc. 77—18860
H^--like ions, electron correlation and Coulomb hole in momentum space 78—86793
H^--positron bound states, CI-Hylleraas calcs. 77—10603
H+He(Ne)(Ar)(Kr)(Xe), low energy elastic scatt. cross section MCSCF calc., van der Waals forces 78—70897
$H+N^{2+}(^2P^0)[N^{3+}(^4S)]$, charge transfer, ab initio CI pot. curves and coupling-matrix elements 80—37878
$H^- + e^-$, bound state calcs., channel coupling array theory 77—19005
H_2, ground state correlations meas. by (e,2e) expt. 77—42413
$H_2{}^{b}Pe^-$, bound state calcs., channel coupling array theory 77—19005
He, $1s^2$ ground state piecewise polynomial CI natural radial orbitals wave functions 80—18805
He, 2^1S and 3^1S, CI expsn., convergence patterns 77—50378
He 2^1S state isoelectronic series, Fermi and Coulomb correlations 78—921
He, and isoelectronic sequence, correlated and HF electron density differences 78—46275
He, autoionisation of highly excited states, config. interaction 78—13445
He, bound states in mag. field, binding anal., variational calcs. 80—42940
He, CI wavefunctions, ang. correl. of electrons 78—62730
He, combined CI and Hylleraas calc. for four lowest ^1S and ^1P states 77—38617
He, Compton defect, high energy electron impact spectroscopy 77—71876
He, correl. contribs. to dipole polarisability, coupled HF-perturbation theory 80—106269
He, correlation energies, Hartree-Fock Hamiltonian 78—41965
He, correlation energy of ground state, pair approx. 78—90065
He, elastic electron scatt. phaseshifts, 2s2p ^3P autoionisation, 1s2s $^3S \rightarrow 1s\varepsilon p$ ^3P triplet continuum photoionisation 79—31480
He, elastic form factors, correlated two-electron-core pots., closed form expressions 79—68195
He, electron affinity of $(1s2s)^3S$ state, CI calc. 79—59591
He, electron angular correlations, CI and Hylleraas wave functions 77—26985
He, electron correl. effects, ang. and radial, in momentum space 77—88399
He, electron impact, ^3P_g and $^{1,3}D_u$ states excitation, electron correlation influence, Rudge-type approx. 78—74771
He, electron impact excitation, ^3P_g and $^{1,3}D_u$ states, electron correlation influence, Born-Oppenheimer approx. 78—74770
He, electronic struct., dilute gas, double excitation CI anal., coupled electron pair approx. 78—21856
He, energy eigenvalues and eigenfunctions, CI method 77—50371
He, energy of S states, appl. of modified interelectronic pot. 78—29736
He excited states, relativistic corrections 78—62734
He, ground state electron correlation visualisation 79—3367
He, ground state radial limit, piecewise polynomial basis functions 78—37560
He, He^--positron bound states, CI-Hylleraas calcs. 77—10603
He isoelectronic sequence, electron correlation effects on one-electron distribs. 77—10598
He isoelectronic series, (H^- to C^{4+}), correl. energy calcs. 79—36543
He isoelectronic series, electron correlation and Coulomb hole in momentum space 78—86793
He like systems, ground state one electron density decay 79—76337

atomic electron correlations continued
He, many electron system, photoionisation and photoexcitation, at. transition strong config. interaction effect 80—47909
He, photoionisation, frozen-core HF perturbation theory, oscillator strength, dipole length and vel. calc. 78—78672
He, S state, electron correl. calcs. 79—49952
He, second order correlation energies, variational-perturbation method, radial basis saturation errors 79—97985
He, self-consistent electron pairs with higher order effects, effect of quadruples 78—46276
He, two-step photoionisation via 4p $^1P_1$ state *(Russian)* 79—59413
He^-, $(1s2s2p)^4P^0$ metastable state, CI calc. 79—59591
He^-, reson. calcs. with correlated target state wave functions, complex coord. method 79—26939
He-like atom, from probability theory 77—3286
He-like ions, ground-state electron impact excitation strengths, close-coupling calcs. 80—23561
He-like ions, radiative 2^3S_1-1^1S_0 transition, correlation effects 79—97989
He-like target+fast projectile, electron capture cross-sections 80—69231
He-like two electron atoms, three-body problem 79—3372
$He+H^+$, 25-3000 keV, electron-capture, continuum distorted wave approx., correl. energy 77—83727
$He+H^+$, electron capture cross sections, electron correlations 77—34758
$He^+ + He$, 150 eV, one-electron excitations, quantal treatment 77—71854
He_2, pot. surface well depth calc. 77—79667
He**, doubly excited, spatial correl. of at. electrons 78—70760
Hg, 5d level open shell interactions, 304 Å photoelectron spectrum 80—87087
Hg, ground state correl., photoelectron spectra, multiconfig. Hartree-Fock calcs. 77—50471
I, photoelectron spectra, strong many electron effects from core levels 77—18862
In I, absorption spectra, 320 to 1000 Å, intersubshell correls. 4d spectrum two-electron detachment 77—10617
In, VUV photoelectron spectra, pseudo-atomic beam technique 80—58225
K II, isoelectronic series, photoionisation, multichannel CI calcs. 79—93931
K, valence p-shell HeIIα photoelectron spectra, final state CI effects 80—14121
Kr, 3p core hole spectrum, many electron description 78—50517
Kr, Compton profile, local density approx., Kohn-Sham self consistent scheme 78—94193
Kr, ESCA, lifetime broadening, CI resonances 77—18853
Kr II, CI calcs. on $4s^2 4p^4 4d + 4s^2 4p^4 5s + 4s4p^6$ configs. 77—3277
$LaCl_3{:}Pr^{3+}$, dipole transition probabilities between states, electron correl. effects 80—23364
Li, $1s2p^2$ $^4P^e$ state, using configuration-interaction wavefunctions 79—3369
Li, $1s2s2p^4P^o$ state, using configuration-interaction wavefunctions 79—3370
Li, and isoelectronic sequence, correlated and HF electron density differences 78—46275
Li atoms, photoexcitation and ionisation cross sections, Stieltjes-Tchebycheff procedure 78—17633
Li, autoionisation states, config. decays and excitation energies 78—13475
Li, correlation energies, Hartree-Fock Hamiltonian 78—41965
Li, even-parity core-excited ^2P states, accurate CI calcs. 79—54782
Li, ground state, radially correl. wave functions 77—75066
Li, isoelectronic sequence, transition probabilities, relativistic effects calcs. 77—27028
Li isoelectronic sequence, quartet states hyperfine consts., Hartree-Fock and CI calcs. 78—919
Li isoelectronic sequence of three electron atoms, pair correlation study 80—74096
Li isoelectronic series, quartet states, HF and CI calcs. 78—17582
Li, positron bound states, CI-Hylleraas calcs. 77—10603
Li, quartet states, absolute term values, CI calcs. 78—58596
Li, quartet states, transition energies, oscill. strengths, CI calcs. 78—58597
Li^-, and isoelectronic sequence, correlated and HF electron density differences 78—46275
Li^-, core excited bound states in beam foil expts., CI calcs. 80—78559
Li^+, elastic form factors, correlated two-electron-core pots., closed form expressions 79—68195
Li^+, electron correl. effects, ang. and radial, in momentum space 77—88399
Li^+, isoelectronic series, electron correlation and Coulomb hole in momentum space 78—86793
Li-like ions, electron impact excitation, config. and parentage mixing effects 77—58176
Li+Li(Be), London coeffs. for long range interaction, CI variation-perturbation method 78—5310
Lw, ground state config., relativistic prediction, multiconfig. Dirac-Fock calcs. 80—106277
Mg, Auger spectra, CI calcs., spin-orbit interactions 77—14558
Mg, electron scatt. cross sections, close coupling calc. with CI 80—43180
Mg, isoelectronic sequence, excitation energies and line strengths, MC Hartree-Fock calcs. 77—83658
Mg, K Auger transition rates, orbital relax. and interchannel interaction effects 78—50521
Mg*+He(Ne), model pot. curves, including CI 78—42154
Mn, fine struct. levels fitting, config. interaction effect, spin-orbit and electrostatic interaction parameters 80—69248
Mn III to VI, struct. and transition probabilities, ab initio calc. using Thomas-Fermi central pot. 79—3360
Mn^{2+}, Hartree-Fock calcs., exchange pot. simplification 77—75054
N, $^4S^0$ ground state, photoionisation calcs. 79—85909
N, 1st order Compton profiles, momentum distribs., correlation effects 77—88429
N, bremsstrahlung by electrons, configuration interaction 78—13483
N IV, excited states, transaction oscill. states and wavefunctions 79—59367
$N^{2+}(^2P^0)+H$, charge transfer, ab initio CI pot. curves and coupling-matrix elements 80—37878
$N^{3+}(^1S)+H$, charge transfer, ab initio CI pot. curves and coupling-matrix elements 80—37878
Na, Auger spectra, CI calcs., spin-orbit interactions 77—14558
Na, photoionisation cross-section, electron correls. Brueckner-Goldstone calcs. 77—6742

atomic electron correlations continued
- $Na+H^+$, configuration interaction potentials and rainbow angle scatt. cross section 80—37745
- ^{23}Na, S states, HFS by Hartree-Fock calcs. 77—68023
- Nd I and II, isotope shifts in spectrum, 3900 to 4760 Å, config. mixing 77—30812
- Ne, 1st order Compton profiles, momentum distribs., correlation effects 77—88429
- Ne, 40 keV electron scatt., 7-200 mrad, relativistic and electron correlation effects 77—34760
- Ne, atomic struct. calc., symmetry adapted pair functions, Rayleigh Schrodinger HF variational perturbation theory 80—42944
- Ne, Auger energies, intensities, for initial K vacancy, many body calc. 77—18869
- Ne, Auger spectra, correl. effects, energies and wavefunctions, ab initio CI calc. 80—14125
- Ne, CI-Hylleraas variational calc. of ground state 77—18798
- Ne, Compton profile, local density approx., Kohn-Sham self consistent scheme 78—94193
- Ne, converged $E^{(2)}$ values 78—66479
- Ne, correl. contribs. to dipole polarisability, coupled HF-perturbation theory 80—106269
- Ne, correlation energy, many-body Rayleigh-Schrodinger perturbation theory calc. 78—894
- Ne, electronic struct., universal STO basis sets 79—10021
- Ne, even-parity levels, double excited energy levels, frozen-core superposition, config. calcs. 80—106273
- Ne, Fermi correlation, for parallel-spin electrons in momentum space 77—10602
- Ne, ground state, configuration interaction, iterative variational method calcs. 78—55127
- Ne ions, isoelectronic series, correlation energy and size, empirical relationship 77—79546
- Ne, isoelectronic sequence, excitation energy and oscillator strength, level crossing anomaly, relativistic RPA calc. 80—14077
- Ne, pair excitation correl. numerical coupled cluster method 80—47906
- Ne, second-order correl. energy calcs. 78—33436
- Ne, triply-excited states contributing to correl. energy, diagrammatic perturbation theory 79—81161
- Ne VII, excited states, transaction oscill. states and wavefunctions 79—59367
- Ne^+, converged $E^{(2)}$ values 78—66479
- Ne^{3+}, CI calc. of at. energy levels 80—5624
- Ni III to VI, struct. and transition probabilities, ab initio calc. using Thomas-Fermi central pot. 79—3360
- Ni XXI, XXIII, spectral energy levels, relativistic corrections, config. superposition method 80—32616
- Ni+Ni, exchange interactions and exchange integrals 80—37849
- Ni+Ni interaction, ab initio HF and CI calcs. 79—59535
- O, 2-photon excitation, cross-section calcs. 78—58641
- O, electron impact ionisation, differential and total cross-sections 80—18935
- O, first order Compton profiles, momentum distribs., correlation effects 77—88429
- O II, relative intensities and lifetimes in nebulae, conventional radiation theory 80—109513
- O III+e, low energy reson. struct., distorted wave approx. 77—75307
- O V, E1 transition probabilities, lifetimes, CI calc. 80—83321
- O V, excited states, transaction oscill. states and wavefunctions 79—59367
- Pb, 5d level open shell interactions, 304 Å photoelectron spectrum 80—87087
- Pb, photoelectron spectra, electron correlations and spin-orbit interaction influence 80—102495
- Pr^{3+}, elec. multipole polarisabilities, discrete basis set calcs. 80—91456
- Rb, oscillator strength ratios for principal series, relativistic and correlation effects 79—784
- Rb, valence p-shell HeIIα photoelectron spectra, final state CI effects 80—14121
- S IV, P-, D-, S-states, oscillator strengths, transition strengths, CI calcs. 80—922
- S V, config. interactions effect on radiative lifetimes 77—30973
- SI odd parity levels, configuration interaction effects 79—72246
- Sc I, arc spectra, energy levels assignment *(French)* 77—83522
- Sc I, hyperfine struct., far-config.-mixing effects 77—42240
- Si (III), excitation thresholds and oscillator strength calc. using CI wavefunctions 80—91496
- Si isoelectronic sequence, CI calcs. of oscillator strengths, L-S framework 80—14089
- Si, Rydberg series electronic struct. 79—22614
- Si, Rydberg series electronic struct. 79—22615
- Si^-, ground state, photodetachment cross section calc., low energy 79—63970
- Sn II, cool plasma, isolated lines, Stark broadening, semi-empirical impact approx. calcs. 80—59186
- Sr, Auger spectra, strong correl. in 3d-spectrum 78—50522
- Sr I, strong configuration interaction, multiconfiguration Hartree-Fock calcs. 77—67987
- Sr I excitation series, potential barrier effects, single configuration HFC 80—78558
- Tb I, $4f^85d6s^2$ config., hyperfine struct. analysis 78—62732
- Te, photoelectron spectra, strong many electron effects from core levels 77—18862
- Ti, fine struct. levels fitting, config. interaction effect, spin-orbit and electrostatic interaction parameters 80—69248
- Ti I, hyperfine struct., far-config.-mixing effects 77—42240
- Ti, neutral and ion val. states, electron correlation, ab initio effective val. Hamiltonian calc. 80—99449
- Tl, 5d level open shell interactions, 304 Å photoelectron spectrum 80—87087
- Tl, photoionis. cross section, spin polaris. and ang. distrib. of photoelectrons, RPA calc. 78—13478
- Tl, VUV photoelectron spectra, pseudo-atomic beam technique 80—58225
- Tl, vacuum UV absorpt. spectra, at. consts. 77—57917
- U, high-lying levels in vapour near ionisation limit 78—21842
- U, isotope shift and configuration interaction 79—31468
- U^{n+} ($n=0$ to 6), electronic struct., multiconfig. Dirac-Fock calcs. 79—45646
- V, fine struct. levels fitting, config. interaction effect, spin-orbit and electrostatic interaction parameters 80—69248
- Xe, $4d^{10}$ subshell photoionisation cross section, electron shell rearrangement 77—14400
- Xe, $5p^6$ subshell, photoelectron ang. distrib., ionisation cross section 77—14401
- Xe, 5s, 5p ESCA spectrum, photoionisation many electron description 78—50516
- Xe II, $5p^46s$ and $5p^45d$ configs., config. interaction effects 78—66478
- Xe, intershell correlation, double electron ejection from outer shell 78—42019
- Xe, N-shell Coster-Kronig transitions 79—13691
- Xe, photoelectron spectra, strong many electron effects from core levels 77—18862
- Xe, photoelectron spectra, intershell correl. effects 77—18863
- Xe, photoelectron-Auger electron post collision interaction, Auger peak shift obs. 77—27039
- Zn, Fermi correlation, for parallel-spin electrons in momentum space 77—10602
- Zn, ground state correl., photoelectron spectra, multiconfig. Hartree-Fock calcs. 77—50471
- Zn, L and M Auger spectra, CI effects, anomalies 78—33488
- Zn^{2+}, closed shell ion, 3d electron pair correl. energies calcs. 79—31417
- Zn^{2+}, electron pair correlation energies 79—93927

atomic electron impact excitation
see also electron spectra
- ab initio methods for atomic and molecular processes 80—63550
- absolute cross sections meas. 77—42411
- adiabatic approximation, energy-modified 79—59523
- AES trace analysis non-thermal excitation, comparison with AAS 80—30312
- alkali atoms, electron impact excitation of autoionis. states 79—54971
- alkali atoms, electron inelastic scatt. in intense laser field 79—72427
- alkali metal, thermal plasma, data on collisional transition probabilities from 1000 to 8000K 77—72406
- alkali metal atom, autoionising levels excitation by electron impact 77—19085
- alkali metal atoms, integrated cross-section calc. 78—62921
- alkaline earth atom, electron impact double electron excitation and autoionisation calcs. 77—68121
- analyticity and dispersion relations in forward e-atom scatt. 77—23561
- atmospheric gases, electron impact cross-sections 78—28398
- atom in resonant EM field, elastic and inelastic scatt. cross sections 77—14574
- ATOM programme package for atomic calculations 79—10010
- atomic electron (positron) elastic (inelastic) scatt., 5-500 eV, perturbations treatments, review 77—30997
- Bethe approx. modifications, impact radiation polarisation 79—31695
- Bethe approximation 79—18249
- Bethe theory, inelastic collisions of fast charged particles 78—58783
- binary collisions, inverse bremsstrahlung absorpt. in strong radiation field 79—89788
- binary inelastic collisons, inverse bremsstrahlung absorpt. in large radiation field, Born approx. calcs. 78—42222
- Born partial wave amplitude for any electrostatic multipole field 80—53128
- bremsstrahlung, atomic electron contrib. *(Russian)* 77—79694
- bremsstrahlung, role of atomic electrons *(Russian)* 77—88575
- bremsstrahlung, series expsn. for intensity components 78—50648
- bremsstrahlung cross-section, near HF limit 79—18288
- bremsstrahlung for electrons 0.4-5 keV *(Russian)* 78—37744
- bremsstrahlung intensity calc., static approx. *(Russian)* 77—75308
- bremsstrahlung of electrons, allowing for polarisability *(Russian)* 77—3475
- bremsstrahlung orientation and alignment parameters 78—33628
- cascade effects on polarisation of radiation, electronic or atomic collisions 80—18917
- close-coupling formalism, perturbative treatment, electron impact excitation 80—48091
- coherence effects, quantum mechanical excitation amplitudes 77—42419
- collisional cross-sections determ. for low and intermediate energy processes 80—99579
- Compton defect in X-ray and electron scatt. in 1st Born approx., Compton shift 77—88428
- computational atomic and molecular physics, conf., Nottingham, England, (Sept. 1978) 79—59567
- conference, electronic and atomic collisions, Paris (July 1977) 78—58758
- conference, physics of ionised gases, Dubrovnik, Yugoslavia, (Aug.-Sep. 1976) 77—42961
- conference on ionised gas physics, Dubrovnik, Yugoslavia (Aug.-Sept. 1978) 80—36779
- continuum orbital approx. weak-coupling theories, inelastic scatt. 78—33417
- continuum state, electron scatt. in intense radiation field, time-independent methods 78—25705
- correlation effects 78—58842
- coupled channels optical model, total reaction cross-sections 80—18929
- cross section, calc. using effective Feynman diagrams, in plasma 80—38566
- dielectric gas, breakdown strength, electron impact ionis. and scatt. cross section 79—82031
- distorted wave approx. for excitation 78—22033
- distorted wave calcs. for Io plasma torus 80—82262
- distorted wave expansion with off diagonal pots., local approx. 79—31694
- distorted-wave approximation, higher-order methods, s-s excitation 79—27088
- eikonal theory, at. electron (positron) scatt., review 78—25707
- electron bremsstrahlung energy spectra, 1 to 2000 keV, neutral atoms $Z=2$ to 92 78—62920
- electron bremsstrahlung energy spectra above 2 MeV, partial wave interpolation 79—72416
- electron impact spectroscopy, low-energy aspects, book contrib. 80—14243
- electron ion collisions, distorted wave theory, Auger ionis. and excitation fluoresc. 79—7018
- electron plasma relax. characts., 3-30 eV 80—79612
- electron scattering, free free processes 80—63834
- electron-collision cross-section data for atom or molecule, rel. to radiation physics 80—63829
- electron-ion bremsstrahlung with shielding 78—66667
- electron-ion collisions, crossed beam expts. 78—58843

atomic electron impact excitation continued
  electron-photon angular correlation in atomic physics 79—64109
  electron-photon coincidence expts., interpretation 80—83489
  electronic and at. collisions, conf., Kyoto, Japan (Aug.-Sept. 1979) 80—57011
  electronic and at. collisions, conference, Kyoto, Japan (Aug.-Sept. 1979) 80—62394
  elementary atomic processes, threshold behaviour 80—23546
  exchange excitation of atoms by high angular momentum electrons *(Russian)* 77—88576
  exchange matrix element evaluation from Coulomb interaction operator 80—18905
  excitation function measurement, three-channel electronic apparatus *(Russian)* 78—25456
  excited atom, electron scattering, low energy, quasidegenerate case 79—76515
  fast electron and positron scatt. 78—62918
  fixed scatterer approx. simple form 77—50544
  free-free transition due to laser beam in electron-atom scatt. process 78—9262
  gas in SEM sample chamber, electron scatt., appl. to N_2 79—49342
  gas mixture, self sustained volume photoionisation discharge existence conditions 80—79610
  gas optical breakdown, quantum kinetic eqn. for electrons *(Russian)* 79—60092
  gases, low energy positron interactions, review 78—50651
  Glauber theory modification, including multiple scatt. *(Russian)* 78—29855
  Glauber wavefunction, without nonmoving bound particle assumption 79—18250
  Glauber-Ochkur exchange amplitude, validity 77—23562
  glow discharges, atomic and ionic spectral line excitation in cathodic region *(Russian)* 78—63611
  H Lyman α in solar chromospheric flares, direct collisional excitation rel. to profile and polarisation 80—41780
  high Rydberg atoms, dipole transitions, impact parameter method 78—62922
  high-energy electron impact spectroscopy, book contrib. 80—14244
  high-momentum transfer, amplitudes form, Faddeev-Watson approx. 80—23555
  HV electron microscopy, total scatt. cross-section obs. 79—21859
  hydrogenic atom, 1s-2s excitation, generalised Coulomb-projected Born approx. cross-sections 78—17803
  hydrogenic atoms and ions, degenerate state transitions, plasma waves, Stark effect 79—72389
  hydrogenic ions, electron impact excitation, modified Coulomb-Glauber approximation 79—81285
  hydrogenic ions, ground state, electron impact excitation, first-order Coulomb exchange approx. calcs. 79—59581
  hydrogenlike ions, electron impact excitation, Coulomb-Born-Oppenheimer calcs. 79—10211
  inelastic exchange kernels, semiclassical exchange approximation theory 78—50642
  inelastic scattering in laser field, Green's function method calcs. 79—94086
  inelastic transitions between close at. levels, cross sections, rate coeffs. 77—3467
  inert gas, electron beam pumping for dye vap. excitation 77—42535
  inert gas atoms, electron impact excitation to high Rydberg states 79—89790
  inert gas electron beam excited plasma UV absorpt. by diatoms 79—68907
  inert gas hollow cathode arc, mol. beam sampling of metastable atoms as electron temp. probe 80—43967
  inert gas nuclear pumped lasers, electron impact cross section meas. 80—63985
  inert gas-positron total cross-sections at intermediate energies meas. 77—3456
  inert gases, electron beam excited, absorpt. characts. 78—82948
  inert gases, electron impact ionisation cross-sections for excited states 80—9742
  inert gases, optical model, differential and inelastic cross-sections, spin polarisation 77—75299
  inner shell generalised oscill. strengths, with outer shell effects 78—50507
  inner shell ionisation phenomena, conf., Freiburg, West Germany, (Mar.-Apr. '76) 77—27040
  intermediate coupling strengths from LS coupled R-matrix elements 79—18292
  ion+electron collision, resonant electron bremsstrahlung *(Russian)* 80—102580
  ion+electron scatt., static exchange approx. Schwinger variational principle, photoionisation cross section 80—43192
  ion electron impact detachment, ionisation, excitation, dissociation and recombination 80—63832
  ionised gas, slow electron momentum transfer cross section in mag. field, RF cond. meas. 79—82030
  ionosphere, electron cooling rates, discrepancy with heating rates 77—29564
  ions, electron impact, 1 to 100 keV, bremsstrahlung emission, theory 78—22005
  ions, electron impact, direct excitation and ionisation, distorted wave theory 78—25722
  ions, electron impact, nonrelativistic bremsstrahlung intensity components 79—72426
  laser excitation mechanisms for atomic and ionic lasers, book contrib. 80—106512
  laser field, photon correl. effects 80—83481
  laser field atomic electron scatt. without optical pumping, reson. state coupling, theory 78—17804
  laser field photon absorption by reson. scatt. electron 79—859
  laser induced free-free transitions, differential sum rule, anal. 80—23372
  laser-atom system, laser field effects 77—10768
  lasing below 1000 Å, electron pumping of C and He like ions 77—65589
  lifetime meas. in atoms, mols., ions 77—30832
  light atoms, intermediate energy, review 79—856
  light element microanalysis 79—61935
  line radiation, polarisation, long-range electron correls. effects 80—91683
  long optical lifetimes meas., distortion effects 78—9276
  many-electron atom-unbound electron system, normalisation of wave function 77—68123

atomic electron impact excitation continued
  many-electron correlations 77—42409
  matrix variational calcs. of electron-atom scattering, review 79—59577
  metal atom, collision cross sections 77—42410
  Ne IX, electron impact excitation cross section calcs. using nonrelativistic Coulomb-Born approx. 77—42414
  neutral atom electron impact, calculation of certain second Born integrals 79—59578
  neutral atom lines, Stark broadening, adiabatic theory, classical trajectories of electrons 80—18936
  neutral atoms, bremsstrahlung of low-energy electrons, polarisation effects 80—102577
  neutral atoms, electron interaction, free-free radiative transitions, review 78—90295
  $nl \rightarrow (n+1)l'$ collisional transitions, inelastic form factors and Born cross sections 80—58390
  open-shell target, electron scatt., orthogonality constraints 77—71869
  optical excitation function, struct. 80—43189
  optical model for electron spin polaris. 78—50646
  optical oscillator strengths calculation, slope of generalised oscill. strength vs. momentum transfer curve 79—98155
  partial resonance widths, Siegert eigenvalues, basis-set calc. 80—37880
  photoelectric effect and electron diffusion in gases 78—81745
  plasma, electron energy loss by ionisation and excitation of atoms 80—33732
  plasma, electron impact excitation coeff. for highly ionised ions 77—7510
  polarisation effects for change in at. spin, triplet state excitation *(Russian)* 77—46645
  polarisation potential for electron-atom scatt. 78—42228
  polarised electrons, book 77—46679
  positive ions, evaluation of radial integrals in Coulomb-Born approx. 78—74768
  positive ions, one- and two-electron, distorted-wave polarised-orbital model 77—83741
  positron annihilation in heavy at. shells, nuclear orientation *(Russian)* 79—49602
  positron collisions in gases, low energy 78—13609
  post collision interactions from collisions between electrons and atoms *(Dutch)* 78—5357
  potential scatt. in low freq. laser field, perturbation theory 80—43191
  potential scattering, refined Born approx. 80—77
  R-matrix method, application to atoms and ions 78—58833
  R-matrix method, basic concepts, rel. to other theories electron scatt. 78—58832
  relativistic effects in excitation and ionis., $Z\alpha$ and v/c depends. 79—860
  resonance obs. optical excitation functions 78—58841
  resonant electron scatt. by atoms in laser field, negative ion formation, polarisability 77—19089
  resonant phenomena, complex stabilisation method 80—78515
  resonant scattering, complex-coordinate method, using variational principle 79—86070
  retarded radiation from fast electrons, dynamic polarisability *(Russian)* 78—22036
  review, of expt. and theory 78—25699
  rotated coordinate method use, rel. to stabilisation method 80—37845
  Rydberg angular momentum transfer, stochastic model for induced consecutive transitions 78—46429
  Rydberg atom, electron collisions 80—63833
  Rydberg atoms, cross sections, theory 77—58172
  Rydberg states, Schwinger's variational principle 80—78713
  Rydberg states, transitions following electron impact excitation *(French)* 80—78711
  Schwinger variational principle 79—45780
  semiclassical approximation calcs. 80—23563
  slow electron scatt., correlation effects 77—42299
  solar atmosphere, spectral line intensity, electron impact excitation 80—36605
  spin dependent phenomena in electron-atom collisions 80—63830
  spin polarisation, density matrix formulation *(Russian)* 77—31003
  spontaneous superradiance in plasma flow 77—3470
  system of N charge particles in external Coulomb field, asymptotic form of wave function 77—71871
  T-operator, general quasiclassical approx., appl. to $H(1s) \rightarrow H(2s,2p)$ 79—50134
  target atom decay, scatt. projectile and photon coincident detect coherence effects 80—63791
  theoretical models, review 77—58166
  total inelastic scatt. cross section, detector solid angle depend., approx. bounds 78—17798
  two-body model atom, excitation by fast particles in high momentum transfer limit 78—17780
  two-electron ions, distorted-wave program 77—88570
  upper atmosphere, electron impact yield spectra 78—28401
  variable phase method in multichannel electron-atom or electron-ion scatt. 77—19082
  variational method in ion-atom collisions 77—23547
  variational methods, appl. to at. scatt., review 78—86951
  variational principle for scatt. length, target ground-state wave functions imprecisely known 77—58164
  wave packets, radial, appl. to target distortion 80—87234
  X-ray spectra of impact excit. highly charged ions, dielectronic satellites 78—62762
  μ^-p, electron scatt. length determ. 79—36801
  Ag electron excited Lα emission spectra 80—102481
  Ag, population mechanism, highly-excited states, hollow cathode discharge *(Russian)* 78—63610
  Al, electron impact excitation cross sections calc. *(Russian)* 78—55240
  Al, electron scatt., transitions, oscill. strengths, config. superposition calcs. 77—6732
  Al, excitation cross sections 79—54972
  Al, fast electron beam scatt. calcs. 77—65534
  Al I, electron impact line broadening in arc spectra 79—26919
  Ar, 40 keV electron scatt. 7-200 mrad, relativistic and electron correlation effects 77—34760
  Ar, autoionising states excitation by electron impact, threshold effects 78—62923
  Ar electrical discharge, electron-collisional excited-state kinetics 77—24226
  Ar, electron impact, L X-ray spectrum, radiative Auger transitions 80—58227

atomic electron impact excitation continued
Ar, electron impact, near threshold UV-emitting level excitation 78—25711
Ar, electron impact excitation, extreme VUV reson. lines 77—6937
Ar, electron impact excitation, L-MM, LM-M^3 Auger linewidths, L, S and J dependence 77—14588
Ar, electron impact excitation, continuous spectrum radiation mechanism 79—3395
Ar, electron impact excitation, 23 to 37 eV, metastable yield 80—9739
Ar, electron ionisation, Ar^+ metastable cross section, laser fluoresc. 77—3465
Ar, electron ionisation and excitation coeffs. in low E/N region 80—48090
Ar, electron momentum transfer cross-sections 0.4 eV 77—35308
Ar, electron scatt., free-free transition meas. 77—3464
Ar, electron scatt. and ejection, electron energy loss spectra 80—58394
Ar, electron scatt. in intense IR field, multiphoton free-free transitions 79—81289
Ar, electron scatt. multiphoton process effects, laser-induced free-free transitions 77—79595
Ar, electron-atom bremsstrahlung continuum, afterglow decay *(German)* 78—83626
Ar, electron-photon coincidence obs., reson. lines, polarisation correls. 79—31697
Ar, electron-photon coincidence measurements for Ar excitation 80—37886
Ar, excitation by energetic electrons, appl. to Mars atmosphere 77—31420
Ar, excitation by pulsed electric discharge, luminescence obs., time resolved spectra meas. 80—102482
Ar fluoresc., polarisation of reson. lines, 104.8 and 106.7 nm, electron impact excitation 77—83739
Ar, fluoresc. following slow electron impact, 380-710 nm 79—22646
Ar, gas, slow positron annihilation and momentum transfer rates 79—22828
Ar glow discharge, line radiation of plasma in early afterglow 80—38745
Ar II, line-continuum interference effect in Lorentzian wings 79—18147
Ar jet, supersonic, electron beam-excited, continuous VUV emission spectrum origins 79—6964
Ar, L-excitation by electron and proton impact, Auger multiplets, excitation probabilities 77—14589
Ar L-shell, X-ray emission spectra prod. by 0.3-3 keV electron impact, line intensities 79—45666
Ar, metastable, electron impact excitation cross-sections calcs. 78—94323
Ar, multiple-collision diffr. theory 78—82844
Ar, positive column, 4S and 4P levels populations, rel. theory with recomb. 77—10766
Ar, positron annihilation decay rates, high temp. behaviour 80—58389
Ar, production of Ar_2*, kinetic behaviour and energy transfer 79—68305
Ar supersonic jet, ultrasoft X-ray emission 77—27015
Ar, total electron impact excitation cross section, first Townsend coeffs. 77—536
Ar, total scatt. cross section, 20-3000 eV 79—36778
Ar, weakly ionised, energy transfer at high press. 78—58845
Ar XVI, lithiumlike ions, excitation by electron impact 78—13606
Ar^+, electron impact excitation, extreme VUV reson. lines 77—6937
Ar^+, upper laser levels collisional excitation and de-excitation, rate coeffs. 79—7112
Ar^{n+}, electron impact inner-shell excitation/ionis. cross section 77—23564
Ar-Cu, Cu diffusion coeff. determ. volatile salt dissoc. in pulsed discharge 80—33721
Ar-Kr jet, electron excited, VUV emission spectra 80—933
Ar+HCN(H_2O), electron excitation of Ar* and Ar_2*, fluoresc. and dissoc. energy transfer collisions 77—14580
Ar+Xe→Xe*, electronic energy transfer, emission spectra, electron beam excitation 77—38722
^{37}Ar, L-shell internal excitation accompanying L-capture 80—95726
^{79}Au, electron impact, relativistic, L-shell ionis., $L\beta/L\alpha$ branching ratio energy depend. 79—98228
B^+, collision strength for 2p state, close-coupling calc. 78—55247
B^{3+}, cross-sections, modified Oppenheimer approx. 78—82843
Ba, electron impact step-wise excitation *(Russian)* 80—83497
Ba, electron scatt., elastic and inelastic (5^1D, 6^1P) cross sections, 20-100 eV 78—74769
Ba, electron scatt. cross sections, close coupling calc. with CI 80—43180
Ba, emission spectra, 50 to 90 nm 78—82846
Ba, excited state lifetime, delayed coincidence meas. 77—3315
Ba, scatt. from excited atoms, 30 and 100 eV, inelasic and superelastic 78—86933
Be isoelectronic sequence, electron impact excitation 79—81286
Be isoelectronic sequence, electron impact excitation of reson. transitions 80—63825
Be^+, 2p state, cross sections, Coulomb-Born and close-coupling approxs. 77—75303
Be^+, absolute cross sections and polarisation of electron-impact excitation of resonance multiplet 80—99577
Be^+, resonance lines electron impact excitation, polarisability 78—42225
Be^{2+}, cross-sections, modified Oppenheimer approx. 78—82843
Be^{3+}, electron scatt. near ionis. threshold, ang. momenta 79—31698
Be-like ions, electron impact excitation, config. mixing 77—58175
^{83}Bi, electron impact, relativistic, L-shell ionis., $L\beta/L\alpha$ branching ratio energy depend. 79—98228
C, $^3P \rightarrow {}^1D$ electron impact excitation, distorted wave approx., exchange and polaris. effects 77—34764
C, cross sections 77—50538
C, electron excitation cross section calc., Born approx. with Slater wave functions 80—69243
C, electron scatt., at. field bremsstrahlung, photon linear polaris. 78—62927
C II, electron impact induced fine struct. transitions, collision strength 77—50540
C III, electron collisional excitation, R-matrix calc. 77—58169
C III, electron collision rates rel. to solar emission line ratios interpretation 78—28598
C III, excitation cross sections, Coulomb-Born approx. 77—75302
C IV, lithiumlike ions, excitation by electron impact 78—13606
C, low energy elastic and inelastic scatt., Bethe-Goldstone and pseudostate approx. 77—68112
C V, electron impact collision rates, reinterpretation of solar emission line ratios 80—98624

atomic electron impact excitation continued
C V, electron impact excitation cross section calcs. using nonrelativistic Coulomb-Born approx. 77—42414
C^{3+}, electron impact, inner shell excitation cross-sections 79—59580
C^{3+}, electron impact 2s-2p excitation, absolute cross sections 78—13605
C^{3+}, lithium like ion, excitation, resonance tabulation, cross sections 78—33616
C^{3+}, relativistic Coulomb-Born approx. 79—68318
C^{4+}, cross-sections, modified Oppenheimer approx. 78—82843
C^{5+}, electron impact, continuum orbital approx., weak coupling theory 78—33417
C^{n+}, electron impact inner shell excitation/ionis. cross sections 77—23564
Ca, 2 keV electron excitation and ionis., ejected electron spectra 77—3466
Ca, $3p^6$ subshell excitation by electron impact 80—1070
Ca, electron impact, $3p^6$ subshell excitation, VUV spectra *(Russian)* 78—90117
Ca II, identification of low energy autoionising levels 79—31703
Ca^+, resonance lines electron impact excitation, polarisability 78—42225
Cd, 5^3P_1 autoionising state, 150 eV electron impact excitation, (e, 2e) ang. distrib. study 80—83495
Cd, AES, $M_{4,5}N_{4,5}N_{4,5}$, vap. and solid, solid state effects 77—61857
Cd, electron impact, 6^2D_2 and 7^1P_1 level mixing 80—37889
Cd electron impact ionisation, of autoionising levels, ejected electron spectrum 78—5356
Cd, electron impact ionisation cross-sections for excited states 80—9742
Cd, electron scatt., negative ion form., shape resonances, electron affinity 77—14581
Cd, excitation by slow electrons 79—72428
Cd II, $4d^95s^2\ {}^2D_{5/2}$ level broadening in ion laser 77—19239
Cr ions in Tokamak plasmas, spectroscopy and atomic physics 80—53938
Cs, ejected electrons from autoionis. levels excited by electron impact 77—88573
Cs, electron excitation cross sections for six autoion. config., Born approx. calc. 78—25713
Cs, electron impact excitation velocity consts. for reson. levels, meas. *(Russian)* 78—1086
Cs, electron-atom momentum transfer cross sections, from plasma electron thermal conductivity 78—42224
Cs, optical reson. line electron impact excitation cross sections, polaris. 78—55244
Cs plasma in vacuum diode, pre-discharge, electron impact excitation line emission polarisation 78—47170
Cs, reson. lines, slow electron excitation cross section, low-lying D level coupling 77—23563
Cs^{2+}, electron impact excitation studies by intersecting beam method 80—69239
Cs(Ar-Cs) plasmas, electron momentum transfer cross section, cyclotron reson., temp., cond., and vel. meas. 80—106930
^{131}Cs, L-shell internal excitation accompanying L-capture 80—95726
Cu, absolute effective electron impact excitation cross sections, spectral obs. 80—53147
Cu, ang. distrib. for 98.6 keV electrons 79—18295
Cu, atom, electron impact cross section, elastic and ^2P and ^2D states, inversion ratios 78—9256
Cu, electron impact, excitation function (maxima, cross-sections) 78—50650
Cu, electron impact ionisation cross-section, calc. *(Russian)* 79—89789
Cu isoelectronic series, collision strengths and Gaunt factors 79—98227
Cu, population mechanism, highly-excited states, hollow cathode discharge *(Russian)* 78—63610
D, electron impact, coherent excitation in longit. elec. field, Balmer-α flux 78—22035
^{165}Er, L-shell internal excitation accompanying L-capture 80—95726
Eu, autoionising states excitation in electron collisions *(Russian)* 79—86073
Eu, electron impact excitation of spectral lines 79—3579
Eu, electron impact excitation cross section, Born and Ochkur approx. 80—87230
Eu, VUV emission spectra, 5p electron excitation by electron impact 77—68007
Eu^+, resonant line excitation 78—82847
F^{q+}+He, (q=1-9), X-ray prod. by electron excitation, ionisation and capture 79—76379
Fe II permitted emission, excitation mechanism in Seyfert 1 galaxies and QSOs 79—21412
Fe III, Fe VI, electron impact excitation cross sections and gaseous nebulae Fe abundances 78—53806
Fe ions in Tokamak plasmas, spectroscopy and atomic physics 80—53938
Fe, Kα satellite lines following electron bombardment 80—69097
Fe XII, in solar corona, excitation of spectrum 77—17458
Fe XXIV, oscillator strengths, electron impact excitation collision strengths, solar flare spectra appl. 80—32647
Fe XXVI, and isoelectronic ions, electron impact excitation cross section calcs. 78—9257
Fe^{19+}, electron collision strengths calcs. 80—67545
Fe^{23+}, relativistic Coulomb-Born approx. 79—68318
Fe^{5+}, electron impact collision strengths and forbidden Fe VI emission under nebular conditions 79—8970
^{55}Fe, L-shell internal excitation accompanying L-capture 80—95726
Ga, electron impact excitation cross sections calc. *(Russian)* 78—55240
Ga, excitation cross sections 79—54972
Ga, reson. states lifetimes, electron-at. crossed beams expt. 77—68013
^{77}Ge, L-shell internal excitation accompanying L-capture 80—95726
H, 1s-2s exchange scatt., exchange corrected eikonal approx. 78—9252
H, 1s→2s transition, electron impact excitation, exact second Born amplitude 80—102572
H, 2p state, electron impact excitation, distorted wave approx. 77—10771
H, 2p state orientation by fast electrons 77—71874
H, 2s and 2p electron scatt. excitation, second Born term 77—538
H, 2s state, differential cross section, plane-wave approx. 78—86953
H, (1s-2s) excitation, dynamic polaris. pot. 78—78818
H and hydrogenic ions, cross-sections and rates 78—50649
H, angular momentum transfer 77—30999
H, asymptotic Glauber cross sections 80—9741
H, Born and classical cross-sections, comparison *(German)* 78—86952
H, coherent-state multipole moments, final state interactions 77—83742
H, complex optical pot. methods 79—22844
H, cross section calc., Crothers and McCarroll method 78—25715
H, cross sections, second Born approx. *(Russian)* 79—36780

atomic electron impact excitation continued
H, cross sections 77—50538
H, cross-section, two-pot. eikonal approx. 79—22847
H, differential cross-section and oscillator strength, 136-300 eV 79—36774
H, distorted wave approx. 78—22033
H, distorted wave expansion with off diagonal pots., local approx. 79—31694
H, e$^+$ scatt., two-pot. eikonal approx., 50-200 eV 79—31685
H, elastic scatt. and n=2 states excitation, fixed-scatterer approx. 77—50544
H, electron and positron bremsstrahlung, differential cross sections 79—18294
H, electron elastic scatt. at low intermediate energies 80—106393
H, electron exchange scatt., generalised Coulomb-projected Ochkur-Born approx. 77—83730
H, electron impact, 1s-2s and 1s-2p excitation, electron-photon coincidence meas. 80—87233
H, electron impact, coherent excitation in longit. elec. field, Balmer-α flux 78—22035
H, electron impact, coupled channels optical model, total reaction cross-sections 80—18929
H, electron impact, in laser field, Born-Oppenheimer approx. calcs. 79—54973
H, electron impact, inelastic scatt. semiclassical exchange approximation theory 78—50642
H, electron impact coincidence, even-odd parity coherence effects, polarisation ang. distrib. 78—9253
H, electron impact excitation, differential scatt., semiclassical calcs. 77—14583
H, electron impact excitation of n=3 levels, polaris. fractions in Glauber theory 77—34765
H, electron impact excitation of resons. below n=3 levels, algebraic variational calc. 78—9254
H, electron impact excitation, 1s-2p, ang. correl. parameters, distorted wave approx. calcs. 78—9258
H, electron impact excitation in presence of intense laser beam 78—9261
H, electron impact excitation, coherent state multipole moments, model calcs. 79—76518
H, electron impact excitation 80—18909
H, electron impact excitation in circ. polarised laser field 80—18927
H, electron impact excitation, modified Glauber theory calcs. 80—18934
H, electron impact excitation, cross-sections, multipole moments, quasiclassical calcs. 80—63828
H, electron impact excitation, electron-photon coincidence, large angle expt. 80—83500
H, electron impact excitation of n=2 to n=3 transition, algebraic variational method close coupling calcs. 80—91678
H, electron impact ionisation, electron-photon coincidence meas. 78—55242
H, electron inelastic scatt., effective exchange potentials 78—90300
H electron scatt., lowest ^{1}S resonance 77—58177
H, electron scatt., lowest ^{1}S resonance, Feshbach formalism corrections 77—58178
H, electron scatt., orthogonality constraints 77—71869
H, electron scatt., polarisation potential 78—42228
H, electron scatt. at intermediate energies, fixed scatter approx. 80—9740
H, electron scatt. information obtained using symmetrically coupled partial differential eqn. 80—102574
H, electron scatt. total spin quantum number changes 79—54969
H, electron scattering, inhomogeneous eqn. method 77—27:82
H, electron scattering, low-energy, 1S-approximation channel coupling array 77—10756
H, electron-photon ang. correl., for H(2p) 79—31699
H, electron-photon excitation, high-energy resonant cross sections 78—70938
H, electronic stopping power calcs. 80—2104
H, equivalent exchange pots., algebraic variational method, 2p-2p and 2s-2p transitions 80—18931
H, exchange amplitude, Glauber-Bonham-Ochkur approx., differential cross sections 77—19078
H, exchange polarisation effects 77—42417
H, excited state electron and ion quantum scatt. cross sections, dipole approx. *(Russian)* 79—6996
H, form factors and cross sections for nl→n′l′ direct collisional transitions 79—31636
H, gas discharge source for electron scatt. expts. 78—94332
H, Glauber amplitudes from low to highly excited states 77—68122
H, Glauber exchange effect 78—25720
H, high-energy behaviour of elastic and 2s excitation scatt. cross-sections 77—10763
H, in homogeneous mag. field, transition amplitude from 1st Landau level 79—10218
H, inelastic electron scatt., relativistic calcs. *(Russian)* 77—83737
H isoelectronic series, electron impact ionisation, electron ang. momentum exchange 78—78820
H, matrix elements by Faddeev approach 80—78714
H, modified Glauber method with exchange calc. 78—37751
H, n-changing transitions, Glauber approx. 77—79686
H, n=2 level, generalised two-pot. distorted wave model calcs. 78—37748
H, n=3 level, coherent excitation by electron impact, density matrix anal. 78—78817
H plasma, departures of electron energy distrib. from Maxwellian rel. to excitation rates 77—80266
H, positron P-wave scatt., elastic and positronium form. cross sections 77—3468
H, positron scatt., analytic model, complex scaling 79—18257
H, positron scatt., Feshbach resonances, close-coupling calc. 77—6940
H, positron scatt., S-wave reson., generalised scatt. length 78—42226
H, scattering length calc. with imprecise target wave function, variation principle 79—72375
H, simplified model, low and medium energy 78—86954
H, source theory 78—46415
H, transitions between degenerate states at low energies 77—79685
H, transitions between excited states 77—58168
H$^-$ ^{1}P resonances, pseudostate expansion calcs. 80—32841
H^{2-}, Z-Z 80—28104
H-like atoms, electron exchange scatt., high impact vels. 79—22846

atomic electron impact excitation continued
H-like ions, electron impact excitation, Coulomb-Born-Oppenheimer calcs. 77—6938
H-like ions, electron impact excitation, distorted-wave approx., accuracy 78—5351
H-like ions, electron impact excitation, resonances, collision strengths 78—33612
H-like ions, electron impact excitation to S states exchange effects 78—58835
H-like ions, electron impact excitation to s state 78—58836
H-like ions, electron impact excitation, Coulomb Born approx. 78—58840
H-like ions, electron impact excitation, Coulomb modified Glauber approx. calcs. 78—94324
H-like ions, excitation cross sections and rates, Coulomb-Born and Born approx. 77—71873
H-like ions, Glauber exchange amplitudes for electron scatt. 78—74772
H-like ions, n=2→1 transitions, collision strength Z-dependence 80—91675
H+atom(ion)(electron), general excitation cross section theory 80—37869
H(1s) electron scattering, variable-charge Coulomb-projected Born approximation 80—58392
H(1s), excitation to 2s and 2p, Glauber theory modification *(Russian)* 78—29855
He, ^{1}S(1s,3s) state excitation by electron impact, Glauber approx. 79—31696
He, ^{1}2P$_1$ electron scatt. excitation, second Born term 77—538
He, ^{3}S→2^{1}S transition probability, electron collisions 78—5358
He, 1^{1}S→2^{3}S, 2^{3}P, R-matrix method extension 79—64107
He, 2^{1}P state, eikonal-Born series approx. 78—17799
He, 2^{1}P state excitation, 80 eV electron impact, λ and χ parameters meas. 80—32839
He, 2^{1}P-state electron impact excitation, 40 to 500 eV, alignment and orientation 80—83499
He, 2^{1}S, 2^{1}P and 2^{3}P states excitation and ionisation yields, energy deposition efficiency 77—31002
He, 2^{1}S and 2^{3}S excitation cross sections, partial wave anal. 78—90301
He, 2^{1}S and 2^{3}S states excitation 77—42412
He, 2^{1}S-state, electron impact excitation, intermediate energy calcs. 79—59583
He 2^{3}S-3^{3}S electron impact excitation, first Born and Glauber cross sections 78—55243
He, 2^{3}S-state, electron impact excitation, reson. form. mechanism 80—99463
He, 3^{3}P level, excitation and decay study up to high press. pumped by intense relativistic electron beam 80—74250
He, 3^{3}P level, spontaneous decay probability, expt. and theoretical values 78—50501
He, (1^{1}S-2^{1}P) excitation, coincidence meas. 77—46641
He, (2^{3}S$_1$) state excitation by electron impact, at. time of flight meas. 77—19083
He (2^{3}S), resons. below n=3 doubly excited states, electron impact excitation 77—50543
He, (2p^2)^{3}P doubly excited state, electron impact excitation XUV emission 79—86071
He, (2p^2)^{3}P state, electron impact excitation, parity unfavoured transition 80—91680
He, absolute total scatt. cross sections, 0.5 to 50 eV 78—74765
He and He$^+$, 3^{3}P and 4^{2}F levels excitation with electron beams, radiation decay obs. 80—43188
He, coherent excitation of 2^{1}P state, large momentum transfer 79—36775
He, Compton defect, high energy electron impact spectroscopy 77—71876
He, cross section calc., Crothers and McCarroll method 78—25715
He, cross sections, second Born approx. *(Russian)* 79—36780
He, cross-sections, modified Oppenheimer approx. 78—82843
He, electron and neutral collisions, Rydberg level transitions 79—45821
He, electron elastic and inelastic scatt., Glauber eikonal series 80—43183
He, electron excitation functions for 2^{3}S, 2^{1}S, 2^{3}P and 2^{1}P states, R-matrix methods 78—25716
He, electron impact, ^{3}P$_g$ and ^{1,3}D$_u$ states excitation, electron correlation influence, Rudge-type approx. 78—74771
He, electron impact, 1^{1}S→2^{1}S and 1^{1}S→2^{1}P excitation 80—91679
He, electron impact, induced transitions between high Rydberg levels 78—21877
He, electron impact, low energy, post collision interaction, ejected electron energy distrib. 79—72423
He, electron impact calcs. using R-matrix and linear algebraic methods 79—59579
He, electron impact double excitation, Glauber amplitude calcs. 78—1083
He, electron impact excitation, correl. effects near ionisation threshold 77—10764
He, electron impact excitation, photon emission, ang. 77—14584
He, electron impact excitation cross-section, Born-Ochkur approx. calcs. 77—19088
He, electron impact excitation, in autoionisation region, parametrised close-coupling calcs. 77—54612
He, electron impact excitation of 2^{3}S level, differential cross section in second Born approx. *(Russian)* 78—1087
He, electron impact excitation, near threshold, UV emitting levels obs. 78—5170
He, electron impact excitation, 2nd order pots. method calcs. 78—13608
He, electron impact excitation, Born-Oppenheimer exchange amplitude and local exchange pot. 78—29854
He, electron impact excitation of 2^{1}P state, first-order many-body theory 78—42223
He, electron impact excitation, ^{3}P$_g$ and ^{1,3}D$_u$ states, electron correlation influence, Born-Oppenheimer approx. 78—74770
He, electron impact excitation of 1^{1}S→2^{1}P(3^{1}P), excitation cross section and polarisation fractions, XUV emission 79—22841
He, electron impact excitation, resons., near n=3 threshold 79—36773
He, electron impact excitation, intermediate energies calcs. 79—76517
He, electron impact excitation, distorted wave theory of electron interaction 80—23554
He, electron impact excitation, electron-photon angular correlation meas. 80—63826
He, electron impact fluoresc., polarisation of visible and UV lines 77—88568
He, electron impact fluorescence, polarisation of 5876 line 78—82848

atomic electron impact excitation continued
He, electron impact metastable excitation, resonance struct. 77—27184
He, electron impact spectroscopy for Compton profile meas. 78—90299
He electron impact threshold excitation of n=2 state 80—83490
He, electron scatt., inelastic Feshbach resons., quasi projection operator calc. 80—58395
He, electron scatt., ionisation, elastic and inelastic collisions, many body theory appl. 80—48093
He, electron scatt., near 2^1S-state threshold, S-matrix obs. 77—10761
He, electron scatt., total cross-sections, meas. apparatus 77—54628
He, electron scattering total cross sections, 0-3000 eV 78—25709
He, electron-photon ang. correl. meas., 80 eV 78—42229
He, electron-photon ang. meas. for 2^1P state 80—102575
He, electron-photon coincidence meas. quantum mech. excitation amplitudes phases determ. 77—10762
He, exchange polarisation effects 77—42417
He, excitation cross sections rel. to photon interactions 80—27985
He, excitation of $^3P(2p)^2$ state, integral form of close-coupling approx. 77—539
He, excitation of 2^1P and 2^3S states, distorted-wave model 79—31701
He, excited, optically-allowed, long-range interaction pots. with electrons, protons and atoms 77—14520
He, excited S, D and F state radiative lifetimes, electron impact method 78—94325
He, excited state, excitation, long-range force effects 79—10170
He gas, electron energy loss function in range 50 eV to 1 keV 77—61859
He, Glauber scatt. amplitude, numerical method in Lommel function 79—22795
He ground state, electron impact excitation, alignment and orientation parameters calcs. 79—36772
He, ground state to n^3S states (n=2, 3, 4), 200 and 300 eV, calc. 80—14235
He, ground→$3^1S,4^1S$, intermediate energy calc. with exchange 80—53143
He, high Rydberg state, dipole transitions, impact parameter method 78—62922
He I, transfer excitation energy between n=5 levels 78—70942
He I, triplet state, excitation energy transfer among upper levels 79—26901
He I $2^3S \rightarrow 2^3P$ transition, rate coeff. for electron impact excitation 79—48664
He I spectral lines, radiation trapping in electron beam spatial distrib. of line intensity 77—79572
He II excited states in optically thin plasmas, role of direct ionisation-excitation 80—102579
He in transient plasma, excitation transfer between excited states 78—70914
He, low energy excitation of high Rydberg states, cross-sections and distribs. of quantum states 77—83744
He metastable 2^3S state, electron impact excitation cross-sections calc. *(Russian)* 80—53149
He, metastable atoms beam prod. with good vel. resolution 77—14609
He, metastable state excitation, high resolution study 77—6935
He, n=3 levels excitation, cross sections, angular correlation parameters 77—61855
He, n=3 states, polarisation and excitation functions 77—6934
He, polarised state electron excitation, electron photon coincidence 77—6930
He, positron diffusion in gas, annihilation and scatt. 77—19074
He, positron inelastic scatt. at intermediate energies, time of flight spectra 80—18932
He, positron s-wave scatt., total cross sections 77—42406
He, resonances, cusp effects, virtual state 78—25712
He, resonant states, high resolution study via electron excitation 77—6936
He, Schwinger variational principle, including exchange 79—81277
He, sensitivity of cross-section and ang. correl. to scatt. parameters 80—5596
He$_-$, electron impact, post-collision interaction, reson. states 77—10767
He$^-$ resons. in 56 to 64 eV electron collisions, autoionising states and spectral line polarisation 80—53145
He$^+$, detection of $6D_{5/2}$-$6S_{1/2}$ double quantum transition 77—61858
He$^+$, electron impact excitation, Coulomb-Born-Oppenheimer calcs. 77—6938
He$^+$, electron impact excitation, five-state model calcs. 77—10770
He$^+$, electron impact excitation to S states exchange effects 78—58835
He$^+$, electron impact excitation cross-sections, reson. parameters calcs. 80—91686
He$^+$, electron impact ionisation, in threshold region, three body theory 77—19087
He$^+$, electron impact ionisation, electron ang. momentum exchange 78—78820
He$^+$, electron inelastic scatt., effective exchange potentials 78—90300
He$^+$, electron scatt., 1s-2s transition, Coulomb-Born and Coulomb-Born Oppenheimer calcs. 77—50539
He$^+$, electron scatt., Glauber exchange amplitudes 78—74772
He$^+$, electron scatt., reson. state assoc., incomplete spectrum of Hamiltonian matrix 80—99568
He$^+$, electron scatt. near ionis. threshold, ang. momenta 79—31698
He$^+$, excitation in hollow cathode discharge, rel. to plasma electron density and temp. 77—7589
He$^+$, ion+electron scatt., static exchange approx. Schwinger variational principle, photoionisation cross section 80—43192
He$^+$, n=2, 3, electron impact excitation, Coulomb-Glauber-Ochkur approx. appl. 80—69238
He$^+$, n=2 level, generalised two-pot. distorted wave model calcs. 78—37748
He$^+$, n=2 state electron impact excitation, hybrid algebraic close coupling approx. 80—18930
He-Cd II hollow-cathode laser, 4416 Å pulse oscillation 79—7122
He-Cd positive-column laser discharge, excitation mechanisms from radial profiles 77—68205
He-Cd$^+$ hollow cathode laser, He(2^3S) densities and excitation mechanisms 80—48220
He-like ions, electron impact, collision strengths for fine-struct. transitions 78—62925
He-like ions, electron impact excitations 80—78712
He-like ions, ground-state electron impact excitation strengths, close-coupling calcs. 80—23561

atomic electron impact excitation continued
He-like ions, highly charged, electron impact, intermediate-coupling strengths for fine struct. transitions 80—32837
He-like ions, n=2→1 transitions, collision strength Z-dependence 80—91675
He-like ions, triplet-state, electron impact excitation cross sections obtained by Coulomb Ochkur Rudge approx. 80—102576
He-like positive ions, electron impact excitation, electron exchange, CBO approx. calcs. 79—36771
He+e$^-$(H$^+$)(pion), specific primary excitation by fast accelerator particles 80—23559
HeI, 3^3D-2^3P transition, light polarisation depend. on time and exciting electrons energy 80—37891
^{3}He(^{4}He) clusters, metastable electronic states, electron impact excitation, time of flight spectra 80—106411
^{4}He, Rydberg states, fine struct., D, F and G states meas. 77—50418
He(2^1S, 2^3S), threshold to 0.10 eV, energy-integrated total cross section ratio 80—37885
He($2^{1,3}S$), electron impact excitation and ionis., cross sections 77—31001
He($2^{1,3}S$), inelastic scatt., RPA and 1st Born approx. calcs. 80—53148
He(2^3S_1), metastable state electron impact excitation differential cross section meas. 79—10210
He($2p^2\ ^3P$), electron impact parity unfavoured excitation, trapped electron data reinterpretation 77—58180
Hg, 5.2 eV resonance in electron impact excitation 79—10208
Hg, $6^3P_{0,2}$-state, electron impact excitation, optical detect. 77—50546
Hg 6^3P_1 states, detection impact excitation cross section meas., using self calibrating apparatus 79—50135
Hg, 6^3P_2 state, stepwise excitation, effective cross-section *(Russian)* 78—5348
Hg, absolute total cross section 79—59570
Hg, cross sections for electron impact excitation in visible and UV 78—17801
Hg electrical discharge, electron-collisional excited-state kinetics 77—24226
Hg, electron depolarisation depend. on coupling type *(Russian)* 79—89792
Hg, electron drift vel., momentum cross-section, theory 78—30404
Hg, electron impact ionisation cross-sections for excited states 80—9742
Hg, electron impact spectra, intermediate energy 78—82842
Hg, electron inelastic scatt., spin-polarisation, differential cross-section, DWBA 78—50644
Hg, electron scatt., negative ion form., shape resonances, electron affinity 77—14581
Hg, excitation of $^3D^0_3$, metastable state 78—5350
Hg, hyperfine effect on polarisation of 6^3P_1-6^1S_0 intercombination line excited by electron impact 78—37750
Hg I, II, electron impact excitation, absolute emission cross sections, 284.7 and 479.7 nm 77—19086
Hg II, excitation cross sections, transition probabilities, by electron impact 79—3580
Hg, $N_{6,7}O_{4,5}O_{4,5}$ Auger electron spectrum, electron impact excitation 77—57958
Hg, slow electron collision effective cross section, quenching probability 78—50627
Hg, spin polaris. and differential cross section 78—17800
Hg(6^3P_1), slow electron scatt. stepwise excitation function to 6^3P_2 state 79—858
In, electron impact excitation cross sections calc. *(Russian)* 78—55240
In, excitation cross sections 79—54972
In, excited state lifetime, delayed coincidence meas. 77—3315
K, absolute optical electron-impact excitation functions 80—18933
K, electron collision cross sections determ. from plasma DC conductivity 77—3469
K, electron elastic and inelastic scatt., 54.4-217.7 eV, 2-145° 80—1067
K, electron excitation cross sections for six autoion. config., Born approx. calc. 78—25713
K, electron impact excitation velocity consts. for reson. levels, meas. *(Russian)* 78—1086
K, electron impact excitation cross sections, Vainshtein approx. 78—25721
K, electron impact excitation, combined classical theory and free fall model 79—98229
K, electron impact reson. transition excitation, unitarised distorted-wave polarised-orbit model 78—25710
K, electronic excitation cross-section determ. method 77—540
K I, identification of low energy autoionising levels 79—31703
K I, K II, ejected electrons from autoionis. levels excited by electron impact 77—88572
K, normalized momentum-transfer, differential and integral cross-sections, 6.7, 16 and 60 eV 77—68117
K, optical reson. line electron impact excitation cross sections, polaris. 78—55244
K$^+$, dielectronic recomb., in crossed beams, UV emission obs. *(Russian)* 79—10212
K$^+$, direct excitation of levels, transition probs. and cross sections 80—37890
K$^+$, electron impact excitation of reson. levels *(Russian)* 79—45852
Kr, $4p^55s$ state, electron excitation fine struct., neg. on reson. 77—14585
Kr, electron energy loss spectra, energy-depend. multichannel quantum defect theory anal. 77—61860
Kr, electron impact, near threshold UV-emitting level excitation 78—25711
Kr, electron impact excitation, rel. differential cross-section meas., 15 to 100 eV *(French)* 78—13602
Kr, electron impact excitation of autoionis. states 78—90302
Kr, electron ionisation and excitation coeffs. in low E/N region 80—48090
Kr, large angle elastic and inelastic electron scatt. differential cross section, exchange corrections 80—28111
Kr, metastable, electron impact excitation cross-sections calcs. 78—94323
Kr supersonic jet, electron beam excited, vac. UV spectrum 77—88414
Kr, threshold excitation spectra 78—70936
Kr, total electron impact excitation cross section, first Townsend coeffs. 77—536
Kr, total scatt. cross section, 20-3000 eV 79—36778
Li, electron excitation cross section calc., Born approx. with Slater wave functions 80—69243
Li, electron impact excitation, 2nd order pots. method calcs. 78—13608
Li, electron impact excitation cross sections, Vainshtein approx. 78—25721

atomic electron impact excitation continued
Li, electron impact excitation, 15-190 eV, generalised oscill. strengths, differential cross sections 80–23556
Li, electron impact excited high-l Rydberg states 77–65535
Li, electron impact reson. transition excitation, unitarised distorted-wave polarised-orbit model 78–25710
Li, electron impact total excitation cross section, first order exchange approx. 79–31692
Li, electronic excitation cross-section determ. method 77–540
Li electronic impact excitation, energy level calcs. *(Chinese)* 80–83488
Li, emission spectra in 10 to 25 nm range excited by electron-atom collision *(Russian)* 77–83526
Li excitation mechanisms, Auger and autoionisation spectra 77–19042
Li, excitation of autoionis. state, ejected electron intensity 78–5352
Li I, autoionising levels, electron impact excitation, ejected electron spectrum 78–9259
Li II, electron impact excitation, distorted wave approx. 80–91689
Li, S and D state electron impact excitation, emission line intensity obs. 80–23560
Li^{+}, cross-sections, modified Oppenheimer approx. 78–82843
Li^{+}, electron scatt., inelastic Feshbach resons., quasi projection operator calc. 80–58395
Li^{+}, polarised state electron excitation, electron-photon coincidence 77–6930
Li^{2+}, electron impact ionisation, electron ang. momentum exchange 78–78820
Li^{2+}, electron scatt. near ionis. threshold, ang. momenta 79–31698
Li-like ions, electron impact excitation, config. and parentage mixing effects 77–58176
Li-like ions, electron impact, ionisation cross section including excitation-autoionisation contributions 80–28105
Li^{+}(2^{3}P), electron impact excitation, absolute 548.5 nm emission cross-section 79–10209
Mg, 2p-electron excitation and ionisation by electron impact, autoionising states, electron spectra 77–14590
Mg, 4snl autoionising states ejected electron spectra, low energy impact two electron excitation 80–83494
Mg, cross sections 10, 20, 40 eV 78–70940
Mg, electron impact two-electron excitation, ejected electrons from autoionis. levels 77–88571
Mg, electron scatt., negative ion form., shape resonances, electron affinity 77–14581
Mg, electron scatt. cross sections, close coupling calc. with CI 80–43180
Mg, hollow cathode discharge, excitation mechanisms of triplet state atoms and decay obs. 80–44015
Mg I, ^{3}p triplet system, lifetime meas. 80–47946
Mg ions in low density plasma, dielectronic recomb., ionization equilib. and radiative energy loss, solar corona appl. 79–68903
Mg isoelectronic sequence, electron impact excitation of reson. transitions 80–63825
Mg, L-shell ionisation and excitation, electron spectra 77–10765
Mg, radiative lifetimes on excitation by electron impact *(Russian)* 77–50408
Mg^{+}, resonance lines electron impact excitation, polarisability 78–42225
Mo^{24+}, electron impact ionis., dominant Auger process 77–68120
Mo^{39+}, relativistic Coulomb-Born approx. 79–68318
N, cross sections 77–50538
N, electron impact excitation, near threshold, cross-sections for (2s^{2}2p^{2}3s)^{4}P and (2s2p^{4})^{4}P states 80–91684
N II, electron impact excitation cross sections, rel. to solar corona abundance 80–58391
N III, electron impact excitation cross sections, generalised oscillator strengths, Born approx. 80–18928
N IV, excitation cross sections, Coulomb-Born approx. 77–75302
N isoelectronic sequence ions, atomic struct. and electron scatt. data 80–51649
N, low energy elastic and inelastic scatt., Bethe-Goldstone and pseudostate approx. 77–68112
N VI, electron impact excitation cross section calcs. using nonrelativistic Coulomb-Born approx. 77–42414
N^{4+}, 2s-2p excitation absolute cross sections by electron impact, rate coeffs. temp. depend. 79–94087
N^{4+}, electron impact, inner shell excitation cross-sections 79–59580
N^{5+}, cross-sections, modified Oppenheimer approx. 78–82843
N^{n+}, electron impact inner-shell excitation/ionis. cross sections 77–23564
N$_2$, electron scatt., total cross-sections, meas. apparatus 77–54628
N(^{2}D,^{2}P) metastable atoms prod. in N$_2$ DC glow discharge 80–38758
Na, 3^{2}P$_{1/2,3/2}$ reson. levels, electron impact excitation, differential cross-section calcs. 79–59584
Na, Auger and autoionisation spectra, collisional excitation mechanisms 77–19042
Na, ejected-electron spectrum of autoionis. levels excited by 35-400 eV electrons 77–14582
Na, electron drift vel., momentum cross-section, theory 78–30404
Na, electron impact, crossed beam study 80–91672
Na, electron impact excitation of 3^{2}S-3^{2}P transition 77–58173
Na, electron impact excitation, 2nd order pots. method calcs. 78–13608
Na, electron impact excitation cross sections, Vainshtein approx. 78–25721
Na, electron impact excitation, polarised photon emission, delayed coincidence meas. 79–98225
Na, electron impact excitation, combined classical theory and free fall model 79–98229
Na, electron impact reson. transition excitation, unitarised distorted-wave polarised-orbit model 78–25710
Na, electron impact total excitation cross section, first order exchange approx. 79–31692
Na, electron inelastic scatt. in intense laser field 79–72427
Na, electron scatt., theory 77–58172
Na, electronic excitation cross-section determ. method 77–540
Na, ground-4s(5s)(6s) state cross-sections, Percival's combined classical theory 77–75301
Na, high resolution inelastic electron scatt. at zero angle, oscillator strengths 78–9255
Na isoelectronic sequence, electron impact excitation, transition probabilities, oscill. and collision strengths 78–25718
Na, L-Auger, autoionisation spectrum after electron impact excitation 77–14591
Na, L-Auger and autoionis. spectra 78–5354

atomic electron impact excitation continued
Na, laser-excited, electron collision-induced alignment in 3P to nS transitions 77–19084
Na, overlapping autoionisation lines, interference effects 80–91677
Na^{+}, autoionising 2s2p^{6}ns, np states, electron reson. scatt. calc. 80–53142
^{23}Na, optical excitation function and polarisation meas. of spectral resolved D-lines 79–3575
Na(3^{2}P$_{3/2}$), electron total cross section, at. beam recoil technique 77–27186
Ne, 18.5 to 18.7 eV resonances, fine struct. resolved by reson. free-free radiative absorptions 79–3576
Ne, 2p^{5}3s and 2p^{5}3p states excitation by slow electrons, H^{+}, H$_2^{+}$, and He^{+} 80–43185
Ne, 2p^{5}3s^{3}P$_2$ to ground state, electron collisions of the second kind, rate consts. 79–27090
Ne, 2p^{6}(^{1}S$_0$) ground state electron impact excitation cross sections 80–23558
Ne, 40 keV electron scatt., 7-200 mrad, relativistic and electron correlation effects 77–34760
Ne, autoionisation region states, differential excitation function resons. obs. 77–6939
Ne, autoionising states, scatt. electron spectra, post collision interaction effects 78–58819
Ne, electron beam excited states population, press. depend., fluoresc. obs. 78–17802
Ne, electron impact, near threshold UV-emitting level excitation 78–25711
Ne, electron impact, resonances, autoionising states 77–58170
Ne, electron impact excitation, photon emission, ang. correl. 77–14584
Ne, electron impact excitation of autoionising states by fast electrons 79–72425
Ne, electron impact excitation of 2s2p^{6}3s and 2s2p^{6}3p configs., energy loss obs. 80–91685
Ne, electron impact K-shell excitation, EELS 80–106396
Ne, electron scattering, elastic and inelastic, reson. spectra, R-matrix calcs. 79–72421
Ne, electron-atom bremsstrahlung continuum, afterglow decay *(German)* 78–83626
Ne, energy exchange between scatt. and ejected electrons following 2s2p^{6}3s(^{1}S) state autoionis. 78–46448
Ne III, excitation cross-sections, electron impact with simultaneous ionisation 77–68119
Ne ions, multiply charged, IV and V, excitation by electron impact, sections of lines meas. *(Russian)* 77–6941
Ne ions in low density plasma, dielectronic recomb., ionization equilib. and radiative energy loss, solar corona appl. 79–68903
Ne, metastable and pseudo-metastable states destruction by electron impact *(French)* 78–9260
Ne, metastable electronic states, electron impact excitation, time of flight spectra 80–106411
Ne, metastable form. by electron impact *(French)* 78–33611
Ne, metastable level deactivation by electron collision in low press. discharge 78–83520
Ne, multiple-collision diffr. theory 78–82844
Ne, population inversion mechanism between 4p→3d, laser generation conditions 80–1185
Ne positive column, 3S and 3P level populations, rel. theory with recomb. 77–10766
Ne, positive column, excited level decay at high electron temp. 77–23442
Ne, total cross section below ionisation threshold *(French)* 80–43187
Ne, total scatt. cross section, 20-3000 eV 79–36778
Ne V forbidden lines, collision strengths for electron impact excitation, astrophys. appl. 79–50138
Ne VII, excitation cross sections, Coulomb-Born approx. 77–75302
Ne VIII, electron impact excitation 77–537
Ne, weakly ionised, energy transfer at high press. 78–58845
Ne^{+}, electron scatt., relativistic R-matrix calc., fine-struct. level transition cross sections 78–13604
Ne^{4+}, collision strength calc. 80–5624
Ne^{4+}, electron impact calcs. using R-matrix and linear algebraic methods 79–59579
Ne^{7+}, electron impact, continuum orbital approx., weak coupling theory 78–33417
Ne^{n+}, electron impact inner-shell excitation/ionis. cross sections 77–23564
Ne-Ar (1%), 250 kV pulsed electron beam-excited, at. line rel. intensities 79–89646
Ne+e^{-}(H^{+})(pion), specific primary excitation by fast accelerator particles 80–23559
^{21}Ne, ground state, electronic pumping, alignment transfer with multiple diffusion *(French)* 78–50643
Ni ions in Tokamak plasmas, spectroscopy and atomic physics 80–53938
O, cross section, close coupling expsn. 77–83740
O, cross sections 77–50538
O, electron impact, collision freq. in ionospheric F-region 79–53641
O, excitation cross section, Born approximation 77–10772
O I, O II, permitted lines excitation cross-sections, rel. to auroral emissions 78–37745
O I 630 nm predawn airglow, excitation by conjugate photoelectrons 78–49196
O III, electron impact excitation of semi-forbidden transitions 80–48092
O III, electron impact excitation cross sections, independent particle model calcs. 80–63823
O III, low energy reson. struct., distorted wave approx. 77–75307
O IV, electron-impact excitation cross sections 80–14236
O, inelastic electron scatt., 100-500 eV, ^{3}P→^{3}S^{0} oscill. strength 79–81282
O, low energy elastic and inelastic scatt., Bethe-Goldstone and pseudostate approx. 77–68112
O, low-energy electrons integral scatt. cross section 78–69556
O V, electron collision rates rel. to solar emission line ratios interpretation 78–28598
O V, electron collisional excitation, R-matrix calc. 77–58169
O V, electron impact excitation, resons. converging to n=3 thresholds 79–50136
O V, Z 77–75302
O VII, electron impact collision rates, reinterpretation of solar emission line ratios 80–98624

atomic electron impact excitation continued

- O VII, electron impact excitation cross section calcs. using nonrelativistic Coulomb-Born approx. 77—42414
- O VII electron impact excitation, reson. effects 79—41243
- $O^{+,4+}$, electron impact calcs. using R-matrix and linear algebraic methods 79—59579
- O^{+}, electron impact excitation, ionisation, rel. to auroral spectral intensities 79—84563
- O^{2+}, collision strengths, radiative transition probabilities, solar atm. appl. 79—86069
- O^{5+}, electron impact, inner shell excitation cross-sections 79—59580
- O^{6+}, cross-sections, modified Oppenheimer approx. 78—82843
- O^{n+}, electron inner shell excitation/ionis. cross sections 77—23564
- $O^{+}(^{2}D)$ in thermosphere, quenching by electrons 80—94630
- Pb, electron impact excitation, visible and UV spectra, excitation cross sections anal. 80—32840
- Pb, electron impact excited, spectrum in 54-126 nm range 79—63942
- ^{82}Pb, electron impact, relativistic, L-shell ionis., $L\beta/L\alpha$ branching ratio energy depend. 79—98228
- ^{193}Pt, L-shell internal excitation accompanying L-capture 80—95726
- Rb, ejected electron spectrum of autoionis. levels excited by electron impact 77—58174
- Rb, electron excitation cross sections for six autoion. config., Born approx. calc. 78—25713
- Rb, electron impact excitation velocity consts. for reson. levels, meas. *(Russian)* 78—1086
- Rb, electron impact excitation, combined classical theory and free fall model 79—98229
- Rb I, 4p subshell excitation spectra, 15 to 19 eV, a new interpretation 79—777
- Rb, optical reson. line electron impact excitation cross sections, polaris. 78—55244
- Rb^{+}, electron impact excitation, absolute cross-sections 78—82849
- Rb^{2+}, crossed beam electron impact excitation, cross sections 80—43190
- S II, fine-structure transitions by electron impact 78—65493
- S II in Io Na cloud, excitation rel. to Jupiter magnetosphere thermal electron density 79—40133
- S ions in low density plasma, dielectronic recomb., ionization equilib. and radiative energy loss, solar corona appl. 79—68903
- SI III, electron impact excitation of $3s^{2}\ ^{1}S$-$3s3p\ ^{3}P^{0}$ transition 80—102578
- Si $^{3}P \rightarrow {}^{1}D$ electron impact excitation, distorted wave approx., exchange and polaris. effects 77—34764
- Si VI-XIV, line strengths, collision strengths and excitation rates, calcs. 78—5174
- Sm, VUV emission spectra, 5p electron excitation by electron impact 77—68007
- Sr, 2 keV electron excitation and ionis., ejected electron spectra 77—3466
- Sr, ejected-electron spectrum, Auger levels, autoionisation 79—22843
- Sr, electron impact ionisation cross-section, calc. *(Russian)* 79—89789
- Sr, electron scatt., autoionis. states electron spectra *(Russian)* 79—36779
- Sr, excited state lifetime, delayed coincidence meas. 77—3315
- Sr, from metastable states, stepwise and direct excitation 78—1084
- Sr III (IV), UV spectra, 40-100 nm, crossed electron and atomic beams *(Russian)* 78—37580
- ^{179}Ta, L-shell internal excitation accompanying L-capture 80—95726
- ^{157}Tb, L-shell internal excitation accompanying L-capture 80—95726
- Tl, $7^{2}S_{1/2}$, $6^{2}D_{3/2,5/2}$ cross sections, threshold to 1500 eV 77—54614
- Tl, atoms and ions, lifetimes, electron impact excitation excited state lifetimes of atoms and ions 77—79581
- Tl, electron drift vel., momentum cross-section, theory 78—30404
- Tl, electron impact excitation of vacuum UV spectral lines 77—3471
- Tl, electron impact excitation cross sections calc. *(Russian)* 78—55240
- Tl, excitation cross sections 79—54972
- Tm, VUV emission spectra, 5p electron excitation by electron impact 77—68007
- U, atomic model 79—41095
- U I, gf-values, level mean lifetimes, electronic excitation and delayed coincidence meas. 78—21878
- U^{+}, atomic model 79—41095
- ^{235}U, lifetime meas. of electron excited states, rel. to laser isotope separation 77—34591
- W, electron impact ionisation, L-subshell cross-sections, X-ray obs. 79—76519
- W, fast electron beam scatt. calcs. 77—65534
- W^{71+}, relativistic Coulomb-Born approx. 79—68318
- Xe, $^{3}P_{2}$ metastable, deexcitation by slow electrons *(Russian)* 78—13607
- Xe, $5p^{5}5s$ state, electron excitation fine struct. neg. ion reson. 77—14585
- Xe, afterglow, metastable atom deactivation, electron collision effects 77—23441
- Xe atom, electron inelastic interaction, two-grid thyratron expts. 77—83747
- Xe, electron beam excited, VUV radn. emission 79—27089
- Xe, electron energy loss spectra, energy-depend. multichannel quantum defect theory anal. 77—61860
- Xe, electron impact, L-shell excitation, characteristic X-ray spectra, relative cross sections 77—19094
- Xe, electron impact, near threshold UV-emitting level excitation 78—25711
- Xe, electron impact polaris. and excitation functions 78—66665
- Xe, electron ionis., Xe^{+} metastable cross section, laser fluoresc. 77—3465
- Xe, electron ionisation and excitation coeffs. in low E/N region 80—48090
- Xe, electron scatt., optical model for electron spin polaris. 78—50646
- Xe, excitation by low energy electrons, IR spectra obs. 80—27974
- Xe I, electron impact excitation in 18-24 eV autoionis. region 77—58171
- Xe I, indirect level population in electron excitation *(Spanish)* 77—3461
- Xe, N-shell Coster-Kronig transitions 79—13691
- Xe, total excitation cross-section 79—4198
- Xe, total scatt. cross section, 20-3000 eV 79—36778
- Xe-I_{2} mixtures, electron beam excitation, XeI* emission spectrum 77—6843
- Yb, 5p ionisation, 40 to 120 nm 78—82845
- Yb, electron impact excitation cross section, Born and Ochkur approx. 80—87230
- Zn, electron scatt., negative ion form., shape resonances, electron affinity 77—14581

atomic electron impact excitation continued

- Zn I,II, excited state lifetimes, electron-photon delayed coincidence meas. 78—25478
- Zn isoelectronic sequence, electron impact excitation of reson. transitions 80—63825
- ^{30}Zn, electron bombardment, $K\alpha$ satellites 80—47932

atomic electron impact ionisation

- *see also electron spectra*
- adiabatic approximation, energy-modified 79—59523
- alkali metal ions, electron impact ionisation, binary encounter model 80—23557
- atmospheric gases, electron impact cross-sections 78—28398
- atmospheric gases, yield spectra calcs. 78—28401
- atom, autoionisation intersecting terms of collisions, electron spectra interference struct. *(Russian)* 78—1070
- atoms, one-photon decay of two-hole states *(Russian)* 77—79592
- autoionisation state excitation near threshold, post-collision interactions *(Russian)* 77—68125
- autoionising states, electron impact ionisation obs., distortion effects calcs. 80—83491
- autoionising transitions excited in atom+ion (electron) collisions 77—42390
- binary approximation, appl. full cross-section calcs. *(Russian)* 77—31004
- Born approx., $55 \leq Z \leq 102$ scaled electron ionisation cross sections 79—94089
- Born approx., ionisation cross-section, $Z=19$-54, generalised oscillator-strength formulation 77—83745
- bremsstrahlung, role of atomic electrons *(Russian)* 77—88575
- bremsstrahlung of electrons, allowing for polarisability *(Russian)* 77—3475
- coherence and correlation in atomic collisions, book 80—90615
- coincidence measurements 77—42420
- collisional cross-sections determ. for low and intermediate energy processes 80—99579
- conference, physics of ionised gases, Dubrovnik, Yugoslavia, (Aug.-Sep. 1976) 77—42961
- Coulomb-Born-exchange calcs., ionisation from 3p and 3d sublevels of highly charged ions 80—37887
- dielectric gas, breakdown strength, electron impact ionis. and scatt. cross section 79—82031
- discharge, RF, gamma regime, ionis. balance and plasma characts., model 80—44022
- 'displaced thresholds' in ejected electron spectrum 78—5349
- dynamic structure, determ. using electron impact ionisation 77—3460
- (e,2e) knockout reactions, electron momentum states 77—88117
- (e,2e) offshell impulse approx., electronic momentum distribs. 77—88565
- effective ionisation cross section determ. for H, Li, Na, Cu, Ag, Au and Fr, classical theory *(Russian)* 77—30998
- ejected electron orbital-bound target orbital orthogonalisation procedure, appl. to He 79—72429
- electron beam ion source, charge, state distrib. of multiply charged ions, balance model 77—18726
- electron beam ion source for multiply charged ions 79—30608
- electron coincidence ionisation spectra, Green's function anal. 79—31714
- electron coincidence spectroscopy, binding energy charge density meas. 80—63817
- electron coincidence spectroscopy, orbital shape, charge density, mol. struct. determ. appls. 79—27113
- electron impact detachment, ionisation, excitation, dissociation and recombination 80—63832
- electron ion collisions, distorted wave theory, Auger ionis. and excitation fluoresc. 79—7018
- electron plasma relax. characts., 3-30 eV 80—79612
- electron spectroscopy, coincidence experiments, two-parameter 78—20135
- electron wave function pair Fourier transforms, at., mol. and solids, by $(\gamma,2e)$ and (e,3e) *(Russian)* 77—71878
- electron wavefunctions for $(\gamma,2e)$ and (e,3e) processes at high energy, double Fourier transform 78—17628
- electron-ion collisions, crossed beam expts. 78—58843
- electronic and at. collisions, conf., Kyoto, Japan (Aug.-Sept. 1979) 80—57011
- electrostatic electron energy analysers, cylindrical mirror appls., review 78—21265
- fast electron collision, K, L, M-shell generalised oscillator strengths and ionisation cross section, Hartree-Slater calc. 80—53141
- fast electron ionisation or attachment transition probabilities, extended statistical law 77—54613
- fifth-row elements, L_{1} electron ionisation cross section, relativistic plane wave Born approx. 80—87229
- group VA and VIA, single ionisation calc. 77—68118
- $H(1s)+e^{+} \rightarrow (e^{+}e^{-})(nlm)+H^{+}$, highly excited states rearrangement collisions 79—59564
- high-Z atoms ($Z=48$-104), electron impact, K-shel ionisation cross sections calcs. 80—63827
- highly charged ions, ionis. from 3s sub-level 78—90297
- hydrogenic ion, mutual ang. and energy distribs. near ionis. threshold 79—64108
- hydrogenic ions, break-up processes, eikonal approach 80—91676
- hydrogenic ions, highly charged, electron ionisation of 4s, 4p, 4d and 4f sublevels 80—91681
- inert gas, electron impact double ionisation, binary encounter approx. calcs. 78—90294
- inert gas, s- and p-electron double ionisation, soft X-ray emission *(Russian)* 77—34766
- inert gas-halogen mixture, ion form., ion-mole. reactions, mass spectra 77—61841
- inert gases, (e,2e) reactions 200 to 2600 eV as probe of atomic and molecular struct. 77—88566
- inert gases, absolute ionisation cross section, 0.5 to 5.0 keV 80—53146
- inert gases, cross section ratios 78—94326
- inert gases, metastable, electron impact ionisation cross-section calcs. 77—46644
- inert gases, primary ionisation by ~2 MeV relativistic electrons *(Russian)* 77—75309
- inner atomic shells, coincidence expts. theory 78—58837
- inner shell (e, 2e) symmetric reacts. 77—19092
- inner shell generalised oscill. strengths, with outer shell effects 78—50507
- inner shell ionisation, coincidence exptl. method, theory 80—1066

atomic electron impact ionisation continued

- inner shell ionisation by electron, positron and proton impact 77—19090
- inner shell ionisation by relativistic electrons and positrons 77—19091
- inner-shell ionis. cross section meas. system, Cockcroft-Walton accelerator 77—68116
- innershell ionisation, positron impact 78—62930
- innershell ionisation, proton and electron impact equivalence at high vel. 77—14556
- innershell ionisation, relativistic electron impact 78—62930
- interstellar medium, local, electron impact rel. to ionisation state 80—90502
- Io atmosphere, electron impact ionisation rate rel. to interaction with plasma torus 80—98604
- ion gun, for UHV microbalance, absolute meas. of sputtering yield *(Japanese)* 80—17951
- ion source, of mass spectrometer, EI/FI modes pot. distrib. calcs. 77—74553
- ions, electron impact, direct excitation and ionisation, distorted wave theory 78—25722
- ions, highly charged, $Z=\infty$ method 78—33614
- ions, multicharged, cross sections for electron impact ionis. 78—37746
- isoelectronic sequence, electron impact ionisation cross section 80—91688
- K- and L-shell ionization of atoms by relativistic electrons 79—7017
- K-shell electrons, single quantum annihilation of positrons 79—89791
- K-shell ionisation by Coulomb excitation, plane-wave Born-approx. 79—18272
- K-shell ionisation by relativistic electron impact, X-ray emission 77—23565
- K-shell ionisation by relativistic electrons, scaling law 77—75306
- K-vacancy production by relativistic H^+ or e^- 79—50126
- L_1-shell ionisation, high-energy impact, relativistic plane-wave Born approx. 79—54970
- low ionised anisothermal plasma, ionising electron collision kinetics *(German)* 80—33730
- low temp. plasma ionisation by fast electron beam, effective cross section calc. 79—14572
- metal vapour, autoionising and ionising processes 78—58830
- metal vapour, ejected-electron spectra from autoionising levels 80—37893
- momentum wave function determ. in atomic, molecular and nuclear systems 77—88556
- negative ion, ionisation by electron impact near threshold, classical approx. *(Russian)* 77—68124
- $np^6(n+1)s^2$ state, atomic resonant autoionisation, photoelectron spectra 77—18980
- outer shell ionisation, ang. distribs. and polaris. of charact. X-rays and Auger electrons 79—10205
- outer shell rearrangement effect on inner shell oscill. strength 77—42418
- plasma, electron energy loss by ionisation and excitation of atoms 80—33732
- plasma, thermal ionisation, single-step ionis. role, diffusion approx. 80—43843
- polarization phenomena in electronic and atomic collisions, review 80—83501
- positive ions, electron impact ionis. cross-sections 77—46642
- positive ions, electron impact ionisation, Coulomb-Born approx. 80—74249
- positive ions, electron impact ionisation, cross-sections calc. 78—70943
- positron annihilation on atoms, δ function operator method 79—94088
- post collision interaction *(Russian)* 79—50140
- post collision interactions from collisions between electrons and atoms *(Dutch)* 78—5357
- post collision interactions in at. excitation processes 78—58803
- potential scattering, refined Born approx. 80—77
- R-matrix appls., quantum defect, frame transportation 78—58761
- radiative attachment coeffs., 10-10^4K *(Japanese)* 77—42415
- rate coefficients and ionisation cross sections 77—50547
- relativistic effects in excitation and ionis., $Z\alpha$ and v/c depends. 79—860
- relativistic electron impact, K-shell ionisation, Z and E depend., scaling behaviour 78—42227
- review, of expt. and theory 78—25699
- review 77—34762
- RF quadrupole ion trap, singly charged ion prod. 79—98224
- Rydberg atom, electron collisions 80—63833
- Schwinger variational principle 79—45780
- semiclassical approximation calcs. 80—23563
- subshell ionisation, He to Ar, scaled cross-sections by Born approx. 77—83746
- system of N charge particles in external Coulomb field, asymptotic form of wave function 77—71871
- total inelastic scatt. cross section, detector solid angle depend., approx. bounds 78—17798
- transition metals, ionisation pot. meas. 79—45849
- two-electron Fourier amplitudes of atomic and mol. wavefunctions using the (γ,2e) and (e,3e) processes 79—3419
- two-particle-hole Tamm-Dancoff approximation (2ph-TDA) equations for closed-shell atoms and molecules 78—70937
- variational methods, appl. to at. scatt., review 78—86951
- wave packets, radial, appl. to target distortion 80—87234
- X-ray and Auger spectra, ang. distrib., polaris. 77—75305
- X-ray production, ang. distrib. obs. 80—1069
- X-ray production, cross-sections for inner shell ionisation by electrons, positrons, protons and α-particles 77—46643
- X-ray transitions, K_α/K_β ratio 80—27972
- yield spectra, continuous-slowing-down approx. 77—88569
- Z=12-92, inner shell ionisation by relativistic electron impact 80—23562
- Z=13 to 92, inner shell ionis., by ultrarelativistic electrons, scaling law 77—54615
- Ag, electron (positron), impact, K- and L-shell ionisation, $K\alpha$ and L X-rays meas. 80—99575
- Ag, electron impact ionis., X-ray obs., 3000 to 6000 keV, measuring system 77—68116
- Ag, electron impact ionisation, K-shell, doubly differential cross section meas. 79—98226
- Ag, K-shell ionis. by electron impact, cross-sections, 300-600 keV 78—29853
- Ag, photoionisation cross sections, electron-impact inverse mean free paths, and stopping powers for each subshell 80—69113
- Al, K-shell ionisation by ultrarelativistic electrons, density effect 80—99576
- Al, photionisation and electron impact ionisation relationship, mean free paths 79—22672

atomic electron impact ionisation continued

- Ar, (e,2e) coplanar symmetry reaction, factorised distorted-wave approx., 400-1200 eV 78—55246
- Ar, electron impact, struct. near $L_{2,3}$ edges 77—75083
- Ar, electron impact autoionisation, cross-section parametrisation 77—6932
- Ar, electron impact ionis., L_3-shell alignment, Auger electrons ang. distrib. 78—58838
- Ar, electron impact ionis., differential cross sections 78—58839
- Ar, electron impact ionis. of inner shells, coincidence expt. theory 78—58837
- Ar, electron impact ionisation, $2p_{3/2}$-shell alignment, Auger investig. 77—14587
- Ar, electron ionisation, Ar^+ metastable cross section, laser fluoresc. 77—3465
- Ar, electron ionisation and excitation coeffs. in low E/N region 80—48090
- Ar, electron scatt. and ejection, electron energy loss spectra 80—58394
- Ar, energetic electron degradation spectra and initial yields 80—95724
- Ar, energy deposition, Monte Carlo calcs. 80—69242
- Ar, energy resolution and ang. correl. of scatt. and ejected electrons 78—70939
- Ar, free ats. electron bombard., subsequent X-radiation ang. distrib. 80—53144
- Ar glow discharge, line radiation of plasma in early afterglow 80—38745
- Ar, high resoln. pulsed electron beam time-of-flight ejected electron spectra 77—3462
- Ar II, (e,2e), photoelectron and conventional spectroscopies 78—90298
- Ar, inner shell alignment calc. in electron impact ionisation 77—14586
- Ar, inner shell alignment following electron impact ionisation, distorted wave approx. calcs. 80—91682
- Ar, ionisation by energetic electrons, appl. to Mars atmosphere 77—31420
- Ar ions, electron impact ionisation, trapped ion cyclotron resonance spectroscopy 80—53140
- Ar L-shell, X-ray emission spectra prod. by 0.3-3 keV electron impact, line intensities 79—45666
- Ar L-shell ionisation, post-collision interaction, electron impact, energy loss meas. 77—19093
- Ar, low-energy, triple-differential cross section 78—74773
- Ar neutral system, complete saturation phase excited state population density 80—106284
- Ar, positron scatt., positronium form. cross-section calcs. 78—9283
- Ar, secondary electron energy distrib. on fast electron impact 77—34763
- Ar, singly charged ion formation, near L-shell ionis. threshold, inter-shell correl 77—88567
- Ar, slow electron ionis., calc. for $3s^2$ subshell 79—31700
- Ar supersonic jet, ultrasoft X-ray emission 77—27015
- Ar, total scatt. cross section, 20-3000 eV 79—36778
- Ar, weakly ionised, energy transfer at high press. 78—58845
- $Ar^{+,2+,3+}$, electron impact, <800 eV, multiple ionis., L-shell contribs. 80—37892
- Ar^+, electron impact ionis. cross section 78—50647
- Ar^{i+}, (i=1, 2, 3, 4, 5), absolute electron impact ionisation cross section 80—83496
- Ar^{n+}, electron impact inner-shell excitation/ionis. cross section 77—23564
- Ar-Cu, Cu diffusion coeff. determ. volatile salt dissoc. in pulsed discharge 80—33721
- ^{37}Ar, L-shell internal excitation accompanying L-capture 80—95726
- As, electron impact ionisation, in RF ion source, effective cross-sections 78—22034
- Au, electron impact ionisation, K-shell, doubly differential cross section meas. 79—98226
- Au, electron impact L-shell ionis., 300-600 keV 77—50542
- Au, electron impact M-shell ionisation, 60-600 keV, absolute cross sections meas. 80—83493
- Au, inner-shell ionis. by relativistic electron and positron impact 77—6933
- Au, L-shell electron impact ionisation, X-ray production cross sections 77—19095
- Au, photionisation and electron impact ionisation relationship, mean free paths 79—22672
- B, electron impact ionisation, in RF ion source, effective cross-sections 78—22034
- Ba, electron spectra of autoionisation states, electron-atom collisions *(Russian)* 78—1085
- Ba II, 5p excitation, relativistic anal., multiconfig. Dirac-Fock calcs. 80—69240
- Bi, electron impact ionisation, characteristic X-radiation ang. distrib. obs. 80—1069
- Bi, electron impact M-shell ionisation, 60-600 keV, absolute cross sections meas. 80—83493
- Bi, keV electron impact, L X-ray prod. cross section 79—18293
- C, 7-1000 eV, cross-section 78—86956
- C, cross sections 77—50538
- C, electron impact, C K-ionisation, Auger and X-ray meas. 77—19096
- C III, C IV, electron impact ionisation 78—70941
- C IV, electron ionisation cross sections of excited atoms and ions 80—43186
- C, ionis. cross-section, accuracy of fast at. beam method 79—81283
- C, ionis. cross-section, accuracy of crossed at. beam method 79—81284
- C^-, electron impact detachment, cross-section, 10-1000 eV 79—31702
- C , electron impact detachment cross sections 79—89787
- C^+, C^{2+}, electron impact ionisation cross section in hollow beam trap 78—25717
- C^+, electron impact ionisation cross sections, autoionisation contrib. at low temp. 80—32838
- C^{2+}, electron impact ionis. cross-section meas. 79—3577
- C^{3+}, cross section measurement, contribution due to excitation-autoionisation 79—45850
- C^{3+}, electron impact ionis. cross sections 79—22845
- C^{n+}, electron impact inner shell excitation/ionis. cross sections 77—23564
- Ca, 2 keV electron excitation and ionis., ejected electron spectra 77—3466
- Ca, electron impact ionis., ejected electron spectrum from autoionis. levels 78—33613
- Cd, $4d^{-1}5p^1P$ autoionising state, electron impact ionisation obs., distortion effects calcs. 80—83491

atomic electron impact ionisation continued
  Cd, Auger electron spectra, electron impact excited, vap. and solid state differences 78—52603
  Cd, electron impact, ejected electron spectrum of autoionis. levels 77—27185
  Cd, electron scatt., negative ion form., shape resonances, electron affinity 77—14581
  Cl, K-shell ionisation by ultrarelativistic electrons, density effect 80—99576
  Co, 300 to 600 keV, K_α/K_β X-ray intensity ratios, K-shell ionis. cross sections 78—37747
  Cr, double K-shell ionisation by electron impact, X-ray spectra 78—62928
  Cr, double K-shell ionisation by electron impact 78—62929
  Cs, 1st reson. level, effective electron-ionis. cross sections, plasma discharge method 78—13603
  Cs, $5p^5 6s^2\ ^2P_{3/2}$ autoionising level, ejected electron excitation function, reson. 77—58167
  Cs, ejected electrons from autoionis. levels excited by electron impact 77—88573
  Cs^{2+} formation during electron-ion collisions, ultrasoft X-ray spectroscopic study *(Russian)* 80—43193
  ^{131}Cs, L-shell internal excitation accompanying L-capture 80—95726
  Cu, 300 to 600 keV, K_α/K_β X-ray intensity ratios, K-shell ionis. cross sections 78—37747
  Cu, K-shell ionisation cross sections, slow electron impact 80—83498
  Er, keV electron impact, L X-ray prod. cross section 79—18293
  ^{165}Er, L-shell internal excitation accompanying L-capture 80—95726
  Eu, autoionising states excitation in electron collisions *(Russian)* 79—86073
  Eu III, two-electron single-photon transition in electron-atom collisions *(Russian)* 79—68319
  F , electron impact detachment cross sections, test of classical scaling theory 79—31693
  F^{q+} + He, (q=1-9), X-ray prod. by electron excitation, ionisation and capture 79—76379
  Fe, 300 to 600 keV, K_α/K_β X-ray intensity ratios, K-shell ionis. cross sections 78—37747
  Fe, double K-shell ionisation by electron impact, X-ray spectra 78—62928
  Fe, double K-shell ionisation by electron impact 78—62929
  Fe, inner-shell vacancies, cascade decay, multiple ionisation and X-ray emission calcs. 80—87072
  Fe ions, Li-like Auger contribs. to electron impact ionisation 80—87231
  Fe XVI, autoionisation contrib. to total ionisation rates 80—9738
  Fe^{14+}, Fe^{15+}, ionis. from 3s sub-level 78—90297
  ^{55}Fe, L-shell internal excitation accompanying L-capture 80—95726
  ^{77}Ge, L-shell internal excitation accompanying L-capture 80—95726
  H, complex optical pot. methods 79—22844
  H, Coulomb ionisation, Glauber scatt. amplitude, integral representation 77—6915
  H, cross sections 77—50538
  H, cross sections for ionisation, calc. 79—76516
  H, eikonal exchange amplitude in Coulomb break-up processes 80—87232
  H, electron coincidence ionisation spectroscopy, rel. to impulse approx. calcs. 79—31715
  H, electron impact, coupled channels optical model, total reaction cross-sections 80—18929
  H, electron impact, ionisation, angular correls. of outgoing electrons 78—5355
  H, electron impact ionisation, in RF ion source, effective cross-sections 78—22034
  H, electron impact ionisation, 100 to 250 eV, triple differential cross-section 79—59582
  H, electron impact ionisation, polarised Coulomb-projected Born approx. 80—106395
  H, electron scatt., atomic optical potential model 80—99578
  H, expt. and theoretical cross sections 79—22842
  H, gas discharge source for electron scatt. expts. 78—94332
  H I, electron ionisation cross sections of excited atoms and ions 80—43186
  H II regions, effect of collisional ionisation time evolution 77—53664
  H, inelastic electron scatt., relativistic calcs. *(Russian)* 77—83737
  H, multiple stage cluster beam ionizer 79—67425
  H plasma, departures of electron energy distrib. from Maxwellian rel. to ionisation rates 77—80266
  H plasma, departures of electron energy distrib. from Maxwellian rel. to ionisation 77—80274
  H, positron impact ionisation, charge exchange problem 79—50139
  H, positron scatt., forming $(e^+e^-)(1s) + H^+$, first-order approx. 79—55006
  H, source theory 78—46415
  H, spin effects, Born exchange calcs., expt. results, interference term, a comparison 78—37749
  H, spin exchange effects, 15-197 eV 77—71877
  H, triple differential cross section 79—36776
  H, with multiphoton absorption in intense laser beam 78—46449
  H^-, electron detachment by electron impact, 1s state product, Born approx. 78—78816
  H^{2-}, existence, alternative explanation of results, electron effects 77—19079
  H^{2-}, existence, expt. evidence 77—19081
  H^{2+}, existence, alternative explanation of results, ion intensities 77—19080
  H-like ions, highly charged, Born exchange or Coulomb-Born-Oppenheimer approx. 77—71875
  H-like ions, scaled Coulomb-Born-Oppenheimer collision strengths 79—22839
  $H + e^+$, moment T-matrix approach, ang. distrib., total cross section, below pickup threshold 79—3573
  $H + e^-$, moment T-matrix approach, elastic scatt., total cross section, intermediate energy 79—3582
  H + positron, charge exchange, excited positronium states form. 78—58873
  H_2, ground state correlations meas. by (e,2e) expt. 77—42413
  H_2-Ne, positron annihilation involving low energy positrons, lifetime spectra 79—94091
  H_2-Ne, positron annihilation, positron form. 79—94092
  He, 100 and 200 eV, secondary electron emission, doubly differential cross-sections 77—83743

atomic electron impact ionisation continued
  He, 2^1S, 2^1P and 2^3P states excitation and ionisation yields, energy deposition efficiency 77—31002
  He, 35 eV, triple differential cross section 79—36777
  He, 7-1000 eV, cross-section 78—86956
  He, (e,2e), absolute double- and triple-differential cross sections, 0.2-2.8 keV 80—5623
  He, (e,2e) coplanar symmetry reaction, factorised distorted-wave approx., 200-1200 eV 78—55246
  He, absolute (e,2e) differential cross section, meas. in coplanar conditions 78—25719
  He atoms, electron impact ionisation, Glauber amplitude 77—83748
  He, autoionisation states, electron impact, electron ejection, distribs. 77—50545
  He, autoionising S states, electron-atom collision resons. theory calcs. 77—58179
  He, autoionising transitions interference 77—42390
  He, distorted wave approx., 80-250 eV 78—86955
  He, distorted-wave model, 100-400 eV 79—45824
  He, electron Compton profiles from energy loss spectra 79—7013
  He, electron impact ionis., post-collision interaction anal. from ejected electron spectra 77—42416
  He, electron impact ionis., triple differential cross section 78—62924
  He, electron impact ionisation, energy and ang. distrib. calcs. 77—6914
  He, electron impact ionisation, emitted electron ang. distrib. 78—55241
  He, electron impact ionisation, decay modes investig. 79—72422
  He, electron impact ionisation cross sections using RF quadrupole ion trap 79—98224
  He, electron scatt., interaction with electrons ejected from impact excited autoionis. states 78—42221
  He, electron scatt., ionisation, elastic and inelastic collisions, many body theory appl. 80—48093
  He, electron scatt. at intermediate energy, quantum mechanical treatment 80—91687
  He, electron scattering total cross sections, 0-3000 eV 78—25709
  He, fast electron retardation, ionisation cascade, degradation spectra, anal. *(Russian)* 79—27741
  He flow discharge, intermediate press., positive column conc. of ions and metastables 80—44017
  He gas, electron energy loss function in range 50 eV to 1 keV 77—61859
  He, Glauber scatt. amplitude, numerical method in Lommel function 79—22795
  He, high resoln. pulsed electron beam time-of-flight ejected-electron spectra 77—3462
  He hollow-cathode discharge, Ba^+ and Sr^+ formation 78—67527
  He II, electron ionisation cross sections of excited atoms and ions 80—43186
  He, ionis. cross-section, accuracy of fast at. beam method 79—81283
  He, ionis. cross-section, accuracy of crossed at. beam method 79—81284
  He, mechanism of (e,2e) reaction 78—62926
  He, metastable, electron impact ionisation atomic metastable states [-] cross-section meas. 77—6931
  He, metastable states, electron and proton impact ionisation, autoionisation 80—102573
  He, near threshold ionisation 79—3578
  He, positron inelastic scatt. at intermediate energies, time of flight spectra 80—18932
  He, secondary electrons from gas, doubly differential cross-section, 50-300 eV 79—59585
  He, triple differential cross section, DWA calc. 77—88574
  He, triple-differential three-dimens. cross sections 77—31000
  He^+ ions, electron impact ionisation 78—66666
  He-Cd discharge, principal Cd ionis. mechanism, radial profiles meas. 77—27758
  He + e, generalised differential oscillator strengths 78—55239
  $He + e^-(H^+)$(pion), specific primary excitation by fast accelerator particles 80—23559
  $He(2^{1,3}S)$, electron impact excitation and ionis., cross sections 77—31001
  $He(2^3S)$, electron impact ionis. to 1s, 2s, and 2p state, autoionis. 80—1068
  $He(2s2p)^1P$ autoionised transition, ang. correl. function (e,2e) fast coincidence technique 77—83738
  Hg, absolute total cross section 79—59570
  Hg electron resonant elastic and inelastic scatt. *(Russian)* 80—78710
  Hg, electron scatt., negative ion form., shape resonances, electron affinity 77—14581
  Hg, $N_{6,7}O_{4,5}O_{4,5}$ Auger electron spectrum, electron impact excitation 77—57958
  Ho, keV electron impact, L X-ray prod. cross section 79—18293
  In, K-shell ionis. by electron impact, cross-sections, 300-600 keV 78—29853
  K, 1st reson. level, effective electron-ionis. cross sections, plasma discharge method 78—13603
  K I, K II, ejected electrons from autoionis. levels excited by electron impact 77—88572
  K, polarised, ionis. by polarised electrons in crossed beam expt. 78—50645
  Kr, 3d-shell electron impact ionis., Auger electrons ang. distrib. 77—27183
  Kr, electron impact, struct. near $M_{4,5}$ edges 77—75083
  Kr, electron impact autoionisation, cross-section parametrisation 77—6932
  Kr, electron impact ionis. of inner shells, coincidence expt. theory 78—58837
  Kr, electron ionis. cross section, Born approx. 77—83745
  Kr, electron ionisation and excitation coeffs. in low E/N region 80—48090
  Kr, free ats. electron bombard., subsequent X-radiation ang. distrib. 80—53144
  Kr, inner shell alignment calc. in electron impact ionisation 77—14586
  Kr, total scatt. cross section, 20-3000 eV 79—36778
  Li, electron impact excitation of autoionis. state, ejected electron intensity 78—5352
  Li III, electron ionisation cross sections of excited atoms and ions 80—43186
  Li isoelectronic sequence, electron impact ionisation cross section 80—91688
  Li, laser excitation and ionisation, autoionising states obs. 77—61699
  Li^{2+}, mutual ang. and energy distribs. near ionis. threshold 79—64108

atomic electron impact ionisation continued
- Li-like ions, electron impact, ionisation cross section including excitation-autoionisation contributions 80—28105
- Li+positron, positronium formation in highly excited states, first Born approx. 80—58420
- Mg, 2p-electron excitation and ionisation by electron impact, autoionising states, electron spectra 77—14590
- Mg, Auger electron spectra, electron impact excited, vap. and solid state differences 78—52603
- Mg, electron impact two-electron excitation, ejected electrons from autoionis. levels 77—88571
- Mg, electron scatt., negative ion form., shape resonances, electron affinity 77—14581
- Mg I, fluoresc. lines polarisation and mag. depolarisation *(German)* 77—6719
- Mg I, Mg II, ejected electron spectrum from autoionis. levels after electron impact 77—75304
- Mg I, Mg II autoionisation state radiative decay *(Russian)* 80—5509
- Mg, K-shell ionisation by ultrarelativistic electrons, density effect 80—99576
- Mg, L-shell ionisation and excitation, electron spectra 77—10765
- Mg, negative ion form. and post-collision interaction *(Russian)* 79—54974
- Mg, single and double ionisation by electron impact, absolute cross section meas. 78—25714
- Mg+H$^+$(He$^+$) and electron impact ionis., Auger study of collisionally induced alignment 78—90279
- Mn, elastic and inelastic electron scatt. 10 to 100 eV 78—70934
- Mn, K-shell ionisation cross sections, slow electron impact 80—83498
- Mo^{24+}, electron impact ionis., dominant Auger process 77—68120
- N, 7-1000 eV, cross-section 78—86956
- N, cross sections 77—50538
- N IV, N V, electron impact ionisation 78—70941
- N, ionis. cross-section, accuracy of fast at. beam method 79—81283
- N, ionis. cross-section, accuracy of crossed at. beam method 79—81284
- N V, electron ionisation cross sections of excited atoms and ions 80—43186
- N^{2+}, electron impact ionisation cross sections, autoionisation contrib. at low temp. 80—32838
- N^{4+}, cross section measurement, contribution due to excitation-autoionisation 79—45850
- N^{4+}, electron impact ionis. cross sections 79—22845
- N^{4+}, electron-impact ionisation rate coeffs. in theta-pinch plasma 79—41878
- N^{n+}, electron impact inner-shell excitation/ionis. cross sections 77—23564
- Na, electron impact ionisation, reson. and nonreson. electron distrib. 78—33615
- Na, electron ionis., ejected electrons ang. distrib. 77—50541
- Na I in Io Na cloud, ionisation rel. to Jupiter magnetosphere thermal electron density 79—40133
- Na, K-shell ionisation by ultrarelativistic electrons, density effect 80—99576
- Na$^+$, autoionising 2s2p^{6}ns, np states, electron reson. scatt. calc. 80—53142
- Ne, (e,2e) coplanar symmetry reaction, factorised distorted-wave approx., 400-1200 eV 78—55246
- Ne, autoionisation region states, differential excitation function resons. obs. 77—6939
- Ne, electron degradation spectra, inner-shell contribs. 77—3474
- Ne, electron impact, resonances, autoionising states 77—58170
- Ne, electron impact ionis., differential cross sections 78—58839
- Ne, electron impact ionisation cross-section 78—58844
- Ne, electron impact ionisation, ang. correl., first Born approx. 79—22840
- Ne, electron impact ionisation yield model 79—45851
- Ne, electron impact ionisation, coplanar symm. cross-sections for valence orbitals 79—86072
- Ne, electron impact ionisation, eikonal approx., shell-averaged, distorted-wave impulse approx. 80—37888
- Ne, electron or photoionisation, electron shake-off, continuum states interaction 78—29766
- Ne, electron shake-off following electron or photon bombardment, continuum states interaction 77—14403
- Ne III, excitation cross-sections, electron impact with simultaneous ionisation 77—68119
- Ne, K-L$_{2,3}$L$_{2,3}$, post-collision interaction Auger effects 79—45686
- Ne, low ionised anisothermal plasma, ionising electron collision kinetics *(German)* 80—33731
- Ne, noncoplanar symmetric (e,2e) reaction, factorised distorted-wave approx., 0.4-2.5 keV 78—55245
- Ne plasma, electron collision ionisation, electron kinetic behaviour during elec. field perturbation *(German)* 80—64676
- Ne, positron scatt., positronium form. cross-section calcs. 78—9283
- Ne, total scatt. cross section, 20-3000 eV 79—36778
- Ne VIII, X, electron ionisation cross sections of excited atoms and ions 80—43186
- Ne, weakly ionised, energy transfer at high press. 78—58845
- Ne$^+$, absolute electron impact ionisation cross section 80—83496
- Ne^{n+} (n=1-4), electron impact ionisation cross-section 78—58844
- Ne^{n+}, electron impact inner-shell excitation/ionis. cross sections 77—23564
- Ne+e$^-$(H$^+$)(pion), specific primary excitation by fast accelerator particles 80—23559
- Ni, 300 to 600 keV, K$_\alpha$/K$_\beta$ X-ray intensity ratios, K-shell ionis. cross sections 78—37747
- O, 7-1000 eV, cross-section 78—86956
- O, cross sections 77—50538
- O, electron impact ionisation, differential and total cross-sections 80—18935
- O I 5577 Å meteoric forbidden line collisional quenching 77—17448
- O, ionis. cross-section, accuracy of fast at. beam method 79—81283
- O, ionis. cross-section, accuracy of crossed at. beam method 79—81284
- O ions, Li-like Auger contribs. to electron impact 80—87231
- O, low-energy electrons integral scatt. cross section 78—69556
- O, triple differential cross sections 79—10207
- O VI, electron ionisation cross sections of excited atoms and ions 80—43186
- O$^-$, electron impact detachment, cross-section, 10-1000 eV 79—31702
- O$^-$, electron impact detachment cross sections 79—89787
- O$^+$, absolute electron impact ionisation cross section 80—83496

atomic electron impact ionisation continued
- O$^+$, electron impact excitation, ionisation, rel. to auroral spectral intensities 79—84563
- O$^+$, O^{2+}, electron impact ionisation cross section in hollow beam trap 78—25717
- O^{4+}, electron impact ionisation, close coupling calcs. 80—106293
- O^{5+}, cross section measurement, contribution due to excitation-autoionisation 79—45850
- O^{5+}, electron-impact ionisation rate coeffs. in theta-pinch plasma 79—41878
- O^{n+}, electron inner shell excitation/ionis. cross sections 77—23564
- Pb, electron impact L-shell ionis., 300-600 keV 77—50542
- Pb, electron impact M-shell ionisation, 60-600 keV, absolute cross sections meas. 80—83493
- Pb, L-shell electron impact ionisation, X-ray production cross sections 77—19095
- Pd, K-shell ionis. by electron impact, cross-sections, 300-600 keV 78—29853
- ^{193}Pt, L-shell internal excitation accompanying L-capture 80—95726
- Rb, 1st reson. level, effective electron-ionis. cross sections, plasma discharge method 78—13603
- Rb^{2+} formation during electron-ion collisions, ultrasoft X-ray spectroscopic study *(Russian)* 80—43193
- Se, 300 to 600 keV, K$_\alpha$/K$_\beta$ X-ray intensity ratios, K-shell ionis. cross sections 78—37747
- Se, electron impact ionisation, characteristic X-radiation ang. distrib. obs. 80—1069
- Sm, keV electron impact, L X-ray prod. cross section 79—18293
- Sn, K-shell ionis. by electron impact, cross-sections, 300-600 keV 78—29853
- Sr, 2 keV electron excitation and ionis., ejected electron spectra 77—3466
- Sr, ejected-electron spectrum, Auger levels, autoionisation 79—22843
- Sr, electron scatt., autoionis. states electron spectra *(Russian)* 79—36779
- ^{179}Ta, L-shell internal excitation accompanying L-capture 80—95726
- ^{157}Tb, L-shell internal excitation accompanying L-capture 80—95726
- Xe, electron impact, struct. near N$_{4,5}$ edges 77—75083
- Xe, electron impact autoionisation, cross-section parametrisation 77—6932
- Xe, electron impact ionis. of inner shells, coincidence expt. theory 78—58837
- Xe, electron ionis., Xe$^+$ metastable cross section, laser fluoresc. 77—3465
- Xe, electron ionis. cross section, Born approx. 77—83745
- Xe, electron ionisation and excitation coeffs. in low E/N region 80—48090
- Xe, free ats. electron bombard., subsequent X-radiation ang. distrib. 80—53144
- Xe, noncoplanar symmetric (e,2e) reaction, factorised distorted-wave approx., 0.4-2.5 keV 78—55245
- Xe, total scatt. cross section, 20-3000 eV 79—36778
- Xe, valence orbital, electron impact ionisation, absolute cross-section 80—69241
- Xe$^+$, absolute electron impact ionisation cross section 80—83496
- Y, 300 to 600 keV, K$_\alpha$/K$_\beta$ X-ray intensity ratios, K-shell ionis. cross sections 78—37747
- Yb, electron impact L-shell ionis., 300-600 keV 77—50542
- Zn, Auger electron spectra, electron impact excited, vap. and solid state differences 78—52603
- Zn, electron impact ionisation cross sections, 40 eV 77—3472
- Zn, electron impact ionisation efficiency curve, threshold of 12.7 eV 79—50137
- Zn, electron scatt., negative ion form., shape resonances, electron affinity 77—14581

atomic electron scattering *see atomic electron impact excitation; atomic electron impact ionisation; elastic scattering of electrons by atoms and molecules*

atomic emission spectroscopy
- acetylene flame, Na and MgO concs. meas., saturation vs. absorption spectroscopy 79—29425
- aerosol aerodynamics effects 78—48709
- AES, quantitative, parameters, appls. 79—43697
- air, elemental anal. at sub parts per trillion concs. via SONRES 78—81465
- air pollution, particulate matter, heavy metal analysis 77—41151
- alkali halides, electron stimulated dissoc. 80—34301
- alkaline impurity, source function in combustion products flow *(Russian)* 77—56301
- alloy steel welds, distrib. of Cr, Ni, Mn, Si, Ti, laser emission microanal. method 78—61110
- alloys, using laser plasma obtained without supplementary elec. discharges *(Russian)* 77—29081
- analytical, sensitivity and detection limit, review *(Japanese)* 80—11990
- analytical physico-chem. methods, characts. *(French)* 79—48033
- aqueous atomic species, subpicogram detection by fluorescence spectroscopy with dye laser excitation 77—90671
- arc discharge utilisation in uniform mag. field *(Russian)* 77—56303
- arc intensity distortion by transverse oscills., method of statistical regularisation *(Russian)* 77—48746
- arc spectrography, applic. of equidensitometry *(German)* 77—1962
- arc spectrum, correlation between anal. signals, plasma parameter changes 79—52828
- atomic spectrometry, using vidicon tube detectors, sensitivity 77—41695
- atomisation of solns., US method, aerosol dispersion, sensitivity, reproducibility *(Russian)* 77—1964
- background corrections obtained with oscillating refractor plate, modulation waveform effect 77—90653
- background fluorescence spectra, in continuum source at. fluoresc. spectrometry 77—81430
- biological materials, inductively coupled plasma-atomic emission spectroscopic anal. 78—31725
- blackening transformation parameters and computers use *(German)* 80—30300
- combustion diagnostics, laser Raman and fluoresc. techniques 78—88635
- continuum source atomic fluorescence spectrometer, wavelength modulated, appls. 78—70190
- continuum source fluoresc. spectroscopy 78—11578
- correlation of signals, internal standardisation 80—55749
- data processing systems *(Japanese)* 78—88685

atomic emission spectroscopy continued
- DC arc plasma, alterations in spectral line intensities due to external mag. fields 80—79621
- DC plasma atomic emission spectrometry system, characterisation of interelement enhancement effect 80—89549
- DC plasma excitation source, interference effects 80—86434
- DC plasma multielement spectrometer, spectral interferences 79—100459
- discharge characteristics, electrolyte filled narrow channel *(Russian)* 77—52726
- discharge lamps, electrodeless, for at. fluoresc. spectrometry, twin-port power divider 79—43681
- discharge localisation with oxidised electrodes *(Russian)* 77—52728
- droplets produced by pneumatic nebulisers, size meas. method 80—71992
- dry residues from solutions, additive chem. comp. effect on intensity distrib. of arc *(Russian)* 79—34419
- electrode erosion, pulse discharge on various materials *(Russian)* 77—51255
- electrodeless discharge lamps, pulsed RF excited, for at. absorpt. and at. fluoresc. spectrosc. 79—21816
- electronic spark source, adjustable-waveform, thyratron-diode switch element 77—63998
- emulsion calibration curve 79—43650
- environmental materials, multielement analysis by inductively coupled Ar plasma excitation and direct reading spectrometry 79—92028
- exploding foil excitation, parametric investig., Cd, Ni anal. appl. 77—12840
- flame, improvements in methods for trace element analysis 79—16066
- flame and plasma type, trace analysis, spectral instrument choice 80—35613
- flame emission, atomic absorption, and atomic fluorescence spectrometry, review of literature 1975-1977 78—85224
- flame emission anal., apparatus for teaching 77—29976
- flame emission analysis, sample matrix ionisation interference and spectral background determ. 77—9144
- flame emission spectrometry; calibration plot systematic errors 79—43648
- flame spectrometer, multigrating, for simultaneous determ. of five elements 77—21455
- flame spectrometry, theoretical model 77—36803
- flame spectrometry using CW dye laser 78—3409
- flame spectroscopy, absorpt. and emission, analogue data processing system 77—36804
- flameless atomisation systems, sensitivity enhancement by rigid W collar 78—35770
- flameless atomisers, diffusion process anal. 79—87925
- flames, anal., small vol. temp. meas. by two-line at. fluoresc. 77—40594
- fluorescence, analytical appls. 79—43668
- fluorescence spectrometry, inductively coupled plasmas as excitation sources 80—43999
- fluorescence spectrophotometry, review 77—66780
- free radicals, in flame, with low press. counterflow, spectrosc. and probe obs. *(Russian)* 77—36755
- gas jet source, emission spectrographic analysis appl. *(French)* 79—34390
- glass bubbles, form., condensate trace quantities determ., spectral anal. techniques *(Russian)* 77—36852
- glow discharge lamp, sputtering process, comparison with ion microprobe 77—52730
- graphite, impurity analysis, laser emission spectroscopy, material evaporation, auxiliary spark gap effects 79—87924
- graphite arc method, anal. signal axial distrib. rel. to additives, atms. 79—87922
- graphite electrode, mass transfer in channel, effect on calibration graph *(Russian)* 77—86428
- graphite furnace AES, anal. appls. 78—27837
- grating double monochromator, GDM 1000, spectral anal. of low intensity emissions 79—80701
- halogens, determ., by emission spectrograph, surrounding gas effects *(German)* 77—44571
- hard water, trace element determ. by multielement ICP-AES method 78—23992
- high voltage high frequency spark, with electronic control, for emission spectral anal. *(Russian)* 78—35771
- high-intesnity arc, anal. appls. *(Russian)* 78—35772
- hollow cathode lamp, pulsing conditions optimisation 78—65972
- ICP plasma source, axially viewed, for atomic emission spectroscopy 80—22434
- ICP-AES, prominent spectral lines listing 79—83519
- ICP-atomic emission spectroscopy, line broadening and radiative recomb. background interferences 80—22435
- image dissector echelle spectrometer use in flame atomic fluoresc. and emission meas. 80—11993
- impedance matching network and impedance meas. for inductively coupled plasma 79—43678
- Inconel 600, surface composition depend. on H atom influx, AES 79—5192
- inductively coupled plasma, detection limits rel. to spectral props. of injected elements *(French)* 77—66776
- inductively coupled plasma, multi-element method for liquids and dissolved solids 79—96395
- inductively coupled plasma, spectral line shapes 77—43083
- inductively coupled plasma, with CW dye laser 79—43646
- inductively coupled plasma and atomic absorption spectroscopy combined 80—104478
- inductively coupled plasma and DC atomic emission spectrometry, tabulation of spectral interferences 80—71991
- inductively coupled plasma-AES, present and future position in analytical chem., review 80—7887
- inelastic mean free paths of solids, data tables 78—84686
- instrumentation, review of current developments *(Japanese)* 78—86356
- interference filter, stray light reduction 79—43645
- intracavity atomic spectroscopy, fluoresc. detection of narrow absorpt. lines 79—52830
- IR, double-beam reflectance measuring device 79—80704
- laser emission spectrochem. anal., data reduction, KSR 4100 small process control computer 77—48707
- laser emission spectroscopy, quantitative microanalysis of reactor graphites 80—81384
- laser excited at. fluoresc. flame spectrometry, improvement of detection limits 78—61073

atomic emission spectroscopy continued
- laser excited atomic fluoresc. spectrosc., appl. to determ. of Ni and Sn 80—93811
- laser microemission spectroscopy for local determ. of impurities in graphite reactor material *(German)* 78—7161
- laser microprobe analyser assessment for quantitative analysis in AES 80—30313
- laser microprobe emission spectroscopy, matrix effects, appls. 77—16870
- laser microspectral analyser, LMA 10, combined atomic absorption and emission 79—79344
- laser plasma obtained without supplementary elec. discharges *(Russian)* 77—29081
- laser-cum-discharge source for spectrochemical analysis *(Russian)* 77—21464
- light sources, reproducibility for emission spectroscopy 78—3429
- liquid nitrogen cooler, for specimen manipulator of LEED-AES experiment *(Japanese)* 78—45639
- liquid sampling and use of inductively coupled plasma 79—43679
- lubricating oils, spectrographic anal. of wear metals 78—20114
- luminescence spectroscopy, image devices and photomultiplier detectors, signal-noise calcs. 77—81433
- luminescence spectroscopy for gases excited by products of neutron nuclear reactions 80—26074
- metal, emission analysis using glow discharge, Grimm lamp struct. and discharge characts. *(Japanese)* 78—27867
- metal, laser initiated combustion, time-resolved spectroscopy 78—7207
- metal foils, electric detonation in vac., Xe, He, N_2 atoms., discharge rad. characts. *(Russian)* 77—11435
- metal oxides, electron stimulated dissoc. 80—34301
- metal sample preparation furnace for remelting prior to spectrochem. analysis 77—44556
- metals and alloys, thermodynamic props., evaporation, optical spectral method appls., review *(Russian)* 78—75822
- metastable transfer emission spectroscopy, for trace materials in gas flows detection 78—85257
- microwave induced He plasma excitation source for trace metal anal., excitation mechanism 77—56262
- microwave-induced He(Ar) plasma cavity, excitation source for optical emission spectroscopy 77—44567
- microwave-induced plasma, improvements to TM_{010} cavity 79—43680
- multielement atomic emission/fluoresc. spectrometer system, computer-controlled 80—45587
- multielement determination, using at. emission echelle spectrometer with image dissector and vidicon tubes 78—61081
- multielement flame spectrometry, flame condition optimisation 78—31723
- multielement simultaneous analysis using C furnace and optical MCA 77—40607
- Nimocast, diffusion of Cs, AES, SIMS depth profile study *(German)* 78—84008
- on-line dual-wavelength spectrometer for automatic correction of light scattering interference in atomic fluorescence analysis 77—70377
- optical, using inductively-coupled plasma light source *(Japanese)* 79—48020
- optimum conditions, theoretical problems 79—87918
- photodiode array for radiation detection in AES and analytical appl. *(German)* 80—11992
- plant materials, trace elements emission spectrographic determ. 77—4953
- plasma, inductively coupled, atomisation cell for at. fluoresc. spectroscopy, appls. 77—12839
- plasma discharge, spatially-resolved spectrometry, radial emission line profiles, Abel inversion 77—12841
- plasma jet, discharge current and gas flow rate influence on spectral characts. *(Czech)* 80—26081
- plasma jet and aerosol desolvation system, appl. to emission spectroscopy 77—86425
- plasma jet light source, intensity distribs., OH band rot. temp. 77—44555
- plasma quantometer, quantitatively coupled, for emission spectrochem. anal. *(Japanese)* 78—83624
- plasma source, inductively coupled, analyte excitation temp. and electron density distribs. 77—40592
- plasma source 80—26068
- plasma spectral line intensity rel. to plasma temp., composition, anal. appl. *(Russian)* 77—36851
- plasma wall sputtered metal density meas. by atomic fluorescence spectroscopy 78—67422
- plasmatron, bilateral emission, as radiation source *(Russian)* 77—48744
- powdered mixtures, optimum conditions for emission spectral anal. using AC arc *(Russian)* 77—16894
- powdered samples blown into arc discharge, improvement of accuracy of spectral anal. *(Russian)* 77—32851
- Pu nondestructive assay, gamma-spectrometric method 79—81068
- pulsed EIMAC source, for at. fluoresc. spectrometry 77—61144
- pulsed excitation sources, signal-to-noise ratio effects 77—79158
- quantitative elemental analyses by plasma emission spectroscopy 79—57337
- quantometric meas. of spectra of controlled arc, spark generators, correls. 79—66382
- quartz, synthetic single crystal, impurity content 77—11583
- radio-frequency excited pulsed hollow-cathode lamp, absorpt. and emission characteristics 80—89550
- rare earth metal impurities in PuO_2, PuO_2-UO_2 determ. by chem. separation, at. emission anal. 77—52723
- refractory refinement during prep. by self propagating high temp. synthesis 78—60634
- resonance flame fluorescence with CW dye laser excitation 77—21438
- review 1976-1977 78—80797
- review of advances in past 25 years 79—34381
- review of principles, instrumentation, methodologies, appls., teacher education appl. 78—69927
- RF inductively coupled plasma, interference effects for simultaneous multielement analysis 77—1963
- river water, Na determ. by flame emission meas. 77—36850
- saline water, trace element determ. by multielement ICP-AES method 78—23992
- saturated optical non-resonant emission spectroscopy for detection of atoms 77—90672
- saturation in laser excited atomic fluoresc. spectrometry, expt. verification 79—79330
- saturation of energy levels 78—65980

atomic emission spectroscopy continued
sediment leachates, trace element anal., multielement-direct reading method 78−69514
selectivity evaluation 80−89561
signal-to-noise ratio improvement and data processing *(Japanese)* 77−21448
single atom detection, by 1- and 2-photon SONRES 78−85282
single atom detection by saturated optical nonresonant emission spectroscopy 78−31741
soft water, trace element determ. by multielement ICP-AES method 78−23992
soil, inductively coupled plasma-atomic emission spectroscopic anal. 78−31725
solid sample direct excitation sources *(French)* 78−3426
solution, use of discharges in narrow channels *(Russian)* 77−56304
source profiling using Reticon photodiode array 77−63999
spark, high-voltage, effect of strong transverse blowing 80−3441
spark discharge spectrum, correlations rel. to matrix effect *(Russian)* 77−86427
spark source, 323 MHz quarter-wave, stable discharge prod. 77−80394
spark source, linear Si photodiode array detector, appl. to Cu determ. in Al alloys *(German)* 79−87926
spectral decomposition, generalised algorithm, appl. to UV, IR, at. emission spectrometry 77−12842
spectral line intensity, arc plasma temp. depend. 77−29079
spectral line recording in presence of intense background, techniques, appls. *(Russian)* 77−40613
SpectraScan III system using high-energy Ar plasma excitation and high-resolution spectrometry 79−96382
spectrochemical analysis with glow-discharge lamp *(Japanese)* 78−85262
spectrophotometric methods applied to pharmaceutical analysis 79−96397
steel, austenitic stainless, oxidation of (100)-plane, LEED-AES obs. *(German)* 78−68841
steel, emission spectrochemical analysis of Nb, effect of Mn, interference for Nb II 3194.977 Å 77−21457
steel, liquid state, spectrochemical anal. 79−16096
steel, stainless, oxidised, sputtering yield meas. by atomic fluoresc. spectroscopy 80−80922
steel sheets, surface layer composition charact. by glow discharge spectrometry *(French)* 79−87923
steels, determ. of C, Si, Cr, Mn, Ni by spectrographic method using combined discharge 79−57327
steels, Si determination by at. emission spectroscopy using steeloscope 79−57330
sulphate residues of fresh waters, elemental, anal., spectrographic technique *(Russian)* 77−12868
synthetic calibration standards 79−24850
trace analysis non-thermal excitation 80−30312
trace element detection from static thermal induction plasma, anal. curves, detection limits 79−87919
trace element determination, using emission flame type spectrometer with automatic spectral interference registration *(Russian)* 78−35775
trace metal analysis in water, accuracy in AAS and AES using graphite furnace 78−69510
trace metal conc. in waste water, spectrochem. anal. 78−61106
transport of atoms in arc electrode channel *(Russian)* 77−52725
trifluoromethane plasma etching of SiO_2, optical spectroscopy appl. 80−87940
vacuum far-ultraviolet light source, hypersonic dense plasma *(Russian)* 77−49789
water pollution by metals monitoring, instrument survey 79−74580
water quality testing, inductively coupled plasma atomic emission spectrometry 79−83520
water vapour, spectrochem. anal., effect on HF torch discharge *(Japanese)* 77−44554
wavelength modulation, using CW dye laser 78−61083
wavelength modulation spectrometry, computer modelling 77−63974
Ag, Auger spectra, 4d bandwidth effect 80−89093
Al, spectral anal. in HV impulse discharge sensitivity limit 79−29420
Al-Cu-Si, effect of sample conditions on sputtering and intensities, emission spectrochem. anal. using glow discharge *(Japanese)* 80−21349
AlAg, Auger spectra, 4d bandwidth effect 80−89093
Ar atmosphere, controlled, line intensities of metals *(Russian)* 77−56300
Ar ICP plasma, excitation source for flame at. fluoresc. spectrometry 80−37089
Ar plasma, RF, multi-element anal. 78−3410
Ar plasma source in TM_{010} cavity, for soln. anal. 79−48032
As continuum source, for atomic fluorescence spectrometry 78−45716
Au, analysis of trace elements using vidicon spectrometer 77−21453
C furnace method, atomisation temp. effects 77−40583
C_2, conc. meas. in oxyacetylene flame rel. to saturation spectroscopy 77−60148
Cd, $5,6,7^1D_2 \rightarrow 5^1P_1$ transition probabilities meas. be US pulverisation/flame emission *(French)* 80−42995
Cs, picogram detection in aq. soln., nonflame atomic fluoresc. spectroscopy with dye laser excitation 77−44528
Cu, lines in hollow cathode discharge, radial inhomogeneities in excitation and profile 77−4974
Cu-Au, surface anal. by LEED and AES 77−69153
Cu-Zn-Sn-Pb (5, 5, 5 wt.%) alloy, analysis in glow discharge lamp and in ion microprobe, sputtering processes 77−52730
Eu, determ. by at. fluoresc. anal. with pulsed dye laser excitation *(Russian)* 78−35774
Fe and steel, centrifugal casting method and high frequency induction melting, sample prep., emission spectral anal. 77−48367
Fe, P determination by at. emission spectroscopy using steeloscope 79−57330
Fe-Ni-Co(Cu) alloy components, dynamics of arrival to arc discharge during roasting *(Russian)* 77−16895
He-Ne lasers nondestructive analysis 80−1210
Ir, determ. by at. fluoresc. anal. with pulsed dye laser excitation *(Russian)* 78−35774
Li, at. emission obs. using modified graphite furnace at. absorpt. spectrometer 78−31727
MgAg, Auger spectra, 4d bandwidth effect 80−89093
MgO in acetylene flame, saturation spectroscopic determ. 79−29425
Mn, determ. by plasma jet emission spectroscopy, using desolvation system with US nebuliser 78−68960

atomic emission spectroscopy continued
Mo, diffusion of Cs, AES, SIMS depth profile study *(German)* 78−84008
N_2, N_2-He, barrier discharge, struct., spectral anal. *(Russian)* 77−21463
N_2, plasma, pulsed discharge, component conc. radial distrib. determ. *(Russian)* 77−21462
N_2O-acetylene flame, background compensation in differential atomic emission spectrometry *(French)* 78−7296
Na, detection limit, using CW dye laser spectroscopy *(Japanese)* 78−44435
Na, flame absorption and fluorescence, laser saturation broadening 78−88661
Na, in acetylene flame, saturation spectroscopic determ. 79−29425
Na in air-acetylene flame, harmonic saturated spectroscopy for at. fluoresc. detect. 80−104472
Na in flames, saturated fluoresc. meas. 77−79571
Na, near-resonant Rayleigh scattering and atomic flame fluorescence spectroscopy 79−92033
Na, reson. line, laser excitation, combustion Rayleigh scatt., at. flame fluoresc. spectroscopy 80−42972
Na, single atom detection by laser fluoresc. *(Russian)* 80−35620
Na, trace detection in furnace atm., 1000°C, fluoresc. 77−4955
Ni, determ. using laser excited atomic fluoresc. spectrosc. 80−93811
Ni, diffusion of Cs, AES, SIMS depth profile study *(German)* 78−84008
O_2 $^1\Sigma_g^+$ lifetime obs., in corona discharge *(French)* 77−24230
Pt, determ. by at. fluoresc. anal. with pulsed dye laser excitation *(Russian)* 78−35774
Si, semiconducting, determ. of traces of Br and Cl using hollow cathode of special design *(Russian)* 77−29083
SiO_2-GeO_2-B_2O_5-P_2O_5, optical waveguide glass, comp. determ., plasma emission spectra 80−87446
Sn, determ. using laser excited atomic fluoresc. spectrosc. 80−93811
TZM, diffusion of Cs, AES, SIMS depth profile study *(German)* 78−84008
Ta, determ. in ore, spectrochem. method 79−16075
Ta-Re-Y-La alloy, Y, La determ., spectrochem. method 79−16076
Ti alloys, elemental distrib., emission microspectral anal. *(Russian)* 78−35773
TiO_2, sputtering defects, associated surface electron states, UPS, XPS and AES obs. 80−60755
U, atom form. in chem. reaction, conc. determ. by laser fluoresc. excitation *(Russian)* 77−9156
Y impurity in PuO_2, PuO_2-UO_2 determ. by chem. separation, at. emission anal. 77−52723

atomic energy *see nuclear power*

atomic excited states
see also atomic metastable states; atomic resonant states
1s2p^{3}P levels, theoretical lifetimes and fluoresc. yields 80−27975
1s hole states of 3- and 4-electron systems, generalised Brillouin theorem-multiconfig. method 77−23443
3d^N ions, free and in crystals, Slater parameters, 3d-4s excitation energy 78−33433
4d states, atoms in compounds, model with two-well potential 77−26989
^{1}D isoelectronic series, Sternheimer valence shielding and antishielding factors 80−18807
adsorption on Sc and Lu surfaces, effect on reflection EELS 80−20742
advances in electron physics, book 80−8742
alignment in gas discharge, Hanle effect 80−23378
alkali, metal, Rydberg state emission oscill. strength minima 80−32662
alkali atoms, excited state, laser photoionisation theory, hyperfine coupling effect 80−102493
alkali atoms, highly excited Rydberg states, fine struct. 80−58402
alkali metal, dynamic polarisability, variational calcs. with mode pot. *(Russian)* 78−902
alkali metal, dynamic polarisability dispersion eqn., dispersion interaction of atoms 79−26902
alkali metal, excited state lifetime var. along isoelectronic series *(French)* 77−46538
alkali metal, high ang. momentum Rydberg states, quantum defect core polaris. depend. 77−18808
alkali metal, radial matrix elements and radiative lifetimes 79−59375
alkali metal, transition oscillator strengths in discontinuous and continuous spectra, review 80−52937
alkali metal atom, Rydberg state Stark struct. 80−37754
alkali metal atom Rydberg state quantum defects, semiclassical calc. 77−38621
alkali metal atoms, excited hyperfine and Stark parameters, meas. and calc. 78−86814
alkali metals, excited states energy levels ordering 77−67968
alkali metals, Rydberg states, Stark ionisation 80−52933
alkaline earth atoms, multiphoton spectra of high Rydberg states 77−68022
alkaline earth metals doubly excited, autoionising states and interference profiles 80−52949
alkaline earths, high Rydberg states, multichannel quantum defect theory 79−72250
approximate and exact state wavefunctions, ionisation potentials, energy difference calcs. 79−97967
atom, 5d6p$^1F_3$-state lifetime meas. 79−89633
atom, multiconfigurational time-dependent Hartree-Fock approach 79−85889
atom+atom, potential well depth estimation method 79−86034
atom+charged particle, autoionisation state decay 80−9565
atom+molecule rot. effect on polar mol. collisional ionis. 77−83702
atom+neutral particle, Rydberg state transitions 78−9213
atom-molecule collisions, rotational transitions, classical cross sections, sudden approx. calcs. 79−89751
atomic shell rearrangement during electron capture 79−75921
autoionisation electrons, photons emitted from collisionally aligned states, angular correl. 77−14385
autoionising states, nonexponential decay to continuum, possibility of obs. 77−42288
b_n factors at low temperatures, appl. to interstellar C II regions 80−36696
beam-foil excitation, level population concept, depend. on exptl. parameters 80−14206
beam-foil interaction process, quantum beats, alignment and orientation obs. 80−14252

atomic excited states continued
beam-foil lifetime measurement, cascading problem, ANDC method use and error limits 80—14249
beam-foil spectroscopy, lifetime meas. from decay curves, book contrib. 77—38747
beam-foil spectroscopy measurement techniques, review 77—50563
beam-target interaction, atomic orientation prod. by electron capture, semiclassical model 80—9723
blackbody radiation interaction with LF atomic transitions, Zeeman, Stark and stimulated emission 79—41127
bound and free, inner charge defect method calcs. 80—78511
bound state decay in external field in semiclassical approx. 80—12941
bound states, beam-foil excitation and decay near ionis. limit 80—9552
C III, excited states, transaction oscill. states and wavefunctions 79—59367
calculation for atoms with one or two external electrons 77—14374
cascade effects on polarisation of radiation, electronic or atomic collisions 80—18917
Cd+molecules collisions 80—58338
coherent non-stationary superpositions of atomic eigenstates, beam-foil spectroscopy 77—38748
coherent populations, RF elec. field reson. interactions, quantum beats 77—46542
collisional excitation transfer, with small reson. defect, mag. field effects 77—3449
Coloumb excitation of atoms by fast protons, proton energy loss depend. on impact parameters *(Russian)* 80—53123
complex atom*+inert gas atom, model pot. curves, including CI 78—42154
Coulomb approximation oscillator strengths and multipole radial integral calc. 79—63959
crystal lattices, atomic collisions of channelled ions, resonant coherent excitation 80—15170
decay, radiative emission-autoionisation interference 79—26945
decay time coincidence spectra, anal. 77—38575
degenerate atomic level perturbation by neutral particles 79—792
double vacancy states, correl. photon and electron transition, perturbation theory 80—27968
doublet state, ionis. pots., electron affinities, using electron propagator, appl. to Li, Na, and BeH 79—63933
doubly ionised K-shell system, radiative decay of excited state, branching ratio calcs. 77—54521
education, Na Rydberg states, anomalous fine struct., perturbation model 80—57035
education, spontaneous emission and superradiance, coherence effects, semiclassical 77—82347
education, two-electron atom, 1snl excited levels, ionisation energy calc., perturbation, Schrodinger eqn. methods 80—17728
effective excitation cross-sections for atoms in meteors 80—101565
electric field ionisation, highly excited state, linearly polarised field, freq. (amplitude) depend. 80—32630
electron+ion scattering, Schwinger's variational principle, Rydberg states 80—78713
electron impact excitation of 2^3S level, differential cross section in second Born approx. *(Russian)* 78—1087
electron scattering, low energy, quasidegenerate case 79—76515
electronic and at. collisions, conference, Kyoto, Japan (Aug.-Sept. 1979) 80—62394
electronic energy transfer, in excited atom collisions, review, book contrib. 77—40543
electronic transition probabilities and lifetimes, expt. determ. 80—23369
elementary atomic processes, threshold behaviour 80—23546
EM field effects, strong, review 79—49955
energy level ordering 78—21863
energy levels calc. of atoms in $1s^22s^22p^N3p$ and $1s^22s^22p^N3d$ configs. 77—46509
eqn. of motion-Green's function and config. interaction methods comparison, appls. 80—47841
excitation energies calc., using renormalised Green's function method *(Japanese)* 80—83295
excitation energy, eqn. of motion method calcs., approxs. and error anal. 79—36501
excitation energy, validity of excited minus ground state calcs. using HF/pair correlation 77—38620
excitation of simple atomic and mol. systems, long-range force effects 79—10170
excited atom ionisation due to collisions in their own gas *(Russian)* 80—91654
excited state collisional relax., line broadening, interat. interactions, review 80—43149
excited state structure, electron correl., var. collapse theory 79—6890
excited states of closed-shell systems, SCF scheme 79—6885
fast ion double collision spectroscopy, polarisation obs. of emitted photons 80—16134
fast ion excited levels produced in foil or surface collisions, orientation and alignment 80—14214
fast projectile electron loss forward peak oscill. struct. as autoionisation 80—69227
fast projectile electron spectroscopy, autoionizing ion levels and lifetimes 77—38749
fast projectiles, electron capture into n,l excited states 80—23543
fast reactions of excited atoms, absorption spectrophotometry 79—52667
field ionisation mechanisms 78—70761
field theoretic Green's functions, excited states transitions, appl. 79—68199
field-ionisation of Rydberg states, depend. on $|m_l|$ 78—58856
first row atoms and multiply excited states, SO(4) theory for electron correlation 79—22608
force on atom in electrostatic field, Feynman-Hellmann theorem and oscillator strengths 80—65275
form factors and cross sections for $nl \rightarrow n'l'$ direct collisional transitions 79—31636
four subshells of equivalent electrons, matrix elements of relativistic energy operator 78—33407
four-electron ions, excited states, one-electron approximation calcs. 79—10049
fourth row element ions, relativistic Dirac-Fock-Slater orbital binding energies, one-electron transition energies 79—25778
gas discharge, photoionis. at low illumination intensity, nonlinearities, effective cross section 78—87517

atomic excited states continued
gas phase reaction consts. for electronically excited species, relax. processes, data tables 80—16644
generalised Brillouin theorem multiconfig. method 77—67993
giant Rydberg state, theory, behaviour, applications *(French)* 79—26903
grazing incidence ion beam-surface interaction, mechanism and uses 80—14251
ground and excited states, polarisability and scaling, oscillator strengths, continuum spectrum contribution 80—27923
Group IVA elements, excited states, quadrupole moments, Sternheimer shielding factors 78—82630
$H(1s)+e^+ \rightarrow (e^+e^-)(nlm)+H^+$, highly excited states rearrangement collisions 79—59564
hadronic atom level shifts, multiple scat. expansion 78—70978
halogen, negative ion form. in dissoc. attachment by 0-8 eV electrons 78—74776
halogen atom (^2P)+inert gas atom (^1S), coupled channel study, rel. to elastic approx. 79—81255
Hartree-Fock equations derivation, N-body excited states 79—93934
He, ions recomb. and level populations, resolution of ang. momentum states 77—45529
heavy ion, beam-foil spectra from 20 to 238 MeV energy, 5 to 60 nm, lifetime meas. problems 80—9722
heavy ion+atom collisions, small impact parameters, K-vacancy prod., molecular theory 80—69229
heavy ion collisions, adiabatic basis for inner shell excitations 79—89759
high Rydberg atom+neutron atom (molecule), collisional quenching, theory 79—86051
high Rydberg atom+polar molecule, l-changing collision 79—10185
high Rydberg electron interaction with core, retardation effects 79—6888
high Rydberg states, expansions in inverse principal quantum no. 79—36551
high Rydberg states with long range correl., single photon double excitation amplitudes 79—72251
high-Rydberg atom+inert gas atom, thermal collision, l-changing cross section calc. 80—14190
high-Rydberg atom+polar molecule, state-changing collisions 80—9727
high-Rydberg state high-impact-velocity forward charge transfer as classical process 79—22824
highly excited atoms, acted on by EM radiation, oscillator stochastic instability theory *(Russian)* 79—31487
highly excited atoms, blackbody radiation effects 80—58176
highly excited atoms, collision processes, review 77—58146
highly excited atoms, review 80—58174
highly excited atoms, review of recent expts. 80—23325
hydrogen-like ions, beam-foil excitation, relative initial populations, lifetime curves 80—14210
hydrogenic ion + H^+, electron capture in highly excited s-state 79—45839
inert gas, at. excited states in discharge, Hanle effect 79—76394
inert gas, photoionis. cross sections of excited levels, quantum defect method calcs. 80—37795
inert gas+H^-, charge transfer, ejected electron spectra 79—45828
inert gas atom, first excited config., intermediate coupling coeff. 80—83450
inert gas atom+halogen mol., halide form., relax. and quenching 80—81314
inert gas collisional perturbation of 6^3D_1, 6^1D_2 Hg levels 80—74223
inert gas plasma, free-bound continuum determ. using photoionis. cross sections calc. 80—43878
inert gases, atomic alignment in positive column *(Russian)* 80—87981
inert gases, electron impact ionisation cross-sections for excited states 80—9742
inert gases, photoionisation cross sections of excited atoms and dimers 78—66523
inner shell ionisation phenomena, conf., Freiburg, West Germany (Mar.-Apr. '76) 77—27040
inner-shell excitation in heavy ion collisions, variational method 79—31428
ion, singly-charged, sufficient conditions for finite no. of bound states 79—10047
ion+atom collision produced highly excited states, decay spectra 80—63780
ion+atom collisions, K-shell hole, multiple hole production, charge transfer and antisymmetry 80—43168
ion+atom collisions, X-ray polarisation 79—45810
ion collisions, electron capture, atomic excited state polarisation, optical detection 80—58377
ion excited state lifetimes meas. using orientation transfer in Penning collisions *(French)* 78—50621
ion-Rydberg atom collision cross sections, classical trajectory Monte Carlo calcs. 80—43174
ionisation and excitation energies, ΔE SCF, transition functional method 77—88404
ionisation in EM field by electron diffusion *(Russian)* 78—86798
ionised atoms, quantum numbers, filling order of ionic electron shells, statistical model 80—52884
ions, electronic transition probabilities and lifetimes, expt. determ. 80—23369
ions, multiply charged, highly excited states, parity nonconservation effects 80—52898
ions in $1s^22s^n2p^{4-n}$ configurations, term-energy calcs. using perturbation theory 77—42229
ions resembling Li, Be and B, spectra calcs. 77—42260
isoelectronic series, excited state ions energy level ordering 78—21863
k-ordering, l-patterns, ats. and isoelectronic ions 77—88406
Landau condensation in atomic physics 80—74098
lanthanide atomic vapours, (Sm, Eu, Dy, Ho, Er, Tm, Yb,) photoabsorption spectra 77—88417
lanthanides, Rydberg spectra and ionisation thresholds, time resolved resonant multistep technique 78—82701
laser atom interaction, phase diffusion model, Lorentzian laser lineshape, detuning 80—944
laser excited, reactive collisions 80—66793
level crossing, using laser excitation *(Rumanian)* 78—50510
lifetime determinations, errors using pulsed dye lasers 77—42281
lifetime meas., cascade-free, fast-beam-spectroscopy by combined gas cell-laser excitation 77—61714
lifetime meas. astronomical applications, beam-foil method 77—41313
lifetime meas. in atoms, mols., ions 77—30832
local-density theory of multiplet structure 80—18776

atomic excited states continued
magnetic scattering of neutrons on excited atoms or mols., cross sections, neutron polarisation *(Russian)* 78−55249
many-body perturbation theory, eqns. of motion formulation 77−88373
many-electron systems, time depend., complex scaling and resons. calcs. 79−22612
metal surface, excited atom emission, survival probabilities 78−48266
metal vapour laser, upper and lower laser states population densities, simultaneous determ. method 78−87042
metals, refractory, excited state radiative life time, sputtering techniques 78−17602
microwave ionisation of highly excited states, and excitation 79−31482
molecules, eqn. of motion-Green's function and config. interaction methods comparison, appls. 80−47841
multichannel threshold structures in scattering theory 80−58334
multiphoton ionisation, theory of two strongly interacting resons. 80−52955
multiphoton ionisation from excited states 77−88433
multiple quantum transitions, excited states in presence of static electric field 78−37618
multiplet lines emitted after beam-surface interaction, polarisation calc., time development 80−14216
multiply charged ion, electron capture into different excited states in plasma 80−64679
muonium hyperfine structure of ground state, magnetic moments, muonium-antimuonium conversion, excited states 80−69273
N-electron system, Schrodinger eqn. soln. using antisymmetrisation 80−106246
neutral+high Rydberg atom, thermal collisions, review 80−63756
neutral particle balance in nonequilib. plasma, excited atoms effect 79−27747
neutral particles, electrostatic trapping 80−102485
nondegenerate optical transitions of excited atom in buffer gas, line shape kinetic theory 80−42997
one electron excited atom ionisation collisions at high energy, improved impulse approx. 79−94072
one-electron atom in strong light field 79−63946
open shell excited states, perturbation effects, restricted Hartree-Fock calcs. 78−86770
operator manifolds, expansion and completeness theorems 79−59331
optical pumping of gaseous atoms, review *(Japanese)* 78−25489
orbital angular momentum transfer to nucl. spin polarisation in external mag. fields 80−14217
ordering of energy levels, quantum defect and the quantity $k=n+l$ 79−81162
orientation and alignment, collisional transfer, single-mode laser-excited atom. 80−23495
orientation of excited atoms in elec. field *(German)* 78−25472
oscillator strengths, core relax. effects calcs. 79−10050
oscillator strengths calcs., influence of wave function determ. method 80−99478
perturbation and SCF calcs. 80−102455
photoemission, many-electron theory, in electron spectroscopy book 78−17714
photoionisation, quantum beats, origin 80−52954
photoionisation from low or high excited states, radial transition integrals 80−18832
photoionisation processes, expt. techniques, theory, review 77−14402
photon emission by N-independent excited atoms, wave functions 77−57895
picosecond excited state meas. using tunable laser induced grating 77−10786
planetary atoms, energies of states 77−30799
plasma, population distrib., electron-density variation influence 78−87431
plasma, rapidly varying, excitation temp., electron density variation influence 80−38537
polarisability of atoms, freq. depend., Hartree-Fock theory 79−45652
polarised excited atom, freq. depend. polarisation of emitted radiation 77−61705
population densities of excited states of H-like ions, computer program 77−39402
positronium formation in highly excited states, first Born approx. 80−58420
quasi-hydrogenic atoms, Rydberg states 78−90098
radiative collisions and two-photon transitions 77−46552
radiative decay of atom with two coupled excited states, line hole shift 77−18834
rare earth elements, atomic partition functions, Chebyshev approximations 80−67544
rare earth films, Auger emission from excited atoms 77−20967
resonant electron scatt. by atoms in laser field, negative ion formation, polarisability 77−19089
retardation effects on high Rydberg states, retarded R^{-5} polarisation pot. 78−82629
rotationally induced atomic excitation, quasimolecular orbital rot. coupling, uniform Airy approx. 78−25644
row element ions 79−25778
Rydberg, extrapolation to high principal quantum numbers of radial integrals in Coulomb approx. 79−3380
Rydberg, use as spectroscopic probe for resonances in mol. electron elastic scatt. 77−58162
Rydberg atom, electron collisions 80−63833
Rydberg atom+atom, l-changing collision, rel. to low-energy electron scatt. 79−50112
Rydberg atom+atom (photon), separation of Rydberg electron and ion core 80−63754
Rydberg atom+atom collision, expts. 78−62908
Rydberg atom+ground state atom, slow collision, excitation and deexcitation processes 80−23508
Rydberg atom+ion, collision theory 78−62909
Rydberg atom+molecule, reaction channels, expt. vs. theory 80−63755
Rydberg atom+Rydberg atom, ionisation cross sections 79−81267
Rydberg atom+Rydberg atom, ionisation cross-section calcs. 79−31664
Rydberg atom microwave and far IR spectroscopy 80−63564
Rydberg atoms, expts., metastable states, multiphoton ionisation, spectroscopy, Stark struct., collisions, polarisability *(Dutch)* 78−5160
Rydberg atoms, high-resolution laser spectroscopy of at. beams *(Dutch)* 79−50166
Rydberg atoms, microwave ionisation and excitation 78−94217
Rydberg atoms, teaching approach 80−77570

atomic excited states continued
Rydberg autoionising states, props. in elec. fields, appl. to Fe^{23+} dielectronic recomb. 79−59405
Rydberg electron-ionic core nonadiabatic long-range forces, nucl. charge depend. 80−23328
Rydberg state atom+ion, electron capture, asymptotically high impact vel. 79−54965
Rydberg states, Auger and radiative transition probabilities 79−6923
Rydberg states, autoionisation with large orbital angular momentum 80−87052
Rydberg states, Coulomb and Yukawa pot., wave functions and quantum defects, Schwinger's var. principle 80−63549
Rydberg states, cross sections for collisional ang. momentum transfer 79−6997
Rydberg states, fine struct. splitting, quantum beat and double reson. spectroscopy 78−86979
Rydberg states, selections from 1977 Comments on Modern Physics, book 79−30181
Rydberg states, transitions following electron impact excitation *(French)* 80−78711
Rydberg states in condensed matter, appl. to doped solid rare gases and H_2 79−69425
Rydberg-valence mixing, oscillator strengths 79−31492
SCF theory, hole states of free atoms 77−10610
SCF treatment of higher excited states, method and its appl. to Si II 78−82658
SCF wavefunctions 78−90099
second-row elements, low lying levels, excitation equilib. and line intensities 79−12401
single-term atomic state props., variationally optimised local central pot. calcs., $2<Z<55$ 79−41123
singly excited states, oscillator strengths, ab initio calcs. 80−920
singly ionised atom, excited state struct., electron correl., oscill. strengths, theory 79−6889
solar coronal ions, proton excitations approximation, erratum and extension 79−35118
spontaneous emission from excited atoms, mechanism 79−35586
sputtered atoms in excited states, vel. meas. 80−63561
Stark splitting, optical dynamic, Zeeman degeneracy 80−37774
stimulated transitions betweeen highly excited levels, rel. to anomalous Balmer decrement 78−5176
superexcited atoms, radiowave scatt. in ionospheric plasma, quantum model 80−32677
superfluorescence initiation, master equation study, microscopic description 80−63577
superradiant, excitation by pulse of quantum field 80−87359
three-electron atom systems with two vacancies in K-shell excited states and autoionis. state energies *(Russian)* 79−31429
time-resolved laser fluorescence spectroscopy for atomic and mol. excited states obs., review, book contrib. 80−9760
transition metal, atom, ion, solid, $M_{2,3}$ excitation spectra 78−91653
transition metal atoms, neutral and ion val. states, electron correlation, ab initio effective val. Hamiltonian calc. 80−99449
transition metals, 1st period, at. correlation energies, perturbation calc. 79−36508
transition metals, 3d, M III excited states, radiative lifetimes, beam-foil obs. 77−30979
transitions, excitation by monochromatic laser radiation, Doppler-broadened transitions 80−78582
two electron atom, energy levels, classical first order perturbation theory 80−58118
two K-shell vacancy systems, excited states, radiative decay 79−10048
two photon excitation, time depend. emitted light spectra, perturbation theory 80−63605
two-atom interaction, decay rate, dynamical operator treatment 77−42272
two-electron atom, dipole approx. for electron-electron interaction, autoionisation widths *(Russian)* 77−61691
two-electron atom, doubly excited states, classification 77−14373
two-electron atoms, doubly excited resonances assoc. with $N=4$ hydrogenic threshold 80−106283
two-electron ats. and ions, low lying S states, pairwise correlated generalised VB method 77−65427
two-electron doubly excited states, rotor-like spectra 79−18128
two-electron systems below $N=2$ threshold, widths and config. mixing 79−18129
two-k-shell-vacancy systems, excited states, radiationless decay probability calcs. 78−41993
two-level atom, interaction with radiation, photon number time evolution 80−58216
two-level atom plane, one-dimens. $\delta l=1$, $\Delta m=0$ decay, soluble semiclassical model *(Portuguese)* 80−18809
two-level atoms, effect of high-power coherent radiation on spontaneous emission 79−55094
valence correlation energies, contributions of triply- and quadruply excited states determ. using perturbation theory 80−78545
vapours, three-level system, collisional effects in saturation spectroscopy, appl. to Na 80−78579
weakly excited system, neoclassical theory of radiation test calcs. 77−6737
yrast state cascade population of atomic levels, power law 80−18808
Ag, excitation by FKα and AlKα ESCA sources 78−53301
Al, electron impact excitation cross sections calc. *(Russian)* 78−55240
Al II, $^3F^0$ Rydberg series, energy levels, multiconfigurational HF procedure 80−47882
Al II to Al VI, beam-foil obs. from 1100 to 1900 Å, lifetimes and oscillator strengths 80−14108
Al II to Al VI, beam-foil obs. from 300 to 2000 Å, mean lives and oscillator strengths 80−14109
Al IV, lifetimes of $n=3$ and 4 levels meas. and calc. *(French)* 80−9554
Al IV, Ne-like, atomic lifetimes, second order calc. and beam-foil meas. 79−59422
Al IX to Al XI, beam-foil obs. of lifetimes and oscillator strengths, 300 to 1000 Å 80−14110
Al ions, 720 keV beam foil spectra 1800 to 7000 Å, excited state cascades and lifetimes 77−23450
Al, lowest S-state lifetime meas. 77−65436
Al, plasma, transfer eqn. soln. using freq. and angle averaged photon escape probabilities 80−64688
Al, vacuum arc, excited state density from line intensities 80−96404
Al, vacuum arc, excited state density theory 80−100107

atomic excited states continued
- Ar, $3p^5 5p$ config. aligned in discharge, interf. signals, lifetimes and collision cross sections 78−70796
- Ar arc discharge atomic excitation, effect of ion conversion *(Russian)* 79−10731
- Ar atomic excited states collision radiative destruction in glow discharge 79−3528
- Ar discharge, population processes of 4p levels, perturbation influence 80−38565
- Ar, emerging from C foil, excited ion Auger decay 77−3333
- Ar high density plasma, highly excited atomic levels, spectral-line-blending study 80−48969
- Ar I arc plasma, excited atom density meas., Saha-Boltzmann equilib. 80−926
- Ar II, lifetime meas. using photon-photon delayed coincidence 77−14389
- Ar II, transition probabilities, lifetimes, intermediate coupling semiempirical calcs. 79−789
- Ar IV to Ar XII, beam-foil obs. of lifetimes and oscillator strengths, spectral identifications, 400-2000 Å *(French)* 80−9555
- Ar, multiply excited, inner level X-ray emission spectra, line widths and Auger transition rates 79−36575
- Ar neutral system, complete saturation phase excited state population density 80−106284
- Ar, optical gas breakdown, reduced threshold in two-freq. field 80−64819
- Ar, outer $p_{1/2}$ subshell photoionisation, polarised electrons, relativistic RPA calcs. 80−83331
- Ar, photoionisation cross sections for excited states, rel. to KrF laser 77−75110
- Ar plasma, inelastic collisions between excited states, Chapman-Engskog procedure, electron energy distrib. 79−68902
- Ar, plasma column of hollow cathode arc, collisional model of ion system 80−38749
- Ar, positive column, 4S and 4P levels populations, rel. theory with recomb. 77−10766
- Ar, production of Ar_2*, kinetic behaviour and energy transfer 79−68305
- Ar, Rydberg states, nearly zero energy electron source 79−72433
- Ar^{2+}, multiple open shell configs. calcs., modified HF method 77−50356
- Ar^{2+}, single photon decay of $(2s)^{-2}$ and $(2p)^{-2}$ double hole states 77−34606
- Ar^{5+}, Ar^{6+}, excited state lifetimes, beam-foil meas. 77−10750
- Ar+Kr, $(4p^5 5p)$ and $(4p^5 5p')$ states, radiative lifetimes and two-body collisional deactivation rate consts. 80−95572
- Ar^{2+}+Ar (Kr)(Xe), single electron capture excitation, photon emission, VUV spectroscopy 80−58379
- Ar^{2+}+Na, Ar^+ form, electron capture, Ar^+ excited states relative population distrib. 80−23544
- Ar^{2+}+Na collision, single electron capture into Ar^+ excited states, 0.2-12 eV, emission cross section 80−48071
- Ar^{2+}+Na collision, single electron capture into Ar^+ excited states, relative population distrib. 80−48072
- $^{40}Ar^+$, excited state polarisation transfer due to optical cascades 78−9238
- Ar*, electron excited in Ar-CO_2 mixture, transfer reaction kinetic study 80−63824
- Ar*$(3p^5 4p)_i$+Ar$(^1S_0)$, collisional population transfer rate coeffs., 300K 79−10177
- As, $np^2(n+1)s$ excited-state config. quadrupole moments, Sternheimer shielding factor 80−37755
- Au, excitation by FKα and AlKα ESCA sources 78−53301
- Au+H^+ ionisation, induced L-shell alignment 80−32813
- B, excited in single gas collisions, high-resolution Auger spectra 80−9717
- B I and II, high spin and mixed states 77−61709
- B IV, doubly-excited states, energy levels, calc. and expt. *(French)* 78−41971
- B ion, equilib. charge state distrib., in C foil and doubly excited states *(French)* 77−27171
- B^+, beam-foil excitation, absolute Auger yield meas. 80−14203
- B^{2+}, ^2S, $^2P^0$ and ^2D autoionising states, positions and widths 79−26944
- B+He(Ne)(Ar), ground and excited states interaction, B spectral line breadth 77−68092
- Ba, $(6p_J 20s_{1/2})_J$ state, autoionisation, ejected electron energy anal. 80−43009
- Ba, autoionis. spectrum, pair splittings 79−13684
- Ba, autoionisation and Auger decay, collective excitation effect 80−43008
- Ba, excited state lifetime, delayed coincidence meas. 77−3315
- Ba, hyperfine splitting and isotope shift of high lying levels, Doppler-free 2-photon laser spectroscopy 80−58215
- Ba II, 5p excitation, relativistic anal., multiconfig. Dirac-Fock calcs. 80−69240
- Ba II, Hanle effect, $^2P_{3/2}$ lifetime determ. 77−18852
- Ba, multiphoton ionis. spectroscopy of even- and odd-parity states 78−86973
- Ba, photoexcitation spectrum, discrete autoionising states interferences 80−5508
- Ba, quadratic Zeeman effect, diamagnetic shift, Rydberg series, strong field mixing 78−946
- Ba, quantum defect param., ab initio calcs. 80−78525
- Ba, two-photon spectroscopy, highly excited even levels, J=0 spectrum anal. 79−31447
- Ba^+, excited state lifetimes, fluoresc. decay meas. 77−79574
- Ba+N_2O, reaction, electronic branching, statistical and dynamical influences 78−92451
- Ba+Tl, dipole-quadrupole radiative collisional fluoresc. 80−83315
- Ba+Tl, radiative collisional fluoresc. obs. from thermally excited atoms 80−102480
- $Ba^+(^2P_{3/2})$, coherently Penning ionis.-excited, with He(2^3S_1), Hanle effect 80−5520
- Ba$(^1S,^3D)$+ halogenated methanes, laser induced fluorescence 79−66270
- Be, excitation energies and transition moments in a second order polarization propagator approach 79−10051
- Be, excitation energy calc., improved virtual orbitals 77−46491
- Be, excited in single gas collisions, high-resolution Auger spectra 80−9717
- Be II, autoionising core-excited states, alignment prod., Be^++He(methane) collision excitation 80−14204
- Be III, doubly excited states, triplet spectra 80−87069
- Be isoelectronic sequence, mag. quadrupole transitions, multiconfig. HF calcs. 78−33420

atomic excited states continued
- Be isoelectronic sequence, highly ionised, beam-foil obs. of oscillator strengths for E1 transitions 80−14112
- Be isoelectronic series, excited states, transaction oscill. states and wavefunctions 79−59367
- Be isoelectronic series, excited states, oscill. strengths calcs., influence of wave function determ. method 80−99478
- Be like ion, radiative decay of 2 $^3P_0{}^o$ level 80−27984
- Be, multiconfig. HF procedure, 2nd- and approx. 2nd-order, convergency 79−93907
- Be, optical beam-foil spectra, relative level population 80−14207
- Be, pair excitation correl. numerical coupled cluster method 80−47906
- Be, SCF ion improved virtual orbitals, excited configs. calc. 77−10585
- Be^+, ^2S, $^2P^0$ and ^2D autoionising states, positions and widths 79−26944
- Be^+, formed in laser-produced plasma, absorpt. from excited states 78−17594
- Be^{2+} quantum defects rel. to angular momentum, nuclear charge, Coulomb-Born approx. method *(Japanese)* 77−50534
- Bi, $6p^3(^2D_{3/2}{}^0)$ and $6p^3(^2D_{5/2}{}^0)$, collisional deactivation 77−61702
- Bi I, excited configs., mag. hyperfine splitting factors, interferometric determ. near 200 nm 80−32852
- Bi Rydberg series from Bi_2 three photon excitation 80−106280
- Br+HCN, electronic-vibr. energy transfer, Br$(4^2P_{1/2})$ quenching and HCN (001) deactivation, fluoresc. obs. 77−518
- Br+O_2(NO), quencher paramagnetism, deactivation rate const., spin-orbit relax. study 80−21263
- Br*+N_2O, electronic-vibr. energy transfer, time-resolved fluoresc. obs. 79−89753
- Br*$(4^2P_{1/2})$ yield, in Br_2(IBr) photodissoc., wavelength depend., collisional release 78−64857
- Br$(4^2P_{1/2})$+CO_2(COS)(CS_2), electronic to vibrational energy transfer rates 78−29839
- β^{3+} quantum defects, rel. to angular momentum, nuclear charge, Coulomb-Born approx. method *(Japanese)* 77−50534
- C, excited electronic states contrib. to transport props. 80−23326
- C, excited in single gas collisions, high-resolution Auger spectra 80−9717
- C, first-principles pseudopotential in the local-density-functional formalism 79−59328
- C, ground and excited states, atomic polarisability calc. 77−83756
- C II and III, mean lifetimes of astrophysically important excited levels 77−46528
- C II line excitation by C I photoionisation 80−58223
- C II to C VI, beam-foil excitation functions for optical transitions 80−14209
- C III, IV, V Auger lines obs., beam-foil excitation, ab initio calcs. 77−54601
- C IV (CV), UV line identifications and lifetime meas. 80−106288
- C, optical oscillator strengths, independent particle model, excited state wave functions, LS coupling and Born approx. 80−32674
- C, photoionisation cross section, CI calcs. 79−98050
- C, theoretical ionis. energies and oscill. strengths, excited s-, p- and d-levels 78−86823
- C^+, beam-foil excitation, absolute Auger yield meas. 80−14203
- C^{3+}, ^2S, $^2P^0$ and ^2D autoionising states, positions and widths 79−26944
- CO, photoelectron ang. distrib., photon energy depend. , 16-25 eV 80−53046
- CO+K, atom electronic excitation, vibr. to electronic energy transfer, seeded mol. beam studies 80−47919
- $C^+(^4P)$+H_2, reaction, energy and ang. distrib., energy spectra 77−1918
- ^{13}C III, $1s^2 2s3p$ $^3P^0$ state,, HFS, beamfoil expt., CI and Hartree-Fock calcs. 77−75276
- Ca, $3p^6$ subshell excitation by electron impact 80−1070
- Ca, 4s4p $^1p_1$ level Hanle effect density depend., lifetime 80−91494
- Ca, atoms and ions, radiative lifetimes of excited states *(Russian)* 78−13472
- Ca, direct meas. of excited state lifetimes 77−65435
- Ca I excitation series, potential barrier effects, single configuration HFC 80−78558
- Ca II, Hanle effect, $^2P_{3/2}$ lifetime meas. 77−18852
- Ca II, lifetime extraction from beam-foil decay curves 80−14107
- Ca, multiphoton ionis. spectroscopy of even- and odd-parity states 78−86973
- Ca, oscillator strengths and excitation energy, valence shell states 78−17611
- Ca, quantum defect param., ab initio calcs. 80−78525
- Ca, Rydberg states and microwaves, spectroscopy, masers and superradiance study 80−53248
- Ca^+ cyclic laser, double-pulse excitation expts. 79−55118
- Ca+inert gas, collision-induced dipole transitions assoc. with high-lying states 80−37866
- Ca+$O_2(CO_2)(N_2O)$, reaction, electronic branching, statistical and dynamical influences 78−92451
- $Ca^+(^2P_{3/2})$, coherently Penning ionis.-excited, with He(2^3S_1), Hanle effect 80−5520
- $Ca_2{}^+(^2\Sigma_u{}^+$ and $^2\Sigma_g{}^+)$, ab initio SCF and CI pot. energies 79−27055
- Ca*+Cl_2, collision and reaction cross section meas. 79−59537
- Ca*+He(Ne), model pot. curves, including CI 78−42154
- Ca**+Ca^+, Rydberg levels collision cross sections, $Ca_2{}^+$ pot. energies 79−27055
- Ca$(4p\ ^3P_J)$+Ba, collisional deactivation and optical lifetime 80−48070
- Ca$(4s4p\,^3P)$+N_2O, absolute chemiluminesc. cross-section and photon yield 78−53208
- Cd, ^1S, ^3P, ^1P states, dipole polarisabilities from compact variational trial functions 80−63568
- Cd, (5s7s), (5s6d), (5s7d) configs., triplet state lifetimes *(French)* .77−3326
- Cd, electron impact ionisation cross-sections for excited states 80−9742
- Cd I, absorption spectrum, simultaneous excitation of two electrons 78−58614
- Cd I, excited states radiative lifetimes 80−942
- Cd II, Hanle effect, $^2P_{3/2}$ lifetime determ. 77−18852
- Cd, n^1S_0 and n^1D_2 levels lifetimes, time-resolved spectrosc. obs. *(French)* 80−102456
- Cd, photoionisation, alignment, linear polarisation 77−83556
- Cd^+ excited state prod., Penning and charge exchange reactions in He-Cd afterglow 77−15252
- Cd+alkane hydrocarbon, $^3P_{0,1,2}$ state distrib., E to V,R transfer 80−28088
- Cd+Cs, excitation energy transfer in sensitized fluoresc. 79−98210

atomic excited states continued
$Cd+N_2$, vap., creation of inverse population of atomic Cd 6^3S and 5^3P_2 levels 80—58219
$Cd(^1P_1)$ excited state quenching by mols., cross sections, chem., phys. exit channels 79—779
$Cd(^1P_1)+NO(X^2\Pi)\rightarrow NO(A^2\Sigma^+, \nu=0)$, electronic energy transfer react., collisional fluoresc. quenching 77—14548
$Cd(^3P_J)(^1P_1)+H_2(HD)(D_2)$ reacts., CdH(CdD) yields, quenching cross sections 79—1948
$Cd(5^3P_1)$, (5^1P_1), and mag. sublevels, excitation in $Na^+ + Cd$ collisions 80—9710
Ce, F states, radiative lifetime and g-factor determ. 79—41138
Ce, $fds^2\rightarrow d^2s^2$, theoretical calc. of energy 77—62639
Cl, $4s$-$3p^5$ transitions, oscillator strengths 77—46537
Cl ions, multiply-charged, beam-foil obs. of allowed L-shell transitions 80—14113
Cl, XVI, $1s2s\ ^3S$-$1s2p\ ^3P$ transitions, Lamb shift, VUV beam foil spectra obs. 80—52919
Cl^{6+}, Cl^{7+}, excited state lifetimes, beam-foil meas. 77—10750
$Cl+O_3(H_2O_2)$(methane), reaction kinetics, temp. depend., reson. fluoresc. obs. 77—4903
$Cl_2+Ca(4s4p^3P)\rightarrow CaCl+Cl$, chemiluminescent reaction, state-to-state cross-section, beam-gas expt. 80—45510
Co I, excited level lifetime meas. 78—5178
Co I, radiative lifetimes of atomic excited states, delayed coincidence technique 77—27030
Co I and Co II, beam-foil obs. of lifetimes 80—14111
^{59}Co, excited states lifetimes, Doppler shift attenuation meas. 78—42009
Cr XVIII, XIX, spectral energy levels, relativistic corrections, config. superposition method 80—32616
^{35}Cr, ^7P states HFS, level crossing technique, core polarisation, spin orbit interaction, config. mixing 78—78668
Cs, $^2P_{1/2}$ and $^2P_{3/2}$ levels lifetimes, Xe collisional effect 77—3307
Cs, 5^2D-n^2F series fine and hyperfine struct. 80—43201
Cs, 7^2P excited states, photoionisation cross section meas. 77—18858
Cs, $7P_{3/2}$-$6S_{1/2}$ transition, photon-echo quantum beats obs. 80—23373
Cs atom, direct meas. of 7P doublet state lifetimes by pulsed dye laser 79—786
Cs, atomic excited states population in arc 78—26368
Cs, collisional and radiative relax., eigenvalue problem 78—29827
Cs, collisions between excited atoms, highly excited states excitation 78—17771
Cs, cooperative cascade emission transitions 80—14120
Cs, discrete level raising into far continuum, oscillator strength to shape reson. transfer 78—78624
Cs, excited np states, fine struct., core electrons effect 77—18807
Cs, excited S- and D-states, Stark interaction by laser spectroscopy, polarisability 77—50404
Cs, excited state, laser photoionisation theory, hyperfine coupling effect 80—102493
Cs, excited state, two-photon ionisation by ruby laser light 78—74621
Cs, excited states photoionis. cross-section, quantum defect method 78—25494
Cs, fine-struct. of excited nd and nf states, at. core effect 78—58606
Cs, forbidden M1 transitions, parity nonconserving effects 78—21844
Cs, four-photon ionis., strongly interacting resons. theory 80—52955
Cs, He IIα $5p^{-1}$ photoelectron spectrum, config. interaction effects 80—5510
Cs II, radiation lifetimes of excited states 80—9558
Cs, natural and effective lifetimes meas. for 10 P states 79—26934
Cs, P,D,F, and G Rydberg states, quantum defects and fine struct. 80—5496
Cs, plasma conductivity, effect of elastic electron scatt. by at. excited states 78—42715
Cs Rydberg atom-blackbody radiation interactions 80—37761
Cs, Rydberg S and P states, hyperfine struct., RF spectroscopic meas. 77—57911
Cs, Rydberg states, diamag. and collisional perturbations 80—58181
Cs, Rydberg states collisional ionis. 79—64097
Cs^+ excited levels, hyperfine struct. and lifetimes 80—63590
$Cs+Cs$, Rydberg states collisional disalignment determ. by fluoresc. quantum beat damping 79—13789
$Cs+F_2$, electronic excited states, chemiluminesc. in flame, spectra 77—52643
^{133}Cs, first excited D-level, hyperfine struct. meas. by cascade, fluoresc. spectrosc. 80—69101
^{133}Cs, Rydberg S and D states, hyperfine struct., lifetimes, depopulation cross sections 77—42270
^{133}Cs, time-resolved fluoresc. spectra, collisional perturbation of Rydberg states 77—83529
Cu, atom, electron impact cross section, elastic and ^2P and ^2D states, inversion ratios 78—9256
Cu, electron impact, excitation function (maxima, cross-sections) 78—50650
Cu, excited states population in high-current hollow-cathode discharge *(Russian)* 77—35421
Cu, isoelectronic series, semi-empirical oscillator strengths, lifetime, transition probability 80—32672
Cu, lines in hollow cathode discharge, radial inhomogeneities in excitation and profile 77—4974
Cu^{18+}, $3^2P_{1/2}$ level decay, time-resolved obs., intensity modulations 77—61704
Cu-like ions, E1 transitions, wavelengths, oscillator strengths and transition probabilities, data tables 80—37780
$Cu+N_2$, Cu^*, preferential energy transfer from N_2 to specific Cu energy levels 80—43152
^{63}Cu, excited states lifetimes, Doppler shift attenuation meas. 78—42009
^{65}Cu, excited states lifetimes, Doppler shift attenuation meas. 78—42009
$D+N_2$, fast collision, electron scatt. resons., ionisation, deexcitation 79—81268
$D^{**}+N_2$ fast collisions, impulse approx. 80—106281
$^{161,163}Dy$, hyperfine struct. and hyperfine anomaly for fine transitions, high resolution meas. 77—88416
Dy I excited states, lifetime meas. using single photon counting method 78—70793
Dy, lifetime meas. using cw dye-laser 79—89636
$Dy+H^+$ ionisation, induced L-shell alignment 80—32813
Eu, excitation transfer cross section, luminesc. meas. *(Russian)* 77—61706
Eu, lifetime meas. using cw dye-laser 79—89636
Eu^*+Sr, light-induced collisional energy transfer 78—50614

atomic excited states continued
$Eu^*+Sr+h\omega\rightarrow Eu+Sr^{**}$, photon assisted collisional energy transfer 78—90285
F VIII, $1s2p\ ^3P_0$ and $^3P_2$ levels, lifetimes, hyperfine quenching effects, UV beam foil spectra 80—47931
$F+H_2$, reactive collision, semiclassical dynamics on multiple electronic surfaces, 3-dimens. calcs. 78—27746
$F(^2P_{1/2})+H_2(j=0)$ quenching, quantum mech. study, ortho-para mixing role 79—76485
F^*+H_2, quenching of excited state, semiclassical studies, comparison between reactive and nonreactive processes 80—106375
Fe I, $a^5D_{0,1,2}$ levels, relative oscillator strengths precision meas. 77—438
Fe I, excited levels measured lifetimes compared with calcs. from oscillator strengths 79—36586
Fe I, precision oscillator strengths from levels $a^5F_{1\text{-}5}$ and $a^5D_{0\text{-}4}$, comparison 79—36584
Fe I transition from levels $a^5F_{1\text{-}5}$, relative oscillator strengths precision meas. 79—36585
Fe I transitions from levels $a^5D_{0\text{-}4}$, relative oscillator strengths precision meas. 79—36583
Fe V, VI, beam-foil level populations, charge state fractions 80—52913
Fe XIX, XXI, spectral energy levels, relativistic corrections, config. superposition method 80—32616
Fe XXII, allowed transition CI wave functions, oscill. strengths and transition probabilities 80—32664
Fe^+, excited config. position and level struct., review 80—32621
$Fe^+(Fe^{2+})$, Rayleigh and Compton scatt., differential cross section determ. 80—52912
Ga, electron impact excitation cross sections calc. *(Russian)* 78—55240
Ga, lowest S-state lifetime meas. 77—65436
H, 2S level population calc. in turbulent plasma *(Russian)* 78—25451
H, 2p state production by H_2 photolysis in Ne matrix 80—93372
H (2s) elec. field-quenched radiation polaris., Bethe-Lamb theory justification 78—17603
H atom, energy level calcs. in superstrong mag. field 80—37737
H atom, highly excited states in static elec. field 77—61707
H, backscatt. by Cu or Mo, 4-30 keV, O_2 effect 78—15268
H, backscatt. from Mo in the presence of O 79—3388
H, Balmer-β line intensity, backscattered from $H^+(H_2^+)(H_3^+)$-metal impact 77—23470
H, beam foil excitation, n=2 density operator and prod. probability meas., transition probabilities 80—14219
H, beam-foil excitation of 2P-state, alignment meas. 80—14215
H, beam-foil excited, zero-field quantum beats in H_β emission, polarisation energy depend. 80—14218
H, charge exchange involving excited states, Born cross sections 79—45836
H, electron impact coincidence, even-odd parity coherence effects, polarisation ang. distrib. 78—9253
H, electron impact excitation 80—18909
H, excited atom Lyman-α and Balmer fluoresc. from H_2 photodissoc. 79—86018
H excited atoms, charge transfer processes, perturbed stationary state method 79—89770
H, excited S-states, static dipole polarisabilities, Green's function calcs. 77—6696
H, excited state, $J=3/2$-$J=5/2$ transition, fine struct. interval meas. 77—46542
H, excited state electron and ion quantum scatt. cross sections, dipole approx. *(Russian)* 79—6996
H, excited state interaction with photon field, simultaneous eqns. 78—66481
H, excited states, pseudopotential calcs., teaching approach 79—84893
H, excited states, Rayleigh-Schrodinger perturbation theory, Pade approximants calcs. 79—98024
H, excited states prod. by near threshold photodissoc. 79—86019
H, form factors and cross sections for $nl\rightarrow n'l'$ direct collisional transitions 79—31636
H, ground and first excited states in homogeneous magnetic field 78—925
H, highly excited, multiphoton ionisation rates, perturb. theory calcs. 77—54542
H, in elec. field, semi-classical approx. *(Russian)* 78—86797
H, in Ne-H_2 h.f. pulsed discharge *(French)* 77—433
H in quasars, excited-state population equilib. rel. to line and continuum emission 80—27003
H in spherical box, hyperfine energy, effect of excited state admixture 80—906
H, ionisation threshold for excited states in uniform elec. field 78—37607
H, ions recomb. and level populations, resolution of ang. momentum states 77—45529
H, longit. excited states in intense mag. fields, rel. to pulsars 80—91469
H, multilevel atom, excitation and decay 80—9530
H, multiple quantum transitions, in the presence of static electric field 78—37618
H, parity mixing, relativistic neutral current interactions and nonrelativistic pots. 79—26908
H, population inversion obs. in FM-1 spherator 77—7048
H, produced by electron impact dissociation of H_2, velocity distrib. *(Russian)* 77—10779
H, relax. rates in glow discharge 79—7001
H Rydberg level selective excitation by three-photon absorption 80—58640
H, Rydberg levels, selective excitation by three-photon absorpt. 80—5518
H, Rydberg Stark ionis. threshold scaling laws 77—6721
H, self-interaction of excited at. with radiation field 78—86794
H, Stark effect, asymptotic expansion for level width 78—70783
H, Stark effect, high orders of perturbation theory for excited states 80—87079
H, third-order optical harmonic coeffs., R-matrix calc. 77—57955
H^-, double excited states below N=3 threshold, arrangement of resonances in series converging exponentially 80—99462
H^-, energy levels, doubly excited states, three particle Coulomb problem, hyperspherical coords. framework 80—52875
H-like atom, spin-orbit interaction and single electron excitations rel. to mag. dielectrics 79—54780
H-like ions, one-photon decay rates, general theory of radiative corrections 78—46282
$H+Ar$, $H\alpha$ and $H\beta$ emission cross sections 80—63782
$H+H$, cross-section for excitation of high-lying levels, quasiclassical approx. *(Russian)* 77—79676

atomic excited states continued
H+H, excited atom ionisation collision, excitation transfer effect 79-81272
H+H, excited states, ionisation collision cross-section energy depend., semiquantal theory 78-42160
H+H$^+$, charge exchange probability 79-98216
H+H$^+$, excited atom collisions, transitions between degenerate states 77-30976
H+H$^+$, H excitation, angular differential cross sections 80-63784
H^0+N^{3+}, electron loss cross section 80-63805
H$^+$+Ar, Hα and Hβ emission cross section 80-63783
H$^+$+H, gas-phase collisions, intermediate and high velocities, excitation 80-32822
H$^+$+H(1s)$\rightarrow$H(nlm)+H$^+$, highly excited states rearrangement collisions 79-59564
H$^+$+He(Ar)(O$_2$), charge transfer to H(n=2), mixed parity elec.-dipole oscillations 79-31678
H$^+$+Na(K), excited state form. by inelastic processes, energy partitioning 78-82833
HCl+Ca(4s3d^{1}D)$\rightarrow$CaCl+H, chemiluminescent reaction, state-to-state cross-section, beam-gas expt. 80-45510
HF+I*(5^{2}P$_{1/2}$), electronic-vibr. energy transfer fluoresc. decay meas. 77-71846
^{2}H pionic atom, energy shift off-shell contribs., zero energy approx. validity 79-76537
H*, prod. by H+Br$_2$ or H+HBr reaction 79-100336
H*, radiative magnetic energy shift, H in 2p state 78-58601
H*+H(Li), resonant ionisation, cross section and ionisation probability 80-63785
H(1s, 2s, 2p), approx. Dirac eqn. soln., partitioning technique 80-23284
H(2S)+He(N)(Ar), excitation and ionisation contributions to sum-rule Born cross sections 80-99551
H(3p), excitation in electron impact dissoc. of methane Lyman β and Balmer α obs. 78-46450
He, ^{1}S(1s,3s) state excitation by electron impact, Glauber approx. 79-31696
He, 2^{1}S and 3^{1}S, CI expsn., convergence patterns 77-50378
He, 2^{3}S-state, electron impact excitation, reson. form. mechanism 80-99463
He, 2p3d ^{1,3}L^0 doubly excited state, soln. of Hartree-Fock eqns. 77-75072
He, (2p^2)^{3}P doubly excited state, electron impact excitation XUV emission 79-86071
He, (2p^2)^{3}P state, electron impact excitation, parity unfavoured transition 80-91680
He and He$^+$, 3^{3}P and 4^{2}F levels excitation with electron beams, radiation decay obs. 80-43188
He, double excited states, lifetime meas. by beam-foil technique 78-74590
He, doubly excited, supermultiplet energy levels, classification as rot.-vibr. spectrum 80-52900
He, doubly excited states classification, for intermediate quantum nos. 79-10046
He, elastic electron scatt. phaseshifts, 2s2p ^{3}P autoionisation, 1s2s ^{3}S$\rightarrow$1sεp ^{3}P triplet continuum photoionisation 79-31480
He, electron and neutral collisions, Rydberg level transitions 79-45821
He, electron impact, ^{3}P$_g$ and ^{1,3}D$_u$ states excitation, electron correlation influence, Rudge-type approx. 78-74771
He, electron impact, induced transitions between high Rydberg levels 78-21877
He, electron impact excitation, ^{3}P$_g$ and ^{1,3}D$_u$ states, electron correlation influence, Born-Oppenheimer approx. 78-74770
He, electron impact excitation, electron-photon angular correlation meas. 80-63826
He, electron impact ionisation, decay modes investig. 79-72422
He, electronic struct., dilute gas, double excitation CI anal., coupled electron pair approx. 78-21856
He energy levels, classical first order perturbation theory 80-58118
He, energy levels, doubly excited states, three particle Coulomb problem, hyperspherical coords. framework 80-52875
He, excitation energy calc., improved virtual orbitals 77-46491
He, excited S, D and F state radiative lifetimes, electron impact method 78-94325
He, excited state formation from He$_2$$^+$ in afterglow, theory 79-22802
He excited states, relativistic corrections 78-62734
He, first excited state, electron Hamiltonian, effective one-body, with correct asymptotic behaviour 79-45619
He, Galerkin-Petrov method, nonlinear parameters 78-78619
He glow discharge, low press., excitation transfer and quenching of n=3 excited states 80-38743
He glow discharge, n=3 sublevel quenching and energy transfer, laser perturbation method 80-44060
He, high-L states, laser driven forbidden transitions, line shapes 79-22638
He, hollow-cathode type discharge, spectroscopic obs., laser light source appl. 80-59335
He I, beam-foil excitation, temp. depend., linear polarisation of transitions 80-14213
He I, beam-foil excited, 70-400 keV, relative initial populations 80-14211
He I, excited states decay, lifetime meas., lab. mag. field effects 77-10640
He I, heavy ion impact excitation, alignment relax. of nonresonant levels *(French)* 77-61842
He I, heavy ion impact excitation, orientation by anisotropic relax. of 4 ^{1}D level *(French)* 77-61844
He I, II excited state population densities in non-LTE plasmas 78-67328
He I, in solar flare, levels populations calc. 77-53538
He I glow discharge, low-press., quenching of singlet states by N$_2$ 80-49030
He I transitions, polarisation meas. using beam-foil excitation, foil tilt angle depend. 80-14212
He, isoelectronic sequence, 2^{1}S states, analytic wave function 80-9525
He isoelectronic sequence to Z=10, D and F states fine struct. 77-544
He isoelectronic sequences, screening constants, ground and excited states 78-62701
He isoelectronic series, energy level and classifications of doubly-excited states 78-62736
He, laser spectroscopy in intense magnetic fields 80-62738
He, long-lived states population decay 79-54954

atomic excited states continued
He, N-body excited states, Hartree-Fock eqns. derivation 79-93934
He, optically-allowed, long-range interaction pots. with electrons, protons and atoms 77-14520
He, photoionisation cross section from excited state ^{4}p^{1}P$_1$ *(Russian)* 77-61722
He, polarised light emission after HeH$^+$ impact on C foil 80-58361
He quantum defects rel. to angular momentum, nuclear charge, Coulomb-Born approx. method *(Japanese)* 77-50534
He, S state, electron correl. calcs. 79-49952
He, SCF ion improved virtual orbitals, excited configs. calc. 77-10585
He sequence, 2p3d ^{1,3}L^0 doubly excited state, soln. of Hartree-Fock eqns. 77-75072
He, subDoppler lineshape obs., of IR mag. reson. Rydberg transitions, using motional Stark effect 78-947
He, third-order optical harmonic coeffs., R-matrix calc. 77-57955
He, two-electron excited states 78-58605
He, variational energies for highly excited states 78-62737
He$^+$, electron scatt., elastic, ^{1}P continuum phaseshift, 2s2p^{1}P autoionising state 77-88561
He-Cd vapour excitation in hollow cathode discharge 80-64815
He-like atoms, n=2 states radiative transition rates, oscill. strengths, RRPA extension 77-34584
He-like ions, He through Mg^{10+}, 2^{1}S, 2^{3}S, 2^{1}P and 2^{3}P states variational wave functions 77-34546
He+atom, He upper states, excitation energy transfer mechanisms 80-28102
He+B(C)(N)(O)(F) bare nuclei, electron capture to excited states, X-ray cross-sections 77-71814
He+H$^+$, determ. of He excited state populations by two-photon reson. ionisation spectroscopy 78-82707
He+H$^+$, electron capture into ground and 2s states, cross sections 77-27177
He+He, Rydberg states ang. momentum transfer, singlet-triplet anticrossing 77-88543
He+He$^+$, (Ne)(Li), gas-phase collisions, intermediate and high velocities, excitation 80-32822
He+He$^+$, low energy collisions, excitation of 2 ^{1}S, 2 ^{1}P and 3 ^{1}P, 3 ^{3}P levels 80-58342
He+He$^+$(Ne), tensor polarisabilities of 1snd ^{1}D level, fluoresc. depolarisation obs. 80-69099
He+Ne$^+$, impact excitation, cascade-fluorescence spectroscopy, level-crossing techniques 80-23357
He$^+$+He, 150 eV, one-electron excitations, quantal treatment 77-71854
He$^+$+He(Ne), model pot. for law energy scatt. 78-66642
He$^+$+Mg(Zn), inelastic collisions, 2-800 eV, excited state form. 78-94312
He$^+$+Na(K), excited state form. by inelastic processes, energy partitioning 78-82833
He$^+$+Ne, 10-150 keV, Rydberg-state total cross section, oscillatory behaviour 77-83716
He$_2$$^+$+Mg(Zn), inelastic collisions, 2-800 eV, excited state form. 78-94312
^{3}He, hyperfine-induced singlet-triplet mixing obs. 80-106399
^{3}He-Xe nuclear pumped laser, small signal gain coeff. and power output, theory comparison with expt. 80-63983
^{3}He$^+$, 2s state, HFS, improved electrostatic device and microwave state selection 77-83757
^{4}He, 3p ^{3}P state alignment and orientation as function of foil tilt angle, quantum heat spectra 79-94071
^{4}He$^+$+H, electron transfer calc., electron ionization calc., Monte Carlo method, 79-72387
He*, collisional transfer rates between excited levels 79-22793
He*, Rydberg state charge transfer reactions, time of flight mass spectrometric obs. 77-71867
He*+Ar, complex potential from elastic differential cross sections 77-23534
He*+Ar, Penning ionis., multichannel calcs. 80-53111
He*+He, (*=excitation or charge), differential scatt. inversion procedure, symmetric exchange, classical, semiclassical theory 79-13802
He*+He, excitation exchange and collisional relax. 80-69226
He*+Ne, (3^{1}S, 3^{3}S, 3^{1}P, 3^{3}P) de-excitation cross section temp. depend., time resolved spectra 80-28100
He*(^{3}S)+Ar+$\hbar\omega\rightarrow$He+Ar$^+$(^{2}P)+e$^-$, intense laser radiation assisted collisional ionis. 79-76497
He**, doubly excited, spatial correl. of at. electrons 78-70760
He**(2p^2 ^{1}D), collisionally excited, autoionisation electron ang. distrib., interference struct. 80-32819
He*(2^{3}S)+F, Penning ionisation and excitation transfer, unified treatment 78-25672
He(2s-3p transitions), beam foil spectra, emitted light polarisation, depend. on foil tilt angle 80-63786
He(5^{3}D)+He, collisional quenching probability, 2-250 mtorr 78-25679
Hg, ^{1}S, ^{3}P, ^{1}P states, dipole polarisabilities from compact variational trial functions 80-63568
Hg, 5d spin-orbit X-ray excitation, 21-2700 eV, by ESCA sources 78-53301
Hg 6^{3}P$_1$ states, detection impact excitation cross section meas., using self calibrating apparatus 79-50135
Hg, electron impact ionisation cross-sections for excited states 80-9742
Hg electron resonant elastic and inelastic scatt. *(Russian)* 80-78710
Hg, electronically excited, form. by electron impact dissoc. of Hg halides 79-18296
Hg II, excitation cross sections, transition probabilities, by electron impact 79-3580
Hg, laser stepwise excitation of 6s6d6^{3}D$_1$ level, transition probabilities and collisional excitation transfer 78-55146
Hg, metastable and excited states, pulsed dye laser absorption spectroscopy 79-26924
Hg, two photon excitation, time resolved spectroscopy 80-87075
Hg+He(Xe), collisionally induced coherence, orientation and alignment, transfer among 6s6d levels 78-74747
Hg+N$_2$, 6(^{3}P$_0$)$\rightarrow$6(^{3}P$_1$) excitation, double modulation obs. 79-27072
Hg+N$_2$, inelastic collision, 6^{3}D$_1$ population transfer to other 6s6d Hg levels, fluoresc. obs. 78-78791
Hg(6^{3}P)+O$_2$, photosensitised reaction, excited intermediates, energy transfer detect. 78-73030
Hg(6^{3}P$_2$)+Cd(5^{1}S$_0$), spectral width of Cd(5^{3}P$_1$) line *(French)* 77-50397
H(n=2) excitation by ion impact, precision doubly differential cross section meas. 79-45811

atomic excited states continued
$H(n=3)+H_2O$, radiation quenching in pulse radiolytically excited water vap. 79−89738
$H(n=4)$, s-d coherence, quantum beats obs. in $H^+ + He(Ar)$ 80−32676
Ho I, Ho II, excited level lifetimes and oscillator strengths, visible spectra 80−63573
I, $^2P_{1/2}$ state, relax. between hyperfine levels 80−18880
I $(5^2P_{1/2})$, quenching by mols. with C-I bonds 79−64076
I VI and I VII, beam-foil obs. of lifetimes, spectral assignments, 400 to 1300 Å 80−9556
I VII, beam-foil lifetime meas., cascading problem 80−14249
I+methane d_0(d_3),(d_4), excited atoms, quenching, isotope effects, time resolved reson. fluoresc. 80−32656
IBr:CO_2 photolysis, electron-vibr. pumping, 2.7 μm Br and 4.3, 10.6 μm CO_2 laser transitions 80−28196
$I^* + H_2O(D_2O)(HDO)$, $5^2P_{1/2}$ electronic to vibr. energy transfer, quenching and time resolved IR fluoresc. 79−3537
$I^* + I_2(Br_2)(Cl_2)(IBr)(ICl)(BrCl)$, collisional deactivation and reaction rate consts., obs. 78−80738
$I(5^2P_{1/2})$, prod. by ICN photodissoc. 79−94047
$I(5^2P_{1/2})+Br_2$, deactivation kinetics, time-resolved spectrosc. obs. 78−95916
$I(5^2P_{1/2})+Br_2$, deactivation kinetics, $Br(4^2P_{1/2})$ prod., time-resolved spectrosc. obs. 78−95917
$I(5^2P_{1/2})$+HBr(DBr)(methane)(propane), collisional deactivation, rate consts. meas. 77−86300
$I(5^2P_{1/2})$+HCl(HBr)(NO), electronic-vibrational energy transfer, fluoresc. obs. 78−66579
$I(5p^5(^2P_{1/2}))$, time-resolved kinetics, mean radiative lifetime, radiation trapping, HFS 78−5171
In, electron impact excitation cross sections calc. *(Russian)* 78−55240
In, excited state lifetime, delayed coincidence meas. 77−3315
In I, $6^2S_{1/2}$ state lifetime meas. by Hanle effect method 78−90097
In ions, analytical HF solns. for ground and excited states 77−72835
In, lowest S-state lifetime meas. 77−65436
^{215}In, $8P^2P_{3/2,1/2}$, HFS and lifetimes, fluoresc. decay and quantum heats, beam 80−32657
Ir I, radiation lifetimes, beam-sputtering technique meas. 79−18142
K, absolute optical electron-impact excitation functions 80−18933
K, collisional depopulation of high-lying P state 77−3447
K, excited np states, fine struct., core electrons effect 77−18807
K, excited states field ionis., p states spin-orbit interaction 79−59592
K, fine-struct. intervals, polarisabilities, highly excited d states 79−27100
K I, lifetime meas. of lowest ^{2}D-states, elec. quadrupole excitation 78−42004
K, isotope shifts of individual nS and nD levels 80−102489
K, photorecomb., mol. ions form. *(Russian)* 79−89779
K, Rydberg states, two photon absorption, decay fluoresc. 77−71787
K, s and d state radiative lifetimes, time and wavelength resolved fluoresc. spectra 80−14104
K, two-step photoionisation, triple crossed beam obs. 78−66616
K^+ in molecular complexes, K-edge absorpt. spectra, Z+1 analogy, theory-expt. comparison 80−47935
K+He, 4^2P state $j_1m_1 \rightarrow j_2m_2$ Zeeman transition, total cross section energy depend. 80−83475
$K+N_2$, $K(4^2P)$ electronic excitation and energy transfer, time of flight spectra 80−43151
^{39}K, first excited D-level, hyperfine struct. meas. by cascade, fluoresc. spectrosc. 80−69101
^{39}K, weakly excited, hyperfine struct. transitions obs., neoclassical theory 77−6737
K^*+molecule, assoc. ionisation, mass spectra *(Russian)* 77−42393
Kr, 6p levels, two-photon excitation, time resolved fluoresc., quenching, lifetimes and photoionisation cross section 80−78587
Kr afterglow plasma, electron energy distrib. funtion 80−38748
Kr, discharge, non-self-maintained, ionis. instability of excited ats. and excimers *(Russian)* 77−84557
Kr, g-factors meas. by optical pumping and mag. reson. 80−14246
Kr I, 5871 Å line, transition probability meas. 77−3291
Kr II, excited states lifetime meas., photon-photon delayed coincidence technique 77−68011
Kr, outer $p_{1/2}$ subshell photoionisation, polarised electrons, relativistic RPA calcs. 80−83331
Kr, photoionisation cross sections for excited states, rel. to KrF laser 77−75110
Kr plasma, of positive column, at. alignment, radiative lifetimes, collision cross sections 79−4203
Kr VII, beam-foil excitation, 4s4p $^1P_1{}^0$ level decay simulation 80−78578
Kr VIII, excited state energies and lifetimes, beam foil spectra 80−63591
$Kr+F_2$, KrF form., relax. and quenching 80−81314
Kr^{**}+HCl rot. effect on collisional ionis. 77−83702
La I, extension of even energy level system 77−3285
La I, lifetimes of $z^2F_{5/2}$, $z^2D_{3/2}$, $z^4G_{5/2}$ and $y^2D_{3/2}$ states 78−66489
^{138}La/^{139}La nuclear electric quadrupole moment ratio, laser RF double reson. obs. 80−23447
Li, ^2S, $^2P^0$ and ^2D autoionising states, positions and widths 79−26944
Li, $1s2p^2$ $^4P^e$ state, using configuration-interaction wavefunctions 79−3369
Li, $1s2s2p^4P^o$ state, using configuration-interaction wavefunctions 79−3370
Li, 2P level lifetime, at. beam-laser expt. *(Russian)* 77−79575
Li, $3d^2D$ level, lifetime meas., fast-beam spectroscopy 77−61714
Li, core charge polarisation, HF calcs. 79−45627
Li core excited even parity ^2P states, fluoresc. 80−69100
Li, doublet open-shell restricted SCF eqns. 79−59350
Li, electron impact excited high-l Rydberg states 77−65535
Li, even-parity core-excited ^2P states, accurate CI calcs. 79−54782
Li, excitation energy calc., improved virtual orbitals 77−46491
Li, excited in single gas collisions, high-resolution Auger spectra 80−9717
Li, excited-state lifetime meas. using disc-shaped heat-pipe oven 80−52941
Li, hyperfine coupling, in ground and excited states, Green's function calcs. 77−6692
Li I, $2s^2sp$ and $1s2s^2$ decay rates many-body perturbation theory calc. 79−59376
Li I and Li II, beam-foil excited, 70-400 keV, relative initial populations 80−14211
Li I to Li III, beam-foil obs. of 2000-5500 Å spectra 80−9548

atomic excited states continued
Li I to Ne VIII isoelectronic sequence, quartet spectra, Hylleraas method calcs. 80−9524
Li I to Ne VIII isoelectronic sequence, term level diagrams of doubly excited states 80−14093
Li isoelectronic sequence, 1s2s3p $^4P^0$ state, nuclear charge expansion 78−37569
Li isoelectronic sequence, doubly-excited states, relative ordering 79−31424
Li isoelectronic sequences, screening constants, ground and excited states 78−62701
Li, isoelectronic series, doubly excited states, Hartree-Fock energy 79−22613
Li, isoelectronic series, model potential field, pseudopotential calcs. 79−59339
Li isoelectronic series, quartet states, HF and CI calcs. 78−17582
Li, laser excited beam, Ta and Re surface ionis., quantum yield 79−87540
Li, lifetimes, differential meas. using atomic ionoluminesc. 79−13672
Li, optical beam-foil spectra, relative level population 80−14207
Li, plasma conductivity, effect of elastic electron scatt. by at. excited states 78−42715
Li, SCF ion improved virtual orbitals, excited configs. calcs. 77−10585
Li, seeded flames, excitation, laser radiation absorpt., sound vel., opto-acoustic effects obs. 80−43345
Li^-, core excited bound states in beam foil expts., CI calcs. 80−78559
Li^-, optical transition between bound states, beam-foil spectrosc. obs. 80−91476
Li^+, ^3P and ^3S states, fine (hyperfine) struct., dye laser saturation spectroscopy, beam expt. 80−58169
Li^+ 2p3d $^{1,3}L^0$ doubly excited state, soln. of Hartree-Fock eqns. 77−75072
Li^+ quantum defects rel. to angular momentum, nuclear charge, Coulomb-Born approx. method *(Japanese)* 77−50534
Li-like atoms, $^4S^e$ doubly excited states, orbital config. assignment 79−41118
Li-like ions, fine struct. in $1s2p^2$ ^4P and 1s2s2p $^4P^0$ states 78−66471
Li-like ions, highly charged, innner shell excitation, intermediate coupling collision strengths 80−1074
$Li+F_2(Cl_2)(NO_2)$, $4^2S_{1/2}$ excited atom crossed beam collisional ionisation 79−64087
$Li+H^+(H_2{}^+)(He^+)(He^{2+})(He_2{}^+)$, excited state form. obs. 80−9686
Li+He, gas-phase collisions, intermediate and high velocities, excitation 80−32822
$Li+Li^*(H^*)$, resonant ionisation, cross section and ionisation probability 80−63785
$Li^+ +He$, 10-50 keV, mol. promotion, many-electron aspects 79−50124
Li^*+He(Ar), Li principal series line broadening and shift, interat. pot. consts. 78−42165
$Li(2^2P_{1/2,3/2})$, laser induced flame chemistry, saturated mode fluoresc. meas. 80−89491
$Li(2p)+H_2(N_2)$, Li(2p) excitation, alignment and orientation obs. 80−63794
Mg, $3s3d^3D$ and $3s4d^3D$ states, fine-struct. meas. by level crossing spectra 79−36572
Mg, direct meas. of excited state lifetimes 77−65435
Mg, hollow cathode discharge, excitation mechanisms of triplet state atoms and decay obs. 80−44015
Mg I, $^3F^0$ Rydberg series, energy levels, multiconfigurational HF procedure 80−47882
Mg I, Mg II autoionisation state radiative decay *(Russian)* 80−5509
Mg I, press. shifts of $^1D_2$ Rydberg states 77−61711
Mg I to Mg III, beam-foil excitation, Rydberg states, relative populations 80−14208
Mg II, Hanle effect, $^2P_{3/2}$ lifetime meas. 77−18852
Mg ions, foil-excited, EUV spectrum 80−42976
Mg, isoelectronic series, oscill. strengths and excitation energy, RRPA calcs. 78−13471
Mg, Kα radiation, X-ray photoelectron spectroscopy resolution 80−18888
Mg, radiative lifetimes on excitation by electron impact *(Russian)* 77−50408
Mg, valence shell states, calc. 78−17611
Mg^{9+}, beam-foil excited, spin orbit-forbidden X-ray transition obs. 80−23537
Mg^*+Cl_2, collision and reaction cross section meas. 79−59537
Mg^*+He(Ne), model pot. curves, including CI 78−42154
Mn I, collisional and radiative excited, lifetime meas. 80−91501
Mn V, forbidden transitions laboratory wavelengths and excitation potentials 78−50496
Mo, excited at. emission from 40 keV Ar^+ bombarded surface 80−11481
Mo I spectrum, lifetime meas. of excited states of $4d^55p$ and $4d^45s5p$ config. 79−13683
Mo XV, electronic struct. of complex ion, relativistic perturbation theory 79−22610
N, electron impact excitation, near threshold, cross-sections for $(2s^22p^23s)^4P$ and $(2s2p^4)^4P$ states 80−91684
N, ground and excited states, atomic polarisability calc. 77−83756
N, high Rydberg states, radiative decay rates, TOF meas 78−46302
N I (^{2}D) in auroral zone, prod. 79−21090
N IV, excited states, transaction oscill. states and wavefunctions 79−59367
N, mean lifetimes of astrophysically important excited levels 77−46528
N, $np^2(n+1)s$ excited-state config. quadrupole moments, Sternheimer shielding factor 80−37755
N V, beam-foil decay curves, mean lives determ. 80−9553
N^+, beam-foil and beam-gas excitation, Coulomb explosion effects, Auger spectra obs. 80−14220
N^+, beam-foil excitation, absolute Auger yield meas. 80−14203
^{14}N II, 2p3p $^1P_1$, hyperfine struct. after ion beam surface impact at grazing incidence 80−58403
N_2, photoelectron ang. distrib., photon energy depend. , 16-25 eV 80−53046
N_2+K (Na), atom electronic excitation, vibr. to electronic energy transfer, seeded mol. beam studies 80−47919
$N^{2+}(^2P^0)+H$, charge transfer, ab initio CI pot. curves and coupling-matrix elements 80−37878
Na, ^2D highly excited states, fine struct. splitting, field ionisation quantum interference 80−18835

atomic excited states continued
Na, $3^2S_{1/2}$-$3^2P_{3/2}$, spectral distrib. and collisional depolarisation of laser light, D_2-fluorescence 80−58209
Na 4D level, relax. by inert gas collisions, expt. 79−68307
Na 4D level, relax. by inert gas collisions, theory 79−68308
Na, atom, excited p-states radiative lifetimes, laser cascade fluoresc. meas. 77−27022
Na, atomic states highly excited by laser radiation, Stark effect 79−13669
Na, D-doublet in H_2-O_2-Ar flame, excitation profiles 77−88436
Na, detection of nF Rydberg levels by photoionisation *(French)* 77 71785
Na, diabatic field ionisation of highly excited at. states 80−43202
Na, doublet open-shell restricted SCF eqns. 79−59350
Na, energy transfer with 3P-excited atom high density, mol. form., fluoresc. 77−88422
Na, energy transfer with 3P-excited atoms, fluoresc. spectrum 78−66498
Na, excitation energy calc., improved virtual orbitals 77−46491
Na, excited, electron scatt. at low energy, total cross section 80−63821
Na, excited 4D and 5S state, absolute photoionisation cross-section 80−99488
Na, excited np states, fine struct., core electrons effect 77−18807
Na, excited state photon echo relax. 78−37606
Na, fine-struct. of excited nd and nf states, at. core effect 78−58606
Na, first excited states, non-resonant emission spectra *(Chinese)* 80−42971
Na, high ang. momentum Rydberg states, quantum defect core polaris. depend. 77−18808
Na, high Rydberg states, quenching in strong 1.06 μm laser field 80−95559
Na, high-lying Rydberg states, field ionisation 79−45683
Na, highly excited, f-state fine struct., microwave reson. obs. 77−83535
Na, highly excited d states, elec. field ionisation 77−6658
Na, highly excited p and d states, fine struct. intervals and polarisabilities, RF reson. meas. 77−67999
Na, ionisation and energy pooling in laser-excited vapour 79−795
Na, ionisation of high-lying states by pulsed laser field *(Russian)* 77−75113
Na isoelectronic sequence, electron impact excitation, transition probabilities, oscill. and collision strengths 78−25718
Na isoelectronic sequence, Bethe excitation cross-sections 78−82657
Na, nonequilib. excited-level population in inhomogeneous plasma 77−3917
Na, photofragment of NaBr, non-Gaussian line shape, level shifting and velocity inversion 80−58182
Na, positron energy levels, rel. to Rydberg levels of Na, NO 79−86089
Na, Raman transients obs. in Doppler free two-photon excitation 77−61728
Na, Rydberg atoms, photoionisation, 300K background radiation effects 79−68271
Na, Rydberg states, diamag. struct. 78−50484
Na, Rydberg states, fine struct. and Zeeman beats 79−14044
Na, Rydberg states, high resolution spectroscopy 80−52901
Na, Rydberg states, millimeter spectra, quantum defect, fine struct., polarisability, field ionis. obs. 78−82672
Na, Rydberg states, millmetre spectrosc. 80−99469
Na, Rydberg states, nd$\rightarrow$(n+1)p intervals meas. 78−33629
Na, Rydberg states, optically pumped, electric field ionis. *(Russian)* 79−27095
Na, Rydberg states and microwaves, spectroscopy, masers and superradiance study 80−53248
Na, Rydberg transitions to detect far IR radn. 80−4763
Na seeded flames, excitation, laser radiation absorpt., sound vel., opto-acoustic effects obs. 80−43345
Na, single atom detection by laser photoionisation *(Russian)* 78−33487
$Na+H^+$, $2p^53s^{22}P_{3/2}$ state alignment, collisionally induced, impact parameter calc. 80−83474
$Na+H^+(He^+)$, Na $2p^53s^2\ ^2P_{3/2}$ state alignment by 5-30 keV excitation 80−14200
Na+H(Ne)(Kr) vel.-changing collisions, effect on 2 photon and stepwise absorpt. line shape 80−87221
$Na+He^+$, crossed beams, l-changing collisions, n-depend. 80−58345
Na+He(Ar)(Xe), excited state, collisional depopulation cross-sections meas. 79−86057
Na+He(Ne)(Ar), Rydberg states, collisional angular momentum mixing meas. 77−68093
Na+He(Ne)(Ar), Rydberg S and D state relax., trilevel echo effect 79−72409
Na+Hg, collision processes, laser excitation, fluoresc. 79−94059
Na+inert gas, Rydberg states, collisional ang. momentum mixing theory 77−10748
Na+inert gas, Rydberg states transitions, broadening cross-sections meas. 80−69110
$Na+N_2$, higher Na s and manifold states deactivation cross sections 79−10176
Na+Na, electronic-field pot. curves determ. for large interatomic distances, excitation cross sections calc. 80−95704
Na+Na, excited atoms, coupling terms, asymptotic pot., excitation energy transfer 80−23530
Na+Ne(CO), 13d-13f transition, collisional dephasing, Ramsey method investig. 79−54791
Na+Xe, nonreson. two-photon absorpt., 4s excited states and pot. energy curves, close coupled eqns. 80−48068
$Na(^2P)+Hg$, differential cross section, orbiting backward peak, obs. 79−76482
$Na(^2P_{3/2})+Hg$, laser excited atoms, differential cross sections 78−62905
^{22}Na, Rydberg states, fine struct. splitting, quantum beat and double reson. spectroscopy 78−86979
$Na^*(3p)+Na_2$, collisional and radiative processes, fluoresc. decay obs. 78−66638
Na^*(nd,nf)+He, ang. momentum mixing 79−10175
$Na(3^2P)+CO(X^2S^+)$, electronic-vibr. energy transfer reaction 79−64084
$Na(3^2P_{1/2,3/2})$, laser induced flame chemistry, saturated mode fluoresc. meas. 80−89491
$Na(3p^2P_{3/2})+N_2(O_2)(CO)(NO)$, electronic energy quenching dynamics, crossed beam expt. 80−9683
$Na(n^2D)+N_2(CO)$, collisional l-mixing, highly excited states, fluoresc. obs. 77−83686
Ne $^3P_1$ state, radiative decay time 79−72277
Ne, 2p levels prod. by dissoc. recomb. in afterglow, recomb. coeffs., level population 80−43855

atomic excited states continued
Ne, $2p^53p$-$2p^55s$ emission lines, press. broadening, with Ne(He), rel. to repulsive forces 80−9692
Ne, $2p^53s^3P_2$ to ground state, electron collisions of the second kind, rate consts. 79−27090
Ne, atomic deexcitation effects of X-rays, X-ray preionisation in TEA lasers 79−793
Ne, charge-state distributions and the population of X-ray emitting states 79−68311
Ne, collisional transfer coeffs. between 2p levels, in afterglow, laser excitation obs. 80−43856
Ne, discharge, low-press., atom densities of first excited state 80−38750
Ne, doubly excited energy levels, subshell ang. momenta coupling, frozen core superposition of config. method 80−52874
Ne, electron beam excited states population, press. depend., fluoresc. obs. 78−17802
Ne, even-parity levels, double excited energy levels, frozen-core superposition, config. calcs. 80−106273
Ne, foil excited, 6 to 10 MeV, equilibrium K-shell excitation 79−22817
Ne I, beam-foil excitation, Rydberg states, relative populations 80−14208
Ne I to Ne IV, excitation in ion-atom collisions, 100 keV region, emission spectra obs. 80−14205
Ne II, transition probabilities, lifetimes, intermediate coupling semiempirical calcs. 79−789
Ne II-VIII L-shell excit. by highly ionised heavy ion impact 78−1074
Ne isoelectronic series, $2s^22p^53l$ and $2s^22p^63l$ configs., excited state energy levels 79−54781
Ne, optical-optical double reson., $2p_4$ and $2s_2$ level g_J-values by mode crossing 77−50411
Ne, pair excitation correl. numerical coupled cluster method 80−47906
Ne positive column, 3S and 3P level populations, rel. theory with recomb. 77−10766
Ne, positive column, excited level decay at high electron temp. 77−23442
Ne, positive column, radial distrib. of excited atoms *(French)* 78−14237
Ne, reson. level lifetimes, Zeeman coherence radiative and collisional transfer between excited states 77−23466
Ne, single photon decay of $(2s)^{-2}$ double hole state 77−34606
Ne, triply-excited states contributing to correl. energy, diagrammatic perturbation theory 79−81161
Ne VII, excited states, transaction oscill. states and wavefunctions 79−59367
Ne, with 1s-hole, wave function calcs. using radial orbitals, orthogonality 77 67971
Ne-Xe-$F_2(NF_3)$, excited states quenching 79−18406
$Ne+H^+$ 80−18916
Ne+He, 2p-levels, excitation obs. 80−9712
$Ne+He^+$, $He(3^1P)$ level excitation, total emission cross section, fast oscills. obs. 80−58362
Ne+heavy ion, few-electron states prod. K X-rays obs. 80−9718
Ne+Ne(He), 7d′ states, isotope shift, press. shift, press. broadening, two-photon spectra obs. 78−55155
Ne^++He, 10-150 keV, Rydberg-state total cross section, oscillatory behaviour 77−83716
Ne^++Kr, low vel. collision, enhanced K-L vacancy sharing ratios, X-ray prod. cross section 78−78790
Ne^++Ne, (He^+), gas-phase collisions, intermediate and high velocities, excitation 80−32822
$Ne^{2+}+Ar$ (Kr)(Xe), single electron capture excitation, photon emission, VUV spectroscopy 80−58379
$Ne^{2+}+Xe$, electron capture collisions, 15 to 50 keV, excitation 80−102566
$^{21}Ne^{n+}$, $5/2^+$ state, hyperfine interactions and mag. moment of 0.350 MeV 78−17583
$^{21}Ne^*$, produced in $^2H(^{20}Ne,p)^{21}Ne^*$, degree of atomic excitation within nuclear lifetimes 78−41631
$Ne^{2+}(2s2p^5\ ^1P,^3P)$, singlet/triplet population ratio, in 100 keV ion impact excitation, ion Z depend. 78−37733
Ni I, in solar spectrum, effect of parity of spectral terms on curve of growth 77−53539
Ni XXI, XXIII, spectral energy levels, relativistic corrections, config. superposition method 80−32616
^{61}Ni, $3d^94p\ ^3D_2$ level, hyperfine struct., level crossing obs. *(French)* 78−41997
O, ground and excited states, atomic polarisability calc. 77−83756
O I, 15-level model for chromospheric spectrum of α Bootis (Arcturus) 77−56923
O I, 3s′ $^3D^0$ and 3d $^3D^0$ levels excitation and radiative decay 79−80064
O I, lifetimes of 2s2p $^3P^0$ state 77−27027
O II, III, IV, beam-foil spectra, mean lives, 270-490 angstrom 78−55223
O II and III, mean lifetimes of astrophysically important excited levels 77−46528
O III, electron impact excitation cross sections, independent particle model calcs. 80−63823
O, two-photon absorpt., auroral transition relax. obs. *(Japanese)* 80−47954
O V, E1 transition probabilities, lifetimes, CI calc. 80−83321
O V, excited states, transaction oscill. states and wavefunctions 79−59367
O VII and VIII, beam foil excited, alignment effects 77−34605
O^+, beam-foil excitation, absolute Auger yield meas. 80−14203
O^{n+}, n=1 to 4, gas and foil-excited, 2-18 MeV, projectile Auger spectra 79−59414
$O+N_2$, excitation and deactivation at above-thermal energies 80−43171
O_2, photoelectron ang. distrib., photon energy depend. , 16-25 eV 80−53046
$O(^1D)$, excited states prod. by O_2 photodissoc., quantum yield 78−33557
$O(^1D)+CO$, deactivation rate consts. temp. depend., 113-333K 78−88629
$O(^1D)+Xe(Kr)(Ar)$, deactivation rate consts., 110-330K 78−88628
$O^{7+}(O^{8+})+He$, p-state alignment, X-ray emission polaris. obs. 79−50123
$O(^1S)+CO_2(H_2O)(NO)(N_2O)$, product channels 78−46422
^{16}O ions, mag. hyperfine interactions, PAC meas. 80−95734
O** Rydberg state translational energy spectra in dissoc. electron impact excitation by CO_2 79−54979
$O(2^1D_2)$, prod. by O_3 photolysis, collisional deactivation 79−20384
$O(3p^3P)$, population and depopulation of $O(3P^5P)$ in supersonic freejet of O_2-seeded Ar plasma 80−42958

atomic excited states continued
$O(3p^3P)+H_2O$, radiation quenching in pulse radiolytically excited water vap. 79—89738
P, excited config., Hulthen and Slater type 2d functions 78—41972
P, highly ionised, beam foil radiative lifetimes and EUV spectrum 80—32671
P, $np^2(n+1)s$ excited-state config. quadrupole moments, Sternheimer shielding factor 80—37755
P V, beam foil excited, alignment effects 77—34605
Pb, $^3P_1{}^0$ state reson. radiation, collisional quenching cross-sections 77—435
Pb, electron impact excitation, visible and UV spectra, excitation cross sections anal. 80—32840
Pb, L-shell photoelectric photon absorpt. cross section, energy depend. 80—106279
Pb Rydberg series from Pb_2 three photon excitation 80—106280
$PbO+C \rightarrow CO+Pb$, chemiluminesc. from gas phase reaction 79—8426
$Pb(^3P_1{}^o)+H$, spin-orbit relax., fluoresc. intensity meas. 78—82681
^{210}Po, nucl. alpha decay, electron inner shell vacancy creation, semi quantal approach 80—68607
Pt I, radiative lifetimes, beam-sputtering technique meas. 79—18142
Ra, Rydberg series, ionisation limit derivation from multichannel quantum defect theory, UV absorpt. spectra 80—52918
Rb, ^2D states, fine struct. 78—90098
Rb, 6^2D excited levels, assoc. ionisation efficiency 77—10747
Rb, excited np states, fine struct., core electrons effect 77—18807
Rb, excited S- and D-states, Stark interaction by laser spectroscopy, polarisability 77—50404
Rb F states, highly excited, natural radiative lifetime meas. 79—3404
Rb, fine struct. intervals in 6^2F and 7^2F states, RF spectroscopic meas. 77—71766
Rb, high lying Rydberg states, atomic beam laser spectra 79—94101
Rb, highly excited P-states natural radiative lifetimes 77—6727
Rb I, lifetime meas. of lowest ^2D-states, elec. quadrupole excitation 78—42004
Rb in Xe, collision-induced dipole transitions, absorpt. meas. 80—95718
Rb, isotopically selective ionisation through Rydberg states 78—5186
Rb, n^2D states, fine struct. near ionisation limit, two-photon spectra 77—30843
Rb, oscillator strengths of 5s-4d first forbidden lines 78—86824
Rb, quenching cross sections, highly excited states 79—89761
Rb, radiative lifetimes up to $n=12$ excited states, pulsed dye laser and superradiance excitation 80—83322
Rb, radiatively excited states, ionis. rate coeffs. in two atom collisions 80—43160
Rb, Rydberg levels, Stark patterns, expt. and central pot. calc., positions and intensities 79—93953
Rb Rydberg levels in intense mag. field, diamag. struct. 79—26958
Rb, Rydberg S and P states, hyperfine struct., RF spectroscopic meas. 77—57911
Rb, Rydberg states, detection using freq. doubled CW dye laser 78—17592
Rb^+, levels direct excitation, cross sections and transition probabilities determ. 80—52899
$^{85,87}Rb$, high Rydberg levels, press. broadening and shifts 80—52902
Rb+atom, Rb Rydberg states, collisional ionisation, rate consts. 80—32817
Rb+He, quasielastic and inelastic collisions in S and D Rydberg states 80—83462
Rb+Rb, radiatively excited states, chemi-ionisation, ionisation rate consts. determ. 80—58363
Rb+Rb**, freq. shift, line broadening, phase interference effects, Doppler free two photon spectra 80—58200
RbHe(Ne), spin relax., Rb hyperfine interaction in Van der Waals mol. 78—94201
Rb*+He(Xe), thermal, 5p $^2P_{1/2}$ state depolarisation cross-sections 77—71852
$^{85,87}Rb$, first excited D-level, hyperfine struct. meas. by cascade, fluoresc. spectrosc. 80—69101
$Rb(6^2P_{1/2})$ polarisabiliyt, mag. scanning obs. 80—27977
Rb(nP)+Rb(inert gas), collisional depopulation Rydberg P state 77—75281
$Rb(nS, nD_{3/2})+Rb$(ground state), collisional quenching cross sections 80—43146
S, excited config., Hulthen and Slater type 2d functions 78—41972
S XV, 1s2s ^3S-1s2p ^3P transitions, Lamb shift, VUV beam foil spectra obs. 80—52919
$S+CS_2(OCS)(CH_4)$, electronically excited atom, reson. fluoresc. 80—99476
$S^+ +Ar$, double K-vacancy prod., X-ray X-ray coincidence and fluoresc. yields obs. 78—55230
$S(^1S)$, in OCS laser, collisional electronic energy transfer, for fusion research 78—59003
$S(^1S)$, photolytic prod. from OCS 79—13775
Sb, excited state lifetimes, crossed at. electron beams obs. 79—790
Sb, $np^2(n+1)s$ excited-state config. quadrupole moments, Sternheimer shielding factor 80—37755
SbI, ^2D state radiative lifetimes 79—3381
SbII, ^3P, ^3D state radiative lifetimes 79—3381
Sc I to Sc XXI, energy level tables derived from atomic spectra anal. 80—101672
Sc II, 3d4p ^1P and ^3F levels, beam-foil mean-life meas. 77—3306
Sc^+, excited config. position and level struct., review 80—32621
$Se(^3P_1)$+inert gas, gas phase flash photolytic deexcitation obs., 1000K *(Russian)* 78—50626
$Se(^1S)$, quenching of high concs. prod. by photolysis 79—6904
Si $3p^2(^1D_2)$ state collisional quenching 79—22806
Si (III), excitation thresholds and oscillator strength calc. using CI wavefunctions 80—91496
Si, excited states lifetimes, fluoresc. decay curves 80—58175
Si, highly ionised, beam-foil lifetime obs. 80—32670
Si II, transition probabilities between excited states, SCF treatment 78—82658
Si III, $^3F^0$ Rydberg series, energy levels, multiconfigurational HF procedure 80—47882
Si IV, V, VI, beam-foil level populations, charge state fractions 80—52913
Si ions, multiply-charged, beam-foil obs. of $1s2p^3P_1$ lifetime 80—14114
Si, Rydberg series electronic struct. 79—22614
Si, Rydberg series electronic struct. 79—22615

atomic excited states continued
Si XIII, 1s2s ^3S-1s2p ^3P transitions, Lamb shift, VUV beam foil spectra obs. 80—52919
Si^{12+}, 1s2s $^3S_1$-1s2p $^3P_{0,2}$ transition wavelengths, by beam-foil 80—32649
Si^{n+}, excited state population density in p and p^5 configs., temp. depend. 80—31273
SiO^+, vac. UV photoelectron spectra, ab initio mol. orbital and $X\alpha$ calcs., $(X^1\Sigma^+)$ state 78—46395
$Si(Si^+)(Si^{2+})(Si^{3+})$, excited levels, radiative lifetimes, beam foil spectra 80—58368
Sm, excited state lifetimes, oscillator strengths 77—83531
Sm, excited states hyperfine struct., isotope shifts, laser-RF double reson. obs. 79—41140
Sn I, Sn II, Sn III, atomic partition functions 77—26955
Sn ions, analytical HF solns. for ground and excited states 77—72835
Sr, 5^1P state quenching cross sections in $CO\text{-}N_2O^1$ flames 77—18836
Sr, $5p^2$ $^1D_2$ level lifetime 79—63960
Sr, associative ionisation of laser-excited Rydberg states, mass spectrometry obs. 78—94303
Sr, direct meas. of excited state lifetimes 77—65435
Sr, excited state lifetime, delayed coincidence meas. 77—3315
Sr I, lifetime meas., stepwise excitation by pulsed dye lasers 77—83536
Sr I, Rydberg and autoionisation levels, laser ionisation spectroscopy 77—3331
Sr I and II, excited states radiative lifetimes 79—98042
Sr I excitation series, potential barrier effects, single configuration HFC 80—78558
Sr II, Hanle effect, $^2P_{3/2}$ lifetime determ. 77—18852
Sr, multiphoton ionis. spectroscopy of even- and odd-parity states 78—86973
Sr, quadratic Zeeman effect, diamagnetic shift, Rydberg series, strong field mixing 78—946
Sr, quantum defect param., ab initio calcs. 80—78525
$Sr^+(^2P_{3/2})$, coherently Penning ionis.-excited, with $He(2^3S_1)$, Hanle effect 80—5520
$Sr(^1S,^3P)+$ halogenated methanes, laser induced fluorescence 79—66270
Sr^*+Cl_2, collision and reaction cross section meas. 79—59537
$Sr^*(^3P_1)+HCl(HF)$, laser-excited atom reaction, energy deposition 78—85134
$Sr^+(5p^2P_{3/2})$ alignment in $He(2s^3S_1)+Sr$ Penning collisions, polarised emission obs. 80—23533
Te I, UV line rel. oscill. strengths and unexcited atom conc., AAS meas. *(Russian)* 78—31749
$Te(^3P_1)$+inert gas, gas phase flash photolytic deexcitation obs., 1000K *(Russian)* 78—50626
Ti, $4s3d^3$ and $3d^4$ states, HF descriptions, alternative orbital config. 80—63534
Ti atoms sputtered from Ti, Ti oxides, photon emission, nonradiative transition effects 80—58208
Ti, neutral and ion val. states, electron correlation, ab initio effective val. Hamiltonian calc. 80—99449
Ti, Tokamak plasma, atomic struct., highly ionized states 80—75086
Ti^+, excited config. position and level struct., review 80—32621
TiXIV(TiXV)(TiXVII), Tokamak discharge, ground state, mag. dipole transitions, UV spectra obs. 80—63575
Tl, atoms and ions, lifetimes, electron impact excitation 77—79581
Tl, electron impact excitation cross sections calc. *(Russian)* 78—55240
Tl ions, analytical HF solns. for ground and excited states 77—72835
Tl, lowest S-state lifetime meas. 77—65436
Tl, obs. of Dicke superradiance at 1.30 μ 77—441
Tl+Ba, radiative collisional fluoresc. obs. from thermally excited atoms 80—102480
$Tl+CO_2$, relax. of $6^2P_{3/2}$ and $7^2S_{1/2}$ states 79—64094
$Tl(7^2P)$ states, isotopic forms, HFS, press. self-broadening, two-photon spectra 77—18879
Tm I, hyperfine struct., high resolution spectrosc. meas. 80—87238
U, excited state radiative lifetime, sputtering technique 78—17602
U I, relative branching ratios for excited level decay 77—57922
U, Rydberg levels, time-resolved stepwise laser photoionisation obs. 77—27038
$U+{}^3He({}^4He)(Ne)$, collisional relax. of highly excited states, laser-induced fluoresc. obs. 80—58205
U+molecule, collisional relax. of highly excited states, laser-induced fluoresc. obs. 80—58205
^{235}U, ground and 1st excited states, hfs, laser fluoresc. and laser-RF double reson. spectroscopy 80—58170
^{235}U, lifetime meas. of electron excited states, rel. to laser isotope separation 77—34591
^{238}U I, lifetime, branching ratio and absolute transition probability of 6395.42 Å transition 79—3402
V, hyperfine struct., laser-RF double-reson. obs. 79—41141
W, first-principles pseudopotential in the local-density-functional formalism 79—59328
Xe, $5d(3/2)_1$ photoexcited state radiative decay 78—74605
Xe, $5p^5ns$, $5p^5np$, $5p^5nd$ and $5p^54f$ config., HF calc. 77—23468
Xe, excited levels Lande factors *(French)* 79—68326
Xe, g-factors meas. by optical pumping and mag. reson. 80—14246
Xe, ground state, two-photon excitation spectra, fluoresc, decay 77—75115
Xe, high Rydberg states, radiative lifetimes and transition probabilities 78—86817
Xe I, indirect level population in electron excitation *(Spanish)* 77—3461
Xe II, $5d^4D_{7/2}\text{-}6p^4P_{5/2}{}^0$ transition, isotope shift, h.f.s., laser-ion beam expt. 79—93945
Xe II, beam-foil spectroscopy, radiative lifetimes 80—18825
Xe II, excited states lifetime meas., photon-photon delayed coincidence technique 77—68011
Xe II, influence of relativistic effects, excited states 79—72274
Xe II $5s5p^6$ $^2S_{1/2}$ state, lifetime meas. 79—13670
Xe III, $5s^25p^3(^4S)nl$ levels, ionis. pot., from spectral data 80—47920
Xe, in gas discharge, collisional excitation, radiation lifetimes, macroscopic alignment obs. 80—33734
Xe, ionisation of high Rydberg states by collision with molecules 77—88545
Xe, on dissoc. recomb. of Xe_2, electron temp. depend. 77—46647
Xe, outer $p_{1/2}$ subshell photoionisation, polarised electrons, relativistic RPA calcs. 80—83331
Xe, photoionis. from excited states 79—10078
Xe, Rydberg atoms, field ionisation, 300K background radiation effects 79—68271
Xe, single photon decay of $(4d)^{-2}$ double hole state 77—34606

atomic excited states continued

- Xe, three level systems, obs. of isotope shifts 78—82670
- Xe, united atom rare gas spectra analogy with mol. Rydberg states 80—32700
- Xe VIII, beam-foil lifetime meas., cascading problem 80—14249
- Xe^+, $5p^45d^4D_{7/2}$ and $5p^46p^4P^0{}_{5/2}$ levels, HFS, ion-beam laser fluoresc. 77—75319
- $Xe\text{-}Br_2$ discharge, atomic state density determ. 79—36573
- $Xe+Cl_2(F_2)$, XeCl(XeF) form., relax. and quenching 80—81314
- $Xe+H^+$ ionisation, induced L-shell alignment 80—32813
- $Xe+NH_3(H_2S)(SO_2)(HCl)$, ionis. cross sections calc. 77—68103
- $Xe^+(7s^2P_{1/2,3/2})$, charge exchange excitation in Ne-Xe glow discharge 80—38857
- $Xe(nf)+NH_3$, at. Rydberg state further excitation by rot. transfer, field ionis. obs. 78—58795
- Xe(nf Rydberg state)$+NH_3$, n- and l-changing and ionising collisions 80—58360
- Y I, Y II, lifetimes of excited states, rel. to solar abundance determ. 78—86815
- Yb, autoionisation and Auger decay, collective excitation effect 80—43008
- Yb, HFS in 6s6p $^1P_1$ state, level-crossing and anticrossing spectroscopy 77—27036
- Yb, highly excited levels, odd and even parity spectra, multichannel quantum defect anal. 80—58133
- Yb highly excited levels, reson., visible two photon absorpt. spectra obs. 80—58228
- Yb I, high Rydberg levels of $4f^{14}$ 6snd configs., very high resolution obs. 80—106300
- Yb I, Yb II, excited states radiative lifetimes 79—76386
- Yb, isomers and hyperfine struct., selective detection through Rydberg states 80—52903
- Yb, lifetime meas. using cw dye-laser 79—89636
- Yb, Rydberg states, optically pumped, electric field ionis. *(Russian)* 79—27095
- Yb, single atom detection by selective laser excitation and field ionisation from Rydberg states 79—18159
- ^{A}YbI, A=170,171,173, 6s6p $^1P_1$-$6s^2$ $^1S_0$ transition, spectrosc., isotope shifts and hyperfine structure 80—23368
- $Yb(6^3P_1)$, Zeeman splitting, high-resolution time-resolved quantum beat spectra 78—58640
- Zn, ^1S, ^3P, ^1P states, dipole polarisabilities from compact variational trial functions 80—63568
- Zn, electron impact ionisation efficiency curve, threshold of 12.7 eV 79—50137
- Zn I,II, excited state lifetimes, electron-photon delayed coincidence meas. 78—25478
- Zn I isoelectronic series, $4s4p^1P$ lifetimes meas. 80—42998
- Zn II, Hanle effect, $^2P_{3/2}$ lifetime determ. 77—18852
- Zn II, lifetime extraction from beam-foil decay curves 80—14107
- Zn^+-He, positive column laser discharge, upper and lower state densities, Penning collision 80—32964
- ZnI, II, excited states, radiative lifetimes, multi-channel delayed-coincidence method 80—32669
- $Zn(^1P_1)+NO(X^2\Pi)\rightarrow Zn(^1S_0)+NO(A^2\Pi^+, \nu=0,1)$, near-resonant electronic energy transfer, fluoresc. quenching 77—14549
- Zr, excited state radiative lifetime, sputtering technique 78—17602
- Zr I, lifetimes of excited states, rel. to solar abundance determ. 78—86815
- Zr XIII, electronic struct. of complex ion, relativistic perturbation theory 79—22610

atomic explosions *see nuclear explosions*

atomic fine structure

- ^2P fine struct. interval of $2s^22p^5$ and $2s^22p$ configs., Z-depend. 79—22634
- alkali atoms, highly excited Rydberg states, fine struct. 80—58402
- alkali metal, high ang. momentum Rydberg states, quantum defect core polaris. depend. 77—18808
- alkali metal, quantum beats in photoionis. by fine struct. levels coherent superposition 79—6922
- alkali metal+inert gas, role of different interactions in intramultiplet relax. at nonresonant interactions 77—6902
- alkali metal atom, Rydberg state Stark struct. 80—37754
- atom+atom collisions, fine-struct. transition cross sections, eigenphase formulation 78—25651
- atomic elastic scatt., fine struct. transitions at thermal energies, collision cross section calc. 78—25652
- autoionising states, electron angular distribution, fine and hyperfine struct. 80—58222
- cascade quantum beats, intensity profile calculation 79—89630
- constant determination, measurement accuracy, atomic metastable beam method 77—68105
- constant variation, summary of obs. evidence 79—12759
- Cu isoelectronic sequence, fine structure separations for ^2D terms 79—89804
- education, Na Rydberg states, anomalous fine struct., perturbation model 80—57035
- eight-electron ions, $2p^k$ and $2p^k$ ^13l config. transitions calcs. 78—933
- electron polarisation produced by reson. ionisation by intense EM field *(Russian)* 78—50518
- EXAFS, theory and technique appl. in atomic environment *(French)* 79—26927
- Feynman diagrammatic calc. 77—26981
- inert gases, fine struct. of atomic levels in field of intense reson. wave 78—9099
- interstellar gas, fine struct. levels population ratios 79—35351
- ions in $1s^22s^n2p^{4-n}$ configurations, term-energy calcs. using perturbation theory 77—42229
- ions resembling Li, Be and B, spectra calcs. 77—42260
- k ordering of atomic and ionic energy levels 80—74095
- many-electron atom-unbound electron system, normalisation of wave function 77—68123
- metastable autoionising states, ang. distrib. of electrons which decay via fine and hyperfine struct. interactions 80—102492
- multiple anticrossings in atomic spectrosc. 80—87091
- neutral atoms, slow collisions, fine struct. transitions 79—841
- nonlinear resonances of accelerated atoms and molecules *(Russian)* 78—50488
- one electron atom, Dirac energy, αZ expansion procedure 78—9053
- one-electron atoms, corrected for fine struct., lamb shift and QED shift, tables 77—79529

atomic fine structure continued

- P-S state atomic collisions, quantum mechanical treatment, decoupling approx. 80—99542
- P-state collisions, quantum mechanical treatment, angular momentum coupling 80—99541
- pionic Ti, Klein-Gordon eqn., relativistic fine struct. term, verification 79—22868
- positronium, ground state, fine struct. interval, NMR meas. 77—34787
- positronium$+N_2$ (inert gas), fine struct. interval, collisional density shifts 77—34788
- ps configuration parametrization 79—97988
- quantum beats in light absorption from atoms, expression for fine levels 78—25499
- reactance matrices, fine struct. cross sections, JAJOMPRE program 78—90312
- resonance scattering spectrum, fine struct. in external field 77—83533
- Rydberg states, fine struct. splitting, quantum beat and double reson. spectroscopy 78—86979
- seven-electron ions, $2p^k$ and $2p^{k-1}3l$ config. transitions calcs. 78—933
- six-electron ions, $2p^k$ and $2p^{k-1}3l$ config. transitions calcs. 78—933
- spectroscopy, high-resolution, by at. beam-laser beam interaction *(Dutch)* 79—50166
- transition probability, semiclassical multichannel scatt. matrix 80—37854
- two-level atoms, Dicke superradiance and superluminosity, fine struct. and time evolution 77—65438
- two-level system, spontaneous emission in bichromatic reson. field 80—69093
- two-photon spectroscopy, Doppler-free *(Dutch)* 79—50167
- $(\mu^{-4}He)^+$ ion, meas. of $2S_{1/2}$-$2P_{3/2}$ splitting, QED vacuum polarisation 77—34785
- Ω hyperon atoms, Coulomb level fine splitting *(Russian)* 79—22871
- $\pi\mu$ atom, energy levels, fine struct. and Lamb shift calc. *(Russian)* 79—31744
- $^4He(3^3P)$, fine struct., level crossing obs. 78—82686
- Al I, fine struct. splittings in some highly ionized n=3 doublets 80—43200
- Al_2Cl_6, matrix isolated, vibr. spectra, isotopic fine struct. and valence force field calcs. 80—58258
- Ar, absorpt. spectra, field induced autoionisation near ionisation threshold 80—106301
- Ar^{16+}, radiative decay from 2^3P_2 and 2^3P_0 levels, beam-foil time of flight meas. 77—68015
- $Ar+Ar^+$, charge exchange, Σ oscill. and spin change 80—74247
- Ar^++Ar, charge transfer, fine-structure transitions 80—63808
- Ba I, extended average level calcs. 78—37568
- Ba I, quasi-Landau spectrum, semiclassical strong field mixing models 80—63847
- Ba II, $6p^2P$ fine struct. g-values, laser excitation of fast ion beam 77—10645
- Ba, X-ray spectra, high energy $L\gamma$ satellites 80—102474
- Be I isoelectronic sequence, radiative props. determ. by model-pot. method 78—70788
- Be I-like spectra, low configs., isoelectronic consistency 79—93940
- C, fine struct. excitation by H impacts 77—42384
- C, ground state fine struct., laser mag. reson. obs. 80—87062
- C II, electron impact induced fine struct. transitions, collision strength 77—50540
- C^{3+}, fine struct. and lifetimes, doubly excited quartet system 78—78827
- C^++H, fine struct. excitation cross section 77—38724
- C^++H, fine structure transition of C^+, collision cross section calc., validity of current approx. 78—25652
- C^++H_2, C^+ fine-struct. excitation, interstellar cloud cooling 78—25675
- C^++H_2, fine struct. transition excitation 77—42389
- $Ca^{14+}+H^+$, collisional excitation of fine struct. transitions in ground state 77—19017
- Cl, $3p^5$, $^2P_{1/2}\leftarrow{}^2P_{3/2}$ fine struct., tunable IR diode laser detection 80—23348
- Cl I, fine struct. splittings in some highly ionized n=3 doublets 80—43200
- ^{35}Cl XVI, beam-foil excitation, Lamb shift and fine struct., QED test 80—9549
- ^{35}Cl XVI, n=2, Lamb shift, fine struct. 79—13675
- Co I, fine struct. splittings in some highly ionized n=3 doublets 80—43200
- Co^-, photoelectron spectra, electron affinity and fine-struct. interval 79—68212
- Cs, 5^2D-n^2F series fine and hyperfine struct. 80—43201
- Cs, Doppler-free two-photon spectrum, recorded using thermionic detector 78—46465
- Cs, excited np states, fine struct., core electrons effect 77—18807
- Cs, fine-struct. of excited nd and nf states, at. core effect 78—58606
- Cs, four-photon ionis., strongly interacting resons. theory 80—52955
- Cs, highly excited F states, fine struct. meas. 78—21871
- Cs, P,D,F, and G Rydberg states, quantum defects and fine struct. 80—5496
- Cs, resonant multiphoton ionis. 79—36589
- Cs, Rydberg states, diamag. and collisional perturbations 80—58181
- Cs^+ dipole and quadrupole polarisability fine struct. intervals and g-factor interval 80—91477
- $Cs(8^2P)+He(Ar)(Xe)$, fine-struct. transition cross sections, semiclassical calcs. 77—30972
- Cu I isoelectric sequence, fine struct. separations for reson. transitions 78—17588
- Cu, $K\beta_{1,3}$ intensity distribution, line strength calcs., single vacancy scheme 80—32650
- F, spin-orbit splitting and $^2P_{1/2}$ radiative lifetime, absorpt. spectrosc. meas. 80—87063
- $F(^2P_{1/2})+H^+(Xe)$, nonadiabatic collision processes, electronic degrees of freedom, classical model 79—64062
- Fe, fine struct. levels fitting, config. interaction effect, spin-orbit and electrostatic interaction parameters 80—69248
- Fe, highly ionised, 1s to 3p $K\beta$-like X-ray spectrum 77—50394
- Fe, X-ray absorpt., spectra, far fine struct., multiple scatt. terms contrib. 80—40184
- Fe XXI, relativistic energy levels, Dirac-Fock multiconfig. calc., triplet state fine struct. and Lamb shift 80—23315
- Fe XXII, intercomb. transitions, oscill. strengths, transition probs., rel. to solar spectra 80—52935
- Fe XXIV, oscillator strengths, electron impact excitation collision strengths, solar flare spectra appl. 80—32647

atomic fine structure continued
Fe^-, electron affinity, nonstatistical fine-struct. detachment intensities at 488 nm, laser electron spectra 79—41144
$Fe^{20+}+H^+$, collisional excitation of fine struct. transitions in ground state 77—19017
Ga, atom and ion, k-ordering props. and fine struct. inversion 79—59388
Gd, isotope shifts and deform. obs. 77—65433
H , Rydberg consts., saturated absorpt., spectroscopy meas. 80—105604
H atom, many-photon excitation spectra, fine structure 79—59419
H Balmer-α fine struct. lines, anomalous shifts, in He-H_2 DC discharge 79—45677
H, Dirac equation calcs. 80—46760
H, excited state, J=3/2-J=5/2 transition, fine struct. interval meas. 77—46542
H fine structure $3^2S_{1/2}$-$3^2D_{5/2}$ interval, separated oscillatory field meas. 80—99482
H, fine structure levels, Stark component radiative widths 77—3302
H I, in solar chromosphere, substates populuIation rel. to Hα seven components and 9873 MHz line 78—89151
H, n=2 levels, Lamb shift and fine struct. reson. meas. 80—23321
H, relativistic, in strong mag. field 80—9518
H, two-photon transition, $3^2S_{1/2}$-$3^2D_{5/2}$, precision meas. 78—17642
H^+, gyromag. ratio and fine struct. meas. by meas. distance between wires, using laser interferometer 80—74253
H-like atom, fine struct. and HFS levels, Zeeman effect, relativistic corrections 80—37776
H-like atom, Stark effect on fine struct. 79—26929
H-like ions, radiative level widths in low electric fields 78—37589
H-like ions, reson. doublet component intensities in optically thin laser plasma *(Russian)* 78—38458
H-like ions in laser-produced plasma, Balmer fine struct. (broadening) 80—48860
H-like problems, spinor and scalar QED calcs. in Euclidean formulation 77—88378
$H^++N^+(O^{2+})(Ne^{4+})(Na^{5+})$ (Mg^{6+}), ^3P_J fine structure transitions 80—37864
H_α Balmer line emission fine struct., Stark effect *(German)* 78—82673
H_α line shape, plasma broadened, fine struct. effects at low electron densities 78—62765
Hα line, fine struct. meas. Rydberg const. determ. 79—54093
He, 3^3D level, fine struct. changing collisions in glow discharge 80—58346
He, electron impact excitation of high Rydberg state, impact parameter method 78—62922
He, fine structure, 2nd order contribs. from all intermediate states 79—3354
He, fine structure intervals, elec. field-induced anticrossing meas. 78—42031
He fine structure interval 2^3P_0-2^3P_2, optical microwave atomic beam mag. resonance meas. 80—102585
He, forbidden radio lines, 2^3P state fine struct. 77—23447
He I, fine struct. of triplet term of 1s3d config. 79—3595
He I, saturated absorpt. on 587.5 nm line, cross-over reson. 77—23448
He isoelectronic sequence to Z=10, D and F states fine struct. 77—544
He plasma, satellites of He 492.2 nm line, fine struct. interpretation 80—59235
He Rydberg states, mag. and elec. fine struct. calcs. 79—76333
He, singlet-triplet anticrossing, elec. field induced 77—14404
He, triplet P state splittings, higher order corrections of theoretical calc., book contrib. 78—82632
He^+, fine struct. obs. by beam-gas spectroscopy, level crossing resonances 80—9719
He^+, n=4 level, fine struct., level-crossing and anti-crossing reson. obs. *(French)* 78—25488
He-like atoms, n=2 states radiative transition rates, oscill. strengths, RRPA extension 77—34584
He-like ions, electron impact, collision strengths for fine-struct. transitions 78—62925
He-like ions, highly charged, electron impact, intermediate-coupling strengths for fine struct. transitions 80—32837
^4He, 3^3P-state fine struct. 80—23568
^4He, fine structure intervals in 3^3P and n^3D states, level crossing meas. 77—14396
^4He II, widths of Stark components calc., beam-foil data comparison *(French)* 80—9545
^4He, Rydberg states, fine struct., D, F and G states meas. 77—50418
^4He, Rydberg states, fine struct. obs. 80—23350
$^4He^+$ II, H-like, fine struct. Stark effect *(French)* 78—943
Hg, IR arc spectrum, fine struct., HFS and isotope shifts 77—79559
Hg, IR arc spectrum, fine struct., HFS and isotope shifts 77—79560
Hg(6^3P_0), $^3P_1$-$^2P_0$ fine struct. obs., CO_2 laser mag. res. 77—61696
K, ^2P fine struct. splittings, Hartree-Fock calcs. 77—10606
K, 5^2P to 4^2S resonance line, rare gas perturbations, broadening, shift and dipolaris. 78—9126
K, excited np states, fine struct., core electrons effect 77—18807
K, fine struct. splittings of 5d and 6d states, energy level crossing expts. 79—76396
K, fine-struct. intervals, polarisabilities, highly excited d states 79—27100
K I, fine struct. splittings in some highly ionized n=3 doublets 80—43200
K+He, fine struct. transitions, energy depend. crossed beam determ. 79—86035
K(4p)+He, fine struct. transitions, vel. depend., interatomic pots. 77—42388
Kr, $4p^55s$ state, electron excitation fine struct., neg. on reson. 77—14585
Kr, absorpt. spectra, field induced autoionisation near ionisation threshold 80—106301
Kr VIII, excited state energies and lifetimes, beam foil spectra 80—63591
Li, $1s2p^2$ $^4P^e$ state, using configuration-interaction wavefunctions 79—3369
Li, $1s2s2p^4P^o$ state, using configuration-interaction wavefunctions 79—3370
Li 3^2D state, level crossing meas. 79—13832
Li, 4^2D state, fine-struct. splitting, level-crossing spectroscopy 77—83552
Li, A=6,7 two-photon intracavity dye laser spectroscopy 78—82706
Li, microwave fine-struct., Rydberg states 78—13451
Li^+, ^3P and ^3S states, fine (hyperfine) struct., dye laser saturation spectroscopy, beam expt. 80—58169

atomic fine structure continued
Li^+, at. fine struct. and HFS, meas. by Doppler tuned hyperfine spectrosc. 79—81292
Li-like ions, fine struct. in $1s2p^2$ ^4P and $1s2s2p$ $^4P^0$ states 78—66471
Li+He, $P_{1/2-3/2}$, fine-structure transition probability, semiclassical multichannel scatt. matrix 80—37854
$Li^*(2^2P_J)+H_2(D_2)$, collision induced quenching and fine struct. transition rate coefficients meas. 80—74221
$Li^*(2^2P_J)$+He(Ne)(Ar)(Kr)(Xe), collision induced fine struct. transition rate coefficients determ. 80—74220
Mg, $3s3d^3D$ and $3s4d^3D$ states, fine-struct. meas. by level crossing spectra 79—36572
Mg II, fine struct. of ^2D and ^2F sequences by level crossing and anticrossing spectroscopy 79—6919
Mg, intercombination line oscill. strength, including core-polaris. and relativistic effects 78—25475
Mn, fine struct. levels fitting, config. interaction effect, spin-orbit and electrostatic interaction parameters 80—69248
Mn I, collisional and radiative excited, lifetime meas. 80—91501
N, active condensed, thermolum. meas. *(French)* 80—11484
N^{4+}, fine struct. and lifetimes, doubly excited quartet system 78—78827
Na, ^2D highly excited states, fine struct. splitting, field ionisation quantum interference 80—18835
Na, ^2P fine struct. splittings, Hartree-Fock calcs. 77—10606
Na, ^2P photodissoc. product, fine struct. anal. 80—78665
Na, excited np states, fine struct., core electrons effect 77—18807
Na, fine-struct. of excited nd and nf states, at. core effect 78—58606
Na high ang. momentum Rydberg states, quantum defect core polaris. depend. 77—18808
Na, highly excited, f-state fine struct., microwave reson. obs. 77—83535
Na, highly excited p and d states, fine struct. intervals and polarisabilities, RF reson. meas. 77—67999
Na I, fine struct. splittings in some highly ionized n=3 doublets 80—43200
Na, Rydberg states, fine struct. and Zeeman beats 79—14044
Na, Rydberg states, high resolution spectroscopy 80—52901
Na, Rydberg states, IR Stark spectra, term energy, fine struct. 77—57910
Na, Rydberg states, millimeter spectra, quantum defect, fine struct., polarisability, field ionis. obs. 78—82672
Na, Rydberg states, nd→(n+1)p intervals meas. 78—33629
Na, Stark effect study, S and D excited states struct., two-photon spectra 77—54547
Na+Ar, fine structure transition cross-sections, emission spectra, NaAr form. 78—9085
Na+inert gas, fine struct. state changing cross-sections, crossed beam determ. 77—50496
Na+inert gas atom, 4^2D fine struct. transition 79—850
Na+N_2, rot. excitation and fine struct.-changing collisions 78—42176
Na+Ne(Ar)(Kr)(Xe)(N_2)(CO_2), fine struct. changing collisions, vel. depend. 79—22803
NaI isoelectronic sequence, 3s-3p and 3p-3d transitions, ionisation energy 78—70773
$Na(3^2P_J)+Na(3^2S_{1/2})$, collisional excitation transfer, pot. symm. rules and cond. function 80—9690
Ne, atom, isotopic shift and fine struct. for $2p^54d$ and $2p^55s$ config., Doppler-free two-photon spectroscopy 80—23387
Ne, Doppler-free two-photon spectra, fine struct. and hyperfine consts. of 4d′ level 77—61725
Ne, electron impact, fine struct. resolved by reson. free-free radiative absorptions 79—3576
Ne, fine struct. obs. by beam-gas spectroscopy, level crossing resonances 80—9719
Ne^+, electron scatt., relativistic R-matrix calc., fine-struct. level transition cross sections 78—13604
Ne^+ mobility in Ne, fine struct. splitting effect 77—39400
Ni^-, photoelectron spectra, electron affinity and fine-struct. interval 79—68212
$Ni^{14+}+H^+$, collisional excitation of fine struct. transitions in ground state 77—19017
O, 2^3P_2-2^3P_1 fine struct. splitting by laser mag. resonance 79—98010
O, fine struct. excitation by H impact 77—42384
O, He-like, $1s3s^3S$-$1s3p^3P$ transition 79—89637
O^-, photodetachment, fine struct. transitions, photoelectron spectra 78—55151
O^{5+}, fine struct. and lifetimes, doubly excited quartet system 78—78827
$P^-(^3P_{2,1,0})+h\nu$, P electron affinity, P^- fine struct. interval 77—79590
Pt, ground state configs., isotope shifts and fine struct. anal., visible and UV spectra 80—42987
Rb, ^2D states, fine struct. 78—90098
Rb, ^2P photodissoc. product, fine struct. anal. 80—78665
Rb, atom and ion, k-ordering props. and fine struct. inversion 79—59388
Rb, excited np states, fine struct., core electrons effect 77—18807
Rb, fine struct. intervals in 6^2F and 7^2F states, RF spectroscopic meas. 77—71766
Rb, fine-struct. splittings in visible region, ^2D states 78—50656
Rb, high lying Rydberg states, atomic beam laser spectra 79—94101
Rb, multiphoton ionis. processes, fine struct., hybrid reson. 77—18877
Rb, n^2D states, fine struct. near ionisation limit, two-photon spectra 77—30843
$^{85,87}Rb$, high Rydberg levels, press. broadening and shifts 80—52902
$Rb(6^2P)$+He(Ar)(Xe), fine-struct. transition cross sections, semiclassical calcs. 77—30972
S II, fine-structure transitions by electron impact 78—65493
S^-, photodetachment, fine struct. transitions, photoelectron spectra 78—55151
SeO, mol., mm wave spectra, $X^3\Sigma^-$ state 79—85959
Si, EUV beam foil spectra, highly resolved, fine struct. splittings 79—31448
Si^{12+}, $1s2s^3S$-$1s2p$-^3P transitions 79—22632
Sr, atom and ion, k-ordering props. and fine struct. inversion 79—59388
Sr I, quasi-Landau spectrum, semiclassical strong field mixing models 80—63847
Sr II, ^2F states, fine struct. splitting 78—50494
$Te^-(^2P_{1/2,3/2})+h\nu$, Te electron affinity, Te^- fine struct. interval 77—79590
Ti, fine struct. levels fitting, config. interaction effect, spin-orbit and electrostatic interaction parameters 80—69248
V, fine struct. levels fitting, config. interaction effect, spin-orbit and electrostatic interaction parameters 80—69248
Xe, $5p^55s$ state, electron excitation fine struct. neg. ion reson. 77—14585

atomic fine structure continued

- Xe, electron impact, L-shell excitation, characteristic X-ray spectra, relative cross sections 77—19094
- Xe subshell photoionisation, multichannel k-matrix calc., spin orbit interactions 80—63600
- Zr IV, energy levels, spectrum obs. 440 to 2670 Å 80—99470

atomic fluorescence

- 1s2p^{24}P levels, lifetimes and line fluoresc. yields 78—74612
- 1s2p^{3}P levels, theoretical lifetimes and fluoresc. yields 80—27975
- absorptive optical bistability, transmitted and fluoresc. light spectrum 79—49981
- AC Stark effect, fluoresc., in modulated laser beams, two-photon stepwise excitation 80—42989
- acetylene-air flames, local temp. profiles and at. fluoresc. intensity profiles meas. 77—52680
- actinides, K-shell fluorescence yields from Auger electrons and X-rays, precision meas. 79—31462
- air-H$_2$ flame, temp. profile, two-line at. fluoresc. method meas. 77—71328
- alkali metal vapour, nonresonant excitation of fluoresc. *(Russian)* 77—10633
- anti-Stokes luminescence, quantum statistics 79—915
- antibunching phenomena on single-scatterer fluorescence in weak-field limit 80—63580
- astrophysical magnetic field determ. from polarization by atomic fluorescence 77—25938
- asymmetric resonance fluorescence spectra, in partially coherent fields 78—66503
- atom, 5d6p^{1}F$_3$-state lifetime meas. 79—89633
- atom+atom collisional intense-field fluoresc., Zeeman degeneracy effects 80—99477
- atom+charged particle, autoionisation state decay 80—9565
- atom+molecule reaction rate meas. 80—16676
- atomic and laser spectroscopy, book 77—79554
- Ba I, lifetime meas. of Rydberg states in 6snd ^{1}D$_2$ series 78—33472
- beam, arbitrary angle in uniaxial cryst., emission energy spectrum 77—57923
- cascade quantum beats, intensity profile calculation 79—89630
- Cl, shock heated, radiative recombination under nonequilib. expansion in supersonic nozzle *(Ukrainian)* 79—37421
- colliding atoms, optical excitation to state of quasibound motion *(Russian)* 78—58784
- colliding particle system, two-photon transition, stimulated Raman scatt. 80—9663
- collision and Doppler broadening of fluorescence and Raman scatt. 78—13465
- collision induced, high incident laser intensity effect 78—86811
- collision processes, laser excitation, fluoresc. 79—94059
- collisional depolarisation, impact and quasistatic limit 77—65439
- collisional redistribution of fluorescence radiation 78—13464
- collisional relax. of highly excited states, laser-induced fluoresc. obs. 80—58205
- collisionally aided fluoresc., for heating or cooling 78—37584
- collisionally aided radiative excitation, three level system, interference effect 79—98022
- collisions, radiative electron transitions *(Russian)* 79—98212
- collisions in intense light beams, quantum aspects *(Russian)* 79—6903
- cooperative resonance fluorescence, additional sidebands 80—5501
- cooperative resonance fluorescence and atomic interactions 80—91486
- cooperative spontaneous emission, short-range Coulomb interactions 78—58619
- delayed quantum beat subnatural linewidth spectroscopy 80—77879
- dense metal vapour, radiation trapping, multiphoton ionisation and reson. fluoresc. 80—32654
- dipole transition, transient behaviour in intense laser field *(German)* 78—66520
- dipoles, magnetic and electric, close to plane interface, radiation patterns 78—37675
- dipoles, magnetic and electric, close to plane interface, total radiated power 78—37674
- Doppler broadening compensation with laser induced light-shifts 79—3405
- dressed atom system, energy levels and reson. phenomena, universal algorithm 80—69111
- dressed atom system, phase represent. applic. to reson. fluoresc., universal algorithm 80—69112
- electrical analogues for two- and three-level systems, for teaching 77—33793
- electron impact excited line radiation, polarisation, long-range electron correls. effects 80—91683
- electron ion collisions, distorted wave theory, Auger ionis. and excitation fluoresc. 79—7018
- emission spectra of atoms strongly driven by laser light 78—42017
- energy trap, atomic device 77—88604
- ethylene, electron impact dissoc., optical emission from fragments 77—83750
- excitation spectroscopy, time-resolved photoluminescence emission and lifetime meas., synchrotron radiation use 78—66687
- excited state decay, radiative emission-autoionisation interference, fluoresc. yield 79—26945
- exponential decay law, long-time deviations, sensitivity to interaction Hamiltonians 77—46523
- fast atomic beam, optical reson. detect. by at. fluoresc. 80—102479
- fast atomic beams, collinear laser spectroscopy 78—37078
- flame temperature meas., 5 laser-excited fluoresc. methods, theoretical basis 80—101793
- flames, local temperature measurement, by two-line at. fluoresc. and photon counting method 79—71447
- gas laser, atomic constants and collision cross sections determ. by level crossing 78—50763
- gas-phase and ion-surface collisions, optical emission 80—32821
- glow discharge, gas temp. meas. by fluoresc. spectroscopy 78—18467
- heavy ion transitions, beam-foil decay curves, theoretical simulation 78—74755
- high Z atoms, L shell fluorescence yields, K to L transfer of vacancies 78—74606
- hyperfine structure quantum beats, intensity profile, ang. momentum theory graphical method 78—25497
- hysteresis in spectrum for cooperative resonance fluorescence, linewidth narrowing 78—21876

atomic fluorescence continued

- induced coherent emission in spatially separated light fields *(Russian)* 79—50274
- inelastic collisions, calc. of fluoresc. in multilevel system in gas phase 79—98129
- inert gas+Li(Be$^+$)(Na)(Mg$^+$)(K)(Zn$^+$), collision-induced alignment, reson.-line emission polaris. obs. 80—18912
- inert gas discharge, reson. radiation imprisonment model 80—38756
- inert gases, metastable states, laser excitation and fluoresc. 77—57921
- inner shell bound-bound radiative transitions, analytical description 78—82684
- inner-shell ionisation, fluoresc. X-ray ang. depend. 77—10649
- intensity correlations in resonance fluorescence with atomic number fluctuations, photon antibunching 78—50499
- intensity fluctuation spectrum of nonlinear reson. fluoresc. *(Russian)* 77—68009
- ion+atom, low vel., X-ray emission ang. distrib., MO calc. 79—54803
- ion+atom (molecule), slow collisions, K-shell excitation, impact parameter depend. 79—72388
- ion beam, laser-induced resonances, high-resolution expt. 77—6959
- ion beam ejected particles from metallic targets, continuous emission spectra *(Russian)* 78—55140
- ion excited state lifetimes meas. using orientation transfer in Penning collisions *(French)* 78—50621
- ion-beam laser fluorescence meas. of hyperfine struct., applic. to Xe$^+$ 77—75319
- ions, electron impact, 1 to 100 keV, bremsstrahlung emission, theory 78—22005
- isoelectronic series, X-ray line excitation 79—44453
- K and L shell, radiative and radiationless yields 79—76376
- K-emission photons, calc. of number generated by monoenergetic electrons and β-particles 80—63581
- K-series X-ray resonance fluorescence *(Russian)* 78—37587
- K-shell Auger rates, level widths and fluoresc. yields, relativistic Dirac Hartree Slater calc. 80—52957
- K-shell fluorescence yield, outer-shell effects 79—49980
- L-subshell Auger and Coster-Kronig rates and fluorescence yields, relativistic calcs. 79—81180
- laser fluorescence temperature measurements in flames 80—11892
- laser fluorescent detection of single atoms *(Russian)* 78—1108
- laser induced, effect of Gaussian intensity distrib. 78—37581
- laser radiation, interaction with free atoms, review 78—13473
- laser selective detection of ultralow concentrations of atoms 78—3407
- laser selective detection of ultralow concentrations of molecules 77—90669
- laser-atom system, electron impact excitation, laser field effects 77—10768
- laser-induced, review 78—37678
- level crossing, using laser excitation *(Rumanian)* 78—50510
- lifetime determinations via fluoresc. decay, errors using pulsed dye lasers 77—42281
- lifetime meas., cascade-free, fast-beam-spectroscopy by combined gas cell-laser excitation 77—61714
- lifetime meas., time resolved optical precision spectroscopy 77—42444
- lifetime meas. by method of correlated photons in cascade 77—42284
- lifetime meas. in atoms, mols., ions 77—30832
- lifetime measurement using pulse-delay sampling system for nanosecond transient decay analysis 80—37004
- light induced correlations in spontaneous emission 77—71773
- line shape, quantum system master eqn. appl. 79—49154
- luminescence spectrometry, pulsed and continuous wave excitation sources, signal-noise ratios 77—71381
- M-shell radiationless transitions, subshell fluoresc., Coster Kronig yields and X-ray linewidths, relativistic Dirac Hartree Slater calcs. 80—52959
- magnetic hyperfine atomic sublevels multiple anticrossings 80—27986
- metal atoms sputtered by light and heavy particles, velocity distrib. meas. by fluorescence spectroscopy 78—95626
- metal vapours, excitation energy transfer, sensitised fluoresc. 80—23358
- metals, refractory, excited state radiative life time, sputtering techniques 78—17602
- methane electron impact dissoc., optical emission from fragments 77—83750
- methanol, electron impact dissoc., optical emission from fragments 77—83750
- molecule synthesis by ion implantation, laboratory simulation of interstellar process 77—70297
- momentum transfer to atom in resonance fluoresc. 79—72271
- multilevel atom, quantum beat effect on emission rate 77—18840
- multilevel atom, resonance fluoresc. and absorpt. spectra in laser field 77—27018
- multilevel relaxing systems, multitime correl. in scatt. and fluoresc. 80—1166
- multiplet mixing collisions, effect on near resonant light scatt. 79—6908
- multiply ionised ions, fluorescence yields 77—71774
- N two-level atoms, interaction with radiation field in restricted rotating wave approx. 80—5713
- N two-level atoms, quantum theory of nonlinear optical phenomena 80—5790
- n-photon resonance phenomena, finite laser bandwidth effect 80—58230
- N-two level atoms, interaction with radiation field in restricted rotating wave approx., numerical anal. 80—5714
- Na, fluoresc. study, reson. radiation illum. 80—83314
- near resonant scatt. and collision induced *(Chinese)* 80—63582
- neutral atoms, electron interaction, free-free radiative transitions, review 78—90295
- neutron flux energy spectrum meas. from freq. change of luminesc. line 80—23272
- neutron induced X-ray atomic excitation 80—23510
- non-Markovian resonance fluorescence 79—98021
- nonlinear optical phenomena in system of colliding atoms, atomic fluoresc. 80—99788
- nonlinear resonance fluoresc., negative time pair correlation of photons *(Russian)* 79—59750
- nonmonochromatic chaotic field, double optical reson. and reson. fluoresc., AC Stark splitting 80—9547
- nonresonant intermediate state, affecting time depend. spectra after two-photon excitation 79—13664
- optical bistability, photon statistics and spectrum of transmitted light 78—46298
- optical Bloch equation, stochastic incoherences 79—68373

atomic fluorescence continued
optical nutation and free precession, laser-atomic beam reson. fluoresc. 77—18837
oscillatory superfluorescence, statistical props. 80—47938
photoionisation, fluoresc. radiation polarisation 80—87076
photon antibunching in reson. fluoresc. from two-level atom, quantum nature of light 79—85251
photon antibunching in resonance fluorescence in the presence of atomic number fluctuations 80—91764
photon antibunching in single atom fluoresc., rel. to wave packet reduction in detection process 80—52928
photon time-correlated counting, for fluoresc. decay signal analysis 78—49910
polarisation of atomic fluorescence produced by laser-induced dissociation of Na_2 80—78569
polarised excited atom, freq. depend. polarisation of emitted radiation 77—61705
quantum beats in two-photon resonance fluorescence 80—91488
quantum counter, atomic vapour, Stark tuning 80—53242
quantum interference method of distinguishing 0 and 2π rotations 80—91485
radiance expressions, steady-state, for continuum excitation 78—82680
radiation capture in cylindrical volumes of finite dimensions 78—66500
radiative interatomic collisions in bichromatic field *(Russian)* 80—14224
radiative lifetimes, polarisation propagator approach 77—18844
Raman scattered light, Hanle effect influence 80—83323
rare earth ion potential vapour laser systems, spectroscopic props. 78—66812
recoil atoms meas. by laser spectroscopy neutron detect. possibility 79—22864
resonance, canonical dressing by intense radn. fields 80—1173
resonance atomic beam fluorescence, multiat. and transit-time effects on photon-correlation meas. 78—86812
resonance fluoresc., power spectrum of scatt. light, $j=1/2$ to $j=1/2$ transition 77—10632
resonance fluorescence, collective at. effects, dipole-dipole interaction 79—54806
resonance fluorescence, collective atomic effects calcs. 77—57925
resonance fluorescence, collective effects *(Russian)* 80—91490
resonance fluorescence, high resolution technique 78—42244
resonance fluorescence, in phase freq. modulated laser fields 78—37588
resonance fluorescence, in weak radiation field with arbitrary spectral distrib. 80—23356
resonance fluorescence, intensity and phase fluctuating light 78—82683
resonance fluorescence, laser excitation time-dependent spectrum 80—37770
resonance fluorescence, multiatom effects 79—6906
resonance fluorescence, photon antibunching at. no. fluctuations effect 78—21875
resonance fluorescence, photon bunching and antibunching 79—31460
resonance fluorescence, photon correlation laser linewidth effects 80—83316
resonance fluorescence, QED calcs. 78—41995
resonance fluorescence and Rayleigh scattering at high intensities, effect of collisions 80—102478
resonance fluorescence in modulated laser field, stochastic model 78—5169
resonance fluorescence in vacuum UV, detection of low gas densities 78—54341
resonance fluorescence intensity correlation, chaotic pump radn. effect 79—98019
resonance fluorescence of N two-level atoms in a weak EM field, Heitler-Ma approach 79—93950
resonance fluorescence of two level atom, calc. of nonlinear optical susceptibility 79—98436
resonance fluorescence of two-state atom, collisional broadening 80—91484
resonance fluorescence of two-state atoms irradiated by monochromatic light, collisional broadening 80—91483
resonance fluorescence with recoil effects, quantum statistical theory 78—78660
resonance interaction of intense light with atoms, review 79—68216
resonance interactions of atomic and molecular systems driven by strong laser field, theory 80—14097
resonance ionisation spectroscopy for detection of single atoms using tunable narrow-band dye lasers 80—3422
resonance light scattering, spectral props. and photon correls. 80—91510
resonance Raman lineshapes and fluorescence in strong radiation fields 80—87074
resonance Raman scatt. modification in intense laser fields 77—27002
resonance Raman scattering and resonance fluoresc., time and freq. resolved 77—75624
resonance scattering spectrum, fine struct. in external field 77—83533
resonant fluorescence, final state perturbation effect on transition rate 78—941
resonant fluorescence props., in strong field 78—940
resonant light scattering, collisional repopulation of at. levels 79—6907
resonantly absorbing atomic vapour, fluoresc. of light signal for optical filter 79—55216
Rydberg states, Auger and radiative transition probabilities 79—6923
saturated laser-induced fluoresc., rot. redistrib. effect 79—81259
saturation of energy levels in analytical spectroscopy 78—65980
sensitised fluorescence, inverse problem 79—98020
shift of holes in emission lines due to time depend. perturbation 77—18834
sideband prediction in strong-field reson. fluoresc. 78—55139
signal parameters in optical pumping experiments *(German)* 79—59404
single atom detection, laser reson. fluoresc. method 80—26096
single atom photon burst detection in high resolution laser fluoresc. spectroscopy with atomic beam 79—72446
single localised ions, prep., cooling and fluoresc. 80—52929
small volume flames, temp., temporal meas., two line at. fluoresc. technique, Raman scatt. 80—42226
spatially extended medium, oscillating superfluoresc., leading pulse shape and delay 80—23648
spectral density of resonance fluorescence, two level atom in intense radiation fields 78—58961
spectroscopy of atoms near a wall *(Dutch)* 78—70972
spin-polarised atoms, optical emission 77—75094
spontaneous emission and absorpt. of weak wave, radn. capture effect 80—939

atomic fluorescence continued
spontaneous emission by large system of identical atoms, math. treatment 77—50396
spontaneous emission near plane mirror, quantum formalism *(French)* 77—27267
spontaneous emission spectra in strong monochromatic light field 78—25483
sputter-induced optical emission, absolute photon yields 79—45667
sputtered atoms, from metal surface with adsorbed O_2 77—28674
sputtered excited states, secondary photon emission, role of transition probability 80—102483
stimulated collision-induced fluoresc. and stimulated Raman scatt. 78—87103
stratospheric species monitor, review 77—9472
superfluorescence, delay-time statistics and inhomogeneous line broadening 80—99684
superfluorescence, oscill., quantum statistics 79—917
superfluorescence, phase-wave fluctuations 80—23652
superfluorescence, quantum beats 77—42275
superfluorescence, theory and expt. evidence 80—32658
superfluorescence beats, theory incl. quantum fluctuations and finite sample size 80—102686
superfluorescence initiation, master equation study, microscopic description 80—63577
superfluorescence initiation 79—781
superfluorescent decay, large time behaviour 78—46296
temporally limited EM radiation, time integrated spectrum *(German)* 80—37769
three level atom, reson. fluoresc. fluctuation-regression theorem 77—10629
three level atom at high photon densities, reson. fluoresc. interference effects 80—87073
three level atom in two-photon reson. with laser field 77—42273
three-level atom, reson. fluoresc. spectrum 79—54804
three-level atom reson. fluorescence, statistical props. 78—78661
three-level atom resonance fluoresc., polaris. depend. 78—50500
three-level atoms, multitime correlations in scatt. and fluoresc. *(Russian)* 79—10065
three-level system, 2-photon reson. fluoresc. 80—87077
three-level system, cooperative cascade emission 78—78659
three-level system, reson. interaction of opposite waves, relax. consts. of common level 78—50511
three-level system, two-photon transition in two pulsed fields 79—68215
three-level systems, laser fluoresc. spectroscopy 79—36578
time-resolved laser fluorescence spectroscopy for atomic and mol. excited states obs., review, book contrib. 80—9760
transverse effects in superfluorescence 80—37979
two level atom, two-photon reson. fluoresc. 79—780
two level atom system, coherently driven, cooperative fluoresc. 80—87357
two level atoms, reson. fluoresc., cooperative effects, bistability 77—10628
two particle system, spontaneous emission spectrum, collective singularities *(Russian)* 78—33466
two photon excitation, time depend. emitted light spectra, perturbation theory 80—63605
two-atom resonance fluoresc. spectrum, cooperative effects 80—78570
two-atom system, continuously pumped, radiation props., master eqn. 78—86828
two-atom system, cooperative, reson. fluoresc. spectrum. sidebands 80—43000
two-atom two-photon resonance fluorescence 79—22645
two-k-shell-vacancy systems, excited states, radiationless decay probability calcs. 78—41993
two-level atom, active, collisionally aided radiative excitation 79—54805
two-level atom, driven by reson. multimode laser, light scatt., statistical props. 80—91489
two-level atom, influence of relaxation parameters and laser fluctuations 79—72273
two-level atom, intensity effects in reson. fluoresc. 79—59661
two-level atom, multiphoton reson. fluoresc. in strong low-freq. field 78—55154
two-level atom, radiation by intense laser beam, resonance fluorescence, photon antibunching, Doppler shift 80—74146
two-level atom, radiative decay, external static perturbation effect 79—93949
two-level atom, relax. and reson. fluoresc. in phase-modulated laser light, calcs. 77—54535
two-level atom, reson. fluoresc., at. operators 80—937
two-level atom, reson. fluoresc., atomic operators 80—63579
two-level atom, reson. fluoresc., photon recoil shift 77—18839
two-level atom, reson. fluoresc. spectrum of intense amplitude modulated laser light 80—91487
two-level atom, sub-Poissonian photon statistics in resonance fluorescence 79—76650
two-level atom fluoresc. Markovian and non-Markovian behaviour 77—6718
two-level atom saturated by resonant laser beam, at. fluoresc. 77—18835
two-level atom system, reson. fuoresc., photon antibunching, propag. effect 80—9843
two-level atom system, superfluorescence and amplified spontaneous emission 79—85933
two-level atomic system, superfluoresc. fluctuations 80—23651
two-level atoms, Dicke superradiance and superluminosity, fine struct. and time evolution 77—65438
two-level atoms, inhomogeneously broadened, superfluoresc. and amplified spontaneous emission 80—106499
two-level atoms, reson. fluoresc., finite bandwidth excitation effects calcs. 77—68008
two-level atoms assembly, chirping in emitted light 78—37598
two-level resonance fluorescence, in at. beam, anal. calcs. 77—14386
two-level system, reson. fluoresc., laser temporal fluctuations calcs. 77—10630
two-level system, reson. fluoresc., laser temporal fluctuations calcs. 77—10631
two-level system, reson. fluoresc. theory, intensity correl. functions, time factorisation 77—50401
upper atmosphere, in situ reson. fluoresc. meas. 79—53600
vanishing electric dipole transition moment, appl. to fluoresc. 79—59397
Volterra cycles and cooperative fluoresc. crit. point 79—3667
weak polarisation meas. using alternating magnetic field 78—1105
Weisskopf-Heitler effect, intrinsic laser linewidth contrib. 78—70782

atomic fluorescence continued
- Zeeman degeneracies effect on reson. fluoresc. *(French)* 77—61703
- 0 I, 63 μm emission and quenching cross section in thermosphere and ionosphere 79—16732
- Ag electron excited Lα emission spectra 80—102481
- Ag, K-fluorescence yield determ. from K-Auger electron emission rates 80—95569
- Ag, matrix isolated, fluoresc. spectra. excimeric bond effects 78—50498
- Al II-VII, radiative lifetimes, beam-foil spectra 79—49986
- Al, lowest S-state lifetime meas. 77—65436
- Ar, electron impact excitation, continuous spectrum radiation mechanism 79—3395
- Ar, electron pulse radiolysis, 2p levels formation and decay kinetics 78—31665
- Ar, fluoresc. following slow electron impact, 380-710 nm 79—22646
- Ar fluorescent X-rays from sunlit Earth atmosphere during solar flares 77—13142
- Ar glow discharge, line radiation of plasma in early afterglow 80—38745
- Ar I, II, fission fragment excitation of optical radiation, quenching by UF_6 77—23665
- Ar II, lifetime meas. using photon-photon delayed coincidence 77—14389
- Ar jet, supersonic, electron beam-excited, continuous VUV emission spectrum origins 79—6964
- Ar, laser discharge, spontaneous emission, at. line shapes, interferometric obs. 77—30816
- Ar, metastable ion beam, collinear laser spectroscopy, isotope shift, fluoresc. detect. 80—37771
- Ar, metastable state production, microwave and DC discharges in flowing afterglows 78—46463
- Ar, plasma column of hollow cathode arc, collisional model of ion system 80—38749
- Ar, polarisation of reson. lines, 104.8 and 106.7 nm, electron impact excitation 77—83739
- Ar^+, metastable, electron impact cross section, laser fluoresc. 77—3465
- Ar+Ar low energy collisions, K X-ray excitation, impact parameter depend. 80—23539
- Ar+Kr, $(4p^5 5p)$ and $(4p^5 5p')$ states, radiative lifetimes and two-body collisional deactivation rate consts. 80—95572
- $Ar+N_2(SF_6)$, proton excited, time resolved VUV, UV and visible emission 77—14547
- $Ar^+ +C$, beam-foil spectra, Ar^+ ion orientation, ang. variation 78—86944
- Ar*, electron excited in $Ar-CO_2$ mixture, transfer reaction kinetic study 80—63824
- $Ar^*(3p^5 4p)_i+Ar(^1S_0)$, collisional population transfer rate coeffs., 300K 79—10177
- Ar*(4p),(5p) states, lifetimes and two-body rate consts. meas. 78—63058
- As, $(4^4S_{3/2})$ state, kinetic obs. using time resolved reson. fluoresc. 78—94211
- Au, X-ray production cross sections for protons, fluoresc. obs. 80—102476
- B, quenching of reson. radn. by Xe and Kr 77—30820
- Ba, $(5d^3D_J)$state, quenching obs. 80—52926
- Ba, fluoresc. freq. distrib. induced by monochromatic laser beam 78—942
- Ba II $5D_{3/2}$ metastable state, decay rate using ion storage technique 80—18826
- Ba ions, resonance fluorescence and optical sideband cooling of electrodynamically contained ions 79—3422
- Ba, radiative decay of autoionisation states *(Ukrainian)* 78—82682
- Ba, reson. fluoresc., photon burst detection 78—42244
- Ba^+ confined in RF quadrupole trap, optical detection 77—75096
- Ba^+, electrodynamically trapped, saturation dip in fluoresc. 77—65437
- Ba^+, excited state lifetimes, fluoresc. decay meas. 77—79574
- Ba^+ ions, hyperfine struct. reson. determ. from fluoresc. *(French)* 77—432
- Ba^+ ions confined in cylindrical RF trap, lifetime meas., laser probing 80—95573
- Ba^+, laser-induced resonances, high-resolution expt. 77—6959
- Ba+Tl, dipole-quadrupole radiative collisional fluoresc. 80—83315
- Ba+Tl, radiative collisional fluoresc. obs. from thermally excited atoms 80—102480
- Ba^++inert gas atom collision, polarisation of emitted radiation, quasimol. interf. effect *(Russian)* 77—46633
- BaI resonance transitions, hyperfine struct. and isotope shifts, atomic beam laser spectroscopy 80—102141
- $Ba^+(^2P_{3/2})$, coherently Penning ionis.-excited, with $He(2^3S_1)$, Hanle effect 80—5520
- $^{135}Ba^+$, $^{137}Ba^+$, $6p^2P_{3/2}$ level hyperfine struct., Lamb-dip spectroscopy 77—83530
- $^{135}Ba^+[^{137}Ba^+]$ hyperfine structure resonance detection method *(French)* 77—75095
- Be, inner-shell photoionis., fluoresc. yield 77—57945
- Bi, electron impact ionisation, characteristic X-radiation ang. distrib. obs. 80—1069
- Bi, excited in discharge region, new light source of forbidden lines 78—90112
- ^{209}Bi I, tunable CW dye laser spectroscopy, energy levels, lifetimes and hyperfine struct. 79—6905
- Br, in Ar^*+Br_2 lamp, Br atom conc. meas. by line absorpt. 78—46466
- Br, K-fluorescence yield determ. using MWPC 79—18140
- $Br_2+H(d)\rightarrow HBr(DBr)+Br$, reactive cross-section, collision energy depend. obs. 79—11784
- Br^*+N_2O, electronic-vibr. energy transfer, time-resolved fluoresc. obs. 79—89753
- C I, UV fluoresc. from photodissoc. of CO_2 79—13776
- Ca, direct meas. of excited state lifetimes 77—65435
- Ca, electron impact, $3p^6$ subshell excitation, VUV spectra *(Russian)* 78—90117
- Ca, in Ar matrix, multiphonon relax. processes, emission spectra 78—37583
- Ca, intercombination line, at. beam saturation and reson. fluoresc. spectroscopy 79—36580
- Ca, laser saturation broadening in flames, fluoresc. excitation profile obs. 80—95568
- Ca, radiative decay of autoionisation states *(Ukrainian)* 78—82682
- Ca, resonance fluoresc. detection with intracavity at. beam laser spectrometer 77—19107
- Ca resonance line, quenching cross section of Ar atoms 77—19021
- Ca, stable and radioisotopes, hfs, isotope shifts, dye laser saturation spectroscopy, beam expt. 80—58169

atomic fluorescence continued
- Ca, weak intercombination line, Lamb-dips obs. by resonance fluorescence monitoring 79—3392
- Ca+Ca(Mg)(inert gas), metastable ^{3}P-state, quenching reactions, fluoresc. meas. 80—102477
- Ca+Sr, laser-induced collisions, large cross sections meas. 79—64075
- Ca+Sr, laser-induced inelastic collision, fluoresc. obs. 77—54603
- Ca^++inert gas atom collision, polarisation of emitted radiation, quasimol. interf. effect *(Russian)* 77—46633
- $Ca^+(^2P_{3/2})$, coherently Penning ionis.-excited, with $He(2^3S_1)$, Hanle effect 80—5520
- ^{45}Ca, nuclear charge radius, spin, moments, by laserspectroscopy 80—18187
- Cd, 6^3P_1 level, relax. of alignment and population 78—70795
- Cd, P_1 state resonance fluoresc. in rot. mag. field 77—42271
- Cd, slow electron excitation 80—938
- Cd^+, polarised emission of light following photoionis, Cooper-Zare model 79—81179
- Cd-Cs, vapour, sensitised fluoresc. anisotropy transfer 77—57924
- Cd+Cs, excitation energy transfer in sensitized fluoresc. 79—98210
- $Cd+K(+N_2)$, optical excitation, rate consts., collisional energy transfer kinetics 80—32801
- CdI_2, vapour, excited by photodissociation, fluoresc. yields 78—55138
- $Cd(^1P_1)$ excited state quenching by mols., cross sections, chem., phys. exit channels 79—779
- $Cd(^3P_1)$ radiation imprisonment lifetime, inert gas effect, phase-shift method 80—58213
- $Cd(^1P_1)+N_2$(alkanes), laser excitation, absolute quenching cross sections and branching ratios 79—49979
- ^{113}Cd, two-level system, absorption spectrum, intense two-photon excitation obs. *(Russian)* 78—33465
- $Cd(5^3P_{0,1})$+methane $(H_2)(D_2)(N_2)$, absolute quenching cross sections 80—5604
- $Cd(5^3P_1)$+POPOP, vap., electronic energy transfer, laser appl. 77—30980
- Ce, F states, radiative lifetime and g-factor determ. 79—41138
- Cl, form. from HCl dissoc. excitation in afterflow, light emission 78—90115
- Cl, K-fluorescence yield determ. using MWPC 79—18140
- Cl metastable ion beam, collinear laser spectroscopy, isotope shift, fluoresc. detect. 80—37771
- $Cl+O_3(H_2O_2)$(methane), reaction kinetics, temp. depend., reson. fluoresc. obs. 77—4903
- $ClO+O\rightarrow Cl+O_2$, reaction kinetics, 220 to 426K, at. fluoresc. obs. 77—21380
- Co I, radiative lifetimes of atomic excited states, delayed coincidence technique 77—27030
- Cs, 8S hyperfine splitting, two-photon transition and fluoresc. meas. 78—37585
- Cs, 8S level lifetime meas., cooperative effects in EM cascade 77—30818
- Cs atom, direct meas. of 7P doublet state lifetimes by pulsed dye laser 79—786
- Cs, atom single pulse superfluoresc. 77—79573
- Cs cell, laser beam excitation, multipass, optical pumping and weak neutral current parity violation 80—58207
- Cs, collisional and radiative relax., eigenvalue problem 78—29827
- Cs, collisions between excited atoms, highly excited states excitation 78—17771
- Cs, emission meas. in wing of self-broadened reson. line 77—50400
- Cs, fast atomic beams, collinear laser spectroscopy 78—37078
- Cs, fluoresc., far wings profile of self-broadened reson. lines 79—76388
- Cs, HFS of optically inaccesible excited states 78—37582
- Cs I, radiative lifetime of 8S, 9S and 7D levels 77—34588
- Cs I, time-resolved fluoresc., lifetimes 77—58068
- Cs II, hyperfine struct., beam laser technique meas. 79—93951
- Cs, in He-Ne 632.8 nm radiation-induced disintegration of Cs_2 79—76474
- Cs, optical reson. line electron impact excitation cross sections, polaris. 78—55244
- Cs, optically dense vapours excited by resonance lines, distribution of excited atoms *(Russian)* 77—23458
- Cs, resonant 6P state, quenching by CO_2 mols. in $He-CO_2-Cs$ discharge 80—43860
- Cs, superfluorescence *(Dutch)* 78—70780
- Cs, superfluorescence of vapour, effective initial tipping angle 79—22923
- Cs, superfluorescence quantum beats 77—42275
- Cs-He, new absorption/emission bands perturbed Cs transitions assignment, pot. energy curves 78—66486
- Cs+inert gas, three body interaction, fluoresc. spectra principal series lines and secondary satellites 80—83313
- Cs+X, $(X=N_2, H_2$, He, Ar, Xe), collisional relax. and population quenching of Cs 78—25467
- ^{133}Cs, first excited D-level, hyperfine struct. meas. by cascade, fluoresc. spectrosc. 80—69101
- ^{133}Cs, Rydberg S and D states, hyperfine struct., lifetimes, depopulation cross sections 77—42270
- ^{133}Cs, time-resolved fluoresc. spectra, collisional perturbation of Rydberg states 77—83529
- $Cs(6^2P_{3/2})$+He(Ne)(Ar)(Xe), collisional depolaris., nucl. spin depend., by Zeeman scanning 77—19012
- Cu laser lines, broadening, induced emission cross-sections 79—26928
- Cu vapour pulsed laser, spectral comp. of superradiance, stimulated and spontaneous radiation 80—102713
- Cu^{18+}, $3^2P_{1/2}$ level decay, time-resolved obs., intensity modulations 77—61704
- D, fluoresc., Balmer series, from mol. photodissoc. 77—27020
- Dy I, hyperfine struct. and isotope shift, fluoresc. meas. on at. beam 78—9109
- Er^{3+}, luminesc. sensitisation by Yb^{3+}, in liq., efficiency *(Russian)* 78—90116
- Eu, excitation transfer cross section, luminesc. meas. *(Russian)* 77—61706
- Eu, VUV emission spectra, 5p electron excitation by electron impact 77—68007
- Eu, visible superfluorescence cooperative reson. Stokes radiation 80—5500
- Eu^+ metastable states in discharge plasma, anomalously high speed deexcitation, modulation of induced radiation obs. 80—44014
- Eu^{2+} in aqueous solution, multiphoton excitation and emission 78—94222

atomic fluorescence continued
$Eu^{3+} \rightarrow Nd^{3+}(Ho^{3+})$ radiationless energy trnasfer in $EuCl_3.6H_2O$-$NdCl_3.6H_2O(HoCl_3.6H_2O)$ DMSO soln. 80—5499
Eu+Sr, absorptive collisional energy transfer, laser induced excitation spectra 80—63584
F^{n+}, lifetimes and fluoresc. yields calcs. 79—45668
F^{-}+atom (Z=10-57), K-shell ionisation, X-ray prod. in transition region, collision symmetry effects 80—43163
F^{q+}+Ti(V)(Cr)(Fe)(Co), target and projectile cross-sections, X-ray prod. yields 79—81269
Fe II permitted emission, excitation mechanism in Seyfert 1 galaxies and QSOs 79—21412
Fe in solar atmosphere, $K\alpha$ fluoresc. due to flares 80—17569
Fe, K_{α} X-ray line, natural width at energy threshold meas. 78—41992
^{57}Fe metastable states, hyperfine struct. meas. by laser RF double-resonance 80—58404
Ga, isotope shift and HFS, isotope effects, UV spectra obs. 80—42973
Ga, lowest S-state lifetime meas. 77—65436
Ga, reson. states lifetimes, electron-at. crossed beams expt. 77—68013
Gd, populations of metastable levels during electron beam evap. 77—57926
^{155}Gd $L_{2,3}$ subshell X-ray fluorescence and Coster-Kronig yields from ^{155}Eu decay 80—69102
Ge, K-fluorescence yield meas. 77—3300
H (2s) elec. field-quenched radiation polaris., Bethe-Lamb theory justification 78—17603
H atoms reflected from Ni surface, following H^{+} beam impact at grazing incidence 79—63951
H, collisional energy level transition rate, in RF plasma, fluoresc. meas. 77—38726
H detection by reson. fluoresc., coherent tunable VUV generation near Ly-β transition 80—99798
H, diffusion coeff., in H_2, luminesc. intensity meas. 80—103098
H, electron impact, transitions between excited states 77—58168
H, electron impact excitation, electron-photon ang. correl., for H(2p) 79—31699
H, excited atom Lyman-α and Balmer fluoresc. from H_2 photodissoc. 79—86018
H, excited in h.f. discharge, emission spectrum *(French)* 77—433
H, fluorescence, Balmer series, from H_2 photodissoc. 77—27020
H Lyα fluoresc. obs. in $H_2(^1\Pi_u{}^{\pm})$ predissoc. 80—32784
H, s-p coherence quantum beats, following H^{+} electron capture in gas 79—89773
H, sublevel excitation cross sections following mol. dissoc., Stark effect determ. 77—14593
H^{-}, fluoresc. in γ- and UV-irrad. solvent matrices at 77K 78—70779
H^{+}, ion-surface collision with Mo, optical radiation emission 78—95644
H-D discharge, RF, meas. of excitation transfer rate by laser fluoresc. 80—9542
H-like, average spectral lifetime, asymptotic expression 79—45671
H-like atoms, E1-M1 interference in radiative decay, $2S_{1/2}$ metastable state, effect on Lamb shift expts. 78—41994
H-like ions, fluoresc. polarisation of Stark quenched spin-polarised beam 78—66501
H-like ions, reson. doublet component intensities in optically thin laser plasma *(Russian)* 78—38458
$H+Cl_2 \rightarrow HCl+Cl$, rate consts. meas., Lyman-α fluoresc. technique 77—16780
H+He(Ar), collisional coherent excitation, meas. of Lyman α-photons 80—99552
$H+NO_2 \rightarrow NO+OH$ and $H+O_3 \rightarrow O_2+OH$ by atomic resonance fluorescence 77—48618
$H+NO_2 \rightarrow OH+NO$, $H+NOCl \rightarrow HCl+NO$, rate meas. by Lyman-$\alpha$ fluoresc. 77—21353
$H+O_2(N_2)$, collisional coherent excitation, meas. of Lyman α-photons 80—99552
$H+O_3 \rightarrow HO_2+O(^3P)$, reson. fluoresc. obs. 79—70317
$H+PH_3$, abstraction rate consts., 209-495K, time-resolved fluoresc. 77—16807
H_2+D(O)(Cl)(Br), relax. and chem. reaction, time resolved IR fluoresc. and mass spectrometry obs. 80—69177
H_{α}, H_{β}, Balmer line intensity ratios following mol. dissoc. of H_2 and benzene 77—10778
HCl+D(O)(Cl)(Br), relax. and chem. reaction, time resolved IR fluoresc. and mass spectrometry obs. 80—69177
H* translational energy distrib., in HCl electron impact dissoc., optical emission obs. 80—14238
H(2s)/H(2p) branching ratio, H_2 photodissoc. near threshold 78—21983
H(2s)+He $(Ne)(Ar)(Kr)(H_2)(N_2)$, 5-25 keV, H(n=3) excitation, Balmer α emission obs. 80—53113
H(3p), excitation in electron impact dissoc. of methane Lyman β and Balmer α obs. 78—46450
He, 3^3P level, spontaneous decay probability, expt. and theoretical values 78—50501
He, $(2p^2)^3P$ doubly excited state, electron impact excitation XUV emission 79—86071
He and He^{+}, 3^3P and 4^2F levels excitation with electron beams, radiation decay obs. 80—43188
He, collisional excitation transfer for $3^{1,3}P$ and D states 80—106387
He, electron impact, induced transitions between high Rydberg levels 78—21877
He, electron impact excitation, photon emission, ang. 77—14584
He, electron impact excitation, near threshold, UV emitting levels obs. 78—5170
He, electron impact fluoresc., polarisation of visible and UV lines 77—88568
He, electron impact fluorescence, polarisation of 5876 line 78—82848
He, excitation in n=4 levels after laser pumping 77—3324
He, excited S, D and F state radiative lifetimes, electron impact method 78—94325
He glow discharge, low press., excitation transfer and quenching of n=3 excited states 80—38743
He I, excited states decay, lifetime meas., lab. mag. field effects 77—10640
He I, heavy ion impact excitation, orientation by anisotropic relax. of $4\,^1D$ level *(French)* 77—61844
He I glow discharge, low-press., quenching of singlet states by N_2 80—49030
He I singlet transitions, polarisation meas. following beam-filted foil excitation 79—13665

atomic fluorescence continued
He, level crossing signals in inhomogeneous mag. field *(German)* 77—27037
He, optical escape factor, 3^1P-1^1S transition, laser perturbation method 78—37586
He, pulsed microwave discharge, vac. UV emission characts. 77—35408
He^{+}, 195 keV, light emission after focusing and channelling interactions with Ni (101) 78—35240
He^{+}, channelled in Au thin single cryst., coherent electronic excitation 78—22778
He^{+}, fine struct. obs. by beam-gas spectroscopy, level crossing resonances 80—9719
He-like atoms, n=2 states radiative transition rates, oscill. strengths, RRPA extension 77—34584
$He+He^{+}(Ne)$, tensor polarisabilities of 1snd ^1D level, fluoresc. depolarisation obs. 80—69099
$He+Ne^{+}$, impact excitation, cascade-fluorescence spectroscopy, level-crossing techniques 80—23357
$He^{+}+C$, beam-foil spectra, He atom orientation, ang. variation 78—86944
He^{+}+Mg(Zn), inelastic collisions, 2-800 eV, excited state form. 78—94312
$He^{+}+N_2$, $\lesssim$0.1 eV, charge exchange, UV and visible luminesc. spectra 77—83722
$He^{+}+N_2$, collisional excitation processes, visible emission, cross-sections 80—99571
He^{+}+Xe, internal energy distrib. at 100 eV 80—99564
He^{+}+Xe charge transfer, optical emission cross sections 77—61853
$He_2{}^{+}$+Mg(Zn), inelastic collisions, 2-800 eV, excited state form. 78—94312
^3He, hyperfine-induced singlet-triplet mixing obs. 80—106399
$He(3^3S)$ decay rates in high-press. afterglow 79—41898
Hg, $^3P_0$ quenching rates, laser fluoresc. meas. 77—46522
Hg I, II, electron impact excitation, absolute emission cross sections, 284.7 and 479.7 nm 77—19086
Hg ions, relaxation two constants meas. of optically pumped stored Hg ions 80—106287
Hg, spontaneous emission, fluctuation spectroscopy 77—434
Hg, two photon excitation, time resolved spectroscopy 80—87075
Hg, two-photon excitation by photodissoc. of Hg halide 78—90114
Hg-Ar(Kr)(Xe) mixtures, prebreakdown discharges, discharge current depend. on electron mobility 79—77433
Hg-Cd, sensitised fluoresc., anomalous Hanle effect 79—81186
Hg+Cd, quantum beats under transfer of orientation 79—98206
Hg+He, laser excitation of Hg $6s6d6^3D_1$ level, transition probabilities and collisional excitation transfer 78—55146
Hg+He(Xe), collisionally induced coherence, orientation and alignment, transfer among 6s6d levels 78—74747
Hg+Hg*, combination into ungerade dimer states 80—55633
$Hg+N_2$, inelastic collision, 6^3D_1 population transfer to other 6s6d Hg levels, fluoresc. obs. 78—78791
Hg+Tl, excitation energy transfer, excitation rate consts. 80—37772
Hg+Tl, Tl sensitised fluorescence 78—70778
Hg+Tl vap., sensitised fluoresc. 77—88423
Hg+Zn(Cd), sensitized fluoresc., orientation and alignment transfers *(French)* 79—13808
$HgI_2(Br_2)$, vapour, excited by photodissociation, fluoresc. yields 78—55138
$Hg(^3P_0)+N_2$ decay following pulsed laser excitation 77—30817
$^{199}Hg^{+}$ isolated ions, mag. hyperfine spectrum 78—29760
$Hg^{*}+NH_3$, UV emission at low press., pulsed excitation, relax. meas. 77—79570
$Hg(6^3P_1)+Hg(6^1S_0)$, collisional excitation transfer in high mag. fields, fluoresc. obs. 80—9689
$Hg(6^3P_2)+Cd(5^1S_0)$, spectral width of $Cd(5^3P_1)$ line *(French)* 77—50397
$H(n=3)+H_2O$, radiation quenching in pulse radiolytically excited water vap. 79—89738
$Ho+H^{+}(^3He^{+})$, X-ray intensity ratios, projectile energy depend. 80—23535
^{155}Ho $L_{2,3}$ subshell X-ray fluorescence and Coster-Kronig yields from ^{165}Er decay 80—69102
I, collision-induced $5^2P_{1/2}$-$5^2P_{3/2}$ radiative transition 79—31461
I I,II, radiative lifetime meas., rel. to I and He-I^{+} laser transitions 79—54810
I, produced in UV photodissoc. of alkyliodides, time-resolved obs. of $I(^2P_{1/2})$ reactions 80—11940
I, reson. UV fluoresc. and photoionis. obs., in nonlinear I_2 photodissoc. 78—37692
I+methane $^{-}d_0(^{-}d_3),(^{-}d_4)$, excited atoms, quenching, isotope effects, time resolved reson. fluoresc. 80—32656
$I^2P_{1/2} \rightarrow {}^2P_{3/2}$, collision induced emission (Ar)(Xe), dipole transition moment by perturbation theory 77—83528
$I(^2P_{1/2})$+n-iodopropane (iodoethane), quenching rate coeff., in UV photolysis of n-iodopropane (iodoethane) 79—11799
$I^{*}+H_2O(D_2O)(HDO)$, $5^2P_{1/2}$ electronic to vibr. energy transfer, quenching and time resolved IR fluoresc. 79—3537
$I(5^2P_{1/2})$, time-resolved reson. fluoresc., quenching rate coeffs. 78—25466
$I(5^2P_{1/2})$+benzene-d_0(-d_6), fluoresc. quenching, spin-orbit interaction, isotope effect obs. 78—62763
$I(5^2P_{1/2})$+HCl(HBr)(NO), electronic-vibrational energy transfer, fluoresc. obs. 78—66579
$I(5p^5(^2P_{1/2}))$, time-resolved kinetics, mean radiative lifetime, radiation trapping, HFS 78—5171
In, isotope shift and HFS, isotope effects, UV spectra obs. 80—42973
In, K-fluorescence yield determ. from K-Auger electron emission rates 80—95569
In, laser saturation broadening in flames, fluoresc. excitation profile obs. 80—95568
In, Lα X-ray fluoresc. spectra, natural linewidth meas. 79—85934
In, lowest S-state lifetime meas. 77—65436
InI, vapour, excited by photodissociation, fluoresc. yields 78—55138
^{215}In, $8P^2P_{3/2,1/2}$, HFS and lifetimes, fluoresc. decay and quantum heats, beam 80—32657
K, $4^2P_{1/2}$ resonance substate, disorientation cross-section, Zeeman scanning obs. 80—42988
K, absolute optical electron-impact excitation functions 80—18933
K, emission and absorpt. spectra in inert gas matrix 79—54800
K, optical reson. line electron impact excitation cross sections, polaris 78—55244
K, Rydberg states, two photon absorption, decay fluoresc. 77—71787

atomic fluorescence continued
K, s and d state radiative lifetimes, time and wavelength resolved fluoresc. spectra 80—14104
K, Zeeman shift of Rydberg states, fluoresc. detect. of two-photon absorpt. 77—23461
K$^+$, dielectronic recomb., in crossed beams, UV emission obs. *(Russian)* 79—10212
K+He, 93 eV, excitation of K atom, photon-scatt.-atom coincidence study 78—82829
K+He(Ne)(Ar), 0.7-80 keV, K excitation, reson.-line emission and polaris. 80—18911
K+Hg, electronic excitation, integral cross-section, 50-1500 eV 78—62888
K$^+$+H$_2$, dissociative collision, H$_\alpha$, H$_\beta$ emission prod. 77—75093
^{39}K, first excited D-level, hyperfine struct. meas. by cascade, fluoresc. spectrosc. 80—69101
Kr, $^3P_1$ state, reson. fluoresc., Zeeman beats, time-resolved VUV spectra using synchrotron radiation 78—33454
Kr, 6p levels, two-photon excitation, time resolved fluoresc., quenching, lifetimes and photoionisation cross section 80—78587
Kr, electron pulse radiolysis, 2p levels formation and decay kinetics 78—31665
Kr, fluoresc. lifetimes, time resolved VUV spectra 78—17601
Kr II, excited states lifetime meas., photon-photon delayed coincidence technique 77—68011
Kr, L-shell fluorescence yield 80—47937
Kr plasma, of positive column, at. alignment, radiative lifetimes, collision cross sections 79—4203
Kr VIII beam-foil decay curves for resonance transitions 78—74755
Kr, VUV fluoresc. under monochromatic excitation 78—9237
Kr+Ar*, 123.6 nm emission excitation of Kr by metastable Ar, press. depend. 78—5331
Kr+Ti, 200 MeV, collision, quasimol. bremsstrahlung, semiclassical calcs. 77—88530
La II, $y^3F_{4,3,2}^0$ levels, lifetime meas. using beam-laser method 77—30827
^{139}La, hyperfine struct. of excited odd-parity levels, laser at. beam fluoresc. obs. 79—13663
^{139}La, laser at. beam spectrum, HFS resolution at 5930.6 Å 78—9110
Li, 2P level lifetime, at. beam-laser expt. *(Russian)* 77—79575
Li, $3d^2D$ level, lifetime meas., fast-beam spectroscopy 77—61714
Li, autoionisation states, config. decays and excitation energies 78—13475
Li core excited even parity ^2P states, fluoresc. 80—69100
Li, electron impact excited high-l Rydberg states 77—65535
Li, excited-state lifetime meas. using disc-shaped heat-pipe oven 80—52941
Li, isotope shift in 2^2P states and spatially resolved laser-induced fluoresc. 80—14103
Li, lifetime measurement of D-states, by time resolved resonance fluorescence 79—63965
Li, photoexcitation of high levels, reson. radiation at 670.7 nm 79—783
Li, S and D state electron impact excitation, emission line intensity obs. 80—23560
Li, scan of $2^2S \rightarrow 6^2P$ transition using freq. summed UV radiation 79—55182
Li, seeded flames, excitation, laser radiation absorpt., sound vel., opto-acoustic effects obs. 80—43345
Li, sputtered from Li and LiF, kinetic energies 80—66373
Li$^+$, 2^3S_1 metastable state radiative lifetime, fluoresc. meas. 80—42999
Li+H$^+$(H$_2^+$)(He$^+$)(He^{2+})(He$_2^+$), excited state form. obs. 80—9686
Li+inert gas, fluoresc. reson. line broadening 77—6734
Li+inert gas atom, low energy, excitation, emission cross sections and polarisation fractions 80—37867
Li$^+$+H$_2$, dissociative collision, H$_\alpha$, H$_\beta$ emission prod. 77—75093
Li(^{2}P), obs. in laser-excited collision-induced Li$_2$(B$^1\Pi_u$) dissoc. 79—79232
^{A}Li$^+$, A=6,7, $2^3{}_1$-2^3P, dye laser saturation spectroscopy 80—18821
Li$^+$(2^3P), electron impact excitation, absolute 548.5 nm emission cross-section 79—10209
Li($2^2P_{1/2,3/2}$), laser induced flame chemistry, saturated mode fluoresc. meas. 80—89491
Mg, direct meas. of excited state lifetimes 77—65435
Mg, excited in discharge region, new light source of forbidden lines 78—90112
Mg, hollow cathode discharge, excitation mechanisms of triplet state atoms and decay obs. 80—44015
Mg I, fluoresc. lines polarisation and mag. depolarisation *(German)* 77—6719
Mg II 2934 Å emission in QSOs, excitation mechanisms involving fluorescence 78—41073
Mg, radiative lifetimes on excitation by electron impact *(Russian)* 77—50408
Mg XI-S XV ions, 2l3l-1s3l and 2l2l-1s2l radiative transitions and non-radiative decay probabilities 78—70781
Mg$^+$+He,(Ne)(Ar), 3^2P differential excitation, alignment and orientation 79—86053
Mn I, collisional and radiative excited, lifetime meas. 80—91501
Mo^{32+}, dielectronic recomb. rate coeffs. in plasma 80—43853
Mo^{38+}, dielectronic recomb. rate coeffs. in plasma 80—43852
N, ($2^4S_{3/2}$), kinetic study by time resolved atomic resonance fluorescence 80—95557
N, high Rydberg states, radiative decay rates, TOF meas 78—46302
N I (^{2}D) in auroral zone, prod. 79—21090
N+NO, ^{4}(S) state reaction rate, discharge flow and photolysis reson. fluoresc. method 79—5142
N(^{4}S)+O$_3$, rate const. at 298K, upper limit determ. 79—74360
Na, $3^2S_{1/2}$-$3^2P_{3/2}$, spectral distrib. and collisional depolarisation of laser light, D$_2$-fluorescence 80—58209
Na, 3^2S-4^2D two-photon transitions, isolated optical Ramsey fringes 77—83559
Na, anomalous laser fluoresc. scatt. in shock tube 77—10627
Na arc plasma, dense, high-temp., near-reson. light scatt., collision-induced fluoresc. 77—1019
Na, atom, excited p-states radiative lifetimes, laser cascade fluoresc. meas. 77—27022
Na atomic beam, Autler-Townes effect in double optical resonance 78—66499
Na, atomic states highly excited by laser radiation, Stark effect, fluoresc. monitoring 79—13669
Na beam, associative ionisation, resonance fluoresence 79—98215

atomic fluorescence continued
Na beam, laser beam irrad., reson. fluoresc. intensity, Bloch model calcs. 80—58206
Na beam, velocity spectrum determ. from Doppler shifted fluoresc. meas. 77 3210
Na, CW laser excitation, appl. to flame diagnostics 77—79571
Na, D line broadening by inert gases, fluoresc. obs. 80—32663
Na, D$_2$ line, fluorescence freq. distrib. induced by monochromatic laser beam 78—942
Na D$_2$ line, resonance fluorescence, photon antibunching, quantisation of light 78—66791
Na, D-doublet in H$_2$-O$_2$-Ar flame, excitation profiles 77—88436
Na, D-line saturation, under high power laser illumination 80—32653
Na, energy transfer with 3P-excited atom high density, mol. form., fluoresc. 77—88422
Na, energy transfer with 3P-excited atoms, fluoresc. spectrum 78—66498
Na, fast atomic beams, collinear laser spectroscopy 78—37078
Na, flame absorption and fluorescence, laser saturation broadening 78—88661
Na, fluoresc. in flame, saturation curves with pulsed tunable dye laser 79—36579
Na free atom cooling in resonant laser field at scanning freq. *(Russian)* 79—72272
Na, from laser photodissoc. of Na$_2$ 77—18838
Na, highly excited, f-state fine struct., microwave reson. obs. 77—83535
Na, hyperfine interaction in 4D$_{3/2}$ and 4D$_{5/2}$ levels 78—37616
Na, hyperfine splitting, fluoresc. after two-photon excitation 79—18307
Na I $3^2P_{3/2}$ meas. beyond natural linewidth by beam laser quantum beats 77—50399
Na, in acetylene flame, conc. determ. by saturation spectroscopy 79—29425
Na in flames, laser-induced fluoresc. temp. meas. 80—11893
Na, in He buffer gas, collisional freq. redistrib. of scatt. laser light 77—30815
Na, laser excited fluoresc., saturation power, calc. and obs. 77—42276
Na, laser saturation broadening in flames, fluoresc. excitation profile obs. 80—95568
Na, muonic, $2s^1/_2$ level decay channel concurrence, neutral current effects observation *(Russian)* 80—83526
Na, near-resonant Rayleigh scattering and atomic flame fluorescence spectroscopy 79—92033
Na, nonabsorption hyperfine resonances in dye laser irrad. vapour 79—93941
Na, optically excited vapour, evanescent light emission near interface, transient polarisation 78—25468
Na, photon emissions, two-time correls. 79—22647
Na, Raman transients obs. in Doppler free two-photon excitation 77—61728
Na, reson. fluoresc., photon burst detection 78—42244
Na, reson. fluoresc. spectrum in intense monochromatic field 77—34585
Na, reson. line, laser excitation, combustion Rayleigh scatt., at. flame fluoresc. spectroscopy 80—42972
Na, resonance fluorescence, photon antibunching obs. 77—83534
Na resonance line fluoresc. profile, perturbed by He 79—36723
Na seeded flames, excitation, laser radiation absorpt., sound vel., opto-acoustic effects obs. 80—43345
Na, self-collision-induced reson. fluoresc. 77—10616
Na, single atoms, fluoresc. selective detect. by laser radiation 80—83312
Na, spectra, emission and absorpt., inert gas matrix 78—90106
Na, sputtered from NaCl, kinetic energies 80—66373
Na, strongly driven two-level atoms, reson. fluoresc. and absorpt. spectra meas. 79—36581
Na, two-photon excitation in flame, saturation broadening, fluoresc. obs., broad-band excitation 78—74625
Na vapour, transient optical nutations in D$_2$ line 78—66507
Na vapour seeded He hypersonic flow, velocity profile visualisation 78—59530
Na, wing profile of doublet lines, in flames at 1 atm. 79—22660
Na+Ar$\rightarrow$NaAr, quasimol. form., laser spectroscopic obs. 77—57920
Na+He(Ne)(Ar), 3^2P differential excitation, mechanism 79—86052
Na+Kr(Xe), excimer bands, multiperturber interactions 78—66497
Na+Kr(Xe), reson. line broadening, press. depend. 78—66596
Na+N$_2$, collisional deactivation of Na excited states, time resolved fluoresc. 78—42197
Na+N$_2$, higher Na s and manifold states deactivation cross sections 79—10176
Na+N$_2$, Na excitation in non-equilib. conditions behind shock wave 77—23539
Na+Na, excited atoms, electronic energy transfer, doublets obs. 77—3448
Na+Ne(Ar)(Kr)(Xe)(N$_2$)(CO$_2$), fine struct. changing collisions, vel. depend. 79—22803
Na$_2$, laser excited, atomic and molecular fluorescence with long radiative decay times 80—27976
NaK, C$^1\Pi$ state, spectroscopic consts., vibr.-rot. struct., K fluoresc. obs. 77—18901
^{20}Na, D-line absorption, isotope shift determ. *(French)* 78—42008
Na*(3p)+Na$_2$, collisional and radiative processes, fluoresc. decay obs. 78—66638
Na(3^2P), in O$_2$-H$_2$-Ar flame, atm. press., lifetime obs. 79—39149
Na($3^2P_{1/2,3/2}$), laser induced flame chemistry, saturated mode fluoresc. meas. 80—89491
Na(n^2D)+N$_2$(CO), collisional l-mixing, highly excited states, fluoresc. obs. 77—83686
Ne, 1s$_5$, depopulation effects, dye laser fluoresc. obs. *(French)* 78—41996
Ne, 2p levels prod. by dissoc. recomb. in afterglow, recomb. coeffs., level population 80—43855
Ne, 2p$_1$ level relax. and populations of 1s$_2$ and 1s$_4$ in afterglow 78—9111
Ne, collisional transfer coeffs. between 2p levels, in afterglow, laser excitation obs. 80—43856
Ne, discharge, excitation mechanisms investig. using radial distrib. of excited atoms 80—38744
Ne, discharge, low-press., atom densities of first excited state 80—38750
Ne, electron beam excited states population, press. depend., fluoresc. obs. 78—17802
Ne, electron impact excitation, photon emission, ang. correl. 77—14584
Ne, electron pulse radiolysis, 2p levels formation and decay kinetics 78—31665
Ne, fine struct. obs. by beam-gas spectroscopy, level crossing resonances 80—9719

atomic fluorescence continued
Ne, fluoresc. spectra, mol. bands, 0.1 to 6 atm., 3000-8200 Å 79—3394
Ne, g-factors meas. by quantum beat spectroscopy 79—93955
Ne I, lifetimes of levels of $2p^54d$, $2p^55d$, $2p^54p$ and $2p^55s$ configs. 77—50407
Ne II, $2p^43p$ levels, radiative lifetime by delayed coincidence method 77—83545
Ne, in magnetised positive column fluoresc. obs., 4s and 3d levels props. 77—68006
Ne, laser fluoresc. spectroscopy in microwave discharge 79—36578
Ne, optical transitions, Doppler broadening, compensation by vel. depend. light shifts 80—52930
Ne, pulsed discharge, spectral characts. *(Russian)* 78—47201
Ne, reson. interaction of opposite waves, relax. consts. of common level 78—50511
Ne^{7+}, 1s2l3l′ config., Auger and radiative deexcitation, intermediate coupling 77—79567
Ne-like ions, E1 and M2 transitions, HF calcs. 79—59401
Ne^{n+}-Ne, K-shell vacancy prod. cross section, X-ray and Auger electron prod. fluoresc. yield 78—13582
$Ne+H^+$ 80—18916
Ne+He, population transfer between Ne 2p levels *(French)* 77—30975
$Ne+He(Ar)(Xe)(N_2)(CO_2)$, fluoresc. spectra, mol. bands, 0.1 to 6 atm., 3000-8200 Å 79—3394
Ne+ion, 100 keV, excited Ne 2s vacancy singlet/triplet population ratio, ion Z depend. 78—37733
Ne+Kr(Xe) and Ne+Kr+Xe glow discharge, Kr^+ and Xe^+ excitation in negative luminesc. *(Russian)* 77—68883
Ne+Ne, excitation transfer between 2p levels 78—22006
Ne+Ne, excitation transfer, coupling coeffs., temp. depend., fluoresc. meas. 78—58620
$Ne^+ + Ne$, reson. transitions, direct and charge-exchange excitation 77—19020
$Ne^{2+} + Xe$, electron capture collisions, 15 to 50 keV, excitation 80—102566
$Ne^{n+} + Ar(He)$, slow ion and electron prod., VUV radiation 78—5321
Ne^{z+} + inert gas atom (z=1-4), radiative and non-radiative deexcitation after electron capture 79—7008
^{61}Ni, $3d^94p\ ^3D_2$ level, hyperfine struct., level crossing obs. *(French)* 78—41997
O, absolute fluoresc. production cross section, 1304 angstrom, from $CO(CO_2)$ UV photodissoc. 80—32652
O, autoionis., radiative emission, competition in excited state decay 77—75109
O, conc. in lower ionosphere, fluorescence spectra 80—36434
O I, red line, luminesc. amplification by radiowave anomalous absorpt. *(Russian)* 79—29925
$O+N_2$, quenching of $O(^1D)$ state at 300K, semiclassical study 79—45823
$O(^1D)$+haloalkanes, deactivation reactions, absolute rate consts. determ. 79—11783
$O(^3P)$ prod. by O_3 photolysis, quantum yield determ. 80—78568
$O(^3P)$+dimethyl sulphide, fast flow reson. fluoresc. obs. of absolute rate consts. 80—61077
$O(^3P)+H_2S(D_2S)$, reaction rate, flash photolysis-reson. fluoresc. obs. 77—4918
$O(^3P)+O_3^{\dagger}$, bimolecular reaction rate coeff. reactant vibr. excitation depend., reson. fluoresc. obs. 78—76837
$O(^3S)$ prod., reson. radiation 80—53122
$O(^1S)+O_2$, collisional interaction products, reson. fluoresc. obs. 78—46423
$O(3p^3P)+H_2O$, radiation quenching in pulse radiolytically excited water vap. 79—89738
P, ground state $3p^3(^4S_{3/2})$, time-resolved reson. fluoresc. obs. 79—34333
Pb, $^3P_1{}^0$ state reson. radiation, collisional quenching cross-sections 77—435
Pb, electron impact excitation, visible and UV spectra, excitation cross sections anal. 80—32840
Pb, L-shell photoelectric photon absorpt. cross section, energy depend. 80—106279
Pb, laser excited fluoresc., three-level scheme 78—17605
Pb, X-ray production cross sections for protons, fluoresc. obs. 80—102476
$Pb(^3P_1{}^o)+H$, spin-orbit relax., fluoresc. intensity meas. 78—82681
Pt, ground state configs., isotope shifts and fine struct. anal., visible and UV spectra 80—42987
Rb $6^2P_{1/2}$ state, fluoresc. electric scanning method, polarisability 79—76381
Rb, circ. polarised reson. fluoresc. excited with π polarised D_2 line, 0-170 G 79—41133
Rb, Doppler-free superradiance, polarisation characts. 79—782
Rb, fluoresc., far wings profile of self-broadened reson. lines 79—76388
Rb, HFS of optically inaccesible excited states 78—37582
Rb, high resolution laser fluoresc. spectroscopy in deep blue spectral region 77—82622
Rb, highly excited P-states natural radiative lifetimes 77—6727
Rb, laser saturation spectra, collision broadened line struct. *(Russian)* 79—45678
Rb, optical reson. line electron impact excitation cross sections, polaris. 78—55244
Rb, radiative lifetime, time resolved laser induced fluorescence 80—37781
Rb, Stark shift of $6^2P_{1/2}$ to $5^2S_{1/2}$ line, mag. scanning meas. 80—27977
Rb, superradiant cascading effects, Rydberg levels 79—31491
Rb+methane (and deuterates), $5^2P_{1/2} \rightleftarrows 5^2P_{3/2}$ excitation transfer, isotope effects, temp. depend. 80—91630
Rb+Xe, interatomic spectrum, theoret. and exptl. obs. 78—9112
Rb+Xe system, reson. fluoresc., quasimol. states *(Russian)* 79—85935
$^{87}Rb+Kr$, D_1 line broadening and shift 77—38640
$^{85,87}Rb$, first excited D-level, hyperfine struct. meas. by cascade, fluoresc. spectrosc. 80—69101
$S+CS_2(OCS)(CH_4)$, electronically excited atom, reson. fluoresc. 80—99476
$S+He(Ar)(N_2)(H_2)(Kr)(Xe)$, collision-induced emission of $S(^1S)$, 232 and 425K 79—81264
$S^+ + Ar$, double K-vacancy prod., X-ray X-ray coincidence and fluoresc. yields obs. 78—55230
SF_5Cl, multiphoton dissoc., real-time Cl atom fluoresc. detect. 78—86923
Sb, L-shell fluorescence yield, L_2L_3 average yield 80—47936
Se, electron impact ionisation, characteristic X-radiation ang. distrib. obs. 80—1069

atomic fluorescence continued
Se trace amount determ. by hydride generation-nondispersive flame at. fluoresc. spectroscopy 80—89553
Si, excited states lifetimes, fluoresc. decay curves 80—58175
$Si(3p^2(^1S_0))+He(SiCl_4)(O_2)(N_2O)$, attenuation of reson. radiation, time-resolved kinetic obs. 78—5329
Sm, excited state lifetimes, oscillator strengths 77—83531
Sm, excited states hyperfine struct., isotope shifts, laser-RF double reson. obs. 79—41140
Sm I, lifetime meas. by dye laser excitation 78—25465
Sm, VUV emission spectra, 5p electron excitation by electron impact 77—68007
$Sm+H^+(^3He^+)$, X-ray intensity ratios, projectile energy depend. 80—23535
Sn, L-shell fluorescence yield, L_3 subshell yield 80—47936
Sn, Lα X-ray fluoresc. spectra, natural linewidth meas. 79—85934
Sr atomic beam, time correlations between two sidebands of reson. fluoresc. triplet, multiphoton processes 80—95570
Sr, direct meas. of excited state lifetimes 77—65435
Sr I, lifetime meas., stepwise excitation by pulsed dye lasers 77—83536
Sr, laser saturation broadening in flames, fluoresc. excitation profile obs. 80—95568
Sr, radiative decay of autoionisation states *(Ukrainian)* 78—82682
Sr-Cs mixture, laser induced collisional two-photon ionisation, fluoresc. monitoring 80—91515
Sr^+ + inert gas atom collision, polarisation of emitted radiation, quasimol. interf. effect *(Russian)* 77—46633
$Sr^+(^2P_{3/2})$, coherently Penning ionis.-excited, with $He(2^3S_1)$, Hanle effect 80—5520
$Sr^+(5p^2P_{3/2})$ alignment in $He(2s^3S_1)+Sr$ Penning collisions, polarised emission obs. 80—23533
Tb I, HFS laser fluoresc., unclassified lines anal. 79—81178
Tb^{3+}, in $POCl_3:SnCl_4$, $^5D_3 \rightarrow {}^5D_4$ transition, solvent depend. 79—22644
Tb^{3+} in $TbCl_3(AlCl_3)_x$ complex, potential vapour laser system, fluoresc. obs. 78—66812
Tb^{3+}, luminesc. sensitisation by Yb^{3+}, in liq., efficiency *(Russian)* 78—90116
$Tb^{3+} \rightarrow Pr^{3+}(Er^{3+})$ energy transfer mechanism, in $TbCl_3.6H_2O$-$PrCl_3.6H_2O(ErCl_3.6H_2O)$ DMSO soln. 80—5498
Ti atoms sputtered from Ti, Ti oxides, photon emission, nonradiative transition effects 80—58208
Tl, $6^2P_{1/2}$-$7^2P_{1/2}$ M1 transition, parity violation detection in neutral weak interaction 77—30819
Tl, line shape in Ar gas, collisional redistrib. of near-reson. rad. 79—31469
Tl, lowest S-state lifetime meas. 77—65436
Tl, optical excitation, Landau-Ziner nonlinearity, fluoresc. obs. *(Russian)* 80—52948
Tl, sensitised fluoresc. in Hg-Tl vap., Doppler broadening 77—3314
Tl, stimulated Raman scatt. and stimulated collision induced fluoresc. 78—87103
Tl+Ar, stimulated collision-induced fluoresc. and stimulated Raman scatt., simultaneous obs. 78—13463
Tl+Ba, radiative collisional fluoresc. obs. from thermally excited atoms 80—102480
$Tl+H_2$, Tl atomic fluorescence, pressure and Doppler broadening 80—5504
$Tl+N_2$, Hg sensitised fluoresc., quenching 79—22643
TlI, atomic fluorescence, D_2 pressure effect on width and shift 80—99475
TlI, vapour, excited by photodissociation, fluoresc. yields 78—55138
Tm, VUV emission spectra, 5p electron excitation by electron impact 77—68007
U, excited state radiative lifetime, sputtering technique 78—17602
U I, gf-values, level mean lifetimes, electronic excitation and delayed coincidence meas. 78—21878
U I, laser spectroscopy, using stepwise excitation and fluoresc. detect. 79—54802
U I, relative branching ratios for excited level decay 77—57922
U, laser fluoresc. spectroscopy using pulse hollow cathode lamp 80—27973
U, laser isotope separation, atomic spectroscopy requirements 78—33638
U+molecule, collisional relax. of highly excited states, laser-induced fluoresc. obs. 80—58205
^{235}U, ground and 1st excited states, hfs, laser fluoresc. and laser-RF double reson. spectroscopy 80—58170
^{235}U, ground-state hyperfine structure high-precision meas. by laser-RF double reson. 79—26942
^{235}U, high precision meas. of hyperfine struct. of 620 cm^{-1} atomic level 79—45660
^{235}U, lifetime meas. of electron excited states, rel. to laser isotope separation 77—34591
$U(f^3ds^2)$+molecule, collisional relax. of $^5K_5{}^0$ and $^5L_7{}^0$ states, laser-induced fluoresc. obs. 80—52925
V, hyperfine struct., laser-RF double-reson. obs. 79—41141
^{50}V quadrupole moment and atomic ground state hyperfine intervals, laser spectroscopic determ. 79—89234
Xe, $^3P_1$ resonance state, three photon excitation, fluoresc. obs. 78—13481
Xe, $^3P_1$ state, reson. fluoresc., Zeeman beats, time-resolved VUV spectra using synchrotron radiation 78—33454
Xe, $5d(3/2)_1$ photoexcited state radiative decay 78—74605
Xe, $6p_{01}$ level, peculiar signal in Hanle effect 78—25487
Xe, 6s-6p emission, following vac. UV irrad., press. depend. 79—63950
Xe, afterglow, $6s_{12}$ metastable atom density decay rate 78—63612
Xe afterglow, radiative and collisional deexcitation of reson. states, absorpt. and emission obs. 80—38742
Xe, atom and ions, relativistic Dirac-Fock-Slater calc., fluoresc. yield, X-ray energies shift 78—25450
Xe, discharge lamp, RF excited electrodeless, atomic fluoresc. spectrometry 77—86395
Xe, electron impact polaris. and excitation functions 78—66665
Xe, electron pulse radiolysis, 2p levels formation and decay kinetics 78—31665
Xe, excitation by low energy electrons, IR spectra obs. 80—27974
Xe, fast beam of metastable ions, high resolution spectra 77—42274
Xe, fluoresc. lifetimes, time resolved VUV spectra 78—17601
Xe, ground state, two-photon excitation spectra, fluoresc, decay 77—75115
Xe I, indirect level population in electron excitation *(Spanish)* 77—3461
Xe II, excited states lifetime meas., photon-photon delayed coincidence technique 77—68011

atomic fluorescence continued
- Xe II 5s5p^6 $^2S_{1/2}$ state, lifetime meas. 79−13670
- Xe, K-shell fluoresc. yield determ. by proportional counter method 77−27023
- Xe, laser light irrad. in mag. field, light modulation expt. 78−82699
- Xe, lifetimes and cross sections of laser levels, Hanle effect 77−75480
- Xe, metastable ions, 5d$^4D_{7/2}$ state, laser induced fluoresc. 77−14387
- Xe, second continuum fluoresc. excited by synchrotron radn. 78−90113
- Xe, spontaneous emission, fluctuation spectroscopy 77−434
- Xe, VUV fluoresc. under monochromatic excitation 78−9237
- Xe, vac. UV irradiated, near IR emissions 79−3393
- Xe$^+$, 5p^{4}5d$^4D_{7/2}$ and 5p^{4}6p$^4P^0{}_{5/2}$ levels, HFS, ion-beam laser fluoresc. 77−75319
- Xe$^+$, ($^2P_{1/2}$) radiative deactivation in Xe$^+$+NF$_3$ reaction 78−27737
- Xe$^+$, metastable, electron impact cross section, laser fluoresc. 77−3465
- Xe+Xe, near threshold collision, UV emission 79−54799
- Xe$_2$(−Kr,He), time-resolved excitation spectra, 1500 Å region, fluoresc. lifetime 77−75195
- Yb, high resolution laser fluoresc. spectroscopy in deep blue spectral region 77−82622
- Zn, excited states, collisional quenching cross sections and exit channels, fluoresc, quenching obs. 80−18919
- Zn$^+$+He(Ne)(Ar), 1-500 keV, Zn$^+$ excitation, reson.-line emission and polaris. 80−18911
- ZnI$_2$, vapour, excited by photodissociation, fluoresc. yields 78−55138
- Zr, excited state radiative lifetime, sputtering technique 78−17602

atomic fluorescence spectroscopy *see atomic emission spectroscopy*

atomic forces
- alkali atom+H, long-range interaction, S-state alkali atom 79−76480
- alkali atom+inert gas, long-range interaction, S-state alkali atom 79−76480
- alkali ion+inert gas, interaction pots., gaseous ion mobilities 77−54584
- alkali metal, dynamic polarisability dispersion eqn., dispersion interaction of atoms 79−26902
- alkali metal+inert gas, adiabatic pots. 79−81254
- alkali metal+inert gas, role of different interactions in intramultiplet relax. at nonresonant interactions 77−6902
- alkali metal atom, S-state, +H(inert gas), long-range interaction theory 77−50490
- alkali metal atom+ion coupling energy, internuclear separation depend. 77−14523
- alkali metal atoms, calc. of Van der Waals energies, variation-perturbation method 77−510
- alkali metal chlorides, interionic pots. 77−47372
- anharmonically coupled oscillators, semiclassical calcs. of eigenvalues 80−95514
- atom+diatom, anisotropic interaction pot., total cross-section calcs. 78−29835
- atomic ground-state wavefunctions, optimised central pots. 80−32593
- BEBO method calculations 77−19007
- binary gas mixtures, force consts., intermol. pots. calcs. 78−66624
- Bound state vibrational spectrum of the 3-9 atom-surface interaction 78−14615
- bound states of atoms in optical reson. field, interaction potential 79−93958
- chemisorbed atoms, theory of interactions *(German)* 78−31706
- closed-shell systems interaction, exchange-repulsion energy, many-orbital cluster expansion 80−18896
- collision anisotropy and spectral line impact contour *(Russian)* 80−52942
- collisions rotationally induced transitions in two-state model 80−47945
- compressed gases, intermol. interactions, translation absorption spectra, temp. depend. 78−46419
- cooling, trapping and storage of atoms by resonant laser fields 79−59421
- coulombic potentials, two virial theorems 77−3429
- diatomic bonding energy, changes due to Van der Waals interactions with other atoms 78−95012
- diatomic ionic-molecular systems, two centre mol. wave function 77−65524
- diatomic mol. scatt., Schrodinger eqn. phase shift differences for some trigonometrical potentials 80−43132
- diatomic molecule, bound-states, new trigonometric pots. 79−72383
- diatomic mols., electronegativity, bond charge and chemical pot. approach 80−91703
- diatomic systems, interactions, long-range dipoles, quadrupoles and hyperpolarisabilities 80−53161
- dilute atomic gas, weak at.-at. interaction pot. from master eqn. for coupled radiation 80−23484
- dipole properties and dispersion energies additivity, using atoms and small mol. models 80−53091
- Dirac-Slater potential, hole and exchange terms, influence on photoionisation and internal conversion 80−952
- dispersion energies, charge overlap effects, with freq.-depend. polarisability 79−86025
- dispersion energy consts., dipole oscill. strength sums, refractivity, for Li, N, O, H$_2$, N$_2$, O$_2$, NH$_3$, H$_2$O, NO, N$_2$O 77−50492
- dispersion forces, new expansion 77−14521
- dispersion forces between closed shell atoms 77−88522
- DNA, improved definition of A and B forms, atom-atom potential functions method 78−96000
- Drude oscillator model, atomic and molecular props. for different oscillator freq. 80−37846
- dynamic polarisabilities and dispersion force coeffs., bounds 79−68290
- dynamic polarisability of two atoms at large separation, Green's function method *(Russian)* 79−76481
- electrostatic pot.-electronic density relationships 80−69206
- exchange energy, zeroth-order, optimised atomic basis sets in interatomic force calcs. 80−43131
- exchange interactions, generalised Jansen's perturbation theory 79−6981
- exchange interactions of atoms in paired orbital approx. 77−88521
- exchange interactions of atoms with valence s electrons 77−83677
- excitation of simple atomic and mol. systems, long-range force effects 79−10170
- excited state collisional relax., line broadening, interat. interactions, review 80−43149
- few-body methods, stat. mechanics, atomic and molecular physics, nuclear N-body problem 79−85379
- fibrous materials, struct., interatomic forces calcs. 79−22875

atomic forces continued
- ground state atoms, Van der Waals coeffs., polarisabilities and oscill. strengths calcs. 79−93913
- homonuclear diatomic molecule, united-atom projected perturbation theory 78−37705
- hydrogenic ion lines, red shift in plasma 80−103128
- induction energy, coupled Hartree-Fock calcs. 80−43139
- induction energy between neutral spherical S-state atoms, nonexpanded multipoles 80−23485
- inert gas+inert gas, total cross-section, glory struct. meas. apparatus 80−18901
- inert gas crystal, correlation forces *(Russian)* 78−22686
- inert gas halides, emission spectra, open-shell closed-shell interaction, electron gas model 77−30879
- inert gas mixture, collision-induced absorption, exact line shapes, appl. to He-Ar 78−66512
- inert gas mixtures, interatomic pots. and interaction dipole moments, IR spectra calcs. 77−75082
- inert gas pairs, Thomas-Fermi-Dirac interaction pots. 77−75253
- inert gas small clusters, three body interaction effects on thermodynamic props., comparison bulk props. 80−28128
- inert gas solids, lattice dynamics, book contrib. 77−47522
- inert gases, interatomic pots., book contrib. 77−46615
- inert gases, long range forces, book contrib. 77−51347
- inert gases, short and intermediate range forces, book contrib. 77−50494
- interaction dipoles, perturbation theory 80−78680
- interatomic potential between two equal ions 78−94300
- interatomic potentials, semi-empirical, comparison 78−5315
- internal scalar pressure determ. in atom or molecule, density functional theory 80−47857
- ion-atom repulsive potential reconstruction from ion mobility in gas data 80−23486
- ion-ion, ion-dipole, and dipole-dipole interactions, teaching 78−10
- ions in dipolar solvent, potential of mean force, linearised hypernetted chain approx. calcs. 78−55798
- laser-induced atom-atom collision line shape 80−9691
- like atoms in static gravitational field 78−54270
- long range atomic potentials in Thomas-Fermi theory 79−50101
- long-range interaction, effect of strong e.m. fields *(Russian)* 77−10734
- long-range interactions, rel. to internal kinetic and pot. energy variations, chem. bond theory 78−1046
- matter stability despite catastrophic Coulomb forces 80−22212
- microcosm and macrocosm, discrete modelling 80−82643
- minimum potential energy per particle configuration, one-dimens. system 78−70084
- molecular electronic structure, multiple scattered wave method, incl. interatomic forces 79−59325
- n(R)-6 potential model, modification 77−75254
- neutral atoms, stimulated Coulomb interaction in external resonance field 80−83449
- neutral systems, total binding energy, virial theorem appl. 80−47840
- nucleic acids, atom-atom potential parameters, determ. of nonvalent interactions 78−25648
- off-shell t-matrix elements, for interatomic pots., semiclassical calcs., appl. to repulsive pots. 78−9216
- one-electron atoms, interaction between N atoms, biorthonormal basis sets 79−22576
- oscillator strength sums, dynamic polarisabilities, one-term approximations 79−22782
- paraffin oil, aq. emulsion, polyelectrolyte stabilised, mech. props. 79−39223
- photon exchange between neutral neighbours and cooperative radiation 77−27141
- polyatomic mols. in liqs., vibr. energy relax. 80−63611
- potential curve fitting to differential cross section, simple classical method 77−58118
- potential determ. from elastic scatt. phaseshifts, generalised WKB method 77−58116
- potentials with Coulomb tails, eigenenergy calc. 79−58560
- proton hydrogen bond attractive force at different excitation levels *(Russian)* 80−23493
- resonance fluorescence, multiatom effects 79−6906
- retardation effects on high Rydberg states, retarded R^{-5} polarisation pot. 78−82629
- Schwinger and Kohn variational phase shift calculations, comparison 80−78672
- screened Coulomb pot. full continuum wavefunction, analytic perturbation theory 79−64065
- screened Coulomb potential for slow heavy ion scatt. 77−14522
- screened Coulomb pots., perturbation theory approach 80−63524
- second-order MSMA energy, extremal props. and bounds 77−58115
- semiempirical calc. for simple systems 77−27138
- short-range atomic interactions, symmetry and similarity transform. for perturbation theory 77−10722
- SPF-Dunham expansion for interat. pot., systematic anal. of elastic beam scatt. cross sections 77−50491
- surface, adsorbed atoms thermal desorption, one dimens. microscopic model, weak binding case 80−96729
- surface processes, interatomic forces, theories 80−107632
- three-body interatomic forces, electron gas model and SCF calcs. 78−33564
- trapping and cooling of neutral atoms by resonance radiation pressure 79−72291
- trimers, 3-body interactions in binding, semiclassical approx. calcs. 78−21994
- two atom system near metallic surface, cooperative Lamb shift 77−3317
- two-state curve-crossing collision, total cross-sections interatomic attraction effects 79−68297
- Van der Waals interaction, finite size effects, linear response theory 79−81252
- Yukawa potential function, determ. of phase shifts 78−58237
- Al-Al, Thomas-Fermi-Dirac model, inhomogeneity corrections 80−23308
- Ar, adsorbed on Xe-plated graphite, virial coeffs. and interatomic pots. 77−9125
- Ar, force constant props., 12-6 pot. model 78−13563
- Ar, interatomic pot. and transport props. 77−14519
- Ar liquid, empirical anal. of computer expts. on mol. dynamics 78−21995
- Ar-Kr, pair pot. energy functions, gas phase bulk property reproduction 77−27642
- Ar-Kr, pair pot. function calcs. 78−74726

atomic forces continued

- Ar+Ar(He)(Ne), dispersion interaction, series coeffs., variation method 79−3518
- Ar+Ar(Kr)(Xe), total cross section, glory struct. 80−23494
- Ar+N_2(CO), intermolecular pots. from Thomas-Fermi-Dirac functional 77−19009
- Ar+$O^+(^4\Sigma^-)$, differential elastic cross sections, 2-20 eV, interatomic pot. 77−6885
- ArKr, intermol. pots., differential cross-sections inversion calcs. 78−66619
- Ar.HCl bond energy from IR spectra 77−27061
- As_3, 3-body nonadditive interaction, nodal struct. 78−1049
- Be+Be, polarisability and London coeff., ab initio variation perturbation calc. 79−13635
- Be+Be closed-shell system, exchange polarisation energy 78−42155
- Be+Be(Li) 78−5310
- Be+Mg, polarisability and London coeff., ab initio variation perturbation calc. 79−13635
- Be_3, 3-body interactions in binding, semiclassical approx. calcs. 78−21994
- Be_3, 3-body nonadditive interaction, nodal struct. 78−1049
- ^{209}Bi, P violating eN pot., determ. of effects by optical rotation meas. 79−26277
- Ca+Xe, collision-induced dipole transition due to long range interaction, absorpt. obs. 80−63779
- Cl^-, pair polarisability, ab initio SCF MO energies 78−70741
- Cs-He, new absorption/emission bands perturbed Cs transitions assignment, pot. energy curves 78−66486
- Cs^+-Ar, gaseous ion transport, three-temp. theory appl., interaction pot. 80−6202
- Cs+Ar, laser two-photon ionisation, collisional line broadening, atomic forces 77−83543
- D, spin-aligned, stability at low temp. and high mag. field 77−10723
- $Fe^{12+}+H^+$, short range pot. rel. to forbidden lines collisional excitation 77−17457
- H, gaseous, spin aligned, low-density props. 79−18255
- H, hyperfine shift and interatomic pots. in inert buffer gas 80−5491
- H, line profile, Stark broadening, quantum theory, including short-range interactions 78−9114
- H, low density atomic gas props., dil. hard sphere Bose gas model calc. 80−87194
- H, spin-aligned stability at low temp. and high mag. field 77−10723
- H, triple-dipole energy calcs using pseudo spectral theory 78−46418
- H^+, in H_2, tensor forces and intermediate particle exchanges 79−64067
- H+H, diatomic transition operators, numerical calcs., variable phase and amplitude calcs. 78−25653
- H+H, dispersion forces between closed shell atoms 77−88522
- H+H, dispersion forces calc. 77−14521
- H+H, interaction energy, modified perturbation theory calc. 78−9217
- H+H, interatomic retarded dispersion energy, form-factor representation, multipole expansion 77−23532
- H+H, multipole-multipole dispersion interaction, Pade approximants 79−31638
- H+H, two body multipole-multipole Pade approximants, second order dispersion energy 80−28081
- H+H_2, anisotropic interaction pot., total cross-section calcs. 78−29835
- H+H^+, interaction energy, perturbation theory, Pade approximants and convergence 79−31635
- H+H^+ coupling energy, internuclear separation depend. 77−14523
- H+He^+ (Li^{2+}), two-body dispersion interaction, freq. depend. multipole polarisability, variational calc. 80−37758
- H_2, p- and o-, calc. of thermal cond. 77−54587
- H_2, triple-dipole energy calcs. using pseudo spectral theory 78−46418
- H_2^+ bonding, simplest MO approx. 77−30948
- H_2O, triple-dipole energy calcs. using pseudo-spectral theory 78−46418
- He, excited, optically-allowed, long-range interaction pots. with electrons, protons and atoms 77−14520
- He pair, dispersion interaction, independent particle model, polarisabilities 80−37732
- He, thermal conductivity determ., repulsive wall of interatomic pot. 77−54586
- He, triple-dipole energy calcs. using pseudo-spectral theory 78−46418
- He-Ar(Kr)(Xe), intermol. forces, combining rules 78−66622
- He-He, Born Oppenheimer pot. using Hylleraas-type electronic wave functions 80−91442
- He-He, dispersion interaction 77−58114
- He-He, exchange dispersion energy, multiple expansion, rate of convergence 77−46614
- He+Ar, van der Waals pot., from crossed at.-mol. thermal beams scatt. 79−27053
- He+Ar(Kr)(Xe), He*(2^1S) scatt., low energy repulsion systematic struct. 78−22000
- He+H (inert gas atom), long range interactions for (2^1S) and (2^3S) states 78−70895
- He+H_2, anisotropic interaction pot., total cross-section calcs. 78−29835
- He+H_2^+(H^+)(H_3^+), interaction pots. from ion mobility data 77−14518
- He+He, interatomic force calcs., zeroth-order exchange energy for optimised atomic basis set 80−43131
- He+He, low-energy interactions with phenomenological pots. 77−34714
- He+He, weak intermol. interactions, intramol. correl. effects, perturbation anal. 79−86038
- He+He^+ interactions, electronic forces 79−22790
- He+He(Ne)(Ar), dispersion interaction, series coeffs., variation method 79−3518
- He+N_2, intermolecular pots. from Thomas-Fermi-Dirac functional 77−19009
- He+Ne pot., differential cross section, quantum mechanical inversion 78−70896
- He^++He^+(Li^{2+})(H), two-body dispersion interaction, freq. depend. multipole polarisability, variational calc. 80−37758
- He_2, ground state, interaction energy, many-body perturbation theory calcs. 80−69210
- He_2, pot. surface well depth calc. 77−79667
- He_3, 3-body nonadditive interaction, nodal struct. 78−1049
- He_3 three-body interatomic forces, electron gas model and SCF calcs. 78−33564
- $HeCl^+$, interaction potential, HF dissociation energies, LCAO SCF calcs. 77−6880
- ^{4}He, threshold condition for forming atomic trimer 80−63741
- $(^4He)_3$, interaction through realistic diatomic pots., Faddeev-UPE theory 77 23531
- He*+D, Penning and assoc. ionis. with metastable He, 0.01 to 10 eV beams 79−27074
- He(2^3S)+Ar, differential cross-section meas., optical interaction pots. 77−3443
- Hg-Hg potential, relativistic effects on interactions 77−75252
- Hg+inert gas interaction potential *(French)* 78−25647
- Hg+Ne(Na)(K)(Rb), elastic scatt., interatomic pots. 77−58122
- $Hg_2(X^1\Sigma_g^+)$ potential, intra-atomic correl. in HF calcs. 78−5314
- K+inert gas atom, ground-state pots. from elastic cross sections 77−75258
- K^++inert gas atom potential, determ. from total cross section meas. 77−68091
- K(4p)+He, fine struct. transitions, vel. depend., interatomic pots. 77−42388
- Kr gas structure, three-body-contrib., neutron diffr. obs 80−43820
- Kr, interatomic pot. and transport props. 77−14519
- Li, triple-dipole energy calcs. using speudo-spectral theory 78−46418
- Li^+, pair polarisability, ab initio SCF MO energies 78−70741
- Li+Li(Be), London coeffs. for long range interaction, CI variation-perturbation method 78−5310
- Li^++He, interaction pot., direct determ. from gaseous ion mobility 77−10720
- Li^++K, rot. coupling, Fraunhofer diffraction effects 77−65526
- Li^{2+}+Li^{2+}(H), two-body dispersion interaction, freq. depend. multipole polarisability, variational calc. 80−37758
- Li_2, potential curve calc. using $MTX\alpha_R$ method 77−10593
- Mg+Mg, polarisability and London coeff., ab initio variation perturbation calc. 79−13635
- N, triple-dipole energy calcs. using pseudo-spectral theory 78−46418
- N_2, solid, lattice dynamical calcs., use of anisotropic at.-at. pot. functions, α-γ transition 78−71811
- N_2, triple-dipole energy calcs. using speudo-spectral theory 78−46418
- N_π ground state, second virial coeffs. calcs., 6000 to 20000K 77−14524
- NH_3, triple-dipole energy calcs. using pseudo-spectral theory 78−46418
- NO, triple-dipole energy calcs. using pseudo-spectral theory 78−46418
- N_2O, triple-dipole energy calcs. using pseudo-spectral theory 78−46418
- Na, liq., inelastic thermal neutron scatt., interatomic pots. calc. 78−42891
- Na_2, $A^1\Sigma_u^+$ state, spectroscopic consts. and RKR pot. calcs. 77−75130
- NaKr, red wing radiation and pot. 80−87180
- Ne, $2p^53p$-$2p^55s$ emission lines, press. broadening, with Ne(He), rel. to repulsive forces 80−9692
- Ne, atomic interaction energy, basis set effects in SCF calcs. 77−83678
- Ne, interatomic pot. and transport props. 77−14519
- Ne-Ne, Thomas-Fermi-Dirac model, inhomogeneity corrections 80−23308
- Ne+Ar(Kr)(Xe), elastic scatt. absolute total cross section, long range interaction 78−58768
- Ne+Ar(Xr)(Xe), total cross section, glory struct. 80−23494
- Ne+Ne, exchange-repulsion energy, many-orbital cluster expansion 80−18896
- Ne+Ne, pot. curve derived from gas and solid scatt. data, ESMSV pot. 80−1040
- Ne+Ne(He)(Ar), dispersion interaction, series coeffs., variation method 79−3518
- Ne_3, 3-body interactions in binding, semiclassical approx. calcs. 78−21994
- Ne_3, 3-body nonadditive interaction, nodal struct. 78−1049
- Ni+Ni, exchange interactions and exchange integrals 80−37849
- O, triple-dipole energy calcs. using pseudo-spectral theory 78−46418
- O+N_2, intermolecular pots. from Thomas-Fermi-Dirac functional 77−19009
- O_2, triple-dipole energy calcs. using pseudo-spectral theory 78−46418
- O(^3P)+inert gas atom, absolute total cross sections, 0.6-2.0 km sec^{-1}, model pots. 77−19010
- Rb+inert gas atom, ground-state pots. from elastic cross sections 77−75258
- ^{87}Rb+^{129}Xe, spin-exchange cross-section meas. 80−78686
- Tl($^7S_{1/2}$)+inert gas, long-range interaction, spectral line shifts and broadening 79−10174
- Xe, mean force of two atoms dissolved in water 80−54114
- Xe, multiphoton ionisation spectrum, interatomic effects in multiphoton transitions 78−29764
- Xe, thermal cond., 500 to 2400K, interatomic pots. 77−39393
- Xe-Ne, interatomic pots., Ne adatom on Xe-plated graphite 78−18904
- Xe+ion ($1\leq Z_1\leq 90$), 2.5-400 keV, 1-6°, effective interat. pots. 80−23492
- XeF, $X^2\Sigma^+$, energy curve calcs. 77−10719

atomic hyperfine structure

see also Lamb shift

- ^{14}N II ground state hyperfine structure quantum beats via ion-beam surface interaction at grazing incidence 79−10233
- $^ALi^+$, A=6,7, $2^3{}_1$-2^3P, dye laser saturation spectroscopy 80−18821
- alkali atoms, excited state, laser photoionisation theory, hyperfine coupling effect 80−102493
- alkali atoms, hyperfine interactions of excited states, Brueckner and natural orbitals 77−3283
- alkali atoms, review of exptl. methods of hyperfine struct. determ. 77−31019
- alkali metal, resonance levels relax., hyperfine struct. effect 77−38725
- alkali metal atom, Stark effect for hyperfine structure sublevels and splitting of $n^2S_{1/2}$ states *(Russian)* 79−3401
- alkali metal atom+inert gas atom, hyperfine transition spectral line shift, quantum corrections 78−82655
- alkali metal atoms, excited hyperfine and Stark parameters, meas. and calc. 78−86814
- alkali metal atoms, Zeeman coherences relaxation in ground state by spin-exchange and sudden collisions 77−50402
- alkali metal radioisotopes, hyperfine spectroscopy, nucl. props. 80−57677
- alkali metal vapour, optically pumped, longit. relax. in hyperfine states 77−57908
- atomic muon repolarisation by polarised nuclei of arbitrary spin 79−94112
- autoionising states, electron angular distribution, fine and hyperfine struct. 80−58222
- bibliography at. energy levels and spectra, (July 1971-June 1975) 77−71764
- Ca, A=40,42,43,44,46,48, laser spectroscopy, isotope shifts obs. 77−14392

atomic hyperfine structure continued
- calculations, UHF and PHF methods 79—36517
- conference on hyperfine interactions, Madison, NJ, USA (Jun 1977) 78—39076
- de-excitation cascades, influence on time integrated ang. correl. 78—932
- delta-function potential, modified Fermi contact interaction 79—3378
- electron polarisation produced by reson. ionisation by intense EM field *(Russian)* 78—50518
- EPR, at. parameters calc. using Hermann-Skillman wavefunction, He to Bi 78—91956
- EPR of $S={}^1/_2$, $I={}^3/_2$ system, quadrupole effects 79—42827
- excitation regimes in higher shells 78—70955
- excited nuclear levels, polarisation induced by at. orientation 80—91144
- exotic atoms, E2 and E4 nucl. moments from HFS, review 78—37265
- exotic atoms, hyperfine splitting, recoil corrections calcs. 78—50667
- fast atomic beams, high-resolution spectroscopy 78—89557
- first row atoms and ions, LSD approx., density functional calcs. 80—78720
- first row elements, ground state, self-consistent orbitals with uniform long-range behaviour 80—9485
- first-row atoms, ground states, using CI wavefunctions 78—74583
- growth curves for line absorption 79—54812
- H-like atoms, nuclear size and hyperfine struct., theory 80—924
- Hanle effect, level crossover signal distortion by radiation capture 77 - 3327
- heavy atoms, hyperfine structure 79—3375
- highly stripped H-like ions, de-excitation cascades, influence on time integrated ang. correl. 78—932
- impact broadening of spectral lines 77—83541
- ion, free, aligned, static hyperfine interaction, gamma-ray ang. distrib. 79—9508
- kaonic atoms, quadrupole hyperfine structure 80—78726
- $l_1^{n1}l_2^{n2}l_3^{n3}$ configuration, hyperfine struct. theory 77—67964
- laser spectroscopy of unstable isotopes, nucl. props. determ. from atomic spectra using fast beams 80—9720
- laser spectroscopy techniques, review 78—70975
- longitudinal decoupling of free hyperfine interactions, influence of time depend. effects 78—50655
- magnetic fields effect on HFS 78—37759
- magnetic hyperfine atomic sublevels multiple anticrossings 80—27986
- many-body and relativistic effects 78—37565
- many-electron atoms, determination of matrix elements of operators 77—46505
- many-electron atoms, hyperfine struct., relativistic matrix element determ. ^{209}Bi appl. 77—42251
- mesic atoms of light nuclei in field of reson. EM radiation *(Russian)* 77—79713
- metal impurity in plasma, temp. and density determ. from HFS brightness ratios 77—89310
- metastable autoionising states, ang. distrib. of electrons which decay via fine and hyperfine struct. interactions 80—102492
- moment method in stochastic perturbation of angular correlations 77—3268
- multiple anticrossings in atomic spectrosc. 80—87091
- multiplet struct. obtained from HF, statistical exchange and local spin density approx. 80—32619
- muonic atom muon capture probability and laser effect on hyperfine level population *(Russian)* 77—75348
- muonic atoms, conversion Auger transition rate, s-shell electron effects *(Russian)* 77—75349
- muonic He, hyperfine struct., relativistic, radiative and recoil corrections, QED test 80—14256
- muonium, ground state, hyperfine struct. due to exchange and virtual photons 79—36804
- muonium, ground state, muon mag. moment and HFS, Zeeman transition obs. 77—75345
- muonium, hyperfine quadratic shift in electric field, press. depend. 78—13442
- muonium, hyperfine splitting 78—74806
- muonium, hyperfine splitting correction 78—94336
- muonium, hyperfine splitting of ground-state 78—94337
- muonium hyperfine structure of ground state, magnetic moments, muonium-antimuonium conversion, excited states 80—69273
- muonium hyperfine Zeeman freq. meas. via Ramsey reson. 77—14620
- narrowing and deformation of lines in mag. field 79—98238
- neutral atom collisions, hyperfine component broadening and shift of spectral lines 80—74136
- nuclear energy levels, observation by laser technique book contrib. 78—9212
- nuclear orientation, induced by laser, at. and nucl. applications, review 78—37310
- nuclear quadrupole coupling const., relativistic many-body perturbation theory 78—37566
- pionic atoms, quadrupole hyperfine structure 80—78726
- polarised nuclear beam production by reson. at. ionis. 79—13576
- positronium, fermion-antifermion eqn., static interaction limit 78—62963
- positronium, ground state, hyperfine struct. due to exchange and virtual photons 79—36804
- positronium, ground state hyperfine splitting, logarithmic contributions *(Russian)* 79—94114
- positronium, hyperfine quadratic shift in electric field, press. depend. 78—13442
- positronium, hyperfine splitting, contrib. of ground state quasipot. approach 79—59606
- positronium, hyperfine splitting 78—74806
- positronium, hyperfine splitting and decay rates, contrib. from annihilation kernels 79—89812
- positronium, hyperfine structure, order-α^4R_∞ contribs., radiative corrections calcs. 79—76538
- positronium hyperfine press. shift in buffer gas, calc. 77—557
- positronium hyperfine splitting, anomalous contribs., radiation gauge 77 83771
- positronium hyperfine struct., $m\alpha^6$ contribs. from two photon virtual annihilation 78—89642
- positronium hyperfine struct., three-photon virtual annihilation 77—68143
- quantum beats, intensity profile, ang. momentum theory graphical method 78—25497
- quantum beats in light absorption from atoms, expression for hyperfine levels 78—25499

atomic hyperfine structure continued
- radioactive atoms, hyperfine spectrosc., nucleus-electron interactions, review 79—72259
- radioactive atoms, long isotropic chains, on-line spectroscopic techniques 80—37903
- rare earth metal atoms and ions, relativistic effects on core-polarisation contrib. 77—67990
- reduced tensor matrix elements program, AAKP, adaptation for tensor product evaluation 78—17587
- refractory elements, atomic-beam mag. reson. nuclear spin and hyperfine structure meas. 79—776
- relative atomic transition probabilities of Na, Sc, Ti, Cr, Fe, Co and Ni 79—89642
- resonance line intensity ratio, radn. capture effect 79—98040
- resonance scattering methods in atomic spectroscopy 80—53167
- RF superradiance optical pulse generated under photon-echo conditions 80—95858
- s-states, effect on magnetic dipoles 78—28969
- spectral line, collisional broadening and shift of hyperfine components 77—34587
- spectral line shifts and broadening in buffer gas, quantum theory *(Russian)* 78—21881
- spectral lines, hyperfine struct., brightness distrib., form. model verification 77—57928
- spectrometer, high resolution, for meas. of isotope, isomer shifts and hyperfine struct. 77—61141
- spectroscopy, high-resolution, by at. beam-laser beam interaction *(Dutch)* 79—50166
- spectroscopy of Na neutron rich isotopes, nuclear ground state props. 77—22875
- spin exchange collisions, Pauli principle effects 80—99535
- Sternheimer valence shielding and antishielding factors for 2p and 3p ats. and ions 80—18807
- surface wave polarisation in hyperfine dipolar mag. transitions *(French)* 78—50504
- transition metal atoms and ions, relativistic effects on core-polarisation contrib. 77—67990
- transitions, nonstationary RF coherence signals *(Russian)* 79—98011
- two step reson. photoionisation, multimode and level degeneracy effects 80—78583
- two-level system, hyperfine struct. transitions, weak interaction meas. *(Russian)* 80—58196
- two-photon spectroscopy, Doppler-free *(Dutch)* 79—50167
- vanishing electric dipole transition moment, appl. to fluoresc. 79—59397
- weak electron-nucleon interactions, testing Laporte's rule, review 78—37564
- weak field absolute induction meas. HFS magnetometer 78—77949
- X-ray lines involved in K-capture, hyperfine struct. *(Russian)* 79—85931
- Ag electron excited Lα emission spectra 80—102481
- Ag, stabilized atom, contact HFS const., matrix shifts 77—42254
- ^{107}Ag, hyperfine density splitting, density shifts meas. in inert gases 77—54540
- Al I, perturbed HFS, interconfiguration interaction calc. 80—9523
- Al XIII, $1s2p\,^3P_2$ and $1s2p\,^3P_0$ levels, radiative lifetimes and hyperfine induced decay 80—74149
- As, spin magnetic moment density, spin-density functional method calcs. 77—67969
- ^{A}As, A=69-72, $^4S_{3/2}$ ground state hyperfine struct. and nuclear moments 80—32853
- Au, nucl. spin and mag. moment, trends in neutron deficient nuclei 78—37261
- Au, stabilized atom, contact HFS const., matrix shifts 77—42254
- ^{11}B, ground state, two-determinant numerical self-consistent at. orbitals appl. 79—93937
- ^{135,137}Ba , at. beam mag. reson., metastable 6s5d configs. 79—49971
- Ba, atomic beam, optical isotope shifts and hyperfine struct. 79—50154
- Ba, atomic beam and resonance spectroscopy 80—58180
- Ba, hyperfine splitting and isotope shift of high lying levels, Doppler-free 2-photon laser spectroscopy 80—58215
- Ba, hyperfine structure of metastable states, atomic-beam mag. reson. with laser detection exam. 77—79558
- Ba I, isotope shifts, hyperfine struct., neutron deficient nuclei, laser resonance fluorescence study 79—72436
- Ba II, $5d\,^2D_{3/2,5/2}$, isotope shifts, hyperfine struct., collinear fast beam laser spectroscopy 80—83310
- Ba II, $6p\,^2P$ fine struct. g-values, laser excitation of fast ion beam 77—10645
- Ba isotopes, isotope shifts and hyperfine struct. from laser spectroscopy 79—9460
- Ba, radioisotopes, at. beam laser spectroscopy, hyperfine struct., nucl. moments and radii 80—57678
- Ba, two-photon spectra, isotope shift and hyperfine splitting 78—33491
- Ba^+ confined in RF quadrupole trap, optical detection 77—75096
- Ba^+, hyperfine struct. of $5d\,^2D_{3/2}$ to $6p\,^2P_{3/2}{}^0$, laser absorpt. expt. 78—21870
- Ba^+ ions, hyperfine struct. reson. determ. from fluoresc. *(French)* 77 432
- Ba^+, laser-induced resonances, high-resolution expt. 77—6959
- BaI resonance transitions, hyperfine struct. and isotope shifts, atomic beam laser spectroscopy 80—102141
- ^{128}Ba, charge radius determ. using Doppler free laser spectroscopy 77—71558
- ^{131}Ba, magnetic mom. and charge determ. using Doppler free laser spectroscopy 77—71558
- ^{135}Ba, ^{137}Ba Fourier transform NMR, NQR studies 78—94261
- $^{135}Ba^+$, $^{137}Ba^+$, $6p\,^2P_{3/2}$ level hyperfine struct., Lamb-dip spectroscopy 77—83530
- $^{135}Ba^+$ [$^{137}Ba^+$] hyperfine structure resonance detection method *(French)* 77—75095
- Bi, atomic, parity violation in M1 transition 79—85927
- Bi, Faraday effect and magnetic circular dichroism 80—83399
- Bi I, excited configs., mag. hyperfine splitting factors, interferometric determ. near 200 nm 80—32852
- Bi I, hyperfine struct. determ. 78—935
- Bi II ion, relativistic effects in hyperfine splitting of second spectrum 80—23344
- Bi III, 4809.1 Å multipole line, hyperfine struct. splitting factor 77—68004
- Bi, parity nonconservation, light polarisation plane deflection by components of ultrafine splitting *(Russian)* 78—46456

atomic hyperfine structure continued
Bi, vapour, optical activity and HFS, neutral weak currents *(Russian)* 79—13660
^{207}Bi optical HFS intensity profile for nuclear spin determ. 77—54619
^{209}Bi I, tunable CW dye laser spectroscopy, energy levels, lifetimes and hyperfine struct. 79—6905
Bk, emission spectrum, 2540-9800 Å, electrodeless lamp source 80—27970
Bk I, data from IR spectrum 77—68001
Br I, isoelectronic sequence, multiconfiguration HF calc. of sp^6-s^2p^4d interaction 78—9072
C, ^5S-$^3P_2$ and $^5S_2$-$^3P_1$ transitions, ^{13}C isotope shift 80—58201
C^{3+}, lowest $^2P^0$ and $^4P^0$ states, variational Hylleraas-type wavefunction 79—10023
^{13}C III, $1s^22s3p\ ^3P^0$ state,, HFS, beamfoil expt., CI and Hartree-Fock calcs. 77—75276
^{13}C V, high energy hyperfine struct. meas. 77—57915
Ca, hyperfine field of highly stripped atom, recoil distance method 78—37760
Ca, stable and radioisotopes, hfs, isotope shifts, dye laser saturation spectroscopy, beam expt. 80—58169
^{40}Ca, nucl. mag. moment, hyperfine interaction of electron in L, M and N regimes 78—70448
^{41}Ca, atomic beam and resonance spectroscopy 80—58180
^{43}Ca, isotope shift and hyperfine struct. by laser spectroscopy 79—41139
^{43}Ca, nucl. quadrupole moment, HFS in at. beam mag. reson. 79—63940
^{45}Ca, nuclear charge radius, spin, moments, by laserspectroscopy, splitting of $4s4p\ ^3P_1$, state 80—18187
Cd, $5s5p^3P_1$-$5s^2\ ^1S_0$ intercombination line, press. broadening and shift 80—95564
Cd, optical isotope shifts and hyperfine struct. 77—3316
Cd, triplet states, hyperfine struct. obs., project expt. 77—33737
^{113}CdII, hyperfine level crossing, saturation induced in laser 79—18160
^{107}Cd, heavy ion nucl. alignment, recoil in vac., time-differential meas. 78—37304
Ce, optically oriented, hyperfine transition struct. parametric reson. *(Russian)* 77—54522
Cl I, isoelectronic sequence, multiconfiguration HF calc. of sp^6-s^2p^4d interaction 78—9072
Co I, hyperfine struct. rel. to excited levels lifetime meas. 78—5178
Co I, odd levels, hyperfine structure by level crossing and optical methods 77—83551
^{59}Co, mag. hyperfine struct. analysis, spectral lines 4000 to 4300 Å 78—62752
^{35}Cr, ^7P states HFS, level crossing technique, core polarisation, spin orbit interaction, config. mixing 78—78668
Cs, 5^2D-n^2F series fine and hyperfine struct. 80—43201
Cs, $6^2S_{1/2}$-$6_2P_{3/2}$ transition ($\lambda=8521$ Å) with hyperfine splitting, curves of growth 78—66513
Cs, $6S_{1/2}$-$7P_{1/2}$ transition, photon echo polarisation rotation in mag. field 78—22180
Cs, $7^2P_{3/2}$ sublevels, hyperfine struct., multiphoton elec. dipole transitions anal. 80—32692
Cs, $7P_{3/2}$-$6S_{1/2}$ transition, photon-echo quantum beats obs. 80—23373
Cs, 8S hyperfine splitting, two-photon transition and fluoresc. meas. 78—37585
Cs atomic beam, optical pumping and detection of 0-0 transition 79—18158
Cs atomic beam optical pumping, appls. 77—75108
Cs atomic beam tube operation at HFS level transition in absence of Zeeman splitting 77—82482
Cs, coherence of HFS excitations in optically oriented ats. mag. field modulation *(Russian)* 77—54530
Cs, excited state, laser photoionisation theory, hyperfine coupling effect 80—102493
Cs, forbidden M1 transitions, parity nonconserving effects 78—21844
Cs, HFS, isotope shift related to nucl. charge rad. 78—78826
Cs, HFS of first doublet, He, Ne and Ar press. effects 77—38638
Cs, HFS of optically inaccesible excited states 78—37582
Cs HFS pressure effect determ. from absorption coeff. profiles 80—106299
Cs, hyperfine struct. density and temp. shift coeffs., at high buffer gas densities 79—18138
Cs II, HFS determ. by collinear laser-ion beam 80—52914
Cs II, hyperfine struct., beam laser technique meas. 79—93951
Cs, nucl. spin and mag. moment, trends in neutron deficient nuclei 78—37261
Cs, optically oriented, RF coherency on HFS transition excitation by AM UHF mag. field *(Russian)* 77—42278
Cs, Rydberg S and P states, hyperfine struct., RF spectroscopic meas. 77—57911
Cs, spin relax., effect of optical pumping in high mag. field 77—88430
Cs, transverse, relax. in strong reson. RF field 78—5323
Cs, two-photon ionis. via $6^2P_{3/2}$ state, photoelectron spin polarisation 77—3328
Cs^+ excited levels, hyperfine struct. and lifetimes 80—63590
Cs+inert gas, D_2 line collisional broadening and shift, and HFS 79—22664
Cs+inert gas, hyperfine struct., broadening and shift calcs. 77—58153
^{A}Cs, A=133, 135, 137, isotope shifts and hyperfine struct. of 5s-7p transitions 79—13677
^{A}Cs, A=133, 137-139, hyperfine struct., isotope shifts, nuclear moments and radii, laser spectroscopy 79—10071
^{A}Cs, A=138 to 142, nucl. moments and charge radii changes from hyperfine struct. and isotope shifts 79—17804
^{133}Cs, filter cells for hyperfine optical pumping, optical detect. of 0-0 transition *(French)* 77—443
^{133}Cs, first excited D-level, hyperfine struct. meas. by cascade, fluoresc. spectrosc. 80—69101
^{133}Cs, Rydberg S and D states, hyperfine struct., lifetimes, depopulation cross sections 77—42270
Cu, Doppler-free laser spectroscopy in hollow cathode discharge 80—9537
Cu, stabilized atom, contact HFS const., matrix shifts 77—42254
D, hyperfine quadratic shift in electric field, press. depend. 78—13442
^{161,163}Dy, hyperfine struct. and hyperfine anomaly for fine transitions, high resolution meas. 77—88416
Dy, hyperfine structure of odd isotopes, two step photoionisation, mass filtration *(Russian)* 77—46550
Dy I, hyperfine struct. and isotope shift, fluoresc. meas. on at. beam 78—9109

atomic hyperfine structure continued
Dy, isotope shifts and hyperfine structs. 78—37600
Dy, visible spectra obs., hyperfine struct., mag. dipole and electric quadrupole interaction const. anal. 80—91698
^{161}Dy, ^{163}Dy, HFS, isotope shifts and hyperfine splittings 78—37595
Er, hyperfine structure of odd isotopes, two step photoionisation, mass filtration *(Russian)* 77—46550
Eu, HFS, many-body and relativistic effects 78—37565
Eu, hyperfine interaction calc., relativistic many-body approach 77—46504
Eu I, high resolution study of $4f^76s^2 \rightarrow 4f^76s6p$ 79—54790
Eu I, isotope shift meas., level classification in $4f^65d6s^2$ and $4f^75d6p$ configs. 77—30831
F VIII, $1s2p\ ^3P_0$ and $^3P_2$ levels, lifetimes, hyperfine quenching effects, UV beam foil spectra 80—47931
Fe, hyperfine interaction parameters, effect of local exchange, $X\alpha$ and HF calcs. 78—78622
Fe series atoms and ions, LSD approx., density functional calcs. 80—78720
^{57}Fe, configuration interaction, SL-dependent, effect on hyperfine structure 80—37749
^{57}Fe metastable states, hyperfine struct. meas. by laser RF double-resonance 80—58404
Fr, nucl. spin and mag. moment, trends in neutron deficient nuclei 78—37261
Ga, ground-state hyperfine struct., differential Stark effect 80—42990
Ga, isotope shift and HFS, isotope effects, UV spectra obs. 80—42973
Ga+inert gas atom, diffuse series head lines, hyperfine components, broadening calcs. 80—32632
Gd^{3+}, hyperfine interactions, relativistic CI using many-body calcs. 78—78638
^{157}Gd, splitting factor determ. by computer fit in Gd II spectrum 79—31723
H, 1s-state hyperfine interaction, Blinder operator calcs. 80—14072
H Balmer-α fine struct. lines, anomalous shifts, in He-H_2 DC discharge 79—45677
H, beam, $2^2S_{1/2}$ metastabld ats., nonadiabatic transition in mag. field 78—55157
H, double-quantum saturation spectroscopy, laser and RF 80—77880
H, He atmosphere, hyperfine press. shift, MCSCF-variational procedure 77—6735
H, hyperfine freq. and wall shift, 4.2K gas in solid H_2 coated bulb 79—50155
H, hyperfine freq. meas. of ground state 78—78984
H, hyperfine shift and interatomic pots. in inert buffer gas 80—5491
H, hyperfine shift in He buffer, exchange perturbation theory 77—6736
H hyperfine splitting inside paraboloidal surfaces 80—99445
H in spherical box, hyperfine energy, effect of excited state admixture 80—906
H, in spherical box, SCF calcs. 77—54508
H, linear shifts as function of pressure 78—13442
H, mag. reson. transitions between hyperfine levels, 4.2-77K 79—50053
H, nonrelativistic calc., delta function contributions 77—14368
H, scatt. in reson. line wings and hyperfine struct. levels excitation *(Russian)* 77—57930
H, second-order hyperfine splitting with Blinder-type contact operator 80—23319
H-He, H hyperfine struct. shift, commutator computational method 78—78608
H-like atom, fine struct. and HFS levels, Zeeman effect, relativistic corrections 80—37776
H-like ions, excitation regimes, nucl. orientation due to hyperfine interaction 78—70928
H+D, close coupling calc., resonant spin-flip process, Ramsauer-Townsend effects 80—99547
H+He, H Balmer-α fine-struct. line shift and broadening 80—37783
He, 2^3P-3^3D transitions, Doppler free intermodulated optogalvanic spectroscopy obs. 80—52333
He, Doppler-free two-photon high resolution spectroscopy 80—58197
He isoelectronic series, Z=2-10, hyperfine struct. calcs. 77—31018
He neutral muonic atoms, ground state hyperfine splitting 79—68334
^{3}He, nucl. mag. moment, ratio of precession freqs. of gas phase helions-proton mixture- *(Russian)* 79—17803
^{4}He, muonic, formation and hyperfine struct. 80—91707
He-F, doublet series laser lines near 700 μm, hyperfine splitting and broadening meas. 78—63070
He-like ions, excitation regimes, nucl. orientation due to hyperfine interaction 78—70928
He+Cs(Rb), interatomic pots., hyperfine shifts, diffusion coeffs., perturbation exchange theory 79—41220
^{3}He and ^{4}He superimposed spectra, isotope shift, mass and vol. effect, Fe arc spectrum calibration, teaching 80—46763
^{3}He atom forbidden singlet-triplet anticrossings, D levels 80—99491
^{3}He, hyperfine splitting, using Doppler-free intermodulated optogalvanic spectrosc. 79—50169
^{3}He, hyperfine-induced singlet-triplet mixing obs. 80—106399
$^3He^+$, 2s state, HFS, improved electrostatic device and microwave state selection 77—83757
^{179}Hf, hyperfine struct. in ground multiplet ^3F and nucl. quadrupole moments of ^{177}Hf and ^{179}Hf 77—83520
Hg, hyperfine effect on polarisation of 6^3P_1-6^1S_0 intercombination line excited by electron impact 78—37750
Hg II, hyperfine struct. of 194.2 line, $^2S_{1/2}$-$^2P_{1/2}$ transition *(French)* 77—27009
Hg, IR arc spectrum, fine struct., HFS and isotope shifts 77—79559
Hg, IR arc spectrum, fine struct., HFS and isotope shifts 77—79560
Hg isotopes, nuclear ground state props. via atomic spectra 77—22874
Hg, short-lived isotopes, HFS and isotope shift 78—37594
$^{191}Hg^m$, and $^{190m\text{-}185m}$Hg, nucl. spins, on-line quantum beat spectrosc. determ. 80—9562
$^{199}Hg^+$, hyperfine separation of ground-state, optical double-reson. 78—78828
$^{199}Hg^+$ isolated ions, mag. hyperfine spectrum 78—29760
$^{199}Hg^+$ trapped ion frequency standard 78—57914
Ho III, energy levels, parametric anal. of spectrum 77—46519
Ho, IR emission spectra and hyperfine struct. *(French)* 78—13452
Ho, spectra, energy levels and hyperfine struct., parametric calcs. *(French)* 78—41984
^{165}Ho, pionic atom, quadrupole hyperfine interactions, nucl. moment 78—37772
I, $^2P_{1/2}$ state, relax. between hyperfine levels 80—18880

atomic hyperfine structure continued
I atomic vapour, self-induced transparency and reson. self focusing 80–64114
I, ESR spectra, broadening by He, O_2 and HI 79–68205
I I, isoelectronic sequence, multiconfiguration HF calc. of sp^6-s^2p^4d interaction 78–9072
I, laser 1.315 μm transition line struct. 78–59000
^{127}I atoms in Xe matrices, ESR spectrum 80–1005
$^{127}I_2$, B-X electronic transition, systematic hyperfine struct. meas. 78–9267
^{129}I, hyperfine struct. and isotope shift of 1.3 μm transition 80–102486
I($5p^5(^2P_{1/2})$), time-resolved kinetics, mean radiative lifetime, radiation trapping, HFS 78–5171
In, 451.1 nm transition, HFS and ^{113}In-^{115}In isotope shift 78–82674
In, isotope shift and HFS, isotope effects, UV spectra obs. 80–42973
In+inert gas atom, diffuse series head lines, hyperfine components, broadening calcs. 80–32632
^{215}In, $8P^2P_{3/2,1/2}$, HFS and lifetimes, fluoresc. decay and quantum heats, beam 80–32657
Ir, hyperfine interaction parameters, effect of local exchange, Xα and HF calcs. 78–78622
^{191}Ir, magnetic hyperfine struct. 78–934
^{192}Ir ground state spectroscopic quadrupole moment, g-factor, hyperfine quadrupole splitting 79–89235
K, hyperfine struct. density and temp. shift coeffs., at high buffer gas densities 79–18138
K, spin magnetic moment density, spin-density functional method calcs. 77–67969
^{39}K, first excited D-level, hyperfine struct. meas. by cascade, fluoresc. spectrosc. 80–69101
^{39}K, ground-state g-factor, rel. to ^{87}Rb, spin-exchange optical pumping meas. 77–34596
Kr I, laser spectroscopy, isotope shifts, hyperfine struct. *(French)* 78–33457
^{83}Kr, $4p^55p$ config., HFS meas. using level crossing technique 80–18827
^{83}Kr I, hyperfine structure in arc spectrum 78–41988
^{83}Kr, weak hyperfine component detect., time averaging using dye laser spectrometer 80–101850
^{138}La/^{139}La nuclear electric quadrupole moment ratio, laser RF double reson. obs. 80–23447
^{139}La, hyperfine struct. of excited odd-parity levels, laser at. beam fluoresc. obs. 79–13663
^{139}La II $5d^2\ ^3F_4 \rightarrow 5d4f\ ^3F_4^0$, hyperfine structure, $\Delta F = \pm 2$ transitions, three-quantum process 80–63848
^{139}La, laser at. beam spectrum, HFS resolution at 5930.6 Å 78–9110
Li, ^{2}P-state, hyperfine structure, UHF and PHF methods calcs. 79–36517
Li, $1s2p^2\ ^4P^e$ state, using configuration-interaction wavefunctions 79–3369
Li, $1s2s2p\,^4P^o$ state, using configuration-interaction wavefunctions 79–3370
Li, A=6,7 two-photon intracavity dye laser spectroscopy 78–82706
Li, core charge polarisation, HF calcs. 79–45627
Li ground state, HFS 80–91699
Li, hyperfine coupling, in ground and excited states, Green's function calcs. 77–6692
Li, hyperfine splitting and isotopic shift, Doppler-free two-photon spectroscopy 79–36592
Li isoelectronic sequence, quartet states hyperfine consts., Hartree-Fock and CI calcs. 78–919
Li, spin magnetic moment density, spin-density functional method calcs. 77–67969
Li, unrestricted and projected Hartree-Fock methods 79–63924
Li^+, ^{3}P and ^{3}S states, fine (hyperfine) struct., dye laser saturation spectroscopy, beam expt. 80–58169
Li^+, at. fine struct. and HFS, meas. by Doppler tuned hyperfine spectrosc. 79–81292
$^6Li^+$, hyperfine structure, Doppler-tuned ion beam laser spectroscopy 79–89627
^{7}Li, HFS using Doppler-tuned HFS spectroscopy 79–13831
^{7}Li, level-crossing method for HFS and at. lifetimes 78–66678
^{A}Lu, A=175,176, $5d6s^{2\,2}D_{3/2}$-$5d6s6p\,^4F_{3/2}$ transition, isotope shift and hyperfine struct. 80–83309
^{176}Lu, hyperfine struct. and isotope shift of 605.5 nm line by laser spectroscopy 79–41137
Mg I, hyperfine struct., brightness distrib., form. model verification 77–57928
Mg I, isotope shift, hyperfine struct. 78–42011
Mg^+ laser cooled ions bound in Penning trap, high-resolution optical spectra 80–102487
Mn, $3d^64s\,^6D_{1/2\cdots9/2}$ hfs from laser-RF double reson. spectroscopy 80–57682
Mn, HFS, many-body and relativistic effects 78–37565
Mn I laboratory hyperfine struct. for astrophysical interest 78–17818
Mn, spin magnetic moment density, spin-density functional method calcs. 77–67969
^{55}Mn, metastable states, hyperfine struct., laser RF double reson. study 79–72260
^{95}Mo, ^{97}Mo, quadrupole moments, hyperfine B factors, laser-Rf double reson. meas. 78–33452
N, HFS and g_J factor, precision meas. ground state 77–88412
N, nucl. quadrupole coupling const., relativistic many-body perturbation theory 78–37566
N, spin magnetic moment density, spin-density functional method calcs. 77–67969
^{14}N II, 2p3p $^1P_1$, hyperfine struct. after ion beam surface impact at grazing incidence 80–58403
^{14}N II-$2p3p\,^3$D-state, nuclear spin polarised ion beam use 77–42396
^{14}N III, hyperfine struct. of quadruplet levels *(French)* 77–19103
^{14}N, spherical ground state nuclear quadrupole interaction, Breit interaction, relativistic perturbation theory 80–42939
^{15}N, highly ionized, atomic transition polarisation by beam-foil interaction, 3-8 MeV 80–18908
Na, (3s-4d), Doppler free spectra, 4d fine struct. splitting=1028±0.4 MHz 78–41356
Na, ($4^2P_{1/2}$, $5^2{}_{1/2}$ states), mag. dipole interaction consts., RF spectroscopy 78–37577
Na, Autler-Townes effect in two-step optical resonance 77–38648
Na, electron impact excitation, polarised photon emission, delayed coincidence meas. 79–98225

atomic hyperfine structure continued
Na free atom cooling in resonant laser field at scanning freq. *(Russian)* 79–72272
Na gas, polarisation spectroscopy and forward scatt. 80–52336
Na, hyperfine interaction in $4D_{3/2}$ and $4D_{5/2}$ levels 78–37616
Na I, interstellar lines, in α Cygni direction 78–24542
Na I, possible detect. of 17 cm hyperfine emission in W 51 region 78–8139
Na I $3^2P_{3/2}$ meas. beyond natural linewidth by beam laser quantum beats 77–50399
Na I D_2-line at 5890 Å, laser obs. of ground-state hyperfine structure 80–931
Na, nonabsorption hyperfine resonances in dye laser irrad. vapour 79–93941
Na, optical heterodyne spectra, hyperfine struct. 77–30841
Na, quantum beats of hyperfine levels observed in photoionisation 80–32690
Na, reson. two-photon ionis., photoelectron ang. distrib. and polaris., nucl. spin influence 79–10083
Na, reson. two-photon ionisation via $3p^2P_{3/2}$ state, photoelectron ang. distrib. 80–43016
Na, spin magnetic moment density, spin-density functional method calcs. 77–67969
Na, Stark effect study, S and D excited states struct., two-photon spectra 77–54547
Na, Stark shifts, absolute and differential, coherent optical transient meas. 80–37773
Na vapour, superradiance, quantum beat spectra 80–106311
^{23}Na, hyperfine splitting, fluoresc. after two-photon excitation 79–18307
Na-Ne, gas phase, absorption, D-line profiles, dye laser meas. *(French)* 78–42007
^{A}Na, A=21-31, hyperfine struct., mag. moments and isotope shifts, laser spectroscopy 79–10072
^{22}Na and ^{23}Na, isotope shift, HFS, saturation spectroscopy 77–50409
^{22}Na, spectrometer for meas. of isotopic, isomeric shifts and hyperfine structure 79–6191
^{23}Na, P sequence, quantum beat spectroscopy 79–89632
^{23}Na, S states, HFS optical double-reson. techniques 77–68023
^{143}Nd, ^{145}Nd, visible spectra, relative isotope shift, odd-even staggering parameters 77–10615
Ne, Doppler-free two-photon spectra, fine struct. and hyperfine consts. of 4d′ level 77–61725
^{21}Ne, $2p^53p$ config., hyperfine mag. const. by laser level-crossing technique 78–50509
^{21}Ne, hyperfine interaction in 4d subconfiguration, Doppler-free two-photon spectroscopy meas. 80–18944
$^{21}Ne^{n+}$, $5/2^+$ state, hyperfine interactions and mag. moment of 0.350 MeV 78–17583
^{61}Ni, $3d^94p\ ^3D_2$ level, hyperfine struct., level crossing obs. *(French)* 78–41997
Np I, spectrum, 4000-40000 cm^{-1}, term analysis 77–38629
^{16}O ions, mag. hyperfine interactions, PAC meas. 80–95734
^{192}Os, muonic, dynamic hyperfine effect, model independ. anal. 78–22057
P I, IR spectra and HFS 80–91478
P, spin magnetic moment density, spin-density functional method calcs. 77–67969
^{201}Pb, nuclear spin, metastable atomic states, hyperfine struct. meas. 78–25110
^{203}Pb, nuclear spin, metastable atomic states, hyperfine struct. meas. 78–25110
Pr, metastable, $F=7 \rightleftharpoons 6$ Hfs, laser-RF double reson. spectroscopy 80–58170
Pt group, even atom config., parametric calcs. 78–82631
Rb, 4^2D-state, hyperfine struct. calcs. 77–67970
Rb $5^2P_{3/2}$ state, Hanle effect intensities 78–66521
Rb, Doppler-free two-photon absorpt. spectrum 80–42975
Rb, ground state, hyperfine struct., relativistic many-body calcs. 80–23322
Rb, HFS, many-body and relativistic effects 78–37565
Rb, HFS of optically inaccesible excited states 78–37582
Rb, hyperfine struct. density and temp. shift coeffs., at high buffer gas densities 79–18138
Rb, lowest metastable autoionising level identification by RF spectroscopy 77–426
Rb, nucl. spin and mag. moment, trends in neutron deficient nuclei 78–37261
Rb, Rydberg S and P states, hyperfine struct., RF spectroscopic meas. 77–57911
^{85,87}Rb, high Rydberg levels, press. broadening and shifts 80–52902
Rb^{85}, Rb^{87}, quantum beat between transitions $6^2P_{1/2}$ to $6^2S_{1/2}$ 79–45691
Rb+inert gas, D_2 line collisional broadening and shift, and HFS 79–22664
Rb+inert gas, hyperfine struct., broadening and shift calcs. 77–58153
RbHe(Ne), spin relax., Rb hyperfine interaction in Van der Waals mol. 78–94201
^{85}Rb, ground state dipole HFS diamagnetic shift, high field optical pumping expt. 78–90129
^{85}Rb, HFS affected by strong mag. fields 78–37759
^{85}Rb, hyperfine struct., diamag. shift obs. 77–61717
$^{85}Rb^+$($^{87}Rb^+$), hyperfine struct., in-flight saturated absorption laser spectrosc. 78–78650
^{87}Rb, ground state g-factor, rel. to ^{39}K, spin-exchange optical pumping meas. 77–34596
^{87}Rb, hyperfine transition, light shifts, buffer gas shifts, rel. to maser freq. stability 79–98029
^{87}Rb, surface wave polarisation in hyperfine dipolar mag. transitions *(French)* 78–50504
^{87}Rb+inert gas, D_1-line hyperfine components perturbation, interferometer obs. 80–32635
^{85,87}Rb, first excited D-level, hyperfine struct. meas. by cascade, fluoresc. spectrosc. 80–69101
Re I, isotope shift meas. by HFS, methods, $5d^46s^26p$ level classification 79–49988
Ru, A=99, 101, hyperfine struct. and nucl. moments determ. 77–26575
Ru, hyperfine interaction parameters, effect of local exchange, Xα and HF calcs. 78–78622
^{A}Sb, A=121, 123, elec. and mag. hfs. 79–10224
Sc, HFS and g_J-values, calc. 78–21860
Sc I, hyperfine struct., far-config.-mixing effects 77–42240

atomic hyperfine structure continued
Sm, (A=147,149), hyperfine struct. second order effects on isotope shifts 78−25476
Sm, and isotopes, hfs, laser-RF double reson. spectroscopy 80−58170
Sm, excited states hyperfine struct., isotope shifts, laser-RF double reson. obs. 79−41140
Sm, hyperfine interactions, decoupling meas. 78−37761
Sm I spectrum from laser-atomic-beam spectroscopy 78−37578
SmI, laser atomic beam spectroscopy, isotope shifts, hyperfine struct., transitions 80−102468
^{A}Sm, A=144-154, charge distrib. and hyperfine splitting from muonic X-rays 79−40838
Sn, oscillator strengths and hyperfine splitting of $5^3D_1{}^0$ and $6^3P_2{}^0$ levels, line absorpt. meas. 80−18818
^{87}Sr, $^3P_2$ metastable state, hyperfine struct. at. beam mag. reson. obs. 78−17590
T, hyperfine quadratic shift in electric field, press. depend. 78−13442
TC I, HFS from spectra, mag.-dipole and electric-quadrupole hyperfine consts. 77−68002
^{181}Ta, magnetic hyperfine struct. 78−934
^{181}Ta, pionic atom, quadrupole hyperfine interactions, nucl. moment 78−37772
Tb I, $4f^85d6s^2$ config., hyperfine struct. analysis 78−62732
Tb I, HFS laser fluoresc., unclassified lines anal. 79−81178
^{160}Tb, hyperfine interaction parameters in Gd matrix 80−18240
Ti I, hyperfine struct., far-config.-mixing effects 77−42240
Tl atomic beam tubes, freq. pulling effect with mag. double reson. 80−37802
Tl, ground state population ‘freezing’ effect in hyperfine structure *(Russian)* 78−937
Tl, ground-state hyperfine struct. tensor polarisability 77−6708
Tl, HFS resonance lines anomalous intensity ratios 79−63961
Tl, hyperfine struct. optical pumping, O-O transition perturbation 80−949
Tl I, $6s^26d^2D_{3/2}$ state, hyperfine struct. interaction const., mean lifetime 77−42286
Tl, in gas discharge, optical self pumping, hyperfine struct., microwave-optical spectroscopy 80−32680
Tl, parity nonconserving effects in $6^2P_{1/2}$-$7^2P_{1/2}$ transition 78−13458
Tl, reson. lines, perturbing gas and self-broadening, temp. effects 80−42979
Tl+inert gas atom, diffuse series head lines, hyperfine components, broadening calcs. 80−32632
Tl(7^2P) states, isotopic forms, HFS, press. self-broadening, two-photon spectra 77−18879
Tm I, hyperfine struct., high resolution spectrosc. meas. 80−87238
Tm I, hyperfine struct. for various configs. 78−939
U, 4 eV odd levels, hyperfine struct., double reson. spectrosc. 79−81171
U I, hyperfine struct. meas. of high-lying levels 79−54796
^{235}U, ground and 1st excited states, hfs, laser fluoresc. and laser-RF double reson. spectroscopy 80−58170
^{235}U, ground-state hyperfine structure high-precision meas. by laser-RF double reson. 79−26942
^{235}U, high precision meas. of hyperfine struct. of 620 cm^{-1} atomic level 79−45660
^{235}U, hyperfine struct. and isotope shift meas., laser separation by two-step photoionisation 78−78822
^{235}U isotope separation enhancement with RF hyperfine transitions 79−41249
^{238}U, muonic, non-axiality effects in quadrupole hyperfine splitting 77−46107
V, hyperfine struct., laser-RF double-reson. obs. 79−41141
^{50}V quadrupole moment and atomic ground state hyperfine intervals, laser spectroscopic determ. 79−89234
W, at. beam mag. reson., for HFS and contact interaction 79−68207
W, isotope shifts in visible region and HFS 78−82694
^{183}W, magnetic hyperfine struct. 78−934
Xe, $^3P_2$ metastable, deexcitation by slow electrons *(Russian)* 78−13607
Xe, fast beam of metastable ions, high resolution spectra 77−42274
Xe, γ-γ PAC following nucl. electron capture, cascades perturbed by hyperfine coupling 78−37303
Xe II, $5d^4D_{7/2}$-$6p^4P_{5/2}{}^0$ transition, isotope shift, h.f.s., laser-ion beam expt. 79−93945
Xe, K X-ray energy shifts following electron capture beta decay, role of nucl. hyperfine struct. 78−5166
Xe^+, $5p^45d^4D_{7/2}$ and $5p^46p^4P^0{}_{5/2}$ levels, HFS, ion-beam laser fluoresc. 77−75319
^{129}Xe and ^{131}Xe, HFS of 6p, 7p, 4f and 5f levels *(French)* 79−68211
$^{129}Xe^+$, hyperfine struct., ion-beam mag reson., laser induced fluoresc. for signal detect and state selection 78−41986
^{131}Xe*, hyperfine struct., ion-beam mag reson., laser induced fluoresc. for signal detect and state selection 78−41986
^{133}Xe, nuclear moments and optical isotope shift 78−33118
Yb, HFS in 6s6p $^1P_1$ state, level-crossing and anticrossing spectroscopy 77−27036
Yb I, high Rydberg levels of $4f^{14}$ 6snd configs., very high resolution obs. 80−106300
Yb, isomers and hyperfine struct., selective detection through Rydberg states 80−52903
Yb, optical isotope shifts and hyperfine splittings 79−93943
^{A}YbI, A=170,171,173, 6s6p $^1P_1$-$6s^2$ $^1S_0$ transition, spectrosc. 80−23368
^{173}Yb, 6s6p$^1P_1$ state, level crossing with additional pumping of ground state 77−34595
^{91}Zr, hyperfine struct. and nucl. elec. quadrupole moment. at. beam mag. reson. meas. 78−55133
^{91}Zr, magnetic hyperfine struct. 78−934

atomic inelastic collisions
see also atom-atom collisions; atom-ion collisions; atom-molecule collisions; atom-molecule reactions; beam-foil spectra; ionisation of atoms
accelerator-based atomic physics expts. 77−68141
adiabatic analysis, velocity-coupled channels 77−58129
adiabatic approximation, energy-modified 79−59523
alkali metal, ground state coherence, transversal relaxation rates, Zeeman shifts 77−6888
alkali metal, modulated optical absorption transients weights, transversal relaxation effects 77−6887
alkali metal+N_2, thermal ionis. rate coeff. 77−30982
alkali metal scattering at high-energies, intermol. potential determ. 77−46609
analysis using charact. noise of strong EM wave 80−99492

atomic inelastic collisions continued
angular correlations, summary of review papers 80−63757
anisotropic collisions, direct meas. method 80−23498
approximate classical scatt. method for power law potential 80−5597
approximate wavefunctions, radial couplings calcs. 78−42163
Ar, light scattering, collision induced, low density limit, mol. dynamics and memory function approach 80−43841
asymmetric scattering, spin-1 particle by non-central field 78−55214
atom, autoionisation intersecting terms of collisions, electron spectra interference struct. *(Russian)* 78−1070
atom, coherent transients, spherical tensor treatment 79−26940
atom+charged particle anisotropic collision, spectral line shift and broadening, polarisation depend. 78−82695
atom+diatom scattering, field theoretic calcs. 77−50484
atom+foreign gas, absorpt. spectrum shift near series limit, K-matrix anal. 77−10731
atom+harmonic oscillator, radial Schrodinger eqn., propag. method, appl. to close coupled eqns. 80−42096
atom+heavy particle, inelastic scatt. differential cross-section calcs. 77−10730
atom+muon, ionisation loss formula derivation using covariant method of equivalent photons 78−29337
atom+neutral particle, Rydberg state transitions 78−9213
atom+oscillator, collinear collision, distorted wave perturbation theory 78−74731
atom+rigid rotor, rot. inelastic scatt., semiclassical 79−18264
atom-surface scatt., inelastic, quantum theory, eikonal approx. 80−50499
atomic, molecular and solid-state theory, conf., Flagler Beach, Florida, USA (Mar. 1978) 79−31356
atomic and molecular collisions, book 80−27058
atomic collisions in solids, book contrib. 78−75697
atomic gas, laser irrad., field avoided crossings, new transition channels 78−33477
atomic physics, conf., Riga, USSR (Aug. 1978) 80−22141
atoms, general adiabatic-diabatic transformation matrix, electronic non-adiabatic transitions 80−93751
atoms in solids, focusing and defocusing collisions model 80−82618
Auger process in atomic collisions 78−62899
Auger transitions, three-electron, in ats. with two inner-shell vacancies 77−19049
autoionisation electrons, photons emitted from collisionally aligned states, angular correl. 77−14385
Bethe theory, inelastic collisions of fast charged particles 78−58783
Born inelastic cross sections, Pade approximants 78−17742
born-Huang expansions in the generator coordinate method of molecular dynamics 79−31646
cascade effects on polarisation of radiation, electronic or atomic collisions 80−18917
charge transfer cross sections of highly-ionised atoms, Coulomb-Born calc. 77−10752
charged particle scattering, Schwinger variational principle 79−45780
chemical ionisation, classical description, complex interaction pot., exponential representation 80−99570
classical many-body collision model incorporating Heisenberg and Pauli principles 80−63511
classical trajectory theory, choice of phase 77−50486
close, slow collisions, Σ-Π transitions united-at. approx. 79−22794
coherence and correlation in atomic collisions, book 80−90615
coherent non-stationary superpositions of atomic eigenstates, beam-foil spectroscopy 77−38748
colliding-beam studies of atomic collision processes 79−31742
collinear, quantum mech. sudden vibr. approx. calcs. 79−98193
collision effects on nonreson. interactions, nonlinear spectrosc. obs. 80−23496
collision induced line shapes, hard sphere model calcs. 79−81182
collision reorientation in resonant light field *(Russian)* 80−14192
collision spectroscopy, book 79−27065
collisional and radiative damping effects in Rayleigh and reson. fluorescence scatt. at high intensities 80−102478
collisional ionisation in intense laser field, quasimol. state reson., quantum mechanical anal. 78−33589
collisional ionization rate coefficients 79−14518
collisional processes, nonreson. laser field effects 77−60093
collisionally perturbed atoms, saturated near-reson. light scatt., spectral line strengths 80−23345
complex scaling transformations in stationary and scattering problems 79−18124
computational atomic and molecular physics, conf., Nottingham, England, (Sept. 1978) 79−59567
conference on ionised gas physics, Dubrovnik, Yugoslavia (Aug.-Sept. 1978) 80−36779
cooling/heating rates for collision in light fields *(Russian)* 78−62874
coupled equations solution method in adiabatic approx. 79−3524
cross section, calc. using effective Feynman diagrams, in plasma 80−38566
crossing electronic term problem, influence of motion 79−76499
data inversion, interaction function recovery, appl. to He^++Ne 79−89741
deflection functions for curve-crossing collisions 79−94051
diabatic and adiabatic representations 79−45795
diabatic correl. diagrams 77−14517
diatomic transition operators, L^2 basis expansions 80−63519
dielectronic recombination amplitudes, scaling props. 78−58781
differential cross-sections, factorisation, sudden approx. calcs. 80−18902
direct Coulomb ionisation, origin and nature of universality 79−45791
disorienting collisions, nonlinear resonance induction 80−37900
distorted wave perturbation theory, higher order, accuracy and convergence 78−74731
distorted-wave amplitudes, sensitivity of cross-section and ang. correl. to scatt. parameters 80−5596
Doppler line profile, saturation, influence of atomic collisions 78−70792
eikonal approximation, reson. charge exchange ang. distrib. and atom refl. *(Russian)* 77−34759
electron ang. distrib. from autoionising states with unresolved fine struct. 80−43007
electron scattering, free free processes 80−63834
energy level transitions, Doppler broadening, phase-destroying collisions 80−9561
exchange matrix element evaluation from Coulomb interaction operator 80−18905

atomic inelastic collisions continued
- excitation, target atom decay, scatt. projectile and photon coincident detect., coherence effects 80—63791
- excitation cross section oscillations, unequal spacing 79—27079
- excitation transfer in high mag. fields, theory 80—9688
- excited harmonic oscillator+atom, high-energy, energy transfer 79—68296
- excited state collisional relax., line broadening, interat. interactions, review 80—43149
- excited state processes, collision rates obs. using single at. or mol. beam 78—13567
- experiments, review 79—81256
- exponential model, two-state, comment on Stueckelberg phase calcs. 79—3514
- Faddeev equations, off-shell matrix elements evaluation 77—67336
- fast heavy ion+atom, and solid targets, ionis. and excitation states 78—70927
- fast particle electron emission, line shape, acceptance function effects 80—37787
- flame collisional processes, coherent optical transient spectroscopy 79—39147
- fluorescence, collisional depolarisation, impact and quasistatic limit 77—65439
- fluorescence, collisional redistribution of radiation 78—13464
- fluorescence, collisionally aided, for heating or cooling 78—37584
- fluorescence and Raman scattering, collisional and Doppler broadening 78—13465
- form factor, squared, integral over momentum transfer 80—1039
- four-body problems, Faddeev eqns., appl. to ^{6}Li 79—59569
- free atom, polarisation moments decay 80—23513
- gamma-ray incoherent scatt., meas. of ang. distrib. 77—54538
- gas mixture, laser irradiated, anisotropy of inelastic scatt. and selective diffusion 80—53907
- gas with fast disturbance, slowing down, nonlinear Boltzmann eqn. 79—98196
- gases, coherent neutron scatt. length meas. 79—72435
- gases, collision induced absorpt. spectra, integral data 79—81202
- Glauber approx. for particle-atom collisions 77—10716
- Glauber wavefunction, without nonmoving bound particle assumption 79—18250
- heavy ion collision, delta electrons as probe of high mag. fields 79—13810
- heavy ion collisions, adiabatic basis for inner shell excitations 79—89759
- heavy ion collisions, inner and outer shell contribs. to charge state distribs. 80—14228
- heavy ions, in air, energy loss, high-energy calcs. 77—6891
- heavy particle scatt., independent electron approx., semiclassical derivation 77—83673
- heavy particles, reson. scatt., pseudocrossing problem 79—49412
- high momentum transfer, semiclassical model cross sections 77—19004
- highly excited atoms, collision processes, review 77—58146
- highly excited atoms, review of recent expts. 80—23325
- hydrogenic atoms and ions, degenerate state transitions, plasma waves, Stark effect 79—72389
- induced moments in at. and mols., polarisability density concept limitations 78—70964
- inert gas atom+atom, excited state-ground state interactions 79—18259
- inert gas excimer lasers, at. and mol. collision processes 80—53263
- inert gas halide lasers, at. and mol. collision processes 80—53263
- inert gas mixtures, collision-induced translational absorpt., line shape 77—439
- inert gas mixtures, interatomic pots. and interaction dipole moments, IR spectra calcs. 77—75082
- inner shell ionisation, semiclassical approx. method calcs. 80—43162
- inner shell ionisation by heavy particles, conf., Linz, Austria (May 1979) 80—41938
- inner shell ionisation phenomena, conf., Freiburg, West Germany (Mar.-Apr. '76) 77—27040
- inner shells, Coulomb ionisation, semiclassical description 80—42938
- inner-shell ionisation, semi-classical theory 78—62896
- in intense light beams, quantum aspects *(Russian)* 79—6903
- interatomic force calcs., zeroth-order exchange energy for optimised atomic basis set 80—43131
- intermolecular potential well depth role in collision-induced state changes 79—81257
- interstellar medium, collisional excitation rel. to fine struct. levels population ratios 79—35351
- interstellar medium, effect of collisions on b_n factors at low temps. 80—36696
- ion+H^+, in solar corona, approximations for fine struct. excitation 77—17463
- ion+ion, reson. charge exchange collisions 77—1921
- ion channelling, coherent excitation 79—46727
- ion-induced dipole pot. scatt. calcs., electronic and nuclear contribs. to mol. polarisability 77—50488
- Laguerre uniform approximation for vibrational transition probabilities 77—71849
- laser spectroscopy, atom and mol. interactions, conf., Zarogoza, Spain (June 1979) 80—27041
- laser-assisted excitive Penning ionisation 79—41232
- laser-assisted inelastic collisions, impulse approximation theory 80—18904
- laser-induced atom-atom collision line shape 80—9691
- lasers, atomic and molecular, appl. to collision physics 80—63596
- light scatt., near-reson., from collisionally perturbed atoms and molecules, theory 80—1045
- light scattering, near-reson., by collisionally perturbed ats. time and freq. depends. 79—72281
- lineshape analysis for collision induced spectra 78—70787
- low energy atomic collisions, ionisation processes, chemi-ionisation, review 78—22024
- low-energy, review 77—30958
- low-energy scattering, resonances 79—72384
- magnetic and laser fields simultaneously influencing potential scattering 79—81248
- magnetic scattering of neutrons on excited atoms or mols., cross sections, neutron polarisation *(Russian)* 78—55249
- many channel scattering model, exactly soluble 80—43127
- metal vapours, excitation energy transfer, sensitised fluoresc. 80—23358
- mixing and quenching cross-sections for atomic collision processes 77—61821

atomic inelastic collisions continued
- monatomic gas, collision-induced light scatt. at intermediate density, integrated intensity, appl. to Ar 80—24124
- multistate mol. treatment, impact parameter approx., computer program 77—38705
- muon transfer in gas targets 77—42445
- muonic D+Y, muon transfer mechanism from free muonic deuterium 80—69218
- muonic H+Y, muon transfer mechanism from free muonic hydrogen 80—69218
- near-adiabatic collisions, theory, electron translation factor method 78—81889
- near-adiabatic collisions, theory, scatt. coord. method 78—81890
- neutral atom scatt. at long range from metal surface 78—13572
- neutral atoms, slow collisions, fine struct. transitions 79—841
- neutron induced X-ray atomic excitation 80—23510
- nonlinear optical phenomena in system of colliding atoms, atomic fluoresc. 80—99788
- nonlinear spectroscopy, collision induced resonant four photon parametric generations 77—3627
- nonreactive scatt., classical differential cross sections in Legendre polynomials 79—836
- one-electron atom, rearrangement collisions in laser radiation field 80—74225
- optical Bloch equation, stochastic incoherences 79—68373
- optical collisions, solvable model 80—91638
- outer-shell excitation, electron promotion model, 1-10 keV, closed-shell-closed-shell interaction 79—27073
- pair polarisabilities, continuum electrostatic theory 78—86769
- partial-wave two-cluster atomic scattering amplitudes 79—44763
- photon echoes in standing-wave fields: time separation of spatial harmonics 80—9759
- photon-atom sections, 100 eV to 100 GeV 77—54536
- photon-bound-electron scatt. meas. 77—14394
- photorecombination emission reaction mechs. during atomic collisions 80—18914
- plasma, atomic processes for mag. fusion research, review 80—42851
- plasmas, low density, H to Ca, Cr, Mn, Fe, Ni, ionization equilib. 78—17768
- polarisation in atomic and nuclear physics 80—63162
- positronium+SO_2(benzaldehyde), spin conversion 77—31030
- potential scatt., separable expansion method, off-shell T matrix 78—93564
- potentials, anisotropic, from rotationally inelastic and elastic cross sections, direct inversion method 80—69090
- pressure broadened spectral line shape, effect of turning points 79—22655
- protonium formation in flight, $\bar{p}p$, antiproton+neutral and negatively ionised hydrogen atoms 79—85319
- quantum system, jarring and corresponding stimulated transitions 80—17839
- quasimolecular states, coherent population *(Russian)* 77—10718
- quasimolecule as atomic collision intermediate, superheavy, X-ray emission empirical scaling rule 79—76502
- quasiresonant atomic collisions, asymptotic calcs. 80—23512
- quenching rate const. for metastable $Ne(^3P_2)$, flowing afterglow 78—46295
- radial coupled equation solution, fast numerical method, applic. to collision processes 77—14545
- radiative collisions, line shape in external mag. field 79—22665
- radiative collisions, solvable model 80—91638
- radiative collisions, with impact level shifts 79—54951
- radiative excitation, collisionally aided, three level system, interference effect 79—98022
- rainbow scattering, Regge pole anal. 78—58774
- Rayleigh spectrum, collision-induced, intermediate density, second freq. moment, appl. to Ar 80—24125
- reduced phase space approach calcs. 80—83438
- relaxation coefficients, meas. method *(French)* 78—58771
- relaxed sudden approx., moderate collision energies 78—70902
- resonance broadening due to collision-induced vel. change *(Russian)* 77—46540
- resonant transfer of electronic excitation, eqns. of classical system interacting with quantum system 79—76498
- rotationally induced transitions in two-state model 80—47945
- rotationally inelastic scattering, sudden approximation, theory 77—71843
- Rydberg angular momentum transfer, stochastic model for induced consecutive transitions 78—46429
- Rydberg atoms, expts., metastable states, multiphoton ionisation, spectroscopy, Stark struct., collisions, polarisability *(Dutch)* 78—5160
- Rydberg states, use as spectroscopic probe for resonances in mol. electron elastic scatt. 77—58162
- scattering amplitude, Glauber approx. 79—59531
- scattering amplitudes, Regge representation calcs. 78—58770
- semiclassical scatt. matrix, Massey parameter expansion 78—58759
- slow heavy ion scattering, screened Coulomb pot. 77—14522
- spectral line, collisional broadening and shift of hyperfine components 77—34587
- spectral line collisional broadening, classical and quantum theories, radiator motion effect 78—86822
- spectral line shapes, linear and nonlinear, atom or mol. cross sections 78—70899
- spectral lines, impact broadening HFS considerations 77—83541
- spectroscopy of atoms near a wall *(Dutch)* 78—70972
- statistical model of inner-shell vacancy production in atomic collisions 79—45792
- stripping in gaseous targets, equilib. charge state distrib., statistical anal., appl. to Cl, I and Br data 80—5610
- supernovae, Type I, He energy and charge transfer collisions rel. to spectra 78—49467
- surface evanescent wave-moving atom interaction, exchanged momentum meas. *(French)* 78—37603
- theory, review 78—1043
- three body problems with Coulomb interaction, adiabatic representation, two-level approx. 80—47861
- Three-electron Auger transitions in atoms with two inner shell vacancies 78—62900
- three-level atomic system, saturation spectroscopy including collisional effects 80—37099
- three-level system, velocity changing collisions, saturation spectroscopy, internal coherences 78—42245

atomic inelastic collisions continued
three-photon ionisation, collision-induced 80—23384
three-state atom, saturated two-photon absorpt. in perturber gas 80—106310
Tokamak impurity problems, atomic and mol. struct. and collision data, review 80—43959
transformation theory, translation factors 77—61831
transition probability amplitudes quasiclassical approx. *(Russian)* 77—79676
two-atom system, with weakly bound electron, s-term passing through continuum parabolic boundary 79—72392
two-body model atom, excitation by fast particles in high momentum transfer limit 78—17780
two-level atom, active, collisionally aided radiative excitation 79—54805
two-level atom, interatomic force depend. on intense radiation fields 80—53100
two-level atomic dynamics, damped Bloch eqns., quantum mech. form 77—23530
two-photon transition in colliding particle system, stimulated Raman scatt. 80—9663
two-state atom, resonance fluoresc. spectra, collisional broadening 80—91484
two-state atoms irradiated by monochromatic light, reson. fluoresc. spectra, collisional broadening 80—91483
two-state collision problems, distorted-wave formula for transition probabilities 80—69212
two-state curve-crossing collision, total cross-sections interatomic attraction effects 79—68297
vacancy sharing process, Nikitin two-state model 80—9684
vapours, three-level system, collisional effects in saturation spectroscopy, appl. to Na 80—78579
X-ray and electron spectra excited by atomic collisions, beats mechanism *(Russian)* 79—94075
X-ray and UV lasers appls. 80—64787
X-ray satellites, multiple inner shell vacancies from collision processes 77—83527
μ+atom, e^+e^- pair prod., energy spectrum, screening effects *(Russian)* 78—55250
Ag, loss of K-electron by proton-atom collision *(Russian)* 77—50523
Al transitions, Stark broadening and oscillator strengths 78—29761
Ar, collision induced light scatt. spectra, pair polarisability 78—55135
Ar, collision processes, photoionisation mass spectra obs. 79—31479
Ar, gas, electron thermalization time and position distribution meas. 80—93771
B, X-ray spectral line broadening in solid and gas targets 77—6713
Ba discharge, dipole-dipole pair absorpt. obs. using optogalvanic detect. 80—54064
$Be^+ + H_2$(He)(Ne)(methane), Be Auger spectra 77—57951
Bi, $6p^3(^2D_{3/2}{}^0)$ and $6p^3(^2D_{5/2}{}^0)$, collisional deactivation 77—61702
Br+HCN, electronic-vibr. energy transfer, $Br(4^2P_{1/2})$ quenching and HCN (001) deactivation, fluoresc. obs. 77—518
C, excited electronic states contrib. to transport props. 80—23326
$C^+ + H_2$, fine struct. transition excitation 77—42389
Ca I 6102, 6122, 6162 Å multiplet, collisional broadening 80—37777
$Ca^{14+} + H^+$, collisional excitation of fine struct. transitions in ground state 77—19017
Cd, $5s5p^3P_1$-$5s^2\ {}^1S_0$ intercombination line, press. broadening and shift 80—95564
$Cl^{n+} + Ne(SiH_4)(H_2S)(HCl)(Ar)$, K X-ray cross section, projectile charge depend. 77—19029
$Cs + Cl_2(Br_2)(I_2)(ICl)(IBr)$, negative ion prod. cross sections 77—531
Cu laser lines, broadening, induced emission cross-sections 79—26928
(D,T), reaction rate parameter, temp. dependence, fusion process in Maxwellian DT plasma 80—59254
$D^0(D^+)$+Cs, D^- formation, ang. distrib., total cross sections 77—529
^{151}Eu (^{153}Eu) excitation transfer, effect on selective photoionisation 80—99538
Eu+noble gas, spin relaxation of Eu $^8S_{7/2}$ ground state 77—58131
Eu*+Sr, light-induced collisional energy transfer 78—50614
$F^{7+,8+} + H_2$(He), 20-56 MeV, F K X-ray cross sections, inner shell Coulomb excitation 77—19025
Fe I low excitation lines, collisional broadening 80—37778
$Fe^{11+} + H^+$, collisional excitation cross-sections for ground configuration 78—33582
$Fe^{12+} + H^+$, forbidden lines collisional excitation, importance of short-range pot. 77—17457
$Fe^{20+} + H^+$, collisional excitation of fine struct. transitions in ground state 77—19017
H atoms in cylindrical hydrogenic plasma, transport code 78—51284
H, collisional energy level transition rate, in RF plasma, fluoresc. meas. 77—38726
H, electron-photon angular correlation meas. for excitation of 2P state 80—91636
H generator, freq. shift due to atomic collisions with storage flask walls 78—77870
H, in galaxies active nuclei, inelastic collisions rel. to spectra 77—45599
H like atom alignment due to electron capture in particle-atom collisions *(Russian)* 80—106379
H loss of K-electron by proton-atom collision *(Russian)* 77—50523
H, productive form factor *(Russian)* 77—79675
H, Stark effect, scatt. theory methods obs. 80—63586
H^-, target polarisation rel. to free-free transitions 79—66917
H^+, in H_2 gas, energy loss, high-energy calcs. 77—6891
H-D discharge, RF, meas. of excitation transfer rate by laser fluoresc. 80—9542
H-like excited atom interaction with charged particle, dipole approx. *(Russian)* 78—22007
H-like ions, excitation regimes, nucl. orientation due to hyperfine interaction 78—70928
$H + e^-$ interactions in intense EM field, one photon absorpt., 1s-2s transition 79—36765
H+H, pair polarisabilities, continuum electrostatic theory 78—86769
$H^- + H_2(N_2)$, collisional detachment cross-sections, high-energy obs. 77—3442
H_2+H(2S), metastable atom total quenching 77—46628
He, 3^3D level, fine struct. changing collisions in glow discharge 80—58346
He, collision induced scattering of depolarised light 80—14118
He, collisional excitation transfer for $3^{1,3}$P and D states 80—106387
He, emission line profile, hollow cathode source 77—23469

atomic inelastic collisions continued
He I 2^3P-3^1D intercombination line, collision-induced, obs. by laser absorpt. spectroscopy 80—58194
He-Ba discharge, dipole-dipole pair absorpt. obs. using optogalvanic detect. 80—54064
He-like ions, excitation regimes, nucl. orientation due to hyperfine interaction 78—70928
He-Ne, 632.8 nm line broadening, perturbation energies additivity 79—54941
He^+-$H_2(N_2)(O_2)$, electron capture, loss and de-excitation 77—6904
He^3-He^4 mixture, relax. of 2^3S_1 metastable atoms 80—102469
He+H_2(HD)(HT), interaction second virial coeff. nonspherical pot. terms effects 77—3432
He+H_2(He)(N_2)(Ne)(Ar), 25-450 keV, metastable ion beam electron loss and deexcitation cross section 77—34745
$He^- + H_2(N_2)$, collisional detachment, cross-sections, high-energy obs. 77—3442
^{3}He and ^{4}He microdroplets, momentum transfer in collisions with Xe and CO_2 beams 79—50113
$^3He^{2+}(^4He^+)$+C foil, electron vel. distrib., nonexistence of wake bound states 78—13571
Hg vapour, absorpt. spectrum, 1849 Å line, self-broadening, interatomic interaction *(French)* 80—32661
Hg+H(H_2), resonance scatt., HgH potential determ. 77—61830
$Hg(6^3P) + O_2$, photosensitised reaction, excited intermediates, energy transfer detect. 78—73030
I radical recombination in dense liquids, stochastic trajectory simulation 80—45487
$I(5p^2P_{1/2}) + I_2$, metastable relax., rate const. 77—19022
K, $4^2P_{1/2}$ resonance substate, disorientation cross-section, Zeeman scanning obs. 80—42988
K, collisional depopulation of high-lying P state 77—3447
K, photosensitised assoc. ionisation, excited from reson. levels 77—83710
K Rydberg states, optical excitation, collision ionisation processes 80—102561
$K + Cl_2(Br_2)(I_2)(ICl)(IBr)$, negative ion prod. cross sections 77—531
K^++molecule, total cross section anal. method, mol. quadrupole moment determ. 77—50495
Kr, gas, electron thermalization time and position distribution meas. 80—93771
Kr I, saturated absorpt. profile of 557 nm line, collision effects 78—9121
Li-like ions, highly charged, innner shell excitation, intermediate coupling collision strengths 80—1074
Li(^{2}P), quenching cross-sections, energy depend. 79—63952
Mg ($^3P_1$) metastable atom afterglow quenching rate consts. with various mols. 77—6720
Mg I, press. shifts of $^1D_2$ Rydberg states 77—61711
N, $3p^4S^0$-state quenching in low-press. glow discharge 80—23355
N, $(2p^3\ {}^2P^0)$ state, form. and depletion in N afterglow 79—49951
$N^+ + NH_3(H_2O)(Ne)$ symmetric collisions, double K-shell ionisation, two-electron-one-photon transitions 77—19067
Na D_2 resonance line broadening in atom and molecule collisions *(Russian)* 80—14119
Na, D-lines, inert gas broadening, photon echo meas. 80—91475
Na, photosensitised assoc. ionisation, excited from reson. levels 77—83710
Na, self-broadening of 3S-5S and 3S-4D two-photon transitions 79—26955
$Na + Cl_2(Br_2)(I_2)(ICl)(IBr)$, negative ion prod. cross sections 77—531
Na+H(He)(Ne), D2 reson. linewidth 79—31647
Na+Ne, potential curves from a model potential *(French)* 80—78685
Na^++Ne, excitation and charge transfer, 0.2-12 keV collision 79—68314
Na(^{2}P), quenching cross-sections, energy depend. 79—63952
Nb+Nb, X-ray ang. distrib., 35-75 MeV 2 pΣ MO calc. 79—76380
Nd, relaxation in weakly ionised expanding plasma 79—41222
Ne, $1s_3$ metastable, velocity-changing collisions, study by time resolved saturated absorption 80—82832
Ne, collision-induced light scatt. of low density 77—71765
Ne, gas, electron thermalization time and position distribution meas. 80—93771
Ne, reson. broadening at low densities 79—31452
Ne, reson. level lifetimes, Zeeman coherence radiative and collisional transfer between excited states 77—23466
Ne, spectral line broadening due to reson. interaction 79—22654
Ne, velocity diffusion, saturated absorpt. obs. of Hanle effect 77—61716
Ne, X-ray spectral line broadening in solid and gas targets 77—6713
Ne+Kr, K-L vacancy sharing process, Nikitin two-state model 80—9684
$Ne^+ + NH_3(H_2O)(Ne)$ symmetric collisions, double K-shell ionisation, two-electron-one-photon transitions 77—19067
Ni+Ni, continuum X-ray radiation, collision broadening 80—9539
$Ni^{14+} + H^+$, collisional excitation of fine struct. transitions in ground state 77—19017
O IV 1402.5 Å semi-forbidden line, collisional cross section from identification in quasi-stellar objects 80—12825
O^{q+}, electron loss, forward peak oscill. struct. 78—78796
$O^+ + NH_3(H_2O)(Ne)$ symmetric collisions, double K-shell ionisation, two-electron-one-photon transitions 77—19067
Pb, $^3P_1{}^0$ state reson. radiation, collisional quenching cross-sections 77—435
Rb+Kr, STS components shift and broadening 77—68014
Rb+N_2, spin relax. rate 77—19027
Rb+Rb(Cs), continuum- and bound-state pair absorption, 2300-3100 Å, 410-540°C 80—42970
^{85}Rb cell filtering action, press. shift and broadening by foreign gases 79—3403
^{87}Rb, hyperfine transition, light shifts, buffer gas shifts, rel. to maser freq. stability 79—98029
$^{87}Rb + {}^{129}Xe$, spin-exchange cross-section meas. 80—78686
$S^{n+} + Ne(SiH_4)(H_2S)(HCl)(Ar)$, K X-ray cross section, projectile charge depend. 77—19029
Se, loss of K-electron by proton-atom collision *(Russian)* 77—50523
Si^{q+} electron loss, forward peak oscill. struct. 78—78796
Sr, 4607.33 Å line, broadening and shift in H_2-O_2-Ar flames 77—18849
Sr, 5^1P state quenching cross sections in CO-N_2O^1 flames 77—18836
Sr-Cs mixture, laser induced collisional two-photon ionisation, fluoresc. monitoring 80—91515
Tl, 535.0 nm line shift by H_2 perturber 80—91506

atomic inelastic collisions continued
Tl, reson. lines, perturbing gas and self-broadening, temp. effects 80—42979
Xe, gas, electron thermalization time and position distribution meas. 80—93771

atomic magnetic moment
see also gyromagnetic ratio
Lamb shift, anomalous mag. moment, relativistic Dirac eqn. 80—42954
many-electron calc. 77—57884
multipole interaction between two nonoverlapping charge distributions 79—89731
muonium, ground state, muon mag. moment and HFS, Zeeman transition obs. 77—75345
muonium hyperfine structure of ground state, magnetic moments, muonium-antimuonium conversion, excited states 80—69273
paramagnetic electronic props. of atoms and mols., orbital mag. moments, paramagnetic currents 77—46476
paramagnetic gas in radiation field, magnetisation 78—78667
refractory elements, atomic-beam mag. reson. nuclear spin and hyperfine structure meas. 79—776
two-level spin system, mag. moment dynamics in mutually perpendicular mag. fields, of arbitrary freq. 79—3415
Bi, Faraday effect and magnetic circular dichroism 80—83399
Co, atomic magnetic moments comparison to values of ferromagnetic metal 78—52244
^{161,163}Dy, hyperfine struct. and hyperfine anomaly for fine transitions, high resolution meas. 77—88416
Fe, atomic magnetic moments comparison to values of ferromagnetic metal 78—52244
H atom, form factor for arbitrary states, dipole moment component matrix element calcs. *(Russian)* 80—58143
^{4}He, muonic, formation and hyperfine struct. 80—91707
^{4}He, electronic g_J-value of 2^3S_1 state, by atomic beam mag. reson. method 77—23446
I atomic vapour, self-induced transparency and reson. self focusing 80—64114
^{95}Mo, ^{97}Mo, quadrupole moments, hyperfine B factors, laser-Rf double reson. meas. 78—33452
Na, ($4^2P_{1/2}$, $5^2{}_{1/2}$ states), mag. dipole interaction consts., RF spectroscopy 78—37577
Ne, reson. four-photon parametric mixing conditioned by multipole relax. rates difference 79—89959
^{21}Ne^{n+}, $5/2^+$ state, hyperfine interactions and mag. moment of 0.350 MeV 78—17583
Ni, atomic magnetic moments comparison to values of ferromagnetic metal 78—52244
Ni-Pd, mag. form. factor, polarised neutron diffr. meas. 80—29525
O II, relative intensities and lifetimes in nebulae, conventional radiation theory 80—109513
Rb, induced mag. moment by laser excitaion *(Russian)* 79—68327
Tc I, HFS from atomic spectra, mag. dipole hyperfine consts. 77—68002
TiXIV(TiXV)(TiXVII), Tokamak discharge, ground state, mag. dipole transitions, UV spectra obs. 80—63575
U I, hyperfine struct. meas. of high-lying levels, mag. dipole and elec. quadrupole consts. 79—54796

atomic mass
see also isotopes; mass spectra; nuclear mass
alkali metal, phonon frequencies, depend. on atomic mass 79—14901
alloys, effective atomic number from β-ray produced bremsstrahlung meas. 78—22046
data tables 80—1076
differences, for wide doublets determ. with Manitoba II mass spectrometer 77—42432
experimental values of nucl. masses 77—6218
gram atomic volume, density, atomic mass, packing factor, eqns. for calc. 79—95066
heavy nuclei, Z=68-72, nucleon separation, pairing and decay energies and mass defect 77—79301
mass spectrometer determination, collector slit system 78—8463
optimum atomic mass formula from nuclear mass shell and parity corrections *(Russian)* 80—37902
reaction with time and expansion of Universe 80—90588
relative mass evaluation, input values 78—70949
sputtering yield, mass dependence, rel. to boundary effect 79—24398
table, mass excesses, total BEs, β-decay energies: at. mass evaluation 1977 78—4894
XY_6-type molecules, Coriolis coupling consts., at. mass effect, XCl_6 appls. 78—66684
Ca, atomic weight and isotope fractionation on Earth and in solar system 79—20835
^{37}Cl-^{35}Cl mass differences, for wide doublets, determ. with Manitoba II mass spectrometer 77—42432
^ER, A=167,168, absolute atomic masses 79—89228
Ga atomic weight from GaAs stoichiometry meas. 78—42234
Ga, atomic weight from solid-source mass spectra 77—541
^Hf, A=179,180, absolute atomic masses 79—89228
Ne, mass spectrometer determ., collector slit system 78—8463
^Os, A=189,190, absolute atomic masses 79—89228
Pd, isotopic comp. and at. wt., using solid source mass spectrometry 79—864
Re, atomic masses and mass differences, mass spectrometric obs. 77—42433
^{47,48}Ti, precise atomic mass determ. 79—31718
W, atomic masses and mass differences, mass spectrometric obs. 77—42433
Zr, isotopic composition, at. wt., rock standards, chondrite composition 79—3591

atomic metastable states
$1s2p^{2\,4}P$ levels, lifetimes and line fluoresc. yields 78—74612
atom+metastable atom collisions, ionis. processes 78—62907
autoionising and inner shell vacancy states, decay, time independent multichannel scatt. theory 80—47854
binary collisions, form. of He^+ and $He_2{}^+$ in afterglow, mass spectra obs. 80—54046
detection by microchannel plate 77—82618
discharge, running striation excitation, metastable atoms lifetime influence 80—38760
Doppler-free linear single-photon spectroscopy 78—50487
excitation function measurement, three-channel electronic apparatus *(Russian)* 78—25456

atomic metastable states continued
gas laser, at. and mol. vibr. and electronic metastable states, book contrib. 77—50653
glow discharge plasma, corpuscular diagnostic method of metastable atoms, review *(Czech)* 80—24241
He, Rydberg, series transitions, opto-galvanic spectroscopy 79—54779
heavy ion, one and two electron systems, Lamb shift and radiative decays 77—38643
heavy ion+at. collisions using GSI linear accelerator, X-ray production, appls. 77—19041
hydrogenic atoms, metastable, Raman-like two-photon scatt., calc. 80—47953
hydrogenic ions, radiative decay of $2S_{1/2}$ metastable state 77—67992
hydrogenic ions, selections from 1977 Comments on Modern Physics, book 79—30181
inert gas, metastable atoms, scatt. 78—62906
inert gas, metastable composition of inert gas beam from ion-neutral reaction 77—29008
inert gas collisions, intermediate energies 78—62904
inert gas hollow cathode arc, mol. beam sampling of metastable atoms as electron temp. probe 80—43967
inert gas ion beam, metastable fraction determ. by W surface impact, secondary electrons obs. 79—28873
inert gas metastable atoms, photoionisation rel. to laser development 78—13476
inert gas plasma, weakly ionised, photon echo relax. obs. in RF discharge 80—43986
inert gases, metastable atom diffusion, state decay, VUV obs. from discharge afterglow 80—44061
inert gases, metastable states, laser excitation and fluoresc. 77—57921
ionisation in positive column, unified electron temp. characts. 77—11419
metastability exchange collisions, Pauli principle effects 80—99536
metastable atoms in arc burning in argon, local densities meas. *(French)* 77—4017
metastable autoionising states, ang. distrib. of electrons which decay via fine and hyperfine struct. interactions 80—102492
multicharged Li-like ions, decay of metastable autoionised state *(Russian)* 78—25455
multiphoton transition detection 80—58231
parity nonconservation meas. sensitivity and level crossings role 80—43005
particle beam excited state populations, preparation, measurement and control, review 79—30607
Penning ionisation processes investig. by electron spectroscopy 80—58364
positive column, metastable atom radial transport, effect of wall boundary conditions 78—67493
positive column, metastable atom radial transport at various electron distribs., atom+atom collision effects 80—44037
positive column, metastable atom transport, excitation rate radial variation, flux to wall calc. 80—44038
properties, energy transfer mechanisms and exptl. techniques 80—27921
Rydberg atoms, expts., metastable states, multiphoton ionisation, spectroscopy, Stark struct., collisions, polarisability *(Dutch)* 78—5160
$n \rightarrow ep\bar{\nu}$, H atom spectra and metastable state *(Russian)* 80—37262
Al, in metal-halide arc, laser Raman scatt. determ. of local density 77—11424
Al^-, metastable, electron affinity calcs. 79—31439
Ar, 1s states deactivation by N_2 and SF_6, pulsed afterglow, kinetic absorption obs. 77—50398
Ar, ($^3P_2$) and ($^3P_0$) states, quenching mechanisms and rate consts. 79—13801
Ar (metastable)+dichloroethylene (dichlorobenzene), mol. ionis., collisional energy depend. 79—54950
Ar, electron impact excitation, 23 to 37 eV, metastable yield 80—9739
Ar, electron ionisation and excitation coeffs. in low E/N region 80—48090
Ar, hydrogenlike, Lamb shift meas. by motional elec. field quenching time-of-flight expt. 80—9550
Ar ions, electron impact ionisation, trapped ion cyclotron resonance spectroscopy 80—53140
Ar, metastable, electron impact excitation cross-sections calcs. 78—94323
Ar, metastable $^3P_2$ deactivation in afterflow, plasma characts. 78—55769
Ar metastable atom concentration, expts. determ. inside hollow cathode arc discharge *(French)* 77—31540
Ar, metastable atom density changes during arc interruption 77—51250
Ar, metastable ion beam, collinear laser spectroscopy, isotope shift, fluoresc. detect. 80—37771
Ar plasma, RF surface wave form., metastable atom density meas. 77—58890
Ar plasma, radial distrib. of excited atoms prod. by surface wave *(French)* 80—96349
Ar, sputtering glow discharge, metastable and reson. states density meas. *(French)* 80—14955
Ar, stationary afterglow obs. of singly charged atomic ions, three-body rate coeffs. 80—38757
Ar^+, metastable, electron impact cross section, laser fluoresc. 77—3465
Ar^{15+} and Ar^{16+}, beam-foil obs. of lifetimes of metastable states 80—14116
Ar^{x+}, high resolution spectroscopy of prompt and metastable decaying levels 78—33462
Ar-Br_2, positive column at. state densities 80—44007
Ar-Ti hollow cathode afterglow, energy transfer mechanisms and excited metallic ion prod. 80—43857
$Ar+Ar(^3P_2)(^3P_0)$, flowing afterglow metastable decay rates, diffusion, two- and three-body rate consts. 78—73027
$Ar+H_2$, metastable state breakdown, temp. depend. 79—98211
$Ar+H_2O(D_2O)$, ($^3P_{0,2}$) state quenching cross sections 78—70912
$Ar+HCN(H_2O)$, electron excitation of Ar^* and $Ar_2{}^*$, fluoresc. and dissoc. energy transfer collisions 77—14580
Ar+He, Penning ionis., ejected electrons energy and ang. distrib. 79—81266
$Ar+He^*(1s2s,{}^3S)$, coupled channel calcs. of chemi-ionisation 77—27166
$Ar+Kr(^3P_2)$, flowing afterglow metastable decay rates, diffusion, two- and three-body rate consts. 78—73027
$Ar+N_2$, 0.06-0.41 eV, metastable at. electronic excitation transfer 79—64071
$Ar+N_2$, pulsed microwave discharge, early afterglow and radiative transitions, Penning ionisation 78—9874
Ar+Xe, relaxation processes of $Xe^*(^3P_2)$ metastable atoms 78—50624
$Ar+Xe(^3P_2)$, flowing afterglow metastable decay rates, diffusion, two- and three-body rate consts. 78—73027

atomic metastable states continued

$Ar+Xe \rightarrow Xe^*$, electronic energy transfer, emission spectra, electron beam excitation 77−38722
$Ar(^3P_{0,2})$, excitation of $N_2(C^3\Pi_u)$, symmetry, propensity rules and alternation intensity, rot. spectrum 80−87135
$Ar(^3P_{0,2})+H(^2S)$, energy transfer rate const. and mechanism 78−37727
$Ar(^3P_{0,2})+H(^2S)$, energy transfer collisions, Lyman-α emission profile obs., in microwave discharge and reaction cell 80−58359
$Ar(^3P_{2,0})$, collision with chlorine atoms and molecules 77−46537
$Ar(^3P_2)$+fluorine containing molecules, quenching rate consts. 77−9072
$Ar(^3P_2)+H(^2S)$, energy transfer, Lyman-α line obs. 79−64085
$Ar(^3P_2)+N_2(C^3\Pi_u)$ excitation transfer cross section, radiative lifetimes, in N_2 laser, transitions 79−27246
Ar^*, quenching by $O(2p^4\ ^3P)$, population and depopulation of $O(3p^5P)$ 80−42958
Ar^*+CS_2, Penning ionisation and dissoc. fluoresc, collisional energy depend. 78−33584
$Ar^*+Fe(CO)_5$, chemiionisation and chemiluminescence reactions, Penning ionisation and fluoresc. obs. 80−97689
Ar^*+formaldehyde thermal collisions, $CH(A^2\Delta=X^2\Pi)$ emission 77−86304
Ar^*+H, assoc. ionis., rovibronic struct. in electron energy spectrum 80−106380
Ar^*+H, collisional quenching rates 80−95548
Ar^*+Kr^*, metastables, chemi-ionis., merging beams, 0.01-10 eV 80−14198
Ar^*+N_2, excitation transfer collision, vibronic energy partitioning 77−75264
Ar^*+N_2, metastable mol. form., emission spectra 77−19019
$Ar^*+N_2(H_2)(D_2)$, de-excitation processes, by pulse radiolysis optical emission obs. 77−65529
$Ar^*+N_2 \rightarrow Ar+N_2^*$, electronic to vibr. energy transfer, time depend. theory 80−23514
Ar^*+O_2, ion pair form. explained by charge transfer model 80−99546
$Ar^{*+}+Kr$, flowing afterglow, energy transfer reaction and quenching rates 80−23529
$Ar^*(^3P)+CO_2(X^1\Sigma_g{}^+)$, differential elastic and quenching cross-sections 78−58773
$Ar^*(^3P)+Co_2(X^1\Sigma_g{}^+)$, T-R and T-V energy transfer, collisional energy depend. 79−18262
$Ar^*(3p^54p)_i+Ar(^1S_0)$, collisional population transfer rate coeffs., 300K 79−10177
$Ar^*(4s^3{}_{2,0})+Kr(Xe)$, elastic and reactive scatt., ang. distribs. 77−6919
$Ar(3p^5, 4p)$ and $(3p^5, 4p')$ states, radiative lifetimes, two-body deactivation rate consts. 79−10068
$Ar(4s^3P_{2,0})+Xe\ (O)(Cl)$, exit channel distribution 77−46627
B^-, metastable, electron affinity calcs. 79−31439
$^{135,137}Ba$, HFS of metastable 6s5d configs., at. beam mag. reson. 79−49971
Ba, $(5d^3D_1)$state, quenching obs. 80−52926
Ba $(5d6p)^3D_3$ state, lifetime meas. by dye laser spectrosc. 80−78577
Ba, atomic beam and resonance spectroscopy 80−58180
Ba, Hanle effect in reson. line, density depend. 77−23473
Ba, hyperfine structure of metastable states, atomic-beam mag. reson. with laser detection exam. 77−79558
Ba II $5D_{3/2}$ metastable state, decay rate using ion storage technique 80−18826
Ba, time-resolved saturated absorption expt., collisions effects 78−29758
Ba vapour gas discharge laser excited by dual-pulse, lasing characts. 79−89895
Ba^+ ions, hyperfine struct. reson. determ. from fluoresc. *(French)* 77−432
Ba+Ba(Tl), laser induced collisional and radiative energy transfer 80−53108
$Ba+F_2$, crossed beam chemilum., kinetics and mechanisms 80−21264
Bi beams excited passing discharge region, new light source of forbidden lines 78−90112
Bi, metastable states collisional quenching, temp. depend. 77−88526
C^-, near-threshold photodetachment, IR meas. 77−42290
C^++N_2, luminescent charge transfer, metastable and ground state ions 78−42202
$C(^1D)$, prod. in cometary coma, detect. in comet west (1976 VI) 79−16885
$C(2^1S_0)+H_2(O_2)$(ethylene), collisional behaviour, kinetic study 80−74241
Ca, forbidden transitions, radiative lifetimes, MCSCF and CI calcs., time of flight spectra for metastable state 80−91498
Ca, metastable, prod. in N_2O-CO flame, u.v. spectra 77−9081
Ca+Ca(Mg)(inert gas), metastable ^3P-state, quenching reactions, fluoresc. meas. 80−102477
$Ca+F_2$, crossed beam chemilum., kinetics and mechanisms 80−21264
$Ca+O_2(CO_2)$, CaO form., product states obs. 78−92450
Ca+Sr, laser induced collisional and radiative energy transfer 80−53108
$Ca(^3P)+SF_6$, F_5S-F bond energy bounds from chemiluminesc. obs. 79−86081
^{43}Ca, atomic beam and resonance spectroscopy 80−58180
$Ca^*+Cl_2(HCl)$, luminesc. reactive collisions 77−16816
Ca^*+HCl, reaction performed under high resolution, luminescence obs. 80−95662
Cd metastable state, Li^+ charge transfer 80−48084
Cd+Cs, excitation energy transfer in sensitized fluoresc. 79−98210
$Cd(^3P_0)+CO(CO_2)(NO)$, absolute quenching cross section, phase-shift method 80−58340
Cl, foil excitation, K-vacancy bearing metastable states yield, 30-50 MeV 77−54600
Cl metastable ion beam, collinear laser spectroscopy, isotope shift, fluoresc. detect. 80−37771
Cl, metastable states, form. from Cl_2 dissoc. excitation, time of flight spectra 78−1094
Cl^{16+}, Lamb shift meas. using beam-foil excitation, QED test 80−9551
^{35}Cl XVI, beam-foil excitation, Lamb shift and fine struct., QED test 80−9549
$Cl(3p^5(^2P_{1/2}))$+carbon tetrachloride $(Cl_2)(He)$, VUV metastable state quenching, absolute rate const. 77−79641
Cu, absolute effective electron impact excitation cross sections, spectral obs. 80−53147
Cu, ground and metastable populations, buffer gas effect 78−82955
Cu, high current hollow cathode tube production 80−10445
Cu-vapour-He laser discharge, metastable decay rates 79−86164
CuCl pulsed laser, time depend. of Cu-atom conc. in ground and metastable states 78−66806

atomic metastable states continued

D, muonic atom initial population of 2S metastable state 77−27207
D(2S), form. by electron impact from $D_2(HD)$, time of flight obs 79−86079
Dy, isotope shift meas. using laser atomic beam technique specific mass shift determ. 80−91497
Dy^+ spectra, exam. of $4f^{10}6s$ and $4f^{10}5d$ configs. *(French)* 77−50385
Eu^+ in discharge plasma, anomalously high speed deexcitation, modulation of induced radiation obs. 80−44014
F^{7+}, $1s2p^3P_1$ collisional quenching, perturbation theoretic calc. 77−54602
Fe III, metastable states in Be star ϕ Persei rel. to mass loss 79−5832
^{57}Fe metastable states, hyperfine struct. meas. by laser RF double-resonance 80−58404
Gd, populations of metastable levels during electron beam evap. 77−57926
H, $2^2S_{1/2}$ state F=1 hyperfine component, Majorana transitions, LZS model 77−57959
H $(2^1S_{1/2})$, two-photon decay, Laplace transform method 79−10084
H (2s) metastable state elastic electron scatt. 78−55238
H atom, many-photon excitation spectra, fine structure 79−59419
H atoms, 1s-2s excitation in collisions with H and H_2 79−89764
H, beam, $2^2S_{1/2}$ metastabld ats., nonadiabatic transition in mag. field 78−55157
H, form. by charge exchange in $H^++Mg(Ba)$ collision 79−81275
H like, metastable 2S state in weak elec. field, radiative decay, bound state QED 80−42959
H, metastable fraction of n=2 populations in H^++Cs electron capture 77−30988
H, metastable quenching, subsequent photoionis., polarised proton prod. *(Russian)* 78−46202
H metastable states; polarised, ion form., charge exchange in ion source *(Rumanian)* 77−46445
H, muonic, metastable 2s state fraction at 150 and 600 Torr 78−13631
H, muonic atom initial population of 2S metastable state 77−27207
H, subnatural linewidth resolution $2^2S_{1/2}$, $2^2P_{1/2}$ level crossing, Lambshift, pulse technique 79−22669
H , metastable, electron affinity calcs. 79−31439
H^+, isoelectronic sequence, quenching radiation anisotropy calcs. 77−27021
H^{2-}, metastable, electron affinity calcs. 79−31439
H^2 , metastable state 77−18805
H-like atoms, E1-M1 interference in radiative decay, $2S_{1/2}$ metastable state, effect on Lamb shift expts. 78−41994
H-like metastable ions, de-excitation in laser plasma *(Russian)* 77−7597
$H+A^{7+}$, charge transfer for ground and metastable states 77−42399
$H_2+He(2^3S_1)$ mol. ionis., optical atom orientation method *(Russian)* 78−13591
$H(1^2S)+H_2$ (inert gas), electron capture, electron loss and deexcitation cross sections meas. 78−22025
H(2S), form. by electron impact from $H_2(HD)$, time of flight obs. 79−86079
$H(2S)+H_2(N_2)(NH_3)$(acetone)(methanol), collisional quenching, mass spectral obs. 78−25685
H(2S)+inert gas, collisional quenching, mass spectral obs. 78−25685
$H(2S)+Kr(Ne)(Xe)(H_2)$, metastable atom total quenching 77−46628
$H(2^2S)+H_2$(inert gas), electron capture, electron loss and deexcitation cross sections meas. 78−22025
H(2s), optical model approach to elastic scattering of electrons, polarisation effects 80−58382
$H(2s)+H_2(He)(Ne)(Ar)(Kr)$, collisional de-excitation, 5-26 keV 79−59546
$H(2s)+H(H_2)$, electron capture, loss, and collisional destruction, 5-26 keV 80−5611
$H(2s)+He\ (Ne)(Ar)(Kr)(H_2)(N_2)$, 5-25 keV, H(n=3) excitation, Balmer α emission obs. 80−53113
H(2s)+inert gas, electron capture, H form., 4-25 keV 80−9729
He, $^3S \rightarrow 2^1S$ transition probability, electron collisions 78−5358
He, 2^1S and 3^1S, CI expsn., convergence patterns 77−50378
He, 2^1S state, two-photon ionisation, multipole interference 79−22675
He 2^1S state isoelectronic series, Fermi and Coulomb correlations 78−921
He, 2^3S_1 metastable state, interactions, optical pumping investig. 80−23377
He, 2^3S_1 and 2^1S_0 metastable states, static dipole polaris. meas. 78−1098
He 2^3S-3^3S electron impact excitation, first Born and Glauber cross sections 78−55243
He 2S metastable state, three-photon ionis. 79−18167
He, 2S metastable states, singlet and triplet; two and three photon ionisation cross section, absolute determ. 80−83329
He, $2(^{1,3}S)$ excited states, dynamic polarisabilities 77−34772
He, $2(^{1,3}S)$ excited states and ground state, dynamic polarisabilities, van der Waals force consts. 77−34773
He $(2^3P)+Ca(Sr)$, collisional quenching of metastable states, excitation transfer cross sections 78−66653
He, (2^3S_1) state excitation by electron impact, at. time of flight meas. 77−19083
He, afterglow, intermediate press., plasma discharge parameter time depend. calc. 79−19102
He, autoionising S states, electron-atom collision resons. theory calcs. 77−58179
He beam, electron impact excitation with good vel. resolution retention 77−14609
He, discharge, level populations, time resolved spectra 77−80391
He, Doppler-free two-photon high resolution spectroscopy 80−58197
He, electron impact metastable excitation, resonance struct. 77−27184
He flow discharge, intermediate press., positive column conc. of ions and metastables 80−44017
He glow discharge, laser-induced 569 and 637 Å Raman emission source 79−46024
He I 1s3d levels, cascade-free lifetime meas., using He^++He 35 keV collisions 78−58607
He low-current discharge, metastable atoms, radial density distrib. obs. and calc. 78−67495
He, metastable, deexcitation process on Mo [110] impact 78−95642
He, metastable, multiphoton transition detection, n^3S-n^3D splitting meas. 80−58231
He, metastable, two-photon ionisation, multipole interference effects 80−23466

atomic metastable states continued
He, metastable 1s2s^{1}S state, photoionisation, perturbation theory calcs. 78–78759
He metastable 2^{3}S state, electron impact excitation cross-sections calc. *(Russian)* 80–53149
He, metastable and ground state electron loss cross section, collisions with gases and metal vapours 80–53117
He metastable beam, form. by alkali metal vap. charge exchange, composition 79–89775
He, metastable beam source for surface spectroscopy 77–36334
He metastable state, two- and three-photon ionisation 80–91518
He, metastable states, electron and proton impact ionisation, autoionisation 80–102573
He, metastable states, high resolution study via electron scatt. 77–6935
He, metastable thermal atoms, interaction with solid surface, obs. of He$^+$ ion creation *(French)* 77–79684
He, Penning ionisation electron spectroscopy, metastable He impact, electron energy distrib. 79–52060
He plasma, cryogenic, oscill. excitation by hot electrons 79–55493
He, positive column plasmas, metastable atom density meas. by improved self absorpt. method 80–87968
He, three-photon ionisation from metastable states, cross-sections 77–42296
He, two-photon ionisation calc. for linearly and circularly polarised laser light 79–797
He, Voigt profile, line absorpt. calcs. of 388.9 nm triplet, 501.6 nm singlet lines 78–90123
He$^-$, (1s2s2p)^{4}P^0 metastable state, CI calc. 79–59591
He$^-$, binding energy of metastable 1s2s2p ^{4}P^0 state 80–9524
He$^-$, isoelectronic sequence, triply excited bound state, variational calc. 80–9526
He$^-$, metastable, electron affinity calc. 79–31439
He$^+$, ion+electron scatt., static exchange approx. Schwinger variational principle, photoionisation cross section 80–43192
He$^+$ Lamb-shift measurement by the quenching-radiation anisotropy method 80–18824
He-Cd hollow cathode laser, He singlet and triplet metastable number densities 78–29938
He-Cd laser, 8067 Å, He metastable atoms effect on power 78–33722
He-Cd laser, hollow cathode type, quasi-metastable state excitation 78–33721
He-like atoms, 2^{3}S$_1$-state nonexponential decay profile 77–88407
He-Ne lasers levels, modulation spectroscopy 78–46572
He-Zn laser, 7588 Å, He metastable atoms effect on power 78–33722
He^3-He^4 mixture, relax. of 2^{3}S$_1$ metastable atoms 80–102469
He+Ar(Kr)(Xe), He*(2^{1}S) scatt., low energy repulsion systematic struct. 78–22000
He+CS$_2$, metastable atoms, energy transfer processes 80–83466
He+H (inert gas atom), long range interactions for (2^{1}S) and (2^{3}S) states 78–70895
He+H$_2$O(D$_2$O), chemi-ionisation and secondary ion reactions, ^{3,1}S He metastables 77–40531
He+H$_2$(He)(Ar)(N$_2$), fast metastable at. collisional destruction cross section 78–74760
He+H$_2$(He)(N$_2$)(Ne)(Ar), 25-450 keV, metastable ion beam electron loss and deexcitation cross section 77–34745
He+He, (2^{3}S) and (2^{1}S) metastable states, direct and assoc. ionisation rate consts. in afterglow, electron energy spectra 79–13812
He+He, metastable atoms, collisional ionisation cross-sections 78–70911
He+Hg, metastable He, collision rate consts. in pulsed discharge afterflow 78–50627
He+N$_2$(O$_2$), He(2^{3}S) quenching reactions 78–22014
He+Ne, afterglow, metastable state energy transfer, spectra 80–43167
He+Xe, electron-loss cross section struct., 0.05-4 MeV 78–9236
He$^+$+Ar(H$_2$)(He)(Kr)(N$_2$)(O$_2$), metastable ion electron capture, loss and de-excitation 77–6904
He$^+$+atom, metastable state deexcitation, 2S- and 2P-state mixing and Penning ionisation 77–42394
He$^+$+Na(K)(Cs), 5-100 keV, electron capture form. of fast metastable He 78–74760
He$^+$+Ne*$\rightarrow$He*+Ne$^+$, cross sections 79–22821
He(He$_2$)+Ar, metastable destruction rates 78–37728
He(^{1}S$_0$)+Na(Li) radiative Penning ionis., photoionis. cross section depend. of continuum radiation 77–19034
He(S^{3}S)+alkali metal atom, Penning ionisation by slow collisions 77–50512
^{3}He-^{4}He isotope mixtures, mag. resonance line widths of 2^{3}S$_1$ states, metastability exchange cross sections *(Russian)* 77–10614
^{3}He+^{4}He, metastability exchange, coherency transfer *(Russian)* 78–13594
^{3}He(^{4}He) clusters, metastable electronic states, electron impact excitation, time of flight spectra 80–106411
^{4}He, electronic g$_J$-value of 2^{3}S$_1$ state, by atomic beam mag. reson. method 77–23446
He*, impact on Mo surface, clean and gas covered, deexcitation, pot. energy transfer mechanism 80–60743
He* impact on Pd (111) surface, clean and CO covered, electron emission, energy and ang. distrib. 80–60744
He*-Ne*, Penning ionisation of metastable He* 80–83472
He*+Ar, Penning ionisation, laser modified collisional effects in electron energy spectrum 78–90278
He*+Ar(Kr)(Xe), elastic scatt., repulsive rainbows and optical pots. 79–840
He*+D, Penning and assoc. ionis. with metastable He, 0.01 to 10 eV beams 79–27074
He*+D$_2$(Ar)(Kr) interaction pots. 77–83674
He*+H(H$_2$)(Ar), metastable state, ionis. processes 78–62907
He*+He, collisional ionisation, cross-section meas. 77–46631
He*+He, collisional ionisation, He$_2$ $^1\Sigma_g{}^+$ state pot. curve calcs. 77–46632
He*+He, inelastic collision, 1-5 keV, autoionising states 78–13581
He*+N$_2$, Penning ionisation, ejected electron spectra obs. 80–48074
He*+Ne*$\rightarrow$He+Ne$^+$+e, Penning ionisation, merging beams obs. 78–33585
He*Ar(Kr)(Hg), Penning and assoc. ionisation, correl. diagrams calcs. 77–50521
He*(1s2s,^{3}S)+Ar, Penning ionis., discrete-continuum states coupling 79–10193
He*(2^{1}P)+Ar$\rightarrow$He+Ar$^+$+e$^-$, anisotropic interaction potential, impact parameter method 77–68102

atomic metastable states continued
He*(2^{3}S), (2^{1}S)+O$_2$, ion pair form., ion beam neutralisation reionisation spectroscopy 80–53120
He*(2^{1}S)+Ne, elastic and reactive scatt., ang. distribs. 77–6919
He(2^{1}S, 2^{3}S), elastic electron scatt., 7-500 eV Glauber cross sections 77–19077
He(2^{1}S,2^{3}S)+Ne(Ar)(Kr)(Xe), Van der Waals forces, one-electron model pot. calcs. 80–14094
He(2^{3}S, 2^{1}S)+Ba(Y)(Ce), Penning process, double ionisation 77–3439
He(2^{3}S,2^{1}S)+H, Penning ions. 79–64089
He(2^{1,3}S), electron impact excitation and ionis., cross sections 77–31001
He(2^{1,3}S), inelastic scatt., RPA and 1st Born approx. calcs. 80–53148
He(2^{3}S), bi- and ter-mol. deexcitation reaction rate coeffs. meas. in afterglow 79–36748
He(2^{3}S) bubble in liq. He, phenomenological model 77–20147
He(2^{3}S) collisions, elastic scatt., Penning ionisation, polarisations *(Russian)* 78–70922
He(2^{3}S) population in fast beam formed by 25-90 keV He$^+$ neutralisation 79–31740
He(2^{3}S), quenching rates meas., in pure afterglow 77–75206
He(2^{3}S), singlet and triplet metastable number densities and excitation mechanisms in He-Cd$^+$ hollow cathode laser 80–48220
He(2^{1}S)+Ar, optical interaction pots. from differential cross sections 77–30956
He(2^{3}S)+Ar, differential cross-section meas., optical interaction pots. 77–3443
He(2^{3}S)+CS$_2$, CS$^+$ and CS fluoresc. spectra assignments, vibr. populations, transition moments 77–14473
He(2^{3}S)+H$_2$O(H$_2$S), energy transfer processes, reaction products, UV and visible obs. in flowing afterglow 78–85138
He(2^{3}S)+H(D), Penning and assoc. ionis. cross sections, vel. depend. 79–22815
He(2^{3}S)+molecule collisions, exit channels rate consts. 79–13800
He(2^{3}S$_1$) in alkali-He quantum magnetometer 80–17965
He(2^{3}S$_1$), metastable state electron impact excitation differential cross section meas. 79–10210
He(2^{3}S$_1$)+Ca(Sr)(Ba), coherent ^{2}P$_{3/2}$ levels excitation by Penning ionis., Hanle effect 80–5520
He(2^{3}S$_1$)+e$\rightarrow$He(1^{1}S$_0$)+e+KE, in afterglow, rate const., electron energy distrib. 78–71571
He(2^{3}S$_1$)+Hg$_0$$\rightarrow$He$_0$+Hg$^+$+e, in afterglow, rate const. meas. 78–17785
He(2^{3}S$_1$)+Na(K)(Rb)(Cs), Penning ionis. in stationary afterglow 78–42184
He(2^{3}S and 2^{1}S)+H$_2$(D$_2$), Penning, rearrangement and total ionis. cross sections, vel. depend. 79–22816
He(2s^{3}S$_1$)+Sr, alignment of ions in Penning collisions, polarised emission obs. 80–23533
He(metastable)+dichloroethylene (dichlorobenzene), mol. ionis., collisional energy depend. 79–54950
^{179}Hf, hyperfine struct. in ground multiplet ^{3}F and nucl. quadrupole moments of ^{177}Hf and ^{179}Hf 77–83520
Hg, 6^{3}P$_{0,2}$-state, electron impact excitation, optical detect. 77–50546
Hg, diffusion coeffs. temp. depend. in Ne and Ar 77–68731
Hg, metastable and excited states, pulsed dye laser absorption spectroscopy 79–26924
Hg, odd isotopes, Lande factor of 6^{3}P$_0$ metastable level *(French)* 78–5162
Hg+He, metastable ccts., in afterglow, Hg$^+$(7^{2}P$_{1/2}$) excitation rate const. *(Russian)* 78–29848
Hg+Hg*, combination into ungerade dimer states 80–55633
Hg+Tl, excitation energy transfer, excitation rate consts. 80–37772
Hg(^{3}P$_0$)+Br$_2$$\rightarrow$HgBr(B)+Br, crossed mol. beam chemiluminesc., cross section 78–31622
Hg(6^{3}P$_0$), ^{3}P$_1$-^{2}P$_0$ fine struct. obs., CO$_2$ laser mag. res. 77–61696
Hg(6^{3}P$_0$)+Hg(6^{3}P$_2$), line excitation and population decay in afterglow 80–74242
Hg(6^{3}P$_0$)+Na, energy transfer, rate consts. *(Russian)* 79–54952
Hg(6^{3}P$_{2,0}$)+inert gas, diffusion in low-current discharge 78–63618
Hg(6^{3}P$_2$), Pt surface impact, in Hg(6^{3}P$_1$) stepwise electron excitation function meas. 79–858
Hg(6^{3}P$_2$)+Hg, aligned metastable ats., longitudinal and transverse relax. times, simultaneous meas. 78–13585
I, prod. from He-I$_2$, quenching rate const. by I$_2$ mols. 78–13691
I, produced in UV photodissoc. of alkyliodides, time-resolved obs. of I(^{2}P$_{1/2}$) reactions 80–11940
I(^{2}P$_{1/2}$)+n-iodopropane (iodoethane), quenching rate coeff., in UV photolysis of n-iodopropane (iodoethane) 79–11799
I*(5^{2}P$_{1/2}$)+HF(HCl)(HBr)(HI), collisional quenching rate consts. meas. 77–3299
I(5p^{2}P$_{1/2}$)+I$_2$, metastable relax., rate const. 77–19022
In, in metal-halide arc, laser Raman scatt. determ. of local density 77–11424
Kr, at. beam, partially metastable, composition, charge exchange 79–85914
Kr, DC glow discharge excited atoms, radial conc. distrib. obs. 78–67494
Kr, electron ionisation and excitation coeffs. in low E/N region 80–48090
Kr I, laser spectroscopy, isotope shifts, hyperfine struct. *(French)* 78–33457
Kr, in afterglow, spectra collisions 77–427
Kr, metastable, electron impact excitation cross-sections calcs. 78–94323
Kr, stationary afterglow obs. of singly charged atomic ions, three-body rate coeffs. 80–38757
Kr$^+$, Kr$_2{}^+$, ^{2}P$_{1/2}$ and ^{2}P$_{3/2}$ states, mobilities in Kr, spin state depend. 77–3913
^{86}Kr, discharge, metastability-exchange cross section 80–99464
^{86}Kr-^{78}Kr, discharge, metastability-exchange cross section 80–99464
Kr+Ar*, 123.6 nm emission excitation of Kr by metastable Ar, press. depend. 78–5331
Kr+H$_2$O(D$_2$O), (^{3}P$_{0,2}$) state quenching cross sections 78–70912
Kr(^{3}P$_2$), quenching mechanisms and rate consts. 79–13801
Kr(^{3}P$_2$)+fluorine containing molecules, quenching rate consts., KrF* formation branching ratios 77–9072
Kr(^{3}P$_1$)(^{1}P$_1$)+CO, A$^1\Pi$-X$^1\Sigma^+$ and b$^3\Sigma^+$-a$^3\Pi$ sensitised fluorescence, isotope effects 78–82761
Kr*+Ar*, metastables, chemi-ionis,, merging beams. 0.01-10 eV 80–14198
Kr*+He, ^{3}P$_2$ metastable state, disorientation cross-sections 77–71853
Kr*+He, persistence of velocity following elastic collisions 78–78779

atomic metastable states continued
$Kr^*+He(Ar)$, vel. changing collisions studied by saturated absorpt. 78–62892
Kr^*+Kr, $^3P_2$ state, metastability-exchange and depolarisation, press. broadening of mag. reson. curves 77–71853
Li, quartet states, absolute term values, CI calcs. 78–58596
Li, quartet states, transition energies, oscill. strengths, CI calcs. 78–58597
Li^-, core-excited bound states 80–91468
Li^+, 2^3S_1 metastable state radiative lifetime, fluoresc. meas. 80–42999
Li^+, $2(^{1,3}S)$ excited states, dynamic polarisabilities 77–34772
Li^+, $2(^{1,3}S)$ excited states and ground state, dynamic polarisabilities, van der Waals force consts. 77–34773
$^6Li^+$, hyperfine structure, Doppler-tuned ion beam laser spectroscopy 79–89627
$^ALi^+$, A=6,7, $2^3{}_1$-2^3P, dye laser saturation spectroscopy 80–18821
Mg ($^3P_1$) metastable atom afterglow quenching rate consts. with various mols. 77–6720
Mg beams excited passing discharge region, new light source of forbidden lines 78–90112
Mg I, ^3p triplet system, lifetime meas. 80–47946
Mg, metastable, prod. in N_2O-CO flame, UV spectra 77–9081
$Mg+F_2$, crossed beam chemilum., kinetics and mechanisms 80–21264
$Mg(^3P)+K(Ca)$, energy transfer and excimer form. in flowing afterglow 77–60049
^{55}Mn, metastable states, hyperfine struct., laser RF double reson. study 79–72260
^{95}Mo, ^{97}Mo, quadrupole moments, hyperfine B factors, laser-Rf double reson. meas. 78–33452
N, $(2p^3\ ^2P^0)$ state, form. and depletion in N afterglow 79–49951
$N+O(^3P)$, endoergic assoc. ionisation, merged beam obs. 79–100348
$N^++H_2(DH)$, >6 eV reaction dynamics 77–32779
N^+ +inert gas, electron capture (loss) by metastable (ground-state) ions, 2-30 keV 78–25695
N^++N_2, luminescent charge transfer, metastable and ground state ions 78–42202
$N_2+Ar^*(He^*)$, sensitised fluoresc., vel. depend. 77–10744
$N(^2D,^2P)$ metastable atoms prod. in N_2 DC glow discharge 80–38758
$N(^2D,^2P)$ metastable production by electron collisions in DC glow discharge 80–59274
$N(^2D)+O_2$, chemiexcited NO form., 90-180K IR obs. 78–90163
$N^+(^5S)$+inert gas, de-excitation cross section, 2-30 keV 78–25695
$N_2(X^1\Sigma_g{}^+)+Ar(^3P_{2,0})\rightarrow Ar(^1S)+N_2(C^3\Pi_u)$, sensitised fluoresc., vel. depend. 78–90204
$Na+Ar^*$, Penning, associative and total ionis. cross sections 77–79683
$Na+Na^*$ resonant collisions mechanisms, excitation transfer in strong mag. fields between Zeeman sublevels 77–83712
Nd, relaxation in weakly ionised expanding plasma 79–41222
Ne, $1s_3$ metastable, velocity-changing collisions, study by time resolved saturated absorption 80–82832
Ne, $2p_1$ level relax. and populations of $1s_2$ and $1s_4$ in afterglow 78–9111
Ne, $2p^53p$ level, stepwise excitation, effective cross section 77–83550
Ne, $2p^53s^3P_0$ state, optical pumping, g-factor, metastability exchange cross section 80–947
Ne $(2p^53p)$ states, radiative lifetimes, collisional deactivation rate consts. 80–69107
Ne, atom, isotopic shift and fine struct. for $2p^54d$ and $2p^55s$ config., Doppler-free two-photon spectroscopy 80–23387
Ne, beam-foil excited ^4P state, delayed coincidence Auger electron lifetime meas. 80–14117
Ne, discharge, excitation mechanisms investig. using radial distrib. of excited atoms 80–38744
Ne discharge positive column in longitudinal mag. field, metastable atom radial density distrib. obs. 78–67496
Ne, Doppler-free linear single-photon spectroscopy 78–50487
Ne, hollow cathode discharge, role of Penning ionisation of minor species 79–86633
Ne, metastable, photoionis. cross section calc. 78–33485
Ne, metastable and pseudo-metastable states destruction by electron impact *(French)* 78–9260
Ne metastable atom concentration, expts. determ. inside hollow cathode arc discharge *(French)* 77–31540
Ne, metastable electronic states, electron impact excitation, time of flight spectra 80–106411
Ne, metastable form. by electron impact *(French)* 78–33611
Ne, metastable level deactivation by electron collision in low press. discharge 78–83520
Ne, metastable state ratio in fast beam, laser-induced fluoresc. obs. 79–54801
Ne, optical pumping of metastable $(2p^53s^3P_0)$ state 78–25486
Ne positive column plasmas, metastable atom density meas. by improved self absorpt. method 80–87968
Ne, Townsend discharge afterglow, decay rate of metastable ats. 80–44011
Ne-N_2 AC discharge, pulse to continuous mode transition, Ne metastable effects *(German)* 80–84011
$Ne+CS_2$, metastable atoms, energy transfer processes 80–83466
$Ne+H_2$, metastable state breakdown, temp. depend. 79–98211
$Ne+H_2O(D_2O)$, chemi-ionisation and secondary ion reactions, $^3P_{2,0}$ Ne metastables 77–40531
Ne+Ne(He), 7d′ states, isotope shift, press. shift, press. broadening, two-photon spectra obs. 78–55155
$Ne+SF_6(N_2)$, metastable state de-excitation, rate consts., radiolysis obs. 80–40709
Ne^++H, Penning ionisation, electron energy spectrum 79–72406
$Ne(^3P_{0,2})+Ne$, differential cross sections 80–58370
$Ne(^3P_2)$ elastically scattered, metastable, ang. distrib., conventional rel. to Doppler shift methods 80–58418
Ne^* 5882 Å line, Doppler free spectra, press. broadening and shifts, saturation spectroscopy 80–78565
Ne^*+Ar, associative ionisation studied by merging-beams technique 80–91646
Ne^*+Ar, Penning and assoc. ionisation, correl. diagrams calcs. 77–50521
Ne^*+Ar^*, Penning ionisation studied by merging-beams technique 80–91646
$Ne^*+Fe(CO)_5$, chemiionisation and chemiluminescence reactions, Penning ionisation and fluoresc. obs. 80–97689
Ne^*+H, assoc. ionis., rovibronic struct. in electron energy spectrum 80–106380

atomic metastable states continued
Ne^*+H_2O, pot. energy surfaces, MO and CI calcs., Penning ionisation electron spectra 80–106376
$Ne^*+He^*\rightarrow He+Ne^++e$, Penning ionisation, merging beams obs. 78–33585
Ne^*+Kr, Penning and associative ionisation 77–6910
Ne^*+Ne, differential elastic scatt., rainbow max., mol. states 77–38710
Ne^*+Ne, metastability exchange by optical pumping *(French)* 77–61845
Ne^*+Xe, chemiionis. in metastable state collisions 79–68306
Ne(metastable)+dichloroethylene (dichlorobenzene), mol. ionis., collisional energy depend. 79–54950
O, autoionis., radiative emission, competition in excited state decay 77–75109
O, beam-foil excited ^4P state, delayed coincidence Auger electron lifetime meas. 80–14117
O I 5577 Å meteoric forbidden line collisional quenching 77–17448
O, metastable ^5S-state, optical pumping 80–32678
O^+ +atmospheric gases, thermal energy reaction rates 78–92443
O^++N_2, luminescent charge transfer, metastable and ground state ions 78–42202
$O^++N_2(O_2)$, excited ion reactions, charge transfer coeffs. at thermal energy 80–95721
$O^+(^2D)$ in thermosphere, quenching by electrons 80–94630
$O^+(^2D)$ metastable state, temp. depend. of rate coeff. for charge exchange with N_2 80–77179
$O(^1D)$, energy transfer contrib. to heating of low nighttime ionosphere 79–44288
$O(^1D)$ metastable beam form. in O^- +inert gas scatt. 80–32829
$O(^1D)+H_2(HCl)(NH_3)(N_2O)$(methane), rate consts., temp. depend. 78–27747
$O(^1D)+O_3$, UV photolysis, $O(^3P)$ prod., rate consts. determ. 80–55636
$O(^1D_2)+CO(^1\Sigma^+)$, collisional quenching, energy transfer processes 80–23501
$O(^3S)$ prod., reson. radiation 80–53122
$O(^5S)$ impact on Cu-Be-O surface, secondary electron yield 78–58797
$O(^5S)$ metastable state, radiative lifetime determ. 78–74614
$O(^5S)$+inert gas, de-excitation cross sections 80–53118
$O(^5S)+Ne(Ar)(Kr)(Xe)$, total cross sections 78–42188
$O(^5S_2)$ metastable state g_J factor, TOF at. beam mag. reson. obs., rel. to $He(^3S)$ 79–3593
O(Se)(S)+inert gas, ^1S-^1D collision-induced transitions 78–33588
$O^{+*}+N_2(O_2)$, metastable ion reactions, rate consts. and ion mobility at 300K 80–95722
$O(2^1D_2)+Cl_2$, reaction kinetics, vac. UV at. spectra 77–21365
$O(2^1D_2)+N_2(O_2)(N_2O)(CO_2)(H_2O)$(methane), collisional deactivation meas., 295K, rel. to atmospheric processes 80–16663
P , metastable, electron affinity calcs. 79–31439
Pb, chemiexcitation of ^3P metastable states, during combustion of acetylene and C_2H_2 78–3339
Pb, laser excited fluoresc., three-level scheme 78–17605
Pr, metastable, F=7⇌6 Hfs, laser-RF double reson. spectroscopy 80–58170
Rb, lowest metastable autoionising level identification by RF spectroscopy 77–426
S, foil excitation, K-vacancy bearing metastable states yield, 30-50 MeV 77–54600
S, He-like, 2^3P_1 state lifetime, X-ray emission 77–18851
Si, foil excitation, K-vacancy bearing metastable states yield, 30-50 MeV 77–54600
Si, He-like, 2^3P_1 state lifetime, X-ray emission 77–18851
$Si+H_2(O_2)(He)(SiCl_4)$, $3p^2(^1D_2)$ state behaviour, at. absorpt. spectra 78–29846
$Si(3p^2(^1S_0))+He(SiCl_4)(O_2)(N_2O)$, attenuation of reson. radiation, time-resolved kinetic obs. 78–5329
Sm, excited states hyperfine struct., isotope shifts, laser-RF double reson. obs. 79–41140
Sr, electron impact excitation, from metastable states 78–1084
Sr, metastable, prod. in N_2O-CO 77–9081
$Sr+F_2$, crossed beam chemilum., kinetics and mechanisms 80–21264
$Sr(^3P)+SF_6$, F_5S-F bond energy bounds from chemiluminesc. obs. 79–86081
^{87}Sr, $^3P_2$ metastable state, hyperfine struct. at. beam mag. reson. obs. 78–17590
Sr^*+HCl, reaction performed under high resolution, luminescence obs. 80–95662
$Sr^*+N_2O\rightarrow SrO^*+N_2$, visible chemiluminescence, absolute cross section and photon yields 78–92463
$Ti(^5F)+N_2O(O_2)(NO_2)$, chemiluminesc., TiO dissoc. mechanisms, confirmation of $D^\circ{}_0$(TiO) 77–40534
Tl, $6^2P_{3/2}$-$6^2P_{1/2}$ transition, population inversion 80–950
Tl, $(6p^2P_{3/2})$, from selective photodissoc. of TlBr 78–90243
Tl, metastable atoms quenching, diffusion and decay in buffer gases 79–54953
Tm I, hyperfine struct., high resolution spectrosc. meas. 80–87238
^{235}U, high precision meas. of hyperfine struct. of 620 cm^{-1} atomic level 79–45660
$U(f^3ds^2)$+molecule, collisional relax. of $^5K_5{}^0$ and $^5L_7{}^0$ states, laser-induced fluoresc. obs. 80–52925
Xe, $^3P_2$ metastable, deexcitation by slow electrons *(Russian)* 78–13607
Xe, afterglow, $6s_{12}$ metastable atom density decay rate 78–63612
Xe, afterglow, metastable atom deactivation, electron collision effects 77–23441
Xe, electron ionisation and excitation coeffs. in low E/N region 80–48090
Xe, fast beam of metastable ions, high resolution spectra 77–42274
Xe, gas discharge, laser beam polarisation plane rot. near reson. 77–1024
Xe, line transition probabilities, in afterglow plasma, light absorpt. obs. 77–30807
Xe, metastable ions, $5d^4D_{7/2}$ state, laser induced fluoresc. 77–14387
Xe^+, metastable, electron impact cross section, laser fluoresc. 77–3465
Xe^+, $Xe_2{}^+$, $^2P_{1/2}$ and $^2P_{3/2}$ states, mobilities in Xe, spin state depend. 77–3913
Xe-Br_2 discharge, atomic state density determ. 79–36573
$Xe+Br(CCl_4)$, excitation functions and rotational polarisation, chemiluminesc., crossed beam study 80–76491
$Xe+H_2$ 79–98211
Xe+Ne, quenching of excited $Xe^*(^3P_2, ^3P_1, ^1P_1)$ states 80–63578
Xe+Xe(6s′(1/2)), (6p(1/2)), energy transfer, rate coeffs. 78–33573

atomic metastable states continued
- $Xe^{+}(^{2}P)+Ca(Sr)$, collisional quenching of metastable states, excitation transfer cross sections 78—66653
- $Xe(^{3}P_{0,2})+Br_2 \rightarrow Xe^{*}+Br$, excitation function 78—40028
- $Xe(^{3}P_2)$, quenching mechanisms and rate consts. 79—13801
- $Xe(^{3}P_2)$ + fluorine containing molecules, quenching rate consts., XeF^{*} formation branching ratios 77—9072
- $Xe^{*}+Xe$, $^{3}P_2$ state, metastability-exchange and depolarisation, press. broadening of mag. reson. curves 77—71853
- $Xe(6s,^{3}P_2)+Cl_2(PCl_3)(CCl_4)(COCl_2)$, vibr. energy disposal from XCl^{*} spectrum 79—100345
- $Xe(6s,^{3}P_2)+RCl$, reactive quenching, XCl^{*} emission spectrum obs. 79—100344
- $Xe(nf)+SF_6$, l-changing collisions obs. 80—91633
- $Zn(4^{3}P_2)+Zn(4^{1}S_0) \rightarrow Zn(4^{3}P_{0,1})+Zn(4^{1}S_0)$, metastable Zn depopulation, diffusion coeff. determ. 77—23542

atomic orbitals *see atomic structure*

atomic orbitals calculations
- *see also GO calculations; GTO calculations; STO calculations*
- 1s hole states of 3- and 4-electron systems, generalised Brillouin theorem-multiconfig. method 77—23443
- 2p-h TDA equations, superoperator derivative 79—31372
- ab initio effective core pots., reduction of all electron to valence electron calcs. 77—14361
- Aitken's δ^2 transformation generalisation, summing perturbation series 78—24652
- alkali anions, autodetaching sub $^{2}P_{1/2}$ threshold states 79—22611
- alkali atoms, hyperfine interactions of excited states, Brueckner and natural orbitals 77—3283
- alkali metal atom Rydberg state quantum defects, semiclassical calc. 77—38621
- ATOM programme package for atomic calculations 79—10010
- atomic dynamic polarisability, variational calcs. with mode pot. *(Russian)* 78—902
- atomic ionisation by heavy ion impact, inner-shell ionis., binary collision model 79—54962
- atomic-integral calculations using spatial symmetry, efficient permutational approach 79—63888
- Auger decay theory at. orbital non-orthogonality, Wentzel Ansatz 77—18871
- Auger effect, semi-empirical models for electron energy calcs. 78—50519
- beam-foil spectra oscillator strengths, neutral and ionised atoms, non-closed shell many electron theory 77—38612
- Bethe-Goldstone time-depend. first-order theory, short range correl., transition moments 78—25449
- binding and transition energies, expt. and theoret. comparison, review 78—50497
- bond orbital model, atomic charges calcs., fully localised SCF method 80—42923
- Born approx., $55 \leq Z \leq 102$ scaled electron ionisation cross sections 79—94089
- bound state quantum fluctuations and variational method, relativistic HF calc. with radiative effects 80—42918
- Breit-type three-electron eqn., Pauli approx. 79—10044
- central potential models, energy eigenvalues 77—54511
- central potential models 77—54510
- CI calculations, virtual orbitals for rapid convergence, perturbational method 79—85906
- closed-shell configurations of isoelectronic ions and atom, SCF and STO energies 79—89598
- closed-shell systems interaction, exchange-repulsion energy, many-orbital cluster expansion 80—18896
- cluster expsn. of wavefunction, closed-shell orbital theory 79—10004
- collective dynamics, hydrodynamic approach and many body approach based on RPA calcs. 80—47855
- Compton bound electron state scatt., binding and off-mass shell effects, relativistic anal. 78—17637
- Compton profile, Fourier anal. 79—89588
- configuration interactions, appl. of unitary group methods 80—27958
- contour calcs., teaching approach 78—93500
- correlated electronic wavefunctions, Schrodinger eqn. variational form, generalised k-particle Brillouin conditions 79—81146
- correlated wave functions anal. gradients from two particle density matrix and unitary group 80—78548
- correlation coefficient and electron correlation 80—78552
- Coulomb integral and quantum mechanical exchange redefinition from atomic and molecular orbitals 79—44787
- coupled cluster many electron theory, unitary group formulation 80—52859
- coupled pair theory, exact and approx. methods and quasi-degeneracy 80—14074
- d-orbitals importance in calc. of effective interactions and excitation spectra 79—6823
- density function method 79—41091
- density functional formalism, linear response theory, appl. polarisability 80—42924
- diagrammatic many-body perturbation theory for general model spaces 80—18780
- Dirac operator, essential self adjointness anal. 80—18794
- dynamic multipole polarisability, dispersion forces and oscillator strengths, Coulomb approx. 80—63520
- education, classical and quantum uncertainties, particle in box, harmonic oscill. and atom 79—25789
- education, Na Rydberg states, anomalous fine struct., perturbation model 80—57035
- education, two-electron atom, 1snl excited levels, ionisation energy calc., perturbation, Schrodinger eqn. methods 80—17728
- electric field variant orbitals, STO field gradient depend., atomic quadrupole polarisability 80—23295
- electric-field-variant orbitals, Slater- and Gaussian-type 78—37543
- electron + ion scattering, Schwinger's variational principle, Rydberg states 80—78713
- electron affinity, MNDO semi-empirical SCF-MO calcs. for atoms, mols., negative ions 78—74578
- electron integrals transformation method, program in FORTRAN IV H 78—82603
- electron shakeoff accompanying beta-decay, probability for K- and L-shells 78—94204
- electron transfer collisions time independ. quantum theory with nonorthogonal basis and R-matrix propag. 79—89769

atomic orbitals calculations continued
- electron-electron interactions, radiative effects, canonical transformation calcs. 77—3275
- electronic energy of atoms and mols., $(N+1/N)$ Pade approximants in Rayleigh-Schrodinger perturbation theory 77—71738
- electronic wavefunctions in a space of constant curvature 80—5466
- energy levels calc. of atoms in $1s^{2}2s^{2}2p^{N}3p$ and $1s^{2}2s^{2}2p^{N}3d$ configs. 77—46509
- equations of motion Green's function methods, higher order terms, ionisation pots. 80—52891
- equations of motion Green's function methods, higher order terms, ionisation pots., CI comparison 80—52892
- ESCA photoionisation cross section, relative intensities calcs., comparisons 78—50464
- ethane, CH bond orbitals, internal rot. barriers, antisymmetrization effects 80—63529
- ethane, shift of electronic spectrum during dissoc., CNDO calc. 80—37759
- excited atomic states, bound and free, inner charge defect method calcs. 80—78511
- excited states, hypervirial relations, off-diagonal 80—37728
- extended Numerov method for the numerical solution of the Hartree-Fock equations 80—83245
- fast electron collision, K, L, M-shell generalised oscillator strengths and ionisation cross section, Hartree-Slater calc. 80—53141
- few-charged particle problem 77—26977
- Feynman diagrammatic technique 77—26981
- first row atoms, real STOS, parameter optimiation method 78—41929
- first row elements, ground state, self-consistent orbitals with uniform long-range behaviour 80—9485
- first-row atom, uniformly balanced constrained gaussian basis tests 77—65423
- first-row elements, model pots., STO calcs. 77—408
- formic acid, harmonic force consts., ab initio calcs. and uniqueness problem 79—6834
- fourth row element ions, relativistic Dirac-Fock-Slater orbital binding energies, one-electron transition energies 79—25778
- Gaussian basis sets, Ga, Ge, As, Se, Br, and Kr, HF calcs. 77—38611
- Gaussian orbitals, multi-centre integrals, Racah algebra, Talmi transformation 79—45626
- Gaussian-lobe orbitals, ang. depend., anal. of standard p- and d-orbitals 79—6851
- Gaussian-lobe orbitals, ang. depend., axial GLO sets, theory 79—6852
- Gaussian-lobe orbitals, ang. depend., polyhedric lobe edifices 79—6853
- generalised hydrogen-type wave functions, momentum representation 77—6674
- generalised quantum defect, energy and radius depend. 80—14067
- ground-state wavefunctions, optimised central pots. 80—32593
- groups II and III, doubly charged negative ions, analytical radial orbitals 77—6668
- Hamiltonian, zero-order, for many-body perturbation theory 80—9483
- Hartree Fock atomic orbitals, approximation by Gauss functions 77—67985
- Hartree-Fock approximation with pseudowavefunctions 79—3357
- Hartree-Fock energies, scaled $1/Z$ expansion, integral eqns. 80—47886
- heavy atom, L-shell Auger and Coster-Kronig intensities from relativistic theory 79—93962
- heavy ion + atom collisions, small impact parameters, K-vacancy prod., molecular theory 80—69229
- HF function determ. in case of term mixing 79—63911
- HF model, nucl. charge rel. to orbital contribution to values $\langle r_{12}{}^{n} \rangle^{-1/n}$ 80—58115
- highly charged ion, $1s^{2}2s^{2}2p^{5}3d$ configuration, energy spectra in relativistic approx. 80—14082
- Hund's rules in atomic spectra, frozen electron core and valence electrons in nucl. field 77—67967
- hybridisation for arbitrary orbital 77—57852
- hydrogenic atom, model perturbation theoretic calculations with finite continuum basis sets 78—25412
- hydrogenic atoms, hybrid orbitals and Runge-Lenz vector, matrix elements 77—38606
- hydrogenic functions, Gaussian expansions involving few variational parameters 80—91420
- hydrogenic Gaussian lobe functions 80—74102
- hydrogenic one particle Green's function power moments, 1s-type orbital reduction 78—9051
- incomplete basis set problem, Hartree-Fock energy, perturbative corrections 78—70744
- INDO theories, rotational invariance, with d-orbitals included in basis set 78—41954
- inert gases, collision induced polarisabilities, perturbation treatment 78—86778
- inert gases, photoabsorption to bound state and photoabsorption to continuum state (ionisation), comparison, HF calcs. 80—47910
- inert gases, quantum defects, photoionisation cross-sections, central pot. model calcs. 77—54510
- inner electron shell, change in atomic quantities when vacancy occurs 79—63909
- inner shell electron props., relativistic effects 77—18803
- inner shell ionisation phenomena, conf., Freiburg, West Germany (Mar.-Apr. 1976) 77—27040
- integral expression, for $(nl|n'l')$ with $n, n'=3, 4$ 77—30769
- interaction between N one-electron atoms, biorthonormal basis sets 79—22576
- interorbital pair correl. energies and absolute overlap integrals, 1s and 2s HF orbitals 77—46501
- inverse Gaussian transforms, general props., Slater type orbitals appl., coord. and momentum representation 78—37549
- inverse matrix diagonal and off diagonal elements, self energy perturbation theory 78—82607
- ionisation potential, X_{α} eigenvalues and Slater transition state 79—31394
- ionisation potentials, natural transition orbital theory, perturbation theory anal. 77—34541
- ionised atoms, quantum numbers, filling order of ionic electron shells, statistical model 80—52884
- $K\alpha_1/K\beta_1$ X-ray intensity ratio rel. to at. number for $Z=20$ to 90 77—23457
- K-LL Auger spectra in intermediate-coupling scheme with CI, relativistic Dirac Hartree Slater calc. 80—52958
- K-shell Auger rates, level widths and fluoresc. yields, relativistic Dirac Hartree Slater calc. 80—52957

atomic orbitals calculations continued

- Kepler problem, classical limit 78−17553
- Koopmans atomic valence electron ionisation energy, $1/Z$ expansion method, reorganisation corrections 78−78623
- Langer uniform approx. average trajectory approx. weak-coupling theories, inelastic electron scatt. 78−33417
- ligand fields calcs., strong and intermediate fields, tensor algebra 80−42922
- lower bound Hamiltonians for atoms and mols., projection operator method 78−82602
- M-shell radiationless transitions, subshell fluoresc., Coster Kronig yields and X-ray linewidths, relativistic Dirac Hartree Slater calcs. 80−52959
- many centre basis, electron population anal. and nonorthogonality problem *(Russian)* 78−29730
- many-body perturbation theory with radially restricted basis functions 80−78526
- many-electron spin degeneracy, recursive formula for Young's orthogonal representation 77−38596
- many-electron systems, oscill. strengths, Bates-Damgaard approx. calcs. 77−3311
- MC-SCF theory, modified one-electron Hamiltonian, iteration convergence 79−6871
- modified virtual orbitals, for config. interaction calc. 80−58163
- molecular photoionisation cross sections, at. extrapolation, ground state inversion method appl. 80−18787
- moment method in stochastic perturbation of angular correlations 77−3268
- momentum eigenfunctions in complex momentum plane, Hartree Fock functions 80−63517
- momentum eigenfunctions in complex momentum plane, secondary singular points 79−68179
- Mossbauer atoms, electron densities at nuclear centre and surface, calcs. using Dirac-Fock eqn. 80−74100
- multiconfiguration Hartree-Fock procedures, 2nd and approx. 2nd. order, convergency 80−47901
- multiconfigurational reference states, orbitals optimisation 79−10002
- multiplet ratios for photoionisation and electron attachment, shell model, LS coupling and correl. 78−17636
- n-electron atomic wavefunction, Schrodinger inequalities, many-electron densities 78−94191
- n-electron atoms, compactness proof for infinite systems of linear equations 79−72247
- negative quantum chemical calcs. 78−62703
- nonhydrogenic atoms, radial transition integrals, Coulomb approx. calcs. 79−45625
- nonlinear differential equations, similar to Schrodinger eqn., variational principle application 79−63065
- one electron atom, Dirac energy, αZ expansion procedure 78−9053
- one-electron operators in atomic systems, inequalities among expectation values 79−89590
- open shell orbital theory with electron correl., wavefunction cluster expansion 79−13647
- open shell restricted HF eqns., role of coupling operators 79−758
- open-shell atom, electron density calc., approx. differential eqn. 80−47864
- optimised one-electron wave functions, determ. ionisation energies of atoms 77−38599
- orbital amplitudes of nuclei, extrapolation procedure, gaussian basis set and nucl. cusp eqn. 78−74560
- orbital functional theory for exchange and correl., local spin density approx., self interaction correction 79−76347
- orbital symmetry conservation, chem. appl. of field theory *(Chinese)* 79−63884
- organic chemistry courses, unified approach to teaching of struct. and bonding 80−17732
- oscillator strength sum rule, hydrodynamic analogy to quantum mechanics 79−26873
- oxygen-type atoms, subdivision of 2p-shell 78−82609
- p-block ats., energy levels, position orbital calcs., electron repulsion integrals, teaching appl. 78−93494
- paramagnetic electronic props. of atoms and mols., orbital mag. moments, paramagnetic currents 77−46476
- perturbation var. calc. with contact interaction, effect of approx. zero order wavefunctions 80−58107
- perturbed boundary conditions, for differential equations in theory of atoms 78−33432
- perturbed Rydberg series, quantum defect and CI theories 80−23300
- photoelectric cross section, fixed-orientation atomic orbitals, rel. to plane-wave final state approx., angle-resolved photoemission 79−28891
- photoionisation from low or high excited states, radial transition integrals 80−18832
- polarisability and London coeff., ab initio variation perturbation calc. 79−13635
- polarisability of atoms, freq. depend., Hartree-Fock theory 79−45652
- polarization Green's function with multiconfiguration self-consistent-field reference states 80−37724
- population optimised basis function in semiempirical atomic state energy calcs. 78−914
- positive atomic ions, orbital SCF energies, rel. to total SCF energies 79−3350
- pseudo pot. model Hamiltonian, spin-orbit splitting, intercombination and relativistic orbital reorganisation 78−25424
- pseudo-orbital theory, cluster expansion of wavefunction 78−62706
- pseudopotentials, improved three parameter, Li to Kr and hydrides, PSIBMOL algorithm 77−26963
- quadrupole shielding factors calc. using elec. field variant orbitals 80−106276
- quantum defect theory, general form 79−68177
- quasi-energetic spectra of quantum systems in classical monochromatic fields 78−78981
- R-matrix method, atomic continuum processes calc., program 78−74558
- rare earth elements, extended calculation method 77−6667
- relativistic atomic wave functions, Hartree-Fock calcs. 79−10009
- row element ions 79−25778
- scalar relativistic approximation 79−26899
- Schrodinger eqn., random walk soln., electron spin effects 77−18780
- Schrodinger-Infeld-Hull factorisation, quantisation condition, matrix elements and selection rules 78−41909
- screened Coulomb pot., perturbation theory and hypervirial theorem, sixth order atom energy levels 80−14071

atomic orbitals calculations continued

- screened Coulomb pot., Schrodinger eqn. with Hulthen pot., variational soln. 77−23427
- screened Coulomb potentials, energies calcs. 80−31452
- screened potential model, oscill. strength and energy levels 79−63896
- second row atoms, contracted Gaussian basis sets for mol. calcs. 80−83264
- second-row atoms, SCF loge localised wave functions 78−41932
- shell occupation number, rel. to coeff. for radial integrals of energy of electrostatic interaction of atomic electrons 79−63906
- single-term atomic state props., variationally optimised local central pot. calcs., $2<Z<55$ 79−41123
- singlet-triplet energy difference and singlet generalised oscillator strength, Lassettre-Dillon relation 80−63508
- Slater's calculations, improved screening-loss parameter calc. 80−83271
- Slater orbital translation in j-j coupling scheme *(French)* 78−41922
- Slater-type orbitals, hybrid and Coulomb integrals, anal. evaluation 78−13432
- spherical harmonics problems, identities 80−63515
- spin and charge density determ., relativistic Dirac-Fock, review 77−75045
- spin density, first row ats., wavefunction cluster expansion, pseudo-orbital calc. 77−54502
- spin factoring for spectroscopic term determ. 77−61695
- spin-density gradient expansion for kinetic energy of electron gas, variational calc. 79−93917
- spin-other orbit and spin-spin interactions 80−913
- Stark resonances, calc. from complex-rotation technique applied to variational principle 78−33549
- STO atomic basis sets, orbital exponents for $3<Z<18$ 78−29738
- Sturm expansions in the Hartree-Fock method 78−25409
- superheavy elements E116 and E114, theoretical chem. 77−32824
- total electronic energy, atoms and mols., SCF binding energy, Z^{-1} perturbation theory 80−83268
- total Hartree-Fock energy-eigenvalue sum relationship 79−59338
- transition elements, higher types, electronic config. and nucl. quadrupole interaction, atomic SCF Hartree-Fock calcs. 79−60777
- transition metal atom, many-config. approx. in X-ray and electronic spectra interpret. 80−32615
- transition metal atoms, neutral and ion val. states, electron correlation, ab initio effective val. Hamiltonian calc. 80−99449
- transition metal ion, superposition of quasidegenerate configurations, principal quantum number $N=3$ 80−14079
- transition metal systems, ESR studies, polarised absorption, ligand field model, group theory applications 80−43077
- trial wave functions, by off-diagonal hypervirial theorem 79−22578
- two electron atom, energy levels, classical first order perturbation theory 80−58118
- two electron systems, coupling schemes, transition energies and probabilities of autoionising states 80−18828
- two-electron atom, Kinoshita expansion 79−59351
- two-electron atom, momentum distrib. and Compton profiles, Fourier integral calcs. 77−3276
- two-electron atom, Schrodinger local energies 79−41090
- two-electron wave functions with monopole interaction, asymptotic forms 80−78528
- two-parameter exponential-type basis functions for atomic calculations 79−63889
- two-valence electron systems, valence Rydberg and continuum orbitals 77−3259
- unified atom limit, adiabatic approx. for transitions between $l=2$ states 79−22781
- unitary group generators and permutations, CI matrix elements, algebraic method 80−37725
- unitary group generators and permutations, CI matrix elements, graphical method 80−37726
- unitary group irreducible representation subduction coeffs. 80−37723
- unitary variational method 77−71743
- universal atomic basis sets, light atom HF ground state energies 78−78605
- universal basis set concept, Slater-basis 79−36502
- unlinked cluster corrections for configuration interaction calculations 79−3368
- valence electrons local-density theory of exchange and correlation energies 80−52854
- variation-iteraction soln. of Hartree Fock eqns., Green's integral operator, SCF formalism 79−6842
- variational method, metric-constrained 79−22579
- variational technique,73 variational technique, for two-electron atom, for teachers 79−21505
- variations preserving orthonormality, parameter representation for first and second-order variation 79−76326
- velocity parameters of atomic HF wavefunctions 77−71744
- weak exchange interaction between atoms or ions orbitally degenerate ground states, atomic second quantisation method 80−32604
- X_α optimised STO exponents 78−62721
- $X\alpha$ method with pseudopotentials 80−83282
- yrast state cascade population of atomic levels, power law 80−18808
- $Z=100$ to 173, Dirac-Fock-Slater calcs. of energy eigenvalues and total eigenvalues 77−71739
- $Z=11$ to 103, theoretical, L-shell Coster-Kronig energies 77−83524
- $Z=95$ to 130, calc. of K- and L-X-rays binding energies 77−83525
- Ag, semiempirical, relativistic oscillator strengths including core polarisation for p-, s-, d-series 78−74609
- Al, electron impact excitation cross sections calc. *(Russian)* 78−55240
- Al, Raffenetti-type atomic basis set calcs. 79−97974
- Ar, electron scattering, elastic, at low-energy, polarised orbital calc. 78−82840
- Ar, electron scattering, elastic, low-energy, polarised-orbital calcs. 80−37882
- Ar, first order density matrix, effective core pot. valence electron UHF method 77−30786
- Ar IX, Ne I like reson. and Na I-like satellite lines, relativistic HF calc., beam-foil spectra 78−94210
- Ar isoelectronic series, orbital binding energies within statistical exchange approx. 79−85895
- Ar, KLL and KLM Auger electron spectra, obs. and relativistic multiconfigurational Dirac-Fock calc. 78−50524
- Ar, momentum eigenfunctions in complex momentum plane, Hartree Fock functions 80−63517
- Ar, nonempirical calc. of X-ray K-absorpt. spectra 77−88465

atomic orbitals calculations continued

- Ar, vacancy, electronic structure, Green's function theory 80 – 39525
- Ar^{2+}, multiple open shell configs. calcs., modified HF method 77 – 50356
- Au, semiempirical, relativistic oscillator strengths including core polarisation for p-, s-, d-series 78 – 74609
- B, ground state wave function, 2s-2p electron promotion effect 78 – 86779
- B, ground state wavefunction, SCF HF calc. 78 – 90070
- B^{3+}, few-parameter two-electron wavefunction of ground state 77 – 75051
- Be, ^{1}S, Schrodinger eqn., random walk soln., electron spin effects 77 – 18780
- Be, coupled pair theory, exact and approx. methods and quasi-degeneracy 80 – 14074
- Be, electronic struct., universal STO basis sets 79 – 10021
- Be, ground state, CI and many-body perturbation theory 79 – 68198
- Be, ground state energy determ., Galerkin-Petrov method 79 – 769
- Be, ground state reduced first order density matrix CI calc., mag. shielding const. and diamagnetic susceptibility 79 – 6872
- Be, ground state wavefunction, SCF HF calc. 78 – 90070
- Be, ionisation energies and oscillator strengths, polarised frozen core approx. 79 – 36524
- Be, multiconfig. Hartree-Fock calcs. convergency 80 – 47901
- Be, one-particle ionis. energy, correlated wavefunction 79 – 45639
- Be sequence, (Z=4 to 10, 14), $^3P_1 \rightarrow {}^1S_0$ intercombination line, CI calc., Breit interaction 78 – 78641
- Be^{2+}, elastic form factors, correlated two-electron-core pots., closed form expressions 79 – 68195
- Be^{2+}, few-parameter two-electron wavefunction of ground state 77 – 75051
- Be^{2+}, numerical Hartree-Fock calc. of 1s^2 ground state 79 – 81155
- Be+Be closed-shell system, exchange polarisation energy 78 – 42155
- Bi, neutral current-induced parity nonconserving optical rot., Dirac-HF calcs. 80 – 47948
- C, effective valence shell Hamiltonian, ab initio calcs. 78 – 82611
- C, ground state wavefunction, SCF HF calc. 78 – 90070
- C, one-centre integrals of semiempirical theories of valence, ab initio calcs. 80 – 102441
- C, optical oscillator strengths, independent particle model, excited state wave functions, LS coupling and Born approx. 80 – 32674
- C$^-$, effective valence shell Hamiltonian, ab initio calcs. 78 – 82611
- C^{4+}, few-parameter two-electron wavefunction of ground state 77 – 75051
- C^{5+}, electron impact, continuum orbital approx., weak coupling theory 78 – 33417
- C^{n+}, (n=1,2,3) effective valence shell Hamiltonian, ab initio calcs. 78 – 82611
- Cl, photoionisation cross section and reson. theory, many body perturbation theory, 3p and 3s subshells 80 – 69114
- Cl, Raffenetti-type atomic basis set calcs. 79 – 97974
- Cl VIII, Ne I like reson. and Na I-like satellite lines, relativistic HF calc., beam-foil spectra 78 – 94210
- Cl$^-$, contracted Gaussian basis sets for mol. calcs. 80 – 83264
- Cr IV, semiempirical calc. of energy spectra 77 – 46499
- Cr XVIII, XIX, spectral energy levels, relativistic corrections, config. superposition method 80 – 32616
- Cs, discrete level raising into far continuum, oscillator strength to shape reson. transfer 78 – 78624
- Cs, excited np states, fine struct., core electrons effect 77 – 18807
- Cu, ionisation energy, multiplet strengths, diagrammatic MBPT theory calcs. 80 – 9500
- Cu, semiempirical, relativistic oscillator strengths including core polarisation for p-, s-, d-series 78 – 74609
- Eu, electron impact excitation cross section, Born and Ochkur approx. 80 – 87230
- F, ab initio effective valence shell Hamiltonian for neutral and ionic valence states 80 – 74117
- F, energy levels of $1s^22s^22p^N3d$, (N=2,3,4) configurations 77 – 46509
- F, Raffenetti-type atomic basis set calcs. 79 – 97974
- Fe group ions, spectra, calcs., allowance for d^n shell pair excitations 77 – 42261
- Fe, hyperfine interaction parameters, effect of local exchange, Xα and HF calcs. 78 – 78622
- Fe, model potential method, in Roothaan's open-shell scheme 79 – 36513
- Fe X (XI), energy levels and oscill. strengths, Slater radial integrals 77 – 79583
- Fe XIX, XXI, spectral energy levels, relativistic corrections, config. superposition method 80 – 32616
- Fe XXI, relativistic energy levels, Dirac-Fock multiconfig. calc., triplet state fine struct. and Lamb shift 80 – 23315
- Fe^{3+} isoelectronic series, radial charge distrib. calc. 80 – 9507
- Ga, electron impact excitation cross sections calc. *(Russian)* 78 – 55240
- H, ^{2}P, Schrodinger eqn., random walk soln., electron spin effects 77 – 18780
- H, dipole static polarizability for any state, modified Coulombic Green's function Sturm expansion 79 – 7031
- H, elastic electron scatt., modified Glauber theory, intermediate states 80 – 53139
- H, electron elastic scatt., exchange perturbation theory 80 – 78709
- H, electron impact excitation of resons. below n=3 levels, algebraic variational calc. 78 – 9254
- H, one-, two-, three- and four photon absorpt., truncated model semiclassical calcs. 78 – 17644
- H, quadratic Zeeman effect, perturbative approach 79 – 22649
- H, relativistic Dirac eqn., for teachers 78 – 62019
- H, Stark and photoabsorption spectrum, density of oscillator strengths, atom c.f. semiconductor spectra 80 – 83318
- H, Stark spectrum and field ionisation, density of continuum states, normalised wavefunctions 80 – 83317
- H, uniform mag. field, low lying levels below 10^9 G, adiabatic approx. 79 – 72235
- H$^-$, autoioniation states, below N=3 hydrogenic threshold, complex-rot. calc. 77 – 67966
- H$^-$, elastic form factors, correlated two-electron-core pots., closed form expressions 79 – 68195
- H ion bound state, extensions to finite nuclear mass 78 – 29743
- H$^-$, many-body perturbation theory with radially restricted basis functions 80 – 78526
- H$^-$, numerical Hartree-Fock calc. of 1s^2 ground state 79 – 81155
- H$^-$, photodetachment cross section, dynamic polarisability calc., sum rules, basis set depend. 78 – 17635
- H^{2-}, Z-Z 80 – 28104

atomic orbitals calculations continued

- H-like atoms, Stark effect and perturbation approxs. 80 – 52932
- H-like problems, spinor and scalar QED calcs. in Euclidean formulation 77 – 88378
- H$^+$ + H, 1s charge exchange amplitudes, impact parameter calcs. 77 – 534
- H$_2$ electron scatt., equivalent exchange pots., algebraic variational method, 2p-2p and 2s-2p transitions 80 – 18931
- H$_2$-like at. orbitals, shape, teaching appl. 78 – 93496
- HD, perturbation var. calc. with contact interaction, effect of approx. zero order wavefunctions 80 – 58107
- He, 1s^2 ground state piecewise polynomial CI natural radial orbitals wave functions 80 – 18805
- He, 1s3d config., Zeeman sublevel energies, anticrossing and degeneracy 77 – 23417
- He, autoionising resons., complex-coord. anal. 79 – 49992
- He, autoionising resons., complex rot. method, non- and degenerate perturbation theory 79 – 72283
- He, doubly excited, supermultiplet energy levels, classification as rot.-vibr. spectrum 80 – 52900
- He, elastic form factors, correlated two-electron-core pots., closed form expressions 79 – 68195
- He, electron affinity of (1s2s)^{3}S state, CI calc. 79 – 59591
- He, electron scattering, elastic, at low-energy, polarised orbital calc. 78 – 82840
- He, electronic struct., dilute gas, double excitation CI anal., coupled electron pair approx. 78 – 21856
- He energy levels, classical first order perturbation theory 80 – 58118
- He, excited states, Galerkin-Petrov method, nonlinear parameters 78 – 78619
- He, freq. depend. polarizability, LCAO SCF perturbation theory 79 – 31387
- He, ground state, Galerkin-Petrov method calc. 77 – 46485
- He ground state, Hylleraas six parameter wave function, minimisation method 80 – 27925
- He, ground state wavefunction, SCF HF calc. 78 – 90070
- He, Hartree eqn. variational method 79 – 49941
- He, Hartree operator, upper and lower bounds to critical values 77 – 23426
- He, Hartree-Fock energy, perturbative corrections, incomplete basis set problem 78 – 70744
- He isoelectronic sequence, few-parameter wavefunctions of ground state 77 – 75051
- He, isoelectronic sequence, 2^{1}S states, analytic wave function 80 – 9525
- He isoelectronic series, ground state, Coulomb holes and correl. pots. 79 – 89594
- He, isoelectronic series, ground state specific mass shift, HF variation perturbation calc. 80 – 47889
- He, l-limit energies for ground state atoms using hyperspherical basis sets 80 – 14076
- He like systems, ground state one electron density decay 79 – 76337
- He, numerical Hartree-Fock calc. of 1s^2 ground state 79 – 81155
- He, orbitals calculations, using extended STO basis sets 79 – 6844
- He pair, dispersion interaction, independent particle model, polarisabilities 80 – 37732
- He, path integral formalism of perturbation theory, simple mols. and atoms 79 – 6841
- He, photoionisation, frozen-core HF perturbation theory, oscillator strength, dipole length and vel. calc. 78 – 78672
- He, positron scatt., polarisation effects, orbitals calcs. 77 – 3457
- He, S state, electron correl. calcs. 79 – 49952
- He to Ne, STP basis sets 77 – 3262
- He$^-$, (1s2s2p)^{4}P^0 metastable state, CI calc. 79 – 59591
- He$^-$, wave function structure, complex coord. method 78 – 94190
- He$^+$, n=2 state electron impact excitation, hybrid algebraic close coupling approx. 80 – 18930
- He-He, Born Oppenheimer pot. using Hylleraas-type electronic wave functions 80 – 91442
- He-like atoms, oscillator strength calc., allowed np-n'd and nd-n'f transitions 79 – 31467
- He-like ions, H$^-$ through Mg^{10+} 1^{1}S state variational wave functions 77 – 34545
- He-like ions, He through Mg^{10+}, 2^{1}S, 2^{3}S, 2^{1}P and 2^{3}P states variational wave functions 77 – 34546
- He$^+$ + alkali metal atom, ionisation cross sections, binary encounter approx. with HF electron vel. distrib. 78 – 55225
- Hg$_{1-x}$Cd$_x$Te, mixed crysts., band struct. and optical transitions, distorted atomic orbitals 77 – 69224
- I, model potential method, in Roothaan's open-shell scheme 79 – 36513
- In, electron impact excitation cross sections calc. *(Russian)* 78 – 55240
- Ir, hyperfine interaction parameters, effect of local exchange, Xα and HF calcs. 78 – 78622
- K, electronic excitation cross-section determ. method 77 – 540
- K, excited np states, fine struct., core electrons effect 77 – 18807
- K$^+$ in molecular complexes, K-edge absorpt. spectra, Z+1 analogy, theory-expt. comparison 80 – 47935
- K^{2+}, photoionisation cross-section, R-matrix theory 78 – 82702
- Kr, 3p core hole spectrum, many electron description 78 – 50517
- Kr, elastic positron scatt., phaseshifts and elastic, diffusion and annihilation cross section 80 – 53134
- Kr, electron scattering, elastic, low-energy, polarised-orbital calcs. 80 – 37882
- Kr, large angle elastic and inelastic electron scatt. differential cross section, exchange corrections 80 – 28111
- Li, at. HFS, unrestricted and projected Hartree-Fock methods 79 – 63924
- Li, doublet open-shell restricted SCF eqns. 79 – 59350
- Li, electron impact total excitation cross section, first order exchange approx. 79 – 31692
- Li, electronic excitation cross-section determ. method 77 – 540
- Li electronic impact excitation, energy level calcs. *(Chinese)* 80 – 83488
- Li ground state optimised one-electron wave functions 77 – 38597
- Li, ground state wavefunction, SCF HF calc. 78 – 90070
- Li isoelectronic sequence, self-consistent relativistic density-functional theory 80 – 91441
- Li, isoelectronic series (Be,B,C) best optimised one-electron wave functions 77 – 38598
- Li, s^{2}S and 2^{2}P states, spin-optimised SCF general spin orbitals 78 – 82617
- Li to Ne, coreless Hartree-Fock pseudopotential method 79 – 68188
- Li$^-$, core excited bound states in beam foil expts., CI calcs. 80 – 78559

atomic orbitals calculations continued
  Li^{+}, elastic form factors, correlated two-electron-core pots., closed form expressions 79—68195
  Li^{+}, few parameter two-electron wavefunction of ground state 77—75051
  Li^{+}, numerical Hartree-Fock calc. of 1s^{2} ground state 79—81155
  Mg, polarisability and London coeff., ab initio variation perturbation calc. 79—13635
  Mg^{2+}, 2p^{5}np-2p^{5}ms (n=3, 4; m=3,4,5) transition probabilities calc. 79—6915
  Mn I inner shell absorpt. spectrum, 3d wavefunction collapse 77—23455
  Mn V, semiempirical calc. of energy spectra 77—46499
  Mn^{2+}, Fermi contact interaction, spin density distrib., X$_{\alpha}$ calc. 77—54514
  Mo XXXIII, dielectronic recombination rate calc. 80—14232
  N, ab initio effective valence shell Hamiltonian for neutral and ionic valence states 80—74117
  N, energy levels of 1s^{2}2s^{2}2p^{N}3d, (N=2,3,4) configurations 77—46509
  N III, electron impact excitation cross sections, generalised oscillator strengths, Born approx. 80—18928
  N^{5+}, few-parameter two-electron wavefunction of ground state 77—75051
  ^{14}N, spherical ground state nuclear quadrupole interaction, Breit interaction, relativistic perturbation theory 80—42939
  Na, doublet open-shell restricted SCF eqns. 79—59350
  Na, electron impact total excitation cross section, first order exchange approx. 79—31692
  Na, electronic excitation cross-section determ. method 77—540
  Na, excited np states, fine struct., core electrons effect 77—18807
  Na isoelectronic series, wave functions and effective pots. of valence electron 80—47873
  Na, oscill. strengths, Bates-Damgaard approx. calcs. 77—3311
  Na+H^{+}, 2p^{5}3s^{2} ^{2}P$_{3/2}$ state alignment, collisionally induced, impact parameter calc. 80—83474
  NaI-SVI isoelectronic series, radiative lifetimes calc. 79—72276
  Ne, atomic struct. calc., symmetry adapted pair functions, Rayleigh Schrodinger HF variational perturbation theory 80—42944
  Ne, Auger spectra, correl. effects, energies and wavefunctions, ab initio CI calc. 80—14125
  Ne, doubly excited energy levels, subshell ang. momenta coupling, frozen core superposition of config. method 80—52874
  Ne, electron impact ionisation, ang. correl., first Born approx. 79—22840
  Ne, electron scattering, elastic, at low-energy, polarised orbital calc. 78—82840
  Ne, ground state wavefunction, SCF HF calc. 78—90070
  Ne, isoelectronic sequence, excitation energy and oscillator strength, level crossing anomaly, relativistic RPA calc. 80—14077
  Ne, isoelectronic series, ionisation pots., Ritz law and Edlen formula 80—32854
  Ne isoelectronic series, orbital binding energies within statistical exchange approx. 79—85895
  Ne, momentum eigenfunctions in complex momentum plane, Hartree Fock functions 80—63517
  Ne, nonempirical calc. of X-ray K-absorpt. spectra 77—88465
  Ne, photoionisation, complex amplitudes at low energy singly and doubly excited resons. 78—78673
  Ne, triply-excited states contributing to correl. energy, diagrammatic perturbation theory 79—81161
  Ne, vacancy, electronic structure, Green's function theory 80—39525
  Ne, with 1s-hole, wave function calcs. using radial orbitals, orthogonality 77—67971
  Ne^{+}, electron scatt., relativistic R-matrix calc., fine-struct. level transition cross sections 78—13604
  Ne^{2+}, energy levels of 1s^{2}2s^{2}2p^{N}3d, (N=2,3,4) configurations 77—46509
  Ne^{7+}, electron impact, continuum orbital approx., weak coupling theory 78—33417
  Ne^{x+}, (x=3-7), K-LL Auger transition energies calc. 79—54823
  Ne+Ne, exchange-repulsion energy, many-orbital cluster expansion 80—18896
  Ni (001), chemisorption of H, O and CO, localised orbital approach 77—69166
  Ni, pseudopotential calculations, parameter fitting scheme appls. 78—41928
  Ni XXI, XXIII, spectral energy levels, relativistic corrections, config. superposition method 80—32616
  Ni+Ni interaction, ab initio HF and CI calcs. 79—59535
  O, ab initio effective valence shell Hamiltonian for neutral and ionic valence states 80—74117
  O, pseudopotential calculations, parameter fitting scheme appls. 78—41928
  O V, E1 transition probabilities, lifetimes, CI calc. 80—83321
  P, ab initio effective valence shell Hamiltonian for neutral and ionic valence states 80—74117
  P, excited config., Hulthen and Slater type 2d functions 78—41972
  P^{-}, contracted Gaussian basis sets for mol. calcs. 80—83264
  PH$_{5}$, rearrangements, CI calcs. in large at. orbital basis 79—94106
  Pt (001), chemisorption of H, O and CO, localised orbital approach 77—69166
  Pt, L-shell Auger and Coster-Kronig intensities from relativistic theory 79—93962
  Rb, excited np states, fine struct., core electrons effect 77—18807
  Rb, Rydberg levels, Stark patterns, expt. and central pot. calc., positions and intensities 79—93953
  Ru, hyperfine interaction parameters, effect of local exchange, Xα and HF calcs. 78—78622
  Ru^{3+} isoelectronic series, radial charge distrib. calc. 80—9507
  S, ab initio effective valence shell Hamiltonian for neutral and ionic valence states 80—74117
  S, excited config., Hulthen and Slater type 2d functions 78—41972
  S, pseudopotential calculations, parameter fitting scheme appls. 78—41928
  S^{-}, contracted Gaussian basis sets for mol. calcs. 80—83264
  Si, ab initio effective valence shell Hamiltonian for neutral and ionic valence states 80—74117
  Si, first order density matrix, effective core pot. valence electron UHF method 77—30786
  Ti, 4s3d^{3} and 3d^{4} states, HF descriptions, alternative orbital config. 80—63534
  Ti, neutral and ion val. states, electron correlation, ab initio effective val. Hamiltonian calc. 80—99449
  Tl, electron impact excitation cross sections calc. *(Russian)* 78—55240
  Tl, oscill. strengths, Bates-Damgaard approx. calcs. 77—3311

atomic orbitals calculations continued
  U, ab initio effective core pots., relativistic corrections 78—50483
  U, L-shell Auger and Coster-Kronig intensities from relativistic theory 79—93962
  U, valence energy levels, SCF relativistic Xalpha calc. 79—85912
  ^{92}U, self-consistent relativistic density-functional theory 80—91441
  V III, semiempirical calc. of energy spectra 77—46499
  V, model pots., STO calcs. 77—408
  W(100), chemisorption of H, localised orbital approach 77—69165
  Xe, 5p subshell photoelectron branching ratio, Dirac-Fock calcs. 78—42021
  Xe, 5p^{5}ns, 5p^{5}np, 5p^{5}nd and 5p^{5}4f config., HF calc. 77—23468
  Xe, 5s, 5p ESCA spectrum, photoionisation many electron description 78—50516
  Xe, atom and ions, relativistic Dirac-Fock-Slater calc., fluoresc. yield, X-ray energies shift 78—25450
  Xe, elastic positron scatt., phaseshifts and elastic, diffusion and annihilation cross section 80—53134
  Xe, electron scattering, elastic, low-energy, polarised-orbital calcs. 80—37882
  Yb, electron impact excitation cross section, Born and Ochkur approx. 80—87230

atomic polarisability
  additive-orbital scheme for calculating atomic and molecular polarizabilities 77—3273
  Aitken δ^{2} transformation, geometric approx. 77—10595
  alkali metal, dynamic polarisability, variational calcs. with mode pot. *(Russian)* 78—902
  alkali metal, dynamic polarisability dispersion eqn., dispersion interaction of atoms 79—26902
  alkali metal, high ang. momentum Rydberg states, quantum defect core polaris. depend. 77—18808
  alkali metal+inert gas, role of different interactions in intramultiplet relax. at nonresonant interactions 77—6902
  alkali metal anions, photodetachment cross-sections and multipole polarisabilities, extended asymptotic model 78—42028
  alkali metal atoms, static polarisability, lower bounds, oscill. strength calcs. 77—75074
  alkali metal atoms, Van der Waals energies calcs., variation-perturbation method 77—510
  alkali metal ion, with filled shell, dipole polarisability 80—9501
  alkali metals, calc. using Laplace method *(Russian)* 79—89803
  alkaline earth atoms, static polarisability, lower bounds, oscill. strength calcs. 77—75074
  atom+atom collisional intense-field fluoresc., Zeeman degeneracy effects 80—99477
  atoms, polarisation of electrons and nuclei in resonant multiphoton ionisation 80—99486
  bremsstrahlung of electrons on atoms allowing for polarisability *(Russian)* 77—3475
  Cauchy moments calc. using recurrence procedure 80—48097
  classical fluid, collision-induced and multiple light scatt. 80—53919
  colloid, electro-optical characterisation methods 77—24821
  contact term, link with polarisability, use of local spin density functional method 80—58158
  correlation with atomic dimensions 80—23288
  density functional formalism, linear response theory, appl. polarisability 80—42924
  dipole, of first row atoms and ions, multiconfig. approach 77—42435
  dipole polarisability 80—58148
  dispersion energies, charge overlap effects, with freq.-depend. polarisability 79—86025
  dynamic, model pot. calcs. 77—31017
  dynamic multipole polarisability, dispersion forces and oscillator strengths, Coulomb approx. 80—63520
  dynamic multipole polarisability, functional calcs. 78—74595
  dynamic multipole polarisability, hydrodynamic model, variational approximations 80—23340
  dynamic polarisabilities and dispersion force coeffs., bounds 79—68290
  dynamic polarisability, variational calc. 78—22047
  dynamic variational calc. method, below 1st excitation freq. 77—50552
  effective potential approximation method 77—88587
  electric field variant orbitals, STO field gradient depend., atomic quadrupole polarisability 80—23295
  electric-field-variant orbitals, Slater- and Gaussian-type 78—37543
  electron-atom scatt., polarisation potential 78—42228
  electrostatic pot. energy of atoms in mols., electronegativity, charge transfer and polarisation 79—63885
  excitation of simple atomic and mol. systems, long-range force effects 79—10170
  ferrocene, quantum mechanical delta-function potential study 77—23571
  first row atoms, static quadrupole and mixed dipole-octupole polarisabilities 79—22857
  first-row atoms, SCF calcs. using cusped-Gaussian basis sets, polarisation effects 80—74118
  first-row elements, s-shell spin polarisation calcs. 77—75318
  frequency dependent polarisability, time depend. Hartree-Fock calc. 79—45652
  ground and excited states, polarisability and scaling, oscillator strengths, continuum spectrum contribution 80—27923
  ground state atoms, Van der Waals coeffs., polarisabilities and oscill. strengths calcs. 79—93913
  halogen ion, with filled shell, dipole polarisability 80—9501
  halogens, positron, scatt., low energy, semiempirical polarisation pot. calcs. 80—9736
  highly ionised atoms, dipole and quadrupole polarisabilities, extrapolation method calcs. 80—9534
  hydrogenic atom, nonrelativistic, linear response to external linear polarised EM wave 78—8258
  hydrogenic atom in weak mag. field, polarisability, ground-state energy 79—3594
  independent particle pots. comparison, appl. to Be(Ne)(Ar)(Kr)(Xe)(O V)(Ae IV) 80—52846
  inert gas, at. polarisability variation with density 77—68131
  inert gas isoelectronic series, polarisabilities and shielding factors 79—98008
  inert gases, collision induced polarisabilities, perturbation treatment 78—86778
  inert gases, polarisabilities, linear and nonlinear, screening consts. effects 79—31435

atomic polarisability continued
- inert gases, positron scatt., low energy, semiempirical polarisation pot. calcs. 80−9735
- inert gases, relation between diamag. susceptibility and electronic polarisability 77−14597
- interacting atoms, retarded energy shift and pair polarisability, field theoretical perturbation theory 80−102560
- interacting systems, oscillator strength sums, dynamic polarisabilities, one-term approximations 79−22782
- ion+atom collisions, asymmetric, polarisation and binding of inner-shell electrons, recoil in close encounters 80−18915
- ion collisions, electron capture, atomic excited state polarisation, optical detection 80−58377
- ions, closed-shell cryst. field and self-consistency effects on dipole and quadrupole polarisabilities 79−87072
- Kirkwood relation in at. diamag., satisfaction by Thomas-Fermi model 78−9266
- Kirkwood-Pople-Schofield method, appls. to polarisabilities calcs. 80−83272
- l-shell Coulomb ionization by heavy charged particles, polarisation effects 79−94073
- long-range potentials, vac. fluctuations and retardation effects 79−3522
- macromolecular soln., electro-optical characterisation methods 77−24821
- measurement using field electron microscope, appl. to Pb *(French)* 77−543
- metals, surface atom polarisation energy, effect of depolarisation 79−60620
- monatomic gas, collision-induced light scatt. at intermediate density, integrated intensity, appl. to Ar 80−24124
- multipole electric polarisability, variational calc. *(French)* 77−542
- multipole polarisability, extended Coulomb approx., for mono and divalent atoms and ions 78−33451
- negative ions, dynamic polarisability, many-centre short-radius model pots. 78−25735
- nonuniform arbitrary elec. field-induced moments polarisability density concept limitations 78−70964
- open-shell ions, coupled HF calc., static dipole polarisabilities and shielding factors 79−6862
- optical pumping with lasers, atomic polarisability, coherence between Zeeman sublevels 77−83549
- pair of atoms, long range effects, intrinsic polarisability rel. to hyperpolarisability 78−78824
- pair polarisabilities, continuum electrostatic theory 78−86769
- pair polarisability, retardation effects 77−30744
- photoionisation, fluoresc. radiation polarisation 80−87076
- physisorbed atoms on metallic surfaces, atomic size effect on polarisability 78−43242
- polarisability and London coeff., ab initio variation perturbation calc. 79−13635
- polarisation potential, quasiadiabatic, for elastic electron-atom scatt. 77−6929
- polarisation propagator calculations of frequency-dependent polarisabilities, Verdet constants, and energy weighted sum rules 78−58647
- quadrupole polarisability, using elec. field variant GTO basis set 79−76359
- quantum static multipole polarisabilities 78−82859
- quantum systems, at. or spin two level, reson. EM wave excitation, free induction decay oscills. 80−63562
- quinazolines, enzyme inhibitory, structure-activity quantitative study 80−78540
- R-matrix method, appl. to atoms and mols. 78−58833
- R-matrix method, atomic continuum processes calc., program 78−74558
- rare earth metal atoms and ions, relativistic effects on core-polarisation contrib. to HFS 77−67990
- resonant electron scatt. by atoms in laser field, negative ion formation, polarisability 77−19089
- retardation effects on high Rydberg states, retarded R^{-5} polarisation pot. 78−82629
- ring laser, collision model, averaged, in active medium polarizability theory 80−95924
- ring laser, nonlinear polarisability of two-isotope active medium 80−14369
- Rydberg atoms, expts., metastable states, multiphoton ionisation, spectroscopy, Stark struct., collisions, polarisability *(Dutch)* 78−5160
- second-row atoms, static dipole polarisabilities, finite perturbation calcs. 77−6690
- second-row elements, s-shell spin polarisation calcs. 77−75318
- SI system units, rel. to field ion theory 77−58191
- single-term atomic state props., variationally optimised local central pot. calcs., $2<Z<55$ 79−41123
- spin waves and spin polarisability 77−65538
- static dipole, Thomas-Fermi model calc. 79−49965
- surface-atom polarisability derivation from field-ion energy deficits 80−76155
- Thomas-Fermi and Thomas-Fermi-Dirac model calcs. of at. polarisabilities 77−57876
- transition metal atoms and ions, relativistic effects on core-polarisation contrib. to HFS 77−67990
- two atoms at large separation, Green's function method *(Russian)* 79−76481
- two-electron atoms with rigorous upper and lower bounds, dynamic polarisabilities calc. 77−14599
- two-electron ions, ground state, quadratic Stark effect 80−37775
- two-level atom, spontaneous polarisability, Dicke model 80−1167
- Ag, semiempirical, relativistic oscillator strengths including core polarisation for p-, s-, d-series 78−74609
- Al, static quadrupole polarisability and shielding factor, Hartree-Fock calc. 78−41950
- Ar, atomic polarisabilities and shielding factors, coupled HF approx. 78−22048
- Ar, collision induced light scatt. spectra, pair polarisability 78−55135
- Ar, pair polarisability determ. from collision induced light scatt. spectrum 79−13678
- Ar+Ar(He)(Ne), dispersion interaction, series coeffs., variation method 79−3518
- Au, semiempirical, relativistic oscillator strengths including core polarisation for p-, s-, d-series 78−74609
- B^+, dynamic multipole polarisability, coupled Hartree-Fock 78−82858
- B^{2+}, multipole polarizabilities and shielding factors, calcs. on open shell ions 78−46263
- Ba I, Stark quantum beats under pulsed dye laser excitation 77−42277

atomic polarisability continued
- Ba^{2+}, free-ion polarisability, empirical values 77−20792
- Be, correl. contribs. to dipole polarisability, coupled HF-perturbation theory 80−106269
- Be, dynamic multipole polarisability, coupled Hartree-Fock 78−82858
- Be, electric dipole polarisabilities and hyperpolarisabilities, perturb. theory calcs. 78−17563
- Be, freq.-depend. polarisabilities and Verdet consts., calcs. 78−62781
- Be, HF polarisability, second order correlation correction 78−25429
- Be I, energy level calcs. using model pot. and cores approxs. 77−14353
- Be I isoelectronic sequence, radiative props. determ. by model-pot. method 78−70788
- Be, many-electron calc. 77−57884
- Be, quadrupole polarisability, using elec. field variant GTO basis set 79−76359
- Be^+, multipole polarizabilities and shielding factors, calcs. on open shell ions 78−46263
- Be^+, resonance lines electron impact excitation, polarisability 78−42225
- Bi, Dirac eqn. calc. 79−22620
- Br^-, free-ion polarisability, empirical values 77−20792
- C, ground and excited states, atomic polarisability calc. 77−83756
- C III, atoms, static polarisability, lower bounds, oscill. strength calcs. 77−75074
- C^{2+}, dynamic multipole polarisability, coupled Hartree-Fock 78−82858
- Ca dipole polarisability, in $Ca_2{}^+$ pot. energies calcs. 79−27055
- Ca, static electric dipole polaris., ground state, electric beam deflection technique 77−10780
- Ca^+, resonance lines electron impact excitation, polarisability 78−42225
- Cd, ^1S, ^3P, ^1P states, dipole polarisabilities from compact variational trial functions 80−63568
- Cd, Stark interaction in nspz$^3P_1$ levels, optical double resonance obs. 79−63941
- Cd(^1S), dipole polarisability, relativistic effective core pot. calc. 79−76362
- Cl, static quadrupole polarisability and shielding factor, Hartree-Fock calc. 78−41950
- Cl^-, free-ion polarisability, empirical values 77−20792
- Cl^-, pair polarisability, ab initio SCF MO energies 78−70741
- ^{35}Cr, ^7P states HFS, level crossing technique, core polarisation, spin orbit interaction, config. mixing 78−78668
- Cs gas, optically pumped, spatial distrib. of polaris. 79−76392
- Cs polarisability constant, Stark interaction for excited states, laser spectroscopy 77−50404
- Cs^+ dipole and quadrupole polarisability fine struct. intervals and g-factor interval 80−91477
- Cs^+, free-ion polarisability, empirical values 77−20792
- $Cs(6^2P_{3/2})+He(Ne)(Ar)(Xe)$, collisional depolaris., nucl. spin depend., by Zeeman scanning 77−19012
- Cu isoelectronic series, dipole polarisability, numerical Coulomb approx. 80−43199
- Cu, semiempirical, relativistic oscillator strengths including core polarisation for p-, s-, d-series 78−74609
- F^-, free-ion polarisability, empirical values 77−20792
- F^-, static electric dipole polarisability 79−76332
- Ga, ground-state hyperfine struct., differential Stark effect 80−42990
- H, dipole static polarizability for any state, modified Coulombic Green's function Sturm expansion 79−7031
- H, dynamic multipole polarisability, functional calcs. 78−74595
- H, dynamic polarisability, variational calc. 78−22047
- H, electron scatt., polarisation potential 78−42228
- H, excited S-states, static dipole polarisabilities, Green's function calcs. 77−6696
- H, freq. depend. multipole polarisability and dispersion energy between interacting pairs 79−18306
- H ground state, dynamic polarisability, laplace transform method in two-photon spectroscopy theory 79−10084
- H, ground-state, freq.-depend. multipole polaris., reduced Green's functions 78−1097
- H, imaginary frequency mutipole polarisability and long-range dispersion consts, functional calcs. 78−74596
- H interacting with EM vacuum fluctuations, ground state energy in multiply connected universes 80−87050
- H, multipole polaris. and shielding factors Wiener Askar perturbation treatment 77−34774
- H, multipole polarisability and shielding factors, hydrodynamic analogy to quantum mech. 78−66677
- H, polarizability, evaluation of generalised sum rules 77−68132
- H, positron scatt., low energy, semiempirical polarisation pot. calcs. 80−9735
- H, quadrupole polarisability, using elec. field variant GTO basis set 79−76359
- H, third-order optical harmonic coeffs., R-matrix calc. 77−57955
- H^-, bound states in mag. field, binding anal., variational calcs. 80−42940
- H^-, dynamic polarisability 79−76526
- H_-, dynamic polarisability calc. 77−14599
- H^-, photodetachment cross section, dynamic polarisability calc., sum rules, basis set depend. 78−17635
- H-like atoms, dipole polarisability of arbitrary hybrid bound states 80−87237
- H-like atoms, multipole polarisability, dynamic, for S state, closed-form expression 78−82857
- H+H, pair polarisabilities, continuum electrostatic theory 78−86769
- H+H, two body multipole-multipole Pade approximants, second order dispersion energy 80−28081
- $H+He^+$ (Li^{2+}), two-body dispersion interaction, freq. depend. multipole polarisability, variational calc. 80−37758
- H(2s), optical model approach to elastic scattering of electrons, polarisation effects 80−58382
- He, 2^3S_1 and 2^1S_0 metastable states, static dipole polaris. meas. 78−1098
- He, $2(^{1,3}S)$ excited states, dynamic polarisabilities 77−34772
- He, $2(^{1,3}S)$ excited states and ground state, dynamic polarisabilities, van der Waals force consts. 77−34773
- He, atomic polarisabilities and shielding factors, coupled HF approx. 78−22048
- He, bound states in mag. field, binding anal., variational calcs. 80−42940
- He, correl. contribs. to dipole polarisability, coupled HF-perturbation theory 80−106269
- He, dynamic multipole polarisability, functional calcs. 78−74595

atomic polarisability continued
He, dynamic polarisability, 2^3S_1 and 2^1S_0 states var. perturbation calcs. 77—54507
He, dynamic polarisability, variational calc. 78—22047
He, dynamic polarisability, CHF method 78—50472
He, dynamic polarisability calc. 77—14599
He, electric dipole polarisabilities and hyperpolarisabilities, perturb. theory calcs. 78—17563
He, electron scatt. at intermediate energy, quantum mechanical treatment 80—91687
He, freq. depend. multipole polarisability and dispersion energy between interacting pairs 79—18306
He, freq. depend. polarizability, LCAO SCF perturbation theory 79—31387
He, freq.-depend. polarisabilities and Verdet consts., calcs. 78—62781
He, imaginary frequency mutipole polarisability and long-range dispersion consts, functional calcs. 78—74596
He isoelectronic series, static dipole polarisability, reduced Green's functions, HF calcs. 77—71750
He, isoelectronic series 79—3358
He, n=3 states, polarisation and excitation functions 77—6934
He pair, dispersion interaction, independent particle model, polarisabilities 80—37732
He, positron scatt., polarisation effects, orbitals calcs. 77—3457
He, quadrupole polarisability, using elec. field variant GTO basis set 79—76359
He, static and dynamic dipole, dynamic quadrupole 77—18810
He, static multipole polarisabilities, integral equation approach to scaled 1/Z expansion 80—63846
He, third-order optical harmonic coeffs., R-matrix calc. 77—57955
He through Ne, static polarisabilities and hyperpolarisabilities, numerical SCF method 79—36567
He triplet states, doubly excited, spectrum and polarisation 80—99472
He^+, dynamic multipole polarisability, functional calcs. 78—74595
He^+, imaginary frequency mutipole polarisability and long-range dispersion consts, functional calcs. 78—74596
$He+He^+(Ne)$, tensor polarisabilities of 1snd ^1D level, fluoresc. depolarisation obs. 80—69099
He+He(Ne)(Ar), dispersion interaction, series coeffs., variation method 79—3518
$He^++He^+(Li^{2+})(H)$, two-body dispersion interaction, freq. depend. multipole polarisability, variational calc. 80—37758
He_2, pair polarisability correl. effects, SCF-CI-GTO-SO calc. 78—82651
Hf IV, 6s $^2S_{1/2}$-6p $^2P°_{1/2,3/2}$ transition, relativistic oscillator strengths, influence of core polarisation 80—58132
Hg, ^1S, ^3P, ^1P states, dipole polarisabilities from compact variational trial functions 80—63568
Hg(^1S), dipole polarisability, relativistic effective core pot. calc. 79—76362
I^-, free-ion polarisability, empirical values 77—20792
In^{2+}, emission spectrum, 340 to 6500 Å, ionisation pot. and dipole polarisability 78—78654
K, fine-struct. intervals, polarisabilities, highly excited d states 79—27100
K^-, photodetachment and at. polarisability 80—91522
K^+, free-ion polarisability, empirical values 77—20792
Li, dipole (quadrupole) polarisabilities, shielding factors, using hydrodynamic analogy 80—52905
Li, isoelectronic sequence, photoionisation cross section, core polarisability effects 77—57944
Li isoelectronic series, dipole polarisability, numerical Coulomb approx. 80—43199
Li, microwave fine-struct., polarisability of Li^+ core 78—13451
Li, multipole polarisabilities, shielding factors calc., hydrodynamic analogy to quantum mechs. 77—68134
Li^+, 2($^{1,3}S$) excited states, dynamic polarisabilities 77—34772
Li^+, 2($^{1,3}S$) excited states and ground state, dynamic polarisabilities, van der Waals force consts. 77—34773
Li^+, dynamic multipole polarisability, functional calcs. 78—74595
Li^+, dynamic polarisability calc. 77—14599
Li^+, imaginary frequency mutipole polarisability and long-range dispersion consts, functional calcs. 78—74596
Li^+, pair polarisability, ab initio SCF MO energies 78—70741
$Li^{2+}+Li^{2+}(H)$, two-body dispersion interaction, freq. depend. multipole polarisability, variational calc. 80—37758
$Li(2p)+H_2(N_2)$, Li(2p) excitation, alignment and orientation obs. 80—63794
Lu III, 6s $^2S_{1/2}$-6p $^2P°_{1/2,3/2}$ transition, relativistic oscillator strengths, influence of core polarisation 80—58132
Mg isoelectronic sequence, static dipole quadrupole polarisabilities and shielding factors calc. using HF scheme 80—99450
Mg, polarisability and London coeff., ab initio variation perturbation calc. 79—13635
Mg^+, resonance lines electron impact excitation, polarisability 78—42225
N, ground and excited states, atomic polarisability calc. 77—83756
Na, atomic states highly excited by laser radiation, Stark effect 79—13669
Na high ang. momentum Rydberg states, quantum defect core polaris. depend. 77—18808
Na, highly excited p and d states, fine struct. intervals and polarisabilities, RF reson. meas. 77—67999
Na isoelectronic series, dipole polarisability, numerical Coulomb approx. 80—43199
Na, Rydberg states, millimeter spectra, quantum defect, fine struct., polarisability, field ionis. obs. 78—82672
Na, saturation spectra, crossover signals, effect of atomic alignment, optical pumping 80—58202
Na, Stark effect study, S and D excited states struct., two-photon spectra 77—54547
Na, Stark shifts, absolute and differential, coherent optical transient meas. 80—37773
^{23}Na S states, HFS by Hartree-Fock calcs. 77—68023
Ne, atom, calculation from optimised potential model 79—6895
Ne, atomic polarisabilities and shielding factors, coupled HF approx. 78—22048
Ne, correl. contribs. to dipole polarisability, coupled HF-perturbation theory 80—106269
Ne, dipole dynamic polarisabilities and two-photon photoionisation cross section calc., R-matrix approach 80—102444
Ne, optical transitions, Doppler broadening, compensation by vel. depend. light shifts 80—52930

atomic polarisability continued
Ne+Ne(He)(Ar), dispersion interaction, series coeffs., variation method 79—3518
O, ground and excited states, atomic polarisability calc. 77—83756
$P(P^+)(P^{2+})$, static quadrupole polarisability and shielding factor, Hartree-Fock calc. 78—41950
Pb, Dirac eqn. calc. 79—22620
Pr^{3+}, elec. multipole polarisabilities, discrete basis set calcs. 80—91456
Rb $6^2P_{1/2}$ state, fluoresc. electric scanning method, polarisability 79—76381
Rb, high lying Rydberg states, atomic beam laser spectra 79—94101
Rb, polarisability constant, Stark interaction for excited states, laser spectroscopy 77—50404
Rb^+, free-ion polarisability, empirical values 77—20792
Rb($6^2P_{1/2}$) polarisabiliyt, mag. scanning obs. 80—27977
S, static multipole polarisability, frozen core approx. 79—36791
$Si(Si^+)$, static quadrupole polarisability and shielding factor, Hartree-Fock calc. 78—41950
Th, tensor polarisabilities of levels, level crossing method 79—10223
Tl, Dirac eqn. calc. 79—22620
Tl, ground-state hyperfine struct. tensor polarisability 77—6708
Tl, tensor polarisability calc. 79—76525
Xe+ inert gas, Xe three level system, collisional transfers, disalignment cross section 80—53098
Yb, $4f^{14}6s6p$ $^3P_1$ and $^1P_1$ levels, Stark effect, tensor polarisabilities 80—87080
Yb II, 6s $^2S_{1/2}$-6p $^2P°_{1/2,3/2}$ transition, relativistic oscillator strengths, influence of core polarisation 80—58132
Zn, ^1S, ^3P, ^1P states, dipole polarisabilities from compact variational trial functions 80—63568
Zn, Stark interaction in nspz$^3P_1$ levels, optical double resonance obs. 79—63941
Zn(^1S), dipole polarisability, relativistic effective core pot. calc. 79—76362

atomic positron scattering *see atomic electron impact excitation; atomic electron impact ionisation; elastic scattering of electrons by atoms and molecules*

atomic power *see nuclear power*

atomic reactors *see fission reactors*

atomic resonant states
absorption notch in spectrum of transform limited pulse 77—18817
AC Stark splitting in doubly reson, three-photon ionisation, nonmonochromatic field 78—94220
adsorption, selective, correlation of intensity features with at.-surface pot. Fourier components 79—15013
alkali anions, autodetaching sub $^2P_{1/2}$ threshold states 79—22611
alkali atom collisions, photon absorpt. cross-section and quasimol. transitions *(Russian)* 77—75285
alkali metal, resonance levels relax., hyperfine struct. effect 77—38725
alkali metal, two-photon ionis. via reson. intermediate state 78—42023
alkali metal atom, resonant multiphoton ionis. *(Russian)* 79—3401
alkali metal atoms, excited hyperfine and Stark parameters, meas. and calc. 78—86814
alkali metal atoms, resonance interaction, resonance lines self-broadening, adiabatic pot. curves 77—83676
alkali metal Stark profiles, of reson. lines, model microfield method appl. 79—26931
angular momentum depend. of laser-induced birefr. and dichroism in atomic reson. lines 79—10367
asymmetric resonance fluorescence spectra, in partially coherent fields 78—66503
atom, reson. lines relative oscill. strengths, hook technique using wall-stabilised arc 78—13628
atom, two-photon resonant ionis. 78—58631
atom+atom near-resonant processes, excitation transfer cross sections 77—3446
atom resonant scattering by light, quantum struct. *(Russian)* 80—78580
atom-surface impact, electron tunnelling in external electric field, atomic resonant ionis. and field ionis. 77—52208
atomic gas with resonant levels, mag. rot. of ellipse of polarisation of propagating rad. 79—50340
atomic resonance interaction, photon echo meas. 79—27061
Autler-Townes effect, coupled 1- and 2-photon resons., theory 77—83649
autoionising resonance, relativistic multichannel RPA 80—47925
autoionising resonances, density of states calc. 77—18857
autoionising resonances, vac. UV nonlinear optical props. 77—50565
axisymmetric medium, at. reson. level population meas., emission method *(Russian)* 77—68140
beam cooling, manipulation and trapping by CW reson. radiation 78—45751
Block-Siegert shifts and multi-quantum transitions, spin-one systems, RF and DC fields 77—75103
bound states of atoms in optical reson. field, interaction potential 79—93958
bound-continuum decay, AC Stark splitting 80—5502
bremsstrahlung, high frequency cross section limit for neutral ats. and ions 79—27142
channelled ions, reson. coherent excitation 79—51178
charge exchange in laser field, secondary emission 79—27081
charged particle scatt., resonant transitions, theory 77—58172
coherent transients, spherical tensor treatment 79—26940
coherent two-photon pulse propagation, solitary wave solns. 78—21891
collisional excitation transfer, with small reson. defect, mag. field effects 77—3449
collisions in intense mag. field, quasi-resonant *(French)* 77—527
collisions in strong light field, reson. broadening *(Russian)* 77—27149
complex scaling method, theory 79—18123
complex scaling transformations in stationary and scattering problems 79—18124
crossed electric and magnetic fields 79—85943
cumulative resonance in atomic ground state induced by modulated light field 78—66518
DC discharge, isotope enrichment by reson. trapping and cataphoresist. 77—27752
dielectronic recombination amplitudes, scaling props. 78—58781
dilation analyticity in constant electric field, two-body Stark problem 79—26900
Doppler-free two-photon resonances, interference fringe form. 77—42305
dressed atom system, energy levels and reson. phenomena, universal algorithm 80—69111

atomic resonant states continued
dressed atom system, phase represent. applic. to reson. fluoresc., universal algorithm 80—69112
elastic scattering, reson. width, stabilisation method, variational calc. 77—19011
electric field ionisation, highly excited state, linearly polarised field, freq. (amplitude) depend. 80—32630
electron+atom resonance scattering in laser field 79—859
electron elastic scatt., angle depend. resonance profile parameter 77—88563
electron elastic scatt., Feshbach resonances 78—58831
electron multichannel scatt., variable phase method 77—19082
electron scatt., optical excitation functions 78—58841
electron scatt. reson. using dilatation transforms., dilatation stability condition 78—46445
electron scatt. resonances during dilatation transformations, reson. eigenvalues stability 79—18291
electron scatt. using dilatation transforms., restricted perturbation methods 78—50639
electron scattering, reson. laser induced negative ion production 79—64104
electron scattering from ats.(mols.), partial resonance widths, Siegert eigenvalues, basis-set calc. 80—37880
electrostatically induced, pertubation theory 1-D model 77—75077
EM wave, reson., standing, at. beam deflection 79—26959
excitation and ionisation by strong EM field, threshold features *(Russian)* 79—85940
Feshbach reson. classification, relation to ionis. pots., appl. Ne, Kr, Ar, Xe 77—54519
fifth order atomic optical nonlinearities in multiphoton resonances 80—28275
final state channel, partial cross-sections, branching ratios 77—83555
fluctuating resonant laser radiation-produced at. motion 80—43310
fluorescence, canonical dressing by intense radn. fields 80—1173
fluorescence, nonlinear, intensity fluctuation spectrum *(Russian)* 77—68009
fluorescence, photon bunching and antibunching 79—31460
fluorescence, QED calcs. 78—41995
fluorescence, reson., in at. beam, multiat. and transit-time effects on photon-correlation meas. 78—86812
fluorescence, resonance, in vacuum UV, detection of low gas densities 78—54341
fluorescence, resonance, j=1/2 to j=1/2 transition 77—10632
fluorescence, resonance, with recoil effects, quantum statistical theory 78—78660
fluorescence, scattering spectrum, fine struct in external field 77—83533
fluorescence intensity correlation, chaotic pump radn. effect 79—98019
Fokker-Planck eqn. for resonant interaction with light wave 77—18854
Hamiltonian, complex-rotated, reson. props. 79—31427
heavy ion transitions, beam-foil decay curves, theoretical simulation 78—74755
heavy ions, beam-foil decay curves for reson. transitions, simulation 80—9721
high-resolution laser spectroscopy with minute samples 78—17822
hole-burning in at. vel. distrib. by EM radiation 80—64674
hydrogenic ions of high-Z, expt. and calc. of Lamb shift, review 77—54534
hyperfine structure quantum beats, intensity profile, ang. momentum theory graphical method 78—25497
inert gas, oscill. strength determ. from resonance radn. self-absorpt. 77—18847
inert gas+Li(Be$^+$)(Na)(Mg$^+$)(K)(Zn$^+$), collision-induced alignment, reson.-line emission polaris. obs. 80—18912
inert gas discharges, reson. radiation imprisonment model 80—38756
inert gases, fine struct. of atomic levels in field of intense reson. wave 78—9099
inert gases, photoabsorption to bound state and photoabsorption to continuum state (ionisation), comparison, HF calcs. 80—47910
inert gases, reson. widths, anomalous variation 79—31478
intense beam of radiation, resonant scatt. 77—57936
ion beam, laser-induced resonances, high-resolution expt. 77—6959
ion channelling, coherent excitation 79—46727
ionisation, resonant, under adiabatic level inversion conditions *(Russian)* 80—32691
ionisation spectroscopy, reson. chem.-physics appls. 80—68259
ions, H-, He-like, Z=4 to 34, wavelengths, radiative transition probabilities, autoionisation rates 79—25776
isotope separation by resonance scattering 77—61825
J-dependence of intensity-dependent polarization change in atomic reson. lines 78—70775
lanthanide sequence, 5p spectra collective excitation 77—50387
laser field atomic electron scatt. without optical pumping, reson. state coupling, theory 78—17804
laser induced one-photon transitions between two short-lived negative ion states 80—9731
laser radiation, interaction with free atoms, review 78—13473
laser-atom system, electron impact excitation, laser field effects 77—10768
laser-induced line shifts and double-quantum Lamb dips 78—86825
level splitting in strong mag. field and intense reson. EM waves *(Russian)* 77—27032
light scattering, resonant Voigt effect, analysis 79—76390
light scattering in strong monochromatic light field 78—25483
light scattering spectrum, relax. process effect 79—98046
light wave resonant interaction with atoms and molecules *(Ukrainian)* 78—66515
low-energy scattering, resonances 79—72384
many-electron systems, complex-coord. method extension 78—74591
many-electron systems, time depend., complex scaling and resons. calcs. 79 22612
metal vapour coherent two photon reson. third and fifth harmonic VUV generation 79—72627
momentum transfer to atom in resonance fluoresc. 79—72271
multi-level atom with Raman reson., time-delayed laser scatt. 80—48343
multi-level atomic systems, reson. lineshapes and shifts in rot. mag. field 77—68010
multi-level excitation theory, analytic approximations 78—29922
multichannel threshold structures in scattering theory 80—58334
multicharged ion thermal charge exchange reaction, rel. to astrophysics 80—63815

atomic resonant states continued
multilevel atom, resonance fluoresc. and absorpt. spectra in laser field 77—27018
multilevel systems, nonlinear reson. freq. shifts and saturation effects 78—78675
multiphoton ionisation, doubly resonant 78—42024
multiphoton ionisation, line profile as Fano profile with background struct. 79—72290
multiphoton ionisation, photon correl. effects, near reson. levels 80—43020
multiphoton ionisation, resonance peaks strengths 77—42293
multiphoton ionisation, resonant, in strong EM wave field 79—10079
multiphoton ionisation, resonant, with intense monochromatic laser 80—32689
multiphoton ionisation, resonant *(Russian)* 79—3421
multiphoton ionisation, short-time behaviour 79—59418
multiphoton processes of laser radiation interaction 80—37800
multiphoton resonant ionis., model calc. 78—62773
multiphoton resonant ionis. in incoherent field 79—26952
multiphoton transitions, continuum level shift effects 79—26956
multiphoton transitions, perturbation theory, atomic ionisation and intermediate reson., dissoc., review 79—41145
multiphoton transitions to continuum, via multiple resons. 77—10650
multiple quantum transitions, excited states in presence of static electric field 78—37618
N-electron atoms, resons., complex coord. calcs. 79—18125
N-level atom (molecule), coherent dynamics, two- and three-level behaviour 80—23649
N-level atomic system, reson. excitation by strong coherent radiation 79—68374
N-level atoms, coherent dynamics, anal. solns. 78—22105
N-level atoms, coherent dynamics, numerical expts. 78—22104
n-photon resonance phenomena, finite laser bandwidth effect 80—58230
near-resonant atomic interaction with intense radiation field 80—23375
negative ions, autodetachment, spectroscopy 80—23385
neutral atom reson. lines, Stark widths and shifts, regularities from He to Ca 80—47939
neutral atoms, bremsstrahlung, high freq. limit, effect of resonance scatt. 79—31473
non-Markovian resonance fluorescence 79—98021
nonlinear Faraday effect in resonant media 79—32001
nonlinear Ramsey resonance of excited atoms, Doppler-broadened transition 79—10074
nonlinear resonance fluoresc., negative time pair correlation of photons *(Russian)* 79—59750
nonlinear resonance for transitions to continuum 77—750
nonlinear resonances of accelerated atoms and molecules *(Russian)* 78—50488
nonmonochromatic chaotic field, double optical reson. and reson. fluoresc., AC Stark splitting 80—9547
optical Bloch equation, stochastic incoherences 79—68373
optical diffraction and refl. 79—63969
optical nutation and free precession, laser-atomic beam reson. fluoresc. 77—18837
optical nutation in gases *(Russian)* 79—27225
Paschen-Back effect in reson. radiation field 78—17607
perturbation of the atomic spectrum by a strong light field 79—10073
phase modulation *(Chinese)* 80—37801
photoionisation, multistep resonant, coherence versus incoherence 77—18859
photoionisation, nuclear polaris. *(Russian)* 79—49997
photoionisation, resonant and direct 77—83553
polarised nuclear beam production by reson. at. ionis. 79—13576
population inversion, anomalous resonance-radiation press. 80—52946
potential electron scattering in LF laser field 80—23545
quantum mechanical theory of resonance in chem. 77—75038
quantum motion in reson. field of standing light wave *(Russian)* 78—50508
quantum systems, at. or spin two level, reson. EM wave excitation, free induction decay oscills. 80—63562
quasiresonance EM field, vel. distrib. of atoms *(Russian)* 77—23472
radiation capture in cylindrical volumes of finite dimensions 78—66500
radiative atom collisions involving excitation transfer with small reson. defects *(Russian)* 80—53101
Raman X-ray scattering, reson., K vacancy excited state widths, appl. to Zr, Mo, Rh, Ag and Sn 79—45661
resonance calculations for arbitrary potentials 79—22779
resonance eigenvalues, accuracy criteria 80—91423
resonance energies, complex, diverging wave functions, least squares bivariational method 78—17741
resonance fluorescence, collective at. effects, dipole-dipole interaction 79—54806
resonance fluorescence, photon antibunching at. no. fluctuations effect 78—21875
resonance fluorescence in modulated laser field, stochastic model 78—5169
resonance levels prediction, stabilisation technique 77—61818
resonance partial widths and partial photodetachment rate using the rotated-coordinate method 80—91428
resonances, S-wave pot. scatt., coord. rot. method 80—28104
resonant electron scatt. by atoms in laser field, negative ion formation, polarisability 77—19089
resonant energies and width from discrete states in spherical box 80—47918
resonant ionisation by intense EM field 77—71784
resonant multiphoton absorption, transients, interference effects 79—85942
resonant two-photon ionisation in partially coherent radiation field 78—66525
rotated coordinate method use, rel. to stabilisation method 80—37845
rotated-coordinate method, rel. to stabilisation method 80—74097
Rydberg formula, modified 77—26957
Rydberg spectra, Landau standing wave form. 80—102466
Rydberg states in electric and magnetic fields: near-zero-energy resonances 79—36552
Schrodinger equation solution for atom near metallic surface, resonant state, jellium model 78—80033
selective atomic excitation by self-induced resonance 80—28189
semiclassical two electron atom, appl. of semiclassical equivalent of Hylleraas var. method 80—58111
Siegert wavefunctions, partial widths calcs. 80—5507

atomic resonant states continued
single atom detection, laser reson. fluoresc. method 80—26096
soft photon approx. accuracy for resonances in electron scatt. in laser field 78—70935
solar flar spectra, high dielectronic satellite lines analysis for plasma props. calc. 80—12728
spectral line intensity ratio, radn. capture effect 79—98040
spin transition, nonadiabatic, in time-depend. mag. field 80—9576
sputtered atoms from SiO_2, neutralisation and de-excitation 77—16446
Stark resonances, stabilisation method calcs., convergence 80—91492
stimulated collision-induced fluoresc. and stimulated Raman scatt. 78—87103
stochastic field, saturation and Stark splitting 80—9546
surface wave, momentum exchange with moving atom 79—64359
three level atom, reson. fluoresc. fluctuation-regression theorem 77—10629
three level atom in two-photon reson. with laser field, fluoresc. spectrum 77—42273
three-level atom, continued fraction transition theory, reson. lineshape 78—33473
three-level atom, reson. fluoresc. spectrum 79—54804
three-level atom in radn. field, resonance processes *(Russian)* 79—45687
three-level atom reson. fluorescence, statistical props. 78—78661
three-level atom resonance fluoresc., polaris. depend. 78—50500
three-level system, reson. interaction of opposite waves, relax. consts. of common level 78—50511
three-photon ionisation, collision-induced 80—23384
transition rate in reson. field, final state perturbation effect 78—941
transitions in laser field, reson. light press. forces 79—98045
two level atom, two-photon reson. fluoresc. 79—780
two level atom in low freq. EM field, quasienergetic states *(Russian)* 80—91471
two level atoms, reson. fluoresc., cooperative effects, bistability 77—10628
two level system, relax. consts. meas., two travelling waves reson. interaction 77—38644
two- and three-photon resonances, Doppler-free power broadening 78—5308
two-atom system, cooperative, reson. fluoresc. spectrum. sidebands 80—43000
two-atom two-photon resonance fluorescence 79—22645
two-level atom, in strong reson. field, fluoresc. props. 78—940
two-level atom, intensity effects in reson. fluoresc. 79—59661
two-level atom, multiphoton reson. fluoresc. in strong low-freq. field 78—55154
two-level atom, radiation by intense laser beam, resonance fluorescence, photon antibunching, Doppler shift 80—74146
two-level atom, reson. fluoresc., at. operators 80—937
two-level atom, reson. fluoresc., atomic operators 80—63579
two-level atom, reson. fluoresc., photon recoil shift 77—18839
two-level atom, reson. pulse excitation, ionisation 78—42029
two-level atom, sub-Poissonian photon statistics in resonance fluorescence 79—76650
two-level atom in resonant bichromatic field *(Russian)* 79—36588
two-level atom in resonant EM wave, atomic motion 79—18155
two-level atom system, reson. fuoresc., photon antibunching, propag. effect 80—9843
two-level atoms, cooperative resonance fluorescence, linewidth narrowing 78—21876
two-level resonance fluorescence, in at. beam, anal. calcs. 77—14386
two-level system, fluctuations and mean value, intense nonmonochromatic rad. 77—68018
two-level system, hyperfine struct. transitions, weak interaction meas. *(Russian)* 80—58196
two-level system, optimal control of resonance radiation processes 80—106498
two-level system, resonance properties, intense photon beam interaction, QED calc. 77—27033
two-level system, two-photon transverse reson. in RF spectra 77—79594
two-photon absorpt. of super-narrow pulses, narrow resonances 77—18876
two-photon ionis., polarisation effects *(Dutch)* 78—5185
two-photon reson. ionis. with sub-ns laser pulses 78—9131
two-photon resonant ionisation saturation and Rabi oscills. 77—79589
two-photon resonant three-photon ionisation with ultrashort pulses, optical nutation effect 79—89654
two-photon S-S transitions, reson. broadening *(Russian)* 79—26957
ultrahigh-Q isotropically sensitive optical filter employing atomic reson. transitions 79—55216
variational calc. of energies and widths of reson. 77—83506
variational calculation of reson. width and energy 78—33445
variational development of reson. theory, appl. to two-level at. S autoionising states 80—23329
variational method for reson. width and energy calc. 77—30798
variational method for reson. width and energy calc. 77—61690
wavefunctions of complex coord. method 80—106282
widths, purely L^2 method 78—46283
X-ray absorption spectra, resonance formation, role of surrounding potential 78—9168
Zeeman degeneracies effect on reson. fluoresc. *(French)* 77—61703
Zeeman resonance lineshapes, motional narrowing, analytical results 77—46524
Zeeman resonance lineshapes, motional narrowing, expt. 77—46525
^{4}He(3^{3}P), fine struct., level crossing obs. 78—82686
Ag I, resonance level, radiative lifetime, dye laser excitation 78—46300
Al, autoionisation reson. determ. from photoelectron polarisation meas. 80—58221
Al I, 4s^{2}S$_{1/2}$ reson. level, mean life 79—59400
Al I, resonance level, radiative lifetime, dye laser excitation 78—46300
Al I resonance line profiles, influence of boundary layer of Al-seeded shock heated plasma 80—43876
Al ions, He-like, satellite lines to higher-order reson. series lines in laser-prod. plasma 79—85930
Ar, 1s$_2$ and 1s$_4$ levels excit. via He$^+$ 100-1000 keV impact 77—10611
Ar, elastic electron scatt., resonance struct. 77—50532
Ar, electron impact, near threshold UV-emitting level excitation 78—25711
Ar, electron impact excitation, extreme VUV reson. lines 77—6937
Ar, electron scatt. in laser radiation field, free-free cross sections, reson. struct. 78—74763

atomic resonant states continued
Ar, electron-photon coincidence obs., reson. lines, polarisation correls. 79—31697
Ar fluoresc., polarisation of reson. lines, 104.8 and 106.7 nm, electron impact excitation 77—83739
Ar IX, Ne I like reson. and Na I-like satellite lines, relativistic HF calc., beam-foil spectra 78—94210
Ar line broadening by at. collisions, meas. of oscillator strength of ArI lines reson. *(French)* 78—5172
Ar, oscillator strengths, determ. from self-absorption of reson. radiation 79—89641
Ar, Paschen (1s) reson. state, decay mechanism and kinetics 79—27021
Ar, photoelectron angular-distribution β parameters, resonance parameters 78—21886
Ar plasma jet, weakly ionised, collisional line broadening 77—75106
Ar, Raman scatt., single particle HF approx. and RPA many-electron correlations calcs. 80—23374
Ar, reson. transition oscill. strengths, rel. to electron impact 80—27985
Ar, sputtering glow discharge, metastable and reson. states density meas. *(French)* 80—14955
Ar VIII, beam-foil lifetime meas. using ANDC anal. for reson. doublet 79—93964
Ar$^+$, electron impact excitation, extreme VUV reson. lines 77—6937
Ar+Ar, low-energy collision induced UV radiation 79—50125
Ar+Ca, quenching cross section of Ar atom for Ce reson. line 77—19021
Ar+N$_2$, bimol. and three body quenching, reson. state ^{1}P$_1$, ^{3}P$_1$ and excimer Ar atoms 79—3540
As I, rel. oscill. strengths, 193.8 and 197.3 nm lines 79—791
B, quenching of reson. radn. by Xe and Kr 77—30820
Ba, diamag. quasi-Landau spectrum near ionis. threshold, two-photon ionis. spectra obs. 78—58642
Ba, electron-correlation satellites, selective reson. enhancement 80—9569
Ba, Hanle effect in reson. line, density depend. 77—23473
Ba I, 5p spectra collective excitation, rel. to double photoionis. 77—50387
Ba I, quasi-Landau spectrum, semiclassical strong field mixing models 80—63847
Ba II resonance level lifetime meas. by pulsed laser excitation of ion beam 78—25480
Ba, reson. lines, emission and absorpt. core profiles 77—50389
Ba, reson. transition, laser saturation spectroscopy with optical pumping 80—52334
Ba vapour gas discharge laser excited by dual-pulse, lasing characts. 79—89895
Ba$^+$, inert gas atom collision, spectral line polarisation 79—13811
Ba$^+$ ions, hyperfine struct. reson. determ. from fluoresc. *(French)* 77—432
Ba$^+$, laser-induced resonances, high-resolution expt. 77—6959
Ba-inert gas, Ba reson. lines broadening, absorpt. cross sections anal. 80—32642
Be, ^{2}P shape reson., electron scatt. calc. 79—41240
Be, highly excited states, electronic struct., oscillator strengths and resons., HF calcs. 77—46506
Be$^-$, ^{2}P shape resonances, shift potential calcs. 80—69089
Be$_+$, ^{2}P^0 shape resonance, complex-coord. method calc. 78—74591
Be$^+$, resonance lines electron impact excitation, polarisability 78—42225
Br, ESCA, lifetime broadening, CI resonances 77—18853
Br, in Ar*+Br$_2$ lamp, Br atom conc. meas. by line absorpt. 78—46466
Br, reson. line emission attenuation following Br$_2$ photodissoc. 79—64059
C, ground state fine struct., laser mag. reson. obs. 80—87062
C, reson. transitions, Stark widths and shifts of UV and VUV Lines 77—88425
C^{3+}, electron impact 2s-2p excitation, absolute cross sections 78—13605
C^{3+}, excitation by electron impact, resonance tabulation, cross sections 78—33616
C$^{5+,6+}$+C reson. charge transfer, population inversion, in laser generated plasma 77—50526
Ca I, inner shell absorpt. spectrum, 3d wavefunction collapse 77—23455
Ca II H-K solar lines, non-mag. polarisation 80—63569
Ca, intensities of reson. lines *(French)* 77—57912
Ca, intercombination line, at. beam saturation and reson. fluoresc. spectroscopy 79—36580
Ca, resonance fluoresc. detection with intracavity at. beam laser spectrometer 77—19107
Ca stable isotopes, nucl. charge distrib. from isotope shift in Ca I resonance line 79—9461
Ca$^+$, inert gas atom collision, spectral line polarisation 79—13811
Ca$^+$, resonance lines electron impact excitation, polarisability 78—42225
Cd, electron scatt., negative ion form., shape resonances, electron affinity 77—14581
Cd I, 326.1 nm line absorpt. growth curve 79—76375
Cd, P$_1$ state resonance fluoresc. in rot. mag. field 77—42271
^{114}Cd λ326.1 nm reson. line, self-broadened, temp. depend. of parameters 79—63964
^{114}Cd+He, collisional effects on 326.1 nm line rel. to temp. and conc. 78—5336
Cl, photoionisation cross section and reson. theory, many body perturbation theory, 3p and 3s subshells 80—69114
Cl VIII, Ne I like reson. and Na I-like satellite lines, relativistic HF calc., beam-foil spectra 78—94210
Cl^{16+}, Lamb shift meas. using beam-foil excitation, QED test 80—9551
Co, 3p excitation spectra 79—22633
Cs, 16^{2}P states, reson., 3-photon ionisation, DC Stark effect 78—42026
Cs, 1st reson. level, effective electron-ionis. cross sections, plasma discharge method 78—13603
Cs, 7^{2}P$_{3/2}$ sublevels, hyperfine struct., multiphoton elec. dipole transitions anal. 80—32692
Cs atoms, exp. multiphoton ionisation through 9D$_{3/2}$ resonant level 77—34602
Cs, elastic electron scatt., 0.8-20 eV, Cs autoionis. state 78—5353
Cs, electron impact excitation velocity consts. for reson. levels, meas. *(Russian)* 78—1086
Cs, fluoresc., far wings profile of self-broadened reson. lines 79—76388
Cs, four-photon ionis., near 6F reson., rate theory 80—9568
Cs, four-photon ionisation, new resonances 78—5187
Cs I, pulsed 4-photon 6f-reson. ionis. 80—18831
Cs I, three-photon 16p reson. ionis. and DC Stark effect 80—14124
Cs, multiphoton ionisation, reson. shift obs. 77—445
Cs, multiphoton ionisation, reson. peak amplitude, temporal effects 78—78760

atomic resonant states continued

- Cs, optical reson. line electron impact excitation cross sections, polaris. 78—55244
- Cs, optically dense vapours excited by resonance lines, distribution of excited atoms *(Russian)* 77—23458
- Cs, photoplasma, optical excitation in radiation diffusion conditions 78—55227
- Cs, reson. lines, slow electron excitation cross section, low-lying D level coupling 77—23563
- Cs, reson. multiphoton ionisation by ultrashort laser pulsers, 1.06 μm 78—58630
- Cs, reson. multiphoton ionis. 79—41146
- Cs, reson. multiphoton ionisation near 6f reson., effective nonlinearity order 80—32688
- Cs, resonant 6P state, quenching by CO_2 mols. in He-CO_2-Cs discharge 80—43860
- Cs, resonant multiphoton ionis. *(Russian)* 79—3421
- Cs, resonant multiphoton ionis. 79—36589
- Cs, resonantly excited in cylindrical discharge plasma, effective lifetimes 78—79413
- Cs, self-broadened first reson. lines, near-wing asymmetries 80—9535
- Cs, three-photon ionisation, reson. and AC Stark effects 77—68020
- Cs, two-photon ionisation, 6s-6d quadrupole resons., ion asymmetry and spin polarisation 79—72286
- Cs^-, multichannel photodetachment 78—42027
- Cs-H_2 vapour, resonant character of laser induced formation of particles 80—89481
- $Cs+Cs^+$, charge exchange cross-section, temp. depend. 78—9244
- CsI, four-photon ionisation near 6f resonance 78—70801
- $Cs^*(6D_{3/2})+Cs(6S_{1/2})$, preferential excitation transfer from laser populated state 78—37732
- Cu, 3p excitation spectra 79—22633
- Cu, (100) surface, UPS, two-electron reson. at 3p threshold, rel. to Ni 80—25522
- Cu, absolute effective electron impact excitation cross sections, spectral obs. 80—53147
- Cu I isoelectric sequence, fine struct. separations for reson. transitions 78—17588
- Cu, intensities of reson. lines *(French)* 77—57912
- Cu isoelectronic sequence, 4s-4p reson. transition in highly charged ions 77—75087
- Cu, isoelectronic series, oscillator strengths of reson. transitions 79—22666
- Cu, resonance line, degree of coordination of clusters in metallic vapours *(French)* 77—58218
- Cu, resonance lines, relative oscill. strengths, absorpt. spectra 78—42005
- Cu vapour laser, energy conversion efficiency, reson. levels excitation 80—99715
- Cu^+, reson. transition, effect of correl. in $3d^n$ core, HF calcs. 80—47911
- $D+H^+(D^+)(He^+)(Ne^+)(Ar^+)(Kr^+)$, reson. charge charge transfer from photoexcited donor state 79—22820
- Eu I, 5p spectra collective excitation, rel. to double photoionis. 77—50387
- F, electron scatt., d-wave resonances, close coupling calcs. 78—33610
- F, electron scatt., low energy d-wave resonances 78—33609
- F^-, near threshold electron detachment cross section, effect of resons. 77—42403
- ^{19}F IX, high n states, laser induced resonances 77—83548
- Fe, 3p excitation spectra 79—22633
- Fe, UV photoionisation cross-section, resons. 77—14398
- Fe XXIII and XXIV, reson. and intersystem transitions, oscill. strength, lifetime, beam-foil spectra 78—82685
- ^{57}Fe metastable states, hyperfine struct. meas. by laser RF double-resonance 80—58404
- Fr I, wavelength estimate of first and second resonance lines 78—58617
- Ga, isotope shift and HFS, isotope effects, UV spectra obs. 80—42973
- Ga, reson. states lifetimes, electron-at. crossed beams expt. 77—68013
- H 1s reson., stabilisation method calcs., convergence 80—91492
- H detection by reson. fluoresc., coherent tunable VUV generation near Ly-β transition 80—99798
- H, double-quantum saturation spectroscopy, laser and RF 80—77880
- H, effect of metallic surface 77—35979
- H, electron elastic scatt. phaseshifts H continuum, frozen-core Hartree-Fock approx. perturbation theory 77—75295
- H, electron impact excitation of resons. below $n=3$ levels, algebraic variational calc. 78—9254
- H electron scatt., lowest ^1S resonance 77—58177
- H, electron scatt., lowest ^1S resonance, Feshbach formalism corrections 77—58178
- H, electron scatt. in EM field, reson. emission and absorpt. of photons 79—27087
- H, electron-photon excitation, high-energy resonant cross sections 78—70938
- H, highly excited resonant states, Stark effect, nonperturbative regime 78—70786
- H, ionisation, by microwave-stimulated multiphoton excitation, resons. obs. 77—68019
- H maser, effects on long-term freq. stability 77—75465
- H, multiple quantum transitions, in the presence of static electric field 78—37618
- H, photoionisation, two- and three-photon, calc. methods comparison 78—956
- H, positron scatt., Feshbach resonances, close-coupling calc. 77—6940
- H, positron scatt., S-wave reson., generalised scatt. length 78—42226
- H, quasibound states, Stark effect, variational 77—3251
- H, resonant pole trajectories in complex scaling, stationarity 79—18126
- H simultaneous mag./elec. microwave resonance transition, parity nonconservation, Weinberg-Salam theory test 77—54066
- H, Stark effect resons., strongly asymptotic approximants 80—52931
- H, two-photon absorpt. of ultrashort pulses, reson. intensities 78—59077
- H^- ^1P resonances, pseudostate expansion calcs. 80—32841
- H^-, $^1P_0$-reson., DC Stark effect calcs. 78—42000
- H^-, $^1p^0(1)$ and $^3p^0(1)$ resonances associated with $n=3$ hydrogenic threshold 80—78557
- H , autoioniation states, below $N=3$ hydrogenic threshold, complex-rot. calc. 77—67966
- H^-, autoionising states, electric field effect 78—50528
- H^-, energies and widths of $^1P^0(1)$ and $^1S(2)$ resonant states 79—18130
- H , $n=4$ resonances, complex rot. meas. calcs. 79—97995
- H , photodetachment, Feshbach and shape resons. 77—23480
- H photodetachment, Feshbach resonances 80—37753

atomic resonant states continued

- H^-, photodetachment cross section, Feshbach and shape reson. elec. field depend. 78—37614
- H^- photodetachment cross section, narrow resonances near $n=3$ threshold 80—27988
- H^- resonances in electric field 80—63607
- H^-, S reson. state, appl. of improved line width expression 80—5505
- H-like ions, electron impact excitation, resonances, collision strengths 78—33612
- H-like ions, reson. doublet component intensities in optically thin laser plasma *(Russian)* 78—38458
- H+D, near-resonant excitation transfer cross sections 77—3446
- H+positron, S-wave scatt., lowest reson. calc. 78—37743
- $H^++H(D)$, elastic scatt. and charge exchange, resonances 78—78777
- H(2s)+energetic projectile ion, charge exchange, cross-sections calcs. 79—59554
- He, 2^3S-state, electron impact excitation, reson. form. mechanism 80—99463
- He, 2p3d $^{1,3}L^0$ doubly excited state, soln. of Hartree-Fock eqns. 77—75072
- He (2^3S), resons. below $n=3$ doubly excited states, electron impact excitation 77—50543
- He, appl. of semiclassical equivalent of Hylleraas var. method appls. 80—58111
- He, autoionising resons., complex-coord. anal. 79—49992
- He, autoionising resons., complex rot. method, non- and degenerate perturbation theory 79—72283
- He, elastic electron scatt., resonance struct. 77—50532
- He, electron elastic scatt., p-wave reson., Breit-Wigner formula calc., perturbation method 77—38731
- He, electron elastic scatt., angle depend. resonance profile parameter 77—88563
- He, electron impact excitation, resons., near $n=3$ threshold 79—36773
- He, electron impact metastable excitation, resonance struct. 77—27184
- He, electron scatt., resonances, cusp effects, virtual state 78—25712
- He, electron scatt. resonances during dilatation transformations, reson. eigenvalues stability 79—18291
- He I, heavy ion impact excitation, relax. of 3 ^1P level *(French)* 77—61843
- He I, saturated absorpt. on 587.5 nm line, cross-over reson. 77—23448
- He, metastable, deexcitation process on Mo [110] impact 78—95642
- He, $n=3$ states, polarisation and excitation functions 77—6934
- He, $n=4$ resonances, complex rot. meas. calcs. 79—97995
- He, purely L^2 method for calculating resonance widths 78—46283
- He, resonance photoabsorption in (3s3p) ^1P reson. region 79—45659
- He, resonant states, high resolution study via electron excitation 77—6936
- He, S reson. state, appl. of improved line width expression 80—5505
- He, spectral lines, singlet, self-broadening, resonant interaction 80—63574
- He, two-step photoionisation via 4p $^1P_1$ state *(Russian)* 79—59413
- He^-, electron impact, post-collision interaction, reson. states 77—10767
- He^-, highly excited states, electronic struct., oscillator strengths and resons., HF calcs. 77—46506
- He^-, inelastic Feshbach resons., quasi projection operator calc. 80—58395
- He^-, purely L^2 method for calculating resonance widths 78—46283
- He^-, reson. calcs. with correlated target state wave functions, complex coord. method 79—26939
- He^-, resonances in post collision interaction 79—13820
- He^- resons. in 56 to 64 eV electron collisions, autoionising states and spectral line polarisation 80—53145
- He^-, resons. near doubly excited states thresholds, close coupling calcs. 77—54612
- He^+, electron scatt., reson. state assoc., incomplete spectrum of Hamiltonian matrix 80—99568
- He^+, fine struct. obs. by beam-gas spectroscopy, level crossing resonances 80—9719
- He^+, multiphoton RF reson. meas. 77—448
- He-like ions, multiple charged, reson. photoionis. 79—54818
- He-like ions in laser prod. plasma, anomalous intensity ratios of reson. to intercombination lines 79—23454
- He-like three-electron atoms and ions, inelastic-reson. quasiprojection operators 79—3581
- $He+He^+$, resonant charge transfer cross sections, 2 to 100 eV 78—66655
- He+Ne, scatt., orbiting reson. total cross-sections 78—5320
- $He^++Ar(N_2)(He)$, up to 70 keV, symmetric (antisymmetric) reson. charge transfer cross sections *(Korean)* 78—50636
- He^++He, $He(2^3S)$ formation, elastic and resonance charge exchange perturbations 77—42386
- He^++He, reson. charge transfer, merging-beam technique 79—41235
- He^++He, symmetric reson change transfer, 0.1-3 keV, 3-state close-coupled calcs. 77—50524
- $He(2S)^2$, autoionising reson., appl. of complex-rotated Hamiltonians 79—31427
- $He(2^{1,3}S)+H$, autoionising system, Siegert eigenvalues, variational calcs. 79—50106
- Hg, 5.2 eV resonance in electron impact excitation 79—10208
- Hg, electron elastic scatt., 4-6 eV, reson., scatt. ang. and spin polaris. spectra 78—25702
- Hg, electron scatt., absolute total cross section $(6s^26p_{1/2})^2P_{1/2}$ shape reson. 79—59570
- Hg, electron scatt., negative ion form., shape resonances, electron affinity 77—14581
- Hg, four-photon resonance ionis. 77—42289
- Hg, photoelectron angular distrib. resonance 79—13687
- Hg resonance line, 253.7 nm for atomic absorpt. meas. 80—78556
- $Hg+H(H_2)$, resonance scatt., HgH potential determ. 77—61830
- $Hg(6^3P_1)$ resonance level population, in vap. and inert gas modulated discharges 77—83532
- I II, reson. lines, oscill. strengths determ. by absorption method 80—58214
- $I(^2P_{1/2})$+n-iodopropane (iodoethane), quenching rate coeff., in UV photolysis of n-iodopropane (iodoethane) 79—11799
- $I(5^2P_{1/2})$, time-resolved reson. fluoresc., quenching rate coeffs. 78—25466
- In, isotope shift and HFS, isotope effects, UV spectra obs. 80—42973
- In, two-photon laser spectroscopy 79—6925
- K, 1st reson. level, effective electron-ionis. cross sections, plasma discharge method 78—13603

atomic resonant states continued
- K, 5^2P to 4^2S resonance line, rare gas perturbations, broadening, shift and dipolaris. 78—9126
- K, associative ionis. from resonance levels 77—30978
- K atom, stimulated multipole Raman scatt. between opposite-parity states 79—76753
- K discharge plasma, K_2 excited mols. form. by K(4P) collisions 80—44013
- K, electron elastic and inelastic scatt., 54.4-217.7 eV, 2-145° 80—1067
- K, electron impact excitation velocity consts. for reson. levels, meas. *(Russian)* 78—1086
- K, electron impact reson. transition excitation, unitarised distorted-wave polarised-orbit model 78—25710
- K, excitation cross sections in collisions with alkali ions 77—27167
- K, fine-struct. intervals, polarisabilities, highly excited d states 79—27100
- K I, inner shell absorpt. spectra, 3d wavefunction collapse 77—23455
- K, multiphoton excitation, Rydberg transitions, ionisation detection 77—42304
- K, optical reson. line electron impact excitation cross sections, polaris. 78—55244
- K, photosensitised assoc. ionisation, excited from reson. levels 77—83710
- K, reson. line polarisation, 2-photon excitation 77—54546
- K, resonance spectral lines, Stark broadening and shift 77—75097
- K, resonantly excited in cylindrical discharge plasma, effective lifetimes 78—79413
- K, two photon excitation by opposing light beams, reson. lines polarisation studies 78—82705
- K^-, multichannel photodetachment 78—42027
- K^+, electron impact excitation of reson. levels *(Russian)* 79—45852
- K+He(Ne)(Ar), 0.7-80 keV, K excitation, reson.-line emission and polaris. 80—18911
- K+inert gas atom, resonance levels relax. 77—83684
- $K^*+K^*\rightarrow K^*_2+h\nu$, in discharge plasma, anomalous K_2 5725Å band, photorecomb. 79—50088
- Kr, $^3P_1$ state, reson. fluoresc., Zeeman beats, time-resolved VUV spectra using synchrotron radiation 78—33454
- Kr, $4p^55s$ state, electron excitation fine struct., neg. on reson. 77—14585
- Kr, DC glow discharge excited atoms, radial conc. distrib. obs. 78—67494
- Kr, ESCA, lifetime broadening, CI resonances 77—18853
- Kr, electron impact, near threshold UV-emitting level excitation 78—25711
- Kr, reson. levels relax. consts. determ. by alignment method in discharge 79—26936
- Kr, self-broadening of first reson. line 79—26933
- Kr, twelve-photon ionis. at 10^{13} W cm^{-2} laser field 80—32687
- Kr VIII, beam-foil decay curves for reson. transitions simulation 80—9721
- Kr VIII, beam-foil lifetime meas. using ANDC anal. for reson. doublet 79—93964
- Kr VIII beam-foil decay curves for resonance transitions 78—74755
- Kr, VUV fluoresc. under monochromatic excitation 78—9237
- Kr XXXIII and Kr XXXIV, beam-foil obs. of transition wavelengths and oscillator strengths 80—14115
- Kr+Kr, low-energy collision induced UV radiation 79—50125
- La, intense 4d-f resons., cross-sections, spectra, calcs. 79—31426
- Li, electron impact reson. transition excitation, unitarised distorted-wave polarised-orbit model 78—25710
- Li, highly excited states, electronic struct., oscillator strengths and resons., HF calcs. 77—46506
- Li, inelastic Feshbach resons., quasi projection operator calc. 80—58395
- Li, photoionisation, two- and three-photon, calc. methods comparison 78—956
- Li, resonance spectral lines, Stark broadening and shift 77—75097
- Li, saturated three-step resonance ionisation spectroscopy 79—81189
- Li, spin-polarisation by dual-freq. optical pumping 80—43003
- Li, wings of resonance lines perturbed by inert gases, intensities 78—37596
- Li^+, 2p3d $^{1,3}L^0$ doubly excited state, soln. of Hartree-Fock eqns. 77—75072
- Li^+, autoionising, and quasibound states, Feshbach calcs. 77—54505
- Li^+, doubly excited autoionis. resons., laser prod. plasma absorption spectra obs. 77—50392
- Li^+, n=4 resonances, complex rot. meas. calcs. 79—97995
- Li+He(Ne), excitation cross sections, Li I resonance line emission and polarisation 77—61846
- Li+inert gas, fluoresc. reson. line broadening 77—6734
- Li^++Ar, up to 70 keV, symmetric (antisymmetric) reson. charge transfer cross sections *(Korean)* 78—50636
- Mg, ^2P shape reson., electron scatt. calc. 79—41240
- Mg, and isoelectronic sequence, relativistic effects on transition probabilities 77—54532
- Mg atoms, cooling to broad band reson. light press. 80—48835
- Mg, electron scatt., negative ion form., shape resonances, electron affinity 77—14581
- Mg I, $3^1P_1{}^0$ level reson. broadening and lifetime 77—57916
- Mg ions, He-like, satellite lines to higher-order reson. series lines in laser-prod. plasma 79—85930
- Mg, reson. line, Hanle effect, density depend. 79—6917
- Mg^-, purely L^2 method for calculating resonance widths 78—46283
- Mg^-, shape resonances, shift potential calcs. 80—69089
- Mg^+ laser cooled ions bound in Penning trap, high-resolution optical spectra 80—102487
- Mg^+, resonance lines electron impact excitation, polarisability 78—42225
- Mg-inert gas, Mg reson. lines broadening, absorpt. cross sections anal. 80—32642
- Mg^++Mg and Mg^{2+}+Mg, resonant charge transfer, phase interference effect 79—10199
- Mg^++Na(K)(Rb)(Cs), charge exchange and excitation processes 78—17772
- Mn I inner shell absorpt. spectrum, 3d wavefunction collapse 77—23455
- Mo, reson. Raman X-ray scatt., evidence for K-M scatt. 79—61466
- Mo^{12+}, VUV reson. lines, transition probabilities calcs. 78—41989
- Mo^{30+}, VUV reson. lines, transition probabilities calcs. 78—41989
- N, $^4S^0$ ground state, photoionisation calcs. 79—85909
- N, coherent radn. excited by external field 79—81184
- N, electron elastic scatt. resonance, neutral bremsstrahlung 77—46639
- N, reson. lines shapes determ. by Zeeman scans 77—6723
- N^-, $^3P^e$ shape reson. in absorpt. coeff. 77—424

atomic resonant states continued
- N^-, continuous absorption coeffs., from elastic e-N scatt. data, target wavefunction effect 78—9128
- NE, disalignment collision cross sections of $2p_4$, $2s_2$ levels, mode crossing determ. 79—18162
- Na, $^2P_{3/2}$-$^2S_{1/2}$ reson., light scatt. polarisation change 78—55144
- Na, $3^2P_{1/2,3/2}$ reson. levels, electron impact excitation, differential cross-section calcs. 79—59584
- Na, 3^2P-states, orientation and alignment relax. 79—76395
- Na, 3s-5s transition, Doppler-free two-photon excitation by multiple light pulses 77—42306
- Na, 5890/96 Å resonance emission lines, wing profile meas. 77—46534
- Na beam, associative ionisation, resonance fluoresence 79—98215
- Na beam deflection by reson. standing wave radiation 79—98056
- Na, D_1 and D_2 reson. lines, intensity dependent polarisation change 78—5163
- Na, depolarisation obs. of near-resonant scattered light 80—52921
- Na, electron impact ionisation, reson. and nonreson. electron distrib. 78—33615
- Na, electron impact reson. transition excitation, unitarised distorted-wave polarised-orbit model 78—25710
- Na, electron ionis., ejected electrons ang. distrib. 77—50541
- Na, electron scatt., theory 77—58172
- Na, four- and six-photon resonance spectra *(Russian)* 80—91527
- Na I reson. line broadening by collisions with dipolar mols. 80—941
- Na I solar D-lines, non-mag. polarisation 80—63569
- Na, laser temporal coherence effects in two-photon resonant three-photon ionisation 80—32686
- Na, near-resonant Rayleigh scattering and atomic flame fluorescence spectroscopy 79—92033
- Na, photoionis. cross section resons., time-dependent HF theory 80—32684
- Na, photosensitised assoc. ionisation, excited from reson. levels 77—83710
- Na, Rayleigh scatt. near $A^2P_{3/2,1/2}$-$^2S_{1/2}$ reson. doublet, polarisation reversal 77—10616
- Na, reson. multiphoton ionisation, broadband laser AC Stark splitting 78—70808
- Na, reson. transition, laser saturation spectroscopy with optical pumping 80—52334
- Na, reson. two-photon ionis., photoelectron ang. distrib. and polaris., nucl. spin influence 79—10083
- Na, reson. two-photon ionisation via $3p^2P_{3/2}$ state, photoelectron ang. distrib. 80—43016
- Na resonance line fluoresc. profile, perturbed by He 79—36723
- Na, resonance spectral lines, Stark broadening and shift 77—75097
- Na, resonant collisions in laser beam 78—78782
- Na, resonant three-photon ionis., saturation effects 78—58632
- Na, Rydberg levels mm resonances detected by field ionis., quantum defects, Stark shifts 77—42262
- Na, Rydberg states, high resolution two-photon mm spectroscopy, metrology appl. 80—43018
- Na, Rydberg states, millimeter spectra, quantum defect, fine struct., polarisability, field ionis. obs. 78—82672
- Na, strongly driven two-level atoms, reson. fluoresc. and absorpt. spectra meas. 79—36581
- Na, two and three photon resonances in strong nonmonochromatic field 77—34908
- Na, two-photon absorption reson. in spatially separated fields 78—21890
- Na, wings of resonance lines perturbed by inert gases, intensities 78—37596
- Na^+, autoionising $2s2p^6ns$, np states, electron reson. scatt. calc. 80—53142
- Na-like ions, transition probabilities for reson. transitions 78—66494
- Na+H(He)(Ne), D2 reson. linewidth 79—31647
- Na+He(Ne), excitation cross sections, Na I resonance line emission and polarisation 77—61846
- Na+inert gas, collisional redistrib., two-photon absorpt. with near-reson. intermediate state 80—23505
- Na+inert gas atom collisions, optical emission cross section, reson. lines 78—13584
- Na+Kr(Xe), reson. line broadening, press. depend. 78—66596
- Na+Na* resonant collisions mechanisms, excitation transfer in strong mag. fields between Zeeman sublevels 77—83712
- Ne, $1s_2$ and $1s_4$ levels excit. via He^+ 100-1000 keV impact 77—10611
- Ne, $2p_1$ level relax. and populations of $1s_2$ and $1s_4$ in afterglow 78—9111
- Ne, autoionisation region states, differential excitation function resons. obs. 77—6939
- Ne, autoionising resons. near 575 Å, ab initio relativistic RPA calc. 80—32681
- Ne, discharge, excitation mechanisms investig. using radial distrib. of excited atoms 80—38744
- Ne, elastic electron scatt., resonance struct. 77—50532
- Ne, electron impact, fine struct. resolved by reson. free-free radiative absorptions 79—3576
- Ne, electron impact, near threshold UV-emitting level excitation 78—25711
- Ne, electron impact, resonances, autoionising states 77—58170
- Ne, electron impact excitation, photon emission, ang. correl. 77—14584
- Ne, electron scattering, elastic and inelastic, reson. spectra, R-matrix calcs. 79—72421
- Ne, fine struct. obs. by beam-gas spectroscopy, level crossing resonances 80—9719
- Ne II, III, and IV ground state, photoionis. cross sections, close coupling calcs. 80—5513
- Ne, oscillator strengths, determ. from self-absorption of reson. radiation 79—89641
- Ne, photoelectron angular-distribution β parameters, resonance parameters 78—21886
- Ne, photoionisation, complex amplitudes at low energy singly and doubly excited resons. 78—78673
- Ne, photoionization mass spectroscopy using synchrotron radiation, reson. width meas. 79—31478
- Ne, reson. broadening at low densities 79—31452
- Ne, reson. free-free absorpt. by electrons in at. field, negative ion form. 77—3463
- Ne, reson. interaction of opposite waves, relax. consts. of common level 78—50511
- Ne, reson. level lifetimes, Zeeman coherence radiative and collisional transfer between excited states 77—23466
- Ne, reson. obs. in saturated absorpt. spectroscopy 79—89972

atomic resonant states continued
Ne, reson. transition oscill. strengths, rel. to electron impact 80−27985
Ne superradiation propagation through reson.-absorbing positive column plasma, pulse shape change 79−4117
Ne transitions, 1.52 μm and 633 nm, mode crossing resonance shape 79−18163
Ne$^-$ scatt. electron spectra, distinction from neutral autoionising states 80−83482
Ne$^+$+Ne, reson. transitions, direct and charge-exchange excitation 77−19020
Ni, 3p excitation spectra 79−22633
Ni, UPS, two-electron reson. at 3p threshold, rel. to Cu (100) expt. 80−25522
O III+e, low energy reson. struct., distorted wave approx. 77−75307
O V, electron impact excitation, resons. converging to n=3 thresholds 79−50136
O VI, $2s^2S$-$2p^2P$ reson. lines, wavelength determ. 80−102470
O VII electron impact excitation, reson. effects 79−41243
Pb, VUV photoelectron spectra, spin polarisation autoionis. reson. 78−33483
Rb, 1st reson. level, effective electron-ionis. cross sections, plasma discharge method 78−13603
Rb, $5^2P_{1/2} \rightarrow 5^2S_{1/2}$ resonance line perturbed by inert gases, depolaris., broadening and shift 78−21880
Rb, circ. polarised reson. fluoresc. excited with π polarised D_2 line, 0-170 G 79−41133
Rb, electron impact excitation velocity consts. for reson. levels, meas. *(Russian)* 78−1086
Rb, first reson. line oscillator strength, phase matching condition determ. 77−10638
Rb, fluoresc., far wings profile of self-broadened reson. lines 79−76388
Rb I, D_2 resonance line ^{85}Rb-^{87}Rb shift, mean square charge distrib. values inversion *(French)* 77−57931
Rb induced radiation in multiphoton excitation above ionisation limit *(Russian)* 79−3425
Rb, multiphoton ionis. processes, fine struct., hybrid reson. 77−18877
Rb, optical reson. line electron impact excitation cross sections, polaris. 78−55244
Rb, photoionis. cross section, elec. field depend. 80−37796
Rb, photoionisation from ground state in DC elec. field, narrow resonances *(French)* 77−61718
Rb, resonance lines 7800.23 and 7947.6 Å, Stark broadening obs. 78−66508
Rb, resonance spectral lines, Stark broadening and shift 77−75097
Rb, resonantly excited in cylindrical discharge plasma, effective lifetimes 78−79413
Rb, self-broadened first reson. lines, near-wing asymmetries 80−9535
Rb, situated in external elec. field, near zero energy reson. anal. 80−63563
Rb, vap., 1.06 micron conversion to 420 nm range 79−14040
Rb, Zeeman resonance lineshapes, motional narrowing 77−46525
Rb+Rb, ^2P states, near IR spectra, collision induced features 77−10637
Rb+Xe system, reson. fluoresc., quasimol. states *(Russian)* 79−85935
^{87}Rb atomic frequency standard, resonant frequency change, due to spectral profile of pumping light 78−45590
^{87}Rb, Stark effect on $5^2P_{3/2}$ state 79−3399
Sb VI, reson. lines, UV spectra 77−46515
Se I, $4p^3nl$ levels determ. from reson. lines meas. 78−938
$Si(3p^2(^1S_0))+He(SiCl_4)(O_2)(N_2O)$, attenuation of reson. radiation, time-resolved kinetic obs. 78−5329
Sn V, reson. lines, UV spectra 77−46515
Sr, 4607 Å reson. line shape, width and shift in Ar, press. depend. 79−22653
Sr, 4607 Å resonance emission line, wing profile meas. 77−46534
Sr, 4607.33 Å resonance line, spectral width depend. on at. density in flame 77−46535
Sr, autoionisation reson. states elec. field depend., three-photon ionisation 78−33478
Sr, diamag. quasi-Landau spectrum near ionis. threshold, two-photon ionis. spectra obs. 78−58642
Sr I, quasi-Landau spectrum, semiclassical strong field mixing models 80−63847
Sr II, resonance level lifetime meas. by pulsed laser excitation of ion beam 78−25480
Sr, reson. lines, emission and absorpt. core profiles 77−50389
Sr, Rydberg states, $^1D_2 \rightarrow {}^1F_3$ microwave transition meas. using selective reson. ionisation 79−72258
Sr$^+$, inert gas atom collision, spectral line polarisation 79−13811
Sr$^+$, inversion and lasing on optically pumped reson. line 78−70798
Sr+He(Xe), Sr reson. line width, 4607 Å, press. effects, pot. well depths 79−89643
Th, reson. localised 5,εf continuum state, giant reson. 80−91467
Tl, autoionisation reson. determ. from photoelectron polarisation meas. 80−58221
Tl HFS resonance lines anomalous intensity ratios 79−63961
Tl, photoionis. cross section, spin polaris. and ang. distrib. of photoelectrons, RPA calc. 78−13478
Tl, reson. lines, perturbing gas and self-broadening, temp. effects 80−42979
Tl($^7S_{1/2}$)+inert gas, long-range interaction, spectral line shifts and broadening 79−10174
Tm, intense 4d-f resons., cross-sections, spectra, calcs. 79−31426
U atomic beam, two laser irrad., two photon reson. effects., visible spectra 80−63604
U, reson. absorption meas. using Zeeman tuned arc lamp 78−17593
Xe, $^3P_1$ resonance state, three photon excitation, fluoresc. obs. 78−13481
Xe, $^3P_1$ state, reson. fluoresc., Zeeman beats, time-resolved VUV spectra using synchrotron radiation 78−33454
Xe, $5p^55s$ state, electron excitation fine struct. neg. ion reson. 77−14585
Xe afterglow, radiative and collisional deexcitation of reson. states, absorpt. and emission obs. 80−38742
Xe, autoionising reson., Stark effect 80−58198
Xe, collective excitation spectra, schematic model 78−41981
Xe, discharge lamps, 147 nm resonance line production 77−39497
Xe, electron impact, near threshold UV-emitting level excitation 78−25711
Xe I, 147 nm resonance line, wavelength stability 77−17948
Xe, line transition probabilities, in afterglow plasma, light absorpt. obs. 77−30807
Xe, photoionis., $\sigma 3/2:\sigma 1/2$ branching ratio in $5s5p^66p(^1P_1)$ resonance 77−42292
Xe, radiation imprisonment of $1s_4$ resonance line 79−82115
Xe, reson. levels relax. consts. determ. by alignment method in discharge 79−26936
Xe, reson. line excitation, Auger decay 78−70804
Xe, resonantly enhanced multiphoton ionis., photoelectron energy anal. 80−63597
Xe, self-broadening of first reson. line 79−26933
Xe VIII, beam-foil lifetime meas. using ANDC anal. for reson. doublet 79−93964
Xe, VUV fluoresc. under monochromatic excitation 78−9237
Xe+Xe(6s′(1/2)), (6p(1/2)), energy transfer, rate coeffs. 78−33573
Xe$^+$+Xe, XeI reson. line excitation 80−87220
Yb highly excited levels, reson., visible two photon absorpt. spectra obs. 80−58228
Yb, two-photon laser spectra, hybrid resonances 79−31489
Zn, electron scatt., negative ion form., shape resonances, electron affinity 77−14581
Zn I isoelectronic series transitions, theoretical oscillator strengths 78−74616
Zn isoelectronic sequence, 4s-4p reson. transition in highly charged ions 77−75087
Zn isoelectronic sequence, RRPA calcs. of resonance transitions from $4s^2$ $^1S_0$ 78−17612
Zn isoelectronic sequence, resonance oscill. strengths 79−3413
Zn, isoelectronic series, oscillator strengths of reson. transitions 79−22666
Zn$^+$+He(Ne)(Ar), 1-500 keV, Zn$^+$ excitation, reson.-line emission and polaris. 80−18911
Zr VIII, reson. transitions in UV 80−91479

atomic scattering factors *see crystal atomic structure; crystallography; lattice dynamics*

atomic spectra
see also atomic fluorescence; atomic hyperfine structure; atomic spectral line breadth; atomic structure; beam-foil spectra; conversion electron spectra; radiative corrections; Russell-Saunders coupling; Stark effect; Zeeman effect
3d photoabsorpt. spectra, continuum and discrete states 79−81176
^2P fine struct. interval of $2s^22p^5$ and $2s^22p$ configs., Z-depend. 79−22634
A=1-257, nuclear excitation by atomic electron transitions, nuclear levels 80−78191
absorption, collision-induced, at. electronic transitions 78−33594
absorption, emission, linebreadths, EM radiation interaction with atoms and mols. 78−13448
absorption coeff. in weakly ionised gas *(Russian)* 79−93939
absorption notch in spectrum of transform limited pulse 77−18817
absorption profile of at. beam nonorthogonal to laser light, optical freq. standard appl. 78−74940
absorption spectra in 100-900 Å region, device design 79−54202
absorption spectrum windows, of oscillator ensemble with embedded impurity oscill. 79−6045
actinides, and positive ions, non-relativistic Hartree-Fock X-ray scatt. factors 78−37602
adiabatic following coherent pulse propag. eqns., exact soln. 77−34579
air, plasma, optical absorpt. coeff. at 1000 atm, 13000K, N_2^- photodissoc. 80−64691
alkali+inert gas collisions in laser beam, transition probability 79−50120
alkali atom, in inert-gas solid, at level struct. calc. pseudopot. method 80−9532
alkali isoelectronic series, transition probabilities, oscill. strengths, lifetimes, branching ratios 78−33470
alkali metal, transition oscillator strengths in discontinuous and continuous spectra, review 80−52937
alkali metal atom, perturbed by rare gases, dipole moments of S-P transitions 80−27979
alkali metal vapour flash lamp, absolute spectral distrib. and radiant output 78−66510
alkali metals, Stark and photoabsorption spectrum, density of oscillator strengths, atom c.f. semiconductor spectra 80−83318
alkaline earth atom, correl. lines, Rydberg excitations and ionisation pots. 77−6705
alkaline earth atoms, multiphoton ionisation spectroscopy 78−82703
anomalous dispersion meas. by interference fringe shift 77−71891
arc plasma electron density meas., high-pressure, use of strioscopy and IR absorption *(French)* 80−19620
arc spectra, energy levels assignment *(French)* 77−83522
astrophysical X-ray spectra, limitations, comments and reply 77−56824
astrophysical X-ray spectra, usefulness 77−56823
atom+diatomic molecule, collinear collision, light absorption 79−76486
atomic and laser spectroscopy, book 77−79554
atomic collisions, absorption spectrum oscill. struct. due to quasimol. states 79−64093
atomic motion in resonant radiation, Ehrenfest's theorem 79−93957
atomic physics, conf., Riga, USSR (Aug. 1978) 80−22141
atomic scatt. factors and momentum densities, asymptotic form 80−74105
atomic spectra, two-electron matrix elements in Hylleraas coords., ang. integrals, radial recurrence relations 79−3386
atomic spectra and radiative transitions, book 80−22159
atomic spectroscopy using synchrotron radiation, book contrib. 80−4779
atoms, $70 \leq Z \leq 82$, Kα X-ray linewidths and relative intensities, energy dispersive meas. 80−99483
atoms, reson. radiation force, quantum mech. fluctuations, influence on at. motion 80−58233
autoionising and inner shell vacancy states, decay, time independent multichannel scatt. theory 80−47854
autoionising resonances, vac. UV nonlinear optical props. 77−50565
autoionising states, bounds on energy levels and widths 78−21885
Balmer wavelength calc. with hand calculator, student project 78−12512
beam-foil interaction, electron capture by protons, prod. of circular polarisation 77−3453
bibliography at. energy levels and spectra, (July 1971-June 1975) 77−71764
bibliography on experimental optical isotope shifts, (1918 to October 1976) 77−57932
blackbody radiation interaction with LF atomic transitions, Zeeman, Stark and stimulated emission 79−41127
bound-continuum decay, AC Stark splitting 80−5502
chemistry and spectroscopy 78−89556

atomic spectra continued
  classification, pattern recognition method, appl. to Cm energy levels 78−41983
  classification, pattern recognition method, H model appls. 78−41982
  closed-subshell atom, correl. lines, Rydberg excitations and ionisation pots. 77−6705
  coherent light scatt., two-photon Doppler-free transition amplitude 77−57954
  coherent two-photon pulse propagation, solitary wave solns. 78−21891
  cold atoms, trapping and storage in laser field 78−86826
  collective atomic system in external field, exact steady state density operator 79−76391
  collective excitation spectra, schematic model 78−41981
  collision systems $\alpha(Z_1+Z_2)\gtrsim 1$, quasimolecular 1 $s\sigma$ orbital, excitation and spectroscopy 80−87199
  collisional radiation redistrib. in spectral line nonimpact region 79−22667
  collisionally aided radiative excitation, three level system, interference effect 79−98022
  collisionally perturbed atoms, saturated near-reson. light scatt., spectral line strengths 80−23345
  complex specta, theory, tableau matrix elements, vector coupling approach 77−67996
  complex spectra; Gel'fand states for pure and mixed configs. 77−75079
  compressed gases, intermol. interactions, translation absorption spectra, temp. depend. 78−46419
  computational atomic and molecular physics, conf., Nottingham, England, (Sept. 1978) 79−59567
  Condon-Shortley coefficient, storage algorithm 79−49929
  conference, Leningrad, USSR (Feb. 1977) 79−10059
  cooling and trapping of atoms and mols., by reson. laser field 77−3321
  cooling and trapping of atoms and mols. by reson. light field *(Russian)* 77−46544
  cooperative system, light scatt. spectrum, coherent-state representation, numerical results 80−23650
  Coulomb de-excitation of neutral exotic atoms, μ^-p and π^-p H atoms 78−25757
  curve of growth, approx. 79−41126
  decaying atomic states, behaviour in applied fields, Lamb shift expt. 79−63963
  dense atomic fluids, variable polarisability, depolarised light scatt. 79−64823
  diffusion pulling in and pushing out by light field *(Russian)* 79−98047
  dipole K-L_{23} transitions, matrix elements 79−76368
  dipole transition, transient behaviour in intense laser field *(German)* 78−66520
  direct obs. of the transversal Doppler-shift 79−18151
  discharge radial distrib. of line intensities 78−18473
  double beam two-photon absorption spectra, off-diagonal matrix elements 80−5517
  double radiooptical resonance, signal propag. and shape 80−87360
  double vacancy states, correl. photon and electron transition, perturbation theory 80−27968
  doublet interference pattern, Nl determ. 79−63937
  doubly ionised K-shell system, radiative decay of excited state, branching ratio calcs. 77−54521
  dye laser with modes locked to atomic absorption lines, spectral characts. 80−9881
  educational push-button exhibit 77−57127
  eight-electron ions, $2p^k$ and $2p^{k-1}3l$ config. transitions calcs. 78−933
  electric dipole radiation interaction, length vs. vel. form, gauge invariance 79−41142
  electric multipole transitions, theory 78−41980
  electron pair prod., by intermediate and low energy photons, screening corrections 79−49991
  emission from hypersonic plasma-plane obstruction zone *(Russian)* 77−84449
  emission line profiles, ultrarelativistic charged particle EM field effects 77−3313
  emission spectra, semiclassical descriptions, extension to damping and line widths 79−59399
  energy level and Grotrian diagrams, S I to Ti XXII, book 79−3387
  energy level and transition array distribs. variance, Mo VX-XIV appl. 80−37767
  energy level transitions, Doppler broadening, phase-destroying collisions 80−9561
  excitation and ionisation by strong EM field, threshold features *(Russian)* 79−85940
  excitation by coherent pumping, induced Raman scatt. 78−66519
  excitation profile, effect of radiative emission-autoionisation interference of excited state decay 79−26945
  exotic atoms, with monopoles, spectral line intensities and selection rules *(Chinese)* 79−36800
  Faraday effect, analytical appl. 80−9538
  fast atomic beams, collinear laser spectroscopy 78−37078
  fine-structure transition probability, semiclassical multichannel scatt. matrix 80−37854
  first-row elements, low lying levels, excitation equilib. and line intensities 79−12401
  flame atomic absorption lines, appl. as background reduction method in plasma emission spectroscopy 79−16069
  forbidden decay modes of one- and two-electron ions, book contrib. 78−82679
  fourth row element ions, relativistic Dirac-Fock-Slater orbital binding energies, one-electron transition energies 79−25778
  fractional-parentage coefficients, reduced in quasi-spin space, submatrix elements of tensor operators 80−4578
  free atoms, diagram Auger electron spectra 80−78585
  free atoms in high magnetic fields, review 77−50383
  galvanic detection of optical absorpt. in gas discharge 77−15251
  gas lasers, computer modelling, at. and mol. processes 80−23661
  gaseous molecules, persistence of p, d, f and g orbitals, ang. functions, Schrodinger's eqn. and cardinal number anal. 80−102426
  gases, collision induced absorpt. spectra, integral data 79−81202
  ground and excited states, polarisability and scaling, oscillator strengths, continuum spectrum contribution 80−27923
  ground state shift, limited nonreson. moderately strong laser field 79−18157
  group IV homologous ions, oscillator strength trends 80−42991
  heavy atom, parity non-conserving E1 matrix elements, many body calcs. 80−47924

atomic spectra continued
  heavy atom valence shells, transition probability of valence shells, relativistic pseudopot. calc. 78−86803
  heavy atoms, strongly forbidden M_1 transitions, g-factor anomalies *(Russian)* 78−78648
  heavy elements, $74<Z<93$, L-subshell vacancy relative radiative decay rates 78−55137
  heavy metal vapours, optical activity as indication of electron-nucleon weak interactions *(Russian)* 77−10618
  Heisenberg's work on anomalous Zeeman effect and multiple spectra of atoms 78−70784
  high resolution two-photon FM laser spectroscopy of gas atoms, free of Doppler broadening 80−95748
  high-resolution laser spectroscopy with minute samples 78−17822
  high-Z electronic and muonic atoms, QED, strong and supercritical fields, book contrib. 78−74193
  highly charged ion, $1s^22s^22p^53d$ configuration, energy spectra in relativistic approx. 80−14082
  highly excited atoms, review 80−58174
  highly-charged ions, spectral characts., relativistic effects, theory 79−10061
  homologous ions series, Stark broadening trends 80−105157
  hook spectra, evaluation limitations 80−90905
  Hund's rules in atomic spectra, frozen electron core and valence electrons in nucl. field 77−67967
  hydrogenic atom, nonrelativistic, linear response to external linear polarised EM wave 78−8258
  hydrogenic atoms, metastable, Raman-like two-photon scatt., calc. 80−47953
  hydrogenlike ions, induced $2s_{1/2}\rightarrow 2p_{1/2}+$one photon transition, rate calcs. 77−50384
  hyperfine struct. transitions, nonstationary RF coherence signals *(Russian)* 79−98011
  inert gas, electron beam pumped, visible absorpt. rel. to visible laser development 78−63057
  inert gas atom, correl. lines, Rydberg excitations and ionisation pots. 77−6705
  inert gas atom adsorbed on graphite surface, excitation spectrum 78−71943
  inert gas atoms, adsorbed on metal surface, excitation spectrum 79−23832
  inert gas flash lamp, absolute spectral distrib. and radiant output 78−66510
  inert gas mixture, collision induced light absorpt., density effects 77−42258
  inert gas mixture, collision induced microwave absorpt. spectra 80−74216
  inert gas mixtures, interatomic pots. and interaction dipole moments, IR spectra calcs. 77−75082
  inert gas plasma, free-bound continuum determ. using photoionis. cross sections calc. 80−43878
  inert gases, electron beam excited, absorpt. characts. 78−82948
  inert gases, electron beam excited, transient absorpt. at XeF laser wavelengths 80−32644
  inert gases, fine struct. of atomic levels in field of intense reson. wave 78−9099
  inert gases, lifetimes from collision induced absorption spectra, IR line broadening 78−33554
  inert gases, mixtures, dipole moments, IR absorpt. spectra obs. 80−28903
  inert gases, photoabsorption to bound state and photoabsorption to continuum state (ionisation), comparison, HF calcs. 80−47910
  inner level spectroscopy with synchrotron radiation, theoretical aspects, book contrib. 80−4778
  inner shell excitation processes in heavy ion-atom collisions, review 80−37874
  inner shell ionisation phenomena, conf., Freiburg, West Germany, (Mar.-Apr. '76) 77−27040
  inner shell two-electron one-photon transition probabilities 77−14557
  interaction between atoms and RF fields, averaging method 79−81172
  interaction of atom with inhomogeneous plane wave 80−37786
  interferometer calibration for atomic and molecular transition wavelength meas. 79−80696
  ion, highly-stripped, quantum defects 79−41147
  ion, multiply charged, two-electron, parity nonconservation in spectra 79−10087
  ion+atom collision produced highly excited states, decay spectra 80−63780
  ion beam, from saddle-field ion source, gas depend. characts., at. spectroscopy appls. 78−78039
  ionised atoms, prod. by low inductance vacuum spark, spectroscopy *(Japanese)* 80−52911
  ionised atoms, quantum numbers, filling order of ionic electron shells, statistical model 80−52884
  ions, H-, He-like, $Z=4$ to 34, wavelengths, radiative transition probabilities, autoionisation rates 79−25776
  ions, highly ionised, review 78−62755
  ions, supermultiplet lines excited by beam surface interaction 78−13459
  ions in $1s^22s^n2p^{4-n}$ configurations, term-energy calcs. using perturbation theory 77−42229
  ions resembling Li, Be and B, spectra calcs., fine struct., transition energies 77−42260
  ions with $Z=2$ to 137, probability of $1s^2\ {}^1S$-$1s2p^3p_2$ and $1s^2\ {}^1S_0$-$1s2s^3S_1$ radiative transitions 79−63939
  IR spectral lines, 10000-40000 Å 78−50490
  irreducible spin precession theory applied to atomic and nuclear RF spectroscopy 80−27969
  J-dependence of intensity-dependent polarization change in atomic reson. lines 78−70775
  k ordering of atomic and ionic energy levels 80−74095
  k-ordering of atomic energy levels rel. to spectroscopic quantum defects 79−89657
  K-shell bound electrons, photon scatt. cross-sections, energy and ang. depend. 78−21882
  K-shell photoeffect, radiative corrections 77−57940
  kaonic H atom X-rays obs. 79−86088
  L^2 discretisation of atomic and mol. electronic continua, review 79−59425
  lanthanide atomic vapours, (Sm, Eu, Dy, Ho, Er, Tm, Yb,) photoabsorption spectra 77−88417
  lanthanide sequence, 5p spectra collective excitation 77−50387

atomic spectra continued

- lanthanides, 4d spectra in atoms rel. to solids 79—31450
- lanthanides, doubly ionised, f-d interaction 78—90102
- lanthanides, Rydberg spectra and ionisation thresholds, time resolved resonant multistep technique 78—82701
- laser atomic motion control, vel. selection, cooling, trapping, spectroscopy appl. 77—30833
- laser interaction, high intensity, Faisal's theory refinement *(Chinese)* 80—58195
- laser interaction with matter, nature of light, nonlinear spectroscopy 77—50712
- laser spectroscopy, multiphoton and multistep methods, review 79—35842
- laser spectroscopy 79—55002
- laser spectroscopy of unstable isotopes, nucl. props. determ. from atomic spectra using fast beams 80—9720
- laser-induced line shifts and double-quantum Lamb dips 78—86825
- level crossing signals, for at. and nucl. parameters 79—3416
- level splitting in strong mag. field and intense reson. EM waves *(Russian)* 77—27032
- level-band quantum system interaction with quasireson. monochromatic field *(Russian)* 79—26915
- level-crossing and line-crossing in atomic spectroscopy, appl. of terms 78—70799
- light ion lines sensitive to LTE departure in early type stars *(Russian)* 79—92770
- light scattering, near-reson., from collisionally perturbed at., time and freq. depends. 79—72281
- light shifts on atomic energy levels, non-resonant irradiation effect, appls. 77—75107
- line identification lists bibliogrpahy, August 1978 supplement 79—54787
- line wings, polarized radiative transfer, excited state interference 80—105158
- m-scheme configuration interaction calcs., interaction integrals 79—45645
- strong magnetic field effects, theory rel. to spectra of dense stars 80—105160
- magnetic null line tables for elements of astrophys. interest 77—70998
- magnetic scanning method, for at. parameters obs., accuracy 79—27116
- magnetoactive plasma, high-freq. electric effect on atomic spectra 78—9761
- many-electron atom, spectra calcs. 80—23347
- many-level atoms, Raman scatt. resons. in separated fields 79—31449
- matrix isolated atoms, matrix influence, theory 78—46288
- matrix isolated metal atoms, matrix influence, theory 78—46290
- mesonic atom and nuclear E1 transitions, dynamic electron screening 78—55260
- metal atoms, matrix isolation spectra 78—46287
- metallic species, ionised and neutral, high intensity resonance lines provided by flow lamp light source 79—27355
- metastable states, Doppler-free linear single-photon spectroscopy 78—50487
- microwave-atomic beam resonance interactions, standing wave effects 78—41985
- monochromatic laser radiation, excitation of atomic, mol. energy level transitions, inhomogeneous and mixed line broadening 78—55147
- monochromatic laser radiation, excitation of atomic or mol. energy level transitions, strictly homogeneous line broadening 78—58629
- monopole H atom, spectra, energy levels, transition probabilities *(Chinese)* 78—90322
- Moseley's expts.: $K\alpha$ line freqs., rel. to at. number, reinterpretation 80—82616
- moving atom-surface wave interaction, EM field momentum very close to plane interface 79—13936
- multi-level atom with Raman reson., time-delayed laser scatt. 80—48343
- multifrequency resonance transitions between quasi-energy states 80—43019
- multilevel atom, resonance fluoresc. and absorpt. spectra in laser field 77—27018
- multilevel atomic system, thermally relaxing, coherent radiation reson. scatt. and absorpt. 79—81401
- multiphoton bound-bound transition rates in hydrogenic atoms 77—23483
- multiphoton ionisation, r-photon resonant, theory 79—49998
- multiphoton transitions, choice of gauge 79—31488
- multiphoton transitions, continuum level shift effects 79—26956
- multiple anticrossings in atomic spectrosc. 80—87091
- multiply charged ions, autoionisation states 77—31434
- multiply charged ions, spectra calcs. 80—23347
- multiply charged ions, superposition of quasidegenerate configurations 80—42956
- multiply charged ions, X-ray spectroscopy 77—31434
- multipole radiation transitions, theoretical and experimental investigations *(Polish)* 78—13447
- multipole transitions in complex config., matrix elements for operators inc. relativistic corrections 78—5150
- muonic atoms, Dirac-Fock method 78—74805
- muonic atoms, nuclear polarisation energy shifts, phenomenologically extended microscopic calcs. 78—94335
- muonic atoms, parity violating neutral current effects, E1-E2 interference 79—41254
- muonic atoms, X-ray emission 79—86087
- muonic atoms, X-ray emission polarisation *(German)* 80—69268
- muonic X-rays, circular polarisation *(German)* 80—69266
- n-electron atom, transition probabilities, relativistic calcs. 77—14391
- N-level atoms, coherent dynamics, anal. solns. 78—22105
- N-level atoms, coherent dynamics, numerical expts. 78—22104
- near threshold struct. in K-shell spectra, photoionisation or fast charged particle ionisation 80—87064
- negative ions, autodetachment, spectroscopy 80—23385
- neutral atoms, bremsstrahlung, high freq. limit, effect of resonance scatt. 79—31473
- neutral atoms, bremsstrahlung, high frequency limit 79—31472
- noble metal, matrix-isolated, matrix-induced changes in opt. spectra 77—57913
- non-Rydberg atomic spectroscopy, review 78—90127
- nonlinear laser spectroscopy, book 77—71894
- nonlinear polarisation resonances in a continuum, optical activity, spin-orbit interactions *(Russian)* 80—53391
- nonlinear resonance for transitions to continuum 77—750
- nonlinear resonances of accelerated atoms and molecules *(Russian)* 78—50488

atomic spectra continued

- nonlinear spectroscopic determ. of g-factor difference between atomic transition levels 80—23346
- nonresonance perturbation in strong light field, review 77—46543
- np^q ions, forbidden lines, balance and line intensity ratios 80—83305
- one-electron atom in strong light field 79—63946
- one-electron systems, photoabsorpt. and dispersion profiles, moment theory 77—6709
- open-shell atom, 1st order transition matrices calc., graphical method in RPA 80—47846
- optical dispersion using nonresonant light beam *(Spanish)* 79—23394
- optical transitions, radiation induced, choice of gauge 77—27001
- optically active atoms in perturber gas in radiation field, master eqn. 77—30834
- oriented atoms, electronic Raman reson. scatt., statistical theory 80—102467
- oscillator strength, meas. using stimulated electronic Raman scatt. polarisation flip method 79—31471
- oscillator strength interpolation formulae for ground state transitions for H to Al isoelectronic sequences 77—71778
- oscillator strengths, relative, determ. by combined absorption/emission meas., Ti appl. 80—37784
- parity nonconservation effects, possible obs. 77—13889
- parity nonconservation effects, review 77—13890
- parity nonconservation in atomic transitions 79—36574
- parity violation in atomic processes 77—22657
- parity-violating weak interaction of electrons with nuclei, atomic spectroscopy search 79—36571
- perturbation of the atomic spectrum by a strong light field 79—10073
- photoelectron spectroscopy, review *(French)* 77—34599
- photoionisation, selective, use in laser isotope separation and spectros., review 80—83332
- photon emission by N-independent excited atoms, wave functions 77—57895
- photon total cross sections, 5 to 1100 keV, $6 \leq Z \leq 92$ elements 77—57935
- photon-bound-electron scatt. meas. 77—14394
- pionic atoms, electron screening and inner shell refilling, X-ray 80—78729
- pionic X-ray transitions, strong interaction line widths and shifts 77—23586
- in planetary nebulae, theory of physical processes rel. to emission line spectra 80—109527
- plasma, dense, quantum defect method modification, Ar appl. 80—38570
- plasma, Jeffries' level population ratios and Seaton's cascade matrix 80—52934
- plasma, Stark effect and four-quantum transitions, very strong stochastic electric fields 78—9760
- plasma spectral transitions, 50 to 150 Å, Fe to Br range ions with 15-24 lost electrons 77—80369
- polarisation propagator calculations of frequency-dependent polarisabilities, Verdet constants, and energy weighted sum rules 78—58647
- polyelectron atom He-Xe, strength sum evaluation method 77—75229
- protonium, atomic X-ray yields 1s and 2p level shifts and widths, cascades, calc. 80—78730
- quadrupole transition moment meas. by interference of quadrupole and DC field-induced sum freq. generation 77—30830
- quantum motion in reson. field of standing light wave *(Russian)* 78—50508
- quasi-classical quantisation of multidimens. systems, adiabatic invariants *(Russian)* 79—3343
- quasiresonance EM field, vel. distrib. of atoms *(Russian)* 77—23472
- quasistationary states decay, electron and photon spectra *(Russian)* 79—49969
- Rabi oscillations, double-pole decay 79—86151
- radiation distrib. and polarisation, of near-reson. radiation 78—37575
- radiation field interaction, Kramers-Heisenberg dispersion relation from QED 78—42015
- radiation lifetime laws in spectral series of atoms and ions 80—74150
- radiation pressure in gas for possible spectroscopic use 77—79164
- radiation trapping, analysis using charact. noise of strong EM wave 80—99492
- radiative portion of electronic transitions, continuum-field description 78—82894
- radiative transitions, classical theory appl. 78—74597
- radioactive atoms, hyperfine spectrosc., nucleus-electron interactions, review 79—72259
- Raman effect, spontaneous, three-level system in intense laser fields 78—86802
- random velocity fields, radiative transfer and line form., intensity moment transfer eqn. derivation 80—52967
- rare earth elements, atomic energy levels, data tables 78—86805
- rare earth ions, optical transitions, hypersensitivity to environment, mechanism 79—72255
- rare earth metals, photoionisation thresholds and Rydberg spectra 78—66522
- rare earth metals, spectra analysis, present state and trends 78—62749
- rare earths, atomic props. and electronic struct., review 79—68204
- rare gas adsorbates on simple metals, optical excitation, configurational switching, charge transfer 80—107643
- relativistic transition operators, matrix elements 77—30822
- relaxation shift by laser action freq. 79—18150
- resonance interactions of atomic and molecular systems driven by strong laser field, theory 80—14097
- resonance ionization spectroscopy with amplification 79—54996
- resonance light pressure, anal. of forces and applications, reviews 79—18156
- resonance light scatt. and spontaneous emission spectra in strong monochromatic light field 78—25483
- resonance line intensity ratio, radn. capture effect 79—98040
- resonance properties, intense photon beam interaction, QED calcs. 77—27033
- resonance Raman scatt. modification in intense laser fields 77—27002
- resonance scattering methods in atomic spectroscopy 80—53167
- resonance scattering spectrum, relax. process effect 79—98046
- resonances in crossed electric and magnetic fields 79—85943
- resonant atoms, optical diffraction and refl. 79—63969
- resonant EM wave affecting atomic motion, two-level atom 79—18155
- resonant interaction with light wave, Fokker-Planck eqn. 77—18854
- resonant line satellites, abnormal intensity in laser plasma emission *(Russian)* 77—3995

atomic spectra continued
- resonant scatt. of intense beam of radiation 77—57936
- resonant scattering of laser pulses by a system of N atoms 78—74617
- resonant transitions in laser field, reson. light press. forces 79—98045
- RF, nonlinear and parametric effects, review 80—18816
- row element ions 79—25778
- Rydberg atoms, expts., metastable states, multiphoton ionisation, spectroscopy, Stark struct., collisions, polarisability *(Dutch)* 78—5160
- Rydberg constant, using a hand-calculator, for teachers 78—81765
- Rydberg spectra, Landau standing wave form. 80—102466
- Rydberg states, simultaneous strong elec. and mag. fields 78—78663
- Rydberg states, spectrosc. and ionis. props. 80—23303
- Rydberg-Schuster law, at. spectrum anal., teaching 78—16591
- Rydberg-valence mixing, oscillator strengths 79—31492
- scattering by EM field 78—954
- selection rules for spectra and photochemical reactions *(Chinese)* 80—21308
- seven-electron ions, $2p^k$ and $2p^{k-1}3l$ config. transitions calcs. 78—933
- singly-ionised atoms of Fe group, oscillator strengths for $3d^N4p \rightarrow 3d^N4s$ dipole transitions 77—71780
- six-electron ions, $2p^k$ and $2p^{k-1}3l$ config. transitions calcs. 78—933
- soft photon approx. accuracy for resonances in electron scatt. in laser field 78—70935
- solar coronal ions, proton excitation of fine struct., approximations 77—17463
- solar emission lines of NeV, MgVII, SiIX, SXI, population levels as function of electron density and temp. 80—21963
- solar line intensities, OSO-7 obs. of limb brightening in EUV range 78—69759
- spatial frequency response of a nonlinear absorbing medium 79—27314
- spectrochemical anal., line pair intensity ratio stability, internal standard variability 79—39247
- spectroscopy quantum chem. teaching, fluctuating elec. dipoles, light absorpt. 78—73802
- spin factoring for spectroscopic term determ. 77—61695
- spontaneous emission fluctuations, data extraction 77—434
- spontaneous radiation, near field calcs. 80—99493
- sputtered atoms from SiO_2, neutralisation and de-excitation 77—16446
- Stark effect in Lyman α-line wings 79—22648
- stellar UV spectral line identifications 78—16371
- stochastic destruction of bound states in interaction with radiation field *(Russian)* 77—10644
- stochastic field, saturation and Stark splitting 80—9546
- sum-rule functions, parametrized, C_6 consts. 77—27000
- superexcited atoms, radiowave scatt. in ionospheric plasma, quantum model 80—32677
- superheavy elements, Z=114, 126, 134, 145, 164, 173, electronic transition rate calc. 77—26999
- surface wave polarisation in hyperfine dipolar mag. transitions *(French)* 78—50504
- survey for analysis of stellar spectra *(Spanish)* 79—75099
- synchrotron radiation, techniques and appls., book 80—5668
- temporally limited EM radiation, time integrated spectrum *(German)* 80—37769
- Thomas-Fermi model, atoms in strong mag. field 78—62724
- three-level atom, multilevel laser excitation dynamics 77—57941
- three-level atom, optically dressed, in spectroscopy 78—962
- three-level system, interacting with two strong EM fields, steady-state population distrib. and complex susceptibility 80—37978
- three-state atom, saturated two-photon absorpt. in perturber gas 80—106310
- time-dependent spectra, alternative definition 79—89625
- transition cross section meas. by saturation flux with laser oscill. 79—27114
- transition integral, Z-representation 77—27029
- transition matrices, higher approx. 78—33458
- transition metal, many-config. approx. in X-ray and electronic spectra interpret. 80—32615
- transition probabilities, bibliography (1914-1977) 78—74598
- transition probabilities, conf., Lund, Sweden, (March 1977) 77—79555
- transition probabilities meas. by time resolved optical pumping 77—46545
- transitional probabilities in quasiclassical case *(Russian)* 79—26914
- transitions, a-parameter and optical collisional cross-sections calcs. 77—83518
- transitions induced by gravitational radiation *(French)* 78—29026
- translational motion, coherent radiation effect *(Russian)* 77—27035
- two internal-vacancy atoms, Green function calcs. *(Russian)* 78—50451
- two K-shell vacancy systems, excited states, radiative decay 79—10048
- two k-shell vacancy systems, one-electron and two-electron one-photon transitions 78—58775
- two level atom, coherent and Raman scatt. spectra, secondary emissions 80—69449
- two level atoms, absorption spectra of optical bistability with dispersion 80—102757
- two level system, relax. consts. meas., two travelling waves reson. interaction 77—38644
- two-electron systems, photoabsorpt. and dispersion profiles, moment theory 77—6709
- two-internal-vacancy atoms, characts., Green's function calcs. *(Russian)* 78—50450
- two-level atom, in radiation field, level shifts and transition amplitudes calcs. 77—34592
- two-level atom, interaction with laser pulse 78—86827
- two-level atom, interaction with radiation, photon number time evolution 80—58216
- two-level atom, relax. and reson. fluoresc. in phase-modulated laser light, calcs. 77—54535
- two-level atom, spin-$^1/_2$ RF spectroscopy, saturation effects, semiclassical calcs. 77—67998
- two-level atom, strongly driven, absorption spectrum 79—54789
- two-level atom interaction with EM field, quasi-classical approx. *(Russian)* 77—27031
- two-level atom problem, Rosen-Zener solution 78—41937
- two-level atomic system, weak probe field absorption spectra in coherent laser field 80—23758
- two-level atoms, effect of high-power coherent radiation on spontaneous emission 79—55094
- two-level system, hyperfine struct. transitions, weak interaction meas. *(Russian)* 80—58196

atomic spectra continued
- two-level system, interaction with polarised light, Floquet's theorem 77—57939
- two-level system, resonance properties, intense photon beam interaction, QED calc. 77—27033
- two-level system, strongly coupled, induced transition probabilities and energy 78—66598
- two-level system in coherent field, quantum description 79—64053
- two-level system in two periodic fields, kinetics 79—64188
- two-photon absorpt., collisionally perturbed, reson. profile and strengths, degeneracy and Doppler shift 78—55156
- two-photon absorption, photon statistics and time depend. 78—13480
- two-photon resonant processes, conserved quantity 79—45688
- two-photon spectroscopy, ultra-high-resolution, Doppler-free 78—49909
- ultra-soft X-ray emission spectroscopy, correl. with electron spectroscopy 78—50558
- ultrahigh resolution spectroscopy using light echo effect *(Russian)* 78—70774
- unstable atomic targets, power broadening effects in reson. scatt. 80—32633
- UV photoelectric spectra from microwave lamps for calibration of spectroscopic instruments 77—45899
- vacuum UV emission and absorption from laser-induced plasmas, target geometry effects *(Russian)* 77—47164
- velocity distribution of photo-excited atoms, reson. radiation trapping 79—22668
- weak resonance radiation, collisional redistrib. function 79—794
- weakly excited system, neoclassical theory of radiation test calcs. 77—6737
- weakly inductive vacuum discharge, multiply ionised Fe ion spectra *(Russian)* 77—76224
- Wigner-Weisskopf atom in one-dimens. radiation field, relax. to equilib. 78—62769
- Wolf-Rayet stars, calc. of oscillator strengths of transitions for ion spectra C III, N IV, and O V *(Russian)* 78—57566
- X-ray, configurational interaction effects in region of 4f and 3d shell build up 77—27012
- X-ray absorption edge-shifts, empirical relations, effective ionic charge for isoelectronic series 78—55136
- X-ray emission from Z=37 to 56 atoms, Coster-Kronig transition thresholds 79—68214
- X-ray lasers, plasma, production, optical transitions of multiply charged ions, population inversion, review 77—19227
- X-ray satellite line spectra, spin doublet emission, common doublet levels 77—10621
- X-ray satellites, multiple inner shell vacancies from collision processes 77—83527
- Z=46-54, $L_{\gamma2,3}$ emission spectra, breadth, dynamical effects 80—32645
- Z-dependence of the intensity of $|\Delta n|=2$ pionic X-rays 79—94111
- Zeeman coherence in saturated absorpt., velocity changing collisions study 77—46527
- zeolite-Y, continaing Ag atoms, ions and clusters, optical absorption spectra 79—36569
- zeroth approximation, formally exact perturbation theory, transition energies calc. 77—42259
- H atoms, two-photon transition matrix elements, group theory calc. 78—62776
- $n \rightarrow ep\bar{\nu}$, H atom spectra and metastable state *(Russian)* 80—37262
- 0 I, 63 μm emission and quenching cross section in thermosphere and ionosphere 79—16732
- Ag, 4d-subshell absorpt. spectra, ab initio Hartree-Fock calcs. 79—18139
- Ag I, absorption spectrum, 1540-1850 Å 78—13453
- Ag in SiO_2 isolation matrix, XPS, atomic electronic struct., gas phase type spectra 79—89655
- Ag isoelectronic sequence, UV spectra (60-600 Å), resonance line identifications 78—33455
- Ag, isolated in mol. matrix, absorption spectra 79—22724
- Ag, oscillator strengths, relativistic HF, core-polarisation model pot. 78—86818
- Ag plasma, laser produced soft X-ray spectra, transitions 77—15171
- Ag, polarised photoelectron yields in VUV region 80—106307
- Ag, VUV absorption spectrum 79—49973
- $Ag+H^+$, excited X-ray polarisation, Born approx. calcs. *(Russian)* 80—78566
- Al, bombard. by Ar ions, impact-parameter depend. of K- and L-X-rays 79—76501
- Al I, electron impact line broadening in arc spectra 79—26919
- Al I, II, III, photon emission from secondary ions 77—59660
- Al I, relativistic and cancellation effects in line strength ratios 78—82689
- Al I isoelectronic sequence, forbidden transition probabilities for ground terms 77—2376
- Al II, energy levels, spectrum obs. 8640 to 683 Å 79—54797
- Al IV, autoionising transitions $ns^2np^6-nsnp^6mp$ 77—88419
- Al IV, transition probabilities and radiative lifetimes 79—76372
- Al ions, 720 keV beam foil spectra 1800 to 7000 Å, excited state cascades and lifetimes 77—23450
- Al ions, He-like, satellite lines to higher-order reson. series lines in laser-prod. plasma 79—85930
- Al ions, in plasma, spectral line intensity rel. to composition *(Russian)* 77—36851
- Al, muonic atom, Lyman series, muon transfer effect 79—7040
- Al plasma, simplified spectra obtained by electro-optic gating of radiant emission 78—22561
- Al sequence, $4s^2S$-$4p^2P$ transition, f-values 78—78651
- Al spectral line, hollow cathode discharge, pulse feeding 80—64797
- Al, sputtered by He^+, photon emission, dose depend. 77—8695
- Al, vacuum arc, excited state density from line intensities 80—96404
- Al XII, He-like ion, oscillator strengths of transitions between low-lying S and P states 78—13470
- Al XIII, hot pinched plasma, Lyman series Stark profiles, electron density determ. 78—51348
- Al^{5+}, $2s2p^5$-$2s2p^43s$ transition, spectroscopic investig. 79—59384
- Al^{n+} foil-excited ion, X-ray spectra and satellite classification 80—95567
- Al+He(C)(O)(Ne), K-shell ionising collisions, average L-shell ionisation probability, K_α spectra 79—72408
- $^{240}Am^m$, spontaneously fissioning isomer optical shift in pumped $^8S_{7/2} \rightarrow {}^{10}P_{7/2}$ transition, nuclear deformation 80—27971
- Ar,K inner-shell level energies, absorpt. spectroscopy with synchrotron radiation 80—99583
- Ar, absorpt. spectra, field induced autoionisation near ionisation threshold 80—106301

atomic spectra continued
Ar, and mixtures, photon mass attenuation and mass energy-absorpt. coeffs., 0.1 keV to 20 MeV 77−61715
Ar arc plasma, transition probabilities, continuum emission coeffs., electron density 77−51228
Ar atom, K-absorption spectrum, core electron rearrangement effect 80−47880
Ar, collision induced light scatt., three- and four-body spectra 79−18260
Ar, collision-induced light scatt., spectral features 78−13493
Ar, electron impact, L X-ray spectrum, radiative Auger transitions 80−58227
Ar, electron impact excitation, extreme VUV reson. lines 77−6937
Ar, electron scatt., free-free transition meas. 77−3464
Ar, electron-photon coincidence obs., reson. lines, polarisation correls. 79−31697
Ar, free ats. electron bombard., subsequent X-radiation ang. distrib. 80−53144
Ar I, probabilities of $np^5n'p \rightarrow np^5n's$ dipole transitions, two config. approx. calcs. 77−71779
Ar I and II transition probability determ. from improved branching ratio obs. 78−66514
Ar I arc plasma, excited atom density meas., Saha-Boltzmann equilib. 80−926
Ar II, transition probabilities and level lifetimes calc. 79−26935
Ar II arcs, transition probabilities, statistical inference 80−106357
Ar IX, Ne I like reson. and Na I-like satellite lines, relativistic HF calc. and expt. 78−94210
Ar ions, electron impact ionisation, trapped ion cyclotron resonance spectroscopy 80−53140
Ar ions, spectral classification in θ-pinch plasma 79−6896
Ar, line strength calcs. for 6s-5p and 3d-4p transitions 77−14384
Ar plasma radiation obs., line and continuous spectra *(French)* 80−19619
Ar, radiative level lifetime, photoionisation and photoexcitation rates, in shock tube 77−34594
Ar, Raman scatt., single particle HF approx. and RPA many-electron correlations calcs. 80−23374
Ar, three-body collision-induced light scatt. spectrum moments 78−9226
Ar, two-electron one-photon transition rate 77−71772
Ar XI, excited level populations, line intensity ratios, solar corona appl. 80−32637
Ar XIII, Ar XIV in solar flares, atomic data rel. to XUV electron density diagnostics 79−88633
Ar^-, free-free radiative absorpt. coeff. calcs. 77−423
Ar^{15+}, Ar^{16+}, $^3P_2$ and $^4P_{5/2}$ states lifetimes meas. 79−63966
Ar^{16+}, radiative decay from 2^3P_2 and 2^3P_0 levels, beam-foil time of flight meas. 77−68015
Ar^{5+}, Ar^{6+}, excited state lifetimes, beam-foil meas. 77−10750
Ar-Kr jet, electron excited, VUV emission spectra 80−933
Ar-Kr(Xe), UV absorption spectra, induced lines and line-shift meas. *(French)* 77−61697
Ar+Ar, low-energy collision induced UV radiation 79−50125
Ar+Ar, optical emission spectra 77−14551
$Ar+Xe \rightarrow Xe^*$, electronic energy transfer, emission spectra, electron beam excitation 77−38722
$Ar^{2+}+Na$ collision, single electron capture into Ar^+ excited states, 0.2-12 eV, emission cross section 80−48071
$Ar^{2+}+Na$ collision, single electron capture into Ar^+ excited states, relative population distrib. 80−48072
$Ar(^3P_2)+H(^2S)$, energy transfer, Lyman-α line obs. 79−64085
As, $4p^3 \rightarrow 4p^25s$, transition probabilities 80−47943
As I, level identification and Zeeman effect obs. 80−95571
As, L-shell soft X-ray emission spectra, oscillator strengths 80−32651
As VI, VII, spectra 100 to 300 and 500 to 1200 Å ranges 80−83307
As XXV, 2p-4d and 2p-4s transition arrays, wavelengths and oscillator strengths 80−47933
Au I, absorpt. spectrum obs., 1300 to 1900 Å 78−62751
Au in SiO_2 isolation matrix, XPS, atomic electronic struct., gas phase type spectra 79−89655
Au, incoherent γ-ray scatt. by K-shell electrons 77−83560
Au, isolated in mol. matrix, absorption spectra 79−22724
Au, K-shell X-rays, energy shifts and excitation mechanism 78−41990
Au, oscillator strengths, relativistic HF, core-polarisation model pot. 78−86818
Au, sputtering yields of D^+ and Ar^+ ions using matrix isolation spectroscopy 79−78809
Au, transition probability of valence shells, relativistic pseudopot. calc. 78−86803
Au, VUV absorption spectrum, photoionis. cross section, Fano parameters 79−93947
$Au+H^+$, L X-ray production cross sections, 0.3-1.8 MeV, expt. rel. to PWBA prediction 80−53115
$Au+H^+$ ionisation, induced L-shell alignment 80−32813
B I isoelectronic sequence, forbidden transition probabilities for ground terms 77−2376
B III, IV, laser produced plasma, satellite spectra 78−5165
B, spectra and energy level data tables 79−59386
B-like ions, EUV emission density sensitivity 79−16910
B-like ions, highly ionised, up to Fe XXII, Breit-Pauli approximation 78−53810
Ba $(5d6p)^3D_3$ state, lifetime meas. by dye laser spectrosc. 80−78577
Ba, atoms, high-lying levels, optogalvanic detection by laser excitation 79−98055
Ba, bound odd-parity J=1 spectra, multiphoton excitation 79−54795
Ba discharge, dipole-dipole pair absorpt. obs. using optogalvanic detect. 80−54064
Ba, emission spectra, 50 to 90 nm, electron impact excitation 78−82846
Ba, even-parity autoionising levels, multiphoton ionisation spectroscopy 79−59417
Ba, even-parity J=2 spectra, multichannel quantum-defect anal. 79−31445
Ba, even-parity states, one- and two-photon absorpt. 77−42303
Ba, excited state lifetime, delayed coincidence meas. 77−3315
Ba, high-resolution laser spectroscopy with minute samples 78−17822
Ba I, 440 to 830 Å, 5p absorpt. spectra 79−31455
Ba I, 5p spectra collective excitation, rel. to double photoionis. 77−50387
Ba I, absorption spectrum, 1560 to 1770 Å 78−66487
Ba I, hook method, gf values of intercombination line, 7911.38 Å 78−66511
Ba I, laser-excited, absorpt. spectra, press. shifts 77−27007

atomic spectra continued
Ba II, $5d^2D_{3/2,5/2}$, isotope shifts, hyperfine struct., collinear fast beam laser spectroscopy 80−83310
Ba II, vac. UV absorption, 350-1100 Å 77−30809
Ba isotopes, isotope shifts and hyperfine struct. from laser spectroscopy 79−9460
Ba, laser spectroscopic anal. of Rydberg series, multichannel quantum defect theory 80−18815
Ba, reson. absorpt. transitions, laser saturation spectroscopy with optical pumping 80−47121
Ba, reson. lines, emission and absorpt. core profiles 77−50389
Ba, reson. transition, laser saturation spectroscopy with optical pumping 80−52334
Ba, saturation spectroscopy with laser optical pumping 80−83324
Ba, time-resolved saturated absorption expt., collisions effects 78−29758
Ba, transition probability of valence shells, relativistic pseudopot. calc. 78−86803
Ba^+, hyperfine struct. of $5d^2D_{3/2}$ to $6p^2P_{3/2}{}^0$, laser absorpt. expt. 78−21870
Ba^+, inert gas atom collision, spectral line polarisation 79−13811
Ba^+, optical pumping and saturable absorpt. of fast ion beam superimposed on continuous laser beam *(French)* 78−5179
Ba^+, transition probability of valence shells, relativistic pseudopot. calc. 78−86803
Ba^{2+}, 3d photoabsorpt. spectra, continuum and discrete states 79−81176
Ba+Ba, atomic pair absorpt. obs. with white-light source 79−63944
Ba+Kr, collision induced dipole transition, elec. quadrupole transition, oscillator strengths 79−41128
Ba+Tl, atomic pair absorpt. obs. with white-light source 79−63944
$^{138}Ba^+$, lifetime of $6p^2P_{3/2}$ level using superimposed ion and laser beams 77−57933
Be, 4-wave sum mixing around H Lyman-α 80−23747
Be, freq.-depend. polarisabilities and Verdet consts., calcs. 78−62781
Be I, B I, C I, N I and O I isoelectronic series, tables of oscillator strengths of transitions 80−37779
Be I isoelectronic series, $2p^2$-2s2p and 2s2p-$2s^2$ transitions, oscill. strengths, transition probabilities 77−46532
Be I-like spectra, low configs., isoelectronic consistency 79−93940
Be II, III, laser produced plasma, satellite spectra 78−5165
Be III, doubly excited states, triplet spectra 80−87069
Be, isoelectronic sequence, transition probabilities, relativistic effects calcs. 77−27028
Be isoelectronic sequence, mag. quadrupole transition probabilities calcs. 78−21865
Be isoelectronic sequence, mag. quadrupole transitions probabilities 78−37592
Be isoelectronic series, Z=22-34, spectral lines from laser prod. plasma 77−50388
Be lines formation, non-LTE calc., rel. to solar Be I 2650 Å line misidentification 80−32636
Be sequence, (Z=4 to 10, 14), $^3P_1 \rightarrow {}^1S_0$ intercombination line, CI calc., Breit interaction 78−78641
Be^+, electron impact excitation, Bethe approx. modifications, impact radiation polarisation 79−31695
Be^+, formed in laser-produced plasma, absorpt. from excited states 78−17594
Be-like ions, $2s2p(^3P_1{}^0) \rightarrow 2s^2(^1S_0{}^e)$ transition probabilities, CI calcs. 79−36544
Be-like ions, oscill. strengths and transition probabilities, Breit-Pauli approx. calcs. 79−36570
^7Be, gamma ray lines from $\alpha\alpha$ reactions 77−87248
Bi, $6p_J{}^3$-$6p_J{}^3$, search for optical rot. induced by weak neutral currents 78−82710
Bi, atomic, parity violation in M1 transition 79−85927
Bi I, hyperfine struct. determ. 78−935
Bi I, transition probabilities in 195-600 nm range 79−6898
Bi II ion, relativistic effects in hyperfine splitting of second spectrum 80−23344
Bi III, 4809.1 Å multipole line, hyperfine struct. splitting factor 77−68004
Bi, optical activity, search for parity nonconservation 79−36574
Bi, optical transitions, struct. of weak neutral currents *(Russian)* 77−88420
Bi, parity violation, optical activity of vap. 79−26938
Bi, pionic $4f \rightarrow 3d$ X-ray transition 79−86085
Bi, UV absorption spectrum, flash photolysis method 78−90105
Bi, vapour, optical rot., parity nonconservation 80−23353
Bi, vapour, optical rot., parity nonconservation expts. 80−23354
$Bi+H^+$, L X-ray production cross sections, 0.3-1.8 MeV, expt. rel. to PWBA prediction 80−53115
^{209}Bi, P violating eN pot., determ. of effects by optical rotation meas. 79−26277
^{209}Bi, transitions, parity nonconservation due to neutral weak currents 77−13913
Bk, emission spectrum, 2540-9800 Å, electrodeless lamp source 80−27970
^{249}Bk, IR spectrum, 3700-12000 cm^{-1} 77−68001
Br II, visible spectrum, shock tube time-resolved photographic photometry, transition probabilities 77−23449
Br II levels, NF values meas. in Ne-Br_2 mixtures 78−62753
Br, L-shell soft X-ray emission spectra, oscillator strengths 80−32651
C, ^5S-$^3P_2$ and $^5S_2$-$^3P_1$ transitions, ^{13}C isotope shift 80−58201
C, and mixtures, photon mass attenuation and mass energy-absorpt. coeffs., 0.1 keV to 20 MeV 77−61715
C, ground state fine struct., laser mag. reson. obs. 80−87062
C I, interstellar, UV lines obs. in ζ Puppis and ζ Ophiuchi 79−35332
C I 1101 Å absorpt. edge in A-type stars, effect of $C+H^+ \rightleftharpoons C^++H$ charge transfer 80−90423
C I isoelectronic sequence, forbidden transitions calc. 79−31444
C I transition probabilities and oscillator strengths, rel. to H I regions 77−49448
C II, Zeeman splitting of high-n recomb. lines 80−58210
C II and III, mean lifetimes of astrophysically important excited levels 77−46528
C II line excitation by C I photoionisation 80−58223
C III, solar emission line ratios interpretation 78−28598
C III, transition probabilities 78−41987
C IV, V, laser produced plasma, satellite spectra 78−5165
C IV (CV), UV line identifications and lifetime meas. 80−106288
C IV doublets in QSO spectra rel. to absorption redshift 79−35417
C lines, charge exchange reaction effect 79−58243

atomic spectra continued
C plasma, spectral and absorpt. coeffs. 80—69985
C, radiative lifetimes of visible and near IR transitions, solar abundance 78—50506
C V, electron impact collision rates, reinterpretation of solar emission line ratios 80—98624
C, vac. UV spectral line broadening parameters meas. 80—23352
C^-, free-free transitions, continuous absorpt. estimation 78—9098
C^{5+}, plasma expansion, Balmer spectrum intensity inversion, charge transfer pumping 78—34371
C^++Ne, energy loss collision spectrosc. 79—86037
$C^{5+,6+}$+C reson. charge transfer, population inversion, in laser generated plasma 77—50526
Ca, $4p^2\ {}^1S_0-4s4p\ {}^1P_1-4s^2\ {}^1S_0$ cascade rate, two photon coincidence meas. technique 80—95576
Ca, 6573Å line photon recoil struct. 79—85925
Ca, A=40-48, isotope shift meas. using enriched isotopes in atomic beam 78—17610
Ca, bound odd-parity J=1 spectra, multiphoton excitation 79—54795
Ca, bound-even parity spectra, multichannel quantum defect theory anal. 77—34600
Ca I, emission spectrum, level struct. 77—79562
Ca I, inner shell absorpt. spectrum, 3d wavefunction collapse 77—23455
Ca I 6573 Å and Ca II 7324 Å forbidden line, centre-to-limb behaviour 79—25572
Ca I absorption spectrum, 1430-1340 Å 80—47930
Ca I absorption spectrum in vac. UV, excitation of 3p-subshell 77—75085
Ca II, in fast sporadic meteor spectrum, low-energy electron excitation 78—93170
Ca II emission from stellar chromospheres 79—30061
Ca II H- and K-line complex structure in HD 190073 (A0ep-type) 77—60775
Ca II H-K solar lines, non-mag. polarisation 80—63569
Ca II H-line emission from Sun observed as star *(Russian)* 77—64727
Ca II solar K-line network, giant cell circulation pattern 77—53546
Ca III, autoionising transitions $ns^2np^6-nsnp^6mp$ 77—88419
Ca, intensities of reson. lines *(French)* 77—57912
Ca ions, dielectronic recombination excitation in solar X-ray lines 80—51725
Ca, laser spectroscopic anal. of Rydberg series, multichannel quantum defect theory 80—18815
Ca, photon recoil splitting, line widths, Doppler effects, saturated absorpt. optical interference spectroscopy 80—52922
Ca, Rydberg states and microwaves, spectroscopy, masers, and superradiance 80—53248
Ca stable isotopes, nucl. charge distrib. from isotope shift in Ca I resonance line 79—9461
Ca, Stark mixing of high-lying calcium levels by laser-produced charges 78—25469
Ca, two-electron one-photon transition rate 77—71772
Ca XV, Ca XVI in solar flares, atomic data rel. to XUV electron density diagnostics 79—88633
Ca XV, proton collisional excitation of fine struct. transitions in ground state 77—19017
Ca XV III, line identification in solar corona radiation 77—79569
Ca XVII, energy levels and transition 79—59383
Ca^+, inert gas atom collision, spectral line polarisation 79—13811
Ca^+, transition probability of valence shells, relativistic pseudopot. calc. 78—86803
Ca+inert gas, collision-induced dipole transitions, absorpt. study 80—37865
Ca+inert gas, collision-induced dipole transitions assoc. with high-lying states 80—37866
Ca+Xe, collision-induced dipole transition due to long range interaction, absorpt. obs. 80—63779
CaI, inner shell absorpt. spectrum, 3d wavefunction collapse 77—23455
^{43}Ca, isotope shift and hyperfine struct. by laser spectroscopy 79—41139
Cd, $5s5p^3P_1-5s^2\ {}^1S_0$ intercombination line, press. broadening and shift 80—95564
Cd, absolute photoabsorption. cross section, 40-250 eV 78—58613
Cd, absorpt. spectra in nonreson. biharmonic radiation field 79—3400
Cd I, 326.1 nm line absorpt. growth curve 79—76375
Cd I, absorption spectrum, simultaneous excitation of two electrons 78—58614
Cd IV, $4d^9 \rightarrow 4d^85p$ transitions, UV spectra 77—46515
Cd IV, UV spectral analysis 80—83306
Cd, nonadiabatic transitions in two-level system 79—98014
Cd, optical isotope shifts and hyperfine struct. 77—3316
Cd, Stark interaction in $nspz^3P_1$ levels, optical double resonance obs. 79—63941
Cd, triplet states, hyperfine struct. obs., project expt. 77—33737
^{114}Cd, resonance line contant., effect of Xe temp. and conc. 79—63945
Ce, isotope shift in IR spectrum *(French)* 77—54523
^{249}Cf, IR spectrum, 3700-12000 cm^{-1} 77—68000
Cl, $4s-3p^5$ transitions, oscillator strengths 77—46537
Cl I, wall-stabilised arc, absolute transition probabilities, 5300-6850 Å 78—9105
Cl I isoelectronic sequence, forbidden transition probabilities for ground terms 77—2376
Cl, kinetic spectroscopy in far vacuum UV, oscillator strengths of transitions 78—13457
Cl, L X-ray emitting levels, lifetimes 78—66493
Cl VIII, Ne I like reson. and Na I-like satellite lines, relativistic HF calc., beam-foil spectra 78—94210
Cl^-, far UV spectra in solns. 78—94208
Cl^{6+}, Cl^{7+}, excited state lifetimes, beam-foil meas. 77—10750
Cl+He(C)(O)(Ne), K-shell ionising collisions, average L-shell ionisation probability, K_α spectra 79—72408
^{244}Cm, emission spectrum, 2400-11200 Å, wavelengths, rel. intensities, Zeeman effect 77—46514
Co, 3p excitation spectra 79—22633
Co (VII), semiempirical investigation of spectra 78—33434
Co II, wavelengths and estimated intensities 1020 to 9500 Å *(Spanish)* 80—52920
Co, n=2-2 transitions in XUV spectra, anal. 80—102472
Co V spectrum analysis 79—72266
Co, X-ray transitions in laser produced plasma 80—100093
Co XI-XVII solar $3s^23p^n-3s3p^{n+1}$ transition arrays, UV spectra classification 80—63570
Co(VIII), resonance transitions, classification 80—42985

atomic spectra continued
^{59}Co, mag. hyperfine struct. analysis, spectral lines 4000 to 4300 Å 78—62752
Cr, atomic transition probabilities, oscill. strengths 78—74601
Cr from Tokamak-produced plasma, $2s^22p^k-2s2p^{k+1}$ transitions in F I to Be I isoelectronic sequences 80—37765
Cr I, discrepancies between theoretical and experimental oscillator strengths 77—83539
Cr I, inner shell absorpt. spectrum, 3d wavefunction collapse 77—23455
Cr I, vapour phase absorpt. spectrum, 30-400 Å, excitation of 3p-subshell 78—21866
Cr I excited levels, lifetime meas., oscill. strengths 77—71777
Cr I in photospheric spectra, solar abundance and oscillator strengths 78—69757
Cr I lines, 200-541 nm, oscillator strengths determ. from hook-method and absorpt. meas. 77—79582
Cr I to XXIV, energy levels, ionis. pots., g-factors, from spectral data review 77—79556
Cr II lines, A_{mn} transition probabilities 80—14099
Cr II to VI, struct. and transition probabilities, ab initio calc. using Thomas-Fermi central pot. 79—3360
Cr III, spectra obs. in low-voltage sliding-spark discharge 77—6710
Cr, $K\alpha^h$ hypersatellite spectra and double photoionisation cross-section 79—85922
Cr, multiphoton ionisation and absorpt. 80—95575
Cr, n=2-2 transitions in XUV spectra, anal. 80—102472
Cr VII, autoionising transitions $ns^2np^6-nsnp^6mp$ 77—88419
Cr, X-ray transitions in laser produced plasma 80—100093
Cr XV, mag. quadrupole lines, in TFR600 Tokamak plasma, 10-20 Å 79—13662
Cr XVIII, XIX, spectral energy levels, relativistic corrections, config. superposition method 80—32616
Cr(II) lines, oscill. strengths in 2413-2718 Å wavelength range 80—106294
Cs, 6S-7S, parity violation search in highly forbidden mag. transition 78—82709
Cs, 6s-9p doublet, Xe perturbations, simultaneous additive effect on multiple satellite lines 79—76389
Cs atomic beam, optical pumping and detection of 0-0 transition 79—18158
Cs atomic clock using laser optical pumping of Cs beam 80—101785
Cs, fast atomic beams, collinear laser spectroscopy 78—37078
Cs, fine struct. meas. of highly excited F states 78—21871
Cs, hook spectra, evaluation limitations 80—90905
Cs I, 560 to 1050 Å 79—31455
Cs II, HFS determ. by collinear laser-ion beam 80—52914
Cs, multiphoton ionisation spectroscopy, molecular satellites of 6^2S-7^2P doublet 78—17632
Cs, one-atom detection by reson. photoionisation spectroscopy 77—38742
Cs, optical transitions, struct. of weak neutral currents *(Russian)* 77—88420
Cs, oscill. strengths of principal series doublets 79—13671
Cs, oscillator strengths in principal series, Rozhdestvenskii hook obs. 80—37760
Cs, P,D,F, and G Rydberg states, quantum defects and fine struct. 80—5496
Cs, parity violation in atomic electrons and electron-electron interaction effects 79—54788
Cs, photoabsorption oscillator strengths, $17<n<\infty$ transitions, interpolation formula 80—9559
Cs, photoplasma, optical excitation in radiation diffusion conditions 78—55227
Cs Rydberg atom-blackbody radiation interactions 80—37761
Cs, Rydberg S and P states, hyperfine struct., RF spectroscopic meas. 77—57911
Cs, Rydberg states, principal series doublets, intensity ratio anomalies 79—18148
Cs, self-broadened first reson. lines, near-wing asymmetries 80—9535
Cs, spectral line relative intensity, determ. of hypersonic wake excitation temp. 80—43732
Cs, transition probability of valence shells, relativistic pseudopot. calc. 78—86803
Cs, transverse, relax. in strong reson. RF field 78—5323
Cs, two photon ionisation, destructive interference effect 80—74153
Cs, two-photon ionis., profiles of $6^2S_{1/2}-7^2P_{1/2,3/2}$ lines 80—958
Cs vapour, coherent anti-Stokes Raman scatt. 78—71146
Cs, Xe collision-induced 6s-ns transitions in absorpt. spectrum 78—9101
Cs^+, 3d photoabsorpt. spectra, continuum and discrete states 79—81176
Cs^+ excited levels, hyperfine struct. and lifetimes 80—63590
Cs^{2+}, electron impact excitation studies by intersecting beam method 80—69239
Cs^{2+} formation during electron-ion collisions, ultrasoft X-ray spectroscopic study *(Russian)* 80—43193
Cs-He, new absorption/emission bands perturbed Cs transitions assignment, pot. energy curves 78—66486
Cs+F_2, electronic excited states, chemiluminesc. in flame, spectra 77—52643
Cs+He, interaction pot. and oscill. strength 80—91645
Cs+Xe, broadened Cs principal series lines, absorption meas., Cs-Xe pots. 77—79584
Cu, 3p excitation spectra 79—22633
Cu, absolute effective electron impact excitation cross sections, spectral obs. 80—53147
Cu, crossing effect in 3249Å emission line, mag. field strength depend. 78—25491
Cu, Doppler-free laser spectroscopy in hollow cathode discharge 80—9537
Cu, electron configs., isotope shifts, visible and UV spectra 80—32641
Cu, from moving arc, microcrater current and spectral fluctuations, simultaneous meas. 80—38828
Cu, ground and metastable populations, buffer gas effect 78—82955
Cu, highly ionised, spectral classifications below 55 Å 79—13658
Cu hollow-cathode emission spectra, 200 to 430 nm 79—72264
Cu I, high-dispersion absorpt. spectrum obs. 1570 to 2500 Å 80—78564
Cu I isoelectric sequence, fine struct. separations for reson. transitions 78—17588
Cu II, vacuum UV wavelength standards 77—82619
Cu IV, wavelength region 700-1200 Å, extended analysis 80—99473
Cu in SiO_2 isolation matrix, XPS, atomic electronic struct., gas phase type spectra 79—89655
Cu, intensities of reson. lines *(French)* 77—57912

atomic spectra continued
Cu isoelectronic sequence, 4s-4p reson. transition in highly charged ions 77−75087
Cu isoelectronic series, Hartree-Fock line strengths 78−9122
Cu, isolated in mol. matrix, absorption spectra 79−22724
Cu, L-shell soft X-ray emission spectra, oscillator strengths 80−32651
Cu, oscillator strengths, relativistic HF, core-polarisation model pot. 78−86818
Cu, resonance line, degree of coordination of clusters in metallic vapours *(French)* 77−58218
Cu, two-electron one-photon transition rate 77−71772
Cu V, spectra, config. levels 77−18820
Cu XXI, 2p-4d and 2p-4s transition arrays, wavelengths and oscillator strengths 80−47933
Cu XXI, spectra and energy levels of F isoelectronic series 79−93948
Cu$^+$, reson. transition, effect of correl. in 3d^n core, HF calcs. 80−47911
Cu-like ions, 4s-4p reson. lines and transitions obs. by means of laser prod. plasma, appl. to Tokamaks 80−99468
Cu+Cu collisions, Kα X-ray energy shifts, target thickness depend. 80−83311
Cu+N$_2$, preferential energy transfer from N$_2$ to specific Cu energy levels 80−43152
Cu(X), resonance transitions, classification 80−42985
D, adsorbed on graphite (0001), vibr. spectrum, at. beam scatt. obs. 80−92779
^{161,163}Dy, hyperfine struct. and hyperfine anomaly for fine transitions, high resolution meas. 77−88416
Dy II spark spectrum, isotope shift, config. mixing 78−58628
Dy III lines in spectra of Ap and Bp stars 80−12764
Dy, isotope shift meas. using laser atomic beam technique specific mass shift determ. 80−91497
Dy, visible spectra obs., hyperfine struct., mag. dipole and electric quadrupole interaction const. anal. 80−91698
Dy$^+$ spectra, exam. of 4f^{10}6s and 4f^{10}5d configs. *(French)* 77−50385
Dy+H$^+$ ionisation, induced L-shell alignment 80−32813
Er, absolute oscill. strengths of spectral lines 79−85928
Er, spectral lines, relative oscill. strengths determ. 77−83657
Eu, absorpt. spectrum, 1300-2200 Å 80−932
Eu, absorpt. spectrum in Schumann region, 1750-2200 Å 77−34581
Eu absorption spectrum, 2100-7200 Å, wavelengths, intensities, J- and g$_J$-values determ. 77−14383
Eu, electron impact excitation of spectral lines 79−3579
Eu I, 5p spectra collective excitation, rel. to double photoionis. 77−50387
Eu I, high resolution study of 4f^{7}6s^2$\rightarrow$4f^{7}6s6p 79−54790
Eu I, isotope shift meas., level classification in 4f^{6}5d6s^2 and 4f^{7}5d6p configs. 77−30831
Eu, in inert gas matrix, pseudolocalised vibr. modes, UV/vis. spectra 78−46289
Eu, L$_{II}$N$_{II}$ forbidden transition obs. in L-emission spectrum 77−23451
Eu$^+$, IR transition probability meas. 79−6897
Eu^{3+}, intracavity enhancement of absorpt. in nanosecond regime 78−78839
F I, isoelectronic series, Fe XVIII, Zn XXII, Ge XXIV, Se XXVI, spectral line identification 79−72230
F I isoelectronic sequence, forbidden transition probabilities for ground terms 77−2376
F II to VIII, mean lives, beam-foil spectrum in far UV 79−59389
F III, IV, beam-foil spectra, mean lives, 2150-3200 angstrom 78−55224
F isoelectronic sequence, spectra and energy levels 79−93948
F isoelectronic series, transitions between 1s^{2}2s^{2}p^5-1s^{2}2s^{2}2p^{4}3d and 1s^{2}2s^{2}2p^5-1s^{2}2s^{2}2p^{4}3s configs. 79−26925
F, kinetic spectroscopy in far vacuum UV, oscillator strengths of transitions 78−13457
F, Raman scatt. cross section for transitions between ground fine-struct. electronic states 80−23349
F, spin-orbit splitting and ^{2}P$_{1/2}$ radiative lifetime, absorpt. spectrosc. meas. 80−87063
F V, F VI, transition probabilities calcs. 79−54792
F VI, intercombination lines, transition probabilities determ. 79−89645
F+He+Ar, VUV spark emission spectra 79−3457
^{19}F, pionic 2p-1s X-ray transitions 79−18319
Fe, 3p excitation spectra 79−22633
Fe, fine struct. levels fitting, config. interaction effect, spin-orbit and electrostatic interaction parameters 80−69248
Fe from Tokamak-produced plasma, 2s^{2}2p^k-2s2p^{k+1} transitions in F I to Be I isoelectronic sequences 80−37765
Fe group ions, spectra, calcs., allowance for d^n shell pair excitations 77−42261
Fe, highly ionised, 1s to 3p Kβ-like X-ray spectrum 77−50394
Fe, hollow-cathode emission spectra, 200 to 430 nm 79−72263
Fe I, a^{3}F$_{2\text{-}4}$ levels, relative oscillator strengths 80−63572
Fe I, excited levels measured lifetimes compared with calcs. from oscillator strengths 79−36586
Fe I, gf-values rel. to metal-poor dwarf stars abundance anals. 79−92760
Fe I, isoelectronic sequence, abnormal intensities in multiplets 79−22635
Fe I, new levels and classification for 1.3-2.5 μm range 77−18819
Fe I, precision oscillator strengths from levels a^{5}F$_{1\text{-}5}$ and a^{5}D$_{0\text{-}4}$, comparison 79−36584
Fe I 5250 Å line magnetic field meas. of polar regions of Sun *(Russian)* 77−64724
Fe I even-odd and odd-even transitions, difference in curves of growth 77−25996
Fe I in solar spectrum, 300 to 900 nm lines interpretation using precise oscillator strengths 79−40155
Fe I lines limb shift in solar atmosphere, pressure shifts effect 78−89150
Fe I solar spectrum, 300 to 900 nm, microturbulence, Fe abundance, damping, oscillator strengths 77−5516
Fe I transition from levels a^{5}F$_{1\text{-}5}$, relative oscillator strengths precision meas. 79−36585
Fe I transitions from levels a^{5}D$_{0\text{-}4}$, relative oscillator strengths precision meas. 79−36583
Fe II, 3000-12000 Å, forbidden transitions, excitation pot. and transition probability 77−79563
Fe II, identification in IR spectrum of η Carinae 77−45463
Fe II, oscillator strengths derived from solar spectrum, choice of solar model atmosphere 80−56791
Fe II, spectrum, term system 79−778
Fe II emission line spectra in Be-stars 77−56978

atomic spectra continued
Fe II permitted emission in Seyfert 1 galaxies and QSOs, obs. 79−35361
Fe II permitted lines in spectra of type 1 Seyferts and quasars 79−44602
Fe III, Fe VI, electron impact excitation cross sections and gaseous nebulae Fe abundances 78−53806
Fe III, metastable states in Be star ϕ Persei rel. to mass loss 79−5832
Fe III in astronomical sources, multiplet table 80−41732
Fe III to VI, struct. and transition probabilities, ab initio calc. using Thomas-Fermi central pot. 79−3360
Fe IV, spectrum, term anal., rel. to RR Telescopic 78−82677
Fe IX, autoionising transitions ns^{2}np^6−nsnp^{6}mp 77−88419
Fe IX, Fe X, forbidden transitions, solar coronal spectrum appl. 78−77537
Fe IX lines in solar corona, appl. as plasmas density indicators 79−44429
Fe IX radiative and collisional data rel. to solar coronal emission spectrum 77−49350
Fe, incoherent γ-ray scatt. by K-shell electrons 77−83560
Fe ions, transition energies, inner-shell electron effects 77−42259
Fe, Kα satellite lines following electron bombardment 80−69097
Fe, Kα^h hypersatellite spectra and double photoionisation cross-section 79−85922
Fe lines in solar spectrum, wing shapes anal. 80−4317
Fe, n=2-2 transitions in XUV spectra, anal. 80−102472
Fe plasma, simplified spectra obtained by electro-optic gating of radiant emission 78−22561
Fe, revised lifetimes of energy levels 77−65440
Fe, two-electron one-photon transition rate 77−71772
Fe VI, forbidden emission under nebular conditions 79−8970
Fe VI spectrum 3d^3-3d^{2}4p transition, wavelengths and energy levels 77−42264
Fe VIII to Fe XXVI, wavelength tables *(Japanese)* 79−13661
Fe vapour, line strengths, energy-level structure for 3p-edge absorption spectrum 79−45673
Fe X, 3p^{4}4s levels, population processes 80−47926
Fe X, Fe XIV, unsuccessful search for forbidden emission in HD 153919 (3U 1700−37) 80−4358
Fe X and XIV, solar line intensity ratio and coronal temp. determ. 78−73697
Fe X and XIV forbidden line emission from supernova remnants 79−44580
Fe XI, 3p^{3}3d configuration transitions in solar corona, 1175 to 1965 Å 79−25559
Fe XII, excitation in solar corona 77−17458
Fe XII and XIII, energy levels and oscillator strengths for XUV transitions 78−46277
Fe XIII, IR lines of solar corona, polarisation degree calc. 77−45373
Fe XIII and XIV emission lines in solar corona 77−13299
Fe XIV 5303 Å coronal emission line polarisation obs. during 1973, June 30 eclipse 77−49352
Fe XIV 5303 Å forbidden line emission from Puppis A SNR 80−26962
Fe XIX, Fe XX, Fe XXI, forbidden lines obs. in solar flares 78−57519
Fe XIX, XXI, spectral energy levels, relativistic corrections, config. superposition method 80−32616
Fe XIX and isoelectronic ions 2p^4-2p^{3}3d transition array 77−42267
Fe XIX-XXII blend at 1.9 Å in flare X-ray spectra 79−96979
Fe, XUV emission lines in solar corona rel. to temps. and Fe abundances 78−4180
Fe XV, line intensity and linewidths at high electron density, generalised population ratio 80−99481
Fe XV, transition probabilities and collision strengths 80−78562
Fe XV 284 Å spectroheliograms and rot. characts. of EUV coronal holes 77−53547
Fe XV solar coronal EUV line intensities 80−51731
Fe XVI, L-series satellite spectra 79−98012
Fe XVII, mag. quadrupole lines, in TFR600 Tokamak plasma, 10-20 Å 79−13662
Fe XVII-XXIV X-ray line complex obs. of M87 galaxy halo 79−21425
Fe XVIII, spectra and energy levels of F isoelectronic series 79−93948
Fe XVIII and XIX 2s^{2}2p^n-2s^{2}2p^{n-1}4d classification, for laser produced plasmas and solar spectra 77−42268
Fe XVIII-Zn XXII, transitions between 1s^{2}2s^{2}p^5-1s^{2}2s^{2}2p^{4}3d and 1s^{2}2s^{2}2p^5-1s^{2}2s^{2}2p^{4}3s configs. 79−26925
Fe XX, in solar flares and tokamak plasmas, new atomic data 80−67545
Fe XX and isoelectronic ions, 2p^3-2p^{2}3d transition array 77−65434
Fe XXI, Fe XVII, identifications in solar flares XUV spectra 78−49406
Fe XXI, proton collision of excitation of fine struct. transitions in ground state 77−19017
Fe XXI and isoelectronic spectra 2p^2-2p3d transition array 77−38632
Fe XXII,XXIII, Be I and B I like spectra from laser-produced plasma, classification 78−67410
Fe XXIII, energy levels and transition 79−59383
Fe XXIII, Fe XXIV, new line obs. in laser-produced spectra 79−81175
Fe XXIV, dielectronic satellite spectra calc., solar flare spectra appl. 79−35123
Fe XXIV, dielectronic satellite spectra, solar flares appl. 80−32646
Fe XXIV, line identification in solar corona radiation 77−79569
Fe XXIV, spectra, radiative corrections 79−98015
Fe XXIV, XXV, line wavelengths in 1.85 to 1.87 Å region in solar flare X-ray spectra 80−21973
Fe XXV, dielectronic satellite line spectra as measure of nonthermal electron energy distribs. 80−21911
Fe XXV, Fe XXVI, astrophysical X-ray and gamma-ray lines prod. by nonthermal ions 78−36725
Fe XXV, He-like, dielectronic satellite spectrum, electron temp. diagnostics in plasma 79−82098
Fe XXV, He-like ion, oscillator strengths of transitions between low-lying S and P states 78−13470
Fe XXV, XXVI, X-ray spectral lines profile evolution due to Comptonisation, Monte Carlo computations 79−66916
Fe XXV-XXVI resonance lines region, laboratory reproduction of solar flare X-ray spectra 80−18819
Fe$^+$, Fe^{++}, synthetic spectra rel. to radioactive excitation source model for late time spectra for Type I supernovae 80−105264
Fe$^+$, gf values determ. in laboratory, for solar studies 80−42994
Fe^{12+}, forbidden lines collisional excitation, importance of short-range pot. 77 17457
Fe^{19+}, forbidden line in UV, Tokomak plasma diagnostics 78−83602

atomic spectra continued
Fe^{25+} line emission in Hercules X-1 (HZ Herculis), theory of emission during X-ray source low state 80−105393
Fe-group elements, L spectra interpretation 77−27013
Fe-group spectra, superposition configurations in semiempirical calc. 78−920
Fe+I, Fe K-α X-ray emission, high-resolution meas. 80−37871
FeVIII-XXVI energy level tables and Grotrian diagrams 80−74142
Fr, emission spectra measurements *(French)* 79−26918
Fr I, wavelength estimate of first and second resonance lines 78−58617
Ga, atom and ion, k-ordering props. and fine struct. inversion 79−59388
Ga I, absorption spectrum 320-1000 Å, intersubshell correls., simultaneous ejection of two photoelectrons 77−50391
Ga I, relativistic and cancellation effects in line strength ratios 78−82689
Ga I, Rydberg series, disctete levels and continua of finite bandwidth 78−74603
Ga II, 4s4d^{1}D and 4p$^{2\,1}$D energies and lifetimes 79−59391
Ga, isotope shift and HFS, isotope effects, UV spectra obs. 80−42973
Ga, L-shell soft X-ray emission spectra, oscillator strengths 80−32651
Ga XXIII, 2p-4d and 2p-4s transition arrays, wavelengths and oscillator strengths 80−47933
Ga$^+$, photon coherent scatt., cross sections 77−50410
Gd I and II spectra, 3930 to 4140 Å, isotope shift meas. 77−61713
Gd, isotope shifts and deform. obs. 77−65433
Gd, sputtered vapour, neutral ground state population, laser obs., appl. to isotope separation *(Russian)* 78−29759
Ge I, absorption spectra of outermost d-subshell 77−75086
Ge I, absorption spectrum, 1500-1900 Å 77−71769
Ge I, transition probabilities, 4p^2-4p4d and 4p^2-4p5s, 1900-4700 Å *(French)* 78−74600
Ge IV spectra, nonrelativistic oscillator strengths calc. 77−83538
Ge XXIV, 2p^5-2p^{4}3s(2p^{4}3d) transitions in laser produced X-ray spectra 78−13460
Ge XXIV, spectra and energy levels of F isoelectronic series 79−93948
Ge XXIV, transitions between 1s^{2}2s^{2}p^5-1s^{2}2s^{2}2p^{4}3d and 1s^{2}2s^{2}2p^5-1s^{2}2s^{2}2p^{4}3s configs. 79−26925
Ge^{2+}, photon coherent scatt., cross sections 77−50410
H , Rydberg consts., saturated absorpt., spectroscopy meas. 80−105604
H, 3^{2}S$_{1/2}$-3^{2}D$_{5/2}$ interval, two-photon lineshape theory 79−54825
H, 3^{2}S$_{1/2}$-3^{2}D$_{5/2}$ interval, double quantum RF meas. 79−54826
H, adsorbed on graphite (0001), vibr. spectrum, at. beam scatt. obs. 80−92779
H, and mixtures, photon mass attenuation and mass energy-absorpt. coeffs., 0.1 keV to 20 MeV 77−61715
H, appl. of lasers 79−72267
H atom, relativistic, in superstrong mag. fields 78−90095
H atom, spectrum in strong mag. field, effect of proton mass 79−59387
H atom energy spectrum in expanding Robertson-Walker universe 78−73869
H atom spectra, homogeneous mag. field, variational approach 79−22629
H, backscatt. by Cu or Mo, 4-30 keV, O$_2$ effect 78−15268
H, backscatt. from Mo in the presence of O, ion form., line emission 79−3388
H, backscattered from H$^+$(H$_2{}^+$)(H$_3{}^+$)-metal impact, Balmer-β line intensity 77−23470
H, Balmer spectrum at line merging region, statistically extended recomb. continuum and line dissolution 77−27006
H, Balmer-α line 80−52915
H, beam-foil spectroscopy, stray electric field due to high C foil resistance 80−42978
H early Balmer lines emission in solar prominences *(Russian)* 80−12718
H, electron impact coincidence, even-odd parity coherence effects, polarisation ang. distrib. 78−9253
H, electron impact excitation, Bethe approx. modifications, impact radiation polarisation 79−31695
H emission spectrum, last observable line, rel. to solar obs. through Earth atm. 78−77536
H, emission-line spectra in quasars and active galactic nuclei 78−96557
H, excited atom interacting with reson. oscill. EM field 79−76371
H, exponential decay law for $2P_{1/2}\rightarrow 1S_{1/2}$ transition 78−78649
H fine structure 3^{2}S$_{1/2}$-3^{2}D$_{5/2}$ interval, separated oscillatory field meas. 80−99482
H, gaseous, high-resolution mag. reson. study, 1 to 1.3K 80−95560
H I Balmer lines, formation in bright prominences spectra *(Russian)* 80−77377
H I Lyman α emission meas. at solar minimum 79−12417
H I radio recombination lines, in interstellar H II regions, quasiclassical anal. 78−28511
H II, Zeeman splitting of high-n recomb. lines 80−58210
H, in H$_2$-Ne(He) glow discharge, Balmer lines, recomb. excitation *(Russian)* 77−46516
H, induced $2s_{1/2}\rightarrow 2p_{1/2}$+one photon transition, rate calcs. 77−50384
H, infinitely magnetised, spectrum rel. to props. of pulsar crust 80−77282
H L$_\alpha$ line breadth, Cherenkov line radiation, QSO emission-like spectra *(Chinese)* 80−105378
H like atom, splitting and coalescence of photons *(Russian)* 79−54815
H, line and continuum emission in quasars 80−27003
H, line spectrum, relativistic red shift phenomenon 80−32675
H, Lyman-α emission from photodissoc. of H$_2$O 79−10158
H, maser hyperfine transition, affected by coherently excited Zeeman transitions 79−72544
H, mesic, atomic X-ray yields 1s and 2p level shifts and widths, cascades, calc. 80−78730
H, n=3 level, coherent excitation by electron impact, density matrix anal. 78−78817
H, nonresonant two-photon absorption, gauge interaction calcs. 78−37617
H, parity nonconservation in emission spectra 79−10086
H, Rydberg levels, selective excitation by three-photon absorpt. 80−5518
H simultaneous mag./elec. microwave resonance transition, parity nonconservation, Weinberg-Salam theory test 77−54066
H, spectra, quasistationary states due to CO$_2$ laser radiation 77−67997
H, Stark and photoabsorption spectrum, density of oscillator strengths, atom c.f. semiconductor spectra 80−83318
H to Ca, leading atomic lines, solar spectra 79−25560
H, transition probabilities and expectation values, in intense mag. field 79−10066

atomic spectra continued
H, two-photon radiation rel. to planetary nebulae continuous UV spectra 79−92843
H with quark embedded in nucleus, at. spectral lines 78−62965
H$^-$ affinity radiation, theoretical study of negative absorption 80−38001
H$^-$ free-free transitions, target polarisation effects 79−66917
H$^-$, grazing incidence collision with surface, Balmer radiation, elliptical polarisation 78−86804
H , in solar atmosphere, bound-free electron transitions, review 78−33563
H$_-$, photoabsorpt. and dispersion profiles, moment theory 77−6709
H$^-$ vac. UV spectra, narrow reson. at 1129.5 Å, H-arc spectra 78−66490
H$^+$, grazing incidence collision with surface, Balmer radiation, elliptical polarisation 78−86804
H-like atom, interacting with EM field, matrix elements and transition probabilities 78−37533
H-like atom, photon coalescence and splitting at 1s electron, low-energy limit 79−10082
H-like atoms, dipole transitions, asymptotic expansion of radial-dipole integral 78−82667
H-like atoms, weakly bound charged particle system, interacting with EM field 79−68332
H-like ions, departure coeffs. from thermodynamic equilib., rel. to radiosources recomb. lines 79−76369
H-like ions (Mg XII to S XVI), anal. of satellites to reson. lines in X-ray region 77−88421
H-like ions in solar corona, reson. lines fine struct. components intensity ratios 80−101581
H-Xe atom, oscillator strength sum S(2) evaluation using Roothaan-Hartree-Fock method 77−75230
H+e, free-free electron transitions in solar atm., review 78−33563
H$^+$+H, 1-7 keV, H(2s) form. and Lyman-α polarisation 80−14221
H$_2{}^+$, polarised Balmer radiation due to scatt. from Nb surface, adsorbed O$_2$ effects 80−99569
H$_2$+D$_2$, exchange reaction, at. vs. mol. mechanism, at. absorpt. spectrometry 78−7190
H$_\alpha$ Balmer line emission fine struct., Stark effect *(German)* 78−82673
H$_\alpha$, polaris. spectroscopy, Rydberg const. determ. 79−9202
H(D), ground state Lamb shift, isotope shift and relativistic nuclear recoil correction 78−82696
H(D), H$_\alpha$, H$_\beta$ emission from electron impact dissoc. of H$_2$(D$_2$) 78−25729
^{1}H, pionic, pion mass high accuracy meas. from transitions 80−106406
^{165}H muonic X-rays, K- and L-transitions energies meas. 77−79711
H50α, detect. in interstellar mol. clouds 77−60808
Hα emission line asymmetry in solar limb flares *(Russian)* 77−64728
Hα, in solar chromosphere, seven components rel. to 9873 MHz line 78−89151
He, $_j$K and LS coupling between states, transition probs., depend. on elec. field 80−37782
He, 2^{1}S$_0$-1^{1}S$_0$ transition, transition matrices higher approx. 78−33458
He, 3^{3}P level, excitation and decay study up to high press. pumped by intense relativistic electron beam 80−74250
He, collision induced scattering of depolarised light 80−14118
He, continuous emission spectrum *(Russian)* 77−84508
He, electron impact excitation of $1^1S\rightarrow 2^1P(3^1P)$, excitation cross section and polarisation fractions, XUV emission 79−22841
He, electron impact excitation, Bethe approx. modifications, impact radiation polarisation 79−31695
He, emission line profile, hollow cathode source 77−23469
He, excitation by photon or electron scatt., long range force effects 79−10170
He, forbidden radio lines, 2^{3}P state fine struct. 77−23447
He, freq.-depend. polarisabilities and Verdet consts., calcs. 78−62781
He, high-L states, laser driven forbidden transitions, line shapes 79−22638
He I, 10830 Å line obs. of HR 1105, cold giant star *(Russian)* 80−17586
He I, rate coeff. for $2^3S\rightarrow 2^3P$ transition electron impact excitation 79−48664
He I 2^{3}P-3^{1}D intercombination line, collision-induced, obs. by laser absorpt. spectroscopy 80−58194
He I beam-foil excitation, 60-180 keV, alignment production, foil temp. depend. 79−54956
He I in solar flare, lines optical depths and levels populations calcs. 79−62809
He II, spectral lines branching ratios 77−46518
He II, Zeeman splitting of high-n recomb. lines 80−58210
He II 304 Å line, intensity in solar corona 77−91510
He II 4686 Å emission in spectrum of HDE 226868 (Cygnus X-1) 79−21328
He II 4686 Å line phase shift from spectrophotometry of DQ Herculis 79−21296
He II recombination lines, calc. intensities in UV 78−94212
He, isoelectronic series, dipole matrix elements derivation 77−83519
He, isoelectronic series, transition moments, exchange and core polarisation effects 77−54531
He, Lande g-factor determ. from free radn. beats 77−18880
He, light scattering spectra of gas, collision-induced scatt. 79−18137
He like ions Z=12-19, 1s^2 ^{1}S$_0$-1s3p^{1}P$_1$ lines satellites obs. in laser 79−22640
He, many electron system, photoionisation and photoexcitation, at. transition strong config. interaction effect 80−47909
He, metastable states, high resolution study via electron scatt. 77−6935
He, muonic, 3p-3d transitions calcs., energy splittings 80−87253
He muonic atoms, 2S$_{1/2}$-2P$_{3/2}$ level splitting, test of QED predictions on electronic vacuum polarisation 77−3494
He, n=3 states, polarisation and excitation functions 77−6934
He, optical excitation function of 5876Å line near threshold 78−70797
He parity-violating elec. dipole transitions 80−69094
He, photoabsorpt. and dispersion profiles, moment theory 77−6709
He plasma, satellites of He 492.2 nm line, fine struct. interpretation 80−59235
He positive column discharge, IR optogalvanic spectrosc. using F-centre laser 80−78563
He, radiation from hollow-cathode discharge in weak mag. field 78−70789
He, resonance photoabsorption in (3s3p) ^{1}P reson. region 79−45659
He, resonant states, high resolution study via electron excitation 77−6936

atomic spectra continued
He, shift of 4^3S-2^3P line by CW CO_2 laser beam 77—30829
He, spectrogram using moderate-resolution spectrometer with interf. selective amplitude modulation 79—30588
He, Stark broadening satellite transitions, in turbulent plasma 77—61759
He, subDoppler lineshape obs., of IR mag. reson. Rydberg transitions, using motional Stark effect 78—947
He triplet states, doubly excited, spectrum and polarisation 80—99472
He, Voigt profile, absorpt. line calcs. for the 396.5, 361.4, 318.7, 492.2, 587.6 and 447.1 nm lines 80—99471
He^- resons. in 56 to 64 eV electron collisions, autoionising states and spectral line polarisation 80—53145
He-Ar mixture, collision induced far IR absorption at high press. 78—5161
He-Ar mixture HP collision-induced translational far IR absorption obs. 77—38628
He-Ba discharge, dipole-dipole pair absorpt. obs. using optogalvanic detect. 80—54064
He-Cd positive-column laser discharge, excitation mechanisms from radial profiles 77—68205
He-like ions, $2^3P_1{}^0$-1^1S_0 and $2^1P_1{}^0$-1^1S_0 freqs. and transition rates, relativistic calc. 79—68210
He-like ions, line intensities for stationary plasmas 78—53811
He-like ions, line intensities for non-stationary plasmas 78—53812
He-like ions, line intensities results 78—89051
He-like ions, oscillator strengths of transitions between low-lying S and P states 78—13470
He-like ions, $P_1{}^0$-1^1S_0 and $^3P_1{}^0$-1^1S_0 intercombination-line transitions 78—70771
He-like ions, radiative 2^3S_1-1^1S_0 transition, correlation effects 79—97989
He-Ne, 632.8 nm line broadening, perturbation energies additivity 79—54941
He-Ne travelling wave laser, spontaneous emission spectra, 3.39 μm region 80—37995
He+Ar(Kr), translation band spectral moments, induced dipole moments 78—55218
He+He, (Ne), (Ar), optical emission spectra 77—14551
He+Ne, afterglow, metastable state energy transfer, spectra 80—43167
$He+Ne^{n+}$ (n=1,2,3,4), excitations, emission cross-sections 77—57914
He^++H_2, charge transfer, appl. of atom-photon coincidence meas. 79—45829
He^++He, charge transfer, appl. of atom-photon coincidence meas. 79—45829
He^++He, interference struct., optical emission interpretation 79—45816
He^++Xe, internal energy distrib. at 100 eV 80—99564
HeI 2s-2p transition at He^+ and HeH^+ impact on C foil 80—58343
HeI, 3^3D-2^3P transition, light polarisation depend. on time and exciting electrons energy 80—37891
HeI, beam-foil mean life meas. of 1s 3p ^1P level 77—3320
^3He, pionic, X-ray transitions obs. 77—65549
^4He, beam foil and quantum beat spectra *(Chinese)* 80—32638
^4He, Rydberg states, fine struct. obs. 80—23350
$(^4He+\mu^-)^+$ muonic ion, $2S_{1/2}$-$2P_{1/2}$ energy transition meas. 78—33641
He*+Ne, (3^1S, 3^3S, 3^1P, 3^3P) de-excitation cross section temp. depend., time resolved spectra 80—28100
Hf IV, 6s $^2S_{1/2}$-6p $^2P°_{1/2,3/2}$ transition, relativistic oscillator strengths, influence of core polarisation 80—58132
Hf XLV X-ray spectra from laser produced plasmas 80—42981
HfI, at spectrum, g-values, Zeeman effect, LS-coupling, ionisation pot. 77—3292
Hg, 1849 Å absorption line broadening and shift in inert gases *(French)* 77—30825
Hg, 2537 Å line satellites, Kr broadening 77—83523
Hg, 435.8 nm spectral line, stigmatic imaging with spherical concave grating 77—38808
Hg, $6^3P_{0,2}$-state, electron impact excitation, optical detect. 77—50546
Hg continuous spectra at series limit 6p′ $^3P_2$ *(French)* 77—88413
Hg I 4047 Å night sky contamination and Simkin effect 78—41032
Hg II, excitation cross sections, transition probabilities, by electron impact 79—3580
Hg II, hyperfine struct. of 194.2 line, $^2S_{1/2}$-$^2P_{1/2}$ transition *(French)* 77—27009
Hg, IR arc spectrum, fine struct., HFS and isotope shifts 77—79559
Hg, IR arc spectrum, fine struct., HFS and isotope shifts 77—79560
Hg, in aq. soln., transient spectra 79—6899
Hg, transition probabilities, 238-1530 nm 78—13455
Hg, transition probability of valence shells, relativistic pseudopot. calc. 78—86803
Hg, vap., high density, optical absorpt. edge, density depend. 79—72985
^{199}Hg, 6^1S_0-6^3P_0 forbidden transition absorpt. at 265.6 nm, A coeff. and self-press. broadening determ. 80—95562
Hg+Ar, spectral line broadening of Hg in UV, interaction pot. 79—26937
$Hg+N_2$, $6(^3P_0)\rightarrow6(^3P_1)$ excitation, double modulation obs. 79—27072
^AHg, A=198-202,204, muonic X-ray transitions, nuclear state quadrupole moments and charge distrib. 79—41253
^{190}Hg, isotope shift by on-line laser spectroscopy 77—34589
$Hg(6^3P_2)+Hg$, aligned metastable ats., longitudinal and transverse relax. times, simultaneous meas. 78—13585
Ho I, Ho II, excited level lifetimes and oscillator strengths, visible spectra 80—63573
Ho I, II spectra in photographic IR region 77—14382
Ho III, energy levels, parametric anal. of spectrum 77—46519
Ho, IR emission spectra and hyperfine struct. *(French)* 78—13452
Ho, incoherent γ-ray scatt. by K-shell electrons 77—83560
Ho, spectra, energy levels and hyperfine struct., parametric calcs. *(French)* 78—41984
HoI, relative oscill. strengths 79—98038
H^+(spin polarised)+atom, inner-shell ionis., subsequent radiation ang. distrib. 80—53114
I excited atom ($5^2P_{1/2}$) quenching by mols. with C-I bonds 79—64076
I II, reson. lines, oscill. strengths determ. by absorption method 80—58214
I, spectral transition probabilities, 500-1050 nm 78—82676
I VI, beam-foil spectrum, 400 to 1300 Å 79—86059
I VII, beam-foil spectrum, 400 to 1300 Å 79—86059
I^-, 3d photoabsorpt. spectra, continuum and discrete states 79—81176
$I(^5P_{1/2,3/2})$, from ICN A-state photolysis, branching ratio wavelength depend. 80—81335
^{129}I, hyperfine struct. and isotope shift of 1.3 μm transition 80—102486
In, 451.1 nm transition, HFS and ^{113}In-^{115}In isotope shift 78—82674

atomic spectra continued
In, excited state lifetime, delayed coincidence meas. 77—3315
In I, absorption spectra, 320 to 1000 Å, intersubshell correls. 4d spectrum two-electron detachment 77—10617
In, I, relativistic and cancellation effects in line strength ratios 78—82689
In I, Rydberg series, disctete levels and continua of finite bandwidth 78—74603
In, L X-ray yields from double-vacancy states 79—49977
In, s^2p-$sp(^3P)np$ transitions, absorpt. spectra in 100-150 nm region 80—87067
In, sputtering in Ar-N_2 discharge, mechanism, optical spectra study 80—89107
In sputtering in N_2-O_2 discharge, mechanism, optical spectra study 80—89108
In V, spectrum, levels in $4d^86s$ and $4d^85d$ configs. 78—62748
In V fifth spectrum, $4d^85s$ and $4d^85p$ configurations, UV spectra (270 to 2400 Å) 78—33456
In^{2+}, emission spectrum, 340 to 6500 Å, ionisation pot. and dipole polarisability 78—78654
Ir II, term anal. of spectrum 79—6902
K, absolute optical electron-impact excitation functions 80—18933
K atom, stimulated multipole Raman scatt. between opposite-parity states 79—76753
K, emission and absorpt. spectra in inert gas matrix 79—54800
K I, inner shell absorpt. spectra, 3d wavefunction collapse 77—23455
K I 769.9 nm line obs. of solar 5-min. oscills. 80—26838
K I to K XIX, energy levels, tabulated data 80—51966
K, reson. line polarisation, 2-photon excitation 77—54546
K, vapour, absorpt. spectra 79—21509
K^+, direct excitation of levels, transition probs. and cross sections 80—37890
K^+ in molecular complexes, K-edge absorpt. spectra, Z+1 analogy, theory-expt. comparison 80—47935
^{39}K, weakly excited, hyperfine struct. transitions obs., neoclassical theory 77—6737
^{41}K, isolated in Ar matrix, optical absorpt. spectra 77—10619
Kr, $^3P_1$ state, reson. fluoresc., Zeeman beats, time-resolved VUV spectra using synchrotron radiation 78—33454
Kr, absorpt. spectra, field induced autoionisation near ionisation threshold 80—106301
Kr, absorpt. spectrum, using vacuum UV storage ring source 77—7165
Kr arc spectrum, isotope shifts in near IR lines 79—72257
Kr, even isotopes, isotope shifts of 557 nm transition 77—61710
Kr, free ats. electron bombard., subsequent X-radiation ang. distrib. 80—53144
Kr I, 5871 Å line, transition probability meas. 77—3291
Kr I, (A=78 to 86), isotope shift, saturated absorpt. technique 77—75102
Kr I, high resolution polarisation spectroscopy of 557 nm transition 78—74602
Kr I, laser spectroscopy, isotope shifts, hyperfine struct. *(French)* 78—33457
Kr I, theoretical transition probabilities and lifetimes, data tables 79—54793
Kr I 6058 Å line, asymmetry rel. to cause of anomalous astron. redshifts 77—13458
Kr II, absorption spectrum in vac. UV region, ionisation energies 79—49972
Kr II, calcs. of radiative lifetimes, absolute transition probabilities and oscillator strengths 77—50405
Kr IV emission spectral lines, classification 80—95563
Kr, K inner-shell level energies, absorpt. spectroscopy with synchrotron radiation 80—99583
Kr, line strength calcs. for 7s-6p and 4d-5p transitions 77—14384
Kr, metastable ats. in Kr and Kr-N_2 afterglow 77—427
Kr, optical and Auger spectra, discrepancies anal. 79—93944
Kr, reson. levels relax. consts. determ. by alignment method in discharge 79—26936
Kr, rotation of plane of polarisation close to reson. 79—41129
Kr supersonic jet, electron beam excited, vac. UV spectrum 77—88414
Kr, three-body collision-induced light scatt. spectrum moments 78—9226
Kr V, emission spectral lines, classification 80—95563
Kr VIII, excited state energies and lifetimes, beam foil spectra 80—63591
Kr XI-XIV, X-ray and UV spectra, 30-300 Å range 80—95566
Kr XXXIII, energy levels and transition 79—59383
Kr+Kr, low-energy collision induced UV radiation 79—50125
Kr(-He) arc, wall-stabilised, atm. press. 79—46503
KrI, p-s lines, transition probabilities meas. 80—23366
^{83}Kr, $4p^55p$ config., HFS meas. using level crossing technique 80—18827
^{83}Kr I, hyperfine structure in arc spectrum 78—41988
La I, lifetimes of $z^2F_{5/2}$, $z^2D_{3/2}$, $z^4G_{5/2}$ and $y^2D_{3/2}$ states 78—66489
La IV, spectrum and energy levels 79—72261
La, intense 4d-f resons., cross-sections, spectra, calcs. 79—31426
La^{3+}, 3d photoabsorpt. spectra, continuum and discrete states 79—81176
^{139}La II $5d^2\ ^3F_4\rightarrow5d4f\ ^3F_4{}^0$, hyperfine structure, ΔF=±2 transitions, three-quantum process 80—63848
Li, absorpt. spectra, high mag. field, quasi-Landau reson. 78—90109
Li, autoionisation spectrum, theory *(Spanish)* 79—89647
Li, even-parity core-excited ^2P states, accurate CI calcs. 79—54782
Li I, doubly-excited $^4P^0$ terms calcs. 78—9100
Li I, II, absorption spectra in grazing incidence region, 215-160 Å 78—5164
Li I, IR emission spectrum, extended anal. 78—62747
Li I 6708 Å twilight emission enhancement following rocket release 77—53255
Li I to Li III, beam-foil obs. of 2000-5500 Å spectra 80—9548
Li I to Ne VIII isoelectronic sequence, quartet spectra, Hylleraas method calcs. 80—9524
Li I to Ne VIII isoelectronic sequence, term level diagrams of doubly excited states 80—14093
Li I-like spectra, energy struct., accurate semiempirical formulae 79—49970
Li isoelectronic sequence, oscill. strengths 77—3309
Li, isoelectronic sequence, transition probabilities, relativistic effects calcs. 77—27028
Li, isoelectronic sequence, radiative transition probabilities calcs. 77—83544
Li, isoelectronic series, Hartree-Fock line strengths 78—9122
Li isoelectronic series, quartet states, HF and CI calcs. 78—17582

atomic spectra continued
- Li isoelectronic series, relativistic pseudopot. appl. in HF calcs. 80−27960
- Li, isoelectronic series, transition moments, exchange and core polarisation effects 77−54531
- Li, laser excitation and ionisation, autoionising states obs. 77−61699
- Li, laser photoionisation cross-section obs. 77−71782
- Li, lifetime measurement of D-states, by time resolved resonance fluorescence 79−63965
- Li like ions, oscillator strength calc. for inner shell transitions 77−30821
- Li, microwave fine-struct., Rydberg states 78−13451
- Li, motional Stark effect in high mag. field 79−63958
- Li, quartet states, transition energies, oscill. strengths, CI calcs. 78−58597
- Li, vap., multiphoton absorption, space-charge ion detect. 79−54827
- Li, vapour, absorpt. spectra 79−21509
- Li$^-$, optical transition between bound states, beam-foil spectrosc. obs. 80−91476
- Li-like ions K...Fe, survey table of wavelengths in X-ray region 77−79569
- Li-like multiply charged ions, spectra, radiative corrections 79−98015
- Li+He, $P_{1/2\text{-}3/2}$, fine-structure transition probability, semiclassical multichannel scatt. matrix 80−37854
- ^{6}Li$^+$, hyperfine structure, Doppler-tuned ion beam laser spectroscopy 79−89627
- ^{7}Li, gamma ray lines from $\alpha\alpha$ reactions 77−87248
- ^{7}Li, HFS using Doppler-tuned HFS spectroscopy 79−13831
- ^{7}Li I 6708 Å line in stellar spectra, Li interstellar abundance 78−49494
- Lu I, 5d6s6p-config., laser spectrosc. investig. 80−69096
- Lu III, 6s $^2S_{1/2}$-6p $^2P^\circ{}_{1/2,3/2}$ transition, relativistic oscillator strengths, influence of core polarisation 80−58132
- Lu V, spectrum anal., 500-2100 Å 79−26920
- ^{A}Lu, A=175,176, 5d6s$^{22}D_{3/2}$-5d6s6p$^4F_{3/2}$ transition, isotope shift and hyperfine struct. 80−83309
- ^{176}Lu, hyperfine struct. and isotope shift of 605.5 nm line by laser spectroscopy 79−41137
- Mg break arc, LV, low current, electron density, temp., local thermodynamic equilib. 78−9878
- Mg I, extensions to the doubly excited spectra in the vacuum uv 79−6901
- Mg I, photoabsorpt. spectrum 225-170 Å 79−72262
- Mg I isoelectronic sequence, intercombination line oscillator strengths 80−23360
- Mg I isotope shifts 77−71771
- Mg I sequences for elements Cr to Zn, $n=3\rightarrow n'=4$ transitions 79−26922
- Mg, I-XII, energy levels and optical spectra 80−87065
- Mg II 2934 Å emission in QSOs, possible identification 78−41073
- Mg II solar UV doublet obs. *(Japanese)* 78−61831
- Mg III, autoionising transitions ns^{2}np^6−nsnp^{6}mp 77−88419
- Mg III-V, beam-foil spectra, 100-450 Å 80−83308
- Mg ions, foil-excited, EUV spectrum 80−42976
- Mg ions, He-like, satellite lines to higher-order reson. series lines in laser-prod. plasma 79−85930
- Mg, isoelectronic sequence, excitation energies and line strengths, MC Hartree-Fock calcs. 77−83658
- Mg isoelectronic sequence, mag. quadrupole transitions probabilities 78−37592
- Mg, Kα^h hypersatellite spectrum, K-shell electron double ionisation cross section, binding energy 79−36577
- Mg, pionic X-ray transitions, strong interaction line widths and shifts 77−23586
- Mg plasma, simplified spectra obtained by electro-optic gating of radiant emission 78−22561
- Mg, polarisation of light emitted from sputtered Mg atoms 77−27008
- Mg VII, UV lines, theoretical intensity ratios 78−90108
- Mg XI, He-like ion, oscillator strengths of transitions between low-lying S and P states 78−13470
- Mg XI resonance lines, dielectronic satellite lines atomic parameters calcs. 80−78567
- Mg$^+$ laser cooled ions bound in Penning trap, high-resolution optical spectra 80−102487
- Mg$^+$, Penning trap, laser cooling, optical spectrum from laser freq. sweeping 80−52916
- Mg^{2+}, 2p^{5}np-2p^{5}ms (n=3, 4; m=3,4,5) transition probabilities calc. 79−6915
- Mg^{4+}, 2s2p^5-2s2p^{4}3s transition, spectroscopic investig. 79−59384
- Mg^{n+}, foil-excited ion, X-ray spectra and satellite classification 80−95567
- Mg-like V XII, Cr XIII, Mn XIV and Co XVI, level struct. and predicted intercombination lines 80−14098
- Mn, atomic transition probabilities, oscill. strengths 78−74601
- Mn, fine struct. levels fitting, config. interaction effect, spin-orbit and electrostatic interaction parameters 80−69248
- Mn I, absorpt. spectrum, 1305-2040 Å, ionis. energy 79−26921
- Mn I, UV absorption spectra, 3d and 4s excitation spectra, spectator electron model validity 79−85926
- Mn I inner shell absorpt. spectrum, 3d wavefunction collapse 77−23455
- Mn III, revision and extension of spectrum, fundamental configs. *(Spanish)* 79−22637
- Mn III to VI, struct. and transition probabilities, ab initio calc. using Thomas-Fermi central pot. 79−3360
- Mn, M$_{2,3}$ absorpt. spectra in UV, single-config. Hartree-Fock multiplet theory 78−78656
- Mn, n=2-2 transitions in XUV spectra, anal. 80−102472
- Mn, UV absorpt. spectra, 3p-excitation, super Coster-Kronig decay 79−13659
- Mn V, 3d^{2}4s-3d^{2}4p transition 79−63943
- Mn V, 3d^3-3d^{2}4p transition obs. energy level assignments 78−55134
- Mn V, forbidden transitions laboratory wavelengths 78−50496
- Mn VI, classification of absorption lines, 800-1550 Å 78−9103
- Mo, beam-foil spectra, 5-55 nm, using 22-200 MeV beams, rel. to Tokamak impurities 79−46481
- Mo IX, 4p-5d,6d and 4p-6s,7s transitions, grazing incidence spectrograms 79−36576
- Mo IX, 4p-5s transition 77−27010
- Mo IX, energy levels, 4s^{2}4p^4 to 4s4p^5 transitions obs. 77−3288
- Mo IX, X, XI, 4p-4d transitions obs. 78−82669
- Mo VI, 4p^{6}4d-4p^{5}4d5s transitions, level assignments 79−22631
- Mo, visible emission from excited ats. emitted from 40 keV Ar$^+$-bombarded surface 80−11481

atomic spectra continued
- Mo XIII and XVII, spectra, perturbation theory with model pot. 78−58579
- Mo XIII-XVIII, spectrum 20 to 90 Å from laser-prod. plasma and low-inductance vac. spark 80−102473
- Mo XIV, spectrum and energy levels, ionisation energy 79−49954
- Mo XIV to Mo XXIX, extreme UV spectra 80−87068
- Mo XXX to Mo XXXII, XUV spectra in laser prod. plasma 78−50493
- Mo XXXI-XXXIV spectra from exploded Mo wire plasmas 79−1295
- Mo XXXIII, XXXIV, XXXV, transition identification X-ray spectra 80−32648
- Mo XXXIX, energy levels and transition 79−59383
- Mo X(XI), 4p-5s transitions 77−23453
- Mo^{12+}, VUV reson. lines, transition probabilities calcs. 78−41989
- Mo^{13+}, determination of spectrum using low-inductance spark and laser-produced plasma 80−19610
- Mo^{13+}, energy levels for transition probabilities, oscillator strengths, rad. lifetimes 78−17589
- Mo^{30+}, VUV reson. lines, transition probabilities calcs. 78−41989
- N, (2$^4S_{3/2}$), kinetic study by time resolved atomic resonance fluorescence 80−95557
- N, and mixtures, photon mass attenuation and mass energy-absorpt. coeffs., 0.1 keV to 20 MeV 77−61715
- N, far vac. UV spectra, oscillator strengths for 3s, 4s, 5s, 3d and 4d ^4P_J-2p^3 $^4S_{3/2}{}^0$ 80−74178
- N, HFS and g_J factor, precision meas. ground state 77−88412
- N I, forbidden radiative transition probabilities rel. to NGC 7027 low-excitation emission 77−64823
- N I, spectra in Ar inductively coupled plasma 80−91474
- N I isoelectronic sequence, density-sensitive line ratios and electron densities in solar corona 79−16906
- N I resonance lines, oscillator strengths 79−5741
- N I transition probabilities and absolute oscillator strengths, rel. to H I regions 77−49448
- N II 2144 Å, emission feature obs. in UV aurora 78−88963
- N III, optical oscill. strengths meas. 79−98031
- N III, VUV spectrum *(Chinese)* 80−42974
- N III intersystem multiplet as density indicator for solar plasmas 80−31264
- N III lines for solar diagnostics 79−30031
- N IV, absorption spectra, 4f electron localisation effects in collapsing shell 77−3290
- N IV, intercombination lines, transition probabilities determ. 79−89645
- N IV, transition probabilities calcs. 79−54792
- N IX to Ni XII, wavelengths of transitions between lower configurations 80−99474
- N ions, in plasma spectral line intensity rel. to composition *(Russian)* 77−36851
- N isoelectronic sequence ions, level populations and EUV line intensities for solar coronal conditions 80−51649
- N, mean lifetimes of astrophysically important excited levels 77−46528
- N, radiative lifetimes of visible and near IR transitions, solar abundance 78−50506
- N, Rydberg-valence mixing, oscillator strengths 79−31492
- N, Stark broadened VUV lines in wall-stabilised arc, 1100-1800 Å 78−90107
- N, UV, visible spectra in Ar plasma, 230-620 nm 78−13456
- N V, absorption spectra, 4f electron localisation effects in collapsing shell 77−3290
- N V, VI, laser produced plasma, satellite spectra 78−5165
- N$^-$, continuous absorption coeffs., from elastic e-N scatt. data, target wavefunction effect 78−9128
- N$^-$, free-free absorpt., multichannel theory 77−18816
- N$^-$, reson. in i.r. spectrum 77−424
- ^{14}N II, 2p3p $^1P_1$, hyperfine struct. after ion beam surface impact at grazing incidence 80−58403
- ^{15}N, beam foil and quantum beat spectra *(Chinese)* 80−32638
- Na, (4$^2P_{1/2}$, 5$^2{}_{1/2}$ states), mag. dipole interaction consts., RF spectroscopy 78−37577
- Na, absorpt. notch in spectrum of transform limited pulse 77−18817
- Na, absorption D-line shape, rel. to single-mode laser intensity 78−66491
- Na, anomalous emission in blue wings 77−46517
- Na, D_1 and D_2 reson. lines, intensity dependent polarisation change 78−5163
- Na, D_1 line, optical coherent transients by laser freq. switching 78−42391
- Na D_1 line profile, Zeeman scanning 80−47928
- Na, D-lines, inert gas broadening, photon echo meas. 80−91475
- Na, depolarisation obs. of near-resonant scattered light 80−52921
- Na, fast atomic beams, collinear laser spectroscopy 78−37078
- Na, first excited states, non-resonant emission spectra *(Chinese)* 80−42971
- Na, first reson. doublet, anomalous dispersion meas. 77−71891
- Na, four- and six-photon resonance spectra *(Russian)* 80−91527
- Na, high Rydberg states, quenching in strong 1.06 μm laser field 80−95559
- Na, high-resolution laser spectroscopy with minute samples 78−17822
- Na, highly excited p and d states, fine struct. intervals and polarisabilities, RF reson. meas. 77−67999
- Na I, atomic spectrum, series formulas 80−99466
- Na I, even-parity autoionising states, photoabsorpt. 350 to 400 Å, laser excitation 79−59390
- Na I isoelectronic sequence, K IX to Mn XV, wavelengths and energy levels, spectral obs. 77−428
- Na I solar D-lines, non-mag. polarisation 80−63569
- Na II, spectrum, config. superposition and transition probabilities calcs. 80−87082
- Na, in Xe matrix, 3s excitation, UV and vis. spectra 78−46291
- Na, intracavity laser spectroscopy sensitivity, saturation absorpt. influence 79−63312
- Na, isoelectronic series, Cu XIX-Br XXV, laser-produced at. spectra 79−49974
- Na isoelectronic series, Hartree-Fock line strengths 78−9122
- Na isoelectronic series, spectroscopy, review 79−10060
- Na, laser photoionisation cross section obs. 77−71782
- Na, matrix isolated in Ne, absorpt. and emission spectra 80−99465
- Na, optical heterodyne spectra, hyperfine struct. 77−30841
- Na, oriented vapour, RF transitions and laser beat reson., expt. technique 77−27005

atomic spectra continued
Na, pionic X-ray transition strong interaction line widths and shifts 77—23586
Na, quadrupole transition moment meas. 77—30830
Na, quantum defects and ionis. pots., graphical procedure for students 80—7
Na, Rayleigh scatt. near $A^2P_{3/2,1/2}$-$^2S_{1/2}$ reson. doublet, polarisation reversal 77—10616
Na, reson. absorpt. transitions, laser saturation spectroscopy with optical pumping 80—47121
Na, reson. light scatt., theory of correl. meas. 78—42014
Na, reson. transition, laser saturation spectroscopy with optical pumping 80—52334
Na, rotation of plane of polarisation close to reson. 79—41129
Na, Rydberg levels mm resonances detected by field ionis., quantum defects, Stark shifts 77—42262
Na, Rydberg states, diamag. struct. 78—50484
Na, Rydberg states, IR Stark spectra, term energy, fine struct. 77—57910
Na, Rydberg states, millimeter spectra, quantum defect, fine struct., polarisability, field ionis. obs. 78—82672
Na, Rydberg states, millmetre spectrosc. 80—99469
Na, Rydberg states and microwaves, spectroscopy, masers and superradiance study 80—53248
Na, Rydberg transitions to detect far IR radn. 80—4763
Na, saturation spectra, crossover signals, effect of atomic alignment, optical pumping 80—58202
Na, spectra, emission and absorpt., inert gas matrix 78—90106
Na, strongly driven two-level atoms, reson. fluoresc. and absorpt. spectra meas. 79—36581
Na, two-photon absorpt. processes, polarisation selection rules 80—9574
Na, two-photon optical free-induction decay 78—90138
Na, vap., two-photon echo, quantum beats, superposition relax. 78—83041
Na, vapour, absorpt. spectra 79—21509
Na vapour, saturation holes meas. using FM spectrosc. 80—42262
Na-He-N_2 dense vapour system, optical pumping, RF spectrum analyser appl. 79—76393
Na-like ions, transition probabilities for reson. transitions 78—66494
Na+Ar, fine structure transition cross-sections, emission spectra, NaAr form. 78—9085
Na+H(Ne)(Kr) vel.-changing collisions, effect on 2 photon and stepwise absorpt. line shape 80—87221
Na+inert gas, collisional redistrib., two-photon absorpt. with near-reson. intermediate state 80—23505
Na+inert gas atom collisions, optical emission cross section, reson. lines 78—13584
Na+Kr collisions in laser beam, transition probability 79—50120
Na+Ne(CO), 13d-13f transition, collisional dephasing, Ramsey method investig. 79—54791
Na^++Hg, low-energy collision, quantum mech. phase interference and optical polarisation 77—42385
Na_x, matrix-isolated, formed in supersonic nozzle beam, 400-800 nm absorption and mass spectra obs. 79—76439
NaI isoelectronic sequence, 3s-3p and 3p-3d transitions, ionisation energy 78—70773
^{A}Na, A=21-31, hyperfine struct., mag. moments and isotope shifts, laser spectroscopy 79—10072
^{23}Na, P sequence, hyperfine structure using quantum beat spectroscopy 79—89632
^{23}Na, pionic 2p-1s X-ray transitions 79—18319
Nb IX (X), 4p-5s transitions 77—23453
Nb V, $4p^64d$-$4p^54d5s$ transitions, level assignments 79—22631
Nb VIII, 4p-5s transition 77—27010
Nb VIII, energy levels, $4s^24p^4$ to $4s4p^5$ transitions obs. 77—3288
Nb VIII, IX, X, 4p-4d transitions obs. 78—82669
Nb XIII, energy levels, spectrum obs. 80—63571
Nb XXXII, XXXIII, XXXIV, transition identification X-ray spectra 80—32648
Nb XXXIX and XL, X-ray spectrum weak line detection 80—5497
Nd I, isotope shifts in energy levels of neutral Nd atom 80—69095
Nd I and II, isotope shifts in spectrum, 3900 to 4760 Å, config. mixing 77—30812
Nd, new lines, 3930-6450 Å, isotope shifts 80—47929
Nd^+, branching ratios and transition probabilities, solar abundance 78—9104
^{143}Nd, ^{145}Nd, visible spectra, relative isotope shift, odd-even staggering parameters 77—10615
Ne, 2p-1s transition, time-resolved spectroscopy 78—90103
Ne, $3s_2$-$2p_4$ transition relax. consts. using cross saturation of travelling waves in ring laser 79—76374
Ne atom, K-absorption spectrum, core electron rearrangement effect 80—47880
Ne, collision-induced light scatt. of low density 77—71765
Ne, Doppler-free two-photon spectra, fine struct. and hyperfine consts. of 4d′ level 77—61725
Ne, electron scattering, elastic and inelastic, reson. spectra, R-matrix calcs. 79—72421
Ne, few-electron states prod. K X-rays obs. 80—9718
Ne, ground level isotope shift between ^{20}Ne and ^{22}Ne, obs. 79—31451
Ne I, $3d^1(3/2)_2$ level, absolute transition probabilities 78—13454
Ne I, at. state densities meas. in Ne-Br_2 mixture 78—62753
Ne I, probabilities of $np^5n'p \rightarrow np^5n's$ dipole transitions, two-config. approx. calcs. 77—71779
Ne I, transition probabilities for 3p to 4d array 77—437
Ne I, transition probabilities for 3s-4p transitions 77—88415
Ne I isoelectronic sequence, X-ray spectra, K X to Fe XVII 79—22641
Ne I to Ne IV, excitation in ion-atom collisions, 100 keV region, emission spectra obs. 80—14205
Ne II 12.8 μ fine-struct. line in Nova Cygni 1975, contrib. to 10 micron excess 78—93269
Ne II 12.8 μm emission and NGC 253 galactic dynamics 79—92844
Ne III, excitation cross-sections, electron impact with simultaneous ionisation 77—68119
Ne III, UV spectra excited by He^+ impact 79—6900
Ne ions, multiply charged, IV and V, excitation by electron impact, sections of lines meas. *(Russian)* 77—6941
Ne isoelectronic sequence, level energies and lifetimes 79—89644
Ne, isoelectronic series, dipole matrix elements derivation 77—83519
Ne, L-shell photoabsorption cross-section, moment theory and finite basis pseudospectra calcs. 79—63938

atomic spectra continued
Ne, Lamb-dip structure anal., linear and helicoidal polaris. 78—25852
Ne, magnetorotation of 6328 Å line, absorpt. coeff. for $3s_2$-$2p_4$ transition 77—71768
Ne, metastable states, studied by Doppler-free spectrosc. with vel. selective pumping 79—81304
Ne microballoon spectra, density-sensitive dielectronic satellite lines 79—72270
Ne, near IR lines, transition probabilities 78—13450
Ne, nonlinear laser spectroscopy, inside Doppler line *(Russian)* 78—21231
Ne, one-electron and two-electron one-photon transitions 78—58775
Ne, radiation from hollow-cathode discharge in weak mag. field 78—70789
Ne, reson. broadening at low densities 79—31452
Ne, reson. free-free absorpt. by electrons, negative ion form. 77—3463
Ne, spectral line relative intensity, radial depend. in low press. discharge 80—37764
Ne, thermalisation of level populations 78—66649
Ne, two-electron one-photon transition rate 77—71772
Ne VII, transition probabilities calcs. 79—54792
Ne, velocity diffusion, saturated absorpt. obs. of Hanle effect 77—61716
Ne-Ar (1%), 250 kV pulsed electron beam-excited, at. line rel. intensities 79—89646
Ne-Ar Penning mixture, pulsating discharge, emission spectra, Ne state population 79—55594
Ne-Kr mixture, collision-induced microwave absorpt. 77—88411
Ne-O_2, DC glow discharge, Ne I spectral line intensities 78—74610
Ne+$^4He^{2+}$, optical transition excitation function and cross sections 80—63787
Ne+Ar(Kr), translation band spectral moments, induced dipole moments 78—55218
Ne+Mg^{2+} collisions, 2p-3p excitation, optical spectroscopy investig. 77—19064
Ne+Ne^+ collisions, satellite struct. of 2s-subshell ionisation of Ne 77—19065
Ne+Ne(Ar), optical emission spectra 77—14551
Ne^{2+}+Xe, electron capture collisions, 15 to 50 keV, excitation 80—102566
^{20}Ne, ^{22}Ne, 1.15 μm line isotopic shift, phase-polarisation nonlinear high-resolution spectroscopy in longit. mag. field 79—41423
^{21}Ne, ground state, electronic pumping, alignment transfer with multiple diffusion *(French)* 78—50643
Ne* 5882 Å line, Doppler free spectra, press. broadening and shifts, saturation spectroscopy 80—78565
Ni, 3p excitation spectra 79—22633
Ni (VIII), semiempirical investigation of spectra 78—33434
Ni atoms, Xe matrix isolation, photoemission 80—27987
Ni from Tokamak-produced plasma, $2s^22p^k$-$2s2p^{k+1}$ transitions in F I to Be I isoelectronic sequences 80—37765
Ni I, in solar spectrum, effect of parity of spectral terms on curve of growth 77—53539
Ni I, UV lines, oscillator strengths from hook method and absorpt. meas. in furnace 80—83319
Ni I isotope shift for stable isotopes, nuclear charge radii 80—99484
Ni III to VI, struct. and transition probabilities, ab initio calc. using Thomas-Fermi central pot. 79—3360
Ni IV spectrum anal., energy level classification 77—61700
Ni, $K\alpha^h$ hypersatellite spectra and double photoionisation cross-section 79—85922
Ni, $L\alpha$ and $L\beta_1$ emission spectra structure 77—27013
Ni, n=2-2 transitions in XUV spectra, anal. 80—102472
Ni, UV matrix freq. shifts, ionis., pot., assignments, appl. to Ni_2, Ni_3 77—75178
Ni V spectrum, 990 to 1400 Å, ionisation pot. 77—30811
Ni, X-ray transitions in laser produced plasma 80—100093
Ni XI, Ni XII, forbidden transitions, solar coronal spectrum appl. 78—77537
Ni XII, XIII, XIV, XV, 3s-3p and 3p-3d transitions, oscillator strength and energy levels calcs. 80—83251
Ni XII-XVIII solar $3s^23p^n$-$3s3p^{n+1}$ transition arrays, UV spectra classification 80—63570
Ni XIX, mag. quadrupole lines, in TFR600 Tokamak plasma, 10-20 Å 79—13662
Ni XV, proton collisional excitation of fine struct. transitions in ground state 77—19017
Ni XVII solar coronal EUV line intensities 80—51731
Ni XVII transition probabilities and collision strengths 80—78562
Ni XVIII solar XUV flare lines, oscillator strength meas. 79—5796
Ni XX, spectra and energy levels of F isoelectronic series 79—93948
Ni XXI, XXIII, spectral energy levels, relativistic corrections, config. superposition method 80—32616
Ni XXV, Ni XXVI, line classifications in laser-produced spectra 79—81175
Ni XXVII, He-like ion, oscillator strengths of transitions between low-lying S and P states 78—13470
Ni^{2+}, in zeolites, reduction, UV spectroscopic obs. 77—77738
Ni(IX), resonance transitions, classification 80—42985
NiVI, sixth spectrum analysis 220-335 and 890-1325 Å regions 80—95565
Np I, 4000-40000 cm^{-1}, term analysis 77—38629
Np I, first ionisation pot., radiative lifetimes, high-lying energy levels, laser spectroscopy 79—76370
Np, UV emission spectra, Fourier transform spectroscopy appl. 78—58060
O, 2^3P_2-2^3P_1 fine struct. splitting by laser mag. resonance 79—98010
O, and mixtures, photon mass attenuation and mass energy-absorpt. coeffs., 0.1 keV to 20 MeV 77—61715
O, atom or ion sputtered from SiO_2 and oxidised Al surfaces, light emission 80—58199
O, beam-foil spectra, multiply ionised O 80—42977
O, He-like, $1s3s\,^3S$-$1s3p\,^3P$ transition, Lamb shift and fine structure 79—89637
O I, $3s'\,^3D^0$ and $3d\,^3D^0$ levels excitation and radiative decay 79—80064
O I, 5577 Å emission from meteor wakes, plasma column dynamic and reaction processes 77—82176
O I, anal. of chromospheric spectrum in α Bootis (Arcturus) 77—56923
O I, auroral 989 Å and 1027 Å emissions 78—28367
O I, new absorpt. lines 79—26923
O I 5577 Å and 6300 Å, laboratory discharge lamp source for lines of known width 80—4148

atomic spectra continued
- O I 5577 Å emission of meteors, vel. dependence 78—20758
- O I 5577 Å forbidden line rel. to $O_2$and OH band atmospheric spectra 78—61639
- O I 557.7 nm forbidden line emission structure in airglow 79—35027
- O I 6300 Å emission in twilight airglow, thermospheric temperature depend. 77—45215
- O I 6300 Å line meas. of $O(^1D)$ quenching coeff. by molecular collision, optical meas. 79—2419
- O I 7774 Å multiplet obs. of nightglow over Arecibo during magnetic storm 80—72663
- O I 7990 Å and 11287 Å branching ratios, astron. appl. 79—41134
- O I 7990 Å branching ratio, lab. study, rel. to airglow and auroral emissions 79—775
- O I auroral emissions, ground-based photometric meas. 78—77387
- O I forbidden line nightglow intensity var. 77—73899
- O I lines in A-type stars, non-LTE anal. 77—41378
- O I transition probabilities and oscillator strengths, rel. to H I regions 77—49448
- O I-like ions, solar emission lines density depend. 79—40165
- O II, III, IV, beam-foil spectra, mean lives, 270-490 angstrom 78—55223
- O II and III, mean lifetimes of astrophysically important excited levels 77—46528
- O III, forbidden lines in quasars and active galaxies, theory 78—93408
- O III, optical oscillator strengths for astrophysically interesting lines 80—32660
- O III 1666 Å line used in electron density determ. for quiet Sun and polar coronal holes 79—21245
- O III 5007 Å forbidden line splitting, NGC 7293 (Helix Nebula) obs. 79—25694
- O III 51.8 μ forbidden emission line obs. of Orion Nebula 78—65510
- O III forbidden lines in Seyfert galaxy Markarian 335, intensities rel. to gas props. *(Russian)* 79—101204
- O IV, intersystem multiplet as density indicator for solar plasmas 80—31264
- O IV, optical oscillator strengths 79—98043
- O IV 1402.5 Å semi-forbidden line, identification with 1400 Å emission feature in quasi-stellar objects 80—12825
- O IV solar intersystem line obs. in EUV, electron density at 10^5K 78—53903
- O, in thermosphere, 63 μm radiation field and influence on H temp. 79—80066
- O, isoelectronic sequences, energy spectra inc. relativistic corrections 78—924
- O, Kα spectrum, intensity of high energy peak as function of oxide layer thickness 80—936
- O, ns ^3S-$2p^4\ ^3P_2$ transitions, for VUV, oscill. strengths 77—34580
- O, radiative lifetimes of visible and near IR transitions, solar abundance 78—50506
- O, two-photon absorpt., auroral transition relax. obs. *(Japanese)* 80—47954
- O V, $2s^2S_0$-$2s2p^3P_1$° intercombination line wavelength determ. 80—102470
- O V, intercombination lines, transition probabilities determ. 79—89645
- O V, solar emission line ratios interpretation 78—28598
- O V, transition probabilities calcs. 79—54792
- O VI, $2s^2S$-$2p^2P$ reson. lines, wavelength determ. 80—102470
- O VI, O VII, O VIII, energy levels and multiplet tables 80—930
- O VII, electron impact collision rates, reinterpretation of solar emission line ratios 80—98624
- O VII, laser produced plasma, satellite spectra 78—5165
- O VII line intensity ratios depend. on temp. and ionization balance 79—16903
- O^-, free-free absorpt., multichannel theory 77—18816
- O^-, spectra in pure O arc plasma, 2000-9000 Å, 9000K 79—32750
- O^{2+}, collision strengths, radiative transition probabilities, solar atm. appl. 79—86069
- O^{4+} to Be isoelectronic series, transition values and energies, transition-operator method 77—30826
- O^{5+}, spectra, 7-32 nm, doubly excited quartet system 78—62757
- O^{n+}, n=1 to 4, gas and foil-excited, 2-18 MeV, projectile Auger spectra 79—59414
- O-like ions, Fe to Zn, intercombination lines, lab. obs. 77—3289
- OI, spectra in Ar inductively coupled plasma 80—91473
- $O(^3P_J)$ state, direct obs. from O_3 photolysis at 248 nm 80—101028
- $O(^1S)$, prod. and props. in liq. Ar and N_2, by N_2O photodissociation 80—43063
- $O(^1S)$ yield from O_3 photodissoc. at 1700-2000 Å 80—97714
- $O(2^1D_2)+Cl_2$, reaction kinetics, vac. UV at. spectra 77—21365
- $O(2^1D_2)+N_2(O_2)(N_2O)(CO_2)(H_2O)$(methane), collisional deactivation meas., 295K, rel. to atmospheric processes 80—16663
- P, highly ionised, beam foil radiative lifetimes and EUV spectrum 80—32671
- P I, IR spectra and HFS 80—91478
- P I, spectra and term anal. 80—91481
- P III, UV and vis. spectrum, ionisation limit calcs. 78—936
- P IV, 200-9800 Å, spectral line classification and term system 77—79564
- P, muonic allotropes muonic Roentgen intensities *(German)* 80—53168
- P VI, UV spectrum, anal. 78—17595
- Pb atom, optical activity near suppressed M1 transition *(Russian)* 78—46292
- Pb, electron impact excited, spectrum in 54-126 nm range 79—63942
- Pb I, absorption spectrum, 1350-2041 Å 78—9102
- Pb I, interchannel interactions and series quenching in 5d and 6s spectra 77—88418
- Pb, muonic high-lying states transitions, electron screening effects 77—34786
- Pb muonic isotopes, A=204, 206, 207, 208, nuclear polarisation energy shifts, RPA calcs. 78—94334
- Pb, optical transitions, struct. of weak neutral currents *(Russian)* 77—88420
- Pb stable isotopes, 2-photon spectroscopy, isotope shift of $6\text{-}^2\ ^3P_0$-$7p\ ^3P_0$ transition 80—87070
- Pb, transition probabilities, 200-700 nm 79—31454
- Pb, X-ray L shell emission spectra *(Spanish)* 79—98016
- PbI, $np^2 \rightarrow np(n+1)s$ transition array, relativistic oscill. strengths 79—31465
- ^{207}Pb, laser isotope separation using nuclear spin induced elec. dipole transitions 77—61877

atomic spectra continued
- Pd isoelectronic sequence, UV spectra (60-600Å), reson. line identifications 78—33455
- ^{103}Pd, K-electron capture decay, double K-shell vacancy creation 80—22773
- Pr IV, $4f^2$ config., semiempirical eqns. for deciphering spectrum 77—24874
- PrIV, change of spectra under free state to cryst. transition 79—33271
- Ra, Rydberg series, ionisation limit derivation from multichannel quantum defect theory, UV absorpt. spectra 80—52918
- Rb, anomalous emission in blue wings 77—46517
- Rb, atom and ion, k-ordering props. and fine struct. inversion 79—59388
- Rb, Doppler-free two-photon absorpt. spectrum 80—42975
- Rb, fine struct. intervals in 6^2F and 7^2F states, RF spectroscopic meas. 77—71766
- Rb, fine-struct. splittings in visible region, ^2D states 78—50656
- Rb, forbidden quadrupole lines, oscill. strengths meas. 77—50390
- Rb I, 4p subshell excitation spectra, 15 to 19 eV, a new interpretation 79—777
- Rb II, lifetimes in $4p^55p$ config., precision meas. and calc. 80—102488
- Rb in Xe, collision-induced dipole transitions, absorpt. meas. 80—95718
- Rb, L-shell soft X-ray emission spectra, oscillator strengths 80—32651
- Rb, lowest metastable autoionising level identification by RF spectroscopy 77—426
- Rb Rydberg levels in intense mag. field, diamag. struct. 79—26958
- Rb, Rydberg S and P states, hyperfine struct., RF spectroscopic meas. 77—57911
- Rb, Rydberg states, detection using freq. doubled CW dye laser 78—17592
- Rb, self-broadened first reson. lines, near-wing asymmetries 80—9535
- Rb vapour, IR stimulated Raman scatt. 79—27325
- Rb^{2+} formation during electron-ion collisions, ultrasoft X-ray spectroscopic study *(Russian)* 80—43193
- $Rb+H^+$, single photon emission following double K-shell ionisation, contrib. to superheavy element search data 78—50625
- Rb+Kr, STS components shift and broadening 77—68014
- Rb+Rb, ^2P states, near IR spectra, collision induced features 77—10637
- Rb+Rb(Cs), continuum- and bound-state pair absorption, 2300-3100 Å, 410-540°C 80—42970
- ^{85}Rb, unperturbed hyperfine transition freq. meas. 77—17954
- $^{85}Rb^+(^{87}Rb^+)$, hyperfine struct., in-flight saturated absorption laser spectrosc. 78—78650
- ^{87}Rb, freq. displacement meas. by passing pumping light through ^{85}Rb filter cell 77—41702
- ^{87}Rb, surface wave polarisation in hyperfine dipolar mag. transitions *(French)* 78—50504
- ^{87}Rb+inert gas, D_1-line hyperfine components perturbation, interferometer obs. 80—32635
- Re I, isotope shift meas. by HFS, methods, $5d^46s^26p$ level classification 79—49988
- Re, pionic 4f$\rightarrow$3d X-ray transition 79—86085
- Re XLVIII X-ray spectra from laser produced plasmas 80—42981
- S, emission spectra in Ar plasma, lines above first ionisation limit 78—25462
- S I ground configuration, wavelengths of observed transitions between levels 78—50489
- S II forbidden line emission from thermal plasma of Jupiter 78—93146
- S II-VII, spectra, 1050-5500 Å, beam-foil expt. with 100-700 keV ions 78—50495
- S III, forbidden 18.71 micron emission obs. in galactic H II regions 79—97046
- S III, S IV in Io plasma torus, Voyager 1 EUV emission lines obs. 80—26792
- S III-IV, beam-foil study, 500 to 1200 Å 78—66488
- S IV, $3s^23p^2P$-$3s3p^2\ ^4P$ multiplet, energy levels and transitions, appl. to solar atm. 80—87028
- S IX, excited level populations, line intensity ratios, solar corona appl. 80—32637
- S, in CS_2 and SCO, $L_{II,III}$-absorption spectra 78—86807
- S, L X-ray emitting levels, lifetimes 78—66493
- S VI, spectrum, 100-8000 Å, ionis pot. 79—93946
- S X, ground configs., forbidden line intensities calcs. 80—23362
- S X in solar corona, density-sensitive line ratio and electron densities 79—16906
- S XI, UV lines, theoretical intensity ratios 78—90108
- S XV, He-like ion, oscillator strengths of transitions between low-lying S and P states 78—13470
- S^{6+}, spectra, 500-1200 Å, lifetimes 78—62756
- $S^{q+}+O_2(Ar)(He)$, (q=8-19), K X-ray prod., charge-state depend. 80—106391
- $S(^1S)$, prod. and props. by OCS photodissociation in liq. Ar and N_2 80—43064
- Sb I, ratio of oscillator strengths for 217.6 and 231.1 nm lines *(Russian)* 79—31457
- Sb, new autoionised series, flash pyrolysis IR absorption obs. 79—85937
- Sb VI, $4d^95d$ and $4d^96s$ configs., UV spectrosc. obs. 80—18817
- Sb VI, $4d^95s$-$4d^95p$ transitions, UV spectra 79—93942
- Sb VI, reson. lines, UV spectra 77—46515
- Sb VI, spectra, ionisation limits 79—54794
- Sb VII, $4d^9$-$4d^85p$ transitions, spectra, least squares calcs., Hartree Fock calcs. 79—54794
- Sb VII, $4d^9 \rightarrow 4d^85p$ transitions, UV spectra 77—46515
- Sb VII, spectrum obs. 600 to 2100 Å, analysis of $4d^85s$-$4d^85p$, $4d^9$-$4p^54d^{10}$ transitions 80—102471
- Sc, arc spectra, Zeeman effect *(French)* 77—83521
- Sc I to Sc XXI, energy level tables derived from atomic spectra anal. 80—101672
- Sc II, visible spectra and ionisation limit 80—74143
- Sc IV, autoionising transitions $ns^2np^6-nsnp^6mp$ 77—88419
- $Sc+Ar^+$, charge exchange obs. through spectral line enhancement 79—7005
- Se, 1897 to 9271 Å region spectrum 78—21869
- Se I resonance lines, new meas. 78—938
- Se, muonic allotropes, muonic Roentgen intensities *(German)* 80—53168
- Se VI, 2400 to 90 Å spectrum anal. 78—58616
- Se VII, VIII, $3p^53d^{10}$ config., spectrum, 100-1200 Å 77—65431
- Se XXVI, $2p^5$-$2p^43s(2p^43d)$ transitions in laser produced X-ray spectra 78—13460
- Se XXVI, spectra and energy levels of F isoelectronic series 79—93948
- Se XXVI, transitions between $1s^22s^2p^5$-$1s^22s^22p^43d$ and $1s^22s^22p^5$-$1s^22s^22p^43s$ configs. 79—26925

atomic spectra continued
Se(4^1D_2) atoms, electronically excited, direct obs., quenching by inert gases 78—25461
Si I lines in far UV spectra of G-type dwarf stars 80—56829
Si I sequences for elements Cr to Zn, $n=3 \rightarrow n'=4$ transitions 79—26922
Si I UV spectrum, series from 3000 to 1200 Å, identifications in solar spectrum 77—56882
Si II 1533 Å identifications in QSO spectra rel. to absorption redshift 79—35417
Si II lines in shell spectrum of ζ Tauri 77—60774
Si IV, 1122 and 1128 Å lines in solar spectrum 78—4170
Si IV, spectra, nonrelativistic oscillator strengths calc. 77—83538
Si IV radial wave functions of discrete spectrum calcs., dipole and quadrupole polarisation 80—5476
Si IV/C IV ratio for Be-stars, Skylab UV obs. 77—56987
Si IX, UV lines, theoretical intensity ratios 78—90108
Si, K_α X-ray emission spectra chemical shifts, linewidths and intensities 78—13461
Si, L X-ray emitting levels, lifetimes 78—66493
Si lines as spectral diagnostics for astrophysical plasmas, effect of charge transfer 80—41717
Si V, line obs. and classification 77—27011
Si VI, $2p^43s$, $2p^43p$ and $2p^43d$ configs., UV spectrum anal. 78—21868
Si VI-XIV, line strengths, collision strengths and excitation rates, calcs. 78—5174
Si VII, excited level populations, line intensity ratios, solar corona appl. 80—32637
Si XIV, X-ray spectral lines profile evolution due to Comptonisation, Monte Carlo computations 79—66916
Si^{12+}, $1s2s\ ^3S_1$-$1s2p\ ^3P_{0,2}$ transition wavelengths, by beam-foil 80—32649
Si^{6+}, $2s2p^5$-$2s2p^43s$ transitions, spectroscopic investig. 79—59384
$Si+H_2(O_2)(He)(SiCl_4)$, $3p^2(^1D_2)$ state behaviour, at. absorpt. spectra 78—29846
Si+He(C)(O)(Ne), K-shell ionising collisions, average L-shell ionisation probability, K_α spectra 79—72408
Sm I $^{144}Sm^{152}Sm$ isotope shift J depend., in ground term. 77—75101
Sm I spectrum from laser-atomic-beam spectroscopy 78—37578
Sm II, transition probability, 3000-7000 Å, solar abundance 79—31453
Sm, in inert gas matrix, pseudolocalised vibr. modes, UV/vis. spectra 78—46289
Sm, optical isotope shifts, optical heterodyne method 79—22630
Sm, spectra, 2900 to 7100 Å relative oscill. strengths, Rozhdestvenskii hooks 77—75084
SmI, laser atomic beam spectroscopy, isotope shifts, hyperfine struct., transitions 80—102468
^{A}Sm, $A=144$-154, charge distrib. and hyperfine splitting from muonic X-rays 79—40838
Sn, bombard. by Ar ions impact-parameter depend. of K- and L-X-rays 79—76501
Sn I, absorption spectra of outermost d-subshell 77—75086
Sn I, absorption spectrum, 1580-2040 Å 77—71770
Sn I, Sn II, wall-stabilised arc, absolute transition probabilities, 5300-6850 Å 78—9105
Sn, incoherent γ-ray scatt. by K-shell electrons 77—83560
Sn, oscillator strengths and hyperfine splitting of $5^3D_1{}^0$ and $6^3P_2{}^0$ levels, line absorpt. meas. 80—18818
Sn V, reson. lines, UV spectra 77—46515
Sn VI, $4d^85p \rightarrow 4d^85s$ transitions, near IR spectra 78—13449
Sn VI, $4d^9 \rightarrow 4d^85p$ transitions, UV spectra 77—46515
SnI, $np^2 \rightarrow np(n+1)s$ transition array, relativistic oscill. strengths 79—31465
^{50}Sn, $L\gamma_{2,3}$ X-ray emission spectra, line breadth 78—62760
$Sn[5p^2(^3P_0)]$, kinetic studies of ground state atoms, by resonance line absorpt. 78—85128
Sr, atom and ion, k-ordering props. and fine struct. inversion 79—59388
Sr, bound even-parity $J=0$ and $J=2$ states, multiphoton ionisation spectra 77—71789
Sr, bound odd-parity $J=1$ spectra, multiphoton excitation 79—54795
Sr, excited state lifetime, delayed coincidence meas. 77—3315
Sr I, oscillator strengths for certain transitions 79—18143
Sr I, principal absorpt. series near threshold, 5s-p and 4d-p interf. 77—30810
Sr I, strong configuration interaction, multiconfiguration Hartree-Fock calcs., transition probability 77—67987
Sr II, ^2F states, fine struct. splitting 78—50494
Sr III (IV), UV spectra, 40-100 nm, crossed electron and atomic beams *(Russian)* 78—37580
Sr, L-shell soft X-ray emission spectra, oscillator strengths 80—32651
Sr, laser spectroscopic anal. of Rydberg series, multichannel quantum defect theory 80—18815
Sr, reson. lines, emission and absorpt. core profiles 77—50389
Sr, Rydberg series, absorpt. by selectively laser-excited atoms 79—3390
Sr^+, inert gas atom collision, spectrai line polarisation 79—13811
Sr^{3+}, spectra, 250-6500 Å 78—62754
Ta IV, 2900 to 200 Å spectrum anal. 78—58615
Ta, pionic $4f \rightarrow 3d$ X-ray transition 79—86085
Ta XLVI X-ray spectra from laser produced plasmas 80—42981
^{181}Ta, L X-ray spectrum, L_1 subshell yield 79—49608
Tc I, mag.-dipole and electric-quadrupole hyperfine consts. 77—68002
Te II, vis. spectral lines, relative isotope shifts 78—37579
Te VII, $4d^95s$-$4d^95p$ transitions, UV spectra 79—93942
Te VII, $4d^96s$ configuration spectrum obs., line identifications 80—106289
Te VII, spectra, ionisation limits 79—54794
Te VIII, $4d^85s$, $4d^85p$ and $4d^54d^{10}$ config. spectrum obs., line indentifications 80—106289
Te VIII, $4d^9$-$4d^85p$ transitions, spectra, least squares calcs., Hartree Fock calcs. 79—54794
^{52}Te, $L\gamma_{2,3}$ X-ray emission spectra, line breadth 78—62760
Th, X-ray L shell emission spectra *(Spanish)* 79—98016
Ti, energy level data tables, Ti I to Ti XXII 79—59385
Ti, fine struct. levels fitting, config. interaction effect, spin-orbit and electrostatic interaction parameters 80—69248
Ti I, transition probabilities rel. to solar Ti abundance 77—29743
Ti III, IV, V, radiative lifetime meas. using beam-foil technique, 700 to 1900 Å 80—78574
Ti, $K\alpha^h$ hypersatellite spectra and double photoionisation cross-section 79—85922
Ti, pionic, pion mass high accuracy meas. from transitions 80—106406
Ti, sputtering yields of D^+ and Ar^+ ions using matrix isolation spectroscopy 79—78809

atomic spectra continued
Ti V, autoionising transitions $ns^2np^6-nsnp^6mp$ 77—88419
Ti XII, L-series satellite spectra 79—98012
$Ti^{q+}+O_2(Ar)(He)$, ($q=8$-19), K X-ray prod., charge-state depend. 80—106391
TiXIV(TiXV)(TiXVII), Tokamak discharge, ground state, mag. dipole transitions, UV spectra obs. 80—63575
Tl, $6^2P_{1/2}$-$7^2P_{1/2}$ transition, parity nonconservation obs. 79—31446
Tl, $6p_{1/2}$-$6p_{3/2}$, search for optical rot. induced by weak neutral currents 78—82710
Tl, absorpt. and emission spectra, in inert gas matrix 77—57909
Tl atom, optical activity near suppressed M1 transition *(Russian)* 78—46292
Tl, electron impact excitation of vacuum UV spectral lines 77—3471
Tl, ground state, population 'freezing' effect in hyperfine structure *(Russian)* 78—937
Tl HFS resonance lines anomalous intensity ratios 79—63961
Tl, hyperfine struct. optical pumping, O-O transition perturbation 80—949
Tl I, relativistic and cancellation effects in line strength ratios 78—82689
Tl I, Rydberg series, disctete levels and continua of finite bandwidth 78—74603
Tl, ionisation limit and oscill. strength in VUV absorpt. spectra 80—74152
Tl, $\lambda_{max}=251.3$ nm absorption band, rel. to Tl atom conc., temp. and disturbing gases 80—42980
Tl, optical transitions, struct. of weak neutral currents *(Russian)* 77—88420
Tl, parity nonconserving effects in $6^2P_{1/2}$-$7^2P_{1/2}$ transition 78—13458
Tl, reson. lines, perturbing gas and self-broadening, temp. effects 80—42979
Tl, self-broadening of 377.6 reson. line 78—82692
Tl, two-photon laser spectroscopy and ionisation 78—55153
Tl, vacuum UV absorpt. spectra, at. consts. 77—57917
^{205}Tl, transitions, parity nonconservation due to neutral weak currents 77—13913
Tm I, hyperfine struct., high resolution spectrosc. meas. 80—87238
Tm I, hyperfine struct. for various configs. 78—939
Tm, intense 4d-f resons., cross-sections, spectra, calcs. 79—31426
U, 4 eV odd levels, hyperfine struct., double reson. spectrosc. 79—81171
U atomic beam, two laser irrad., two photon reson. effects., visible spectra 80—63604
U, emission spectrum, visible region, wavenumber meas. by Fourier transform spectroscopy *(French)* 77—57407
U I, hyperfine struct. meas. of high-lying levels 79—54796
U I, isotope and relative isotope shifts for ^{234}U, ^{236}U and ^{238}U 77—30823
U I, visible spectrum, ^{238}U-^{233}U isotope shift 79—788
U II, oscillator strengths for calibration 77—42280
U III, IV, line identification on relative intensity basis 80—95561
U III, in hexamethyl phosphoric triamide soln., absorption spectrum, intensities, oscill. strengths 78—74599
U, isotope shift and configuration interaction 79—31468
U, laser isotope separation, atomic spectroscopy requirements 78—33638
U, matrix isolation studies with Fourier transform IR 78—45740
U, neutral atomic, oscill. strengths, 2289.8-2860.3K, 355.2-359.4 nm 79—10069
U, reson. absorption meas. using Zeeman tuned arc lamp 78—17593
U, sputtered, absorpt. spectra in hollow cathode glow discharge 80—32643
U vapour, 5758.143 Å transition probability and branching ratio, laser absorpt. meas. *(French)* 79—82107
U, X-ray L shell emission spectra *(Spanish)* 79—98016
$U+H^+$, L X-ray production cross sections, 0.3-1.8 MeV, expt. rel. to PWBA prediction 80—53115
UI, precision isotope shifts meas. in visible, near IR 80—63587
UV, energy levels and UV spectral anal. 80—106290
$^{238}U\ (^5L^0{}_6)$ from hollow cathode lamp, laser absorpt. spectroscopy *(French)* 79—59402
^{238}U I, lifetime, branching ratio and absolute transition probability of 6395.42 Å transition 79—3402
^{238}U I, transition probabilities meas. by time resolved optical pumping 77—46545
^{238}U vapour, hollow-cathode generator, energetic yield 80—47724
V, atomic transition probabilities, oscill. strengths 78—74601
V, fine struct. levels fitting, config. interaction effect, spin-orbit and electrostatic interaction parameters 80—69248
V I, IR emission spectrum meas. 78—62746
V I, photographic emission spectrum remeas. 78—62750
V II, spectrum, $3d^35s$ and $3d^34d$ config. *(Spanish)* 79—22636
V III, absolute oscill. strengths determ. 78—82691
V IV, $3d^2$-$3d4f$ tranistions obs. 190 to 650 Å 78—62758
V V, 100-8500 Å 77—65432
V VI, autoionising transitions $ns^2np^6-nsnp^6mp$ 77—88419
V VII, VIII, IX, X, 3s-3p and 3p-3d transitions, oscillator strength and energy levels calcs. 80—83251
V XX, Be I like spectra from laser-produced plasma, classification 78—67410
W ion emission from PLT Tokamak, W ion soft X-ray emission effects 78—83537
W, isotope shifts in visible region and HFS 78—82694
W, multiphoton ionisation and absorpt. 80—95575
W XLVII X-ray spectra from laser produced plasmas 80—42981
Xe, $^3P_1$ state, reson. fluoresc., Zeeman beats, time-resolved VUV spectra using synchrotron radiation 78—33454
Xe, $5d_{7/2} \rightarrow 6p_{5/2}$ transition struct., laser spectrosc. and double reson. obs. 78—1210
Xe, 6s-6p emission, following vac. UV irrad., press. depend. 79—63950
Xe, atom-diatom paradox, phenomenological description of spectroscopic props. 78—78766
Xe, Autler-Townes effect, i.r. laser transitions 77—425
Xe, autoionising reson., Stark effect 80—58198
Xe, collective excitation spectra, schematic model 78—41981
Xe, free ats. electron bombard., subsequent X-radiation ang. distrib. 80—53144
Xe, gas discharge, laser beam polarisation plane rot. near reson. 77—1024
Xe I, 147 nm resonance line, wavelength stability 77—17948
Xe I, theoretical transition probabilities and lifetimes, data tables 79—54793

atomic spectra continued
Xe II, 5d^{4}D$_{7/2}$-6p^{4}P$_{5/2}$^{0} transition, isotope shift, h.f.s., laser-ion beam expt. 79—93945
Xe II, optical and Auger spectra, discrepancies anal. 79—93944
Xe II, transition probabilities for 5p^{4}6p to 5p^{4}6s array 77—436
Xe, L$_1$,L$_2$,L$_3$ inner-shell level energies, absorpt. spectroscopy with synchrotron radiation 80—99583
Xe, line strength calcs. for 8s-7p and 5d-6p transitions 77—14384
Xe, line transition probabilities, in afterglow plasma, light absorpt. obs. 77—30807
Xe, photoabsorption, local field effects 80—74151
Xe, reson. levels relax. consts. determ. by alignment method in discharge 79—26936
Xe, s-p transitions, Stark consts. and oscill. strengths, shock tube meas. 80—18822
Xe, three level systems, obs. of isotope shifts 78—82670
Xe, three-body collision-induced light scatt. spectrum moments 78—9226
Xe, time resolved spectra, UV and near UV continuums 78—78653
Xe, united atom rare gas spectra analogy with mol. Rydberg states 80—32700
Xe VI, emission spectral lines, classification 80—95563
Xe VII, VUV line classifications and energy levels in triplet system 80—37763
Xe VIII, one-electron spectrum in theta pinch discharge, line identification 80—32640
Xe-Br$_2$ discharge, atomic state density determ. 79—36573
Xe-Kr, UV absorption spectra, induced lines and line-shift meas. *(French)* 77—61697
Xe-Kr-Ar mixtures, VUV continuous spectrum prod. in low volt. lamp *(Russian)* 78—75451
Xe-rare gas mixtures, far UV absorpt., at. and quasimol. spectra 77—61698
Xe+^{4}He^{2+}, optical transition excitation function and cross sections 80—63787
Xe+H$^+$ ionisation, induced L-shell alignment 80—32813
Xe+He, saturated absorpt. of 3.51 μm line, vel. changing collisions by line width 78—86819
XeI, transition probabilities of optical lines 79—89626
XeI, visible lines, absolute transition probabilities 80—69108
Y III, 4p^{6}4d-4p^{5}4d5s transitions, level assignments 79—22631
Y VI, 4p-5s transition 77—27010
Y VI, VII, VIII, 4p-4d transitions obs. 78—82669
Y VII (VIII), 4p-5s transitions 77—23453
Yb, 1060-1700 Å 78—82675
Yb, 4f^{14}6s6p ^{3}P$_1$ and ^{1}P$_1$ levels, Stark effect, tensor polarisabilities 80—87080
Yb, atomic energy level classification, ground state to two-electron level 77—68003
Yb, electron impact excitation, 40 to 120 nm, 5p ionisation 78—82845
Yb, highly excited levels, odd and even parity spectra, multichannel quantum defect anal. 80—58133
Yb highly excited levels, reson., visible two photon absorpt. spectra obs. 80—58228
Yb I, high Rydberg levels of 4f^{14} 6snd configs., very high resolution obs. 80—106300
Yb I isotope shift studies in 3900 to 6500 Å region 80—74144
Yb II, 6s ^{2}S$_{1/2}$-6p ^{2}P°$_{1/2,3/2}$ transition, relativistic oscillator strengths, influence of core polarisation 80—58132
Yb II, III to Bi XV, XVI isoelectronic sequences, wavelengths and ionisation energies 77—429
Yb, optical isotope shifts and hyperfine splittings 79—93943
Yb, Schumann region absorpt. spectrum, oscill. strengths, line profiles, collisional and autoionis. broadening 77—18818
Yb, two-photon laser spectra, hybrid resonances 79—31489
Yb, VUV absorpt. spectrum, 4f^{14} subshell excitation 79—76373
Yb, VUV spectra, 6s^2 shell excitation 79—72265
Yb^{3+}, spectrum and energy levels 79—26916
YbI, emission spectrum, extended anal. 79—85923
YbI, first spectrum, wavelengths and intensities, Zeeman effect 79—3389
^{A}YbI, A=170,171,173, 6s6p ^{1}P$_1$-6s^2 ^{1}S$_0$ transition, spectrosc., isotope shifts and hyperfine structure 80—23368
^{70}Yb, L X-ray emission spectrum, new satellites 78—46293
Zn, highly ionised, spectral classifications below 55 Å 79—13658
Zn I, relative populations in arc, sputtering and gas phase collisions 80—934
Zn I,II, excited state lifetimes, electron-photon delayed coincidence meas. 78—25478
Zn isoelectronic sequence, 4s-4p reson. transition in highly charged ions 77—75087
Zn, L-shell soft X-ray emission spectra, oscillator strengths 80—32651
Zn, metastable state depopulation, diffusion coeff. in Zn afterglow determ. 77—23542
Zn simultaneous excitation of two electrons 78—21867
Zn, Stark interaction in nspz^{3}P$_1$ levels, optical double resonance obs. 79—63941
Zn XIX, XX, spectral lines 20 to 50 Å 77—18822
Zn XXII, 2p-4d and 2p-4s transition arrays, wavelengths and oscillator strengths 80—47933
Zn XXII, 2p^5-2p^{4}3s(2p^{4}3d) transitions in laser produced X-ray spectra 78—13460
Zn, XXII, spectra and energy levels of F isoelectronic series 79—93948
Zn, Zn$^+$, Zn^{2+}, photon coherent scatt., cross sections 77—50410
Zn-like ions, 4s-4p reson. lines and transitions obs. by means of laser prod. plasma, appl. to Tokamaks 80—99468
^{68}Zn, 2s-2p muonic X-ray transition obs. 80—74264
^{68}Zn muonic atom, dynamical E0 excitation, E0 resonances, muonic X-rays 80—95749
Zr, absorption spectra, isolated in rare gas matrices 78—78652
Zr II and III, oscillator strengths for certain transitions 79—18143
Zr IV, 4p^{6}4d-4p^{5}4d5s transitions, level assignments 79—22631
Zr IV, energy levels, spectrum obs. 440 to 2670 Å 80—99470
Zr IX, 4s^{2}4p^2-4s4p^3 transitions, in VUV 80—91480
Zr V, energy levels, spectrum obs. 200 to 2670 Å 79—54798
Zr VII, 4p-5s transition 77—27010
Zr VII, energy levels, 4s^{2}4p^4 to 4s4p^5 transitions obs. 77—3288
Zr VII, VIII, IX, 4p-4d transitions obs. 78—82669
Zr VIII, reson. transitions in UV 80—91479
Zr VIII (IX), 4p-5s transitions 77—23453
Zr XI and XV, spectra, perturbation theory with model pot. 78—58579

atomic spectra continued
Zr XII, energy level system, spectrum obs. 70 to 630 Å 80—37766
Zr XXXI, XXXII, XXXIII, transition identification X-ray spectra 80—32648

atomic spectral line breadth
absorption, emission, linebreadths, EM radiation interaction with atoms and mols. 78—13448
absorption line profiles, instrumental spectral resolution effects 77—6726
AC Stark splitting in doubly reson, three-photon ionisation, nonmonochromatic field 78—94220
alkali atom+inert gas, three-body interaction, secondary satellites of alkali line 77—83683
alkali metal, two-photon S-S transitions, press. broadening and shift by rare gases 79—6916
alkali metal+inert gas, collisional shifts and broadening of Voigt contour 80—27983
alkali metal+inert gas, line profiles, width, shift and asymmetry, square well pot. approx. 80—52936
alkali metal atom+inert gas, collisional broadening and shifts, semiempirical pots. calcs. 77—10727
alkali metal atom+inert gas atom, hyperfine transition spectral line shift, quantum corrections 78—82655
alkali metal atoms, resonance interaction, resonance lines self-broadening, adiabatic pot. curves 77—83676
alkali metal Stark profiles, of reson. lines, model microfield method appl. 79—26931
alkali metals, Rydberg states, Stark ionisation 80—52933
anisotropic collisions, spectral line breadth and shift, polarisation depend. 78—46305
Ar, light scattering, collision induced, low density limit, mol. dynamics and memory function approach 80—43841
arc plasma electron density meas., high-pressure, use of strioscopy and IR absorption *(French)* 80—19620
asymmetries in photospheric lines of α Bootis (Arcturus) and Sun 80—51753
asymmetries in sunspot penumbral spectra 80—51715
atom, Schumann region absorpt. spectrum, oscill. strengths, line profiles, collisional and autoionis. broadening 77—18818
atom, two-photon absorption resonance, transit effects 79—10085
atom+charged particle anisotropic collision, spectral line shift and broadening, polarisation depend. 78—82695
atom-atom collisions, use of multipole expansions in spectral line broadening theory 78—74611
atomic collisions, at. vel. effect on relax. processes 79—49985
atomic radiative collision, in external mag. field 79—22665
atomic systems, coherent transients theorem 80—99808
atoms, 70≤Z≤82, Kα X-ray linewidths and relative intensities, energy dispersive meas. 80—99483
atoms, natural line widths, K and L X-rays, XPS and KLL Auger lines 79—76383
Beals' Type III P Cygni line profiles 80—51771
Beer's law, deviations due to relative lineshape functions 77—68012
bibliography on atomic line shapes and shifts (June 1975-June 1978) 79—49990
Block-Siegert shifts and multi-quantum transitions, spin-one systems, RF and DC fields 77—75103
broadening in turbulent plasma, retardation effects in motion of quantum systems 77—60975
Ca II K line emission widths in solar and stellar spectra 77—41373
Ca II K-line in α Bootis (Arcturus), Wilson-Bappu effect rel. to temp. minima 79—62825
cadmium, Lα X-ray spectra, $_{40}$Zr to $_{48}$Cd, linewidths 79—41131
CARS spectroscopy, laser linewidth effects 79—89012
catalogue of stellar absorption lines in β Lyrae components *(Russian)* 78—28725
collision and Doppler broadening of fluorescence and Raman scatt. 78—13465
collision anisotropy and spectral line impact contour *(Russian)* 80—52942
collision broadening in gases 77—88426
collision damping consts. rel. to stellar atmospheres 77—42279
collision induced line shapes, hard sphere model calcs. 79—81182
collisional broadening 79—26932
collisional broadening by H, appls. to stellar spectra 77—13237
collisional broadening by neutral H, simple formula 79—92665
collisional line broadening, classical and quantum theories, radiator motion effect 78—86822
complex spectral bands, separation into components, Alentsev-Fock method *(Russian)* 78—90229
complex spectral bands, separation into components, Alentsev-Fock method *(Russian)* 78—90230
Compton K-electron line contour *(Russian)* 79—93959
conversion from freq. to wavelength widths, for teachers 78—32632
cumulative resonance in atomic ground state induced by modulated light field 78—66518
decaying atomic states, behaviour in applied fields, Lamb shift expt. 79—63963
degenerate atomic level perturbation by neutral particles 79—792
delayed quantum beat subnatural linewidth spectroscopy 80—77879
dense atomic fluids, variable polarisability, depolarised light scatt. 79—64823
discharge, high-freq., excited atoms concentration determ., Ne or Ar, using spectral method *(German)* 80—70053
discharge radial distrib. of line intensities 78—18473
dispersion-absorption plots, for spectral line shape anal. for RF and microwave spectrometry 78—89511
dispersive optical bistability with inhomogeneous broadening, exact soln. 80—53360
Doppler broadening compensation with laser induced light-shifts 79—3405
Doppler line profile, saturation, influence of atomic collisions 78—70792
Doppler spectrum saturation kinetics *(Russian)* 77—38641
Doppler-free laser-induced dichroism and birefringence 78—82711
Doppler-free two-photon spectra 79—59416
double radiooptical resonance, signal propag. and shape 80—87360
early B-type stars, UV lines damping consts. and LTE line blanketing 78—16419
electron scatt. broadening, pure absorption *(Russian)* 78—25473
emission and absorpt. line shapes 79—49154

atomic spectral line breadth continued
- emission line asymmetry in novae, QSOs and Seyfert galaxies 79—101214
- emission line profiles, ultrarelativistic charged particle EM field effects 77—3313
- emission spectra, semiclassical descriptions, extension to damping and line widths 79—59399
- emission spectra of atoms accelerated by stationary external field *(Russian)* 77—3319
- energy level transitions, Doppler broadening, phase-destroying collisions 80—9561
- EUV emission line nonthermal broadening near quiet solar limb 79—48748
- excited state collisional relax., line broadening, interat. interactions, review 80—43149
- exotic atom excited state lifetime calc. using Bethe-Salpeter eqn. 77—27208
- flameless AAS, anal. response shape and position 78—92545
- fluids, atomic and molecular, collision induced light scatt. *(German)* 79—27057
- fluorescence, collisional redistrib. 78—13464
- fluorescence of multilevel system in gas phase, calc. including inelastic collision 79—98129
- foreign gas broadening, translational heat-bath model, variational methods 78—9124
- foreign gas broadening, translational heat-bath T-approx. model 78—9125
- foreign gas broadening WKB approx. for satellite bands 78—46304
- foreign gas induced line shifts, thermodynamics 80—106295
- Fraunhofer line profiles for 1973 period *(Russian)* 79—92743
- Fraunhofer line profiles interpretation 78—7976
- Fraunhofer lines, profiles in 4226-7700 Å range *(Russian)* 78—28606
- Fraunhofer lines, progressive sound waves effect on profiles *(Russian)* 78—73689
- gases, line profile calcs., evolution operator of interfering atomic states *(French)* 78—9119
- growth curves for line absorption 79—54812
- H Lyman α in solar chromospheric flares, direct collisional excitation rel. to profile and polarisation 80—41780
- H Lyman-α line core, effect of emitter ion dynamics 77—47161
- H radio recombination lines from multiple-component H II regions, press. broadening 80—4419
- hadronic atoms, absorptive line shape 77—83767
- heavy ion collisions, radiative electron capture, line profiles 77—14565
- hyperfine components of spectral line, collisional broadening 77—34587
- hyperfine structure, brightness distrib., form. model verification 77—57928
- hyperfine structure lines, narrowing and deformation 79—98238
- hyperfine structure quantum beats, intensity profile, ang. momentum theory graphical method 78—25497
- hyperfine transitions in buffer gas, quantum theory *(Russian)* 78—21881
- impact broadening of nonlinear reson. due to collision-induced vel. change *(Russian)* 77—46540
- impact broadening of spectral lines, HFS, considerations 77—83541
- inert gas, spectral line width and shift in shock-tube plasma 77—23467
- inert gas atom adsorbed on graphite surface, excitation spectrum 78—71943
- inert gas ion-atom collisons, momentum transfer rate consts., energy depend., polarisation pots. 77—75260
- inert gas mixture, collision-induced absorption, exact line shapes, appl. to He-Ar 78—66512
- inert gas mixtures, collision-induced translational absorpt., line shape 77—439
- inert gas recombination afterglow, spectral line shapes 80—940
- inert gases, lifetimes from collision induced absorption spectra, IR line broadening 78—33554
- instrumental response deconvolution for asymmetric spectral lines 79—58802
- interstellar medium Lyman α emission, line profile, temp. and polarisation from geocoronal absorpt. 77—67120
- ion-atom collisions, two-electron rearrangement X-ray transitions, theory 77—38633
- ionisation, resonant, under adiabatic level inversion conditions *(Russian)* 80—32691
- ionisation broadening under action of intense pumping wave *(Russian)* 77—42283
- ionised emitters in plasma, electron impact broadened lines, quantum mech. interference effects 77—42282
- irreducible spin precession theory applied to atomic and nuclear RF spectroscopy 80—27969
- K-shell Auger rates, level widths and fluoresc. yields, relativistic Dirac Hartree Slater calc. 80—52957
- laser and accel. beam method for narrowed optical lines 78—37770
- laser beam surface evaporation, spectral-line absorption 79—19951
- laser spectroscopy conf., Jackson Lake Lodge, WY, USA, 1977 July 78—82666
- laser-induced atom-atom collision line shape 80—9691
- level shift and width in light field, higher order perturbation theory *(Russian)* 79—3414
- lidar observations of atmosphere at Kingston, Jamaica 78—36284
- light shifts on atomic energy levels, non-resonant irradiation effect, appls. 77—75107
- line sources, freq. modulated, appl. to small mol. detect. by mag. tuning 79—59508
- lineshape, orientation and vel. relax. contribs., low press. region 80—5503
- lineshape analysis for collision induced spectra 78—70787
- Lorentzian Raman lines, eqn. for correcting finite slit width effect 80—63593
- M-shell radiationless transitions, subshell fluoresc., Coster Kronig yields and X-ray linewidths, relativistic Dirac Hartree Slater calcs. 80—52959
- magnetic hyperfine atomic sublevels multiple anticrossings 80—27986
- magnetoactive plasma, high-freq. electric effect on atomic spectra 78—9761
- many-level atoms, Raman scatt. resons. in separated fields 79—31449
- mesic atoms of light nuclei in field of reson. EM radiation *(Russian)* 77—79713
- modified Voigt function, speed dependent, for at. absorpt. spectrosc. 78—35765
- molecule-molecule collision, effect on linear and non-linear spectroscopic line shapes 79—36735

atomic spectral line breadth continued
- monochromatic laser radiation, excitation of atomic, mol. energy level transitions, inhomogeneous and mixed line broadening 78—55147
- monochromatic laser radiation, excitation of atomic or mol. energy level transitions, strictly homogeneous line broadening 78—58629
- monopole H atom, spectra, energy levels, transition probabilities *(Chinese)* 78—90322
- multi-level atomic systems, reson. lineshapes and shifts in rot. mag. field 77—68010
- multimode radiation, many-photon atomic excitation 80—74154
- multiphoton ionisation, resonant, in strong EM wave field 79—10079
- multiplet line-centre fluxes, effects on temp. models 79—5806
- multiply charged ions, $2p_{1/2}3p_{3/2}$ config., level widths, relativistic calc., S-matrix method 80—63546
- n-photon resonance phenomena, finite laser bandwidth effect 80—58230
- negative ion+neutral atom, autoionisation states investigation by Rydberg series broadening and displacement *(German)* 79—85938
- neutral+high Rydberg atom, thermal collisions, review 80—63756
- neutral atom collisions, hyperfine component broadening and shift of spectral lines 80—74136
- neutral atom lines, Stark broadening, adiabatic theory, classical trajectories of electrons 80—18936
- neutral atom reson. lines, Stark widths and shifts, regularities from He to Ca 80—47939
- NGC 6853 (Dumb-bell Nebula), emission line profiles rel. to neutral and inoised gas motions 78—24539
- niobium, Lα X-ray spectra, ${}_{40}$Zr to ${}_{48}$Cd, linewidths 79—41131
- nondegenerate optical transitions of excited atom in buffer gas, line shape kinetic theory 80—42997
- nonlinear Ramsey resonance of excited atoms, Doppler-broadened transition 79—10074
- nonmonochromatic chaotic field, double optical reson. and reson. fluoresc., AC Stark splitting 80—9547
- O-type stars, UV reson. lines profiles rel. to coronae possible existence 79—21293
- optical Autler-Townes effect, time depend., finite bandwidth laser appl. theory 80—91499
- optical bistability, photon statistics and spectrum of transmitted light 78—46298
- optical Ramsey fringes in two-photon spectroscopy, time delayed pulsed Doppler free technique 78—82708
- optical triple resonance, semiclassical anal. 79—93963
- orientation and vel. relax. contributions 79—49984
- oscillator strength absolute value, collision broadened absorption linewidths method 77—10639
- perturbation of the atomic spectrum by a strong light field 79—10073
- pionic atoms, 2p level shifts and widths 78—46469
- pionic X-ray transitions, strong interaction line widths and shifts 77—23586
- plasma, atomic absorption spectra, high freq. Stark effect 80—23359
- plasma, axially symmetric, Doppler broadened optical line emission interpretation model 78—75276
- plasma, Gaunt factor temp. depends., from Ar II and Ca II Stark widths 78—87491
- plasma, H line Stark broadening, role of ion dynamics simulation 80—24144
- plasma, line width variation within Stark broadened multiplets 78—91073
- plasma, nonequilib., kinetic theory of spectral line broadening 80—59187
- plasma, of theta pinch, $N^{+,2+,3+}$ lines Stark broadening, He(II) line diagnostics 80—24249
- plasma, photon escape probabilities for Stark-broadened Lyman series lines 80—24143
- plasma lines, electron impact width of multiply ionised ats. semiclassical formula 80—43972
- plasma negative ions, broadening of free-bound radiation threshold, quasistatic theory 80—53941
- plasma reson. lines regularities in Stark widths and shifts, He^+-Ca^+ 80—43881
- polarised excited atom, freq. depend. polarisation of emitted radiation 77—61705
- power broadened two-photon ionisation, reson. lineshape and photoelectron spectra 80—58229
- pressure broadened spectral line shape, effect of turning points 79—22655
- pressure broadening, adiabatic theory, low density approxs. 79—22628
- pressure broadening, quantum-path theory 79—31470
- pressure broadening optical cross section, change due to intense laser field, anal. 78—42006
- pressure effects on spectral lines 78—82690
- profiles in Orion Nebula, intensity and vel. calibrations 80—62243
- protonium, atomic X-ray yields 1s and 2p level shifts and widths, cascades, calc. 80—78730
- quantum systems, at. or spin two level, reson. EM wave excitation, free induction decay oscills. 80—63562
- radiative atom collisions involving excitation transfer with small reson. defects *(Russian)* 80—53101
- radiative collisions, with impact level shifts 79—54951
- radio recombination lines from galactic centre direction and galactic sources, profiles 78—32589
- rare gas adsorbates on simple metals, optical excitation, configurational switching, charge transfer 80—107643
- redistribution of scattered radiation by collisions in nonimpact region of spectral line profile 79—35109
- relative atomic transition probabilities of Na, Sc, Ti, Cr, Fe, Co and Ni 79—89642
- resonance broadening in strong light field *(Russian)* 77—27149
- resonance fluorescence, in weak radiation field with arbitrary spectral distrib. 80—23356
- resonance interaction of intense light with atoms, review 79—68216
- resonance line polarisation, non-LTE, absence of magnetic fields, solar models 79—80293
- resonance spectral broadening in high density gas, many body shielding 77—79579
- resonant Raman X-ray scattering, K-vacancy excited state widths, appl. to Zr, Mo, Rh, Ag and Sn 79—45661
- resonant states, improved line width expression, appl. to H^- and He 80—5505
- rotational line broadening, wavelength depend. rel. to rapidly rotating B stars 77—45416

atomic spectral line breadth continued
Rydberg states, use as spectroscopic probe for resonances in mol. electron elastic scatt. 77—58162
saturation spectroscopy, with delayed pulses, Lamb dip profiles 78—21221
selective refl. from atomic vapour, narrowing of level crossing curves 77—18856
self reversal contours, use in determ. of line broadening and shift consts. 80—52940
solar atmosphere, emission line profiles of phenomena with different porosity *(Russian)* 78—40891
solar C I multiplets at 1560 and 1657 Å, overlapping emission peaks obs. and theory 78—93178
solar chromosphere line profiles from OSO-8 satellite 80—67690
solar flares spectral diagnostics for turbulent elec. fields 77—17493
solar He I, D_3-line profile meas. with birefringent filter 78—4177
solar inhomogeneous emission formations, line profiles calc. 79—25562
solar Lyman α line, wavelength and profile meas. 79—8896
solar photosphere, line profile displacement rel. to line formation in unresolved magnetic element 79—48750
solar photosphere spectral line profiles for Na I and O I, acoustic wave effects 80—17558
solar spectral line asymmetries, radial movement effects 80—41792
solar spectral line profiles, acoustic wave effects 80—46517
solar spectrum, asymmetry of selected Fraunhofer lines *(Russian)* 78—40892
solar spectrum, weak absorpt. lines profiles appl. to photosphere total vel. field determ. *(Russian)* 78—40894
spectral line shapes, linear and nonlinear, atom or mol. cross sections 78—70899
spectroscopy of atoms near a wall *(Dutch)* 78—70972
spontaneous emission, exponential decay law, long-time deviations, sensitivity to interaction Hamiltonians 77—46523
Stark broadening of neutral lines 78—46299
Stark widths of neutral lines, simple estimating formula 79—3397
stars, line profiles in expanding envelopes 79—44464
stellar chromospheric scaling laws, width-luminosity correls., Wilson-Bappu effect 79—40177
stellar photosphere line profiles, thick circumstellar dust shell effect 79—30058
stellar spectra, profile calc. method *(Russian)* 79—92684
stochastic field, saturation and Stark splitting 80—9546
subnatural linewidth spectra by optical double reson. with two-photon pumping 80—74200
superfluorescence, delay-time statistics and inhomogeneous line broadening 80—99684
three-level atom, continued fraction transition theory, reson. lineshape 78—33473
three-level atomic system, saturation spectroscopy including collisional effects 80—37099
three-level spectra, lineshapes in intense laser field, theory 80—69109
three-state atom, saturated two-photon absorpt. in perturber gas 80—106310
transient line narrowing, laser spectroscopic technique yielding resolution beyond natural linewidth 80—82834
transition arrays in X-ray, UV spectra, mean wavelength and spectral width 79—6913
transition metals, gas phase, photoelectron spectra, photoionisation cross section 79—98051
trapped particle in anharmonic potential, lineshape 80—23361
two level model theory, extended, appl. to Doppler-, laser and collision-broadened bound-bound multiphoton absorption 79—3423
two particle system, spontaneous emission spectrum, collective singularities *(Russian)* 78—33466
two photon absorption, time varying perturbation theory *(Rumanian)* 78—46311
two- and three-photon resonances, Doppler-free power broadening 78—5308
two-atom resonance fluoresc. spectrum, cooperative effects 80—78570
two-atom system, cooperative, reson. fluoresc. spectrum. sidebands 80—43000
two-level atom, active, collisionally aided radiative excitation 79—54805
two-level atom, EM radiation interaction, elec.- and mag.-dipole contribs., reaction field 78—94215
two-level atom, phase shifts in weakly amplitude modulated light scatt., linewidth effect 78—50505
two-level atom, radiative decay, external static perturbation effect 79—93949
two-level atomic system, spectral line depend. on number of atoms 79—49981
two-level atoms, cooperative resonance fluorescence, linewidth narrowing 78—21876
two-level atoms, dynamics and spontaneous radiation in bichromatic EM field 80—91502
two-level atoms, inhomogeneously broadened, superfluoresc. and amplified spontaneous emission 80—106499
two-level Doppler-broadened medium in Fabry-Perot, optical bistability 80—102759
two-level system, saturated lineshape, collisional and radiative damping effects 77—58124
two-photon absorpt., laser linewidth effect 78—46310
two-photon resonant absorpt. line profile, quadratic Doppler effect 77—34590
two-photon S-S transitions, reson. broadening *(Russian)* 79—26957
two-photon spectra, Doppler-free, occurrence of split spectra 78—292
ultrahigh resolution spectroscopy using light echo effect *(Russian)* 78—70774
unresolved components, interferometric meas. 79—98039
unstable atomic targets, power broadening effects in reson. scatt. 80—32633
UV line blending and wavelengths, spectral resolution influence in solar spectrum 80—56811
van der Waals interaction, spectral line broadening, growth curves 80—102548
vapours, three-level system, collisional effects in saturation spectroscopy, appl. to Na 80—78579
Voigt effect, reson. absorpt. description 80—30302
Voigt lines, random array, curve-of-growth function 78—89055
Voigt profile, analytical approximation for spectral profile analysis *(Spanish)* 79—76384

atomic spectral line breadth continued
Voigt profile, reson. parameters determ., finite energy resolution effects, folding problem 80—32673
X-ray K and L line widths determ. 77—42265
X-ray line shape broadening anal., least squares method 80—63588
Zeeman atomic absorption spectrosc. anal. curve shapes 80—22437
Zeeman line profile, mag. field determ., appl. of radiative transfer problem soln. 80—82221
Zeeman resonance lineshapes, motional narrowing, analytical results 77—46524
Zeeman resonance lineshapes, motional narrowing, expt. 77—46525
Ag, VUV absorption spectrum, autoionised level Fano parameters, photoionis. 79—49973
Al I, 1932 and 1936 Å autoionisation lines profiles during solar flare, Skylab obs. 80—26829
Al I, electron impact line broadening in arc spectra 79—26919
Al I line broadening and shifts by van der Waals interaction with Ar and He atoms 79—6912
Al I line profiles, Stark broadening meas. 78—9115
Al I resonance line profiles, influence of boundary layer of Al-seeded shock heated plasma 80—43876
Al II line profiles, Stark broadening meas. 78—9115
Al, plasma, transfer eqn. soln. using freq. and angle averaged photon escape probabilities 80—64688
Al transitions, Stark broadening and oscillator strengths 78—29761
Al XII, electron density meas. using Stark profiles 79—81181
Ar, $3p^5 5p$ config. aligned in discharge, interf. signals, lifetimes and collision cross sections 78—70796
Ar atomic excited states collision radiative destruction in glow discharge, spectral line profiles 79—3528
Ar, DC magnetron discharge, spectroscopic obs. 80—44010
Ar, electron impact excitation, L-MM, LM-M^3 Auger linewidths, L, S and J dependence 77—14588
Ar, electron scatt. and ejection, electron energy loss spectra 80—58394
Ar I, emission line profile analysis, Fabry-Perot spectrometer instrumental function determ. *(Spanish)* 80—52322
Ar I 3949 Å, Stark width in medium electron density plasma 79—63954
Ar II, electron impact width, UV-region 79—22661
Ar II, line-continuum interference effect in Lorentzian wings 79—18147
Ar II, lower laser levels, natural lifetime determ. 77—6724
Ar, $L_{2,2}M_{2,3}M_{2,3}$ Auger spectra, using cylindrical mirror spectrometer 79—63326
Ar, laser discharge, spontaneous emission, at. line shapes, interferometric obs. 77—30816
Ar, lifetimes of L and LM vacancy states, X-ray emission linewidth 78—17621
Ar line broadening by at. collisions, meas. of oscillator strength of ArI lines reson. *(French)* 78—5172
Ar, multiply excited, inner level X-ray emission spectra, line widths and Auger transition rates 79—36575
Ar, oscillator strengths, determ. from self-absorption of reson. radiation 79—89641
Ar, photoionisation, Auger processes, decay lifetime, line shift, profile, X-ray photoelectron spectra 80—37798
Ar plasma, wall stabilised arc, spectroscopic temp. and radiation standard 77—76199
Ar plasma jet, weakly ionised, collisional line broadening 77—75106
Ar, spectral line collisional broadening and line shift 77—10641
Ar, Stark shift and splitting in visible spectra 80—32659
$Ar(^3P_2)+H(^2S)$, energy transfer, Lyman-α line obs. 79—64085
As I, rel. oscill. strengths, 193.8 and 197.3 nm lines 79—791
B, X-ray spectral line broadening in solid and gas targets 77—6713
B+Ar(Kr)(Xe), B emission line broadening in glow discharge lamp 77—3304
B+He(Ne)(Ar), ground and excited states interaction, B spectral line breadth 77—68092
Ba, $5p_{3/2}$ level broadening, ligand field splitting, photoelectron spectra 80—47950
Ba, atomic beam and resonance spectroscopy 80—58180
Ba, autoionis. spectrum, pair splittings 79—13684
Ba II 4554 Å solar resonance line formation, empirical NLTE analysis 78—53907
Ba II in solar photospheric spectrum, partial redistrib. rel. to line profiles 79—101128
Ba II lines in solar spectra, non-mag. polarisation, centre-to-limb var. 80—67678
Ba in shock heated Ar, absorpt. line broadening obs. *(Japanese)* 80—83464
Ba, line shape obs. in CW dye laser intracavity absorpt. 80—47120
Ba, photoexcitation spectrum, discrete autoionising states interferences 80—5508
Ba, reson. lines, emission and absorpt. core profiles 77—50389
Ba, spectral line contour broadened by Xe collisions 78—25477
Ba, two-photon spectra, isotope shift and hyperfine splitting 78—33491
Ba^+, electrodynamically trapped, saturation dip in fluoresc. 77—65437
Ba-inert gas, Ba reson. lines broadening, absorpt. cross sections anal. 80—32642
Be, Doppler effects in X-ray spectra excited by accelerated ions 78—86808
Be IV, line broadening and self-absorpt. in laser prod. plasma 78—17615
^{209}Bi, pionic 4f→3d transition, pionic 3d state strong interaction level shift and width 79—98251
Br, ESCA, lifetime broadening, CI resonances 77—18853
C I, C II, C III, C IV in solar flare, line profiles rel. to upper chromosphere model 79—40148
C II, UV lines Stark widths 79—6910
C II lines in A-type star α Lyrae (Vega), Copernicus UV obs. 80—8627
C III 5696 Å in OB-type stars, transition from absorpt. to emission 79—67006
C IV, reson. line in O-type stars of open cluster IC 1805, P Cygni profiles 80—31296
C IV 1548 Å line profiles of impulsive EUV bursts, OSO-8 obs. 80—90401
C IV 1548 Å profile in quiet solar region, interpretation 79—96980
C IV (C V), UV line identifications and lifetime meas. 80—106288
C plasma, spectral and absorpt. coeffs. 80—69985
C, reson. transitions, Stark widths and shifts of UV and VUV Lines 77—88425
C, vac. UV spectral line broadening parameters meas. 80—23352
Ca 657.3 nm line saturated absorption spectroscopy, photon-recoil component resolution 80—86457

atomic spectral line breadth continued
- Ca and Ca$^+$, spectral lines collision broadening and shifts 78—58624
- Ca I, Ca II lines in solar spectra, non-mag. polarisation, centre-to-limb var. 80—67678
- Ca I, Ca II lines in Sun, line profiles rel. to upper photosphere models and Ca abundance 77—33445
- Ca I 6102, 6122, 6162 Å multiplet, collisional broadening 80—37777
- Ca II, reson. line broadening in shock tube plasma 77—35393
- Ca II, solar H and K line profiles vars. at solar minimum and cycle 21 onset 79—16907
- Ca II, unique interstellar K-line profile in 30 Doradus direction 80—51850
- Ca II H and K line profiles rel. to temperature and electron density of solar chromosphere 78—53908
- Ca II H and K line profiles of active solar limb filament 79—44446
- Ca II H and K lines in F0 to M2-type stars, high resolution absolute flux profiles 80—26842
- Ca II H and K lines in late-type stars, line width-luminosity relation for wing emission lines 77—78766
- Ca II H and K lines in late type stars; photoelectric calibration 80—36617
- Ca II IR triplet lines, profiles and halfwidths in RW Aurigae 79—92768
- Ca II K-line, formation of optically thick solar, profile 80—94767
- Ca II K-line asymmetry in A-type star Sirius unconfirmed 79—30062
- Ca II K-line asymmetry in A-type star Sirius, comments 79—30063
- Ca II K-line in dwarf stars, profiles rel. to chromospheric models and activity 79—48773
- Ca II K-line in quiescent solar prominence, influence of spatial resolution on line width and shift 80—77364
- Ca II line width in late type stars, Wilson-Bappu effect 79—12464
- Ca II stellar emission line, V/R ratio rel. to mass loss 78—93208
- Ca in shock heated Ar, absorpt. line broadening obs. *(Japanese)* 80—83464
- Ca, photon recoil splitting, line widths, Doppler effects, saturated absorpt. optical interference spectroscopy 80—52922
- Ca+He(Ne), press. broadening, line shifts 78—5290
- Cd, $3d_{3/2,5/2}$ photoelectron spectrum, using cylindrical mirror spectrometer 79—63326
- Cd, $5s5p\,^3P_1$-$5s^2\,^1S_0$ intercombination line, press. broadening and shift 80—95564
- Cd, broadening of 5^1P_1 level 80—83479
- Cd, N-shell vacancy state widths, X-ray photoelectron Auger spectra 77—18875
- ^{114}Cd λ326.1 nm reson. line, self-broadened, temp. depend. of parameters 79—63964
- ^{114}Cd+He, collisional effects on 326.1 nm line rel. to temp. and conc. 78—5336
- Cl III, Stark broadening of isolated lines by plasma 78—9116
- Cl$^-$ (Br$^-$) (I$^-$), in plasma, broadening of free-bound radiation thresholds 80—53940
- Co I, excited levels lifetimes meas., influence of exciting reson. lines profiles 78—5178
- Cr, pulse hollow cathode discharge, time resolved high resolution spectroscopy 80—38759
- Cs, 16^2P states, reson., 3-photon ionisation, DC Stark effect 78—42026
- Cs, $6^2S_{1/2}$-$6_2P_{3/2}$ transition (λ=8521 Å) with hyperfine splitting, curves of growth 78—66513
- Cs, 6s-9p doublet, Xe perturbations, simultaneous additive effect on multiple satellite lines 79—76389
- Cs atom, oscillator strength meas. by tunable laser interferometry 80—105697
- Cs, emission meas. in wing of self-broadened reson. line 77—50400
- Cs, fluoresc., far wings profile of self-broadened reson. lines 79—76388
- Cs, four-photon ionis., strongly interacting resons. theory 80—52955
- Cs, HFS of first doublet, He, Ne and Ar press. effects 77—38638
- Cs HFS pressure effect determ. from absorption coeff. profiles 80—106299
- Cs principal series lines, self-broadening 77—46541
- Cs, quadrupole lines, oscillator strengths, broadening 77—18846
- Cs, self-broadened first reson. lines, near-wing asymmetries 80—9535
- Cs, self-broadening of Doppler-free two-photon lines 79—41135
- Cs, Xe perturbed emission lines, satellites in square well pot. approx. 78—46303
- Cs-He, new absorption/emission bands perturbed Cs transitions assignment, pot. energy curves 78—66486
- Cs+Ar, laser two-photon ionisation, collisional line broadening, atomic forces 77—83543
- Cs+Ar, two-photon ionisation spectra, satellites, absorption line shape 78—82668
- Cs+Ar(Kr)(Xe), spectral line breadth and shift, Van der Waals pot. calc. 78—90126
- Cs+Ar(Xe)(He), shift, halfwidth, satellite and absorpt line in square-well pot. 80—42993
- Cs+He(Ne)(Ar), optical pumping, spectral line shape *(Spanish)* 79—22662
- Cs+inert gas, D_2 line collisional broadening and shift, and HFS 79—22664
- Cs+inert gas, hyperfine struct., broadening and shift calcs. 77—58153
- Cs+inert gas, three body interaction, fluoresc. spectra principal series lines and secondary satellites 80—83313
- Cs+Xe, broadened Cs principal series lines, absorption meas., Cs-Xe pots. 77—79584
- Cs+Xe, Cs spectral line profile and absorpt. transitions 80—47944
- Cs+Xe (neopentane), Cs line shape broadening, satellite data inversion, interaction pot. 78—74608
- Cs($5D_{5/2,m=1/2}$)+inert gas, dipole-induced transitions, pot. curves, oscillator strength 80—32816
- Cu alloys, time and spatially resolved at. absorpt. anal. 80—40760
- Cu, CC K$\beta_{1,3}$ emission spectrum, double vacancy transitions 79—59393
- Cu laser line structure at 510.6, 578.2 nm 80—53274
- Cu laser lines, broadening, induced emission cross-sections 79—26928
- Cu, lines in hollow cathode discharge, radial inhomogeneities in excitation and profile 77—4974
- Cu vapour pulsed laser, spectral comp. of superradiance, stimulated and spontaneous radiation 80—102713
- Eu, Kα line widths, precise meas. 78—62761
- Eu+Sr, absorptive collisional energy transfer, laser induced excitation spectra 80—63584
- F II, Stark broadening of isolated lines by plasma 78—9116
- Fe I 3719.94 Å line broadening by He, line width and shift meas., astrophys. significance 77—73942

atomic spectral line breadth continued
- Fe I 5383 Å line width, Stark broadening 79—31463
- Fe I line profiles and magnetic field in quiet network regions of solar photosphere 78—69758
- Fe I lines, equivalent widths and microturbulent vels. determ. for solar photosphere *(Russian)* 80—51719
- Fe I lines in solar spectrum, statistical anal., mag. line broadening 77—74028
- Fe I lines in solar spectrum, damping const. determ. preliminary results *(Russian)* 80—72900
- Fe I low excitation lines, collisional broadening 80—37778
- Fe I weak Fraunhofer line profiles rel. to absorption coeff. *(Russian)* 78—20783
- Fe II 4520.2 Å, in mag. Ap star α^2 Canum Venaticorum, polarisation and intensity profiles 78—40951
- Fe II lines, permitted, in type 1 Seyfert galaxies and quasars, form. and relative intensities 80—62278
- Fe II lines in quasars and Seyfert galaxies, excitation and line strength 80—67896
- Fe II multiplet anomalous line contours in α Cygni spectrum *(Russian)* 78—93243
- Fe, K$_\alpha$ X-ray line, natural width at energy threshold meas. 78—41992
- Fe lines, equivalent widths in cool standard stars spectra 77—78771
- Fe lines in solar spectrum, wing shapes anal. 80—4317
- Fe, X-ray line emission in Cygnus X-3, line intrinsic width 78—8153
- Fe XV, line intensity and linewidths at high electron density, generalised population ratio 80—99481
- Fe XXI 1354 Å in solar flares, line width obs. from Skylab rel. to ionisation equilib. calcs. 80—21956
- Fe XXIII, Fe XXIV, new line obs. in laser-produced spectra 79—81175
- Fe XXIV, dielectronic satellite spectra, solar flares appl. 80—32646
- Fe+Ar, Fe I reson. line, collisional broadening at high temp. *(German)* 80—106298
- Fe+I, Fe K-α X-ray emission, high-resolution meas. 80—37871
- Ga+inert gas atom, diffuse series head lines, hyperfine components, broadening calcs. 80—32632
- H 137β/109α intensity ratio in H II regions, interpretation 80—31344
- H, $3^2S_{1/2}$-$3^2D_{5/2}$ interval, two-photon lineshape theory 79—54825
- H, $3^2S_{1/2}$-$3^2D_{5/2}$ interval, double quantum RF meas. 79—54826
- H and D, UV lamp, microwave discharge, Lyman-α line shapes 79—80698
- H, Balmer emission line decrement in HR 1099, evidence for nonthermal excitation 79—21342
- H, Balmer line profiles in G, F, A, B and O stars from model atmospheres 79—80298
- H Balmer lines, plasma-broadening in wall-stabilised arc, low electron density 80—43891
- H, Balmer lines equivalent widths in stars of upper Scorpius region 79—88647
- H, Balmer lines in southern young emission-line stars, YY Orionis profiles 78—8016
- H, Balmer lines produced in sputtering glow discharge *(French)* 77—24229
- H emission line intensities from dense plasmas, appl. to quasar spectra 80—51900
- H fine structure $3^2S_{1/2}$-$3^2D_{5/2}$ interval, separated oscillatory field meas. 80—99482
- H, Hα line profile as plasma density meas. 80—43987
- H, He II, in Of-type stars, theoretical line profiles 78—40950
- H I, galactic subsystem, 21 cm line profile rel. to galactic rot. curve *(Russian)* 80—36724
- H I, hot, interstellar between Sun and Earth, Lyman α absorpt. line width 80—31185
- H I, interstellar Lyman lines profiles, implications of high-vel. absorpt. features 79—48891
- H I, line profiles in Nova Vulpeculae (1979) 79—48820
- H I, line widths in elliptical galaxies (NGC 2974, 4105, 5846) 79—62906
- H I, solar Lyman-α and Lyman-β calibrated full disc profiles 78—93185
- H I 21 cm, line profiles in clumpy irregular galaxies (Markarian 296 and 297) 79—44608
- H I 21 cm line widths in galaxies, correl. with absolute magnitude and type 79—5900
- H I ($3^1P^0-2^1S$) line, Stark broadening parameters, modified adiabatic theory, electron scatt. phase shifts 80—43879
- H I and HeI lines in ν Eridani, β Cephei type star, visible obs. 80—67739
- H I at high galactic latitudes, time variable 21 cm line profiles correction 80—51844
- H I Balmer α and β line profile rapid vars. in Be-stars *(Russian)* 79—16992
- H I Balmer α and β lines in O6 to G2 stars, equivalent widths and narrow-band photometry 80—8621
- H I Balmer α emission line core formation in chromosphere of T Tauri-type variables 80—94792
- H I Balmer β profile of Markaryan 372 Seyfert galaxy 80—26972
- H I Balmer γ line profiles and masses of DA white dwarf stars 80—77399
- H I Balmer line strengths, profiles and equivalent widths in white dwarfs 79—96998
- H I Balmer lines, formation in bright prominences spectra *(Russian)* 80—77377
- H I Balmer series limit, line blurring 80—23351
- H I emission line profiles obs. in o Ceti spectrum *(Russian)* 79—16990
- H I in galactic centre direction, 21 cm emission line profiles 77—78853
- H I in interacting galaxy NGC 2623, emission and absorpt. profile 79—17087
- H I in Seyfert galaxies, anomalous line profiles 79—8988
- H I line profiles in RY Persei spectra, visible obs. 80—67795
- H I line strength var. in HD 184905, Ap-star 79—16987
- H I Lyman α chromospheric emission line profile in UV spectrum of giant star α Bootis 78—81620
- H I Lyman α Doppler line profiles in geocorona 80—12579
- H I Lyman α line profile of active solar limb filament 79—44446
- H I Lyman α profile in interplanetary space 80—8586
- H I profile width distances for disc galaxies rel. to Hubble constant 78—41050
- H I profiles of nearby galaxies, obs. 80—41895
- H I regions, N.galactic hemisphere 80—17643
- H II regions, narrow radio recomb. lines prod. around X-ray source 79—8972

atomic spectral line breadth continued
H, in hot plasma, elementary excitation spectrum, exchange and polarisation effects 80—43892
H L_α line breadth, Cherenkov line radiation, QSO emission-like spectra *(Chinese)* 80—105378
H line broadening and shift due to plasma ions *(Russian)* 80—96350
H, line profile, Stark broadening, quantum theory, including short-range interactions 78—9114
H, line profiles in planetary corona, collisional model 78—77508
H lines in plasma, electron width and shift *(Russian)* 78—67421
H Lyman α, astronomical, profile rel. to H_2 reson. fluoresc. 79—8821
H Lyman α, solar line profile modification in propag. through interplanetary medium 79—66973
H, Lyman α and β lines, in solar spectra, exptl. obs. and theoretical profiles 79—8888
H, Lyman α asymmetry in solar flares, rel. to proton/electron energy flux ratio 79—8887
H Lyman α line profile in Ar plasma 79—22658
H maser, atomic resonance effects on long-term freq. stability 77—75465
H, mesic, atomic X-ray yields 1s and 2p level shifts and widths, cascades, calc. 80—78730
H, multiphoton absorpt., reson. shift and power broadening, truncated model semiclassical calcs. 78—17644
H, plasma, spectral line broadening, ion dynamic effects 79—46432
H, spectral broadening by low-freq. elec. field in dense plasma 79—98026
H spectral lines, Lyman series asymm. 77—38639
H, Stark broadening by ion impact on moving emitter, Doppler H shift, theory 80—47940
H, subnatural linewidth resolution $2^2S_{1/2}$, $2^2P_{1/2}$ level crossing, Lambshift, pulse technique 79—22669
H^-, DC Stark broadening of $^1P^0$ shape reson. 80—63585
H^- vac. UV spectra, narrow reson. at 1129.5 Å, H-arc spectra 78—66490
H-like atoms, Stark broadening, ion dynamics correction to unified classical path theory 79—76382
H-like excited atom interaction with charged particle, dipole approx. *(Russian)* 78—22007
H-like ions, radiative level widths in low electric fields 78—37589
H-like ions, spectral broadening in plasma 79—46431
H-like ions in laser-produced plasma, Balmer fine struct. (broadening) 80—48860
H+Ar, $H\alpha$ and $H\beta$ emission cross sections 80—63782
H+D, excitation transfer, spectral line broadening and shift 77—46531
H+He, H Balmer-α fine-struct. line shift and broadening 80—37783
H+He(Ar), press. effects on H_α and H_β Balmer series 77—18845
H^++Ar, $H\alpha$ and $H\beta$ emission cross section 80—63783
H_A line width in at. H atmosphere, shock tube absorption meas. 79—64834
H_α and H_β line profiles in high density plasma *(Japanese)* 77—43065
H_α and H_β spectral profiles from neutral beams and plasmas in high mag. fields 80—83999
H_α line shape, plasma broadened, fine struct. effects at low electron densities 78—62765
H_β line Stark broadened spectrum obs. in pulsed relativistic magnetron intense elec. field 79—89635
H_β, Stark broadening, wings calc. 79—31464
$H_\alpha(D_\alpha)$ Stark broadening in Ar arc plasma 79—36582
$H(^2S)+Ar(^3P_{0,2})$, energy transfer collisions, Lyman-α emission profile obs., in microwave discharge and reaction cell 80—58359
H* translational energy distrib., in HCl electron impact dissoc., optical emission obs. 80—14238
H*(3), D*(3) Balmer-α emission, obs. of $H_2O(D_2O)$ electron impact dissoc. excitation 79—31706
H166α, H239γ recombination lines in W51, impact broadening detect. 78—28741
H8 equivalent width rel. to Heζ line in spectrum of solar chromospheric spicules 78—40904
$H\alpha$ and $H\beta$, Stark profiles, ion-motion effect 80—63592
$H\alpha$ emission in Cygnus X-1, line profile during (1977) 80—51919
$H\alpha$ emission line in active binary star II Pegasi (HD 224085), equivalent width vars. and profile 80—90480
$H\alpha$, emission line profiles in Nova Vulpeculae 1976 in November to December, (1976) *(Russian)* 78—40971
$H\alpha$ emission profile in RS Canum Venaticorum binary HR 1099, vars. obs. 79—21343
$H\alpha$, in Cygnus Loop nebula, halfwidth correl. with filaments brightness *(Russian)* 78—41028
$H\alpha$ in dwarf stars, profiles rel. to chromospheric models and activity 79—48773
$H\alpha$ in giant extragalactic H II regions, line widths rel. to vel. dispersion 79—44606
$H\alpha$, in γ Cassiopeiae, profile and polarisation rel. to circumstellar envelope model 78—40952
$H\alpha$ in HR 9076 (ε Tucanae), shell profile 78—36583
$H\alpha$ in O-type stars, line-profile anals. rel. to winds and coronae struct. 78—40947
$H\alpha$, in T Tauri, line profile vars. 78—40944
$H\alpha$ in variable supergiant HR 8752 (V509 Cassiopeiae), rapid line profile vars. 80—36645
$H\alpha$ line profile in star T Tauri, obs. of fast var. *(French)* 78—61859
$H\alpha$ profile in HR 1099 during February 1978 radio flare, spectrophotometry 79—21344
$H\alpha$ profile in He weak and He strong stars, vars. 79—40201
$H\alpha(D\alpha)$ plasma red shift meas. in Ar arc, ion dynamic depend. 80—10364
$H\beta$ in Be shell stars, high-resolution polarisation struct. meas. by digicon spectropolarimeter 79—44485
$H\delta$ equivalent width in long-period variable stars, correl. with phase 79—88685
He 504.7 nm line, use of hollow cathode discharge for determ. *(Russian)* 77—46529
He, 504.7 nm line excited in discharge 77—18848
He, high-L states, laser driven forbidden transitions, line shapes 79—22638
He I, 10830 line in R Coronae Borealis at pre-max. phase, P Cygni profile 79—16975
He I, 4471 Å line profile in various plasmas, ion perturbation effects 78—94214
He I, exptl. line profiles near 4471.5 Å 77—6725
He I, saturated absorpt. on 587.5 nm line, pressure effects 77—23448

atomic spectral line breadth continued
He I, Stark broadening of 3965 Å line in plasma jet 79—98023
He I 4^3D, ^3F-2^3P line struct., in low-press. linear discharge 79—14523
He I 4026 Å in He weak and He strong stars, line variability 79—40201
He I 584 Å, solar line profile modification in propag. through interplanetary medium 79—66973
He I 584 Å, solar reson. line profile and intensity meas. 79—40153
He I 584 Å in quasars, line strength prediction 80—67550
He I 58.4 nm line profile, monitoring using resonance absorption spectrometer 80—62019
He I 6678 Å in ζ Ophiuchi, profile vars. rel. to rot. 80—22000
He I emission lines in T Tauri stars, singlet to triplet ratio 78—28680
He I line profiles, ion motion effect in low electron density plasma 80—43877
He I line profiles in RY Persei spectra visible obs. 80—67795
He I line profiles with forbidden components induced by fluctuating fields in small theta pinch plasma 77—80353
He I lines in spectra of QSOs and Seyfert galaxies 78—36717
He I overlapping lines, model microfield method Stark profiles, ion dynamics effect 79—82049
He I plasma lines, Stark broadening, quantum mechanical calcs. 80—43880
He I spectral lines, radiation trapping in electron beam, spatial distrib. of line intensity 77—79572
He II, 4686 Å line, Stark broadening, meas. and calcs. 80—91504
He II, plasma polaris. red shift, Stark profile, temp. depend. 77—18842
He II, Stark broadening of VUV transitions at 304, 1215, 1640 Å 78—66506
He II 4686 Å in OB-type stars, line profiles and equivalent widths obs. 79—67006
He II plasma reson. line Stark broadening and plasma polarisation shift 77—1020
He, interplanetary, 584 Å reson. scatt., dynamical effects 80—8509
He plasma, Stark shift and line broadening in 3-D stochastic laser field 78—50502
He, press. broadened (2^1P-2^1S) line, 0.3-20 torr. 79—13673
He, spectral lines, singlet, self-broadening, resonant interaction 80—63574
He, Stark profile in arc plasma, heavy-particle temp. 79—46484
He, Voigt profile, absorpt. line calcs. for the 396.5, 361.4, 318.7, 492.2, 587.6 and 447.1 nm lines 80—99471
He, Voigt profile, line absorpt. calcs. of 388.9 nm triplet, 501.6 nm singlet lines 78—90123
He with bound quark, atomic spectral lines calc. 79—86092
He^-, reson. calcs. with correlated target state wave functions, complex coord. method 79—26939
He-Ar, Ar I TEA lasers, energy characteristics 80—63977
He-Cu discharge, Cu ion laser, at. emission obs. of plasma props. 80—19021
He-F, doublet series laser lines near 700 μm, hyperfine splitting and broadening meas. 78—63070
He-Kr, Kr I TEA lasers, energy characteristics 80—63977
He-like ions, spectral broadening in plasma, theory, high-Z 80—6223
He-Ne, 632.8 nm line broadening, perturbation energies additivity 79—54941
He-Ne laser plasma, line profiles meas. by optogalvanic spectroscopy 78—62233
He-Xe, Xe I TEA lasers, energy characteristics 80—63977
He^+-like atoms, subordinate line profiles in spherically expanding stellar atmospheres 78—28499
^{3}He, dynamical Hanle effect, line halfwidth, sensitivity threshold, signal to noise ratio *(Russian)* 77—54541
^{3}He-^{4}He isotope mixtures, mag. resonance line widths of 2^3S_1 states, metastability exchange cross sections *(Russian)* 77—10614
^{4}He, kaonic and pionic X-rays, strong interaction widths and shifts 79—98253
^{4}He, laser mag. reson., 7^1S-9^1P energy separation, motional Stark effect, Zeeman tuning parameters 79—6911
^{A}He, A=3,4, pionic 1s state energy shift and line broadening *(German)* 80—48107
He(2^1S, 2^3S), threshold to 0.10 eV, energy-integrated total cross section ratio 80—37885
He(2^3S), quenching rates meas., in pure afterglow 77—75206
Heζ equivalent width rel. to H8 line in spectrum of solar chromospheric spicules 78—40904
Hg, 1849 Å absorption line broadening and shift in inert gases *(French)* 77—30825
Hg, 2537 Å line satellites, Kr broadening 77—83523
Hg 6 $^1S_0$-Hg 6 $^1P_1$, Van der Waals term in interaction, blue satellite line *(French)* 80—37848
Hg, line profile and shift at 546.1 nm, high-press. discharge *(French)* 79—785
Hg, metastable and excited states, pulsed dye laser absorption spectroscopy 79—26924
Hg, spectral line width, in high freq. spectroscopic light source *(Russian)* 78—4708
Hg, vap., high density, optical absorpt. edge, density depend. 79—72985
Hg vapour, absorpt. spectrum, 1849 Å line, self-broadening, interatomic interaction *(French)* 80—32661
Hg vapour, resonance line shape in presence of Hg(6^3P_1)-Hg(6^1S_0) interactions 80—78572
^{199}Hg, 6^1S_0-6^3P_0 forbidden transition absorpt. at 265.6 nm, A coeff. and self-press. broadening determ. 80—95562
Hg+Ar, spectral line broadening of Hg in UV, interaction pot. 79—26937
Hg+inert gas interaction potential *(French)* 78—25647
Hg+Xe, pressure broadened absorption profiles *(French)* 79—98033
HgMn stars, line asymmetries rel. to diffusion 78—40948
$^{199}Hg^+$, hyperfine separation of ground-state, optical double-reson. 78—78828
$^{199}Hg^+$ isolated ions, mag. hyperfine spectrum 78—29760
Hg(6^3P_2)+Cd(5^1S_0), spectral width of Cd(5^3P_1) line *(French)* 77—50397
H(n=4) Balmer-β emission, Doppler profile, in HCN electron impact dissoc. 80—28106
Hnα radio recombination lines, profile in static ion field 77—78629
Hnα, recomb. line profiles in W49A, high-sensitivity obs. 80—26998
I, laser 1.315 μm transition line struct. 78—59000
In, Lα X-ray fluoresc. spectra, natural linewidth meas. 79—85934
In normal atom conc. determ. by resonance line broadening with Hg press. 80—43883

atomic spectral line breadth continued
In+Hg, spectral-line contours in high-press. arcs 79—3412
In+inert gas atom, diffuse series head lines, hyperfine components, broadening calcs. 80—32632
K, 5^2P to 4^2S resonance line, rare gas perturbations, broadening, shift and dipolaris. 78—9126
K, resonance lines broadening and shift by noble gases 79—10070
K+He(Ar)(Ne)(Xe), K 5^2P level broadening and collisional relax., quantal, semiclassical and expt. comparison 80—18903
Kr, 3p X-ray photoelectron spectrum, many-electron effects 78—50513
Kr, $4p^5$5s state, electron excitation fine struct., neg. on reson. 77—14585
Kr, ESCA, lifetime broadening, CI resonances 77—18853
Kr I, saturated absorpt. profile of 557 nm line, collision effects 78—9121
Kr I, Stark broadening in visible spectra 78—37590
Kr, self-broadening of first reson. line 79—26933
Kr$^+$ mode-locked ion laser, pulse width and linewidth meas. 80—102696
Kr-Xe, absorpt. spectra line-narrowing, with reson. excitation transfer 79—89973
Kr(-He) arc, wall-stabilised, atm. press. 79—46503
Li, wings of resonance lines perturbed by inert gases, intensities 78—37596
Li+He, press. broadening, line shifts 78—5290
Li+inert gas, Doppler and collisional broadening, correls. 77—14530
Li+inert gas, fluoresc. reson. line broadening 77—6734
Li$^+$+He, excitation, optical emission line shapes 80—18820
Li*+He(Ar), Li principal series line broadening and shift, interat. pot. consts. 78—42165
Mg, Doppler effects in X-ray spectra excited by accelerated ions 78—86808
Mg I, $3^1P_1^0$ level reson. broadening and lifetime 77—57916
Mg I, hyperfine struct., brightness distrib., form. model verification 77—57928
Mg I, Mg II, solar reson. lines obs. in active region 79—40163
Mg I, Mg II lines, broadening and shift by van der Waals interactions and electron impact 77—3303
Mg I 2852 Å line in solar spectrum, sensitivity to partial redistrib. effects 78—7951
Mg I and II in Sun, line profiles comparison with theoretical spectra, visible obs. 80—82320
Mg I λ2852, in Sun, supergranular line profile var. 79—40164
Mg II, solar reson. lines, first emission features obs. in wings 78—32429
Mg II 280 nm line in Persei, profile, calcs. and UV obs. 80—82421
Mg II flux profiles in cool stars, obs. rel. to chromospheric radiative loss rates 80—36611
Mg II h and k line profiles of active solar limb filament 79—44446
Mg II interstellar resonance doublet absorption, equivalent widths and column density 78—45391
Mg II k chromospheric emission line profile in UV spectrum of giant star α Bootis 78—81620
Mg II k-line formation of optically thick solar chromospheric line, profile 80—94767
Mg II lines in quasars and Seyfert galaxies, excitation and line strength 80—67896
Mg, pionic X-ray transitions, strong interaction line widths and shifts 77—23586
Mg, reson. line, Hanle effect, density depend. 79—6917
Mg-inert gas, Mg reson. lines broadening, absorpt. cross sections anal. 80—32642
Mg+Xe(Ar)(Ne)(He)(Kr), collisional broadening of 285.2 nm line 77—79580
Mo, $N_2N_3N_{45}$ super Coster Kronig processes 80—106303
Mo, X-ray spectra, Kα hypersatellites 80—63576
Mo^{32+}, dielectronic recomb. rate coeffs. in plasma 80—43853
Mo^{38+}, dielectronic recomb. rate coeffs. in plasma 80—43852
N I, resonance line broadening in low press. He discharge lamps 78—9123
N II 6584 Å forbidden line profiles of giant H II regions 79—67081
N, reson. lines shapes determ. by Zeeman scans 77—6723
N, Stark broadened VUV lines in wall-stabilised arc, 1100-1800 Å 78—90107
N$^+$, stark broadening of high orbital ang. momentum states 79—22650
N_2:N, dynamically induced electronic transitions of matrix isolated atom 78—63825
Na, 3S-4D and 3S-5S two-photon lines, broadening and shift by inert gases 77—75105
Na, 5890/96 Å resonance emission lines, wing profile meas. 77—46534
Na, absorption D-line shape, rel. to single-mode laser intensity 78—66491
Na atomic vapour, Doppler-broadened system, degenerate four-wave mixing, line shape and strength angular depend. 80—43391
Na beam, optical amplification without population inversion 77—50645
Na, D line broadening by inert gases, fluoresc. obs. 80—32663
Na D_2 resonance line broadening in atom and molecule collisions *(Russian)* 80—14119
Na D-line emission from Io, comparison of observed and theoretical line profiles 78—93145
Na, D-lines, inert gas broadening, photon echo meas. 80—91475
Na, Doppler-free two-photon linewidths, 3S-4D press. broadening coeffs. 78—25481
Na, flame absorption and fluorescence, laser saturation broadening 78—88661
Na, fluoresc. study, reson. radiation illum. 80—83314
Na I, reson. line broadening in shock tube plasma 77—35393
Na I $3^2P_{3/2}$ meas. beyond natural linewidth by beam laser quantum beats 77—50399
Na I 8190 Å absorption feature in M31 and M32, equivalent widths 80—51862
Na I D-line obs., Doppler width from intensity integral 80—41782
Na I lines in solar spectra, non-mag. polarisation, centre-to-limb var. 80—67678
Na I reson. line broadening by collisions with dipolar mols. 80—941
Na I twilight and nightglow, interferometric studies of D-line profiles 78—36353
Na, in He buffer gas, collisional freq. redistrib. of scatt. laser light 77—30815
Na, laser excited fluoresc., saturation power, calc. and obs. 77—42276
Na, Lorentzian power broadening by optical pumping 78—17613
Na, narrowed optical lines, laser and accel. beam method 78—37770
Na normal atom conc. determ. by resonance line broadening with Hg press. 80—43883

atomic spectral line breadth continued
Na, oriented vapour, line broadening meas. in atoms following optical pumping, new technique 77—27005
Na, photofragment of NaBr, non-Gaussian line shape, level shifting and velocity inversion 80—58182
Na, photoionis. cross section resons., time-dependent HF theory 80—32684
Na, pionic X-ray transition strong interaction line widths and shifts 77—23586
Na, reson. multiphoton ionisation, broadband laser AC Stark splitting 78—70808
Na, Rydberg states, high resolution two-photon mm spectroscopy, metrology appl. 80—43018
Na, self-broadening of 3S-5S and 3S-4D two-photon transitions 79—26955
Na, Stark shifts, absolute and differential, coherent optical transient meas. 80—37773
Na, three-photon ionisation, laser bandwidth and intensity effects 80—52956
Na, total absorpt. of 3S→nP transitions 78—46306
Na, two-photon absorption reson. in spatially separated fields 78—21890
Na, two-photon excitation in flame, saturation broadening, fluoresc. obs., broad-band excitation 78—74625
Na, two-photon transition broadened by Ar impact 79—22681
Na vapour, saturation holes meas. using FM spectrosc. 80—42262
Na, wing profile of doublet lines, in flames at 1 atm. 79—22660
Na, wings of resonance lines perturbed by inert gases, intensities 78—37596
Na-Ne, gas phase, absorption, D-line profiles, dye laser meas. *(French)* 78—42007
Na+Ar, Na spectral lineshape, orientation and vel. relax. contribs., low press. region 80—5503
Na+H(He)(Ne), D2 reson. linewidth 79—31647
Na+H(Ne)(Kr) vel.-changing collisions, effect on 2 photon and stepwise absorpt. line shape 80—87221
Na+He, Na ($3S_{1/2}$-$3P_{1/2}$) photon echo, collision vel. changes and dissimilar electronic states superposition 80—32803
Na+He (Ne), two-photon optical free induction decay meas. by broadband excitation in unidirectional beams 79—76489
Na+He(Ar)(N_2), collision broadening and shift of 3S-4D and 3S-5S lines 79—3406
Na+inert gas, non-Lorentzian spectral line shape 80—106297
Na+inert gas, Rydberg states transitions, broadening cross-sections meas. 80—69110
Na+Kr(Xe), excimer bands, multiperturber interactions 78—66497
Na+Kr(Xe), reson. line broadening, press. depend. 78—66596
Na+Ne(Ar)(Xe), 3^3P-3^2D line broadening obs. 80—78684
Na$^+$+Ti(Ni)(Zn)(Fe), 0.2-3.0 MeV, united-at. limits, mol.-orbital continua 77—19030
Nb, $N_2N_3N_{45}$ super Coster Kronig processes 80—106303
Ne, $2p^5$3p-$2p^5$5s emission lines, press. broadening, with Ne(He), rel. to repulsive forces 80—9692
Ne, atomic, selfbroadened collision widths 77—38637
Ne, autoionising resons. near 575 Å, ab initio relativistic RPA calc. 80—32681
Ne, broadening of $2p^5$3p-$2p^5$4d spectral line by He 79—18145
Ne, Doppler broadening compensated by light shifts 79—41136
Ne, excited atoms reactions in pure afterglow, plasmas using resonance absorpt. spectrometry 80—33835
Ne, g-factors meas. by quantum beat spectroscopy 79—93955
Ne I, isotopic component separation by numerical method 78—21227
Ne II lines from pulsed arc plasma, Stark broadening 78—66504
Ne, Lamb-dip structure anal., linear and helicoidal polaris. 78—25852
Ne, optical transitions, Doppler broadening, compensation by vel. depend. light shifts 80—52930
Ne, oscillator strengths, determ. from self-absorption of reson. radiation 79—89641
Ne, photoionisation, complex amplitudes at low energy singly and doubly excited resons. 78—78673
Ne, reson. broadening at low densities 79—31452
Ne, self broadening of $2p^5$3p-$2p^5$4d spectral line 79—18144
Ne, spectral line broadening due to reson. interaction 79—22654
Ne transitions, 1.52 μm and 633 nm, mode crossing resonance shape 79—18163
Ne V, forbidden 3426 Å emission in nebula NGC 6302, broad wings obs. rel. to energetic stellar wind 80—67835
Ne, X-ray spectral line broadening in solid and gas targets 77—6713
Ne+Ne, (He) low pressure broadening and shift of Ne line, Lennard-Jones pot. 80—102554
Ne+Ne(He), 7d′ states, isotope shift, press. shift, press. broadening, two-photon spectra obs. 78—55155
^{20}Ne $3s_2-2p_4$ 6328 Å line wavenumber determ., laser induced line narrowing technique 79—76385
Ne* 5882 Å line, Doppler free spectra, press. broadening and shifts, saturation spectroscopy 80—78565
Ni, $M_{II,III}$ spectrum, ab initio calculation 80—83276
Ni XXV, Ni XXVI, line classifications in laser-produced spectra 79—81175
Ni+Ni, 39 MeV, X-ray emission spectra, nonLorentzian shape of atomic line tail 78—21872
Ni+Ni, continuum X-ray radiation, collision broadening 80—9539
Np, M-series X-rays, energies and widths 77—75092
O I, resonance line broadening in low press. He discharge lamps 78—9123
O I 1302 Å line profile in ζ Ophiuchi spectrum and interstellar O abundance 79—44583
O I 5577 Å and 6300 Å, laboratory discharge lamp source for lines of known width 80—4148
O I 5577 Å and 6300 Å forbidden emissions during aurora, line profile vars. 78—45081
O I 630 nm airglow profile, daytime thermospheric temps., wind vels. and emission intensities 79—58144
O I 630 nm nightglow line profiles, thermospheric temps. and winds 79—58143
O I 6300 Å airglow, interferometer meas. rel. to global model of exospheric temp. 77—53265
O I 6300 Å forbidden line high resolution obs. in dayglow 77—41252
O I 7774 Å line in O6 to G2 stars, equivalent widths and narrow-band photometry 80—8621
O I lines in A-type stars, non-LTE anal. of profiles and equivalent widths 77—41378

atomic spectral line breadth continued

- O III 5007 Å forbidden line profiles from M16 H II region 79—8976
- O III forbidden line in Seyfert galaxy NGC 1068, high-resolution profile 80—46665
- O, in supernova remnant in NGC 4449, forbidden emission line widths rel. to nucleosynthesis 80—56895
- O, line shape following dissociative excitation of O_2, CO_2, CO and NO 80—105097
- O, metastable ^{5}S-state, optical pumping 80—32678
- O VI in OB-type stars stellar winds, P Cygni line profiles obs. 80—8630
- O VI interstellar survey, UV spectra of OB stars 78—36679
- O^{n+}, n=1 to 4, gas and foil-excited, 2-18 MeV, projectile Auger spectra 79—59414
- ^{A}O, A=16,18, pionic 1s state energy shift and line broadening *(German)* 80—48107
- Pb I and II, transition probabilities, Stark broadening parameters 80—23367
- Pd at. N-shell vacancy state widths, X-ray photoelectron, Auger spectra 77—18875
- Pd, Lα X-ray spectra, $_{40}$Zr to $_{48}$Cd, linewidths 79—41131
- Rb, $5^{2}P_{1/2}\rightarrow 5^{2}S_{1/2}$ resonance line perturbed by inert gases, depolaris., broadening and shift 78—21880
- Rb, 5^{2}S-n^{2}S transitions, Rydberg levels, high resolution two photon spectra obs. 80—52923
- Rb Doppler-free two-photon lines, self-broadening and shift meas. 80—5506
- Rb, fluoresc., far wings profile of self-broadened reson. lines 79—76388
- Rb, laser saturation spectra, collision broadened line struct. *(Russian)* 79—45678
- Rb, self-broadened first reson. lines, near-wing asymmetries 80—9535
- Rb spherical electrodeless lamp, spectral profile of D_1 line 77—50744
- Rb, Stark shift of $6^{2}P_{1/2}$ to $5^{2}S_{1/2}$ line, mag. scanning meas. 80—27977
- Rb vapour, spectral profiles of D-lines, spherical lamp case *(French)* 78—18032
- Rb, Zeeman resonance lineshapes, motional narrowing 77—46525
- ^{85,87}Rb, high Rydberg levels, press. broadening and shifts 80—52902
- Rb+Ar(Kr)(Xe), spectral line breadth and shift, Van der Waals pot. calc. 78—90126
- Rb+inert gas, D_2 line collisional broadening and shift, and HFS 79—22664
- Rb+inert gas, hyperfine struct., broadening and shift calcs. 77—58153
- Rb+inert gas, mag. scanning technique for broadening and shift 79—22663
- Rb+Kr, STS components shift and broadening 77—68014
- Rb+Rb, ^{2}P states, near IR spectra, collision induced features 77—10637
- Rb+Rb**, freq. shift, line broadening, phase interference effects, Doppler free two photon spectra 80—58200
- ^{85}Rb cell filtering action, press. shift and broadening by foreign gases 79—3403
- ^{87}Rb+Kr, D_1 line broadening and shift 77—38640
- ^{87}Rb+inert gas, D_1-line hyperfine components perturbation, interferometer obs. 80—32635
- Re, pionic 4f$\rightarrow$3d transition, pionic 3d state strong interaction level shift and width 79—98251
- Rh, Lα X-ray spectra, $_{40}$Zr to $_{48}$Cd, linewidths 79—41131
- Rh, $N_2N_3N_{45}$ super Coster Kronig processes 80—106303
- Ru, Lα X-ray spectra, $_{40}$Zr to $_{48}$Cd, linewidths 79—41131
- Ru, $N_2N_3N_{45}$ super Coster Kronig processes 80—106303
- Se, Doppler effects in X-ray spectra excited by accelerated ions 78—86808
- Si II, Si III, chromospheric line profiles, spectrum synthesis 78—36543
- Si II lines in A-type star α Lyrae (Vega), Copernicus UV obs. 80—8627
- Si II solar lines 1808-1817 Å, observed and theoretical profiles 78—49412
- Si III, IV, Stark line broadening in pulsed arc, plasma diagnostics 78—944
- Si IV 1393 Å, line width in quiet Sun and coronal hole, OSO-8 obs. 77—91511
- Si, K_{α} X-ray emission spectra chemical shifts, linewidths and intensities in SiC, SiO_2, Si_3N_4 78—13461
- Si line profile vars. in B-type stars 79—5823
- Si XI 303 Å, solar line profiles 79—12452
- Si^{+}, Stark broadening, shock tube meas. 78—17614
- Si^{12+}, 1s2s $^{3}S_{1}$-1s2p $^{3}P_{0,2}$ transition wavelengths, by beam-foil 80—32649
- Sn, at. N-shell vacancy state widths, X-ray photoelectron, Auger spectra 77—18875
- Sn II, cool plasma, isolated lines, Stark broadening, semi-empirical impact approx. calcs. 80—59186
- Sn, Lα X-ray fluoresc. spectra, natural linewidth meas. 79—85934
- Sn, Sn^{+}, transition probabilities and Stark-broadening parameters, shock tube meas. 79—93956
- ^{50}Sn, L$\gamma_{2,3}$ X-ray emission spectra, line breadth 78—62760
- Sr, 4607 Å reson. line shape, width and shift in Ar, press. depend. 79—22653
- Sr, 4607 Å resonance emission line, wing profile meas. 77—46534
- Sr, 4607.33 Å line, broadening and shift in H_2-O_2-Ar flames 77—18849
- Sr, 4607.33 Å resonance line, spectral width depend. on at. density in flame 77—46535
- Sr, reson. lines, emission and absorpt. core profiles 77—50389
- Sr+He(Xe), Sr reson. line width, 4607 Å, press. effects, pot. well depths 79—89643
- Ta, Kα line widths, precise meas. 78—62761
- ^{181}Ta, pionic 4f$\rightarrow$3d transition, pionic 3d state strong interaction level shift and width 79—98251
- Tc, Lα X-ray spectra, $_{40}$Zr to $_{48}$Cd, linewidths 79—41131
- Te VII, 4d^{9}6s configuration spectrum obs., line identifications 80—106289
- Te VIII, 4d^{8}5s, 4d^{8}5p and 4d^{5}4d^{10} config. spectrum obs., line indentifications 80—106289
- ^{52}Te, L$\gamma_{2,3}$ X-ray emission spectra, line breadth 78—62760
- Tl, 377.5 nm line, broadening by Xe 77—71781
- Tl, effect of intrinsic vapour pressure on shape of 258 nm line 77—46539
- Tl, line shape in Ar gas, collisional redistrib. of near-reson. rad. 79—31469
- Tl, λ_{max}=251.3 nm absorption band, rel. to Tl atom conc., temp. and disturbing gases 80—42980
- Tl, normal atom conc. determ. by resonance line broadening with Hg press. 80—43883
- Tl, reson. lines, perturbing gas and self-broadening, temp. effects 80—42979
- Tl, self-broadening of 377.6 reson. line 78—82692

atomic spectral line breadth continued

- Tl, sensitised fluoresc. in Hg-Tl vap., Doppler broadening 77—3314
- Tl+H_2, Tl atomic fluorescence, pressure and Doppler broadening 80—5504
- Tl+Hg, spectral-line contours in high-press. arcs 79—3412
- Tl+inert gas atom, diffuse series head lines, hyperfine components, broadening calcs. 80—32632
- TlI, atomic fluorescence, D_2 pressure effect on width and shift 80—99475
- Tl($^{7}S_{1/2}$)+inert gas, long-range interaction, spectral line shifts and broadening 79—10174
- Tl(7^{2}P) states, isotopic forms, HFS, press. self-broadening, two-photon spectra 77—18879
- Tm, Kα line widths, precise meas. 78—62761
- U, atomic model 79—41095
- U, M-shell X-ray emission obs. by photoelectron spectrosc. 77—54529
- U^{+}, atomic model 79—41095
- UI, absorption line shape change, pulsed hollow cathode source *(French)* 80—47927
- W, X-ray $L_{\alpha 1}$ line width meas. *(French)* 77—50393
- Xe, 3.51 μm broadening due to velocity-changing collisions 78—37597
- Xe 3.51 μm laser amplifiers, spectral narrowing and saturation induced rebroadening optical heterodyne obs. 80—63976
- Xe, 3.51 μm laser transition, phase-changing broadening, inert gas perturbers 78—82949
- Xe, 3.51 μm line press. broadening 77—14390
- Xe, 5p^{5}5s state, electron excitation fine struct. neg. ion reson. 77—14585
- Xe, AC Stark effect, on saturated absorption line shape in partially Doppler-compensated system 79—45669
- Xe, discharge lamps, 147 nm resonance line production 77—39497
- Xe, extravalence excitations, VUV spectra, solvent perturbations 77—50386
- Xe I, arc spectrum, press. shifts and broadenings in visible and near i.r. 77—440
- Xe I three-level system, level splitting within natural width, saturation spectrum 80—106291
- Xe in inert gases at high press., extravalence excitation solvent perturbation 77—75099
- Xe, self-broadening of first reson. line 79—26933
- Xe three-level system, collisional effects on optical coherence 79—93954
- Xe+Bi, Bi Kα X-ray lines, Doppler broadening 78—62759
- Xe+He, saturated absorpt. of 3.51 μm line, vel. changing collisions by line width 78—86819
- Xe+Kr, excitation transferred populations, absorpt. profile analysis 78—74748
- XeI, visible lines, absolute transition probabilities 80—69108
- Y^{10+}, spectrum and energy levels 80—32639
- Yb, 4f levels, hole lifetime and chemical shift, UHV study 80—20762
- Yb vapour, Mα line width 77—27014
- Zn, optimisation of pulse parameters in pulsed supply hollow cathode discharge 78—33471
- Zn, self-broadened 3075.9 Å line, temp. effects 77—3318
- Zr, Lα X-ray spectra, $_{40}$Zr to $_{48}$Cd, linewidths 79—41131

atomic structure

see also atomic electron correlations; atomic excited states; atomic fine structure; atomic orbitals calculations; atomic polarisability; atomic spectra; nuclear screening; Russell-Saunders coupling; triplet state

- 1-matrix energy functionals, extension to all ensemble representable 1-matrices 80—99442
- 2p-h TDA equations, superoperator derivative 79—31372
- 3d^{5}, 4f^{6} configurations, partial level density, statistical props. of atomic energy levels 78—70732
- 3d photoabsorpt. spectra, continuum and discrete states 79—81176
- 4d^{9}4f configuration, 4f electron localisation, rel. to N ion spectra 77—3290
- π electron Hamiltonian, ab initio derivation by nonperturbative open shell formalism 78—21846
- actinide atoms and ions, electronic struct. *(Japanese)* 79—6856
- adatom, valence shell energy level shift *(French)* 78—67900
- adsorption of atoms on metals, Green's function formalism for studying electronic struct., local density of states calc. 80—107884
- alkali metal atom, valence electron ground states, model potentials 78—50476
- alkali metal excited states, radial matrix elements and radiative lifetimes 79—59375
- alkali metals, excited states energy levels ordering 77—67968
- alkali metals, positive ion Rydberg states, pseudopotentials, local exchange approx. calcs. 77—14337
- alkaline earth positive ions, valence electron ground states, model potentials 78—50476
- alloys, binary substitutional, determ. of local atomic configurations 79—86739
- angular momentum coefficients in relativistic atomic struct., Fortran program MCP75 77—10605
- approximate energy differences from average electron densities 79—36505
- approximate energy relationships, Z^{1} perturbation expansion 79—13620
- arc spectra, energy levels assignment *(French)* 77—83522
- asymptotic expansions in motion of two electrons in nuclear field 78—66459
- atom, multiconfigurational time-dependent Hartree-Fock approach 79—85889
- atom-diatom collinear reaction, potential classical transition collinear state theory 79—98191
- atom-excess electron systems, negativity of ground state interaction energies 79—13619
- atomic, molecular and solid-state theory, conf., Flagler Beach, Florida, USA (Mar. 1978) 79—31356
- atomic excited terms generator program 79—54759
- atomic physics, conf., Riga, USSR (Aug. 1978) 80—22141
- atomic physics in nuclear experiments, conference, Haifa, Israel, Aug. 1976 78—70947
- atomic scatt. factors and momentum densities, asymptotic form 80—74105
- atomic spectra and radiative transitions, book 80—22159
- atoms, 5f^{N} and 5f^{N}7s config., parametric study 80—91444
- Aufbau, principle, low-cost classroom demonstration 80—42011
- average electron density, isoelectronic changes, rel. to X-ray scatt. intensity 80—91424

atomic structure continued
b_n factors at low temperatures, appl. to interstellar C II regions 80–36696
Be, Rayleigh-Schroedinger perturbation calculations 78–9064
bibliography at. energy levels and spectra, (July 1971-June 1975) 77–71764
binding energies, determ. from fund. theorems involving electron density, $\langle r^{-1}\rangle$ and Z^{-1} perturbation expansion 80–63521
binding energy and rest mass of constituents, total symmetry effects *(French)* 80–63068
Bohr's 1913 atomic theory, chem. aspects 77–67170
book, atomic data handbook 77–23398
Born-Oppenheimer approx., physics of new derivation 79–9997
Born-Oppenheimer energy, energy states of one electron, two nuclei interaction 78–90052
bound and quasi-bound states in continuum 77–14329
bound s-state energies for exponential cosine screen Coloumb potential, Ecker-Weizel approx. 79–97965
bound s-state energies for static screened Coulomb pot. 77–18771
bound s-state of electron in screened Coulomb field 78–58581
bound state problems, many-body scatt. theory, arrangement channel 77–75044
bound-state energy, 1/Z perturbation expansion, analytic behaviour 77–50344
bound-state energy, 1/Z perturbation expansion, singularity 77–50343
bound-state properties calcs., theoretical error estimates 80–102425
Breit interaction between electrons, calc. angular coeffs., computer program 80–18779
Brillouin-Wigner type perturbation series summation 79–81149
central analytic potential with three parameters 77–71737
channeled ions, electronic states calcs. 80–24517
charge distribution, chem. effects, total valence-electron energy/nucl.-electronic interaction energy relation 79–3347
charged particle scatt. in quantising mag. field 80–46853
classical many-body collision model incorporating Heisenberg and Pauli principles 80–63511
closed-shell atoms, Jastrow wave functions, var. calcs. 80–83249
clustering of levels in regular spectrum 77–71237
cold atoms, trapping and storage in laser field 78–86826
collective core electron-valence electron model, props. 77–83476
collision, two-centre one-electron, nonadiabatic couplings for ionising transitions, switching functions determ. 79–22813
combinatorial computation of atomic terms for equivalent electrons 78–17549
complex energy eigenvalues of a zero-range atom in a uniform electric field 79–72227
compressed-atom model, macroscopic parameters calc. 77–47136
Condon-Shortley coefficient, storage algorithm 79–49929
conference, Boulder, Colorado, USA, June 1978 79–36511
conference, Leningrad, USSR (Feb. 1977) 79–10059
configuration rearrangement effects on beam-foil projectile K X-rays 77–46634
configurational interaction, for impurity ions with d^2 and d^3 configurations, corrections 79–54829
contact interactions, parity-violating and parity-conserving, new evaluation techniques 79–26872
convex structure of electrons 78–62685
core charge polarisation effects, dipolar contributions 79–45631
correlation energy for closed and open shells, approx. calcs. 80–42942
Coulomb energy bounds, rel. to local density functional theory 80–47839
Coulomb Hamiltonian, one-dimensional, spectral props. 80–47859
Coulomb potential, modified, S-wave energy levels 78–41918
Coulomb potential with cut-off, exact eigenvalues 78–62692
Coulombic integrals, approximated, error bounds 77–3247
coupled stationary states, analogy using triple pendulum 78–16598
covariant photon interaction 79–3342
critical nuclear charge for levels crossing lower continuum *(Russian)* 77–50338
deep levels, energies and wave functions, correl. corrections *(Russian)* 77–14364
delocalisation, statistical and stochastic aspects 77–30759
delocalisation, statistical and stochastic aspects 77–30760
density functional calculations for atoms, molecules and clusters 80–47850
density functional theory, quantum mech. system, accurate pot. and energy functionals 80–52849
diagrammatic many-body perturbation expansion, computer program 78–50454
diagrammatic many-body perturbation expansion, ladder energies, computer program 78–50455
diagrammatic many-body perturbation expansion, ring energies, computer program 78–50456
dimensions, correlation with polarisability 80–23288
Dirac type essentially self adjoint operators 78–16957
double antisymmetrisation 78–21836
doublet state, ionis. pots., electron affinities, using electron propagator, appl. to Li, Na, and BeH 79–63933
dressed atom system, energy levels and reson. phenomena, universal algorithm 80–69111
dynamical groups in atomic and molecular physics 80–42362
educational model 77–26110
effective valence shell Hamiltonians, generalised perturbation theory 79–36509
eigenvalue sum rel. to total SCF energy for ats. and mols. 79–9993
electron coincidence spectroscopy, orbital shape, charge density, mol. struct. determ. appls. 79–27113
electron density, spherically averaged, exponentially decreasing upper bounds 77–18772
electron density contours from FSGO model wave functions, nonbonded radius of atoms, mol. anisotropy of polarisability 79–85897
electron density partitioning 77–30749
electron density studies, quantum chem., basic concepts 78–70731
electron energy levels deform. in strongly compressed plasma *(Russian)* 80–53931
electron gas exchange and Fermi hole density, HF calcs. 78–17565
electron Hamiltonian, effective one-body, with correct asymptotic behaviour, appl. to He 79–45619
electron momentum densities, expt. determ., review 77–76776
electron momentum densities, theory, review 77–75039
electron shell, types of collective motion 79–63886

atomic structure continued
electronegativity scale determ. from effective nuclear charges and X-ray spectra 77–75037
electronic 4s, 3d energy levels, textbook diagram, teaching 78–73801
electronic degrees of freedom, classical models 80–63507
electronic densities, analytic expressions 80–99437
electronic energies, homogeneity prop. 80–63539
electronic levels, near crystal surface, pot. drop effects 78–19123
electronic structure calcs., self-consistent, accelerating convergence of iterative process 80–87037
electrostatic pot.-electronic density relationships 80–69206
elements with $Z\leq30$, core electron binding energies in free and standard state 77–43168
energy density functional approach, kinetic energy model 79–31357
energy level and Grotrian diagrams, S I to Ti XXII, book 79–3387
energy level and transition array distribs. variance, Mo VX-XIV appl. 80–37767
energy level isotopic shifts and nuclear polarisation *(Russian)* 78–13444
energy levels lower bounds, matrix Pade approximants 78–41905
exchange energy as function of electron density 80–91426
exchange energy density functional, gradient expansion, rel. to at. energy functional 80–99441
excitation operators and extended RPA 78–13412
excited state structure, electron correl., var. collapse theory 79–6890
excited states, k-ordering, l-patterns, ats. and isoelectronic ions 77–88406
exotic atoms containing monopoles, energy levels and stationary states *(Chinese)* 78–86982
expectation values, rigorous and approx. relations 80–74099
in external AC and DC fields, complex dressed states determ. 80–63585
Fermi contact interaction, by finite nucleus model 79–63887
fermion interaction theory of nuclear and atomic struct. models, singlet paired fermions 79–9180
few body methods in atomic and molecular structure calcs. 79–76330
Feynman diagrams, open shells, f_κ and g_κ coeffs. *(Russian)* 77–46480
field isotope shift off-diagonal parameter in $(5d+6s)^N$, ab initio evaluation 80–47912
filled shells symmetry 77–23400
first-row atoms, local density formalism calcs. using pseudopots. 77–75047
first-row atoms (ions), valence region electron energies calcs. 78–899
Fock, V., development of ideas in atomic phys. and quantum theory 80–22183
form factor, squared, integral over momentum transfer 80–1039
form factors, relativistic Hartree-Fock, tables for Z=1-100 79–59381
form factors for atoms and ions with $Z\leq54$ 77–10582
form factors for large momentum transfers, relativistic SCF calc. 77–83504
form-factors, l-dominant, analytical formulae, appl. to $Ar+N_2$ 80–1052
four subshells of equivalent electrons, matrix elements of relativistic energy operator 78–33407
fractional parentage coefficient identities, atomic, molecular spectroscopy applications 80–69050
fractional parentage coefficients and submatrix elements of transposition operators for spin and quasispin quantum numbers 77–71736
free ions, electron density near nucleus, isoelectronic change, nonrelativistic calcs. 79–54768
gaseous molecules, persistence of p, d, f and g orbitals, ang. functions, Schrodinger's eqn. and cardinal number anal. 80–102426
ground state, energy functional of first-order reduced density matrix 79–10003
ground state atoms, Van der Waals coeffs., polarisabilities and oscill. strengths calcs. 79–93913
ground state charge density, asymptotic behaviour 79–22575
ground state energy, atomic shell model 78–50460
ground state energy, relativistic and radiative corrections *(Russian)* 77–67991
ground state kinetic energy functional, gradient expsn. 77–6665
hadronic atoms, Coulomb levels shift *(Russian)* 79–45870
handedness of atoms, and parity non-conservation 78–29757
Hartree problem, iterative diagonalisation soln. 79–6829
Hartree-Fock expectation values, systematic behaviour 79–3365
heavy atoms, collective oscillations, of individual shell 79–45674
heavy elements, electron config. rel. to chem. behaviour *(German)* 78–29727
heavy positive ions, total energy, rel. to eigenvalue sum and chem. pot. 80–47858
Heisenberg equation of motion, operator level and function level 79–6826
HF coreless pseudopots. for atoms K through Zn 78–55121
high-Z atoms (Z=48-104), electron impact, K-shel ionisation cross sections calcs. 80–63827
high-Z electronic and muonic atoms, QED, strong and supercritical fields, book contrib. 78–74193
highly correlated particle densities and idempotent one-densities 79–6815
highly ionised atoms, relativistic effects, book contrib. 78–74588
HKS theory, occupation nos. role, rel. to density functional theory 80–52851
homologous ions series, struct.-related trends in line strengths and Stark widths 80–105157
Hund's rules in atomic spectra, frozen electron core and valence electrons in nucl. field 77–67967
hydrocarbon catalysis 78–11550
hydrogenic and atomic observables, time resolved spectra, time reversal symm. 80–91418
hydrogenic atom, Dirac eqn. approx. soln., Moore's method appl. 80–42926
hydrogenlike atoms, spin-orbit terms derivation 80–73148
independent particle pots. comparison, appl. to Be(Ne)(Ar)(Kr)(Xe)(O V)(Al IV) 80–52846
inert gas atom+degenerate atoms, pairwise additivity, DIM calc. 79–89728
inert gases, (e,2e) reactions 200 to 2600 eV as probe of atomic and molecular struct. 77–88566
inert gases, He to Xe, Hartree-Fock electron density, kinetic energy functional 79–26879
inner electron shell, change in atomic quantities when vacancy occurs 79–63909

atomic structure continued
inner shell ionisation by electron or proton impact, coincidence exptl. method, theory 80—1066
inner shell vacancy influence on atomic props. 77—26956
inner shells, Coulomb ionisation, semiclassical description 80—42938
inner shells, physics, quantum mech. appls., history 77—18773
inner-shell vacancy system, saddle point calcs. 80—23292
integral calculations, permutational approach using spatial symmetry 79—36515
intermediate states, far off-reson., temporal coherence in multiphoton absorpt. 78—50458
ion, Thomas-Fermi eqn., anal. soln., Araldi correction *(Russian)* 77—18790
ion, three-electron, 2s2p1s config., intermediate coupling state, energy level calcs. 79—3353
ionisation potential, using Slater's value of at. screening parameters 80—912
ionisation potential, X_α eigenvalues and Slater transition state 79—31394
ionisation pots. in EM field, Kramers-Henneberger transformation, QED and semiclassical 77—23481
ions, positive, dielectronic recomb. in plasma generalised cascade theory 80—43851
ions, positive or negative, electron density, semi-statistical model 78—21850
ions with partly filled L-shells, relativistic Hartree-Fock energy calcs. 78—82656
isoelectronic changes, energy density eqn. 78—70768
isoelectronic series, electron density relation between adjacent members 79—72222
isoelectronic series, Politzer's energy rel. determ. using HF data 80—91425
isoelectronic series (2-36 electrons) energy-density relationships 80—9486
j-j coupling between two equivalent electrons, J and M_J states determ. 80—37752
jj-coupling, submatrix elements of operators derived from unit tensors 77—422
k-ordering of atomic energy levels rel. to spectroscopic quantum defects 79—89657
K-shell ionisation by H^+, electronic final states description 77—38723
K-shell vacancy production, by charged particles, relativistic effects calc. 78—58600
kaonic ^{12}C, coupled channel formalism, role of $\Lambda(1405)$, binding effect, Pauli blocking 78—55261
Kelvin-Thomson atom, the one- to six-electron atoms 77—88367
Kelvin-Thomson atom, theory for teachers, expt. simulation 78—4439
kinetic energy, bound on lowest order gradient correction 78—62709
Kirkwood-Pople-Schofield method, appls. to polarisabilities calcs. 80—83272
l-splitting of energy levels for almost Coulombic central pots. 77—6659
Landau condensation in atomic physics 80—74098
lanthanide series properties, double peaks effect *(Chinese)* 78—29740
level shift and width in light field, higher order perturbation theory *(Russian)* 79—3414
light atoms, large-q form factors, calcs. for ^3Li to ^{19}K, ^{22}Ti 78—58589
light atoms, large-q form factors for momentum transfer 78—70734
light hydrogen-like atoms, nuclear size corrections to energy levels 79—36549
local density functional theory of atomic and mol. ground electronic states 80—23286
local exchange potential, numerical tests 80—18784
local exchange potential giving correct asymptotic behaviour 79—45618
local-density theory of multiplet structure 80—18776
magnetic interactions of electrons *(German)* 78—82610
many body theory, appls. review of development 80—46968
many electron atomic Hamiltonians spectral props., method of configuration interaction 79—59368
many electron theory, state vectors and propagators, unified approach 79—6822
many-body theory, collisions and interactions calc. method 80—46726
many-electron, energy calc. by diagrammatic method *(Russian)* 77—14332
many-electron atom, tensorial props. of operators in quasi-spin space 80—42925
many-electron atoms, energy levels, quantum statistical theory of recomb. continuum *(Russian)* 79—63907
many-electron atoms, foundations of relativistic theory, Hamiltonian H_+ and h_+ and related relativistic HF eqn. derivation 80—99458
many-electron atoms, generalised spherical functions 77—46483
many-electron atoms, one-electron operators, Z-expansion of matrix elements 80—9489
many-electron atoms, orthogonal multidimensional ang. functions 79—13628
many-electron atoms, use of generalized spherical functions 77—38601
many-electron atoms in mag. fields, total energy and atom spin calcs., spin rearrangement 80—83267
many-electron atoms with different coupling types, transform. of wave functions 77—67956
many-electron autoionising states, Z-expansion energy calcs. 80—909
many-electron systems, electron density, Schrodinger inequalities and asymptotic behavior 78—21845
many-electron theory, multidimens. angular Coulomb functions 79—54756
many-fermion systems, partial level density for widely varying values of the range of interaction 80—58120
matrix elements of relativistic energy operator, complex electronic configs. 77—30792
model potentials, constructive theory 79—26869
model potentials soluble in closed form 80—23287
modern atomic and nuclear physics (book) 80—11
molecular internal stresses, stress tensor, one electron system 78—62686
momentum distributions via (e,2e), offshell impulse approx. 77—88565
momentum single particle states via (e,2e) knockout reactions 77—88117
momentum wave function determ. in atomic, molecular and nuclear systems 77—88556
Moseley's expts.: $K\alpha$ line freqs., rel. to at. number, reinterpretation 80—82616
multi-configuration Hartree-Fock program 78—50471
multicentre multielectron system, wave function construction 78—893
multichannel quantum defect theory, derived from config.-mixing approach 78—41919

atomic structure continued
multicharged ions, transitions between energy levels in strong external field, relativistic calcs. *(Russian)* 80—63547
multiconfiguration Dirak-Fock program, appl. to Ba X-ray levels and 5p excited spectra 80—47865
multiconfiguration Hartree Fock method, appl. to at. energy levels and transition probabilities calcs. 80—23318
multiconfiguration optimised central pot. method calcs. 80—9515
multiconfigurational Hartree-Fock calcs., radial orbitals anal. approxs. 79—54760
multielectron configuration, evaluation of matrix elements of energy operator 79—63895
multiply charged ions, $2p_{1/2}3p_{3/2}$ config., level widths, relativistic calc., S-matrix method 80—63546
multiply charged ions, energy calcs., coupling schemes, diagram technique appls. 79—10007
multipole transitions in complex config., matrix elements for operators inc. relativistic corrections 78—5150
muonic atom energy levels 79—76533
muonic atoms, electron screening calculations in O, Al, Fe, In, Ho, Au, Th 78—94339
muonic atoms, energy levels of light hydrogen like and muonic atoms, nuclear size corrections 79—36549
muonic atoms, energy-level values, electrodynamic corrections 78—62956
N-electron atomic Hamiltonian first eigenvalue, Hartree-Fock approx. method 78—90062
N-electron zero-momentum energy expressions, approx. wave function accuracy assessment criterion 79—3348
near threshold struct. in K-shell spectra, photoionisation or fast charged particle ionisation 80—87064
negative energies, teaching approach 77—13553
negative ions, electronic structure, stabilisation calcs. using big mol. Gaussian SCF/CI program 79—18121
neutral atom and isoelectronic ions, non-relativistic binding energies 79—59334
neutral atoms, gradient expansion of at. kinetic energy functional 80—42932
neutral atoms, total energy and eigenvalue sums 78—21835
neutral atoms in plasma background, strong EM radiation effects 80—103157
neutral systems, total binding energy, virial theorem appl. 80—47840
nonlocal pseudopotentials, density functional formalism calcs. 79—41096
nonrelativistic atomic and ionic binding energies 78—90054
nonrelativistic atomic orbital calc. program using Slater functions 79—49930
nonrelativistic atomic states matrix element generator program 79—54758
nucl. vol. isotope shift theory, many electron effects 80—47851
nuclear screening parameters, using Hartree-Fock energy 79—6883
numerical HF radial function during SCF iteration, convergence 78—58574
one-electron atom in curved space-time 80—78509
one-electron atoms, corrected for fine struct., lamb shift and QED shift, tables 77—79529
one-electron density, spherically averaged, upper bounds calc. 78—25415
one-electron density at nucleus, expectation values 78—90053
one-electron eigenenergies for class of atomic model pots., exact calcs. 77—23399
open shell systems, wave operator hierarchy eqns. 79—41087
open-shell atom, effective electron-electron interaction, many-body perturbation theory, C appl. 80—47843
open-shell systems, many-body perturbation theory, coupled cluster approach 79—31360
orbital cross-sections, bonding interactions, spring model, teaching aid 78—93503
orbitals, max. and min. overlap, localised, and hybrid, orthonormality-constrained variation method 79—6830
and oscillator strengths, book contrib. 77—26959
parity breaking, implications for unification of weak and EM interactions 77—57479
parity non-conservation, weak neutral current, relativistic many-body perturbation theory 78—923
parity violation effects 77—71457
parity violation in atomic processes 77—22657
partially-filled shell atom, relativistic theory, secular operator renormalisation *(Russian)* 80—52896
periodic table, struct., at. orbital energies, screened Coulomb pot. theory 77—75035
perturbation, periodically time-depend., quasi-states theory *(German)* 78—82601
perturbation expansion, diagrammatic, of electronic energy, 4th-order terms 79—85882
perturbed Rydberg series, quantum defect and CI theories 80—23300
phase integral approximations, advantages over JWKB approx. 80—87027
pi systems representation, efficient computer manipulation 79—81148
Politzer-Parr partitioning, electron correl., isoelectronic, isonuclear, spin and excitation aspects 80—78522
positive ion behaviour in strong mag. field 79—35978
positron+H(He), second-order nonadiabatic polaris. pot. for elastic scatt. 79—22836
positron annihilation in rare gases, Doppler broadening meas., electron mom. distribs. 78—55131
post-collisionally Stark mixed states, autoionisation electron energy and ang. distrib. 80—18829
quantum chemistry, conf., Kyoto, Japan, 29 Oct.-3 Nov. 1979 80—101659
quantum defect theory, general form 79—68177
quantum defect theory, positive ion+electron system 79—13621
quantum mechanical perturbation problems, resolution using integral eqn. 80—58112
quantum mechanical system, energy spectra calc. using trajectory integrals 78—21838
quasibound states, variational principle 77—3251
quasiclassical approximation, Thomas-Fermi method, for $Z>137$ nuclei *(Russian)* 78—17547
quasiclassical corrections to Thomas-Fermi model, electron density, eqns. of state 78—25404
quasiparticle formalism, atomic shell operators, Lie algebra 80—91414
quasiparticle picture, at. and mol. systems, breakdown for inner valence electrons 78—5112

atomic structure continued
- qunatum beats in atomic and nuclear physics 78−70772
- radial wave functions, approx. relativistic corrections 77−421
- rare earth chlorides, glass transition temp. meas., inner-sphere coordination number change effect on soln. props. 80−83239
- rare earth elements, atomic energy levels, data tables 78−86805
- rare earth elements, atomic partition functions, Chebyshev approximations 80−67544
- rare earth metal orbital radii, quantum-mech. calcs. rel. to inner series contraction 77−83514
- rare earth perchlorates, glass transition temp. meas., inner-sphere coordination number change effect on soln. props. 80−83239
- rare earths, atomic props. and electronic struct., review 79−68204
- rare earths, valency, ionicity and electronic config. 80−18775
- relativistic atomic structure calculations, review 79−59379
- relativistic corrections, estimation method 80−14091
- relativistic corrections, review 80−47914
- relativistic HF eqn. from QED bound states 79−21992
- relativistic theory of P violation in many-electron atoms 80−91042
- relativistic two-electron atom, level shifts, transition probabilities, perturbation theory 79−22001
- representation of reduced density (transition density) operators, symmetry role 80−52858
- rotated-coordinate method, rel. to stabilisation method 80−74097
- Rydberg constant, using a hand-calculator, for teachers 78−81765
- Rydberg formula, modified 77−26957
- Rydberg states, spectrosc. and ionis. props. 80−23303
- scalar particle in Coulomb and uniform mag. field *(Russian)* 79−3385
- scalar relativistic approximation 79−26899
- scaling and Pade approximants, perturbation theory 80−91429
- Schrodinger eqn., soln. using model statistical potential *(Russian)* 77−22444
- screened Coulomb potentials, energies calcs. 80−31452
- screened Coulomb potentials, energy levels, nonperturbative approach 78−41917
- screened Coulomb potentials, energy levels, perturbation theory appl. 78−25406
- screened photoeffect cross-sections, anal. calcs. 77−10643
- screened potential model, for at. energy levels and oscill. strengths 79−36516
- screening constants calc. 77−3252
- Singer polymals, evaluation of matrix elements 79−6813
- single-term atomic state props., variationally optimised local central pot. calcs., $2<Z<55$ 79−41123
- singly ionised atom, excited state struct., electron correl., oscill. strengths, theory 79−6889
- solar coronal ions, proton excitations approximation, erratum and extension 79−35118
- spatially degenerate levels, transitions, quasiclassical theory of atomic collisions 80−43150
- spin density of open-shell systems, pseudo-orbital theory 78−62706
- spin permutation group for transpositions, elements of representation matrices 79−31358
- spin-adapted vector method, alternative to conventional CI approach 79−54777
- spin-degenerate system, Martin-Schwinger functional differentiation method 77−30765
- spin-density functional formalism, correl. energies calcs., appls. and corrections 80−91433
- spin-dependent correlated atomic pseudopotentials 80−107686
- spin-dependent operators in the spin-free quantum chemistry 79−6817
- spin-flip dipole transitions 79−63936
- statistical model with piecewise exponentially decaying electron densities 78−13408
- strong field QED in atomic phys., Dirac eqn., autoionisation model, QFT 77−54495
- structure and collisions of ions and atoms, book 78−74554
- subshell filling order, method for determining 77−26111
- supercritical nuclei, $Z>137$, relativistic Thomas-Fermi eqn. soln. *(Russian)* 78−29748
- superheavy and intermediate atomic collision systems, UNILAC expts. 80−63751
- superheavy elements, $118<Z<138$, electronic spectra, anomalous levels 77−14331
- supermultiplets, dynamical group anal. 80−8836
- swift ions, electron state energy shift in passing through solids 80−65107
- symmetric deorthogonalisation, constrained variation method 78−37540
- symposium, Florida, USA (March 1979) 80−51946
- teaching, from Compton effect to quarks, at., proton, and nucl. struct. 78−24596
- ten-electron positive ions, ionic size rel. to Koopmans' ionisation pot. 79−85892
- tensor operators, reduced matrix elements for L-S coupled, N-electron configurations 79−13625
- theory, history of developments in USSR 79−9069
- theory, relativistic corrections 77−57891
- thermochemical properties of atoms and molecules in specific quantum states 78−68911
- Thomas Fermi model, free boundary 79−93906
- Thomas precession, new simple deduction 77−67281
- Thomas-Fermi and Thomas-Fermi-Dirac model calcs. of at. polarisabilities 77−57876
- Thomas-Fermi model, asymmetric pot., spherically symmetric solns. 77−26978
- Thomas-Fermi model, Dirac exchange and relativistic corrections, effective EM potential 79−89614
- Thomas-Fermi model, review 77−84
- Thomas-Fermi positive ions in extremely strong mag. field, $1/Z$ expansion for total energy 80−52855
- Thomas-Fermi theory, many-body atomic theory 78−21849
- Thomas-Fermi theory, stability of matter, review 77−5696
- Thomas-Fermi theory, stability of matter anal. 77−5678
- Thomson and Bohr atomic models 77−45668
- three-body problem, effective pots. in adiabatic representation 79−6819
- three-electron atoms, ground state third-order energy, Z-depend. perturb. calcs. 77−46484
- three-electron dynamics, hyperspherical coord. anal. 80−83241
- Tokamak impurity problems, atomic and mol. struct. and collision data, review 80−43959
- total energies, virial-statistical method 78−62696

atomic structure continued
- total HF SCF energy, of ats. and ions, approximation methods comparison 79−31366
- transition matrix, for arbitrary pots., matrix element calcs. 77−3249
- transition metal, 3-d, density functional theory 78−58578
- transition metal, atom and ions, mixing of $3d^n4s^k$ configurations 79−63910
- 3d-transition metal ions, s-doublet struct., appl. of exchange correlation mass operator approx. 80−106266
- transition probabilities in sudden vacancy formation in electron shell 80−37788
- transverse electron-electron interaction calc. 80−91430
- two internal-vacancy atoms, Green function calcs. *(Russian)* 78−50451
- two-body correls., variational approach 80−91455
- two-electron atom, exchange and correlation pots., density functional theory, He appl. 80−52848
- two-electron atom, long-range electron density, function reliability test 79−26875
- two-electron atom, lower band to ground state decay 80−78508
- two-electron atom, three-body problem, Feshback-Rubinow approx., nucl. screening 77−18777
- two-electron atom, trial wave function for ground state 80−78510
- two-electron atoms, autoionisable states decay, parity violation effects 79−72231
- two-electron atoms, channel invariants and SU(3) classification 78−41906
- two-electron atoms, exponential decay of sub-continuum wave functions 77−46477
- two-electron atoms, ground-state energy, Darboux functions, perturbative theory 77−23402
- two-electron atoms, nucl. charge correl. with $(r_{12}{}^n)^{-1/n}$ function 79−68178
- two-electron ions, autoionisable states decay, parity violation effects 79−72231
- two-electron systems, ground-state energy, var. calcs. 77−61679
- two-electron systems, pair function calcs. 80−32590
- two-electron systems, RPA eigenvalue eqns., excitation frequencies and oscillator strengths 78−17570
- two-internal-vacancy atoms, characts., Green's function calcs. *(Russian)* 78−50450
- two-level atom problem, Rosen-Zener solution 78−41937
- two-parameter exponential-type basis functions 80−52847
- two-parameter statistical model 78−55124
- unified theory of atoms and atomic aggregates, self consistent theory 80−102418
- unitary group generators representation matrices calcs. 78−78610
- universal atomic basis sets, light atom HF ground state energies 78−78605
- universal variational functionals of electron densities, first-order density matrices, and natural spin-orbitals and solution of the ν-representability problem 80−95516
- valence electrons local-density theory of exchange and correlation energies 80−52854
- variation-iteration procedure, by numerical integration scheme 78−17551
- variational computations, containing nonlinear parameters, nonexistence of maxima 79−6816
- variational method, metric-constrained 79−22579
- virtual levels, in three-level atoms, definition 79−44671
- volume characts., and electron correlations, one- and two-electron systems 77−3286
- wave function asymptotic coeff. for electron in atom or ion 79−26871
- weakly ionised nonrelativistic atom, props., exchange effects 79−10008
- $Z=118$, 172, 226, symm. and stability of $2(2l+1)$ electron configurations of elements 80−1100
- Z-expansion scheme, generalisation 79−36500
- (γ, e) reaction, determ. of atomic wave function, electron energy levels *(Russian)* 78−957
- Ag in SiO_2 isolation matrix, XPS, atomic electronic struct. 79−89655
- Al I to XIII, energy levels and ionisation energies, data compilation 80−14100
- $Al(^2P_{3/2})$, at. quadrupole shielding factor 79−10222
- AlS, $B^2\Pi$-$X^2\Sigma^+$ transition, assignment of UV bands, vibr. and rot. anal. 80−58278
- Ar,K inner-shell level energies, absorpt. spectroscopy with synchrotron radiation 80−99583
- Ar, $1s2s3p^4P_{5/2}{}^o$-state, relativistic effects and config. mixing 79−45640
- Ar, $2p^6$ shell, oscillator strength, photoionisation cross sections, electron shell alterations determ. *(Russian)* 80−58144
- Ar, 40 keV electron scatt. 7-200 mrad, relativistic and electron correlation effects 77−34760
- Ar atom, K-absorption spectrum, core electron rearrangement effect 80−47880
- Ar, correlation energies, second-order, by variational-perturbation study 80−908
- Ar, inner shell alignment following electron impact ionisation, distorted wave approx. calcs. 80−91682
- Ar, momentum density of electrons, two-gamma positron annihilation determ. 77−69211
- Ar, Thomas-Fermi model with Fermi-Amaldi correction 79−81156
- Ar^{2+}, levels of $2p^53p^5$ 78−74574
- Ar(I), $3p^54p$ config., level lifetimes meas. 80−102490
- As, $(4^5S_{3/2})$ state, kinetic obs. using time resolved reson. fluoresc. 78−94211
- Au, ab initio effective core pot., Dirac-Hartree-Fock and Hartree-Fock calcs. 78−33426
- Au, atomic form factor, meas. using Bragg scatt. of 412 keV gamma-radiation 79−14734
- Au in SiO_2 isolation matrix, XPS, atomic electronic struct. 79−89655
- Au, relativistic effective core pots., appl. to AuH and AuCl ab initio calcs. 78−86767
- ^{79}Au, electron impact, relativistic, L-shell ionis., $L\beta/L\alpha$ branching ratio energy depend. 79−98228
- B, spectra and energy level data tables 79−59386
- B^+, Hund's first rule, new interpretation 78−78620
- B-like ions, highly ionised, up to Fe XXII, Breit-Pauli approximation 78−53810
- ^{11}B, ground state, two-determinant numerical self-consistent at. orbitals appl. 79−93937
- Ba, $4d^{10}$ shell, photoionisation cross sections, electron shell alterations determ. *(Russian)* 80−58144
- Ba^{2+}, 3d photoabsorpt. spectra, continuum and discrete states 79−81176

atomic structure continued
- Be, exchange energies, Born-Oppenheimer exchange amplitude, Bonham series calcs. 78—29854
- Be, ground state energy, split valence GO basis set SCF calc. 77—34554
- Be, Hund's first rule, new interpretation 78—78620
- Be I, energy level calcs. using model pot. and cores approxs. 77—14353
- Be I, energy level calcs. term systems, convergence to Be II 2s limit 77—14354
- Be, isoelectronic sequence, pot. energy relationships 79—22584
- Be isoelectronic sequence, mag. dipole transition contrib. 79—81153
- Be, optical beam foil spectra, relative level populations 80—23540
- Be-type atoms in $1s^2 2s^2$ ^1S state, soln. of Hartree-Fock eqns. with nonorthogonal radial orbitals 77—46493
- Be_4 (Be_4^-), atomic clusters, electronic struct., LCAO-MO-SCF and HF calcs. 80—63880
- Bi, parity nonconservation, weak electron-electron interaction, light polarisation, vapour optical activity *(Russian)* 78—55132
- Bi, radial integral, polarisability and oscillator strength, Dirac eqn. calc. 79—22620
- ^{83}Bi, electron impact, relativistic, L-shell ionis., $L\beta/L\alpha$ branching ratio energy depend. 79—98228
- Bk, emission spectrum, 2540-9800 Å, electrodeless lamp source 80—27970
- Bk I and Bk II, lowest levels, from IR spectrum 77—68001
- Br_2-Ar, positive column at. state densities 80—44007
- C, asymmetric atom, case history for independent discovery, inductivistic model 79—25821
- C I, m-representation approach 79—45645
- C, structure, multiconfiguration optimised central pot. method calcs. 80—9515
- C^{2+}, Hund's first rule, new interpretation 78—78620
- Ca, $4p^2$ $^1S_0 - 4s4p$ $^1P_1 - 4s^2$ $^1S_0$ cascade rate, two photon coincidence meas. technique 80—95576
- Ca I to XX, energy levels and ionisation energies, data compilation 80—14101
- Ca III, atomic structure determ. by model pot. method 78—86777
- Ca, isotopes 40, 42, 44, 48, charge distrib., Hartree-Fock anal. *(Russian)* 78—70747
- Ca, quantum defect theory of oscill. strength density 79—81183
- Cd, ^1S, ^3P, ^1P states, dipole polarisabilities from compact variational trial functions 80—63568
- Ce, $fds^2 \rightarrow d^2s^2$, theoretical calc. of energy 77—62639
- Ce II, isotope shift and screening, pseudo-relativistic HF calc. 78—90096
- Cl^-, atomic core states, antishielding effects calcs. 80—83299
- Co (VII), semiempirical investigation of spectra 78—33434
- Co V spectrum analysis 79—72266
- Co^+, Rayleigh and Compton scatt., differential cross section determ. 80—52912
- Cr I to XXIV, energy levels, ionis. pots., g-factors, from spectral data review 77—79556
- Cs, $4d^{10}$ shell, photoionisation cross sections, electron shell alterations determ. *(Russian)* 80—58144
- Cs, $5p^5 6s^2$ level, Hartree-Fock calcs. 79—59349
- Cs, core charge polarisation effects, dipolar contributions 79—45631
- Cs I, $n^2S_{1/2}$ and $n^2D_{3/2,5/2}$ states, energies 80—87066
- Cs^+, 3d photoabsorpt. spectra, continuum and discrete states 79—81176
- Cu III, calc. of configurations, CI effects 77—42228
- Cu in SiO_2 isolation matrix, XPS, atomic electronic struct. 79—89655
- Cu^{2+}, in Zn (II) complex, ground state ion wavefunction calcs. 78—895
- D_3 Rydberg states, spectroscopic B_0 consts. 80—74109
- ^{160}Dy ion, electronic config. after β-decay of ^{160}Tb in $TbSi_2$ 79—59340
- Er III $4f^{12}$ configuration, spectra calcs. by configuration superposition *(Russian)* 80—14080
- Eu coexistence of 'collapse' and 'blow' states 80—32587
- F I, and isoelectronic series, Z=10-100, L-shell energy struct. and level classification 78—55129
- F II, $2p^3nl$ terms, beam-foil lifetime meas. 79—81173
- F IV, m-representation approach 79—45645
- $F^-.e^+$, positron energy levels, rel. to Rydberg levels of Na, NO 79—86089
- Fe, $3d^6 4s^2$ and $3d^7 4s$ configs., Rayleigh and Compton scatt., differential cross sections 80—52912
- Fe group ions, spectra, calcs., allowance for d^n shell pair excitations 77—42261
- Fe I levels, mean radiative lifetimes determ. 79—49987
- Fe, valence electronic struct., pseudopot. method 79—68184
- Fe X (XI), energy levels and oscill. strengths, Slater radial integrals 77—79583
- Fe XII and XIII, energy levels and oscillator strengths for XUV transitions 78—46277
- Fe XXI, relativistic energy levels, Dirac-Fock multiconfig. calc., triplet state fine struct. and Lamb shift 80—23315
- Fe XXII, coupling energy levels, oscillator strengths, electron collision energies 80—69068
- Fe^{19+}, new atomic data rel. to solar phase spectra 80—67545
- Fe^{n+}, valence electronic struct., pseudopot. method 79—68184
- Fe-group spectra, superposition configurations in semiempirical calc. 78—920
- Fe^+(Fe^{2+}), Rayleigh and Compton scatt., differential cross section determ. 80—52912
- Ga, J_1J_2 transition from LS, revised assignments for $d^9s^2p^2$, $d^9s^2p^3$ 79—45630
- Ge, J_1J_2 transition from LS, revised assignments for $d^9s^2p^2$, $d^9s^2p^3$ 79—45630
- H, 2p state alignment, influence of surface electric fields after beam foil excitation 78—29849
- H, appl. of Schrodinger eqn. *(Hungarian)* 79—3339
- H atom, Dirac and Klein-Gordon relativistic eqns., energy level splitting 80—77938
- H atom, energy level calcs. in superstrong mag. field 80—37737
- H atom, form factor for arbitrary states, dipole moment component matrix element calcs. *(Russian)* 80—58143
- H atom, relativistic model of spin 1/2 particles interacting with external EM field 78—70756
- H atom, strongly magnetised, quantum number assignments, semi-classical approach 78—90055
- H atom in box, 2-D Schroedinger equation, influence of constant elec. field, finite-element method 80—31544
- H atom theory, Schrodinger-Dirac spaces of entire functions 77—54494
- H atoms, energy levels and bound-bound transitions in strong mag. field 80—58134

atomic structure continued
- H atoms on liquid He surface, interaction and bound states 79—18131
- H bound states in strong mag. field 80—99438
- H, degenerate 3s-3d levels, in mag. field, eigenvalues, Bender-Wu formulas 80—83275
- H, electron-photon angular correlation meas. for excitation of 2P state 80—91636
- H, energy levels in strong mag. field 78—90071
- H, ground state energy in interacting system 79—18255
- H, in spherical box, SCF calcs. 77—54508
- H, in static multipole field, logarithmic perturbation expansion 80—91431
- H, in uniform electric field, level energies and widths 77—14378
- H, infinitely magnetised, energy levels rel. to props. of pulsar crust 80—77282
- H, multipole sum rules 77—42257
- H, n-dimensional atom, Kepler problem, dynamical symmetries 80—58121
- H, nonrelativistic high order perturbation theory corrections to energy levels, infinite series representation 77—34564
- H, parity mixing, relativistic neutral current interactions and nonrelativistic pots. 79—26908
- H, photon emission, Bohr theory covariant eqns., teaching 80—105482
- H, quasi-stationary states in field of strong monochromatic wave, perturbation theory calcs. *(Russian)* 80—58145
- H, relativistic energy levels in strong mag. fields 80—102454
- H, relativistic spin 1/2 particle dynamics 78—70001
- H, scalar relativistic approximation 79—26899
- H, spin-aligned atoms, theoretical props., expt. prep. 80—42969
- H, strongly bound states in intense mag. field 80—37721
- H, symmetry algebra, group theoretical derivation of Hughes-Yadegar algebra 77—17766
- H to Xe, relative sizes, density distrib. 77—75036
- H, uniform mag. field, low lying levels below 10^9 G, adiabatic approx. 79—72235
- H, wavefunctions, parabolic, polar, unitary transform. coeffs. *(Russian)* 79—3344
- H^-, $(2p^2)^3P$-state, CI series convergence 80—27955
- H^-, electronic structure, stabilisation calcs. using big mol. Gaussian SCF/CI program 79—18121
- H^- free-free transitions, target polarisation effects 79—66917
- H^-, ground state energy, post-adiabatic approx. calcs. 78—58827
- H^-, magnetic interactions of electrons *(German)* 78—82610
- H^-, multipole sum rules 77—42257
- H^-, proof of only one bound state, fixed nucleus approx. 77—30805
- H-He, H hyperfine struct. shift, commutator computational method 78—78608
- H-like atom, interacting with EM field, matrix elements and transition probabilities 78—37533
- H-like atom near metal surface, quasi-stationary spectrum 79—18132
- H-like atoms, bound states, so(2,1) algebra 79—10016
- H-positron bound state, effective one-body pot. to prove absence 78—82871
- H+ charged particle, Glauber approx. scatt. amplitude 80—14191
- H_2, magnetic interactions of electrons *(German)* 78—82610
- $H_2 + C^+(N^+)(O^+)$, reactant ion electronic states, effect on charge transfer cross sections 80—63809
- H_3, Rydberg states, spectroscopic B_0 consts. 80—74109
- ^{A}H, A=1,2,3, muonic atoms, ground state energy levels from quasipot. eqn. 80—87251
- H(1s, 2s, 2p), approx. Dirac eqn. soln., partitioning technique 80—23284
- He, 2^3P-3^3D transitions, Doppler free intermodulated optogalvanic spectroscopy obs. 80—52333
- He, channel coupling array cals. 79—31362
- He, diamag. suscept., form factor, variational method 77—18813
- He, doubly excited, supermultiplet energy levels, classification as rot.-vibr. spectrum 80—52900
- He, energy density functional, gradient corrections 78—25428
- He, energy of S states, appl. of modified interelectronic pot. 78—29736
- He, exchange energies, Born-Oppenheimer exchange amplitude, Bonham series calcs. 78—29854
- He I in solar flare, levels populations calc. 79—62809
- He isoelectronic sequence, electron correlation effects on one-electron distribs. 77—10598
- He, isoelectronic sequence, pot. energy relationships 79—22584
- He, isoelectronic sequence, Schrodinger eqn. finite difference soln. 79—31373
- He isoelectronic series, energy level and classifications of doubly-excited states 78—62736
- He isoelectronic series 79—85894
- He, l-limit energies for ground state atoms using hyperspherical basis sets 80—14076
- He, magnetic interactions of electrons *(German)* 78—82610
- He, muonic three-particle system with Coulomb interaction, correl. wavefunctions calcs. 77—68144
- He, one-dimensional atom, bound states, for teachers 79—40317
- He, RPA eigenvalue eqns., excitation frequencies and oscillator strengths 78—17570
- He to Xe, radial density functions, HF calcs. 77—42238
- He^-, 1s2s2p config., nonrelativistic energy *(Russian)* 77—75048
- He^+, neutralisation, reionisation in O_2, ion pair form., differential cross sections determ. 80—53120
- He-like ions, X-ray form factors and total scatt. X-ray intensities 79—10063
- $He + H^+$, double He ionis., polarised electron vel. distrib. effect 80—53109
- $He^+ + e^-$ system, complex quantum defects 79—13622
- Hf IV, one-electron spectra energy levels and line lists 79—49953
- Hf, neutral atom, partial level density, statistical props. of atomic energy levels 78—70732
- Hg, ^1S, ^3P, ^1P states, dipole polarisabilities from compact variational trial functions 80—63568
- Hg, 6D levels excited by dye laser, lifetimes 80—42996
- $Hg(6^3P_1) + Li^+(Na^+)(K^+)$, excitation, optical polarisation fractions and mag. sublevels obs. 78—50619
- Hγ energy levels and Debye screening, no evidence for red shift 79—31369
- Ho III, energy levels, parametric anal. of spectrum 77—46519
- Ho, K X-rays, energy shifts, role of atomic struct. 78—70777
- Ho, spectra, energy levels and hyperfine struct., parametric calcs. *(French)* 78—41984

atomic structure continued
I, state determ. following photodissoc. of KI, time of flight meas. 79−18105
I^-, 3d photoabsorpt. spectra, continuum and discrete states 79−81176
In, J_1J_2 transition from LS, revised assignments for $d^9s^2p^2$, $d^9s^2p^3$ 79−45630
In, L X-ray yields from double-vacancy states 79−49977
In V, spectrum, levels in $4d^86s$ and $4d^85d$ configs. 78−62748
K, $4^2P_{1/2}$ resonance substate, disorientation cross-section, Zeeman scanning obs. 80−42988
K I to K XIX, energy levels, tabulated data 80−51966
K, state determ. following photodissoc. of KI, time of flight meas. 79−18105
K+He(Ar)(Ne)(Xe), K 5^2P level broadening and collisional relax., quantal, semiclassical and expt. comparison 80−18903
Kr, 4p asymmetry parameter and cross section photoelectron energy depend. pseudopot. method 78−9130
Kr, atomic form factor, calculation from optimised potential model 79−6895
Kr I atom, $4p^5$ nd (n=4,5,6,7) configurations, experimental lifetimes 80−27981
Kr II, graphical multichannel quantum defect analysis 79−49972
Kr, K inner-shell level energies, absorpt. spectroscopy with synchrotron radiation 80−99583
Kr, Thomas-Fermi model with Fermi-Amaldi correction 79−81156
KrI, $4p^55p$ and $4p^56p$ configs., level radiative lifetimes meas. 78−58625
La coexistence of 'collapse' and 'blow' states 80−32587
La^{3+}, 3d photoabsorpt. spectra, continuum and discrete states 79−81176
Li, 1s2s2p config. nonrelativistic energy *(Russian)* 77−75048
Li atom, effective potentials, energy levels 80−106263
Li I, and isoelectronic series, Z=10-100, L-shell energy struct. and level classification 78−55129
Li, isoelectronic sequence, pot. energy relationships 79−22584
Li, isoelectronic series, model potential field, pseudopotential calcs. 79−59339
Li isoelectronic series, semiempirical prediction of energy levels 79−72243
Li isoelectronic series, wave functions, effective pots. and energy values 79−68182
Li, optical beam foil spectra, relative level populations 80−23540
Li, optical oscill. strengths calcs. 80−91495
Li, quartet states, absolute term values, CI calcs. 78−58596
Li^+, S-autoionising states, energy calcs. 79−36520
Li-like atoms, $^4S^e$ doubly excited states, orbital config. assignment 79−41118
$Li+H^+$, Li core excitation cross section, correlation and reorganisation effect 80−87215
$Li(^2S)$, open shell polarisation propagator, for doublet-doublet transitions calcs. 80−27939
Lu I, 5d6s6p-config., laser spectrosc. investig. 80−69096
Mg (Mg^+), lifetime meas., beam foil spectra, comparison with numerical coulomb approx. calc. 80−58367
Mg, atom, solid and MgO, electronic relax., Friedel model, KLL′ AES 77−65444
Mg, correlation energies, second-order, by variational-perturbation study 80−908
Mg, I-XII, energy levels and optical spectra 80−87065
Mg, optical beam foil spectra, relative level populations 80−23540
Mg XI resonance lines, dielectronic satellite lines atomic parameters calcs. 80−78567
Mg^{2+} atomic core states, antishielding effects calcs. 80−83299
Mg-like V XII, Cr XIII, Mn XIV and Co XVI, level struct. and predicted intercombination lines 80−14098
$Mg_4(Mg_4^-)$, atomic clusters, electronic struct., LCAO-MO-SCF and HF calcs. 80−63880
Mg^{n+}(n=9,10,11,12), ionic config. via $^{24}Mg(^{32}S,^{32}S\gamma)^{24}Mg$ 67 MeV 77−67762
Mn, energy levels, Mn I to Mn XXV, review 78−21841
Mn V, $3d^3$-$3d^24p$ transition obs. energy level assignments 78−55134
Mo XIII and XVII, spectra, perturbation theory with model pot. 78−58579
Mo XIV, spectrum and energy levels, ionisation energy 79−49954
Mo XV, electronic struct. of complex ion, relativistic perturbation theory 79−22610
Mo^{32+}, dielectronic recomb. rate coeffs. in plasma 80−43853
Mo^{38+}, dielectronic recomb. rate coeffs. in plasma 80−43852
N II, m-representation approach 79−45645
N III, VUV spectrum *(Chinese)* 80−42974
N IV, dipole lengths, dipole vels. and transition probabilities 79−35113
N isoelectronic sequence ions, atomic struct. and electron scatt. data 80−51649
N type atoms, separation effect in 2p shells *(Russian)* 77−14333
Na, $2s2p^63s^2$ term position and width 79−59347
Na atom, effective potentials, energy levels 80−106263
Na, core polarisation effect on oscillator strengths and energy level locations 78−82688
Na I, atomic spectrum, series formulas 80−99466
Na, Rydberg levels mm resonances detected by field ionis., quantum defects, Stark shifts 77−42262
Na, Rydberg states, IR Stark spectra, term energy, fine struct. 77−57910
Na^+, atomic core states, antishielding effects calcs. 80−83299
Ne, 40 keV electron scatt., 7-200 mrad, relativistic and electron correlation effects 77−34760
Ne atom, K-absorption spectrum, core electron rearrangement effect 80−47880
Ne, atomic structure determ. by model pot. method 78−86777
Ne, electron degradation spectra, inner-shell contribs. 77−3474
Ne, electron impact excitation of $2s2p^63s$ and $2s2p^63p$ configs., energy loss obs. 80−91685
Ne, energy density functional, gradient corrections 78−25428
Ne, exchange energies, Born-Oppenheimer exchange amplitude, Bonham series calcs. 78−29854
Ne, statistical model with piecewise exponentially decaying electron densities 78−13408
Ne, Thomas-Fermi model with Fermi-Amaldi correction 79−81156
Ne V, m-representation approach 79−45645
Ne^- scatt. electron spectra, distinction from neutral autoionising states 80−83482
Ni (VIII), semiempirical investigation of spectra 78−33434

atomic structure continued
Ni films, electronic struct. calc., effects of chemisorption; contact pot. and surface magnetisation 80−103734
Ni I isotope shift for stable isotopes, nuclear charge radii 80−99484
Ni IV spectrum anal., energy level classification 77−61700
Ni XII, XIII, XIV, XV, 3s-3p and 3p-3d transitions, oscillator strength and energy levels calcs. 80−83251
Ni^{2+}, Rayleigh and Compton scatt., differential cross section determ. 80−52912
Ni-Fe, electronic struct. calc., effects of chemisorption; contact pot. and surface magnetisation 80−103734
O III, electron impact excitation of semi-forbidden transitions 80−48092
O III, m-representation approach 79−45645
O ions, non-equilibrium charge state distrib. charge exchange cross-sections in solid targets 80−65109
O, isoelectronic sequences, energy spectra inc. relativistic corrections 78−924
O, two-photon absorpt., auroral transition relax. obs. *(Japanese)* 80−47954
O V, O VI, dipole lengths, dipole vels. and transition probabilities 79−35113
Os VIII, one-electron spectra energy levels and line lists 79−49953
P VI, UV spectrum, anal. 78−17595
Pb, J_1J_2 transition from LS, revised assignments for $d^9s^2p^2$, $d^9s^2p^3$ 79−45630
Pb, muonic high-lying states transitions, electron screening effects 77−34786
Pb, parity nonconservation, weak electron-electron interaction, light polarisation, vapour optical activity *(Russian)* 78−55132
Pb radial integral, polarisability and oscillator strength, Dirac eqn. calc. 79−22620
^{82}Pb, electron impact, relativistic, L-shell ionis., $L\beta/L\alpha$ branching ratio energy depend. 79−98228
^{208}Pb, muonic atom, 2Z 79−64123
Pt, ground state configs., isotope shifts and fine struct. anal., visible and UV spectra 80−42987
Pt group, even atom config., parametric calcs. 78−82631
Pt group elements, singly ionised, $(5d+6s)^N$ electronic configs. *(French)* 79−22594
Rb, 5^2S-n^2S transitions, Rydberg levels, high resolution two photon spectra obs. 80−52923
Rb I, D_2 resonance line ^{85}Rb-^{87}Rb shift, mean square charge distrib. values inversion *(French)* 77−57931
Re_3Br_9, atomic clusters, electronic struct. and photoelectron spectra 80−69287
$(Re_3Cl_{12})^{3-}$, atomic clusters, electronic struct. and photoelectron spectra 80−69287
Re_3Cl_9, atomic cluster, electronic struct. and photoelectron spectra 80−69287
reactant ion electronic states, effect on charge transfer cross sections 80−63809
Rn, Thomas-Fermi model with Fermi-Amaldi correction 79−81156
S atom, van der Waals radius, mean statistical value 77−83515
S I ground configuration, wavelengths of observed transitions between levels 78−50489
S IV, $3s^23p^2P$-$3s3p^2\ ^4P$ multiplet, energy levels and transitions, appl. to solar atm. 80−87028
SI odd parity levels, configuration interaction effects 79−72246
Sb VI, $4d^95d$ and $4d^96s$ configs., UV spectrosc. obs. 80−18817
Sb VII, spectrum obs. 600 to 2100 Å, analysis of $4d^85s$-$4d^85p$, $4d^9$-$4p^54d^{10}$ transitions 80−102471
Sc II, visible spectra and ionisation limit 80−74143
Sc IV, atomic structure determ. by model pot. method 78−86777
Si VI, $2p^43s$, $2p^43p$ and $2p^43d$ configs., UV spectrum anal. 78−21868
Sn I, Sn II, Sn III, atomic partition functions 77−26955
Sn, J_1J_2 transition from LS, revised assignments for $d^9s^2p^2$, $d^9s^2p^3$ 79−45630
$Sn^+(5s5p^2)^4P_{1/2}$ level, lifetime and Lande g-factor *(French)* 80−52938
Sr I, 5s-p and 4d-p channel interactions, quantum defect model 77−30810
Sr, Rydberg series, absorpt. by selectively laser-excited atoms 79−3390
Ta II, even-parity states, partial level density, statistical props. of atomic energy levels 78−70732
Te VII, $4d^95d$ config., UV spectrosc. obs. 80−18817
Ti, energy level data tables, Ti I to Ti XXII 79−59385
Tl, J_1J_2 transition from LS, revised assignments for $d^9s^2p^2$, $d^9s^2p^3$ 79−45630
Tl, parity nonconservation, weak electron-electron interaction, light polarisation, vapour optical activity *(Russian)* 78−55132
Tl, radial integral, polarisability and oscillator strength, Dirac eqn. calc. 79−22620
Tm IV $4f^{12}$ configuration, spectra calcs. by configuration superposition *(Russian)* 80−14080
U, atomic model 79−41095
U, high-lying levels in vapour near ionisation limit 78−21842
U I, electronic configs., HF relativistic calc., spin-orbit const.-Slater integral relation 77−18793
U, relativistic Dirac-Slater calcs. *(Japanese)* 77−42252
U^+, atomic model 79−41095
U^{4+} electron configuration from nuclear information 80−58146
U^{n+} (n=0 to 6), electronic struct., multiconfig. Dirac-Fock calcs. 79−45646
UV, energy levels and UV spectral anal. 80−106290
^{234}U, isotope shifts and inherent quadrupole moments *(French)* 79−7032
V, atom and ions, shell energy struct., SCF calc. by Dirac-Fock-Slater method 80−52877
V, energy levels in all stages of ionisation, data anal. 78−94207
V VII, VIII, IX, X, 3s-3p and 3p-3d transitions, oscillator strength and energy levels calcs. 80−83251
W VI, one-electron spectra energy levels and line lists 79−49953
Xe, $4d^{10}$ and $3d^{10}$ shell, photoionisation cross sections, electron shell alterations determ. *(Russian)* 80−58144
Xe, $5s^2$ shell, oscillator strength determ. *(Russian)* 80−58144
Xe, ab initio effective core pot., Dirac-Hartree-Fock and Hartree-Fock calcs. 78−33426
Xe compounds, Xe chemical and isomer shifts, electron valence struct. *(Russian)* 80−53056
Xe, L_1,L_2,L_3 inner-shell level energies, absorpt. spectroscopy with synchrotron radiation 80−99583

atomic structure continued
Xe like ions (I^-, Cs^+, Ba^{2+}, La^{3+}) $3d^94f$ config., collapse of 4f electron, X-ray spectral obs. *(Russian)* 80—58204
Xe, Thomas-Fermi model with Fermi-Amaldi correction 79—81156
Xe VII, VUV line classifications and energy levels in triplet system 80—37763
Xe VIII, one-electron spectrum in theta pinch discharge, line identification 80—32640
Xe+ inert gas, Xe three level system, collisional transfers, disalignment cross section 80—53098
Y^{10+}, spectrum and energy levels 80—32639
Yb, scalar relativistic approximation 79—26899
Yb^{3+}, spectrum and energy levels 79—26916
Zn, ^1S, ^3P, ^1P states, dipole polarisabilities from compact variational trial functions 80—63568
Zn XX, energy levels and one electron transitions, relativistic calculations 80—87051
Zr XI and XV, spectra, perturbation theory with model pot. 78—58579
Zr XIII, electronic struct. of complex ion, relativistic perturbation theory 79—22610
atomic structure, crystals *see crystal atomic structure*
atomic weight *see atomic mass*
atoms
see also exotic atoms; helium atoms; hydrogen neutral atoms; positronium
history, nineteenth century British atomism, A.W. Williamson and atomic theory 78—32637
parity nonconservation effects in ats. and ions 79—10086
realism and instrumentalism in 19th-century atomism 79—97172
velocity meas. in real time using laser time-of-flight velocimeter 78—46467
attaching *see joining processes*
attenuation *see absorption; dispersion (wave); scattering; transmission*
attenuation equalisers
see also attenuators
bidirectional fibre-optic data bus with T-couplers 77—19451
radiowaves, troposcatter channels and appls. of adaptive equalization techniques, statistical anal. 79—29841
step-index fibre baseband equalisation 78—1371
attenuation measurement
atmospheric, radiometer use for satellite link system *(Czech)* 78—36351
atmospheric attenuation of 1.25 and 2.0 mm waves, radiotelescopic obs. 79—34897
attenuator monitoring, computational tables and computers for efficiency improvement 77—79073
backscattering technique, appl. in fibre diagnostics and attenuation meas. 80—33188
bone, 2 to 8 MHz US attenuation obs. 79—57701
compressional wave attenuation in deep ocean sediments 80—79033
duct noise active attenuation meas. 78—90592
Earth-space path rain attenuation at 11 and 14 GHz, Darwin, Australia, satellite communications appl. 79—62541
enclosed dielectric microstrip, Schelkunoff analysis *(Spanish)* 80—45005
fibre optical cable, buried, transmission characts. meas. *(German)* 78—33865
fibre-optic cable pulse dispersion and attenuation meas. *(German)* 78—33859
frequency scaling of attenuation above 10 GHz due to rain, use of COMSAT satellites 79—5595
graded-index fibre differential mode attenuation meas. 78—1403
graded-index optical waveguide mode-dependent attenuation meas. 78—46774
MF radiowave field strength digital measurement equipment *(Japanese)* 77—82051
microwave at 36.8 GHz in sea ice, freshwater ice and snow *(Russian)* 77—5209
microwave attenuation by atmospheric water vapour at 0.869 mm *(Russian)* 77—5277
microwave meas. in human torso, 1.8-2.7 GHz 77—70517
microwave path- and area-integrated rainfall meas. 78—65414
microwave propagation at 10, 11 GHz, radiometric measurement of rain attenuation 80—67397
mm wave radar, measurements of effective sea reflectivity and attenuation due to rain at 81 GHz 79—80001
mm waves, attenuation due to rain at 74 GHz 79—80002
mm waves, rain attenuation measurements at 94 GHz 79—80000
nonsteady mag. field induction meas. by prerecorded tape signal attenuation 79—67355
optical attenuator metrological certification methods 80—91941
optical fibre, graded index, differential mode attenuation meas. 78—13797
optical fibre, immersed in high index surrounding medium 77—42614
optical fibre, measurement of attenuation, numerical aperture and input-output radiation profile 80—33186
optical fibre, measurement of attenuation and dispersion 80—33185
optical fibre attenuation, bandwidth, and refractive index meas. methods compared 80—64190
optical fibre attenuation and dispersion meas. techniques and interpretation pitfalls 78—1399
optical fibre attenuation meas., backscatter method modified for endfire launching *(German)* 78—33868
optical fibre attenuation meas. instrument 78—59138
optical fibre attenuation measurement comparison among USA manufacturers 80—58747
optical fibre backscatter attenuation measurements, optimised technique 80—53447
optical fibre cables for field trials, meas. methods *(German)* 78—50922
optical fibre characterisation techniques compared 80—64202
optical fibre insertion loss measuring set for field use 79—64357
optical fibre joint loss measurements with OTDR 79—64354
optical fibre total loss spectra, precise meas., automatic meas. system 80—64169
optical fibre variable attenuator, calibrated, expt. 77—39047
optical fibre waveguide and cable parameter meas. techniques *(German)* 78—33860
optical fibres, backscatter meas. theory *(German)* 80—91921
optical fibres, backscattering method for attenuation and connection insertion loss meas, anal. 80—58675
optical fibres, bandwidth and backscatter measurements, review 79—64356

attenuation measurement continued
optical fibres, fault location and backscattering meas. 80—64183
optical fibres, graded index, observation of differential mode attenuation using OTDR 79—46085
optical fibres, numerical aperture depend. spectral loss meas. 78—66942
optical fibres, spectral and length-depend. attenuation meas. using two-channel backscatter anal. 80—33159
optical fibres, using time-domain reflectometer 79—64355
optical fibres *(German)* 79—76864
optical fibres 80—43458
optical fibres characteristics, by improved backscattering technique 77—75669
optical fibres using bench equipment 80—58695
optical waveguides, power decay evaluation using backscatter technique 80—106599
Polish conversion to SI system of units, technical aspects *(Polish)* 77—74346
radiowave propagation at X, K bands, microwave radiometers for rain attenuation measurement 80—68254
radiowave propapation attenuation due to water vapour, microwave radiometer study at 22.235 GHz 80—72610
rain, radar and distrometer results compared with radiometer measurements, microwave transmissions appl. 79—62542
RF instrumentation based on superconducting quantum interference 78—57995
satellite Earth path, in the freq., bands 20 to 30 GHz 78—7822
satellite radio path at 20 GHz, measuring ATS-6 satellite and radar system 79—20912
satellite relay signals, 30 GHz, attenuation due to weather *(Dutch)* 78—7741
seismic Rayleigh waves, inversion of global average group vels. and attenuation coeffs. 79—12090
seismic Rayleigh waves attenuation and group vel., regionalisation and pure path models 79—12091
swept-frequency technique, for attenuator calibration 77—18021
thin film optical waveguide, attenuation due to roughness-induced mode coupling 79—10408
underground optical cable transmission meas. 78—50942
US propagation in paper fibre suspension, modelling 77—27447
vacuum gauge calibration, attenuation meas. on buffer gas scatt. of mol. beam *(French)* 79—58669
very-low-dose ion implantation by scatt. attenuation 79—77617
VSWR indicator, type 6953A, ICs, performance, specification 77—53935
$LiNbO_3$, aluminum-coated YZ, measurements of SAW attenuation 80—74619

attenuators
see also waveguide attenuators
active, for medical US pulse-echo systems 77—40835
calibration, swept-frequency technique 77—18021
optical, for TEM_{00} mode laser beam, using collimators and iris diaphragm *(Japanese)* 79—98378
optical, review *(Japanese)* 79—98475
optical attenuator metrological certification methods 80—91941

attitude control
aircraft, ballistic descent, stabilisation transient processes 77—53395
artificial Earth satellites, low-altitude, appl. of altitude control techniques 79—25441
artificial satellite, spin-stabilised, nutation damping *(Russian)* 77—64626
artificial satellite equipped with two gyroscopes, planar oscills. 79—62714
artificial satellite stabilization system optimal parameters allowing for atm. resistance 79—62715
artificial satellite with gravitational attitude control, dynamics 77—25905
astronomical telescopes, computer appls. 78—4111
biaxial optical guider for rocket-borne solar obs. *(Polish)* 78—61744
control moment gyroscopes, single-gimbal, geometric theory 79—21738
dual-spin satellite magnetic attitude control system, geomag. field effects 78—65484
Earth resource satellite attitude meas. and control requirements 78—65482
Earth satellite, combination turning manoeuvre of orbital plane with constraints on motion 77—64592
Earth surface obs. satellite remote sensor/attitude control system interface 78—65481
Earth surface obs. satellites and remote sensor/attitude control interface 78—45182
geomagnetic aspect horizontal component sensor *(Japanese)* 78—24421
geostationary satellite, semi-passive attitude control and trajectory stabilisation 77—41282
gyroscope speed-optimal EM correction of magnetized rotor *(Russian)* 79—9227
gyrostabilized platform, nonlinear response to transient input 78—30219
HEAO-B X-ray telescope orbiting observatory, aspect system providing absolute referencing to celestial sphere 78—40791
INTELSAT IV, in-orbit liquid slosh tests, anal. 78—81516
Large Space Telescope, optimal manoeuvring and fine pointing control with annular momentum storage device 77—22078
Large Space Telescope optimal fine pointing control using Annular Momentum Control Device 77—73934
magnetic damper for satellite stability, asymptotic theory *(Russian)* 79—30496
magnetic sensor in Bhaskara satellite 80—72746
Multipurpose Utility Pointing and Stabilisation System *(Italian)* 77—82114
and orbit control systems, conference, Noordwijk (1977) 78—65480
orbital station, two-stage force gyroscopes system *(Russian)* 79—30458
orientation stability of double spin satellite 77—53398
Quadrant Photosil Autoguider for Cambridge Schmidt telescope 77—60612
rigid body attitude control in inertial space *(Russian)* 79—9101
rocket, monoaxial controlled solar pointer for atmospheric occultation meas. *(Japancse)* 78—32312
rocket attitude control, solar sensor system pointing accuracy *(Japanese)* 78—24420
rocket solar sensor data processing cct. *(Japanese)* 78—24423
SAS-3 X-ray astronomical satellite, system using gyro 77—2326
satellite, gravitational stabilization system, optimum parameters 77—41280
satellite, spinning notion, optimal nutation damping by flywheel 77—53396

attitude control continued

- satellite orientation, optimal parameters of passive systems 77—41279
- satellite stabiliser system with 2-stage suspension, dynamics *(Russian)* 79—32222
- satellite stabilizer system, rate-optimal parameters 78—69641
- satellite under aerodynamic torque, total stability anal. 77—56805
- satellite-gyrostat reorientation, optimal attitude control 80—61980
- satellites, gyrodampers in passive control system 78—96379
- satellites attitude control, inertially fixed pitch stabilisation by solar radiation press. 80—101523
- SIRIO satellite dynamics and control in geostationary orbit *(Italian)* 77—82108
- Skylark rocket, using magnetometers and Moon sensor 79—25436
- solar radiation pressure and orientation control of rotating spacecraft 77—53397
- solar radiation pressure induced orbital perturbation analysis 78—89041
- sounding rocket, attitude sensing using albedo sensor 79—101044
- sounding rocket attitude estimation using star sensor data 79—25435
- sounding rocket attitude stabilisation H_2O_2 jet system *(Japanese)* 78—28482
- sounding rocket three-axis attitude control system *(Japanese)* 78—24422
- space station motion, mechanical model, rotational stability *(Russian)* 79—35095
- space telescope, low-cost, pointing control system 77—5430
- Space Telescope pointing control fine guidance subsystem design 80—82201
- space vehicle descent to surface of atmosphere-less planet, optimal control 78—16265
- space vehicles, star pattern recognition using CCD star sensors 78—96380
- space vehicles, thrust-aided sub-orbits 78—45181
- space vehicles station-keeping manoeuvre, operational requirements and geometry 78—45180
- spacecraft, meteoroid impacts effect on attitude motion, analytical model 78—73608
- spacecraft, optimal aerodynamic attitude control 80—77250
- spacecraft, rotation control by mass ejection 77—41278
- spacecraft instrum. package reliability enhancement technique 77—29623
- Spacelab Instrument Pointing Subsystem 79—25447
- Spacelab passive atm. sounders, attitude control and stabilisation 78—65483
- telescope, orbiting, celestial object sighting accuracy anal. 78—4057
- telescope pointing and stabilisation by fine control of secondary mirror 77—82124
- undirected Earth satellite, estimate of attitude precision 77—64593
- X-ray telescope, balloon-borne, attitude control system for telescope pointing *(Japanese)* 79—80220

audio acoustics

- *see also audio recording; audio systems; hearing; speech*
- acoustical communication theory, computation of modulation and carrier functions of an arbitrary audio signal 80—79064
- application of communication theory to acoustics, separation of sound carrier and modulating signal 80—79063
- auditoria speech amplification space and electro-acoustics study *(Dutch)* 77—68330
- auditoriums sound insulation *(Japanese)* 79—81635
- concert halls, hearing impressions of loudspeaker reproductions and orchestras *(German)* 78—94485
- domestic room acoustics, speaker positioning for optimum frequency response 77—54845
- earphones, stereophonic reproduction with control of special transfer functions through head movements *(German)* 78—20182
- equalisers as universal sound quality control instruments *(German)* 79—64399
- finite element simulation of acoustic transmission system with radiation 79—3862
- frequency analyzer for room quality meas. for HiFi *(German)* 79—46140
- Hi-Fi sound reproduction, listening tests in preference to acoustic measurements 79—83792
- interior acoustics CAD *(Polish)* 78—59205
- mobile sound reinforcement system for musical performances in New York City parks 78—1509
- psychoacoustic and sound recording, book 77—826
- room acoustics and subjective sound perception, computer simulation *(Polish)* 79—7258
- sound diffusion systems, fundamentals calc. *(Spanish)* 79—3855
- stereo perception space, in intensive stereophony (quadrophony) *(Czech)* 79—68491
- TV and motion picture stages, noise and insulation 78—79169

audio amplifiers *see audio-frequency amplifiers*

audio equipment

- *see also audio-frequency amplifiers; gramophones; loudspeakers; microphones; pick-ups*
- AC-DC comparator, for AF current and voltage meas. 77—18024
- architectural aspects, intelligible and uniform sound production in Westphalen Hall, Dortmund *(German)* 79—1029
- audiometer, Bekesy-type, for clinical use 78—3499
- cinema industry Soviet, survey *(Russian)* 78—29201
- clinical device for simultaneous multiple auscultation, portable 77—56507
- decibel, definition, meter calibration and hi-fi equipment *(Spanish)* 79—54092
- digital reverberation and echo apparatus *(German)* 79—50554
- distortions of audio instrums., pulse response and transient nonlinearities *(Japanese)* 79—18658
- earphones, comparison of DT 48, TDH 49, and TDH 39 types 79—94438
- earphones, stereophonic reproduction with control of special transfer functions through head movements *(German)* 78—20182
- electronic 80—106682
- four-channel percussion synthesiser using 5700 type modules, construction details 80—106681
- HP3582A spectrum analyser using digital signal processing 80—43567
- Hungarian developments, BEAG activities 78—46860
- metronome, accentuated beat, ETI, using 555 timers 78—46864
- mobile sound reinforcement system for musical performances in New York City parks 78—1509
- multichannel audio monitor for detecting electrical signals, neurophysiological expt. appl. 79—20694
- oscillator, modified transistor radio, for teachers 78—81772

audio equipment continued

- polymer piezoelectric transducer appls. 79—32169
- production association Ecran, 25 years of achievement in cinematographic, TV industry *(Russian)* 80—62770
- real time system for acoustic measurement and analysis and its applications *(Japanese)* 79—68522
- reverberation changes in concert halls, using electroacoustic method *(Czech)* 78—1514
- sound recording equipment for use in cinematography *(Russian)* 77—74540
- spatial hearing problems, stereophony, quadraphony appl. *(German)* 79—16213
- stereophony, reproduction of sound effects using microphone and headphones *(German)* 79—37106

audio-frequency amplifiers

- auditory training apparatus, individual for persons suffering from severe hearing loss 79—39590
- compensating circuit for audio system functions *(Japanese)* 80—53566
- differential capacitance displacement transducer with low power lock-in amplifier 77—49710
- digital lock-in amplifier simulation 77—151
- high-gain, narrow-band, amplifier using active filters for ionosphere measurement 77—56760
- medium-scale live concert sound reinforcement system requirements 80—92012
- outdoor classical music sound reinforcement systems compared 80—92011
- power matching with loudspeakers *(Japanese)* 79—90106

audio recording

- acoustical research laboratory design for the Rensselaer Polytechnic Institute 77—80036
- broadcasting and recording studios, computer-aided method for acoustical design 79—64402
- cinecameras, Super 8 appl. *(German)* 79—80707
- cinefilm, acoustoelectric data on 35 mm magnetic tapes, magnetic tracks for 70, 16 and S8 mm film prints *(Russian)* 79—18665
- cinefilm sound track quality improvement *(Russian)* 80—288
- cinematography, anamorphic super-8 wide-screen prints with stereophonic sound 80—282
- cinematography, magnetic sound records release print KMP-23 *(Russian)* 80—90918
- cinematography, post-synchronization recording equipment KZM-24 *(Russian)* 80—86482
- cinematography, recording equipment for 35, 32 mm film *(Russian)* 79—89024
- cinematography rerecording panel 70K-21, modernisation of indicator desk *(Russian)* 80—37114
- commentary to photographic slides, signal level drop operates automatic slide changer 77—65060
- digital coding of high-quality musical sound 80—5883
- digital photographic sound track recording optimisation *(Russian)* 78—89580
- digital systems for use in cinematography *(Russian)* 79—27487
- dual message tape preparation, for dichotic listening research 78—57010
- dual track sound, picture recording, mixing system, cinematography appl. *(Russian)* 79—17532
- dummy head design comparisons 79—18656
- editing 16 mm film and magnetic tape sound recording by time-code system 78—24875
- educational aids, synchronising visual to audio material 77—57135
- electronic modification of room acoustics in a concert hall 77—3702
- equipment and services, 1979 video yearbook 79—14197
- film projection, sound track synchronisation, new system *(German)* 79—67402
- film sound tracks, electronic cutting, thyristor appl. *(Russian)* 78—21252
- film soundtracks, low-cost pure, undistorted sound 79—27476
- Fourier transform recording and playback system, hypothetical cct. and characts. 79—3879
- head-related stereophonic recording techniques, dummy head method 78—61286
- holographic, general principles 77—34844
- holographic disc with high data transfer rate, audio response memory appl. 80—58477
- holographic recording on photographic film *(German)* 78—22101
- holography, sequential information retrieval 77—7024
- impulsive noise reduction on gramophone records 80—87689
- laser modulating device 6 record sound track of variable width *(Russian)* 80—1399
- limiter, frequency-selective, for correction of speech sound track defects *(Russian)* 79—27486
- Macquarie University lectures, tape recording via dual channel microphone amplifier 79—71210
- magnetic tape recording synchronisation with 16 mm film, time-code system appl. 78—24874
- magnetic tapes, electroacoustic characteristics, multiple printing appl. *(Russian)* 77—38048
- microphone techniques, practical and aesthetic 80—5885
- microphone techniques for recording and broadcasting symphonic music, comments and reply 80—53595
- motion picture sound recording and reproduction using a holographic method *(Russian)* 79—10273
- motion picture sound track, freq. distortion and two dimens. sound record scatt. *(Russian)* 80—95175
- motion picture sound track films, appl. of computer program simulation of recording and reproducing system 80—62767
- noise eval. in motion picture studio recording room *(Russian)* 78—55518
- PCM audio disc *(Japanese)* 79—27484
- peak level meter with LEDs *(Spanish)* 77—37936
- photographic, computer simulation 78—78022
- photographic sound negative film, Eastman sound recording II film, 5373/7373 80—62768
- photographic sound tracks, increasing quality for release prints, direct positive recording process *(Russian)* 79—9255
- physics homework solutions, recording methods 80—77573
- psychoacoustic and sound recording, book 77—826
- purported Bigfoot vocalisation record pitch and vocal tract length estimates 79—94418

audio recording continued
  read head for magnetic tape recorders using magneto-resistance principle 80—87688
  recent magnetic sound recording tape *(Japanese)* 80—33406
  sound stage, cinema acoustics *(Russian)* 79—18609
  stereophonic, head-related, special artificial head design *(German)* 78—40199
  stereophonic transmission, head-related method, technical problems *(German)* 78—38156
  stereophony, artificial head, tone meas. *(German)* 80—106702
  studio specification and design, Supreme Being Studios 79—64400
  studios, shortcomings of apparently improved acoustic designs 80—69601
  symphonic music, practical and aesthetic microphone techniques, comments 80—79073
  transformations in acoustical transduction based on optical principles 80—53594
  Zimdex audio indexing system, efficiency 79—92915
  Te film and trilayer antireflection structure for optical recording 79—94329
audio systems
  see also acoustic devices; acoustic equipment
  acoustic feedback's influence on speech intelligibility 80—23859
  audiometric tests, automatic operation using a programmable system, hardware *(Italian)* 77—5006
  Bayerischer Rundfunk carnival, acoustical problems, measurement and audience comparisons *(German)* 78—13860
  club noise control by electronic power reduction 78—51004
  concert hall sound system for touring quartet 80—92013
  digital, future prospects *(Japanese)* 80—83725
  digital signal processing, spurious signals and their suppression *(Czech)* 79—98555
  echo and reverberation generation, electronic ccts. *(German)* 79—32138
  loudspeaker system amplitude and phase response rel. to driver alignment on baffle 80—92010
  medium-scale live concert sound reinforcement system requirements 80—92012
  multidesktop distributed sound system in large room, in-depth time delay spectrometry study of early late arrivals 80—38179
  outdoor classical music sound reinforcement systems compared 80—92011
  psychosomatic clinic audio-visual communication system 79—83997
  room acoustics and audio visual design for board rooms 79—37092
  room influence on music rendering, unified sound field anal. *(German)* 77—11092
  sound diffusion systems, fundamentals calc. *(Spanish)* 79—3855
  sound reinforcement, for large multi-purpose rooms *(German)* 77—80019
  sound system design aid, HP 97 program 78—75015
  source elevation illusions, created by spectral manipulation using monaural hearing 78—3510
  stereophony, auditory cues, importance of transients 79—88090
  system function, design of compensating cct., state-space methods *(Japanese)* 80—53566
  technical laboratory, Toshiba Audio Center 79—55284
  transmission function in rooms rel. to acoustic amplification systems 78—59204
  triphonic sound reproduction system using coincident microphones 80—28405
auditory activity *see hearing*
auditory perception *see hearing*
Auger effect
  A15-superconductor, surface characterisation by energy loss spectra, AES and HEED 77—24635
  acetylene, mol. and cluster Auger spectrum calc., SCF core-valence-valence spectra 80—48045
  actinides, K-shell fluorescence yields from Auger electrons and X-rays, precision meas. 79—31462
  adhesion, surface anal. techniques appl. 80—65381
  adhesion measurement, locus of failure, bond failure in adhesive joints 80—50801
  admiralty brass, stress corrosion cracking, aqueous $CuSO_4$ 77—59961
  adsorbates, thermal desorption and conversion kinetics, AES study 78—71959
  adsorbates deep level spectroscopy, many body effects 80—39441
  adsorbed layers, photoelectron spectra, review 79—52072
  adsorbed monolayer, quantitative analysis 77—85851
  adsorption on Pt electrode surface, struct. and comp. exam. by LEED and AES 79—70342
  AES, anal. techniques 79—43691
  AES, electronics design 79—30615
  AES, ESCA and SIMS analysis of thin films, expt. *(Hungarian)* 77—4952
  AES, ionisation enhanced diffusion effect obs. 80—71497
  AES, microarea anal. system with submicron anal. capacity, performance tests 78—73106
  AES, quantitative, parameters, appls. 79—43697
  AES depth profiling, appl. of tailored modulation techniques 77—15702
  AES of surfaces 78—85277
  AES-LEED, satellite vac. system with sample transfer capability 77—7639
  AES/APS self-convolution inversion, FFT and digital signal processing 79—71430
  airborne particles, surface toxic elements, ion microprobe and Auger electron spectrometric anal. 78—7753
  alkali graphite intercalation cpds., selection rules and restricted valence band self-convolution for KVV Auger transition 80—29832
  alkali halide, coloured crystal, possibility of Auger effect as result of positron capture 78—14381
  alkali halide, with oppositely charged defect centres, autoionisation-tunnel relax. of electron excitation 78—72112
  alkali halides, photoelectric yield spectra, 10 to 40 eV photon energy 79—28887
  alkali intercalated graphite, C XVV Auger lineshape anal. 80—104019
  alkaline earth vapour, soft X-ray gain 77—23655
  alloy, binary, calibration line introduction for comp. determ. by AES 79—56892
  alloy, binary, surface phase diagram, electron spectroscopy 77—24469
  alloy, chemical induced segregation, obs. by Auger fine struct. anal. 78—15416
  alloy systems, sputtering and AES 80—50503
Auger effect continued
  alloys, binary, surface composition, regular soln. theory 78—10265
  alloys, embrittling residuals categorisation by Auger electron spectroscopy 80—66739
  alloys, oxidation, spectral lineshapes and shifts 78—14600
  alloys, with second phase precipitates, transient sputtering characteristics, glow discharge optical spectroscopy meas. 77—44156
  amino acid overlayers, static SIMS exam. 79—83074
  angle resolved Auger surface spectroscopy, for chemisorbed atoms on metal surface 77—28694
  angular resolved Auger emission, expt. results and predictions from simple model 78—39635
  apparatus for low energy in scatt. spectroscopy, LEED and AES *(Japanese)* 80—20746
  appearance pot. spectrometer design, demonstrations 80—105477
  appearance potential spectroscopy, apparatus 80—101888
  appearance potential spectroscopy, core level spectroscopy *(Japanese)* 80—50473
  APS, extended fine struct. analysis 79—28863
  atom, electron impact ionis., X-ray and Auger spectra, ang. distrib., polaris. 77—75305
  atom, free, modified $Z/(Z+1)$ approx. for Auger electron energies 77—42300
  atom, inner-shell ionisation, fluoresc. X-ray ang. depend. 77—10649
  atom, inner-shell multiplet, Auger transition rate calc. 77—6743
  atom, inner-shell photoionis., anisotropy of X-rays and Auger electrons 78—58633
  atom, intermediate and heavy, relative probabilites of KLM and KLN Auger transitions 78—17639
  atom, KLL Auger spectrum, new developments, line energies, intensities 77—18868
  atom, L-subshell Auger and Coster-Kronig rates and fluorescence yields, relativistic calcs. 79—81180
  atom, multielectron, correlated transitions in decay of two inner-shell vacancies 80—37799
  atom, outer shell ionisation, ang. distribs. and polaris. of charact. X-rays and Auger electrons 79—10205
  atom, post-collision interactions, near-threshold inner-shell photoionisation 77—68021
  atom, with two inner-shell vacancies, correlated transitions 80—23386
  atom, $Z=37$-56, Coster-Kronig transition thresholds 79—68214
  atom+heavy ion, K-shell excitation, absolute cross section, $0<Z<11$, 40-600 keV 79—41231
  atom Breit interaction between electrons, calc. angular coeffs., computer program 80—18779
  atomic collision, coherence and correlation, book 80—90615
  atomic collisions, fast particle electron emission, line shape, acceptance function effects 80—37787
  atomic collisions, quasi-molecule Auger decay 78—62899
  atomic inner shell electron props., relativistic effects 77—18803
  atomic inner shell ionisation phenomena, conf., Freiburg, West Germany (Mar.-Apr. '76) 77—27040
  atomic inner-shell ionisation, post-collision photoelectron-Auger electron interactions 77—18870
  atomic orbital non-orthogonality, Wentzel Ansatz 77—18871
  atomic screening model for solid-state effects 77—73194
  atoms, K and L shell, radiative and radiationless yields 79—76376
  atoms, natural linewidths of KLL Auger lines 79—76383
  atoms, one-photon decay of two-hole states *(Russian)* 77—79592
  atoms with two inner-shell vacancies, three-electron Auger transitions 77—19049
  Auger radiation effect with γ-ray emission 77—50417
  backscattering factor, estimation for low atomic number elements and their alloys 78—72649
  backscattering factor, Monte Carlo method calc. 80—7449
  ball bearings, surface comp., AES and ion sputter profiling 77—40465
  beam brightness modulation, in Auger scanning microscopy 79—16097
  beam foil spectroscopy, extensions, lifetime meas., book contrib. 78—74758
  benzene, adsorbed on Pt (111) surface, Auger spectra 79—52077
  benzene, chemisorption on (111) surface of Pt, LEED and Auger spectroscopy obs. 78—30823
  bimetallic strip, interface struct., scanning Auger microprobe study 80—34322
  binary alloy, relative sensitivity factors for quantitative Auger analysis 77—32861
  binary alloys, detection of compositional homogeneities using ion-induced Auger electron spectroscopy 80—25514
  binary alloys, homogeneous, surface anal. using quantitative AES 79—24395
  binary alloys, relative sensitivity factors by quantitative Auger analysis 77—60151
  binary metal alloys, quantitative analysis *(Polish)* 78—76967
  blanking resistive heating for Auger spectroscopy and LEED using retarding field analyzer 78—54509
  brass, Auger spectral anal. of oxide corrosion films, quantitative methods 78—35557
  brass, nondestructive determ. of in-depth profile 80—93836
  α-brass, stress corrosion fracture surface anal. by AES 80—104321
  α-brass stress corrosion cracking in nontarnishing ammoniacal environment, fractography, chemical anal. 77—40466
  bremsstrahlung-induced Auger peaks, utility in spectroscopy 79—30618
  bremsstrahlung-induced Auger peaks 80—45199
  bronze, Al, wear on 13% Cr steel in presence of aviation fuel, Auger electron spectroscopy study 80—11781
  bronze P, friction with steel, boundary lubrication conditions, element conc. anal. of films 78—85001
  carriers bound to centres involving phonons, Auger recomb. 80—107805
  cascade background correction, Auger peaks, Cu(110) surface appl. 79—43079
  catalyst, polycryst., oxidation, spectral lineshapes and shifts 78—14600
  cathode workshop, conf., Washington, DC, USA (Jan.-Feb. 1978) 79—43068
  ceramics SEM and anal. techniques *(German)* 78—56832
  chemical information from Auger spectra, gas and solid phase investigs. 80—3434
  chemical state effects in AES 78—72687
  chemical state effects in AES 78—92566
  chemisorbed mol. and cluster Auger spectrum calc., SCF core-valence-valence spectra 80—48045
  chloromethanes, Auger electron spectra and chem. shift 78—90231

Auger effect continued
coating characterisation 77—31919
coating chemical characterisation by surface and near-surface sensitive techniques 79—15053
cobalt phthalocyanine film, sorption of O_2 and water, AES obs. 78—91531
codeposited with S on (111) surface, AES and photoelectron spectra 78—71957
composition and structure of engineering and industrial materials, instrumentation 77—4882
composition depth profiling sputtering times, conc. gradient effect *(French)* 80—76116
compositional depth profiling by Auger electron spectroscopy 79—52053
computer control of spectrometers in microanalysis lab. *(German)* 77—52686
configuration with incomplete shell, Auger transition probability, LS and JJ coupling cases 77—42302
contact resistance probing and Auger analysis of contaminants, combined technique 80—39662
core hole relaxation energies 78—80439
corrosion science, surface analytic techniques 80—31929
crystalline solids, electronic industry, chem. anal. instrumental methods progress 80—66903
cylindrical mirror analyser 78—24899
cylindrical mirror analyser system for AES, Auger electron appearance pot. spectroscopy and disappearance pot. spectroscopy 78—23986
cylindrical mirror electron spectrometer, for gas and metal vapour obs. 79—63326
data acquisition of Auger and line optical information 78—63019
deconvolution, electron loss data as unit impulse response function 79—9265
degenerate semiconductor, phonon-assisted Auger recomb. 77—59292
depth profile analysis, influence of impurity gases in UHV systems 78—76958
depth profile determ. using spherical erosion and scanning Auger electron spectroscopy 80—11994
depth profiles by sputtering in SIMS and AES 79—56891
depth profiling, line shape changes correction 77—40605
depth profiling techniques for thin film interdiffusion and interfacial reactions, book contrib. 79—1564
depth profiling with ${N_2}^+$ ion sputtering 77—16889
diamond, inelastic scatt. differential cross-sections 77—76652
diamond, total secondary electron emission spectrum 77—72759
diamond-Si heterostructure, Auger spectra electron microscopy study 80—34340
diffusion in grain boundaries, determ. using surface anal. 77—11742
digital acquisition and processing, of Auger spectra 79—43698
digital scanning Auger electron microscope 78—12797
dilute alloy, matrix effects in quantitative Auger analysis 79—69927
dimethyl ether, condensed multilayers, electron bombard. effects, AES line-shape anal., XPS, and desorption meas. 80—7450
Dirac-Slater potential, hole and exchange terms, influence on internal conversion coeffs. 80—952
double vacancy states, correl. photon and electron transition, perturbation theory 80—27968
Earth ionosphere and plasmasphere, fluxes and spectra of Auger electrons and photoelectrons 78—45094
elastic and inelastic contribs. to secondary electron yield struct. 78—72642
electrode-electrolyte interface, solid film props., review of expt. techniques 77—77780
electron emission from nuclear accelerator targets *(Russian)* 79—49335
electron energy loss struct. in Auger anal. 79—47559
electron gun use of glow discharge lamp for Auger spectroscopy 77—31027
electron interactions with solids, conf., Southampton, England (Apr. 1976) 77—44570
electron ion collisions, distorted wave theory, Auger ionis. and excitation fluoresc. 79—7018
electron meas. with double proportional counter 79—81129
electron microprobe Auger spectrometer with ultra high vac. SEM capability *(Japanese)* 78—27849
electron rearrangement in K X-ray spectra due to heavy ion bombardment 77—85846
electron spectrometer with microcomputer-based multiplexer for performing depth profiling 79—67435
electron spectroscopic quantitative surface analysis 78—92552
electron spectroscopy appls., review *(Japanese)* 79—40645
electron spectroscopy blanking resistive heating cct. 77—29078
electron spectroscopy of crystals, book 80—36786
electron stimulated desorption data, chemisorbed systems, reinterpretation in Auger decay model 79—42375
electron-hole droplet phonon wind 80—107707
electron-hole drops, non-radiative recombination by phonon-assisted Auger recomb. 79—60716
electronic and at. collisions, conf., Kyoto, Japan (Aug.-Sept. 1979) 80—57011
electronic material and device characterisation using surface-sensitive analytical techniques 80—65341
elements, Auger electron emission, relax. energies, excited atom model 80—40192
elements $10 \leq Z \leq 100$, semiempirical Auger electron energies 78—62774
energy referencing of AES from charging samples by implanted inert gas spectra 80—40196
epitaxial growth, vapour phase, growth mode characterisation 78—87885
epitaxial growth mode, numerical confirmation of Palmberg's criterion 77—11812
epitaxy, growth modes, exp. techniques, book contrib. 80—49558
ESCA, principles and appls. 78—27375
ESCA studies of Ga, As, GaAs,Ga_2O_3, As_2O_3 and As_2O_5 78—92171
ESCA using X-ray photons >1500 eV, Au M_α X-rays (2123 eV) 78—72683
ethylene, adsorbed on Pt (111) surface, Auger spectra 79—52077
ethylene, mol. and cluster Auger spectrum calc., SCF core-valence-valence spectra 80—48045
EXAFS in photoelectron yield spectra 80—16123
EXAFS-Auger process for surface struct. anal. 77—51580
exploding wire photon sources induced electron emission spectra, yield and energy meas. 78—31299
extra-atomic relax. energies, rel. to Auger parameters 80—87090

Auger effect continued
fast projectile electron spectroscopy, autoionizing ion levels and lifetimes 77—38749
field emission micro SEM, for UHV surface anal. 80—86519
film analysis using computer-controlled Auger spectrometer, digital methods 77—56268
film sandwich structures Auger anal. 78—72030
film-substrate bond strength, meas. by laser spallation 80—50821
fracture, ionisation wave generation, microbreakdown mechanism 79—33032
free atoms, diagram Auger electron spectra 80—78585
free metal atoms photoelectron and Auger spectra, core level energies 78—50522
free surfaces, apparatus for Mossbauer effect emission and AES, appl. to ^{57}Co on Ni (111) 79—80735
GaAs, Schottky barrier, effect of oxide composition on elec. behaviour, AES meas. 79—87141
GaP/In_xGa_{1-x}P/GaAs:(Cs-O) high sensitivity transmission photocathodes, photosensitivity, electron diffusion length 79—78832
gas-surface interactions, mol. beam apparatus 78—72675
geometrically induced structure on SXAPS and Auger electron appearance potential spectra 79—38695
glass, adsorption of Au, AES study, electron bombardment effects 80—65380
glass envelope for H_2 dissociator, used in atomic clock, AES obs. of degradation 77—61876
glass surface anal. by AES 78—60013
glass-metal seals, Auger spectroscopy study of interface 80—76587
glasses, high vol. low cost, as solar reflectors, compositions and weathering effects 80—106589
grain boundary segregation, critical assessment 80—75362
graphite, AES/APS self-convolution inversion, FFT and digital signal processing 79—71430
graphite, Auger electron appearance potential spectroscopy *(Japanese)* 80—50473
graphite, energetic ion sputtering, appl. of AES-SIMS (IMA)-FDS combined systems to physical and chemical processes 78—95636
graphite, sintered powder, energy losses, secondary electron spectra, AES, and EELS 79—99997
graphite, surface cleaning, air cleavage and UHV cleavage, obs. using Au decoration 78—80665
graphite, XPS and Auger KVV valence band spectra 78—11028
graphite (0001), Xe adsorption and desorption kinetics 77—72782
graphite monolayer on Ni (110) surface, oxidation mechanism 80—101037
graphite surface, adsorbed Cs, dissolution, lamellar cpd. form. *(French)* 80—100399
graphite-alkali metal intercalation cpds., electronic props. 80—45202
gridless cylindrical mirror analyser for electron energy meas. 79—71563
guanidinium aluminium sulphate hexahydrate, surface obs., SEM and AES expts. 80—71362
Hastelloy, H_2 embrittlement in H_2S environment impurity segregation effects, AES study 80—71724
Hastelloy B-2, corroded surface, electron bombardment effect during Auger electron anal. 80—61014
Hastelloy B-2, decomposition of metal oxide films under electron bombardment 78—19928
Hastelloy C-276, cold worked, annealed, surface segregation, Auger spectroscopy study 79—83204
heavy atom, L-shell Auger and Coster-Kronig intensities from relativistic theory 79—93962
heavy ion+at. collisions using GSI linear accelerator, X-ray production, appls. 77—19041
heavy ion beam-foil spectra, ion equilib. excitation, density effect 77—19056
heavy ion-atom collisions, inner shell ionis. X-ray emission and Auger spectra obs., appls. *(Japanese)* 78—9240
high resolution Auger photoelectron spectrometer 77—48704
high resolution spectroscopy in SEM, electron sources 77—25330
high-resolution AES in diffusion-pumped SEM 77—40515
hole states of free atoms, SCF theory 77—10610
hydrocarbons, substituted, chemisorbed monolayers on Pt (100) surface, AES quantitative anal., calibration 78—31724
II-VI semiconductors surface struct., LEED and AES *(Japanese)* 78—22943
III-V semiconductor, oxide coatings by thermal and anodic oxidation 77—32706
III-V semiconductor, surface protection by KCl layer, obs. 77—89628
III-V semiconductors, Auger coeffs. calc., appl. to GaSb 79—15160
impact ionisation thresholds, as generalisation of van Hove singularities 77—77295
impurity flux in scrape off layer of Tokamaks TFR 400 and 600 79—652
$In_{1-x}Ga_xSb$ film, epitaxial growth by multitarget RF sputtering, composition determ. by AES 77—44157
Incoloy 800, high temp. oxidation in low O_2 pressures, SEM obs. of oxide morphologies, Auger spectra 79—47844
inelastic electron reflection role, model, and expt. check for Al 78—11027
inert gases, inner-shell optical photon excitation, Auger, autoionisation, photoionisation processes 77—18867
inner shell electron excitation by heavy ion collisions 80—37875
inner shell excitation processes in heavy ion-atom collisions, review 80—37874
inner shell ionisation by electron or proton impact, coincidence exptl. method, theory 80—1066
inner-shell vacancy creation, ionised fragments probability distrib. 80—83274
n-InP, magneto-impurity resonances, obs. of central cell struct. 78—95303
instrumental distortion of Auger spectra, cylindrical energy analyzer construction 78—8469
insulating film, Auger depth profiling by angle lapping 78—53287
insulators, chemical state identification, Auger and photoelectron lineshapes and chem. shifts 77—32855
integral Auger spectra, tailored waveform modulation calc. 77—32860
interface composition determ. methods 79—70396
internal photoemission peaks 78—52621
ion+atom (molecule), slow collisions, K-shell excitation, impact parameter depend. 79—72388

Auger effect continued

- ion+atom collision, nonadiabatic transitions between decaying states *(Russian)* 77—10754
- ion+atom collisions, Auger spectra, book contrib. 78—74756
- ion Auger spectroscopy and chemical binding of atoms in a compound 80—11528
- ion beam material characterisation, conf., Aleria, Corsica (Sept. 1976) 79—96403
- ion bombarded surfaces, energy analysed SIMS with Auger and XPS meas. 79—4457
- ion bombardment induced, main features 80—100730
- ion bombardment of solid surfaces, appl. to surface anal. *(French)* 77—66563
- ion deposition techniques, AES exam. of surface cleaning methods 79—15878
- ion desorption by core hole Auger decay 78—48262
- ion impact induced in metals 80—71545
- ion induced Auger spectroscopy for surface anal. 80—55756
- ion irradiated solids, energy spectra of Auger electrons, possible surface diagnostic method 79—69946
- ion microprobe analysis using ion-induced AES 80—30305
- ion-atom collisions, high resolution spectroscopy of Auger electrons 77—83558
- ion-bombardment Auger spectroscopy for studying surfaces of solids 79—20497
- ion-etch profiles, interface position determ., nomographic method 77—89658
- ion-excited Auger emission from sample trays in Auger-sputter profiling study 78—52607
- ion-induced X-ray prod., solid-effects 77—77326
- ionically bonded surfaces, stability in ionising environments, core hole Auger decay mechanism 80—29457
- ions, photon stimulated desorption obs. 79—82459
- ions, positive, dielectronic recomb. in plasma generalised cascade theory 80—43851
- ions emerging from C foils, mean charge, inner-shell vacancy effects 80—87219
- K-LL Auger spectra in intermediate-coupling scheme with CI, relativistic Dirac Hartree Slater calc. 80—52958
- K-LL Auger spectrum, relativistic calc. 77—18872
- K-shell Auger rates, level widths and fluoresc. yields, relativistic Dirac Hartree Slater calc. 80—52957
- K-shell ionisation, X-ray or Auger-electron prod. by ion impact, cross section tables 79—54947
- Kane model, three-band, Auger recombination overlap integrals, kp approx. *(Russian)* 78—87897
- keratin-NaCl, Na Auger electron spectra 78—53339
- kinetic and relax. energies in atoms and solids 78—15297
- KLL Auger transition energies, relativistic multiconfig. calcs. 77—18873
- KLL O Auger lines, intensity ratios in different cpds. 79—87531
- L-LM Coster-Kronig processes, role in Auger spectroscopy 78—56548
- laser fusion targets, vapour deposited coatings, surface finish obs. 78—60863
- LEED-AES system, three-grid type *(Japanese)* 79—55618
- LEED/Auger spectroscopy system, retractable rear viewing system 80—57434
- light atom collisions, $2p\pi$ orbital transitions Auger study *(Russian)* 80—91639
- light elements, $Z>10$, K-LL Auger process, review 78—50523
- light metal, surface effects on X-ray level widths 79—47147
- lineshape anal. of molecules and solids 80—76113
- lineshape determ. by numerical integration background subtraction 79—74469
- (LMM) Auger electron emission by keV Ar$^+$ bombardment 79—95880
- LSI surface analytical techniques applied to electronic components [Si LSI chip inspection] 80—81392
- lubrication, spectroscopic methods for surface anal. *(French)* 80—26095
- lunar soil, relationship between surface chemistry and albedo, Auger electron spectroscopy 77—60677
- M-shell radiationless transitions, subshell fluoresc., Coster Kronig yields and X-ray linewidths, relativistic Dirac Hartree Slater calcs. 80—52959
- MBE, obs. by LEED-AES *(Japanese)* 78—91564
- mesic and muonic mol. ion formation in liq. He, X-ray intensities, Auger and Stark transitions 78—94338
- metal, narrow band, quasiatomic Auger spectra 78—60536
- metal, narrow-band, quasiatomic Auger spectra and electron correl. effects 77—81183
- metal, oxidation, Auger electron, X-ray fluoresc. spectroscopy appls. 77—44412
- metal, valence band Auger spectra, effect of edge anomaly 79—69908
- metal embrittlement, Auger electron spectrographic anal. *(Chinese)* 79—38982
- metal film and foil, surface IR wave propag. distance, imperfection and oxidation effects 77—28641
- metal nuclei evaporated on to C, SiO$_2$ films, atm. contamination, AES meas. 77—4264
- metal oxidation, O Auger peak studies 77—1769
- metal oxide ultrathin layers by reactive sputtering, controlled deposition and characterisation, AES 79—78887
- metal oxides, Auger quantitative anal. 78—73104
- metal silicides, fabrication technique and characterisation *(Japanese)* 80—60779
- metal substrate, thin film form., appl. of AES and ESCA *(French)* 80—50903
- metal surface, AES anal. in adhesion, friction and wear 78—53179
- metal surface, chemisorption, vac. UV photoelectron spectrometer for study *(Japanese)* 78—62264
- metal surface, reactivity, review of electron spectra 77—62748
- metal surfaces, clean, AES anal., contamination effects obs. 78—53293
- metal vapours, at. inner-shell optical photon excitations, Auger, autoionisation, photoionisation processes 77—18867
- metal-InP contacts, intermediate adsorbed layer effect on electronic props. 80—39674
- metal-oxide system characterisation by high-resolution electron spectroscopy 77—40624
- metal-semiconductor contact, Auger depth profiling 79—78177
- metal-semiconductor interfacial reaction, AES study *(Japanese)* 80—96701
- metal-semiconductor system, interfacial reaction, dynamical obs. at room temp. using AES 80—10798

Auger effect continued

- metal-semiconductor thin film preparation under UHV conditions 78—72733
- metallic film continuity, observations by Auger spectroscopy 78—64433
- metallic glass, bulk and surface properties, review 80—44147
- metallic thin film, multilayered, depth profiling, improved depth resolution by reactive ion sputtering 79—91557
- metallography appl. 79—91883
- metallurgical applications of XPS, AES, and SIMS *(French)* 80—81253
- metallurgy, use of combined ion-, electron-beam techniques 79—43700
- metals, alloys and oxides, AES investigation of corrosion and growth nature of surface layers 77—77330
- metals, chemisorption of gases, book 79—69370
- metals, in hostile environments, oxidation, in situ meas. method 78—44277
- metals, narrow-band, Auger line shape 80—60719
- methane, mol. and cluster Auger spectrum calc., SCF core-valence-valence spectra 80—48045
- methane+X^{n+}, (X=Ar,Kr,Xe,U), Auger emission line shape after dissoc. 78—86838
- methanol, condensed multilayers, electron bombard. effects, AES lineshape anal., XPS, and desorption meas. 80—7450
- micro Auger analysis, using field emission source 80—104020
- micro-Auger analysis, ratio technique 77—32862
- micro-organisms irradiated with monoenergetic X-rays, biological consequences of Auger effect 79—11969
- microanalysis, general principles, experiments and appl. *(French)* 79—8468
- microanalysis, high resolution, review 80—40792
- microanalysis, in SEM 80—101058
- microanalysis, sample sandwiched between anode and converter *(French)* 79—74471
- microanalysis of solid matter in a scanning electron microscope *(Czech)* 79—8465
- microbeam anal., conf., Ann Arbor, MI, USA (June 1978) 79—39258
- microcomputer controlled Auger microprobe 80—81414
- microscopy, Auger electron, instrumental capabilities 78—70227
- microscopy, scanning Auger, backscattered electron lateral resolution effects 78—15262
- MIS solar cells, interface problems, AES, SIMS and XPS study 80—89627
- MIS structures, AES depth profiles, factors affecting depth resolution 79—15567
- MNOS structure, Auger depth profiling and ion sputtering of interfaces 77—20200
- MNOS structure, depth chem. profiling by AES 77—89875
- MNOS structures, Auger depth profiling by Ar ion sputtering 77—55613
- molecular break-up in mol. ion collision with solid and gaseous targets 79—45814
- molecule, electron impact, K-shell electrons excitation with high energy resolution, review 80—37899
- monolayer coverage, determ. by AES, appl. to C on Pt 79—46916
- monolayer overgrowth obs. in Auger electron spectra 77—85081
- multialkaline antimonides, (Sb, Na, K, Cs) type, photoemission rel. to chem. struct. *(French)* 78—39655
- multicentre Auger matrix element, ang. depend. calc. for solids and adsorbate systems 78—92151
- muonic atom cascade program, X-ray calcs. and cataloguing 78—90323
- muonic atoms, conversion Auger transition rate, s-shell electron effects *(Russian)* 77—75349
- narrow gap semiconductors, recombination mechanisms, review 80—96905
- Ni, oxidation in air, 50-150°C, film growth obs. using AES and contact resist. 80—3242
- Ni (100) surface, adsorption of H$_2$S and S, ang. distrib. of S Auger emission 77—32475
- Ni-Co, H$_2$ embrittlement, heat treatment and impurities effect, Auger anal. 80—76331
- nonrelativistic K Auger transition probability calcs. 77—30840
- organo tin polymers, glow discharge formed, interface composition and adhesion 79—82467
- organo-tin polymer films, glow discharge prep., comp. determ. by XPS and AES 80—35109
- oxidation induced by ion or electron bombardment, AES-SIMS study 80—108606
- oxide surface, in-situ obs. using galvanic cells 78—19615
- oxide thickness measurements up to 120 Å on silicon and aluminium using the chemically shifted Auger spectra 78—23586
- oxides of third-row elements, Auger LVV transitions, X-ray photoelectrons and emission spectra 78—21978
- p$^+$-n$^-$-n$^+$ pulsed diodes, forward pulsed case, voltage transient response 80—60071
- p-i-n structure, forward biased, with band to band Auger recombination, numerical simulation 79—7879
- PDX vacuum vessel, glow discharge conditioning 80—79607
- peak-height ratios, EM field effects 77—86424
- Permalloy, magnetic head wear resistance and surface charact. against magnetic tape *(Japanese)* 80—35335
- Permalloy film, corrosion induced defects, scanning Auger microscopy 77—40464
- Permalloy film, oxidation, quartz cryst. microbalance, AES and XPS obs. 78—27676
- Permalloy film oxidation, microbalance, AES, ESCA and sputter profiling 78—15600
- Permalloy films, oxidation effects on atmospheric corrosion, AES, XPS and ion sputtering anal. 80—11829
- Permalloys, wear by magnetic tape, AES *(Japanese)* 78—39916
- phosphosilicate glass, AES quantitative anal., electron irrad. induced surface comp. changes 77—48709
- photoelectron spectra, Auger electron spectra of atomic Fano resonances 80—93454
- photoelectron spectra formation in upper atmosphere, role of Auger processes 79—2403
- photon-induced Auger emission, deep-hole interferences 79—43098
- photovoltaics and absorber/reflectors, diffusion, chemical reactions, contamination, AES and SIMS 80—72066
- pionic atom, X-ray intensity, at. no. variation, Z=5-90 80—43212
- pionic atoms, Auger electron emission from C, N, O, Ag, Br *(Russian)* 80—69271
- pionic atoms, electron screening and inner shell refilling, X-ray 80—78729

Auger effect continued
plasma anodisation, mass transfer from cathode to anode, Auger spectra 78—35583
plasmon effects in electron spectroscopies of valence state 78—56098
pollutant particles, characterised by AES and XPS 79—43694
poly(alkyl methacrylate) films, chemical characterisation from C Auger spectra, appl. of pattern recognition and factor anal. 79—79347
polyacetylene: AsF$_5$, X-ray and UV photoemission spectra, Auger spectra 79—98150
polyacetylene:AsF$_5$, AES, XPS, UPS, and X-ray induced 80—66400
polyacetylene X-ray and UV photoemission spectra, Auger spectra 79—98150
polymer film on Pt, energy losses, secondary electron spectra, AES, and EELS 79—99997
positive ions, photoionisation and Auger effect 78—90135
prep. by evap. and ion plating, AES determ. of comp. profiles 77—89675
principles, developments and applics. of Auger electron spectroscopy 78—35781
pseudobinary systems, internal calibration technique for quantitative analysis, AES 77—36834
pyrographite, surface struct., amorphisation, secondary electron spectra and AES 79—43077
qualitative and quantitative surface analysis appls. of AES, review 77—90704
quantitative, spectroscopy, background determ. method 77—1968
quantitative AES, backscattering effects, review 80—81398
quantitative AES, Monte Carlo calc. 80—84813
quantitative anal. of impurities *(Japanese)* 78—91356
quantitative depth profile, by AES *(Japanese)* 80—16751
quantitative spectrometry, applic. to impurity segregation and depth profiling 78—19611
quantitative spectrometry, formalism for surface conc. calcs. 78—19612
radiationless Auger-recombination of electrons on three centres *(Russian)* 79—78114
radioisotope Auger electrons, use in low energy electron range meas. 80—70257
rare earth films, Auger emission from excited atoms 77—20967
rare earth fluorides, as antirefl. coatings, evaluation 77—61963
rare earth hexaborides, thermoelectronic props. rel. to surface state *(French)* 79—69950
rare earth hydrides, form. by rare earth reaction with H$_2$O vapour 80—76504
RHEED-AES combined system, simultaneous struct. and comp. information 78—47216
Rydberg states, Auger and radiative transition probabilities 79—6923
S and S^{2-} states, identification from Auger line shapes 79—92034
scanning Auger electron microscope, analytical techniques 79—79359
scanning Auger electron microscope, calc. of effects of backscattered electrons on spatial resolution 80—81412
scanning Auger electron microscope, Monte Carlo calc. of spatial resolution 78—41383
scanning Auger electron microscope, spatial resolution, Monte Carlo calcs., Ag edge on W profiles 79—85204
scanning Auger electron microscopy, appl. of square wave modulation technique 78—14257
scanning Auger electron microscopy, Monte Carlo calc. 78—19610
scanning Auger microanalysis, charge buildup reduction technique 79—17569
scanning Auger microanalysis, review 79—43699
scanning Auger microscopy, appl. of new integral field emission gun with small spot size 79—75663
scanning Auger microscopy, developments 80—101909
scanning Auger microscopy, effect of backscatt. electrons on resolution 79—2898
scanning Auger microscopy, effects of backscattering on resolution 80—104021
scanning Auger microscopy, resolution, quantification and sensitivity 80—81411
scanning Auger microscopy for analysis of biological material 80—73535
scanning Auger microscopy of Pd on UHV-cleaved mica substrate 80—80149
scanning electron excited AES, appl. to cathode studies 79—40643
scanning electron microscope with field emission gun for solid surface studies *(Czech)* 79—6240
scanning microprobe, approach to damage-free anal. 80—89581
scanning microprobe, backscattered electron images, tailored modulation techniques appl. 80—68305
scanning microprobe, with computerised image processing 80—68304
scanning microscope using microprobe with thermal field emission source 80—68297
scanning microscopy, S/N aspects 80—71993
secondary electron emission spectroscopy of solid surfaces, review 77—36326
SEM, edge effect, Monte Carlo simulation 79—1801
SEM, spatial resolution *(Japanese)* 78—21278
SEM, synchronous modulation technique 79—17570
SEM, with beam brightness modulation *(Hungarian)* 78—29210
SEM microanalysis techniques, review 80—71995
SEM voltage contrast mode at semiconductor surfaces and Auger electron spectroscopy, anal. of conditions *(Czech)* 79—35897
SEM with ultrahigh vacuum system for surface physics expts. 78—38925
SEM-AES-IMA combination with SIM spectrometer, Si device anal. appls. *(Japanese)* 78—85249
semi-empirical models for electron energy calcs. 78—50519
semiconductor, Auger recombination, carrier density depend. 79—38089
semiconductor, Auger recombination cross sections associated with deep centres 78—47810
semiconductor, Auger recombination rate, nonequilib. carrier distrib. 80—65578
semiconductor, Auger transition probability, phonon-assisted 79—15120
semiconductor, bound excitons, review, book contrib. 80—44519
semiconductor, dimaond-like narrow-gap, Auger recomb. calc. 78—63978
semiconductor, highly doped and highly excited, Auger coefficients 79—19606
semiconductor, highly excited, photomagnetoelectric effect under Auger recombination 80—44664
semiconductor, indirect band gap, Auger recomb. of electron-hole drops 78—39600
semiconductor, narrow gap, mag. quantum oscills. of Auger transition rate 77—69340

Auger effect continued
semiconductor, phonon-assisted Auger recomb., scatt. mechanisms 77—85804
semiconductor, phonon-assisted Auger recomb. transition probability 77—44064
semiconductor, photodesorption, role of C 77—36787
semiconductor, recombination enhanced defect reactions 79—38094
semiconductor substrate, work function rel. to AES *(French)* 80—50479
semiconductor substrate surface, low loss electron and Auger images correl. 78—22944
semiconductor thin films and heterojunctions, grain boundary and interdiffusion studies, AES and SIMS 79—77842
semiconductor wafer defects, study by ASLEEP, SEM and scanning AES 79—19256
semiconductor-oxide interface and Schottky barriers, photoemission and Auger spectroscopy 80—50536
semiconductors, Auger and radiative recombination of acceptor bound excitons 79—47023
semiconductors, Auger recombination processes 79—38091
semiconductors, Auger recombination with traps 80—49763
semiconductors, cryst. growth and defects, appl. of analytical techniques for observation 80—73546
semiconductors, impact ionisation, Auger recombination involving traps 80—80912
semiconductors, impact ionisation theory 80—49752
semiconductors, intervalley electron-electron scattering effect on optical transitions 80—108267
semiconductors, nonradiative recombination, combination of Auger and many-phonon processes 79—87111
semiconductors, phonon assisted electron impact ionisation and Auger recombination, theory 80—39591
semiconductors, recombination processes, review 79—38088
semiconductors, scatt. influence on Auger transitions depend. of impact ionisation on electron energy 80—44608
Sendust alloy, magnetic head wear resistance and surface characts. against mag. tape *(Japanese)* 80—35335
sheet steels, carbonaceous residue, chemical characterisation from C Auger spectra, appl. of pattern recognition and factor anal. 79—79347
Si:H amorphous layers, ion bombard., AES study, $L_1L_{23}V$ Coster-Kronig transition 79—99992
SiC (6H) thermal oxide layers, AES *(Japanese)* 79—96386
silane layers, reactive ion etching and Auger electron spectra 79—24394
SIMS-AES-X-ray photoelectron spectral analysis system, for solids anal. 79—39268
SIMS/AES, instrumentation and appls. in Japan 79—35883
single crystals with lowered work function, secondary and Auger electron emission anisotropy 80—100716
soda-lime glass, depth profiles of Na and Ca by SIMS and AES 78—51805
soft X-ray induced electron emission, yield and energy spectrum prediction 78—31297
solar cell, Auger recombination limit on efficiency at high level of illumination 80—108797
solid, density of states of two interacting holes 77—1348
solid, photon-induced Auger emission, deep-hole interferences 79—95900
solid, semi-empirical Auger electron energies 77—73193
solid laser dynamics, Auger recombination effects 80—69398
solid surface, Auger electron spectroscopy, review 79—92043
solid surface, Auger neutralisation of slow protons 78—72668
solid surface and thin film anal. methods, review 79—34410
solid surface and thin film analysis 78—80825
solid surface characterisation techniques, review 78—22945
solid surfaces meas. appl., in combination with threshold-potential spectrometer 80—52365
solid-solid interface chemistry, characterisation, theory 80—75448
solids, two hole reson. in XVV Auger spectra 78—11029
solids Auger XVV spectra, many body effects in incompletely filled bands, theory 80—7448
specimen charging control for SIMS and AES of insulators 80—101875
spectral, convolution and deconvolution 78—52601
spectral analysis, by computer *(French)* 80—7890
spectrometer, with electrostatic prism electron optics 79—29437
spectrometer for surface studies, including AES 79—58849
spectrometry, analytic approach 80—50474
spectrometry, electron gun beam current control for improved stability 80—84814
spectroscopy, Au-refractory film interdiffusion obs., in combination with other scattering techniques 80—65308
spectroscopy, data acquisition control using HP 9845 desktop computer 79—21726
spectroscopy, directional effects, review *(French)* 80—47153
spectroscopy, instrument function of cylindrical energy analyzer in raster Auger spectroscopy 80—42886
spectroscopy, low-energy detectability enhancement 80—22477
sputter, depth profile improvement using two ion guns 80—71964
sputtered atoms from SiO$_2$, neutralisation and de-excitation 77—16446
sputtering, preferred, phenomenological model for SIMS and Auger profiling 80—55254
sputtering yield meas. on first wall materials of thermonuclear fusion devices *(Japanese)* 77—85865
stainless steel, austenitic, surface, interaction with O$_2$, AES and work function obs. 80—65364
stainless steel passivating film, comp., AES obs. 77—48571
static AES, appls. to surface reaction and submonolayer adsorption 78—84685
steel, alloy, HY130, temper embrittlement due to Si intergranular segregation, effect on H$_2$ induced cracking 78—76735
steel, alloy, Ni-Cr-Mn, type 4340 intergranular brittle fracture, exam. by impact testing and Auger spectroscopy 78—52978
steel, austenitic, Cr-Ni, ion-implanted N, chem. state study by AES and XPS 80—79825
steel, austenitic stainless, Cr-Ni-Mo (21,6,9 wt.%), N$_2$-strengthened, surface segregation of B, Auger and XPS spectra 79—90854
steel, austenitic stainless, grain boundary segregation studies, intergranular fracturing technique for stress corrosion cracking investigation 79—39057
steel, austenitic stainless, high temp. oxidation, high temp., in low O$_2$ press., surface anal., impurity diffusion effects 77—56142
steel, austenitic stainless, temper embrittled, type 304, Auger spectroscopic exam. of grain boundary surface phases 78—76741

Auger effect continued

- steel, austenitic stainless type AISI 304, surface comp. after different surface treatments 80—3253
- steel, austenitic stainless type AISI 316, L sheet and LN plate surface comp. after different surface treatments 80—3253
- steel, austenitic type 304, temper embrittlement and surface segregation an AES and ionization loss spectroscopy study 79—43372
- steel, bearing, type AISI 52100, tricresyl phosphate treated, Auger anal. 79—52413
- steel, C (1 wt.%), intergranular segregation of C and P in as-quenched state, AES *(Japanese)* 78—19764
- steel, C (1 wt.%), intergranular segregation of Cr, Mn, Sn in as-quenched state, AES *(Japanese)* 78—19764
- steel, C-Mo-P, intergranular fracture and grain boundary segregation, P, H, Mo effects *(Japanese)* 79—15775
- steel, C-Ni-Cr (0.6, 1, 1 wt.%), grain boundary segregation of S, N, P, As, Sb and Bi *(Japanese)* 78—15405
- steel, cold-rolled, good and bad paintability, AES, SEM and X-ray diffr. characterisation of surfaces 79—42344
- steel, cold-rolled sheet, surface chemistry 80—61146
- steel, continuously cast, segregation at halfway cracks 80—60869
- steel, Cr (1.7 and 2.5 wt.%), segregation of S and P to prior austenite grain boundary, stress effect *(Japanese)* 77—55962
- steel, Cr (9 wt.%), oxidation in CO_2, early stages study by AES 78—7080
- steel, Cr-Mo:P (2.25, 1 wt.%), stress relief cracking, effect of P segregation 80—89324
- steel, Cr-Ni (2.25, 1 wt.%), role of Mo in P-induced temper embrittlement 80—35316
- steel, Cr-Ni-Mo, 'spots' *(Chinese)* 80—104248
- steel, ferritic stainless, Cr-Mo, Mo effect on pitting pot., AES anal. 78—95852
- steel, ferritic stainless (26 wt.% Cr) passivation, cathodic reduction and AES anal. 77—90500
- steel, galvanised, interface struct., scanning Auger microprobe study 80—34322
- steel, high strength, sulphide stress cracking props., density and distrib. of intergranular sulphide effects 79—74291
- steel, industrial, surface chem. characterisation by SIMS, glow discharge spectrometry and other techniques 80—66907
- steel, low alloy, crack form. during stress relief in heated zones *(German)* 79—74242
- steel, low alloy, Mn determ. by AES and APS 79—48001
- steel, low alloy, rel. between over-heating embrittlement and behaviour of S, Auger spectroscopy anal. *(Japanese)* 79—79088
- steel, low alloy Mn-Sb(2, 0.12 wt.%), reversibility of temper embrittlement, studied by XPS and AES 77—32667
- steel, low C, cold rolled, graphite precip. and S segregation, AES investigation *(Japanese)* 80—89222
- steel, low-C, structural, with Zr impurities, grain boundaries, AES 79—24524
- steel, maraging, Ni (18 wt.%), grain boundary precipitation, scanning Auger electron obs. 78—3132
- steel, mild, surface analysis rel. to annealing *(French)* 77—32857
- steel, Mn and Mn-Ti, cryogenic mech. props. and intergranular brittleness *(Korean)* 79—70164
- steel, Ni-Cr, (4,1, wt.%), isothermal embrittlement, AES exam. of grain boundary segregation 78—60814
- steel, Ni-Cr, cast, tempering embrittlement due to impurities, Auger spectroscopy exam. 80—11683
- steel, Ni-Cr, intergranular segregation of P in austenite, grain boundary coherency depend. 78—84761
- steel, Ni-Cr, temper embrittlement, intermediate tempering treatments 80—60944
- steel, Ni-Cr, temper embrittlement by Sb, Ni, Cr effects 77—36628
- steel, Ni-Cr, temper embrittlement by Sn 77—86149
- steel, Ni-Cr temper embrittlement by P 77—40448
- steel, room temp. O_2 adsorption in ultra-high vacuum system 77—20188
- steel, stainless, corrosion and grain boundary penetration on exposure to coal gasification environment 80—61003
- steel, stainless, Cr, Mo effects on passivation AES and electrochemical anal. 79—74292
- steel, stainless, Cr-Mn (21, 14 wt.%), grain boundary precipitation and fracture *(Japanese)* 79—100149
- steel, stainless, depth profiling of passive film by quantitative AES 78—19611
- steel, stainless, EN58E, Auger spectra and interpretation 78—27354
- steel, stainless, heat treated, oxide comp. and corrosion susceptibility of grades 410 and 430, AES study 80—66692
- steel, stainless, N-implanted, type 304, surface hardness and abrasive wear resist. 80—50746
- steel, stainless, O_2 desorpt. during laser irrad., etching, AES study 80—66338
- steel, stainless, quantitative AES with computer evaluation 78—76949
- steel, stainless, sputtering yield meas. using AES 80—18654
- steel, stainless, surface cleaning by H^+ bombard., AES study 78—53022
- steel, stainless, type 304, sputtering yield of first oxide layers by substrate Auger meas. 79—95889
- steel, stainless, type 304, surface treatment effect on protium uptake, AES anal. 77—59984
- steel, stainless, type 316, surface comp. rel. to crevice corrosion initiation 80—93680
- steel, stainless 304, Auger electron appearance potential spectroscopy *(Japanese)* 80—50473
- steel, stainless 316, ion sputtered, surface anal. by Auguer effect and SEM 78—95632
- steel, stainless casts, creep ductility, Auger spectroscopy study 80—60917
- steel, stainless type 304, AES of stoichiometric Cr carbides and carbide precipitates at grain boundaries 80—3055
- steel, stainless type 304, surface cleanup and sputtered ion production, AES and SIMS obs. 79—66209
- steel, stainless wear by magnetic tape, Auger spectroscopy exam. *(Japanese)* 78—39916
- steel, ultra high strength, P induced 350°C embrittlement 79—57099
- steels, stainless, surface characterisation rel. to adhesive bonding chem. etching, SEM, AES, XPS and electron probe microanal. 80—88416
- STEM, UHV, for thin foil anal. *(German)* 78—12794
- surface, density of states, information from self-deconvolution of Auger band-type spectra 78—92150
- surface, use of vacuum ultramicrobalance 79—71465
- surface AES with secondary emission imaging 78—11475

Auger effect continued

- surface anal., deconvolution of exptl. curves *(French)* 80—16153
- surface analysis, AES and ESCA combined with SEM *(French)* 80—47154
- surface analysis, appl. to lubrication problems, review *(French)* 80—45616
- surface analysis, electron probe methods, AES, electron stimulated desorpt. 77—44098
- surface analysis, electron-excited core level spectroscopies, book contrib. 77—63503
- surface analysis, in space exploration, analytical appls. of Auger and XPS 78—35756
- surface analysis, low beam current density Auger spectroscopy 78—15748
- surface analysis, review of AES technique and applications 78—68946
- surface analysis, spectroscopic methods, review *(Chinese)* 79—34414
- surface analysis, system, modular combined ESCA, UPS, AES, and SIMS 78—73107
- surface analysis by synchrotron radiation and sputter Auger techniques 78—61130
- surface analysis of thin films *(Hungarian)* 80—54537
- surface analysis techniques, AES, ESCA, and photoelectron spectroscopy 79—95252
- surface analysis techniques 79—70411
- surface analysis techniques and appls., symposium, Dayton, USA (Jun. 1979) 80—62363
- surface analytical techniques, quantification, review 80—65342
- surface and bulk microanalysis, electron spectroscopy apparatus *(French)* 80—47151
- surface and thin film, chemical analysis, comparative survey of methods, book contrib. 79—66393
- surface characterisation, multiple technique instrument, ESCA, scanning Auger, UPS and SIMS 78—73108
- surface characterisation, physical methods, review *(French)* 80—7889
- surface characterisation, XPS and AES techniques 77—32495
- surface chemical analysis, direct comparison of AES and ESCA 77—1969
- surface chemical bonding, electron spectroscopy, book contrib. 80—24992
- surface cleaning and depth profiling, effects due to probing electrons and sputtering 77—90706
- surface comp. profiles by Auger spectroscopy and ion etching 77—90223
- surface composition, quantitative anal., review 79—24854
- surface composition quantitative analysis, effect of electron escape depth 77—21452
- surface EXAFS study of adsorbate Auger electron intensity on single cryst. surfaces 78—66562
- surface impurities, in ISX-A Tokamak, AES obs. 79—82097
- surface impurities during start up and early operation of ISX-A, surface anal. with sample transfer 79—654
- surface impurity spectral analysis 77—15671
- surface layers, photon induced ion desorption, surface atom core ionisation, Auger decay 80—59809
- surface microstructure determ. and microanalysis by ultrahigh vacuum field emission gun SEM 80—96423
- surface problems, in materials science and technology, conference, Gothenburg, Sweden, June 1979 80—51950
- surface science, conf., York, England (March 1977) 78—14540
- surface segregation, effect on metallurgical props, SIMS, XPS and AES *(French)* 80—80045
- surface struct. anal. using extended X-ray absorpt. fine struct.-Auger process 77—11768
- surface structure analysis at high press. 78—73103
- surface techniques, AES, ESCA and SIMS 77—56187
- surface topography development during depth profiling in AES, sputter-etching effects 79—46900
- surface trace analysis *(Japanese)* 78—40102
- surfaces and interfaces, analysis by combined Auger, X-ray and SEM studies 80—81413
- surfaces and thin film studies by combined system of SIMS, AES and XPS 80—86536
- surfaces and thin films, combined ion, electron and X-ray beams for anal. and struct. determ. 77—86412
- synchrotron radiation techniques for studying atomic physics 80—63583
- synchrotron sources for low energy AES 80—77913
- tensile fracture device for Auger electron spectroscopy 80—73530
- tetrachloromethane, Auger emission anomalous spectra and yield, chemical species depend. 78—55152
- tetrafluoromethane, Auger emission anomalous spectra and yield, chemical species depend. 78—55152
- tetrafluoromethane, Auger transition energies, transition state approx. SCF Xα calc. 77—65426
- thin film, and surface anal., modern methods 80—54486
- thin film, sputter profiling, combined Auger-X-ray anal. 80—66909
- thin film analysis and characterisation, conf., Les Arcs, France (Jan. 1978) *(French)* 79—8466
- thin film fabrication for photothermal solar convertors 80—11573
- thin film growth mode determination *(Japanese)* 78—22975
- thin film structures, chemical anal. by Auger spectroscopy *(Russian)* 78—92581
- thin films, surface anal., survey of ESCA, AES, SIMS, and ISS *(Hungarian)* 80—70544
- thin films and surfaces, ultra-high vacuum system for preparation and anal. 79—69986
- thin foils, chem. anal. by electron microscopy *(French)* 80—50899
- three electron Auger transitions at K-vacancies *(Russian)* 78—959
- Three-electron Auger transitions in atoms with two inner shell vacancies 78—62900
- tinplate surfaces, Auger depth profiling and anal. 80—59768
- Tokamak, ISX-A, wall conditioning by low power discharge, AES and residual gas anal. 79—90438
- Tokamak discharge chamber, AES anal. *(Russian)* 79—4163
- Tokamak first-wall characterisation by in situ Auger electron spectroscopy 78—5022
- Tokamak gettering, Ti thin films, H absorption and desorption, Auger electron spectrosc. 80—75092
- transition energies, frozen orbital calc. method 79—18168
- transition energies calcs., contributions from beyond relativistic HF limit 77—18874
- transition intensities, calc. for quantitative solid surface analysis using AES *(German)* 79—34400

Auger effect continued
transition metal, 3d, electron-electron interaction, X-ray excited Auger spectra 78—91631
transition metal, 3d, energy parameter, Auger spectra, quasi-atomic behaviour 77—20966
transition metal, CO adsorpt. obs. 77—35818
transition metal carbides, coated emitters, thermionic emission props., rel. to surface composition *(Japanese)* 77—40322
transition metal carbonyl complexes, UV and X-ray photoelectron spectra, effect of adsorbed CO 79—4897
transition metal oxides, surface oxidation, study by AES 80—45175
transition metal oxides, UPS, LEED and AES studies of mol. adsorption 79—4480
transition metals, 3d, electron delocalisation and characterisation of L_3MN Auger spectra 77—48315
transition metals, Auger relaxation energy theory 80—7446
transition metals, first row, high resolution LMM AES 78—15263
transition metals, $K \rightarrow M^2$ radiative Auger effect, low energy satellites meas. 80—45174
transition potentials, for ESCA and Auger spectra, equiv. cores and Hellmann-Feynman calcs. 77—61724
ultra-high vacuum SEM technique exam., secondary electron emission dependence on electron beam density dose 80—61209
ultrathin film thickness meas. by AES 79—35663
upper atmosphere, Auger electrons fluxes and spectra 78—28376
upper atmosphere, ionisation due to X-ray pulse, Auger electrons form. 78—53767
upper atmosphere, photoelectron spectra allowing for Auger effect 78—69557
vacuum improvement technique for electron spectroscopy 80—27381
vacuum vessel wall surface conditions, long term changes, PLT appl. 79—653
velocity analysers response function, Auger electron spectrometry appl. 77—14298
W (110), chemisorption of N, surface diffusion, scanning Auger spectroscopy exam. 77—55452
water, condensed multilayers, electron bombard. effects, AES line-shape anal., XPS, and desorption meas. 80—7450
water at interfaces, mol. struct. and dynamics, LEED-Auger obs. 77—31873
wear study, analytical surface tool, review 78—64718
worn surfaces, lubricant additive effects, AES appl. 77—44445
X-ray induced, model 77—59669
X-ray spectra, energy-dispersive, radiative Auger-like satellites 78—5168
X-ray spectra, K, origin of low-energy satellites, α-region 80—55229
X-ray spectroscopy, book 80—2899
X-Y recorder for Auger spectrometer using pulse height analyser, computer interfaces 78—49942
XPS Auger lines, generation by bremsstrahlung 80—87174
XPS spectrometer, consistent calibration method, rel. to Pd Fermi level 77—16458
zinc blende structured semiconductor surface analysis by X-ray photoelectron spectroscopy *(Japanese)* 78—88672
zinc phthalocyanine, resonant two hole bound state at 3p core threshold 80—60750
β-Zircaloy, O_2 diffusion 78—6181
$AR+N^+(O^+)$, electron emission, double differential cross sections, Auger spectra 79—45684
Ag, 4d bandwidth influence on $M_{4,5}N_{4,5}N_{4,5}$ Auger spectra 79—100017
Ag (100) surface, angle-resolved Auger emission 78—72650
Ag (110), ethylene-O_2 interaction, LEED and AES obs. 80—89520
Ag (110) surface, adsorption and surface structural chemistry of Na and $Na+O_2$ 77—31883
Ag (110) surface, clean and Na dosed, chemisorption and surface reactivity of NO 77—31882
Ag (111), adsorbed layers of $O_2(N_2)(S)$, electronic props., XPS and UPS 78—10279
Ag (111), adsorpt., coadsorpt., and reactivity of Na and NO 78—38948
Ag (111), adsorpt.-desorpt. props. and surface struct. chem. of Cl 77—89648
Ag (111), clean or Na-covered, adsorpt.-desorpt. props. of Br_2 78—38944
Ag (111), ordered and damaged surfaces, O_2 adsorption, O_2+CO interaction 78—14583
Ag, AES, valence band spectra, solid-state and atomic features 78—72646
Ag, adsorbed on Si (111), electronic and cryst. struct., Schottky barrier form. obs. 78—84091
Ag, adsorption of pyridine, UPS, AES and flash desorption meas. 80—92776
Ag, Auger depth profiling limitations 79—61473
Ag, Auger $M_{4,5}$-VV spectrum, quasi-atomic final states 78—72688
Ag, cluster growth and nucleation on Mo (100), UHV-SEM, AES/(RHEED or LEED) obs. comparison 78—63956
Ag, deposition on Si(100) surface, LEED and AES meas. 77—35833
Ag, epitaxial growth on electron bombard. NaCl(111) surfaces, RHEED and AES 80—15419
Ag film, epitaxial growth on Pd, AES and LEED obs. of growth modes and substrate influences *(French)* 80—84408
Ag film, initial stages of growth on Si (111) 7×7, LEED, AES and UPS expts. 78—38988
Ag film, on Au substrate, monolayer overgrowth, quantitative AES method 80—10813
Ag film, vacuum deposited on NaCl, microstructure and orientation, surface condition influence 79—82486
Ag film, vacuum deposition on Pb (111), substrate diffusion effects, RHEED, LEED, AES 80—65410
Ag film growth on KCl, LEED, AES meas. 77—35834
Ag film growth on Pd substrate, interface cpd. form., AES study *(French)* 80—80131
Ag films, electrodeposited and vac. deposited, AES depth profiling anal. 77—59232
Ag in SiO_2 isolation matrix, XPS, atomic electronic struct., Auger energy calc. 79—89655
Ag, ion beam plating using mass analysed ions, SIMS and AES expts. 78—19673
Ag ion plated film on permalloy, Cu and Vicalloy substrate, AES, SEM and X-ray study *(Japanese)* 78—11128
Ag, K-fluorescence yield determ. from K-Auger electron emission rates 80—95569
Ag, L-X-ray emission spectra, hypersatellite origin 79—89629
Ag, $M_{4,5}VV$ Auger spectrum interpretation 78—23562

Auger effect continued
Ag monolayer on (111)Si surface, Schottky barrier, interface electronic nature and epitaxy 79—77934
Ag, N-shell vacancy state widths, X-ray photoelectron, Auger spectra 77—18875
Ag on Pt electrode, underpotential deposition, XPS and AES 77—77770
Ag, solid state and atomic features in the valence band Auger spectra 78—76563
Ag surface, clean and oxidised, $M_{4,5}VV$ Auger spectra, anal. based on self-convolution of measured UPS 77—77332
Ag surface, production of Na Auger electrons by Na^+ bombardment 77—63515
Ag, thin sub-monolayer film, Auger emission coeffs. meas. 80—55236
Ag, XPS and $M_{4,5}N_{4,5}N_{4,5}$ Auger spectra 79—61472
Ag-(100)InP contacts, interface struct. 79—60922
Ag-Au, calibration line introduction for comp. determ. by AES 79—56892
Ag-Au, composition changes under ion bombardment, scanning Auger microprobe obs. 79—83076
Ag-Au, surface layer, effect of Ar^+ bombardment, AES and SIMS 80—25504
Ag-Au alloy, Auger exam. of preferred sputtering 77—44106
Ag-Au alloy, ion irrad., surface segregation and selective sputtering, AES expts. 79—7740
Ag-Au alloy, surface after sputtering, AES obs. 77—55858
Ag-Au alloy, surface enrichment, AES meas. 77—1283
Ag-Au-Cu, sputtering and AES 80—50503
Ag-Cu alloy, surface comp. after sputtering, AES obs. 77—55858
Ag-Ni solid solution, reversible surface segregation, radioactive tracer, LEED, and AES expts. *(French)* 77—69155
Ag-Pd, surface comp. changes under ion bombardment, AES study 80—55250
Ag-Pd alloy, surface comp., AES expts., correl. with O_2 heat of chemisorpt. data 78—34684
Ag-Pd alloys, inert gas ion bombardment, dynamic surface composition changes, AES obs. 80—60745
Ag-Pt interface formed by electrodeposition, depth profile 77—16512
AgCuSe, X-ray photoelectron and Auger spectra 78—56561
$AgGaSe_2$, and Ag_9GaSe_6, XPS, Auger and direct electron spectra 78—52620
AgO and Ag_2O, ESCA spectra, Auger effect, initial and final states effect 78—15280
Ag_2S-K_2SO_4 mixtures, surface comp., AES and XPS obs. 80—81386
Ag_2Se, X-ray photoelectron and Auger spectra 78—56561
Al (100) surface, prep. and props. of Pb and Sn monolayers 79—15018
Al (111), chemisorpt. of O 78—14593
Al (111) and (100) surfaces, initial interaction with O_{21} LEED and AES meas. 79—83383
Al, AES study of Sn diffusion and surface segregation in limit of small conc. 79—82384
Al, adsorbed S(O)(N)(C), internal and external sources of electrons 77—44097
Al, adsorption of NH_3, KVV Auger spectra, deconvoluted spectra 80—50508
Al, adsorption of O_2, AES, XPS, and LEED obs. 79—46938
Al, adsorption of O_2 and CO, interatomic Auger transition spectroscopy 80—11521
Al alloy, 2024-T3, adherend surface, chem. comp., effects of chem. and thermal treatments 78—39939
Al alloys, 7075-T6, H_2 effects and Cd segregation to grain boundaries 78—84764
Al and Al alloy anodised oxide films, for adhesive bonding appls., AES and SEM study 80—66689
Al and Al alloys, Auger spectroscopy produced in glow discharge *(Russian)* 78—14545
Al, annealed and powder sintered (SAP 895), sputtering under D^+ and $^4He^+$ bombardment, microstruct. effects study 80—84821
Al, anodic oxide films, AES exam. *(French)* 77—36324
Al, Auger electron microscopy, edge effect, Monte Carlo simulation 79—1801
Al, Auger electron prod. by Ne^+ bombard. 80—7460
Al, Auger electron prod. by Ne^+ bombard., origin of Ne Auger peaks *(French)* 80—7461
Al, Auger electron production by noble gas ion bombardment 77—1778
Al, Auger emission target, contrib. of reflected electrons 78—92152
Al, Auger spectra, KLL and KLV, screening effects and plasmon gains 80—80913
Al, Auger spectra, plasmon satellite intensity 78—64432
Al, Auger spectra induced by 100 keV Ar^+ impact 80—84820
Al, Auger spectrum, KLL, plasmon gain satellite obs. 78—76562
Al, bulk and surface plasmon loss intensities in XPS, Auger and electron energy loss spectra 79—38012
Al, characteristic energy losses on C contaminated surfaces, secondary electron spectra, AES, and EELS 79—99997
Al, chemisorption of CO, interatomic Auger transition spectroscopy 79—7747
Al, chemisorption of O_2, on (111) and (100) faces, AES and work function obs. 77—35822
Al, clean and oxidised surfaces, secondary electron spectrum, EELS and AES, comparison 80—55237
Al, corrosion-protective chromate coatings, characterisation 79—47798
Al, diffusion of Zn along grain boundaries, effect of grain boundary struct. *(Japanese)* 77—15628
Al, film, initial oxidation, AES, work function and gravimetric meas. 78—7087
Al film on GaAs, plasma oxidation, AES and TEM 77—77621
Al, initial interaction of O with single cryst. faces, LEED, AES and work function study 80—84392
Al, initial oxidation, interatomic Auger transition spectroscopy 79—7746
Al, initial oxidation exam. by inter-atomic Auger yield spectroscopy 78—11419
Al, ion bombarded, photon and ion emission, simultaneous meas. 78—15276
Al, ion impact excited, ang. resolved Auger emission 79—61475
Al, ion-induced Auger electron emission, depend. on ion energy 79—78814
Al, L_{23} shell ionisation cross section under He^+ impact, Auger spectra obs. *(French)* 77—69956
Al, L_{23} shell ionisation cross-section under H^+, heavy-ion impact, Auger spectra *(French)* 79—24406
Al, oxidation, in water, oxide growth rate and struct. 78—76783

Auger effect continued
  Al, oxide films, metal and O_2 transport, AES and inert marker, techniques 80−97641
  Al, proton-excited Auger electrons, attenuation lengths of low-energy electrons 78−11058
  Al, role of inelastic refl. in Auger electron formation, expt. check of model 78−11027
  Al, scanning Auger electron microscopy, Monte Carlo calc. 78−19610
  Al sheet surfaces, chem. characterisation by SIMS, glow discharge spectrometry and other techniques 80−66907
  Al, specimen transfer device for combined AES/RHEED and TEM obs. 80−70093
  Al surface, Ar^+ and e^- excited Ar Auger electron emission 79−47560
  Al target, Auger spectrum, meas. by new retarding field spectrometer 78−23564
  Al, valence band Auger spectra, surface effect 80−80915
  Al/Cr thin films, interdiffusion meas., AES and ion beam sputtering 79−82391
  Al/GaAlAs, film, epitaxial growth on (100) GaAs by hot vac. deposition and characterisation 79−56085
  Al/NiSi/Si system, high temp. interaction study, elec. and struct. characts., AES meas. 79−24075
  Al/Pd thin film couples, thermal reactions 80−59830
  Al-base alloys, semiquantitative anal. with SIMS, AES and wet chemical anal. 77−48291
  Al-Cu, surface enrichment of Cu due to Xe sputtering, AES and He ion backscatt. meas. 77−4250
  Al-Cu (4.2 wt.%), precipitation strengthened, solute depletion at fatigue facets, AES study 79−38973
  Al-Cu films, DC sputtered, Cu distrib. 80−80113
  Al-Cu thin film couple, interdiffusion, AES obs. 80−6569
  Al-InP Schottky barrier, increase 80−15603
  Al-Mg, alloy, surface activity of Mg, XPS and AES meas. 79−86975
  Al-Mg/Al_2O_3 composites, interface phase, Auger and electron diffr. study 80−25646
  Al-O (100), extended appearance potential fine struct. anal., LEED study 80−50467
  Al-Pd, preferred sputtering on surface, mass difference and chemical bonding difference effects, AES obs. 79−83078
  Al-Pd_2Si contacts on Si, elec. and structural characterisation 77−43695
  Al-Pd(Si) film, preferred sputtering on surface, mass and bonding difference effects, AES obs. 79−87552
  Al-Si, preferred sputtering on surface, mass difference and chemical bonding difference effects, AES obs. 79−83078
  Al-SiO_2 film-substrate interface, obs. of Al_2O_3 and free Si 78−91571
  Al-SiO_2 interface, chem. struct., deposition conditions depend. 78−72007
  Al-SiO_2-Si structure, Auger depth profiling and ion sputtering of interfaces 77−20200
  Al-silicide-Si systems with $CoSi_2$, $Pt_xNi_{1-x}Si$, and $MoSi_2$ as silicide, diffusion, compound form., and microstructure 80−34253
  Al-Ta-poly-Si interdiffusion, Ta barrier effect, Auger anal. 78−71888
  Al-Zn-Mg, grain boundary surfaces, plasmon loss satellites in Auger spectra 78−15261
  Al-Zn-Mg, grain boundary segregation, AES meas. 78−72781
  Al-Zn-Mg alloy (6, 3 wt.%), grain boundary segregation, AES exam. 78−39783
  Al+heavy ion, X-ray spectra, one-photon two-electron rearrangements 77−6712
  (AlGa)As DH laser degradation due to facet oxidation 78−42336
  $Al_{0.5}Ga_{0.5}As$-GaAs minimum heterojunction width determ. by sputter Auger techniques, interface broadening 79−69586
  $Al_xGa_{1-x}As$ epitaxial layers on GaAs, struct. study by scanning Auger electron microscopy 80−80110
  $Al_xGa_{1-x}As$, LPE, quantitative analysis by AES 77−89667
  $Al_xGa_{1-x}As$ layers, graded band gap, growth and properties 79−60645
  $Al_xGa_{1-x}As$, MBE grown film, in situ surface characterisation by RHEED, SIMS and AES 77−43410
  $Al_xGa_{1-x}As$-GaAs, heterojunction, interface width, AES obs. 80−20290
  $Al_xGa_{1-x}As$-GaAs abrupt LPE heterojunction, Auger profiling 77−85101
  $Al_xGa_{1-x}As$-GaAs interface, Auger depth profiling 77−89657
  $Al_xGa_{1-x}As$-GaAs n-n heterojunction, LPE, Auger profiling and absence of rectification 78−95349
  $Al_xGa_{1-x}As$-GaAs n-n heterojunction, interface width determ. 80−49887
  Al_2O_3, adsorption of NH_3, KVV Auger spectra, deconvoluted spectra 80−50508
  Al_2O_3 anodic layer formation in H_3PO_4 solns., surface charact. 78−15603
  α-Al_2O_3, colour centres, AES, electron energy loss, and optical spectroscopy obs. 78−35176
  Al_2O_3, dense, steam-enhanced Ca segregation, AES and SEM obs. 79−83352
  Al_2O_3, interatomic Auger transitions XPS exam. 77−8692
  Al_2O_3, valence band density of states from self-deconvolution of $L_{23}VV$ Auger spectrum 79−47561
  Al_2O_3:Ni anodised films, electrolytically coloured, spectrally selective surface 80−11490
  Al_2O_3-Al interface, AES depth profiling, appl. of tailored modulation techniques 77−15702
  β-Al_2O_3-Na_2O, colour centers, AES, electron energy loss, and optical spectroscopy obs. 78−35176
  Ar, Auger electron emission during 3-15 keV Ar^+ bombardment of Si 77−59654
  Ar, Auger electron emission from ion-solid collision *(French)* 79−33876
  Ar, electron impact, L X-ray spectrum, radiative Auger transitions 80−58227
  Ar, electron impact excitation, L-MM, LM-M^3 Auger linewidths, L, S and J dependence 77−14588
  Ar, electron impact ionis., L_3-shell alignment, Auger electrons ang. distrib. 78−58838
  Ar, emerging from C foil, excited ion Auger decay 77−3333
  Ar film, on Ag, Auger spectrum film thickness depend. 77−8691
  Ar, heavy ion induced LMM Auger electron spectra 77−6907
  Ar, inner shell alignment calc. in electron impact ionisation 77−14586
  Ar ions+C foils, emergent Ar-L Auger electron absolute yields 77−19061
  Ar, K-MM radiative Auger transition rates, photon spectral distrib. 77−446
  Ar, KLL and KLM Auger electron spectra, obs. and relativistic multiconfigurational Dirac-Fock calc. 78−50524

Auger effect continued
  Ar, $L_{2,2}M_{2,3}M_{2,3}$ Auger spectra, using cylindrical mirror spectrometer 79−63326
  Ar, L-excitation by electron and proton impact, Auger multiplets, excitation probabilities 77−14589
  Ar L-shell ionisation, post-collision interaction, electron impact, energy loss meas. 77−19093
  Ar, multiply excited, inner level X-ray emission spectra, line widths and Auger transition rates 79−36575
  Ar, photoexcited LMM Auger processes, post-collision interaction 80−32682
  Ar, photoionisation, Auger processes, decay lifetime, line shift, profile, X-ray photoelectron spectra 80−37798
  Ar, total state energies, L-, M-electron processes, ab initio CI investig. 77−18801
  Ar, two and three-electron Auger transition, with vacancies in 2p-shell 79−63972
  $Ar^{+,2+,3+}$, electron impact, $<$800 eV, multiple ionis., L-shell contribs. 80−37892
  Ar^{15+} and Ar^{16+}, beam-foil obs. of lifetimes of metastable states 80−14116
  Ar^{n+}, electron impact inner-shell excitation/ionis. cross section 77−23564
  Ar+Ar(Ar^+) collisions, multielectron excitation energy calcs. 78−1071
  Ar+H^+ ions, K-Auger spectra, relative satellite line intensities, X-ray spectra 77−19066
  Ar^++Ar, 1-500 keV, inelastic energy loss, ionis. phenomena, theoretical model 77−34747
  Ar^++Ar, L-vacancy production, close collisions, 50-375 keV 77−54599
  Ar^++Ar, quasimol., Auger transition probability, internucl. distance effect *(Russian)* 77−75116
  ArC, nondifferentiated Auger electron spectrum 79−69929
  AsF_3 X-ray and UV photoemission spectra, Auger spectra 79−98150
  AsF_5, X-ray and UV photoemission spectra, Auger spectra 79−98150
  Au, 4f-subshell photoionisation cross section, energy depend. from Auger and photoelectron spectra 80−35057
  Au (100), characterisation of reordered and normal surfaces by LEED, AES and EELS 78−34687
  Au (111), chemisorption of O_2, AES investig. 77−55446
  Au (111)/Ag (111) thin films, system, diffusion processes, AES meas. 79−77843
  Au, (320) and (311) surfaces, Pb adsorption, LEED and AES obs. 79−86998
  Au, AES, valence band spectra, solid-state and atomic features 78−72646
  Au, AES and characteristic energy loss spectra, expt. and interpretation 78−27354
  Au, adsorption of O_2, Auger spectra 78−87879
  Au, adsorption of Xe and CO on (100) 77−15691
  Au, Auger spectra, $N_{4,5}N_{6,7}N_{6,7}$ and $N_{4,5}N_{6,7}O_{4,5}$ 80−89094
  Au, chemisorption of O_2, catalytic effect of Ca, AES study 79−15021
  Au coins, surface anal. by X-ray fluoresc., SEM and scanning Auger spectroscopy 80−89552
  Au, Coster-Kronig N_{45}-$N_{67}X$ transitions, semi-empirical Auger electron model and obs. 77−85889
  Au, Cu diffusion, 75-150°C, AES, device appls. 77−1262
  Au epitaxy on W (110), LEED and AES 77−69198
  Au film, diffusion of Ag along grain boundaries, scanning Auger microscopy obs. 78−22897
  Au film, epitaxially grown, struct., LEED, AES, resist. and X-ray diffr. analysis 77−59223
  Au film, ionic sputtering and AES anal. *(French)* 78−76959
  Au film, on Ni, AES anal., influence of ion bombardment on depth resolution 77−20210
  Au film, on Si (100) substrate, growth and struct., LEED and AES obs. 79−51457
  Au film, vacuum deposited on Cu, sputtering yield by substrate Auger meas. 79−95889
  Au film growth on Mo (110) surface, AES, LEED, thermal desorption study 80−80130
  Au film sandwiches, recovery kinetics and early stages of diffusion, DC resist. expts., correl. with AES 79−77971
  Au films on Si substrate, solid-solid reactions 78−95369
  Au, foil, X-ray induced electron emission 77−4713
  Au, growth on clean and contaminated GaAs (001) surfaces 78−26785
  Au, high current density plated, Co diffusing out, oxidation kinetics, AES meas. 78−92393
  Au in SiO_2 isolation matrix, XPS, atomic electronic struct., Auger energy calc. 79−89655
  Au, ion beam plating using mass analysed ions, SIMS and AES expts. 78−19673
  Au, $M_{4,5}VV$ Auger spectrum, analysis 77−59649
  Au, Ni and Cu diffusion, relative rates 77−80652
  Au, solid state atomic features in the valence band Auger spectra 78−76563
  Au surface, chemisorption of I, AES and LEED study 80−100405
  Au thick film surface, Cu and Ag contamination, AES obs. 80−24763
  Au, thin film, electrotransport-induced failure site, minor constituents effects 79−23763
  Au, vac. deposited thin film, Auger spectroscopy 80−2952
  Au very thin film on MgO (001) surface, AES obs. 79−33870
  Au, XPS, electronic struct. 80−7464
  Au-Ag, thin film, double layer system electron beam effects during sputter profiling AES obs. 79−65347
  Au-Ag bilayers, conc. profile by AES, interdiffusion coefficient determ. *(French)* 78−84077
  Au-Ag film system grain-boundary diffusion at low temp., meas. by surface accumulation method 79−77839
  Au-$Al_xGa_{1-x}As$ interface, Auger depth profiling 77−89657
  Au-Co electrodeposits, Co hardened, high temp. film formation 79−91848
  Au-Cr alloy, quantitative Auger electron anal., sputter-yield ratio 77−44096
  Au-Cr alloys, Cr conc., quantitative Auger electron analysis 77−85852
  Au-Cu alloy, surface comp. as function of temp., AES expts. 78−95212
  Au-Cu-O surface, quantitative Auger analysis using relative sensitivity factors 78−7295
  Au-Cy alloy, surface comp. after sputtering, AES obs. 77−55858
  Au-InP, Schottky diode, heat treatment in N_2 and O_2, distrib. profiles of elemental species 79−78172

Auger effect continued
Au-Ni-O surface, quantitative Auger analysis using relative sensitivity factors 78—7295
Au-Ni(Pd)(Pt), surface composition determ. 79—69328
Au-Pd, surface comp. changes under ion bombardment, AES study 80—55250
Au-Pd alloy, surface comp., polishing, cleaning and Ar sputtering effects 77—72763
Au-semiconductor system, room temp. interfacial reaction, AES obs. 78—18913
Au-Si interface, critical Au-film thickness obs. for room temp. interfacial reaction 80—75390
Au-Si interface, electron energy loss and AES meas. 80—89096
Au-Si Schottky contact elec. props. rel. to AES 77—85322
Au-Sn alloys, surface comp. by Auger spectroscopy, sputter cleaning 77—59648
Au-$Ti_{0.3}W_{0.7}$, thermal annealing study of metallisation on Si 80—80134
Au-TiC, multilayer struct., microhardness and elec. resist. 80—2950
Au-W-GaAs Schottky barrier, elec. and chem. props., AES 80—96973
Au(III) and polycrystalline surfaces, O_2 adsorption, LEED, AES and energy loss spectra 80—34310
$AuPb_2$, epitaxial layer, formation during Pb absorpt. on Au, LEED, AES study of Au/$AuPb_2$ interface 78—71988
AuSn, XPS, electronic struct. 80—7464
Au(111)/Ag(111) thin film system, diffusion processes, diffused Ag composition profile 79—90832
B, B_4C, BN, Auger and energy loss spectra *(French)* 78—23565
B, excited in single gas collisions, high-resolution Auger spectra 80—9717
B, K-shell binding energy, Auger spectra after collision with He and methane 78—50525
B, X-ray laser, inner-shell photoionis. pumped, practicability 77—58319
B^+, beam-foil excitation, absolute Auger yield meas. 80—14203
B^+, beam-foil excitation; absolute Auger yield meas. 79—45685
B^+ ions, beam foil excitation, L-Auger decays, autoionisation 77—14569
$B+C^{2+}(N^{2+})(O^{2+})$, K Auger electron spectra 79—89758
B+He (methane), collisional excitation, prompt decay line energy, projectile Auger spectrosc. 79—85941
B^++CH_4, 200 keV, Auger spectra, single and double K-vacancy states 77—83706
BN, chem. bonding and electronic struct., AES and SIMS meas. 80—50512
BN, pyrolytic, in contact with various metals, friction and transfer behaviour 78—88535
B_2O_3, chem. bonding, electronic struct., ESCA, Auger, and SIMS spectra 80—50512
Ba, adsorbed layers on W, Auger and work function meas., impregnated W cathode model 79—43073
Ba, autoionisation and Auger decay, collective excitation effect 80—43008
Ba, electron-correlation satellites, selective reson. enhancement 80—9569
Ba film, multilayer and monolayer, an W substrate, AES and work function meas. 77—24921
Ba film, on SiO_2, interfacial chemistry, AES obs. 80—44434
Ba getter film, initial reaction probability with O_2, water, CO and CO_2, AES obs. 80—61153
Ba, strong correl. in 4d-Auger spectrum 78—50522
Ba-O system, adsorbed layers on W, Auger and work function meas., impregnated W cathode model 79—43073
BaB_6, work functions from thermionic and field emission retarding pot. methods 79—65537
BaO film, multilayer and monolayer, on W substrate, AES and work function meas. 77—24921
BaO films on Ir, thermionic props., Auger, LEED, and emission microscopy 79—43089
BaO, single cryst. on Ir, chemical structural effects examination 78—14790
BaO surface, AES peak height calibrations 79—43072
BaO, XPS valence bandstruct. 80—89117
$BaT{:}O_3$, surface microrelief revealed by ion irradiation 80—54485
$BaTiO_3$ film, ferroelec., composition profiles by Auger electron spectra anal. 79—66391
$BaTiO_3$ film, surface layer nature, AES obs., and effect on permittivity 77—24498
$BaTiO_3$, pure and doped crysts., surface and domain struct., AES and SEM expts. 80—71363
$BaTiO_3$, surface study using AES and ion scatt. spectroscopy 80—65339
$BaTiO_3$ surface voids, Auger spectrochem. anal., organic contamination 79—24467
$BaTiO_{3-x}$, ferroelec., Auger spectroscopy of surface layers 79—42343
$BaTiO_{3-x}$, single cryst. and film, Auger spectra, surface comp. 78—27353
Be (0001) surface, work function and purity, AES, LEED and photoelectron spectra meas. 78—68606
Be, Auger emission target, contrib. of reflected electrons 78—92152
Be, Auger spectra, initial state screening effects 80—50476
Be, Auger spectra induced by 100 keV Ar^+ impact 80—84820
Be, Auger spectrum, high energy plasmon satellite 79—82538
Be, Auger transitions, fluoresc. yield calcs., correl. effects 77—18869
Be, excited in single gas collisions, high-resolution Auger spectra 80—9717
Be film, on Cu substrate, monolayer overgrowth, quantitative AES method 80—10813
Be film, on W (110), growth mode, work function, thermal desorption, and struct. 80—75477
Be II, autoionising core-excited states, alignment prod., Be^++He(methane) collision excitation 80—14204
Be, K-shell binding energy, Auger spectra after collision with He and methane 78—50525
Be, proton bombarded, Auger electron attenuation length meas., $E_p=160$ keV 77—44101
Be, proton-excited Auger electrons, attenuation lengths of low-energy electrons 78—11058
Be, slowly oxidised, secondary electron yield changes, and AES characterisation 80—71524
Be, thick film, amorphous, RF magnetron sputtering 80—80971
Be thick film or Au substrate secondary electron emission 80—104022
Be^+ ions, beam-foil excitation, L-Auger decays, autoionisation 77—14569
Be:Ar, ion-implanted, high resolution LMM Auger spectra 79—83066

Auger effect continued
Be-Cu, calibration line introduction for comp. determ. by AES 79—56892
Be+He (methane), collisional excitation, prompt decay line energy, projectile Auger spectrosc. 79—85941
Be^++H_2(He)(Ne)(methane), Be Auger spectra 77—57951
Bi (0001), chemisorption of O_2, LEED, AES and electron loss meas. 79—77908
Bi, and Bi_2O_3, AES and characteristic energy loss spectra, expt. and interpretation 78—27354
Bi film, on Sb_2Te_3, mean scatt. length of low energy electrons meas. 77—36370
Bi film, on Si(111) substrate, MBE deposition kinetics 80—10817
Bi, oxidation, charge transfer obs. from final state changes 77—51703
Bi, X-ray excited, $N_{6,7}O_{4,5}O_{4,5}$ spectra 77—85886
Bi, XPS, electronic struct. 80—7464
BiF_3 thin films, optical props. 79—32005
C, electron impact, C K-ionisation, Auger and X-ray meas. 77—19096
C, excited in single gas collisions, high-resolution Auger spectra 80—9717
C film, atomic comp. at electrode interface 78—6457
C films, surface struct., graphitisation, secondary electron spectra and AES 79—43077
C III, IV, V Auger lines obs., beam-foil excitation, ab initio calcs. 77—54601
C, in methane (acetylene)(CO_2), heavy-ion induced K-shell Auger effect 77—6908
C, K-shell binding energy, Auger spectra after collision with He and methane 78—50525
C layers on W, Auger signal intensity in differential and energy distrib. mode spectra 79—78799
C microneedles, grown on W wires under intense elec. fields, X-ray diffr. and AES 80—54580
C, oxidation kinetics on Ni (110), AES meas. 79—79291
C vacuum deposited coatings for prosthetic devices 77—40374
C^+, beam-foil excitation, absolute Auger yield meas. 80—14203
C^+, beam-foil excitation; absolute Auger yield meas. 79—45685
C^+, from exploding fast mol. ions, Auger spectra 80—32781
C^+ ions, beam-foil excitation, L-Auger decays, autoionisation 77—14569
C^{n+}, electron impact inner shell excitation/ionis. cross sections 77—23564
C:Ni, X-ray photoemission studies 80—76138
C+C, K-shell excitation, Auger electron spectrosc. obs. 80—9714
$C+H^+(He^{2+})$, K-shell Auger electrons ang. distrib. 79—89756
C+He (methane), collisional excitation, prompt decay line energy, projectile Auger spectrosc. 79—85941
C+N(O), K-shell excitation, Auger electron spectrosc. obs. 80—9715
C_2N_2, adsorbed on Pt (111) surface, Auger spectra 79—52077
CO, adsorbed on Pt (111) surface, Auger spectra 79—52077
CO, adsorbed on stepped Ni, thermal decomposition, LEED, AES, thermal flash desorption study 78—71984
CO, adsorpt. on Mo(110) face, Auger yield attenuation interpret. *(French)* 77—85077
CO, electron impact K-shell ionis., ionic fragmentation, Auger decay post-collision interaction 77—75316
CO, hydrogenation on Fe foil, AES and XPS study 80—7858
CO, reaction with adsorbed O_2 on Pd, kinetic behaviour, AES obs. 77—90640
CO, reaction with O_2 chemisorbed on Pt, AES expts. 77—90639
CO^+, exploding fast mol. ions, Auger spectra 80—32781
CO_2, on Rh(110), chemisorpt., surface struct. chemistry, electron-impact props. 78—6225
CO_2+X^{n+}, (X=Ar,Kr,Xe,U), Auger emission line shape after dissoc. 78—86838
CU, solid state and atomic features in the valence band Auger spectra 78—76563
Ca compounds, Auger spectra, shake-up satellites 78—27369
CaO epitaxial layer, on Mo, secondary electron emission, struct. effects, LEED and AES expts. 78—2959
CaO, optimum composition of dielectric materials for AC-operated plasma display panels 80—14945
CaO surface, AES peak height calibrations 79—43072
CaO, XPS valence bandstruct. 80—89117
Cd (0001), oxidation, LEED and AES obs. 79—87756
Cd, AES, $M_{4,5}N_{4,5}N_{4,5}$, vap. and solid, solid state effects 77—61857
Cd, AES and XPS, vapour-metal electron energy shifts 80—16142
Cd, Auger electron spectra, electron impact excited, vap. and solid state differences 78—52603
Cd, Auger MNV lineshapes, hole-hole interaction 80—45177
Cd deposited layers on Ti (0001), LEED and AES determ. of struct. 77—72804
Cd deposited layers on Ti (0001), LEED and AES determ. of structure 77—76688
Cd, N-shell vacancy state widths, X-ray photoelectron Auger spectra 77—18875
Cd, XPS and $M_{4,5}N_{4,5}N_{4,5}$ Auger spectra 79—61472
$Cd+H^+(He^{2+})$, L- and M-shell Auger electrons 79—27076
Cd_xHg_{1-x} Te, photodetectors, recomb. processes, photoconductive decay obs. 79—38129
$Cd_xHg_{1-x}Te$, Auger effect, temp. depend. of Auger lifetime 79—38097
n-$Cd_xHg_{1-x}Te$ crystals, carrier recomb. in extrinsic conduction range 80—70722
CdO, Auger MNV lineshapes, hole-hole interaction 80—45177
CdO, ESCA spectra, Auger effect, initial and final states effect 78—15280
CdS, Auger effects in donor acceptor pair spectra 80—20707
CdS, Auger excitation mech. of 1.6-2.0 micron luminesc. band 79—8184
CdS, Auger interaction between luminescence centres and donor-acceptor pairs 77—63458
CdS, clean surface, AES and LEED exam. 80—10762
CdS, compensated, characts. of Auger excitation spectra of photoluminesc. and photocurrent 77—90194
CdS, electron beam induced desorption of O, AES meas. 79—77921
CdS film, surface stoichiometry rel. to CdS-Cu_2S cell performance 78—2956
CdS, single cryst., polar (0001) and $(000\bar{1})$ surfaces, comparison of AES signals 80—16130
CdS sprayed film, prep., optical props., struct. and comp. 79—78875
CdS, surface energy levels, O(C) adsorpt., AES study *(Japanese)* 78—88008

Auger effect continued

- CdS:In(Cl) concentration quenching mechanism of luminescence 80—97336
- CdS:Li, pure and doped, green edge luminesc., complex nature of centres 80—60671
- CdS:Li, TSC and optical photocurrent quenching spectra, Auger excitation of recomb. centres 79—33294
- CdSe $(11\bar{2}0)$, surface electronic struct. and chem. struct. 78—14788
- CdSe film, laser annealing effects on surface struct. and elec. characts. 79—73605
- CdSe film, vac. deposited, elec. resist. and surface changes by laser annealing 80—2491
- CdSe film polycryst., thermal diffusion of Cr, 240-400°C 80—80001
- Cd_2SnO_4 and Cd_2SnO_4:CdO, thin film electrodes in H_2SO_4 electrolytes, reduction, AES and SEM 80—65674
- n-CdTe-electrolyte solar cells, interface changes during operation, AES, electrolum. and electroreflectance meas. 79—100525
- ^{109}Cd, LX-, LX-coincidences during decay 78—17149
- ^{111}Cd, KLM- and KLN-Auger transitions 77—18884
- CeB_6, single cryst. work function, thermionic emission, evaporation 77—24922
- CeB_6, thermionic emission rel. to surface state 78—39654
- CeB_6, work functions from thermionic and field emission retarding pot. methods 79—65537
- CeO_2:Y_2O_3, bias sputtering, film growth and characts. 77—40366
- CeO_2-Y_2O_3 film, surface characterisation, XPS, ESCA, and AES expts. 78—72028
- Cl compounds, chemical shifts of X-ray electron and Auger lines 78—86912
- Cl, two and three-electron Auger transition, with vacancies in 2p-shell 79—63972
- Cl, X-ray and Auger transition probabilities to 2p level 78—17640
- Cl-containing systems, core Auger and core electron binding energy shifts, ab initio LCAO SCF MO UHF calcs. 77—30777
- Co (0001), adsorption and reactivity of NO, LEED, AES, and thermal desorption study 80—80090
- Co (0001), chemisorption of O_2, surface oxidation and CO oxidation 79—60631
- Co (0001) surface, LEED and AES meas. 77—31857
- Co (100), clean and C-covered, LEED-Auger expts. 78—38921
- Co $(10\bar{1}2)$, struct. and CO chemisorption obs. 79—4474
- Co and its oxides AES meas. 77—36323
- Co, Auger spectrum, ab initio MO LCAO SCF CI calc. many electron contribs. 80—87169
- Co ferrite film prep. by vac. evaporation and annealing 77—85939
- Co, monolayer, oxidation, quasisimultaneous SIMS, AES, XPS 78—72919
- Co, radiative Auger effect, $K \to M^2$ 80—71522
- Co-Mo, multilayer films, depth resolution determ. in Auger depth profiling meas. 79—78800
- Co-Ni, surface chemical comp. changes due to ionic bombardment *(Russian)* 77—1776
- Co-Si, surface physicochemical state, Auger electron spectroscopy study 80—100715
- Co-Sn alloy, electroplated, oxide films, XPS/AES expts. 79—15862
- CoAl, compositional depend. of oxidation rates 79—8393
- $Co_{1-y}Fe_{2+y}O_4$ ferrite, $-0.1 \leq y \leq 0.1$, surface composition, AES 78—14557
- $Co_{20}Ni_{80}$, oxidation study by Auger electron spectroscopy *(Ukrainian)* 80—7711
- CoNiZn ferrites, Fe excess, complex permeab. var. with annealing temp. 77—89979
- CoO, ESCA and Auger lines, chem. shifts 78—6817
- Co_3O_4, ESCA and Auger lines, chem. shifts 78—6817
- ^{57}Co complexes, phenanthroline and ethylenediamine ligands, Auger processes, Mossbauer obs. 77—12277
- ^{57}Co, disintigrating nucleus, energy absorpt. by mol. environment 78—80775
- Cr (100), adsorption of O_2 and initial oxidation at room temp. 80—20034
- Cr, (100) surface, clean $(\sqrt{2}\times\sqrt{2})R45°$ struct. 80—2255
- Cr, AES meas. of soft X-ray emission threshold potential *(Russian)* 79—33866
- Cr and its oxides, AES meas. 77—36323
- Cr containing Cr_2O_3, film struct., oxide percentage determ. and temp. coeff. of resist. 80—103607
- Cr film, reversal etching in gas plasma, reaction mechanism, AES and XPS obs. 80—16564
- Cr, oxidation, combined AES and threshold potential spectroscopy 78—11026
- Cr, oxidation, Cr-O bonding, characterisation by high resolution AES *(French)* 79—100468
- Cr, oxidation in pure CO_2, AES 77—86224
- Cr, oxide film form., combination anal. using ESCA, AES and SIMS 79—16092
- Cr, surface atom electron binding energy depend. on composition, Auger spectra, APS spectra 80—39655
- Cr-Au, matrix sensitive and insensitive factors evaluation using quantitative AES 79—24395
- Cr-C(N) coating, deposited by hollow cathode discharge, characterisation 78—11371
- Cr-Cr_2O_3 black, electroplated solar collector coatings, high temp. optical and struct. degradation 80—66995
- Cr-Cr_2O_3 black chrome, commercial, solar absorber coating characterisation 80—80111
- Cr-O system, initial oxidation, combination anal. using ESCA, AES and SIMS 78—72924
- Cr_3C_2, final-state effects in C Auger spectra 78—6818
- $CrCl_2$, epitaxial relationships studied by RHEED and Auger emission spectra *(French)* 78—22990
- $Cr(NO)_4$, XPS and UV photoelectron spectra, compared to NO data 80—58317
- Cr_2O_3-Cr film, electrodeposited, optical degradation rel. to surface morphology, SEM and AES obs. 79—79401
- $CsSn_2I_5$, surface props., Auger study, elec. cond. meas., photochem. study 80—66339
- Cu (001), chemisorption of S, thermodynamics, AES study 79—82452
- Cu (100), adsorbed layers of N, O and S, electronic props., UPS, XPS and Auger spectra 77—66088
- Cu (100), adsorpt. of O and S, ang. resolved AES and LEED 78—18908
- Cu (100), coadsorption of Pb and Bi, LEED and AES meas. 79—15017

Auger effect continued

- Cu (100), L_3VV Auger emission spectra, angular resolved 77—81182
- Cu (100), linearized secondary-electron cascades, line-shape synthesis, appl. to AES anal. 79—74035
- Cu, (100), oxidation, electron spectroscopic study 78—64782
- Cu, (100) surface, Auger emission ang. depend., overlayer effects 78—39637
- Cu (100) surface, interaction with O_2, AES, EELS, LEED and work function studies 80—24731
- Cu, (100) surface, UPS, two-electron reson. at 3p threshold, rel. to Ni 80—25522
- Cu (110), N implanted, temp. depend. evolution, Auger line shape anal. 78—2376
- Cu (110) surface, O_2 and N_2O interactions, CO reaction with adsorbed O_2, AES study 80—6635
- Cu (111), adsorpt.-desorpt. props. and surface struct. chem. of Cl 77—89648
- Cu (111), chemisorpt, of CO on differently prepared surfaces 78—6223
- Cu (111), interaction of O_2 and N_2O and reaction of CO with adsorbed O_2, AES, LEED and ellipsometric meas. 79—65317
- Cu, (111) and (100) surfaces, Sn segregation 78—14554
- Cu (210) surface, adsorption of O_2, LEED and AES meas. 78—71998
- Cu, AES, valence band spectra, solid-state and atomic features 78—72646
- Cu, AES excited by X-rays, satellite lines 79—33893
- Cu adsorption of O_2, N_2O on (100) surface, reaction with CO 80—103583
- Cu, adsorption of Pb on stepped and low index surfaces, LEED, AES and desorption anal. 79—46942
- Cu, ang. distrib., final state effects 77—66580
- Cu, Auger M_1VV line shape, bandlike and atomiclike features 79—43075
- Cu, Auger spectra, comparison with multiplet struct. calc. 78—31287
- Cu, Auger-photoelectron coincidence measurements 79—19968
- Cu, chemisorpt. of CO, SIMS, AES, desorpt. meas. 78—87875
- Cu, chemisorption of P and P compounds, Auger spectra 78—43248
- Cu, chemisorption on low-index and stepped surfaces, LEED, AES and UPS obs. 80—84391
- Cu compounds, chemical shifts of X-ray electron and Auger lines 78—86912
- Cu, corrosion, noble metal additions effect, Auger spectra 78—35579
- Cu dilute alloys, compositional changes in oxide thin films, Auger electron microanalysis *(Japanese)* 77—21319
- Cu film, vacuum deposition on Pb (111), substrate diffusion effects, RHEED, LEED, AES 80—65410
- Cu, film growth on graphite and amorphous C, electronic struct. by photoemission and Auger obs. 79—77947
- Cu film on Ni, AES comparison of ion plated and vacuum evaporated films 79—28250
- Cu films on Ru (0001), growth, struct. and electronic props. 79—77958
- Cu in SiO_2 isolation matrix, XPS, atomic electronic struct., Auger energy calc. 79—89655
- Cu, $L_{2,3}VV$ and MVV Auger spectra 78—68583
- Cu, L_{23}-$M_{4\,5}M_{4\,5}$ principal and satellite Auger spectra 78—42030
- Cu, $L_3M_{23}M_{23}$ Auger energy calc. using XPS, effect of 3d-4s admixed screening on relax energies 77—1782
- Cu, $L_3M_{4.5}M_{4.5}$ and $M_{2.3}M_{4.5}M_{4.5}$ Auger line shapes, independent electron calc. 77—63500
- Cu, LMM Auger spectra, rel. to L_{23} photoelectron spectra 77—77348
- Cu, LMM Auger spectra, transition probabilities, term splittings and effective Coulomb interaction 77—44126
- Cu, MVV Auger spectra, atomic model and valence band features 78—72644
- Cu, meas. final state CI effects 78—33488
- Cu, molten surface layer thickness, emissivity and AES meas. 80—39261
- Cu molybdates, valence band X-ray induced Auger spectra and XPS 78—80813
- Cu, oxidation in controlled clean air and standard laboratory air, 50-150°C, contact resist. and AES meas. 79—70202
- Cu oxides, valence band X-ray induced Auger spectra and XPS 78—80813
- Cu, secondary electron emission, spurious peaks from grid of retarding field analyser 77—20968
- Cu, slip ring, spectroscopic obs. of elemental surface composition as function of temp. 80—66901
- Cu surface, relative intensities of $L_{2.3}M_{4.5}M_{4.5}$ principal and satellite Auger spectra 79—52054
- Cu surface, surface cleaning by H^+ bombard., AES study 78—53022
- Cu, surface contaminant anal. by ion-electron spectroscopy 80—54490
- Cu, surface film of 2-mercaptobenzothiazole and 2-mercaptobenzimidazole, XPS and X-ray induced Auger spectra obs. 80—40600
- Cu, thin film, sputtering yields due to Ar^+ milling, He^+ Rutherford backscattering and AES obs. 79—65969
- Cu, vac. deposited thin film, Auger spectroscopy 80—2952
- Cu/Ni multilayer films, electron beam induced diffusion during AES depth profiling 80—19993
- Cu/Sn-Ni/Au tricouples, electrodeposited, interdiffusion obs. 80—84331
- Cu-Ag, Auger spectroscopy, effect of composition on matrix parameters *(German)* 79—11489
- Cu-Ag, surface segregation of S, Auger spectral study diffusion 80—76549
- Cu-Al, surface segregation during adsorption and low pressure oxidation *(French)* 78—75932
- Cu-Al (0.05 wt.%), dil. alloy, anisotropic oxidation, electron microprobe Auger spectroscopy 77—12748
- Cu-Al(Sn), effect of Al and Sn on friction and wear 78—11348
- Cu-Au thin film system, interdiffusion coeff. from cond. and Auger anal., 25 to 250°C 77—59154
- Cu-Au-Cu, thin films, sandwich struct., bombarded by 3-15 keV Ar^+ at angle of incidence of 30°, sputtering yield coeff. AES obs. 79—65968
- Cu-Be, dynode surface, SEM and Auger microanalysis 80—100384
- Cu-Be(2 wt.%), tarnish surface films, formed in ammoniacal Cu(II) solns. 80—97624
- Cu-Co-Si (0.36, 0.11 wt.%), surface layer struct. on annealing, SIMS and AES exam. 80—88415
- Cu-Ga, ion bomard. effect on surface comp., reflectometry AES 77—81190
- Cu-Ga alloys, effect of ion bombardment on surface composition using differential reflectometry and AES 77—59189

Auger effect continued
Cu-Mn (3, 5, 10 at.%) alloys, surface segregation of Mn and oxide film form., AES study *(French)* 79−66065
Cu-Mn(Ti)(Sn)(Si), dil., oxide film form. in ammoniacal Cu(II) solns., AES obs. 80−45415
Cu-Ni, chemisorpt. of CO, SIMS, AES, desorpt. meas. 78−87875
Cu-Ni, clean surface, surface segregation and growth process of altered layer *(Japanese)* 80−24720
Cu-Ni, film, preferential sputtering due to altered layer struct., AES meas. 78−76573
Cu-Ni, initial oxidation study by microprobe-AES method *(Japanese)* 79−15867
Cu-Ni, preferential sputtering Auger electron spectra obs. 79−33880
Cu-Ni, quantitative AES anal. of M_1 VV transition, computer simulation 79−91542
Cu-Ni, sputter-induced subsurface segregation, Auger electrons obs. 80−10757
Cu-Ni, surface layer, effect of Ar^+ bombardment, AES and SIMS 80−25504
Cu-Ni (110), adsorption of CO and H_2, UPS, thermal desorption, AES,and LEED study 80−80087
Cu-Ni (50 wt.%), preferential sputtering, thickness and in-depth comp. profile of altered layer, AES 78−39649
Cu-Ni (50 wt.%) alloys, estimation of sublimation energy of Cu atoms, evaporation rate and surface composition, AES meas. *(Japanese)* 80−49352
Cu-Ni alloy, oxidised with NO, surface comp., AES obs. 77−20176
Cu-Ni alloy, sputtered altered layers, in-depth profile, model 78−19613
Cu-Ni alloy, sputtered and sputter-deposited surfaces, in-situ AES meas. 77−48296
Cu-Ni alloy surfaces, chemisorption of CO, LEED, AES, thermal desorption, and work function meas. 79−90879
Cu-Ni alloys, surface comp. and catalysis, AES and thermal desorption meas. 79−46898
Cu-Ni alloys, surface segregation and in-depth profile, AES 77−31856
Cu-Ni alloys 706 and 715, corrosion in flowing sea water, dissolved sulfide effect 80−35379
Cu-Ni film, coevaporated, AES anal. and ion sputtering effects 79−15044
Cu-Ni textured alloys, grain boundary effusion of Ni to surface 79−90680
Cu-Ni-Sn (9, 2 wt.%), surface comp., Auger electron spectroscopy study, manufacture and storage influence 80−65348
Cu-Ni-Zn (18, 27 wt.%), surface comp., Auger electron spectroscopy study, manufacture and storage influence 80−65348
Cu-Ni-Zn alloy, surface comp., outdoor exposure influence 80−59770
Cu-Ni; preferential sputtering, Auger meas. 78−27358
Cu-Pd, surface comp. changes under ion bombardment, AES study 80−55250
Cu-Pd, surface struct. from LEED and AES meas. 79−77882
Cu-Sn, exam. of surface segregation equilibrium and kinetics, by Auger spectroscopy *(Russian)* 79−56981
Cu-Sn, ε and η phases, surface struct. changes due to sputtering 77−73206
Cu-Sn, Sn surface segregation in monolayer regime, model of kinetics and equilib., AES data explained 79−7739
Cu-Sn alloy, surface comp., outdoor exposure influence 80−59770
Cu-Sn-P (5, 1-5 wt.%), effect of P on friction and wear characts. 80−16494
Cu-Zn alloys, surface comp., outdoor exposure influence 80−59770
Cu+He ion, neutralisation and ionisation of low energy He ions scatt. from (100) face 78−23572
$CuAl_2$, chemical effects on Al and Cu AES 77−59651
$Cu_{0.7}Al_{0.3}$, chemical effect on valence electronic states, AES and SXAPS meas. 79−47558
CuCl, XPS and Auger spectroscopy, elec. struct. 80−29852
Cu_5FeS_4, bornite, AES investig. of surface struct., O_2 adsorpt. effects 77−15669
Cu_5FeS_4, S and S^{2-} states, identification from Auger line shapes 79−92034
$CuInS_2$ films prod. by RF sputtered Cu-In films exposure to H_2S 79−95926
$CuInS_2(Se_2)(Te_2)$, thin films and photovoltaic devices, AES evaluation 78−67928
$CuInS_2(Se_2)(Te_2)$, thin film, bulk polycryst. and single cryst. samples, AES 78−72648
$CuInSe_2$ film, MBE growth, AES and optical absorpt. obs. 79−78903
$CuInSe_2$, Zn implantation profiles by AES 77−31692
$CuInTe_2$, vac. deposited film, growth, struct. and elec. characts. 77−69995
$Cu_xNi_yO_z$, protective oxide film on Cu-Ni alloy, AES 79−39035
CuO, on Cu, identification by electron spectroscopic methods 80−60747
CuO-Ag film solar absorbers, mechanism of high-temp. instability 78−22971
Cu_2O, Auger quantitative anal. 78−73104
Cu_2O, on Cu, identification by electron spectroscopic methods 80−60747
Cu_2O solar cell, low barrier heights, Auger spectra obs. 79−15224
Cu_2O, solar cells, space-charge layer chemical origin, AES investigations 79−70449
Cu_2O-Au(Mg)(Mn)(Yb) Schottky barrier solar cells, surface anal. using AES 79−43759
$Cu_{0.75}P_{0.25}$, chemical effect on valence electronic states, AES and SXAPS meas. 79−47558
CuPd, chemical shift effects and origin of Pd 3d core level satellite 80−104039
$Cu_{0.67}S_{0.33}$, chemical effect on valence electronic states, AES and SXAPS meas. 79−47558
Cu_2S, S and S^{2-} states, identification from Auger line shapes 79−92034
Cu_2S-CdS heterojunction interface, depth distribution profiles, Auger spectra 80−88622
$Cu_{2-x}S$ on CdS, low temp. growth, AES obs. 79−28924
CuSe, X-ray photoelectron and Auger spectra 78−56561
Cu_2Se, X-ray photoelectron and Auger spectra 78−56561
$Cu_{0.9}Si_{0.1}$, chemical effect on valence electronic states, AES and SXAPS meas. 79−47558
Cu(100), adsorption of Xe monolayers, thermodynamics and kinetics, LEED and AES obs. 79−99423
D, thermal desorption meas. of H-isotope retention in Alcator-A Tokamak 80−79588
Dy, effect of mode of d-hole formation *(French)* 77−36356

Auger effect continued
Er, film, reaction with H_2O vapour, spectroscopic and X-ray diffr. obs. 77−40575
ErD_2, thin film, reaction with H_2O vapour, spectroscopic and X-ray diffr. obs. 77−40575
$ErRh_4B_4$, film, sputter deposition and low temp. props. 80−2948
^{165}Er decay parameters and whole-body dose, for radioisotope scanning 77−70529
EuO (100), disordered, LEED and electron spectroscopy 79−28178
F K_α X-ray satellite struct. and KLL Auger electron spectra, solid-state effects 80−89089
$F+C^{2+}(N^{2+})(O^{2+})$, K Auger electron spectra 79−89758
Fe (001) surface, initial reaction with water vap. 77−69173
Fe (100), adsorption of Br_2, AES, LEED, work function, and thermal desorption study 80−15375
Fe (100), adsorption of carbon tetrachloride, AES, LEED, work function, and thermal desorption study 80−15376
Fe (100), adsorption of Cl_2, AES, LEED, work function, and thermal desorption meas. 79−82465
Fe (100), adsorption of I_2, AES, LEED, thermal desorption, and work function study 80−15374
Fe (100), adsorption of tetrabromomethane, AES, LEED, work function, and thermal desorption meas. 80−39422
Fe (100), equilib. surface segregation of dissolved C, N and S 77−62723
Fe, (100) surface, S segregation and 2D compounds precipitation *(Japanese)* 80−35188
Fe (11O), coadsorption of K and 0_2, XPS, UPS, AES, and LEED study 80−80084
Fe (110), adsorption and decomposition of ammonia, LEED, AES, UPS, work function and desorption meas. 79−69345
Fe (110), adsorption of C, N, O, S, CO, NO and C_2H_2, UPS and LEED/Auger meas. 77−72773
Fe (110), adsorption of K, LEED, AES, UPS and XPS meas. 79−77919
Fe (110), K promoted, adsorption of CO, UPS, XPS, AES, and flash desorption obs. 79−82463
Fe (111) surface, S segregation, LEED, AES and work function changes 80−15350
Fe and Fe alloys, passive films studied using AES combined with ion sputtering technique 80−35378
Fe and its oxides AES meas. 77−36323
Fe, atomically clean, N_2 treatment, corrosion inhibition 78−19954
Fe, Auger transitions, two-electron-one-photon radiative rate calc. 77−18869
Fe based alloys, solute segregation to grain boundaries, AES 78−72780
Fe, cast, spheroidal graphite form., role of interphase boundary adsorption 77−63657
Fe compounds, radiative Auger transition, $K \rightarrow M^2$ weak X-ray emission lines 78−33556
Fe desorption of H into ultrahigh vac. system, using permeation cell 80−86326
Fe epitaxial growth on Cu(111), supersaturation and mode of growth, LEED and AES exam. 78−18929
Fe film, thermally evaporated, contamination effects obs. 80−49545
Fe, free surface and grain boundary O_2 and S chemistry 80−75410
α-Fe, grain boundary segregation of C, N_2 and C Auger spectroscopy 78−72778
Fe, intergranular corrosion in NO_3 solns., electrochem. and AES study 80−50751
Fe ions, Li-like Auger contribs. to electron impact ionisation 80−87231
Fe, oxidation in CO_2, early stage obs. by AES 78−48570
Fe, oxidation of (001) surface, first monolayer at. struct. 78−34706
Fe, plastic deform. and fracture, H_2 effect, studied by electron microscopy and Auger spectrography *(French)* 77−77545
Fe, pure, Auger anal. of passive films in neutral aqu. soln. 80−16605
Fe, reaction with methane at 750 C micro Auger anal. 80−104020
α-Fe, S and C diffusion, AES obs. 77−51543
Fe surface, (111) and (100), adsorpt. and decomp. of NH_3 78−40077
Fe surface, form. and decomp. of nitrides 79−24831
Fe, surface atom electron binding energy depend. on composition, Auger spectra, APS spectra 80−39655
Fe, surface films formed in inhibitive solns., optical props., protective quality 79−20260
Fe, surface segregation of Sn, AES obs. 77−20172
Fe surfaces, adhesion, effect of adsorbed atoms, AES study 80−39456
Fe surfaces, adsorption, segregation and reactions of non-metal atoms, LEED and AES obs. 80−59783
α-Fe-(Ni,Mn,Cr,Mo,W)-P (1 wt.%). grain boundary segregation, temper brittleness, AES study *(Japanese)* 79−78981
Fe-C (0.25 wt.%), austenitising temp. effect on proeutectoid ferrite reaction kinetics, scanning Auger microprobe exam. 78−44144
Fe-CR alloys, ion-etched, surface comp., effect of adsorbed CO, AES obs. 79−46896
Fe-Co, surface comp. and surface segregation 80−34280
Fe-Cr, Auger electron and appearance pot. spectroscopic study of surfaces 80−11520
Fe-Cr, high-temp. oxidation, borate inhibitors 80−66705
Fe-Cr, surface atom electron binding energy depend. on composition, Auger spectra, APS spectra 80−39655
Fe-Cr, surface segregation of impurities (C,N and S) *(French)* 77−56192
Fe-Cr alloy, (100) and (110) surfaces, lateral lattice spacings, simultaneous LEED and AES 77−20174
Fe-Cr alloy, (100) and (110) surfaces, initial oxidation stages, simultaneous LEED and AES obs. 77−20175
Fe-Cr alloy, sputter etching oxide film, comp. profile, quantitative AES 80−81383
Fe-Cr oxide, quantitative depth profile, by AES *(Japanese)* 80−16751
Fe-Cr-Mo, sputtering effect on surface comp., AES obs. 80−6601
Fe-Cr-Mo(Ni)(Mo-NI), AES using peak-to-peak value *(Japanese)* 79−20485
Fe-M-(I) (M≡Ni, Cr, V, Ti, Mo; I≡Sb, P), co-segregation at free surfaces studied by Auger spectroscopy 80−59767
Fe-Mn (3 wt.%), Sn diffusion along grain boundaries, micro-Auger spectroscopy 77−11740
Fe-Mn (8 wt.%), quenched, exam. of intergranular embrittlement 78−76745
Fe-Mo (5 wt.%), Auger anal. of passive films in neutral aqu. soln. 80−16605
Fe-Ni, sputtered using Hg^+ and Ar^+ beams, variation as function of ejection angle, AES exam. 77−44105
Fe-Ni, surface comp. obs. by AES 78−10266

Auger effect continued
Fe-Ni (3 wt.%), grain boundary segregation microanal. using X-ray (STEM) and AES 78−87685
Fe-Ni (50 wt.%), surface comp. and oxide film thickness after various surface treatments, AES study 80−66693
Fe-Ni alloy, anodic oxide film formed in H_3BO_3-$Na_2B_4O_7$ soln., exam. of in depth profile by AES and sputter etching 79−20247
Fe-Ni-Cr, oxide film form., combination anal. using ESCA, AES and SIMS 79−16092
Fe-Ni-Cr (30.6, 21.3 wt.%), Alloy 800, high temp. oxidation at low O_2 press., SEM, AES and electron probe microanal. study 80−93688
Fe-Ni-Cr-C, ferritic, P segregation to free surface, 723 to 823K, AES 78−48411
Fe-Ni-Mn, martensite, aged, grain boundary embrittlement 79−96144
Fe-O system, initial oxidation, combination anal. using ESCA, AES and SIMS 78−72924
Fe-Si, (3wt.%) alloys, grain boundary anal.,, scanning AES 79−43256
Fe-Si (1%), LEED-Auger exam. of $(1\bar{1}0)$ surfaces 78−71915
Fe-Si (2.35 wt.%), misorientation dependence of grain boundary segregation, Auger spectroscopy exam. 78−76629
Fe-Si (3 wt.%), containing B, grain boundary segregation, AES evidence 77−86046
Fe-Si-Al, surface oxide layer struct., AES study 80−89396
Fe-Si(Al), oxide layer form. during annealing, AES in-depth anal. *(German)* 80−16576
α-Fe-Sn alloy, grain boundary hardening and segregation 80−55417
Fe-Zr, dilute solid solution, surface segregation, AES exam. 77−43413
$FeB_5C_{15}SSi_{15}Cr_5$, amorphous, exam. of metalloid atom mobility by Auger spectroscopy 78−47575
$FeO \rightarrow Fe_3O_4$, in-situ AES using galvanic cells 78−19615
$Fe_{1-x}O$ powder, wustite, AES study, ion and electron bombard. effects 80−76114
α-Fe_2O_3 powder, hematite, AES study, ion and electron bombard. effects 80−76114
Fe_3O_4, film, quantitative sputter rates, AES, ellipsometry determ. 78−72661
Fe_3O_4 powder, magnetite, AES study, ion and electron bombard. effects 80−76114
Fe_xO_y film, thermally evaporated, contamination effects obs. 80−49545
$FeP_{13}C_7$, amorphous, exam. of metalloid atom mobility by Auger spectroscopy 78−47575
$Fe_{1-x}Pd_x$ film, air-exposed, comp. profiles by AES, ESCA and ion sputtering 78−95245
$Fe_{1-x}Pd_x$ film, vac. deposited, oxidation and corrosion, AES, XPS and STEM obs. 79−100286
FeS, S and S^{2-} states, identification from Auger line shapes 79−92034
$Fe_{1-x}S$, soft X-ray emission and AES study 79−91535
FeTi, hydrogen energy storage, surface segregation *(German)* 79−77872
FeTi, surface and mag. props., heat treatment and hydrogenation effects 80−75447
FeTi, surface segregation and catalytic effect on hydrogenation, AES and XPS study 79−11626
α-Fe(111), adsorption of water under the influence of 2.5 keV electrons 79−28199
Ga, effect of $L_1L_{2,3}M$ Coster-Kronig processes on $L_{2,3}MM$ Auger spectrum 78−72681
Ga, L_{23}-$M_{4\ 5}M_{4\ 5}$ principal and satellite Auger spectra 78−42030
Ga, LMM Auger spectra, rel. to L_{23} photoelectron spectra 77−77348
Ga, LMM Auger spectra, transition probabilities, term splittings and effective Coulomb interaction 77−44126
Ga, reson. photoemission shake-up and Auger processes at 3p photothreshold 80−100748
GaAlAs-GaAs heteroepitaxial devices, interstitial impurities and degradation, Auger obs. 80−99730
GaAlAs-GaAs heterostruc. lasers, interstitial impurities and degradation, Auger obs. 80−99730
$Ga_{0.64}Al_{0.36}As$, plasma grown oxide, phys. and elec. props. 78−48550
$Ga_{1-x}AlAs$ (110) oxide-free Schottky barriers, surface comp. and characts., AES obs. 79−82661
$Ga_{1-x}Al_xAs$-GaAs, abrupt quantum-well heterostruct. grown by metalorganic chemical vapour deposition 79−56933
$Ga_{1-x}Al_xAs$-GaAs heterojunctions grown by metallorganic CVD 80−15599
$Ga_xAl_{1-x}As$, Schottky barrier, effect of oxide composition on elec. behaviour, AES meas. 79−87141
GaAs (001) surface, thermal treatment before MBE growth, RHEED-AES meas. 79−61754
GaAs, (100), comp. and struct. of differently prepared surfaces, LEED and AES 78−91524
GaAs (100), Sb desorption props. 80−80074
GaAs (110), adsorpt.-desorpt. processes and phase transitions in alkali halide adsorbed layers 78−2361
GaAs (110), adsorption of Cs 77−72794
GaAs (110), adsorption of O_2, oxide form., XPS/UPS study 80−49497
GaAs (110), initial oxidation, XPS and AES study 80−11542
GaAs (110), struct., elec. props., effects of illumination, O_2 absorpt., electron bombard. *(French)* 78−34690
GaAs (110), surface struct., LEED and AES study, comparison of MBE and ion bombard. surface prep. 80−54496
GaAs (110), valence band Auger spectra 78−35230
GaAs (110), valence band Auger spectra, from Ga and As CCV transitions 78−92149
GaAs, acceptor bound exciton Auger and radiative transition rates, radiative recomb. 80−6733
GaAs, adsorpt.-desorpt. of Zn, thermal desorpt., at. beam adsorpt., AES, SEM, RHEED 78−14591
GaAs, adsorption enhancement by electron beam excitation of gas mols. 78−43238
GaAs, adsorption of O_2, adsorption states and Ga depletion, UPS, AES, and thermal desorption meas. 79−46952
GaAs anodic oxide, quantitative chem. depth profiles 77−72799
GaAs anodic oxide chem. depth profiles, neutron activation analysis and Auger spectroscopy 77−77619
GaAs, anodically oxidised, conc. ratio of O, As and Ga using Auger spectroscopy 79−66188
GaAs, Auger de-excitation of metastable state 79−65410
GaAs, Auger recombination, luminesc. meas. 77−85850
n-GaAs, Auger transitions, nonlinear extrinsic luminesc. study sublinear emission 79−95833
GaAs, chem. etched surface, Auger characterisation 77−25169

Auger effect continued
GaAs, chem. prep. of surfaces, and AES and XPS characterisation 77−90477
GaAs, chemisorption of O_2, effect of surface index and atomic disorder AES, LEED and optical ellipsometry 79−60638
GaAs cleaved (110) face, interaction with O_2, influence of cleavage defects, AES study 80−66684
GaAs, deep radiation centres from heat treatment, γ-irrad., deform., probability of nonradiative electronic transitions 80−50408
GaAs, electronic surface structure Cs(Rb)(Na) adsorpt. processes, AES, LEED, EELS, study 78−68068
GaAs, epitaxially grown (001), (111) and $(\bar{1}\bar{1}\bar{1})$ surfaces, LEED, AES, photoemission 78−38924
GaAs, excitation by 2-4 KeV Ar^+ ions, electron energy spectra 80−11529
n-GaAs, heavily doped, non-linear extrinsic luminesc., role of Auger recombination 79−52010
GaAs, homoepitaxy and epitaxy, surface anal., using RHEED and Auger spectroscopy 80−66433
GaAs, impurity centres ionis. by Auger electrons, carrier relax. *(Russian)* 79−51594
GaAs interface with anodic and thermal oxides, comparison of AES and ESCA 78−95980
GaAs, ion bombardment, composition changes, AES 78−72662
GaAs, laser alloying of Au-Ge ohmic contacts, Auger depth profiling 79−73583
GaAs, luminesc. emitted by deep centres, illumination-induced change in internal quantum efficiency 79−91495
GaAs, MBE grown film, in situ surface characterisation by RHEED, SIMS and AES 77−43410
GaAs, multiple insulator layers studied by Auger anal. 79−83345
GaAs on GaAs and Ge, epitaxy, mechanism, effect of substrate surface struct. 77−51614
GaAs oxide, passivated layers, quantitative in-depth profile, AES-SIMS thermal, anodic and plasma oxidations 78−84087
GaAs oxide, plasma grown, semiquantitative chemical depth profiles, Auger spectroscopy and neutron activation anal. 78−53284
GaAs, oxide layers prepared by anodic, thermal and plasma oxidation, in-depth profiles and annealing effects 79−61768
GaAs, plasma anodisation in DC discharge, AES and MIS diode expts. 78−95826
GaAs, plasma-grown oxides, physical props., Auger and IR spectral anal. 79−91821
GaAs, polycryst., wet and dry oxides, comparative study by AES, SIMS and XPS 80−80116
GaAs, polycrystalline, carrier transport at grain boundaries 80−29411
GaAs solar cell, polycryst., grain boundary passivation by oxidation, AES, SIMS and XPS obs. 80−81467
GaAs substrate, Pd/Ge film sintering, Auger spectra, Schottky barrier energy 79−69581
GaAs, substrate for homoepitaxy, vicinal surfaces characterisation 77−20207
GaAs surface, during vapour phase epitaxial growth, characterisation techniques and meas. *(French)* 77−1817
GaAs, surface (111), $(\bar{1}\bar{1}\bar{1})$, (110), XPS, photo-Auger ionisation cross section, electron mean free paths 78−56558
GaAs, surface segregation of implanted alkali metals, photoemitter prep. and characts. *(French)* 78−60544
GaAs, surface studies during MBE growth 79−90899
GaAs thermally oxidised surface, in-depth comp. profile, Auger analysis 77−89621
GaAs VPE growth, in situ surface anal. 79−95937
GaAs:Ba^+, Auger electron and charact. electron energy loss spectra 80−55235
p-GaAs:Ge, (111) surface, LPE grown, cryst. struct., phys. and chem. props. by Auger obs. 79−73386
GaAs:S, implantation depth profiles of S^+ and S_2^+ using AES 79−55774
GaAs:Se, implanted, annealing with O-free CVD Si_3N_4 encapsulant 78−83834
GaAs:Sn, surface segregation of Sn during MBE, SIMS and AES 78−72031
GaAs:Sn films, MBE grown, doping profiles, carrier mobilities, RHEED and AES obs. 79−1447
GaAs:Te(Cd)(Mg)(B), ion implant depth distribs., AES and glow discharge optical spectroscopy meas. 80−65028
GaAs/Au and GaAs/Au-Ge/Ni, Schottky barrier energy var. with interdiffusion 77−20435
GaAs-Al interdiffusion, 250-450°C, AES meas. 77−1263
GaAs-Au Schottky barriers, PES and depth profiling obs. 79−42641
GaAs-Au(Ag) Schottky barrier solar cells, interface problems, AES, SIMS and XPS study 80−89627
GaAs-Cs-O film, polycryst., secondary emission props., activating coating effects 78−2957
GaAs-metal ohmic contacts, solid phase epitaxy formation, AES and channelling meas. 79−60658
GaAs-Pd junction, contact reactions 79−56308
GaAs$(\bar{1}\bar{1}\bar{1})$As surface, 3 states, comp., struct., surface states and O_2 sticking coeffs. 77−66080
$Ga_xIn_{1-x}As$, alloy film surface processes controlling growth by MBE RHEED and AES exam. 78−84084
p-$Ga_xIn_{1-x}As$, Auger recomb., theory and luminesc. expts. 78−56518
$Ga_xIn_{1-x}P$ alloy films, surface processes controlling growth by MBE, RHEED and AES exam. 78−84084
Ga_2O_3 thin films, reactively evaporated, props. *(Japanese)* 79−99648
GaP (100), prep. of negative electron affinity surface by Cs adsorption 80−10768
GaP (110), initial oxidation, XPS and AES study 80−11542
GaP, adsorption and desorption of Cs, LEED, AES, and photoemission meas. 80−70532
GaP, impact ionisation theory, Auger processer 80−49752
GaP, O_2 adsorpt. monitoring by Auger spectroscopy, electron beam effects 77−72777
GaP, O_2 adsorpt. monitoring by Auger spectroscopy, electron beam effects 78−6218
GaP, overlap integrals and Auger recomb. coeff. direct calc. 79−69524
GaP, reson. photoemission shake-up and Auger processes at 3p photothreshold 80−100748
GaP, single-crystal, anodically oxidised layers, AES measurements 78−91556
GaP surface, Ar^+ and e^- excited Ar Auger electron emission 79−47560

Auger effect continued
- GaP, surface cleaning by oxidation and heating, characterisation for electron emitter appl. 78-35548
- GaP:Cs-O simultaneous adsorption, oxidation interface chemical struct. 80-103584
- GaP:Zn,O, Auger coeff. from luminesc. decay and Hall effect 77-48226
- GaP:Zn,O, Auger coeff. from luminesc. efficiency and Hall effect 77-48227
- GaP-Pd contact system, low temp. alloyed contact formation 80-100519
- GaSb, adsorption and desorption of Cs, LEED, AES, and photoemission meas. 80-70532
- GaSb, Auger recombination, luminesc. meas. 77-85850
- GaSb-Au Schottky barriers, PES and depth profiling obs. 79-42641
- GaSb-Pb junction, Ar ion bombard. effect on tunnelling props. 80-54783
- $GaSb_{1-x}As_x$, disorder-enhanced Auger recomb. 79-43014
- Gd, AES, by computer *(French)* 80-7890
- Gd, resonance recomb. lines in AES and photoelectron spectra 80-97390
- Gd-Fe amorphous film, atomic diffusion of deposited Co 79-73346
- GdF_3, chemically reacted film on ferroelectric-ferroelastic $Gd_2(MoO_4)_3$, characterisation 79-15057
- $GdFe_2$ films, electron beam deposited, amorphous and cryst., mag. and struct. props. 79-4710
- GdFe(Co), amorphous film, XPS meas. 79-87295
- $Gd_2(MoO_4)_3$, domain structure obs. by GdF_3 decoration, AES meas. 78-84544
- $Gd_2(MoO_4)_3$, surface study using AES and ion scatt. spectroscopy 80-65339
- Ge (100), surface structure and chemical state 77-15670
- Ge (111), oxygen adsorption, electron-beam enhanced reaction, AES meas. 77-4256
- Ge, (111) cleavage face, struct. changes, LEED and Auger spectroscopy study 79-95249
- Ge, Auger processes, impact ionisation theory 80-49752
- Ge, Auger recombination probability calc. for degenerate carriers 80-24944
- Ge, Auger spectra, comparison with multiplet struct. calc. 78-31287
- Ge, direct gap recombination, at high excitation level and low temp. 79-38650
- Ge, electron-hole drops, Auger recomb. 77-48240
- Ge, electron-hole drops, phonon lifetime and acoustic attenuation due to phonon-assisted Auger recomb. 80-34462
- Ge, electron-hole liquid, range of energetic Auger electrons 79-90970
- Ge, excitons bound to acceptors, Auger transition rates 78-34778
- Ge, film, amorphous, contamination anal. by AES 77-36828
- Ge, internal photoelectric effect, spectral depend. of quantum efficiency 78-39150
- Ge, LMM Auger spectra, rel. to L_{23} photoelectron spectra 77-77348
- Ge, LMM Auger spectra, transition probabilities, term splittings and effective Coulomb interaction 77-44126
- Ge, oxidation of clean cleaved (111) surfaces, EELS and AES 80-3230
- Ge, phonon assisted Auger recomb. in indirect gap semiconductors 78-39126
- Ge surface, (111), ion-bombarded and annealed, spectroscopic ellipsometry study 80-103543
- Ge:As, recomb. of donor bound excitons, luminesc. intensity decay 80-25441
- GeS (001) surface, electronic struct., Auger and electron energy loss spectra meas. 77-59314
- ^{71}Ge, energy release accompanying electron capture 78-17148
- ^{71}Ge, LX-, LX-coincidences during decay 78-17149
- H, backscatt. by Cu or Mo, 4-30 keV, O_2 effect 78-15268
- $H^+ + O_2(N_2)(Ne)$, K-shell capture cross-section, Auger effect 78-33602
- H_3BO_3, chem. bonding, electronic struct., ESCA, Auger, and SIMS spectra 80-50512
- HCl, mol., XPS and KLL Auger effect, line shifts 79-31602
- HF, ab initio HF-STO perturbation Auger transition rate calc. 79-72368
- HF, Auger spectra, correl. effects, energies and wavefunctions, ab initio CI calc. 80-14125
- HF, Auger transition energy calcs. 77-34704
- $H^+(H_2O)_n$, secondary electron emission from charged clusters on 2.4 keV Ar bombarded surfaces 79-15580
- $H^+(NH_3)_n$, secondary electron emission from charged clusters on 2.4 keV Ar bombarded surfaces 79-15580
- H_2O, double hole states POCI calc., Auger spectrum 78-78630
- H_2O, KLL Auger electron spectrum, semi-internal correl. 80-48038
- H_2S, double hole states POCI calc., Auger spectrum 78-78630
- H_2S, gaseous 1s binding energy and S $KL_2L_3(^1D_2)$Auger energy, XPS obs. 77-3416
- H_2S, KLL Auger spectrum, obs. and ab initio SCF CI calc. 78-50654
- H_2S, KLL spectra of S, ab initio LCAO SCF calcs. 77-65515
- H_2S, $L(S_2)$-MM Auger energies, MC SCF calcs. 78-21977
- H_2S, mol., XPS and KLL Auger effect, line shifts 79-31602
- H_2S, S K-LL Auger energies and chemical shifts 80-28069
- H_2SO_2, S K-LL Auger energies and chemical shifts 80-28069
- H_2SO_4, S K-LL Auger energies and chemical shifts 80-28069
- H_4SO_2, S K-LL Auger energies and chemical shifts 80-28069
- He, Auger radiation effect with γ-ray emission 77-50417
- He, metastable, deexcitation process on Mo [110] impact 78-95642
- $HfAl_3$, anomalous growth in thin films, AES, TEM and He backscatt. meas. 77-43462
- p-(Hg,Cd)Te, carrier lifetime, dominant Auger transitions comparison 80-49768
- Hg, $N_{6,7}O_{4,5}O_{4,5}$ Auger electron spectrum, electron impact excitation 77-57958
- HgCdTe, recomb. effects, mag. quantum oscills. in Auger transition rate 79-82610
- $Hg_{1-x}Cd_xTe$, acceptor bound exciton Auger and radiative transition rates, radiative recomb. 80-6733
- $Hg_{1-x}Cd_xTe$, recombination processes using impact ionization capture cross sections 80-75577
- $nHg_{1-x}Cd_xTe$, single-phonon and plasmon recomb. lifetime effect, with magnetically tuned bandgap 79-38098
- n-$Hg_xCd_{1-x}Te$, narrow band gap, Auger effect under high mag. fields 79-82609
- Hg_2Cl_2, surface composition, electron impact, mass spectrometry, AES and LEED meas. 79-60607
- H^-(spin polarised)+atom, inner-shell ionis., subsequent radiation ang. distrib. 80-53114

Auger effect continued
- I, $M_{4,5}N_{4,5}N_{4,5}$ Auger spectra, kinetic energy shift rel. to I_2 80-5516
- I_2, adsorbed on Ag(111), Cu(111), and Cu(110), surface EXAFS study 80-40186
- I_2, $M_{4,5}N_{4,5}N_{4,5}$ Auger spectra, kinetic energy shift rel. to I 80-5516
- I_2, $M_{4,5}N_{4,5}X$ Auger electron spectra, many-body effects 79-59415
- III-V alloys, disorder-enhanced Auger recomb. 79-43014
- ^{125}I in partially blocked thyroid of rats, testis damage 78-3565
- ^{125}I-iododeoxyuridine, effect of ^{125}I-decay, mol. consequences of Auger effect 77-4982
- In, adsorption of O_2, CO, CO_2, and water, AES study 79-82451
- In, Auger electron spectra, solid state effects 80-20739
- In, K-fluorescence yield determ. from K-Auger electron emission rates 80-95569
- In surface, impurity precipitation and resolution at melting point 78-14553
- In ultrathin films on TbTe and Te, prep. and characterisation 77-7995
- In, XPS and $M_{4,5}N_{4,5}N_{4,5}$ Auger spectra 79-61472
- In-In_xO_y-Pb tunnel-junction barriers, evidence for chemical annealing effects 79-42701
- InAs and solid solutions, recombination mechanisms of excess carriers, luminesc. obs. 80-97337
- p-InAs, Auger recomb., theory and luminesc. expts. 78-56518
- InAs, impact ionisation and Auger recomb. 77-20329
- InAs, on GaAs, heteroepitaxial layers, compositional profile, AES 77-20212
- $InAs_{1-x}Sb$, disorder-enhanced Auger recomb. 79-43014
- $In_xGa_{1-x}As$, MBE layers on InP substrates, elec. props., photoluminesc., X-ray and Auger obs. 79-51450
- InGaAsP LPE heterostructs., interface grading, Auger depth profile 80-103585
- InGaAsP-InP heterojunction, LPE, lattice mismatch, Auger depth profile 79-87005
- $In_xGa_{1-x}As_ySb_{1-y}$ laser, nonequilibrium carrier recombination, luminesc. study 80-50431
- In_2O_3-InN film growth by reactive sputtering in N_2-O_2 discharge, mechanism 80-89108
- InP, (100) surface, Auger depth profiling limitations 79-61473
- InP (100) surfaces, chem. treatment effects on comp. and nature 79-47794
- InP (110) surfaces, cleaved and polished-sputtered-annealed, LEED and AES study 80-103550
- InP, anal. of anodically oxidised (111) layers by MeV $^4He^+$ channelling effect meas. and AES 79-4492
- InP epitaxial layers, (100)-orientated, vapour phase deposited in closed-tube system, surface comp. variation 80-24752
- InP, excitation by 2-4 KeV Ar^+ ions, electron energy spectra 80-11529
- InP interface with anodic and thermal oxides, comparison of AES and ESCA 78-95980
- InP surface, interaction with Cl, electron spectroscopic obs. 78-56036
- InP/anodic oxide interface, Auger analysis 77-90478
- InP/$In_xGa_{1-x}As_yP_{1-y}$ interfaces, sputter-profiled, depth resolution degradation by cone form. 80-80094
- InP-Ag contact system, evaluation of Auger depth profiling technique 79-56893
- InP-Al interface struct., low temp. interaction, AES study 80-107661
- InP-Au Schottky barriers, PES and depth profiling obs. 79-42641
- InP-Cu contact system, low temp. alloyed contact formation 80-100519
- InP-metal ohmic contacts, elec. and metallurgical props., heat treatment effects 80-34514
- InSb (110), clean, O_2 adsorption, AES, LEED, RHEED and field effect meas. 80-49501
- InSb (110), initial oxidation, XPS and AES study 80-11542
- InSb (110), ion bombard. effect on surface struct. and electronic props. 80-6923
- InSb, (111) surface, anal. by low energy ion scattering spectroscopy, LEED and AES *(Japanese)* 80-20746
- InSb, Auger-governed decay of laser-induced plasma, optical probing 80-76105
- InSb, electronic surface struct., Cs(Rb)(Na) absorpt., AES, LEED, EELS study 78-68068
- InSb film, MBE apparatus and AES 78-47875
- InSb film, synthesis by 2-source mol. beam technique and AES characterisation 78-72729
- InSb IR detector array, AES anal. of localised contaminants at interfaces 77-57391
- InSb, intrinsic, photoinjected electron hole pairs, Auger lifetime, photoconductive decay obs. 80-39629
- InSb, recombination processes using impact ionization capture cross sections 80-75577
- InSb-Au contact system, low temp. alloyed contact formation 80-100519
- $In_{2-x}Sn_xO_{3-y}$-Si solar cells, SiO_2 detection of interface, Auger anal. 79-87991
- Ir (100), chemisorption of acetylene, benzene and ethylene, geometric and electronic effects 77-55457
- Ir (110), adsorption of CO, O_2, H_2, N_2, ethylene and benzene 78-38961
- Ir (110), chemisorption of CO, preexponential factor and desorption energy 78-71963
- Ir (110), chemisorption of O_2, sorption and dissoc. kinetics 79-33186
- Ir (110), chemisorption of O_2, AES, LEED, thermal desorption mass spectra, and contact pot. difference meas. 79-77901
- Ir (111), of benzene and pyridine, electronic transitions sensitivity to molecule-surface orientation, energy loss spectra 80-45184
- Ir (111) surface, chemisorption of O_2, dynamics, AES 77-59211
- Ir, Auger spectra, $N_{4,5}N_{6,7}N_{6,7}$ and $N_{4,5}N_{6,7}O_{4,5}$ 80-89094
- Ir, chemisorption of CO on clean and oxidised (110) surfaces 79-11015
- Ir surface, chemisorption of H_2 and hydrocarbons, LEED, AES, and thermal desorption meas. 77-1297
- Ir-W (0.3 wt.%): Al(Fe)(Th)(Ni)(Rh), effect of additions on grain boundary composition 79-83309
- $Ir_4(CO)_{12}$ EELS, AES, comparison with XPS and UV absorpt. spectra obs. 80-35021
- Ir(110)-(1×2) reconstructed, adsorption, of S, AES study 79-42384
- Ir(111), chemisorption of O_2, LEED-Auger expts. 77-20191
- Ir(111) surface, electron beam induced desorption and dissociation of chemisorbed CO, LEED and AES 78-56043
- K compounds, Auger spectra, shake-up satellites 78-27369
- KCl, LEED-AES study of oriented adsorption of TCNE 77-62737
- $KNbO_3$ catalysts, ferroelectric, for reactions involving CO and NO , and adsorption of NO 80-30282

Auger effect continued

K_2O-CaO-SiO_2 glasses, Auger analysis, alkali signal decrease 80−61189
K_2O-SiO_2, glass, influence of electric charge phenomena on AES *(French)* 80−50478
K_2O-SiO_2 glass, AES obs. of K^+ electromigration to surface under electron bombardment *(French)* 79−33869
K_2O-SiO_2 glasses, Auger analysis, alkali signal decrease 80−61189
K_2SO_3-Ag_2SO_4 mixtures, surface comp., AES and XPS obs. 80−81386
Kr, 3d-shell electron impact ionis., Auger electrons ang. distrib. 77−27183
Kr, heavy ion induced MNN Auger electron spectra 77−6907
Kr, inner shell alignment calc. in electron impact ionisation 77−14586
Kr, optical and Auger spectra, discrepancies anal. 79−93944
$Kr+Ar^+(Kr^+)$ collisions, quasimol. Auger transitions 77−19070
Kr_2^+, formed in 50 keV $Kr^+ + Kr$ collisions, Auger transitions obs. by electron-scattered-ion coincidence method 80−74243
$KrAr^+$, quasimolecule Auger spectra 79−68269
LaB_6 (001) surface, struct., initial oxidation, XPS, UPS, LEED, AES, work function meas. 79−99403
LaB_6, clean and oxidised (100) surface, LEED, AES, work function, evaporation meas. 78−71989
LaB_6, direct recomb. and Auger deexcitation channels of La 4d to 4f reson. excitations, photoemission spectra 80−66395
LaB_6, high temp. interaction with 0_2, AES and mass desorption expts. 80−7698
LaB_6, single cryst. work function, thermionic emission, evaporation 77−24922
LaB_6, thermionic emission rel. to surface state 78−39654
LaB_6, work functions from thermionic and field emission retarding pot. methods 79−65537
LaB_6:C, AES, LEED and energy-loss spectra study of C layer on (100) surface 77−62715
$LaNi_5$, surface segregation induced by O_2, LEED and AES exam. 79−11009
Li, $2s^22p$ double Auger rate 80−99489
Li, Auger and autoionisation spectra, collisional excitation mechanisms 77−19042
Li, Auger line shape KVV, energy band theory 79−43074
Li, Auger widths of core levels calc. using diagrammatic many-body technique 77−43544
Li, Auger widths of core levels using renormalised many-body perturbation theory 79−74033
Li, chemisorption of O_2, KVV Auger spectrum of oxidised Li 77−55454
Li, excited in single gas collisions, high-resolution Auger spectra 80−9717
Li I, $2s^2sp$ and $1s2s^2$ decay rates many-body perturbation theory calc. 79−59376
Li, transition density of states, AES meas. 77−36325
Li, valence band Auger spectra, surface effect 80−80915
Li+He (methane), collisional excitation, prompt decay line energy, projectile Auger spectrosc. 79−85941
$Li_2^+ + \rightarrow$, $2(1s^2)Li^+ + e$, Auger electrons energy width 77−23443
$LiNbO_3$:Ti optical waveguide diffusion profile, AES obs. *(German)* 78−33876
$LiNdP_4O_{12}$ laser, relaxation oscillations and mode spectra, high density pumping effect 80−69396
Li_2O-Al_2O_3-SiO_2 glass, aq. corrosion 79−61753
$Li_2O.2SiO_2$ glass and glass ceramic, Auger electron signal decay, crystn. effects 80−25503
Li_3PO_4, Auger lineshape determ. by numerical integration background subtraction 79−74469
Li_2SO_4, Auger lineshape determ. by numerical integration background subtraction 79−74469
LuH_2, electronic struct., photoelectron spectra study 80−50527
MO-B, B effects, rolled, segregation of implanted elements, Auger spectroscopy exam. *(Russian)* 78−35389
Mg, AES, KLL spectra, and plasmon struct. 79−15592
Mg, adsorbed S(O)(N)(C), internal and external sources of electrons 77−44097
Mg, adsorption of O_2, at 100 and 300K, XPS, UPS and X-ray AES meas. 78−18901
Mg, atom, solid and MgO, electronic relax., Friedel model, KLL′ AES 77−65444
Mg, Auger electron prod. by Ne^+ bombard. 80−7460
Mg, Auger electron prod. by Ne^+ bombard., origin of Ne Auger peaks *(French)* 80−7461
Mg, Auger electron production by noble gas ion bombardment 77−1778
Mg, Auger electron spectra, electron impact excited, vap. and solid state differences 78−52603
Mg, Auger spectra, CI calcs., spin-orbit interactions 77−14558
Mg, Auger spectra, KLL and KLV, screening effects and plasmon gains 80−80913
Mg, Auger spectrum, KLL, plasmon gain satellite obs. 78−76562
Mg, free at., electron-excited, K-Auger spectrum, including K-LM and K-MM transitions 80−5519
Mg I, Mg II, ejected electron spectrum from autoionis. levels after electron impact 77−75304
Mg I, Mg II autoionisation state radiative decay *(Russian)* 80−5509
Mg, ion-induced Auger electron emission, depend. on ion energy 79−78814
Mg, K Auger transition rates, orbital relax. and interchannel interaction effects 78−50521
Mg, L_{23} shell ionisation cross-section under H^+, heavy-ion impact, Auger spectra *(French)* 79−24406
Mg, L_{23} shell ionisation-cross section under He^+ impact, Auger spectra obs. *(French)* 77−69956
Mg, $L_{23}VV$ Auger spectrum 78−39634
Mg, lineshape of $KL_2L_3(^1D_2)$ line 78−60535
Mg, plasmon-loss intensities in XPS, EELS and Auger spectra 80−10902
Mg, polycryst., adsorpt. of O_2 at 100 and 300K, XPS, UPS, XAES 78−18906
Mg surface, Ar^+ and e^- excited Ar Auger electron emission 79−47560
Mg, transition energies calc. 79−18168
Mg, X-ray excited L Auger spectra, double ionisation satellites 77−32497
Mg, XPS, plasmon gains as monitor of incomplete relax., interference effects and sudden to adiabatic limits transition 80−66390
Mg-Cd, plasmon loss and plasmon gain, X-ray photoemission and AES 79−23918
Mg-MgF_2, sputtered films, opt. props. 78−80430

Auger effect continued

$Mg+H^+(He^+)$ and electron impact ionis., Auger study of collisionally induced alignment 78−90279
Mg+heavy ion, X-ray spectra, one-photon two-electron rearrangements 77−6712
MgAg, 4d bandwidth influence on $M_{4,5}N_{4,5}N_{4,5}$ Auger spectra 79−100017
Mg_2Cu polycrystals, surface study by AES, XPES and X-ray induced AES 80−65346
MgF_2 coated Al mirrors, AES, UV irrad. effect 77−72047
MgF_2, interatomic Auger transitions, XPS exam. 77−8692
MgO (100), ang. depend. of Auger electron emission 79−61474
MgO, adsorption of Cs and Li, AES, LEED, work function, and secondary electron emission meas. 80−44407
MgO, KLL′ Auger spectra, electronic relax., Friedel model 77−65444
MgO, low-energy Auger transitions 79−61476
MgO, photostimulated electron emission, manifestation of Auger processes 77−52225
MgO, XPS valence bandstruct. 80−89117
MgO:Al(Li)(F)(Sn), hole processes in photostimulated luminesc., electron emission, X-ray irrad., ESR relaxation 79−69889
MgO-ZnO, solid soln., surface comp., Auger and XPS investig. 78−51806
Mn and its oxides AES meas. 77−36323
Mn-Zn ferrites, grain boundary exam. using TEM and AES 80−107268
MnZn ferrites, doped; determ. of grain boundary composition, using Auger spectroscopy *(German)* 79−23618
MnZn ferrites, Ti substituted, mag. permeab. meas., grain boundary comp. AES obs. 78−95473
Mo (100), adsorption of CO_2 and trimethylamine, adsorbed O effect, LEED and AES obs. 80−39443
Mo (100), adsorption of O_2, AES, LEED, work function, and desorption meas. 80−6654
Mo (100), early stage condensation of Cu and Ag, comparison with W (100) 80−80072
Mo (100), orientation effects in Auger electron spectroscopy 79−69928
Mo (110), oxidation of adsorbed C, electron diffr., contact pot. difference, and AES obs. *(Russian)* 79−52430
Mo {100}, anisotropy of secondary electron emission from oblique incidence of electrons 79−99999
Mo, AES and characteristic energy loss spectra, expt. and interpretation 78−27354
Mo, adsorption and dissoc. of CO on (100) surface, comparison with carburised surface 77−15689
Mo, and oxides, AES expts., chem. shift and beam effects 79−15566
Mo, coadsorption of CO_2 and O_2, AES and SIMS obs. 79−46928
Mo, competition between interstitial atoms during segregation at grain boundaries, AES obs. *(Russian)* 77−25008
Mo, monolayer, oxidation, quasisimultaneous SIMS, AES, XPS 78−72919
Mo, RF sputtered, diffusion barrier props. 78−71887
Mo, sintered, thermally induced surface composition variations 79−5078
Mo, sputtering yield meas. by AES 78−95633
Mo, surface struct. changes due to ionic bombardment *(Russian)* 77−1775
Mo^{24+}, electron impact ionis., dominant Auger process 77−68120
Mo^{32+}, dielectronic recomb. rate coeffs. in plasma 80−43853
Mo^{38+}, dielectronic recomb. rate coeffs. in plasma 80−43852
Mo^{n+}, photoionisation and Auger effect 78−90135
Mo:C (110) surface, segregation, precip. and desorpt. of C, AES and LEED study *(French)* 80−103480
Mo-Ca, ion implanted, range distrib. of Ca^+ ions, work function and AES obs. 78−27365
Mo-O system, initial oxidation, combination anal. using ESCA, AES and SIMS 78−72924
Mo-Si, film deposition by reactive sputtering, characteris. *(Japanese)* 80−93485
Mo-W, calibration line introduction for comp. determ. by AES 79−56892
Mo-Zr, nitride form. in N_2 atmos. *(Russian)* 78−19938
MoO_x, AES expts., chem. shift and beam effects 79−15566
MoS_2, adsorption of Cs and O_2, LEED, Auger and work function meas. 78−71994
MoS_2, clean surface, AES and LEED exam. 80−10762
$MoSi_2$ sputtered films, protective layer form. on oxidation, Auger anal. and backscatt. meas. 79−15029
Mo_xSi_y films, magnetron DC reactive sputtering, struct. and props. 80−80966
Mo(100), adsorpt. of CO, LEED, AES, study 78−87873
N, in $NH_3(N_2)$, heavy-ion induced K-shell Auger effect 77−6908
N^+ and N_2^+, beam-foil and beam-gas excitation, Coulomb explosion effects, Auger spectra obs. 80−14220
N^+, beam-foil excitation, absolute Auger yield meas. 80−14203
N^+, beam-foil excitation; absolute Auger yield meas. 79−45685
N^+, from exploding fast mol. ions, Auger spectra 80−32781
N^{n+}, electron impact inner-shell excitation/ionis. cross sections 77−23564
$N+H^+(He^{2+})$, K-shell Auger electrons ang. distrib. 79−89756
N+N, K-shell excitation, Auger electron spectrosc. obs. 80−9714
N+O(C), K-shell excitation, Auger electron spectrosc. obs. 80−9715
N_2^+, exploding fast mol. ions, Auger spectra 80−32781
N_2^+ $X^2\Sigma_g^+$-state, vibr. states asymmetry parameter and photoelectron spectrum 80−95591
$N_2+H^+(He^+)$, K-shell ionisation, AES meas. 77−10749
N_2+X^{n+}, (X=Ar,Kr,Xe,U), Auger emission line shape after dissoc. 78−86838
NH_3, Auger spectrum, resolved peak assignments 77−42362
NH_3, electron excited Auger emission 77−88518
NH_3, gas-phase Auger electron spectrum 77−31005
NH_3, solid, AES excited by X-rays 79−33894
NH_3+X^{n+}, (X=Ar,Kr,Xe,U), Auger emission line shape after dissoc. 78−86838
NO, chemisorbed on Pt(100), vibr. spectra, electron energy loss, LEED and Auger investig. 79−90866
Na (111) surface, epitaxial film, electron induced dissociation 80−6646
Na, AES, KLL spectra, and plasmon struct. 79−15592
Na, Auger and autoionisation spectra, collisional excitation mechanisms 77−19042
Na, Auger electron emission from ion-solid collision *(French)* 79−33876
Na, Auger electron emission due to ion collisions with solid targets *(French)* 80−104031

Auger effect continued
- Na, Auger spectra, CI calcs., spin-orbit interactions 77–14558
- Na, Auger spectra, KLL and KLV, screening effects and plasmon gains 80–80913
- Na, Auger widths of core levels calc. using diagrammatic many-body technique 77–43544
- Na, Auger widths of core levels using renormalised many-body perturbation theory 79–74033
- Na clusters, electronic relaxation energies in $KL_{2,3}L_{2,3}$ Auger transitions, SCF-Xα-SW calcs. 78–90334
- Na, electron impact excitation, L-Auger and autoionis. spectra 78–5354
- Na K_α X-ray satellite struct. and KLL Auger electron spectra, solid-state effects 80–89089
- Na, KLV Auger line shape, one-orthogonalised plane wave calc. 77–48316
- Na, L-Auger, autoionisation spectrum after electron impact excitation 77–14591
- Na, lineshape of $KL_2L_3(^1D_2)$ line 78–60535
- Na, metallic, Auger cross relaxation energy, SCF cluster model calc. 79–46945
- Na, transition energies calc. 79–18168
- Na, XPS, plasmon gains as monitor of incomplete relax., interference effects and sudden to adiabatic limits transition 80–66390
- Na+H^+ collisions, L-Auger electron emission, autoionising states, line broadening effects 77–14568
- Na_3AlF_6 film, evaporated, electron bombard. effect on secondary electron emission, Auger peak shifts 80–2903
- NaCl (100), adsorption of Xe, AES and LEED meas. 77–11792
- NaCl, interatomic Auger processes 77–85892
- NaCl, mechanoluminesc. peaks, microbreakdown mechanism, generation of ionisation waves 79–33032
- NaF, AES, surface composition of surface layers, for TSEE 78–6836
- NaF, interatomic Auger transitions, XPS exam. 77–8692
- β-Na_2O-CaO-Al_2O_3, impurity conc. at grain boundaries, AES obs. 77–35570
- Na_2O-CaO-SiO_2 glasses, Auger analysis, alkali signal decrease 80–61189
- Na_2O-SiO_2 glass surface anal., effect of electron bombardment during AES on composition 79–83065
- Na_2O-SiO_2 glasses, Auger analysis, alkali signal decrease 80–61189
- Na_xWO_3, cubic single cryst., LEED/Auger obs. 78–19614
- Na_xWO_3, surface props., AES meas. 80–71767
- Nb (110) and (750), interaction with O_2, LEED, AES, SIMS, and EELS obs. 80–44408
- Nb, adsorption of O_2, continuous meas. of surface pot. variations using mirror electron microscope 77–47680
- Nb, adsorption of O_2 and N_2, on (100) planes, LEED-AES obs. 77–69186
- Nb foil, oxidized, electron irradiation damage, AES study 79–28015
- Nb foils, coated with H-permeable Pd film 79–52467
- Nb, for supercond. microwave cavities, secondary electron emission and AES meas. 79–56895
- Nb, impurity conc. monitoring during single cryst. production 78–31337
- Nb, interaction with O_2, AES and low-energy SIMS meas. 79–47832
- Nb, oxide growth and oxide coatings, XPS and AES studies 80–50765
- Nb, sputter deposited film, O contamination, Auger anal. 78–52669
- Nb sputtered film analysis, comparison with X-ray diffr. and electron diffr. *(Czech)* 79–51448
- Nb, sputtering yield, SEM and scanning Auger microprobe obs. 79–87545
- Nb superconducting cavities, AES depth profile meas. on oxide layer 77–8984
- Nb thin foils, surface segregation during sputtering at elevated temps., Auger study 80–54386
- Nb-N, superconducting layers, sputtering in high vacuum apparatus *(German)* 80–89147
- Nb-Nb_2O_5-Pb(In) Josephson junctions, props. of Nb_2O_5 thermally grown tunnel barriers 80–100568
- Nb-NbO system, single- and two-phase, sputtering yield, SEM and scanning Auger microprobe obs. 79–87545
- Nb-O, exam. of surface segregation equilibrium and kinetics, by Auger spectroscopy *(Russian)* 79–56981
- Nb_3Ge films, prep. by DC sputtering and solid state diffusion, supercond. props. and struct. 79–38212
- Nb_3Ge, high T_c films, electron tunnelling and AES anal. 79–28471
- Nb_3Ge, sputter-deposited, superconducting T_c and phase relationship 79–56344
- Nb_3Ge sputtered films, Ge surface segregation exam. by AES 79–56084
- Nb_3Ge, supercond. sputtered film, ion scatt., AES, depth profiling 77–11806
- Nb_3Ge superconducting films, quantitative Auger anal. 80–55740
- NbN, for supercond. microwave cavities, secondary electron emission and AES meas. 79–56895
- NbN, supercond. RF reactively sputtered films, deposition parameter effects on props. 80–80972
- NbN superconducting reactively sputtered film, Auger anal. 78–72297
- Nb_2O_5, electron irradiation damage, AES study 79–28015
- Nb_2O_5, for supercond. microwave cavities, secondary electron emission and AES meas. 79–56895
- α-Nb_2O_5, reduction in H_2 discharge, AES and SEM anal. 77–59708
- Nb_3Sn, for supercond. microwave cavities, secondary electron emission and AES meas. 79–56895
- Ne atom with 1s-hole, wave function calcs. using radial orbitals, orthogonality 77–67971
- Ne Auger electron decay, final charge states, beam-foil investig. 77–19060
- Ne, Auger electron emission from ion-solid collision *(French)* 79–33876
- Ne, Auger electron emission due to ion collisions with solid targets *(French)* 80–104031
- Ne, Auger energies, intensities, for initial K vacancy, many body calc. 77–18869
- Ne, Auger rates, X-ray transition energies and fluoresc. yield calcs. 77–6714
- Ne, Auger spectra, correl. effects, energies and wavefunctions, ab initio CI calc. 80–14125
- Ne, beam-foil excited ^4P state, delayed coincidence Auger electron lifetime meas. 80–14117
- Ne, electron degradation spectra, inner-shell contribs. 77–3474
- Ne, electron impact ionisation yield model 79–45851
- Ne, foil excited, 6 to 10 MeV, equilibrium K-shell excitation 79–22817
- Ne, foil-excited, KLL-Auger spectrum 77–34604

Auger effect continued
- Ne, heavy-ion induced K-shell Auger effect 77–6908
- Ne, highly-ionised, heavy ion impact, selective electron capture effects 80–14202
- Ne ion, energy of metastable K-LL Auger transition *(Russian)* 78–82704
- Ne, ionisation potential, KLL Auger energies, SCF transition operator calcs. 78–41925
- Ne, K-$L_{2,3}L_{2,3}$, post-collision interaction Auger effects 79–45686
- Ne, KLL Auger transition rates, effect of interchannel interaction 77–42301
- Ne, Li-like X-ray and Auger populations and line intensities from Cl^{13+} collisions 77–10625
- Ne, orbital relaxation and final-state channel mixing, in Auger effect 78–50520
- Ne, transition energies calc. 79–18168
- Ne^{7+}, 1s2l3l′ config., Auger and radiative deexcitation, intermediate coupling 77–79567
- Ne^{n+}, electron impact inner-shell excitation/ionis. cross sections 77–23564
- Ne^{x+}, (x=3-7), K-LL Auger transition energies calc. 79–54823
- Ne^{n+}-Ne, K-shell vacancy prod. cross section, X-ray and Auger electron prod. fluoresc. yield 78–13582
- Ne+$H^+(He^+)$, K-shell ionisation, AES meas. 77–10749
- Ne+$H^+(He^{2+})$, K-shell Auger electrons ang. distrib. 79–89756
- Ni (001), adsorption of N_2, c(2×2) struct. form 80–80083
- Ni (001), chemisorption of S, thermodynamics, AES study 79–82452
- Ni (001), geometrically induced structure in SXAPS and Auger electron appearance potential spectra 79–38695
- Ni (001) surface, adsorbed N_2, p(2×2) struct., LEED and AES study 80–54515
- Ni (001) surface, Ar ion bombarded, enhancement of oxidation, AES study 80–97644
- Ni (001) surface, electronic struct. of ordered S overlayers 80–84835
- Ni, (100), (111) clean and H_2S, S-adsorbed surfaces, angular distributions of Auger electron emission *(Japanese)* 78–43963
- Ni (100), adsorption of CO, EELS and concomitant surface anal. 80–7453
- Ni (100), adsorption of O_2 and reduction of surface oxide by H_2 80–108741
- Ni (100), ang. resolved meas., compared with electron multiple scatt. calc. 77–32476
- Ni (100), catalysis of CO+H_2, reaction rate, AES and UPS obs. 79–79290
- Ni (100), chemisorption of NO, LEED, AES, UPS, and thermal desorption study 80–39449
- Ni (100), clean and chalcogen-covered, electron ejection by metastable He atom impact 79–8217
- Ni (100), dissociative chemisorption and mol. adsorption of NO 80–65373
- Ni (100), initial oxidation process, angle-resolved AES and LEED obs. 79–52463
- Ni (100), initial oxidation, electron energy loss spectra, LEED, AES, and work function meas. 79–61795
- Ni (100), interaction with methane, diffusion of deposited C, AES-LEED study 79–99418
- Ni (100), kinetics of C deposition from adsorbed CO 80–76553
- Ni (100) and polycrystalline surfaces, CO chemisorption, low energy SIMS and AES 80–34309
- Ni (100) surface, ang. resolved Auger emission and LEED Kikuchi intensities at 850 eV 80–66340
- Ni (100) surface, coadsorption of Sn on Pb, P or O contaminated surface, AES study 80–88437
- Ni, (100) surfaces, Si-, P- and Cl-chemisorbed, LEED and angle-resolved AES obs. 79–95258
- Ni (100)-p(2×2)C, decomp. of formic acid and adsortion/desorption of H_2, CO, and CO_2 79–91995
- Ni (110), adsorption of CO and CO_2, electron bombard. effects, AES and electron stimulated ion desorption obs. 79–51430
- Ni (110), adsorption of O_2, obs. by electron microscopy, AES and LEED *(French)* 77–62732
- Ni (110), chemisorption of O_2 and initial oxidation, AES, EELS, and work function meas. 80–54523
- Ni (110), dissolution of C adlayer, 600-913K 80–49504
- Ni (110), effect of surface O on catalytic and chemisorptive behaviour, LEED and AES 77–85066
- Ni (110), interaction with O_2, electron energy loss spectra and AES obs. 79–47826
- Ni (110), NO chemisorption and dissoc. 77–15695
- Ni, (110) and (111) surfaces, oxidation exam. at room temp. by combined SIMS-AES/LEED method 79–20241
- Ni, (110) surface, methane interaction kinetics, AES-LEED-ellipsometry 77–62756
- Ni (111), adsorption of acetylene and ethylene, surface structs., LEED and AES obs. 79–60636
- Ni (111), adsorption sites of CO using IR reflection-absorption spectroscopy and AES 79–69355
- Ni (111), adsorption sites of CO, LEED, AES, thermal desorption, work function, and IR system meas. 79–77903
- Ni (111), C monolayer phase condensation, LEED and AES obs. 79–46960
- Ni (111), dehydrogenated adsorption of ethylene, thermal desorption and AES study 80–29274
- Ni (111), Mossbauer effect emission spectroscopy and AES 79–91329
- Ni (111) surface, adsorption of Cl, LEED, AES, work function and flash desorption meas. 77–85069
- Ni, AES meas. of soft X-ray emission threshold potential *(Russian)* 79–33866
- Ni, adsorbed S(O)(N)(C), internal and external sources of electrons 77–44097
- Ni and its oxides, AES meas. 77–36323
- Ni, binary alloy, irrad. with heavy ions, non-equilib. segregation phenomena 80–19950
- Ni, chemisorpt. of CO, SIMS, AES, desorpt. meas. 78–87875
- Ni, clean and gas-adsorbed surfaces, ang. distribs. 78–39636
- Ni, coadsorption of Pb or Sn iwth P or C, AES study 80–54521
- Ni, deposited, on stress/annealed pyrolytic graphite, binding, AES 77–59210
- Ni dissolution of C through (110) surface, LEED and AES meas. 78–63932
- Ni, EXAFS in photoelectron yield spectra 80–16123

Auger effect continued
Ni, epitaxial film on NaCl, struct. and purity 78−72047
Ni, epitaxial growth, on NiO(100), by low pressure hydrogen reduction *(French)* 80−11578
Ni film, interaction with O_2, AES, EELS, work function, and gravimetric meas. 80−75433
Ni film, layer mode growth on Fe (001) surface, AES study 80−49540
Ni, film growth on graphite and amorphous C, electronic struct. by photoemission and Auger obs. 79−77947
Ni films, adhesion on graphite 80−80141
Ni films on Pyrex, AES, purity 77−8755
Ni, integranular precipitation after annealing, ion imaging microanalysis *(French)* 79−61594
Ni, $L_3M_{23}M_{23}$ Auger energy calc. using XPS, effect of 3d-4s admixed screening on relax energies 77−1782
Ni, $M_{II,III}$ spectrum, ab initio calculation 80−83276
Ni, Medicus matrix cathode, surface characts. 80−66378
Ni, oxidation, chemisorption and oxide nucleation stages, low-energy SIMS and AES obs. 79−43083
Ni, oxide films, metal and O_2 transport, AES and inert marker, techniques 80−97641
Ni passivation, S influence study by Auger and electron spectroscopy 80−65347
Ni, photoelectric effect in paramag. and ferromag. states, Auger spectra 78−95649
Ni, photoelectron spectra, threshold Auger emission 80−29849
Ni plating, surface props. of Ni after each step of activation process 78−95243
Ni, polycryst., bulk-to-surface precip. and surface diffusion of C, AES data interpretation 78−34713
Ni pseudodiffusion in single crystal Si during RF sputtering, Auger spectroscopy 78−2396
Ni, sputtered, on Si, annealing effects on transmission electron diffr. patterns, silicide form. 78−91562
Ni stepped surface, morphology exam. by LEED and ARS 78−71913
Ni, stress corrosion susceptibility, S segregation effect, Auger spectrosc. study 80−61019
Ni sulphide surface, oxidation studied by AES 79−83505
Ni surface, adsorbed S, H_2^+ ion induced desorption, AES meas. 78−84069
Ni surface, adsorpt. and decomp. of formic acid, obs. using combined SIMS-FDS-AES system 78−40076
Ni surface, electron stimulated interaction of H_2O, AES obs. 77−31902
Ni surface, S and O_2 covered, polycrystalline, initial sticking coeff. of H_2, LEED and AES 78−63937
Ni surface with adsorbed S, oxidation studied by AES 79−83505
Ni, tarnishing in air, 23-200°C, relative humidities from ambient to 95%, monitoring 78−19940
Ni, UPS, two-electron reson. at 3p threshold, rel. to Cu (100) expt. 80−25522
Ni:C, bulk-to-surface precip. and surface diffusion, AES meas. 77−11784
Ni/Au-Ge/GaAs contact system, alloying behaviour, microprobe AES and X-ray diffr. 80−54548
Ni/Cr multilayers, AES depth profiling by sputtering with N_2^+ ions 79−95881
Ni/Fe interfaces sputter profiling, by AES 79−15572
Ni/Fe layers, interdiffusion, Auger sputter profiling obs. 79−46848
Ni/GaAs film contact system, alloying reaction 80−96747
Ni-Al(Ti)(Mo)(Si), effect of solute misfit and temp. on irradiation induced segregation 78−72779
Ni-Au, dil., orientation depend. of surface segregation, AES and SEM obs. 78−71908
Ni-Au alloy, oxidation in air, 50-150°C, film growth obs. using AES and contact resist. 80−3242
Ni-Au alloys, surface segreg., surface energy and solute strain energy effects 77−72760
Ni-base alloy, semiquantitative anal. with SIMS, AES and wet chemical anal. 77−48291
Ni-Cr film, electrical props. rel. to AES conc. depth profile 77−32092
Ni-Cr film, resistance stabilisation by surface oxide formation 79−78214
Ni-Cr film, vac. deposition, elec. props. and comp. struct. 79−77966
Ni-Cr films, vac. deposited, comp. and temp. coeff. of resist., AES obs. 79−91161
Ni-Cr multilayer structs., sputter profiling, depth resolution and surface roughness effects, AES obs. 77−76694
Ni-Cr-Fe, Inconel, effects of heat treatment on surface segregation, Auger spectroscopic exam. 80−7602
Ni-Cu, sputtered using Hg^+ and Ar^+ beams, comp. variation as function of ejection angle, AES exam. 77−44105
Ni-Cu, surface composition, AES 78−14558
Ni-Cu diffusion couple surface, epitaxial, AES and CO chemisorption 77−31891
Ni-Fe reed contact, Au-plated, submicron Auger spectroscopy exam. 79−15027
Ni-Mo, multilayer films, depth resolution determ. in Auger depth profiling meas. 79−78800
Ni-O system, initial oxidation, combination anal. using ESCA, AES and SIMS 78−72924
Ni-O system, oxidized polycryst. Ni films, H_2 reduction, AES 77−12472
Ni-Pd (1 at.%), surface comp. and surface segregation, AES obs. 79−51404
Ni-pigmented anodic Al_2O_3, for selective absorpt. of solar energy, optical and struct. props. 80−55892
Ni-S, dil. alloy, AES of grain boundaries *(French)* 80−50477
Ni-Si, Cs ion-bombarded, surface Cs concs., AES meas. 79−83073
Ni-Sn alloys, oxidation, AES obs. 77−48575
Ni-Th (1 at.%), surface comp., temp. and O_2 exposure effects, AES study 80−80914
Ni-W (2%), Mg diffusion meas., 970-1330K, appl. of vapour collect and AES method 78−75876
β-NiAl, oxide films, metal and O_2 transport, AES and inert marker, techniques 80−97641
Ni_3Al and $Ni_3(Al, Ti)$, S segregation to grain boundaries 78−48410
Ni_3C film, thermal decomposition, AES meas. 78−56056
Ni_3C films, form. by carburisation, characterisation 80−34337
Ni_3C films, on graphite, thermal decomp., AES lineshape study 79−79293
Ni_3C formation and decomposition during evaporation of Ni onto graphite 79−15055
NiO (100), ang. depend. of Auger electron emission 79−61474

Auger effect continued
NiO (100) surface, sulphurisation by H_2S, AES, LEED, RHEED structural study *(French)* 78−64888
NiO, (100) surface interaction with SO_2, electron diffr. and Auger spectrosc. obs. *(French)* 80−97728
NiO, Auger quantitative anal. 78−73104
NiO film, formed by Ni galvanic oxidation in borate buffer soln., struct. 80−100948
$Ni_{0.96}Sb_{0.04}$, surface segregation, XPS and AES obs. 80−76135
Ni_3Sn, surface composition determ. 79−69328
Ni_3Ti, electronic struct., Xα calc., photoelectron and AES spectra 80−20769
Ni(100), chemisorption of unsaturated hydrocarbons, LEED and AES obs. 77−31904
Ni(110) surface, AES *(Dutch)* 79−1802
Ni(110)(2×1)C surface, kinetics of D_2 desorption, LEED and AES meas. 77−47683
Ni(111), adsorpt. of CO, absolute coverage determ., AES and LEED 77−76661
Ni(111) surface, CO, CO_2, carburisation, AES meas, electron beam-induced effects 77−48588
O adsorbed on Ni (111), order-disorder transition 79−82447
O, beam-foil excited ^4P state, delayed coincidence Auger electron lifetime meas. 80−14117
O III, production by Auger effect, astrophysical appls. 78−20633
O ions, Li-like Auger contribs. to electron impact 80−87231
O^+, beam-foil excitation, absolute Auger yield meas. 80−14203
O^+, beam-foil excitation; absolute Auger yield meas. 79−45685
O^+, from exploding fast mol. ions, Auger spectra 80−32781
O^{n+}, electron inner shell excitation/ionis. cross sections 77−23564
O^{n+}, n=1 to 4, gas and foil-excited, 2-18 MeV, projectile Auger spectra 79−59414
O+C(N), K-shell excitation, Auger electron spectrosc. obs. 80−9715
$O+H^+(He^{2+})$, K-shell Auger electrons ang. distrib. 79−89756
O+O, K-shell excitation, Auger electron spectrosc. obs. 80−9714
O_2, electron impact ionis., mean energy expended per ion pair 78−74777
O_2+X^{n+}, (X=Ar,Kr,Xe,U), Auger emission line shape after dissoc. 78−86838
P, two and three-electron Auger transition, with vacancies in 2p-shell 79−63972
P^+, beam-foil excitation; absolute Auger yield meas. 79−45685
PH_3, mol., XPS and KLL Auger effect, line shifts 79−31602
PLZT, thin film epitaxial growth and characteris. 79−28918
PZT, ferroelec. film, elec. props., composition anal., AES 78−84530
Pb, Auger emission target, contrib. of reflected electrons 78−92152
Pb chalcogenides, Auger recomb., theory 80−65586
Pb, deposition on Au, quantitative Auger electron spectroscopy, substrate and instrumental effects 80−71523
Pb, double-vacancy states, L X-ray fluoresc., K Auger electrons 77−27016
Pb, epitaxial growth on Ag (111) and Cu (111) LEED, RHEED, AES study 78−84090
Pb, LL-vacancy states produced by KLL Auger transitions, X-ray fluoresc. yield 77−18832
Pb monolayer, double layer with Sn, growth on Al (111), struct. 80−70567
Pb, muonic high-lying states transitions, electron screening effects 77−34786
Pb on Cu, Auger electron spectroscopy 77−85851
Pb overlayers, on Cu substrate, oxidation, AES and XPS obs. 79−47833
Pb ultrathin films on PbTe and Te, prep. and characterisation 77−7995
Pb, X-ray excited, $N_{6,7}O_{4,5}O_{4,5}$ spectra 77−85886
Pb-In(-Au) base electrode film Josephson junctions, tunnel barrier oxide struct. 80−65750
$PbO-SiO_2$ glass, leaching behaviour in dil. HNO_3, ellipsometry and AES obs. 78−23846
PbO_2, Auger quantitative anal. 78−73104
PbS, clean surface, AES and LEED exam. 80−10762
PbS film, soln. grown on Si, struct. and comp. of heterojunction 80−54530
PbS-Si heterojunction, chem. struct., AES anal. 80−76115
$Pb_{1-x}Sn_xSe$ epitaxial layers, radiative and nonradiative recomb. processes 80−60670
PbSnTe-like semicond., Auger recomb., nonparabolic approx. 79−15161
$Pb_{0.78}Sn_{0.22}Te$, $Pb_{0.91}Sn_{0.09}Se$, radiative and nonradiative recombination 80−80849
$Pb_{0.8}Sn_{0.2}Te-Pb$, Schottky barrier form., Auger depth profiling and I-V meas. 80−49903
$Pb_{1-x}Sn_xTe$, epitaxial layers, carrier lifetime meas. 79−42559
$Pb_{1-x}Sn_xTe$ film on BaF_2, electron beam delineation effect on MBE growth, LEED and AES obs. 79−99434
$Pb_{1-x}Sn_xTe$, MBE, O_2 uptake, AES, XPS and UPS expts. 78−95227
$Pb_{1-x}Sn_xTe$, small-gap, recomb. mech. 79−38099
PbTe (111) epitaxial films, localised electron irrad. effects on elec. props. and O_2 sorption 80−49472
PbTe, epitaxial layers, carrier lifetime meas. 79−42559
PbTe p-n junction, minority carrier lifetime, step pulse recovery 77−11995
PbTe-In contacts, fabrication and props. 80−60078
Pd (110) surface, adsorption of S, characterised by LEED *(French)* 80−88422
Pd (111), chemisorption of Cl_2, LEED, AES, thermal desorption, and work function meas. 80−75444
Pd (111), interaction with O_2, EELS, AES and LEED obs. 79−86985
Pd, adsorption of NH_3, NH_x and N, decomposition of NH_3 and hydrogenation of N, AES 77−1315
Pd at. N-shell vacancy state widths, X-ray photoelectron, Auger spectra 77−18875
Pd cluster, adsorption/desorption of CO, AES and thermal desorption meas. 80−75436
Pd, film, on ZnO, struct., elec. props., AES, UPS study 78−76168
Pd, film growth on graphite and amorphous C, electronic struct. by photoemission and Auger obs. 79−77947
Pd, influence of surface environment on Auger peak, $M_{45}N_{45}N_{45}$ transition 80−7447
Pd on Al_2O_3 catalysts, surface atomic composition by AES 77−86377
Pd surface, segregated S state, AES, EELS, UPS and XPS study 80−93452
Pd, XPS, electronic struct. 80−7464
Pd/Si, Schottky-barrier type devices, chemical and polarisation characteristics, comparative study 79−78173

Auger effect continued
Pd/Si interface, chem. and struct. props. during silicide form., AES and TEM obs. 80—49430
Pd/SiO_x/Si, Schottky-barrier type devices, chemical and polarisation characteristics, comparative study 79—78173
Pd-Ag, surface segregation, Auger studies 78—87849
Pd-Ag (Cu) alloys, epitaxial growth and surface characterisation 78—14638
Pd-amorphous Si thin film interaction, metal rich Pd-silicide formation 80—2284
Pd-Ba (1.5 wt.%), thermionic emitter, Auger spectrum fine struct. 78—2954
Pd-Ba alloy emitter, thermionic emission props. and Auger spectrum 78—11066
Pd-Cu-Si metallic glass, energy loss spectra and Auger spectra 78—23563
Pd-Ni, Auger sensitivity factors 78—43964
Pd-Ni alloys, surface comp. and catalysis, AES and thermal desorption meas. 79—46898
Pd-Ni-P metallic glass, energy loss spectra and Auger spectra 78—23563
Pd-Si structure, epitaxial silicide growth, LEED and AES study 80—103590
Pd-silicate transport in Si-Pd_2Si-Si, correl. with C contamination 79—4491
PdH(D), energy loss spectra and Auger spectra 78—23563
PdSb, XPS, electronic struct. 80—7464
$Pd_{0.81}Si_{0.19}$, amorphous, partial densities of states, XPS, UPS and AES meas. 79—95315
Pd_2Si, Cs ion-bombarded, surface Cs concs., AES meas. 79—83073
Pd_2Si, on Si substrate, thermally induced Si accumulation, AES study 80—24718
^{106}Pd, KLM- and KLN-Auger transitions 77—18884
Pd(110) surface, adsorption of Xe, AES study 80—6633
^{210}Po, ^{211}Po, KLM- and KLN-Auger transitions 77—18884
Pt (100), adsorption of acteylene or ethylene , intermolecular forces and kinetics of adsorption 78—75930
Pt (100), adsorption of H_2S, intermolecular forces and kinetics of adsorption 78—75930
Pt (100), adsorption of NO, 40-400°C LEED, AES, XPS and UPS obs. 77—35820
Pt (100) chemisorption of acetylene and benzene, LEED, AES, HPS and temp. programmed dehydrogenation exam. 77—55456
Pt (100) surface, chemisorption of acetylene and benzene, AES, UPS, LEED and flash dehydrogenation 77—59216
Pt (110), acetylene adsorption, desorption and surface dissoc. 77—62749
Pt (110) reconstructed surface, LEED-AES study, O_2 treatment effect 80—39398
Pt (111), adsorbed H_2 and O_2 interaction investig. 77—55461
Pt (111), adsorption of NO, EELS, thermal desorption, LEED, and AES study 80—80086
Pt (111), at. steps role in H interaction 77—15690
Pt (111), chemisorption of Cl_2, LEED, AES, thermal desorption, and work function meas. 80—75444
Pt (111), clean and oxidised, binding states and sticking coeffs. of CO and H_2 77—72787
Pt (111), O_2, CO and C_2H_2 adsorption and cooxidation, AES *(German)* 78—14619
Pt (111) and (100) superlattices formed by dissociative adsorption of HI, LEED, AES, and thermal desorption studies 80—55715
Pt (111) and Pt (S)-12(111)X(111)surfaces, adsorption of 0, thermal desorption, AES, XPS, and LEED study 80—70534
Pt (111) stepped surface, adsorption of O_2, CO, C_2N_2 and ethylene 78—71992
Pt, adsoprtion of H, electrode surface exam. by LEED and AES 77—47665
Pt, adsorption and desorption of O_2 on (110) surface, thermal desorpt., LEED/AES obs. 77—72788
Pt, adsorption of CO, O_2, NH_3, surface composition, AES and temp. programmed desorption meas. 80—34313
Pt, adsorption of H_2 and CO, AES and flash desorpt. mass spectrometry 77—28078
Pt, adsorption of O_2, AES, LEED and thermal desorption spectroscopy exam. 78—79891
Pt, adsorption of O_2, surface struct. depend., LEED, AES, and electron energy loss spectra 79—46934
Pt, Auger spectra, $N_{4,5}N_{6,7}N_{6,7}$ and $N_{4,5}N_{6,7}O_{4,5}$ 80—89094
Pt, binding states of CO, flash desorption mass spectrometry and AES 77—85065
Pt, chemisorption of acetylene, characteristic loss spectrum and AES 77—55458
Pt electroplated film, Schottky barrier metallisation, Au diffusion, AES obs. 79—14968
Pt film, growth on amorphous Si:H, AES and LEED study 80—88447
Pt film on Si, PtSi form. kinetics, AES, SIMS, EPMA 77—11800
Pt films, high-purity, sputtered onto Si, PtSi and Pt_2Si form. 77—76676
Pt, hydrocarbon reactions catalysed by surfaces with variable kink concs., surface O_2 effects 80—35576
Pt, L-shell Auger and Coster-Kronig intensities from relativistic theory 79—93962
Pt, low index surface, O_2 reduction exam. using LEED and AES 79—70343
Pt, single cryst., oxidation, spectral lineshapes and shifts 78—14600
Pt, sputtered film, Al and Mg contamination, AES, SIMS 77—11822
Pt, stepped surface, adsorpt. and decomp. of NO and NH_3, LEED, AES, and thermal desorption expts. 78—38943
Pt surface, adsorption of H_2, rel. to electrocatalysis 78—38935
Pt surface, kinetics of NH_3 decomposition, AES meas. 77—1948
Pt, surface struct. and electronic props., CO_2, O_2 and H_2 chemisorption, LEED, AES 77—1300
Pt, XPS, electronic struct. 80—7464
Pt:C, C layer formation on (111) surface, temp. depend., LEED, AES study 78—71911
Pt-Au film couple, diffusion of Au, depend. on annealing ambient, AES exam. 77—1261
Pt-Ba alloy, elemental comp. and chem. state of surface during thermal activation, AES obs. 78—2345
Pt-Cr(Fe)(Ni) dilute alloys, surface segreation, equilib. surface composition, AES meas. 77—85039
Pt-Ir alloys, surface composition 79—19433
Pt-Pb fibre, CO adsorption and oxidation, AES and ESCA obs. 79 52469

Auger effect continued
Pt-Pd alloy, surface composition determ. by AES 78—79869
Pt-Pd(Au) alloys, surface comp. and catalysis, AES and thermal desorption meas. 79—46898
Pt-Si, Cs ion-bombarded, surface Cs concs., AES meas. 79—83073
Pt-$SrTiO_3$ (100) interface, struct. and electronic props., AES, LEED, EELS, and UPS study 80—24986
Pt-$SrTiO_3$ (100) interface, Auger and photoemission studies, relax. and chem. shift effects 80—54749
PtBi, XPS, electronic struct. 80—7464
Pt(S)-[9(111)×(111)] face, adsorption of O_2, flash desorption, LEED and AES obs. 77—69182
Pt_2Si, and PtSi, growth rate for form. by Pt film deposition under ultrahigh vac. and controlled impurity atm. 80—65388
Pt_2Si film formation, AES exam. to characterise impurity effects 79—15054
Pt(111), adsorption of Br, irreversible order-disorder transition, LEED AES, thermal description and work function meas. 79—69361
Pt(111) surface, adsorbed Br, $M_{2,3}M_{4,5}V$ and $M_{4,5}VV$ Auger spectra 79—69926
Pu, oxidation, binding energies, Auger and X-ray photoelectron spectra study 80—76550
Re, adsorpt. of CO on basal (0001) and stepped $|14(0001)\times(10\bar{1}1)|$ planes 78—14594
Re, dissociative and mol. adsorption of NO and H_2O, XPS, AES and SIMS study *(French)* 79—69344
Re, O_2 adsorption, effect of struct. defects, steps and kinks 80—29269
Re vicinal faces, adsorption of O_2, mirror electron microscopy, LEED and AES obs. 79—65323
Re:C, work function, graphitic layer formation 80—96966
Rh (110), chemisorption of CO and NO, LEED, AES, XPS, UPS, and desorption obs. 79—77899
Rh (111), adsorption of O_2, AES, LEED, and thermal desorption mass spectra meas. 79—77900
Rh (111), chemisorbed CO, dissociation probability, isotopic exchange and AES meas. 80—40743
Rh (111), coadsorption of O_2 and H_2 below 140K 80—29276
Rh (111), interaction with O_2, thermal desorption spectra, AES and LEED obs. 79—51428
Rh (111) and (100) surfaces, chemisorption of H_2, O_2, CO, CO_2, NO, C, ethylene, acetylene, LEED, AES and thermal desorption meas. 78—38951
Rh, (111) surface, chemisorbed O_2, catalytic reaction between adsorbed O_2 and gaseous H_2 79—83503
Rh (755), (331), chemisorption of H_2, O_2, CO, CO_2, NO, C_2H_2, C_2H_4 and C, AES and TDS obs. 79—65318
Ru (0001) surface, adsorption and desorption of NH_3, effects of electron beam 78—38955
Ru (001), adsorption of H_2S and S, LEED, UPS, AES, and thermal desorption meas. 79—99420
Ru (001), adsorption of NO, KPS, UPS, and X-ray AES meas. 80—6655
Ru (001), chemisorption of O_2, uptake meas., thermal desorpt. spectroscopy and AES 80—108739
Ru (001), coadsorption of O_2 and CO, uptake and flash desorption meas. 80—39450
Ru (001), dissociation of adsorbed H_2S, chemisorption and electronic struct. of S layer 79—79292
Ru (001) surface, adsorbed layer of CO, electron induced dissociation, X-ray AES 77—59215
Ru $(10\bar{1}0)$, adsorption of NO and CO 77—72783
Ru $(10\bar{1}0)$, dissociative adsorpt. of NO, LEED and AES expts. 77—90642
Ru (101), O_2 chemisorption, CO+O_2 interaction 77—73471
Ru (110), kinetics of C deposition from adsorbed CO 80—76553
Ru (~001) stepped surface, O_2 chemisorption, LEED and AES obs. 80—11947
Ru layer, 2-3 μm thick, ion plating and characterisation 78—11131
Ru(101), chemisorption of CO, surface structural chemistry and electron impact props. 77—1312
S compounds, one-electron binding and Auger energies 80—52872
S, one-electron binding and Auger energies 80—52872
S, two and three-electron Auger transition, with vacancies in 2p-shell 79—63972
S, X-ray and Auger transition probabilities to 2p level 78—17640
S^{n+}, fast highly charged ions, passing through foil, multiplet states equilib. population 77—10746
S-metal interactions 80—55710
SF_6, Auger emission anomalous spectra and yield, chemical species depend. 78—55152
SF_6, gaseous 1s binding energy and S $KL_2L_3(^1D_2)$ Auger energy, XPS obs. 77—3416
SF_6, KLL Auger spectrum, obs. and ab initio SCF CI calc. 78—50654
SF_6, KLL spectra of S, ab initio LCAO SCF calcs. 77—65515
$SF_6+H^+(He^+)$, F K-shell ionisation, AES meas. 77—10749
$SF_6+H^+\rightarrow SF_6^{+}+e^-+H^+$, 0.3-1.8 MeV, electron energy and ang. distrib. 78—22015
SO_2, double hole states POCI calc., Auger spectrum 78—78630
SO_2, gaseous 1s binding energy and S $KL_2L_3(^1D_2)$ Auger energy, XPS obs. 77—3416
SO_2, KLL Auger spectrum, obs. and ab initio SCF CI calc. 78—50654
SO_2, KLL spectra of S, ab initio LCAO SCF calcs. 77—65515
SO_2, S K-LL Auger energies and chemical shifts 80—28069
Sb, Auger electron spectra, solid state effects 80—20739
Sb, Sb_2O_3 and Sb_2S_3, AES and characteristic energy loss spectra, expt. and interpretation 78—27354
Sb, XPS, electronic struct. 80—7464
Sb_4, vap., $M_{4,5}N_{4,5}N_{4,5}$ Auger electron spectra 79—50089
Sc surface, single cryst., segregation of impurities, AES meas. 79—65299
ScH_2, electronic struct., photoelectron spectra study 80—50527
Se compounds, chemical shifts of X-ray electron and Auger lines 78—86912
Se compounds, LMM Auger spectra, relative intensity and relaxation energy 80—69115
Se film, metal ion diffusion during memory switching 78—26976
Se, $L_2M_{4,5}M_{4,5}$ Auger spectrum following photoionisation, post collision interaction, chemical shifts 79—22678
Se, LMM Auger spectra, relative intensity and relaxation energy 80—69115
Si, 1-10 keV H^+, He^+ irrad., role of Auger processes in electron emission 79—15579

Auger effect continued
Si, 3-15 keV Ar$^+$ induced Auger electron emission 77—59654
Si (100), oxides formed in Cs-O adsorbed films, ionisation loss spectra, Auger spectra 79—69365
Si (100), transition density of states from $L_1L_{2\ 3}V$ and $L_{2\ 3}VV$ Auger spectra 77—40314
Si, (100) surface, Auger emission ang. depend., overlayer effects 78—39637
Si (100) surface, LEED and AES meas. 78—60016
Si (110), chemisorption of Cl, LCAO calcs., Auger line shapes, localized density of states 78—56202
Si (111), (100) and (110) ideal surfaces, valence-band Auger lineshape theory 77—48286
Si (111), adsorpt. of O and stimulated oxidation by electron bombardment, AES 78—14599
Si (111), condensation of Au, AES obs. of very first stages 78—14633
Si (111), ion bombard., struct. changes, AES obs. 80—79842
Si (111), nitridation, AES and LEED results 80—80041
Si (111), with and without H chemisorption, Auger surface spectroscopy 80—50472
Si (111) 7×7 clean surface and O chemisorbed stage valence band density of states from $L_{23}VV$ Auger spectra 80—100717
Si (111) 7×7 surface, chemisorption of H_2O, AES, EELS and UPS 80—10792
Si (111) 7×7 surface, H_2S interaction, LEED and AES 78—38966
Si (111) 7×7 surface states, comparison with low-energy electron loss spectroscopy 79—60891
Si (111) surface, 1-3 keV He$^+$, Ne$^+$, Ar$^+$, Xe$^+$ bombard., AES obs. 79—33877
Si, (111) surface, Ag interaction, AES 78—14589
Si (111) surface, anal. by ion-electron spectroscopy 78—72670
Si (111) surface, clean and O_2-chemisorbed, electron states by AES 80—54747
Si, (111) surface, electronic density of states changes during O adsorption, AES obs. 79—65528
Si (111) surface, heating effects on ellipsometric parameters 77—72764
Si (111) surface, O_2 adsorption, atomic steps and residual gas effects 80—54517
Si, (111) surface, oxide formation, AES and EELS meas. 80—3232
Si (111) surfaces, cleaved, electronic structure following Al adsorption 80—75610
Si (111)/Au deposit, 2-dimens. condensed phase characterisation 77—69181
Si, AES examination of Ar$^+$ ion retention during Ar sputtering 78—56552
Si, adsorption of O_2, early stages, AES, LEED, and XPS obs. 79—46937
Si, amorphous, hydrogenated, work function and Auger spectroscopy of initial oxidation 78—76132
Si, amorphous, sputtered, Auger surface spectroscopy 80—50472
Si, amorphous film, sputtering by 0.5 to 5 keV Ar$^+$ ions 79—91550
Si, Ar ion etching, carbide form. 80—81222
Si, Auger band-to-band recomb. temp. depend. 80—29416
Si, Auger electron emission, ion induced and secondary ion emission 80—71546
Si, Auger electron prod. by Ne$^+$ bombard. 80—7460
Si, Auger line shape $L_{2,3}$ VV, energy band theory 79—43074
Si, Auger lineshape, one-electron theory for $L_{23}VV$ and $L_1L_{23}V$ 78—72645
Si, Auger recomb. coeff. meas. using laser excitation 79—38654
Si, Auger recombination, localized and free carrier comparison 79—38090
Si, Auger recombination 78—26883
Si, Auger spectra, KLL and KLV, screening effects and plasmon gains 80—80913
Si, Auger spectra induced by 100 keV Ar$^+$ impact 80—84820
Si, bound exciton-dopant Auger lifetimes 78—18970
Si, CF_3^+ ion bombardment, XPS and Auger study 79—70367
Si, CVD, surface anal. during growth, using RHEED and Auger spectroscopy 80—66433
Si, chemisorption of XeF_2 and SiF_4, XPS and Auger spectra, surface chemistry 80—81358
Si compounds, free mol. chemical shift, binding energy and Auger spectra 80—32782
Si, core and valence electron excitations, AES, chemical shift and line shape 80—2365
Si, Cs ion-bombarded, surface Cs concs., AES meas. 79—83073
Si diode, Auger recombination coefficient at very high injection rates 78—47863
Si diode, transient switching duration, linear carrier lifetime, emitter efficiency and Auger recomb. coeff. determ. 79—11207
Si, dry etching induced surface contamination, SIMS, AES, and XPS obs. 80—11810
Si, early oxidation stages, AES study *(French)* 79—8379
Si, electron-hole drops, Auger recomb. 77—48240
Si, energy losses on C contaminated surfaces, secondary electron spectra, AES, and SEM 79—99997
Si, epitaxial film growth on Si(111) and sapphire $(1\bar{1}02)$, simultaneous RHEED/AES study 80—10833
Si, epitaxial growth on sapphire by partially ionised vapour deposition, RHEED-AES obs. 80—80985
Si, epitaxial regrowth and grain struct. of Al metallisation on ⟨100⟩Si 78—79901
Si, excitons bound to acceptors, Auger transition rates 78—34778
Si, F-enhanced plasma growth of native layers, Auger profiles 80—93662
Si film, epitaxial growth by partially ionised vapour deposition, RHEED-AES-QMS study 79—83136
Si films, electron-beam-deposited on W substrates, growth and struct., AES and SEM obs. 79—46972
Si, grain boundary elec. props./impurity correl. using surface anal. of multigrained samples by SIMS and AES 80—79816
Si, growth and thermal evaporation kinetics of oxide film on Si surface 78—3246
Si heavily doped shallow-emitter p-n junction solar cells, diodes and transistors, Auger recombination 79—96445
Si, highly doped and highly exerted, Auger coeffs., radiative band to band recomb. lifetime meas. 77—85764
Si, hole localisation, solid solubility, excitonic Auger lifetime of acceptors 80—20216
Si, hole-hole-electron Auger recombination 80—70720
Si, internal photoelectric effect, spectral depend. of quantum efficiency 78—39150

Auger effect continued
Si, ion-excited L-shell Auger spectra, characts. 79—87533
Si, ion-induced Auger electron emission, depend. on ion energy 79—78814
n-Si, ionisation of low donor levels and recomb. of hot electrons at low temp. 79—51596
Si KLL Auger peaks, bremsstrahlung-induced 80—45199
Si, $L_{2,3}$ AES, local probe of atomic charge 78—48261
Si, LVV Auger spectra 79—52055
Si layer, on buried SiO_2 layer formed by high-dose, O ion implantation, TEM, AES, and XPS obs. 80—88172
Si MOS device, electron optical identification of precipitations 80—16309
Si, multigrained, grain boundary elec. and compositional props., surface anal. 80—76575
Si, multigrained, impurity segregation to grain boundaries, AES and SIMS obs. 80—65027
Si, nonradiative recombination and luminesc. 79—33770
Si, oxidation, AES photoelectron spectra exam. of early stages 79—74272
Si p^+-i-n^+ field induced junction solar cells, conversion efficiency limit in concentrated sunlight 80—85282
Si, phonon assisted Auger recomb. in indirect gap semiconductors 78—39126
Si, phonon-assisted Auger recomb., direct calc. of overlap integrals 80—107808
Si, semi-insulating polycrystalline CVD layers, AES and XPS characterisation 80—16129
Si, single cryst., oxidation, spectral lineshapes and shifts 78—14600
Si solar cells, fundamental efficiency limitations 80—93963
Si solar cells, ion-implanted 80—81452
Si solar cells, unified model of fundamental limitations 80—81448
Si, spectral, convolution and deconvolution 78—52601
Si, struct. of $L_{2,3}VV$-Auger line, rel. to soft X-ray spectra 78—2953
Si surface, Ar$^+$ and e$^-$ excited Ar Auger electron emission 79—47560
Si, surface, Auger spectrum, high energy plasmon satellites 78—2955
Si surface, planar and O_2 etched, CO adsorption, SEM, AES, and desorption meas. 78—63934
Si, surface, plasma etching in CF_4-H_2 glow discharge, AES meas. 79—98922
Si surface, valence band Auger line shape, corrected numerical results 78—52602
Si, surface cleaning by pulsed laser irrad. 80—45173
Si, surface contamination during high dose ion implantation, AES obs. 79—70374
Si, surface inversion layers, intersubband optical absorpt., Auger-type transition 80—29741
Si surfaces, amorphous, hydrogenated, and monocryst., AES and LEED, comparative study *(French)* 80—44398
Si, temp. depend. of Auger recomb. coeff. 80—24942
Si, thin sub-monolayer film, Auger emission coeffs. meas. 80—55236
Si, two and three-electron Auger transition, with vacancies in 2p-shell 79—63972
Si, work function and Auger spectroscopy of initial oxidation 78—76132
Si:Al, polycryst. film, grain boundary diffusion, Auger sputter profiling 80—75388
Si:Ar, ion-implanted, high resolution LMM Auger spectra 79—83066
Si:As, segregation and desorption kinetics for evaporation of As 79—99410
Si:B, diffusion from BN source with H_2 injection, AES study 80—19986
Si:B, ion implantation using B_2O_3-B mixture, Auger spectra, channelling anal. 79—4317
Si:B, polycrystalline, ion implanted, AES analysis 77—31690
Si:B deposition diffusion from B_2H_6, AES analysis 78—6085
Si:B diffusion at Si-SiO_2 interface, Auger spectra, Rutherford backscattering 80—70471
Si:H, amorphous, Auger electron spectrosc. obs. 80—76112
Si:H, amorphous, sputtered, Auger surface spectroscopy 80—50472
Si:O, comparision of depth profiling techniques 80—29048
Si/Al interfaces, chemical bonding states, low energy AES 80—6985
Si-Al-O-N ceramic, single-phase, prep. by hot-pressing, microstruct. investig. 77—8792
Si-Au, (LMM) Auger electron emission by keV Ar$^+$ bombardment 79—95880
Si-Au-Si, Auger line intensity, contrib. of backscattered electrons 79—65962
Si-H, amorphous, H three-dimens. distrib., ion-induced AES and Rutherford backscattering 80—44132
Si-Ni, (LMM) Auger electron emission by keV Ar$^+$ bombardment 79—95880
Si-Pd, (LMM) Auger electron emission by keV Ar$^+$ bombardment 79—95880
Si-Pd, preferred sputtering on surface, mass difference and chemical bonding difference effects, AES obs. 79—83078
Si-Pd film, preferred sputtering on surface, mass and bonding difference effects, AES obs. 79—87552
Si-refractory metal structs., interface modification by ion implantation 80—70475
Si-SiO_2 (111) interface, H_2 effects, AES study 80—65688
Si-SiO_2 film, crater-edge profiling in interface anal., ion beam etching and AES 77—1323
Si-SiO_2 interface, Auger sputter profiling and photoelectron spectroscopy obs. 78—10287
Si-SiO_2 interface, Auger sputter profiling 78—43254
Si-SiO_2 interface, Auger-sputter profiling obs. of P pileup 78—95240
Si-SiO_2 interface, effect of oxidation time and temp. using AES 80—35359
Si-SiO_2 interface, form. and struct., AES obs. 79—56314
Si-SiO_2 interface, intermediate chem. state of Si during sputter profiling, Auger spectra 79—11230
Si-SiO_2 interface morphology, P pileup effect, Auger sputter profiling 78—72006
Si-SiO_2 interfacial region on TCE/O_2 and CCl_4/O_2 oxidised Si, struct. and comp. 80—50741
Si-SiO_2-Si_3N_4 MNOS structure, chem. comp. and electronic states, Auger and energy loss spectra obs. 80—92999
Si-transition metal silicide interface, chemical state, AES expts. 78—91767
Si+heavy ion, X-ray spectra, one-photon two electron rearrangements 77—6712

Auger effect continued
  SiC, (LMM) Auger electron emission by keV Ar$^+$ bombardment 79—95880
  SiC, attritious wear in ginding, TEM, SEM and AES meas. 77—32696
  SiC coatings for first-wall candidate materials by RF sputtering 80—25563
  SiC, energetic H and Ar ion sputtering, AES-SIMS-FDS combined obs. 78—80444
  SiC, energetic ion sputtering, appl. of AES-SIMS (IMA)-FDS combined systems to physical and chemical processes 78—95636
  SiC, sputtered, comp. and struct. props., effect of target materials 80—54549
  SiC, sputtering processes by energetic ions, combined SIMS-AES study 80—40201
  SiC, struct. of $L_{2,3}$VV-Auger lines, rel. to soft X-ray spectra 78—2953
  SiC, surface characterisation by combined AES-IMA system, for first wall material of fusion devices *(Japanese)* 79—74039
  SiC, thermal oxide layers, AES depth-profiling anal. 79—43454
  SiC-SiO_2 interface, Auger anal. 78—95375
  $Si_{1-x}C_x$:H glow discharge films, local atomic struct., XPS and AES study 80—93448
  SiH, (LMM) Auger electron emission by keV Ar$^+$ bombardment 79—95880
  SiH_4, $L_{2,3}$MM Auger spectrum, line width and intensities 80—58325
  SiH_4, mol., XPS and KLL Auger effect, line shifts 79—31602
  SiH_4, SiH_3F, SiH_2F_2, CH_3SiH_3, core Auger shifts, ab initio,LCAO MO SCF calcs. 78—904
  Si_5H_{12} cluster, Si valence band Auger spectrum, cluster approach, comparison with experimental spectrum 80—40191
  Si_3N_4 amorphous film, CVD, core and valence electron excitations, low energy electron loss spectroscopy and AES 80—2365
  Si_3N_4, encapsulant for annealing of GaAs, photolum. and AES evaluation 78—27657
  Si_3N_4 film, amorphous, AES and EELS characterisation 79—90905
  Si_3N_4 film, diffusion of Al, AES and depth profiling 78—51744
  Si_3N_4 film, with varying refr. index, AES and XPS 78—72029
  Si_3N_4, LVV Auger spectra 79—52055
  Si_3N_4 layers, on GaAs, encapsulation, low-energy ion beam sputtering 79—78882
  Si_3N_4 off-stoichiometric plasma-deposited layer, AES evaluation of comp. 78—26781
  Si_3N_4, Si(LVV) Auger spectra, ion bombardment, electron energy loss spectra 80—80911
  Si_3N_4-MgO (5 wt.%), microstructural changes during gas pressure sintering *(Japanese)* 77—12589
  SiO film and powder, effect of heat treatment on chemical and electronic struct., electron spectroscopy 77—48320
  SiO_2 amorphous film, Si(LVV) Auger spectra, ion bombardment, electron energy loss spectra 80—80911
  SiO_2 amorphous film, thermal, core and valence electron excitations, low energy electron loss spectroscopy and AES 80—2365
  SiO_2, Auger line shapes, final state correlation effects 80—89095
  SiO_2, Auger lineshapes Si L_{23}VV, Si L_1L_{23}V, O KVV, contributing factors 79—83064
  SiO_2, calculated and measured Auger line shapes 79—83067
  SiO_2 coating on $MoSi_2$, effect on oxidation, AES study *(German)* 79—74298
  SiO_2 coatings on SiO_2 substrate, cathodoluminescence spectra, electron irrad. 80—76085
  SiO_2, dry etching induced surface contamination, SIMS, AES, and XPS obs. 80—11810
  SiO_2, encapsulant for annealing of GaAs, photolum. and AES evaluation 78—27657
  SiO_2, film on Si, electron beam damage, obs. using scanning AES 80—2070
  SiO_2, fused, slide glass surface, Ca^{2+} ion deposition as inhibitor to alkaline attack 80—50737
  SiO_2 glass, AES anal. *(French)* 79—39236
  SiO_2, LVV Auger spectra 79—52055
  SiO_2, struct. of $L_{2,3}$VV-Auger line, rel. to soft X-ray spectra 78—2953
  SiO_2, surface, plasma etching in CF_4-H_2 glow discharge, AES meas. 79—98922
  SiO_2, surface defect studies, AES, theoretical model, and expt. 79—7738
  SiO_2 surfaces, charging and dissociation, AES meas. 77—59650
  SiO_2, valence band density of states from self-deconvolution of L_{23}VV Auger spectrum 79—47561
  SiO_2:B film, on Si, AES meas. 77—39951
  SiO_2/InP film/substrate system, interface formation during CVD, modelling 80—24764
  SiO_2-Al_2O_3-Fe_2O_3-CaO-MgO, basalt glass, AES obs. 79—91543
  SiO_2-Si, cathodoluminesc. and AES rel. to struct. 78—43937
  SiO_x film, amorphous, AES and EELS characterisation 79—90905
  SiO_x, phase comp., electron spectroscopy obs. 78—60042
  SiO_x semi-insulating polycryst. films, AES and PES studies 80—107939
  SiO_x thin films, deposition and characterisation study 80—80133
  SiON/GaAs film/substrate system, interface formation during CVD, modelling 80—24764
  $Si_xO_yN_2$ films, chemical struct. using AES 79—77945
  Si_2Te_3, surface exam. by Auger spectroscopy 77—69150
  Si_2Te_3 surface reaction, AES exam. 78—63931
  SiX_4 (X=Cl,H,F), chemical shifts, relax., X-ray spectra, SCF Xalpha calcs. 80—27928
  Si(111), adsorption of HBr(Cl), AES, electron energy loss spectra and electron impact desorption exam. 78—43243
  Si(111), of Ag, cohesive energy and 2-dimens. phase diagram, AES exam. 78—43246
  Si(111) surface, Auger spectra intensity var. due to diffr. 77—85849
  Si; Ar ion bombarded, projectile energy depend. and line shape of Ar-L AEs 80—16139
  SmB_6, work functions from thermionic and field emission retarding pot. methods 79—65537
  ^{152}Sm, KLM- and KLN- Auger transitions 77—18884
  Sn, (100) surface, clean and O_2 exposed, slow positron studies, positronium formation 80—93429
  Sn, at. N-shell vacancy state widths, X-ray photoelectron, Auger spectra 77—18875
  Sn, Auger electron spectra, solid state effects 80—20739
  Sn, chemisorption of O_2, AES and EELS study 79—46917
  Sn, clean and oxidised, Auger spectra expt., fine structure anal. 80—29831
  Sn diffusion in Cu, via surface segregation 77—7905

Auger effect continued
  Sn, internal conversion coeffs. for inner shells of atomic ions and relativistic ionic potentials 80—68600
  Sn, monolayer, double layer with Pb on Al (111), layer growth, struct. 80—70567
  Sn, XPS, electronic struct. 80—7464
  Sn, XPS and $M_{4,5}N_{4,5}N_{4,5}$ Auger spectra 79—61472
  Sn/CU electroplated bimetallic films, interfacial reaction 80—96765
  SnO_2 thin films, analytical characterisation 80—20053
  SnO_2:Sb film, DC sputtered, correspondence between Sb content and targets 79—23847
  Sr, ejected-electron spectrum, autoionisation 79—22843
  Sr, strong correl. in 3d-Auger spectrum 78—50522
  SrO epitaxial layer, on Mo (110), secondary electron emission and struct., LEED and AES expts. 78—2958
  SrO, optimum composition of dielectric materials for AC-operated plasma display panels 80—14945
  SrO surface, AES peak height calibrations 79—43072
  SrO, XPS valence bandstruct. 80—89117
  $SrTiO_3$ (100) surface, struct. and electronic props., AES, LEED, EELS, and UPS study 80—24986
  $SrTiO_3$ (111), surface struct., electronic props., LEED, AES, UPS study, photoelectrochem. cell anode appl. 78—84035
  $SrTiO_3$ film, surface layer nature, AES obs., and effect on permittivity 77—24498
  $SrTiO_3$, surface defects, electronic struct., LEED, AES, UPS study 78—84273
  $SrTiO_3$, surface microrelief revealed by ion irradiation 80—54485
  $SrTiO_{3-x}$, single cryst. and film, Auger spectra, surface comp. 78—27353
  Ta, AES at very low energies, caesiation 77—69946
  Ta film, determ. of thickness and O, N content 78—80824
  Ta film, RF sputtered, thermoelec. power, Hall coeff. and struct. props. 77—43743
  Ta films, H$^+$ and D$^+$ sputtering in energy range 0.6 to 15 keV 79—78808
  Ta, foil, reaction with acetylene gas, periodic chemical var. effect on mech. props. 79—91590
  Ta foils, coated with H-permeable Pd film 79—52467
  Ta, KLL Auger emission, de-excitation of double L vacancy states 77—18886
  Ta, X-ray fluoresc. yields in KLL Auger emission 77—54525
  TaC surface, effect of C oxidation on work function, 1250-2000K, AES 79—24054
  TaO_n, combined SIMS, AES and XPS investigation 79—33199
  Ta_2O_5, anodic, sputtered, equilib. surface comp., mass and energy depend. 79—19472
  Ta_2O_5, oxidised Ta foil, electron bombardment effects on surface composition, Auger spectroscopy, electron desorption measurements 79—77874
  Ta_2O_5, preferential sputtering by Ar$^+$ ions, AES obs. 79—83083
  ^{182}Ta-containing Ta sheet, radioactive electron emission spectrum (exoelectrons), surface elec. field and Auger effects 78—72705
  Te and U/Te thin film junctions, combined electron, proton and X-ray beam obs. 77—85041
  Te, Auger electron spectra, solid state effects 80—20739
  Te, coefficient of Auger recomb. 77—72884
  Te, film, AES, LEED, XPS, energy loss spectra studies oxidation effects 78—73086
  Te, photoconductivity under pulse excitation conditions, carrier relaxation by Auger recomb. 80—2425
  Te, relax. energies for photoionisation 77—20988
  Te, Te cpds., Auger spectra 78—58638
  Te_2, vap., $M_{4,5}N_{4,5}N_{4,5}$ Auger electron spectra 79—50089
  $TeF_6 + H^+ \rightarrow TeF_6^+ + e^- + H^+$, 0.3-1.8 MeV, electron energy and ang. distrib. 78—22015
  TeO_2, film, AES, LEED, XPS, energy loss spectra studies 78—73086
  ^{125}Te, KLM- and KLN-Auger transitions 77—18884
  Te(1$\bar{2}$10) face, epitaxial growth of Se, LEED and AES meas. 77—1328
  Th (111), struct., Debye temp., and oxidation, LEED and AES obs. 77—89625
  Th, ion irrad., surface C and O, AES obs. 78—71775
  $ThNi_5$, methanation catalyst, AES and characteristic energy loss spectra 78—56915
  Ti (0001) surface, oxidation, LEED and AES meas. 77—31851
  Ti, AES meas. of soft X-ray emission threshold potential *(Russian)* 79—33866
  Ti alloy, TA6V, surface segregation, AES exam. *(French)* 78—22941
  Ti, and alloys, intergranular precipitation after annealing, ion imaging microanalysis *(French)* 79—61594
  Ti atoms sputtered from Ti, Ti oxides, photon emission, nonradiative transition effects 80—58208
  Ti, Auger electron appearance potential spectrum, elastic and inelastic contribs. 78—35231
  Ti, Auger electron appearance potential spectroscopy *(Japanese)* 80—50473
  Ti, chemisorption of N_2, O_2 and CO on polycryst. surfaces, secondary electron yield obs. 78—71971
  Ti, chemisorption of N_2 on {0001}, at. underlayer form. 77—15693
  Ti, corrosion inhibition in acid medium, electrochem., Auger investigs. *(French)* 78—44430
  Ti, electronic structure, appl. of Auger and characteristic loss spectroscopies 77—77331
  Ti, electropolishing in perchloric acid-acetic acid soln., AES study of anodic films 79—5072
  Ti film, effect of surface and bulk oxidation on charact. electron energy loss spectra *(French)* 78—39641
  Ti film, ultra-thin, AES and XPS anal. 78—91573
  Ti film electrode, oxidation, electrochem. and surface analytical characterisation 79—39034
  Ti film on Si, induced interface interaction by ion implantation, AES exam. 79—77625
  Ti, for supercond. microwave cavities, secondary electron emission and AES meas. 79—56895
  Ti, monolayer, oxidation, quasisimultaneous SIMS, AES, XPS 78—72919
  Ti, oxidation in monolayer range, SIMS, AES and XPS meas. 77—86215
  Ti oxide films, anal. by AES *(French)* 80—44440
  Ti, polycryst., chemisorption, of N_2, O_2 and CO, secondary electron yield spectrum obs. 78—38933
  α-Ti, S, C and Cl diffusion, AES meas. 78—51735

Auger effect continued

- Ti surface, Ar^+ and e^- excited Ar Auger electron emission 79—47560
- Ti, surface anal. using digital scanning Auger electron microscope 78—12797
- Ti, surface impurity segregation, quantitative AES 78—19611
- Ti:D, implanted, deuteride imaging using scanning Auger spectroscopy 80—89092
- Ti/Cu/(Au) thin films thermocompression bonds degradation by thermal ageing 80—66546
- Ti-Al, surface segregation, AES exam. *(French)* 78—22941
- Ti-Al-V-Sn (6,6,2 wt.%), H_2 induced crack growth, in-situ scanning Auger anal. 79—8355
- Ti-Cu thin films, oxidation kinetics in air at 100 to 300°C, meas. 80—40590
- Ti-Mo alloy, thin anodic oxide, AES depth profile 80—71801
- Ti-Permalloy films, interdiffusion, Auger anal. and X-ray diffr. obs., degradation of mag. props. 80—34251
- Ti-sapphire interface, solid-state reaction 78—72008
- Ti-W film, bias-sputtered, resist. and comp. 80—25023
- Ti-W films, bias-sputtered, quantitative anal. 80—80114
- Ti-W/Au, Auger depth profile anal. 79—23868
- TiC, CVD and activated reactive evaporation on WC-TiC-Ta(Nb)C-Co, substrate-layer interactions, AES obs. 79—24679
- TiC, CVD coating on Co-bonded multicarbide substrate, SEM, RHEED, AES interface study 79—77927
- TiC, final-state effects in C Auger spectra 78—6818
- TiC, RF sputtered film on steel, transition region 78—39956
- TiC_x film, formation by hollow cathode discharge reactive deposition process, on mild steel sheet 79—24451
- TiD_2, clean and contaminated films, fabrication and AES 78—52600
- TiD_2, film, AES detection of decomp. 79—91937
- TiH_x and $TiD_{0.9}$, surface characts., AES, EELS, SIMS, and XPS study 80—65343
- TiH_x film electrode, oxidation, electrochem. and surface analytical characterisation 79—39034
- TiN film as protective coating for vacuum deposition chamber, Auger electron spectroscopy study 80—25922
- TiN, for supercond. microwave cavities, secondary electron emission and AES meas. 79—56895
- TiO_2 (100), chemisorption of H_2, O_2, and H_2O, electron spectroscopy, evidence for Ti^{3+} photogeneration 78—38940
- TiO_2, (110) and (100) surfaces, LEED and electron spectra 77—72757
- TiO_2 (rutile), (001) and (110) faces, UPS and LEED obs. 80—45206
- TiO_2, chemisorption of O_2 and H_2O, electron stimulated desorption, AES and charact. loss spectra 78—22963
- TiO_2, electronic structure, appl. of Auger and characteristic loss spectroscopies 77—77331
- TiO_2, H species characterisation by electron-stimulated desorption 80—34305
- TiO_2, reactive- and chemical-sputter deposition from Ti and TiC target 79—100051
- TiO_2, rutile, electron mean free path, four-step transition and Auger spectra investig. 80—97389
- TiO_2-Ni (100) interface, electronic props., struct., comp., chemical bonding 80—84499
- TiO_x, surface film on plasma anodised Ti, comp. determ. 77—48591
- Ti_xO_y film, AES, with and without simultaneous sputtering, beam effects 77—90224
- Ti_yO_x on Ti film electrodes, AES, XPS and electrochem. characterisation 78—7086
- Tl, epitaxial growth on Ag (111) and Cu (111), LEED, RHEED, AES study 78—84090
- Tl, X-ray excited $N_{6,7}O_{4,5}O_{4,5}$ spectra 77—85886
- U, AES and loss spectra, changes on oxidation 77—20965
- U, L-shell Auger and Coster-Kronig intensities from relativistic theory 79—93962
- U/Te thin film junctions, combined electron, proton and X-ray beam obs. 77—85041
- UF_4, AES and loss spectra 77—20965
- UF_4 optical interference layers, electron-beam decomposition 78—34541
- UIr_3, (100) surface reconstruction, LEED, AES, electron energy loss spectra study 78—75918
- UO_2 ($\sim$100), vicinal surfaces, LEED and AES expts. 79—4464
- UO_2, and U_3O_8, AES and loss spectra 77—20965
- UO_2-zircaloy-4, reaction kinetics at high temps., O_2 diffusion 80—16667
- V, extended fine struct. above 2s appearance potential edge, AEAPS spectra 78—72647
- V, extended fine struct. above L-shell appearance pot. thresholds 78—92148
- V foils, coated with H-permeable Pd film 79—52467
- V, H_2 permeability, surface impurity layer effect 77—24440
- V oxides, XPS and AES study, electron correl. effects, semicond.-metal transition 80—7467
- VC, final-state effects in C Auger spectra 78—6818
- VC-Ni, fracture mode determination, using Auger electron spectroscopy 80—7680
- VO_2 films, chemically deposited, chemical transition layers at interface with substrate, AES and SEM obs. 79—95533
- V_2O_5 and lower oxides, defect structures and related props. 80—59454
- W (011), adsorption of Ag, LEED, AES, and work function meas. 79—86990
- W (100), adsorpt. of acetylene, room temp., electron spectroscopy obs. 79—7749
- W (100), adsorption and decomposition of ethylene, AES obs. 79—66353
- W (100), adsorption of Cl_2, LEED and AES study 79—90878
- W (100), adsorption of O_2, AES, desorption, LEED and work function obs. 77—1317
- W (100), adsorption of Zr, AES, LEED, thermal desorption, and work function meas. 80—39444
- W (100), CO/H_2 surface complex, flash desorption and AES obs. 78—73083
- W (100), chemisorption of Hg, AES, LEED, work function and thermal desorption expts. 78—34709
- W (100), coadsorption of CO and H_2, CO/H surface complex obs. 79—4478
- W (100), coadsorption of Zr and O_2 at high temp. 80—6653
- W (100), desorption of O_2, electron desorption cross sections 79—46944
- W (100), early stage condensation of Cu and Ag, comparison with Mo (100) 80—80072
- W (100), reconstruction in presence of O half monolayer, struct. props. 80—44421

Auger effect continued

- W (100) and (110) surface, chemical effects in N_7 VV Auger spectra 77—32474
- W (100) photocathode, monitoring of Cs and O_2 coadsorption 77—55862
- W (110), adsorpt. of N_2, N_2O, and NO_2/N_2O_4, 300K and 100K, XPS, UPS, and XAES 79—28203
- W (110), adsorpt. of NO, 300K and 100K, XPS, UPS and XAES 79—28204
- W (110), chemisorption of CO, LEED, XPS and Auger meas. 77—89647
- W (110), codeposition of Cs and O, Cs_2O form. 80—44425
- W (110), O_2 and WO_2 adsorption by LEED AND AES 80—34317
- W (110), oxygenated and oxidised, Cs absorption 80—44424
- W (110) surface, adsorbed Pd, growth, struct., stability, desorption 80—59794
- W (110) surface, adsorption of O_2, LEED, AES and thermal desorption meas. 78—38957
- W (110) surface, NO adsorption, chemical changes detected by AES 80—10787
- W (111), 0_2 and CO adsorption, angle resolved electron stimulated desorption, LEED and AES 80—6645
- W (111), adsorption of O_2, AES, LEED and electron stimulated desorption obs. 79—46935
- W {001} $(1\times1)\rightarrow(\sqrt{2}\times\sqrt{2})R45°$ surface struct. transition, LEED, AES, and work function meas. 79—42348
- W {100}, chemisorbed CO, electron beam effects, AES obs. 77—31897
- W {100}, coadsorption of N_2 with O_2 or C, AES obs. 77—35821
- W {110}, chemisorption of β-N_2, underlayer mechanism 80—39432
- W, adsorption and early stages of condensation of Ag and Au on single cryst. surface 78—6212
- W, adsorption of C(O), Auger signal comparison using differential and integral Auger spectra 78—76561
- W, adsorption of O_2, N_2 and CO, on (100) planes, LEED-AES obs. 77—69186
- W, clean and oxidised, mol. binding states of SiO 79—7750
- W, competition between interstitial atoms during segregation at grain boundaries, AES obs. *(Russian)* 77—25008
- W, electron induced Auger spectrum, double ionisation satellite 79—87532
- W, impregnated thermionic cathode, surface props. exam. using AES and work function meas. 77—8715
- W, monolayer gas adsorption, relax., electron contrib. to chemisorption, Auger shift study 80—20738
- W ribbon, with adsorbed CO, CO_2, or methane electron beam induced C deposition, AES obs. 77—89651
- W stepped surface, O adsorption and desorption, AES obs. 77—47675
- W surface, (100), photon and electron stimulated desorpt. of O 80—100397
- W, surface diffusion of adsorbed Pd and Au layers, spreading behaviour 79—99421
- W, surface diffusion of Pd, anisotropy effects due to substrate struct. 79—99422
- W, surface struct. changes due to ionic bombardment *(Russian)* 77—1775
- W, surfaces (100) and (110), adsorbed O electron stimulated desorption, combined method using LEED and AES 79—33181
- W, transitions, yield curves, line energies, UV Auger spectra obs. 80—35022
- W, wire, exam. of grain boundary segregation, using Auger spectroscopy, new technique 78—80551
- W-Ni-Fe(Cu), liquid phase sintered, interfacial embrittlement 79—57101
- WC-Co, fracture mode determination, using Auger electron spectroscopy 80—7680
- WC-Co cemented carbides, effect of Co form and distrib. in prep. starting mixture 78—44072
- WC-Co composite, ion scatt. spectrometry and AES 77—60150
- WC-Co composite, surface anal. by quantitative AES 78—76622
- WC-Co composite chemical characterisation by AES and ISS 78—76621
- WC-Co DC and RF sputtered coatings, bias effect, struct., X-ray-Auger study 80—70565
- WC-Co sputter deposited film, struct. and comp. 78—72023
- WC_x, (3×5) struct. on W (110) surface, at. beam diffr. and scatt., surface characteris. 79—78819
- W_6Co_6C cemented carbide, with CVD TiC coating, structure, composition and hardness exam. 78—11425
- WO_3, oxidised W foil, electron bombardment effects on surface composition, Auger spectroscopy, electron desorption measurements 79—77874
- WO_3 powder, electron bombardment effects on surface composition, Auger spectroscopy, electron desorption measurements 79—77874
- WSi_2, steam-oxidized, Auger sputter profiling studies 80—107663
- W(100), adsorption of O_2, H_2, N_2, CO, NO and water, AES and flash desorption meas. 77—1320
- W(100), clean thermally induced $c(2\times2)$ surface struct. 77—62714
- W(100), I adsorption at room temp., LEED and AES study 80—84389
- W(100), NVV Auger spectra, $O_2(H_2)$ adsorption effects, comp. to band struct. calcs. 78—72643
- W(100) surface, chemisorption of CO and N_2, AES and electron energy loss spectra 77—1313
- W(110), adsorbed CO, adsorbate characterisation by UPS, XPS and X-ray AES 77—15683
- W(110), Cs and O_2 coadsorption, surface anal. 77—89656
- W(111), chemisorption of ethane, AES and LEED pattern exam. 79—15005
- W{100} surface, co-adsorption of Cu and O_2, AES, thermal desorption, LEED and work function meas. 78—38950
- Xe adsorbed on Cu, NaCl, stepped and disordered surfaces, two-dimens. phase transformations 80—103580
- Xe II, optical and Auger spectra, discrepancies anal. 79—93944
- Xe, K-MM, Auger transitions, calc. within intermediate coupling framework 77—34601
- Xe, $M_{4,5}N_{4,5}X$ Auger electron spectra, many-body effects 79—59415
- Xe, N-shell Coster-Kronig transitions 79—13691
- Xe, photoelectron-Auger electron post collision interaction, Auger peak shift obs. 77—27039
- Xe, reson. line excitation, Auger decay 78—70804
- Xe^+ + Xe collisions, Auger electron ionisation, inelastic energy loss meas., multiple inner shell excitation 77—19055
- Xe^{31+} + Ne, 200 MeV collision, Auger emission 77—57952
- ^{131}Xe, KLM- and KLN-Auger transitions 77—18884
- $^{131}_{54}Xe$, K-Auger transitions 77—18883
- YH_2, electronic struct., photoelectron spectra study 80—50527

Auger effect continued
Yb, autoionisation and Auger decay, collective excitation effect 80−43008
Yb-Al, valence changes during autoionisation and Auger electron emission 80−50475
Zircaloy-4, heat treated in SiO_2 capsules, Zr and Si vapour transport surface struct. anal. of deposits 80−55437
Zn, AES and XPS, vapour-metal electron energy shifts 80−16142
Zn, adiabatic to sudden regime transition for $M_3M_{4,5}M_{4,5}(^1G)$ Auger excitation 80−45176
Zn, atomic and metallic, photoelectron and L_{23}-MM Auger spectra, binding energies 77−90238
Zn, Auger electron spectra, electron impact excited, vap. and solid state differences 78−52603
Zn, Auger spectra, comparison with multiplet struct. calc. 78−31287
Zn, $L_{2,3}M_{4,5}M_{4,5}$ Auger spectra, solid state and oxidation effects 77−63501
Zn, L_{23}-$M_{4\,5}M_{4\,5}$ principal and satellite Auger spectra 78−42030
Zn, L_3-MM Auger spectrum, multiplet struct. 77−48285
Zn, $L_3M_{23}M_{23}$ Auger energy calc. using XPS, effect of 3d-4s admixed screening on relax. energies 77−1782
Zn, LMM Auger spectra, rel. to L_{23} photoelectron spectra 77−77348
Zn, LMM Auger spectra, transition probabilities, term splittings and effective Coulomb interaction 77−44126
Zn, meas. final state CI effects 78−33488
Zn on Be, zincating conditions, film characts. 77−40397
Zn, oxidation, MVV Auger spectra, line shape, relax. energies 77−73195
Zn, resonant two hole bound state at 3p core threshold 80−60750
Zn, surface oxidation, Auger spectrosc. obs. 80−97388
Zn, XPS and Auger spectra, many-body calcs. 79−49995
$Zn+H^+(He^{2+})$, L- and M-shell Auger electrons 79−27076
ZnO $10\bar{1}0$ surface, reaction of O_2, AES, LEED, EPR, desorpt., surface cond. and work function expts. 78−95950
ZnO $(000\bar{1})$, adsorption of alkali metal, anomalous behaviour of Na 78−79883
ZnO $(000\bar{1})$ and $(10\bar{1}0)$ surfaces, clean and contaminated, reactivity to Cl_2 79−61904
ZnO, (0001) surface, clean and O adsorbed, AES and refl. electron energy loss spectra 79−46927
ZnO, ceramic varistor, physical props. of elec. barriers by AES and electron microscopy 77−20326
ZnO, electron beam induced decomposition and desorption, AES and contact pot. difference meas. 78−79893
ZnO, electronic surface and bulk transitions exam. by electron energy loss spectra 78−30964
ZnO, nonpolar surface, interaction with CO and CO_2, thermal desorption, AES, EELS and LEED obs. 79−65321
ZnO on Zn (0001), oxide film growth, at. and electronic struct. 78−15587
ZnO, photodesorption of CO_2, rel. to surface cond. and AES, band-bending model 77−47671
ZnO, powder, adsorption of methanol, electron spectrosc. obs. 79−52076
ZnO, prismatic surface, O_2 interaction obs. 77−31899
ZnO-Si(SiO_2) interface, XPS and Auger LMM anal. 79−90893
ZnS 80−35096
ZnS, chemisorption of O_2 after illumination and in presence of CO and O_2 78−87877
ZnS, clean surface, AES and LEED exam. 80−10762
ZnSe (100) surfaces, surface states meas. *(Japanese)* 79−99599
ZnSe (110), LEED intensity anal. and electron spectroscopy 77−43678
ZnTe (110) and (111) surfaces, O_2 adsorption, electron energy loss and Auger spectra 79−47568
ZnTe clean and adsorbed O_2 (110) surfaces, UV photoemission spectra *(Japanese)* 80−93456
Zr, adsorption and absorpt. of CO, NO, N_2, O_2, and D_2, dissoc. and diffusion 80−80085
Zr, UPS constant final state energy spectra, direct emission and Auger decay from multiplet final states 77−44131
$ZrNi_5$, methanation catalyst, AES and characteristic energy loss spectra 78−56915
ZrO_2:Y_2O_3, bias sputtering, film growth and characts. 77−40366
ZrO_2:Y_2O_3 film, preferential sputtering, Auger and XPS spectra obs. 79−52071
ZrO_2-Y_2O_3 film, surface characterisation, XPS, ESCA, and AES expts. 78−72028

Auger electrons *see Auger effect*
Auger showers *see cosmic ray showers and bursts*
Auger spectra *see Auger effect*
Auger spectroscopy *see Auger effect*
augmented plane wave calculations *see APW calculations*
aural null direction finders *see radio direction-finding*

aurora
see also airglow; atmospheric electron precipitation; atmospheric proton precipitation; atmospheric spectra
17th and 18th centuries, auroral freq. rel. to Maunder min. 79−66856
17th century solar activity from auroral and sunspot obs. *(French)* 77−29747
1972, August, optical diagnostics of polar cap absorpt. event 77−29567
1978 May 1 to 2, auroral storm obs. 80−56664
acceleration region, altitudinal double-layer criterion 80−94656
afternoon sector, obs. of pulsating aurora after twilight 78−81486
albedo profile over snow-covered ground, rocket obs. 78−77384
ARAKS and electron beam injection expts. 78−36405
ARAKS Project 79−21021
arc formation, particle accel, by MHD surface waves 77−9621
arc structure, numerical simulations 79−53607
arc structures, rel. to two-dimensional inertial turbulence in magnetospheric plasma 78−36399
arcs, equipotential model, laminar electrostatic shocks 80−41594
arcs, relation to 100 and 500 kHz noise, field-aligned current and electrons accel. 79−66859
arcs location near substorm onsets 78−88968
artificial, optical equipment for detection during ARAKS expt. 79−21075
artificial aurora, conjugate to a Hawaiian launched electron accelerator 80−82124
artificial aurora, optical emission excited by electron ejection from rocket 80−51592
artificial aurora initiated by rocket electron injection, optically observed from ground 80−41559

aurora continued
artificial aurora prod. by electron beam injection 79−62638
artificial aurorae obs. in conjugate region during ARAKS expt., TV system 79−21074
artificial auroral streaks during Echo 4 electron beam expt., beam magnetospheric interactions 78−89036
artificial polar aurora region, external airglow meas. 78−16227
artificial stimulation of electron precipitation by Cs doped explosion 80−17436
auroral activity, 1962-1978 period 79−39999
auroral arcs formation and V-potential double layers 80−103185
auroral electric field, description based on plasma interaction with geomag. field 80−46342
auroral hiss, source regions of fine struct. 77−87203
auroral oval, dynamics during double substorm in midnight sector 77−53330
auroral oval dynamics, influence of interplanetary mag. field B_2 component 79−62641
auroral oval motions during substorm development 77−2295
auroral oval size, effect on mag. substorm occurrence probability 78−32298
austral auroral oval, empirical eqn. for max. probability contour 78−28363
BDI position and plasmapause position during Feb. 1972 mag. storm 80−56666
Birkeland current systems, anomalous resistivity effects 77−9591
Birkeland currents and auroral structure 80−77209
Birkeland currents occurrence in ionosphere during aurora *(Norwegian)* 80−31158
borealis, origin of metaphor 79−58512
bremsstrahlung X-ray flux comp. 77−60508
brightness fluctuations at mid-latitudes 77−87150
brightness monitoring, rocket studies, using 2972 Å photometer 79−25334
brightness obs. from satellites, atmospheric absorption effects 80−12538
brightness pulsations, assoc, with electrostatic ion cyclotron waves 77−73900
bulge expansion features during substorms 80−41597
catalogue of auroras from European sources, 450-1466 AD period 79−75010
characteristics of auroral forms 79−8738
coordinated rocket and satellite obs., Atmosphere Explorer C 77−70908
cryogenic spectrometry in 1-2.5 μm range 77−70886
curl and shear instability 78−77433
current convective instability in auroral F-region 80−72680
current convective instability in diffuse aurora 79−70907
currents, magnetometer array and radar backscatt. joint obs., N.Scandinavia 78−85768
cyclotron soliton theory of Earth's kilometric radiation 80−94657
D-region, NO prod. rel. to winds and electron densities time vars. correl. 79−25389
D-region electron density and energy distrib., heating by high energy protons 77−82078
dayside 5577 A and 3914 A characts. 78−28364
dayside arcs and convection 78−81484
dayside aurora, relevance to substorm current systems and dayside merging 79−96852
dayside aurora, response to interplanetary mag. field transitions and magnetospheric substorms 77−87148
dayside aurora, rocket-borne meas. of particles and ion convection 78−77391
dayside aurora in F-region assoc. with magnetospheric cusp 80−90273
dayside auroral morphology, from large scale obs. at 6300 Å, 5577 Å and 3914 Å 80−85786
dayside auroral oval, elec. fields meas. 80−98501
dayside auroral oval, evidence for parallel elec. field particle accel. 80−98503
dayside cleft aurora and ionosphere effects, review 80−94633
dayside cleft emission, Dec. 1976 obs., 6300 Å photometry 80−46332
dayside emissions, obs. from Scandinavia 78−85755
dayside magnetospheric cleft, N_2^+ 3914 Å, O I 5577 and 6300 Å emissions obs. 77−2294
daytime auroral zone, proton source in magnetosheath 77−33240
detached arcs and patches, equatorward of auroral oval, Isis 2 obs. of particle precip. 79−70911
detached auroral arcs in ionosphere trough region, obs. 78−88965
diffuse aurora, Birkeland current determ. from plasma line meas. of Chatanika 80−98507
diffuse aurora, excitation by proton precip. due to magnetospheric proton-cyclotron instabilities 80−90286
diffuse aurora equatorward boundary, 6300 Å obs. 80−72668
diffuse auroral precipitation mechanisms 79−12327
diffuse auroral zone, form. and dynamics of polar edge of ionospheric trough 79−8743
discrete and diffuse aurora, simultaneous obs. by Isis 2 satellite and airborne instruments 77−29532
discrete and diffuse aurorae, observed microstruct. 80−77188
discrete aurora mechanisms, review 79−8737
discrete auroral arc, energy source for electron accel. and field-aligned currents 77−9593
discrete auroral arcs, prod. by electrostatic shocks 78−45153
discrete auroral arcs and currents, review 80−77190
discrete auroras near midnight, occurrence and lifetimes 80−67447
displays recorded by low-light sensor, DMSP nighttime images 78−88942
DMSP data calibration 80−8443
DMSP photographs, rel. to new auroral pattern 77−13146
Doppler vel. meas., radio aural spectral characts. and incident incoherent scatter meas. 80−56663
double layer formation and discrete aurora 80−12607
double plasma layers, simulation 80−12590
double-layer criterion, trapped electrons and streaming speed 80−82123
E_s-layer, large-scale inhomogeneities 80−4171
E_s-layer ionisation at high latitude, quiet and disturbed conditions 80−61941
E-layer, auroral, seasonal vars. 79−8746
E-region, plasma lines meas. 79−25386
E-region, possible nature 78−45088
E-region fine structure obs. in substorm 80−36452
E-region ion comp. and NO profile 77−41258

aurora continued
eastward electrojet and field-aligned current flow at dusk meridian 79—80076
education, auroral science role and physics textbooks contrib. 80—4493
effect on fair weather electric field 79—44285
electric currents and potentials, generation by magnetosphere correction elec. field divergence 80—67453
electric currents in power transmission lines induced by auroral activity, meas. 79—62640
electric currents over auroral arc, theory 77—33296
electric field, model 79—53608
electric field, non-neutral field-aligned current sheet, theory 80—77196
electric field of auroral arc, radar obs. 80—72692
electric field oscills. meas. near auroral arc, assoc. with MHD wave 78—65457
electric fields, comparison of F-region plasma drifts and E-region irregularity drifts 77—33262
electric fields, conductivities and currents in auroral zone, latitudinal distrib. 78—77399
electric fields, energetic particles and suprathermal electrons obs. near active auroral arc 77—70912
electric fields, meas. in diffuse aurora 77—82077
electric fields, potential and inductive, in magnetosphere during auroras 80—21878
electric fields and currents, origin and structure *(German)* 78—32196
electric fields and currents assoc. with auroral arcs, radar obs. 78—28396
electric fields in auroral zone at 1 R_E altitude 78—57397
electrodynamics of an arc, auroral vector electric field and particle comparisons 77—70907
electrojet, curvature rel. to interpretation of azimuth-scan radar Doppler data 77—41266
electrojet, gravity waves and infrasound generation, Joule heating and Lorentz force 79—66866
electrojet, spectral struct. estimate of elec. field 78—40732
electrojet, two-stream irregularities, nonlinear states 78—28403
electrojet activity, rel. to LF/MF transmissions non-linear demodulation and ELF signals generation 80—94639
electrojet as infrasonic wave source *(Japanese)* 80—17434
electrojet boundary definitions using energetic electron spectra and magnetometer data 79—75026
electrojet in morning sector, rel. to field-aligned currents 77—29573
electrojet parameters, Chatanika radar meas. compared with Anchorage VHF backscatt. obs. 78—12048
electrojet region, combination freq. radiation generation *(Russian)* 77—41268
electrojet region, elec. fields and mag. effects of solar flares 78—69576
electron accel. by electrostatic double layers, discrete auroral forms prod. 77—25809
electron acceleration, in array of auroral arcs 78—36357
electron accelerator expt. on POLAR-5 sounding rocket, for use within aurora 80—77170
electron and auroral simultaneous meas., discussion of differences 77—53271
electron beam, electrostatic noise generation 78—85759
electron bunching near artificial electron beam 80—98511
electron diffuse surge zone, equatorial boundary model 78—69610
electron energy distrib. above aurora, secondary peaks driving instability 80—82135
electron flux, rel. to field aligned elec. pot. difference 80—72684
electron flux measurements rel. to auroral emission calcs., comparison with obs. 77—9592
electron modulation at 2.2 Hz, geomagnetic equatorial origin 80—94632
electron modulation by electrostatic waves, freq. anal. of 4-6 keV electrons 78—45086
electron precipitation, energy distrib. from incoherent scatter radar and photometric meas. 78—77390
electron precipitation, field-aligned suprathermal fluxes below 270 km 77—33278
electron precipitation, high resolution energy spectra, 1976 Mar. 26 mag. storm onset 77—33257
electron precipitation, inverted-V event characteristics 79—75019
electron precipitation, rel. to NO densities in lower thermosphere 77—37467
electron precipitation, role of mag. mirroring 78—20572
electron precipitation pulsating aurora 80—85794
electron precipitations and polar auroras 79—29932
electron spectra meas. 20 eV to 18 keV 79—62642
electron velocity distribution function, 25 eV to 15 keV 78—45085
electrons, pitch angle and energy distrib., ESRO 4 satellite obs. 79—29921
electrons, spatial distrib. rel. to high-latit. ionosphere cond. 79—12334
electrons acceleration, role of turbulent generation of electrostatic fields in magnetosphere 78—28439
electrons acceleration by electrostatic V-shocks, approximate equipotentials 80—21870
electrons acceleration mechanisms 80—77210
electrons and positive ions in auroral arc 77—33246
electrons precipitating in assoc. with diffuse aurora, origin in plasma sheet 80—41614
electrostatic ion cyclotron waves, modulational instability 79—62643
electrostatic noise damping by warm auroral electrons 80—41668
electrostatic turbulence, appl. of transverse Kelvin-Helmholtz instability 77—53287
electrostatic waves assoc. with intense vel. shear near auroral arc 77—70911
EM radiation bursts during substorms rel. to auroral electron beam 79—88557
energetic ions and EM radiation in auroral regions 78—81490
energy dissipation due to ionospheric currents, high-resolution altitude profiles 78—88978
equatorial aurora, EUV Apollo-Soyuz obs. of mag. quiet conditions 80—12591
equatorial latitude of auroral activity from DMSP satellite electron and visible obs. 80—98499
equatorial obs. and ring current composition change 78—36401
equatorward auroral boundary characts. near midnight from DMSP images 79—16733
equatorward extent (1973-4) of auroral activity 79—12328
equatorward shift during mag. storm, D_{st} contrib. 79—75013
European Incoherent Scatter (EISCAT) project for auroral ionosphere study *(French)* 79—2437

aurora continued
EUV spectrum, 750-120 Å region 77—33242
evening diffuse aurora and conjugate electron fluxes near magnetospheric equator, electron precipitation 79—101008
evening sector, relationship of radar and visual aurora and auroral electrojets 77—25810
evening sector auroral oval dynamics, from DMSP photographs 79—96853
Excede 2 test, artificial auroral expt., ground-based optical meas. 78—89038
F-region scintillation, rel. to aurora 77—87158
fading before breakup, obs., rel. to substorm expansion 79—2420
field aligned current above auroral arc, e^- and H^+ precipitation obs. 80—77215
field aligned currents carried by suprathermal electrons, relation with auroral arc 78—28362
field-aligned current closure and Joule heating near Harang discontinuity 80—72682
field-aligned current system assoc. with structured auroral arc 77—33243
field-aligned currents, effect on ionosphere currents and elec. fields 78—96339
field-aligned elec. fields and currents in rays and arcs 80—41593
filamentary auroral arc, as source of travelling ionospheric disturbance obs. by radar 79—48610
flare processes, problems, rel. to solar flares 77—17270
geomagnetic bays, rel. to auroral and geomag. activity and interplanetary mag. field in (1968) 79—53654
global formation of auroral arcs, numerical simulation 80—67446
gravity waves in neutral comp. and temp., auroral origin 79—74998
ground level electric potential gradient, auroral effects on slow vars. and short-period pulsations 79—12188
H emission oval, temporal variation 77—13145
Harang discontinuity, electric field meas. by auroral radar and rocket double-probes 78—88971
Harang discontinuity, electron flow and visual aurora 80—8475
HF radio noise study during auroral substorms, freq. range 8 to 25.5 MHz 80—41670
HF radiowave absorption prediction 79—58132
HF radiowave propagation at high latitudes, geomagnetic activity influence *(Russian)* 77—29551
hiss at $L\approx4$ on the ground 77—70931
historical aurorae, Latin terminology 80—62437
historical records, occurrence correl. with solar activity long-period vars. *(French)* 78—73695
history of auroral research, the less known contributors 80—73157
IAGA/IAMAP symposium on auroral processes (Seattle, August 1977) 79—88521
infrasonic substorm obs. with Chatanika radar 77—17269
infrasonic wave emission, multiplicity of wave forms 77—29534
infrasonic wave emissions, temporal and spatial changes rel. to polar substorms 79—100996
infrasonic wave emissions on night of low geomag. disturbance 77—25811
infrasonic waves and auroral electrojet 79—35023
infrasonic waves in substorm area, source regions *(Japanese)* 80—85788
infrasound, asymmetry in generation by travelling aurora 77—87152
instantaneous optical auroral distrib. by ISIS-2 satellite 80—56662
intensity and electron flux, in situ rocket meas. 79—39998
intensity correlations and excitation theories 77—70913
interplanetary magnetic field B_y component influence on auroral dynamics 79—62689
interplanetary magnetic field effects on auroral oval and plasmapause 79—80186
interplanetary magnetic fields, midday gap and substorm photographs 80—12592
inverted V event, electron flux fluctuations, Nov. 5 1975 obs. 80—41618
inverted-V precipitation events and parallel electric fields, rel. to high-latit. convection field 77—33297
ion composition and energy spectrum vars. 77—64509
ion precipitation events in morning auroral oval, evidence for solar wind ion injections 80—98502
ion velocity distributions for polarisation collision model 77—45241
ionic structure near auroral arc, meas. 77—2292
ionosphere, auroral, radio turbidity coeff. 78—45112
ionosphere, auroral acceleration regions, energetic particle meas. 79—53644
ionosphere, auroral electron flux obs. 80—67466
ionosphere, differences between regions of inflowing and outflowing auroral current 79—100999
ionosphere, heating during aurora 77—21973
ionosphere, radio investigations via VHF bistatic Doppler system 78—28387
ionosphere, time-depend. auroral model with comp. meas. 80—12609
ionosphere absorption event, lower ionosphere ion prod., density and comp. 80—36443
ionosphere collisional ion cyclotron waves, appl. to auroral irregularities 77—29574
ionosphere electric field obs., comparative rocket obs. 80—85789
ionosphere electron density and temp. meas. by sounding rockets 79—8760
ionosphere F-region ionisation, role of auroral particle precip. 79—44296
ionosphere irregularities in auroral zone, simultaneous rocket probe, scintillation and incoherent scatter radar obs. 80—94640
ionospheric perturbations, SW radio noise level variation obs. *(Russian)* 77—91359
IR emissions, auroral enhancement 80—12586
IR emissions in auroral regions, origin 77—33247
IR enhancements assoc. with bright auroral breakup, 1.5-5.3 μm 78—12036
Jupiter, $H\alpha$ auroral activity obs. 77—45350
Kelvin-Helmholtz instability and aurora 77—29558
kilometric radiation, ISIS 1 obs. at source 79—84558
kilometric radiation, theory 79—70900
kilometric radiation coherent generation by nonlinear beatings between electrostatic waves 80—26691
kilometric radiation correl. with inverted-V electron precip. 80—26692
kilometric radio emission, obs. during JIKIKEN (EXOS-B) satellite initial phase *(Japanese)* 80—94675
km radiation ang. distrib., satellite obs. 77—60530
large scale structure observed by riometer radiowave absorpt. 80—72670

aurora continued
latitudinal distribution, vars. during 18th and 19th centuries rel. to solar wind and sunspot activity long-term 80—98498
latitudinal variation of auroral ionization, radar meas. 77—5385
location, visual and radio emission 80—82122
longitudinal dependence, effects of pitch-angle diffusion with asymmetric loss cones 77—13162
low energy electrons, energy dissipation 77—45217
luminosity rel. to geomag. field changes 80—77187
lunar influence on occurrence freq. 77—87149
magnetic and auroral substorm development at mag. midnight 79—66888
magnetic disturbances indicated by auroral kilometric radiation 77—70909
magnetic field, closed lines and auroral forms 78—36356
magnetic field aligned electric fields rel. to downward electron energy fluxes 79—53606
magnetic field line merging and slippage in auroral arcs 78—77393
magnetic field lines in auroral zone, electrostatic wave measurements 79—88555
magnetic mirroring and auroral phenomena 77—73901
magnetosphere, auroral particles adiabatic motion in presence of dipole mag. field 77—60547
magnetosphere, substorms, mag. merging rel. to auroral phenomena 77—17301
magnetosphere auroral absorption substorm, onset obs. 78—96362
magnetosphere auroral radiation, theory of generation 79—75051
magnetosphere morning sector, auroral electron discontinuity location meas. by Molniya-1 satellite 79—8778
magnetospheric physics, review of selected topics 78—65466
magnetospheric substorms, onset and intensification, Pi 2 micropulsations as indicators 79—88552
Maunder Minimum, catalogues of auroral obs. 80—51722
mesopause, H_2O dissoc. during auroras rel. to ionosphere winter absorpt. anomaly 79—58152
meteoric aurora, review of historical obs. 80—94761
MF waves over strong aurora, rocket obs. 78—45082
microburst precipitation phenomena in auroral zone 80—77208
micropulsations, auroral effects 78—28424
midday discrete auroral gap 79—2421
midnight sector, discrete auroras in oval and polar cap and continuous auroras 78—12037
midnight sector, electrojet and precip. particle characts. 78—12039
midnight sector, F-layer irregularity zone and O I 6300 Å emission meas. 78—12038
modification of auroral zone due to geomag. excursions, minimum-effect model 77—78101
molecule, O_2, $(b^1\Sigma_g{}^+\text{-}X^3\Sigma_g{}^-)$ system in auroras, vibr. development 77—2293
monochromatic observation of all-sky auroral images, using intensified TV camera 77—73859
morning sector, eastward movement of auroral radio absorption events 77—56792
motion and mag. variation associated with auroral substorm onset 80—51593
multiple auroral arcs, electron meas. 77—49210
$N_2{}^*+NO(H_2O)$, vibr. excited quenching temp. depend., flowing afterglow 77—54595
narrow auroral arc widths, high resolution meas. in O I 5577 Å and $N_2{}^+$ 3914 Å line emissions 77—56787
near IR spectrum, 0.83 to 1.67 μm obs. 77—53272
neutral atmosphere interaction, obs. of neutral wind profiles in dayside auroral oval 80—98494
neutral wind in upper atmosphere, rel. to magnetospheric disturbances in aurora borealis zone *(Norwegian)* 78—24399
nightside auroras, distrib. rel. to field-aligned currents and auroral electrojets 78—32267
nightside km radiation origin and polarization 78—45161
nighttime auroral zone scintillation, struct. of localised enhancements 80—98506
north-south movement of irregularities, 42 MHz obs. 80—67449
optical auroral arcs and low-energy electron precip., DMSP 32 obs., comment 77—60507
optical emission features in aurora and nightglow, satellite obs., ground scatt. effect 78—77385
optical emission height profiles of medium intensity aurora 79—40002
optical emissions, near steady state conditions obs. rel. to precip. and high-latit. ionosphere 79—40000
optical observation systems for the ARAKS experiment 79—21073
optical phenomena, review including airglow and aurora 77—70831
oral size diurnal var. assoc. with geomag. pole precession 80—26661
palaeofield weak dipole epochs, nondipole component effect on auroral zone config. 80—105098
parallel electric field, signature in ion and electron distribs. in vel. space 78—89005
particle acceleration by paired electrostatic shocks in polar magnetosphere 77—29601
particle acceleration in auroral magnetosphere 80—31171
particle distrib. rel. to mag. field perturbations assoc. with field-aligned currents 80—41596
particle dumping into ionosphere, Ariel 2 obs. 80—109313
particle fluxes during substorm, rel. to magnetosphere global fine structural forms. development 79—58190
particle instantaneous energy deposition, determ. from optical emissions 78—81491
particle precipitation, high latit., relationship with auroral forms 80—77189
particle precipitation, rel. to turbulence at 500 mb level 80—77218
particle precipitation, stratified struct. development during magnetospheric convection 78—28377
particle precipitation effects on ionospheric and atm. props. 78—4021
particle precipitation region rel. to position of eastward electrojet and energetic electrons trapping boundary 77—25822
particle precipitation rel. to convection in plasma sheet 79—88544
particles acceleration, by mag. field-aligned pot. drops due to electrostatic ion cyclotron turbulence 78—45155
particles energy spectra and magnetospheric convection 77—49234
particles precipitation, electrodynamic processes in injection region 78—45095
particles precipitation, influence of ring current and plasma sheet drift instabilities 79—12351
patches caused by energetic particle precip. near plasmapause 77—33241

aurora continued
Pc 5 micropulsation resonance region, examination by dual auroral radar system 78—65454
perturbation magnetic fields and current systems associated with eastward drifting auroral structures 79—75009
photographic observations from Skylab 77—60505
photometric observations, ground-based and topside, correl. with electron spectra meas. 78—32266
photometric systems, comparison at observatories in Arecibo and Stara Zagora 79—48575
Photozavr modulation photometer for artificial aurorae/airglow 79—21076
physics of auroral zone, review 77—17268
plasma, turbulent acceleration by electrostatic waves *(Russian)* 80—53952
plasma parameters, incoherent scatt. of EM waves, EISCAT project *(French)* 80—82142
plasma wave emissions from auroral field lines 79—88556
polar cap, intense uniform low-energy electron precip., interplanetary origin 77—70910
polar cap aurora, proton-induced, secondary electron flux 79—53605
polar cap sun aligned arcs, Isis 2 obs. 78—28366
polar luminance struct. depend. on plasma collective effects *(Russian)* 80—90274
polar substorms, equatorial-auroral ionosphere coupling 78—32291
poleward leaps of auroral zone activity rel. to plasma sheet recoveries 79—25401
Precede, artificial auroral expt., summarised results 78—89037
precipitating particle dynamics and auroral morphology, photometric data interpretation 80—82141
premidnight convection topology, auroral vector electric field and particle comparisons 77—70906
primary ions, above diffuse midnight aurora 80—41595
propagation condition anticipation for radio amateurs 77—64529
proton bursts struct. during mag. quiet times and substorms 77—29531
proton precipitation, energy spectra and pitch angle distrib. 77—9596
proton precipitation and electrostatic ion-cyclotron instability during quiet times 77—33256
protons energy and pitch angle spectra vars. in upper atm. 79—75032
protons origin at dayside auroral oval 77—9597
pulsating aurora, 3 Hz modulation rel. to pitch angle diffusion instabilities 79—25391
pulsating aurora, comments and reply on morphology 79—25383
pulsating aurora, induction by atmospheric Ba releases 77—49211
pulsating aurora, local and global morphology 78—28365
pulsating aurora, optical-particle characteristics 78—88969
pulsating aurora, review 78—73562
pulsating aurora, the importance of the ionosphere 80—85787
pulsating aurorae, evidence for limiting electron flux 80—72666
pulsating auroral structures, implications of extreme vertical thinness 80—72667
pulsating auroras, evidence for noncollisional thermalisation of precipitating electrons 79—96851
pulsating patches periodicity, latit. effect 80—31155
pulsation caused by magnetosphere self-modulated VLF wave-electron interactions 80—41658
pulsations, harmonic anal. 79—8736
pulsations caused by pressure waves in neutral atmosphere 80—12588
pulsations of electron and ion intensity 80—61934
quantitative spectroscopy, 8800 to 11400 Å 77—13144
quiet auroral arc, electrostatic model 80—72669
quiet auroral arcs, feedback instability in ionosphere-magnetosphere system 78—57379
quiet auroral belt, delineation of poleward boundary 77—33244
quiet time arc pattern rel. to interplanetary magnetic field 79—25382
quiet-time patterns and magnetospheric convection, comparison 80—17433
radar aurora, per-unit-vol. RF scatt. cross section calc. 78—45079
radar aurora, Stare obs. of Pc 5 geomag. pulsations 79—96862
radar auroral substorms, signatures of auroral east-west motions 77—29535
radar auroral substorms, signatures of expansive and recovery phases 77—25812
radar echoes drift meas. using radar auroragraph 78—65436
radiation transport, multidimensional, in plane-parallel atmosphere, appl. to 4.3 μm auroral arc 78—88917
radio, ion-acoustic plasma waves and two-stream instability 78—36355
radio absorption, spike events 80—12589
radio absorption obs. by riometers rel. to 10-80 keV electron precip. at geosynchronous orbit 79—48606
radio aurora, 398 MHz echoes, depend. on electron density and elec. field 79—66854
radio aurora, spatially ordered structure, spaced radar obs. 78—73561
radio aurora (diffuse), rel. to field-aligned currents and particle precipitation 80—105119
radio aurora dynamics as seen by Doppler radar 79—62639
radio aurora in dayside auroral oval, rel. to field-aligned currents and energetic particles 78—88966
radio auroral signals, maximum entropy spectral anal. 78—93006
radio backscatter at 42 MHz, amplitude rel. to Doppler shift 80—61955
radio echo, ion-acoustic, short term characts. 78—45080
radio emissions in 2.5-6 MHz range 79—70906
radio scattering anisotropy, from 42 MHz polarisation investig. 77—21968
radio-aurora, rocket borne radar study of ion-acoustic waves 79—100995
radiometry methods (Soc. Photo-Optical Instrum. Engrs., Proc. vol.91, San Diego, 26-27 Aug. 1976) 77—70880
radiowave absorption at mid-latitude coupled to auroral activity 80—61945
radiowave generation, by auroral electron beams, mechanism *(Russian)* 78—40724
radiowave propagation, foreshortened scatt. by auroral inhomogeneities *(Russian)* 77—64519
rapid auroral fluctuations, obs., classification 80—77186
review 78—77386
review of current knowledge 79—84564
RF emission, in electron beam-plasma and beam-beam interactions 78—45137
ring current unstable waves, role of charge exchange 77—49225
rocket obs. and analysis in coordinated rocket/satellite meas. 79—75011
rotational electric field of auroral origin 78—45102

aurora continued
SAR arc event, soft electron flux as excitation source 80—77217
SAR arc formation, proton obs. supporting ion cyclotron wave heating theory 78—49197
satellite auroral photometry, Earth albedo effects 77—56737
satellite auroral photometry, spectral albedo corrections 77—49208
secondary electrons spectrum at low altitudes, collisionless effects 79—40008
sheet-like auroral ionospheric irregularities 79—35033
simultaneous particle precipitation and auroral emission obs. by Isis 2 77—70905
sky background elimination with stellar chopping photometer 80—72776
soft auroral bremsstrahlung and K_α line emission 77—87153
solar activity cycle during classical antiquity, rel. to auroral cycle 79—92736
solar cycles during 1540-1700 period, from solar and auroral obs. 79—21267
solar terrestrial event, 1971 December 14 to 21, polar cap 6300 Å emission pattern 79—75012
southern oval, spherical harmonic analysis 78—81487
space-time pattern, rel. to sunspot turning points since (AD 1510) 80—21980
spectral feature at 2150 Å, contrib. from N II lines 78—61645
spectral intensity, rel. to at. and mol. electron impact excitation and ionisation 79—84563
spectroscopic observations, appl. of matched tandem etalon camera (MATEC) 80—101442
spectrum vars. at latit. of polar cleft 79—25384
stable auroral red arc, 1978 Sept. 25/26, atmos. temp. 80—12594
stable auroral red arc, 4th Aug. 1972, obs. during ring current growth 80—51594
stable auroral red arcs, rel. to ionosphere scintillation producing irregularities horizontal struct. 79—12339
STARE: a new radar auroral backscatter experiment in northern Scandinavia 79—39977
statistical auroral ovals, comparison of all-sky camera photographs and satellite photographs 79—48599
steady diffuse aurora forms, 10 eV to 25 keV electrons energy spectra 77—29536
storm time auroral ionosphere, anomalous transport coeffs. effect on thermal struct. 79—16743
subauroral ionosphere, persistent scintillation enhancement obs. in Alaska 78—20573
subauroral ionosphere, rapid ion drifts obs. by Atmosphere Explorer C 80—4188
subauroral red arc event caused by kinetic Alfven waves 78—93026
substorm, trapped electrons dynamics in auroral zone 78—40767
substorm absorption events, at low auroral latits., apparent equatorward propag. 79—8769
substorm and auroral activity, development after southward turning of interplanetary mag. field 78—28435
substorm expansion phase, ionospheric currents and elec. field vars. assoc. with absorpt. spikes 79—35039
substorms, 1970, March 6, auroral struct. rel. to plasma sheet thinning 77—25874
substorms, electron flux intensity rel. to form of auroral absorpt. bays 78—69619
substorms, ground magnetogram timing of onset 79—88553
substorms, HF signals statistical characts. 78—69583
substorms, high-latit. ionospheric currents prod. by vars. of asymmetric ring current 77—21971
substorms, morphology of N and NO 79—48607
substorms, multiple-satellite studies of polar mag. substorms and convection bays 78—45159
substorms, small scale auroral absorpt. events 77—56791
substorms correl. with terrestrial kilometric radiation 78—28450
sunspot period stability investigation by periodic anal. of aurora and earthquake records in ancient China *(Chinese)* 79—21253
thermosphere, auroral energy deposition and neutral comp. changes, simultaneous satellite obs. 77—53264
thermosphere, effect of auroral energy input on neutral and ion drifts 78—65446
thermosphere, N and NO density in polar regions under auroral perturbs. 77—73897
thermosphere, solar and auroral heating rel. to zonal mean circulation vars. 78—32262
thermosphere at. O content, spectral method for 100-160 km altitude 80—41578
thermosphere heating, rel. to midlatit. F-region quiet time depressions 78—36385
time-dependent modelling 80—72672
topside ionosphere, anomalous resistivity of auroral plasma 77—5389
transverse Kelvin-Helmholtz instability, suppression by lower hybrid turbulence 77—65861
travelling arcs, prod. of infrasonic waves 78—12040
trough region auroral patches and detached arcs characts., Isis 2 obs. 79—70910
type A aurora rays, O I 6300 Å emission intensification 80—4163
type-B, obs. and interpretation of spectra and rapid time vars. 79—40001
UBV photometry, at geographic latat. 69°22′ north 79—44376
UBV stellar photometry from N.Norway during auroral activity, technique and results 79—40084
UHF diffuse radar aurora, rapid scan Doppler vel. maps 78—77388
ULF elec. fields and particle precip., rocket meas. 78—96337
upper atmosphere emissions during 1974, March 16 magnetic storm 77—49209
UV aurora, spectrum between 2100 Å and 2300 Å 78—88963
UV spectrum, 1200-3200 Å, OGO-4 obs. 77—9594
UV spectrum, 2000-2800 Å region 79—70908
VHF radar aurora and strong HF backscatt. comparison 80—61960
VHF solar activity and auroral effects 77—67004
visible arcs, precip. primary electrons and bremsstrahlung X-rays, satellite correlated obs. 79—35029
visible aurorae and field-aligned currents, satellite obs. 80—12593
visible spectrum, detection and study 77—70903
visual, radio and mag. events 1976-1977, UK obs. 80—12587
visual obs. from space 79—96850
visual observations from space 80—21825
VLF hiss from auroral zone, direction find method and obs. 80—85777
VLF propagation in auroral zone, essential height determ. 79—53631

aurora continued
VUV global observations made by satellite, 110-290 nm region 80—90272
westward electrojet, rel. to Pc 5 activity in morning sector 78—61685
westward travelling surges and low-energy electron precip. obs. 78—45084
X-ray aurorae prod. by energetic electrons precip., imaging from Spacelab 78—61608
X-ray bremsstrahlung rel. to VLF emissions 78—45106
X-ray source region determ. by high-altitude balloon obs. over Thompson, Canada *(Japanese)* 78—61644
X-rays, balloon obs. in Canada rel. to X-ray illuminating regions determ. 80—31156
Zarnitsa.2 electron injection expt., circumrocket glow spectral obs. *(Russian)* 80—12596
CO_2 4.3 μm aurora and related phenomena 77—70904
H aurorae and sporadic-E ionization 79—62659
$H+N_2$, excitation of Hα and Lα emissions, rel. to aurora 79—68309
$H+O_2$, excitation of Hα and Lα emissions, rel. to aurora 79—68309
N and O radiative recomb., source of NO γ and δ bands auroral emission 77—91343
N I 1.04 μm forbidden multiplet relative intensity, auroral forms mean height indicator 79—70909
N I (^{2}D) 5200 Å emission, prod. in auroral zone 79—21090
N_2 15300 Å high-resolution electronic emission spectrum, lab. meas. 78—66549
N_2, band emission as source of 1027 Å aurora 79—80064
N_2 bands in proton-induced poalr cap aurora, intensities 78—77389
N_2 dissociation by electron impact and EUV photoabsorpt., rel. to aurora and airglow 78—58847
N_2, identified as source of 2150 Å emission feature rather than NO 78—45083
N_2, N_2^+ bands, airborne spectroscopic studies 77—29533
N_2, spatial yield spectra for electron energy degradation 79—100992
N_2 Vegard Kaplan bands in bright auroral displays, ground-based photometry 77—33245
N_2, vibr. populations of excited states under auroral conditions 78—42035
N_2, vibrational distrib. in aurorae 79—80068
N_2^+ 1 NG emissions from proton aurora, anomalous vibr. distrib. 80—67448
N_2^+ 4278 Å emission and electron flux comparison in auroral zone 77—87151
N_2^+ excitation of 3914 Å band by proton impact 77—68101
N_2^+ first negative (0-1) band temp. height profile in auroral arc 78—40725
N_2^{2+}, auroral ionosphere spectral emission process 80—41577
$N_2^+(A^2\Pi_u)$ Meinel band deactivation cross sections 78—66635
$N_2^+(A^2\Pi_u\text{-}X^2\Sigma_g^+)$ system, vibr. development and quenching effects 78—88967
$N_2(B^3\Pi_g\text{-}A^3\Sigma_u^+)$ system, vibr. development and quenching effects 78—88967
N(^{2}D) emission and ion chemistry, satellite obs. 80—72673
N(^{2}D)+O_2 as source of O(^{1}D) atoms 79—35028
NO concentrations, theory 77—2291
NO densities, horizontal winds effects 80—26656
NO, γ (1,0) band emission at 2150 Å probably N_2 feature 78—45083
NO_2, continuum emission in aurora 79—2422
N(^{2}P), excitation and collisional deactivation processes in auroral arc 80—72658
N(^{2}P) metastable atoms, UV spectra obs. 80—77185
O I, O II, permitted lines excitation cross-sections, rel. to auroral emissions 78—37745
O I 5577 Å and 6300 Å forbidden emissions, line profile vars. 78—45081
O I 5577 Å forbidden line and O_2 7620 Å band auroral excitation 78—88964
O I 6300 Å, ionospheric luminesc. amplification by radiowave anomalous absorpt. *(Russian)* 79—29925
O I 6300 Å emission production efficiency by energetic electrons 80—72671
O I 7990 Å branching ratio, lab. study, rel. to airglow and auroral emissions 79—775
O I (989 Å) and O I (1027 Å) emissions 78—28367
O I aurora, 3s′ $^3D^0$ and 3d $^3D^0$ levels excitation and radiative decay 79—80064
O I emissions, ground-based photometric meas. 78—77387
O I forbidden emission, Fabry-Perot interferometer obs. for thermosphere wind and temp. meas. 80—101441
O II forbidden line emission, 7320-7330 Å, intensity ratio and centre wavelengths 79—44284
O, O_2 and N_2 emissions, rocket meas. and anal. 78—57380
O_2 1.27μ emission, auroral enhancement 78—81485
O_2 7619 Å band in aurora, rocket obs. 77—25813
O_2 ($^1\Delta_g$) emission, vibr. excitation process 80—82125
O_2^+, 1NG bands spectral synthesis, for auroral obs. anal. 77—2296
O_2^+ dissociative recombination in auroral region 80—41581
O_2^+, second negative bands excitation cross-sections, rel. to auroral emissions 78—37745
O_2^{2+}, auroral ionosphere spectral emission process 80—41577
O(^{1}S) production and loss processes, artificial auroral expt. Precede meas. 79—66855
O(^{1}S) production indirect mechanism in aurora 79—48597
O(^{1}S) production sources determ. from rocket and satellite meas. 80—26662
O(^{1}S) source in aurora, energy transfer from excited N_2 and O_2 79—48598

auroral ionisation *see aurora*

austenitic stainless steel
304, intergranular H_2 assisted fracture, exam. of mechanism 78—80644
304, plasticity and creep anal., fraction model 77—3743
304, rupture of tubes, appl. of fracture mechanics 77—3794
316 trapping up to 7 eV D, depth profiles 78—71751
A302B, neutron damage, ductile-brittle transition temp. 77—3109
acoustic emission during cyclic deformation *(Japanese)* 79—43314
acoustic emission during tensile tests, H_2 assisted fracture 79—100257
advanced reactors, materials and design 78—78452
ageing at high temp., effect on creep props. SEM 80—97516
AISI 304, plane sheet, surface comp. after different surface treatments 80—3253

austenitic stainless steel continued
alloying element influence on struct. and mechanical props. 40Kh12G14N10F(13F), types *(Russian)* 80−35256
anelasticity and creep transients in type 316 stainless steel 78−84880
anodic polarization, Cr content effect 80−35382
anodically polarised, Cl ion effect on passive film 80−97621
anticorrosion props., heat treatment effects, in type 00Kh18N20S3M3D3B 80−30168
austenite stabilisation by H cathodic impregnation *(German)* 79−47680
austenite transformation kinetics, steels 12Kh13 and 15Kh11MF 79−87612
bimetal faced with low alloy steel, fracture toughness *(Russian)* 78−35482
bimetal with alloy steel, H permeability 80−107572
blister initiation inclusion, heat treatment and thermomechanical treatment effects *(French)* 80−35224
boiler tubes, use of mag. field intensity meter to detect magnetic oxide 78−76794
bulk and grain boundary diffusion of Fe, Cr, Ni, effect of Si content 78−38875
carburisation, X-ray microanalysis *(French)* 80−11981
cast struct., determination of origin using etching techniques 78−39985
cathodically charged, H_2 embrittlement, α' martensite effect 80−71725
cavitation erosion resistance, martensitic transform. effect *(Russian)* 78−35524
chloride corrosion in hot acidic media 78−35552
chloride pitting corrosion, effect of autogenous welding 79−91842
cladding, in LWR primary circuit, stress-corrosion cracking 79−20293
cladding on carbon steel, creep-rupture strength in corrosive environment *(Russian)* 77−52533
coarse grained Kh18N9T, US amplitude inspection, efficiency estimation 78−48592
cold worked, 20%, heat treatment effects on mech. state, load-relaxation expts. 77−52350
cold worked, AISI type 304 L and 316 L, pitting resistance in NaCl solns. 80−35393
cold worked type 304 and 316, fatigue and creep crack growth 78−48524
cold working type, heat treated, tool wear during cutting 79−47782
constructional, self lubricating composite, frictional props., Ag-Cu-Zn-Cd lubricant 78−11340
cooling sensitization, continuous, exam. in type 304 79−29098
corrosion, and electrochem. behaviour of cold work-hardened types AISI 304L and 316L 80−50757
corrosion, and mass transfer in liq. Na of type 304, metallurgical factors influence *(Japanese)* 80−71804
corrosion, cold working effect on corrosion behavior 79−74299
corrosion, crevice, rel. to surface comp., in type 316 80−93680
corrosion, in high temp. Na, influence of steel comp. 78−80675
corrosion, in molten SO_4 deposits of types AISI 316, 347 and Esshete 1250 80−97625
corrosion, intergranular, evaluation 77−16741
corrosion and electrochem. behaviour in NaOH soln. containing ClO_3^- *(Japanese)* 78−72928
corrosion behaviour in reducing environment of coal fired MHD generator 80−104322
corrosion by Li and Li:LiH at 873K 80−35397
corrosion by molten Cs_2O_3-CsO_2 of type 304 79−57141
corrosion cracking in chloride and alkaline solutions, 12Kh18N10T and 15Kh17N2 80−55576
corrosion fatigue fracture of Kh17N13M3T, in carbamide production *(Russian)* 78−31574
corrosion in acidic chloride soln. at 25°C 77−70202
corrosion in hot conc. aqu. NaOH soln. 80−7710
corrosion in hot conc. caustic soda, NaCl addition effects *(Japanese)* 77−8990
corrosion inhibition, of Li by AP additions 80−108646
corrosion mechanism in hot flowing Na, computer simulation for type 316 80−3251
corrosion of pressurised tubes in liquid Na, 873K and 973K 77−57722
corrosion performance in automobile exhaust environments 78−7091
corrosion pits, specimen position effect on shape 78−11387
corrosion product in hot conc. NaOH, effect of container material 77−63834
corrosion rate expressions, for type 304L in liq. Li, 600-100°C 80−93682
corrosion resistance *(Russian)* 78−15572
corrosion resistance in passive state, cold work effects *(Czech)* 77−59987
corrosion resistance of cold deformed Cr-Ni austenitic stainless steel in N_2O_4 media at 433K *(Russian)* 80−76422
corrosion resistance testing, urea plant applications *(Czech)* 80−61012
corrosion resistant welded joints, cold working effects on mech. and corrosion props. *(Hungarian)* 78−52838
corrosion studies of materials for nucl. reactor applic. 77−34402
corrosion susceptibilities in synthetic geothermal brines of types of 304 and 316 77−86223
corrosion testing, slow rate strain of type 55 23 33, under electrochem. control in high temp. water 80−97650
corrosion-resistant, strengthening by alloying with N_2 78−95757
crack growth behaviour, under creep and fatigue conditions, environment effects, on types 304 and 316 80−85035
crack growth behaviour at elevated temp., freq. effects in 304, 316 79−83326
crack growth of X6CrNi1811 and X6CrNiMo1713 under Na cooled fast breeder reactor conditions *(German)* 78−56798
crack growth-tertiary creep relation 77−28863
crack obs. and specimens low-cycle fatigue at high temps. 77−1874
crack propag. rates under high-temp. low cycle fatigue conditions 80−21088
crack propagation 78−60797
cracking, environment-sensitive, metallurgical variables influence 80−35391
creep, cyclic, type 304, unbalanced tension-compression loading at elevated temp. 80−97545
creep, effect of temp. and dose-rate variations on En58B, E, J, FV548 and type 316 in Dounreay fast reactor 80−93603
creep, irrad. induced, 60 MeV alpha particles 80−92597
creep, irrad. induced, deuteron bombarded type 316 80−93606
creep, irradiation induced, type 316, climb induced glide model 80−89292
creep, performing effect under tensile and compressive load, rel. to Bauschinger effect 79−96103
creep, rel. to radiation swelling and stacking fault energy *(Russian)* 78−27562
creep and fatigue fracture, of plate with crack, expts. and finite element analysis *(Japanese)* 80−50694
creep crack growth, environmental sensitivity 80−85030
creep crack propag. at elevated temps. 78−19862
creep curve jumps, in type 304 and 316 80−30037
creep deform. effect on struct. of twin boundaries 79−8332
creep deformation, effect on grain boundary struct. on type 800 alloy at 800°C, TEM study 79−38885
creep deformation, under reversed cyclic stresses in type SUS 304 *(Japanese)* 80−81114
creep dependence on electron irrad., in type SS316 steel, dislocation motion *(Russian)* 80−108495
creep fracture, under constant sustaining load 79−83311
creep of pressurised tubes in liquid Na , 873K and 973K 77−57722
creep under irrad. of type 316 in HVEM 80−97523
creep-fatigue crack propagation, in thermally aged type 316 80−89326
creep-fatigue interaction in types 304 and 316 77−70113
current maxima in passivity range 79−66200
cyclic strain induced creep, relation between modes of stress and strain superposition 78−60733
cylindrical specimens with crack. fracture characts. in inelastic strain, test methodology 80−25839
defect structure, N content depend. *(Russian)* 77−59022
deformation and fracture rel. to grain-boundary reaction nodules 78−80591
deformation by hydroforming, heat treatment effects *(French)* 78−35450
deformation induced cavitation, exam. 79−43363
deformation process, stage-by-stage nature investigation using acoustic emission *(Russian)* 80−40434
deformation temp. determ. for high yield strength 78−44177
deformed, phase comp. and props. after prolonged heating in type 12Kh18N10T 80−30040
deformed plate, X-ray line profile anal. *(Japanese)* 78−7144
diffusion coefficients of D, ion beam meas. technique 80−75382
DIN 1.4970, influence of He on high temp. mech. props. 79−7636
dislocation damping, H pinning 78−15501
dislocation struct., carbides, deform. mech. map 77−16650
dislocation substruct., carbide precipitation and deform. mech. map. 77−70116
dynamic recrystallization kinetics 79−47731
elastic constant variability, in type 304, US vel. meas. 80−55446
elastic constants, for N-alloyed steels, and low temp. sound vels. 80−108490
elastic moduli exam. after thermomechanical treatment in 13Khi8N10G3S2M2 *(Russian)* 79−24558
electrochemical behaviour in Ringer's soln., composition effects, SCC 77−90485
electrolytic deep etching 78−31604
electron beam welding effect, on mech. props. of steels 310L, 316, 21-6-9 78−48498
electron microprobes and scanning electron microscopy, conf., Orsay, France, Dec. (1978) 80−11979
electron transmission microscopy, microstructural zones *(Spanish)* 79−39059
embrittled by α-particle irrad. 77−69015
embrittlement by He in ^3H handling facilities 80−102285
equivalent alternating stress from two-level multiple-step wave *(Japanese)* 78−92333
even elongation and relative hardening, effects of struct., comp. and testing temp. 78−52926
explosively welded, orientation relationship in martensitic transform. 80−104158
extrinsic grain boundary dislocation spreading 79−57004
extrinsic grain boundary dislocations, effect on $M_{23}C_6$ precipitate nucleation 79−51118
faceted fracture surfaces, selected area channelling patterns for type 304 77−77565
fast neutron irrad., effect on mech. props. 78−92309
fatigue, effect of struct. and work hardening rate *(French)* 77−63783
fatigue, low cycle, temp. and strain rate effects *(Japanese)* 79−29198
fatigue and cyclic stress-strain characts. austenite-martensite transform. effect 80−21109
fatigue behaviour, influence of stressing conditions *(French)* 78−68776
fatigue behaviour, of soln. annealed and thermally aged type 304 80−100923
fatigue crack growth and threshold measured at very high frequencies, for type 304 steel 80−71742
fatigue crack growth in PWR environment in type 304 and 316 79−66170
fatigue crack growth rates in type 316, effects of overloads on growth rate 78−64688
fatigue crack growth under mixed loading conditions in AISI 304 tubes 77−3114
fatigue crack propag., stable and unstable, role of precipitation 80−40534
fatigue crack propagation, effect of neutron irradiation 80−97583
fatigue crack propagation, influence of neutron irradiation 80−97584
fatigue crack propagation in single crysts., orientation depend. 79−29167
fatigue cracks, steel 07Kh25N12G2T US monitoring of growth rate 78−60917
fatigue damage, under sawtooth wave strain cycling at elevated temp. *(Japanese)* 78−84977
fatigue damage indicators, non-destructive 80−25932
fatigue design curves using modified Langer eqn. for pressure vessels 80−30107
fatigue endurance rel. to test piece size, corrosive environment effects *(Russian)* 79−29270
fatigue life of type 316, effect of hold times, explanation in terms of grain boundary sliding damage 78−72851
fatigue mechanistic model, time-dependent, for type 304 80−100925
fatigue properties, low cycle, in vac. of type 316 80−85021
fatigue resistance, high-temp. low-cycle, under superimposed stresses at two freqs. 80−25832
fatigue strength, low cycle, reduction factor for type SUS 304 *(Japanese)* 80−104259

austenitic stainless steel continued
fatigue tests, low cycle, frequency effect on notch sensitivity at elevated temps. *(Japanese)* 80—104260
fatigue under static and cyclic heating fractographic peculiarities, electron microscope obs. *(Russian)* 77—52465
fatigued, deform. subsruct. and annealing stacking fault tetrahedra form 80—107282
FCC, fractographic obs. of SCC 78—64786
ferrite volume fraction, high-speed determ. by XDXRD 78—76628
ferritic, prep. with fine grains by cold rolling and recrystallisation, superplasticity *(French)* 78—35406
ferritic, single phase ferritic solidification in welds, exam. 80—7546
ferritic/austenitic high Cr, development, mech. props. and corrosion resist. 80—45422
fibre reinforced porous mat. prod., mat. props. 77—59723
flow cavitation erosion, initial part of incubation period 78—44224
foil, in situ oxidation in HVEM 80—104354
fracture toughness and transition temp., T_{50}, effect of cooling rate and supercooling temp. 78—84987
fracture-mechanisms, tensile specimens types 304 and 316 80—85039
fretting corrosion of orthopaedic implant materials by bone cement 80—104813
fretting wear in air and CO_2 at elevated temps. 80—21119
friction, wear and microstruct. of unlubricated 304, 316 and Nitronic 60 80—108589
friction in vacuum, at elevated temps., steel Kh18N9T 80—55542
fusion reactor blanket struct. material, low cycle fatigue behaviour 80—30073
fusion reactor environments, mech. props. correl. methodology development 80—29068
fusion reactor first wall material, radiation damage by simultaneous accelerator microscope irrad. 79—45402
fusion reactor first-wall and blanket material, mech. props. 80—34074
fusion reactor materials, material requirements exam., review 78—50257
gas liberation, 20°C, surface oxide effects *(Russian)* 80—3286
grain boundaries, interfacial structure effects on high temp. mechanical behaviour 80—59480
grain boundary as dislocation source during high temp. deform. *(Russian)* 78—15453
grain boundary dislocation interaction with TiC precip. during high temp. creep 80—16384
grain boundary migration during high temp. creep, TEM exam. 78—88509
grain boundary segregation studies, intergranular fracturing technique for stress corrosion cracking investigation 79—39057
grain boundary struct. changes during initial stages of recrystallisation 77—36559
grain boundary structure, during recrystn. and grain growth 80—76270
grain growth, annealing twins role 79—57016
grain growth, time dependence and activation energy 78—72787
grain growth kinetics, effect of C content and rolling *(French)* 77—81269
grain size effect on softening *(Russian)* 78—23731
heat conductivity, low temp. mag. susceptibility meas. *(Chinese)* 79—47080
heterogeneous duplex grain structure in 304 austenitic stainless steel, US spectroscopy 80—30204
high Mn, thermally induced segregation 79—4971
high N, heat treatment effect on struct. and props., N solubility 80—29994
high N, plasma arc remelting, processing parameters and props. 80—16336
high strength, for cryogenic appl., tensile testing, room temp. and 4K 77—25119
high temp. alternating torsion behaviour, saturation state phenomenology 79—70111
high tensile X 3 CrNiMoNbN 23 17, creep at room temp., effect of Bauschinger effect *(German)* 77—1852
hot plasticity, Y additions effect 79—83270
hot-worked precipitation kinetics and struct. of dispersed phases, Ti effect on type 08Kh18N10T 80—29964
HVEM irrad., point defect trapping influence on void swelling 79—23652
hydride phases rel. to SCC 80—35385
hydride study by X-ray diffr., rel. to martensitic transform. *(Japanese)* 77—81263
hydrogen embrittlement and SCC, austenite stability effect 79—100291
hydrogen embrittlement of type 316, exam. by tensile testing 80—7671
hydrogen permeation characteristics in types 316-SS and 321-SS 79—69295
hydrogen permeation characts. 79—67948
hydrogenated, Mossbauer effect 77—7758
implanted with N, type 304, surface hardness and abrasive wear resist. 80—50746
induced martensites morphology 80—104153
interaction of annealing twins in fcc metals and alloys 78—68712
intercrystalline corrosion, hot rolling effect in 12Kh18N10T 79—79010
intercrystalline corrosion, stressed state effect 80—55582
intercrystalline corrosion in low and high oxidizing environment *(Russian)* 79—43477
intergranular corrosion and pitting corrosion of 308 stainless steels, mech. 79—91846
internal friction due to H_2 *(Japanese)* 77—48469
internal friction due to H_2 gas molecules 80—71682
ion beam irradiation of type 316, effects study by HVEM 80—103396
ion irradiated type 316, 46.5 MeV Ni^{6+} ions, soluble C effect on void swelling and low dose dislocation structs. 80—49280
irradiated OKh16M15M3B, reactor structural material, low-cycle fatigue study 79—91793
irradiation creep data, obtained in fast and thermal neutron spectra correlation with displacement cross-sections in types M316, FV548, 304 80—84993
irradiation induced creep, AISI 316, 20% cold worked effect of temp. change 78—72816
irradiation induced creep by alpha particles, in type 316 steels *(French)* 78—72791
life prediction of high temp. low cycle fatigue, strain rate effect 79—8360
liquation cracking during welding, comp. influence 80—66645
LMFBR performance, effects of irradiation creep and swelling 78—78482

austenitic stainless steel continued
LMFBR primary piping materials, mech. props., review 77—25151
load relaxation data, comparison with Hart's deform. model 77—70091
low alloy 316, high temp. plasticity, B addition effects *(Russian)* 77—28852
low cycle fatigue, effect of mean plastic strain and stress factor 77—63766
LWR austenitic stainless steel coolant tubing, bending props. *(Czech)* 79—67851
LWR piping, intergranular stress-corrosion cracking 80—81234
magnetic phase content determ. via permeability meas. using MF-10F probe 77—77648
magnetic susceptibility and magnetisation, low temp. 80—25102
martensite transformation of type 304, acoustic emission identification, opt. microscopy obs. 80—81062
martensitic transform. effect during static and fatigue loading 77—52325
martensitic transformation, effect of H in a 18-8 type *(Chinese)* 80—55394
matrix precipitation of Cr_2N, due to P addition, TEM exam. 79—4973
mechanical behaviour of type 316 stainless steel from 760 to 1204 C 78—86604
mechanical properties in liq. Na, review 79—20150
metallic second phases, effect on steel behaviour, review 78—31503
metastable, alloy 000Kh18N10 creep at low temps. 77—1861
metastable, determ. of strain-deform. martensite content 78—3282
metastable, fatigue damage, static and dynamic simultaneous obs. *(French)* 78—88516
metastable, transform. depend. ductility, temp. and deform. effects 78—3185
microarcing studies in low temp. RF-plasma 80—96407
microdeformation measurement using method of grids 80—55615
microstructural distribution of cathodic H_2 in Z2CN1810 steel *(French)* 79—99234
microstructural effects on US attenuation 78—11455
microstructure and transient creep 79—61675
microstructure evolution, neutron induced, He role 80—29064
mild, fretting fatigue, shot-peening effect 79—87733
monolayer on cladded low alloy steel, heavy section, residual stresses *(German)* 78—35420
mottling on radiographs of weldments and castings 80—16614
multiaxial creep equations for nonlinear and volume-nonconservative in-reactor creep 79—59164
NbC precipitate particles, size distrib., TEM study of grain to grain variations 79—29066
Neel temperature and max. susceptibility calcs. 77—43833
neutron irrad., He release kinetics, 600 to 850°C 78—79638
neutron irrad., swelling due to gamma prime and $M_{23}(C_1Si)_6$ form. 78—51590
neutron irradiated, mag. props. 80—29067
neutron irradiated, Si-rich phase occurrence of M_6C phase 80—15156
neutron irradiated, type 316, ferrite formation, study by mag. meas. and TEM 79—37742
neutron irradiation on fatigue crack propag. 80—29069
neutron radiation damage simulation, effect of the preinjection on swelling 80—44236
neutron-irradiated, gamma-alpha transformation 79—96027
nitriding, accel. for type 12Kh18N10T 79—96204
nonsensitized, fatigue strength, intergranular corrosion effect *(Japanese)* 80—85027
nuclear power reactor appl., in primary and auxiliary systems 77—3102
nuclear power reactor appl., props. 77—3101
nuclear reactor structural material, effect of irrad. and other factors on fatigue crack propagation 79—20194
nucleation, of $M_{23}C_6$ carbides, from directly aged 18 Cr-11 Ni *(Polish)* 78—52806
oxidation, high temp., in low O_2 press., surface anal., impurity diffusion effects 77—56142
oxidation, high temp., obs. using $^{18}O(p,\alpha)^{15}N$, ^{18}O distrib. determ. 79—87912
oxidation and spalling resistance 80—30133
oxidation in CO_2, charged-particle nuclear techniques 80—61022
oxidation of (100)-plane, LEED-AES obs. *(German)* 78—68841
oxidation resistance, Cl and H_2S effect on types AISI 304, 320, 316, 321 80—45418
oxide film morphology, irradiation effects in N_2O_4 *(Russian)* 79—33209
partial dislocations separation and dislocation substructure, effect of applied stress 78—22727
pearlitic, type Kh18N9T, study of long term cyclic strength under soft asymmetric and rigid loading 79—57076
phase diagrams, multicomponent, at 600 and 650°C 79—78937
phase identification, $2^1/_2$D imaging techniques 80—96424
phosphide analysis using nonaqueous electrolyte potentiostatic etching method *(Japanese)* 80—89221
pipe welds, US inspection pattern recognition reflector classification feasibility study 80—16615
pipes, electro-thermal method, for NDT of welds 80—35447
piping cracks, JPDR, stress corrosion and fatigue tests 79—66204
pitting and crevice corrosion, effect of Mo, Si and N *(Japanese)* 78—92399
pitting corrosion, effect of Cr, Mo and N content on resist. 78—80668
pitting corrosion susceptibility, non-metallic inclusion effect 80—11816
pitting resistance, in low salinity brine 80—93681
plastic deform. build-up during low cycle fatigue *(Russian)* 77—25207
plastic deformation, TEM obs. *(French)* 77—44302
plastic deformation generalised constitutive rels. for type 304 80—104219
plastic deformation under hot working conditions, two-phase austenitic-ferritic 77—48466
plastic loosening and deform. defect healing during recovery annealing of 12Kh18N10T *(Russian)* 80—66530
pool metal, solidification kinetics in welding with electromag. stirring 80—71636
porous fibre, sintered and compacted, mech. props. 79—15623
porous gauzes, hydraulic resist. in laminar filtration 80—100034
potentiostatic tests, on type 317L, use of free-corrosion potential time transients to distinguish between pitting and crevice corrosion 79—39058
powder, sintering behaviour 78—44051
precipitates and grain orientation, by non aqueous electrolyte potentiostatic etching method *(Japanese)* 80—15102
precipitation behaviour under high temp. conditions, photoemission electron microscope obs. 80—108456

austenitic stainless steel continued
precipitation hardening and N_2 effects obs. *(Rumanian)* 77—55973
precipitation of $M_{23}C_6$ carbide by ageing *(French)* 79—52216
precipitation of $M_{23}C_6$ type carbide on twin boundaries 80—89226
radiation-induced swelling in BOR-60 reactor 79—97814
radiational swelling of two-phase austenitic-ferritic stainless steels 80—65063
reactor fuel assemblies, postirradiation mechanical props. of honeycomb spacer grids 79—36324
recrystallisation, TEM obs. *(Japanese)* 79—52269
recrystallisation *(Japanese)* 77—52346
recrystallisation transformation energies, α' to γ, effect of Si content and deformation by rolling *(French)* 77—48433
recrystallization after hot rolling 79—47734
repassivation kinetics study in Ct media 80—97614
replication, NDT anal. and inspection technique 78—11467
sensitisation assessment, Jominy bar technique 80—60887
sensitivity of intergranular corrosion, effect of Mo content, heat treatment and degree of stabilization *(Czech)* 79—70095
sensitized, type 304, intergranular corrosion fatigue crack growth in oxygenated pure water at 85°C 79—47814
sensitized forgings, corrosion resistance restoration, computer calc. *(German)* 79—66074
solution annealed, 304 tensile flow behaviour after exposure to flowing Na, between temp. 550 to 700°C 78—35463
stability, deform. rel. to $\gamma \rightarrow \alpha$ transform. kinetics 79—24522
stability under deform., magnetisation meas. 77—1579
stabilized, creep improvement, effect of B precipitation and hyperquenching *(French)* 78—23784
stacking fault effect on martensitic transform. during plastic deform. *(Russian)* 80—25696
stacking fault energy, composition depend. 78—38733
stacking fault energy, effect of C, exam. 78—80553
stacking fault energy, effect of N 80—107279
stacking fault energy measurement, by weak beam electron microscopy 78—18661
stacking fault energy rel. to mech. props. *(French)* 79—43339
stacking fault tetrahedra and dihedra 77—84768
steam generator tubing, stress corrosion cracking in NaOH soln. 78—60866
steel, austenitic, type 316, in $MgCl_2$, acidity and applied potential effect on stress corrosion cracking 80—85076
steel, austenitic stainless, dislocation transport and H_2 embrittlement 80—30087
steel, austenitic stainless, Ni-alloyed, Cr_2N precipitation, interface struct. and morphology 80—11644
steel, austenitic stainless, nitrided, type 03kh17N8G5MFAB, alloying characts. and phase comp. 80—30166
steel, austenitic stainless, stress corrosion crack growth, electrochem. aspects 80—97620
steel, austenitic stainless, texture influence as through thickness strength 79—91771
steel, austenitic stainless, type 304, exam. of continuous cooling sensitization 79—29098
steel, austenitic stainless, type 321S12, fatigue cycling in R=−1 loadings 80—35317
steel, austenitic stainless sheet, texture anisotropy influence on deformation forming limits 79—91706
steel, austenitic stainless type 304L, temp. depend. of acoustic emission accompanying plastic deform. 79—74217
steel, austenitic stainless type AISI 316, L sheet and LN plate surface comp. after different surface treatments 80—3253
steel, austenitic stainless type-316, fracture mechanics study of stress corrosion cracking 80—16580
steel, austenitic stainless weld, US inspection, focusing probe significance *(German)* 77—73397
steel, stainless, type 316, modelling effects of fast neutron irradiation in mech. behaviour 80—84234
steels, stainless, accelerated test for susceptibility to Cl_2 stress corrosion cracking 80—21199
strain growth, due to thermal stress ratcheting, exam. 78—92354
strain hardened containing N_2, low temp. props. 79—66128
strength properties, dispersity of struct. effect, steel Kh18N10T 80—55486
strengthening by modified ausforming 78—76665
stress corrosion crack growth 77—90484
stress corrosion cracking, alloying and environmental variation effects on cracking susceptibility 78—31563
stress corrosion cracking, analysis of fracture surface *(Japanese)* 80—16573
stress corrosion cracking, and K_{ISCC} in boiling $MgCl_2$ solns., effect of alloying elements on type 304 *(Japanese)* 80—93692
stress corrosion cracking, classification in various environments *(Japanese)* 80—71805
stress corrosion cracking, comparison with mech. tests in neutral environment *(French)* 77—70222
stress corrosion cracking, correl. between electrochem. and mech. parameters 80—97613
stress corrosion cracking, effect of Cl^- content, pH, test soln. temp. 78—11388
stress corrosion cracking, environments responsible 79—20242
stress corrosion cracking, exam. of inhibiting action of Pb^{2+} 79—20249
stress corrosion cracking, factors influencing susceptibility 80—97617
stress corrosion cracking, high voltage electron metallography 79—52425
stress corrosion cracking, in $MgCl_2$ soln., temp. effect *(Korean)* 80—93694
stress corrosion cracking, mechanisms *(Japanese)* 80—104336
stress corrosion cracking, mixed mode, fractographic evidence in surgical implant 80—30156
stress corrosion cracking, rel. between polarisation behaviour and susceptibility, in type 304 *(Japanese)* 80—93693
stress corrosion cracking, role of H_2, state of art review 80—61017
stress corrosion cracking *(German)* 78—19953
stress corrosion cracking and electrochem. behaviour in $(NH_4)_2SO_4$-Cl^- solns., for AISI 304 80—55566
stress corrosion cracking and stacking fault energy, N_2, P and Ni effects *(Czech)* 78—60875
stress corrosion cracking at low stress intensity factors 77—73362
stress corrosion cracking at low stress intensity factors 79—29264
stress corrosion cracking by polythionic acid *(Korean)* 80—21179

austenitic stainless steel continued
stress corrosion cracking critical potential, determination *(Czech)* 79—91850
stress corrosion cracking in boiling MgCl solution *(Japanese)* 78—92400
stress corrosion cracking in boiling solutions of $CaCl_2$, $MgCl_2$ and LiCl *(French)* 77—81342
stress corrosion cracking in concentrated chloride solution 78—56825
stress corrosion cracking in H_2SO_4-NaCl soln., Ni and N_2 effects *(Japanese)* 79—100289
stress corrosion cracking in high temp. water, effect of environmental factors 79—1924
stress corrosion cracking in high temp. water, heat and cooling rate effects 79—61800
stress corrosion cracking in high temp. water, surface prep. effect 79—5088
stress corrosion cracking in $MgCl_2$ soln., cold working effect, in type 304 *(Japanese)* 80—104339
stress corrosion cracking in various environments, fractography, of type SUS 304 *(Japanese)* 80—93690
stress corrosion cracking inhibition, insensitized type 304 80—100939
stress corrosion cracking problems in chemical plants 79—96190
stress corrosion cracking susceptibility, effect of strain-induced α'-martensite *(Japanese)* 80—104335
stress corrosion testing, slow strain rate, elevated temp. and high press. study 80—97615
stress intensity factor, reliability of values 80—55530
stress relaxation, model, experiment confirmation of model 78—92293
stress-strain relationships, uniaxial and biaxial, FBR containment 80—81122
stressed state blistering 78—95085
structural alloys for superconducting magnets in fusion energy systems, props. at 4K 80—86976
structural inhomogeneity in rolled steel, electron and optical microscope exam. 78—72827
structure and mech. props. under low temp. deform. under linear and plane stress conditions 79—1902
structure phase transitions due to high energy electron irrad. *(Russian)* 80—7553
sulphidation, rel. to Fe-Ni-Cr-S phase relations 79—38800
superconducting magnet, large system, structure, insulators, conductors 80—32471
supersaturated, recrystallisation 77—77506
surface, interaction with O_2, AES and work function obs. 80—65364
surface films grown in Cl^- solns., ellipsometric investig. 79—20261
surface hardening by electrohydraulic forming *(Japanese)* 80—16571
surgical implant ion beam textured, stress/strain relations, fatigue characts. 78—73297
swelling in fission reactors, dose rate dependence 80—104233
temper embrittled, type 304, Auger spectroscopic exam. of grain boundary surface phases 78—76741
tensile and creep data evaluated for 304 and 316 steel 77—77552
tensile ductility in air and H_2 77—66687
tensile fracture, phase transform. effect, comparison of stable and metastable phases 78—60798
tensile prestrained, X-ray elastic const. meas. *(Japanese)* 79—66093
tensile properties, exposure to Li and LiH at 600°C, effect on types 304, 316 80—35219
tensile stress effect on He bublbe growth 79—87684
tensile test at elevated temp., high velocity 77—73302
testing for chemical plants, use of electrochemical methods, corrosion rate forecast automatic instrumentation *(German)* 78—44289
texture effects in rods, in series tests, elastic props. *(German)* 78—15439
thermal cycling, low temp., effect on principal mech. props. 77—81322
thermal fatigue, fractographic features of failure 80—76349
thermal fatigue of sodium mixer *(French)* 79—91789
thermal passivation of type AISI 316 steel in controlled vacuum 80—76276
thermal treatment for spectrally selective surface fabrication 80—35752
Tokamak fusion reactor, blanket structural material selection and development *(Japanese)* 79—97901
Tokamak vacuum vessel, H plasma effects on mech. props., embrittlement 80—21111
tool, Kh18N9T, self lubricating composite, frictional props., Ag-Cu-Zn-Cd lubricant 78—11340
transformation, H_2 induced, charging temperature, specimen thickness and aging time dependences obs. *(Japanese)* 80—11640
transformations during continuous cooling 77—44245
transgranular slip obs. 78—80595
TRIP, fretting corrosion of surgical implant material, electrochemical investigation 79—66197
tube carburised layer metallographic determ. 78—85077
twinning and martensitic phases on hydrogen-charging, TEM 77—21222
type 304, LMFBR, creep rupture modee of failure, reliability anal. 77—3113
type 304 with He distrib., foil, effect of momentum transfer, damage energy gradient, on He distrib. 78—71773
type 304N, machining induced deformation transformation, mag. evaluation 79—83195
type 316, σ phase precipitation during long term high temp. creep, fracture 79—74157
type 316, D-T fusion neutron and Ni^{2+} ion damage 78—14388
underclad cracking mechanism, effects of residual strain and heat affected zone ductility 77—25158
US examination, of type SIS 2343 butt welds 80—93710
US fatigue meas. 80—40489
US propagation in austenitic stainless steel weld metal, effect of anisotropy 80—45452
US wave velocity meas., rel. to cold working in type 304, 304L, 316L 80—99908
US weld testing, false indications, cause and influence 78—31599
V alloyed, creep inhibition at grain boundaries, dislocation struct., TEM study 79—43346
vacancy porosity, effect of Soviet BR-5 reactor operating conditions 79—32990
VASCOMAX 300, struct. transforms. on tempering 77—86058
viscoplastic behaviour, strain rate sensitivity, creep, relaxation, tensile tests 80—66727
viscoplastic behaviour under hot working conditions, constitutive eqns. 79—57024
viscoplastic deformation under hot working conditions, struct. model for type AISI 316 L 79—83278

austenitic stainless steel continued
- void volume, swelling, errors in determ. by TEM 80—84208
- void-swelling, in type FV 548 20% cold worked irradiated with 22 MeV C^{2+} ions or 46 MeV Ni^{6+} ions 79—37744
- wedge crack nucleation in type 316 77—73339
- weld, ferritic-austenitic solidification mode 80—89214
- weld metal defect detection, shear-wave polarisation effect 78—44337
- weld metal magnetic testing, delta ferrite content measurement 78—31600
- weld metals, austenitic and austenitic ferritic, rel. between solidification and microstructs. 79—61579
- weldments, creep fracture, correlation with time-temperature parameters 79—29219
- welds, exam. of austenitic solidification mode 80—7545
- welds, time domain approach to crack location and sizing 80—50781
- welds, US inspection 80—71821
- welds, US longitudinal wave examination 80—50784
- wires, type 301-304, phenomenology of cold twisted deformation *(French)* 80—21030
- X-ray elastic constants, determination by ψ_0 oscillation method *(Japanese)* 78—64575
- X-ray line profile analysis 77—86048
- X-ray meas. of residual stress in ground surface layer *(Japanese)* 77—48491
- X-ray microanalysis of C *(French)* 80—11981
- X-ray stress anal. by new position sensitive proportional counter with uniform angular resolution *(Japanese)* 80—30190
- X-ray stress meas., accuracy and method of data treatment *(Japanese)* 80—104365
- yield strength, effect of N_2 additions and grain size, solid soln. strengthening 77—52430
- Zircaloy-4/stainless steel type 304 diffusion junction, hydriding behaviour 79—65200
- B effect on corrosion resistance 78—35569
- B-containing decomp. of solid solns., effect of cooling conditions 77—44256
- C heterogeneities demonstration by high-resolution autoradiography *(French)* 77—66729
- Cl^- stress corrosion cracking, forming process of fan-shaped pattern 79—20287
- Cr tracer diffusion coeffs. for AISI 321 80—2193
- Cr-Mn, austenite stability during deform. 77—70050
- Cr-Ni, ^{51}Cr tracer diffusion coeffs. 80—34225
- Cr-Ni, ^{59}Fe self-diffusion in ferrite/austenite interface *(French)* 80—19975
- Cr-Ni, 316 type, electron irradiated, void swelling 79—42104
- Cr-Ni, effect of boron on nucleation of $M_{23}C_6$ carbides *(Polish)* 78—84808
- Cr-Ni, elec. resistivity and struct.-mag. transitions at low temp. 79—99527
- Cr-Ni, resist. damage rate during neutron irrad. at 23K 80—96571
- Cr-Ni, sp. ht., 4-300K 77—24416
- Cr-Ni, stability, tensile and compressive strain depend., 4-373K 77—25052
- Cr-Ni, X5CrNiN19.7 and X5CrNi18.10 corrosion in HNO_3 *(German)* 78—44253
- Cr-Ni (16, 16 wt.%), in-pile rupture strength, cold work and soln. annealing effects 77—63687
- Cr-Ni (16,14 wt.%), Si effect on texture, grain growth after rolling or recrystallisation *(French)* 77—55986
- Cr-Ni (18, 15 wt.%), oxidation resist., metallic alloying additions effect 79—52419
- Cr-Ni (18,11 wt.%), corrosion resistance in urea *(Czech)* 77—70220
- Cr-Ni (18,12 wt.%), containing coarse irregular carbide precipitates along grain boundaries, ductility 78—60718
- Cr-Ni (18,8 wt.%), stress-corrosion cracking in conc. $MgCl_2$ soln. 78—85057
- Cr-Ni (18.22, 8.87 wt.%), welded joint, polarisation behaviour, boiling $MgCl_2$ soln. *(Japanese)* 80—93695
- Cr-Ni (20, 25 wt.%), Nb stabilized, oxidation behaviour in CO_2, surface ion implantation effect 80—71791
- Cr-Ni (25, 20 wt.%), grain size, temp. and stress influence on creep 80—30021
- Cr-Ni-Mn (21, 4, 9 wt.%), heat resistant, grain boundary reaction, effect of alloying elements *(Japanese)* 77—52331
- Cr-Ni-Mn-Mo, mechanical properties rel. to treatment, Mn and Mo effect 79—96039
- Cr-Ni-Mo, Mo effect on lattice parameters and chem. comp. of σ-phase and $M_{23}C_6$ carbides 77—70072
- Cr-Ni-Mo (21,6,9 wt.%), N_2-strengthened, surface segregation of B, Auger and XPS spectra 79—90854
- Cr-Ni-Mo (25, 28, 20 wt.%), containing N_2, electron microscope obs. of Cr_2N precipitates *(Japanese)* 78—15404
- Cr-Ni-Mo-Mn, Mo, Mn and ageing effects of hardness 78—35413
- Cr-Ni-Mu-V, biphase, ferritic, ageing and thermomech. treatment effects on struct. and props. 80—35226
- Cr-Ni-Nb, intergranular precipitation, predicted behaviour 79—100148
- Cr-Ni-Ti, creep deform. effects on intergranular TiC dispersion stability 78—84912
- Cr-Ni-Ti(20,25,1.5 wt.%), dispersion-strengthened, threshold stress for creep 80—93626
- Cr-Ni-(Mo), intercrystalline corrosion sensitivity, electrochemical determ. *(Czech)* 77—59989
- Cr-Ni(18.8 wt.%), X-ray stress meas., accuracy and method of data treatment *(Japanese)* 80—104365
- Cu-Mn substituted 18/8 type, austenitic stability 79—91716
- D depth distrib. determ. using $D(^3He,p)^4He$ 79—4326
- GCFR fuel pin claddings, oxidation behaviour in He environment 80—16594
- H trapping studies in fusion first wall materials 79—45407
- H_2 induced strain in single crystal *(Japanese)* 77—48530
- He implanted 1.4970, high temp. fracture 77—86186
- Mn alloy, sound vel. anomalies near spin glass transition 79—82795
- Mn-Cr, austenite decomposition by deform., rel. to mech. props. *(Russian)* 78—27515
- Mn-N interaction, internal friction obs. 78—84883
- Mo effect on mech. behaviour in inert medium and hot Cl^- medium *(French)* 79—43482
- Mo-bearing, ellipsometric meas. of passive films, optical constants *(Japanese)* 78—85041
- N diffusion 77—62677

austenitic stainless steel continued
- N-alloyed, room temp. elastic consts. and low temp. sound vels. 80—108490
- NbC particle growth and dissolution, in aged and deformed state 78—39782
- Ni-Al, γ-phase, fracture mechanical aspects of abrasive friction, wear, chip formation 78—72865
- Ni-Cr, heat resist. and comp. of non-metallic inclusions, effect of La, Nd, Pr and Ce 80—76315
- Ni-Cr machine steel, austenite grain size effects on mech. props. *(Russian)* 77—44292
- Ni-Cr type, creep deformed, dislocation multipole obs. 80—107258
- Ni-Cr-Fe, AISI 316, irradiation effects on phase stability 79—11566
- Ni-free austenitic stainless steel, corrosion obs. 79—24652
- Si additions effect on unlubricated adhesive wear, oxidation resistance, solid soln. hardening 77—59949
- $Te/O_2/Cs$ corrodents attack, on tubing 316 80—50770
- Ti stabilised MC precipitate comp., APFIM study 80—104161
- V alloyed, creep mechanism 77—36591
- V alloyed, creep mechanism 77—48514

austenitic steel
- *see also austenitic stainless steel*
- 10R6M5, atomised powders *(Russian)* 80—97446
- 10R6M5K5, atomised powders *(Russian)* 80—97446
- 30Kh3SNMBF, α-phase nucleation of growth, influence of supercooled austenite state *(Russian)* 77—48435
- 800H, effect of hardening processes on initial stress-strain curve 78—84846
- abrasive wear, fracture toughness effects on friction force *(German)* 77—4860
- aged, stress induced martensitic transform., mech. props. *(Russian)* 79—87632
- ageing after deform. in pre-martensitic state, internal friction meas. *(Russian)* 77—77477
- ageing and plastic deform. effect on struct. and mech. props. of N15Kh5G3T3 *(Russian)* 80—71691
- AISI 310, creep damage and rupture 79—20127
- AISI 4340, effect of step quenching on microstruct. and fracture toughness 78—84834
- alloy, Cr or Mo, metallography study of high temp. decomposition 79—61559
- alloy, grain size, tempering effect on brittle fracture susceptibility 80—55534
- alloy steel, austenitic, Ni free, TEM exam. of corrosion process 78—85029
- annealed, Ni ion bombardment, swelling temp. depend. effect of He implantation 80—29080
- austenitic and ferritic steel in contact with liq. Na, C transfer 80—22945
- austenitic solid solution, chem. evaluation of B and its correlations with hardenability and hardness *(German)* 79—39230
- austenitic-martensitic, phase comp., struct. and mech. props. 80—29974
- bainite, formed from deformed austenite, morphology and mech. props. 79—43345
- bainite substructure changes during HTMTI 78—23742
- bainite transform., US strain effects *(Russian)* 77—13269
- bainitic, morphological characteristics 78—68682
- Bauschinger effect, structural sensitivity *(Russian)* 79—52303
- blistering after 40 keV He ion bombard. 80—39175
- carbide transformations on precipitation of C from austenite *(Russian)* 80—97487
- carbonitriding, high-temp., saturation kinetics *(Russian)* 79—52450
- carburising in vac., rate, austenite grain size, C distrib. 79—20277
- cast iron, hypereutectic, transform. of cementite to austenite 77—52318
- cavitation failure in liq. O_2 77—44405
- Charpy type bars of AISI 4340, varying notch root radii, fracture initiation and propag. at notch root 80—85050
- cladding material, deform., failure, rigid loading scheme 79—91765
- cladding stability of fuel element for gas-cooled fast reactors *(Russian)* 77—83042
- cold brittleness structural depend., fracture mechanisms in type 70 steel *(Russian)* 80—97571
- cold rolling, effect of transformations during quench hardening and tempering 77—55989
- cold worked, derivation of simple void-swelling equation 79—7631
- cold worked 10Kh11N23T3MR, structural transformations, aging effect, electron microscope obs. 80—40402
- cold working of steel 12 Kh18N10T after prolonged operation at −183°C, struct. and props. 77—55988
- constructional, austenite grain shape eval. method 78—35607
- corrosion effects of Li 80—35398
- corrosion resistance and degradation of mechanical props., influence of N, in liquid Na 80—16567
- corrosion resistant, review of heat treatment, mech. and corrosion resist. characts. *(Korean)* 79—24653
- corrosion under boiled conditions, Mossbauer spectroscopy study 79—47800
- crack determ. using mag. permeability probe *(German)* 79—52549
- crack resistance, high-temp., B and Mo influence *(Russian)* 80—16435
- cracking resistance, high-temp., approx. method of estimation 78—23914
- creep, low-temp., during dynamic relaxation, effect of dislocation struct. *(Russian)* 77—25103
- creep, radiation induced, fundamental mechanisms *(Italian)* 80—55457
- creep and cyclic loading at 823K *(German)* 77—90435
- creep cavities, nucleation and growth in type 347 80—40513
- creep exposure, partial recovery of mech. props. by subsequent annealing *(German)* 77—59886
- creep exposure, propag. rate of intercryst. cracks *(German)* 77—59887
- creep failure in 316 at 625°C, grain size effect 78—27631
- creep fatigue cycling, electric crack growth 79—29209
- creep rupture testing between 400 and 700°C const. stress, accel. temp. method 78—31495
- creep-fatigue interaction, creep effect in type SUS 304 *(Japanese)* 79—83264
- critical strain rate in type 30KhGSA 80—16399
- damping, logarithmic decrement meas. by torsion pendulum *(German)* 79—74195
- damping capacity, magnetomechanical, phase transform. effects 78—31445
- decomposition, controlled rolling rel. to substruct., props. 79—29014
- decomposition, effect of struct. of initial state *(Russian)* 77—48442

austenitic steel continued
decomposition, exam. of phase transformation kinetics, using new method 79−52509
decomposition kinetics, crack sensitivity, H_2 effect *(Russian)* 80−20885
decomposition of solid solution in steel alloyed with N 78−23712
deformable solids, fracture and hardening kinetics 80−35210
deformation, struct., transform. kinetics hot working effects *(Russian)* 77−52361
deformation under modified ausforming *(Japanese)* 79−11673
deformed, struct., texture and mech. props. of product of transform. 78−92273
diffusion couple with C steel, diffusion of C, 773-1373K 79−19392
diffusion of C after high-temp. thermomechanical treatment *(Russian)* 78−39813
diffusion saturation with Cr in closed reaction space, kinetics and mechanisms 79−52458
disc, biaxial fatigue testing under changing temps. *(German)* 80−71759
dislocation density effect on form., $\alpha \rightarrow \gamma$ transform. temp. *(Russian)* 77−8813
dislocation struct. formed by interstitial diffusion of C 77−4223
dislocation structural changes on hot rolling *(Russian)* 77−59805
displacement energy determ. of 316, HVEM obs. and electron bombardment 78−6100
dissolution kinetics of carbide $Cr_{23}C_6$ in steel 40Kh13N8G8 *(Russian)* 78−48369
ductile, fatigue limit during bending, inelastic strain effects 77−44355
ductile fracture of austenitic-martensitic 0Kh15N5M 78−3226
eddy current testing of welds, cladding and cast materials *(German)* 78−44293
electron beam welded, Charpy test expts. *(Hungarian)* 80−104252
electron irradiated type FV548, influence of pre-injected He on void nucleation and growth 80−34054
emissivity, integrated normal with low heat conductivity coeffs. of type Kh23N18 80−103504
eutectoid decomposition, effect of liquation of alloying elements *(Russian)* 78−19708
explosive-thermal treatment, sulphide cracking decrease, hydrogen embrittlement *(Russian)* 80−108477
fatigue, scale effect, structural parameter effect in rotary bending *(French)* 78−23822
fatigue after plastic deform. sequences *(French)* 79−20131
fatigue crack development at normal and low temps., struct. effects *(Russian)* 78−35480
fatigue in hot water 77−4871
fatigue life diagrams plotting of type VNS-2 79−70246
ferritic, fatigue, effect of struct. and work hardening rate *(French)* 77−63783
ferritic weld metal, austenitising and ferritising effects of elements 79−87614
ferritic welded transition joint, type 316, thermal fatigue life *(Japanese)* 79−83307
fission reactor component reliability, non-destructive testing and flaw evaluation *(French)* 79−24711
fracture state in creep *(Czech)* 80−30081
fracture toughness, tempering effects in 30 KhGSA 77−90463
fracture toughness meas. by Charpy impact testing, welding, heat treatment, neutron irrad. effects 79−5062
fracture toughness props. of A533B, prior austenite grain size effect 78−60780
friction in vacuum of type U8 steel under microshock loading *(Russian)* 80−108583
fusion material, continuous gas generation effects in neutron and simulation environments 80−34068
fusion reactor first wall materials, surface resist. 80−42853
gas implantation effects to simulate fusion reactor first wall damage 80−29079
grain boundary sliding, creep strain and stress depend. 77−25109
grain boundary sliding, exam. by tensile creep tests 78−76715
grain boundary sliding, grain size depend. 77−25108
grain boundary sliding, temp. depend. 77−25110
grain formation in structural recrystallisation 77−55990
grain growth, melting procedure effects 77−12650
grain growth in 16G2S, 16G2SF, and 09G2SF, As effect 77−70060
grain size before quenching rel. to mech. props. of type 30KhGSA 79−24553
grain size eval. technique 80−25933
grain size meas. of austenitic thin gauge plates by US backscattering *(German)* 79−91878
grain size rating methods, comparison 78−85074
Hadfield, cast and crystallised, deform. resist. of grain boundaries *(Russian)* 77−21216
Hadfield, containing Ni, carbide precipitation, heat and cold work effects *(Korean)* 77−77484
Hadfield, Mossbauer spectra meas., 25-250°C *(Russian)* 77−51994
Hadfield steel, hollow cathode sputtering 78−11433
hardened by thermomechanical treatment with ageing, influence of stabilisation on mech. props. *(Russian)* 77−52356
hardening, effect of quenching and ageing temps. *(Russian)* 77−81267
heat resistant, mag. permeability increase, measurement method 78−53039
heat resistant, zig-zag grain boundaries strength 77−73308
heat resistant Kh15N24VChT, microscopic intergranular crack form. prediction in high temp. deform. 77−81325
heat resisting, creep rupture props., effect of grain- and grain boundary-strengths 80−97573
heat treatment, preliminary, cold deform., elec. heating rel. to mech. props. of type 30KhGSA 79−24554
high alloyed, low C, polarization resistance meas. in boiling HNO_3 80−16557
high C, 80Kh5G5 and 120N12, austenite hot deform. effect on martensitic transform. *(Russian)* 77−48434
high Mn, abrasive wear resistance *(Korean)* 77−25162
high speed, supercooled, austenite decomposition kinetics 78−92233
high speed, tempered, etching reagents for austenite grain boundaries 78−80704
high strength, treatment effect on ductility and strength 80−60880
high strength X 3 CrNiMoNbN 2317, Bauschinger effect and creep at room temp., effect of heat treatment *(German)* 77−36543
high-alloy die steel, heat resistance and crushing strength, low-temp. thermomech. treatment effects 77−52372

austenitic steel continued
high-Si corrosion-resistant steel, 02Kh8N20S6, mech. props. and heat treatment 77−56003
high-speed, austenite grain growth, W addition effects 79−20085
high-temperature materials, technological requirements, R and D, report 80−45222
hot deformation influence on phase transformations 80−7606
hot isostatically pressed superalloy A286, fracture path 78−23824
hot rolling, microalloyed with V and N 77−52364
hot-worked, formation of high-C martensite, struct. *(Russian)* 78−6950
hot-worked, kinetics of austenite grain growth, rel. to deformation degree, for steel 18H2N4WA *(Polish)* 80−45322
hot-worked, struct., post-deform. ht. treatment effects *(Russian)* 77−8859
hot-worked, subgrain struct., X-ray diffr. and electron microscope obs. *(Russian)* 79−15698
hydrogen embrittlement behavior of unirrad. steels for nuclear reactor press. vessels 79−8340
hydrogenation, different stability characts. 78−35383
hypereutectoid steels, 120G4 and U15 type, with initially pearlitic struct., mechanism of structural inheritance *(Russian)* 77−52329
Inconel 718 cladding possibility for gas-cooled fast breeder reactor fuel 77−18667
intercrystalline corrosion, N_2, C and Cr effects 79−83374
intergranular defectiveness determ. using inductive instruments 78−53075
intermittent loading effect on creep *(Japanese)* 79−29147
internal stress meas. and anelasticity in creep *(Czech)* 79−38909
lattice, X-ray diffr. study in KL12M and 40G5 near martensitic-transform. *(Russian)* 79−1868
lattice stability loss near $\gamma \rightarrow \alpha$ and $\gamma \rightleftarrows \varepsilon$ transitions *(Russian)* 79−61584
law-C, hot deform., austenite strengthening and weakening 80−76282
LMFBR steam generators, mass transfer props., test *(Japanese)* 77−348
low C, struct. charact. of dynamic recrystallisation *(Czech)* 77−59813
low cycle fatigue in 30KhGSA high strength steel 79−87724
low-alloy, case carburised, retained austenite effect on contact fatigue strength 80−30096
martensite formation and reversion, effect on void swelling, on type En58B 80−11641
martensite formation and reversion, effect on void swelling on type M316 80−11641
martensite lattice struct. obtained by deform. of steel 70Kh5G4 *(Russian)* 78−88464
martensite transformation mechanism, position of C atoms in cryst. lattice *(Russian)* 77−8820
martensitic transform., alternating elastic stressing effects 77−86029
martensitic transform., mechanism and kinetics, TEM, X-ray and optical obs. *(Rumanian)* 78−19746
martensitic transform. at crack tip 77−70051
martensitic transform. at propagating fatigue crack 78−19745
martensitic transform. during low temp. alternating torsion *(Russian)* 78−23706
martensitic transform. temp., singularities in 50Kh2N22 *(Russian)* 78−68689
mechanical instability in premartensitic state *(Russian)* 77−73273
mechanical properties, −196 to +250°C, and kinetics of phase transforms., for steel 0Kh14AG12M *(Russian)* 78−92297
mechanical properties, effect of high temp. thermomechanical treatment and post-deform. ageing *(Russian)* 78−39809
mechanical props. of DIN X8 CRNIMONB 1616 and DIN X2 CRNI 189, FBR safety anal. 78−60966
mechanical strength, effect of mech. and heat treatment 77−12659
metastable, 0Kh14AG12M, Cr-Mn and Cr-Mn-Ni, phase transform. kinetic effect on mech. props. *(Russian)* 79−34024
metastable, fatigue, effect of deformation-induced martensitic transformation *(Japanese)* 78−15514
metastable, fatigue testing machine and fatigue strength temp. dependence *(Japanese)* 80−71842
metastable, hardening by cycling of martesitic transform. during rapid heating, in 30N24M4 and 50N21M3 *(Russian)* 79−20074
metastable, microneckíng deform. in tension, singularities *(Russian)* 80−30017
metastable, resistance to failure 77−4852
metastable formation of martensite under load, effect on mech. props. *(Russian)* 77−86026
microdefect accumulation during creep, effects of heat treatment, hardening 79−24550
Mn-Cr-Ni-N, N effect on relaxation behaviour, internal friction temp. depend. *(Russian)* 78−52872
neutron irradiated, He absorption 77−51414
neutron irradiation, effect on intercrystallite corrosion 78−688
neutron irradiation induced embrittlement, review 79−65120
neutron irradiation of BOR-60 reactor shim-rod sockets, Kh18N9 steel 79−46716
neutron-irradiated weld toughness rel. to ferrite content 79−83327
nitrided, creep, effect of N_2 and Ti and prior deform. 78−23789
nitrided layer depth meas. by eddy current instrument 79−34242
nitriding and nitride composition, Ti addition effects 79−20278
non-oxidising B and by secondary ion emission and X-ray microanal. *(French)* 80−11985
overheated, ESR, low alloy, fatigue crack growth rate 79−34141
oxidation of structural steels in gas-cooled reactors 80−45447
paraprocess magnetostriction near martensitic point in mag. field for steel 40Kh2N20 *(Russian)* 79−82850
pearlite transform. kinetics, effect of US deform. *(Russian)* 77−21136
pearlitic, weld, US testing, frequency and beam angle choice 78−60950
pearlitic and bainitic transformations in austenite, processes during incubation period 80−40348
pearlitic and bainitic transforms., effect of austenitisation conditions *(Russian)* 79−38820
pearlitic transformation incubation effect, Mossbauer spectra *(Russian)* 79−70061
phase composition of Kh 14N16 with Zr, Ti, Nb and N additions after quenching and tempering 77−90378
phase transform to pearlite and martensite, kinetics, stresses due to quenching, anal. *(Japanese)* 78−27508
pipe, ultrasonic testing of grain size 78−44313
plastic deformation influence on internal friction, relaxation processes *(Russian)* 80−100870

austenitic steel continued

- porous fibres, oriented struct., strength props. 78−3199
- post deformation holding at deform. temp. effect on struct. and strength of austenite and martensite, in 45Kh2N12GS *(Russian)* 79−1880
- precipitation behaviour under high temp. conditions, photoemission electron microscope obs. 80−108456
- precipitation hardenable, friction and wear under abrasive conditions *(German)* 77−59951
- precipitation hardened, ductility of grain boundaries and crack propag. *(German)* 78−52834
- precipitation hardened Kh15N27T3MR, exam. of elasticity props. 78−56687
- precipitation hardening, effect on fatigue strength 78−84829
- precipitation hardening by VC in 37Kh12N8G8MFT, hardness meas. and electron microscope exam. *(Russian)* 79−38843
- precipitation of spherical misfitting VN$_x$ particles along dislocations, diffr. contrast 77−16595
- precipitation strengthened, Cr-Ni, anomalous stress-depend. of creep rate 80−11712
- preliminary strengthening inheritance in 110G13L, strength testing and microstruct. anal. 78−44137
- pressure vessel, fatigue design criteria 78−60758
- proof stress meas. in N28G1.5, by internal friction 78−56638
- quenched, adsorption of P on austenite grain boundaries rel. to tendency to delayed fracture of type 18Kh2N4VA *(Russian)* 80−45378
- quenched state, impact strength, influence of austenite stability *(Russian)* 80−81146
- quenching, press. effect, distrib. of temp. fields analysis 79−38860
- radiation damage, γ and neutron irradiation, Mossbauer spectra anal. 78−692
- recrystallisation diagrams, heating, plastic deform. rel. to struct. 79−20067
- relaxation processes, alloyed with N, model *(Russian)* 79−11650
- rod, coupled flexural and torsional vibrs., energy dissipation 80−89281
- rupture of steel Kh17N13M3T, activation characts., microalloying effects *(Russian)* 79−5033
- self diffusion of Fe, Cr and Ni *(Czech)* 80−107464
- sheet deformation, criteria for determ. of deformation limit G *(German)* 80−21000
- solid solution decomposition at defects, TEM meas. 77−12656
- stabilisation of austenite during $\alpha\rightleftarrows\gamma$ transition *(Russian)* 78−44117
- stacking fault energy of austenite, high resolution electron microscopy *(Russian)* 80−44219
- steel, austenitic, age-hardening kinetics, study by resistivity, Young's modulus and internal friction *(Czech)* 80−29970
- steel, austenitic, ageing and plastic deform. effect on struct. and mech. props. of N15Kh5G3T3 *(Russian)* 80−71691
- steel, austenitic, intercrystn. corrosion and mech. props., inflence of Cr, N and Nb *(German)* 80−50747
- steel, austenitic, types A533B and A508, acoustic emission and deformation processes during tensile tests 79−74212
- steel, ferritic and austenitic, microstruct. study by means of replicas taken from components at 100°C 80−81256
- steel, stainless, LWR appl., US and AE testing of welds 79−36330
- steel alloyed with carbide formers, retained austenite determ. 80−20551
- strength, ductility and fracture toughness, N and Cr effects 80−100878
- stress, variation coeffs., at low temps. 80−16402
- stress intensity factor, reliability of values 80−55530
- structural, austenite decomposition, 500 to 450°C 77−16593
- structural steel, microstruct. and brittleness, rel. to austenizing and heat treatments 77−56091
- structural steel, quenched and tempered, effect of bainitic decomp. products on mech. props. 77−56007
- structure and loss of strength after hot deform. by rolling *(Russian)* 78−39794
- structure steels 4Kh4VMFSSh and 45Kh3V3MFSSh, grain size, hot deform. and austenitising effects 80−76286
- submicroscopic structure of Kh12N20T3R, and role in dispersion hardening *(Russian)* 78−64549
- substructure change in hot deform. process *(Russian)* 77−16617
- supercooled, decomposition by heat treatment, carbide particle morphology *(Russian)* 77−70076
- supercooled, sintered at various temps., isothermal decomposition 77−12617
- supercooled, transformation kinetics into spheroidised pearlite *(Russian)* 78−95742
- supercooled ShKh15, stability, effect of spheroidising carbides *(Russian)* 77−25074
- surface, He blistering at high irradiation doses 79−51167
- surface hardening, mechanism 78−85048
- tempering cavity condensation *(French)* 80−55442
- tensile props. after corrosion by UO_{2+x} and fission products *(German)* 77−70216
- tensile strength, elec. current impulse effect down to 4.2K 80−81131
- tension tests in high speed gaseous streams 77−63761
- thermal expansion, of heavily doped steels and alloys 80−103501
- thermodynamic props. of C in austenite, relationship with cryst. lattice anomalies of martensite *(Russian)* 78−59781
- thermomechanical treatment, high temp., effect of austenite deform. on martensite stability during low temp. tempering 80Kh5 79−57018
- thermonuclear reactor walls, ferromagnetic layer form. magneto-optical testing method 80−35465
- tool, thermal treatment effect on abrasive wear resistance 78−92369
- toughness evaluation inconsistency of AISI 4340 austenitised at increasing temp. 78−52982
- transform. kinetics of supercooled austenite in 12Kh1MF, structural method 78−52801
- transform. kinetics rel. to temp., deform., struct., mech. props. 79−24519
- transformation kinetics and structure of 17G1S type, under influence of deform. *(Russian)* 79−70060
- transformation temp. and crack prevention in weld cooling 79−83200
- tubing, heavy walled, US inspection 79−39107
- type 316, neutron irradiation induced embrittlement, review 79−65120
- type FV548, Ni and Si rich phase, energy dispersive X-ray anal. of precipitates 79−66063
- type Kh15N15M, high content of low melting additives, high temp. neutron irradiation embrittlement *(Russian)* 79−73218
- type Kh18N9, high content of low melting additives, high temp. neutron irradiation embrittlement *(Russian)* 79−73218
- ultrasonic testing of austenitic collars in a computer controlled immersion test-plant *(German)* 79−96256

austenitic steel continued

- US absorpt. at large strain amplitudes 80−19192
- US test equipment and practice *(German)* 79−74316
- US testing, optimum freq. *(German)* 80−30195
- void swelling, role of bulk point-defect recombination, calcs. for type 316 79−42105
- weld, morphology, effect of ferrite content 77−36521
- weld, with natural flaws, US test techniques *(German)* 78−27713
- weld joints and surface claddings, eddy current testing *(German)* 77−1895
- weld testing review *(German)* 78−53068
- white phases structure after heat treatment, steel 30KhGSA 80−76281
- wire rod, austenite transform. kinetics accompanying interrupted cyclic cooling *(Russian)* 79−70064
- X-ray elasticity constants *(German)* 80−30004
- yield point, temp. depend. anomaly for steel OKh18N10T, subjected to low temp. thermal cycling *(Russian)* 78−48489
- yield point temperature depend. of alloys undergoing martensitic transform. during deform. *(Russian)* 77−66677
- Al-C, microstruct., Mossbauer obs. *(Russian)* 80−29655
- C and low-alloy steel inherent austenitic grain size determ., exam. of methods used 78−85071
- C diffusivity, computer simulation 79−77803
- C-Mn-V-Al-N, fine grained steel, relationship between ferrite and austenite grain size 80−3001
- Cr (2%), austenite decomp., phase diagrams and struct. form. kinetics 80−76223
- Cr, deform. on decomp. of austenite, carbide precipitation 80−84938
- Cr, mech. props, carbide phase struct. 79−15702
- Cr, post-hotforming recrystallisation condition, use of NEOPHOT 2 and EPIQUANT 80−84949
- Cr with metastable austenite, wear resist., temp. effect 80−76370
- Cr-Mn, effect of composition, plastic deformation, and heat treatment on martensitic transformation 79−100141
- Cr-Mn, Kh4G18F, microstruct. and mech. props. during tensile deform. *(Russian)* 79−20114
- Cr-Mn, $M_{23}C_6$ carbide precipitates comp., heat and thermomech. treatment influence *(Russian)* 80−40361
- Cr-Mn, martensitic transform. effect on hardening kinetics and fracture resist. of friction surface of type 45Kh12G8 *(Russian)* 80−50727
- Cr-Mn, metastable, plasticity, contrib. of martensitic transform. during deform. *(Russian)* 80−30018
- Cr-Mn, N_2-alloyed, Me_2N separation estimation, X-ray microanalysis of electron microscope extraction replicas *(Bulgarian)* 78−40012
- Cr-Mn steel, X-ray diffr. exam. of fine struct. during deform. *(Russian)* 78−38661
- Cr-Mn type, optimum rate of martensite transform. during loading *(Russian)* 77−16579
- Cr-Mn-B-N, phase composition and struct. transformations 80−104171
- Cr-Mo-V low-alloy, prior austenite grain boundary embrittlement by B 80−66657
- Cr-Mo-V rotor steel, austenite to bainite transformation under cooling conditions, effect on creep 80−3033
- Cr-Mo-W, splat quenched, formation of metastable austenite 80−84974
- Cr-Mo-(V), creep resist., high-temp. props. residuals effect 80−66600
- Cr-Ni, bulk and intergranular autodiffusion of ^{59}Fe *(French)* 79−55921
- Cr-Ni, intergranular damage parameters in creep *(Czech)* 80−89342
- Cr-Ni, ion-implanted N, chem. state study by AES and XPS 80−79825
- Cr-Ni, microstructural distrib. of cathodic H_2, autoradiography *(French)* 79−99234
- Cr-Ni, nonmetallic inclusions modification using rare earth metals *(Russian)* 80−40369
- Cr-Ni, SCC and pits in $MgCl_2$ solns. at 40-90°C 80−50748
- Cr-Ni, type 304, temper embrittlement and surface segregation an AES and ionization loss spectroscopy study 79−43372
- Cr-Ni, X5CrNiTi26.6, ferrite-austenitic struct., optical and electron microscopy 78−84848
- Cr-Ni (18, 11 wt.%), creep rupture *(German)* 78−11297
- Cr-Ni (18,12 wt.%), containing coarse grain boundary precipitates, thermomechanical treatment 78−27545
- Cr-Ni (18%, 12(8)%), martensite formation and reversion, effect on void swelling 80−11641
- Cr-Ni (20, 25 wt.%), containing B and Ti additions, splat quenching, X-ray and TEM study 79−74186
- Cr-Ni (25, 20 wt.%), recrystallisation and sigma phase formation 80−35211
- Cr-Ni (32.8 wt.%), tensile props. and fracture of two phase Fe alloy austenite and ferrite *(Japanese)* 79−8344
- Cr-Ni alloyed, Ti stabilised, corrosion props., nuclear reactor pipeline appl. *(Hungarian)* 77−18658
- Cr-Ni steel, austenitic, effect of Si on carburising mechanism at 930°C 77−56155
- Cr-Ni steel, carburised, effect of atm. during heating to quenching temp. on austenite decomp. 77−56157
- Cr-Ni-Be, cellular precipitation *(Japanese)* 78−11229
- Cr-Ni-Cu (14, 5, 2 wt.%), phase transform. and props., preliminary heat treatment effect 79−79011
- Cr-Ni-Mn-V, X-ray anal. of carbide phases formed during ageing *(Russian)* 80−20936
- Cr-Ni-Mo, for boiler tubes, austenisation conditions effect obs., on structure and mechanical props. 80−3151
- Cr-Ni-Mo-V, quenched, morphology, structural constitution after austenite form. by heating *(Russian)* 78−68709
- Cr-Ni-Ti, X5CrNiTi18.10, corrosion in HNO_3 *(German)* 78−44253
- Cr-Ni-Ti (08KH18N10T), heat treatment for fission reactor appls. 80−66454
- Cr-Ni-(Mo) (25, 28, 2 wt.%), lattice dilation by N_2 77−16592
- CrNi, high Mo, corrosion, effect of struct. *(German)* 77−90481
- Fe-C, determ. using high temp. vacuum metallography *(Russian)* 77−15677
- Fe-C alloys, thermodynamics of proeutectoid ferrite transform. re-exam. 78−84763
- Fe-C-Al, low of variation of cryst. lattice parameters X-ray diffr. analysis *(Russian)* 77−52322
- Fe-C(0.47 wt.%) austenite, obs. of morphology and crystallography of proeutectoid ferrite 77−8837
- Fe-Cr-Ni (17.20, 7.34 wt.%), transform.-induced plasticity 78−23774
- $\alpha+\gamma$Fe-Cr-Ni alloy, stress-induced α'-martensite occurrence 78−23704
- Fe-Cr-Ni-Nb-C, austenitic, splat quenching 78−72798
- Fe-Mn-C, Mossbauer spectra interpretation allowing for at. interaction in lattice *(Russian)* 77−69738

austenitic steel continued
Fe-Mn-C austenitic steel, deform. twinning and mech. props. 77—59868
Fe-Mn-Cr-V-C, carbide strain hardened, strength and plasticity, effect of Mn content *(Russian)* 80—97500
Fe-Mn-V-C, carbide strain hardened, strength and plasticity, effect of Mn content *(Russian)* 80—97500
Fe-Mn-V-C austenitic steel, discontinuous precipitation, morphological changes 80—3078
Fe-Mn-V-C type, ageing characts., discontinuous precip. nature 80—84940
Fe-Ni, inverted casting process for very rapid growth of large crystals 78—84791
Fe-Ni-C, inverted casting process for very rapid growth of large crystals 78—84791
Fe-Ni-C (24, 0.5 wt.%), recovery and recrystallisation of stable austenite after hot rolling *(German)* 77—32591
Fe-Ni-Cr austenitic steel, martensitic transform. kinetics, metastability criterion *(French)* 78—68690
Fe-Ni-Ti, inverted casting process for very rapid growth of large crystals 78—84791
Mn (high), creep rupture, p addition and two-step soln. heat treatment effects *(Korean)* 80—93646
Mn alloy, martensitic transform. effect on hardening kinetics and fracture resist. of friction surface of type 110G13 *(Russian)* 80—50727
Mn, existence of carbide M_5C_2 phase, electron microdiffr. analysis *(Russian)* 78—23727
Mn strain hardening at room and low temps. *(German)* 79—38845
Mn-Al, low temp. appl. explosion test of fracture mode *(Chinese)* 78—31496
Mn-Al-V, NDT of nitrided layer depth 79—11750
Mn-base, for LNG storage and transportation systems, tensile and yield strength 79—70133
Mn-Cr, austenitic and austenitic-ferritic, stress corrosion cracking resist. *(Czech)* 80—45437
Mn-Cr, austenitic struct. stability and low-temp. toughness *(Japanese)* 80—76356
Mn-Cr-C(20, 4, 0.5 wt.%), intrinsic stacking fault energy, temperature variation 77—31679
Mn-Ni ageing, alloying element influence on struct. and mechanical props. *(Russian)* 80—35256
Mn-Ni-Cr-C, supercooled, influence of constant mag. field on diffusional decomp. *(Russian)* 79—4964
Mn-V-C, discontinuous precipitation, grain boundary struct. effect 79—29068
N alloyed, internal friction relaxation model *(Bulgarian)* 78—19806
Nb modified, HSLA, interaction between recrystallisation and precipitation during high temp. determ. 79—100187
Ni (17 wt.%), martensitic deform. temp., cryst. struct. effect *(Russian)* 80—66576
Ni, N22, X-ray diffr. study of austenite lattice near martensitic transform. *(Russian)* 79—1868
Ni, struct. change of hot-worked austenite during post-deform. holding 80—35228
Ni-Cr, corrosion tests with stray currents after manufacturing operation and welding *(German)* 77—86274
Ni-Cr, intergranular segregation of P 78—84761
Ni-Cr, microstruct. effects in low-cycle fatigue tests 77—56108
Ni-Cr, neutron-irradiated solute segregation and void swelling 79—60407
Ni-Cr, precipitation strengthened, anelasticity, plastic creep limit, 823K 79—1899
Ni-Cr-Fe base, radiation enhanced precip. and dissolution of precipitates, point defect kinetics and dislocation obs. 80—108467
Ni-Cr-Mo, (En 24) deform. effect on decomp. of austenite, carbide precipitation 80—84938
Ni-Ti, alloy N35T5, ageing, magnetisation and Curie temp. depend. on plastic deform., Mossbauer studies *(Russian)* 79—69669
Ni-Ti, high-alloy, precipitation hardening, fatigue strength 79—79103
V, deform. effect on decomp. of austenite, carbide precipitation 80—84938

autoionisation
see also Auger effect
acetylene, ionis. efficiency curves by electron impact, $CH_2^+(C_2H^+)$ form., $\sim$10 eV 78—62935
adsorbed layers, autoionisation bands due to one-centre resonances, theory 80—59790
alkali anions, autodetaching sub $^2P_{1/2}$ threshold states 79—22611
alkali atoms, electron impact excitation of autoionis. states 79—54971
alkali metal atom, autoionising levels excitation by electron impact 77—19085
alkaline earth atom, electron impact double electron excitation and autoionisation calcs. 77—68121
alkaline earth metals doubly excited, autoionising states and interference profiles 80—52949
all-metal autoionisation microscope construction and equipment 79—67433
atom, autoionis. transitions excited in atom+ion (electron) collisions 77—42390
atom, collisionally excited, electron ang. distrib. from autoionising states 80—43007
atom, electron excitation of autoionisation states near threshold, post-collision interactions *(Russian)* 77—68125
atom, electron spectra interference struct., for intersecting terms of collisions *(Russian)* 78—1070
atom, Rydberg autoionising states, props. in elec. fields, appl. to Fe^{23+} dielectronic recomb. 79—59405
atom, Rydberg formula, modified 77—26957
atom, Schumann region absorpt. spectrum, oscill. strengths, line profiles, collisional and autoionis. broadening 77—18818
atom, two-step autoionis., double photoionis. 77—50415
atom+charged particle, autoionisation state decay 80—9565
atomic autionisation, astronomically oriented bibliography 78—32340
atomic collisions, fast particle electron emission, line shape, acceptance function effects 80—37787
atomic density of states involved in autoionising resonances 77—18857
atomic excited state decay, radiative-emission autoionisation interference, fluoresc. yield 79—26945
atomic K- and L-shell shakeoff probability, following β-decay, hydrogenic wave function 78—94204
atomic photoionisation anal. using relativistic random phase approximation and multichannel quantum defect theory 80—63602

autoionisation continued
atomic states, autoionising, electron impact ionisation obs., distortion effects calcs. 80—83491
atomic systems, many-electron autoionisation states, transition probability and autoionisation rate, perturbation theory Z-expansion 80—52863
atomic systems, many-electron autoionising states, Z-expansion energy calcs. 80—909
atoms, autoionising resonances, vac. UV nonlinear optical props. 77—50565
atoms, ejected electron spectra, displaced thresholds 78—5349
atoms, excited, collisionally aligned, angular correl. of autoionisation electrons, photons 77—14385
atoms, four-wave parametric process, resonant enhancement study 77—41697
atoms, Rydberg states, autoionisation with large orbital angular momentum 80—87052
atoms and molecules, review of autoionisation processes and expt. methods 78—29763
autoionising states, mean-square deviation formula derivation 77—57943
azulene, multiphoton ionisation, mass spectra 80—63717
complex ion-electron recomb. models, autoionisation states *(Russian)* 77—46638
decay state interactions, autoionisation bands *(Russian)* 80—75486
dielectronic recombination and ionisation equilib., influence of autoionisation and excitation 77—15160
electron correlation effects, two electron autoionising resonances 79—89648
electrons from autoionising states, angular distribution, fine and hyperfine struct. 80—58222
energy levels and widths, bounds, autoionising states of atoms 78—21885
ESCA, principles and appls. 78—27375
ethylene, autoionisation and photoemitted electron ang. distrib., cylindrical mirror analyser study 80—18049
excited atom thermal energy collisions, electron spectrometric studies 80—63788
fast projectile electron loss forward peak oscill. struct. as autoionisation 80—69227
fast projectile electron spectroscopy, autoionizing ion levels and lifetimes 77—38749
group VI atoms, $(np)^4$ $^1S_0$-level photoionisation via autoionising levels 79—76398
heavy particle collisions, electron spectroscopy 77—42397
high angular momentum Rydberg states, autoionisation rates calcs 79—81163
impurity photoconductivity and autoionisation calc. 80—44648
inert gases, inner-shell optical photon excitation, Auger, autoionisation, photoionisation processes 77—18867
ion+electron collision, resonant electron bremsstrahlung *(Russian)* 80—102580
ions, H-, He-like, Z=4 to 34, wavelengths, radiative transition probabilities, autoionisation rates 79—25776
ions in low density plasma, dielectronic recomb., ionization equilib. and radiative energy loss, solar corona appl. 79—68903
labile species, electron photoejection, reaction kinetics characterisation 80—26089
lanthanides, Rydberg spectra and ionisation thresholds, time resolved resonant multistep technique 78—82701
metal vapour, electron impact, ionis. and autoionis. 78—58830
metal vapour, excited by electron impact, ejected-electron spectra from autoionising levels 80—37893
metal vapours, at. inner-shell optical photon excitations, Auger, autoionisation, photoionisation processes 77—18867
metastable autoionised state decay of multicharged Li-like ions *(Russian)* 78—25455
metastable autoionising states, ang. distrib. of electrons which decay via fine and hyperfine struct. interactions 80—102492
methane and methane-d_4, low energy electron impact dissoc. autoionisation 80—9744
molecular, resonant, vibr.-excited ions form. in Franck-Condon gaps, threshold photoelectron spectra obs. 79—68262
molecular dissociative recombination, repulsive term, states of products 77—65537
molecular electron impact, autoionising states 78—58852
molecular photoionisation mass spectroscopy, reson. peak shapes 80—42295
molecule, electron impact, K-shell electrons excitation with high energy resolution, review 80—37899
molecules, autoionising resonances, vac. UV nonlinear optical props. 77—50565
multiply charged ion+atom, autoionisation, electron and photon emission 80—63813
multiply charged ions, X-ray spectroscopy 77—31434
naphthalene, multiphoton ionisation, mass spectra 80—63717
negative ion+neutral atom, autoionisation states investigation by Rydberg series broadening and displacement *(German)* 79—85938
nonexponential decay from autoionising states, possibility of obs. 77—42288
nonlinear polarisation resonances in a continuum, optical activity, spin-orbit interactions *(Russian)* 80—53391
$np^6(n+1)s^2$ state, atomic resonant autoionisation, photoelectron spectra 77—18980
parity violating neutral currents in two-photon and autoionisation atomic transitions 80—32034
plasma, attenuation of autoionis. lines, function of electron density 78—18387
plasma, low-density, autoionisation contrib. to total ionisation rates 80—9738
plasma, multiply charged ions, collisional dielectronic recomb. rate, effect on level populations 79—1287
plasma dielectronic satellite spectra, electron collisions, corona model theory 80—59188
post-collisionally Stark mixed states, autoionisation electron energy and ang. distrib. 80—18829
propylene, electron impact ionisation and dissoc. 80—37894
quasimolecule, autoionisation states decay 79—64058
quasimolecules, electron spectra on autoionisation *(Russian)* 77—79690
rate coeffs. for quadruply and quintuply ionised atoms, solar corona appl. 78—74619
relativistic multichannel RPA, appls. 80—47925
Siegert eigenvalues for autoionising electronic states 79—10075
Siegert wavefunctions, partial widths calcs. 80—5507

autoionisation continued
SIMS, secondary ion emission mechanism, autoionis. process model *(Japanese)* 79–26177
slow ion+atom collisions, coherent excitation and decay of autoionising states 79–45789
solar coronal ions, autoionisation rate coeffs. 78–17623
strong field QED in atomic phys., Dirac eqn., autoionisation model, QFT 77–54495
three-electrode autoionisation gun of ion field source for MKh1303 mass spectrometer 77–38055
three-electron atom systems with two vacancies in K-shell excited states and autoionis. state energies *(Russian)* 79–31429
three-electron atomic systems, autoionising states decay calcs. 78–78670
three-electron systems, autoionis. state widths *(Russian)* 79–49993
transition probabilities in sudden vacancy formation in electron shell 80–37788
two electron systems, coupling schemes, transition energies and probabilities of autoionising states 80–18828
two step reson. photoionisation, multimode and level degeneracy effects 80–78583
two-electron atom, dipole approx. for electron-electron interaction, autoionisation widths *(Russian)* 77–61691
two-electron atoms, autoionisable states decay, parity violation effects 79–72231
two-electron atoms, S autoionising states, at. reson. theory appl. 80–23329
two-electron doubly excited systems, truncated diagonalisation method 77–23476
two-electron ions, autoionisable states decay, parity violation effects 79–72231
Ag, polarised photoelectron yields in VUV region 80–106307
Ag, VUV absorption spectrum, autoionised level Fano parameters, photoionis. 79–49973
Al, autoionisation reson. determ. from photoelectron polarisation meas. 80–58221
Al I, 1932 and 1936 Å autoionisation lines in solar flare, Skylab obs. 80–26829
Al IV, autoionising transitions $ns^2np^6-nsnp^6mp$ 77–88419
Ar, $(3s^{-1}4p\,^1P)$ autoionising state decay, triple differential cross section 78–86831
Ar, absorpt. spectra, field induced autoionisation near ionisation threshold 80–106301
Ar, autoionising levels excited by heavy ion impact 79–13804
Ar, autoionising states excitation by electron impact, threshold effects 78–62923
Ar, collision processes, photoionisation mass spectra obs. 79–31479
Ar, electron impact autoionisation, cross-section parametrisation 77–6932
Ar, spin-polarised photoelectrons by circularly polarised synchrotron radiation 80–91516
$Ar+Ar(Ar^+)$ collisions, multielectron excitation energy calcs. 78–1071
$Ar+C^{2+}(O^{4+})(Si^{n+})$, n=10,11,12, intense low energy autoionisation lines 79–31674
Ar_2, photoionisation 77–54578
Au, VUV absorption spectrum, photoionis. cross section, Fano parameters 79–93947
B^+ ions, beam foil excitation, L-Auger decays, autoionisation 77–14569
B^{2+}, ^2S, $^2P^0$ and ^2D autoionising states, positions and widths 79–26944
B-like ions, autoionisation states calcs. 80–43006
B^++methane, single collision, time delayed autoionisation spectra 78–1067
Ba, $(6p_J20s_{1/2})_J$ state, autoionisation, ejected electron energy anal. 80–43009
Ba, autoionis. spectrum, pair splittings 79–13684
Ba, autoionisation and Auger decay, collective excitation effect 80–43008
Ba, electron spectra of autoionisation states, electron-atom collisions *(Russian)* 78–1085
Ba, even-parity autoionising levels, multiphoton ionisation spectroscopy 79–59417
Ba I, absorption spectrum, 1560 to 1770 Å 78–66487
Ba I, two-step autoionisation 80–91513
Ba, photoexcitation spectrum, discrete autoionising states interferences 80–5508
Ba, radiative decay of autoionisation states *(Ukrainian)* 78–82682
Ba, two-step autoionis., double ionis. anomaly 79–22671
Be I like ions, resonant-scatt. contributions to excitation rates 80–58393
Be II, autoionising core-excited states, alignment prod., Be^++He(methane) collision excitation 80–14204
Be^-, $^2P^0$ shape resonance, complex-coord. method calc. 78–74591
Be^+, ^2S, $^2P^0$ and ^2D autoionising states, positions and widths 79–26944
Be^+ ions, beam-foil excitation, L-Auger decays, autoionisation 77–14569
Be^++methane, single collision, time delayed autoionisation spectra 78–1067
$^{210}Bi\rightarrow{}^{210}Po\rightarrow{}^{206}Pb$, L-shell auto -ionisation 77–6739
C III, IV, V Auger lines obs., beam-foil excitation, ab initio calcs. 77–54601
C^+, electron impact ionisation cross sections, autoionisation contrib. at low temp. 80–32838
C^+ ions, beam-foil excitation, L-Auger decays, autoionisation 77–14569
C^{3+}, ^2S, $^2P^0$ and ^2D autoionising states, positions and widths 79–26944
C^{3+}, cross section measurement, contribution due to excitation-autoionisation 79–45850
CO, dissociative ionisation 77–54616
CO, ejected electron spectroscopy of autoionising states using electron-electron coincidence technique 79–3587
CO, electron impact, reson. vibr. excitation calcs. 77–14595
CO, photoelectron ang. distributions, wavelength and vibr. state depend., reson. effects, asymmetry parameters 80–91602
CO, photoelectron spectra ang. distrib., vibr. transitions, autoionis. state 79–31609
CO, $X^2\Sigma^+$, vibr. levels, UPS electron attachment obs. 80–95683
CO_2, high resolution UV photoelectron spectra 80–91603
CO_2, threshold photoelectron and photoionisation spectra 77–14491
COS, high resolution UV photoelectron spectra 80–91603
CS_2, electronic autoionisation branching 80–91614
CS_2, high resolution UV photoelectron spectra 80–91603
CS_2^+, and $(CS_2)_2^+$, photoionis. in supersonic mol. beam 79–98165
CSe_2, photoionis. mass spectrum, Rydberg state props. 77–46604

autoionisation continued
Ca, electron impact ionis., ejected electron spectrum from autoionis. levels 78–33613
Ca I absorption spectrum, 1430-1340 Å 80–47930
Ca II, electron impact excitation, identification of low energy autoionising levels 79–31703
Ca III, autoionising transitions $ns^2np^6-nsnp^6mp$ 77–88419
Ca, radiative decay of autoionisation states *(Ukrainian)* 78–82682
Cd, $4d^{-1}5p\,^1P$ autoionising state, electron impact ionisation obs., distortion effects calcs. 80–83491
Cd, 5^3P_1 autoionising state, 150 eV electron impact excitation, (e, 2e) ang. distrib. study 80–83495
Cd, electron impact, ejected electron spectrum of autoionis. levels 77–27185
Cd electron impact ionisation, of autoionising levels, ejected electron spectrum 78–5356
Cl VII, in laser heated plasma, emission intensity anomalies, 58-78 Å *(Russian)* 77–46521
^{36}Cl, beta decay, K-shell electron ejection 77–18888
Cr VII, autoionising transitions $ns^2np^6-nsnp^6mp$ 77–88419
Cs, $5p^56s^2\ ^2P_{3/2}$ autoionising level, ejected electron excitation function, reson. 77–58167
Cs, ejected electrons from autoionis. levels excited by electron impact 77–88573
Cs, elastic electron scatt., 0.8-20 eV, Cs^- autoionis. state 78–5353
Cs, electron excitation cross sections for six autoion. config., Born approx. calc. 78–25713
Cs, polarised photoelectrons produced by circ. polarised synchrotron radiation 80–18830
Cu, low energy He^+ ion bombardment, origin of autoionisation electron emission 77–20973
Cu vapour, conc. determ. in hollow-cathode discharge from autoionised line intensity *(Russian)* 77–84547
CuCl, reson. coherent nonlinear scatt., biexciton autoionising states 79–51978
^{64}Cu β^- decay, K-shell autoionis. 80–956
$D+He(2^1S)(2^3S)$, associative and Penning ionisation, autoionisation, calcs. 78–25674
D_2, electron impact dissoc. to D^+, from autoionising state 79–54980
DF, threshold photoelectron spectra, photoionis. threshold, resonant autoionis. 77–499
Eu, autoionising states excitation in electron collisions *(Russian)* 79–86073
F_2, threshold photoelectron spectra, photoionis. threshold, resonant autoionis. 77–499
FHF ion, H-bond excited electronic states, CI calc., dissoc. and autoionising states 80–5489
Fe IX, autoionising transitions $ns^2np^6-nsnp^6mp$ 77–88419
Fe XVI, autoionisation contrib. to total ionisation rates 80–9738
Gd atom, long-lived autoionisation state *(Russian)* 78–94216
H^-, autoioniation states, below N=3 hydrogenic threshold, complex-rot. calc. 77–67966
H_-, autoionising states, electric field effect 78–50528
H^- photodetachment cross section, narrow resonances near n=3 threshold 80–27988
H^-, S autoionising states, time stability theory 78–90130
H^-, S reson. state, appl. of improved line width expression 80–5505
H+He (2^3S), pot. energy surfaces and autoionisation lifetimes calcs. 77–34740
$H+He(2^1S)(2^3S)$, associative and Penning ionisation, autoionisation, calcs. 78–25674
H_2, autoionising states, complex scaling method calcs. 80–9527
H_2, chemiionisation by $He(2^3S)$ and $He(2^1S)$, pot. surfaces, autoionisation widths, cross sections 77–36739
H_2, dissociative photoionis. at 26.9 eV 77–3423
H_2, dissociative photoionisation, 19.8-40.8 eV, proton kinetic energy spectra 79–68273
H_2, electron impact dissoc., vel. distrib. of H(2s), $^1\pi_u$ autoionising state 77–79696
H_2, electron impact dissoc. ionisation, energetic protons for autoionising states 78–25728
H_2, electron impact dissoc. to H^+, from autoionising state 79–54980
H_2, photoionisation, resonant, dissociative 79–68272
H_2, vibr. autoionisation and H_2^+ vibr. state distrib. depend. 77–48628
H_2^-, autoionising states, complex scaling method calcs. 80–9527
H_2+ He (metastable), Penning ionisation *(French)* 80–1060
$H_2+He(2^3S)$, pot. energy surfaces and autoionisation lifetimes calcs. 77–34740
HCN^-, SCF ab initio ground state pot. energy surface, geometry, rel. to HCN 78–78646
HF, threshold photoelectron spectra, photoionis. threshold, resonant autoionis. 77–499
$H(2s)+He(Ne)(Ar)(Kr)(H_2)(N_2)$, 5-25 keV, H(n=3) excitation, Balmer α emission obs. 80–53113
He, autoionisation states, electron impact, electron ejection, distribs. 77–50545
He, autoionising resons., complex-coord. anal. 79–49992
He, autoionising resons., complex rot. method, non- and degenerate perturbation theory 79–72283
He, autoionising S states, electron-atom collision resons. theory calcs. 77–58179
He, elastic electron scatt. phaseshifts, 2s2p ^3P autoionisation, 1s2s $^3S\rightarrow 1s\varepsilon p\ ^3P$ triplet continuum photoionisation 79–31480
He, electron impact, low energy, post collision interaction, ejected electron energy distrib. 79–72423
He, electron impact excitation, in autoionisation region, parametrised close-coupling calcs. 77–54612
He, electron impact ionisation, decay modes investig. 79–72422
He, electron ionisation, autoionising transitions interference 77–42390
He, electron scatt., interaction with electrons ejected from impact excited autoionis. states 78–42221
He, highly excited states, config. interaction 78–13445
He, isoelectronic spectra autoionisation states n=3 hydrogenic threshold, complex rot. method 79–31477
He, lifetimes of doubly excited states, autoionisation and radiative decay 79–18146
He, metastable states, electron and proton impact ionisation, autoionisation 80–102573
He, photoionisation cross sections up to n=2 excited state, evidence of autoionisation 80–91520
He, resonance photoabsorption in (3s3p) ^1P reson. region 79–45659

autoionisation continued
He, S reson. state, appl. of improved line width expression 80—5505
He triplet states, doubly excited, spectrum and polarisation 80—99472
He$^-$, reson. calcs. with correlated target state wave functions, complex coord. method 79—26939
He$^-$ resons. in 56 to 64 eV electron collisions, autoionising states and spectral line polarisation 80—53145
He$^+$, electron scatt., elastic, ^{1}P continuum phaseshift, autoionis. state 77—88561
He+He$^+$, autoionising transitions interference 77—42390
He+Li$^+$ autoionisation, electron spectra 80—91653
He$^+$+Ca(Ba), 2-1000 eV, spontaneous ionis. mechanisms 79—64090
He$^+$+He, autoionisation electrons and scatt. ions, ang. correl. determ. 80—63792
He$^+$+He, autoionising state excitation, ion-electron coincidence, electron azimuthal depend. 78—37734
He$^+$+He, scattered ion-autoionisation electron ang. correl. determ. 80—9725
He$^+$+He(2p^2 ^{1}D), collisionally excited, autoionisation electron ang. distrib., interference struct. 80—32819
He$_2^{2+}$, autoionising states, adiabatic pot. energy curves calcs. 78—42140
He*+He, inelastic collision, 1-5 keV, autoionising states 78—13581
He(2S)^2, autoionising reson., appl. of complex-rotated Hamiltonians 79—31427
He(2^{3}S), electron impact ionis. to 1s, 2s, and 2p state, autoionis. 80—1068
He(2^{1,3}S)+H, autoionising system, Siegert eigenvalues, variational calcs. 79—50106
He(2^{3}S)+H(D), Penning and assoc. ionis. cross sections, vel. depend. 79—22815
He(2s2p)^{1}P autoionised transition, ang. correl. function (e,2e) fast coincidence technique 77—83738
Hg+He^{2+}, autoionisation, 5-20 eV, electron and ion ang. distrib. 78—78795
K, electron excitation cross sections for six autoion. config., Born approx. calc. 78—25713
K, electron impact excitation, 3p inner shell, autoionis. features 77—68117
K I, electron impact excitation, identification of low energy autoionising levels 79—31703
K I, K II, ejected electrons from autoionis. levels excited by electron impact 77—88572
K, Rydberg autoionisation state lifetime calc. 77—444
K^{2+}, photoionisation cross sections calc., R-matrix theory 77—18865
K^{2+}, photoionisation cross-section, R-matrix theory 78—82702
K$_2$, supersonic mol. beam, isotope selective two-step photoionisation study 80—74203
Kr, 4p^{5}5s state, electron excitation fine struct., neg. on reson. 77—14585
Kr, absorpt. spectra, field induced autoionisation near ionisation threshold 80—106301
Kr, electron energy loss spectra, energy-depend. multichannel quantum defect theory anal. 77—61860
Kr, electron impact autoionisation, cross-section parametrisation 77—6932
Kr, electron impact excitation of autoionis. states 78—90302
Kr II, absorption spectrum in vac. UV region, ionisation energies 79—49972
Kr, spin-polarised photoelectrons by circularly polarised synchrotron radiation 80—91516
Kr$_2$, photoionisation 77—54578
Li, ^{2}S, ^{2}P^0 and ^{2}D autoionising states, positions and widths 79—26944
Li, Auger and autoionisation spectra, collisional excitation mechanisms 77—19042
Li, autoionisation spectrum, theory *(Spanish)* 79—89647
Li, autoionising states, config. decays and excitation energies 78—13475
Li core excited even parity ^{2}P states, fluoresc. 80—69100
Li, electron impact excitation of autoionis. state, ejected electron intensity 78—5352
Li I, autoionising levels, electron impact excitation, ejected electron spectrum 78—9259
Li ion soft X-ray laser, 199 Å, autoionising state effect 77—34876
Li laser, 207 Å, proposal for construction 80—43324
Li, laser excitation and ionisation, autoionising states obs. 77—61699
Li$^+$, autoionising, and quasibound states, Feshbach calcs. 77—54505
Li$^+$, doubly excited autoionis. resons., laser prod. plasma absorption spectra obs. 77—50392
Li$^+$, S-autoionising states, energy calcs. 79—36520
Li-like ions, electron impact, ionisation cross section including excitation-autoionisation contributions 80—28105
Li$^+$+He, 10-50 keV, mol. promotion, many-electron aspects 79—50124
Li$^+$+He, <5 keV, autoionised electron spectra 80—32823
Li$^+$+He collisions, Li-K shell excitation, autoionisation spectra meas., total cross sections 77—19053
Li$^+$+methane, single collision, time delayed autoionisation spectra 78—1067
Li$^+$+Ne collisions, vel. dependence of Ne 2s and 2p, vacancy production, electron spectroscopy 80—58344
Li$_2$, core-excited states, UV photoabsorpt. and ejected electron spectra 78—37655
LiI, electron-mol. beam collisions, autoionising states, electronic spectra *(Russian)* 78—22023
Mg, 2p-electron excitation and ionisation by electron impact, autoionising states, electron spectra 77—14590
Mg, 4snl autoionising states ejected electron spectra, low energy impact two electron excitation 80—83494
Mg, electron impact negative ion form. and post-collision interaction *(Russian)* 79—54974
Mg, electron impact two-electron excitation, ejected electrons from autoionis. levels 77—88571
Mg I, Mg II, ejected electron spectrum from autoionis. levels after electron impact 77—75304
Mg I, Mg II autoionisation state radiative decay *(Russian)* 80—5509
Mg III, autoionising transitions ns^{2}np^6—nsnp^{6}mp 77—88419
Mg ions in low density plasma, dielectronic recomb., ionization equilib. and radiative energy loss, solar corona appl. 79—68903
Mn, giant-resonance autoionisation 79—89649
N$^-$ autoionisation from N$_2$ electron impact dissoc., EELS 80—106397
N^{2+}, electron impact ionisation cross sections, autoionisation contrib. at low temp. 80—32838
N^{4+}, cross section measurement, contribution due to excitation-autoionisation 79—45850

autoionisation continued
NO, ang. distrib. valance photoelectron spectra, vibr. depend., autoionisation and Franck-Condon factors 79—72356
NO, autoionisation struct. at first ionisation limit, photoionis. data 78—58748
NO, ionic ground state, photoelectron spectra vibr. intensity, Franck-Condon factors 77—79650
NO, photoionisation and ionisation pot., mol. beam meas. 77—10709
NO, UV irrad. photoionisation, NO$^+$ high vibr. excitation, photoelectron spectra 77—71830
NO, UV photoelectron spectrum, autoionisation from Rydberg state, vibr. progressions, Franck-Condon factors 78—50583
N$_2$O, electronic autoionisation branching 80—91614
N$_2$O, non-Franck-Condon transitions in resonant autoionization 79—50092
N$_2$O, photoelectron spectrum, vibronic interaction and autoionis. effects 80—95680
N$_2$O, X$_2\Pi$ state, Ne I photoelectron spectra 77—30924
Na, Auger and autoionisation spectra, collisional excitation mechanisms 77—19042
Na, ejected-electron spectrum of autoionis. levels excited by 35-400 eV electrons 77—14582
Na, electron impact excitation, L-Auger and autoionis. spectra 78—5354
Na I, even-parity autoionising states, photoabsorpt. 350 to 400 Å, laser excitation 79—59390
Na, L-Auger, autoionisation spectrum after electron impact excitation 77—14591
Na, overlapping autoionisation lines, interference effects 80—91677
Na$^+$, autoionising 2s2p^{6}ns, np states, electron reson. scatt. calc. 80—53142
Na+H$^+$ collisions, L-Auger electron emission, autoionising states, line broadening effects 77—14568
Na+H$^+$(He$^+$), Na 2p^{5}3s^2 ^{2}P$_{3/2}$ state alignment by 5-30 keV excitation 80—14200
^{95}Nb, beta decay, K-shell electron ejection 77—18888
^{95}Nb, K-shell autoionisation in β-decay 77—298
Ne, autoionisation region states, differential excitation function resons. obs. 77—6939
Ne, autoionising Ne levels excited in 5-10 keV collisions 78—22017
Ne, autoionising resons. near 575 Å, ab initio relativistic RPA calc. 80—32681
Ne, autoionising states, scatt. electron spectra, post collision interaction effects 78—58819
Ne, beam-foil excited ^{4}P state, delayed coincidence Auger electron lifetime meas. 80—14117
Ne, electron impact, resonances, autoionising states 77—58170
Ne, electron impact excitation of autoionising states by fast electrons 79—72425
Ne, energy exchange between scatt. and ejected electrons following 2s2p^{6}3s(^{1}S) state autoionis. 78—46448
Ne$^-$ scatt. electron spectra, distinction from neutral autoionising states 80—83482
Ne+He$^+$(Li$^+$)(Mg$^+$)(Na$^+$)(Ne$^+$), autoionising level excitation, electron spectra 77—14554
Ne+He$^+$(Ne$^+$), coherent excitation and decay of autoionising states 79—45789
Ne$^+$+Ba, 2-1000 eV, spontaneous ionis. mechanisms 79—64090
Ne^{n+}+Ar(Kr), (n=1, 2, 3, 4), energy spectra of electrons produced 79—45822
Ni, M$_{\rm II,III}$ spectrum, ab initio calculation 80—83276
O, autoionis., radiative emission, competition in excited state decay 77—75109
O, beam-foil excited ^{4}P state, delayed coincidence Auger electron lifetime meas. 80—14117
O II, autoionisation probabilities rel. to O III prod. by Auger effect 78—20633
O^{4+}, resonant-scatt. contributions to excitation rates 80—58393
O^{5+}, cross section measurement, contribution due to excitation-autoionisation 79—45850
O$_2$, I and I′ resonance series, vibr. level populations in autoionisation, photoelectron spectra, bond length determ. 80—91612
Pb, VUV photoelectron spectra, spin polarisation autoionis. reson. 78—33483
^{147}Pm, β-decay, branching ratio and K-shell autoionisation 80—42598
Rb, ejected electron spectrum of autoionis. levels excited by electron impact 77—58174
Rb, electron excitation cross sections for six autoion. config., Born approx. calc. 78—25713
Rb, lowest metastable autoionising level identification by RF spectroscopy 77—426
Sb, new autoionised series, flash pyrolysis IR absorption obs. 79—85937
Sc IV, autoionising transitions ns^{2}np^6—nsnp^{6}mp 77—88419
Si, dielectronic recomb. and ionization equilib., autoionization and excitation influence 78—1077
^{151}Sm, β-decay, branching ratio and K-shell autoionisation 80—42598
Sr, autoionisation reson. states elec. field depend., three-photon ionisation 78—33478
Sr, bound even-parity J=0 and J=2 states, multiphoton ionisation spectra 77—71789
Sr, doubly excited Rydberg states 78—33479
Sr, ejected-electron spectrum, Auger levels 79—22843
Sr, electron scatt., autoionis. states electron spectra *(Russian)* 79—36779
Sr I, Rydberg and autoionisation levels, laser ionisation spectroscopy 77—3331
Sr, radiative decay of autoionisation states *(Ukrainian)* 78—82682
Sr, Rydberg states, ^{1}D$_2$→^{1}F$_3$ microwave transition meas. using selective reson. ionisation 79—72258
^{99}Tc, β-decay, branching ratio and K-shell autoionisation 80—42598
Ti V, autoionising transitions ns^{2}np^6—nsnp^{6}mp 77—88419
Tl, autoionisation reson. determ. from photoelectron polarisation meas. 80—58221
Tl, ionisation limit and oscill. strength in VUV absorpt. spectra 80—74152
Tl, photoionis. cross section, spin polaris. and ang. distrib. of photoelectrons, RPA calc. 78—13478
Tl, vacuum UV absorpt. spectra, at. consts. 77—57917
^{204}Tl, β-decay, branching ratio and K-shell autoionisation 80—42598
^{204}Tl β-decay, K-shell autoionisation accompanying internal bremsstrahlung 80—57745
Tm, intense 4d-f resons., cross-sections, spectra, calcs. 79—31426

autoionisation continued
- V VI, autoionising transitions $ns^2np^6-nsnp^6mp$ 77−88419
- Xe, $5p^55s$ state, electron excitation fine struct. neg. ion reson. 77−14585
- Xe, autoionising reson., Stark effect 80−58198
- Xe, electron energy loss spectra, energy-depend. multichannel quantum defect theory anal. 77−61860
- Xe, electron impact autoionisation, cross-section parametrisation 77−6932
- Xe I, electron impact excitation in 18-24 eV autoionis. region 77−58171
- Xe, united atom rare gas spectra analogy with mol. Rydberg states 80−32700
- Yb, autoionisation and Auger decay, collective excitation effect 80−43008
- Yb highly excited levels, reson., visible two photon absorpt. spectra obs. 80−58228
- Yb, photoemission, valence-charge-induced Fano reson. 80−55267
- Yb-Al, valence changes during autoionisation and Auger electron emission 80−50475
- Zn, electron impact ionisation efficiency curve, threshold of 12.7 eV 79−50137
- Zn, Kβ X-ray spectra and autoionisation following β-decay of ^{64}Cu 78−13029

automata theory
- *see also finite automata; stochastic automata*
- EMG signal generation, quantification using automata theory 77−29132
- neural automaton model I/O characteristic for semi-Markov impulse sequences *(Japanese)* 80−16917
- prokaryote epigenetic control mechanisms, distributed model 77−77879

automatic control
- abdominal cavity organs, circulation hydrodynamics in presence of extracoporeal perfusion 77−29172
- active vibration-suppression systems, automation 78−18098
- aerosol filter sampler, automatic time sequence, for proton induced X-ray emission anal. 77−60171
- analyser automatic, for melting point of paraffin wax determ. 79−14223
- arc-welding seam US defectoscope *(Russian)* 80−43564
- artificial blood circulation system, thermoelectric heat exchanger control unit 79−25149
- artificial heart, automatic control system 77−44841
- aviation and astronautics, conference, Tel Aviv (1977) 78−81517
- bipedal walking, linear stabilisation *(Russian)* 78−51055
- blood O_2 affinity variability, automated meas. method 79−39544
- blood pressure cuff control unit, automatic multi-function device 78−36013
- bubble chamber film analysis, semiautomatic measuring system 80−58105
- BWR, automatic protection system *(German)* 78−4989
- C-CD based control system for Si cryst. growth 78−68623
- camera automatic focusing mechanism principles and designs 79−30595
- camera exposure time, design and operation *(German)* 78−21249
- cancer problem cell kinetic study using digital simulation 77−40639
- CANDU nuclear power reactors, automated chemistry control system development 80−42738
- CANDU secondary coolant circuit chemistry control, automated system development 78−66359
- ceramic suspension, ferromagnetic filtration apparatus improvement 78−11561
- ceramic ware manufacture, mechanisation and automation 79−61548
- chart recorder timer control, pen overload protection systems, at. absorpt. appl. 77−73481
- chromatography, nonlinear detector response quantification with lab. automation system 80−40775
- cine cameras, high speed *(Russian)* 80−285
- clinical electrophysiolgy laboratory automatic control system 78−57110
- cold light production by high vacuum deposition of multilayer interference coatings *(German)* 80−53486
- conductometer to record rapidly varying electrical conductivity 80−61184
- corneal mechanised trepan control 79−29659
- coulometer, controlled-potential, design, operation, anal. appls. 77−25335
- crack length automatic recording in sheet samples 78−60907
- crystal diameter system design and operation 77−1797
- crystal growth, Czochralski and related methods, diameter control, review 78−31328
- crystallizer for growing single crystals from solutions with precision control of supersaturation 78−80465
- cyclotron, vacuum chamber pumping system automatic control *(Japanese)* 79−85842
- Czochralski crystal growth, automatic, weighing method 77−85929
- Czochralski crystal growth, automatic, weighing method 77−85930
- Czochralski growth of alkali halides, dynamical aspects, use of optical diameter controller 78−31332
- defibrillator, miniaturised implantable, automatic, heart monitoring appl. 77−81645
- deformation, cyclic, static, meas., recording, automatic system 79−15893
- densitometer system for photographic spectral sensitivity meas. 78−29190
- dynamic radiography, automatic control system design 77−60244
- electrochemical voltage indicators, production, voltage response, resist. 77−1936
- electromechanical actuator, vibr. linearisation of mag. hysteresis charact. *(Russian)* 79−12789
- electrophotographic dry powder toner concentration control *(Japanese)* 78−24878
- ellipsometer, null-setting type design and performance 77−45884
- ethylene, polymerisation plant, high-press. equipment design 79−24746
- extracorporeal circulation equipment 80−3865
- fatigue testing, low cycle, automation of installation control 79−15926
- Febry-Perot interferometer, with automated data acquisition and stabilisation system 78−70180
- film printing, processing, automatic control system structure *(Russian)* 77−61149
- flute oscillation suppression by automatic EM control *(Russian)* 78−30464
- force/tension transducer for small muscle meas. 80−41281
- gamma-ray irradiator for dosimeter calibration, automatic irrad. time control *(Japanese)* 78−66452
- gas anal. of ^{14}C-labelled compounds using piston-type counter tube, automated 77−56281
- gas chromatography, online, improvements *(Spanish)* 77−32865

automatic control continued
- gas flow control, automated, transducer 78−59508
- gas nitriding, automatic control of NH_3 dissociation 77−70223
- geodesy, appl. of modern automatic drafting system *(German)* 78−15952
- glass balls production, drop feeders automation 79−61556
- glass melting furnace, gas consumption through ports, monitoring and control system 79−58692
- graphite furnace anal., autosampling system, timing circuit for baseline absorbance monitoring 77−73482
- heat treatment apparatus 79−79005
- HTGR fuel reprocessing pilot plant, solids handling and fluidised-bed combustion techniques development 79−45397
- impulse stochastic control on 3D crystallographic lattice 77−22499
- in-series cardiac assist devices, expt. and theoretic observations 78−36063
- indicator-setting operator terminal for physical instruments 78−32804
- ion source electron beam modulator automatic control system 79−72173
- Ionosphere sounding satellite control, automated system 77−60572
- Ionospheric Sounding Satellite, automated control system *(Japanese)* 77−78607
- Ionospheric Sounding Satellite, summary of control centre *(Japanese)* 77−78606
- laser absorption calorimeter automation 78−74084
- laser level-control circuit for high-bit-rate system using slope detector 79−18430
- laser radiation level control in He-Ne laser *(Russian)* 77−46716
- lasers with unstable cavities, automatic adjustment system 77−50693
- lathe during metal removing, vibration control systems reviews *(Russian)* 78−70118
- liquid N_2, automatic level controller, transfer system for cold traps 78−24805
- magnetic field, 0.1 to 2 T, automatic control, performance improvement *(French)* 79−30450
- magnetic induction, stabilised source 78−94360
- mass spectra, automatic recording microphotometer modification 77−12845
- mechanical properties, of materials and structural members, rating quality of automated systems 79−15928
- mechanical testing of materials in complex stressed condition, automatic unit 79−15898
- medical engineering, appl. of automatic meas. and automata 79−62381
- microscope, system for automatic tracking of white blood cells 77−78064
- monochrome photographic print exposure control cct. *(Danish)* 80−62748
- neutron spectrometer, angular-displacement precision control with fast error-signal transducer 78−186
- nitriding system for Si_3N_4 fabrication, automated 79−24468
- NMR spectrometer, pulse, controlled by programmable digital unit *(Czech)* 78−77952
- non-destructive assay technology and automated 'real-time' materials control 79−26721
- nuclear reactor, IRT-M, automatic control using in-core detector system 77−50264
- nuclear reactor fuel consumption determ., automated techniques *(German)* 77−14236
- odour analyser, automatic, for atmospheric sulphide anal. *(Japanese)* 80−50924
- optical adjustment and control subsystem, for OMEGA-10 multibeam laser system 78−50847
- optical fibre coupling alignment by fully automatic system 77−79949
- optical prism polishing equipment 77−34968
- optical sensing systems, with automatic light-intensity control, stabilisation 77−54784
- pH, electrolysis, instrumentation, appls. to electrosynthesis, electrode react. stoichiometry meas. 77−63928
- photoelectric control system for large azimuthal telescope 78−16301
- photographic camera films, automatic exposure 78−65992
- photometric determination and control of solution components, automatic method 79−79350
- photomicroscopes with automatic exposure control 80−86475
- plasma, automated diagnostics 79−94820
- plasma diagnostics, automatic system for addition at. conc. meas. in MHD generator 79−50892
- plasma frequency response investigation problem 79−10649
- plasma oscillations, stabilisation of spatial mode, algorithm 80−64721
- plastics sheet blowing and extruding, process identification for automatic process control *(German)* 80−81023
- polymer dynamic mech. loss testing apparatus, automation, review 77−32616
- potentiometric analyser, automated, with selective electrodes, microcomputer control 80−40773
- potentiometric analysis with ion-selective electrodes, computer automation 80−3424
- PVC, radiation destruction, automatic control *(Polish)* 77−29025
- PWR power unit, automatic control and meas. system design lines *(Russian)* 79−30964
- quantum oscillator, phase automatic freq. control parameters, optimal values *(Russian)* 80−77814
- radiation pyrometer, use in automatic control of molten glass temp. in feeders 77−49729
- radio telescope system, fully automatic, for interplanetary scintillation obs. 79−101064
- refractometer, REMAT 20 process-control, of photoelec. differential flow-through type 77−45885
- RF accelerating structures, improved reference cavity design for freq. tracking 77−83176
- Rheovibron viscoelastometer, dynamic, direct reading, automation, appls. to polymer films, fibres 79−3980
- rotating-anode X-ray tube apparatus 78−58100
- sample changer, automatic, for semi-automatic photometric anal. systems 77−48705
- scanning system for grazing-incidence spectrometer 80−14250
- sectional mirror, optoelectronic control system 78−20645
- sedimentation anal., automatic recording system 78−60897
- semiconductor junction laser, electronic stabilisation of radiated power 80−23702
- sintering uranium oxide, resistance furnace appl. and characteristics *(Italian)* 77−81239
- smoke gas purification process control system *(Russian)* 77−52712

automatic control continued

- solar furnace, materials melting process dynamics rel. to automatic control 79—39317
- sound reproduction in cinema *(Russian)* 80—38212
- spacecraft attitude control and navigation systems, instruments reliability enhancement 77—29623
- spectrometer automatic control unit for discrete recording 78—58049
- spectrophotometer, near IR, SPECORD 61 recording-type grating spectrophotometer with LT1 air drier 77—45906
- spectroscopic light source fluctuations, automatic correction, split beam system 77—10115
- SQUID RF sensor, automatic monitoring circuitry 77—18044
- stereoscopic X-ray unit for medical diagnostic sets 80—85467
- stopped-flow systems, automated, for fast react. rate anal. methods, review 78—95971
- surgical aspiration automatic control device for cardiac surgery *(French)* 78—61282
- target position checking by light beam using automatic two-coord. system 78—5564
- telescope, large azimuthal complex, automated control system 78—73641
- thermal convection suppression by distributed automatic regulator *(Russian)* 78—30364
- thermal loading, quick-acting system 77—48609
- threshold following pacemaker concept and application 77—81671
- tilt meters, photoelectric, with negative feedback, block diagrams anal. *(Russian)* 78—88948
- Tokamak, automatic TO-1, plasma concentration control *(Russian)* 78—91160
- TOPOCART-ORTHOPHOT C system for prod. of stereo orthophotos 77—66994
- TOPOMAT all-automatic photogrammetric system for aerial photography 77—66993
- toroidal plasma, ion temp. control by neutral injection 79—37514
- tumour microwave heating with automatic temperature control 77—77963
- US rail-inspection transducers lateral position automatic control 79—57200
- US thickness gauge, Kvarts-6, design of automatic control block 78—73005
- vacuum system backing pressure automatic regulation device 79—49241
- ventilation, artificial, for patients, pulmonary model 77—21556
- vibration meas. using gel electrocapillary transducers *(Polish)* 78—26094
- voltage stabiliser attachment circuit 78—57981
- wedge compensator for automatic control system 78—13808
- welding, continuous drive, selection of welding conditions 77—114
- X-ray diffr. anal., single cryst. automated technique, comparison with powder method 77—70386
- X-ray fluoresc. spectrograph, automatic computerised, for rock trace elemnt anal. 77—56320
- X-ray fluoresc. spectrometer system, automated, for chem. shift meas. 78—4750
- X-ray images processing, CALTIX system description *(French)* 77—4872
- X-ray residual stress anal., computer controlled, software, precision 78—5712
- X-ray spectrometer, computer controlled, for steel alloying element determs. 77—56318
- X-ray spectrometer control, interactive program for data collection, manipulation chem. anal. appl. 78—7312
- X-ray spectrometer movements, automatic control system 80—69012
- $Ga_{1-x}Al_xAs$ injection laser automatic bias control cct. 78—5498
- HCl automatic control in air by electrochem. methods 79—96491
- H_2SO_4 mist monitor, semicontinuous 80—61495
- O_2 inhalation automatic control for patients with respiratory failure 80—17181
- SO_2 automatic control in air by electrochem. methods 79—96491
- Si, surface, controlled stripping, automated system 78—31557
- Si, VPE growth, in process monitoring and control of doping gas conc. 79—24443
- Zn, corrosion rate monitoring, automatic, in near-neutral soln., using a microcomputer 80—50749

automatic data processing *see data processing*

automatic frequency control

- astable multivibrator freq. control for rapid cond meas. with electrolyte cond. probe 78—37029
- EPR spectrometer, 2 mm band, with re-entrant resonator 78—86311
- frequency standard, passive quantum, static AFC system parameter optimisation 77—9989
- frequency-agile phase lock system for mm wave klystrklystron 77—5446
- gas laser with automatic freq. control, long-term instability and irreproducibility of freq. 79—45962
- IMPATT source, frequency-stabilised, 115 GHz 80—67573
- implantable biotelemetry transmitter for 6 differential signals 77—48968
- quantum magnetometer using optical pumping, broadband freq. multiplier 77—37951
- reference time interval reproduction device 78—77869
- two-laser frequency difference stabilisation electronic system 79—68401
- CO_2 lasers intermode beats appl. 80—48209
- He-Ne laser, zero beat AFC system, two laser injection locking system 77—88737
- He-Ne lasers, stabilised by saturation absorpt. in I_2 78—1270

automatic gain control

- biomedical instrumentation, digitally controlled 77—56493
- blind children's CW FM sonar 79—70708
- dichrograph, control unit construction 78—21122
- double-beam single-detector wavelength-modulating spectrometer, appln. 80—86447
- ECG computerised acquisition, compression, and retrieval 78—36019
- heart rate module, implantable, for animal use 78—44753
- lateral motion analyser sensitivity stabilisation along ranging line 79—72694
- linear feedback AGC with input-level-invariant response times for sonar signal processing 78—30130
- optical path electronic simulator GaAlAs laser power control loop *(German)* 78—82987
- phase-stable amplifier, with automatic gain control, input stage 78—4633
- photomultipliers, logarithmic scale using AGC *(Czech)* 77—5884
- plasma, grooved instability, self-adjusting feedback system for stabilisation *(Russian)* 77—68767

automatic gain control continued

- pulse processing automatic gain control circuit for photomultiplier tube 79—97955
- radiometers, multichannel, digital control *(Russian)* 77—26399
- radiometry defectoscope with feedback, charact. of operation 78—44321
- radiopolarimeters for solar patrol at microwave freqs., receiver gain attenuation control 79—101065
- scintillation probe containing long plastic scintillator, AGC circuit 77—57833
- scintillation spectrometer, computer controlled gain stabilizing system using LED, processor in feedback 78—17473
- seismic recording equipment, digital automatic amplitude control unit parameters choice *(Russian)* 79—39964
- seismometer digital automatic amplitude controller with preliminary smoothing, parameter selection *(Russian)* 79—74985
- signal amplitude digital auotmatic control system, instrumental realisation algorithm *(Russian)* 79—39924
- US inspection of cast explosive billets for air voids 78—3287
- GaAs signal processing optical electronic devices 80—33242

automatic test equipment

- abrasion testing, automatic device for discrete batching small amounts of abrasive suspension 79—87782
- AC/DC transfer measurements, wideband, automated 77—18035
- acoustic emission analysis system with programmed control *(Russian)* 78—46866
- admittance bridge, microcomputer controlled, for passive network testing 77—18037
- aerosol particle size spectrometer, microcomputer-modified 79—39329
- airtightness, total lack of, automatic system for measurement 79—52593
- analyser, automatic, for melting point of paraffin waxes meas. 79—14223
- audiometer, digital, for mass hearing examinations 80—33379
- automatic defect signaller for the ASNK-U assembly system for nondestructive testing 79—39101
- automatic magnetic inspection system for oil country tubular goods 77—81361
- babbitting tester, semiautomatic, for US inspection 79—66245
- Battery Energy Storage Test facility, test programs and data processing 80—30449
- birefringence measurement of system for characterisation of polarisation props. of optical fibres 79—93205
- blood cell leukocytes, automatic recognition and classification systems *(Italian)* 80—81780
- bonded joints, device for automatically recording internal stresses 80—25963
- brittle material, surface energy determ. from AE, automatic system 79—91899
- building product, nonmetallic, first crack determ. device, during load test *(Czech)* 80—45471
- BUS-2 scan control unit for automatic interference reduction 79—5126
- calculator-based instruments, meas. accel. due to gravity 80—73336
- calibration of resistance thermometers, thermodiodes and thermocouples, 4.2-300K range 78—45624
- calorimeter, without use of computer, 80 to 320K 79—88957
- calorimeters, high temperature, automatic measurement of electrical energy 79—71451
- capacitance to voltage convertor, for automatic test set 78—24818
- ceramic, electrical transducers for automatic recording of mechanisms occurring during drying 77—52561
- channel separating system for multichannel radiometer *(Russian)* 80—58094
- chemical analysis of solution components, automatic photometric method for determining and controlling concs. 79—79350
- cineangiocardiograms, automatic anal. using TV system on line with minicomputer 78—92699
- coercive field strength of soft magnetic particles meas. *(German)* 80—22395
- coercive force, automatic meas. by remote means, for ferromag. metals and alloys 79—24690
- computer controlled test equipment for eval. of Pb-acid batteries for electric vehicles 80—30445
- computer peripheral pressure transducer calibration and metrological servicing 77—57314
- computerised for plastic and rubber tensile properties 77—26284
- crack detect. in electrically cond. materials, pulsed elec. meas. method *(French)* 79—29324
- crack growth recording using PSR-1-19 potentiometer 78—39971
- crack length determ. by electric potential meas., automatic instrument *(German)* 79—96258
- crack propagation testing machine using Shimadzu Servopulser Dynatec *(Japanese)* 80—25973
- creep and long-term strength tests, system for automatic temp. regulation 77—63853
- creep testing in complex stressed condition, programmed automatic unit 77—56208
- CROs developments 78—24821
- cylindrical articles of small diameter, monitoring by automatic X-ray apparatus 79—70280
- Daresbury Laboratory automated magnet field meas. facility 79—30509
- data processing from static tests on constructional materials 77—4885
- dead weight machines, instrumentation for load cells, with compensators and computerized data processing 79—37266
- deformation, cyclic, static, meas., recording, automatic system 79—15893
- deformation recording instrument 78—7122
- dielectric loss of polymers determ., at 100 MHz to 300 MHz and 2°C to 40°C 80—68219
- dielectric polarisation studies in ferroelectrics using automated, programmable system 79—67268
- digital automatic thermodynamic enthalpy and specific heat determ. equipment 78—57951
- digital circuit for selecting information bearing components of output voltage of electromagnetic transducer 79—2760
- digital computer control of mech. tests 79—43508
- digital equipment for recording acoustic emission signals 80—102948
- dimensional nonuniformities, refractive index profiles of optical fibres 79—18541
- dioptometer with projection readout system 79—50455
- disc-on-disc apparatus, for adherence, wear resist. and thermal shock meas. of thin films 78—72943
- dust meter, EIP-9M, with optical and inductive-charge transducers 79—17595

automatic test equipment continued
- echo signal amplitude of US flaw detector, automatic measuring instrument 79−79212
- eddy current fastener hole tester, improved design 80−30194
- eddy current inspection of fastener holes, computer automation, exam. 78−53040
- eddy current testing of wire and bar 80−71819
- eddy-current phase thickness gauge with automatic error corrections 79−9204
- electrical conductance of concrete meas., automatic instrument 77−77659
- electromagnetic device for loading and measuring wear in vacuum 78−56841
- fatigue, low cycle, charact. determ. using digital computers 79−100263
- fatigue crack growth testing, decreasing stress intensity technique, computer-controlled 78−72949
- fatigue failure testing 77−56209
- fatigue testing, low cycle, automation of installation control 79−15926
- fatigue testing, low-cycle, adapted hydraulic machine 79−57175
- fatigue testing machine, stress amplitude stabilising system 79−52501
- fatigue testing unit, varying temp., automatic control 77−77667
- fatigue tests, programmed, two-frequency, using EM resonance machine 79−96232
- ferromagnetic probe inspection unit for automatic inspection of welded tubing 78−56860
- ferromagnetic probe unit, MD-10F, automatic 78−56861
- ferroprobe tube testers, automatic checking system 79−79211
- fibre to fibre coupling loss due to displacement, separation, misalignment, automatic measuring technique 79−32036
- fluctuating noise measurement system *(French)* 80−64316
- friction test machine SMTs-2, automatic loading device 79−70257
- galvanostatic potential meas. apparatus for automatic accumulator testing 77−30185
- gas analyser, meas. errors due to gas-water interaction *(German)* 78−44438
- gas chromatograph capillary column, computerized testing 79−16067
- gas parameter measuring system, temperature and relative humidity testing 79−67318
- gas turbine blades, exam. using automated vibrating bench 78−64800
- gel permeation chromatography, automated system using laboratory automation system 80−71961
- glasses, automatic recording dilatometer *(Japanese)* 79−70291
- hardness testing apparatus display for time dependent hardness test on plastics *(German)* 80−66742
- hearing aid test system, signal processing techniques 78−30131
- image analysers, use of Saltykov corrective method 78−31362
- impact machines, pendulum, energy meas. using optical system 80−69746
- implanted cardiac pacemaker function analyser 77−81717
- implanted pacemaker performance parameter assessment appl. 78−11778
- inhomogeneous material structural characts. NDT 78−48586
- intelligent, programmable, instruments produced using microprocessors 77−33998
- intelligent oscilloscopes used for production testing, dynamic analysis 77−37929
- interferometer, microcomputer based automatic heterodyne 79−85174
- intrinsic semiconductor IR detector array data acquisition system 78−77991
- karyotyping automatic image processor *(French)* 77−40953
- laboratory complex for fatigue testing with variation of low-temp. conditions 78−27723
- Large Coil Test Facility, instrumentation system design 80−95446
- leak test, automatic, nondestructive, design, evaluation and implementation for IC assemblies 78−53180
- light and water exposure apparatus 79−15914
- liquid chromatography, high performance, with CRT display 79−57321
- liquid-flow measurement system using positron active tracer, microcomputer-controlled 80−24113
- long-path light absorption cell meas., automation, optical alignment 79−17491
- low-loss solid dielectric meas., automated resonance substitution systems 80−15957
- machines, crank driven, electromech. system for stabilisation and programming static load 78−64801
- macrostress in deposits, spontaneous, dilatometric method 77−36709
- Macsym One, automated measurement and control system based on 'real world' signals 79−17402
- magnet testing using digital apparatus with incompletely closed mag. system 79−9226
- magnetic characts. of permanent magnets meas., temperature dependences in −150 to 300°C range 80−31809
- magnetic induction measuring device for superconducting solenoids, using NMR 80−57344
- magnetodynamic method of part inspection 79−96272
- mass spectrometrer, double collecting, device for automatic digital measurement of isotopic ratios 80−31932
- mass spectrometric leak detection, automation of prep. operations 79−52597
- mass-measuring device, automatic digital, 0 to 9.99 g 79−71417
- material inspection techniques using lasers 80−66734
- material properties determination, quality control automatic test equipment 77−86236
- materials testing, programmed loading unit for test machines 78−23900
- measurement of thermoelectromotive force and resistance, study of kinetic phenomena of charge transfers 80−57330
- measurement-computation complexes, general principles, introduction to the USSR 80−52177
- measuring-channel characteristics measurements, process control systems, compound and element-by-element methods 80−62612
- mechanical oscillation damping characts., apparatus for examining, based on amplitude-frequency relationship resonant trough 78−64803
- mechanical properties, of materials and structural members, rating quality of automated systems 79−15928
- mechanical testing of materials automation, using 500 kN and 2.5 MN ATE *(Czech)* 80−66710
- mechanical testing of materials in complex stressed condition, automatic unit 79−15898
- metal sheet parity, pressed, X-ray TV system for automatic analysis *(German)* 77−90536
- microcomputer-based blood-pressure recorder *(Japanese)* 80−67139

automatic test equipment continued
- microscope-spectrophotometer, computer processed, for measurement of absorption spectra of rock-forming minerals 80−18010
- microspot CRT, non-deflected spot position stability testing device 77−82500
- microwave resonator monitor, resonant freq. and bandwidth meas. 77−22567
- multichannel instrum. for measuring energy of pulsed laser radiation 79−76731
- multimeter, automatic PM 2517 80−22347
- NDT, data processing and acquisition for product quality control 80−11862
- NDT, vehicle reliability improvement on structural and motor parts 79−91859
- network parameter automatic meas. methods and systems 77−57363
- neutron sensor performance testing, automatic counting channel and analysis system 79−13612
- nitroglycerine, in waste water, monitoring continuous electrochem. analyser 77−60147
- noise suppression circuit for automatic flaw indicator 79−5111
- nondestructive testing, solar cell welds, system selection 78−35629
- nuclear fuel pins, computer controlled meas. 80−5300
- optical fibre parameters, dimensional nonuniformity, refractive index profile *(Japanese)* 78−37982
- optical fibre testing using digital processing oscilloscope 78−22188
- optical fibres measurement system 78−50909
- optical heterodyne interferometer, appl. to surface inspection 77−90529
- optical stimulator for vision expts. 80−26423
- pacemaker automated test system developments 80−30944
- pacemaker testing automation using microcomputer *(German)* 78−81068
- pacemaker testing in vivo, computerised system 80−94412
- partial discharge amplitude spectra, acquisition and automatic processing system *(Italian)* 79−93108
- particle size distrib., on-line measurement techniques, instruments *(German)* 78−60895
- PDP 11/40 minicomputer dynamic analysis system, noise analysis of fluid power equipment, graphical presentation of results 80−64327
- photo-optic measuring systems using bifurcated fibre-optic probe 79−81569
- photoelectronic spectrometer and coincidence instrum., use of pulse height analyzer and D/A convertor 80−22473
- photographic materials inspection by IR laser beam 79−30593
- photometric system for human blood clotting time determination, digital display *(Danish)* 77−90826
- physical expt. automation, coupling device for small computers to external device 80−31722
- pipe end crack detection, by magnetic particle device *(German)* 77−90535
- plastic pipe inspection by rotational ultrasonics 79−20323
- plastics testing, automation 80−76443
- pneumatic test equipment for plate testing under alternating flexure 78−7119
- point defect concentration monitoring during low-temp. irradiations and anneals 80−7741
- polymer, viscofluid, extensional vibrorheometer 77−70257
- polymer relaxation props., automatic assembly for exam. over wide range of temp., and medium moisture contents 80−7739
- polymers, atuomatic device for measuring elec. direct current props. *(German)* 78−45647
- portable digital reactivity meter for power reactors PWR, BWR appls. *(German, English)* 77−82999
- positive displacement measurement system for diesel pump and injector performance testing, microcomputer-controlled 80−24112
- potentiometer, semiautomatic, webermeter testing appl. 77−74464
- precision tubes, US inspection system *(German)* 77−90539
- programmable semiautomatic instruments for quantitative struct. anal., geometric eval. in materials lab. *(German, English)* 78−64798
- programmed controlled, for inorganic material internal friction meas. 77−90541
- progressive wave apparatus for measurement of dynamic material constants of rubber compounds 79−91866
- pulmonary blood flow, noninvasive meas. using PDP 12 digital computer 79−70685
- pupil responses, human, instrumentation for automated study 80−36164
- Q multiplier technique, microcomputer-controlled for wide-range dynamic complex dielec. const. measurements 80−22383
- quantum frequency store and Cs atomic transition frequency comparison system 77−79064
- radiation flaw detection, automatic control systems 78−48596
- radiograph processing 79−66242
- radiometric flaw detection with X-rays on series prod. parts *(German)* 80−21240
- rail flaw detection, US wheel probe variation problems 79−47862
- reactor pressure vessel, remote-controlled compound scanning US inspection system 77−1892
- real time system for acoustic measurement and analysis and its applications *(Japanese)* 79−68522
- reflectance microscopy of coal, considerations involved in automation 80−18001
- regulation of CO_2 conc. in climatic cabinets for corrosion testing *(German)* 78−53069
- reproducible adjustment of test equipment, procedure utilising computer controlled electronics *(German)* 78−60927
- resistance thermometer automatic calibration oven 80−98914
- reverberation time digital meas. instrum. for auditoria and studios *(Japanese)* 80−64321
- RF, synthesised signal generator design 77−53875
- rotary-vane attenuator, automatic calibration on modulated subcarrier system 77−18022
- roughness of periodically shred surfaces, on-line meas. technique using He-Ne laser *(German)* 80−33014
- scanner development, for surface inspection of cold rolled sheets *(German)* 79−43533
- scrapping of soldered pipes, automatic, device 79−29308
- semiautomatic portable coercimeter 79−34250
- semiautomatic ultrasonic flaw detector for studs 79−66247
- semiconductor device evaluation, CV and GV characts. at HF, automatic accurate display 77−26329
- semiconductor wafer diagnostics, using computer automated scanning low-energy electron probe 79−4214

automatic test equipment continued
  - semiconductors temperature dependences meas., of electric conductivity, Hall coeff. and magnetoresistance 80—31792
  - shearing interferometer with scanned photodiode array and microcomputer for automatic transparency distortion measurements 79—80675
  - single sheet tester for Fe sheet loss meas. at 20 Hz-20 kHz *(Japanese)* 77—70251
  - spectrometer, anti-Stokes Raman, microcomputer-controlled 80—24111
  - spent nuclear fuel burn-up level determ., computerised equipment *(Polish)* 80—32582
  - stamped disc surface inspection by automated eddy current unit 78—92430
  - standard cell intercomparison system for reference groups, microcomputer-controlled 80—22384
  - steel, ball, fatigue life prediction, fully automatic X-ray diffr. apparatus *(Japanese)* 79—39076
  - steel, ball bearing rods, inspection installation 80—81268
  - steel, billet, high speed automatic surface inspection, MIDAS 79—83420
  - steel, circular hot rolled stock, magnetic inspection of external surface, zond automated installation 79—79210
  - steel, cold rolled strip, surface defects, online automatic system, design study 79—34231
  - steel, non metallic inclusion eval. using Quantinet systems 79—15923
  - steel, pearlitic atom probe microanal., computer controlled 77—66781
  - steel, strip components, automatic US macrostruct. monitoring 79—79203
  - steel, US internal flaw detection system 77—66717
  - steel tubes, ferromag., complex of devices for automatic nondestructive testing 78—53092
  - steel weld fatigue life estimation, multichannel NDT monitor 78—56846
  - stopwatch, electrical, testing device, semiautomatic 79—30424
  - stress-strain diagram, automatic plotting during mech. testing 78—27724
  - submarine periscope optical test equipment 80—78943
  - surface finish automatic inspection by laser scanning *(German)* 78—170
  - surface flaw inspection of nuclear fuel pellets 79—30939
  - surface roughness meas., hand-held instrument with in-built data processor *(German)* 80—57255
  - suspension, automated meas. of viscosity 79—37258
  - system to monitor effluent tank contents, HPLC analysis 80—71982
  - temperature and humidity monitor for biological exposure chambers, microprocessor-controlled 79—49239
  - temperature difference meas. by automatic thermistor bridges 77—22547
  - tensile test diagram remote recording device 78—7139
  - tensile testing, control of test cycles, data logging and data processing *(German)* 80—97648
  - tensile testing, microcomputer for automatic meas. and data treatment *(German)* 77—44433
  - tensile testing machine with automatic null-balancing load meas. instrument, dynamic behaviour and optimal adjustment *(German)* 77—60005
  - tensile testing machine with automatic null-balancing load meas. instrument, dynamic behaviour investig. and control *(German)* 77—60006
  - tests control and evaluation, using 500 kN and 2.5 MN ATE, fracture toughness and fatigue strength determ. *(Czech)* 80—66710
  - thermal conductivity apparatus for sedimentary rocks, using needle probe and microcomputer control 79—100970
  - thermal fatigue test apparatus with automatic heating and cooling for welded joints 78—3278
  - thermal loading, automatic control system, quick-acting 77—48609
  - thermal meas. using data logger and computer 78—81966
  - thermocouples and meas. line inspection, based on capacitor discharging method *(German)* 80—13079
  - thermoelectric heating and cooling device, creep test appl. 80—21218
  - thermoelectric thermometer checking unit with programmed control 77—22548
  - thermophysical testing device, rate of change of temp. in time *(Russian)* 80—208
  - thin film adhesion meas., semiautomatic installation 79—96245
  - thin film thickness meas., automatic Brewster angle spectrophotometer 79—6078
  - three-coordinate measuring machine, dynamic acquisition and automatic reduction of data 79—75507
  - time-average electronic speckle pattern interferometry system for measurements of HF vibrations of piezoelec. transducer 80—37966
  - titrometric liquid analyser for determining oxidisability of water 79—79441
  - torque magnetometer for vacuum-to-high-pressure H_2 environments 80—4746
  - torque meters, electromechanical indicators application 77—87757
  - torsional oscillation test instrument with process computer control *(German)* 77—21344
  - total oxygen demand meter for use in waste-water treatment plant 79—96399
  - toxic gas microconcentration determ. by automatic belt photometer *(Russian)* 78—28347
  - transformer bridge cct., for resist. thermometer testing, industrial appl. 77—53906
  - TV analyzer for material structure studies 78—27696
  - two-probe synchronized sampling technique for measuring flows behind rotors, calibration 80—14865
  - ultrasonic testing of austenitic collars in a computer controlled immersion test-plant *(German)* 79—96256
  - US, online inspection, steel plate manufacture appl. 78—80702
  - US adhesive bond eval., computer controlled 79—96253
  - US automatic inspection of tubing 78—56865
  - US automatic monitoring of tube butt welds, sensitivity and reliability 79—79205
  - US basic instrument crack and flaw detection, basic instrument 79—5108
  - US crack detection and heat treatment monitoring system 77—90542
  - US echo pulse flaw detectors, use of auxiliary sensitivity regulation 78—60951
  - US equipment for monitoring drill and casing tubes 78—53085
  - US evaluation, computer-assisted, review 79—43536
  - US fault detection, MatEval computerised test system *(French)* 79—52564
  - US flaw detection for welded seams, with automatic registration of flaw parameters 77—90570
  - US flaw detector, pulse-to-analogue convertor 79—39102
  - US flowmeter, microcomputer-controlled 80—24111
  - US inspection system, automatic, for welding seams 79—29310
  - US inspection unit, UDM-1M, modernisation 79—39106

automatic test equipment continued
  - US shadow immersion exam. of defects, dimension determ., error anal. 78—44305
  - US sing-around system, high-speed, for vel. of sound measurement 79—90101
  - US tester for steel plate circular stampings 79—15949
  - US testing, instrument limitation, flaw detection instruments, programmed automatic corrections 78—7103
  - US testing by digital scanning, adjustable step technique 77—90574
  - US units for inspecting thin walled tubing 78—88606
  - US wall thickness meas., test equipment *(German)* 78—18136
  - US wave propag. vel. and attenuation measurement system for solids, precision test installation *(German)* 79—50549
  - vacuum tightness monitoring in components with unclosed cavities, automatic mass spectrometer 79—52592
  - vector cardiographic assessment of implanted pacemaker, PDP 11/40 computer, disc storage 78—11771
  - velocity measurement in rotating liquids, two-dimensional, using automatic analysis of trace particle motion 79—64810
  - vibration decrement recording as function of amplitude with fully automatic system 78—15630
  - vibration processes, automatic system for measuring, recording, analysing 77—53895
  - vibration test rig for wear meas. of granules 78—56840
  - viscoelastic material, automatic system for short-time stress relaxation 77—63710
  - viscosimeter, high-temp. device for melt viscosity determ. 80—79418
  - weight-measuring instruments, Russian types 990VN and 959DN, accuracy improvement 80—52166
  - wire in torsion, installation for automated determination of yield strength 80—21221
  - X-ray fluorescence anal., automated fusion device for making fusion tablets *(German)* 77—90512
  - X-ray quality control, automatic exposure relay 78—95893
  - X-ray TV-computer unit for measuring defect parameters in weld seams 79—67451
  - Al-Mg alloy AMg5, welded structures, machine for fatigue life investigation 79—52566
  - C content in Fe_3C melt, measurement using automatic device 79—39252
  - H^+ concentration meas. *(German)* 79—16083
  - HCl, gas monitoring ion-selective electrode analyser 77—60146
  - Hg barometer, digital, 710 to 770 torr 80—47046

automatic testing
  - aerospace test meas. symposium, San Diego (1976) 77—41284
  - airtightness inspection using halogen leak detector, automation 79—52595
  - automatic anomalous noise meas. for ferroelectric capacitor parameters, not in equilib. *(French)* 78—74029
  - ceramic, automatic US defect detection for tile grading and packing processes 78—23885
  - composite structures, multipoint moments meas. by optical struct. anal. 79—15910
  - concrete, automatic testing installation *(German)* 77—48604
  - conference on analysis instrumentation, Charleston, West Virginia, USA (May 1977) 79—16100
  - crack growth recording, automatic, elec. resist. method 79—39070
  - crack growth recording using PSR-1-19 potentiometer 78—39971
  - critical evaluation of test results, representation, processing *(German)* 78—7145
  - cupping, sheet material, automation of standard testing 79—57172
  - defect reconstruction, from US methods, mathematical model *(German)* 78—44295
  - defect-marking system, position-delay, pulse signals of scanning defectoscope conversion 77—90566
  - destructive examination of materials with data processing, microprocessor application *(German)* 80—93714
  - digital computer control of mech. tests, review 79—43508
  - digital voltmeters, pulse-counting, automatic checking method 80—57240
  - displacements, angular, linear, simultaneous use primary transducers 79—6084
  - dosimeter, exoemissive, automation of testing 79—6770
  - electric machines, digital measurement, of rotational speed *(Czech)* 79—71419
  - electrodynamic vibration test beds, feedback signals for correcting characteristics 80—53543
  - engineering metrology, measurements by optically generated patterns 79—3648
  - experimental control system, exam. of mech. props. under complex stress conditions 78—64802
  - fatigue tests, short-term, methodological problem of automating data computer processing 79—15931
  - ferrite materials and components, laboratory meas. automation *(Polish)* 80—101789
  - ferroelectric material, dielectric aftereffect meas. with digital data acquisition 77—43952
  - fission reactor safety channel system with on-line testing capability 77—65278
  - flowmeters, low liquid flow rate, based on dynamic weighing 77—55111
  - fluorescence microscope photometry data processing and display *(German)* 80—86369
  - fracture toughness, automation of method of forming and measuring circular crack depth in cylinders 79—43531
  - glass, raster technique for automatic checking in sheets 78—23883
  - halfsecond levels, investigations using atuomatic comparator *(Russian)* 78—40675
  - hardness testing, depth of impression meas., automated 79—15892
  - hardness testing apparatus display for time dependent hardness test on plastics *(German)* 80—66742
  - holographic store automated test using BASIC M-400 interpreter *(Russian)* 79—94180
  - industrial resistance thermometers testing using incomplete bridge balancing technique 78—73998
  - lamps, standard temperature-calibrated, integrated arc optoelectronic spectral comparator method 77—53907
  - luminescence, automatic meas. of SO_2 and oxides of nitrogen, optical technique *(Dutch)* 80—3565
  - materials testing applications of microcomputers *(German)* 77—32744
  - microhardness testing on PMT-3 tester, automatic loading device 77—77668
  - multifaceted prism test automation 79—72724

automatic testing continued
nondestructive hardness test, determ. of elastically homogeneous struct. elastic limit 77—66719
nuclear materials, use of US identified seals 79—85677
nuclear power plant at Obrigheim, inservice inspection of primary components *(German)* 77—34406
nuclear reactor fuel consumption determ., automated techniques *(German)* 77—14236
nuclear steam generator tubes testing and evaluation, using CIS/DASIO system *(Czech)* 80—63301
partial discharge long-time testing using automatic data acquisition and computation *(German)* 79—71432
particle size distrib., on-line measurement techniques, instruments *(German)* 78—60895
phasemeter, flip-flop type, modulation method 77—53939
photolithographic mask linewidth meas. by diffraction pattern analysis 77—37960
piezoelectric transducer automatic setup, for continuous meas. of internal friction and elastic moduli of solids 80—108652
pipe, thick walled, increasing efficiency of automated ultrasonic inspection of segregate defects 79—11755
pipes, hot-rolled, automatic mag. quality control on prod. line 80—108661
plastic materials, process computers for control and meas. of laboratory testing *(German)* 79—61821
plastics, short-time testing using process computers *(German)* 79—61822
plastics testing, automation 80—76443
polymer cyclic deformation amplitude, automatic meas., apparatus design 78—85082
pressure instrument calibration 77—53880
PWR power unit, automatic control and meas. system design lines *(Russian)* 79—30964
radiochemical purity quality control by rapid feedback system 77—90900
radiography, automatic reading systems, estimation of performance time 78—40005
real time interferogram simulation by analogue device, aberration generation, CRT display 79—54181
refractories, strength and thermal properties, automated test system 80—100986
sheet materials, heat stability, small automatic device for rapid testing 77—77672
solar cell, automated electronic analysis system 80—93952
steel bars, type 3102 bright steel, combined NDT inspection line 77—77714
tensile testing methods, metallurgical industries appl. *(German)* 78—35598
testing for chemical plants, use of electrochemical methods, corrosion rate forecast automatic instrumentation *(German)* 78—44289
thermocouples, base metal, temperature range 600 to 1300K 77—53908
thermoelectric thermometers. automatic testing, structural method for improving precision 79—35744
three-coordinate measuring machine, dynamic acquisition and automatic reduction of data 79—75507
torque measurement, electromechanical indicators application 77—87757
trace analysis using injection method of at. absorpt. spectrometry 79—34382
u.s. automatic inspection system, computer aided *(German)* 77—4877
US evaluation, computer-assisted, review 79—43536
US in-service inspection for reactor pressure vessels *(German)* 77—90538
US inspection, automatic, thin walled large diameter pipes, flaw size classification 78—60949
US inspection of heated objects by SGK-2Ts system 78—95894
US installations for weld testing on tubes and tanks *(German)* 77—1894
US materials testing, SARD-1 automatic system with digital recording 77—77712
US tank test systems for crystal defects location *(German)* 79—83406
vacuum gauges, absolute pressure, combined method 80—22378
vibration installations, certification results processing 80—22336
visual inspection of moving steel surface 77—81349
volt-ampere meters, pointer-type, digital representation errors 77—53937
voltmeter, digital, error determination algorithm 77—53938
weighing, automatic, application in ceramics industry 80—95074
Pb powder, automatic image analysis for charact. of size and shape distrib. 78—11473

automation, social aspects *see social aspects of automation*

automobile industry
acoustic noise measuring techniques, exterior, interior noise in automobile development *(German)* 78—79178
automatic induction hardening equipment 78—92284
electron beam appl., to metal treatment *(French)* 80—66558
low flow meas., Flo-Tron microflow meter 78—14118
motor-car corrosion protection improvement, primer paint appl. by electrocoating effect *(Dutch)* 80—71915
polyurethane foam, processing machines and systems, motor car components appl. *(German)* 80—71955

automobiles
acoustic measurements in automobile development *(German)* 78—87219
acoustic soundlevel meter ELMOT improvements 78—42506
air-intake flowmeter using corona discharge principle 80—33716
anti-collision equipment, microwaves non-conventional appl. survey *(Italian)* 80—13093
audibility and effective loudness of sirens and speech in automobiles 77—16935
chrysler's electronic lean burn system 80—16868
drag force, air and rolling resistance effects 77—11
electric car, physical principles 77—41440
exhaust, multigas analyser 77—49198
exhaust emission meas. and testing procedures, error statistics, survey *(German)* 77—73839
exhaust gas catalysts, radiometric determ. of Pt and Pd attrition 78—31740
exhaust pollution, data reliability 80—3559
exhaust system, procedures for evaluation of acoustical performance 79—18645
exhaust system design, finite element acoustic analysis 78—51003
exhaust systems, measurement of acoustic parameters 80—53591
hybrid drives with flywheel energy storage, appls. *(German)* 80—30563
ignition RFI suppression at distributor rotor gap 79—55586
interior noise levels running in city streets 79—23127

automobiles continued
motor vehicle racing and shooting noise 78—55510
noise annoyance from power drive train 79—90077
noise legislation 79—34465
planetary surface transport vehicles, stability in weak gravity field 77—64594
pollution meas. and testing procedures, for exhaust emissions limitation *(German)* 77—56299
propulsion, H_2-powered and battery-powered, comparison 80—45819
propulsion batteries, current designs and their limitations 79—66405
propulsion using H_2 and electric power, comparative evaluation 80—16769
structural analysis using hybrid stress finite elements 78—30176
tetra-alkyl Pb compounds in urban air 78—16149
H cryogenic storage and refuelling for automobiles 80—30604
H fuel, survey of liquid hydrogen container technology for highway vehicle fuel system applications 80—30607
H storage by metal hydrides for automotive propulsion 80—40922
H_2 automotive fuel, technico-economic feasibility of storage, transportation, distrib. 80—16766
H_2, liquid automobile fuel, cryogenic storage, and semiautomatic refueling station 80—40926

autoresonant accelerators *see collective accelerators*

autotransformers
four-terminal high capacitance standard 77—5869

avalanche diodes
see also avalanche photodiodes; IMPATT diodes
2 km 20 Mb/s optical fibre transmission system 78—42437
avalanche radiation detector, large-area, high-gain, using transmutation doped Si 77—23367
avalanching statistics, strong electric field *(Russian)* 77—66171
breakdown process as nonlinear wave of soliton type 77—47824
digicons, image detection with semicond. array for multichannel photon counting 77—83989
n-GaAs, intrinsic avalanche response time, orientation depend. 79—51587
III-V semiconductors, p-n heterostructures, epitaxial growth techniques, appl. to electronics, review 80—54770
microwave P-N avalanche diode as gamma-ray dosimeter 77—54408
photodetector, characts. *(Swedish)* 78—89545
photodiode, avalanche multiplication of electron beam generated carriers 77—80833
photodiode, double epitaxial, for optical fibre communications 77—54782
photodiode, model, fibre optic receiver optimisation 77—792
photodiode, n^+-p-π-p^+, epitaxial Si diode for optical fibre communication at 800 to 900 nm 77—79961
photodiode, operating conditions in phase optical rangefinding 77—13799
photodiode, semiplanar mesa-type passivation by slightly conductive chalcogenide film 78—2556
photodiode receiver, for fibre optic transmission system 77—19455
photodiode receiver sensitivity, specification and testing *(German)* 78—38015
photodiodes for 400 MHz optical fibre communication systems, construction and characts. 77—11011
reach-through photodiodes, Si, avalanche buildup time 77—15892
surface avalanched p-n junctions, localised charge injection and trapping 77—76907
wideband 1064 nm laser communications detector evaluation 77—18097
AlGaSb, growth and characts. for 1.0-1.8 μm heterojunction devices 78—6870
GaAs, electroabsorpt. avalanche photodiode, waveguide detector for 1.06 μm 78—16842
GaAs, epitaxial growth for microwave devices *(French)* 77—48360
GaAs high speed avalanche photodiode design 78—8446
p-$(GaAs)_x(ZnSe)_{1-x}$-nn^+.GaAs, avalanche heterojunctions, inverse branch of volt ampere characts. *(Russian)* 80—6974
$Ga_{0.47}In_{0.53}As$, homojunction avalanche photodiode, exam. of props. 78—37072
GaInAsP on InP substrate, epitaxially grown, fabrication of avalanche photodiode 78—37071
InAs, noise meas. 77—4431
$In_xGa_{1-x}As$, noise meas. 77—4431
Si avalanche photodiode, microplasma sites in n^+-p junction SEM and TEM characterisation 77—43702

avalanche photodiodes
conference on measurement techniques for optical fibre systems, London, England (May 1979) 79—64348
detectors, 1.0 to 1.4 μm region, for high data rate fibre optic systems 79—54188
electrical parameters, optical derivative meas. 80—2455
fibre communication devices, directional couplers, atennuators, switches development 79—3782
guided-wave optical signal processing, diode laser sources and photodetectors 80—48465
III-V semiconductor heterostructure, high speed response, high quantum efficiency 79—80682
InGaAsP leakage current, shot noise, quantum efficiency, gain saturation 79—67381
laser low-level pulse meas. system at 1.064, transfer standards 80—86253
low-noise multistage avalanche photodetector using heterojunctions 79—88999
MIS photodetector linear array 79—63308
MIS structure based pulsed avalanche photodetector with stable internal amplification, feasibility 79—58794
n^+-p-π-p^+, carrier multiplication and noise in avalanche devices 80—15579
optical communication channel, error probability calc. charact. function method, intersymbol interference 80—53227
optical fibre communication, cabling, light source and receiver technology, review 78—59125
for optical fibre communication *(Japanese)* 80—78977
optical fibre sources and detectors *(Italian)* 80—69390
optical fibre transmission system devices *(Japanese)* 80—58693
optoelectronic devices and optical imaging techniques, book 80—27059
SEM, electron beam induced cond. of defects, rel. to TEM 80—107027
short-pulse photodiode receiver quasioptimal filtering 79—26132
transmission system, semiconductor device reliability tests 80—58573
GaAlAsSb, for LW optical communication systems 80—10043
GaAlAsSb/GaSb alloys, prep. and optoelectronic device appl. 80—25587
GaAlSb, for LW optical communication systems 80—10043
$Ga_{0.72}Al_{0.28}Sb$ avalanche photodiodes, ionization coeff. 79—17488

avalanche photodiodes continued
  GaAs, electroabsorpt. avalanche photodiode waveguide detectors 78−65965
  GaAs, electroabsorpt. avalanche photodiode waveguide detector, freq. demultiplexing 79−17486
  GaAs, p-i-n, temp. depend. characts. 79−35835
  GaAs, planar ion-implanted avalanche photodiodes 80−22431
  GaAs, reach-through APDs, temperature dependent characteristics 79−95482
  GaAs signal processing optical electronic devices 80−33242
  $Ga_{0.47}In_{0.53}As$ homojunction photodiode, avalanche photodetector for 1.0-1.6 μm region 79−6179
  GaInAsP-InP avalanche photodiode, fabrication and characts. 78−54454
  GaInAsP-InP avalanche photodiode IR detectors, 1.1 to 1.3 μm, fibre optics appls. 80−14360
  GaInAsP-InP lasers and detectors, for fibre optic communications at 1.0-1.6 μm 79−3803
  Ge avalanche photodiode, cryst. orientation depend. of multiplication noise 79−80680
  Ge for graded-index fibre cables, transmission meas. in 1.2 to 1.6 μm range 80−10037
  Ge, ionisation rates, cryst. orientation depend. 80−103700
  Ge, non-repeatered 50 km transmission experiment using low-loss optical fibres 78−79108
  Ge, p-i-n, temp. depend. characts. 79−35835
  Ge, reach-through APDs, temperature dependent characteristics 79−95482
  p^+-n Ge shallow junction avalanche photo diodes, noise and quantum efficiency 79−87143
  $In_{0.53}Ga_{0.47}As$/InP avalanche photodetector 80−4764
  $In_{0.53}Ga_{0.47}As$-InP avalanche photodiode with guard-ring struct., characts. 80−96939
  $In_{0.53}Ga_{0.47}As$-InP avalanche photodiode structure for 1 to 1.6 μm region 80−98978
  $In_xGa_{1-x}As$, planar photodiodes made by VPE 79−49286
  InGaAsP avalanche photodiode, 1.3 μm, noise performance, −190°C 80−57370
  InGaAsP avalanche photodiodes, breakdown mechanism, donor conc. effect 80−70710
  InGaAsP, for LW optical communication systems 80−10043
  InGaAsP:Be, avalanche photodetectors annealing temp. effect on photolum. spectra 79−69872
  InGaAsP:Be ion-implanted avalanche photodiode, struct. and characts. 79−17487
  InGaAsP/InP, for LW optical fibre communication 80−9885
  InGaAsP/InP avalanche photodiode, ionisation coeff. 80−15590
  InGaAsP-InP photodiodes, microplasma-limited avalanche multiplication at 1 to 1.3 μm 79−26128
  InP, ions coeffs. of electrons and holes 80−2394
  InP, microplasmas, investigation 80−60018
  InP planar guarded avalanche diode prod. by ion implantation 79−95473
  InP:Cd(Zn), avalanche photodiode characts., impurity diffusion effects 80−70709
  InP/InGaAsP, with guard ring structure 80−100506
  InP-InGaAsP p-n junction avalanche photodiodes, surface passivation techniques 80−100508
  n^+-n-pGe avalanche photodiode, noise factors, internal quantum efficiency 80−70803
  Si film double-mesa reach-through avalanche photodiode with large gain-bandwidth product 79−12845
  Si, lightwave sources and detectors 80−64068
  Si, p-i-n, temp. depend. characts. 79−35835
  Si p-n junctions, electron emission from depletion layers 80−100509
  Si photodiode, avalanche, $n^+p\pi p^+$-type, primary photocurrent anal. by noise measurements *(French)* 80−88624
  Si, reach-through APDs, temperature dependent characteristics 79−95482
  Si, stress enhanced diffusion of B, using SiO_2 diffusion masks, photodiode fabrication 78−67865
  Si:B, low noise avalanche photodiode fabrication by channelling implantation 79−35827

avalanches, carrier *see impact ionisation*

avalanches, electron *see electron avalanches*

avalanches, electron-hole *see impact ionisation*

avionic systems *see aircraft instrumentation*

avogadro's number *see constants*

axicons *see lenses*

axiomatic field theory
  (1/N) expanded nonrenormalisable interactions, nonlocality investigation 79−30652
  1/N expansion in two-dimensional lattice gauge theory 80−86559
  $\eta\phi^6$ theory, 1/N expansion and instantons, gauge theory extension 80−47180
  $(\theta^4)_4$ field, Borel summability, renormalization group, perturbation theory 78−16922
  θ^4 quantum fields, ground state energy per particle 80−68064
  $\lambda{:}\Phi^4{:}/4!$ massive Euclidean field theory, perturbation expansion, cutoff bounds on n-point Schwinger function 79−71630
  $\lambda_0\Phi^4$ field theory, 3 space-time dimensions, renormalisation, analytical continuation to imaginary time 80−86563
  $\lambda\pi^4$ field theory with internal symm., string representation 78−70266
  $\lambda\phi_2{}^4$, Glimm-Jaffe-Spencer expansion for classical boundary conditions and phase coexistence 79−54245
  $\lambda\phi_3{}^4$ QFT, relativistic field eqn. 77−87893
  $\lambda\Phi_4{}^4$, Euclidean loop expansion 77−65068
  $\lambda\phi_6{}^3$ field theory, renormalisation group and ladder approx. 79−97524
  $\lambda\phi^{2N}$ theory, Green's function approximation scheme 77−13862
  $\lambda\phi^3_{(4,6)}$ field theory in curved spacetime 80−86556
  $\lambda\phi^3$, deep inelastic struct. functions for bound states, ladder approx. 79−35952
  $\lambda\phi^4_d$ and continuous spin Ising model, high temp. anal. 79−63161
  $\lambda\phi^4$, extended objects in quantum systems and soliton solns. 79−35945
  $\lambda\phi^4$, momentum space renormalisation in curved space time 80−37158
  $\lambda\phi^4$ field theory, canonical struct., Kijowski-Szczyrba formalism appl. 80−52427
  $\lambda\phi^4$ field theory, renormalisation in curved space-time 80−42320
  $\lambda\phi^4$ field theory at finite temp., Casimir effect and topological mass 80−57479
  $\lambda\phi^4$ field theory renormalisation in curved space-time 80−42319

axiomatic field theory continued
  $\lambda\phi^4$ self interaction theory, symmetry breaking and mass generation by space-time topology 80−82892
  $\lambda\phi^4$ theory, conformal symmetry breaking, cosmological particle creation 80−90998
  $\lambda\phi^4$ theory, dual string theory from Feynman graph expansion 78−54544
  $\lambda\phi^4$ theory, dynamical mass generation in $S^1 \times R^3$ 80−99046
  $\lambda\phi^4$ theory, renormalisation in nonsimply connected spacetime 80−90999
  $\lambda\phi^4$ theory with tachionic mass term, metastable states 79−97501
  $(\lambda\phi^4\text{-}\sigma\phi^2\text{-}\mu\phi)_3$ quantum field models, Euclidean approach 77−5978
  $\lambda\phi^n$ theory, exact solns. 79−45012
  $(\lambda|\phi|^4)_2$ quantum field model, soliton mass and surface tension 78−58109
  $\lambda P(\phi)_2$ model, bound states and irreducible kernels 80−73569
  $\lambda P(\phi)_2$ weakly coupled model, spectral props. and bound-state scatt. 77−22629
  $\lambda P(\phi)$ lattice theory, coupling const. analyticity 80−99035
  $\mu\phi^3 + \lambda\phi^4$ model, second order phase transiton 78−24752
  ν-dimensional Yang-Mills and (ν-1)-dimens. nonlinear σ-model connection, quark confinement, dual strings 80−90978
  $\pi^{3,4}$ theories, Regge-pole behaviour 80−18081
  σ model, linear in SU(n), $n \geq 4$, renormalisation in one loop approx. 79−97516
  σ model, SU(3) linear, renormalisation in one loop approx. 80−68368
  σ model, two and four-dimens., classical solns., instantons and merons 80−86548
  σ models of nonlinear evolution equations 80−57487
  σ-model, classical solns., stability props. 80−77954
  σ-model, nonlinear, n-component, on lattice of arbitrary dimensions, 1/n expansion 80−73576
  σ-model, nonlinear, order-parameter relaxation from renormalisation group 80−57504
  σ-model, nonlinear, superconformal invariance in 4-dimens. space-time 80−37154
  σ-model, O(2k+1), Euclidean, nonlinear, local theory of solutions, Euler-Lagrange eqns. 80−52387
  σ-model appl. to nuclear physics in one dimension, fission, Hartree approx. 79−80890
  σ-models, nonlinear, classical two dimens., dual symmetry 79−80750
  σ-models with dynamical charges, two-dimensional, renormalisation 79−85223
  $\phi_2{}^4$, perturbation expansion, Borel summability, improvement on Watsons theorem 80−52394
  $\phi_2{}^4$ theory, mass and S-matrix Borel summability 79−89054
  $\Phi_3{}^4$ weakly coupled model, nontriviality of scatt. matrix 77−87891
  $\Phi_4{}^4$ model anal. using perturbation theory anharmonic oscillator strong coupling 78−89622
  $\phi_6{}^3$ theory, anomalous dimension, Regge cut effect on structure function 80−62847
  Φ^{2k} theory in d-dimensions, strong coupling expansion 80−99054
  $(\phi^2)_3{}^2$ model with O(N) symmetry, phase transition 77−6007
  ϕ^2 field, scaling limit in anharmonic oscillator 79−63341
  ϕ^2 theory, renormalisation, Nelson's symmetry and energy densities 79−40671
  $\phi^{3,4}$ theory, conformal anomalies for interacting scalar fields in curved spacetime 79−49396
  ϕ^3, ϕ^4, planar Feynman diagrams in perturbation theory 77−61189
  ϕ^3, conformally invariant amplitudes and field theory in a spacetime of constant curvature 79−49395
  $(\phi^3)_6$, theory, inclusive annihilation processes, jet evolution 79−71640
  $(\phi^3)_6$ field theory, deep inelastic lepton-headron scatt., cut vertex theory and reciprocity relation 80−57466
  $(\phi^3)_6$ theory, composite particle form factor, asymptotic behaviour 80−86595
  $(\phi^3)_6$ theory, IR behaviour, gluon confinement mech., nonperturbative approach 78−24954
  ϕ^3 4-D model, existence 79−97261
  ϕ^3 field theory, vacuum instability in scalar field theories 79−58872
  ϕ^3 field theory with internal Potts symmetry, exactly soluble limit 79−45004
  ϕ^3 interaction, four-dimensional Green's function model *(Russian)* 78−77775
  ϕ^3 theory scatt. amplitude extrapolation between Regge region and fixed angle region 77−74596
  $\phi^4{}_3$ field theory, transform. props. of normal operators and Hamiltonians 78−8526
  $\phi^{4,6}$ self-interacting theory, three well potential, block spin renormalization 80−57490
  ϕ^4, large order behaviour of perturbation theory and mass terms 79−45018
  ϕ^4, mass divergences of wide angle scatt. amplitudes 79−49402
  ϕ^4, massive and massless, elliptic function methods 80−4829
  ϕ^4, vacuum tunnelling, effective potential 79−54262
  $(\phi^4)_3$ renormalised theory, phase transition 77−6007
  $(\phi^4)_4$ theory, semiclassical infrared emission processes 78−29257
  ϕ^4 asymptotic free theory, renormalisation-group method 77−22652
  ϕ^4 Euclidean field theory, scale limit of ϕ^2 80−333
  ϕ^4 field theory, manifestly finite, renormalisable, scatt. amplitudes 78−41407
  ϕ^4 field theory, scatt. amplitude asymptotic behaviour, renormalisation group and slope parameter 79−49389
  $g\phi^4$ field theory, strong coupling expansion, appl. to $g\phi^{2N}$,$g(\bar{\psi}\psi)^2$ and QED 79−58880
  ϕ^4 field theory dual transforms., extension to 4-dimens. using renormalisation group eqns. 79−49393
  ϕ^4 fields, critical exponents and elementary particles 77−26243
  ϕ^4 Grinzberg Landau Wilson model, dispersion theory and ε expansion for $T > T_c$ 79−12753
  ϕ^4 kink behaviour in presence of inhomogeneous perturbation 79−75692
  ϕ^4 lattice field theory, d-dimens., thermodynamic props. near Ising limit 80−82860
  ϕ^4 lattice field theory, kink soln. 77−22651
  ϕ^4 lattice field theory as an asymptotic expansion about Ising limit 80−31967
  ϕ^4 model, Altman's contractor techniques, appl. to nonlinear integral eqns. for Green's functions 79−45005
  ϕ^4 model, four-loop approx. 79−89070
  ϕ^4 model, large order perturbation coeffs., asymptotic evaluation 80−82867
  ϕ^4 model, Pade approximants, EM form factor, pseudoscalar particles 78−74122

axiomatic field theory continued
- ϕ^4 model, strong coupling and infrared struct., renormalisation 80−101921
- ϕ^4 model, strong-coupling expansion in the large-N limit 80−346
- ϕ^4 models, 't Hooft transformation, explicit solns. 80−345
- ϕ^4 operators, anomalous dimensions, universality in percolation problem 77−79045
- ϕ^4 quantum field theory, crit. point existence 77−10170
- ϕ^4 renormalisable field theory, virtual heavy particle effects 80−22513
- ϕ^4 theories, orthogonal transforms 80−82898
- $g\phi^4$ theory, asymptotic series sum of perturbation theory, Green's function method *(Russian)* 79−54271
- ϕ^4 theory, asymptotically free, finite local field equation 79−35944
- ϕ^4 theory, bound states and irreducible kernels 80−73569
- Φ^4 theory, conformal-invariant, massive scalar, tadpole diagram, Ward identity 80−73593
- ϕ^4 theory, Euclidean, local existence of Borel transform of Schwinger functions 80−77932
- ϕ^4 theory, renormalisation anal. 77−10168
- ϕ^4 theory, renormalisation anal. and methods of calc. many loop diagrams 79−58885
- ϕ^4 theory, renormalisation groups transformation explicit construction 80−4832
- ϕ^4 theory, spontaneous symmetry breakdown in finite systems 79−45011
- ϕ^4 theory, three dimens. second order phase transitions, infrared singularities 80−37161
- ϕ^4 two-dimens. model, kink-antikink collisions 79−85218
- ϕ^4 type bag model of hadrons, rubber bag model theory *(Chinese)* 79−49479
- ϕ^4-model, dimensional regularisation and instantons, scalar field theory model 80−4830
- ϕ^4-theory, soliton soln., fluctuation renormalisation and extended particles 77−5996
- ϕ^6 operators in scalar systems near four dimensions, tricritical scaling and renormalisation 79−58863
- ϕ^6 theory in three dimens., global ground state 77−6015
- ϕ^6 three-dimens. theory, consistency of 1/N expansion anal. 77−26456
- $(\psi\psi)^2/N$ interaction in 4-dimens., nonlocal theory for Thirring model 79−21940
- $P(\phi)_2$ field theory, non-relativistic limit for two particle phenomena 78−16906
- *-algebra, decomposition of families of unbounded operators 77−10159
- Abelian Higgs model, lattice version, phase transitions and confinement 79−49398
- Abelian Higgs two-dimens. model, continuum and lattice version, dual transforms 80−4860
- Abelian lattice gauge theories, θ-vacua construction in compact gauge theories 79−58874
- Abelian lattice gauge theories, Monte Carlo anal. 80−18079
- Abelian magnetic monopoles in Euclidean lattice model, improved Schwinger-Zwanziger Lagrangian 79−97515
- aesthetic field equations, behaviour of solutions, pulse and oscillatory solns. 80−68346
- aesthetic theory, increased complexity 77−45933
- analytic regularization in an arbitrary number of dimensions 79−26215
- anticommuting massive Thirring model, generalised prolongation struct., Backlund transform. 78−32972
- arbitrary N critical phenomena in three dimens., critical exponents 79−80746
- asymptotic estimate of perturbation theory at large orders, anharmonic oscillator, Φ field theory 80−4585
- asymptotic estimates in perturbation theory, Yukawa and g0^4 theory 80−4873
- asymptotically free gauge theories, higher-order effects, anomalous dimensions of Wilson operators 78−4771
- axial symmetry in lattice theories 79−9280
- axially symmetric multi-instanton solutions generated by conformal mappings in SU(2) Yang-Mills field 80−42337
- baglike struct., ϕ and ψ interacting scalar fields 79−22046
- bell's inequalities from the field concept in general relativity 80−105771
- Bethe-Salpeter model, scaling reconstruction using renormalisation group, Callan-Symanzik eqn., $\phi_6{}^3$ theory *(Russian)* 80−42351
- binding energy in model classical field theories 80−4927
- Bogoliubov approach, current functional, reduction formula *(Russian)* 79−279
- Bogoljubov axiomatic approach, global axioms and S-functional *(Russian)* 78−54572
- Bogoljubov axiomatic approach, necessary classes of generalised functions *(Russian)* 78−54571
- Bogolyubov approach for nonlocal field theory CSL topologization *(Russian)* 80−47202
- Bogolyubov axiomatic approach to nonlocal QFT microcausality and broken microcausality *(Russian)* 79−12972
- book, PCT, spin and statistics 78−78102
- boson field theory, isolated one-particle states 77−38079
- bound state spectra in ϕ^4 theory and Gross-Neveu model, temp. depend. 78−4770
- boundary effects in quantum field theory 80−42331
- C*-algebra applications, conference, Varenna, Italy (July-August 1973) 77−17753
- C*-algebras of two body interactions, existence of scatt. theory of time automorphism groups 80−31972
- Casimir effect for a self-interacting scalar field 79−97497
- Casimir effect in quantum field theory 80−42330
- causal A-statistics 80−22504
- chiral invariant SU(N) Thirring model, exact S-matrix 79−21911
- chiral SU(N) Thirring model, S-matrix bound state poles fixing 80−360
- classical massive Thirring model, quasiperiodic solns. of field eqn. 78−41418
- closure of cones in algebra of test functions 79−278
- cluster operator bound states 80−8899
- collective coordinates with non trivial dynamics, review 79−26232
- collision amplitudes, structural anal. 77−10188
- complex ϕ^4 theory, Euclidean path integrals and Feynman-Dyson-Wick perturbation expansion 78−49957
- conditioning of states 79−6008
- confinement criteria for gauge invariant, lattice, and Abelian models 79−22023
- confinement in SU(N) lattice gauge theories 80−57493
- confinement in Z_n lattice gauge theories implies confinement in SU(n) lattice Higgs theories 79−58930

axiomatic field theory continued
- conformal invariance in quantum field theory 79−63377
- conformal invariant, convergence of operator product expansion on vac. 77−41749
- conformal invariant four point functions, analytical props. 77−30263
- conformal symm. in quantum field theory 77−65069
- conformally invariant soln. of QFT, tensor fields and Ward identities 77−87894
- conservation laws, infinite set for Thirring model, massive and quantum sine Gordon model 78−29226
- conserved currents and symmetries of the S-matrix 80−9110
- convergence properties of the Pade approximants on a lattice 79−17615
- cosmological quantum theory, a general framework 79−9043
- coupling of logics 78−62104
- covariance principle in quantum physics 78−4496
- covariant representations of nuclear *-algebra, C*-algebra comparison, Wightman axioms 78−58120
- CP_{n-1} models and non-Abelian HP_{n-1}, quantum props., σ relation, renormalisation 80−13210
- CP^1 model, instanton interaction with fermion field 79−97514
- CP^{N-1} model (D=2,3), UV renormalisation and phase transition 80−31989
- CP^{n-1} models, effective lagrangian with no U(1) current problem 79−89066
- CP^{n-1} nonlinear σ-model, lattice formulation 79−58870
- critical exponents in three dimensions, derivation from ϕ^4 field theory with Gaussian propagator 80−4686
- critical exponents to order ε^3 for ϕ^3 models of critical phenomena in 6-ε dimensions 80−86547
- critical indices, conformally invariant bootstrap method 79−12955
- current conservation in perturbative sine-Gordon and massive Thirring models 79−9273
- curved space-time quantum stochastic processes, covariant Kolmogorov-Klein-Fock eqn. 80−18083
- cut vertices and their renormalisation, generalisation of Wilson expt. 79−21929
- cutoff and lattice models, construction of renormalised field theories 78−4787
- de Sitter space-time, QFT, relativistic wave eqns. *(German)* 77−82666
- Debye screening in dilute classical Coulomb systems 78−41170
- degree of freedom, cutoff and space time struct. 78−66031
- derivative analyticity relations, high-energy status 78−66043
- Dirac fermion fields in (3+1) dimensions, boson representation 79−26243
- discrete and Abelian lattice gauge theories 79−9279
- discrete lattice gauge fields, duality transformation, review 79−26236
- discrete lattice gauge theories with matter fields, 1/N expansions phase diagram 80−73603
- discrete space structure dynamics 80−52392
- dissipative systems with a Liapounov function, quantum rules 78−89611
- divergent series summation by order depend. mappings 79−88819
- double scaling limit of one-dimens. XY model in monodromy preserving deformation theory 80−47194
- duality for non-abelian lattice fields 80−42431
- duality in field theory and statistical systems, review 80 -73610
- dynamic renormalisation group in the large-n limit 80−4842
- dynamical lattice theory 79−21933
- dynamical symmetry and asymptotic scale invariance in ladder models 79−21959
- Dyson eqn. and Ward-Takahashi identities of closed time path Green's functions *(Chinese)* 79−80759
- electrons and gravitational instantons 79−25961
- elementary particle classification, selection maps for quantum logics 78−29320
- elementary particle modeling in axiomatic relativistic field theories *(German)* 80−91009
- elementary particle symmetries, axiomatic approach 79−21897
- elementary particle theory, mathematical method, conf., Liblice, Czechoslovakia (June 1978) 79−21891
- embedding lattice field theory in continuum field theory 80−77972
- equations of motion in asymptotically free theories 79−26247
- ergodic theory in von Neumann algebras 80−9104
- Euclidean, projective limits 80−27209
- Euclidean 0^4 theory, simple Feynman graph evaluation 78−41404
- Euclidean $\phi_3{}^4$ theory, phase space cell expansion, Borel summability 78−8501
- Euclidean (super ϕ^3)$_4$, Wess-Zumino model, asymptotic behaviour in perturbation theory 79−30645
- Euclidean approach in curved spacetime, functional anal. 80−27181
- Euclidean boson quantum field theory, two dimens., translation invariant ground states 78−21314
- Euclidean classical field eqns. with unique vacuua 80−32017
- Euclidean Dirac field, local structure, Green's function method 80−68347
- Euclidean field theories, singular classic solns. 79−97510
- Euclidean field theory, nonlinear elliptic eqn., classical solns. 79−21569
- Euclidean fields, low momentum behaviour scale limit 80−62834
- Euclidean fields, uniqueness, global Markov property in trigonometric interaction case 79−89053
- Euclidean formulation, external field depend. of magnetisation and long range order 77−10165
- Euclidean functional determinant, bounds 80−32019
- Euclidean Green functions, quantum fluctuations of instantons 79−26220
- euclidean image of soliton coherent state 78−32989
- Euclidean lattice Yang-Mills theory in two spacetime dimensions *(German)* 80−37157
- Euclidean light cone gauge, 1/N expansions with non-isoscalar gluons 80−47169
- Euclidean manifolds, N-dimensional instantons and monopoles 80−42321
- Euclidean Markov massive fields of higher integer spin 77−201
- Euclidean measures and Schwinger functionals 77−5976
- Euclidean $P(0)_2$ model, quasiclassical expansions 80−47200
- Euclidean QED$_2$ on lattice, continuum limit, Schwinger functions, vacuum expectation values 80−73624
- Euclidean QED$_2$ on periodic lattice, continuum limit 80−18092
- Euclidean QFT, n-particle irreducible functions 80−13199
- Euclidean quantisation of gauge theories, Weinger integral and nonstandard analysis 80−68358
- Euclidean quantum field theory, 1/n expansion 80 −82864

axiomatic field theory continued
- Euclidean quantum fjeld theory, n-point functions, renormalised G-convolution 80—68341
- Euclidean scalar field eqns., action minima among solns. 78—29229
- Euclidean scalar field theories, UV stability 80—37155
- Euclidean self-dual Yang-Mills field configurations, set of linear algebraic eqns. 80—73587
- Euclidean space, spherically symmetric self-dual eqns., representation theory and integration 80—77936
- Euclidean theory, embedding in relativistic Hilbert space 77—2724
- Euclidean Yang Mills eqns., self-dual solns. 79—26230
- Euclidean Yukawa quantum field theory in two dimens., cluster expansion 77—10164
- Euclidean-Markov field theory, Nelson axioms, connection with stochastic quantisation 77—17877
- evaluation functionals, products, convolutions, distribution integrals 80—57498
- exponential clustering for long-range integer-spin systems 79—80744
- exponential interactions and quantum sine-Gordan eqn., two space-time dimens. 77—65072
- extended hadrons, functional eqns. soln. by stochastic methods 78—21376
- extended meson model, Euler-Lagrange eqn. bilocal field theory conservation laws 79—21938
- extended n-point tube 77—49859
- extended structures described by Z(N) spin and gauge models, applications 79—67479
- extrapolation method for perturbative expansion of S-matrix, high energy hadron collisions, ϕ^4 model calcs. 78—394
- factorised S-matrices in 2-dimens., relativistic QFT model exact solns. 79—93274
- Fermi quantisation of EM field, model for quantum field theory 77—79208
- fermionic and boronic descriptors, equivalence in two-dimens. 80—22505
- Feynman amplitudes, zero-mass behaviour 80—68353
- filter theory and covering law 79—58860
- finite Lorentz transformation applications 77—45976
- finite-particle approximations of local field, rel. to local saturation 77—30270
- five dimensional QFT, generalised free fields conformal group 80—4837
- forward scattering amplitude high energy behaviour, renormalisation group eqns., ϕ^3 model 77—57448
- four fermion field theory, renormalisation in mean field expansion, Yukawa coupling 79—21939
- Fourier hyperfunctions appl. 77—38084
- free automorphic quantum field theory, gauge transformations and field algebras 80—86546
- free Euclidean field, struct. of translation operators in phase space 79—30662
- free massless scalar field in two-dimens. space-time, quantum theory, positivity conditions 77—41754
- Froissant bound saturation for two particle elastic scatt. 79—75680
- $g\phi_d^4$ theory, $g\to\infty$, vacuum energy density 79—40657
- $g\phi^3$ model, supersymmetric, massive and massless, renormalised supercurrent and anomalies 79—6267
- $g\phi^3$ theory, ladder graph scatt. amplitudes, bounds at their boundary 77—71420
- $g\phi^4+f\phi^6$, massless limits, anomalous dimens. from renormalisation group, Callan-Symanzik eqns. 77—65091
- $g\phi^4$ field theory, strong coupling expansion, extrapolation scheme improvement 79—89063
- $g\phi^4$ model, asymptotic freedom and discontinuities for $g\to0$ 77—41771
- $g\phi^4$ model perturbation theory, anal. continuation to $g\geq1$ region 79—97525
- $g\phi^4$ quantum field theory, clusterlike expansion based on static ultralocal approx. 80—62839
- $g\phi^4$ renormalised field theory in limit $g\to\infty$, effective potential 80—99058
- $g\phi^4$ static ultralocal field, path integral anal. of spontaneous breakdown of symmetry 79—54249
- $g\phi^4$ theory, strong coupling limit of Green functions, anharmonic oscillator appl. 78—78071
- $g\Phi^4/4!$ theory, asymptotically nonfree theories with vanishing anomalous dimens. 79—97506
- G-convolution of n-point functions in quantum field theory 80—18065
- gauge invariant fermion theories, path-integral measure 79—54267
- gauge theories, facts and prospects, conf., Schladming, Austria (Feb.-Mar. 1978) 79—26203
- gauge theory, Z(2), renormalisation group calc. 80—22514
- gauge theory phases 79—97486
- Gaussian stochastic Euclidean covariant fields, Markov property 78—21322
- Gell-Mann-Low function and Borel summations in renormalizable theories 79—40670
- Gell-Mann-Loy function in scalar field theory, $g\phi^4/4!$ appl. *(Russian)* 78—82116
- general, nonlinear program, many-particle struct. anal. in complex momentum space 77—10189
- Gibbs lattice field, clustering operator invariant subspaces 80—4658
- global Markov property for Euclidean and Lattice fields 79—67469
- goldstone modes in vacuum decay and first-order phase transitions 80—77941
- gravitational instantons, self-dual soln. to Euclidean gravity 80—68118
- Green's function in nonrenormalisable massless $\phi^6{}_{3+\epsilon}$ theory, removal of cutoff, vertex functions expansion 78—45772
- Green's functions, nonperturbative generating functionals 80—73588
- Green's functions in nonrenormalisable massless $\phi^6{}_{3+\epsilon}$ theory, renormalisation of regularised theory 78—45771
- Gross-Neveu model, irrelevant operators and equivalent field theories 79—21912
- group theory solution to problem of particle motion, field of two Coulomb centres *(Russian)* 79—92992
- Haag-Ruelle formulation of scattering in hyperfunction quantum field theory 80—57497
- hadron+hadron elastic scatt., >100 GeV, asymptotic theorems review *(Czech)* 78—29357
- hadron form factors, axiomatic local constraints *(Russian)* 78—58190
- hadron scatt. amplitude, axiomatic restrictions 78—32967
- hadron scattering amplitudes, integral axiomatic inequalities *(Russian)* 77—79224
- hadron scattering amplitudes, integral axiomatic restrictions *(Russian)* 77—82685

axiomatic field theory continued
- hadronic wave eqns. from lattice gauge theory, breathing modes 79—97586
- Hawking effect, temp. relativity, axiomatic field theory 80—109456
- Heisenberg eqns. on C* algebra of quasilocal observables, boson and fermion systems 78—57854
- Higgs lattice abelian model, finite temp. behaviour 80—13260
- Higgs-Villain model, exponential clustering for long-range integer-spin systems 79—80744
- high-mass diffraction in the supercritical region 79—22081
- Holder continuity of sample paths in Euclidean field theory 80—9085
- holonomic fields, density matrix of impenetrable Bose gas 80—62576
- holonomic quantum fields, classical scatt. in Minkowski space time 79—80472
- holonomic quantum fields, deformation model 79—25907
- holonomic quantum fields, deformation theory, matrix step function limit 79—97519
- holonomic quantum fields, deformation theory in 2 space-time dimens. 79—97518
- holonomic quantum fields, form for any space-time dimension 79—67193
- holonomic quantum fields, global monodromy structs. for monodromy preserving deformation 79—45019
- holonomic quantum fields, model 79—25908
- holonomic quantum fields, model 79—25909
- holonomic quantum fields, Riemann-Hilbert problem 79—75690
- holonomic quantum fields, Riemann-Hilbert problem on complex sphere 79—25910
- holonomic quantum fields, symplectic version of 2-dimens. operator theory 79—49102
- holonomic quantum fields 79—25911
- Hubbard model with half filled band, fermion mass spectrum 79—21955
- hyperscaling and the critical exponent ν 79—80747
- inclusive processes, analytic structure of the $3\to3$ forward amplitude 80—68376
- indefinite metric theories, reconstruction theorem, Wightman functions, Hilbert space structure 78—12609
- independent value models, renormalisation of nonperturbative functional integral 78—12810
- instanton system weakly interacting with anti-instanton system, external electric fields, structure and stability 80—77956
- instantons, dynamical role in quarkless chromodynamics, bag model test 80—47246
- instantons in field theory 79—71642
- instantons in the presence of a fixed density of massless fermions in two dimensions 80—62853
- integral representation for the dimensionally regularized massive Feynman amplitude 79—71592
- intertwiner calculus, algebraic struct. of superselection sectors 77—18185
- IR singularities for arbitrary Euclidean external momenta 79—58861
- irregular operations in quantum field theory, distrib. multiplication for axiomatic set-up 79—54270
- Ising chain in transverse magnetic field, SLAC renormalisation group approach 79—67476
- Ising field theory, Z_2 duality algebra in $D=2$ quantum field theory 79—75685
- Ising model-gauge field analogues, universality 80—18068
- Jost-Lehmann-Dyson representation, scale invariance breaking and spectral function 80—13316
- Klauder augmented theory, Green function formalism, ϕ^4 model 78—78094
- Klein-Gordon nonlinear problems, existence of standing waves *(French)* 79—63339
- Klein-Gordon theory, classical limit in coherent state representation, holomorphic solns. 79—49372
- Klein-Gordon-Schrodinger coupled eqns. 79—35955
- Lagrangian, exact solutions in field thory 79—75677
- Lagrangian formalism for the theory of spin-3 fields 79—26224
- Lagrangian theory of anti-self-dual fields in 4-D Euclidean space, nonlinear σ-model 80—52386
- Laplace transform. inversion, non-unitary representations of MH(2) and group ax+b 80—4866
- large-N lattice gauge theory, third-order phase transition 80—52418
- lattice and continuum gauge theories, rigorous results 80—4880
- lattice fermions, Dirac fields and Thirring fields, spontaneous breaking of chiral symm. 78—24962
- lattice field theories, anharmonic anal. procedure 80—4859
- lattice field theories, energy levels, semiquantum approx. appl. 80—42343
- lattice formulation of general relativity 79—40426
- lattice gauge theories, boxiton scatt. cross section 80—82890
- lattice gauge theories, chiral symmetry dynamical breaking 80—99061
- lattice gauge theories, extrapolation to continuum limit 80—349
- lattice gauge theories, improved strong coupling expansions and matrix Pade approximants 79—71628
- lattice gauge theories, selfduality and topological-like props. 80—22506
- lattice gauge theories, strong coupling phase, large space-time dimension, Ising model 80—27397
- lattice gauge theories, two dimens., static quark confinement 79—35916
- lattice gauge theories, U(N) and SU(N), non-planar diagrams in large N limit 80—47187
- lattice gauge theories, vortex free energy, strong and intermediate coupling string tension 80—105786
- lattice gauge theories, Z(N) system phase struct., dual variables 80—62848
- lattice gauge theories with Higgs fields, phase diagrams 79—85231
- lattice gauge theory, 4-D Z_2 gauge, verification of first order phase transition 79—58876
- lattice gauge theory, local struct. Kirkwood-Salzburg eqn., recursive eqns., critical behaviour 79—26207
- lattice gauge theory, map between corner and link operators, QCD relation 79—35926
- lattice gauge theory, strongly coupled, confinement of fermions 79—2905
- lattice gauge theory *(Chinese)* 79—63336
- lattice gauge theory and spin systems, review 80—22528
- lattice gauge theory with fermions, renormalised phases, vacuum polarization 80—13198
- lattice Hamiltonian field theory, finite-size scaling 80—73580
- lattice Hamiltonian models, connected diagram expansion 79—21916
- lattice Hamiltonian models, estimation of eigenvalues 79—40669
- lattice Higgs models, (non)Abelian, diamag. and crit. props. 79—67465
- lattice massive dual fields for gravity 80—105779
- lattice models of quark confinement at high temperature 80—32082

axiomatic field theory continued
- lattice models with a solvable symmetry group 79—17616
- lattice QCD$_2$, Wilson's loop eqn. soln. for large N limit 80—78030
- lattice QCD, hadron mass spectrum, effective Hamiltonians, degenerate perturbation theory 80—102003
- lattice QCD, mass levels of boxiton (glueball) states 79—54259
- lattice quantisation of Sine-Gordon system, single-site approx. 79—17603
- lattice regularised field theory, renormalised and bare coupling constants 80—77960
- lattice SU(N) gauge theory, vacuum structure, large-scale 80—57470
- lattice theory, reconstruction of Euclidean fields from plane rotator models 79—97509
- lattice theory for fermions, Adler anomaly nonexistence 79—71667
- lattice-limit definition of functional integrals 80—27396
- Lie-admissible local powers, incompatibility with Wightman axioms and spin statistics theorem 78—93793
- linear field equations on self-dual spaces 80—42328
- linear SU(4) meson σ-model, one-loop approx., spin zero mass spectrum and leptonic-decay 80—47278
- linearised gravitational pot., Euclidean and Minkowski space formulations 80—121
- local, general props. of n-point functions 77—13877
- local charge densities in quantum field theory, conserved local currents 77—2718
- local field theory, n-point functions 77—10190
- local field theory, universal singular functions 78—32969
- local props. in field theories without strict locality 78—86401
- local Z(2) lattice gauge theory, gauge and matter screening 79—89065
- Luttinger-Thirring model on lattice, real space-time renormalisation 80—62590
- macrocausality of S-matrix, LSZ asymptotic condition 77—26452
- Mandelstam graph, deep inelastic asymptotics 79—85244
- many-body scattering processes in one-dimens. boson system, nonrelativistic $|\phi|^4$ theory 77—30093
- Markov fields in noncommutative probability theory on W* algebras 79—97260
- Markov representations of current algebra, T-positivity 77—18199
- mass, physical, in ϕ^4-model, renormalisation group and mass generation 80—77948
- massive field theories, low energy behaviour in Euclidean space 80—27385
- massive Thirring model, complete S-matrix, sine-Gordon solitons 78—16936
- massive Thirring model, explicit diagonalisation of Hamiltonian 79—21918
- massive Thirring model, inverse scattering transformation, correl. with exact quantum eigenstates 79—58873
- massive Thirring model, multisoliton solns. in Pohlmeyer-Lund-Regge system 80—47195
- massive Thirring model, particle scatt. in perturbation theory 77—82674
- massive Thirring model, quantized renormalized, dynamical charges, soliton, antisoliton, breather states 77—18171
- massive Thirring model, repulsive case, new effects 80—27415
- massive Thirring model, S-matrix calcs., required number of conserved currents 80—42329
- massive Thirring model, sine-Gordon eqn., soliton struct., Coleman correspondence 78—8509
- massive Thirring model, stability *(Russian)* 78—45800
- massive Thirring model, struct. and soln. 79—85230
- massive Thirring model potential, reflectivity of solns. 77—74597
- massive Thirring model with bosons, asymptotic scale invariance 78—93799
- massless $(\phi^3)_6$ theory, exponentiation of IR logarithms 80—31965
- massless $g\phi^4/4!$ theory, finite UV fixed point freedom 80—47181
- massless limit in the ladder approximation 79—21953
- massless Schwinger model, indefinite metric QFT axioms 78—29227
- massless Thirring model, saturating field configurations for two point Green's function 79—35923
- massless Thirring model is curved space, black holes, thermal states, conformal anomaly 79—26221
- massless $[g\phi^4]_4$ theory, functional integrals, complex instantons and asymptotic perturbation series 80—86571
- Maxwell's equations in axiomatic QFT, field tensor and pots. 77—71421
- Mayer equations for Bose field theoretical models 79—71593
- membrane models and generalized Z_2 gauge theories, renormalisation props. 80—86587
- meron and meron pair analogs in XY model 80—32010
- meron solutions in a non-Abelian, conformal invariant Higgs model 79—17610
- Minkowski-space formulation of two-pseudoparticle processes 80—95220
- model U(N) lattice gauge theories, exactly soluble, $N=\infty$ phase transition 80—86583
- model with anomalous dimensionalities in four-dimensional space 80—101934
- models and mathematics of quantum dynamics, conf., Bielefeld, Germany (Sept. 1975) 77—10158
- modified Wilson equation, appl. *(Chinese)* 79—71594
- multicomponent $\lambda(\phi^2)^2$ model, symmetry breakdown absence, vacuum uniqueness 79—12926
- multiparticle S-matrix factorisation in two dimens. space-time models 79—281
- multiparticle S-matrix in field theory two dimens. space-time models, factorisation 78—62324
- multiple vacua for non-Abelian lattice gauge theories 79—35929
- n-point functions, renormalised G-convolution, convergence in Euclidean case 80—77930
- non-Abelian lattice fields, duality 79—93280
- non-Minkowskian space-times, mass generation by self-interaction 79—45014
- non-perturbative quantum field theory, lattice renormalisation construction 80—9098
- nonAbelian lattice gauge theories, phase structure critical temp. 80—86592
- noncausal effects in relativistic wave eqns., Wightman fomulation 77—41750
- nonlinear Klein-Gordon eqn. related to Riemannian geometry, localised solns. 79—26223
- nonlocal QFT within Bogolyubov axiomatic approach, mapping abstract classes *(Russian)* 80—22530
- nonlocal structures, shell effects 80—52391
- nonlocal Wightman fields, PCT and spin statistics 79—35915

axiomatic field theory continued
- nonperturbative renormalizability for a class of gradient-free models 79—49392
- nonrelativistic ϕ^3 field theory in two spatial dimens., automation, FORTRAN system 78—8502
- nonrelativistic persistent model, Schrodinger and Klein Gordon interacting fields with Chew-Low coupling, renormalisation props. 79—54250
- nonrenormalisable model, non-cutoff Euclidean Green's function in four dimens. space-time 79—21898
- null plane field and algebra struct. 77—18154
- $(O^3)_6$, scale breaking for quark and gluon distribs., diagrammatic anal. 79—71706
- O(2) Heisenberg gauge invariant model, eigenfunctions and energy spectrum 79—58875
- O(5) gauge field coupled system with massless scalar fields in Euclidean space, exact classical solns. 79—97499
- O(N) invariant $(\phi^2)_3^2$ model, chiral field model and universality in 3-dimens. space 80—105796
- O(N) nonlinear σ-model, analyticity of solns. 80—52384
- one dimensional gauge field theories, at finite temp. and densities, props. and quark confinement 79—49468
- one-dimensional ϕ^4 and double quadratic systems, kinks, quantum statistical mechanics 80—47197
- order, disorder and generalized statistics 80—99055
- order/disorder quantum field operators associated with 2—D Ising model in continuum limit 79—9276
- $P(\phi)_2$, two-dimens. model, existence of three phases 78—49951
- $P(\phi)_2$ Euclidean field theory, boundary conditions rel. to ferromagnetic spin systems 77—54036
- $P(\phi)_2$ field theory, time ordered operator products and S-matrix 77—10162
- $P(\phi)_2$ Green's functions 77—10160
- $P(\phi)_2$ models, soliton solns. 80—42333
- $P(\phi)_2$ QFT, periodic boundary conditons, energy-momentum spectrum 78—365
- $P(\phi)_2$ quantum field theory, asymptotic perturbation expansion 77—10161
- para-Bose coherent states 79—96
- particle creation in curved space-time, back reaction effect 77—49645
- pathological lattice field theory for interacting strings 80—47186
- perturbation theory, large-order behaviour, critical exponents, Callan-Symanzik eqns. 79 —30397
- planar Feynman diag. enumeration 79—26239
- planar model electrodynamics, phase diagram, continuum limit, and mass spectrum 79—63426
- probabilistic techniques in field theory 78—49952
- propositional systems in local field theories 80—105799
- $Q^2\bar{Q}^2$ states, mass levels in (3+1) dimens. lattice gauge theory 79—58942
- QCD, lattice and continuum, Λ parameters connections 80—82945
- QCD lattice gauge theory, matrix Pade approximants, ratio of hadron to nucleon mass 80—4928
- QCD perturbation theory of hard processes in asymptotically free field theory, ϕ^3 80—13263
- QED, indefinite metric axioms, Markov property failure 78—41444
- QED, scale and conformal covariance 77—6067
- QED on lattice, Hamiltonian variational approach to physics of weak-coupling region 79—35979
- QED on lattice, vacuum polarisation in one-loop approx., SLAC fermion lattice action 79—85249
- quantised gauge field construction, lattice approx. convergence 80—37156
- quantised lattice gauge field construction, mass generation and Abelian Higgs models 80—4831
- quantum axiomatics 80—76
- quantum chirality, Wilson expansion for chiral field 79—71644
- quantum field construction from Markov fields 78—8504
- quantum fields in Fock space, construction 79—2911
- quantum theory evolution law approach appl. *(Russian)* 79—80866
- quark confinement in 2-D lattice Higgs-Villain model 79—26289
- random fields, characteristic functionals construction 80—31599
- random magnetic systems, gauge symmetries, Ising and X-Y models anal. 79—38295
- random spin systems, gauge symm., phase transitions *(Russian)* 80—77929
- real-space renormalization-group scheme for spin and gauge systems 80—32008
- reflection positivity in quantum field theory, some remarks 79—21900
- Reggeon field theory on a lattice, critical behaviour, Monte Carlo calc. 80—18126
- relativistic, reconstruction of local observable algebras from Euclidean Green's functions 78—54522
- relativistic many body theory, finite temp. and density., elementary particle symmetries 79—49403
- renormalised field products, Wilson expansion in dimens. regularised form 77—65066
- renormalised Thirring model, massless scalar field in 2-space-time dimensions 79—12929
- renormalized operator form of quantum action principle 80—42314
- resonances and field theory 79—2907
- S-matrix in boson theory, probability struct. in Euclidean domain 79—89071
- S-matrix in constructive quantum field theory of self-interacting bosons *(Russian)* 77—209
- scalar field theories, finite amplitudes in perturbation theory, ϕ^n models, pass. renormalisation 78—93794
- scalar field theory in lattice space, analogy to random walk 78—21325
- scalar neutral field, with self-interaction $g\phi^4$, strong coupling expansion for ground-state functional 77—30271
- scattering operator, analyticity in nonlinear relativistic classical and pre-quantised field theories 80—73611
- Schrodinger equation, nonlinear field equations, quantum inverse scattering transform method, 2-D ice and ferroelectric lattices 80—68348
- Schwinger functionals, positive extensions, moment problems, representations 78—8505
- self-generating discrete-space structure, lattice model in QFT 79—93276
- semiquantum approximation for the Reggeon field theory on a lattice 79—35968
- sequential events and objectivistic probabilities, quantum logic 80—94973
- sine-Gordon equation, discrete, on SU(2) lattice, group theory aspects 80—57486

axiomatic field theory continued
sine-Gordon equation, discretisation 79−21931
sine-Gordon equation, nonlinear field equations, quantum inverse scattering transform method, 2-D ice and ferroelectric lattices 80−68348
sine-Gordon equation and nonlinear σ model on a lattice 79−21932
Sine-Gordon field theory, ferromag. model, existence and renormalisation in all dimensions 79−26248
sine-Gordon field theory Coulomb gas equivalence, classical gas with logarithmic pot. 80−4850
singularities of Borel transform in renormalisable theories, massive $g\phi^4$ theory 78−62304
solitary solutions collision in nonlinear field theory, variational anal., ϕ^4 appl. 79−35922
solitary wave exchange potential in pseudoscalar and scalar meson fields 79−71617
soliton conservation laws, S-matrix bootstrapping approach *(German)* 79−9274
spatial inversions in aesthetic field theory, complex fields, computer solns. 80−68350
spin system, critical, in random mag. field, supersymmetry, neg. dimensions 79−97533
spin-statistics theorem, asymptotic, for composites containing electric and magnetic charges 80−68342
static Euclidean SU(2) solns., global struct. 80−4862
static ultralocal solutions, 1/N expansion of O(N) symmetric theories 80−52401
stress tensor of conformally invariant field in conformally flat spacetime, axiomatic renormalisation 78−29034
strong coupling lattice theory, approx. scheme 80−42342
SU(2)×U(1) six quark model, uniquely determined discrete symmetry 79−93360
SU(2) theory with four fermion interaction and asymptotic freedom, exact soln. 80−4858
SU(4) broken lattice gauge theory spectrum 79−49474
SU(N) lattice gauge model, weak coupling, monopole condensation and quark confinement 79−75683
SU(N) lattice gauge theories, weak to strong coupling crossover 80−95212
SU(N) Thirring model and 1/N expansion, chiral symmetry breaking 79−12977
(super-ϕ^3)$_4$, Euclidean model, normalisation of Schwinger functions 79−89060
(super-ϕ^3)$_4$, model, Euclidean formulation 78−93797
(super-ϕ^3)$_4$, regularisation of Euclidean model, supersymmetry Ward identity derivation 79−89059
superrenormalisable interactions, struct. of infrared divergences 79−40663
superselection rules, commutativity 79−240
supersymmetric Ising field theory, ‘doubled’ model, and supersymmetric sine-Gordon kink struct. 79−71614
Symanzik’s approach to nonrenormalizable theories for massless models 79−26212
symmetry generator struct. for Wightman field theory 79−71587
tachyons in field theories, conventional treatment book contrib. 79−58888
test function algebra positive elements, symmetrisation 77−37715
thermodynamic limit for correlation functions in $P(\phi_\varepsilon)_d$ models 79−93271
thinning degrees of freedom in lattice field theories 80−57492
Thirring and Schwinger models, operator solns. in terms of asymptotic fields 77−57449
Thirring massive SU(N) model, factorisation 79−12951
Thirring model, iterative variational anal., fermion field theory on lattice 78−41426
Thirring model, massive, static localised soln. 78−16930
Thirring model, phase transitions 80−18067
Thirring model, renormalisation and sine-Gordonisation 78−37135
Thirring model coupled to gravity, classical solns. in generally covariant model with fermions 80−9091
Thirring model Lagrangian, generalised, interacting fermions, interacting solitons 77−45937
Thirring model massive phase, dynamic mass generation 80−4851
Thirring model S-matrix, exact soln., agreement with perturbation theory 77−54049
Thirring model SU(1,1) group representation theory algebraic struct. *(German)* 79−89055
Thirring model with SU$_n$ symmetry, scale invariance 79−9288
Thirring-Weiss model, massless, saturating field configurations 79−35953
time-ordered products and Schwinger functions 79−26216
trace anomaly of a conformally invariant quantum field in curved spacetime 78−54278
transition rates at finite temperatures, instanton solns. 80−42336
translationally noncovariant conserved local currents in Wightman’s axiomatic field theory 78−32971
transverse lattice QCD, hadron mass spectrum 80−57568
tricritical behavior in a two-dimensional field theory 80−77726
trilocal structures, expansions 80−57460
twisted lattice gauge fields, local order parameter, phase transitions 80−77966
two dimensional field theories with infinite number of conservation laws and Backlund transformations 80−9095
two-dimens. U(1)-Goldstone model, QFT on lattice 78−74158
two-dimensional theory containing massless scalar theory 77−65079
two-Reggeon cut in the ordered phase of Reggeon field theory 80−52422
U(1) lattice gauge model, phase transition in four-dimensional compact QED 80−105820
U(1) lattice gauge theory, four dimens., nonconfining phase, existance proof 80−73602
U(N) lattice gauge QCD, complete integration in large-N limit 80−42338
U(N) lattice gauge theory as N→∞, planar diagram sums in terms of statistical ensembles 80−99052
U(n) symmetric Thirring model in indefinite metric space, boson representation 79−12942
ultradistributions, Fourier-Laplace transforms, boundary values 80−57496
vacuum polarization effects in lattice gauge theories 80−13211
vector boson and graviton propagators in the presence of multipole forces 79−85207

axiomatic field theory continued
von Neumann theorem extension to unreproducible meas. *(Ukrainian)* 77−71415
Ward identity, conformally invariant form, Green’s function and two conserved currents 78−86421
Weyl and conformal covariant field theories 79−80749
Wick square, infinite divisibility 77−30230
Wightman axiomatic scheme for concentratable field, local commutativity axiom *(Russian)* 77−61201
Wightman axiomatic scheme for concentratable field, polynomial cluster props. *(Russian)* 79−12971
Wightman distributions, globally conformal invariant quantum field theory, conformal superworld 77−49824
Wightman field operators, linear independence at different space-time points 77−18164
Wightman fields, algebra of test functions 77−18186
Wightman formulation, nontranslationally covariant currents and symm. of S-matrix 78−58133
Wightman function, two-point, asymptotic behaviour 80−73614
Wightman functions, decomposition in Euclidean framework 78−54566
Wightman functions for interacting spinor fields on a lightlike plane 79−93284
Wightman scheme construction for concentratable field *(Russian)* 77−49863
Wightman scheme for concentratable field, VR-field *(Russian)* 78−21343
Wightman theories, consequences of weakening positivity property 80−62833
Wightman theory, all spontaneously broken symmetries for noncovariant currents 80−31975
Wilson’s lattice, local chiral symmetry for gauge theories 80−105774
Wilson loop critical point behaviour in gauge and lattice guage theories 80−90993
WKB approximation for quantum theory on a lattice 80−32009
X-Y model, gauge theory analogue, 4-D self-dual gauge model, phases and transitions 80−27399
Yang-Lee edge singularity, field theoretic formulation 79−17354
Yang-Mills lattice theories, comparison with gauge groups SU(2) and Z_2 80−31966
Yang-Mills theory, lattice gauge theory, Gaussian transformation into string field theory 80−32003
Yukawa$_2$ quantum field theory, boson-fermion interactions 77−10163
Yukawa$_2$ quantum field theory, connection between spectrum condition and Lorentz invariance 78−21317
Yukawa$_2$ quantum field theory, FKG correlation inequality 80−68357
Yukawa, field theory, energy-momentum spectrum 78−16905
Yukawa, mass divergences of wide angle scatt. amplitudes 79−49402
Yukawa field theory model, boson field fluctuations and FKG inequalities 80−77712
Yukawa potentials, finite sum S-matrix 80−101940
Yukawa quantum field theory, Matthews-Salam integral representations 80−327
Yukawa quantum field theory in 2D space-time, linear N_τ bound, locally Fock property 80−326
Yukawa weakly coupled model in two dimens., Wightman axioms 77−13837
Z_2 lattice gauge Higgs theories, Monte-Carlo calcs. 80−86593
Z_n four dimensional lattice gauge theories, series anal. 80−99050
Z_n lattice gauge theory coupled to Higgs field, phase diagrams 80−57485
Z_N lattice gauge theory phases, Lagrangian formulation 80−42323
Z_N symmetric models phase transitions 80−101922
Z(2)(3) Ising spin systems, Hamiltonian formulation in 1+1 dimens. 80−57491
Z(2) gauge theories, hidden fermions 80−82899
Z(2) gauge theory, phase transition, variational calcs. 80−99049
Z(2) lattice gauge theory, variational approach, two phase struct., phase transition 80−68361
Z(2) lattice gauge theory in 2+1 dimens., fermion representation 80−82900
Z(N) and U(1) lattice theories in three-dimens., phase diagram 80−82901
Z(N) lattice gauge theories, Hamiltonian approach 79−85233
Z(N) strings and hadron structure 80−86572
Z(N) topological excitations in Yang-Mills theories: duality and confinement 79−12938
0^4 spontaneously broken theory, quantisation of classical moving extended object 77−79217
$e^+e^-\rightarrow$hadrons$+X$, structure functions in next to leading logarithm approx., ϕ^3 field theory 80−37268
$e^+e^-h\rightarrow e^-X$, h=hadron, structure functions in next to leading logarithm approx., ϕ^3 field theory 80−37268
NN scattering, effective interaction in the Blankenbecler-Sugar equation in ϕ^3 theory 79−21914
ϕ^3 field theory in $6+\varepsilon$ dimensions, anomalous dimens. calc. 78−134
ϕ^4 3-D field theory, IR behaviour and connection with critical phenomena 79−71601
ϕ^4 model, free energy, spontaneous symmetry breaking 80−101925
ϕ^4-field model with image mass, spontaneous coherent state transition 80−99057
ϕ^6_2 theory, Gell-Mann and Low renormalisation group appls. 78−29224
$\phi^2\phi_0$ 79−67579
π N forward scattering amplitudes high energy, integral axiomatic upper bounds for coupling const., logarithmic sensitivity *(Russian)* 77−13984
π^0 condensation in σ-model, chiral symmetry 79−80895
$\pi\pi$ scatt. lengths, rigorous phenomenological anal. 80−102070
$\pi^0\pi^0$ amplitudes, construction from axiomatic requirements 77−38201
ψ^{2N} field theory, asymptotic graphs counting techniques 79−17608
$\bar{\psi}\psi\bar{\psi}\psi$ model, two dimens., relationship with Yukawa-type model 79−35948
$\Theta_2{}^4$ quantum field theory, numerical methods, anharmonic oscillator approx. 80−52390
$g\phi^4$ model, large-order behaviour of the 1/N expansion in zero and one dimensions 79−58862
$\Lambda\phi^4$ theory, high temp. expansion without lattice, strong coupling expansion 78−58124
$\lambda\phi^4{}_2$, quantum field as limit of sine Gordon field 78−82094
$(\lambda\phi^4-\sigma\phi^2-\mu\phi)_3$, quantum field model, convergence of lattice approxs., infinite vol. limit 77−49823
ϕ^3, six-dimens., struct. of high-energy jets 78−29248

axiomatic field theory continued
ϕ^4_4 scaling limit, crit. exponents and renormalisation 77—10166
ϕ^4_2 multiphase field theory, asymptotic perturbation expansion 77—10167

backplane wiring *see wiring*

backscatter
see also particle backscattering
absorbing-scattering layered material, light beam diffusion obs. method 78—62215
acoustic, backscattering, from thin air-filled spherical shells in water 78—13838
acoustic backscatter in GATE, effect of wind shear and moisture fluctuations 80—85709
acoustic backscattering cross-sections of live fish, probability density function and aspect 80—64260
acoustic backscattering from a plate with a thickness discontinuity 80—96056
acoustic backscattering from very rough water surfaces 79—41499
acoustic backscattering measurements in laboratory waveguide 80—64259
acoustic LF backscattering by wind-generated air bubbles undersea with large-scale roughness 79—86285
acoustic monitoring of industrial chem. waste at deep water dump site 79—34466
acoustic transducer, backscattering formula 80—96064
acoustic wave scattering from rough surface with 2 types of roughness 80—14505
acoustic waves, surface roughness and frequency dependence of backscattered field *(French)* 80—53506
active and passive remote sensing of Earth terrain, effects of scattering 80—101435
active remote sensing with radar, radiative transfer theory, half-space random media appl. 79—8721
aerosols, high relative humidity, optical backscattering, extinction coeffs. 77—34825
Arctic sea ice, surface-based radar scatterometer results 79—92544
Arecibo radar meas. of tropical winds 79—100975
atmosphere, finite plane-parallel, forward and backward scatt. effect on spherical albedo 79—92592
atmospheric boundary layer, acoustic backscatter, beamwidth effects 79—70859
atmospheric remote sensing by aerosol lidar backscatter *(Dutch)* 80—4110
auroral currents, magnetometer array and radar backscatt. joint obs., N.Scandinavia 78—85768
auroral E-layer, plasma lines meas. 79—25386
auroral electrojet, Chatanika radar meas. compared with Anchorage VHF backscatt. obs. 78—12048
auroral radio echo, ion-acoustic, short term characts. 78—45080
bidirectional optical fibre, Rayleigh scattering freq. depend. meas. 79—64317
broadband integrated backscatter approach to tissue characterization in vivo 80—74635
calorimeter, BB2, for high-power CW laser energy meas. 78—54372
cerebral tissue, freq.-dependent US backscatter obs. and correl. 79—79620
chemical identification of substances fixed on silica gel, using Raman spectroscopy *(French)* 78—88664
cirrus clouds, lidar backscatter meas. rel. to visible and IR optical props. calc. 80—82060
clouds, radar reflectivity rel. to cloud dynamics and microphysics 80—61877
coated hollow cylinder in water, sonar cross section 77—46844
conducting rectangular corrugations, radar appls. 79—18332
cosmic radio noise absorpt. events meas. on riometers, due to backscatt. by E-region irregularities 77—25831
densely distributed scatterers, picosecond pulse backscatt. 80—14281
density monitoring by back scattering of single energy electrons 79—97362
dielectric spheroids, backscatter matrix 78—66716
differential scatter lidar system, for atm. aerosols remote anal. 78—69524
directional sea spectrum determ. using HF Doppler radar techniques 77—17229
directional sea wave spectrum determ. using HF Doppler radar techniques 77—29476
Doppler acoustic sounding of lower atm., convective plumes detect. *(French)* 78—40603
Doppler processing of HF backscatter radar and mode structures of ionospheric propagation 79—16753
Doppler US blood velocity meas., phase-locked loop technique 78—61234
drops of water, ice or mixed phase, backscatt. at 633 nm 77—64426
duroral zone ionospheric modification, incoherent scatter radar obs. 77—82083
effective scattering area of objects, average-value estimation in real-time *(Russian)* 77—83790
elastic scattering large-ang., approx. classical theory, for teaching 79—25801
electron beam, relativistic, unmagnetised, stimulated scatt. anal. of HF incident pump wave 79—77345
electron beam, surface thickness monitoring, object accessible from one side 78—60944
EM, cross-sections, precision meas. as function of freq. 77—18014
EM back scattering effects due to diffusion by the Earth's surface *(French)* 78—24289
EM plane waves, scattering by metal cone, near its symmetry axis 80—106426
EM scattering from large rotating conducting cylinder of arbitrary cross section 79—18331
EM sounding method using spatial and spectral sampling, for investigation of inhomogeneities in ionospheric plasma *(French)* 79—29911
EM wave backscatter, from relativistic electron beam front 77—27235
EM wave from metallic sphere in radially inhomogeneous plasma sheath, anal. *(Russian)* 77—7558
EM wave in bounded dissipative plasma, stimulated backscattering nonlinear theory 77—7547
EM waves, multiple backscattering from randomly fluctuating media 77—50593
emulsive foams, UHF radiation scatt. *(Russian)* 77—6978
F-region, equatorial, backscatter obs. rel. to irregularity patches localised origin 78—77404

backscatter continued
finite plates, nonspecular acoustic backscattering 79—72736
fogs, optical probing, homogeneous particle model 79—66790
foil, surface density meas. method using back-scattered low energy γ-rays *(Czech)* 77—50323
hailstone trajectories determ. from crystallography, D content and radar backscatt. 78—61614
heat radiation, two-dimens. isotropic scatt. in semiinfinite medium 78—42521
heavy ion neutralization behaviour in the 30-130 keV energy regime 80—71542
heterodyne optical radar S/N ratio in atmospheric turbulence 80—106558
HF radar sea-echo Doppler spectra, extraction of wave height and period 77—78474
HF radio scatter appl. to sea studies 77—17230
HF radio wave backscatter by artificial ionised clouds 77—56788
HF sea-echo Doppler spectra, statistics 77—17231
hydrometeor backscattering cross sections, meas. at 6328 Å 78—49135
ice samples, backscatter matrix rel. to hail identification by radar 79—58046
incoherent backscatter from rough surfaces, two-scale model re-examined 78—71013
infinitely long circular cylinder, backscatter of arbitrarily polarised EM wave 80—9778
inverse scattering methods for EM fields 77—31048
ionosphere, backscatter leading edge ionograms inversion method 77—41265
ionosphere, backscatter radar data rel. to O I 6300 Å nightglow intensity 78—77401
ionosphere, equatorial, backscatter data rel. to irregularity patch form., motion and decay 80—67456
ionosphere, equatorial radar backscatter plumes spatial relationship with plasma bubbles 80—67457
ionosphere, incoherent scatt. radar spectrum, plasma line intensity as aeronomical diagnostic 78—32271
ionosphere, low-altitude plasma line anisotropy theory 78—77414
ionosphere, oblique-backscatter sounding signal fluctuations and accumulation method of reception 77—60521
ionosphere, stimulated Brillouin scatt. and incoherent backscatter 77—78552
ionosphere, stimulated Brillouin scatt. theory 77—37478
ionosphere, stimulated reson. line scatt. with Eiscat radar 78—57389
ionosphere electron density meas., using radio wave scattering, from artificial plasma inhomogeneities 79—75074
ionosphere EM wave propagation, backscatter echo spectral analysis and radio transmission forecasts *(French)* 79—29912
ionosphere equatorial spread F, radar backscatter obs. 77—29566
ionosphere equatorial spread-F, VHF and UHF backscatter from high freq. drift waves 78—88973
ionosphere HF signal, group path variations from modulation envelope measurements 80—51597
ionosphere oblique-backscatter sounding on multihop path, HF signal intensities 78—45113
ionosphere temperature latitude E_s-layer, skywave backscatter studies 78—85761
Kirchhoff approximation in horizontally polarized backscatt. from random surface 79—7061
lakes, ice-covered (North Slope, Alaska), radar return differences 79—2298
laser backscattering from dense water-droplet clouds 79—53513
laser backscattering from turbid water-nigrosin black dye-Teflon spheres dispersion 80—1129
lidar, heterodyne, signal-to noise ratio in presence of atmospheric turbulence 79—100949
lidar backscatter from horizontal ice crystal plates 78—92984
lidar investigation of inhomogeneous atmosphere optical parameters *(Dutch)* 79—80026
lidar return, simulated, from one-dimensional stratospheric aerosol model 79—44247
Lidar return from fogs, effect of non-uniform extinction coeff. on double scatt. contrib. 79—100952
lidar target calibration, backscatter refl. for circularly polarised radiation 80—102750
Loran-A (1.85 MHz) radio wave backscatter from ocean waves, Doppler spectra *(Japanese)* 78—85737
magnetised plasma, backscatt. of laser beam from electrostatic waves 80—33779
mammography, backscatt. factors, var. with field diameter and half-value layer 78—3593
mesosphere, lower, O_3 abundance from backscattered solar radiances 78—69414
meteors, bright, radar backscatter meas. of ionisation columns initial radii 80—94762
MF/HF backscatter radar for sea surface meas. *(Japanese)* 78—16210
microwave, effect of induced current, investigation with wind-wave tank 77—17111
microwave backscatter from intense relativistic electron beam 77—38794
microwave backscatter modulation by shoaling ocean waves 78—57212
microwave by sea waves, meas. at 8 mm and 30 mm *(Russian)* 77—5210
microwave scatterometer, backscatter optimisation using complex charact. polarisation concept 79—100966
microwave sea backscatter intermittency at extreme grazing angles, model 78—24307
microwaves attenuation by rain for Earth-space links, comparison between radar- and radiometer-derived data 78—24343
Milne problem and spherical albedo, law of darkening, forward and backward scatt. effects 78—77483
modulated backscatter from reed switch loaded dipole 77—75386
multimode fibre waveguides, optical characts. meas. by backscatt. 80—23801
multiple atmospheric parameter meas. laser radar system 78—4009
multiple scatt. between a rigid steel cylinder and plane, underwater 77—23793
multiple scattering effect on backscattering from random medium 77—19137
myocardial and hepatic tissue US backscatter comparison 79—48310
nearfield array for use in acoustic backscattering cross section meas. 77—14862

backscatter continued
- nonhomogeneous layer above reflecting surface, scattering of waves 80−58449
- North Sea, surface film, 13.9 GHz radar backscatter cross section meas. 79−39764
- ocean, Doppler sonar backscatter from strongly nonlinear internal motion in open sea 80−51422
- ocean, microwave scattering signature, aircraft measurements 77−17112
- ocean surface, radar backscatter rel. to wind speed and fetch 78−77247
- ocean surface wind obs., SeaSat scatterometer/scanning radiometer/altimeter comparison 80−46249
- ocean wave height statistics, dual freq. correl. radar meas. 77−29478
- ocean wave meas. using pulse compression radar scatterometer system, expt. 77−29483
- ocean wave spectra derivation by integral inversion of second order radar echoes 77−78475
- oceanography, acoustic backscatter monitoring of natural suspensates and slope/shelf water intrusions 79−2241
- oil spills remote detection using laser-excited Raman backscatt. and backscatt. fluoresc. 78−32242
- optical fibre attenuation, bandwidth, and refractive index meas. methods compared 80−64190
- optical fibre attenuation charact. meas. by backscatter technique *(Italian)* 80−106600
- optical fibre attenuation meas., backscatter method modified for endfire launching *(German)* 78−33868
- optical fibre attenuation meas. by backscattering method, effect of noise 80−102824
- optical fibre attenuation measurements performed by backscattering technique 80−64152
- optical fibre backscatter attenuation measurements, optimised technique 80−53447
- optical fibre connector loss evaluation by backscattering 80−58721
- optical fibre loss estimation using backscatter technique, time domain reflectometry theoretical assumptions 80−74508
- optical fibre mean splice loss meas., applying backscattering method 80−19091
- optical fibre measurements, separation of power decay from imperfection contribution 79−76827
- optical fibre splice insertion loss meas., backscattering method 80−58720
- optical fibre transmission characteristics measurement appl. 80−53409
- optical fibres, backscatter meas. theory *(German)* 80−91921
- optical fibres, backscattering method for attenuation and connection insertion loss meas, anal. 80−58675
- optical fibres, bandwidth and backscatter measurements, review 79−64356
- optical fibres, time-domain reflectometer for attenuation measurement and fault location 79−64355
- optical fibres attenuation characteristics obs., improved experimental approach 77−75669
- optical glory, theory, physical effects 77−60468
- optical heterodyne line-scan imagery, speckle noise model 79−50337
- optical single-mode fibres, backscattering method analysis 80−106610
- optical time domain reflectometry by photon counting 80−95122
- optical wave backscattering amplification during large intensity fluctuations 80−18994
- optical waveguides, power decay eval. using backscattering technique 80−106599
- periodic surface characterisation by US diffraction spectroscopy 78−60974
- plasma, Brillouin backscatt. depend. on density scale lengths near crit. density 80−43888
- plasma, collisionless, enhanced Raman backscatt. of Gaussian laser beam from plasma wave 79−86566
- plasma, laser prod., z-depend. absorpt. and stimulated backscatter processes 80−43944
- plasma, stimulated Raman and Brillouin backscattering along mag. field 80−69983
- plasma, stimulated Raman backscattering of circ. polarised EM waves 79−37465
- plasma, weakly inhomogeneous laser-produced, stimulated Brillouin back-scatt. losses 80−19561
- plasma target, underdense, Brillouin backscatt. saturation 80−14886
- polycrystalline structure testing by US backscatter meas. 77−21347
- precipitating electrons, atmospheric backscatter program rel. to loss cone struct. 78−40774
- prolate spheroids, EM vs acoustic backscattering 78−46854
- radar, backscatter from scatt. cells located in random medium 77−39428
- radar backscatter from lunar surface, results from automatic stations 77−53438
- radar cross-sections of ocean surface, friction vel. depend. 78−77246
- radar imaging of ocean surface waves, models 77−25689
- radar meas. of surface roughness, soil moisture and texture with vegetation cover 79−62534
- radar remote sensing of sea state, HF sea-echo Doppler spectra statistical props. 77−29312
- radar scatterometer discrimination of sea ice types 77−41198
- radiowave scattering from meteoric ionisation, theory 77−87337
- raindrop induced forward and backward scattering amplitudes, tabulations 79−34884
- random media, active remote sensing, depolarisation effects 80−82090
- random media, spatial correlation function of backscattered field 78−25779
- Rayleigh surface waves, submerged Al cylinders 79−86276
- remote sensing, scatter model for leafy vegetation 79−12193
- remote sensing of vegetation layer, scatt. model 79−29880
- ring lasers, solid-state, synchronisation modes of colliding waves and beats 79−72602
- rough surface, average impulse response, satellite radioaltimeter appl. 77−25791
- scatterometer, pulse compression system, experimental study 77−17240
- sea echo radar spectra resolution limitation inferred from ionospheric Doppler broadening 78−81489
- sea return, CW dual-freq. X-band radar studies 77−25687
- sea return studies with CW dual-freq. X-band radar 77−17232
- sea roughness investigations, radiophysical, Ukrainian Academy of Sciences 77−17233
- sea roughness radio measurement at Ukrainian Academy of Sciences 77−29313
- sea surface, microwave backscatter rel. to remote sensing using one and two freq. microwave techniques 80−94622

backscatter continued
- sea surface scattering theory for large incident angles 77−86911
- sea surface wind speed and significant wave height measurement using pulsed radar 77−29477
- sea wave meas. using HF radio scatter 77−25789
- sea wave space and time structure measurement from Doppler frequency shift 77−29482
- sea waves, low-angle backscatter of microwave radar, long-period feature origin 78−57218
- sea-wave space and time params. determ. from freq. characts. of RF signal scattered by sea 77−17239
- side scan sonar data, adaptive sample set construction 80−43554
- single-mode optical fibres, backscattering signal anal. utilising wave optics approach 80−64151
- single-strand fibre couplers 77−68283
- Skylab scatterometer meas. of hurricane Ava, anomalous data correction 79−29881
- slurry conc. and particle size determ., on-line light backscattering method, fibre optic appl. 79−58674
- snow, radar backscatter in 1-8 GHz range, MAS expt. 77−86946
- snow penetration and backscatter of millimetric waves 77−21877
- soil moisture measurement, active microwave remote sensing, surface roughness and texture effects 79−12295
- soil moisture sensitivity of cross-polarized radar backscatt. 79−25282
- solar hard X-rays, backscatter, anisotropy and polarisation 78−28594
- solar resonance radiation multiply scattered by nearby interstellar medium, backscattered intensity 80−41874
- sonar 77−817
- sound backscattering by disturbed sea surface 77−11077
- sounding technique for study of the ionosphere *(Spanish)* 79−100998
- sporadic-E (E_3) layer over Japan, sky-wave backscatter obs. 79−44298
- STARE: a new radar auroral backscatter experiment in northern Scandinavia 79−39977
- stimulated light scatt., wavefront reconstruction 80−64107
- stimulated Raman scatt., backscatter in an optical fibre 80−64109
- suspension, particle size and concentration, determ. by light backscatter technique 78−85214
- tapered fibre coupler for optical pulse backscatter meas. 77−7212
- thin stiffened Al plate, underwater acoustic backscattering and echo struct. characts. 78−55492
- tissue characterisation by US backscattering 79−70595
- tissue characterisation by US scatt. frequency and angular dependence 77−64118
- tissues, fixed and unfixed, US propagation, backscattering coeffs. and speech determ. 80−41109
- topography and backscatter analysis of Geos 3 data 80−3915
- underwater sound, backscattering spectra of preserved zooplankton 77−79994
- underwater sound scattering from fluid sphere, appls. to marine organisms 77−46846
- upper-hybrid reson. absorpt. of laser in plasma focus, backscatter 80−28621
- US diffraction scanner for in vivo tissue characterisation 78−61226
- US pulses, short, backscattering 80−43502
- US radiation, from human tissue 77−86576
- US tissue characterisation by backscattered field space-time processing 79−48305
- UV backscatter expt., airborne, for O_3 distrib. determ., error anal. 78−92985
- UV backscatter meas. in tropical stratosphere, O_3 profiles 78−49091
- UV backscattering rel. to vertical O_3 profile in atmosphere 78−7762
- VHF, from E-region 77−33248
- VHF backscatt. from blanketing E_s-layers in equatorial electrojet, gradient instabilities 77−29577
- VHF coherent radar sounding of lower atmosphere 78−28281
- VHF radar aurora and strong HF backscatt. comparison 80−61960
- VHF radar echoes from equatorial E-region irregularities, sudden disappearance 78−40738
- water, backscatter and absorption coeffs., simultaneous determ. 80−82074
- wave propagation in inhomogeneous media, backscatter folding series *(Russian)* 78−73862
- wave reflected from randomly inhomogeneous layer description, by series satisfying causality condition 80−106420
- Z-pinch plasma, interaction with CO_2 laser radiation 80−48919
- ^{241}Am 60 keV γ backscatter meas. of solid powder mixture composition 77−52695
- BO_2, Doppler free spectra, backscatter fluoresc. line narrowing, theory and obs. 80−53034
- CO_2-laser (long pulse)-plasma interactions, classical absorpt. and heat conduction in low-irradiance 80−75059
- ^{60}Co skyshine, continuous γ-spectra unfolding 79−81118
- Fe slab *(Japanese)* 80−18595
- H^+, neutralisation in low energy surface scatt. by polycryst. graphite 80−71541
- He^+ reflection from Pt surface, 10 to 35 keV 80−71543

backward wave oscillations *see backward wave tubes; electromagnetic oscillations*

backward wave tubes
- *see also carcinotrons*
- BWO for 110 to 170 GHz, using Sm-Co using magnets, design and appl. *(German)* 80−105684
- EM waves generation and amplification based on Doppler effect 80−63902
- one-dimensional wire grid and BWT spectrometers 77−38040
- p-Ge, free-carrier reson. investigation using backward-wave tube spectrometer 79−15353

bagging *see packaging*

balance (physiological) *see mechanoception*

balanced amplifiers *see differential amplifiers*

balanced input amplifiers *see differential amplifiers*

balances
- *see also weighing*
- acceleration compensation of force transducers and weighing systems *(German)* 79−35733
- accuracy class increase, using several standard weights of equivalent mass *(Rumanian)* 80−47022
- animal and organ weighing, automatic balance *(Japanese)* 79−25173
- automatic, Russian types 990VN and 959DN, accuracy improvement 80−52166

balances continued
beam microbalance for microweighing in vacuum and controlled environments, book 80—62401
Cahn electrobalance adaption for solid-gas reactions at high temps. 77—79084
capacitance-torsion balance for measuring small stresses and strains 78—73988
corrosion kinetics, mass and resist. change techniques, comparison, for Permalloy film 78—27675
deadweight standard machines, 100 kN, investigation of parasitic effects 79—35731
dynamic wind-tunnel, two-component, for mounted flying insects 80—22350
education, spring-mass oscillator, parametric instability 77—78921
electro-mechanical, evaluation of limits of resolution using characteristic values of load cells *(German)* 79—71445
electrobalance, used in thermogravimetric system for investigating gas-metal reactions at elevated temps. 80—229
electromechanical balance type-test results *(German)* 77—79059
electromechanical weighing machines, testing of strain gauge load cells *(German)* 79—35682
electronic, reasons for slow sales and review of recent models 79—21706
electronic balance ED series *(Japanese)* 80—22330
electronic balance with integral microprocessor 79—67255
electronic microbalance and precision balance design *(German)* 78—57935
electronic scales and precision instrum. *(German)* 78—70100
equal-arm balance for masses up to 1 g 77—22531
Faraday balance for teaching appl., strong mag. field rel. to react. rates 80—57043
Faraday balance susceptometer, computer controlled 78—65946
Faraday magnetic balance for metalloprotein solns. in 6.5-300K range 78—70170
flat spring strip elasticity characteristics *(Polish)* 78—21129
force and meas. measurement, conf., Braunschweig, W.Germany (Sept. 1978) 79—35725
force standard machines, calibration using mass standards *(German)* 79—35735
general purpose, program for state acceptance testing 79—80581
glass-ceramic beam, for 1 kg balance, props. *(German)* 78—89472
granular material crushing strength determ. apparatus 79—70260
hydrostatic weighing, solid density standards 80—77758
inertial, direct reading, for student demonstrations, experiment 78—86081
laser interferometer for measuring beam oscill., construction *(German)* 77—79090
lever balance error calc. with adjustability consideration 77—30131
lever balance errors caused by knife edge height displacement 79—35680
liquid density meas., analytical one panned scales appl. based on solid body density standards *(Croatian)* 79—26033
load cell, automatically controlled using capacitive and US sensors *(German)* 79—35715
load cells and indicators for weighing machines, permissible number of digits *(German)* 79—35681
loading machines, comparison with German PTB force scale *(German)* 79—35734
magnetic, for weight of body in closed vessel 77—22529
mass change meas., automatic recording system, exam. 78—57901
mass standard error limits and accuracy class determ. *(German)* 77—74364
mass standards (1000 kg) for electromech. balance testing *(German)* 77—79060
mechanical, with electronic displacement sensor, precision 78—77866
metal surface oxidation study, vacuum microbalance investigation 80—76552
metrological balance automatic recorder and printer 77—22530
microbalance, Cahn-RG, mass artifacts in water vap. 78—65909
microbalance techniques, conf., Boston, USA (Nov. 1977) 78—65905
microprocessor, laboratory weighing appl., capabilities 80—13067
microprocessor based electronic scale 77—74421
mutual disposition of working edge of prisms, deviation effect on accuracy 78—4594
piezoelectric microbalance, for respirable aerosol mass conc. meas. 78—69518
piezoelectric quartz cryst. microbalance for sorption studies under dynamic conditions 80—73323
ponderomatic meas. for fluid detection in chem. anal. 78—68953
precision, electronic methods *(French)* 80—62660
precision, read-off automation with aid of computer, use of Michelson interferometer 77—5809
pressure, effective area at low press. 80—86332
pressure, improved floating-element spinning mechanism 80—86331
quartz crystal microbalance, reson. freqs., influence of mass loading outside electrode area 77—82491
quartz crystal microbalance, response to liq. deposit 79—30422
quartz crystal microbalance sensing elements in cascade impaction instrument, particle size meas. 78—65904
quartz crystal microbalance with coatings of finite viscosity, transmission line analogy 80—17933
quartz oscillator microbalance, high resolution, appl. to Al oxidation 77—70219
quartz spring vacuum microbalance 79—49204
radiation balance for US power meas. 79—83863
reliability and performance testing 79—80579
scale single flat spring fulcrum deformation, second approximation *(Japanese)* 79—184
self-balancing bridge as a micro-balance 77—2644
shipboard weighing techniques 78—45595
single pan balance method, adjustment of weights to OIML conditional density 77—41572
single-pan analytical, liquid density meas. using solid density standards *(German)* 80—52167
skin-friction balance measurement, error sources 77—65828
small weight, automation problems *(Polish)* 78—70099
strain gauge load cells, small dead weight machines with compensator and computerized data processing 79—37266
substance amount, precise meas. and dosage 80—90819
surface balance, Langmuir-type, monolayer parameters meas. in radiation field 78—82092
thermal noise effect on meas. appls. 78—65906

balances continued
thermo-balance method for expts. under controlled vapour press. 80—47021
thermobalance, high sensitivity for macro samples, construction, performance *(Japanese)* 80—47023
thin films, vac. deposited, mass change, optical transmittance, and reflectance, simultaneous meas. apparatus 79—75501
three-chip digital scale zeroes tare weight, cct. 80—27282
torsion, sat up by welding fused quartz rods and fibres *(Japanese)* 80—31738
torsion vacuum microbalance appl. to sputtering yield meas. *(Japanese)* 78—19622
torsional, operational principles *(Polish)* 79—80583
two-string balance microprocessor operation *(German)* 78—57936
UHV microbalance, with ion gun, absolute meas. of sputtering yield *(Japanese)* 80—17951
vacuum microbalance, Cahn RG-2000, improvement in sensibility 80—77794
vacuum microbalance, cryopump 80—77803
vacuum microbalance, Knudsen forces, theory 77—74366
vacuum microbalance, props., characts., applications 80—73322
vacuum microbalance of physical adsorption studies 80—76551
vacuum thermogravimetric apparatus for evaporation kinetics determ., design of weighing device 77—37865
vacuum ultramicrobalance, for surface studies 79—71465
vibration isolation cantilevered bench 80—68183
weighbridge and heavy-goods weighing machines, changes in standards 79—6096
weight and cost read-out balances *(Polish)* 80—90820
wind-tunnel balance, 6-component, using load cell techniques *(German)* 79—37268

ball lightning *see lightning*

ballistics
see also impact (mechanical); military equipment
aircraft, ballistic descent, stabilisation transient processes 77—53395
anomalous dispersion methods, for meas. in hypersonic wakes of ballistic devices 79—82014
armour material, selection criterion 78—53063
artillery shell, experimental determination of mass-property/trajectory-drift relationship 80—8779
bouncing ball experiment, theory of time of flight, for teachers 79—71196
collision of aimed and initially stationary balls, for teachers 79—21506
dynamic pressures, shock wave parameters, high speed bodies collisions 77—68491
education, ballistics, max. range at elevated launch height, expt. and BASIC program 79—97156
education, ballistics pendulum 77—78914
equivalence principle, monkey and hunter demonstration 80—67984
gas gun with rectangular bore, appl. to impact expts. 77—41588
Gurney's ballistics calc. 80—67946
handwriting a Japanese letter to investigate the patternization of motion 78—12555
high speed photography, in aeroballistic range, track facilities of von Karman gas dynamics facility 78—37094
hypersonic ballistics experiment, application of laser light source 78—38433
hypersonic target material, subject to impact with water droplet, holographic investigation 78—42306
instrumentation for impact, erosion and fracture studies 77—81383
intercontinental ballistic paths, pencil of orbits with variable launching direction 80—26723
interferometer appl. to ballistic expts., use of commercial shadowgraphic instrument 80—47093
interferometers, polarization and grating, used in ballistic experiments 79—97426
Kelvin, background, teaching motivation, demonstrations 80—42025
Keplerian paths, pencil, with two common points, nongravitational foci 80—52005
local inertial frame of reference, demonstration 80—67982
Mach one impact test apparatus utilizing He-driven gas gun 79—75673
missile trajectory algorithm, analytic, including Earth oblateness 78—4476
monkey/hunter problem and possible solutions 79—75306
nanosecond hydrodynamic diagnostics, streaking camera, fibre optic probes 78—37096
optimum re-entry configuration via the method of steepest decent 79—37339
pairs of focal curves in orthogonal planes and movable bar frames *(German)* 77—60927
penetration mechanics, theoretical and experimental study 78—30173
photographic techniques, high-speed and other methods 80—9068
plastic plate velocity measurement, as continuum, by streak camera technique 78—37095
polarisation interferometer, appl. to ballistic expt. 79—55435
projectile range, generalised launching point solution, for teaching 79—62965
projectiles, penetration into targets, mechanics 78—18159
ricochet of dumb-bell shaped projectiles off sand 78—30172
ricochet of spheres and cylinders from water surface, including spin 77—11122
ricochet of spherical projectile off water and sand 77—17804
ricochet of spherical projectiles off sand 78—26025
rocket trajectories, intermediate thrust arcs in rotating potential force fields 80—52007
shot put, maximum range, for teachers 78—61985
snowballs and ICBM's, teaching 79—58465
spacecraft braking problem in Jupiter atmosphere, ballistic and navigation aspects 80—61981
steel, liquid bath, shooting methods for projecting buoyant alloy additions, expt. and mathematical eval. 77—21047
supersonic aircraft simulation using high speed jets, sonic-boom press. signature 78—79156
synchroballistic camera, synchrospeed 78—41366
thick target penetration model based on pressure bar force meas. 78—30174
thin plate response to ballistic impact 78—30193
two-phase reacting flow, heterogeneous, balance eqns. and soln., interior ballistic phenomena modelling 79—94737
valcanic eruptions, external ballistics 80—46159

ballistics continued
- X-ray cinematographic systems for diagnostic methods 80—13194
- Pb target, multiple interior impacts, hard target high vel. impact simulation 77—72145
- Ti-Al-V (6, 4 wt.%), targets, metallographic features after ballistic tests 79—79046

balloons
- *see also aircraft*
- air, buoyancy demonstration 80—67988
- ascent meter *(Japanese)* 78—61567
- astronomical balloon-borne equipment, data communications 79—16793
- astronomy, transatlantic self-ballasting balloons appl. 80—21917
- astronomy and atmosphere programs, conf. Bournemouth, England (1980, Aug.) 80—105433
- Atmosat balloon for tropospheric research, flight history and appls. 78—7775
- atmosphere IR mosaic background obs. from balloon altitude expt. 80—90222
- atmosphere sounding, self-contained tethered balloon system 78—28343
- Balloon Altitude Mosaic Measurements Program 78—81455
- balloon-borne solar telescope viewfinder, narrowband TV system appl. *(Japanese)* 78—24464
- boomerang, programming *(Japanese)* 77—82017
- Buoyant Venus Station placed by inflated balloon entry 78—4058
- cosmic rays new particles, balloon meas. *(Japanese)* 79—80112
- data storage, prior to transmission to ground via satellite 80—46263
- double theodolite measurement of balloon height, control of inherent uncertainties 80—77160
- endocardial balloon-tipped pacing catheter 77—81752
- far IR calibration source for balloon-borne telescopes 80—62027
- galactic gamma-ray lines, balloon obs. with high resolution Ge(Li) spectrometer *(Japanese)* 79—80353
- galactic IR radiation, balloon borne obs. *(Japanese)* 79—80351
- galactic IR radiation, balloon obs. *(Japanese)* 79—80350
- Galaxy IR surface brightness obs. *(Japanese)* 77—82308
- high-altitude, magnetic survey at Northeastern Japan *(Japanese)* 77—82019
- hot-air, mile-long, space research and solar power generation appl. 79—48583
- hot-air balloon, lecture sized 79—75308
- intra-aortic balloon pumping apparatus trials 79—48368
- lunar occultation obs., of Crab Nebula X-ray source *(Japanese)* 77—82319
- magnetic measurement at high altitude, by high-sensitivity balloon-borne ring-core magnetometer *(Japanese)* 80—94608
- meteorological pilot balloons, tropospheric temp. lapse rate effect on ascent rate 77—2204
- meteorology, boundary layer data acquisition and analysis system 77—60471
- orbital variations caused by radiation press. 77—78612
- oscillations in stratosphere, cosmic ray and pressure obs. *(Japanese)* 80—31182
- PAGEOS, shape determ., theory of light refl. from regular specular surface 79—68363
- Pageos 1 balloon satellite, orbital effects of direct solar and Earth albedo radiation pressure 79—88566
- paired tetroon flights, comparison of vertical motions 78—16111
- patrol *(Japanese)* 77—82018
- patrol balloon, long duration flight *(Japanese)* 79—80218
- pilot balloon ascent rate, tropospheric temp. lapse rate effect, further comments 77—17175
- planetary probes for hostile atmospheres and surfaces 78—4065
- rawinsonde balloons, wind profiles meas. comparison with Doppler radar 78—44916
- rise rate calcs. for constant lapse-rate layer 77—64387
- rubber balloon, internal press. eqn., for teachers 79—14
- rubber balloon bursting under biaxial strain, tear behaviour 80—19287
- satellite solar cell calibration using high-altitude balloon *(Japanese)* 78—61700
- Schumann resonances, balloon meas. *(Japanese)* 79—79919
- scientific, Japanese 1966 to 1975 activities *(Japanese)* 77—82016
- slow-scan TV camera performance test *(Japanese)* 80—12635
- solar faculae and sunspots, direct photographs with balloon-borne 10 cm telescope *(Japanese)* 79—80292
- solar stratospheric station, automatic, construction, selection of variant *(Russian)* 79—96913
- solar telescope, balloon-borne, narrow band TV system appl. as viewfinder *(Japanese)* 79—80228
- space obs. (1966-76) *(Japanese)* 78—24419
- space research using stratospheric balloons *(Italian)* 79—48683
- space shuttle-tethered balloon subsatellite, current collection by long wire 77—25859
- space shuttle-tethered balloon subsatellite for ionospheric plasma studies and power generation 77—25912
- spheroidal balloon satellite, orbital perturbations due to direct solar radiation press. 80—4219
- stratosphere, ion sampling package 78—69497
- stratosphere extensible balloons, buoyancy control expts. 77—87113
- stratosphere superpress. balloon, used as radiometry sensor 80—85763
- stratospheric balloon, ceiling altitude var. compensation for stellar occultation meas. *(French)* 78—11947
- stratospheric balloon trajectory analysis for long-term missions *(Italian)* 77—82055
- stratospheric balloons flight behaviour 77—13138
- stratospheric tethered system, feasibility study *(Italian)* 79—44251
- superpressure balloon, orbital simulator of stratospheric photochem. 79—29966
- superpressure balloon sounding of meso- and microscale phenomena in atmosphere 79—66815
- superpressure balloons for airflow circulation obs. over Arabian Sea during summer monsoon 77—17192
- tethered, for multispectral radiometric monitoring of plants and soils 78—3958
- tethering system, for very low altitude meteorological obs. 80—36430
- tethersonde system for remote meas. of wind and temp. 79—80038
- tropical constant-level balloon system 80—17395
- Tropical Wind, Energy Conversion and Reference Level Experiment (TWERLE), results 78—40605
- vertical oscills. of constant volume balloons 79—53545
- X-ray astronomy balloon, microprocessor-controlled payload 79—62716

balloons continued
- X-ray telescope, balloon-borne, for Crab Nebula imaging *(Japanese)* 79—80220
- He balloon in stratosphere, atm. and astron. research 77—37435

band gap *see energy gap*

band model of magnetism
- *see also Hubbard model*
- actinide elements, cpds. and alloys, mag. props., review 79—4649
- actinide intermetallic cpds., cubic, var. from localised to itinerant magnetism 77—20534
- actinide metals and intermetallics, localised versus itinerant character of 5f electron states 77—28138
- actinide systems, nearly ferromag., coupled d- and f-band model 77—63211
- actinide systems, spin fluctuations effect, model approach 77—28404
- alloy, local moment to itinerant magnetism transition with comp. 77—72984
- alloys, crystalline and amorphous mag. props. from Rhodes-Wohlfarth plot 78—52190
- amorphous alloys, Curie temp. comp. depend. 80—84597
- amorphous ferromagnets, itinerant electron model, Invar anomalies, review 78—95413
- amorphous ferromagnets, itinerant electron model 79—73664
- amorphous metals, mag. anisotropy, spin glass like phase 77—66295
- amorphous system, cluster effective lattice method, mag. and electron props. 77—66242
- amorphous systems with dense random packed hard sphere structure, density of states and itinerant ferromagnetism 78—34950
- anisotropy, temp. and field dependence, anisotropy constant meas., review *(Rumanian)* 80—25125
- antiferromagnet, collinear *(Russian)* 78—2646
- antiferromagnet, itinerant, effect of imperfect nesting of band struct. 78—31045
- antiferromagnet, itinerant, paramag. impurity effects on Neel temp., calc. 80—60257
- antiferromagnet, itinerant electron, dynamic magnetisation as internal Josephson effect 78—47931
- antiferromagnet, itinerant electron, mag. excitations 78—56305
- antiferromagnet, itinerant electron, spin wave spectrum calc. 77—36063
- antiferromagnet, itinerant model, spin density wave transition, impurities effect 77—72986
- antiferromagnetic solution of extended Hubbard model, CPA treatment 78—19208
- antiferromagnetism in system if itinerant electrons 80—2547
- antiferromagnetism itinerant electron theory, spin susceptibilities 78—6504
- antiferromagnetism of strongly correlated electrons in narrow bands 78—76218
- band model, mag. susceptibility of exchange-enhanced paramagnet Pd, band model, mag. susceptibility of exchange-enhanced paramagnet 78—2644
- $CeAg_xIn_{1-x}$, cubic to tetragonal phase transform., conc. dependence by resist. meas. 78—2252
- charge-transfer organic salts, strongly correlated, interband absorpt., long-range Coulomb interaction 79—4525
- charge-transfer salts, strongly correlated, interband absorpt., long-range Coulomb interaction 79—4525
- conduction electron-localised electron interaction mechanism 77—59377
- crystal with strong s-d exchange, mag. susceptibility and Curie-Weiss law *(Russian)* 80—25068
- dilute magnetic alloys, crystal fields for mag. ions from itinerant electrons 80—39537
- disordered system, orbital mag. susceptibility of conduction electrons 78—76217
- domain structure, theory, band model of ferromagnetism approach 77—80954
- effective exchange interactions and magnetic ground state of strongly correlated electrons 79—61036
- elastic properties of magnetic materials, review 80—7142
- electron-hole paired systems, ferromagnetic ordering phase diagram 80—97097
- electron-magnon interaction effects on Ward-Takahashi identities in itinerant electron ferromag. 80—39730
- exciton ferromagnet, spin-lattice relax., light and US absorption *(Russian)* 79—7960
- Fermi surface, electronic props., book 80—105445
- ferromagnet, disordered itinerant-electron, spin waves 78—95427
- ferromagnet, domain struct. 77—69608
- ferromagnet, inter-atomic interaction effect on dynamic susceptibility, RPA calcs. 79—65662
- ferromagnet, itinerant, electron-magnon interactions 79—99673
- ferromagnet, itinerant, inhomogeneity corrections to ground-state props. 78—14921
- ferromagnet, itinerant, mag. props., temp. depend., functional integral approach 80—60170
- ferromagnet, itinerant, spin waves, appl. of self consistent many-body theory 79—73702
- ferromagnet, itinerant, spin waves, surface effects, RPA calc. 80—60226
- ferromagnet, itinerant electron, magnetoelastic contribs. to US vel., elastic consts., and susceptibility 80—75829
- ferromagnet, itinerant electron, magnetoresist. and anomalous Hall effect due to electron-phonon interactions 80—70680
- ferromagnet, itinerant electron, magnon spectrum just below T_c, theory 80—65833
- ferromagnet, itinerant electron, surface spin waves, tight-binding Hubbard model 80—39763
- ferromagnet, itinerant electron, temp. depend. of angle-resolved photoemission 80—76142
- ferromagnet, itinerant electron model, spin wave stiffness temp. depend. 77—20535
- ferromagnet. with itinerant electrons, domain struct. stability 77—20629
- ferromagnet-Al_2O_3-Al superconductor, spin polarisation of tunnelling electrons, band model 77—72947
- ferromagnetic 3d metal film, rel. to linear mag. birefr. dispersion interpretation 77—69807
- ferromagnetic alloys, itinerant electron model, spin wave stiffness const. calc. 80—34613
- ferromagnetic alloys, itinerant electrons, magnon stiffness const. 77—63155

band model of magnetism continued
- ferromagnetic conducting cryst., dynamics of s-d model in alternating mag. field *(Russian)* 80—65825
- ferromagnetic Fermi liquid, stability conditions 79—47224
- ferromagnetic film, band model of domain struct. 77—36105
- ferromagnetic metal, band struct. contribs. to shear consts., deform. pot. formalism and Stoner model 79—91280
- ferromagnetic metal, exciton condensation effects on props., Hubbard model 80—60171
- ferromagnetic metal, impurity resist., band model calcs. 77—39830
- ferromagnetic metal, itinerant electron model, for US propagation and structural instabilities 78—95508
- ferromagnetic metal, nearly and weakly ferromag., freq. depend. elec. cond., Drude's formula deviation 79—47091
- ferromagnetic metal, two-band model ordinary Hall effect and spin-depend. phenomena 79—19577
- ferromagnetic metal, two-site interaction model 79—82744
- ferromagnetic metal, uniaxial, anisotropic spin fluctuations and anisotropic band struct. effects on resist. near T_c 80—65543
- ferromagnetic metal surface, Fermi level shift by charging, mag. moment and hyperfine splitting 77—20677
- ferromagnetic metals, itinerant electron, theory of crit. US propag. 77—69655
- ferromagnetic metals, thermodynamic props. 79—91245
- ferromagnetic s-d model, electronic spectrum struct., moments method 80—97052
- ferromagnetic semiconductor, electronic excitation spectrum 80—11149
- ferromagnetic semiconductor, electronic spectra, s-d model, method of moments 80—7070
- ferromagnetic semiconductor, electronic spectrum, influence of finite carrier conc. 78—76220
- ferromagnetic semiconductor, magnon coupling to plasmons and LA phonons, s-d model 80—29536
- ferromagnetic semiconductor, theory review 80—20369
- ferromagnetic semiconductor, two-band s-d model hybridization 80—65446
- ferromagnetic semiconductor s-d model, electronic struct. from lowest six momenta 80—39732
- ferromagnetic semiconductors, electronic quasiparticle spectrum 80—97051
- ferromagnetic transition metal alloys, CPA appls. 77—72983
- ferromagnetic transition metal alloys, mag. props. review 80—44823
- ferromagnetic transition metals, electron spin polarisation, review 78—76591
- ferromagnetic transition metals, electron spin polarisation, review 78—76592
- ferromagnetism, band model, pseudodipolar theory of magneto crystalline anisotropy 77—36068
- ferromagnetism, basic models, classification of theories *(Rumanian)* 78—91840
- ferromagnetism, itinerant, and density of states, off-diagonal disorder effects 77—28360
- ferromagnetism, itinerant, effective Hamiltonian 80—11150
- ferromagnetism, itinerant, local band theory, Fermi-liq. theory 78—31040
- ferromagnetism, itinerant, local band theory, nonlinear Landau Lifshitz eqns. 78—31042
- ferromagnetism, itinerant, local band theory, spin waves 78—31041
- ferromagnetism, itinerant electron magnetism in two dimensions 77—63065
- ferromagnetism, itinerant electron model, contrib. of Conyers Herring in 1930s 80—57056
- ferromagnetism, itinerant electron model, spin quantization direction fluctuations, short range order. 80—34582
- ferromagnetism, itinerant electron theory, local moment approach, review *(Japanese)* 80—25071
- ferromagnetism, origin of magnetostriction, review *(Rumanian)* 80—34747
- ferromagnetism and ferroelectricity, coexistence in systems with electron-hole pairing 80—7310
- ferromagnets, itinerant electron, lattice props. depend. on cond. electron magnetisation, elastic props. 79—61035
- graphite, low temp. magnetisation in strong mag. fields, filled band contrib. 77—32157
- Hall effect, AC, ferromag., in electron-impurity system, itinerant electron model 77—47796
- heavy rare earth metals, RKKY theory of magnetism, electron-electron interactions 79—73667
- Hubbard model, itinerant antiferromagnetism 78—91841
- Hubbard model, partly filled narrow band, electron correlation and mag. props. 78—67968
- Hubbard model, static approx., mag. phase transitions 77—1558
- induced moment systems, effect of spin fluctuations 80—2585
- inhomogeneous electron system, gradient expansion in density-functional approach 77—89721
- inhomogeneous itinerant electron ferromagnet, mag. and thermal props. 79—7964
- interacting electron system, mag. props., momentum dependent interaction 77—72976
- Invar, itinerant electron character 77—66240
- Invar alloy, thermodynamic properties, effects of forced magnetostriction 79—11331
- Invar alloys, bulk modulus anomaly, rel. to itinerant electron model of ferromag. 77—48025
- Invar problem, conf., Nagoya, Japan (Sept. 78) 79—56481
- itinerant antiferromag., partially disordered, electronic density of states 77—4494
- itinerant antiferromagnetism, s-band Hubbard model, zero temp. props. 77—4493
- itinerant antiferromagnetism and density waves at surface 79—82743
- itinerant electron antiferromag., localised mag. states 79—28500
- itinerant electron antiferromagnet, effects of paramagnetic impurities on Neel temperature 79—4678
- itinerant electron antiferromagnet, localised spin coupling 78—68142
- itinerant electron antiferromagnetic matrix, local moments, spin Hamiltonian 80—34626
- itinerant electron antiferromagnetism, effect of mag. field 78—27013
- itinerant electron ferro- and antiferromagnetism, spin fluctuations 79—7961
- itinerant electron ferromag., spin fluctuation *(Japanese)* 78—47936
- itinerant electron ferromag., Ward-Takahashi identities, zero temp. case 79—73669

band model of magnetism continued
- itinerant electron ferromagnet, effective Lorentz force and Landau level 78—80120
- itinerant electron ferromagnet, two magnon bound states 77—20537
- itinerant electron ferromagnet with domain struct., spin waves 78—64182
- itinerant electron ferromagnetic alloys, magnon energy, effect of ordering 79—7986
- itinerant electron ferromagnetism, linear response theory 77—72989
- itinerant electron ferromagnetism, local exchange model 77—72994
- itinerant electron ferromagnetism, press. effects on mag. props. 77—66241
- itinerant electron ferromagnetism, single-site functional integral approach 79—65637
- itinerant electron ferromagnetism, spin fluctuation theory 78—80151
- itinerant electron ferromagnetism at zero temp. 78—56285
- itinerant electron ferromagnetism of two dimensional system 77—24666
- itinerant electron ferromagnets, elastic props. and electronic struct. 80—66001
- itinerant electron ferromagnets, magnetisation fluctuations, Landau-Lifshitz eqn. 79—73729
- itinerant electron ferromagnets, magneto-volume effects 80—60397
- itinerant electron magnet, low temp. resist., collective excitations 77—72851
- itinerant electron magnetism, conf. Oxford, England (Sept. 1976) 77—72973
- itinerant electron magnetism, neutron scatt. 78—68194
- itinerant electron magnetism, thermodynamic aspects 77—72992
- itinerant electron magnets, effect of spin fluctuations on elec. field gradient 78—39078
- itinerant electron magnets, spin fluctuations 77—72990
- itinerant electron magnets, spin fluctuations and thermodynamic props. 79—65687
- itinerant electron magnets, theory of spin fluctuations 77—63064
- itinerant electron model, mag. props. under press. *(Japanese)* 80—20444
- itinerant electron model for ferro- and antiferromag. systems, dynamic susceptibility 77—72988
- itinerant electron paramagnets, coupled charge and spin fields 77—72991
- itinerant electron system, coexistence of antiferro- and ferromagnetism 78—2645
- itinerant electron system, cond. transition to antiferromag. metallic phase 77—72980
- itinerant electron system, helical spin structure appl. to MnSi 78—23234
- itinerant electron system, mag. excitations, neutron scatt. studies 80—44838
- itinerant electron system, weakly ferromagnetic ground state, Fermi liquid theoretical study 79—4646
- itinerant electron systems, mag. excitations, study by inelastic neutron scatt. 79—47264
- itinerant ferromagnet, effect of planar defects on electronic struct. and mag. ordering 79—99672
- itinerant ferromagnet, neutron inelastic scatt. 79—7970
- itinerant ferromagnet, sloppy spin waves above T_c 77—72979
- itinerant ferromagnet, spin-wave dispersion and linewidth 79—4668
- itinerant ferromagnet, surface spin waves 77—69480
- itinerant ferromagnet, thermodynamics 79—4645
- itinerant ferromagnet, tight-binding metal, Einstein temp. 79—24126
- itinerant ferromagnet in disordered phase, energy band struct. 78—68141
- itinerant ferromagnet with helical spin struct., US attenuation 79—78497
- itinerant ferromagnetism, local-band theory, equivalent Heisenberg model 79—82745
- itinerant ferromagnetism, statistical mechanics of spin waves 79—82746
- itinerant ferromagnetism with at. ordering 78—14920
- itinerant magnetism, quasispin model, effect of short-range order 78—68144
- itinerant magnetism 79—73668
- itinerant magnets, anomalous sound attenuation near mag. transition temp. 78—15004
- itinerant magnets, band struct., mag. props. and local moments 80—70929
- itinerant magnets and superconductors, structural instabilities, phase diagrams 78—14922
- itinerant strong ferromagnetism, effect of electron correlations 79—7962
- itinerant strongly interacting fermion system, uniform paramagnon theory 77—69577
- itinerant system of coupled diamagnetic pairs of electrons, electronic and magnetic correlations 79—61033
- itinerant-electron antiferromagnet, effect of mag. field on crit. temp. 78—60293
- itinerant-electron ferromagnet, US propag. and struct. instabilities, screening effects 77—69653
- itinerant-electron ferromagnetic film on nonmagnetic metallic substrate, mag. props. 80—20371
- itinerant-electron ferromagnetism, possible coexistence with itinerant-electron antiferromagnetism 78—39286
- liquid transition metal, mag. susceptibility rel. to theories of electronic structure 77—1536
- magnetic semiconductor, doping effects on exchange interaction mechanism 78—31064
- magnetic semiconductors, excitation spectrum, temp. and band occupation depend. 80—49588
- magnon relaxation, spin-orbit interaction, itinerant electron ferromagnets 80—11179
- metal, cond. electron polarisation, magnetisation densities, neutron mag. form factors 77—72981
- metal, electron-phonon interaction, magnetism influence 77—73040
- metal, electron-phonon interaction effects on spin susceptibility 80—93108
- metal, indirect coupling between localised mag. moments by narrow band electrons 80—70942
- metal surface, spin susceptibility, density-functional approach 77—90011
- metallic magnetic materials, high mag. field effects, interpretation of expt. results 80—60272
- metals, crystalline, disordered ferromagnetism 78—19207
- metals, narrow-band, magnetism and mag. excitations 77—69478
- narrow band electron systems, unified theory of magnetism 80—70928
- narrow conduction bands, allowance for correl. effects 78—47933
- narrow-band s-d magnetic materials, ground state and thermodynamic parameters, cond. electron density depend. 78—47934
- nearly ferromagnetic semiconductor, spin fluctuation theory 79—65636
- nonequilibrium semiconductor with electron-hole pairing, mag. moment quantum oscills. *(Russian)* 77—28131

band model of magnetism continued
  orbital magnetic susceptibility, effects of impurities 77—47962
  orbital ordering 77—89923
  paramagnetic exchange enhanced alloy, double d-band model 77—66238
  paramagnetic metal, band struct. contribs. to shear consts., deform. pot. formalism and Stoner model 79—91280
  paramagnetic metal with nonmag. impurities, spin-flip scatt. 77—4497
  paramagnets, itinerant electron, spin wave like modes 77—63067
  paramagnon theories below three dimensions for itinerant strongly interacting fermion system 79—38298
  periodic Anderson Hamiltonian, alloy analogy treatment for mixed valence states 80—75527
  quasispin model of itinerant magnetism 77—66239
  rare earth cobalt alloy, RCo_2, itinerant system, weak ferromagnetism 78—52191
  rare earth intermetallics, mag. props. 78—84380
  rare earth intermetallics, RCo_2, itinerant metamagnetism, Van Vleck model 79—78297
  rare earth metal, magnetic properties, nonlinear s-f exchange interaction effect 80—15711
  rare earth metals, ferromag. ordering *(Russian)* 78—60262
  rare earth orthocobaltites, $R_{1-x}Sr_xCoO_3$ and $La_{1-x}M_xCoO_3$, itinerant ferromags., electronic and mag. props. 78—10660
  rare earth-Co alloys, spin wave spectra 78—56304
  rare earth-Co intermetallics, RCo_2, itinerant ferromag., magnetovolume effects 79—8038
  rare earth-transition metal alloy, disordered, model of localised spins d-band interaction 77—20515
  rare earth-transition metal alloys, cryst. and amorphous, mag. props. 77—73008
  rare earths, heavy, mag., electronic struct., book 78—60259
  resistance critical behaviour, temp. and mag. field depends. 77—73037
  resistivity anomalies of ferromag. metals near Curie temp., itinerant mag. electron theory 78—95292
  s-d electron model, finite temp. diagram technique, perturbation theory 78—67932
  s-f model with electron-hole reson., antiferromag. behaviour and phonon spectrum 78—47992
  semiconductor, doped, electron struct. and indirect exchange mechanisms 80—25123
  semiconductor, ferromag., electronic props., effect of electron-ion spin coupling 77—28359
  semiconductor, ferromagnetic, electronic quasiparticle spectrum in sf-model 78—52188
  semiconductor, narrow band gap, ferromagnetism of electrons in filled band *(Russian)* 79—78300
  single-site spin fluctuation theory of itinerant-electron systems with narrow bands 80—97049
  spin polarons in narrow almost half-filled s-band, appl. to BCC ^3He 77—62703
  spin systems, coupled itinerant localised systems, dynamic magnetic response 80—34583
  spin-density-functional formalism 78—68140
  Stoner ferromagnetism, criteria in doped semimetals, uncompensated metals, derivation 78—68145
  Stoner glass, disordered itinerant-electron system, spin-glass condensation 79—78424
  strong ferromagnetic 3d alloys, electron correls. 77—40030
  susceptibility, local exchange approx. calc. in itinerant electron magnets 80—60169
  susceptibility of cryst. with strong s-d exchange *(Russian)* 78—56283
  symmetric Wolff model, weak-coupling—long-time—zero-temp limit 77—80907
  ternary compounds, supercond., p-state pairing and magnetism 80—54819
  transition metal, 3d, giant internal mag. press. and compressibility anomalies 77—16034
  transition metal, band model, mag. susceptibility of exchange-enhanced paramagnet 78—2644
  transition metal, chemisorption of H, effect of surface spin fluctuations 80—75613
  transition metal, d-d electron correlations in cohesion and ferromagnetism 77—62810
  transition metal, ferromag., band theory of linear magnetostriction 80—71141
  transition metal, itinerant-localised electron model 78—14918
  transition metal, mag. susceptibility, spin wave spectrum for improved itinerant-localised electron model 79—1654
  transition metal, magnetic ground state props., simple one-electron theory 77—63063
  transition metal, magnetic moment near surface, one-electron band model 79—82747
  transition metal, nonmag., possibility of mag. monolayer formation 78—15009
  transition metal, Stoner theory 78—34757
  transition metal 3d alloys, neutron spin wave scatt., itinerancy 77—73018
  transition metal 3d monoxides, specific vol. and mag. moment calcs. 80—65822
  transition metal alloy, ferromag., local environment effect on atomic moments, itinerant model 78—68188
  transition metal alloys, dilute ferromagnetic, itinerant d-electron(hole) degenerate, spin stiffness constant 80—70930
  transition metal alloys, local environment effect on magnetic states 79—56491
  transition metal alloys, mag. props. *(Japanese)* 78—47935
  transition metal alloys, spin glass behaviour, simple itinerant model 78—84436
  transition metal intermetallic cpds., H absorption and mag. props. 80—60224
  transition metal itinerant magnets, neutron scatt. expts. 77—73002
  transition metals, 3d, ferromag. props., book contrib. 80—75724
  transition metals, 3d ferromag., itinerant electron magnetism, magnetic excitation props., theory 80—34581
  transition metals, conf., Toronto, Canada (Aug. 1977) 78—91577
  transition metals, double d-band model, dynamic susceptibilities calc. 77—1535
  transition metals, itinerant ferromagnetism theory 79—78301
  transition metals, magnetism, interacting virtual state approach 77—72987
  transition metals, paramagnetic state, itinerant electron model 80—65769
  transition metals, role of electron correlation 77—72974

band model of magnetism continued
  transition metals, Stoner model in spin density functional formalism 77—72993
  transition metals, theory of ferromagnetism involving crystal field effects, connection with band theory 80—2541
  TTF-TCNQ, single cryst., mag. susceptibility in phase transition region, two-gap model 78—6511
  two-dimensional layer, model, electron-correlated density-wave states 78—51919
  Wannier functions for Bloch electron in mag. field 77—80906
  weak itinerant electron ferromagnet, spin fluctuation curvature of Arrott plot 79—8012
  weak itinerant magnetism as inhibited supercond. 79—51715
  Wolff model, effective mag. interactions between impurity and conduction electrons 78—68143
  Au-Ni, magnetisation and sp. ht., ferromag., paramag. and crit.-conc. regions 79—38330
  Au_4V single crystal, ordered, mag, props., domain models 80—39770
  $CeSn_3$, polarised neutron study of induced magnetisation 80—34594
  Co, bulk modulus and thermal expansion coefficient, mag. contributions 79—8039
  Co, FCC, itinerant ferromagnetism 78—23238
  Co film, amorphous, rel. to magnetoresist. in fields up to 80 kG 77—39823
  Co, magneto-volume effects calc., rel. to itinerant electron model 78—43621
  Co, Stoner model, mol. field coeff., temp. and field depends. 77—72975
  Co-Al_2O_3Al superconductor, spin polarisation of tunnelling electrons, band model 77—72947
  Co-V, solid and liq., mag. susceptibility and electronic struct. 80—39738
  CoS_2, itinerant ferromagnet, ferromag. reson. and EPR meas. 80—66044
  $CoTi_{1-x}Al_x$, mag. and electronic props., ferromag. and paramag. state 80—65814
  Cr and alloys, itinerant antiferromagnetism and density waves at surface 79—82743
  Cr, critical coeff. of resistivity near Neel temp. 77—59417
  Cr, electronic struct., spin-density functional calcs. 80—88476
  Cr, electronic structure model, Invar effect, antiferromagnetic-non mag. transitions 80—20370
  Cr, Fermi surface, stress depend., from quantum oscill. effects, rel. to itinerant antiferromagnetism 78—91597
  Cr, inelastic neutron scatt. expts., spin density waves 80—44818
  Cr, mag. susceptibility calc. two band model for electronic spectrum 78—10663
  Cr, magnetic phase transition at Neel temp. 78—2681
  Cr, phase transition at T_N 79—4676
  Cr, spin density wave, Nambu-Eliashberg eqns. for k-state electron-hole pairing 80—97050
  Cr, spin density wave, stress and impurity conc. depend. 77—73029
  Cr, spin density wave, temp. depend. of second and third harmonics 77—12094
  Cr, spin-density-wave antiferromagnet, uniaxial anisotropy 78—10640
  Cr-Fe, low conc. alloys, coexistence of itinerant antiferromagnetism with paramagnetism 78—84386
  Cr-Fe alloys, itinerant antiferromag. effect of mag. impurities 77—32186
  Cr-Pt, dil., effect of Pt on itinerant antiferromagnetism 78—64191
  Cr-V, itinerant electron antiferromag., spin fluctuations, low temp. specific heat 80—107439
  CrAs, high press. paramag. antiferromag. transitions, elec. props., band model development *(Russian)* 80—60277
  CrB_2, itinerant antiferromag., sping fluctuations, NMR study 80—108119
  $Cr_{0.98}Mn_{0.02}$, rel. to spin dynamics and spin wave form factor 77—40047
  $CrTe_{1+x}$, rel. to thermal expansion and spontaneous magnetostriction *(Russian)* 78—48017
  Cu-Mn (7 at.%), magnetic susceptibility, clustering, band model of heterogeneous magnetics 77—43823
  Cu_2MnAl, alloy, energy band calc. by nonrelativistic SAPW method 79—4507
  EuO(s), mag. semicond., s-f model, intermediate coupling theory 79—95326
  Fe alloys, amorphous, mag. saturation, spin wave stiffness, temp. depend. 80—75741
  Fe alloys, amorphous, saturation magnetisation, Curie temp. and size effect 80—65815
  Fe, BCC, high field Knight shift and hyperfine anisotropy of ^{57}Fe 80—71205
  Fe, band theoretic interpretation of neutron scatt. expts., spin wave modes 80—44791
  Fe, Curie temp. calc. using model containing five bands 79—56536
  Fe, density of states, photoemission expts. above and below T_c, rel. to magnetism model 77—20536
  Fe dilute alloys, itinerant 3d electron spin density oscills. around solute atoms 77—72978
  Fe, energy of mag. anisotropy, band calcs. *(Russian)* 77—20583
  Fe, ferromag., dynamic susceptibility calc. 80—80488
  Fe, ferromag., evidence for itinerant electron model, angle resolved photoemission from surface 79—24414
  Fe, ferromag., spin wave energies and intensities calc. 77—8293
  Fe ferromagnetism, transition metal valence electron struct. explanation 78—47932
  Fe, magnetic moments, local short range order, high temp. effects 80—65902
  Fe, magnetisation, spin wave and Stoner contribs. 77—73017
  Fe, magnetism at high temps., total electronic band struct. energy calc. 80—75721
  Fe, magneto-volume effects calc., rel. to itinerant electron model 78—43621
  Fe, photoelectron spin polarisation and itinerant magnetism 78—68602
  Fe, photoemission study of (100), (110) and (111) surfaces, ferromag. band struct. 79—38714
  Fe, spin polarisation in electron field emission, surface magnetism 78—68607
  Fe, Stoner model, mol. field coeff., temp. and field depends. 77—72975
  γ-Fe, Stoner theory support for two-state hypothesis 77—69477
  Fe, theory of magnetism 79—78299
  Fe-Al_2O_3-Al superconductor, spin polarisation of tunnelling electrons, band model 77—72947
  Fe-Cr-Al alloys, localised mag. moment determ. and electron struct. 77—66268

band model of magnetism continued
Fe-Mn(0 to 80 wt.%), paramagnetic susceptibility by Faraday method, band model interpretation *(Russian)* 77–20545
Fe-Ni, Invar problem, vibronic state model 79–56492
Fe-Ni alloy, FCC, high-field susceptibility and spin wave spectrum 79–56493
Fe-Ni alloys, electronic struct. by XPS obs. 79–33226
Fe-Ni Invar alloy, effect of hydrogenation, Mossbauer spectra 79–56641
Fe-Ni Invar alloy, thermal expansion coeff. at low temp. 79–86911
Fe-Ni Invar alloys, Arrott plots rel. to itinerant electron characts. 77–73009
Fe-Ni Invar alloys, thermodynamic props. 79–56560
Fe-Ni Invar anomalies, explanation in terms of itinerant electron magnetism 80–75705
Fe-Ni(Co), solid and liq., paramag. susceptibility and electron struct., 800-1800°C *(Russian)* 80–25081
Fe-Pt Invar alloy, magnetocryst. anisotropy energy, itinerant electron model 80–54884
Fe-Si (7.5, 14.3 at.%), mag. moments and form factors, neutron diffr. obs., d-band electron redistrib. 79–51751
Fe-Ti, mag. moment distrib. and environmental effects around Ti impurity 80–7092
Fe_2Al, mag. moment determ., role of local environment, self consistent calcs. 80–44815
$Fe_3Al(Si)$, electronic structure, magnetic moments 80–107695
$(FeCoNi)_8B_{20}$, glass, evidence supporting split-band model from magnetostriction 78–95509
$Fe_{2-x}M_xP_{1-y}As_y$, (M=Mn,Fe, Co,Ni), band model of mag. props. 77–40029
$(Fe_{0.5}Ni_{0.5})$-Co, solid and liq., paramag. susceptibility and electron struct., 800-1800°C *(Russian)* 80–25081
$(Fe_xNi_{1-x})_{80}P_{10}B_{10}$, amorphous, weak itinerant ferromag., Arrott plots 77–73007
$(Fe_{0.2}Ni_{0.8})_{1-y}(SiO)_y$, Permalloy material, magnetisation, temp. and impurity atom conc. depend., band model calcs. *(Russian)* 80–93088
Fe_3Pt, Invar alloy, theory of elastic-anomalies, rel. to Stoner theory of band magnetism 78–95505
FeRh, antiferromag., band structure and effect of Fe impurity on mag. props. 77–28377
Gd, band structure and Fermi surface using KKR formalism 79–77993
Gd, ferromag. Fermi surface and band struct., press. effects, dHvA expts. 78–14656
Gd, self consistent relativistic ferromag. band struct. 78–91609
GdMg, noncollinear mag. struct., nonlinear band behaviour 80–75706
LaMg, Pauli paramagnet, mag. susceptibility, nonlinear band behaviour 80–75706
$La_{1-x}Sr_xCoO_3$, $(0.5 \leq x \leq 0.9)$, ferromag., elec. props., itinerant electron model 80–107785
α-Mn, electronic structure model, Invar effect, antiferromagnetic-non mag. transitions 80–20370
Mn, FCC, itinerant antiferromag., spin susceptibilities and collective excitations, many band effects 77–63140
β-Mn-Fe-Sn alloys, weak itinerant electron antiferromagnetism, Mossbauer spectra meas. 77–36158
τ-MnAl, estimated theoretical limit of mag. moment 80–97072
$(Mn_{1-x}Cr_x(Fe_x))B$, Invar charact. 77–15602
MnSi, weak itinerant ferromag., mag. excitations, neutron scatt. obs. 78–34969
MnSi, weak itinerant ferromagnet, mag. excitations 79–7985
MnSi, weak itinerant magnetic compound, paramagnetic response function, polarised neutron scattering 80–107982
Ni (001), spin polarised photoemission theory 79–15584
Ni (100), electron field emission, positive spin polarisation and band model of magnetism 77–52226
Ni (111), band struct. and temp.-depend. mag. exchange splitting, angle resolved photoemission obs. 78–60546
Ni, APS and band theory of magnetism 77–40303
Ni, and its alloys, rel. to spin polarised tunnelling 78–39372
Ni, anomalous resistivity near Curie temp., band theoretical calc. 78–56127
Ni, band structure, μSR Knight shift meas. 79–56663
Ni, band theoretic interpretation of neutron scatt. expts., spin wave modes 80–44791
Ni, Curie temp. calc. using model containing five bands 79–56536
Ni, density of states, photoemission expts. above and below T_c, rel. to magnetism model 77–20536
Ni, dynamical spin susceptibility, noninteracting spin band model 78–31059
Ni, effective Coulomb interaction momentum depend. 79–78298
Ni, electron field emission, spin polarisation positive sign 77–73220
Ni, exchange splitting of 3d bands, angle-resolved photoemission meas. 80–71568
Ni, ferro- to paramag. transition, angular resolved photoemission 78–68603
Ni, ferromag., dynamic susceptibility calc. 80–80488
Ni, ferromag., self-consistent calc. of energy bands 77–39774
Ni film, few atomic layers thick, transition from Pauli paramag. to band ferromag. 80–44885
Ni, magnetisation in pulsed field up to 320 kOe, 283 to 693K, band theory *(Russian)* 77–80920
Ni, magnetisation spin wave and Stoner contribs. 77–73017
Ni, magneto-volume effects calc., rel. to itinerant electron model 78–43621
Ni, magnetocrystalline anisotropy energy, temp. and magnetisation depend. 78–6525
Ni, paramag., model calc. of dynamical spin susceptibility 77–69489
Ni, paramagnetic, mag. form factors in Stoner-like model 80–97061
Ni, photoelectron spin polarisation 77–32501
Ni, spin polarisation in electron field emission, surface magnetism 78–68607
Ni, spin polarisation of field-emitted electrons, theory 77–44134
Ni, Stoner model, mol. field coeff., temp. and field depends. 77–72975
Ni-Au film, amorphous, rel. to magnetoresist. in fields up to 80 kG 77–39823
Ni-Co, solid and liq., paramag. susceptibility and electron struct., 800-1800°C *(Russian)* 80–25081
Ni-Co alloy, stiffness const., interpretation within band model 79–42748
Ni-Cr(V)(Co)(Mn)(Mo)(Ru)(Fe), spin wave stiffness consts., RPA CPA band model 79–61088
Ni-Fe, split bands rel. to sp. ht., g-factor and magnetostriction data 77–72977

band model of magnetism continued
Ni-Mn, spin wave stiffness const., low temp. neutron scatt. meas. 79–51768
Ni-Mn-H solid solutions, mag. props. 80–88753
Ni-Pt alloy, spin susceptibility, temp. variation, band model calc. 77–28365
Ni-Rh alloys, disordered, vol. paramagnetostriction calc. 77–80985
Ni-Ru ($\leq$4 at.%), influence of alloying on mag. anisotropy, itinerant electron model 80–71010
Ni-Ti, mag. moment distrib. and environmental effects around Ti impurity 80–7092
Ni-Ti(Mn)(Cu), tunnelling electron spin polarisation 77–73058
Ni-V, solid and liq., mag. susceptibility and electronic struct. 80–39738
Ni_xPt_{1-x}, disordered alloy, itinerant system, induced magnetism 78–52191
$Ni_{0.991}S$, antiferromagnetism due to itinerant electrons 77–40077
Ni(alloy)-Al_2O_3-Al superconductor, spin polarisation of tunnelling electrons, band model 77–72947
$NpOs_2$, band magnetism due to f-electrons, T_c 77–73039
$NpOs_2$, itinerant ferromagnet, sp. ht., 3-25K 77–63212
$NpSn_3$, band magnetism due to f-electrons, T_N 77–73039
Pd, confined geometry, p-wave supercond. or itinerant ferromag. 80–11129
Pd-Rh alloys, disordered, vol. paramagnetostriction calc. 77–80985
Pd-Rh-Ag, magnetic susceptibility press. depend., d-band deform. and exchange var. 77–47967
Pd-transition metal, dil., itinerant versus localised magnetism 78–64188
Pt, band model, mag. susceptibility of exchange-enhanced paramagnet 78–2644
Pt-Ni alloys, disordered, vol. paramagnetostriction calc. 77–80985
Sc_3In, itinerant electron ferromagnet, spin fluctuations 77–73096
Sc_3In, itinerant electron ferromag., NMR and relax. 78–6586
Sc_3In, itinerant electron ferromag., low temp. sp. ht., mag. field depend. 79–42765
Sm-Hf-Co alloy, rare-earth electron transfer 77–40028
$Sm_2(Co_{1-x}M_x)_{17}$, bulk magnetisation and magnetocryst. anisotropy, interpretation 77–40055
$Sm_2(Co_{1-x}M_x)_{17}$, magnetocryst. anisotropy 77–40054
$TiBe_2$, cubic Laves compound, sp. ht. rel. to intinerant antiferromag. 79–82356
$TiBe_2$, itinerant antiferromagnetism, mag. susceptibility obs. 79–15288
$TiBe_{2-x}Cu_x$, C-15 lower phase, itinerant ferromagnetism 80–15723
$TiFe_{1-x}Co_x$, electronic struct. and mag. moment calcs. 80–65821
$Ti(Fe_{1-x}Co_x)$, ferro- to paramag. transition, press. depend. 77–73028
UAL_2, band magnetism due to f-electrons, T_{sf} 77–73039
UPt, valence bands, XPS spectra, itinerant 5f electron behavior 80–50520
$(U_xTh_{1-x})S$, mag. props. rel. to elec. struct., 1.5-300K 77–1557
V, magnetic moment near surface, one-electron band model 79–82747
V_nO_{2n-1} Magneli phases, elec. and mag. props. 79–37990
$Y_2(Co_{1-x}M_x)_{17}$, bulk magnetisation and magnetocryst. anisotropy interpretation 77–40055
$Y_2(Co_{1-x}M_x)_{17}$, magnetocryst. anisotropy 77–40054
YMg, Pauli paramagnet, mag. susceptibility, nonlinear band behaviour 80–75706
YNi_3, magnetism resurgence, neutron diffr. and mag. props. study 80–65819
YRh_4B_4, supercond., anomalous cond.-electron polaris. 80–25047
$ZrZn_2$, itinerant electron ferromag., NMR exam. of effect of spin fluctuations 77–16192
$ZrZn_2$, weak itinerant electron ferromagnet, resistivity 77–72850

band-pass filters
see also crystal filters; vocoders
acoustic radiation coupling of disc to plane and back or to disc, exact soln. 77–46828
acoustically coupled SAW grating resonator filter synthesis 77–23821
active band-pass filter for infralow freqs. 80–53578
amplifier, lock-in, with synchronous filter, construction *(Japanese)* 80–28362
analogue filters, in ocean wave spectrum analyser system for operational buoys 79–5662
bandpass filters, technique, construction, appl. *(German)* 79–50544
cascaded SAW gratings as passband filters 77–68333
contrast enhancing filter for banded chromosomes 78–92755
controlled filter for bioelec. pots. 78–40357
digital bandpass filters, filter type and operator parameters selection for instrumental realisation *(Russian)* 79–74984
digitally controlled, spectral analyser for EEG signals 77–44792
dye laser tuning by dielectric interference filter-coated prism 79–10322
earthquake foci, parameters determ. using spectral theory of seismic sources 77–21687
EMG biofeedback device 79–96706
far IR narrow band-pass filter construction 77–39065
far IR narrow-bandpass interference filters, prod. and performance 78–5558
feedback optical system using liquid crystal light valves 78–66924
fibre-optic band-pass attenuator 79–37003
flexible band-pass filtering using coherent optical feedback 79–94166
frequency anal., optimized octave, half-octave and third octave bandpass filters *(German)* 79–64470
grooved reflective array SAW compressor and resonator performance 77–23820
image Fourier transform correlator using US light modulator *(Russian)* 77–58264
image processing appl. of multiple bandpass filters 80–109002
interdigital transducers for one-port SAW resonators, narrow band filters appl. *(Japanese)* 79–27478
interference filters for 1-3 mm window, far IR astronomy 80–109368
low-temperature narrow-bandpass interference filter construction 79–32049
lumped parameter equiv. ccts. for HF transducers, quarter-wave matching characts. 80–1397
metallic mesh interference filters, low temp. narrowbandpass 80–14430
microcomputer based digital filter for electroencephalogram processing 78–73278
narrowband optical wave filter with stacked directional coupler 79–7226
one-port SAW resonators using long IDTs and their application to narrow band filters 79–76934
operation details, hearing analysis appl. *(Italian)* 80–94218
optical, narrow, via nearly degenerate four-wave mixing 79–23013

band-pass filters continued
optical filters for visible region, glass characts. 77−75659
parallel-channel SAW filter bank transfer function synthesis 77−23828
peripheral auditory system, anal., noise appls. 78−80888
precision TV demodulator using high-performance SAW transversal filters 79−49258
PS booster at CERN, longit. active damping system electronics, tracking band pass filters 77−83297
quadrature sampled digital bandpass filters 77−23816
quartz temperature-stable shallow bulk acoustic wave devices 79−55293
reflective dot array SAW filter 77−23825
ripple noise pitch detection by human, adaptive model 78−73166
SAW, approx. parameter anal. *(Russian)* 80−23858
SAW, characteristics 77−68332
SAW, combined bandpass and rejection filters, design and eval. *(Russian)* 80−83718
SAW, design and expt. results *(Czech)* 80−19201
SAW, manufacturing inaccuracies influence on transmission characts. 79−10434
SAW, signal sorting in military high density signal receivers 79−18615
SAW, transversal, principle, design and performance 78−38147
SAW, two-port model 77−62117
SAW, use of charge distribution model 80−74678
SAW, with −50 dB sidelobes using unweighted interdigital transducers 78−71244
SAW, with three-transducer configuration 80−74610
SAW, withdrawal weighted, CAD 78−66991
SAW and CCD transversal filtering technology 77−27440
SAW bandpass filter using fanned multistrip coupler 77−50837
SAW bandpass filters, TV receiver appls. 78−51008
SAW broad-band filters, tap weight enhancement 78−22239
SAW Butterworth contiguous filters, design, fabrication and testing, 248.8 to 401.2 MHz 79−68493
SAW devices props. and appl., ZnO thin-film, for HF range *(Japanese)* 80−53598
SAW digital filter design using optimum pulse response techniques 77−46872
SAW filter design using linear programming technique *(Japanese)* 77−23839
SAW filter design with arbitrary phase and amplitude characteristics 77−23826
SAW filter synthesis, asymptotic and Fourier transform. methods *(Russian)* 77−58510
SAW filters, narrow pass-band, for transmission system appls. 79−50517
SAW filters exhibiting arbitrary phase and amplitude response characts., design 77−80021
SAW filters with quarter wave reflections, design 80−19183
SAW grating resonators, reflection-dependent coupling 77−23822
SAW narrow pass band, frequency stability study *(Japanese)* 78−90603
SAW narrow pass band, transmission systems appl. *(Japanese)* 78−90602
SAW quartz resonator, two-port design 77−23819
SAW resonator bandpass filter design for various coupling mechanisms 78−33967
SAW resonator reflector and transducer characteristic effects 77−39168
SAW ring filter geometry 77−39175
SAW transducer with capacitive electrode weighting, band-pass filters 80−48544
SAW X-ray topographical representation 79−47870
seismic surface waves, freq. filter anal., fast method 79−48573
semiconductor-compatible SAW devices 77−80044
sleep EEG activity and hormonal change correlation 77−9314
spatial filtering properties of volume holograms 79−27211
speech noise suppression filter for narrowband vocoder 80−91977
surface skimming bulk wave filters using Y-rotated quartz 80−74583
synthetic aperture radar image coherent-optical simulation 77−50632
whistler analyser, semiautomated, using spectrum analyser and programmable tracking filter 79−74975
white light optical processor for edge enhancement and spectral filtering 79−76599
withdrawal weighted SAW filter design from electric field interactions in finite arrays 77−23827
zero crossing and FFT speech recognition systems compared 79−76917
LiNbO$_3$ crystal acousto-optical tunable filter 77−19434
LiNbO$_3$ SAW filter bulk wave suppression by triangular metal film overlay 77−23830
LiTaO$_3$ crystals for commercial SAW TV IF filters, fabrication 80−80961
LiTaO$_3$ rotated Y-cuts for SAW launching 79−56060
LiTaO$_3$ temperature-stable shallow bulk acoustic wave devices 79−55293

band structure
see also band structure of crystalline metals; band structure of crystalline semiconductors and insulators; band structure of semimetals; band theory models and calculation methods; Brillouin zones; conduction bands; degenerate semiconductors; electron energy states of amorphous solids; electron energy states of liquid metals; electron energy states of liquid semiconductors; energy gap; Fermi surface; many-valley semiconductors; valence bands
A-15 compounds, supercond. props., band struct. calcs. 79−33388
alloys, disordered, band edge position, tight-binding Hamiltonian *(French)* 78−10324
angle resolved photoemission obs. and band struct. 79−33899
angle-resolved photoemission, review 80−45214
band modification caused by impurities and magnetophonon effect 79−42562
band tailing due to zero-point vibrs. in perfect cryst. 79−28267
binary alloys, random, quantum percolation 80−80156
binary alloys, structural aspects of energy 77−39556
Bloch electron continuous spectrum instability, N-band Stark ladder 77−57220
Bloch electrons, closure of bands in a mag. field 78−79918
Bloch Hamiltonians, analytic props. determ. 78−22995
Bloch reduced Hamiltonians, spectral props. and bands 77−24509
Bravais-lattice operator in one band of solid 80−10519
chalcogenide glass/n-GaAs heterojunctions, elec. props. and band diagram 79−99609
channelling in Kronig-Penney pot., band struct. and Bloch wavefunctions 80−65112
cluster calculation, fast self-consistent, for large systems, appl. to electronic struct. of solids 79−82513

band structure continued
conducting π-electron systems, electronic struct., one-electron band theory 80−65450
covalent and ionic solids, determ. of electronic struct. 78−2409
crystals, matching Green function method 77−85129
crystals, Schrodinger eqn. calcs. variational cellular method, general formulation 78−94192
cummulene type infinite chain cryst., energy bands, ab initio Hartree-Fock orbital calc. 78−60066
diamagnetic band structure, first principles calc. 80−88470
diamagnetic band structure, second order calc. using Landau functions 80−24784
diamond-like structure, interatomic matrix elements between s- and p-like states, LCAO calc. 80−10857
dielectric band structure, of solids 79−47034
disordered solid, l-depend. pseudopot. in theory of band struct. 78−84124
disordered system, density of states calc. using augmented space formalism, comment 80−2322
electron band structure, optically induced in external plane wave field 80−106432
electron eigenstates in ordered and disordered ensembles of scatterers 79−99466
electron scattering by atomic planes in single crysts., and band struct. with intrinsic values of transverse energy *(Russian)* 78−39639
electron spectroscopy of crystals, book 80−36786
electronic system with two-fold degenerate band, free energy change due to electron-phonon coupling 79−42500
electrons in helical mag. fields, quantum theory 79−80470
energy spectrum in periodic magnetic field, band struct., surface states anal. *(Russian)* 80−39645
energy sub-bands in polar model of crystal *(Russian)* 80−80183
rel. to excitonic molecule theory 77−69238
FCC, BCC and SC crysals, electronic struct. tight binding model 78−84123
Fermi surface studies of pure cryst. materials, review 78−10334
field emitted electrons, effects of band struct. on energy distrib. 77−24932
film, linear APW method, muffin-tin potential, appl. to Cu monolayers 78−87899
finite diffraction models for electron bandstructures 79−87034
free charge carriers in solids, high order harmonic generation 77−76804
graphite, electron energy loss meas. 77−51688
graphite, layered, electronic band struct., direct evaluation by angle resolved photoemission 77−51652
graphite compound, metallic electronic props. and correl. with chemistry 80−44567
graphite intercalated with AsF$_5$, quantum oscillatory phenomena 80−107823
graphite intercalation compounds, band struct. model, dynamical dielec. function, reflectivity 80−34348
graphite intercalation compounds, C$_n$K, electronic struct. and elec. props. 80−44471
graphite intercalation compounds, galvanomagnetic and optical data, electronic structure 77−51634
graphite intercalation compounds with K and Cs, sp. ht., XPS 78−26693
graphite intercalation cpd., C$_6$Li, charge distrib. 78−34743
graphite intercalation cpd., C$_6$Li energy band struct. 78−30861
graphite intercalation cpds., electronic props. 78−34744
graphite nitrate, $(C_{3.24})^+(NO_3)^-3HNO_3$, DTA, NMR and refl. meas., dynamical and electronic props. 77−59478
graphite-alkali metal intercalation cpds., electronic props. 80−45202
group-V layer compounds, 2H-polytypes, origin of CDW, elec. susceptibility, electron-phonon interactions 77−51679
hard sphere problem on lattice, moment method, uniform chain 79−97311
Hartree-Fock energy bands using OPW method 80−10856
HEED, cross-grating, atomic string approx., dispersion surface and Bloch waves 80−49056
HEED atomic string approximation use in obtaining dispersion surfaces 80−100143
helical systems, energy band calcs. using Hartree-Fock SCF-LCAO formulae 78−10329
HF field energy absorpt. in strong parallel mag. and elec. fields 79−73801
Hubbard model, doubly degenerate, functional integral approach 79−99711
Hubbard model, half-filled, charge-ordered ground state 80−39487
ice, UPS study 79−43101
impact ionisation thresholds, as generalisation of van Hove singularities 77−77295
interband absorpt. in strong parallel mag. and elec. fields 79−78063
ionicity and struct., interrelation, appl. to zincblende, rocksalt and wurtzite structs. and amorphous semiconductors 77−1093
layered compounds, book 77−39757
layered compounds, optical props., book contrib. 77−44023
LCAO model, self-consistent numerical-basis-set, local density formalism 77−76725
Leman-Weaire-Thorpe theorem generalisation 79−95308
localisation in impurity bands 80−20114
magnetic semiconductors, long-range exchange interactions 77−69531
metal-insulator transition region, narrow energy bands, electron correlation, Gutzwiller variational method 80−84426
momentum space formalism, total energy of solids, calc. 80−15468
Mott transitions, temperature induced, Hubbard model theory 80−29326
muffin-tin phase shift parametrisation scheme 77−55473
one dimensional polymers, compositional disorder, approx. band struct., self consistent virtual crystal approx. 80−39486
one-dimensional conductor, model system, polymer-bridged metal complex, MO theory 79−90940
one-dimensional conductors, Peierls transition temp. and 0K energy gap, mean field theory calc. 80−24782
one-dimensional disordered systems, electron transmission and wave propag. 80−24907
one-dimensional molecular crystals, electronic struct., mol. orbital theory 80−54588
optical oscillator strengths and excitation energies in liquids, solids and mols. 78−6648
organic molecular solid, space group C_{2h}^5, triplet excitons energy band struct. 78−6276

band structure continued
- organic solids, energy band theory problems due to narrow bandwidths 80—44469
- organic solids, one-dimens. conductor, dimer level splitting, hopping integral calc. using PPP Hamiltonian 80—24890
- p-n heterojunction solar cells, band structure and photocurrent collection 80—21402
- periodic stratified medium, EM propag., general theory 77—65565
- photoemission, angle-resolved, from bulk bands of solids 79—4895
- photoemission from bulk bands of solids, electron-phonon interaction effects 80—20767
- photoemission in solids, book 80—12860
- polar crystal model, instabilities in electron energy spectrum, metallic state stability criterion 79—82524
- polar crystal model, instabilities in electron energy spectrum, max. polarity state 79—82534
- polyacetylene, bond length alternation and energy gap, intermediate exciton formalism 80—29305
- trans-polyacetylene, electronic energy band struct., extended Huckel and MNDO studies 80—20065
- polyacetylene, electronic energy states and charge density contours studied muffin tin orbitals technique 80—80164
- polyacetylene, electronic struct., one-electron band theory 80—65450
- polyacetylene type infinite chain cryst., energy bands, ab initio Hartree-Fock orbital calc. 78—60066
- polycytosine, ab initio energy band struct. 77—70415
- polydiacetylene polymer crystals, optical nonlinearities, chain pairing effects, one dimens. band model 77—69851
- polydiacetylenes, electronic struct., cyclic vs. linear models 80—54587
- polyene, energy bands, ab initio Hartree-Fock cryst. orbital calcs. 77—89717
- polyene band struct. calc., excitons in polyene chain 78—26816
- polyethylene, electronic band struct., tight-binding approx. with MNDO 77—89691
- polyethylene, electronic energy states and charge density contours studied muffin tin orbitals technique 80—80164
- polyyne, linear infinite chain, ground-state props., ab initio studies 79—95306
- PTFE, electronic energy states and charge density contours studied muffin tin orbitals technique 80—80164
- quasi-one-dimensional organic conductor, chem. trends and stabilisation of nearly one-dimens. state, review 78—10328
- rare earth monochalcogenides, electronic transitions 77—43496
- rare earth ternary borides, RRh_4B_4, supercond., re-entrant magnetism, energy band calcs. 78—52140
- $(Sn)_x$ chain, energy band struct., Hartree-Fock and CDW solns. 79—23885
- solid, new Hartree-Fock energy band struct. determ. using LCAO basis, appl. to diamond 77—35848
- solid, semi-infinite, electronic instability of surface 77—43682
- solid state physics, book 80—101676
- solids, optical absorption under laser irrad. 80—34940
- spectroscopy using synchrotron radiation 77—20882
- superlattice, electronic band struct. in mag. fields 79—65355
- superlattice, one-dimensional, band structure instability under strong population inversion 77—43470
- surface study using photoelectron spectroscopy *(French)* 80—50519
- symmetry-adapted Wannier functions, variational procedure 80—2323
- synchrotron radiation applications 77—51283
- TCNQ, infinite stacks, all valence electron band struct. 78—39001
- TCNQ complexes, $Qn(TCNQ)_2$, NMePh.TCNQ, and Li^+TCNQ^-, rel. to extrinsic and intrinsic mag. susceptibility 78—43556
- TCNQ salt, $(N\text{-methylphenazinium})_x(\text{phenazine})_{1-x}$, 1 band filling, carrier mogility and disorder effects 80—24904
- TCNQ salt, $(NMP)_x(Phen)_{1-x}(TCNQ)$, band filling and disorder 78—87968
- TCNQ salt, $MEM(TCNQ)_2$, phase transition electronic struct. interpretation 80—24781
- TCNQ salt, NMP-TCNQ, realisation of disordered Hubbard model, dielec. props. 78—79917
- TCNQ salt, $Qn(TCNQ)_2$, thermoelec. power and cond., large Coulomb repulsion model 80—24893
- TCNQ salts, electron localized and band motion, IR spectra 77—66487
- tetrazaporphin, coord. polymer with transition metal, one-dimens. conductor, band struct., EHT theory 79—90941
- transition metal, dichalcogenide layer cpds., bonding and phase transitions 80—34186
- transition metal carbides, complex phases with NaCl struct., microhardness rel. to electronic structure 77—90438
- transition metal carbides, high temp. supercond., role of electronic struct. on obs. phonon anomalies 77—24363
- transition metal carbides and borides, electronic structures calc. in conjunction with X-ray photoelectron spectroscopy *(Japanese)* 79—15074
- transition metal compounds, electronically driven lattice instabilities, role of p-d hybridisation 78—63835
- transition metal hydrides, electronic states calc. 79—7769
- transition metal monoantimonides, 3d-states, optical evidence for analogy with transition metals 77—62816
- transition metal-rare earth dil. alloy, hyperfine field of rare earth impurity 79—1588
- TTF, infinite stacks, all valence electron band struct. 78—39001
- TTF-TCNQ, band struct., Fermi surface and density of states, LCAO calc. 78—60048
- TTF-TCNQ, elec. resist., electron-phonon scatt. 80—92884
- TTT_2I_3, charge transfer salt, Coulomb effects 79—46599
- unit-cell scheme in solids, kq representation based 78—87898
- UPS, rel. to band struct., appl. to Cu 79—52080
- X-ray spectroscopy, appl. to studies of band struct. of solids *(Polish)* 79—56887
- $(BHNH)_n$, band structure, ab initio calcs. 79—23895
- $(BH_2NH_2)_n$, band structure, ab initio calcs. 79—23895
- C_8K graphite intercalation compound, band structure calc., charge transfer effect 80—6692
- C_8K, K-graphite intercalation compound, electronic struct. using semi-empirical tight-binding scheme 78—6255
- $Cd_xHg_{1-x}Te$-metal contacts, schematic energy band diag., transport props. 77—47897
- $Co_{0.32}NbS_2$, intercalation compound, struct. and photoemission meas. 77—16453
- $CsPbBr_3$, optical props. and electronic struct. 78—48198
- $CsPbCl_3$, optical props. and electronic struct. 78—48198

band structure continued
- $Cu_{60}Zr_{40}$ glassy metal, photoemission and mag. susceptibility 79—28896
- ErH_2, electronic struct. 79—28268
- $EuMo_6S_8$, Chevrel phase, RE mag. isolation and supercond. 80—44470
- Fe-Al, optical props. rel. to order-disorder transformations 80—29736
- $Fe_{0.33}NbS_2$, intercalation compound, struct. and photoemission meas. 77—16453
- FeO_4^{2-} ion, electronic struct., hyperfine interactions, SCF $X\alpha$ calcs. 79—37951
- $GdMo_6S_8$, Chevrel phase, RE mag. isolation and supercond. 80—44470
- H linear chain of atoms, electronic struct. calc. 78—79969
- H-He, metallic solid alloys, phase separation, electron band struct. and lattice dynamics determ. 77—43333
- H_2, FCC solid, first-order shifts in electronic states 79—82510
- H_2, highly compressed, combined representation method for use in band struct. calc. 77—89685
- H_2, solid, electronic struct., HF calc. using plane wave basis 79—7772
- $(HF)_n$, $n=1\text{-}\infty$, ab initio hydrogen bond and electronic parameters, phonons 77—14342
- n-$Hg_{1-x}Mn_xTe$, quantum transport phenomena, exchange interaction influence 78—76093
- In_2O_3-SnO_2 film, XPS expts., energy band model accounting for phys. props. 77—90241
- InSb-anodic oxide-Ni, energy band diagram, internal photoemission meas. 79—33356
- KC_8, intercalated graphite, electronic and cryst. struct. 80—44472
- $KMnF_3$ film, photoelec. yield spectra, rel. to band struct. 78—43980
- $K_2Pt(CN)_4Br_{0.3}.3H_2O$, Krogmann salt, non-empirical localised orbital cal. of electronic struct. 78—91636
- $KZnF_3$ film, photoelec. yield spectra, rel. to band struct. 78—43980
- LaB_6, metallic, energy bands and bonding 77—43486
- Li chain, disordered system, ab initio cryst. orbital calcs. 77—47715
- Li film, optical absorpt. spectra, rel. to phase struct. 77—4651
- LiAl, semimetallic, B32 struct., electronic props. 78—56062
- LiC_6, intercalated graphite, band struct. determ. by angle-resolved photoemission 80—45203
- LiC_6, intercalation compound, electronic struct., XPS meas. 80—59850
- β'-MgHg, energy bands and Fermi surface calc. 77—43481
- β'-MgTl, energy bands and Fermi surface calc. 77—43481
- $Mn_{0.26}NbS_2$, intercalation compound, struct. and photoemission meas. 77—16453
- Mo ternary chalcogenides, supercond., muffin-tin orbitals and atomic-sphere approx. 78—51871
- MoS_2 intercalation compounds, reaction with alkali and alkali earth metals, band struct., superconductivity 78—26541
- Na_xWO_3, cubic, final-state effects in XPS 77—90251
- Na_xWO_3 enhanced T_c, interband coupling 78—91804
- Nb-H, exam. of electron structure 80—29306
- NbS_2, 2H layer cpd., tight-binding fit to bond struct. 78—39000
- $NbSe_2$, 2H layer cpd., tight-binding fit to bond struct. 78—39000
- $NbSe_2$ (2H), metallic layer cpd., angle-resolved photoemission spectra 79—47593
- $NbSe_2$ (2H), metallic layer cpd., reconstructed band struct. and Fermi surface 79—95312
- $NbSe_3$, two band model and galvanomagnetic study 80—20176
- Nb_3Si, hypothetical, electronic struct., lattice parameters and possible supercond. transition temp. 79—23891
- $Ni_{0.34}NbS_2$, intercalation compound, struct. and photoemission meas. 77—16453
- PbI_2, electronic struct. and exciton problem, photoelectron spectra meas. 77—63540
- Pd-H, dil., electronic states, de Haas Haas-van Alphen effect meas. 77—47718
- $PdH_{0.72}$, Compton profiles, comparison with band struct. calcs. 78—84675
- RbC_8, intercalated graphite, band struct. determ. by angle-resolved photoemission 80—45203
- $(SN)_x$ chain, isolated, effect of $(SCH_2)_2$ impurities, on electronic props., EHT calcs. 79—15067
- $(SN)_x$, electrical cond. at high press., scatt., evidence for semimetallic band struct. 77—43573
- $(SN)_x$, electronic struct., one-electron band theory 80—65450
- $(SN)_x$, electronic struct. by extended tight-binding method, comparison with S_2N_2 precursor 77—76722
- $(SN)_x$, energy band struct., self-consistent calc. by intersecting spheres model 79—28269
- $(SN)_x$, LCAO band struct. calc. for one-dimens. chain and three-dimens. cryst. 77—76723
- $(SN)_x$, mol. cluster and band struct. calc. 77—8004
- $(SN)_x$, polymeric, electronic structure, semi-empirical pseudopotential calc. 77—72812
- $(SN)_x$ single crystals, tunnelling spectroscopy investigation *(Japanese)* 80—49954
- $(SN)_x$, tight-binding SCF MO calcs., interchain interaction 78—30859
- $SnMo_6S_8$, Chevrel phase, RE mag. isolation and supercond. 80—44470
- $SnMo_6Se_8$, Chevrel phase, RE mag. isolation and supercond. 80—44470
- TaS_2 (1T) and (2H), bonding and charge density wave phase transitions 80—44282
- $TaSe_2$ 2H, CDW effect on thermoreflectance spectra 77—52120
- Ti-H exam. of electron structure 80—29306
- TiC, calcs. of 2γ-ang. correlations and Compton profiles 78—39624
- $TiCl_3$, electronic band struct., tight-binding approx. 78—51872
- TiH_2, band model of martensitic phase transition 80—29953
- β-UD_3, electronic props., metallic character 80—6693
- V-H, exam. of electron structure 80—29306
- $VD_{0.77}$, Compton profiles, comparison with band struct. calcs. 78—84675
- $VH_{0.71}$, Compton profiles, comparison with band struct. calcs. 78—84675
- V_3In, hypothetical, electronic struct., lattice parameters and possible supercond. transition temp. 79—23891
- VO_2, metallic, magnetisation distribution and band structure 78—76223
- V_3Si, quasi-one-dimens. band struct. 78—19596
- Y-H, exam. of electron structure 80—29306
- YB_6, metallic, energy bands and bonding 77—43486
- YIG, epitaxial layer, n and p-type, UPS, elec. struct. 77—4710
- ZnO, electronic struct. calc., appl. of O nonlocal ionic pseudopot. 77—51659
- Zr-H, exam. of electron structure 80—29306
- ZrB_2, band struct. and XPS 77—90253
- ZrB_2, self-consistent band struct., XPS, reflectance, NQR, Hall effect and density of states meas. 80—107689

band structure continued
ZrH$_x$ (x=1.55, 1.7), synthesis and electron structure 80—29889
ZrN$_y$H$_x$ (y=0.81 or 0.84, x=0.19 or 0.16) synthesis and electron structure 80—29889

band structure of crystalline metals
A15 compound trends, self consistent band calcs. 78—79925
A15 compounds, band theory, semiself-consistent band calcs. 78—2406
A15 compounds, calc. 79—37970
A15 compounds, high-temp. superconductors, martensitic transform., microscopic theory based on 3-dimens. band struct. 78—19752
A15 compounds, linear muffin tin orbital band results by press. calc. 79—65356
A15 compounds, self-consistent LMTO band calcs. 79—37954
A15 compounds, struct. transform., comparison of Landau theories 78—67824
A-15 compounds, disordered, T_c depression, appl. to Nb_3Ge 80—7020
A-15 superconductors, transition temp., d band relative displacement *(Chinese)* 80—103770
A-15 type superconductor, comment on new 3-dimens. $\bar{k}.\bar{p}$ model for electronic struct. 80—10865
A-15 type superconductor, reply to comment on new 3-dimens. $\bar{k}.\bar{p}$ model for electronic struct. 80—10866
actinide metals and intermetallics, electronic energy band struct., 5f electrons role 77—28107
actinides, band structure and bonding calcs. 80—10871
actinides, band structure Fermi surface, magnetisation density 78—84140
actinides, band theory approach 80—15440
actinides, electronic excitation energies calcs. 80—54592
actinides, electronic structure, role of 5f electrons, Dirac-Slater wave function structure 77—28108
actinides, electronic structure and props., review 77—62813
actinides, Slater-Koster interpolation scheme 80—6708
actinides and alloys, metallurgical props. rel. to electronic struct., energies calc. method 77—20221
alkali metal, local Heine-Abarenkov-type model pot. 79—87031
alkali metals, Fermi surface topological changes due to uniaxial stresses 80—92810
alloy, electronic characts. from thermomodulation spectra 79—87421
alloy, one-dimensional, electronic struct. 79—69391
alloys, binary with long and short range order, electron energy spectrum calcs. *(Russian)* 79—99471
alloys, CPA for props. 80—75493
alloys, density of electronic states, dressed-cluster approx. 78—95249
alloys, disordered, muffin-tin model, electronic struct. and density of states, theory 80—29301
alloys, local density of states and local environment 79—82509
antiferromagnetic solution of extended Hubbard model, CPA treatment 78—19208
band structure, optical cond., Compton profile, self consistent calcs. 80—65435
binary alloy, ordered, electronic struct. in Bethe lattice, exact analytic treatment 80—49582
binary alloys, FCC, with short-range order, electron theory, pair interaction and third-order perturbation theory 79—69404
borides, electronic struct., review, book contrib. 78—47700
borides, hexa- and di-, electronic structs., elec. props., book contrib. 78—47701
borides, nature of chem. bond, book contrib. 78—47276
brass, α and β phases, Hume-Rothery rules for phase stability 79—99292
Cu_cNi_{1-c}, soft X-ray emission spectra 78—95620
cubic metal binary alloys for H energy storage 80—45787
dilute alloy, electronic config. and vol. of formation 79—90991
dilute alloy, mag. ordering, strong renormalisation of electron spectrum 77—20550
dilute alloys, electron self-energy, Fermi surface changes and generalized golden rule 80—10858
dipole-nuclear acoustic resonance, electron band struct. influence, in cubic metal 79—19787
disordered alloy, band theory, numerical solution of KKR-CPA equations 80—44474
disordered alloy, positron annihilation, Fermi surface study, review 80—44480
disordered simple metal, electronic and cohesive properties, review 80—44475
electric properties calc., book 79—28274
electron energy loss spectra, threshold potentials and X-ray absorption, band struct. determ. *(Russian)* 78—39009
electron momentum distributions, effect of symmetry 78—63962
electrons in disordered metals and at metallic surfaces, conf., Ghent, Belgium (Sept. 1978) 80—41946
elementary excitations in crystals, dielectric theory 78—60076
Fano effect theory, electronic structure, d band metals and alloys 78—2402
FCC binary alloys, short-range order diffuse scattering, Fermi surface imaging *(Japanese)* 79—7776
FCC metal, covalent component of electron density and energy *(Russian)* 80—28945
Fermi surface, electronic props., book 80—105445
ferromagnets, itinerant electron, lattice props. depend. on cond. electron magnetisation, elastic props. 79—61035
films, linearized APW method for electronic band struct., appl. to Fe, Co, Ni, Cu and Al 79—69393
highly conducting material, electroreflectance by deep field penetration 79—19864
itinerant electron ferromagnets, elastic props. and electronic struct. 80—66001
localised versus itinerant character of 5f electron states 77—28138
metal, electronic characts. from thermomodulation spectra 79—87421
metallic compounds, cohesive props., augmented-spherical-wave calcs. 79—94952
metals, electron-deformation interaction, lattice contraction, Hubbard model calcs. *(Russian)* 80—59592
noble metal, electronic structure and d-holes of films and surfaces 78—39180
noble metal alloys, disordered, bulk electronic structure 80—44467
plasmons, APW dispersion relation, rel. to band filling 77—69265
positron annihilation studies of electronic structure *(Japanese)* 78—18951
random alloy, optical absorption and photoemission spectra 80—45216
random metallic alloy, first principles band theory, review 80—44473

band structure of crystalline metals continued
rare earth, 5d energy band widths 78—63971
rare earth alloys, RBe_{13}, XPS, resist. and susceptibility study 80—71565
rare earth metal film, optical cond., rel. to cryst. struct. and electronic config. 77—36303
rare earth metals, band structure calcs. 80—15441
rare earth metals, elastic props., connection with electron struct. *(Russian)* 80—19895
rare earth metals, electronic structure rel. to valence, chem. bonding 80—54601
rare earths, band structure Fermi surface, magnetisation density 78—84140
rare earths, electronic excitation energies calcs. 80—54592
rare earths, electronic structure, calc. methods, review 79—69405
rare earths, heavy, mag., electronic struct., book 78—60259
rare earths and their alloys, photoemission, rel. to electronic struct., book contrib. 80—16157
s-d electron model, finite temp. diagram technique, perturbation theory 78—67932
simple metals, singular struct. in density of levels 79—77997
solids, angular dependent photoemission, book contrib. 79—61500
symmetry props. of energy bands determ. by UPS with unpolarised radiation 78—48275
TC, internal conversion, scattered-wave cluster technique 80—107696
tight-binding metals, electronic struct. and kinetic props. at high temp. 80—59848
transition, rare earth, and normal metals, electronic struct. and magnetism, review 80—70573
transition and noble metal dilute alloys, Einstein's temp. and vibrational entropy, rel. to electronic struct. 78—83900
transition metal, 4d, photoabsorption spectra near K-edge 78—92144
transition metal, 4d, rel. to systematic struct. in K-edge photoabsorpt. spectra 78—43960
transition metal, 4d BCC, electron-phonon interactions 79—95107
transition metal, d-d electron correlations in cohesion and ferromagnetism 77—62810
transition metal, electronic structure and d-holes of films and surfaces 78—39180
transition metal, energy band structure and X-ray emission spectra, calc. *(Russian)* 77—1763
transition metal, field emission, effect of model hybridized energy bands 77—77349
transition metal, fusion entropy, electronic contrib. 79—42217
transition metal, impurities, as probes of critical points, in host band structure 78—91645
transition metal, inner shell photoelectron and photoabsorpt. spectra 79—43091
transition metal, Lorenz number and high-temp. interband transitions 78—26844
transition metal, rel. to bulk props. and cryst. struct. trend 78—34757
transition metal, renormalised atom. calc. of cohesive energy, band struct. inform. 77—43170
transition metal alloy, electronic structure, mag. props. 78—95254
transition metal alloys, BCC crystal struct. dependence on band struct. 78—83778
transition metal alloys, binary, state density curves, relation between short-range order and Fermi level position, CPA calculations 80—107687
transition metal alloys, cohesive properties and press.-vol. relation 80—92476
transition metal alloys, d-band hybridisation, electronegativities, structural stability 79—42007
transition metal alloys, density of states and complex band struct. for one-dimens. model 78—79919
transition metal alloys, disordered, bulk electronic structure 80—44467
transition metal alloys, elastic properties, vol. depend. 78—95103
transition metal alloys, ferromag., with atomic short range order, local environment effects on electronic struct., Fe-V appl. 78—67936
transition metal alloys, heats of formation, tight binding theory, moments approach 79—61891
transition metal compounds, electronically driven lattice instabilities, role of p-d hybridisation 79—7669
transition metal diborides, C32-type, phys., chem. props., appls., review, book contrib. 78—47308
transition metal film, energy band calc. by linear combination of muffin tin orbitals method 77—4283
transition metal impurities in transition and noble metal hosts, electronic struct. 78—75990
transition metal monoantimonides, electronic struct. determ. 77—4290
transition metal silicides, X-ray spectra *(Russian)* 77—28106
3d-transition metal-metalloid cryst. and glassy alloys, electronic struct. from magnetisation and Mossbauer meas. 80—29363
transition metal-simple metal alloys, dil., electronic states, reson. model pot. method 79—77995
transition metals, 3d, systematics of electron momentum distribs. 78—18950
transition metals, 3d electron struct. plasmons 79—77996
transition metals, 3d-, 4d-, 5d-, band struct. from spectral data and theoret. calcs. *(Russian)* 77—8013
transition metals, 4d, energy band and related props., theory 77—62811
transition metals, 4d, energy band parameters and vol. depend. 77—39772
transition metals, 4d, theory of energy bands, s and d contrib. to eqn. of state 78—30865
transition metals, and alloys, energy band filling *(Russian)* 78—6263
transition metals, band struct., parametrisation via Hubbard's scheme 77—31938
transition metals, BCC, 3d series, numerical calc. of orbital mag. susceptibility 79—82764
transition metals, BCC, electronic struct., model Hamiltonian interpolation scheme 77—47723
transition metals, BCC, films, vac. evaporated, optical cond. 80—76100
transition metals, electronic Gruneisen parameter 79—82297
transition metals, electronic structure of interstitials 79—1583
transition metals, interatomic forces, phonon spectra, from band structure charge densities 79—7662
transition metals, local pseudopotential theory 78—30863
transition metals, OPW and MOPW calcs. 79—90942
transition metals, second series, electronic band Brillouin zone APW calc., electronic config. effects 78—51883
transition metals, universal LCAO parameters 80—75503

band structure of crystalline metals continued
  transition metals, X-ray emission spectra, crystal pot., partial state densities 77−28105
  transition metals and alloys, appl. of X-ray spectroscopy to band struct. study *(Polish)* 79−56887
  transition metals and alloys, metallurgical props. rel. to electronic struct., energies calc. method 77−20221
  transition metals and their alloys, photoelectron energy distrib. curves, rel. to band struct., book contrib. 80−16156
  two-band alloy, Green's function from multiband theory 79−37952
  type II superconductor, phase diagrams, exam. in terms of electronic structure 79−8278
  uncompensated, one-particle interband transition, effect on Curie temp. 79−7994
  V-Ru, electronic states calculation 78−95255
  whiskers in MIM diodes, freq. response, effect of d-electrons 77−47898
  X-ray photoelectron and absorpt. spectra, edge singularities in spin-depend. final-state interactions 78−6810
  XPS core line asymmetries in muffin tin approximation 79−69953
  A15 compounds, electronic struct., XPS and SXE spectra calc. 79−42437
  Ag, 4d bandwidth influence on $M_{4,5}N_{4,5}N_{4,5}$ Auger spectra 79−100017
  Ag (001) surface, photoemission, electron escape effect 79−1814
  Ag (100), (110), (111), high resolution photoelectron energy distrib. curves 77−28693
  Ag (100) and (111) epitaxial films, ang. depend. UPS 80−55270
  Ag (111), angle-resolved photoemission, free-electron final state model 79−4896
  Ag, angular resolved photoemission from low index faces 78−48282
  Ag, Auger spectra, 4d bandwidth effect 80−89093
  Ag, empirical parametrisation of electronic structure 78−91585
  Ag, nonlocal model pseudopotential 78−14659
  Ag, thermomodulation spectra of high-energy interband transitions 80−108226
  Ag, valence band Auger spectra 78−76563
  Ag-Cd, α and β phase, XPS, effects of atomic order on band struct. 79−42440
  α-Ag-Cd, dil., electronic struct. determ. from thermoreflectance and XPS 78−39011
  AgH, electronic struct. and supercond., APW calc. 79−95318
  β'-AgMg, de Haas-van Alphen effect, LMTO band struct. and Fermi surface 78−75984
  Al, atomic structure factor calc. from band struct. eigenfunctions 78−6030
  Al, band struct. and density of states, calc. using model pot. method 77−76742
  Al, direct nonvertical interband transitions at large wave vectors, electron energy loss meas. 78−34759
  Al, energy bands, densities of states and X-ray spectra, superposed self-consistent pots. 78−39010
  Al, K X-ray absorption, K-emission spectrum, band struct. using APW method 80−97380
  Al, model pseudopotential 78−91582
  Al, optimised model potential parameters Hartree-Fock-Slater procedure for calc. 77−69214
  Al, plasmon dispersion, effect of band struct., dielec. function calc. 78−26825
  Al, polycryst., anisotropy of plasmon dispersion, pseudopotential method 78−23039
  Al, pseudopot. band struct. calc. 79−56119
  Al, self-consistent energy band calc. 78−6266
  Al, singular struct. in density of levels 79−77997
  Al, soft X-ray spectrum, Al core state transition probabilities, band struct. calc. 77−77325
  Al, valence band Auger spectra, surface effect 80−80915
  Al, XPS theory, valence band spectra band struct. 78−72702
  Al-3d transition metal, dil., electronic states, reson. model pot. method 79−77995
  Al-based 3d-transition metal alloys, soft X-ray absorpt., electronic struct. 79−38690
  Al-Ge(Mg)(Zn)(Ga), dil., electronic transport coeffs. for point defect scatt., 4-OPW calc. 79−42531
  AlAg, Auger spectra, 4d bandwidth effect 80−89093
  AlB_2, density of states and band struct., metallic props. 77−59249
  Al_2Cu, de Haas-van Alphen effect and LMTO band struct. 79−69396
  AlH_x, electronic struct. and electron-phonon interaction, hydrogenation effect, rel. to supercond. 80−107694
  Am, 5f-electron delocalisation 80−70595
  Au, energy band structure, X-ray N-emission spectra, relativistic APW calcs. 80−70596
  Au, energy band structure, X-ray emission spectra, APW calc. 80−92811
  Au, Fermi surface orbit integrals, tetrahedron method, cyclotron mass orientation depend. 80−44476
  Au, nonlocal model pseudopotential 78−14659
  Au, photoelectron spectra, occupied surface-state bands in sp gap 79−43094
  Au, photoelectron spectra, bulk and surface, rel. to band struct. 80−20770
  Au, photoemission study of bulk and surface electronic struct. 79−4894
  Au, self-consistent relativistic band struct. 80−75501
  Au, thermomodulation spectra of high-energy interband transitions 80−108226
  Au, UPS, band struct. 77−16455
  Au, ultrathin island films, band struct. formation 77−85893
  Au, valence band Auger spectra 78−76563
  Au, XPS, D-orbital directed emission 77−40328
  Au, XPS, electronic struct. 80−7464
  Au-Cd(Ga)(In) alloy, UPS exam. of valence bands 79−19511
  Au-Ga dil. alloys, electronic struct. 79−37974
  β'-Au-Mg, de Haas-van Alphen effect, relativistic LMTO bandstructure, Fermi surface 79−37959
  Au-Mn, band profile, density of states, quantum defect-Green's function calcs. 80−54599
  $AuCu_3$, ordered, band struct. and optical props. at 30K 79−60696
  AuSn, XPS, electronic struct. 80−7464
  Au(111), Λ-line valence bands, angle-resolved photoemission determ. 80−108323
  Be, anisotropy, theoretical investigation by K-emission, APS, and Compton profiles 78−63970
  Be, Auger spectra, initial state screening effects 80−50476

band structure of crystalline metals continued
  Be, BCC, high-temp. resist. and band struct. 79−51551
  Be, electronic struct., NMR study 80−108085
  Be, HCP metals, K-emission valence bands, structure and bonding 80−7438
  Be metal, electron distribution and momentum density, Compton scatt. 80−11502
  Be, XPS theory, valence band spectra band struct. 78−72702
  Be-Mg, two-band alloy, electronic and optical props., multiband theory 79−37952
  BeB_2, density of states and band struct., metallic props. 77−59249
  BeNi, dil., electronic struct., NMR study 80−108085
  Bi (0001) surface, angle resolved UV photoemission spectra 77−66578
  Bi, deformation calculations, band struct. variation, electron phase transitions due to deform. *(Russian)* 80−65137
  Bi, XPS, electronic struct. 80−7464
  Bi-Sb, dil., magnetothermal oscillation and spin splitting of electrons 78−43362
  Bi-Sb(-As), band struct., effects of Sb and As, mag. susceptibility meas. *(Russian)* 80−65775
  Bi-Sn, maximum diamagnetism rel. to electron density 80−54865
  $Bi_{1-x}Sb_x$, deformation calculations, band struct. variation, electron phase transitions due to deform. *(Russian)* 80−65137
  Ca, FCC, ground-state props. 78−75989
  $CaAl_2$, Laves phase, soft X-ray spectrum, band struct. calc. 77−77325
  CaSb, resist., susceptibility and thermopower rel. to electronic struct. 78−67935
  Cd, band structure, density of states and Fermi surface, APW calc. 77−20232
  Cd, photoelectron spectra, 4d spin-orbit splitting, crystal field and band-broadening effects, CNDO calcs. 78−76577
  $Cd_{1-x}Mg_x$, energy spectrum pseudopotential calcs., mag. props., impurity scatt. *(Russian)* 80−65430
  Ce, density functional theory 80−15442
  β-Ce, electronic energy band calcs. by KKR method 79−95317
  Ce, electronic structure, 4f band *(German)* 77−55479
  Ce, electronic structure, Compton profile meas. 80−10867
  Ce, electronic structure vol. depend., rigorous cellular method, γ- and α-forms 77−20233
  Ce, p core states calc., linear muffin-tin orbitals method 78−91607
  γ-Ce, photoelectron spectra, 4f level position 80−25519
  $CeBe_{13}$, intermediate valence state, XPS, resist. and susceptibility study 80−71565
  $CeRh_{3-x}Pd_x$, powdered alloys, catalytic behaviour correlation with electronic struct., lattice struct. and surface comp. 79−82181
  $CeSn_3$, mixed valence cpd., electronic struct. and mag. props. 80−70649
  $CeSn_3$, polarised neutron study of induced magnetisation 80−34594
  Co, Co alloys, electrical resistivity and specific heat meas., anomalies rel. to thermally excited states 80−6809
  Co, energy band dispersion and mag. exchange splitting, angle-resolved photoemission meas. 80−71567
  Co, energy band dispersions and mag. exchange splitting 80−76146
  Co, ferromag., HCP, electronic struct. calcs., band props. 78−39012
  Co, ferromag., spin subband level position determ. by de Haas-van Alphen meas. under press. *(Russian)* 79−90947
  Co, HCP, low energy interband absorption, electronic struct. exam. 79−73930
  Co, Kerr equatorial effect freq. spectra anisotropy, dielectric permeability tensor *(Russian)* 80−55072
  Co, tunnelling electron spin polarisation rel. to band struct. 78−68095
  Co, UPS, single cryst. and polycryst. film, electronic struct. 78−11081
  Co-Al, band struct. and density of states, KKR method and X-ray meas. 80−10863
  Co-Pd, transfer phenomena and association with electronic struct. *(Russian)* 79−91017
  Co-Si-Ge system, X-ray diffr. exam., band struct. *(Russian)* 78−56623
  Co_3B, crystalline, photoemission and electronic struct. 80−2926
  $Co_{92}Fe_8$, FCC, electronic struct., ang. correlation of positron annihilation γ-quanta, meas. 80−10864
  CoGe, and TiCoGe, X-ray K- and L-spectra obs. *(Russian)* 78−11022
  CoGe, Co_2Ge and $CoGe_2$, X-ray spectrum analysis, energy band struct. *(Ukrainian)* 77−52200
  CoSb, at. struct. and mag. susceptibility 77−39561
  CoSi, and TiCoSi, X-ray K- and L-spectra obs. *(Russian)* 78−11022
  CoSi, electronic struct. determ. by XPS and X-ray emission spectra 77−85147
  Co_3Ti, electron energy spectrum calcs. by supplementary plane wave method 80−6711
  Cr, band struct. and Fermi surfce, ang. correlation of positron annihilation radiation 78−6260
  Cr, band structure and Fermi suface of paramag. solid *(Russian)* 79−65375
  Cr, electronic density of states, X-ray emission bands, self-consistent calc. 77−28104
  Cr, electronic struct., spin-density functional calcs. 80−88476
  Cr, Neel temperature and Fermi energy, nonmag. impurity effects 80−65888
  Cr, paramagnetic, elastic moduli meas., comparison with Ti-V, V-Cr, rel. to bandstructure 80−7615
  Cr, paramagnetic, Hartree band struct., Fermi surface, nesting wave vector 80−49583
  Cr, rel. to optical absorpt. spectrum, 0.25-21 μm *(Russian)* 77−81118
  Cr, single Q-state, antiferromag. phase, rel. to band struct. 77−15759
  Cr, spin density wave, Nambu-Eliashberg eqns. for k-state electron-hole pairing 80−97050
  Cr-Al, band struct. and density of states, KKR method and X-ray meas. 80−10863
  Cr-Al, disordered alloy, effect of high press. on resistivity 78−95286
  Cr-Co (4 wt.%) alloy, antiferromag. transitions effect on opt. props. 77−12371
  Cr-Fe, electronic struct., Mossbauer and positron annihilation study 79−82518
  Cs, electronic transition from self consistent APW Xα calcs. 78−51884
  Cs, isostructural transition and lattice vibrs., relativistic LMTO calc. 80−20074
  Cs, supercond., elec. resist. and phase transforms. under high press. *(German)* 80−107763
  Cs-Ag, dil., electronic struct., density functional approach 80−44492
  Cs-Au alloy, cryst., UV photoemission investig. of band struct. 77−24923

band structure of crystalline metals continued
CsAu, band struct. and charge distrib., semicond. and metallic behaviour 77—20238
CsAu, electronic struct., XPS meas. 79—69403
Cu (001) monolayer, electronic struct., self-consistent LCAO calc. 79—4606
Cu (100) and (111), angle-resolved photoemission and band struct. 79—95904
Cu, (100) and (111), surface states, d-band, angle-resolved photoemission spectra obs. 80—20768
Cu (110), surface angle resolved photoemission 79—83097
Cu (110), valence bands, angle-resolved photoemission spectra meas. 79—74056
Cu (110) film, energy bands, tight binding calc. 77—15761
Cu (111), angle-resolved UPS, free electron final state model calcs. 78—31302
Cu (111), final state band gap effects in UPS 80—89120
Cu (111) film, energy bands, tight binding calc. 77—15760
Cu (111) surface, PES and band struct. calcs. 80—89118
Cu, angle-resolved photoemission, band struct. 78—95680
Cu, band structure and high-resolution normal emission UPS 80—6712
Cu, band structure calcs., optimised LCAO version, appl. to Wannier states 79—33220
Cu, Bloch states, photoelectron spectra, angle resolved 78—92175
Cu, bulk and (001) films, extended tight-binding calcs. 80—70592
Cu, electronic struct., linear APW method 79—51467
Cu, electronic structure and d-holes of films and surfaces 78—39180
Cu, empirical parametrisation of electronic structure 78—91585
Cu, energy band calc. by model-pseudopotential method 79—7779
Cu, energy band dispersions, absolute determ. using ang.-resolved photoelectron spectrosc., symmetry method 79—15590
Cu, energy band dispersions and lifetimes using angle-resolved photoemission 79—77998
Cu, Fermi surface, electron mass enhancement, orthornormal function enhancement 80—96777
Cu, Fermi surface orbit integrals, tetrahedron method, cyclotron mass orientation depend. 80—44476
Cu, Fermi surface orbit integrals, tetrahedron method, Dingle temps. for 3d transition metal impurities 80—44477
Cu film, APW band struct. calc., muffin-tin potential 78—87899
Cu, final energy bands, high energy, angle resolved photoemission 80—2327
Cu halides, reflection spectra, 4.5-7.5 eV, bond struct. scheme 79—61402
Cu, multipole wave functions for photoelectrons, constant-energy-surface harmonics, s-d band appl. 79—37955
Cu, nonlocal model pseudopotential 78—14659
Cu on Ag (001), ultrathin film electronic states calc. 78—6318
Cu, parametrised, separable potential for band structure calculations 78—79912
Cu, photoemission spectra and band struct., extensions of combined interpolation scheme 79—78844
Cu, point-geometry ang. correl. curves, enhancement in positron annihilation 79—95873
Cu, thermomodulation spectra of high-energy interband transitions 80—108226
Cu, UPS, rel. to band struct. 79—52080
Cu, valence band Auger spectra 78—76563
Cu, XPS, D-orbital directed emission 77—40328
Cu/Ni coherent modulated structures, electronic struct. and magnetism 80—103620
Cu-Al, optical composition modulation spectra, dielec. const. var., Fermi surface and electronic level shifts 80—6707
Cu-Au film, optical props. of ordered and disordered alloys 77—20945
Cu-Ni, optical absorption and photoemission spectra 80—45216
Cu-Pd, mag. susceptibility and electronic struct. of ordering *(Russian)* 80—11161
Cu-phthalocyanine, photoemission multielectron effects from quasi atomic Cu 80—93458
Cu-transition metal dil. alloy, virtual bound states 79—37975
Cu-Zn, optical composition modulation spectra, dielec. const. var., Fermi surface and electronic level shifts 80—6707
α-$Cu_{0.7}$ $Zn_{0.3}$, point-geometry ang. correl. curves, enhancement in positron annihilation 79—95873
CuAu, mag. susceptibility and electronic struct. of ordering *(Russian)* 80—11161
Cu_3Au, mag. susceptibility and electronic struct. of ordering *(Russian)* 80—11161
Cu_2Mg, electronic struct. volume depend. 79—65366
Cu_2MnAl, alloy, energy band calc. by nonrelativistic SAPW method 79—4507
Cu_2Ni_{1-c}, solutions of KKR-CPA equations for paramagnetic alloys 78—95256
Cu_cNi_{1-c}, Fermi surface of concentrated paramag. alloys 78—95257
Cu_xNi_{1-x}, bulk electronic structure, comparison of CPA and ATA techniques 80—44467
Cu_xNi_{1-x}, disordered alloy, muffin-tin model, electronic struct. and density of states calc. 80—29302
$Cu_xNi_{1\ x}$, paramag., electronic struct., atomic sphere approx. to KKR-CPA 79—19502
Cu_xNi_{1-x} random alloy, angle-resolved photoemission 78—95683
Cu_2Sb, linear muffin-tin calc. for Fermi surface 77—62802
Cu_xZn_{1-x}, disordered alloy, muffin-tin model, electronic struct. and density of states calc. 80—29302
Cu(110), photoemission, bulk versus surface effects 78—52626
Cu(111), (100), temp. depend. of bulk and surface energy bands using angle-resolved photoemission 79—69572
Cu(111), bulk s orbital bands, sensitivity to oxidation, photoelectron spectra 79—47597
de Haas-van Alphen freq. and Fermi surface anisotropy press. depend. 80—59856
$ErRh_4B_4$, supercond., electronic struct. and reentrant magnetism 78—10340
Eu, band struct. and Fermi surface 77—62814
Eu, electronic struct. investigation by electron spectroscopy method 80—92812
Eu, Fermi surface and helical spin ordering 77—4291
Eu intermetallic compounds, valence fluctuations, role of charge screening 78—51944
Eu, relativistic band struct. calcs., unoccupied 4f level calc., Fermi level, atomic configuration 80—49584
Eu-transition metal intermetallics, valence fluctuations 78—91649

band structure of crystalline metals continued
$Eu_{1-x}La_xS$, electron struct., lattice consts., X-ray spectral study *(Russian)* 80—100432
Fe, BCC, low energy interband absorption, electronic struct. exam. 79—73930
Fe, electronic band struct., generalised k.p. interpolation method 80—6709
Fe, electronic structure, positron annihilation meas. 79—91524
Fe, energy band dispersion and mag. exchange splitting, angle-resolved photoemission meas. 80—71567
Fe, energy bands, tight binding calc. *(Korean)* 79—51479
Fe, FCC, electronic struct. at Earth core press. 77—1356
Fe, ferromag., effect of pressure on electron struct. *(Russian)* 79—77987
Fe, ferromag. nonrelativistic LCAO energy band calc. 78—10343
Fe, interband optical conductivity, self energy correction 80—2792
Fe, magnetism at high temps., total electronic band struct. energy calc. 80—75721
Fe, photoemission and electronic spectra, exchange splitting 77—4717
Fe, photoemission study of (100), (110) and (111) surfaces, ferromag. band struct. 79—38714
Fe rich binary alloys, effect of transition impurities on structural stabilisation, rel. to band struct. 77—76552
Fe, spin dependent momentum distrib., APW calc. 78—2416
Fe, tunnelling electron spin polarisation rel. to band struct. 78—68095
Fe-Al, band struct. and density of states, KKR method and X-ray meas. 80—10863
Fe-Al, directional Compton profiles, self-consistent APW band struct. calc. 80—25476
Fe-Al, X-ray emission spectra 80—25489
Fe-Al (8 at.%), XPS investig. of cond. band region 77—16456
Fe-Al systems, band struct. and cluster calcs. 79—51480
Fe-based alloy, effect of sp-3d impurity interactions in resistivity 79—46696
α-Fe-based dil. solid solutions, electronic struct., hyperfine interactions 78—79968
Fe-C, electronic structure of interstitials 79—1583
Fe-C-Cr(Al), electronic structure, thermodynamics of structure formation 79 99475
Fe-Co, electron energy spectrum calc. by Green function method *(Russian)* 77—35860
Fe-Co films, optical props. order-disorder transformation influence, absorpt. band existence *(Russian)* 79—65942
Fe-Cr, Auger electron and appearance pot. spectroscopic study of surfaces 80—11520
Fe-Mn-Cr(Ni), mag. and crystallographic transformation depend. on Cr-Ni addition *(Russian)* 79—83334
Fe-Ni alloys, electronic struct. by XPS obs. 79—33226
Fe-Ni alloys, electronic struct., XPS study 80—29842
Fe-Ni alloys, thermal expansion rel. to X-ray emission spectra *(Russian)* 77—32470
Fe-Rh alloy, nonmag. and mag., band theory 79—37973
Fe-V(Cr)(Mo)(W)(Ti)(Nb) alloys, split bands evidence from sp. ht. and elec. transport data 77—24515
FeAl, B2-cpd., band struct. and density of states, KKR calc. 78—63969
Fe_2Al, mag. moment determ., role of local environment, self consistent calcs. 80—44815
Fe_3Al, super-lattice, band theory 77—15758
$Fe_3Al(Si)$, electronic structure, magnetic moments 80—107695
$FeGe_2$, antiferromagnet, de Haas-van Alphen effect 79—4505
$Fe_{1\ x}(P,B)_x$, amorphous and crystalline, photoemission and band structure 80—60754
$Fe_{1-x}P_x$ dilute alloys, electronic struct., mag., elec. and struct. props. 79—37971
FeRh, antiferromag., band structure and effect of Fe impurity on mag. props. 77—28377
FeRh, antiferromag., band struc., off-stoichiometry effects 78—10341
$Fe_3Si(Al)$, electronic structure, X-ray spectra comparison with band struct. calcs. 80—97383
Ga, liquid and solid, photoemission, conduction electrons 79—87566
Ga-La, energy band struct. and atomic radius 79—73434
Gd, band structure and Fermi surface using KKR formalism 79—77993
Gd, ferromag. Fermi surface and band struct., press. effects, dHvA expts. 78—14656
Gd, HCP, ferromag. band struct. and Fermi surface, KKR band calcs. 77—62815
Gd, photoabsorpt. spectra, band structure at. ionisation mechanisms, electron energy loss spectra 77—24909
Gd pnictides, APW calc., semicond.-metal trend 77—28111
Gd, relativistic spin polarised calc. 77—85128
Gd, self consistent relativistic ferromag. band struct. 78—91609
Gd-Fe, mag. moment of Fe, multiplet splitting in photoemission 79—78846
$GdCo_5$, spin polarised energy band struct., APW calc. 78—10342
H_2, metallic, electron-phonon interaction and superconductivity, APW calcs. 78—14854
H_2 metallic, electronic band struct. using θ-function basis 79—37976
H_xWO_3 bronzes, Anderson transition, XPS 80—107705
Hf, electron structure and soft X-ray emission spectrum, RAPW calcs. 79—91536
$HoRh_4B_4$, electronic struct. and reentrant magnetism 78—10340
In, lattice dynamics, pseudopot. computation *(Russian)* 80—92617
In, relativistic energy bands, density of states, and optical spectra, KKRZ calc. 79—51478
β-In_3Sn, band struct. and Fermi surface calc. using model pseudopot. 77—28103
Ir, (111) surface states, surface Umklapp effects, photoelectron spectra 80—93457
Ir, electronic struct., double beam photoemission 79—83098
Ir, electronic struct. determ. from optical refl. meas. 77—62812
Ir, energy band structure, X-ray emission spectra, APW calc. 80—92811
K, MAPW calcs. using nonlocal screened exchange pot. 77—1359
La, band struct., linear APW method 79—51467
La, density functional theory 80—15442
La, electronic structure, 4f band *(German)* 77—55479
La, electronic structure vol. depend., rigorous cellular method 77—20233
La, FCC, ground-state props. 78—75989
La, p core states calc., linear muffin-tin orbitals method 78—91607
La-In alloys, cohesive and superconducting props. from electronic struct. calcs. 79—99113

band structure of crystalline metals continued

- LaAg, band calcs., rel. to mag. and electronic props. and martensitic transform. 77—8014
- LaAg, electronic struct., susceptibility, sp. ht. and Knight shift meas. 77—43485
- LaAg, electronic struct., NMR relax. times meas. 79—51871
- $LaAl_2$, calc. of energy band-structure and Fermi surface by APW method 80—70590
- $LaAl_2$, electronic struct., APW method and local-spin-density approx. 80—65434
- $LaAl_2$, magnetoresist. and de Haas-van Alphen effect, Fermi surface model 79—15069
- LaB_6, electronic struct., APW method and local-spin-density approx. 80—65434
- LaB_6, metallic, energy band structure and Fermi surface, self-consistent APW method 77—69221
- Li, Auger line shape KVV, energy band theory 79—43074
- Li, Auger widths of core levels using renormalised many-body perturbation theory 79—74033
- Li, BCC, cryst. pot. 77—89693
- Li, cryst. wave function deter., muffin-tin method 80—65436
- Li, electronic structure and lattice const. determ. using orthogonalised modulated plane wave method *(Ukrainian)* 79—42436
- Li, local orbital energy bands using Kohn-Sham and near Hartree-Fock exchange 78—30866
- Li, phonon spectrum from first principles band struct. 78—6134
- Li, valence band Auger spectra, surface effect 80—80915
- Li, X-ray K-edge transitions, band theory 77—16426
- $Li_2Ag_{2-x}In_x$, optical props., struct., energy bands, interband transitions 78—72539
- $Li_2Cd_{2-x}In_x$, optical props., struct., energy bands, interband transitions 78—72539
- Lu, band structure, influence of relativistic effects 78—75991
- Lu, Compton profiles, electronic configurations 80—11501
- Mg, bandstruct. using potentials with exchange and correlation, KKR methods 79—11060
- Mg, Fermi surface, stress induced changes, kinetic, pot. energy contrib. 79—60683
- Mg, HCP metals, K-emission valence bands, structure and bonding 80—7438
- Mg, XPS theory, valence band spectra band struct. 78—72702
- MgAg, 4d bandwidth influence on $M_{4,5}N_{4,5}N_{4,5}$ Auger spectra 79—100017
- MgAg, Auger spectra, 4d bandwidth effect 80—89093
- MgB_2, density of states and band struct., metallic props. 77—59249
- γ-Mn, antiferromagnetic, self-consistent bandstructure calcs. 80—88475
- δ-Mn, paramag., antiferromag. and ferromag., magnetic moment calcs. 80—60223
- Mn pnictides, energy bands, electron correl. effects 78—14688
- $MnAu_2$, helical antiferromagnetic compound, optical props. and electronic struct., visible and IR obs. *(French)* 80—45101
- MnP, metallic, band struct., X-ray spectral obs. 78—11019
- MnP, spin polarised energy band struct., electronic specific heat, APW calcs. 80—65431
- MnSb, electronic state, neutron diffr. study 78—87906
- MnSb, resist., susceptibility and thermopower rel. to electronic struct. 78—67935
- MnSi, electronic energy band struct., self-consistent APW calc. 80—65433
- Mn_3Si, electronic structure, X-ray spectra comparison with band struct. calcs. 80—97383
- Mo, band struct. and Fermi surface angular correl. of positron annihilation radiation 78—6260
- Mo, electronic and struct. props., nonlocal pseudopot. calc. 80—34349
- Mo, electronic density of states, X-ray emission bands, self-consistent calc. 77—28104
- Mo, electronic props., first-principles nonlocal pseudopot. approach 79—95319
- Mo, Fermi surface, homogeneous strain response 78—34753
- Mo, thermoreflectance spectra, 0.3 to 6 eV, rel. to band struct. calcs. 77—66521
- Mo_cNb_{1-c}, is the rigid-band model valid? 78—95258
- Na, Auger widths of core levels using renormalised many-body perturbation theory 79—74033
- Na, equilibrium struct. and phys. props., pseudopot. method 80—96778
- Na, variational cellular method, electronic struct. calcs. 80—54591
- Na, X-ray edge shape, band struct. role 77—16425
- Na, XPS theory, valence band spectra band struct. 78—72702
- Na_xWO_3, $(0.22\leq x\leq 0.84)$, ^{183}W NMR, electronic struct. near metal-semicond. transition, Knight shift 78—48063
- Nb (001) ideal surface, self-consistent pseudopot. calcs. 77—76894
- Nb, band struct., deformation potentials calc. by Green's function method 79—1568
- Nb, band structure, self-consistent pseudopot. calc. 77—43487
- Nb, Compton profile anisotropy 77—73182
- Nb, de Haas-van Alphen study of Fermi surface, cyclotron effective masses, mag. breakdown effects, KKR calcs. 78—43288
- Nb, electron-phonon interaction, relativistic, APW calc. 80—92837
- Nb, electronic and optical properties 78—91612
- Nb, electronic density of states, X-ray emission bands, self-consistent calc. 77—28104
- Nb, electronic struct. with non-muffin-tin pot., self-consistent relativistic APW calc. 77—66108
- Nb, electronic structure, APW calcs., self-consistency and exchange effects 77—66109
- Nb, electronic structure, self-consistent mixed-basis approach 79—69394
- Nb, Fermi surface, electron mass enhancement, orthornormal function enhancement 80—96777
- Nb, high-temperature nonlinear electrical resistivity, supposed failure of Boltzmann eqn. 78—91664
- Nb, optical properties and electronic props. 79—42439
- Nb, optical spectroscopy, for investigation of electronic struct. 78—91611
- Nb, thermoreflectance studies 80—76047
- Nb-Co, X-ray emission spectra investigation of electron struct. of Laves phases *(Russian)* 78—23554
- Nb-Fe, X-ray emission spectra study of electron struct. of Laves phases *(Russian)* 78—23555
- Nb-Mo, electronic struct., thermoreflectance meas. 0.5-5.0 eV 80—45050
- Nb-Mo BCC, press. derivatives of elastic moduli, Fermi surface topological changes 79—61639

band structure of crystalline metals continued

- Nb-Sn, A15 cpd., Hall coeffs., effect of tetragonal distortion on band struct. 79—33281
- Nb-Zr, effect of band structure on elastic constants and superconductivity 79—8313
- Nb_3Al, band struct. and density of states from self-consistent pseudopotentials 79—69401
- $Nb_3Al(Ga)(Si)(Ge)(Sn)$, electronic struct. calcs. 79—47005
- NbC, electronic structure, PES study 80—70594
- $NbD_{0.6}$, Compton profile meas. 77—4698
- Nb_3Ge, band struct. and density of states from self-consistent pseudopotentials 79—69401
- $NbH_{0.453}$, influence of H on bulk band struct., optical absorptivity spectra obs. 77—89692
- $Nb_{0.5}Mo_{0.5}$, soft X-ray spectra, theoretical considerations 80—11511
- $NbS(Se)_2$, polymorphism at high press. and temps., T_c and band struct. 78—26528
- $NbSe_3$, electronic props. variation with struct. 79—42438
- Nb_3Si, Nb_3Sn, Nb_3Ge, Nb_3Ga, Nb_3Al, electronic struct., electron-phonon interactions, X-ray spectra 78—91613
- Nb_3Sn, A-15 cubic phase, band calc. using APW method 79—56120
- Nb_3Sn, electronic struct., APW method 78—72066
- Nb_3Sn, electronic struct. from three-dimens. k.p model 78—84139
- $Nb_3(Sn-Al)$ system, X-ray spectroscopic studies of electronic struct. of A15 cpds. 80—2900
- Ni (001) film, electronic struct. by self-consistent numerical-basis-set LCAO discrete variational method 79—60938
- Ni (100), angle resolved photoemission, final-state effects 78—56565
- Ni (100) films, spin density by self-consistent linear APW method 80—65710
- Ni (110) and (111), two-photon photoemission 80—76150
- Ni (111), band struct. and temp.-depend. mag. exchange splitting, angle resolved photoemission obs. 78—60546
- Ni (111) surface, clean and with CO absorbed layer, angle-resolved photoemission meas. 77—16463
- Ni and Ni alloys, tunnelling electron spin polarisation rel. to band struct. 78—68095
- Ni, angle-resolved photoemission, band struct. 78—95680
- Ni, band struct., angle-resolved photoemission meas. 80—71569
- Ni, band struct., cryst. pot. anisotropy effect *(Russian)* 80—88474
- Ni, band struct. and multielectron excitations, angle-resolved photoemission determ. 80—76147
- Ni, band structure, μSR Knight shift meas. 79—56663
- Ni band structure, rel. to lattice const., spin polarised APW calc. 80—20073
- Ni, correlation effects on energy bands 79—60697
- Ni, d-band width, angle-resolved UPS meas. 77—20234
- Ni, electronic structure, photoelectron spectra, theory 80—80168
- Ni, electronic structure and optical consts. by inelastic electron scatt. 80—7451
- Ni, energy band dispersion and mag. exchange splitting, angle-resolved photoemission meas. 80—71567
- Ni, energy-band dispersions and exchange splitting, angle-resolved photoelectron spectroscopy 79—69402
- Ni, ferromag., effect of pressure on electron struct. *(Russian)* 79—77987
- Ni, ferromag., self-consistent calc. of energy bands 77—39774
- Ni, ferromagnetic, electron-magnon interactions 78—68205
- Ni, ferromagnetic, electronic struct. by real space approach 80—65432
- Ni, ferromagnetic, Fermi surface and band struct. 78—6267
- Ni, ferromagnetic, photoemission spectra and band struct., spin polarisation of bulk photoemission 79—78843
- Ni film (111), ferromag., energy bands and planar densities of states, LCAO calc. 79—4509
- Ni, interband optical conductivity, self energy correction 80—2792
- Ni, metallic particles, stability and electronic struct. *(French)* 80—80155
- Ni, near-Fermi part of energy band struct. from PES 80—2328
- Ni, optical absorption in near IR 79—38539
- Ni, optical consts., influence of temp. and relation to bandstruct. 80—25403
- Ni, optical spectrum, anomalous temp. depend. around T_c, band struct. 80—40128
- Ni, photoemission near Curie temp. 79—78841
- Ni, polarisation-dependent angle-resolved photoemission for band structure studies 78—95678
- Ni, quasi-particle energies, two-hole XPS satellite 80—66399
- Ni surface (111), photoyield near theshold negative-positive spin polaris. crossover 80—2922
- Ni, valence-band photoemission spectra, self-energy corrections effect 80—11534
- Ni-Al, band struct. and density of states, KKR method and X-ray meas. 80—10863
- Ni-Al, electronic, mag., and cohesive props. 80—44491
- Ni-Al alloys, XPS for band struct. 79—33889
- Ni-Co(Fe)(V)(Ti), dil., optical absorpt., electronic struct. 80—108227
- Ni-Cr, residual resist., CPA calc. to muffin tin pot. 77—62892
- Ni-Fe, residual resist., CPA calc. to muffin tin pot. 77—62892
- Ni-Mn alloys, ferromagnetism-to-spin glass phase transition and strong mag. field effect 80—75773
- Ni-Re, dil. alloys, two-band Mott conductivity *(Russian)* 78—60118
- Ni-Zn alloys, XPS for band struct. 79—33889
- β'-NiAl, electronic struct. and optical props. 80—97228
- β'-NiAl, self consistent embedded cluster model for Fe, Co, Ni mag. impurities 80—2549
- NiC, electronic structure of interstitials 79—1583
- $Ni_{1-x}Cu_x$ $(x=0.03, 0.16, 0.24)$, photoemission study, surface, bulk electronic struct. 78—48281
- NiGe, Ni_2Ge and Ni_3Ge, X-ray spectrum analysis energy band struct. *(Ukrainian)* 77—52200
- NiH_x, electronic band struct. and interatomic bond 78—43295
- Ni_2MnSn, ferromag. Heusler alloy, electronic struct., spin polarisations, theory 80—54598
- NiSb, at. struct. and mag. susceptibility 77—39561
- NiSb, resist., susceptibility and thermopower rel. to electronic struct. 78—67935
- NiTi, search for electronic phase transition, soft X-ray appearance potential spectra 79—24391
- Ni_3Ti, electronic struct., Xα calc., photoelectron and AES spectra 80—20769

band structure of crystalline metals continued
Ni(001) surface states, surface magnetisation, electron spin polarisation 80—88612
$NpAl_4$ clusters, band struct., variational $X\alpha$ calc. 79—4508
Os, correlation effect of crystal pot., RAPW calcs. 78—6265
Os, electronic energy band struct. 80—107697
Pb, ab initio band struct. calcs. 80—75502
Pb and Pb-Mg, dil., resistivity, multiple plane wave calc., Fermi surface, vel. and band struct. 77—51723
Pb, band structure, and electron-phonon interaction, supercond. transition temp. determ. 79—19512
Pb, Fermi surface and non-muffin-tin energy bands, calc. 80—20072
Pb, pseudopot. band struct. calc. 79—56119
Pb, single and polytextured thin films, band struct., tunnelling spectroscopy 80—80169
Pd (100), $(\sqrt{2}\times\sqrt{2})R45°$ s layer, adsorbate induced surface reson. obs. in photoemission 80—7470
Pd (111) surface, angular-resolved UPS meas. 79—95902
Pd and Pd-Ag(Cd)(In)(H), electronic struct. from annihilation quanta ang. distribs. 77—66107
Pd, Compton profiles, comparison with band struct. calcs. 78—84675
Pd, dil. alloy, electronic struct. calc. using KKR method 80—15438
Pd, electronic band struct. and photoemission 80—97410
Pd, electronic states, effect of hydrostatic press. 79—11055
Pd, electronic struct., double beam photoemission 79—83098
Pd, electronic struct., field-induced magnetisation density and mag. form factor 77—4496
Pd, electronic struct. determ. by relativistic APW method, rel. to UV spectroscopy 77—4289
Pd, electronic structre, Compton scatt., soft X-ray emission and X-ray photoelectron spectra 79—77999
Pd, electronic structure, self-consistent mixed-basis approach 79—69394
Pd, g tensor of d holes, sub-bands and energy splitting 79—23890
Pd, generalised susceptibilities and phonon anomalies, band struct. calcs. 79—90953
Pd, hydride and alloys, electronic band struct., comparative study of electric and mag. props. 78—95259
Pd on Ag (001), ultrathin film electronic states calc. 78—6318
Pd, thermomodulation spectra of high-energy interband transitions 80—108226
Pd, XPS, electronic struct. 80—7464
Pd-Co, normal Hall effect *(Russian)* 80—103676
Pd-Cu compound, KKR electronic struct. 80—59864
Pd-Fe, normal Hall effect *(Russian)* 80—103676
Pd-H, electronic states from de Haas-van Alphen measurements 79—7777
Pd-H, nature of the 50K anomaly, residual resist. 79—7818
Pd-H system, energy band struct., magnetic susceptibility meas. 78—18953
Pd-H(D), band struct. and supercond. props., APW calc. 79—56354
Pd-Ni, normal Hall effect *(Russian)* 80—103676
Pd-Rh-Ag, mag. susceptibility, pressure effect up to 4000 atms. 77—16142
Pd-Rh-H and Pd-Ag-H, band struct. and supercond. props., APW calc. 79—56354
Pd_cAg_{1-c}, possibility of superconductivity 80—10862
$Pd_{1-x}Ag_xH_n$, positron annihilation examination of electronic structure *(German)* 77—69931
$Pd_{1-y}Ag_yH_x$, electronic struct. and supercond., APW calc. 79—95318
$Pd_{1-y}Ag_yH_x$, superconducting transition temp., APW band struct. calcs. 78—95393
PdH, electronic struct. and proton spin-lattice relax. calc. 78—67937
PdH, electronic struct. and supercond., APW calc. 79—95318
$PdH_x(D_x)$, band struct., supercond. props., APW calcs. and neutron scatt. 78—43511
PdIn, refractive index, reflectivity and band struct., APW calcs. 80—40139
Pd_2MnSn, ferromag. Heusler alloy, electronic struct., spin polarisations, theory 80—54598
$Pd_{1-y}Rh_yH_x$, electronic struct. and supercond., APW calc. 79—95318
PdSb, electronic struct., optical transitions, Fermi surface 78—51885
PdSb, XPS, electronic struct. 80—7464
$PdTe_2$, bandstructure, Fermi surface, LMTO method 78—6264
Pt, 5d band structure effects on line shapes and intensities of core electron excitations 78—92177
Pt band-structure determ., angle-resolved photoemission 80—66398
Pt, electronic struct., double beam photoemission 79—83098
Pt, energy band structure, X-ray emission spectra, APW calc. 80—92811
Pt, generalised susceptibilities and phonon anomalies, band struct. calcs. 79—90953
Pt, paramagnetic, induced magnetic form factor, 73 kOe at 78K 79—33454
Pt, thermomodulation spectra of high-energy interband transitions 80—108226
Pt, XPS, electronic struct. 80—7464
Pt-Cu alloys, ESCA determ. of electronic struct. 80—34352
PtBi, XPS, electronic struct. 80—7464
Pt_3Mn, mag. excitation dispersion relation 80—25090
Pt_3Sn, electronic struct., calc. using linear-muffin-tin-orbitals method 77—24516
Pt(111), Λ-line valence bands, angle-resolved photoemission determ. 80—108323
α-Pu, 5f electron distrib. analysis by X-ray emission spectra 77—28663
Pu, α and δ phases, 5f states modification obs., X-ray absorpt. spectra 77—28649
$PuAl_4$ clusters, band struct., variational $X\alpha$ calc. 79—4508
Rb, elec. resist. and phase transforms. under high press. *(German)* 80—107763
Re, electronic struct. and CO adsorption characts., XPS, UPS, and thermal desorption study 80—71571
Re-based HCP-BCC binary systems, electronic struct. and supercond. *(Russian)* 79—33375
Rh, band structure and photoemission from low index surfaces 80—24790
Rh, band structure calc., ground state and effects of change of volume 79—77994
Rh, electronic struct., double beam photoemission 79—83098
Rh, electronic struct. determ. from optical refl. meas. 77—62812
RhH, electronic struct. and supercond., APW calc. 79—95318
Ru, electronic struct. and X-ray emission band intensities 77—20960
Sb, XPS, electronic struct. 80—7464

band structure of crystalline metals continued
Sc, band structure, density of states, absorpt. spectra, KKRZ calc. 80—70593
Sc, electronic struct. and X-ray emission band intensities 77—20960
Sc, HCP, optical examination of electronic struct. 77—89694
Sc, photoabsorpt. spectra, at. ionisation, band struct. mechanisms, electron energy loss investig. 77—24909
Sc, sp. ht. data rel. to electronic props. 78—83971
Sc-Ag(Cu)(Pd)(Rh)(Ir)(Ru), electronic struct., susceptibility, sp. ht. and Knight shift meas. 77—43485
ScM (M=Cu, Ag, Pd, Rh, Ir, Ru), electronic struct., NMR relax. times meas. 79—51871
ScM, (M=Ru,Rh,Pd,Ag), electronic struct., self-consistent local density functional calcs., LMTO method 79—11059
Se, trigonal, electronic props. under press. 77—31939
$SmCo_5$, spin polarised energy band struct., APW calc. 78—10342
$Sm_{1-x}La_xS$, electron struct., lattice consts., X-ray spectral study *(Russian)* 80—100432
SmS film, energy band struct. of metallic phase 77—32098
Sn, band structure using modified Vejkovic, Slavic pseudopot. form factor 79—56121
Sn film, thermoreflectance meas. 77—28640
Sn, UPS, 7.7-10.8 eV, and band struct. calc. 78—15282
Sn, white, band masses and deformation pots., OPW pseudopotential model 80—100430
Sn, XPS, electronic struct. 80—7464
Ta, and α-TaH_x, thermoreflectance studies 80—76047
Ta, BCC, band struct., generalised APW method using variational expression 80—6695
Ta, electron-phonon interaction, relativistic, APW calc. 80—92837
Ta, electronic props. and reflectivity, iterative empirical pseudopot. calc. 77—76745
Ta, electronic structure, APW calcs., self-consistency and exchange effects 77—66109
Ta film, photoemiss. from conduction band and core levels 77—16464
Ta, optical properties and electronic props. 79—42439
Ta, optical spectroscopy, for investigation of electronic struct. 78—91611
Ta, photo field emission characteristics, band struct. influence 78—27373
Ta, photo field emission spectroscopy of band structure by He-Ne laser irrad. 80—55276
Ta, photofield emission spectroscopy of band struct. 78—35261
Ta white-lines at L_{III} and L_{II} edges due to transitions from $2p_{3/2}$ and $2p_{1/2}$ levels to 5d levels 79—61469
Ta-Fe, X-ray emission spectra study of electron struct. of Laves phases *(Russian)* 78—23555
Ta-W, BCC, press. derivatives of elastic moduli, Fermi surface topological changes 79—61639
$TaH_{0.257}$, influence of H on bulk band struct., optical absorptivity spectra obs. 77—89692
$TaSe_3$, electronic props. variation with struct. 79—42438
Tc, band structure calc., effect of correlation 79—60699
Tc, rel. to superconductivity and Fermi surface calcs. 80—70873
Te, monoclinic, electronic states above high-press. phase transition 79—99476
Th, correlation effect of crystal pot., RAPW calcs. 78—6265
Th, density functional theory 80—15442
Th, electronic states under press. 80—54600
Th, FCC, ground-state props. 78—75989
Th, interband structure and role of 5f electronic states, optical reflectivity meas. 77—76744
Th, p core states, linear muffin-tin orbitals method 78—91607
Th, photoelectron spectra study, core and valence levels 80—66394
Th, valence and 5f states, XPS and bremsstrahlung isochromat spectroscopy 80—66393
Ti alloys, Fermi sphere limiting electronic capacitance, Brillouin zones *(Russian)* 80—92808
Ti, band struct., cryst. pot. anisotropy effect *(Russian)* 80—88474
Ti, band struct. correlation with TiC, APW calc. *(Japanese)* 78—23017
Ti, electronic struct. and X-ray emission band intensities 77—20960
Ti, electronic structure of omega and alpha phases, nonrelativistic APW method 79—90952
Ti, X-ray $K_{\beta 5}$ emission band, effect of struct. change on alloying *(Russian)* 77—59645
Ti-based HCP-BCC binary systems, electronic struct. and supercond. *(Russian)* 79—33375
Ti-Co, X-ray emission spectra investigation of electron struct. of Laves phases *(Russian)* 78—23554
Ti-Ni, martensite transform. B2-B19′, optical props. and electron struct. *(Russian)*, 80—34878
Ti-Ni alloys, energy band structures, X-ray spectra obs. *(Ukrainian)* 77—32469
Ti-V, elastic moduli, comparison with paramag. Cr, V-Cr, rel. to bandstructure 80—7615
Ti-V-Cr, BCC, press. derivatives of elastic moduli, Fermi surface topological changes 79—61639
Ti_2, electronic structure of five and ten atom chains SCF-$X\alpha$-SW calcs. 80—5483
$TiBe_2$, de Haas-van Alphen effect, Fermi surface, theory 80—103614
TiC, electronic structure, PES study 80—70594
TiCo, and TiCoSi(Ge), X-ray K- and L-spectra obs. *(Russian)* 78—11022
$Ti_{1-x}Co_x$, electronic struct. and anomalies of elec. and mag. props. 80—6710
$TiFe_{1-x}Co_x$, electronic struct. and mag. moment calcs. 80—65821
TiGe, and TiCoGe, X-ray K- and L-spectra obs. *(Russian)* 78—11022
TiH, electronic structure of five and ten atom chains SCF-$X\alpha$-SW calcs. 80—5483
$Ti_{1-x}Nb_xH_{1.94}$, electronic struct. MNR meas. 80—15439
$Ti_{1-x}Ni_x$, electronic struct. and anomalies of elec. and mag. props. 80—6710
TiP, metallic, band struct., X-ray spectral obs. 78—11019
TiSi, and TiCoSi, X-ray K- and L-spectra obs. *(Russian)* 78—11022
Tl, band struct. by LMTO method 77—39773
Tl, band structure and fermi surface using relativistic APW calc., optical spectra interpretation 77—20231
Tl, polycryst. film, photoelectron spectra, UV incident 78—2986
Tl, relativistic Green's function theory 79—82512
α-U, electronic band struct. and props. 80—10861
U, photoelectron spectra study, core and valence levels 80—66394
U, valence and 5f states, XPS and bremsstrahlung isochromat spectroscopy 80—66393

band structure of crystalline metals continued
UAl_4, clusters, band struct., variational Xα calc. 79—4508
UGe_3, de Haas-van Alphen effect, band struct. calc. 78—72068
UGe_3, spin fluctuation phenomena, band struct. calcs. and de Haas-van Alphen meas. 77—20225
V, Compton profiles, comparison with band struct. calcs. 78—84675
V, electronic density of states, X-ray emission bands, self-consistent calc. 77—28104
V, electronic density of states, effective mass, electron-phonon interaction, Coulomb pseudopot. *(Russian)* 78—26804
V, electronic structure, APW calcs., self-consistency and exchange effects 77—66109
V, electronic structure, model potential calcs. *(Russian)* 80—100431
V, electronic structure, X-ray spectra and XPS meas. 77—85842
V, energy bands, Compton profile, optical cond., SCF LCAO calcs. Gaussian orbitals 78—47698
V, optical properties and electronic props. 79—42439
V, rel. to optical absorpt. spectrum, 0.25-14 μm *(Russian)* 77—81118
V, thermoreflectance studies 80—76047
V, X-ray band spectra calcs. 79—33860
V-Al, band struct. and density of states, KKR method and X-ray meas. 80—10863
V-Cr, elastic moduli, comparison with paramag. Cr, Ti-V, rel. to band-structure 80—7615
V-D alloys, positron annihilation radn. angular correlation, electronic struct. study 79—43058
$V_3Al(Ga)(Si)(Ge)(Sn)$ electronic struct. calcs. 79—47005
V_3Ga, self-consistent APW band struct. calc. 78—47697
VO_2, metallic, electronic struct., lattice instability 78—14664
VO_2, metallic phase, electronic props., plasma freq., Hall coeff. 78—84195
V_2O_3, metallic differential refl. spectra and band struct. 77—1699
VRu, soft X-ray emission, photoelectron spectra and electron structure 79—37978
VSe_2, angle-resolved UPS, Fermi surface determ. 80—55257
V_3Si, EFG and band struct. 77—35861
V_3Si, electronic struct., electron-phonon interaction and high temp. superconductivity, APW calc. 78—14871
V_3Si electronic struct. from three-dimens. k.p model 78—84139
V_3Si, V_3Sn, V_3Ge, V_3Ga, V_3Al, electronic struct., electron-phonon interactions, X-ray spectra 78—91613
V_3Si, X-ray emission spectra, XPS 77—48278
V_3Si, XPS and APS of valence band 77—20994
$(V_{1-x}Ti_x)Ge$, pseudobinary A15 compound, supercond. transition temp. 80—49970
W (001), clean and H_2 chemisorbed, angle resolved photemission, symmetry-related polarisation effects 78—56566
W (001), surface resonance bands 78—47843
W (001), surface resonance band fine struct. in LEED 78—47844
W (100), optical magnetisation from spin polarised photoemission 79—78830
W, electronic and struct. props., nonlocal pseudopot. calc. 80—34349
W, Fermi velocity calc., linear muffin-tin orbital method 79—28272
W films, (010), energy band calc. including spin-orbit interactions 80—20274
W, photo field emission spectra of optical transitions, band struct. 77—16467
W, photoemission of spin polarised electrons 78—35248
W, polarisation-dependent angle-resolved photoemission for band structure studies 78—95678
W, semi-infinite cryst., secondary electron emission, obs. of electronic struct. 79—33871
W, thermoreflectance spectra, 0.3 to 6 eV, rel. to band struct. calcs. 77—66521
W(100), NVV Auger spectra, $O_2(H_2)$ adsorption effects, comp. to band struct. calcs. 78—72643
Y, electronic struct. and X-ray emission band intensities 77—20960
Y, photoabsorpt. spectra, at. ionisation, band struct. mechanisms, electron energy loss investig. 77—24909
YCo_5, spin polarised energy band struct., APW calc. 78—10342
YRh, electronic struct., susceptibility, sp. ht. and Knight shift meas. 77—43485
YRh_4B_4, supercond., electronic struct. and reentrant magnetism 78—10340
YZn, self-consistent energy bands and Fermi surface 77—72814
Zn, band structure, density of states and Fermi surface, APW calc. 77—20232
Zn, electromigration, electron wind force calc. 78—6183
Zn, electronic band struct., pseudopotential calcs. 79—19510
Zn, HCP metals, K-emission valence bands, structure and bonding 80—7438
Zn, HCP struct., selection rule, electron momentum distrib. rel. to positron annihilation 80—39495
ZnS(Se), wavelength-modulated refl. spectra, 2.5 to 8 eV 77—20877
Zr, band struct. correlation with ZrC, APW calc. *(Japanese)* 78—23017
Zr, electronic struct. and X-ray emission band intensities 77—20960
Zr, electronic structure of omega and alpha phases, nonrelativistic APW method 79—90952
Zr, X-ray K-absorpt. spectra 78—76558
Zr-Co, amorphous and crystalline, d-band struct., alloying effects 80—59862
Zr-H alloy, soft X-ray emission spectra, electronic struct. 79—65959
Zr-Nb-Mo, phonon spectra anomalies, lattice dynamics calculations, superconductivity parameters 79—7655
Zr-Ni, amorphous and crystalline, d-band struct., alloying effects 80—59862
$ZrRh_{3-x}Pd_x$, powdered alloys, catalytic behaviour correlation with electronic struct., lattice struct. and surface comp. 79—82181
ZrV_2, Laves-phase, cubic to rhombohedral transition, lattice electron instability 78—92261
$ZrZn_2$, de Haas-van Alphen effect, Fermi surface, theory 80—103614

band structure of crystalline semiconductors and insulators
see also conduction bands; energy gap; valence bands
abrupt heterojunction, energy band lineup 78—10541
actinide, compounds, f-electron systems with fluctuating valence, phase transitions 80—6789
actinide compounds, band structure and bonding calcs. 80—10871
actinide compounds, electronic configurations correlation 80—6385
actinide compounds, specific heat meas., review 80—6524

band structure of crystalline semiconductors and insulators continued
actinide compounds, spectroscopic techniques for electronic props. meas. 80—11427
actinide dioxides, electronic struct. and ionicity 80—10872
actinide oxides, chem. bonding, mol. cluster theory 80—10526
actinide oxides, electronic props., review 77—28115
alkali graphite intercalation compound, evidence for alkalilike cond. bands 80—45201
alkali halides, Doppler broadening meas. of positron annihilation 78—26806
alkali halides, thermoreflect. spectrum, 5 to 9 eV, electronic struct. 77—81123
alkali tungsten bronzes, struct. and supercond. 79—82703
alkali-trihalogeno-plumbates, $M[PbX_3]$, cryst. growth struct. and spectra *(German)* 79—90632
alkaline earth oxides, point defect props., band struct., lattice simulation calc. 80—19797
alkanes, band struct. evolution and electronic relax. in photoemission *(French)* 77—36358
n-alkanes, conduction band struct., LEED, secondary electron emission and UPS study 80—70601
alkanes, linear, elec. struct., evolution of electronic level towards band struct. *(French)* 78—5282
alkanes, linear, electronic struct., electronic relax. during photoemission *(French)* 78—5283
n-alkanes, solid, core electron relax. energies and valence band form., XPS exam. 77—36372
alloy semiconductor, two-band, band struct. calc. 79—37952
anthracene, excess electron and excess hole cryst., band struct., drift and Hall mobilities, depend. on press. 79—60709
anthracene, isotopically mixed cryst., exciton dynamics 80—29329
auramine, photocond. and intermol. electron interaction, tight binding approx. 77—15765
benzene-diazonium salts, absorption band *(Ukrainian)* 79—78001
borate glasses, effects of clusetring and transition metal ions on electronic struct. 78—10347
borides, electronic struct., review, book contrib. 78—47700
borides, hexa- and di-, electronic structs., elec. props., book contrib. 78—47701
borides, nature of chem. bond, book contrib. 78—47276
Cd_3As_2, energy band parameter calc., temp. and press. depend. 77—31943
CdS film, polycryst, optical spectra, 0.5-6.5 eV 80—55212
chalcopyrites, for electrolum. device appl., props. and technology, book contrib. 77—73175
chlorophyll-a, crystalline film, energy levels and carrier generation by photocond. and fluoresc. 77—16909
cluster type effect on band struct. 77—28109
compound semiconductor, electronic polarisability rel. to energy gap 80—10524
conjugated polymers, one- and two-dimensional, band structs. and band gap sizes 79—47008
copper phthalocyanide, cryst. struct. sensitivity of band struct. 79—42444
corundum, electronic struct., determ. by X-ray spectroscopy 79—8210
cubic semiconductors, bulk hot-electron props., review 79—99553
current fluctuations in quantizing elec. field, rel. to band struct. *(Russian)* 77—28175
defect tetrahedral cpd. semiconductors, band struct. trends 79—90956
degenerate materials with position depend. band struct. carrier densities and emitter efficiency calc. 78—43378
degenerate semiconductors, impurity band struct. for dense donors and acceptors 80—29348
diamond, band structure of diamond like crystals, cluster-Bethe lattice model calc. 80—6713
diamond, Compton profiles, X-ray struct. factors, band struct., LCAO calc. 78—51889
diamond, electronic energy bands of diamond-type crysts., appl. of EHT method 78—87907
diamond, energy band calcs. using intersecting spheres model 77—66110
diamond, ground-state, electronic properties, ground-state in local-density formalism 77—69223
diamond, large unit cell semiempirical mol. orbital approach to props. of solids 79—87036
diamond, momentum density, Compton profile 77—20235
diamond, natural, anisotropy and saturation of hot carrier drift velocity 80—6867
diamond, natural, electron effective mass and lattice scatt., Monte Carlo anal. 80—44484
diamond, nonlinear optical susceptibility, tight binding bonding orbital model 80—5784
diamond, photoionisation cross-sections of valence s- and p-electrons *(Ukrainian)* 77—73211
diamond, pseudopotential method of band struct. anal. 78—51886
diamond, quasiparticle states, quantitative calc. 80—88499
diamond, semiconducting, band gap temp. depend, dilation and vibr. contribs. determ. 80—10868
diamond, surface electronic struct., self consistent pseudopotential calc. 78—47842
diamond energy band struct., elec. and optical props., review 77—35862
diamond semiconductors, electronic structure, self consistent local description 80—20067
diamond-like crysts, electro-optic effects due to the Stark splitting of energy bands 79—82950
diamond-type crystals, LCAO band structure, overlap and distant neighbour effects 80—49585
dielectric solids, laser damage, conduction-band electron interaction theory 80—35017
dimethyl cadmium, photoelectron spectra, 4d spin-orbit splitting, crystal field and band-broadening effects, CNDO calcs. 78—76577
education, forbidden energy gap meas. in Si and Ge p-n junctions 80—57027
electrode and volume controlled photocurrents 80—6908
electronic structure of solids under laser irradiation 78—91614
elemental semiconductor, electric susceptibility from chemical-bond approach 78—51922
elemental semiconductors, model pseudopotential, band struct. calcs., liquid semicond. resistivity calcs. 80—20075
$(ethylene)_x$, mol. crystals, quantum theory, mol. tight binding method calcs. 80—49572
Ewald method, convergence of reciprocal lattice sums 77—11834
excitonic insulator, tunnel breakdown theory *(Russian)* 80—29686

band structure of crystalline semiconductors and insulators continued
ferroelectric, calc. using Euwema PWG method with $X_\alpha$approx. 78—15106
ferroelectric semiconductor, electron theory 78—43801
ferroelectric semiconductor, vibronic, interband light absorption 78—72555
ferroelectric semiconductors, props., book 80—82590
ferroelectricity, vibronic theory, developments 79—33620
ferroelectrics, vibronic, band struct. temp. depend. 80—70598
ferromagnetic semiconductor, doped, electron spin polarisation and conduction band struct. 80—65449
ferromagnetic semiconductor, electronic excitation spectrum 80—11149
ferromagnetic semiconductor, electronic spectrum, influence of finite carrier conc. 78—76220
ferromagnetic semiconductor, spectral density approach for s-f model quasiparticle concept 80—80173
ferromagnetic semiconductor, two-band s-d model hybridization 80—65446
$(\text{formamide})_x$, mol. crystals, quantum theory, mol. tight binding method calcs. 80—49572
four-photon transitions, perturbation theory calc. 80—96786
gapless semiconductor, effect of nonlocal pot. on hole energy spectrum in mag. field 78—39017
gapless semiconductor valence band in mag. field 80—49600
$GaSe_{1-x}Sx$, exciton spectrum nature and anisotropy of electron bands near absorption edge *(Russian)* 79—51483
p-GaSe, relaxational oscillations of photoconductivity and dark conductivity 77—69379
graphite, band parameters, depend. on temp. press. and acceptor conc. 77—62818
graphite, band struct. determ. by angle-resolved photoemission 80—45203
graphite, calc. based on rigorous cellular method 77—15762
graphite, electronic props., self-consistent LCAO calc. 78—51887
graphite, electronic struct. exact exchange HF calcs. 80—65438
graphite, heteroatom doped, electronic struct., energy spectrum, HMO LCAO calcs. 77—43539
graphite, magnetoreflection under press., Landau level transitions 80—50303
graphite, neutron irradiated, effect on quantum limit Shubnikov-de Haas oscills. 78—95304
graphite, polycryst., EPR meas. rel. to temp., crystallite orientation, paramag. suscept. 78—35023
graphite, pressure-depend. conducting calcs. using band model 77—28171
graphite, thermoelec. and thermomag. props., cylindrical band model 80—39616
graphite, various modifications, electronic props. 80—49592
graphite, Wannier functions and density matrix determ. in terms of localised orbitals 78—2408
graphite acceptor compounds, band struct. model and electrostatic effects 80—92814
graphite intercalation compound, interaction between one or two s orbitals *(French)* 80—65440
graphite monofluoride, self-consistent semi-empirical LCAO calcs. of electronic band struct. 77—85142
group IV semiconductors, cryst. binding and band struct. 80—24791
heterojunctions, discontinuities predicted from bulk band structs. 77—20409
hexamethylbenzene, exciton band struct. for first singlet state 77—55483
hexatriacontane, polycryst., UPS, 11.4-21.2 eV, polyethylene model compound 77—66570
high pressure solid state physics, review 79—90729
HMTSF-TCNQ, metallic state at He temps., elec. props. and band struct. 79—65462
hot electrons, Monte Carlo calc. of transport characts. and distrib. functions of hot electrons 80—6853
Hubbard antiferromag. semiconductor, electron correlations, weak coupling 78—67969
$I\text{-}III\text{-}VI_2$ chalcopyrite compounds, d-level struct. and p-d coupling 79—42451
ice, cubic, LCMO calc. of energy bands 77—51656
ice, electronic structure investig. by XPS, UPS and UV absorpt. spectra 77—16452
ice, UPS, valence band struct. 79—33890
II_3V_2 semiconductors, spin-orbit and cryst. field splittings of valence band 78—63980
$II\text{-}IV\text{-}V_2$ semiconductors, electronic band struct., general model pseudopot. 78—39020
$II\text{-}IV\text{-}V_2$ semiconductors, heat of formation from spin-orbit splitting in valence bands 77—31985
III-V semiconductor, transferred electron effect 77—39855
III-V semiconductors, Auger coeffs. calc., appl. to GaSb 79—15160
III-V semiconductors, cond. band struct. and transport parameters, review 79—19587
III-V semiconductors, conduction-band struct. from reflectivity meas. when subject to mechanical strain 79—42449
III-V semiconductors, ionic tetrahedral, electrical susceptibility, chemical bond approach 78—87931
III-V semiconductors, k.p perturbation theory 77—43484
III-V semiconductors physical properties and importance *(German)* 79—56127
inert gas crystals, excitons exam. 78—51898
inert gas solids, band struct. and excitons, book contrib. 77—47731
inert gas solids, collective excitations and EELS, calc. 80—92842
inorganic binary iono-covalent compounds, cryst., inorganic static effective charge calcs. *(French)* 80—2331
interband light scattering in semimetals and semiconductors *(Russian)* 78—60485
intrinsic semiconductor, quantum theory of transverse galvanomag. phenomena, model of two standard bands *(Russian)* 77—62945
isoelectronic series 77—89696
IV-VI compounds, interaction of outer s states 79—10825
IV-VI compounds, orthorhombic, atomic pseudopots. 79—42453
IV-VI compounds, structural transitions, rel. to many-band model of electronic struct. 77—51497
IV-VI mixed compounds, structural phase transition 80—15242
IV-VI semiconductors, cubic dielectric constant from band struct. calc. 80—15463
IV-VI semiconductors, transverse effective charge from one dimens. band struct. calc. 80—15038
IV-VI semiconductors, transverse effective charge from three dimens. band struct. calc. 80—15039

band structure of crystalline semiconductors and insulators continued
Kane semiconductor, many photon electron spin orientation, EM wave absorption 80—44506
Kane semiconductor films, thermomag. and thermoelec. effects, theory 80—70864
KKR calc. of energy bands 80—34355
laser-modulated photoemission, technique for band struct. determ. of semicond. 77—28686
layered semiconductors, high pressure effects 77—51654
leucosapphire, electronic band struct., optical props. 79—95329
light pulse propagation, high-power, transitions between bands with different effective masses 80—34871
magnetic semiconductors, electron spectrum, light absorpt. spectrum, calcs. 80—2793
many-valley semiconductor, relative displacement of D_1 and D_2' bands under shear deform. influence 79—15080
many-valley semiconductors, localised impurity states with low binding energy 80—24835
metal-dielectric transition, two-band model, Coulomb interactions, self consistent calcs. *(Russian)* 80—80185
metal-GeS-metal system, current-voltage characts., band struct. effects in field emission region 79—42667
mixed crystals with indirect band struct., no-phonon struct. from Wannier exciton model 78—43898
modulation spectroscopy, two-ray methods, appl. to band struct. determ. *(Russian)* 78—54469
molecular crystal, band structure, excitonic processes, trap distrib. 80—6720
molecular crystals, compositional disorder, approx. band struct., self consistent virtual crystal approx. 80—39486
monocarbides of subgroups IVa and Va, kinetic props., review 78—47613
Moss relation between refr. index and energy gap of semiconductors 80—11357
multivalley semicond., biexciton props. 77—66120
narrow band gap semiconductors, conference, Warsaw, Poland (Sept. 1977) 79—82582
narrow band gap semiconductors, conference, Warsaw, Poland (Sept. 1977) 80—49703
narrow band gap semiconductors, multiphoton absorption in crossed fields *(Russian)* 80—60553
narrow-gap ferroelectric, phase transition due to strong mag. field 80—103924
narrow-gap semiconductor, heavy holes, energy spectrum in mag. field, effect of nonlocal pot. 79—90959
narrow-gap semiconductors, energy spectrum, three band model 77—89699
narrow-gap semiconductors, externally induced band population effects on electroreflectance 77—66114
nickel phthalocyanide, cryst. struct. sensitivity of band struct. 79—42444
nonequilibrium semiconductor with electron-hole pairing, mag. moment quantum oscills. *(Russian)* 77—28131
nonspherical band semiconductor, optical absorpt. in crossed elec. and mag. fields 77—40264
one-dimensional homonuclear molecular systems, nature of energy gap 79—11063
one-dimensional semiconductor, delocalisation and superalternation effects in nonlinear susceptibilities 77—11840
optical orientation of electronic and nuclear spins 78—79928
oxide semiconductor crystals, with forbidden energy gap, review of spectroscopic props. 78—2876
passive layer, on Fe electrode, semiconductor model, appl. to electrochem. reactions, review 80—26022
Peierls one dimensional model, exact solution, electron spectra, static lattice deformation *(Russian)* 80—70609
perovskite oxides, point defects, elec. cond., and electron energy spectra 80—70706
perovskites, d-band, model for X-ray photoelectron distrib. 79—61491
perylene, energy structure, photocond., photoemission and absorpt. spectra meas. 77—39895
phenazine, charge carrier transport rel. to cryst. and band struct. 79—95403
piezoelectric, calc. using Euwema PWG method with X_α approx. 78—15106
piezoelectric nondegenerate semicond., magnetoacoustic effects of nonparabolic band struct. 80—96948
bis cantena pol methylarsenide, energy gap depend. on As electron delocalization *(German)* 78—43296
polar semiconductor, conduction states, pseudopot. and tight-binding calcs. 80—24785
poly(p-phenylene), electronic struct., one-electron band theory 80—65450
cis-polyacetylene, electronic struct. 79—47012
polyacetylene, pure and doped, electronic props. from one-dimens., tight-binding LCAO-SCF-MO calcs. 79—56123
polyacetylene, pure and heavily doped, optical and IR studies, electronic struct. calcs. 80—7347
polydiacetylene, extended chains with realistic model side groups, self-consistent electronic band structs. 77—39776
polydiacetylene, model chain, band struct. calcs. 77—8016
polydiacetylene, photoconduction in multilayer structs. and single cryst. 78—80024
polydiacetylene backbone sequence, electronic structs., unrestricted HF approach 78—63975
polydiacetylenes, ab initio 'exact' exchange Hartree-Fock cryst. orbital method 78—26811
polyethylene, conduction band struct., LEED, secondary electron emission and UPS study 80—70601
polyglycine chain, electronic struct. and transport props., ab initio Hartree-Fock crystal orbital calc. 79—42448
polypyrrole, electronic struct., one-electron band theory 80—65450
population-inverted, resonant Brillouin scatt., photoelastic consts. 80—89016
pseudobinary semiconductors, energy band calc., compositional disorder effect determ. 79—42442
pyrene, band structure, excitonic processes, trap distrib. 80—6720
α-quartz, electronic energy band struct. calc. 79—23894
α-quartz, electronic struct., local disorder influence 80—59870
α-quartz electron states, self-consistent pseudopot. calc. 77—62823
rare earth borides, higher types, phys. props. and electronic struct., group orbitals-LCAO calcs. 80—20077
rare earth chalcogenides, compositions, props., computer prediction 79—42429

band structure of crystalline semiconductors and insulators continued
rare earth compounds, binary, regression eqns., for calc. props. from electron struct. 80—39498
rare earth cpds., photoemission, rel. to electronic struct., book contrib. 80—16157
rare earth hydrides, props., book contrib. 80—45291
rare earth monophosphides, K-emission bands, electronic struct. 78—15250
rare earth oxides, electronic structure rel. to valence, chem. bonding 80—54601
rare earth trifluoride film, optical props., 5 to 34 eV 79—38687
rare earth tungstates, elec. cond. and thermoelec. power meas., band theory 80—20191
rare earths cpds., Fano-resonances, surface and bulk effects in photoemission 80—97405
semicond. alloy, spin splitting and effective g-factor of T-holes *(Russian)* 77—51643
semiconducting oxides, interband transitions determined from photoelectrolysis spectra 79—65378
semiconducting solid solutions, optical transitions, review 78—2908
semiconductor, carrier number and effective bandwidths *(Spanish)* 78—18954
semiconductor, complex energy band under optical excitation, high-frequency negative cond. and population inversion 80—107858
semiconductor, covalent, molecular cluster model 78—43283
semiconductor, electron quantum states, nonequilibrium current fluctuations in quantised mag. fields *(Russian)* 80—107704
semiconductor, electron spectra in mag. and US fields *(Russian)* 77—62801
semiconductor, electronic props. 79—95490
semiconductor, energy spectrum of discrete centre in high inhomogeneous electric field of space charge region 80—10873
semiconductor, heavy hole spectrum in mag. field 79—15079
semiconductor, local fields, nonuniform charge distrib. 80—24826
semiconductor, microwave magnetoconductivity in large quantising mag. field, effect of band non-parabolicity 79—47112
semiconductor, photoemission meas. of surface and bulk states 80—25527
semiconductor, spin-orbit splitting, tight binding calc. 77—85184
semiconductor, test of electronic band struct. by laser-induced reson. 78—37949
semiconductor, Wannier-Mott polaritons in mag. fields, review 78—2437
semiconductor, zero-gap props. correlated to Γ_8 symmetry, review 80—6717
semiconductor alloys, effect of lattice const. variation in band theory 80—49596
semiconductor film, size-quantised with tilted valleys, two-photon absorpt. 79—95869
semiconductor heterojunction, amorphous/cryst., energy band diagram construction 77—55602
semiconductor morphotropic and isomorphic series, cryst. struct. stability 77—51353
semiconductor neutral point defect electronic struct., self consistent method 78—91641
semiconductor physics, conf., Edinburgh, Scotland (Sept. 1978) 79—95303
semiconductor solid soln., bending parameters calc. by pseudopot. method 78—26813
semiconductor thin film, energy spectrum in mag. field, size effect, calc. 80—70865
semiconductor tunnelling, bound levels and band struct., rel. to inelastic electron tunnelling spectroscopy 79—4597
semiconductor wire, quantised monochromatic wave absorpt., indirect transitions due to surface roughnesses *(Russian)* 79—91397
semiconductor wire, two-photon interband absorpt., quantum size effect *(Russian)* 79—95721
semiconductor with nonspherical bands, diamag. excitons and Franz-Keldysh effect 78—72554
semiconductor with position depend. band struct., electron and hole currents 78—43377
semiconductor with superlattice, two-photon absorpt. 77—16331
semiconductors, antiferromagnetic, magnetoelec. effect, magnetization and ferroelec. props. 80—25180
semiconductors, band shape, k.p perturbation theory *(Korean)* 78—23020
semiconductors, band states temp. depend., book contrib. 80—80182
semiconductors, degenerate, energy band structure effect on transverse magnetoresistance 80—88580
semiconductors, energy states under high press. *(Chinese)* 79—56128
semiconductors, ferromagnetic multivalley anisotropic, electron autolocalisation *(Russian)* 80—92848
semiconductors, free carrier optical props., book contrib. 80—80738
semiconductors, impact ionisation theory 80—49752
semiconductors, optical props. above band edge, book contrib. 80—84425
semiconductors, photoelectron spectra and band struct., book contrib. 80—16155
semiconductors with grain-boundary barriers, boundary states' energy struct. influence on elec. cond. 79—11147
semiconductors with optically anisotropic energy bands, antiresonance states of diamagnetic excitons 79—51500
singularities of the small polaron effective mass 78—63989
solid solution, density of states in forbidden band and band edge smearing 79—73418
solid state physics rel. to solar cells, review 80—49601
solids, angular dependent photoemission, book contrib. 79—61500
sp-hybrid crystals, energy bands calc. by many-neighbour approximation 77—35846
sphalerite-type crystals, effect of effective charges on X_5^v and L_3^v 77—35847
spin depend. wave functions and band parameters 77—72818
structure stability ot morphotropic and isomorphic series 77—51353
superlattice, cond.-valence band interactions, subband struct. 77—72815
surface, generalised tridiagonal Hamiltonian resolvent matrix, exact soln. 80—29307
TCNQ complexes with N-methyl derivatives of pyridine, cond. and thermoelec. power meas., band model anal. 80—10952
TCNQ salt, K^+TCNQ^-, spin polarised band struct., effective Coulomb repulsion 77—15734
ternary alloy semiconductor, band struct., CPA calc. based on linear combination of bond orbitals 79—87035
ternary alloy semiconductors, disorder effects on electronic props. *(Japanese)* 80—49709

band structure of crystalline semiconductors and insulators continued
ternary chalcopyrite semiconductors, energy band struct. 78—34767
ternary diamond-like semiconductors, charact. features of electronic spectrum and stability 79—33230
ternary semiconductor, $A^{II}B_2^{III}C_4^{VI}$, crystal structure effects in electronic states 80—20085
ternary semiconductor, struct. effects on energy band struct. 78—39021
ternary system compound formation, comp. and props. w.r.t. component electron struct., computer prediction 80—103444
tetracyanoplatinates, energy band calcs. 77—39780
tetrahedral crystal, electron localisability by LCAO band theory, Pauling ionicity 77—47776
tetrahedral semiconductors, exciton binding energy, Haben methods for single isotropic parabolic energy bands 79—56140
tetrahedrally coordinated semiconductors, electronic struct. and Fourier transformed Compton profiles 79—38689
tetraselenotetracene, electronic structure, conductivity studied by ESCA 79—4889
tetrathionaphthalene, electronic structure, conductivity studied by ESCA 79—4889
tetrathiotetracene, cond. mechanisms and refined energy level spectrum *(Russian)* 78—52103
tetrathiotetracene, electronic structure, conductivity studied by ESCA 79—4889
tetravalent, fundamental absorpt. spectra, direct interband transitions 78—63972
three-band semiconductor, absorpt. of weak EM wave in presence of intensive one 79—61325
TiO, local density of states, X-ray spectra, Hartree-Fock and Xα calcs. discrepancies 79—77980
transition metal borides, higher types, phys. props. and electronic struct., group orbitals-LCAO calcs. 80—20077
transition metal carbide, d-band effects in lattice dynamics contrib. to acoustic phonon freqs. 78—2207
transition metal carbide, X-ray emission band exam. and electronic struct. 77—8689
transition metal carbides, 3d metal, interatomic interaction 79—1569
transition metal carbides, d-metal, band struct. calc., Fermi level *(Russian)* 78—39019
transition metal chalcogenides, struct. and mag. props., book contrib. 77—43808
transition metal cpds., photoelectron energy distrib. curves, rel. to band struct., book contrib. 80—16156
transition metal diborides, 3d metal, interatomic interaction 79—1569
transition metal dichalcogenides, electronic struct. and band theory 80—44497
transition metal dichalcogenides, layered, electronic band struct. and bonding by atomic orbitals methods 79—15077
transition metal dichalcogenides, phys. props. *(Japanese)* 77—69225
transition metal dichalcogenides, physical props., review *(Japanese)* 80—33969
transition metal dihydrides, band struct. and electronic props., electron-phonon coupling 79—47011
transition metal dioxides, elec. struct. props., two-band model calcs. 78—67934
transition metal hydrides, electronic struct., heat of formation, single particle lifetimes, Dingle temp. meas. 78—51923
transition metal mononitrides, 3d metal, interatomic interaction 79—1569
transition metal monoxides, 3d, ground state electronic struct., atomic sphere approx. 80—59855
transition metal nitrides, X-ray emission band exam. and electronic struct. 77—8689
transition metal oxides, 3d metal, interatomic interaction 79—1569
transition metal-metalloid band structure, nonorthogonality and tight-binding fit 80—59852
transition metalloids, d-bandwidth contraction 79—87041
transiton metal oxide perovskites, UPS, XPS, X-ray absorpt. spectra, band struct. study 79—56885
TTF-TCNQ, TCNQ and TTF bandwidths, extended Huckel and CNDO/2 calcs. 79—7771
two band model with electron-phonon interactions for narrow-gap electron spectra 79—90961
uranium monopnictides, NaCl struct., band struct. 80—6714
V_2VI_3 compounds, electronic struct., X-ray emission, XPS, UPS obs. 78—52638
variable gap semiconductors, carrier transport and fluctuation effects due to changes in gap width 80—107793
wurtzite-type semiconductor, exciton binding energy, effect of electron-hole exchange and valence bands 79—51494
zero gap semiconductor, magnetooptical and impurity effects 80—6721
zero-gap semiconductors, dynamic dielec. function in mag. field, appl. to magnetoreflection spectra 79—15108
zero-gap semiconductors, electronic energy spectrum 77—66118
zinc blende structure semiconductors, cyclotron reson. *(German)* 78—10337
zincblende compounds, electronic struct. and atomic config. at cleavage surface 77—62974
α-$ZnIn_2S_4$, and related polytypes, electron band struct. 79—51485
Ag halides, quadrupolar deformability theory by tight binding method 80—10614
$AgAsS_2$, $AgSbS_2$ and $AgBiS_2$, cryst. and vitreous, refl. spectra, energy spectrum 77—8596
$AgAsS_2$, band struct. photoemission and refl. spectra obs. 77—66581
$AgFeSe_2(S_2)(Te_2)$, elec. props., band gap *(Russian)* 79—11116
$AgGaSe_2$ wavelength-modulated reflectance, optical electronic transitions, 1.5-5.5 eV 78—35170
Ag_8GeS_6, fundamental absorpt. edge changes due to polymorphic transitions 77—20240
$Ag_8GeS_6(Se_6)(Te_6)$, Ag_8SiSe_6, $Ag_8SnS_6(Se_6)$, absorpt. edge investigs. at phase transitions 78—35149
Ag_8GeSe_6, fundamental absorpt. edge changes due to polymorphic transitions 77—20240
AgI, FCC and γ phase, electronic struct., relativistic KKR calc. 77—85140
AgN_3, optical absorpt. spectra, and photoemission, electron band scheme 79—100015
β-$AgSbS_2$, phase transitions, electrophysical props. 80—44316
Ag_8SnS_6, fundamental absorpt. edge changes due to polymorphic transitions 77—20240
Ag_8SnSe_6, fundamental absorpt. edge changes due to polymorphic transitions 77—20240

band structure of crystalline semiconductors and insulators continued
AlAs-GaAs (001) interface and superlattice, electronic props., band struct. 79—95485
AlAs-GaAs (100) superlattices, band struct. 78—30868
AlB_2 electronic struct. calcs. 78—2417
$Al_xGa_{1-x}As$, energy band struct. calc. 78—23019
AlGaSb, growth and characts. for 1.0-1.8 μm heterojunction devices 78—6870
$Al_xGa_{1-x}Sb$, solid soln., depend. of forbidden-band width on composition 78—39602
$Al_2In_{12}S_{21}$, preparation, struct. and elec. props. 77—59685
AlN, excitation, luminescence, reflection spectra in fund. absorpt. region 78—10956
AlN, luminesc. excitation spectrum and band struct. 80—84783
AlN, rel. to photocond., 6-12 eV 77—89796
Al_2O_3, band structure and stored charge 80—49589
Al_2O_3, corundum, calc. using semiempirical Mulliken-Rudenberg method 80—80177
AlP(As)(Sb), APW calc. of electronic structure and optical props. 79—99479
AlSb solar cell material, epitaxy, ionicity and bond struct. 80—61367
Ar film, electron MFP, vacuum UV photoemission data 77—28690
Ar, lattice dynamics calc. using energy band theory 80—49320
Ar, solid, energy bands, depend. on choice of exchange-correlation pot. 80—70607
As, band structure and cryst. energy, pseudopot. calc. 79—90954
As_2S_3, As_2Se_3, optical props., electronic struct., photocond., book contrib. 77—44024
As_2S_3 layered crystal and amorphous analogues, XPS valence band spectra, electronic struct. 77—52218
As_2Se_3, monoclinic, chem. bonds rel. to electronic and vibr. states 80—64951
As_2Se_3, polarised light reflectance spectra, band struct. 78—63979
As_2Se_3, single crysts., fine struct. of direct gap from electrorefl. spectra 80—93280
B modifications exam. of physical props. and electron structure 79—94954
$B_{12}C_x$, phonon energies and electronic props., x depend., refl. spectra and thermoelec. power meas. 80—16052
BN, chem. bonding and electronic struct., AES and SIMS meas. 80—50512
BN, cubic, ab initio SCF calcs., band struct., ground state props. 78—51891
BN, cubic, energy band and piezoelec. calcs. 78—72071
BN, electronic energy band struct., X-ray spectra, pseudopotential calcs. 79—78008
BN, electronic struct., exact exchange HF calcs. 80—65438
BN, hexagonal, electronic struct. from X-ray emission and XPS 79—47009
BN, Wannier functions and density matrix determ. in terms of localised orbitals 78—2408
BN, wave-vector depend. energy loss functions and dielec. functions 77—51688
B_2O_3, chem. bonding, electronic struct., ESCA, Auger, and SIMS spectra 80—50512
BP-BAs, quasi-binary system, X-ray emission and electron spectra of solid soln. *(Russian)* 77—1764
$BaTiO_3$ and $BaTi_{1-x}Fe_xO_{3-x}F_x$, electrical, optical and mag. props., photoelectrolysis 77—47856
$BaTiO_3$, band struct. calc., interpretation of XPS and UPS spectra 80—70597
$BaTiO_3$, electronic props., SCF-MS-Xα calc. 80—54607
$BaTiO_3$, electronic struct., XPS and band struct. calc. 79—38708
$BaTiO_3$, photoelectron and optical spectra derived from self-consistent charge MO and band calcs. 80—96785
$BaTiO_3$, UV refl. spectra, optical consts. 0 to 32 eV Kramer-Kronig anal., band struct. calcs. 78—43903
$BaTiO_3$, XPS, band struct., density of states, photoionisation cross sections 78—52629
BeO, ceramic, sintered, thermoluminesc., EPR, emission spectra, energy level diagram 77—81163
BeO, cryst., local centres, electronic struct. calcs. 80—100433
BeS, electronic energy bands, APW and LCAO calc. 77—20236
BeSe, electronic energy bands, APW and LCAO calc. 77—20236
BeTe, electronic energy bands, APW and LCAO calc. 77—20236
Bi, electron tunnelling and band struct., mag. field effect 79—37979
Bi-Sb, semiconducting, lattice dielec. const., comp. depend. 80—39516
Bi-Sb, semiconducting solid solution, forbidden band width Sb-conc. depend. 77—66117
γ-Bi-Se phase, electronic props. 77—43493
$Bi_{12}GeO_{20}$, reflectivity spectrum and band struct. 79—47474
BiI_3, empirical pseudopotential calc. 77—15766
BiI_3, octahedrally coordinated, layer cpd., electronic struct. using synchrotron-radiation photoemission spectroscopy 79—74058
$Bi_{0.89}Sb_{0.11}$, effect of band structure on the dispersion of magnetoplasma waves 77—47845
n-$Bi_{0.924}Sb_{0.076}$, energy spectrum variation under strong uniaxial tension 79—73432
$Bi_{1-x}Sb_x$, deformation calculations, band struct. variation, electron phase transitions due to deform. *(Russian)* 80—65137
$Bi_{1-x}Sb_x$, far IR magnetoabsorption, band struct. study 80—50351
$Bi_{1-x}Sb_x$, semicond.-semimetal transition, temp. and press. depend. of transport props. 78—76120
$Bi_{1-x}Sb_x$ semiconducting alloy, band struct. study, Shubnikov-de Haas effect *(Russian)* 80—80181
$Bi_{1-x}Sb_x$:Te(Sn), band struct., plasma refl. spectra and galvanomag. tensor 77—16315
$Bi_4Si_3O_{12}$, eulytine, change in band structure on transition to amorphous state 79—15081
Bi_2Te_3, layered semiconductor, angle resolved photoemission 79—28893
Bi_2Te_3, Shubnikov-de Haas effect, high press. effect on band struct. 77—51767
Bi_2Te_3-Sb_2Te_3 film, cond., galvanomag. Seebeck and Nernst-Ettingshausen effects under press., band model 77—47907
C, pregraphitic, diamag. suscept. rel. to temp., energy level calcs. *(French)* 78—34951
CaB_6, electronic struct. APW and muffin-tin calcs. 80—29320
CaF_2, band struct. determ. by adjoint plane wave method 77—76750
CaF_2, electronic band struct. determ., combined OPW and tight binding calc. 77—85145
CaF_2, electronic energy bands calc. 78—34762

band structure of crystalline semiconductors and insulators continued
CaO, band struct. calc. rel. to high press. metallisation 80—84427
CaO, electronic band struct., combined tight-binding and pseudopot. approach 77—47728
CaO, electronic structure 80—2332
Cd_3As_2, band struct. and g-factor, Shubnikov-de Haas oscills. meas. 80—49598
Cd_3As_2, band struct. from Shubnikov-de Haas and de Haas-van Alphen effects 80—49597
Cd_3As_2, band structure, Kane model, magneto-Seebeck and Hall data 77—62821
Cd_3As_2, effect of annealing on elec. transport props. 80—49739
Cd_3As_2, electron conc. temp. depend. heavy hole-cond. band energy gap 79—69410
Cd_3As_2, energy band structure calc. 80—75504
Cd_3As_2 film, band struct. model, rel. to transmission spectra, 0.6-15 μm 78—11013
Cd_3As_2, inverted band struct. 79—90958
Cd_3As_2, pressure dependence of galvano- and thermo-magnetic effects 80—6722
Cd_3As_2, valence band struct., optical absorpt. meas. 80—50293
$Cd_3(As_xP_{1-x})_2$, $0 \leq x \leq 1.0$, band struct. calc. near Brillouin zone centre 80—107703
$Cd_3(As_xP_{1-x})_3$, thermoelectric power and Hall effect., mag. field depend. 78—10484
$CdCr_2S_4(Se_4)$, ferromagnetic semiconductors, spinel-type, resonance Raman scattering and electronic structure *(Japanese)* 79—47421
$CdCr_2S_4(Se_4)$, pure and Ag doped, electronic struct., mixed valence 80—70612
$CdCr_2S_4(Se_4)$, spin depend. phonon Raman scatt., band struct. 78—68491
$CdCr_2Se_4$, energy band struct calc. by augmented plane wave method 80—103621
$CdCr_2Se_4$, energy structure, magnetooptic effects 80—71394
$CdCr_2Se_4$, magnetic red shift origin, specular reflectivity, band struct. 80—40127
$CdCr_2Se_4$, modulated piezoreflection spectra 80—97237
$CdCr_2Se_4$, narrow conduction band, crit. behaviour of resistivity 79—78096
$CdCr_2Se_4$, optical absorption due to transitions between bands and local levels 79—38537
$CdCr_2S_4(se_4)$, ferromag. semicond., band struct., EHT calc. 80—54608
CdF_2, electronic band struct., combined tight-binding and pseudopotential calc. 77—43495
CdF_2, electronic energy bands calc. 78—34762
CdF_2, electronic structure of outermost levels, UPS study 80—7468
CdF_2, UPS and XPS spectra, rel. to optical props. 80—66386
$Cd_xFe_{3-x}O_4$, collective electron states, ^{57}Fe Mossbauer meas. 77—69748
$CdGa_2S_4$, direct excitons, refl. spectra 79—90972
$CdGaS_4(Se_4)$, absorption and refl. spectra anisotropy, band struct. 77—69840
$CdGa_2(S_{1-x}Se_x)_4$ solid solns., band struct. behaviour w.r.t. comp. *(French)* 80—107699
$CdGa_2S_4(Se_4)$, band struct., and optical spectra 78—19511
$CdGa_2S_4(Se_4)$, band struct., pseudopot. method 80—92816
$CdGa_2Se_4$, struct. of valence band, photocond. and reflection spectra meas. 80—6719
$CdGa_2Se_4$, thermoreflectance and visible absorpt. spectra, energy gap, cryst. field splitting 80—34945
$Cd_{1-x}Hg_xGa_2S_4$ solid solns., band struct. behaviour w.r.t. comp. *(French)* 80—107699
$Cd_xHg_{1-x}Te$, band struct. and optical props. 80—15450
$Cd_xHg_{1-x}Te$, disorder scatt. 78—39137
$Cd_xHg_{1-x}Te$, epitaxial graded-gap layers, elec. transport props. 77—85358
$Cd_xHg_{1-x}Te$, film, optical props., struct. depend. 77—1751
$Cd_xHg_{1-x}Te$, solid solns., role of stoichiometry defects 77—47813
$Cd_xHg_{1-x}Te$ solid solns., dimensional resonances of HF helicons, band struct. and electron mobility 77—47846
$Cd_xHg_{1-x}Te$, strong elec. field effect on galvanomagnetic effects 79—11159
$Cd_xHg_{1-x}Te$, $x=0$, $x=1$, effective mass of heavy holes, 4.2 to 300K 77—1353
$Cd_xHg_{1-x}Te$, zero gap semiconductor, interband optical-phonon scattering 80—6846
CdI, tight binding calcs. and photoemission expts. 78—23018
CdI_2, ang. depend. electron energy loss meas. 79—95884
CdI_2, electronic struct., tight-binding calcs. 80—15446
CdI_2, UV reflectivity meas., band struct., LCAO calcs. 78—72545
$CdIn_2S_4$ cubic spinel, electronic band struct. and chem. bonds 78—34768
$CdIn_2S_4$, electronic states, sensitivity to cryst. struct., UPS study 80—45209
$CdIn_2S_4$, fund. reflectivity, 2 to 6 eV, band struct. implications 78—39574
$CdIn_2Se_4$ defect tetrahedral crystal, pseudopotential scheme 77—11850
α-$CdIn_2Se_4$, defect zincblende struct., electronic props. 77—15767
$CdIn_3Se_4$, cryst. growth, photoresponse and optical props. 78—39165
$CdIn_2Te_4$ defect tetrahedral crystal, pseudopotential scheme 77—11850
CdMnTe, semimagnetic semiconductor, band structure, optical properties 79—95331
$Cd_{0.6}Mn_{0.6}Te$ crystals, $Mn(3d^5)$ band, photoemission evidence 80—11535
$Cd_{1-x}Mn_xTe$, effect of Mn $3d^5$ states on band struct., exciton refl. struct. in mag. field 79—11094
CdO, point defect props., band struct., lattice simulation calc. 80—19797
CdP_2, role of metal d states in valence band formation 79—65380
CdP_4, role of metal d states in valence band formation 79—65380
Cd_2P_3, role of metal d states in valence band formation 79—65380
Cd_3P_2, band struct., $D_{4h}{}^{15}$ space group symmetry props. 80—34357
Cd_3P_2, energy band struct. and electron mobility at low temp. 79—37984
Cd_3P_2, energy band structure for real $D_{4h}{}^{15}$ symmetry 79—56124
Cd_3P_2, free carrier and interband absorption 78—23446
Cd_3P_2, role of metal d states in valence band formation 79—65380
Cd_3P_2, X-ray spectra determ. 78—35225
CdS, cubic, ab initio band struct. calcs. within local density functional formalism 78—87910
CdS, explanation for total current spectrum 77—8693
CdS, photocond. on supplementary X-irrad. *(Russian)* 77—28212
CdS, photoemission due to direct transition near L- and M-points in Brillouin zone 77—16451
CdS, surface electronic struct., slow electron reflection, total current spectroscopy *(Russian)* 80—54759

band structure of crystalline semiconductors and insulators continued
CdS, up-conversion and optical storage, spatially modulated band struct. 78—64397
CdS, XPS, secondary illumination effects, band bending, level shifts 80—108324
CdS(Se), optical spectroscopy, absorpt. coeff., lattice vibr. modes, band gap, acoustic approach 77—69822
CdS(Se), single cryst., band parameters from optical exciton spectra 79—47021
CdS_xTe_{1-x}, emission spectra at high excitation levels *(Russian)* 79—74004
CdSb, energy spectrum, influence of chem. bonds, LCAO calc. 80—34356
CdSb:Ge, anisotropy of elec., mag. props. 78—34829
$CdSe_xTe_{1-x}$ film, polycrystalline, deposition and physical props. 77—4741
$CdSiP_2$, pseudodirect chalcopyrite semicond., electronic band struct. 80—20079
$CdSiP_2$, thermoreflectance spectra 77—81122
$CdSnAs_2$, hydrostatic press. effect on resist. and Hall coeff., band struct. 77—47808
n-$CdSnAs_2$, optical absorption rel. to energy spectra *(Russian)* 78—75994
$CdSnAs_2(P_2)$ single crysts., refl. spectra, band struct., dielec. consts. 77—44022
$CdSnP_2$, optical props., band struct. calcs., real space atomic potential parameters 79—95325
CdTe, bulk and surface states anal. using synchrotron radiation 77—66574
CdTe, energy bands and optical props. calc., tight-binding model with spin-orbit interaction 80—65448
CdTe, suitability for solar photocells, photovoltaic conversion props., band gap 77—43652
CdTe:Ti^{2+}, Jahn-Teller effect on $^3T_1(^3F)$ state, resonance on $^3T_1(^3P)$ state 78—27271
CdTe-HgTe superlattice on CdTE layers, evanescent states, tight binding calcs. 80—70611
CeN, electronic struct., XPS exam. 78—6269
CeSb, forbidden band gap and electrotransfer parameters 80—39497
CmO_2, band struct., cryst. binding and ESCA spectra, X_α cluster calc. 78—64443
$CoBr_2$, UV reflectivity spectra for band struct. calc. 77—20878
$CoCl_2$, cryst., self-consistent band struct., intersecting spheres model 80—75505
$CoCl_2$, UV reflectivity spectra for band struct. calc. 77—20878
$Co_{1-x}Fe_xSi$, elec. and optical props. 80—49740
CoO, electronic struct. calc. 78—43297
CoO, self consistent energy band calc. 78—23022
CoO, valence band struct., cryst. field anal., photoelectron data 79—47007
$CoS_2(Se_2)$, electronic struct., UPS and XPS study 80—80935
CrAl, semicond. solid solns., temp. depend. of elec. resist. at high temp. 78—67941
$CrBr_3$, self consistent band struct., intersecting spheres model 79—37985
$CrCl_3$, electronic struct. and struct. phase transition 80—59644
$CrCl_3$, self consistent band struct., intersecting spheres model 79—37985
CrH, electronic props., H alloying effects, book contrib. 79—82522
CrN, electron struct. calc. 80—49587
CrO_2, optical conductivities and dielec. functions in 0.2-6 eV range, rel. to band struct. 79—42938
Cr_2O_3, electron structures calc. using models, ESCA and X-ray spectral data 77—35863
Cr_2O_3, electronic struct. study by XPS 80—25518
CsAu, band struct. and charge distrib., semicond. and metallic behaviour 77—20238
CsI, optical props. in vacuum UV 77—24861
$CsPbBr_3$, electronic and optical props. 80—25414
$CsPbCl_3$, electronic and optical props. 80—25414
$CsPbCl_3$, electronic struct. and optical props. in fundamental absorpt. region 80—93367
$Cu_{1-y}Ag_yInS_{2-x}Se_{2x}$, for solar photovoltaic cells 80—10982
CuBr(Cl)(I), energy bands, relativistic KKR method, UV absorpt. spectra 80—39501
CuBr(I), reflectance and thermoreflectance spectra, electronic struct. 80—71444
CuCl, absorpt. coeff., 0.4-25 μm, band struct. determ. 77—73155
CuCl, band struct., OPW calc. and X-ray spectra meas. 80—75506
CuCl, band struct. calc. using layer method 79—60704
CuCl, biexciton resonant two-photon absorption 78—23491
CuCl, electronic struct., ab initio HF SCF MO calcs. of $CuCl_4^{3-}$ cluster 78—95262
CuCl, electronic struct., self consistent all electron approach 80—2333
CuCl, electronic struct. by LCAO and LMTO methods, direct gap semiconductor 80—59868
CuCl, energy bands and effective mass 80—10859
CuCl, refl. spectra, 4.5-30 eV, vel. to band struct. 80—103969
CuCl, self-consistent energy-band study 79—69408
CuCl, self-consistent zonal struct. calcs., electron spectrum gap *(Russian)* 80—34359
CuCl, XPS and Auger spectroscopy, elec. struct. 80—29852
CuCl(Br), charged excitons, band struct., electron-hole exchange interaction 77—69233
CuCl(Br)(I), optical props., 4 to 30 eV, band struct. 77—90166
$CuCr_2S_4(Se_4)$, electronic struct., mixed valence 80—70612
$CuCrSe_2$, influence of excess Cu on physical props. 80—103836
$CuFeS_2$ single crystal, optical reflectivity spectrum 80—40129
$CuGaS_2$, tetragonal distortion, crystal field splitting, temp. depend. 79—47060
$CuGaSe_2$ film, optical props. near and above fundamental absorption edge 78—35215
$CuGaTe_2$ and $CuInTe_2$, electroreflectance data, direct gap obs., cryst. field splitting and hybridisation degree 78—39557
$CuGaTe_2$ film, flash evaporated, growth and optical props. 79—95296
CuH, electronic struct., heat of formation, single particle lifetimes, Dingle temp. meas. 78—51923
$CuInS_2$, fund. reflectivity, 2 to 6 eV, band struct. implications 78—39574
$CuInSe_2$ semicond. films, optical props., 1-3 eV 78—27346
Cu_2O, energy band interactions under uniaxial compression 80—25412
Cu_2O, relationship between interband transitions and spectrum of diagmagnetic excitons in moderate mag. fields 79—91412
Cu_2O, self-consistent energy bands 80—59869

band structure of crystalline semiconductors and insulators continued
CuP_2, Cu_3P, electronic struct. of valence bands, X-ray spectra and XPS 78—92176
Cu_2S, electromechanical props. *(Russian)* 79—11117
Cu_2S-CdS heterojunction characteristics and CdS polarity *(Japanese)* 78—23154
Cu_2S-CdS heterojunctions, electron trap characterisation by capacitance transient meas. 79—78163
$CuS_2(Se_2)$, electronic struct., UPS and XPS study 80—80935
$Cu_{2-x}Se$, elec. props. and band struct. 79—73513
Dy_2S_3, optical props. and electronic struct. in fund. absorpt. region 80—80817
ErP, energy spectrum calcs. in one-electron approx. 78—15250
Eu chalcogenides, cond. band spin struct. 80—71577
Eu solid solutions with lanthanides, monosulfides, and oxides, vacant d states, X-ray absorpt. 80—103623
EuB_6, electronic struct., transport and mag. props. 80—96782
$EuMo_6S_8$, Chevrel phase, mag. interactions, LMTO energy band studies 80—70606
EuO, band struct., linear combination of muffin-tin orbitals calcs. 78—2407
EuO, electronic struct. investigation by electron spectroscopy method 80—92812
EuO, electronic structure, octahedral clusters, determ. by X_α method 78—10350
EuO magnetic semiconductor, quasiparticle lifetimes, CPA study 80—65443
EuO(S)(Se)(Te), cryst. and electronic struct., mag., elec., and optical props., book contrib. 80—39760
EuO(Se), complex elec. cond. anomalies 80—107812
EuO(s), mag. semicond., s-f model, intermediate coupling theory 79—95326
EuS, pure and Gd doped, electronic struct., mag. exchange and elec. transport props. 78—87974
EuSe:Gd, mag. props. explained by band struct. 78—43324
$EuSi_2$, valence band struct. *(Russian)* 79—15076
$Eu_xSr_{1-x}M_4O_{11}$, M=Nb, Ta, electrophys. and mag. props. 77—89760
$FeCl_2$, cryst., self-consistent band struct., intersecting spheres model 80—75505
$FeCl_3$-graphite intercalation compound, dielec. function, band struct. EELS study 80—49643
$FeCr_2S_4$, ionic distrib. and band struct., Mossbauer study 80—80646
$FeCr_2S_4$, pure and doped, CVD grown, surface struct., elec. props. and band struct. 79—4905
FeO, electronic struct. calc. 78—43297
FeO, Fe_3O_4, Fe_2O_3, absorption spectra, 0.1-6 eV, one electron energy level diagram 78—52487
FeO, self consistent energy band calc. 78—23022
Fe_3O_4, rel. to photocond., 70-130K, temp. range including metal-semicond. transition *(Russian)* 78—56178
FeS_2, ionisation loss spectra, density of unoccupied states 80—55241
FeS_2, mag. susceptibility press. depend., bandstruct. calcs. 78—19212
(Ga, Al, As) heterostructures and compounds, electronic props., empirical pseudopot. calc. 80—80366
Ga-group V semiconductors, electroreflectance spectroscopy using synchrotron rad. 78—10912
$Ga_{0.5}Al_{0.5}As$, heterostructure, cation order, effect on energy bands 79—1570
$Ga_{1-x}Al_xAs$, alternate monolayer crysts., MBE and props. exam. 78—10289
$Ga_{1-x}Al_xAs$, band struct. from I-V, C-V meas. on Schottky diodes 80—96989
$Ga_{1-x}Al_xAs$, deep levels, pressure effects 80—49651
$Ga_{1-x}Al_xAs$ epitaxial layer, elec. cond., Hall effect, band struct. 80—49964
$Ga_{1-x}Al_xAs$, non-shallow levels and cond. band struct. from Hall carrier conc. meas. 80—39607
n-$Ga_{1-x}Al_xAs$:Si, room-temp. cond. and band struct. 80—96869
$Ga_{1-x}Al_xAs$-GaAs solar cells, computer anal. of cell characts. incl. band gap variation 80—55866
$Ga_{1-x}Al_xP$, bending parameters calc. by pseudopot. method 78—26813
$Ga_xAl_{1-x}P$ high-temp. solar cell with 0.3 eV band gap 80—21400
GaAs (110), double-dangling-bond defects and band bending 79—69411
GaAs, (110) surface structure, rotational relaxation, cluster model *(Chinese)* 80—107621
GaAs, angle-resolved photoemission and valence band dispersions 80—7469
GaAs anodic oxide, states, electrochemical meas. 80—80176
GaAs, band structure under high stress, nonperturbative calc. 78—10344
GaAs, conduction band mapping by angle-resolved photoemission 79—83105
GaAs, deep level trap emission identification by indirect conduction minima technique 78—84163
GaAs, degenerate, impurity band struct. for dense donors and acceptors 80—29348
GaAs, degenerate, nonequilib. electron distrib. functions 77—63394
GaAs, direct energy gap, press. depend. up to 180 kbar 77—8020
GaAs, EHT calcs. of energy bands and pressure dependences *(Japanese)* 78—34747
p-GaAs, electronic props. 78—68040
GaAs, electronic struct., mol. cluster model, SCF multiple scatt. method 79—42446
GaAs, electronic structure, self consistent local description 80—20067
GaAs, energy bands and wavefunctions, localised orbital description 78—18942
GaAs, field penetration in FIM, band bending 79—87567
GaAs, heavily doped, electron effective mass, Kane equation calcs. 79—77989
GaAs, hot carrier impact ionisation, band struct. depend. 78—30934
GaAs, indirect band edge, determ. by quantum-well bandfilling 78—92120
GaAs, ion-bombarded, energy band struct., electrorefl. obs. 79—19517
GaAs, k-linear coupling, E_1' transitions 78—91583
GaAs, LMTO self consistent band struct. calc. 80—20078
p-GaAs, magnetoluminesc. of cond. band to acceptor transition 77—1716
GaAs, modulation spectroscopy, two-ray methods *(Russian)* 78—54469
GaAs, optical inhomogeneity, physical basis 79—15430
GaAs, Raman scattering absolute cross section band struct. model calcs. 80—7349
GaAs, refr. index and induced birefringence dispersion 80—2717

band structure of crystalline semiconductors and insulators continued
GaAs, Schottky barrier electrorefl. under uniaxial stress, band struct. 77–48193
GaAs, Schottky barrier ellipsometric electroreflectance spectra, energy band parameters 79–99853
GaAs, self-consistent localised electronic struct. 79–42445
n-GaAs, three valley band struct., high temp. Hall mobility 80–29318
GaAs, UV photoemission, polarisation-depend., angle-resolved spectroscopy 77–66573
GaAs, valence band struct. obtained by magnetophonon effect 77–76748
GaAs, XPS, secondary illumination effects, band bending, level shifts 80–108324
GaAs:Cr (Cr-Te), and undoped, transverse-acoustoelec.-voltage spectroscopy 79–99586
GaAs:Cu melt grown, 1.36 eV band luminescence studies, edge emission 79–87510
GaAs:O, electronic struct., multiple-scatt. Xα mol. cluster model 80–15445
GaAs:Se(Zn) polycrystalline film, Hall effect, resistivity meas. 80–96911
n-GaAs:Te, elec. cond. and Hall coeff. temp. depend. meas., three band model 79–33287
GaAs-$\mathrm{Ga_{1-x}Al_xAl}$ superlattice, reson. Raman scatt., 2-D quantum states 77–8577
GaAs-$\mathrm{Ga_{1-x}Al_xAs}$, semiconductor superlattices by MBE 79–95939
n-GaAs-$\mathrm{Ga_{1-x}Al_xAs}$, superlattice, subband struct. and optical spectra, self-consistent calc. 80–15443
GaAs-$\mathrm{Ga_{1-x}Al_xAs}$ heterostructures, quantum size effect in superlattices, electronic props. 80–29471
GaAs-GaSb, threshold energies for impact ionisation by electrons and holes 78–6390
$\mathrm{(GaAs)_n}$-$\mathrm{(AlAs)_n}$, multilayer heterostructure, cation order, effect on energy bands 79–1570
$\mathrm{GaAs_{1-x}P_x}$, bending parameters calc. by pseudopot. method 78–26813
$\mathrm{GaAs_xP_{1-x}}$, band struct., CPA calc. based on linear combination of bond orbitals 79–87035
$\mathrm{GaAs_xP_{1-x}}$, energy band struct., CPA based on LCBO *(Japanese)* 80–44495
$\mathrm{Ga_{0.08}In_{0.92}As_{0.18}P_{0.82}}$, band struct., optical studies 79–47013
$\mathrm{Ga_xIn_{1-x}As_yP_{1-y}}$, electron effective mass, cyclotron reson. and magnetophonon effect meas. 80–103618
$\mathrm{Ga_xIn_{1-x}P}$, band struct. enhancement of indirect transitions, piezoreflectance meas. 77–20823
$\mathrm{Ga_xIn_{1-x}P}$, film, energy band struct., photolum. meas. 79–7784
$\mathrm{Ga_{1-x}In_xSe}$, energy bands near absorpt. edge, transmission and photoluminesc. spectra 79–83022
$\mathrm{Ga_{1-x}In_xSe}$, energy spectrum and struct., X-ray diffr. and light absorption 79–11437
$\mathrm{Ga_{1-x}In_xSe}$, exciton spectrum nature and anisotropy of electron bands near absorption edge *(Russian)* 79–51483
GaN, electron struct., ESCA study 80–89116
GaP complex band semicond. photogalvanic effect mechanism 80–11036
GaP, deformation potentials of direct and indirect absorpt. edges 79–69854
GaP, density of states effective mass and cond. band energy minima 77–28101
GaP, EHT calcs. of energy bands and pressure dependences *(Japanese)* 78–34747
GaP, ion-bombarded, energy band struct., electrorefl. obs. 79–19517
n-GaP, many-valley semiconductor, relative displacement of D_1 and D_2', bands under shear deform. influence 79–15080
GaP, optical inhomogeneity, physical basis 79–15430
n-GaP, optical rectification and photon drag, rel. to band struct. 77–36224
GaP, overlap integrals and Auger recomb. coeff. direct calc. 79–69524
GaP, polar semicond., radiative recomb., electron-phonon interaction effects, calc. 80–49631
GaP, stress-induced X_{1c}-X_{3c} conduction band mixing 79–19515
GaP-InAs solid solns., energy band struct., edge absoprtion spectra 78–39018
GaS, photoemission props. of III-VI layer compounds 79–65976
GaS, polarisation selection rules for photoemission spectra, test of band struct. calcs. 77–52216
GaS, semiconductor layer cpds., band struct. calc. using tight-binding method 79–65376
GaS(Se), $\mathrm{GaS_{0.6}Se_{0.4}}$, angle resolved UPS, energy band dispersion curves determ. 79–100022
$\mathrm{GaS_xSe_{1-x}}$, valence band states, composition depend., photoemission spectra study 80–100434
$\mathrm{GaS_xSe_{1-x}}$, wavefunction symm. and binding energies, synchrotron radiation photoemission spectroscopy 80–50532
GaS(Se)(Te), electronic struct., tight-binding calcs. 80–15448
GaSb, E_1 and $E_1+\Delta_1$ edges using electroreflectance, Franz-Keldysh oscills., high mag. fields 77–66518
n-GaSb, fundamental absorpt. and energy relax., elec. field induced changes 77–1688
n-GaSb:Te(Se), forbidden optical band gap, Moss-Burstein effect 78–88335
GaSb-InAs superlattices, two-dim. electronic structure 78–75995
GaSb-InSb solid solns., heavily doped, electronic props. 77–80727
GaSe, band struct. and electron density of states in two-dimens. approx. 79–37987
GaSe, band struct. from ang. resolved photoemission 77–59673
GaSe, band structure calc., semi-empirical tight-binding method 77–47726
GaSe based layer crystals, three dimensional electron state nature near absorpt. edge 79–90960
GaSe, direct exciton excited state hot luminescence, band struct. props. 80–55183
GaSe, electron beam excited free exciton luminesc., rel. to band struct. 79–19940
GaSe, exciton spectra at 4.2K rel. to layer struct. 77–16336
GaSe, interlayer interaction and exciton spectra study 77–52165
GaSe, layer, upper valence bands using bond-orbital model 79–15078
GaSe, layered, electronic band struct., direct evaluation by angle resolved photoemission 77–51652
GaSe layers, band struct. and state density calc. by empirical tight-binding method 79–42443
GaSe, photoemission props. of III-VI layer compounds 79–65976
GaSe, polarisation selection rules for photoemission spectra, test of band struct. calcs. 77–52216

band structure of crystalline semiconductors and insulators continued
GaSe polytypes, electronic band struct. calcs. 77–51650
GaSe polytypes, tight binding study of electronic states 79–60705
GaSe, semiconductor layer cpds., band struct. calc. using tight-binding method 79–65376
GaSe, thin film, photoelectrical props. at high electric field *(Russian)* 79–11247
GaSe, tight-binding calc. 77–80729
GaSe, two and three dimensionality of electron states, normal photoemission obs. 77–32503
$\mathrm{GaSe_xS_{1-x}}$, layered semicond., electroabsorpt. in fundamental absorpt. edge region 77–52043
GaSe(Te), optical spectra in 2 to 50 eV range 78–10915
$\mathrm{GaSe_{1-x}Te_x}$, energy bands near absorpt. edge, transmission and photoluminesc. spectra 79–83022
GaTe, single cryst. prep. and electroabsorpt. spectra investig. 80–103968
$\mathrm{GaTe_{1-x}Se_x}$, exciton spectrum nature and anisotropy of electron bands near absorption edge *(Russian)* 79–51483
Gd pnictides, APW calc., semiclassical-metal trend 77–28111
$\mathrm{Gd_2O_3}$ photoabsorpt. spectra, band struct., at ionisation mechanisms, electron energy loss spectra 77–24909
GdP, electronic struct., mag. exchange and elec. transport props. 78–87974
GdS, electronic struct., mag. exchange and elec. transport props. 78–87974
Ge (111) surface, n-channel inversion layer, subband energies 80–11063
Ge, band structure of diamond like crystals, cluster-Bethe lattice model calc. 80–6713
Ge, band structure under high stress, nonperturbative calc. 78–10344
Ge, band structure using modified Vejkovic, Slavic pseudopot. form factor 79–56121
Ge, crit. points in E′ region from ellipsometric data 77–80726
Ge, doped, D^- band width, influence of resonances 79–11061
Ge, E_1-optical struct. from electroreflectance spectra 78–43897
Ge, EHT calcs. of energy bands and pressure dependences *(Japanese)* 78–34747
Ge, electronic and struct. props., nonlocal pseudopot. calc. 80–34349
Ge, electronic energy bands of diamond-type crysts., appl. of EHT method 78–87907
Ge, electronic struct. from SCF calc. using intersecting spheres model 78–51888
Ge, electronic structure, self consistent local description 80–20067
Ge, electroreflectance spectra, nonparabolicity effects of bands *(Russian)* 79–4791
Ge, energy band gap dilation and vibr. contrib. determ. 79–60703
Ge, energy bands and wavefunctions, localised orbital description 78–18942
Ge, energy-gap narrowing and state filling under laser irrad. 79–42441
Ge, Faraday rotation and ellipticity, interband transitions, comparison with Si 77–52048
p-Ge, IR light free hole absorpt., nonvertical optical transitions *(Russian)* 80–80802
Ge, indirect exciton excited states 78–30873
Ge, interband Faraday ellipticity 78–92052
Ge, LCAO band structure, overlap and distant neighbour effects 80–49585
Ge, nonlinear optical susceptibility, tight binding bonding orbital model 80–5784
Ge, optical excitation of dislocation states 77–85265
Ge, phonon energy variation under high press. band struct. changes, tunnel spectroscopy study *(Russian)* 80–2134
Ge, photoionisation cross-sections of valence s- and p-electrons *(Ukrainian)* 77–73211
Ge, piezoresistance, energy and momentum relax. of charge carriers 78–47786
n-Ge, piezoresistance under mechanical stress, rel. to cond. band minima 80–6836
Ge, piezospectroscopy of group V impurities, conduction band deformation potential 79–99915
Ge, pseudopotential method of band struct. anal. 78–51886
Ge, Schottky barrier electrorefl. under uniaxial stress, band struct. 77–48193
Ge, self-consistent localised electronic struct. 79–42445
Ge, surface electronic struct., self consistent pseudopotential calc. 78–47842
p-Ge, test of electronic band struct. by laser-induced reson. 78–37949
p-Ge, theory of photon-drag effect, parabolic and anisotropic band-struct. approx. 78–47825
Ge, valence band struct. obtained by magnetophonon effect 77–76748
Ge, X-ray spectra and energy band struct. 79–69407
Ge:As, NMR, conduction electrons in impurity band, metal-nonmetal transition 79–78544
Ge:Li, Cu p-n junctions, current stimulated LiCu complex formation, photocurrents 80–107897
Ge-Si, electronic structure, short-range order effects, calc. 80–92861
Ge-Si alloys, electronic struct. comp. depend., X-ray spectral obs. 77–81178
GeAsS, X-ray photoelectron spectra, valence electrons density of states *(Russian)* 79–15583
$\mathrm{GeO_2}$, band struct., tight-binding calc. 80–24796
$\mathrm{GeO_2}$, electronic struct., photoemission spectra calc. 77–35865
$\mathrm{GeO_2}$, electronic struct. and densities of states, tight-binding calcs. 80–15447
GeS, angular resolved UV photoemission and band structs. 77–85144
GeS, orthorhombic, atomic pseudopots. 79–42453
$\mathrm{GeSe_2}$, exciton absorpt., transmission spectra of cryst., glasses and amorphous samples 79–15485
$\mathrm{Ge_xSe_{1-x}}$, bonds and band struct. determ., tight-binding model 78–18959
$\mathrm{Ge_xSi_{1-x}}$, solid solution, single crystal, photoconductivity *(Russian)* 79–11170
GeTe, bond orbital model of band struct. 80–59853
GeTe, effective masses for cond., density of states 80–88472
GeTe, electron-phonon interactin induced phase transition 79–82338
GeTe-$\mathrm{Sb_2Te_3}$, solid solutions, cond., density of states 80–88472
α-$\mathrm{Ge_{1-x}Te_x}$, anisotropy of elec. props. rel. to cubic phase transition and band struct. 77–76820
$\mathrm{H_3BO_3}$, chem. bonding, electronic struct., ESCA, Auger, and SIMS spectra 80–50512
$\mathrm{(HCN)_x}$, mol. crystals, quantum theory, mol. tight binding method calcs. 80–49572

band structure of crystalline semiconductors and insulators continued
- HCl, infinite chain, ab-initio electronic band struct., MUNICH-CHAIN program 77—8017
- HF chain, ab initio cryst. orbital calcs., basis set depend. 78—34746
- $H_{1.6}MoO_3$, electronic props., mag. susceptibility and spectra 80—80266
- H_xWO_3 bronzes, Anderson transition, XPS 80—107705
- H_xWO_3, crystalline, band struct., XPS meas. 77—59667
- HfC, quasi-self-consistent energy band structures using relativistic KKR calcs. chemical bonding 79—51484
- HfC_x, electron energy spectrum and phys. props. in homogeneous region *(Russian)* 77—31941
- HfN, electronic struct., relativistic energy band struct. calc. 80—34354
- $Hg_{2.86}AsF_6$, linear chain compound NMR exam. 78—19359
- $Hg_{0.985}Cd_{0.015}Se$, interband $\Gamma_6 \rightarrow \Gamma_8$ magnetoabsorption and band parameters 79—82960
- $Hg_{1-x}Cd_xSe$, IR absorpt. spectra, band struct., refr. index 80—50337
- $Hg_{1-x}Cd_xSe$, zinc blende structure, optical and electronic properties 80—6723
- HgCdTe, interband magnetoabsorption and band struct. 79—82959
- HgCdTe, recomb. effects, mag. quantum oscills. in Auger transition rate 79—82610
- $Hg_{0.75}Cd_{0.25}Te$, single crystal, reflection spectra 80—40140
- $Hg_{1-x}Cd_xTe$, interband magnetoreflectance 78—19448
- $Hg_{1-x}Cd_xTe$, magnetooptical and impurity effects 80—6721
- $Hg_{1-x}Cd_xTe$, magnetoreflection studies 79—82963
- $Hg_{1-x}Cd_xTe$, mixed crysts., band struct. and optical transitions, distorted atomic orbitals 77—69224
- $Hg_{1-x}Cd_xTe$ mixed crysts., magneto-opt. obs., semicond. config., semimetal-semicond. transition 77—73131
- $Hg_{1-x}Cd_xTe$, optical absorpt., quasilocal acceptor level effects, theory 80—92853
- $Hg_{1-x}Cd_xTe$, props. and appls., book contrib. 77—39834
- $Hg_{1-x}Cd_xTe$, quasi-local acceptor levels and electron mobility 78—67974
- $Hg_{1-x}Cd_xTe$, recombination processes using impact ionization capture cross sections 80—75577
- $Hg_{1-x}Cd_xTe$, semimetallic state, magneto-optical investig. of Landau levels and band parameters 77—63410
- $Hg_{1-x}Cd_xTe$, transverse magnetoresist. in quantum limit, band struct. nonparabolicity effect 77—39885
- $Hg_{1-x}Cd_xTe$, zero-gap semicond. with nonparabolic band struct., hot electron mobility and conc. 78—76080
- n-$Hg_xCd_{1-x}Te$, narrow band gap, Auger effect under high mag. fields 79—82609
- HgF_2, electronic structure of outermost levels, UPS study 80—7468
- $HgGa_2S_4$, energy band struct. calc., empirical pseudopot. method 80—24793
- $HgGa_2Se_4$, anisotropic photocond., pleochroism, and band struct. 78—19094
- $HgGa_2Se_4$, energy band struct. calc., empirical pseudopot. method 80—24793
- $Hg_{1-x}Mn_xSe$, band struct. from anomalous Shubnikov-de Haas effect 80—20080
- HgMnTe, interband magnetoabsorption and band struct. 79—82959
- HgMnTe, semimagnetic semiconductor, band structure, transport phenomena 79—95331
- $Hg_{1-x}Mn_xTe$, energy levels at Γ-point in intense mag. fields, Shubnikov-de Haas effect meas. 80—24951
- $Hg_{1-x}Mn_xTe$, magnetooptical and impurity effects 80—6721
- α-HgS, electronic energy level calcs. 80—6718
- HgSe, band struct. and spin splitting Shubnikov de Haas study 80—65445
- HgSe, interband absorpt. and Γ-point band structure parameters 79—47010
- HgSe, interband $\Gamma_6 \rightarrow \Gamma_8$ magnetoabsorption and band parameters 79—82960
- HgSe, magnetooptical and impurity effects 80—6721
- HgSe, optical determ. of Γ-point band struct. parameters 79—82523
- HgTe, energy bands and optical props. calcs., tight-bonding model with spin-orbit interaction 80—65448
- HgTe, magnetooptical study of Γ_8 bands anisotropy 79—82984
- HgTe, magnetophonon oscills. of thermoelec. power 80—49789
- HgTe, optical absorption 77—28572
- HgTe, uniaxially compressed, anomalous magnetoresist. and band crossing 79—65501
- HgTe, zero gap semiconductor, review 77—31944
- HgTe-HgSe film, optical spectra in fundamental absorption edge 79—74012
- $HgTe_xSe_{1-x}$, solid soln., intrinsic carrier density and energy band struct. 78—39134
- IV-VI small gap semiconductor alloys, band edge parameters 80—49594
- InAs, band gap and effective mass, depend on impurity conc. 79—69412
- InAs, heavily doped, Burstein-Moss effect and near-band-edge luminesc. 79—47525
- N-InAs, Moss-Burstein effect, S, Sn, Te dopants 78—64389
- n-InAs, Shubnikov-de Haas oscills., conduction electron density, phonon scatt. 77—15768
- n-InAs, transport props., influence of higher energy bands, calcs. 79—19598
- InAs/GaSb (001) superlattices, electronic struct., two dimensional effects 80—11064
- InAs-GaSb (100) superlattice, electronic struct., self-consistent pseudopot. method 80—49884
- InAs-GaSb superlattices, two-dim. electronic structure 78—75995
- InAs-GaSb superlattice energy struct. and semiconductor-semimetal transition 79—23893
- InAs-GaSb superlattice, electronic struct., self-consistent pseudopot. calc. 80—29470
- $InAs_{1-x}P_x$, evidence for reduction in momentum matrix element P^2 due to alloy disorder 79—65853
- InBi, Fermi surface and band struct., press. effects 77—39779
- $In_{1-x}Ga_xAs$-$GaSb_{1-y}As_y$ superlattice, optical absorption 79—19887
- $In_{1-x}Ga_xAs$-$GaSb_{1-y}As_y$, semiconductor superlattices by MBE 79—95939
- $In_{1-x}Ga_xAs$-$GaSb_{1-y}As_y$ heterostructure devices 79—42624
- $In_{1-x}Ga_xAs_yP_{1-y}$, oscillatory magneto-transmission, band parameters 79—60707
- $In_xGa_{1-x}As_yP_{1-y}$, valence band struct., CPA calc. 79—73435
- $In_{1-x}Ga_xP$, temp. depend. of forbidden band width, photoluminesc. meas. 78—19556
- $In_{1-x}Ga_xP_{1-z}As_z$, lattice matched to InP, electroreflectance obs. 80—93416

band structure of crystalline semiconductors and insulators continued
- $In_{1-x}Ga_xSb$ alloy system, interband magnetooptical study using Schottky barrier 79—8124
- $In_{1-x}Ga_xSb$, band parameter variations 80—20084
- InN film, refl. and transmission spectra, band struct. 78—72625
- n-In_2O_3 film, RF sputter grown, substrate bias effect on elec. and optical props. 78—64150
- In_2O_3:Sn films, RF reactive sputtered, optical props. rel. to band struct. 79—91515
- In_2O_3-SnO_2/SiO_x/Si diode solar cells, loss mechanisms, characts., band struct. 80—26135
- InP, cleaved surface, angle resolved photoelectron spectroscopy 80—55258
- InP, deep level trap interaction with lowest and upper cond. minima 80—49654
- n-InP, high field props. under high press. 78—26872
- InP, III-V semicond., electronic struct. of valence and conduct. bands 77—28110
- InP, transferred electron effects under high press. 80—34453
- InP-Au, Schottky barriers, electroreflectance spectra 77—43698
- InP-$Ga_xIn_{1-x}As_{1-y}P_y$ heterojunctions, energy band diagram 77—16400
- n-InSb, acoustoelectric instability, effect of nonparabolic band struct. 79—60875
- InSb, band nonparabolicity, rel. to low temp. electron mobility 77—89759
- n-InSb, cond. electron spectra in quantised mag. field, impurity resonance scatt. *(Russian)* 80—93178
- n-InSb, conduction band effective mass anisotropy and nonsphericity 79—69414
- n-InSb, conduction-band struct. from reflectivity meas. when subject to mechanical strain 79—42450
- n-InSb, directional temp. of hot electrons under elec. and mag. fields 78—84135
- n-InSb film, degenerate, electron conc. and resist. temp. depend., band struct. 77—76971
- n-InSb, highly doped semicond., enhancement of magnetoresistance due to nonparabolic bands 79—56246
- InSb, intensity depend. interband Faraday rot. obs., saturation and reson. enhancement effects 80—108186
- InSb, Landau level struct., magneto-electroreflectance 80—25349
- InSb, recombination processes using impact ionization capture cross sections 80—75577
- InSb, semiconductor, Brillouin zone spin dependent wave functions calcs. 79—56126
- p-InSb, stress induced k-linear terms in band struct. 80—49595
- n-InSb, transverse magnetoresist. in strong mag. fields 79—4571
- InSb, valence band struct. obtained by magnetophonon effect 77—76748
- InSb, zincblende and rocksalt type struct., semiempirical LCAO band struct. calc. 77—72816
- InSe, band structure, pseudopotential calc. 80—24799
- InSe, band structure, XPS, UPS and tight-binding calc. 77—47727
- InSe, band structure calc., semi-empirical tight-binding method 77—47726
- InSe, electronic struct., tight-binding calcs. 80—15448
- InSe, energy band structure, chem. bond polarity, photoemission, semiempirical tight binding method 80—44504
- InSe, layer semicond., electronic props. 79—28275
- InSe, photoemission props. of III-VI layer compounds 79—65976
- InSe, polarisation selection rules for photoemission spectra, test of band struct. calcs. 77—52216
- InSe, reflectivity and low energy absorption 80—34944
- InSe, semiconductor layer cpds., band struct. calc. using tight-binding method 79—65376
- InSe, spin orbit split off valence bands, exciton transitions, Hopfield's quasicubic model, visible absorpt. spectrum 80—50370
- InSe, two and three dimensionality of electron states, normal photoemission obs. 77—32503
- InSe, two-dimensional band struct., XPS meas. and tight-binding calc. 78—2419
- In_6Se_7, single cryst. prep. and electrophys. props. 79—43129
- $(In_2Te_3)_x$-$(Hg_3Te_3)_{1-x}$, photoelec. and luminesc. props. 77—39889
- In_2Te_5, energy band struct., localisation of interband transitions in Brillouin zone 80—20642
- Insb, doped, electron scatt. by deform. pot. 77—72860
- K-intercalated graphite (stage-1), electron energy loss expts. and band struct. theory 79—100001
- KCl, band struct. and charge densities, intersecting spheres model 80—49591
- KCl, band struct. calc. by mixed LCAO and OPW method 77—8019
- KCl, large unit cell semiempirical mol. orbital approach to props. of solids 79—87037
- $KCoF_3$, XPS of band struct. 77—11851
- $KCuF_3$, XPS of band struct. 77—11851
- $KFeF_3$, XPS of band struct. 77—11851
- KH_2AsO_4, ferroelec., electronic struct. study *(Japanese)* 79—87463
- KH_2PO_4 and related substances, electronic structures study *(Japanese)* 79—87463
- $KMnF_3$, XPS of band struct. 77—11851
- $KNbO_3$, complex electronic dielectric const. from tight binding energy bands 78—60054
- $KNbO_3$, electronic props., SCF-MS-Xα calc. 80—54607
- $KNbO_3$, electronic struct., XPS and band struct. calc. 79—38708
- $KNbO_3$, XPS, band struct., density of states, photoionisation cross sections 78—52629
- $KNiF_3$, rel. to XPS data 77—20871
- $KNiF_3$, XPS of band struct. 77—11851
- K_3Sb, and Na_2KSb, photocathode materials, empirical pseudopotential calc. 78—10346
- K_3Sb, optical and dielectric props., energy spectra, density of states calcs. 80—20083
- $KTaO_3$, complex electronic dielectric const. from tight binding energy bands 78—60054
- $KTaO_3$, electronic props., SCF-MS-Xα calc. 80—54607
- $KTaO_3$, electronic struct., XPS and band struct. calc. 79—38708
- $KTaO_3$, quantum magnetoresist. results, using pulsed fields up to 35 T 79—73528
- $KZnF_3$, XPS of band struct. 77—11851
- Kr film, electron MFP, vacuum UV photoemission data 77—28690
- La silicides, valence band struct. *(Russian)* 79—15076
- LaB_6 (001), surface state exam. by angular resolved UPS 78—19114
- LaB_6, synthesis and props. *(Japanese)* 80—40255

band structure of crystalline semiconductors and insulators continued

- $LaFe_{1-x}Co_xO_3$, UPS, XPS, X-ray absorpt. spectra, band struct. study 79−56885
- $La_{1-x}M_xCrO_3$, M = Mg, Sr, electronic struct. study by XPS 80−25518
- $LaNi_{1-x}Fe_xO_3$, UPS, XPS, X-ray absorpt. spectra, band struct. study 79−56885
- $LaNi_{1-x}Co_xO_3$, UPS, XPS, X-ray absorpt. spectra, band struct. study 79−56885
- La_2O_3, electronic struct. study by XPS 80−25518
- LaOF, features of formation of band structure 79−33232
- La_2S_3, optical props. and electronic struct. in fund. absorpt. region 80−80817
- $La_{1-x}Sr_xVO_3$, high-temp. transport meas., band model 77−11917
- LiC_6, and LiC_{12}, intercalation cpds., electronic struct. calcs. 80−70613
- LiC_6, band struct., density of states and Fermi surface props. 79−37982
- LiC_6, intercalated, charge-transfer and non-rigid-band effects 80−44496
- LiC_6, Raman spectrum, rigid band model anal. 79−4800
- LiC_6, spatial distribution of valence electrons 79−37983
- LiCL, band struct. calc. by mixed LCAO and OPW method 77−8019
- LiF, band struct. and charge densities, intersecting spheres model 80−49591
- LiF, Ewald method, convergence of reciprocal lattice sums 77−11834
- LiF, ground and excited state props., local density formalism 78−10349
- LiF, Hartree-Fock eqns. and two-centre approx. validity 77−76726
- LiF, large unit cell semiempirical mol. orbital approach to props. of solids 79−87037
- LiF, selective adsorption of He, band struct. effects 79−73402
- LiH, electronic struct., equation of state, insulator-metal phase transition 79−33234
- LiH, electronic struct. and equation of state up to 100 Mbar 77−1361
- LiH, single crysts., refl. photolum., cathodolum., and photocond. meas. 77−52186
- LiH, solid. Hartree-Fock energy band calc. using OPW method 80−10856
- α-$LiIO_3$, energy band struct., nonlinear optical absorpt. obs. 79−64277
- $LiNbO_3$, band struct. and spontaneous polarisation calcs. 78−95261
- $LiNbO_3$, energy band struct., nonlinear optical absorpt. obs. 79−64277
- $LiNbO_3$-Si, acoustoelectronic memory, effect of band-bending 80−70771
- $LiSnS_2$, Li intercalation effects on electronic struct. 79−78004
- $LiTiS_2$, intercalation complex, band struct., tight-binding calc. 79−95323
- Li_xWO_3, band struct., XPS meas. 77−59667
- LuH_2, electronic struct., optical studies, 0.2-5 eV, 4.2-340K 79−78005
- LuH_2, electronic struct., photoelectron spectra study 80−50527
- $LuH_{2.05}$, Compton profiles, electronic configurations 80−11501
- $MNbO_3$, orthorhombic, electronic struct., SCF-MS-Xα calc. 80−70600
- $MNbO_3$, tetragonal, electronic struct., optical anisotropy 80−70599
- MgB_2, LCAO calc. 79−90957
- $MgCl_2$, electronic structure by intersecting spheres model 79−99482
- MgF_2, band struct., tight-binding calc. 80−24796
- MgF_2, electronic struct. and densities of states, tight-binding calcs. 80−15447
- Mg_2Ge, semicond., electronic band struct., reson. Raman scatt. meas. 77−12384
- MgO, bonding, pressure effects in lower mantle 80−72491
- MgO, compressed, SCF electronic struct. calcs., necy. press. for conversion to metallic state 78−43300
- MgO, electronic band struct., combined tight-binding and pseudopot. approach 77−47728
- MgO, electronic struct., approx. SCF calcs. 79−56125
- MgO, electronic struct. calc. 79−78003
- Mg_2Si, semicond., electronic band struct., reson. Raman scatt. meas. 77−12384
- Mg_2Sn, semicond., electronic band struct., reson. Raman scatt. meas. 77−12384
- $Mg_xZn_{1-x}Te$, band struct. refl. spectra meas. 80−80813
- $MnCl_2$, cryst., self-consistent band struct., intersecting spheres model 80−75505
- MnO, electronic struct. calc. 78−43297
- MnTe, optical props. and electronic struct. 78−6682
- MnZn ferrites, thin struct. of $K\beta_5$ and $L\alpha_{1,2}$ emission bands of Fe *(Ukrainian)* 79−78790
- MoO_2, optical conductivities and dielec. functions in 0.2-6 eV range, rel. to band struct. 79−42938
- MoS_2, electronic struct. by photoelectron spectroscopy using line and synchrotron sources 79−87560
- MoS_2, KKR calc. of energy bands 80−34355
- MoS_2 molybdenite band structural props. rel. to supercond. and semicond. 80−96781
- MoS_2, surface electronic struct., slow electron reflection, total current spectroscopy *(Russian)* 80−54759
- MoS_2, UPS meas. band struct. determ. 78−35250
- Mo_6S_8 Chevrel phases with group IIIa metals, Nb, Hg, Pb and Cu, synthesis, stability and characts. 80−71608
- $MoS_2(Se_2)$, 2H polytype, low energy electron energy loss spectra 79−95885
- $MoS_2(Se_2)(Te_2)$(2H) polytypes, Kramers-Kronig anal. of reflectivity spectra, 0-30 eV, band model 79−51976
- $MoSe_2$:Nb(Re), layered, elec. props., semicond.-metal transition 77−11922
- $MoSe_{2-x}$, transport meas. and band structure 77−69361
- Mo_3Si, Mo_5Si_3 and $MoSi_2$, ultrasoft X-ray emission bands, empirical band schemes 78−15249
- α-$MoTe_2$, band struct. photoelectron spectroscopy 77−51653
- α-$MoTe_2$, electronic struct. by photoelectron spectroscopy using line and synchrotron sources 79−87560
- α-$MoTe_2$, KKR calc. of energy bands 80−34355
- $MoTe_{2-x}$, thermoelec. power and resist. meas. 77−1438
- NH_3, solid, UPS, valence band struct. 79−33890
- $NH_4H_2PO_4$, ferroelec., electronic struct. study *(Japanese)* 79−87463
- NaCl (100) face, angle-resolved photoemission 78−56567
- NaCl, band struct. calc. by mixed LCAO and OPW method 77−8019
- NaCl, conduction band struct. from first principles 79−65379
- NaCl, electronic struct., SCF cryst. cluster model 80−24792
- NaCl, electronic structure calculation, CNDO semi-empirical methods *(Russian)* 80−10909
- NaF, band struct. and charge densities, intersecting spheres model 80−49591
- NaF, quasimolecular struct. characts. of $NaL_{II,III}$ absorpt. edge 80−93436
- $NaNO_2$, band struct., polarisation and piezoelec. consts. calc. 78−52448

band structure of crystalline semiconductors and insulators continued

- Na_3Sb, and Na_2KSb, photocathode materials, empirical pseudopotential calc. 78−10346
- NaV_6O_{15} monocrystal, electronic struct. and X-ray emission spectra anisotropy 80−84807
- Na_xWO_3, band struct., XPS meas. 77−59667
- Na_xWO_3, band struct. calcs. 77−62824
- Na_xWO_3, optical props. 79−38515
- Nb chalcogenides and chalcogenide halides, geometrical struct. and metal-metal bonding 80−80172
- NbC, band struct. and X-ray emission spectra, APW and Xα calc. 80−70605
- NbC, self consistent APW-Xα calc. 77−20237
- NbC_x, stoichiometric and defective phases, electronic energy spectrum and physical props. *(Russian)* 77−35868
- NbN, band structure, nonorthogonality and tight-binding fit 80−59852
- NbN, self consistent APW-Xα calc. 77−20237
- NbO, electronic struct. from photoelec.- and X-ray emission spectra and X_α calcs. of NbO_6^{-10} cluster 79−23892
- NbO_2, electronic band struct., optical props., generalised susceptibility, struct. transition 79−95328
- Nb_2O_5, electron energy spectrum by optical and thermal methods 79−69418
- Nb_4Si, Nb_5Si_3 and $NbSi_2$, ultrasoft X-ray emission bands, empirical band schemes 78−15249
- Nd_2S_3, optical props. and electronic struct. in fund. absorpt. region 80−80817
- NdSb, forbidden band gap and electrotransfer parameters 80−39497
- Ne, lattice dynamics calc. using energy band theory 80−49320
- Ne, solid, energy bands, depend. on choice of exchange-correlation pot. 80−70607
- Ne, solid, hole band struct., Bratsev wave function calcs. *(Russian)* 80−65437
- $NiBr_2$, self consistent band struct., intersecting spheres model 79−37985
- $NiCl_2$, cryst., self-consistent band struct., intersecting spheres model 80−75505
- $NiCl_2$, self consistent band struct., intersecting spheres model 79−37985
- $Ni_{1-x}Co_xS_2$, anomalous elec. props., polaron transport in highly correl. narrow bands 77−85222
- NiH_x, electronic band struct. and interatomic bond 78−43295
- NiO, electronic struct. calc. 78−43297
- NiO, self consistent energy band calc. 78−23022
- $NiS_2(Se_2)$, electronic struct., UPS and XPS study 80−80935
- Pb chalcogenide mixed crystals, intraband absorption due to chemical disorder 79−56789
- Pb chalcogenides, interband absorpt., optical absorpt. coeff., two- and six-band models 79−33728
- Pb chalcogenides, interband transitions, absorpt. coeff., multiband calc. 80−29738
- $Pb_{1-x}Ge_xTe$, band struct., tunnelling obs. in MIS struct. 80−54795
- $Pb_{1-x}Ge_xTe$, n- and p-type, effective masses 80−44481
- PbI_2 (2H), angular depend. magnetoluminesc. 79−43029
- PbI_2, electronic struct., tight-binding calcs. 80−15446
- PbI_2, layered, electronic band struct., direct evaluation by angle resolved photoemission 77−51652
- PbI_2, octahedrally coordinated, layer cpd., electronic struct. using synchrotron-radiation photoemission spectroscopy 79−74058
- PbI_2, semicond., band struct., angle resolved photoemission meas. 78−15296
- PbI_2, tight binding band structure using scaled parameters 78−79927
- PbI_2, UV reflectivity meas., band struct., LCAO calcs. 78−72545
- $PbMo_6S_8$, Chevrel-phase, electronic struct., LCAO calc. for idealised Mo_6S_8 cluster 77−43494
- PbO_2, electronic struct. and densities of states, tight-binding calcs. 80−15447
- PbS, (100), angular resolved UV photoemission 78−2989
- PbS, band struct., angle resolved photoemission obs. 79−33899
- PbS, energy gap anomaly, relativistic band struct. calc. 79−4510
- PbS, film, total current spectrum and energy struct. 80−100719
- p-PbS, struct. of valence band, transport processes study 80−20081
- PbS-Si, photosensitive p-n heterojunction, energy band diagram 79−95489
- PbS(Se)(Te), angle resolved UPS and electronic band struct. 79−37981
- PbS(Se)(Te), bond orbital model of band struct. 80−59853
- PbS(Se)(Te), photoemission interpretation 80−25531
- PbSe, band struct. angle resolved photoemission obs. 79−33899
- PbSe, energy gap anomaly, relativistic band struct. calc. 79−4510
- n-PbSe, pressure induced transition to gapless state 78−2533
- $PbSe_{0.5}S_{0.5}$, valence band struct., absorpt. spectra, elec. props. 80−44505
- $(PbSe)_{1-x}(SnTe)_x$ solid solution, band struct. and some optical props. *(Russian)* 77−76752
- $PbSe_{1-x}Te_x$, symmetry change in cond. levels, photovoltaic effect and reflectivity obs. 78−34766
- n-$Pb_{0.94}Sn_{0.06}Se$ solid solns., Burstein-Moss effect and energy band struct. 80−40118
- $Pb_{1-x}Sn_xSe$, (x = 0.125), pressure induced band inversion, effect on energy spectrum *(Russian)* 78−39007
- $Pb_{1-x}Sn_xSe$, band struct. parameters, thermoelectric power meas. in strong mag. fields 79−51474
- $Pb_{1-x}Sn_xSe$, band struct. and transport props., hydrostatic press. effects 80−15452
- $Pb_{1-x}Sn_xSe$, energy band parameter determ. from Shubnikov-de Haas effect 77−69227
- $Pb_{1-x}Sn_xSe$ solid solns., photoluminesc. spectra, energy band parameter determ. 80−71484
- PbSnTe/PbTe inverted heterostructure mosaics, long wavelength, energy gap-Fermi level temp. depend. 79−85182
- $Pb_{0.72}Sn_{0.28}Te$, Hall effect and elec. cond., 77 to 480K, energy band struct. 77−76817
- $Pb_{0.8}Sn_{0.2}Te$, susceptibility effective mass, carrier conc. depend. 80−20069
- n-$Pb_{0.82}Sn_{0.18}Te$, conduction band struct., determ. by Shubnikov-de Haas meas. 78−2504
- $Pb_{0.82}Sn_{0.18}Te$, film, effect of hydrostatic pressure on props. 80−70862
- $Pb_{0.82}Sn_{0.18}Te$ solid solution, energy band spectrum characts., Hall effect meas. 77−76737
- $Pb_{1-x}Sn_xTe$, band struct. and phonon energies, tunnelling spectroscopy 78−72070
- $Pb_{1-x}Sn_xTe$, band struct. changes due to displacive phase transition, Hall coeff. meas. 80−10671

band structure of crystalline semiconductors and insulators continued
- Pb$_{1-x}$Sn$_x$Te, basic electrons energy spectrum near mag. phase transition *(Russian)* 79—90955
- Pb$_{1-x}$Sn$_x$Te, displacive phase transition, effect of interband hybridisation 79—33233
- Pb$_{1-x}$Sn$_x$Te, electroreflectance, Faraday rot., elec. band struct. parameters 77—66113
- Pb$_{1-x}$Sn$_x$Te, energy band parameters from IR Faraday rotation 78—48154
- Pb$_{1-x}$Sn$_x$Te, energy band parameter determ. from photoluminescence. spectra in mag. field 79—11066
- Pb$_{1-x}$Sn$_x$Te, energy spectrum under hydrostatic pressure 79—65381
- Pb$_{1-x}$Sn$_x$Te, epitaxial layers, photolum. in mag. field 79—83033
- Pb$_{1-x}$Sn$_x$Te films, size quantisation, optical orientation of free carriers 80—20725
- Pb$_{1-x}$Sn$_x$Te, lattice and electronic props. and g-value 80—80161
- p-Pb$_{1-x}$Sn$_x$Te, pressure-induced transition to zero-gap state, changes in energy band parameters 79—69413
- Pb$_{1-x}$Sn$_x$Te:In, energy spectrum under combined effect of mag. field and hydrostatic press. 79—65382
- Pb$_{1-x}$Sn$_x$Te:In, Hall const. depend. on temp., autocompensation, band gap temp. depend. explanation 79—69527
- Pb$_{1-x}$Sn$_x$Te:In, semiconductor-metal-semiconductor transitions under press. 80—34491
- Pb$_{1-x}$Sn$_x$Te-Pb$_{1-y}$Sn$_y$Te, p-n heterojunction, prep. and props. 79—51662
- Pb$_{1-x}$Sn$_x$Y (Y=Te, Se, S), interband absorption under linearly polarised light excitation 78—92089
- PbTe, band struct., angle resolved photoemission obs. 79—33899
- PbTe, electron-phonon interactin induced phase transition 79—82338
- PbTe, electronic struct. near band gap 77—69226
- p-PbTe, energy band struct. and scattering of holes 80—10874
- PbTe, energy gap anomaly, relativistic band struct. calc. 79—4510
- PbTe epitaxial film, many valley semicond., band population effects, intraband magneto-optical props. 79—78007
- PbTe epitaxial films, quantum size effect, optical meas. 80—11121
- PbTe epitaxial layers, submillimetre spectroscopy 79—83048
- PbTe, far IR magnetorefl., band struct. 80—76010
- PbTe, far IR spin flip reson. 79—82979
- p-PbTe, MIS struct. inversion layer sub-bands, IR magnetoreflectance obs. 80—44731
- PbTe, magneto-optical transitions and band parameters 79—82961
- n-PbTe, noncubic (111) oriented epitaxial films, weak field magnetoresistance 80—75584
- PbTe, resonant scattering, photocond. 80—6910
- p-PbTe, thermorefl., 1.0-4-6 eV 78—76492
- PbTe:Bi-PbSmTe-PbTe, epitaxial laser struct., growth, p-n junction position and lasing region 79—89908
- PbTe-InTe, solid solns., anomalies in electron mobility 77—80772
- PdH, electronic struct., heat of formation, single particle lifetimes, Dingle temp. meas. 78—51923
- PdH$_{0.72}$, Compton profile, electronic struct. *(German)* 78—92140
- PdH$_x$, electronic props., H alloying effects, book contrib. 79—82522
- PdH(D), superconducting props., effect of hybridisation, band struct. determ. 79—69628
- PdH$_x$(D$_x$), band struct., supercond. props., APW calcs. and neutron scatt. 78—43511
- PdO, electronic struct., XPS and UPS study 80—35061
- PrSb, forbidden band gap and electrotransfer parameters 80—39497
- γ-PtPc, Pc=phthalocyanine, single crystals, energy band structures and carrier mobilities 77—72817
- PtTe, electronic struct., self-consistent and non-self-consistent band calcs. 80—44499
- Rb-halide, UPS exam., band struct. determ. 77—40330
- ReB$_2$, electron struct., Fermi energy and surface, bonding 80—20076
- SMS, band struct. and semicond. metal phase transition 80—80180
- S$_2$N$_2$, electronic struct. by extended tight-binding method, comparison with (SN)$_x$ 77—76722
- S$_2$N$_2$, LCAO band struct. calc. 77—76723
- Sb (III) compounds, Mossbauer spectra, direct population of solid-state bands 80—15905
- SbSBr, electronic and optical props. 78—34763
- SbSI, electronic and optical props. 78—34763
- SbSI, energy band struct. from modulation spectra 78—43892
- Sb$_2$Se$_3$ single crysts., phys. prop. anomalies, 400-450K *(German)* 79—38072
- SbSeI, electronic and optical props. 78—34763
- Sb$_2$Te$_3$, mag. and elec. props., carrier excitation 78—43395
- Sc silicides, valence band struct. *(Russian)* 79—15076
- ScH$_2$, electronic struct., optical studies, 0.2-5 eV, 4.2-340K 79—78005
- ScH$_2$, electronic struct., band theory 79—78006
- ScH$_2$, electronic struct., photoelectron spectra study 80—50527
- ScH$_2$, self-consistent bond struct., charge transfer 80—49590
- ScH$_2$, self-consistent energy bands, KKR method with Hedin-Lundqvist approx. 80—49593
- Sc$_2$O$_3$ photoabsorpt. spectra, at. ionisation, band struct. mechanisms, electron energy loss investig. 77—24909
- ScP, electronic struct., self-consistent Hedin-Lundqvist and Xα APW calcs. 80—29322
- ScP, energy band struct., exchange-correl. pot. effects, APW calcs. 80—29321
- Se, charge density, self-constent OPW and pseudopot. calcs. 80—92813
- Se, Compton profile, charge and momentum density 80—55220
- Se, electronic struct. of cryst. phases and hydrostatic press. effects 80—59865
- Se, trigonal, electronic props. under press. 77—31939
- Se, trigonal, electronic states, tight-binding model Hamiltonian 77—59250
- Se, trigonal, electronic struct., near metal transition, press. depend. 78—34758
- Se, trigonal, luminesc. identification of indirect transition 80—55189
- Se, trigonal, NMR chem. shift, tight-binding calc. 78—2759
- Se, trigonal and amorphous, Compton profiles 77—32464
- Se, trigonal and amorphous, electronic struct. and nonempirical calc. of struct. props. 80—59866
- Se, X-ray K-shell absorpt. discontinuity 79—61467
- Si, (001) (2×1) reconstructed surface, dimer model self consistent calcs. 80—88613
- Si (111), chemisorption of H$_2$(Cl), conduction-band surface resonance 78—52051
- Si, (111) surface, ang.-resolved photoemission, matrix element effects 79—69957

band structure of crystalline semiconductors and insulators continued
- Si, ab initio self consistent calcs., charge density and band struct., Wannier function scheme 79—69409
- Si, amorphous and cryst., electronic and optic props. 78—39013
- Si, amorphous and cryst. K X-ray spectra of band struct. 79—87525
- Si, atomic wave functions localisation and band struct., LCAO calcs. 77—51648
- Si, Auger line shape L$_{2,3}$ VV, energy band theory 79—43074
- Si, Auger lineshape, one-electron theory for L$_{23}$VV and L$_1$L$_{23}$V 78—72645
- Si, band struct. and valence charge density, self consistent pseudopot. method with Gaussian orbitals 79—90928
- Si, band structure of diamond like crystals, cluster-Bethe lattice model calc. 80—6713
- Si, band structure selfconsistently determined with X$_\alpha$ potentials using MAPW method 79—33227
- Si, band structure under high stress, nonperturbative calc. 78—10344
- Si, band structure using modified Vejkovic, Slavic pseudopot. form factor 79—56121
- P-Si, conductivity and carrier lifetime, high injection effects 80—70719
- Si, defects, divacancy and split 100 interstitial, electronic structure calc. 80—65494
- n-Si, deform. pot. shear const. determ. 77—15763
- Si, determ. from line-shape anal. of electro- and thermo-reflectance spectra 79—24296
- Si, EHT calcs. of energy bands and pressure dependences *(Japanese)* 78—34747
- Si, effective mass from Kramers-Kronig analysis for various doped crysts. 77—31942
- Si, electron energy loss spectra, direct nonvertical interband transitions 77—85856
- Si, electronic and struct. props., nonlocal pseudopot. calc. 80—34349
- Si, electronic energy bands of diamond-type crysts., appl. of EHT method 78—87907
- Si, electronic energy levels strain depend., pseudopot. method 77—39775
- Si, electronic struct., non-spherical local pseudopotential calcs. 80—39496
- Si, electronic struct. from SCF calc. using intersecting spheres model 78—51888
- Si, electronic structure, self consistent local description 80—20067
- Si, electronic structure at high press. near semicond.-metal transition 80—49586
- Si, energy band gap dilation and vibr. contrib. determ. 79—60703
- Si, energy bands and wavefunctions, localised orbital description 78—18942
- Si, exchange and correlation pot., band struct. calc. 78—56068
- n-Si, Faraday rot. temp. depend., effective mass determ. 80—71392
- Si, Faraday rotation and ellipticity, interband transitions, comparison with Ge 77—52048
- Si, field penetration in FIM, band bending 79—87567
- Si, Hartree-Fock eqns. and two-centre approx. validity 77—76726
- Si, heavily doped, bandgap narrowing and diffusion length meas. 79—7781
- Si, heavily doped, characts. of distrib. of density of states 79—15072
- p-Si, heavily doped, intra- and interband Raman scatt. by free carriers 80—108208
- Si, hole mobility temp. depend., valence bandstruct. 77—80771
- Si, IR photoresponse at 1.15 microns, band-gap narrowing effects 79—7864
- Si inversion layer electronic transitions for voltage-tunable far IR emission 77—39962
- Si, Jahn-Teller distorted vacancy, electronic struct. 80—10869
- Si, large unit cell semiempirical mol. orbital approach to props. of solids 79—87036
- Si, lattice energy, pseudopotential calc. 78—23002
- Si, local pseudopotential, Gaussian band charge model 80—88477
- n-Si, many-valley semicond., relative displacement of D$_1$ and D$_2'$ bands under shear deform. influence 79—15080
- Si modulation spectroscopy, two-ray methods *(Russian)* 78—54469
- Si, momentum density, Compton profile 77—20235
- Si, neutral point defect electronic struct., self consistent method 78—91641
- Si, neutral vacancy electronic struct. 77—62865
- Si, nondiagonally screened model potential appl. to band struct. calc. 78—14651
- Si, nonlinear optical susceptibility, tight binding bonding orbital model 80—5784
- Si on sapphire, residual strain effect on elec. props. *(Japanese)* 80—84522
- Si, optical spectroscopy, absorpt. coeff., lattice vibrs. modes, band gap, acoustic approach 77—69822
- Si, optical spectrum, many particle effects, band struct. 80—89024
- Si, p-n junc. solar cell, forward bias capacitance and current meas. for lifetime and band narrowing detn. 79—7892
- Si, photoionisation cross-sections of valence s- and p-electrons *(Ukrainian)* 77—73211
- Si, piezoresistance, energy and momentum relax. of charge carriers 78—47786
- Si polymorphs, optical props., orthogonalized LCAO calc. 78—10345
- Si, pseudopotentials for band struct. and cryst. energy calcs. 79—82514
- p-Si, Raman spectra, pseudopot. calc. of discrete-continuum interference 80—2747
- Si, screening of ions, band struct. calcs. with screening variants 78—67938
- Si, self-consistent pseudopotential *(Japanese)* 77—43491
- Si, semi-empirical APW calc. of band structure 80—84424
- Si, SiO$_2$ electronic energy, structure calc. using tight binding approximation 77—69215
- Si surface, ideal and 2xl chain-reconstructed, electronic struct. determ. 78—52050
- Si surface (100), vicinal plane surface band struct. electron inversion layers, minigaps 78—68062
- Si, technology and physics, review 80—34353
- Si, transverse effective mass of E$_1$ and E$_1$+Δ$_1$ transitions, rel. to band struct. 77—80725
- Si, with non-spherical pots. for two basis atoms, electronic struct. 78—72069
- Si:Ar(B), implantation-doped, energy band struct., variation with depth 79—51983
- Si:O, semi-insulating polycryst. film, cond. through localised and extended states 77—28268

band structure of crystalline semiconductors and insulators continued
- Si:P, impurity cond., hopping conduction and the Coulomb gap 80—44605
- Si:P, polycryst. films, elec. props., EPR, defect states, doping effects 80—75660
- n-Si:P(B), elec. cond. oscills., electron instability effects due to dislocations 80—103704
- Si-SiO_2, electron photoemission from Si, band struct. effects 79—19977
- SiAs, monoclinic OPW calc. 77—59255
- SiAs-Au surface barrier diodes, optical props. of SiAs 79—8145
- SiC (6H), semicond. with one-dimens. electron superlattice, interband optical absorpt. 79—15483
- SiC crystal, energy band struct. and optical spectra 78—18962
- β-SiC, cubic, conduction band minima location and shape determ. 77—85141
- SiC, momentum density, Compton profile 77—20235
- SiC polymorphs, widths of first minibands and effective masses, resist. anisotropy 80—20071
- SiC polytypes, localisation of cond. band minima in Brillouin zone 80—20082
- $Si_{0.5}Ge_{0.5}O_2$, band struct., photoemission spectra calc. and meas. 77—35865
- SiO_2, amorphous and α-cristobalite cryst., band struct., photoelectron and X-ray spectra interpret. 80—24787
- SiO_2, amorphous and cryst., XPS electronic band struct. interpret. 77—16454
- SiO_2, Auger line shapes, final state correlation effects 80—89095
- SiO_2, crystalline and amorphous density of states, bulk electronic struct., tight binding calcs. 80—44502
- SiO_2, electronic energy, structure calc. using tight binding approximation 77—69215
- SiO_2, electronic struct., photoemission spectra calc. 77—35865
- SiO_2, electronic struct., review of spectroscopic and theoretical data 77—76749
- SiO_2, electronic structure, theory 78—95260
- SiO_2, ideal β-cristobalite struct., one-electron energy bands determ. 79—42452
- SiO_2, new interpretation of structure 78—84120
- SiO_2 selections from 1977 Comments on Modern Physics, book 79—30181
- SiO_x, electronic struct., mixed-crystal and random-bonding models 79—65029
- Si(111), conduction-band surface resonance 78—52051
- Sm monochalcogenides, electronic struct., optical props. 0.03 to 12 eV 77—28594
- Sm monochalcogenides, semicond.-metal phase transition 79—47017
- SmB_6, mixed valent semicond., transport props. and electonic struct., review 80—96877
- $Sm_{1-x}Ca_xS$, XPS, electronic struct. excitonic effects, insulator to metal transition 78—43988
- $Sm_{1-x}Gd_xS$, XPS, electronic struct. excitonic effects, insulator to metal transition 78—43988
- $Sm_{1-x}M_xS$, M = transition metal, valence charges, band struct. 80—20131
- $Sm_{1-x}R_x^{3+}S$, (R is rare earth metal), semicond.-metal phase transition 79—47017
- SmS, electronic phase transition, mechanism, trivalent metal impurity effects 80—49604
- SmS, optical props. and electronic struct., Kramers-Kronig model anal. 79—69859
- SmS, semicond. thin film, absorpt. and refl. spectra, fine struct., cond. band extremum 79—69897
- SmSb, forbidden band gap and electrotransfer parameters 80—39497
- $SmSi_2$, valence band struct. *(Russian)* 79—15076
- $Sm_{1-x}Th_xS$, XPS, electronic struct. excitonic effects, insulator to metal transition 78—43988
- $Sm_{1-x}Y_xS$, XPS, electronic struct. excitonic effects, insulator to metal transition 78—43988
- $Sm_{1-x}Yb_xS$, simultaneous Sm^{2+}-Sm^{3+} and Yb^{2+}-Yb^{3+} electron transitions *(Russian)* 79—60711
- Sn (II) compounds, Mossbauer spectra, direct population of solid-state bands 80—15905
- α-Sn, band structure of diamond like crystals, cluster-Bethe lattice model calc. 80—6713
- α-Sn, electronic energy bands of diamond-type crysts., appl. of EHT method 78—87907
- Sn, semicond., pseudopotential method of band struct. anal. 78—51886
- $SnBr_2$, UPS, 40.81 eV, valence band struct. 79—33891
- $SnCl_2$, UPS, 40.81 eV, valence band struct. 79—33891
- SnI_2 band struct., layer model 80—44501
- $Sn_{1-x}Mn_xTe$, electronic struct., transport props., mag. ordering effects 80—65441
- $SnMo_6S_8$, Chevrel phase, mag. interactions, LMTO energy band studies 80—70606
- SnO_2, band struct., tight-binding calc. 80—24796
- SnO_2, electronic struct. and densities of states, tight-binding calcs. 80—15447
- SnO_2, rutile, band gap assignment by two-photon spectroscopy 79—19513
- $Sn_xPb_{1-x}Te$ mixed cryst., cryst. growth and assessment 78—80463
- SnS_2 (2H), band struct. press. depend. 78—43292
- SnS_2, band struct., effect of polytypism 78—43293
- SnS_2, conduction and valence band density of states 77—62817
- SnS_2, octahedrally coordinated, layer cpd., electronic struct. using synchrotron-radiation photoemission spectroscopy 79—74058
- SnS_2, optical props. and band struct. 78—2880
- SnS_2 press. effects on optical absorpt. edge 77—52119
- SnS_2, refl. using Kramers-Kronig anal., optical functions 79—95798
- SnS_2, UV reflectivity meas., band struct., LCAO calcs. 78—72545
- $SnS_2(Se_2)$, electronic struct., tight-binding calcs. 80—15446
- $Sn(S_xSe_{1-x})_2$, valence band states, composition depend., photoemission spectra study 80—100434
- SnSe, electron states anal. by pseudopotential method 77—66115
- SnSe, electronic band struct. determ. 78—51890
- SnSe, orthorhombic, atomic pseudopots. 79—42453
- $SnSe_2$, band struct., angle resolved photoelectron spectra meas. 78—72680
- $SnSe_2$, intercalated with cyclopropylamine, photoelectron spectra study of electronic struct. 78—84698
- $SnSe_2$, optical props. and band struct. 78—2880
- $SnSe_2$, press. effects on optical absorpt. edge 77—52119

band structure of crystalline semiconductors and insulators continued
- $SnSe_2$, refl. using Kramers-Kronig anal., optical functions 79—95798
- $SnSe_2$, single crystal, reflectivity, XPS, UPS, and band struct. 78—6701
- SnTe, bond orbital model of band struct. 80—59853
- SnTe, electron-phonon interactin induced phase transition 79—82338
- SnTe, self-consistent relativistic energy bands 80—10870
- $(SnTe)_{1-x}(PbSe)_x$ films on glass-ceramics, struct. and elec. props. 77—52251
- Sr, monochalcogenides, electronic energy band struct., APW calcs. 80—65439
- SrF_2, band struct. determ. 77—89700
- SrF_2, UPS and XPS spectra, rel. to optical props. 80—66386
- $SrTiO_3$, energy band struct., two-photon absorption spectra study 80—15453
- n-$SrTiO_3$, magnetoresist. meas., band struct. exam. 77—85242
- $SrTiO_3$, non-orthogonal orbitals and recursion method 78—43284
- $SrTiO_3$, semicond., free carrier optical absorption and scatt. *(Korean)* 78—23489
- $SrTiO_3$, UV refl. spectra, optical consts. 0 to 32 eV Kramer-Kronig anal., band struct. calcs. 78—43903
- $SrTiO_3$, XPS, band struct., density of states, photoionisation cross sections, theoretical determ. 78—52629
- TCNQ, ab initio SCF LCAO band struct. calc. 80—70608
- TTF, ab initio SCF LCAO band struct. calc. 80—70608
- TaC, quasi-self-consistent energy band structures using relativistic KKR calcs. chemical bonding 79—51484
- TaN, electronic struct., relativistic energy band struct. calc. 80—34354
- TaN, energy band struct. calc., symmetrised APW method 80—96784
- TaN_x metastable FCC, band struct. calc. 79—33231
- TaS_2, 1T, quasi-octahedral layer compound, band struct. and Fermi surfaces 77—76747
- TaS_2 (1T), generalised electronic suscept. and CDW 77—43471
- 4Hb-TaS_2, Fermi surfaces, charge transfer and charge density waves 78—79926
- $TaSe_2$, 1T, quasi-octahedral layer compound, band struct. and Fermi surface 77—76747
- $TaSe_2$ (1T), generalised electronic suscept. and CDW 77—43471
- $TaSe_2$ (2H), optical absorpt., band struct., plasmons, and CDW 80—45104
- $TaSe_2$(2H), plasmon behaviour at charge density wave onset 80—10900
- TcB_2, electron struct., Fermi energy and surface, bonding 80—20076
- Te (IV) compounds, Mossbauer spectra, direct population of solid-state bands 80—15905
- Te, Compton profile, charge and momentum density 80—55220
- Te, cyclotron reson. in pulsed high mag. fields, cond. band struct. 80—59867
- Te cyclotron resonance, transport and surface phenomena 77—40132
- Te double-beam photoemission, electronic structure 77—66576
- Te, electronic struct. of cryst. phases and hydrostatic press. effects 80—59865
- Te, hole susceptibility anisotropy, spin contrib. and total 77—85413
- Te, intervalence band absorption, press. and defects influence 80—55149
- Te, laser-modulated photoemission expts. 77—28686
- Te, opt. props. under high press., band struct. transform. 80—55112
- Te, optical activity, de Haas-van Alphen oscillations and cond. band parameters 80—54605
- Te, optical activity rel. to band struct., 4 to 300K 77—77165
- Te, oriented films, semiconducting props., Hall coeff., band structure 80—70854
- Te, trigonal, ^{129}I Mossbauer obs. at high press. 80—55005
- Te, trigonal, electronic states, tight-binding model Hamiltonian 77—59250
- Te, trigonal, electronic struct., near metal transition, press. depend. 78—34758
- Te, trigonal, NMR chem. shift, tight-binding calc. 78—2759
- Te, trigonal, self-consistent ground state, X_α calcs. 80—54604
- Te, trigonal and amorphous, electronic struct. and nonempirical calc. of struct. props. 80—59866
- Te, uniaxially stressed, submm. cyclotron reson., deform. pots. and k.p coeffs. 80—54606
- TeO_2, band struct., tight-binding calc. 80—24796
- TeO_2, electronic struct. and densities of states, tight-binding calcs. 80—15447
- ThH_2, electronic struct., photoelectron spectra meas. 77—85143
- Th_4H_{15}, electronic struct., photoelectron spectra meas. 77—85143
- ThN, photoelectron spectra study, core and valence levels 80—66394
- ThO_2, electronic struct. and bonding, molecular cluster approx. 77—51657
- Ti-H, proton spin-lattice relaxation time, band struct. 78—56395
- TiC, band struct. correlation with Ti, APW calc. *(Japanese)* 78—23017
- TiC, electronic struct. and XPS, cluster method and band struct. 79—60710
- TiC, energy schemes 77—39778
- TiC, LCAO band struct., Compton profile 77—85138
- TiC, one-centre exchange pot. superposition 77—15738
- TiC, soft X-ray emission, excitation pot. spectra, excited level binding energy 80—35009
- TiC_x, electron energy spectrum and phys. props. in homogeneous region *(Russian)* 77—31941
- TiC_xN_{1-x}, (O_{1-x}), electronic struct., KKR-ATA method 80—65447
- TiCl, band structure and optical spectra, local field and exchange effects 80—24798
- $TiCl_3$, electronic struct. and struct. phase transition 80—59644
- $TiCl_3$, lattice instability, d-electron-lattice interaction 80—44276
- $TiCl_3$, layer compound, theoretical study of phase transition, energy bonds calc. 79—10945
- TiH_2, electronic density of states and tetragonal distortion, APW calc. 79—37986
- TiN, soft X-ray emission, excitation pot. spectra, excited level binding energy 80—35009
- TiN-CrN system solid solns., electrophys. and galvanomag. props., energy spectra 77—15847
- TiN_xO_{1-x}, electronic struct., KKR-ATA method 80—65447
- TiO, electron struct. calc. 80—49587
- TiO, energy band struct. and density of states *(Russian)* 80—44493
- TiO, Hartree-Fock and local exchange energy bands, disagreement of results 77—76724
- TiO, soft X-ray spectra and XPS, Xα and Hartree-Fock calcs. discrepancies 79—77979
- TiO_{1+x}, conduction band determ. 78—60055

band structure of crystalline semiconductors and insulators continued
TiO_2 (rutile), (001) and (110) surfaces, surface and bulk density of states calcs. 80−49858
TiO_2, cond. and valence band struct., gap anisotropy 77−47729
TiO_2, electronic energy levels, electrorefl. spectra 77−24870
TiO_2, energy band struct., uniaxial stress depend. 80−2334
TiO_2, indirect forbidden transitions, band struct. enhancement 80−44503
TiO_2, rutile, optoelectronic props., band struct., theory 80−80175
TiO_2 single cryst., refl. and electrorefl., energy levels 78−2871
TiO_2, Ti^{4+} XPS, band struct. investig. 79−38707
TiO_2, uniaxial stress depend. of direct-forbidden and indirect-allowed transitions, absorpt. edge obs. 79−42990
TiO_x, X-ray Ti K spectra and band struct. 77−77320
Ti_2O_3, crystal and band struct. calcs. 80−49858
Ti_2O_3, electron structures calc. using models, ESCA and X-ray spectral data 77−35863
Ti_2O_3, electronic structure from single crystal thermoreflectance spectroscopy 79−87420
Ti_2O_3, semicond., effect of stress on elec. resist. 78−34832
Ti_2O_3, XPS, band states 77−20986
Ti_2O_3:V_2O_3, XPS, band states 77−20986
Ti_2O_3:V(Al)(Sc), crystal struct. and metal-metal distance, rel. to electronic struct. 77−47431
Ti_4O_7, semicond.-semicond. transition, lattice gas model 77−1364
$(Ti_2O_3)_{1-x}(V_2O_3)_x$, lattice polarisability, electronic contribs. IR refl. obs. 78−59904
TiP, TiP_2, electronic struct. of valence bands, X-ray spectra and XPS 78−92176
TiS_2, band struct., angle-resolved photoemission studies 80−70610
TiS_2, carrier-lattice coupling 78−63822
TiS_2, electronic struct. and props., self consistent numerical basis set LCAO calc. 77−89698
TiS_2 layer compound, electronic ground state, band struct. calcs. 77−51651
$TiS_2(Se_2)$, core states, energy bands, and valence densities of states 79−95322
$TiS_2(Se_2)$, modelling contrasting semimetallic characters 78−43393
$TiSe_2$ layer compound, electronic ground state, band struct. calcs. 77−51651
$TiSe_2$, structural distortion, band Jahn-Teller type mechanism 77−62875
$TiSe_2$, UPS, excitonic instability indicated from study of band struct. 78−56069
$TiSe_2(S_2)$ (1T), electronic and vibronic struct. 80−44500
$Ti_xV_{1-x}C$, electronic struct. and X-ray emission spectra, cluster MO calc. 80−65444
$Ti_xV_{1-x}Cy$ solid solutions, mag. susceptibility and band struct. 79−51739
$Ti_{1-y}V_yH_x$, electronic props., H alloying effects, book contrib. 79−82522
$(Ti_{1-x}V_x)_2O_3$, semicond. to semimetal electrical transition, lattice parameter changes 79−60714
TlCl, ground-state props., Wannier functions, and electronic struct., ab initio self-consistent calc. 80−80178
TlCl, self-consistent electronic struct. and ground state props. 80−15451
$TlCl_xBr_{1-x}$, $TlBr_xI_{1-x}$, polymorphous mixed cryst. layers, opt. props. 78−23490
$TlGaS_2$, optical and photoelec. props. 77−55571
p-TlInSe, piezoresist. effect 77−35942
$TlInSe_2$, single cryst., elec. cond., photocond. and IR spectra absorpt. spectrum 79−47097
TlTe, empty lattice band struct. *(Japanese)* 77−51660
U chalcogenides, electronic struct., relativistic single-site scatt. model 79−87040
U compounds, NaCl struct. type, relativistic energy bands, LMTO calcs. 80−65442
U pnictides, electronic struct., relativistic single-site scatt. model 79−87040
UC, partially filled f bands, configurational and relativistic effect sensitivity 79−78002
UC, quasi-self-consistent energy band structures using relativistic KKR calcs. chemical bonding 79−51484
$UC_{1-x}N_x$, NMR of ^{13}C and ^{15}N, 5f electrons nature, mag. susceptibility, spin fluctuations 77−20736
UF_5, electronic struct. calc. 80−6716
UN, band struct., SAPW calcs. 78−26810
UN, band struct. and density and states, PES meas. 79−42454
UN, density of states calc. 80−6715
UN, electronic struct., relativistic energy band struct. calc. 80−34354
UN, photoelectron spectra study, core and valence levels 80−66394
UO_2 and U_4O_9 single crysts., optical props. rel. to chem. bonding 77−28598
UO_2, electronic distributions by X-ray spectroscopy 80−97407
UO_2, electronic struct. and bonding, molecular cluster approx. 77−51657
UO_2, electronic struct. contribs. to excess enthalpy at 3000K and in liq. phase 80−15265
UO_2, electronic transitions, crystal field effects and phonons, phase transition 80−97303
UO_2, photoelectron spectra study, core and valence levels 80−66394
UO_2, U_2O_5, U_3O_8, and UO_3, bonding and valence obs. by ESCA and EPR 77−28696
UO_2, U_3O_8, U_2O_5, shake-up satellites and band struct. 77−55861
$(UO_8)^{12-}$, electronic struct., variational Xalpha cluster calc. 80−39499
$U_xPu_{1-x}O_2$, theoretical study of electronic thermodynamic and valence props. 79−37655
US, band struct., SAPW calcs. 78−26810
US, band struct. and density and states, PES meas. 79−42454
US, density of states calc. 80−6715
US, electronic struct. calc. 78−91615
US, NaCl struct., band struct. 80−6714
US, optical props. and electronic struct. 80−25410
US(Se)(Te), electronic struct. and exchange band splitting, optical refl. meas. 80−66226
US(Se)(Te), photoelectron energy distrib. and spin polarisation, electronic and mag. props. 80−16146
US(Se)(Te), spin polarisation and magnetism, photoelectron study 80−40219
USb, reflectivity spectrum, band struct. 80−7368
USb, UPS and XPS, surface oxidation 80−7465
UTe, electronic and spin struct. negative spin polarisation of photoelectrons 79−19514
UTe_xSb_{1-x}, photoemission energy distrib. curve and density of states 79−52074

band structure of crystalline semiconductors and insulators continued
$U_xTh_{1-x}As$ (Sb), electronic struct., relativistic KKR-averaged T-matrix approx. method 80−107702
$(UX_6)^{n-}$, X=N,O,S, electronic struct., variational Xalpha cluster calc. 80−39499
VC, energy band struct., chem. bonding 78−18958
VC, energy schemes 77−39778
VC, soft X-ray emission, excitation pot. spectra, excited level binding energy 80−35009
VC_x electron band struct. and X-ray spectra *(Ukrainian)* 79−51482
VCl_3, electronic struct. and struct. phase transition 80−59644
$VD_{0.77}$, Compton profile, electronic struct. *(German)* 78−92140
$VH_{0.71}$, Compton profile, electronic struct. *(German)* 78−92140
VH_x, electronic props., H alloying effects, book contrib. 79−82522
VN, soft X-ray emission, excitation pot. spectra, excited level binding energy 80−35009
VN-CrN system solid solns., electrophys. and galvanomag. props. 77−24567
VO, energy band spectrum, APW and Green's function method calcs. 79−7783
VO, energy band struct. and density of states *(Russian)* 80−44493
VO, octahedral clusters, electronic struct., $X\alpha$ discrete variation and SW methods 78−63976
VO_2 clusters in metallic and semiconductor phases, electronic struct., $X\alpha$ calcs. 78−63977
VO_2, metal-insulator transition and electronic struct., ion bombard. effects 80−92948
VO_2, nonstoichiometry influence on electron struct. and metal-insulator phase transition 80−44507
V_2O_3, electron structures calc. using models, ESCA and X-ray spectral data 77−35863
V_2O_5 and lower oxides, electronic, optical, structural and surface props., review 80−88120
V_2O_5, energy band structure, tight-binding method 80−70602
V_2O_5, energy band structure, bonding props., projected density of states anal. 80−70603
V_2O_5-Si, sandwich system, photocond. in range 380-1000 nm 77−32034
V_3O_5, high-temp. phase transition, resistivity, valence photoelectron spectra 80−49357
V_nO_{2n-1} Magneli phases, elec. and mag. props. 79−37990
$VS_2(SE_2)$ (1T), electronic struct. using nonspherical cryst. pot. 80−44498
VSe_2, 1T, band struct. calc. 79−95324
VSe_2, 1T, quasi-octahedral layer compound, band struct. and Fermi surface 77−76747
V_3Si, electronic struct., charge distrib. and X-ray emission spectra 79−51481
$V_xTi_{1-x}S_2$, elec. and mag. props. 79−65504
WO_2, optical conductivities and dielec. functions in 0.2-6 eV range, rel. to band struct. 79−42938
WO_3, optical props. 79−38515
WO_3:H^+, optical and elec. props., suggested band struct. model 77−4654
Xe crystal, photoelectron spectroscopy, hole-electron valence bound state 77−36369
Xe film, electron MFP, vacuum UV photoemission data 77−28690
Xe, single crystal, photoemission exam. 79−78845
Xe-Ar system, band formation exam. by photoelectron spectroscopy 77−66116
Y silicides, valence band struct. *(Russian)* 79−15076
YH_2, electronic struct., optical studies, 0.2-5 eV, 4.2-340K 79−78005
YH_2, electronic struct., band theory 79−78006
YH_2, electronic struct., photoelectron spectra study 80−50527
YH_2, self-consistent energy bands, KKR method with Hedin-Lundqvist approx. 80−49593
YH_2, synchrotron XPS obs., rel. to theory for metal dihydrides 80−55275
YIG, thermoreflectance spectra 80−20616
Y_2O_3, fundamental absorpt. 79−8161
Y_2O_3, photoabsorpt. spectra, at ionisation, band struct. mechanisms, electron energy loss investig. 77−24909
YOF, band structure formation, valence band 79−33232
YOF, electronic stuct. calcs. from XPS and X-ray emission spectra 80−35056
YS, band struct. and X-ray emission spectra, APW and $X\alpha$ calc. 80−70605
YS, electronic instability and phonon softening, APW calc. 80−29323
YbSb, forbidden band gap and electrotransfer parameters 80−39497
Z+C, band struct. correlation with Zr, APW calc. *(Japanese)* 78−23017
ZnCdS:(Cu+Ag) binder layer for electrophotography 80−4797
$Zn_xCd_{1-x}S$ monocrystal, optical and nonlinear optical characts. *(Russian)* 79−98442
$Zn_xCd_{1-x}S$, reflectivity spectrum, excitons and energy band struct. 77−55804
$Zn_xCd_{1-x}Se$, vacuum condensates, forbidden band width determ. from transmission spectra 77−8670
$Zn_xCd_{1-x}Te$, reflection spectra, energy band struct. comp. depend. *(Russian)* 78−56500
ZnF_2, electronic structure of outermost levels, UPS study 80−7468
$Zn_xFe_{3-x}O_4$, collective electron states, ^{57}Fe Mossbauer meas. 77−69748
$ZnGa_2S_4$, band struct., pseudopot. method 80−92816
$ZnGeAs_2$, photoelectron spin polarisations, electron level struct. 79−87557
$Zn_xHg_{1-x}Se$, band struct. and scattering mechanism, determ. from transport coeffs. 77−59254
$Zn_xHg_{1-x}Se$, band struct. from Shubnikov de Haas effect and hydrostatic press. meas. 80−49599
$Zn_xHg_{1-x}Se$, galvanomagnetic effects, Shubnikov-de Haas oscill. determ. of band struct. 80−6884
$ZnIn_2S_4$, cond. and valence band states, photoemission study 80−35054
$ZnIn_2S_4$, fund. reflectivity, 2 to 6 eV, band struct. implications 78−39574
$ZnIn_2Se_4$ defect tetrahedral crystal, pseudopotential scheme 77−11850
$ZnIn_2Te_4$ defect tetrahedral crystal, pseudopotential scheme 77−11850
ZnO on Zn (0001), oxide film growth, at. and electronic struct. 78−15587
ZnO-CdSe thin film n-n heterojunctions, prep. elec. and optical props. *(Korean)* 77−28244
ZnP, Zn_3P_2, electronic struct. of valence bands, X-ray spectra and XPS 78−92176

band structure of crystalline semiconductors and insulators continued
Zn_3P_2, absorption edge meas. 78—80380
Zn_3P_2, direct and indirect optical transitions, metal-Zn_3P_2 contact photovoltage response 80—25402
Zn_3P_2, single crystal, growth, electronic and device props. 80—25551
ZnS bulk and surface states anal. using synchrotron radiation 77—66574
ZnS, elec. struct., piezoelec. consts. *(Chinese)* 79—56122
ZnS, self energy effects of valence and conduction electrons 79—37980
ZnSb, band struct. calc. 78—39015
ZnSe, band-edge photoluminesc., far-below band-gap excitation 80—76063
ZnSe, bulk and surface states anal. using synchrotron radiation 77—66574
ZnSe, electronic structure, self consistent local description 80—20067
ZnSe, polar semicond., radiative recomb., electron-phonon interaction effects, calc. 80—49631
ZnSe, self-consistent localised electronic struct. 79—42445
$ZnSiAs_2$, photoelectron spin polarisations, electron level struct. 79—87557
$ZnSiP_2$, band struct. calc., empirical pseudopotential method 77—1362
$ZnSiP_2$, pseudodirect chalcopyrite semicond., electronic band struct. 80—20079
$ZnSiP_2$-In Schottky diode, photovoltaic spectra 80—2423
$ZnSnAs_2(P_2)$ single crysts., refl. spectra, band struct., dielec. consts. 77—44022
ZnTe, band parameters from bound exciton, donor-acceptor pair excitation luminescence 78—92111
ZnTe, bulk and surface states anal. using synchrotron radiation 77—66574
ZnTe films, internal stress effect on fund. refl. spectra 80—60701
ZnTe(Se), optical circular polarisation correl. in secondary radiation, resonant light excitation 77—69885
Zr compounds, X-ray K-absorpt. spectra 78—76558
ZrBr(Cl), electronic struct., self-consistent and non-self-consistent band calcs. 80—44499
ZrC, electronic struct. and XPS, cluster method and band struct. 79—60710
ZrO_2 films on Zr alloys, exoelectronic emission props. and energy-band parameters 79—91571
ZrS, electronic struct., bonding effects, photoelectron spectroscopic and low temp. heat capacity cal. 80—96780
ZrS_2 layer compound, electronic ground state, band struct. calcs. 77—51651
$ZrS_2(Se_2)$, core states, energy bands, and valence densities of states 79—95322
$ZrSe_3$, electronic props, variation with struct. 79—42438
ZrSi and $ZrSi_2$, ultrasoft X-ray emission bands, empirical band schemes 78—15249

band structure of semimetals
degenerate, quantum theory of transverse galvanomag. phenomena, model of two standard bands *(Russian)* 77—62945
doped, one-particle interband transition, effect on Curie temp. 79—7994
film, quantised, in high mag. field, thermodynamics of electrons *(Russian)* 79—56341
graphite, magnetoreflectivity in high fields under press., energy band parameters 79—61346
group V semimetals, cryst. binding and band struct. 80—24791
two-dimensional, electron-hole rearrangements in high mag. fields 79—87028
As, band structure on Jones zone boundary, pseudopot. calc. 80—54603
As, electrical resist., thermal cond. and thermopower, low temp. transport props. 80—49708
As, interband, magnetorefl. for circularly polarised radiation 78—2840
As, magnetoreflection of circularly polarised IR radiation, band struct. 77—52094
As, orthorhombic and rhombohedral, comparison of electronic band struct. 78—23016
As, pseudopotential, self-consistent, band struct. 78—84141
As, rhombohedral, electronic struct. and optical props. var. with internal displacement parameter 79—60702
Bi, acoustic waves, giant quantum attenuation at high mag. fields, angular depend. *(Japanese)* 79—4585
Bi, band structure model parameters, deformation theory *(Russian)* 78—56067
Bi, Bi-Pb and Bi-Sn, elec. cond. and thermal EMF at press. up to 12 kbar 77—47806
Bi, electrical resist., thermal cond. and thermopower, low temp. transport props. 80—49708
Bi, empirical pseudopot., temp. and press. depend. 78—18955
Bi, energy spectrum changes under strong uniaxial compression, Shubnikov-de Haas effect 77—28098
Bi, energy spectrum variation under strong uniaxial tension 79—73432
Bi film, quantum size effect and band struct. Bi-dielec.-metal system obs. 80—54811
Bi, giant quantum attenuation of sound, anomalous temp. depend. 77—76728
Bi, intravalley electron-phonon scatt. non parabolicity, thermoelectric power 79—99539
Bi, longitudinal magnetoacoustic effects on energy bands 77—28095
Bi, magnetoreflectance, L-pt. band parameters 80—25344
Bi, magnetoreflection of circularly polarised IR radiation, band struct. 77—52094
Bi, magnetoreflectivity in high fields under press., energy band parameters 79—61346
Bi, magnetoresistance, high temp. oscills., props. *(Russian)* 80—65606
Bi, review of electronic props. 77—15742
Bi, superconducting transition temp., two-band model 80—25034
Bi:Sb, semimetallic alloy, microwave spectroscopy 78—87908
Bi-Sb, magnetic susceptibility, 4.2 to 270K, field and band parameter depend. 77—36051
Bi-Sb, semimetallic alloy, cyclotron reson. and quantum oscillations 77—28096
Bi-Sb alloy film, rel. to amorphous nature, AC and DC cond. and Hall coeff. obs. 80—11114
Bi(-Sn), hydrostatic press. effect on band struct., thermoelec. power meas. 79—69406
BiSb, alloys, semimetallic, camera, dispersion relations 80—59854
$CsSnBI_3$, electronic struct., XPES and band theory calc. semimetallic behaviour 79—78837

band structure of semimetals continued
$CsSnCl_3$, electronic struct., XPES and band theory calc. semimetallic behaviour 79—78837
EuB_6, ferromag., spin-polarised energy band struct., APW calc. 80—96779
EuB_6, pure single crystals, magnetic and electric props. 80—11260
$Hg_{1-x}Cd_xTe$, optical absorpt., quasilocal acceptor level effects, theory 80—92853
$Hg_{1-x}Cd_xTe$, quasi-local acceptor levels and electron mobility 78—67974
$Hg_{a-x}Cd_xTe$, single-LO-phonon and -plasmon recombination channels narrow-bandgaps 78—91728
LiAl, transport props., rel. to semimetallic band struct. 80—88581
$NbSe_3$ and related cpds. bands, bonds and charge density waves 79—95327
$NbSe_3$, chemical bonding and dimensionality 78—75992
PbPo, electronic struct., relativistic band struct. calc. 79—4510
Sb, electrical resist., thermal cond. and thermopower, low temp. transport props. 80—49708
Sb, electronic band struct. changes due to plane straining effects *(Russian)* 80—54602
Sb, electronic structure change with press., pseudopot. calcs. *(Russian)* 79—47006
Sb, energy spectrum variation under strong uniaxial tension 79—73432
Sb, magnetoreflection of circularly polarised IR radiation, band struct. 77—52094
Sb, partial Fermi levels of electrons and holes, press. depend. 77—43490
$TiSe_2$, band struct., angle-resolved photoemission studies 80—70610
$TiSe_2$, carrier-lattice coupling 78—63822
$TiSe_2$, semimetal, electronic props., superlattice form. 77—15532
$TiSe_2$, semimetallic behaviour band struct. from local-density functional approach 78—56070
$TiSe_2$, UPS, excitonic instability indicated from study of band struct. 78—56069

band theory models and calculation methods
see also APW calculations; band model of magnetism; band structure; cellular method; free-electron approximation; Hubbard model; KKR calculations; k.p calculations; Kronig-Penney model; muffin-tin potential; nearly-free-electron approximation; OPW calculations; pseudopotential methods; relativistic band structure calculations; tight-binding calculations
A-15 compounds, X-point model for mag. susceptibility 78—23014
adsorption, surface band theory and surface transport props. 77—43680
alloy, concentrated, electrical resist. and Hall coefficient, temp. depend. 78—39093
alloy, disordered, energy band struct. and elec. cond., effect of short-range order 80—10860
alloys, binary with long and short range order, electron energy spectrum calcs. *(Russian)* 79—99471
alloys, disordered, charge density function calculation method 79—42433
alloys, short-range order, electronic theory using pseudopot. approx., review 79—47004
amorphous compound semiconductor, thermoelectric power and transport models 78—10482
amorphous covalent semiconductor, random two-band Weaire model, localisation theory 77—15788
amorphous solid, two-band model, Thorpe-Weaire type, localisation near band edges 78—23050
aperiodic materials, recursion method 78—34739
binary disordered alloy with long range order, elec. cond., single band model 77—28154
binary semiconductors, general model pseudopot. 77—62800
Bloch Hamiltonian one-dimens. bands by fibres 77—31934
Bloch wave packet group vel., in external field, reciprocal mass tensor 77—35843
Bloch wavepackets, instantaneous velocity 78—18937
Bloch waves, Lame eqn. interpretation 80—39489
bounded crystal, dispersion law for electrons, Tamm sub-bands *(Russian)* 77—43468
Brillouin scattering, resonant, analogy to modulation spectroscopy *(Japanese)* 78—68526
Cain model, two-band, dispersion and iso-energy surfaces of valence and conduction bands *(Russian)* 80—24783
canonical method for one electron energy states, closely packed cryst. 77—72811
chalcogenide glass, optical transitions and electronic struct., review 77—76741
charge ordered crystals, mag. props., energy spectrum, triplet excitations 78—18979
Cohen model, approx. to electron spectrum in Bi 77—15742
continued fraction approach, numerical determ. of 1-D band struct. 80—6694
Coulombic interaction summation in Gaussian basis 80—70575
covalent semiconductor, valence band calc. using many-electron theory 80—15434
cubic crystal electronic energy band calc. by LCGO method, FORTRAN IV program 78—75977
cubic crystals, non-Bloch electron states determ. 77—1352
cubic crysts., perfect, nonBloch electron state density 80—75487
deep impurities, large unit cell approach 78—23046
Density-functional pseudopotential approach to crystal phase stability and electronic structure 78—72058
diagonal vertex approx. for Gaussian random systems 78—23003
dielectric spheres, three dimensional lattice model, photon energy band, low energy photon diffr. 79—78795
disordered binary substitutional alloys, elec. cond., two band model 78—14699
disordered system electron energy system, calc. methods 80—75485
EHT calcs. of energy bands and pressure dependences of Si, Ge, GaAs, GaP *(Japanese)* 78—34747
electron state density calcs. by linearly analytical tetrahedron method *(Russian)* 79—82507
electrons in disordered metals and at metallic surfaces, conf., Ghent, Belgium (Sept. 1978) 80—41946
elemental semiconductors, model pseudopotential, band struct. calcs., liquid semicond. resistivity calcs. 80—20075
empirical parametrisation of electronic structure 78—91585
energy bands, low-lying, Mathieu and Kronig-Penney potentials comparisons 80—70583
exchange potential construction by superposition of effective one-centre exchange pots. 77—15738

band theory models and calculation methods continued
- FCC clusters, size and shape depend., tight binding approximation 78—79920
- Fermi integral calculation by complex var. procedure *(Russian)* 77—69206
- Fermi level, density of states, normal systems 78—23004
- Fermi surface, cubic harmonics product representation 77—13588
- Fermi-Dirac integral $\mathcal{I}_{1/2}(\eta)$ approx. 78—22997
- ferromagnetism, band model, pseudodipolar theory of magneto crystalline anisotropy 77—36068
- film, crystalline, band theory of size-quantised electron states 78—75976
- Fourier method, symmetrized for interpolating band-structure results 79—73419
- generalised tridiagonal Hamiltonian resolvent matrix, exact soln., appl. to semicond. surface 80—29307
- graphite, pressure-depend. conducting calcs. using band model 77—28171
- Hartree-Fock equations with localised set of basis functions, two-centre approx. 77—76726
- HEED, branch points, critical voltage effect, band theory models 78—1961
- heterojunction superlattice, energy spectrum 78—6259
- holes, in degenerate bands, variational principle for Landau levels, const. mag. field 79—33219
- hybridised conduction band, intrinsic upper limit of electron-phonon coupling *(Chinese)* 80—54589
- hybridized energy bands, effect on field emission from transition metals 77—77349
- integral characteristics of the electron structure of crystalline surfaces 78—64078
- interface plasmons, longitudinal optical phonons, multilayer struct. 78—19118
- intermediate valence, theory, electronic sp. ht. calc. 80—79956
- ionic crystals, large unit cell calc. of band struct., Mulliken-Ruedenberg approx. 78—39003
- ionicity, Pauling's and Phillips' comparison by empirical LCAO band theory 78—51464
- Kane model, three-band, Auger recombination overlap integrals, kp approx. *(Russian)* 78—87897
- KKR-CPA equations, numerical soln., appl. to band theory of disordered alloys 80—44474
- large unit cell semiempirical mol. orbital approach to props. of solids, Si and diamond appl. 79—87036
- large unit cell semiempirical mol. orbital approach to props. of solids, LiF and KCl appl. 79—87037
- layer materials, SXAPS interpret., cond. band self-convolution model, cryst. field splitting 78—23558
- LCAO method, optimised version appl. to Cu 79—33220
- LCAO Slater-type orbital band structure calcs., computable expressions, derivation 80—24776
- LCBO, pseudobinary semiconductors energy band calc., compositional disorder effect determ. 79—42442
- linear Brillouin zone integration method, generalised susceptibility calcs. 80—88462
- local potential problems, improved Pauli Hamiltonian 79—19499
- magnetic semiconductors, conference, Montpellier, France (Sept. 79) 80—94916
- many-neighbour approximation, energy bands of sp-hybrid crystals 77—35846
- metal, lattice stability, perturbation formalism for comparison of crysts. with different lattices 77—51631
- metal, new method for solving Boltzmann equation for electron 78—72127
- metal-insulator transition in disordered system, two band model 77—51662
- metallic alloy, random, first principles band theory, review 80—44473
- metals, electron theory and cond. props., contrib. of Sir Rudolf Peierls, 1928-1935 80—57054
- molecular crystals, compositional disorder, approx. band struct., self consistent virtual crystal approx. 80—39486
- molecular crystals, electronic excitation energy transfer, external elec. field effect 80—84431
- muffin tin orbital method for surface and films 78—95331
- multiple scattering eqn. for bond theory with general non muffin-tin potentials 79—95309
- multipole wave functions, singular points in band struct. and Wannier function tails, Cu cond. band appl. 79—37956
- multipole wave functions for photoelectrons, constant-energy-surface harmonics, Cu s-d band appl. 79—37955
- narrow-gap semiconductors, energy spectrum, three band model 77—89699
- one dimensional polymers, compositional disorder, approx. band struct., self consistent virtual crystal approx. 80—39486
- one-dimensional band calculations using perturbation theory 80—44460
- one-electron approximation, effect of correls. and defects 78—63960
- operator recursion analysis, electronic struct. determ. 78—14644
- parametrised, separable potential for band structure calculations 78—79912
- partially filled s band, strong intraatomic interaction 79—28271
- periodic function integration over Brillouin zone 78—6251
- periodic function integration over Brillouin zone 78—6252
- phase shift changes effect, sensitivity factor 77—72810
- photoelectrons in crystals, scatt. by impurity centre, multipole wavefunctions 79—42490
- polyacetylene:$ASF_5(AsF_6)(SbF_6)(PF_6)$, metallic, band theory 80—49570
- polydiacetylene, extended chains with realistic model side groups, self-consistent electronic band structs. 77—39776
- polydiacetylene polymer crystals, optical nonlinearities, chain pairing effects, one dimens. band model 77—69851
- polymer, band structure calc. using symm. considerations and line groups 77—51636
- polymer, conjugated and saturated chain, electronic struct., review 80—59860
- polymers, fragment method, nonempirical, electronic struct. determ. 77—89684
- pseudopotentials from self-consistent atomic calcs., appl. to band struct. determ. 80—59846
- recursion method and non-orthogonal orbitals 78—43284
- relativistic Green function 77—20214
- rigorous cellular method, appl. to graphite 77—15762
- s-d electron model, finite temp. diagram technique, perturbation theory 78—67932

band theory models and calculation methods continued
- semiconductor, electronic polarizability as function of Penn gap 80—49638
- semiconductor, energy spectrum restructuring and light absorption in intense EM field 79—56111
- semiconductor, Falicov-Kimball model, intermediate valence states, metal-insulator transition 78—51897
- semiconductor, impurity band props. 79—23888
- semiconductor, short range impurities in two band model 78—34803
- semiconductor, two-band model, appl. to double reson. in two-phonon Raman scatt. by longitudinal optical phonons 77—24852
- semiconductor, zero gap, collisionless, anomalous Hall effect 79—23988
- semiconductor, zincblende-type, valence band effective mass strain depend. 78—51880
- semiconductor heterojunction, interface states, two-band-narrow gap approximation 79—24059
- semiconductors, polycrystalline, electrical conductivity theories *(Czech)* 79—42537
- semiconductors, temp. depend. electronic cond. 80—59975
- Slater-Koster integrals, general expressions in two-centre approx. 80—70585
- solid, linear combination of Gaussian orbital basis sets 78—6258
- solid, orthogonalised augmented plane wave method, appl. to ZnS 77—66105
- solid state physics, 1933-40, contrib. of Sir Nevill Mott 80—57055
- solid state physics, contrib. of Conyers Herring in 1930s 80—57056
- solids, self-consistent mixed-basis approach to electronic struct., appl. to Nb, Pd 79—69394
- sphalerite-type crystals, effect of effective charges on X_5^v and L_3^v 77—35847
- spin depend. wave functions and band parameters 77—72818
- superconducting ground state of quasi-orbital electrons 78—39252
- surface electronic wave functions in semi-infinite, muffin-tin lattice, spherical-wave method 79—42603
- surface properties, two dimens. Brillouin zone and Wigner-Seitz cell integrations, special point formulae generation 80—70783
- symmetry projection technique, for linear combination of muffin-tin orbitals method 78—2407
- p-Te, impact ionization rate of holes at 77K 80—10993
- tetrahedron method for evaluating spectral props. of solids 80—10855
- theta function-modulated plane wave appl. to band theory models 77—39763
- theta-function modulated plane-wave bases, reciprocal relations 77—85130
- thin disordered film, electronic energy spectrum calcs. extended Halpern Green's function technique 80—20066
- transition metal, one-electron theory, atomic sphere approx. to KKR and LMTO methods 78—91584
- transition metal alloys, Wolff model of origin of localised mag. moments 79—61049
- transition metal compounds, band struct. calc. 78—18956
- transition metal cpds., electronic spectrum calc. by GO-LCAO method *(Russian)* 79—73420
- transition metal monoantimonides, electronic struct. determ. 77—4290
- transition metals, 3d-, 4d-, 5d-, band struct. from spectral data and theoret. calcs. *(Russian)* 77—8013
- transition metals, double d-band model, delocalisation of electrons 77—76743
- TTF-TCNQ, two-chain inverted band model 78—6313
- TTT_2I_3, charge transfer salt, Coulomb effects 79—28308
- tunnelling in crystal for arbitrary band widths ratio *(Russian)* 78—14650
- two-band alloy, Green's function from multiband theory 79—37952
- two-band alloy model, self-consistent cluster Bethe lattice study 80—29303
- two-phonon transitions, phonon assisted, in mag. field, four-band model 77—36260
- variational cellular method, electronic struct. calcs. 80—54591
- wave functions, symm. transformation, computer programs, symmetrisation procedure 78—10315
- Ag-Au, order-disorder transforms., s-band model 79—60502
- Bi, band structure model parameters, deformation theory *(Russian)* 78—56067
- Bi, energy band model, resolution of theoretical discrepancy 77—11849
- Bi, energy band model for electrons 77—35849
- Bi-type crystal, deformation model of carrier spectrum, holes 79—60680
- CrAs, high press. paramag. antiferromag. transitions, elec. props., band model development *(Russian)* 80—60277
- Cu, Brillouin zone integration special directions, electronic density of states calcs. application 80—49569
- Cu-Ag, order-disorder transforms., s-band model 79—60502
- Cu_3Au and $CuAu_3$, band theory of order-disorder transforms. 79—60501
- Fe, itinerant model of spin polarised field emission 78—95685
- GaAs, k-linear coupling, E_1' transitions 78—91583
- GdM_x, M=3d transition metal, hyperfine interactions 78—19401
- Ge, valence band effective mass strain depend. 78—51880
- GeTe, bond orbital model of band struct. 80—59853
- $Hg_{1-x}Cd_xTe$, mixed crysts., band struct. and optical transitions, distorted atomic orbitals 77—69224
- HgSe(Te), dynamic dielectric function, IR absorpt. meas. 78—68508
- InSb-type semiconductor, spatial dispersion of permittivity 78—67967
- Mo_cNb_{1-c}, is the rigid-band model valid? 78—95258
- Nb, $NbH_{0.76}$, rigid band treatment of Compton profile anisotropies 77—73182
- $Nd_2(WO_4)_3$, elec. transport and mag. props. meas. 77—24668
- Ni and Ni alloys, tunnel currents, spin polarisation, simple band theory interpretation 79—78451
- $NiWO_4$, AC elec. conductivity, thermoelec. power and dielec. const. 80—70736
- Pb chalcogenides, interband absorpt., optical absorpt. coeff., two- and six-band models 79—33728
- PbS(Se)(Te), bond orbital model of band struct. 80—59853
- PbTe, electronic struct. near band gap 77—69226
- Pd, dielec. screening and phonon frequencies using isotropic noninteracting s-d-band model 79—19343
- Pd, Fermi surface, extremal cross section, press. derivative, band struct. calc., LMTO method 79—11055
- Pt, dielec. screening and phonon frequencies using isotropic noninteracting s-d-band model 79—19343
- ScM, (M=Ru,Rh,Pd,Ag), electronic struct., self-consistent local density functional calcs., LMTO method 79—11059

band theory models and calculation methods continued
  Si, nondiagonally screened model potential appl. to band struct. calc. 78—14651
  Si:H, amorphous, electronic states of hydrogenated Si, theory 79—42494
  SiC polytypes, electrolum. in anodic oxidation, band model *(Russian)* 80—50429
  SnTe, bond orbital model of band struct. 80—59853
  TiCl, band structure and optical spectra, local field and exchange effects 80—24798
  $TiSe_2$, structural distortion, band Jahn-Teller type mechanism 77—62875
  $(Ti_{1-x}V_x)_2O_3$ solid soln., struct. changes comp. depend. 77—55275
  UO_2, localised versus itinerant 5f electrons exam., reflectivity meas. 79—19905
  USb, localised versus itinerant 5f electrons exam., reflectivity meas. 79—19905
  V, dielec. screening and phonon frequencies using isotropic noninteracting s-d-band model 79—19343
  ZnS photocells, thickness depend. of interband transition photovoltaic voltage and short circuit photocurrent 77—76871
bands (kink) *see kink bands*
bandwidth compression
  see also vocoders
  ADPCM and ADM, and speech digitization *(Korean)* 79—55273
  effect on military target observers' detection and recognition performance 80—106484
  frequency variant optical signal processing 77—71934
  frequency-variant signal waveform processing using 2-D optical processors 80—48178
  hearing aids, limitations of voiced portion of speech 79—29668
  image bandwidth compression, scene analysis algorithms and rule-based controller 80—95819
  LANDSAT multispectral sensor image adaptive coding techniques 78—45060
  low bit-rate robust vocoder with special envelope estimator and pitch estimator 79—59883
  narrowband linear predictive coding speech transmission over noisy channels, vocoder 79—55276
  optical image anal. and digital simulation 78—94373
  phased array US imaging delay line bandwidth reduction 79—50552
  Pioneer Venus occultation expt., bandwidth reduction for radio science data generation 80—67492
  polystyrene, compressed, TEM obs. of coarse shear bands 79—70117
  quantiser algorithm for real-time block quantising 79—64449
  Raman laser, CW fibre, bandwidth reduction using prisms, gratings and etalons 80—53366
  SAW pulse compression filter using reflective dot array 77—75749
  SAW/CCD hybrid signal processor 79—32163
  SPAC speech processing system using autocorrelation function, operation and characts. 79—68510
  speech compression system with vector quantizing, two-step 79—59881
  speech digitisation and bandwidth compression techniques, ADPCM and ADM *(Korean)* 79—59876
  speech intelligibility improvement for ski-slope hearing impaired person, signal processing 77—11091
  speech signals, time-domain algorithms for harmonic bandwidth compression 79—46125
  underwater acoustic transducers, bandwidth extension by FM signal correl. methods 77—62086
  vector ECG meas., bandwidth limitation effects 78—36001
  He speech, translation via segmentation, partial-rejection and expansion 78—31823
bang-bang control
  see also on-off control
  nuclear reactor, Xe spatial oscillation, time optimal control 80—32320
  sounding rocket attitude stabilisation H_2O_2 jet system *(Japanese)* 78—28482
  sounding rocket three-axis attitude control system *(Japanese)* 78—24422
Bardeen-Cooper-Schrieffer theory *see BCS theory*
BARITT diodes
  minority and majority mobilities, transit time effects determ. 78—14753
  p^+np^+ diode below reach through, current voltage characteristics 79—56292
  Schottky BARITT devices, boundary conditions, RF performance 80—49955
barium
  see also nuclei with ......
  abundance determ. in stony meteorites 78—65557
  abundance in Ap and Am stars 77—33505
  adsorbed layer on Mo (011), surface diffusion *(Russian)* 80—6658
  adsorbed layers on W, Auger and work function meas., impregnated W cathode model 79—43073
  adsorbed on 4d or 5d metal, work function, O_2 coadsorpt. effects, thermionic emission obs. 78—11064
  adsorbed on Ir (111), thermionic emission obs. 77—85881
  adsorption, on (110), (121) and (111) faces of W 80—100411
  adsorption on ZnO, effect on low-energy cathodolum. 78—60522
  Atlantic Ocean Ba profiles, GEOSECS expedition 77—81918
  atom, $4d^{10}$ shell, photoionisation cross sections, electron shell alterations determ. *(Russian)* 80—58144
  atom, $4d^{10}$ subshell photoionisation cross section, electron shell rearrangement 77—14400
  atom, 4d subshell spectra, strong interaction regime 79—18165
  atom, $5d6p\,^1F_3$-state lifetime meas. 79—89633
  atom, $(5d6p)\,^3D_3$ state, lifetime meas. by dye laser spectrosc. 80—78577
  atom, $(5d\,^3D_J)$state, quenching obs. 80—52926
  atom, $(6p_J20s_{1/2})_J$ state, autoionisation, ejected electron energy anal. 80—43009
  atom, at. beam mag. reson., ^{135,137}Ba HFS, of 6s5d configs. 79—49971
  atom, Auger spectra, strong correl. in 4d-spectrum 78—50522
  atom, autoionis. spectrum, pair splittings 79—13684
  atom, autoionisation and Auger decay, collective excitation effect 80—43008
  atom, Ba I, absorption spectrum, 1560 to 1770 Å 78—66487
  atom, bound odd-parity $J=1$ spectra, multiphoton excitation 79—54795
  atom, diamag. quasi-Landau spectrum near ionis. threshold, two-photon ionis. spectra obs. 78—58642
  atom, diamagnetic Zeeman effect, 20-40 kG, induced config. mixing 78—17608
  atom, double ionisation, 20-25 eV photoionisation cross sections 80—83328

barium continued
  atom, efficient ionis. by reson. laser pumping 80—32085
  atom, electron impact step-wise excitation *(Russian)* 80—83497
  atom, electron scatt., elastic and inelastic ($5\,^1D$, $6\,^1P$) cross sections, 20-100 eV 78—74769
  atom, electron scatt. cross sections, close coupling calc. with CI 80—43180
  atom, electron scatt. from excited atoms, 30 and 100 eV, inelasic and superelastic 78—86933
  atom, electron scattering, above ionisation threshold *(Russian)* 79—68317
  atom, electron spectra of autoionisation states, electron-atom collisions *(Russian)* 78—1085
  atom, electron-correlation satellites, selective reson. enhancement 80—9569
  atom, even-parity autoionising levels, multiphoton ionisation spectroscopy 79—59417
  atom, even-parity states, one- and two-photon absorpt. 77—42303
  atom, excited state lifetime, delayed coincidence meas. 77—3315
  atom, fluoresc. freq. distrib. induced by monochromatic laser beam 78—942
  atom, Hanle effect in reson. line, density depend. 77—23473
  atom, high-resolution laser spectroscopy with minute samples 78—17822
  atom, hyperfine structure of metastable states, atomic-beam mag. reson. with laser detection exam. 77—79558
  atom, in shock heated Ar, absorpt. line broadening obs. *(Japanese)* 80—83464
  atom, laser excited, ionisation studies 80—83330
  atom, light-shift induced zero-field level crossing, optical Hanle effect 80—52947
  atom, line shape obs. in CW dye laser intracavity absorpt. 80—47120
  atom, multichannel quantum defect theory anal. to predict Ra states 80—52918
  atom, multiphoton ionis. spectroscopy of even- and odd-parity states 78—86973
  atom, multiphoton ionisation spectra of $msnp\,^3P^0$ states 77—83554
  atom, photoelectron spectra, 20-25 eV, 5p ionis. 79—81188
  atom, photoelectron spectra, strong many electron effects from core levels 77—18862
  atom, photoexcitation spectrum, discrete autoionising states interferences 80—5508
  atom, quadratic Zeeman effect, diamagnetic shift, Rydberg series, strong field mixing 78—946
  atom, radioisotopes, at. beam laser spectroscopy, hyperfine struct., nucl. moments and radii 80—57678
  atom, reson. absorpt. transitions, laser saturation spectroscopy with optical pumping 80—47121
  atom, reson. fluoresc., photon burst detection 78—42244
  atom, reson. lines, emission and absorpt. core profiles 77—50389
  atom, reson. transition, laser saturation spectroscopy with optical pumping 80—52334
  atom, saturation spectroscopy with laser optical pumping 80—83324
  atom, spectra even-parity $J=2$, multichannel quantum-defect anal. 79—31445
  atom, spectral line contour broadened by Xe collisions 78—25477
  atom, Stark struct. of Rydberg states 78—25471
  atom, term dependence of position of 4f electron in $4d^9 4f$ configuration 77—26973
  atom, time-resolved saturated absorption expt., collisions effects 78—29758
  atom, transition probability of valence shells, relativistic pseudopot. calc. 78—86803
  atom, two-photon spectra, isotope shift and hyperfine splitting 78—33491
  atom, two-photon spectroscopy, highly excited even levels, $J=0$ spectrum anal. 79—31447
  atom, two-step autoionis., double ionis. anomaly 79—22671
  atom, UV photoelectron spectra, config. interaction effects 77—50413
  atom, X-ray levels, 5p excited spectra, using multiconfiguration Dirak-Fock program 80—47865
  atom 80—47950
  atom X-ray spectra, mass absorpt. coeffs. in ultrasoft region, spectral depend. 77—10622
  atomic beam, optical isotope shifts and hyperfine struct. 79—50154
  atomic electron collision cross sections 77—42410
  atomic $np^6(n+1)s^2$ state, atomic resonant autoionisation, photoelectron spectra 77—18980
  atomic photoionisation, ion alignment, many electron correl. effect 78—74622
  atomic polarisability, effective potential approximation method 77—88587
  atomic quasi-Landau spectrum, semiclassical strong field mixing models 80—63847
  atoms, emission spectra, 50 to 90 nm, electron impact excitation 78—82846
  atoms, high-lying levels, optogalvanic detection by laser excitation 79—98055
  atoms, hyperfine splitting and isotope shift of high lying levels, Doppler-free 2-photon laser spectroscopy 80—58215
  atoms, quantum defect param., ab initio calcs. 80—78525
  atoms, X-ray spectra, high energy $L\gamma$ satellites 80—102474
  auroral oval, dayside, Ba plasma injection rel. to rocket-borne VLF and ELF waves meas. 80—98504
  axons, giant, squid, interaction of Ba^{2+} with K^+ channels 80—85379
  Ba^+ + inert gas, ($^2P_{3/2}$) states relax. cross sections 78—13595
  Ba I, lifetime meas. of Rydberg states in 6snd $^1D_2$ series 78—33472
  Ba II stars, spectral energy distribs. from DDO photometry 79—92757
  BCC, superconductivity under press. 78—14858
  bremsstrahlung resonances and APS near 3d threshold 77—69937
  characteristic energy loss, ang. depend., surface plasmon excitation 78—2962
  chemi-ionisation reactions of Ca, Sr, Ba, and Yb with halogens and interhalogens 77—32791
  chemisorption on W (100), inelastic tunnelling spectra 78—47664
  chemisorptive luminescence systems for surface reaction obs. 78—7236
  coadsorption with Cs on W (100), work function of surface under equilibrium conditions 79—15025
  coadsorption with Cu on W faces, work function changes 80—65378
  coating on W tip, photoemission in electric field *(French)* 78—80458
  desorption from Ir (111), conc. depend. of kinetic characts. of thermal desorption 78—2377
  desorption from polycryst. W ribbon, electron stimulated 77—11793

barium continued
desorption from river-borne sediments in Hudson estuary 79—79877
desorption from W (121) in strong electric fields 80—29280
determination, in seawater, matrix effects in graphite furnace AAS 78—85230
determination, in Si:Ba, Geiger counter neutron activation anal. 79—52816
determination in biological materials, by thermal NAA 78—27854
diffusion in Bi, mechanism 79—77819
diffusion in KCl, light scatt. meas., dipole mechanism *(Russian)* 78—22900
discharge, dipole-dipole pair absorpt. obs. using optogalvanic detect. 80—54064
elastic properties, Debye temp., 20°C, 20 to 70 kbar, US wave velocity meas. 78—87735
electrical resistivity; 1-1000K, data tables 79—78073
electrical resistivity and thermopower meas., high-purity liq. and solid phases 77—47799
eye rod photoreceptors, vertebrate, opposing effects of Ca^{2+} and Ba^{2+} 79—24990
F-region plasma clouds, high altitude limit of gradient drift instability 78—88984
F-region striated Ba clouds, electron density struct. meas. 78—88974
field desorption from W (011), conc. depend. 80—25533
film, deposited on W (100), struct. determ. using LEED 79—90902
film, growth on (111) face of Ir covered with graphite monolayer 78—26791
film, multilayer and monolayer, an W substrate, AES and work function meas. 77—24921
film, on SiO_2, interfacial chemistry, AES obs. 80—44434
film, semitransparent, opt. props. in 2-5.6 eV range, electronic transitions, thickness depend. *(French)* 80—108289
film, structure effects on work function, electron micrographs and photoemission meas. 79—83107
film, vapour-quenched, unsuccessful search for supercond. above 0.3K 77—12053
film, work function and struct. 78—80040
film on Ir (111), growth of 2-dimens. islands in presence of activation barriers at island boundaries 78—43274
fission product, solubility and migration in oxide fuel 79—19373
forced-flow chromatography, detection by photometric method 80—71965
gas laser, pulse repetition frequency scaling law 78—82954
geochemistry, non-conservative behaviour during mixing of Mississippi River and Gulf of Mexico waters 78—32120
getter film initial reaction probability with O_2, water, CO and CO_2, AES obs. 80—61153
ion beam, plasma optical diagnostics 79—94815
ion polarisation and point defect resistivity in metals 80—103672
ionosphere, Tordo 1 polar cusp Ba plasma injection expt. 78—77402
ionospheric clouds, assoc. striations form. 77—9607
ions, resonance fluorescence and optical sideband cooling of electrodynamically contained ions 79—3422
isotopic anomalies in Allende meteorite 78—32409
laser, discharge heating, power and performance 78—46580
laser, discharge-heated, 1.5 μm, improved performance by vol. scaling 77—88778
laser, energy characts. at 1.5 μm 79—13953
laser, gas discharge, excited by dual-pulse, lasing characts. 79—89895
laser, vap. in heat pipe oven, 1.5 μm monomode emission *(French)* 77—3570
laser, vapour, pulsed lasing due to 1.13, 1.5 μm atomic transitions 80—53276
laser spectroscopic anal. of Rydberg series, multichannel quantum defect theory 80—18815
liquid, density meas. at intermediate temps., method employs Archimedes' Principle 78—22784
liquid, thermophysical properties, up to 1800K 78—30767
monoatomic film on W (110), characteristic electron energy loss 80—100720
monolayer, conc. depend. of characteristic loss spectrum 77—15938
monolayer on W(110) surface struct. transformation stages 77—47681
muonic atom, QED valdity test precision meas. of 4-3 transition 78—33642
muonic atom transition energy meas., tests of high-order vac. polarisation corrections 77—71895
nerve cells, Ba-treated, generation of long pot. waves 80—56002
nerve cells, reduced systems, qualitative anal. of model generating long potential waves 80—26213
neutron yield calcs., electron beam incidence 78—95622
phase transformation in high-press. chamber *(Russian)* 77—76544
phase transitions under high press. 80—96641
photo-stimulated field emission, effect of light polarisation, pure and Ba covered W *(French)* 80—7480
photoneutron yields released by incident electrons, improved calc. 80—27630
plasma clouds, magnetosphere injection via front-end electroreactive accelerators 77—53400
plasma ionospheric injection, ion cyclotron wáves generation 79—53648
plasmon excitation by oblique incidence of primary electron beam of medium energy 78—18987
radiative decay of autoionisation states *(Ukrainian)* 78—82682
rail gun for plasma injection 80—59255
Raman conversion of XeCl-laser radiation in metal vapours, up to 40% efficient 79—23025
recrystallisation of wires and filings by thermal processing encapsulated in metal tubulation 77—59810
resonant photoemission, time-depend. density-functional technique 80—89114
seawater, Ba concs. in Atlantic and Pacific Oceans, comparison with ^{226}Ra 77—5222
seawater content, as pot. indicator of marine drilling contamination 77—2180
solution in liq. ammonia, conductance at −62.37°C 78—91459
submonolayer film on Mo(011) face, surface diffusion, manifestation of phase states *(Russian)* 78—91539
superconducting film, A1-type quench-condensed, prep. and crit. temp. 77 69443
superconductivity, pressure dependence, ion core 78—91805
transport properties, elec. resist., thermoelec. power, thermal cond. deviations from Matthiessen's rule 78—39086

barium continued
upper atmosphere Ba^+ clouds, early time striation struct. due to presence of BaO flow 77—25833
vapour, efficient Raman conversion of XeCl excimer laser radiation 78—79069
vapour, efficient Raman conversion of XeF laser output, 351 to 585 nm 77—58377
vapour, laser excited, anomalous conical emission and self focusing 80—43411
vapour, level populations, laser pumping effects 80—91507
vapour laser, high average output power 79—72593
vapour releases in upper atmosphere, induction of pulsating aurora 77—49211
XPS, in BaS and $BaSO_4$ 80—43104
$AgCl:Ba^{2+}$, plasticity, impurity hardening effect 78—47466
β-Al_2O_3-Na_2O:Ba, dopant effect on ionic cond. and phase comp. 79—65242
Ba, atomic beam and resonance spectroscopy 80—58180
Ba I, 440 to 830 Å, 5p absorpt. spectra 79—31455
Ba I, 5p spectra collective excitation, rel. to double photoionis. 77—50387
Ba I, hook method, gf values of intercombination line, 7911.38 Å 78—66511
Ba I, isotope shifts, hyperfine struct., neutron deficient nuclei, laser resonance fluorescence study 79—72436
Ba I, laser-excited, absorpt. spectra, press. shifts 77—27007
Ba I, light shift induced zero-field level crossing 80—58220
Ba I, low-lying, even-parity levels, ab initio relativistic SCF MCDF calcs. 78—37568
Ba I, oscillator strength meas. 78—74607
Ba I, Stark quantum beats under pulsed dye laser excitation 77—42277
Ba I, two-step autoionisation 80—91513
Ba I-Ba II phase boundary, Ba I fusion curve peak at high press. *(Russian)* 80—2165
Ba II, $5d^2D_{3/2,5/2}$, isotope shifts, hyperfine struct., collinear fast beam laser spectroscopy 80—83310
Ba II, 5p excitation, relativistic anal., multiconfig. Dirac-Fock calcs. 80—69240
Ba II, $6p^2P$ fine struct. g-values, laser excitation of fast ion beam 77—10645
Ba II, ab initio calc. of isotope shifts 78—37555
Ba II, even isotopes, optical isotope shifts, Lamb-dip spectrosc. obs. 78—78666
Ba II, Hanle effect, $^2P_{3/2}$ lifetime determ. 77—18852
Ba II, Stark half-widths, line shifts, calcs. *(Russian)* 78—62764
Ba II, vac. UV absorption, 350-1100 Å 77—30809
Ba II 4554 Å solar resonance line formation, empirical NLTE analysis 78—53907
Ba II $5D_{3/2}$ metastable state, decay rate using ion storage technique 80—18826
Ba II lines in solar spectra, non-mag. polarisation, centre-to-limb var. 80—67678
Ba II metal rich stars, Ba abundance implications 79—71024
Ba II resonance level lifetime meas. by pulsed laser excitation of ion beam 78—25480
Ba II star HR 774, Reticon spectra rel. to Mg isotopes and s-process elements 79—25594
Ba isotopes, isotope shifts and hyperfine struct. from laser spectroscopy 79—9460
Ba, oxidation, SXAPS 77—73189
Ba X, UV spectra, 60-600 Å reson. lines 78—33455
Ba^+ confined in RF quadrupole trap, optical detection 77—75096
Ba^+, electrodynamically trapped, saturation dip in fluoresc. 77—65437
Ba^+, electron and ion Stark effects in plasma, widths and shifts 77—46526
Ba^+, excited state lifetimes, fluoresc. decay meas. 77—79574
Ba^+, hyperfine struct. of $5d^2D_{3/2}$ to $6p^2P_{3/2}{}^0$, laser absorpt. expt. 78—21870
Ba^+ ion cloud containment in RF trap, <50 ions, optical sideband cooling 78—75407
Ba^+ ions, hyperfine struct. reson. determ. from fluoresc. *(French)* 77—432
Ba^+ ions confined in cylindrical RF trap, lifetime meas., laser probing 80—95573
Ba^+, laser-induced resonances, high-resolution expt. 77—6959
Ba^+, optical pumping and saturable absorpt. of fast ion beam superimposed on continuous laser beam *(French)* 78—5179
Ba^+, transition probability of valence shells, relativistic pseudopot. calc. 78—86803
Ba^{2+}, 3d photoabsorpt. spectra, continuum and discrete states 79—81176
Ba^{2+} $3d^94f$ config., collapse of 4f electron, X-ray spectra obs. *(Russian)* 80—58204
Ba^{2+} effect on neuromuscular junction transmitter release during repetitive stimulation 78—3469
Ba^{2+}, effects on toad rod dark-adapted intensity-response curve 79 - 79531
Ba^{2+}, free-ion polarisabilities, empirical values 77—20792
Ba^{2+} induced contracture in rabbit papillary muscle, elec. phenomenon 79—83732
Ba^{2+}, on calcite surface, ESCA, calibration 77—81432
Ba-Al-Si, exam. of phase diagram, confirmation of $BaAl_2Si_2$ and $Ba(Al,Si)_2$ *(Russian)* 79—29019
Ba-BaO coated cathode, role of surface donor centres 78—11063
Ba-H_2 system, equilib. H_2 press. and enthalpy of forml of BaH_2 79—86893
Ba-inert gas, Ba reson. lines broadening, absorpt. cross sections anal. 80—32642
Ba-N_2O flame, candidate chem. laser reactions, intracavity dye laser absorpt. meas. 78—63108
Ba-Tl laser optically pumped by pair-absorption transitions, 1.5 μm emission obs. 80—58517
Ba^{2+}-methyl propionate mixtures, in DMSO, acetonitrile solns. IR, assoc., solvent, catalytic effects *(French)* 79—87827
Ba + Ba, atomic pair absorpt. obs. with white-light source 79—63944
$Ba+Ba^+$, $6p^2P$ level lifetimes, depolaris. cross-sections, Hanle effect obs. 79—26943
Ba + Ba(Tl), laser induced collisional and radiative energy transfer 80—53108
$Ba+Br_2(I_2) \rightarrow BaBr(BaI)+Br(I)$, time-of-flight chemiluminesc., mol. bond energies determ. 78—40051

barium continued
- $Ba+CCl_4 \rightarrow BaCl_2+CCl_2(\bar{A})$, chemiluminesc. spectrum and ang. distrib. obs. 79−15962
- $Ba+CF_3I \rightarrow BaI+CF_3$, products translational distrib., crossed beam reaction 78−31629
- $Ba+CH_3I \rightarrow BaI+CH_3$, products translational distrib., crossed beam reaction 78−31629
- Ba+CO, radiation quenching of metastable Ba (5d ^1D) in gas 79−85932
- $Ba+CO_2(O_2)$, crossed beam kinetics, BaO recoil velocity spectra 80−76500
- $Ba+CO(CO_2)$, flame spectra, 500-1150 nm mechanism 77−48646
- $Ba+Cl_2$, 10^{-5} torr, dynamics, chemiluminesc. ang. depend., radiative lifetime 77−40539
- $Ba+Cl_2 \rightarrow BaCl^++Cl^-$, chemi-ionis. reaction, mol. beam obs. 80−104434
- $Ba+D_2$, radiation quenching of metastable Ba (5d ^1D) in gas 79−85932
- $Ba+F_2$, crossed beam chemilum., kinetics and mechanisms 80−21264
- $Ba+H_2$, radiation quenching of metastable Ba (5d ^1D) in gas 79−85932
- $Ba+H^+$, electron capture, single and double, 1-100 keV 79−68313
- $Ba+H^+$, metastable H form. by charge exchange 79−81275
- Ba+HBr, laser induced fluoresc. study at different collision energies 80−91632
- Ba+HCl, beam-gas reaction, multiphoton ionisation, product identification 78−23946
- Ba+HCl, laser induced fluoresc. study at different collision energies 80−91632
- Ba+HF, product rot. and vibr. distributions and reaction cross sections depend. on reagent translational energy 80−93745
- $Ba+HF \rightarrow BaF+H$, dual mol. beam excitation difference spectroscopy, state-to-state vibr. resolved dynamics 80−89474
- $Ba+He(2^3S_1)$, coherent $^2P_{3/2}$ levels excitation by Penning ionis., Hanle effect 80−5520
- Ba+Kr, collision induced dipole transition, elec. quadrupole transition, oscillator strengths 79−41128
- $Ba+N_2$, radiation quenching of metastable Ba (5d ^1D) in gas 79−85932
- $Ba+N_2O$, chemiluminescent flame, BaO states population 79−39153
- $Ba+N_2O$, crossed mol. beams, BaO recoil vel. spectra 78−7184
- $Ba+N_2O$ reaction, intracavity dye laser spectroscopy 77−86293
- $Ba+N_2O \rightarrow BaO+N_2$, chemiluminesc., ang. distrib. 78−44361
- $Ba+N_2O \rightarrow BaO^*+N_2$, model electronically nonadiabatic reaction, large quantum effects 77−4897
- $Ba+NO_3(N_2O)$, chemiluminesc., absolute photon yields determ. 77−86317
- $Ba+Ne^+(He^+)$, 2-1000 eV, spontaneous ionis. mechanisms 79−64090
- $Ba+O_2$ flame, chemilum. from three-body recombination reactions 77−77759
- $Ba+S_2Cl_2 \rightarrow S_2^*+BaCl_2$, rearrangement reaction, crossed-beam chemiluminesc. 77−29009
- $Ba+SO_2 \rightarrow BaO+SO$, reaction kinetics, BaO recoil velocity spectra 79−74361
- $Ba+SO_2 \rightarrow BaO+SO$ reaction, laser-induced fluoresc. obs., vibronic distrib. of BaO, collisional energy depend. 80−11917
- Ba+Tl, atomic pair absorpt. obs. with white-light source 79−63944
- Ba+Tl, dipole-quadrupole radiative collisional fluoresc. 80−83315
- Ba+Tl, radiative collisional fluoresc. obs. from thermally excited atoms 80−102480
- Ba+trifluoromethyl iodide, BaI vibr. states bimodal distrib. 78−27743
- Ba^++Ba, $6p^2P$ level lifetimes, depolaris. cross-sections, Hanle effect obs. 79−26943
- $Ba^++D_2 \rightarrow D+BaD^+$, sequential impulse model, prod. bond dissoc. energy and cross section 80−81295
- Ba^++inert gas atom collision, polarisation of emitted radiation, quasimol. interf. effect *(Russian)* 77−46633
- Ba^++Kr, quasimolecular states interference, degree of polaris. oscill. *(Russian)* 77−6917
- Ba_2, low-lying states binding energy, local spin density functional formalism calcs. 79−97994
- Ba_2^{2+}, very long lived vibr. states, lifetimes, WKB calc. 80−78560
- BaF_2, force consts., mean amplitudes of vibr. 78−17647
- BaI resonance transitions, hyperfine struct. and isotope shifts, atomic beam laser spectroscopy 80−102141
- $Ba(^1S,^3D)+$ halogenated methanes, laser induced fluorescence 79−66270
- ^{133}Ba separation from $BaCO_3$ by method of internal reduction 77−14613
- ^{135}Ba, ^{137}Ba Fourier transform NMR, NQR studies 78−94261
- $^{135}Ba^+$, $^{137}Ba^+$, $6p^2P_{3/2}$ level hyperfine struct., Lamb-dip spectroscopy 77−83530
- $^{135}Ba^+[^{137}Ba^+]$ hyperfine structure resonance detection method *(French)* 77−75095
- $^{135}Ba^{2+}$, $^{137}Ba^{2+}$, aq. ions, nucl. quadrupole relax. 78−64287
- $^{138}Ba^+$, lifetime of $6p^2P_{3/2}$ level using superimposed ion and laser beams 77−57933
- ^{139}Ba, γ-ray emission profitabilities and half-life obs. 80−57723
- ^{140}Ba, airborne short-lived radionuclides of unknown origin in Sweden (1976) 78−32219
- ^{140}Ba, diffusion behaviour in SiC, 1650 to 1850°C 78−79814
- ^{140}Ba, volatile fission product, diffusion in Mo, 1400-2000K *(Russian)* 78−91485
- $^{140}Ba/^{140}La$ radio-nuclide generator, separation methods *(German)* 77−25298
- Ba^*+Ba^*, radiative collisional fluoresc. at sum freq. 79−18261
- ^{137m}Ba, internal conversion decay, double K-hole creation 77−18887
- $CaF_2{:}Ba^{2+}$, localised vibrs. due to substitutional impurities 78−22803
- $Ca(4p\ ^3P_J)+Ba$, collisional deactivation and optical lifetime 80−48070
- Cs-Ba, high current Knudsen arc discharge, spontaneous extinction, optical diagnostics 80−44044
- Cs-Ba discharge, high-current, low-press., spontaneous current cutoff 80−19626
- Cs-Ba Knudsen thermionic converter performance optimisation 79−27840
- Cs-Ba triode arc switch, high-current, low-voltage, pulsed control 78−71551
- $GaAs{:}Ba^+$, Auger electron and charact. electron energy loss spectra 80−55235
- Ge:Ba, Ca, recomb. props. 78−56156
- Ge:Ba, elec. props. and effect of impurities on γ-radiation defect formation 78−10088
- Ge:Ba distrib. pattern, partition coeff., limiting solubility and energy levels 77−15444
- Ge:Be, positron annihilation angular distrib. 80−45165
- He hollow-cathode discharge, Ba^+ and Sr^+ formation 78−67527

barium continued
- He-Ba discharge, dipole-dipole pair absorpt. obs. using optogalvanic detect. 80−54064
- $He(2^3S, 2^1S)+Ba(Y)(Ce)$, Penning process, double ionisation 77−3439
- KCl:Ba, defect struct., dark-field microscopy, anal. of decoration patterns 79−23506
- KCl:Ba, γ-irrad., point defect form. and interaction, X-ray and optical studies 79−65078
- KCl:Ba, γ-irrad. effects on intensity distrib. of diffuse X-ray scatt. 77−24329
- KCl:Ba, γ-irradiation, defect struct., X-ray and chemical etching exam. 77−84793
- KCl:Ba, microcrystalline powders, role of Z-centres in stabilizing coloration 80−54227
- KCl:Ba, negative photoplastic effect, photodestruction of Z-centres 77−43272
- KCl:Ba, structural changes due to γ-irradiation *(Russian)* 77−76460
- KCl:Ba, symm. of elastic fields due to defect displacements, diffuse X-ray scatt. 80−70256
- KCl:Ba (0.005 at.%), spatial diffuse X-ray scatt. intensity distrib. 77−7757
- KCl:Ba effect of doping on dislocation distrib., in melt grown cryst. 80−6410
- KCl:Ba solid solution decomposition, elastic ordered structure formation 79−86896
- $KCl{:}Ba^{2+}$, localised stress relaxation in excess vacancy system, prismatic loops *(Russian)* 80−88160
- $KCl{:}Ba^{2+}$, precipitation kinetics, supersaturation effects, geometry of formed heterophase struct. *(Russian)* 78−84824
- KCl:Ba(Ca)(Sr), microstruct. and hardness, impurity distrib. effects 79−24529
- KCl:Ba(Sr), Z-centre, luminesc. and absorpt. spectra obs. 80−49221
- $KCl{:}Br^{2+}$, solid solution periodic precipitation in inhomogeneous conc. field 80−103485
- $KCl{:}CO_3^{2-}$, Ba^{2+}, shift and broadening of local vibr. bands, temp. depend. 78−87755
- KCl-Ba, X-ray irrad. cryst., thermoluminescence spectra 80−20719
- $KCl(Br){:}Ba^{2+}$, BeF_4^{2-}, IR absorpt. spectra, impurity cation rel. to degenerate vibr. splitting *(Russian)* 80−2807
- $KNbO_3{:}Ba^{2+}$, dopant effect on domain struct., etching study 79−56749
- $Mo{:}Ba^+$, secondary electron coefficients, temp. depend. 77−69947
- NaCl:Ba, Ba precipitation at dislocations, kinetics, ionic cond. meas. 79−60510
- $NaCl{:}Ba^{2+}$, dopant aggregation and precipitation 80−107306
- $Ni{:}Ba^+$, ion implantation, effect on inelastic refl. and energy losses of fast primary electrons 78−55900
- $O_2+Be(Mg)(Ca)(Sr)(Ba)$, reaction kinetics in diffusion flame 77−90579
- $Pb_5Ge_3O_{11}{:}Ba,O$, impurities, static central peak 78−92079
- $Pb(Zr,Ti)O_3{:}Ba$, paraelectric ceramic, giant electrostrictive effect 79−91378
- $Pb(Zr,Ti)O_3{:}Ba$, paraelectric ceramic, electrostrictive effect 80−80701
- Pd-Ba (1.5 wt.%), thermionic emitter, Auger spectrum fine struct. 78−2954
- Pt-Ba, elemental comp. and chem. state of surface during thermal activation, AES obs. 78−2345
- $RbBr{:}Ba^{2+},Sn^{2+}$, thermal depolarisation meas., relax. processes 78−23389
- Si:Ba, Geiger counter determ. of Ba by neutron activation 79−52816
- W-Ba, type B impregnated cathode, operation mechanism 78−15278
- ZnO:Ba varistors, microstructure-prop. relations 80−100249

barium alloys
- *see also barium compounds*
- Ba-Al-Si system, phase diagrams construction by simplex designing method 78−6899
- Ba-Cd, variation in interatomic interaction and lattice parameters during ordering, numerical calc. *(Russian)* 77−81255
- Ba-Cd system, short-range order calc. *(Russian)* 79−23566
- Ba-Eu, phase diag. *(Russian)* 78−80514
- Ba-Mg, liq. alloys, thermodynamic activities determ. 80−50604
- Ba-Nd, phase diagram, microstruct., X-ray, chemical and thermal diffusion anal. *(Russian)* 78−52761
- Ba-Pb system, intermediate phases, equilib. phase diagram, cryst. struct. 77−44213
- Ba-Ti, phase diagrams *(Russian)* 78−80513
- Ba-Yb, phase diag. *(Russian)* 78−80514
- BaCu, X-ray cryst. struct. determ. 80−92478
- $Ba_{10}Ga$, cryst. struct. *(French)* 80−79749
- $BaNiSn_3$, cryst. struct. rel. to $ThCr_2Si_2$ type *(German)* 78−51470
- BaPd, gaseous, dissoc. energies, obs. and calc. values 78−58864
- $BaPdSn_3$, prep. and crystal structure *(German)* 80−84138
- $Ba_{0.67}Pt_3B_2$, cryst. struct. and supercond. props. 79−38231
- $BaPtSn_3$, cryst. struct. rel. to $ThCr_2Si_2$ type *(German)* 78−51470
- BaRh, gaseous, dissoc. energies, obs. and calc. values 78−58864
- Ba_2X, X=Si, Ge, Sn, Pb, occurrence, struct. 78−38663
- $Eu_{0.95}Ba_{0.05}Pt_2$, ^{151}Eu Mossbauer studies at high press. 80−39923
- Pt-Ba cathode, vaporisation expts., heat of adsorpt. and migration of Ba on Pt 78−10272
- Sr-Al-Si system, phase diagrams construction by simplex designing method 78−6899

barium compounds
- *see also barium alloys*
- aluminate:Eu, effect of non-stoichiometry on luminesc. 78−68550
- arsenates, $BaM^{IV}(AsO_4)_2$, (M^{IV}=Ge,Ti,Sn,Zr,Hf), IR and Raman spectra, cryst. struct., chem. bonding 77−36225
- barium acid oxalate, lacunary phase, thermodynamic and crystallographic characts. 79−55731
- barium formate, γ-irrad., ESR of free radicals 79−65737
- barium methylsulphonate, X-ray powder cryst. data 80−59451
- barium stearate, in MIM struct., internal voltage work function meas. 79−82684
- barium stearate, in MIM symmetric junction, internal voltage due to Al_2O_3 film on electrodes 79−78202
- barium stearate film, low energy electron range meas. using radioisotope Auger electrons 80−70257
- baryta crystal gas-liquid inclusion meas. with microscope heating stage 80−76967
- celsian, with CaF_2 and ZnO additives, props. obs. *(Bulgarian)* 80−50579
- α-celsian-leucospherite-tuhualite-milarite series of cpds., struct. types 79 19223

barium compounds continued
  dicalcium barium propionate, ferroelec. in press. induced phase VI 79—91393
  ferrite, FMR in uniaxial crystal plate with bubble domain lattice 80—93182
  ferrite, hexagonal, with M, W and Y structures containing Fe^{2+} and Fe^{3+} mag. ions, saturation moment and anisotropy 80—71009
  ferrite, modulated struct. phenomena, survey 79—95033
  ferrite, plastic magnet appl., based on moulding ferromagnetic powder material with plastics *(Japanese)* 80—60829
  ferrite compounds, microsyntactic intergrowth and cryst. defects, TEM obs. 79—10858
  ferrite platelets in multidomain state and at saturation, FMR absorpt. 79—42841
  ferrite powder, effect of lattice defects on coercivity *(German)* 79—24194
  ferrites, lattice imaging 78—30522
  formate, cryst., Raman scatt. 79—4804
  hectorite, Ba ion position, water effect *(French)* 77—72593
  hexaferrites, mech. and mag. props. 79—70151
  illite, vacancy ordering, transition state cluster model, electron diffr. 77—47547
  KCl-$BaCl_2$ system, solid solns., phase diagram, enthalpy of soln., vibr. entropy. 78—39751
  mordenite, dehydrated, position of cations and molecules, electron probe anal. 78—51509
  oxalatte, lacunary phase form., morphological and kinetic characts. 79—60299
  oxides, Ba_2MO_4, M=Tc, Sn, Zr, Pb, Hf, K_2NiF_4 structure, study by method of invariants *(French)* 80—33959
  perovskites, $A_2^{2+}B^{3+}U_{5/6}^{6+}\nu_{1/6}O_6$, struct., cation vacancies, X-ray diffr. study *(German)* 80—107147
  perovskites, ordered cubic, cationic effect on intramolecular forces, stretching force const. 80—88979
  phosphate and silicate glasses, Nd^{3+} luminesc. quenching by transition metal and rare earth ions 80—25449
  phosphates, $BaM^{IV}(PO_4)_2$, (M^{IV}=Ge,Ti,Sn,Zr,Hf), IR and Raman spectra, cryst. struct., bonding 77—36225
  plaster, X-ray absorption coefficients, from 100 to 400 keV 78—31283
  psilomelane type structures, rel. between rutile, β-gallia, hollandite and $Ga_4Ti_{x-4}O_{2x-2}$ type structs. 79—37664
  sodalites, aluminogermanate- and aluminate-, IR spectra rel. to T-O bond length and T-O-T ang. 79—91445
  stearate film, between Al electrodes, intrinsic voltage 78—72277
  stearate film, in $Al/(Al_2O_3)$-BaSt/Sn struct., internal voltage temp. variation 80—20326
  stearate film, thickness measurement using Talbot effect 78—9321
  stearate multilayer films on EDF glass, interference colours, thin film thickness step gauge 77—5900
  stearate single-layer Langmuir films, elastic and inelastic tunnelling 80—80403
  tienshanite, cryst. struct. determ. 78—83800
  traskite, Ba mineral of variable comp., X-ray diffr. struct. anal. 77—44981
  Al-Ba stearate-Sn struct., internal voltage, thickness depend. 77—72920
  Al_2O_3:$BaTiO_3$, sintering temperature effect of titanate additions 80—60808
  Al_2O_3-BaO, fracture *(German)* 77—28882
  Al_2O_3-BaO-SiO_2 glass coatings in fission and fusion reactors, permeation, elec. cond. and dielectric breakdown 80—18439
  Al_2O_3-$BaTiO_3$, sintering *(Polish)* 79—100096
  $Al(PO_3)_3$-BaF_2-Al_3 glasses, opt. props., group I-III fluorides effect 80—66143
  BCl_3, excitation by steady-state and pulsed laser radn. 77—50476
  BH^+, spin-extended Hartree-Fock ab initio calculations for small radicals 78—70746
  B_2O_3-BaO, liquid immiscibility region, equilibration and quenching expts. 80—45288
  $B_{0.65}Ru_{2.7}Cr_{1.3}O_8$, short axis tripling, X-ray and electron diffr. study 79—77576
  (Ba, Ca)(Ti, Zr)O_3, segregation of $CaTiO_3$ and effect on dielec. props. 78—38849
  (Ba,Gd)TiO_3, flux growth and chem. characts. 78—23595
  (Ba,La)TiO_3, defect chemistry and elec. cond., thermogravimetric meas. 77—39580
  (Ba,Pb)$Al_{12}O_9$, LPE growth 79—100064
  (Ba,Sr)$Fe_{12}O_{19}$, Ferroxdure, developments and research 78—84455
  (Ba,Sr)TiO_3, ferroelec. solid solution, dielec. nonlinearity in nonpolar phase *(Russian)* 77—32317
  (Ba, Sr)TiO_3 ferroelectric film, phys. props. in weak elec. fields 78—35098
  (Ba,Sr)TiO_3, ferroelec. props., press. depend., anharmonic oscillator model 80—80716
  (Ba,Sr)TiO_3 polycrystalline solid soln., electrostriction constants, reson.-antireson. meas. *(Russian)* 78—10849
  (Ba,Sr)Nb_2O_6 monocrystal optical homogeneity requirement for light beam control 79—82952
  Ba ferrite crystals, etch pitting, of hard magnetic ferrite crystals *(German)* 78—26568
  Ba hexaferrite, irradiated by fast neutrons, mag. props. 80—97116
  Ba-ferrite, Hall effect and electrical conductivity 79—42564
  Ba-ferrite, Hall effect caused by remanent magnetisation 79—38109
  Ba-H_2 system, equilib. H_2 press. and enthalpy of forml of BaH_2 79—86893
  Ba-O system, adsorbed layers on W, Auger and work function meas., impregnated W cathode model 79—43073
  Ba-Se(Te) systems, phase diagrams 77—36472
  Ba-Sr-Pb hexaferrites, prep. by cernet procedure, mag. props. 77—32174
  Ba+N_2O, reaction, electronic branching, statistical and dynamical influences 78—92451
  $Ba_{0.25}$ $Sr_{0.75}Nb_2O_6$, inhomogeneous ferroelec., photorefractive effect 79—42935
  $Ba_{3x}A_{2-2x}Ti_{6-x}O_{13}$, (A=Na, K, Rb), $0<x<0.2$, struct. evolution, tunnel struct. 79—65049
  $Ba_2AgNb_5O_{15}$, $Ba_2AgTa_5O_{15}$, ferroelec. and ferroelastic props. *(French)* 79—24266
  $BaAgP_3O_9.4H_2O$, cryst. struct. determ. *(French)* 77—80464
  $BaAl_4$ type structure, role of elongated rhombic dodecahedron in alloy structures 79—32946
  $BaAl_2Ge_2O_8$, feldspar, crystal atomic struct. 78—14312
  $BaAl_{12}O_{19}$, refr. index and optical absorpt. 80—66139

barium compounds continued
  $BaAl_{12}O_{19}$, single crysts., Czochralski growth, Al_2O_3-BaO phase diagram, cryst. quality 79—24428
  $BaAl_{12}O_{19}$:Mn, phosphor, vac. UV excitation spectra, appl. to gas discharge display 80—2816
  $BaAl_2O_4$-Ba_2SiO_4-$BaZrO_3$, fusibility diagram 79—83184
  $BaAl_2Si_2O_8$-SiO_2, celsian solid solns., effects on polymorphic transform. kinetics 78—68677
  BaB_6, (La,Ba)B_6, (Ea,Ba)B_6, single crystal growth for thermionic emission 78—92183
  BaB_6 powder, surface struct. effects on thermionic emission characts. and vapour pressure *(Japanese)* 80—50506
  BaB_6 powder prep., thermionic emission charact. *(Japanese)* 80—11610
  BaB_6, thermionic emission, O_2 adsorption effects 77—8711
  BaB_6, work function, thermionic and field emission retarding pot. meas. 77—90233
  BaB_6, work functions from thermionic and field emission retarding pot. methods 79—65537
  $BaB_{12}H_{12}.10H_2O$, struct. dehydration, intermediate phases and thermooxidative degradation 80—33951
  $BaB_{12}H_{12}.6H_2O$, cryst. growth from soln. and morphology 77—44145
  BaB_2O_4-RF_2, R=Mg, Ca, Sr, Ba, glass form., struct. and props. 80—84077
  $Ba_x(Ba_{1-x}Al_x)Fe_2S_6[S_{1-y}(S_2)_y]$, cryst. struct., Mossbauer and mag. behaviour 77—55273
  $BaBe(PO_4)F$, babefphite, cryst. struct. determ. using $P\bar{1}$ automatic diffractometer 80—107179
  $Ba_2Bi^{3+}Bi^{5+}O_6$, structure and elec., mag., thermal props. vs. temp. X-ray and neutron powder diffr. study 79—19189
  $Ba_2Bi^{V}Bi^{III}O_6$, struct. determ. by powder neutron diffr. 78—34468
  $BaBiMTeO_6$, M=Li, Na, antiferroelectric, synthesis and charact. 77—55758
  Ba_2BiRuO_6, perovskites, prep., struct., emission control catalysts 77—68957
  $BaBi_6Ti_3Nb_2O_{21}$, cryst. struct. 77—47428
  $BaBi_4Ti_4O_{15}$, SHG, temp. depend. ferroelec.-ferroelec. transition 78—15121
  $BaBi_8Ti_7O_{27}$, cryst. struct. 77—47428
  BaBr, BaCl gas equilib. mass spectra, dissoc. energy 77—65543
  BaBr, visible spectrum, $C^2\Pi_{1/2,3/2}-X^2\Sigma^+$ transition, laser induced fluorescence 79—98072
  $BaBr_2$, absorpt. and refl. spectra 79—82994
  $BaBr_2$, F-centre localisation, absorpt. spectra calc. and EPR spectra analysis 77—48203
  $BaBr_2$, mol., He(II) photoelectron 79—59509
  $BaBr_2$:K^+, X-irradiated, perturbed F-centre, EPR and optical absorption 77—68966
  $BaBr_2$:Sm^{2+}, radiationless coupling, $4f^5 5d$ band effects, spectra 77—8627
  $BaBr_2$:Sm^{2+}, spectra, ^5D states, Lauer-Fong formula and SCC model 79—15513
  $BaBr_2$-$BaCl_2$, vap. mixture, ion-mol. equilib., heat of form. of ions 80—26039
  BaBrF, cryst. at. struct. by X-ray diffr. 78—75641
  $BaBr_2.H_2O$, dehydration, kinetic parameters from thermogravimetric data 79—61859
  $BaBr_2.2H_2O$, dehydration kinetics, isothermal and nonisothermal kinetics 79—57227
  $BaBr_2.2H_2O$, pure and deuterated, low temp. IR and Raman spectra *(German)* 79—19874
  $BaBr_2.2H_2O$, X-ray cryst. struct. redeterm. and refinement *(German)* 80—39025
  $BaBr_2.2H_2O$:VO^{2+}, EPR meas. 77—16145
  $BaCO_3$, decomp., rel. to CO_2 transport in BaO 79—23780
  $BaCO_3$, electric quadrupole interaction, TDPAC meas. 78—39455
  $BaCO_3$, excited Ba emission by Ar^+ impact 80—100727
  $BaCO_3$, growth in silica gel medium in test tube 77—36379
  $BaCO_3$, precipitation induction errors, a method for determ. 79—5175
  $BaCO_3$, soln. kinetics and activation heat *(German)* 79—16031
  $Ba^{14}CO_3$ gel suspension scintillation counting problems 79—3283
  $BaCO_3$-BaF_2-$TiO(OH)_2$, coprecipitated, use in prep. of polycryst. $BaTiO_3$ 77—24996
  $BaCO_3$-$PbCO_3$ systems, solid soln. form., regions of existence 79—11581
  $BaCO_3$-$SrCO_3$-$CaCO_3$, phase inhomogeneity effects on oxide cathode props. 78—52614
  $BaCO_3$-$SrCO_3$-$TiO_2(ZrO_2)$, ternary systems, solid-phase synthesis 78—52733
  $BaCO_3$+BaO+SiC react., contact phenomena at SiC grain boundary 79—43193
  $BaCO_3$+Ti(Zr)(Hf)O_2, reacts., mechanism, effect of polymorphic transitions 79—11605
  $BaCaLu_2F_{10}$, single cryst. X-ray struct. determ. and refinement 79—69084
  $BaCaLu_2F_{10}$, site occupancy from excitation and emission spectra *(French)* 77—81145
  $BaCa_2Mg[SiO_4]_2$, synthesis and struct. characterization 78—22698
  $Ba_{15}Ca_{27-x}Nd_xAl_{31}Be_{27}F_{231+x}$, $0\leq x<8$, optical props. and vitreous domain 79—65820
  $Ba_{0.8}Ca_{0.08}Pb_{0.12}TiO_3$, piezoelectric ceramic solid soln. *(Polish)* 77—55755
  Ba_2CaReO_6, ordered or perovskite type struct., magnetic and elec. props. 79—65053
  $BaCa_{1/2}Ru_{2/3}O_3$, biquadratic exchange interaction between Ru^{5+} ions in (Ru_2O_9) clusters 77—20580
  $BaCa_{1/3}Ru_{2/3}O_3$, crystal struct., mag. susceptibility and exchange integrals *(French)* 77—16037
  $Ba_2CaTe_{1-x}W_xO_6$, tungstate luminescence 77—69904
  $Ba_{0.92}Ca_{0.08}TiO_3$ ceramic, uniaxial stress effects, US dilatometric and dielec. meas. 78—52454
  $Ba_{0.95}Ca_{0.005}TiO_3$, piezoelectric ceramic solid soln. *(Polish)* 77—55755
  $(Ba_{0.95}Ca_{0.05})TiO_2+CaCO_3$ (0.75%), piezoelectric ceramic solid soln. *(Polish)* 77—55755
  Ba_2CaUO_6, luminescence and energy migration 79—4837
  $BaCd_{1/3}Ru_{2/3}O_3$, crystal struct., mag. susceptibility and exchange integrals *(French)* 77—16037
  BaCl, fluoresc. spectra, dye laser excited 79—68260
  BaCl+Ar(He)(N_2), intermultiplet energy transfer 79—27063
  $BaCl_2$, absorpt. and refl. spectra 79—82994
  $BaCl_2$ aq. soln., vel. correls., time integral calcs. 80—59360
  $BaCl_2$, conc. solns., vel. correls. calcs., diffusion, cond. and transference props. 78—85166

barium compounds continued
$BaCl_2$, F-centre localisation, absorpt. spectra calc. and EPR spectra analysis 77—48203
$BaCl_2$ film, non-cryst., very-low-freq. inelastic light scatt. 80—25367
$BaCl_2$ film, UPS exam. 79—38716
$BaCl_2$, ionic crystal, possible high-temp. thermometer using elec. cond. changes 80—52203
$BaCl_2$, mol., He(II) photoelectron 79—59509
$BaCl_2$, molten, struct. determ. by neutron diffr. 78—42883
$BaCl_2$, non-crystalline film, disorder-induced Raman scatt. 80—11387
$BaCl_2$, photoelectron spectra, geometry 78—29816
$BaCl_2$, positron annihilation ang. correl., bonding depend. 77—20951
$BaCl_2$, Sn-activated, luminescence studies 80—108246
$BaCl_2$, solns. in methanol, conductance data anal., assoc. consts. 78—71875
$BaCl_2$, sp. ht. meas., Schottky-type diffuse phase transitions, defect form. energies and entropies 80—107441
$BaCl_2:Eu^{2+}$, fluorescence lifetime and quantum efficiency for 5d→4f transitions 80—100681
$BaCl_2:Gd^{3+}(Eu^{2+})$, EPR, electrostatic versus superposition model 78—23337
$BaCl_2$:Pb, absorption and emission spectra *(Russian)* 78—23527
$BaCl_2$:Pb crystal phosphor, emission spectra 80—66298
$BaCl_2:Sm^{2+}$, radiationless coupling, $4f^55d$ band effects, spectra 77—8627
$BaCl_2:Sm^{2+}$, spectra, ^5D states, Lauer-Fong formula and SCC model 79—15513
$BaCl_2$-$BaBr_2$, vap. mixture, ion-mol. equilib., heat of form. of ions 80—26039
$BaCl(C^2\Pi_{3/2}, \nu=0)+Ar$, intermultiplet energy transfer, laser induced fluoresc. obs. 78—9227
$BaCl(C^2\Pi)+He(Ar)(N_2)$, collisional quenching, laser induced fluoresc. decay meas. 79—27075
BaClF, cryst., elastic consts. 80—19863
BaClF, localised vibr. of U-centres 78—75779
BaClF, long wavelength dynamics, shell model calc. 80—29134
BaClF, two types of F-centres, identification by ENDOR 78—60355
$BaClF:Sm^{2+}$, energy levels, optical props. 78—84631
$BaClF:Sm^{2+}$, radiative and radiationless transition rate meas. using tunable pulsed dye laser 77—24891
$BaClF:Sm^{2+}$, radiationless processes 79—33792
$Ba(ClO_4)_2$, anhydrous, phase transition obs. *(French)* 78—83939
$Ba(ClO_4)_2$, soln. in liq. ammonia, conductance at −62.37°C 78—91459
$Ba(ClO_4)_2$, solutions in amides and esters, structure *(French)* 80—7343
$Ba(ClO_3)_2H_2O$, γ-irradiated, resonant Raman effect of O_3^- centres 78—48178
$Ba(ClO_3)_2.D_2O$, D quadrupole coupling, temp. depend. 79—31551
$BaClO_3.H_2O \rightarrow BaClO_3$, dehydration process 78—59932
$BaClO_3.H_2O$, force fields and normal coords. of H_2O mols. 79—31500
$Ba(ClO_3)_2.H_2O$, ^{35}Cl NQR meas. 77—66435
$Ba(ClO_3)_2.H_2O$, cryst., O-H bond lengths, H-O-H angles, corrections 79—32945
$Ba(ClO_3)_2.H_2O$, Γ-irrad. defects, ^{35}Cl NQR, 77 and 300K 78—91981
$Ba(ClO_3)_2.H_2O(HDO)(D_2O)$, hydrate group vibr., IR spectra, isotope effects 77—8557
$Ba(ClO_3)_2.2H_2{}^{17}O$, fine struct. in quad. reson. of ^{17}O, DNMR 77—8453
$Ba_5Cl(PO_4)_3$, X-ray cryst. struct. determ. and refinement 80—1974
$BaCl_2.2H_2O$, artificial production of growth twins 78—30641
$BaCl_2.2H_2O$, cryst. struct. determ. by neutron diffr. 78—75639
$BaCl_2.2H_2O$, ferroelastic effect obs. 79—28033
$BaCl_2.2H_2O$, polycryst. hydrates, librational motion of H_2O mols., neutron diffr. exam. 80—10604
$BaCl_2.2H_2O:VO^{2+}$, EPR meas. 77—16145
$BaCl_2.2H_2O(D_2O)$, lattice vibr., IR and Raman spectra 79—15443
$BaCo_2(AsO_4)_2$, mag. model, 0K phase diagram, spin wave spectrum 79—87273
$BaCo_2(AsO_4)_2$, magnetic field effect on mag. ordering neutron diffr. obs. 80—50053
$BaCo_2(AsO_4)_2$, planar X-Y model, mag. ordering 77—66256
$BaCo_2(AsO_4)_2$, quasi 2D XY helimag., sp. ht. meas. 79—61151
$BaCoF_4$, low temp. magnon effects on polarisation 79—42905
$Ba_2Co_{1.65}Fe_{0.35}{}^{2+}Fe_{28}{}^{3+}O_{46}$, temp.-mag. field phase diagram, torque method 80—60276
$BaCo_{1.5}Fe_{16.5}O_{27}$, type W ferrite, spin reorientation 78—60301
$BaCo_{1.65}Fe_{16.35}O_{27}$, spin reorientation obs. using magneticaloric effect *(Russian)* 77—32195
$BaCoO_3$, cryst. struct. determ. 77—47394
$BaCo_2(PO_4)_2$, crystal growth from melt, optimal conditions for crystn. 77—59683
$BaCo_2(PO_4)_2$, dielectric permittivity and elec. resist., temp. depend. 77—59502
$BaCo_2(PO_4)_2$, quasi 2D XY helimag., sp. ht. meas. 79—61151
Ba_2CoReO_6, seignettomagnets with perovskite struct. 79—38459
Ba_2CoS_3, linear chain antiferromag., mag. susceptibility meas. and Mossbauer spectra 80—107992
$Ba_3Co_{2+x}Ti_xFe_{24-2x}O_{41}$, z-type ferroxplan, effect of Co^{2+} ions 77—36094
$Ba_2Co_{1.75}Zn_{0.25}Fe_{12}O_{22}$, trigonal ferrite, mag. anisotropy 79—73709
$Ba_2Co_{2x}Zn_{2-2x}Fe_{12}O_{22}$, mechanically oriented, topotactic prod. technique, mag. props. 80—35140
$BaCrO_3$, 27 layer polytype, struct. determ. 80—107162
$BaCrO_4$, diffuse reflectance spectroscopy 78—88326
$BaCrO_4$, precip. from aq. solns. with slow supersat. development 77—28707
$BaCrO_4$, precipitation from aq. soln., cryst. growth kinetics 77—72574
$BaCr_2O_7$, α and β form, powder data, cryst. struct. *(French)* 80—39032
α-$BaCr_2O_7$, X-ray cryst. struct. determ. *(French)* 80—15064
$Ba_{1-p}Cr_2S_{4-p}(Se_{4-p})$, modulation of intergrowth struct. 79—94967
$BaCuO_2$, prep. and props. *(French)* 77—43201
$BaCuO_{2+x}$ ($0 \leq x \leq 0.12$), study of mag. and elec. props. rel. to the non-stoichiometry *(French)* 78—95051
$Ba_2Cu(OH)_6$, EPR, g-values 79—19770
$Ba_3Dy_4O_9$, synthesis, thermal stability, emissivity, reduction processes 77—8791
$Ba_3Er_4O_9$, synthesis, thermal stability, emissivity, reduction processes 77—8791
Ba_2EuNbO_6, luminescence Raman spectra, means for localisation of binding energy levels *(German)* 78—88304
Ba_2EuTaO_6, luminescence Raman spectra, means for localisation of binding energy levels *(German)* 78—88304
BaF, excited state spectroscopic consts., dissoc., chemilum. obs. 80—21264

barium compounds continued
BaF windows, process for vacuum tight joints prod. 77—26312
β-BaF_2, ⟨111⟩ single cryst., behaviour under room temp. shock compression 77—62585
BaF_2 and fluorite large crystal, block orientation determ. from light scatt. pattern 79—50964
BaF_2, anharmonicity vibrs. and correlation effects, neutron diffr. 78—55915
BaF_2, barrier instability in strong elec. fields 79—69522
BaF_2, Brillouin scatt. and high temp. disorder 78—80365
BaF_2, colour centre thermal stability 78—83811
BaF_2, crack propag., cryst. props. effects 78—75720
BaF_2 crystal, refr. index temp. increments meas. 80—33098
BaF_2 crystal, selective etching and dissolution kinetics 80—71775
BaF_2 crystal windows, transmission in vac. UV region, heat treatment effect 77—31137
BaF_2, current oscills. in elec. field of $\sim 10^6$ Vm^{-1} *(Russian)* 77—20334
BaF_2, dielec. const., 5.5 to 400K 80—50249
BaF_2, dielectric const. and polarisability strain derivatives 77—73125
BaF_2, disorder at high temp., Brillouin scatt. 78—2866
BaF_2, dispersion calcs. of cubic nonlinear susceptibility near Raman resonance 79—94292
BaF_2, elec. cond. of shock-compressed monocrystals 77—9404
BaF_2, electronic polarizability and dielectric const., strain derivatives 78—19406
BaF_2, Eu^{2+} isomer shift, Mossbauer studies 79—56649
BaF_2, F^- interstitial and substitutional trivalent cations, phonon reson. and IR absorpt. 80—84752
BaF_2, F-centres, muffin-tin approx. inadequacy 78—63761
BaF_2 film, contamination by 1 MeV proton bombardment, backscatt. obs. 77—11811
BaF_2 film, UPS exam. 79—38716
BaF_2, fluorine K absorpt. spectra using APS technique 79—99986
BaF_2, fluorite-struct. compound, high-temp. elasticity, US pulse meas. 77—81878
BaF_2, formation and growth of oxidation centres result of O^{2-} diffusion 80—7706
BaF_2 IR window refractive index var. with temp., −180° to +200°C obs. 79—14052
BaF_2, illuminated over large area, optical strength 77—75593
BaF_2, influence of O_2 on elec. cond., 450-1150°C *(French)* 77—47619
BaF_2, ionic cond., activation vols., freq. depend. cond., press. effects 80—100354
BaF_2, ionic conductivity meas., computer anal. point defect parameters 80—54429
BaF_2, large optical crystals, quality 80—33097
BaF_2, laser window coating material, damage at 10.6 μm 77—61991
BaF_2, laser window material, refr. index, temp. and stress effects 77—46771
BaF_2, laser window material, surface and bulk absorpt., photoacoustic meas. 78—25912
BaF_2, linear thermal expansion coeff., capacitance method meas. 78—16772
BaF_2, long wavelength behaviour, elastic consts. 79—87441
BaF_2, mag. hyperfine const. and lattice distortion of V_k-centre 77—62864
BaF_2, melting curve, press. up to 40 kbar, rel. to high press. melting systematics 77—51475
BaF_2, mid IR laser window material, absorption props. 77—46770
BaF_2, muon Coulomb capture ratio 78—62959
BaF_2, NMR relax., ionic cond. and self-diffusion 78—23362
BaF_2, optical breakdown threshold, illuminated spot dimension effects 78—68582
BaF_2, optical ceramic, hot pressing in vacuum, rel. to spectral transmission 78—52730
BaF_2, piezo-optical coeffs. meas. at 0.6328, 1.15 and 3.39 μm 80—34888
BaF_2, planar channelling, minimum yields determ. 80—70280
BaF_2, polarised Raman scatt. in fluorite crysts., anharmonicity, high-temp. disorder 78—35132
BaF_2, polycryst., laser window material, IR thermooptic coeff. meas. 77—36208
BaF_2, powder, elec. cond. transition under high press. *(Russian)* 77—20370
BaF_2, prism coupling efficiency optimisation for surface IR wave excitation 77—75708
BaF_2 purification for laser components, selective ion filter design and construction 79—14051
BaF_2, Raman spectra, 15 to 1300K, anharmonic vibr. effects 77—43990
BaF_2, rare-earth and transition ion doped, far IR absorption and Zeeman effect 77—40246
BaF_2, refr. index, 20-85°C, temp. depend. 77—8536
BaF_2, single cryst., linear thermal resistance temp. depend. 77—66048
BaF_2, single cryst. windows for high power lasers, stress-induced birefr. elimination 77—88818
BaF_2 solid electrolyte, n-type electronic cond., 700-900°C 80—29448
BaF_2, sp. ht. meas., Schottky-type diffuse phase transitions, defect form. energies and entropies 80—107441
BaF_2, spectral diffusion, coherent effects in ESR of Gd^{3+} 79—51852
BaF_2, strain induced splitting and oscillator strength anisotropy of IR transverse optic phonon 80—92625
β-BaF_2, stress wave profiles 80—96593
BaF_2, superionic conductor, theoretical investigation of Raman scatt. 78—80351
BaF_2, synthetic single crystal, etching 79—95018
BaF_2, thermal props. *(German)* 80—81355
BaF_2, thermoluminesc. and F-centre annealing, after neutron irrad. 80—7422
BaF_2, third-order elastic consts. from Lundqvist pot., many-body effects 80—39201
BaF_2, U-centre, electronic struct. and optical transition energies, SCF MS Xα calc. 79—4532
BaF_2, ultralow loss optical fibre material, loss mechanism 80—78920
BaF_2, undoped, H-centre prod. by reactor neutron irrad., optical absorpt. meas. 77—59010
BaF_2, undoped and U-doped, neutron irrad., absorpt. band attributed to F_2- centres 80—7380
BaF_2, vibr. anal., kinetic consts. method 80—18838
BaF_2, vol. depend. of refr. index 78—88275
BaF_2, width of upper valence band, tight-binding calc. 78—26814
BaF_2, XPS, core-electro peaks, satellite and loss structs. 77—66571
BaF_2: rare earth, far IR electronic transitions 77—4657
$BaF_2:Cd^{2+}$, X-irrad., ESR of Cd^+ centres 77—59459

barium compounds continued
$BaF_2:Ce^{3+}$, EPR of low-symmetry sites 79–47332
$BaF_2:Cm(Bk)$, fluorite-struct., self-luminesc. 78–27309
$BaF_2:Co^{2+}(Mn^{2+})(Ni^{2+})$, far IR absorpt. spectra peaks 78–27265
$BaF_2:Dy^{3+}$, far IR absorption 80–40143
$BaF_2:Er^{3+}$, fluoresc., importance of defect clustering 79–33827
$BaF_2:Er^{3+}$, fluoresc. spectra of charge compensated cryst., multiphonon and energy transfer relax. 79–87496
$BaF_2:Er^{3+}$, single-site multiphonon and energy transfer relax. 78–52547
$BaF_2:Eu^{2+}$, ENDOR of ^{19}F ligands, under uniaxial stress 77–16207
$BaF_2:Eu^{2+}$, fluorescence lifetime and quantum efficiency for 5d→4f transitions 80–100681
$BaF_2:Eu^{2+}$, spin-lattice coeffs., meas. using uniaxial stress method 77–36129
$BaF_2:Gd^{3+}$, dielectric relax. and EPR line broadening 79–56608
$BaF_2:Gd^{3+}$, high-order EPR transitions of Gd^{3+} centre 78–23335
$BaF_2:Gd^{3+}$, spin-lattice coeffs., EPR study 80–66032
$BaF_2:Gd^{3+}$ film, Gd^{3+} luminesc. spectrum and kinetics 78–6763
$BaF_2:Gd^{3+}$-m^+ complex, cryst. field parameters, EPR 78–10768
$BaF_2:K^+$, cryst., thermal depolarisation 79–82912
$BaF_2:K^+(La^{3+})$, nuclear spin relax. orientation depend., point defect self-diffusion mechanism 77–48078
$BaF_2:La^{3+}$, relaxation processes, studies by ionic-thermocurrent techniques 79–69769
$BaF_2:La^{3+}$, thermal depolarisation of La^{3+}-F_i^- defect dipoles 80–75926
$BaF_2:Mn^{2+}$, far IR absorption spectra 78–76507
$BaF_2:Pb^{2+}$, band struct., Jahn-Teller effect, UV luminesc. and optical absorpt. spectra 80–66243
$BaF_2:Pr^{3+}$, wavelength and temp.-modulated UV absorpt. 80–2799
$BaF_2:R$, R=rare earth, dopant effect on superionic state transition 79–60547
$BaF_2:R^{3+}$, far IR Stark and Zeeman splitting 77–48190
$BaF_2:R^{3+}$ (R=rare earth) dipole reorientation, ionic thermocurrents obs. 79–95705
$BaF_2:RF_3$, cryst., absorpt. spectra, γ-ray effects 77–12409
$BaF_2:Sm^{2+}(Tm^{2+})$, vibronic spectra and dynamics of impurity-contaiing lattice 79–1787
$BaF_2:Tb^{3+}$, cubic Tb^{3+} centres, energy level and cryst. field parameters 77–52181
$BaF_2:Tb^{3+}$, thermally, stimulated polarisation currents, 80 to 400K 79–51900
$BaF_2:Ti^{2+}$, electronic struct. and EPR of Ti^{2+} 78–76034
$BaF_2:Tm^{2+}$, EPR, optical recording in weak mag. field 78–68376
$BaF_2:Tm^{2+}$, EPR meas. of Tm^{2+} ion pair interactions 79–95641
$BaF_2:Tm^{2+}(Yb^{3+})$, axial g-values of $4f^{13}$ ions with trigonal symmetry *(Korean)* 79–24135
$BaF_2:Tm^{2+}(Yb^{3+})$, trigonal centres, point-charge approx. 78–39072
$BaF_2:U$, absorption band spectra following neutron irrad. 80–29763
$BaF_2:U^{3+}$, single crystal, superhyperfine interaction of tetragonal centres 79–42834
$BaF_2:Y^{3+}$, diffusion of bound and free $F_{(i)}^-$ interstitials, NMR meas. 79–78542
$BaF_2:Y^{3+},Gd^{3+}$ production and mech. props. 79–72638
BaF_2-CaF_2-$SrF_2:Gd^{3+}$, luminescence spectrum of Gd^{3+} ion and solid solution region obs. 78–84638
BaF_2-MnF_2-FeF_3 system, X-ray investigation, struct. relations, liquid-solid equilibria diagram, study by DTA *(French)* 79–34017
BaF_2-MnF_2-$M'F_3$ (M′=V,Cr), comparative study of barium fluorides rel. to 1st transition series elements *(French)* 79–69090
BaF_2-NiF_2-CrF_3, X-ray crystallography study, phase identification at 700°C, cryst. symm. *(French)* 78–95733
BaF_2-UF_4-CeF_3 solid soln., surface degradation, complex admittance analysis 78–55980
BaF_2-xBaO.ySiO_2 freezing point depression meas., effect of SiO_2 compound additions 77–28798
BaF_2-YF_3 system, phase diagram 78–35363
BaF_2+BCl_3, crossed beam metathesis, total cross sections 77–21354
BaFBr, absorpt. and refl. spectra 79–82994
BaFBr, cryst. struct. determ. 77–80465
BaFBr, single cryst. growth by flux method, dislocation etch pits on dissoln. 79–56925
BaFBr, X- and γ-irrad., thermolum. and optical absorpt. spectra 79–95857
BaFCl, absorpt. and refl. spectra 79–82994
BaFCl, cryst., anisotropic ionic cond. 78–43171
BaFCl crystals, F-centres, X- and γ-irradiation, thermoluminescence and optical absorption spectra 80–45155
BaFCl film, non-cryst., very-low-freq. inelastic light scatt. 80–25367
BaFCl, luminesc. and ionic conduction 79–28829
BaFCl, non-crystalline film, disorder-induced Raman scatt. 80–11387
BaFCl, thin film, in vacuo Raman spectra using prism-film coupler 78–24873
BaFCl:Eu X-ray intensifying screen 78–11735
$BaFCl:Eu^{2+}$, fluorescence lifetime and quantum efficiency for 5d→4f transitions 80–100681
$BaF_{2-x}H_x$, synthesis and struct. determ. using neutron diffr. *(French)* 80–24425
$BaFHF_2$, ^1H and ^{19}F NMR 78–2753
BaFI, absorpt. and refl. spectra 79–82994
BaFI, cryst. struct. determ. 77–80465
$(BaF_2)_{1-x}(YF_3)_x$, crystal growth and struct. 77–12520
$(BaF_2)_{1-x}(YbF_3)_x$ and $(BaF_2)_{1-x}(NdF_3)_x$, crystal growth and struct. 77–12520
$(BaF)_2[Zn_{1-x}Cu_xF_4]$, statistics of ion distrib. 80–49167
$Ba_3Fe_2BO_9$ (B=Re, Te, W, Mo), siegnette magnets with hexagonal barium titanate structure 78–76397
$BaFe^{2+}{}_2Fe^{3+}{}_{16}O_{27}$, metal deficient, hexagonal with W struct., chemical instability 78–27662
$Ba_3Fe_{2-x}Ho_xUO_9$, $O \leq x \leq 1.2$, perovskites, struct. and mag. props. *(French)* 78–18612
$Ba_3Fe_{2-x}Lu_xUO_9$, crystallographic and mag. props. *(French)* 77–15380
$BaFe_{12-x}M_xO_{19}$ (M=Al, Ga, Sc, In) ferrites, mag. props. and struct. 80–15690
$BaFe_{12-2x}M_xTi_xO_{19}$ (M=Co, Ni, Zn), mag. props. determ. 80–75759
$BaFeO_{2\ 79}$, 6H polytype, perovskite related phase, electron microscope obs. 77–51391
$BaFe_{12}O_{19}$, bubble and stripe lattice domain wall oscills. 80–97115
$BaFe_{12}O_{19}$, Ca^{2+} substitution effect on hexaferrite lattice and mag. props. 80–60243
$BaFe_{12}O_{19}$, discontinuous growth, effect of equilib. segreg. at boundaries 77–51336

barium compounds continued
$BaFe_{12}O_{19}$, effect of impurity concentrations, and sintering conditions on grain size *(German)* 79–23630
$BaFe_{12}O_{19}$, ferrite, DC cond., dielec. props., lattice consts. 80–80272
$BaFe_{12}O_{19}$, formation, dilatometric investigs. 78–27459
$BaFe_{12}O_{19}$, Hall effect, magnetisation and elec. resist., 30 to 80°C 77–51766
$BaFe_{12}O_{19}$, hexagonal ferrite, local lattice distortions, use of Mossbauer effect 78–43745
$BaFe_{12}O_{19}$, high field Mossbauer effect on ^{57}Fe at room temp. and 4.2K 79–24238
$BaFe_{12}O_{19}$, M type hexaferrite, Fe ion dynamic characts. in bipyramidal position, nucl. γ reson. 79–95697
$BaFe_{12}O_{19}$, nucl. spin-lattice and spin-spin relax. in domain walls 77–69610
$BaFe_{12}O_{19}$ particles, magnetic domain study by colloid-SEM method 80–97120
$BaFe_{12}O_{19}$ plate, with cylindrical domain struct., ferromag. reson. at arbitrary magnetisation 77–81017
$BaFe_{12}O_{19}$ powder, chemical plating with Co, Co-P, Ni-P and Cu 80–25593
$BaFe_{12}O_{19}$ powder, hysteresis of microwave absorpt. and magnetisation reversal 80–75814
$BaFe_{12}O_{19}$, powder, milled and annealed, phase composition, lattice conts. and crystallite size 80–71677
$BaFe_{12}O_{19}$ powders, fast reaction presintering 80–97445
$BaFe_2O_4$ amorphous film, prep. by RF sputtering, crystallisation 80–76183
$BaFe_2O_4$, formation, dilatometric investigs. 78–27459
$BaFe_2O_4$, free energy of form. 77–4924
δ-$BaFe_2O_4$ room-temp. formation and polymorphism *(German)* 80–44192
$BaFe_2O_4$-Fe_2O_3-$ZnFe_2O_2$ system, phase relations at 1200°C 78–72767
$Ba_2Fe_{18}O_{27}$, hexagonal ferrite, W-struct., Mossbauer spectra of Fe^{3+} and Fe^{2+} 78–88242
$Ba_2Fe_6O_{11}$, cryst. struct. *(French)* 79–86755
$Ba_2Fe_7O_{11}$, antiferromagnet, exam. of mag. props. by mag. meas., and Mossbauer spectroscopy 78–52256
Ba_2FeReO_6, seignettomagnets with perovskite struct. 79–38459
β-$BaFe_2S_4$, cryst. struct., X-ray diffr. obs. 80–84153
$Ba_{0.5}FeS_2$ cathodes for nonaqueous Li batteries 80–3506
$Ba_{1+x}Fe_2S_4$, electron diffr. study, orientation anomaly 80–107152
Ba_2FeS_3, linear chain antiferromag., mag. susceptibility meas. and Mossbauer spectra 80–107992
$Ba_9(Fe_2S_4)_8$, cryst. struct. 77–35512
β-$Ba_9Fe_4S_{15}$, and low temp. α polymorph., cryst. struct. 78–67690
Ba_2FeSbO_6, siegnette magnets with hexagonal barium titanate structure 78--76397
$Ba_3Fe_3Se_7$, stella quadrangula as struct. building unit 80–15055
$Ba_3Fe_{0.2}Si_{0.8}S_5$, stabilisation of tetravalent Fe 79–60326
$Ba_3FeTa_2O_9$, Mossbauer and X-ray diffr. studies 80–103905
$BaFe_4Ti_2O_{11}$, R-type hexaferrite, spin struct. and mag. props. 78–52216
$Ba_2Fe[Ge_2O_7]$, hydrothermal growth, struct. and opt. props. 77–65971
$BaGaF_5$, X-ray cryst. struct. anal., lattice energy *(German)* 79–69094
$BaGa_2Ge_2O_8$, ordered synthetic feldspar, cryst. struct. 78–34469
$Ba_2Ga_2GeO_7$, gehlenite struct., synthesis and physicochem. props. 79–43181
$BaGa_2Si_2O_8$, ordered synthetic feldspar, cryst. struct. 78–34469
$BaGd_4X_5O_{17}$ (X=Si,Ge), cell consts., luminesc. of various rare-earth activators 80–93376
$BaGe_2$, superconducting temperature depression due to mag. field 80–54820
$BaGeF_6$, Group IV hexafluoride anion radical γ-irrad., EPR spectra 78–72411
$BaGeF_6$, Raman spectra at press. up to 25 kbar 78–6670
$BaGeO_3$-$(0.25MgF_2.0.75YF_3)$-Ga_2O_3 glass, synthesis and props. 80–25648
$BaGeO_3$-CaF_2MgF_2-$Ca_2Al_2GeO_7(CaTiGeO_5)$ systems, glass forming and props. 80–19717
$Ba_3Ge_9O_{20}(OH)_2$, cryst. struct. determ. 77–11524
BaH, 3800 angstrom absorption band, concave grating spectrograph obs. 80–14154
BaH, new absorpt. band at 2991 Å, electronic transition, rot. consts. 77–83616
BaH_2, proton chemical shift tensor, heavy ion effects 79–19791
BaH_2, XPS spectra, crystalline potentials 77–77344
$BaH_6As_4O_{14}$, cryst. struct. exam., new cyclic anion *(French)* 78–2080
$BaHCr_2PO_{10}.H_2O$ and $BaHCr_2PO_{10}.3H_2O$, cryst. struct. determ. *(French)* 77–47407
$BaHPO_4$, high temp. conversion to $Ba_2P_2O_7$, X-ray diffr. meas. 78–44371
$Ba(H_2PO_4)_2$, antiferroelectric, phonon spectra 77–62592
$Ba(H_2PO_4)_2$, crystal. struct. 77–31649
$Ba(H_2PO_4)_2$, dielectric const. and polarisation, antiferroelectricity 77–59526
$Ba(H_2PO_4)_2$, orthorhombic, crystal struct. 78–10005
$Ba(H_2PO_4)_2$, orthorhombic, cryst. struct. determ. 78–26515
$Ba(H_2PO_4)_2$, triclinic, cryst. struct. *(French)* 78–55848
$Ba(H_2PO_4)_2$, X -ray cryst. struct. determ. 79–7589
$BaH[AsCr_2O_{10}]$, X-ray cryst. struct. determ. 79–42019
$BaHfO_3$, high-density ceramics prep. and elec. props. 80–60812
$BaHg_{11}$ type structure, role of elongated rhombic dodecahedron in alloy structures 79–32946
$Ba_3Ho_4O_9$, synthesis, thermal stability, emissivity, reduction processes 77–8791
BaI, mol. dissoc. energy, high temp. mass spectra 78–58863
BaI molecule UV band systems 79–22728
BaI, visible emission spectrum, vibr. consts. 77--34643
BaI, visible spectra, 5200-5700 Å, vibr. consts. 78–25549
BaI_2, absorpt. and refl. spectra 79–82994
BaI_2 aqueous solution, US study of apparent molar compressibility 78–10125
BaI_2, mol., He(II) photoelectron 79–59509
BaI_2, photoelectron spectra, geometry 78–29816
$BaI_2+Cl_2(HCl)$(1,1-dichloroethane)(chloroethene), crossed beam metathesis, total cross sections 77–21354
Ba_xI_y cyclodextrin, quasi-one-dimens. cpd., synthesis, elec. and mag. props. 80–2380
$Ba(IO_3)$, complex salts, phase transitions, cryst. struct. *(Chinese)* 80–70171
$Ba(IO_3)_2$, cryst. struct. determ. by X-ray diffractometry 80–107139

barium compounds continued

- $BaIn_2Se_4$, cryst. struct. *(German)* 80-79760
- $Ba_2KNb_5O_{15}$, Raman scatt. experiments in tetragonal tungsten bronze compounds 80-40113
- $BaKP_3O_9.H_2O$, cryst. struct. *(French)* 78-51480
- $Ba_xLa_{1-x}CoO_3$, $x=0$ to 0.5, structural, elec. and mag. props., Zener double exchange and Goodenough's model 79-65663
- $Ba_{1-x}La_xF_{2+x}$, enhanced ionic motion in solid solutions 80-107491
- $BaLa_2Fe_2O_7$, Mossbauer exam. of mag. struct. 77-40157
- $BaLaGa_3O_7$, melilite struct., synthesis 77-81236
- $BaLaMRuO_6$, ($M=$Mg, Fe, Co, Ni, Zn), cubic ordered perovskites, Mossbauer and mag. susceptibility meas. 80-75889
- $BaLaMTeO_6$, $M=$Li, Na, antiferroelectric, synthesis and characts. 77-55758
- $BaLaMnO_4$, and $Ba_{1+x}La_{1-x}MnO_4$, cryst. struct. determ. *(French)* 78-6042
- $Ba_6La_2Na_2(PO_4)_6F_2$, cryst. structure 79-60332
- $Ba_2LiNb_5O_{15}$, Czochralski growth, crystn. 80-35081
- $Ba_3Lu_4O_9$, synthesis, thermal stability, emissivity, reduction processes 77-8791
- $Ba_2M_{II}M_{III}'F_9$, ($M_{II}=$Fe, Co, Ni, Zn; $M_{III}'=$V, Cr, Fe), solid state synthesis and cryst. chem. study *(French)* 79-41988
- $Ba_3M_{4-4x}Ti_{4+5x}O_{21}$ $(O\leq x\leq 0.3)$, $M=$Nb,Ta, synthesis and struct. anal. *(French)* 80-44185
- $Ba_3(M_4Ti_4)O_{21}$, $M=$Nb, Ta, Sb, effects of Sb substit., synthesis and cryst. chemistry 77-76379
- $BaMg_2Al_{16}O_{27}:Eu^{2+}$ phosphor, for low press. fluoresc. lamp, luminesc. characts. 78-10960
- $Ba_2MgCr(PO_4)_3$, cryst. data 77-39564
- $BaMgF_4$, low temp. phonon effects on polarisation 79-42905
- $BaMgF_4:Mn^{2+}$ ferroelec., EPR and ENDOR study, cryst. field tensor 80-71162
- $Ba_2Mg_2Fe_{12}O_{22}$, hexagonal ferrite, with anisotropic g-factor, ferromag. reson. 77-69700
- $BaMg_2(PO_4)_2$, crystal growth from melt, optimal conditions for crystn. 77-59683
- $BaMg_2(PO_4)_2$, dielectric permittivity and elec. resist., temp. depend. 77-59502
- $BaMg_{1/3}Ru_{2/3}O_3$, crystal struct., mag. susceptibility and exchange integrals *(French)* 77-16037
- $Ba_{1-x}Mg_xSO_4:Eu^{3+}$ phosphor, thermolum. characts. 77-90203
- Ba_2MgTeO_6, ferroelec. behaviour, microwave dielec. props. meas. 77-43948
- $BaMgTi_7O_{16}$, hollandite struct. electron-optical imaging at 3 Å resolution 77-65939
- $BaMn_{0.99}Co_{0.01}F_4$, magnetoelec. phenomena, dielec. behaviour near Neel temp. 80-71151
- $BaMnF_4$, anisotropic order parameter phase fluctuations, light scatt. and thermal diffusivity meas. 80-80807
- $BaMnF_4$, anomalous acoustic phonon dispersion 77-47523
- $BaMnF_4$, antiferromag., dielec. anomalies at low temp. obs. 77-20791
- $BaMnF_4$, dielec. anomaly, mechanism, spin canting 78-10744
- $BaMnF_4$, dielectric props. near 250K phase transition 77-12335
- $BaMnF_4$, ESR linewidth and reson. field for Mn^{2+}, 25 to 300K, spin diffusion 77-69681
- $BaMnF_4$, ferromag. ferroelectrics *(Japanese)* 79-65804
- $BaMnF_4$, incommensurate phase, Brillouin spectra 79-42981
- $BaMnF_4$, incommensurate transition, Brillouin scatt. investigation 79-87406
- $BaMnF_4$, low temp. dielec. props. and phase transitions 77-20790
- $BaMnF_4$, low temp. phonon, and exciton effects on polarisation 79-42905
- $BaMnF_4$, luminesc., emission from localised traps 79-33777
- $BaMnF_4$, mag. and structural phase transitions, neutron scatt. obs. 79-87259
- $BaMnF_4$, magnetic neutron scatt. from structurally distorted cryst. 80-93086
- $BaMnF_4$, magnetoelec. phenomena, dielec. behaviour near Neel temp. 80-71151
- $BaMnF_4$, phase transitions, review 79-78378
- $BaMnF_4$, pure and Co doped, ferroelec. antiferromag., dielec. anomalies 80-71288
- $BaMnF_4$, spectroscopy, ferroelectric/ferromagnetic coupling 79-19845
- $BaMnF_4$, spectroscopy near ferroelec. transition, dielec. anomalies near mag. ordering temp. 80-75965
- $BaMnF_4$, struct. and mag. transitions, magnon dispersion curves, nearest neighbour exchange consts. 79-42760
- $BaMnF_4$, struct. phase transition, optical parameters obs. 80-100328
- $BaMnO_{3-x}$, O_2 deficiency induced polymorphs 78-26531
- $BaMnO_4$, ferroelectrically induced ferromagnetism 77-73067
- Ba_2MnReO_6, seignettomagnets with perovskite struct. 79-38459
- Ba_2MnS_3, linear chain antiferromag., mag. susceptibility meas. and Mossbauer spectra 80-107992
- $BaMo_4$, $M=$Mo,W, EPR spectrum, temp. depend. of zero field splitting 79-15346
- $BaMoO_3$, perovskite-type cmpd., metallic conductivity, room temp. to 2.5K 79-65483
- $BaMoO_4$ crystals, growth in SiO_2 gel under influence of elec. field 80-93469
- $BaMoO_4$, Davydov splitting of vibr. levels, short range interaction 80-71418
- $BaMoO_4$, external lattice vibr. modes and elastic wave vels., dispersion relations 79-33050
- $BaMoO_4$, growth in silica gel medium in test tube 77-36379
- $BaMoO_4$, luminesc. props. 80-11459
- $BaMoO_4$, precipitation from neutral equivalent solns., cryst. numbers, final morphology and sizes 78-23597
- $BaMoO_4$, single crystals, habit modification, growth kinetics in silica gel 80-20777
- $BaMoO_4$-$CdO(PbO)(ZnO)$ and $BaMoO_4$-$CdMoO_4(PbMoO_4)(ZnMoO_4)$ systems, phase diagrams 77-25034
- Ba_2MoO_5, Ba_3MoO_6, electrophys. props., effects of thermophys. props. of medium in synthesis 77-48375
- $Ba_2Mo_{15}Se_{19}$, superconducting chalcogenides containing Mo_6 and Mo_9 clusters 80-103804
- $Ba(N_3)_2$, thermal decomp., role of defects 78-73033
- $BaNB_2O_6$, IR and Raman spectra, vibr. anal. *(French)* 79-91446
- $Ba(NO_3)_2$, Born-Mayer interaction pot. and lattice props. 79-37858
- $Ba(NO_3)_2$, dynamical props., IR reflection spectra meas., 10-300K 77-1676
- $Ba(NO_3)_2$, electric field gradient, quadrupole coupling consts. 77-89740

barium compounds continued

- $Ba(NO_3)_2$, IR reflection spectra, dynamical props. 77-16303
- $Ba(NO_3)_2$, isomorphous crysts., growth defects, X-ray topography 80-70188
- $Ba(NO_3)_2$, low temp. struct. changes, elec. props. 79-87377
- $Ba(NO_3)_2$, Nd laser second harmonic stimulated Raman scatt., efficiency in calcite, nitrate crysts. 80-95949
- $Ba(NO_3)_2$, press. derivatives of elastic-moduli, ultrasonic velocity meas. 78-95102
- $Ba(NO_3)_2$, Raman spectra temp. depend. anomalies in symmetric stretch region 79-61361
- $Ba(NO_3)_2$, vibrations of isotopic impurities, IR reflection and Raman spectra meas. 77-51465
- $Ba(NO_3)_2$, X-ray Debye temp. determ. 77-59088
- BaN_2O_3, vibr. spectra, assignments 77-38670
- $Ba(NO_2)_2.H_2O$, crystal gyrotropy, meas. in IR region 80-88957
- $Ba(NO_2)_2.H_2O$, hexagonal, piezoelec., electro-optic, dielec., elastic, thermoelastic props., space groups 78-76388
- $Ba(NO_2)_2.H_2O$, nonlinear optical props. and polariton scatt. spectra 77-75616
- $Ba(NO_2)_2.H_2O$, pyroelectric IR radn. detector 79-80685
- $Ba(NO_2)_2.H_2O$, pyroelec., room temp. cryst. struct. 80-96491
- $Ba_2Na(Nb,Ti)_5O_{15}$, prep. and electro-opt. props. 78-76432
- $Ba_2Na(NbO_3)_5$, intracavity cryst., thermo-optical distortion, effect on freq. doubled Nd:YAG laser 77-71998
- $Ba_2NaNb_3O_{15}$, struct. phase transitions, light scatt. meas. 79-95774
- $Ba_2NaNb_5O_{15}$, absorption loss effects on frequency-doubled operation of Nd:YAG laser 79-36957
- $Ba_2NaNb_5O_{15}$, birefr. material, thermal cond. determ. by optical method 78-18851
- $Ba_2NaNb_5O_{15}$, cryst. comp. effect on low temp. phase transition 80-71346
- $Ba_2NaNb_5O_{15}$ crystal, high optical quality, and optical absorption coeff. meas. 78-30036
- $Ba_2NaNb_5O_{15}$ crystal domains, amplitude modulation of light by diffr. 79-59832
- $Ba_2NaNb_5O_{15}$ crystals, in Nd^{3+}:YAG laser cavity, AM of optical second harmonic 80-78908
- $Ba_2NaNb_5O_{15}$, dispersion of quadratic optical susceptibility *(Russian)* 77-3635
- $Ba_2NaNb_5O_{15}$, effect of substituting Gd, Cr on lattice parameters 78-47291
- $Ba_2NaNb_5O_{15}$, electrooptic coeffs. and refractive indices 79-33673
- $Ba_2NaNb_5O_{15}$, electrooptical diffr. by periodic domain struct. 80-40090
- $Ba_2NaNb_5O_{15}$, ferroelastic transition with increasing symm. on cooling 77-16265
- $Ba_2NaNb_5O_{15}$, ferroelastic transition sequence, cooperative pseudo-Jahn-Teller model 77-35689
- $Ba_2NaNb_5O_{15}$, ferroelec., cathodlum. spectral and temp. depend. 78-84665
- $Ba_2NaNb_5O_{15}$, ferroelec. conversion to single domain, elec. and photoelec. props. 78-88271
- $Ba_2NaNb_5O_{15}$, ferroelec. phase, thermally stimulated light flashes, surface elec. props. effects 79-73885
- $Ba_2NaNb_5O_{15}$, ferroelectric, local states, thermoluminesc. study 80-60690
- $Ba_2NaNb_5O_{15}$, Gd substitution, effect on linear thermal expansion, possible BSN replacement 78-43153
- $Ba_2NaNb_5O_{15}$, growth layer form., crystallization conditions effect, light diffr., Curie temp. 80-100778
- $Ba_2NaNb_5O_{15}$, high press. phase transitions, Raman scatt. studies 80-71402
- $Ba_2NaNb_5O_{15}$, high-pressure phase transitions, ferroelastic phase 79-7687
- $Ba_2NaNb_5O_{15}$, incommensurate refls. near ferroelastic transition, neutron and X-ray precession obs. 80-70395
- $Ba_2NaNb_5O_{15}$, ionic grouping theory of electro-optical and nonlinear optical effects of crystals *(Chinese)* 78-27183
- $Ba_2NaNb_5O_{15}$, kinetics of low temp. conversion into single domain form 77-43953
- $Ba_2NaNb_5O_{15}$, low temp. ferroelectric transitions, birefr. and dielec. meas. 79-38499
- $Ba_2NaNb_5O_{15}$, optical mode softenings, Raman scatt. meas., 1.5 to 600K 79-33631
- $Ba_2NaNb_5O_{15}$, phase transition at high press., Raman scatt. obs. 79-55884
- $Ba_2NaNb_5O_{15}$, Raman spectra, soft oscillations, temp. depend. 78-31203
- $Ba_2NaNb_5O_{15}$, Raman spectra in elec. field 79-1763
- $Ba_2NaNb_5O_{15}$, Raman scatt. experiments in tetragonal tungsten bronze compounds 80-40113
- $Ba_2NaNb_5O_{15}$, refr. index, equal-deflection method, UV laser rad. 78-29145
- $Ba_2NaNb_5O_{15}$, two-stage internal SHG in coupled resonators of Nd:YAG laser *(German)* 79-98438
- $Ba_2NaNb_5O_{15}$, X-ray powder diffraction data determ. *(Chinese)* 80-70170
- $Ba_2NaNb_5O_{15}:Fe,Mo$, photorefraction mechanism and photoelec. props. 80-71381
- $Ba_{2.09}Na_{0.72}Nb_{5.02}O_{15}$, cryst. growth, monodomenisation, detwinning, optical homogeneity, composition, dielec., spectral props. 77-44151
- $Ba_{4+x}Na_{2-2x}Nb_{10}O_{30}$, tetragonal tungsten bronze structure ferroelec. mech. for ferroelec. transition 79-38481
- $Ba_2NaNb_{5-x}Ti_xO_{15-x}F_x$ and $Ba_{2-x}Na_{1+x}Nb_5O_{15-x}F_x$, ferroelectric props., F substitution effect 77-12331
- $Ba_2NaNb_50_{15}$ ferroelec. crystals for electrooptics and nonlinear optics, optical inhomogeneities, review *(Japanese)* 77-65613
- $Ba_{2.09}Na_{0.72}O_{15}$, ferroelec., photocond. and optical absorpt. spectra. 77-8149
- $BaNb_2O_6$, solid-phase formation reaction, thermographic, X-ray phase and chemical anal. 77-12783
- $Ba_3Nb_{10}O_{28}$, diffuse ferroelec. phase transition, dielec. const. and X-ray diffr. meas. 78-23419
- $Ba_5Nb_4O_{15}$, 5H polytype, perovskite related phase, electron microscope obs. 77-51391
- $Ba_4NbRu_3O_{12}$ $(Ru_3O_{12})^{13-}$ cluster obs. in presence of orbital degeneracy and spin-orbit coupling *(French)* 80-70655
- $Ba_3Nb_6Si_4O_{26}$-$Ba_3Nb_4Ti_4O_{21}$, intergrowth, nonstoichiometry, struct. obs. *(French)* 77-19932
- $(Ba_3Nb_6Si_4O_{26})_n.Ba_3Nb_4Ti_4O_{11}$, $n=3/2$ to $29/2$, intergrowth series, electron microscope obs. *(French)* 78-83762

barium compounds continued
$(Ba_3Nb_6Si_4O_{26})_n.Ba_3Nb_4Ti_4O_{21}$, multiple intergrowth and microdomains obs. by electron diffr. and microscopy *(French)* 78−95160
$BaNb_x{}^{V}Ti_x{}^{III}Ti_{1-x}{}^{IV}O_3$, A and C-domain crysts., elec. cond. and absorption spectra 77−47805
$Ba_3Nb_{8-x}X_xO_{21}$ (X=Nb, Ti, Cr, Fe, Ni, Mg, Zn), X-ray diffr., layer struct. *(French)* 77−15368
$BaNdMnO_4$, cryst. struct. determ. *(French)* 78−6042
$BaNd_2(MoO_4)_4$, X-ray cryst. struct. determ. 80−88128
$Ba_4Nd_3Na_3(PO_4)_6F_2$, cryst. structure 79−60332
$BaNiF_4$, low temp. magnon effects on polarisation 79−42905
$BaNiF_4$, obs. of anomalous pyroelec. behaviour due to cooperative mag. singularity 77−59517
Ba_2NiF_6, obs. of short range order by optical birefringence 79−11318
Ba_2NiF_6, quadratic layer antiferromag., optical spectra obs. 77−16326
Ba_2NiF_6, specific heat capacity, critical amplitude, cross-over from 2-D Ising to Heisenberg behaviour 80−39791
$Ba_2Ni_3F_{10}$, cryst. struct. and antiferromag. props. 80−107153
$BaNi_2M_xFe_{16-x}O_{27}$, effect of $M=Sc^{3+}$ or In^{3+} on props. 77−47978
$BaNiO_3$, form. entropy and tolerance factor 80−34204
$BaNi_2(PO_4)_2$ and $BaNi_2(AsO_4)_2$, mag. props., neutron diffr. and sp. ht. meas. 80−70948
$BaNi_2(PO_4)_2$, crystal growth from melt, optimal conditions for crystn. 77−59683
$BaNi_2(PO_4)_2$, dielectric permittivity and elec. resist., temp. depend. 77−59502
Ba_2NiReO_6, mag. and cryst. struct. 77−20554
$BaNpO_2(H_3C_2O_2)_3.2H_2O$, structure and bonding study 77−27868
BaO, $A\ {}^1\Sigma^+$ state, dipole moment, MODR Stark effect 77−46584
BaO, $A\ {}^1\Sigma^+$ state, dipole moment, level crossing spectroscopy obs. 79−94040
BaO adsorbed on Si photofield cathode, work function and emission props. *(Russian)* 78−68608
BaO, association with $N_2O_4 \rightleftharpoons 2NO_2 \rightleftharpoons 2NO+O_2$ system, 350-650K *(Russian)* 79−20363
BaO, at. charge densities, X-ray struct. factors 78−79566
BaO, atomic interaction effects in X-ray emission spectra *(Russian)* 79−69905
BaO, $C^1\Sigma^+$-level, perturbation, extra lines, assignment 79−18213
BaO, CO_2 transport kinetics following $BaCO_3$ decomp. 79−23780
BaO coating, on W cathode, struct. transforms., LEED obs. 78−11061
BaO, cohesive and thermophysical props., role of three-body interactions 80−92477
BaO core glass/multicomponent clad glass optical fibres 80−78949
BaO crown and flint glasses, Ag and Cu diffusion for optical waveguide fabrication 78−59166
BaO, cryst., Debye characteristic temp. calcs. 79−37796
BaO, cubic NaCl-type cryst., Debye temp. 80−54333
BaO, determ. in glass, at. absorpt. method *(Polish)* 79−24872
BaO, dielectric behaviour 79−91343
BaO, dissociation energy 77−550
BaO, effect on crystallisation of $Na_2O-CaO-Al_2O_3-SiO_2-F-B_2O_3-ZrO_2$ glaze 79−60279
BaO, effect on props. of PbO containing cryst. glass 80−24637
BaO, effect on viscosity of PbO containing crystal glasses 80−19973
BaO, electron energy loss and secondary emission mechanisms, plasmon losses 78−76565
BaO, electronic struct. of V^- and related centres 80−2355
BaO epitaxial films, cathode poisoning due to O_2, CO_2, and S, surface anal. 79−42600
BaO, excited electronic states, lifetimes and transition moments 80−87177
BaO film, depend. of struct. on thickness 78−2391
BaO, film, emission props. in relation to struct. 80−100501
BaO, film, initial struct., field electron emission microscopy and LEED determ. 79−11033
BaO film, multilayer and monolayer, on W substrate, AES and work function meas. 77−24921
BaO film on W surface, struct. of crit. nuclei in heterogeneous crystn., LEED and FEM 77−11817
BaO films on Ir, thermionic props., Auger, LEED, and emission microscopy 79−43089
BaO, fluoresc. spectra, dye laser excited 79−68260
BaO, ground state vibr. pop. distribs. from photoluminesc. in $Ba+O_2$ and $Ba+N_2O$ 77−34731
BaO, high refractive index core glass for high NA optical fibres *(Japanese)* 79−59853
BaO, in upper atmosphere, flow rel. to striation struct. in Ba^+ clouds 77−25833
BaO, lattice dynamics calc., three-body force shell model 77−1195
BaO, logarithmic derivative reflectance spectra 80−11429
BaO, lowest triplet state, photoluminesc. optical-optical double reson. obs. 79−68254
BaO, meas. of time-resolved spectra of fluorescence using photon correlator 80−87250
BaO, microwave-laser double reson. spectra 78−82757
BaO, mm wave spectrum, spectroscopic consts. 78−37629
BaO, modified three-body shell model, lattice dynamics 77−4165
BaO, Mollwo-Ivey relation between peak-colour absorption energy and average O ion spacing 77−90179
BaO, monolayer on W (110), film struct. and electron state 80−100498
BaO, NaCl struct., elastic props., US meas. 78−18697
BaO optical waveguides, Fresnel lenses 80−96034
BaO, optical-optical double reson. of excited states, Parkinson band system 78−70857
BaO produced in $Ba+SO_2$ reaction, vibronic distrib., collisional energy depend., laser-induced fluoresc. obs. 80−11917
BaO, recoil velocity spectra from crossed-beam spin-forbidden $Ba+SO_2$ reaction 79−74361
BaO, recoil velocity spectra from form. in crossed beam system 80−76500
BaO, reduction by C, kinetics and mechanism *(Russian)* 80−93743
BaO reversible oxidation energy storage system feasibility 79−83637
BaO, single cryst. on Ir, electron affinity, conduction band edge position, low energy electron reflection spectra 78−14790
BaO single crystal, temp. depend. of bulk modulus 78−27549
BaO, slow-electron-stimulated desorption 79−60623
BaO solubility products in molten NaCl-KCl, potentiometric determ. 80−76488
BaO surface, AES peak height calibrations 79−43072

barium compounds continued
BaO, surface pot. meas., cond. band edge, electron affinity, LEER 77−24606
BaO, surface states, reflectance spectra, impurity effects 77−20873
BaO, temp. depend. of thermal expansivity between 20-300K 79−77778
BaO, transition moment of diatom., ρ-evaluation 79−31612
BaO whiskers, electromech. effect 79−65800
BaO, XPS valence bandstruct. 80−89117
$BaO{:}Mn^{2+}$, impurity pot. well shape calcs. 78−87950
$BaO-Al_2O_3-B_2O_3{:}Ce^{3+}$ glass, EPR spectra, before and after X-irrad. 78−19320
$BaO-Al_2O_3-B_2O_3{:}Ag$, X-ray irrad., atomic centre interactions, EPR spectra 80−25207
$BaO-Al_2O_3-B_2O_3-V_2O_5$ glass, spectra, oxidation-reduction behaviour, DC cond. 77−76814
$BaO-Al_2O_3-GeO_2-MF_2$ ($M=0.45\ CaF_2+0.55MgF_2$), MgF_2 and CaF_2 effect on physicochem. props. 80−34876
$BaO-Al_2O_3-P_2O_5$, struct. energetics and charging under irrad. *(Russian)* 77−84791
$BaO-Al_2O_3-P_2O_5$, exam. of electron beam irrad. effects on physical props. 79−4253
$BaO-Al_2O_3-P_2O_5$, electron beam irrad., temporal change in electric field produced 79−4760
$BaO-Al_2O_3-P_2O_5$ irradiated electret glasses, relax. of external field intensity on heating 80−25282
$BaO-Al_2O_3-SiO_2$ ceramic, chem. resist. and struct. 79−61756
$BaO-Al_2O_3-SiO_2-H_2O$ system, phase transitions during hydrothermal treatment 79−43216
$BaO-Al_2O_3-SiO_2-TiO_2$ glass-crystal material, elec. cond. 79−60876
$BaO-Al_2O_3-SiO_2-Ta_2O_5-Mo$ glass ceramic metal composites, cermet prep. 80−11618
$BaO-Al_2O_3-TiO_2-SiO_2$, glass formation, structure of cations *(Russian)* 80−38933
$BaO-B_2O_3$, composition effects on mean dispersion 78−80313
$BaO-B_2O_3$, glass, refraction, refractive index from 0.365 to 2.50 μm 80−88953
$BaO-B_2O_3$ glass, $Mn^{2+} \rightarrow Nd^{3+}$ energy transfer, fluoresc. obs. 77−8621
$BaO-B_2O_3$ melt, $Fe_2O_3-Fe_3O_4$ equilibrium, ferrite prep. 77−36428
$BaO-B_2O_3{:}\ UO_2{}^{2+}$, Eu^{3+} glass, nonradiative energy transfer 77−59602
$BaO-B_2O_3{:}UO_2{}^{2+}$, Nd^{3+} glass, radiative and nonradiative energy transfer 78−60508
$BaO-B_2O_3{:}UO_2{}^{2+} \rightarrow Er^{3+}$ glass, energy transfer 78−2895
$BaO-B_2O_3-GeO_2$, exam. of glass formation and physicochemical props. 79−4959
$BaO-B_2O_3-SiO_2$ system glass, electronic cond. of Ti ions 78−23095
$BaO-B_2O_3-SiO_2{:}Ti^{3+}$, elec. cond., struct. 78−72148
$BaO-B_2O_3-SiO_2{:}Ti^{3+}$, optical absorpt. spectra 78−72564
$BaO-B_2O_3-SiO_2{:}Ti^{3+}$, Ti^{4+}, glass EPR spectra, variation of g-factor with temp. 79−99757
$BaO-B_2O_3-V_2O_5$ glasses, polaron hopping cond., optical absorpt. and ESR spectra 79−23966
$BaO-B_2O_3-V_2O_5(Fe_2O_3)(Cu_2O)$, glass, resist. and activation energy, reduced valency 77−51749
BaO-Ba coated cathode, role of surface donor centres 78−11063
$BaO-BaCO_3$, thermal dissociation 77−86297
$BaO-BaX_2-P_2O_5$ glass, X=F, Cl, Br, conductivity 78−67862
BaO-CaO, amorphous film, Cu-electrodes, elec. props. 77−35997
$BaO-Fe_2O_3$, chemically coprecipitated, mag. props., orientation 80−15763
$BaO-Fe_2O_3$, splat quenching struct. and crystn. mechanism *(French)* 78−51426
$BaO-Fe_2O_3$ system, splat cooled phases struct., magnetisation and susceptibility 300-1100K *(French)* 77−48017
$BaO-Fe_2O_3-B_2O_3$ glass system, mag. struct., Mossbauer study 78−39485
$BaO-Fe_2O_3-B_2O_3$ glass, Mossbauer study of struct. and mag. props. 79−47369
$BaO-Fe_2O_3-B_2O_3$ glass, struct. and mag. props., Mossbauer spectra 80−7226
$BaO-Fe_2O_3-B_2O_3$ glass, splat cooled, low temp. micromagnetism 80−34660
$BaO-Fe_2O_3-B_2O_3(Na_2O)$ glasses, high Fe_2O_3 content, mictomagnetic props. 80−65916
$BaO-Fe_2O_3-Na_2O$ glass, mag. props. 78−88123
$BaO-Fe_2O_3-(Na_2O)$ glass, rapidly quenched, mag. and ferrimag. props. 80−75744
$BaO-GeO_2$ system, phase equilibrium diagram 79−70047
$BaO-GeO_2-Na_2O$ borosilicate core glasses for high numerical aperture fibres 80−69534
$BaO-GeO_2-Na_2O-H_2O$ system, hydrothermal crystn., phase formation laws 79−46636
$BaO-In_2O_3$ system, stability of synthesized compounds 77−36487
$BaO-K_2O-Na_2O-ZnO-SiO_2$, corrosion and microhardness, effect of detergents 80−16518
$BaO-K_2O-VO_2-SiO_2$, glass, elec. cond. rel. to ion polarisability, polarons 80−49729
$BaO-La_2O_3-B_2O_3$, glass, refraction, refractive index from 0.365 to 2.50 μm 80−88953
$BaO-La_2O_3-GeO_2$, exam. of glass forming region, properties and crystallisation 78−88454
$BaO-M_xO_y-B_2O_3$ glass, UV absorpt., inherent absorpt. wavelength and oscill. strength, cation effects 78−80374
$BaO-MMOo_4$, M=Cd,Pb, phase diag. cross sections and reactions 78−27487
$BaO-Mn_2O_3-B_2O_3$, amorphous mag. oxide, field-cooling effect *(Japanese)* 80−84615
$BaO-MoO_3$, solid phase reaction, thermal analysis 80−55639
$BaO-Nd_2O_3-P_2O_5$ ultraphosphate glasses, Nd^{3+} conc. quenching of luminesc. effect 79−19931
$BaO-Nd_2O_3-TiO_2-Bi_2O_3$ system ceramics, high stability low loss dielectric preparation 80−81008
$BaO-OsO_2$ system 79−24739
$BaO-P_2O_5$, glass, US velocity rel. to elastic props. 80−103425
$BaO-P_2O_5$ glass, diffusion of Cu^+, fluoresc. meas. 78−59980
$BaO-P_2O_5$ glass, ESR of VO^{2+} ions 80−100610
$BaO-P_2O_5$ glasses, Cu^+ ion electromigration at 400°C, luminesc. meas. 77−76610
$BaO-P_2O_5{:}Mo^{5+}$ glass, EPR spectra, computer simulation 80−88872
$BaO-P_2O_5-SiO_2$ glasses, photoelastic consts. and polarisability 79−65839
$BaO-PbO-GeO_2-MF_2$ ($M=0.45CaF_2+0.55MgF_2$), MgF_2 and CaF_2 effect on physicochem. props. 80−34876

barium compounds continued

BaO-SiO_2, and KF-BeF_2 systems, complex ionic liquids, corresponding-state principle *(Japanese)* 77−56245

BaO-SiO_2, molten, corresponding state principle with KF-BeF_2 and appl. 79−11589

BaO-SiO_2 glass, effect of high-dose X-rays and reactor radiation 80−19838

BaO-SiO_2 glass ceramic, nucleation, effect of electric fields 78−83742

BaO-SiO_2 glass ceramic, growth and nucleation kinetics 80−7528

BaO-SiO_2 glass-ceramic, crystallisation mechanism 79−90559

BaO-SiO_2 glasses, morphology effects on props. 80−49118

BaO-SiO_2-Fe_2O_3 permanent mag. ceramics, exam. of phase diagram, using X-ray analysis, optical microscopy, electron probe anal., and thermal analysis *(German)* 79−29012

BaO-SiO_2-P_2O_5, effect of thermal history on crystallisation of glasses 77−80424

BaO-SiO_2-TiO_2, molten, ionic elec. cond., TiO_2 effects *(Japanese)* 77−51532

BaO-SrO-Al_2O_3-TiO-SiO_2 glass ceramics, cryst. phases form., BaO/SrO ratio influence 80−19705

BaO-TeO_2, cryst. chem. study, X-ray diffr. powder data *(French)* 80−15080

BaO-TeO_2 glass, struct. and props. *(Japanese)* 79−32917

BaO-TiO_2-Al_2O_3 system, subsolidus equilibria, X-ray powder diffr. 80−108413

BaO-TiO_2-Cr_2O_3, new compound, phase relations *(Japanesè)* 78−6911

BaO-TiO_2-GeO_2, subsolidus equilibria 77−86014

BaO-TiO_2-Nd_2O_3, exam. of compositional and dielectric props. 79−33601

BaO-V_2O_5-CuO glass, EPR, Cu impurity effect on elec. props. 79−51849

BaO-V_2O_5-CuO semiconducting glasses, impurity effects, elec. resist. and EPR study 80−103692

BaO-WO_3, solid phase reaction, thermal anal. 80−55639

BaO-WO_3-P_2O_5 glass, struct. and IR spectra 80−64914

BaO+Ar(CO_2), in Ar flame, rot. and translational relax. by sub-Doppler optical-optical double reson. 80−95583

BaO+$BaCO_3$+SiC react., contact phenomena at SiC grain boundary 79−43193

BaO_3, visible absorpt. and reson. Raman spectra in Ar and N_2 matrices 77−65487

BaOH, (BaCl), mol. dissoc. energies calc. by high temp. mass spectrometer 80−83514

BaOH, fluoresc. spectra, dye laser excited 79−68260

$Ba(OH)_2+2K_2O.11TiO_2.3H_2O$ fibre hydrothermal reaction to form $BaTiO_3$ fibres *(Japanese)* 80−93527

Ba_3OSiO_4, struct. refinement 78−34479

$BaO(X^1\Sigma^+)$, vibr. relax., laser-induced fluoresc. meas. 77−83631

BaO*, quenching of excited species formed by Ba+NO_2 chemiluminesc. reaction 77−58140

$BaO.Al_2O_3.2SiO_2$, hydrothermal synthesis, phase transitions 77−48378

$BaO.GeO_2.5H_2O$, X-ray cryst. struct. determ. *(German)* 79−69067

$BaO.2SiO_2$, glass, spherulitic growth and recrystallisation 77−4046

$BaO.3B_2O_3.5H_2O$, thermal dehydration 78−43132

$3BaO.5SiO_2$ glass, nonisothermal devitrification kinetics 80−92465

$BaO.6Fe_2O_3$, ferrite polycryst., depend. of domain width on sample thickness 80−108031

$BaO.6Fe_2O_3$, solubility of CaO 80−100333

BaO.n Fe_2O_3, magnet, effect of SiO_2 on texture and densification behaviour *(German)* 79−24631

$Ba(PO_3)_2$ based fluorophosphate glasses, alkali free, and crystallisation products, struct and IR spectra 79−94913

$Ba(PO_3)_2$, hydrolytic decomp. 80−21271

$Ba(PO_3)_2$, vitreous, microhardness 80−25864

$Ba(PO_3)_2$-AlF_3-BaF_2 glasses, elec. cond., density, and IR spectra 79−95215

$Ba(PO_3)_2$-AlF_3-CaF_2, glass, elec. cond. and IR spectra 80−89005

$Ba(PO_3)_2$-AlF_3-MgF_2, glass, elec. cond. and IR spectra 80−89005

$Ba(PO_3)_2$-alkaline earth fluoride and $Ba(PO_3)_2$-YF_3 glasses, pseudobinary, elec. cond. and dielec. losses 77−7890

$Ba(PO_3)_2$-BaF_2, IR absorption spectra exam. of hydrolytic stability 80−39291

$Ba(PO_3)_2$-BaF_2-$BaCl_2(BaBr_2)$ glasses, elec. cond., mixed anion effect 80−15300

$Ba(PO_3)_2$-CaF_2, IR absorption spectra exam. of hydrolytic stability 80−39291

$Ba(PO_3)_2$-$CsPO_3$ system, equilibrium diagram *(French)* 77−28789

$Ba(PO_3)_2$-fluoride glass, elec. cond., struct. 80−88056

$Ba(PO_3)_2$-MgF_2, IR absorption spectra exam. of hydrolytic stability 80−39291

$Ba(PO_3)_2$-MgF_2, vitrification region 77−35676

$Ba(PO_3)_2$-$MgF_2=0.4AlF_3.0.6CaF_2$ glass system, vsicosity and energy parameters of rheological props. *(Polish)* 79−73331

$Ba(PO_3)_2$-SrF_2, IR absorption spectra exam. of hydrolytic stability 80−39291

$Ba(PO_3)_2$-WO_3, electron-absorpt. spectra and structure of W centres 80−88873

α-$Ba_2P_2O_7$, Raman, IR spectra, factor group anal. and band assignment 78−35126

$Ba_3(PO_4)_2$ glass, phase equilibrium data 79−27923

$Ba_3(PO_4)_2$ glass, phase equilibrium data 79−27922

$Ba_3(PO_4)_2$ phosphor, ionisation of capture centres, thermolum. spectra 80−11487

$Ba_3(PO_4)_2$, recomb. luminesc. mechanisms 80−2874

$Ba_3(PO_4)_2$ transition metal ion, optical and magnetic props. 78−64196

$Ba_3(PO_4)_2$, vib. of PO_4^{3-} 77−51457

$Ba_3(PO_4)_2$:Eu, X-ray phosphor, study of emission and trapping centres 79−8197

$Ba_5(PO_4)_3Cl$ with substituted CrO_4^{3-}, ESR study 80−2629

$BaPO_3F$, prep. from $BaCO_3$, H_3PO_4 and NH_4HF_2, props. 79−52147

$BaPO_3F$-Al_2O_3-B_2O_3 glasses, phys. props. 78−63676

$BaPO_3F$-Al_2O_3-B_2O_3 glasses, viscosity in the softening region and crystn. range 80−29105

$BaPO_3F$-Al_2O_3-B_2O_3 system, liq. phase separation, IR spectra, microstruct. 80−29940

$Ba_{10}(PO_4)_6F_2$, cryst. structure 79−60332

$Ba_{10}(PO_4)_6(OH)_2$, cryst., IR spectra, band assignments 78−60442

$Ba_{10}(PO_4)_6(OH)_2$, IR spectra, stretching and librational bands of OH groups, and hindered rotation 78−2841

$Ba(Pb,Bi)O_3$ perovskites, resputtering effects 80−80969

barium compounds continued

$BaPb_{1-x}B_xO_3$, critical temp. depend. on band gap for dielectric-supercond. transition *(Russian)* 79−65578

$BaPb_{1-x}Bi_xO_3$ film, RF sputtered, T_c as function of comp. and annealing conditions 79−24100

$BaPb_{1-x}Bi_xO_3$, semiconductor-metal transition and supercond., IR absorpt. and struct. meas. 77−28278

$BaPb_{1-x}Bi_xO_3$, struct. determ., X-ray and neutron diffr. study 79−42039

$BaPb_{1-x}Bi_xO_3$, supercond. T_c and crit. fields, comp. depend. 79−73623

$BaPb_{1-x}Bi_xO_3$, superconducting thin films, RF sputtering prep. 80−76181

$BaPb_{1-x}Bi_xO_3$, superconducting props., Hall coeff. and elec. resist. meas. 80−84531

$BaPbF_6$, Group IV hexafluoride anion radical γ-irrad., EPR spectra 78−72411

$BaPt(CN)_4.4H_2O$, cryst. struct., neutron diffr. 77−35521

$BaPt(CN)_4.4H_20$, energy band calcs. 77−39780

$BaPtO_3$, synthesis and struct. 77−80486

$Ba_3Pt_2O_7$, struct. model 77−72597

Ba_2RF_7, (R=Dy, Ho, Er, Tm, Yb, Lu, Y), superstructure phases, prep., thermal characterisation and X-ray powder diffr. 80−96494

$BaR_2(MoO_4)_4$, R=rare-earth, struct., optical, mech., spectral and physico-chem. props. 80−84161

BaR_2O_4, luminesc. on activation by Eu^{3+}, Nd^{3+}, Eu^{3+}-Tb^{3+} 77−52156

$Ba_4R_6(SiO_4)_6F_2$, (R=Nd, Y or Yb), synthesis and characterisation 77−24992

$Ba_3Re_2O_9$, cryst. struct., mag. and semicond. props. 79−10836

$Ba_5(ReO_5)_3Cl$, X-ray cryst. struct. determ., $(ReO_5)^{3-}$ content *(French)* 79−90601

$Ba_{10}(ReO_5)_6X$(X=Br, I), single cryst. X-ray struct. refinement *(French)* 79−77578

$Ba_3Ru_2MO_9$, (M=Mg, Ca, Sr, Co, Ni, Cu, Zn, Ca), Mossbauer spectra 80−108136

$Ba_4Ru_3MO_{12}$, (M=Ta, Nb), Ru oxidation state, Mossbauer study 80−44965

BaS, Ba and S XPS 80−43104

BaS, dielectric behaviour 79−91343

BaS, press. induced phase transform., X-ray diffr. study 80−39283

BaS:Bi phosphors, polycrystalline, effect of grain size on thermolum. 79−61446

BaS:Cu, thermoluminesc. and decay 78−80426

BaS:Cu phosphor, photo- and electro-luminescence 79−43030

BaS-CaS:Cu phosphors, X-ray diffr. and fluoresc. spectra 80−40148

$BaSO_2$, suspension, light scatt., optical anisotropy determ. by polarisation ratio 79−1772

$BaSO_4$, Ba and S XPS 80−43104

$BaSO_4$, barite, crystal struct. and sulphate force consts. 78−83784

$BaSO_4$, barite, periodic bond chains, computer determ. *(French)* 78−26474

$BaSO_4$, barytes, with large magnitude of emitted light, thermolum. curves 78−88368

$BaSO_4$, crystal growth, effect of nitrilotri (methylenephosphonic acid) adsorption 78−88417

$BaSO_4$, crystallisation, seeded growth kinetics, inhibitor effects 79−37644

$BaSO_4$, crysts., coagulative growth from a strongly supersaturated aq. soln. 80−2937

$BaSO_4$, electric quadrupole interaction, TDPAC meas. 78−39455

$BaSO_4$, growth curves, growth affinity presentation, for growth from soln. 79−27936

$BaSO_4$, microscopic grains, optical Cherenkov radiation 79−56880

$BaSO_4$, natural barite, thermoluminesc. glow curves after γ-ray irrad., low doses 77−63471

$BaSO_4$ natural barites, mech. of thermolum. 79−78763

$BaSO_4$, new high density powders for radiography 79−74745

$BaSO_4$, polarised IR refl., absorpt. and laser Raman spectra 77−43997

$BaSO_4$ powder, flashlamp reflectors for I photodissoc. laser 77−79848

$BaSO_4$ powder pressed tablets, Helmholtz reciprocity theorem for diffuse refl. *(German)* 77−79753

$BaSO_4$, precip. from aq. solns. with slow supersat. development 77−28707

$BaSO_4$, pressed powder Eastman White reflectance standard, absolute refl. meas. 78−25939

$BaSO_4$, single cryst., SO_4^{2-} vibr. levels, cryst. field effects, laser Raman spectroscopy 78−43847

$BaSO_4$, single cryst., neutron bombard. effect on struct. 78−63793

$BaSO_4$, solubility in water, effect of ^{35}S tracer, particle size and imperfection 78−43126

$BaSO_4$, $SrSO_4$ surface crystn. 80−34332

$BaSO_4$, TSEE and surface charging, simultaneous meas. 80−29864

$BaSO_4$ tablet, reciprocity of reflection values for geometries 45/0 and 0/45 *(German)* 80−71370

$BaSO_4$ white reflectance standard, Kubelka-Munk optical props. 77−42581

$BaSO_4$ white reflectance standard, Kubelka-Munk optical props. 78−4675

$BaSO_4$, with small retrapping factor, thermolum. glow curve 77−52188

$BaSO_4$, X-ray irrad., electron and holes traps, g-factors, ESR obs. 80−50183

$BaSO_4$, X-ray L-emission spectra of S *(Japanese)* 78−15254

$BaS_2O_3.H_2O$, X-ray powder data 79−14767

$Ba_2Sb^{V}Bi^{III}O_6$, struct. determ. by powder neutron diffr. 78−34468

$Ba_4Sb_3LiO_{12}$, Li sites determ., using method based on bond-strength calcs. 79−7514

$Ba_3Sb_2NiO_9$, 6H, cation ordering, powder neutron diffr. obs. 78−55852

$Ba_4Sb_4S_{11}$, cryst. struct., selenoantimonate (III) anions *(German)* 80−103305

$(Ba_xSb_{1-x})TiO_3$ 80−60514

$(Ba_xSb_{1-x})TiO_3$, ferroelectric films, dielectric and semicond. props. 79−91388

$BaSc_2O_4$, synthesis, thermal stability, emissivity, reduction processes 77−8791

$Ba_3Sc_4O_9$, $Ba_3Sc_2WO_9$ and Ba_2ScTaO_6, elec. cond. nature, depend. on comp. and medium thermodynamic parameters 80−70773

$Ba_3Sc_4O_9$, synthesis, thermal stability, emissivity, reduction processes 77−8791

$BaSi_2$, semicond.-metal transition, high-press. and temp. 78−43299

$BaSi_2$, trimorphic, transform. of three-connected Si nets, press.-temp. phase diagram, 40 kbar and 1000°C 80−75198

$Ba_3SiAl_{10}O_{20}$, Ce^{3+} activated, X-ray diffr. and luminesc. props. 80−49199

barium compounds continued
$BaSiF_6$, Raman spectra at press. up to 25 kbar 78−6670
$BaSi_{2\ y}Ge_y$, solid solution with type $SrSi_2$ struct., lattice parameters at high press. 80−54203
$BaSiO_3$, solid state reactions, thermodynamics and kinetics *(German)* 80−76236
$BaSiO_3$-$BaGeO_3$, phase diag. 77−48404
Ba_2SiO_4, gamma-irrad., ESR spectra 79−51853
Ba_2SiO_4, solid state reactions, thermodynamics and kinetics *(German)* 80−76236
Ba_2SiO_4:Eu^{2+}, activated phosphors, luminesc. efficiency, temp. and high-press. 78−23508
Ba_3SiO_5, solid state reactions, thermodynamics and kinetics *(German)* 80−76236
$Ba_5SiO_4Br_6$:Eu, blue emitting X-ray luminescent material for intensifying screens *(French)* 80−66260
$Ba_5SiO_4Cl_6$:Eu, blue-emitting phosphor high quenching temp. 80−16076
$Ba_2Si_2TiO_8$, elastic consts., thermal expansion and piezoelec. props. 77−85651
$Ba_2Si_2TiO_8$, fresnoite, SAW props., expt. and calc. 78−43229
$Ba_2Si_2TiO_8$, fresnoite single cryst. SAW characts. 79−37913
$Ba_2Si_2TiO_8$ fresnoite, characts. for SAW devices 79−82430
$Ba_{1-x}Sm_xB_6$, prep., elec. cond. and thermoelec. props. 80−49697
$Ba_{1-x}Sm_xS$, electron config. of Sm ions, X-ray L-absorpt. spectroscopy 80−60715
$Ba_{0\ 7}Sn_{2.6}Cr_{1.4}O_8$, short axis tripling, X-ray and electron diffr. study 79−77576
$Ba_{0.7}Sn_{2.6}Cr_{1.4}O_8$, X-ray cryst. struct. and composition determ., new hollandite phase 79−14750
$BaSnF_4$, thermal expansion and phase transitions 79−77781
$BaSnF_6$, Raman spectra at press. up to 25 kbar 78−6670
$BaSnO_3$, high-density ceramics prep. and elec. props. 80−60812
$BaSnO_3$, powder, electron scatt. from ^{119}Sn, effective range, Mossbauer obs. 77−63345
$Ba^{119m}SnO_3$ Mossbauer source, resonant self-absorpt. correction 77−28498
$Ba_{0.5}Sr_{1.5}Al_4Si_{12}O_{32}.10H_2O$, brewsterite cryst. struct. refinement 77−80471
$BaSr_xCa_{1-x}Fe_4O_8$, substituted hexagonal ferrites, mag. split Mossbauer spectra obs. and X-ray struct. data 80−71250
(BaSrCa)O, cathodes, thermionic emission characts., X-ray struct. obs. 78−48270
$Ba_{0.725}Sr_{1.775}Li_xNb_{5-x}Ti_xO_{15}$, solid soln., prep., struct., dielec. props. *(French)* 77−69782
$Ba_{0.1}Sr_{0.9}MnO_{2.96}$, 4H polytype, perovskite related phase, electron microscope obs. 77−51391
$Ba_{1.35}Sr_{0.65}NaNb_5O_{15}$ crystals, struct., dielec. and pyroelectric characts. 79−51913
$Ba_{0.25}Sr_{0.75}Nb_2O_6$, anomalous photovoltaic effect and photocond. 79−38122
$Ba_{0.25}Sr_{0.75}Nb_2O_6$, fast-response pyroelec. cryst. detector 78−49904
$Ba_{0.25}Sr_{0.75}Nb_2O_6$, ferroelec., photocond. and optical absorpt. spectra 77−8149
$Ba_{0.25}Sr_{0.75}Nb_2O_6$, ferroelec., influence of temp. on Raman scatt. spectra 77−69842
$Ba_{0.25}Sr_{0.75}Nb_2O_6$, ferroelectric, anomalous photovoltaic effects 79−7861
$Ba_{0.25}Sr_{0.75}Nb_2O_6$, photoresponse in transition region 77−1451
$Ba_{0.25}Sr_{0.75}Nb_2O_6$, photovoltaic current, temp. and spectral depend. 78−47828
$Ba_{0.25}Sr_{0.75}Nb_2O_6$, quadratic susceptibility dispersion meas., oscillator model including structure 78−59078
$Ba_{0.25}Sr_{0.75}Nb_2O_6$, spontaneous electroopticabsorption effect 78−19443
$Ba_{0.25}Sr_{0.75}Nb_2O_6$, thermal and spectral variations in the photovoltaic current in ferroelectrics 78−91719
$Ba_{0.39}Sr_{0.61}Nb_2O_6$, electro-optical props. 80−2728
$Ba_{0.50}Sr_{0.50}Nb_2O_6$:$La_2O_3(Tm_2O_3)(Y_2O_3)$, Raman spectra 79−78678
$Ba_{0.5}Sr_{0.5}Nb_2O_6$, electronic props. and photoresponses 80−92925
$Ba_{0.5}Sr_{0.5}Nb_2O_6$, temp. depend. of Raman spectra 78−72524
$Ba_{0.54}Sr_{0.46}Nb_2O_6$, line broadening effect in Rayleigh scatt. of Mossbauer radiation 80−50238
$Ba_{0.54}Sr_{0.46}Nb_2O_6$:Y(La)(Tm), dielectric and electrooptic props. 78−68466
$(Ba_{1-x}Sr_x)_{1-y}(Nb_2O_6)_y$:$CeO_2$ crystals, photoelectric and photorefractive props., hologram recording 80−53239
$Ba_xSr_{1-x}Nb_2O_6$ (x=0.27 to 0.54) exam. of freq. dependence of permittivity diffuse ferroelectric phase transition kinetics 80−2703
$Ba_xSr_{1-x}Nb_2O_6$, anomalous photovoltaic effect and photocond. 78−52449
$Ba_xSr_{1-x}Nb_2O_6$ crystals, struct., dielec. and pyroelectric characts. 79−51913
$Ba_xSr_{1-x}Nb_2O_6$ crystals, optical defects and edge dislocation distributions 80−19806
$Ba_xSr_{1-x}Nb_2O_6$ crystals, defects and their characteristic features 80−88138
$Ba_xSr_{1-x}Nb_2O_6$, ferroelec., cathodlum. spectral and temp. depend. 78−84665
$Ba_xSr_{1-x}Nb_2O_6$, ferroelectric with diffused phase transition, photoelectret states 80−20583
$Ba_xSr_{1-x}Nb_2O_6$, growth defects 78−38640
$Ba_xSr_{1-x}Nb_2O_6$, nonequilibrium processes 78−48124
$Ba_xSr_{1-x}Nb_2O_6$, photoelectretic states in real time spatial light modulators, photorefractive effect 80−80676
$Ba_xSr_{1-x}Nb_2O_6$, reduced, elec. cond., effect of oxygen vacancies 77−35939
$Ba_xSr_{1-x}Nb_2O_6$, single crystal, Mossbauer diffraction *(Russian)* 79−56644
$Ba_xSr_{1-x}Nb_2O_6$, struct. and dielec. props., isomorphic substitution effect 78−27165
$Ba_xSr_{1-x}Nb_2O_6$:Ce, pure and doped, photoelec. props. and photorefraction 80−60538
$Ba_{1-x}Sr_xNiO_{3-y}$, Sr substitution effect, powder X-ray diffr. 78−51498
(BaSr)O on Ni, cathode, oxide thickness depend. of emission 77−48299
$Ba_{1-x}Sr_xPb_{0.75}Bi_{0.25}O_3$, superconductivity, rel. to lattice const. 80−49966
Ba_2SrReO_6, ordered or perovskite type struct., magnetic and elec. props. 79−65053
$BaSr_{1/3}Ru_{2/3}O_3$, crystal struct., mag. susceptibility and exchange integrals *(French)* 77−16037
$(Ba_xSr_{1-x})SO_4$:Eu mixed crystal series, X-ray diffr. study of miscibility 80−2168
$Ba_{1-x}Sr_xSi_2$, solid solution with type $SrSi_2$ struct., lattice parameters at high press. 80−54203

barium compounds continued
$(BaSr)TiO_3$ film, ferroelec., dielec. props. in strong elec. fields 78−27163
$BaSrTiO_3$, model for 1/f excess noise 79−99591
$BaSrTiO_3$, semiconducting, excess noise characts. exam. 78−19110
$Ba_{0.4}Sr_{0.6}TiO_3$, ferroelec. thin film, fabrication, props. 77−28521
$Ba_{0.4}Sr_{0.6}TiO_3$ films, DC conductivity, strong microwave field effect 80−65727
$Ba_{0.60}Sr_{0.40}TiO_3$, sputtered film on Pt, pyro-effect for laser registration *(Russian)* 77−20804
$Ba_{1-x}Sr_xTiO_3$ ceramic pyroelec. responsivity, −140° to +160°C obs. 78−23405
$Ba_xSr_{1-x}TiO_3$, disordered ferroelec., dielec. const. and spontaneous polarisation meas. 78−48130
$Ba_xSr_{1-x}TiO_3$, ferroelec. thin film, elec. characts. *(Russian)* 78−23406
$Ba_xSr_{1-x}TiO_3$, ferroelec., with impurities, lattice dynamics 79−28061
$Ba_xSr_{1-x}TiO_3$, ferroelec. film, heteroepitaxial growth in cathode sputtering 80−93486
$Ba_xSr_{1-x}TiO_3$, thin ferroelec. layers 79−42912
$Ba_{2-x}Sr_xTiSi_2O_8$, piezoelec. crysts., SAW characts. 80−84354
BaT:O_3, surface microrelief revealed by ion irradiation 80−54485
BaT:O_3:Mn, ferroelec. domain stabilisation by bulk ordering of defects 79−42925
$Ba(TCNQ)_2$, electronic absorpt. spectra, vibronic struct., charge transfer bands 79−24331
$BaTa_2O_6$, structural study X-ray diffr., IR absorpt. and Raman spectra *(French)* 80−107173
$Ba_4TaRu_3O_{12}$, $(Ru_3O_{12})^{13-}$ cluster obs. in presence of orbital degeneracy and spin-orbit coupling *(French)* 80−70655
$BaTbO_3$, perowskite struct., Tb^{4+} EPR obs., cryst. field parameters determ. *(Italian)* 78−52350
$BaTe_2O_6$, X-ray cryst. struct., O_2 coordination no. of Te *(German)* 79−69075
$Ba(Ti,Sn)O_3$, thin film elec. and photoconductivity 79−33366
(BaTi) citrates, thermal decomp., thermal anal., IR and X-ray diffr. obs. 79−24735
$BaTiF_6$, Raman spectra at press. up to 25 kbar 78−6670
$Ba_2TiGe_2O_8$-$Ba_2TiSi_2O_8$, pseudobinary system, pyroelectricity and related props. 78−95553
BaTiO, mosaic struct. charge at ferroelec. phase transition *(Russian)* 77−32335
$BaTiO_2$, Fe-Co-Ti-Ba-O, composites, ferroelectric, magnetoelectric effects *(Russian)* 80−20440
$BaTiO_3$, 3d element doped, phase stability, phase transition temp., mag. susceptibility meas. 78−38835
$BaTiO_3$, 90° electric domain processes, mech. stress, X-ray diffr. 78−72478
$BaTiO_3$ (001), LEED and UPS studies 80−100747
$BaTiO_3$, A_1 and E optical phonons obs. in temp. range 10 to 132°C 77−27963
$BaTiO_3$, A_1-modes reflectivity meas. 79−65875
$BaTiO_3$, A_1(TO) phonon spectrum, ferroelectric phase transition, Raman scatt. meas. 78−56478
$BaTiO_3$ a-domain crystals, domain struct. influence on physical consts. 79−69798
$BaTiO_3$, acceptor doped, exam. of electrical conductivity 130 to 300°C 79−33286
$BaTiO_3$, acceptor-doped defect equilibria, elec. cond. 77−39579
$BaTiO_3$, acoustic wave interaction with microwave radiation field 80−6913
$BaTiO_3$, adsorpt. of O_2, mechanism calc. 78−63927
$BaTiO_3$, adsorption of $O_2(H_2)$, effect on work function and spontaneous polarisation *(Russian)* 78−6211
$BaTiO_3$ and $BaTi_{0.08}Sn_{0.02}O_3$ films, pyroelectric response to step radiation signals 80−7302
$BaTiO_3$ and $BaTi_{1-x}Fe_xO_{3-x}F_x$, electrical, optical and mag. props., photoelectrolysis 77−47856
$BaTiO_3$, anisotropic emission of exoelectrons ferroelec. phase transitions *(Russian)* 78−48291
$BaTiO_3$, anomalous photovoltaic effect and photocond. 78−52449
$BaTiO_3$, anomalous photovoltaic effect and photocond. 79−38122
$BaTiO_3$, antireson. in EPR spectra of Fe^{3+} ions *(Russian)* 80−11257
$BaTiO_3$, automatic anomalous noise meas. for ferroelectric capacitor parameters, not in equilib. *(French)* 78−74029
$BaTiO_3$, band struct. calc., interpretation of XPS and UPS spectra 80−70597
$BaTiO_3$, based ceramics with large permittivity, electrostriction consts. 77−66457
$BaTiO_3$, broadening of ferroelec. transition, heterophase fluctuations theory 77−81073
$BaTiO_3$, $BuTi_4O_9$, Ba_2TiO_4, synthesis from coprecipitation products 77−48382
$BaTiO_3$, bulk photovoltaic effect in ferroelecs. 79−15181
$BaTiO_3$, c-domain cryst., HF dispersion of permittivity 78−60379
$BaTiO_3$ ceramic, degradation under high AC elec. field 80−60499
$BaTiO_3$, ceramic, effect of grain size on nonlinear dielec. props. 77−8522
$BaTiO_3$ ceramic, electromechanical coupling caused by electrostriction, reson. props. meas. 77−20802
n-$BaTiO_3$, ceramic, expt. and theoretical investigation of grain-boundary resist. 79−56235
$BaTiO_3$ ceramic, PTC-type, voltage contrast imaging for low and high Ti excess 77−28183
$BaTiO_3$ ceramic, piezoelectric effect due to polarisation *(Polish)* 77−77151
$BaTiO_3$ ceramic, positive temp. coeff. resistivity, investigation as function of Ti-Ba ratio 78−72151
$BaTiO_3$ ceramic, semiconductive sintering 77−36430
n-$BaTiO_3$, ceramic, systematic expt. and theoretical investigation of grain-boundary resist. 79−56236
$BaTiO_3$ ceramic dielectric capacitor, processing prop. relations, hysteresis, permittivity 80−80730
$BaTiO_3$ ceramic films, dielec. strength, statistical anal. 80−75935
$BaTiO_3$ ceramic semiconductors, principle and appl. *(Chinese)* 79−73523
$BaTiO_3$ ceramic surface, neutralisation of bombarding ion beam 80−71528
$BaTiO_3$ ceramics, calcination effects, TiO_2 powder eval. *(Japanese)* 78−64516
$BaTiO_3$ ceramics, grain boundary pot. barriers, cathodoluminesc., electron probe anal. 80−2864

barium compounds continued
$BaTiO_3$ ceramics, PTC-type, grain boundary study using TEM 80–107267
$BaTiO_3$, charges effect on form. of nucleation centres of ferroelec. phase 79–65810
$BaTiO_3$, chemically precipitated, exam. of sintering behaviour by isothermal shrinkage *(German)* 79–4935
$BaTiO_3$, Clausius-Mossotti formula and irreducible susceptibility *(Japanese)* 79–65802
$BaTiO_3$, cluster surface states, LCAO calc. 77–43686
$BaTiO_3$, Co substituted, ferroelec., diffuse behaviour 79–38475
$BaTiO_3$, coherent excitation of soft polariton mode 79–15464
$BaTiO_3$, controlled surface layers 78–48120
$BaTiO_3$, coupled acousto-optic modes 80–96093
$BaTiO_3$, coupled electroacoustic eqns. 80–96092
$BaTiO_3$, critical hyper-Raman scattering 78–76466
$BaTiO_3$, crystallisation from melt, nucl. and final cryst. sizes 77–24951
$BaTiO_3$ crystals, mechanically compressed, dielec. const. 79–56711
$BaTiO_3$ crystals, octahedral TiO_6^{8-} cluster atomic population, ionisation energy, SCF MS Xα calcs. 79–72244
$BaTiO_3$, crystn. from melts, comparison of different prospective oxy-anion solvents 80–71583
$BaTiO_3$, cubic, optical modes meas. by neutron scatt. 79–69213
$BaTiO_3$, cubic-tetragonal phase transition, birefringence meas., surface distortion effects 78–95564
$BaTiO_3$, defect chem., elec. cond. obs. 77–4097
$BaTiO_3$, defect chemistry and elec. cond. improved positive temp. coeff. model 77–39859
$BaTiO_3$, deform. and stress relax. of single crysts. 77–59542
$BaTiO_3$, dielec. and elastic consts., temp. depend. *(Russian)* 78–64307
$BaTiO_3$, dielec. and optical props. using shell model 79–33654
$BaTiO_3$, dielectric ceramic, interaction with metallic film during sintering 79–33958
$BaTiO_3$, dielectric const. and polarisation, fluctuations, catastrophes 77–8491
$BaTiO_3$, diffr. of Mossbauer radiation near Curie point *(Russian)* 79–8079
$BaTiO_3$ disc in axial mag. and radial elec. fields, unusual EM surface force 77–26185
$BaTiO_3$, displacive ferroelectric, effective charge determ. 80–97212
$BaTiO_3$, displacive type ferroelectric, SHG 79–36955
$BaTiO_3$, domain structure obs. using SEM 77–1647
$BaTiO_3$, domain struct. characts. of unipolar ferroelec., photocarrier effects 78–19435
$BaTiO_3$, domain struct., formation at phase transitions 79–38510
$BaTiO_3$, donor doped, elec. props., effect of kinetic processes 78–64042
$BaTiO_3$, donor doped, exam. of heterogeneous microstructure *(German)* 79–24632
$BaTiO_3$, doped, defect chemistry and elec. cond. kinetics of equilib. restoration 77–39700
$BaTiO_3$, doped, loss mechanism and domain stabilisation 78–84542
$BaTiO_3$, Doppler-broadened positron annihilation 78–64428
$BaTiO_3$, dynamic Rayleigh light scatt. in region of ferroelectric-paraelectric transition 78–64371
$BaTiO_3$, effect of phase transformation on fracture behaviour 78–48507
$BaTiO_3$, elastic props., singularities near tetragonal-cubic phase transition 80–70303
$BaTiO_3$, elastooptic effect near ferroelec. transition, temp. depend. 80–97233
$BaTiO_3$, elec. and thermoelec. props. of grains and grain boundaries 78–43382
n-$BaTiO_3$, elec. transport props., theoretical discussion and expt. 78–84215
$BaTiO_3$ electrode, surface comp. changes during photoelectrolysis, XPS obs. 79–7894
$BaTiO_3$ electrodes, photocurrent efficiency, photo-oxidation of water 77–12000
$BaTiO_3$, electron energy loss spectra, 0.02-2 eV 78–39642
$BaTiO_3$, electron exoemission unipolarity associated with phase transitions 80–97415
$BaTiO_3$, electron microscopy investigs. of ferroelec. substances, review *(Japanese)* 80–71366
$BaTiO_3$, electronic props., SCF-MS-Xα calc. 80–54607
$BaTiO_3$, electronic struct., XPS and band struct. calc. 79–38708
$BaTiO_3$, electrostatic energy calc. by planewise summation method 79–23564
$BaTiO_3$, epitaxial ferroelectric, appl. of electron microprobe methods 80–44443
$BaTiO_3$, epitaxial films and single domain crysts., exoelectron emission obs. of phase transition 79–74069
$BaTiO_3$, epitaxial vacuum condensates struct. 79–95290
$BaTiO_3$, exam. of anomalous pyroelectric effect above Curie point 79–33613
$BaTiO_3$, exam. of PTC effect as function of Ti excess *(German)* 79–23960
$BaTiO_3$, exoelectron emission during phase transition, orientational depend. 79–69786
$BaTiO_3$ family, unified phenomenological theory, spherical system of transition parameters 77–31751
$BaTiO_3$, ferroelec., appl. of pseudo-ionic model for ionic cryst. 79–33049
$BaTiO_3$, ferroelec., crit. X-ray scatt. 79–33636
$BaTiO_3$, ferroelec., elec. field in 90° domain walls 80–2713
$BaTiO_3$, ferroelec., nonlinear optical susceptibility calc. 78–9409
$BaTiO_3$, ferroelec., repolarisation in SEM 79–15424
$BaTiO_3$, ferroelec., reduction of hysteresis losses 79–42926
$BaTiO_3$, ferroelec., susceptibility of eight site order-disorder model calcs. 77–8523
$BaTiO_3$, ferroelec., X-ray diffr. topographic study of polarisation reversal 79–38442
$BaTiO_3$, ferroelec. ceramic, mech. strength, for single crysts. and Ca and Co modified specimens 78–64332
$BaTiO_3$, ferroelec. ceramic, 90° domain rot. in fixed elec. field 80–7315
$BaTiO_3$, ferroelec. cryst., IR and Raman spectra, mode coupling 80–66194
$BaTiO_3$, ferroelec. domain boundary struct., TEM 77–24806
$BaTiO_3$, ferroelec. domain form., X-ray topography 79–78638
$BaTiO_3$, ferroelec. inhomogeneous impurity distrib., distrib. of spontaneous induction 77–28530
$BaTiO_3$, ferroelec. phase transition, soft phonons, Raman scatt. obs. *(Japanese)* 79–65880

barium compounds continued
$BaTiO_3$, ferroelec. temp. depend. of broad A_1 (TO) phonon Raman linewidth 78–2857
$BaTiO_3$, ferroelec. thin films, r.f. sputtering, X-ray and microprobe obs. 79–47627
$BaTiO_3$, ferroelec. to paraelec. transform., influence of domain boundaries on interface struct. 79–95718
$BaTiO_3$, ferroelectric domain struct. and cryst. struct. changes, X-ray diffr. 77–24803
$BaTiO_3$, ferroelectric transitions rel. to Earth and planetary interiors 77–53045
$BaTiO_3$, ferroelectric ceramic, dielec., piezoelec. and elastic props., orientational contrib. 78–68468
$BaTiO_3$, ferroelectric polydomain crysts., piezoresonance effects, appl. as transducer 79–4779
$BaTiO_3$, ferroelectric domains, X-ray topography 79–65815
$BaTiO_3$, ferroelectric-paraelectric transform., basic struct. and characts. 79–95717
$BaTiO_3$, ferroelectric semicond. anomalous photovoltaic effect due to ionising radiation 80–29437
$BaTiO_3$, ferroelectric ceramic, internal stress and strength, failure mechanism 80–66128
$BaTiO_3$, ferroelectric mechanisms, anharmonic couplings by scanning IR interferometry 80–75978
$BaTiO_3$, ferroelectric, polarisation reversal, electric field induced phase transform. 80–103925
$BaTiO_3$, ferroic materials, fracture processes 80–79869
$BaTiO_3$ fibres synthesised from $Ba(OH)_2+2K_2O.11TiO_2.3H_2O$ fibre hydrothermal reaction *(Japanese)* 80–93527
$BaTiO_3$ film, dielectric props. depend. on sinusoidal elec. field 80–71318
$BaTiO_3$ film, ferroelec., composition profiles by Auger electron spectra anal. 79–66391
$BaTiO_3$, film, ferroelectricity of vap. deposited coating 79–69781
$BaTiO_3$ film, prep. by hydrolysis of organometallic cpds. 77–59702
$BaTiO_3$ film, sputtered, refr. index, 0.3-1.0 μm, substrate temp. effects 77–55840
$BaTiO_3$ film, sputtered, elec. props. 79–42676
$BaTiO_3$ film, struct. and dielec. props. 80–60514
$BaTiO_3$ film, surface layer nature, AES obs., and effect on permittivity 77–24498
$BaTiO_3$ film, unstable modulated struct. near ferroelec. phase transition 78–27164
$BaTiO_3$, film deposition by HF cathode sputtering 77–36398
$BaTiO_3$ films, ferroelec., effect of elec. field on dielec. props. 79–33642
$BaTiO_3$, form. entropy and tolerance factor 80–34204
$BaTiO_3$, fractographic features of fatigue 79–52374
n-$BaTiO_3$, grain boundary resistivities 77–80782
$BaTiO_3$, H_2-reduced, elec. cond. mechanism, EPR, resist. and Seebeck coeff. meas. 80–10976
$BaTiO_3$, head to head and tail to tail domains 78–43826
$BaTiO_3$, hologram storage, book contrib. 78–25834
$BaTiO_3$, holographic storage props. 80–87354
$BaTiO_3$, intrinsic luminesc. 80–71467
$BaTiO_3$, isotropic dielectric, US vel. and longit. elec. field *(Russian)* 78–38785
$BaTiO_3$, K-edge X-ray absorpt., cond. band states 80–97382
$BaTiO_3$, LF relaxational polarisation 78–68460
$BaTiO_3$, laminar domains, periodic motion under const. elec. field 78–15133
$BaTiO_3$, light emission during repolarisation 77–36299
$BaTiO_3$, light scatt., Comes Lambert Guinier model 79–15471
$BaTiO_3$, line broadening effect in Rayleigh scatt. of Mossbauer radiation 80–50238
$BaTiO_3$, logarithmic velocity variations for longitudinal US waves near ferroelec. transition 78–72472
$BaTiO_3$, magnetochemical exam. of phase transition, mag. suscept. meas. 78–88265
$BaTiO_3$, martensite type phase transition 78–64326
$BaTiO_3$, mean square atomic displacement temp. depend., sublattice vibration anharmonicity 80–79890
$BaTiO_3$, melt grown, drift mobility meas. 79–19596
$BaTiO_3$, molecular field statistical model, ferroelectric materials, props. *(French)* 79–69793
$BaTiO_3$, monocrystalline, dielectric loss after superposition of unidirectional electric field time depend. *(Slovak)* 78–52435
$BaTiO_3$, Mossbauer spectrum, isomer shift and quadrupolar splitting, internal elec. field effects 79–56648
$BaTiO_3$, Mossbauer spectroscopy, sample prep. and results 80–66078
$BaTiO_3$, nonpiezoelec. dielec., light-sensitive Rayleigh wave generation by surface piezoelectricity 78–43228
$BaTiO_3$, nonstoichiometry of vac. condensates, effect on dielectric props. 77–16260
$BaTiO_3$, O K_α X-ray emission band spectra *(Russian)* 79–15563
$BaTiO_3$, OH^- impurity IR spectra meas. 80–20679
n-$BaTiO_3$, ohmic contact form. 80–92969
$BaTiO_3$, ohmic noble metal contacts using In_2O_3 layer 79–42638
$BaTiO_3$ on Si substrate, prep. and elec. props., expt. 77–20460
$BaTiO_3$, optical wave reflectance *(Japanese)* 78–87012
$BaTiO_3$, oxygen vacancies and partial pressures 77–84938
$BaTiO_3$, para to ferroelec. transition, strong Rayleigh scatt. 78–76486
$BaTiO_3$, paraelec. cryst., electro-optical absorpt. near Curie temp. 77–1657
$BaTiO_3$, paraelec. phase, stabilisation of soft mode 80–75985
$BaTiO_3$, paraelectric crystal, nonlinear props. 80–84699
$BaTiO_3$ particulates coagulation in solar nebula 77–53434
$BaTiO_3$, periodic domain struct. and opalescence at tetragonal to orthorhombic transition 80–66131
$BaTiO_3$, permittivity, temp. depend., submm. spectroscopy 77–176
$BaTiO_3$, permittivity, low freq. and lattice contribs. 78–15105
$BaTiO_3$, perovskite structure, semiconductor props. *(Polish)* 78–56437
$BaTiO_3$, phonon scatt. surfaces obs., by neutron film methods 79–46761
$BaTiO_3$, phonon spectroscopy, amorphous versus crystalline material 78–83898
$BaTiO_3$, photo-ferroelectric noise effect *(Russian)* 78–52450
$BaTiO_3$, photocond. of doped single cryst., photoexcitable levels 77–4391
$BaTiO_3$, photoelectron and optical spectra derived from self-consistent charge MO and band calcs. 80–96785
$BaTiO_3$, photoferroelec., lighting effect on deform. and stresses 78–43802
$BaTiO_3$ photorefractive material for real-time edge enhancement 80–99642

barium compounds continued
$BaTiO_3$, piezoceramic, nonlinear piezoeffect 79—42900
$BaTiO_3$, piezoceramic, elastic normal wave propagation, phase transitions *(Russian)* 80—40067
$BaTiO_3$, piezoelectric ceramic solid soln. *(Polish)* 77—55755
$BaTiO_3$, piezoelectric ceramic, secondary electron emission yield 79—91546
$BaTiO_3$, planar phase boundaries and domain struct. 79—69795
$BaTiO_3$, polarisation reversal and surface neutralisation 78—27169
$BaTiO_3$, polarisation switching, influence of charges arising from defects 79—69796
$BaTiO_3$, polariton freq. meas. by Raman scattering and permittivity 78—76006
$BaTiO_3$, polycryst., elec. resist. anomaly in phase transition region 78—43381
$BaTiO_3$, polycryst., form. from coprecip. products 77—24997
$BaTiO_3$, polycryst., prep. from coprecipitated $BaCO_3$-BaF_2-$TiO(OH)_2$ 77—24996
$BaTiO_3$, polycryst., phase transition obs. in −170 to 220°C range *(Russian)* 80—103474
$BaTiO_3$, polycrystalline, exam. of effect of freq., temp. and DC electric field strength, on elastic consts. 79—1890
$BaTiO_3$, polycrystalline, X-ray diffraction, Curie temp., lattice defects, phase changes 79—99830
$BaTiO_3$, polycrystalline, dielec. nonlinearity coeffs. difference in free and clamped specimens *(Russian)* 80—25314
$BaTiO_3$, polycrystalline ferroelectric, grain-size dependent props. 80—71352
$BaTiO_3$ polydomain crystals, dielec. props. 78—43827
$BaTiO_3$, polydomain ferroelec. crysts., phys. consts., self consistent calcs. 80—88942
$BaTiO_3$ polymorph, hexagonal, low temp. and surface CO_3 adsorption and desorption 80—80713
$BaTiO_3$, pot. functions of ions 80—19885
$BaTiO_3$, powder, anomalous particle size effect, demonstration with high resolution energy dispersive diffractometer using synchrotron radiation 79—14640
$BaTiO_3$ powder, dispersion effect on meas. in electrical sensing zone particle size counter 79—17383
$BaTiO_3$ powder, US dispersed, SEM study *(German)* 80—33860
$BaTiO_3$, powder compacts, sintered, physical and chem. inhomogeneities 79—87594
$BaTiO_3$, powders, Bragg reflection integral intensities due to structural anomalies 80—107098
$BaTiO_3$, pseudo-ionic model applic. to dynamics 77—59077
$BaTiO_3$, pure, dielec. behaviour at ultralow freq. 79—38425
$BaTiO_3$, pure, dielectric const. and elastic compliance temp. depend. for various phases 79—19830
$BaTiO_3$, pure and doped, cryst. growth and chemical composition 77—40349
$BaTiO_3$, pure and doped, photocurrent kinetics 79—42576
$BaTiO_3$, pure and doped crysts., surface and domain struct., AES and SEM expts. 80—71363
$BaTiO_3$, pure and Fe doped, X-ray induced luminesc. 79—69885
$BaTiO_3$, pure and Fe doped, ferroelec., switching and electrolum. 80—76079
$BaTiO_3$, quadratic electro-optic effect, incident light wavelength depend. 80—16010
$BaTiO_3$, RF sputtered amorphous films, phys. and elec. characterisation. 79—83119
$BaTiO_3$ RF sputtered ferroelectic film on Si substrate, ferroelectric props. 80—80697
$BaTiO_3$, RF-sputtered tetragonal films on Si, ferroelec. and insulating props. 79—78888
$BaTiO_3$, radiation spectra during pulsed repolarisation 79—95804
$BaTiO_3$, Raman intensity analysis, symmetry coords., optical modes, electro-opt. consts. 79—95740
$BaTiO_3$, rare earth doped ceramics, thermolum. and microwave induced thermolum. fading 79—1792
$BaTiO_3$, Rayleigh wave generation by surface piezoelectricity 78—71925
$BaTiO_3$, reduction inhibition by impurity ions 80—101018
$BaTiO_3$, SCL currents, carrier mobility and trapping 77—15863
$BaTiO_3$, secondary struct. periodic motion 80—15993
$BaTiO_3$, semiconducting ceramic, AC thermopower measurement 80—44624
$BaTiO_3$, single cryst., dielec. const., var. with applied AC field and temp. 78—2787
$BaTiO_3$, single cryst., dielec. breakdown and electroluminesc. 78—2917
$BaTiO_3$, single cryst., elec. cond., 800-1200°C, nonstoichiometric disorder 78—51989
$BaTiO_3$, single crysts., electron microscope study of domain and defect structs. 79—15425
$BaTiO_3$, single crysts., dielec. spectrum 80—25275
$BaTiO_3$, soft mode dielec., anomalous low temp. sp. ht. 78—14423
$BaTiO_3$, soft mode exam. 79—37799
$BaTiO_3$, soft mode spectroscopy IR refl. meas. 80—88982
$BaTiO_3$, solubility of Al estimation by conductivity meas. 79—69250
$BaTiO_3$, spontaneous polarisation, low temp. meas. 80—75921
$BaTiO_3$, stoichiometric excess of TiO_2, thermodynamic characterisation, case of extensive defect association 77—47445
$BaTiO_3$, struct. changes due to cubic-tetragonal phase transition 78—60407
$BaTiO_3$, struct. phase transitions, light scatt. meas. 79—95774
$BaTiO_3$, surface layer exam. 78—43805
$BaTiO_3$, surface microrelief after ion irrad. 80—59774
$BaTiO_3$, surface pot. between ferroelec. domains 78—15132
$BaTiO_3$, surface spark discharge, channel spreading and substrate vaporisation 77—89336
$BaTiO_3$, surface study using AES and ion scatt. spectroscopy 80—65339
$BaTiO_3$ surface voids, Auger spectrochem. anal., organic contamination 79—24467
$BaTiO_3$, synthesis by solid-solid reactions 79—38776
$BaTiO_3$, synthesis by solid-solid reactions 79—38777
$BaTiO_3$, synthesis from barium titanyloxalate 77—48381
$BaTiO_3$, tetragonal, model for temp. depend. of dielec. const., ferro-paraelectric transition 78—43771
$BaTiO_3$, tetragonal, over-damped soft E-polariton and dielec. dispersion 78—15111
$BaTiO_3$, thermodynamic props. 77—39680
$BaTiO_3$, thin film, obtained by modified doctor blade method grain orientation *(Japanese)* 77—77455

barium compounds continued
$BaTiO_3$, thin film elec. and photoconductivity 79—33366
$BaTiO_3$ thin film microwave complex permittivity meas. 79—73879
$BaTiO_3$, transform. of cryst. struct., at cubic-to-tetragonal phase transitions 79—37827
$BaTiO_3$, transport and optical props., small polaron hopping theory 79—47096
$BaTiO_3$, tricrit. point 77—63378
$BaTiO_3$ type crystal, thermodynamic analysis of struct. phase transitions *(Russian)* 80—103473
$BaTiO_3$ type crystals, determ. of phase transitions using symmetry breaking theory *(French)* 78—83950
$BaTiO_3$ type perovskite ferroelectric, neutron irradiated, amplification of freq. dispersion of permittivity *(Russian)* 78—52419
$BaTiO_3$ type vibronic ferroelectric, light induced refractive index change *(Russian)* 79—91399
$BaTiO_3$, UV refl. spectra, optical consts. 0 to 32 eV Kramer-Kronig anal., band struct. calcs. 78—43903
$BaTiO_3$, undoped and Cu doped, Γ_{15} phonon freezing, electronic instability, LCAO calc. 80—25318
$BaTiO_3$, uniaxial pyroelectric, nonlinear optical susceptibility 77—23705
$BaTiO_3$, unipolar cryst., topography of defect. and thermodepolarisation currents 77—43954
$BaTiO_3$, vacuum condensates on US irrad. substrates, props. 77—66466
$BaTiO_3$, vacuum condensates, epitaxial growth on $SrTiO_3$ crysts., electron diffr. and TEM anal. 79—15051
$BaTiO_3$, vacuum UV spectra and electro-optical prop. *(Japanese)* 79—65900
$BaTiO_3$, valence band UPS and partial p and d density of states 80—71560
$BaTiO_3$, vibronic ferroelec., spontaneous birefringence calc. 78—68473
$BaTiO_3$, vibronic theory and opt. props. 80—103939
$BaTiO_3$, X-ray diffr. intensities, anomalous temp. depend. *(Russian)* 79—1484
$BaTiO_3$, X-ray irrad. effect on dielec. props. 78—15082
$BaTiO_3$, XPS, band struct., density of states, photoionisation cross sections 78—52629
$BaTiO_3$, XPS and UPS from surface defects 80—76136
$BaTiO_3$, XPS satellite spectra, mol. orbital study 80—43100
$BaTiO_3$:^{89}Zr, electron capture decay lifetime, struct. environment effects 77—28523
$BaTiO_3$:Al, 0.05-0.3 wt.%, ceramic dielectric, dielec. and mech. props. 79—8091
$BaTiO_3$:$BaTi_3O_7$, dielec. props. and microstruct. 80—60481
$BaTiO_3$:C, solubility of C at low O_2 potentials, 800°C 80—100334
$BaTiO_3$:Co, charact. behaviour of spontaneous polarisation and dielec. const. 78—60382
$BaTiO_3$:Co, trap recomb. consts., photocurrents 78—43435
$BaTiO_3$:Co, tricritical point, X-ray diffr. meas. 80—71341
$BaTiO_3$:Co, voltaic current appearance on proton irrad. 80—104032
$BaTiO_3$:Cr^{3+} crystal, radiationless relax., photoacoustic spectra 78—27264
$BaTiO_3$:Cu, photoferroelec. props., Jahn-Teller effect, laser irrad. effect on pyroelec. props. 78—60400
$BaTiO_3$:Dy ceramic, sintering, grain size, characterisation and props. 77—55923
$BaTiO_3$:Eu(Sm), absorption spectra, Ti^{3+} ion and Z-centre formation 77—24871
$BaTiO_3$:Fe, photoinduced Rayleigh scatt. and bulk photovoltaic effect 79—38554
$BaTiO_3$:Fe, short circuit photocurrent, depend. on polarization 79—38121
$BaTiO_3$:Fe ceramic, dopant distrib., STEM obs. 79—82255
$BaTiO_3$:Fe^{3+}, local position of Fe^{3+} in ferroelec. phases, EPR study 80—25196
$BaTiO_3$:Fe^{3+}, local position determ. by EPR 80—108057
$BaTiO_3$:Fe^{3+} bulk photovoltaic effect and photoinduced Rayleigh scatt. 77—77226
$BaTiO_3$:Gd, positron lifetime spectra meas. 78—43956
$BaTiO_3$:Hf, crystal field distortion by stacking faults, PAC meas. 80—11306
$BaTiO_3$:La, Sb, second phase effect on elec. and mag. props. 80—60986
$BaTiO_3$:La and undoped, defect chemistry elec. cond. at high temp. meas. 77—39858
$BaTiO_3$:La_2O_3 and $BaTiO_3$:La_2O_3.3TiO_2 capacitor, permittivity ageing obs. *(Korean)* 80—25325
$BaTiO_3$:Mn, polycrystn., annealing effect on transition temps. 80—3100
$BaTiO_3$:Mn^{2+}, electrooptical effect, charge transfer mechanism, defect. pair form. 79—38519
$BaTiO_3$:Nb, elec. props., contact material influence 80—70848
$BaTiO_3$:Nb, ferroelec. and paraelec. phases, props. 79—42919
$BaTiO_3$:SnO_2, transition temperature shift, resistivity anomaly obs. *(Korean)* 77—39856
$BaTiO_3$:X(X=Cr, Mn, Fe, Co, Ni, Zn, Ga), annealed in H_2 and O_2, valence change in phase stability 80—20600
$BaTiO_3$:ZrO_2, dielec. loss tangent and const. 79—4769
$BaTiO_3$/SiO_2 charge storage memory films for IGFETs 80—11566
$BaTiO_3$-$Ba_{1/2}NbO_3$, defective solid solns., reduction 77—81395
$BaTiO_3$-$BaNb_2O_6$, semiconducting ferroelectric ceramic, nonlinearity of dielectric layer capacitance 79—8098
$BaTiO_3$-$BaNb_2O_6$ system, solid solns. of tungsten bronze struct. of type $BA_{5+x/2}Nb_{10-x}Ti_xO_{30}$ 77—52021
$BaTiO_3$-$BaNbO_3$ system, solid solns., thermal ionic relaxation, vacancy form. 77—8499
$BaTiO_3$-based ceramics, impurity atoms chem. state, Mossbauer spectra 80—15902
$BaTiO_3$-based nonpiezoelectric ceramic, acoustic convolution in paraelectric phase 80—6467
$BaTiO_3$-$BiFeO_3$ solid solns., ferroelec.-antiferromag., magnetoelectric effect at ferroelec. transition 80—100637
$BaTiO_3$-CeO_2 liquid immiscibility region, X-ray diffr. anal. 80—50611
$BaTiO_3$-$CuO(TiO_2)(ZrO_2)$ mixture, exam. of liquid phase sintering, densification 79—33979
$BaTiO_3$-$KNbO_3$, ferroelec. Curie temp., theory 80—7313
$BaTiO_3$-metal contact, surface barrier Rayleigh wave transducer 79—98578
$BaTiO_3$-$NaNbO_3$, ferroelec. Curie temp., theory 80—7313
$BaTiO_3$-Ni ferrite, piezoelectric-piezomagnetic sintered two-phase composite, magnetoelec. conversion 77—12181
$BaTiO_3$-$Ni(Co, Mn)Fe_2O_4$, ceramic, exam. of prep. and physical props. 78—68655

barium compounds continued

- $BaTiO_3$-PbO-B_2O_3, liquid phase sintering, effect on props. *(German)* 79—33980
- $BaTiO_3$-type ferroelectrics, existence of noncommensurate phases due to gradient term in free energy 79—69792
- $BaTiO_{3-x}$, ferroelec., Auger spectroscopy of surface layers 79—42343
- $BaTiO_{3-x}$, single cryst. and film, Auger spectra, surface comp. 78—27353
- $BaTi_4O_9$ effect of chemical treatment on loss quality, at microwave wavelengths 79—34159
- Ba_2TiO_4, $Ba_6Ti_{17}O_{40}$, standard Gibbs free energy of formation, EMF meas. at 673K 80—85207
- $Ba_2Ti_{5.5}O_{13}$, X-ray cryst. struct. determ. *(French)* 79—73148
- $Ba_2Ti_9O_{20}$, effect of chemical treatment on loss quality, at microwave wavelengths 79—34159
- $Ba_2Ti_9O_{20}$ single crysts., prep. and unit-cell parameters 80—103302
- $BaTiO_3Fe_2O_3$, photoacoustic effect, first order phase transitions at increasing and decreasing temp. 80—70320
- $BaTi(PO_4)_2$, cryst., luminesc., struct. interpretation 79—47489
- $Ba_2TiSi_2O_8$, fresnoite, Czochralski growth and phys. props. 78—3026
- $Ba_2TiSi_2O_8$, fresnoite, unsuitability for phase matched SHG 78—46721
- $Ba_2TiSi_2O_8$, luminescence of TiO_5 group, decay time, IR and Raman spectrosc. 80—2819
- $Ba_{100}Ti_{101-x}Sn_x$+0.3 at.%Sb, intergranular capacitor, effect of microstructure on electrical props. 79—34160
- $BaTi_{0.98}Sn_{0.02}O_3$, ferroelec. film, switching process 80—60518
- $Ba(Ti_{0.98}Sn_{0.02})O_3$ film, ferroelec., switching process in elec. field with rectangular impulses 80—2714
- $Ba(Ti_xSn_{1-x})O_3$ film, struct. and dielec. props. 80—60514
- $Ba(Ti_xSn_{1-x})O_3$ thick film, ferroelec., phase transitions and dielec. props. 80—97215
- $Ba_3Tm_4O_9$, synthesis thermal stability, emissivity, reduction processes 77—8791
- $Ba_{1-x-y}U_xCe_yF_{2+2x+y}$, solid soln., ionic cond. 79—99356
- $Ba_2UO_2(HPO_3)_2$, synthesis and comp. 80—35516
- BaV_2O_6:Cr, EPR spectra temp. depend., paramagnetic ion point symm. 80—71166
- $Ba_{0.15}VO_2$, electrical cond., thermo-EMF, and lattice consts. 80—54685
- $Ba_2V_2O_7$, cryst. struct. determ. and bond strength anal. 79—23576
- $Ba_2V_2O_7$, V-O-V bridge stretching freq. correl. with bond angle 78—74636
- Ba_xVO_2, oxygen vanadium bronze, phase comp., heating in air 77—40417
- BaVO(EDTA).$6H_2O$, cryst. and mol. struct., X-ray diffr. obs. *(Russian)* 78—30601
- $Ba_3(VO4)_2$, determination of enthalpies of formation, from heats of solution 80—2182
- $BaVS_3$, annealing influence on lattice constants, neutron diffr. profile anal. 80—1976
- $BaVS_3$, elec. resist., mag. susceptibility, structural transition amd Mossbauer effect meas. 77—84923
- $BaVS_3$, exam. of ferromagnetic, antiferromagnetic behaviour, depending on stoichiometry 78—52233
- $BaVS_3$, mag. and elec. props. 79—91214
- $BaVS_3$, mag. transition and hyperfine interaction, neutron spin-flip scatt. obs. 80—97093
- $BaVS_3$, magnetisation and neutron study 80—84588
- $BaVS_3$, polycrystalline, elastic behaviour, 40 to 350K 79—60498
- $BaVS_3$:Fe, Mossbauer and mag. studies, electronic state of Fe 80—108130
- $BaVSe_3$, one-dimensional, struct. and mag. props. 80—28993
- $Ba(V_{1-x}Ti_x)S_3$, synthesis and struct. phase transitions 80—107415
- $BaV_xTi_{1-x}S_3$, mag. and elec. props. 79—91214
- $Ba_3WFe_2O_9$ and $Ba_3WFe_2O_{8.42}$, crystallographic and mag. props., comparative study 80—103303
- $Ba_3WFe_2O_9$-$Ba_3WCo_2O_{9-x}$ system, struct. evolution *(French)* 80—88110
- $BaWO_4$, crystallization kinetics from saturated Na_2WO_4 solns. 79—99093
- $BaWO_4$ crystals, X-irradiated, EPR, TSC and thermoluminescence spectra meas. 79—1791
- $BaWO_4$, Davydov splitting of vibr. levels, short range interaction 80—71418
- $BaWO_4$, external lattice vibr. modes and elastic wave vels., dispersion relations 79—33050
- $BaWO_4$, flux- and gel-grown, comparative microtopography 77—31852
- $BaWO_4$, refr. index, single crystals having scheelite struct. 78—79082
- $BaWO_4$, single cryst. growth by Czochralski method and U incorporation, effective distrib. ratios, luminesc. characts. 79—42094
- $BaWO_4$, slow neutron inelastic scatt. spectra, Debye temp. calcs. *(Russian)* 80—59347
- $BaWO_4:Er^{3+}$, spin-lattice and spin-spin relax. times, electron spin echo obs. 79—28609
- $BaWO_4$:Mo, P, thermoluminesc. traps, EPR meas. 77—90032
- Ba_3WO_6, Ba_2WO_5, and $BaWO_4$, chem. thermodynamics, galvanic cell study 80—21315
- $Ba_3W_2O_9$, X-ray powder struct., face shared octahedra with W(VI) 80—64974
- Ba_xWO_3, ($0.01<x<0.33$) series form. 79—65046
- BaX_2, X=Cl, Br, I, valence shell electronic struct., ab initio SCF calc., photoelectron spectra 79—31383
- Ba_5X_3, α, intermediate phases, cryst. struct. (X=IIb, IIIb, IVb, Vb element) 78—83793
- Ba_2XRuO_6(X=La,Eu), ^{99}Ru Mossbauer spectra and other techniques 80—29659
- BaY_2F_8, energy transfer from Eu^{2+} to trivalent rare earth ion 79—91490
- $BaY_2F_8:Nd^{3+}(Ho^{3+})(Er^{3+})(Yb^{3+})$, ESR spectra and spin-lattice relax. 80—11263
- Ba_2YRuO_6, perovskites, prep., struct., emission control catalysts 77—68957
- $(Ba_{1-x}Y_x)TiO_3$ ceramic, resistivity rel. to donor dopant content 79—65474
- $BaY_4X_5O_{17}$ (X=Si,Ge), cell consts., luminesc. of various rare-earth activators 80—93376
- $BaYb_2F_8:Ho^{3+}$, stimulated emission at 2 μm, Nd laser radiation freq. conversion 80—95902
- Ba_2YbF_7 single crystals, electron diffr. cryst. struct. anal. *(French)* 80—92507
- $Ba_3Yb_4O_9$, synthesis, thermal stability, emissivity, reduction processes 77—8791

barium compounds continued

- $BaZn_{1.38}Co_{0.62}Fe_{16}O_{27}$, W-type hexaferrite cryst., first order magnetisation processes 78—95472
- $Ba_2Zn_{2-2(x+y)}Cu_{2x}Cd_{2y}Fe_{12}O_{22}$, mag. props. and Mossbauer spectrum 80—75765
- $Ba_2Zn_{2-2x}Cu_{2x}Fe_{12}O_{22}$, hexagonal ferrites, prep. and mag. characterisation 79—1727
- $BaZnF_4$, low temp. phonon effects on polarisation 79—42905
- $BaZn_2Fe_{16-x}Al_xO_{27}$, saturation magnetisation, anisotropy field and Mossbauer meas. 77—69508
- $BaZn_2Fe_{16-x}M_xO_{27}$ (M=Al, Ga, In, Sc), mag. props. and Mossbauer effect 80—75766
- $Ba_2Zn_2Fe_{12}O_{22}$, anisotropic magnetisation and susceptibility 78—84411
- $Ba_2Zn_2Fe_{12}O_{22}$, model for low mag. moment, magnetisation meas., 5-1375K 78—2655
- $Ba_3Zn_2Fe_{24}O_{41}$, ferromag. reson., low power nonlinear effects 80—75861
- $BaZnGeO_4$, revised cryst. data 80—100210
- $BaZn_2(PO_4)_2$, dielectric permittivity and elec. resist., temp. depend. 77—59502
- Ba_2ZnS_3, cryst. struct. determ., X-ray powder diffr. data 77—76365
- Ba_2ZnS_3, prep. by solid state reaction and melt growth, X-ray anal. 77—73226
- Ba_2ZnS_3:Mn, luminescent props. 77—77292
- (BaZnSr)TiO_3 ferroelectric film, parameters at upper end of centimetre band *(Russian)* 77—40185
- x— $BaZrF_6$, synthesis and characterisation *(French)* 80—92506
- α-$BaZrF_6$ with $[Zr_2F_{12}]^{4-}$ complex, cryst. struct. *(French)* 78—51477
- $\alpha(\beta)$— $BaZr_2F_{10}$, synthesis and characterisation *(French)* 80—92506
- $Ba_{0.65}Zr_{0.35}F_{2.70}$, synthesis and characterisation *(French)* 80—92506
- Ba_3ZrF_{10}, synthesis and characterisation *(French)* 80—92506
- $Ba_{1-x}Zr_xF_{2+2x}(0\leq x\leq 0.1)$, synthesis and characterisation *(French)* 80—92506
- $Ba_{1-x}Zr_xF_{2+2x}(0.333\leq x\leq 0.361)$, synthesis and characterisation *(French)* 80—92506
- $BaZrO_3$, cryst. growth and thermoluminesc. *(Russian)* 78—23604
- $BaZrO_3$, form. entropy and tolerance factor 80—34204
- $BaZrO_3$, high-density ceramics prep. and elec. props. 80—60812
- $BaZrO_3$, high-temp. enthalpy and specific heat, method of mixtures 77—35712
- $BaZrO_3$, perovskite type, X-ray K-absorpt. edge, chem. shift 79—91529
- $BaZrO_3:Pb^{2+}$, $Ba_2ZrO_4:Pb^{2+}$, cryst. struct. effs. on luminesc. 77—16376
- $BaZrO_3$-$LaAlO_3$ systems, sintering conditions, elec. props. 79—43184
- $BaZrO_3$(s), evaporation and standard ht. of formation 77—25302
- ^{133}Ba separation from $BaCO_3$ by method of internal reduction 77—14613
- $Ba[Fe(CN)_5NO]_2.2H_2O$, NMR, H_2O orient. *(French)* 78—52366
- $Ba[Pt(CN)_4Br_2]4.5H_2O$, single crystal neutron diffr. struct. exam. 78—2082
- $Ba[Pt(CN)_4].4H_2O$, polarised time-resolved emission spectra 79—33811
- $Ba[Pt(CN)_4].4H_2O$, DC elec. cond. props. 79—51582
- BeO_2-Al_2O_3-SiO_2-BaF_2 system glass, role of fluoride cations during crystn. 79—65176
- $Bn(IO_3)_2$, radiolysis in Portland cement, rel. to immobilisation of long lived ^{129}I 79—59208
- C_6Ba intercalation compounds, three dimensional continuous melting 80—59631
- $CaAl_2O_4$-$SrAl_2O_4$-BaA_2O_4, binary and ternary systems, solid solubility *(Japanese)* 80—35174
- $CaBaFe_4O_8$, Mossbauer study 79—38414
- $CaBaFe_4O_8$, overlap contribution to $^{57}Fe^{3+}$ isomer shifts, nuclear size change 80—39903
- $CaBa(PO_3)_4$, struct. from IR spectra 77—47421
- $Ca_{0.2}Ba_{0.8}TiO_3$:Nb, conductive single cryst. growth by Verneuil method 77—85928
- $CaCl_2$-$BaCl_2$-H_2O ternary system, 45°C isotherm *(French)* 79—96004
- CaO, CO_2 transport kinetics following $CaCO_3$ decomp. 79—23780
- $(CaO_{1-x}BaO_x.6Fe_2O_3)_{97}(La_2O_3)_3$ ferrite magnets, anisotropic, BaO substitution effect on mag. props. *(Japanese)* 79—99697
- Ca_2SiO_4-BaO, conditions and mechanism in cryst.-chemical stabilisation of unstable phases 80—39302
- $Ca_{1-y}Sr_{y/2}Ba_{y/2}Zr_{1-x}Ti_xO_3$, ceramic system, dielectric props., microwave resonator application 80—80674
- $CdBa(PO_3)_4$, struct. from IR spectra 77—47421
- $Co_{1.8}BaFe_{0.2}{}^{2+}Fe_{16}{}^{3+}O_{27}(Co_{1.8}W)$, magnetoelastic props. under spin-reorientation conditions 79—69709
- CsCl-$BaCl_2$ molten binary mixtures, thermal cond. 79—86931
- CsCl-$BaCl_2:U^{3+}$, melt, diffusion coeffs. and mechanisms 79—73330
- Cu-GeO_2/BaO-Cu thin film, amorphous, effect of electroforming on conductance and capacitance 80—34537
- γ-$DBa(PO_3)_2$, polyphosphate, crystal structure determination *(French)* 78—91314
- dibarium cobalt formate tetrahydrate Cu^{2+} doped, EPR of Cu-Co interactions 78—60334
- $Eu_{0.5}Ba_{0.5}TiO_3$, ferromag., ferroelec., ceramic, Curie temps. determ. 78—68230
- $Fe_2NaBa_6Ge_8O_{24}.4(OH,H_2O)$, growth and struct. 77—65971
- Fe_2O_3-BaO-B_2O_3, magnetic props. of Fe-rich amorphous oxide *(French)* 80—80511
- Fe_2O_3-BaO-B_2O_3 glass, Mossbauer spectra, ^{57}Fe hyperfine interactions 80—39969
- Fe_2O_3-BaO-CoO system, phase comp. and mag. props., Bi_2O_3 additions effect 79—29032
- Fe_2O_3-Na_2O-BaO glass, mag. props. 4.2-295K, mictomagnetism *(French)* 80—39782
- GdF_3-BaF_2-ZrF_4 glass fibres, IR transmission, losses, fabrication 80—87516
- HfF_4-BaF_2-LaF_3 glass system, IR transmitting, synthesis and props. 80—71623
- HfF_4-BaF_2-ThF_4-(ZrF_4) glass system, IR transmitting, synthesis and props. 80—71623
- $KAlSi_3O_8$-$BaAl_2Si_2O_8$ hyalophane, natural and heat treated, cryst. struct. refinement 78—2072
- $K_{6-2x}Ba_xM_6Si_4O_{26}$, M=Nb,Ta, IR spectra, appl. to nonstoichiometry in cpds. with $(M_6X_4O_{26})$ layers (X=Si,Ge) *(French)* 79—11418
- $K_2Ba(NO_2)_4$, ferroelastic, Raman spectra and phase transition 79—56800
- $K_2Ba(NO_2)_4$, new ferroelastic, phase transitions, optical and electrical props. 79—55887
- $K_{6-2x}Ba_xTa_6Sl_4O_{26}$, struct. determ. *(French)* 77—27866
- KCl-$BaCl_2$ supersaturated solid soln., deformed, $BaCl_2$ precipitation kinetics, metastable region *(Russian)* 78—60673
- KCl-$BaTiO_3$, composite cryst., F-centres, thermoluminesc., DC field and X-irrad. effects 78—2926

barium compounds continued
$(K_{0.5}La_{0.5})_xBa_{1-x}TiO_3$, cryst. struct., dielec. and IR spectral meas. 79−46614
K_2O-Al_2O_3-$2SiO_2$-BaO plasma emitter 80−96368
K_2O-BaO-B_2O_3 glasses, ESR detection of immiscibility rel. to Cu II ions 80−20916
K_2O-BaO-CaO-SiO_2 glass-Nichrome-CaF_2 multicomponent self-lubricating coating, prep. by plasma spraying, and props. 80−40604
K_2O-BaO-SiO_2 glass, rare earth ion activated, spectral intensity, effect of number of 4f electrons 78−84602
K_2O-BaO-SiO_2:Nd^{3+} glasses, absorption and fluoresc. spectra, density 80−25417
K_2O-BaO-SiO_2-Ti(Ce)O_2 laser glasses, TiO_2 and CeO_2 antisolarisation additive effects 79−94309
K_2O-CaO-BaO-B_2O_3, glass, refraction, refractive index from 0.365 to 2.50 μm 80−88953
K_2O-CaO-BaO-SiO_2 (B_2O_3) (GeO_2), calc. of network refraction and exam. of glass structure 79−4783
K_2O-Na_2O-BaO-SiO_2 glass, corrosion kinetics in aqn. KOH, transition metal oxide addition effects 77−56125
$La_{1-x}Ba_xCoO_3$, electronic and mag. props., itinerant ferromagnetism obs. 78−10660
$La_{0.003}Ba_{0.66}Sr_{0.34}TiO_3$ ceramic, positive TCR near Curie temp. rel. to charge dispersion *(Russian)* 80−16511
LaF_3-BaF_2-ZrF_4(-MF), M=Na, Li, glassy transition, refr. index, density and molar refr. 80−1937
$LiBaAlF_6$:Eu^{2+}, luminesc., band emission and line emission 79−28810
$Li_2Ba_4O_7$ non-universality of TL-LET response, effect of high-temp. TL 80−99348
$LiBaPO_4$, vibrational spectra and cryst. struct. 78−39536
LiF-BaF_2, densities of binary molten salts *(Japanese)* 79−7644
LiF-BaF_2 binary molten salt, elec. cond. *(Japanese)* 77−76588
$(Li_{0.5}La_{0.5})_xBa_{1-x}TiO_3$, cryst. struct., dielec. and IR spectral meas. 79−46614
$LiNbO_3$:Fe, calc. of photorefraction *(Russian)* 78−92032
Li_2O-BaO-SiO_2 glasses, elec. cond., room temp. to 450°C 80−107473
MgO-BaO-Al_2O_3-SiO_2, glass, IR absorpt. spectra and solid struct. exam. 78−88314
NaBaZn glass, Eu^{3+} centre symm. 80−100447
NaCl:$BaCl_2$, oriented growth of $BaCl_2$ phases, platelet-matrix interface structure and energy 78−87793
NaCl-$BaCl_2$ 1%, oriented growth of $BaCl_2$ phases, morphology 77−80627
$(Na_{0.5}La_{0.5})_xBa_{1-x}TiO_3$, dielec, and IR spectra exam., ferroelec. transition 78−23418
Na_2MoO_4-$BaMoO_4$, phase diagrams 77−36467
$NaNbO_3$-$BaTiO_3$, unidirectionally solidified transparent ceramics 80−25677
$NaNbO_3$-$BaTiO_3$ solid soln. form. and props. *(Russian)* 78−48378
Na_2O-BaO-Al_2O_3-SiO_2, glass, nucleation, crystn., ceramic form. 80−84082
Na_2O-BaO-SiO_2 based oxide glasses, ion-bombarded, optical line intensities 80−35037
Na_2O-BaO-SiO_2 glass, chemical durability of surface, heat treatment effect 79−52405
Na_2O-BaO-SiO_2 glasses, elec. cond., room temp. to 450°C 80−107473
Na_2O-BaO-SiO_2:Nd^{3+} glasses, absorption and fluoresc. spectra, density 80−25417
$(Na_2Ti_6O_{13})_n.(BaTi_4O_9)_m$, tunnel struct. intergrowth, electron, microscopy investigations 80−100218
$NaVO_3$-BaV_2O_6-SrV_2O_6, phase diagrams, simple eutectic system 78−48379
$NiFe_2O_4$-$BuTiO_3$, in situ composite growth, phase diag., melting relns. 77−21132
$NpBa_6Zr_{12}F_{64}$ glass, Mossbauer spectrum, evidence for charge states 3+ and 4+ *(French)* 78−88231
$NpBa_6Zr_{12}F_x$ glass, Mossbauer spectrum 80−11304
$(Pb,Ba)_5Ge_3O_{11}$ ferroelectric crystals, influence of Pb replacement by Ba on props. 79−87402
$(Pb,Ba)Nb_2O_6$, polycryst., orientational polarisation and phase comp. in strong field 78−27157
$(Pb,Ba)(Zr,Ti)O_3$, diffuse phase transitions, Curie temp., dielectric props. 80−75979
$(Pb_{1-x}Ba_x)_5Ge_3O_{11}$, ferroelec. phase transition, dielec. const. and quasi-elastic light scatt. 80−71289
$Pb_{5-x}Ba_xGe_3O_{11}$, Raman spectra, temp. depend. of ferroelec. soft A-mode 79−33682
$(Pb_xBa_{1-x})_5Ge_3O_{11}$, electrogyration, and dielectric props. 78−19444
$(Pb_{1-y}Ba_y)_{1-x}La_xNb_{2-x/5}O_6$, transparent ferroelec. ceramic, optical transmittance, electrooptic props. and Curie temp. 77−32395
$(Pb_{1-y}Ba_y)_{1-x}La_xNb_{2-x/5}O_6$, ferroelec., phase transitions 79−38487
$Pb_{2-x}Ba_xLi_{0.5}Nb_{1.5}O_6$, elec. resistivity, Curie temp., x=0-0.15, 50-350°C 78−2478
$Pb_{2-x}Ba_xLi_{0.5}Nb_{1.5}O_6$, dielectric const., temp. and Ba conc. 78−64308
$Pb_{1-x}Ba_xMoO_4$, refr. index. and photoelastic consts. 77−63393
$Pb_{0.94-x/2}Ba_{0.6}Nb_xZr_{1-x}O_3$, Nb dopant morphology effect on microstructure 80−81005
$Pb_{1-x}Ba_xZrO_3$, electric quadrupole interaction meas., by PAC 77−4591
$(Pb_{0.715}Ba_{0.285})_{0.991}(Zr_{0.707}Ti_{0.293})_{0.981}Bi_{0.019}O_3$, slim loop ferroelec. ceramic, shock wave compressed, elec. response 78−80293
$(Pb_{0.8}Ba_{0.2})(Zr_{0.8}Ti_{0.2})O_3$, ferroelec. ceramic, pulse-like voltage generation using polarisation reversal 78−2809
$2PbFe_{1/2}Ta_{1/2}O_3$-Ba_2FeReO_6, comp., struct., dielec. and mag. props. 80−2704
$PbFe_{2/3}W_{1/3}O_3$-$BaTiO_3$ system ferroelec., antiferromag., ESR and dielec. props. meas. 77−40172
PbO-BaO-SiO_2 system, melt, viscosity meas. in temp. range 950 to 1250°C *(Japanese)* 79−77663
Pd-Ba alloy emitter, thermionic emission props. and Auger spectrum 78−11066
perovskite, Ba_2XReO_6, (X=Li, Mg, Ca, Mn, Fe, Co, Ni), new seignettomagnets and ferroelectrics 78−19425
Si, commercial, nitridation, effect of BaF_2 80−81359
SiO/BaO complex, new switching effect in MIM thin-film structures 78−80067
SiO_2-Al_2O_3-B_2O_3-MgO-CaO-Na_2O, strengthened by ion exchange, exam. of internal stresses using polarising microscope 78−88549
SiO_2-Al_2O_3-CaO-BaO-SrO-ZnO-Na_2O-K_2O-B_2O_3, glaze effect of P_2O_5 additions 80−60824
SiO_2-Al_2O_3-Na_2O-BaO-TiO_2, glass ceramic interaction with Pb borosilicate glaze 80−84398

barium compounds continued
SiO_2-K_2O-Na_2O-BaO-SrO-ZnO system glass, props. optimisation 79−91611
SiO_2-MgO-BaO ceramic, steatite, glass-ceramics technology appl. 80−104097
SiO_2-TiO_2-Al_2O_3-SrO(BaO), glasses, ceramic form. rel. to Al_2O_3 content 77−25005
$(Sr,Ba)Nb_2O_6$:Ce, high sensitivity holographic storage 77−71953
$(Sr/Ba)(Fe/Al/Ga)_{12}O_{19}$ solid soln. crystal for hexaferrite layer substrate *(German)* 78−23672
$SrAl_2O_4$-$BaAl_2O_4$ system, solid solubility, α-β transition 78−63860
$SrBaNaNb_5O_{12}$, X-ray powder diffraction data determ. *(Chinese)* 80−70170
$Sr_{0.61}Ba_{0.39}Nb_2D_6$, photoinduced birefr. 80−7325
$Sr_{0.25}Ba_{0.75}Nb_2O_6$ film, growth and electrophys. props. 79−42928
$Sr_{0.5}Ba_{0.5}Nb_2O_3$ piezoelectric transducer, SAW props. 80−79037
$Sr_{0.5}Ba_{0.5}Nb_2O_6$ crystals, ferroelec., dislocation free, pyroelec. props. 79−42907
$Sr_{0.5}Ba_{0.5}Nb_2O_6$, ferroelec., primary pyroelectricity 77−63371
$Sr_{0.5}Ba_{0.5}Nb_2O_6$, ferroelec., dielec. behaviour 78−80309
$Sr_{0.5}Ba_{0.5}Nb_2O_6$ film, pyroelectric effects, origin 78−88258
$Sr_{0.5}Ba_{0.5}Nb_2O_6$:Fe(Mn)(Cr)(La), ceramic, additive effects on ferroelec. and pyroelec. props. 77−16256
$Sr_{0.61}Ba_{0.39}Nb_2O_6$, electromechanical props., permittivity, elastic compliance, piezoelectric moduli 80−29691
$Sr_{0.65}Ba_{0.35}Nb_2O_6$, internal field distrib. and photorefraction 79−99843
$Sr_{0.75}Ba_{0.25}Nb_2O_6$, ceramic ageing, dielec. props. 80−88940
$Sr_{0.75}Ba_{0.25}Nb_2O_6$ single cryst., electro-optical hysteresis curves and phase transitions *(German)* 79−28717
$Sr_{1-x}Ba_xNb_2O_6$, and Nd doped growth of low dislocation density cryst., dislocation struct. 77−40348
$Sr_{1-x}Ba_xNb_2O_6$ crysts., defect-free growth 80−108346
$Sr_{1-x}Ba_xNb_2O_6$, photorefraction in space charge field, phase transitions 80−97229
$Sr_{1-x}Ba_xNb_2O_6$, tetragonal tungsten bronze structure ferroelec. mech. for ferroelec. transition 79−38481
$Sr_xBa_{1-x}Nb_2O_6$, appl. in sub-100 ps pyroelec. detectors, 10.6 μm damage threshold meas. 80−77859
$Sr_xBa_{1-x}Nb_2O_6$, domain struct. influence on electrooptical props. 80−93283
$Sr_xBa_{1-x}Nb_2O_6$, high press. phase transitions, Raman scatt. studies 80−71402
$Sr_{0.75}Ba_{0.25}O_6$, photorefractive effect, spectral characts. 78−43829
$Sr_{1-x}Ba_xZrO_3$, struct., X-ray powder diffr. study 80−1989
SrF_2-BaF_2, interdiffusion 77−7912
$Sr(NO_3)_2$, X-ray Debye temp. determ. 77−59088
U-Ba-C FBR nuclear fuels, phase anal., 1400°C 80−66487
V_2O_5-As_2O_3-BaO, semicond. glass, electronic props. 80−88557
V_2O_5-BaO-K_2O-ZnO glasses, elect. props. and struct. 80−15547
V_2O_5-CuO-BaO glass, unpaired electron localisation, ESR study 80−66026
V_2O_5-P_2O_5-BaO system glasses, phase separation, crystn. and EPR spectra 77−76321
V_2O_5-V_2O_4-$BaZnO_2$ glass, V ion states, mag. and elec. props. 80−88556
WO_3-BaO film, electrochromic coloration and decoloration, BaO additive effects 78−72620
Y_6WO_{12}:BaO, polycryst., elec. cond., 800-7400°C 80−15517
$Zn_2Ba_2Fe_{12}O_{22}$, phase transition, mag. props. *(Russian)* 79−51837
$ZnCl_2$-$BaCl_2$, molten, viscosity coeff. meas. *(Japanese)* 79−77662
ZrF_4-BaF_2-MF_n (M=Na, Ca, Ln, Th, n=1, 2, 3, 4), vitreous phases, network formers, modifiers and stabilisers *(French)* 80−64909
ZrF_4-BaF_2-NdF_3 glass, vitreous domain, prep. and optical props. 78−27304
ZrF_4-BaF_2-ThF_4-NaF(RF_3) (R=rare-earth) glass system, anion cond. 80−70460
ZrF_4-BaF_2-ThF_4(LaF_3)(NdF_3)(PrF_3), F^- ion cond. glasses, cond. process 80−107477
ZrF_4-ThF_4-BaF_2:V^{3+}(Cr^{3+}) glasses, absorpt. spectra *(French)* 79−99918
(ZrF_4-BaF_2-ThF_4)-EuF_2 system, glass forming region, prep. and props. 79−91633
ZrF_4ThF_4-BaF_2 system, new fluoride glass, optical props. *(French)* 77−36443

Barkhausen effect
anisotropic materials, magnetisation reversal, 1/H law 78−84454
Bloch walls, history 80−86065
diamagnetic susceptibility meas., thermal, Nyquist and Barkhausen noise 77−13782
ferroelectric, contrib. to repolarisation process *(Russian)* 77−32330
ferromagnet, Barkhausen discontinuities in model of rigid domain boundaries *(Russian)* 77−51922
ferromagnet, irreversible magnetising processes, random propag. 80−88818
ferromagnet, magnetisation noise and power loss 79−24197
ferromagnetic alloys, amorphous, sputter-deposited, soft mag. props., magnetostriction 80−34696
ferromagnetic irreversible Bloch wall jumps and static losses 78−19276
ferromagnetic rods, irreversible and reversible magnetising processes, impressed propag. 80−88819
ferromagnets, nondestructive inspection by magnetic noise method 78−72997
film, general behaviour and stationarity along hysteresis loop 78−56357
guanidine aluminium sulphate hexahydrate, ferroelec. cryst., growth, domain struct., dielec., switching props. 77−43950
machined surface layer structure determ. using Barkhousen noise probe *(German)* 79−24710
magnetic noise meas. method based on periodicity of Barkhausen jumps 79−17452
magnetic thin films, statistical anal., instrumentation, computer interfacing 78−82008
magnetizing device for inspection of products of ferromagnetic materials according to paramcters of Barkhausen discontinuity 80−89457
magneto inductive pick-up for Barkhausen noise spectra meas. *(Russian)* 78−65945
magnetoresistive head Barkhausen noise voltage meas. 79−82821
magnetostrictive pulse-producing wire plating 80−2618
NDT appl. 79−70261
Nyquist noise in mag. and dielec. materials 77−1569
pulse sequence with correl. between shape and separation time, power spectrum 78−4556

- **Barkhausen effect** continued
  - soft magnetic material, analysis by means of Barkhausen noise cross spectra 79−24199
  - soft magnetic materials, effect on static losses *(Slovak)* 79−4695
  - statistical theory for jumps assoc. with irreversible displacement of domain boundaries *(Russian)* 77−8346
  - steel, magnetisation transitions, Barkhausen noise 78−91894
  - steel, mild, fatigue softening and hardening detected from Barkhausen noise 80−76428
  - steel, mild, plastic deform. during fatigue, detection by Barkhausen noise meas. 79−43524
  - steel, mild, tensile and cyclic loading effect in Barkhausen noise 80−40560
  - steel 42NKhTYuA wire, hysteresis loop and differential permeab. after US and conventional drawing 79−15818
  - steel struct. testing from anal. of Barkhausen noise statistics 77−77647
  - TGS, Barkhausen jump, elec. pulse shapes 77−66465
  - TGS, ferroelec. crystal, Barkhausen effect study 79−38507
  - TGS, polarisation reversal, cryst. defects effect 78−27156
  - TGSe, ferroelec. crystal, Barkhausen effect study 79−38507
  - weak magnetic samples, conduction of flux 79−28560
  - welds, residual stresses, evaluation by Barkhausen noise meas. 80−76436
  - Co-Fe-Ni semi-hard mag. alloy, 3-D Barkhausen effect meas. 77−69623
  - Co-Fe-Ni semihard magnetic alloy, directional distrib. of magnetisation changes 78−14985
  - Co-Ni-Fe, semi-hard magnet, irreversible magnetisation changes, directional distrib. 79−24196
  - DyCu film, amorphous, asperomagnetic domains, Barkhausen jumps in hysteresis loop 80−75822
  - Fe, Barkhausen effect, grain size depend. at 300K and 77K *(German)* 77−16113
  - Fe, irreversible magnetisation changes, directional distrib. 79−24196
  - Fe polycrystalline, two ferromag. methods for eval. of fatigue limit 80−89438
  - Fe, remagnetisation processes, temp. and grain size depend. *(German)* 78−14987
  - Fe thin layers, vacuum coated on PMMA, mag. behaviour during mech. stress cycles *(German)* 80−80581
  - Fe-Al-Co-Ni, Alnico alloys, irreversible remagnetisation processes in rotating fields *(Russian)* 79−8015
  - Fe-Ci (3 wt.%), local magnetisation losses, grain orientation effect 80−88817
  - Fe-Ni alloy, low-noise, for cores of ferromag. probes and mag. modulators 79−8017
  - Fe-Si, 180° Bloch wall motion, Barkhausen jumps *(French)* 78−23294
  - Fe-Si, Bloch wall motion, irreversible processes 79−78431
  - Fe-Si, irreversible Barkhausen jumps *(French)* 77−1568
  - Fe-Si, stress and plastic deform. effect on Barkhausen effect, instrumentation 78−52313
  - Fe-Si, strips and rods, spatial extent of flux due to irreversible changes of mag. polarisation 79−33506
  - Fe-Si (3 wt.%), Barkhausen effect meas. 77−85492
  - Fe-Si (3 wt.%) laminations, grain oriented, plastically deformed, anomalous losses 80−88853
  - Fe-Si (3.5 wt.%), Barkhausen noise, strain depend., interaction of dislocations and domain walls 77−12155
  - $(Fe_{0.06}Co_{0.94})$-B, amorphous, ferromag., mag. instability rel. to struct. 79−99729
  - $Fe_{40}Ni_{40}P_{14}B_6$, $Fe_{35}Ni_{32}Cr_{15}P_{12}B_6$, amorphous ferromagnets, Barkhausen noise and core losses 77−69618
  - $GdCo_5$, large Barkhausen discontinuities, effect of dynamic elastic stresses *(Russian)* 78−39364
  - $Gd_2(MoO_4)_3$, domain wall motion dynamics 80−108030
  - $LiNbO_3$:Fe, spontaneous polarisation reversal and photorefractive effect 78−31163
  - MgMn ferrite, mag. noise features at low temps. *(Russian)* 78−27060
  - $NaH_3(SeO_3)_2$, domain struct. realignment and Barkhausen effect 80−71361
  - $NaH_3(SeO_3)_2$, ferroelec. crystal, Barkhausen effect study 79−38507
  - Ni, simultaneous obs. of Barkhausen and magnetoplastic effect 79−28583
  - Ni-Fe film, Barkhausen noise spectra meas. 77−16131
  - Ni-Fe wire, hard-drawn, increased Barkhausen noise at low temps. 77−16114
  - NiCo ferrite, induced mag. anisotropy, hysteresis loops, Barkhausen effect *(Russian)* 78−64203
  - NiFe film, stationarity and behaviour of Barkhausen noise 79−24198
  - SbSi, SbSI, contrib. to repolarisation process *(Russian)* 77−32330
  - Si-Fe, freq. spectrum of Barkhausen noise of moving 180° domain wall 77−16115
  - $SmCO_5$, etched microparticles, Barkhausen discontinuity, nucleation, and domain wall pinning 79−87288
  - $SmCo_{4.3}Cu_{0.7}$, highly anisotropic ferromag., mag. state after large Barkhausen jump *(Russian)* 79−4699
  - SmYGa garnet, bubble motion depend. on wall pinning 79−78455
  - U_3P_4, single cryst., Barkhausen effect 77−28410
  - YIG, interconnection of Bloch walls *(German)* 78−14986
  - YIG:Si, photo-induced low freq. mag. permeab. *(Russian)* 78−39368
- **Barnett effect** *see gyromagnetic effect; magnetisation*
- **barometers**
  - barometer, Hg, precision, 710 to 770 torr 80−47046
  - buoy-mounted barometric pressure instrument as wave height sensor 78−36321
  - demonstration model 80−73156
  - digital, description and applics. 77−41208
  - IC barometer using op. amps. and pressure transducer 79−35709
  - microbarometer with capacitive detector, highly sensitive 80−109261
  - NCAR digital barometer 77−29453
  - ocean wave height barometric sensor 77−78487
  - sensor for constant-level balloon expt., boundary layer to 100 mbar level 79−21047
  - vapour pressure thermometric barometer for remote locations and data buoys 80−46300
  - Hg, automatic, precision 710 to 770 torr 80−47046
  - Hg, primary standard appl., comparison with gas-operated pressure balance 80−13090
- **barometric pressure** *see atmospheric pressure and density*
- **barrages** *see dams*
- **barrel distortion** *see aberrations*
- **barretters** *see thermistors*
- **barrier injection transit-time diodes** *see BARITT diodes*
- **baryon-baryon interactions**
  - *see also baryon-baryon scattering; hyperon-nucleon interactions; nucleon-nucleon interactions*
  - baryon+antibaryon, baryonium dual S-matrix approach 80−52526
  - baryon+antibaryon annihilation model, high energy, multiperipheral interpretation of dual unitarity diagrams 77−18253
  - coupled channels method, applicability to nuclear physics with Ns and Δ's, book contrib. 79−97667
  - inclusive single-particle distribution function structure, urbaryon model 77−18343
  - infinite finite temperature baryon matter, Green's function formalism, quantum correction 78−13000
  - quark fragmentation distribs., meson, baryon and photon reactions 77−74655
  - $SU(4)_W$ symmetry, dibaryon coupling constants for γ, π and baryon interactions *(Russian)* 80−13329
  - SU(4), symmetry breaking effects on strong coupling const., charmed and uncharmed $\bar{B}$ BP couplings calc. 80−105802
  - total cross sections, semiempirical formulae, three component model with SU(3) components 78−41600
  - $\bar{B}B$ states, rest mass parameterisation 77−87992
  - $\Lambda\Lambda$, hypernuclei studies in nuclear emulsions 77−22923
  - $\bar{\Lambda}\Lambda$, OBE pot. calc., bound state and reson. energies, widths in 1.6 to 2.7 GeV range 77−49931
  - $\bar{p}d \to e^+e^- + n_s$, proton EM form factors, $p\bar{p}$ annihilation *(Russian)* 80−68457
  - $\bar{\Sigma}\Sigma$, OBE pot. calc., bound state and reson. energies, widths in 1.6 to 2.7 GeV range 77−49931
  - $\bar{\Xi}\Xi$, OBE pot. calc., bound state and reson. energies, widths in 1.6 to 2.7 GeV range 77−49931
- **baryon-baryon scattering**
  - *see also baryon-baryon interactions; hyperon-nucleon scattering; nucleon-nucleon scattering*
  - chiral invariance for asymptotic momenta, elastic scatt. of hadrons, helicity amplitudes 78−4800
  - differential cross section ang. depend., constituent interchange model 77−255
  - diffractive scatt., field theoretic model with quark field operators 79−26318
  - gauge-dual-topological approach to soft hadronic reactions, trajectory slopes 80−18142
  - line reversal symmetry breaking, simple rearrangement and absorption models 78−62326
  - p+baryon elastic scattering, polarisation phenomena in hadron collisions at small momentum transfer *(Russian)* 78−58196
- **baryon decay**
  - *see also baryon hadronic decay; baryon leptonic decay; hyperon decay*
  - algebraic formulation, vector and axial vector operators, SU(3), form factors 77−71512
  - asymptotically free SU(5) grand unification, proton stability, renormalisation group 80−82929
  - baryon+antibaryon bound states, $N\bar{N}$, quasinuclear levels, annihilation, influence of decay channels, multichannel model 79−2912
  - baryon number nonconservation limits, grand unified theory nucleon decay modes 80−411
  - baryon resonances, complex mixing, decays and mass splittings, Wigner-Weisskopf simultaneous treatment 80−62977
  - baryonia, decay properties and L=1 state width approx. 79−75773
  - baryonia decay props., L=1 state widths 79−75772
  - charmed, parity violating and conserving decays, $(1/2^+ \to 3/2^+ + 0^-/1^-)$ in Abe, Fujii and Sato model 79−97623
  - charmed baryon semi-leptonic decay and quark effective masses, SU_4 symmetry 78−58185
  - charmed baryons, semileptonic decays, SU(4) breaking, mag. moments, suppression factors 79−387
  - charmed baryons in a quark model with hyperfine interactions 79−97601
  - charmed particle weak semileptonic decays, free parton model 79−75766
  - charmed particles, masses and decay consts. in SU(4)×SU(4) broken chiral symmetry 79−40686
  - conference, baryon resonances, Oxford, England (July 1976) 77−22750
  - effective lagrangian flavour struct. and renormalisation, grand unification 80−27447
  - even-wave harmonic oscill. theory of baryon decay 78−45853
  - form factors, semi-leptonic weak interactions, book contrib. 78−78162
  - free neutron decay, fundamental phys. expts. with reactor neutrons and neutrinos, summary 79−67543
  - gravitational annihilation, radioactive decay 77−6075
  - hadron resonance decay, intermediate vector boson and high energy weak interaction detect. 79−22012
  - hadronic charmed particle decays, quark and particle helicities, charm changing current chirality 80−37256
  - heavy fermions in the standard sequential scheme 79−71748
  - multiquark baryons and the MIT bag model in SU(6), coupling const. and decay modes 79−97600
  - neutral charmed particle decay, direct observation in ν-emulsion interactions 80−9165
  - neutron half life meas., p registration method *(Russian)* 78−93879
  - neutron mean lifetime meas. using EM trap 80−73703
  - neutrons, ultracold, use for lifetime meas., collision loss calcs. *(Russian)* 80−52504
  - nucleon decay, T violation possibility and consequences in superunified theories 80−82917
  - nucleon decay operator anal., superunified theories selection rules 80−13302
  - nucleon stability testing, radiochemical and geochemical method limits 79−22093
  - nucleons, symmetry relations, effective Hamiltonian and inclusive decay rates, kinship hypothesis 80−78060
  - O(10), SU(4) colour subgroup, fractional charged gauge boson, proton half-life 80−73644
  - proton semileptonic decay in nuclei, pion attenuation 80−47286
  - Q^6 dibaryon resonances, orbitally excited mass spectrum, decays 80−73670
  - relativistic heavy ion collisions, pion volume emission from Δ (1232) decay 79−93651
  - resonance decays and $SU(6)_W$ models 77−22700

baryon decay continued
- resonances, radiative decay in relativistic harmonic oscillator model 79−85277
- semileptonic, applic. of SU_3 theorems 80−32030
- strange baryonium, spectrum, decay, production 78−93854
- straton model of $1/2^+$ baryon semileptonic decays and high energy neutrino-nucleon reactions *(Chinese)* 78−12873
- string-junction model, hair pin line rule and baryonium decay 80−27487
- SU(3) symmetry breaking in baryon resonance decay 78−89712
- SU(5) and SO(10) grand unification, flavour mixing and proton instability *(Russian)* 80−68413
- SU(5) grand unification, p lifetime and branching ratio, bag model wavefunctions 80−78004
- SU(5) grand unification, superheavy fermions and proton lifetime *(Russian)* 80−91036
- SU(5) grand unified theories, proton decay, flavour mixing effects 80−377
- SU(5) grand unified theory, proton lifetime estimate accuracy 80−101967
- $SU(6)_W$ decay anal. of $[70, 1^-]$ and $[56, 2^+]$ multiplets 77−22733
- subcomponent models of quarks and leptons in SU(3) subcolour, proton decay 80−78035
- ultracold neutron accumulation, above-barrier neutron effects, lifetime determ. 80−102227
- ultracold neutrons, lifetime in traps, film-substrate model calcs. 80−106098
- universe ultimate fate, effect of finite proton lifetime 80−82560
- $B_c \rightarrow e^+e^- +$hadrons, decay due to weak neutral currents *(Russian)* 79−22146
- $D_{15} \rightarrow \rho\gamma$, SU(6) selection rule violation from quark hyperfine interactions 79−6329
- $\Delta(1232)$ decay width using little bag dynamics and axial vector current 79−75771
- Δ-isobar decay products ang. distrib. *(Russian)* 78−45932
- $\Delta^+ \rightarrow P\gamma$, ground and radially excited states, broken symmetry treatment 80−9174
- $K^- p \rightarrow \pi^- Y^*(1385)$, 11.5 GeV/c, line reversed reaction, $Y^*(1385)$ diff. cross section and decay ang. distribs. 79−89193
- n, decay, weak interaction meas., coincidence type ion electron converter detector obs. 80−58100
- n, polarised, spin-electron correlation coeff., G_A/G_V ratio *(Russian)* 79−97625
- N,N* resonances, radiative decays, static quark bag model *(Russian)* 80−47299
- $n \rightarrow ep\bar{\nu}$, H atom spectra and metastable state *(Russian)* 80−37262
- $n \rightarrow H\bar{\nu}$, atomic decay, scalar and tensor interaction effects *(Russian)* 80−68455
- N stability, geochem. test independ. of decay mode 78−8667
- p, baryon number nonconservation, expt. status 80−57594
- p, decay, confirmation of unification of forces, book contrib. 80−42383
- p, decay, search techniques for lifetimes of order 10^{34} years 80−47287
- P decay, baryon number-lepton number conservation or violation, grand unification implications 80−27425
- p decay, flavour gonimetry 80−99100
- $\bar{p}$ decay and baryon number of universe 77−49964
- p decay lifetime in SU(5) grand unified theory 79−71749
- $\bar{p} \rightarrow e\pi^0$, lifetime meas. using counter technique at ICE 79−93413
- $\pi^+ p \rightarrow K^+ Y^*$, 11.5 GeV/c, line reversed reaction, $Y^*(1385)$ diff. cross section and decay ang. distribs. 79−89193
- $\pi^+ p \rightarrow \pi\pi N$, 1.4-1.7 GeV, isobar model partial wave anal., baryon resonance decay 80−86750
- $\Sigma^- n$ dibaryon decay in exotic atoms 80−9762

baryon hadronic decay
- $1/2^+$ baryon nonleptonic weak decays, pseudo connected line diagrams 78−45917
- baryon, charm changing weak decays $1/2^+ \rightarrow 3/2^+ + 0^-/\gamma$ in SU(4) and $SU(8)_w$ 79−3021
- Bethe-Salpeter formulation for baryon matrix elements in hadronic weak decays 79−386
- bottom hadrons, masses and allowed decays, SU(5) quark model 80−62954
- charm changing radiative weak decays in AFS model 80−47285
- charm-changing decay, derivation of selection rules 79−13120
- charmed baryon decay time 79−67548
- charmed baryon decays, EM and weak, U- and V-spin generalisations 80−47284
- charmed baryon decays, nonleptonic, parity-violating, single-quark and two-quark transitions 80−68453
- charmed baryon decays, weak hadronic, SU(3) dynamical scheme 80−68454
- charmed baryon hadronic decays, parity violation in SU(8) 79−89077
- charmed baryon non-leptonic weak decays 77−2829
- charmed baryon non-leptonic weak decays in SU(8) 77−49963
- charmed baryon nonleptonic decays, sum rules for $\Delta C = \Delta S = 1$ S-wave decays 79−58957
- charmed baryon weak nonleptonic multibody decay interpretation of $\bar{\Lambda}$-multi π peaks in photoprod. data 77−34153
- charmed baryons, $\Delta C = \Delta S = 1$ nonleptonic decays, amplitude relations 79−54339
- charmed baryons, nonleptonic decays 78−66118
- charmed baryons, quark-diquark model of nonleptonic decays 79−13120
- charmed baryons, weak decays, quark model framework 80−62976
- charmed hadrons $\Delta C = \Delta S$ decays, sum rules, internal symm. props. 77−30376
- charmed multiplet decay, $3/2^+$ decuplet isobars in SU(3) symmetry, dynamical assumption 79−26333
- charmed-baryon nonleptonic decays, parity-violating amplitudes 78−62398
- fundamental physics with reactor neutrons and neutrinos [conf. ILL, Grenoble, France (Oct. 1977)] 79−59112
- harmonic oscill. covariant model matrix element calcs. 77−61284
- hyperon, absolute magnitude and EM hyperfine splittings 78−17016
- hyperon decays, theoretical description, and sum rules for $NN\pi$ amplitudes 79−17663
- hyperon nonleptonic decay, SU_3 symm., second class currents in effective Hamiltonian 77−41842
- hyperons, octet enhancement, MIT bag model 77−10249
- hyperons, quark-diquark model of nonleptonic decays 79−13120
- light-like reduction formula and derivation of PC and PV Lee-Sugawara relation 80−32032

baryon hadronic decay continued
- M_2 baryonium state decays, baryonium assignment scheme 79−71691
- N resonance electroproduction, helicity structure and quark motion effect 78−398
- non leptonic hyperon decay amplitudes, calc. without arbitrary parameters 80−13300
- non-leptonic hyperon decays and the baryon spectrum, S- and P-waves, quark model description 79−36073
- nonleptonic hyperon decays, final state interactions with inelastic effects, comments 80−99099
- nonleptonic hyperon decays, QCD corrections 80−91087
- nonleptonic hyperon decays and lightlike chiral struct. of hadrons 79−36074
- parity violating non-leptonic hyperon and charmed baryons in SU(8) 77−26523
- penguins in $\Delta S = 1$ nonleptonic weak decays 80−91086
- pionic decays, anal. of baryon reson. photocoupling signs 79−22094
- pionic transitions in MIT bag model using PCAC hypothesis 80−37228
- pseudo-connected line diagrams, $1/2^+$ baryon nonleptonic decay 78−45918
- pseudoscalar transition between spin-J and spin 5/2 baryon 78−50032
- QCD model for internal structure, pseudoscalar-meson and photon emission 80−68452
- radially excited states in baryon resonance pionic decays, relativistic quark model 80−95268
- resonance decay, broken SU_3 and total reduced width 78−17017
- resonance decay, l-broken $SU(6)_W$ model equivalence to relativistic harmonic oscillator quark model 78−41546
- resonance decay, unified interactions in relativistic quark model 78−41547
- resonances, binary decays, centrifugal effects *(Russian)* 78−17012
- selection rules in $B\bar{B}$ harmonic oscill. pot. model 77−49930
- single quark transition model, parity violating charmed hadron decays, current-current interaction 78−12907
- SU(3) quark sectors, weak hadronic and radiative decays of nonstrange charmed baryons 79−22092
- $SU(6)_w$ analysis of sums of baryonic partial widths 77−30378
- $SU(6)_w$ and $\{70, 1^-\}$, $\{56, 2^+\}$ decays 77−6122
- two-quarks transition amplitude, mesonic decays, taking baryons as symmetric three quark states 78−17013
- vector mesonic decay of $1/2^+$ baryons, charm changing mode 80−47283
- weak hadronic decays of uncharmed baryons in SU(3)−dynamical considerations 79−75769
- weak radiative decay, sum rules, octet/sextet and 20-plet dominance 78−62400
- weak radiative decay of baryons, SU(3), SU(4) anal. 78−33069
- weak radiative decays in SU(4) and SU(8) 77−87977
- $C_0{}^+$ prod. and decay, test of charmed current struct. 77−61271
- $C_1 \rightarrow C_0{}^+ \pi$ decay width calc. 78−25011
- $D_{05} \rightarrow \bar{K}N$, SU(6) selection rule violation from quark hyperfine interactions 79−6329
- $D_{13}(1510) \rightarrow P_{11}(940) + \gamma$, Melosh transform, $[70.1^-] \rightarrow [56.0^+] + \gamma$ *(Russian)* 78−66116
- Δ, $I = 3/2$ high mass enhancement in 10.3 GeV/c $\pi^+ p$ interactions 78−66117
- $\Delta(3,3)$ phase shift, current algebra model, πN decay channel 77−79232
- $\Delta^{++} \rightarrow p\pi^+$, decay widths calc. in MIT bag model 77−74681
- η decay modes of $1/2^-$ baryons, hadronic interaction symm. 77−30379
- Λ decay, absolute magnitude determ. 77−30377
- $\Lambda_c{}^+ \rightarrow p\pi^+ k^-$, lifetime of charged charm particles 79−67548
- $n \rightarrow pe^- \bar{\nu}$, neutron lifetime, expt. determ. using storage of decay protons 79−58959
- $n \rightarrow pe\bar{\nu}$, experimental determination of the neutron lifetime 79−58958
- $n \rightarrow pe\bar{\nu}$, expt. determ. of correlation coefficients in neutron β-decay 79−58960
- $\Omega \rightarrow \Lambda K$, QCD and valence quark approx. 80−105893
- Ω^-, charm changing weak decays $1/2^+ \rightarrow 3/2^+ + 0^-/\gamma$ in SU(4) and $SU(8)_w$ 79−3021
- $\Omega^- \rightarrow \Lambda K^-$, current algebra calc. with phenomenological modification of nonleptonic decay amplitude 77−67650
- $\Omega^- \rightarrow \Lambda K^-$, Ω^- lifetime, spin from $K^- p \rightarrow \Omega^- + X$, 8.25 GeV/c 78−93877
- $\Omega^- \rightarrow \Xi^0 \pi^-$, $\Xi^- \pi^0$, or $\Lambda^0 k^-$, nonleptonic decay rates, $\Delta I = {}^1/_2$ contrib. 78−62399
- $\Omega^- \rightarrow \Xi^* \pi(\Xi^0 l^- \nu_l)$, nonleptonic hyperon decays, QCD description, PCAC anal. 80−95269
- $\Omega_3{}^{*++}$, charm changing weak decays $1/2^+ \rightarrow 3/2^+ + 0^-/\gamma$ in SU(4) and $SU(8)_w$ 79−3021
- $\Sigma^- \rightarrow \Lambda K$, QCD and valence quark approx. 80−105893
- $\Sigma^+ \rightarrow p\gamma$, $1/2^-$ resonance poles to parity-violating amplitude, two-quark weak transitions 80−78062
- $\Sigma^\pm$, lifetimes and longitudinal accel. 80−86709
- $\Sigma_c{}^+$, production and decay obs. 80−105894
- $\Sigma^- n$ dibaryon, decay particles momenta 79−85298
- $C_0{}^+$ prod. and decay, test of charmed current struct. 77−61272
- π emission decay of baryon resonances, quark model, widths, amplitudes, sum rules 77−57534

baryon interactions *see baryon-baryon interactions; lepton-hadron interactions; meson-baryon interactions; photon-hadron interactions*

baryon leptonic decay
- β-decay, neutrino-free, theory, weak interaction const. derivation 79−13254
- charmed baryons, weak decays, quark model framework 80−62976
- neutron β-decay, first order radiative corrections to e, ν and e-ν asymmetry coefficients 78−58254
- neutron beta decay characteristics 79−6338
- neutron decay, radiative corrections to proton recoil spectrum 79−13119
- nonlocal quark model of leptonic decays and mag. moments *(Russian)* 80−86711
- $C_0{}^+$ charmed baryon weak decays 79−9369
- m, polarised, false effects in decay triple correlation, time-parity violation search *(Russian)* 78−78180
- n decay, model independ. form of certain observables 78−33068

baryon mass
- *see also hyperon mass*
- 1^- baryon multiplet mass splitting anal. 77−2832
- baryonia mass spectra calc. incl. spin-dependent forces 79−26309
- baryonium narrow states in QCD 77−57494
- baryonium spectrum, SU(4) mass formulae, degenerate clustering 79−93393

baryon mass continued
bottom hadrons, masses and allowed decays, SU(5) quark model 80−62954
charm baryons, mass splitting and weight diagrams 79−26314
charmed, baryon spectrum due to chromomagnetic and electromagnetic hyperfine interaction 79−13123
charmed, EM mass differences in charmed quark model 77−71515
charmed, mass spectrum, 15-plet dominance of SU(4) symmetry breaking 77−74663
charmed, mass splitting by weight diags. 77−49915
charmed, one parameter mass formula 77−10232
charmed, SU(1,4) as a dynamical group, analysis of all discrete representations 77−45982
charmed, tensorial mass operators 77−54091
charmed baryon EM mass splitting 79−93311
charmed baryon mass and F/D ratio, colour magnetic interaction 80−62957
charmed baryon mass formula 77−79257
charmed baryons, mass spectrum from $SU_{1,3}$ dynamical group theory 80−62956
charmed baryons, mass splitting sum rules 79−89083
charmed baryons in a quark model with hyperfine interactions 79−97601
charmed baryons of $J_{\pi}=e^{-},7/2^{+}$ *(Russian)* 77−61258
charmed hadron masses, from effective quark masses, sum rules 80−4965
charmed hadrons, SU(4) mass-breaking, mass sum rules 80−62959
charmed particles, masses and decay consts. in SU(4)×SU(4) broken chiral symmetry 79−40686
charmed-hadron masses and electromagnetic mass differences in a broken-SU(8) quark model 77−61256
EM mass differences, one gluon exchange contrib. 79−3024
ground state, combined effects of internal quark motion and SU(6) breaking 77−38128
ground-state baryons in a quark model with hyperfine interactions, masses 80−4944
hadron spectroscopy with covariant Coulomb and confining interactions 80−32090
horizontal-quantum-flavor-dynamics approach to the fermion mass spectrum in $[SU(2)\times U(1)]_{WS}\times U'(1)$ gauge 80−52474
large transverse momenta selection to enhance high-mass resonances 77−2871
meson and baryon mass formula, chromodynamics consideration *(Russian)* 80−91071
naive quark model predictions for meson mass and baryon mass and mag. moment 80−78036
narrow multiquark baryons, masses and decay modes 79−89119
negative parity baryons, spectrum and mixing angles, QCD type quark model 79−26307
neutron, ratio of mass to Plancks const. *(German)* 79−6077
neutron mass determ. method 79−59294
QCD, hadron masses, behaviour of constituent quarks 80−57557
quark confinement, Dirac equation with relativistic linear potential, baryon properties, SU_6 representations 80−47261
quark model and hadron spectroscopy, review 79−80808
quasi-stable baryons *(French)* 77−57533
resonances of even parity 77−10224
s-wave baryon spectrum, phenomenological quark-quark interaction 80−101984
SU(5) symmetry with beauty quark, baryon and meson mass spectra 79−45079
SU(6) symmetry, mass relations for $^{1}/_{2}^{+}$-baryons 80−82962
SU(8) symmetry and the baryon mass spectrum 79−80814
symmetry-breaking, current algebra quark masses 80−42436
three quark oscillator model for baryon spectrum 77−22698
Δ, M=1871 MeV obs. in 10.3 GeV $\pi^{+}p$ interaction 78−66117
δ(3,3) phase shift 77−79232
Δ^{+} isobar in $\pi p \rightarrow N\pi$ expts., M=1208.5 MeV *(Russian)* 78−86453
$K^{+}p \rightarrow \Lambda pn\pi^{+}$, reson. peak at 2.46 GeV 78−89744
N, mass estimation from $\nu n \rightarrow \mu^{-}p$ 80−18128
N-Δ mass difference 77−67653
n-p mass difference, semiclassical approach 77−6123
N* resonances, prod. in $\pi^{-}p \rightarrow \Lambda k^{+}+X$ and $\pi^{-}p \rightarrow \Lambda^{\phi+X\phi}$ 77−6159
p̄, mag. moment and mass meas. 78−45990
p mass, reln. to ρ meson liftime 77−22716
p/e mass ratio, limits to past variability set by quasar absorpt. line redshifts 77−61338
p-n mass difference and causality 77−61286
pp effective mass distrib. in $C+\pi^{-}$ at 5 GeV/c *(Russian)* 80−9316
$\bar{p}p \rightarrow p(slow)+X$, 22.4 GeV/c, associative multiplicity *(Russian)* 80−5031
X(2244) data from symmetry breaking SU(4) mass formula 78−89690
X(2430) data from symmetry breaking SU(4) mass formula 78−89690
Y* prod. in Σ^{-}-nucleus reacts. 77−50183
Δ(1236)-N(939) mass difference from deep inelastic scatt. quark wave functions, hyperon masses 80−47289

baryon photoproduction
see also hyperon production; neutron production; proton production
charmed hadrons, assoc. prod. by 9.3 GeV photons 77−18301
radiative transitions of baryons in the MIT bag model 79−40722
resonance photocouplings using mixed nucleon and even-wave harmonic oscillator theory of baryonic states 77−82752
Δ(1232), production in N photo-excitation, multipole amplitudes, dispersion relations 80−5002
Δ(1232) production by virtual photons, Δ^{++} and Δ^{0} prod. 79−9383
Δ_{33} energy region, electroproduction, simple-pole model, $\gamma\mathcal{N}\Delta_{33}$ vertex 80−22625
$\gamma d \rightarrow np$, 300 MeV, dibaryon resonance manifestation, pseudoindependent amplitude elimination *(Russian)* 80−57612
$\gamma d \rightarrow pn$, proton polarisation energy depend., 400-700 MeV *(Russian)* 80−63000
$\gamma D \rightarrow pp\pi^{-}$, π rescatt. through Δ(1236) for nucleon high momentum 77−57547
$\gamma N \rightarrow K^{+}\Sigma$, meas. of asymmetries and cross sections using 16 GeV linearly polarised photons 80−13318
$\gamma N \rightarrow \pi\Delta$, Δ-isobar density matrix *(Russian)* 78−45932
$\gamma N \rightarrow \pi\Delta$, meas. of asymmetries and cross sections using 16 GeV linearly polarised photons 80−13318
$\gamma p \rightarrow K^{+}\Lambda$, meas. of asymmetries and cross sections using 16 GeV linearly polarised photons 80−13318

baryon photoproduction continued
$\gamma p \rightarrow \pi^{0}p$, 450 to 800 MeV, proton polarisation, Walker-type anal., $P_{11}(1470)$, $D_{13}(1470)$, $S_{11}(1535)$ resonances 80−73721
N(1420), $SU(6)_{W}$ fits in baryon photo- and electroproduction 77−46057
$\gamma p \rightarrow K^{+}\lambda(\Sigma^{0})$, $\pi^{+}n$, $\pi^{-}p$, $K^{+}\Lambda$, $K^{+}\Sigma^{0}$ final state comparisons above resonance region 80−105906

baryon production
see also baryon photoproduction; hyperon production; neutron production; proton production
additive quark model in quasi-two-body hadronic reactions, Δ and vector meson prods. relation 78−41494
baryon number generation in grand unified theories 79−26279
charmed baryon diffractive prod. at ISR energies 77−41818
charmed baryons, ground state, production by neutrino interactions 79−93400
charmed production in electron positron annihilations 79−49530
conference, baryon resonances, Oxford, England (July 1976) 77−22750
cosmological baryon production, expanding Universe, baryon to entropy ratio, number nonconservation 79−44652
cross sections, high mass particles 78−25018
diquark and quark jet fragmentation model, meson and baryon production 79−2979
dual unitarisation scheme, dynamical threshold for baryon resonance prod., baryon exchange 78−45884
grand unified theories, baryon production through primordial black holes 80−101970
high-transverse-momentum symmetric-particle-pair spectra and correlations 80−95250
hydrodynamic theory of multiple hadron production, new approach *(Russian)* 79−6332
inclusive prod. in $e^{+}e^{-}$ annihilation, meas. of inclusive antiproton, Λ and $\bar{\Lambda}$ prod. cross section charmed baryon prod. 78−17034
inclusive prod. in quark cascade model in pp, πp and $e^{+}e^{-}$ 77−50025
nucleon production in quark parton model, $e^{+}e^{-}$, ep and large $p_{\perp}$ reactions 78−21391
pair prod. with large decay Q-value 79−58992
photoproduction, and Compton scatt., formalism 79−9384
primordial baryons, generation by black holes 80−98750
primordial black hole evaporation, baryon prod. and excess 80−41852
QCD predictions for large momentum transfer baryon prod. 79−89125
quark recombination model, meson and baryon prod. sum rules 80−4922
resonance electro- and photoproduction, EM transitions, multipole moments in single quark transition model 80−62985
resonance electroproduction, review of expt. information 77−22745
spectroscopy, experimental trends and problems 77−22754
spectroscopy, history, trends, outlook 77−22751
spin-parity test using polarised proton targets or beams 79−9427
superconducting early Universe, cosmological baryon prod., CP invariance grand unification 80−90592
weak charmed-baryon resonance prod., neutrino inclusive interactions, scaling behaviour 78−8645
weak production of charmed baryons by neutrinos, relativistic quark model 78−41496
C_{0}^{+} prod. and decay, test of charmed current struct. 77−61271
d breakup, exotic final state interaction, intermediate Δ, ΔN threshold parameters 78−50043
Δ(1232) production in deep inelastic electron-nucleus scatt. 80−57772
Δ(1236) inclusive prod., absorpt. corrections in triple-Regge region 77−87956
Δ(1236) production by high energy neutrinos, straton model *(Chinese)* 78−12900
Δ(1236) production in νp reactions, multipole struct. of weak prod. by charged currents 78−29328
Δ prod., spin-3/2 polarisation density matrix determ. 77−87965
Δ prod. and spin depend. of pp total cross sections 77−82794
Δ production probability in d breakup, isobar model, static NN-ΔΔ mixing pot. 78−29438
Δ^{++}, prod. in $\nu p \rightarrow \mu^{-}\Delta^{++}$, 5-100 GeV 78−93873
Δ^{++}, production in $pp \rightarrow p\pi^{+}n$, 800 MeV 78−70385
$\Delta^{++}(1232)$, mag. dipole moment calc., from πp data 79−22133
$\Delta^{++}(1232)$ inclusive prod. in $\pi^{+}p$, $\pi^{-}p$, $K^{-}p$ at 16 GeV/c 78−66169
$\Delta^{++}(1232)$ inclusive prod. in $\pi^{-}p$ interactions at 147 GeV/c 79−17772
$\Delta^{++}(1236)$, $\bar{\Delta}^{++}$ inclusive prod. in p̄p, interaction mech. 79−3054
ed→ed*, dibaryon resonance production 80−78070
$e^{+}e^{-}$ annihilation, prod. of orbitally charmed hadrons, free quark model anal. 79−22120
$e^{+}e^{-}$ annihilation, ratio of secondary baryon and meson yields and quark combinatorics *(Russian)* 79−49532
$e^{+}e^{-} \rightarrow$charmed hadrons, quark mass effect on fragmentation functions 80−91098
$e^{+}e^{-} \rightarrow \Delta X$, polarisation effects in nonperturbative parton model, scaling 80−105912
$e^{+}e^{-} \rightarrow$hadrons, weak interaction effects, ang. distrib. charge asymm. baryon longitudinal polarisation *(Russian)* 77−30397
$e^{+}e^{-} \rightarrow p^{-}X$, charmed baryon pair prod. cross section, pole-dominated form factor 78−12922
$e^{+}e^{-} \rightarrow q\bar{q} \rightarrow BX$, weak-neutral current effects 80−42480
$eN \rightarrow e\pi\Delta$, low energy, ΔN axial form factors soft-pion theory 78−70380
$\gamma N\Delta_{33}$ form factors in πN collisions 79−63515
$K^{-}d \rightarrow \Lambda p\pi^{-}$, Λp invariant mass distrib., ΣN bound state 77−30428
$KN \rightarrow K^{*}\Delta$, positivity conditions in joint vector-meson Δ prod. 77−13975
$K^{-}N \rightarrow \bar{K}^{*}\Delta$, energy depend. 79−63524
$K^{-}n$ reactions, quasi two-body final states at 8.25 GeV/c 79−22139
$K^{+}N \rightarrow K^{*}\Delta$, energy depend. 79−63524
$K^{-}p \rightarrow \Delta^{++}X$, 32 GeV, inclusive and total cross sections 80−105936
$K^{-}p \rightarrow \pi^{-}Y^{*}(1385)$, 11.5 GeV/c, line reversed reaction, Y*(1385) diff. cross section and decay ang. distribs. 79−89193
$K^{+}p$, 147 GeV/c, inclusive Δ^{++} prod., cross section energy depend. 80−57651
$K^{+}p \rightarrow \Delta^{++}(1232)+X^{0}$, 32 GeV/c 80−52540
$K^{+}p \rightarrow K^{0}\Delta^{++}$, cross-sections below 2 GeV/c, data compilation 77−22780
$K^{+}p \rightarrow X\Delta^{++}$, absorption corrections to three Reggeon formulas *(Russian)* 79−9423
$K^{\pm}p \rightarrow K^{\pm}(\Delta^{++}\pi^{-})$, 8.25 GeV/*c*, proton diffraction region 79−9405
$Ld \rightarrow l'\Delta X$, deep inelastic scatt., isobar admixture possibility *(Russian)* 80−91095
NN→Δ(1236)Δ(1236), 4-25 GeV/c, Reggeised absorption model 77−6170

baryon production continued
$\bar{\nu}$ induced dimuon events, V^0 yield, possible beautiful baryon prod. 80−105882
νH_2, possible new meson or baryon reson. decay 77−240
$\bar{\nu}H_2$-Ne, possible new meson or baryon reson. decay 77−240
$\bar{\nu}p\to\mu^+n$ or $\mu^+\Lambda$ or $\mu^+\Sigma^0$, bounds on outgoing baryon transverse polarisation, T-odd effects 77−87966
(p,N*), high energy reactions, Glauber scatt. theory study *(Chinese)* 79−93626
pp, 147 GeV/c, inclusive Δ^{++} prod., cross section energy depend. 80−57651
$\bar{p}p$, azimuthal correlations at 22.4 GeV, ρ^0, Δ^{++} reson. prod. 79−67611
pp, probabilistic quark-model approach to p fragmentation 80−63049
$pp\to$baryons by diquark-quark fusion model 80−102065
$pp\to\Delta^{++}\Delta^0$ up to 1500 GeV/c, Reggeised-absorption model 77−6170
$\bar{p}p\to\Delta^{++}(1236)X$, 22.4 GeV/c, inclusive and semiinclusive cross sections, one pion exchange contrib. 79−49548
$pp\to\Delta^{++}p\pi^-$, 4 GeV/c, mass spectra, ang. distribs. and momentum transfer *(Russian)* 80−42489
$pp\to\Lambda K_3^0X^{++}$, 19 GeV, strong dynamic correlations 79−93468
$pp\to n\Delta^{++}$, 6 GeV/c, polarised p, spin density matrix elements, beam polarisation induced effects 79−93451
$pp\to pX$, 6 GeV/c, π exchange, depolarisation parameter 80−78088
$pp\to pX$, diquark fragments, large transverse momentum baryon production 80−47330
$\bar{p}p\to\bar{p}p\pi^+\pi^-$, 7.2 GeV/c, diffraction dissociation and double resonance prod. 79−89177
$p\pi\to$baryons by diquark-quark fusion model 80−102065
$\pi^-d\to\Delta^-p$, high energy, backward Δ^- prod. mech., Δ^{++}-Reggeon exchange *(Russian)* 79−97637
$\pi^{+4}He\to\pi^-4p$; 1.5 to 2.0 GeV/c, cross sections, momentum spectra, ang. distrib. Δ resonances prod. 77−65237
πN elastic scatt. in dual model, baryon reson. 77−18318
$\pi N\to N(1360)\Gamma<67$ resonance, dibaryon pp resonance systematics 80−68481
πp, quark-diquark elastic scatt., diquark fragments, large transverse momentum baryon production 80−47330
π^-p, 2-14 GeV/c, total cross section, narrow baryon search 80−105922
$\pi^-p\to\Delta^{++}X$, 100, 200, 360 GeV/c, δ^{++} inclusive and semi-inclusive prod. cross sections 79−40817
$\pi^-p\to\Delta^{++}(1232)$, 15 GeV/c, multiplicity distrib. determ. 78−45982
$\pi^-p\to\Delta^+(1236)\pi^-$, 3.0 to 5.5 GeV/c, differential cross section, fluctuations 77−22774
π^-p elastic scatt., 3.42-5.03 GeV, narrow baryon search in differential cross section 80−105921
π^-p inclusive reactions, 147 GeV/c, average charged particle multiplicities 79−40818
$\pi^-p\to n\pi^-\pi^-\pi^+\pi^+$, 12 GeV/c, Δ^-, ρ and f prod., baryon exchange 79−423
$\pi^-p\to\pi^+\pi^-n$, 1.33-1.38 GeV, isobar prod. near threshold, isobar model partial wave anal., bag model 79−93456
π^+p, 32 GeV/c, slow proton and $\Delta^{++}(1236)$ inclusive prod. *(Russian)* 80−63046
$\pi^+p\to(\pi^+\pi^-\pi^0)\Delta^{++}$, 16 GeV/c, partial wave anal., ω^* and A_2^0 80−63033
$\pi^+p\to(\rho^0,\omega)\Delta^{++}(1238)$, $q_L=7.1$ GeV/c, role of new exchanges *(Russian)* 79−54355
$\pi^+p\to K^+Y^*$, 11.5 GeV/c, line reversed reaction, Y*(1385) diff. cross section and decay ang. distribs. 79−89193
$\pi^+p\to\pi^+\pi^-\Delta^{++}$, polarization measurements and a narrow $\varepsilon(750)$ 79−63514
π^+p radiative scatt., bremsstrahlung peak in Δ^{++} resonance region, mag. moment from low energy theorem 78−45944
$\pi^+p\to\rho^0\Delta^{++}$ or $\omega\Delta^{++}$, positivity conditions in joint vector-meson Δ prod. 77−13975
$\pi^+p\to\rho^0\Delta^{++}(1236)$ or $\omega\Delta^{++}(1236)$, 10.3 GeV/c, cross-section meas. 78−82248
$\pi^{\pm}p$, 147 GeV/c, inclusive Δ^{++} prod., cross section energy depend. 80−57651
$\bar{\Sigma}^{\pm}$ prod., 4-7 GeV e^+e^- annihilation 79−9387
C_0^+ prod. and decay, test of charmed current struct. 77−61272
D+hadron, inclusive π, N spectra in high energy hadronic reactions, d fragmentation region *(Russian)* 78−54809
$\bar{p}p$, 5.7 GeV/c, nonannihilation channels Δ^{++}, $\bar{\Delta}^{++}$, Δ^0, $\bar{\Delta}^0$ prod. cross sections 80−27515

baryon resonances
see also hyperon resonances
$3/2^+$ charmed baryons, mass splitting by weight diagrams, parallelogram law sum rules 77−49915
Δ(1232) isobar propagation in nuclear matter 77−10349
Δ(3,3) role in low energy πN elastic and photoproduction models 77−6146
additive quark model in quasi-two-body hadronic reactions, Δ and vector meson prods. relation 78−41494
bag-quark model, spectroscopic applications, baryon excitations 77−22699
baryon+antibaryon bound states, $N\bar{N}$, quasinuclear levels, annihilation, influence of decay channels, multichannel model 79−2912
baryon couplings and 'missing resonance' in quark model with chromodynamics 80−57558
baryon spectroscopy and photoproduction couplings using new baryon wavefunctions 80−102016
baryonia, decay properties and L=1 state width approx. 79−75773
baryonia decay props., L=1 state widths 79−75772
baryonia mass spectra calc. incl. spin-dependent forces 79−26309
baryonium, exotic nuclear state or four quark boson resonance? 79−325
baryonium, importance of isospin *(French)* 79−85260
baryonium, mass and selection rule, string model 78−29319
baryonium, review of QCD, duality, string models and bag models 78−78135
baryonium, Schwinger partial symmetry, quark flavour EM interaction 79−93335
baryonium, spectrum and prod. mechanisms 78−74295
baryonium and dibaryon, quark shell model 78−41479
baryonium interaction, dual amplitudes 78−25022
baryonium interactions, string model, dual amplitudes *(Russian)* 78−54620
baryonium mass spectrum in planar bootstrap model 78−25020
baryonium model from $qq\bar{q}\bar{q}$ hadron spectrum, T- and M-diquonium 78−58172

baryon resonances continued
baryonium Regge trajectories exchange in medium and high energy scatt., expt. evidence 78−50022
baryonium spectrum, SU(4) mass formulae, degenerate clustering 79−93393
baryonium spectrum classification based on duality and unitarity 78−45869
baryoniums coupled directly to photon 79−17694
binary decays, centrifugal effects *(Russian)* 78−17012
Brayshaw and Peierls mechanisms for generating hadron peaks, N*(1470), 0(1020) and charm 79−404
broken $SU(6)_w$ analysis of electroproduction 79−93436
centrifugal barriers and Ω^- spin, quantisation of l=0 levels 77−18221
charm particle spectroscopy 80−73680
charmed baryon prod. by neutrinos, quark-model calc. 78−45909
charmed baryon reson. prod. cross-sections in νN reactions 77−26513
charmed baryons, mass splitting, derivation using weight diagrams 80−27481
charmed baryons in a quark model with hyperfine interactions 79−97601
colour model, mass splittings of heavy mesons and baryons *(Chinese)* 78−78146
complex mixing, decays and mass splittings, Wigner-Weisskopf simultaneous treatment 80−62977
conference, baryon resonances, Oxford, England (July 1976) 77−22750
cosmological baryon production, expanding Universe, baryon to entropy ratio, number nonconservation 79−44652
coupled channels method, applicability to nuclear physics with Ns and Δ's, book contrib. 79−97667
DC K^+p, 32 GeV/c, resonance inclusive prod. cross sections, quark model comparison 78−93913
decay, l-broken $SU(6)_W$ model equivalence to relativistic harmonic oscillator quark model 78−41546
decay, unified interactions in relativistic quark model 78−41547
decays and $SU(6)_W$ models 77−22700
di-baryon resonances and new N-N Regge trajectory scheme 77−67633
di-nucleon exotics and quark statistics 79−13071
dibaryon resonance existence, pp scatt. data 78−45939
dibaryon resonance existence in ΔΔ system, potential model investigations 79−85285
dibaryon resonances, quark cluster model 79−13081
dibaryon resonances in πNN and $\pi\pi NN$ dynamics 79−13177
dibaryons, SO_4 symmetry for classification 79−97531
diquark constituents of baryons and baryonium 79−93383
dispersion sum rules and exotic baryon resonances, reggeon scatt., E_{55} resonance *(Russian)* 80−101955
dual unitarisation scheme, dynamical threshold for baryon resonance prod., baryon exchange 78−45884
dual unitarisation scheme for baryon and baryonium states with string junctions 78−25021
electroproduction, review of expt. information 77−22745
elementarity of baryon resonances in nuclear matter 79−97666
EM mixing of narrow baryon-antibaryon states 77−87979
EM transitions, multipole moments in single quark transition model 80−62985
exotic baryon interpretation of narrow mass enhancement at 1360 MeV, diffr. dissociation 78−12888
exotic baryon resonance with isospins ≥5/2, existence, sum rule in Reggeon field theory *(Russian)* 78−93824
exotic NN resonances, joined spring model, Bose quark model anal. 79−89120
extended Regge trajectories, modified Chew-Frautschi plot for meson and baryon resonances 78−82176
field current relations, appl. in weak form to radial excited states *(Chinese)* 79−49420
finite-range effects in the πNN, $\pi N\Delta$ and $\pi\Delta\Delta$ vertices 79−22129
for meson-nucleus physics 77−10327
gluon perturbed linear potential 77−46023
hadron induced multiparticle reactions, S-1500 GeV, resonance prod. correlations, jet model *(German)* 80−91118
hadron lepton model interpretation of particle resonance states 80−4957
hadron resonance decay, intermediate vector boson and high energy weak interaction detect. 79−22012
hadronic decay, broken SU_3 and total reduced width 78−17017
hadronic decay matrix elements in covariant harmonic oscill. model 77−61284
hadronic resonance props., consideration as compound of bradyons and tachyons 78−58163
heavy fermions in the standard sequential scheme 79−71748
heavy meson exchange effect on $^1D_2$ and $^3F_3$ N-N partial waves, dibaryon resonances 80−105874
heavy triply charmed spin $3/2^+$ baryon, radial excitation spectrum 80−27482
isobar components of nuclei, experimental tests, review, book contrib. 79−97668
isobar model and $\pi N\to\pi\pi N$ analyses 77−22776
M_2 baryonium state decays, baryonium assignment scheme 79−71691
magnetic moments in higher symmetry schemes, charm particles 77−57538
mass spectrum anal. using quark shell model 78−4833
mesons in nuclei, nuclear forces, baryon reson. effects, book 79−97661
MIT bag model and Roper resonance 77−82705
multibaryon resonances, coloured quark-cluster model, possible 3-baryon state 79−6318
multiquark baryons and the MIT bag model in SU(6), coupling const. and decay modes 79−97600
multiquark dibaryon resonances 79−67518
multiquark states: Q^3 baryon resonances, mass spectrum from MIT bag model 79−67510
multiquark states, obs. in $p\bar{p}$ formation and prod. expts. 80−9153
N resonances in NN interaction 78−25066
narrow multiquark baryons, masses and decay modes 79−89119
narrow resonance in an open channel 78−66099
narrow states in $\bar{p}p$, $qq\bar{q}\bar{q}$ mesons, $\bar{B}B$ bound states, duality, expt. 78−62378
new particle searches in e^+e^- interactions at LEP energies 79−97617
new particles and weak interactions, models *(Chinese)* 79−93334
NP11 radially excited baryon states, MIT bag model predictions at 1525, 1631 MeV 79−89127
nuclear charge form factors, effect of N* (1688) resonance 79−93501
nuclear forces and isobar configs. in nuclei, review 78−50093

baryon resonances continued
nuclear interactions of strange particles and resonances, conf. Warsaw, Poland (lct. 1976) 78—70406
nuclear matter binding energy, Δ(1236) effect, lowest order reaction matrix calc. 77—6278
in nuclei, review 77—79364
nucleon excited states in nuclei, expts. on ^{2}H and ^{3}He *(French)* 79—3179
nucleon fluid, excitation to N*(1234) state, lowest order constrained variational calcs. 79—40864
nucleon isobars in nuclear struct., Δ (1236) role in exchange currents 79—26378
p-p resonance, possible existence in the $^3F_3$ state 78—4869
photocoupling anal. in relativistic quark model 78—66086
photocouplings, single quark transition anal. 77—82751
photocouplings using mixed nucleon and even-wave harmonic oscillator theory of baryonic states 77—82752
photoproduction, and Compton scatt., formalism 79—9384
photoproduction, experimental review 77—22738
pion prod. in resonant decay, correl. *(Russian)* 77—228
pionic decays, anal. of baryon reson. photocoupling signs 79—22094
Pomeron coupling diag. to order 1/N 80—47263
potential model, harmonic oscill. theory, orbital matrix elements and selection rules 77—49930
pseudobaryons, narrow bound states of qq with $qq\bar{q}$ 78—45870
pseudoresonance Argand loops *(Russian)* 79—9354
pseudoresonances, nonresonant Argand loops 77—61264
pseudoscalar transitions between high-spin reson. 78—8666
Q^6 dibaryon resonances, orbitally excited mass spectrum, decays 80—73670
QCD, effective quark pot. in baryon reson. 78—16910
QCD, resonance props. from sum rules 79—26301
quark bag model, spectroscopic appls., baryonium, gluonium, quark phase of matter, review 78—50008
quark cluster, model of ordinary and exotic hadrons 79—40759
quark model of resonances, $SU_6 \times O_3$, form factors, review 77—67624
quark string model, hadron spectrum, semiclassical approach, baryons and exotic hadrons 79—40747
radially excited states in baryon resonance pionic decays, relativistic quark model 80—95268
radiative decay in relativistic harmonic oscillator model 79—85277
relativistic corrections to baryon resonance photoexcitation amplitudes, harmonic oscillator quark model 77—13935
relativistic hadron couplings, unified framework, symms., quark models *(German)* 78—50012
resonance photoproduction, Melosh transformation 77—46059
Roper resonance photocoupling in relativistic quark model with scalar confining pot. 80—4936
s-channel resonance model based on peripheral resonances, exotic peaks 80—91069
s-channel resonance prod. in πN scatt., amplitude zeros in Mandelstam plane 80—73686
s-wave pion-nucleon phase shifts in Pade approximation using ε, ρ, f, N, Δ 79—67603
spectroscopy, experimental trends and problems 77—22754
spectroscopy, history, trends, outlook 77—22751
spin-parity test using polarised proton targets or beams 79—9427
strange baryonium, spectrum, decay, production 78—93854
SU(3) symmetry breaking in baryon resonance decay 78—89712
$SU(4)_W$ symmetry, dibaryon coupling constants for γ, π and baryon interactions *(Russian)* 80—13329
SU(4) broken symm., baryon reson. 77—71455
SU(4) broken symm., duality, baryon+baryon and baryon+antibaryon exotic mesons prod. 78—89629
SU(4) symmetry predicted $^1/_2{}^+$ charmed baryons, $C_1{}^{++}$, $C_1{}^+$, $C_1{}^0$, $X_u{}^{++}$, $X_d{}^+$, possible observation 79—40758
$SU(6)_w$ and $\{70, 1^-\}$, $\{56, 2^+\}$ decays 77—6122
$SU(6)_W$ decay anal. of $[70, 1^-]$ and $[56, 2^+]$ multiplets 77—22733
$SU(6)_W$ structure of baryonic reson. photocouplings duality constraint 79—71649
SU(8) mass relations among $J^P = 112^+$ and $3/2^+$ baryons 77—71499
three quark oscillator model for baryon spectrum 77—22698
three-body mechanism for narrow resonances 77—74654
transition mixing model, even parity baryon reson. classification 77—10224
two-nucleon interaction isobar contributions from noncovariant perturbation theory 79—478
two-nucleon system, Δ resonance, excitation spectrum 78—41649
weak charmed-baryon resonance prod., neutrino inclusive interactions, scaling behaviour 78—8645
weak hadronic $\Delta S = 0$ baryon-π amplitudes, Melosh transformation 78—12857
$b\bar{b}$ baryons, mag. moment sum rules, in Su(S) 80—78065
$B\bar{B}$ channel narrow widths, use of 'mock' diquoniums, quark-pair-creation model 79—75734
$B\bar{B}$ narrow states in QCD 77—57494
$C_1 \rightarrow C_0{}^+\pi$ decay width calc. 78—25011
d breakup, exotic final state interaction, intermediate Δ, ΔN threshold parameters 78—50043
$D_{05} \rightarrow \bar{K}N$, SU(6) selection rule violation from quark hyperfine interactions 79—6329
$D_{35}(1925)$, evidence from πp data, 0.8-2.0 GeV/c, $[56,1^-]SU(6) \times 0(3)$ supermultiplet 77—22771
$^1D_2$ (2.17 GeV) pp resonance, phase shifts 79—58970
$^1D_2$ diproton, resonance criteria 77—18312
Δ, I=3/2 high mass enhancement in 10.3 GeV/c π^+p interactions 78—66117
Δ(1226) effect in NN scatt., nucleaar and neutron matter 77—14051
Δ(1230) isobars, transition potentials, short-range repulsion in NN interaction 77—34235
Δ(1232), contrib. to e-nucleus quasielastic scatt. 77—79366
Δ(1232), contrib. to nuclear (γ, p) reactions at intermediate energies 77—18522
Δ(1232), differential cross section for $\pi^- p \rightarrow \pi^0 n$ near Δ resonance 78—17045
Δ(1232), intensification of pion beams by highly excited nuclear matter with inverse population *(Russian)* 79—49595
Δ(1232), mass calc. by inverse scatt. procedure 78—403
Δ(1232), momentum distrib. in nuclei 77—18444
Δ(1232), nucl. double beta decay and resonances 78—54722

baryon resonances continued
Δ(1232), production in N photo-excitation, multipole amplitudes, dispersion relations 80—5002
Δ(1232), πN scatt., separable interactions for three-body problems 78—78113
Δ(1232) excitation in $ep \rightarrow en\pi^+$ 79—22115
Δ(1232) from $NN \rightarrow N\Delta$, π production in $^{40}Ca(^{40}Ca,x)$, relativistic, compression and pion distrib., Monte Carlo calc. 80—73853
Δ(1232) isobar, role in $^{16}O(\gamma,p)$ 79—85451
Δ(1232) isobar in nuclei, one-boson-exchange and straton model anal. *(Chinese)* 78—78275
Δ(1232) pole position, stabilized bias free method 78—24968
Δ(1232) production by virtual photons, Δ^{++} and Δ^0 prod. 79—9383
Δ(1232) production in deep inelastic electron-nucleus scatt. 80—57772
Δ(1232) region, $^1H(\pi^-,\gamma n)$ radiative capture 79—93665
Δ(1232)-N(938) mass difference, determ. of πN coupling const. in MIT bag model 78—78149
Δ(1233) resonance region, P-odd effects in reaction $\Gamma p \rightarrow p\pi^0$ *(Russian)* 79—93435
Δ(1236), anal. cold matter at super-nuclear densities including pion condensates 78—17128
Δ(1236), bound states, single particle energies, wave functions in ^{16}O *(Chinese)* 80—52562
Δ(1236), neutral current prod., vector axial-vector ambiguity 77—74636
Δ(1236), virtual isobar admixtures in complex nuclei, OBE approx. 78—17107
Δ(1236) degree of freedom in interacting nuclei fireball model 78—17233
Δ(1236) effect on imaginary component of NN phase shifts 78—70398
Δ(1236) inclusion in ALS model of π^0 condensation 79—71814
Δ(1236) inclusive prod., absorpt. corrections in triple-Regge region 77—87956
Δ(1236) isobar prod., $pN \rightarrow pn\pi^+$ (and similar) 78—21443
Δ(1236) isomer, charged and neutral current prod. 79—17711
Δ(1236) M1 and E2 photoexcitation $N \rightarrow \Delta$ in $\gamma N \rightarrow \pi N$ 78—70377
Δ(1236) νN neutral current prod., quark model anal., isovector vector and axial-vector neutral-current couplings 77—61278
Δ(1236) production by high energy neutrinos, straton model *(Chinese)* 78—12900
Δ(1236) production in νp reactions, multipole struct. of weak prod. by charged currents 78—29328
Δ(1236) resonance, effect on NN scatt., nuclear and neutron matter 77—41909
Δ(1236) states, three nucleon clusters in nuclear matter 78—17112
Δ(1236)-resonance effects in nucl. matter 78—82302
Δ(1950) enhancement by large transverse momenta selection 77—2871
Δ(3,3) phase shift, current algebra model, πN decay channel 77—79232
Δ(33) interaction with nucleus, effective shell model pot., pion scatt. test 80—32202
Δ electroproduction cross section in deuteron scatt. *(Russian)* 77—67737
Δ inclusive production, Mueller-Regge model 79—17767
Δ isobar production, multiple pion exchange in nonstatic theory 77—34236
Δ mass, three quarks bound state, variational method calcs. 78—21396
Δ mass splitting in $\pi^\pm$p elastic scatt., charge exchange, partial wave anal., P_{33} resonance 78—29348
Δ prod., spin-3/2 polarisation density matrix determ. 77—87965
Δ prod. and spin depend. of pp total cross sections 77—82794
Δ production in $\pi^{+4}He \rightarrow \pi^- 4p$, 1.5 to 2.0 GeV/c 77—65237
Δ production probability in d breakup, isobar model, static NN-ΔΔ mixing pot. 78—29438
Δ resonance admixtures in NN problem, OBE model, d electrodisintegration 78—70373
Δ resonance inclusion in one-boson-exchange potential, Brueckner-Hartree-Fock calcs. for ^{16}O 77—54155
Δ resonance shifts, simple model 77—82829
Δ resonances, π^+p elastic scatt. partial wave anal. up to 10 GeV/c with impact parameter approach 77—22769
Δ spreading potential in pion-nucleus scatt., optical model approach 79—85422
Δ-Δ resonance in nonrelativistic quark model 80—86692
Δ-Δ system, deeply bound, one boson exchange potl. model 77—30501
Δ-isobar, exclusion principle effects, Chew Low theory 77—6275
Δ-isobar contribution to meson condensation in nuclear matter *(Russian)* 80—5086
Δ-isobar density matrix in $\gamma N \rightarrow \pi\Delta$ *(Russian)* 78—45932
Δ-isobar dynamics in finite nuclei, (π,π) scatt. in 3,3 region 77—34347
Δ-N interaction and π photoproduction on few body systems 79—71842
Δ-nuclear states excited in $^4He\text{-}\pi^-$ scatt. 77—88093
Δ-nucleon virtual state, evidence of existence in $pd \rightarrow npp$ at 1.65 $(GeV/c)^2$ 77—10274
Δ^+, in $pp \rightarrow pp\pi^0$, 800 MeV, Δ^+ prod., π and ρ exchange 79—85316
Δ^+ isobar mass and total width, $M^{3/2}{}_{1+}$ amplitude pole position from $\gamma p \rightarrow N\pi$ *(Russian)* 78—86453
$\Delta^+ \rightarrow P\gamma$, ground and radially excited states, broken symmetry treatment 80—9174
Δ^+ pole parameters from multichannel N/D model fit to π photoprod. data 77—10265
Δ^{++}, bremsstrahlung peak in resonance region of π^+p radiative scatt., mag. moment 78—45944
Δ^{++}, prod. in $\nu p \rightarrow \mu^- \Delta^{++}$, 5-100 GeV 78—93873
Δ^{++}, production in $pp \rightarrow p\pi^+ n$, 800 MeV 78—70385
Δ^{++}(1232), effect on $\pi^+ p \rightarrow \pi^+ p\gamma$, 165 MeV, spectrum 80—68476
Δ^{++}(1232), mag. dipole moment calc., from πp data 79—22133
Δ^{++}(1232), spin density matrix, production in $\nu p \rightarrow \mu^- p\pi^+$ 79—9362
Δ^{++}(1232) inclusive prod. in π^+p, π^-p, K^-p at 16 GeV/c 78—66169
Δ^{++}(1232) inclusive prod. in π^-p interactions at 147 GeV/c 79—17772
Δ^{++}(1236), $\bar{\Delta}^{++}$ inclusive prod. in $\bar{p}$p, interaction mech. 79—3054
Δ^{++}(1236), prod. in K^+p, and pp interactions *(Russian)* 79—9423
Δ^{++}(1236) prod. in π^+p at 16 GeV/c, cross-sections, spin density matrix elements determ. 78—21467
Δ^{++}(1236) resonances in $K^+ p \rightarrow K^0 p\pi^+$ reaction at 5, 8.25 and 16 GeV/c 78—12931
Δ^{++}(1238), role of new exchanges in $\pi^+ p \rightarrow (\rho^0,\omega)\Delta^{++}(1238)$ at 7.1 GeV/c *(Russian)* 79—54355
$\Delta^{++} \rightarrow p\pi^+$, decay widths calc. in MIT bag model 77—74681
Δ^{++} prod. in $K^+ p \rightarrow K^0 \Delta^{++}$, cross-sections below 2 GeV/c, data compilation 77—22780
Δ^{++} prod. in $\pi^+ p \rightarrow \Delta^{++}\pi^0\pi^0$ at 4 GeV/c 78—82232
Δ^{++} prod. obs. in $^+$p at 10.3 GeV 78—21453

baryon resonances continued
Δ_{33} energy region, electroproduction, simple-pole model, $\gamma\mathcal{N}\Delta_{33}$ vertex 80−22625
Δ_{D35}(1925) baryonic degrees of freedom, nonrelativistic, harmonic oscillator quark model mass formula 80−91066
$\Delta^{++}-\Delta^{0}$ pole parameter determ. 80−13303
ΔD35(1925) reson. and $(56,1_3{}^-)$ baryonic supermultiplet 77−82718
ΔΔ and NN channels in six-quark model, isobaric component of d 78−21377
ΔΔ content of deuteron 77−22680
(ΔΔ) isobar admixtures in two-nucleon continuum 77−10335
ΔΔ prod. in $\bar{p}p$ interactions at 32 GeV/c 78−4881
$\Delta^{++}\Delta^{0}$ prod. in $pp \to (p\pi^+)(p\pi^-)$ 79−6350
$\Delta_1{}^0\Delta^{++}$ production from $\pi^{\pm}p$, partial wave anal., T-matrix poles and residues 80−63018
Δππ system, study in 4.5 GeV $\pi^- p \to \pi^- p\pi^+\pi^-\pi^0$ interaction 79−93453
$\Delta^{++}\pi^0\pi^0$ events in 4 GeV/c $\pi^+ p$ interactions 79−22132
ed→ed*, dibaryon resonance production 80−78070
ed inelastic scatt., electrodisintegration at high energy and momentum transfer, exchange currents 79−6342
$e^-e^+ \to N^*\bar{N}^*$, weak neutral current effects for polarised e^+e^- pair 80−37287
$e^+e^- \to$ baryon-antibaryon pairs, vector meson dominance model 78−21442
eN→eπΔ, low energy, ΔN axial form factors soft-pion theory 78−70380
$e^-N \to e^-\Delta(3/2, 3/2)$, P-odd asymmetry, P nonconserving neutral current interaction 80−57611
ep, deep inelastic scattering on π-pole Regge *(Russian)* 78−12918
F_{37}(1950), magnetic excitation in $\gamma p \to \pi^0 p$ 80−42476
γd→ηd, resonance model including S_{11}(1535) and P_{11}(1470) 79−93432
γd→np, 300 MeV, dibaryon resonance manifestation, pseudoindependent amplitude elimination *(Russian)* 80−57612
γd→pn, 400 to 650 MeV, ang. depend. of proton polarisation and partial wave anal. of possible dibaryon resonances 79−58967
γd→pn, EM properties of πNN system, virtual π reabsorption 79−22109
$\gamma D \to pp\pi^-$, π rescatt. through Δ(1236) for nucleon high momentum 77−57547
γN→Δ magnetic dipole photoexcitation, singular integral equations 78−50040
γN→Nπ, instability of anal. results near Nπ reson. region *(Russian)* 79−9385
γN→πΔ, low energy prod. and Δ-N axial transition vertex 77−49981
γN→πΔ, meas. of asymmetries and cross sections using 16 GeV linearly polarised photons 80−13318
γN→πΔ reaction amplitude, equivalence theorems *(Russian)* 80−52522
$\gamma p \to e^+e^- p$, reson. struct. obs. background process *(Russian)* 78−89722
$\gamma p \to \pi^0 p$, 450 to 800 MeV, proton polarisation, Walker-type anal., P_{11}(1470), D_{13}(1470), S_{11}(1535) resonances 80−73721
$\gamma p \to \pi^+\pi^- p$, Lagrangian model, ε(700), ρ(770), f(1260), Δ(1236) resons. 78−17028
$\gamma^+ p\Delta^+$(1231) vertex transition form factor from ep→eNπ *(Russian)* 80−37269
$K^-d \to \Lambda p\pi^-$, 680 to 840 MeV/c, Λp enhancement near ΣN threshold 77−67672
$K^-d \to \pi^-\Lambda p$, pole in $^3S_1$ hyperon-nucleon scattering amplitudes 80−102068
KN→K*Δ, positivity conditions in joint vector-meson Δ prod. 77−13975
KN scatt., Z_0^* resonance generalisation in SU(3) symmetry 78−37230
$\bar{K}N$ system, new reson. evidence in $SU(6)_W \times O(3)$ harmonic oscill. model 79−13178
$\bar{K}N$ two-body data multichannel anal. in resonance region 77−88006
$K^-p \to K^*$ (890) Δ (1236), 10 GeV/c, multidimens. anal., reaction sub-channel separation 80−32127
$K^-p \to \pi^- Y^*$(1385), 11.5 GeV/c, line reversed reaction, Y*(1385) diff. cross section and decay ang. distribs. 79−89193
K^+p, phase shift anal., exotic reson. Z_1^* 78−62456
$K^+p \to K^0\Delta^{++}$, 3 to 16 GeV/c, resonance production, cross sections and density matrix elements 78−17048
$K^+p \to \bar{\Lambda}pn\pi^+$, 12 GeV/c, narrow resonant state in $\bar{\Lambda}\Delta^{++}$(1232) and $\bar{\Sigma}^+$(1385)p combinations 78−89744
K^+p scatt., Z_1^*(1800) resonance from elastic spin-rotation angle 79−63523
N, N*, evidence for core of valence quarks 79−36025
N,N* resonances, radiative decays, static quark bag model *(Russian)* 80−47299
N(1360)$\Gamma<67$ resonance, πN channel, dibaryon pp resonance systematics 80−68481
N(1420), $SU(6)_w$ fits in baryon photo- and electroproduction 77−46057
N and Δ resonances in nuclei, coupled channel eqns. soln. for nuclear matter 79−17845
N→Δ(1232) electromagnetic transition form factor and pion-nucleon dynamics at moderate energies 80−57598
N-Δ reson. with T=1, $J^P=2^-$ obs. in pp scatt. 78−17041
N-Δ system, bag model, quark-quark interaction anal. 78−33029
N-N* EM transition form factors 77−22735
N*, production in high energy p+nucleus reactions, Glauber scatt. study *(Chinese)* 79−93626
N*(1232) from pp inclusive process, π exchange, depolarisation parameter 80−78088
N*(1234) saturating effect on binding of light nuclei 78−58231
N*(1238), high energy neutrino reactions for weak interaction props. and hadron struct. investigation, book contrib. 79−30727
N*(1470), intensification of pion beams by highly excited nuclear matter with inverse population *(Russian)* 79−49595
N*(1470), Roper resonance, quark pair creation model soln. 80−47252
N* EM transition form factors 80−102049
N* prod. in $\pi^-n \to \pi^-\pi^-p$, 15 GeV/c 77−41865
N* prod. in $\pi^-p \to \Lambda K+X$ at 4.35 and 4.85 GeV *(Russian)* 77−6159
N* weak prod. in ν-N, quark oscill. model *(Russian)* 77−220
NΔ(1232) state contrib. to $pp \to \pi^+d$, K matrix theory anal. 80−5013
NΔ conversion, two-channel formalism and three-body forces approaches 78−8733
(NΔ) isobar admixtures in two-nucleon continuum 77−10335
(NΔ) quasi bound state, T=J=2 79−45007
$N\bar{N}$, baryonium, internal struct. *(Norwegian)* 79−36032
$\bar{N}N$, OBE pot. calc., bound state and reson. energies, widths in 1.6 to 2.7 GeV range 77−49931
$\bar{N}N$ and $\pi\bar{N}N$, $\pi\pi\bar{N}N$ bound states from $\bar{N}N$ potentials 80−62951
NN→Δ(1236)Δ(1236), 4-25 GeV/c, Reggeised absorption model 77−6170

baryon resonances continued
NN inelastic processes, SU(3) breaking, N(1688), Λ(1815) and Σ(1915) states 77−71526
NN→NNπ, lowest order Feynman diagram calc. 79−63508
NN negative-parity reson., six-quark bag 78−74210
$N\bar{N}$ resonance, Goldberger-Treiman relation corrections 78−463
$N\bar{N}$ resonances 78−62431
$N\bar{N}$ system, positions of resonances found by applying Faddeev's equations *(Russian)* 79−93529
NN systems, resonances due to annihilation, baryonium states, many channel N/D method 78−66143
(NN*) isobar admixtures in two-nucleon continuum 77−10335
$NN\bar{N}$ system, bound and reson. states using Fadeev eqns. *(Russian)* 78−89804
NNρ couplings, parity-violating, QCD and MIT bag model, $1/2^-$ resonance contribs., $SU(6)_w$ symmetry 80−57540
np→pX, 800 MeV, proton spectra, πN(1232) resonance 78−62437
$np \to p\pi^+\pi^+\pi^-\pi^-n$, 5.1 GeV/c, $p\pi^+\pi^+(n\pi^-\pi^-)$ combination effective mass distrib. singularity *(Russian)* 79−67569
Nπ→N*π, Gribov-Morrison rule as kinematic effect 77−49999
ν, $\bar{\nu}$ charged current induced one pion weak prod., I=1/2 resonant contrib. 80−47274
νH_2, possible new meson or baryon reson. decay 77−240
$\bar{\nu}H_2$-Ne, possible new meson or baryon reson. decay 77−240
$\nu N \to \mu\bar{N}\pi$, PCAC anal. in 1st reson. region 77−82730
$\nu N \to \pi^{\pm}\Delta$, dynamical model 79−401
νN S_{11}(1335) resonance in gluon perturbed linear potential 77−46023
p+n nucleon diffractive 19.2 GeV/c excit., 2- and 3-particle decays *(Russian)* 78−473
pd→d′N* collisions, backward N* prod., 1.0 to 5.0 GeV, exam. of N* exchanges 78−21448
$pd \to d\pi^+n$, 585 MeV, Glauber theory, NN and NΔ amplitudes 78−62525
$pn \to \Delta^{++}\Delta^-$, quasi eikonal model anal., πP cut contribution, enhancement coefficients *(Russian)* 79−40798
pn→np, charge exchange processes, baryonium trajectories, Regge pole description 80−9180
pN→NπΔ(1236) above 6 GeV, crossed channel isospin amplitude anal. 79−6346
$\bar{p}n \to \bar{p}p\pi^-$, 2.98 GeV/c, $\bar{\Delta}^{--}$ prod. in additive quark model framework 80−52529
pp, 1.5 GeV/c, phenomenological anal., dibaryon resonances 79−17750
$\bar{p}p$, 400-850 MeV/c, annihilation and elastic cross-sections meas. reson. obs. at 1939 MeV 77−46082
pp, 69 GeV/c, charged backward π prod., inclusive baryon resonance prod. cross section *(Russian)* 79−30760
pp $^3F_3$ resonance as resonance in πNN system 78−45940
pp bremsstrahlung, Δ isobar excitation and radiative decay 79−67586
$pp \to d\pi^+$, differential cross-section and polarisation 78−8683
$pp \to d\pi^+$, polarised beam and target, NΔ intermediate states, coupled channel method 79−9392
$pp \to \Delta^{++}\Delta^0$ up to 1500 GeV/c, Reggeised absorption model 77−6170
$\bar{p}p \to \bar{\Delta}^{++}\Delta^{++}$, quasi eikonal model anal., πP cut contribution, enhancement coefficients *(Russian)* 79−40798
$\bar{p}p \to \Delta^{++}X$, 9.1 GeV/c, topological and channel cross-sections 77−30415
$pp \to \delta^{++}$(1236), Λ^0, 100 GeV/c, one-meson-exchange mechanism anal. 78−8712
$pp \to \Delta^{++}n$, polarised proton, spin effects in SU(3) and quark model 77−30399
$pp \to \Delta^{++}\pi^-p$, polarised proton, spin effects in SU(3) and quark model 77−30399
pp elastic scatt., diproton reson. 78−4871
pp inelastic scatt. in Δ(1232) prod. region, parity violation 78−62435
$pp \to K^0(\Lambda)(\Delta^{++})X$, 6 GeV/c, polarised proton 77−30400
$pp \to K^+K^+$+missing mass, stable six quark state search, mass range 2.1-2.4 GeV 78−89742
$pp \to n\Delta^{++}$, 6-1500 GeV/c, differential cross-section 78−8700
$pp \to n\Delta^{++}$, quasi eikonal model anal., πP cut contribution, enhancement coefficients *(Russian)* 79−40798
$\bar{p}p \to \bar{n}n$, charge exchange processes, baryonium trajectories, Regge pole description 80−9180
$pp \to pp\bar{p}_{\text{forward}}$+anything, observation of qq with $qq\bar{q}$ bound states, pseudobaryons and baryonium 78−58219
$pp \to pp\bar{p}p$, 11.75 GeV/c, baryonium states, cross section and branching ratio 80−95288
$\bar{p}p \to \bar{p}p\pi^+\pi^-$, 100 GeV/c diffraction and Δ^{++} prod. in exclusive interactions 78−93909
$\bar{p}p \to \bar{p}p\pi^+\pi^-$, 7.2 GeV/c, diffraction dissociation and double resonance prod. 79−89177
$pp \to \pi^+d$, 400-800 MeV, anal. by neutron exchange, ΔN intermediate states, diproton resonances 80−27518
$pp \to \pi^+d$, di-proton resonances 80−22631
pp scattering, dibaryon resonance behaviour, nonadiabatic rotational bands in light nuclei 80−13353
pp spin observables, possible dibaryon resonance 78−78224
pp total cross section, spin dependence, relativistic model of Δ(1232) prod. 78−62436
pp total cross-section difference of pure helicity states, 2100 to 2500 MeV, obs. of structs. 78−78206
(π^+,p) reaction in (3,3) resonance region proceeding through Δ-hole states 78−41778
π field relaxation in nuclear materials *(Russian)* 78−8764
π resonances, Peierls-Yoccoz projection applied to satellite meson coherent state 79−26345
π-baryon resonance scattering interaction region, props. of baryon resonances 77−41856
π+d→2N in Δ-resonance region, 100-300 MeV *(Russian)* 78−33083
$\pi^-A \to \pi^0X$ with Δ(1240) slow isobar intermediate prod. in heavy nuclei, cross section *(Russian)* 78−89917
πd system, resonances near ΔN threshold, Argand diagrams 78−62582
$\pi^+d \to p(N^*,\Delta^+)$, 1-5 GeV, inclusive cross-sections 77−6157
πN coupling in Δ(1231) isobar region, pion index of refraction, self-energy in low density limit 80−42554
πN low energy partial wave anal., cross sections, Δ^0 and Δ^{++} 80−52531
πN low energy scatt. from N, Δ poles, low energy theorems 80−86751
πN→Nππ, 1.65-1.97 GeV/c^2, πN resonance coupling to Δπ and ρN channels 78−66149
πN P11 ground state potential, meson probability density 80−27558
πN partial wave anal. 1.6 to 10 GeV, possible high spin resonances in Argand plots 78−70403

baryon resonances continued
  πN scatt., isospin violation from π^0-η mixing, partial wave anal., N*(1540) struct. 80—27426
  $\pi^+ n \to \pi^+ \pi^- p$, 15 GeV/c, longit. phase space anal., ρ^0, f^0, Δ^0, N* 77—74727
  πNN dynamics, Faddeev approach, 0-1200 MeV pp scatt. 80—57625
  πNN form factor, $\Delta(1236)$ contrib., calc. 80—22609
  πNN form factor; relativistic calc. of $\Delta(1232)$ contribution to imaginary part *(Korean)* 80—47292
  $\pi^- p$, 2-14 GeV/c, total cross section, narrow baryon search 80—105922
  $\pi^- p$, 200 GeV, inclusive $\Delta^{++}(1232)$ prod. 78—21478
  $\pi^- p \to \Delta^{++}X$, 100, 200, 360 GeV/c, δ^{++} inclusive and semi-inclusive prod. cross sections 79—40817
  $\pi^- p \to \Delta^+(1236)\pi^-$, 3.0 to 5.5 GeV/c, differential cross section, fluctuations 77—22774
  $\pi^- p$ elastic scatt., 3.42-5.03 GeV, narrow baryon search in differential cross section 80—105921
  $\pi^- p \to K^0 \Lambda^0$, up to 1334 MeV/c, baryon resonance parameters 79—412
  $\pi^- p \to n\pi^+\pi^-$, 8 GeV/c, backward meson and baryon reson. prod. 79—415
  $\pi^- p \to pF\bar{p}n$, M^- state in $\bar{p}n$ search, M^0 state decay 79—36108
  $\pi^- p \to pp\bar{p}\pi^-$, narrow $p\bar{p}$ reson. at 2020 MeV, 2200 MeV 77—67682
  $\pi^- p \to \pi^0 n$, charge exchange polarisation parameter meas., 617 to 2267 MeV/c 78—82231
  $\pi^+ p$, angular correl. reson. prod. effect at 16 GeV/c 77—88014
  $\pi^+ p \to (\pi^+ p\bar{p})p$ 50 GeV/c, narrow baryonium states, diffractive prod. cross sections 80—442
  $\pi^+ p \to \Delta_f^{++} \bar{p}p$, 9.8 GeV/c, narrow $\bar{p}p$ state search 80—57636
  $\pi^+ p \to \Delta^{++}(1236)$, Λ^0, 100 GeV/c, one-meson-exchange mechanism anal. 78—8712
  $\pi^+ p \to$four prong final states, 10.3 GeV/c, resonance prod. cross-sections 78—74276
  $\pi^+ p \to K^+ Y^*$, 11.5 GeV/c, line reversed reaction, Y*(1385) diff. cross section and decay ang. distribs. 79—89193
  $\pi^+ p \to \omega\Delta^{++}(1236)$ 16 GeV/c, cross-sections, spin-density matrix elements 77—10284
  $\pi^+ p \to \pi^+ p\pi^0$, 1 GeV, N^{*+}, N^{*+} and ρ^+ prod., single π distribs. 77—74716
  $\pi^+ p \to \pi\pi N$, 1.4-1.7 GeV, isobar model partial wave anal., baryon resonance decay 80—86750
  $\pi^+ p \to \rho^0 \Delta^{++}$, quasi eikonal model anal., πP cut contribution, enhancement coefficients *(Russian)* 79—40798
  $\pi^+ p \to \rho^0 \Delta^{++}$ or $\omega\Delta^{++}$, positivity conditions in joint vector-meson Δ prod. 77—13975
  $\pi^+ p \to \rho^0 \Delta^{++}(1236)$ or $\omega\Delta^{++}(1236)$, 10.3 GeV/c, cross-section meas. 78—82248
  $\pi^+ p \to \Sigma^+(1385)K^+(K^{*+}(890))$ 10.3 GeV.c, Y*K and Y*K* prod. 79—49544
  $\pi\Sigma$ resonances, asymptotic restrictions and sum rules *(Russian)* 79—22137
  $Q^2\bar{Q}^2$ resonances in baryon-antibaryon systems, $N\bar{N}$ scattering and $\bar{N}N \to \pi^+\pi^-$ 78—58171
  $\bar{\Sigma}^\pm$ prod., 4-7 GeV e^+e^- annihilation 79—9387
  $\Sigma^*(1385)$, prod. in Σ^--nucleus reactions at 23 GeV/c 77—50183
  $\Sigma^{*-}(1385)$, prod. in Σ^--nucleus reactions at 23 GeV/c 77—50183
  $\Sigma^- n$ dibaryon, decay particles momenta 79—85298
  $\Sigma^- n$ dibaryon decay in exotic atoms 80—9762
  $\Sigma^- p$ systems, possible resonance existence 80—47340
  Υ, QCD, three gluon jets as test 78—25001
  Υ(9.5 GeV), prod. cross section at ISR energies in pp collisions 78—25085
  Υ (9.5), heavy quark charge 78—37180
  Y* prod. in Σ^--nucleus reactions at 23 GeV/c 77—50183
  $Ca(\pi^\pm,X)$, stopped π^-, fast $\pi^\pm$, 180, 220 MeV, interactions near $\Delta(1232)$ resonance 79—6712
  $^3F_3$ (2.22 GeV) diproton, obs. in pp scatt. 79—36093
  ^{2}H ground state, N* configurations 77—18436
  $^2H(\pi,\pi)$, dibaryon resonances in Glauber model anal. *(Russian)* 79—89331
  $^3He(\pi,\pi)$, role of spin isospin effects in $\Delta(1236)$ resonance domain *(Russian)* 78—78423
  ^{4}He (p,p), effective channel approach, N* resonance effects 79—9570
  ^{4}He isobar configurations, impulse approx. 77—46114
  ^{4}He, N*-^{3}H configurations 79—17822
  $^4He+\pi^+ \to \pi^+\pi^- ppd$, 1.7 GeV/c, cross section, $\Delta(1232)$ and $\rho(770)$ resonance prod. 78—89911
  N*(1236) propagator, momentum depend. in N*-excitation current 80—27559
  $\bar{p}p$, 5.7 GeV/c, nonannihilation channels Δ^{++}, $\bar{\Delta}^{++}$, Δ^0, $\bar{\Delta}^0$ prod. cross sections 80—27515
  pp, polarised p, resonant like structs. in mass region 2100 to 2800 MeV 78—89745
  π emission decay of baryon resonances, quark model, widths, amplitudes, sum rules 77—57534
  $\pi^- p \to \eta n$, 724-2723 MeV/c, differential cross sections, baryon resonance non-zero couplings 79—71761

baryon scattering *see baryon-baryon scattering; lepton-hadron scattering; meson-baryon scattering; photon-hadron scattering*

baryon spin and parity
  see also hyperon spin and parity
  baryon pion amplitudes, strangeness conserving and weak parity violating 78—12857
  baryon spin-parity tests using polarized proton targets or beams 79—9427
  charied hadrons, parity violating nonleptoric decay in quark model 78—12907
  charmed high spin states, quark model calcs. 77—61258
  even parity resonances, transition mixing in 2 GeV mass region 77—10224
  exotic baryon resonances with isospins $\geq {}^5/_2$ 78—93824
  field equation for arbitrary hadrons and parity operators 80—37263
  hadron resonance prod., parity violating effects 79—22012
  micrononcausal Euclidean wave functions, G^1-parity 79—45030
  nonleptonic hyperon decay, CP violation 78—70367
  reactor neutrino parity violating reactions 79—67543
  s-channel resonance prod. in πN scatt., amplitude zeros in Mandelstam plane 80—73686
  spin, isospin, strangeness and charm relations 80—37183
  Z*/SUB 1/(1800) and spin-rotation parameter measurements 79—63523
  A inclusive prod., spin depend. 78—21402

baryon spin and parity continued
  δ, spin 3/2 polarisation density matrix in $\nu N \to l\delta$ 77—87965
  $\Delta^{++}(1236)$ spin density matrix elements from $\pi^+ p \to \Delta^{++}X$ 78—21467
  Δ^{++} spin density matrix from $\nu p \to p\pi^+\mu^-$ 79—9362
  $\gamma N \to \pi\Delta$, density matrix, parity exchange contribs. 78—45932
  K*(890) prod. in K^+p, parity exchange contrib. 78—17048
  K^-P, 10,16 GeV/c, Λ polarisation, spin-parity exchanges 78—62466
  $\Lambda(1520)$ spin density matrix elements from K^-p 79—40801
  Λ and $\bar{\Lambda}$ spin from pN interactions 78—82253
  n, dipole moments and spin rots. 78—74296
  n, polarised, decay, time-parity violation 78—78180
  n, spin rots. and dipole moments 79—36080
  n β-decay, n-spin-e-momentum and n-spin-ν-momentum correlation 79—58960
  N* resonance prod. in $\bar{\pi} \to \Lambda K^+$ 4.35-4.85 GeV 77—6159
  NN elastic scatt. at high P_{T1} spin spin forces 78—78216
  Ω^-, lifetime and spin from K^-p interactions 78—93877
  Ωyperon, spin and lifetime 78—29333
  $\bar{p}$, parity confirmation in $\bar{p}p \to \pi^-\pi^+$ interaction 77—2860
  $\bar{p}p \to \bar{\Delta}^{++}\Delta^{++}$ parity exchange contnts. 79—13146
  pp inelastic scatt., parity violation 78—62435
  $pp \to N\Delta(1232)$, total cross section spin depend. 78—62436
  $pp \to pp$ pure spin total cross section 78—62439
  $\bar{p}p \to \pi^+\pi$ polarised target, charge parity determ. 77—57567
  $p\bar{p} \to \pi^+\pi^-$ 78—4889
  pp spin observable struct. 78—78224
  pp total cross section for parallel and antiparallel longitudinal spin states 78—78206
  πN scatt. up to 10 GeV/c, high spin resonances 78—70403
  $\pi^+ p \to (p|,\omega)\Delta^{++}$ 10.3 GeV/c, spin density matrix eleme 78—82248
  $\Sigma^+(1385)$ spin density matrix elements 79—49544
  $\Xi^*(1820)$ resonance, spin determ. 78—89767

baryons
  see also baryon resonances; baryon spin and parity; hyperons; nucleons
  antibaryons in Universe, hiding place in primordial black holes 80—22126
  asymmetry in Universe, thermodynamic equilib. departure *(Russian)* 79—48975
  baryon number generation mechanism in expanding universe 80—51931
  baryon number of the Universe 79—30163
  baryonic matter, transition to quark matter, appl. to neutron stars 77—5424
  baryonic state even wave harmonic oscillator theory, structure functions versus form factor 79—393
  bound state in two-dimens. SU(N) gauge theory 77—13918
  bound states composed of the baryon and the monopole *(Chinese)* 79—63340
  charmed, discoveries during 1974-7, and associated theory *(Czech)* 78—86103
  charmed, elec. and mag. quarks rel. to Dirac mag. monopoles 80—402
  charmed, hadronic props., superconvergence sum rules 80—78043
  charmed, mag. dipole moments and mag. quarks 79—97573
  charmed, spectrum in SU(4) breaking 15-plet dominance scheme 77—74663
  charmed, static and transition magnetic moments in quark model 77—46050
  charmed baryon, EM mass differences in charmed-quark model 77—71515
  charmed baryon EM mass differences 77—65155
  charmed baryon mass formulae via SU(4) Regge trajectory anal. 77—79257
  charmed baryons, binding to single nucleon, finite nuclei, exam. 78—21511
  charmed baryons, dipole mag. moments, new U_3 scheme using u, d, c quarks 78—58165
  charmed baryons, magnetic moments by SU_3 and SU_4 symmetry 78—82209
  charmed baryons, one-parameter mass formula 77—10232
  classification in SU(4) charm symm. model, mag. moments 77—61257
  coloured SU(3) scheme of three quarks binding in baryons, mass formulae 78—12876
  composite models, mag. moments of quarks, leptons and hadrons 80—32081
  configuration mixing in 70 1^- multiplet of $SU(6)\times O(3)$, decoupling conditions 77—38142
  cosmological baryon asymmetry, rel. to x-boson asymmetric decay 80—4464
  cosmological baryon asymmetry origin, unification mass 80—31398
  cosmological baryon production, expanding Universe, baryon to entropy ratio, number nonconservation 79—44652
  cosmology, baryon symmetric big bang 78—61945
  cosmology, baryon-symmetric, cosmic microwave background distortions 78—65727
  cosmology origin of baryons in Universe 79—62938
  diquark constituents of baryons and baryonium 79—93383
  diquark contribs. to scaling violation and deep inelastic σ_L/σ_T, structure functions, QCD 80—22573
  dual unitarisation and baryon processes, S-matrix topological expansion 77—74662
  dual unitarisation scheme for baryon and baryonium states with string junctions 78—25021
  duality, diagram topological expansions incorporating baryons and mesons 77—57505
  dynamics description in dual and gauge theories 77—65138
  early Universe, baryon number generation due to CP- and B-violating interactions 80—109571
  electric and magnetic confinement schemes for mesons and baryons 80—4960
  electric dipole moments in CP noninvariant Kobayashi-Maskawa theory *(Russian)* 80—105897
  exotic atoms, conf., Erice, Sicily, (1979) 80—67939
  f-quark, five quark models and baryon magnetic moments 79—13020
  field equation for baryons with arbitrary spin, generalisation of Dirac eqn., group scheme 80—73615
  five quark models and mag. moments of baryons 79—26297
  geometrodynamic quark model, baryon states 77—61254
  geometrodynamical model of extended baryons 77—79251
  gluon exchange corrections in model with confining potentials 78—21379
  grand unified theories, baryon asymmetry of the Universe, SO(10) model 80—4619

baryons continued
gravitational baryon annihilation as type of radioactive decay *(Russian)* 77—26470
ground state properties, effects of internal quark motion and SU(6) breaking 77—38128
heavy baryon spectroscopy in the QCD bag model 80—105866
Higgs boson critical mass, baryon asymmetry from boson pair decay 80—90590
independent quark model, baryon model based on Dirac eqn. with confining pots. 78—425
isospin classification, same finite group for mesons and baryons *(Chinese)* 80—62887
Jeans mass in eary Universe, rel. to cosmic inhomogeneities physical origin 80—56986
leptonic decays and mag. moments in nonlocal quark model *(Russian)* 80—86711
low lying baryons, anomalous mag. moment contrib. from quarks 80—42462
magnetic moment, incorrect value from static compound quark models 80—9169
magnetic moment, reln. to charmed meson hyperfine splitting 80—47293
magnetic moment calculation in quark models 80—27505
magnetic moments, current status, additional symmetry breaking assumptions 80—4995
magnetic moments, ground-state, SU(6) symmetry 80—78064
magnetic moments, implications for quark model 80—13290
magnetic moments calc. using quark confinement ideas 77—57539
magnetic moments in broken SU(4), ordinary and charmed baryons 80—18136
magnetic moments in higher symmetry schemes, charm particles 77—57538
magnetic moments is broken SU(6) model 79—49417
many worlds cosmology, entropy per baryon 77—53714
mass, charmed states with high spin, unified calc. *(Russian)* 77—61258
mass relations for π, K and baryons 78—41520
matter-antimatter symmetry breaking, rel. to Universe initial regularity 80—22124
micrononcausal Euclidean wave functions for baryons by assuming 'Yukawa type' couplings and G′-parity 79—45030
multibaryonic systems, 3n-quark systems, MIT bag model 78—70321
multiplicative baryon number conservation, $H \rightarrow \bar{H}$ oscill. upper limit, baryon to lepton transform. 79—298
multiquark baryons, masses and decay modes 79—89119
negative parity, spectrum and mixing angles, QCD type quark model 79—26307
neutron stars, hadronic matter components, leptons and baryons *(Polish)* 79—88587
nonrelativistic quark model with one gluon exchange pot., baryon spectroscopy in $SU(6) \otimes O(3)$ 78—78147
octet baryons in SU_3, EM mass difference, u, d and c quark sectors 78—29334
parton distribs. consistent with naive quark model and QCD 80—62937
planar baryon model based on duality and unitarity 78—17000
positive parity excited baryons in quark model with hyperfine interactions 78—82161
properties, review from particle data group 80—67944
QCD, two dimens., soln. of Bars-Durgut model for baryons 79—75741
quark constituents, binding energy and rest mass of constituents, total symmetry effects *(French)* 80—63068
quark diagrams for baryons 77—87939
quark geometrodynamics, baryon struct., current and meson couplings 79—6320
quark linear string model, flavour symmetry, exchange degeneracy and spin structure 79—89118
quark masses and structure functions, $1/2^+$, $3/2^+$ baryons 80—22585
quark model relativistic generalisation minimal boosting of SU(6) scheme, meson, baryon props. 77—41814
quark structure of baryons involving the u, d, s quarks 79—63414
quark-baryon phase transition, asymptotic freedom studied using renormalised coupling constant 78—4830
quasinuclear systems containing baryons and antibaryons 80—22709
relativistic model for baryons with scalar raising pot. 80—37231
relativistic quark model, confining force saturation 79—93336
spectral function sum rules for quark and baryon fields, using lightlike charges 78—93822
spectrum, P-wave excitations of quarks in bag model 77—13925
spin $1/2^+$ baryons, mag. moment sum rule, in SU_3 for u-, d- and c-quark sector 78—21428
stable dibaryon in QCD, Λc^0 bound state 79—67519
string model, string geometrical shape and overlapping functions 79—13073
strongly interacting system, finite temp. many body theory, phase transition 77—65210
structure functions, dynamic relationship to baryonium trajectories 79—40763
SU_3 dynamical model, gravit. bound linear rotator 77—49904
SU(1,4) dynamical group, anal. of discrete representations, mass formulae 77—45982
SU(4), EM props. and mesonic couplings of baryons 77—22663
SU(4) symmetry breaking pattern and baryon masses 78—89690
SU(5) grand unification, cosmological baryon asymmetry 80—86640
SU(6) breaking of baryon wave functions, chromodynamic spin-spin force 79—340
SU(8) broken symmetry, baryon masses 79—290
SU(8) mass relations among $J^P = 112^+$ and $3/2^+$ baryons 77—71499
three quark operators, anomalous dimensions, baryon form factors and quantum numbers 80—22568
three-quark systems, dynamics, linear mass spectra baryon models 80—42390
topological expansion for baryons and mesons, reaction diagrams using coloured quark lines 77—82700
topological expansion for baryons and mesons, Veneziano scheme 78—70335
transition mixing, mass splitting, degenerate perturbation theory model 77—2832
universal baryon density, constraint from ^7Li abundance 78—4420
Universe, baryon number nonconservation rel. to isotropy and homogeneity 80—22125
very early Universe, baryon asymmetry 79—40309
wave functions, SU_n representation transformations and phase *(Chinese)* 79—93313

baryons continued
Y-shaped baryon, baryon models and the planar bootstrap condition 79—3005
$B \rightarrow \psi p K^-$, search for b flavoured baryons 80—42450
b-quark baryons, magnetic moments, broken SU(5) symmetry 80—95257
$\bar{p}$ decay, baryon number of universe 77—91422

barysphere *see Earth core*

BASIC
holographic store automated test using BASIC M-400 interpreter *(Russian)* 79—94180
light interferometry, 3D orthographic projection plotting program 79—85172
overlay for CAMAC data and command handling 80—18772

batch processing (computers)
distributed computing system THESEUS for mag. field analysis 79—41293

batch processing (industrial)
chemical reactions, appl. bench scale calorimeter 80—52214
glass raw materials and batch prep. 78—3085
laser mirror manufacture, ion beam/plasma chemical etching mixed batch process *(French, English)* 77—83880
LPE pure melt batch production in sliding apparatus 78—44028
polymerisation of styrene, bulk, thermally initiated, optimal temperature policies determ. 79—87845
quartz crystals production, synthetic, using large autoclaves with 400 kg/batch capacities 79—91576
Tarapur Atomic Power Station radioactive waste discharge monitoring 78—89989

batteries *see cells (electric); primary cells; secondary cells; solar cells*

Bauschinger effect
AE peak detection of back stress component in flow stress *(Japanese)* 78—6977
alloys of two ductile phases of unequal strength, deform. *(Japanese)* 78—11284
BCC and FCC polycrystals, selection of active slip system 79—90665
α-brass, Bauschinger AE peak detection of back stress component in flow stress *(Japanese)* 78—6977
brass, burst acoustic emission during Bauschinger effect 77—48475
α-brass, polycrysts., deformed in tension or rolling, anneal hardening *(Japanese)* 80—93564
α-β-brass, two phase bicrysts., deform. and fracture at 150K 80—16388
β-brass, uniaxial tension and compression, cyclic stress-strain behaviour 80—97551
β-brass bicrystals, shear-incompatible, grain boundary contrib. to Bauschinger effect 80—97550
cell wall and lattice misorientation origin during deform. 80—71712
compressible materials, flow behaviour 78—55573
cyclic plasticity and masing behaviour in metals and alloys 78—64616
cylinder, plastic flow rules and Bauschinger effect parameters 78—6984
dislocations model, compatibility with transient and steady state creep *(Italian)* 80—33487
energy based theory 78—63316
grain boundary contribution, to Bauschinger effect 79—47759
Incoloy 800H, high temp. low cycle fatigue, ageing and cold working effect 79—43277
kinematic hardening models, use in multi-axial cyclic plasticity 80—25717
metal, model of elastic-plastic deformation *(Russian)* 77—48484
metal, polycryst., Bauschinger effect and mutual restriction between grains 78—52895
metal, prediction by constitutive eqns. 77—62162
metal and alloy, deformation strengthening and anisotropy prediction *(Russian)* 78—27533
metallic media, varying loads, elevated temp. inelastic anal. using state variable theories 78—83264
metallic structures, elastic/plastic bodies with work hardening, general shakedown theorem 77—3746
metals, Bauschinger effect, review 80—21025
Orowan's explanation 77—32656
orthotropic compressible plastic yielding, derivation of elementary equation *(German)* 78—84902
overstrained spring strip 77—7320
plastic anisotropy, descriptive eqn. *(German)* 77—84154
plastic anisotropy, general formulation, comparison with expt. yield curves *(German)* 77—20006
plastic flow rules and Bauschinger effect parameters 78—6984
plastic material, rate type, with kinematic work hardening 78—15450
plastic torsion elongation due to Bauschinger effect *(German)* 77—72184
prestrain dependence 78—27582
reverse torsion testing for Bauschinger effect investig. 78—7133
rigid work hardening structures optimum design 78—13917
sheet material, determ. using tension-tension loading cycle 77—52570
sign-reversing loading *(Russian)* 79—23224
simulation of inelastic material behaviour in struct. anal. 78—34041
steel, austenitic, high tensile X 3 CrNiMoNbN 23 17, creep at room temp., effect of Bauschinger effect *(German)* 77—1852
steel, austenitic and martensitic, structural sensitivity of Bauschinger effect *(Russian)* 79—52303
steel, austenitic stainless, creep, performing effect under tensile and compressive load, rel. to Bauschinger effect 79—96103
steel, Bauschinger effect minimization by dynamic strain ageing 78—48469
steel, C, thermal stresses in submerged arc welded joint, consideration of phase transformations 79—61683
steel, Fe-Si (3 wt.%), Bauschinger effect, computerised evaluation method 80—93625
steel, medium C, fatigue behaviour of NiAl precipitation hardening 78—84983
steel, Nb-Mn, Molytor 53, Bauschinger effect, computerised evaluation method 80—93625
steel, residual stress influence on mech. props. *(German)* 78—27587
steel, spheroidized, Bauschinger effect and work hardening 78—64596
steel, stainless SUS 304, Bauschinger AE peak detection of back stress component in flow stress *(Japanese)* 78—6977
steel, structural, Bauschinger effect *(French)* 78—23787
steel, type 20 and Kh18N10T, Poisson ratio, prestrain effects 79—70103
steel high strength X 3 CrNiMoNbN 2317, Bauschinger effect and creep at room temp., effect of heat treatment *(German)* 77—36543

Bauschinger effect continued
steels, high-strength low-alloy, Bauschinger effect, computerised evaluation method 80—93625
tensors of anisotropic component of yield condition *(German)* 77—23901
Al, and Al alloys 6061 and 2024, burst acoustic emission during Bauschinger effect 77—48475
Al, Bauschinger AE peak detection of back stress component in flow stress *(Japanese)* 78—6977
Al, Bauschinger effect, temp. influence, combined tension-torsion testing machine 80—45453
Al single crystal, Bauschinger effect, orientation depend. 77—21237
Al-Cu, Bauschinger effect 79—61646
Al-Cu-(Mg), precipitation strengthened, Bauschinger effect 77—36585
Al-Ni(Ca)(6 and 7.6 wt.%), polycrystalline containing coarse particles, Bauschinger effect 77—48480
Al-Si (1.2 and 0.6 wt.%), single crystal, dispersion hardened with SiC, Bauschinger effect and work hardening 79—43360
Al-Zn-Mg, precipitation strengthened, Bauschinger effect 77—36585
Cu, Bauschinger AE peak detection of back stress component in flow stress *(Japanese)* 78—6977
Cu-Al (7.9 wt.%), burst acoustic emission during Bauschinger effect 77—48475
Fe, Armco, Bauschinger effect, computerised evaluation method 80—93625
Mg alloys, strain rate effects during reverse torsional shear 77—4143
Mg, burst acoustic emission during Bauschinger effect 77—48475
α-Ti alloy, rolled, elastic stiffness and Bauschinger effect accompanying anisotropic hardening *(Russian)* 80—40435
Ti-Al-V, rolled, elastic stiffness and Bauschinger effect accompanying anisotropic hardening *(Russian)* 80—40435
α, $\alpha+\beta$, β-Ti-Mn alloys, Bauschinger effect during cyclic straining 79—43310
Ti-V, cyclic stress-strain response 78—60700
W fibre reinforced Cu composite, hardening in two-phase material 77—52448

Bayard-Alpert gauges *see ionisation gauges*

Bayes methods
astronomical images optimal classification into stars or galaxies, Bayesian approach 80—21920
atmospheric science, radiative transfer modelling techniques extension using Bayes' rule 77—78443
Bayesian deconvolution, convergent props. 78—57861
Bayesian deconvolution, noise props. 78—57862
cervical cancer automatic cytoscreening, atypical cells classification 78—73289
charged particle mass, confidence density method for parameter estimation *(Chinese)* 78—81811
data base, classification, comparison of pattern recognition methods 80—199
decision analysis, appl. to nuclear fuel reprocessing analysis, USA policy 79—85737
deconvolution, appl. and algorithm implementation 78—70103
earthquake prediction, long-range, based on single predictor 80—26454
earthquake prediction, probabilistic significance 77—56589
EM noiselike radiation, noncoherent polarimetry anal. 80—1111
fission reactor system reliability prediction 77—67797
flow prediction, Monte Carlo and Bayesian probability techniques 78—30256
myocardial imaging with ^{201}Tl, clinical usefulness analysis based on Bayes theorem 79—88170
myocardial-stress perfusion scintigraphy, predictive value in patients without previous infarction 78—73205
nuclear fuel cycle facility safety evaluation physical security assessment results synthesis 79—85740
nuclear fuel reprocessing plant, optimal installation program 77—46370
nuclear plant specific risk studies, data specialisation, Bayes' theorem 80—47601
ophthalmology diagnosis, computer assisted 78—92739
optimum filter for image restoration *(Ukrainian)* 78—55308
P wave detection and identification using statistical signal analysis 80—8202
pattern classification of patients with essential hypertension 77—25583
radioactive isotopes, probability determ. of number of atoms at end of production 79—63637
random signal detection in noise, accounting for polarisation 77—61672
rivers, synthetic streamflow, Bayesian generation of multivariate model 77—78274
statistic inference, subjective Bayesian approach 78—57729
SO_2 air pollution, decomposed model design for assessment of utility measure 79—66426

bays (magnetic) *see geomagnetic variations*

BCS theory
see also many-body problems
$\lambda\phi^4$, spontaneous symmetry breakdown, approx. ground state, variational approach 77—79229
A15 compounds, microscopic model of supercond. and martensitic transform. 77—8226
A-15 superconductors with defects, transition temp. 78—14857
coherent-state formalism in supercond. and Josephson-junction calcs. 79—51723
collective excitations, appl. of generalized self-consistent field method 78—10598
collective quantum fields for many body systems, appl. to BCS, ^{3}He and type II superconductors *(German)* 79—35917
deformed nuclei, first monopole excitation energies in systems with pairing forces 77—61364
electron-ion system, multiplicity and pseudomultiplicity 77—1389
electronic and spin Peierls transition, gap eqns. 80—24801
Eliashberg gap equation, approx. BCS-like soln. 77—1513
even-even rare earth nuclei, rotational energies, moments of inertia 77—54133
Fermi superfluid hydrodynamics, time-depend. BCS formalism, compared with He II, finite nuclear systems 78—22920
general commutator equation in the algebra of spin operators 79—4638
helical order of spins in supercond. 80—70888
Josephson motor, rotational solns. in BCS theory 78—72310
Josephson tunnel junction, Q-factor and reson. amplitude, calc. 78—10617
layer crystals, superconductivity using BCS model 79—15254

BCS theory continued
linear fermion systems, molecular field models, and the KMS condition *(German)* 79—9178
microscopic mechanism for the macroscopic asymmetry of superconductivity 79—19687
neutron star matter, $^3P_2$ pairing near transition temp. 78—57571
non-equilibrium superconductivity 80—44762
nonequilibrium superconductor, high-freq. AC process dynamics 80—88674
nonequilibrium superconductors, transients, phonon distrib., supercond. gap, Boltzmann-BCS formulation 78—52149
nonthermal quasiparticle distribs., energy gap instability 78—39256
nuclear collective energy dissipation, into internal energy superfluid wall formula 80—63108
nuclear matter, thermodynamic model, shear viscosity temp. dependence 78—62499
nuclear moment of inertia, particle-number-projected BCS wavefunctions 77—22830
nuclear semiempirical liquid drop model, shell correction formula 77—6267
open BSC model, dynamics in weak coupling limit 79—2738
pairing vibration model of meson states, supercond. model of hadrons *(Chinese)* 77—10217
proton-neutron multiplets, odd-odd nuclei, parabolic Regge trajectories, exchange of quadrupole phonon 80—52590
proximity-effect sandwiches BCS-like term in local density of states 79—1646
response functions of superconductors and ^{3}He(B), density and current correlation functions 80—49448
retarded Josephson equation 79—19697
self-consistent selection of a superconducting representation for the BCS model 78—88067
shell model, application and results 79—89249
superconducting metal, reliability of tunnel density of states 79—28483
superconducting transition critical temperature, BCS theory, phonon spectra, review *(Spanish)* 80—84535
superconductivity, basic principles *(German)* 77—89896
superconductivity, complete Lagrangian formulation 77—89897
superconductivity, derivation of relativistic Bogoljubov eqns. 79—73627
superconductivity, magnetic impurity effects, Anderson model 78—52148
superconductivity, microscopic theory, nonequilibrium and high T_c supercond. 79—65591
superconductivity, pseudopotential, Bragg planes, effect on superconducting pairing and crit. temp. 80—15648
superconductivity theory, introductory remarks recent developments *(Chinese)* 79—47192
superconductor in EM field, nonlinear behaviour *(Russian)* 78—68108
superconductor with magnetic impurities, coexistence of superconductivity and ferromag., BCS and Zener models 80—88676
superconductors, nonequilibrium, BCS-Boltzmann and Ginzburg-Landau descriptions 79—65589
superconductors, relaxation and collective motion two-fluid theory 79—73625
superfluid, anisotropic, BCS ground state ang. momentum 79—90840
thermal expansion in supercond. state based on weak coupling BCS theory 78—80094
transition metal alloy, binary, conc., superconductivity and electron-phonon interactions, theory 78—14868
transition metals, d-band superconds., s-electron current density calc. 77—47926
transitional odd-odd mass nuclei, gamma deformed rotor model 79—93498
TTF-$CuS_4C_4(CF_3)_4$, quasi-one-dimens. antiferromag., spin-lattice dimerisation, X-ray scatt. obs. 77—85464
two-band systems, BCS pairing and Peierls distortion compatibility 78—88068
weak-coupling superconductor, effect of electron-phonon renormalisation on thermodynamics 79—99655
Woods-Saxon potential spectrum, pairing force strength, Nilsson model comparison 80—57704
Al film, crit. temp. enhancement *(Russian)* 80—93021
Al-formvar superconductive junction, Ginzburg's generalised jellium model 80—15663
Cs, deformed nuclei, low-lying positive parity states 77—6240
CuCl, high-temp. supercond., BCS strong-coupling limit for transition temp. 80—2511
^{158}Er, number conservation, effect on energy spectra, deform. and B(E2) values 79—36122
^{160}Er, number conservation, effect on energy spectra, deform. and B(E2) values 79—36122
Ge, A=64, 66, 68, 70, Lipkin-Nogami method, ground state props. 78—50103
^{3}He, anisotropic superfluid phases, book contrib. 79—99387
^{3}He, superfluid, multipole pair vibrs. 78—47627
^{3}He, superfluid, transport parameters, Kubo formulae and BCS-Green's functions 80—88382
^{3}He, superfluid A phase, intrinsic angular momentum value in BCS theory 79—51340
^{3}He, superfluid B-phase, microscopic evaluation of transport parameters 79—51354
^{3}He, superfluid B-phase, sound dispersion and neutral superfluids with BCS pairing at $T=0$ 79—51345
In films, crit. temp. enhancement *(Russian)* 80—93021
In-Bi(Tl)(Pb), small κ supercond., phase transitions higher than second order 80—88668
Nb-NbO_x-Pb, miniature tunnel junction, gap voltage calc. 79—7939
$NbSe_2$, charge density wave state, NMR meas., BCS model 77—8430
$NbSe_3$, non-ohmic transport props. near phase tranistions 78—72213
Nb_3Sn, fast neutron irradiation, effect on critical current density 78—19197
Ni, A=58. 60, 62, 64, 66, Lipkin-Nogami method, ground state props. 78—50103
Pb-formvar-Al tunnel junction, excitonic superconductivity, BCS theory, generalised jellium model 80—75684
Pd, electron-phonon parameters and supercond. p-state pairing 80—25041
Sn film, crit. temp. enhancement *(Russian)* 80—93021
Sn-Bi(Sb), small κ supercond., phase transitions higher than second order 80—88668
V_3Si, A15 compound, microscopic model of supercond. and martensitic transform. 77—8226

BCS theory continued
V$_3$Si, normal, mixed and supercond. state, specific heat meas., thermodynamic and superconducting props. 80−49987
Zn, A=60, 62, 64, 66, 68, Lipkin-Nogami method, ground state props. 78−50103

beam choppers
correlation chopper for TOF neutron scatt., deconvolution, triangular signal function 77−61158
correlation chopper for TOF neutron scatt., deconvolution theory 77−61157
cryogenic booster linac, heavy ion beam dynamics in chopper, buncher, mag. lenses 77−67919
electron, systems comparison and universal system development 80−68306
linac injection system beam dynamics, computer simulation 80−13989
neutron time of flight anal., non-conventional methods, expt. capability study 79−44985
neutrons, reverse Fourier TOF anal. with mech. beam choppers 79−6788
RF ion beam choppers with fringing fields, theory 77−13822
scanning electron microscope, beam chopping by electrostatic deflection 77−22619
time of flight spectrometer with correlation chopper, elastic neutron scatt. on powdered samples 77−62447

beam-foil spectra
16 to 110 MeV beam energy, 20 to 350 nm wavelength 78−78655
anisotropic excitation at large inclination angles, foil angle depend. 79−45820
atomic coherent populations, RF elec. field reson. interactions, quantum beats 77−46542
atomic inner shell ionisation phenomena, conf., Freiburg, West Germany (March.-Apr. '76) 77−27040
atomic orientation production by electron capture in beam-target interaction, semiclassical model 80−9723
bound states, beam-foil excitation and decay near ionis. limit 80−9552
cascade effects on Zeeman quantum beats 79−89631
conference, Lyon, France (Sept. 1978) 80−9754
electron capture, model for prod. of circular polarisation 77−3453
excitation mechanism, investig. using C II-C VI projectiles 79−86060
fast ion excited levels produced in foil or surface collisions, orientation and alignment 80−14214
fast projectile electron loss forward peak oscill. struct. as autoionisation 80−69227
fine structure control determination, atomic metastable beam method 77−68105
forbidden decay modes of one- and two-electron ions, book contrib. 78−82679
heavy atoms, charge-state distribs., beam foil populations, independent electron model 77−19035
heavy ion, beam-foil spectra from 20 to 238 MeV energy, 5 to 60 nm, lifetime meas. problems 80−9722
heavy ion+C coil collisions, electron emission, energy distribs., solid state effects 77−19062
heavy ion beam-foil spectra, ion equilib. excitation, density effect 77−19056
heavy ions, charge state fraction on emerging from solids, K-shell vacancies effects 78−25686
heavy ions moving in solids, vacancy config. determ. 77−69019
heavy ions passing through C foils and gases, charge-state distrib. 78−42191
high angular momenta levels 79−54918
hydrogen-like ions, beam-foil excitation, relative initial populations, lifetime curves 80−14210
introduction and review 78−70925
ion-atom and ion-solid collisions, continuum electron capture and loss, cusp spectroscopy of forward peak 80−14201
ion-induced electron distributions, experimental resolution and background effects 79−36749
ion-neutral atom, in foil, inner-shell processes, oscill. X-ray spectra excitation 77−54565
ions emerging from C foils, mean charge, inner-shell vacancy effects 80−87219
level population concept, depend. on exptl. parameters 80−14206
lifetime meas. in atoms, mols., ions 77−30832
molecule, Dicke photon trapping effects 78−42149
multimolecular system, two-level mols., coherent trapping of single excitation 79−89875
multiplet lines emitted after beam-surface interaction, polarisation calc., time development 80−14216
nuclear spin polarised ion beam, quantum beat expt. 77−42396
orbital angular momentum transfer to nucl. spin polarisation in external mag. fields 80−14217
projectile K X-rays, configuration rearrangement effects 77−46634
second-row elements, K-shell X-ray prod. by H(He) ion bombardment 79−47550
surface interactions, nuclear hyperfine interactions 77−23544
third-row elements, L-shell X-ray prod. by H(He) ion bombardment 79−47548
Tokamak plasma, heavy metal contaminants, rel. abundance and charge stable comp. diagnostics 79−46480
transition metals, 3d, M III excited states, radiative lifetimes, beam-foil obs. 77−30979
5^{n+}, beam-foil UV spectra, elec. dipole transition probabilities, radiative lifetimes 77−6730
Al II to Al VI, beam-foil obs. from 1100 to 1900 Å, lifetimes and oscillator strengths 80−14108
Al II to Al VI, beam-foil obs. from 300 to 2000 Å, mean lives and oscillator strengths 80−14109
Al II-VII, radiative lifetimes, beam-foil spectra 79−49986
Al IV, lifetimes of n=3 and 4 levels meas. and calc. *(French)* 80−9554
Al IV, Ne-like, atomic lifetimes, second order calc. and beam-foil meas. 79−59422
Al IV, V, beam foil spectra, 1100-1900 Å, lifetime meas. 78−70919
Al IX to Al XI, beam-foil obs. of lifetimes and oscillator strengths, 300 to 1000 Å 80−14110
Al ions, 720 keV beam foil spectra 1800 to 7000 Å, excited state cascades and lifetimes 77−23450
Al V-VII, between 85 and 135 Å 78−9134
Al^{10+}, $^4P^0{}_{5/2}$ state excitation energy, X-ray spectra 77−27017
Al^{7+}, 2s2p^3 terms, mean lives, from beam-foil spectra 78−37601
Al^{n+} foil-excited ion, X-ray spectra and satellite classification 80−95567

beam-foil spectra continued
Ar, cascade effects on Zeeman quantum beats 79−89631
Ar, emerging from C foil, excited ion Auger decay 77−3333
Ar, hydrogenlike, Lamb shift meas. by motional elec. field quenching time-of-flight expt. 80−9550
Ar II, beam-foil spectra, lifetimes meas. 78−42167
Ar III, beam-foil spectra, lifetimes meas. 78−42167
Ar IV to Ar XII, beam-foil obs. of lifetimes and oscillator strengths, spectral identifications, 400-2000 Å *(French)* 80−9555
Ar IX, Ne I like reson. and Na I-like satellite lines, relativistic HF calc. and expt. 78−94210
Ar ions+C foils, emergent Ar-L Auger electron absolute yields 77−19061
Ar VIII, beam-foil lifetime meas. using ANDC anal. for reson. doublet 79−93964
Ar$^+$ orientation angular depend., beam-tilted foil interaction 78−5335
Ar$^+$, orientation by collision with tilted surface, appl. to zero-field level crossing 77−3452
Ar^{15+} and Ar^{16+}, beam-foil obs. of lifetimes of metastable states 80−14116
Ar^{15+}, Ar^{16+}, population of $^3P_2$ and $^4P_{5/2}$ states by cascading process 79−63966
Ar^{15+}, population of $^4P_{5/2}$ state meas. by cascading processes 78−94315
Ar^{16+}, radiative decay from 2^3P_2 and 2^3P_0 levels, beam-foil time of flight meas. 77−68015
Ar^{5+}, Ar^{6+}, excited state lifetimes, beam-foil meas. 77−10750
Ar^{x+}, high resolution spectroscopy of prompt and metastable decaying levels 78−33462
Ar$^+$+C, beam-foil spectra, Ar$^+$ ion orientation, ang. variation 78−86944
Ar^{2+}+Al(Sn), impact-parameter depend. of K- and L-X-rays 79−76501
^{40}Ar$^+$, excited state polarisation transfer due to optical cascades 78−9238
As III, radiative lifetimes, calcs. and beam-foil spectra 77−75223
Au, radiation from beam-foil excitation and Tokamak produced plasmas 79−54828
^{79}Au+^{19}F(^{28}Si), target Lα X-ray prod., projectile charge state depend. 79−47549
B, excited in single gas collisions, high-resolution Auger spectra 80−9717
B I and II, high spin and mixed states 77−61709
B IV, doubly-excited states, energy levels, calc. and expt. *(French)* 78−41971
B IV, V, beam-foil meas. of mean lives below 450 Å 78−90120
B ion, equilib. charge state distrib., in C foil and doubly excited states *(French)* 77−27171
B$^+$, beam-foil excitation, absolute Auger yield meas. 80−14203
B$^+$, beam-foil excitation; absolute Auger yield meas. 79−45685
B$^+$ ions, beam foil excitation, L-Auger decays, autoionisation 77−14569
Be, excited in single gas collisions, high-resolution Auger spectra 80−9717
Be II, beam-foil spectra assignment, compared with HF energies, isoelectronic sequence 79−31424
Be III, doubly excited states, triplet spectra 80−87069
Be isoelectronic sequence, highly ionised, beam-foil obs. of oscillator strengths for E1 transitions 80−14112
Be, optical beam foil spectra, relative level populations 80−23540
Be, optical beam-foil spectra, relative level population 80−14207
Be$^+$ ions, beam-foil excitation, L-Auger decays, autoionisation 77−14569
Br V, VI, VII, radiative lifetime meas., 450 to 1000 Å 77−54524
BrVI(VII), reson. line oscill. strengths, beam-foil spectra 77−38630
C, excited in single gas collisions, high-resolution Auger spectra 80−9717
C foil, charge state distrib. of heavy ions 78−5334
C foil+H$_2^+$(H$^+$), 0.5-2.5 MeV, forward electron vel. distrib., peak shape 78−78794
C II, III, IV, radiative mean life meas. by beam-foil technique 78−90121
C II and III, mean lifetimes of astrophysically important excited levels 77−46528
C II to C VI, beam-foil excitation functions for optical transitions 80−14209
C III, IV, V Auger lines obs., beam-foil excitation, ab initio calcs. 77−54601
C IV, beam-foil spectra assignment, compared with HF energies, isoelectronic sequence 79−31424
C, K-shell X-ray yield, following H$^+$ bombardment of foil 77−10624
C$^+$, beam-foil excitation, absolute Auger yield meas. 80−14203
C$^+$, beam-foil excitation; absolute Auger yield meas. 79−45685
C$^+$, beam-tilted C foil interactions, charge-state distrib., photon emission, 100-400 keV 79−22814
C$^+$ ions, beam-foil excitation, L-Auger decays, autoionisation 77−14569
C^{3+}, fine struct. and lifetimes, doubly excited quartet system 78−78827
C-foil, secondary electron yield from heavy ion beam-tilted-foil expts. 78−62889
C+C(N)(O) ions, 4 to 40 MeV, beam-foil K-shell X-ray prod. cross sections 78−33461
CO$_2{}^+$, thin foil impact, dissoc. struct. effects in ionic fragment energy spectra 78−50631
^{13}C III, 1s^{2}2s3p $^3P^0$ state,, HFS, beamfoil expt., CI and Hartree-Fock calcs. 77−75276
^{13}C V, high energy hyperfine struct. meas. 77−57915
Ca II, lifetime extraction from beam-foil decay curves 80−14107
Cl (IX-XV) allowed intra L-shell transitions, oscill. strengths and radiative lifetimes meas. 79−13676
Cl, foil excitation, K-vacancy bearing metastable states yield, 30-50 MeV 77−54600
Cl, ion-foil interaction, K-shell vacancies and residual excitation 77−50519
Cl ions, multiply-charged, beam-foil obs. of allowed L-shell transitions 80−14113
Cl, multiply-ionised, radiative electron capture on impact with Ca and Ni foils 77−6916
Cl VIII, Ne I like reson. and Na I-like satellite lines, relativistic HF calc., and expt. 78−94210
Cl XIII-XV, Δn=0 transitions, lifetime meas. beam-foil spectra 78−78798
Cl, XVI, 1s2s ^{3}S-1s2p ^{3}P transitions, Lamb shift, VUV beam foil spectra obs. 80−52919
Cl^{16+}, Lamb shift meas. using beam-foil excitation, QED test 80−9551

beam-foil spectra continued
Cl^{6+}, Cl^{7+}, excited state lifetimes, beam-foil meas. 77—10750
Cl^{n+}+Cu, effect on projectile charact. X-rays and REC of target thickness 79—45662
Cl^{n+}+Cu film on C foil, X-ray production, radiative electron capture 77—19063
^{35}Cl XVI, beam-foil excitation, Lamb shift and fine struct., QED test 80—9549
Co I, multichannel anal. techniques, appl. to beam-foil spectroscopy, 3000-3950 Å, lifetimes 77—58206
Co I and Co II, beam-foil obs. of lifetimes 80—14111
Cr, gas-phase, plasma, sputtering and beam-foil excitations 80—32820
Cs L-shell X-ray prod. by H(He) ion bombardment 79—47548
Cs+H^+, 4 MeV beam-foil X-ray production cross-section 79—7003
Cu^{18+}, $3^2P_{1/2}$ level decay, time-resolved obs., intensity modulations 77—61704
Cu^{18+}, Na-like, low-lying levels, radiative lifetimes, f-values obs. 78—25482
Cu+Ni foil target, 50-65.5 MeV, K-vacancy production, impact parameter depend. 79—54958
D^+, $D_2{}^+$ and $D_3{}^+$ fragments traversing thick foils, correls. in motions, integral ang. distribs. 80—16136
F II, $2p^3nl$ terms, beam-foil lifetime meas. 79—81173
F II to VIII, mean lives, beam-foil spectrum in far UV 79—59389
F III, IV, beam-foil spectra, mean lives, 2150-3200 angstrom 78—55224
F, ion-foil interaction, K-shell vacancies and residual excitation 77—50519
F VI, intercombination lines, transition probabilities determ. 79—89645
F VIII, 1s2p $^3P_0$ and $^3P_2$ levels, lifetimes, hyperfine quenching effects, UV beam foil spectra 80—47931
Fe 16 to 110 MeV beam energy, 20 to 350 nm wavelength 78—78655
Fe II, Fe III, lifetimes, VUV beam-foil spectroscopy 79—22657
Fe V, VI, beam-foil level populations, charge state fractions 80—52913
Fe XXIII and XXIV, reson. and intersystem transitions, oscill. strength, lifetime, beam-foil spectra 78—82685
FeV and VI, beam-foil lifetime meas., 1100-1900 Å 80—23532
Ga I, radiative lifetimes, calcs. and beam-foil spectra 77—75223
Ga II, $4s4d{}^1D$ and $4p^{21}D$ energies and lifetimes 79—59391
Ge II, radiative lifetimes, calcs. and beam-foil spectra 77—75223
H, 2p state alignment, influence of surface electric fields after beam foil excitation 78—29849
H, beam foil excitation, n=2 density operator and prod. probability meas., transition probabilities 80—14219
H, beam-foil excitation of 2P-state, alignment meas. 80—14215
H, beam-foil excited, zero-field quantum beats in H_β emission, polarisation energy depend. 80—14218
H, beam-foil spectroscopy, stray electric field due to high C foil resistance 80—42978
H, excited state, J=3/2-J=5/2 transition, fine struct. interval meas. 77—46542
H, line spectra, Doppler shift, of ions after traversing thin C foil, vel. meas. 78—16778
H, Stark-induced quantum beats in H_β 80—9757
H^+, beam-tilted C foil interactions, charge-state distrib., photon emission, 100-400 keV 79—22814
H^+, $H_2{}^+$ and $H_3{}^+$, beam-foil excitation, optical radiation obs. 80—9724
H^+, $H_2{}^+$ and $H_3{}^+$ interactions with thin foils, electronic polarisation wake effects, dissoc. of mol. ions 80—16135
H-like ions, excitation regimes, nucl. orientation due to hyperfine interaction 78—70928
$H_2{}^+$, energy spectra of emergent dissoc. and recomb. products from C film 79—45819
$H_3{}^+$ expt. determ. struct., foil-induced dissoc. fast mol.-ion beam 78—74752
$H_3{}^+$+C foil, 2.2 MeV, ion survival during traversal 79—64103
$H^+(H_2{}^+)$+C foil, $v_i=v_e$ electron prod., charge transfer to continuum theories 78—13583
He, coherence meas. of light polarisation from 60 keV ions 77—71863
He, double excited states, lifetime meas. by beam-foil technique 78—74590
He I, $2s{}^1S$-$3p{}^1P$ excitation, linear polarisation fraction, foil material effects 78—21893
He I, beam-foil excitation, temp. depend., linear polarisation of transitions 80—14213
He I, beam-foil excited, 70-400 keV, relative initial populations 80—14211
He I, lifetime meas. by beam-foil spectra 77—75104
He I beam-foil excitation, 60-180 keV, alignment production, foil temp. depend. 79—54956
He I singlet transitions, polarisation meas. following beam-filted foil excitation 79—13665
He I transitions, polarisation meas. using beam-foil excitation, foil tilt angle depend. 80—14212
He^+, beam-foil excitation, alignment, 50 to 500 keV 78—22022
He^+, fine struct. obs. by beam-gas spectroscopy, level crossing resonances 80—9719
He-like ions, excitation regimes, nucl. orientation due to hyperfine interaction 78—70928
He^++C, beam-foil spectra, He atom orientation, ang. variation 78—86944
He^{2+}+C foil collisions, electron emission, energy distribs., solid state effects 77—19062
HeI, beam-foil mean life meas. of 1s 3p ^1P level 77—3320
^{4}He, 3p ^3P state alignment and orientation as function of foil tilt angle, quantum heat spectra 79—94071
^{4}He, beam foil and quantum beat spectra *(Chinese)* 80—32638
^{4}He II, widths of Stark components calc., beam-foil data comparison *(French)* 80—9545
$^4He^+$, quantum beats in C foil interaction *(French)* 79—59544
$^4He^+$ II, H-like, fine struct. Stark effect *(French)* 78—943
He(2s-3p transitions), beam foil spectra, emitted light polarisation, depend. on foil tilt angle 80—63786
Hg II, $6p^2P$ and $6p^2D$ levels, radiative lifetimes meas. 80—78576
^{67}Ho-^{19}F(^{28}Si), target Lα X-ray prod., projectile charge state depend. 79—47549
I VI, beam-foil spectrum, 400 to 1300 Å 79—86059
I VI and I VII, beam-foil obs. of lifetimes, spectral assignments, 400 to 1300 Å 80—9556
I VII, beam-foil lifetime meas., cascading problem 80—14249
I VII, beam-foil spectrum, 400 to 1300 Å 79—86059
In I, radiative lifetimes, calcs. and beam-foil spectra 77—75223

beam-foil spectra continued
Kr I-VIII, beam foil mean life meas., f-values 77—30974
Kr ions, high energy stripping by solid foil, charge state distribs. 77—6912
Kr VII, beam-foil excitation, 4s4p $^1P_1{}^0$ level decay simulation 80—78578
Kr VIII, beam-foil decay curves for reson. transitions simulation 80—9721
Kr VIII, beam-foil lifetime meas. using ANDC anal. for reson. doublet 79—93964
Kr VIII, excited state energies and lifetimes, beam foil spectra 80—63591
Kr VIII beam-foil decay curves for resonance transitions 78—74755
Kr VII(VIII), reson. line oscill. strengths, beam-foil spectra 77—38630
Kr XXXIII and Kr XXXIV, beam-foil obs. of transition wavelengths and oscillator strengths 80—14115
Kr^+, beam-tilted C foil interactions, charge-state distrib., photon emission, 100-400 keV 79—22814
Kr^+, equilib. charge state distribs. and multiple scatt. angles in C foil 80—59532
Li, coherence meas. of light polarisation from 60 keV ions 77—71863
Li, excited in single gas collisions, high-resolution Auger spectra 80—9717
Li I and Li II, beam-foil excited, 70-400 keV, relative initial populations 80—14211
Li I to Li III, beam-foil obs. of 2000-5500 Å spectra 80—9548
Li I to Ne VIII isoelectronic sequence, term level diagrams of doubly excited states 80—14093
Li, optical beam foil spectra, relative level populations 80—23540
Li, optical beam-foil spectra, relative level population 80—14207
Li^-, core excited bound states in beam foil expts., CI calcs. 80—78559
Li^-, optical transition between bound states, beam-foil spectrosc. obs. 80—91476
Mg (Mg^+), lifetime meas., beam foil spectra, comparison with numerical coulomb approx. calc. 80—58367
Mg I to Mg III, beam-foil excitation, Rydberg states, relative populations 80—14208
Mg III-V, beam-foil spectra, 100-450 Å 80—83308
Mg ions, foil-excited, EUV spectrum 80—42976
Mg, optical beam foil spectra, relative level populations 80—23540
Mg^+, beam-tilted C foil interactions, charge-state distrib., photon emission, 100-400 keV 79—22814
Mg^{6+}, $2s2p^3$ terms, mean lives, from beam-foil spectra 78—37601
Mg^{9+}, beam-foil excited, spin orbit-forbidden X-ray transition obs. 80—23537
Mg^{n+}, foil-excited ion, X-ray spectra and satellite classification 80—95567
MnI, transition probability and solar abundance, beam foil TOF meas. 79—40154
Mo, EUV spectra 5 to 55 nm using 22 to 200 MeV beams 79—46481
Mo XIV to Mo XXIX, extreme UV spectra 80—87068
N IV, intercombination lines, transition probabilities determ. 79—89645
N, mean lifetimes of astrophysically important excited levels 77—46528
N V, beam-foil decay curves, mean lives determ. 80—9553
N^+ and $N_2{}^+$, beam-foil and beam-gas excitation, Coulomb explosion effects, Auger spectra obs. 80—14220
N^+, beam-foil excitation, absolute Auger yield meas. 80—14203
N^+, beam-foil excitation; absolute Auger yield meas. 79—45685
N^+, beam-tilted C foil interactions, charge-state distrib., photon emission, 100-400 keV 79—22814
N^{4+}, fine struct. and lifetimes, doubly excited quartet system 78—78827
$NH_3{}^+$, fast mol., dissoc. in thin C foils, Doppler broadening obs. 78—22019
NII, NIII level lifetimes, beam-foil method meas. 78—94314
N_2O^+, thin foil impact, dissoc. struct. effects in ionic fragment energy spectra 78—50631
^{14}N III, hyperfine struct. of quadruplet levels *(French)* 77—19103
^{15}N, beam foil and quantum beat spectra *(Chinese)* 80—32638
^{15}N, highly ionized, atomic transition polarisation by beam-foil interaction, 3-8 MeV 80—18908
Na V(VI)(VII), beam-foil spectra, extreme UV mean lifes and oscillator strengths 79—31456
Na^+, beam-tilted C foil interactions, charge-state distrib., photon emission, 100-400 keV 79—22814
$^{23}Na^+$ polarised beam, beam foil technique for polarisation determ. 79—13843
^{60}Nd+^{19}F(^{28}Si), target Lα X-ray prod., projectile charge state depend. 79—47549
Ne (II-VI), 209-602 Å, mean lives and oscill. strengths beam-foil spectroscopy 77—79561
Ne Auger electron decay, final charge states, beam-foil investig. 77—19060
Ne, beam-foil excited ^4P state, delayed coincidence Auger electron lifetime meas. 80—14117
Ne, charge-state distributions and the population of X-ray emitting states 79—68311
Ne, fine struct. obs. by beam-gas spectroscopy, level crossing resonances 80—9719
Ne, foil excited, 6 to 10 MeV, equilibrium K-shell excitation 79—22817
Ne, foil-excited, KLL-Auger spectrum 77—34604
Ne I, beam-foil excitation, Rydberg states, relative populations 80—14208
Ne^{4+}, $2s2p^3$ terms, mean lives, from beam-foil spectra 78—37601
Ne+Al foil, projectile K-vacancy production cross section, X-ray production rel. to target thickness 77—19059
Ne+heavy ion, few-electron states prod. K X-rays obs. 80—9718
Ni+Ni, beam-foil collisions, X-ray transitions between correl. many electron quantum states 77—79689
O, beam-foil excited ^4P state, delayed coincidence Auger electron lifetime meas. 80—14117
O, beam-foil spectra, multiply ionised O 80—42977
O I, lifetimes of 2s2p $^3P^0$ state 77—27027
O II, III, IV, beam-foil spectra, mean lives, 270-490 angstrom 78—55223
O II and III, mean lifetimes of astrophysically important excited levels 77—46528
O IV(VI), circular polarisation of light emitted in beam-foil collisions, cascade free lifetimes 78—55228
O V, intercombination lines, transition probabilities determ. 79—89645
O VII, beam foil lifetimes in 10-100 ps range 77—23471
O VII and VIII, beam foil excited, alignment effects 77—34605
O^+ and $O_2{}^+$, beam-foil excitation, optical radiation obs. 80—9724

beam-foil spectra continued
O^{+}, beam-foil excitation, absolute Auger yield meas. 80−14203
O^{+}, beam-foil excitation; absolute Auger yield meas. 79−45685
O^{+}, beam-tilted C foil interactions, charge-state distrib., photon emission, 100-400 keV 79−22814
O^{5+}, fine struct. and lifetimes, doubly excited quartet system 78−78827
O^{5+}, spectra, 7-32 nm, doubly excited quartet system 78−62757
O^{n+}, n=1 to 4, gas and foil-excited, 2-18 MeV, projectile Auger spectra 79−59414
OH$_2{}^{+}$, and OH$_3{}^{+}$, fast mols., dissoc. in thin C foils, Doppler broadening obs. 78−22019
^{16}O, recoil, γ-ray ang. distrib. spin rot. 77−23545
P, highly ionised, beam foil radiative lifetimes and EUV spectrum 80−32671
P V, beam foil excited, alignment effects 77−34605
P^{+}, beam-foil excitation; absolute Auger yield meas. 79−45685
S, foil excitation, K-vacancy bearing metastable states yield, 30-50 MeV 77−54600
S, He-like, 2^{3}P$_1$ state lifetime, X-ray emission 77−18851
S, He-like ions, X-ray emission passing through thin foils 77−3293
S II-VII, spectra, 1050-5500 Å, beam-foil expt. with 100-700 keV ions 78−50495
S III-IV, 500 to 1200 Å 78−66488
S, ion-foil interaction, K-shell vacancies and residual excitation 77−50519
S ion+target (Z=4-40), single and double K-shell excitation, X-ray satellites, hypersatellites 77−19058
S ions, multiplet state equilib. population in beam-foil excitation 77−19057
S V, VI, radiative lifetimes, oscillator strengths 77−30973
S VII, vuv beam-foil spectrum, lifetimes 79−81174
S XIV, splitting and oscillator strengths for 2s^{2}S-2p^{2}P^0 doublet 77−49348
S XV, 1s2s ^{3}S-1s2p ^{3}P transitions, Lamb shift, VUV beam foil spectra obs. 80−52919
S^{+}, beam-tilted C foil interactions, charge-state distrib., photon emission, 100-400 keV 79−22814
S^{11+}, charge state fraction on emerging from solids, K-shell vacancies effects 78−25686
S^{12+}, S^{13+}, in-shell dipole transitions, oscill. strengths, beam-foil spectra 77−71861
S^{15+}, charge state fraction on emerging from solids, K-shell vacancies effects 78−25686
S^{6+}, spectra, 500-1200 Å, lifetimes 78−62756
S^{n+}, fast highly charged ions, passing through foil, multiplet states equilib. population 77−10746
Sb III, radiative lifetimes, calcs. and beam-foil spectra 77−75223
Sc II, 3d4p ^{1}P and ^{3}F levels, beam-foil mean-life meas. 77−3306
Se IV, radiative lifetimes, calcs. and beam-foil spectra 77−75223
Si, atom, highly ionised beam foil lifetimes 77−57934
Si, EUV beam foil spectra, highly resolved, fine struct. splittings 79−31448
Si, foil excitation, K-vacancy bearing metastable states yield, 30-50 MeV 77 −54600
Si, He-like, 2^{3}P$_1$ state lifetime, X-ray emission 77−18851
Si, highly ionised, beam-foil lifetime obs. 80−32670
Si III, IV, radiative lifetimes, oscillator strengths 77−30973
Si IV, V, VI, beam-foil level populations, charge state fractions 80−52913
Si ions, extreme UV spectra 77−6711
Si ions, H-like, He-like and Li-like, X-ray spectra after foil excitation 79−59545
Si ions, multiply-charged, beam-foil obs. of 1s2p^{3}P$_1$ lifetime 80−14114
Si V, VI, beam-foil meas. of lifetimes, 500 to 1300 Å 78−9118
Si XI, allowed transitions, radiative lifetimes and oscill. strengths meas. 78−78797
Si XII, allowed transitions, radiative lifetimes and oscill. strengths meas. 78−78797
Si XIII, 1s2s ^{3}S-1s2p ^{3}P transitions, Lamb shift, VUV beam foil spectra obs. 80−52919
Si^{12+}, 1s2s ^{3}S$_1$-1s2p ^{3}P$_{0.2}$ transition wavelengths, by beam-foil 80−32649
Si^{12+}, 1s2s^{3}S-1s2p-^{3}P transitions 79−22632
Si^{12+} from Au, C foils, population in ^{3}S$_1$ metastable state, 15-60 MeV 78−17776
Si^{n+}, foil excited, satellite lines in X-ray spectrum 79−85929
Si+F^{q+}, q=3-9, Si K-shell ionis., electron transfer cross sections, solid targets 79−10192
Si(Si^{+})(Si^{2+})(Si^{3+}), excited levels, radiative lifetimes, beam foil spectra 80−58368
Sn II; radiative lifetimes, calcs. and beam-foil spectra 77−75223
Te IV, radiative lifetimes, calcs. and beam-foil spectra 77−75223
Ti III, IV, V, radiative lifetime meas. using beam-foil technique, 700 to 1900 Å 80−78574
W, radiation from beam-foil excitation and Tokamak produced plasmas 79−54828
Xe II, radiative lifetimes 80−18825
Xe VIII, beam-foil lifetime meas. using ANDC anal. for reson. doublet 79−93964
Xe VIII, beam-foil lifetime meas., cascading problem 80−14249
Y I, Y II, lifetimes of excited states, rel. to solar abundance determ. 78−86815
Zn, gas-phase, plasma, sputtering and beam-foil 80−32820
Zn I isoelectronic series, 4s4p^{1}P lifetimes meas. 80−42998
Zn II, beam excited levels, population inversion 79−18161
Zn II, lifetime extraction from beam-foil decay curves 80−14107
Zn I(II), low lying level lifetimes, beam foil spectra 79−36751
Zr I, lifetimes of excited states, rel. to solar abundance determ. 78−86815

beam-foil spectroscopy
astrophysical applications, oscill. strengths meas. 79−50168
atomic beam, improved light collection 77−75337
atomic systems, beam-foil interaction process, quantum beats, alignment and orientation obs. 80−14252
book 77−38744
characteristic features and comparison with other light sources, book contrib. 77−38746
coherence, alignment and orientation phenomena 77−38748
collectively accelerated protons, nucl. activation, time-of-flight, and foil activation meas. 79−4195
conference, Lyon, France (Sept. 1978) 80−9754

beam-foil spectroscopy continued
continuum, effect on cascades in beam-foil spectroscopy 78−9133
Doppler shifted X-ray refl. 77−18821
electron emission from nuclear accelerator targets *(Russian)* 79−49335
experimental methods, book contrib. 77−38745
fast ion beam (Z≤18), semi-empirical determ. of charge states *(French)* 79−45867
fast ion double collision spectroscopy, polarisation obs. of emitted photons 80−16134
fast projectile electron spectroscopy, autoionizing ion levels and lifetimes 77−38749
grazing incidence ion beam-surface interaction, mechanism and uses 80−14251
grazing-incidence spectral region, beam-gas and beam-foil excitation obs. 80−14250
heavy ion, decay curves influence of cascades, theoretical simulation 78−74755
heavy ion, one and two electron systems, Lamb shift and radiative decays 77−38643
heavy ions, beam-foil decay curves for reson. transitions, simulation 80−9721
large M0 K X-ray, anisotropy from Ne on Al foil 78−55254
laser spectroscopy of unstable isotopes, nucl. props. determ. from atomic spectra using fast beams 80−9720
level population concept, depend. on exptl. parameters 80−14206
life time measurements, review 80−14248
lifetime extraction from beam-foil decay curves 80−14107
lifetime meas., extension of techniques, book contrib. 78−74758
lifetime meas. astronomical applications 77−41313
lifetime meas. from decay curves, book contrib. 77−38747
lifetime measurement, cascading problem, ANDC method use and error limits 80−14249
light intensity from beam-foil source, non-depend. of foil temp. 78−37736
measurement techniques, review 77−50563
molecular effects 79−50127
multi-exponential beam-foil decay curves, spatial resolution function 77−23580
multichannel analysis techniques appl., Co I meas. 77−58206
nuclear spectroscopy techniques in at. and mol. physics, review 78 22055
oscillator strengths, neutral and ionised atoms, non-closed shell many electron theory 77−38612
quantum beats observation technique 80−9757
review of advances 80−9756
solar UV emission spectrum, beam-foil spectroscopy appls. 77−41314
target ion spectroscopy as method of overcoming Doppler limitation in beam foil spectroscopy 77−83720
University of Liege beam-foil facility 79−45866
C foil, ion irrad., graphitisation rel. to lifetime, relevance to beam-foil spectroscopy 80−15166
C, stripper foil prepared by cracking hydrocarbon vapour in glow discharge 79−31286
C thin foil breakage times under Ar^{+} bombardment 78−25753

beam handling equipment
see also particle beam diagnostics
3 GeV proton synchrotron magnet design and meas. 79−31303
14 UD Pelletron accelerator terminal, ion optics, high energy acceleration tube 78−33321
30 T pulsed solenoid construction and life tests 79−31297
180° electron scatt. magnet system, characts. and performance 80−23238
180° mass spectrometer, mag. field effects on ion source 77−30216
aberrational quadrupole lens system, for charged particle beam focusing, with finite emittance 79−26180
accelerator grid assemblies, 120 keV, fabrication and brazing 78−66379
accelerator magnet systems, piggy back power supplies advantages 77−83365
ALA, high luminosity e^{+}e^{-} storage ring, 1.2 GeV, design study 79−72066
ALFA, electron pulse stretcher to increase Frascati Linac duty factor, feasibility study 80−23237
analog wire chambers for beam tuning 79−3267
ANL ZGSynchrotron, 1 to 12 GeV beam transport for polarised protons 79−72056
antiproton high-intensity low-momentum separated beam for annihilation at rest study 77−14292
atomic O$_2$ supersonic nozzle beam source development 80−58016
AVF-cyclotron at Vrije Univ., timing expts., burst suppression 78−21793
axisymmetric high flux secondary particle channel 79−45502
beam, 70 GeV, channel, shaping system, for Protvino Inst. neutrino expts. 78−37476
beam buncher improvement at Univ. of Manitoba cyclotron 77−88308
beam direct conversion for fusion injection at energies above 100 keV 78−13330
beam direct conversion for fusion reactor appl. 78−13329
beam induced e.m. fields, coupling impedance struct. above tube cutoff frequency 77−375
beam optical components, anal. of misalignment effects 78−13355
beam profile monitor using Rutherford backscatt., emittance and luminosity meas. 79−45497
beam pulsing system for cyclotron beams 77−10514
beam scanning 3-dimens. systems for radiation therapy 77−86589
beam swinging magnet at neutron scatt. facility in 20-40 MeV range 77−26888
BEAMSCOPE, device for meas. of emittances and betatron amplitude distribs. 79−72145
betatron, 5 MeV, bremsstrahlung radiation ang. distrib. and penetrating power 78−70657
betatron bremsstrahlung field shaping apparatus for teletherapy 78−57062
Bevalac radiotherapy facility, dosimetry and beam handling apparatus 79−79630
BLIP at AGS beam transport 200 MeV line 78−25362
BNL AGS, high field superconducting beam transport 79−76203
BNL AGS, polarised proton acceleration 79−72055
BNL AGS slow extraction improvements 79−72045
BNL AGSynchrotron, 1.5 GeV/c multiturn shaving extraction and its transport line 79−72062
BNL short separators, modernisation and improvement 79−22525

beam handling equipment continued
- Bonn isochronous cyclotron, beam stabilisation and automatic energy variation 79—54705
- booster synchrotron, 100 to 700 MeV, for BNL National Synchrotron Light Source 79—67973
- bunched beam neutralization by Gabor lenses 79—72132
- buncher cavity, resonant at 1st and 2nd harmonic of ANL low beta linac 79—72134
- buncher waveguides, engineering design 77—83399
- Calcutta 224 cm variable energy cyclotron, initial operating experience and beam transport 79—54629
- cascaded 800 MeV normal conducting CW race track microtron, design 77—6583
- CERN ISR, revised skew quadrupole system for coupling compensation 79—72097
- CERN ISR, supercond. quadrupole magnets, wire dimension meas. and short circuit detection 79—31255
- CERN ISR, superconducting high luminosity insertion 79—72049
- CERN ISR collimator system 79—72119
- CERN ISR operation with antiprotons, project description 79—72064
- CERN PS booster, simultaneous dynamic stopband compensation and correction lens location 79—76191
- CERN SPS, external proton beams and splitter system 77—83386
- CERN SPS, high freq. longitudinal and transverse pick-ups 79—72152
- CERN SPS, supercond. bending magnets CESAR 79—31251
- CERN SPS, target stations and beam dumps 77—83385
- CERN SPS, zer flux DC current transformer 77—88306
- CERN Super Proton Synchrotron beam-splitting steel septum magnets 79—31295
- CERN Super Proton Synchrotron extraction channel septum magnets 79—31296
- CESR, synchrotron radiation exit ports, thermal design 79—68035
- CESR electron storage ring, ultra fast pulsed magnets for beam manipulation 77—83239
- CESR injection linac, electron beam modulator, design, performance 77—83374
- channel for high-current beam transportation, design parameters 79—59291
- charged particle beam position detectors, dielectric use 79—26794
- chopper for neutron pulse propagation experiments 78—13362
- chromaticity correction in KEK main ring 80—74049
- chromaticity corrections, second order effects in sextupole-corrected SPS lattice 79—76196
- coaxial diode electron beam system for excimer laser excitation 80—86509
- cold neutron beam polarising supercond. hexapole magnet 79—31300
- collective accelerators, helix controlled collective ion acceleration 80—14009
- collective ion acceleration in reflecting electron systems 80—14010
- colliding ring solenoidal detector magnetic system design and fabrication 79—31298
- collimator system for fast neutron scattering experiments 80—52802
- communication network within hierarchical control system, appl. to Fermilab beam line 79—45610
- compact versatile beam steering unit for cyclotron beam guiding system 78—21799
- comparison apparatus for bunch excited fields and energy loss meas. 79—72164
- conference on cryogenic engineering, London, England, (July 1978) 79—54137
- conference on cyclotrons and their appl., Bloomington, USA (Sept. 1978) 79—54626
- conference on nuclear spectroscopy of fission products, Grenoble, France (May 1979) 80—77546
- conference on particle accelerator engineering and technology, San Francisco, USA (Mar. 79) 79—67979
- counterstreaming 10 MeV electron beam profile and position monitor 77—83403
- CPS at CERN, pulse to pulse modulation, extraction modes, beam intensity 77—83277
- CPS continuous transfer, modulated fast bump 77—83240
- cryogenic booster linac, heavy ion beam dynamics in chopper, buncher, mag. lenses 77—67919
- crystal channelling measurements, experimental system, components, capabilities 77—22617
- Cs, pulsed sputter negative ion source 78—33347
- CTR neutral beam source, SCR series switch and impulse crowbar 78—66395
- current to frequency converter for digitization of millisecond beam signals 79—72160
- cyclotron, supercond., trim coi! power requirement minimisation method 79—54665
- cyclotron separated sector type, model magnet *(Japanese)* 80—874
- cylindrical diode, magnetically insulated, cathode plasma props., electron beam prod. *(Russian)* 77—74550
- cylindrical magnetic lens, 100-300 kOe, use of Li 79—9257
- Darmstadt linear accelerator electron scatt. facility, beam transport and spectrom. 78—70679
- deflecting plates, using elec. field, energy change, theory 79—71192
- deflecting septum magnet for cyclic accelerator 78—78525
- deflection system for SEM 78—58096
- deuteron beam production, by localised source in focused discharge 78—58093
- diameter of glass tubing meas., using radionuclide methods *(Czech)* 77—5803
- dipole magnets for 180° electron scatt. 79—49891
- direct current accelerator for 14 MeV neutron prod., thermal-mech. design 78—66383
- disc and washer structure, RF props. 79—72170
- double focusing bending magnet, meas. of optical props. with thin alpha source 78—55073
- double-drift beam bunching systems 79—45495
- edge effect in beam monitor 77—88317
- eight-magnet spin precession snakes, survey for new configurations 80—91352
- electron beam deflection system for scanning microprobe 79—2878
- electron beam extracted from microtron, transportation system 77—65061
- electron beam injection, inflectorless system for betatron 78—825
- electron beam lithography, triple slit scheme for high current variable-shaped beam forming 80—68290

beam handling equipment continued
- electron beam production, by localised source in focused discharge 78—58093
- electron beams, in-line energy monitoring by C and graphite monofilaments 77—61159
- electron beams, intense, in ultrahigh vacuum, possible method of neutralisation 80—47145
- electron collimation system for use with electron cones of Varian Clinac 18 accelerator 78—11725
- electron gun system, pulsed, for use with superconducting accelerator and free-electron laser 80—68989
- electron injection system into collective accelerator model compressor 77—14277
- electron linac, 600 MeV, Saclay, 40000 hrs. of operation, recent improvements *(French)* 79—688
- electron linear accelerator prebuncher design calcs. 79—54624
- electron microscope, mag. energy filter, for error-free image, second order approx. *(German)* 77—191
- electron storage ring, Be windows for synchrotron radiation beam lines 79—68026
- electron storage ring, horizontal wiggler, modelling of effect on beam parameters 79—68029
- electron storage ring, vacuum control system for synchrotron radiation beam lines 79—68027
- electron storage ring VEPP-3, proposal to install supercond. wiggler magnet, synchrotron radiation prod. 78—62671
- electron test accelerator, computer control of beam transport system 78—25359
- electrostatic analyser, spherical, focusing using supplementary electrodes 77—9155
- electrostatic inflector and extractor for cyclic accelerators, HV expts. 78—50421
- electrostatic ion microprobe system 80—47144
- electrostatic lens, coaxial, hollow charged particle beam focusing appls. 77—82640
- electrostatic lenses, accelerating, decelerating heavy ion beams focusing 78—89588
- electrostatic lenses, cylindrical, optical characts. 78—8473
- electrostatic lenses, lens properties and computational techniques 79—44983
- electrostatic lenses for control of ion or electron beams 80—32897
- electrostatic mirror for heavy ion handling 77—18136
- electrostatic mirrors for heavy-ion manipulation and focusing 77—10520
- electrostatic particle guide, parameter anal. using radioactive recoil ions 78—33343
- electrostatic prism, electron optics for Auger spectrometer 79—29437
- electrostatic wire septums, leakage field 80—5423
- EN-tandem, foil stripper *(German)* 79—36437
- energy doubler dipole, sensitivity to beam induced quenches 79—68084
- energy doubler magnets, AC loss meas. 79—31277
- energy doubler magnets, production characts. 79—31276
- energy doubler magnets, recent meas. results 79—68087
- ESCAR, tests of superconducting bending magnets 79—76202
- ESCAR magnet cooling system 79—30485
- ESCAR superconducting fully cryogenic accelerator 77—83236
- Faraday double transmitting cup, ion optical control device 78—82556
- fast beam scraper, stepping motor control 79—71562
- fast electrostatic chopper of low power consumption 79—31284
- fast particle beam differential scatt. instrument 78—86381
- fast pneumatic transfer system for neutron activation anal., time and fluence meas. *(German, English)* 77—38576
- Fermilab, 100 GeV beam storage, improved chromaticity control 79—76187
- Fermilab, magnetisation effects in superconducting dipole magnets 77—83229
- Fermilab antiproton cooling ring, injection, magnet and vacuum systems 79—72139
- Fermilab Booster, design of additional extraction/injection area 79—72047
- Fermilab booster accelerator, mag. system modification, increased energy 77—83222
- Fermilab booster beam damping system, high-speed RF data transmitter 77—88296
- Fermilab Booster synchrotron, broadrange beam signal limiter 79—72082
- Fermilab booster synchrotron, transverse instability damping electronics 77—83318
- Fermilab Doubler warm Fe supercond. dipole, stress anal. 80—58012
- Fermilab energy doubler, supercond. magnets, mag. field meas. 79—31258
- Fermilab energy doubler correction magnets, construction 79—68042
- Fermilab energy doubler magnets, support design and cryostat system 79—31257
- Fermilab energy doubler/saver project, ring of superconducting mags., status report 77—83212
- Fermilab main accelerator quadrupole transistorised regulators 77—83243
- Fermilab main ring magnets, operational reliability 79—72044
- Fermilab neutrino focusing horn, 10 msec. 150 kA pulsed power supply 79—68092
- Fermilab neutrino focusing horn, pulse stretching in high current power supplies 77—83367
- Fermilab switchyard, superconducting dipole 79—76204
- ferrite ring, 2000 NN type, self-accel. caused by high-current electron beam interruption 80—4809
- ferromagnetic gates for ultracold neutrons 77—46440
- field reversing E-layers, translation and compression in magnetically insulated diode 80—14017
- filtered neutron beam facility, 2, 24 keV neutron beams prod., filter comps. and configs. 77—6597
- filtering of the six-dimensional phase volume of a beam in a linear ion accelerator 79—67994
- floating deck modulators for high voltage protection of ion beam accelerators 78—66392
- FMIT deuteron accelerator, proposed RF system 79—67981
- FMIT deuteron linac, Alvarez section geometry choice 79—72130
- focusing systems for intense beams, instabilities, electron model expt. 79—68066
- FODO struct., dispersion suppression with missing magnets, appl. to CERN antiproton accumulator 79—72162
- foil strippers, remote control system 78—29670

beam handling equipment continued
football coil, absolute minimum mag. field prod., heavy ion isochronous cyclotron synergic focusing 77—83364
Frascati linac, feasibility study of electron pulse stretcher to increase duty cycle 79—72135
free electron laser-electron storage ring system, basic characteristics and possible developments 79—68019
fusion expt., multimegawatt beam dump 77—83356
fusion reactor, ASDEX, neutral beam injection, beam line design 80—99395
fusion reactor, Doublet III beamline, review, component relation and config., design constraints 80—99382
fusion reactor, Doublet III beamline calorimeter, three dimens. heat transfer anal. 80—99381
fusion reactor, ISX-B, neutral beam system 80—99388
fusion reactor, MFTF, ion and neutral beams dumps, design 80—102317
fusion reactor, PDX, 6 MW Neutral Beam Project, overview 80—106223
fusion reactor, TFTR, high energy heat sink, ion beam dump and calorimeter 80—99394
fusion reactor, TFTR, neutral beam injector prototype, construction and performance 80—99390
fusion reactor, TFTR, neutral beam line final design 80—99309
fusion reactor, TFTR, neutral beam-torus connecting duct 80—99302
fusion reactor, TMX, injector system mech. design and installation 80—99393
fusion reactor 150 kV negative ion test stand, electronics system 78—54934
fusion reactor coil design, cost anal., for neutral beam magnets 78—55005
fusion reactor neutral beam injector, beam line studies 78—54969
fusion reactor neutral beam transport system 78—54968
fusion reactor PDX, ORNL prototype neutral beam injection system, ion source development 80—99391
fusion reactors, neutral beam design for plasma heating 80—13836
fusion reactors, TFTR neutral beam support system 80—102376
Gabor lenses, configurations and beam optical performance 79—68070
GANIL heavy ion accelerator facility, status report on injector, magnets and RF system 79—54630
GANIL heavy ion beam tuning by secondary emission multiwire chamber 79—54733
gas foil stripper system, Daresbury heavy ion Van de Graaff 79—67988
general purpose 1 GeV/c separated beam at Argonne ZGS, operation and design 77—10516
Giessen polarisation facility, multi-detector analysing system 77—65373
gradient septum magnet, effect of pole gradient 78—25369
Grenoble separated sector booster cyclotron, SARA, current machine status 79—54634
gyrocon, microwave oscillator for charged particle accel. 79—72176
Hanford FMIT linear accelerator, high energy beam transport 79—76159
harmonic beam interceptor, increased cyclotron beam intensity 77—381
Harwell, neutron diffractometers, spectrometers and ancillary equipment 79—45527
heavy ion beam buncher control system 79—72148
heavy ion facility for radiation therapy 77—86588
heavy ion generator, 150 keV, for sputtering 79—697
heavy ion implanter, 400 keV 80—31943
heavy-ion 300 kV accelerator design 77—75010
heavy-ion beam buncher for ion pulsing into tandem accelerator 79—31280
Heidelberg proton microprobe, for PIXE anal. of small, 4 μm^2, size samples 79—5239
helical electrostatic quadrupole, line charge system 78—25363
hexapole magnetic lens, for ultracold neutrons *(Russian)* 78—21273
HF magnetic chopper for polarised neutrons 77—14293
high current beams, accelerating structure with on-axis couplers 79—93862
high flux muon channel incorporating a high quality spectrometer field 79—72136
high power RF amplifiers, recent advances 79—68082
high-current electrostatic scanner-deflector 77—13820
HV generator for accelerator beam control 79—26797
Hyperon-1 supercond. magnet for high-energy physics expts. 79—31302
ILL HFR, Grenoble, fundamental phys. expts. with neutrons and ν, beam tubes, neutron guides, UCN and VCN sources 79—67932
intense low energy ion beam transportation, space charge blow up 79—44982
Intense Pulsed Neutron Source (IPNS-1) accelerator 500 MeV fast kickers 79—72131
Intense Pulsed Neutron Source (IPNS-1) accelerator RF system 79—67998
interferometric chopper for neutrons and X-rays 78—82088
ion beam alignment and energy meas. analyser 79—6781
ion beam dump, design and development 77—83441
ion beam stepping motor driven scanner 77—83416
ion beams, intense, production and postaccel. in magnetically insulated gaps 80—74041
ion implantation extractor accel plate, beam intensity optimisation 78—37103
ion implanter, semiconductor device processing 80—31944
ion pulse stacking for prod. of intense current pulses 80—23209
ion source electron beam modulator automatic control system 79—72173
ion source fission product separators 80—78479
ion source light link control system 79—68093
ion source with electron bombardment, power-supply block 78—8467
iris loaded waveguide relativistic electron beam interaction, electron energy distrib. space charge effects 78—46190
iris-loaded waveguide, inhomogeneous ferrite filled, autoacceleration 78—79441
ISABELLE, lattice status 79—76189
ISABELLE insertion quadrupoles 79—76197
ISABELLE magnet support and adjustment system 79—76198
ISABELLE ring magnets, design, construction, operational update 79—68088
ISABELLE storage ring magnets, mag. field meas. 79—68089
ISOLDE as a source of neutron-rich nuclei 80—78480
ISR absorber blocks for high intensity beams 79—68060
JET, extraction element design for long pulse multi-megawatt neutral beam 80—102373
K17 beamline for stopping kaons, Nimrod, design, construction, operation 77—3205

beam handling equipment continued
K=500 superconducting cyclotron, beam extraction system 79—54666
kaon intense low-momentum beam at Argonne ZGS, design and operation 77—10515
KEK, 750 keV beam line construction 77—38438
KEK, minicomputer assisted function generator for the dynamic control of chromaticity correction sextupoles 79—68009
KEK 12 GeV proton synchrotron, beam profile meas. 77—83404
KEK booster to main ring beam transfer system, construction operation 77—83264
KEK main ring, prototype multipole magnets, design, field uniformity 77—83220
KEK photon factory storage ring lattice, design principle 79—68033
KEK synchrotron, low energy kaon beam line characts. 79—72053
KVI cyclotron, dee voltage and beam RF phase stabilisation 79—54688
LAMPF biomedical channel, beam shaping section tuning 77—86591
LAMPF H^+ beam chopper 79—72158
LAMPF linac, Monitor remote-handling system, status, improvements and accomplishments 79—71997
LAMPF line D fast deflector system 77—38501
LAMPF line D fast kicker system, operating experience 79—72010
LAMPF particle separator 77—83388
LAMPF primary beam line protection system 79—72014
LAMPF stopped muon channel 79—68115
large area DC ion beam formation with multiple electron beams 80—305
laser polarimeter for $e^+ e^-$ beam polarisation meas. in storage ring 80—14019
lenses, electrostatic, focusing of GeV particle beams 80—74061
LEP storage ring, C-shaped laminated magnets, implication of low field levels 79—72051
LEP storage ring, control system design 79—72050
linac beam loss monitoring by long radiation detector 77—88310
linear accelerator, Unilac beam diagnostic system 77—38489
linear accelerators, plasma waveguides appl. as accelerating structures 80—9438
linear accelerators, recent progress and plans for heavy ion fusion 79—71992
linear high current ion accelerators utilising electron neutralisation 79—72016
liquid jet vacuum seal, inflow, rel. to electron beam emergence into atmosphere 80—78469
liquid ultrasonic meter for the intensity of pulsed beams of charged particles 79—68110
longitudinal feed back system, for PEP accelerating cavities 79—72144
Los Alamos Meson Physics Facility proton irradiation port 79—9935
low current DC beam line magnets, supercond. coil manufacturing method 77—82575
LSI-11 based auxiliary crate controller for beam line and experiment control 79—89565
magnet and cryostat design 79—31252
magnetic electron deflection system, high accuracy, shielding ferrite tube 80 102602
magnetic lens, wide-angle focusing device for low energy π collection 78—70664
magnetic optical achromat, second order, design 79—72161
magnetic spectrograph, fast resolution optimization 79—6792
magnetically isolated annular relativistic electron beam 78—78037
magnetostatic system of the collective electron ring accelerator 80—5407
magnets in the PEP injection lines 79—68103
Mainz 300 MeV linear accelerator, energy loss system of electron scatt. facility 78—58524
mass-separator beam, quadrupolar focusing lens system 80—47801
mechanical interrupter-monochromator with changeable rotors for slow neutron beam, 3 to 60 MeV 77—46442
MIMAS, low energy accumulator-injector for SATURNE, project description 79—71985
Mirror Fusion Test Facility, neutral beam injection, optimisation by computer graphics 78—66376
moderator, MgO coated, for slow positron beam prod. 79—17557
MP-Tandem at Munich, light link coupled current monitor 78—33311
multichannel focusing collimator, computation of efficiency distrib. functions 77—10519
multiple magnet test program, Fermilab 79—68085
multiple superconducting energy doubler accelerator magnets, series operation 77—83214
Munich MP tandem, beam optical components, anal. of misalignment effects 78—13355
muon beam channel, 40 GeV/c, Serpukhov, lens, guide reflector, filter 77—18729
MWPC for beam definition in precision total cross section meas. 79—3268
NAC cyclotron, proposed transfer beamline preliminary design 79—72061
nanosecond pulse generators, wave processes 77—18730
neutral atomic beam source, power supply system 78—66393
neutral beam high power injector cryopumps, design and performance, for fusion reactor 78—74494
neutral beam injection system, for TFTR 78—54971
neutral beam injection system cryopump, liq. He-cooled, for fusion reactor H_2 pumping 78—74495
neutral beam injection vac. components, for fusion reactor 78—74493
neutral beam injector, monoenergetic, power flow and gas flow models 78—66398
neutral beam injector for tandem mirror fusion reactor, delivering 1.2 MeV D atoms 79—22509
neutral beam injectors, electrostatic energy recovery system 78—66400
neutral beam injectors, for Princeton Large Torus, component design 78—54966
neutral beam injectors for mirror reactors, arc snubbers 78—13333
neutral beam line upgrade for laser initiated target expt. 78—13334
neutral beam lines, for Princeton Large Torus, development and testing 78—54967
neutral beam system, 120 keV, for fusion reactor ignition 78—66377
neutral beam system, for ignition Tokamak 78—54973
neutral beam system for TFTR Tokamak 78—13331
neutral beam test stand, 120 keV, computer based diagnostic and control system 78—66389
neutral beams, continuously operating, mech. design criteria 78—66380
neutral injection beam line, parameter studies, computer programme 78—66390

beam handling equipment continued
- neutral injection system, for JAERI experimental fusion reactor 78—54972
- neutrino beam focusing system, Protvino Inst. 78—37477
- neutrino channel monitoring system, acquisition of digital information 77—3199
- neutron 2 keV filtered beam facility 77—23346
- neutron curved monochromators, reflectivity data 79—45515
- neutron double monochromator for diffraction studies 78—1957
- neutron double monochromator with periodically bent single Si crystals 77—58927
- neutron energy spectra at intermediate energy, measuring apparatus 79—54738
- neutron guide tube, axial peaking of ultra cold neutrons 77—14295
- neutron guides for pulsed sources, geometry optimisation and simulation 80—47802
- neutron monochromator, curved Cu comb 80—63427
- neutron monochromator, development of Institut Laue Langevin 79—45514
- neutron monochromator, moving cryst., design and operation 77—74552
- neutron monoenergetic beams from sector focusing isochronous cyclotron 77—26917
- neutron multilayer monochromator-polariser *(Russian)* 80—27854
- neutron polarisation filter, cryogenic, construction 77—23341
- neutron polarising monochromator with Fe/Ge multilayers 77—19841
- neutron super mirrors, reflectivities calc. 79—45320
- neutron time of flight facility with mag. beam swinger, time, energy resolutions 77—57796
- neutrons, ultracold, zone mirrors for high resolution image form. 78—87003
- Nevis proton synchrocyclotron extraction system, design, operation 77—83265
- noncylindrical symmetric space-charge flow, Coriolis and centripetal accel. 78—91182
- normal incidence monochromator, 2m high throughput, for SURF II storage ring 80—90951
- nuclear filters, prep. from polymers using Ar ions 78—86714
- nuclear reaction-emitted charged particle mag. spectrograph, multi-ang. 80—5429
- nuclear studies with tagged photons 80—23245
- optimal magnetic multipole for Na beam polarisation 77—30684
- Orsay 200 MeV synchrocyclotron, machine parameters, beam handling and extraction, current status 79—54635
- Osaka RCNP 230 cm cyclotron, recent development and proposal for new ring accelerator 79—54632
- particle beams, monitoring at high frequencies 77—88316
- Pelletron, 14 UD, subnanosecond chopper buncher 78—33322
- PEP chopper magnet power supply system 79—76208
- PEP injection line, sensitivity to perturbations 79—72096
- PEP insertion quadrupole design features 79—68105
- PEP interaction region quadrupole magnets, meas. and corrections 79—68104
- PEP magnet power supply systems 77—83216
- permanent quadrupole magnets 77—38498
- PETRA storage ring control system, applications and future developments 79—72083
- PETRA storage ring control system, control console for man machine communication 79—72084
- PIGMI, linear pion generator, mechanical technologies 79—72008
- pion$^-$ radiotherapy, dynamic rangeshifter for modifying depth-dose distribs. 78—3595
- pion beam, hydraulic servomechanism for shifting range 77—83358
- PLT toroidal field coils, operational deflection meas. 78—62627
- polarised ion sources and low energy collector rings, H$^-$, D$^-$ beams 78—58515
- polarised proton beams, higher energy, conf., Ann Arbor, MI, USA, Oct. 1977 78—58514
- polarising neutron guide using laminated mirror 78—9012
- polarising Soller guides for cold neutrons 78—54501
- position stabilisation system for electron storage ring 79—68079
- pressure measurement system for beam expts., 0.5-10^{-2} Pa 79—88971
- profile monitor providing multiple profile during beam spill, Fermilab 77—57784
- proton, non-destructive bunch length monitor 77—376
- proton accelerator, target and collimator precision position control and monitoring via CAMAC 77—67927
- proton accelerator beam scraper, photon dose rate calc. 80—99367
- proton beam diffusing system for PIXE analysis 79—85848
- proton beams, scattered, intensity distrib. monitor 80—74062
- proton microbeam scanner facility for trace element anal. in biological samples by p induced X-ray fluoresc. 79—5431
- proton microprobe, feasibility study and design 79—54226
- proton radiography beam line establishment at Fermi National Accelerator Laboratory 78—65121
- pulse selection and shortening system for cyclotrons 79—54690
- pulsed electron gun systems, 1 ns pulse width 79—67977
- pulsed plasma injector, for intense mol. beam prod. 77—65548
- pulsed RF systems for large storage rings 79—72141
- pulsed septum magnet for extraction from Fermilab booster synchrotron 77—83219
- quadrupole —1 system with aberration correction octupoles 79—68068
- quadrupole gradient-length product meas. device 79—76232
- quadrupole mass filter, adaptor unit for secondary ion anal. *(German)* 79—75650
- quadrupole triplet, electrostatic, for 10 mA MeV ion beam focusing, construction and performance details 79—3621
- radiotherapy, design principles of telecobalt collimators 78—15888
- rapid cycling synchrotron magnet with separate AC and DC circuits 79—68101
- RCNP AVF cyclotron, outline of RF system and latest developments 79—54686
- recoil deuteron polarimeter for polarised ^{3}He beam 77—34529
- recuperator, with deep stopping of electron beam 77—65562
- reflex triode, unidirectional ion generation and geometric focusing 79—76235
- remote handling equipment, LAMPF 77—83389
- RF contact for superconducting cavities 80—63429
- RF deflector, HV, reduction of cyclotron beam repetition rates 77—57789
- RF ion beam choppers, ion motion *(Chinese)* 80—99371
- RF quadrupole beam dynamics 79—71986

beam handling equipment continued
- RF separated hadron beams to BEBC, on-line control system 77—38530
- RF separators, review 77—13821
- RF superconducting resonators for booster linac 79—54623
- ring-type state selector and space focuser for mols. with positive induced dipole moment, appl. to mol. beam maser 78—54503
- S.African National Accelerator Centre, accessory design, current status 79—54631
- Saturne II, beam liner computerised control system, organisation, function, hardware 77—83400
- Saturne II, secondary emission detector system for beam profile monitoring 77—83402
- scan-forming unit for controlling coupled beams from an electron-beam probing device 80—52366
- scanning microprobe, digitally controlled for p and heavy ions 79—13571
- scanning system, automatic computer-controlled, for merged beams expts. 77—13818
- scanning systems, electrostatic 80—31939
- scintillation hodoscope counter for beam meas. in CERN SPS 79—36472
- SCR-type magnet power supplies, subharmonic ripple reduction 79—68094
- secondary beam profile monitor based on MWPC 79—6783
- secondary electron imaging system for a nuclear microprobe 79—26799
- septum magnet, new design Ar beam injection/extraction in ultra-high vacuum system 79—68095
- series III high current industrial ion implanter, performance 80—31941
- SIN, pion beam line πE3 modifications 80—74054
- SIN π-channel and spectrometer, technical aspects of pion scatt. facility 79—13574
- SIN high resolution pion channel and spectrometer 79—22517
- SIN injector cyclotron, RF system improvements 78—90005
- single wavelength standard wiggler, for 4-18 GeV PEP storage ring 79—68080
- single-cavity double-frequency buncher 79—68076
- SIRIUS facility for neutron rich fission fragment studies 80—78484
- SLAC, beam containment electronics operational experience 77—83466
- SLAC, microwave developments, beam-test results 77—83405
- SLAC beam, feedback system for steering and energy correction in beam switchyard 79—93852
- slit nozzle, for cluster beam generation with strong flux intensity *(Japanese)* 80—52361
- slow neutrons, superconducting mag. storage ring 79—59293
- soft X-ray microscopy/lithography branch line at SSRL 80—91344
- Soller collimators, appl. to small angle neutron scatt., Monte-Carlo simulation 78—29701
- space charge lens development, electrode geometries and current status 79—68071
- space charge lens for high current ion beams 78—55075
- SPEAR, synchrotron radiation beam ports, installation and thermal design 79—68034
- SPEAR storage ring, initial operation of mag. wiggler 79—68025
- SPEAR transport line toroids, intensity monitors calib. system 77—88295
- spin flipper with prolonged working area for non-monochromatic neutron beams 80—37673
- spin precessor for polarised proton beam prod. 79—68097
- SPS beam instrumentation, closed orbit correction 77—83305
- SPS magnet system, nonlinear fields and their compensation 77—83268
- stochastic beam cooling, slot type pick-up and kicker 78—33332
- storage rings, free electron laser amplifier operation 79—68399
- storage rings, ISABELLE, superconducting dipole prototypes, operational parameters 77—83215
- stressed parabolic magnetic lens, thermal effects 79—27151
- stripper foils, energy straggling of heavy ion beams at tandem energies, C foil appl. 78—33353
- stripper foils for electrostatic accelerator, new mounting method 78—33355
- stripping foil design from electron loss cross section for H$^-$ on C 79—67976
- stripping foils for multiturn charge exchange injection into the Fermilab booster 79—68099
- strong rare earth cobalt quadrupoles, general props. and configurations 79—68083
- subnanosecond chopper-buncher system for heavy ions 79—72159
- superconducting accelerating cavities for high energy e$^+$e$^-$ storage ring, DORIS appl. 79—72140
- superconducting accelerating cavities for high-energy e$^+$e$^-$ storage rings 79—97924
- superconducting accelerator and beam-line mags., mech. and thermal stresses 77—83362
- superconducting accelerator magnets, magnetization effects on field shape 79—31253
- superconducting accelerator struct., performance figures 79—68078
- superconducting beam line magnets, fast energy dump 79—68091
- superconducting bending magnets, 10.8 T.m, design and construction 78—82559
- superconducting bending magnets, large aperture design for Brookhaven AGS 77—26910
- superconducting coil for beam transport dipole magnet 79—31256
- superconducting dipole magnet models of combined type 79—31301
- superconducting dipole magnets, stress and strain distrib. 79—31250
- superconducting dipole magnets for CERN beam line 79—31294
- superconducting dipole models for accelerator-storage ring complex 79—31259
- superconducting dipole ultra stable window frame magnet 77—83235
- superconducting dipole window-frame type high precision magnets at BNL 77—83228
- superconducting dipoles, 2.5 T window-frame type, for small synchrotrons 79—54224
- superconducting heavy ion cyclotron, Chalk River, movable steel trim rods, orbit dynamics 77—83267
- superconducting heavy-ion cyclotron at Chalk River, extraction system, design 77—83266
- superconducting hexapole magnet construction and design 79—30503
- superconducting magnet energy doubler central liquefier 77—82530
- superconducting magnets, aperture limitation due to coil block errors 77—386
- superconducting magnets, high-energy physics appl. 80—68990
- superconducting magnets, pulsed and DC types, appl. *(German)* 78—21834
- superconducting magnets in synchrotron, quench thresholds after proton beam exposure 79—31254

beam handling equipment continued
superconducting quadrupoles used in CERN hyperon-beam, cryogenic design and performance 79—54220
superconducting RF particle separator, negative 16 to 37 GeV beam, results 78—89589
superconducting RF separator at CERN 79—81113
superconducting solenoid field magnet for large polarised target, 2.6 T field 79—54221
superconducting solenoid for intense meson beam channel *(Czech)* 77—38527
superconducting solenoid SUPER-SOLO, switch and cryostat, for heavy ion source 79—54222
superconducting warm Fe dipoles, stress anal. 79—68041
superconducting wiggler magnet, 5T design for dedicated synchrotron radiation source at Daresbury 78—62672
SURF II, 250 MeV storage ring for UV synchrotron radiation, progress report 79—68032
synchronisation of neutron beam, ultracold neutron spectrometer 79—721
synchrophasotron, system for meas. spatial characteristics of extracted beam 79—26793
synchrotron miniature pulse deflector construction 78—82545
synchrotron radiation, expt. enclosures and beam line safety components 80—91341
synchrotron secondary emission chamber, stability tests in high flux photon beams 79—72077
tanked tube for open air accelerators 80—99356
targets for energetic ion beams, design 79—54218
TFTR neutral beam injector, calorimeter and beam dump design 78—66382
TFTR type neutral beam system, ion accelerator design and fabrication 78—66381
thermal neutron non adiabatic spin flippers 78—70668
thermal neutron traps for nuclear pumped laser 80—64041
thermomagnetic gates for ultracold neutrons, accumulation in closed vessels 80—87005
thyristor modulator with periodically interrupted supply, microtron appl. 78—55061
TNS fusion reactors, negative-ion neutral-beam system design for plasma heating 80—13837
Tokamak Fusion Test Reactor neutron collimator design 79—9876
toroid monitors, beam charge meas. at Bates Linac 80—14026
Torus accelerator, transport of high current relativistic electron beams in large vols. *(Russian)* 78—82544
transformer septum magnet for intense pulsed neutron source 79—68102
transport of low energy divergent H_2 beam at 300 eV by permanent magnets 80—69001
transport systems with optically axisymmetric transfer props., comments 77—79495
travelling wave kicker magnets with sharp rise and less overshoot 79—68057
triple focusing mass separator using Wien filter 78—45748
triple-focusing magnet for the collection of nuclear recoils 80—102363
trirotron, RF vacuum tube amplifier, electron accel. appl. 79—68086
TRISTAN II mass separator, ion source, beam optics, computer system 80—78481
TRISTAN II mass separator at Brookhaven HFBR, research programme for fission products 80—78482
twinned neutron monochromator 78—840
UHF klystron, high efficiency, high power, performance at SLAC PEP storage ring 77—83296
UHV beam line at SSRL for spectral range 4-4000 eV, monochromatised radiation 78—62673
ultra-cold neutrons, transporting apparatus for storage in pulsed reactor *(Russian)* 77—3204
ultracold neutron beams from ultracold neutron gas 77—26913
ultracold neutrons, multilayer ferromag. shutter 80—91354
undulator design for ACO storage ring 80—91334
undulator for the 700 MeV VUV-Ring of the National Synchrotron Light Source 80—91337
undulators, quasi monochromatic synchrotron radiation, spectra for strong and weak fields 78—63000
Unilac injector for stable elements 77—34481
University of Liege beam-foil facility, computer controlled system 79—45866
unslowed fission product separators, gas filled JOSEF, parabola LOHENGRIN 80—78478
UV beamlines for National Synchrotron Light Source 80—91342
VICKSI beam line instrumentation and control system 77—83401
VUV beam line instrumentation for National Synchrotron Light Source storage ring 80—91343
water trap, polarised-neutron beam shut-off 80—87004
Wendelstein VII-A, neutral beam injectors, performance 80—99389
Wien filter, inhomogeneous field, theory and expt. of ion optics 79—45510
wiggler magnet, Adone, status report 79—68081
wiggler magnets, standard, effects on synchrotron radiation spectrum and storage ring operation 78—62670
wiggler magnets, use as synchrotron radiation source at SPEAR storage ring 80—91332
wigglers, conference on synchrotron radiation instrumentation, Orsay, France (Sept. 1977) 78—62999
wigglers and undulators, interaction with stored electron beam 80—91331
X-ray monochromator development for synchrotron radiation facilities 80—91351
X-ray synchrotron source, design status 79—68024
ZGS, low level beam diagnostics for polarised proton operation 77—83311
ZGS beam transport for transverse and longitudinally polarised protons 78—55074
zoom lens quadrupole magnets for Colorado Univ. energy-loss spectrograph 77—83410
B fibre/Al laminates, use in neutron collimators 79—45506
C foils, stripping of heavy ions with energy 0.4-0.9 MeV/A, straggling, foil behaviour 78—33351
C stripper foil irradiation lifetime, preparation by hydrocarbon cracking 79—76249
C stripper foils, ethylene cracking in glow discharge, irradiation lifetimes 80—23207
C stripper foils, lifetime enhancement, heavy ion bombardment 78—94156
C stripper foils, tests with 4.8 MeV Ar ions 79—76240
C stripper foils for heavy ions, preparation method 79—22516
C, stripper foils under 4.8 MeV Ar^{++} ion bombardment, shrinkage, rupture, lifetime 78—33352
C thin foil breakage times under Ar^+ bombardment 78—25753
Cu-Ge neutron monochromator 78—71643
D beam, polarised, short compression magnet for intensity increase 80—18732
Fe analysing magnet, fast precise field control 79—45883
Fe beam stop for 500 MeV protons, secondary flux, beam intensity meas. 79—85850
Fe lenses for muon beam transport 77—30685
Fe/Ge multilayer neutron polarizing monochromator 79—45513
H^- beam 90° bending magnet, pole face configuration study 79—68090
H^- multiturn charge exchange injection system for Fermilab Booster accelerator 79—67971
H^- polarised beam production by 800 MeV spin precessor 79—68096
He-jet chopper for meas. half-lives of short-lived nuclei 77—38532
MgO scintillator prep. for viewing accelerator beam spots 79—6803
Mo, extraction grid for high power ion source 80—102372
Nb_3Sn multifilamentary dipole magnets, supercond. props., 4.2 to 15K 79—31275
O_2 filtered neutron beam of 2.35 MeV 80—27848
^{32}S 96 MeV heavy ion ps pulses, rebunching of MP Tandem pulses by spiral resonator 78—33357
Si:As ion implanter system, high current, architecture and control 80—31942

beam handling techniques
see also mass spectroscopy; particle beam diagnostics; particle optics
40 kV multimegawatt neutral beam line, power flow and ion source 79—76238
β-ray interference elimination by mag. deflection, for X-ray meas. following neutron activation 78—74101
accelerated electron cluster in synchrotron, rot. disc, method investig. of synchrotron radiation 79—3264
AGS slow extracted beam, size meas. 80—37672
Amsterdam 500 MeV high duty factor electron scatt. facility, status report 80—23191
anastigmatic electron deflection system between beam-shaping lens and probe target 79—27155
ANL ZGSynchrotron, high energy polarised deuteron beams 79—72054
atomic beam, focused with laser beam, Na beam and dipole forces 79—7066
atomic beam cooling, manipulation and trapping by CW reson. radiation 78—45751
atomic/molecular beam interrogation in Ramsey cavity, two freq. separated oscillating fields technique 78—89596
ballistic focusing of intense neutralised beam in pinched electron beam diode 78—9859
beam handling and detection system matching for optimum resolution in nucl. physics 79—45504
beam line magnet misalignment effects 77—30688
beam loss in initial acceleration in KEK booster 79—76182
beam matching problems, improved analytic starting points 79—72163
beam transfer from AGS to ISABELLE, momentum stacking method 79—76188
bending magnet for energy doubler, prototype test 77—83366
bending of high energy beams using axial and planar channeling 80—88225
Berkeley 88 inch cyclotron, systematics in the control settings, beam parameter prediction 78—78526
beta particles deflection by magnetic field, radioisotope thickness gauge appl. 77—79054
betatron, electron beam rapid extraction by parametric reson., analogue computer anal. 77—18731
betatron oscillation reduction, low-noise wide-band power amplifier system 80—58011
BEVALAC, high purity radioactive beam prod. 79—72129
bit-slice microprocessor appl. 79—89566
Bonn isochronous cyclotron, external ion sources, inject lines, description 79—54675
bunch recombination, CERN proton synchrotron booster rings 79—76192
bunched beams, transport, second order aberrations 80—52801
bunching in cyclic focusing channel 80—23229
centrifugal electrostatic shaping of high intensity electron beams 80—13183
ceramic vac. chamber, bunched beam EM field penetration 77—83368
CERN ISR, at 31.4 GeV, phase displacement acceleration, operating techniques and beam diagnostics 79—68003
CERN ISR control scheme for acceleration by phase displacement 79—72213
CERN proton synchrotron, automatic procedures 79—72074
CERN PS, collective phenomena at very high intensity 79—76193
CERN PS, computer controlled beam local radial perturbation and rotation 79—72072
charge transfer cross sections in high-flux, low-energy accelerators 79—30609
charged particle beam focusing, collimation and deflection 80—48132
charged particle beam focussing by cryst. film for colliding beam expt. *(Russian)* 79—67426
charged particle beams, 2-dim., invariance of order of focusing 79—94140
charged particle beams, energy spread reduction, laser pulse technique 80—87279
charged particle trajectory steering by a bent Si crystal 80—32557
Cherenkov radiation focusing, electric piston effect, appls. 79—55041
chromaticity correction in KEK main ring 80—74049
circular beam tube, longitudinal coupling impedance of step discontinuities 79—72115
cluster beam generation of strong flux intensity using a slit nozzle *(Japanese)* 80—52361
coasting particle beam, RF fields due to Schottky noise 77—88632
collective acceleration, relativistic stabilised electron beam in toroidal geometry 80—5401
collective acceleration of heavy ions, problems and prospects 80—14013
collective accelerators, autoacceleration process for generation of high current relativistic electron beams 80—14011
collective accelerators, autoaccelerator dynamics and stability 80—14012

beam handling techniques continued
  collective accelerators, ion burst accel. and prefocusing using rel. electron beam interactions 80—14008
  collective focusing ion accelerator based on HIPAC concept 80—14014
  collective ion acceleration, dielectric guide controlled rel. electron beam propag. 80—14001
  collective ion acceleration, relativistic electron beam interaction with apertured solid dielec. anode 80—14007
  collective ion acceleration and intense electron beam propagation within an evacuated dielectric guide 80—14002
  collective ion acceleration and intense electron beam propag. in vacuum dielectric channels 80—14003
  collective ion acceleration in diode with insulated anode 80—14005
  collective ion acceleration using space charge waves on electron beams 80—13995
  collective ionisation front accelerator using intense relativistic electron beam, experimental feasibility program 80—13998
  collective linear acceleration of ions 80—5402
  collective methods of acceleration, conference, Irvine, CA, USA (May 1978) 80—4479
  collective-effect electron acceleration 80—14016
  colliding beam arrangement using laser linac, feasibility study, laser accelerator problems 78—78521
  combined fixed freq. and freq. modulated cyclotron, mag. field design 79—54726
  compensated ion beams, handling and expts. *(Russian)* 79—46461
  conference, ion implantation equipment, Povo-Trento, Italy (Aug., 1978) 80—31413
  conference on particle accelerator engineering and technology, San Francisco, USA (Mar. 79) 79—67979
  cooling by electrons, expts. on proton beam 77—23334
  Cornell electron ring, high resolution digital time base 79—76215
  coupled Marx-Tesla circuit for production of intense relativistic electron beams 79—17558
  coupling resonance $2\nu_H$-$2\nu_V$, in KEK proton synchrotron 79—76185
  crossing of depolarization resonances in strongly modulated structures 79—72057
  cyclotron, TRIUMF, beam props. improvements 77—83397
  cyclotron acceleration process and its influence on beam quality, theory 80—74051
  cyclotron beam automatic centring and matching 79—54708
  cyclotron resonance, Doppler effect, anomalous, amplification of slow waves in electron beam, obs. 80—78463
  cylindrical diode for charged particle beam generation and focusing 77—67532
  cylindrical-mirror electrostatic analyser for beta spectroscopy of beams 80—63446
  DCI storage rings, status report, space charge compensation, and 3- and 4-beam behaviour 79—76190
  decay proton-storage, for neutron lifetime expts. 79—58959
  Dee, bevelled, for beam centering in AVF cyclotron 80—63428
  deflecting magnet for external beam of 150 keV accelerator, influence of magnetic fringing field 78—46195
  delayed coincidence techniques with accelerator beams, anal., optimisation rules 78—78598
  delivery of single accelerated particles 79—703
  depolarisation during acceleration and storage of polarised protons and deuterons 78—58519
  doubly-ionised beams, nucl. backscatt. anal. of energy and ion impurities 77—75017
  duopigatron, preacceleration effects on ion beam transmission effects 78—87005
  E×B filter with improved velocity-separating capability, design 77—41728
  effusive beam source, heterogeneous reaction type, chem. equilib. 80—52362
  Eindhoven AVG cyclotron, on-line determ. of acceptances and emittances of beam guiding system 77—38515
  electron and positron depolarisation suppression in storage rings and cyclic accelerators 80—42882
  electron beam, 400 keV; spot radius and beam divergence 80—877
  electron beam, high υ/γ, magnetic compression and electrostatic refl. 77—83398
  electron beam, intense, ns, production in linear accelerator, space charge and radiation field effects 78—70654
  electron beam, nonrelativistic, injection into drift space 79—895
  electron beam, relativistic, focusing limitations in low-press. gas 79—41322
  electron beam guiding system including automatic capture circuitry 80—99005
  electron beam in microtron, orbit correction scheme 77—65366
  electron beam polarisation in storage ring by laser beam interaction 79—93860
  electron beam propag., Z-pinch plasma 77—87874
  electron beam self-acceleration expts., regulation of magnetization of ferrite 80—63425
  electron beam shaping by multichannel gate voltage selection 79—50204
  electron beam trasnport for inertial fusion, high current density generation 77—67870
  electron beams, intense, ion focusing and mag. self-focusing 78—331
  electron beams, point focusing through different vacuum lines 79—45499
  electron beams, relativistic, intense, guiding with axial mag. field 80—87006
  electron bremsstrahlung on thin diamond monocrystals, polarisation *(Russian)* 77—6603
  electron bunch energy losses, along circular waveguide with periodically perturbed wall 79—76564
  electron cooling and new possibilities in elementary particle physics, review 79—68118
  electron cooling of beams in heavy particle storage rings, kinetics 77—67922
  electron cooling of proton beam in storage ring 77—14281
  electron cooling of protons at CERN 80—9443
  electron cooling with magnetic field 80—58013
  electron diffraction by gases, use of rotating sector for electron intensities obs. 77—55214
  electron image deflection system, crossed elec. and mag. field, intensity modulation 78—89592
  electron linac, reduction in energy spread of nanosec. relativistic beam 80—5397
  electron linear accelerator prebuncher design calcs. 79—54624

beam handling techniques continued
  electron polarisation by circularly polarised EM waves in storage ring 80—14020
  electron polarisation by radiative separation in inhomogeneous mag. field practicality 78—82076
  electron probe forming systems, optimisation with respect to aberrations and vertical beam landing 80—68291
  electron ring accelerator, nonneutral electron layer trapping 80—5409
  electron ring formation and trapping, using resistive walls and static mirror coils 78—45752
  electron-ion ring, stationary state 80—106217
  electronic collimation of neutrons using Ge(Li) detector, for $(n,n'\gamma)$ cross section meas. 77—6591
  electronic cooling, developments *(Russian)* 78—86712
  electrons in synchrotron, beam lifetime increase using pulsed mag. field 79—3265
  electrostatic accelerators, beam transmission problems during design, operation, upgrading 78—33320
  electrostatic lens, for acceleration and deceleration of high intensity ion beams 78—89595
  electrostatic mirror, ion beam focusing for low energy heavy ion accelerator 77—14654
  electrostatic quadrupole focusing of heavy ions in low beta linac 79—72005
  electrostatically focused ions, spherical potential profile, meas. 80—64762
  elliptical beam inside non-confocal elliptic vacuum chamber, potential 80—47799
  EM fields in resonance systems used in charged-particle accelerators 80—37641
  energy distribution control technique for proton synchrotron 79—72128
  energy loss of charged particles, review 79—95060
  energy monochromation of relativistic proton beam using laser 78—90010
  energy resolution improvements in scatt. expts. using highly divergent accelerator beams 77—384
  energy spread, cancellation by current loading 78—9007
  fast ion beam contamination, gas neutraliser design 78—25368
  fast neutron filter of liquid O_2, effect of antiresonance of 2.37 MeV beam prod. 77—79494
  fast resonant extraction from CERN SPS 79—72137
  Fermilab, beam intensity and efficiency display system 79—72218
  Fermilab, high energy electron cooling 79—72090
  Fermilab antiproton cooling ring, initial operation 79—68004
  Fermilab booster beam, longitudinal dipole oscills., effects, damping 77—83259
  Fermilab booster main ring beam transfer phase lock cct. 79—72073
  Fermilab electron cooling expt., design and construction of electron beam 79—72138
  field emitter electron beam exposure system for semiconductor fabrication 79—30624
  filamentation instability of electron and positron colliding beams in storage rings 80—872
  fission product ionisation by He jet rapid transport technique 79—63831
  fluorocarbon stripping of low beta heavy ions 79—72168
  fusion by particle beam, laser beam with retractable focus, ionis. path form. in gases 79—18992
  fusion reactor, TMX, neutral beam control systems 80—99323
  GANIL, beam stripper interaction studies 79—54721
  gas stripping, charge changing cross sections for heavy ions at 8.5 MeV/amu 79—68073
  gas-jet recoil transport system for short-lived spallation and fission reactions 77—23338
  general orbit theory for accelerated particles in cyclotrons, appl. to synchrocyclotrons and omegatrons 80—74052
  gyrocon, computer modeling, electron eqns. of motion, beam losses 79—68100
  heavy ion beam prod., ionisation 78—843
  heavy ion beam source, high charge and intensity beam prod. 79—12884
  heavy ion beams, transport of intense bursts 77—83352
  heavy ion focusing system with large number of magnets, optimisation method 79—68074
  heavy ions, pellet fusion 77—83354
  heavy particle beam, electron cooling, magnetisation effects *(Russian)* 78—70219
  heavy particle beam, electron cooling 77—71713
  heavy particle beam cooling in an electron flux, mag. field effects 78—82557
  heavy-ion intense beam, periodic focusing, mag. channels 78—55079
  helical electron beam shaping using synthesis of axially symmetrical systems 80—309
  helix resonators, supercond., elec. freq. control 79—72169
  HEPI accelerator, active filter of annular electromagnet 78—33338
  HFEF/N, handling equipment for neutron radiography facility 79—45443
  high current vacuum diode, breakdown, electron beam prod. 77—82641
  high energy deposition from pulsed electron beams 78—54500
  hollow cathode discharge, with quadrupole mass filter, ion form. and handling 79—12878
  hollow-beam accelerator, with phase focusing, limiting current 79—18065
  inertial confinement fusion, generation, focusing and transport of light ion and electron beams 80—5323
  intense negative ion beams from N_2 cluster ions, size specification 78—87006
  intense neutral beam, species composition meas. method 80—308
  intense particle beams, production and handling 79—76117
  intense transported ion beams, stability of K-V distrib. 79—76224
  ion acceleration, by electron beam, in gas-filled waveguide, in mag. field, theory 78—9316
  ion acceleration by rotation and scanning of electron beam 77—593
  ion beam, intense, adiabatic wall focusing for thermonuclear microexplosion ignition 77—61611
  ion beam, overneutralisation, by electrons in mag. field 79—10256
  ion beam accelerator, multimegawatt, high-voltage power system, design philosophy, for fusion reactor 78—62613
  ion beam current stabilisation 77—79491
  ion beam deviation, plasma boundary neutralisation surface depend. *(Russian)* 78—59613
  ion beam focusing and acceleration by high electron currents in betatron *(Russian)* 77—6601
  ion beam focusing from quadrupole mass filter using electrostatic lens 79—229

beam handling techniques continued
ion beam focusing in intense mag. insulated ion diode, particle diagnostics 78—9858
ion beam image transformation using magnetic quadrupole lenses 78—55071
ion beam in vacuum system, rel. to atomic collisions in solids, review 80—54290
ion beam intensity measurement, noninterceptive method *(German)* 77—387
ion beam material characterisation, conf., Aleria, Corsica (Sept. 1976) 79—96403
ion beam production and manipulation, general considerations 79—93256
ion beam steering by aperture displacement for tetrode accelerating structure 78—82075
ion beamlet steering by aperture displacement in 2-stage accelerator, experimental study 80—68998
ion beamlet steering by aperture displacement in ion sources with large acceleration-deceleration ratio 80—63430
ion beams, divergence, effect of preacceleration voltage 78—66743
ion beams, factors affecting shape and quality 77—19160
ion beams for pellet fusion, focusing and prod. 77—83353
ion imaging for ion implantation and micromachining *(French)* 80—34027
ion implantation system, high current, design of end station, appl. to Si:As, ion implantation system, high current, design of end station 80—34030
ion source, accelerator system computer solns. 77—88309
ion transport in linear accelerators by electron neutralisation 80—58014
ionic motion, 3-D quadrupole electric field, charge exchange collisions 78—9315
IPCR separated sector cyclotron, injection 79—54614
isochronous cyclotron, energy variation, microcomputer control 79—13565
ISR, CERN, stochastic cooling of vertical betatron oscills. 77—83373
ISR, stochastic cooling in initial cooling expt. 79—72089
ISR at CERN, beam stability, coupling impedance, meas. by RF excitation 77—83269
ISR at CERN, high luminosity operation, 26 GeV/c proton beams, loss rates, background control 77—83276
ISX-B neutral beam injector expt. on prototype beam line 80—74039
jet target intense neutron source 78—66384
KEK beam line magnets control by CAMAC serial highway 79—68007
KEK proton synchrotron, closed orbit control system for main ring 79—68008
KEK proton synchrotron, synchronous beam transfer from booster to main ring 77—83263
KEK-PS main ring, slow beam extraction schemes 79—72046
Kiev 240 cm cyclotron facility, present status and accelerated beam characts. 79—54628
Kiev isochronous cyclotron, beam extraction and transportation 79—54717
LAMPF, secondary beam line phase space meas. and modelling 79—72157
LAMPF line-D fast deflector system 77—83157
laser accelerator, phase-adjusted focusing 80—63434
laser pumped ring accelerator, particle focusing with rectified light 80—42879
laser-plasma ion source for ion implantation in solids 80—78474
LEP storage ring, polarised $e^{\pm}$ beams, Siberian Snake scheme 79—63827
linac, pion generator for medical applications, beam dynamics 77—38475
linac injection system beam dynamics, computer simulation 80—13989
linear electron accelerator, efficiency of calorimetric method 79—6778
low energy ion beams, conference, Salford, Sept. 1977 78—66444
luminosity optimisation for e-p collisions 79—76230
magnetic focusing of proton beams by single dipole coil 79—40642
magnetic insulation wave, propag. in vacuum coaxial line 79—27144
magnetoelectrostatic traps, charged particle injection *(Russian)* 78—37102
mass dependent molecular beam focusing by cross-jet deflection 79—93257
mass filter performance, quadrupolar field distortion effects 79—35887
mass separator, with 3-parameter focusing, plasma optical model 78—9855
mass spectrometer molecular beam mass spectrometer, sampling nozzle, gas dynamics 79—49330
mechanical scanning, applic. to ion implantation 80—31940
MEIRA isotope separator, deflection radius and operational characteristics 77—19161
metal neutral beams, low energy (0.1 to 10 eV) prod. by laser vaporisation of metals 80—77910
microwave deflector for cryogenic phase selector of electrons 80—27845
misaligned beam transport elements, ion beam optics, IONBEAM program 77—65564
mitigation of residual space charge ion optics effects in gas cell by adjustment of beam perveance 78—74105
molecular and atomic beams, vel., intensity and particle density, using mass spectrometer 79—67428
molecular beam, discharge characteristics from multichannel nozzle *(French)* 79—30603
molecular beam, electrostatic space focusing 80—28118
molecular beam, in inhomogeneous mag. field, electron impact detect. 77—6963
molecular beam, modulated, detect. by electron bombard. detect. 79—2885
molecular beams, sources, gasdynamic, use of lasers, time-of-flight and detection techniques 80—69264
MSU K=800 superconducting cyclotron, injection studies 79—54616
multimegawatt neutral beams for Tokamaks, review 79—76234
multiple scatt. displacement reduction by parallel mag. field 79—81110
multiple scatt. of particle beams, axial mag. field effect 78—70712
muon channel, axisymmetric high flux 79—54727
muon low momentum surface beam for LAMPF 78—70672
muonic beam, polarised, variable helicity, for parity nonconservation studies 77—6598
Na atomic beam focusing and defocusing using reson. radiation press. 80—47143
NAP-M, meas. of momentum cooling rates with electron cooling 79—72095
NAP-M proton storage ring, equilib. beam orbit meas. 78—831
NBS positron annihilation in flight facility, positron beam calibration 79—31306

beam handling techniques continued
negative ion based neutral systems, generation, handling and acceleration 79—44981
negative ion beam, generation, transport and accel., fusion reactor appl. 78—66378
negative ion beam in gas, space-charge neutralisation 79—55048
neutral beam, increased divergence due to transverse mag. field 80—95494
neutral beam divergence due to imperfect mag. shielding 80—91349
neutral beam generation, negative ion revolving multiple beam instabilities *(French)* 80—47798
neutral beam injectors, continuously operated, grid convective He cooling 79—81083
neutral beam injectors, multi-aperture extraction systems 80—42301
neutral beam injectors, spectroscopic diagnostics, on-line data acquisition, anal. 77—82643
neutral beam line for plasma heating, stray particle loss near deflection magnet 80—47794
neutral beam proximity operation of cryopump, meas. relating to safety, pumping speed and radiation outgassing 79—88968
neutral beam systems, computerised, development and operation 79—93849
neutral particle beam, controlled energy distrib., prod. method 78—78038
neutralizer gas evolution due to beam interaction, coupled nonlinear Euler level equations 80—47800
neutrino, beam channel characts., Protvino Inst. 78—37474
neutrino beam, monitoring systems, at the Protvino Institute of High-energy physics 79—9929
neutron, effects of imperfect beam modulation using mechanical correlation choppers 77—57798
neutron beam, 25 keV, filtering technique 77—23348
neutron beams at NBS reactor, prod. for calibration standards using reson. scatt. and filters 77—38539
neutron depolarisation meas., exptl. set up and process program 80—18771
neutron electric dipole moment, expt. determ. of non-zero value employing ultra cold neutron storage methods 79—58963
neutron filtered beams, 2 keV, 24 keV, 144 keV, calibration and use 79—9937
neutron guide tubes, effect of sharp bend on transmission 77—385
neutron guides for pulsed sources, geometry optimisation and simulation 80—47802
neutron polarised beam prod. using ferromag. doubly bent neutron guide *(Russian)* 77—46446
neutron rich nuclei, beta decay half lives, expt. techniques 80—78224
neutron spin echo, matrix anal. 78—86715
neutrons, dead time distortions in reverse Fourier TOF spectrometry 79—6789
neutrons, longwave, monochromatic intense beam, prod. by polycryst. scatterers in open tangential reactor channel 77—71712
neutrons, polarised, mass determ. method 79—59294
non K-V beams, space charge limited transport and bunching in heavy ion fusion 79—76227
noncylindrical symmetric space-charge flow, momentum eqns. 78—91181
on-line isotope separators 77—23337
ondulator as EM radiation source in synchrotron orbit 79—72174
optimum resolution by matching beam handling and detection systems 79—45494
overlap knockout resonances with colliding bunched beams in CERN ISR 79—76195
overneutralised electron beams in metal vapour, ion focusing theory and expt. 78—75366
parametric focusing of charge- and current-neutralised proton beams 77—57421
particle beam, flux control, charge exchange method *(Russian)* 78—70662
particle beam cooling, by channelling in monocrystals *(Russian)* 80—52806
PEP beams line components, bench meas. of loss impedance 79—68055
phase displacement accel. in presence of RF noise, efficiency 79—76231
phase space acceptance and emittance, appl. to tandem accelerators 77—31058
phase space meas. at 2 MHz particle rate 77—54383
photodisintegration and π photoprod. coincidence expts. at Bonn 500 MeV synchrotron 80—22815
photon beam fast neutron contamination detection using $^{19}F(n, \alpha)^{16}N$ 77—10570
pinched beam diode, geometrical focusing of intense ion beams 78—58898
plasma lens for ion-beam, focusing and form. of intensive beam *(Russian)* 78—21270
plasma-optical mass separator, double focusing, 'nontransitive' cylindrical model 79—67423
PLT, neutral beam test stand, data acquisition system 78—62622
Polarised beam from the University of Manitoba spiral ridge cyclotron 78—70660
polarised beams, acceleration and storage 78—58518
polarised neutron production and appls., book contrib. 79—58843
polarised proton beam production in high energy hyperon decay 78—58517
polarised proton beams, higher energy, conf., Ann Arbor, MI, USA, Oct. 1977 78—58514
positron beam, relativistic, collimation in single cryst. 79—23669
positrons, slow, time bunching for annihilation lifetime and pulsed laser photon absorpt. expts. 80—95492
prebuncher design calculations for 150 MeV electron linac 79—68075
proton (antiproton) beam in storage ring, stochastic cooling anal. 80—5420
proton (antiproton) storage ring, incoherent motion damping by dissipative elements 80—5419
proton beam, 20 GW, geom. focusing using magnetically insulated diode 77—67533
proton beam 70 GeV, for Protvino Inst. neutrino expts., characts. 78—37475
proton beam characts. control by laser-induced selective multistep processes 80—61122
proton beam diffusing system for PIXE analysis 79—85848
proton beam focusing to micrometer dimensions 77—46444
proton beam for neutrino experiments, focusing, pulsed power supply 79—9974

beam handling techniques continued
proton beam in storage ring or synchrotron, monitoring by narrow band synchrotron radiation 77—83293
proton beam of neutrino experiments facility, particle loss and radiation environment 79—9930
proton beams, prod. of narrow band visible synchrotron radiation 77—58241
proton double extraction for irradiation of Mirabel and Lyudmila bubble chambers 78—839
proton LINAC—injector I-2 operation for several users 79—45480
proton recapture and moderation on magnetic field decay in proton synchrotron 79—68062
proton synchrotron booster, CERN, longit. active damping system 77—83371
proton synchrotron booster RF accelerating system, dynamic closed loop control 77—83379
pulse-power particle beam sources as fusion drivers, review 79—18066
pulsed linear accelerators for inertial fusion driver appls. 80—13842
Pustarex device, trapping and compression of electron rings 80—5403
quadrupole ion store, of mass spectrometer, ion ejection expts. 79—89033
quadrupole ion store, of mass spectrometer, phase synchronised ion ejection study 79—89034
radial damping by octupole for zero gradient synchrotron beam 77—83383
relativistic beam injection, into strong mag. field, cross-section limiting 80—5427
relativistic charged-particle beam, collimation by coherent radiation *(Russian)* 77—61156
relativistic electron beam, magnetic compression of high current beams 77—87876
relativistic electron beam, propag. in air, exploding beam preformed plasma column 77—87875
relativistic electron beam, transport to thermonuclear target *(Russian)* 78—38552
relativistic electron beam acceleration accompanied by beam focusing, for pulsed fusion 77—34054
relativistic electron beam generation, in foil-less diodes 78—89593
relativistic electron beam in plasma, coherently radiating, radiation press. at surface 78—9314
relativistic electron beam transmission through strong mag. field in gases 80—48900
relativistic electron beams, high current, pulse length adjustment 78—65997
relativistic electron beams, mag. focusing, equilib. surface ripples 79—3618
relativistic electron beams, transport in laser prod. plasma channel 78—71568
relativistic electron ring, retarding force of image currents in resistive cylinder, stopping length 77—67918
relativistic electron rings, translation and stacking 77—87877
relativistic particle beam in crystal, collimation, cooling 80—42885
RF ion source, 15 cm diameter, stable working conditions calcs. 78—86388
RF ion source, modified extraction geometry 78—33349
RF quadrupole accelerating struct. research at Los Alamos 79—71988
RF superconducting resonators for booster linac 79—54623
rotating proton beam, generation and propag. 79—6217
Saturne, improvement in 20 MeV beam brightness 77—38500
Saturne 2 synchrotron, strong focusing and polarised beam acceleration in strongly modulated structures 79—72057
secondary-electron time pickoff for pulsed charged-particle beams 79—97957
separated sector cyclotrons, chromatic correlations at injection and ejection 79—72110
sextupole magnets with nonlinear lattice, computational methods for dispersion, betatron functions, closed orbit distortion 79—68028
Siberian Snake configuration, efficient configuration 79—63849
SIN meson factory, computer control strategies 79—54701
slow neutron polarisation by polarised proton filter using ethylene glycol 78—90046
Soller slit collimators for thermal neutrons 77—45916
space charge in beam transport 79—30610
space charge limitations on transport of max. power beams 77—83355
spin precession of polarised proton beam in quadrupole lens, analytic soln. 77—30692
SPS, CERN, damping of longit, instabilities 77—83372
stability of the longitudinal oscillations of a bunched beam propagating in a vacuum chamber with reactive impedance 79—85849
Stanford Synchrotron Radiation Laboratory, operation and development, review 79—68020
stochastic cooling techniques for heavy particle beams 79—72175
stochastic cooling tests on proton beams, initial cooling expt. 78—90006
strong focusing colliding beams for electric power generation 79—18032
superconducting cyclotron in Milan, beam extraction studies 77—83361
supersonic molecular beam source, simple calibration method 80—82845
surface structure anal., discussion of ion optics 79—46902
synchrocyclotron beam intensity monitoring using Ni and Cu foils 77—38578
synchrotron, calc. of finite Q-jump magnitude in intrinsic depolarisation resonance crossing 79—72058
synchrotron, methods of increasing heavy ion beams intensity 79—26790
synchrotron beam RF phase lock loops, effect of large delays 79—68046
synchrotron radiation, review of props., facilities, and source parameters and optimisation 79—68018
thermal neutron monochromators, Monte-Carlo simulation of mechanical velocity selectors 78—24886
thermal neutrons, spin-flipping methods for polarised beams 78—25370
thermal particle motion effect on autoresonance acceleration process *(Russian)* 80—69007
TMX injector system, mech. design 78—66403
TOKAMAK and other fusion reactor realisation, plasma beam control, Boltzmann eqn. 79—97903
toroidal collective focusing accelerator for heavy ion acceleration 80—14015
transfer maps for linear and nonlinear beam elements 79—72107
TRANSPORT, design program for charged particle beam transport systems 80—106220
transport experiments with neutralized and space charge dominated deneutralized 2 mA 80 keV Xe^{+1} beams 79—72133
trapping dynamics, in weak cold beam plasma instability, DC elec. field effects 78—83581

beam handling techniques continued
travelling wave periodic struct. props., computer calcs. 79—72165
TRIUMF biomedical negative pion beam line, tuning 78—96113
TRIUMF cyclotron, variable energy polarised proton beam 79—72059
TRIUMF cyclotron improved beam quality 79—72060
two component ion beam accelerator system, for interactive surface effect studies 79—49880
ultra cold neutron extraction from high flux reactor SM-2 77—57787
ultracold neutron beams from ultracold neutron gas 77—26913
ultracold neutron diffusion along guide tube 78—33237
ultracold neutrons, extraction, transportation and storage 77—26826
very high current beams, transport calcs. computer program 79—76226
VICKSI cyclotron, automatic isochronisation and computer aided centering 79—54706
VICKSI facility, running in period and initial operating experience 79—54627
water trap, polarised-neutron beam shut-off 80—87004
wedge type ion beam divergence profile calc. 78—82555
XTU tandem of Lab. Nazionali di Legnaro (Padova) 78—13354
ZGS polarised proton beam splitting 78—13366
$\bar{p}$ beams cooling and storage, high energy collisions with protons 78—54654
π^- biomedical beam line, CAMAC control 77—90886
Be monochromator grain identification by neutron topography 79—76244
Cs beam deflection system for time and freq. primary standard 78—89453
Cs beam standard, Ramsey cavity and beam optics design, expt. 78—89456
H^- short bunch shaping at entrance of linear accelerator, calcs. 79—700
H^- stripping, neutrals scatt. angle 78—5340
H^+ beam, control using laser radiation 79—27112
H_n^+ multispecies beam, particle species evolution in neutral-beam injection lines 79—85846
He^+ shutter controlled microbeam, with scanning system, for 2-dimens. backscatt. images 79—2879
^{127}I ions, 20 MeV, emerging from gas stripper, absolute charge state yields 78—55066
K atom clusters, cluster beam Stern-Gerlach mag. deflection 78—54504
N ion collective acceleration expts. at JINR 80—5406
S ion charge distrib., 70-140 MeV, through C and Be foils 78—13364
^{149}Sm polarising filter for thermal neutrons 78—54502
U, 50 keV beam prod. by charge exchange in gas and metal vapour targets 78—70675
^{238}U filtered beam of 186 eV neutrons, development 77—88318
^{238}U, single charged, numerical anal. of longitudinal motion of 9.5 GeV 79—54737

beam-trapping *see self-trapping*
bearings (machine) *see machine bearings*
behavioural sciences *see social and behavioural sciences*
behavioural sciences computing *see social and behavioural sciences computing*

bells
see also musical instruments
acoustics, in review for teaching 77—57128
eccentric, vibr. meas., discussion of warble suppression 78—90612
forced damped harmonic oscillators, meas. separation and half-width of components of doublets, high-Q systems 80—74590
Japanese bell, effect of changing striking rod on timbre *(Japanese)* 77—7266
Japanese bell, striking rod effect on timbre *(Japanese)* 77—14860
ornamented, warble occurrence 79—23149
ornamented bells, group theoretical approach to warble 77—80032

bending
see also bending strength; buckling; stress analysis; torsion
1 MN combination load/bending moment transducer *(German)* 77—79080
acrylic plastic, deform. of rigidly clamped specimens subject to one sided cyclic heating 77—59932
adhesive bonded lap joints, elastic stresses theory 78—55563
Al alloy 2024-T81, adhesive bonded multi-ply laminate, effective remote stresses and stress intensity factors 77—73328
alloy steel samples, spherical, fatigue testing *(Croatian)* 77—36712
alloy V93, fatigue strength, effect of residual stresses and cold working 77—56101
alloys, shape memory effect, device for testing in bending 80—66723
anisotropic composite cantilever, bending and torsion, mathematical formulation 79—18708
anisotropic reinforced plate, stress distrib. near recesses, variational anal. *(Russian)* 79—27521
annular and sector plates, finite element anal. 77—46950
arches, curved beams, rings, treatment of extensional deformations for bending 77—58556
automotive struct. analysis using hybrid stress finite elements 78—30176
axisymmetric elastic bodies with arbitrary boundary conditions, semianal. boundary integral 80—102969
bar, curved, in-plane vibrs., shear deform. and rotatory inertia effects 80—43646
bar, localised damage region effect on parametric excitation 78—30215
bar (tube), compressible, combined loading, elastic-plastic problem 78—63311
bar of linearly work hardening material, critical load *(Russian)* 77—89053
bar undergoing bending oscillations, shape optimisation *(Russian)* 79—37210
beam, fixed ended, exptl. behaviour under simulated uniformly distributed load 79—27540
beam, impulsively loaded, clamped end bending moment, Bessel function eval. 79—92937
beam, internal damage induced instability 77—7341
beam, large deflection in four point bending 77—11130
beam, nonuniform cross section, influence of shearing deformation and rotatory inertia on lateral vibr., pt.II *(Japanese)* 77—68518
beam, nonuniform cross section, influence of shearing deformation and rotatory inertia on lateral vibr., pt.III *(Japanese)* 77—68519
beam, prismatic, unsymmetrical, pure bending anal. 77—80091
beam, rotating slender, bending vibrs., Galekin method anal. 80—1465
beam, slip line development 80—58928
beam, thin wall, bending stiffness 80—28425
beam bending on Pasternak foundation, reciprocal variational inequalities 80—92091

bending continued
  beam design, HIFIX performative method 78—26064
  beam formation, eccentric, error anal. 79—3920
  beam inelastic bending including transverse shear finite element anal. 79—90148
  beam modelling, linear shape function for axial displacement approx., finite element anal. 80—69665
  beam of stepped thickness, Timoshenko theory 78—94600
  beam on nonlinear spring support, random vibr. 78—55585
  beam on nonlinear spring support, random vibr. 80—33515
  beams, crack effects on vibr. frequency *(Japanese)* 77—27487
  beams, dynamic plastic behaviour, rot. inertia and transverse shear influence 80—48601
  beams, effect of secondary terms 78—79237
  beams, inelastic bending under time varying moments, state variable approach 80—28439
  beams, nonlinear bending, finite element anal. 78—26068
  beams, optimal layouts, allowance for cost of shear and bending 79—68566
  beams, straight, homogeneous and isotropic, linear flexural theory *(French)* 80—74743
  beams and plates, active suppression of flexural vibrs. 77—27422
  beams in pure bending, distributed damage theory, cracks, fracture 80—64474
  bending free toroidal shell shapes for Tokamak fusion reactors 79—64503
  bi-material, elastic composite, Southwell's analogues for plane and bending problems 78—87265
  biaxial flexure test, exam. of loading factors 78—80695
  bimetallic plates, deflection meas. during high-temp. heating 78—7134
  bituminous mixes, fatigue strength, effect of mix and test variables 77—63881
  bone, compact, fatigue damage, residual strength and stiffness 77—90834
  bone, distrib. of induced elec. activity in bent long bone 78—3541
  bone, distrib. of piezoelec. effects in bent long bone, anal. model 77—36983
  bone, elastic and damping props. of human femur 77—25489
  bone, human, ulnar bending stiffness, mineral content, geometry and strength 78—3537
  bones, long, struct. anal., appl. to human tibia 77—21551
  brass, anisotropic bend ductility in single phase alloys 78—60726
  γ-brass, brittle to ductile transition under high hydrostatic pressure and high temp. *(Japanese)* 80—35305
  brass, crack propagation properties in rotating bending fatigue tests 77—32669
  α-brass, dislocation structure around crack tips in early stage of fatigue 78—60830
  brass, stress corrosion cracking, in ammoniacal atmosphere, surface stress change and crack growth *(Japanese)* 77—59986
  brittle coating, ductility meas., four point bend test 78—48577
  bronze, anisotropic bend ductility in single phase alloys 78—60726
  cantilever beam, nonlinear bending and torsion deform. 77—58571
  cantilever beam, rot., bending freq. calc. 79—68637
  cantilever beam, stability on viscoelastic foundation with shear layer subjected to circulatory force 79—86374
  cantilever beam method to investigate J_{Ic} and J_{Iscc} *(Chinese)* 78—15488
  cantilever beam with shear and longitudinal deformations, nonlinear bending 79—72822
  cantilever beams, free transverse bending vibrs., secondary effect influence *(French)* 79—18785
  CBOOA, nematic, mag. field depend. of laser light scatt., interf. rings 78—26434
  ceramics, polycrystalline, stress-relaxation technique for deformation studies in four point bending 79—100200
  ceramics, tensile and compressive creep behaviour, bend tests 78—48455
  cilia and flagella, displacement and sliding of twisted filaments 77—32929
  circular cylinder, with straight crack, in grooved and ungrooved shafts, stress intensity factor calc. 77—56061
  circular cylinders, plastic buckling in pure bending 79—90158
  circular membrane reflector made by surface bending due to electrostatic tension 80—91876
  circular plate, thin, with single eccentric circular holes, bending stresses 77—3721
  circular plate bending under eccentric loads, elastic buckling eigenfunction method *(Japanese)* 78—22285
  circular plate of variable thickness, bending with symmetrical loading 80—69699
  circular plate on elastic foundation, bending and contact problems 80—96235
  circular plate resonse to central pulse loading 78—18187
  circular plates, nonuniform, finite element analysis 77—7316
  circular tube fibre reinforced sector, elastic deform. 77—72164
  circular tubes under transverse loading, expt. anal. of large deformations 77—19543
  clamped hyperbolic paraboloid shell, bending analysis 77—11129
  clamped rectangular plates, bending anal. 77—68435
  coil winding, plastic over bending, and over springing *(German)* 79—90156
  composite, shell, rotation under axisymmetrical strain, elastoplastic edge effect 79—94509
  composite, steady creep bending stresses 78—71280
  composite beams, effects of fibre orientations on free vibrations 80—87734
  composite materials, fibre reinforced, rectangular rods, elastic wave propagation *(French)* 80—83749
  compressed bar, secondary plastic deformation influence beyond yield stress *(Russian)* 79—37199
  comressible circular block, bending into a spherical shell 80—1437
  concrete, prestressed hollow beams in combined torsion and bending 79—96087
  concrete, reinforced, failed slabs, nonlinear analysis by finite element method *(Japanese)* 77—42785
  concrete plates, cracked, and beams existence of critical strain energy release rate 78—76765
  concrete reinforced members, limit index point and flexural capacity *(Japanese)* 79—83283
  concrete reinforced rectangular membranes, torsional stiffness 80—65131
  concrete slabs, subjected to biaxial moments, optimum design of steel bars reinforcement, using analytical and graphical methods 80—50664

bending continued
  constained plates, Rayleigh-Ritz method using Lagrange multipliers 77—68502
  constructional material fatigue resistance test under asymmetric loading 78—85083
  contactless temp. meas. in circular cyclic bending, using thermoelectric radiation sensors 78—57947
  continuous beams with concrete slabs under load, method for crack prevention in slab *(Japanese)* 80—83760
  countersunk hole in flat bar in tension and transverse bending, stress concentration factors 79—46274
  coupled bending-torsion flutter in cascades, aeroelastic stability boundaries 80—64424
  crack, oblique edge, in semi-infinite plate, stress anal. 80—64463
  crack anal., frictional contact 80—1475
  crack emanation, from circular hole in infinite sheet, Green's function methods 80—92084
  crack extension angle, influence of specimen's geometry 80—99965
  crack test, for fatigue crack propag. laws determ. *(French)* 77—51007
  cracked cylinder, transverse bending effect on stress intensity factor 78—30237
  cracked plates, symmetric bending by reflected caustics method 80—19283
  cracks, plastic, in bending, tension, anal. 79—41623
  creep const. determ. from stress-relaxation meas. in bending and torsion 78—9572
  creep in circular specimen subject to pure bend, ultimate tensile and compressive strength *(Russian)* 80—74768
  crystals pulled from melt, thermal stresses and struct. defects 78—2041
  curved plate bending problem solved with nonconforming finite elements 79—37202
  curved sandwich beam, five point loading test, bending and shear stiffness determ. *(German)* 77—16765
  curved structural members, large displacement theory, applic. to lateral-torsional buckling anal. of circular arches 80—23924
  curves of strengthening construction from bend tests, deformation curves *(Russian)* 79—59928
  cylinder, hollow with external annular crack, bending, stress intensity coeff. *(Russian)* 79—27537
  cylinder, thin, deformation due to band press. 78—94595
  cylinders, anisotropic homogeneous circular, Saint-Venant's problem and bending 80—53622
  cylinders, elastic doubly connected hollow, min. weight design for given torsional, flexural rigidities 78—18172
  cylindrical elastic tubes, collapse and buckling under combined bending and pressure loads 78—83277
  cylindrical notched specimen, four-point bending, crack resist. tests 80—53735
  cylindrical shell, heated, large deflection 78—63289
  cylindrical shell, stretching, bending, twisting and flexure 77—11125
  cylindrical shell, transverse shear effect on axial crack 78—67090
  cylindrical shell with circular cut out, uniform bending, strength and flexural rigidity 78—87282
  cylindrical shell with small circular cutout subject to asymmetric bending, stress anal. 77—46920
  cylindrical shells, mildly sloped, with circular aperture, bending problem 79—18704
  cylindrical shells, stiffened, min. weight design for pure bending *(Japanese)* 80—64381
  cylindrical specimen with external crack reaching surface of annular stress concentrator, tension and bending 79—14349
  damping props. investigation, material in bending oscillations, new method 77—21340
  deep circular notches, plane strain general yielding under loads and bending 79—18809
  deflection analysis of cylindrical shell, with end plate subjected to centrifugal force, finite element method appl. *(Japanese)* 79—1104
  deflection contour generation by white light projection speckle method 80—98881
  deformable media, equivalence of force systems *(Russian)* 77—50886
  disc, axisymmetric nonuniform quickness distrib., influence of shearing deformation and rotatory inertia on lateral vibr., pt.II *(Japanese)* 77—68518
  disc, axisymmetric nonuniform thickness distrib., influence of shearing deformation and rotatory inertia on lateral vibr., pt.III *(Japanese)* 77—68519
  disc, axisymmetrically variable thickness, deflection by conc. lateral load *(Japanese)* 80—96194
  disc with variable thickness, cross-section warping and corres. stress quantities *(German)* 78—18206
  displacement derivative meas., image-shearing interferometric camera 80—33549
  double cantilever beam, fracture behaviour, quasistatic energy anal. 79—18817
  doubly clad W-type, microbending losses 77—88899
  Duralumin D16T, creep, energy variant of theory expt. verification 78—6993
  dynamic fracture toughness determination, by instrumented impact tests 78—68861
  dynamic laser speckle interferometry, appl. to transient flexure 78—32861
  Earth lithosphere bending at trench, elastic-perfectly plastic anal. 78—81135
  eight node solid element for pure bending 79—44734
  elastic beams, 1-D, stability in torsional extension *(German)* 78—87270
  elastic beams subjected to successive loading, bending, stability eqns. *(German)* 78—26045
  elastic elbow, in-plane bending behaviour, finite element anal., pipeline design 78—18166
  elastic layer, dynamics, approx. eqns. 79—7326
  elastic members, thin-walled, displacement theories for straight and circ. curved members *(Japanese)* 80—43615
  elastic optimal plates, of rectangular form *(Russian)* 77—23882
  elastic plate, crack closure in bending, sixth order anal. 80—96231
  elastic plate problems, novel finite element method 77—35063
  elastic plates, resolution of elliptic problems 79—64538
  elastic plates and shells, bending, small parameter method 80—99930
  elastic prisms, minimum energy, St. Venant's solns. 80—52027
  elastic solid with annular crack, bending effect 79—72806
  elastic springback in beams and plates 80—38256
  elasticity, fundamental theory, and applications, book 80—22158

bending continued
- elastoplastic anal. using ASKA program system, bending, isotropic/kinematic hardening 78—63312
- elastoplastic bending of thick-walled tube, approx. determ. 77—882
- elastoplastic circular plates, nonlinear behaviour equilibr. eqns. 79—14279
- electrotechnical porcelain, bend tests, fracture stress distrib. at various loading rates 78—15529
- elliptical punch, elastic contact problems 78—9613
- epoxy resin, E-glass fibre reinforced, flexural fatigue properties 79—66138
- epoxy resins, correlation between valence energies and low temp. flexibility 80—25815
- fast reactor subassemblies, irrad. swelling induced bow 79—93724
- fatigue crack, low cycle, test machine rigidity effect on kinetics 78—15632
- fatigue limit under combined stress 77—73314
- fatigue strength criterion, of a round bar, subject to combined static and repeated bending and torsion 80—40496
- fatigue surface crack propagation in bending 77—72238
- fatigue test machine, low-cycle, far sheet material bending to —196°C 80—55616
- fatigue testing machine, materials in pure bending 77—1906
- fibre reinforced concrete beam, load-deflection curves in flexure 78—35437
- fibre reinforced organic matrix composite, use of unidirectional flexural tests, to assess environmental behaviour 79—20301
- fibre reinforced plastics, bent thin-wall constructions, rupture 80—64472
- fibre-optic index-difference dispersion and bending loss/wavelength relationships 78—1367
- finite elastic, existence-uniqueness results 77—75811
- fission reactor core system, bowed, NUBOW-3D program for static anal. including irrad. creep and swelling 80—5215
- fission reactor pipework integrity assessment 79—22431
- flagella bend propagation, derivation of eqns. of motion and simulation 78—77074
- flat elliptical crack, in infinite solid, mixed boundary value problems 78—9602
- flat shells, bending stresses, parametric study *(German)* 79—86365
- flexible tie, problems connected with body blow *(Russian)* 78—42541
- flexural vibration mode shape change by defects 79—7335
- flexure of clamped rectangular plates resting on Winkler foundations 80—5934
- force meas. rod bending moment compensation by parallel resistors *(German)* 77—79078
- forming limit curve for bending processes 80—7627
- fracture mechanics stress intensity calibration in four-point bending, expt. determ. 77—77558
- fracture toughness determ. from fatigue test results in circular bending 78—15526
- frame, two-bar, with tangential load, snap-through buckling 80—64406
- frame structs., large deflection anal. by fictitious forces 78—83249
- fusion reactor, toroidal field coil in-plane bending stress, struct. support design 80—106164
- fusion reactor coil, multilayer structs., laminated beam theory anal. 78—55011
- glass, silicate, EM pulse radiation, under symmetrical bending 80—45350
- glass beam, brittle bending fracture and emitted stress waves 77—73329
- glass fibre, loss, mechanically induced periodic bends effect 77—3668
- glass fibre reinforced poly- and vinyl ester thermoset moulding, cure cycle effect on mech. props. 80—45369
- glass fibre reinforced polyester, epoxy-polyamide, single lap joint, tension-shear strength *(Japanese)* 78—11494
- glass fibre reinforced polyester, single lap joint, tension-shear strength *(Japanese)* 78—11494
- glass fibre reinforced polymer, fatigue life, determ. from reheat temp. 79—61724
- glass-plastic AG-4c, fatigue resistance under bending in H_2SO_4 *(Russian)* 79—34163
- graphite, fracture criterion 77—48552
- graphite reinforced epoxy laminate, cantilever shells and late, natural modes 79—91737
- graphite reinforced epoxy/Al laminate, cantilever shells and late, natural modes 79—91737
- graphitised viscose fibre, fluorination, change in struct. 80—88039
- head, spheroidal model, effect of bending on axisymm. vibrs. 77—29168
- heat resistant materials, high temp. fatigue testing machine 80—25954
- heavy fabric sheets, fabric folding obs. 79—18756
- 'heterosis' finite element for plate bending 79—3933
- hologram interference fringe bending analysis and expt. 80—106494
- holographic optical elements, third-order aberration theory and generalised aplanatic condition 80—74314
- hybrid composite material beams, exam. of shear stress correction factors 78—46899
- hydraulic lines, wave phenomena, coupled vibrations in bending and branching lines 80—14778
- ice, transverse flexure, refined Reissner anal. 80—88247
- image moire method for determination of partial slopes in fixed plates 80—14645
- impact bending, specimen parameter effect on crack propag. 77—86242
- impact tester attachment, for bending impact tests, method of obtaining asymmetric cycles 80—16628
- impact three point bend testing for notched and precracked specimens, testing and data analysis procedures 78—53053
- Incoloy 800, fatigue crack behaviour in bending and pull-push modes 77—81315
- infinite plate, axisymmetric interaction with elastic halfspace, influence of Mindlin force 78—38193
- infinite plate with doubly periodic hole array, transverse bending, Poisson-Kirchhoff theory 80—58920
- initial flaw shape, effect on cracks emanating from fastener holes under combined stress 78—64694
- inorganic particle reinforced thermosetting resins, chem. bonding, mech. bonding and compression tests 77—59735
- n-InSb, acceptor effect of plastic bending 80—6885
- internal fixation plate, effect on long bone remodelling 77—48935
- internal fixation plates, evaluation of 1-, 2- and 3-dimens. finite element and exptl. models 77—48934
- isoparametric linear bending element and one-point integration 79—3919
- isotropic circular plate bending into paraboloidal shell 79—41592

bending continued
- isotropic elastic circular plate, flexural vibrs., Mindlin's theory 80—43650
- isotropic plane sandwich plates, constant shear theory 80—99943
- isotropic semiinfinite plate heated by moving point source of heat, temperature stresses 80—43628
- jute filament, bending rigidity at various delignification stages 78—19817
- laminated cylindrical shell, coupling effect under internal press. *(Japanese)* 80—55449
- laminated magnetostrictive plates, bending vibrs., reson. excitation 78—10746
- laminated plates, symmetric, specially orthotropic, thermoelastic anal. 80—92058
- laminated plates flutter and buckling anal. 77—65698
- laminates, multilayer, thick, hybrid-stress finite element formulation 80—92043
- at large deflections as elastic moduli meas. method 78—27699
- large plane bending deformation anal., approx. solution *(German)* 78—5674
- lateral buckling by bending, and by torsion 77—42763
- life calc. under combined torsion and bending 77—11148
- light gauge steel diaphragms, buckling, bending anal. under concentrated loads 79—23233
- linear elastic beams, shells and plates, elementary theories review 80—69677
- linear plate bending, finite difference energy techniques 79—55330
- liquid crystals, piezoelectric effect use as light modulator 80—83679
- lithosphere, elastic-perfectly plastic bending under generalised loading, appl. to Kuril Trench 78—73341
- LMFBR assembly, fuel pin deformations, analytical method, computational code (SHADOW) 78—54829
- LMFBR fuel channels, measurement of irradiation creep in bending 80—104406
- LMFBR piping components, resistance to bending moments 77—6505
- load stability problems, power method modification *(Russian)* 80—28444
- LORA—an accurate four node stress plate bending element 79—27527
- low-cycle pure bending tester for several specimens simultaneously 80—55607
- lumbar vertebra cortical surface strain distribution tests 78—11692
- machine, four-point assessment, steel bar deform. meas. by holographic interferometry 79—34266
- matrix analysis of composed bar of open cross section 80—83736
- MBBA, nematic liq. cryst., transverse electrooptic effect 79—94897
- membrane, prestressed, dynamic loading 78—51068
- mesh analysis processes, convergence *(German)* 78—87257
- metal, ductile fracture criterion 78—60817
- metal, fatigue and inelasticity testing apparatus in symmetrical bending mode, 36 to 330 Hz 78—27722
- metal, fatigue damage accumulated by combination of alternately applied over- and under-stresses *(Japanese)* 80—35306
- metal sheeting, profiled, shear deformation, stressed-skin anal. 79—1121
- metal tubes, crushed between rigid plates, large deformation compression 80—66579
- metal-composite rods, compressed, delamination 80—64396
- metallic bending springs at small mech. stress, non-elastic props. *(German)* 77—77532
- metallic thin spring strip, bending test device 80—61052
- micromachine for low-frequency fatigue testing of materials by pure bending 79—29317
- micropolar elastic plates and rods, eqns. of motion *(German)* 80—53643
- micropolar plates, stress concentration around hole 77—3731
- microstrains distrib. in macroinhomogeneous fields *(Russian)* 80—21018
- Mindlin plates, finite element displacement formulation 80—10154
- mineral-fibre composites that resist fracture and cracking 77—8798
- mitral valve vibration anal. to detect first heart sound freq. 78—40233
- monomode optical fibre dimensions, dispersion, and losses *(German)* 78—33866
- mortar specimens, repeated impact bending load study *(Japanese)* 80—93622
- moving load in initially stressed thick plates attached together by a flexible core 79—81752
- multi-layer beam assembly bending, appl. to leaf spring *(Russian)* 79—81718
- multilayer cylindrical shell, with elastic core, bending under local radial load 77—27474
- multilayer plates, optimum design for cylindrical bending 79—87698
- multimode focusing fibre with random bends, optical power loss 79—7214
- nematic liquid crystals, flexoelectric bending, e_{1z}/e_{3x} meas. 77—72555
- Nimanic 80A, inhomogeneity effect of cyclin strain on crack initiation 78—48532
- non-linear optimized fibre reinforced plates in bending 79—27550
- nonlinear bending of elastic plates, lumped mass approx. *(Japanese)* 77—78984
- nonlinear thermal bending of shallow sandwich shells and flat plates, numerical anal. 80—5936
- nonlinearity of rectangular convertor foils *(German)* 80—33489
- notched and bend specimens with equivalent geometries, cyclic deform. *(German)* 77—86271
- notched rectangular bars, stresses at plastic deflection *(German)* 78—34025
- notched specimen, brittle fracture characts. under impact bending 78—23810
- nuclear fuel can designs for Safety Test Facility, structural analysis 77—46310
- oceanic plate bending at trenches, mechanical models constraints from earthquakes 80—41426
- open cylindrical shell, buckling under combined compression and bending stress 77—65697
- open shells, prebuckling state, bending stability, contour deformation effect 79—94519
- optical fibre, fundamental mode microbending loss 77—23762
- optical fibre, microbending eqns., exact time-dependent, solns. 80—87530
- optical fibre, single mode, bending induced birefringence 80—87537
- optical fibre, single-mode, dependence of optical losses on bending effects 79—50417
- optical fibre, single-mode, for current meas. system, birefr. induced by bends and twists 80—99832
- optical fibre, single-mode, misalignment and bend losses 79—10411
- optical fibre bandwidth limitations and bend losses 80—87553

bending continued
- optical fibre cables, single-mode and parabolic-index multimode, random-bend loss 80—78951
- optical fibre coating structure for microbending loss minimisation 80—28346
- optical fibre packaging in loose fitting tubes of orientated polymer 78—1338
- optical fibre waveguides and cables, microbending losses, depend. on numerical aperture 80—96025
- optical fibres, Al coated, empirical formula for induced excess loss 79—46074
- optical fibres, coated, strain-induced excess loss 79—50418
- optical fibres, deformation of cable sheath by bending in plastic range, loss anal. 80—43477
- optical fibres, single mode, curvature and microbending losses 79—27418
- optical fibres, single-mode, splicing and bending losses 79—18505
- optical fibres, single-mode step-index, practical microbending loss formula 79—81534
- optical fibres, two dimens., microbending theory, role of nonadjacent mode coupling 79—27415
- optical fibres for communication, fibre technology and props. *(German)* 79—81564
- optical materials, Twyman effect theory based on Van der Waals interactions *(Russian)* 79—77890
- optical multimode W-type fibre, periodi bending loss 79—76848
- optical single mode fibers, microbending loss evaluation, core index profile effects 80—48412
- optical single mode fibres, arbitrary index, microbending loss evaluation 80—48411
- optical single-mode fibres, simplified bending loss formula 79—59800
- optimal design of bending elements 79—10470
- orthotropic annular plates, general nonsymmetric postbuckling anal. 79—7307
- orthotropic cylindrical shell acted upon by local load 80—43617
- orthotropic plate bending anal. with identification method 78—26071
- orthotropic plate flexure, theoret. considerations, expt. investigations *(German)* 79—10463
- orthotropic plates, large deflection behaviour anal. 79—98605
- orthotropic sandwich plates, large deflection governing eqns. 79—7301
- orthotropic strip, stress intensity factors and crack opening displacements 80—53710
- parabolic isometric plate element, laminated composites flexural analysis 77—14921
- peeling mechanics of elastic strip from rigid substrate, large bending 77—80122
- piezoceramic microwelding transducer component oscillation amplitudes 79—26046
- piezoceramic plates, bending strains, electromechanical transformation, energetic method of calc. *(Ukrainian)* 80—71320
- piezoelectric elements with passive substrate layer, static force/deflection calc. *(German)* 77—77152
- piezoelectric multilayer plates with uniform elec. field, anal. 80—40064
- piezoelectric thin plate with elliptic opening, flexure, twisting *(Russian)* 77—66456
- piezoelectric thin plates, integer polynomial solns. *(Russian)* 78—52444
- piezoresistive accel. transmitter mech. designs *(German)* 79—12792
- pipe, curved, in creep, flexibility 78—34039
- pipe, curved, thin-walled, steady creep problem, stress distrib. *(Russian)* 80—23905
- pipe bend in-plane bending, shell theory anal. 77—6516
- pipe bends, flexibility and stress factors, finite ring method 77—75828
- pipe bends, short radius, creep bending 77—6517
- pipe bends with flanged tangents, bending and pressurising 79—94516
- pipe elbow element, linear anal., bending axial and torsional displacements, ovalisation 80—79177
- pipe expansion bend, Na-H_2O heat exchanger, bending-loadings determ. 77—80085
- plane bending-and-torque supporting grids, numerical plastic collapse anal. 79—68594
- plane homogeneous curved beam 80—69697
- plane stress crack problems, fully plastic soln. and large scale yielding estimates 77—19573
- plastic bending and torsion of simple geometries, subjected to cyclic loading, stress-strain analysis 78—90734
- plastic collapse, mm. cost in elastoplastic structs. 78—30197
- plastics, bending fatigue, exam. of new method of testing 78—53056
- plate, and plane elasticity, finite element analysis 77—35033
- plate, annular, bending anal., closed form solns. 80—38263
- plate, annular, non-uniform thickness, partial arc loading effects 80—74774
- plate, annular, uniformly stressed, with variable rigidity, axisymmetric bending problem 79—32295
- plate, bending vibrations and acoustic pressure *(Russian)* 80—23949
- plate, cantilever, strain meas. from holographic data 79—20303
- plate, circ., large deflection anal., with nonuniform Jacobi polynomial load 79—37184
- plate, circ., with initial deflection, nonsymmetrical bending under mid-plane forces 78—79238
- plate, circ. isotropic, compressible, bending into ellipsoidal shell 79—32252
- plate, circular, flexural response on bilinear foundation 79—32238
- plate, circular, nonlinear analysis using Chebyshev polynomials 77—49597
- plate, circular thin hinged, bending, Hertz-Timoshenko hypothesis 80—33482
- plate, containing crack, resting on elastic base *(Russian)* 79—86364
- plate, elastic circular cylindrical, with arbitrary transference, stress-strain state *(Russian)* 80—23895
- plate, finite difference variational method 80—92045
- plate, increase of first natural freq. and buckling load by optimal fields of initial stresses 78—13945
- plate, notched, plane strain general yield due to combined axial force and bending 78—18197
- plate, numerical soln. by general boundary integral formulation 80—1422
- plate, optimal design under dead weight and surface loading 79—3915
- plate, out of plane bending, steady state crack propagation, rotatory inertial effects 79—7340
- plate, prestressed elastic, homogeneous solns. for bending and stability 80—43610
- plate, rectangular, deflections, bending moments, nodal line anal. 79—32366

bending continued
- plate, rectangular, finite bending in creep conditions *(Russian)* 80—79169
- plate, rectangular with asymmetrically reinforcing beams, contact interaction 80—99975
- plate, rectangular with two opposite edges supported and partially loaded *(Japanese)* 78—34004
- plate, semi-infinite, with strip mound, stress analysis 80—10139
- plate, simply supported, shear and bending moments by hydrodynamic analogy, results 79—64524
- plate, state of stress and strain near crack vertex in nonlinear bending 80—5991
- plate, static geometric and elastic stiffness matrices of finite element hybrid displacement models 78—18173
- plate, symmetrically notched, plane-strain general yield due to combined axial force and bending 78—18198
- plate, temp. bending, generalised eqns. WRT transversal mech. characts., stress conc. problems *(Ukrainian)* 77—54876
- plate, thick, containing eccentric spherical cavity, transverse bending stresses 78—63288
- plate, thin, homogenisation, periodic and symm. structure *(French)* 77—39222
- plate, thin, under elastic bending, optical method for slope and curvature contours 79—37259
- plate, thin circular, bending, parabolic loading over concentric elliptic limacon 78—59299
- plate, three-layered, weakened with cylindrical cavities, stressed state determ. for bending problem *(Russian)* 78—22263
- plate, variable thickness, on elastic foundation, bending, closed form soln. 80—79179
- plate, viscoelastic, heated, bending, Kelvin Voigt model 80—106731
- plate and shell bending, finite elements by mixed formulations 78—38217
- plate bending, finite element anal. 78—46
- plate bending, penalty finite element method 77—35062
- plate bending, powerful finite element method for computing 78—1583
- plate bending, reduced and selective integration techniques in finite element analysis 78—42552
- plate bending, simplified Reissner theory 78—18202
- plate bending, transient problem, variational and reciprocity principles 77—50898
- plate bending analysis using extended field method 80—38311
- plate bending theory, optimal thickness distrib. *(Russian)* 78—63295
- plate bent with clamped edges, polyharmonic functions in elasticity theory 78—13927
- plate boundary and extension problems, stress intensity factors, finite element anal. 79—55341
- plate contiguous to fluid, shock loading, bending 78—90765
- plate deflection theory, soln. of biharmonic eqn. 77—80068
- plate integration of triangular finite elements 77—13591
- plate vibrating in water, stress meas. by interferometric holography 79—3653
- plate with aperture, bending moments, exact. soln. 78—94598
- plate with bend interaction, numerical calc. method for stress and deflection *(Japanese)* 80—23919
- plate with circular hole reinforced with strained annulus, stress distrib. *(Ukrainian)* 79—50591
- plate with crack, effect of couple stresses *(Ukrainian)* 77—31258
- plate with rectilinear thin walled elastic inclusion, bending stress state *(Russian)* 79—81736
- plate with sharp angled holes, bending *(Russian)* 78—34045
- plate-beam interaction, bending in plane of plate *(Russian)* 80—1428
- plate-bending elements, first- and second-order, variational principles, numerical convergence 80—48576
- plates, annular, clamped edges, asymmetric bending, Ritz method 80—58907
- plates, circular, variable thickness, numerical solution for flexure 80—99951
- plates, elastic, optimum bending and extension *(Russian)* 80—38259
- plates, laminated, cylindrical bending, random loading, dynamic response 80—58902
- plates, laminated anisotropic composite, penalty plate bending element 80—96200
- plates, laterally loaded, expt. soln. by method of caustics 77—65724
- plates, micropolar, complex variable treatment of bending 78—9565
- plates, orthotropic curved, bending behaviour, nonhomogeneity effects 80—23903
- plates, rectangular, with internal rigid support, bending vibration 80—102981
- plates, rectangular and circular, bending, singularity function method 80—74740
- plates, ridigity matrix, triangular finite elements *(Russian)* 80—74739
- plates, simply supported, under uniform loading, caustics 78—22277
- plates, thick, bending anal. *(Russian)* 79—10485
- plates, thick, thermally loaded, 3-D anal. 80—33459
- plates, thin, finite element anal., variational principle, simplified modified potential energy technique 80—52029
- plates, thin and moderately thick, serendipity cubic displacement hybrid stress element 80—96202
- plates, thin rectangular elastic, bending, finite difference anal. 79—46181
- plates, variable thickness annular, axisymmetric bending 79—46193
- plates of arbitrary contour 77—54902
- plates of arbitrary shape, limit anal. for plastic bending 80—14584
- plates with flows or cracks; twisting and bending theory 79—64545
- PMMA/PVC, cracking in layered composites 78—95808
- polycarbonate, criterion for craze nucleation 78—19881
- polycarbonate blends, yield and deform. behaviour, impact modification 77—36572
- polyester polymer concrete, longitudinal deform. modulus study is creep conditions *(Bulgarian)* 80—71685
- polyethylene, low density, SEM exam. of environmental stress cracking 78—53011
- polyethylene, pyramidal crysts., soln.-grown, collapse mechanics 78—76713
- polymer, soln.-grown cryst., diffr. line-broadening, bending contrib. 78—75574
- polymer composite anisotropic plates, stress conc. around holes with shear strain taken into account 80—43618
- polymer cyclic deformation amplitude, automatic meas., apparatus design 78—85082
- polymeric joist, bending calcs. *(Rumanian)* 77—68396
- polymers, fatigue life, determ. from reheat temp. 79—61724

bending continued
polymers, hydrostatic extrusion effects on subsequent mechanical behaviour 77—90392
polystyrene, fracture toughness eval. with surface crack specimens 79—15777
polyvinylidene fluoride, bending piezoelectricity 77—12319
porcelain-metal cermet, stress determ., meas. method *(German)* 80—76425
portal frame, elastic-perfectly plastic behaviour under column axial force variations 79—7296
post yield fracture mechanics analysis of 3-pt bonding specimens rel. to toughness testing 77—56168
prebending measurement methods, plate, compression osteosynthesis appl. *(German)* 77—40895
prefracture zone, similarity conditions in vicinity of contour of microcrack *(Russian)* 78—30233
pressure-shaping components, glass bending monitoring 77—796
prestressed beam, dynamic bending response 77—39230
prism bending to helical form, formal perturbation scheme 78—55558
quarter plate support, planar flexibility depend. on fillet radius 80—5944
quartz crystal plate, elastically bent, diffr. of pulsed thermal neutron beam 77—43116
quasi-static deflection of thin rectangular plate due to transient heating 77—72199
rapidly rotating compressed rods, stability 80—79189
rectangular plate, superpower degeneration of boundary layer of angular points *(Russian)* 80—74776
rectangular plate of variable thickness, bending under normal variable loads 79—37205
rectangular plate resting on Pasternak-type elastic foundation, large deflection 78—38215
rectangular plate with fins, stress anal. under bending, approximation theory *(German)* 79—90144
rectangular plate with mixed fixing conditions on the outline 80—69696
rectangular plates, flow-induced bending 77—80088
rectangular prisms, galloping in smooth and in turbulent flow 77—75840
red blood cell elastic deforms. 77—56400
reinforced concrete, lower bound anal. for torsion 78—35436
reinforced concrete curved beam, expt. investigation of collapse 77—90404
reinforced cylindrical shell, tranverse bending rel. to rigidity of local insertions 79—90154
reinforced open cylindrical shells, bending stability 79—41581
reinforced plastics, failure of thin walled flexural structures 80—10209
reinforced polymer, fatigue testing machine, materials in pure bending 77—1906
reinforced ring, shear failure mechanism in bending 77—72189
reinforced shell of revolution, failure in bending 79—90185
reinforced tube, bending and flexure 78—51076
residual stress formation in explosive welding 79—83285
resonant bending fatigue apparatus for approx. determ. of dislocation density 77—86279
rhombic plates uniformly loaded over concentric circle, Taylor series expansion of Schwarz-Christoffel transformation 80—5962
rigid-plastic beam, shear to bending response to blast type loading 77—54891
ring of micropolar elastic material, displacement soln. 77—19535
ring subjected to distributed impulsive load, dynamic response 78—13946
rings with circular cross section, vibrations 79—90172
rocks, form and stress state of high-amplitude longit. folds 77—9382
rod, elastoplastic, dynamic bending and residual deformation *(Russian)* 80—75293
rod and plate, fatigue strength in bending, small number load cycles 77—86183
rod in penetrating liquid, exam. of lengthwise bending 80—5955
rod with distributed load, lateral buckling as spatial bifurcation problem, Mathieu eqn. solns. 77—50940
rod with nonlinear curvature, dynamic stability theory, lateral bending problem under torsion *(German)* 78—54
rods, elastic, large deflections and rots., asymptotic anal. 79—50584
rods, ideally elastic, nonlinear bending, discrete anal. 77—46953
rods, second order theory for bending and torsion *(German)* 79—68598
rods with thin perforated walls, bending, finite element method *(German)* 80—14591
rotational shells, geometric stiffness matrices for finite element anal. *(French)* 77—68464
rotor blades, flapwise and chordwise bending, and torsion 77—39251
Saint Venant's solns. in rod and beam theories 80—69676
Saint-Venant pure bending problems, transient creep bounds 80—19249
sandwich circular cylindrical shell, natural vibrations 77—89062
sandwich composite beams, stress distrib. meas. under four-point bonding, multilayer builtup theory 80—96190
sandwich plate, modified Berger method, large thermal bending anal. 78—63297
sandwich type shells, elastic Cosserat surfaces, small bending and stretching 78—22264
satin woven glass cloth fibre reinforced plastic, fatigue life under random loading *(Japanese)* 80—55509
saturated elastic half-space with partially embedded elastic bar, quasi-static bending 80—79145
screw connections, bend and tension loaded, hysteresis *(German)* 78—87312
semielliptical surface cracks, stress intensity factors in bending *(Japanese)* 78—26089
semiinfinite strip with clamped sides, bending, Papkovich-Fadle eigenfunction completeness 80—58929
shadow methods, reflected, transmitted, obs. of sharp V-notched plates, under pure bending 78—90777
shafts, endurance subject to bending and torsion *(Russian)* 79—72831
shafts, with abrupt changes of section, flexibility of shafts 78—90711
shallow anisotropic shells of double curvature, weakened by hole, bending problem 79—90151
shallow shell bending, mixed variational eqn. 80—77618
shear stress bounds in Saint-Venant's theory of flexure 77—13608
sheet bending of additional deformation zone loading 77—23899
sheet materials, bend testing unit 77—25214
sheet metal, roll bending on machine with elastic element, bending moment determ. 78—6948
sheets and beams, blank maximal deformations, length and thickness in plastic bending 77—19550

bending continued
shell, circular cylindrical, infinite, dynamic stresses under conc. impulsive loads 77—42765
shell, cylindrical, cantilever, dynamic deforms. and stresses under impulsive loads 79—27504
shell, cylindrical, elastoplastic plastic buckling in pure bending 80—19257
shell, cylindrical, isotropic, elastic stability, critical load analysis 80—83744
shell, cylindrical, with spiral groove, Kirchhoff's boundary conditions deduced from energy principle 80—74741
shell and surface rigidity, pseudobending, vibrs. and stability loss *(Russian)* 80—33470
shell bending, static geometric analogy in classical shell theory *(Russian)* 79—37159
shell buckling rigidity characts. *(German)* 80—48608
shell of double curvature, bending in zone of elliptical loading area, stress anal. *(Russian)* 79—50593
shells, axisymmetric, unsymmetrical bending, elastoplastic anal. 80—92065
shells, bending waves 77—50971
shells, long cylindrical, plastic buckling under pure bending 80—64409
shells, oval cylinder, orthogonally stiffened, buckling under axial compression 80—74777
shells, thin, doubly curved, numerical integration of triangular finite element 80—92044
shells, thin orthotropic elliptical cylindrical, elastic collapse under combined bending and press. 80—48589
shells, thin walled, elastic, Rayleigh method anal., energy calcs. 77—65677
shells, toroidal, quasibending of surfaces *(Russian)* 80—79170
shells of revolution, bending, physical and geometrical nonlinearity, finite element method *(Russian)* 80—33471
Si crystal, elastically bent, strain distrib. determ. by X-ray intensity meas. 79—50928
simple plate bending theory, approx. stress intensity factors 80—43612
simplified hybrid displacement method, critical assessment 77—14920
simply supported circular, cylindrical panel, vibration with initial bending 79—32343
simply supported orthotropic elliptical plate, bending, straight normals hypothesis 79—86354
single crystal, equilib. face, surface relief form. during annealing 78—47651
single mode and graded-index multimode fibre cable random bend losses 80—58741
single-mode optical fibre microbending loss and pulse distortion analysis 78—1395
sitall cylindrical shell reinforced with internal stiffening ribs, stress-strain state under external press. 80—71684
skin wrinkling, human, using model of thin elastic shell on continuum foundation 77—52819
smooth circular pipe bends, under combined in-plane bending/internal press. creep anal. 77—46936
smooth circular pipe bends, under combined in-plane bending/internal press. creep anal. 77—50927
smooth curved pipes, external bending, effect of thickness variations 80—69702
smooth pipe bend, plastic limit moment under in-plane bending 80—23906
splint making materials, comparative study 79—39606
square box sections—experimental behaviour under combined bending and compression 79—61657
stability of parallel cracks in solids reinforced by bars 80—43671
static-geometric analogy in thin shell struct. eqns. 77—80087
steatite, ceramic, exam. of thermal damage by strength meas. 78—84997
steel, 15G2AFDps and boiler steel, fracture toughness determ. from fatigue test results in circular bending 78—15526
steel, 17KhG2SAFR, 45 and fatigue cracking under cyclic bending, 40 kH *(Russian)* 78—31506
steel, 18% Ni maraging, fatigue strength, effect of ageing treatment 78—23805
steel, 30KhGSA, fracture toughness, tempering effects 77—90463
steel, 40, elastoplastic bending of beams of various cross section 78—3196
steel, 4340, H_2 embrittlement, stress state, thickness and delayed failure in bending 80—71746
steel, 45, depth length relationship of fatigue crack developing in circular specimens during bending 79—11705
steel, 45, EHI961, EHI437B, fatigue strength, effect of residual stresses and cold working 77—56101
steel, age-hardenable, relation between fatigue S-N and P-N charact., definite fatigue limit *(Japanese)* 77—8938
steel, alloy, C-Cr-Mo-V, exam. of fracture toughness and critical flow anal. 78—72848
steel, alloy, fracture and fracture energy, subject to static, impact and repeated impact bending 77—63799
steel, alloy, rectangular beam, stress-strain anal. of cyclic plastic bending and torsion 78—90734
steel, alloy, type 36NKhTYu, plastic deformation, effect of surface condition on initial stage 78—84929
steel, C, and high strength, fatigue crack propag. under periodic overstressing, design criterion *(Japanese)* 79—20166
steel, C, bainitic, microstruct. and cleavage resistance 77—52481
steel, C, fatigue crack exam. using slip initiation phenomena *(Japanese)* 77—8930
steel, C, prestrain effect on non ductile transition temp. and bending speed relationship *(Japanese)* 78—84919
steel, C, rotating bending fatigue strength, high tensile load effect during stress cycling *(Japanese)* 77—52477
steel, C, rotating bending fatigue strength, periodic high tensile load effects *(Japanese)* 78—11313
steel, C, S15C, S35C, S55C, rotating bending fatigue strength, annealing in vacuum effects *(Japanese)* 78—11314
steel, C, unnotched, fatigue life estimation, under combined torsion and bending *(Japanese)* 80—93647
steel, C and alloy, restricted durability, subject to pure bending with rotation 77—90431
steel, C and low alloy, size effect in bending fatigue strength and its prediction 79—43411
steel, carburized, fractography of fatigue fractures 77—86137

bending continued
- steel, carburized fatigue, non-martensitic struct. effect, rel. to mean stress and residual stress *(Japanese)* 78—7024
- steel, case hardening and carbonitriding treatment, mech. props. testing *(French)* 77—59991
- steel, cast, plain C, C-Mn and low-alloy fatigue from notches 77—16678
- steel, Ck 45 alternating bending, fracture surface appearance *(German)* 78—52995
- steel, Cr, high strength, hot dip galvanized delayed fracture *(Japanese)* 78—15512
- steel, Cr (13 wt.%), tempered, quenched, fatigue resistance in corrosive medium *(French)* 78—23870
- steel, Cr-Mo, high tension, delayed fracture, fundamental study *(Japanese)* 77—48531
- steel, Cr-Mo-V (0.5, 0.5, 0.25 wt.%), creep crack growth in notched bend test, microstruct. effect 77—21261
- steel, crack propagation properties in rotating bending fatigue tests 77—32669
- steel, CrMo, cast, fatigue tests under varying stress amplitude and varying temp., amplitude damage *(Japanese)* 78—27605
- steel, dynamic fracture toughness meas. by instrumented impact bend and compact K testing 77—36718
- steel, effect of side-grooving on K_{IC} meas. by bending *(Japanese)* 78—35614
- steel, electroless Ni plated, fatigue strength, effect of P content of Ni film *(Japanese)* 77—52478
- steel, eutectoid, fatigue crack tip props. in rotary bending and cyclic torsion 77—32668
- steel, fatigue, low cycle, test results, least square deviation method 77—63796
- steel, fatigue limit estimation when subject to bending loads 77—21281
- steel, fatigue strength, statistical prop. *(Japanese)* 79—20169
- steel, fatigue strength with stress concentrator, mean compressive stress effect 77—21264
- steel, ferritic-pearlitic, low C, low alloy, low temp. effects on fatigue strength 79—5057
- steel, flat bars, stress meas. and calc. around drilled hole, with hole-gage-rosettes aid *(German)* 80—25757
- steel, hardened and casecarburized, fatigue crack initiation, propag. and termination, notch depth effects *(Japanese)* 78—7022
- steel, heat treated SCM3, SNCM8 and SUS403, statistical fatigue props. *(Japanese)* 77—48532
- steel, high strength, low alloy, fatigue crack growth from a surface flaw 78—68803
- steel, high strength, strain concentration and occurrence of fatigue cracks in welded joint *(Japanese)* 77—90452
- steel, high-strength, fatigue crack growth rate and crack tip shapes, cyclic bending *(Russian)* 80—71740
- steel, high-strength and mild, fatigue of V-bent specimens 77—16681
- steel, high-strength maraging, N18K9M5T, improvement in mech. props. under applied stress influence during ageing 80—20985
- steel, high-strength plate with soft cladding layer, failure resistance during repeated static bending 77—44406
- steel, hypereutectoid, thermomech. treatment, Fe_3C distrib. and yield point *(German)* 79—52243
- steel, low alloy, 10KhSND, 16G2AF, welded joint low-cycle fatigue during crack form. and propag. during biaxial bending 79—11704
- steel, low alloy, press. vessel, fracture toughness in post yield regime 77—16671
- steel, low alloy, radiation embrittlement, heat treatment effects 78—19893
- steel, low C, fatigue crack propagation in smooth specimen, strain ageing effect *(Japanese)* 79—20163
- steel, low C, fatigue life under programmed loading including stress lower than fatigue limit *(Japanese)* 77—8934
- steel, low C, fatigue strength under rotating bending and torsion, understressing effects *(Japanese)* 78—44201
- steel, low C, fractographic study of stage 1 cracking, endurance limit *(Japanese)* 77—8936
- steel, low C, transition behaviour, bending speed effect *(Japanese)* 78—11222
- steel, low C, tufftrided, fatigue strength ahd microstructure change by reversed stressing *(Japanese)* 78—15511
- steel, low C, type 17G2SF, crack critical opening evaluation using plasticity diagram 80—45382
- steel, low C, under rotating bending and torsion, overstressing effects *(Japanese)* 77—8935
- steel, low-alloy, testing cracked specimens for impact bending, expt. planning method appl. 80—71831
- steel, low-C, sheet, thin, residual stresses determ. after bending 78—60708
- steel, maraging, Ni-Co-Mo (18, 8, 5 wt.%), fatigue strength charact. *(German)* 77—21241
- steel, martensitic and austenitic, fatigue, scale effect, structural parameter effect in rotary bending *(French)* 78—23822
- steel, medium C, behaviour under combined fatigue and wear 78—3236
- steel, medium C, difference between strain energy changes during repeated bending and rotatory bending fatigue tests *(Japanese)* 78—39894
- steel, medium C, tempered, normalised or quenched, statistical property of fatigue limit, press-fitted axles *(Japanese)* 77—12693
- steel, medium C, type 45, sheet, working life, effect of dynamic loading type 77—21278
- steel, metastable austenitic, resistance to failure 77—4852
- steel, mild, exam. of fatigue damage, using thermography 78—92356
- steel, mild, fatigue crack growth from a surface flaw 78—68803
- steel, mild, fatigue strength, effect of grinding surface *(Japanese)* 77—48533
- steel, mild, friction welded joint, strain distrib. and fatigue damage under rotary bending *(Japanese)* 80—30076
- steel, mild, programmed fatigue crack propag., crack tip residual stresses 77—36644
- steel, mild cylindrical shells, limit loading under loop bending moment 78—80581
- steel, Mn-Cr, blank hardened, shot peening effect on bending fatigue strength *(German)* 78—35402
- steel, Mn-Cr, normalised, shot peening effect on bending fatigue strength *(German)* 78—35401
- steel, nuclear pressure vessel, type A533B-1, three point bending, yield stress, exam., Charpy V-notch and precracked specimens 78—92310
- steel, perforated bent sections, microstruct. near holes 78—23725
- steel, plain C, X-ray diffr. study of low cycle fatigue damage 77—66700

bending continued
- steel, plastic deform., density changes *(German)* 80—60908
- steel, pressurised tubes under dynamic bending and torsional loading, inelastic deform. 77—77549
- steel, rolled, effect of inclusions on torsional fatigue 78—92314
- steel, rotating bending fatigue tests in hydrostatic environment 77—21343
- steel, sheet, thermomechanical bending, induction heating calc. 79—52280
- steel, sintered constructional, resistance to cyclic impact loads 77—77583
- steel, spring leaf retainer with variable ductility, processing error, cold working error *(German, English)* 79—70267
- steel, stainless, 20% cold worked 316, in-reactor stress relaxation in bending 77—42079
- steel, stainless, 304, bend test ductility of irrad. specimens for LMFBR appls. 80—104235
- steel, stainless, AISI 316, irrad. creep in bending at low fluence, LMFBR fuel duct deform. 79—61680
- steel, stainless, corrosion fatigue cracking in NaCl aqueous solution, fractographic anal. *(Japanese)* 78—53023
- steel, stainless, global bending response analysis of elastic and viscoplastic nuclear shipping cask structures subjected to impact loading 80—76301
- steel, stainless, irradiation creep in bending 77—42078
- steel, stainless, martensitic SUS 403-B, high temp. rotating bending fatigue *(Japanese)* 77—59906
- steel, stainless, martensitic SUS 403-B, high temp. rotating bending fatigue 78—60756
- steel, stainless, reinforced glass matrix, vibr. damping anal. rel. to internal friction 80—40413
- steel, stainless, ring notched samples, charge in fatigue crack growth rate 80—50716
- steel, stainless, SUS 304B, tufftrided, fatigue strength *(Japanese)* 77—77572
- steel, stainless 304, creep and fatigue crack propag. at elevated temps., fract. mech. and fractography 77—21279
- steel, stainless 304, stress crack initiation in chloride soln., role of corrosion pits *(Japanese)* 78—92397
- steel, statistical fatigue props. of SM50A for welded structures *(Japanese)* 79—20168
- steel, structural, low temp. fatigue strength 77—21273
- steel, structural, sharp notched bending specimens, fracture stress, temp. depend. anal. 77—56062
- steel, structural, type St 37, microstruct. rel. to fracture toughness and fracture load of bending specimens *(German)* 80—89352
- steel, structural bending moments and tensile creep, relaxation bending test device 79—70245
- steel, transforms CC types M6 and M3N, elastoplastic bending, insulating coating influence on magnetic losses *(Russian)* 79—100284
- steel, tubing, viscoplastic bending 78—35464
- steel, tufftrided, fatigue strength estimated from heat generation in specimen *(Japanese)* 77—52476
- steel, tufftrided, residual stress and fatigue crack propag. *(Japanese)* 77—48536
- steel, type 20, fatigue, low cycle, exam. of damage accumulation rule', for loading in air and H impregnating medium 78—64649
- steel, type SAE 1008, finite fatigue life distribs., various load-time histories 80—97589
- steel, unnotched C-35, cumulative damage rule based on knee point of S-N curve 77—25156
- steel, welded joints, durability in repeated impact loading, low temp. effects 77—63800
- steel 45, fracture surface obs. during fatigue failure 77—86185
- steel 45G2, fracture resistance, from impact bending tests and oscillograms 80—61047
- steel C, fatigue life and cumulative fatigue damage under const. stress cycling, plastic strain range effect *(Japanese)* 77—8940
- steel Kh18N10T, substructure after low-endurance fatigue in pure bending *(Russian)* 77—81311
- steel Kh18N9T, fractographic features of rupture, rel. to struct. changes 77—63801
- steel reinforced concrete beams, mech. strength determ. under combined bending and tension 78—60749
- steel sheet, hot and cold rolled, cold formability, notched tensile test and stretch bend test *(German)* 80—61031
- steel structural bars, subjected to plastic bending, random fatigue analysis *(Japanese)* 78—27619
- steel tube eversion, effect of material and geometrical parameters 79—15690
- steel tubes, 12 Kh1MF, cross-section shape change, during creep of bent tubes loaded with internal pressure 78—31485
- steel tubes, square section, collapse in bending 80 -25792
- steel-Cu M3 bimetal, eutectic alloy, crack development, failure energy capacity *(Russian)* 80—40480
- steel-steel bimetal rolled plate, low-cycle fatigue in bending 79—91794
- steels, C, H_2 embrittlement after patenting and cold deform. *(Russian)* 79—29175
- steels, S 45 C, SK 5 SCM 3, SNCM 8 and SUS 403, heat treated JIS, statistical fatigue props. 78—44222
- steels, wide plate and V-notch bending tests evaluation on basis of materials mechanics *(German)* 80—66571
- step-index optical fibre and cable transmission characteristics 78—1404
- stiff bending plates, stress-strain states, finite element effectiveness, polynomial approx. *(Russian)* 80—58921
- stiffness formulation of unbalanced anisotropic sandwich plates 77—84168
- strain diagram plotting from data obtained during elastoplastic bending or torsion 77—81371
- strain in plates, direct determ. using projected gratings 79—32420
- stress analysis of cylindircal shell with rigid circular inclusion 79—14267
- stress corrosion testing device, lab. and autoclave testing 79—52502
- stress relaxation in bending, alternative eqns. 79—7294
- stress relaxation in complex system, apparatus for investigation 77—23922
- strip with semi-elliptic notches or cracks, stress anal. by rational mapping function 79—14257
- structural anal., soln. by orthogonal collocation 78—51063
- structural anisotropic domes composed of cylindrical shells, numerical anal. 80—19260
- structural element design calc. under creep conditions 80—48598
- structural elements, mechanical calc. of bending *(Chinese)* 79—72834

bending continued

- structures of discontinuous shape, finite element analysis *(Japanese)* 78—83238
- struts, plain channel section, beyond local buckling load 77—46947
- submarine optical fibre cable unit design and test results 78—46799
- substrate bending during thin film evaporation due to temp. difference between substrate faces 80—54571
- substrates, instantaneous bending during thin film deposition, intrinsic stresses, cantilivered plate method anal. 80—54570
- superconductor, multifilamentary, flexibility and elec. characts. 77—24990
- surface crack in a clamped circular plate subjected to uniform lateral pressure, bending stress anal. 80—74811
- surface crack shape change in bending fatigue, resonant fatiguing apparatus 78—72950
- surfaces, Beilby layer generation, plate distortion by heat *(German)* 77—73370
- tail-wheel struct. of light aircraft, large deflection anal. 78—83272
- telescope secondary mirror, flexure, elasticity theory *(French)* 77—14789
- test apparatus for high press., high temp. 80—85126
- test machine for fatigue cracking kinetics in pure bending *(Russian)* 79—52477
- thermal bending of thick rectangular plates 79—94517
- thermal bowing of wire-wrapped fuel pins in the fast test reactor 80—42770
- thermal flexure of an infinite plate with a doubly periodic array of holes 79—68586
- thermobimetal, specific bending, effect of functional parameters and stabilizing heat treatment 77—89555
- thermoelastic deformation, second order effects 80—92051
- thermoplastic materials, flexure testing 77—86087
- thick cylinders, static and dynamic instability 80—23923
- thick membrane strip, effect of shearing prestress, static case 80—10137
- thick plate, with elliptical hole, subjected to simple out of plane bending, photoelastic anal. to determ. stress distrib. 79—37187
- thick plate, with spherical cavity, stresses under transverse bending 77—23874
- thick plate flexure by arbitrary load *(Russian)* 78—22287
- thick plates, 3-dimens. refined elasticity theory, bending and torsion 80—64375
- thick rectangular plate bending under own weight *(Japanese)* 78—22284
- thick-walled cylinder subject to internal press. and bending, full plastic anal. at collapse stage 78—22275
- thin annular plate, inner clamp carrying bending moments 77—89031
- thin beams of cambered section, bending stiffness props., pretwist effects 80—48605
- thin circular quadrant, singularly loaded, with clamped radial edges and free circular edge 78—63300
- thin elastic layer, bending by rigid die 80—14627
- thin elastic plate, bending problem soln. in fracture mech. using specialized finite element technique 79—77011
- thin orthotropic plates, bending stability and free vibration 79—3961
- thin plate, interpolation of function of two variables *(French)* 77—45700
- thin plates, bending anal. hybrid stress finite element model 80—96201
- thin plates, limit load and elasto-plastic bending, finite element anal. 79—27544
- thin plates, optimal loading calc. by duality theory *(Russian)* 78—63409
- thin shell, 9-node Lagrangian element 80—23888
- thin walled bar, elastic-plastic behaviour, expt. *(Croatian)* 77—35060
- three point bend tests, notched or precracked specimens, load displacement measurement and work determ. 78—53054
- three point bending tests, calc. of yield stress, review 78—92310
- tibia flexural wave propagation, discontinuous model and in vitro study 77—29169
- Timoshenko beam, coupled bending and twisting vibration 77—58584
- Timoshenko beam, shear coeff. *(German)* 80—106729
- toroidal field coils, bending-free, for Tokamak reactor 78—55012
- toroidal shells and tubes, flexible shell theory and buckling 79—23231
- transient problems, bounds and approx. solns. 80—43623
- transversally isotropic plate, bending by smooth stamp, contact problem *(Ukrainian)* 80—38346
- transversely isotropic plate with hole, edge supported, shear compliance in bending and torsion 77—2543
- trapezoid plate, freely rotating, mechanical effects, calc. method *(German)* 80—106728
- triangular plate bending element, fast calc. algorithm 79—72830
- tube, semimomentless theory and complete thin shell eqns. *(Russian)* 77—23903
- tube, viscoelastic, containing flowing fluid, bending vibrs. 79—94521
- tubes, circular cylindrical, critical bending moment 77—68468
- tubes, infinitely long cylindrical elastic, collapse under bending, press. and axial loads 78—18204
- tubes, simply supported, surface stress meas. 77—46932
- variable-thickness conical shell, transient stresses in clamped section 77—89051
- VC-EVAC graft copolymer, mech. props., effect of heat treatment *(German)* 77—63702
- vibrating isotropic beams, Timoshenko's correction for shear 77—72226
- vibrating plate like struct., displacement and strain meas. using time average holography 79—46272
- vibrations in their plates layer potential method of solution *(French)* 78—59336
- viscoelastic flat strip, stationary bending plane determ., under moving load *(German)* 80—1446
- viscoelastic orthotropic rectangular plates conformal orthotropy concept 78—38204
- viscoplastic materials, elastic, rate-independent limit of constitutive eqns. 80—74753
- von Karman plate bending equations approx. 79—50598
- wedge shaped notches with large flank angles, plane strain general yielding under loads and bending 79—18808
- wind-induced bending torsional galloping vibration of rigid body, minimal wind velocity determ. 80—48623
- wood, set, force induced from moisture recovery of drying set *(Japanese)* 77—77537
- wound wires, enamel insulated, elongation plus flexibility 80—20999
- Zircaloy 4, stress relaxation in bending 78—68719
- Zircaloy-4, stress-relieved and cold-worked, stress relaxation in bending at 673K 80—93609
- Ag film, intrinsic stress meas. 80—71696
- Ag, surfaces, dislocation climbing, etch pit investig. 79—19260

bending continued

- Al, adhesively bonded and weld bonded aircraft struct. subjected to acoustic excitation, determ. of sonic fatigue life 78—92351
- Al alloy 01205, mech. props. at cryogenic temps. 79—29206
- Al alloy 2017-T3, part-through crack propagation, by alternating bending stress *(Japanese)* 78—27607
- Al alloy 2024, loading sequence, normal and reversed sequence effect 78—68791
- Al alloy 2029-0, circular plates with work hardening, nonlinear behaviour, experimental deflection and strain data 79—38893
- Al alloy 5056, fatigue crack growth in ultrahigh vacuum *(Japanese)* 77—56088
- Al alloy 7075, precipitation hardening, toughness and microstruct. *(Japanese)* 78—15509
- Al alloy D16, elastoplastic bending of beams of various cross section 78—3196
- Al alloy D16, fatigue props. eval. 79—15750
- Al alloys, fatigue crack propag. under periodic overstressing, design criterion *(Japanese)* 79—20166
- Al alloys A5083 and A7075, statistical fatigue props. 79—5060
- Al, alternating bending of single crysts., shear strain accumulation and microstrain distrib. *(Russian)* 78—60706
- Al beam, exam. of elastoplastic contact strength law, using impact bending *(German)* 79—43365
- Al bicrystals, isoaxial, fatigue crack initiation in grain boundary affected regions *(Japanese)* 80—89338
- Al bronze, anisotropic bend ductility in single phase alloys 78—60726
- Al, cold rolled, X-ray diffr. and optical microscope exam. of fatigue damage *(Japanese)* 78—84976
- Al crystal, lattice rotation during tensile deform., X-ray diffr. meas. 80—49231
- Al, fatigue damage, test temp. effects *(Japanese)* 77—52475
- Al film, intrinsic stress meas. 80—71696
- Al, high-temp. internal friction peaks, deformation and annealing effects 77—32615
- Al, laminate, free-free plates, predicted and expt. natural modes 79—10520
- Al, polycrystalline, fatigue damage detection by exoelectron emission meas. *(Japanese)* 77—55871
- Al, stiffness and damping in creep 78—23780
- Al, surface fatigued single crystal, inhomogeneous positron trapping 77—90216
- Al-Cu-Mg alloy D16T, fatigue cracking under cyclic bending *(Russian)* 78—31506
- Al-Cu-Mg-Mn-Si-Fe, endurance with cyclic bending, effect of loading conditions 80—50724
- Al-Cu-Mg-Si-Mn alloy AK8, fatigue strength, effect of residual stresses and cold working 77—56101
- Al-Fe-Si commercial alloy, elevated temp. low cycle fatigue behaviour under rotating bending 79—47766
- Al-Zn-Mg-Cu, alloy 7075, fatigue, loading sequence, normal and reversed sequence effect 78—68791
- AlN, thermal cond. and stability at high temp. 78—47610
- Al_2O_3, ceramic, delayed fracture 77—44342
- Al_2O_3, evaluation of crack resistance and crack velocity, using controlled fracture experiments 78—72881
- Al_2O_3, polycrystalline, fracture probability under static bending and tensile loading at 800°C *(German)* 78—23806
- Al_2O_3 rods, quenched, exam. of contact induced strength degradation 78—76731
- Al_2O_3 strength-size relation 77—21255
- Al_2O_3, stress value determination by bending tests, comparison with crack tip theory 78—67154
- Al_2O_3-AlN, creep 77—21235
- Al_2O_3-SiO_2 (3 wt.%), J-integral meas. at high temps. *(German)* 80—93624
- Al_2O_3-SiO_2 fibre/mineral wool fibre composites, exam. of strength and shrinkage characts. rel. to Al_2O_3-SiO_2 fibre content effects 79—20105
- Al_2O_3-SiO_2 glasses, thermally toughened, residual compressive stresses evaluation 78—31523
- Al_2O_3-TiO_2 (1 wt.%), with and without α-Al_2O_3 laminar crystals, bend tests 77—16531
- Au/Ag couple, diffusion induced stresses and plastic deform. 78—26736
- Be-Cu alloy stress relaxation in bending, 63° to 343°C 80—50693
- C fibre reinforced epoxy phenol plastic, resistance to interlayer shear and elec. resistivity 78—68752
- C fibre reinforced epoxy resin, transverse creep compliance, time and temp. depend. *(Japanese)* 80—45358
- C fibre reinforced plastics with mixed fibres, exam. of fracture toughness and shear strength 79—20151
- C fibre reinforced plastic, fractography of fracture surface under three-point bending *(Japanese)* 80—55506
- C, pyrolytic, high-temp. deform. under mech. loads 77—16644
- C steel, type 45, inelasticity under cyclic strain in active media 78—80613
- $Co_{80}B_{20}$, amorphous metal ribbon, stresses, magnetoelastic anisotropy and zero-field mag. domain struct. 80—44896
- Cr-Mo, structural carbonitrided at low temps., rotating bending fatigue strength *(Japanese)* 77—48534
- Cr-Ni, fatigue, low cycle, test results, least square deviation method 77—63796
- Cu alloys, flat spring, mechanical props. in bending, stress relax. test, 23 to 232°C 78—72806
- Cu, dislocation density in fatigue, approx. determ. by resonant bending fatigue apparatus 77—86279
- Cu plates, thin, dislocation-dislocation interaction inducing cross-slip, X-ray topographic anal. 80—49233
- Cu, single crystals, effect of stacking fault energy on extrusion and intrusion development 78—72826
- Cu single crystals, positron trapping by edge dislocations, produced by bending 78—80606
- Cu-Al (10.5 at.%), dislocation generation and displacement in single crystal in bending 79—60368
- Cu-Ni (20 wt.%) alloy, contour plate for relay appl. use of Larson-Miller method *(Japanese)* 80—55454
- Cu-Ni tubing, viscoplastic bending 78—35464
- α-Cu-Zn (5.3 to 21.8 wt.%), single crystals, effect of stacking fault energy on extrusion and intrusion development 78—72826
- Er-Tb, elasticity modulus, ΔE-effect, internal friction, magnetic transformations *(Russian)* 79—91723
- Fe, Armco, cyclic deform. in presence of H_2 *(Russian)* 77—16728

bending continued
Fe, Armco, inelasticity when under cyclic strain, in active media 78—80613
Fe, casting, fatigue strength, section size and surface struct. effect *(Japanese)* 79—20170
Fe chromised layers, fatigue fracture kinetics study by reverse bend tests *(Russian)* 78—31511
Fe-Al-Si (6.22, 9.63 wt.%), bending test under high press., high temp. 80—85057
Fe-Co-Ni-Al (35, 14.5, 7.2 wt.%), high-coercivity, substructure and texture change during bending and upsetting 80—21037
Fe-Ni-Co-Ti, shape memory effect after appl. of bending moment *(Russian)* 80—45305
Fe-Si (3 wt.%), magnetisation variation during bending oscills., rel. to ΔE effect *(Russian)* 80—65983
Fe-Si-Al, Sendust, ribbon-form, prep. by rapid quenching, mech. and mag. props. 80—71611
Fe-Ti(Nb), internally nitrided, mech. props. 77—44307
$Fe_{81.5}B_{14.5}Si_4$, amorphous metal ribbon, stresses, magnetoelastic anisotropy and zero-field mag. domain struct. 80—44896
$Fe_{32}Ni_{36}Cr_{14}P_{12}B_6$ Metglas, bending deform., shear band form., high-speed cinematographic obs. 80—89322
$Fe_{40}Ni_{40}P_{14}B_6$, metallic glass, bending tests, evidence of ideal elastic-plastic deform. 80—97543
GaAs-$Ga_{0.7}Al_{0.3}As$ (001), (211), threading dislocation in single layer heteroepitaxial struct., bowing 79—65341
GaAs-$Ga_{1-x}Al_xAs$, DH, dark line defects induced by mech. bending 77—683
GaP, birefringence observations of strain and plastic deform. 80—50678
Gd-Tb, elasticity modulus, ΔE-effect, internal friction, magnetic transformations *(Russian)* 79—91723
InSb, plastically bent single crysts., dislocation struct. obs. 78—59816
LiF film, intrinsic stress meas. 80—71696
$LiNbO_3$, Fi diffused, single-mode waveguide, comparison of bending losses in integrated optical circuits 80—83684
Mo alloys, fusion reactor first wall and blanket material, props. for struct. appl. 80—30071
Mo, block boundary dislocation struct. singularities under high temp. steady state creep conditions *(Russian)* 79—90670
Mo, irrad. between 425 and 1000°C, ductility in bending 80—39164
Mo, recrystallised sintered sheet, C addition effect on ductility 79—8319
Mo-Hf-B-C, low C, sheet, strength 77—1859
Mo-Ti, irrad. between 425 and 1000°C, ductility in bending 80—39164
Mo-Zr-C (0.08, 0.02 wt.%), struct. and banding tendency, thermomechanical treatment effects 77—86063
NaCl, bent single crystal, equilib. face, surface relief form. during annealing 78—47651
Na_2O-CaO_2-SiO_2 glass, stressed, chemical reaction in water vapour 79—91819
Na_2O-CaO-SiO_2, evaluation of crack resistance and crack velocity, using controlled fracture experiments 78—72881
Nb alloys, fusion reactor first wall and blanket material, props. for struct. appl. 80—30071
Nb, mixed state, Abrikosov vortices orientation depend. of elastic props. *(Russian)* 77—40007
Nb_3Sn, composite superconducting wire, critical current-bend strain relationships 80—93063
Nb_3Sn multifilamentary composite superconductor, reaction treatment, crit. current, transition temp. and bend props. 79—33430
Nb_3Sn, multifilamentary supercond., flexibility and elec. characts. 77—24990
Nb_3Sn, multifilamentary supercond., crit. current, bend tests 77—28335
NbTi, superconducting multifilamentary conductors, crit. current density, bending effects *(German)* 80—39727
Ni alloy, high temp., fatigue strength, temp. depend. 77—56100
Ni-Nb-Al, unidirectionally solidified γ/γ'-δ eutectic, fatigue crack propag. 79—29184
Ni-Zn ferrite, high temp. behaviour of grain boundaries under bending stress *(Japanese)* 77—1875
Ni_3Al-Ni_3Nb, eutectic alloy, crack development, failure energy capacity *(Russian)* 80—40480
$Ni_{0.5}Zn_{0.5}Fe_2O_4$ coarse grain polycryst. ferrite, diffusional creep *(Japanese)* 80—104238
PLZT ceramics, stress-induced ferrelec. transition, pseudoelasticity and shape memory, bending meas. 79—24274
Pb-Sb-Te-Cu-Sn, influence of specimen and grain size on mech. props. *(Russian)* 77—81297
$Pb_3(PO_4)_2$, ferroelastic, bending stress effect on domain struct. *(Russian)* 77—39623
Pd_2Si and PdSi films, on Si, stress obs. 80—80145
PtSi films, on Si, stress obs. 80—80145
Si, dislocation motion from indentation rosette 80—79798
Si, monocrystalline, effect of notch root radius on fracture behaviour 78—76751
Si, polycryst., on oxide-covered single cryst. Si substrate, deform. 78—26778
Si, single crystal, brittle fracture in axisymmetric bending, study at room temp. 80—81180
Si wafer, bending by thin polycrystalline Si film deposition and by film doping using B diffusion 79—95276
Si wafer, Ta sputtered induced stress meas., X-ray transmission topography 79—24434
Si wafers, process-induced in-plane distortion and wafer bowing 79—11048
Si:P, heavily doped wafer, anomalous bending obs. 78—10074
Si-SiO_2 interface metallisation induced stress meas., X-ray transmission topography 79—24434
SiC, hot pressed, brittle fracture and subcritical crack growth 78—72885
Si_3N_4, hot pressed, slow crack growth from controlled surface flaws 78—80632
Si_3N_4, sintering under high press., modulus of rupture tests 77—44202
TZM, irrad. between 425 and 1000°C ductility in bending 80—39164
Ti alloy AT-3, crack development in air, H_2, aq. H_2SO_4, electrochem. charact. *(Russian)* 77—70209
Ti alloy VT20, endurance in cyclic bending 77—63798
Ti, fatigue cracking, initial stage under bending and torsion *(Japanese)* 79—20165
Ti, fatigue fracture surface microstruct., electron microscope obs. 78—60834
Ti-A-V (6, 4 wt.%), castings, fatigue crack initiation 79—29186

bending continued
Ti-Al-Mn, endurance with cyclic bending, effect of loading conditions 80—50724
Ti-Al-Sn (5, 2.5 wt.%) alloy, fatigue under combined alternating bending and torsional stresses 77—8923
Ti-Al-U (6,4 wt.%), low and high cycle fatigue rupture at same load 78—3217
β-Ti-Mo-V-Fe-Al (8, 8, 2, 3, wt.%), exam. of stress induced H_2 migration 78—87823
U-Mo (10 wt.%), commercial alloys, influence of metallurgical factors on fracture processes *(French)* 78—60751
U-Nb-Zr (7.5, 2.5 wt.%), elastically bent, ageing induced shape instability 77—16622
U-Nb-Zr (7.5, 2.5 wt.%), texture development role in shape memory effect 79—87661
UO_2, superplastic creep 79—15730
V alloys, fusion reactor first wall and blanket material, props. for struct. appl. 80—30071
W, block boundary dislocation struct. singularities under high temp. steady state creep conditions *(Russian)* 79—90670
WC-Co, rupture of bending specimens, use of quantitative metallography and stereology *(French)* 77—28899
WC-Co, rupture stress, microstructure and other effects 77—73343
WC-Co, VK type hard alloy, influence of residual stresses on static strength 77—1862
WC-Co, various combinations, fracture characts. in bending, compression, and toughness tests 78—60808
WC-Co (10 wt.%), elevated temp. bend deform. and fracture, effect of C 77—59877
WC-Co (10 wt.%), vacuum sintered, short-time bending creep rupture strength *(Japanese)* 78—15508
WC-Co (6 to 20 wt.%), bend deform. and fracture up to 1000°C 77—48510
W_2C and WC, plastic deform. under bending, 800-2200°C *(French)* 80—55482
Y_2O_3-AlN, creep 77—21235
Zn, alternating bending of single crysts., shear strain accumulation and microstrain distrib. *(Russian)* 78—60706
Zn, single crystals, positron trapping by edge dislocations, produced by bending 78—80606
ZnS film, intrinsic stress meas. 80—71696
α-Zr and Zircaloy 2, fatigue, 20 to 700°C 77—70154
Zr, foil bending by in situ ion irrad., neutron damage simulation, room temp. oxide growth 80—107342
ZrO_2, stabilised microspheres, sintered, temp. depend. of strength, 20 to 1700°C *(Russian)* 78—23766
ZrO_2-Zr cermet composite, hot pressed, fracture toughness 78—27604

bending of light *see gravitation; light*

bending strength
adhesive joint strength testing under normal rupture and shear stresses 79—52500
beam (plate) pure bending, dynamic fracture, axial force effect 78—63385
beam element in space, geometrical stiffness, virtual work approach 80—14567
beam with different moduli of elasticity in tension and compression, three-point bending 79—81729
bench scale prebaked anode fracture, coke and formulation variables effect during Al smelting 79—52371
biaxial strength tests, finite element anal. 80—89431
bitumous mixes, complex modulus calc. *(French)* 79—20092
bone, fresh and preserved by freezing 77—25488
bone, human, ulnar bending stiffness, mineral content, geometry and strength 78—3537
bone, impact loading, anisotropy of compact bone tissue 77—25491
bone, long, prediction from bending stiffness and bone mineral content meas. 78—11787
bone, whole tubular, rigidity comparison technique 80—3881
bone elastic and strength props., 3-point bending tests using canine long bones 77—64080
borides, metallic, sintering, review, book contrib. 78—48359
borsic fibre reinforced Ti, unidirectional, K-calibration and compliance curves 78—88518
cement and mortar, flexural strength, loading rate effect on crack growth 77—77556
cement based on $Ca(OH)_2$ and polymethylphenylsiloxane, high-temperature high-strength props. 77—36439
cemented carbides, hardmetal, bending strength and fracture toughness 79—20181
ceramic, tensile strengths, uniaxial and equibiaxial in bending statistical comparison 80—25775
ceramic and glass ceramic, AE meas. under maintained load *(German)* 79—43315
ceramic rods, arrangement type 2037/ZT-10 for testing flexural resistance *(Polish)* 80—35455
ceramic rollers for conveyor lines, bending strength as func. of wall thickness 80—11699
ceramics, bending test results processing 80—97672
ceramics, error sources in mech. testing of tensile and bend strength *(German)* 78—35421
ceramics, mech. test apparatus for up to 2200°C *(French)* 80—104372
ceramics, strength and deformation testing, wide temp. range, universal apparatus 79—57177
ceramics containing metastable tetragonal ZrO_2, grinding induced tempering 80—89260
chamotte concrete, alumina-based cement, thermomech. props. 78—35455
cohesive strength of constructional components with crack-type defects, stress intensity coeff. *(Russian)* 78—30234
combined bend mode specimens, calc. of stress intensity factors 78—79284
combined mode bend specimens, calc. of stress intensity factors, 3 alternate methods 79—77025
composite, multimodulus material, apparent flexural modulus and strength 77—28845
composite beams, shearing stresses distrib. under three point flexure, fracture due to surface peeling 78—44183
composite material cylindrical shells, stability during nonsteady heating and transverse flexure 80—40445

bending strength continued
- composites, multicomponent layered, time depend. of flexibilities 80−39205
- concrete, beam with mixed type of reinforcement, shear and bending strength 79−20124
- concrete, glass or steel fibre reinforced 79−87706
- concrete, high strength, made with a special cement admixture, mech. props. *(Japanese)* 80−89297
- concrete, impact bending capacity *(Japanese)* 80−89341
- corundum, polycrystalline, creep under low partial pressure of O_2, 1200-1600°C 80−35255
- crack tip stress and strain *(Chinese)* 79−73249
- cyclic elastoplastic bending, recording deform. curves and working life 79−52499
- diaphragm for loudspeaker, using carbon reinforced olefin polymer, with high specific modulus, flexural rigidity and loss factor *(Japanese)* 80−53596
- double lapped composite joints, efficiency in bending, of steel/B reinforced Al or epoxy adherends 78−68870
- ductile crack extension, evaluation of resistance in single notch edge specimens 78−68807
- E-glass epoxy beams, dynamic mech. behaviour, meas. and analysis 77−28844
- elastic springs, thin, of constants cross section, elastic behaviour calc. and obs. *(German)* 78−87269
- epoxy, mech. props., 20 to 300°C *(French)* 77−56018
- epoxy Al bonded, adhesive joints under complex loading, development of failure criterion 78−92344
- epoxy resin, mech. and thermal props., amine hardeners, added softeners and filter effects *(Polish)* 78−68741
- epoxy resin, powder filled, exam. of mech. props., thermal contraction 80−25821
- epoxy resin based composites, superconducting magnet insulators, gamma-ray radiation effects 80−24495
- epoxy resin composite, powder-filled, of adjustable thermal contraction, mech. props., for construction of superconducting magnets 79−61691
- epoxy resin systems, synthesis review, phys. and mech. props. at low temps. 80−25650
- epoxy resins, relationship between struct. and mech. props. *(Japanese)* 78−31438
- equine long bone forces and moments, in vivo and anal. studies 78−40216
- ethylene propylene/polyolefin blends, radiation cross linking 80−66801
- FCC crystal, grip effect and bend gliding during uniaxial tensile deform. *(Japanese)* 79−52314
- femoral shaft, human, age and sex-related changes in struct. and strength 77−56401
- femur strength, rat, rel. to growth, bone-length, gravity 80−16978
- fibre reinforced cement, mech. and rheological props. *(German)* 79−20129
- fibre reinforced composites, flexural strength, denture base appl. *(Japanese)* 78−40409
- fibre reinforced plastic laminates, US evaluation of hygrothermal effects 80−7730
- fibre reinforced plastics, temp. increase under uniform plane bending fatigue test *(Japanese)* 78−44200
- fibreglasses, long-term strength evaluation, parametric methods efficiency 80−40662
- films and tissues multiple bending testing device 80−21225
- flexural fatigue and surface abrasion 78−15504
- flexure of composite laminates using thick finite strip method 77−42739
- flexure tests, 3 and 4 point, strain rates 80−16379
- float glass 78−23767
- glass, chemically strengthened, ion exchange temp. and time influence on stress profiles and strengths 78−31417
- glass, devitrified technical, bending strength, scale effect 80−89311
- glass, flat, strength and durability levels 80−66608
- glass, strength under linear tension, bending, torsion and compression of type K8 79−14062
- glass, technical, STL10, A-1, A-3, A-6, 13V, statistical features of strength characts. 79−43353
- glass, tensile and impact strength, effect of surface damaging and annealing *(Czech)* 79−74227
- glass components, life testing under flexing load *(French)* 80−89432
- glass fibre bricks, synthesis, strength 80−40304
- glass fibre reinforced cement, durability in wet and dry conditions, fibre length and content effect 80−71726
- glass fibre reinforced concrete, flexural strength 78−11288
- glass fibre reinforced epoxy, deterioration in water, hydraulic press. effect *(Japanese)* 80−55470
- glass fibre reinforced epoxy, deterioration in water, immersion time effect *(Japanese)* 80−55471
- glass fibre reinforced epoxy, epoxy matrix, strength in twisting, stretching and transverse bending 80−11622
- glass fibre reinforced epoxy, fatigue damage in cyclic bending 79−100256
- glass fibre reinforced Kinel, mech. props., 20 to 300°C *(French)* 77−56018
- glass fibre reinforced plastic, bending tests, specimen size and shape selection 77−52575
- glass fibre reinforced plastic, failure under compression, tension and bending 79−96142
- glass fibre reinforced plastic, flexural fatigue props. *(Japanese)* 79−20171
- glass fibre reinforced plastic/polyurethane foam/Al sandwich, flexural props. *(Japanese)* 78−56707
- glass fibre reinforced plastics, ageing by boiling in water, effect on physicomech. props. 80−60892
- glass fibre reinforced plastics, cylindrical shells, compressive and flexural strength *(Japanese)* 80−81115
- glass fibre reinforced plastics, damage summation in nonstationary cyclic loading 80−60969
- glass fibre reinforced plastics, laminates, load carrying capacity, interlaminar imperfections influence *(German)* 79−100218
- glass fibre reinforced poly- and vinyl-ester, fatigue and flexural strength 79−8364
- glass fibre reinforced polyester, behaviour under bending load *(Japanese)* 79−38904
- glass fibre reinforced polyester, plate struct., skeletal member effect on stiffness and strength, finite element anal. 79−91733

bending strength continued
- glass fibre reinforced polyester resin laminate cantilever, bending fatigue strength, cyclic freq. effect *(Japanese)* 80−55507
- glass fibre reinforced thermoplastic, injection moulding, flexural anisotropy 79−61659
- glass plate, flexure crack propag., expt. and anal. 78−80620
- glass sheets, large scale, exam. of bending strength under uniformly distributed load 79−29135
- glass shell, built-up, local strengthening influence on supporting capacity 80−71714
- glass wool reinforced polymer, relationship between Young's modulus and dissipation of energy *(German)* 79−96064
- glass-ceramic, effects of moisture-assisted slow crack growth 78−27593
- glass-ceramic composite, internal stress effects on mech. props. 77−21250
- glass-epoxy laminate, superconducting magnet insulators, gamma-ray radiation effects 80−24495
- glass/C fibre reinforced plastic, hybrid effects between interlaminar and translaminar config., mech. props. 79−52351
- graphite, bending strength, surface roughness effect at high temp. *(Japanese)* 79−70131
- graphite, bending strength testing, quality improvement 79−52581
- graphite, irradiated ultimate tensile bending and compressive strength charact. 78−15479
- graphite, isotropic, nonlinear stress/strain relationship effect on band strength 79−20119
- graphite, oxidation, corrosion resistance, bend strength, assessment for rotary glass fibre making apparatus 78−64753
- graphite, polygranular, flexural strength after heat treatment porosity correl. 80−84996
- graphite, pyrolytic, structural factor effect on strength 79−66135
- graphite, pyrolytic commercial, high-temp. thermal and mech. props. 80−75372
- graphite fibre filled polyimide composite prepreg laminates, room-temp. ageing effect 80−81093
- graphite reinforced epoxy laminate, fracture by three point bend 79−83297
- gypsum, strength changes on setting *(Japanese)* 77−36619
- gypsum casts, improvement in impregnation method, exam. of mech. props. 78−48503
- hard metal, tensile strength meas., bend test-piece geometry effect 80−30184
- heat resisting, types EhI598, ZhS6KP, and 1, fatigue under mech. and thermal stress 79−66164
- high-C steel, strength characts. with controlled hardenability after bulk-surface hardening 77−56156
- ice shelves, floating, tidal flexure cracks, fracture mechanics 78−69368
- illuminating fibre bundles, improved characts. due to glasses type VS 1637 and VO 720 80−102844
- impact bending, investig. by load-time oscillograms 77−63849
- kaolin bodies, effect of mineralizers on firing shrinkage, microstruct. and strength 80−97488
- Kevlar aramid fibre reinforced composites, flexural strength 79−11671
- Kevlar-29, flexural fatigue and surface abrasion 78−15504
- Kinel 5504, mech. props. 20 to 300°C *(French)* 77−56018
- laminated beam, 3 component, strength props. *(German)* 80−35269
- low-alloy steel, bending, effect of strain rate on dynamic stress factors 77−56046
- LWR austenitic stainless steel coolant tubing, bending props. *(Czech)* 79−67851
- metacarpi, equine, fracture toughness 80−3694
- metal bending spring, effects of stress, temp., thermal and mech. treatment on non-elasticity *(German)* 77−77531
- metal vacuum-deposited coatings on glass, strength 80−55505
- MgO-ZrO_2 ceramic reinforced with filamentary crystals, mech. and thermal props. 80−45262
- mineral wool fibre composites, mech. props., effects of thermally induced phys. and chem. changes 77−59884
- mineral-fibre composites that resist fracture and cracking 77−8798
- mortar specimens, repeated impact bending load study *(Japanese)* 80−93622
- mullite ceramic rollers, heat treatment effects 79−61616
- mullite fibre reinforced mullite, in vitro degradation, bending strength, Young's modulus, density meas. 78−85011
- multi-support sandwich beams, calc. *(German)* 79−98612
- natural rubber vulcanisate, network changes during physical testing 80−60936
- nephrite, mech. props. 77−44295
- nonmetallic material, mech. props., testing installation, +600 to −190°C 78−15633
- notched beam, fatigue crack emanates from notch root, fracture strength 78−72866
- notched rectangular bars, notched bend test specimens, strain meas., plastic deform. *(German)* 78−11451
- Nylon 6, unidirectionally reinforced, mech. props. and fracture 77−21252
- optical glass, K8, bending strength, sample dimension effects 80−9975
- optical glass, reproducibility of symm. bending mech. strength values 78−46737
- optical glass ceramic, (sital) surface operation parameters, selection using bending strength tests 79−32101
- optical waveguide fibre coating technology, overview 80−58828
- orthotropic laminates, torsion strength and shear modulus determ. 80−92587
- PA6, loss factor rel. to fatigue strength *(Polish)* 77−28904
- perlite, low temp., processes occurring during firing 80−11607
- phenol formaldehyde resin, (Novolak) with filler, mech. props. determ. *(German)* 78−84933
- phenol formaldehyde resin (Novolak), with and without feldspar filler, mech. and thermal props. determ. *(German)* 78−84828
- phenol resin (Resol), with and without feldspar filler, mech. and thermal props. determ. *(German)* 78−84828
- phenolic resin filled and unfilled, mech. relaxation behaviour, effects of temp. and time *(German)* 78−6963
- phenylone, deformability in physiological salt soln. 80−12305
- piezoelectric ceramic, bend and compressive strength, stressing rate effect 77−52409
- plastic, flexural fatigue props. *(Japanese)* 79−20171
- plastics, tensile and flexural testing device, incorporating an impacter *(German)* 80−3276

bending strength continued
plate testing under alternating flexure, pneumatic test equipment 78—7119
plates, rectangular thin, effect of different edge flexibility coeffs. on transverse vibrs. 78—83294
plates stiffened, large amplitude flexural vibrs. 78—83307
PMMA-mortar composite, thermocatalytically polymerised, fracture morphology and mech. props. 78—27595
poly(butadiene-co-styrene), rubber, radiation cured, dynamic phys. props. 77—69003
polyamidoimide film, thermomech. props. rel. to mol. struct. *(Russian)* 79—57029
polyester laminates, glass fibre-reinforced, due to natural weathering 79—66107
polyester resin, unsaturated, $CaCO_3$ system, $CaCO_3$ addition effect on degradation in boiling water *(Japanese)* 78—11281
polyester resin, unsaturated, chalk filled, props. *(German)* 80—104228
polyester resin, unsaturated $CaCO_3$ system, $CaCO_3$ addition effect on water absorption in boiling water *(Japanese)* 78—11282
polyester resin concrete, effects of styrene-unsaturated polyester ratio on props. *(Japanese)* 80—89299
polyester resin mortar, degradation in boiling water *(Japanese)* 78—11280
polyester resin-filler system, resistance to degradation in boiling water *(Japanese)* 78—11283
polyethyl acrylate modified mortars, inner struct. and flexural props., suspension and emulsion studies *(Japanese)* 77—86092
polyethylene, high density, strength props. *(German)* 79—100219
polyethylene, high mol. wt., deformability in physiological salt soln. 80—12305
polymer films, superconducting magnet insulators, gamma-ray radiation effects 80—24495
polymer impregnated gypsum cast, mech. props. 79—100107
polymer-metal laminate, bone fixation plate fabrication 79—79685
polymer-TiO_2 composite, dielec. props. *(Japanese)* 78—95540
polymide 6, glass fibre reinforced and unreinforced, fatigue under rotary bending *(German)* 79—15782
polyphenylene oxide, with and without impact resisting polystyrene, photo-oxidative ageing, Cu and Fe trace effects *(German)* 79—100191
polypropylene fibre reinforced cement based beams, flexural strength, fibre pull-out 77—56020
polypropylene/peanut-hull flour composite, strength 79—8365
polystyrene, impact resisting *(German)* 79—100219
polyurethane foam, rigid integral, effect on flexural and compressive strength, due to tall oil oligoether 78—68743
polyurethane foam/glass reinforced plastic/Al, sandwich construction, nonsymmetric, flexural fracture 79—74233
porcelain, elec., comparative assessment of methods of determ. strength 80—40429
power transmission cables, pipe-type, low-cycle fatigue tests 80—7731
pure bending, four-point loading design instrument 77—40498
PVC, asbestos reinforced, CIR/Palram process preparation, mechanical and thermal properties measurements 79—66106
refractories, castable, X-ray powder diffr. meas. of phase composition, and flexural strength 80—3449
refractory, flexural creep 79—29155
reinforced concrete containment model behaviour under thermal gradients and internal pressure 80—42837
rim of semi infinite plate, crack originating from triangular notch under transverse bending 79—77009
sandwich composite beam, four point bending stress, multilayer built-up theory anal. *(Japanese)* 79—8322
sandwich composite beam, impact bending behaviour *(Japanese)* 80—55468
sapphire, white, three-point bending test, dislocation climb *(Japanese)* 79—96104
sapphire fibres, meas. of bending strength 80—25964
sea ice flexural strength meas. *(Japanese)* 77—81915
ship propeller shaft dynamics, forces between shaft and bearings, root bearing rigidity depend. 79—81801
Si_3N_4-Ce_2O_3-SiO_2 materials: phase relations and strength 80—97465
sisal fibre reinforced cement, flexural strength 80—11692
sital, structural glass component, strength in complex stress state 79—91763
sital, technical, compressive and bending strength 77—70131
soft-interlayer welded joint bending and torsion endurance, residual stress effects 79—83287
stainless steel, bending, effect of strain rate on dynamic stress factors 77—56046
static bend testing by unit with energy accumulator 77—86251
static bend testing of cracked samples until failure, −60 to 20°C 78—23893
static bending testing device for samples at different temps. in aggressive media 78—39972
steel, 0.54% C, fatigue crack accel. and closure in rotating bending tests, in annealed or quenched/tempered state 79—43383
steel, alloy, quenched, high strength, shot blast hardening effect on repeated impact bending 79—1914
steel, austenitic, precipitation hardening, effect on fatigue strength 78—84829
steel, C, fatigue, residual stress and crack growth expts., notch and surface treatment effects 79—8356
steel, C, fracture criterion determination, using 3-point bending 79—29216
steel, C, non-propagating microcrack, opening and closing behaviour in rotating bending and torsional fatigue *(Japanese)* 80—25846
steel, C, type 45, crack form. mechanism during fatigue 79—38957
steel, C and alloy, notched beam, fatigue crack emanates from notch root, fracture strength 78—72866
steel, C-Mn-V and Cr-Mo-V, power station component, fracture toughness and fatigue characts. 79—20192
steel, cantilever bend specimen, side grooving effect on compliance relationships 78—35472
steel, case hardened, MnCr, shot peening effect on bending fatigue strength *(German)* 78—56777
steel, casecarburized and hardened, relationship between fatigue strength and case hardness distrib. *(Japanese)* 79—61782
steel, cast, SC49, rel. between rotating and flexural bending strengths *(Japanese)* 80—81117
steel, constructional, fracture toughness in cyclic loading 78—72860

bending strength continued
steel, Cr-Cu-Mn, fatigue crack propag. rate eval. by J integral method *(Japanese)* 79—8346
steel, Cr-Mo, notched specimens, statistical eval. of fatigue life and fatigue limit and life distrib. *(Japanese)* 79—61702
steel, Cr-Mo (2.25, 1.0 wt.%), temper embrittlement, effect of P, Sn, comp. and carbide precip. 80—85036
steel, Cr-Mo (2.25, 1 wt.%), strain hardening shakedown load during bending 80—20958
steel, Cr-Ni, effect of tempering under load on mech. props. 80—16354
steel, Cr-V, hardened sping, surface finish effect on fatigue strength *(Japanese)* 79—61708
steel, CrMo and CrMoV, creep resistant, ductile-brittle transition temp., precipitation effects *(German)* 78—19856
steel, deformability characts. in surface-active medium at decreasing temp., mech. working effect *(Russian)* 77—59851
steel, deformation and fracture resistance due to low-cycle fatigue in plane bending 79—66166
steel, electric arc sprayed coating on wire, elastic and elastic-plastic props. *(German)* 79—34089
steel, fatigue fracture after Fe and Ce diffusion coating, microstruct. investigation *(Russian)* 79—52446
steel, fracture ductility, determ. in bending tests and US emission 78—23899
steel, fracture toughness and dynamic strength, surface active agent effects *(Russian)* 78—56812
steel, fracture toughness eval. by equivalent energy method *(Slovak)* 79—43402
steel, hard, high speed and tool, linear elastic fracture mech. appl. 78—48518
steel, high C, quenched and tempered, hydrostatic press. effect on brittle fracture stress 79—61727
steel, high speed, sintered, and wrought, type T6 strength and toughness 80—30102
steel, hollow cylinder, thick walled, effect of thermomech. treatment 80—11674
steel, induction hardened, static bending strength and correlation between static strength and endurance limit *(Japanese)* 77—70108
steel, low alloy, fatigue crack nucleation under high cycle fatigue and uniaxial loading 79—79060
steel, low alloy, type 10KhN1M, heat-treated, struct. and resist. to thermal embrittlement 79—15788
steel, low C, effect of grain size on transition behaviour and bending speed correl. *(Japanese)* 79—8345
steel, low C, fatigue strength, effect of loading type, cross section shape, and specimen edge finish *(Japanese)* 79—8343
steel, low C, gas nitrocarburized, cyclic stressing 79—57098
steel, low C, impact strength and crit. brittleness temp., sample thickness and notch radius influence 80—85018
steel, low C, specimens with notch and fatigue crack, fracture surface features 79—43417
steel, low C, thin walled tube, fatigue behaviour, low endurance, under bending and torsion 77—86129
steel, martensitic, impact bending failure resistance, initial crack length and tempering effects 78—31530
steel, mild, hot shortness mechanism, surface enrichment of residual elements and oxidation *(Chinese)* 79—74230
steel, mild, subject to three point bending and tensile load, acoustic emission 80—3154
steel, Mn-Cr, tempered, case hardened, shot peening effect on bending fatigue strength *(German)* 79—24645
steel, Mn-Si, St 52-3, cleavage fracture toughness, temperature and notch sharpness influence *(German)* 80—35291
steel, MnCr (16, 5 wt.%), bending fatigue behaviour improvement by surface treatment *(German)* 78—84957
steel, Ni, cross girder connections, fatigue strength, design stress 78—64700
steel, Ni-Cr-Mo, cleavage fracture toughness, temperature and notch sharpness influence *(German)* 80—35291
steel, Ni-Cr-Mo, fracture toughness determ. from yield strength and cleavage fracture strength *(German)* 80—35292
steel, Ni-Si-Nb (1.5,0.02,0.03 wt.%), fatigue crack growth under bending *(French)* 80—21089
steel, pearlitic, heat treatment effects on mech. props. and microstruct. *(German)* 77—8857
steel, rare earth additions, effect on physicomechanical props. 77—12639
steel, short-cycle, fatigue, stress concentration effect 78—95859
steel, silver, elastic limit, bending strength, and ductility rel. to tempering temp. after quenching 78—95764
steel, sintered, diffusion treatment with B, Si, Cr and C, corrosion and wear improvement 77—77642
steel, spheroidized AISI 1095, ductile fracture of U-notched bend specimens 79—24616
steel, spring, 60C2A, tempered under stess, influence of tempering conditions on mech. props. *(Russian)* 79—47724
steel, St.3ps, 18 Gps, 09 G2S, fatigue crack resistance, temp. effect 79—52375
steel, stainless, physicomechanical and wear props., influence of ion implantation and overlay coatings 80—40603
steel, stainless, porous sheet, mech. strength, bend and reverse bend tests *(Russian)* 80—93595
steel, structural 15Kh2NMFA, use of linear and nonlinear fracture mech. for crack propagation resist. determ. 79—5056
steel, tensile prestrained strength of anisotropic rolled steel, rot.-bending fatigue tests, slip bands 78—27590
steel, tufftrided, fatigue strength under reversed torsion *(Japanese)* 79—61707
steel, types A533B and KAS, fracture toughness meas. using elect. potential method *(Japanese)* 80—93722
steel, W, high C, amorphous, rapidly quenched from melt, mech. and thermal props. 79—38874
steel bar, in four point bending machine, measurement using holographic interferometry 79—34266
steel bar deformation meas. by holographic interferometry using four point bending machine 78—60721
steel beams, inelastic, mild, flexural behaviour and lateral buckling anal. under cyclic loads *(Japanese)* 78—87283
steel beams with bracket plates welded to tension flange 78—7008
steel fibre reinforced cement based beams, flexural strength, fibre pull-out 77—56020

bending strength continued

steel fibre reinforced concrete, vibr. compaction, pressure compaction and curing *(Japanese)* 80—89179

steel reinforced concrete, computer expt. on slender beam columns 79—70127

steel shafts testing 80—3184

steel stretch-bend test strain distribution obs. 77—70243

steel-concrete composite T-beam, third point loading tests, ultimate flexural strength determ. 77—86252

steels, tool, cold hydrostatic extrusion rel. to struct., props. 79—20068

straight bar bending strength, brittle fracture energy conditions *(Russian)* 80—58974

test apparatus under high press. and temp. *(Japanese)* 78—76795

thermoplastic based composites, mean stiffness 80—11693

thermoplastic-based sheet materials, flexural anisotropy and stiffness assessment 80—76442

tibia, meas. using tibiometer, eval. from postmortem findings 77—37063

tile, resistance to fracture, Weibull statistics *(German)* 77—7338

Timoshenko rod, straight axis, free bending oscillations investigation *(Hungarian)* 80—89327

Tokamak fusion reactor supercond. toroidal coil bending moment computation 79—41867

tubes, thin wall, long-time strength, steady creep conditions *(Russian)* 78—46900

two step program loading involving impact load, fatigue strength and damage accumulation *(Japanese)* 79—66148

W, static deform., removal of surface layer effect on mech. props. in single crystal 79—43359

white cast iron, plasticity in impact toughness, bending angle tests 77—56039

wood fibre reinforced cement, coupling agent effect on strength 80—35295

wood stud walls, rel. between maximum compressive load and width *(Japanese)* 80—3124

Al alloy, 51S, modified by misch metal, for space appl. 80—55466

Al alloy, deformation and fracture resistance due to low-cycle fatigue in plane bending 79—66166

Al, bicrystal, fatigue crack initiation along crystal boundaries *(Japanese)* 79—70163

Al, mech. props., 20 to 300°C *(French)* 77—56018

Al, physicomechanical and wear props., influence of ion implantation and overlay coatings 80—40603

Al, torsional fatigue and bending tests 79—43521

Al/polyethylene/Al sandwich construction, flexural fatigue props. *(Japanese)* 78—56751

Al-Mg alloy AMg6, mech. props. of welded joints, impurity effects 78—95789

Al-Mg-Mn alloy AMG-6M, endurance determ. by dimensionless damageability curves 79—96141

Al-steel mixture, wear resistant, produced by compaction by discrete shock waves 80—84882

AlB_2 flake reinforced composites, prep., props. rel. to aspect ratio, book contrib. 78—48366

AlN, hot pressed, effect of O_2 content on flexural strength and compact density 79—11668

AlN-Mo cermets, ZrO_2 and mullite whisker reinforced, strength var. with temp. 80—104232

AlO_2, corrosion resistance of phosphate bonded castable, and dense fired types in steam CO at 199°C 79—20222

Al_2O_3, bending strength, surface roughness effect at high temp. *(Japanese)* 79—70131

Al_2O_3, ceramic Sinoksal, strength variation dependence on type of loading and temperature 79—57080

Al_2O_3, chemically-strengthened polycryst. mat., flexural strength at high temps. 77—21302

Al_2O_3, glass resistant, plasma coating props. 79—34164

Al_2O_3 rod, damaged, mech. strength, surface defects effect, appl. as insulators *(German)* 80—76330

Al_2O_3 sintered, effects of moisture-assisted slow crack growth 78—27593

Al_2O_3 substrates, tape-casted, fracture strength analysis 80—60948

Al_2O_3, vitreous-bonded, mech. behaviour under various stress-time schedules 79—38968

Al_2O_3:MgO, diffusion creep examined under three-point bending *(Japanese)* 79—96104

Al_2O_3-Mo cermets, ZrO_2 and mullite whisker reinforced, strength var. with temp. 80—104232

β-Al_2O_3-Na_2O, hot pressing and phys. props. 79—4940

Al_2O_3-polymethylsiloxane composite, thermoreactive compaction 80—20879

Al_2O_3-TiC, composite, fracture behaviour in three-point bending 80—60951

Al_2O_3-TiO_2 (1 wt.%), with and without α-Al_2O_3 laminar crystals, bend tests 77—16531

$3Al_2O_3.2SiO_2$-ZrO_2 composites, sintered, in situ-reacted, fracture props. 80—81158

B fibre reinforced Al, impact behaviour under fatigue 80—7661

B fibre reinforced Al, unidirectional, K-calibration and compliance curves 78—88518

B fibre reinforced epoxy resin laminate, fatigue damage, stiffness/strength comparison 77—90451

B-B_4C materials, hot-pressed, elastic modulus and flexural strength rel. to grain size and porosity 79—79018

C fibre, flexural fatigue and surface abrasion 78—15504

C fibre reinforced Al, formed by ion plating and vacuum hot pressing 78—11165

C fibre reinforced Al, mech. props. 80—11708

C fibre reinforced Al composite, CVD fibre coating, diffusion barrier and wetting agent 77—40458

C fibre reinforced C, processing, room temp. mech. props., and low temp. expansion 80—25820

C fibre reinforced epoxy, epoxy matrix, strength in twisting, stretching and transverse bending 80—11622

C fibre reinforced epoxy, deterioration in water, hydraulic press. effect *(Japanese)* 80—55470

C fibre reinforced epoxy, deterioration in water, immersion time effect *(Japanese)* 80—55471

C fibre reinforced Kinel, mech. props., 20 to 300°C *(French)* 77—56018

C fibre reinforced plastics, use in orthopaedic implants, exam. of mech. props. 79—20706

C fibre reinforced plastic, tensile testing using ring specimens *(Japanese)* 79—29148

bending strength continued

C fibre reinforced plastics, failure under compression, tension and bending 79—96142

C fibre reinforced plastic, fractography of fracture surface under three-point bending *(Japanese)* 80—55506

C fibre reinforced plastics, strength props., effect of SiC coating on fibre 80—104224

C fibre reinforced polyethylene, for medical appls., tensile and flexural props. 78—31969

C fibre-Kevlar 49 fibre epoxy laminate, impact props. 78—44164

C fibres with large breaking strain, prep., mech. props., struct., appl. 78—44077

C glass fibre hybrid plastics, review of mech. props 79—20107

C, glassy, size effect on bending strength 79—52309

C materials, bend strength testing, bench assembly with strain recording 79—57176

C, polygranular, flexural strength after heat treatment porosity correl. 80—84996

C steel, bending, effect of strain rate on dynamic stress factors 77—56046

C steel, crack initiation lives at stresses near endurance limit, probability distribs. 77—86127

C steel, fatigue, residual stresses, surface cracks *(Japanese)* 77—25121

C/C composite with S-modified pitch binder precursor, carbonisation and mech. props. *(German)* 77—44183

C-C composite material, syntactic-foam type properties 78—44169

C-fibre reinforced epoxy resin, laminated structs. mech. props. 80—50672

$CaAl_2O_4$ cement bond phases, corrosion in steam-CO at 199°C 79—29234

Cr-Mo-V, steamline bends, restorative heat treatment effects 78—68716

Cu-BeCo (1.85, 0.29 wt.%), type CA172 (TH04), strengthened by spinodal decomp., stress relax. in bending 80—7616

Cu-Ni-Sn (4-15, 4-8 wt.%), strip strengthened by spinodal decomp., stress relax. in bending 80—7616

Dy_2O_3-based ceramic, preparation, mech. props. 77—24998

Fe, cast, grey, electric arc sprayed coating on wire, elastic and elastic-plastic props. *(German)* 79—34089

Fe, water atomized powder, compaction, bending strength *(French)* 80—40287

Fe-Al-Si, bending test, mech. props. under high press. and temp. *(Japanese)* 78—76711

Fe-B alloy reinforced polysulphone exam. of tensile and flexure props. 78—72823

σ-Fe-Cr, brittle fracture stresses under high hydrostatic press. and high temp. *(Japanese)* 79—43397

Fe-Ni-Al-Co-Cu-Ti YuNDK type, S effect on mech. props. 80—60927

Fe-Ni-Al(Ti)(V)(Nb), cryogenic toughness, strength, rel. to reactive metal addition 78—39885

Fe-Ni-C (9, 0.1 wt.%), effect of intercritical tempering on impact energy, exam. of mech. props. 78—52861

Fe-Ni-WC hard alloy, struct. and props. 79—79007

Fe-Si (3 to 5 wt.%) sinters, mag. props., Si and Fe-Si additions effect 80—71104

$Fe_{32}Ni_{36}Cr_{14}P_{12}B_6$, shear band form. 78—68756

HfC-$HfBr_2$, preparation and high temp. antifriction props. 79—1918

KCl:RbCl, $SrCl_2$, IR window material, cryst. growth and props. 78—31333

Mg-Al spinel ceramics, mech. strength, non-stoichiometry and microstruct. *(Japanese)* 80—21054

Mo, electric arc sprayed coating on wire, elastic and elastic-plastic props. *(German)* 79—34089

Mo-Hf-B-C, low C, sheet, strength 77—1859

Mo-Ti-La-C, influence of high pressure on mech. preps. after nitriding *(Russian)* 79—57137

Mo-Ti-Zr (0.5, 0.7 wt.%) alloy TZM, props. and appl. *(German)* 80—21040

Na_2O-B_2O_3-SiO_2 glass fibre, plastic-coated, liq. N_2 strength 80—58707

Na_2O-B_2O_3-SiO_2 glass-Ni compact, indented, strength and fracture toughness 80—93636

Na_2O-CaO-SiO_2, glass, surface indentation effect on mech. strength, and thermal stress resistance 78—48463

Na_2O-CaO-SiO_2 sheet glass, pristine and scratched, fracture behaviour during bending 78—23829

Na_2O-SiO_2 glass, OH^- content effect on mech. and other props. 80—89337

Nb alloy, VN2AE, influence of nitriding on heat resist. and brittleness *(Russian)* 79—8380

NbC, NbC-ArC, right-through sat. prep., strength and plasticity, temp. depend. 77—40432

Ni carbonyl powder, sheet filtration materials with metallic gauze backing layers, bending strength and ductility 78—60613

Ni, electrodeposited in sulphamate bath, cyclic stress, meas. at 160-180°C 80—19295

Ni-based-Ta(Cn,N) hard metals, isostatic hot pressing influence on mechanical properties 78—92219

Ni-Cr-Al sintered alloy, hot vac. pressure, fracture and mech. characts. 80—66667

Ni-Cr-Co alloys, relax. resist. exam. by bending and tension 79—24564

Ni-Cr-Ta-Ti-Si, EP557 precipitation hardening alloy, mech. props., heat treatment effect 80—60877

Ni_3Al-B, $L1_2$ type intermetallic cpd. room temp. ductility improvement by B addition *(Japanese)* 80—35263

$NiO^{-}CaF_2$, hot-pressed, mech. props., thermal expansion rel. to CaF_2 additive 79—43321

PVC-Cu, particulate composite, mech. props. effect of particle size 78—95799

$PbBi_2Nb_2O_9$, bend strength, grain orientation effects 80—40375

$Pb(Zr,Ti)O_3$, effect of spherical pores on strength 77—70103

$Pb(Zr,Ti)O_3$ polycrystalline ceramic, fracture and strength, surface treatment effects 80—11704

S, S mortars, S Concretes, effect of H_2S 77—4818

Se glass, flexural strength in transition range 77—56032

Si wafers, scribing and subsequent fracture 80—11743

Si/SiC ceramic composite, elastic moduli and bend strength meas., anisotropy 77—59838

Si/SiC ceramic composite, room temp. props., effect of SiC content and orientation 78—27599

SiC containing material, deform. props. investigation by pure bending 78—19823

SiC, controlled nucleation thermochemical deposition, charact. and props. 80—108355

bending strength continued
SiC, dense, joining by hot pressing, and bond strength 80—66458
SiC fibre reinforced Al, synthesis by liquid pressing method 80—100816
SiC filament reinforced phosphate foam ceramics, bending strength 80—11716
SiC, hot pressed, bending strength *(German)* 79—24571
SiC, impact resistance, instrumented drop weight test 78—11265
SiC, pressureless-sintered, high temp. strength *(Japanese)* 80—104299
B SiC, sintered, effect of Al trace amounts on specimen props. 79—83289
SiC-fibre reinforced glass, fabrication, thermal expansion, flexural and fracture toughness 80—40319
Si_3N_4, bending strength, deformability, elastic moduli and brittleness 80—81191
Si_3N_4, HS-130, dynamic mode I fracture toughness and flexural strength 77—21248
Si_3N_4, hot pressed with different grain struct., mech. props. 79—61700
Si_3N_4, hot-pressed, fracture in bending *(Japanese)* 79—79113
Si_3N_4, hot-pressed, impact resistance, instrumented drop weight test 78—11265
Si_3N_4, hot-pressed, strength anisotropy origins 80—89330
Si_3N_4, reaction bonded, bending strength meas., influence of loading conditions, proof testing and anal. methods *(German)* 78—31451
Si_3N_4, reaction bonded, effect of Si powder grain size on microstructure, and mech. props. *(German)* 79—4998
Si_3N_4, reaction bonded, pore size and distrib. effect on strength 79—29165
Si_3N_4, reaction sintered, time depend. strength degradation 79—29235
Si_3N_4, reaction-bonded, added oxides effect on strength after oxidation 79—39012
Si_3N_4, reaction-bonded, strength, effect of Si purity in production 80—100902
Si_3N_4, reaction-sintered, elastic moduli, fracture mechanics parameters, and strength 77—28889
Si_3N_4-Y_2O_3 (8.0 wt.%), hot pressed, mech. props. 79—70134
Si_3N_4-Y_2O_3(CeO_2), hot pressed, sintered, microstruct., flexural strength and fractographic anal. 80—40293
SiO_2 glass fibre, plastic-coated, liq. N_2 strength 80—58707
SiO_2, vitreous, strengthening by coating application 77—32636
SiO_2-Al_2O_3-CaO-MgO-Na_2O (1.58, 7.16, 3.59, 14.9 mole.%), polished sheet, strength in commercial state and after strengthening by ion exchange 79—1904
SiO_2-Na_2O-$CaCO_3$ sheet glass, rupture upon local contact loading 80—50725
$Sm_{1-u}Ce_u(Co_{1-x-y-w}Fe_xCu_yCr_w)_z$, permanent mag., improved mech. props. 79—87593
Ti, mech. props., 20 to 300°C *(French)* 77—56018
Ti, physicomechanical and wear props., influence of ion implantation and overlay coatings 80—40603
Ti-Al-Mo-Cr (4.5, 5, 1.5 wt.%), weld metal, α/β interace sliding 80—108512
TiC-Mo_2C-Ni cermets, influence of anomalous phases on strength 78—92228
TiC-steel composite, effect of method of Cr additions on props. 78—15341
TiC-TiB_2, preparation and high temp. antifriction props. 79—1918
TiC-TiB_2, strength and antifriction props. over wider range of concs. 80—50673
TiO_2 based construction ceramics, fibre-like cryst. reinforced, mech. props. 80—55341
TiO_2, sintered ceramic, props. rel. to additives, impurities 78—35329
UO_2 fuel pellet, bending strength, fabrication and microstruct. effect 80—2986
W fibre reinforced Ni-Cr alloys, Ni, Co, Co alloys, and Ni alloys, effect of alloying on structural stability, mech. props. 78—56600
W, sintered, brittle fracture, statistical anal. 80—11744
W-Re wire, CVD coatings of SiO_2 and Mo, for neurological electrode, elec. cond. and bending props. 78—11752
WC-Co cemented carbide, bending strength, surface roughness effects *(German)* 77—8947
WC-Co hardmetal, defect initiated fracture and bond strength 78—11319
Y_2O_3 ceramics, strength under mech. and thermal actions 80—97554
Yb_2O_3-based ceramic, preparation, mech. props. 77—24998
ZrC, NbC-ZrC, right-through sat. prep., strength and plasticity, temp. depend. 77—40432
ZrC-ZrB_2, preparation and high temp. antifriction props. 79—1918
ZrC-ZrB_2, strength and antifriction props. over wider range of concs. 80—50673
ZrO_2, metastable, tetragonal, strengthening by surface grinding 80—71777
ZrO_2, partially stabilised ceramics, strengthening, post-sintering heat treatment 80—97518
ZrO_2, partially stabilized, props. and appl. to extrusion dies 80—97507
ZrO_2, partially stabilized, processing defects 80—97558
ZrO_2 stabilised with Y_2O_3, ultrafine grained, fabrication and flexural strength 77—1829
$ZrSiO_4$ zircon ceramic with glass-forming additives, sintering and mech. props. 80—60814

berkelium
see also nuclei with ......
atom emission spectrum, 2540-9800 Å, electrodeless lamp source 80—27970
separation with phosphororganic extractants 77—26854
target prpe. for synthesis of transactinide elements 80—23206
BaF_2:Bk, fluorite-struct., self-luminesc. 78—27309
^{245}Bk, K-shell fluorescence yields from Auger electrons and X-rays, precision meas. 79—31462
^{249}Bk determination in samples of transuranium elements by neutron activation analysis 79—100473
^{249}Bk, IR spectrum, 3700-12000 cm^{-1} 77—68001
$SrCl_2$:Bk, fluorite-struct., self-luminesc. 78—27309

berkelium compounds
aqueous solution, electrochem. props., thermodynamic props., radiopolarography 77—29040
BkO, and BkO_2, electronic struct. and chem. bonding and XPS line shape calcs. 79—33264
BkO_2, XPS meas. 77—48314
^{249}BkN, prep. and cryst. struct. 79—99115

beryllium
see also nuclei with ......
abundance in α Centauri A, constraints on Be form. 77—41379
abundance in main sequence stars 77—13332
abundance in meteorites rel. to interstellar grain synthesis 79—16894
abundance in subgiant stars rel. to post-main sequence evolution 77—13333
adsorbed layers on W(110) and (100), work function and loss spectra meas. 80—6638
adsorbed on cubium cluster, relax. energy calc., for XPS 78—15283
adsorption on W, crystallites growth, FEM obs. 78—26799
adsorption on W(211), work function changes and scatt. electron energy losses 79—46947
amorphous, reflection of D and T, Monte Carlo study 80—40197
anisotropy, theoretical investigation by K-emission, APS, and Compton profiles 78—63970
anodised, emissivity in 400-1000K range on function of oxide layer struct. 77—35726
atom, ^{1}S, Schrodinger eqn. random walk soln., electron spin effects 77—18780
atom, ^{2}P shape reson., electron scatt. calc. 79—41240
atom, and isoelectronic sequence, correlated and HF electron density differences 78—46275
atom, and isoelectronic sequence, oscillator strengths, relativistic RPA calcs. 77—57929
atom, approximate relativistic Hartree-Fock eqns., soln. using Slater-type functions 80—58168
atom, Auger transitions, fluoresc. yield calc., correl. effects 77—18869
atom, beam-foil populations, charge state distribs., independent electron model 77—19035
atom, CI and many-body perturbation theory for ground state 79—68198
atom, closed shell, Jastrow wave functions, var. calcs. 80—83249
atom, Compton profile, electronic energy calc. 80—37822
atom, correl. contribs. to dipole polarisability, coupled HF-perturbation theory 80—106269
atom, correl. energy, Gaussian geminal basis set calcs. 77—57885
atom, correl. energy, modified bielectronic potential method calcs. 79—59365
atom, correlation energies, Hartree-Fock Hamiltonian 78—41965
atom, coupled pair theory, exact and approx. methods and quasi-degeneracy 80—14074
atom, Doppler effects in X-ray spectra excited by accelerated ions 78—86808
atom, dynamic multipole polarisability, coupled Hartree-Fock 78—82858
atom, elec. dipole polarisability, many-electron calc. 77—57884
atom, electronic struct., universal STO basis sets 79—10021
atom, exchange energies, Born-Oppenheimer exchange amplitude, Bonham series calcs. 78—29854
atom, excitation energies and transition moments in a second order polarization propagator approach 79—10051
atom, excitation energy and transition moment anal. of electronic transitions 78—25620
atom, excitation energy calc., improved virtual orbitals in extended basis function space 77—46491
atom, Fermi correlation, for parallel-spin electrons in momentum space 77—10602
atom, freq.-depend. polarisabilities and Verdet consts., calcs. 78—62781
atom, ground state, accurate CI wavefunction 77—42245
atom, ground state energy, split valence GO basis set SCF calc. 77—34554
atom, ground state energy determ., Galerkin-Petrov method 79—769
atom, ground state reduced first order density matrix CI calc., mag. shielding const. and diamagnetic susceptibility 79—6872
atom, ground state static polarisability and hyperpolarisability, numerical SCF method 79—36567
atom, ground state wavefunction, SCF HF calc. 78—90070
atom, Hartree-Fock density matrix equation, soln. 77—14339
atom, HF polarisability, second order correlation correction 78—25429
atom, Hund's first rule, new interpretation 78—78620
atom, independent particle pots. comparison 80—52846
atom, inner-shell photoionis., fluoresc. yield 77—57945
atom, ionisation energies and oscillator strengths, polarised frozen core approx. 79—36524
atom, isoelectronic series, Coulomb holes and correl. coeffs. 77—88398
atom, isoelectronic series, dipole matrix elements derivation 77—83519
atom, K-shell ionis., double and single, cross section meas. by ion bombardment 78—50629
atom, kaonic X-ray meas., strong interaction widths, shifts, yields 77—58210
atom, magnetic hypersusceptibility *(Russian)* 77—14598
atom, many electron autoionisation states, perturbation theory Z-expansion, numerical results 80—52863
atom, min. basis of Slater-transform-Preuss functions 79—59343
atom, model pots., STO calcs. 77—408
atom, multiconfig. Hartree-Fock calcs. convergency 80—47901
atom, multiconfig. HF procedure, 2nd- and approx. 2nd-order, convergency 79—93907
atom, multiconfigurational time-dependent Hartree-Fock approach 79—85889
atom, muonic X-ray intensities in low-Z elements and their hydrides 80—9761
atom, numerical many-body perturbation calcs. using multiconfig. model space 80—47907
atom, one-particle ionis. energy, correlated wavefunction 79—45639
atom, optical beam foil spectra, relative level populations 80—23540
atom, optical beam-foil spectra, relative level population 80—14207
atom, optimised one-electron wave functions 77—38598
atom, oscillator strengths, generalised RPA with exchange calcs. 79—98030
atom, pair excitation correl. numerical coupled cluster method 80—47906
atom, photoionisation, relativistic RPA calcs. 77—61719
atom, polarisability and London coeff., ab initio variation perturbation calc. 79—13635
atom, quantum mech. energy spectra calc. using trajectory integrals 78—21838
atom, Rayleigh-Schroedinger perturbation calculations 78—9064
atom, real STOS, parameter optimisation method 78—41929
atom, SCF electron-gas local-spin-density model including correlation 80—9488
atom, SCF ion improved virtual orbitals, excited configs. calcs. 77—10585

beryllium continued
atom, second order correlation energies, variational-perturbation method, radial basis saturation errors 79—97985
atom, self-consistent electron pairs with higher order effects 78—46276
atom, total nonrelativistic ground state energy, CI STO calc. 77—18800
atom, X-ray spectra, chemical bonding and multiple ionis. effects 78—50630
atom, zero-order Hamiltonian, for many-body perturbation theory 80—9483
atomic clusters, nonadditive interactions, SCF energy anal. 78—25765
atomic correlation energies, perturbations and near degeneracy 79—3371
atomic displacements, and antisymmetric atom vibrations, neutron data 80—49180
atomic polarisability, correlation corrections finite field method 77—71889
atomic polarisability, quadrupole, using elec. field variant GTO basis set 79—76359
atoms, electric dipole polarisabilities and hyperpolarisabilities, perturb. theory calcs. 78—17563
atoms and ions, excited in single gas collisions, high-resolution Auger spectra 80—9717
Auger electrons, proton-excited, attenuation lengths of low-energy electrons 78—11058
Auger emission target, contrib. of reflected electrons 78—92152
Auger spectra, initial state screening effects 80—50476
Auger spectra induced by 100 keV Ar$^+$ impact 80—84820
Auger spectrum, high energy plasmon satellite 79—82538
BCC, high-temp. resist. and band struct. 79—51551
blisters due to He irrad., proton backscatt. study 80—75273
brittle-ductile transition, intergranular embrittlement *(Russian)* 78—3208
brittleness problems, elevated plasticity and superplasticity, temp. depend. *(Russian)* 79—15758
cast, crystallographic orientation of columnar grains 77—59774
casting, produced in zero gravity environment, BeO particles uniform distrib. 78—72753
CESR linewidth and g-shift in presence of spin-orbit perturbation, spin-phonon scatt. 77—63285
channelled-ion scatt. yield, oscillatory, for 1.9 MeV ^{4}He$^+$ 78—52610
charge-density from X-ray structure factors 77—19893
chemisorption, of H atoms, mol. orbital cluster theory 79—15002
cluster, multibody expansions, convergence 80—23594
clusters, chemisorption of H$_2$, ab initio calcs. 80—3404
coatings, α-radiation meas. of thickness 78—82600
concentration determ. in rainfall, Katowice, Poland *(Polish)* 79—16558
conduction electrode hole coupling, XPS obs. 77—28135
conduction-electron spin flip by phonons, expt. data anal. 79—61219
containerless grain refinement using BeO in space environment, melting and solidification 79—47673
core electron distribution, X-ray diffr. and γ-ray Compton profile obs. 80—1958
core electron expansion, kinetic energy in Compton profiles 78—72628
cosmic ray ^{10}Be, abundance rel. to cosmic ray age 77—60554
cosmic ray isotopes meas., 200-1500 MeV/nucleon 79—12366
creep mechanism 77—36586
crystal, failure energy 80—81192
crystal defects, study with muon probes 78—47314
crystal indicator, single, for high magnetic field measurements 79—63280
CTR blanket materials, neutron multiplication factor studies 80—18628
deformation strengthening, microstruct. and impurity effects 77—4791
determination in biological materials, by flameless atomic absorption spectrometry *(Japanese)* 80—26428
determination in simulated aerosol samples, proton scatt. anal. 79—5217
dielectric function calc. 77—1358
dielectric function from APW calcs. 79—65817
diffusion and solubility of Al 77—35758
diffusion coefficients and solubility of V, Nb, Ce 77—35757
diffusion in Al-Mg-Zn alloy surface, depth profiling by ion microprobe with high mass resolution 79—46894
diffusion in Ti, temp. depend., radioactive tracer method *(Russian)* 80—10703
diffusion of Co, 1250 to 1493K, radioactive tracer method *(Russian)* 80—24668
dopant for GaP, behaviour on crystallisation from melt 77—84772
double excitation wavefunctions, multiconfigurational SCF method 77—10604
electric field gradient, magnitude and sign 77—80755
electric field gradient at nucleus calc. 78—39079
electric field gradients of recoil-implanted ^{19}F via ^{9}Be(^{12}C, np)^{19}F 77—8471
electrical and thermal cond. at low temp. in mag. field, use as heat switch 77—35923
electrical resistivity; 1-1000K, data tables 79—78073
electron density and bonding, Fourier method study 78—26481
electron distribution and momentum density, Compton scatt. 80—11502
electron mean free path, stopping and straggling 78—91367
electron microprobe local anal. of light elements, ultrasoft X-ray spectroscopy 80—99027
electronic struct., NMR study 80—108085
electronic surface states, (001) surface, Brillouin zone 79—24047
emittance at 400 to 850K and normal spectral reflectance at room temp. 77—20813
energy loss of 120 keV heavy ions, range and range straggling determ. 79—45595
equation of state, solid-state models, comparison 80—75332
equation of state from statistical electronic free energy 79—99495
failure on basal plane 78—15525
fast electron multiple scattering, and inner secondary electron generation 77—1160
Fermi surface, stress-induced changes 80—96770
Fermi surface stress induced changes calcs., principal cross sectional areas 79—60684
fibre reinforced Ti-Al-V (6.4 wt.%), synthesis and mech. props. 77—32544
field ion appearance spectroscopy, ion generating processes at field emitter surface 79—52086
film, inelastic-elastic scatt. ratio of 80 keV electrons use for radiation damage monitoring 77—4127
film, on Cu substrate, monolayer overgrowth, quantitative AES method 80—10813
film, on Pt substrate, range of primary electrons 77—4134

beryllium continued
film, on W (110), growth mode, work function, thermal desorption, and struct. 80—75477
film, ultra-thin, fabrication 79—33933
film, vapour quneched, mech. stresses and elec. cond. 79—73414
film as opt. filter in He discharge lamp, for photoelectron spectroscopy 78—79115
foil, ion bombardment, secondary photon emission, ion energy depend. 80—97346
foil, rolling procedures 80—23225
forest dislocation effect on single twin layer development in single crystals 78—63775
fracture and strength properties, dynamic ageing effects 80—81202
fracture initiation location in disc under biaxial tension, statistical distrib. 77—58607
fracture mechanics test, electrical potential method, unusual potential drop 77—16761
fracture of hot-extruded samples in impact, static tensile and fatigue tests *(Russian)* 77—52458
fracture toughness of high-strength specimens 77—73336
fusion reactor blanket material, neutron multiplication meas. 79—59255
fusion reactor first wall protection, Be coated limiters 80—32483
fusion reactor material, 100 keV He ion irrad., surface due to blistering 77—35600
fusion reactor material, low energy ion erosion expts., Kaufman source appl. 80—68942
fusion reactor material, range profiles of Li$^+$, appl. of (n,p) and (n,α) reactions 80—61200
fusion reactor material, response to He$^+$ bombardment determ. 78—86691
galactic Be abundance, rel. to cosmic-ray nucleosynthesis and extragalactic matter infall rate 79—17084
gamma-ray buildup factors 80—27822
HCP, electron-phonon interaction, thermal effects 79—33057
HCP metals, K-emission valence bands, structure and bonding 80—7438
in Hyades stars, abundance meas. 77—53584
implanted D and He, interaction and radiation enhanced oxidation 80—39120
inelastic electron scattering near K-edge 78—52606
ingot, high-purity, TEM obs. of BeO dispersion 80—104165
internal friction, temperature spectrum and dislocation damping, anelastic relaxation *(Russian)* 80—2118
ion, radiative decay of 2 ^{3}P$_0^\circ$ level 80—27984
ion bombarded, chemical effects on secondary photon and ion emission 78—95637
ion bombarded, D trapping 79—19291
ion implantation in InP and In$_{1-x}$Ga$_x$As$_y$P$_{1-y}$, p-n junction diode fabrication 79—47156
ion irradiated, Auger electron spectra struct., possible surface diagnostic methods 79—69946
ion recombination laser 78—17923
ion-implanted, impurity lattice location, channelling meas., Monte Carlo calc. 80—107291
ions, isoelectronic series, correlation energy and size, empirical relationship 77—79546
isoelectronic sequence, electron impact excitation 79—81286
isoelectronic sequence, electron impact excitation of reson. transitions 80—63825
isoelectronic sequence, highly ionised, beam-foil obs. of oscillator strengths for E1 transitions 80—14112
isoelectronic sequence, ionization equilib. balance, solar and stellar atms. appl. 79—36587
isoelectronic sequence, mag. dipole transition contrib. 79—81153
isoelectronic sequence, mag. quadrupole transition probabilities calcs. 78—21865
isoelectronic sequence, multiconfig. HF calc. of mag. quadrupole transitions 78—33420
isoelectronic sequence, pot. energy relationships 79—22584
isoelectronic sequence, relativistic transition probability calcs. 77—54533
isoelectronic sequence, transition probabilities, relativistic effects calcs. 77—27028
isoelectronic series, atom + H$^+$, low-lying ^{3}P term excitation, cross-sections and rate consts. 79—94069
isoelectronic series, electric field variant orbitals, STO field gradient depend., atomic quadrupole polarisability 80—23295
isoelectronic series, excited states, oscill. strengths calcs., influence of wave function determ. method 80—99478
isoelectronic series, excited states, transaction oscill. states and wavefunctions 79—59367
isoelectronic series, inner-shell photoionis. cross sections 78—74623
isoelectronic series, valence, Rydberg and continuum orbitals 77—3259
kaonic X-ray spectra, strong interaction widths 77—10796
Knight shift of μ^+ 79—56657
lattice dynamical props., unpaired forces, phonon dispersion relations 79—19336
lattice dynamics, phonon dispersion relations and Debye temp. 79—42171
lattice location results for implanted impurities, Rutherford backscatt./channelling technique 79—4329
lattice site Be electric field gradients, gamma-spectral study 80—80224
lightweight optical substrate fabrication 79—23107
low oxide, isostatically pressed block, factors affecting tensile strength, elongation, impact resistance 77—16610
machining damage, SEM exam. 78—39990
magnetic suscept. anomalous temp. depend. *(Russian)* 79—4650
magnetoacoustic quantum oscills. due to mag. breakdown orbits, and derivative of magnetisation meas. 77—43479
magnetoresistance at low angles between current and mag. field *(Russian)* 78—68012
magnetothermal switch, electrocaloric refrigeration for 4 to 15K 79—80624
main-sequence stars, Li, Be and B abundances rel. to envelopes hydrodynamical instabilities 78—93202
metallic clusters, size fluctuations of work function 78—14792
mirror, fabrication, metal and dielec. coatings 77—62034
mirror, surface quality and thermal props. 80—23762
mirrors, props. and fabrication procedures 80—38138
moderator in thermionic reactor with ^{233}U fuel, neutron physics analysis 77—50281
monochromator grain identification by neutron topography 79—76244
muon location and diffusion, μSR 79—56693
muonic X-ray transitions, nuclear charge radii 80—99589

beryllium continued

muscle membrane, insect, permeation of Mn, Cd, Zn and Be through Ca channels 77—56357
neutron diffusion in finite blocks, flux synthesis method for 3D multigroup eqn. 77—34366
neutron focus in synchrotron radiation *(Russian)* 78—33344
neutron forces in relativistic electron radiation field in crystal, channelling *(Russian)* 80—70287
neutron irradiated, annealed, tensile props. and swelling, effect of the bubbles 78—22765
neutron irradiated, gas porosity, Brownian motion 79—73222
neutron wave propagation across discontinuity, two group calcs. 78—89931
noncubic crystal, temp. depend. of elec. field gradient 79—99515
nuclear bombardment target, chemical procedure for preparation 79—63854
optical components, electroless Ni coated Be, comparison with glass 80—69473
orbital magnetism, effect of energy spectrum features *(Russian)* 77—85414
oxidised surfaces (0001), internal electron source contrib. to TSEE trap population 80—16161
phase struct. *(Russian)* 78—15401
phonon dispersion calc. 79—51218
phonon spectrum from inelastic coherent scattering of cold neutrons 80—10617
photoemission theory, book contrib. 80—16159
plasma, dense, nondegenerate, electron transport, thermal cond. *(Russian)* 79—98865
plasma, laser-produced, recombination effects 78—94935
plasma, spectral lines 77—7515
plasma, stigmatic obs. with grazing-incidence spectrograph 79—73041
plasma spray/sinter technique, Ar, satellite support structures, appls. 78—7079
plasma sprayed coating, erosion rates under H$^+$ ion bombard., fusion reactor appls. 80—39179
plasma-sprayed coatings on Cu and stainless steel, fusion reactor appl. 80—18619
plastic strain mech., effect of impurities *(Russian)* 79—34101
polycrystalline, metallographic observation of cleaved grains 78—72824
polycrystalline, plasticity, cleavage strength, ductility transition temp. 80—44250
polycrystalline, plasticity and cleavage, yield and flow stresses 80—44249
porous, shrinkage during sintering, kinetics, photographic method 79—15622
powders, gas evolution during heating from 20-700°C 79—61796
projected range distrib. of 5-25 keV ^{4}He$^+$ 80—65094
proton bombarded Auger electron attenuation length meas. $E_p=160$ keV 77—44101
proton energy stagggling in ion backscatt. expt. 79—37750
proton stopping power, 20 to 120 keV 80—91411
quadrupole interaction for ^{100}Rh, ^{111}Cd, and ^{181}Ta, temp. depend. TDPAC obs. 77—20772
quadrupole interaction of ^{100}Rh, ^{111}Cd, ^{181}Ta, temp. depend. 77—8466
quadrupole interaction of ^{12}B and ^{12}N 78—47750
quantum oscillations of thermal EMF under mag. breakdown conditions *(Russian)* 77—69305
reaction with graphite and Zr and Nb carbides, Be_2C layer formation 77—36786
reflector redesign effect on ATR power distrib. and control element reactivity 80—9363
resistance, anomalous temp. depend. of impure samples *(Russian)* 79—51552
resistivity, temp. depend. minimum obs. *(Russian)* 77—35919
resistivity minimum temp. depend., 4.2 to 40K *(Russian)* 79—87077
RF sputtered film, props. rel. to deposition conditions 77—39965
rod, thermal expansion meas. using holographic interferometry 77—31073
rolled ingot, with duplex microstruct., basal texture of two grain size distrib. 77—36556
seawater, bulk viscosity and l.f. sound attenuation, Be and B influence 77—3696
secondary photon emission following ion bombard. 80—71493
sintered, physicomech. props. anisotropy, BeO inclusions effect 80—60804
soft X-ray emission and absorpt. edges, self-absorpt. studies 80—40183
soft X-ray emission edge, temp. depend. 80—89090
Soft X-ray emission edge self absorption and effect of exciting voltage 77—90220
solubility, partition coeff. in SiC 79—10951
solubility of Cu at low temps. 77—62646
spectrophotometric determination, in aq. organic medium using eriochrome cyanine R 77—36829
spin susceptibility, electronic effective mass, spin density functional calcs. 78—43291
sputtered atoms, ion bombardment induced line radn. 79—91553
sputtering by H$^+$, D$^+$, He$^+$, weight loss measurements 80—35028
stopping power for 28 MeV α-particles, re-evaluation 78—79651
stopping power for 6.75 MeV protons 80—34107
stopping powers for 28.8 MeV α-particles 77—80556
strain hardened metal and microalloys, low temp. brittleness 79—96140
substrate for Ag films deposited from hot hollow-cathode source, adhesion 77—8754
sum mixing, 4-wave, around H Lyman-α 80—23747
superconductive device to provide reference temps. below 0.5K 79—63220
surface, (0001), work function and purity, AES, LEED and photoelectron spectra meas. 78—68606
surface, clean and O covered, secondary-ion emission energy depend. 80—50502
surface, contact angs. meas., aq. ethanol (glycerine) solns., 20-70°C 78—56025
surface, O and H covered, secondary ion emission, coverage dependence 80—35043
surface, slowly oxidised, secondary electron yield changes, and AES characterisation 80—71524
surface damage, due to 20 keV He$^+$ irradiation, gas trapping profile meas. *(French)* 80—84218
surface hardening by B ion implantation 80—16604
surface morphology, effect on low energy H ion erosion yield 79—42121

beryllium continued

target, microwave laser irrad., plasma form., inhibited electron thermal cond., laser intensity threshold Z-depend. 80—48928
thermal neutron scatt. anisotropy anal. 80—552
thermal neutron wave propagation 78—58320
thick film, amorphous, RF magnetron sputtering 80—80971
thick film or Au substrate, secondary electron emission 80—104022
thin foil thickness meas. using ^{148}Gd and ^{241}Am alpha-particles 79—30417
transformation enthalpies for α-β and β-liquid transitions 77—35690
twin and stacking fault energies 79—38018
twin boundaries, computer simulation 80—39109
twinning dynamics of single crystal 77—4115
ultra fine-grained, recrystallisation after deform. 79—52239
welded, acoustic emission 78—39976
wire, elec. cond., heat treatment and strain effects *(Russian)* 80—24870
wires and strips, elec. resist. at 77K, size factor *(Russian)* 80—24867
X-ray emission spectra, effect of short range order and deep vacancy screening, multiple-screening theory 77—28651
X-ray emission spectrum, double plasmon high energy satellite 78—72639
X-ray K emission spectrum, high energy double plasmon satellite intensity calcs. 78—2944
X-ray plasmon scatt., electron exchange energy influence 79—56884
X-ray scattering, Wannier function calcs. 80—87988
X-ray spectra, K-shell, produced by heavy ion bombard., chem. effects 77—36314
X-ray spectra, polarised K-emission valence bands 77—16429
X-ray spectra, separation of K-emission and absorpt. edges 79—33864
X-ray spectroscopy of single crysts., use of polarised radiation 78—8481
XPS, plasmon struct. of core lines 77—63530
XPS investigation of density of states 78—6829
XPS theory, core level spectra, plasmon creation 78—72701
XPS theory, valence band spectra band struct. 78—72702
yield strength, struct. factors effects 77—63749
zero-temperature equation of state, statistical model with density gradient correction 80—15215
zincating, deposition conditions, film characts. 77—40397
Al-Be, two-layer foils, mech. props. *(Russian)* 78—51858
p-$Al_xGa_{1-x}As$:Be layer, MBE growth, Be doping and diffusion 77—51397
Am-Be, neutron fluence-to-dose conversion factors 79—6771
B$^+$, electron impact excitation of 2p state, close-coupling calc. 78—55247
B$^+$ + He(Ne), charge transfer and excitation, differential cross sections, 2-5 keV 79—36764
B^{5+} + He, electron capture and impact-ionis. cross sections, Monte Carlo calcs. 79—27083
Be atoms, double-photoionisation cross section, core polarisation effects 78—17626
Be, grain size effect on mech. props. *(Russian)* 79—47749
Be, highly excited states, electronic struct., oscillator strengths and resons., HF calcs. 77—46506
Be I, energy level calcs. using model pot. and cores approxs. 77—14353
Be I, energy level calcs. term systems, convergence to Be II 2s limit 77—14354
Be I, spectra calcs., fine struct., transition energies 77—42260
Be I, weighted oscillator strengths for elec. dipole and forbidden transitions, data tables 80—37779
Be I isoelectronic sequence, radiative props. determ. by model-pot. method 78—70788
Be I isoelectronic series, 2p^2-2s2p and 2s2p-2s^2 transitions, oscill. strengths, transition probabilities 77—46532
Be I like ions, resonant-scatt. contributions to excitation rates 80—58393
Be I-like spectra, low configs., isoelectronic consistency 79—93940
Be II, autoionising core-excited states, alignment prod., Be$^+$ + He(methane) collision excitation 80—14204
Be II, III, laser produced plasma, satellite spectra 78—5165
Be II, optical oscillator strengths for excitations from 1s^{2}2s(^{2}S) ground state 79—98044
Be III, doubly excited states, triplet spectra 80—87069
Be III, X-ray lasers pumped with synchroton radiation and low-energy photons 79—41371
Be IV, line broadening and self-absorpt. in laser prod. plasma 78—17615
Be isoelectronic sequence, mag. quadrupole transitions probabilities 78—37592
Be isoelectronic series, transitions involving 2s3l^{3}L states, oscill. strengths 77—3308
Be isoelectronic series, Z=22-34, spectral lines from laser prod. plasma 77—50388
Be lines formation, non-LTE calc., rel. to solar Be I 2650 Å line misidentification 80—32636
Be sequence, (Z=4 to 10, 14), $^3P_1 \rightarrow {}^1S_0$ intercombination line, CI calc., Breit interaction 78—78641
Be$^-$, ^{2}P shape resonances, shift potential calcs. 80—69089
Be$^-$, low-energy ^{2}P^0 shape resonance, complex-coord. method calc. 78—74591
Be$^+$, ^{2}S, ^{2}P^0 and ^{2}D autoionising states, positions and widths 79—26944
Be$^+$, 1s3s3p ^{4}p^0 state, Hartree-Fock function, third-order energy 78—37569
Be$^+$, absolute cross sections and polarisation of electron-impact excitation of resonance multiplet 80—99577
Be$^+$, electron impact excitation cross sections of 2p state 77—75303
Be$^+$, electron impact excitation, Bethe approx. modifications, impact radiation polarisation 79—31695
Be$^+$, formed in laser-produced plasma, absorpt. from excited states 78—17594
Be$^+$ ions, beam-foil excitation, L-Auger decays, autoionisation 77—14569
Be$^+$, multipole polarizabilities and shielding factors, calcs. on open shell ions 78—46263
Be$^+$, reson. line regularities in plasma Stark widths and shifts 80—43881
Be$^+$, resonance lines electron impact excitation, polarisability 78—42225
Be^{++}, ground state energy via correl. wave function calc. 77—23439
Be^{2+}, elastic form factors, correlated two-electron-core pots., closed form expressions 79—68195
Be^{2+}, electron impact excitation, cross-sections, modified Oppenheimer approx. 78—82843
Be^{2+}, few-parameter two-electron wavefunction of ground state 77—75051
Be^{2+}, numerical Hartree-Fock calc. of 1s^2 ground state 79—81155

beryllium continued
- Be^{2+} quantum defects rel. to angular momentum, nuclear charge, Coulomb-Born approx. method *(Japanese)* 77–50534
- Be^{2+}, three-particle atomic system, binding energy, Faddeev method calcs. 77–57858
- Be^{3+}, electron scatt. near ionis. threshold, ang. momenta 79–31698
- Be:Ar, ion-implanted, high resolution LMM Auger spectra 79–83066
- Be:Li, ion-implanted, interstitial props. 79–37876
- Be:Li, lattice location of implanted ^{6}Li, ion beam channelling study 79–37730
- Be:Os, anomalous displacement of Os atoms from substitutional site 77–59039
- Be:Zn, lattice location of implanted Zn, ion-beam channelling meas. 77–68992
- Be/Au/Be layer configuration 77–24338
- Be-Au, ohmic contact to GaP, metallurgical struct. 77–1485
- Be-diamond support, for high-pressure X-ray diamond-anvil cell 78–30515
- Be-Li-V, phase diagram, metallurgical aspects for fusion blanket use 80–32467
- Be-like ions, $2s2p(^{3}P_{1}^{0})\rightarrow 2s^{2}(^{1}S_{0}^{e})$ transition probabilities, CI calcs. 79–36544
- Be-like ions, electron impact excitation, config. mixing 77–58175
- Be-like ions, multiply charged, laser plasmas, 1.5-15 Å 78–13462
- Be-like ions, oscill. strengths and transition probabilities, Breit-Pauli approx. calcs. 79–36570
- Be-like ions, photoionisation, 2-channel relativistic random phase approx. calcs. 79–59407
- Be-SiO-p-Si, MIS solar cell, performance figures 78–88030
- Be-type atoms in $1s^{2}2s^{2}\ ^{1}S$ state, soln. of Hartree-Fock eqns. with nonorthogonal radial orbitals 77–46493
- Be+Ar(Kr)(Xe), chemiluminesc. associative ionisation mechanisms 77–32781
- Be+Be closed-shell system, exchange polarisation energy 78–42155
- Be+Be(Li) 78–5310
- $Be+FH\rightarrow BeF+H$, collinear, pot. energy surface study 79–11782
- $Be+H^{+}(He^{+})$, double K-shell ionis., projectile Z depend. 78–25680
- Be+He (methane), Be atom K-shell binding energy by Auger spectra 78–50525
- Be+He (methane), collisional excitation, prompt decay line energy, projectile Auger spectrosc. 79–85941
- $Be^{+}+H_{2}(He)(Ne)$(methane), Be Auger spectra 77–57951
- $Be^{+}+He(Ne)$, ns-np excitation, alignment and orientation, impact, parameter theory 80–91648
- $Be^{+}+He(Ne)(Ar)$, Be II $2^{2}P$ excitation, alignment and orientation 80–91647
- $Be^{+}+He(Ne)(Ar)$, Be^{+} collision-induced alignment, reson.-line emission polaris. obs. 80–18912
- Be^{+}+methane, single collision, time delayed autoionisation spectra 78–1067
- $Be^{+}+Ne$, 180 degree phase jumps for Be^{+}(2s-2p) excitation amplitudes, coherence obs. 80–63793
- $Be^{+}+Ne$, $2s\rightarrow 2p$ excitation probability for Be^{+}, coherence parameters 79–54955
- $Be^{2+}+H\rightarrow Be^{+}+H^{+}$, charge transfer total cross-sections 79–3559
- $Be^{4+}+H$, electron capture into n, l levels, 100 keV/amu 79–22826
- $Be^{4+}+He$, electron capture and impact-ionis. cross sections, Monte Carlo calcs. 79–27083
- Be_{2}, electronic structure, SCEP theory calcs. 77–10579
- Be_{2}, ground state, multiple scatt. $X\alpha$ calcs. 80–58149
- Be_{2}, low-lying states binding energy, local spin density functional formalism calcs. 79–97994
- Be_{2}, multipole expansion of diatomic overlap, MEDO calcs. 78–46264
- Be_{2}, polarisability, generalised London formula for dispersion coeff. 78–82662
- Be_{2}, pot. curve, coupled-pair many electron theory, quadrupole excitation 79–36538
- Be_{2}, pot. curve of ground-state, many-body perturbation theory and SCF-CI method 79–36563
- Be_{3}, 3-body interactions in binding, semiclassical approx. calcs. 78–21994
- Be_{3}, 3-body nonadditive interaction, nodal struct. 78–1049
- Be_{4} (Be_{4}^{-}), atomic clusters, electronic struct., LCAO-MO-SCF and HF calcs. 80–63880
- Be_{4}, Be_{2}, dissoc. energy, electron correlation effect, self-consistent electron pair calc. 77–30790
- Be_{n}^{-} (n=2,3,4), electronic struct., ab initio calcs. 78–17560
- $BeO(Be_{2}O)$-TiO_{2}-$P_{2}O_{5}$, electrical resistivity *(Japanese)* 77–12719
- $Be(^{1}S)$ excitation energy, eqn. of motion method calcs., approxs. and error anal. 79–36501
- $Be(^{1}S)$, total X-ray scatt., two-electron density functions 78–70889
- $Be^{2+}(^{1}S)$, correlation energy calc. of at. in spherical box 79–97984
- $Be_{2}(^{1}\Sigma_{g}^{+})$, binding energy, ab initio pot. curves, interacting correlated fragments method 80–63557
- ^{7}Be aerosols content increase over Pacific Ocean during strong jet stream 77–78373
- ^{7}Be, atmospheric, distrib. within high-press. systems in E.United States 80–4072
- ^{7}Be bearing aerosols mean residence time in troposphere 77–87018
- ^{7}Be, electron capture decay, internal ionisation 77–18892
- Be, electron capture radioactive decay probabilities in atoms and ions 79–59556
- Be, impurity in Li liq. in fusion reactor, control system 80–32466
- $^{7}Be/^{9}Be$ data rel. to cosmic ray acceleration mechanisms 80–31183
- ^{9}Be, nuclear mag:spin-lattice relaxation times 78–86889
- $^{9}Be^{2+}$, aq. ions, nucl. quadrupole relax. 78–64287
- ^{10}Be abundance in cosmic rays rel. to age, balloon meas. technique 77–29602
- ^{10}Be conc. vars. search in marine sediment core 80–26511
- ^{10}Be, concs. in environment rel. to cyclospectrometry dating techniques *(French)* 80–21859
- ^{10}Be dating using cyclotron as mass spectrometer 77–64489
- ^{10}Be deposition rates at Earth surface, seasonal vars. 80–26707
- ^{10}Be geochemistry in North Pacific during Pliocene 80–101356
- ^{10}Be in 1000 and 5000 yr old Antarctic ice, meas. 79–2305
- ^{10}Be in Arctic Ocean sediments 77–81865
- ^{10}Be in marine sediments rel. to geophysical events and cosmic ray var. 79–29748
- ^{10}Be in Mn nodules, meas. using tandem Van de Graaff accelerators 79–74967
- ^{10}Be in ocean surface layer, conc. and residence time 79–66714

beryllium continued
- ^{10}Be in seawater rel. to oceanic residence times of dissolved Be 79–34856
- ^{10}Be, use in meas. Mn nodule growth rate 78–40537
- $^{10}Be/^{9}Be$ ratio meas. using electrostatic tandem accelerator 80–76579
- $Be(1^{1}S)$-$Be(1^{1}S)$, dispersion energies, charge overlap effects, with freq.-depend. polarisability 79–86025
- $Be(2^{3}P)$+methane, reaction, ab initio MO calcs. 79–8431
- C diffusion, in metal-ceramic Be *(Russian)* 80–19984
- CdTe:Be, impurity modes and IR absorption 78–76506
- Cu:Be, alloy formation kinetics at solid cathodes, metal electrodeposition from molten salt electrolytes 80–26028
- Cu-Be-O surface, $O(^{5}S)$ impact, secondary electron yield 78–58797
- (GaAl)As:Be implanted DH stripe geometry laser 80–64044
- GaAlAs/GaAs solar cells, Be and Zn behaviour 80–101111
- $Ga_{1-x}Al_{x}As$ low threshold stripe geometry DH laser, Be implanted, on semi-insulating substrate 80–69409
- GaAs:Be, annealing effect during MBE 78–79898
- GaAs:Be, deep levels 80–29358
- GaAs:Be, implantation and annealing, elec. props. 79–99540
- GaAs:Be, implanted, determ. of Be concentration profiles by $^{9}Be(p,\alpha)$ reactions and SIMS anal. 79–4335
- GaAs:Be, implanted, low temp. photolum. spectra 78–39583
- GaAs:Be, ion implanted, elec. profiling and optical activation expts. 77–89457
- p-GaAs:Be, ion implanted, annealing characts., defect cond. profiling, electron diffr. obs. 79–4318
- GaAs:Be, ion-implanted, photolum. spectra, effects of implantant depth distrib. 78–27293
- GaAs:Be, ion-implanted, IR refl. and transmission meas. 80–34908
- GaAs:Be, MBE layers, photoluminesc. 80–29803
- GaAs:Be,Se VPE layers, ion implanted, donor-acceptor pair radiative recomb. 79–91489
- p-GaAs:Be layer, MBE growth, Be doping and diffusion 77–51397
- GaAs:Be MBE films, elec. characterization 79–91168
- GaAs:Be planar p-n junction, Be ion implantation, fabrication and characts. 78–88022
- GaAs:Cr, Be, ion-implanted, semi-insulating, carrier mobility and conc. temp. depend. 77–76808
- GaAs:Cr, Be^{+} implantation, atomic conc. and defect density profiles after annealing 80–39123
- GaAs-$Ga_{2.2}Al_{0.8}$As:Be, LPE, diffusion of Be into GaAs substrate 80–103517
- GaInSb, Be ion implantation, device appl. 80–24478
- Ge:Be, P, absorption of radiation, 0.6-2.8 mm, 4.2 to 20K 80–66332
- Ge:Be, positron annihilation angular distrib. 80–45165
- Ge:Be single crystals, grown by Czochralski method, exam. of Be distribution ratios and solubility 79–95043
- $H+Li^{3+}(Be^{4+})(B^{5+})(C^{6+})$, charge transfer cross sections, distorted wave Born approx. 79–72415
- $He+Be^{+}(Mg^{+})$ high energy, excitation cross sections, impact radiation polaris., models comparison 78–1069
- I_{2}-Be, doping effect on elec. cond., semicond. props. 80–49732
- InAsSb, Be ion implantation, device appl. 80–24478
- InGaAsP:Be, avalanche photodetectors annealing temp. effect on photolum. spectra 79–69872
- InGaAsP:Be ion-implanted avalanche photodiode, struct. and characts. 79–17487
- $In_{1-x}Ga_{x}As_{y}P_{1-y}$:Be, ion implantation, hole conc. and mobility, junction depth 79–46685
- InP:Be, ion implantation, hole conc. and mobility, junction depth 79–46685
- InP:Be, LPE, Be distrib. coeff., carrier conc. 79–90694
- n-InP:Be, p-n junction formation by ion implantation 80–29474
- InP:Be, planar reactive deposition on CdS, heterostruct. formation and elec. evaluation 78–72738
- LiF:Be, Maxwell-Wagner relax. induced by impurity clouds around dislocations, ionic thermocond. meas. 80–7281
- MgO:Be epitaxial layers, vacuum UV luminescence 80–11480
- γ-Mn electrodeposition influence of Cu, Ag, and Be impurities *(Russian)* 79–47938
- $Ne+Be^{+}(Mg^{+})$, high energy, excitation cross section, impact radiation polaris., models comparison 78–1069
- Ni, blistering model, correlation between blister diameter and skin thickness 78–95067
- O_{2}+Be(Mg)(Ca)(Sr)(Ba), reaction kinetics in diffusion flame 77–90579
- Pu-Be neutron source, for activation anal., β-ray meas. 78–73114
- ^{32}S ions+Be(C)(Ni), radiative electron capture, X-ray ang. distrib. 77–38729
- Si:Be, ion implanted, correl. of atomic distrib. and implantation induced damage profiler 80–88199
- Si:Be ion implanted, channelling and random equivalent depth distrib. 80–100293
- SiC:Be, dislocation induced deceleration of impurity diffusion 77–28043
- p-SiC:Be, Fermi level, Fermi distrib. and activity coeff. calc. 77–1365
- SiC:Be, film donor impurity, diffusion influence on elec. and optical props. 78–87942
- SiC:Be, gas-phase equilib. comp., thermodynamic analysis rel. to cryst. growth and doping 77–85909
- α-SiC:Be, piezoresist. rel. to acceptor levels 78–60129
- n-TiO_{2}:Be electrodes, photoassisted oxidation of water 80–30502
- V-Be diffusion couple, ion backscatt. anal. 77–35752
- W, containerless melts in terrestrial and space environment, thermodynamic props. calc. from solidification and cooling curves 79–70052
- YIG:Be^{2+} LPE film, microwave relaxation props. 79–65741
- $Zn_{3}P_{2}$-Be, diode, spectra response meas. of minority carrier diffusion length 79–78131
- ZnS:Be, far IR lattice absorpt., Green's function calc. 78–43865
- ZnS:Be, impurity modes and IR absorption 78–76506

beryllium alloys
- *see also beryllium compounds*
- bronze, Be, elastic elements made from spring alloy bands 79–87678
- bronze, struct. and props. after ageing under load 78–84932
- bronze matrix, Be alloying addition effects on supercond. props. of $Nb_{3}Sn$ monofilament wires 79–87222
- depth profile meas. in alloys, using d and α detection in $^{9}Be(p,d)$ and $^{9}Be(p,\alpha)$ 79–5203
- dilute metastable, produced by ion implantation, lattice location of impurities 79–51132
- dilute metastable alloy formation by ion implantation 80–15130

beryllium alloys continued
distribution of Be in metals, using ^{9}Be(d,p) and ^{9}Be(α,n) 79—5204
magnetic susceptibility meas., Faraday method 77—47969
metastable alloy form. by ion implantation 79—82252
metastable alloy formation by ion implantation 79—14828
metastable microalloys, equilib. form. criteria 78—30762
rare earth alloys, RBe$_{13}$, XPS, resist. and susceptibility study 80—71565
steel austenitic Cr-Ni-Be, cellular precipitation *(Japanese)* 78—11229
struct. and form. of metastable phase m-TiBe 78—48375
superconducting high Debye temperature material, theoretical upper limit of crit. temp. 80—60129
Al-Be-Mg (30, 5wt.%) alloy, weld solification parameters 79—24511
Al-Li-Mg-Be alloys, phase composition of surface films, oxidation protection mechanism *(Russian)* 80—65417
Al-Mg-Be, solid soln. decomposition, metallographic study 77—16577
Al-Si-Cu-Be alloys, phase equilib. *(Russian)* 77—59748
Al$_{1.1}$Be$_{0.6}$B$_{22}$, metal distrib., X-ray diffr. study 80—75204
Al$_4$C$_3$.3Be$_2$C, X-ray difr. and TEM study 80—14973
Au-Be, contact form. for semicond. devices by ionised-cluster beam deposition 77—32528
Be bronze, BrB2 grade, heat treatment quality evaluation, using eddy current device 77—90562
Be bronze, electrolytic polishing using cylindrical stationary electrode 78—64783
Be bronze, electropolishing using cylindrical electrode moving forwards 78—64784
Be bronze BrB2, quenched deformed, substruct. and props., effect of prerecrystallisation annealing *(Russian)* 78—60677
Be-Al-Fe, phase equilibria and diffusion using high energy ion beams 77—16542
Be-Al-Fe system, phase equilibria using high energy ion beams 79—43203
Be-Au, dil., quadrupole interactions and lattice location, ^{197}Hg TDPAC and Mossbauer expts. 78—43726
Be-Au, ohmic contact to p-InP, low contact resist. 80—65677
Be-B, ion implanted surface hardened layer on Be 80—16604
Be-bronze BrB2, struct. and phase transform. during mechano-thermal treatment *(Russian)* 80—11667
Be-Co (0-50 at.%) alloys, thermal, metallographic and X-ray anal., phase diagram *(Russian)* 78—56611
Be-Co phase diagram *(German)* 77—59759
Be-Co-Ni, phase relations *(German)* 79—43209
Be-Cu, calibration line introduction for comp. determ. by AES 79—56892
Be-Cu, ductile erosion, prediction, mechanistic model 77—12709
Be-Cu, optical elements, US cleaning, deleterious effects 77—42631
Be-Cu, props., precipitation hardening effects and appl. *(Italian)* 79—83207
Be-Cu, seawater corrosion protection, of repeater housings 78—15583
Be-Cu, thermal expansion, vibr. characteristics at low temp., effect of substitution impurities *(Russian)* 80—103439
Be-Cu alloy stress relaxation in bending, 63° to 343°C 80—50693
Be-Cu dynode, depth profiling anal. of surface layer 80—2253
Be-Cu high-strength alloy characteristics for electrical components 78—48547
Be-Cu K-band high-pressure cell for EPR-ENDOR studies 79—67336
Be-Cu mill-hardened strip stress relaxation obs. 78—48485
Be-Cu strip surface quality and preparation 80—50779
Be-Cu surface, secondary electron yield, for electron multiplier ion detector 78—74094
Be-Cu surface preparation for Au electrodeposition 78—7100
Be-Cu wire for high-speed matrix printers, wear resistivity obs. *(Japanese)* 80—55540
Be-Hf, dil., ^{178}Hf Mossbauer transition, electric quadrupole interaction 80—39928
Be-Hg, dil., quadrupole interaction and lattice location for Hg 78—48086
Be-Ir, dil., elec. field gradient, Mossbauer meas. 80—80665
Be-Mg, two-band alloy, electronic and optical props., multiband theory 79—37952
Be-Nb-Zr, glassy and partially crystalline, supercond. T_c and struct. props. 78—60239
Be-Ni(Y)(Al), plastic deform., flow stresses, fracture *(Russian)* 80—108496
Be-Ru, dil., quadrupole interactions at ^{99}Ru, TDPAC meas. 78—91996
Be-Si(Al), solubility of Cu at low temps. 77—62646
Be-Zr, glassy, quenched from melt, supercond. props. 78—26983
BeCu pressure clamp cell, for low temp. specific heat and magnetisation meas. 80—17956
Be$_5$(Fe$_{1-x}$Mn$_x$), mag. and calorimetric props. 77—63083
Be$_{1-x}$Mn$_x$, Be-rich, NMR and paramag. susceptibility 80—71206
Be$_2$Mn$_{1-x}$Fe$_x$, mag. props., giant moment clusters 79—28508
BeNi, dil., electronic struct., NMR study 80—108085
Be$_{40}$Ti$_{50}$Zr$_{10}$, metallic glass, thermoelectric power and resist. 78—95289
CeBe$_{13}$, intermediate valence state, XPS, resist. and susceptibility study 80—71565
CeBe$_{13}$, lattice spacings and susceptibilities 80—65778
(Ce$_x$La$_{1-x}$)Be$_{13}$, mag. intermediate valence behaviour 79—24131
Cu-Be, age hardening characts. *(Japanese)* 78—35398
Cu-Be, condensation *(Russian)* 78—44014
Cu-Be, dil., electron high dosage source for residual resistance specimens and irradiation expts. *(German)* 78—21274
Cu-Be, dilute, electron irradiated, Be segregation 79—77637
Cu-Be, dynamic segregation, ESCA obs. 77—8718
Cu-Be, dynamic strain age hardening 77—52375
Cu-Be, dynode surface, SEM and Auger microanalysis 80—100384
Cu-Be, elastic interaction energy calcs. for Guinier-Preston zones 79—11617
Cu-Be, electrical resist. of Guinier-Preston zones during age-hardening 77—72848
Cu-Be, explosive loading, depend. of struct. on deform. *(Russian)* 78—3177
Cu-Be, impurity concentration effects 78—75777
Cu-Be, quasiperiod struct. form. mechanism in eutectoid dissoc. 77—44257
Cu-Be, SCC in NH$_3$ 80—104326
Cu-Be, solute atom displacement in mixed dumbbell interstitials for FCC lattice 78—79631
Cu-Be, study of internal oxidation using central diffusion of X-rays *(French)* 79—37839

beryllium alloys continued
Cu-Be, Young's modulus and yield point obs., dependence on heat treatment *(Czech)* 80—55448
Cu-Be (0.0182 at.%), radiation induced Be segregation 78—23710
Cu-Be (0.25 at.%), channelling meas. of trapping efficiencies of solute atoms for self-interstitials 79—86829
Cu-Be (0.25 at.%), cryst., Cu self-interstitial atom, trapping, nucl. reactions and ion channelling obs. 78—14384
Cu-Be (0.99 wt.%), direct obs. of small Guinier-Preston zones 78—72776
Cu-Be (1.8 wt.%), discontinuous precip. form. and growth, TEM, obs. 80—104169
Cu-Be (2 at.%), plastic deform. and dislocation substruct. 80—76307
Cu-Be (2 wt.%), alloying addition effects on grain boundary reaction *(Japanese)* 80—49236
Cu-Be (2 wt.%), plastic deformation influence on ageing, granular microhardness *(Russian)* 80—55474
Cu-Be (2 wt.%), precipitation sequence, TEM obs. 80—108450
Cu-Be (2.1 wt.%), discontinuous precipitation *(Japanese)* 78—19766
Cu-Be (6.2, 9.3, 13.4 at.%), cell growth of discontinuous precipitation *(Japanese)* 79—24525
Cu-Be alloy, CA 172, flat spring, mechanical props. in bending, stress relax. test, 23 to 232°C 78—72806
Cu-Be alloy, notched specimen, static and dynamic behaviour 78—27634
Cu-Be alloy, X-ray diffr. pattern singularities *(Russian)* 78—67682
Cu-Be alloys, ageing kinetics, ultrasonic effects *(Russian)* 79—78997
Cu-Be alloys, CuBe precipitation 80—29966
Cu-Be alloys, relationship between discontinuous precipitation and continuous precipitation 79—100144
Cu-Be search coil for measurement of magnetisation and susceptibility in pulsed magnetic field 79—63281
Cu-Be solid solutions, local oscill. conc. depend., impurity bands *(Russian)* 80—75318
Cu-Be-Co, cuboid (Co, Cu, Ni, Fe)Be inclusions, metallography, ageing effects 80—11645
Cu-Be-Co, discontinuous reaction, analytical TEM 80—100842
Cu-Be-Co (1.8, 0.2 wt.%), TEM obs. of precipitates, ageing charact. *(Korean)* 77—66648
Cu-Be-Co (2,0.3 wt.%) alloy, heat treatment, influence of tempering on hardness, tensile props. transform diagram *(French)* 78—31384
Cu-Be-Co(0.1,0.2 wt.%), discontinuous precipitation *(Japanese)* 80—55402
Cu-Be-Ni (1.9, 0.32 wt.%) solution treated alloy, age induced vol. changes in structural transformations *(Russian)* 79—100179
Cu-Be-Ni-Ti-Mg (2, 0.3, 0.2, 0.02 to 0.4 wt.%), multiple step ageing *(Russian)* 78—19786
Cu-Be-Ni-Ti-Mg bronze, alloying element influence on minimum thermo EMF, cold working *(Russian)* 80—34426
Cu-Be-Ni-Zr, anodic behaviour of intermetallic phase 78—72895
Cu-BeCo (1.85, 0.29 wt.%), type CA172 (TH04), strengthened by spinodal decomp., stress relax. in bending 80—7616
Cu-Be(2 wt.%), tarnish surface films, formed in ammoniacal Cu(II) solns. 80—97624
Cu-Be(25 wt.%), discontinuous precipitation *(Japanese)* 80—55402
Cu-Be(30 at.%), eutectoid decomp., elastic interaction between precip. phase particles *(Russian)* 77—8833
Cu-Ni-Be (30, 0.5 wt.%), grain boundary reaction after ageing and quenching, obs. *(Japanese)* 79—70089
Cu-Ni-Be-(Al) (30,0.5,(0.2-2) wt.%), Al addition effect on grain boundary reaction *(Japanese)* 80—54254
Cu-Zn-Be, precipitation hardening 77—16599
CuBe, electron emission following ion bombardment of electron multiplier dynode 78—23576
CuBe, SIMS quantitative anal. of Be distrib. in vicinity of oxidation boundary *(French)* 80—11984
CuBe, secondary electron emission coeffs. for multiply charged ion bombard. 78—11051
Er$_x$La$_{1-x}$Be$_{13}$, ESR studies 80—108064
Er$_x$La$_{1-x}$Be$_{13}$, mag. sp. ht. and ESR, cryst. field interactions 80—60290
EuBe$_{13}$:Gd, Van Vleck paramagnet, exchange parameters, ESR determ. 77—4557
Fe-Be, formation of quasi-periodic distrib. of precipitates during ageing *(Russian)* 78—56642
Fe-Be, magnetic transition effect on alloying element solubility *(Japanese)* 79—42256
β-Fe-Be, pseudotwinning and pseudoelasticity 79—96056
Fe-Be (16.5 or 19.5 at.%), four-phase model of struct. in initial ageing stages *(Russian)* 78—48430
Fe-Be-Co, solubility anomaly due to magnetic transition, Co effect *(Japanese)* 79—42257
Fe$_5$(Fe$_{1-y}$Co$_y$), mag. and calorimetric props. 77—63083
Gd$_x$Ce$_y$La$_{1-x-y}$Be$_{13}$, high electron lattice relax., Gd EPR meas. 78—2736
Gd$_x$La$_{1-x}$Be$_{13}$, $0.001 \lesssim x \lesssim 1$, EPR, indirect exchange, bottleneck effect 77—16171
Gd$_x$La$_{1-x}$Be$_{13}$, high electron lattice relax., Gd EPR meas. 78—2736
Hf-Be, coupled phase diagrams and thermochemical descriptions 80—25656
LaBe$_{13}$, lattice spacings and susceptibilities 80—65778
LaBe$_{13}$:Er, ESR spectra, Er spin-spin exchange broadening 78—23338
LaBe$_{13}$-Er(Dy), dil., ESR, crystalline elec. field splitting, exchange parameters 78—52348
LuBe$_{13}$, lattice spacings and susceptibilities 80—65778
LuBe$_{13}$-Er, dil., ESR, crystalline elec. field splitting, exchange parameters 78—52348
Mg-Be, reactor fuel element cladding, corrosion resistance in K$_2$Cr$_2$O$_7$ aq. soln. 79—76074
Mo-Be solid solutions, superconducting transition, temp. changing peculiarity due to press. *(Russian)* 80—70878
NbBe$_{12}$, by diffusion saturation in vacuum, resistance to heat 78—44259
NbMo$_2$Be, predicted A15 struct. and T_c=30K 78—76182
Ni-Be, annealed under load, spatial distrib. of precips. *(Russian)* 77—59790
Ni-Be (2 wt.%), high-temp. radiation embrittlement, mechanical tests and TEM *(Russian)* 77—44331
Ni-Be alloy, precip. sequence 78—80549
Ni-Be alloys, struct. and phase stability in neutron bombardment field *(Russian)* 77—76467
Ni-Be bronze, Fe and Si alloying addition effect on phase composition *(Russian)* 78—15360
Ni-Be system, radiation induced solute segregation and precipitation study by means of Johnson-Lam kinetic model 79—43252

beryllium alloys continued
  $PrBe_{13}$, hyperfine enhanced nuclear mag. cooling 79−63216
  $PrBe_{13}$:Gd, Van Vleck paramagnet, exchange parameters, ESR determ. 77−4557
  $SbBe_{13}$, cryst. struct. determ. 77−24291
  $TABe_{12}$, by diffusion saturation in vacuum, resistance to heat 78−44259
  $TbBe_{13}$, mag. struct., neutron diffr. meas., 4.2K 78−47953
  $TbBe_{13}$, magnetic structure at low temps., antiferromagnetic, neutron diffraction study *(French)* 80−39743
  $(Tb_cLa_{1-c})Be_{13}$, mag. struct., cryst. field effects, neutron diffr. study 80−65789
  $ThBe_{13}$, lattice spacings and susceptibilities 80−65778
  Ti-Al-V-Be-B, melt-extracted polycryst., mech. props. 80−76360
  Ti-Be, coupled phase diagrams and thermochemical descriptions 80−25656
  Ti-Be, metallic glass form. and props. 80−16219
  Ti-Be-Si glass ribbons, physical and mech. props. 78−95767
  Ti-Be-Zr, coupled phase diagrams and thermochemical descriptions 80−25656
  Ti-Be-Zr base, glassy, temp. depend. of resist., rel. to resist. thermometer appl. 77−82532
  $TiBe_2$, de Haas-van Alphen effect, Fermi surface, theory 80−103614
  $TiBe_2$, itinerant antiferromag., mag. susceptibility and elec. cond. meas. 79−19726
  $TiBe_2$, neturon diffr. study of mag. ordering 80−44811
  $TiBe_2$, weak itinerant magnetism as inhibited superconductivity 79−51715
  $TiBe_{1.8}Cu_{0.2}$, ferromag., magnetisation density 80−103817
  $TiBe_{2-x}Cu_x$, C-15 lower phase, itinerant ferromagnetism 80−15723
  $TiBe_{2-x}Cu_x$, high press. study of Curie temp. and mag. susceptibility 80−84600
  $Ti_{50}Be_{40}Zr_{10}$, amorphous, thermopower meas., Nordheim-Gorter relations 79−99535
  $Ti_{50}Be_{40}Zr_{10}$, amorphous, crystn. temp., press. and heating rate depend. 80−70132
  $Ti_{50}Be_{40}Zr_{10}$ glass, mech. props., X-ray diffr. exam. 78−11292
  $Ti_{50}Be_{40}Zr_{10}$, Metglas 2204, stability, crystallisation, ductility meas. 78−47246
  $TiFe_{0.8}Be_{0.2}$ alloys for H_2 storage 80−97817
  $TmBe_{13}$:Gd, Van Vleck paramagnet, exchange parameters, ESR determ. 77−4557
  UBe_{13}:Gd, Van Vleck paramagnet, exchange parameters, ESR determ. 77−4557
  V-Ti-Be, 4 MeV Ni^{++} irrad., He gas bubble form. 80−29085
  VBe_{12}, coated limiters, first wall protection 80−32483
  VBe_{12} coating, erosion rates under H^+ ion bombard., fusion reactor appls. 80−39179
  VBe_{12}, fusion reactor material, low energy ion erosion expts., Kaufman source appl. 80−68942
  YBe_{13}, lattice spacings and susceptibilities 80−65778
  YBe_{13}-Mo, solid state reaction, 1000 to 1400°C *(Russian)* 78−18845
  Zr-Be, coupled phase diagrams and thermochemical descriptions 80−25656
  Zr-Be, metallic glass form. and props. 80−16219
  Zr-Ti-Be metallic glass, phase separation 80−97464
  Zr_xBe_{1-x} noncrystalline alloy, phonon-electron scatt., superconducting temp. 80−54330

beryllium compounds
  see also beryllium alloys
  beH_2 as a moderator in minimum critical mass systems 80−83151
  beryl, natural and synthetic, ion channelling transmission ratios 80−75277
  beryll, synthetic, cryst. growth, review *(German)* 79−33926
  diatomic molecules, linear, substituted fragment series, electronic struct. transferability, mutual at. influence 78−9066
  electronic structure, configs., energy, bonding, of small mols. and complexes 78−13420
  inorganic molecules, ultrasoft X-ray spectra, chemical binding and surrounding symm. effect on Be photoelectric yield 77−27086
  neutron scatterer in open tangential reactor channel, intense monochromatic beam prod. 77−71712
  rare earth beryllogallates with melilite struct., synthesis 77−81236
  silicates, entropy estimates at 298K from molar vols. 77−1243
  triatomic molecules, linear, substituted fragment series, electronic struct. transferability, mutual at. influence 78−9066
  $AlBeB_{24}$, and β-$(Al,Be)B_{12}$, prep. and struct., book contrib. 78−47277
  $Al_2Be_3Si_6O_{18}:Cu^{2+}$, synthetic beryl, ESR, optical spectra and X-ray diffr. meas. 77−16166
  Al_4C_3-Be_2C-SiC system, phase equilibria 80−45284
  Al_4C_3-Be_2C-SiC system, phase analysis and TEM struct. obs. 80−108420
  AlN-Si_3N_4-Be_3N_2 system, phase equilibria 80−60844
  $(Be, Al)B_{12}$, wide-gap semicond., elec. cond., refl. and absorpt. spectra 80−20188
  Be complexes, binding and orbital energies, biological systems ab initio calc. 80−102442
  Be metaphosphate glass, crystallization *(Japanese)* 77−72566
  Be^{2+}, ion compexes with HF, H_2O, and NH_3 solvent molecules, structural and electronic props. calc. 77−57873
  Be-Si-Al-O-N ceramic, phase assemblages, relationships with props. 80−60848
  Be-Si-N system polytypes, struct. obs. using TEM 80−107192
  Be-Si-O-N polytypes, X-ray study 78−27496
  Be-Si-O-N system, polytype periodicities, direct obs. 78−18662
  $Be^{2+}+H_2O$, mol. complex struct. and interaction energy, CI calc. 79−18133
  $BeAl_2O_4$, chrysoberyl, solubility of α-Fe_2O_3, Mossbauer studies 77−7867
  $BeAl_2O_4$, Czochralski grown single crystal, hardness, thermal expansion, concl., elastic const. 79−52353
  $BeAl_2O_4$ film on Al-Li-Mg-Be alloy, phase composition, oxidation protection mechanism *(Russian)* 80−65417
  $BeAl_2O_4:Cr^{3+}$, alexandrite, potential laser material, stimulated emission and absorpt. spectrum 79−33734
  $BeAl_2O_4:Cr^{3+}$ alexandrite laser, high gain performance 80−53299
  $BeAl_2O_4:Cr^{3+}$ alexandrite laser, wavelength-tunable CW laser action 80−53300
  $BeAl_2O_4:Cr^{3+}$; tunable laser performance, 701 to 794 nm, long-pulse and Q-switch operation 79−72573
  $Be_3Al_2(SiO_3)_6$, beryls, optical absorpt. spectra in the near IR (900-2500 nm) 80−89004

beryllium compounds continued
  $Be_3Al_2(SiO_3)_6$, thermal expansion study 79−37857
  $Be_3Al_2(SiO_3)_6:Cr^{3+}$, Raman effect to probe dynamical processes of Cr^{3+} photoexcited states 80−2740
  $Be_3Al_2Si_6O_{18}$, beryl, 350 keV proton irrad., superchannelling effects 79−4344
  $Be_3Al_2Si_6O_{18}:Cr^{3+}$, EPR spectra, exchange-coupled pairs 79−28596
  $Be_3Al_2(Si_6O_{18}):Cr^{3+}$, synthetic emerald crystal, quantum paramag. amplifier with resonator 79−89878
  $Be_3Al_2[Si_6O_{18}]:Cr^{3+}$, artificial emerald, distrib. of Cr^{3+} impurity 80−59505
  $BeAr^+$, long range pot., pot. inversion method 78−21992
  $BeAr^+(X^2\Sigma^+)$, spectrosc. determ., near-dissoc. expansions 80−83513
  $BeAs_2$, high temp. cryst. type, space groups and lattice parameters *(French)* 77−68948
  BeB_{12}, prep. and struct., book contrib. 78−47277
  BeB_2, band struct. and density states, metallic behaviour 77−59249
  BeB_x, borides, lightweight ceramic armour appls., ballistic tests, computer simulation, book contrib. 78−48556
  $BeBH_5$, H bridged system, floating spherical Gaussian model 80−78518
  $Be_2(BO_3)F$, cryst. struct. 79−42026
  Be_2C-graphite-UC_2 fuel development for pulsed reactors 79−67856
  BeCl, ${}^2\Sigma^+$ predissoc. state, vibr. and rot. calcs. 77−42363
  $BeCl_2$, valence shell electronic struct., ab initio SCF calc., photoelectron spectra 79−31383
  $BeCl_2.4H_2O$, IR and Raman spectra *(French)* 80−20618
  BeF, A ${}^2\Pi$ state config., ab initio MO calcs. 80−95532
  BeF, spin orbit coupling const., ab initio calcs. 80−63537
  BeF_2, aq. glass, 76K, solvated electron spectrum evolution, following ns radiolysis 78−88295
  BeF_2 aqueous solns., mag. and quadrupole relax. 80−71226
  BeF_2 glass, durability in water 79−95171
  BeF_2 glass, glass transition temp. and thermal expansion 80−64902
  BeF_2 glass, IR and UV transmission spectra 80−89019
  BeF_2 glass, nonlinear refr. index, meas. of electronic and nucl. contribs. 78−50866
  BeF_2 glass transition, Monte Carlo study 80−75343
  BeF_2, K-emission spectra, optical effects 78−64431
  BeF_2, melting curves at high press., rel. to SiO_2 extended phase diagram 77−11672
  BeF_2, molten, symm. stretching freq. calc. using mol. dynamics method 77−71790
  BeF_2, optical fibres, material dispersion 79−27377
  BeF_2, radiation induced defects, nuclear Hanle effect 78−43734
  BeF_2, thermal conductivity, 1.5-30K *(French)* 77−39704
  BeF_2, vitreous, band limits and vibrational spectra 79−73935
  BeF_2, vitreous, IR and reduced Raman spectra, weak Raman bands 78−68498
  BeF_2, vitreous, ionic transport and defect struct. 80−107472
  BeF_2, vitreous, Raman and IR spectra 78−39549
  BeF_2, vitreous, Raman spectra meas. 77−20858
  BeF_2^-, electron binding, extended basis SCF calc. 79−49944
  BeF_2 , ground state, conform., electron affinity, extended basis SCF calcs. 79−72253
  $BeF_2:Eu^{3+}$ glass, luminesc. of Eu^{3+}, transition probabilities 80−80845
  $BeF_2:Eu^{3+}$ glass, struct. and optical props. 80−84067
  $BeF_2:Eu^{3+}$ glass, struct., Monte Carlo simulations 80−96448
  $BeF_2:Pr^+$, glass, optical homogeneous linewidths 80−7395
  BeF_2-KF-CaF_2-$AlF_3:Nd^{3+}$ (Er^{3+}) glass, multiphonon relax., fluoresc. obs. 78−15219
  BeF_2-KF-CaF_2-AlF_3-EuF_3 fluoroberyllate glass, Eu^{3+} fluoresc. linewidth 80−66285
  BeF_2-LiF, thermodynamically predicted miscibility gap 78−11209
  BeF_2-LiF molten mixtures, mass transport, chronopotentiometry 77−21391
  BeF_3, water free vitreous, preparation and props. 79−66033
  BeF_4^{2-}, pseudo-exact force consts., force fields 77−31022
  BeH, ${}^2\Sigma^+$ states, spin-coupled valence bond theory of molecular electronic struct. 80−83285
  BeH, BeD, linewidth, indirect predissoc., anomalous isotope effect, ab initio calc. 77−58101
  BeH, doublet state, ionis. pots., electron affinities, using electron propagator 79−63933
  BeH radical, hyperfine splitting const., electronic energy, UHF-type, CCI calcs. 80−52909
  BeH, spin-extended Hartree-Fock ab initio calculations for small radicals 78−70746
  BeH^+, electronic structure, SCEP theory calcs. 77−10579
  BeH^+, PNO-CI and CEPA calcs. of electron correl. effects 77−34561
  BeH_2, force consts., ab initio calcs. with differentiated estimation of integrals 77−67974
  BeH_2, ionic nature of chem. binding, positron annihilation obs. 78−18581
  BeH_2, localisability in MO calcs., measured by absolute overlap and 2nd moment dispersions 78−74557
  BeH_2, muonic X-ray intensities in low-Z elements and their hydrides 80−9761
  BeH_2, pot. energy curve, minimal basis ab initio VB calcs. 78−50477
  BeH_2, potential energy surface, DIM method 79−18110
  $(BeH_2)_n$, energy band structure 80−5478
  $(BeH_2)_x$, polymer, ab initio calcs., cryst. orbital method 79−37659
  BeH_3, FSGO model of mol. struct., energy terms 79−63904
  $BeHHe^+$, from BeHT β-decay potential energy curves 78−56910
  $Be^{2+}(H_2O)_n$, (n=1,2,3,4,6), FSGO-pair-pot. calcs. *(German)* 80−74277
  BeI, reinvestigation of $A^2\Pi$-$X^2\Sigma^+$ band system 77−23503
  $BeKr^+$, $A^2\Pi_r$-$X^2\Sigma^+$ system, rot. anal., Λ-doubling consts. 77−27078
  Be_3N_2-$BeSiN_2$ system, crystallography and phase relationships, TEM and electron diffr. study 80−92502
  BeO, anodic film, trapping of ${}^3He$ and ${}^4He$ ions at room temp. 80−84221
  BeO, anomalous exoemission, laser irrad., electron trap ionisation *(Russian)* 77−1792
  BeO, arc spot heat impact degradation *(Japanese)* 78−39819
  BeO black tarnish film, on Cu-Be alloy, Auger electron spectroscopy anal. 80−97624
  BeO cathodoluminescence with/without Al, Zn, Mg admixtures, TV picture tubes appl. *(Polish)* 80−2869
  BeO ceramic, appl. as material for US delay lines 77−51447
  BeO, ceramic, sintered, thermoluminesc., EPR, emission spectra, energy level diagram 77−81163
  BeO, ceramic, thermolum. glow curves 79−47527

beryllium compounds continued
BeO ceramic, unlapped and lapped with diamond powder, thermally stimulated exoelectron emission 78—11086
BeO, ceramic and single cryst., EPR-ENDOR study of [Li]° centre 77—85569
BeO ceramic discharge tube for waveguide CO_2 laser amplifier 80—33027
BeO ceramic plates, exposed to ultrasoft X-rays, thermal luminesc. and electron emission 79—8192
BeO ceramic TLD, gamma ray response 80—23153
BeO ceramic TLD, operational characts. and problems 77—42216
BeO ceramics, thermally stimulated exoelectron max., effect of H_2 adsorption 79—43109
BeO, ceramics, thermally stimulated exoelectron emission *(German)* 79—100028
BeO ceramics, thermostimulated exoemission and adsorption centres 78—27386
BeO, chemical effect, influence on stopping power 80—47830
BeO coating, on Cu-Be, atomic composition depth distrib. by energetic ion anal. 80—35617
BeO, cryst., local centres, electronic struct. calcs. 80—100433
BeO, dielec. breakdown mechanism determ. acoustic signature anal. techniques 80—11337
BeO discharge tube for sealed-off high press. CO_2 laser amplifier 79—18397
BeO discs, thermally stimulated exoelectron emission and thermolum. sensitisation 78—35277
BeO, dissociation energy 77—550
BeO, effect on dynamical mechanical props. of polyester resin POLIMAL 190 *(Polish)* 79—96074
BeO, emission of free charge carriers in vacuum as symptom of pyroelec. props. 79—42908
BeO, excited state MCSCF wave functions appl. 80—47916
BeO, exoelectron emission and radiation dosimetry *(Japanese)* 79—83110
BeO, exoelectron emission from hydrated and dehydrated surfaces 80—11545
BeO, F-centre exam., pseudopotential calc. 78—43328
BeO, field-assisted thermally stimulated exoelectron emission 80—100761
BeO film, 5 keV D implantation 80—100268
BeO film, amorphous or polycryst., dielec. function, refl., from electron energy loss meas. 78—43947
BeO, film, TSEE, low energy electron impact excitation 77—12505
BeO, finite assemblies, thermal neutron wave propagation 78—58320
BeO, flux process for large cryst. growth 78—31316
BeO, free film and Au substrate, transmission spectra and photoemission characts. 77—24925
BeO, grain refining agent for Be containerless processing in space 79—47673
BeO, heated on W, thermal anal. using mass spectrometric, technique, vaporisation behaviour 80—79932
BeO in TLD, for low exposure of personnel, sensitivity, accuracy 77—29209
BeO inclusions in sintered Be, effect on physicomech. props. anisotropy 80—60804
BeO, induced lung carcinogenesis in rats, high-fired oxides 78—96077
BeO, K X-ray spectra produced by heavy ion bombard., chem. effects 77—36314
BeO, K-emission spectra, optical effects 78—64431
BeO, low-Z material, outgassing expts. 79—209
BeO, MCSCF and CI calcs. 80—95526
BeO, Mollwo-Ivey relation between peak-colour absorption energy and average O ion spacing 77—90179
BeO, molten, specific elec. resist., melting temp. to 3000K, ionic character 79—82366
BeO, neutron wave propag., space and angle depend. study 80—106096
BeO, optical second-order nonlinear polarisability 78—25919
BeO, particles uniform distrib. in Be casting prod. in zero gravity expt. 78—72753
BeO, phonon-polariton modes for freq. chirped optical pulse compression 78—46689
BeO, photostimulated exoelectronic emission under discontinuous stimulation 80—108329
BeO, polycrystalline, stress-strain data up to 1.25 GPa 80—100899
BeO powder, sinterable and unsinterable, sintering processes, electron microscope exam. 79—33986
BeO reactively evaporated film, elec. and optical props. 77—32512
BeO, reduction by C, kinetics and mechanism *(Russian)* 80—93743
BeO, small crystal, surface phonon modes, IR transmission spectra 80—11398
BeO, solubility of α-Fe_2O_3, Mossbauer studies 77—7867
BeO specimen supporting films for high resolution electron microscopy of single Au particles 77—27793
BeO, sputtering by H^+, D^+, He^+, weight loss measurements 80—35028
BeO, sputtering by low energy H and D 78—95630
BeO supporting films in high resolution electron microscopy of ferritin particles 78—12792
BeO, T diffusion 77—55391
BeO TLD, comparison with Lif 80—26357
BeO, TLD materials, kerma for monoenergetic neutrons, theory, expt. comparison 77—5086
BeO, TSEE, effect of surface SiO_2 80—76159
BeO, tetrahedrally bonded valence crystals, SCF perturbation theory appl. 79—37658
BeO, thermally stimulated exoelectron emission, influence of desorption processes 77—85906
BeO, thermoelectret props. 80—7269
BeO, thermoelectret state, effect of gamma radiation 80—7270
BeO, vacuum UV luminesc., excitation by X-ray synchrotron radiation 79—8168
BeO, valence force fields and lattice dynamics 77—7799
BeO with Ge film, surface polariton dispersion relations 77—69390
BeO, wurtzite-type crystals, lattice dynamics including the effect of electronic extension 80—59586
BeO, $X^1\Sigma^+$ state pot. energy curve, ground state dissoc. energy 78—41977
BeO, X-ray emission spectra, double plasmon high energy satellites 80—29829
BeO, X-ray spectra, chemical bonding and multiple ionis. effects 78—50630

beryllium compounds continued
BeO:Li, ceramics, thermally stimulated exoelectron emission *(German)* 79—100028
BeO-Al_2O_3 V_2O_5, mixture kinetics and mechanism of formation of cryosoberyl 79—11535
BeO-P_2O_5 glass, ESR of VO^{2+} ions 80—100610
BeO-P_2O_5-$RO(R_2O)$ (R=Li,Na,K,Mg,Ca,Sr,Ba) glasses, gamma irrad., cation modifier effect on radiation centre formation 80—40720
BeO-P_2O_5-SiO_2 glasses, photoelastic consts. and polarisability 79—65839
BeO-TeO_2 glass, struct. and props. *(Japanese)* 79—32917
BeO-UO_2, ceramic fission reactor fuels, fabrication and performance, review 78—58392
BeO-UO_2 fuel testing, annular core pulse reactor 78—86593
$BeO+SiO_2+V_2O_5$, reaction kinetics and mechanism, phenakite formation 78—23608
BeO_2, and anion, dimerisation energy and binding of electron, ab initio calc. 79—45628
BeO_2 , electron binding, ab initio calc. 79—45628
BeO_2-Al_2O_3-SiO_2-MF_2 (MF) glasses, M=Mg, Ca, Sr, Ba, Li, Na, fluoride ion role during crystn. 79—65176
BeO_4 tetrahedra, variabilities in interatomic distances and angles 79—46594
BeO(BeO), electron affinity and dipole moment, ab initio calc. 78—41938
BeOH, struct. and electronic props., ab initio calcs. 80—74113
$Be(OH)_2$ black tarnish film, on Cu-Be alloy, Auger electron spectroscopy anal. 80—97624
$(Be(OH)(NH_3)_2)^+$ model for biological active sites, ab initio calcs., comparison with Zn complex 80—104551
BeP_2, tetrahedral struct. of order-disorder type, coordination rule for short-range order 77—15370
$Be(PO_3)_2(II)$, crystal struct. *(French)* 78—14317
BeS, electronic energy bands, APW and LCAO calc. 77—20236
$BeSO_4$ soln., high press. conductance meas., transfer mechanism 77—76586
$BeSO_4$ soln. in H_2O, methanol-H_2O, US dispersion, 3-60 MHz *(German)* 78—59862
$BeSO_4.2H_2O$, composition of saturated solutions from 360 to 570K 78—22857
$BeSO_4.4H_2O$ and deuterated analogue, IR spectra, 110K, 1200 to 250 cm^{-1} 77—8582
$BeSO_4.4H_2O$, IR and Raman spectra *(French)* 80—20618
$BeSO_4.4H_2O$, p-p vector orient., PMR obs. 78—52361
$BeSO_4.4H_2O$, SHG at 2660 angstroms 78—90451
BeSe, electronic energy bands, APW and LCAO calc. 77—20236
BeSiN ceramics, glass free grain boundary 79—90671
$Be_9Si_3N_{10}$, TEM, direct obs. of cryst. struct. 79—60339
Be_2SiO_4, determ. of electronic polarisabilities of ions 79—7570
Be_2SiO_4, gamma-irrad., ESR spectra 79—51853
Be_2SiO_4, phenakite, flux grown single crysts., twinning study by hydrothermal etching and X-ray diffr. 80—107271
Be_2SiO_4:P, EPR and ENDOR 78—76295
$Be_4(Si_2O_7)(OH)_2$, bertrandite, cryst. struct. determ. 77—76380
BeTe, electronic energy bands, APW and LCAO calc. 77—20236
Be_4TeO_7, cryst. growth by solid-state reaction and struct. *(German)* 78—18603
$Be_4{}^tTe^0[O_7\square]^c$, singularities of atomic arrays as compared with $Al_2{}^0Mg^5[O_4]^c$ spinel struct. type 79—19242
$BeUO_4$, thermochem. of uranium compounds, comment on non-existence of $BeUO_4$ 78—27811
CsF-BeF_2 glass, anion conductivity, transport number radiometric meas. 79—86923
$KBr:BeF_4{}^{2-}$, IR absorption spectra of impurity anions *(Russian)* 80—2807
$KCl:BeF_4{}^{2-}$, IR absorption spectra of impurity anions *(Russian)* 80—2807
KF-BeF_2, and BaO-SiO_2 systems complex ionic liquids, corresponding-state principle *(Japanese)* 77—56245
KF-BeF_2-DyF_3, crystalline and vitreous phases of cross sections 78—44096
KF-BeF_2-DyF_3, phase diagrams, intensification region 78—44097
KF-BeF_2-DyF_3 system, KBe_2F_5-DyF_3 cross section phase diagram, vitreous phases struct. 77—24383
$K_2Zn_2Be_2(SiO_4)(Si_2O_7)$, cryst. struct. determ. 80—88121
LiBe, ${}^2\Sigma^+$ and ${}^2\Pi$ states, mol. binding energy curves 80—58189
Li_2BeF_4-$Na(K)BF_4$, phase diagram 77—21119
LiF-BeF_2, and MgO-SiO_2 systems, complex ionic liquids, corresponding-state principle *(Japanese)* 77—56245
LiF-BeF_2, molten, corresponding state principle with MgO-SiO_2 and appl. 79—11589
LiF-BeF_2, molten, self-diffusion coeff. of F *(Japanese)* 77—47610
Li_2O-BeO-SiO_2, X-ray diffr. exam. of phase equilibrium 78—80522
$MgAl_2O_4$ crystals, flux grown, artificial spinel twin form. by $BeAl_2O_4$ addition 80—96542
$(NH_4)_2BeF_4$, γ-irrad. cryst., $F_2{}^-$ ions, ESR meas. 80—34770
NaF-BeF_2, and CaO-SiO_2 systems, complex ionic liquids, corresponding-state principle *(Japanese)* 77—56245
NaF-BeF_2 glass, anion conductivity, transport number radiometric meas. 79—86923
$Nd:BeF_2$ glass lasers for fusion expts. 78—46661
Si-Al-Be-C-N system, phase equilibria 80—60839

Bessel differential equation *see Bessel functions*

Bessel functions
annular and circular fan duct noise, radial and circumferential mode meas. 79—68529
asymptotic approx., scatt. theory appl. 80—31562
beam, impulsively loaded, clamped end bending moment, Bessel function eval. 79—92937
cylinders, deform. anal. in modified Bessel functions *(Russian)* 79—10478
deflection, large, of circ. plate, produced by nonuniform Jacobi polynomial load 79—37184
diffraction theory, table associated with integral transform 79—97185
dilute mag. alloy, density of energy states in lower energy region in terms of modified Bessel function 79—19741
education, spiral spring, (nonhelical) simple harmonic motion, Bessel functions, closed form solns. 80—57026
Einzel-type electrostatic field with rot. symmetry, Fourier-Bessel soln. 78—82878

Bessel functions continued
electrostatic triple cylinder lenses, accurate expression for potential by Bessel function expansion 79—72474
EM radiation scattering modified Bessel function distribs. 78—37794
fermion systems, integral evaluation 79—40449
ferrite rod phase shifter, azimuthally magnetised, soln. of differential eqns. in terms of Bessel and Neumann functions 79—55025
geoelectric soundings, direct interpretation using filtered Bessel functions 79—74965
graded-index slab waveguide TE mode analysis 77—72087
graded-index slab waveguide TE modes, exact soln. 79—81568
heat conduction in tube wall, transfer functions determ. 77—7287
higher monotonicity properties of certain Sturm-Liouville functions 78—57750
impulse response of Lorentz medium 80—59242
inelastic molecular collisions appl. of non-integer Bessel uniform approx. 79—36733
infinite system of eqns. characterising zeros of Bessel functions 79—12570
integer order and complex argument, $J_n(z)$, $Y_n(z)$, $H_n^{(2)}$ and $H_n^{(2)}(z)$ calc., program 79—63004
integrals associated with Gauss's hypergeometric function and Bessel polynomials 77—74191
ISO(n), explicit determ. of representation functions 80—31561
$J_0(z)$ and $J_1(z)$ of complex argument, code for calc. 77—64923
$J_\nu(x)$, of real order and argument, calc. prog. 80—8776
lossy plasma half-space, transient refl. for TM polarisation 79—98916
numerical Bessel transformation calc. program 79—49016
open electron optical system with rotational symmetry, Fourier-Bessel series soln. for pot. and field intensity 79—76570
optical film, non-homogeneous, oblique light incidence *(Russian)* 79—13905
plate, thin, circ., quasistatic normal deflection due to time depend. heat-source distrib. 79—37145
polaron theory, Bessel function integral, asymptotic evaluation 78—56082
recurrence formulas for phases and amplitudes of free wave spherical functions 78—56
recurrence relations for phase shifts of certain classes of potentials 78—89364
reduced Bessel functions, three dimens. convolution integrals evaluation 78—32654
semiclassical collision theory, non-integer Bessel uniform approx. 79—36730
spherical Bessel function $j_l(r)$, Chebyshev series 80—8775
spherical Bessel functions j_n and y_n of integer order and real argument 78—89321
squares of positive zeros, infinite nonlinear algebraic eqns. 78—20942
squares of positive zeros, nonlinear eqns. and sum rules 78—49639
synchrotron radiation, angular and spectral distrib., modified Bessel functions of fractional order 80—91738
thermal conductivity meas. by comparative longit. ht. flux, use of generalised Bessel functions 78—26741
torsional vibrs. of spherical shell, numerical results 78—59322
turbulent irradiance probability distrib. in saturation regime 79—76588
wave diffraction by thin phase grating, difference eqn. solns. 78—54198
weakly absorbed particles, modified Austern-Blair theory, DWBA 80—86867
wedge field, composite truncated, Dirichlet problem, point source appl. 77—5676
$Y_\nu(x)$, of real order and argument, calc. prog. 80—8776
zeros, a theorem 78—4466
zeros, for finite orders 78—36797
zeros, obtained as infinite systems of nonlinear equations 80—46786
zeros of Bessel functions, algebraic eqns. 78—49640
zeros of classical polynomials and Bessel functions, diophantine props., review 79—35530

beta-decay
see also beta-decay theory; beta-ray spectra; nuclear electron capture
^{173}Lu decay scheme determ. 77—82868
β-active nuclei, neutrino exchange and long range interactions 80—73826
β-active superdense nuclei search in (p,X), (d,X) reactions *(Russian)* 80—42535
A=116-140 fission products far from β-stability, Q_β-values 77—22949
A=12 polarised β-decay, nuclear Dirac wave function test 80—5060
A=135-143, odd A fission products, delayed n, decay studies and Q_β meas. 80—78227
A=144 to 147 short-lived fission products, β-decay energies 77—22948
A=215, nuclear data sheets, decay characteristics and level struct. 78—58224
A=219, nuclear data sheets, decay characts. and level struct. 78—58225
A=223, nuclear data sheets, decay characts. and level struct. 78—58226
A=227, nuclear data sheets, decay characts. and level struct. 78—58227
A=354, Z=126, spontaneous fission, α-decay, β-decay half-lives calc. 77—6469
A=45-153, β^+-decay strength function maximum 79—75914
A=75-93 fission products far from β-stability, Q_β-values 77—22949
A=79-145, β-delayed neutron emission probabilities, half-life 80—52634
A=90 to 101 short-lived fission products, β-decay energies 77—22948
A>70, review of beta-delayed particle emission 77—22972
alkanes, tritiated, fragmentation by β-decay, dissoc. of daughter species 78—31669
atomic K- and L-shell shakeoff probability, following β-decay, hydrogenic wave function 78—94204
atomic mass evaluation 1977: mass table, mass excesses, total BEs, β-decay energies 78—4894
baryon β transitions, EM characteristics, bag model *(Russian)* 79—93380
beta strength function, half life and delays, nuclear- and astro-physics consequences 80—102149
beta strength function structures, nuclear- and astro-physics consequences 80—99152
biological and chemical consequences 78—28018
Cabbibo fit, generalised, appl. to quark mixing angs. in sequential Weinberg-Salam model 79—17655
CANDU reprocessed fuel and high level waste radioactive decay props. 77—71656
conference on nuclear physics, Mikolajki, Poland (2-14 Sept. 1979) 80—101662
conference on nuclear spectroscopy of fission products, Grenoble, France (May 1979) 80—77546

beta-decay continued
conserved vector current hypothesis, weak magnetism and second-class currents 78—554
Coulomb corrections to weak decay transition amplitudes, comments 79—59037
delayed fission produced in synthesis induced by heavy-ion beams and neutron currents *(Russian)* 79—89341
determ. of bulk α and β radioactivity *(Rumanian)* 79—88346
double β-disintegration, search for expt. evidence *(French)* 79—36202
double beta decay, lepton number conservation 78—58256
element formation *(Russian)* 79—8818
energies of separation and alpha- and beta-decay, 1977 at. mass evaluation tables 78—4895
even-even neutron-rich fission products, de-excitation spectra, β-decay, deformation 80—78203
explosive r process cooling process 78—69791
$f_{7/2}$ shell nuclei, shell model study in pure $f_{7/2}{}^n$ config. 79—36162
far unstable nuclei, beta delayed two neutron emission, nuclear structure 80—68606
fission prod. β decay in nucl. reactor, $\bar{\nu}$ energy distrib. 79—75924
formic acid dimer-t_1, H bonding, β^--decay effects, ab initio calcs. 79—54763
free neutron decay, e^--ν ang. correl. coeff., determ. from proton recoil spectrum 79—22242
Gamow Teller matrix elements and nuclear mag. moments, configuration mixing v. mesonic effects 79—26400
Gamow-Teller β transition quenching in mirror nuclei A=3, 15, 17, 39, 41 79—17860
Gamow-Teller $(ft)^+/(ft)^-$ values and second class currents 77—26626
Gamow-Teller matrix element, axial currents in nuclei, quenching mechanism 79—17859
heavy nuclei, Z=68-72, nucleon separation, pairing and decay energies and mass defect 77—79301
K-shell internal ionisation, many electron effect, relativistic theory 77—18890
K-shell internal ionisation and excitation in β decay 78—556
labelled molecules, chem. and biological consequences 78—11541
laser induced nucl. orientation, at. and nucl. applications, review 78—37310
light nuclei, delayed proton precursors 77—22971
LMFBR burnup calc., allowance for ^{239}Np 78—89936
longitudinal polarisation meas., β^+ decay 78—8781
many electron effect on K-shell internal ionisation accompanying β-decay 78—86839
methane, and -t_1, β-decay, ab initio SCF MO calcs. 77—71842
mirror decays in $f_{7/2}$ shell, use of He-jet chopper 77—38532
mirror nuclei, iso-vector mag. moments in 1p-shell, β-decay ft values 77—88084
mixed Fermi and Gamow-Teller β-transitions, data tables 79—54407
natural substances *(Rumanian)* 77—49067
neutron decay, radiative corrections to proton recoil spectrum 79—13119
neutron rich nuclei; β^--emitters, deformation and spectroscopy 80—78223
neutron rich nuclei, beta decay half lives, expt. techniques 80—78224
neutron star metter, β-decay and nucleosynthesis during decompression 77—33544
neutron stars, β-decay of π condensates as cooling mechanism 78—4271
neutron-rich nuclei in A~100 region, decay props. 77—22961
nuclear far from β-stability, delayed neutron energy spectra, structure effects 80—78226
nuclear isotopes far off stability line, production, props., review *(Hungarian)* 79—9927
nuclear matter, β-stable, electrically neutral, constrained variational calc. 78—58243
nuclei far from stability, β-decay energies, γ-rays, Q_β values and masses 80—78225
parity nonconservation, coupling constants, intermediate boson mass ratio 79—9516
polarised neutrons, polarization effects of β decay in intensive electromagnetic field *(Russian)* 79—22243
probabilities of α-, β- and γ-transitions accompanied by changes in nuclear shape *(Russian)* 78—89820
pseudoscalar mesons, in spectrum-generating SU(3), beta-decay 78—4858
pseudoscalar mesons, muonic double β-decay, tree and box diagram approx., K^- and F^- 79—17717
Q-values of β^- decay, rapid meas. from electron and gamma energy decays 80—78220
Quelccaya tropical ice cap, Peru, beta radioactivity meas. for climatic ice core records 80—8345
radiative corrections to lifetime, spectra, ang. distrib., values for ^{12}B, ^{12}N 77—38249
radioactive nuclide decay data for reactor calcs., activation products and related isotopes 78—82426
radiotracer diffusion rates in ionic solid, influence of transmutation products 77—89568
rare-earth isotopes, neutron deficient, β-decay and delayed protons 77—22953
reactor neutrino expts., fission fragment ν radiation, neutral currents, inverse β-decay, $\bar{\nu}$ scatt. *(Russian)* 80—42736
rotational invariance in beta-ray ang. distrib. 78—66252
Rumanian primary standard *(Rumanian)* 80—68603
s-process isotopes, nonthermal isomeric branching, importance of long-lived states 78—7983
second class current upper limit from β-decay data 80—47404
second-class weak currents, experimental progress, few-body aspects 77—22665
semi-leptonic weak interactions 78—555
semileptonic weak and EM interactions, multipole operators, HO single particle matrix elements 80—73840
semileptonic weak and EM interactions, nuclear current operators 79—6515
serial decay, transient equilib. and secular equilib. 79—80901
shape isomer prod. in nuclear reactions and β-decay 79—6377
shell model calcs. A=24, mass, spectra and β decay 78—4903
statistical model of β-decay of fictional nuclide, Pandemonium 78—8779
stellar hot dense matter, beta transition rates 78—73699
stratosphere, residence times from β activity of Antarctic and Greenland snows 79—79421
super-allowed Fermi beta-decay 77—38248

beta-decay continued
surface contamination monitoring probes, comparison of response between detectors 78−25398
T-invariance, EM simulation 79−30807
time reversal invariance and second class weak currents, review 78−37309
transitional odd-mass nuclei, beta decay log ft values from asymmetric rotor model 79−67715
unification of EM and weak interaction *(French)* 79−89270
URCA process, in stellar convective degenerate C cores 77−22203
virtual pions, Yukawa field and effects on μ-capture, β-decay, mag. moment etc. 79−26379
weak decays, EM effects and form factor renormalisation 79−54411
weak interactions, conf., Bloomington, USA, (May, 1977) 78−414
Wigner scheme, Γ-decay of analogue states, β-decay 77−41930
Z=37-43, neutron rich fission products, mass energy surface, decay props. 80−78228
β^{+} decay, Q-value atomic excitation corrections 79−40918
β^{+}-decay, e^{+} annihilation in atomic K-shell, nuclear excitations *(Russian)* 80−42602
^{3}H labelled compounds, β decay fragmentation potential energy curves 78−56910
$\Lambda \rightarrow pe^{-}\nu$, meas. of ang. correl. parameters 77−38166
(p,n), 120 MeV, 0° cross sections, Gamow-Teller matrix elements for A=7-90 80−86860
^{99}Tc^{m} compounds, chemically induced decay constant variation 78−93968
^{94} Rh isomers, beta decay, ^{94}Ru level structure, spin and parity 80−57747
$^{32, 33}$P incorporated in DNA, transmutation effects 80−26283
$^{105}\rightarrow^{105}$Pd, polarised nuclei, ^{105}Rh mag. moment, E2/M1 mixing ratios 77−6315
^{230}Ac decay, ^{230}Ra levels, J^{π} and transitions, Nilsson assignments 80−68543
^{230}Ac, identification and β-decay meas. 77−22963
^{230}Ac, prod., decay characts. 78−54724
^{A}Ag, A=104,104m, characts. of the excited levels of ^{104}Pd 79−9515
^{A}Ag, A=113, 115, β-decay, $^{113, 115}$Cd low lying $7/2^{-}$ state lifetime, triaxial rotor interpretation 80−47432
^{A}Ag, A=97, 98 and $99^{g,m}$ decay spectral meas. 78−93976
^{100}Ag^{g,m} decay, ^{100}Pd levels and γ-transitions 80−83077
^{101}Ag, $T_{1/2}$ meas., decay scheme, ^{101}Pd levels 78−37311
^{103}Ag$\rightarrow^{103}$Pd, β-ground state feedings and branchings 80−102147
^{104}Ag, β^{+} decay, ^{104}Pd energy levels, spins, parities 78−13018
^{105}Ag β decay, ^{105}Pd level scheme 77−82849
^{105}Ag decay, energy levels, spin, parities, of populated ^{105}Pd states 78−37306
^{110}Ag^{m} disintegration, scheme of ^{110}Cd *(French)* 78−58248
^{110}Ag^{m} orientated, β-ray asymmetry, Fermi/Gamow-Teller matrix element ratio 79−93562
^{111}Ag$^{m}\rightarrow^{111}$Cd decay 78−541
^{113}Ag, 5.3 h decay scheme, ^{113}Cd level scheme 78−46028
^{115}Ag, 20 min decay scheme, ^{115}Cd level scheme 78−46029
^{122}Ag decay, struct. of neutron rich even-even Cd nuclei 78−66249
^{24}Al, ^{24}Al^{m}, decay to γ-ray and α-particle emitting ^{24}Mg states 79−49607
^{24}Al, 1^{+} isomer decay 79−85414
^{24}Al, β-transitions, weak magnetism, nuclear struct., matrix elements 79−13253
^{26}Al, as planetoid heat source in early solar system 78−65511
^{26}Al, decay in marine sediments, meas. with cyclotron, dating technique 79−71819
^{26}Al, in interstellar medium, galactic source of γ-ray line emission 77−33692
^{26}Al, stellar weak interaction rates, supernova appl. 80−82336
^{26}Al^{m}, super-allowed Fermi β decay, lifetime meas. 77−79336
^{29}Al, mag. moment quadrupole coupling const. β-ray detected NMR in Al_2O_3 cryst. 78−37267
^{31}Al, radioactive half-life and branching ratios 79−22240
^{26m}Al populated in ^{26}Mg(^{3}He,t), precise Q-value, β decay energy, half life 77−30618
^{A}Ar, A=43,44, β-decay, ^{43,44}K levels, spin and parity assignments, decay scheme 79−13210
^{A}Ar, A=45,46, β-decay, ^{A}K, A=45,46, levels, lifetimes and transitions 80−42597
^{32}Ar, isobaric analogue states via β-delayed protons 78−558
^{35}Ar, β-decay, recoil ion energy spectrum anal. 78−21525
^{35}Ar$\rightarrow^{35}$Cl β^{+} decay and anomalous Cabbibo angle 77−74807
^{35}Ar$\rightarrow^{35}$Cl superallowed decay, branching ratio meas., Cabibbo angle anomaly 79−26399
^{40}Ar(γ, xp yn), 9-29 MeV, cross sections in giant resonance region, particle decay modes 80−13462
^{44}Ar β decay into ^{44}K, neutron rich isotopes, weak coupling predictions, γ-ray meas. 78−74336
^{45}Ar, β-decay scheme and half life, K deduced energy levels 78−78319
^{46}Ar, β-decay scheme and half life, K deduced energy levels 78−78319
^{68}As β-decay, γ coincidence and singles spectra, spin, parity assignments, half-life meas. 77−79333
^{69}As β-decay, struct. determ. of ^{69}Ge 79−22245
^{74}As decay, branching ratios and $T_{1/2}$ meas., K-fluorescence yield of Ge 77−3300
^{76}As, dynamic orientation in n-Si crystals, ang. momentum, forbidden β transition 79−501
^{76}As, level scheme for ^{76}Se from $\gamma\gamma$ coincidence meas. 80−22754
^{85}As, β-decay delayed n emission, simple statistical model description 79−67714
^{85}As, β-strength function energy struct., effect on delayed neutron emission prob. 79−75915
^{85}As, investigation of beta-strength functions by neutron and γ-spectroscopy 79−45209
Au isotopes, A=184-197, β^{+}-decay, single particle and collective degrees of freedom 77−22956
^{191}Au positron spectra, Fermi-Kuri diags. 77−22960
^{193}Au positron spectra, Fermi-Kuri diags. 77−22960
^{203}Au, evidence for existence, β-decay to ^{203}Hg 79−63635
^{8}B β^{+}-decay, β-α angular correlations, final state energy depend., current test 80−102151
^{11}B, +ve parity states in weak coupling model, E1 and β strengths 77−34228
^{12}B, aligned, β ang. distribs., second class currents 78−50126

beta-decay continued
^{12}B, aligned, β-ang. distrib. and alignment correction coeffs., axial vector currents 80−5097
^{12}B, aligned, β-ang. distrib. asymmetry coeffs., pseudotensor interaction, T=1 isospin triplet decay 80−106021
^{12}B, beta decay, PCAC and vector current conservation 79−93561
^{12}B, beta-ray spectra and conserved vector current 79−54409
^{12}B β^{-} decay, conserved vector current, elementary particle approach 78−66246
^{12}B, β-ray branching and $T_{1/2}$ 78−41674
^{12}B, improved impulse approx. treatment of allowed weak and analogue EM transitions in ^{12}C 78−41662
^{12}B, oriented nuclei, β-γ ang. correl., G-parity nonconservation 78−54723
^{12}B, polarised, asymm. of β-ray ang. distrib., second class currents 77−41919
^{12}B, polarised, β-decay asymm., G-parity nonconservation, second class currents 77−41920
^{12}B, polarised, higher order effects in determ. of asymmetry parameters 79−22247
^{12}B spin polarisation meas. in ^{100}Mo(^{14}N,^{12}B) 77−71562
^{12}B spin polarisation meas. from β-decay, product of ^{100}Mo(^{14}N,^{12}B)^{102}Ru 78−50196
^{12}B, weak magnetism and beta spectra 77−6314
^{12}B$\rightarrow$B^{-}+^{12}C, second-class current search, alignment correlation meas. by Zeeman technique 78−37313
^{12}B$\rightarrow\beta^{-}$+^{12}C, alignment correlation meas. by Zeeman technique, vector currents and form factors 78−37312
Ba, A=117, 119, 121, delayed proton emitters, positron-proton coincidence meas. 78−78326
Ba, A=144, 145, short lived fission product, Q_{β}-value 78−37317
Ba and rare-earth neutron deficient isotopes, β^{+} strength $T_{1/2}$, X-ray, γ-ray spectra 77−34260
Ba heavy isotopes, $T_{1/2}$ determ. 77−26633
Ba isotopes, neutron deficient, β-decay and delayed protons 77−22953
^{A}Ba, A=143,146, expt. β-decay energy of neutron-rich nuclides 79−30808
^{A}Ba, A=143 to 148, β-decay half life meas. 79−67718
^{126}Ba$\rightarrow^{126}$Cs$\rightarrow^{126}$Xe, meas. of decay spectra 77−6316
^{131}Ba, decay, electric monopole transitions 80−22752
^{139}Ba β^{-} decay into ^{139}La, γ-rays, energy levels 78−70492
^{139}Ba, first order forbidden β-decay, quasi-particle-phonon interaction calcs. 79−9514
^{143}Ba decay to ^{143}La, β-branching and log ft values 78−50129
^{143}Ba, nuclear spectroscopy of neutron rich A=143 nuclei 79−59039
^{144}Ba, beta and gamma spectra, level scheme 77−22962
^{145}Ba, fission product, β-decay anal. 78−78323
^{147}Ba, neutron rich nucleus identification, $T_{1/2}$ meas. 77−26633
^{148}Ba, neutron rich nucleus identification, $T_{1/2}$ meas. 77−26633
^{12}Be core excited T=2 levels, spin, half life from ^{10}Be(t,p), 12 MeV 78−66210
^{194}Bi$\rightarrow^{194}$Pb, $T_{1/2}$ meas. and ^{194}Pb excited level scheme determ. 77−6306
^{196}Bi$\rightarrow^{196}$Pb, $T_{1/2}$ meas. and ^{196}Pb excited level scheme determ. 77−6306
^{199}Bi$\rightarrow^{199}$Pb, spectra meas. 78−78316
^{201}Bi$\rightarrow^{201}$Pb, spectra meas. 78−78316
^{207}Bi, γ-γ directional correls., mag. perturbation obs. 77−74796
^{208}Bi(1+), β-decay to ^{208}Pb(0+), collective particle-hole states 77−61388
^{210}Bi β-decay, longitudinal polarisation of electrons at 900 keV, precision meas. 77−71592
^{210}Bi$\rightarrow^{210}$Po β-ray ang. distrib. asymm., mag. moment 77−41926
^{210}Bi$\rightarrow^{210}$Po$\rightarrow^{206}$Pb, decay chain, L-shell ionisation investig., X-ray emission during β, α decay 77−18891
^{210}Bi$\rightarrow^{210}$Po$\rightarrow^{206}$Pb, L-shell auto -ionisation 77−6739
^{248}Bk, spectroscopic studies 78−78314
^{250}Bk, β^{-} decay, half life and ^{250}Cf energy levels, bands and transitions 79−22205
^{A}Br, A=85 to 89, total β-decay energies and atomic masses of neutron-rich isotopes 79−40889
^{A}Br, A=89-91, delayed neutron emission probabilities, β-decay half-lives 80−83078
^{70}Br, half life of Fermi superallowed β^{+} activities from ^{58}Ni(^{14}N,2n) 79−9518
^{84}Br decay, ^{84}Kr levels, γ-cascades, J^{Π}, mixing ratios and correlations 80−63134
^{87}Br, β-decay delayed n emission, simple statistical model description 79−67714
^{87}Br, β-decay into ^{87}Kr, delayed neutrons, high energy γ spectra, energy levels 78−25155
^{87}Br, β-strength function energy struct., effect on delayed neutron emission prob. 79−75915
^{87}Br, investigation of beta-strength functions by neutron and γ-spectroscopy 79−45209
^{88}Br β-decay, ^{88}Kr level scheme and transitions, delayed neutrons 80−42600
^{88}Br$\rightarrow^{88}$Kr, γ-ray spectrum, transitions 77−295
^{90}Br, experimental Q_{β}-values 78−93974
^{12}C, β-transitions, weak magnetism, nuclear struct., matrix elements 79−13253
^{12}C(μ^{-}, ν)^{12}B, polarisation studies, muon capture, weak interaction aspects 80−68655
^{14}C, natural beta-decay rel. to origin of biological chirality 77−86445
^{14}C$_{g.s.}$ β-decay, mesonic exchange currents, weak process microscopic treatment 80−57742
^{14}C(^{6}Li,^{6}He)^{14}N and Gamow-Teller strength distrib. 77−6430
^{14}C$\rightarrow^{14}$N $e^{-}\bar{\nu}_{e}$, rate calcs. using elementary particle and macroscopic treatments 78−29429
^{15}C beta decay transition rates and half life, ^{15}N excited states and transitions 80−18248
^{39}Ca β-decay Gamow-Teller interaction renormalisation constant from ^{39}K(p,n) 7480-7530 keV 79−6601
^{45}Ca, internal bremsstrahlung photon intensity and energy yield 78−86509
^{103}Cd decay, ^{103}Ag levels and spectra 79−22235
^{103}Cd$\rightarrow^{103}$Ag, β-ground state feedings and branchings 80−102147
^{115}Cd^{g} 852 keV first forbidden β-transition, ^{115}In 597 keV level J^{π} assignment 79−80900
^{115}Cd^{m,g}, decay to ^{115}In, decay scheme, unified model description of odd mass In nuclei 78−66251

beta-decay continued
^{117}Cd isomer decay, ^{117}In level scheme, J^{π} and transitions 80-32193
^{126}Cd, mass separated, decay scheme and half life, ^{126}In levels 79-3117
Ce, A=145, 147, 148, short lived fission product, Q_{β}-value 78-37317
Ce isotopes, half-life meas. 77-6311
Ce isotopes, neutron rich, decay properties 78-13032
^{A}Ce, A=124-127, half lives, low energy γ-data, β decay probabilities 79-499
^{133}Ce, 5-h isomer β-decay, ^{133}La level struct., parity levels, decoupled band struct. 79-9476
^{141}Ce, half-life determ. 77-34498
^{143}Ce, shape of 1110 keV β transition to ^{143}Pr 351 keV level, spin, parity 77-50085
^{144}Ce, 284.3 D, decay scheme, energy levels and transitions in ^{144}Pr 77-14070
^{144}Ce, e-γ and e-e coincidences, improved detection system 80-52605
^{145}Ce, β^{-} decay scheme and $T_{1/2}$ determ. using γ coincidence counting techniques 79-93558
^{145}Ce, fission product, β-decay anal. 78-78323
^{149}Ce, β-decay half life meas. 79-67718
^{A}Cf, A=244, 248, fission barrier heights from β-delayed fission, β-strength functions struct. 80-5184
^{252}Cf fission fragments, positron activity *(Russian)* 77-6474
^{252}Cf spontaneous fission, symm. and asymm., fragment yields, β-decay chain lengths *(Russian)* 77-50181
^{32}Cl, β^{+} decay, delayed particle emission, ^{32}S levels and J^{π} 80-22772
^{34}Cl populated in ^{34}S(^{3}He,t), precise Q-value, β decay energy, half life 77-30618
^{34}Cl superallowed beta-decay Q-value via ^{34}S(p,n) threshold meas. 77-34298
^{35}Cl, stellar weak interaction rates, supernova appl. 80-82336
^{36}Cl, beta decay, K-shell electron ejection 77-18888
^{36}Cl, internal bremsstrahlung spectra, accompanying second forbidden β-decay 78-8776
^{240}Cm, fission barrier heights from β-delayed fission, β-strength functions struct. 80-5184
^{251}Cm beta decay, ^{251}Bk level struct. 79-36200
^{54}Co populated in ^{54}Fe(^{3}He,t), precise Q-value, β decay energy, half life 77-30618
^{54}Co, super-allowed Fermi β decay lifetime meas. 77-79336
^{56}Co β^{+}-decay, ^{56}Fe low lying levels, J^{π}, γ-γ coincidences, internal conversion 80-86815
^{56}Co in Type II supernovae, decay rel. to supernova light curves 80-77427
^{56}Co, limit on time-reversal violation from β-γ correl. meas. 77-34261
^{58}Co, half-life determ. 77-34498
^{60}Co, 2505 keV gamma ray intensity in β-decay 79-13249
^{60}Co beta decay to ^{60}Ni, 2506 to 2159 keV γ transition 77-22929
^{60}Co, decay to ^{60}Ni, aero-phonon, $4_{1}^{+} \rightarrow 2_{2}^{+}$ γ-ray transition 78-17136
^{60}Co, half-life determ. 77-34498
^{60}Co nuclei polarised in iron foils cooled by dilution refrigeration 77-34263
^{60}Co, oriented, β-decay asymm., positron ang. distrib. meas., matrix elements 77-2951
^{60}Co polarised nuclei, β-ray emission, directional distrib. and asymmetry factor 80-95315
^{47}Cr, β-decay GT matrix elements, $T_{1/2}$ 78-557
^{47}Cr, β-decay half-life and GT matrix element 77-22950
^{57}Cr mass excess, half life, ground state spin and parity, from ^{48}Ca(^{11}B, pn) 78-70436
^{57}Cr, new isotopes of interest to explosive nucleosynthesis, β-decay scheme and mass determ. 79-45208
Cs, A=114-118, neutron deficient isotopes, half lives, β^{+},γ, delayed p and α meas. 78-70489
Cs, A=118,120,122, ground isomeric states, β-decay, $T_{1/2}$, γ- and CE-spectra 77-57601
Cs β-decay, ^{A}Xe, A=122,124,126,128, 0^{+} excited state spin assignments and transitions 79-67649
Cs, fission fragment, delayed neutron branches from γ-spectroscopy 80-78230
Cs heavy isotopes, $T_{1/2}$ determ. 77-26633
Cs isotopes, delayed neutron Pn-values, beta+neutron+gamma decay modes 77-26639
Cs neutron deficient isotopes, beta-decay energies and masses 77-22946
Cs neutron deficient isotopes, beta-decay, Xe low lying levels 77-22947
Cs, neutron rich isotopes, $Q_{\beta}$and direct mass meas. 80-78132
Cs precursors, half lives and delayed neutron emission probabilities 79-49610
^{A}Cs, A=139-144, beta endpoint energy measurements 78-93975
^{A}Cs, A=142-146, β-decay half life meas. 79-67718
^{A}Cs, A=147, 148, $T_{1/2}$ determ. 79-9524
^{114}Cs β-decay, half life and branching ratio, ^{114}Xe excited states and γ-rays 80-47436
^{116}Cs decay, ^{116}Xe quasi-rotational bands, levels J^{π} and $T_{1/2}$ 80-83021
^{116}Cs, delayed particle emission in β^{+} decay 78-8778
^{118}Cs, delayed particle emission in β^{+} decay 78-8778
^{123}Cs$\rightarrow$^{123}Xe$\rightarrow$^{123}I, generator prod. for radiopharmaceutical appls., high energy alpha reactions 77-37053
^{124}Cs, decay scheme, ^{124}Xe energy levels 78-13033
^{127}Cs$\rightarrow$^{127}Xe, study of γ-rays, ^{127}Xe level scheme 77-299
^{128}Cs$\rightarrow$^{128}Xe, ^{128}Xe levels, spin-parity assignments, log ft values 77-54189
^{134}Cs, as potential radiotherapy radionuclide, prod. and decay scheme 77-90875
^{137}Cs, beta-decay, internal bremsstrahlung meas. 77-79338
^{137}Cs β-decay, β_{1} component discrepancies for β- spectrum 79-75918
^{137}Cs decay determ. by β-ray spectrometry 79-26397
^{139}Cs β-decay, ^{139}Ba level scheme, J^{π} and γ-transitions 80-42590
^{142}Cs decay, ^{142}Ba, $\gamma\gamma$ ang. correlations, levels, spins and mixing ratios 80-57734
^{143}Cs, delayed neutrons, energy spectra 80-99153
^{143}Cs, nuclear spectroscopy of neutron rich A=143 nuclei 79-59039
^{144}Cs, beta and gamma spectra, level scheme 77-22962
^{59}Cu(β^{+})^{59}Ni, γ-spectra and levels 77-22935
^{61}Cu, ^{61}Ni multiparticle configs., transition probabilities from shell model 78-70496
^{62}Cu decay to ^{62}Ni excited levels, half life, log ft *(Spanish)* 77-67716
^{64}Cu, autoionisation of K-shell following β-decay 78-13029
^{64}Cu β^{-} and β^{+}-decays. K-shell ionisation probabilities, X-ray spectra 80-42592
^{64}Cu β^{-} decay, K-shell autoionis. 80-956

beta-decay continued
^{64}Cu, electron density determ. in Cu-Au alloys, β-decay expts. 79-54408
^{67}Cu, multiparticle configs. in ^{67}Zn 78-70496
^{153}Dy$\rightarrow$^{153}Tb mass difference from β^{+} spectrum *(Russian)* 79-13257
^{166}Dy decay, ^{166}Ho low lying levels and transitions, 54.24 keV level mag. moment 80-13380
^{167}Dy, β^{-} decay, level scheme of ^{167}Ho obs. 77-26580
^{159}Er decay populating ^{159}Ho levels, γ-singles and electron conversion spectra 78-547
^{165}Er decay, ^{155}Ho $L_{2,3}$ subshell X-ray fluorescence and Coster-Kronig yields 80-69102
^{169}Er, β-decay half-life, γ-ray spectra 77-79330
^{169}Er, internal bremsstrahlung photon intensity and energy yield 78-86509
^{256}Es 7.6 hr β-decaying high-spin isomer, discovery following ^{254}Es(t,p) 77-22964
Eu decay, $^{152,\ 154}$Gd γ-transition energy and intensity meas. 80-73818
^{A}Eu β-decay, A=152, 154, $^{152,\ 154}$Gd negative parity states and β-γ-γ correlations 79-97676
^{143}Eu^{m}, decay obs., struct. determ. 78-50130
^{146}Eu decay, spin-parity assignment of ^{146}Sm levels *(Russian)* 77-14062
^{148}Eu decay, ^{148}Sm energy levels, struct. interpretation from boson expansion model *(Russian)* 78-78261
^{150}Eu decay, ^{150}Sm nucl. struct. determ. *(Japanese)* 77-41888
^{152}Eu, decay, gamma transitions and probabilities of beta transitions 80-22768
^{152}Eu, K-forbidden beta transition, spectral shape anal. 78-74335
^{152}Eu, X-ray emission probabilities per decay 80-14027
^{156}Eu decay, γ-γ directional correls., ^{156}Gd transitions from second $K^{\pi}=0^{+}$ band 78-25150
^{156}Eu$\rightarrow$^{156}Gd, elec. monopole transitions from excited 0^{+} states in ^{156}Gd 77-18478
^{141g}Eu, ^{141m}Eu β-decay props., J^{π}, decay energy, $T_{1/2}$ 77-82876
^{17}F, populated in ^{16}O(d,n), half life meas. 77-88085
^{20}F, β-γ directional correlation meas., search for second class currents 79-13245
^{20}F β-spectra, cf conserved vector current predictions 78-50131
^{20}F, β-transitions, weak magnetism, nuclear struct., matrix elements 79-13253
^{20}F decay, β-γ ang. correlation, second class current contrib. 79-22236
^{20}F$\rightarrow$^{20}Ne+e^{-}+$\bar{\nu}_{e}$, CVC test in $2^{+}\rightarrow 2^{+}$ transitions 79-6514
^{20}Fe, β-γ directional correlation, second class current 78-50127
^{51}Fe, β-decay GT matrix elements, $T_{1/2}$ 78-557
^{51}Fe, β-decay half-life and GT matrix element 77-22950
^{52}Fe^{M} decay, ^{52}Mn yrast state properties, transitions and decays 79-67631
^{52}Fe$\rightarrow$^{52}Mn^{m}$\rightarrow$^{52}Cr, γ-ray spectra, ^{52}Cr levels 78-21529
^{53}Fe half life from ^{54}Fe(n,2n) 79-3142
^{59}Fe nuclei polarised in iron foils cooled by dilution refrigeration 77-34263
^{248}Fm, fission barrier heights from β-delayed fission, β-strength functions struct. 80-5184
^{224}Fr$\rightarrow$^{224}Ra, γrays, internal conversion, eγ coincidence spectra meas. 80-78216
^{62}Ga superallowed Fermi β^{+} decay half life from ^{58}Li(^{6}Li,Zn) 79-54410
^{62}Ga, superallowed Fermi β-transition, half life and β-ray end point energy 78-78320
^{67}Ga, multiparticle configs. in ^{67}Zn 78-70496
^{68}Ga decay, positron polarisation, precision meas. using new polarimeter 77-46144
^{70}Ga, β-decay to excited states, β- and γ-ray meas. 77-41933
^{72}Ga, 3^{-}-2^{+} first forbidden beta transitions, β-γ ang. correlation, nuclear matrix elements 80-42599
^{73}Ga, β-decay rate for estimation of ultra-high pressure 78-77927
^{143}Gd^{m+g}, β^{+} and EC decay 78-50130
^{145}Gd EC/β^{+}-decay branching ratio anomalies, ^{145}Eu level and transition effects 80-32244
^{145}Gd, ε/β^{+} anomalous values, reinvestigation 77-79332
^{147}Gd, γ-transitions, internal conversion electron spectra meas. 79-6475
^{153}Gd decay, EM transitions of ^{153}Eu, internal conversion coeffs. *(Russian)* 80-63121
^{69}Ge, transitions, spin and parity, and mag. moments determ. from β-decay of ^{69}As 79-22245
^{75}Ge, beta decay of 83 min ground state, decay characts. and scheme 79-67713
^{76}Ge double beta decay expt., Monte Carlo evaluation 79-49892
^{1}H, inverse β-decay fission $\bar{\nu}$ induced reaction cross sections 79-22273
^{2}H, inverse β-decay, fission $\bar{\nu}$ induced reaction cross sections 79-22273
^{3}H β-decay spectrum, $\bar{\nu}$e mass *(Russian)* 80-91159
^{3}H β-polarisation at low vel., C_{V}'/C_{V} and C_{A}'/C_{A} 77-10369
^{3}H β-spectrum in valine molecule, νe mass 80-91158
^{3}H, β-spectrum meas., refining of upper limit of $\bar{\nu}$ rest mass 78-17144
^{3}H decay, electron spectra rel. to neutrino rest mass and astronomical consequences *(Russian)* 80-109575
^{3}H low-dose β-ray relative biological effectiveness 80-12190
^{3}H ν-decay, ρ exchange current, weak axial vector current low energy theorem 79-40886
^{3}H$\rightarrow$^{3}He, in $TiH_{1.8}$, NMR investig. of radiation damage, ageing 77-24751
^{6}He, β decay cross sections 80-27880
^{6}He, β-decay, recoil ion energy spectrum anal. 78-21525
^{172}Hf, gamma-ray spectra of ^{172}Yb, excited level struct. 78-33140
Hg isotopes, A=184-197, β^{+}-decay, single particle and collective degrees of freedom 77-22956
^{187}Hg decay, ^{187}Au energy states, parities, γ spectra, triaxial nuclear deform. *(French)* 78-33143
^{191}Hg positron spectra, Fermi-Kuri diags. 77-22960
^{193}Hg positron spectra, Fermi-Kuri diags. 77-22960
^{A}Ho, A=148, 149, identification and β-decay from ^{144}Sm+^{10}B, ^{148,149}Dy levels 79-36166
^{153}Ho$\rightarrow$^{153}Dy, decay scheme, lifetimes 80-22765
^{154}Ho decay, ^{154}Dy N=88 nuclei quasirot. bands and J^{π} 80-83025
^{157}Ho$\rightarrow$^{157}Dy decay, internal conversion electron spectra and eγ coincidences *(Russian)* 80-68604
^{166}Ho, β- and γ-spectra meas. 77-6310
^{166}Ho, internal hyperfine field obs. using β-γ directional correl. 80-32229
^{166}Ho, radioactive decay, ^{166}Er level population *(French)* 78-545
^{170}Ho, 43 s and 2.76 min states, energies and intrinsic structs. 78-78321

beta-decay continued
^{170}Ho β^--decay, $T_{1/2}$ meas., ^{170}Er level struct. 78−41675
I β^+ decay force function resonance struct., level populations *(Russian)* 80−102154
^{A}I, A=139-141, delayed neutron emission probabilities, β-decay half-lives 80−83078
^{126}I β-decay, 0^+ states of ^{126} Te anal. 77−74810
^{128}I decay ^{128}Xe, collective excitations obs. 79−45143
^{132}I decay, weak transition energies and intensities, γ-spectrum, ^{132}Xe levels 79−9521
^{132}I decay ^{132}Xe level struct., J^π, transitions and multipole mixing ratio 80−91134
^{136}I β-decay, ^{136}Xe levels anal. neutron particle-hole states 77−74811
^{137}I beta delayed neutrons, ^{137}Xe neutron unbound states, high energy X-rays 80−86856
^{137}I, β-decay delayed n emission, simple statistical model description 79−67714
^{137}I, investigation of beta-strength functions by neutron and γ-spectroscopy 79−45209
^{138}I, β-decay scheme, population of ^{137}Xe and ^{138}Xe levels, delayed neutron obs. 80−27600
In isomeric decays, ^{A}Sn, A=120,122,124,126,128, levels, transitions and J^π values 79−75851
In light isotopes, studied with LISOL on-line mass separator 77−23361
^{A}In, A=104, 106, β-decay half lives and decay schemes 78−74333
^{A}In, A=120-129, total β-decay energies and masses of strongly neutron rich isotopes 78−86512
^{12}In, β-decay obs., decay scheme, half-lives 79−45207
^{103}In decay, ^{103}Cd levels and spectra 79−22235
^{113}In decay to ^{113}In, decay scheme, unified model description of odd mass In nuclei 78−66251
^{114}In isomer decay, spin, excitation function, T_{112} γ-X-ray and γ-γ coinc. 77−6312
^{115}In, β^- decay spectrum, measured $T_{1/2}$, E_β 79−40888
^{118}In^{g} decay scheme, excited states of ^{118}Sn 77−54187
^{120}In, β-decay, half life and decay schemes, ^{120}Sn level struct. 78−86510
^{181}Ir, γ-ray spectra, half-life, decay scheme 78−41672
^{186}Ir decay into ^{186}Os, K=0 rot. band collective states 77−82803
^{192}Ir β decay into ^{192}Pt 4^+ and 3^+ levels, spectral shapes, ground state parity 77−50086
^{192}Ir β decay into ^{192}Pt 3^+ and $4_1{}^+$ states, lifetime meas. by β-γ coincidence 78−25153
^{192}Ir$\rightarrow{}^{192}$Pt, lifetimes of first four excited states of ^{192}Pt 77−294
^{194}Ir, spectral shapes of $1^-\rightarrow2^+$ and $1^-\rightarrow0^+$ beta transitions 77−30515
^{197}Ir decay studies, prod. in fast neutron reactions 77−23011
K, A=48, 49, 50, half lives, γ meas. 78−74341
^{35}K decay, ^{35}Ar levels, transitions and β-delayed protons 80−91156
^{35}K decay, ^{35}Ar lowest T=3/2 state excitation energy 79−85407
^{36}K, beta delayed emission of protons and α-particles 80−83074
^{36}K, β-decay, delayed proton and alpha emission ^{36}Ar levels, J^π, transitions 80−52629
^{38}K^{m}, β and γ spectra meas., determ. of isomeric ratios *(Russian)* 77−74771
^{38}K^{m} superallowed Fermi β-decay half lives 78−82318
^{38}K$^{m}\rightarrow{}^{38}$Ar, superallowed $0^+\rightarrow0^+$ β transition, spectrum shape 78−37316
^{45}K β-decay, ^{45}Ca levels, excitation functions and J^π 80−105978
^{38m}K, end point energy of superallowed Fermi decay 78−46030
Kr isotopes, A=88 to 91, decay rate determ. for ground state beta-branching 77−26634
^{85}Kr^{m,g} decay, ^{85}Rb levels, J^π and transitions 80−78162
^{90}Kr β-decay, ^{90}Rb level scheme, transitions, J^π assignments and internal conversion coeffs. 79−67663
^{93}Kr, experimental Q_β-values 78−93974
La, A=144, 145, 147, short lived fission product, Q_β-value 78−37317
La, A=144-6, β-decay, γ-ray singles and coincidence meas. 78−4913
La heavy isotopes, $T_{1/2}$ determ. 77−26633
^{A}La, A=123-125, half lives, low energy γ-data, β decay probabilities 79−499
^{A}La, A=144-149, β-decay half life meas. 79−67718
^{128}La decay scheme populating ^{128}Ba levels 77−82806
^{129}La β-decay, struct. of ^{129}Ba 79−22244
^{131}La$\rightarrow{}^{131}$ decay scheme, γ, X-ray and conversion electron spectra *(Russian)* 80−32241
^{134}La, half-life meas. 77−6311
^{138}La, radioactive decay meas., half life, γ energies 80−13418
^{140}La, beta decay half life 80−47435
^{143}La, decay, gamma-ray spectra *(French)* 77−30517
^{143}La, gamma-ray spectra, half-life 77−82859
^{144}La, beta and gamma spectra, level scheme 77−22962
^{144}La, radioactive decay meas., half life, ^{144}Ce levels 80−13417
^{145}La, fission product, β-decay anal. 78−78323
^{146}La, expt. β-decay energy of neutron-rich nuclides 79−30808
^{8}Li β^--decay, β-α angular correlations, final state energy depend., current test 80−102151
^{8}Li β-decay half life from ^{7}Li(d,p) 80−13483
^{8}Li(β)^{8}Be*(α)α, obs. of ^{8}Be state at ~6 MeV 78−93938
^{9}Li, β decay cross sections 80−27880
^{11}Li beta decay, γ activity 80−106018
^{11}Li, β-delayed two neutron radioactivity 80−18247
Lu β^+ decay force function resonance struct., level populations *(Russian)* 80−102154
^{A}Lu, A=160-163, decay and $T_{1/2}$, $^{160\text{-}163}$Yb transitions 80−102146
^{164}Lu, β-decay , half-life, populating ^{164}Yb levels 77−82805
^{167}Lu$\rightarrow{}^{167}$Yb, spin-parity determ. for ^{167}Yb levels 79−6380
^{169}Lu allowed hindered β^+ decay, ^{169}Yb ${}^{7}/_{2}{}^{+}[404]\rightarrow{}^{7}/_{2}{}^{+}[633]$ transition ft value 80−102148
^{169}Lu, internal conversion electron spectrum $E_\gamma<100$ keV, ^{169}Yb ground state population probability 79−6497
^{169}Lu, positron decay spectrum 79−6504
^{169}Lu, radioactive decay, gamma ray and conversion electron spectra 80−22766
^{169}Lu, radioactive decay scheme 80−22767
^{170}Lu$\rightarrow{}^{170}$Hf, beta decay, reduced transition probabilities 77−22945
^{171}Lu, positron decay 79−6505
^{172}Lu decay, identification of γ-spectra unplaced energies by delayed coincidence meas. 80−78221
^{172}Lu, decay scheme, γ-ray, conversion electron spectra 79−75913
^{172}Lu, gamma-ray spectra of ^{172}Yb, excited level struct. 78−33140
^{172}Lu, radioactive decay, γ-ray spectra, internal conversion electron spectra 79−75912

beta-decay continued
^{173}Lu$\rightarrow{}^{173}$Yb e.m. consts. of lower rot. bands of ^{173}Yb determ. 77−82802
^{176}Lu β-decay half life 80−52633
^{177}Lu decay, beta spectral shapes 78−74337
^{179}Lu, level struct. of ^{179}Hf 77−54185
^{A}Mg, A=29-32, radioactive half-life and branching ratios 79−22240
^{20}Mg, β-delayed proton obs., mass excess of T=2 state in ^{20}Na 79−22234
^{28}Mg $\Delta T=1$ $0^+\rightarrow0^+$ β-decay, isospin forbidden branching ratio to ^{28}Al 79−93560
^{28}Mg, isospin forbidden β-decay 78−78315
^{49}Mn, β^+-decay superallowed branch, ^{49}Cr levels, transitions, and Gamow-Teller matrix elements 80−57746
^{50}Mn populated in ^{50}Cr(^{3}He,t), precise Q-value, β decay energy, half life 77−30618
^{52}Mn half-life meas. 78−17152
^{52}Mn, oriented, β-decay asymm., positron ang. distrib. meas., matrix elements 77−2951
^{52}Mn$^{g}\rightarrow{}^{52}$Cr, γ-ray spectra and ^{52}Cr levels 78−21529
^{57}Mn half life 78−82321
^{59}Mn, β-decay scheme, mass, branching ratios 77−82873
^{59}Mn, β-decay scheme, $T_{1/2}$ and mass meas., astrophysical significance 77−26635
^{59}Mn, new isotopes of interest to explosive nucleosynthesis β-decay scheme and mass determ. 79−45208
^{60}Mn, mass and β-decay half life, ^{60}Fe struct. and mass excess 78−78317
^{60}Mn, new isotopes of interest to explosive nucleosynthesis, β decay scheme and mass determ. 79−45208
Mo, A=103-5, half-lives and γ-ray energies of short-lived isotopes following ^{235}U fission 78−17137
Mo neutron rich isotopes, excited 0 states 77−22937
^{A}Mo, A=103, 104, ^{252}Cf fission fragment β-decay, X-ray-β particle coincidence technique 80−74094
^{99}Mo beta decay, gamma-ray obs., 0.1-1 MeV, ^{99}Tc 920 keV level spin 77−54145
^{102}Mo, β-decay, T1/2, ^{102}Tc deduced levels, tentative J^π and transitions 80−52630
^{102}Mo fission product decay, ^{102}Tc decay scheme and γ-intensities 80−78229
^{93m}Mo$\rightarrow{}^{93}$Nb, high-spin three-quasiparticle states of ^{93}Nb 77−34262
NH_2T, β-decay, ab initio SCF MO calcs. 77−71842
^{12}N, aligned, β ang. distribs., second class currents 78−50126
^{12}N, aligned, β-ang. distrib. and alignment correction coeffs., axial vector currents 80−5097
^{12}N, aligned, β-ang. distrib. asymmetry coeffs., pseudotensor interaction, T=1 isospin triplet decay 80−106021
^{12}N, beta decay, PCAC and vector current conservation 79−93561
^{12}N, beta-ray spectra and conserved vector current 79−54409
^{12}N, β-ray branching and $T_{1/2}$ 78−41674
^{12}N, β-transitions, weak magnetism, nuclear struct., matrix elements 79−13253
^{12}N, oriented nuclei, β-γ ang. correl., G-parity nonconservation 78−54723
^{12}N, polarised, asymm. of β-ray ang. distrib., second class currents 77−41919
^{12}N, polarised, β-decay asymm., G-parity nonconservation, second class currents 77−41920
^{12}N, polarised, higher order effects in determ. of asymmetry parameters 79−22247
^{12}N, weak magnetism and beta spectra 77−6314
^{12}N$\rightarrow{}^{12}$C(g.s.), second-class axial current, meas. alignment-positron-momentum correl. 78−82317
^{14}N(γ,π)^{14}O, 145-325 MeV, Gamow-Teller suppression and M1 radiative widths 80−52609
^{14}N(γ,π^+), anomalous $^{14}N_{gs}\rightarrow{}^{14}C_{gs}$ transition, Kroll Ruderman terms 80−63167
^{16}N* beta-decay, elementary particle treatment 78−8800
^{16}N*(0^-) beta decay, calculated decay rate 79−59036
^{16}N(0^-)$\rightarrow{}^{16}$O(0^+)+β, nucl. wave functions and mesonic exchange currents 79−40887
^{16}N(0^-)$\rightarrow{}^{16}$O(0^+)+$\bar{\nu}$e+e^-, one pion exchange current problem for ^{16}O(0^+)$\rightleftarrows{}^{16}$N(0^-) 79−85375
^{17}N, β-decay delayed neutron emission, ^{17}O levels, T1/2 meas. 77−18481
Na neutron rich isotopes, β-delayed emission of n, 2n, α, t 78−74343
^{A}Na, A=22, 24, β-transitions, weak magnetism, nuclear struct., matrix elements 79−13253
^{A}Na, A=27-32, radioactive half-life and branching ratios 79−22240
^{A}Na, A=30,31,32, beta-delayed two-neutron emission 80−95316
^{20}Na, β-γ directional correlation, second-class current search 77−88083
^{20}Na, β-γ directional correlation meas.. search for second class currents 79−13245
^{20}Na, positron decay, β-α ang. correl. meas. 77−46138
^{22}Na, anomalous electron capture/β^+ decay ratio, second forbidden corrections 79−22238
^{22}Na, EM corrections for electron capture to β^+ decay ratio 79−89269
^{24}Na half-life determ., $T_{1/2}=(14.964\pm0.015)$ h 80−95311
^{24}Na^{m}, polarised, β-decay asymmetry and mag. moment from Na(n,γ) 80−91157
Nb isotopes, A=95, 97, 99, beta-decay schemes, level struct. 77−26631
^{90}Nb giant particle hole resonances, Gamow-Teller strength from ^{90}Zr(p,n) 80−86877
^{92}Nb^{g}, cross-section and half-life from ^{83}Nb(n,2n), 14.8 MeV 78−70491
^{95}Nb, beta decay, K-shell electron ejection 77−18888
^{95}Nb, K-shell autoionisation in β-decay 77−298
^{103}Nb, experimental Q_β-values 78−93974
Nd decay, ^{A}Pm, A=149,151, shape coexistence, deformed states 80−78135
^{147}Nd, beta decay, ^{147}Pm $\gamma\gamma$ cascade angular correlations 79−63624
^{147}Nd, beta spectrum, hard component 80−22769
^{147}Nd, β decay, ^{147}Pm level scheme 80−83073
^{147}Nd β-decay, ^{147}Pm energy levels and γ-ray transitions E2/M1 mixing ratio 79−67655
^{147}Nd decay, ^{147}Pm levels, transitions, $\gamma\gamma$-coincidences and IC electrons 80−18243
^{149}Nd$\rightarrow{}^{149}$Pm, energy level study 80−27592
^{149}Nd$\rightarrow{}^{149}$Pm, γ-ray spectra and Pm level scheme 79−63628
^{19}Ne, β-decay, recoil ion energy spectrum anal. 78−21525
^{19}Ne$\rightarrow{}^{19}$F+e^++ν, test of time reversal symmetry 77−30521

beta-decay continued
^{19}Ne$\rightarrow$^{19}Fe+e^{+}+ν_e, limit on Fierz interference 78−560
^{20}Ne, from ^{16}O(α,γ), 10.27 MeV, first T=1,2^{+} state radiative width meas. rel. to analogue β-decays 78−549
^{55}Ni, β-decay GT matrix elements, T$_{1/2}$ 78−557
^{55}Ni, β-decay half-life and GT matrix element 77−22950
^{242}Np β-decay, half life, ^{242}Pu level scheme 79−67664
OHT, β-decay, ab initio SCF MO calcs. 77−71842
^{14}O, superallowed Fermi β-decay half lives 78−82318
^{14}O$_{g.s.}$ β-decay, mesonic exchange currents, weak process microscopic treatment 80−57742
^{14}O(β^{+})^{14}N*, Q-value 77−26625
^{14}O$\rightarrow$^{14}N e^{+}ν_e, rate calcs. using elementary particle and macroscopic treatments 78−29429
^{16}O(0^{+})$\rightleftarrows$^{16}N(0^{-}), beta decay and muon capture rate ratio, mesonic exchange currents 80−42594
^{16}O(0^{+})$\rightleftarrows$^{16}N(0^{-}) β decay and μ capture reactions, mesonic exchange correction 78−58257
^{19}O β-decay, Fermi to Gamow Teller mixing ratio meas., ^{19}F isospin mixing 79−9520
^{177}Os$\rightarrow$^{177}Re decay scheme, lower excited states of ^{177}Re obs. 78−17145
^{179}Os$\rightarrow$^{179}Re decay scheme, lower excited states of ^{179}Re obs. 78−17145
^{185}Os, γ-ray spectra obs., first forbidden beta decay anal. 78−559
^{194}Os beta decay, X-ray/gamma relative intensities, L$_{1}$ subshell yields 78−4919
^{196}Os, identification and β-decay meas. 77−22963
^{196}Os, T$_{1/2}$ and partial decay scheme 78−21527
^{28}P, β^{+} decay, delayed particle emission, ^{28}Si levels and J$^{\pi}$ 80−22772
^{30}P, stellar weak interaction rates, supernova appl. 80−82336
^{31}P(p,n)^{31}S, 6.38 to 13 MeV, polarised protons, β-decay asymmetry meas. 77−18482
^{32}P, β^{-} decay, energy spectra of positron pairs 79−6506
^{32}P, half-life and mean beta distintegration energy determ by low-temp calorimetry 80−5094
^{32}P, transmutation doping of ^{30}Si, residual radioactivity 79−33009
^{A}Pa, A=236, 238, β strength function struct., influence on β-delayed fission 78−89826
^{17}Pa A=236, 238, strength function of β-transitions, probability of delayed fission 80−22764
^{236}Pa, β-delayed fission, search *(Russian)* 78−46033
^{238}Pa, β-delayed fission, search *(Russian)* 78−46033
Pb region, forbidden charge exchange collective modes, β- and γ-decay processes 80−86784
^{193}Pb$\rightarrow$^{193}Tl, ^{193}Tl structure 77−6587
^{210}Pb ground state decay 80−47429
^{97}Pd β^{+}-decay, ^{97}Rh levels and γ-transitions, 3QP model anal. 80−102120
^{109}Pd, ^{238}U fission product, gamma-ray spectra, half-life determ. 77−50084
^{111}Pd, isomer decay populating ^{111}Ag levels 78−551
^{111}Pd^{g,m}, γ-ray decay, ^{111g}Pd half-life, ^{111}Ag levels and decay 78−541
^{112}Pd, ^{238}U fission product, gamma-ray spectra, half-life determ. 77−50084
^{109g}Pd, gamma-ray decay, gamma-gamma coincidences 78−29417
^{139}Pm decay, states in N=79 ^{139}Nd 77−41929
^{147}Pm, β-decay, branching ratio and K-shell autoionisation 80−42598
^{147}Pm decay, K-orbital shake off electrons and X-ray spectra 77−46141
^{147}Pm fuelled betavoltaic pacemaker system status 77−81733
^{147}Pm, internal bremsstrahlung photon intensity and energy yield 78−86509
^{149}Pm, β^{-} decay, ^{149}Sm level scheme 80−22750
^{149}Pm, β-decay, nucl. matrix elements, calc., γ-transitions 80−52628
^{149}Pm first forbidden β-decay, β-γ ang. correlation, ^{149}Sm 286 keV level J$^{\pi}$ character 79−49609
^{149}Pm, shape factor anal. of β-transitions 78−21532
^{149}Pm$\rightarrow$^{149}Sm, beta decay matrix elements 78−70488
^{150}Pm, decay, ^{150}Sm nucl. struct. determ. *(Japanese)* 77−41889
^{151}Pm$\rightarrow$^{151}Sm, β-decay, level scheme of ^{151}Sm 77−74792
^{152}Pm decay, β and γ rays, spins, half lives, ^{152}Sm levels 78−542
^{140}Pr, P$_{K}$/P$_{\beta+}$ ratio for allowed decay 77−61386
^{143}Pr, internal bremsstrahlung 77−82879
^{144}Pr^{m}β-decay, ^{144}Nd levels and transitions, γ-ray spectra *(French)* 80−18250
^{146}Pr β-decay, ^{146}Nd level scheme and transitions 78−86476
^{146}Pr$\rightarrow$^{146}Nd, decay scheme and energy levels, log ft values 78−4912
^{148}Pr, β^{-} decay scheme and T$_{1/2}$ determ. using γ coincidence counting techniques 79−93558
^{148}Pr decay to ^{148}Nd, energy levels, isomerism 80−5096
^{148}Pr, short lived fission product, Q$_{\beta}$-value 78−37317
^{149}Pr decay, β-branching and log ft values determ. 77−71591
^{150}Pr decay into ^{150}Nd vibr. levels 78−89817
^{183}Pt fast β-transition, ^{183}Ir levels, J$^{\pi}$ assignments, Nilsson states for N=105 isotones 79−22206
^{185}Pt^{m+g} decay, population of ^{185}Ir levels 80−9269
^{200}Pt decay studies, prod. in fast neutron reactions 77−23011
^{232}Pu, fission barrier heights from β-delayed fission, β-strength functions struct. 80−5184
^{239}Pu, fission product beta decay, $\bar{\nu}$ spectra 80−102150
^{239}Pu(n,γ), thermal, fission product $\bar{\nu}_e$ spectrum, β-decay characts. 80−78340
^{228}Ra-^{228}Ac decay and ^{228}Th decay chain, gamma ray energies 79−85857
^{230}Ra decay, ^{230}Ac levels, J$^{\pi}$ and transitions, Nilsson assignments 80−68543
^{230}Ra, identification and β-decay meas. 77−22963
^{230}Ra, prod., decay characts. 78−54724
Rb decay, ^{A}Sr, A=98, 100 rot. struct. sudden onset, gamma transitions 80−73777
Rb decay, ^{94,96}Sr direct and skip cascades, $\gamma\gamma$ ang. correlations, levels, mixing ratios 80−86851
Rb, fission fragment, delayed neutron branches from γ-spectroscopy 80−78230
Rb, fission products, precise Q$_{\beta}$ values *(German)* 80−37354
Rb heavy isotopes, T$_{1/2}$ determ. 77−26633
Rb isotopes, A=88 to 91, decay rate determ. for ground state beta-branching 77−26634
Rb isotopes, delayed neutron Pn-values, beta+neutron+gamma-ray decay modes 77−26639
Rb neutron deficient isotopes, beta-decay energies and masses 77−22946
Rb, neutron rich isotopes, Q$_{\beta}$and direct mass meas. 80−78132
Rb odd isotopes, β^{-} strength functions, ‘pygmy’ resonances 79−93559

beta-decay continued
Rb precursors, half lives and delayed neutron emission probabilities 79−49610
^{A}Rb, A=88-94, beta endpoint energy measurements 78−93975
^{A}Rb, A=91 to 98, β-decay half life meas. 79−67718
^{A}Rb, A=93,94,95, delayed neutrons, energy spectra 80−99153
^{A}Rb, A=96,98, β-decay schemes and total energies, mass excess and separation energies 80−27601
^{A}Rb, A=96 to 100, half-lives and neutron emission probabilities in neutron rich isotopes 79−17864
^{74}Rb, N=Z nucleus with T=1, I$^{\pi}$=0^{+}, half life 77−26627
^{74}Rb, Z=N nuclide, superallowed beta decay meas. 77−22952
^{78}Rb β-decay half lives of isomeric and ground state from (^{16}O,3n) 80−27534
^{79}Rb β^{+} decay, ^{79}Kr excited states, J$^{\pi}$ assignment, transitions, level lifetimes 79−17810
^{87}Rb, decay constant determ., Rb-Sr dating appl. 78−29424
^{87}Rb$\rightarrow$^{87}Sr+neutrals, nucleon charge conservation, improved test 80−5098
^{88}Rb$\rightarrow$^{88}Sr, Gamow-Teller β-transition, matrix elements and log ft values calc. 78−21531
^{90}Rb, β,γ, conversion electron spectra obs. 77−71583
^{92}Rb decay, ^{92}Sr $\gamma\gamma$ ang. correlations, levels, J$^{\pi}$, mixing ratios 80−57725
^{94}Rb β-delayed n decay, ^{93}Sr excited state depopulation γ-rays, n coincidence 80−52631
^{98}Rb decay, ^{98}Sr very low lying 0^{+} state, shape coexistence bands, T$_{1/2}$, transitions 80−78148
^{100}Rb β-decay, ^{100}Sr ground state rot. band transitions, deformations and lifetimes 79−93550
^{A}Re, A=186,188, β-decay, weak magnetism effects, triaxial rotor model 80−91155
^{182}Re isomer decay mag. moment, ^{182}W high spin states, J assignments and mixing ratios 80−42593
^{183}Re, γ-ray spectra obs., first forbidden beta decay anal. 78−559
^{186}Re$\rightarrow$^{186}Os, absolute log ft values, beta spectra, directional correlation coeff. and WS potential parameters calc. *(Rumanian)* 78−82316
^{187}Re, decay const. determ. from ^{187}Re-^{187}Os systematics in meteorites 80−41778
^{188}Re, first forbidden 1.98 MeV beta decay, matrix elements 77−61385
^{189}Re, beta-decay, ^{189}Os scheme 79−54388
^{182m}Re β-decay, rot. and intrinsic struct. of ^{182}W determ. 77−41914
^{100}Rh, γ-ray spectrum and ang. $\gamma\gamma$ correlations, ^{100}Ru level struct. study 79−6510
^{100}Rh short lived isomer, decay scheme from (α,pn), (p,n) and (p,3n) 79−75920
^{103}Rh, β-γ-γ directional correl., J$^{\pi}$ determ. 77−26628
^{106}Rh^{g}, decay, excited states and transitions in ^{106}Pd 77−79324
^{106}Rh^{g}, decay, gamma-gamma ang. correlation meas. in ^{106}Pd 77−79325
^{108}Rh, level structure and half life 77−82827
^{109}Rh, 79.8 sec., β-decay to ^{109}Pd, γ and γ-γ meas. 79−3116
^{208}Rn$\rightarrow$^{208}At, γ-ray, conversion electron spectra 80−83072
^{224}Rn$\rightarrow$^{224}Fr±^{224}Ra, γ−rays, internal conversion, eγ coincidence spectra meas. 80−78216
^{224}Rn$\rightarrow$^{224}Fr$\rightarrow$^{224}Ra decay, γ-rays IC electrons and eγ coincidences 80−18239
^{97}Ru, K-capture probability for β-transition to 216 and 324 keV levels of ^{97}Tc 79−6511
^{103}Ru$\rightarrow$^{103}Rh, polarised nuclei, ^{103}Ru mag. moment, E2/M1 mixing ratios 77−6315
^{105}Ru$\rightarrow$^{105}Rh, polarised nuclei, ^{105}Ru mag. moment, E2/M1 mixing ratios 77−6315
^{106}Ru β-decay, e^{+} spectra, ^{106}Pd levels and E0 transitions 79−75894
^{A}S, A=31,32,33, stellar weak interaction rates, supernova appl. 80−82336
^{29}S β^{+}-delayed proton decay, half life, ^{29}P deduced levels 79−22241
^{34}S, half-life 77−54188
^{35}S, beta-decay, internal bremsstrahlung spectrum meas. 77−50089
^{35}S compounds, beta decay, transition probabilities, ab initio calcs. 77−61387
^{35}S, internal bremsstrahlung photon intensity and energy yield 78−86509
^{39}S decay, half life, ^{39}Cl excited states and transitions 80−42595
Sb, A=128,130,131,134, total β decay energies, mass excesses, β-γ coincidence study 77−82870
Sb, neutron rich isotopes, half-lives, fission yields, and neutron emission probabilities 77−67721
^{118}Sb, study of ^{118}Sn excited states 77−54187
^{122}Sb, 2^{-}(1.41 MeV β^{-})2^{+} negatron decay, numerical values of matrix elements 77−41925
^{122}Sb(2^{-})$\rightarrow$^{122}Te(2^{+}), comparison with pairing-plus-quadrupole model 77−10370
^{122}Sb$\rightarrow$^{122}Te second 2^{+} excited state, β-γ ang. correls., β-ray spectrum shape 77−38250
^{124}Sb, beta-decay to ^{124}Te, level struct. determ. 79−54387
^{124}Sb, first forbidden β-transitions, β-γ circular polarisation correlations 79−9517
^{125}Sb$\rightarrow$^{125}Te, γ-ray spectra of ^{125}Te 79−71816
^{134}Sb, expt. β-decay energy of neutron-rich nuclides 79−30808
^{135}Sb, β-decay delayed n emission, simple statistical model description 79−67714
^{135}Sb, β-strength function energy struct., effect on delayed neutron emission prob. 79−75915
^{135}Sb, investigation of beta-strength functions by neutron and γ-spectroscopy 79−45209
^{42}Sc, β^{+} decay, isospin symm. hindered, branching fraction 78−21526
^{42}Sc, ground state β-decay, weak non-analogue Fermi branch, branching ratio upper limit 78−70495
^{42}Sc populated in ^{42}Ca(^{3}He,t), precise Q-value, β decay energy, half life 77−30618
^{46}Sc, beta decay half life 80−47435
^{48}Sc Gamow-Teller strength, ang. distribs., from ^{48}Ca (^{3}He,t) 80−42589
^{48}Sc spin-flip isovector giant resonance, T$_{>}$ Gamov-Teller strength from ^{48}Ca(p,n) 80−106019
^{51}Sc$\rightarrow$^{51}Ti, γ-ray spectra, β-branching ratios, ^{51}Ti levels 77−6318
^{A}Se, A=71, 73 decay, ^{A}As, A=71, 73, levels, J$^{\pi}$, transitions, T1/2 80−57684
^{A}Se, A=85, 86, experimental Q$_{\beta}$-values 78−93974
^{69}Se, decay, T=1/2 β-delayed proton precursor 77−88082
^{69}Se, delayed proton decay 77−22971
^{75}Se, decay, electric monopole transitions 80−22752
^{83m}Se, decay scheme refinement, ^{83}Br levels 78−17147

beta-decay continued
^{32}Si, half life determined from varved Gulf of California sediment core 80—91153
^{32}Si half life from tandem accelerator mass spectrometry 80—95313
^{32}Si half life via accelerator mass spectrometry 80—95314
^{141}Sm^{g} decay scheme, ^{141}Pm level struct. 77—46142
^{145}Sm decay, low-lying levels of ^{145}Pm anal. 78—29420
^{151}Sm, β-decay, branching ratio and K-shell autoionisation 80—42598
Sn, A=127 to 131, total β decay energies, mass excesses, β-γ coincidence study 77—82870
^{106}Sn β^{+}/EC decay, ^{106}In level scheme determ. 78—93971
^{113}Sn, decay to levels of ^{113}In 77—38247
^{121}Sn$^{m}\rightarrow^{121}$Sn$^{g}\rightarrow^{121}$Sb, branching fraction, K-shell IC coeff. 78—82319
^{123}Sn^{m} decay scheme, γ-ray, X-ray and electron spectra, ^{123}Sb transitions 77—88073
^{125}Sn^{9}, ^{125}Sb high spin levels, gamma transition energies and intensities 80—73819
^{130}Sn$\rightarrow^{130}$Sb, decay scheme, log ft values, spin-parity assignments 77—34264
^{131}Sn beta decaying isomer, ^{131}Sb partial level scheme, half life 77—50091
^{131}Sn, expt. β-decay energy of neutron-rich nuclides 79—30808
Sr, fission products, precise Q_{β} values *(German)* 80—37354
Sr heavy isotopes, $T_{1/2}$ determ. 77—26633
Sr isotopes, A=95, 97, 99 beta-decay schemes, level struct. 77—26631
Sr isotopes with A=96, 98, 100, decay scheme, level scheme of Y 77—26632
^{A}Sr, A=94 to 98, β-decay half life meas. 79—67718
^{A}Sr, A=96,98, β-decay schemes and total energies, mass excess and separation energies 80—27601
^{85}Sr, β-decay, γ-ray weak transitions, intensities 77—79326
^{91}Sr$\rightarrow^{91}$Y, decay scheme, gamma-ray spectra 77—71587
^{92}Sr, gaseous fission products, β-decay energies 79—9519
T compounds, beta-decay, transition probabilities, ab initio calcs. 77—61387
T decay, dissociation of HT molecules 77—63941
T decay, storable conc. of atomic H in T-impregnated crystalline solid H_2 80—30594
^{166}Ta, isotope identification in ^{159}Tb(^{16}O,9n) reaction, half-life and decay scheme 77—79331
^{180}Ta^{m}, β^{-} and EC branching ratios, K-internal conversion coeff., γ-intensities, T 1/2 80—68601
^{182}Ta β-decay, ^{182}W 100 keV E2-transition, L-subshell internal conversion coeff. 79—75909
^{146}Tb decay and T1/2, ^{146}Gd lowest 2^{+} state, J^{π} and transitions 80—105979
^{150}Tb, β-decay, ^{150}Gd vibr. levels anal. 78—8772
^{151}Tb, positron decay, γ-ray coincidence spectra 79—9513
^{153}Tb, meas. of positron spectrum 79—6509
^{154}Tb, beta-decay, ^{154}Gd matrix elements determ. 77—57626
^{160}Tb β-decay, oriented nuclei, γ transitions multipole mixing parameters 80—18240
^{160}Tb decay, ^{160}Dy anomalous γ-L X-ray directional correlations 80—52610
^{160}Tb in TbSi$_2$, electronic config. of ^{160}Dy ion produced 79—59340
^{160}Tb$\rightarrow^{160}$Dy, $A_2{}^{\beta}$ ang. correl. coeff., β-γ-γ ang. correl. studies 79—13255
^{162}Tb β-decay, γ-spectra, $T_{1/2}$, deduced ^{162}Dy levels 77—34246
Tc decay, ^{104,106,108}Ru level scheme and transitions, collective model anal. 80—78166
Tc decay ^{106,108}Ru levels, transitions, J^{π} and shape 80—57744
^{94}Tc$\rightarrow^{94}$Mo, level spins and multipole mixing ratios from γ-γ correlation meas. 78—21517
^{95}Tc^{m,g} decay populating ^{95}Mo levels, cluster-vibr. model 77—82856
^{99}Tc, β-decay, branching ratio and K-shell autoionisation 80—42598
^{99}Tc^{m}, β-decay rate for estimation of ultra-high pressure 78—77927
^{99}Tc^{m} β-decay, β-branching, ^{99}Ru decay scheme 80—42596
^{99}Tc^{m} decay constant, chemical state effect 80—42591
^{102}Tc^{g}, β^{-} decay, deduced ^{102}Ru levels 78—86513
^{103}Tc, β-decay, ^{103}Ru level scheme determ. 79—85413
^{103}Tc, decay scheme to ^{103}Ru 79—9470
^{103}Tc, experimental Q_{β}-values 78—93974
^{104}Tc, β^{-} decay, γ-spectra, ^{104}Ru level scheme determ. 78—82313
^{104}Tc decay, ^{104}Ru level energies, B(E2) ratio, mixing ratios, γ-ang. correlations 79—493
^{99m}Tc, beta-decay and dose calcs. 80—91154
Te, A=134,135, total β decay energies, mass excesses, β-γ coincidence study 77—82870
^{127}Te decay, ^{127}I γ cascade, 360.3-57.6 keV γ-γ directional correl. 78—25151
^{128}Te $\beta\beta$ decay ratio of ^{128}Te/^{130}Te half lives 78—66250
^{129}Te^{m+g} decay, ^{129}I time depend. quadrupole interactions, γ-γ correlations 80—78145
^{130}Te double β-decay, lepton charge conservation *(Russian)* 80—102153
^{136}Te (20.9 s), ^{136}I level scheme 77—82877
^{119m}Te decay, population, ^{119}Sb levels, γ-γ and γ-e correls. 78—546
^{231}Th β decay and ^{235}U α decay, γ-radiation study, energy level scheme *(Russian)* 78—17160
^{232}Th, fission barrier heights from β-delayed fission, β-strength functions struct. 80—5184
^{234}Th β^{-} decay into ^{234}Pa isomers, low energy γ-spectrum 78—70493
^{53}Ti, β-decay scheme, $T_{1/2}$ and mass meas., astrophysical significance 77—26635
^{53}Ti β-decay scheme 77—46139
^{53}Ti, new isotopes of interest to explosive nucleosynthesis, β-decay scheme and mass determ. 79—45208
Tl isotopes, A=184-197, β^{+}-decay, single particle and collective degrees of freedom 77—22956
^{184}Tl, half-life 79—97652
^{186}Tl decay, γ, conversion electron spectra and coincidences, ^{186}Hg bands, shape coexistence 78—25156
^{186}Tl, isomer and ground state half-lifes 79—97652
^{188}Tl, half-life 79—97652
^{189}Tl$\rightarrow^{189}$Hg$\rightarrow^{189}$Au, gamma spectra, ^{189}Au shape coexistence 77—6587
^{190}Tl$\rightarrow^{190}$Hg$\rightarrow^{190}$Au, decay spectra and periods 77—6317
^{204}Tl 80—42588
^{204}Tl, beta-transition, spectral shape, small-order deviation 78—74338
^{204}Tl, β-decay, branching ratio and K-shell autoionisation 80—42598
^{204}Tl β-decay, K-shell autoionisation accompanying internal bremsstrahlung 80—57745
^{204}Tl^{+}, diffusion in KCl, transmutation effect 77—89589

beta-decay continued
^{155}Tm$\rightarrow^{155}$Er, level scheme for ^{155}Er *(French)* 77—57630
^{156}Tm, (β^{+}+EC), level struct. of ^{156}Er 77—22957
^{157}Tm$\rightarrow^{157}$Er, level scheme for ^{157}Er *(French)* 77—57630
^{157}Tm$\rightarrow^{157}$Er, Nilsson model anal. of low-lying scheme 77—22958
^{158}Tm, (β^{+}+EC), level struct. of ^{158}Er 77—22957
^{163}Tm, ^{163}Er excited state obs. 78—17146
^{166}Tm decay, ^{166}Er level population 79—93556
^{170}Tm nucleus, form factors coeffs. calc. *(Rumanian)* 79—80899
^{A}U, A=235,238, fission product beta decay, $\bar{\nu}$ spectra 80—102150
^{235}U fission ^{235}U products, β-spectra and total β-energy 78—25158
^{235}U(n,γ), thermal, fission product $\bar{\nu}_e$ spectrum, β-decay characts. 80—78340
^{242}U β-decay, half-life, ^{242}Np levels, J^{π} and transitions 79—67664
^{46}V populated in ^{46}Ti(^{3}He,t), precise Q-value, β decay energy, half life 77—30618
^{46}V(β^{+})^{46}Ti, superallowed Fermi decay half-life 77—34259
^{46}V(β^{+})^{46}Ti superallowed Fermi decay, ft value 77—10371
^{50}V, half lives of β-decay and e^{-}-capture in $\Delta J=4$ transitions 79—22246
^{50}V, half-life limits for β-decay and electron capture 77—79334
^{52}V$\rightarrow^{52}$Cr, γ-ray spectra and ^{52}Cr levels 78—21529
^{52}V$\rightarrow^{52}$Cr, γ-ray spectrum, energies and intensities, ^{52}Cr level scheme *(French)* 77—14066
^{54}V, β-decay scheme and $T_{1/2}$ determ. 78—21528
^{55}V β-decay scheme and $T_{1/2}$ determ., mass excess meas. 78—21528
^{55}V, new isotopes of interest to explosive nucleosynthesis, β-decay scheme and mass determ. 79—45208
^{185}W, beta spectrum, shape factor meas. 77—2947
^{187}W decay, ^{187}Re low lying level struct. and transitions, E2/E1 mixing ratios 80—27557
^{190}W, identification and β-decay meas. 77—22963
Xe, yield curves for cyclotron prod. of ^{123}I, ^{125}I and ^{121}I from ^{127}I(p,xn)Xe reactions 78—44611
^{A}Xe, A=113,5, β-delayed p and α branch ratio, fluctuation function role 79—71820
^{137}Xe β decay into ^{137}Cs, γ spectra, coincidences, excited levels, branching logft values 77—54186
^{139}Xe β-decay, ^{139}Cs level scheme, J^{π} and γ-transitions 80—42590
Y, fission products, precise Q_{β} values *(German)* 80—37354
Y heavy isotopes, $T_{1/2}$ determ. 77—26633
Y isotopes, A=95, 97, 99, beta-decay schemes, level struct. 77—26631
Y isotopes with A=96, 98, 100, decay scheme, level scheme of Zr 77—26632
^{A}Y, A=96 to 98, β-decay half life meas. 79—67718
^{83}Y β^{+}-decay, ^{83}Sr nucl. energy levels, γ-ray coincidence meas. 77—6309
^{90}Y internal bremsstrahlung, evidence for detour transitions in β-decay processes 78—66247
^{91}Y, beta ray generated bremsstrahlung yield consts. 80—42588
^{96}Y from ^{235}U fission, spectroscopic meas. *(German)* 77—67726
^{98}Y, β-decay, level scheme of ^{98}Zr determ. 77—41934
^{98}Y from ^{235}U fission, spectroscopic meas. *(German)* 77—67726
^{98}Y^{g}, β-decay schemes and total energies, mass excess and separation energies 80—27601
^{99}Y$\rightarrow^{99}$Zr, half life and beta decay investigation 79—17863
^{100}Y β-decay, $T_{1/2}$, γ-spectra, low lying O^{+} state in ^{100}Zr 77—82878
^{90m}Y, ^{90g}Y decays, weak β transitions, γ-ray emission 77—34265
Yb isotopes, A=160-165, decay spectra meas. 77—22959
^{160}Yb decay, cc ^{160}Tm doubly odd deformed nucleus, excited states and state lifetimes 79—13209
^{175}Yb, levels of ^{165}Tm and decay scheme, γ-ray and conversion electron spectra 78—74334
^{195}Yb, matrix elements in $7/2^{-}$-$9/2^{+}$ beta-decay 77—41932
^{71}Zn^{m} decay, ^{71}Ga ang. correlations, level spin assignments and multipole mixing ratios 78—78305
Zr isotopes, A=95, 97, 99, beta-decay schemes, level struct. 77—26631
Zr neutron rich isotopes, excited 0 states 77—22937
^{85}Zr$\rightarrow^{85}$Y, decay scheme, half-life 77—34258
^{89}Zr allowed β-decay, K-electron capture/e^{+} emission ratios 79—93557
^{89}Zr, electron capture to positron emission ratios determ. 77—18896
^{97}Zr β decay into ^{97}Nb, level struct., spins, parities, from γ ang. correls. 78—29418
^{97}Zr, β-γ ang. correlation, ^{97}Nb 1251 keV level investig. 77—22879
^{99}Zr$\rightarrow^{99}$Nb, half life, level schemes and β-decay investigation 79—17863

beta-decay theory
see also beta-decay; beta-ray spectra
2p-1f shell nuclei quadrupole pairing, l-forbidden β-transitions 80—22770
A=24-28 nuclei, reliability of calculated decay props. 78—93970
A=6-14 nuclei, OPE current effect on allowed β-decays in the 1p shell nuclei 79—54413
A=8 mirror asymmetry, existence of second class weak currents 77—6307
A=8 systems, second class current problem 77—41921
atomic electron excitation probabilities during orbital electron capture by the nucleus 79—45211
atomic excitation effects on nuclear resonances and Q values 79—45226
atomic rearrangement processes 78—54725
average beta-particle energies and spectra, accurate approximations 77—50087
closed shell ± one nucleon nuclei, axial vector coupling const. quenching 78—89824
composite neutron containing proton+low-mass scalar meson, decay mechanism 77—2948
Coulomb and charge dependent effects in nuclei 77—54131
Coulomb correction to beta-ray ang. distrib. formulae 78—46031
Coulomb corrections, elementary particle approach 77—2946
CVC hypothesis and ^{12}N e^{+} energy spectra, weak magnetism 77—54190
double beta decay, electronic lepton number conservation law, ^{48}Ca 78—17150
double-beta decay, electron-neutrino pair emission via Δ(1232) resonance 78—54722
electron capture in nuclear statistical equilibrium 79—92663
electron capture to positron ratios, recent developments, review 77—18895
exchange current effects on orbital g-factor and E1 sum rule 77—41950
exchange effects in radioactive decay theory based on many body scatt 79—9525
excited states, β-decay and electron capture rates, gross theory, astrophysics implications 77—41927
extended PCAC+Veneziano type model, Goldberger Treiman relations, $\eta\rightarrow\gamma\gamma$or $\pi^{+}\pi^{-}\gamma$ 78—21354

beta-decay theory continued
- extended Siegert theorem, review 77−41924
- Fermi superallowed decay, scalar coupling const. upper limit 77−57631
- first-forbidden decays, hindrance factors, medium and heavy nuclei 77−41922
- fission product β-ray mean energy calcs. *(Russian)* 78−561
- fission products, short lived, estimation of nuclear decay heat 77−71594
- fission products of ^{235}U(n,f) in secular equilib., theoretical β-spectra 80−500
- G-parity nonconservation, ev ang. correlation for allowed beta-decay 78−17151
- Gamow Teller giant resonance struct., consequences for delayed neutron spectra and nucleosynthesis 77−2950
- Gamow Teller transition between collective and single-particle states, spherical odd mass nuclei 77−41923
- Gamow-Teller matrix elements of $T=1/2$ nuclei, axial-vector coupling const. renormalisation 77−74809
- gross theory, shell effects, strength function and half-lives 77−38251
- gross theory and shell effects 77−22954
- historical introduction, weak interactions, book 78−78133
- isoelastic processes, one-body density matrix formalism 77−18528
- isospin forbidden beta decays, collective model, Fermi matrix elements, appl. to ^{8}Li, ^{134}Cs 77−67722
- K-shell internal ionisation, excitation, K-shakeoff probabilities 77−18889
- l-forbidden transitions, phonon-quasiparticle interaction *(Russian)* 77−82875
- low energy β-decay to bound states, probability expression 77−88080
- matrix element calc. numerical results via new approximate meth. 77−88053
- meson dominance model and second class currents 80−63132
- meson exchange currents, configuration mixing, role in nucl. mag. moment, beta decay, review, book contrib. 80−478
- neutrino orbital angular momentum 77−50038
- neutrino-free β-decay theory, new aspects 79−13254
- neutron, first order radiative corrections to e, ν and e-ν asymmetry coefficients 78−58254
- neutron beta decay characteristics 79−6338
- nonleptonic weak interactions, irregular G_u-parity term, hadronic currents 77−2770
- nuclear form factors of 0^{+}-0^{-} transition in $A=16$ system, nuclear struct. effects 80−18246
- nuclear magnetic field, Cabibbo angle, and CP violation 77−41918
- nuclear matrix element $\int\gamma_5$ calc., commutation method 77−61383
- odd nuclei, second forbiddeness order, matrix element determ. 79−6508
- odd-odd neutron deficient nuclei, spectra of delayed protons and α-particles in β^{+} decay *(Russian)* 78−46034
- one-body Gamow Teller β-decay matrix elements for 1s-0d shell, empirical renormalisation 78−66248
- proton decay, β-delayed proton radioactivity, book contrib. 78−82322
- second class axial vector currents with mesonic effects, beta-decay 77−30520
- second-class currents and matrix elements in renormalisable field theory 77−10197
- superallowed beta-decay, charge depend. anal. 78−29427
- superallowed Fermi β transitions, induced scalar interaction 78−33154
- superallowed Fermi β-decay, analogue symmetry breaking 77−65215
- superallowed Fermi β-decay, mismatch problem 77−2949
- superallowed Fermi β-decays, current state of investigation 79−93563
- superheavy region, neutron drip line, energy density mass formula extrapolation 78−93932
- V-A theory, neutron beta-decay *(Russian)* 78−58255
- weak interaction treatment, modifications to $Re/R_{\beta+}$ ratio from finite size and Coulomb corrections 77−46143
- Weinberg model and fundamental nature of work interaction *(Hungarian)* 77−26482
- β-delayed neutron decay, statistical model, Monte Carlo techniques, fictional pandemonium nucleus calcs. 78−89830
- n decay, model independ. form of certain observables 78−33068
- ^{8}B, isospin symmetry breaking in $A=8$ mirror decays 78−93973
- ^{12}B, beta-spectra reanalysis, shape-factors and CVC theory 77−67724
- $^{12}\mathrm{B}\rightarrow{}^{12}\mathrm{C}e^{-}\bar{\nu}_e$, data anal., second-class currents and CVC 77−82874
- ^{8}Be, level feeding via β and γ transitions, role of spatial quantum numbers 77−67723
- $^{12}\mathrm{C}(\mu^{-},\nu_{\mu})^{12}\mathrm{B}$, Hartree Fock wavefunction, correlations, pseudoscalar coupling constant, capture rates, recoil nuclear polarisation 80−22774
- $^{14}\mathrm{C}(^{6}\mathrm{Li},^{6}\mathrm{He})$, 62 MeV, Gamow-Teller sum rules and ground state wave function 80−106073
- $^{48}\mathrm{Ca}\rightarrow{}^{48}\mathrm{Ti}+2e^{-}$, neutrinoless double β decay, matrix elements and lepton conservation 77−30518
- Cs, $A=116$-120, spectra of delayed protons and α-particles in β^{+} decay *(Russian)* 78−46034
- ^{124}Cs, β-decay props. of collective 1^{+} states 78−13028
- ^{126}Cs, β-decay props. of collective 1^{+} states 78−13028
- ^{17}F, axial vector decay, exchange corrections 79−36201
- ^{66}Ga deformation parameter determ. from beta decay Fermi matrix element 79−75923
- $^{145}\mathrm{Gd}\rightarrow{}^{145}\mathrm{Eu}$, weak interaction treatment, modifications to $Re/R_{\beta+}$ ratio from finite size and Coulomb corrections 77−46143
- ^{3}H, meson exchange contrib., and mag. moment 77−6249
- ^{6}He β-decay from three body model of $A=6$ system, α-N, N-N interactions 78−46032
- ^{6}He, G-parity nonconservation, ev ang. correlation for allowed beta-decay 78−17151
- ^{8}Li, isospin symmetry breaking in $A=8$ mirror decays 78−93973
- $^{8}\mathrm{Li}\rightarrow{}^{8}\mathrm{Be}+\beta$, β-decay strength calcs., microscopic continuum wave function 78−62503
- ^{12}N, beta-spectra reanalysis, shape-factors and CVC theory 77−67724
- $^{12}\mathrm{N}\rightarrow{}^{12}\mathrm{C}e^{+}\nu_e$, data anal., second-class currents and CVC 77−82874
- $^{16}\mathrm{N}(0^{-})\rightleftharpoons{}^{16}\mathrm{O}(0^{+})\beta$-decay and μ-capture, mesonic exchange correction 78−41673
- ^{A}Nb, $A=90,92,94$, Gamow-Teller strength distrib., RPA calcs. 80−78218
- ^{15}O, axial vector decay, exchange corrections 79−36201
- ^{208}Pb-^{208}Bi, statistical role of β^{-} strength function 77−22955
- ^{A}Rb, $A=89$ to 99, structure in beta strength function 79−93564
- $^{122}\mathrm{Sb}(2^{-})\rightarrow{}^{122}\mathrm{Te}(2^{+})$, comparison with pairing-plus-quadrupole model 77−10370

beta-particles *see beta-rays*

beta-radiation *see beta-rays*

beta-ray absorption
- *see also electron absorption*
- dew meter, appl. to meas. on soil and plant surfaces 78−24803
- energy distributions in homogeneous media 80−109033
- inhomogeneous medium, density determ. by β-ray attenuation, calcs. and meas. 80−98182
- introductory experiment, using 1-ply toilet paper 77−22358
- lung, beta-emitting particles, fraction of energy absorbed, rat obs. 80−104641
- radioisotope inner shell ionisation, X-ray chemical analysis 79−57323
- ^{147}Pm fuelled betavoltaic pacemaker system status 77−81733

beta-ray angular distribution
- *see also beta-ray spectra*
- $A=12$, decay of $T=1$ isospin triplet, β-ray anisotropy 78−78322
- Coulomb correction to beta-ray ang. distrib. formulae 78−46031
- rotational invariance in beta-ray ang. distrib. 78−66252
- β-decay, radiative corrections 77−38249
- ^{12}B, aligned, β ang. distribs., second class currents 78−50126
- ^{12}B, aligned, β-ang. distrib. asymmetry coeffs., pseudotensor interaction, $T=1$ isospin triplet decay 80−106021
- ^{12}B, aligned, existence of G-parity irregular induced tensor current 78−29384
- ^{12}B β-decay, polarised nucleus, asymm. of β-ray ang. distrib., second class currents 77−41919
- ^{12}B, polarised, β-decay asymm., G-parity nonconservation, second class currents 77−41920
- ^{12}B spin polarisation meas. from β-decay, product of $^{100}\mathrm{Mo}(^{14}\mathrm{N},^{12}\mathrm{B})^{102}\mathrm{Ru}$ 78−50196
- $^{210}\mathrm{Bi}\rightarrow{}^{210}\mathrm{Po}$ β-ray ang. distrib. asymm., mag. moment 77−41926
- ^{60}Co, oriented, β-decay asymm., positron ang. distrib. meas., matrix elements 77−2951
- ^{119}Cs, spin of neutron deficient nucleus by β radiation detected optical pumping 78−8782
- ^{166}Ho, internal hyperfine field obs. using β-γ directional correl. 80−32229
- ^{8}Li, in $LiTaO_3$, multiple quantum NMR transitions obs., quadrupole moment determ. 77−73090
- ^{52}Mn, oriented, β-decay asymm., positron ang. distrib. meas., matrix elements 77−2951
- ^{12}N, aligned, β ang. distribs., second class currents 78−50126
- ^{12}N, aligned, β-ang. distrib. asymmetry coeffs., pseudotensor interaction, $T=1$ isospin triplet decay 80−106021
- ^{12}N, aligned, existence of G-parity irregular induced tensor current 78−29384
- ^{12}N, polarised, β-decay, asymm. of β-ray ang. distrib., second class currents 77−41919
- ^{12}N, polarised, β-decay asymm., G-parity nonconservation, second class currents 77−41920
- ^{76}Rb, spin of neutron deficient nucleus by β radiation detected optical pumping 78−8782
- ^{103}Rh, β-γ-γ directional correl., J^{π} determ. 77−26628
- $^{122}\mathrm{Sb}\rightarrow{}^{122}\mathrm{Te}$ second 2^{+} excited state, β-γ ang. correls., β-ray spectrum shape 77−38250

beta-ray detection and measurement
- *see also beta-ray spectrometers; radioactivity measurement*
- $4\pi\beta$-γ coincidence method for radioactive source standardisation *(Rumanian)* 77−46472
- $4\ \pi\beta$-γ coincidence counting, source prep. using $AlCl_3$ 78−838
- absorbed dose rate, direct meas. using plastic scintillator *(Japanese)* 77−73589
- absorber position on particle attenuation 79−54753
- absorption method for β emitters identification, absorpt. coeff. in Al, accuracy 77−57837
- acoustic detector for beta and gamma radiation *(German)* 79−63876
- air ionisation probe for α, β, γ hand and shoe monitor 80−58084
- air pollution control at Nuclear Research Institute *(Czech)* 78−88906
- asymmetry in oriented ^{52}Mn and ^{60}Co β-decay, positron ang. distrib. meas. 77−2951
- automated Rn-Th monitor for earthquake prediction research 78−73532
- beta-gamma survey meter with numerical display 77−64134
- biological and ecological samples *(French)* 78−5052
- cameras, gas replacement monitor 80−95502
- channel multiplier made of phosphate glass 77−34522
- channel plate electron multipliers, single electron detection and timing 80−9458
- Cherenkov counting of beta emitter isotope pairs using performance number criterion 77−83471
- Cherenkov counting of plants for β-emitter radioassay, sample prep. 78−81088
- Cherenkov radiation, activity meas. of low beta emitters *(Czech)* 77−46450
- Chinese nuclear weapon tests, fresh fallout anal. using beta counting technique 79−92106
- complex spectra, meas. and processing *(Rumanian)* 80−9451
- constant fraction timing discriminator for channel plate electron multipliers 79−59316
- cylindrical proportional counter, gas multiplication factor dependence on anode wire attachment 78−78560
- detector with ring-type conical phosphor 80−27881
- determ. of bulk α and β radioactivity *(Rumanian)* 79−88346
- diamond, elec. props and performance for α- and β-particles 79−36481
- diamond detectors, beta/gamma ratio 77−54431
- differential ionization chamber for the determination of small differences in decay rates of beta emitters 79−76256
- direct meas. of β absorbed dose rate by discriminator and filter *(Japanese)* 78−74511
- dose rates in mixed beta-gamma fields, scintillation counter method 77−60254
- dosimeters, integral, calibration for personal dosimetry *(Czech)* 80−27825
- dosimeters, protection-level, calibration quantities 77−52888
- dosimeters, thermolum., supralinearity 77−10495
- dosimetry, comparison of laboratory standards 77−66858
- double focusing $\pi\sqrt{2}$ spectrometer, Fe-free, spectral distortion 79−26810
- environmental samples, spectrometric method for meas. of hard β-emitters 80−94135
- environmental source monitoring 77−38429

beta-ray detection and measurement continued
- fission products, short lived, light, beta decay energies using online mass separator 78—8783
- gas-chromatography, beta radio effluents, window flow counter 80—93824
- Ge, hyperpure, β end-point-energy meas. 78—78587
- GM counter for millisec. β activity cross section meas. 80—27880
- graphite calorimeter, multisection, for energy distrib. in high current relativistic electron beam 77—46456
- high-current beams, meas. of energy spectrum 77—46470
- highly stabilized hybrid spark chamber for β-ray imaging 80—102398
- holographic gas discharge track chamber 77—10551
- hybrid spark chamber for radioisotope distrib. meas. 78—46227
- ionisation chamber perturbation correct. factor 80—37704
- ionisation chamber with solid Ar 77—30720
- lightguide equiangular spiral, for beta-ray detector 77—3212
- linear position sensitive proportional line scanner for β-emitters 79—31330
- liquid column chromatography, scintillation counters, review *(Czech)* 80—27885
- liquid effluent beta monitor 77—61656
- liquid scintillation counting of ^{3}H or ^{14}C amino acids, optimisation factors 80—30951
- liquid scintillation instrumentation development 78—86728
- liquid scintillation system ^{32}P Cherenkov effect detect. efficiency meas. using ^{60}Co external source 78—25387
- liquid scintillator determ. of dose rates from homogeneously distrib. β,γ- and EC,γ-emitters in phantom organs 78—53501
- low activity beta-ray measurements, us Pu-Be neutron source and beta spectrometer 78—73114
- low temperature detectors using high-purity Ge diodes 77—30724
- low-level beta counting with an automatic sample changer 80—31147
- magnetic electron spectrometers and their in-beam use, review 79—68128
- mixed β-γ dosimetry, ionisation and scintillation counters 80—57975
- modern atomic and nuclear physics (book) 80—11
- monitoring beta and photon radiations for radiation protection purposes 78—15908
- multielement proportional counters for low-level ^{3}H and ^{14}C counting 79—76287
- MWPC, beta-ray imaging device for radiochromatography 80—102387
- MWPC, pressurised, for electron detection 77—14312
- needle counter, small size low-level 80—58075
- nuclear excited states, 10^{-10} to 10^{-6} s, lifetime meas. by time spectrometer system 79—31313
- particle detectors, microprocessor-controlled data acquisition system for temporal/angular correl. between β- and γ-ray emission *(Spanish)* 80—106238
- particulate contamination monitoring, recent developments 80—57985
- personnel dosimeters based on film badges and TLDs, appl. *(Russian)* 78—20293
- plastic scintillator survey meter for directly absorbed dose meas. *(Japanese)* 80—848
- pocket Geiger counter for β detection *(Spanish)* 80—14051
- positron annihilation, spatial factors 77—54396
- positron detection, using Penning trap 78—21812
- Q_{β} value determ. from endpoint energies of β-spectra 80—27864
- Q-values of β^{-} decay, rapid meas. from electron and gamma energy decays 80—78220
- radioactive plume in atmosphere, depletion calc., and exposure from deposited activity 79—66561
- radioisotope thickness gauge, beta particles deflection by magnetic field 77—79054
- real-time environmental α-β-γ radiation monitoring system 78—94152
- retro-dispersion, coating thickness meas. appl. *(Spanish)* 78—12672
- scintillation β-spectra, nucleus identification 79—26805
- scintillation coordinate sensing detector, space and time resolution meas. 77—6621
- scintillation counting of ^{90}Y(^{90}Sr), improved method with reusable phosphors 78—9024
- scintillation quenching curves, solns. by second-order polynomial regression 77—3220
- 4π scintillation system for low activity beta counting 77—65405
- seawater density determ., possible use of beta-emitting radioisotopes *(Russian)* 78—65423
- SEM autoradiography for location and study of microscopic β-active particles 77—57425
- soil and vegetation, surface β-activity caused by nuclear explosion products, depend. on isotope vertical migration 78—86700
- solid sample activity meas., use of plastic scintillator in liq. scintillation counter 77—88333
- source deposit uniformity, meas. techniques 79—26792
- stack gas monitor, β scintillation detector+Ge(Li) detector system, environmental γ dose *(Japanese)* 79—3246
- surface barrier detector for beta dosimetry 80—57973
- survey meter for meas. of absorbed dose rate independently of energy 80—106203
- telemetric system, with external storage, for detect. of radionuclide tracers in humans 77—12995
- thick sample total counting, review 79—36488
- thickness gauge, ^{14}C β-ray, for measurement of target foil thickness 79—26030
- TLD evaluation of internal beta-dose rate for archaeological dating 80—98478
- transition and synchrotron radiation, electron and particle discrimination 77—10568
- ultra-thin bonded TLD for skin dose meas. complying with ICRP recommendation 78—92709
- wholebody autoradiography, B-radioluminescence method for tritium detection 77—52945
- β-ray point source dosimetry using variable cavity chamber, appl. to protection instrument response 80—13942
- e-γ delayed coincidences using magnetic lens spectrometer and Ge(Li) detector 79—710
- (n,γ) total cross sections of 14 MeV neutrons, from activated nuclei β-ray counting 79—3156
- ^{A}Ar, A=37,39, simultaneous activity meas. 80—23270
- ^{14}C counter system using proportional counters of plastic scintillator 77—60491
- ^{14}C dating, apparatus for β-counting 79—80048
- ^{14}C, influence of quenching on the background of liquid scintillation counters 79—18082

beta-ray detection and measurement continued
- ^{14}C meas. in proportional counter, continuous examination of counting efficiency 78—58548
- ^{14}C, multiwire proportional counter for low-level counting 79—6800
- CaF_2(Eu) and NaI(Tl) scintillators in phoswich config., low background β counting 78—37521
- CaF_2(Eu) Phoswich detector, evaluation for ^{90}Sr in situ anal. 80—58067
- $CaSO_4$:Dy Teflon TL dosimeters, thin, development for β-dosimetry in personnel monitoring 80—63399
- $CaSO_4$:Dy Teflon TLD discs, graphite-mixed, for beta dosimetry 77—86639
- $CaSO_4$:Tm composite TLD for γ-rays, X-rays, β-rays, and thermal neutrons 78—28076
- ^{109}Cd nuclear transformation rate meas. using 4π proportional counter 78—21826
- ^{252}Cf fission fragment β-decay, X-ray-β particle coincidence technique 80—74094
- ^{137}Cs decay determ. appl. 79—26397
- Ge detector, in supercond. solenoid, iterative technique for detector distorted data anal. 79—13583
- Ge detectors, use at low temps. 77—65398
- Ge radiation detectors, recording power at 4.2K 77—67936
- ^{76}Ge double beta decay expt., Monte Carlo evaluation 79—49892
- ^{3}H counting efficiencies and sample time stabilities in a Triton X-100/toluene scintillant 80—52813
- ^{3}H, influence of quenching on the background of liquid scintillation counters 79—18082
- ^{3}H-filled glass microspheres, assay by liquid scintillation counting 80—63481
- ^{129}I coincidence counting, efficiency extrapolation technique, methane 4π counter efficiency 77—88354
- ^{131}I in milk, extreme low level determ. 78—92703
- ^{85}Kr conc. determ. at high pressures using β-ray count, CaF_2 scintillation counter activated with Eu 78—13385
- Ne flash tube chambers for electron and photon detection 78—58552
- ^{144}Pr, effect of maximum β energy on colour quenching of Cherenkov radiation *(Spanish)* 79—76268
- Pu-Am survey instrument, β-α-γ-X-ray scintillation detect. probe 78—33376
- ^{74}Rb, Z=N nuclide, superallowed beta decay meas. 77—22952
- Si surface-barrier detector in lava or teflon housing, production 78—17481
- Si:Au use in weakly absorbed nucl. radiation detectors 77—67947
- Si(Li) detectors, unfolding procedure for slowly varying pulse height spectra of β-particles 78—50430
- ^{90}Sr-^{90}Y beta source absorbed dose, thermolum. dosimetry, appl. to dating 77—90911
- T in water, flow cell type detector for continuous monitoring in high γ-background 78—82524
- T monitoring with proportional counters 80—27874
- ^{204}Tl, effect of maximum β energy on colour quenching of Cherenkov radiation *(Spanish)* 79—76268
- U activity, liquid scintillation counting 80—27873
- ^{88}Y solution, standardisation using efficiency extrapolation method, β-γ coincidence meas. 78—21832

beta-ray effects
- *see also electron beam effects*
- aerosol particle charging using beta sources, elect. and mag. fields 79—36429
- alloys, effective atomic number from β-ray produced bremsstrahlung meas. 78—22046
- beta-rays from ^{14}C, biological hazards, cell killing effects, E. coli expts. 80—89805
- blood plasma antiheparin activity changes after irradiation 79—57717
- bone marrow of Indian desert gerbil, effects of ^{45}Ca 80—45971
- carcinogenesis, beagle dogs exposed to ^{226}Ra and ^{90}Sr 79—66487
- cell survival dependent dose rate effects, radiation carcinogenesis theory 79—11973
- chromatographic support materials decomposition by ionising radiation *(German)* 78—92587
- death due to inhalation of β-emitters, probability estimation 80—89801
- dielectrics, fast electron effects, space charge build up, range reduction 77—72636
- dosimetry, dose function calc., eye applicators 77—60260
- E. coli, damage induced by T decay, secondary lethality under nongrowth conditions 80—104654
- E. coli B_{s-1}, response to tritium-β particles rel. to 7 MeV electrons 79—57714
- goose barnacle, effects of tritiated seawater on development 79—66486
- liver, giant cell formation after ^{45}Ca administration, desert gerbil 79—92299
- liver, mouse, effects of tritiated water 79—57719
- lung irradiation, beagle dogs, early damage indicators 80—17018
- lung tumourigenesis from particulate sources of ^{147}Pm β-radiation 80—72247
- mesenteric blood vessels, response to β-irrad., mouse expts. 80—36009
- optical purity origin in living beings, effects of β-decay 78—40459
- ovary of fetal mouse, effect of ^{90}Sr rel. to time administered during pregnancy 80—51163
- prenatal brain development, effects of chronic ingestion of ^{3}HOH, rat expts. 80—36004
- pulmonary collagen turnover after β-emitting radionuclide inhalation 79—25049
- radioactive waste, Magnox, development and radiation stability of glasses for vitrification 77—61554
- skin, pig, response to ^{137}Cs-irrad. 80—67161
- skin, radiation fibrosis after β-irrad. and attempt at suppression, guinea pig expts. 80—72243
- skin, senescent, increased susceptibility to β-irrad., mouse obs. 80—104656
- sodium aluminium tartrate, β-particle effects on crystallisation from aq. solns. 77—36387
- spent fuel, bremsstrahlung spectra and average energies, analytic calc. method 80—22985
- spleen of Indian desert gerbil, ^{45}Ca injection 80—8106
- superlinear filling of traps in crystals due to competition during irradiation 79—33850
- thymus of Indian desert gerbil, ^{45}Ca injection 80—8106
- toxic air ion effects due to tachyon magnetoelectric dipoles and beta rays 80—35999

beta-ray effects continued
α-autoradiography of irrad. nuclear fuel, effect of β radiation *(German)* 78−78466
Al bremsstrahlung, β generated, spectral shape depend. on target thickness 78−56545
Al, bremsstrahlung from β-rays in thick target, 30-1300 keV 79−83049
Al-SiO$_2$-Si structures, on fast surface states and space charge 77−55610
Ar, condensed, luminescence decay under α- and β-particle excitation 79−38678
^{137}Cs-irradiation, fractionated high dose-rate and continuous low dose-rate effect on pig skin 80−41127
Cu, bremsstrahlung, β generated, spectral shape depend. on target thickness 78−56545
^{3}H low-dose β-ray relative biological effectiveness 80−12190
^{85}Kr source, use for liq. phase radiation chem. 77−60091
LiF, dosimeter material, thermolum. non-linear response to sequential irrad. at different dose rates 79−1793
Pb, bremsstrahlung, β generated, spectral shape depend. on target thickness 78−56545
Sn, bremsstrahlung, β generated, spectral shape depend. on target thickness 78−56545
Sn-Pb composition anal. of PCBs using beta-backscatter gauge 80−16631
T_2, solid, radiation-catalyses ortho-para transition 79−73832
^{204}Tl β-particle excitation of external bremsstrahlung spectra from thick targets 80−84797

beta-ray polarisation
electron source, high intensity polarised, illum. of GaAs with polarised light 77−38520
natural beta-decay, rel. to origin of biological chirality 77−86445
polarised electron source PEGGY at SLAC 77−38519
$\mu^+ \rightarrow e^+ \bar{\nu}\nu$, pol. meas. 80−73760
^{210}Bi β-decay, longitudinal polarisation of electrons at 900 keV, precision meas. 77−71592
^{68}Ga decay, positron polarisation, precision meas. using new polarimeter 77−46144
^{3}H β-polarisation at low vel., C_V'/C_V and C_A'/C_A 77−10369
^{147}Pm, emitted β-ray polarisation 79−85412

beta-ray scattering *see beta-ray effects; collision processes; energy loss of particles; particle backscattering; potential scattering; transport processes*

beta-ray spectra
see also beta-decay theory
average beta-particle energies and spectra, accurate approximations 77−50087
background radiation, energy distrib. rel. to vessels for liq. scintillation spectrometers 77−26920
backscattering from thick targets 80−32567
complex, meas. and processing *(Rumanian)* 80−9451
complex, processing method, 'Betarz' programme 78−41884
cylindrical-mirror electrostatic analyser for electron spectroscopy of beams 80−63446
fission product β-ray mean energy calcs. *(Russian)* 78−561
fission product ENDF/B data, processed, rapid spectral and decay heat calcs. 79−67797
fission products, short lived, light, beta decay energies using online mass separator 78−8783
fission products of ^{235}U(n,f) in secular equilib., theoretical β-spectra 80−500
fission products of ^{252}Cf, masses, β decay energies, halflives, He jet TOF mass spectrometer 77−23355
nuclear magnetic moment determ. of recoil nuclei polarised by fast polarised beams 77−28502
odd nuclei, matrix element determ., spectra shape 79−6508
sheet material surface density nonuniformity, effect on energy spectrum 77−77717
β-decay, radiative corrections 77−38249
^{A}Ag, A=97, 98 and $99^{g,m}$ decay spectral meas. 78−93976
As, β-decay energies and masses, A=80, 81, 83 77−74808
^{206}At$\rightarrow$^{206}Po, EC-β^+ decay, Po excited levels 77−79340
^{12}B, beta-spectra reanalysis, shape-factors and CVC theory 77−67724
^{12}B, hyperfine interactions in Mg, decoupling by external mag. field 77−24756
^{12}B, meas. of weak magnetism term in β spectra 78−4917
^{90}Br, experimental Q_β-values 78−93974
^{14}C, energy distrib. rel. to vessels for liq. scintillation spectrometers 77−26920
^{143}Ce, 1404 keV beta transition, spectral shape, ^{143}Pr 57 keV state 78−74339
^{143}Ce, shape of 1110 keV β transition to ^{143}Pr 351 keV level, spin, parity 77−50085
^{144}Ce, $0^- \rightarrow 0^+$ beta transition spectral shape anal. 77−38246
^{252}Cf fission fragment hard β-radiation 79−45306
^{252}Cf spontaneous fission, fission product β spectra *(Russian)* 80−91204
Cs isotopes, short-lived, determ. of nucl. spins by β radiation detected optical pumping 78−37262
^{A}Cs, A=139-144, beta endpoint energy measurements 78−93975
^{119}Cs, spin of neutron deficient nucleus by β radiation detected optical pumping 78−8782
^{152}Eu, K-forbidden beta transition, spectral shape anal. 78−74335
^{154}Eu, $3^- \rightarrow 2^+$ β transition, shape anal. 77−30516
^{20}F, β-decay, recoil-order matrix elements 77−79337
^{20}F β-spectra, cf conserved vector current predictions 78−50131
^{20}Fe, β-γ directional correlation, second class current 78−50127
Ga, β-decay energies and masses, A=76-79 77−74808
^{72}Ga$\rightarrow$^{72}Ge, gamma and beta-ray spectra, intensities, branching ratios, spin and parity assignments *(Korean)* 78−50128
Ge, β-decay energies and masses, A=79, 80 77−74808
^{3}H, β-spectrum meas., refining of upper limit of $\bar{\nu}$ rest mass 78−17144
^{166}Ho, beta decay 77−6310
^{A}In, A=104, 106, β-decay half lives and decay schemes 78−74333
^{192}Ir β decay into ^{192}Pt 4^+ and 3^+ levels, spectral shapes, ground state parity 77−50086
^{194}Ir, spectral shapes of $1^- \rightarrow 2^+$ and $1^- \rightarrow 0^+$ beta transitions 77−30515
^{38}K^m, β and γ spectra meas., determ. of isomeric ratios *(Russian)* 77−74771
^{93}Kr, experimental Q_β-values 78−93974
^{7}Li, liq., nucl. spin-lattice relax. of β-emitter ^{8}Li 77−51985
^{177}Lu decay, beta spectral shapes 78−74337
^{12}N, beta-spectra reanalysis, shape-factors and CVC theory 77−67724
^{12}N e^+ energy spectra, CVC hypothesis and weak magnetism 77−54190

beta-ray spectra continued
^{12}N, meas. of weak magnetism term in β spectra 78−4917
^{20}N, β-decay, recoil-order matrix elements 77−79337
^{103}Nb, experimental Q_β-values 78−93974
^{147}Nd, beta spectrum, hard component 80−22769
^{142}Pr, $2^- \rightarrow 2^+$ β spectrum, shape meas. 77−50083
^{144}Pr, 935 keV beta transition, spectrum shape 78−4918
Rb isotopes, short-lived, determ. of nucl. spins by β radiation detected optical pumping 78−37262
^{A}Rb, A=88-94, beta endpoint energy measurements 78−93975
^{76}Rb, spin of neutron deficient nucleus by β radiation detected optical pumping 78−8782
^{186}Re$\rightarrow$^{186}Os beta decay *(Rumanian)* 78−82316
^{109}Rh, half-life and decay props. 78−25154
^{221}Rn, decay scheme, α-, β-, γ-spectra meas. 79−6507
^{122}Sb$\rightarrow$^{122}Te second 2^+ excited state, β-γ ang. correls., β-ray spectrum shape 77−38250
^{132}Sb, doubly closed shell nuclide, β-spectra, total binding energy determ. 77−50046
^{A}Se, A=85, 86, experimental Q_β-values 78−93974
^{132}Sn, doubly closed shell nuclide, β-spectra, total binding energy determ. 77−50046
^{79}Sr, mass excess values from beta and gamma spectra from ^{32}S+^{54}Fe(^{58}Ni) 80−63137
^{103}Tc, experimental Q_β-values 78−93974
^{204}Tl, beta-transition, spectral shape, small-order deviation 78−74338
^{235}U fission ^{235}U products, β-spectra and total β-energy 78−25158
^{235}U(n,f), thermal, fission product decay spectra calcs., comparison with expt. results 79−93674
^{A}Y, A=82, 83, mass excess values from beta and gamma spectra from ^{32}S+^{54}Fe(^{58}Ni) 80−63137
^{167}Yb$\rightarrow$^{167}Tm mass difference, from positron spectrum, level transition branching ratio 79−6376
Zn, β-decay energies and masses, A=75-78 77−74808

beta-ray spectrometers
see also beta-ray spectra; electron spectrometers
$4\pi\beta$(CP)-γ coinc. counter for radioactive source calibration 77−38545
book, development of magnetic β-ray spectroscopy 77−61647
combination intermediate-image magnetic plus Si(Li) electron spectrometer for in-beam experiments 79−31308
complex spectra, meas. and processing *(Rumanian)* 80−9451
delay line for position readout in wire chambers 80−18757
differential ionization chamber for the determination of small differences in decay rates of beta emitters 79−76256
double focusing $\pi\sqrt{2}$ spectrometer, Fe-free, spectral distortion 79−26810
double focusing crossed field electron spin polarimeter, theory, construction, and operation 78−86761
double tube electron optics, slow electron preliminary accel. 77−23356
double-focusing electron spectrometer, new effective transmission determ. from focalization props. 78−17463
electron spectroscopy, reln. to EM isotope separation 77−23329
electrostatic prism design, exact eqns. 77−27239
fission products, short lived, light, beta decay energies using online mass separator 78−8783
Ge, hyperpure, β end-point-energy meas. 78−78587
high resolution beta spectrometer, BILL, optimal demagnetisation 77−23354
hybrid spark chamber for radioisotope distrib. meas. 78−46227
immersible Si Li-drift alpha- and beta-radiation detector, fabrication 77−65386
internal pair transition ion beam studies, combined mag. lens plus Si(Li) spectrometer 80−74073
internal target β-spectrometer with transport solenoid, background suppression, luminosity increase, (n,e) studies 77−6612
International Committee for Radionuclide Metrology, report 77−23357
liquid scintillation counting of aqueous and non-aqueous samples, solgel characts. 77−38546
liquid scintillation spectrometers, vessels 77−26920
magnetic, processing method for complex spectra 78−41884
magnetic, response function correction 78−74532
magnetic analysis of charged particles, α-, β- and mass spectrometers *(Russian)* 80−87011
magnetic electron spectrometers and their in-beam use, review 79−68128
magnetic lens, adjustable current-supply stabiliser 78−74528
magnetic lens coinc. spectrom. with reduced spherical aberration 77−10529
magnetic lens spectrometer and Ge(Li) detector combined apparatus for e-γ delayed coincidences 79−710
multistrip β semicond. detectors for magnetic spectrometers 78−78545
nuclear excited states, 10^{-10} to 10^{-6} s, lifetime meas. by time spectrometer system 79−31313
plastic scintillator, Q_β value determ. from endpoint energies of β-spectra 80−27864
position sensitive proportional counter for a β-ray spectrom. 78−86732
pulse-shaping cct. for low background scintillation spectrometer with compound detector 80−23243
scintillation β-spectra, nucleus identification 79−26805
scintillation counting using polyethylene mini-vials, construction of permanent standards 77−38550
short lifetime meas., β-spectrometer, plastic scintillator, effects of light guide and mag. field *(Japanese)* 78−90016
standard spectrometric source conversion peak half-width determ. 77−79499
β-γ-γ coinc. spectrom. using GM-Ge(Li)-Na(Tl) counter combination 78−46210
e-γ coincidence spectrometer 77−23390
Fe-free coil arrangement for spectrom. with azimuth depend. field 78−17470
Ge detector, in supercond. solenoid, iterative technique for detector distorted data anal. 79−13583
Ge detector in superconducting solenoid, semi-empirical beta-ray response function 79−13584
Si, detector response functions for radioisotopes complex β spectrometry *(Slovenian)* 78−21802
Si detectors, high resistivity p-type, for β-ray and X-ray spectrometry, advantages 77−88329
Si(Li) detectors, unfolding procedure for slowly varying pulse height spectra of β-particles 78−50430
Si(Li) electron spectrometer on-line with an automatic irradiation apparatus 78−90014

beta-rays
- *see also electrons*
- radiation chemistry research, β source laboratory apparatus 79—34340

beta spectrometers *see beta-ray spectrometers*

betatrons
- bremsstrahlung energy flux unit, 0.8 to 8 pJ, USSR special standard 77—30730
- bremsstrahlung field shaping apparatus for teletherapy 78—57062
- bremsstrahlung radiation, ang. distrib. and penetrating power 78—70657
- charge equations of motion in perturbation theory quadratic approx., betatron oscills. 80—37661
- circulating electron current meas., ionisation method *(Russian)* 78—5069
- comparison circuit for energy varying and stabilisation 77—6581
- current pulse generator, to direct prolonged burst of betatron-accelerated electrons onto target 78—5072
- design and performance of 5 MeV betatron, X-ray prod. 80—63421
- dose field monitoring by independent detectors in cassette 77—81578
- dynamic measurement of radial dimensions of electron beam *(Russian)* 78—13359
- electromagnet pulsed power supply 78—82546
- electron beam injection, expt. 78—5076
- electron beam injection, inflectorless system 78—825
- electron beam parameter measurement by determining ionisation of residual gas 79—97915
- electron beam structure, determ. via synchrotron radiation 77—65368
- free electron devices for light prod., history, book contrib. 79—27147
- gamma bremsstrahlung from thin target 80—86999
- improved PMB-6 78—46194
- injector, with field emission cathode for betatron 78—5064
- ion beam focusing and acceleration by high electron currents in betatron *(Russian)* 77—6601
- magnetically excited, enhanced electron energies 80—86998
- NDT application in industrial products inspection 80—81267
- NDT flaw detection, signal-processing algorithm 77—81375
- neutron dose levels of 8 MeV linear accelerator and 18 MeV betatron used in radiotherapy *(German)* 78—69221
- orbit expansion and beam extraction, simulation 80—91353
- oscillations, frequency shift in nonlinear mag. fields 78—1137
- photon beam fast neutron contamination obs. 79—59284
- pulsed, 2 MeV electron injector 78—824
- pulsed air cored betatron powered from magnetocumulative generator 77—67924
- radiation protection meas. 79—29636
- radiotherapy, 25 MeV, fast neutron component and patient dose 78—3592
- radiotherapy, dose levels due to neutrons 77—13008
- radiotherapy, secondary radiation from supervoltage accelerators rel. to patient protection 77—56471
- radiotherapy accelerator neutron leakage survey 80—51269
- radiotherapy accelerator primary beam neutron contamination 80—51268
- radiotherapy arc technique for total-body irrad. by 42 MV betatron 78—24134
- radiotherapy using high energy electrons *(Japanese)* 77—70544
- rapid extraction by parametric reson., analogue computer anal. 77—18731
- redundant solid-state controller 79—88163
- single-particle dynamics, linear theory of perfect machines 78—78879
- stochastic beam cooling expts., low-noise wide-band power amplifier system 80—58011
- stochastic betatron cooling, slot type pick-up and kicker 78—33332
- synchrobetatron resonances at SPEAR 77—83327
- synchrotron radiation depend. on betatron oscillation linear coupling 80—91345
- synchrotron radiation formation, role of betatron vibrs. *(Russian)* 78—50684

Bethe-Salpeter equation
- $\lambda\phi^3$, deep inelastic struct. functions for bound states, ladder approx. 79—35952
- $\lambda(\phi^6-\phi^4)$ bound state in weak coupling, Bethe Salpeter eqn. 77—5992
- $\lambda P(\phi)_2$ weakly coupled model, spectral props. and bound-state scatt. 77—22629
- $P(\phi)_2$ field theory, non-relativistic limit for two particle phenomena 78—16906
- bare Pomeron in four-dimensional quantum chromodynamics 79—336
- baryon matrix elements in hadronic weak decays, formulation for quark model 79—386
- charmonium and similar two fermion systems, effective Hamiltonian 78—21381
- coherent function of radiation source field in unbounded scattering medium *(Russian)* 78—1160
- composite system, relativistic, light-front wave functions 80—73592
- connected-kernel multifermion Bethe-Salpeter equations 80—32005
- crossed diagrams effect in Bethe Salpeter eqns. 77—2725
- deuterons, current conservation and off-shell effects with arbitrary interaction 79—45183
- dimensional continuation for relativistic bound state problems 77—18159
- Dirac one-body effective eqn. from Bethe Salpeter eqn. 77—54040
- dressed fermion bubble, real-space equivalent calcs. 80—101751
- dressed fermions in Abelian gauge theories 78—82093
- dressing the nucleon propagator, nested bubbles approx. in Bethe Salpeter eqn. 77—6032
- dynamical theory of quark confinement and hadron spectrum 77—82701
- eigenvalue, asymptotic expansion, weak binding approx. of Wick-Cutkosky model 79—2925
- electron conductivity in random pot., diffusive mode existence 79—65421
- electron deep inelast. scatt. processes, Ward identities, struct. functions *(Chinese)* 79—93431
- exact three dimens. reduction, off mass shell amplitudes 78—70247
- fermion+vector gluon systems, Bethe-Salpeter eqn. 77—13868
- fermion pair with instantaneous interactions, relativistic bound-state equations 80—13200
- fermion-antifermion bound states, deep inelastic struct. functions, ladder approx. 79—35952
- gauge theory, dressed quark-gluon vertices, instantaneous approx. 78—78091
- hyperfine struct. in relativistic fermion-antifermion system 77—71432
- integral transform and relativistic radial eqns. 80—4835
- IR singularities, spin $^1/_2$ quark confinement in three dimens. 79—337

Bethe-Salpeter equation continued
- IR singularity quark confinement model, coloured bound state absence 79—338
- Klein paradox absence 80—27384
- ladder approximation with effective propag. and vacuum stability, Bethe-Salpeter bound state 80—47168
- Lagrangian bound state formalism, dynamical vacuum instability 78—74146
- light cone behaviour of pion Bethe Salpeter wave function in ladder model 77—18176
- lightlike wave function and wave eqn. on null-plane using Bethe Salpeter eqn. 78—41412
- Lorentz deformation of Bethe-Salpeter eqn. 79—54246
- massless chromodynamics, vacuum rearrangement 78—70327
- meson bound state eqn. and solutions 78—78101
- meson decay; weak, EM, strong, Bethe-Salpeter model, effective quark mass 78—70336
- meson mass spectrum, planar bootstrap, and Regge approach 80—22581
- meson quark relativistic model with instaneous interaction, spectra, mag. moments 77—61255
- meson structure wave functions, instantaneous interaction approx. straton+antistraton pair *(Chinese)* 77—10216
- meson structure wave functions in relativistic straton model, Bethe-Salpeter eqn. *(Chinese)* 78—50011
- meson theory with internal coords., Dirac eqn., Bethe Salpeter eqn., quark model 77—13937
- meson wave functions, spinor struct., inter-straton potentials 79—12969
- meson wave functions, straton model, Bethe-Salpeter eqn., SU_6 symm. *(Chinese)* 77—34125
- mesonic Bethe-Salpeter eqn. for different mass straton and antistraton, SU(4) mass relations *(Chinese)* 79—58934
- mesons, bound state wave function, probability interpretation, form factors, Bethe-Salpeter eqn. *(Chinese)* 80—101930
- modified Bethe-Salpeter equation from the matrix Pade approximants 79—93286
- multiperipheral cluster model based on Bethe-Salpeter eqn., comparison with pp and π^-p data *(Russian)* 77—10230
- numerical soln. to spinor Bethe-Salpeter eqn. and Goldstein problem 78—86400
- one particle lines, partial resummation for weak coupling cluster expansion 79—71589
- one photon exchange pot. in configuration space from Bethe-Salpeter eqn. 79—67527
- parton model and Bethe-Salpeter wave function 77—41820
- plasma two-particle bound state, lifetimes and level shifts 78—75265
- positronium, Bethe-Salpeter equation, Coulomb like kernel 78—93831
- positronium hyperfine splitting, anomalous contribs., radiation gauge 77—83771
- QCD, 2-dimens., IR structure, EM form factors and inelastic struct. functions *(Chinese)* 79—58935
- QCD, effective quark pot. in baryon reson. 78—16910
- QCD, parton distrib. function, transverse momenta, axial gauge ladder model 80—27467
- quantum chromodynamics, short distance Regge singularities, renormalised gluon ladder 77—49909
- quark theory with internal coords., Dirac eqn., Bethe-Salpeter eqn. 77—18224
- quark-gluon model, approx. soln. 77—54080
- quark-gluon model, approx. soln. of Bethe-Salpeter eqn. 77—41816
- quark-gluon model, eqn. soln. 77—87940
- quarkonia from charmonium and renormalization group equations 79—22055
- quasipotential eqn. derivation *(Chinese)* 80—68370
- reduction to equivalent Schrodinger eqn., appl. to muonium and positronium 79—2933
- relativistic Bethe-Salpeter harmonic oscillator 80—32006
- relativistic deuteron wave function *(Chinese)* 80—47411
- relativistic equation derivation and associated potentials from field theory 79—12954
- relativistic harmonic oscillator for spin-1/2 particles in the Bethe-Salpeter formalism 80—91001
- relativistic radial equations following from the Salpeter equation, leptonium and quarkonium 79—63333
- relativistic radial equations for two spin-1/2 particles consistent with the hole theory 79—93272
- relativistic single-particle two-body bound-state integral equation, numerical solutions 80—52389
- relativistic two-electron atom, level shifts, transition probabilities, perturbation theory 79—22001
- scalar equation solns., self energy diagram effects 80—86590
- scaling in bound state models 77—38181
- scaling reconstruction using renormalisation group, Callan-Symanzik eqn., $\phi_6{}^3$ theory *(Russian)* 80—42351
- scattering states arising from Bethe-Salpeter eqn. 78—54553
- short distance behaviour of Bethe-Salpeter amplitude, renormalisation constant relation, bound states 79—49387
- soliton, quantised 78—32985
- solution in ladder approx., self energy diagram effects *(Chinese)* 80—52425
- spinor-spinor Bethe-Salpeter eqn. 78—29238
- spinor-spinor Bethe-Salpeter eqn. spherically symm. solns., gauge depend. 77—10176
- spontaneous symmetry breaking in chain approx. 77—5998
- three-dimens. reduction of Bethe-Salpeter eqn. 78—29260
- two fermion EM bound state systems, axial and covariant gauges 78—78058
- two-nucleon system, isobar configs., relativistic model 77—41894
- two-particle system in QED, Dyson-Schwinger eqn. 79—2962
- vacuum instability in massless electrodynamics, Bethe-Saltpeter eqn. tachyon solns. *(Russian)* 79—12993
- Ward identities and Bethe-Salpeter equations, meson and baryon EM current transition matrix *(Chinese)* 79—63375
- wave function asymptotic behaviour as relative time$\rightarrow\infty$ *(Chinese)* 78—82113
- wave function divergence at origin 78—74147
- Wick equation soln. *(Chinese)* 77—71435
- Wick-Cutkosky model, asymptotic behaviour of eigenvalues for large principal quantum no. 77—10177
- Wick-Cutkosky model, eigenvalue refl. symmetry 77—61193
- Yang-Mills theory, tachyon bound state and vac. instability 78—29244
- d, elastic form factor calcs. with Bethe-Salpeter eqn. 79—67554

- **Bethe-Salpeter equation** continued
  - D^+-D^0 mass difference, Bethe-Salpeter eqn. calc. 77−26525
  - e^+e^- inclusive annihilation, leading logarithm sum for struct. functions in QCD 79−71735
  - $\eta^0 \to \gamma + (e^+e^-)$, EM bound states, approx. Bethe-Salpeter wave function *(Chinese)* 80−42448
  - $\eta^0 \to \gamma + (\mu^+\mu^-)$, EM bound states, approx. Bethe-Salpeter wave function *(Chinese)* 80−42448
  - $K \to 2\pi$, decay amplitudes in $SU(2) \times U(1) \times U(1)$ model with new neutral current 80−4986
  - $K \to \pi^+\pi^-e^+\nu$ decay form factors, relativistic quark model 77−38160
  - KN scatt., Blankenbecler-Sugar multichannel eqn., $J={}^1/_2$ partial wave soln. 78−37230
  - $N\bar{N}$ annihilation diagrams, simple model, nonperturbative calcs. 79−67578
  - NN elastic scatt. with one boson exchange, Bethe-Salpeter eqn. 80−42485
  - NN I=1 scattering with one boson exchange, Bethe Salpeter eqn. 77−57455
  - NN interaction, coupling const. singular points for approx. eqns., with nonlocal pseudopotential 78−25062
  - NN potential, meson field theory two-pion exchange anal. 77−208
  - $N\bar{N}$ quasinuclear states and the Bethe-Salpeter equation 79−13212
  - NN scattering, effective interaction in the Blankenbecler-Sugar equation in ϕ^3 theory 79−21914
  - ν, charmonium and strangeonium, linear+Coulomb pot. study, high αs regime 80−62935
  - π EM form factor, large-Q^2 behaviour 77−6002
  - π form factors, in QCD, light cone Bethe-Salpeter eqn. soln. 79−80827
  - π struct., confinement scheme, Bethe-Salpeter wave function 78−45841
  - $(\pi^+\pi^-)$s atoms, relativistic covariant B-S wave-function *(Chinese)* 79−81308
  - qqq confinement, by infrared singularities 79−36028
  - $V \to 3P$, vector meson hadronic decay widths in Bethe-Salpeter model 79−58955
  - Cl, multiply-ionised, radiative electron capture on impact with Ca and Ni foils 77−6916
  - $H+H^+$, nuclear repulsion, contrib. to charge transfer 80−18922
  - ^{3}H binding energy, relativistic calc., Bethe Salpeter eqn. 80−68519
- **Bethe-Uhlenbeck equations** *see quantum statistical mechanics*
- **bevatrons** *see synchrotrons*
- **bicrystals**
  - α/β brass, bicrystal, dynamic obs. of fracture phenomena 79−5040
  - α-brass, bicrystal, grain boundary fracture at intermediate temp. *(Japanese)* 79−15774
  - β-brass, bicrystal and tricrystal stress strain behaviour 77−36607
  - brass, inface segregation in α/β two phase bicrystal *(Japanese)* 79−15675
  - α-β brass, interface segregation 80−89231
  - α-brass, stress corrosion cracking in single and bicrystals 77−4866
  - brass, two phase α/β bicrystal, transgranular slip and fracture across an interface 80−81150
  - α-β brass, two phase bicrystal, deform. and fracture at 450K 80−16409
  - α-β brass, two phase bicrystal, fatigue 80−108520
  - brass, two-phase α/β, diffusion induced twins in α-phase 79−46967
  - brass, two-phase α/β, morphology and crystallographic relationships between phases 79−46966
  - α-β brass, two-phase bicrystals, plastic deform. and fracture mechanism 78−84898
  - brass α-β two-phase bicrystals, interface sliding studies 80−54248
  - β-brass bicrystals, shear-incompatible, grain boundary contrib. to Bauschinger effect 80−97550
  - α/β-brass bicrystals, two-phase, with nearly uniform and thermodynamic equilib. concs. 80−65383
  - brass bicrystals, two-phase (α/β), interphase boundary sliding at high temperature 80−88164
  - α-β brass two-phase bicrystals, activated slip systems during yielding 78−84911
  - dislocation arrays at interfaces, stress fields 79−99432
  - elastic incompatibility stresses *(Japanese)* 80−107361
  - electrical conductivity versus interatomic bond character 80−59948
  - electron diffraction spots, computer indexing *(French)* 78−75507
  - electron diffraction theory 80−75122
  - FCC polycrysts., under hydrostatic pressure 80−107356
  - film, grain boundary electromigration, low temp. theory 77−31799
  - film/substrate interface, misfit dislocation obs. using electron microscopy 80−103605
  - grain boundary anal. using TEM 79−28003
  - grain boundary sliding and intergranular fracture 78−75717
  - ice bicrystal, anisotropy of migration and faceting of grain boundaries 79−60381
  - jimthompsonite and anthophyllite from Swiss Alps, disordered intermediate minerals imaging 80−72518
  - metal, mech. behaviour, continuous theory of dislocations appl. 78−67717
  - metallic, residual resistance theory, diffusivity, disorientation effects *(Russian)* 80−49875
  - metals, FCC, (001) twist boundaries symmetry and struct. 79−82242
  - near-coincidence twist boundaries, electron diffr. obs. 79−90675
  - oriented, sintering prod. technique 80−108371
  - poly(ethylene-oxide), isothermal growth, thickening, melting, bilayer crysts. and chain end effects 80−38939
  - semiconductor, charge carrier interface recomb., photocond. meas. method 79−99431
  - semiconductor, Poole-Frenkel effect, grain boundary barriers 79−11137
  - symmetry and interfacial struct. 80−2274
  - TEM, three zone axis method, indexation of diffusion patterns, grain boundary characterisation *(French)* 79−99038
  - thin film, dislocation interaction, with grain boundaries during plastic deform., electron microscopy technique 80−54281
  - vibrational props., different-interface phonons and low-temp. sp. ht. 77−76656
  - Ag foils, polycryst. and bicrystals, grain boundaries, ^{119}Sn Mossbauer anal. 80−7229
  - Ag, oriented bicrystal, sintering prod. technique 80−108371
  - Ag, thin-film bicrystals, planar lattice defects and migrating grain boundaries interaction 80−79835
  - AgCl, grain boundary slip simulation 78−3176
  - AgMg two phase bicrystal growth, orientation, interface struct. 80−60773
- **bicrystals** continued
  - Al, [011] low angle tile boundaries, high resolution electron microscopy 80−34012
  - Al, bicrystal, $\langle 100 \rangle$ oriented, plastic deform. 78−19812
  - Al bicrystal, estimation of grain boundary torque 77−7736
  - Al, bicrystal, fatigue crack initiation, crystal boundary effects *(Japanese)* 78−92328
  - Al, bicrystal, fatigue crack initiation along crystal boundaries *(Japanese)* 79−70163
  - Al, bicrystal, liquid metal induced grain boundary fracture, relative orientation effects 77−36690
  - Al bicrystal, migration of special $\langle 110 \rangle$ tilt boundary 79−46670
  - Al bicrystal, plastically deformed, slip heterogeneities 80−79858
  - Al, bicrystal, varying purity, breakaway of grain boundary from adsorbed impurity 77−31678
  - Al, bicrystal having $\Sigma 7$ and $\Sigma 21$ coincidence tilt boundary, plastic deform. *(Japanese)* 79−66116
  - Al bicrystals, fatigue crack initiation, cryst. boundary effect 80−55537
  - Al bicrystals, isoaxial, fatigue crack initiation in grain boundary affected regions *(Japanese)* 80−89338
  - Al, cold rolled bicrystal, plane grain growth anisotropy 79−91686
  - Al, cutting of bicrystal to compare mechanism for large crystals and polycrystals *(Japanese)* 78−60871
  - Al, faceting of migrating $\langle 110 \rangle$ coincidence boundaries 79−46680
  - Al, faceting of migrating $\langle 110 \rangle$ coincidence boundaries 80−34013
  - Al, high resolution electron microscopy obs. of dislocations 80−103347
  - Al, isoaxial bicrystal, deformation behaviour, study by photoelastic coating and moire methods *(Japanese)* 78−11294
  - Al, isoaxial bicrystal, Moire investigation of mechanical behaviour 77−16647
  - Al, RF size effect at intercryst. boundary *(Russian)* 80−29431
  - Al, tensile and creep deform. obs. by holographic interferometry *(Japanese)* 77−56197
  - Al-Cu alloy, neutron irrad. effects on grain boundaries, intergranular fracture and precip. 77−48520
  - Au, bicrystal, thin, tilt boundary migration and facet development 78−2379
  - Au, bicrystalline thin films, faceting of [001] grain boundaries 80−70222
  - Au bicrystals, interaction of lattice dislocations with grain boundaries, electron microscope obs. 78−51579
  - Au bicrystals, struct. of grain boundaries using diffr. techniques 80−59478
  - Au, core structs. of misfit dislocations in grain boundaries, TEM 78−14360
  - Au, dislocation networks in twin boundaries, TEM obs. 78−51556
  - Au, epitaxially grown bicrystal on (001) Fe substrate, interfacial dislocation behaviour 77−51622
  - Au, epitaxially grown bicrystalline thin films, preferred inclinations of $\langle 100 \rangle$ grain boundaries 80−103367
  - Au, grain boundary thickness, meas. using X-ray techniques 80−34011
  - Au, large-angle twist grain boundaries, X-ray diffr. obs. 79−90672
  - Au, periodic $\langle 111 \rangle$ twist grain boundary structs., electron diffr. obs. 79−65100
  - Au, serration and dissociation of edge dislocations in low-angle tilt boundaries 77−72621
  - Au, thin film bicrystal, annealing twin form. by boundary dissociation 79−47729
  - Au, thin film bicrystal, diffraction effects from inclined grain boundaries 80−103362
  - Au, tilt boundary, small- and large-angle [001], X-ray diffraction study 79−82238
  - Au/AuPd, bicrysts., in situ relax. of interphase interfaces 80−39455
  - Au/Cu, initial epitaxial growth at room temp. 80−59829
  - Au/Pd, bicrysts., in situ relax. of interphase interfaces 80−39455
  - Au-Ag, bicryst. thin film couples, interphase interfaces, TEM 80−70540
  - Au-Pd, bicryst. thin film couples, interphase interfaces, TEM 80−70540
  - Bi-Sb, rearrangement of grid of nonconformity dislocations on (111) interface during heating 79−28215
  - β-brass, nonisoaxial bicrystal, simultaneous hardening and softening 77−36606
  - Cu, bicrystal, $\{110\}\langle 112 \rangle$, deform. *(German)* 77−48513
  - Cu, bicrystalline thin films, characterisation of [001] tilt boundaries 80−75473
  - Cu bicrystals, effect of grain boundary on tensile deformation *(Japanese)* 78−88495
  - Cu, cutting of bicrystal to compare mechanism for large crystals and polycrystals *(Japanese)* 78−60871
  - Cu, epitaxial, on (111) Au, periodic arrays of misfit dislocations, electron diffr. 78−51857
  - Cu, intergranular fracture 78−39883
  - Cu, oriented bicrystal, sintering prod. technique 80−108371
  - Cu, sintered single crystal on flat single crystal, energy misorientation relationship of grain boundaries 79−60377
  - Cu-Ni bicrystals, epitaxial growth, chemical interdiffusion, X-ray diffr. line profile anal. 79−1527
  - Cu-Ni bimetallic film, Moire patterns, interdiffusion effects 77−51621
  - Cu-Ni bimetallic films, dislocation wall form. during interdiffusion, TEM obs. 78−51856
  - β-Cu-Zn-Al pseudoelasticity 79−29126
  - Fe, bicrystal, vapour grown, statistical analysis of grain boundary angles 77−47470
  - Fe-Au (111) bicrystal films, misfit dislocations obs., for 500°C substrate temp. 77−51624
  - Fe-Au (111) interface, nature of interaction layer 79−99433
  - Fe-Si (3.5 wt.%), cutting of bicrystal to compare mechanism for large crystals and polycrystals *(Japanese)* 78−60871
  - GaAs-GaAlAs bicrystal struct., dislocation half-loops, nucleation and generation 79−95009
  - Ge bicrystal, cond., Hall effect and Shubnikov-de Haas oscills. 80−10984
  - Ge bicrystal cleavage plane, Shubnikov-de Haas oscills. *(Russian)* 78−64094
  - Ge bicrystals, [011] tilt boundary, grain boundary stability 79−82240
  - Ge bicrystals, high angle tilt boundaries, TEM *(French)* 80−70224
  - Ge bicrystals, low angle [011] tilt boundary 79−82239
  - Ge, conductive layer form. at bicrystal boundary *(Russian)* 77−39983
  - Ge, dislocation core structure *(French)* 78−26571
  - Ge, high resolution electron microscopy obs. of dislocations 80−103347
  - Ge, struct. of sessile Lomer dislocations *(French)* 77−55286

- **bicrystals** continued
  - Ge, two-dimensional electronic phenomena at He temp. *(Russian)* 79−56273
  - p-InP, prep. with pure tilt boundaries 77−81211
  - KBr, Ag^+ injection transport and grain boundary mobility, electrodecoration obs. 80−2214
  - LiF bicrystal, high-angle tilt boundary and edge dislocation intersection effects 80−79836
  - MgO bicrystals, formed by welding single crystals with H_3PO_4, exam. 78−56796
  - MgO, fracture mechanism obs. 77−44339
  - NaCl, grain boundary segregation, Au decoration obs. 77−68982
  - NaCl, surface charge meas. in ultra high vac. 80−20287
  - NaCl:Ca crystals, surface recrystn., moisture effect 80−84950
  - Nb, impact strength at 20° and −190°C *(Russian)* 80−45379
  - Nb, supercond., flux pinning by grain boundaries 79−24114
  - Ni, oriented bicrystal, sintering prod. technique 80−108371
  - NiO, ⟨001⟩ tilt boundary relative energy 80−29033
  - NiO, oriented bicrystal growth by floating zone and Verneuil's method *(French)* 78−92186
  - PbS-PbSe epitaxial bicrystals, direct scatt. of channelled He ions at dislocations 80−65110
  - Pd, epitaxial, on (111) Au, periodic arrays of misfit dislocations, electron diffr. 78−51857
  - W bicrysts., crack propag. across grain boundaries, crack speed meas. technique appl. 80−108575
  - Zn, $\langle 10\bar{1}0\rangle$ tilt, misorientation depend. of grain boundary sliding 80−15119
  - Zn, bicrystals, galvanomagnetic phenomena at common boundary, electric field potential distribution *(Russian)* 80−29388
  - Zn, compatible bicrystal, plastic deform. *(Japanese)* 78−31460
  - Zn, crack form. at grain and twin boundaries at low temp. *(Russian)* 80−66620
  - Zn, cutting of bicrystal to compare mechanism for large crystals and polycrystals *(Japanese)* 78−60871
  - Zn, diffusionless motion of grain boundaries, 200-405°C 79−19264
  - Zn, grain boundary detachment from adsorbed impurity, conc. depend. 78−2144
  - Zn, grain boundary slip in deform. 80−34008
  - Zn, incompatible bicrystals, effect of grain boundaries on mech. props. *(Japanese)* 78−39798
- **biexcitons** *see excitonic molecules*
- **big-bang theory** *see cosmology*
- **bimetallic strips** *see bimetals*
- **bimetallic wire** *see bimetals*
- **bimetals**
  - bimetal, high-speed steel + machine steel, chem. comp. influence on magnitude of residual stresses in cooling *(Russian)* 79−74183
  - bimetal Nb-steel Kh18N10T with Cu interlayer, cyclic heating effect 77−16687
  - bronze-steel, phase composition and struct. of diffusional interlayer in fusion zone, X-ray analysis 78−56821
  - contact unit, for liquid N_2 level monitor 80−57309
  - diffraction gratings, theoretical study 80−87525
  - diffusion couple, interdiffusion coefficients and phase width calc. 77−62685
  - explosively welded, dissipation of US oscillations at boundary layers 78−53124
  - explosively welded, US oscillation dissipation at boundary layer 78−53157
  - failure during fatigue testing, electron microscope obs. *(Russian)* 78−23808
  - interchangeable-scale switchboard meters *(German)* 77−82497
  - junction layer, low elec. resist. determ. method 79−49249
  - junctions, interface plasmon modes, theoretical anal. 80−54767
  - metal-metal contacts, positron diffusion, ang. distrib. of annihilation photons meas. 79−8207
  - plates, deflection meas. during high-temp. heating 78−7134
  - rolling, calc. of strains by variational method *(Polish)* 80−45323
  - static and fatigue strength, obtained by facing 77−90457
  - steel, alloy with austenitic stainless, H permeability 80−107572
  - steel, double-layer, adhesion strength determ. method 77−63857
  - steel bimetal, low-alloy austenitic ferritic stainless steel, fracture toughness *(Russian)* 78−35482
  - steel tube with internal Cu coating segmental specimens, tensile testing 79−70255
  - steel-Al bimetallic wire for overhead lines, manufacturing methods 80−16247
  - steel-Babbitt, exam. of structure of transition layer 79−100293
  - steel-bronze bimetal mech. props., diffusional interlayer effects 79−29169
  - steel-Cu M3, eutectic alloy, crack development, failure energy capacity *(Russian)* 80−40480
  - steel-steel, rolled plates, low-cycle fatigue in bending 79−91794
  - steel/Cu bemetallic pipe, determ. of yield, tensile strength 80−25771
  - steel/steel bimetal, creep-rupture strength in corrosive environment *(Russian)* 77−52533
  - thermobimetal, specific bending, effect of functional parameters and stabilizing heat treatment 77−89555
  - thermometer, contact, basic parameters *(Czech)* 78−12692
  - thermometer design principles *(German)* 77−49724
  - tube, residual stress after thermal cycling 77−90465
  - vacuum gauge, temperature difference type *(Japanese)* 80−13089
  - vacuum rolling at high temp. *(Russian)* 79−15708
  - van der Waals interaction in bimetallic junction 79−24048
  - welded joints, heterogeneous, metallographic anal., etcharts and etching regimes 80−40635
  - Al/brass/Al bimetal, three layers, formed by cold rolling, exam. of formation of intermetallic phases at interface 78−56658
  - Al/Cu thin film couples, TEM study of intermetallic nucleation at interface 80−65305
  - Al-Au bimetal thin film interdiffusion zone, intermetallic phase form kinetics, 70-160°C 78−75891
  - Al-Fe, O_2 effect on diffusion inhibition 77−89597
  - Au-Al thermocompressional contacts, diffusional zones, phase growth during annealing *(Russian)* 80−75389
  - CO_2 laser bimetallic mirror coating vacuum sputtering technology 80−35086
  - Cu-Ni, bimetallic film, exam. of diffusion by electrical resistivity meas. *(Russian)* 79−14970
- **bimetals** continued
  - Cu-Ni bicrystal, misfit dislocation config., moire patterns, interdiffusion effects 78−84110
  - Cu-Ni bimetallic film, Moire patterns, interdiffusion effects 77−51621
  - Cu-Ni bimetallic films, dislocation wall form. during interdiffusion, TEM obs. 78−51856
  - Cu-Ni evaporated thin film couple interdiffusion obs. 78−43187
  - Cu-Ni thin film couples, interfacial reactions, contact resistance meas. 78−63882
  - Nb-stainless steel bimetallic strip Cu interlayer struct. during thermal fatigue *(Russian)* 78−15498
  - Pt, on Au, crit. thickness of pseudomorphic film growth, substrate size depend. *(Russian)* 80−29286
  - Pt-Au bimetallic films, electron diffraction on networks of grain-boundary and interphase dislocations *(Russian)* 79−73168
  - Pt-Mo(Re), and Pt-(Re-Mo) bimetal sheet specimens, interdiffusion, 1500°C *(Russian)* 77−62683
  - Re-Mo bimetal sheet specimens, interdiffusion, 1500°C *(Russian)* 77−62683
- **binaries (stellar)** *see binary stars*
- **binary adders** *see adders*
- **binary sequences**
  - *see also number theory*
  - ferromagnetic linear chains of spin 1/2 particles, one-magnon states 78−14946
  - high-resolution blood flow imaging system using binary phase coded pseudonoise sequences 79−57703
  - peripheral auditory system, anal., noise appls. 78−80888
  - pseudorandom binary noise US correlation system for nondestructive evaluation 79−52612
  - signal processing, fibre and integrated optics techniques 77−27379
  - spread-spectrum signal optical processing 79−72518
  - underwater acoustic pulse compression system, signal processing methods 80−56630
- **binary stars**
  - *see also eclipsing binary stars*
  - 2A 0311−27 optical counterpart, identification and spectroscopic obs. 79−25762
  - 16 M⊙ supergiant with 1 M⊙ neutron star companion, double core evolution 78−53980
  - 20,986, new unresolved astrometric binary 78−57594
  - 61 Cygni A, wobble obs. possible massive planet partner 77−71131
  - HR 1099, RS Canum Venaticorum type binary, light and colour curve meas. 80−73004
  - Σ2173 (ADS 10598), improved definitive orbit 77−13400
  - A0620−00, transient X-ray source, intensity variations and evidence for 8 day period 77−13496
  - A0620−00, transient X-ray source, spectrophotometry 78−4400
  - 2A 0042+323 (3U 0042+32), periodic behaviour rel. to binary nature 78−54089
  - 2A 0311−227, AM Herculis type X-ray binary, optical counterpart, radial vel. obs. 80−94890
  - 2A 0311−227, complex emission line structure of spectroscopic binary 80−51915
  - 2 A 0311−227, IR flickering obs. 79−40298
  - 2A 0311−227, optical counterpart identification as AM Herculis type star 79−30149
  - 2A 0311−227 optical counterpart, high speed photometry 80−82547
  - 2A 0311−227 optical counterpart, light curve Fourier anal. 80−82549
  - 2A 0311−227 optical counterpart, possibly AM Herculis type white dwarf 79−35434
  - 2A 0311-227 optical counterpart, spectroscopic and photometric obs. 79−101222
  - 2A 0526−328 optical candidate, high speed optical photometry 80−51917
  - 2A 0526−328 optical counterpart, radial vel. meas. and orbital period 80−90579
  - 2A 0526−328 optical counterpart, spectroscopic obs. 80−77515
  - A 0535+26, transient X-ray source, flare obs. by (Prognoz 6) *(Russian)* 80−51920
  - ZA 0536−328, AM Herculis-like star identification confirmed 79−40296
  - 2 A 1052+606, X-ray and optical variability of RS CVn star 80−31331
  - A- and F-type visual binaries, uvbyβ photometry 79−21346
  - A-type central stars of planetary nebulae, radial vel. study 78−81629
  - absolute luminosity calibrations, consistency 80−62111
  - absolute magnitudes of stars in the same seven colour photometric box 78−28662
  - accreting compact object in binary system, magnetosphere theory, X-ray sources 80−46394
  - accreting main sequence stars, radii 77−17623
  - accreting neutron stars, nuclear burning and X-ray bursts 78−36724
  - accreting nonmagnetic degenerate dwarfs, X-ray and UV radiation 79−40184
  - accretion disc, polarisation effects in emission 79−35128
  - accretion disc inner region model *(Russian)* 78−69843
  - accretion disc interaction with stellar mag. field, plasma diffusion across Alfven surface 78−93461
  - accretion disc model for close binaries 78−4282
  - accretion disc models and cataclysmic variables, H line blocking of UBV colours 79−101155
  - accretion disc stability, viscosity and cooling mechanism effects 78−49476
  - accretion disc stability 77−29796
  - accretion discs, steady, optically thick, convective vertical energy transport 80−62112
  - accretion discs, turbulent energy transport 78−28661
  - accretion discs, viscosity determ. for Hercules X-1 and (SS 433) 80−62110
  - accretion discs *(Polish)* 78−89175
  - accretion discs in close binary systems, tidal torques 78−12296
  - accretion discs in X-ray binaries, structured coronae, model 79−48852
  - accretion discs theoretical photometric and spectroscopic props., cataclysmic variables appl. 79−80312
  - accretion disks, theoretical review *(Polish)* 80−26739
  - accretion disks round neutron stars and white dwarfs, flux distrib. and colours 80−94778
  - accretion magnetosphere stability, adiabatic gas model 77−49368
  - accretion of interstellar material, numerical simulation 79−21358

binary stars continued
accretion onto magnetised neutron stars, normal mode anal. of interchange instability at magnetopause 77−13376
adiabatic mass loss, spin evolution 79−75201
adiabatic pulsations of tidally perturbed rotating stars 78−89172
ADS 11871 (β 648), visual binary star, orbital elements, determ. using two methods 80−51805
ADS 148, visual binary speckle interferometry with linear digicon detector 77−78648
ADS 1538=Σ 168=BDS 1015, orbit of visual double *(French)* 78−8056
ADS 1833 and 6871 AB, visual binaries, orbital calc. *(French)* 80−98690
ADS 4299, 8048 and 9352, parallaxes and masses for visual binaries 80−4402
ADS 5281, visual binary speckle interferometry with linear digicon detector 77−78648
ADS 7251, photographic obs. in 1962-73 period, orbital motion *(Russian)* 78−28726
ADS 7390 (ω Leonis), visual binary, orbital elements and removal of nodal ambiguity 77−13399
ADS 8887, photographically unresolved visual binary, parallax and orbit 78−57593
ADS 9476 (Aitken 14), possible astrometric companion *(French)* 79−44553
ADS 9537 (BV Draconis and BW Draconis), ang. separation and position angle 79−35296
Am stars in spectroscopic binary systems, evolutionary status, statistical anal. 78−93262
Am-type, tidal interaction producing stable atm., evolution 80−67752
ο Andromedae, Be star, spectrographic obs. from (1967 to 1976) 77−71116
FF Andromedae, BY Draconis variable, spectroscopic binary, orbit and active region model 77−33527
λ Andromedae, high-press. transition region in model chromosphere 80−26847
AN Andromedae, light curve of Am binary systems, possible third body 79−58374
BX Andromedae, period increase *(Chinese)* 78−36642
λ Andromedae, radio emission detect. from giant binary 77−22248
CG Andromedae, Si star, spectrum variable, short period radial vel. variability determ. 80−72968
γ Andromedae, speckle interferometry and holography *(German)* 79−75116
ζ Andromedae, spectroscopic binary, photometric and spectroscopic obs. *(Russian)* 78−57588
λ Andromedae, spectroscopic binary, UV and optical obs. of chromospheric lines 79−30087
Z Andromedae, symbiotic star, IUE obs. of UV spectrum 80−109450
Z Andromedae, UV spectra, 1979 Feb. 17, quiescent phase 79−40202
λ Andromedae, UV spectrum obs. by International Ultraviolet Explorer 78−96475
λ Andromedae, V photometric obs. during 1976-77 period 78−40994
angular momentum loss and mass exchange instability 77−49433
angular momentum loss from star with rapidly rot. core in close binary system *(Russian)* 78−93196
Ap and Am stars, primary supernova explosion rel. to anomalies nuclear origin 79−35277
Ap stars in spectroscopic binary systems, chemical anomalies surface distrib. 80−62140
Ap stars in spectroscopic double systems, BV photometry *(German)* 77−17583
appl. to double star attraction *(Italian)* 80−8531
apsidal motion in highly evolved stars 77−45483
AE Aquarii, cataclysmic variable, IUE satellite UV obs. 80−72985
AE Aquarii, cataclysmic variable, rapid light oscills. rel. to white dwarf oblique rotator model 80−36634
R Aquarii, Mira variable, 14.9 GHz obs. 79−75210
AE Aquarii, spectroscopic binary variable, X-ray source, orbital element determ. 80−105288
R Aquarii, symbiotic long-period variable, spectrum of assoc. nebulosity 80−90450
R Aquarii, UBVRI polarimetric obs., orbital motion effect *(Russian)* 80−36646
R Aquarii, UV, visible and 85 GHz continuum obs. 80−85946
R Aquarii, UV obs. of hot component 80−56854
R Aquarii (M7+pec), late type variable star, IUE obs. of circumstellar emission 80−82370
Aquila X-1, photometry and spectroscopy of optical counterpart, model 78−32614
Aquila X-1, UBV photometry during 1978 X-ray outburst *(Russian)* 79−101224
V603 Aquilae, accretion disc radiation of cataclysmic binary 77−91537
V794 Aquilae, AM Herculis-like brightness vars. 79−92804
U Aquilae, Cepheid variable, detect. as long-period binary by radial vel. spectrometer 80−51667
η Aquilae, classical Cepheid, companion star detect. and distance determ. 80−90443
Ariel 0535+26, X-ray binary, refined position meas. and pulse period data 79−44635
Ariel 0620−00, transient X-ray source, spherical model 78−12415
Ariel 1540−53, eclipsing X-ray binary pulsator 78−8151
UX Arietis, co-ordinated UV, optical and radio obs. of RS Canum Venaticorum binary 79−16963
UX Arietis, Copernicus UV obs. of Lyman α and Mg II emission 78−81651
κ Arietis, double-lined Am star, spectroscopic obs. and curve of growth anal. 77−22237
TT Arietis, nova-like cataclysmic variable, photoelectric photometry 80−82382
UX Arietis, radio obs. 77−64793
UX Arietis, RS Canum Venaticorum binary, two-freq. radio polarimetry 79−21335
UX Arietis, RS Canum Venaticorum type binary, UBV photometry, 1974-5 period 77−91569
UX Arietis, RS Canum Venaticorum type star, UV excess, spectrophotometric obs. 78−8043
UX Arietis, V photometric obs. during 1976-77 period 78−40994
β Arietis, var. of highly eccentric spectroscopic binary 79−17026
γ Arietis, visual binary Ap-system, photometry 78−85950

binary stars continued
UX Arietis (H0324+28), RS Canum Venaticorum system as coronal X-ray source 79−16979
astrometry, lateral refr. elimination from micrometric method obs. *(Russian)* 79−96890
α Aurigae, ang. separation and position angle, speckle interferometry *(Russian)* 78−40922
α Aurigae, angular diameter meas. with large altazimuthal telescope *(Ukrainian)* 79−96925
NW Aurigae, eclipsing binary, photoelectric photometry 78−8052
LY Aurigae, eclipsing binary, photometric elements, masses, radii, luminosities 78−28723
α Aurigae, high-press. transition region in model chromosphere 80−26847
α Aurigae, UV spectrum obs. by International Ultraviolet Explorer 78−96475
KW Aurigae (14 Aurigae A), ellipsoidal variable and δ Scuti pulsating star, tidal l=1 p_5-modes 79−97028
α Aurigae (Capella), extra-atmospheric obs. analysis 79−25647
α Aurigae (Capella), intense line emission in soft X-ray spectrum 78−93228
α Aurigae (Capella), orbital motion determ. using phase effect detect. at CERGA stellar interferometer *(French)* 80−36508
α Aurigae (Capella), X-ray line emission obs., corona models 80−26905
axisymmetric accretion discs and flows, thickening 78−40989
B-type and Be-type stars, search for binaries 78−57551
BD+29°3805, K-type giant, spectroscopic binary orbit 80−67790
BD+34°1543, hot subdwarf binary, composite spectral type 78−45323
BD+57° 1942, faint short-period binary, influence of Schwarzschild effect on orbital and system elements *(German)* 80−8653
BD+61°1211, optical counterpart of 2A 1052+606, RS Canum Venaticorum binary system 79−92803
BD+61° 1211 (2A 1052+606), RS Canum Venaticorum binary star, spectroscopic obs. 80−36663
BD+66°1066, nucleus of planetary NGC 6543, lightcurve oscills. 79−75223
BD−7°3007, nova-like variable, simultaneous spectroscopy and photometry 78−12250
BD +11° 4571=ADS 15010, subdwarf binary, history of astrometric obs. 79−62874
BDS 1269, pulsation periods of metal-poor δ Scuti primary star 80−105247
BDS 1269, visual binary, metal abundances and characts. of components 80−4397
Be stars in binary systems, apsidal motion of gaseous rings 78−32521
Be-star duplicity and mass exchange 77−60780
Be-stars, binary detection methods 77−56997
Be-stars, binary hypothesis 77−56998
Be-stars, mass-exchange binary evidence from periodic spectral var. 77−60781
bimetric theory of gravitation, viability, gravitational radiation from neutron star binaries 79−35611
binaries, wide visual, spectral type, age and uvbyβ photometry 80−94833
binary pulsar, secular relativistic change in pulsar period 77−5542
binary pulsar PSR 1913+6, dissipative effects connected with gravitational radiation, indirect evidence 79−75236
binary X-ray sources, relation of type I supernovae 77−57021
binding energy distrib. in cluster, homogeneous cluster model 80−62209
blue supergiant+neutron star, evolution 80−98689
ξ Bootis, active dwarf binary star, chromospheric emission lines obs. 80−12762
UZ Bootis, cataclysmic variable similar to WZ Sagittae, outburst characts. 80−17596
AC Bootis, eclipsing binary, detailed photometric study 78−36637
ξ Bootis, late-type dwarf star, mag. field obs. in primary component 80−72949
XY Bootis, photometric obs. of contact binary, light curves, mass ratio 78−4286
η Bootis, soft X-rays detect. with imaging X-ray telescope 79−48953
bound system of two point-masses, influence of weak gravit. wave 80−21903
bright nearby stars, unseen companions discoveries from Sproul plates astrometric anals. 80−61991
BV 845, contact binary, improved photometric soln. 78−45365
CC 1299 (BD+27°4120), unresolved astrometric binary, orbital anal., mass and parallax 80−109464
53 Camelopardalis, Ap star, radial vels. and binary nature 79−80320
Z Camelopardalis, dwarf nova, spectrophotometry at standstill and in eruption 80−82366
SV Camelopardalis, RS Canum Venaticorum star, identification with X-ray source H0630+82, X-ray obs. 80−101654
SY Cancri, dwarf nova, spectrum obs. and possible duplicity *(Russian)* 80−8638
ζ Cancri, speckle holography meas. of double star 78−93120
FF Canis Majoris, eclipsing binary, possible member of Collinder 132a, UBVβ photometry 78−32540
UW Canis Majoris, eclipsing binary, UV photometry and primary component shape and atmospheric struct. 78−40992
α Canis Majoris, EUV obs., Sirius B model atm. 77−33489
α Canis Majoris, Fourier transform method to determine projected rotational vels. 77−29655
29 Canis Majoris, massive hot binary star, spectrograms, mass loss 78−12299
α Canis Majoris, minimum-flux coronal model for Sirius B rel. to X-ray emission 80−8626
α Canis Majoris, relative positions of components of visual binary 77−82274
α Canis Majoris (Sirius), astrometric study rel. to distance and components masses 79−5858
α Canis Majoris (Sirius), binary star interaction rel. to B abundance 77−53585
α Canis Majoris (Sirius), Ca II K line profile rel. to influence of Sirius B 80−56830
α Canis Majoris (Sirius), constraints on corona model for Sirius B 79−2543
α Canis Majoris (Sirius), possible orbits for third star 78−93312
α Canis Majoris (Sirius), rot. vel. and Ba abundance 78−12218
α Canis Majoris (Sirius), search for surrounding nebulosity 78−93242
α Canis Majoris (Sirius) AB, white dwarf formation 79−44483
α Canis Majoris (Sirius B), EUV obs., evidence against photospheric origin of 0.25 keV flux 78−49481

binary stars continued
  α Canis Majoris (Sirius B), spectral energy distrib. 80—8629
  α Canis Majoris B, photoelectric obs. 78—4220
  α Canis Majoris B (Sirius B), search for far UV emission 79—5821
  β Canis Majoris stars, duplicity rel. to multiperiodicity 77—87424
  α Canis Minoris (Procyon) AB, white dwarf formation 79—44483
  TX Canum Venaticorum, cataclysmic variable, P Cygni type, visible spectral obs. 80—105249
  TX Canum Venaticorum, evolution from cataclysmic to stationary P Cygni stage 79—12479
  AM Canum Venaticorum, orbital period increase 80—12765
  RS Canum Venaticorum, UV excess, spectrophotometric obs. 78—8043
  RS Canum Venaticorum binaries, Mg II flux profiles and chromospheric radiative loss rates 80—36611
  RS Canum Venaticorum binaries, multiple periodic behaviour 77—87479
  RS Canum Venaticorum binaries, observational selection and evolution 78—89208
  RS Canum Venaticorum binaries, possible origins 77—57060
  RS Canum Venaticorum binary stars, introduction to series of papers 79—21329
  RS Canum Venaticorum binary stars, mag. starspot model for photometric and spectroscopic behaviour 80—109488
  RS Canum Venaticorum binary stars, radio luminosities and spectra 79—21333
  RS Canum Venaticorum stars, Hα line variability, visible spectra obs. 80—105277
  RS Canum Venaticorum stars, HEAO 1 X-ray obs. of active coronae 80—72925
  RS Canum Venaticorum stars, out of eclipse light var. 80—109489
  RS Canum Venaticorum systems, candidate list for southern HD stars 80—4395
  RS Canum Venaticorum systems, X-ray emission progress report 79—21345
  RS Canum Venaticorum systems, X-ray obs. and coronal model development 80—56873
  RS Canum Venaticorum type binaries, Hγ line vars., chromospheric diagnostics 80—62181
  RS Canum Venaticorum-type binaries, emission line vars. 78—24527
  RS Canum Venaticorum-type binaries, evolutionary status 77—33570
  β Capricorni, 1977 October 20 lunar occultation results 79—44523
  β Capricorni, ang. dia. and separation from lunar occultation 77—74048
  ζ Capricorni, Ba star, white dwarf+giant, UV spectra obs. 80—105284
  η Carinae, circumstellar ring around close binary, proposal 79—67030
  θ Carinae, radial vel. of chemically-peculiar B-type star 80—8635
  Cassiopeia A, supernova remnant, evidence for illumination by binary neutron star 77—33615
  TV Cassiopeiae, eclipsing binary, period and UBV light curves 78—4287
  DO Cassiopeiae, eclipsing binary, three-colour photoelectric investigation 78—16462
  AZ Cassiopeiae, interacting eclipsing binary, mass loss of cool supergiant component 78—32522
  μ Cassiopeiae, subdwarf binary, spectroscopic orbit 78—8046
  V509 Cassiopeiae (HR 8752), spectrum variable supergiant, Hα emission obs. 79—88672
  cataclysmic binaries, circumstellar material geometrical and photometric parameters 80—109492
  cataclysmic binaries, evolution and origin 80—56885
  cataclysmic binaries, gas flow hydrodynamic calc. 77—57037
  cataclysmic binaries, masses and evolution 77—57031
  cataclysmic binaries, role of white dwarf component 80—82356
  cataclysmic binaries evolution, ang. momentum loss 77—57032
  cataclysmic binary formation through common envelope evolution 80—8651
  cataclysmic binary stars (CBS), critique of polarimetric evidence on physical parameters and orbital inclination 80—109486
  cataclysmic variable stars, multiple periodicities 77—87434
  cataclysmic variables, emission lines from accretion discs 80—51774
  cataclysmic variables, review of structure 77—26018
  cataclysmic variables, short-period light oscills. rel. to non-radial oscills. of rot. stars 78—32477
  cataclysmic variables, stability of non-synchronous stars in close binary systems 79—40223
  cataclysmic variables, visual continuum flux distribs. 80—36636
  CD—42°14462, peculiar white dwarf, noneruptive close binary 77—53630
  CD—42°14462 (V3885 Sagittarii), dwarf nova in permanent outburst 78—53966
  CD—42° 14462, binary nature of nova-like variable 77—87435
  BV Centauri, dwarf nova, identification as spectroscopic binary 80—51775
  V436 Centauri, dwarf nova, no periodic modulation in quiescent state light curve 79—88677
  V436 Centauri, dwarf nova, photometry during superoutburst (May 1978) 80—46570
  ν Centauri, single-lined spectroscopic binary, β Cephei-type star 79—48821
  V810 Centauri (HD 101947), yellow variable supergiant near Cepheid instability strip, VBLUW photometry 80—98672
  α Centauri A and B, IUE spectra and transition region models 80—46543
  α Centauri binary system, spectroscopic chemical anal. 80—62128
  α Centauri rel. to Proxima, radial vels. and bound state 80—41859
  Centaurus X-3, periodicity of extended lows 78—24526
  Centaurus X-3 and related binary X-ray sources, origin 77—29954
  Centaurus X-4, spectroscopic obs. of visual counterpart, companion type 80—82545
  Centaurus X-4, transient X-ray burster, optical counterpart discovered 80—67906
  central binary star in planetary nebula NGC 6853 from proper motion obs. 77—49434
  VV Cephei, complex close binary, linear polarisation during 1977 elcipse 78—40995
  VV Cephei, eclipsing binary, astrometric obs. at Sproul Observatory 78—4290
  VW Cephei, evidence for circumstellar matter 77—33563
  U Cephei, mass transfer from light vars. outside primary eclipse, obs. and anal. 78—36636
  VV Cephei, narrow band photometry during 1976-78 eclipse ingress 78—4296
  VV Cephei, spectroscopic obs. during 1976/77 eclipse ingress phase 78—45359

binary stars continued
  VV Cephei, UB photoelec. obs. 77—17633
  VV Cephei, UBV photometry during ingress phase of 1976-78 eclipse 78—20862
  U Cephei, UV excess, mass transfer in eclipsing binary system 77—33555
  17=ξ Cephei A, speckle interferometry, visual orbital elements 80—56874
  β Cephei stars, duplicity rel. to pulsation excitation 77—87425
  VV Cephei system, distant, in Puppis, spectral classification, UBV photometry and polarimetry 80—51810
  Cepheid binary detection from U-V curve obs. 80—98667
  Cepheid variables, incidence of duplicity 80—90453
  Cepheid variables, intrinsic colours, binary system membership and physical props. 78—28696
  Cepheids, anomalous, in dwarf spheroidal galaxies, binary system model 77—45451
  Cepheids, binary star frequency from UBV photometry 77—45465
  δ Ceti, β Cephei variable, spectroscopic binary, radial vels. and period var. 80—82376
  UV Ceti, anomalous flare activity obs. 78—89202
  WX Ceti, cataclysmic variable similar to WZ Sagittae, outburst characts. 80—17596
  o Ceti (Mira), enhanced activity of B-type component at 1976 light minimum 78—81636
  o Ceti (Mira), mass loss rate determ. 79—48831
  o Ceti (Mira), rapid light vars. of companion star during 1977 light min. 78—96492
  o Ceti (Mira), spectrum of companion star 78—4253
  o Ceti AB, IUE obs. of UV spectrum 80—22027
  γ Ceti AB, occultation by 6 Hebe on 1977 March 5, predictions 77—29702
  Z Chamaeleontis, monitoring of southern dwarf nova, 1954-76 period 78—93272
  Ci 182354, astrometric anal. of unseen companion from 61 cm Sproul refractor plates 78—16459
  Circinus X-1, binary model, orbital eccentricity from X-ray and radio obs. 80—98735
  Circinus X-1, binary model, radio emission 80—98736
  Circinus X-1, changes in optical, IR and radio emission 80—67910
  Circinus X-1, continuation of anomalous X-ray behaviour 78—32606
  Circinus X-1, nature and binary star model 79—75296
  Circinus X-1 (3U 1516—56), obs. of optical and radio counterpart 78—12414
  Circinus X-1 and Cygnus X-1, time variability comparison 80—56974
  Circinus X-1 as gamma-ray source, eccentric orbit binary model 79—97100
  circular binaries, effect of instantaneous mass ejection on orbital elements 77—57026
  circumstellar matter existence, interpretation of obs. 77—57042
  classical and dwarf novae, energy sources and systematics 79—67041
  classical and dwarf novae explosions, review 79—67042
  close binaries, angular vel. distrib. in one component with fast rotating core *(Russian)* 78—28648
  close binaries, components periodic collisions induced by collisions and isolated stars 78—8061
  close binaries, convective energy flux in atm. with gravit. field changes *(Russian)* 78—49422
  close binaries, distortion effects on struct. 78—57584
  close binaries, energy release, flares and particle acceleration *(Russian)* 80—73005
  close binaries, form. by two-body tidal capture 77—33556
  close binaries, gaseous circumstellar discs obs. 77—57043
  close binaries, intermediate mass, mass transfer for different stars within evolutionary scheme 80—109476
  close binaries, light scattering in extrastellar gaseous material, emission line profiles spectropolarimetry obs. 80—109471
  close binaries, mag. fields generation *(Russian)* 77—17591
  close binaries, mass flow, binary X-ray sources appl. 77—57039
  close binaries, mass loss, appl. of nonevolutionary sequences of models in thermal equilib. 78—24508
  close binaries, mass loss and parameters 77—13397
  close binaries, nonradial radiative transfer 77—91567
  close binaries, orbital ang. momentum loss by gravit. radiation, mass transfer rates 78—40991
  close binaries, period distrib. from secondary maxima 80—109467
  close binaries, radio survey at 6 cm wavelength 78—32510
  close binaries, review 77—33573
  close binaries, rotational angular momenta 77—57057
  close binaries, satellite UV obs. 77—57033
  close binaries, separation angle meas. by speckle interferometry *(Russian)* 78—40922
  close binaries, struct. and evolution 77—57019
  close binaries, synchronous systems devel. from tidal are rot. interactions 80—109468
  close binaries, undersize subgiant components 79—44528
  close binaries, unsteady mass loss 77—57049
  close binaries accretion processes rel. to binary X-ray sources 77—57034
  close binaries and the evolution of star clusters 79—5863
  close binaries formation, fission hypothesis 78—32334
  close binaries in globular clusters rel. to nature of cluster X-ray sources 77—41396
  close binaries linear polarisation 77—49435
  close binaries with mass transfer, particle motion 77—5545
  close binary and planetary systems, origin 79—5859
  close binary components, model atms. 79—62869
  close binary stars, H I α and β line photometry 80—109470
  close binary stars, low mass, evolution, gravitational wave emission influence 80—82425
  close binary stars props. before and after mass transfer, obs. and theory comparison 80—62187
  close binary stars with single optical component, ellipsoidality effect on light vars. 79—92806
  close binary system, matter flow around one component, period changes 79—62870
  close binary system with mass and ang. momentum loss, period changes 80—72998
  close binary systems, neutron stars tidal disruption by black holes 77—13387
  close binary systems, polarimetric determ. of revolution directions and spatial orientations 79—35309

binary stars continued
close binary systems, precession and nutation 77—13392
close binary systems, problem of components oblique rot. axes 78—96509
close binary systems, reflection effects evaluation, generalised approach 79—25631
close binary systems in globular clusters, possible existence 79—44530
close binary systems in globular clusters, preliminary report 80—109505
close binary systems in quiet stage, detect. from γ-ray emission 79—67058
close binary systems with elliptical orbits, components shape, ellipsoid-ellipsoid approx. 79—80338
close detached, Ap components, chem. anomalies surface distrib. 80—109475
close low mass binaries evolution and gravit. radiation 77—57030
close low-mass binary system, evolution with mass exchange and gravit. radiation losses 77—53631
close low-mass binary systems, evolution, unsteady mass loss, contracting secondary star 77—17617
close low-mass binary systems, evolution into contact 77—33557
close neutron star binaries, evolution, gravit. radiation and mass transfer 77—78821
close systems, mass transfer and accretion disk flow 77—82280
close systems, orbital angular momentum loss during evolution 79—97033
close systems, synchronism between axial rotation and orbital motion 79—97034
close systems including black hole, circumstellar gas motion 77—17628
close systems with neutron star components, evolution *(Italian)* 79—21354
close visual double stars, electronographic UBV magnitudes and separations 79—67056
close visual doubles, mass meas. using gravit. starlight deflection *(French)* 79—62753
close X-ray binaries, ellipsoidality effects and linear polarisation 77—78898
cluster binaries, dynamics 78—12295
collapsed stars, accretion magnetosphere stability, polar cap dripping motion 78—4194
colliding stellar winds, X-ray emission upper limits 78—65607
collisions, by oscill. orbits of second kind 79—35312
CC Comae, W Ursae Majoris type, spectroscopic orbit 78—12300
35 Comae Berenicis, masses and K-line absolute magnitudes 80—8649
common envelope binaries, evolution 77—57025
common-proper-motion pairs in South Galactic Cap, identifications 78—73734
compact binary systems, tidal interactions 77—57027
compact X-ray sources, masses 78—12430
composite spectra stars, new classification scheme for bright stars of Hynek's (1938) list *(French)* 80—56876
composite spectrum stars susceptible to lunar occultation, identification list of 68 stars 80—26908
conference on close binary stars, Toronto, USA (Aug. 1979) 80—105436
contact binaries, mass and energy flow 79—48850
contact binaries, objection to model of Shu, Lubow and Anderson 78—28720
contact binaries, structure, zero-age models 78—8045
contact binaries, synthetic light curves 78—24528
contact binaries, transport processes in envelopes 78—4279
contact binary star, idealised dynamical evolution *(French)* 80—62199
contact binary stars, struct. of high-mass models 79—48855
Cor 197 multiple system, phys. and orbital elements *(French)* 77—78819
coronae above turbulent accretion discs 77—57038
ιCoronae Borealis, Hg-Mn star, spectroscopic binary, visible spectra obs. 80—72983
α Coronae Borealis, spectroscopic orbit determ. 77—22277
σ Coronae Borealis (=ADS 9979), mass and orbital elements *(French)* 80—77449
σ Coronae Borealis (HD 146361), spectroscopic binary, soft, X-ray obs. with (HEAO-1) 80—56886
cosmic exploration by X-rays, 1978 Bakerian lecture 79—48964
cosmology and binary stars 77—41393
CPD-26°389, central star of NGC 1360, spectroscopic binary within planetary nebula 77—45494
critical surface, influence of radiation pressure, X-rays and asynchronisation 77—29880
CRL 2104, CRL 2179, late WC stars, 2 to 4 μm spectrophotometry and circumstellar dust 78—96491
α^1 Crucis, improved spectroscopic orbit 80—67792
BI Crucis, new symbiotic star, spectrum 80—109442
25 G Crucis (HD 108250), orbital elements from spectrograms 80—82432
SS Cygni, 1896-1975 study of dwarf nova 79—16986
SS Cygni, accretion disc radiation during dwarf nova outburst 77—91537
V389 Cygni, BV photometry of peculiar variable 79—44534
SU Cygni, classical Cepheid and spectroscopic binary, UBVRI photometry 79—62852
61 Cygni, detect. of three invisible companions to visual binary star 78—28730
SS Cygni, dwarf nova, ANS detection of both soft and hard X-ray emission 78—36579
SS Cygni, dwarf nova, rapid optical oscills. phase variability 80—85947
SS Cygni, dwarf nova, soft X-ray pulsation obs. 80—46563
SS Cygni, dwarf nova, spectrophotometry rel. to accretion disc models in erruption and at min. light 80—36635
SS Cygni, dwarf nova during outburst, accretion disk model 77—82247
MR Cygni, eclipsing binary, photoelec. photometry and computer soln. *(Chinese)* 78—28724
θ Cygni, F-type dwarf star, spectral type of faint distant companion 80—90481
V444 Cygni, IR eclipse obs. and Wolf-Rayet wind structure 78—45357
SS Cygni, light curve periodicity 79—21300
CH Cygni, new active period, model, double system with accretion disc *(Russian)* 78—69813
V1016 Cygni, new spectroscopic obs., simultaneous presence of increasing excitation and cool features 80—26874
V389 Cygni, peculiar (Ap-type) binary, spectroscopic obs. 78—85975
Y Cygni, precession period determ. from spectroscopic data 79—67062
9 Cygni, radial. vel. and orbital elements of new spectroscopic binary 78—69826

binary stars continued
57 Cygni, spectroscopic binary, search for systematic radial vel. anomalies 80—17617
SS Cygni, spectroscopic binary variable, X-ray source, orbital element determ. 80—105288
CH Cygni, symbiotic star, 1977 outburst, radial vel. and atm. struct. determ. 80—72969
CH Cygni, symbiotic star, binary model 80—62158
V1016 Cygni, symbiotic star, IR variability obs. from VJHKL photometry *(Russian)* 80—105263
CH Cygni, symbiotic star, IUE obs. during active phase 79—62846
CH Cygni, symbiotic star, rapid and slow light vars. 80—51792
CH Cygni, symbiotic star, spectroscopic obs. during 1977 to 1978 outburst 79—75211
CH Cygni, symbiotic variable, flickering obs. during outburst, binary model 79—8929
V1357 Cygni (Cygnus X-1), brightness var. rel. to disk accretion subphotospheric layers *(Russian)* 79—25764
V1357 Cygni (Cygnus X-1), no long-term light vars. (1928-77) 80—41861
V1357 Cygni (Cygnus X-1), UBVR obs. and accreting disk radiation *(Russian)* 79—25645
V1341 Cygni (Cygnus X-2), halo population binary 79—97099
V1341 Cygni (Cygnus X-2), shortest optical variability *(Russian)* 80—17695
V1341 Cygni (Cygnus X-2), UBV photometry and light vars. 79—5833
V1500 Cygni (Nova 1975), 3.35 hour 1978 light curve, rel. to possible double period 79—67039
V1500Cygni (Nova 1975), 3 hour photometric period stabilisation 79—92776
V1500 Cygni (Nova 1975), binary nature, spectral meas. 77—87446
V1500 Cygni (Nova 1975), review of development *(French)* 80—17598
V1500 Cygni (Nova 1975), short-term light vars. 78—36609
V1500 Cygni (Nova 1975), spectroscopic studies, nebular and central binary system 79—62830
V1500 Cygni (Nova 1975), thirteen-colour photometry and anal. of short period variability 79—92788
V1500 Cygni (Nova 1975), TV photometry 78—36602
V1500 Cygni (Nova Cygni 1975), UBVRI photometry 77—33509
61 Cygni A, B, late-type dwarfs, metal abundances 77—78779
β Cygni A, close companion visual obs. 80—8663
Cygnus OB2 number 12, spectrum rel. to mass loss and possible duplicity 80—51760
Cygnus X-1, 39 day polarization period, Thomson scatt. 78—8166
Cygnus X-1, absence of 39 day period in non-UV data 78—8167
Cygnus X-1, accretion disc corona 78—16569
Cygnus X-1, bimodal behaviour of accretion disc 77—60850
Cygnus X-1, black hole candidate, review 78—16577
Cygnus X-1, critique of polarimetric evidence on physical parameters and orbital inclination 80—109486
Cygnus X-1, evidence for 39 day period 78—8165
Cygnus X-1, evidence for new variabilty in hard X-ray emission 80—27011
Cygnus X-1, extended-bandwidth X-ray obs. 80—17689
Cygnus X-1, hard X-ray intensity and spectrum short term changes 77—9814
Cygnus X-1, intensity transitions obs. by OSO 8 77—64886
Cygnus X-1, inverse Compton model 80—51918
Cygnus X-1, mean blue light curve feature 77—17718
Cygnus X-1, model of neutron star surrounded by massive disc 80—36736
Cygnus X-1, neutron star model from bi-metric theory of gravitation 80—90466
Cygnus X-1, new period in X-ray binary system *(German)* 78—81712
Cygnus X-1, obs. during high state (1980 June 11 to 27) 80—86017
Cygnus X-1, obs. in energy range 100 keV-3 MeV 78—20907
Cygnus X-1, optical and X-ray evidence for 78/39-day period 78—89274
Cygnus X-1, optical polarisation orbital vars. rel. to binary system inclination 78—54077
Cygnus X-1, physical reality of millisecond bursts questioned, shot noise effects 78—45429
Cygnus X-1, polarimetry with OSO-8 X-ray polarimeter 78—12426
Cygnus X-1, possible existence of black hole 79—48842
Cygnus X-1, rapid X-ray flaring obs. 77—57105
Cygnus X-1, Salyut-4 obs. in 0.2-10 keV range *(Russian)* 77—57109
Cygnus X-1, search for rapid optical periodicities 78—24573
Cygnus X-1, search for X-ray polarisation 78—4406
Cygnus X-1, short-term time variability, shot noise model 78—36721
Cygnus X-1, short-term time variability 78—93466
Cygnus X-1, short-term variability in hard X-ray region *(Japanese)* 79—80369
Cygnus X-1, status report 78—77618
Cygnus X-1, transition from high X-ray state to low X-ray state, 1980 June to July 80—98738
Cygnus X-1, variable circular polarisation obs. 77—29952
Cygnus X-1, X-2 and X-3, long-term-studies with Ariel 5 All-Sky Monitor (ASM) 80—17688
Cygnus X-1, X-ray binary, variable star, SHF obs. 80—73071
Cygnus X-1, X-ray flux time variability struct. *(Russian)* 80—51921
Cygnus X-1, X-ray variability in high state 78—28855
Cygnus X-1 (HDE 226868), 78.4 day period search in X-rays and optical polarisation 79—75297
Cygnus X-1 (HDE 226868), accretion disk size 80—51910
Cygnus X-1 (HDE 226868), optical photometry, (1972-1976) 78—32609
Cygnus X-1 (V1357 Cygni), narrow-band photoelec. obs. *(Russian)* 79—88767
Cygnus X-1 (V1357 Cygni), optical light curve vars. rel. to X-ray vars. 80—109560
Cygnus X-1 (V1357 Cygni), optical photometry (1980 May 25 to July 7) 80—90578
Cygnus X-1 (X-2), X-ray polarisation obs. from OSO 8 80—90571
Cygnus X-1 and Circinus X-1, time variability comparison 80—56974
Cygnus X-1 possible existence of black hole in binary system 78—16457
Cygnus X-2, 3-8 keV obs. of possible degenerate dwarf 80—46703
Cygnus X-2, optical variability upper limits 78—96564
Cygnus X-2, polarimetry with OSO-8 X-ray polarimeter 78—12426
Cygnus X-2, radial vel. and orbital elements from visible spectra obs. 80—77519
Cygnus X-2, rapid UV flux vars., IUE obs. 80—12833
Cygnus X-2, spectroscopic obs., orbital period, spectral-type var., X-ray heating 79—9036

binary stars continued
Cygnus X-2, X-ray and optical obs., (1973 to 1977) 79—30148
Cygnus X-2, X-ray binary, optical variability in UBV 77—26027
Cygnus X-3, 34.1 day period, 2-12 keV obs. by COS-B 80—94897
Cygnus X-3, 4.8 hour modulation period change disproved 80—8713
Cygnus X-3, 4.8 hour periodicity in spectra 79—5920
Cygnus X-3, 50-400 keV obs., power law spectrum 80—41913
Cygnus X-3, γ-ray flux meas. above 10^{12} eV 77—53706
Cygnus X-3, binary pulsar age and activity *(Russian)* 78—4413
Cygnus X-3, cocooned X-ray binary pulsar model 78—36723
Cygnus X-3, COS-B X-ray obs., 4.8 hour modulation 78—28856
Cygnus X-3, gamma-ray emission from mag. accretion disc 77—78894
Cygnus X-3, gamma-ray obs. with 4.8 hr periodicity 77—26086
Cygnus X-3, hard X-ray spectrum obs. 80—31388
Cygnus X-3, inverse Compton γ rays 77—41421
Cygnus X-3, model for quiescent radio emission 77—33689
Cygnus X-3, observational constraints, on models 78—16567
Cygnus X-3, period derivative 79—48955
Cygnus X-3, period derivative and asymmetric X-ray light curve from HEAO 2 obs. 80—105394
Cygnus X-3, period stability 77—2489
Cygnus X-3, periodic γ-ray emission obs. *(Russian)* 77—91672
Cygnus X-3, X-ray Fe line emission meas. with Bragg crystal spectrometer 79—12544
Cygnus X-3, young pulsar in binary system model 77—29955
damped rotating polytropes, binary fission 79—71016
degenerate star-red giant interacting binary stars, compressible fluid flow, accretion 80—67779
δ Delphini, spectroscopic binary fine anal. 77—17620
HR Delphini, UV spectrum, stellar wind 80—26880
HR Delphini (Nova 1967), cataclysmic binary spectrum 80—4359
HR Delphini (Nova 1967), photoionisation models, binary system evolution 80—17590
HR Delphini (Nova 1967), simultaneous X-ray, UV and optical obs. 80—109440
HR Delphini (Nova 1967), spectroscopic orbit 79—44510
detached, evolution to contact binaries involving mass flow 80—109477
detection by lunar occultation method 79—44542
digital speckle interferometry 77—53641
disc accretion by mag. neutron stars, model 78—93294
disc accretion onto magnetised compact objects, theory *(Russian)* 79—44467
disc formation in stellar wind accretion *(Russian)* 79—88648
disrupted the star in close binary containing neutron star, model for Crab Nebula 79—25696
double star measures at Lick Observatory, Mount Hamilton, California 78—85979
double star photometry and variability 79—44554
double star system, energy and distrib. *(Chinese)* 79—75249
double stars, focal grating photometer for magnitude difference determ. 80—67567
double stars, micrometer obs. 78—57582
double stars, Nice obs. of 267 objects *(French)* 79—44531
double stars, photographic measures 78—57581
double stars, position angles and separation, Venezuelan obs. *(French)* 80—77450
double stars, rectilinear trajectory errors *(French)* 78—89223
double stars, separation and position angle obs. 80—98691
double stars, visual, new spectral classification on MK system 80—109462
double stars, Webb Society handbook 80—8744
double-lined spectroscopic binaries, uvby Hβ photometry 77—82275
doubles, binaries and multiple stars for amateur study 77—17626
CX Draconis, Be star, UBV obs. 80—82388
BY Draconis, binary spotted flare star, orbital elements and pre-main-sequence nature 80—36633
BY Draconis, dwarf binary, flare star, rotational hypothesis for quasi-sinusoidal light variations 78—4234
TW Draconis, photometric study of Algol-type system 78—45361
ϕ Draconis, Si Ap-star, UV vars. rel. to patchy stellar surface model 77—49389
BY Draconis, slow light variability anal. 77—53629
BY Draconis, spectroscopic binary flare star, BVRI obs. 77—53595
CM Draconis, spotted dM4e eclipsing binary flare star, absolute dimensions and masses 78—12289
BY Draconis stars, out of eclipse light var. and comparison with RS Canum Venaticorum stars 80—109489
BY Draconis-type stars, spectroscopic binary incidence 77—87401
dwarf novae, cataclysmic variables, review of spectroscopic and photometric obs. 77—56959
dwarf novae, eruption types and superhumps, obs. 79—75212
dwarf novae, EUV obs. from Apollo-Soyuz Test Project 78—93252
dwarf novae, hard X-ray emission from 47 objects 78—93275
dwarf novae, outbursts, accretion model 79—88680
dwarf novae, photometry of rise to max. and decline 77—9753
dwarf novae, quasi-periodic oscills. and nonradial pulsations of accretion disks 80—46568
dwarf novae, quasiperiodic luminosity vars. 79—80311
dwarf novae, rapid brightness oscills. obs. 78—40968
dwarf novae, review 77—78799
dwarf novae, search for light oscills. during outbursts 78—40966
dwarf novae, soft X-ray emission 77—45457
dwarf novae, X-ray emission 79—67031
dwarf novae and possibly related objects, IR photometry 78—8015
dwarf novae binaries, theory 77—56962
in E3 (ESO-037-SC 01), dying globular cluster, photometric evidence for binary systems 80—105291
eccentricity of apparent orbit 80—51807
eclipsing, Fourier anal. of light curves, reduction of integrals 78—20856
eclipsing, Fourier anal. of light curves 78—24525
eclipsing binaries, late-type, mass-luminosity and radius relations, chem. composition 78—28728
eclipsing binaries, light curves, Fourier analysis, integral evaluation 78—45236
eclipsing binaries in NGC 6235 globular cluster 78—4305
eclipsing binary light curves anal., linearised limb-darkening coefficients 78—49480
eclipsing variable stars, Fourier anal. of light curves, photometric perturbations for total and transit eclipses 78—12291
eclipsing variables, Fourier anal. of light curves 78—20854

binary stars continued
eclipsing variables, photometric perturbations for partial eclipses, Fourier anal. 78—28717
eclipsing variables in Magellanic Clouds, tabulated light curves 78—16536
education, supernova explosion in binary system, classical mechanics appl. 80—62428
encounters with field stars, statistical effect on wide binaries 79—44562
equilibrium states of nonsynchronous stars in detached binaries 79—53853
equipotential surfaces, modification due to pressure of radiation of component *(French)* 80—56880
equipotential surfaces with very luminous components, different types of configurations *(French)* 80—56881
δ Equulei, improved orbit for visual binary 78—45364
α Equulei, radial vel. vars. from microphotometer scans 78—77581
δ Equulei, three-dimens. orbit 79—53852
CC Eridani, BY Draconis variable, Hα variations 77—87406
AS Eridani, eclipsing binary, photometric elements, masses, radii, luminosities 78—28723
66 Eridani, spectroscopic binary, search for light var. 78—32524
$o^2=40$ Eridani, white dwarf, B component, gravitational redshift 79—62868
40 Eridani BC, white dwarf formation 79—44483
eruptive blue variables at high galactic latit., spectrophotometry 78—32482
eruptive star assoc. with pulsar, gamma-ray source *(French)* 78—20913
evolution, effects of mass and ang. momentum losses from massive stars 79—25591
evolution 77—91571
evolution of close binary systems, collapse theory 80—77389
evolution of close double stars 78—73733
evolution of massive close binaries inc. wind mass loss 79—44527
exchange collisions between binary and single stars 77—91563
extrasolar planet detect. using speckle interferometry 77—41309
faint short-period spectroscopic binaries, influence of Schwarzschild effect on orbital and system elements *(German)* 80—8653
fast nova model evolution from pre-explosion to decline 79—35273
Feige 24, EUV star, spectrophotometry in 3800-8200 Å region 78—4280
Feige 24, intense EUV source in Cetus 77—9746
Feige 24, photometric props. rel. to hot white dwarf distance 77—9747
Feige 24, spectroscopy of EUV source, binary orbit, mass 78—93218
fission in damped rotating polytropes 78—93209
flare stars physical characts. 77—41383
formation, angular momentum considerations 78—69781
formation, by three-body encounters in stellar systems, probability 77—13396
formation, nonaxisymmetric collapse in rotating interstellar clouds 80—85927
formation, statistical model for the initial stellar mass function 79—48851
formation by rotating protostar fragmentation, comparison of two three-dimensional computer codes 80—26850
formtion from rot. interstellar clouds fragmentation, three-dimensional hydrodynamical calcs. 80—62236
Fourier deconvolution of electronographic images 79—75112
G139-29, perturb. from rectilinear motion, astrometric red dwarf binary system with subluminous component 79—8910
G148-36, possible white dwarf-sdM close binary, spectrophotometry 80—12763
G24-16, parallax and astrometric orbit from Sproul plate series 78—53983
G262—21/22, subluminous stars in common proper motion binary 77—33491
G 208-44/45, possible double flare star, spectral obs. 80—67727
G- and K-type giants in short period binaries 77—87394
galactic bulge X-ray sources, models, binary systems 78—81706
galactic X-ray sources, correl. between hardness and pulsation 78—4399
gamma-ray binaries, emission during spherically symmetric accretion onto black hole 80—17608
gamma-ray pulsars without radio emission in binary systems 78—53975
gas accretion, thermodynamics and hydrodynamics 80—67696
gas flow, isothermal accretion, stability 78—49303
γ Geminorum, companion to gamma-ray source CG195+4 78—32459
U Geminorum, dwarf nova, M-type dwarf companion spectral type 79—62851
1 Geminorum B, spectroscopic binary, orbit from photoelectric radial vels. 77—22269
giant stars, G and K-type, Ca II H and K lines emission intensity 80—82420
giant X-ray pulses, mass transfer in eccentric binary model 77—33690
Gleise 490 AB (BD+36°2322), red dwarf binary, flares and starspots, rot. period determ. 80—77423
Gliese 867, flares obs. on both components of visual binary 79—48861
globular cluster X-ray source, evolution of 100 M⊙ black hole in binary 78—61932
gravitational collapse of rot. gas cloud, binary systems form. 78—65494
gravitational radiation, effect on evolution and spins of binary systems 78—12292
gravitational radiation, limits on finite size effect 77—33337
gravitational radiation, relativistic corrections and spectrum fine structure 80—90479
gravitational radiation energy loss, free-fall sources model and quadrupole formula failure 80—51647
gravitational radiation from orbiting point masses, post-Newtonian theory 77—13226
gravitational radiation of dipole sources, Maxwell's eqns. analogue, appl. astrophysics 77—13536
gravitational wave detection, astrophysical sources, resonant mass, laser interferometer and Doppler ranging methods 80—68122
gravitational waves emission, theory and astronomical appls. 79—92664
gravitational waves from binary stars, detection opportunities 79—5746
gravitational waves interaction, tidal reson. 78—93089
gravitational waves tidal generation from orbiting Newtonian stars 78—4284
RS Gruis, dwarf Cepheid in binary system 78—77559
GX 1+4 optical counterpart, symbiotic star, spectrophotometry 77—33498
GX 304—1 (3U 1258—61), X-ray binary, discovery of 272 second periodic var. 78—8152

binary stars continued
- GX 339−4 (4U 1658−48), possible black hole binary, optical studies 79−101220
- H1-36 (3U 1746-37), symbiotic star, radio spectrum 77−82239
- H 2252−035, cataclysmic variable, photometry and spectrum rel. to orbital and rot. periods 80−101651
- H 2252−035, spectrophotometry, no periodic linear polarization (1980 Sept.) 80−105401
- H 2252−035, X-ray flux modulation, compact star rotation 80−101652
- h 4636, visual binary in young cluster NGC 5367, relation to Ariel 1353-40 77−82294
- h 4866 B, vars. in spectral type and radial vel. 78−32518
- hard binaries in large N-body systems, two-body tidal dissipation effects 78−93329
- HD 101584, effective viscosity in accretion disc 77−64804
- HD 102567, optical counterpart to 4U 1145−61, atm. model from UV obs. 80−105396
- HD 102567 (4U 1145−61), X-ray periodicity and orbital motion 78−8160
- HD 105902 (ADS 8448), Ba star in visual binary, spectra and photometry 77−78805
- HD 108078, spectroscopic binary orbit from photoelec. radial vel. meas. 80−77451
- HD 108102 (T111), possible RS Canum Venaticorum system in Coma star cluster 79−67020
- HD 108, spectroscopic runaway binary, possible collapsed companion 77−13369
- HD 113001, photometric separation of visual binary *(French)* 80−105281
- HD 11579, spectroscopic binary orbit from photoelectric radial vels. 80−41862
- HD 118216=HR 5110, radio outburst and UV spectra of RS Canum Venaticorum-type binary 79−62844
- HD 128220, peculiar spectroscopic binary, photometric separation of components *(French)* 77−57014
- HD 133461, spectroscopic binary orbit from photoelec. radial vel. 77−57016
- HD 134439/40, high vel. stars, parallaxes, proper motions and positions 77−71128
- HD 135774-5, radial vel. and orbital elements of new spectroscopic binary 78−69826
- HD 137126 spectroscopic binary orbit from photoelectric radial velocities 79−84824
- HD 13738, spectroscopic orbit from photoelec. radial vels. 78−12297
- HD 13970, photometry of probable close binary component 79−8948
- HD 143313, orbit for double-lined spectroscopic binary from radial vels. 79−62873
- HD 147508, spectroscopic binary, orbit from photoelectric radial vels. 78−69839
- HD 149499, IUE obs. of hottest white dwarf component 80−41828
- HD 14969, IAU radial-velocity standard star, orbit from photoelectric radial vels. 80−56884
- HD 152667 (V861 Scorpii), phys. props. and orbital parameters, supergiant star with black hole companion model 79−71067
- HD 152 667, search for black hole companion 79−48848
- HD 153919, Of supergiant, X-ray binary 3U 1700−37 optical counterpart, light curve anal. 78−32470
- HD 153919 (3U 1700−37), forbidden Fe XIV emission detect. 78−16571
- HD 153919 (3U 1700−37), further spectroscopic obs. 80−4358
- HD 153919 (3U 1700−37), X-ray binary, spectrum variations 78−8158
- HD 153919 (3U 1700-37), binary X-ray source, radial vels. in blue spectral region 78−49556
- HD 153919 (4U 1700−37), SAS-3 obs. of 97 minute periodicity 78−36730
- HD 155989, spectroscopic binary, orbit from photoelectric radial vels. 79−21355
- HD 159176, in HGC 6383, props. and initiation of cluster stars form. 78−41003
- HD 159176, spectroscopic binary radial vel. obs., orbit and masses 79−25644
- HD 159378 (Tr 27-102), yellow variable supergiant near Cepheid instability strip, VBLUW photometry 80−98672
- HD 165052, O-type binary, spectroscopic obs., masses and radii 78−93308
- HD 165590, high eccentricity visual binary, periastron time, radial vel. vars. 78−45363
- HD 165590, visual binary with spectroscopic binary component 78−32519
- HD 166734, Of star, spectroscopic binary orbit determ. from visible obs. 80−82414
- HD 167771, O-type binary, spectrcscopic obs., masses and radii 78−93308
- HD 174237, periodic radial vel. changes, interacting binary with var. mass transfer 79−53818
- HD 175742, spectroscopic binary, orbit determ. with CORAVEL photoelectric radial vel. spectrometer *(French)* 80−36671
- HD 17576, UV subdwarf companion discovery from uvbyβ photometry 78−96479
- HD 179558, spectroscopic binary, orbit from photoelectric radial vels. 79−101177
- HD 181330, spectroscopic binary, orbit from photoelectric radial vels. 78−93320
- HD 187299, spectroscopic binary orbit from photoelectric radial vels. 77−91575
- HD 187299 B, spectroscopic detect., late B-type main sequence star 79−48860
- HD 187399, spectroscopic binary, spectral obs. *(Russian)* 77−49427
- HD 192273, high latitude EUV source, low-mass binary 80−4353
- HD 193793, radio emitting Wolf-Rayet binary star, variable mass flow model 77−45469
- HD 193793, shell condensation around W-R binary, IR obs. 79−12495
- HD 193793, Wolf-Rayet binary, visible and near IR spectra 78−8023
- HD 193793, Wolf-Rayet star, circumstellar dust form. episode 80−31301
- HD 193793, Wolf-Rayet star, photometric evidence for C-rich dust cloud 80−26861
- HD 193793(=BD+43°3571), near IR magnitude increase 77−87413
- HD 193857, metallic-line binary star, orbital elements 79−75250
- HD 197406, Wolf-Rayet spectroscopic binary, radial vels. and orbital elements 80−51812

binary stars continued
- HD 199892, spectrographic binary, spectrograms and orbital elements 79−21359
- HD 200428/9, spectroscopic binary orbit from photoelectric radial vels. 77−5547
- HD 203631, spectroscopic binary orbit from photoelectric radial vels. 80−105285
- HD 214419, Wolf-Rayet spectroscopic binary, light and vel. changes, common envelope model 79−53856
- HD 214686, double-lined spectroscopic binary, orbital elements and masses 79−58376
- HD 216533, Ap star, spectroscopic binary oblique rotator model, spectral var. study 79−101153
- HD 218154, spectroscopic binary, orbital elements 77−87476
- HD 22007 (primary of ADS 16681), spectroscopic binary, radial vel., orbit elements 80−67793
- HD 223969, spectroscopic binary orbit from photoelec. radial vels. 77−82279
- HD 22403, spectroscopic binary with Ca II emission, orbital elements *(French)* 79−53854
- HD 224085, K2e star, long-term variability 79−48849
- HD 224085, spot-covered red dwarf, light curves 77−74093
- HD 224355, spectroscopic binary, revised period and orbital elements *(French)* 77−82278
- HD 226868 (Cygnus X-1), periodicity in optical light curve during X-ray flare 78−81652
- HD 2343, spectroscopic binary, orbit from photoelectric radial vels. 80−8656
- HD 39937, 101379, 155555, 174429, southern RS Canum Venaticorum stars candidates, radial vel. study 80−98686
- HD 4174, symbiotic star, spectroscopic obs. 80−85945
- HD 4174 (=EG Andromedae), peculiar M giant, UV spectra obs. 80−94798
- HD 43930, photoelec. radial vels. and spectroscopic binary orbit 77−33574
- HD 44179, 3.3 micron unidentified feature, high resolution spectra 80−82466
- HD 45088, BY Draconis binary, surface activity from high rot. vel., visible obs. 80−77425
- HD 45088, reticon obs. in red of dK3 spectroscopic binary 80−67778
- HD 45166, dwarf in Wolf-Rayet clothing, spectrum anal. 79−5826
- HD 47129 (Plaskett's star), massive O-star binary system, variable linear polarisation obs. 78−53989
- HD 47732, double-lined binary, spectroscopic orbit 78−57574
- HD 47732, young close binary in NGC 2264, photometry and struct. 78−57575
- HD 49798, H-deficient subdwarf O-type binary, non-LTE spectral anal. 79−16978
- HD 49798, strange composite sdO star, evolution and nature of companion 78−49435
- HD 50896, Wolf-Rayet star, linear polarisation periodic vars. rel. to binary star nature 80−72972
- HD 50896 (WN5), emission-line spectrum and radial vel. vars. 80−51791
- HD 5980, eclipsing W-R binary in SMC, photoelectric light curve 78−45366
- HD 67084, new southern spectroscopic binary, radial vels., orbital elements 78−57592
- HD 67198, new southern spectroscopic binary, radial vels. 78−57592
- HD 698, massive spectroscopic binary, spectral obs., evolutionary state, mass loss 78−57590
- HD 72 754, search for black hole companion 79−48848
- HD 77581 (3U 0900-40), X-ray binary, spectroscopic orbit and masses of components 78−16461
- HD 77581 (=Vela X-1), supergiant+neutron star, X-ray, UV and visible obs. 80−94892
- HD 77581 (Vela X-1), optical pulsations discovery 78−20911
- HD 77581 and 153919, polarimetric obs. of massive X-ray binaries 80−98688
- HD 87892, central star of NGC 3132, as visual binary 78−20859
- HD 90657, Wolf-Rayet spectroscopic binary, spectroscopic obs. 77−13357
- HD 92740, spectroscopic binary WN7 star, spectroscopy and photoelectric photometry 79−8924
- HD 92740, WN star, spectroscopic binary in Carina Nebula association 79−35261
- HD 96953, spectroscopic binary orbit from photoelectric radial vels. 80−56887
- HD 9996, Ap star, precessional effects of mag. field and duplicity 77−2432
- HD 9996, Ap star, spectrsocopic obs. 78−77558
- HDE 226868 (Cygnus X-1), anomalous light curve during X-ray increase of 1975 April-May 78−28850
- HDE 226868 (Cygnus X-1), Hα emission in (1977) 80−51919
- HDE 226868 (Cygnus X-1), He II 4686 Å emission in spectrum 79−21328
- HDE 226868 (Cygnus X-1), line blending effects rel. to black hole candidacy 77−64878
- HDE 226868 (Cygnus X-1), long-term circular polarisation variability 79−9031
- HDE 226868 (Cygnus X-1), orbital period and Hβ light curve 79−48952
- HDE 226868 (Cygnus X-1), orbital period and inclination 78−16579
- HDE 226868 (Cygnus X-1), temporal and spectral var., X-ray rocket obs. 78−8163
- HDE 226868 (Cygnus X-1), UV shot noise upper limit 80−4458
- HDE 226868 (Cygnus X-1), variable linear polarisation, 1974-1975 obs. 77−9810
- HDE 226868 (Cygnus X-1), variable UV polarisation 77−37622
- HDE 226868 (Cygnus X-1), X-ray and UV spectra from HEAO 2 and IUE 80−82543
- HDE 228766, evolved Of system, spectroscopic obs. 78−12237
- HDE 245770, optical counterpart to A 0535+26, dimens. spectral type and luminosity visible obs. 80−72976
- HDE 245770 (A0535+26), spectroscopy and orbital periods 78−93306
- HDE 245770 (A0535+26), UBV photometry during X-ray outburst 79−67024
- HDE 245770 (Ariel 0535+26), optical spectrum of Be star 78−4227
- HDE 283048, evidence for hot subluminous component 78−20823
- Henize 2-38, symbiotic star, steam and CO absorpt. obs. 78−40970

binary stars continued
Henize 788 (Wray 977), counterpart of 3U 1223-62, five colour photometry 77—29846
HZ Hercules, 23 day lo state, Uhuru obs. 77—5594
Hercules X-1, mag. neutron star, cyclotron emission and beaming mechanisms 78—36726
Hercules X-1, X-ray binary, X-ray refl. from neutron star surface 78—28716
Hercules X-1, X-ray spectra, Fe line fluoresc. from subrelativistic shell 78—4405
Hercules X-1, X-ray spectrum of pulse 78—8154
Hercules X-1 (HZ Herculis), 35 day cycle investigation 78—32509
Hercules X-1 (HZ Herculis), hard X-ray obs. 78—36728
Hercules X-1 (HZ Herculis), multiperiod variable star 78—28848
Hercules X-1/HZ Herculis, evaporative winds 77—78888
AK Herculis, atypical W Ursae Majoris type, BV light curves 78—28719
AH Herculis, dwarf nova, changes in rapid oscills. during outburst 79—88686
AH Herculis, dwarf nova outburst, rapid oscills. evolution 80—94805
u Herculis, eclipsing binary, phase-locked polarization 78—4281
HZ Herculis, hard X-ray pulsation obs. 78—12293
AM Herculis, light curves and Fourier analysis 78—49483
α Herculis, location of α^2 Herculis along line of sight 78—73739
α Herculis, mass loss from α^1 Herculis determ. from companion circumstellar absorpt. lines 78—7997
AM Herculis, multicolour photometry, slow optical pulsar 78—28693
HZ Herculis, optical props. of accretion disc 78—28729
AM Herculis, OSO-8 hard X-ray obs. 78—4409
YY Herculis, symbiotic star, radio continuum detect. 79—25615
YY Herculis, symbiotic star, radio emission report refuted 79—35274
AM Herculis, X-ray binary, obs., slow rotator model 78—12408
AM Herculis, X-ray binary, vel. curves for emission lines broad and sharp components 78—32513
AM Herculis (3U 1809+50), IR light curves 78—28727
AM Herculis (3U 1809+50), multicolour linear and circular polarisation obs. and geometrical model 78—8053
AM Herculis (3U 1809+50), soft X-ray results from OSO-8 Wisconsin Expt. 78—36722
AM Herculis (3U 1809+50) system nature, general *(Russian)* 78—4295
HZ Herculis (Hercules X-1), hard X-ray spectrum, strong cyclotron line emission 78—41085
HZ Herculis (Hercules X-1), optical behaviour in (1976) 78—32603
HZ Herculis (Hercules X-1), soft X-ray results from OSO-8 Wisconsin Expt. 78—36722
DQ Herculis (Nova 1934), UBV photometry of visual binary 80—8661
V446 Herculis (Nova 1960), ejecta He abundance 79—92775
V533 Herculis (Nova 1963), 63 sec. oscill., UBV photometry 80—17592
AM Herculis objects, linear polarisation model 78—16460
TU Horologii, ellipsoidal variable, UBV photometry 78—4292
TU Horologii, period and spectroscopic orbit of ellipsoidal binary system 79—58372
hot degenerate stars in steady-state accretion, thermal stability 78—40929
hot main-sequence, eclipsing binaries, masses 78—32514
HR7922, B-type spectroscopic binary, orbital soln. 80—26910
HR8891, B-type spectroscopic binary, orbital soln. 80—26910
HR 1099, 10 GHz radio emission from RS Canum Venaticorum binary 80—82427
HR 1099, Ca II H and K emission enhancement during February 1978 radio flare 79—21341
HR 1099, co-ordinated UV, optical and radio obs. of RS Canum Venaticorum binary 79—16963
HR 1099, flare emission at 2.8 cm (1978 February) 78—32476
HR 1099, Hα region spectrophotometry during February 1978 radio flare 79—21344
HR 1099, H and Ca II, emission during February 1978 radio outburst 79—21340
HR 1099, new bright RS Canum Venaticorum variable, spectrum 77—9754
HR 1099, noneclipsing RS Canum Venaticorum binary, radio flare obs. 77—17632
HR 1099, optical linear polarisation meas. 78—53958
HR 1099, photometric and spectroscopic obs. 1978 Feb. 78—40998
HR 1099, radio flux vars. obs. and optical ephemeris 78—36641
HR 1099, radio obs. 77—64793
HR 1099, RS Canum Venaticorum binary, Hα profile obs. 79—21343
HR 1099, RS Canum Venaticorum binary, nonthermal flare emission during February 1978 outburst 79—21332
HR 1099, RS Canum Venaticorum binary, optical spectrophotometry during major flare outburst 79—21342
HR 1099, RS Canum Venaticorum binary, photoelectric photometry 77—53602
HR 1099, RS Canum Venaticorum binary, rapidly variable polarisation obs. at radio freqs. 79—21336
HR 1099, RS Canum Venaticorum binary, strong radio flaring discovery 79—21330
HR 1099, RS Canum Venaticorum binary, two-freq. radio polarimetry 79—21335
HR 1099, RS Canum Venaticorum binary, VLA radio obs. during 1977 international campaign 79—21334
HR 1099, RS Canum Venaticorum binary star, radio obs. at 8.0 GHz 79—21331
HR 1099, RS Canum Venaticorum star, 4U 0336+01 optical counterpart 78—32475
HR 1099, RS Canum Venaticorum type binary, radio emission detect. 77—9772
HR 1099, RS Canum Venaticorum type binary, strong radio flaring obs. 79—84821
HR 1099, UV spectrum obs. by International Ultraviolet Explorer 78—96475
HR 1099, V photometric obs. during 1976-77 period 78—40994
HR 1099, X-ray outburst obs. from RS Canum Venaticorum star 78—81658
HR 1099 (V711 Tauri), Copernicus UV obs. of Lyman α and Mg II emission 78—81651
HR 1099 (V711 Tauri), JHK photometry of noneclipsing RS Canum Venaticorum type star 80—72995
HR 1099 (V711 Tauri), RS Canum Venaticorum star, Hα line variability, visible spectra obs. 80—105277
HR 1300 spectroscopic binary Am star, orbital elements 77—49438

binary stars continued
HR 2081, double-lined spectroscopic binary, radial vel. orbit and min. masses 80—51811
HR 2142 and 7084, mass loss from UV spectra obs. 80—109485
HR 2172, double-lined binary, radial vels. and equivalent widths *(French)* 77—17625
HR 2317, spectroscopic binary orbit from photoelectric radial vels. 79—40225
HR 4665, spectroscopy of bright long-period RS Canum Venaticorum system 80—36665
HR 5049, spectrogram meas. with digital microdensitometer 77—64655
HR 5110, RS Canam Venaticorum binary, V photometry near radio outburst time 80—90469
HR 5110 (HD 118216), RS Canum Venaticorum binary, radio flaring obs. 79—67053
HR 5161, spectroscopic binary star, radial vel. orbit 80—12781
HR 5999, variable shell star and visual binary, VBLUW, photometry 78—28701
HR 6094, gravit. redshift of white dwarf component (CoD−38°10980) 78—24511
HR 6388, spectroscopic binary, orbit determ. from photoelec. radial vels. 78—49482
HR 6392, double star with very high luminosities 77—45493
HR 6659, spectroscopic binary, radial vel. obs. 80—82430
HR 6902, radial vel. and orbital elements of new spectroscopic binary 78—69826
HR 6940, spectroscopic binary orbit from photoelectric radial vels. 78—4294
HR 7083, spectroscopic binary, orbit from photoelectric radial vels. 78—32517
HR 8752, superluminous star, hot companion discovery by IUE 79—16947
HR 8752 emission feature variability, visible obs. 80—109463
HR 8800, precession period determ. from spectroscopic data 79—67062
HR 9049, new eclipsing binary, discovery and photometry 78—12243
HR 976, Am-type star, soft X-ray source obs. 78—81634
Hubble-Sandage variables, mass accretion model 80—26877
EX Hydrae, U Geminorum type star, possible counterpart of (4U 1249-28) 78—36729
RW Hydrae, UV obs. of hot component 80—56854
χ^2 Hydrae, uvby light curves of double-lined eclipsing binary 78—40996
VW Hydri, dwarf nova, model 79—16977
WX Hydri, dwarf nova, obs. of superhumps during supermaximum 79—88677
VW Hydri, dwarf nova, short period light oscills. 78—20837
VW Hydri, light curves of dwarf nova 78—12245
HZ 29, binary white dwarf system, evolution and gravit. radiation 77—57030
HZ 43, visual binary, photographic measures 77—5548
I-38, probable B-type binary in Norma OB1 assoc. 80—62129
IDS 10275S5312, visual double, rectilinear trajectories calc. *(French)* 79—17023
IDS 19062S3401 (AB), visual double, rectilinear trajectories calc. *(French)* 79—17023
IDS 19465S1036 (AB), visual double, rectilinear trajectories calc. *(French)* 79—17023
interacting binary stars, book 79—8953
interstellar communication, binary stars use as time markers 79—101092
Jeans spheroids with toroidal mag. fields, equilib. and stability 78—45319
JL 76, spectroscopic obs. of DC white dwarf candidate 77—67090
Kuiper 41, orbit and flare activity of visual red dwarf pair 79—97032
16 Lacertae, β Cephei star, light var. anal. and photoelec. photometry 80—77412
AR Lacertae, double-subgiant eclipsing binary, spectra, abundances 78—8044
RT Lacertae, eclipsing double-lined spectroscopic binary, light curve soln. 78—32511
AR Lacertae, Fourier anal. of light curves, gas stream effects 78—20855
5 Lacertae, obs. of second max. for long period spectroscopic binary 78—57591
AR Lacertae, RS Canum Venaticorum type star, UV excess, spectrophotometric obs. 78—8043
AR Lacertae, RS Canum Venaticorum type star, VLA obs. 78—8054
AR Lacertae, RS Canum Venaticorum type variable, soft X-rays detect. 78—45362
CP Lacertae (Nova 1936), ejecta He abundance 79—92775
AR Lacertae-type stars, starspots 78—16443
Lapace equations, partial separability Roche coordinates 79—44524
late B-type stars, duplicity characts. 78—57547
late-type spectroscopic binary stars, search for Ca II H and K lines 77—33551
LDS 678B (EG 131), white dwarf, spectrum 78—40946
LDS 720-BC, visual binary with flare star, orbit calc. 77—13391
LDS 720BC (CD−32° 16135), visual binary, orbit 78—32515
LDS 785A (EG 153), DB white dwarf, discovery of H 77—45425
γ Leonis, masses and K-line absolute magnitudes 80—8649
AD Leonis, X-ray emission from flares, HEAO 1 obs. 80—41837
ω Leonis (ADS 7390), orbital elements and removal of nodal ambiguity for visual binary 77—13399
19 Leonis Minoris, spectroscopic binary, orbital elements and mass ratio 80—62197
δ Librae, Algol-type eclipsing binary, detection of secondary 78—49475
lifetime of binary stars 79—44563
light and velocity curves simultaneous solution, eccentric orbit generalisation 80—36664
LMC X-4, discovery of X-ray eclipses 78—24572
LMC X-4, obs. of X-ray eclipses 78—24571
LMC X-4, X-ray variability obs. 78—4398
long-period close binaries, general relativistic periastron advances 77—91564
low mass close binary evolution, catastrophic mass loss 77—33554
LS I+61°303, variable binary radio star (B1 Ib), X-ray emission detect. 80—105400
LSI+61°303, counterpart of γ-ray source CG 135+1 and highly variable radio source 78—54095
LSS 1916, 3371, new VV Cephei stars, spectra and colours 79—35299
luminous composite stars in the Large Magellanic Cloud 79—58375
lunar occultation obs. from University of Illinois Prairie Observatory (1977-1978) 80—105148
lunar occultations, photoelec. obs. 78—4079

binary stars continued
lunar occultations, photoelec. obs. 79—5819
lunar occultations, photoelectric obs. at McDonald Observatory 77—2331
lunar occultations of Hyades, photoelec. obs. 80—72921
lunar occultations photoelec. obs. 80—72920
β Lyrae, nature of disc around secondary component 78—16458
β Lyrae, nature of secondary component from radio emission 78—36638
β Lyrae, optical and IR photometry, gaseous disc electron density distrib. 78—28722
β Lyrae, photoelectric photometry (in 1971) 78—12294
MV Lyrae, polarisation and spectrum obs., polar class candidate *(Russian)* 78—93322
β Lyrae, UV spectrum 78—8048
β Lyrae primary and secondary, catalogue of absorption lines *(Russian)* 78—28725
in M15, globular cluster, binary stars form. rel. to X-ray source 78—32536
magnetic binaries, charged particle motion 78—69828
magnetic binary problem, charged particle motion stationary solns. for oblate spheroid primaries 80—41697
magnetic field generation by close binary interaction 80—26903
magnetic variables, intrinsic rot. vels. of spectroscopic binaries and single stars 78—40967
magnetic white dwarf in binary system, collapse, mass ejection, nova mechanism 78—32485
main sequence, absolute dimens. determ., errors requirement review 80—109473
main sequence stars, freqs. of binaries 80—26901
main sequence stars in close binary systems, rapid mass accretion effect 77—91578
main-sequence binaries, Roche constants 79—35297
mass accretion onto massive white dwarfs, rel. to thermonuclear runaways 80—41822
mass ratios and freq. in open clusters, rot. effects 78—36639
mass ratios distribution, $q(\alpha)$, in spectroscopic binaries, redeterm. 79—21356
mass transfer and accretion disc flow, numerical simulation 77—57035
mass transfer instability in semidetached binary systems 78—8047
mass-exchanging binary stars, XUV emission *(German)* 80—109372
mass-radius relation, in close binary systems 78—12290
massive accreting white dwarfs in close binary systems, H shell flashes 79—75203
massive binaries, evolution review 80—82343
massive close binaries, evolution of systems with primaries of 10-15 $M_{\odot}$ 77—87473
massive close binaries, post-supernova stage, tidal instability 77—57024
massive close binaries evolution, final considerations for conservative case 78—49479
massive close binaries with OB components, evolutionary calcs. comparison with obs. 80—90474
massive close binary stars, effect of stellar evolution on components synchronous rot. 80—62192
massive close binary systems, evolution 77—57022
massive close binary systems, late evolutionary stages 77—57023
massive spectroscopic binaries, anal. rel. to low eccentricity orbits detect. 79—67060
massive stars, effects of binary evolution on heavy elements prod. 80—46534
massive stars ($M \gtrsim 50\ M_{\odot}$), binary star mass transfer model rel. to evolutionary status *(Russian)* 80—109425
massive X-ray binaries, evolution of optical components 80—41857
massive X-ray binaries, lifetimes 77—45608
massive X-ray binaries, OB stars, evolutionary influence of stellar wind 79—101172
massive X-ray binaries, Roche lobe overflow 79—35301
massive X-ray binary systems, pulsars rot. history 77—49412
metal-poor binaries, He abundance determ. 78—81660
MHD processes near compact superdense objects in binaries 79—40206
Michelson stellar interferometer for binary star obs. 79—44370
AT Microscopii, X-ray emission from flares, HEAO 1 obs. 80—41837
minimum projected distance in eccentric binary orbits, calcs. 80—26904
model for horizontal energy transfer 77—57051
V616 Monocerotis (A 0620—00), UBV photometry 80—56846
multiplicity of solar-type stars 79—44543
θ Muscae, Wolf-Rayet binary, spectrum and photometry 77—22235
MWC 349, IR source optical identification with reddened high-luminosity star 80—56971
MWC 349, possible model of emission line star *(Italian)* 79—48829
MWC 349, separate spectra of components of visual binary 79—48858
MXB 1636-536, binary nature from simultaneous X-ray and optical obs. 80—82548
MXB 1730—333, rapid X-ray burster, accreting rot. magnetised neutron star model 79—84866
MXB 1730—335, comparison with dwarf novae rel. to neutron star model 78—12410
MXB 1837+05 (Serpens X-1), detect. of optical burst coincident with X-ray burst 80—27013
nearby stellar systems, ranking method for exploration 78—81522
nearly collisionless spherical accretion, theory 78—12090
neutron star, accreting, magnetopause struct. 78—65647
neutron star binaries, observational constraints on masses 77—5543
neutron star binaries formation rel. to gravit. radiation 79—35291
neutron star free precession, role of vortex pinning 77—49420
neutron stars, electrodynamics of disk acrretion, magnetic field structure 80—85973
neutron stars, in close binary systems, X-ray source model *(German)* 79—84814
neutron stars, magnetised, accretion, fate of sinking filaments 80—51798
neutron stars, rotating, magnetic, accretion flow inside magnetosphere rel. to rot. rate 78—8037
neutron stars and compact X-ray sources, properties, general description *(Danish)* 77—67106
neutron stars in close binary systems, spindown rates 79—40210
new double stars discovered at Nice, 15th series *(French)* 79—35304
NGC 2281, open cluster, UBV photometry, binary star freq., luminosity function 78—81663
NGC 2287, open cluster, spectral classification of brightest stars 80—26919
in NGC 6231, open cluster, double lined spectroscopic binaries discoveries 80—90492

binary stars continued
NGC 7293 (Helix nebula), complex struct. due to mass losing binary companion 79—48895
non-synchronous stars in close binary systems, stability 79—40223
nonejecting novae as EUV sources 78—12238
Nova Cygni 1975, stellar wind and light vars. 77—82237
Nova Cygni 1975 (V1500 Cygni), spectroscopic developments and kinematics 77—45446
Nova Ophiuchi 1977 (H1705—25), X-ray light curve 78—49453
Nova Ophiuchi 1977 (H1705—25), X-ray nova, HEAO 1 obs. 78—49452
nova-like variables, photometric obs. 77—82245
novae, accretion belts on white dwarfs 78—36582
novae, effect of binary companion on outburst 80—82394
novae, effects of white dwarf rot. on remnants shapes 80—105244
novae, low-temp. photonuclear p-nuclei nucleosynthesis in degenerate H burning zones 78—57540
novae, spectrophotometric estimate of electron density in rapidly rot. accretion discs 79—16968
O-type binaries, binary freq. and anomalous mass ratios 80—109478
O-type binary and stellar wind search 78—89197
O-type stars, kinematics, close binary evolution and ages 79—101145
O-type stars, radial vels. and freq. of spectroscopic binaries 77—56922
OB binary stars, evolutionary sequence to X-ray stars and pulsars, tugboat model 77—56915
OB supergiant X-ray binaries, line distortion effects 78—7995
OB supergiants, mass loss and massive binary evolution 77—57020
OBN, OBC stars, short period binaries frequency 78—53951
old novae, search for rapid photometric oscills. 78—4251
open clusters, dynamics of close binaries and single stars *(Russian)* 78—61890
in open clusters, estimation of freq. of binary stars, comparison of methods 77—49441
in open star clusters, distribs. of secondary masses 77—53626
Y Ophiuchi, anomalous Cepheid, evidence for duplicity 78—53990
XX Ophiuchi, emission line star, near IR spectrum of cool component 77—49404
RS Ophiuchi, recurrent nova, spectrum obs. 79—62848
optical doubles, proper motions from rectilinear trajectories and SAO catalogue *(French)* 79—30089
orbit calculation method for double stars *(French)* 79—92801
orbital eccentricity effect on polarimetric obs. 80—109472
orbital elements and run-away vels. caused by symmetric explosion 77—91570
orbital elements calc. using Fourier transform of eqns. 77—56832
orbital elements for 15 visual binaries 78—85969
orbital inclination, polarimetric determ. for five systems 78—45358
orbital inclinations of spatially close spectroscopic doubles *(German)* 79—44532
orbital solutions with unseen companions, measured coordinates interpretation 78—93313
orbits for 24 visual binaries *(Russian)* 79—25646
δ Orionis, apsidal motion of spectroscopic binary 79—8952
42 Orionis, Copernicus UV spectra and IR photometry 77—49437
χ^1 Orionis, new solar-type astrometric binary, parallax and orbital elements 78—73740
ι Orionis, O VI P Cygni profiles hourly vars. 77—37596
δ Orionis, spectroscopic binary, spectrophotometry *(Russian)* 77—64802
θ^2 Orionis A, 4U 0531—05 optical candindate, Copernicus obs. 79—67050
λ Orionis A, far UV flux, emission line obs. of surrounding H II region 78—93303
δ Orionis A, O VI Cygni profiles hourly vars. 77—37596
θ^2 Orionis A, stellar wind driving of high-vel. features in Orion Nebula 79—8978
σ Orionis E, peculiar eclipsing binary, linear polarization obs. 78—32508
particle acceleration in close binary systems 79—58382
particle discs, infrequently colliding, in binary system, tidal torques and appl. to asteroid belt truncation 80—98596
peculiar bright southern stars, identification and spectral types 77—82225
EQ Pegasi, active dwarf binary star, chromospheric emission lines obs. 80—12762
AU Pegasi, binary Type II cepheid, photometric and spectroscopic study 80—26866
RU Pegasi, dwarf nova, rapid and ultrarapid light vars. 77—53596
AW Pegasi, eclipsing binary, photometric elements, masses, radii, luminosities 78—28723
57 Pegasi, long-period pulsating variable, spectrographic and photometric obs. 79—21305
AG Pegasi, OAO 2 UV obs. of symbiotic binary 79—53814
κ Pegasi, radial vel. meas., visual binary with spectroscopic binary component 78—32520
AG Pegasi, symbiotic binary system, UV and optical spectrum rel. to nature of components 80—109449
AG Pegasi, symbiotic nova, radio emission obs. 77—22232
57 Pegasi, visual binary, radial vel. meas. 79—21347
EQ Pegasi (BD+19°5116), flare active binary system 78—61868
II Pegasi (HD 224085), surface-active binary star, spectroscopic obs. 80—90480
period-finding technique, Fortran IV computer program 79—21195
periodic polarization variations in rotating astrophysical systems 79—88585
periods connection with interstellar cloud rotation rates 77—33584
X Persei, 580 day and other periodicities 78—16435
φ Persei, binary Be star, He II emission obs. rel. to components masses 80—12768
AW Persei, binary cepheid variable, radial vel. meas. 77—74072
X Persei, distance determ., 3U 0352+30 optical counterpart *(Chinese)* 78—69836
UV Persei, dwarf nova, characts. of outbursts 79—71052
X Persei, energy distrib., light vars. 1972-76 period 78—16437
12 Persei, masses and luminosities from speckle interferometric obs. 78—93305
IW Persei, metallic-line close binary star, photometric and spectroscopic obs. 80—62186
φ Persei, model for Be-star binary system 77—60782
X Persei, photometric behaviour, 1964 to 1979, and binary star model 79—53820
1 Persei, photometric variability, possible eclipsing binary 78—32489

binary stars continued
b Persei, UBV photometry and spectroscopic study of ellipsoidal variable 80−36666
X Persei, V-band polarization variability 78−49455
7 Persei, visual binary, radial vel. meas. 79−21347
20 Persei, visual binary, radial vel. obs. 78−73736
GK Persei, X-ray outburst detect. from old nova 79−67033
X Persei, X-ray spectra, binary model 79−25757
X Persei (2U 0352+30), photoelec. obs., light vars. 78−40999
X Persei (2U 0352+30), spectral line variations *(Russian)* 78−65655
X Persei (3U 0352+30), eccentric close binary model 77−29879
X Persei (3U 0352+30), photometry, search for optical 13.9 minute period 78−16426
X Persei (3U 0352+30), reality of massive companion questioned 77−13495
X Persei (3U 0352+30), simultaneous X-ray and ground-based optical obs. 80−17591
X Persei (3U 0352+30), UBVRI photometry 78−8049
X Persei (4U 0352+30), Be star, evidence for 6-year photometric periodicity 80−109446
X Persei (4U 0352+30), light vars., tidal distortion by massive unseen companion 78−36640
β Persei (Algol), anal. of red and IR wide-band photometry 78−20853
β Persei (Algol), gas stream producing absorpt. features in red wings of Mg II reson. lines 78−24524
V400 Persei (Nova Persei 1974), photoelectric obs. 78−4252
perturbation analysis techniques 79−44379
photospheric circulation, nonuniformly heated surface 79−96993
δ Pictoris, β Lyrae-type eclipsing binary, satellite UV obs. 77−57033
RR Pictoris, accretion disc radiation of cataclysmic binary 77−91537
64 Piscium, double line spectroscopic binary, orbital elements *(French)* 79−35305
UV Piscium, RS Canum Venaticorum star, identification with X-ray source H0118+067, X-ray obs. 80−101654
RZ Piscium, UBV photometry, light minima *(Russian)* 78−93323
planet formation, Goldreich-Ward planetesimal accretion 78−61883
planetary companions, statistics 77−91572
planetary nebulae central stars, list of binary systems 80−109435
planetary nebulae formation with close binary nuclei 79−71097
planetary orbit stability, Hill's method appl. 80−94834
planetary orbits in binary stars, stability and habitability 78−4291
planetary systems, spectrographic search of nearby stars 77−78827
point source orbiting Schwarzschild black hole, polarised radiation props. 77−67109
polarisation by Thomson scatt. in optically thin envelopes, appl. to binary inclinations determ. 78−81655
polarised radiation from stars with nonuniform surface brightness distrib. 77−17549
polytropes in central orbits, Roche problem 80−82179
PSR 0329+54, binary motion to explain freq. variations 80−26894
PSR 0820+02, long-period binary pulsar, discovery from timing obs. 80−56867
PSR 1913+16, astrometry and photometry of stars in vicinity of binary pulsar 78−93219
PSR 1913+16, binary pulsar, appl. of bimetric gravit. theory 78−45347
PSR 1913+16, binary pulsar, companion star possible optical obs. 79−84823
PSR 1913+16, binary pulsar, components min. projected distance calc. 80−26904
PSR 1913+16, binary pulsar, confirmation of existence of gravit. waves *(French)* 79−80495
PSR 1913+16, binary pulsar, dipole gravitational radiation, Rosen's theory 77−26021
PSR 1913+16, binary pulsar, general relativistic effects meas. 79−35286
PSR 1913+16, binary pulsar, gravit. radiation in alternative metric theories 77−60589
PSR 1913+16, binary pulsar, nature from observational data 80−77435
PSR 1913+16, binary pulsar, optical pulses upper limit 77−26020
PSR 1913+16, binary pulsar, optical source and general relativistic effects 80−56868
PSR 1913+16, binary pulsar, origin through X-ray binary double core evolution 79−84816
PSR 1913+16, binary pulsar, Poincare gauge theory of gravitation 79−75434
PSR 1913+16, binary pulsar, post-Newtonian timing effects 78−4261
PSR 1913+16, binary pulsar, relativistic observable effects 80−77438
PSR 1913+16, binary pulsar, report 79−75234
PSR 1913+16, binary pulsar, test of new dispersion-removing radiometer 79−35142
PSR 1913+16, binary pulsar obs. at 327, 408, 610 and 1420 MHz 77−78810
PSR 1913+16, binary system, test of relativistic effects *(Dutch)* 80−62172
PSR 1913+16, Hulse-Taylor binary pulsar and gravitational spin precession 78−12264
PSR 1913+16, optical candidate discovery, position, magnitude 78−69819
PSR 1913+16, X-ray and timing meas. correlations, grav. radiation, gas cloud friction 80−62171
PSR 1913+6, binary pulsar, relativistic astrophysics *(German)* 79−80213
PSR 1952+29 and 1929+10, evidence of binary system disrupted by supernova explosion 79−35285
pulsar binary origin and asymmetric supernova explosions 78−69816
pulsar/supernova remnant associations, possible origin in close binary systems 78−85965
pulsars, neutrino emission 79−2550
pulsars, radio and X-ray, review 78−69820
pulsars, relation between speed ups and variation of gravitational constant 78−73728
pulsating X-ray sources, secular period changes 77−45613
pulsating X-ray sources period vars., torque vars. and stellar response 79−9029
VV Puppis, brightening, emission line spectrum 78−40960
V Puppis, eclipsing binary, as main sequence contact binary 78−4293
T Pyxidis, recurrent nova, photoelectric obs. 78−4252
radial velocities, of variable velocity stars previously observed at David Dunlap Observatory 79−101141
radial velocity curves of close binary systems, anal. 80−90470
radial velocity curves of close binary systems, anal. 80−94829

binary stars continued
radiation pressure force influence on critical surfaces 78−96505
radiative tides in accretion disks 79−48853
radio emission survey of variable and peculiar stars 77−22248
recurrent novae, magnitude-frequency relation 78−28699
red degenerate stars pair, parallax 78−12224
red giants, enhancement of mass loss by duplicity 77−56928
red supergiant close binary in open cluster NGC 3105, photoelectric UBV obs. 77−64811
relativistic corrections of gravit. force, radiation damping 79−97272
relativistic effects in many body systems, self acceleration 80−8863
resonances, formal third integral eqn. of motion *(Russian)* 77−57062
Roche and Darwin problems for polytropic stars, numerical study 79−75202
Roche lobe formation in highly eccentric X-ray binary systems 80−41858
Ross 614, parallax, orbit and mass of astrometric binary 77−91565
rotation, ang. moments mass depend. rel. to self-similarity 80−36490
Rst 4036, red-dwarf binary star, orbital period and total mass 80−12780
HM Sagittae, eruptive variable, IR variability rel. to symbiotic binary model 79−25614
V Sagittae, light curve coherent oscills. 78−8022
HM Sagittae, new spectroscopic obs., simultaneous presence of increasing excitation and cool features 80−26874
HM Sagittae, possible symbiotic star, optical and IR obs. 78−36575
WZ Sagittae, recurrent nova, photometric study at minimum light 78−24513
HM Sagittae, symbiotic star, IR variability obs. from VJHKL photometry *(Russian)* 80−105263
V356 Sagittarii, unusual eclipsing binary, model 78−49477
SAO 015338, optical counterpart of 2A 1052+606, RS Canum Venaticorum type binary 79−21352
SAO 015338, possible RS Canum Venaticorum star and counterpart of 2A 1052+606, spectrum 80−22118
SAO 114159, duplicity detect. from occultation by 18 Melpomene 79−16870
SAO 114159, occultation by 18 Melpomene, secondary extinction event obs. 80−56749
α Scorpii, circumstellar absorption lines in UV spectrum 80−51804
V 701 Scorpii, early type eclipsing binary, contact props. 78−8051
α Scorpii, location of α^2 Scorpii along line of sight 78−73739
α Scorpii (Antares), spectrum of nebula 78−41014
V861 Scorpii (OAO 1653−40), near IR obs. of single line spectroscopic binary 80−8652
V818 Scorpii (Scorpius X-1), UV, visible, IR and X-ray obs. 80−82541
β Scorpii A, spectroscopic orbit 79−67059
α Scorpii AB, mass loss and circumstellar absorption lines 79−8916
Scorpius X−1, interstellar extinction and UV flux distrib. 79−25754
Scorpius X-1, extended X-ray obs. with Bragg crystal spectrometer 79−12543
Scorpius X-1, high energy X-ray and SHF radio obs. 80−73067
Scorpius X-1, high energy X-ray obs. with Ariel V 80−17694
Scorpius X-1, light and colour curve of periodic variation 77−49497
Scorpius X-1, linear X-ray polarisation obs. 79−101221
Scorpius X-1, linear X-ray polarisation upper limit 77−49503
Scorpius X-1, linear X-ray polarisation upper limit 78−49557
Scorpius X-1, mass-exchange binary characts. 77−57046
Scorpius X-1, Prognoz-6 obs. of X-ray fluxes and energy spectra *(Russian)* 80−109562
Scorpius X-1, rapid variability simultaneous X-ray and optical obs. 80−62322
Scorpius X-1, X-ray binary, spectrum calc. 77−29881
Scorpius X-1, X-ray obs. from 20 to 250 keV 80−94893
Scorpius X-1, X-ray spectrum 20-75 keV, high sensitivity determ. 80−98741
Scorpius X-1 review 78−16576
VY Sculptoris, novalike variable, precise position 80−101597
VY Sculptoris, novalike variable, spectrum during faint state 80−98675
δ Scuti and RRs stars, duplicity rel. to tidal modulation and amplitudes 77−87432
semi-detached systems, revised photometric elements 78−20858
semi-major axes of binary systems 77−57059
semidetached binaries, mass transfer and impact-driven accretion discs 77−57036
separation meas. using speckle interferometry 77−22102
separation measurements by speckle interferometry 79−40215
Serpens X-1 (4U 1837+04), burster optical binary counterpart visible spectra and photometry 80−94891
RT Serpentis, symbiotic star/nova, possible H_2O maser obs. 79−8932
RT Serpentis (Nova 1909), spectrum in 1964, 1975 and (1978) 80−46566
41 Sextantis A, new metallic line spectroscopic binary 78−53982
shell star, optical counterpart of GX304−1 (4U 1258−61), spectrum 80−46582
short period, X- and γ-ray bursts from mag. reconnection 78−81654
slow nova, evolution of model with Z=0.03 envelope from pre-explosion to extinction 78−32468
slow nova, hydrodynamic study of outburst 78−40954
slow novae and symbiotic stars, late-type components spectral classifications 80−94813
SMC X-1, pulse profile and refined orbital elements 78−8148
SMC X-1, VBLUW photometry, evidence for accretion disc 78−12409
SMC X-1, X-ray binary, spin-up rate meas. 78−41083
SMC X-1 (SK 160), spectroscopic orbit and masses 78−4285
SMC X-2, Be-type optical candidate 78−77619
SMC X-2, UBV photometry of proposed optical counterpart 79−67116
solar companion star effects on orbits of comets 78−81567
solar type stars, relation between metallicity and multiplicity 77−78788
solar-type stars, fraction having stellar or massive nonstellar companions 78−16463
southern double stars, magnitude differences, focal grating photometer obs. 80−67785
southern spectroscopic and eclipsing binaries, cooperative obs. feasibility 78−69681
southern visual binaries, orbits and masses 78−96502
southern visual double stars, meas. at Cerro Tololo Observatory 78−8057
southern visual double stars, measures 79−21360
speckel interferometry of 155 objects 79−17017
speckle, interferometric measurements of binary stars 79−71065

binary stars continued
  speckle interferometric obs., with Haute-Provence 1.93 m telescope 80—90475
  speckle interferometric observations, of spectroscopic and visual binary stars 80—90477
  speckle interferometry, atmosphere turbulence effect ang. depend 79—101080
  speckle interferometry at 5200 Å for 30 objects 78—65656
  speckle interferometry meas. 78—85973
  speckle interferometry of binary stars, computer simulations in photon-counting mode 78—53836
  spectrophotometric identification of late type binaries in open clusters 79—44548
  spectroscopic, Ca II H and K line emissions in late-type giants and supergiants 77—91566
  spectroscopic, in open cluster NGC 6475, radial vels. 77—87488
  spectroscopic, in Seventh Catalogue of spectroscopic Binaries, orbital elements statistical anal. 80—82422
  spectroscopic, spectral obs. with solid state detector 80—109469
  spectroscopic, statistical investigation 80—109466
  spectroscopic and eclipsing binaries, survey for intrinsic linear polarization 78—4288
  spectroscopic binaries, Barr effect anal. 80—8650
  spectroscopic binaries, models for distrib. with respect to primary mass, mass ratio and orbital semiaxis 80—46616
  spectroscopic binaries, precession period determ. from spèctroscopic data 79—67062
  spectroscopic binaries, properties of 826 stars 79—97037
  spectroscopic binaries, single-line, nature of secondary stars from X-ray obs. 80—31329
  spectroscopic binaries, test of circularity of orbits 78—93321
  spectroscopic binaries, thirteenth complementary catalogue *(French)* 77—22112
  spectroscopic binaries in NGC 2516, radial vels. from objective prism plates *(German)* 78—45360
  spectroscopic binaries in young SMC cluster NGC 330, limits on frequency 80—67803
  spectroscopic binaries near southern open clusters, relative radial vel. obs. *(German)* 80—94724
  spectroscopic binaries with Ap star components, characts. *(German)* 77—17590
  spectroscopic binaries with nearly identical components, significance 79—48856
  spectroscopic binary member of visual double, mass determ. method *(French)* 79—44549
  spectroscopic binary orbits, catalogue improvements 77—78665
  spectroscopic binary star orbits solution, Fourier transform method 80—26899
  spectroscopic binary systems, apsidal motion 80—82413
  spectroscopic binary systems orbital elements, seventh catalogue 79—16843
  SS 433, accretion disc viscosity determ. using slaved disc model 80—62110
  SS 433, binary star model including mag. white dwarf 80—4385
  SS 433, early-type binary model 80—56843
  SS 433, light curves, double peak and binary-like period, photometry 80—94804
  SS 433, magnetic X-ray binary model 80—109447
  SS 433, mass loss rates and lifetime from W50 optical filaments 80—12804
  SS 433, nature and evolutionary state *(Russian)* 80—36647
  SS 433, Of star orbited by neutron star, model 80—22025
  SS 433, period and evidence for eccentric orbit from IR light curves 80—8642
  SS 433, review of obs. and theories 80—72987
  SS 433, spectral features interpreted a precessing neutron star with jets, possible binary 80—90447
  SS 433, spectroscopic obs. and probable binary nature 80—51780
  SS 433 model, precessing jets in ultra-close binary system 80—4384
  stability criterion, from influence of nonsphericity and radiation press. on stellar moment of inertia 78—28658
  static two-body problem and attraction law, post Newtonian approx. 78—93574
  static two-body problem and attraction law, post-post-Newtonian approx. 79—117
  statistical distrib. and evolution *(Chinese)* 80—85975
  steady accretion disk, with magnetic field, basic equations 79—40179
  steady disc accretion, ang. momentum transfer 78—65609
  Stein 2051 AB, white dwarf formation 79—44483
  Stein 2051B, temp. and radius of cool white dwarf 77—13338
  Stephenson-Sanduleak 433, nature, special relativistic effects, binary model 79—88679
  Sun, companion influencing comet orbits 80—31260
  Sun, possible existence of companion star 78—12198
  Sun, possible neutron star or black hole companion props. 79—2490
  Sun, reality of companion star questioned 78—57475
  Sun+proto-Jupiter, appl. to solar system origin 79—8856
  supercritical accretion discs winds struct. and appearance, numerical models 80—21984
  supermetallicity and the strong-lined binary systems 79—75204
  supernova explosions in binary systems, rel. to origin of runaway stars 78—32448
  supernovae in binary systems, rel. to HD 108 possible collapsed companion 77—13369
  surface nucl. reactions and origin of mag. fields 80—101616
  suspected unresolved visual binaries, reexamination 78—40993
  symbiotic star candidates in LMC, optical spectroscopy and IR photometry 80—62139
  symbiotic stars, binary model with super-critical accretion 77—45458
  symbiotic stars, evolutionary considerations 80—62144
  symbiotic stars, IR variability and nature 77—49399
  symbiotic stars, models, spectral characts. *(Polish)* 79—88689
  symbiotic stars, origin and evolutionary stage *(Russian)* 77—17616
  symbiotic stars and classical novae, optically thick winds 77—87450
  symbiotic stars and recurrent novae, high speed photometry 77—60799
  symbiotic stars and slow novae, late-type components spectral classifications 80—94813
  V711 Tauri, call for optical and IR obs. during, 1977 Oct. 77—67114
  V711 Tauri, change in nature of light curve, and flare, 1979 October to December 80—26906
  θ^1 Tauri, double star, lunar occultation obs. 79—67052

binary stars continued
  λ Tauri, eclipsing binary, photometric elements, masses, radii, luminosities 78—28723
  δ Tauri, Hyades giant, identification as spectroscopic binary 77—64794
  51 Tauri, Hyades spectroscopic binary, speckle interferometry 77—29876
  ζ Tauri, near UV spectrum of shell star 78—81653
  V711 Tauri, radio flare on 1978 Nov. 6 at 15.5 GHz 79—5836
  V711 Tauri (HR 1099), 1977-1978 photometry before radio outburst 79—21337
  V711 Tauri (HR 1099), 1978 photometry during radio outburst 79—21338
  V711 Tauri (HR 1099), February 1978 radio flare obs. 80—26911
  V711 Tauri (HR 1099), Lyman α H I and D I interstellar absorption 80—8658
  V711 Tauri (HR 1099), RS Canum Venaticorum star, BV light curve during (1978-79) 80—105279
  V711 Tauri (HR 1099) and related Ca II emission binaries, Hα emission survey 79—21339
  T Tauri stars, radial vels. rel. to spectroscopic binaries freq. 77—56921
  BL Telescopii, eclipsing binary, unusual variability of bright supergiant companion 77—64797
  RR Telescopii, slow nova and symbiotic stars 77—82256
  RR Telescopii, symbiotic star, steam and CO absorpt. obs. 78—40970
  thermonuclear flashes on accreting neutron stars 80—31321
  tidal distortion of primary star, oscill. freq., perturb. method 77—22206
  tidal fields, d'Alembert's principle and test rigid rod 78—40812
  tidal torques on accretion discs in binary systems with extreme mass ratios 79—40224
  tidal torques on circumbinary accretion discs, theory, contact binaries appl. 79—70952
  tidally distorted stars, Roche coords. appl. to small oscills. 78—77577
  tidally-distorted stellar models small oscills., Roche coordinates appl., second-order terms effect 79—44462
  transient X-ray sources, eccentric orbit binary model 77—53703
  α Trianguli, radial vel. vars. from microdensitometer scans of photographic spectra 79—25642
  RW Trianguli, short-period close binary, circumstellar material size and brightness vars. 78—32512
  EK Trianguli Australis, peaks in lightcurve during 1979 June outburst 79—75222
  EK Trianguli Australis, SU Ursae Majoris dwarf nova, superhumps, light curve UBV obs. 80—105255
  twisted accretion discs, time-dependent eqns., X-ray binary systems appl. 79—12395
  twisted accretion discs in binary systems 77—53632
  two rigid body motion under mutual gravitational attraction 78—28490
  two-body restricted problem, almost circular orbits in general relativity *(Ukrainian)* 79—101056
  4U 0115+634, X-ray binary, 1980 Aug. photometry and spectroscopy 80—101650
  4U 0115+63, binary X-ray transient, obs. 79—92890
  4U 0115+63, orbital elements and nature of hard X-ray transients 78—93470
  4U 0115+63, pulsating X-ray transient, optical counterpart identification and orbital period 78—61939
  4U 0115+63, transient X-ray binary, absorpt. feature discovery at 20 keV 78—69909
  4U 0115+63, transient X-ray source, optical and X-ray obs. 78—32605
  4U 0115+63, X-ray transient, position and pulse profile 78—93467
  3U 0352+30, evidence for 581 day modulation in X-ray pulse period 77—53708
  3U 0352+30 (X Persei), OSO-7 hard X-ray obs. 77—26085
  3U 0614+09, possible low-mass binary X-ray burst source 78—32610
  4U 0900—40, pulsating X-ray binary, search for periodic behaviour 79—84865
  3U 1223—62, binary X-ray pulsar, Ariel V obs. 78—96566
  4U 1223—62, pulsating X-ray binary, search for periodic behaviour 79—84865
  4U 1223—62, X-ray pulsar, optical counterpart Wray 977, spectra 80—72984
  3U 1538—52, binary X-ray pulsar, orbital elements 78—16573
  4 U 1538—52, optical light curve of X-ray binary 79—35431
  4U 1538-52, binary X-ray source, spectral type of possible optical counterpart 78—36727
  3U 1538-52, eclipsing X-ray source, optical candidates 78—12412
  4U 1626—67, 7.7-second X-ray pulsar, simultaneous X-ray and optical obs. 80—51914
  4U 1626—67, discovery of optical pulsations from proposed candidate faint blue star 79—9034
  4U 1626—67, light pulses from optical counterpart 80—51916
  3U 1626—67, X-ray pulsar, 7.68 sec. periodicity, SAS-3 obs. 78—8157
  4U 1626—67, X-ray pulsar, HEAO 1 obs. 79—92889
  4 U 1700—37 (HD 153919), 97 minute periodicity discovery 79—5921
  4U 1702-36, Scorpius X-1 like source, high energy X-ray obs. with Ariel V 80—17694
  4U 1735—44 (MXB 1735—44), optical identification and similarity to (Scorpius X-1) 78—93468
  3U 1820—30 in globular cluster NGC 6624, binary star model for recurrent X-ray bursts 77—33701
  4U 1907+09, optical identification and OB supergiant binary hypothesis 80—82542
  4 U 2129+47 optical counterpart, spectrum and photometry rel. to 80—17693
  UKS-Ce1, unusual symbiotic C star, spectrum 77—67094
  undiscovered triples, in known binaries, selection effects *(French)* 79—44546
  unitary fields, model of Newtonian theory *(French)* 77—53407
  unresolved binary stars, epochs of speckle interferometric obs., (1975-77) 78—73735
  unseen astrometric companions, mass density, rel. to local mass defect 77—91581
  SU Ursae Majoris, dwarf nova, spectrum obs. and possible duplicity *(Russian)* 80—8638
  XY Ursae Majoris, eclipsing binary, polarimetric obs. 78—28718
  AN Ursae Majoris, nova-like variable, extremely high circular polarisation obs. 78—8018
  SU Ursae Majoris, probable 1980 March super outburst 80—51785
  SU Ursae Majoris, soft X-ray halo around dwarf nova 80—98677
  α Ursae Majoris and close companion star, spectrum synthesis 77—49436

binary stars continued
- SU Ursae Majoris stars, important sub-group of dwarf novae, photometric props. 80—101596
- W Ursae Majoris stars, nonradial radiative transfer, appl. to bolometric refl. effect 77—91567
- W Ursae Majoris stars, role of photospheric convection 78—49478
- γ Ursae Minoris, high dispersion spectroscopy 80—41853
- UV Celescope Catalogue, comparison with IRC, common objects identification 77—9676
- van Bueren 62, 117, 121, dwarf stars in Hyades, spectroscopic orbits 79—5862
- Vela X-1, eclipsing X-ray binary, OSO 8 extended obs. 78—49555
- γ^2 Velorum, bright Wolf-Rayet binary, optical light curve 77—56945
- AH Velorum, Cepheid, radial vel. study, possible binary, coude spectrograms 77—49394
- AH Velorum, classical cepheid, binary detect., UBV obs. 80—109443
- γ_2Velorum, interstellar absorption lines in UV spectrum 79—35324
- γ^2 Velorum, occultation by Earth, upper atm. H_2 and O_2 densities meas. by Copernicus satellite 77—9579
- γ^2 Velorum, WC+O binary, evolutionary model for mass-losing massive He star 80—36615
- γ_2 Velorum, Wolf-Rayet binary, orbital element determ. from spectral obs. 80—85950
- γ_2 Velorum, Wolf-Rayet binary star, UV obs. from TD-1A satellite 80—77447
- γ^2 Velorum, WR binary, photometry and polarimetry 77—29847
- very close binary systems, struct. eqns. including rot. and tidal distortions for ZAMS stars 80—22037
- vibrating white dwarfs, ultra-short var. 79—21287
- vibrational stability of distorted stars, anal. using Clairaut coordinates 80—90408
- 32 Virginis, A-type main-sequence and Am-type star components 79—30091
- 32 Virginis, binary Am star, spectroscopic obs. and curve of growth anal. 77—22237
- EQ Virginis, dwarf binary, flare star, rotational hypothesis for quasi-sinusoidal light variations 78—4234
- DL Virginis, eclipsing binary in triple system, UBV photometry 78—8050
- θ Virginis A, pulsating star of unknown type 79—44555
- visual binaries, correl. between rot. vels. of components 78—20861
- visual binaries, effects of proper motion secular accel. on orbital motion 77—91524
- visual binaries, meas. via speckle interferometry 77—71011
- visual binaries, orbital elements and masses for 18 pairs 80—62180
- visual binaries, orbital elements for 12 systems *(Russian)* 78—69842
- visual binaries, parallaxes, mass ratios and masses for six pairs 77—64795
- visual binaries, radial vel. meas. 79—21347
- visual binaries, radial velocities for objects with astrometric orbits 79—67057
- visual binaries, speckle interferometry with 1 m telescope 78—69831
- visual binaries, spectra, statistical props. 79—97038
- visual binaries containing GK giants, CN strengths, mixing and supermetallicity 77—56930
- visual binaries orbital eccentricities, observational selection 77—74098
- visual binaries with red giant component, mean initial mass determ. 78—49429
- visual binaries with variable components, orbital elements, visible obs. *(Russian)* 80—77455
- visual binary and multiple stars, micrometer and interferometer meas. 79—35303
- visual binary multiplicity 79—44545
- visual binary star orbit, computation method for any eccentricity *(French)* 78—85974
- visual binary star orbits solution, Fourier transform method 80—26899
- visual binary stars, astrometric obs. rel. to gravit. const. var. *(Russian)* 79—44537
- visual binary stars, obs. using phase-grating stellar interferometer *(Russian)* 79—101070
- visual binary stars, orbital elements 80—46607
- visual binary stars, speckle interferometric meas. 77—78820
- visual double star catalogues 77—78669
- visual double stars, astrometric meas. at Nice *(French)* 78—89224
- visual double stars, meas. at Las Campanas Observatory, Chile 78—8058
- visual double stars, micrometer obs., (1975 to 1977) 78—89218
- visual double stars, obs. with Herstmonceux 28-inch refractor, (1963-1970) 80—41863
- visual double stars, orbits determ. *(French)* 78—53986
- visual double stars, period-eccentricity relation *(French)* 78—28721
- visual double stars, photographic meas. of position angles and separations 80—26909
- visual double stars, photographic measures 79—17024
- visual double stars, photographic obs., ang. separations and position angles 78—20860
- visual double stars, rectilinear trajectories calc. *(French)* 79—17023
- visual double stars, relative motion meas. in 17 pairs *(French)* 78—57586
- visual double stars, spectral classification and UBV photometry 77—74084
- visual double stars discovered at Nice, 14th series *(French)* 77—78654
- visual double stars measured at Las Campanas Observatory, Chile 78—85978
- visual doubles, ang. separation and position angles, photographic obs. 78—40997
- visual doubles, Lick obs. of 254 pairs 80—8660
- visual doubles, measures of 120 pairs 80—56878
- 15 Vulpeculae, radial vel. from spectrograms 77—56952
- NQ Vulpeculae (Nova Vulpeculae 1976), photoelectric obs. 78—4252
- W92, possible gravit. contracting binary system in NGC 2264 young cluster 78—32462
- white dwarf, outer layer C and O enrichment from companion 80—109465
- white dwarf binary systems, hard X-ray obs. 78—36732
- white dwarf with mass accretion, H shell flashes rel. to symbiotic stars vars. 78—57550
- white dwarfs, accreting, thermonuclear runaways 78—40937
- white dwarfs, highly magnetised, accretion theory 79—92764
- white dwarfs, rapid mass accretion and extended envelope form. 80—67723

binary stars continued
- white dwarfs undergoing spherically symmetric steady-state accretion, stability 80—77402
- wide binaries in Pleiades, number and distrib. 79—88710
- wide visual double stars, B, A and F type, uvbyβ photometry 79—17025
- Wolf 1062, astrometric anal. of unseen companion from 61 cm Sproul refractor plates 78—16459
- Wolf 1062, red dwarf, astrometric perturbation 77—49439
- Wolf 922, nearby red dwarf, evidence for low-mass unseen companion 80—51809
- Wolf Rayet stars, binary freq., mass ratio, low mass companion evidence 80—109479
- Wolf-Rayet binaries, evolution of mass losing massive He burning stars rel. to comp. 80—36615
- Wolf-Rayet close binaries, X-ray production 77—13401
- Wolf-Rayet stars, CNO abundance var. in massive binaries 80—94802
- Wolf-Rayet stars, evolution and binary freq. distrib. 80—105250
- Wolf-Rayet stars, WC9, optical spectropolarimetry and spectrophotometry 77—64778
- Wolf-Rayet stars in SMC, spectral classification 78—73716
- WRA 977 (4U 1223—62, GX 301—2) orbit determ. from X-ray obs. 80—90570
- WRA 977 (4U 1223—62), lightcurve and radial vel. curve 79—21307
- X-ray, burst sources, thermonuclear flashes in envelope of accreting neutron star 80—109455
- X-ray binaries, accretion of plasma onto neutron stars 80—109452
- X-ray binaries, anomalous periastron positions 79—25756
- X-ray binaries, constraints on apsidal motion 77—87571
- X-ray binaries, cyclotron emissivity in accreting neutron stars 80—90463
- X-ray binaries, cyclotron line form. in magnetised neutron star atmosphere 79—48839
- X-ray binaries, double core evolution 79—84816
- X-ray binaries, effect of vacuum birefringence on X-ray polarisation 78—4408
- X-ray binaries, evidence of noncircular orbits 79—12541
- X-ray binaries, evolutionary history 78—12431
- X-ray binaries, fate of matter and ang. momentum in disc accretion onto magnetised neutron star 78—28715
- X-ray binaries, Fe line emission from Alfven shell 80—98737
- X-ray binaries, intensities from stellar wind flow past compact object 80—22116
- X-ray binaries, limitations on nature and evolution 77—82273
- X-ray binaries, linear radial and nonradial modes of oscillation 78—4213
- X-ray binaries, mass transfer rel. to radio emission 80—62317
- X-ray binaries, models of supercritical accretion discs around black holes 80—105272
- X-ray binaries, neutron stars accretion disc and rot. mag. full interaction 80—62173
- X-ray binaries, optical radiation polarization *(Russian)* 79—58450
- X-ray binaries, radiative effects in supersonic accretion 78—40978
- X-ray binaries, recurrent transients model 80—109565
- X-ray binaries, review *(Italian)* 78—32516
- X-ray binaries, review of new developments 77—71154
- X-ray binaries, review of optical obs. 78—12429
- X-ray binaries, Roche-lobe overflow model 78—32601
- X-ray binaries, spectral lines profile evolution due to Comptonisation, Monte Carlo computations 79—66916
- X-ray binaries, spherically symm. accretion near Eddington limiting luminosity 79—16809
- X-ray binaries, stability of non-synchronous stars in close binary systems 79—40223
- X-ray binaries, steady accretion discs general struct. with mag. field 80—8714
- X-ray binaries, stellar parameters of early type companions 78—36564
- X-ray binaries, test of quark bags and interacting neutrons models 77—78812
- X-ray binaries, variable optical polarization rel. to black hole secondary component 78—20910
- X-ray binaries evolution, accretion onto ZAMS stars and contact binary stage 79—66994
- X-ray binaries in dense stellar clusters, dynamical effects 79—97098
- X-ray binaries in galaxies, contrib. to diffuse X-ray background 79—17141
- X-ray binaries rel. to OB stars and pulsars, tugboat model for evolution 77—56915
- X-ray binary sources, periods 78—12424
- X-ray binary sources, pulsating, spin-up due to accretion from Keplerian disc 80—67904
- X-ray binary sources rel. to old novae 77—87576
- X-ray binary stars, observational evidence for black holes 77—57007
- X-ray binary stars, review of types and props. 80—109564
- X-ray binary system, Fe fluoresc. line struct. 77—78889
- X-ray binary systems, accretion discs, observational appearance *(Russian)* 77—87477
- X-ray binary systems, accretion flows 78—12432
- X-ray binary systems, evaporative winds 77—78888
- X-ray binary systems, K-fluorescence lines in spectra 78—93456
- X-ray binary systems, massive, gas streams and accretion discs 78—93464
- X-ray binary systems, models, X-ray transfer, Monte Carlo study 78—93463
- X-ray binary systems, twisted accretion discs 78—4283
- X-ray bindary systems, X-rays polarisation from mag. accretion disc *(Russian)* 77—87575
- X-ray burst sources, binary star model 78—49566
- X-ray burst sources, magnetised accretion disc model 77—53702
- X-ray burst sources, model, substorm process at accreting neutron star 79—17132
- X-ray burst sources, neutron star thermonuclear runaway model 80—22032
- X-ray burst sources, neutron-star thermonuclear flashes model 78—12417
- X-ray burst sources, properties, binary systems *(Russian)* 78—93477
- X-ray burst sources and convective accretion discs 78—16568
- X-ray bursters, spectroscopic study of optical counterparts 80—46699
- X-ray bursters and soft X-ray transients, different phenomena from same objects 79—25755
- X-ray induced shocks in stellar winds of massive binaries 80—94784
- X-ray pulsar, polarized radiation transfer in analytical solns. 80—94894
- X-ray pulsar as accreting neutron star in compact binary 78—49470
- X-ray pulsar binary, X-ray reflection effects on timing obs. of pulses 79—53935

binary stars continued
- X-ray pulsars, accretion torques 77—49505
- X-ray pulsars, continuum optical pulsation from companions 79—30147
- X-ray pulsars, cyclotron line formation in accretion column 80—67901
- X-ray pulsars, role of Alven surface in X-ray pulses form. 77—78899
- X-ray pulsars, rot. history 79—62871
- X-ray pulsars spectra, possible vacuum signature 80—27015
- X-ray sources, binarity detect. via Doppler effect *(Russian)* 78—77623
- X-ray sources, cyclotron line feature identification 80—90577
- X-ray sources, electron-positron pair prod. in hot unsaturated Compton accretion models around black holes 80—36658
- X-ray sources, pulsating, accretion disc mag. field calc. for oblique mag. dipole configuration 80—94895
- X-ray sources, pulsating, period changes due to rot. mag. neutron stars accretion torques 80—31320
- X-ray sources, review of current knowledge in 0.5 to 10 keV range 78—69915
- X-ray sources, space distrib. and physical nature 80—62316
- X-ray sources, spin up as indicator of normal component evolution *(Russian)* 77—74100
- X-ray sources in binary stars and neutron star spin down *(Chinese)* 78—28857
- X-ray sources in globular clusters, mass-transfer binary model 78—12428
- X-ray sources of galactic bulge, highly compact binary model 79—35430
- X-ray stars in globular clusters 78—20916
- X-ray transient sources, hard and soft transients parameters 79—84867
- X-ray transient sources, new class, cool dwarf+unseen companion with accretion disc 80—101653
- in young galaxies, role in contribution to X-ray background 80—82550
- 1228, nearby red dwarf, evidence for low-mass unseen companion 80—51809
- Ba II giant stars binary nature from visible radial vel. obs. 80—82355
- C star pairs, search of Westerlund's catalogue 78—12301
- C-O dwarf, H and He burning in degenerate envelope *(Russian)* 80—17585
- CH stars in globular clusters, possible binary nature 80—82355
- He white dwarfs rejuvenation by mass accretion 78—73712
- He-accreting degenerate stars of high luminosity, pulsational props. 77—5519
- Hg-Mn binary stars, inhibition of atmos. diffusion 80—62153
- Hg-Mn spectroscopic binaries, high-dispersion spectrograms 77—17629
- HgMn stars, incidence among late B-type stars rel. to duplicity and rot. 78—89199
- Si XIII and Si XIV line emission search with ANS crystal spectrometer 79—17131

binding energy
- *see also lattice energy; nuclear binding energy; nuclear forces*
- AB$_2$X$_4$, crystalline compounds, computation of internal energy 78—75623
- absolute core-level binding energies for gaseous atoms and molecules 80—101670
- acetylene dimer, ab initio HF calc. for 64 conforms. 80—23333
- actinides, expt. and theoret. binding and transition energies, review 78—50497
- adsorption system surface properties variational calcs., binding energy, Lang model 80—29279
- alcohols, modified CNDO calcs., conformations, binding energies 77—6682
- alcohols, saturated, bonded and nonbonded, quantum chem. calcs. 80—9514
- alkaki metal halides, cohesive energies, effect of three body interactions 77—76516
- alkali chloride:Mn^{2+}, spin Hamiltonian parameters, binding energies for cation vacancy complexes 80—96461
- alkali dimer+halogen mol. (IBr)(ICl) thermal chemi-ionisation reactions, products, energies 77—63903
- alkali halide:alkaline-earth cations, defect structs. examined by methods based on Mott-Littleton techniques 80—59487
- alkali halide:Eu^{2+} cation vacancy complexes, binding energies 80—96513
- alkali halide, binding energies of positron to F and F′ colour centres 78—87667
- alkali halide, dipolons, graphical method for binding energy determ. 78—59805
- alkali halide, static and dynamic props., appl. to KCl 77—7798
- alkali halide crystals, binding energy of F$_{e+}$′, M$_{e+}$′ and R$_{e+}$′ centres, positron trapping 79—69460
- alkali halide dibenzo-18-crown-6 complex, ESCA, binding energy 78—50584
- alkali halide molecular clusters, equilib. geom., form. energy and vib. spectrum 78—55269
- alkali halide surfaces, adsorbate binding energies and struct. at surface defects 77—59206
- alkali halides, binding energies of vacancy pairs 78—51533
- alkali halides, binding energy, relativistic effects 77—14370
- alkali halides, crystal binding energy, long and short range forces 80—75200
- alkali halides, mol. dynamics study of melting 80—15220
- alkali halides, three body interaction effects on cohesive props. 78—83770
- alkali hydride molecules, pot. energy function, rot. const., vibr. const., and binding energy 80—99532
- alkali hydrides, crystal binding anal. interatomic force model, cohesive energy, compressibility, Debye temp. 79—65030
- alkali hydrides, lattice props. from interacton pot. energy function 80—100199
- alkali metal, model potential calculation of binding energy and compressibility 78—91632
- alkali metal dimers, $^1\Sigma_g{}^+$ ground state, density functional theory 78—37573
- alkali metal halides, crystal properties, cohesive energy, bulk modulus and press. depend., interionic force model 80—15035
- alkali metals, binding energy calc. *(Chinese)* 80—911
- alkali metals, cohesive energy, calc. based on interatomic approach 80—43209
- alkali metals, cohesive energy, dielectric function calcs. 78—2060
- alkali metals, cohesive energy, teaching 80—90630
- alkali metals, non-parametric calc. of binding energy *(Russian)* 77—27844
- alkali metals, pseudopotential calcs. of binding energy, compressibility and resistivity 79—65025
- alkali trimers, London pot. energy surfaces 79—6893

binding energy continued
- alkaline earth fluorides, orbital binding energy and ionicity relations, XPS meas. 80—97399
- alkaline earth metals, binding energy calc. *(Chinese)* 80—911
- alkaline earth oxides, cohesive and thermophysical props., role of three-body interactions 80—92477
- alkanes, linear, electronic struct., electronic relax. during photoemission *(French)* 78—5283
- alkanes, linear, K-shell ion relax. energy chain length depend. 79—72252
- n-alkanes, methane to n-tridecane, ESCA of core electron relax. and valance bands 77—18978
- alkanes, saturated, ab initio LCAO MO SCF calcs., core ionis., electronic relax. 77—71745
- n-alkanes, solid, core electron relax. energies and valence band form., XPS exam. 77—36372
- alloy, binary, charge transfer and alloy binding, Thomas-Fermi-Dirac approx. 77—76775
- alloy, cohesive energy, semiempirical model, heat of form. expressions 80—70160
- amines, modified CNDO calcs., conformations, binding energies 77—6682
- amines, saturated, bonded and nonbonded, quantum chem. calcs. 80—9514
- amorphous surfaces, energy profile and binding energy, computer simulation 80—100381
- associated liquids, mol. binding energies from US absorpt. and hole theory 78—10124
- atom, binding and kinetic energies, Thomas-Fermi-Dirac-Weizsacker calcs. 77—6680
- atom, heavy and superheavy, K-electron binding, self-energy correction 77—18802
- atom, s-electron binding energy regularities in $1^N S^M$ configs. 78—62731
- atom, X-ray spectra, Z=13 to 103, Sommerfeld screening parameter σ_1 78—25463
- atomic aggregates, small, melting transition characts., random walk Monte Carlo calc. 77—75355
- atomic binding energies, determ. from fund. theorems involving electron density, $\langle r^{-1} \rangle$ and Z^{-1} perturbation expansion 80—63521
- atomic chemisorption, chemical trends, core-hole relax. effects, jellium model 78—76909
- atomic electron binding energies, determ. from relaxed-orbital relativistic Hartree-Fock-Slater calcs. 77—42255
- atomic electron binding energies calcs. 78—86768
- atomic electron l-shell Coulomb ionization by heavy charged particles 79—94073
- atomic inner shell electron props., relativistic effects 77—18803
- atomic neutral systems, total binding energy, virial theorem appl. 80—47840
- atomic nonrelativistic binding energy, statistical theory, agreement with SCF calc. 78—25438
- atomic radiative binding in slow collisions into molecules in a laser field *(Russian)* 80—93753
- atoms and ions, central analytic potential with three parameters 77—71737
- atoms on metal surfaces diffusion parameters, binding energy and dipole moment 79—51422
- Auger electron transition energies calcs., contributions from beyond relativistic HF limit 77—18874
- benzene, monosubstituted, ring protonation and C$_{1s}$ binding energies, STO-3G calc. 79—29336
- benzoate ions on Al$_2$O$_3$ 79—60629
- binary alloy, electron theory of short range order 78—10390
- binary metallic solid solns., thermodynamic quantities rel. to vacancy and diffusion characts. 79—95204
- binary system, A^{N}B^{8-N}, ground state of electron subsystem, quasimolecular model 79—69055
- bound states for the symmetric shifted Coulomb potential 79—6007
- bromoethane, mol. parameters, vibr., pot. barrier height etc., data tables 79—76409
- carbenes, core ionised states, singlet and triplet state binding energy, struct. changes, LCAO-SCF calc. 79—97982
- carbonyls, core ionisaton phenomena, nonempirical LCAO MO SCF investig. 80—37906
- catalyst struct., binding energies, ESCA, applic. to MoS$_2$, MoS$_3$, ultramarine 77—21420
- chalcogenide crystals with FCC structure, Moelwyn-Hughes parameter appl. to calcs. 77—80437
- chemical bond, MO-LCAO scheme for binding energy, correlation correction, physical fragmentation 77—46490
- chemisorbed atom on metal, core electron binding energy 78—10280
- chemisorbed diatomic molecule, indirect coupling contrib. 77—1310
- chemisorption of H$_2$ on graphite, substrate relax. effects 77—7962
- chlorin, UV absorption and photoelectron spectra, CNDO/S3 calcs. 77—75210
- classical field theories, quark confinement anal. 80—4927
- classical systems, minimal specific energy 79—90364
- CO, dissoc. sorption on Pt, XPS obs. 77—16863
- cohesive force and resistivity between electrostatically- precipitated particles 79—86102
- collinear triatomic system, binding, crit. pot. strengths 77—6883
- composites, adhesion between two crystals, theory 80—104417
- contact exciton, screening and quenching 80—29334
- core electron binding energy, prediction with four-parameter equation 77—30745
- core hole relaxation energies 78—80439
- core level binding energy shifts between free and condensed atoms 80—20136
- core replacement energy correlation with nonbonding s electron density 77—30921
- core-level transitions, appl. of modulation spectroscopy with synchrotron radiation 78—4710
- Coulomb bound-state problem, semiquantal approx. 80—99435
- covalent semiconductor, electronic and struct. energies calc. 78—59874
- crystal, Compton X-ray scatt., electron binding energy effect 77—59639
- crystalline materials, sp. ht. rel. to binding energy temp. depend. 80—54403
- cubic crystals, calc. of binding energy of X-ray excitons 78—2435
- diamond, Wigner-Seitz effective quasiparticle pot. 79—50160
- diatom, weakly bound, dissoc. energy for Morse and Lennard-Jones pots. 79—54988

binding energy continued
- diatomic bonding energy, changes due to Van der Waals interactions with other atoms 78—95012
- diatomic hydrides, LiH to HCl, CI calcs. in spin density functional formalism 79—18122
- diatomic molecule, binding and excitation energy, Wigner-Seitz pot. 79—50160
- diatomic molecules, inner-shell ionisation, relax. effects calcs. 77—42351
- diatomic molecules, nucleus-nucleus interaction, Einstein relativistic correction, Born-Oppenheimer approx. 80—91463
- dielectric medium, impurity dispersion self energy calcs. 78—52536
- difluoromethane, binding energy, ionisation pots., overlapping sphere MS $X\alpha$ 77—83499
- dimers of Group IIA, low-lying states binding energy, local spin density functional formalism calcs. 79—97994
- dispersive media, localised states of Wannier exciton type, bound state energy 77—43506
- $e^+e^+e^-$, three-particle atomic system, binding energy, Faddeev method calcs. 77—57858
- education, bubble cohesion in foam, binding energy calc. 78—61978
- electron binding energies accurately determined by X-ray photoelectron spectroscopy *(Chinese)* 79—54821
- electron binding energies reference level problem in photoelectron spectra of solids and adsorbates 78—63936
- electron coincidence spectroscopy, binding energy charge density meas. 80—63817
- electron in electric dipole field 79—98220
- electron propagator theory for mol. electron binding energies and photoionis. intensities 80—47848
- electron-hole drops, surface tension coefficient and binding energy, exciton condensation kinetics 78—10370
- electron-hole liquid, in semiconductors, equilib. props., review *(Russian)* 78—34773
- electron-hole system, interaction with phonons 80—6738
- electronic potential energy and X-ray scatt., relationship 79—28311
- electrostatic potential predictions, basis set depend. 78—74786
- elements, monotonous series based on atomic bond energy, for mech. and phys. props. calc. *(Russian)* 80—19740
- elements with $Z\leq30$, core electron binding energies in free and standard state 77—43168
- endothermic reaction rate enhancement in EM field 80—66852
- ESCA expt., charging and rotational dependence of time position 78—21970
- ESCA shifts and effective charges 80—78648
- ESCA studies of Ga, As, GaAs,Ga_2O_3, As_2O_3 and As_2O_5 78—92171
- ethers, modified CNDO calcs., conformations, binding energies 77—6682
- ethers, saturated, bonded and nonbonded, quantum chem. calcs. 80—9514
- ethyl 4-(4′-methoxybenzylideneamino)cinnamate, mesomorphic compound, cryst. struct. and binding energy 77—80494
- ethylene, electron impact ionis., valence electron momentum distrib. 79—18297
- exchange energy density functional, gradient expansion, rel. to at. energy functional 80—99441
- exciton binding energy and lifetime in free carrier gas 79—33238
- exciton to neutral acceptor, calcs. using atomic-like variable wave function 78—79937
- exciton-ionised donor complex, binding energy, effective electron-hole interaction pot. 78—67949
- exciton-neutral donor complex, binding energy 79—60715
- exciton-neutral donor complexes, dissociation energy 80—34364
- excitonic molecules, binding energy in mag. field *(Russian)* 79—78011
- excitonic molecules, variational calc. 80—10891
- excitons, dynamical screening by free carriers 78—39031
- excitons, small radius, binding energy contrib. of freq. depend. optical phonons 77—69236
- fast ion in solid, oscillatory wake, trapped electron binding energy, RPA calc. 80—96575
- Fenske-Hall LCAO method, inner-shell binding energies and chem. shift calcs. 80—47871
- first-row transition metal ions, core ionised states, ΔSCF MO calcs. 80—78523
- fluoride crystals, rutile-type, interionic pots., cohesive energy, bulk modulus, calc. 80—79741
- fluoromethane, binding energy, ionisation pots., overlapping sphere MS $X\alpha$ 77—83499
- fluoromethanes, ab initio calcs. of K-shell ionisation potentials 77—18784
- fluoromethanes, $X\alpha$ calcs. using ΔSCF formalism 79—6861
- formaldehyde, orbital contribs. to relax. energies accompanying core ionis., ΔSCF HF calcs. 78—82642
- formaldehyde.$H_2S(H_2O)$ complexes, ab initio SCF MO calcs., binding energy dispersion contrib. 80—27967
- formic acid, dimerisation energy, non-empirical MO SCF calc. 79—37656
- $(\text{formyl-H-F})^-$, strong H-bond, using recent difinition 79—98240
- fourth row element ions, relativistic Dirac-Fock-Slater orbital binding energies, one-electron transition energies 79—25778
- frozen core approx. and pseudopotential theory validity for cohesive energy calcs. 80—64949
- GaP, reevaluation of bandgap and free exciton binding energy 78—60061
- glass, alcoholic and aq., 4.2K, trapped electron photocond. and optical spectra following radiolysis 79—29378
- glassy polymer, relationship between activation energy of creep and cohesive energy 79—69188
- globular hydrocarbons, cohesive energy and Gruneisen parameter calcs. 79—19183
- grain boundaries decohesion energy, solute adsorption influence 80—65009
- grain boundary cohesion, segregation effects 78—15411
- grain boundary decohesion, exchange type soft solute segregation in hard hosts 80—54258
- grain boundary segregation, computer simulation using Mie type interatomic pot. 80—54259
- graphite, Van der Waals interactions, in and between layers of atoms 77—84695
- graphite basal plane surface, selective adsorption of ^{3}He and ^{4}He 80—6650
- graphite intercalation cpds., electrostatic interactions and staging, nonlinear Thomas-Fermi eqns. 80—107732
- groups II and III, doubly charged negative ions, analytical radial orbitals 77—6668

binding energy continued
- halides, ionic cryst., cohesive energy calc. 80—6384
- halogens in transition metal coordinate compounds, binding energies from XPS data 78—21973
- heavy elements, $Z=84$-103, at. electron binding energies 79—31735
- heavy ion+atom, K-vacancy production, universal scaling law 79—22811
- heavy ion+atom collisions, K X-ray transition energies, two electron-one photon mechanism 77—18828
- heavy ion collisions, electronic states in rot. two-centre Coulomb systems 77—14561
- heavy ions in strong magnetic field, electron binding energy 79—68176
- heavy metal diatomic halides, Wasastjerna pot. function, force consts. internulcear separations and binding energies 80—14187
- hexagonal layered structure, Van der Waals interactions, in and between layers of atoms 77—84695
- hydrides, ionic cryst., cohesive energy calc. 80—6384
- hydrides, third row, electron binding energies, one-centre expansion method 77—6677
- hydrocarbons, saturated, bonded and nonbonded, quantum chem. calcs. 80—9514
- hydrocarbons, saturated, modified CNDO calcs., conformations, binding energies 77—6682
- hydrocarbons, saturated and unsaturated, ionisation spectral intensities, correlation effects 78—90234
- ice, I_h, water monomer on basal plane, static interaction model 78—18891
- II-VI compounds, acceptor state model 80—2059
- II-VI compounds, doubly ionisable centre binding energy 79—65405
- II-VI semiconductors, impurity and defect centre energy states, luminesc. meas., review 80—55150
- inert gas crystallites of 5, 6, 7, 8 atoms, metastable states, Monte Carlo method 78—22687
- inert gas crystals, dispersion binding energy 77—76351
- inert gas trimers and tetramers, ground state energies, pairwise Morse pot., few-body methods 79—72378
- inert gases, solid, long-range many-body interaction and monovacancy heat of form. 80—38996
- inner shell, Fenske-Hall LCAO method calcs. 80—47871
- inorganic compounds, XPS chem. anal., chem. shift, core binding energy 78—20134
- insulators, XPS, binding energy, surface pot. and work function calcs. 80—89113
- interconversion pot. energy surfaces, geometries, electronic structs. 78—35660
- intermetallic molecules, diatomic, enthalpy of form. by model description 79—83497
- iodoethane, mol. parameters, vibr., pot. barrier height etc., data tables 79—76409
- ion, Thomas-Fermi-Dirac model for mag. susceptibility and binding energy 77—67981
- ion Auger spectroscopy and chemical binding of atoms in a compound 80—11528
- ionic, rel. to nonrelativistic neutral atom 78—90054
- ionic bonding, new elements, incomplete orbitals 77—35893
- ionic crystal, surface stability 80—20016
- ionic polymer, role of electrostatic forces in glass transition temp. 77--84908
- ionic solids, lattice and defect props., modified electron gas approx. 79—42054
- isolated small particles, struct. stability, atomistic studies 79—77957
- jellium, chemisorption, effective-medium theory of chem. binding 80—65367
- L-shell ionisation by heavy charged particles, binding energy correction 77—54604
- ligand binding to macromolecules, allosteric and sequential models of cooperativity 80—12870
- liquid, cohesive energy density, surface and interfacial tension and heat of mixing 77—55431
- lower bounds to ground state eigenvalues, Pade approximants 78—49722
- many-valley semiconductors with anisotropic masses, screened donor impurities 78—10399
- matter stability despite catastrophic Coulomb forces 80—22212
- mesic molecule, using Schrodinger perturbation theory in adiabatic rep. *(Russian)* 77—60976
- metal, core-level binding-energy shifts 78—47740
- metal, d-band, generalized pseudopotential theory, density functional formulation 78—10389
- metal, direct obs. of individual atoms, FIM 77—62724
- metal, electron-lattice interaction effect on equilib. struct. form. *(Russian)* 80—34380
- metal, FCC, homovalent impurity migration energies, fluctuation theory model 79—95219
- metal, formation energy of spherical cavities 77—80499
- metal, inhomogeneous electron system, nonlocal exchange and correlation 78—56097
- metal, Morse parameter calc., elastic const. evaluation 77—7692
- metal, physisorbed inert atoms, polarisation due to short range interaction with substrate 80—39428
- metal, polycryst., rel. to sputtering rate on Ar ion bombard. 80—55245
- metal, simple, adatom geometry and chemisorption energies 77—66093
- metal, simple, non muffin-tin corrections to eqn. of state *(French)* 80—59906
- metal, simple, pseudopot. calc., many electron correl. 77—51393
- metal, simple, vacancy and divacancy form. energies and divacancy binding energy 77—35554
- metal, van der Waals energy estimation 78—91634
- metal aggregates, binding energy calcs. 79—51464
- metal BCC, divacancy binding energy, appl. stress effect, computer simulation 77—15408
- metal halides, bond distances and cohesive energies calcs. 80—18783
- metal surface, influence of submonolayer films on props., calc. *(Russian)* 80—2273
- metal-H system, bond energy calcs. 78—51940
- metallic adhesion 79—73463
- metallic compounds, cohesive props., augmented-spherical-wave calcs. 79—94952
- metallic elements, bond energy rel. to thermal expansion coeff. *(Chinese)* 79—14946
- metallic elements, core-level binding-energy shifts 80—88502
- metallic interfaces, local and nonlocal contribs. to adhesive energies 77—85085

binding energy continued
metals, atomic binding energy and surface energy rel. to prediction of physical props. 80—59434
metals, atomic interaction force characts., association with struct., mech. props. 80—49172
metals, close packed, relationship between cohesive energy, and allotropic transformation temp., exam. 78—52802
metals, cohesive properties, energy density functional-pseudopotential method 79—73462
metals, compressiblities, general pseudopotential approach 80—54631
metals, cubic, cohesion and Cauchy discrepancy 80—54170
metals, d band, reson. model pot. binding energies and elastic consts. calc. 77—69263
metals, Morse potential appl. in molecular-metallic framework 80—79742
metals, narrow band, cohesion energy, intraatomic Coulomb correlations 78—43322
metals, noble, dilute alloys, solute vacancy binding energy, Dingle temp. 80—49177
metals, simple, binding energy, compressibility, interionic pot. and transition temp. using pseudopot. method 79—46598
metals, simple, elastic moduli, chem. trends, pseudopot. method 80—107355
metals, simple, model for vacancies, including ionic pot. in self-consistent density calc. 77—51369
metals, simple, static props., Thomas-Fermi-pseudopotential approach 80—75514
metals, simplified local-density theory of cohesive energy 79—60749
metals, vacancies, corrected spherical model 78—34802
methane, elastic and inelastic electron scatt. differential cross section, obs. and calc., struct., binding energy 80—28110
methane, intermolecular interaction energies calcs. using minimal basis sets 80—78681
methanol, ab initio calcs. of K-shell ionisation potentials 77—18784
methanol, polymers, structs., binding energies, LCAO SCF MO calcs. 77—83498
methylamine, affinities for $H^+(Li^+)(K^+)(CH_3{}^+)$, ab initio SCF calculations 80—102443
molecular cations, heats of formation determ. from core electron binding energies 77—86346
molecular electron binding energies calcs. 78—86768
molecular ionisation energies, self-consistent-charge Hartree-Fock-Slater calcs. 77—6687
molecule, approx. energy formula 79—45629
molecule, quartic potential function with finite BE, props. 79—26913
molecule, self-consistent charge calcs. of core-electron binding energy shifts 80—69084
molecule, semi-empirical MO calc. of atom-pair interactions 80—915
molecule, valence states and binding energies 77—30757
molecule near metal surface, proximity effects 79—36797
molecules, core electron binding energy shifts, σ- and π-relax. energies 78—29750
molecules containing 1st row atoms, K-shell binding energy shifts, NDDO MO calcs. 80—58413
dimolybdenum tetraformate, metal-metal bond energy, SCF-Xα-SW calcs. 80—78538
monohalobenzenes, inner shell excitation and ionis., electron energy loss spectra, XPS, assignments 78—62934
Mott-Wannier exciton in polar crystal, binding energy 77—39786
muffin-tin orbitals and total energy of atomic clusters 77—47708
multiexciton complexes in semiconductors *(Russian)* 78—10372
muonic atom, heavy, $1s_{1/2}$ levels, self-energy corrections 78—55262
nearly closed shell atoms, binding energy and isotope shift correl. 80—27980
negative ion+neutral atom, autoionisation states investigation by Rydberg series broadening and displacement *(German)* 79—85938
negative ions of second and third period 77—3279
neutral atom, nonrelativistic binding energy, rel. to isoelectronic ions 80—18782
neutral atom and isoelectronic ions, non-relativistic binding energies 79—59334
neutral bound excitons, accurate binding energies, variational method calc. 80—107715
p-nitroaniline, binding energy, XPS obs. 80—37833
noble metals, pseudopot. exam. of electronic props. 78—51960
noble metals, Van der Waals contribution to binding energy 78—2062
nucleic acid bases, protonated, anion binding, electrostatic mol. pots. 79—1999
ordered alloy, eqn. of state, applicability of semiempirical function of binding energy *(Russian)* 77—15533
organic molecules, relax. phenomena, following core ionis., LCAO MO SCF calc. 79—10030
organometallics, group V, XPS spectra interpretation, pot. model 78—50587
oxide crystals, rutile-type, interionic pots., cohesive energy, bulk modulus, calc. 80—79741
α-perylene crystal, emission spectra, temp. variation and pair states 78—27300
phlorin, UV adsorption and photoelectron spectra, CNDO/S3 calcs. 77—75210
phonon-magnon bound state, temp. depend. 79—78349
photoelectron spectra in solids, sudden approx. approach *(French)* 77—36355
photoelectron spectrometer, calibration using binding energy scale 80—90930
photoemission, many-electron theory, in electron spectroscopy book 78—17714
plasma electrostatic binding energy, relation to elementary consts. 78—47089
polar molecules, electron affinities, Born-Oppenheimer calcs. 77—75333
polar semiconductor, excitons bound to ionised donors, binding energy calc. 77—28128
polar semiconductors, Wannier excitons, effective Hamiltonians and binding energies 78—34777
polyatomic molecules, electron density, generalised Berlin diagram appl. to H_2O internal modes 79—98001
polydiacetylene-bis(toluenesulphonate), XPS valence band obs., binding energies 77—77339
polymer glass temperature, rel. to cohesion energy and vacancy form. energy *(German)* 78—22670
polymethineimine, cryst. orbital studies by HF methods 80—44148
polyvinyl alcohol-Cu interface, XPS study 79—83093

binding energy continued
porphins, UV absorption and photoelectron spectra, CNDO/S3 calcs. 77—75210
positive ions, nonrelativistic binding energy 77—88365
positron+halide ion, competitive reaction in water, ang. correl. obs. 79—61846
positron binding energies at surfaces, thermal activation meas. 79—95371
positronium oxidation react. in aq. soln., positron hydration energy 78—61039
proton in jellium, self-consistent screening 78—2441
PVC, crystalline syndiotactic, exam. of chain folding, lattice energy 80—24373
quasimolecules, superheavy, binding energy of inner-shell electrons, monopole approx. 78—62949
quasimolecules, superheavy, inner shell electronic states calc. 79—89817
rare earth metals, 3d core electron XPS spectra, low-binding-energy satellites, exception of Eu 80—104040
rare earth metals, 4f level energy position relative to Fermi energy 80—6764
rare earth metals, core electron binding energy study 77—48309
rare earth metals, position of unoccupied 4f levels, APS meas. 80—16125
rare earth oxides, core electron binding energy study 77—48309
rare earth vanadites, X-ray fluoresc., IR and UV spectra 77—77206
rare earths, excitation energies for 4f electrons, relativistic calc. 78—72117
rhodamines, solutions, electronic absorption spectra and dimeric props. 77—88458
row element ions 79—25778
rutile-type compounds, crystal binding energies and electronic polarisabilities 80—75202
semiconductor, anisotropic, binding energy of exciton complexes 79—15088
semiconductor, core excitons, binding energy in effective mass approx. 80—24808
semiconductor, core level spectra, electronic polaris. effects 79—90985
semiconductor, effect of pot. fluctuations induced by cryst. inhomogeneities 80—49780
semiconductor, electron-hole liquid, prod. and props. at low temp. 79—82527
semiconductor, quasi-one-dimens., many-exciton instability condition 77—43507
semiconductor, surface state excitons 77—51799
semiconductor multiple bound excitons, binding energy calc. 78—51900
semiconductor-metal interface, electeon-hole liq., binding energy 78—30985
semiconductors, binding energies of core excitons, effective mass approx. 79—73439
semiconductors, binding energy in exciton-impurity systems, Haynes rule 79—15112
semiconductors, deep defects, contrib. to binding energy 80—70634
semiconductors, excitonic polarons, Pollmann-Buttner variational method, donor and exciton binding energies 79—42469
semimetallic film, Wigner crystal in high magnetic field 79—73456
simple metals, compressibility, Harrison pot. calcs. 80—96460
simple metals, model pseudopot. appl. to various props. 80—59845
solid state atomic props., pseudopotential method *(Russian)* 79—60674
superheavy and intermediate atomic collision systems, UNILAC expts. 80—63751
superheavy atoms from heavy ion collisions, electronic binding energy, wave functions 78—46252
supermolecule calcs. with additive procedure, intermolecular interactions and binding energy 80—52880
surface, adsorbed atoms thermal desorption, one dimens. microscopic model, weak binding case 80—96729
surface biexciton in polar semicond., binding energy calc. 80—96796
surface state excitons 77—66192
$TCNQF_4$, charge transfer complexes and salts, C(1s) and N(1s) XPS anal. of shake-up satellites 77—14492
tetra-n-pentylammonium salts, molten, thermodynamic props., cation struct. 79—55639
tetrafluoromethane, elastic and inelastic electron scatt. differential cross section, obs. and calc., struct., binding energy 80—28110
tetrafluoromethane, valence electron binding energies, molecular symmetry restrictions effect 80—63528
tetrahedral semiconductors, exciton binding energy, Haben methods for single isotropic parabolic energy bands 79—56140
three-body system in mesoatomic physics, adiabatic two level approx. *(Russian)* 79—22870
three-particle atomic system, binding energy, Faddeev method calcs. 77—57858
total electronic energy, atoms and mols., SCF binding energy, Z^{-1} perturbation theory 80—83268
transition metal, 3d, energy parameter, Auger spectra, quasi-atomic behaviour 77—20966
transition metal, 3d and 4d, local density theory, mech. and mag. props. evaluation 78—91630
transition metal, atom and ions, mixing of $3d^n4s^k$ configurations 79—63910
transition metal, BCC, phonon dispersion curves and elastic, calc. using cohesive energy 78—59885
transition metal, chemisorpt. of H, Hubbard-type surface mol. model binding energy calcs. 78—71990
transition metal, cohesive energy, lattice consts. and bulk modulus, renormalised atom method 77—43170
transition metal borides, charge state of B, core electron binding energies *(German)* 78—10391
transition metal borides, secondary ion sputtering, ionisation, energy distrib. characts. *(Russian)* 79—69940
transition metal borides, silicides and germanides, binding energies from X-ray photoelectron spectra 80—49170
transition metal carbides, secondary ion sputtering, ionisation, energy distrib. characts. *(Russian)* 79—69940
transition metal carbonitrides, carboxides and oxynitrides, electronic struct., theoretical approach 80—54584
transition metal clusters, cohesive energy and level statistics 78—95267
transition metal compounds, XPS, anal., approx. mol. orbital theories 77—18975
transition metal hydrides, electronic struct., heat of formation, single particle lifetimes, Dingle temp. meas. 78—51923
transition metal oxides, second and third-row, XPES 80—87170

binding energy continued

transition metal surface (adsorbate), intermediate UPS/XPS synchrotron radiation study 78−52633
transition metal-H dilute solns., pair potential anal., unrelaxed lattice model 79−65070
transition metals, 3d, absolute $2p_{3/2}$ core binding energies and work functions 78−15253
transition metals, Auger relaxation energy theory 80−7446
transition metals, BCC, point defects chem. binding energy 79−82260
transition metals, chemisorption of H, O and CO, interpretation of binding energy data 78−2378
transition metals, core levels between surface and bulk atoms, variation of binding energy shifts 80−88615
transition metals, electronic structure and ordering of sp defects 78−91639
transition metals, energy of cohesion calc., Hubbard Hamiltonian with exchange interaction 77−69261
d-transition metals, impurity integration with large-angle grain boundaries 80−39148
transition potentials, for ESCA and Auger spectra, equiv. cores and Hellmann-Feynman calcs. 77−61724
TTF-TCNQ, cryst. binding energy, enthalpy of form., calorimetric 77−52663
TTF-TCNQ crystal, charge transfer, dipolar polaris. binding energy 77−80754
two-dimensional electron-hole metallic liquid, RPA calc. 77−47743
vacanacy trapping by foreign atoms in FCC crystals 79−90696
very heavy ion-atom collisions, inner shell electron binding energies 80−43169
Wannier exciton binding energy in strong anisotropic crystals 77−28126
XPS binding energy determ. without retarding pot., relativistic mass increase 78−41377
XPS spectrometer, consistent calibration method, rel. to Pd Fermi level 77−16458
Z=95 to 130, calc. of K- and L-X-rays binding energies 77−83525
$e^+e^-e^-$, two-electron at., three-body problem, binding energy 79−3372
Λ well depth with class of equiv. pots., nuclear matter appl. 77−26605
(100), chemisorption of O, molecular orbital theory of bonding 77−85059
Ag cluster 78−33646
Ag halides, van der Waals energy, cohesive energy calc. 77−51343
Ag-Cd, behaviour of Cd d-bands, comparison with Hg and Au alloys 79−37972
Ag-O-Cs surface, oxidation, role of Cs suboxides in low work function surface layers, XPS 80−76131
AgBr, adsorpt. of thiolic anitfoggants 78−32907
AgBr, interionic forces, cohesive energy, bulk modulus calcs. 79−82176
AgCl, interionic forces, cohesive energy, bulk modulus calcs. 79−82176
AgCl(Br), thermal shifts in energy level separations, ESCA 77−8723
AgF, interionic forces, cohesive energy, bulk modulus calcs. 79−82176
AgI surface, adsorption of water, effective pair pot. model 80−100394
AgO and Ag_2O, ESCA spectra, Auger effect, initial and final states effect 78−15280
Al, chemisorption of H_2, calc. of adsorption sites and binding energy 79−46953
Al, elastic properties *(Russian)* 78−56678
Al, metallic, phonon freq., binding energy, compressibility, elastic const. and energy band gap calcs., linear pot. 80−88284
Al, model pot. calc., binding energy and compressibility 79−99650
Al, ultra soft X-ray photoelectron energy loss study, angle and energy dependence 78−23582
Al-transition metal, impurity binding energies 79−42096
Al-Zn changes in inner-electron binding energies during ageing, electronic spectra study 77−28816
$Al_2(Al_2^-)(Al_2^+)$ configurations, ab initio study, LCAO, STO, MO-SCF and CI calcs., binding energy *(French)* 80−91447
AlN, interatomic interactions from XPS 80−49171
α-Al_2O_3, chemisorbed water, electron binding energies, UPS, SCF-Xα-SW calcs. 77−69169
Al_2O_3 monolayer, core excitons and inner well resonances in surface soft X-ray absorpt. spectra 80−40187
alkali halides, interatomic forces, Born model anal. on US data 78−55833
Ar, electron binding energies, one-centre expansion method 77−6677
Ar, inner electron energy characteristics, validity of Hartree-Fock-Pauli approx. 80−42957
Ar, solid, many-body contributions to OK binding energy 80−84135
Ar, total state energies, L-, M-electron processes, ab initio CI investig. 77−18801
$Ar+H^+$, low energy, L-shell ionisation, binding energy correction 77−54604
$Ar_nH(H^+)$, excited and ground state struct. energies and binding energy, vibr. modes, LCAO-SCF-MO calc. 79−3608
$Ar_{N-1}K^+$ clusters, equilib. configs. and binding energies 80−48115
As, X-ray absorption edge, chem. shift, electron binding energy in compounds 78−62822
$As_2S_{2.66}Se_{0.34}$, X-ray photoelectron spectra, electron binding energy, effect of Ag alloying 79−11499
Au clusters on alkali halide surface, size depend. of valence bands, XPS study 80−65647
Au, core level binding energy and density of states from first atomic layer, XPS meas. 79−87563
Au, local pseudopotential, phonon frequencies, binding energy and liq. metal resist. calc. 77−20216
Au organometallics, ESCA core binding energies 78−50586
Au, pseudopotential, fitted to elastic data 78−75705
Au, surface atoms, XPES, core level binding energy, density of states 79−8224
Au-Cd, behaviour of Cd d-bands, comparison with Hg and Ag alloys 79−37972
Au-Si interface, valence band and core levels, Si diffusion, alloy form., photoelectron spectra obs. 80−45205
BN, cubic, ab initio SCF calcs., band struct., ground state props. 78−51891
BN, interatomic interactions from XPS 80−49171
Ba, XPS, in BaS and $BaSO_4$ 80−43104
Be complexes, binding and orbital energies, biological systems ab initio calc. 80−102442
Be, Compton profile, electronic energy calc. 80−37822
Be^{2+}, three-particle atomic system, binding energy, Faddeev method calcs. 77−57858

binding energy continued

$BeBH_5$, H bridged system, floating spherical Gaussian model 80−78518
$Be_2(^1\Sigma_g^+)$, binding energy, ab initio pot. curves, interacting correlated fragments method 80−63557
Br ion+target collisions, K-X-ray yields, $1s\sigma$ excitation 77−19051
$Br(H_2O)_n^-$, geometric and electronic struct., CNDO/2 calcs. 77−79542
C bonding to Tokamak walls, XPS studies 80−80942
C^-, near-threshold photodetachment, IR meas. 77−42290
C_2, pot. curves, binding and ionisation energies and config. variational cellular method 80−32597
CO, adsorbed on Pd, UPS of CO on Pd clusters, binding energy, d-electron emission particle size depend. 79−4888
CO, core ionis., electric field depend. 78−13424
CO, electronic struct., binding energy and interatomic distance, SCF variational cellular calc. 80−9498
CO, orbital contribs. to relax. energies accompanying core ionis., ΔSCF HF calcs. 78−82642
CO, pot. curves, binding and ionisation energies and config. variational cellular method 80−32597
CO_2, elastic and inelastic electron scatt. differential cross section, obs. and calc., struct., binding energy 80−28110
CO_2, ionised states, core and valence, ab initio HF calcs. 77−79597
CO_2, valence shell ionis. spectra, theory and dipole (e-2e) spectra expts. 79−76522
CO_2, valence states study by (e,2e) momentum spectroscopy, binding energy spectrum 78−22039
CO_3^{2-}, molecular orbital anal., anisotropic X-ray emission obs. of components 80−18786
COH^+, orbital contribs. to relax. energies accompanying core ionis., ΔSCF HF calcs. 78−82642
CS_2^+, and $(CS_2)_2^+$, photoionis. in supersonic mol. beam 79−98165
$^{12}C(d,d)$, incident ion binding energy effects on scatt., qualitative anal. 79−9600
Ca, 2 keV electron excitation and ionis., ejected electron spectra 77−3466
Cd, core binding energies, gas phase X-ray photoelectron spectra 78−37611
Cd, electron binding energy and shift, core level XPS 80−87088
Cd, inner core neutral atom binding energy, relaxed-orbital relativistic Hartree-Fock-Slater calc. 78−13433
CdF_2, electronic structure of outermost levels, UPS study 80−7468
CdMnTe crystals, exciton binding energy, magnetoabsorption and magnetoreflectivity 79−38523
CdO, ESCA spectra, Auger effect, initial and final states effect 78−15280
CdS, biexcitonic state existence, 2.5 MeV binding energy *(Russian)* 77−39788
CdS, hydrogenlike donor negative ion, ground and excited states, obs. 80−70645
CdS, spin-polarised electron-hole liquid, theory 78−43307
CdS, Wannier exciton and Wannier-exciton-ionised-donor complex, binding energies of lowest excited states 80−34363
CdS, Wannier exciton-ionised donor complex, binding energy 80−44509
CdS:D^-, binding energy of D^- ion 80−92541
CdS(Se), single cryst., band parameters from optical exciton spectra 79−47021
CdSe, biexcitonic state existence, 1.2 MeV binding energy *(Russian)* 77−39788
γ-Ce, photoelectron spectra, 4f level position 80−25519
γ-Ce, valence band exam. by XPS and UPS 79−37977
Cl-containing systems, core Auger and core electron binding energy shifts, ab initio LCAO SCF MO UHF calcs. 77−30777
ClF_2, CNDO/2 calcs., mol. struct. and props. 77−79543
ClF_3, ESCA chemical shift, energy levels, SCC-MO calcs. 79−64045
Co, ferromag. HCP, electronic struct. calcs., cohesive energy and exchange splitting 78−34791
Co II acetylacetonate, XPS 80−74196
$CoFe_2O_4$, thermally induced surface chemistry and struct., XPS 78−22939
Co(ethylenediamine)$_3$(ClO_4)$_3$, ESCA chem. shift meas., internal standards 78−50585
Cr (100), adsorption of O_2 and initial oxidation at room temp. 80−20034
Cr, electronic struct., spin-density functional calcs. 80−88476
Cr, oxidation, Cr-O bonding, characterisation by high resolution AES *(French)* 79−100468
Cr, single cryst., Compton X-ray scatt., electron binding energy effect 77−59639
$Cr(CO)_6$, LCAO-HFS-STO calc., basis set effects 80−52882
CrN, antiferromagnetic EPR spectra, binding energy, isotropic exchange and ordering *(German)* 80−80604
$Cr(NO)_4$, XPS and UV photoelectron spectra, compared to NO data 80−58317
Cs, adsorbed on Ni (100) surface, electron binding energies of core levels 78−18896
Cs, crystal struct., van der Waals and repulsive interaction 80−84137
Cs, inner core neutral atom binding energy, relaxed-orbital relativistic Hartree-Fock-Slater calc. 78−13433
CsBr, lattice statics and dynamics, deformation shell model 77−20034
Cu, adsorption of CO, angle-resolved UPS and adsorbate induced struct. 78−71983
Cu, at. cluster, EXAFS study of bond length and binding energy 79−81317
Cu, atomic clusters, struct. and electronic props., Mulliken-Walsh diagrams, extended Huckel procedure 78−46479
Cu clusters, valence band and core binding energies, UPS meas. 79−38721
Cu crystal, cohesion and vacancy form., electron statistical model 80−54169
Cu, film, growth on amorphous C, electronic props., UPS and XPS obs. 79−82476
Cu films on Ru (0001), growth, struct. and electronic props. 79−77958
Cu halides, van der Waals energy, cohesive energy calc. 77−51343
Cu molybdates, valence band X-ray induced Auger spectra and XPS 78−80813
Cu, on polystyrene, unusual core level spectra, XPS obs., core electron binding energy 79−24415
Cu oxides, valence band X-ray induced Auger spectra and XPS 78−80813
Cu, pair potentials calcs., elastic props. calc. 80−49176
Cu, sputtering, binding energies 80−108312

binding energy continued
Cu, X-ray absorption edge, chem. shift, electron binding energy in compounds 78—62822
Cu^{2+}-1,5-dimethyl-2,4-hexadiene, fluoresc. quenching method for determ. binding const. 80—89530
Cu_3Au, eqn. of state, applicability of semiempirical function of binding energy *(Russian)* 77—15533
CuCl, excitons bound to neutral donor impurities, magneto absorption spectra 79—56816
$CuFe_2O_4$, thermally induced surface chemistry and struct., XPS 78—22939
CuH, electronic struct., heat of formation, single particle lifetimes, Dingle temp. meas. 78—51923
CuO, on Cu, identification by electron spectroscopic methods 80—60747
Cu_2O, on Cu, identification by electron spectroscopic methods 80—60747
Cu_xZn_{1-x}, sputtering, binding energies 80—108312
Cu(111) frequency depend. photoelectric surface state cross section periodic oscills., PES study 80—50522
D, three-particle atomic system, binding energy, Faddeev method calcs. 77—57858
$Eu_xLa_{1-x}Al_2$, binding energy and workfunction charges using XPES 80—33928
F, binding energy of 1s electrons, rel. to adsorption of fluorobenzene *(French)* 79—69346
F_2, MSXα calc., partial wave expansion, binding energy and orbital energy 80—37738
F_2, pot. curves, binding and ionisation energies and config. variational cellular method 80—32597
$(F\text{-}H\text{-}F)^-$, strong H-bond, using recent difinition 79—98240
F_5S-F bond energy, upper and lower bounds, from chemiluminesc. data 79—86081
Fe atoms and condensed matter in strong mag. fields, var. calc. ground-state energy 77—75046
Fe complexes, Mossbauer isomer shift and core electron binding energies of Fe 78—82620
Fe F2 (Fe F3), electronic struct., binding energy, X-ray emission and photoelectron spectra obs. 80—35008
Fe, ferromagnetic, cluster method, environmental effects 78—95405
Fe, hexavalent, XPS, binding energies calcs. 80—43013
Fe series dimers, bonding, density functional theory calcs. 79—45650
Fe:He, BCC, process of interstitial trapping by impurities 79—46697
Fe-C, electronic structure of interstitials 79—1583
Fe-compounds, K-absorption edge energy shift 79—4870
$Fe_{36}Cr_{32}Ni_{14}B_{12}B_6$, amorphous X-ray absorpt. spectra, effective co-ordination charges 80—84805
Fe_3Si, ordering energy, electron micrography determ. 78—14353
$Ga_{1-x}Al_xAs$, epitaxial, radiative deep states 80—76061
GaAs (110), adsorption of Cs 77—72794
GaAs, exciton ground state and oscillatory absorption spectra in mag. fields, variational calc. 79—11071
GaAs, excitons, diamond like semiconductor, variational calculation of binding energies 78—79938
GaAs, impurity states and core excitons, binding energies, perturb. theory 80—49659
GaAs oxide films grown by anodization in electrolytes, electron spectroscopy exam. *(German)* 79—15837
p-GaAs:Cd, (110) cleaved surface, defect-induced surface states 80—6925
GaN, interatomic interactions from XPS 80—49171
GaP, camel's back induced stabilisation of electron-hole liquids 79—19524
GaP, deep O state, model impurity calc. 80—6780
GaP, electron-hole liquid props., luminescence at high excitation intensity 79—69882
GaP oxide films grown by anodization in electrolytes, electron spectroscopy exam. *(German)* 79—15837
GaP, shallow impurity states, free exciton binding energy 78—79960
GaP:N, electron binding by N pairs 79—90990
GaP_xAs_{1-x}:N, impurity electron states, binding energies and wavefunctions 79—42488
GaS_xSe_{1-x}, wavefunction symm. and binding energies, synchrotron radiation photoemission spectroscopy 80—50532
GaSb oxide films grown by anodization in electrolytes, electron spectroscopy exam. *(German)* 79—15837
GdFe(Co), amorphous film, XPS meas. 79—87295
Ge, electron-hole drop binding energy, optical threshold studies 79—38652
n-Ge, Mott transition, dielec. enhancement and conduction electron screening, donor binding energy 78—72073
Ge, valence band relaxation energies during XPS 78—39657
Ge:B(Al)(Ga)(In)(Tl), binding energy, excited state spectra, photolum., semi-empirical short range pot. 80—44534
Ge_2, multiplet struct. and charge distrib. 79—26881
GeTe, bond orbital model of band struct. 80—59853
H atom, proton spreading in strong mag. field 78—70769
H, atom in strong mag. field, relativistic corrections to binding energies using perturbation calc. 79—68186
H atoms, chemisorbed on cluster, indirect interactions, Grimley-Pisani model and tight-binding calc. 80—65370
H atoms on liquid He surface, interaction and bound states 79—18131
H, binding energy, combined algebra for quantum description 78—8271
H, spin-polarised atom, binding to free surface of liq. ^4He 80—34277
H, strongly bound states in intense mag. field 80—37721
H, transition probabilities and expectation values, in intense mag. field 79—10066
H, uniform mag. field, low lying levels below 10^9 G, adiabatic approx. 79—72235
H, bound states in mag. field, binding anal., variational calcs. 80—42940
H, three-particle atomic system, binding energy, Faddeev method calcs. 77—57858
H-bonded systems, core and valence ionis., nonempirical LCAO MO SCF calcs. 77—67973
H-quark interaction, var. method calcs. 78—37771
H_2, binding energy, MINDO/3 calcs. *(German)* 79—3366
H_2, electron total scatt. intensity, first Born approx. , SCF CI calc. 77—10755
H_2 ground state, bond breaking reaction, MINDO/3 CI *(German)* 78—21852
H_2, metallic, cohesive energy determ. 78—91301

binding energy continued
H_2, pot. curves, binding and ionisation energies and config. variational cellular method 80—32597
p-H_2, solid, anisotropic contribs. to ground state props. 78—83914
H_2^+, binding energy, MINDO/3 calcs. *(German)* 79—3366
H_2^+, electronic energy levels calc. 77—57856
H_2^+, high (10^9 G) mag. fields, dissoc. energy, electron binding energy and equilib. separation 80—52910
H_2^+, in mag. field, LCAO calcs. 78—82628
H_2^+, mol. props. in intense mag. fields 79—81169
H_4^+, ground and excited state pot. energy surfaces and geom. struct., SCF and CI calcs. 78—78769
H_n^- (n=5 to 13), ion-induced dipole clusters, binding energies and geometries 79—41261
HBr^+-HBr, binding energy, mol. beam photoionisation method determ. 79—89622
HCN, vibr. fine struct. accompanying core ionis., STO calcs. 78—62844
HCO^+, orbital contribs. to relax. energies accompanying core ionis., ΔSCF HF calcs. 78—82642
HCl, solid, ferroelec., comparative calcs. 77—8529
HCl^+-HCl, binding energy, mol. beam photoionisation method determ. 79—89622
HF, cryst., CNDO calcs., struct., binding energy, 4K 77—15338
HF, solid, ferroelec., comparative calcs. 77—8529
HF, valence orbitals momentum distribs., (e, 2e) binding energy spectra 80—14237
$(HF)_2$, H-bonding and indirect exchange ('superexchange') in 79—93912
H_2^+He, total energy, interat. dist., geometric configurations, LCAO MO SCF calcs., stability, binding energy 77—42236
H_2O, binding energy, MO momentum distrib., electron impact coincidence spectrometer obs. 77—61869
H_2O, intermolecular interaction energies calcs. using minimal basis sets 80—78681
$H_2O+H_2O(Na^+)(K^+)(NH_4^+)$, supermolecule calcs. with additive procedure, intermolecular interactions and binding energy 80—52880
H_2O_2, gas phase XPS, binding energy 77—34689
$(H_2O)_2$, H-bonding and indirect exchange ('superexchange') in 79—93912
H_2O.HF, H-bonding and indirect exchange ('superexchange') in 79—93912
H_2O...HF complex, force field, vibr. freqs., equilib. geometry bond energy, ab initio calc. 77—65450
H_2S, gaseous 1s binding energy and S $KL_2L_3(^1D_2)$Auger energy, XPS obs. 77—3416
H_2S, valence electron ionisation and momentum distribs. 80—28107
H_2S, valence momentum distribs., binding energies, binary (e,2e) spectrosc. meas. 79—31713
H_2S, valence shell binding energy spectrum, 8-34 eV, electron scatt. simulation of photoionis. 79—10213
He, bound states in mag. field, binding anal., variational calcs. 80—42940
He, quantum-mechanical calculations 77—14350
He, three-particle atomic system, binding energy, Faddeev method calcs. 77—57858
He^-, existence in strong mag. field, binding energy, isoelectronic semicond. impurity trapping 78—9097
$HeCl^+$, interaction potential, HF dissociation energies, LCAO SCF calcs. 77—6880
HeH^+, collisional formation, SCF calcs. 77—6893
He_2H^+, quantum-mechanical calculations 78—33424
^3He, adsorbed on Grafoil surface, ground state, thermodynamic anal. 79—19421
^3He atom, near surface of liq. ^4He, binding energy calc. 79—77853
^3He, Jastrow-type variational calc. methods 79—77854
^3He, liq., binding energy, variational calcs. by Pandharipande's method 80—101752
^3He, liq., binding energy and effective interactions, interactions, variational calcs. 80—107596
^3He liquid, binding energy calcs., Pandharipande method 79—65269
^3He, superfluid, response theory calcs., corrections to mag. susceptibility, binding energies, density 78—67883
$^3He_2$, variational calc. of binding energy 77—54503
$^3He_2{}^4He$, ground state binding energy, Faddeev-UPE method 79—72377
$^3He_3$, ground state binding energy, Faddeev-UPE method 79—72377
^3He-^4He few atom mixed mols., binding energy, size, particle distrib. 80—32864
^4He ground state binding energy, near threshold behaviour in 2 and 3 dimens. 80—91716
^4He, liq., binding energy, variational calcs. by Pandharipande's method 80—101752
^4He liquid, binding energy calcs., Pandharipande method 79—65269
^4He, superfluid, Raman expts., interpretation, two roton bound state binding energy 79—73362
^4He trimer and tetramer, ATMS appl., bounding and ground state energies 79—86026
^4He trimer and tetramer, binding energy, appl. of ATMS 78—94349
$^4He_2{}^3He$, ground state binding energy, Faddeev-UPE method 79—72377
$^4He_3$, Efimov states and binding energies, Faddeev coord. momentum approach 78—46259
$^4He_4$, tetramer bound state binding energy, pot. model 80—63883
$(^4He)_3$, Faddeev theory, binding energy 77—26995
HfC_xN_{1-x}, X-ray valence photoelectron spectrum, 4f signal calc. 80—66391
$HfFe_{2-x}Si_x$, Laves pseudo-binary compound, cubic C15 phase stabilisation 77—39559
Hg, electron binding energy and shift, core level XPS 80—87088
Hg-Cd, behaviour of Cd d-bands, comparison with Au and Ag alloys 79—37972
$Hg_{1-x}Cd_xTe$, photolum. and optical pumping 80—50424
HgF_2, electronic structure of outermost levels, UPS study 80—7468
HgXe, fluoresc. spectra, pot. curves and binding energy 78—66581
I compounds, XPS, binding energies and bond orders 77—18976
I ion+target collisions, K-X-ray yields, 1sσ excitation 77—19051
I_4^{2-}, electronic struct., binding energy, charge distrib. from free electron model *(German)* 78—29741
I_2Ar^*, product state distrib. and binding energy 80—63857
$I(H_2O)_n^-$, geometric and electronic struct., CNDO/2 calcs. 77—79542
I_2He^*, product state distrib. and binding energy 80—63857
I_2Ne^*, product state distrib. and binding energy 80—63857
In, oxidised surface, bonding of Cd arachidate monolayers, XPS 79—15011

binding energy continued
- In, ultra soft X-ray photoelectron energy loss study, angle and energy dependence 78−23582
- InI, orthorhombic, reflection spectra, exciton transition 79−24333
- n-InSb, doping and strain depend. of quantum props. 79−60690
- InSb oxide films grown by anodization in electrolytes, electron spectroscopy exam. *(German)* 79−15837
- Ir, surfaces (111), (100)-(5×1) and metastable (100)-(1×1) struct. depend. 4f-core-level binding energies for surface atoms 80−44406
- k, adsorption on Re $(10\bar{1}0)$ surface, electron-adsorption props. 79−33192
- K, binding energy and equilib. struct., pseudopot. calc. *(Russian)* 79−47037
- K, crystal struct., van der Waals and repulsive interaction 80−84137
- K, electron-ion interaction model pseudopot. calcs. 78−26486
- K, inner core neutral atom binding energy, relaxed-orbital relativistic Hartree-Fock-Slater calc. 78−13433
- K, pair potentials calcs., elastic props. calc. 80−49176
- K surface, clean and O_2-exposed, X-ray and UV photoelectron spectra 78−52636
- $KBr(Cl):Mg^{2+}$, dopant aggregation and precipitation 80−107306
- K_2FeO_4, XPS of hexavalent iron binding energies calcs. 80−43013
- KM_gF_3, bond energy, equilib. distances and compressibility calcs. 80−70159
- KN_3, migration of K^+ and N^0 interstitials, activation energies 79−77813
- KNa_2, binding energy and lattice const., nonparametric calc. *(Russian)* 78−51462
- Kr, inner electron energy characteristics, validity of Hartree-Fock-Pauli approx. 80−42957
- Kr, ion+target collisions, K-X-ray yields, 1sσ excitation 77−19051
- KrAr, photoionisation spectra of ground and excited states 78−5297
- Li, binding energy and atomic radius calc., effect of nonlocalised charact. of pseudopot. *(Russian)* 78−18575
- Li, binding energy and equilib. struct., pseudopot. calc. *(Russian)* 79−47037
- Li complexes $((C_2H_2X_2)_2Li)^n$ where X=S, O, binding and orbital energies, biological systems ab initio calc. 80−102442
- Li^+, ab initio SCF binding energies, with −NCO, −CO, −COO−, O, N, and −CN 77−50352
- Li^+, three-particle atomic system, binding energy, Faddeev method calcs. 77−57858
- Li_2, $X^1\Sigma_g{}^+$ and $A^1\Sigma_u{}^+$ states, electronic struct. and spectra 79−89615
- Li_{2n}, (n=1, 2, 3), stable cluster configs., ionisation pots., binding energies, vibr. freqs., al initio SCF and CEPA calcs. 80−14265
- Li_3, binding energy, Wigner-Seitz pot. calcs. 77−83512
- Li_3, geom. struct. and binding energy, diatomic-in-molecules 78−74785
- Li_4, geom. struct. and binding energy, diatomic-in-molecules 78−74785
- Li_5B_4, molecular and electronic struct. 80−20107
- $LiBH_4$, H bridged system, floating spherical Gaussian model 80−78518
- $LiBeH_3$, H bridged system, floating spherical Gaussian model 80−78518
- LiBe(Mg)(Ca), $^2\Sigma^+$ and $^2\Pi$ states, mol. binding energy curves 80−58189
- LiC_6, intercalated graphite, band struct. determ. by angle-resolved photoemission 80−45203
- $LiCH_5$, H bridged system, floating spherical Gaussian model 80−78518
- LiF, cohesion energy, compressibility and density, ab initio calc. 77−72648
- LiF, ground and excited state props., local density formalism 78−10349
- LiF, selective adsorption of ^3He and ^4He, atomic beam scatt. meas., binding energies 78−63935
- LiH, $LiHe^+$ and $LiHe_2{}^+$ systems, ab initio SCF LCAO calcs. of stability and spectroscopic consts. 77−71748
- LiH_2 and $LiH_2{}^+$ binding energies, LiH_2 ionis. pot. and form. heat 79−94042
- Li_2H, Li_2H^+, binding energies, ionisation pot., mass spectrometric determ. 77−65546
- $^{6,7}LiH(D)$, cryst., cohesive energy, force const., lattice freq., Debye temp., Gruneisen parameters, calc. 78−91293
- $LiNbO_3$, XPS core line intensities, electron escape depth 79−100025
- Lu, binding energies for metal and 4d, 4f atomic levels from XPS data 79−15586
- Lu_2O_3, binding energy from XPS data 79−15586
- Mg, chemisorption of H_2, calc. of adsorption sites and binding energy 79−46953
- Mg, $K\alpha^h$ hypersatellite spectrum, K-shell electron double ionisation cross section, binding energy 79−36577
- Mg-Al(-Zn), solute-vacancy binding energies from hardness meas. 78−39789
- MgO, electronic struct. calc., lattice const., cohesive energy and compressibility 79−78003
- $MgO:M^{2+}$, M=Co, Ni, Cu, next-nearest-neighbour ion effects on impurity 2p levels 77−20987
- Mn-compounds, K-absorption edge energy shift 79−4870
- MnAg alloys, XPS meas. 80−60751
- MnS(Se)(Te), core level binding energies and valence band spectra, XPS meas. 78−80455
- Mo, binding energy, lattice parameters bulk modulus, self-consistent pseudopot. calc. 79−60748
- Mo, $N_2N_3N_{45}$ super Coster Kronig processes 80−106303
- Mo, pair potentials calcs., elastic props. calc. 80−49176
- Mo, pure and He doped, at. config. of $^1/_2\langle 111\rangle$ screw dislocation 79−65081
- Mo, X-ray absorption edge, chem. shift, electron binding energy in compounds 78−62822
- Mo:He, interaction of He with edge dislocation, influence of interatomic pot. 79−33014
- Mo:N single cryst., interaction of N with vacancies 79−82261
- Mo-C dilute alloy defect cluster nucleation and growth under 1250 keV electron microscope *(Japanese)* 78−87663
- Mo-N, bond-strength bond-length relationships 80−91702
- Mo_2 metal-metal bond energy, SCF-Xα-SW calcs. 80−78538
- $Mo_2Cl_8{}^{4-}$, metal-metal bond energy, SCF-Xα-SW calcs. 80−78538
- MoN, interatomic interactions from XPS 80−49171
- $MoO_4{}^{2-}$, valence level electron struct. by XPS 77−4712
- MoS_2, specific surface energy determ. 77−28073
- $Mo(\bar{1}10)$ and (100) surface, surface reson. states and adsorption of 4d atoms 78−71982
- N_2, elastic and inelastic electron scatt. differential cross section, obs. and calc., struct., binding energy 80−28109
- N_2, electronic struct., binding energy and interatomic distance, SCF variational cellular calc. 80−9498

binding energy continued
- N_2, MSXα calc., partial wave expansion, binding energy and orbital energy 80−37738
- N_2, pot. curves, binding and ionisation energies and config. variational cellular method 80−32597
- NH_3, affinities for $H^+(Li^+)(K^+)(CH_3{}^+)$, ab initio SCF calculations 80−102443
- NH_4X, X=halogen, phonon dispersion, cohesive and dielec. props. in three body force shell model 80−79892
- NO, adsorbed on Cu, species identification, struct., dissoc. chemisorption, desorption, UV photoelectron spectroscopy 78−52635
- NO_2, valence shell ionis. spectra, theory and dipole (e-2e) spectra expts. 79−76522
- $(NO)_2{}^+$, binding energy from photoionis. data 77−61811
- NOF and ONF, ab initio calcs. of geometry and electronic struct. 79−76342
- $N_3P_3Cl_6$, ionisation energy and electronic struct., UV photoelectron spectra and Xα calcs. 78−94281
- Na, binding energy and equilib. struct., pseudopot. calc. *(Russian)* 79−47037
- Na, chemisorption of H_2, calc. of adsorption sites and binding energy 79−46953
- Na, electron-ion model pseudopot. calcs. 78−26486
- Na, equilibrium struct. and phys. props., pseudopot. method 80−96778
- Na, inner core neutral atom binding energy, relaxed-orbital relativistic Hartree-Fock-Slater calc. 78−13433
- Na, linear potential and phonons 79−82293
- Na, martensitic phase transition energetics 79−99314
- Na particle, consisting of ats., metallic Na, model, electronic levels 78−50673
- NaAr, intramol. pot. functions of ground and excited state 79−54785
- NaCl type crystal, binding energy of ion on unrelaxed (100) and (110) faces, Madelung and dispersion contrib. 79−77550
- $NaCl:Mg^{2+}(Ba^{2+})$, dopant aggregation and precipitation 80−107306
- NaCl(Br) (F) (I), lattice dynamics and statics, three-body-force shell model 80−49323
- NaF, ab-initio calc. of cohesion energy, compressibility and density 78−71782
- NaF, selective adsorption of ^3He and ^4He, atomic beam scatt. meas., binding energies 78−63935
- NaI, Xe^+ ion bombard., sputtering processes, time of flight meas. 78−88392
- NaNe, intramol. pot. functions of first excited state 79−54785
- Na_2O-SiO_2-Fe_2O_3, glass, X-ray absorpt. spectra, effective co-ordination charges 80−84805
- Na_xWO_3, metallic, XPS, initial and final states, WO_3 binding energy 79−95898
- Na(1s), X-ray photoelectron spectrum, binding energy, at. compared with metal 78−70800
- Nb, binding energies from ESCA *(French)* 77−44541
- Nb, $N_2N_3N_{45}$ super Coster Kronig processes 80−106303
- Nb-V system, H_2 absorpt. 80−59808
- NbN, interatomic interactions from XPS 80−49171
- NbO, binding energies from ESCA *(French)* 77−44541
- NbO_2, binding energies from ESCA *(French)* 77−44541
- Nb_2O_5, binding energies from ESCA *(French)* 77−44541
- Ne, adsorbed on exfoliated graphite, vapour press meas., 15-30K 79−69350
- Ne_2, total energy MS and LCAO Xα calcs., non-muffin-tin corrections, overbinding 78−46266
- Ni (001), chemisorpt. of O_2, MSXα total energy calcs. with non-muffin-tin corrections 77−72795
- Ni (001) and (001)c(2×2)S adsorbed, electronic surface resonances by LEED 79−24051
- Ni (100), adsorbed chalcogen, structure, force consts., binding energies and photoemission, importance of final state multiplet splitting 78−71966
- Ni (100), chemisorption of O, S and Se, struct. and energy levels calc. 77−47663
- Ni (110), chemisorption of N_2, mol. and dissociative mechanisms 80−39431
- Ni, adsorption of CO, binding and energy level shifts, NiCO and Ni_2CO electronic struct. 78−34882
- Ni, at. cluster, EXAFS study of bond length and binding energy 79−81317
- Ni, CO chemisorption, (100) surface, mol. cluster theory 77−69174
- Ni clusters, FCC and icosahedral structs., relax. and stability, cohesive energy minimization 79−42479
- Ni clusters, valence band and core binding energies, UPS meas. 79−38721
- Ni, deposited on stress-annealed pyrolytic graphite, binding 77−59210
- Ni, film, growth on amorphous C, electronic props., UPS and XPS obs. 79−82476
- Ni II acetylacetonate, XPS 80−74196
- Ni, L_{III}-binding energy, absolute determ. from self-absorpt. meas. 80−71519
- Ni surface, (111), chemisorbed CO, bond energies 80−100398
- Ni-Al, electronic, mag., and cohesive props. 80−44491
- Ni-Au alloy, electronegativity and core electron binding energy shifts of Au 77−15346
- $NiFe_2O_4$, thermally induced surface chemistry and struct., XPS 78−22939
- $Ni_{98}M_2$, M=impurity metal, formation of MH(D)-complexes 80−65236
- NiNO, ground and core hole states, config. depend. HF LCAO SCF calc., relax. and binding energy 80−29453
- NiO, H chemisorption, perfect surfaces, cation vacancies, self-consistent HF-VB calcs. 79−69351
- O bonding to Tokamak walls, XPS studies 80−80942
- O^{n-} (n=0 to 2), core binding energy shifts, ΔSCF calcs. 80−95558
- O-containing organic molecules, LCAO-SCF calc. core binding and relax. energies, rel. to polymer surface oxidation 79−76344
- O_2 electron coincidence spectrosc., valence electron momentum distrib. and binding energies 80−102583
- O_2, MSXα calc., partial wave expansion, binding energy and orbital energy 80−37738
- O_2, X-ray spectra determ., agreement with ESCA data 79−41186
- O_3, core electron binding energies, XPS, Xα scatt. wave calcs. 77−75332
- OF_2, core electron binding energies, XPS spectra 77−3417
- ONF, geom. and electronic struct., ab initio calcs. 79−76342
- O(1s), XPS energies from oxidised metal surfaces and powders 77−16457

binding energy continued
OsO_4 , valence level electron struct. by XPS 77−4712
P, black, pseudopotential crystal-struct. stability calcs. as function of press. 79−60503
P_4, core and mol. orbital XPS spectra, binding energies 77−65508
PF_5, ESCA chemical shift, energy levels, SCC-MO calcs. 79−64045
PH_3, bonding by electron impact coincidence expt. 77−65536
PH_3, X-ray K-fluoresc. obs. of electronic struct. 80−37818
P_4S_3, XPS spectra, binding energies, differential photoelec. cross sections ratios 77−65508
Pb, elastic properties *(Russian)* 78−56678
Pb, Gruneisen parameter and binding energy, model pot. calcs. 77−51517
Pb, model pot. calc., binding energy and compressibility 79−99650
Pb, muonic high-lying states transitions, electron screening effects 77−34786
Pb, X-ray absorption edge, chem. shift, electron binding energy in compounds 78−62822
$Pb^+ + Z$ ($42 \leq Z \leq 92$), $1s\sigma$ MO excitation probability and binding energy, X-ray coincidence 78−94316
PbS, (100), angular resolved UV photoemission 78−2989
PbS(Se)(Te), bond orbital model of band struct. 80−59853
Pd clusters, valence band and core binding energies, UPS meas. 79−38721
Pd, metal cluster, calculated structural stability 78−95268
Pd surface, segregated S state, AES, EELS, UPS and XPS study 80−93452
Pd-Ag, ion bombarded, surface segregation, XPES obs. 79−77885
Pd-Au alloy, electronegativity and core electron binding energy shifts of Au 77−15346
Pd-H system containing d impurities, chem. binding energies of point defects 80−107214
PdH, electronic struct., heat of formation, single particle lifetimes, Dingle temp. meas. 78−51923
Pt surfaces, clean and S covered, desorption of CO, binding energy meas. 79−46950
Pt-Au alloy, electronegativity and core electron binding energy shifts of Au 77−15346
Pt-Cu, ESCA study 80−2923
PtO_x, thin film, sputtering deposition, XPS and X-ray diffr. chracterisation 79−78878
rare earth oxides, XPS 80−87170
Rb, crystal struct., van der Waals and repulsive interaction 80−84137
Rb, inner core neutral atom binding energy, relaxed-orbital relativistic Hartree-Fock-Slater calc. 78−13433
RbC_8, intercalated graphite, band struct. determ. by angle-resolved photoemission 80−45203
RbCl(Br)(I), thermal shifts in energy level separations, ESCA 77−8723
RbCl(Br)(I), Xe^+ ion bombard., sputtering processes, time of flight meas. 78−88392
Re surface, interaction with N_2^+ beam, reaction dynamics studied by XPS and thermal desorpt. spectrometry 80−93797
ReO_4 , valence level electron struct. by XPS 77−4712
Rh (111), chemisorbed and condensed CO, energy level shifts 78−87865
Rh, $N_2N_3N_{45}$ super Coster Kronig processes 80−106303
Rh, oxidised surface, bonding of Cd arachidate monolayers, XPS 79−15011
Ru, clean and S covered, adsorption and desorption kinetics of CO 80−6643
Ru, $N_2N_3N_{45}$ super Coster Kronig processes 80−106303
S compounds, one-electron binding and Auger energies 80−52872
S, one-electron binding and Auger energies 80−52872
S to Br, $O^{2+,3+,4+,5+}$ induced K-shell X-ray production cross sections, 7 to 24 MeV 77−61850
S, XPS, in BaS and $BaSO_4$ 80−43104
S_8, X-ray photoelectron spectra, S2s and 2p levels binding energies 77−6844
SF_4, ESCA chemical shift, energy levels, SCC-MO calcs. 79−64045
SF_6, gaseous 1s binding energy and S $KL_2L_3(^1D_2)$ Auger energy, XPS obs. 77−3416
$(SN)_x$, film, brominated, XPS, electronic struct. 78−72678
S_4N_4, film, brominated, XPS, electronic struct. 78−72678
SO_2, gaseous 1s binding energy and S $KL_2L_3(^1D_2)$ Auger energy, XPS obs. 77−3416
Se compounds, LMM Auger spectra, relative intensity and relaxation energy 80−69115
Se, LMM Auger spectra, relative intensity and relaxation energy 80−69115
Si (111) surface, clean, ESCA obs., Ni(Au) surface impurities 78−52640
Si, amorphous, effective mass theory, impurity states in band gap 79−77992
Si, bound exciton-dopant Auger lifetimes 78−18970
Si, CF_3^+ ion bombardment, XPS and Auger study 79−70367
Si compounds, free mol. chemical shift, binding energy and Auger spectra 80−32782
Si, density functional theory, energy calcs., core effects 78−72106
Si, impurity states and core excitons, binding energies, perturb. theory 80−49659
Si, inversion layer binding energy of bound state associated with self-consistent pot. 79−28415
n-Si, Mott transition, dielec. enhancement and conduction electron screening, donor binding energy 78−72073
Si, multiple band excitons, binding-energy calc. 78−34775
Si, oxidised surface, bonding of cadmium arachidate monolayers XPS 79−15011
Si, pseudopotentials for band struct. and cryst. energy calcs. 79−82514
Si, shallow donor states, substitutional donors 79−65403
Si, single cryst., rel. to sputtering rate on Ar ion bombard. 80−55245
Si, structural props., self-consistent calc. 80−28947
Si, structurally related bulk and surface props., self-consistent pseudopot. method 80−54632
Si, total energy calcs. by r-space method, Wannier functions 80−88503
Si, valence band relaxation energies during XPS 78−39657
Si, van der Waals electron correlation energy 78−95013
Si , ground state, photodetachment cross section calc., low energy 79−63970
Si:Au, diffusion of Au anal. 79−23786
Si:B(Al)(Ga)(In)(Tl), binding energy, excited state spectra, photolum., semi-empirical short range pot. 80−44534
Si:H, amorphous, 2p level shift, XPS obs. 80−97401

binding energy continued
Si:Sb(P) (B) homoepitaxial film, interpretation of temp. depend. of partition and sticking coeffs. 77−7756
Si/Al interfaces, chemical bonding states, low energy AES 80−6985
Si-SiO_2, n-type inversion layer, theory of impurity-shifted intersubband transitions 80−20324
n-Si-SiO_2, screening of charged impurity centre localised inside oxide and at interface of inversion layer 79−73563
Si^{q+} +He, q=2-11, K-shell fluoresc. yields, charge-state depend. 78−55231
Si_2, multiplet struct. and charge distrib. 79−26881
Si_2, SCF $X\alpha$ calcs. using pseudopots. and PW basis set 77−34558
SiC (15 R), polytype, many valleyed polar semicond., electron-hole-liquid, obs. from excitation and time delayed spectra 79−28289
α-SiC:H, prepared by reactive sputtering, layer props. *(Japanese)* 80−60695
$Si_{1-x}C_x$:H glow discharge films, local atomic struct., XPS and AES study 80−93448
SiN, interatomic interactions from XPS 80−49171
SiO film, XPS meas. 77−7989
SiO_2 monolayer, core excitons and inner well resonances in surface soft X-ray absorpt. spectra 80−40187
SiO_2, quantity anal. of O ions, meas. of chemical shift in Si2p binding energy, using ESCA *(Japanese)* 78−48274
SiO_4 tetrahedra, semi-empirical molecular orbital model, radiation compaction application 79−73433
SiO_x, chem. shift of Si 2p core level, relax. contrib. 79−47141
SiX_4 (X=Cl,H,F), chemical shifts, relax., X-ray spectra, SCF Xalpha calcs. 80−27928
Si(111), adsorption Ag, cohesive energy and 2-dimens. phase diagram, AES exam. 78−43246
Sn, binding state of atoms segregated at boundary of Fe and Fe alloys, Mossbauer study 80−7232
Sn organometallic cpds., chem. shifts in ESCA and Mossbauer spectra *(French)* 77−28685
Sn, oxidised surface, bonding of cadmium arachidate monolayers, XPS 79−15011
SnO_2 films, cohesive energy, free electron density effect 79−60655
SnTe, bond orbital model of band struct. 80−59853
Sr, 2 keV electron excitation and ionis., ejected electron spectra 77−3466
TaO_6^{7-}, octahedral cluster, ionisation energies and atomic populations, XPS and SCFMS $X\alpha$ calc. 79−93923
Te compounds, X-ray photoemission, core level binding energy shifts rel. to Mossbauer isomer shifts 78−2984
Te, relax. energies for photoionisation 77−20988
Te, X-ray photoemission, core level binding energy 78−2984
Th, adsorption of O_2, XPS study 80−7473
TiC, soft X-ray emission, excitation pot. spectra, excited level binding energy 80−35009
TiC, valence band electron distrib., photoelectron spectra obs. 77−44120
TiC_x, single cryst., core level shifts, valence band struct., ESCA 77−32499
TiN, interatomic interactions from XPS 80−49171
TiN, soft X-ray emission, excitation pot. spectra, excited level binding energy 80−35009
TiNi, soft X-ray spectra, electronic struct. 77−44091
TiO_2-Ni (100) interface, electronic props., struct., comp., chemical bonding 80−84499
TiO_x, interstitial alloy, electronic state, XPS, mag. susceptibility and elec. resist. 77−12486
Tl, core level binding energies, UPS obs. 80−66388
Tl halides, van der Waals energy, cohesive energy calc. 77−51343
TlCl, ground-state props., Wannier functions, and electronic struct., ab initio self-consistent calc. 80−80178
TlCl(Br), Wannier exciton-ionised donor complexes, binding energy calc. 80−49609
TlI, XPS and UPS study of phase transforms. 80−45210
Tl(III) organocompounds, XPS study *(French)* 79−64047
U, adsorption of water and O_2, XPS study 80−7473
U in transition metal coordinate compounds, binding energies from XPS data 78−21973
UO_2, U_2O_5, U_3O_8, and UO_3, bonding and valence obs. by ESCA and EPR 77−28696
V oxides, XPS and AES study, electron correl. effects, semicond.-metal transition 80−7467
VC, soft X-ray emission, excitation pot. spectra, excited level binding energy 80−35009
VN, interatomic interactions from XPS 80−49171
VN, soft X-ray emission, excitation pot. spectra, excited level binding energy 80−35009
V_2O_{5-x}, O_2 equilib. press. as measure of O_2 binding energy in oxide system 79−16030
W (011), field desorption of Ba atoms, conc. depend. 80−25533
W (110) and (100), adsorption of Xe and coadsorption with O, work function and thermal desorption meas. 80−39448
W (121), Ba atom desorption in strong elec. fields 80−29280
W, adsorption of Au, field emission microscopy exam. of work function, correlation with LEED and RHEED meas. 78−35276
W, adsorption of benzene, isothermal ramped field desorption technique 79−82450
W, binding energy, lattice parameters bulk modulus, self-consistent pseudopot. calc. 79−60748
W, chemisorbed CO and acetylene, IR vibration spectroscopy using refl. inelastic electron scatt. 78−14603
W field desorption of K, from (001), (011) and (112) planes 78−34715
W, potential of He atom above field adsorbed He or Ne atoms 78−35267
WO_4^{2-}, valence level electron struct. by XPS 77−4712
Xe adsorbed on Pd (110), anomalous 5p photoemission, electron binding energies 80−100750
Xe, inner electron energy characteristics, validity of Hartree-Fock-Pauli approx. 80−42957
Xe, solid, luminesc. from self trapped excitons (excimers) 79−1785
Xe, solid, zero temp. isotherm, APW calc. 79−73128
Xe_2, near metal surface, proximity effects 79−36797
XeAr(XeKr) photoionisation spectra of ground and excited states 78−5297
$XeCl^-$, well depth of mol., $Xe+Cl^-$ elastic cross-section expt. 79−86027
XeF^-, well depth of mol., $Xe+F^-$ elastic cross section expt. 79−86027

binding energy continued
- ^{136}Xe ion+target collisions, K-X-ray yields, 1sσ excitation 77—19051
- Yb, 4f levels, hole lifetime and chemical shift, UHV study 80—20762
- Zn, atomic and metallic, photoelectron and L$_{23}$-MM Auger spectra, binding energies 77—90238
- Zn, core binding energies, gas phase X-ray photoelectron spectra 78—37611
- Zn, electron binding energy and shift, core level XPS 80—87088
- Zn, inner core neutral atom binding energy, relaxed-orbital relativistic Hartree-Fock-Slater calc. 78—13433
- Zn, sputtering, binding energies 80—108312
- ZnF$_2$, electronic structure of outermost levels, UPS study 80—7468
- ZnO, existence of biexcitons, reson. two-photon Raman scatt. 79—19889
- ZnO, optical gain and induced absorption from excitonic mols. 78—84609
- ZnS:MnF$_2$ films, effect of Mn conc., XPS obs. 79—33886
- ZnSe, exciton emission, halfwidths, thermal and optical activation energies obs. *(French)* 80—66268
- ZnSe, single cryst., electron-hole drops, boundary luminesc. *(Russian)* 78—80412
- ZnTe, single cryst., electron-hole drop conc. *(Russian)* 79—11460
- ZnTe:As(P)(Li), binding energy of shallow acceptors from photoluminesc. excitation spectra for donor-acceptor pairs 79—95809
- ZnTe:P, excitations spectra of donor-acceptor pair photoluminesc. 78—23522
- Zr-Co, amorphous and crystalline, d-band struct., alloying effects 80—59862
- Zr-Ni, amorphous and crystalline, d-band struct., alloying effects 80—59862

Bingham plastics and solids *see rheology*

bioacoustics
- *see also biological effects of acoustic radiation; biomedical ultrasonics; hearing; sonar*
- absorption in tissue, possible mechanisms 80—45951
- Acoustical Soc. Amer. 96th meeting, Hawaii, 1978 Nov. 78—90545
- action potential latencies, narrow-band, in normal and recruiting human ears 79—43929
- airway, collapsible, fluid-dynamic flapping, sound generation and flow limitation 80—94258
- airway geometry determ. by anal. of acoustic pulse response meas. 78—28026
- anaesthesia during tooth hard tissue operations, BN-1 apparatus 78—85350
- aneurysm detection using bioacoustic signal processing techniques 78—28120
- aneurysm detection using one-bit correl. 80—17175
- aortic ejection click and first heart sound description 80—30827
- aortic wall, canine, speed of 10 MHz sound, effects of temp., storage, formalin soaking 80—56112
- arterial low freq. vibrations study 79—92462
- Atlantic bottlenose dolphin, echolocation signal propag. 78—88721
- audiosonology, noninvasive diagnostic possibilities of phonocephalography and phonomyelography 78—48920
- bat, const. freq.-FM sonar signal processing in auditory cortex 77—12940
- bat, moustache, aural representation in Doppler-shifted-CF-processing area of auditory cortex 78—80892
- bat, moustache, target range sensitive neurons in auditory cortex 79—83808
- bat, obstacle avoidance for moving and stationary objects 79—2086
- bat, Pteronotus suapurensis, long-latency ‘subthreshold’ collicular responses to emitted const.-freq. components 79—79562
- bat’s sonar system simulation in anechoic chamber, coherent processor performance estimation appl. *(French)* 80—56072
- bat Doppler echolocator, obs. of surroundings 77—70483
- bat echo-locator, phenomenological model of system of precise determ. of direction to target 77—36962
- bat echolocation system, optimum phase modulation for insensitivity to acceleration 79—53163
- bats, biosonar signals, fine freq. anal. via phase-locked loop device 77—56392
- bats, echolocation, pursuit of prey 79—83807
- bats, response of cricothyroid muscles to FM sounds, Myotis lucifugus 77—21540
- bibliography of diagnostic uses of US in medicine and biology 79—96641
- biomechanical spatial motion, data collection method using sonic digitiser 79—39441
- biosonar signals, moustache bat, auditory information processing 79—11943
- blood, canine, US attenuation and speed, rel. to packed cell vol., 37°C 80—41106
- blood, sickle cell, effect of deoxygenation on US absorpt. coeff. 78—44477
- blood, US backscattering, haematocrit and erythrocyte aggregation depend. 80—45961
- blood, US scattering, theoretical study 80—51147
- blood pressure recording, simple method for fidelity improvement, Korotkoff sounds 80—76811
- bone, anisotropy of Young’s modulus, US meas. 78—11687
- bone, cancellous, US attenuation and dispersion 80—51149
- bone, human, acoustic emission in restressing 80—3704
- bone, human cortical, US properties and microtexture 80—51144
- bone, mammalian, acoustic emission testing 80—76783
- bone, US surface waves for studying props. of human tibia 77—25619
- bone, US velocity meas. in temp. range of room temp. to 90°C 80—76787
- bone elastic moduli measurement using US vel. 77—25623
- bone fracture healing, sonic diagnosis 77—21580
- bone healing monitoring method using microprocessor based system 80—21511
- bone tissue, human, subjected to longit. extension, acoustic emission 77 25495
- bovine blood vessel walls US vel. meas. 78—85333
- brain, normal and abnormal, attenuation, vel. and impedance 80—45955
- breast malignant tumour, freq. depend. US attenuation, fast Fourier transform technique 80—45996
- breath sounds, ventilation regional phase differences demonstration 80—8087
- cardiac acoustic model for computer-aided surface acceleration mapping 78—35791

bioacoustics continued
- cardiac sound and vibration recording, electro-optical sensor 77—21648
- cardiac sound frequency shifting stethoscope 79—29647
- cercal system, cricket, const. representation of position of signal source in space 77—25475
- cercal system neurones, cricket, const. representation of sound source position 77—70482
- cochlear macromechanics, time domain solutions 79—88087
- compact bone sample, distrib. of sonic plesio-velocity 79—96611
- crickets, auditory behaviour of hybrids, evidence for genetic coupling in animal communication 77—32913
- delphinid porpoises, sound production and air recycling, cineradiography 79—48275
- deoxygenated sickle cell blood and haemoglobin S solution props. 78—3453
- diagnostic technique for prosthetic fixation evaluation 80—21510
- diagnostic uses of US in medicine and biology 80—4481
- diastolic semilunar valve vibrations, heart sounds, one-dimensional model 79—79580
- dichotic chords perception, individual differences 79—88082
- dog lungs, input impedance from Fourier anal. of response to transient pulse pressure excit. 79—5309
- dolphin, communication signal types and organisations 77—70485
- dolphin, Phocoena phocoena, props. of low freq. sonar signals *(French)* 77—52809
- dolphin acoustorespiratory system, morphology and function *(Russian)* 77—64060
- dolphin communication signal spectrum, fine struct. anal. 78—20197
- dolphins, importance of isolation and anal. of emotional signals *(Russian)* 79—43934
- dolphins and pinnipeds, echolocation system acoustics and hydrodynamics 77—36963
- echo detecting characts. of inferior colliculus neurons of unanaesthetised bats 77—70484
- echo-locating animal, neurocorrelometer model 78—96059
- echolocation, bat, accuracy of meas. of target angular coords. using equisignal zone 78—77071
- electrophonocardiographic systolic time intervals, influences on 79—34681
- erythrocytes, haemolysing action of u.s. 77—2019
- esophageal multiprobe for temp. ECG and heart and lung sounds meas. 79—57791
- eye, abnormal movements control method using audio feedback 80—41156
- fibrous networks in viscous media, appls. of theory of acoustic motion 77—86733
- fiddler crab auditory and vibrational stimuli receptor, Barth’s myochordotonal organ 77—77921
- first-heart-sound spectra, temporal and heart-size effects 80—41276
- fish backscattering cross section, swimbladder effect in gadoid and mackerel 80—89787
- fish target strength functions, model for averaging 80—43512
- frequency dependence of tissue acoustic parameters 77—40718
- frog entrainment to randomly generated calls, Hyla crucifer species 80—89789
- green tree frog, female discrimination of intermediate sounds in synthetic call continuum 78—69109
- haemodynamic parietal friction meas. by pulse type Doppler velocimeter 80—17206
- haemoglobin, US attenuation and dispersion, Kramers-Kronig relative 78—83135
- heart fourth sound studied by FFT 80—94397
- heart vibration quantitative characterisation by multipolar acoustic heart model, minicomputer method 78—85429
- horseshoe bat echolocator signal, freq. stabilisation model 78—20195
- human response to whole-body vibr. duration effect on comfort 77—17011
- human skull, acoustic losses and vel. meas., rel. to diagnostic imaging 78—69159
- infrasound, atmospheric, detect. by homing pigeons 77—29156
- insects, sound radiating cuticular motion, measurement by irradiance modulation technique 79—84057
- intra-ocular pressure measurement using sonics and coherent optics 77—81548
- intracardiac shunt noninvasive quantitation using cardiovascular sound complexes 78—48918
- intravascular thrombus induction in vivo using localised hydrodynamic shear stresses 80—97997
- knee ligament damage monitoring by acoustic emission, canine model 80—41149
- Korotkoff sounds, model expt. on generation 80—98207
- Korotkoff sounds possible origin from steady press. flow in compressed arteries 80—81639
- laryngeal configurations effect on acoustics of phonation 79—86309
- LF characteristics of tissues 77—25496
- liquids, acoustic interferometer for sound speed meas. 77—50844
- liver, US backscatter from human tissue, depend. of freq. and protein/lipid content 80—45960
- liver tissue, attenuation coefficient slope statistical estimation from refl. US signals 80—46000
- lung, airway network geometry inference, broadband relfection data 79—29560
- lung, amplitude-frequency response of pulmonary air tract 79—20574
- lung, distributed response of complex branching duct networks 78—57027
- lung, modal struct. of asymmetrically branching duct networks 78—57028
- lung sound transmission meas. 78—28149
- lung surface US tissue signature 80—45957
- lungs, sound wave propag. in acoustic ducts 77—12981
- mammalian testes, freq. depend. of US absorpt. coeff. 78—61213
- mammalian tissues, compilation of empirical US props. 78—88727
- marine biological choruses observed in tropical waters near Australia 79—2085
- marine organisms, sound scatt. using fluid-sphere model 77—46846
- monkey vocal sounds, species-specific perceptual processing 79—79563
- mustache bat auditory cortex, amplitude spectrum representation in Doppler-shifted-CF processing area 77—52810
- mynah bird imitation of human speech, comment on first formant resonance 79—43939

bioacoustics continued
myocardial tissue, US attenuation depend. on time after excision and temp. 78—11711
myocardium, acoustic microscopic anal. 80—45995
myocardium, normal and ischaemic, US attenuation 80—45954
narwhals, acoustic echolocation signals 79—88097
narwhals, acoustic signal emission characts. 78—40209
nerve-muscle acoustic props. in rats as function of physiogical state 77—21673
noise and vibration effects on human beings, summary of symposium, Southampton Univ. (Dec. 1978) 80—35958
pathological knee joint cartilage damage, electroacoustic evaluation 79—20702
phonocardiogram automatic classification, linear predictive anal. processing *(Japanese)* 80—36036
phonocardiogram detection algorithm using spectral tracking 80—41151
phonocardiogram quantitative anal. for murmur detect. 80—56270
phonocardiography, Fonokard type instruments 80—56229
phonothyreogram and phonocardiogram frequency spectrum analysis by minicomputer, ECG reference time signal 79—83966
phosphatidylcholine monolayer vesicles, US irradiation formation, quasielastic laser light scatt., dynamics 77—48764
piezoceramic cardiovascular acceleration transducer 79—39536
poly-1-glutamic acid, soln., u.s. absorpt., linear Ising chain kinetics 77—4980
polypeptides, in aq. poly(L-glutamic acid) soln., helix-coil transition, US relax. times 80—45849
pulse echo waveform rel. to acoustic characteristics of continuous medium 80—67145
rat, female, sexual behaviour and US vocalisations 78—40208
rat tissue, freshly excised, freq. depend. 77—86573
red blood cell aggregation detect. during blood flow by US 79—84068
respiratory parameter meas. using 200 Hz acoustic pneumograph 77—48913
respiratory rate monitor using microphone pickup 79—79617
respiratory sounds meas., laser vs. acoustical methods *(German)* 80—98058
scanning laser acoustic microscope, principles and analytical capabilities 79—18655
semilunar valvular motion vibr. model during early diastole, rel. to second heart sound 78—44533
semilunar valvular vibration in early diastole, rel. to second heart sound 78—44544
L-serine, in aqueous solns., US spectra using automatic recording spectrometer 78—75735
sharks, rapid withdrawal from underwater sound source 79—16224
signature information in song of humpback whale 79—88093
skeletal muscle, human, LF sounds from sustained contract. 80—61751
skull, acoustic characteristics 79—96730
skull bones, human, US flexural wave study 80—72277
sound analysis, reversible computer method adapted to bioacoustical expts. 78—57137
sperm whale codas 78—31826
stenotic flow, vascular anal. model 79—79593
striated muscle, frog, longitudinal pulse propag. 79—16246
swimbladder resonance in fish, experimental investigation 79—98531
temperature variation of acoustic speed in excised human tissue, US computerised tomography 80—51150
thoracic sound characterisation by time series anal. using canine model 78—31959
tibial bones, of highly trained athletes phys. stress effect type as measured by US techniques 80—16992
tissue, mammalian, survey of US vel. and attenuation data 80—46744
tissue, mammalian, US attenuation and speed determ. as function of temp. 80—41108
tissue, soft, temp. distrib. monitoring by temp. depend. of US vel. 80—45994
tissue absorption coeffs., automated meas. system using transient thermoelec. technique 80—76817
tissue characterisation, US propag. parameter meas. 80—45953
tissue characterisation, US propag. props. 80—45950
tissue characteristion, static and moving, high spatial resolution US meas. techniques 80—51187
tissue damage and death rel. to mech. props., US interaction 80—51151
tissue equivalent test objects, US transmission tomography and pulse echo imaging compared 80—51154
tissue phantom, human abdominal, for US diagnostic equipment 80—51152
tissue simulation, acoustic attenuation CW meas. in oil-polymer mixture 80—35961
tissue simulators for US diagnostics 80—51153
tissue US backscatter and attenuation distrib. mapping, digital reconstruction 80—51188
tissues, fixed and unfixed, US propagation, backscattering coeffs. and speech determ. 80—41109
tissues, mammalian, US absorpt. and attenuation determ. by thermoelectric method 80—41110
transients generated by laser pulses, mechanism and effects 78—48830
underwater sound, volume scattering strengths and zooplankton distributions at acoustic frequencies between 0.5 and 3 MHz 80—33317
US absorpt. and vel. in mammalian tissue, dependence on constituent proteins 80—61621
US attenuation and backscatt. obs., freshly excised animal tissues 80—51148
US attenuation in tissue, temp. and freq. dependence 80—45949
US attenuation mechanisms in soft tissue 80—45952
US attenuation vs. frequency in soft tissue 80—45956
US effects on catalyse and malate dehydrogenase 80—76788
US imaging, backscatter enhancement from collagen microspheres, dog liver, erythrocyte suspension 80—94281
US propagation in biological tissue, phase and amplitude fluctuations 80—8097
US propagation velocity in tissue, meas. device 80—45993
US props. of mammalian tissues, compilation of literature 80—98007
US pulse propagation in dispersive media, human soft tissues 80—81644
US shear velocity of muscle tissues, mech. props. determ. 80—108930
US tissue characterisation, clinical spectrum anal. techniques 80—45998
US tissue characterisation, conf., Gaithersburg, USA (Jun. 1977) 80—41940
US tissue characterisation by angle scan and freq.-swept scatt. technique 80—45958

bioacoustics continued
US tissue characterization in vivo by differential attenuation measurements 80—45999
US transmission through tissue, time post-mortem effects 78—28025
US velocity meas. in liquids and small biological tissue specimens 80—76786
US velocity rel. to mineral content 80—45962
valve vibrations, aortic and mitral, anal. and role in heart sound production 80—101214
ventilatory phonetory conflict, investigation using glottiscope 80—51145
vertebrae, human, deflected US wave propag. tests 80—61617
Vespa orientalis, sound production by workers facing the queen 79—88094
vocal distinctive features used by gelada monkeys 77—1971
zooplankton, underwater sound backscattering spectra 77—79994

biocommunications
see also biocybernetics; hearing; learning systems; speech
acoustic display development in fiddler crab 80—12325
aid for speechless handicapped persons 77—60306
animal communication, INFO program using information theory for anal. 77—90712
biological information processing, theoretical approach *(Japanese)* 80—12049
bird song, species-specific coding 80—97950
cell contact region during communication, obs. of gap junction 80—45873
crickets, auditory behaviour of hybrids, evidence for genetic coupling in animal communication 77—32913
dolphin, communication signal types and organisations 77—70485
dolphin communication signal spectrum, fine struct. anal. 78—20197
dolphins, importance of isolation and anal. of emotional signals *(Russian)* 79—43934
fiddler crab auditory and vibrational stimuli receptor, Barth's myochordotonal organ 77—77921
harp seal calls, underwater, distinctive characts. during breeding season 80—12324
microwave radiometry, natural emission detection, experimental results 77—32949
microwave radiometry applications 77—81770
mynah bird imitation of human speech, comment on first formant resonance 79—43939
neural lateralisation of species-specific vocalisations by Japanese macaques 79—62268
pheromone of cabbage looper moth, IR emission, candle flame as sexual mimic 78—35871
pheromone of cabbage looper moth, IR emission, tapping modulation 78—35872
purported Bigfoot vocalisation record pitch and vocal tract length estimates 79—94418
rat, female, sexual behaviour and US vocalisations 78—40208
sperm whale codas 78—31826
tactile artificial sensory communications, space and freq. optimal displays 78—36049
termite behaviour influence of biofields 77—44622
underwater, direction finding device for bearing determ. of whale sounds, real-time device 80—96079
vocal distinctive features used by gelada monkeys 77—1971
whales, southern right, sound playback expts. 80—89772
zebra finches, female, long-term recognition of father's song 79—83799

biocontrol
see also biocommunications; biocybernetics
adaptive control mechanisms for complex motor systems 80—81573
adaptive stiffness control in human movement 80—108947
adenylate cyclase regulation, depend. on sugar transport system, review 78—69031
alpha rhythm, human, feedback control from central area 80—40988
alpha wave amplitude and frequency, feedback control *(Japanese)* 77—44626
ambulatory neuromuscular activation control model 79—57638
anaesthetised human subject temperature change model 79—92160
ankle joint reflex response to sinusoidal forces 77—21513
arbitrary movements control theory 79—74641
arm movement control, central integration function model 79—83757
arm movement control processes in monkeys 79—53080
arm movements controlled by peripheral feedback, in humans, simulation 78—80891
arm posture control, spring model and equivalent neural network 80—101196
arterial O_2 tension, generation of variable amplitude sinusoidal changes for freq. response anal. 77—56563
arterial O tension servocontrol in preterm infants 80—17183
arterial pressure-flow relationships in anaesthetised dog 78—69120
arterial system least energy regulation 78—53434
arterial system math. model, press.-flow relationships 78—53435
articulation development, possible nonlinear time varying control in feedback path 78—35870
artificial hand, myoelectrically operated with dynamic control *(German)* 79—8571
artificial hand, myoelectrically operated with dynamic control, practical trial *(German)* 79—12029
artificial heart, driven by automatic driving system 78—7541
atrial and/or arterial blood pressure servo control in expt. animals 78—31986
auditory neural mechanism system properties 78—40200
baroreceptor Na sensitivity mediating reflex changes of blood press. and urine flow 77—48818
biochemical multiple-loop negative feedback control networks, oscills., periodic metabolic systems 78—85285
biochemical systems anal., mol. biology, book 77—21468
biocybernetic multilevel system, nervous regulation of internal organs *(Russian)* 78—48779
biofeedback, physiological responses control appl. *(Japanese)* 77—44830
biofeedback control of skin potential level 80—21572
biofeedback devices for control of unconscious physiological processes 78—35992
biofeedback for alpha monitoring of brain activity 78—20299
biofeedback therapy technique and application *(German)* 79—16341
biological system abnormality, regulation and control *(Japanese)* 77—36970
biped dynamics, feedback on-off model 80—30709

biocontrol continued
bipedal locomotion, inverted pendulums stabilisation algorithm *(Japanese)* 80—81630
bipedal locomotion, simple model of step control 79—11958
blood pressure, volume, heart rate and cardiac function regulation *(Japanese)* 77—40688
blood pressure control, mechanical-chemical balloon implant 79—20712
blood pressure control system dynamic behaviour identification 79—2097
blood pressure or flow control system for unanaesthetised animal 77—48983
blood volume control after haemorrhage, model and implication for intravenous fluid therapy 77—40697
blood volume regulation, effects of space flight, review 80—3826
body control mechanism, human, investigation using analysis of body's period signals 79—66576
body temperature humidification, effect on patient thermal regulation 78—85295
brain functional organisation, methodical approach *(Russian)* 78—35824
brainstem respiratory activity, math. model of computer-simulated neurons 77—44637
breathing control hierarchical goal-seeking model description 78—80899
breathing control hierarchical goal-seeking model performance 78—80900
cancer problem cell kinetic study based on automatic control theory 77—40639
carbohydrate and lipometabolism systems interaction, use of mathematical model 78—31758
cardiac assist system, intrathoracic, self-sufficient instantaneous haemodynamic control 77—44842
cardiac in-series assistance using balloon pump, effects on left ventricular afterload/aortic power dissipation 78—3669
cardiac output control mechanism modelling *(Japanese)* 78—69133
cardiopulmonary control and lung O_2 and CO_2 exchange interaction model, duck 80—3600
cardiovascular control dynamic test method evaluation, model considerations *(German)* 77—52813
cardiovascular system contractility characterisation by programmed premature contractions 79—88113
cell cycle kinetics stability and control, cancer chemotherapy appl. 79—34521
cell functional activity regulation, human, by laser emission 79—43957
cell growth regulation, effects of cell density and metabolite flux on dynamics 78—85296
cell growth regulation, effects of cell density and metabolite flux on dynamics 78—88701
cell permeability polarity and control by phytochrome, red light irrad. of mass 78—77025
cell wall deform. and morphogenesis, local control of viscoelastic deform., Acetabularia 77—56349
cellular control of gene expression by positive feedback, differential eqns. 79—66460
central and peripheral nervous control mechanisms *(German)* 79—5271
central nervous system interaction with peripheral motor system, voluntary human movement 79—8499
cerebral blood flow control in hypercapnia, model 79—100641
chelonian muscle spindles motor stimulation model 77—44636
children's newly acquired phoneme articulation, right-ear auditory feedback control 79—57676
circulation, LF dynamics of external iliac arterial bed, unanaesthetised baboon 77—36998
circulation control physiology study *(Japanese)* 77—36969
circulatory regulation by artificial heart *(Japanese)* 77—36971
colonic electrical control activity, human, computer model 80—61537
control signals and transducers for the control of upper extremities in plegic patients, computer controlled experiment *(Slovak)* 80—109061
coral growth form, light control, computer simulation 77—2076
corneal hydration endothelial control theory 78—35841
crustacean cardiac pacemaker control system, model analysis 77—52766
crustacean cardiac pacemaker control system, simple model 77—52765
dialysis, ultrafiltration, meas. and control using differential flowmeter 77—21657
disturbed cell renewal control system modelling and simulation 79—29510
dopaminergic feedback regulation, rel. to postsynaptic receptors 77—52774
drug-carrying microspheres, intravascular mag. guidance 78—73188
dyslexic visual perception and aculomotor performance 79—83769
early referential speech, linguistic development rel. to sensorimotor attainments 79—57674
effective temperature criterion for exercise heat stress prescription 79—92159
electrical control of development, review 77—86467
electromyogram envelope spectral anal., muscular control study 78—92750
electrophrenic respiration, feedback control of tidal vol. *(Japanese)* 80—41316
EMG envelope spectral anal., muscular control process appl. 79—5390
excitatory-inhibitory visual system organisation evidence from oversaturation *(French)* 77—12922
extracorporeal heart-lung bypass, mechanical support of circulation *(Japanese)* 77—40690
eye, abnormal movements control method using audio feedback 80—41156
eye, accommodation and vergence static behaviour, computer simulation of interactive dual-feedback system 80—94205
eye, aqueous temperature stabilisation, laser induced temp. changes and model 77—40713
eye, error-correcting mechanisms in large saccades 78—61175
eye, pursuit movements of disappearing moving target 78—61174
eye, vergence movements, heuristic feedback system model 77—21517
eye lens accommodation, interpositus neuron control obs. 80—21469
eye long-term growth and shortsightedness model 79—83768
eye movement, eccentric fixation with secondary visual feedback 79—79522
eye movement control during single unit recording in pigmented rat 77—81767
eye movement control in cephalopods, cerebellar-type system 77—12914
eye movement hierarchical control model 77—25429
eye movements while reading, annotated bibliography 78—53394
eye position information accuracy for motor control 77—81491
eye torsional movements, rapid phase, in humans 78—69045
eye vergence control, role of spatial freq. tuned channels 80—101170

biocontrol continued
fine muscular control rehabilitation using ramp threshold feedback 79—83996
finger tapping phase transition curves, human *(Japanese)* 80—56333
firing rate control by inhibitory mechanism in tightly coupled two layer random nerve net 80—61533
flow absorption system, reaction vel. parameters rel. to absorbed solutes conc. profile *(Japanese)* 79—74710
fly head and body movements in flight 77—40664
functional electrical stimulation orthoses, gait parameter variability *(French)* 77—9302
functional electrical stimulators, multisite appls. extremity stimulation 77—48936
gait control, peroneal nerve stimulation sequence effect *(Croatian)* 78—44692
haemopoietic stem cell population and proliferation model 77—44610
hand movement control, role of eye movement 80—26237
hand prosthesis development, electromyograph controlled aid *(Spanish)* 78—15924
hand temperature self-regulation, assessment technique 80—16906
head-neck system mechanics, for visually triggered head movements 77—36977
heart, minimal O_2 consumption and optimal contractility, theoretical approach 79—74694
heart rate, in man, system anal. 77—25478
heart rate and sinus arrhythmia obs. during health-resort treatment 79—43855
heart rate control device, appl. for cardiac rehabilitation 79—83995
heart rate variation during ergometric test, computer interpretation 78—85430
hind-limb reflex movements, chelonian, simulation 79—74642
inspiration, graded inhibition, specific effects of flow rate 79—100647
insulin secretion neural control, math. model 78—31796
interlimb coordination, human, expt. obs., two handed movements 79—57636
intestinal motor activity mathematical model 77—90847
intracellular control and intercellular transfer of molecules, multichannel anal. 79—53073
intracranial pressure regulation, nonlinear parametric feedback model 79—96599
knee-torque controller, electrohydraulic, for prosthesis simulator 78—11779
laryngeal control for pitch change in Japanese word accentuation, neuromuscular model *(Japanese)* 78—40205
laterality effect in isometric and isotonic labial tracking 79—57625
limbs microcomputer control, motion analysis using goniometers 80—51138
lower leg reflex asynchronous control via spinal motor neutron pool 78—27935
lungs long-term forced ventilation control excitation 77—60296
mammal locomotion, role of joint receptors in limb control *(Russian)* 79—43938
microcirculation autoregulation mechanistic theories, computer simulation 78—27995
microcirculation O_2 distrib. during and after arteriolar occlusion 78—44529
motoneuron optimal control model 77—86486
motor activity and movements of extremities, use of elec. stimulation 77—86708
motor neuron, simplistic model of clonus 77—48786
motor neuron firing pattern in Aplysia 79—48244
motor unit recruitment and firing freq. control in elec. stimulated muscles of cat 78—81092
movement detection, one-way, in fruitfly visual system 79—39415
muscle, elec. stimulated, closed-loop control of force 80—76728
muscle, myosin regulated, changes in crossbridge attachment 78—53361
muscle, skeletal, bond graph simulation of glucose metabolism 77—36894
muscle, striated, reversible loss of Ca control of tension assoc. with removal of regulatory light chains, scallop 78—53360
muscle contraction strength control during elec. stimulation, using PWM and FM 77—40929
muscle control system Ia feedback pathway correlations, origin and nature 79—24977
muscle coordination in cat hindlimb during maximal vertical jump, computer model 77—40662
muscle electromagnetic stretch, sensorimotor cortex neurons in behaving primates 79—88073
muscle length and strength control, central co-activation of α and static γ motoneurones 77—25414
muscle length reflex control, servosystem simulation 79—57639
muscle stretch reflex system, multi-channel, focused signal transmission mechanism considerations 79—24978
muscle tension development control by motoneurones 77—66813
muscleforce-freq. curve recording from humans, α excitability evaluation *(Japanese)* 78—3643
muscular activity in pasture maintenance, control mechanisms study via spectral anal. 79—5306
musculo-skeletal system, human, complete set of control eqns. 78—40223
myoelectric control of an artificial hand, sequential movement, tropical climate 80—41323
myoelectrically controlled systems, five-state, error rate obs. 80—72376
neural and cellular control system stability properties 77—40640
neural pacemaker phase control 78—11631
neuromuscular mechanism maintaining extrathoracic airway patency 79—100656
neuromuscular system electrical stimulator using biopotential amplifier 79—48315
neurophysiological models, motor control, muscle representation 78—24057
occipital EEG, feedback delay, amplitude threshold and control 80—21465
ocular following reflex elicited from retinal periphery, cat 77—60206
oculomotor control system, expt. set-up for clinical investigation, visual, acoustic, vestibular stimulations 78—80990
oculomotor control system neurological integrator 77—4993
oculomotor control system signal flow diagram 77—25415
oculomotor control system synthesis photoelectric matrix method appl. *(Korean)* 77—90779
oculomotor slow control, effect of expectations, periodic target steps 79—100604

biocontrol continued
oculomotor slow control, effect of expectations, single target displacements 79—100605
oculomotor system parameter identification, strabismus appl. 78—3478
optomotor control, dipteran giant visual interneurone response props. 78—27940
oscillating control system theory 77—25360
perfusion pulse attenuation in dog autoregulation 78—44545
peripheral polymorphonuclear leucocyte system model, humans 78—56956
perspiration mass transfer coefficients and clothing models 79—92158
phototaxis in walking fly, water balance and phototactic response 79—20577
physiological control system simulation and modelling 77—90848
physiological control systems, oscills. and chaos 77—90715
physiological system stochastic anal. and control., cancer detection and therapy 77—90713
physiology system models, breathing control example 80—41058
pigeon rotation reflex input-output relations and model *(German)* 77—44623
plant respiration control through non-photosynthetic light action 77—44717
postural equilibrium, role of kinematic mobility of human cervical spine 77—52837
posture control system response to random accel. disturbances *(Japanese)* 80—72200
posture-control system, responses to pseudorandom accel. disturbances 80—81640
premotion silent period in rapid voluntary movement 77—21511
prokaryote epigenetic control mechanisms, distributed model 77—77879
pupil noise amplitude control, interaction of sensory and motor mechanisms 78—64998
receptor and neuron encoders dynamic behaviour *(German)* 77—36914
renal autoregulation, math. model of transient adjustments 77—90842
respiration dynamic model eqns., explicit solns. and periodic functions *(French)* 79—79574
respirator, servo-controlled, constructed from positive-press. ventilator 77—13041
respiratory airflow pattern modelling by optimisation criteria 78—80898
respiratory control, human, input stimulus design for model discrimination 79—53183
respiratory control in cats, interactions between central and vagal mechanisms 78—53436
respiratory control system, time series cluster anal. 78—56959
respiratory control system simulation, state-of-the-art 78—53441
respiratory controller model 77—44697
respiratory plant dynamics under open control loop conditions 77—44705
respiratory system, human, modelling and parameter estimation 80—12169
respiratory system, human, modelling and parameter identification 79—39444
rod disc membrane phosphodiesterase control 79—79527
rotation of man in weightlessness, biomechanical models 78—96106
saccades, two-dimens., accuracy in absence of continuing retinal stimulation 78—7341
saccadic eye movement control system, digital analogue simulation 77—44654
saccadic eye movement controller, adaptive considerations 78—27949
saccadic eye movements anal., voluntary nystagmus nature investigation 78—3476
schoolchildrens' mental performance levels, aircraft noise effects 79—70495
seizure discharge autorhythmicity, spike, discharge freq. regulation in focal epilepsy 78—40133
semicircular canal afferent response system identification 78—27927
sensorimotor control and learning model 78—69033
set-point of body temperature regulation *(Japanese)* 78—24032
skeletal muscle general myocybernetic control model 78—53385
skeletal muscle myocybernetic control model 77—12906
skeletal muscle rhythmic oscillation simulation and analysis 78—31806
skin blood flow, reflex control by skin temp., role of core temp. 80—85427
snail feeding musculature, neural net producing rhythmic activity 77—40657
space suit cooling, automatic control of human thermal comfort 80—109046
speech, movement-related tonal signal processing, left hemisphere superiority 80—35913
speech, nasalisation in normal and hypernasal speakers, effects of feedback filtering 80—35921
stance stability of man, investigation using vectorstabilograph 77—44772
stick insect leg movement sensory control 77—12904
stick insect leg position control feedback mechanism open loop analysis 77—36907
stochastic systems theory, appl. to blood pressure control 80—81522
stretch reflex system in human forearm, adaptive control characts. 79—83758
striated muscle contraction, intracellular control of force development 79—48228
structural constitution and function *(German)* 79—5256
swimming control in a cubomedusan jellyfish 80—3637
temperature regulation in man, control theory model 78—35805
thermogenesis control in cold-exposed rabbits, variable open-loop gain 80—97868
thermogenic control during exercise in a cold environment 80—72139
thermoregulation in rhesus monkey, thermal balance study 80—8029
thermoregulation mechanism model, human 80—8028
thermoregulatory responses of unanaesthetised rats, acceleration effects 77—48882
thermoregulatory system structure and function maths. treatment 77—12888
tongue placement task performance of articulate and inarticulate children 79—57670
transepithelial ion transport endogenous regulation, implications of ouabain-like activity in toad skin 78—73147
urethral occlusive techniques for restoration of urinary continence, development 78—7543
vestibular control of oculomotor and postural mechanisms 80—72151
vestibular postural control evaluation in humans using computer-TV interface system 77—44773

biocontrol continued
visceral function voluntary control, electrophysiological concept 78—35827
visual cell membrane cond. control, arthropod 78—15831
visual evoked response shape self-regulation in man 78—31809
visual feedback effects on corrective saccades 78—40150
visual image stabilisation, rel. to eye movement meas. *(French)* 77—36916
voltage clamp of multicellular preps. 77—40955
voluntary temperature control and cold stress tolerance, effects of feedback 80—16905
walking, connections between different legs, quantitative model 80—101161
walking, energy-information performance criteria 79—53181
walking, individual leg control, model 80—101160
water excretion control by antidiuretic hormone, modelling 78—31830
yeast cells, budding, genetic control of X-ray resist. 77—37024
O_2 mass transport and regulation, microelectrode and math. modelling study 78—44534
O_2 transport system, multivariate anal. of blood and air flow data from dogs 77—44706

biocybernetics
see also artificial intelligence; brain models; learning systems; man-machine systems; neural nets
a biological system with random parameters, stability considerations 79—74637
acoustic biotope, neural representation 80—51116
activation and inhibition pattern, rate eqns. 79—92118
adaption model evaluation for vestibulo ocular reflex 79—11931
adaptive neuronlike layer net as a control learning system 79—74631
aerobionic systems in flapping-wing flight, self regulation and energy consumption *(Russian)* 77—64002
albumin transport kinetics in renal cortical interstitium, heterogeneity model 80—30632
animal motion, nonstationary mode near air-water interface *(Russian)* 77—32869
antitumor drug dosage schedule, cell cycle kinetics approach 77—86700
aorta, dog, simulation via adaptive model 79—11964
articular cartilage, viscoelastic properties *(Japanese)* 80—101215
associative information processing structure 78—85300
associative noise-like coding memory, algebraic model 80—76720
auditory function, linear system model 80—51127
auditory nerve data appl. to binaural interaction theory, tone detect. in noise 77—36950
auditory perception nonlinear model with autocorrel. feedback 80—81615
aural signal central spectral pattern anal. based on cochlear neural timing and freq. filtering 79—5300
auto-immunity, math. model of cell dynamics 77—16900
average evoked potentials, a posteriori Wiener filtering theory and practice 78—96038
bacterial diagnostic machine and cybernetics *(French)* 77—9162
basilar membrane, nonlinear model rel. to two-tone suppression 77—48811
basilar membrane nonlinear model assessment, spatial differentiation as auditory second filter 77—36949
bat echo-locator, phenomenological model of system of precise determ. of direction to target 77—36962
biochemical systems anal., mol. biology, book 77—21468
biofeedback, physiological responses control appl. *(Japanese)* 77—44830
biological information processing, theoretical approach *(Japanese)* 80—12049
biological membrane, electrically excited, nonlinear dynamic models for simulation 80—94178
biological motions, bionic modelling of, using artificial muscle polymers *(Russian)* 77—64167
biological populations constraints and orderliness, cybernetical actions 77—44576
biological signal time averaging, digital Wiener filtering and detection statistical aspects 78—35979
biological systems and systems theory *(Japanese)* 78—24018
bionic image analysis using lines and edges 77—36931
biosystems, tracer identification of time varying compartmental parameters 77—40960
biped dynamics, feedback on-off model 80—30709
biped locomotion dynamics, control theoretic study *(Japanese)* 79—11963
bladder smooth muscle impulse propag., math. anal. *(Japanese)* 78—53359
blood cell anal., weighted chi-squared test 80—30925
blood circulation simulation development 77—66825
blood flow in artery, stenosis effects on non-Newtonian flow 80—89775
bone functional adaptation model and thermodynamic consideration *(Japanese)* 78—7316
brain activities, synchronous, spatio-temporal filter approach 80—61503
brain activity EEG anal. using Parcor coeffs. 78—35822
brain mechanism studies using evoked pots. *(German)* 80—61535
brain waves, limit cycle model, Frohlich's model 77—73520
bronchial elasticity and air flow, mathematical anal. 80—45942
Calvin photosynthesis cycle parameter identification 79—92186
cancer chemotherapy, cell kinetics system model 79—48229
capillary counter-current system hydrodynamic effects 77—40695
carbohydrate and lipometabolism systems interaction, use of mathematical model 78—31758
cardiac output control mechanism modelling *(Japanese)* 78—69133
cardiovascular control dynamic test method evaluation, model considerations *(German)* 77—52813
cardiovascular parameter estimation, nonlinear filter statistical parameters optimal choice 79—5308
cardiovascular system, mathematical models and identification problems 80—89780
carrier-facilitated steady-state diffusion problems 80—41360
cat brain subdural structure resonance phenomena 77—16923
catastrophy theory appls., book 78—32665
CECG waveform, statistical algorithm and struct. anal. 80—72341
cell cultures mitotic growth model 78—11619
cell growth appl. of time-optimal control theory 77—40638
cell growth regulation modelling 79—2014
cell kinetic parameters estimation from flow microfluorometry 78—73143
cell motion growth control, diffusion coeff. model 77—40645
cell population auto-activation, math. model 78—77017

biocybernetics continued
- cell population auto-oscillations, influence of delay 77—36892
- cellular biological system appls. of von Neumann cellular automata 78—31754
- central nervous system interaction with peripheral motor system, voluntary human movement 79—8499
- cerebellar cortex model, temporal behaviour study 77—86482
- cerebellar stimulation and eye movement in cats 80—30719
- cetaceans, drag reduction and self regulation of skin damping while swimming *(Russian)* 77—32918
- chemically reacting system, temporal oscillations 77—25359
- circulatory system polynomial model *(Japanese)* 77—70488
- clonus, simplistic model rel. to diagnosis and therapy 77—48786
- colour sensitive neural networks, reaction to intensity and colour steps *(German)* 80—76737
- communication between two self-organizing systems modelled by controlled Markov chains 79—39335
- compartmental analysis in biology, medicine and ecology, mathematical foundations 78—68978
- compartmental models, stochastic, parameter estimation 78—40109
- compartmental system anal., identification method, body tracer kinetics appls. 80—35816
- compartmental systems, multi-input and multi-output, controllability, observability and structural identifiability 78—76978
- compartmental systems controllability, observability and structural identifiability 77—40625
- compartments, stochastic theory, general time-depend. reversible systems 78—64916
- concept shaping and recognition, information processing 79—53016
- coupled biological oscillators, describing function techniques 77—25361
- crayfish stretch receptor neuron excitation and inhibition summation 77—2015
- crayfish stretch receptor neuron inhibitory junction expts. 77—9185
- diffused substance kinetics in biological systems 78—53312
- diffusion approximations to neuronal activity and to the time dependent threshold problem 79—74639
- diploid cell culture mutation models 77—73514
- directed cell locomotion model, turning-angle and run-length distributions 77—21502
- diseases, communicable, anal./control, novel model 80—30634
- dissipative systems, dynamical field theory, hierarchical struct. of field thermodynamics 78—73132
- distributed systems, stability of spatially inhomogeneous states 80—30629
- dual input nonlinear system characterisation using impulse trains 78—31761
- dynamic models class, theoretical tools 80—94143
- dynamic receptor pattern generation model 79—62207
- dynamical interactions, empirical method for identifying observables involved 77—56326
- EEG 80—85504
- EEG alpha and non-alpha intervals alternation, queueing theory model 78—96040
- electrokinetic model of transport through biological barriers 80—45871
- electromyographic activity during brief isometric contractions, model 77—16922
- electroosmotic model of longitudinal transport 80—45870
- electroretinogram P III component model, luminance variations 77—81495
- EMG signal nonstationary model 77—86481
- endocrine and metabolic systems simulation 77—86434
- endocrine tumours, silent, feedback system cell number change effects, steady-state anal. 79—20526
- entropies in living systems, thermodynamic, informational and structural *(Russian)* 79—20511
- enzyme reaction kinetics modelling 77—4979
- evoked response estimation 79—43841
- evolution model 79—12060
- excitable medium diffusion discrete models and spatial patterns 78—93629
- excitable medium model with existence of several stable pulses of different duration 78—77036
- excitable membrane phenomena, mathematical analysis 79—74635
- eye, vergence movements, heuristic feedback system model 77—21517
- eye and hand motor systems, optimal response in pointing at a visual target 80—61567
- eye movement control in cephalopods, cerebellar-type system 77—12914
- eye movements, caloric nystagmus, mathematical model 77—73525
- finger tapping, human, neutral networks studies by phase transition curves 80—8042
- flapping wing propulsive efficiency for plane parallel flow (bionics) *(Russian)* 77—32919
- foveal vision, mental scanning mechanism 79—2066
- free walking insect leg movement coordination model 77—64073
- Gaussian process testing method 79—1993
- genetic net, stable dynamics logical probability models 79—74638
- genetic systems, dynamics of neutral mutation 78—86220
- haemoglobin molecule from cybernetic and thermodynamic viewpoint *(German)* 79—1998
- hearing, nonlinear systems theory appl. 78—40195
- heart disease, haemodynamical parameters optimal control 79—53182
- heart muscle contraction simulation 77—12954
- heart optimal control model, stroke volume determ. *(German)* 78—3631
- hierarchical multilevel system, nervous regulation of internal organs *(Russian)* 78—48779
- Hodgkin-Huxley reduced model, speed of spread of excitation, integral differential eqn. 77—21509
- human body model, health, disease and treatment use 79—48205
- human brain electrical signals systems analysis 77—21504
- human brain functions rel. to foundations of physics, science and technology 78—73823
- human locomotion motor coordination and neuromuscular activities study 77—44635
- human lung airways models, inhaled particle deposition appl. 80—89776
- human pattern perception visual form interaction prediction 77—5003
- human psychophysics: functional interpretation for contrast sensitivity versus spatial frequency curve 79—48265
- human pupil light reflex simulation model 77—70462
- human visual perception inductive colour contrast modelling *(Russian)* 77—52793
- human visual system, spatial characts., nonlinear model 77—25439
- human visual system spatial characts. nonlinear model 77—12929

biocybernetics continued
- hydra, simple nervous system and behaviour 79—83738
- identification, quasi-white random signals optimal use, appl. 77—73528
- identification, quasi-white random signals optimal use 77—73502
- identification of biological systems, survey 78—31753
- information transfer in a chain of model neurones 79—74646
- informational processes, statistical, semantic and pragmatic 80—30631
- insect visual system elementary movement detectors 77—2001
- interdisciplinary aspects and problems 78—53553
- intestinal electrical rhythms model, stability of entrainment conditions for RLC coupled Van der Pol oscillators 77—56361
- kidney process modelling 78—44524
- kinetic depth effect, amplitude, freq. and phase determinants of perceived rotations and rigidity 80—76746
- learning and optimisation, sequential actions model 78—44441
- learning velocity in a biological net, noise effects 79—74636
- left ventricle model parameter estimation, global search algorithms *(French)* 78—3529
- light adaptation in cone photoreceptors, dark glasses model 80—12122
- light adaption model and Weber's law 79—8508
- Limulus ommatidia, resonant response of neural model to double freq. stimulation 80—76734
- living being bio- and neurocybernetic models 79—53018
- living self-organising sysems analysis bionic aspects *(Russian)* 77—52732
- living system information processing studies, association and self-repair models *(Japanese)* 78—44443
- living system organisation level comprehension, SYSTEMA approach *(French)* 77—9163
- local adaption effect simulation with nonlinear spatial filters 77—44657
- lung, nonlinear mathematical model, parameter tracking adaptive algorithm 77—60227
- macromolecular systems, self-reproducing, stability and selection 79—96507
- macromolecules, biological, selection models, with time varying constraints 80—67029
- mammalian lung airways, aerosol deposition in anatomical models, theoretical evaluation 80—81627
- mammalian neuromuscular system energy-optimal controls 77—73522
- Markovian biological system modelling via optimisation operators 79—1994
- martingale model for estimation in nonlinear stochastic physiological systems 77—77865
- mathematical biology meeting, Philadelphia, USA, (Aug. 1976) 78—53311
- mathematical modelling in biological research, role of computers *(Chinese)* 79—1996
- mechano-receptors, model for stimulus processing 79—74633
- mental activity, humans, via EEG, discriminating classes 80—16916
- message operators for expression of information 77—29089
- metabolic regulation and math. models, review 77—90714
- methotrexate effects, cellular response simulation 77—40647
- middle ear systems simulation from physiological data 78—44514
- minimum mixing principle as method of choosing form of dynamic model 77—36857
- model parameter reliability range determ. using hybrid computer 77—44581
- modelling in biomedical research 78—31755
- molecular computer, coding during intracellular processes of information processing 77—70400
- molecular self-organization, dynamics 80—67028
- monaural intensity processing, nonlinear-algebraic approach 78—57012
- morphogenetic fields, chemical patterns 79—96498
- motoneuron firing rates with strong random synaptic excitation 77—9184
- motoneurone cross-correlated firing patterns, recurrent inhibition effects 78—80861
- motoneurones excited by phasic muscle stretches, discharge pattern shaping, recurrent inhibitory feedback effects 78—85303
- motor response of hemiparetic patients, model of hypnosis influence *(Slovenian)* 79—2037
- motor systems, eye and hand, optimal response in pointing at visual target 80—56079
- motor unit action potential study using computer simulation 79—11914
- multicellular development growth, L system strategy 78—27906
- multicompartment system simulation 80—55976
- multisensory orientation stimuli, semicircular canal and otolith information integration 78—20199
- multistate systems, freq. of cyclic processes 80—108834
- muscle, anatomical model, internal pressure effects 80—67103
- muscle, frog skeletal fibres, mesh model of tubular system, elec. props. 77—25395
- muscle, striated, analytical soln. to isometric mechanogram of Hill's model 78—73168
- muscle coordination in cat hindlimb during maximal vertical jump, computer model 77—40662
- muscle mechanics in isometric contraction, linear approx. 77—73535
- muscle system, contractile system, sliding motion anal. 80—67104
- mutlicompartment analysis, direct estimation of parameters, appl. to drug conc. 77—44580
- neocognitron, self-organising neural network model, pattern recognition mechanism unaffected by shift in position 80—76745
- nephron functioning, diffusion and selective osmosis *(French)* 80—45864
- nerve action potential, cybernetic elucidation 79—48243
- nerve action potential model 80—30697
- nerve axon, leading edge approx. 77—12903
- nerve conduction velocity distribution based on compound nerve action pot. 78—40138
- nerve excitation, gating currents and dipole transitions 80—67056
- nerve fibre, substance flow transport *(German)* 80—45878
- nerve fields, topographic maps and columnar microstructure formation 80—56013
- nerve fields, topographic organisation 80—89742
- nerve membrane flicker noise model 77—29125
- nerve signal optimal filtering 77—73616
- nerve signals, dipole theory of interactions 80—81574
- nerve spike trains, Fourier anal. 80—12070
- nerve stimulation, noradrenaline release regulated by α-adrenoceptor mediated negative feedback 77—29139
- neural coding schemes, integrate-to-threshold anal. 80—35868
- neural nets and pattern recognition *(French)* 77—9164
- neural network simulation using fast Fourier transform 77—1986

biocybernetics continued
- neural system, one-dimensional, numerical investigation of kinetic neuronic equations 80—76725
- neural transformations of random signals, Wiener and of functionals of Markov chain 80—76727
- neuron firing sequence stochastic model 77—4992
- neuron model, two-terminal electronic circuit 80—61526
- neuron modelling with extremum control of parameters *(Russian)* 77—29133
- neuron multi-input model diffusion approx. 77—29135
- neuron with shunting inhibition, stochastic modelling 77—9183
- neuronal activity firing pattern evoked by monosynaptic inputs, stochastic model 77—29134
- neuronal activity model, Ornstein-Uhlenbeck process 80—51030
- neuronal waveforms, optimal recognition 80—56003
- neurone compartmental chain model membrane voltage changes 77—29124
- neurone potentials, 2 pulse series anal., histogram of recurrence time intervals 77—60196
- neurons, electrical behaviour, general input-output relations 80—85378
- neurons, synergism and antagonism caused by electrical synapse 80—30696
- neurophysiological models, motor control, muscle representation 78—24057
- neurotransmitter dynamic balance, systems and control theoretic anal. 78—44495
- Noble model, spread of excitation through node of branching 77—16899
- nonlinear analysis for shaping and threshold actions 77—12871
- nonlinear system analysis by Wiener kernel estimation in freq. domain 77—1973
- nonlinear systems, mode-locking, computer simulation 77—12872
- nonprobabilistic measures of information *(French)* 77—9160
- normal and tumour-like cell growth model 77—12894
- object fixation and spontaneous pattern preferences in Drosophila melanogaster 79—43903
- object perception criteria, information theory appl. 78—44444
- oculomotor control system neurological integrator 77—4993
- olfactory pattern recognition modelling by adaptive spatial filter 78—24080
- one-dimensional excitable medium, non-steady processes, excitation front division 77—86475
- optic tract fibers, cat, Markov properties of nonstationary spike trains 80—51077
- optokinetic reflex, mathematical model 80—41008
- oscillators, phase locking model 80—21460
- overlapping-cell clustering algorithm, biomedical appls. 80—30926
- pacemaker synaptic interactions: modelled locking and paradoxical features 80—51069
- parameter estimation appl. to physiological systems, accuracy anal. 78—31762
- parametric linear systems, time delays, optimality, control coordination and entropy *(French)* 77—9161
- Parkinson tremor generation, linear modelling of possible mechanisms 80—3615
- pattern formation in Gierer Meinhardt morphogenesis model 79—62210
- pattern generation in lobster stomatogastric ganglion, pyloric neuron kinetics and synaptic interactions 80—8043
- pattern generation in lobster stomatogastric ganglion, pyloric network simulation 80—12076
- pattern separability in random neural net with inhibitory connections 80—76726
- perception space, dimensionality of informational structs. 78—15817
- peristaltic transport, asymptotic method 80—87805
- permeable tube mass transport simulation using perfectly mixed compartments 77—40696
- phosphenes in the light of bioholographic models 79—74632
- photophobic accumulations model, blue-green algae in light traps 79—11965
- photosensitive neuron, lateral inhibition, and optomotor function expts. *(French)* 80—89705
- physiological control system simulation and modelling 77—90848
- physiological control systems, oscills. and chaos 77—90715
- physiological system, nonlinear, Volterra kernels representation determ. 79—2034
- physiological system stochastic anal. and control., cancer detection and therapy 77—90713
- physiological systems, optimisation concepts in models 79—74591
- physiology, flow problem, one tube 80—89703
- picture distortions compensation of moving patterns typical for time filters 80—76731
- posthaemorrhage blood volume control model for intravenous fluid therapy 77—40697
- primary visual cortex orientation selectivity development kinetics, normally and dark reared kittens 80—41006
- prokaryote epigenetic control mechanisms, distributed model 77—77879
- pulmonary arterial circulation process nonlinearity model 77—12944
- pulmonary blood flow estimation, Ljung's algorithm sensitivity 80—56107
- pulmonary gas transport models, boundary conditions and geometry 80—85426
- pupillary light reflex system, modelling and identification 80—61554
- radiation therapy of malignant growths, optimisation 79—5337
- radioimmunoassay, hypergeometric theory of competitive binding 77—77980
- renal autoregulation, math. model of transient adjustments 77—90842
- renal countercurrent model eqns., numerical soln. 77—40698
- renal counterflow system transient soln. computation 77—40699
- renal counterflow systems differential equation, soln. by numerical method 78—24082
- renal medulla, osmotic equilibration by descending limbs of Henle's loop 77—40701
- renal medulla single loop solute cycling model, transient behaviour 78—73167
- renal medulla solute cycling model soln. by Laplace transforms 77—40694
- renal network flows, a priori bounds 77—40693
- renal solute and water movement models and soln. 77—40692
- renal tubule model injection transient response calc. 77—40700
- repetitive firing mechanism excitation parameters, nerve impulse trains statistical evaluation 80—40986

biocybernetics continued
- respiratory system model, identification via mathematical pattern recognition 79—2096
- reverberations and synthesis of a neural network 79—74634
- rhythm phase response curve study, homotopy theory 79—8491
- rhythm research, second-order correlation functions and bi-spectra 78—3441
- robots and manipulators, symposium, Warsaw (Sept., 1976) 78—53574
- saccadic eye-movement system, processing of direction and magnitude obs. 80—56035
- saccadic ocular dysmetria simulation using sampled-data model 77—56373
- segmental muscle stretch reflex, partitioning into completely decoupled parallel loops 80—41000
- self-organizing systems, nonequilib. ensembles, simulation study 79—24933
- self-reproducing macromolecules, selection, controlled energy fluxes constraint 80—67027
- semicircular canal afferent response system identification 78—27927
- sensorimotor control and learning model 78—69033
- sensory biosystem, teleological explanation of Weber's law and the motor unit size law 79—96501
- sensory information coding, adaptation and differential sensitivity in system of detectors 77—56367
- sensory neuron, second order, summation of excitation and inhibition by computer simulation 80—76769
- sensory processes, information received by receptors 77—73521
- signal focusing in segmented stretch reflex system, auxiliary spinal networks 80—40999
- signal modelling and recognition, system identification approach 80—51286
- skeletal muscle general myocybernetic control model 78—53385
- skeletal muscle myocybernetic control model 77—12906
- spatial contrast visual detection, influence of location in visual field, target extent and illuminance level 79—2067
- spinal motoneurones refractoriness accumulation and secondary range firing model 77—1985
- statistical biomechanics, regularity 77—25483
- stochastic neuron models, multi-input-output information transmission 80—30707
- stretch receptor array reflex inhibition enhanced contrast 77—2016
- stretch reflex system in human forearm, adaptive control characts. 79—83758
- striato-nigral fibres, feedback loop vs. output pathway 77—29136
- structural order and partial disorder 80—76695
- structure-function relationships of biologically active molecules, programs *(Russian)* 79—16137
- symmetry in systems 80—81519
- syncytium, passive three-dimens. and anisotropic, modelled as continuous medium 77—16898
- systems theory *(Japanese)* 78—31756
- systems theory *(Japanese)* 78—73134
- systems theory and biological systems *(Japanese)* 78—31757
- systems theory in biology and medicine, importance and motivations *(Spanish)* 80—104549
- temporal sequence memory model simulation studies 77—9181
- tenuissimus muscle, cat dynamic properties 80—8041
- thermodynamic network analysis of biosystems, book 77—86435
- thermodynamic process applied to biological systems 80—45855
- transformation systems direct and inverse regulation control 78—11606
- transformations theory, dynamical similarity 79—34469
- transinformation functions, constrained, essential features 79—1997
- transmitter kinetics model anal. 78—3465
- 3,3′,5′-triiodothyronine plasma to tissue transport rate estimation from 3-compartment model 78—31792
- tumours, fractionated irrad., math. derivation of optimal treatment schedules 80—98078
- two compartment model parameter estimation, computer expt. study 77—70402
- underwater body of changing shape, vortex-free flow due to arbitrary motion *(Russian)* 77—32916
- variational principles, complementary with Michaelis-Menten kinetics 80—94142
- vascular beds, optimum modelling using indicator-dilution measurements 77—40686
- vestibular nystagmus, Alexander's law model 80—35878
- vision, human recognition system with thinking, model 80—76744
- visual cortex of cat, spectral characts. of stimuli and responses of complex receptive field 77—16927
- visual cortex simple cells, spatial resolution and nonlinearities, cat 77—9187
- visual illusion, geometrical, analysis in terms of perceptual field 77—2002
- visual information processing, multi-input system representation, polynomial algorithm properties 80—101145
- visual information subjective contours shape and model for generation 77—16932
- visual models using second degree polynomials for research and clinical use 77—48804
- visual pattern recognition, transformation and relational-struct. models, random-dot pattern tests 79—53130
- visual pattern recognition assignment of invariant features and feature-relations 77—25445
- visual perception, dynamic theory 79—74681
- visual processor, human colour-vision discrimination, statistical-communications approach 79—5288
- visual response, expected waiting time 80—51091
- visual signal detection by simultaneous observation through multiple channels, decision behaviour 77—90791
- visual system, figure-ground discrimination by relative movement, fly appl. 80—56046
- visual system, human, transient characteristic using masking experiments 80—41009
- visual system, hyperacuity decision model 79—5294
- visual system, moving objects localisation, cats 80—76736
- visual system brightness generation, chromatic signals contribution, model 77—90795
- visual system spatial and temporal information separation model 78—40167
- visual systems, filter performance, inhomogeneous and anisotropic 80—76738

biocybernetics continued
visual systems, fly, response properties 80—41021
visual texture discrimination 79—43902
visual-vestibular interaction during body rotation in man, nonlinear model 80—76735
volume-conductor fields of isolated axon, linear filtering problem 78—3463
walking insect, Carausius morosus, coordination of force oscills. and leg movement 80—76775
walking insect, Carausius morosus, oscillations of force in standing legs 80—76774
white-noise analysis of biological systems 79—1995
Wiener filtration versus averaging of evoked responses 78—3689
Wiener-filtering, a posteriori, statistical properties 79—88045
Na channels, inactivation delay in biological membranes 80—45872
O_2 diffusion and reaction in biological tissue, Michaelis-Menten kinetic model 78—31793

biodiffusion
acetylcholine, diffusion in synaptic cleft of normal and myasthenia gravis human endplates 80—94198
albumin, bovine serum, diffusion, hydration and soln. environment effects 77—19116
albumin, bovine serum, diffusion, hydration effects, finite conc. 77—19115
albumin, bovine serum, diffusion, hydration effects 77—19114
albumin, bovine serum, laminar ultrafiltration, limiting flux numerical calc., variable diffusion coeff. 78—40214
alveolar gas exchange, effect of altered gas diffusivity 80—97970
alveolar membrane, ^{11}CO inhalation for imaging small pulmonary ischaemic lesions 77—2035
aortic tissue, rabbit, convective and diffusive transport of ^{125}I-serum albumin 78—44482
axonal K^+ transport, single-file model for squid giant axon 77—73517
bacteria, diffusing and motile, light scatt. props. calc., RGD approx. accuracy 79—92193
bacteria, motion, quasi-elastic light scatt. 77—23617
bacteriophages T4B and T7, determ. of rotational diffusion coeff. by depolarised dynamic light scattering 80—85549
biomembranes, immobilised protein, intrinsic electric fields and proton diffusion 79—24964
biopolymer Brownian diffusion, fluoresc. correl. spectroscopy 79—62193
blood, shear-induced augmentatin of O_2 transfer 80—94274
blood oxygenator, convective-diffusion model 78—44711
blood supersaturation by counterperfusion and diffusion of inert gases 77—90829
blood tissue gas and nutrient exchange, implications of intermittent capillary flow 79—100649
blood vessel wall ion permeability 77—32934
bovine plasma albumin, high conc. soln., quasielastic light scatt. line breadth meas., diffusion coeffs. 77—1976
breathing process analogue model *(German)* 79—16228
burnt skin heat and water losses, thermal modelling 78—31790
capillary-tissue diffusion in multicapillary system, anal. 79—2095
carotid artery Na kinetics 3-compartment model, incorporation of diffusion effects 78—27996
carrier mediated transport theory, survey of applications 77—89113
carrier-facilitated steady-state diffusion problems 80—41360
carrier-mediated photodiffusion membranes 78—23965
cell, membrane permeability, review 78—15813
cell division control by tension or diffusion 78—64962
cell membrane, electrophoresis and diffusion obs. 79—57599
cell membrane diffusion coeffs. meas. 77—48962
cell motion growth control, diffusion coeff. model 77—40645
cell saturation density, evidence against diffusion-limited process 78—48770
cell surface anisotropic molecular motion 80—97883
cell surface component rotational diffusion, time-resolved phosphoresc. anisotropy 80—97885
cell surface receptors, molecular movements 80—45866
cells, classical diffusion to explain ^{1}H spin relax. in NMR obs. 79—83721
cellular testing potential, membrane pot. rel. to ionic diffusion *(French)* 80—94184
cerebral gas exchange, perfusion and diffusion limitations 80—45940
cholinergic channel without const. field, permeab., phase-boundary pot. and conductance 77—60191
collagen membrane H^+ diffusion-limited binding electromechanics 79—79489
comparative diffusion problem 78—24016
cytochrome b_5 rotational diffusion in lipid bilayers, influence of lipid physical state 79—83693
D-leucine, exchange diffusion in mouse Ehrlich ascites tumour cells, temp. reduction effect 80—67053
decompression model for deep sea diving 77—44709
distributed systems, stability of spatially inhomogeneous states 80—30629
DNA light induced diffusion in solutions due to laser cutting *(Russian)* 80—81646
E. coli, light scatt., ribosomal subunit diffusion coeffs. 80—21438
Ehrlich ascites tumour cell, thymidine transport kinetics and DNA synthesis, X-ray effects 78—20215
electrodiffusion, steady-state, scaling, exact. soln. and phase plane 77—25403
electrolyte-membrane-electrolyte, freq. depend. of capacitance and cond., model 77—21488
enzyme, diffusion-controlled reaction rate to buried active site 78—35796
enzyme-substrate interaction forces influence on reaction rates 78—31765
erythrocyte integral membrane protein lateral mobility, human cells 77—66805
erythrocyte membrane water permeability defect in human epilepsy, NMR 77—29122
erythrocytes, frozen human cells, conc. polarisation effect 78—3460
erythrocytes, gas reactions, shape changes microspectrophotometry obs. 79—8488
excitable membrane, with asymm. behaviour of inner and outer sides, oligomeric transport model *(Japanese)* 77—44611
excitable membranes, nonstationary ion fluxes 77—44599
exhalation in lung model, effect of ventilation and diffusion nonuniformity 80—104603
growth, self-reproduction and autoregulation model, anal. of reactions with stretchable semi-perm. walls 77—81460

biodiffusion continued
haemoglobin, human and Lumbricus terrestris, conc. depend. of self-diffusion 78—68984
haemoglobin, in salt soln., diffusion rel. to intermol. interactions, light scatt. investig. 77—44585
haemoglobin, mutual and tracer diffusion coeffs., photon correl. obs. 80—72123
haemoglobin in solution, conc. depend. of diffusion coeff. 79—29546
immobilised enzyme membrane oscillations and pH fronts 77—25387
intervertebral disc, small solute diffusion, in vivo obs. 79—62276
intracellular water, two-fraction fast-exchange model of spin-lattice relax. 77—60192
intravascular radioactive tracers, calc. of residence time distribs. in fields of external registration 80—72291
ionic channels in excitable membranes, current problems and biophysical approaches 78—53369
isobaric counterdiffusion, middle ear gas exchange 80—81798
isobaric gas counterdiffusion in rabbit eye 80—30718
Krogh tissue cylinder, transient convective mass transfer 80—3598
leaf CO_2 absorption and diffusion, sun vs. shade leaves 78—80850
lechithin-cholesterol interaction, effect of lecithin struct. 78—64922
lecithin translational diffusion, pulsed NMR 77—9176
lipid bilayer diffusion transport modelled by dimeric β-cyclodextrin complexes, cryst. struct. anal. 78—80838
lipid bilayer head group, orientational order and rotational diffusion, NMR obs. 80—21451
lipid planar bilayers, lateral diffusion meas. using fluoresc. correl. spectroscopy 77—36884
lipid-water smectic phase, water and thermal diffusivity, light scatt. meas. 78—96031
lung, analytic model, Green's function for convection-diffusion eqn. 78—11684
lung, diffusing capacity at different lung vols., breath holding and rebreathing obs. 80—30739
lung aerosol deposition, particle settling and diffusion 77—52678
lung alveolar membrane, dog, role of bulk fluid flow in protein permeability 77—52814
lung gas concentrations during air breathing, influence of gas exchange 77—12942
lung gas transport model, derived from human anatomical data 77—5020
lung transport and metabolic processes, indicator-dilution study 77—44711
lysozyme macroradicals, ultraslow diffusion in an aq. matrix, EPR obs. 79 92119
macromolecualr thermodynamics and its possible relevance in physiology 80—53176
macromolecular concentrated systems, molecular transport 79—57567
macromolecular solution, rot. diffusion coeff. calc. method w.r.t. mol. struct., elec. birefringence relax. time data interpret. 80—85331
membrane, molecular motion determ. using periodic pattern photobleaching 79—34719
membrane, thin, ionic transport, jump vs. electrodiffusion description, for steady transfer 77—36895
membrane, thin, ionic transport, jump vs. electrodiffusion description, volt. clamp 77—36896
membrane, thin non-uniform, jump vs. electrodiffusion description, volt. clamp 77—36897
membrane, water transport, NMR methods *(Rumanian)* 80—94435
membrane and near-membrane transport processes, effect of volumetric charges 78—53366
membrane damage caused by light irradiation of fluorescent concanavalin A 80—56123
membrane diffusion measurement by fluorescence photobleaching recovery method, bleaching light effect 80—94434
membrane integral proteins, mobility increase in spherocytic erythrocytes obs. 80—81569
membrane transport, monosubstrate inhibited enzymes, conc. response, multiplicity and memory 80—30679
membrane vesicle permeability, light scatt. meas. 77—12889
membrane-moderated controlled release, dynamics 79—2016
membranes, artificial, permeab. to pluridisperse soln. of ^{125}I-polyvinylpyrrolidone 77—12890
membranes, fluoresc. polarisation decay theory 78—20138
membranes, lateral diffusion on a spherical surface, normal mode anal. 80—61518
membranes, mechanism for 1/f noise in diffusing ion channels 78—27911
membranes containing cholesterol, lateral diffusion calcs. 80—85356
mesentery tissue, burn induced alterations of interstitial diffusion 80—104634
microcirculation O_2 distrib. during and after arteriolar occlusion 78—44529
model chemical reaction bifurcation diagram, time-periodic soln. stability changes 79—47886
morphogenetic fields, chemical patterns 79—96498
moving semipermeable boundary, diffusion transport in liquid solution 77—80639
multibilayer membranes, lateral mobility 80—40975
muscle, Ca diffusion in transient and steady states 78—3457
myoblast membrane lateral transport of lipid probe and labelled protein 77—40646
nephron functioning, diffusion and selective osmosis *(French)* 80—45864
nerve fibres, myelinated, diffusion of ions 79—24965
neuromuscular junction, frog, acetylcholine diffusion barrier 78—7334
neuronal adaptation to osmotic stress and facultative blood-brain barrier in marine osmoconformer 77—29127
neurones of large horse-leech, electrophysiological characts. rel. to intracellular Na^+ conc. 78—53374
nonlinear diffusion in biological systems 79—74589
oscillatory biochemical model, spatial differentiation 78—44476
oxymyoglobin, evidence for conformational and diffusional mean square displacements 80—89713
papillary muscle Na kinetics, diffusional and compartmental models 77—44617
periodic conversions in biological system solns., optical mixing method obs. 78—96029
pesticide uptake into membranes meas. by fluoresc. quenching 78—7323
phase transition in system with diffusion noise-induced 79—100560
photoreception, transmitter-medicated, diffusion and reaction modelling system 79—70547

biodiffusion continued
- photoreceptor, barnacle, upper limit on translational diffusion of visual pigment 80—8053
- plant fibre temperature stability investigation, rotary diffusion, spin label obs. 80—81529
- plasma membrane of mouse egg, effect of fertilisation on lateral diffusion of lipids and proteins 78—44480
- platelet diffusivity estimation in flowing blood 79—25010
- polyelectrolytes, diffusion pots., rel. to biological electrochemical phenomena 77—4978
- potassium p-nitrophenoxide transport across carbohydrate membrane, cyclodextrin induced ionic equilibria perturbation 79—96523
- protein adsorption and immunological reactions at liq./solid interface, ellipsometry obs. 77—52948
- protein secretion by pancreas, accounted for by diffusion-like process 80—21457
- pulmonary diffusing capactiy, anatomic dead space meas. 77—25502
- pulmonary gas transport and mixing, diffusivity effects 80—108927
- pulmonary interdependence of gas transport 80—41076
- red blood cell shape, optimality, O$_2$ diffusion approach 80—30693
- red blood cells, hydrodynamic and diffusion considerations in rapid mix expts. 80—40982
- red cells in dilute suspensions, turbulent flow and effect on O$_2$ uptake kinetics 77—60223
- respiration model analytical soln. 79—48282
- respiratory gas exchange by avian embryo 77—44708
- respiratory system, particle deposition due to turbulent diffusion 79—66478
- retinal diffusion, two-stage, rel. to flicker sensitivity 79—74657
- rod external segment surface membrane, lateral diffusion of rhodopsin 78—15828
- salivary gland cell junction, Ca^{2+} produces graded changes in membrane channel permeab. 77—64016
- Schwann cell layer of squid axon, diffusion models 80—40985
- serum albumin, bovine, mutual and tracer diffusion coeffs., photon correl. obs. 80—72123
- skeletal muscle O$_2$ and lactic acid transport, effet of reactive hyperaemia 78—35817
- skin, human, permeation of scopolamine in vitro 77—21487
- skin, role of diffusion during transport of radioactive substances 78—20158
- skin, transport of radioactive substances, diffusion model 77—81483
- spin labels, water soluble, factors restricting diffusion, rel. to biological use 77—86436
- stratum corneum of rat, surfactant diffusion and sorption phenomena, model for human skin 78—77007
- subcutaneous tissue gas space pressure during superficial isobaric counterdiffusion 80—30968
- substance diffusion in tissue with nonlinear consumption, math. model 80—67326
- tissue inert gas washout, diffusion limited obs. 79—84069
- tissue surrounding single capillaries, substrate concs. 80—97853
- tumour growth simulation, in vitro, with aid of computer 77—86464
- variational principles, complementary with Michaelis-Menten kinetics 80—94142
- venous gas bubble prod. by transient deep isobaric counterdiffusion of He against N$_2$ 78—11790
- water, self diffusion in frog muscle 80—8037
- water adsorbed on proteins, new programme for NMR study of diffusion 79—92139
- water diffusion in wheat grain endosperm tissue, ^{1}H NMR obs. 80—8001
- water diffusion meas. by pulsed gradient NMR, cell struct. size determ. 78—77159
- water diffusion through narrow pores of biomembranes, ^{1}H NMR obs. 79—92194
- yeast cell membrane, water transport study, pulse NMR obs. 80—40981
- yeast cells, translational mobility of water, pulsed NMR obs. 79—57612
- ^{18,19}F ion diffusion in dental enamel at pH 7, obs. 79—29553
- CO diffusion in dog lungs, effect of static or slowing flowing blood 80—30970
- CO, single breath diffusing capacity in man, meas. by rapid CO anal. 80—46115
- CO, single breath diffusing capacity, theoretical anal. 80—67328
- H$_2$O in biological samples, PMR, fast-exchange model interpretation via diffusional kinetics clarified 80—67033
- K$^+$ ion flux through membrane channels, nerve impulses, random walk anal. 78—77045
- K-like channel passage of ions, physical model 77—56356
- Na exchange in tissue, incorporating diffusion effects into multicompartment models using digital simulation 80—3611
- Na-like channel passage of ions, physical model 77—56355
- O$_2$ diffusion and chem. reaction in tissue slices 77—44615
- O$_2$ diffusion and reaction in biological tissue, Michaelis-Menten kinetic model 78—31793
- O$_2$ diffusion distance and necrosis development in multicell spheroids 80—81570
- O$_2$, diffusion in blood, analysis of carrier facilitated transport in heterogeneous media 77—39360
- O$_2$ diffusion in blood plasma, effect of plasma constituents 79—92460
- O$_2$ diffusion into mammalian cells following ultrahigh dose rate irrad. 80—30694
- O$_2$, facilitated diffusion by haemoglobin and myoglobin 77—48747
- O$_2$, facilitated diffusion in muscle tissues 80—56327
- O$_2$, steady state diffusion in red blood cell and model suspension 77—40644
- ^{133}Xe diffusion through frog skin, toad bladder and water boundary layer 77—66803

bioelectric phenomena
- *see also bioelectric potentials; biomagnetism*
- 60 Hz electric field, 240 kV/m, long-term effects on mice 80—89784
- 60 Hz half-cycle sinusoid defibrillating waveforms for low-energy application 78—3664
- 60 Hz high intensity electric fields, behavioural and biological effects in living organisms 80—89740
- Acetabularia cell electrical parameters and equiv. cct. 77—56350
- acetylcholine receptor protein, binding kinetics and Ca ions, rel. to membrane cond. changes of acetylcholine 77—40649
- acetylcholine receptor response to rapid photochem. prod. increases in agonist conc. 77—36909

bioelectric phenomena continued
- acetylcholine responses in Aplysia neurons, effect of tris buffer 77—64020
- action potential propagation, effects of cellular geometry on current flow 80—94196
- acupuncture, search for elec. located skin stimulation points 79—43976
- acupuncture, transient impedance between stimulation points 79—43977
- acupuncture point location using elec. impedance meas., statistical anal. 78—44628
- acute myocardial infarction, electrophysiological aspects 79—43858
- afferent activity in stellar nerves of Octopus vulgaris 79—66467
- afferent elec. nerve stimulation with ref. to prosthesis sensory feedback 77—90962
- afferent visual systems of cat and rhesus monkey, responses to wavelength contrast 80—56030
- α-amino acids, naturally occurring, in aq. soln., Kerr constants 80—85353
- amputated finger tips, children, elec. current obs. during regeneration 80—72404
- amygdaloid kindling phenomenon extended first approx. model 78—53378
- anaesthesiology, characts. of elec. currents 80—46093
- analytical electrophoresis, book contrib. 80—12322
- antagonistic muscles, functional elec. stimulation optimisation, math. modelling, joint motion 80—61730
- arterial impedance plethysmographic signal quantitative interpretation 79—57742
- artificial neural network response characts. 78—40137
- asbestos, piezoelec. and ferroelec. rel. to asbestosis and model of carcinogenesis 77—78075
- atrial septal defect repair, sinus node dysfunction and atrioventricular conduction disturbances 77—81647
- atrial trabecula membrane, frog, accommodation, repeat responses and anode-breaking excitation 78—64956
- atrioventricular and His bundle conduction disorders in noncoronarogenic diseases 79—43848
- atrioventricular block, ventricular overdrive test evaluation 77—81632
- atrioventricular conduction disturbances with permanent pacemakers 77—81672
- atrioventricular region of rabbit heart, passive elec. props. rel. to intercellular link 78—48767
- atrium of bullfrog, tension components and temp. effects 77—52760
- atrium trabecula membrane, changes in elec. props. due to elec. stimulus 77—36891
- auditory cortex, amplitude spectrum representation in Doppler-shifted-CF processing area 77—52810
- auditory cortex of moustache bat, aural representation in Doppler-shifted-CF-processing area 78—80892
- auditory impedance changes elicited by tactile and electrocutaneous stimulation 80—56066
- auditory nerve data appl. to binaural interaction theory, tone detect. in noise 77—36950
- auditory nerve discharge rate, two-tone suppression, phenomenological model 77—16936
- auditory nerve fibre bandwidths and critical bandwidths in cat 77—12932
- auditory neural mechanism system properties 78—40200
- auditory neuron, characts. of digital model 78—3516
- auditory neuron response to pulsed microwave irrad. in cat, microwave hearing 78—40259
- auditory neurons of frog mid-brain, discharge rate density function 78—20191
- auditory-nerve fibre encoding of 2-tone approximations to steady-state vowels 80—61582
- auditory-nerve fibre responses to bandlimited noise, nonlinearities 80—61583
- autorhythmicity and entrainment in excitable membranes 80—108866
- axon, squid giant, compensation of potential changes produced by Er ion with applied potentials 79—16181
- axon, squid giant, transient polarisation currents 77—86477
- axon asymmetry currents and admittance, squid 77—73518
- axon conduction velocity modified by reinnervation of mammalian muscle 78—24062
- axon membrane, squid, freq. domain anal. of asymmetry current 80—51064
- axon membrane admittance change during action pots., squid 79—57621
- axon membrane asymm. current, squid, freq. domain anal. 78—44494
- axon Na conductance and Ca transport, squid, mol. model 78—85305
- axonal K$^+$ transport, single-file model for squid giant axon 77—73517
- axonal K conductance anal., squid giant axons 79—96543
- axonal membrane of mammals (myelinated fibres), K channel conduction 80—61538
- axonal membrane transport, elec. field distrib., ionic selectivity and permeability 79—34532
- bacterial cell wall, surface charge and morphogenesis of regular arrays of macromols. 80—85366
- bacterial photosynthesis, mechs. of charge separation 80—30684
- bacterial suspension, physico-chem. changes on cooling, cell elec. cond. anal. 77—86458
- bacteriorhodopsin, elec. response of a back photoreaction 80—98008
- bacteriorhodopsin, enthalpy changes during photochemical cycle 79—34602
- bacteriorhodopsin, photoelec. conversion in charged synthetic membranes 80—108954
- bacteriorhodopsin generated photocurrents on planar bilayer membranes 80—51050
- bacteriorhodopsin in model membranes, new component of displacement photocurrent 79—43827
- bacteriorhodopsin in planar membranes, elec. response to light 78—35806
- bacteriorhodopsin-containing membrane fragments, quantum yield of flash-induced proton release 79—34601
- barbiturate-induced slow outward currents in Aplysia neurones 78—80866
- barnacle photoreceptors, lateral vs. median, elec. props. and early receptor pots. 77—44651
- baroreceptor Na sensitivity mediating reflex changes of blood press. and urine flow 77—48818
- basilar membrane nonlinear model assessment, spatial differentiation as auditory second filter 77—36949
- behaviour patterns in cod released by elec. stimulation of olfactory tract bundlets 80—97951

bioelectric phenomena continued
bilayer lipid membranes, dimer mechanism of action of nigericin 78—24048
bilayer lipid membranes, effect of stress factors on elec. props. 79—92161
bilayer membrane, galvano-static regime of non-steady process 78—64963
bilayer membrane capacitance voltage depend. 77—4983
bilayer membrane dynamic response on simultaneous exposure to two anaesthetics 78—35809
bilayer membranes, static, dynamic current response effect of local anaesthetic 77—52750
bimolecular membranes, interaction with liposomes, elec. resistance obs. 80—81549
bioelectrochemistry and bioenergetics (book) 80—8749
biofeedback, student demonstration 79—44677
biological effects of ELF electric fields: some US research results 80—94278
biomembrane K channels, influence of Coulomb effects on interaction of unilateral fluxes 78—24047
biomembranes, excited, automatic meas. of ionic current electrophysiological characts. *(Russian)* 80—76865
biomembranes, low noise amplification of voltage and current fluctuations 78—44741
biomembranes, proton transport, mol. mechanisms 78—96035
biomolecules, electric and mag. props. 77—44584
biopolymer negative resistance, rel. to living cell props. 78—64923
bipolar cell, catfish, receptive field and input signals 77—12921
bipolymer, charge carriers origin and mobility, adsorbed water effects 79—92461
birefringence, transient, of macromol. solns. in reversing fields of arbitrary strength and duration 80—84719
blink reflex, afferent pathways, human 79—43864
blink reflex, effects of elec. stimulus freq. during rest and a task 80—61547
blink reflex, peripheral electrical stimulation inhibitory effect, abolition by naloxone *(French)* 80—35880
blood, elec. characts. during flow 80—36053
blood, flowing, electrical resistivity changes *(Japanese)* 79—2015
blood cells conc. meas. by conductometric cytometer 79—92437
blood impedance, effects of pulsatile flow *(Japanese)* 80—21513
blood vessel coagulative commissures, influence of high amplitude elec. impulses on strength 80—104600
blood-brain barrier polarity, neutral amino acid transport 79—57616
bone, AC and DC elec. cond., moisture effects 77—2077
bone, bovine cortical, dielec. relax. 77—40964
bone, comparison of electromech. effects in wet and dry bone 80—97985
bone, distrib. of induced elec. activity in bent long bone 78—3541
bone, fluid-saturated, dielec. props. obs. 80—51316
bone, human cortical, local piezoelec. polarisation as function of stress freq. 77—32933
bone, piezoelectric, dielectric and elastic constants, rel. to temp. and hydration 77—16946
bone, piezoelectric effect on exposure to US, effect of sample rot. 78—80913
bone healing augmentation by electric currents and fields 80—8116
bone healing electrostimulation, clinical aspects 79—83879
bone piezoelectric effect, theoretical anal. 79—70567
bone piezoelectric response obs., freq. depend. 79—92287
bone piezoelectricity, role of stress-gradient effects 80—67113
bone stress wave detection using piezoelec. effect, non-invasive technique 78—31948
bone tissue, dry, piezoelectric model 79—25015
brain, bioelectric activity organisation under nembutal narcosis *(Russian)* 78—31795
brain, elec. stimulation, awakening thresholds in 5 sleep-waking stages, cat expts. 80—85377
brain activity EEG anal. using Parcor coeffs. 78—35822
brain electrical stimulation in grasshoppers, elicitation of singing and courtship movements 79—83731
brain impedance meas., spatial resolution of 4 electrode array 79—84033
brain impedograph, computerised 78—77139
brain stimulation and thalamocortical excitability, index of anticonvulsant effect 80—21461
brain tissue, dog, dielectric props. between 0.01 and 10 GHz 80—16915
brain tissue specific-impedance meas. four electrode method 78—3647
brain wave model, Frolich's, limit cycle collapse and travelling wave onset 78—48780
brain waves limit cycle model 78—3464
burst-generating neuron model, field effect transistor analogue 77—25411
bursting pacemaker neuron, internal Ca^{2+} changes meas. with arsenazo III 77—64021
bursting pacemaker neurons, Ca^{2+} effects modelling 78—44484
cardiac arrhythmias, electrophysiological mechanisms *(German)* 77—44631
cardiac cellular electrophysiologic-clinical correlations using a relational data base 80—89890
cardiac electrical generator integral characts. in period of repolarisation 77—70442
cardiac fibrillation thresholds for 60 Hz currents and voltages directly applied to heart 80—101301
cardiac impedance during elec. stimulation, depend. on electrode, pulse duration and acid-base balance 78—27929
cardiac output estimated by impedance cardiography 79—57741
cardiac pacemaking, role of catecholamines 77—70437
cardiac pacing, aortic shear stress reduction 78—40239
cardiac Purkinje fibre, Na current model 79—43861
cardiac Purkinje fibres, rabbit, Na channels 79—43828
cardiac Purkinje fibres, sheep, intercellular clefts effect on elec. props. 79—34522
cardiac slowing, respiratory gating mechanism 77—12902
cardiac stimulation threshold, time var. 77—25609
cardiac stimulation threshold noninvasive meas., long-term follow-up 77—81711
cardiac tissue, pacemaker activity, phase resetting and annihilation 80—81565
cardiac tissue intramural resistivity, canine obs. 79—92319
cardiac tissue resistivity, intramural meas. 79—39388
cartilage proteoglycan, association with hyaluronic acid, elec. birefringence obs. 80—85332

bioelectric phenomena continued
catalytic reaction model, instability and spread of excitation waves, non-trivial modes 78—20161
cell electric circuit model, alternating signal interaction 78—77011
cell electric circuit model, alternating signal interaction 78—77012
cell impedance transient response characterisation 79—53066
cell membrane, electrophoresis and diffusion obs. 79—57599
cell membrane interaction theory of molecular level mechanics 79—92174
cell representation by an elec. circuit, voltage gain 80—40977
cell separation, local conc. gradient determ. by conductivity meas. *(German)* 79—5411
cell suspension analysis, dielec. theory, interfacial polarisation 80—45563
cell suspension physiology and induced pathophysiology, noninvasive analysis using EM method 79—2125
cell-cell junction membrane form., quantum jumps of cond. 78—73145
cells without highly permeable cell contacts, elec. connection 77—70440
cercal system, cricket, const. representation of position of signal source in space 77—25475
cerebellar cortex model, temporal behaviour study 77—86482
cerebellar cortical current appl. rel. to underlying cellular activity 77—60195
cerebellar model, spatial freq. characts. *(Japanese)* 80—67068
cerebellar Purkinje cells, synaptic action depression by inferior olive destruct. 79—34544
Chagas' disease, sinus node dysfunction obs. 77—81776
charge storage, charge transport and electrostatics conference, Kyoto, Japan (Oct. 78) 80—7252
charge transfer in thin membranes, discrete models, nonsteady state, low polarising volts. 77—70420
charge transfer in thin membranes, discrete models, nonsteady state at high polarising voltages 78—69023
charge transfer reactions in biological systems, mech. of coupling 80—76889
charged disk interactions in various dielectric media, biological cell modelling 78—66706
chelonian muscle spindles motor stimulation model 77—44636
chitin, in lobster shell and apodeme, piezoelec. rel. to remodelling 78—64929
Chlorella microwave photocond., rise/fall kinetics, depend. on physiological state 78—15793
chlorophyll, colloidal solns., elec. charge of particles 80—94438
chlorophyll a film, charge injection and storage 78—53317
chlorophyll a-n-chloranil lamellar system, heat stimulated conductivity 79—53043
chlorophyll adsorption films, electrochem. behaviour 78—31778
chlorophyll-a, conc. quenching rel. to functional charge transfer 80—30666
chlorophyll-a, microcryst., trapped-electron doping in photovoltaic sandwich cells 78—53334
chlorophyll-acceptor and chlorophyll + protein-acceptor lamellar systems, steady photocond. 78—53328
chlorophyll-duroquinone photochemical interaction, photopot. 77—16903
chloroplasts, isolated, broken, fluoresc. changes and involvement of elec. double layer 78—44464
chloroplasts, photoinduced dielectric const. shift *(French)* 78—61147
cholesterol derivatives, piezoelec. rel. to atherosclerosis 77—78076
cholinergic channel without const. field, permeab., phase-boundary pot. and conductance 77—60191
Chorella cell microwave photocond., long wave illum. and Emerson effect 78—15794
chromaffin granule electrophoretic mobility meas. by light scatt., effect of Ca^{2+} and Mg^{2+} 78—53357
chromatophores of Rhodospirillum rubrum, cyclic rel. to non-cyclic electron transport 79—53067
cochlea alternating elec. resist. changes caused by acoustic stimuli in guinea-pig 77—86507
cochlear nucleus neuron tonotopic organisation, evidence from masking of elec. by acoustic stimuli 78—44511
cochlear nucleus neurone response, model of phase struct. of bitonal stimulus 78—80887
coherent electric vibrs. in active microorganisms due to microwave radiation 79—2106
collagen, polarisation, contribution of permanent and induced dipole moments, elec. birefringence 80—85351
collagen membrane H^{+} diffusion-limited binding electromechanics 79—79489
collagen structures, piezoelec. effect, in rel. to mol. struct. 80—41100
colon, turtle, active Na transport via an electrogenic Na-K exchange pump 80—108856
colonic electrical control activity, human, computer model 80—61537
coloured membranes, unsymmetric, rectification and current oscillation *(Japanese)* 77—36871
complex mutual inductance concept for bioelectric impedance transformer bridge 80—63886
computerized tomography imaging using elec. parameters inside a patient 80—8117
conductance fluctuations in cultured spinal neurones induced by γ-aminobutyric acid 78—80867
conductivity distributions imaging, systems limitation 80—89901
cone ionic channel closure, turtle 78—15830
cone voltage-current relationships, turtle, origin of non-linearity 79—74659
cortex ensemble distribution patterns in different functional states 77—48774
cortical electrical phosphene props. 80—12112
cortical periodic complex cells, cat, spatial freq. selectivity 78—69057
Coulter electrical sizing principle, appl. to new multiparameter system 80—89911
crustacean cardiac pacemaker control system, model analysis 77—52766
crustacean cardiac pacemaker control system, simple model 77—52765
current noise parameters in embryonic heart cell aggregates 80—21459
current pulse-induced voltage variations in bilayer membranes, apparatus 80—94420
cylindrical cell with time-variant membrane resist., passive parameter meas. 77—29113
cyprinid retina, model of function at outer plexiform layer 80—12103
cytochrome c$_3$, anhydrous film, elec. cond., temp. and ambient press depend. 80—85327
cytochrome c$_3$ film, anhydrous, elec. cond. 79—66439
cytochrome c anhydrous film, electrical conductivity 77—44879

bioelectric phenomena continued
  cytochrome c interaction with phospholipid membranes 77—25384
  dendrite membrane, steady voltage-current characteristic 79—92203
  dental implant fixation, electrically mediated process, interfacial strength 79—16348
  dental implant fixation by elec. mediated process, tissue ingrowth 80—8115
  development control, review 77—86467
  diadynamic current therapy, portable apparatus 79—57809
  dielectric meas. of biological liquids, reflection meas. of complex dielectric const. 80—101309
  dielectric properties meas. technique using an in vivo probe VHF to microwave freqs. 80—85542
  dielectric properties of biological substances, tabulation for freq. range 10 kHz to 10 GHz 80—108143
  dielectric props. of biological substances, physical meas. 80—94417
  dielectric transient response of some biomolecules following UV irrad. 80—51166
  diffusion neuron model, parameter estimation 77—40654
  digitalis inotropy rel. to enhanced slow inward Ca current 78—61155
  discharges from biological objects, electrographic investigation methods 80—46118
  DNA, calf-thymus Na-DNA aq. solns., dielec. behaviour in 5 kHz to 100 MHz range 80—85330
  DNA, dielectric hysteresis loop 79—83691
  DNA, dye labelled elec. dichroism and birefringence, comparison with mol. props. from polarised fluoresc. 80—84785
  DNA, polyelectrolyte soln., appl. of Poisson-Boltzmann eqn. 79—77483
  DNA, sorption and desorption of water, thermal-stimulated press. and thermogravimetric anal. 80—8008
  DNA costacking nucleotides, γ-irrad., charge-migration phenomena, EPR obs. 80—36015
  DNA solution, elec. birefringence, stabilised induced dipole behaviour 80—85349
  double layer phenomena at particle surface *(Rumanian)* 80—94144
  double-sucrose-gap voltage-clamp method, mathematical model 79—96539
  dystrophic muscle, neuromuscular transmission in abnormal fibres 78—27932
  E.coli strains in aq. suspension, polarisability anisotropy and aminoglycoside antibiotic effects 80—85441
  E.coli suspensions, dielec. anal., interfacial polarisation theory appl. 80—97876
  EEG, decision P350, waveform and neural mechanism, auditory click and elec. finger stimuli 80—61528
  EEG, nonstationary, anal. by approx. canonical expansion method 78—53555
  EEG alpha and non-alpha intervals alternation, queueing theory model 78—96040
  EEG potentials in model of thin membranes of brain, multilayered spherical cable model 77—25408
  egg cell membranes, starfish, inward rectification blocking model 80—61523
  electret occurrence and appl. in mol. biophysics and bioengineering 80—8007
  electrets in biomaterials and biopolymers 80—80686
  electric fields, vertical, 45-Hz, influence on rats 80—76784
  electric shocks, 50/60-Hz AC, ventricular fibrillation tests on animals *(German)* 80—101154
  electrical contact generation by tattooing C into skin tissue 78—77122
  electrical discharges from biological objects, charge image method 80—8238
  electrically excitable membrane, phys. model, voltage-current characts. 77—25382
  electrochemical phenomena, rel. to diffusion pots. of polyelectrolytes 77—4978
  electrocoagulation, monoactive, controlled destruction and temp. distribs. 80—94176
  electroconvulsive shock treatment decreases β-adrenergic receptor sensitivity in rat brain 79—79512
  electrocutaneous nerve stimulation, humans and toads 79—11909
  electrocutaneous nerve stimulation, stimulus waveform selection 79—48236
  electrocutaneous stimulation, energy threshold meas. and channel capacity estimation *(Japanese)* 78—53573
  electrocutaneous stimulation, information transmission characts. *(Japanese)* 80—35872
  electrode-induced bone growth, function of implanted cathodes 80—41312
  electrodiffusion, steady-state, scaling, exact. soln. and phase plane 77—25403
  electrogenic Na pump, role in slow synaptic inhibition 77—48780
  electrokinetic model of transport through biological barriers 80—45871
  electrokinetic phenomena in biology, book contrib. 80—12326
  electrolyte-membrane-electrolyte, freq. depend. of capacitance and cond., model 77—21488
  electromechanical model for human articular cartilage 80—104631
  electromotor system of Torpedo, as model cholinergic system 78—53388
  electromyography measurements, human soleus muscle, stretch and Hoffmann reflexes 79—16193
  electron flow, photosynthetic and respiratory, in dual functional bacterial membrane 80—16914
  electronic neuron model incorporating both active and passive responses 80—8040
  electrons, advantage to low mobility in biological systems 79—39346
  electroosmotic model of longitudinal transport 80—45870
  electrophoresis along cell membranes 77—25405
  electrophoresis of concanavalin A receptors along embryonic muscle cell membrane 77—29121
  electrophoresis of proteins in intercellular bridges 80—89734
  electrophoretic mobility test, diagnosis of malignant tumours 79—79680
  electrophrenic respiration, feedback control of tidal vol. *(Japanese)* 80—41316
  Electrophysiological Data Interface 79—79677
  electrophysiological measuring, unity gain follower with buffer 79—12048
  electrophysiological responses of Didinium nasutum to Paramecium capture and mechanical stimulation 80—56001
  electroreceptor-electric organ system, of elephant nose fish, electronic circuit simulation *(Japanese)* 78—40132

bioelectric phenomena continued
  electroretinogram, human, real-time computer for first- and second-order Wiener kernels 79—12046
  electroretinography, human, psychophysical appl., review 78—35859
  electrosensory afferent, dogfish, adaptation, neuron discharge regression anal. 78—35833
  electrostatic voltage, capacitance and energy storage characts. of human body 77—40954
  electrotactile two point discrimination obs. 79—43975
  electrotonic coupling, effective sign reversal by inhibitory neurons 77—29141
  ELF magnetic field effect on personal vegetative status meas. by elec. resist. between hands 77—81533
  EM boundary-value problem in cylindrical conductor, appl. to limb tissue elec. cond. meas. 79—7055
  embryo primitive streak, chick, strong elec. currents obs. 80—72405
  embryonic skeletal muscle differentiation, electrophysiological and biochem. membrane props. 78—53363
  end plate current quantitative description and reconstruction 77—52770
  endocardial unipolar pacing, long term, importance of stimulation threshold 77—81710
  endosteal implants, alveolar bone growth enhancement by elec. stimulation, dog expts. 80—26413
  endplate acetylcholine-induced channels and transmitter release, humans 78—24063
  endplate channel lifetime and cond. alteration by permeant cations 78—3467
  entomological experiments on teratogenic effects of EM fields 80—85446
  epidural neurostimulation, percutaneous, histological reaction, short and long term study results 80—67285
  epileptic activity modelled as chain reaction within system of interconnecting cells 77—48787
  epithelial cells, of unpoisoned non-depolarised frog skin, intercellular junctions 77—12897
  epithelial membrane conductance rel. to extracellular shunting, rabbit salivary duct 77—77881
  epithelium, leaky, effect of plant cytokinins on microfilaments and tight junction permeab. 77—12899
  epithelium, tight, impedance anal. using distributed resistance model 79—62201
  epithelium intercellular contacts, small intestine, permeab. and mech. props. regulation by Ca ions 77—81482
  erythrocyte membranes, human, elec. cond. characts., ghosts and lipid bimol. membranes 77—9180
  erythrocytes, human, haemoglobin's suspending medium, dielec. props. obs. 80—76716
  Escherichia coli, aq. colloid suspension, electrophoretic mobility and elec. polarisability 78—35813
  eukaryotic cell cycle, long-range dielec. aspects 80—94182
  excitable, surface-charge density when exposed to optical radiation 77—29176
  excitable cell model, numerical method 78—53376
  excitable elements, approx. methods of theroy of networks 77—86479
  excitable fibre, steady speeds of spread of stable and unstable impulses, depend. on membrane ionic currents 78—53382
  excitable medium, 1-dimens., non-steady processes, division of arrested excitation front 77—70401
  excitable medium, auto-oscillatory, 1-dimens., stability complex regimes 78—15752
  excitable medium model with existence of several stable pulses of different duration 78—77036
  excitable medium self-sustained activity, role of inhomogeneity 78—64968
  excitable medium wave vel. calc. 77—56366
  excitable membrane, rapid transient changes in Na ion conductivity 77—44613
  excitable membrane K$^+$ conductance temp. dependence *(Japanese)* 78—24051
  excitable membranes, nonstationary ion fluxes 77—44599
  excitation properties of the squid axon membrane and model systems with current stimulation 80—67054
  excitation spread speed, 2D excitable medium 80—76717
  exercise vectorcardiogram changes rel. to left ventricular function at rest 79—43859
  expansion-contraction behaviour in sea pen, control by conduction systems 78—53387
  experiments, RF losses in elec. conducting samples 80—21580
  extra-retinal photoreceptor model for Aplysia californica 78—44506
  eye, Limulus, circadian rhythm mediation by efferent optic nerve fibres 77—90783
  eye crystalline lens, frog, elec. props. of struct. components 79—24982
  eye movements in paralysed cats induced by drugs and sympathetic stimulation 80—51083
  F-wave and M-response conduction velocity in diabetes mellitus 80—56015
  F-wave in normal man, effect of vibr. 78—20164
  field generation and perception by honey bees 78—15941
  file clam mantle edge mechanical and chemical sensitivity 78—53429
  fish, lorenzinian ampullae detect. of geomag. variations 79—39381
  fish, quasi-constant elec. field near body 79—70730
  Fitzhugh nerve conduction equations, appl. of higher order Hopf bifurcation formula 77—86483
  FitzHugh-Nagumo equations, perturbation anal. of slow periodic wave soln. 78—24060
  flagellate alga, photoinduced bioelec. reactions 79—70579
  food, semi-solid, at low, intermediate and high moisture contents, dielectric behaviour 80—101157
  forward problem of bioelectricity, numerical soln., implementation of a consistency criterion 80—76696
  frog, quasi-static bioelec. field obs. 80—51314
  frozen meat dielectric properties, expt. 80—56332
  functional electrical stimulation of the upper limb, joint moment charting 80—41310
  gastro-intestinal electrical activity model, frequency entrainment of oscillators 77—81489
  gastro-intestinal electrical signals, maximum-entropy correlation and spectral analysis 79—66577
  gastrointestinal electrical rhythm freq. estimation using autoregressive modelling 78—80855
  gating charge immobilisation by inactivation-simulating substance 78—61154

bioelectric phenomena continued
  gating currents, role of nonlinear capacitive currents of electrostrictive origin 77—48771
  gel scanner for location of proteins separated by isoelec. focusing 80—30953
  geniculate neurone spatial resolution, impaired by monocular deprivation in kittens 77—21518
  giant axon of the squid, gating current and K channels obs. 80—56012
  giant lecithin vesicles, alignment and opening by elec. field 80—3708
  glial-neural interaction demonstrated by Na$^+$ and Li$^+$ injection into cortical glia 77—36905
  gramicidin A channel struct., elec. meas. with lipid bilayer membranes 78—15783
  gramicidin A ion channel kinetic behaviour, electrostatic calcs. 78—53368
  gramicidin ion pore, potential variation 79—34506
  gramicidin single-channel currents, rate theory calc. using NMR-derived rate consts. 80—94186
  haematocrit, noninvasive meas. by elec. admittance plethysmography technique 80—56246
  haemoglobin, dielectric props. under UV excitation 80—6912
  hair cell, vertebrate, response to controlled mechanical stimuli 78—15852
  Halobacterium species, passive elec. props., membrane ionic flow 79—24970
  hearing, two-tone suppression in nonlinear model of basilar membrane 77—48811
  heart, muscle cells, Na current, electrophysiological studies, rat 79—43838
  heart, sick sinus syndrome pathology 77—81774
  heart cells of chick embryo, pacemaker current obs. 80—51066
  heart natural pacemaker, modelling as pulse-freq. modulator 78—40135
  heart temporary artificial elec. stimulation 80—56272
  high electric field biological effects on human nervous systems 80—89739
  high-pressure chamber for electrophysiological meas. 80—98185
  hippocampal afterdischarges in rats, activity spread by ^{14}C method 80—26221
  hippocampal perforant path, glutamate as transmitter 78—11635
  hippocampus CA_3 field model, phasic transition, transfer of spikes in statistical neurone ensembles 78—48781
  Hodgkin-Huxley equations for nerve membrane elec. activity, crit. topological test 78—35826
  Hodgkin-Huxley model of electrical excitability novel molecular interpretation 79—2024
  Hodgkin-Huxley reduced model, speed of spread of excitation, integral differential eqn. 77—21509
  human, effects of electric currents 80—56330
  human body, dynamic voltage-current characts. 80—94443
  human body, elec. memory effects 80—94444
  human body, equivalent circuit *(Russian)* 79—53295
  human metabolism, effect of electricity and ion concentration *(Polish)* 77—29192
  HV lines to 800 kV, elec. and mag. field effects on human beings *(French, English)* 80—72209
  hyperthermia production technique using UHF currents in superficial rat tumours 80—30947
  ileal mucosa, human, theophylline-induced changes in ion transport and cond. 77—64017
  immunoelectrophoresis, fluorography of ^{3}H-labelled proteins 80—17220
  impedance, clinical appl. for arterial insufficiency study 79—83878
  impedance, LF 4-probe meas. system 78—7554
  impedance cardiography, problems 80—41285
  impedance computerised tomography, a new imaging technique 79—66500
  impedance plethysmography, origin of impedance changes measured in the human calf 80—56269
  impedance relative to fluid distrib. in living tissues 77—32879
  impulse circulation in excitable medium, critical size of closed circuit 79—92200
  impulse spread in medium with non-monotonic function 79—92201
  influx current of edible snail neurons, dependence on Ca^{2+} conc. and membrane pot. 80—108865
  insect, Periplaneta americana, pyroelectric coeff. and permittivity obs. 80—51315
  insect swarm corona discharge as unidentified flying object 79—96728
  interactive computer program for measurement of data obtained using the extra-stimulus technique during electrode-catheter studies 78—24156
  intestinal electrical rhythms model, stability of entrainment conditions for RLC coupled Van der Pol oscillators 77—56361
  intestinal myoelectrical models, pulse synchronisation expts. 80—67061
  intestinal smooth muscle cells, non-cholinergic excitatory transmission 77—77891
  intestinal tissue, electronic modelling of slow-waves and spike-activity 80—89737
  intestinal-prostatic impedance in bulls at ejaculation 78—40458
  intrahisian block detection, endocavitary exploration classification 77—81623
  ion channel, energy and pot. profiles and interactions between ions 78—53367
  ion transport model, intracellular osmoregulation mechanism 77—25400
  ion transport studies instrument, digital readout 79—74815
  ionic channel formation in living cell membrane, microelectrode obs. 78—53372
  ionic channels and gating currents in excitable membranes, review 77—90764
  ionic channels in excitable membranes, current problems and biophysical approaches 78—53369
  ions, active transport through membranes, elec. events, book contrib. 80—12068
  isoelectric focusing method for human globin chain separation 80—17219
  jejunum short circuit current, rat, effect of serum from pancreatic disease patients 80—8204
  Kerr effect of charged dipolar macromolecules without condensed counterions in conducting solution 80—53171
  L-amino acids, weak neutral currents and biological stereoselection 80—26196
  lateral geniculate body, types of receptive fields and freq. characts. 77—25424
  lateral geniculate nucleus, cat, electrophysiological classification of X- and Y-cells 78—64996
  lateral geniculate nucleus of cat, periodic stimulation, neural activity transient persistence 80—56021

bioelectric phenomena continued
  lateral geniculate nucleus X-cell early development, kitten 78—27946
  lateral reticular nucleus neurone activity on scratching 78—24054
  lateral-inhibition type neural fields, pattern formation dynamics 77—90761
  leaves of rhododendron and encephalarts, pyroelectric coeff. and permittivity obs. 80—51315
  light response and kinetics in Aplysia giant neuron 78—53381
  light scattering, dynamic, by flexible macromols. in fluctuating elec. field 80—84722
  light scattering from macromolecular soln. in alternating elec. field, low angle approx. 80—84721
  lipid bilayer, 1 MHz US effects on cond. and capacitance 78—77082
  lipid bilayer, alkane solubility modified by elec. field 80—97874
  lipid bilayer, elec. cond. in presence of proteolytic enzymes and substrates 78—15779
  lipid bilayer, flat, permeab. in presence of vesicles of sarcoplasmic reticulum 77—21490
  lipid bilayer, hydrophobic ion current noise, autocorrel. anal. 80—30676
  lipid bilayer, planar, light guide effect, bilayer spectrosc. appls. 79—29509
  lipid bilayer electrical breakdown 80—81552
  lipid bilayer electrical strength fall after UV irrad. 78—69002
  lipid bilayer gramicidin A channel cation flux interaction 78—56957
  lipid bilayer membrane, melting point rel. to electrostatic field 78—92602
  lipid bilayer membrane countercurrent cation fluxes 79—70528
  lipid bilayer membrane incremental resistance unaffected by anaesthetics 79—83718
  lipid bilayer membranes, discrete charge effect, dipicrylamine anions surface absorption 79—16159
  lipid bilayer membranes, ionic displacement current 79—34503
  lipid bilayer nonlinear electric effects studied by harmonic anal. 78—24188
  lipid bilayer properties in presence of tetra-alkylammonium salts, effect of surface charge 77—21489
  lipid bilayers, Ca^{2+} transport system of rat liver mitochondria 78—64966
  lipid bilayers, dielec. const. calc. from bond polarisabilities 77—29105
  lipid bilayers, elastic props. changes on exposure to different agents, elec. and chem. 80—81548
  lipid bilayers, evidence against channel form. by nystatin 77—44598
  lipid bilayers, ion transport modification by 2,4-dichlorophenoxyacetic acid 79—83710
  lipid bilayers, K$^+$ transport modification by 2,4-dichlorophenoxyacetic acid 79—83709
  lipid bilayers, planar systems, asymm. charge distribs. 77—29104
  lipid membranes, buried charges, virial expansion 79—16158
  lipid-bilayer-aqueous soln. interface with surface-active ions, double elec. layer 77—36872
  liposome, photoinduced electron transport across phospholipid wall using methylene blue 79—74614
  liver cell, DC elec. excitation 77—56565
  liver cells, regenerating, specific resist. and electrophoretic mobility, effect of RNase and neuraminidase 77—25402
  living tissue electrical excitation theory development *(French)* 78—88703
  living tissue stimulation energy threshold meas. using analogue instrument 79—57745
  locomotion studies, technique for correlating film and EMG 78—24186
  locomotor activity circadian rhythm, cockroach, strong phase response curve 78—11630
  locomotory rhythm generation with recurrent cyclic inhibition, leech 78—35832
  long range coherence in biological systems 78—20137
  lower resistance meridian, meridian distrib. in normal individuals *(Chinese)* 79—79717
  lower resistance meridian investigation, method discussion *(Chinese)* 79—79716
  lumbo-sacral motoneuron pools, human, response patterns to distant somatosensory stimuli 80—108924
  lung irritant receptors and afferent C-fibres, stimulation by prostaglandins 77—12939
  lymphatic heart, frog, elec. props. of spinal centre pacemaker 77—56360
  lysozyme, electric and mag. props. 77—44584
  lysozyme, electron acceptor props. in photosensitized electron transfer, EPR study 79—79469
  lysozyme, search for superconducting regions 80—101149
  lysozyme, sorption and desorption of water, thermal-stimulated press. and thermogravimetric anal. 80—8008
  magnetic. fields produced by steady currents in human body 80—94248
  magnetocardiogram, PR segment theory rel. to current sources within heart 80—101191
  magnetoelectric dipole structure hypothesis, biological and cosmic appls. 80—91124
  magnetoencephalogram genesis mechanisms 78—53432
  Marat, Jean Paul, medical use of electricity, historical note 80—17781
  mast cells, rat, electrophoretic mobility distrib. alteration after immunological activation 80—67047
  median nerve lesion localisation, usefulness of F-wave conduction time, post mastectomy patient 80—56267
  medullary interneurons of goldfish, elec. and chem. inhibition in vertebrate central nervous system 77—36911
  melanin, wet, elec. switching, aggregated electrons emulsion inversion as possible mechanism 79—38139
  membrane, dynamic interfacial electrochem. phenomena, toad urinary bladder membrane system 78—27912
  membrane, elec. excited, nonlinear dynamic models for simulation 80—94178
  membrane, thin, ionic transport, jump vs. electrodiffusion description, for steady transfer 77—36895
  membrane, thin, ionic transport, jump vs. electrodiffusion description, volt. clamp 77—36896
  membrane, thin non-uniform, jump vs. electrodiffusion description, volt. clamp 77—36897
  membrane admittance, integral representation 78—15811
  membrane and near-membrane transport processes, effect of volumetric charges 78—53366
  membrane conductance channels, current-induced coupling, multi-channel interaction and mean field cond. 80—67063
  membrane conductance fluctuations and ionic pores, review 77—90752
  membrane current separation using Paramecium mutant 77—66806
  membrane current-voltage relations, Nernst-Planck anal. 79—83715

bioelectric phenomena continued
membrane dynamic equation solving, practical algorithm 78—77038
membrane electric properties measurement method using glass electrode impaled into single cell 80—89916
membrane electrical double layer theory, through Born-Green-Yvon eqn. 80—35539
membrane electrical relaxation, time-depend. rectification, cellulose acetate model 77—90731
membrane energy transduction probes, review 77—21666
membrane excitability, review 78—15786
membrane excitability mechanisms, book contrib. 80—12062
membrane excitability models, electrostriction and/or cooperativity 79—79487
membrane H$^+$ channels and mol. electrostatic generators 77—21501
membrane ionic channels, dipole cooperative model 79—53054
membrane Na-channel gating current carriers, electronic model 79—70542
membrane noise, spectral props. of physical processes of Markov-correlated events 79—21665
membrane noise analysis by integral spectrum procedure 77—48958
membrane noise spectral density measurement, use of octave filters 77—48957
membrane surface charge distributions, discrete, fluctuations near individual channels 79—16160
membrane surface charge visualisation using SEM 80—85566
membrane transport noise in channels with open-closed kinetics 79—100579
membrane-covered cubes in cubic array at high conc., analogue soln. of elec. capacity 77—40642
membranes, electric and magnetic props. in smectic liquid crystal state *(Russian)* 77—60190
membranes, excitable, statistical theory nonlinear force-flux reln. and fluctuation 77—9179
membranes, mechanism for 1/f noise in diffusing ion channels 78—27911
membranes with TTFB, elec. cond. mechanisms 77—52746
metabolic synapse, comparison of effects of cyclic 3′,5′-AMP and 3′,5′-GMP 78—24058
methylglyoxal-protein complexes, hopping conduction, theory 79—24935
micro-organism electrical characteristics meas., elec. cond. and dielec. props. *(Italian)* 78—3684
micro-organism electroretention effectiveness rel. to electrode type *(Russian)* 80—26419
microelectrode current and voltage clamp cct. for central nervous system neurons 78—24191
microelectrophoresis, intracellular, contrib. of volumetric charge to mobility of nuclei 77—86710
microemulsions, struct. aspects, using dielec. relax. and spin label techniques 80—26199
micropipettes of very low resistance for intracellular meas., production method 80—61738
microwave dielectric relaxation in muscle 80—51146
Millipore-dioleylphosphate model membrane, elec. current stimulus effects 80—67046
miniature endplate current decay, effects of extracellular Ca^{2+} and Mg^{2+} 78—24064
mitochondria, giant, elec. props. study by double impalement technique 79—92446
mitochondrion, elec. props. and struct. transitions 79—24943
modular gating channel and the Cole-Moore effect 80—30708
monoamine neutrotransmitters, du channel point, in raphe nuclei of rabbits, elec. stimulation effect *(Chinese)* 78—20170
monoamine-containing neurone connectivity in leech central nervous system 77—44639
motoneuron firing rates with strong random synaptic excitation 77—9184
motoneuron optimal control model 77—86486
motoneurone model with early inactivation, after hyperpolarisation conductance time-course and repetitive firing 80—40987
motoneurone survival during normal cell death in chick embryo, effect of neuromuscular blockade 78—27933
motoneurone transmitter output rel. to muscle fibre growth, lobster 78—64974
motor conduction velocity and H-reflex in infancy and childhood 78—61164
motor nerve conduction velocity determ. in normal subjects 77—60275
motor nerve conduction velocity measurement, semi automatic method 77—48909
motor nerve endings, hyperosmotic neurosecretion rel. to internal Ca conc. 77—56368
motor nerve impulse, conventional Ca^{2+} channel mediating asynchronous acetylcholine release 78—11638
motor neuron activity patterns of Drosophila, anal. with neural analogues 80—108870
motor unit discharge freq. depend. on isometric muscle tension, humans 77—21510
motor unit recruitment and firing freq. control in elec. stimulated muscles of cat 78—81092
motor unit recruitment and rate coding for isometric contractions production 77—73523
motor unit recruitment order reversal by cutaneous stimulation during muscle contraction, man 78—40136
motor unit sequential stimulation in cats through peripheral motor nerves 79—57635
motorneurons of different geometry and size principle 77—36908
multi-enzyme complex carrying out electron transfer, asymptotic anal. of functioning 80—81523
muscle, Ca transients in frog slow muscle fibres 77—77892
muscle, cat tibialis posterior, motor units, neuro-mechanical props., speed-force relations 78—80856
muscle, elec. stimulated, closed-loop control of force 80—76728
muscle, excitation and contraction processes, book contrib. 79—5262
muscle, excitation-contraction coupling in voltage-clamped cut skeletal fibres, rel. to transparency 77—29138
muscle, frog skeletal fibres, mesh model of tubular system, elec. props. 77—25395
muscle, locust, pot.-depend. transition temp. of ionic channels induced by glutamate 77—77882
muscle, multifibre preparation, intercellular clefts influence on pot. and current distrib. 80—72145
muscle, single ionic channels obs. in tissue cultures 80—30699
muscle, single postsynaptic channel currents in tissue cultures 80—30700

bioelectric phenomena continued
muscle, skeletal, birefringence signals rel. to Ca transients 78—24041
muscle, skeletal, contraction time in normal children 78—61163
muscle, skeletal, K-contractures and membrane pot., rat 77—29117
muscle, skeletal, Na:K rel. to Na:Na exchange by Na pump 77—66807
muscle, skeletal fibres, intramembrane charge movement and Ca transients 79—66453
muscle, smooth, depolarised, tone change due to hyperpolarising current 77—86471
muscle, smooth, depolarised in hyper K medium, spontaneous relax. 77—86470
muscle, smooth, intestinal cell, voltage clamp studies of hyperpolarising inactivation 78—80847
muscle, striated, charge movement in membrane, book contrib. 79—5263
muscle, striated, possible gating signal for K channel 77—64018
muscle cell cultures, skeletal, myosin synthesis increased by elec. stimulation 77—1988
muscle cells in tissue culture, acetylcholine-induced current fluctuations 77—29119
muscle contraction, effect of successivity of activating pulses 77—25418
muscle contraction, math. model with account of excitability 77—25417
muscle contraction elec. induced, meas. of suggestion effects *(Slovenian)* 80—81571
muscle depolarisation and repolarisation obs. 80—3624
muscle fatigue, electrophysiological pattern in healthy humans, effects of artificially induced ischemia 80—97890
muscle fatigue in muscular dystrophy, electrophysiological pattern of development 80—97888
muscle fibre end-plate current pot. depend., effect of phenylalkylamines, frog 78—31799
muscle fibre post-synaptic membrane, ionophore-mediated Ca influx effects 78—11637
muscle fibres, elec. interaction 80—51063
muscle fibres, endogenous elec. field, dependency on Na$^+$-K$^+$ pump 80—108869
muscle fibres, skeletal, resting, Cs$^+$ rel. to volt. depend. block of inward K currents 77—52756
muscle fibres of giant barnacle, cyclic GMP levels associated with contraction 77—56369
muscle Na channel use-depend. block by local anaesthetic, pH effect, frog 78—20160
muscle spindle, mammalian, math. model *(Japanese)* 77—44638
muscle tension development control by motoneurones 77—66813
muscle training effect on single motor unit firing pattern 78—7327
muscle transfer function online evaluation by impulse response transformation, rehabilitation test appl. 79—57637
muscleforce-freq. curve recording from humans, α excitability evaluation *(Japanese)* 78—3643
muscles, smooth, of elastic arteries, biophys. props. 78—69011
muscles, stretched fibres, mechanical activation and voltage-depend. charge movement 80—3630
myelinated nerve fibre, response to short duration biphasic stimulating currents 80—85373
myelinated nerve fibre steady-state/dynamic model, threshold comparison 78—27917
myenteric plexus, mediation of slow synaptic excitation by substance P 78—73153
myocardial damage, induction by open-chest low energy countershock, rabbit expts. 80—72150
myocardial damage from defibrillator discharges at various dosages 80—72368
myocardial excitability evaluation, strength-interval curves generation under computer control 80—41336
myocardial fibre excitation and contraction uncoupling on slow Na-Ca channel block 78—15810
myocardial threshold, pharmacological influence determ. 77—81643
myocardium adjacent portions, mutual elec. influence genesis of arrhythmias 79—92202
myocardium contraction amplitude depend. on freq. of elec. stimulation, frog 78—77027
myocardium of frog, temp. effects on membrane currents 77—52759
myotonia and Ca permeab., math. model 78—11620
myotubes, human, cultured, acetylcholine-induced conductance fluctuations 78—61157
Myxicola axons, Na tail currents compared with membrane asymm. currents 77—66808
nematode oesophagus pumping mechanism 78—69121
nerve, temporal stability of solitary impulse solns. of nerve eqn. 78—35830
nerve and muscle elliptical fibres, physico-math. anal. 78—11639
nerve axon, leading edge approx. 77—12903
nerve axon, phys. model, ionic distrib., pot. profile and resting pot. 77—12901
nerve axon, two-factor two-mode model, travelling waves *(Japanese)* 78—20173
nerve axon adsorption model, action pot. and excitation currents, volt. clamp test 80—56018
nerve bundle conduction velocity distrib. meas. and transfer function anal. 77—44867
nerve conduction in squid axon, Hodgkin-Huxley equations, large amplitude periodic solns. 78—20166
nerve conduction velocity distribution based on compound nerve action pot. 78—40138
nerve conduction velocity variability, effect of averaging and limb warming 77—60274
nerve excitability, interactions between intrinsic membrane protein and elec. field 78—53377
nerve excitable membrane, EM wave effect on surface charge density 78—85334
nerve excitation, gating currents and dipole transitions 80—67056
nerve fibre membrane Na permeab. reversible blockage by increase in temp. of medium above 45°C 80—81576
nerve fibres, mammalian, demyelinated, continuous cond. 77—4995
nerve impulse eqn., periodic solns. 77—66812
nerve impulse interspike interval changes during propagation, quantitative description 77—64023
nerve impulses in 2 parallel unmyelinated fibres, induced excitation and synchronisation calcs. 80—56017
nerve ionic permeability of K, Na and Cl, regulation by fixed charges and pH, crayfish 77—66809
nerve membrane, excitable, charge density due to optical irrad. 79—8526

bioelectric phenomena continued
nerve membrane flicker noise model 77—29125
nerve membrane permeability changes, fluctuation anal. 78—11636
nerve membranes, cell excitation detect. using birefringency changes *(Japanese)* 77—66876
nerve membranes, protein channels for Na and K ions, mol. mechanisms 77—4994
nerve signals derivation from contrast flash data 80—108885
nerve-muscle anisotropic syncytia, spread of flat front of excitation 78—53383
nerve-muscle anisotropic syncytia elec. props., steady form of excitation front 78—69037
nerves, electrochem. theory, steady and transient pots., in book, for teaching 78—8202
nervous system microcircuits involving dendrites 78—53390
nervous tissue damage parameters secondary to elec. stimulation 78—44491
nervous tissues, Ca dependent K activation, book contrib. 79—5266
network thermodynamic two-port element, representation of salt, current coupled flow 79—34505
networks of excitable elements, Hebb nets 78—15820
neural activity recording using collagen fibre electrode *(Japanese)* 77—66879
neural conduction times, central and peripheral, in multiple sclerosis, somatosensory obs. 80—89773
neural excitation detection by real-time detect. of small birefringence change *(Japanese)* 78—15938
neural mechanisms of monkey, elec. stimulation remote control device 77—86719
neural membrane depolarisation, possible role in work of molecular computer 79—53075
neural membrane two-factor two-mode model 78—7330
neural net producing rhythmic activity in snail Helisoma trivolvis 77—40657
neural nets, double-layer, analysis and simulation with mutually inhibiting interconnections 77—12905
neural network simulation using fast Fourier transform 77—1986
neural networks, continuous, with analogue neurons, topological props. 78—48783
neural oscillator, free running, perturbation effect on phase transition curve 79—83737
neural pacemaker phase control 78—11631
neural prostheses, review 80—21576
neural repetitive firing, Hodgkin-Huxley axon modification suggested by crustacean axon results 77—48776
neural signal space entropy, neurodynamic basis of Weber's and Steven's laws 77—73516
neural single unit activity from foetal pig brains, recording method 80—67315
neural unit activity rel. to movement, photographic technique for anal. 80—67310
neuroblastoma cells, quiescent, rapid ionic conductance changes, serum induced 79—74612
neuroblastoma cultured cells, membrane currents under volt. clamp 77—60193
neuromuscular blockade monitoring device, twitch box 78—77132
neuromuscular ectopic synapse, gating props. of acetylcholine receptor 78—27934
neuromuscular frequency-depend. block and temp.-induced seizure in ts mutant of Drosophila 78—56963
neuromuscular information transmission, distortion suppression 80—35871
neuromuscular junction, crustacean, ethanol effect on excitatory postsynaptic current duration 77—48777
neuromuscular junction, frog, acetylcholine diffusion barrier 78—7334
neuromuscular junction, frog, electrostatic screening of neurotransmitter release 80—89741
neuromuscular junction, frog, volt.-depend. effect of curare 77—52775
neuromuscular junction, snake, synaptic channel gating differences at twitch and slow junctions 78—80868
neuromuscular junction channel, in frog, endplate current fluctuations 77—25416
neuromuscular junction endplate current simulation 79—62230
neuromuscular junction of crab, in vitro action of anaesthetic and convulsant ethers 77—29140
neuromuscular junction transmitter release during repetitive stimulation, effect of Sr^{2+} and Ba^{2+} 78—3469
neuromuscular system energy-optimal controls, mammals 77—73522
neuromuscular transmission, prejunctional role of cyclic nucleotides 77—1987
neuromuscular unit discharge during muscle fatigue, structural model anal. 80—67066
neuron, spatially distributed, response to white noise current injection 79—83728
neuron, stochastic electronic model 77—48775
neuron extracellular electric field model 79—62233
neuron late outward current, Ca-dependent depression, snail 78—7335
neuron mathematical model, freq. characts. *(Japanese)* 80—35866
neuron membrane, design of a single electrode voltage clamp 80—72385
neuron membrane Ca channels, displacement currents assoc. with activation of gating mechanism 77—81486
neuron membrane inward Ca current, blocking effect of Cd^{2+} ions 77—81485
neuron model, ICs, teaching aid 78—85301
neuron model, response for density modulated Poisson pulse trains *(Japanese)* 78—35829
neuron model using stochastic syncoder 78—15822
neuron models Volterra-like polynomial representation 77—90754
neuron multi-input model diffusion approx. 77—29135
neuron populations as information processing system, stochastic properties 78—80860
neuron with shunting inhibition, stochastic modelling 77—9183
neuronal activity firing pattern evoked by monosynaptic inputs, stochastic model 77—29134
neuronal activity model, Ornstein-Uhlenbeck process 80—51030
neuronal average firing frequencies, digital display 77—5117
neuronal circuit with recurrent inhibition two-component model *(Japanese)* 77—48784
neuronal discharges, Random-Access Memory-Interval Timer and buffered storage system 79—84066

bioelectric phenomena continued
neuronal firing stochastic model, non-renewal point process properties 77—70447
neuronal spike train separation by improved time amplitude window discriminator 77—86726
neuronal synapses, information processing, electrical neuronal model design *(Korean)* 80—35865
neurone Ca conduction units, Helix aspersa 78—77041
neurone compartmental chain model membrane voltage changes 77—29124
neurone depolarisation by purine and pyrimidine mononucleotides, in explanted amphibian sympathetic ganglia 78—11633
neurone electrical activity modulation by cholesterol, Aplysia 78—7329
neurone local hormonal communication, Aplysia 78—69040
neurone membrane, asymm. displacement currents and effect of internal F anions 77—48773
neurone regeneration in leech, form. of elec. synapse on severed axon segment 77—52776
neurone susceptibility to changes in synaptic inflow, evaluation using stochastic model 78—24059
neurones A and B of mollusc, effect of acetylcholine chloride and chlorocholine chloride on resting pot. and membrane resist. 78—53375
neurons, Aplysia, effects of NH_4^+ and HCO_3CO_2 on intracellular Cl^- level 78—44485
neurons, cat eye, stereotaxic method for recording from single cells 80—89913
neurons, developing, optimal stimulus distrib. model 77—25419
neurons, pigmented, of pond snail, effect of light on electrogenic processes 77—81528
neurophysiological data semiautomatic processing, computer program for data reduction 77—44861
neurophysiology, real-time display techniques 77—2071
nexus, evidence for fixed charge, permeability, obs. 80—94193
nicotinic transmission, role of voltage-sensitive receptors 78—44492
Noble model, spread of excitation through node of branching 77—16899
nonmyelinated nerve fibre conduction vel. 77—90759
nuclei of raphe system, electric stimulation and cooling effects on alertness in cat *(French)* 80—35864
nucleic acid bases, charge-transfer complexes 79—70507
nucleic acid-TCNQ complex, charge transfer interaction 80—3576
nucleic acids, discontinuous mag. field effects, room temp. superconductivity 79—62195
nucleosomes and nucleosomal DNA, electro-optical props., relax. times and chain struct. 80—85350
olfactory bulb model, spatial and temporal charact. freqs. of interactive neural masses 77—25476
olfactory receptor sites location, inferences from latency meas. 80—56068
one-dimensional excitable medium, non-steady processes, excitation front division 77—86475
oocyte membrane, existence of acetylcholine receptor 78—24040
optic tract and lateral geniculate neurons, spectral responsiveness and temporal freq. response 77—36923
optic tract fibre recordings, lateral spread of light adaptation in rat retina 77—44659
oral motor tasks, stutterers' and nonstutterers' neural response times 79—96585
organic substances, electrochemiluminescence as possible source of coherent radiation, and role in biological processes *(Russian)* 80—76093
osteon system piezoelec. polarisation model 78—3540
ovipositor receptor, blowfly, monovalent cation sensitive neurones 77—77922
pacemaker neurons, Aplysia, effects of irradiation with 20 MeV electrons 80—17013
pain control in man, medial thalamic permanent electrodes, electrophysiological and clinical study 80—67282
pain mechanisms, neural network model 78—85307
palmar conduction time of median and ulnar nerves in carpal tunnel syndrome 80—12075
pancreatic acinar cells, acetylcholine null pot., mouse 77—4988
pancreatic acinar cells, acetylcholine-like effects of intracellular Ca^{2+} appl. 77—66801
papillary muscle, rabbit, elec. phenomenon during Ba^{2+} induced contracture 79—83732
papillary muscle fibres, rabbit, effect of preliminary stimulation on repeat responses 78—48768
papillary muscle in rat, dynamic behaviour stochastic model 78—35821
paralysed muscle, treatment by elec. stimulation *(Slovenian)* 80—81771
paralysed upper extremities rehabilitation systems, control signals *(Slovenian)* 80—81772
Paramecium, artificial deciliation causes loss of Ca-depend. responses 77—2017
Paramecium excitation, model anal. 80—61524
paraplegic patient muscles, provision of functional use by elec. stimulation, review 80—101289
paraplegic patients, functional elec. stimulation *(Croatian)* 80—109058
paraspinal muscle intramuscular stimulation, mapping area of muscle activated 77—29144
paroxysmal ischaemia, vectorcardiogram and rheokinetocardiogram relationship 79—44047
pea leaf cells, microwave photolosses, electrophysical process obs. 79—70535
percutaneous elec. stimulation of nervous system for pain relief 78—3668
peripheral nerve, single unit detection by real time correlation 79—12047
peripheral nerve conduction velocities distribution estimation 77—90757
peristaltic reflex dynamics model 80—56080
permittivity measurement method for RF and microwave freqs. 80—52275
phantom hand sensations elicited by afferent nerve stimulation, discrimination in below-elbow amputees 80—97892
phospholipid membranes, conductivity changes on exposure to HF EM field 79--79483
phospholipid vesicles charge asymmetry obs. 79—62202
phospholipids, synthetic, ionic permeability in region of phasic transition 79—53052
photoelectric effects in lipid bilayer membranes containing Schiff bases of retinal *(Japanese)* 78—7322
photoinduced electron transport across protein-containing membranes 80—30768
photoreceptor, Drosophila mutant with phototransduction defect 77—90777

bioelectric phenomena continued
photoreceptor membrane fragment modified artificial lipid membranes, effect of light 77—77898
photoreceptor voltage signal at visual threshold 77—16930
photoreceptors, arthropod, prolonged light-induced cond. change on recovery from anoxia 77—12915
photoreceptors, Limulus ventral eye, effects of removing extracellular Ca^{2+} on excitation and adaptation 77—9190
photostimulator for visual electrophysiology 78—35846
photosynthesis, redox conversion kinetics in the electron transport chain 80—40950
photosynthetic reaction centre functional reconstitution in planar lipid bilayers 80—97881
phthoralocyanin porous films, Becquerel photovoltaic effect 77—16907
Physarum polycephalum, true slime mold, surface membrane simulation using liquid ion-exchange membrane *(Japanese)* 78—31781
piezoelectricity, induced, in isotropic biomaterial 77—13048
pigmented biomembranes, photoelec. and magneto-orientation effects, review 77—48766
pineal unitary response to light stimulation in frog central nervous system 77—52780
placenta, human, detect. of pulsatile flow in situ by impedance meas. 80—104799
plant growth and development, effect of 60Hz elec. field 77—81534
plant sieve tube sucrose loading, role of pH gradient and membrane ATPase 77—52757
plant tissue, elec. conductivity meas. in physiological pot. gradient 79—57838
plant tissues, adsorbed water, detection of OH groups for adsorption centres, dielectric relaxation *(Japanese)* 80—7999
plasmalemma of Nitella flexilis, selective centres of excitable channels of early ionic current 80—81568
plethysmography, elec. admittance, blood flow meas., evaluation of theory and accuracy *(Japanese)* 79—43979
plethysmography, impedance, sampling field in the human calf 79—57740
polar solvent reorganisation energy in inner sphere complex charge redistrib. 80—40730
polyelectrolyte membranes, persistent polarisation in aq. environment, neural model 78—48763
polymers, electro-optical changes, chem. and rotational contribs. 80—85352
polymorphonuclear granulocytes and FL-cells, effect of X-rays on membrane pot. and electrophoretic mobility *(German)* 77—56442
polynucleotide solution, elec. birefringence, stabilised induced dipole behaviour 80—85349
polynucleotide solution, elec. field induced orientation and effects 80—85348
polypeptide, conformational change induced by strong elec. field 80—85336
polyribonucleotides, dye tagged, aqueous solns., elec. induced fluoresc. changes 80—85346
portal currents rel. to intramembrane charge displacement, one-dimens. approx. 78—31789
postsynaptic effects of multiaction gaint interneurone on identified snail neurones 77—70448
power-frequency AC danger zones *(German)* 80—21600
power-line elec. field interaction with human and animal organisms 79—66483
premotion silent period in rapid voluntary movement 77—21511
presynaptic electrical coupling in Aplysia, effects on postsynaptic chem. transmission 77—48782
presynaptic facilitation as mechanism for behavioural sensitisation in Aplysia 77—36912
primary auditory neurons, preferred intervals in spontaneous activity 80—45921
primary T-wave determ., spatial ventricular gradient change factors 79—43850
protein kinases, cAMP-depend., membrane-localised, and regulation, of slow inward current, frog heart 80—81567
protein model chain, aperiodic, electronic spectra, hopping cond. 80—5641
protein periodic models, forbidden band gap calc. indicating insulating behaviour 77—25367
protein-methylglyoxal complex, electronic props., energy band cond. 79—24936
proteins, electrostatic effects on behaviour 79—53027
proteins, hopping conduction, theory 79—24935
proteins, role in electron transport at large distances 79—34480
proton transport across charged membrane and pH oscillations 80—61516
pulmonary stretch receptor dynamic response, dog 78—20194
Purkinje fibers, delay, block, oneway conduction model 80—21462
Purkinje fibres, calf, role of intracellular Ca in transient outward current 77—90748
Purkinje terminal electrical connection with muscle fibres in canine ventricle 77—86460
Purkinje-myocardial junction conduction rel. to ventricular overload 77—81775
purple membrane fragment suspensions, elec. dichroism obs., trimer model interpret. 80—89728
purple membrane suspensions, light-induced conductivity changes, pH and temp. effects 80—51157
pyroelectricity, anomalous behaviour of leaf epidermis of palm-like plant Encephalartos Villosus 78—44755
pyroelectricity and induced pyroelec. polarisation in leaves of palmlike plant Encephalartos villosus 77—77876
quantal size rel. to abrupt changes in nerve terminal vol. 78—31805
quantum chemistry, biology, and pharmacology, conference, Kiev, USSR (Sept.-1978) 79—96499
R. sphaeroides, polarisation of photosynthetic membranes and reaction centres in elec. field 80—94277
random threshold element networks with absolute refractory period 77—29143
Ranvier nodes exposed to DDT, asymm. currents and Na currents 77 48778
ratfish, electroreception, obs. 80—94442
rats, lack of effect of elec. field exposure, data re-evaluation 80—72210
ray, Black Sea, electric organ discharge structure 78—64969
receptive field types in lateral geniculate body and functional model 78—69046

bioelectric phenomena continued
redox conversions, electron transport 79—92179
reflex conditioning effects on motoneuron pool 79—79509
regional electroaerosol deposition model 79—83842
Renshaw cells dynamic properties, freq. response characts. 78—3462
Renshaw spinal interneuron repetitive firing, model 77—90760
repetitive firing mechanism excitation parameters, nerve impulse trains statistical evaluation 80—40986
resistance and facilitation gradient demonstration in cardiac pacing 77—81669
respiration rhythmogenesis model, Lotka-Volterra equations *(German)* 77 48772
respiratory rhythm, synchronisation by electrical stimulation of phrenic nerve 79—11910
retardation currents in excitable membranes and models of flicker noise 78—92618
retina, on-centre bipolar cell, effect on polarisation of horizontal cells in carp 79—16207
retina, pigeon, extensive lateral transmission in inner plexiform layer 77—48794
retina, toad, evidence for passive electrotonic interactions in red rods 78—92627
retina, turtle, modes of chromatic interactions 78—7347
retina of Limulus, spatially synchronised oscillatory response theory 78—73158
retina receptor layer current spatial distribution, frog, electrical model 77—40666
retinal b-wave currents, frog 79—57652
retinal bipolar cell dark noise and stability of rod rhodopsin 78—11644
retinal ganglion cell of cat, refractoriness in maintained discharge 78—64991
retinal ganglion cell responses to flashing and moving stimuli, mudpuppy 77—12917
retinal ganglion cells, abnormal response in Siamese cats 77—90785
retinal ganglion cells, frog, species differences in optimal stimulus sizes 77—21519
retinal ganglion cells, rat, adaptation pools and excitation receptive fields 78—7356
retinal ganglion cells, suppression of maintained activity 79—79537
retinal ganglion cells, surround- to centre-type response transition by receptive field centre darkening 77—44649
retinal ganglion cells of 3 week old kittens, physiological props. 77—36922
retinal horizontal cell receptive field centre/surround interaction model 77—86497
retinal horizontal cells, amplification of graded pots. 77—32889
retinal neuron firing rates, lack of predictability from interspike interval statistics 80—67075
retinal neuronal network, interactions between photoreceptors and horizontal cells 78—11648
retinal neuronal network of photoreceptors and horizontal cells 78—3482
retinal photoreceptor and horizontal cell synaptic connections 77—90787
retinal responsivity compression, V-log I functions and increment thresholds 78—61181
retinal rods, thermal activation of visual transduction mechanism 79—74651
retinular cells, arthropod, light-induced membrane cond. change rel. to membrane pot. 77—5001
rhodopsin-containing bilayer membranes, light induced transmembrane channel form. 77—52784
Rhodospirillum rubrum, chromatophores electron transport chain, functional organisation 80—81555
rhythms represented by coupled synthesized relax. oscillators 80—26218
rod outer segment adaptation anal. based on a simple equiv. cct. 78—73157
rod outer segment membrane current, light-induced fluctuations recorded in single toad rod 77—86493
rod outer segments membrane current fluctuations 79—79530
rod outer segments membrane current obs. 79—79529
rod photoreceptor membrane, pot. regulation by cyclic GMP 79—74654
rod/cone system interactions in goldfish retina 78—35853
rods, toad, effects of Ba^{2+} on dark-adapted intensity-response curve 79—79531
saccadic suppression by corollary discharge in the locust 79—92217
saphenous nerve normal sensory cond. in man 78—61162
sarcoplasmic reticulum, fragmented, voltage-dependent Cs^{+} blockage of K^{+} channel 79—96524
sekeletal muscle dynamics, isometric and isotonic contraction model 78—31807
self-excited oscill. of neuronal circuit with recurrent inhibition and delay *(Japanese)* 78—20172
semiconducting biopolymers and their part in biochemical phenomena, book contrib. 80—12053
sensory fibres, amphibian, spike freq. adaptation due to slow K channels 79—2025
serum albumin, bovine, hydrated, dielec. and elec. props. 80—97854
serum low density lipoprotein, human, anomalous permittivity behaviour 80—81540
short latency potentials from neck and scalp following median nerve stimulation in man 78—31794
single-ion channels in unmodified membrane at phase transition temp. 80—45559
sinus node and AV junction, automaticity model based on weakly coupled relax. oscillators 78—24017
sinus node function electrophysiology rel. to long-term cardiac pacing 77—81673
sinus node of rabbit heart, intercellular coupling 78—20159
sinus node response to premature atrial stimulation, microelectrode analysis 77—81630
skeletal muscle, freq. response characteristics evaluation 79—96594
skeletal muscle const.-vel. contractions by sequential stimulation of muscle efferents 80—41309
skeletal muscle fibre with helicoidal T system, linear elec. props. 78—80852
skeletal muscle general myocybernetic control model 78—53385
skeletal muscle of frog, displacement currents, K cond. channel contrib. 79—39409
skeletal muscle rhythmic oscillation simulation and analysis 78—31806
skin conductance meas. IC operational amplifier cct. 77—25566
skin electric field intensity distribution due to external pot. 77—73553
skin electrical quantities, frog, method for in situ meas. 80—36208

bioelectric phenomena continued
skin electrical resistance, w.r.t. galvanic reaction *(Hungarian)* 78—35982
skin impedance, Laplace plane anal. 79—39458
skin impedance change, equivalent cct. 77—81773
skin impedance parameter dispersion and correlation 79—29518
skin impedance simulation, w.r.t. Cole-Cole circular arc law 77—5101
skin resistance biofeedback, using frequency controlled oscillator detector 80—101156
skin resistance during square-wave elec. pulses of 1 to 10 mA, rel. to nerve stimulation 78—31929
skin resistance measurements, collection and off-line processing *(German)* 80—67273
sleep electrophysiological signals multidimensional anal. 77—52762
sleep spindles, automatic detection with a phase locked loop device 79—16316
slow motor nerve cond. meas. by blocking technique, computer simulation 78—36027
soleus muscle, rat, electrogenic Na^+-K^+ transport obs. 80—21456
somatosensory pathways, assessment of central conduction 80—97949
somatosensory system afferent signals, modulatory effect of prior input 77—90758
spark discharges from body obs., nature and incendiary behaviour 80—72406
spastic patients H-reflexes, factorial anal. of specific electrophysiological parameters 80—72148
spinach chloroplasts, laser photoinduced changes in high freq. dielectric constant 80—85449
spinal cord, electro stimulation for demyelinating and degenerative diseases 79—79621
spinal cord conduction velocity, indirect estimation in intact man 77—25616
spinal cord electrical stimulation, 2D finite element anal. 80—98054
spinal cord seizures elicited by high pressures of He 80—12071
spinal cord to axilla, F-wave conduction vel. 80—97894
spinal motoneurones refractoriness accumulation and secondary range firing model 77—1985
spinal neurones, mammalian, D-α-aminoadipate as selective antagonist. of amino acid-induced and synaptic excitation 78—20171
spruce budworm visible glow as UFO explanation 79—16361
squid giant axon, response of delayed K^+ channels to time-dependent clamping functions 79—39382
stapedial reflex thresholds with and without anxiety, fluent and disfluent speakers 79—96584
static charge sensitive bed, method for recording body movements during sleep 80—3840
stereodynamic interferential current, new electrotherapeutic technique 80—85458
stereodynamic interferential current therapy, fundamentals and initial results 80—85459
stimulation of organs and tissues in clinical medicine 78—35977
stimulator for electrophysiological expts. 77—21663
stimulus artifact suppression, sample and hold amplifier system 78—77163
Stomotoca atra electrical responses induced by extract of Aequorea aequorea 77—64064
streaming potential measurements of biosurfaces 77—2074
stretch receptor array reflex inhibition enhanced contrast 77—2016
stretch receptor neuron excitation and inhibition summation, crayfish 77—2015
striate neurons in area 17 of Siamese cats, response props. 80—12116
striate visual cortex, spatial freq. rows 77—32888
student laboratory apparatus, electronic, modules by Thornton 79—71206
stuttering, laryngeal muscular activity obs. 79—57675
subesophageal ganglion, cricket, descending interneurons, impulse patterns and ventilation 79—29519
suction capillary for holding moving cells during intracellular elec. recording 79—100793
superconductivity, possible mechanism for non-thermal effects of microwaves 77—2022
suspensions of ellipsoidal particles covered with shell, dielec. behaviour, rel. to biological cells 80—51057
sympathetic ganglia stimulated in vitro, effect of temp. on coated vesicle form. in presynaptic terminals, cat 80—85380
sympathetic ganglion cell in bullfrog, oscill. of $[Ca^{2+}]_i$-linked K^+ conductance 80—35867
sympathetic preganglionic neurons, raphe inhibition 79—92211
synapse formation between parasympathetic neurones deprived of preganglionic innervation, frog heart 77—77888
synaptic active zone functional unity, evidence from quantum and amplitude distribs. 78—3468
synaptic and ephaptic transmission, quantum mech. tunnelling model 77—52772
synaptic conductance changes, nonlinear effects 79—2045
synaptic conductivity effect on conditions of spike appearance 79—79507
synaptic facilitation and behavioural sensitisation in Aplysia, role of serotonin and cyclic AMP 77—36913
synaptic membrane, acetylcholine-activated, interaction of fluoresc. probe 77—90762
synaptic proteins after electroconvulsive stimulation, rat brain obs. 80—56011
synaptic transmission modulation and information processing model 77—29142
synaptic transmitter release, modulation by repetitive postsynaptic action pots. 77—4996
synaptic vescles and synaptosomal membranes, electrokinetic props. 80—67055
synaptosomal preparation, depolarisation-induced ATP release, direct detect. 77—48779
syncytium, passive three-dimens. and anisotropic, modelled as continuous medium 77—16898
synthetic voltage-dependent cation-selective transmembrane channel characterisation 78—77009
tachycardia suppression by programmed premature stimulation 77—81650
tenuissimus muscle, cat dynamic properties 80—8041
termite communication by biofields 77—44622
testosteron, dielectric props. under UV excitation 80—6912
thalamocortical non-specific system, auto-oscillatory processes 77—70443
thalamus, cat, stimulus induced and seizure related changes in extracellular K conc. 80—35870

bioelectric phenomena continued
thoracic electrical impedance sensitivity to blood volume changes 79—34543
thymocytes, negative surface charge reduction and thymic phagocytosis after X-irrad. 80—81663
tissue dielectric loss and permittivity spectrometer 79—57743
tissue equivalent bolus, 1 to 10 GHz electrical prop. characterisation 80—3763
tissue impedance meas. by phase-sensitive voltage and current detection 78—53602
tissue LF dielectric dispersion calc. and meas. *(Russian)* 80—21512
tissues, excitable, dipole flip-flop theory for excitation and conduction 80—101153
tonoplast ionic channels in charophyte algae cell, role of Ca ions in excitation 77—81481
trabecula membrane of frog auricle, electrophysiological characts. from ionic currents on pot. clamping 78—24049
trabeculae of frog atrium, Ca^{2+} incoming current obs. 79—79497
tracheal ephithelium, effect of Ca on ion transport and elec. props. 79—34527
tracheal mucosa, canine, interaction between Na^{2+} and Cl^- transport 79—88060
transducer noise in locust photoreceptor, intracellular responses 79—34560
transepithelial current-voltage relationships of toad urinary bladder and colon 79—92195
transepithelial electrical parameters in midgut of Lepidoptera larvae 78—20154
transmission problem in restoration of electrical activity to brain *(French)* 80—45876
transmitter release statistics, applicability of binomial distrib. 77—70450
transthoracic impedance curve processing, patient-computer interface 79—34686
tumour cell chromosomes, effect of electrostatic fields 79—62212
two-tone suppression in cat auditory nerve, rate-intensity and temporal anal. 78—61194
ungulate cardiac electrical activity peculiarities and evaluation methods 79—39394
ureteral elec. activity in unrestrained dogs, telemetric study 77—86664
urethral closing muscle functional electrical stimulation effects 77—60286
vaginal impedance meas., cattle, proposed instrumentation for optimum insemination time determ. 80—36210
vagus nerve cortical projection area, discharge pattern of neuronal units during hypoxia 77—25407
ventricular arrhythmias and depolariation effect of simultaneous biventricular pacing 77—81642
ventricular excitation, digital simulation, computer model evaluation 78—85302
ventricular fibrillation for AC shocks at 50-60 Hz, threshold considerations 80—51065
ventricular muscle excitation threshold current rel. to electrode area, volume effect 77—81670
ventricular myocardial function anal., computer-controlled stimulator 77—60267
ventricular Purkinje fibre, electrophysiological and histological props. 79—39396
Vespa orientalis, photoelec. props. of 'yellow strips' on cuticle, math. model 80—104638
visceral function voluntary control, electrophysiological concept 78—35827
vision, associative learning model, voltage-dependent Ca^{2+} and K^+ conductances 80—72166
vision, pattern recognition functional mechanisms in humans 80—81609
vision with moving eyes, microelectrode studies of single neurons *(German)* 78—53397
visual cell, proposed role of cyclic GMP 78—64997
visual cortex afferent geometry and neuronal trigger features generation, primates 78—35842
visual cortex receptive field spatial freq. characts. rel. to stimulus speed, cat 78—20174
visual cortex simple cells, spatial resolution and nonlinearities, cat 77—9187
visual discrimination between small objects and large textured backgrounds 78—11652
visual flicker sensitivity in primates, psychophysics and electrophysiology 77—29150
visual function in man, electrophysiological techniques, review 78—35843
visual non-spiking interneurone, spike response 78—11645
visual prosthesis design, human factors and electrophysiological considerations 78—53583
visual stimulator, computer-controlled 78—69230
visual system, signal processing in brain *(German)* 78—48792
visual system neuron response to light stimulus, computer monitored method 77—86725
visual thalamus, mammalian, neuronal organisation 78—27948
visual Wulst, barn owl, neurons selective for orientation and binocular disparity 77—1996
visual Wulst, owl, effect of monocular deprivation on binocular neurones 77—16929
vocal fundamental frequency measurement, comparison of contact microphone and electroglottograph 80—109056
voltage clamp of multicellular preps. 77—40955
wheat, pyroelectric props. 77—12322
white noise analysis, coherence improvement by use of repeated random sequence generator 80—36203
wrist actigraphic measures of sleep and rhythms 79—16315
yeast cells, singular, dielec. props. 78—88699
C-fibre microelectrodes, neurophysiology appl. 80—67314
Ca^{2+} conductance of acetylcholine-induced endplate channels 79—70546
Ca^{2+} current in Paramecium, inactivation of Ca channel 79—79488
Ca^{2+} effect on rat cell electrophoretic mobility after X-irrad. 79—92293
Ca^{2+} voltage-depend. facilitated entry into voltage-clamped aequorin injected molluscan neurons 77—90763
Ca-Na channel of cell, reconstruction in lipid bilayer 77—25404
Cl^- active transport inhibition by piretanide, in teleost intestine cell 78—64967
H-bonded model systems, intermolecular charge transfer, biological implications 80—3572
H^+-K^+ exchange and cell enlargement in maize coleoptile segments treated with auxin and fusicoccin 77—86469

bioelectric phenomena continued
K channel ionic interactions, squid giant axon 78—3458
K current components in node of Ranvier membrane frog Rana ridibunda 78—31800
K currents induced by acetylcholine in Aplysia neurones, slow relax. 78—80865
K ion noise currents and inactivation in voltage-clamped node of Ranvier 77—16924
K^+ channels of myelinated nerve, conditioning hyperpolarisation-induced delays 79—88066
K^+ transport of squid axon membrane, internal pH effects 79—62221
K-like channel passage of ions, physical model 77—56356
Na channel, fully coupled excited state model, conductance in volt. clamped case 78—85297
Na channel, graph of states 77—25383
Na channel density in myelinated nerve fibres and nature of axonal membrane 77—52777
Na channel fluctuations, phys. nature, microscopic model 80—35869
Na channels in nerve, evidence for two conductance states 78—11634
Na permeability inactivation in squid giant nerve fibres, review of exptl. work 78—73154
Na pump, electrogenesis in model of boundary transfer 77—25401
Na^+ activity of epithelial cells, liquid-ion exchanger microelectrode estimates, resistive artifacts 80—89909
Na-like channel passage of ions, physical model 77—56355
Na-specific membrane channels of frog skin, pore mechanism, current fluctuation obs. 77—36883

bioelectric potentials
see also contact potential; electrocardiography; electroencephalography
40 Hz activity in sigmoid gyrus, nucleus accumbens and amygdala, cross correl. anal. 80—76730
above-knee prosthesis, myoelectric control system development 78—53575
Achilles tendon reflex potentials, shape of T- and H-pots. 77—86480
acoustic frequency following responses in man, identification and separation 77—48810
acoustically evoked potential, age depend. 80—12163
acoustically evoked potentials in EEG, meas. by adaptive matched filters *(German)* 78—88755
action potential clamp to probe effectiveness of space clamp in axons 78—40441
action potential propagation, effects of cellular geometry on current flow 80—94196
action potential sources and their volume conductor fields 77—44640
action potentials from cultured neurons, recording by extracellular microcircuit electrodes 80—72382
action potentials from two different sources, distinction using dual channel audio monitor 78—61293
action potentials in single axons, effects of hyperbaric air and hydrostatic press. 80—56007
afferent nerves from muscle spindles, signal interpretation method 80—101188
afterpotentials influence on shape and magnitude of extracellular pots. 80—3625
airway transepithelial elec. pot. in vivo, species and regional diffs. 80—98208
alga intracellular potential, effect of ionic composition of external medium 78—20157
alpha frequency rel. to head size, implications for brain wave model 78—69035
alpha wave amplitude and frequency control, feedback learning system *(Japanese)* 77—44626
amacrine cells in Necturus retina, independ. γ-aminobutyric acid- and glycine-releasing neurons 78—35848
amino acid taste and smell, electrophysiological distinctions in catfish 77—44694
amplifier system for voltage clamping, used for tracing membrane potentials *(German)* 78—61285
amplifier-electrode hybrid module for surface EMG pots. meas. 80—41294
anisometropia, cortical evoked potentials, electrophysiological correlate of perceptual suppression 79—53105
antennal flagellum mechanosensory hair response, lobster 78—27974
anterior pituitary cell action pots., stimulation by thyrotropin-releasing hormone 78—48771
anterior semicircular canal units of anaesthetised pigeon, point process anal. 78—24079
arrhythmia detection by RR-interval comparison *(Bulgarian)* 78—15919
arteries, small, isolated, perfused, method for simultaneous elec. and mech. recording 80—101300
articular cartilage, electromechanical props. during compression and stress relaxation 78—92667
artifact-free electrodes for recording biopotentials in strong EM fields 78—40452
artificial membranes, excitable and ion-selective, review of axon and bilayer membrane props. 77—86451
artificial membranes, excitable and ion-selective, review of non-bilayer lipidic membrane props. 77—86452
atrial muscle, cyclic GMP rel. to negative isotropic effect of acetylcholine 77—48781
audition, compound PST histogram rel. to neural activity in cochlear 80—94148
audition, freq. following pot., appl. of least-square-fit technique 80—94149
audition, frequency following response and brainstem evoked response 80—94232
auditory, neuron receptive fields, owl 78—44512
auditory 80—94236
auditory averaged EEG response, stimulus freq. and intensity rel. to middle components 77—52804
auditory averaged electroencephalic response to tone pips in normal-hearing and hearing-impaired subjects 78—65049
auditory brain stem potentials, monkey, mapping following monaural clicks 79—16211
auditory click evoked compound action pots., guinea pig obs. 80—94231
auditory cortex unit response to synthesized formants, cat 80—67098
auditory electrophysiology, spectral analysis of cochlear and brain stem evoked potentials 80—16957
auditory emitted potentials and temporal uncertainty 79—34575
auditory event related potentials due to single stimuli, recognition by discriminant functions 77—9305

bioelectric potentials continued
auditory evoked brainstem response, age and sex diffs. 80—94234
auditory evoked cortical potential online detector 78—31952
auditory evoked potential, as probe of hemispheric differences in cognitive processing 78—15847
auditory evoked potential data acquisition, dual-processor system 79—79712
auditory evoked potential development in early childhood, longit. study 78—77061
auditory evoked potentials, averaged, effects of active attention switching between ears 77—40680
auditory evoked potentials, averaging and FM 79—34574
auditory evoked potentials, dependence of peripheral auditory adaptation on recording site 80—81613
auditory evoked potentials, effectiveness of earphone shielding for artifact control 79—57790
auditory evoked potentials, simultaneous recording of brain stem and freq.-following responses to LF tone 78—11665
auditory evoked potentials and sonomotor responses, evaluation of components and recording techniques 78—3498
auditory evoked potentials in human brainstem, effect of stimulus parameters 77—12935
auditory evoked potentials in normal human subjects, age-related vars. 78—77063
auditory evoked pots., differential changes, mouse obs. 79—100624
auditory evoked pots., technique for separating endogenous from exogenous pots. 79—100794
auditory evoked pots. with pseudorandom noise excitation, spectral anal. 79—83795
auditory evoked response, effects of signal rise time and frequency 79—20552
auditory evoked response, hemispheric differences 77—90801
auditory evoked response, primary inhibited elements, review 80—94235
auditory evoked response, relationship of latency and amplitude with sound intensity 79—20551
auditory evoked response correlate of symbol and significate 79—25000
auditory evoked response due to 3 GHz microwave pulses, mammals 78—53444
auditory evoked response research on animals, exptl. design 77—78068
auditory evoked response system for dogs, in dental instrument noise studies 77—29226
auditory evoked response with homophasic and antiphasic signal and noise, masking level difference quantification 80—41045
auditory evoked responses, computer driven bipolar stimulator 78—57011
auditory evoked sustained potentials, nature of response 79—34572
auditory evoked sustained potentials, stimulus relationships 79—34573
auditory frequency following response sources in man 77—70479
auditory middle component AERs from neonates to low-level tonal stimuli 80—94220
auditory nerve, two-tone suppression, stimulus freq. effect, physiological and psychophysical obs. 78—85317
auditory nerve fibre, insect, latency shift, neuronal time cue of sound direction 79—48274
auditory nerve fibre freq. selectivity in response to broadband noise 77—77906
auditory nerve oscillating summed action potential, spike pattern and synchronisation, insect 78—40181
auditory neural network modelling by computer simulation, spatial firing patterns 79—74686
auditory system evoked potential, human, automated recording and analysing complex 79—57780
auditory time shift evoked potentials, generation technique 79—16354
autoregressive model order selection applied to physiological signals 80—104780
average evoked potentials, a posteriori Wiener filtering theory and practice 78—96038
average evoked potentials, localising technique in aphasia diagnosis appl. 78—31950
average visual evoked response estimation, predictor-subtractor-restorer filter 78—65143
axon, giant squid, current fluctuations obs. 79—24973
axon, motor, reflexes following intranervous regeneration 79—34541
axon, squid, Na channel gates, interactions with quaternary lidocaine and tetrodotoxin 79—83745
axon, squid giant, dispersive structure *(Japanese)* 78—61158
axon, squid giant, exponentiated exponential model g Na^+ and K^+ cond. changes 78—44493
axon, squid giant, poisoned with quaternary strychnine, block of Na conductnace and gating current 79—83746
axon cockroach giant, action potential separation by multiunit analysis 79—83760
axon diameter changes concurrent with action pot., crayfish, laser interferometer meas. 77—64029
axon K^+ channel response to time-dependent clamping functions, squid 79—62229
axon membrane, squid, null space in Hodgkin-Huxley eqns., critical test 79—83747
axon membrane white noise, stimulation, strength-freq. relationship, squid 78—3466
axons, crit. slowing down near transition region from resting to time-ordered states, squid giant axon 78—44486
B-DNA helix, guanine-cytosine base pair, electrostatic pot. 80—8003
bacteria motility, proton pump as molecular engine 78—40130
bacterial chemotaxis, cyanine fluorescent dye membrane probe effects on cell props. 78—35815
bacterial chemotaxis in Escherichia coli, membrane pot. changes 77—44695
bacterial flagella, protonmotive driving force 78—48774
bacterial membrane, light-induced generation of elec. pot. difference 78—28001
bacterial sensory electrophysiology, motility depend. on membrane pot. and chemotaxis 78—53373
bacteriorhodopsin membrane preps. associated with lipid-water interface, form. of elec. pot. diff. 80—81551
barnacle photoreceptors, initiation of light adaption, intracellular recordings 79—20542
biofeedback control of skin potential level 80—21572
biosignal processing, spurious signal detection method *(German)* 78—92722
bladder smooth muscle impulse propag., math. anal. *(Japanese)* 78—53359

bioelectric potentials continued
blastocyst, rabbit, amiloride-sensitive rheogenic Na$^+$ transport 78-15812
blood vessel walls, active and passive transport of Na$^+$ and K$^+$ 77-44618
body surface and epicardial activity, computer-aided meas. system 79-39551
body surface ECG potential mapping, data acquisition system 79-29653
body surface mapping of cardiac field, computer-aided pattern recognition 79-39553
body surface potential distribution map recording and processing 78-57116
body surface potential image recording and processing methods 79-20704
body surface potential maps, high speed semicond. disc memory 77-78014
bone, strain-related potentials, freq. depend., effect of meas. system parameters 80-16991
bone, stress generated potentials at osteon level 78-31837
bone, stress generated potentials rel. to collagen piezoelectricity 77-32932
bone, stress generated pots., linear piezoelec. model 80-3688
bone functional adaptation model and thermodynamic consideration *(Japanese)* 78-7316
bone tissue regeneration process, investigation of elec. characts. 80-51313
brachial biceps, human, extracellular action potential radial decline 79-16192
brain, EEG correlates of higher cortical functions 79-100591
brain, unit and slow-wave field activity, telemetry techniques 77-60310
brain electrical sources, human, 3D localisation, quantitative evaluation 78-92613
brain evoked potentials, processing, computer techniques 78-92728
brain evoked potentials, rel. to perception mechanisms 78-11627
brain evoked potentials, visual and auditory, comparison of signal components 78-44513
brain potential comparison, average evoked, on spectral and coherency function basis 77-2072
brain potentials, synchronous and asynchronous, space-time organisation formal anal. *(Russian)* 77-52767
brain potentials, synchronous and asynchronous, struct. of sets *(Russian)* 77-36904
brain potentials, synchronous and asynchronous, vol. model *(Russian)* 77-40652
brain reflexes meas., using Sredetz device *(Bulgarian)* 80-30909
brain rhythmic activity generation models *(Dutch)* 78-73150
brain stem evoked responses, acoustically depend. wave V latencies 78-85318
brain unit and slow-wave field activity, telemetry with FM pulse subcarrier 77-25625
brain waves, limit cycle model, Frohlich's model 77-73520
brain-stem auditory evoked response in young and old adults, normal variability 78-77064
brainstem auditory evoked pot., human, sources 80-108919
brainstem auditory evoked potentials, human, freq. comp. 80-16956
brainstem auditory on- and off-potentials in humans 80-16954
brainstem auditory on- and off-pots., latency determ. 80-94233
brainstem-evoked response audiometry, combination with otometry 80-85417
bulbar evoked potentials, olfactory bulb and cortex, spatial props. of EEG event 79-16223
capacitance-dynamic electrode for bioelectric potentials 79-57782
captured nerve fibre multiple single-unit recording by tubular electrode array 77-60321
cardiac biopotential distribution laws rel. to functional state 78-65142
cardiac conduction and propag., equiv. cct. 78-31791
cardiac dipole apparent orientation, vol. conductor effects 78-28108
cardiac dipole moment variation with body size, double-layer model 77-56358
cardiac electric field probabilistic model 79-39387
cardiac electrical activity, mag. detect. *(Japanese)* 77-81515
cardiac electromechanical field model and computation, inverse problems 79-39400
cardiac injury potentials, inadequacy of solid angle formulation 77-44633
cardiac intracellular transmembrane action pots., automated anal. 79-70729
cardiac inverse generator, dipole crosstalk 78-92615
cardiac potential distribution, human body surface, digital simulation 77-29221
cardiac potential function represented by chains of maps, analysis 77-37062
cardiac rhythm disturbances, Markov process model *(German)* 79-2019
cardioelectrical field, human, intraindividual variability obs. 79-39404
cat brain subdural structure resonance phenomena 77-16923
cell action pot., birefringence change of Nitellopsis obtusa internodal cell 79-100585
cell electric potentials, ECG, EEG and EMG differences in signal types, propag. and meas. methods 80-40995
cell external elec. fields, Fourier transform anal. 79-62223
cell membrane potential changes on X-irradiation 79-39369
cell membrane potential levels in Acetabularia 77-70427
cell voltage measurement using voltage sensitive dyes 79-57833
cellular resting pot., eqns. according to surface adsorption theory 80-35861
cellular testing potential, membrane pot. rel. to ionic diffusion *(French)* 80-94184
cercal system neurones, cricket, const. representation of sound source position 77-70482
cerebral blindness recovery, evoked pot. and psychophys. meas. 77-40668
cerebral cortex evoked pots. in cat, as electrode safety model 78-31797
cerebral potential impulse response, EEG method *(Japanese)* 78-3661
cerebral potentials preceding unilateral and simultaneous bilateral finger movements 80-26217
charged membrane osmotic transport, generalised flux eqns. 78-24050
checkerboard-evoked multichannel pot. fields, reference-free components identification 80-108887
chemical synapse, feedback mechanism model through elec. current 78-96043
chromatophores of R. rubrum, induction of elec. pot. diff. by laser flash 80-81560

bioelectric potentials continued
ciliary motor responses, intracellularly recorded receptor currents 79-11916
click stimuli, psychophysical magnitude estimates rel. to electrophysiological responses in man 78-31817
click-evoked brainstem potentials in man using high pass noise masking 78-61193
click-evoked electric brainstem responses, use in audiological diagnosis 80-104689
clinical electrophysiolgy laboratory automatic control system 78-57110
cochlea action potential responses to tone bursts, human and guinea pig 77-12930
cochlea hair cell tuning props. 77-64054
cochlea of Sphenodon punctatus, ear anatomy and hearing 77-40681
cochlear compound action pots., tuning curves and delay times 80-94230
cochlear microphonic and sound transmission characts., gerbil and guinea pig 77-32909
cochlear microphonic potentials rel. to cochlear injuries 80-94229
cochlear microphonic responses, far-field, to continuous pure tones, cat scalp recordings 80-97924
cochlear microphonics, middle ear transmission in cats with tympanic membrane perforations 77-32908
cochlear microphonics induced by 918 and 2450 MHz pulsed microwaves, cat and guinea pig 78-40258
cochlear nucleus, combination tones role in phase changes perception 77-36948
cochlear potential, rel. to caecilian ear sensitivity 77-36959
cochlear potentials, effect of ethylendiaminetetraacetate in the scala media 80-16952
cochlear summating potentials, effects of crossed olivocochlear bundle stimulation 77-52800
colon EMG, use of autoregressive-modelling techniques for anal. 80-101146
colon signal multistage decimation and filtering, multiple-input algorithmic processing 77-78069
colour vision physiological measurement facility, monkey detected responses *(Japanese)* 78-92752
comparator with auto reference level, used in physiological research 78-31992
composite bioelectric potential analysis, online hybrid system 77-9313
compound action potentials, volume conductor study, forward problem 79-88067
compound PST histograms, deconvolution 80-94146
cone cell of tiger salamander, hardware model 78-44505
cone specific c-wave in turtle retina 78-69060
contingent negative variation and accuracy of time estimation. A study on cats 80-26216
contingent negative variations, rel. to distraction-arousal hypothesis 77-5002
contour map production for electrophysiology 80-72340
control signals and transducers for the control of upper extremities in plegic patients, computer controlled experiment *(Slovak)* 80-109061
controlled filter for smoothing 78-40357
convolution equation solution, problems arising, auditory appl. 80-94147
corneal-retinal, production of EEG α-rhythm by eye tremour modulation 79-34535
coronary artery disease diagnosis, exercise ECG, VCG and body surface mapping 79-44046
cortex, human, no-stimulus, no-response, event-related pot., motosensory system obs. 80-108923
cortical auditory evoked responses under hyperbaric conditions 80-94237
cortical event-related potential waveform, effect of stimulus sequence 77-2011
cortical evoked response audiometry, portable programmable tape recorder 77-60279
cortical pattern evoked visual pots., estimation of rat eye refr. 77-70455
cortical response to callosal stimulation, model for determ. of safe and efficient stimulus parameters 80-3614
cortical slow negative waves following non-paired auditory and visual stimuli 80-3650
cortical spreading depression, math. model 78-80857
cortical visual evoked potential, normal humans, bibliography of research 79-5278
cortical visual evoked potential, normal humans, main chapters of research 79-20537
crayfish stretch receptor repetitive firing behaviour nonlinear systems anal. 78-80853
cricothyroid muscles of bat, Myotis lucifugus, response to FM sounds 77-21540
curve crossing problem for Gaussian stochastic processes, neural modelling appl. 78-85299
decision making, split-second, electrophysiological signs, auditory stimuli 80-89771
demyelinated nerve fibre conduction failure, effect of prolonging action pot. 78-73152
dendritic membranes, active vs. passive effects on simulated neuron transfer properties 79-24976
digestive tract electrical rhythms simulation 78-64970
digit-wrist sensory compound nerve action pot. obs. in patients with focal nerve injuries 80-3655
digital EMG processor and three-state myoelectric control design 79-53283
dipole sources in conducting tissues 78-64915
dipteran giant visual interneurone response props., rel. to optomotor control 78-27940
duodenal slow waves, human, anal. and modelling. 80-72146
Dutch development of medical physics *(Dutch)* 80-3877
dye indicators of membrane pot., review 80-21594
ear reflex threshold shift in chinchillas following a prolonged exposure to noise 79-100631
ECG, effects of filtering His-Purkinje system pots. 79-48355
ECG preauricular O wave, embryonic origin 79-39390
ECG solid angle interpretation, myocardial fibre orientation implications 79-39397
ECG surface electrode potential recording apparatus 79-83987
ECG surface potential recording electrodes 79-100779
ECG U-wave correlation with repolarisation of Purkinje system 78-28122
EEG, cat, computed unit-EEG correls. and laminar profiles of spindle waves 78-11625

bioelectric potentials continued
EEG, pathological delta waves, cortical electromicrophysiology, cat 78—11626
EEG, pattern-evoked potentials and nerve conduction vel. in family with adrenoleucodystrophy 80—45875
EEG, real-time detection of brain events, expt. 77—44793
EEG alpha rhythm blocking, absence in visuobehavioural deprivation 78—27944
EEG and evoked potentials, intracerebral current contribs. 78—92611
EEG and volume conduction in brain, influence of elec. spread on linear relationship of activity 77—90933
EEG bispectra computation computer program, in FORTRAN 78—92727
EEG data during sleep stages, stationarity and normality 78—92610
EEG in dominant hemisphere, changes during memorising and reasoning 77—70444
EEG patterns optimal display, relative merits of different montages 77—78004
EEG potential in model of thin cerebral membranes, tangentially orientated dipoles 78—15818
EEG potential in model of thin cerebral meninges, radial dipoles and double layers 77—86476
EEG potential model with thin meninges, multilayer flat cable model 77—36903
EEG potential source in model with thin meninges 77—56359
EEG signal stationarity anal., human 78—7461
eel electroplaque, temp. dependence of four ionic processes of spike electrogenesis 77—36899
egg cell membrane elec. props 80—21455
electro oculography, computerised diagnostic system 80—21566
electro-cochleographic methods in the diagnosis of hearing defects *(Dutch)* 80—3855
electro-oculogram, interocular comparison of eye movements while reading, normal and amblyopic subjects 78—53393
electro-oculogram, rapid eye movement automatic detect. system and normative data 79—74771
electro-oculogram light induced amplification effect, time const. 78—15827
electro-oculogram light-induced amplification, quantification in clinical practice 77—90771
electro-oculographic activity, computerised meas. during sleep 79—74781
electro-oculographic amplification induced by macular light adaptation in various retinal diseases 77—90773
electro-oculographic ratio, rod and cone contribution 79—11925
electro-oculographic response, binocular synchronism monitoring, prolonged monolateral occlusion 79—20543
electro-oculographic response, comparison between binocular and monocular recordings 77—48791
electro-oculographic response, diagnostic tool for principal ocular disorders *(Italian)* 79—5391
electro-oculographic response, interocular comparison while reading printed material 79—20536
electro-oculographic response, recording and interpretation review *(Italian)* 78—73156
electro-oculographic response interocular comparison, unpredictability of residual long-term effects 78—53392
electro-oculography, on-line system for quantitative study of ocular kinetics 79—34699
electrocardiology 4th International Congress, Balatonfured, Hungary (Sept. 1977) 79—39384
electrocochleography, tone-burst, interpretation of action pot. off-effect 77—56386
electrocorticogram, automated anal. of sleep in rat 77—90969
electrocutaneous tracking, evaluation of sensory feedback codes 79—25004
electrode design, ventricular fibrillation in animals appl. *(German)* 78—3461
electrode motion artifact, minimisation by skin abrasion 77—40802
electrogenesis, rat liver, Ca balance 79—57608
electromyograph signal characteristics, various muscle tension levels and during fatigue 79—34537
electromyographic activity during brief isometric contractions, model 77—16922
electromyographic activity of jaw muscle and mandible static loading 79—43951
electromyographic analyser and recorder 79—57785
electromyographic biofeedback, facial palsy treatment 79—34701
electromyographic recordings, perioral reflex amplitude variation 79—20558
electromyographic shimmer in normal human muscles 79—34538
electromyographs of limb tremor, normal and alcoholic withdrawal 79—29544
electromyography, clinical, computer anal. 78—80985
electromyography, diagnostic applications 77—44784
electromyography, ulna nerve, slowing of motor conduction vel. in sulcus 79—34548
electromyography and nerve conduction, digital memory recorder 79—43999
electromyography during arm swing in human locomotion, mathematical model 79—39434
electronic feature extractor for action potential parameters 79—84047
electronystagmography signal processing *(French)* 77—37078
electronystagmography system for vestibular testing, microprocessor-based 4-channel 80—41293
electrooculargram recording, single channel method for vertical and lateral eye movements 79—16205
electrooculogram, eye movements of African chameleons, spontaneous saccade timing 78—69053
electrooculographic evaluation of eye movements in target tracking 80—109057
electrophrenic respirator, implantable, Hg battery powered, design, features *(Japanese)* 78—3675
electrophysiological average transients computer, 200 point 80—12284
electrophysiological filtered click responses, short-latency, recorded from vertex and external auditory meatus 79—53156
electrophysiological instrument calibrator 77—48970
electrophysiological recording from behaving animals, 10-channel commutator 79—84050
electrophysiological signal degradation reduction, patient virtual earth and electrical interference monitor 79—57800
electroretinogram, annelid worm vision 77—86496
electroretinogram, automatic meas. of b-wave amplitude and peak latency *(German)* 78—80993
electroretinogram, DC registered, off-responses in humans 77—44647
electroretinogram, E- and b-wave analogue model, retinal expression of inductive reactance 77—48797
electroretinogram, effects of light adaptation, frog 77—44650
electroretinogram, extracellular recordings of cephalopod retina 79—62245
electroretinogram, fly visual receptor adaptation 77—29149
electroretinogram, frog, rod and cone generation of wavelets 78—48799
electroretinogram, human, DC registered, influence of ethyl alcohol 79—2052
electroretinogram, human, nonlinearities reflected by Wiener kernels 79—34556
electroretinogram, human, white noise analysis 79—1995
electroretinogram, increment spectral sensitivities of primate late receptor pot. and b-wave 77—70461
electroretinogram, mechanisms of visual latency in Bufo marinus 79—48255
electroretinogram, photopic, freq. response characts. meas. with synchronous detect. 77—48796
electroretinogram, photoreceptor survival in light-damaged eye of albino rat 77—36927
electroretinogram, primate cone sensitivity to flicker during light and dark adaptation 79—43900
electroretinogram, retinal degeneration in RCS rats raised under ambient light levels 79—43887
electroretinogram, spectral sensitivity and Purkinje shift in lemon shark retina 77—70469
electroretinogram b-wave, transient tritanopia 79—100614
electroretinogram e-wave, frog, rel. to ganglion cell activity and rod responses 79—48254
electroretinogram of albinos 79—53099
electroretinogram P III component model, luminance variations 77—81495
electroretinogram recordings from frogs during rapid dark adaption 79—62253
electroretinogram signals computer anal. 79—8559
electroretinograms of epigeous and cave-dwelling harvest spiders *(French)* 79—53093
electroretinographic observations of insect compound eye 79—53100
electroretinographic response rel. to vars. of visual performance during day 78—77051
electroretinographic sensitivity and rhodopsin content in light-damaged rat retina 77—64033
electroretinographic species difference within the leopard frog complex 79 62254
electroretinography, clinical, use of Mingograph ink-jet recorder 78—92731
electroretinography improved electrode, design and standardisation 79—92401
electrospinogram, human, recorded from intrathecal, epidural and cutaneous levels 79—16182
electrostatic isopotential maps for large biomolecules, STO transferable bond calc. 80—3571
electroureterogram telemetric registration using implantable Nikrothal LX electrode 77—86668
electroureterograph and dynamoureterograph 80—56235
EMG, abdominal, for uterus activity recording *(German)* 78—92712
EMG, analysis of signals, myogram integration, amplitude value determ. 80—40997
EMG, ankle joint reflex response to sinusoidal forces 77—21513
EMG, automated anal. of sleep in rat 77—90969
EMG, computerised, software support in clinical dentistry 79—74780
EMG, correl. with voice tremor, as psychological stress evaluators 77—9214
EMG, cutaneous trunci muscle in spinal reflexes 80—3635
EMG, data for math. model of pelvic forces 77—52818
EMG, dynamic arm movements data, acquisition and anal. 80—36179
EMG, EEG and unit activity in lateral geniculate, arousal and sleep effect in cats 80—40991
EMG, electrode-to-skin contact area and amplifier input impedance selection *(German)* 79—88205
EMG, estimation of normalised gait pattern using computer anal. 77—40819
EMG, evoked, evaluation of Wiener filter 80—3747
EMG, expiratory duration and abdominal muscle responses to elastic and resistive loading 79—100653
EMG, factors affecting interpretation, stochastic process model 77—44825
EMG, fast-recovery electrode amplifier 79—70654
EMG, fatigue characts. of human gastrocnemius and soleus muscles 78—20169
EMG, filter bank analyser for automatic anal. 80—98162
EMG, freq. response of biceps brachii in isometric contraction to fatigue 80—3621
EMG, freq. sweep anal. to meas. neuromuscular junction continuity 79—96686
EMG, functional roles of vastus and calf muscles in humans, synchronised EMG, cinematographic study 77—81488
EMG, hand position and forces during manual work, documentation method 79—74803
EMG, human locomotion motor coordination and neuromuscular activities study 77—44635
EMG, human motor unit dynamics props., Hoffmann-reflex and M responses 78—7331
EMG, human red and pale skeletal muscles, force rel. to fatigability 80—8076
EMG, human skeletal muscle conduction vel. estimation in situ by surface electrodes 80—8196
EMG, in meas. of chest-wall compliance with biofeedback 77—52905
EMG, influence of visual input on monosynaptic reflex 77—60197
EMG, inspiratory diaphragmatic, spectral anal. 79—88071
EMG, instrumentation requirements 80—41301
EMG, integrated, rel. to angular vel. in horizontal elbow flexion 80—3620
EMG, interactive minicomputer system for anal. of twitch waveforms of human motor units *(Japanese)* 78—28103
EMG, miniature skin-mounted preamplifier for surface meas. 78—35990

bioelectric potentials continued
EMG, miniaturised FM-AM transmitter for sleep telemetry in rat 78—48947
EMG, multichannel data acquisition system for the survey of intercostal muscle activity 80—81790
EMG, multiplexing system for measuring physiological responses 80—56292
EMG, myographs design and technical requirements 80—40996
EMG, myophone appl. to functional rehabilitation *(Spanish)* 78—48924
EMG, needle, influence of skeletal muscle atrophy 80—3853
EMG, pattern recognition of multiple signals, appl. to description of human gait 77—44795
EMG, physiology and mathematics 79—74621
EMG, pulsed integrator for anal. 80—61719
EMG, quantitative, value of automatic anal. 80—8203
EMG, rectified surface, time constant in low pass filtering 80—67266
EMG, rel. to skeletal joint torques, for prosthesis control 77—48953
EMG, simultaneous recordings of parts of pectoralis major muscles during swimming 80—72147
EMG, single fibre, microcomputer-based jittermeter 80—46078
EMG, single fibre, selective gain control along oscilloscope sweep 77—44864
EMG, single motor unit action pots. identification by computerised anal. 80—72343
EMG, single pots., anal. by means of multivariate methods 80—98170
EMG, sleep telemetry in rat, automatic identification and recording of vigilance states 78—48948
EMG, slow motor nerve cond. meas. by blocking technique 78—36027
EMG, stimulated activity from close lying and remote muscles 79—79501
EMG, surface, digital simulation, spectral anal. 78—80863
EMG, surface, dT-dL anal. during muscle fatigue, left hand obs. 80—104576
EMG, surface, dT-dL anal. during muscle fatigue, right hand obs. 80—104575
EMG, surface, model for digital simulation 78—80862
EMG, surface, muscle fibre conduction vel., direct on-line estimation 79—100765
EMG, surface, system for meas., recording and digital anal. *(German)* 80—76848
EMG, surface integrated, rel. to isometric contraction force 79—74618
EMG, surface pots. rel. to force transients in muscle, simulation and expt. 77—44642
EMG, surface-recorded, stabilisation of isoelec. line using high-pass filter 78—31917
EMG, use in diagnosis by skeletal muscle tension development meas. 77—40880
EMG, vector, of motor units with short, inclined and curved muscle fibres 77—86689
EMG, weighted sum rel. to total torque, human triceps surae 78—20203
EMG activated spatial morse code general purpose communication device 80—30946
EMG activity as indicator of muscle fibre regeneration after transplantation 80—30701
EMG activity in extraocular muscles, visual display 77—40834
EMG amplifier, wideband isolated, cct. 78—57089
EMG analysis, normal values obtained by automated system 80—3845
EMG analysis of levator scapulae and rhomboideus major muscles in shoulder movements 80—3627
EMG analysis of soft tissue lesions affecting shoulder function 78—35828
EMG and temporal information during gait, clinical telemetry 78—80994
EMG assisted relaxation training with hyperkinetic children 80—21571
EMG biofeedback device 79—96706
EMG biofeedback in hemiplegic patient treatment, comparison of actual and simulated treatment 80—104806
EMG biofeedback in relaxation training 77—81636
EMG biofeedback training in low back pain treatment 80—21570
EMG changes during sustained voluntary isometric contracts. 80—3629
eMG comparison of quadriceps femoris activity during knee extension and straight leg raises 80—8038
EMG control enhancement using predictor feedback technology 77—48952
EMG curves peak detection algorithm 78—96107
EMG data synchronised with cine records by LED display device, rats appl. 77—81754
EMG detection by pasteless electrode 79—92413
EMG digital processor design and performance 79—96712
EMG electrode array for single muscle fibre activity measurement *(Swedish)* 78—24193
EMG electrodes, small-size, meas. of uptake area 79—74799
EMG envelope spectral anal., Parkinson's disease diagnosis and treatment appl. 79—5390
EMG F response, radicular injury evaluation 80—3852
EMG F-wave electrodiagnostic confirmation of upper trunk brachial plexus neuropathies 79—74779
EMG feedback and static stretching, effect on artifically induced muscle soreness 80—12069
EMG feedback in therapeutic aid for disabled children 78—36048
EMG feedback therapy after stroke, efficacy obs. 80—30927
EMG filtered signal in isometric muscle contraction, S/N ratio anal. *(German)* 77—81490
EMG frequency spectrum rel. to shape recognition 78—40207
EMG in alcoholism, nerve conduct. vel. and sensory pot. studies 80—3617
EMG in alcoholism, terminal latencies in superior gluteal, distal peroneal and tibial nerves 80—3618
EMG in moving finger muscle, pattern recognition by linear prediction 79—8555
EMG in quadriparetics and quadriplegics, evoked giant sensory nerve pots. 80—3653
EMG index for localised muscle fatigue 78—57093
EMG investigations of gait 80—8198
EMG investigations of gait in cerebral palsied children 80—72186
EMG jitter, single fibre electronic meas. device 77—40832
EMG jitter effect on single motor unit pots. 79—83960
EMG low freq. power spectra, motor units characts. determ. 80—3626
EMG motor command extraction by pulse counting method *(Japanese)* 78—53546
EMG of biceps brachii muscle, single motor unit action pot. model 78—53386

bioelectric potentials continued
EMG of digastric muscles rel. to mandible opening force 79—74619
EMG of genioglossus muscle, Japanese semivowel /j/ prod. 77—5013
EMG of genioglossus muscle, Japanese vowel prod. 77—5012
EMG of muscular exterior carpi radialis, form recognition by freq. spectrum 78—15939
EMG of temporal muscle in rhesus monkey, spectral anal. 78—69039
EMG of Vastus medialis, power spectral changes for graded isometric torques 80—3622
EMG of Vastus medialis for graded isometric torque tensions, power spectrum distrib. 78—44673
EMG operated electronic artificial-leg controller 78—7545
EMG operated prosthesis controller 77—48954
EMG parameter identification, use in prosthetic limb function discrimination performance 80—8220
EMG pattern of diaphragmatic fatigue 79—88069
EMG period-amplitude analysis, cat locomotion and jumping obs. 80—67057
EMG potential sensing electrodes, types, selection criteria 77—90953
EMG power spectra linking to recruitment and rate coding 80—3616
EMG power spectrum, contrib. of individual motor units 77—29129
EMG power spectrum analysis, in neuromotor speech disorders 77—29161
EMG processing for sleep research 80—67267
EMG quantitative analysis instrument 78—81041
EMG recording computer editing 78—80999
EMG recordings of muscular contract., estimations of active-state, linear systems muscle model 80—3623
EMG rel. to muscle force 78—40231
EMG results from a study of nerve-muscle disorders 77—40811
EMG shimmer in patients with neuropathy and neurogenic atrophy 80—72149
EMG signal generation, quantification using automata theory 77—29132
EMG signal nonstationary model 77—86481
EMG signal onset and termination establishment method 79—83761
EMG signal processing, use in multifunctional upper-extremity prosthesis control signal generation 80—8219
EMG signal processing rel. to human locomotion, optimality criterion 78—92612
EMG signal processor, sequential multistate 79—100763
EMG silent period and muscle mechanics in human soleus muscle 80—67060
EMG silent period before voluntary movement rel. to preparatory phase condition *(Japanese)* 79—74622
EMG silent period measurement, automated system 80—89883
EMG single motor unit potential parameter analysis 77—9290
EMG spectra, effect of motor-unit firing time statistics 78—31804
EMG spontaneous activity in paretic skeletal muscle, LF bizarre discharges 78—80864
EMG spontaneous activity mechanisms in motor neuron disease 78—20162
EMG studies of low back mobility and activity levels 80—41059
EMG studies of temporal firing sequences of antagonistic muscles 80—40984
EMG surface power density spectral bandwidth rel. to electrode parameters 79—29517
EMG technique for percutaneous lateral pterygoid muscle 80—3841
EMG/US transducer for biodynamic research, speech appl. 78—77164
EMGs, reliable derivation and relation to muscle tension 79—79499
endogenous and exogenous activity in molluscan neurone, identification by spike train anal. 80—89735
energy transformation, intracellular, phys. aspects 77—86462
EOG, electronically controlled light sequence bar for eye pursuit movement study *(German)* 80—36058
EOG, sleep research, computerised anal. 79—62377
EOG, three-electrode array, in communication interface for non-vocal physically handicapped 77—25603
EOG and CT obs. in neural disease 80—36070
epicardial activation sequence rel. to body surface maps, right bundle branch block induced in dogs 79—39402
epicardial and body surface pot. meas. in intact dog, transfer coeffs. calc. 78—92614
epicardial and body surface potential distributions related by geometric transfer coeffs. 77—21671
epicardial excitation pattern spherical double layer model, using human multipole data 78—27928
epicardial potential derivation from torso skin potential obs. 77—64148
epileptic seizure spatiotemporal patterns, neuronal network model 77—64019
epiphysis, frog, characts. of slow pots. 80—56029
epithelial cells of Hydra, mechanically dissociated, spontaneous and evoked pots. 77—21499
epithelial K active transport system of insect midgut, pump-mediated efflux 78—80846
ERG, adaptation-overlap model, response to laser stimuli 79—74650
ERG, effects of conducting media inhomogeneities 80—51078
ERG, foveal local, elicited with sinusoidal flicker, component anal. 79—74660
ERG, human, nonlinear kernels 80—61545
ERG, human corneal, frequency domain anal. 80—45888
ERG, oscillatory pots., analogue circuit model and frog obs. 80—89750
ERG, rabbit, dynamic light-dark adaptation 80—35887
ERG, suprafusion, theoretical retinal anal. 80—56020
ERG, surface-recorded, use to meas. eye position 80—26400
ERG, Wiener kernels and freq. response functions, human retina, obs. 80—45887
ERG and psychophysical obs. of cone spectral mechanisms 80—61565
ERG B-wave of ground squirrel, spectral components 80—51082
ERG critical flicker fusion freq., river lamprey 79—74663
ERG photostimulus calibration by standard photometer and photodiode 80—8222
ERG recording, computer assisted standardised quantitative method 80—109048
ERG studies on albino rats, mech. of formation of X-ray induced phosphenes 80—104675
erythrocyte suspension, laser-induced fluoresc. of intact human membrane cell 77—90733
event-related desynchronisation, graphical display and statistical evaluation 78—24192
evoked action potentials, muscular and sensory 79—34530
evoked frequency stabilisation in cat brain electrical activity 79—34533

bioelectric potentials continued
evoked potential analysis, on-line signal optimisation using minicomputer 77—5112
evoked potential and early studies of bioelectricity 80—101158
evoked potential averaging, cross correlation and latency-corrected averaging comparison 79—53268
evoked potential estimation, method for evaluation of Wiener filtering method 78—24190
evoked potential late components in man, effects of selective attention 77—70445
evoked potential multi-channel data acquisition system, microprocessor controlled 78—11750
evoked potential optimal filtering in sequential range *(German)* 78—85401
evoked potential recordings, cancellation of coherent line-freq. noise 80—98161
evoked potential scalp topography in auditory and visual go/nogo tasks 78—31818
evoked potentials, averaged, long-term changes after X-irrad., rabbit 78—11704
evoked potentials, single trial, S/N ratio and response variability 78—61159
evoked potentials, transient, in man, size and orientation specificity 78—69056
evoked potentials, visual and auditory, interlab. vs. intralab. and intersession vs. intrasession variability 77—70570
evoked potentials and EEG freq. in patients undergoing haemodialysis and kidney transplantation 78—61160
evoked potentials in same hand, normal subjects rel. to capral tunnel syndrome patients 79—48231
evoked response averaging for schistosome activity monitoring 79—34613
evoked response estimation 79—43841
evoked response recording, 7-electrode totally-implanted stimulus-monitor unit 78—31996
evoked responses, electrogenesis, models methodology and wavefront reconstruction 77—44627
evoked responses, statistical detect., evaluation of Woody's adaptive filter 77—81757
evoked responses, Wiener filtration vs. averaging 78—3689
evoked signals on nerve surface, rabbit, distinguishability 79—57623
evoked spinal cord and nerve root potentials in humans using a non-invasive recording technique 79—39377
EVOQ: a system configurable for automatic simulation and recording of mean evoked potentials on a minicomputer *(French)* 80—85507
excitable membrane analysis, computer calcs. 80—56004
excitation spread equation boundary conditions for undistorted impulse movement pattern 77—56365
excitatory-inhibitory visual system organisation evidence from oversaturation *(French)* 77—12922
external geniculate body, metric of space of description of images 80—30716
extracellular action potential recording, interference suppression 78—61294
extracellular potentials generated by curved fibres in a vol. conductor, modelling 80—97889
extraocular motor unit activity, electromyographic recording in man during fixation and saccades 79—16203
eye, of horseshoe crab, anal. of adapting bump model 78—73160
eye 79—83775
eye movement monitoring, signal detect. via phase-locked sampling in mag. search coil 79—25124
eye slow cell responses in insects, colour adaptation 78—64988
eyeblink response to startle evoking stimuli in humans, excitatory and inhibitory components 78—77050
ferrocytochrome c_3, anhydrous, ionisation pot., UV photoelectron spectrosc. obs. 80—85328
filters as selective electrodes for synthetic penetrating ions 80—104821
fine muscular control rehabilitation using ramp threshold feedback 79—83996
fixed charge membrane modules, pot. controlled transient gating mechanism, book contrib. 80—12067
flash evoked potentials following unilateral electroconvulsive therapy 80—97906
foveal vision central mechanisms, monkey 80—12108
frequency following potential, 500 Hz, kangaroo rat, evaluation with noise masking 80—108905
frequency-following potential components in man 78—77062
Frohlich brain wave model, limit cycle stability, enzyme-substrate reaction 78—44490
frontalis muscle spontaneous elec. activity as indicator of surgical patient relax. 78—44686
functional electrical stimulation control using volitional EMG signal 78—57128
ganglion cell recordings from pigeon retina 79—57655
ganglion cell response to far violet light, macaque 78—11656
gastro-duodenal zone spike activity, stochastic activity 79—79496
gastro-intestinal electrical rhythms, freq. estimation using auto-correlation and auto-regressive modelling 77—44875
gastro-intestinal tract, physiological signals, spectral analysis, autoregressive technique appl. 80—41269
gastroelectric surface signal analysis, phase-lock system design 79—34687
gastroelectric surface signal analysis, phase-lock system performance 79—34688
gastrointestinal electrical activity, Hodgkin-Huxley type electronic modelling 78—61165
gastrointestinal electrical rhythm frequency estimation by autoregressive modelling 78—56948
gastrointestinal electrical rhythm simulation, differential quadrature method 77—44634
gastrointestinal signals, quantitative analysis 80—41339
giant axons, time-ordered state, spatially organised struct. obs. in squid 78—53380
gramicidin A channel cation permeation interactions and anion binding 78—53370
guard cells, anion, light-sensitive membrane pots. 78—11622
H. halobium, light-induced surface pot. changes in purple membranes and bacteriorhodopsin liposomes 80—98015
hair cell receptor pot., ionic basis in vertebrates, bullfrog obs. 80—26239
hair cell voltage noise during mech. stimulation 77—90817
hand prosthesis myoelectric aid *(Spanish)* 79—84011

bioelectric potentials continued
hearing, analogue of two-tone suppression in whole nerve responses 78—11671
hearing, rational determ. of evoked response audiometry thresholds (window-ERA) *(German)* 77—70477
hearing action potential tuning curves, normal and pathological human ears 78—20184
hearing model, cellular approach 78—44515
heart, electrical activity observability, singular value decomposition 79—11913
heart activity characteristics in terms of membrane potentials *(Dutch)* 80—8034
heart Ca^{2+} transients during excitation-contraction coupling 80—97896
heart conduction system modelling 79—83741
heart contraction kinetics recording using thorax elec. fields *(Czech)* 78—77138
heart electrical generator integral characts. in normal humans 78—69244
heart multipole moments rel. to activated parts of epicardium and endocardium 79—100588
heart polyphase harmonic generator model and application to ECG 77—60278
hemi-retina evoked average multichannel EEG pot. fields, latency differences between upper and lower hemi-retina 78—24067
hippocampus pyramidal cells, somatostatin as excitatory transmitter 78—64973
His bundle analysis in human heart, meas. device *(German)* 77—40831
histamine-containing neurones, synaptic responses 77—64027
homologous displacement resulting from simultaneously applied rostral-caudal tactile stimuli, physiological mechanism 78—20198
human brain electrical signals systems analysis 77—21504
human motion bioelectric control transfer functions 78—27926
5-hydroxytryptamine receptors on visceral primary afferent neurones in rabbit nodose ganglion 77—56364
hypothalamic neurone spontaneous firing over narrow temp. interval 78—56961
impedance plethysmography and appl. of finite-element method, torso model and elec. potential distrib. 80—30958
insect auditory nerve oscillating summed action potential expt. 77—64039
insect mechanoreceptor sensory transduction nonlinear anal. 77—64061
instrumentation elements, electrophysiology appl., review, book contrib. 80—12293
intercellular communications and membrane electrical noise in embryonic heart cells 77—44612
intercellular contact high permeab. 78—48773
interference and motion artifact in recording signal, sources and suppression 77—81634
internodal cell, Nitella, mebrane pot. instability 79—92204
interval data presentation method, visual display of nonstationarities appl. 78—31949
intestinal electrical activity, motility, computer anal. of electrophysiological study on dogs 78—80851
intestinal epithelium, effect of Ca ions and pH on osmotic pot. 78—20156
intestinal mechanical and electrical activity recording transducer 77—44862
intestinal modelling, spectral anal. of coupled non-linear oscillators under modulation conditions 78—44754
intestinal motility study by computerised anal. of sounds and EMG wall pots. *(German)* 78—31944
intestinal myoelectrical activity model 79—70537
intracellular potential amplifier input capacitance determ. errors 77—60320
intracellular recording from pulsating cerebral cortex 77—48960
intramembrane potential jump meas. by potentiodynamic method 80—81778
intramuscular nerve action pot. derived from sensory fibres 80—56071
intraspinal nerve fibres, cat, electrical threshold continuous monitoring method 80—46104
inverse electrocardiology regularisation method, isolated canine heart expt. 79—39393
ion channels in development, book contrib. 79—96549
ion exchange membrane, unstirred layer effects on pot. difference calcs. 77—48680
ionic mechanisms of excitation in Paramecium, review 80—21458
ischaemic myocardium ST segment electrical alternans obs. 79—43857
ischaemic triaxicardiographic changes induced by exercise 79—39407
jellyfish electrically-coupled photosensitive neurons controlling swimming 77—90756
labial muscle EMG analysis and feature extraction by Hanning Cosine Modulated wave function 77—81605
latency meter, digital, for evoked pots. 77—60322
lateral geniculate nucleus of cat, oscillatory neural activity entrainment 79—92216
left ventricular potential quantitative assessment rel. to echocardiographic meas. 79—44042
leg muscle EMG pattern variability on stairs and in level walking 79—53175
limb displacement in man, late EMG response long-loop hypothesis test 79—96544
limb displacement in man, late EMG response muscle and afferent contributions 79—96545
limb muscle dynamic force meas. by surface EMG 79—34689
limbic spindle re-appraisal 78—69036
limbic spindles, cerebral activity or artifact 78—48778
Limulus ventral nerve photoreceptor response height vs. stimulus intensity curve 78—69058
lipid bilayer, hydrophobic ion electrostatic interactions 78—27904
lipid bilayer. interaction of cytochrome c 78—69001
lipid bilayer hydrophobic ion interactions, inner volt. clamping method 78—28129
lipid bilayers, asymmetry, dipole pot. meas. 77—4984
lipid bilayers, peroxide oxidation of lipids coupled with NAD.H oxidation by atm.O 77—36875
lipid bilayers made from monolayers, volt.-depend. capacitance 78—27903
lipid free radical oxidation, UV effect on lipid-protein complexes and membranes 77—36874
liver membrane potential in situ, effect of blood flow changes 78—48772
lumbosacral spinal cord and cauda equina, evoked pots. recording 80—17147

bioelectric potentials continued
m. biceps brachii, human, extraterritorial pots. of high-threshold motor units 80—56005
magnetic recording, FM freq. convertor 78—7469
maxillary gum trigeminal evoked pots. in humans 80—97948
measurement and processing instrument trends *(Croatian)* 78—44665
measurement in living tissue, effect on simultaneous O_2 partial press. determ. *(German)* 78—85453
mechano-sensory receptor of crayfish stretch receptor organ, effect of D_2O 77—44696
mechanoreception, Millipore-DOPH model membrane showing excitation with press. stimulus *(Japanese)* 78—3526
median nerve, transient responses to elec. stimulation, SQUID appl. to somatically evoked field meas. 80—104706
megakaryocytes, guinea pig, membrane elec. responses 78—44472
membrane, elec. excitable, phys. model, excitation mechanism 77—36902
membrane, parchment-supported, thermodynamic parameters, membrane and bi-ionic pot. theories testing 79—92168
membrane potential and active transport, information theory approach 80—35855
membrane potential generation by submitochondrial particles, direct meas. 80—35852
membrane potentials meas. using the dye safranine 79—48386
membrane responsiveness curve automated on-line determ. 78—92761
membranes, bioenergetics and proton-electron systems 79—57596
membranes, effect of carbocyanine dye fluoresc. probes on Ca-depend. K efflux 77—12896
membranes, volt.-depend. tetrodotoxin action 77—44620
microcomputer-aided arm prosthesis using myoelectric pattern recognition 78—53576
Millipore-dioleylphosphate model membrane potential oscillation mechanism 79—57603
miniature endplate potential amplitude online meas., programmable calculator conversion 79—84051
mitochondria and submitochondrial particle membrane pot. generation in anaerobic conditions 78—69015
mitochondrial membrane charging by cytochrome oxidase, role of protons 79—43807
mitochondrial membrane pot., respiratory chain study by method of penetrating ions 78—64951
mitochondrial membrane potential meas. with microelectrodes 77—48769
mitochondrial proton pump coupled to cytochrome c oxidase 77—25406
monosynaptic potentials onset and propagation, discrete-dynamic equations 78—77040
motional EMF, rel. to animal navigation 77—60879
motoneurone cross-correlated firing patterns, recurrent inhibition effects 78—80861
motoneurones excited by phasic muscle stretches, discharge pattern shaping, recurrent inhibitory feedback effects 78—85303
motor nerve conduction vel. and evoked pots. in peripheral nerve lesion localisation 78—31802
motor nerve terminals, cyclic nucleotide-mediated Ca flux 77—73524
motor neuron lesions, EMG positive sharp waves and fibrillation potentials 77—60194
motor unit action potential, influence of sustained contraction 78—31801
motor unit action potential duration meas. by surface electrode EMG 78—81039
motor unit activity and force gradation in human voluntary movements 80—97887
motor unit potential recording using monopolar and bipolar leads 77—81615
motor unit surface pots. spectrum and muscle geometry 80—30704
motor units, no preferential activation of fast units in rapid voluntary contractions in man 77—64025
mu rhythm detect. from human scalp, functional topography 78—48777
multi-microelectrode system for simultaneous recording of closely spaced neurons *(Japanese)* 78—61284
multichannel analyser, microprocessor-controlled, transfer of blood pressures and neural activities for computer anal. 80—72356
multipoint electrode for biological pot. recording 80—104784
multispike signal detection and sorting hardware 79—79711
multispike train, anal. techniques 77—44868
multiunit spike train sampling control by peak discriminator 79—34717
multiunit spike train separation techniques evaluation criteria 78—85422
muscle, cross-striated, effect of uncouplers of oxidative phosphorylation on conc. of ATP 78—20149
muscle, human skeletal, vol. cond., in situ meas. 77—90755
muscle, multifibre preparation, intercellular clefts influence on pot. and current distrib. 80—72145
muscle, skeletal, effect of stretch on EMF *(Japanese)* 77—36886
muscle, smooth, effect of hyperosmolar soln. on elec. connections between cells 78—69027
muscle and nerve fibre electric field resolution for EMG analysis 79—57627
muscle endplate, desensitisation rel. to selective alteration of Na^+ channels 77—77890
muscle fibre membrane pot., effect of eserine, frog 77—56345
muscle fibre resting pot. in cricket, influence of ions 78—24046
muscle fibres, computed extracellular pots. 79—43843
muscle fibres, computed extracellular pots. 79—74620
muscle fibres, slow and twitch type, of frog, contractile activation 77—32884
muscle membrane, insect, permeation of Mn, Cd, Zn and Be through Ca channels 77—56357
muscle potential, monitor for electroconvulsive therapy 77—40899
muscle spindle afferent activity and tone meas. in man, apparatus generating controlled ramp movements 78—77121
muscular electrical and mech. changes due to sustained voluntary isometric contracts. 80—3628
muscular fatigue, EMG meas. and analogue model *(Japanese)* 79—8498
muslce mass potential, stochastic model, NMV activity *(Japanese)* 78—24056
myelinated axon impulse cond. simulation, sensitivity to nodal and internodal parameters 78—35831
myocardial fibre accommodation, role of incoming currents 77—36898
myocardial fibres, ionic nature of repeated responses 77—70441
myoelectric control of an artificial hand, sequential movement, tropical climate 80—41323
myoelectric multistate control systems, operator error 78—81076
myoelectric processor and human operator dynamic error performance 79—96714

bioelectric potentials continued
myoelectric processor sampling rate selection 79—96713
myoelectric signal processing, expt. demonstration of optimal myoprocessor performance 80—89882
myoelectric signal processing, optimal myoprocessor derivation 80—89881
myoelectric signal rel. to physiological props. of deltoid muscle 79—70539
myoelectric signal variance parameter 77—29130
myoelectric signals, improved processor 80—104800
myoelectric signals, power spectra interpretation, model and appls. 77—44641
myoelectric single motor unit potential generation model 77—29131
myoelectrically controlled artificial hand, with sense of touch 79—12035
myoelectrically controlled systems, five-state, error rate obs. 80—72376
myopotential controlled elec. operated hand with sensory feedback 79—57815
myopotentials, prevention of unipolar demand pacemaker inhibition 77—81709
myopotentials and endocardial potentials causing pacemaker malfunction 77—81723
Nernst-Planck analog equations and stationary state membrane electric potentials 79—92196
nerve action pot., lipid bilayer local phase transition 80—89744
nerve action potential, cybernetic elucidation 79—48243
nerve action potential, molecular events and energy changes 78—44497
nerve action potential changes associated with proved lumbosacral root compression 80—56006
nerve action potential model 80—30697
nerve action potentials, low-frequency FM tape recording 79—57832
nerve and muscle isolated preps., 2450 MHz radiation effects 78—53443
nerve biopotential recording by laminated electrodes 78—92760
nerve cell impulse flows, determ. of quantity of useful information 78—69038
nerve cell information conversion mechanisms 79—43862
nerve cell unitary discharge automatic recognition *(French)* 77—37072
nerve conduction model, FitzHugh-Nagumo, repetitive activity and Hopf bifurcation under point-simulation 79—11915
nerve evoked pots., sensory and mixed conduction vel. obs. 79—74693
nerve fibre, active, in finite volume conductor, surface action potentials, model 79—24980
nerve fibre action pots., use in estimation of fibre conduction vel. distribs. 80—3633
nerve fibre compound action pots., use in estimation of conduction vel. distribs. 80—8044
nerve fibre membrane analogue-code conversion, ionic mechanisms 80—81575
nerve field, isolated sciatic nerve in volume conductor 77—21505
nerve impulse, physical mechs., ion transport through membranes, review 78—85306
nerve impulse data treatment for comparison with theory 80—97893
nerve impulse electro-diffusion model 79—53078
nerve impulse encoding, elec. processes 80—76718
nerve impulse equation, dynamic responses of impulse 78—64972
nerve impulse propagation, subthreshold solns. of Hodgkin-Huxley eqns. 78—77044
nerve impulse radial decline in restricted cylindrical extracellular space 78—53379
nerve impulse stability theory, Hodgkin-Huxley eqns. appl. 78—48782
nerve membrane potential, effect of constant mag. field 79—57679
nerve membrane response due to time depend. stimulus 79—24974
nerve or muscle potentials meas., using electromechanical device, with semiautomatic processing of results 77—5115
nerve signal optimal filtering 77—73616
nerve signal recording in awake animals, implantable electrode 77—5119
nerve spike trains, Fourier anal. 80—12070
nerve spike trains, interleaved, in a noisy channel, separation system 80—94424
nerve trunk multifibre activity quantitation 80—76853
nerve trunks, method for determ. of conduction velocity distribs. 79—48241
nerve-muscle anisotropic syncytia, electrotonic membrane pot. distrib. 78—64971
neural modelling and identification, state variable approach 78—35825
neural multiunit signals, educable waveform recognition system for sorting unit discharges 80—51312
neural populations, simplified model eqns. and envelope eqns. 78—31798
neural signal recording using implantable electrode and telemetry system, awake animals *(Japanese)* 80—94427
neural signals, non-stationary, pattern trajectory anal. 78—36082
neural single unit activity recording with photoetched Au multimicroelectrode surface 79—57824
neural spike trains, relationship of post-stimulus time and interval histograms to time characts. 78—69032
neural spike window discriminator confirmation by analogue delay cct. 77—21664
neural systems, receiver operating characts. anal. of sensitivity 77—44629
neuroelectric control of upper-limb prosthesis 78—44704
neuroelectric transmembrane pots., EM radiation effects, possible model of mechanisms 80—26259
neurological signal processing, detection of pathological conditions in man appl. 79—83993
neuromathematical concepts of point process theory 78—27916
neuromuscular block indicator, model INMB-1, EMG amplitude meas. 80—104785
neuromuscular blockade by amantadine by suppression of acetylcholine receptor ionic cond. 78—64975
neuromuscular junction, frog, Ca-depend. presynaptic action 77—52773
neuromuscular junction, membrane surface pot. changes effect on drug interactions 80—3631
neuromuscular miniature endplate potential online acquisition microcomputer system 78—36015
neuromuscular synapse, frog, dual action of Er^{3+} on transmitter release 78—35834
neuromuscular system deterministic neuron models 79—29523
neuromuscular system electrical stimulator using biopotential amplifier 79—48315
neuromuscular system model for small isometric tensions, human 77—52771
neuromuscular system output response, effect of correlated adjacent interspike interval sequences of input, computer simulation 78—80858

bioelectric potentials continued
neuromuscular transmission, locust, modulation by octopaminergic neurone 78—11632
neuron activity, optical monitoring methods, book contrib. 79—2030
neuron firing threshold model, empirical examination 80—56014
neuron inhibitory synapse, influence of presynaptic irregularity on action pots., stretch receptor 77—9185
neuron input current, Helix pomatia, rel. to membrane pot. and extracellular Sr and Ca ion concs. 80—81577
neuron model, excitatory and inhibitory impulse sequence interactions in math. models *(Japanese)* 78—27919
neuron model of burst generation, FET analogue 77—44630
neuron single-unit pots., multi-microelectrodes system for simultaneous recording *(Japanese)* 79—57826
neuron single-unit pots. recording, multi-microelectrode system characts. *(Japanese)* 80—21581
neuronal adaptation to osmotic stress and facultative blood-brain barrier in marine osmoconformer 77—29127
neuronal generation of singing in cicada 78—7328
neuronal interspike time histograms for random input model 78—40134
neuronal membrane DC resting pot., automatic offset cct. 77—40940
neuronal membrane process field potentials anal. and synthesis, computer system 80—85374
neuronal models, spike trains, and the inverse problem 77—52764
neuronal populations, diffusely-connected, computer simulation 78—53384
neuronal response analyser with microprocessor *(French)* 79—20730
neuronal response in rat hippocampus, dynamic model 79—34547
neuronal spike activity discriminator 77—48966
neuronal spike train data, adaptive filtering 80—67265
neuronal spike train sampling, implementation of French-Holden algorithm 78—40440
neuronal spike trains, dependency as estimation measure 77—25357
neuronal spike trains, simulation, multiple Markov sequences 77—25413
neuronal spike-train statistical anal. methods 78—73149
neuronal spikes, peak-detecting window discriminator 77—60323
neurone activity, simultaneous recording from several neurones in invertebrate central nervous system 77—66880
neurone potentials, 2 pulse series anal., histogram of recurrence time intervals 77—60196
neurone stochastic activity models, book 77—44632
neurones of large horse-leech, electrophysiological characts. rel. to intracellular Na$^+$ conc. 78—53374
neurophysiological spike unit data acquisition and reduction system 79—79713
neurophysiology, computer assisted unit data acquisition/reduction 78—61266
neurosurgical patient monitoring computer system 79—88206
neurotransmitter release statistics: moment estimates for inhomogeneous Bernoulli trials 79—62228
Nitella, fluctuation and instability in membrane pot. near threshold 80—89723
node of Ranvier, crit. pot. of repeat responses 79—70538
nonlinear electrotonus problem exact soln. 77—70446
nonlinear filtering technique for identification of biological signals 78—40438
nonspiking neurones, pharmacological evidence for fast Na channels 78—73151
noradrenaline-induced hyperpolarisation of spinal motoneurons 80—56010
occipital evoked potential meas. of contrast sensitivity and acuity of conscious cat 78—48803
occipital potentials, pattern and movement detect. in man and rabbit 78—48805
ocellus of phalangium opilio, electrical response 79—53095
oesophageal diaphragmatic EMG in humans, effects of electrode position 80—81753
olfactometer, environmental odour emission analysis, hospital appl. *(German)* 78—7754
olfactory bulb, 55 counts/sec rhythm anal. and simulation 80—85422
olfactory bulb, caiman, computer anal. of EEG activity 77—81513
olfactory cortex of guinea pig maintained in vitro, effects of cooling 78—3525
olfactory evoked brain pot., correl. anal. of recorded waveforms *(Japanese)* 80—97946
optic tectum extracellular recording, reproducible manufacture of metal-filled microelectrodes 78—69263
optic tectum movement detecting cell response to change of wavelength, pigeon 78—7348
optic tract fibre spike trains, cat, nonstationary anal. on Markov props. *(Japanese)* 77—90780
optic tract of self-respiring fish, method for obtaining single cell response 77—56545
orbicularis oculi reflex, diagnostic significance of reflex amplitude 79—34540
oscillatory neural networks in the rabbit hippocampus 80—89743
pacemaker transmembrane potential generation in fish heart sinoatrial cells 79—39395
pancreatic islet cells, plateau pots. as voltage-dependent action pots. 80—94180
Paramecium membrane potential changes during chemokinesis 80—26209
patient physiological signal on-line anal., multiple microprocessor system 80—26389
pattern recognition of human brain electrical potentials 80—109051
pattern-evoked potential, modifications rel. to stimulated part of visual field 80—26225
pericardial potential simulation and mapping in dog 79—39399
perimetry by visual evoked pot. recording limitations 78—69049
peripheral nerve, generation of unidirectionally propagated action pots. by brief stimuli 80—85546
peripheral nervous system multichannel data anal., frog sartorius muscle mechanoreceptor transducer characts. *(Japanese)* 80—3656
phase-locked responses in Limulus lateral eye 77—86491
phasic pupillary light reflex and visual evokes potentials, simultaneous anal. 80—26226
phospholipid bilayer membrane modified by valinomycin, volt. fluctuations 78—31777
phospholipid vesicle surface charge equilib. distrib., effect of non-electrostatic factors 80—30672
photic one-second stimulation, on/off effects in background EEG activity 78—69047
photic sensitivity of macaque monkey and pulvinar neurons 80—12106

bioelectric potentials continued
photoreceptor, barnacle, effects on prolonged depolarising afterpot. of Mn^{2+}, Ca^{2+} 80—8051
photoreceptor, barnacle, props. of on-transient of intracellular response 80—8052
photoreceptor, invertebrate,, basic mechanisms of excitation and adaptation 80—81593
photoreceptor cell disk membrane, photoinduction of pot. 79—70548
photoreceptor electric potential in phototaxis of alga Haematococcus pluvialis 78—27909
photoreceptor electric response, in invertebrates and vertebrates, quantitative model 77—44656
photoreceptor function, rel. to prolonged depolarising afterpot. 78—15832
photoreceptor membrane interfacial pots., light-induced 80—72161
photoreceptor membrane potential reconstruction from simultaneous intra- and extracellular recordings, S. atlantica 77—86494
photoreceptor mutant of Drosophila, protein role in intermediate steps of phototransduction 77—48799
photoreceptor synaptic activity in isolated frog retina, Co ion effects 78—48797
photoreceptor visual response rel. to metarhodopsin transitions, barnacle 78—69050
photoreceptors of Limulus ventral eye, sensitivity rel. to Ca^{2+} injection and light adaptation 78—44500
photoresponse suppression during anoxia, role of Ca^{2+}, Limulus 79—62252
photosensory membrane of Limulus ventral nerve photoreceptor, effect of extracellular Ca/Na ratio 78—69067
pineal photoreceptors, evidence for vertebrate visual pigment with two physiologically active states 78—44504
piriform cortex neurons, rabbit, fast and slow inhibitory postsynaptic potentials 79—92244
pituitary cell, Na and Ca action potential 77—48770
plant protoplast membrane, osmotically induced changes in elec. props. 78—27910
plants, light-induced intracellular and extracellular bioelec. reactions 77—56422
point processes, time-connectivity patterns quantification 80—21564
polarised spherical cell, ionic conc. profiles and charge distrib. 78—73144
polyphase envelope detection for physiological signals *(Korean)* 79—66565
pontine reticular formation neurons, discharge rel. to motor activity 77—66810
post-operative human gait, EMG mes., pattern recognition appl. 79—34599
postpuerperal maternal α-rhythm increase obs. 79—96534
postsynaptic conductance charge, quantal event at nicotine synapses, numerical reconstruction 79—83748
precision full-wave rectifier/integrator for physiological signals 79—83988
presynaptic membrane, Ca^{2+} current rel. to synaptic transmission, squid giant synapse 77—16926
proton transfer from water to octane coupled with ATP hydrolysis by chloroplast ATPase 77—36876
QRS-T wave simulation based on transmembrane potential of myocardial cell *(Japanese)* 77—90740
radial nerve potential recording at wrist in man *(French)* 77—81756
radial nerves branching quotient, determ. in healthy adults 79—34539
random signal analysis, conf., London (April 1977) 77—44822
recording using surface electrodes, methods of reducing movement interference *(German)* 78—85405
repetitive firing computer models nonlinear systems anal. 78—80854
repetitive muscular contraction, localised fatigue evaluation from EMG power spectrum 78—57103
respiratory muscle EMG anal. by digital computer technique 78—28102
retina, bovine, R2 component of early receptor pot. rel. to metarhodopsin II form. 80—97904
retina, carp, neuronal architecture of on and off pathways to ganglion cells 78—44502
retina, early receptor pot. study of chicken and pigeon visual pigments 77—44667
retina, inner, of teleosts and reptiles, proximal negative response 77—21521
retina, of river lamprey, electroretinogram recordings 77—60205
retina, pigeon, graded pots. accompanying antidromic invasion 79—43882
retina, rat, rod elec. model, early receptor pot. generation 79—57647
retina, significance of antidromic potentiation and induced activity 80—12092
retina, teleost, enhancement of hyperpolarising S-potentials of surround illumination 79—2051
retina early receptor potential, quantum mechanical model 79—57644
retina electrical activity and lipid peroxidation 79—43885
retina of carp, colour coded S-potentials, latency measurement 79—53097
retina of turtle, horizontal cells influence on bipolar cells' membrane pot. 78—88708
retina outer plexiform layer lateral interactions after atropine block of horizontal cells, turtle 77—70457
retinal bipolar cells, struct. basis for on- and off-centre responses 78—44503
retinal class IV ganglion cell luminance and chrominance processing in frog 78—40148
retinal ganglion cell activity in ground squirrel under halothane anaesthesia 78—40147
retinal ganglion cell firing patterns, implications for separate ON and OFF processes goldfish 77—70458
retinal ganglion cell response props. in Siamese cat 80—12115
retinal ganglion cell response to sinusoidal flicker, mudpuppy 78—48798
retinal ganglion cells, goldfish, effects of photic stimulation upon var. of interspike intervals 77—70460
retinal ganglion cells, mudpuppy, hyperpolarising ON/OFF responses 77—25427
retinal ganglion cells, Necturus, responses to stationary and moving stimuli 77—70459
retinal ganglion cells action pots., goldfish, function of lighting conditions 79—43888
retinal ganglion cells of cat, response patterns for moving contours 78—69059
retinal ganglion cells of pigeon, concentric receptive fields 77—44653
retinal horizontal cell reaction to non-uniform illum., model 77—56375

bioelectric potentials continued
retinal light responses, simultaneous recording by extra- and intracellular electrodes in crayfish 78—69055
retinal neuron, variability of interspike intervals during sustained firing, model 77—86492
retinal on-centre bipolar cell, ionic mechanisms of rod and cone signals 78—61177
retinal potentials, cephalopod, dark adaption dynamics 79—79541
retinal R/G horizontal cells, light intensity and response amplitude relation 79—5281
retinal single-photon impulse coding mechanisms *(Russian)* 78—27941
retinal-entrapped membrane, photo-induced potential 78—20148
retinula peripheral cells within Drosophila visual mutants, response to monochromatic white-noise 78—69078
rheoencephalogram parameters vs. mech. props. of cerebral artery walls 78—3547
rhodopsin in model membranes, charge displacements in interfacial layers 77—52785
rhodopsin membrane at oil-water interface, effect of illumination, rel. to cephalopod visual cells 77—44646
rhythmic heart-cell clusters, fluctuations in interbeat interval, membrane voltage noise role 80—30705
rod, Ca-depend. regenerative responses 78—3480
rod early receptor potential isolation from frog retina 78—69066
rod ERG, human, dark-adapted a-wave response function obs. 80—56036
rod ERG, human, rel. to psychophysical responses in light and dark adaptation 78—69063
rod ERG of mudpuppy, effect of dim red backgrounds 78—69062
rod external segment surface membrane, lateral diffusion of rhodopsin 78—15828
rod network in turtle retina, elec. spread 78—80874
rod outer segments pots., frog, local stimulation and adaption obs. 79—79528
rod photoreceptor model sensitivity, depend. on level of background light intensity 78—20179
rod photoresponse, contrib. of Cs$^+$-sensitive cond. increase 78—44501
saccade-related unit activity in monkey superior colliculus 80—12101
saccadic eye movement, accompanying pots. 80—12102
scalp potentials, dipole layer model 78—77035
scalp topography of human somatosensory and auditory evoked pots. 77—25412
scalp topography of pots. in auditory and visual discrimination tasks 77—52797
sciatic nerve, frog, spontaneous and evoked pot. recording by flexible PC probe 79—84049
scotomata, effect on responses to pattern reversal in one half visual field 79—39417
seizure discharge autorhythmicity, spike, discharge freq. regulation in focal epilepsy 78—40133
semicircular canal primary afferents, impulse weight functions, frog 78—69116
sensory evoked potentials in nervous system clinical disorders, book contrib. 79—2029
sensory evoked pots. at the wrist, infants and children 79—79566
serotonergic excitation, unconventional response in Aplysia 77—86484
signal analysis and simulation program 79—79678
signal focusing in segmented stretch reflex system, auxiliary spinal networks 80—40999
signal processing, computerised system *(French)* 77—37112
signal processing using an extended desk computer *(German)* 80—26387
simultaneous telephone transmission of four ECG/EEG signals *(Spanish)* 79—62399
sinatorial node of rabbit heart, vagal stimulation, K$^+$ permeability and extracellular transients 78—92608
single motor unit, recording during strong effort 79—11908
single myocardial fibre model, source-field relationships 79—39385
single unit activity, computer program for generating on-line raster dot displays 78—57087
single-epoch somatosensory evoked vertex potential, time window for electro-ocular monitoring 79—96535
skeletal muscle activity pattern in humans rel. to muscle fibre type composition 78—80869
skeletal muscle motor units, system for rapid acquisition of surface pot. maps 80—46077
skin action potentials, receptor on-line field mapping technique 79—74797
skin electrical responses to tactile and thermal stimuli, instrumentation for 79—74767
skin potential artifact reduction in biopot. recording 77—40873
skin potential motion artifact reduction by skin abrasion 78—40361
skin-electrode processes obs., during medical electrography 77—40828
soma potential of interneurone controls tramsmitter release on monosynaptic pathway in Aplysia 78—56964
somatosensory evoked potential, effects of interaction between large and small diameter fibre systems 79—16188
somatosensory evoked potential, scalp-recorded, normal and neurologically disordered patients 79—16186
somatosensory evoked potential early components in monkey 79—96533
somatosensory evoked potential in man, far field pots. 77—9182
somatosensory evoked potential measurement and analysis on a small laboratory computer 78—92729
somatosensory evoked potentials, conduct. time in central pathways in man 79—39408
somatosensory evoked potentials, cortical and thalamic activity in cat 79—16187
somatosensory evoked potentials, elec. stimulation of fingers in random stimulation 78—11628
somatosensory evoked potentials, in man, cerebral, subcortical, spinal and peripheral nerve pots. 80—16961
somatosensory evoked potentials, recovery function of short latency components, cat 79—34534
somatosensory evoked potentials, review of acquisition and anal. 80—101281
somatosensory evoked potentials, short latency, in man following median nerve stimulation 80—94243
somatosensory evoked potentials obs., human and monkey 79—43842
somatosensory evoked response, multiple sclerosis effects, expt. 77—44628
somatosensory potentials following electroconvulsive therapy 80—97947
somatosensory short latency pots. in humans, mech. evoked 80—67099
speech production, cranial and facial pot. characts. 78—11675

bioelectric potentials continued
speech production, recruitment and discharge patterns of single motor units 78—65054
spike recognition and on-line classification by unsupervised learning system 79—57789
spike separation in multiunit records, multivariate anal. 80—26215
spike transfer in statistical neuronal ensembles, neurone as nonlinear source of spikes 78—15819
spinal and sub-cortical evoked pots. following stimulation of posterior tibial nerve in man 78—69034
spinal evoked potential in man, maturational study 79—79498
spinal field potential, rat, rel. to focal interictal epileptiform discharges 80—94191
spine, evoked elec. response surface recording 78—36028
squid giant axons, oscillatory subthreshold responses and pot. fluctuation obs. 78—27918
squid joint axon membrane potential fluctuations, cross-correlations 78—92616
steady state evoked potentials, recording and appls. review 78—35823
stomach surface and serosal elec. activity meas., autoregressive anal. 79—70656
Streptococcus, effect of ionising radiation on transmembrane pot. 80—36019
striate cortex cat, orientation selectivity of single cells 79—2053
striate cortex single cell response, effects of interacting visual patterns, cat 78—7346
subcellular particle membrane pot. diff., proton channels in oxidative phosphorylation 78—64964
subcellular particle membrane pot. difference, compensation meas. method 77—56547
subcellular particle pot. difference, chemiosmotic and chemielec. generation mechanism 77—52751
subtilisin charge-relay system, electrostatic pot. map, STO transferable bond calc. 80—3571
superior colliculus, eye movement pots. in awake cats 77—60208
superior colliculus and its sensory inputs, primate 80—12100
superior colliculus directional selectivity in hamster rel. to strobe-rearing and dark-rearing 78—69052
surface charge density variation of excitable nerve membrane exposed to optical radiation 79—34542
surface EMG, computer anal. during isometric exercise, muscle tension quantification 80—85505
surface EMG and fatigue, muscle temp. and blood flow 80—94199
surface EMG bipolar recording, influences of electrode geometry 79 53269
surface potentials of stratified spheroidal vol. conductors, bioelec. phenomena elucidation 80—32867
sympathetic ganglia, possible mediation of slow excitatory postsynaptic pot. by cyclic GMP 78—27930
sympathetic ganglia, postsynaptic modulation of excitatory process by cyclic AMP 78—27931
sympathetic ganglia, synaptic potentials and cyclic nucleotides 79—11912
synaptic potential, release of transmitter from locust nonspiking interneurons 80—3632
synaptic transmission, long-lasting potentiation by postsynaptic mechanism 77—32885
syncytia, cylindrical, and muscle fibres, elec. pots. induced by current point source 79—74610
syncytia, spherical, electrical props. 79—24962
syncytial tissues, pot. induced by current point source 79—74609
tactile receptor response to stepped and sinusoidal vibrs. of hair, crayfish 77—70481
taste hair tip recording, insect, non-blocking AC preamplifier 77—90971
tectal cell recordings, frog 79—79525
tectum opticum neuron response characts., Salamandra 79—53092
telemetry, micropowered multichannel PAM/FM system for brain research 77—25618
temporal pattern generation in coupled oscillators, Tritonia mollusc trigger group model 79—96538
thalamo-cortical unspecific system, two-freq. oscillatory process investigation 79—53076
thoracic surface, human, heart potentials distrib. with left bundle branch blocks 79—39403
threshold models of reaction latency, properties 78—44440
tissue regeneration by electric potentials 80—41308
torso model for potential distrib. from VCG data 79—39401
transmitter release quanta, evidence against subunits 78—77042
tree root potential meas. electrode earthing method *(Russian)* 80—26420
tremor state motor unit discharge patterns *(Japanese)* 78—31803
triceps surae motor units, depend. of H-reflex pot. shape on extraterritorial pots. 77—40655
triceps surae muscle, human, vol. conducted motor unit pots. 77—40656
trigeminal motoneuron activity during sleep, intracellular anal., cct. 78—53389
unitary synaptic potentials rel. to behavioural sequence timing 78—61161
unmyelinated nerve Na channels optimum density, analytic treatment 78—24061
urodynamic combination EMG and functional X-ray exam. technique 80—8131
ventricular action potential, mammalian, analysis 79—62227
ventricular muscle, mammalian, slow inward current depression by acetylcholine 79—92210
ventricular myocardial excitation, elec. field theory and integral topogram analysis 79—39386
ventricular surface excitation wave spread and collision obs. in dog 79—39398
vertex short latency acoustic responses ir cat, factors affecting amplitudes and latencies 78—61192
vision, bioelectric recording from human retina and cortex 80—12111
vision, photoconvertible pigment states and excitation, prolonged depolarising afterpot., blowfly 80—8060
vision, photopigment rapid conversions in blowfly visual sense cells, effect on receptor pot., pupillary response 80—8062
vision, prolonged depolarising afterpot., transduction in photoreceptors with bistable pigments 80—8050
vision, spectral sensitivity in goldfish, photochem. and neural correlates 80—81599
visual 80—97905
visual acuity assessment by evoked pots., temporal depend. of spatial freq. selectivity 78—64995

bioelectric potentials continued
- visual behaviour monitoring system, EMG triggered photographic technique 78—31919
- visual cell membrane cond. control, arthropod 78—15831
- visual cell microvilli membrane fragment protonic and ionic processes, cephalopod 78—73159
- visual cortex, critical period interaction, kitten 78—56972
- visual cortex development, kitten, monocular astigmatism effects 78—7345
- visual cortex functional specialisation of rhesus monkey 78—80873
- visual cortex neurones, rabbit, organisation of background activity 78—69044
- visual cortex pattern evoked pots. and single unit responses, cat 78—27947
- visual cortical area 19 of cat, periodic complex cells 78—56974
- visual cortical effects of early visual experience 80—12119
- visual development in humans, animal models 80—12118
- visual electrophysiological examinations of flying personnel 79—11929
- visual event detection, cortical pots. 77—52782
- visual event related potentials of the late positive complex in visual discrimination tasks 79—39416
- visual evoked cortical potential, contrast sensitivity meas. of 6 month old infant 77—12913
- visual evoked cortical potential, rel. to dark adaptation, human 77—9192
- visual evoked cortical potential, removal of alpha by selective averaging 77—81766
- visual evoked cortical potentials, transient response, techniques reviewed 78—35844
- visual evoked cortical potentials in men during compression and saturation in He-O$_2$ 78—61173
- visual evoked neural activity intensity and structure, rel. to visual system modelling 77—25426
- visual evoked potential, cortical, normal humans, bibliography 79—39414
- visual evoked potential, steady state latency determ. 77—21516
- visual evoked potential amplitude rel. to pattern displacement amplitude 77—90778
- visual evoked potential augmentation/reduction by cortical mechanisms, cat 78—27945
- visual evoked potential distribution, half-field pattern-reversal and pattern-onset stimuli 77—12912
- visual evoked potential evidence of adaptation to spatial Fourier components in humans 78—69051
- visual evoked potential in man, detect. of luminosity response *(Japanese)* 77—56374
- visual evoked potential latency, steady-state, phase versus time analysis 78—11643
- visual evoked potential maturation in normal child *(French)* 78—24068
- visual evoked potential on-line evaluation by sliding average form. *(German)* 78—85402
- visual evoked potential recording in high-noise environment, biphasic 60 Hz synchroniser cct. 78—24155
- visual evoked potential recovery, cumulative inhibitory effect of repetitively flashed stimuli 78—69048
- visual evoked potential registration methods *(German)* 78—48916
- visual evoked potential spectrum, short term vars. 77—48795
- visual evoked potential to search in short-term memory, late components 78—61172
- visual evoked potential waveform, effects of head support *(Japanese)* 80—3642
- visual evoked potentials, cortical extracted pattern response with bipolar and monopolar recordings 77—12919
- visual evoked potentials, during hypothermia, prolonged circulatory arrest 79—16204
- visual evoked potentials, human scalp topography 77—40669
- visual evoked potentials, latency and wave form obs. 80—97907
- visual evoked potentials, monocular, recording under binocular conditions 78—81035
- visual evoked potentials, n-hexane induced changes, ERG of industrial workers 80—45886
- visual evoked potentials, rel. to perception of instantaneous and durable 77—25451
- visual evoked potentials, size-specific interocular suppression, rel. to human binocular vision 78—31810
- visual evoked potentials, transient, real-time filtering 78—31940
- visual evoked potentials, usefulness in multiple sclerosis diagnosis *(Italian)* 79—34555
- visual evoked potentials and excitability cycle during simulated diving at −610 m in O$_2$-He 77—5000
- visual evoked potentials and latent chromatic response *(Japanese)* 78—92629
- visual evoked potentials from occipital and precentral cortex in visually deprived humans 78—3479
- visual evoked potentials in 6 to 45 day old infants 77—70456
- visual evoked potentials rel. to pattern reversal stimulus frequency *(German)* 79—16322
- visual evoked potentials to sine wave modulated light in normals and patients, interhemispheric relationships 78—77049
- visual evoked potentials to stimulus trains, normative data and photosensitive seizures appl. 80—94204
- visual evoked response, central visual field contribs. 80—108881
- visual evoked response, defocus effects 77—90768
- visual evoked response, diagnostic tool in demyelinating diseases 79—20538
- visual evoked response, digital inverse filtering 79—53098
- visual evoked response, standard normal determ. 77—1995
- visual evoked response in human albinos, brain abnormality 80—94208
- visual evoked response in strabismic and anisometropic amblyopia, effects of check size and retinal locus 78—61171
- visual evoked response meas. using computerised rapid random flash 79—83776
- visual evoked response meas. using versatile pattern-reversal stimulator 80—17177
- visual evoked response of humans, nonlinear anal. 78—92622
- visual evoked response shape self-regulation in man 78—31809
- visual evoked response to sinusoidal gradients, latency changes, humans 78—7349
- visual function assessment, electrophysiological responses, signal averaging technique 77—44655
- visual neuron-discharges in eye movements 80—12099
- visual pattern reversal evoked pots., infant visual acuity meas. 78—40149

bioelectric potentials continued
- visual pattern-evoked cortical pots., human infants, spatial and temporal interaction 80—101169
- visual pattern-evoked occipital pots. in blind boy with visual assoc. cortex destruction, pattern-evoked occipital pots. 78—40145
- visual pigment system kinetics, bistable system measurements appl. 78—92624
- visual pigment system kinetics, mathematical anal. 78—92623
- visual responses in geniculo-striate and pulvino-extrastriate systems, squirrel monkeys 77—40667
- visual S-potentials, adaption effects in post-receptoral neurons of roach retina 79—79534
- visual single unit recording in pigmented rat, eye movement control 77—81767
- visual system, crayfish, coding and decoding of steady state information by patterned pulse trains 80—12105
- visual system, primate, subdivisions and interconnections 80—12110
- visual tracking, target vel. signals in vermal Purkinje cells, monkey obs. 80—56026
- visual Wulst retinotopic organisation in nocturnal and diurnal raptors 80—12098
- visual-neural correlate of speechreading ability 78—64992
- visually evoked brain potentials, meas. of signal components 77—40946
- visually evoked cortical potentials in renal failure, latency changes 79—16200
- visually evoked cortical pots. during binocular rivalry 78—40153
- visually evoked elec. and mag. response simultaneous recording for diagnosis 78—53558
- visually evoked potential analysis *(Japanese)* 80—12090
- visually evoked potentials, classification for visual stimuli discrimiuation 79—92414
- visually evoked potentials, comparison with behavioural studies for visual acuity assess. 79—53112
- visually evoked potentials, latency and reaction times as power functions of luminance in peripheral field 79—11928
- visually evoked potentials, visual anomalies in human ocular albinos 79—43875
- visually evoked pots., polarity inversion obs. 79—100602
- visually evoked scalp potentials, spatiotemporal mapping for human 78—35845
- volitionally activated low-threshold EDC motor units, firing rate response 78—20163
- volume conducted potentials, averaged multiple unit activity as estimate of local neuronal activity changes 80—89917
- volume conductor electrical source information from elec. and mag. surface data 79—83727
- volume conductor principles in scalp EEG recordings, montage design 77—78003
- volume-conductor fields of isolated axon, linear filtering problem 78—3463
- waveform analysis, computerized method for electronystagmogram anal. *(Croatian)* 79—20697
- weight sensation quantification by EMG meas. 77—90940
- Wiener filtering, estimation of evoked potentials 79—48235
- Ba treated nerve cells, generation of long potential waves 80—56002
- Na$^+$,K$^+$-ATPase generation of pot. jump at octane-water interface 77—81484
- Na channels, one-to-one binding of purified scorpion toxin, tunicate egg membrane 77—32877
- Na current in cardiac and nervous tissues, validity of dV$_{max}$/dt as meas. 78—77037

biographical dictionaries *see biographies*

biographies
- Adams, Roger, his role in American chem. education and research 80—4497
- Airy, G.B., Astronomer Royal 1835-81, contrib. to horology 80—86061
- Albert Einstein, physicist (1879-1955), review of his life and work 79—67132
- Amici, G.B., contrib. to optical microscopy 77—57138
- Anger, Hal O., work at the Donner Lab., nuclear medicine appl. 80—42027
- archives, use as generators of personal notes 77—87618
- Aryabhata, 5th century Indian astronomer and mathematician, life and works 78—65741
- Bacon, Francis 77—13562
- Ball, Sir Robert Stawell, Victorian astronomer and mathematician 79—88783
- Bardeen, John, contrib. to solid state physics 80—57057
- Barnard, Edward E. (1857-1923) and comet discovering machine hoax 80—13
- Beclere, Antoine, pioneer of radiation therapy techniques, biography 79—62982
- Benjamin Franklin, expts., theories and background 77—9845
- Bergeron, Tor (1891-1977), meteorologist 79—2589
- Berson, Solomon A., achievements in nuclear medicine 80—42028
- Bloch, Felix, electron theory of metals, contrib. 80—57053
- Boll, Franz, (1849 to 1879), investigator of retinal pigments 78—20927
- Brahe, Tycho, obs. and deductions of 1577 Great Comet 78—32407
- Bremmer, H., scientific work 79—62984
- Broude, Vladimir L. (1924-1978), Russian physicist 80—82625
- Cailletet, liquefaction of air, from Cailletet and Pictet to microkelvin 79—40
- Campbell, J.D., testing techniques and material behaviour at high strain rates, memorial lecture 80—82627
- Cassini, Jean-Dominque (1625-1712), lunar map 80—8769
- Chamberlin, geological methodology compared with Gilbert 79—17182
- Clap, Rev. Thomas, terrestrial comets theory of fireballs 77—74017
- Cottrell, Frederick Gardner 78—20926
- crystal tuning fork development and biography of Jurgen Staudte *(German)* 79—30182
- Darwin, Charles, meteorological notes from voyage of the Beagle 79—17173
- de Saussure, H.-B., first mountain meteorologist 79—21513
- Driart, Pierre (1484-1535), meteorological events recorded in diary during 1522-35 period *(French)* 78—32199
- Edison the scientist 80—22179
- Einstein, Albert, a correspondence with Adolf Schmidt, an archive discovery *(German)* 79—84924
- Einstein, Albert, contrib. to cosmology 80—77530
- Einstein, Albert, his contribution to cosmology 79—71165

biographies continued
Einstein, Albert, his life and times 79−71212
Einstein, Albert, life and scientific work 79−71211
Einstein, Albert, life and work *(Russian)* 79−84926
Einstein, Albert, relativity theory acceptance in Canada 80−68012
Einstein, Albert (1879-1955), cosmological works *(Czech)* 80−27097
Einstein, Albert (1879-1955), memorable quotations 79−40342
Einstein, character rel. to scientific contributions 80−36828
Einstein's influence on technical sciences *(German)* 80−36827
Einstein and Berlin physicists, 1927 to 1930 *(Russian)* 79−84927
Einstein centenary 80−46782
Einthoven, Willem, (1861-1927), electrocardiological work 79−35514
Ernest Rutherford 80−8768
de l'Estoile, Pierre (1546-1611), meteorological events in journals *(French)* 79−58510
Evans, Thomas Simpson, 1777-1818, mathematician and astronomer 78−89287
F. Klement, investigations in spectroscopy of solid solutions *(Russian)* 80−8767
Faraday and the concept of force 80−57048
Flamsteed, Rev. John (1646-1719), and annual parallax of Pole Star 79−88786
Fock, V., development of ideas in atomic phys. and quantum theory 80−22183
Fox Talbot, W.H., history of photography 78−17
Franklin, Benjamin, exptl. philosopher, theory of electricity, for teaching 78−24630
Fraunhofer, Joseph, contributions to astronomy *(German)* 77−57142
Friedmann, Alexander Alexandrovich, cosmology in modern context *(French)* 79−2581
Frohlich, H., biographical notes rel. to solid state physics develop. 80−57059
Gaede, Wolfgang, memories on 100th anniversary of birth 79−67133
Galileo, satellite predictions for Jupiter 79−88784
Gauss, C.F. Contrib. to astronomy 78−19
Gauss 78−8207
Gay-Lussac, biography 79−25815
Gay-Lussac, J.L., contribution to chemistry *(Russian)* 79−80407
Gay-Lussac, Joseph Louis, achievements in anal. chem. 79−49001
Gibbs (1839-1903) *(Czech)* 80−22180
Gilbert, geological methodology compared with Chamberlin 79−17182
Gilbert, Grove Karl, 1843-1918, life and contribs. to geomorphology 78−45451
Glaisher, James (1809-1903) 79−36
Goodricke, John (1764-86), variable star studies 79−44690
Gray, Stephen (1666-1736), astronomer 80−77601
Grigg, Emanuel Radu Newman, (1916-1976) radiologist and historian 80−42026
Hahn, Otto, discovery of nuclear fission 80−57063
Harriot, Thomas, 1560-1621, biography, astronomical instruments and obs. 79−35512
Heisenberg, the birth of quantum mechanics *(Polish)* 78−89291
Hell, Miksa (1720-92), Hungarian astronomer *(Danish)* 80−8766
Helmholtz, H. von, evolution of empiricism, study of a universalist 78−8212
Henry Norris Russell, and Hertzsprung-Russell (H-R) diagram 78−69957
Herring, Conyers, contrib. to solid state physics in 1930s 80−57056
Herschel, Friedrich Wilhelm, possible obs. of Uranus' rings 79−48733
Herschel, Sir William (1738-1822) and early investigation of nebulae 80−12876
Hirsch, Monroe J., Prentice Memorial Lecture [optometry] 80−27089
historical accounts, solar and lunar 79−80411
Holden, Edward S., founder of Astronomical Society of Pacific, California-Wisconsin astron. connection 79−75310
Holmes, Arthur and continental drift hypothesis 79−12559
Hornsby, Dr. Thomas Hornsby (1733-1810), private records of rainfall in 1767-1814 period 78−44948
Huygens, C., aviation history 80−31475
Infeld, Leopold, research on problem of motion *(Polish)* 79−35513
Jansky, Karl Guthe, and extraterrestrial radio emission detection 79−17144
Jeans, Sir James Hopwood (1877-1946) 78−32635
Jeans, Sir James Hopwood (1877-1946) 79−35
J.J. Thomson, mechanical interpretation of nature 80−57049
John Goodricke and variable stars 79−49005
John Tyndall's demonstrations on sound (1854-82) 77−22362
Joseph Everett, and King's College Observatory, Nova Scotia 79−34
Joseph Henry (1797-1878) *(Czech)* 79−44689
Judd's contributions to colour metrics and eval. of colour differences 80−94945
Kelvin, background, teaching motivation, demonstrations 80−42025
Kepler, Johann (1571-1630), Bibliographia Kepleriana. Supplements and continuation 1975-1978 78−77657
Kepler, Johann (1571-1630) and ephemerides of the early seventeenth century 78−77659
Kittel, Charles, 1978 Oersted medalist of the AAPT 79−97124
Klopsteg, Paul E, 1978 Oersted Medalist of the AAPT 79−97126
Kropotkin, Pyotr Alekseevich (1842-1921), meteorologist *(Russian)* 79−97167
Kuhne, Friedrich Wilhelm, (1837 to 1900), chem. processes in retina 78−20928
Kukarkin, Boris Vasil'yevich (1909-77), Russian astronomer *(Russian)* 80−101701
Lambert, J.H., self-taught scientist, life and work on cosmology 77−82354
Lambert, Johann Heinrich, 1728-1777, contribs. to philosophy, mathematics, astronomy and cartography *(German)* 79−17174
Lambert, Johann Heinrich (1728-77), planetary and cometary orbit determ. 80−42024
Landau, L.D., attitudes and advice to students 77−60885
Landau, Lev D., life and work 80−14
Lavoisier, du Pont families during French Revolution 80−57051
Lemaitre, Georges, cosmology in modern context *(French)* 79−2581
Levi ben Gerson on instrumental errors and transversal scale 78−21
Lise Meitner, nuclear pioneer 79−30184
Lyapunov, M.V. (1820-68), work as third Kazan astronomer (1840-55) *(Russian)* 79−88789
Lyapunov, M.V. (1820-68) and letters of A.M. Lyapunov to Dubiago *(Russian)* 79−88790
Mach, Ernst, autobiographical manuscripts as source material 78−86098

biographies continued
Marat, Jean Paul, medical use of electricity 80−17781
Marconi's scientific activity, role of his discoveries in radio research 79−17172
Marquis de Charbert (1724-1805) and Louisbourg Observatory 80−68010
Max Born, biography, review of contributions to physics 78−86100
Maxwell, development of ideas 80−27087
Maxwell, discoveries relevant to wireless and colour reconstruction 80−27093
Maxwell, diversity of interest across phys. sciences 80−27092
Maxwell, James Clerk, (1831-79) 80−27090
Maxwell, James Clerk (1831-79), EM field theory development 80−16
Maxwell, J.C., scientific contribs. and upbringing role 80−27091
Mayer, Tobias (1723-62), solar diameter obs. (1756-60) study 80−90389
Michell, John and early 'black hole' theory 79−44691
Michelson, Nobel Prize winner, work including Michelson-Morley expt. 77−13563
Millikan, Robert A., contribs. to physics teaching 78−69956
Millikan, Robert A., Nobel prizewinner, cosmic rays and support of science 79−62985
Mott, Sir Nevill, contrib. to solid state physics, 1933-40 80−57055
Mouchot, A.B., solar power harnessing *(French)* 80−105484
Newcomb, Simon, American astronomer, 1835-1909, life and works 78−93504
Newton, Sir Isaac (1642-1727), symposium (Cagliari, Italy, 3-5 October 1977) 79−62986
Newton and mutual gravitation of fixed stars 78−20
Noyce, R.N., technological innovation 80−51997
H.C. Oersted, first spark of electrotechnology, biography *(French)* 78−69955
p.-O. Lowdin's scientific and other activities 78−62023
Parsons, William (Third Earl of Rosse), reflecting telescope technology 78−18
Pauling, Linus 79−21514
Peierls, Sir Rudolf Ernst, solid state physics, 1928-1935 80−57054
Peierls and theoretical physics, symposium, Oxford, UK, (July 1974) 77−64909
Perrine, Charles Dillon (1867-1951) and Argentine National Observatory 77−37702
Perry, Rev. Stephen J. (1833-89), Jesuit priest, astronomer and teacher 80−46781
Perutz, Max, molecular biology origins, autobiographical review 80−57052
photographic researches of Hurter and Driffield 80−22181
Piaget, J., research and theory 79−49000
Pickering, E.C., Henry Draper Memorial and American astrophysics 78−86102
Pictet, liquefaction of air 79−40
Pienkowski, Stefan, scientific activity *(Polish)* 79−75311
Pigott, Edward (1753-1825), variable star studies 79−44690
Planck, Max Karl Ernst Ludwig (1858-1947), quantum and relativity theories 80−68008
Pohl, R., recollections of solid state physics 80−57060
Ptolemy (2nd century astronomer), reassessment 79−67131
Quetelet, A.L.J., life and spread of science in Belgium during 19th century *(French)* 78−65742
Regiomontan, Johannes, astronomer, life and work *(German)* 77−53726
Regiomontanus, Johannes, 15th century astronomer, life and works 78−20929
Romer, Ole (1644-1710), astronomical observatory at Vridslosemagle, Denmark *(Danish)* 80−8765
Rontgen's discovery of X-rays, accidents role in scientific enterprise 80−4502
Rosse, Third Earl of, reflecting telecope technology 78−18
Schmidt, Adolf, a correspondence with Albert Einstein, an archive discovery *(German)* 79−84924
Seitz, Frederick, biographical notes on early solid state physics 80−57058
Smiley, Charles Hugh (1903-77) 78−62024
Smyth, Charles Piazzi (1819-1909) at Cape of Good Hope 80−68011
Soddy, F., nuclear science, economics and social responsibility, holistic approach 80−90640
Stephen Gray, astronomer (1666-1736) 80−22182
Taylor, G.I., contrib. to EHD 78−86099
Ting, personal recollection of ψ meson discovery *(Polish)* 78−73820
Tobias Mayer, contrib. to observational astronomy 80−62438
Towneley, Richard (1629-1707) and regular rainfall meas. 78−36248
Tycho Brahe's solar observations 79−88785
Tyndall, John (1820-1893) 79−35511
Veitch, James (1771-1838) 77−29977
Wolf, M.N., astron. observatory in Gdansk, Poland, in 18th century *(Polish)* 79−88591
Zavoiskii, Evgenii Konstanovich, 1907-1976, life and work 78−24629
Zubov, Nikolai Nikolaevich (1885-1960), oceanologist *(Russian)* 78−86101

biological cybernetics *see biocybernetics*

biological effects of acoustic radiation
see also biomolecular effects of radiation; cellular effects of radiation
aircraft noise, effect on schoolchildrens' mental functions 79−70495
aircraft noise, effects on mental health 79−5316
aircraft noise and premature birth 79−5324
animal experiments on effects other than on hearing, review 79−5314
auditory nerve responses and cochlear microphonics in cats using pulsed US 78−61200
auditory sensitivity, loss following exposure to spectrally narrow impulses 79−96568
autonomic system activities 80−83700
autonomic system activity and performance on a psychomotor task in noise 80−89790
bean roots, non-thermal inhibition of growth and detect. of acoustic emissions, 1 MHz US 80−104643
bleeding, inner-ears of chinchillas, caused by simulated sonic boom 79−16247
blood cell banding in US standing wave field 79−62291
blood pressure, industrial noise effects on man, cardiovascular disease risk factors 79−5321
bone, piezoelectric effect on exposure to US, effect of sample rot. 78−80913
bone regeneration, morphology, effect of US 80−41111

biological effects of acoustic radiation continued
brain hyperthermia, reversible, during audiogenic seizures, rat 80−8098
brain lesion prod. threshold, influence of subarachnoid structures on transmeningeal US propag. 77−16952
cardiovascular function, effects of noise, rhesus monkey study 79−5322
catalyse and malate dehydrogenase, effects of US wares 80−76788
cells and tissues, mouse and human, biochem. effects of US irradiation 80−30764
cells of Chinese hamster, US treatment at high intensities and long exposures 77−5026
cellular inactivation by US, thermal and non-thermal components 77−48835
central nervous struct. stimulation in invertebrates by focused US 79−20576
chamber for microscopical obs. of biophysical effects of US 77−13039
chemotherapy enhancement by US, time/intensity studies using cell suspension and mechlorethamine 77−29175
children, auditory thresholds, noise exposure and biological factors 79−16219
chinchilla, threshold shifts following 3 days noise exposure 78−88712
Chinese hamster ovary cell colony size and giant cell form. after 1 MHz US irrad. 78−28000
Chinese hamster V-79 cells, US lethality obs. 80−85443
chromosome aberrations in vivo effect of US alone and in combination with X-rays 78−20210
cochlear, struct. and functional changes following US irrad. 80−89791
collagen synthesis stimulation, human fibroblasts, role of US-induced cavitation 80−85442
corn seed treatment with ultrasound, changes in production, yield, chemical composition 79−79597
defensive activation toward noise 79−5318
Drosophila eggs, killing on exposure to traveling and standing US wave fields 80−101223
duration subjective impression rel. to ambient noise 78−44554
E. coli, effect of US at 1.5 MHz 80−72212
E. coli B, combined US and gamma irrad. 78−20211
ear, acoustic-reflex dynamics for pulsed signals 79−20549
ear and hearing physical and psychological effects *(Spanish)* 78−15857
ear reflex threshold shift in chinchillas following a prolonged exposure to noise 79−100631
Elodea, cell death thresholds for 0.45-10 MHz US 80−67149
Elodea, US induced pulsations of gas-filled channels 79−53185
environmental noise, conclusions and recommendations of conf. Gothenburg 1977 79−5325
environmental noise, health effects of noise exposure, review 79−5313
environmental noise, medical effects, Conf., Gothenburg, Sweden, 1977 79−5311
environmental noise, review of non-specific responses in humans 79−5315
environmental noise exposure, medical effects, review of basic considerations 79−5312
erythrocyte membranes, US absorpt. in 12 to 68 MHz range 80−89727
erythrocytes, avian, US effects on transport 79−96613
eye and eye socket, short US pulse scatt. 77−37008
fibrosarcoma, hamster, absence of metastases following US treatment 80−35960
fibrous networks in viscous media, appls. of theory of acoustic motion 77−86733
genetically deaf animals, differentiation of infrasonic and sonic effects in mice 78−57037
growth retardation in Chinese hamster V-79 cells by 1 MHz ultrasound 79−62293
haemolysing action on erythrocytes 77−2019
hatching acceleration due to brief auditory stimulation, Japanese quail 77−48836
hearing, threshold shift in chinchilla from daily exposure to noise 77−36954
hearing damage formation as consequence of accumulated noise action *(German)* 77−77902
hearing effects of sports related noise or trauma 77−64057
hearing hazard from occupational noise, obs. on heavy industry workers 77−81512
hearing loss, noise-induced vasoconstriction rel. to pattern A personality 80−35917
hearing loss due to noise and sodium salicylate combined effects, obs. 77−52798
HF audiometry and noise-induced hearing loss 80−16960
high-intensity noise, after-effects of exposure 79−74685
human body, noise exposure effects *(Japanese)* 77−40709
human response to house vibr. caused by sonic booms or air blasts 78−90589
human whole-body, vibrations, biodynamic response and variability 78−92672
hyperthermia, deep local, induction by US and EM fields, problems and choices 80−94283
hyperthermia, nonintrusive meas. by US temperature tomography 79−53282
hyperthermia, US induced in previously X-irradiated sites 79−62315
hyperthermia in tissue-like substances, EM and US induction 80−98012
immunological effects of auditory stress 79−5323
industrial noise, biological effects other than on hearing 79−5320
industrial noise, effect upon hearing threshold 79−83801
infrasonic effects on man and construction of test chamber *(German)* 80−67147
infrasound, exptl. study of levels in transportation 78−88726
infrasound and pressure waveform generator, compact, for small cavity appls., animal research 80−104830
infrasound effects on task performance 77−56421
intracellular temperature distribution produced by ultrasound 80−61623
jet aeroplane noise, effects on facial expression, EEG and manual responses, human subjects 80−98006
leucocytes, human, US effects, sister chromatid exchange anal. 79−96612
LF noise, effect on people, review 78−92673
lipid bilayer, 1 MHz US effects on cond. and capacitance 78−77082
lymphocyte cell DNA damage by US diagnosis 80−67148
lymphocytes, human, effects of US irradiation 79−96609
mammalian cells, in vitro US irrad. at hyperthermic temps. 80−94282
mammalian cells and chromosomes in vitro, 65 kHz 78−40240
mammalian cultured cell survival after US exposure, synergism with X-ray effects 78−11693

biological effects of acoustic radiation continued
mammalian liver structural changes, US thresholds 79−48287
mammalian testes, US propagation 77−25507
mammalian tissue shear properties 77−29174
mechanisms of action of ultrasound on biological media and objects 80−21490
medical ultrasonics conference, Munich (May 1975) 77−32945
medical US and its biological effects 79−96614
microsonation effect on leucocytes, cell destruction critical threshold determ. 78−20212
mouse uterine smooth muscle, US induced contractions 79−25028
neutral response to LF tone-burst stimuli, determ. of freq. following response 79−83796
noise, air conditioning system, subjective responses and meas. 78−83168
noise, asymptotic threshold shift in chinchillas exposed to impulse noise 78−57019
noise, bias assessment in surveys of symptoms 79−3852
noise, effect of intermittent truck noise on deep sleep 79−5310
noise, hearing protection, types and limitations 78−55509
noise, industrial, hazard control programme 78−9490
noise, industrial deafness risk, British Government code of practice 78−55513
noise, statistical estimation of percentage of overexposed noise-impacted workers 78−92671
noise dose criteria for setting hearing loss risk estimates for industrial noise 78−1504
noise effects, specific and nonspecific, human hearing system *(French)* 77−21538
noise from road traffic, rel. to sleep disturbance 77−42659
noise near airport, sleep interference of residents 77−54843
noise of aircraft, effect on sleep of babies 77−77928
noise protection of occupationally exposed workers 79−92392
noise research index, for UK (1975/1976) 77−7257
noise-induced hearing loss, industrial 78−22223
noise-induced hearing loss estimation tables 78−15848
noise-induced threshold shift and cochlear pathology in the Mongolian gerbil 78−65035
nucleic acid component pulse sonolysis obs. 79−53186
nucleic acid components, low-intensity US effects 77−32874
oedema experimentally induced in rats by $AgNO_3$, effect of US on response 80−104642
pea roots, effects of localised US irradiation 79−48285
plant tissue acoustic microstreaming induced by Doppler foetal heart detector 79−62292
platelet aggregation induced by US under specialised conditions in vitro 80−45963
platelet morphology and function modification by US exposure 77−77929
porphyrins, effects of ultrasound on biosynthesis links 79−62184
pregnant mice, acute US exposure at different stages of gestation 80−94284
protein synthesis in human fibroblasts in vitro, US stimulation, role of cavitation 80−8100
pulsed US bioeffects 80−51155
pupa, Drosophila melanogaster survival after 1 MHz US exposure 79−88114
radiation hazards from emissions of thermal and nuclear power stations, comparative study 79−34460
reflex adaptation to combined steady-state and repeated pulse stimuli 78−44555
root growth, Zea mays, combined effect of US and cytotoxics 77−5025
root meristem cells, 2 MHz US effects on DNA, RNA and protein synthesis 77−9218
root meristem cells, Vicia faba, micronuclei induction, X-ray rel. to US exposure 79−96633
root meristem cells of Pisum sativum, increased G_2 duration after sonication obs. 80−56117
sleep, disturbance by noise 78−92645
sleep disturbances, noise induced, effects on health 79−5317
small peptide antibiotic and protein solns., US absorption 79−48286
soft tissue temp. increases due to US Doppler blood flowmeters, thermographic meas. 79−62294
sonoluminescence generation by US therapy equipment, in water and blood plasma 77−77930
squirrel monkey, temporary threshold shift from noise exposure 78−88715
startle reactions to simulated sonic booms, influence of habituation, boom level and background noise 79−39326
subjective analysis of acoustic noise *(German)* 79−46109
testicular tissue, mouse, morphological changes from in vivo US irrad. 80−35959
thermistor probe use to meas. energy distrib. in US fields 80−109075
thermocytes, rat, US-induced changes in rates of influx and efflux of K^+ in vitro 80−89793
thresholds for ultrasonic lesions, rabbit liver, kidney and testicle 77−81527
thyroid substances levels in blood serum of rats exposed to 0.2, 0.6 and 1 W/cm^2 of US energy 78−69134
tissue damaging effects of US 77−21559
transients generated by laser pulses, mechanism and effects 78−48830
transkull transmission of an intense focused US beam, lesion production at 500 kHz 80−89792
tumour irradiation with intense US, hamster 80−8099
tumours, spontaneous, in dogs and cats, treatment by ultrasound-induced hyperthermia 79−62290
ultrasonic waves, postpartum survival of mice exposed 'in utero' 79−96610
underwater noise spectra produced by fishing boats affecting albacore catch, comment 80−58844
urban noise, field study, noise sources, effects on humans 79−5319
US, 1 MHz, lysis and viability of cultured mammalian cells 78−7384
US, 2 MHz, effects on growth and mitotic index of Pisum sativum roots 78−7385
US, bibliography 78−7417
US, review 79−66498
US, status and problems of methods used in microbiology 80−21592
US activation effect on gas-filled intercellular channels of Elodea leave at 1 MHz 78−24093
US beam, intense-focused, transkull transmission props. 78−24090
US cavitation emission from insonated plant tissues 78−59185
US effects on experimental bruising in guinea-pig pinna 79−16248

biological effects of acoustic radiation continued
US effects on plant root growth, cavitation mechanism 80—21489
US effects on pregnant mice and embryos in utero 78—35880
US in medical diagnosis, theory and advantages 78—92682
US in medicine and biology, review 77—66830
US irradiation from diagnostic instruments *(Japanese)* 78—80936
US micro streaming, in vivo intravascular mural thrombi formation, drug screening appl. 78—24091
US perturbation obs. at cellular level 78—61214
US therapeutic level effect on HeLa cells 78—24092
US tissue characterisation practice and risk 79—48309
US tissue model, liq. mixture component selection aid 77—78066
US toxicity, effect on adult mortality and litter size of mouse 78—69135
uterus, mouse, US irradiation at therapeutic intensities in standing wave fields 80—41112
visual field displacements evoked by intense sound exposure, humans 78—85332

biological effects of gamma-rays
see also biomolecular effects of radiation; cellular effects of radiation
abdomen, pig, therapeutics of intense irrads. 80—67167
absorbed dose estimeates in prolonged ^{137}Cs γ-irrad facility for mice 80—101233
acute radiation lethality, evidence for a decreased susceptibility in young lambs 80—108962
adenovirus, decreased repair after γ-irrad. when infecting Xeroderma pigmentosum fibroblasts 80—61650
alcohol dehydrogenases, yeast and horse-liver, radiation chem. evidence for differences in amino acid composition 78—40116
alkaline endonuclease activity in thymus and spleen of irrad. mice 78—28004
alkaline phosphatases in serum, as indicators of radiation damage in rats 77—86556
amino acid, in polycryst., γ-irrad. induced radical pair form., 77K, EPR obs. 78—85292
D-amino acid oxidase, crit. residues, pulse radiolysis and inactivation study 78—27897
amino acid radioracemisation, geochem. and cosmochem. implications 80—45975
amino acid stimulatable transport system in rat liver after hole-body γ-irrad. 78—65098
amino acid transport hormonal control in liver of rats exposed to whole-body γ-irrad. 78—65099
amino acid transport in lymphoid cell lines, differences in ionising irrad. effects 80—72264
amino acid transport in rat liver after whole-body gamma irrad. 77—9232
α-amino acids, γ-irradiated, primary oxidation products, ESR and ENDOR 77—48754
amino acids, aq. solns. EPR of spin-trapped radicals, hydrated electron reactions 78—27796
amobarbital, radiation-prod. free radicals in pyrimidines, EPR 77—25374
dAMP.dTMP costacking complexes, charge migration, computer-assisted EPR 77—86446
aneurysmal bone cyst response to low doses of ^{60}Co gamma radiation with prolonged treatment 78—73196
Asiatic clams, biocide expts. using ^{60}Co source 79—16255
aspartate transcarbamylase, solid, enzyme activity and allosteric characts. after gamma irrad. 78—53341
aspartate transcarbamylase, solid, sedimentation and subunit interactions, after gamma irrad. 78—53342
Aspergillus nidulans, mutation induction by γ-irradiation in presence of O_2 or N_2 80—94297
autotrophic microorganism, repair of potentially lethal γ-ray damage 80—3735
bacteria survival, E. coli effect of membrane fluidity 77—21568
bacterial cells, heavy ion irrad., long range effects, comparison with γ-irrad 80—101236
bacteriophage, gamma-ray induced cross linkage of DNA and protein 77—21485
bacteriophage DNA and protein cross-linkage by ^{60}Co gamma-rays 78—77002
bacteriorhodopsin chromophore, bleaching by ^{60}Co γ-rays 80—30784
barley coleoptile growth behaviour under low LET radiations 79—88122
barley seeds, effects on enzymes 79—83856
barley seeds, interaction of radiation exposure, O_2 and seed water content 80—30778
barley seeds, minimum γ-exposure and O_2 concs. to produce post irrad. O_2 damage enhancement 80—30779
barley varietal differences in repair of induced lesions 80—104647
beams, sensitivity and mutability under gamma rays and EMS 80—26262
beef, irradiated, failure to induce genetic alterations in Drosophila 80—17009
blood, elemental variations following gamma ray injury of mice, PIXE anal. 77—48973
blood adenylate energy charge changes of lymphocytes, platelets, erythrocytes 79—57718
blood extracorporeal irradiation with ^{137}Cs, expt. research and clinical appl. *(German)* 78—69149
blood plasma antiheparin activity changes after irradiation 79—57717
bone marrow cell inactivation with ^{60}Co γ-rays, depth-related differences 78—7406
bone marrow colony-forming units in beagles, response to whole-body γ irrad. 79—25043
bone marrow electronic cell sizing and counting, biological dosimetry of irradiated rat 79—100744
bone marrow-engrafted mice, survival after irrad. 80—104681
bowel muscle, rat, adrenalectomy and whole body irradiation obs. 79—100676
Bowman-Birk soybean proteinase inhibitor, gamma irrad. 78—53343
brain tumour, rat, RBE of cyclotron fast neutrons rel. to ^{60}Co γ-rays 80—76797
Bramley's Seedling apple, positions of mutated sectors in shoots from irradiated buds 80—30777
breast carcinoma, appearance of non-specific suppressor cells in the blood after local irradiation 79—20597
breeding performance of female mice, comparative effects of ^{60}Co γ-rays and ^{239}Pu α-particles 80—72231
breeding performance of guppy, effects of chronic irrad. 77—86546

biological effects of gamma-rays continued
broad bean, low dose effects on growth and yield of 2 cultivars 80—81653
bronchial tumour reaction to combined neutron-telecobalt therapy 79—20642
capillary blood flow, long-term effects of ^{60}Co gamma and fission spectrum neutrons, mouse 78—80927
capillary endotherlial cells, repair of sublethal radiation damage, beagle cornea 79—100672
carcinogenesis, beagle dogs exposed to ^{226}Ra and ^{90}Sr 79—66487
carcinogenicity of inhaled air-oxidised $^{239}PuO_2$, rat obs. 79—66492
cardiac arrhythmias, chronic, produced by focused ^{60}Co γ-irrad. of canine atria 80—41136
cardiac ultrastructural effects, aged mouse, fission spectrum neutrons rel. to γ-rays 80—41138
cell inactivation, depth-related, serum-mediated differences 79—96629
cell nucleoside effect, dependence on LET 80—35980
cell survival, fractionation and dose-rate effects at lowered temps. 78—28013
cell survival, mol. theory anal. of synergistic interaction with Pt complex 77—21565
cells, conference, Tokyo, Japan (Apr. 1979) 80—27034
cells, human, multinucleate and micronucleus formation obs. 80—72219
cells, human, radiosensitivity, comparative study with different statistical models 80—108967
cells, lack of lethality threshold obs. 80—76810
cellular slime moulds, effects on species-specific cell sorting-out 77—44720
cervical spinal cord, radiation myelopathy, time, dose and volume factors 79—20658
cervical stage III carcinoma treatment, two regimes with same TDF but differing morbidity 78—53474
Chinese hamster cell, γ-dose survival, seasonal variations 79—43959
Chinese hamster cells, ^{60}Co-irrad., computer anal. of survival curve data 78—85344
chondromucoprotein, effects of ^{60}Co γ-irrad. 78—7400
chromatin extracted from cultured mammalian cells, gamma radiolysis, DNA alkali-labile strand damage 78—77003
chromatin from cultured mammalian cells, radiolysis, DNA-protein cross-links formation 80—81655
chromosomal proteins from Yoshida ascites tumour chromatin 79—96626
chromosomally aberrant cells, Japanese A-bomb survivors, dose-response relationship of neutrons and γ-rays 80—94295
chromosome aberration form. by gamma irrad. in lymphocytes, protection by free radical scavenging 78—20216
chromosome aberrations, dose-effect relationship, population exposed to increased natural radioactivity 80—72254
chymotrypsin-like proteins, γ-irrad. rel. to UV irrad., unfolding obs. 80—35984
chymotrypsin-like proteins, gamma irrad. induced struct. changes 77—44594
chymotrypsin-like proteins, gamma-irrad., inactivation rel. to struct. changes 77—56341
clonal survival curves with cellular recovery, parameter fitting 77—56352
clonal survival model generalisation for fractionated irrad., Chlorella example 77—2029
Coastcross 1 bermudagrass, induced mutant with improved winterhardiness 80—104645
cockroach, reproductive behaviour, pheromone production and release 78—85341
concanavalin A-carbohydrate interactions, implication of protein aromatic amino acids, radiolysis 78—40110
continuous diploid yeast cultures, radiosensitivity to continuous ^{60}Co gamma-ray exposure 77—52843
corneas, canine, γ and negative pion irradiation of microvasculature 79—43964
coronary arteries and aorta, late ultrastruct. changes after irradiation, mouse 79—57725
corpus luteum, human, influence of therapeutic pelvic irrad. on form. and function 77—5035
cotton fibre grown from γ-irrad. seed, struct. and conform., using spin labels 77—81539
crypt system, mouse, alternating fractionation formula of cumulative radiation effect 80—104652
cumbu seeds, effects on R_1 and R_2 progenies 79—29571
cytidine-5′-monophosphate, γ-irrad. aq. soln., spin-trapped radicals, liq. chromatography and EPR spectroscopy 78—53340
cytosine monohydrate single cryst., ion radical recomb., EPR 78—15776
deoxyribonucleoprotein, gamma-ray protein damage 78—53338
deoxyribonucleoprotein, thin fibres revealed after γ-irrad., calf thymus 80—30794
diploid yeast, liquid-holding recovery, nature of damage 79—16256
diploid yeast, O_2 effect in killing by photon irrads. of different energies 80—36018
diploid yeast cell ribosomal RNA gene inactivation curves and cross-sections 80—26297
DNA, 2-deoxy-D-erythro-pentonic acid isolation from alkali-labile site 78—20144
DNA, γ-irrad. at 77K, effect of visible light, EPR 77—52744
DNA, alkali-stable, lesion excision repair by γ-endonuclease Y enzyme 79—92145
DNA, calf-thymus and superhelical PM2 aq. solns., electro-optic obs. of γ-irrad. damage 80—85452
DNA, cytosine ^{14}C-2 labelled, gamma radiolysis products from N-glycosidic bond rupture 77—9171
DNA, damage from ionising radiation 79—11987
DNA, enzymatic digestion, separation by ion exchange chromatography 78—85290
DNA, Escherichia coli, γ-irradiation induced damage, enzyme labile sites 80—35993
DNA, gamma irradiated biologically active double stranded, alkali labile sites, post irradiation effects 80—35991
DNA, gamma-ray effects on hydration, PMR of frozen and liq. solns. 78—27900
DNA, N-formamido group formed in place of thymine fragment, evaluation method 80—30790
DNA, properties changes caused by UV- and γ-irrad., electrochem. anal. 80—72271
DNA, radiation-induced strand breaks in deoxygenated aq. solns. 80—61649

- **biological effects of gamma-rays** continued
  - DNA, single-stranded, alkali-labile sites and post-irrad. effects induced by H radicals 78—68994
  - DNA, single-stranded, in aq. soln., alkali-labile sites 77—9170
  - DNA, UV and gamma-ray damaged, defective repair in Fanconi's anaemia 77—44725
  - DNA and polynucleotide hydration, NMR of frozen H_2O and D_2O solns. 77—21484
  - DNA break rejoining capacity rel. to mouse age 78—69148
  - DNA chain growth in vivo in intestinal crypt cells, effect of ^{60} gamma and hydroxyurea 77—66795
  - DNA costacking nucleotides, γ-irrad., charge-migration phenomena, EPR obs. 80—36015
  - DNA damage and repair in γ-irrad. rat brain tumour, detect. by S_1 nuclease 78—48838
  - DNA double-strand breaks, temporal local denaturation 78—48754
  - DNA double-strand breaks during γ-irrad. of Micrococcus radiodurans, O_2 effects 78—7393
  - DNA end group characterisation after low dose γ-irrad. of thymocytes 78—11613
  - DNA films, free radical EPR, rel. to X-ray induced luminesc. and optical absorpt. 77—5033
  - DNA hydration characts. in H_2O/D_2O frozen solns., γ irrad. effects, PMR 78—31772
  - DNA inactivation by γ-rays in vitro, O_2 effect in presence of metalloporphyrins 79—92303
  - DNA interaction with nucl. non-histone proteins 78—7401
  - DNA molecule, radioprotection by oxide-reduction coenzymes 78—40274
  - DNA repair after γ-irradiation, action of hyperthermia in HeLa cells 79—100577
  - DNA single strand break yield and survival curves for E.coli B/r 80—26282
  - DNA single-strand breaks, ultra-fast repair in γ-irrad. Chinese hamster cells 77—21569
  - DNA single-strand breaks in preheated cells irrad. under N_2 and N_2O saturation 78—28017
  - DNA single-strand breaks in rat thymocytes due to irrad. histidine and γ-rays 77—56438
  - DNA strand breakage, prod. of monophosphate end groups 77—32873
  - DNA strand breaks in ^{60}Co γ-irrad. thymocytes 78—7395
  - DNA strand breaks in developing rat brain and their repair 80—30786
  - DNA synthesis, nucl., in yeast, UV and gamma-ray effects 77—56428
  - dominant lethality in spermatogonia of mice after acute and chronic gamma-irradiation 79—25039
  - dose assignment criteria, beagles, bilateral exposure to ^{60}Co γ-rays 79—16305
  - dose fractionation in housefly larvae irradiation, effect of caffeine on sparing effect 79—100679
  - dose-rate effects on performance and blood press. in monkeys exposed to ^{60}Co 77—81540
  - dose-response relationship of neutrons and γ-rays to leukemia incidence, atomic bomb survivors 80—36148
  - double strand breaks, protein cross-links, induced by fast neutrons, γ-rays 79—66446
  - Drosophila germ cells, decrease of γ-induced mutations by visible light 80—67159
  - E. coli, photoreactivable component in the mutagenic action of ionising radiations 80—72225
  - E coli, photoreactivation following ionising irrad. rel. to Cherenkov emission 80—108969
  - E. coli, relative rates of repair of single-strand breaks and postirradiation DNA degradation 79—16149
  - E. coli, UV-induced recovery of γ-irrad. bacteriophage DNA 80—72214
  - E. coli, value of photoreactivable component after exposure to ionising radiation 80—72224
  - E. coli B, combined US and gamma irrad. 78—20211
  - E. coli B/r radiosensitisation by paracetamol, mechanisms 77—86544
  - E. coli fatty acid auxotroph, factors influencing survival after γ-irradiation 80—17007
  - E. coli strains, two with lambda lysogens, induced radioresist. 78—69140
  - E.coli, radiation killing, role of membrane fluidity, hypothermia and local anaesthetics 80—104653
  - egg, sea urchin, radiation-induced mitotic delay rel. to S-phase 79—96625
  - eggs, F_1, of Chilo partellus, embryonic development and induced dominant lethality 77—5042
  - Ehrlich ascites tumour cell mitotic activity, H_20_2 and gamma-ray effects 77—52854
  - Ehrlich ascites vital cell UV primary fluoresc. rel. to ^{60}Co γ-ray dose 78—69142
  - embryo survival and development, rats, compared with extended-Bragg-peak He ions 77—12961
  - embryonic bone and cartilage, effects of in vitro gamma irrad. 78—65089
  - embryonic development and nucleic acids in trigeminal neurons, rats 80—72270
  - emesis ED_{50} determination, rhesus monkey obs. 80—104678
  - energy metabolism of blood morphotic elements, ionising radiation effects 80—61645
  - energy transfer in biological model structs. *(German)* 78—15906
  - enzyme activities of kidney after gamma irrad. 77—12976
  - EPR studies using aqueous LiCl glass as neutral matrix 79—96632
  - erythrocyte membrane, spin-label study of γ-irrad. effect 80—51168
  - erythrocyte radiosensitivity for cells with increased level of superoxide dismutase 77—44726
  - erythropoietin action, identification of two components by irrad. in vitro 78—65094
  - Euglena cells, light and dark grown, sensitivity to gamma-irradiation 80—35989
  - Euglena gracilis, differential response in light and dark 79—57710
  - Fasciola gigantica infectivity to hamsters, effect of ^{60}Co γ-irrad. 80—85451
  - fast neutron and photon therapy, randomised clinical trials 79—20638
  - ferric haemoglobin, EPR studies before and after irradiation 79—29503
  - feto-placental tissues, irrad. effects after treatment of material genital carcinoma 80—45964
  - fibrinogen solution, effect of scavengers on radiation-susceptible sites 78—11701
  - fibroblasts human, non-transformed, ionizing radiation effect on life span 80—41125
- **biological effects of gamma-rays** continued
  - fibrosarcoma cells, murine, separated by centrifugal elutriation, radiation sensitivity obs. 80—76808
  - finger-millet, induced mutagenesis obs., chlorophyll mutation freq. and sepctrum 80—30776
  - fish fin regeneration after amputation, effects of prior irradiation 80—30792
  - fish immediate mortality after massive γ-ray exposure, Oryzias latipes 78—48837
  - flour beetle, interaction of hyperthermia and γ-rays 78—31867
  - fluoresceindiacetate hydrolysis and transport in mammalian cells 77—56333
  - foetus, human, effect of a high dose from ^{226}Ra 79—25104
  - food preservation *(Italian)* 80—89799
  - food preservation irrad. systems 77—70508
  - free-ranging animals exposed to 300 R, behaviour and mortality 77—56435
  - gamma-ray dose rate conversion and buildup factors 79—34671
  - gastrointestinal crypt stem cells, murine, single-dose—response curve 77—37022
  - genetic and cytogenetic effects in mice fed on gamma-irrad. wheat 77—86545
  - gliovascular interphase in irrad. brain tissue, horseradish peroxidase transport 80—41119
  - gliovascular interphase in irrad. brain tissue, phosphatases location 80—41120
  - glyceraldehyde-3-phosphate dehydrogenase radiolysis, active-site and SH loss 78—77000
  - gonadal changes in Uta stansburiana lizards 80—36001
  - graft-versus-host reactivity, single irrad., bone marrow reconstitution and continuous irrad. 77—9229
  - gram (cicer arietinum L.), γ irradiation effects 79—34609
  - green alga, 2 species of Sirogonium with different chromosome types 80—81651
  - gustatory function, radiation-induced changes, neutrons rel. to photons 80—12184
  - haematological findings significance for medical exam. of radiation employee *(Japanese)* 79—11971
  - haematopoietic microenvironment, progenitor cells radiosensitivity, mouse expts. 80—45983
  - haematopoietic stem cells, effects of dose rate, mouse bone marrow 79—100674
  - haemodynamics after ^{60}Co exposure in monkeys rel. to performance decrement 77—81541
  - haemoglobin, bovine type A, γ-induced changes obs. 79—43811
  - haemoglobin aqueous solutions, γ-irrad. in air and Ar 80—41135
  - haemopoiesis, kinetic basis for compensation during continuous irrad. with low doses 80—36010
  - head and neck, advanced cancers, low dose rate irradiation 79—34649
  - heart, ultrastruct. changes, fission neutrons vs. ^{60}Co gammas, mouse 77—5047
  - HeLa cells, first postirrad. division obs. 80—72258
  - heritable lesions, radiation induced, in proliferating mammalian cells, review 79—20602
  - herpesviruses, survival and immunological characts. 78—77089
  - high LET constraints on low LET radiation survival 80—12199
  - hormones rel. to drug-metabolising enzymes in liver, whole- and partial-body irrad. 78—48840
  - housefly larvae, radiation-induced biochemical changes 80—30788
  - housefly pupariation, effects of single and fractionated doses 80—30789
  - human marrow, radiation dose deposition calcs. 80—26365
  - human whole body irradiation, fluence- and exposure-to-dose conversion 79—5371
  - hydra, elimination of interstitial cells 80—21495
  - hyperthermia and cancer therapy, 2450 MHz microwave and γ-radiation effects on flour beetle 79—2103
  - hypoxic cell radiosensitisation by respiratory inhibitors in in vitro tumour model 77—52852
  - intenstinal crypt cells, extreme sensitivity to X- and γ-irrad. 77—90864
  - intestinal proliferation after multiple fractions of gamma irrad. 78—20223
  - intestinal stem cells and crypts of γ-irrad. mice, cell-survival characts. 80—72255
  - intestinal tolerance in mice, effect of dose rate, implications in radiotherapy 79—29568
  - intestine, mouse, lack of correl. between villus and crypt irradiation damage 79—62300
  - intestine, protection by 2-mercaptopropionylglycine, mouse 77—90863
  - invertase, S-containing glycoprotein, gamma-irrad., secondary radical reactions, EPR 77—9175
  - irradiation doses, effects and sources of ionising radiations *(French)* 79—66494
  - jejunum, mouse, effect of hyperthermia on radiation response 79—25038
  - kidney enzyme activities, early effects after irrad., rat expts. 80—51162
  - L-cells, γ-irrad. effect on chromatin struct., mouse 80—30793
  - leaves of Kalanchoe daigremontiana, organogenesis delay obs. 80—104650
  - lethal doses, repair of radiation damage, mammals 78—11703
  - lethality of opossum 77—25521
  - life shortening in RFM and BALB/c mice as function of radiation quality, dose and dose rate 80—41134
  - liver, RBE of cyclotron fast neutrons and γ-rays for late hepatic injury in rats 80—108975
  - liver and hepatoma samples, EPR spectral anal. after irradiation 79—92289
  - liver biomembranes of gamma-irrad. animals, postradiation recovery 80—35976
  - liver chromosome aberrations, mice, effect of continuous intake of HTO 77—25518
  - liver microsomes, γ-induced lipid peroxidation and membrane-bound enzymes 80—104660
  - long-term effects on mice, partial body irrad., RBE of pion$^-$ rel. to ^{60}Co gammas 77—81537
  - low dose/dose rate RBE of ^{3}H β-rays and other low LET radiations 80—12190
  - low-dose RBE and quality factor for X-rays and gamma-rays 78—73175
  - low-level chronic irradiation, field irradiator for small mammal population studies 77—5126
  - lung, canine, relative effectiveness of fast neutron and ^{60}Co γ-ray irradiation 80—3737

logical effects of gamma-rays continued
lymphocyte, hog, energy metabolism effect of ionising radiation 79−92301
lymphocyte, human, dicentric yield, γ dose rate dependence calc. 79−92294
lymphocyte B and T cell membrane receptors, human effects of ^{60}Co gamma-rays 77−21575
lymphocyte chromosome aberrations and the Poisson distrib. 79−100675
lymphocytes, comparative radiosensitivity of T and B cells in mice 79−11968
lymphocytes, human, effects of heat and radiation 80−97864
lymphocytes, human, prediction of dose-rate effects for dicentric production by X- and γ-rays 80−72226
lymphocytes, human, sister chromatid exchanges obs. 80−41140
lymphocytes, human peripheral blood grown in γ-irrad. medium, sister chromatid exchanges 80−104658
lymphocytes, in vitro ^{60}Co gamma-ray response of leucoagglutinin stimulated human cells 78−57041
lymphocytes, pig, chromosomal aberrations after neutron and gamma irrad. in vitro 77−64095
lymphocytes and thymocytes, human, radiosensitivyt 77−37026
lymphocytes of man, rabbit and swine, chromosome aberrations induced by ^{60}Co gamma rays 80−56146
lymphoid cells, peripheral, functional changes after breast carcinoma radiotherapy 79−88125
lysosomal enzyme activation in gamma-irrad. mammary tumours 77−5050
lysosomal enzymes, pigeon tissue, effects of sub-lethal dose 80−98022
lysosomal hydrolase redistrib. in rat spleen homogenates 79−88132
lysosomal hydrolases of rat serum and spleen 77−52848
mammal gonads, radiation induced morphological and endocrinological changes *(Russian)* 78−77090
mammalian cell line sensitivities to hyperthermia, γ-rays and UV 77−66800
mammalian cell mutation and activation by radiations of differing LET 77−56431
mammalian cell radiosensitivity, effect of NaCl solns. containing radiosensitisers and radioprotectors 78−69146
mammalian cells, influence of radiation quality on effectiveness of small doses 80−30785
mammalian cells, thermal enhancement of γ-irradiation effectiveness of reproductive death induction 79−34509
mammalian cells in culture, continuous and fractionated irrad., growth rate effect 79−66493
mammalian cells irrad. with π^- and Co γ-rays, cell cycle progression 78−40269
mammary adenocarcinomas, effects on tumor cell survival after irradiation, mice 79−25036
mammary carcinoma C3H response to fractionated irrad., rel. to fractionation number and intertreatment interval 78−53453
mammary tumour, mouse, interstitial ^{226}Ra irradiation 79−57716
melanoma, B16, in mice, effect of hyperthermia alone and in combination with ^{60}Co radiation 80−72138
melanoma cell radiosensitivity in culture rel. to radiotherapy of malignant melanoma 77−73548
melanoma cell strains, human, γ-radiosensitivity and growth parameters 79−29574
melanoma treatment in hamsters using microwave hyperthermia, chemotherapy, and ^{60}Co radiation 77−77931
melanomas, effect of clinical irrad. regimes on human malignant tumours grown in athymic mice 78−24101
melanomas, human malignant, in athymic nude mice, effect of ^{60}Co gammas and DTIC 77−48839
metabolic and thermoregulatory effects of acute ^{60}Co γ-radiation in myomorph rodents 79−88134
microdosimetry, energy deposition distrib. patterns 79−20600
microtubule polymerisation in vitro, effects of ^{60}Co gamma irrad. 78−20222
mitotic accumulation of HeLa cells during continuous irrad., cinemicrography obs. 77−64094
monocytosis observation during ^{60}Co radiotherapy 77−70501
mung bean seeds, induced variation in resulting plant morphology 79−43960
mutations, specific locus, re-anal. of mouse data 77−21570
natural fats, effects on fatty acid composition and lipid peroxide formation 79−96623
natural radioactivity in Southwest France and its possible genetic consequences for mammals 80−36007
neoplastic and nontransformed human cell radiosensitivity 80−12194
neoplastic disease development in mice, dose-rate effects 80−76803
neoplastic disease development in mice, reticular tissue tumours 80−72259
neoplastic disease development in mice, solid tumours 80−76802
neoplastic disease in mice, comparison with neutrons, dose and dose-rate effects 77−12975
neoplastic transformation of 10T1/2 cells by ^{60}Co γ-rays 80−104659
nephropathy, neonatal whole body irrad. in growing dog, plasma renin activity and arterial press. 80−41132
nephropathy, neonatal whole body irrad. in growing dog, renal morphological and functional adaptations 80−41131
neutron radiotherapy, nature and significance of radiation outside beam 78−53477
normal tissue reactions, comparison with protons for fractionated dose schedules 78−31858
nuclear medicine, intrainstitutional mobile, health physics considerations 79−8546
nuclear-dockyard workers, radiation-induced chromosome aberrations 79−34606
nucleoside metabolism effects, Physarum polycephalum 80−30797
OER for bacteria and cultured mammalian cells irrad. in frozen state, γ and neutron irrad. 77−90856
one-hit chromosome exchanges 78−3566
oocyte nondisjunction in aged mice 77−16958
oocytes, bovine, late effects of ^{60}Co gammas, oocyte survival, follicular devel. and reproduction 77−9231
oral function changes in the rat, Na preference and fluid intake obs. 80−35986
ovarian cancer, comparison of ^{32}P and ^{60}Co in treatment of intraperitoneal implants in mice 77−56457
ovarian cortex effect of daily prenatal gamma irrad. in beagle pups 80−85453

biological effects of gamma-rays continued
papain inactivated by OH radicals and H_2O_2, optical density, amino acid composition and fluoresc. 78−53344
penicillamine-treated mice, survival following whole-body irrad. 80−98030
peroxidase, low-temperature radioreduction, MCD and absorpt. spectra 78−31763
photoreactivation in E. coli bacteria 77−29184
pigeons, effect of total-body irradiation 80−3736
pine tree seeds, effect in trees 10 years after germination 79−88119
pith cell, growth in vitro after γ irradiation 79−92295
plasma testosterone levels and hepatic drug metabolism, effects in the rat 80−45985
platelets, human blood, adenine nucleotide content and release reaction after ^{60}Co γ-irrad. 78−28021
pollen tube, pine, growth stimulation by low doses of radiation 79−100677
polygenic variation induced in wheat and rice 79−43962
polynucleotide hydration characts. in H_2O/D_2O frozen solns., γ irrad. effects, PMR 78−31772
polynucleotides, gamma-ray effects on hydration, PMR of frozen and liq. solns. 78−27900
polyribosome distribution in regenerating livers of irrad. adrenalectomised rats 78−7398
positional signalling in chick limb by high doses 78−44565
prairie pepperweed, chronic irrad. effect on production and viability of seed 80−81649
preservation of fruit and veg. 77−37015
preservation of potatoes and onions in Pakistan, feasibility 77−37014
primordial germ cells in embryos of Oryzias latipes 78−48843
primordial germ cells of fish Oryzias latipes, nucl. size changes 78−53451
public health aspects of radiation 79−88141
pulmonary metastases, artificial, of Lewis lung carcinoma, cell radiosensitivity 77−12978
pulmonary metastases of mouse fibrosarcoma, RBE of neutrons rel. to ^{137}Cs gammas 77−81536
purine and pyrimidine, γ-irrad. investig. by diffuse refl. spectrophotometry 77−48756
purine powder, dose-response curves 78−7215
pyri pyriformis,→pyriformis, 80−61648
pyrimidine powder, dose-response curves 78−7215
radiation, risk to health assessment 80−41124
radiation therapy, fractionation in ^{60}Co teletherapy, weekly intervals 79−34650
radiobiological aspects of supralinear photographic emulsions, modelling appl. 79−8549
radiotherapy treatment time and sub-lethal repair, CHO cell obs. 80−30773
radiotherapy with multiple daily sessions with ^{60}Co and 250 kV X-rays, clinical experience 78−53475
radiovaccine of S. typhimurium cells 77−56426
RBE and OER values from Vicia Faba root growth inhibition obs. 80−26271
RBE of megavoltage photon and electron beams for tail necrosis in mice 78−35886
RBE of protons rel. to γ-rays for human cells 80−30798
renal damage following perinatal gamma irrad. in beagle 78−31866
renal function in rat monitored low gamma camera 77−56454
ribosomes, E. coli, form. of covalent linkages between RNA and proteins *(French)* 77−56340
rice seeds, glucose metabolism effects 80−81650
RNA, messenger, synthesis in rat livers, ionising radiation and partial hepatectomy effects 79−92144
RNA of Novikoff Hepatoma ascites cells, effects of sparsely-ionising radiation after in vivo labelling 78−7389
RNA specific activity, Novikoff Hepatoma ascites cells 78−3560
RNA synthesis in regenerating liver of irrad. adrenalectomised rats 77−64087
sarcoma, dose fractionation studies on mice breathing air or O_2+CO_2 78−35889
sea-urchin egg radiosensitivity during early cleavage stages, split-dose ^{137}Cs γ-irrad. 78−7392
seasonal oscillation of radiosensitivity of cells in culture 78−7397
seed radiosensitivity of winter hexaploid triticale 79−20583
seedlings, Vicia faba, effects of different radiation types on growth *(German)* 79−43961
skin, pig, response to ^{137}Cs-irrad. 80−67161
skin γ and neutron responses, dose fractionation effects 79−20593
skin blood volume pulse in humans 77−5029
skin injury, pig, relationship of acute to late injury in fractionated radiation doses 79−34604
skin injury, pig, relative biological effectiveness of neutrons and γ-rays 79−34605
sleeping times induced by hexobarbital in rats, effect of ^{60}Co gamma-rays 77−56441
soft fruit cell walls, histochem. effects 80−81652
soybean plants, changes in export and distrib. of photoassimilated C 80−56139
soybean plants, radiation-stressed, photosynthesis and photophosphorylation rel. to photoassimilate export 80−56140
sperm cells of eri silkmoth, chromosomal breaks obs. 80−41123
spermatocytes, mouse, stage-sensitivity and dose-response 77−29182
spermatogenesis in sugarcane root borer, γ irradiation effects 79−34608
spermatogonia, stem and differentiating cells, ^{60}Co gamma-ray effect, postpuberal rat 77−25515
spheroids, V79, split-dose survival and cycle progression 77−56430
spleen damage by ^{125}I after partial thyroid blockage, rat expt. 79−96631
spores of Bacillus pumilus E601, radiation resist. changes 77−52846
sterilisation, ^{60}Co plant design for developing countries 77−60246
sterilisation of 4-5-day old pupae of Indian meal moth and effect on mating competitiveness 78−44563
sterility among female lizards exposed to continuous gamma irrad. 77−64093
sterility in fish, role of spermatogonia in recovery process 77−5038
sugarcane, evaluation of mathematical methods for optimum γ-dose prediction 79−29630
sweet cherry, ^{60}Co γ-induced mutations 80−56142
synchronous HeLa cells exposed to low LET radiation, OER 77−37019
synchronous HeLa cells in culture, dose-rate effects 78−28010
tapeworm eradication in pork and beef carcasses 77−70506

biological effects of gamma-rays continued
- testes, glucose 6-phosphate dehydrogenase studies following partial body γ-irrad. 78—80924
- testes, glycogen and metabolising enzymes following radiation-induced atrophy 78—15869
- testes, inorganic pyrophosphatase and pyrophosphate following γ-irrad. of rat 78—15868
- testes, isocitrate dehydrogenase studies after partial-body γ-irrad. 78—80923
- testes, mice, comparative effects of various radiations on weight loss and spermatogenic stem-cell survival 80—108976
- testes, monovalent electrolytes rel. to radiation injury of germinal epithelium 78—31862
- testes, morphological changes after long term γ-irradiation in mice *(Russian)* 79—20601
- testes, rat, serum FSH, LH, and testosterone levels after ^{60}Co γ-irradiation 80—21499
- testicle, influence of duration of Ra irrad. 78—3556
- testicles, mice, combined action of acute and chronic gamma irrad. 80—72241
- testicles, rat, comparison of acute and chronic gamma irrads. *(Russian)* 80—72240
- testicular stem cell, mouse, regeneration after γ irradiation 79—25048
- testis, house sparrow, effect of ^{60}Co external irrad. after testosterone propionate administration 80—101232
- testis mass loss, mouse, induced by tritiated thymidine, tritiated water, ^{60}Co γ-irradiation 79—39452
- testis radiosensitivity, rel. to alternating rhythm of cellular mitoses 78—3557
- testis weight loss following high energy neutron or γ irrad., mouse expts. 80—35985
- Tetrahymena, γ-irrad., role of DNA damage and repair in eukaryotic gene function 80—104677
- Tetrahymena pyriformis, γ-irrad., release of thymine base damage from DNA 80—72268
- thymidine, frozen aq. solns., final products of gamma radiolysis 78—77001
- thymidine monophosphate, gamma irradiated, inorganic phosphate release, in presence and absence of O_2 80—67168
- thymidine monophosphate aqeous solution, gamma irrad. effect on base damage, phosphate release 80—89806
- thymidine-5-monophosphate, γ-irrad. aq. soln., spin-trapped radicals, liq. chromatography and EPR spectroscopy 78—53340
- thymine, EPR study of post-radiolysis growth of spin-trapped radicals 79—16155
- thymine aq., and N_2O solns., radiolysis products anal. 80—30257
- thymine fragment damage retained in DNA polynucleotide chain after γ irrad. in aerated soln. 78—31773
- thymocyte membrane props. modification by hyperthermia and gamma-rays 78—69017
- thymus dividing cells, recovery response, in whole-body gamma-irrad. mice 77—12968
- thyroid radiobiological response, sheep cells, single X- and γ-doses 80—41122
- tight junction disruption and recovery after sublethal γ-irrad. 80—36027
- tissue neutron and gamma-ray response function, mid-head, military appl. 80—8185
- tobacco plants, enhanced bud formation after γ-irradiation 79—48293
- tomatoes, effect of presown seeds irradiation on crop yield and productivity 77—70509
- Toxoplasma gondii, effects of ^{60}Co irradiation and its use in expt. immunisation 80—3731
- Tradescantia clone 02, dose-response curve for pink somatic mutations 77—16959
- transcriptase switch-on perturbed by ionising radiation 80—3733
- trypsin, in suspension, radical form. and inactivation 78—3564
- tsetse fly, effects on reproductive biology 79—62303
- tumour and normal tissue of γ-irradiated mice, EPR spectra comparison 79—53193
- tumour cells, Ehrlich ascites, lethal effects of ^{64}Cu-bleomycin complex 79—57709
- tumour cells, human, from pancreatic carcinoma xenograft, in vitro and in vivo radiosensitivity 77—5041
- tumour curability rel. to vol. in murine carcinoma and sarcoma 78—61215
- tumour incidence and longevity in neutron and γ-irrad. rabbits, RBE assess. 80—104661
- tumour model in vitro, repair and reoxygenation following irrad. 77—44727
- tumour recurrences, immunogenic and nonimmunogenic, time distribs. following local irrad. 78—65090
- tumour regrowth after irradiation in rat hepatoma 79—92292
- tumour-bearing mice, selective protection of normal tissues by irrad. in hypoxic hypoxia 77—5051
- UDPG-dehydrogenage, rat liver, struct. alterations and functional vars. 78—15873
- uracil metabolism in golden hamster 77—40714
- uridine 5'-phosphate (Na salt), NO_2 species in an irrad. single crystal, EPR obs. 80—40719
- uridine-5′-monophosphate gamma-irrad. solutions, short-lived radical detect. by spin-trapping method 77—21479
- valyl-h-tRNA synthetase of chick embryo brain, ^{60}Co γ-irrad. obs. 80—72222
- valyl-tRNA synthetase from chick embryo brain, effect of ^{60}Co γ-radiation 79—34490
- Vicia faba, comparative effects of ^{125}I and ^{192}Ir γ-rays 80—51164
- Vicia faba roots, comparison of effect of ^{125}I and ^{182}Ta gamma rays 78—48832
- Vigna sinensis, effect of irrad. on callus growth 80—45966
- water, X- and γ-irrad., electron slowing-down spectra and photon RBE 80—12197
- wheat, germinating, effect on formation of α-amylase isoenzymes 80—56143
- wheat seedlings, effect on growth and abscisic acid concs. 79—29570
- whole-body monitors, shadow-shield, accuracy of person internal contamination determ. *(Czech)* 78—35962
- yeast, diploid, liq.-holding recovery in stationary and log phase cultures 77—2028
- yeast, diploid, radiation sensitive mutants, γ-ray response and recovery obs. 80—101227

biological effects of gamma-rays continued
- yeast, hyperthermic inactivation and interaction of hyperthermic and γ-irradiation damage 79—96518
- yeast cell suspensions, lethal and genetic damage, comparison with vac. UV 77—21573
- yeast cells, elevated temp. effect on radiation sensitivity 79—79610
- yeast cells, reparable and irreparable damage induced by sparsely ionising radiation 80—51167
- ^{252}Cf in radiotherapy, RBE-dose rate relationships 77—5030
- ^{252}Cf in radiotherapy, RBE vs. dose-rate relationships 77—9222
- ^{60}Co dosimetry for beagles in Collaborative Radiological Health Lab., long-term study 77—73585
- ^{66}Ga tumour uptake in rats after whole-body ^{60}Co irrad. 78—65081
- ^{67}Ga, prod. for medical uses using Ruder Boskovic Institute cyclotron 78—20273
- ^{192}Ir, accidental over-exposure to industrial radiography source 77—56472
- ^{192}Ir radiographic source, radiation accident 78—53514
- K^+ permeability of E. coli, membrane lipid role in radiation damage 78—48834
- O_2 effect, rel. to cellular glutathione 78—31861
- O_2 enhancement effect, photo-reactivation of γ-radiation damage 78—77087
- Pu, toxicity, cancer risk. calc. 77—2025
- ^{81}Rb/^{81m}Kr, prod. for medical uses using Ruder Boskovic Institute cyclotron 78—20273

biological effects of ionising particles
- *see also biomolecular effects of radiation; cellular effects of radiation*
- alcohol dehydrogenases, yeast and horse-liver, radiation chem. evidence for differences in amino acid composition 78—40116
- alpha particles, $^{239}PuO_2$, cancer risk, max. permissible conc. in air 79—25108
- alpha radioactivity per cigarette smoke particle 77—29181
- alpha-dose rates, upper limit calc. method for aquatic organisms, re ^{239}Pu, plankton 79—2133
- alpha-emitting radionuclides in bone, particularly ^{226}Ra and ^{239}Pu, dosimetry 77—16993
- D-amino acid oxidase, crit. residues, pulse radiolysis and inactivation study 78—27897
- amino acids, high energy radiation effects and chemical evolution 77—63937
- amoeba, combined effects of thermal neutrons and agents which interact with DNA 78—20219
- amoeba irradiated by thermal neutrons, absorbed dose estimation 78—53449
- anoxic kidney cell sensitivity to 35 MeV electron single pulses 80—26292
- aqueous tissue equivalent soln., alpha particle stopping power, 0.5-8 MeV 78—40334
- Artema eggs, SEM hatching obs. 80—35998
- Artemia eggs, effects of 645 MeV and 9.2 GeV protons 80—45969
- arterial wall damage, fast neutrons vs. X-rays 77—29183
- bacterial cells, heavy ion irrad., long range effects, comparison with γ-irrad 80—101236
- bacterial culture viability under negative ion irrad. in elec. field *(Russian)* 79—83855
- bacterial spores, loss of optical density due to partial cell electron irrad. 77—32943
- bacterial spores, thermorestoration of mutagenic radiation damage 79—20524
- bacteriophage T1 radiosensitivity on various host strain mutants of E. coli 78—20228
- bacteriophage T7, radiation inactivation 78—65083
- barley coleoptile growth behaviour under low LET radiations 79—88122
- beta dose in skin from gaseous radioactive reactor effluents 80—26364
- beta emitters, insoluble, ingested, dose to gastrointestinal tract 78—65134
- beta irradiation of beagle dogs, early lung damage indicators 80—17018
- beta rays, thymus and spleen of Indian desert gerbil, ^{45}Ca injection 80—8106
- beta-decay, chem. and biological consequences 78—28018
- beta-emitting radionuclides from reactor accident, ingestion, acute toxicity 78—65082
- beta-rays, high-energy, hazards to eye lens and gonads 78—65131
- beta-rays from ^{14}C, biological hazards, cell killing effects, E. coli expts. 80—89805
- beta-rays from ^{45}Ca, effects on bone marrow of Indian desert gerbil 80—45971
- bilirubin, aq. soln., pulse radiolysis 78—48761
- blood cell permeability to K^+, Na^+ repair after X-ray, fast-neutron damage 79—57615
- blood plasma antiheparin activity changes after irradiation 79—57717
- bone cancer induction by α radiation 78—15871
- bone marrow, effect of a 600 MeV neutron beam, mouse 79—96630
- bone marrow cell-culture, RBE of different-energy neutrons 79—34508
- bone marrow cellular survival parameters, neutron kerma factors 80—51176
- bone marrow stem cells of C_3H mice, long term radiation effects 80—30787
- brain, caudate nucleus, neutotransmitter activity transient alterations after electron irrad., rat expts. 80—72267
- brain, irradiation with C ions, recovery from pot. lethal damage, rat expts. 80—72234
- breeding performance of female mice, comparative effects of ^{60}Co γ-rays and ^{239}Pu α-particles 80—72231
- bremsstrahlung yield produced by 4 MeV linear electron accelerator calc. rel. to hazard in radiolysis 79—76181
- bronchial cancer induction by α-emitting warm particles 78—96078
- bronchial tumour reaction to combined neutron-telecobalt therapy 79—20642
- cancer deaths among classified radiation workers, obs. and anal., proposed survey 77—2027
- cancer treatment using neutron 77—40733
- cancers, genetic defects, resulting from use of various energy sources 79—16259
- capillary blood flow, long-term effects of ^{60}Co gamma and fission spectrum neutrons, mouse 78—80927
- carcinogenesis, beagle dogs exposed to ^{226}Ra and ^{90}Sr 79—66487
- carcinogenesis, fission neutron produced, influence of chronic environmental stress 77—25516
- carcinogenesis, multiple simultaneous event model 78—11705
- carcinogenesis by fission neutrons, RBE rel. to γ-rays 79—70588

biological effects of ionising particles continued
- carcinogenetic risk estimation, comparison of radiation therapy and chemotherapy 79—20592
- carcinogenicity of inhaled air-oxidised $^{239}PuO_2$, rat obs. 79—66492
- catalase, glucose embedded, measurement and reduction of radiation damage in frozen hydrated crystalline specimens 80—89810
- catalase, solid state, electron microscopy radiation damage, amino acid composition 77—25377
- cell inactivation and mutations, Al ultrasoft X-rays vs. different LET radiations 77—86543
- cell killing by π^- on glass and plastic surfaces 79—92305
- cell progression, in broad bean roots, monoenergetic neutron effects 78—65086
- cell survival, hyperthermia interactions with radiations of different LET, C ions and X-rays 77—48846
- cell survival and cytogenic responses to ^{125}I-, ^{131}I- and ^{3}H-labelled deoxyribonucleosides 77—5046
- cell survival as function of depth, modulated negative pion beams 79—43966
- cell survival dependence on radiation quality, models and exptl. data analysis 80—26287
- cell survival dependent dose rate effects, radiation carcinogenesis theory 79—11973
- cells, human, multinucleate and micronucleus formation obs. 80—72219
- cellular repair mechanism, investigation by high dose rate electron beam 79—53195
- cellular repair rates determined by split-dose and dose-rate methods, comparison 80—104680
- characts., natural occurrences, technological enhancement and health effects 80—46071
- charged particle track evaluation, distance distrib. and intratrack dose 80—26368
- charged particle yields from π^- capture in biologically significant materials 80—12201
- Chinese hamster cell, repair of potentially lethal damage after X- and α-irrad. 78—28014
- Chinese hamster cell sublethal damage repair after fast neutron irrad. with or without X-irrad. 78—20218
- Chinese hamster cell survival and sublethal repair, ultra-high dose rate electron irrad. compared with X-rays 78—40272
- Chinese hamster cells, enhanced killing by ^{238}Pu α-particles in the presence of cordycepin 80—72233
- Chinese hamster ovary cell recovery from damage due to fast neutron radiotherapy beams 78—20231
- Chinese hamster ovary cells, response to fast neutron radiotherapy beams 80—21497
- Chinese hamster V79 cells, mutation and inactivation by heavy ion beams 80—35982
- Chinese hamster V79 cells, synchronised, inactivation with charged-particle track segments 80—108966
- Chlamydomonas reinhardi, dividing, X-ray and proton-induced ultrastruct. changes 78—65085
- Chlorella pyrenoidosa synchronised cultures, effect of extremely low doses of secondary radiation from ^{32}P 78—73176
- chromosomal aberrations for tritiated water dose, Swiss albino mice 79—2112
- chromosome aberration of human lymphocytes, microdosimetric expts. 80—26289
- chromosome aberrations, dose-effect relationship, population exposed to increased natural radioactivity 80—72254
- chromosome aberrations as dosimetric technique for fission neutrons at 0.2 to 50 rad 78—69145
- chromosome aberrations in swine leukocytes after in vitro and in vivo exposure to fission neutrons 78—28011
- chromosome aberrations in Syrian hamster lung cells due to inhaled $^{238}PuO_2$-ZrO_2 particles 77—56440
- contrast and radiation damage in biological specimens, conf., Nancy, France (May 1978) 79—66591
- corneas, canine, γ and negative pion irradiation of microvasculature 79—43964
- coronary arteries and aorta, late ultrastruct. changes after irradiation, mouse 79—57725
- cosmic galactic radiation heavy nuclei, effects on shrimp, flour beetle and stick insect 78—20236
- cosmic high energy loss particles, high precision localisation methods, Biostack expts. 78—20235
- cosmic high energy loss particles, radiobiology using visual track detectors in Biostack expt. 78—20234
- cosmic ray heavy ions, charge and LET distrib. meas., radiation damage in biological objects 80—94664
- cosmic ray high LET particle dosimetry, Biostack III Zea mays expt. 78—20287
- cosmic ray nuclei, $Z=30$-40, fractional cell loss, Earth orbit expt. 80—3828
- cutaneous and spinal cord response to accelerated charged particles 79—20586
- cutaneous telanagiectasia after electron beam radiation, dose-time relationships 78—3552
- cytogenetic dosimetry, human, dose response relationship for ^{241}Am α-particle 80—30895
- death due to inhalation of β-emitters, probability estimation 80—89801
- delta-electrons prod. in water by high-energy electrons and X-rays 77—29178
- dentin, human, effects of irradiation on wear resistance, microhardness and acid solubility 79—96634
- dihydro-6-methyl uracil single cryst., electron and UV irrad., free radicals, EPR 77—29100
- dimethyl sulphoxide radioprotection of mammalian cells, exposed to X-rays, heavy charged-particle beams 79—79609
- diploid yeast, liquid-holding recovery, nature of damage 79—16256
- diploid yeast cell inactivation by accelerated heavy ions 80—26295
- diploid yeast cell ribosomal RNA gene inactivation curves and cross-sections 80—26297
- DNA, double strand breaks, protein cross-links, induced by fast neutrons, γ-rays 79—66446
- DNA, ion beam effects, review *(German)* 79—43968
- DNA, radiation induced mol. size change, electron irradiated, effect of p-nitroacetophenone 80—89807
- DNA, repair mechanisms 79—11987
- DNA, thymine damage production and excision, mammalian cells, high-LET irrad. obs. 80—72261

biological effects of ionising particles continued
- DNA breaks in E. coli and superinfecting phage λ, repair rel. to buffer. 77—25376
- DNA double strand breaks rel. to radiation dose, yeast cell obs. 80—72232
- DNA double-strand breaks in irradiated yeast cells, survival and yield, O_2 influence 80—35992
- DNA electron damage repair in E. coli mutants, appl. of rapid lysis techniques 78—31775
- DNA kinetics in soln., electron pulse radiolysis using light scatt. detect. 77—16910
- DNA non-rejoining break induction by high LET radiation, rel. to cell death 77—44596
- DNA strand breaks, lymphoma cells, detected by hydroxyapatite chromatographic technique 79—43819
- DNA strand breaks induced by ^{125}I in cultured human kidney cells, repair 80—12192
- DNA synthesis by DNA-membrane complexes from electron irradiated E. coli 79—16167
- dose-rate model testing with Chlamydomonas reinhardi 80—21543
- dose-response relationship of neutrons and γ-rays to leukemia incidence, atomic bomb survivors 80—36148
- Drosophila melanogaster, repair of electron irradiation damage 79—11983
- E. coli, damage induced by T decay, secondary lethality under nongrowth conditions 80—104654
- E. coli, DNA repair in radiation resistant and radiation sensitive strains 79—34489
- E. coli, value of photoreactivable component after exposure to ionising radiation 80—72224
- E. coli B_{s-1}, response to tritium-β particles rel. to 7 MeV electrons 79—57714
- E. coli B irrad. with 0.8 MeV electrons in oxygenated and anoxic states, mol. alterations 78—24031
- E. coli photoreactivation after electron irrad., O_2 effect 78—20213
- E.coli AB2463 recA response to fast neutron beams, 4 to 27 MeV, rel. to dosimetry intercomparison 78—65077
- Ehrlich ascites carcinoma cells, effects of pions$^-$ rel. to electrons and X-rays 80—26267
- electron beam therapy of lateralised lesions of oral cavity and oropharynx 80—12215
- electron beams, 10, 20 and 30 MeV, RBE vs. depth for mouse leukaemic cells 77—5037
- electron energy loss spectra, yield calcs. in H_2O, bioligical implications 79—7641
- electron interactions, low-energy, single and twin biological targets 80—12195
- electron irradiated ham, failure to induce genetic alterations in Drosophila 80—17009
- electron microscope superconducting lens system for reduction of radiation damage 79—34718
- electron microscopy, high-resolution imaging of biological specimens, radiation damage, review 79—5331
- electron probe analysis, effects of electron irrad. of sample 79—43969
- electron probe microanalysis, charging effect in electron-irrad. ice 78—57141
- electron radiation damage, knock-on process 80—79840
- electron transport simulation in liq. water, appl. to microdosimetry and radiobiology *(French)* 80—12202
- electrons, O_2 sensitisation of CHO cells at ultrahigh dose rates 80—36000
- embryo C3H10T1/2 cells, mouse, high-energy neon particle irrad., viral transformation enhancement 80—104668
- embryo survival and development, rats, RBE and OER of extended-Bragg-peak He ions 77—12961
- EMT6 cell, RBE, OER and recovery of potentially lethal damage of 645 MeV He ion beam 78—20229
- EMT6 tumour cell response to single fractions of X-rays and cyclotron neutrons 78—20230
- EMT-6 cells in vitro, potentially lethal damage recovery following X-ray or neutron irrad. 79—62308
- energetic heavy ion beam model for radiobiology 80—26293
- environmental actinides, pot. carcinogenic effects 80—30780
- epidermal carcinoma in sheep due to ^{144}Ce-^{144}Pr 77—29180
- epidermic regeneration cytokinetics, β-irrad., guinea-pig 78—15870
- fast neutron and photon therapy, randomised clinical trials 79—20638
- fast neutron effects on multicell spheroids 77—56423
- fast neutron exposure, risk of leukemia 80—30782
- fast neutron irradiation of cells cultured in monolayer, dosimetric aspects 78—69218
- fast neutron RBE comparison for Edinburgh and Hammersmith hospital 78—11698
- fast neutron sublethal damage and cell division delay expts. 79—20588
- fast neutron teletherapy, preliminary clinical results 79—20639
- fast neutron therapy, radiobiological bases 80—35995
- fast neutron therapy beam intercomparison using mouse testes as biological test system 78—20225
- fast neutron therapy with medical cyclotron, clinical results 79—20643
- fast neutrons in normal tissue, early and late damage obs. 79—20590
- fast particle therapy status and prospects in Europe 79—20641
- fast proton track energy deposition and ionisation calc. and obs. 80—12196
- fatty acid synthetase, from yeast, three-dimens. electron microscopy, struct. and image reconstruction 77—12883
- fibroblast cells, human, comparative response to 50 MeV neutrons 79—34512
- fibrosarcoma selected tumour cell populations, fast neutron irrad. in situ 78—44560
- 5-fluorocytosine, electron beam damage assessed by EELS 80—89809
- free plant cell, suspension-cultivated, survival after X-ray and fission neutron irrad. 79—92296
- gerbil, Mongolian, radioresist. to fast neutrons 77—48844
- glycine, electron-irrad. polycrysts., stable products obs. by ^{13}C NMR 78—15775
- goose barnacle, effects of tritiated seawater on development 79—66486
- growth inhibition of Vicia faba roots by neutron (pion) beams, RBE and OER values 80—26276
- gustatory function, radiation-induced changes, neutrons rel. to photons 80—12184
- haematological findings significance for medical exam. of radiation employee *(Japanese)* 79—11971

biological effects of ionising particles continued
haematopoietic stem cells, susceptibility to ^{55}Fe radiation damage 79—11975
haemopoietic stem cells, mouse, proliferative and differentiative ability, ^{226}Ra and X-irrad. effects 79—79611
hair, volatility of Hg in NAA from samples and standards *(Russian)* 80—41128
head irradiation by fast neutrons and X-rays, pathological effects on rabbits 78—31860
heart, ultrastruct. changes, fission neutrons vs. ^{60}Co gammas, mouse 77—5047
heavy ion and He effectiveness on tumour systems 79—20587
heavy ion and He inactivation of mammalian cells, radiobiological characterisation 79—20585
heavy ion peak-to-plateau relative biological effectiveness ratios, fractionation enhancement 79—62309
heavy ion track structure in tissue, microdosimetry 77—2032
heavy ions, high energy, dosimetry for radiobiology expts. 77—66849
heavy particle comparison for therapy, acute and late reactions in mice 78—85338
heavy particle comparison for therapy, cell survival, OER and RBE 78—85337
heavy particle comparison for therapy, cell survival vs. depth 78—85336
heavy-ion and He fractionated radiation therapy, clinical trial 79—20632
heavy-ion radiography and autoactivation techniques 79—20624
Hela cells, recovery from sub-lethal damage when irradiated at ultra high dose rates 79—79608
heritable lesions, radiation induced, in proliferating mammalian cells, review 79—20602
heteroallelic reversion induction, in diploid yeast fission neutron O_2 enhancement ratio 79—88139
human diploid fibroblasts, mutation and inactivation by heavy ion beams 80—35983
immune capacity suppression, mice to intestinal cestode, comparison of fast neutrons to X-rays 79—16257
inhalation carcinogenesis of high-fired ^{244}CmO$_2$ in rats 80—21502
inhalation exposure of miniature swine 79—11976
intestinal cell sublethal damage after mixed treatment with X-rays and fast neutrons, mouse 77—64086
intestine, small, acute and late damage following fractionated neutron and X-irrad. mouse 78—11706
^{125}I-iododeoxyuridine, effect of ^{125}I-decay, mol. consequences of Auger effect 77—4982
ion energy deposition in simulated biological matter, Monte Carlo method 77—81584
irradiation chamber and sample changer for biological samples 80—56198
irradiation doses, effects and sources of ionising radiations *(French)* 79—66494
isocitrate dehydrogenase from Azotobacter vinelandii, essential amino-acid residues identification 80—76538
kidney cells, cultured human, fast neutron effects on reproductive capacity 79—62307
kidney cells, inactivation by high-energy monoenergetic heavy-ion beams 80—72256
leaf, Saintpaula, dose-effect curve shape rel. to radiation-stimulated repair 80—26291
lens opacification in mice exposed to 14 MeV neutrons 78—65097
LET dependent radiosensitivity of E. coli K-12 rec and uvr mutants 78—15874
DL-leucine degradation with longitudinally polarised electrons 79—79474
leukaemia cell reproductive survival and hypoxic protection rel. to ionisation density 77—86554
leukaemia risk from neutrons, rel. to max. permissible dose for occupational exposure 78—53448
leukemia risk from neutron exposure 79—39509
leukemia risk from neutrons 79—70589
life shortening in RFM and BALB/c mice as function of radiation quality, dose and dose rate 80—41134
liver, giant cell formation after ^{45}Ca administration, desert gerbil 79—92299
liver, mouse, effects of tritiated water rel. to age 79—43967
liver beta irradiation effects from tritiated water, mouse 79—57719
liver chromosome aberrations, mice, effect of continuous intake of HTO 77—25518
low dose ionizing radiation, health hazard estimates 80—61646
low-dose radiation carcinogenesis 80—12198
lung, ^{218}Po, ^{214}Po, α-particle effects in Syrian golden hamster 79—16304
lung, canine, relative effectiveness of fast neutron and ^{60}Co γ-ray irradiation 80—3737
lung, carcinogenic effect of localised fission fragment irrad., rat expts. 80—81656
lung, late effects of inhaled ^{253}Es(NO$_3$)$_3$ in rats 80—30781
lung, Syrian hamster, tumourigenic hazard of particulate α-activity 80—41133
lung cancer, expt., effect of dose distrib. of α-particles in Syrian hamster 79—16254
lung carcinogenesis in rats, induced by inhaled high-fired ^{239}PuO$_2$, BeO 78—96077
lung lipids, biochem. effects of inhaled ^{239}PuO$_2$ 77—25510
lung parenchyma irradiated by inhaled ^{238}PuO$_2$ particles, collagen localisation, Syrian hamsters 80—72252
lung tissue localised irrad. using radioactive microspheres, prod. and props. 78—53445
lung tumourigenesis from particulate sources of ^{147}Pm β-radiation 80—72247
lymphocyte, hog, energy metabolism effect of ionising radiation 79—92301
lymphocyte chromosome aberrations, pion$^-$ peak expansion to range of depths useful in radiotherapy 78—20243
lymphocyte chromosome aberrations and the Poisson distrib. 79—100675
lymphocyte chromosome aberrations in humans induced by photon and electron irrad., sublesion interaction model 80—26279
lymphocyte death and transform., effects of X-ray and neutrons 78—69144
lymphocytes, human, chromosome aberration yields due to 15 MeV electrons 77—48843
lymphocytes, human, chromosome aberrations induced by ^{252}Cf neutron radiation 79—16169
lymphocytes, peripheral, function in dog, impairment by chronic pulmonary ^{144}Ce irradiation 79—88135

biological effects of ionising particles continued
lymphocytes, pig, chromosomal aberrations after neutron and gamma irrad. in vitro 77—64095
lymphocytes, stimulated, cell cycle progression perturb. by tritiated thymidine radiation 79—57726
maize disinfestation by electron irrad. 77—70505
mammal gonads, radiation induced morphological and endocrinological changes *(Russian)* 78—77090
mammalian cell, survival of normal and hybrid X-ray resist. lines exposed to X-rays and protons 78—80929
mammalian cell mutation and activation by radiations of differing LET 77—56431
mammalian cells, Chinese hamster, human kidney, radiation studies with modulated C ion beam 79—11978
mammalian cells, cultured, interpretation of mutation and inactivation obs. 80—72229
mammalian cells, drastic G_2 arrest after heavy-ion beam irrad. 80—45979
mammalian cells, dual radiation action of diatomic deuteron beams, interaction distance effects 79—53196
mammalian cells, effects of ultrahigh electron dose from field emission accelerator 79—53194
mammalian cells, heavy ion effects, irrad. facilities and methods 80—35981
mammalian cells, influence of radiation quality on effectiveness of small doses 80—30785
mammalian cells, lethally damaged, proliferation obs. after irrad. by various particles 80—108971
mammalian cells, microdosimetric determ. of radiation quality factors 77—37027
mammalian cells, transformation by α-particles 80—45968
mammalian cells in vitro, 300 keV X-ray, 14 MeV neutron and pion$^-$ effects 78—69155
mammalian cells irrad. with π^- and Co γ-rays, cell cycle progression 78—40269
mammalian cells irradiated at ultra-high dose rates, sublethal damage repair 80—36006
mammalian cellular DNA; breaks induced by accelerated heavy ions, impaired repair capacity 80—41129
mammary tumour, mouse, interstitial ^{226}Ra irradiation 79—57716
medical neutron dosimetry, standards 79—12013
membrane permeability, sheep erythrocytes, O_2 effects 77—5039
mesenteric blood vessels, response to β-irrad., mouse expts. 80—36009
microdosimetry, energy deposition distrib. patterns 79—20600
molecule chirality, origin via natural beta-decay 77—86445
monkey mortality, X-ray and neutron exposure, effect of autologous bone marrow transplantation 79—29572
mortality of radiation workers 80—8108
multicell spheroid low dose-rate irrad. 79—62304
multiple neutron fractions, RBE for late spinal cord injury 79—25051
neoplastic disease in RFM mice, incidence after neutron irrad., dose and dose-rate effects 77—12975
neoplastic transformation in vitro induced by neutrons and X-rays, rel. to radiation quality and repair 80—51178
neutron beam production at Ruder Boskovic Institute for radiobiology and dosimetry appl. 78—20273
neutron capture therapy of cancer in mice, long range effects, dose effect 78—48877
neutron carcinogenesis, dose and dose-rate effects in BALB/c mice 78—53455
neutron collimated beam RBE for cell survival rel. to lineal energy spectral differences 80—12200
neutron contamination of 25 MV photon therapy beam from Varian Clinac-35, evaluation criteria 77—86628
neutron dose distributions across graphite-tissue and polythene-tissue interfaces, air/nitrogen gaps, stopping power data 80—26353
neutron dose measurements in a dummy for test animal irradiation in a reactor 78—61218
neutron dosimetry, international intercomparisons 79—12014
neutron flux density for irradiation of human tissue, max. permissible dose calc. 79—43992
neutron personnel dosimetry, need for improved standards 79—12012
neutron radiation therapy, cyclotron biological intercomparisons 79—20589
neutron radiotherapy, nature and significance of radiation outside beam 78—53477
neutron RBE, rel. to leakage from HV electron accelerators 80—51177
neutron relative biological effectiveness in different exptl. tumours, 15 MeV neutrons 79—20591
neutron spectra at 0° from 83.7 MeV deuterons and 100.2 MeV protons on Be 77—73593
neutron therapy beams, radiobiological intercomparisons 80—3739
neutron therapy clinical trial programme in USA 79—20640
neutron therapy radiobiology, review 77—5076
neutron therapy vs. existing therapy techniques in Switzerland, cost-benefit anal. 78—11718
neutron-irradiated tissue and equivalent material recoil spectra 80—17022
neutrons, 14.1 MeV, estimated dose to bone and whole body via ^{40}Ca and ^{31}P 79—53256
neutrons, 15 MeV, RBE for jejunal crypt cells, oesophagus and lung 77—44728
neutrons, calc. of spectra and linear energy transfer 79—100659
neutrons, cyclotron-produced, repair of radiation damage in cells 80—3740
neutrons, fast, bone-tissue interface, dosimetry 79—25113
neutrons, fast, calcs. of charged particle recoils, slowing down spectra, LET, event-size distribs. 79—25040
neutrons, fast, review of current usage in radiation therapy 79—16270
neutrons, high energy, from Fermilab 500 BeV synchrotron, OER 77—70500
neutrons, high-energy, prod. by 80 MeV deuterons on Be, OER 77—81538
neutrons, system for meas. total body Ca, in man using ^{40}Ca(n,α)^{37}Ar reaction 79—25083
neutrons generated by 70 MeV protons on Li, OER and RBE meas. 78—65079
normal and tumour-like cell growth model 77—12894
nuclear energy industry, impact on human health and safety 77—25508
nuclear therapy, survey *(French)* 78—48889

biological effects of ionising particles continued
nuclear-dockyard workers, radiation-induced chromosome aberrations 79–34606
OER at low dose-rates 77–9223
OER for bacteria and cultured mammalian cells irrad. in frozen state, γ and neutron irrad. 77–90856
osteocytes from mouse proximal tibial metaphysis, early ultrastruct. changes after ^{224}Ra incorporation 77–37020
ovarian cancer, stage III, maximal treatment technique 79–25063
ovarian tumour types and incidence in mice after whole-body exposure 79–57724
ovary of fetal mouse, effect of ^{90}Sr β-rays rel. to time administered during pregnancy 80–51163
pacemaker neurons, Aplysia, effects of irradiation with 20 MeV electrons 80–17013
pathologic effects of neutron and photon exposures of lung and spinal cord, rabbit expts. 80–41126
phage ϕX 174 inactivation by accelerated ions, enhancement by δ-ray effect 80–36008
phosphorylation in simple lipid and chloroplast ATP synthetase system 79–92298
pion$^-$, biomedical experiences, conf., Brugg-Windisch, Switzerland (Dec. 1978) 80–22138
pion$^-$, cell survival over the depth profile after irradiation 80–26268
pion$^-$, central axis depth-dose and stopping rate distrib. for radiobiology studies 77–52879
pion$^-$, chromatid breaks induced in Chinese hamster cells, rel. to X-irradiation 80–26270
pion$^-$, effect on brain vascular permeability of neonatal rats 80–26275
pion$^-$, effects on monolayers and spheroids of Chinese hamster cells 80–26269
pion$^-$, effects on mouse embryo pronuclear zygote stage 80–26274
pion$^-$, genetic and cellular response, depend. on intrinsic props. of reaction systems, RBE 78–3562
pion$^-$, long-term effects on female mice rel. to X-rays 80–26273
pion$^-$, long-term effects on mice, partial body irrad. 77–81537
pion$^-$, OER and RBE for beams of different peak widths, Chinese hamster cells 79–62301
pion$^-$, pre-clinical studies at TRIUMF 80–26264
pion$^-$, radiobiological data for clinical dosimetry in pion tumour therapy 80–26266
pion$^-$, RBE and OER values from Vicia Faba root growth inhibition obs. 80–26271
pion$^-$, suitability for use, in radiotherapy, radiobiological obs. 80–26338
pion$^-$, usefulness of pig for assessing damage in locally treated pelvis and abdomen 78–3554
pion$^-$ biological effectiveness and O_2 enhancement ratio obs. 79–20595
pion$^-$ cancer radiotherapy, RBE in and near large beam 80–12245
pion$^-$ radiotherapy, biological effect prdiction, star distrib. for high LET dose determ. 80–12248
pion beam radiobiology at Rutherford Lab., 1971-76 77–13003
pion radiotherapy facility at TRIUMF, dosimetry and radiobiology 77–70526
polynucleotides, single-stranded, reaction of O_2 with radiation-induced free radicals 78–48759
polynucleotides poly(A+U), double-stranded, radiolysis in presence of O_2 78–48760
prenatal brain development, effects of chronic ingestion of ^{3}HOH, rat expts. 80–36004
protein, electron radiation damage on primary and secondary struct. level 80–89808
proton activation analysis of human dental enamel, radiation damage 79–70608
proton and heavy-ion therapeutic advantages 79–20628
proton RBE for normal tissue reactions and fractionated dose schedules 78–31858
proton relative biological effectiveness, microdosimetric interpretation of biological data 79–62306
proton relative biological effectiveness, microdosimetric parameters 79–62305
proton-exposed Macaca mulatta, mortality and latent effects, 9 year study 77–2026
public health aspects of radiation 79–88141
pulmonary collagen turnover after β-emitting radionuclide inhalation 79–25049
pulmonary metastases of mouse fibrosarcoma, RBE of neutrons prod. by 50 MeV deuterons on Be 77–81536
pulse radiolysis of aqueous systems with deuterons and alphas, LET depend. of transient yields 77–63940
radiation protection needs for ionising rad. and other mutagens 80–51276
radiation protection progress report, EEC, 1978, book 80–22148
radiation quality factor, lineal energy correction for saturation effects 80–26376
and radiation therapy, conference, Berkeley, USA (1976) 79–20619
radiation therapy, electron beam dose distributions, magnetic field modification 79–5376
radiation therapy, electron-dose distrib. in tissue, lung phantoms, magnetic modification 79–5377
radiation therapy, low linear energy transfer alternatives 79–20648
radiation-damage artefacts in biological electron microscopy, technique for visualisation 79–20726
radioactive waste processing, health physics implications 79–57727
radiolyoluminescence, appl. to dosimetry of ionising radiation 79–62374
radionuclides incorporated into mammalian cell DNA, microdosimetry 80–12191
radionuclides incorporated into stem cell DNA, biological damage, radiation protection implications 80–12187
radiotherapy by heavy particle radiations, modern developments *(French)* 78–48890
RBE of megavoltage photon and electron beams for tail necrosis in mice 78–35886
RBE of mouse skin damage, pions$^-$ rel. to X-rays 80–26272
RBE of protons rel. to γ-rays for human cells 80–30798
recoil nuclei specific energy losses in tissue, analytic representation 79–100680
rhabdomyosarcoma, rat, response to Ne and He ion irrad. 79–25042
ribonuclease inactivation cross-sections for slow heavy ions 80–26286
rice, M_1 damage, RBE of thermal neutrons 80–104649
RNA of Novikoff Hepatoma ascites cells, effects of sparsely-ionising radiation after in vivo labelling 78–7389

biological effects of ionising particles continued
RNA specific activity, Novikoff Hepatoma ascites cells 78–3560
RNA synthesis in slime-mould, effects of electrons and neutrons, caffeine modification 77–12962
RNase, damage and energy deposition by low-energy ions 77–9172
RNase inactivation due to elastic nucl. collisions 78–28008
root meristem cells, Vicia faba, subnuclear chromosome aberrations rel. to neutron energy deposition 80–26280
root meristems, Vicia faba, X- and neutron-induced cell progression delay 77–56437
scanning proton elemental microanal., biological and medical specimens 80–56311
seed radiosensitivity of winter hexaploid triticale 79–20583
seedlings, Vicia faba, effects of different radiation types on growth *(German)* 79–43961
skin, α-irradiation, possibility of late effects, U miners 79–20584
skin, pig, response to ^{137}Cs-irrad. 80–67161
skin, radiation fibrosis after β-irrad. and attempt at suppression, guinea pig expts. 80–72243
skin, senescent, increased susceptibility to β-irrad., mouse obs. 80–104656
skin, tumour induction and hair follicle damage rel. to electron penetration, rat 77–5052
skin, X-ray and fast neutron damage, relationship between OER, RBE and no. of fractions 80–35978
skin γ and neutron responses, dose fractionation effects 79–20593
skin acute response, human, pion$^-$ relative biological effectiveness 79–20596
skin injury, pig, relative biological effectiveness of neutrons and γ-rays 79–34605
skin nodules, comparative effects of pion and X-irradiation 79–20659
skin tumour, rat, following proton irradiation 79–11982
slow repair after X-rays and fast neutrons, mouse lung 77–73547
space radiation effects, implications of Li, Be, B production in ^{12}C(p, spallation) reactions, 45-100 MeV 77–23053
spatially correlated ions studies, background and theory 80–36024
spatially correlated ions studies, cell survival obs. using diatomic deuterium 80–36026
spatially correlated ions studies, multiple scatt., expt. facility and dosimetry 80–36025
spermatogenesis of fish Oryzias latipes, fast neutron effects 77–86553
spermatogonial stem cell survival in mouse, split dose neutron and X-irrad. 78–28012
spine and forearm Ca changes, meas. apparatus using ^{252}Cf neutron activation anal. 79–39490
spores exposed to pulsed electron irrad., decay of potentially lethal O_2-depend. damage 78–20217
spores of Bacillus megaterium, wet, anoxic damage enhancement by electron pulses 80–26296
spores of Bacillus subtilis, inactivation by heavy ion irradiation 80–26294
spores of Bacillus subtilis, mutagenic effect of water-t 78–80928
spores of Bacillus subtilis inactivation rel. to heavy ion impact parameters 80–26288
STEM, contrast and radiation damage 79–66592
structural damage at low temps., effects on microanal. 79–39453
sub-lethal damage accumulation site, evidence for location in Chlamydomonas 78–7390
sublesion combination probability, molecular ion expt. 80–26285
sublesion production and interaction, primary ionisation cluster nanodosimetry 80–26278
sublethal damage repair in multi-cell spheroids, fast neutrons vs. X-rays 77–25512
tail re-irradiation to necrosis six months after tolerance X-ray or neutron dose, rat 77–73543
TEM, low-temp., radiation damage, review 78–57147
testes, mice, comparative effects of various radiations on weight loss and spermatogenic stem-cell survival 80–108976
testis damage by ^{125}I in partially blocked thyroid of rats 78–3565
testis mass loss, mouse, induced by tritiated thymidine, tritiated water, ^{60}Co γ-irradiation 79–39452
testis weight loss, mouse, RBE for fast neutrons rel. to X-rays 78–7396
testis weight loss following high energy neutron or γ irrad., mouse expts. 80–35985
thermal neutron beam response of hamster and HeLa cells containing various concs. of ^{10}B 78–73178
thick inhomogeneity effects on charged particle beams 79–25041
thorotrast and ^{224}Ra radiobiological significance 78–96076
thorotrast biological effects, conf., Alta, USA (July 1974) 78–96068
thorotrast cases, bone irradiation meas. results 78–96092
thorotrast patients, α-ray tissue dose 78–96093
thorotrast patients, Danish, malignancies 78–96074
thorotrast patients, endosteal α-particle dose 78–96094
thorotrast patients, German, malignancies and estimated tissue dose 78–96072
thorotrast patients, Portuguese, malignancies 78–96073
tissue neutron and gamma-ray response function, mid-head, military appl. 80–8185
tissue neutron energy deposition spectra from improved cross-section values 80–26300
tissue-equivalent gas, energy loss of H, C, N and O ions for elastic nuclear collisions 78–86759
toxic air ion effects due to tachyon magnetoelectric dipoles and beta rays 80–35999
track structure analysis advantages over classical microdosimetry 80–26284
track theory of survival appl. to neutrons 77–12970
transplantable tumour response to fractionated fast neutrons plus Ro-07-0582 77–86558
transport calculations for poins, neutrons, protons, α-particles, ions 77–25555
5-trifluoromethyluracyl, electron beam damage assessed by EELS 80–89809
triton bombardment of human blood cells, morphological detail of radiation damage 77–60230
tryptophyl peptides, pulse radiolysis, hydrated electron reaction 78–48679
tumour cells, Ehrlich ascites, lethal effects of ^{64}Cu-bleomycin complex 79–57709
tumour cells, interaction of hyperthermia with fast neutrons or X-rays on local tumour response 77–9230

biological effects of ionising particles continued
tumour response to fractionated fast neutron irrad. rel. to X-rays 77—12974
tumour response to neutron radiation therapy, animal expts. 79—20594
tumours in rat skin, split dose recovery, electron irrad. 77—90855
uridine-5′-phosphate.2Na$^+$ single crysts., radiation damage, ESR obs. 80—108964
V79-spheroids, survival and kinetic response after heavy ion beam exposure 80—104651
Vicia faba bean root growth, effects of π and neutrons 78—28003
Vicia faba growth reduction, RBE of d(50)-Be neutrons and 650-MeV He^{2+} 80—98025
visual light flashes, astronaut obs. on Skylab 4, role of nucl. stars 77—5089
visual phenomena in space 78—20297
visual phenomena induced by relativistic ^{6}C$^+$ ions with and without Cherenkov radiation 79—24991
water treatment by high-energy electron beams 77—70507
water vapour electron stopping power and energy degradation 80—23276
yeast, diploid, liq.-holding recovery in stationary and log phase cultures, α-irrad. 77—2028
yeast cells, alpha-irrad., UV-induced reactivation 78—80920
yeast cells, dried, inactivation by accelerated heavy ions of very high LET 80—108965
yeast cells, elevated temp. effect on radiation sensitivity 79—79610
yeast cells, reparable and irreparable damage induced by sparsely ionising radiation 80—51167
π irradiation of Chinese hamster cells, OER 79—88126
Ar ions, high-energy, chromosome aberrations in aerated and hypoxic Vicia faba root meristems 78—7403
Ar ions, high-energy, depth-dose meas. in tissue-equivalent liq. and water 78—3614
Ar ions, high-energy, RBE OER and cell cycle response 78—3558
^{14}C fallout from nucl. weapons testing, human radiation burden 77—64091
^{252}Cf in radiotherapy, RBE-dose rate relationships 77—5030
^{252}Cf in radiotherapy, RBE vs. dose-rate relationships 77—9222
^{137}Cs-irradiation, fractionated high dose-rate and continuous low dose-rate effect on pig skin 80—41127
D$_2^+$, dissociation on impact with mylar foil 80—67164
^{3}H low-dose β-ray relative biological effectiveness 80—12190
He^{2+} 650 MeV beam relative biological effectiveness as function of depth 80—26281
He^{2+} 650 MeV ions study for possible radiation therapy applications *(French)* 77—66835
^{4}He ions, mammalian cell inactivation and mutation, compared with Al ultrasoft X-rays 77—86548
I, radioisotopes, environmental and biological effects from nuclear fuel cycle *(Russian)* 80—52768
5-^{125}I-iododeoxyuridine as prototype for radionuclide therapy with Auger emitters 77—29186
^{131}I in tissue, specific energy calc. in accordance with crit. cell concept 77—2031
^{131}I metabolism in amphibian and reptile thyroid *(Italian)* 79—20579
^{20}Ne, high-LET, effects on brain, eyes and other hand structs., mouse 79—66489
O$_2$ effect fast kinetics in electron irrad. mammalian cells 78—48836
O$_2^-$, in air, effects on environmental hygiene 79—16258
^{238,239}PuO$_2$ inhalation toxicology in Syrian golden hamsters 77—86552
^{238}PuO$_2$ particle inhalation, pulmonary tissue local dose computation 79—92385
^{239}PuO$_2$ inhalation, rat pulmonary connective tissue modification by internal α-irrad. 79—92302
^{238}Pu 4.4 MeV α-particles, mutagenicity and cytotoxicity rel. to X-rays 80—72265
^{238}Pu, factors affecting particle mobility in rats 79—12003
^{238}Pu IV citrate chronic exposure effect on embryonic development of fish eggs 78—53447
^{239}Pu, endosteal cell dose and relative distrib. factors compared to ^{226}Ra 78—96091
^{239}Pu in tissue, specific energy calc. in accordance with crit. cell concept 77—2031
^{239}Pu, subparticle formation expt. by α-decay 79—6520
^{239}PuO$_2$, inhaled particles, toxicity and translocation in baboons 79—2109
^{239}PuO$_2$ alpha-particle freq. in lung cells 78—69151
^{226,228}Ra in humans, radiation induced malignancies 78—96075
^{224}Ra and daughters, radioactive props. and biological behaviour 78—96090
^{224}Ra biological effects, conf., Alta, USA (July 1974) 78—96068
^{224}Ra, endosteal cell dose and relative distrib. factors compared to ^{226}Ra 78—96091
^{224}Ra injections into humans, soft-tissue effects 78—96070
^{224}Ra injections into humans, skeletal effects 78—96071
^{224}Ra preparation, for ankylosing spondylitis therapy 78—96089
^{224}Ra, short-lived α-emitter, late effects after incorporation in mice 78—96069
^{224}Ra usage in radiotherapy and radiobiology, brief history 78—96085
^{224}Ra use in treatment of ankylosing spondylitis and rheumatoid synovitis 78—96086
Rn daughters, low level exposure effects on lung cancer 80—41142
^{222}Rn, props. and behaviour of short lived daughter nuclides in the atmos. *(Japanese)* 80—72339
^{227}Th, short-lived α-emitter, late effects after incorporation in mice 78—96069
U mill tailings pile, health effect estimations 77—40800

biological effects of microwaves
see also biomolecular effects of radiation; cellular effects of radiation
2.45 GHz irradiation effect on rat digestive transit *(French)* 80—3723
9.712 GHz irradiation effect on vagal heat membrane bound acetylcholinesterase 80—3593
10 GHz pulse irradiation effect on bacterial growth 80—3721
27.12 MHz selective heating of cutaneous tumours 78—24179
148 MHz teratogenic potential in pregnant mice 79—70583
915 MHz prenatal irradiation effect on rat foetal and postnatal development 80—3722
918 MHz rat irradiation, thermographic near field effects and behavioural studies, near field effects 78—7386
absorption by biological material, role of water 80—17004
absorption in multilayer cylindrical models of man 80—30767

biological effects of microwaves continued
acoustic signal generation, anal. 78—24095
anechoic chamber, miniature, for chronic exposure of small animals to plane-wave microwave fields 80—67304
animal exposures, perturbation by dielectric restraining materials 77—21665
animals in aerospace activities *(French)* 77—44716
auditory, neuron response to pulsed microwave irrad. in cat, microwave hearing 78—40259
auditory effect, of short rectangular pulses 78—24094
auditory phenomenon, microwave pulse irrad. of animal brain matter 80—35968
auditory responces induced by microwaves, guinea pig 80—61628
auditory responses in mammals, using 3 GHz pulses 78—53444
auditory sensations due to pulsed microwaves 77—2010
auditory sensations evoked by pulsed microwave fields, some pecularities 80—61636
auditory signal freqs. and thresholds 78—40260
Australian hard seed germination induced by 2.45 GHz irradiation 80—3715
bacteria, E. coli B, microwave radiation effects on colony formation and mol. struct. 78—24097
bacterial cell microwave absorption at spectral singularities 77—40712
behaviour disruption in mammals of 3 different sizes 79—100670
behaviour of rats, combined effects of microwaves and dextroamphetamine, expt. obs. 80—61635
behavioural alterations of rats, interaction of ambient temp. and microwave irrad. 80—67153
behavioural and thermal effects at reson. and nonreson. wavelengths 78—40262
behavioural effects in conjunction with chlordiazepoxide, rat expts. 80—3711
behavioural observations of microwave exposed rats and mice 80—61631
blood-brain barrier, effects of microwave-induced hyperthermia, rat 80—61642
blood-brain barrier, problems in quantifying effects, comparison of methods 80—61643
blood-brain barrier, reversal of microwave-induced permeability 80—61641
blood-brain barrier effects, review 80—56121
blood-brain barrier permeability obs., rat 79—74718
bone, granulocyte and macrophage precursor cells, mouse, microwave effects in vitro 80—76789
book 77—90850
Bose condensation, and time threshold for biological effects 79—100664
brain, microwave irrad. effects on blood-brain barrier function, overview 80—35967
brain enzyme inactivation in rodents using high-intensity microwave irrad. 80—41116
brain enzymes inactivation in rats, comparison of microwave radiation at 986 vs. 2450 MHz 79—53188
brain microwave reception, interaction with nerves 77—12958
brain tissue, microwave fixation, neurochemical technique, review 78—20323
brainstem potentials, microwave-evoked, auditory responses, in cats 80—56061
bulk biomaterial thawing, electric field uniformity requirements *(Russian)* 79—83852
cancer treatment appl. of microwave arrays for localised tumour heating 80—94308
cancer treatment by controlled local heating, 915 MHz or 2450 MHz 80—76860
cancer treatment by microwave hyperthermia *(French)* 80—3764
cancerous cell culture, phonons, long-range coherence, microwave effects 78—35816
carcinoma cell metabolism, Ehrlich ascites, effects of microwave radiation 79—2104
cardiovascular disease in North Karelia, Finland 77—12959
cataract formation in rabbits and monkeys 79—5326
cells in vitro, microwave radiation effects study using waveguide exposure chamber 79—5327
cellular, subcellular and molecular effects *(Russian)* 79—16249
cerebrovascular permeability, quantitative method for meas. of alterations 80—61748
CHO cells, comparative effects of water-bath- and microwave-induced hyperthermia on survival 80—55997
cholinesterase, microwave radiation interaction studies 79—39363
chronic exposure, physiological and behavioural effects, rat obs. 80—67152
chronotropic effects in isolated rat heart 78—69137
cochlear microphonics induced by 918 and 2450 MHz pulsed microwaves, cat and guinea pig 78—40258
coherent electric vibrs. in active microorganisms due to microwave radiation 79—2106
complex permittivity meas. bench for 2-10 GHz at 77-300K *(Russian)* 77—32966
conference on EM effects, Amherst, USA (Oct. 1976) 78—40243
conference on microwave power appls., London, England (Nov. 1979) 80—21520
corn seed germination and growth rate, effect of low level radiation 77—77937
cranial structure model exposed to microwaves, heat potential distrib. 79—2105
diathermy, shortwave and microwave, for deep-tissue heating 80—17050
diathermy and suspicion of harmful effects of microwaves and RF radiations 77—77939
diathermy direct-contact applicators, comparative heating patterns 78—40286
dielectric properties of living tissue, 10 MHz to 6 GHz meas. 77—78071
digestive transit of rat, low level radiation effects 80—56122
direct-contact heating of dielec. encapsulated mouse tumour using dual-beam TEM applicator 78—40245
dose rate and O$_2$ consumption rate in mice confined in small holder during 2450 MHz exposure ·78—11697
dose rate relation to time of death and total absorbed dose in mouse 77—2024
dose-response relationship for rat irrad. by 918 MHz microwaves at 2.5 mW/cm^2 78—40248
dosimeter, evaluation of implantable elec. field probe within finite simulated tissues 78—40345

biological effects of microwaves continued
  dosimetry, meas. of energy absorbed by biological systems by anal. of heating and cooling data 78–40343
  dosimetry, meas. of energy absorbed by biological systems by Dewar-flask calorimetry 78–40344
  dosimetry, whole-body, in small animals, effect of body mass and exposure geometry 78–40348
  E.Coli, lambda prophages induction by mm microwaves 79–100663
  E.coli repair-deficient mutant 79–100666
  EEG waveform and behaviour for human subjects, low-power RF and microwave effects 79–96616
  effects of microwave energy on Acacia longifolia 79–53190
  EM energy deposition for realistic model of man, numerical calc. 80–12180
  EM field induced load damage, mechanism 79–74716
  EM field quantifying for radiation safety survey, meas. and instrumentation 78–44618
  embryo early development, chickens, microwave irrad. and body temp. effects 80–56135
  embryo in utero, human, injurious effects of microwaves 79–83850
  embryonic development effects 80–30769
  endocrine function in rhesus monkeys exposed to pulsed microwave radiation 79–96620
  energy absorption by mice, effect of ambient temp. 78–40263
  energy absorption of animals, effect of Plexiglas animal holders 78–92674
  entomological experiments on teratogenic effects of EM fields 80–85446
  enzyme inactivation system, electronic control to reduce dose variability 78–40285
  enzyme-substrate system, potential difference changes 79–29565
  enzymes, membrane-bound, activity on exposure to 2450-MHz microwave radiation 80–56126
  epidemiological investigation of US employees in Moscow 80–3730
  erythrocyte ghost IR spectra in region of amide I and II bands 77–86531
  erythrocyte membranes of rabbit, dog, man, expt. obs. 80–56130
  erythrocytes, investigation of thermal and athermal effects of microwave irradiation 79–70581
  erythrocytes, rabbit, increased passive efflux of ^{22}Na and ^{86}Rb on irrad. 80–108957
  excitable cellular membranes, nonthermal interaction of RF and microwave fields, squid giant axon model 80–67150
  exposure, densitometry and dosimetry techniques 77–78072
  exposure array device for uniform irrad. of multiple animals 77–40941
  exposure biological expts., compact light-weight Gaussian-beam launcher 78–96119
  exposure hazard publicity 79–70582
  exposure limits proposal, in Canada 79–5375
  exposure system for marine animals, dosimetry and reflectometric obs. 80–56319
  exposure system for primates 78–40451
  eye, cataractogenesis, expt. investigations 80–35965
  eye lens, human, microwave-induced hazardous non linear thermoelastic vibrs. 79–83853
  eye lens thermal stresses, humans 78–80914
  fetal growth acceleration and deceleration, rat 79–100669
  fetuses, mouse, obs. after 2.45 GHz irradiation of mothers 79–20578
  fixed interval behaviour of rats exposed at low power densities 78–40265
  Gaussian beam launcher, focal region field aberrations 78–44580
  Gaussian-beam launcher for microwave exposure studies, dielectric hemisphere-loaded scalar horn 80–12206
  glioma cells, cultured, enzymatic and scanning electron microscope study 79–100661
  haemopoietic system of mice, X-irrad., damage repair modification by microwaves 78–24096
  hazard assessment methodology for USA Army Radiation Protection Program 78–85389
  health hazards of environmental microwave radiation 77–77938
  hearing sensation induced by pulsed microwave radiation 77–60229
  heart, isolated, microwave irrad. after treatment with ANS blocking agents 78–40251
  heart rate of embryonic quail, effect of 2450 MHz irrad. 80–89794
  heart rate of frog, insensitivity to p.m. microwave energy 77–2020
  heat dissipation rate after irrad., mice 77–81472
  heating, in treatment of cancer by hyperthermia 77–52859
  heating effect on dog thyroid gland at 2.45 GHz 78–31854
  heating effects of radiowaves and microwaves 80–98011
  heating of tissue, effect of surface cooling and blood flow 78–57038
  heating patterns in spherical tissue models 77–86537
  heating patterns produced by 434 MHz Erbotherm UHF^{69} in tissue-equivalent medium 80–98013
  high power electronic systems, hazards to personnel *(Italian)* 77–21561
  human epidemiologic studies rel. to health effects of microwave radiation 80–35970
  human head EM induced field and power absorption, ellipsoidal model 80–3724
  humoral immunity of Japanese quail irrad. during embryogeny 77–73540
  hyperactivity and disruption of operant behaviour in rats after multiple exposures 78–40264
  hyperthermia, microwave-induced, in cancer treatment, appartus and preliminary results 79–62296
  hyperthermia, rats, classical conditioning obs. 80–61629
  hyperthermia, rel. to visually evoked electrocortical response, guinea pig 80–61627
  hyperthermia and cancer therapy, 2450 MHz microwave and γ-radiation effects on flour beetle 79–2103
  hyperthermia by local EM heating and conductivity change, cancer treatment appl. 77–86578
  hyperthermia dosage definition form in vitro thermal cytotoxicity data 78–24178
  hyperthermia for hamster melanoma treatment, expt. 77–77931
  hyperthermia induced by microwaves, dose definition 79–2135
  hyperthermia induction in small animals using microwave system 79–2118
  hyperthermia of expt. mouse cancers using 2450 MHz microwaves 79–2119
  hyperthermia research with dual-beam microwave applicator 80–17052
  hyperthermia simulation *(French)* 80–3770
  hyperthermia to cancer treatment *(Spanish)* 80–89795

biological effects of microwaves continued
  hyperthermic treatment of tissue, biological effectiveness estimation, minimum inactivated cell ratio 79–100574
  hypothalamic temperatures, rat, effects of low power density microwaves 79–96619
  immune response of mice to 2450 MHz microwaves, lymphoid splenic cells 78–40257
  induced EM field, arbitrary cylinders, anal. by integral eqn. and moment method techniques 77–12957
  induced hyperthermal therapy of tumours in mice, bolusing technique 77–77934
  insect teratogenesis in standing-wave irrad. system 78–40256
  Intern. Microwave Power Symposium, Minneapolis, Minn., USA May 1977 77–70492
  irradiated breast tumour thermal pattern calc. *(French)* 80–3759
  irradiation requirements and role of temperature *(Russian)* 79–83851
  labelled microspheres, localised embedding by microwave heating of tissues of hypothermic dogs 80–61640
  leg, human, elevated temps. induced by microwave diathermy with surface cooling 80–61638
  lipid metabolism disorder in mice *(French)* 79–34600
  lipid metabolism effects in mice 80–56128
  living system biophysical interaction mechanism with RF and microwave radiation 79–79602
  local tumour hyperthermia in animals, microwave system for controlled prod. 79–34624
  long-term effects of 2.45 GHz microwaves on ultrastruct. of cerebral cortex and haematologic profiles of rats 78–40267
  long-term irradiation, methodology and evaluation of ocular and physiologic effects, rabbits 80–101225
  long-term irradiation, rabbits, evaluation of haematological and immunological effects 80–101226
  low-intensity microwave field hazards and alterations induced in mammalian systems 80–3729
  low-power MM-wave interaction with biologically active compounds and polar liquids 80–16707
  lymphocyte function evaluation after 2450 MHz CW microwave exposure, mouse 79–100667
  lymphocyte morphology and chromosomes, effect of 2450 MHz microwaves 78–40252
  lymphocytes, perinatal rats, effects of 2450-MHz CW microwave irrad. 80–56133
  mapping of near-field pattern in simulated biological tissues 79–39445
  medical applications and biological effects *(Spanish)* 80–26260
  membrane level, athermal electrophysiological mechanisms and experimental test 79–2108
  microbial genetic response to 2.45 GHz CW and 8.5-9.6 GHz pulsed microwaves 80–56120
  microtubules and axonal transport in rabbit tissue, 3.1 GHz pulsed irrad. 77–64097
  microwave induced hyperthermia and neurochemical correlates, orientation effects 78–24098
  microwave natural emission, effects of drugs and microwaves 77–32949
  microwave-diathermy, pulsed, expt. obs. 79–83849
  model mouse cancer response to 2.45 GHz free-field hyperthermia 79–70584
  morphologic alterations in brain-blood barrier of hamster 77–77935
  mouse lung tumour growth delay by bleomycin with 2.45 GHz local hyperthermia 79–83894
  mouse sensitivity to curariform drug. 2.45 GHz irradiation effect *(French)* 80–3717
  multibeam microwave therapy with computer control 80–3766
  multiple murine tumours, simultaneous microwave irradiation bolusing technique 78–7422
  murine brain rapid thermal fixation using microwave device 78–92689
  murine ocular lens in vitro, microwave and temp. effects 80–89798
  muscle cell osmotic state and membrane permselectivity repeated microwave irrad. effects quantitation 80–56131
  muscle smooth, contraction in a microwave field, rat obs. 80–56134
  neonatal rats, effect of repeated exposure on plasma corticosterone and adrenal glands 78–40246
  nerve and muscle isolated preps., 2450 MHz radiation effects 78–53443
  neuroelectric transmembrane pots., EM radiation effects, possible model of mechanisms 80–26259
  neuroendocrine effects, microwave-induced, nonspecific stress reaction 80–35969
  neuron response by individual Aplysia pacemakers, CW and pulsed radiation 78–92675
  neurophysiology, microwave biological effects, overview 80–35964
  non-thermal effects, supercond. mechanism phenomena 77–2022
  nonionising electromagnetic radiation bioeffects research and related occupational health aspects 78–73172
  nonionising RF and microwave radiation hazards *(French)* 80–3824
  nonlinear membrane capacity effects, theory 79–29563
  nonthermal effects of radio and microwave fields on biological membranes 77–86534
  observation prerequisite conditions 80–3592
  ocular pathologt absence after 9.3 GHz microwave repeated exposure, unanaesthetized monkeys 79–53191
  operant behaviour and rectal temp. during 2.45-GHz microwave irrad., squirrel monkey obs. 80–61630
  operant behaviour induced by microwave radiation, effect of psychoactive drugs 80–61632
  pea leaf cells, microwave photolosses, electrophysical process obs. 79–70535
  peristaltic activity of isolated segments of rat gut 78–40250
  phantom models of man, head resonance, numerical solns. and expt. results 80–12181
  plasma steroid levels in male rats 77–81530
  plasmonic absorpt. of RF energy, hypothesis 80–72215
  porphin free base, triplet state electron spin echoes, fluoresc. detection 78–70856
  power symposium, Monaco (1979) 80–3758
  primate restraint device, for microwave biological research 77–40945
  probe fibre optic telemetric linked, 0.2 to 12 GHz range hazard evaluation 78–15859
  prostate, dog, microwave localised heat treatment, new applicator 79–100698
  protection standards, American and European 78–80973
  protein coagulation and internal dielec. heating, surgery and cancer therapy appls. 79–5336

biological effects of microwaves continued
  quail embryo exposure to 2.45 GHz microwave radiation during development 78−20214
  R. spheroides, triplet state electron spin echoes, fluoresc. detection 78−70856
  radar antennas field, effects on maintenance and repair personnel investigation 77−81529
  radar irradiation, impact on human systems 77−40710
  radiation pattern meas. 78−48828
  radiation therapy, microwave hyperthermia applicators, development of 79−25059
  radiators, waveguide slot array with const. intensity 78−40450
  rat brain, rapid fixation device 77−81761
  rat brain ATP, ADP and AMP levels after 2.45 GHz whole-body irradiation 80−3718
  rat EEG activity depression by 2.45 GHz whole-body irradiation 80−3720
  rat embryo acute viral infection inhibition by whole-body microwave heating 80−3769
  rat embryo localised microwave heating effect 80−3728
  rat metastatic growth effect of local tumour hyperthermia 78−24115
  rat sleep patterns under chronic low-power microwave irradiation *(French)* 80−3716
  rat thermoregulatory behaviour when subject to microwave irrad. 80−81547
  rats, long-term exposure effects, simulation of chronic exposure of human body 80−35972
  reproductive capacity of Drosophila, effects of microwave radiation rel. to conventional heating 80−21492
  research, international trends 77−77932
  research in Soviet Union and Eastern Europe since 1976, review 80−35971
  reticuloendothelial system, granulopectic activity modification in mice exposed to 1 to 10 GHz fields *(French)* 77−21560
  RF and microwave exposure, USA occupational safety and health standards 80−3727
  Salmonella typhimurium LT2 mutants, effects of microwave radiation and heat 80−108958
  Satellite Power Station microwave health and ecology programme 79 70443
  scattering and absorption efficiencies for nonspherical dielec. objects, biological models 78−40241
  sciatic nerves, frog, isolated, effects on vitality 80−108959
  seed germination improvement, alfalfa plant 77−2023
  serous triglyceride evolution in mice exposed to 2 to 10 GHz radiation *(French)* 77−64083
  skin, pig, combined effects of X-irrad. and microwave heating 80−94290
  skin, pig, response to combined X-irrad. and microwave heating 80−61653
  soft mode transition induction by interaction with radiative fields, rel. to microwave effects in biological materials 78−7421
  soilborne pathogenic fungus population reduction by 2.45 GHz irradiation 80−3719
  sources, potentially hazardous, review 78−73173
  spores of Bacillus subtilis, interdependence of thermal and EM effects 78−15860
  stomatal response to induced thermal stresses, leaves 77−2021
  Temebrio, developmental effects of microwave irrad., culturing protocol and carrier freq. influences 80−61626
  temperature and absorbed energy meas. method, contactless, using fluorescent screens 80−36186
  temperature and corticosterone relationships in rats 78−92676
  temperature distrib. in microwave-irradiated cylinders simulating living tissues 80−3760
  Tenebrio molitor pupae, teratogenic response rel. to intensity of microwave irrad. 80−56136
  teratogenesis in mammals due to microwave exposure, expt. investigations 80−35966
  teratogenic effects and static field perception 77−81532
  teratological study of rat, IR vs. microwaves 78−40255
  thawing of cryogenically preserved canine kidneys 77−5059
  thermal and endocrinological effects of protracted irrad. of rats by 2450 MHz microwaves 78−40249
  thermal and non-thermal, review and German research on cellular effects *(German)* 80−51159
  thermocouple, nonmetallic, differential-temp. probe for use in microwave fields 80−56320
  thermographic observability of tumours with microwave heating 78−73193
  thermographic turnover detect., microwave enhancement with swept-freq. illum. 78−73194
  tissue induced EM power distribution in closed environment 80−3725
  tissue microwave heating models, surface cooling and blood flow effects 78−7388
  tissue sphere temp. profiles due to EM heating 79−100578
  tissue spherical model near-zone microwave exposure 78−7387
  tumour and normal cell microwave transmission 79−2107
  tumour blood flow changes due to microwave hyperthermia 78−24116
  tumour growth inhibition in mice, microwave irradiation, 3000 MHz 79−2101
  tumour growth inhibition in mice by microwave hyperthermia, Streptolysin S and Colcemide 78−40254
  tumour microwave heating for thermographic detection enhancement 79−2124
  tumour microwave heating with automatic temperature control 77−77963
  tumour oncolysis, mouse, local HF hyperthermia, X-irradiation and apathogenic clostridia 79−100662
  vasodilation, peripheral, induced in squirrel monkeys 80−104682
  VHF, UHF and microwave radiation effect on human body 80−8101
  visual-motor performance, skilled, by monkeys in a 1.2-GHz field 80−61634
  waveguide system for chronic exposure of small animals to microwaves 80−56318
  whole-body biological dosimeter using drug-induced ectothermia in small mammals 78−40350
  wild oat weed control appl. 77−81531
  yeast cells, determ. of thermal equivalent to MM microwaves 80−67151
  yeast cells, irrad. by weak microwaves, reson. growth rate response 78−3549
  yeast survival rate obs., millimetre-waves influence *(Russian)* 79−2100

biological effects of microwaves continued
  O$_2$ consumption of mouse, effects of microwaves and environmental temp. 80−51161
  O$_2$ consumption rate of mice, dose-rate depend. 78−40247

biological effects of radiation
  see also biological effects of acoustic radiation; biological effects of gamma-rays; biological effects of ionising particles; biological effects of microwaves; biological effects of ultraviolet radiation; biological effects of X-rays; biomolecular effects of radiation; cellular effects of radiation; dosimetry; radiation therapy
  10MHz to 1GHz, antennas safety, ANSI and EPA recommendations 80−30765
  60 Hz electric field effect on plant growth and development 77−81534
  60 Hz electric field effects on small birds and mammals 77−86538
  60 Hz magnetic field effects on mice activity levels 78−40266
  800 MHz portable transmitters, meas. of energy deposition in simulated human operators, comments and reply 79−57777
  abdominal irradiation, biliary and pancreatic secretions obs. 80−45965
  alpha emitters, health effects, man-made actinides compared with natural radionuclides 80−61647
  antenna, whip, effect on human body *(Czech)* 79−43958
  anthers from cultured barley, effects of light and temp. environments 80−56119
  atomic number dependence of photon and electron interactions 77−37017
  autoimmune reactions, non-organ specific, absence of curative radiotherapy 80−12185
  autopsy studies of Hashimoto's thyroiditis in Hiroshima and Nagasaki 79−92297
  bacteriorhodopsin, elec. response of a back photoreaction 80−98008
  biological systems, photochemical reactions, excitation by pulsed LED *(German)* 79−16250
  bioluminescence of lantern fish, Myctophidae, in response to light intensity by visual monitoring 77−16953
  Biophysical Society, 23rd annual meeting, conf., Atlanta, USA (Feb. 1979) 79−34468
  biosphere and active solar processes link, role of Earth's natural electromag. field 78−61211
  blood, extracorporeal irradiation method for rats 80−72396
  blue light phototherapy of neonatal icterus, comparison of lamps 78−44582
  bone lesions in CBA mice from nanocurie amounts of ^{239}Pu 80−81657
  bone-marrow stroma, vasoformative non-osteogenic sarcomas due to ^{90}Sr 77−12964
  brain, quantitative assess. by computerised tomography scan anal. 80−72306
  brain tissues, temperature rise induced by EM field 79−29564
  breast cancer induction in humans by ionising radiation 78−61217
  breast carcinoma prognostic relevance of radiation induced immune suppression 80−72217
  bronchogenic carcinoma among former U mine workers at Port Radium, Canada 80−89802
  cancer, dose-effect relationship linearity 80−67157
  cancer, statistical method for testing epidemiological results 79−70591
  cancer deaths among classified radiation workers, obs. and anal. 77−9228
  cancer deaths in atomic plant employees rel. to low-level exposure 78−85339
  cancer induction in workers at US Hanford Nucl. Facility 80−35977
  cancer mortality among A-bomb survivors, 1950 to 1972, additive logit model 77−70504
  cancer risks from low-level radiation 79−83857
  cancers and mutations, radiation levels and induced illnesses 80−76791
  capillary microscopic obs. of superficial minute vessels of Hiroshima atomic bomb survivors 78−31871
  carcinogenesis, link between radiation and chemical effects, time factors 78−53446
  carcinogenesis, time and dose factors 79−70590
  carcinogenetic hazard from natural background radiation in Japan 79−57720
  cervical spinal cord, rhesus monkey, effects of 50 MeV (d→Be) neutron irrad. 80−101228
  Chalk River Nuclear Laboratories research in radiation biology, environment and radiation protection 78−61222
  chemical pollutants and radiation, comparative biological hazards 79−25035
  circadian rhythms in humans, role of light, bibliography 77−48985
  civilisations possible self-annihilation through thermonuclear war 78−81562
  coagulation by irradiation with laser light 80−41113
  coagulation in gastrointestinal haemorrhages, using laser endoscope *(German)* 78−69178
  conference, Osaka, Japan (Nov. 1979) 80−98756
  conference on photochem. and photophys. processes, New Delhi, India, (Jan.'72) 78−11694
  coral growth form, light control, computer simulation 77−2076
  corneal epithelium, predictive equation for IR laser damage 79−25031
  corneal temperature range, implications in prediction of laser thermal damage 80−108848
  corneal temperatures, normal and laser injured rabbits 79−11919
  cranial structure exposed to RF radiation, thermal response model 80−94285
  crops, effect of accidental Na release as peroxide aerosol from LMFBR *(French)* 78−8997
  cytogenetical indicator of radiation effect, chromosomal dosimeter *(Hungarian)* 80−94292
  2′-deoxyadenosine in aq. deaerated soln., new radiolysis mechanism 80−81350
  DNA molecule, radioprotection by oxide-reduction coenzymes 78−40274
  dose comparisons in the effects of radiation and of chemical pollutants 79−88115
  dose-effect relationship for quantifying health risks *(German)* 80−61644
  dose-modifying factor, parametric method, low-dose extrapolation limit 77−37018
  dose-mortality relationships, implications for FBR accidental releases 80−46064
  dose-response relationships for female Ra dial painters 80−21545
  education, undergraduate course evaluation on radiation and the environment 78−1

biological effects of radiation continued
EEG of mammalian brains, modulated RF energy effect for acute and chronic irrads. 79—79603
EEG waveform and behaviour for human subjects, low-power RF and microwave effects 79—96616
EEGs of mammals, effects of modulated RF energy irradiation 79—100665
EHV and UHV power overhead line 60 GHz electric field effect on animal and plant growth 77—77933
EHV installation effects 77—81535
EHV transmission line ground level gradient, small plants and animals biological studies 78—31856
electric field, 25 kV/m 60 Hz, behavioral effects in rats 80—56108
electric fields, vertical, 45-Hz, influence on rats 80—76784
electromagnetic fields induced inside biological bodies, experimental and theoretical studies, comment 77—56420
electron microscopy, high-resolution imaging of biological specimens, radiation damage, review 79—5331
electrostatic field effects on human body, HV transmission lines *(French)* 77—21562
ELF electric fields as from EHV/UHV power transmission lines, US research results 80—94278
ELF magnetic field effect on personal vegetative status meas. by elec. resist. between hands 77—81533
ELF submarine communication systems, land-based transmitting antenna elec. and mag. field hazards 80—35973
EM, artifact-free electrodes for recording biopotentials in strong EM fields 78—40452
EM, conf., Amherst, USA (Oct. 1976) 78—40243
EM, coupling between small thin-wire antenna and biological body 78—3548
EM, effects on human body 77—9295
EM, in transmission stations, employees protection, Polish and international regulations *(Polish)* 78—61263
EM, non-ionising, hazards in the laboratory and effects on skin and eyes 78—96064
EM, state of research *(German)* 78—88728
EM absorbed dose in man and animals for plane wave irrad. condition at variable orientations 80—36141
EM and electrostatic fields effects on human body 77—64084
EM bioeffects research, international trends 77—77932
EM dominant reson. freqs. of human body 78—31857
EM dosimetry for human and animal models, numerical techniques review 80—36142
EM energy deposition in animals and human models, grounding and reflector effects 78—40346
EM energy deposition in biological tissue at 900 and 450 MHz 78—69222
EM energy irrad., research review 80—85444
EM field, in HV-power line and switchyard environments 77—5028
EM field cell culture exposure under controlled temp. and field strength conditions 78—40449
EM field effect on living organisms, standard magnetic field measurements methods *(Polish)* 79—39450
EM field effects on man and environment 77—44719
EM field hazard to radio operator, thin wire antenna coupling with human body 77—21563
EM field of overhead power lines, rel. to suicide 80—94287
EM field probe, implantable design for finite biological body 77—21670
EM fields, ELF, metabolic rates in 5 animal populations after prolonged exposure 77—2034
EM fields, range 3-30 MHz, exposure, maximum permissible intensity and duration, physiological effects *(German)* 80—12179
EM fields, review of expt. techniques 80—8239
EM fields in biology, conf., Ottawa, Canada (June, 1978) 79—96618
EM fields induced in human bodies, up to 500 MHz 78—24140
EM irradiation, temp. distrib. in simulated living tissues 80—85354
EM near-field irrad. of prolate spheroidal mammalian models, long wavelength anal. 80—41115
EM non-ionising radiation, influence of quality on bioeffects, exposure standards 78—44558
EM nonionising weak-field interaction with brain tissue, freq. and power windows 80—35974
EM plane wave irradiation of ellipsoidal model of man, long-wavelength anal. 77—9219
EM power absorpt. in dielec. cylindrical tissue models in presence of refl. surface, arm and thigh sizes 80—26258
EM power absorption, long-wavelength, by ellipsoidal models of man and animals 77—12956
EM power absorption in cylindrical tissue models excited by loop antenna 79—39446
EM power deposition in prolate spheroid models of man and animals at resonance 78—31905
EM pulse environment, tests of biological integrity in dogs 79—39448
EM scattering and absorption efficiencies for nonspherical dielec. objects, biological models 78—40241
EM wave absorption and scattering by prolate spherical models of biostructures 77—77941
EM wave biological effects, interdisciplinary and international contribs. 79—48288
EM wave effects and meas. methods 77—16954
EM wave exposure facilities for bioeffects research, survey 78—73174
EM wave heating effects, radiowaves and microwaves 80—98011
embryo, human, radiation effects on pre-natal development 79—29566
encephalic receptors, photostimulation in sparrows, induction of Zugunruhe 79—24985
energy, environment and health, Failla Memorial Lecture, learning from nucl. experience 78—80982
energy deposition in simulated human operators of 800-MHz portable transmitters 79—8525
entomological experiments on teratogenic effects of EM fields 80—85446
environmental effects of radioactive wastes, survey *(French, English)* 77—83064
environmental health hazards, nonionising radiation 78—35883
environmental health hazards, perspective 78—35896
extrapolation from exptl. animal to human *(Japanese)* 79—11972
eye, aqueous temperature stabilisation, laser induced temp. changes and model 77—40713
eye, human, max. permissible exposure to 1.54 μm laser radiation 79—11966
eye maximum permissible exposure to 1.06 μm picosecond laser pulses 79—25033
eye non-ionising radiation absorption, hot spots study, stochastic model 78—35884
eye retina, laser radiation dosimetry 80—12268
fallout effects of Nagasaki atomic bomb 78—85393
fast breeder reactor accidental releases, influence of physico-chemical form on consequences 79—74574
fast neutron facilities for radiobiological irrad. 80—109064
fathead minnow, effect of dose rate on survival time 80—30799
FBR notional accidental releases, effect of duration on consequences 80—94296
fertility in man, influence of radiation 80—56137
fibrosis in the rat gut, protective effect of hypoxia 80—30772
fractionation, math. models 77—5049
fundus oculi tissue, thermal effects on exposure to laser radiation 80—26261
fusion reactor blanket material impurity hazardous activity and dose rates, biological hazard pot. 80—102315
fusion reactor magnetic fields, biological implications 78—768
gastric carcinoma rel. to radiation from atomic bombs of Hiroshima, Nagasaki 79—57721
genetic studies of humans in areas of high natural radiation, mortality, morbidity and sex ratio 78—24102
geomagnetic perturbations, biotropicity due to atmospheric Rn activity induced increase 79—96621
gliomas, malignant, anal. of dose-effect relationship 80—72331
grey matter calcification secondary to radiation therapy, computerised tomography evidence 77—56424
Gribble Limnoria tripinctata, reaction to intensity gradient of mag. fields *(German)* 80—56074
guppy life cycle, effect continuous static mag. field 80—21481
Hanford workers' radiation exposure, review of report 80—8104
Hanford workers dying from cancer and other causes, radiation exposures, Richland USA 78—15893
head heating by EM waves, human and infrahuman models 80—56125
health aspects of low-level radiation, radiation protection standards 80—26375
health of radiation workers 80—98038
hereditary damage [review] after low-level radiation exposure 80—67165
human marrow, radiation dose deposition calcs. 80—26365
human model, multilayered, EM wave absorpt. 79—70580
HV transmission line, electrostatic field effects on human body *(French)* 77—21562
HV transmission line elec. and mag. field exposure effects and hazards 78—77083
hyperthermia by local EM heating and conductivity change, cancer treatment appl. 77—86578
indoor natural radiation environment and dose distribution in man, multicompartment models 79—12015
inhaled hot particle toxicity, recommendations of German Commission on Radiation Protection 78—69150
inhaled radioactive particles, acute effects, prognosis for survival in mammals 77—16956
inhaled radioisotopes effects 80—94288
ionising radiation, current research in Canada, review 80—104683
ionising radiation, positive and negative aspects, hazards assoc. with medical radiology *(Italian)* 77—77942
ionising radiation effects *(Croatian)* 80—104644
ionising radiation effects estimation, BEIR report relative risk and absolute risk models 80—26263
ionising radiation induced behavioural and physiological changes in rats hormonal radioprotection 80—98026
IR, effects on skin, safety *(Japanese)* 78—35882
IR, from GaAs laser diodes, effects on human eye evaluation *(German)* 78—20241
IR. effects on eyes, safety *(Japanese)* 78—35881
K-value determination and applicability of hyperbolic O_2 eqn. 77—12966
kidney transplant patients, effect of local irrad. on acute rejection process 78—24117
laser, tunable, effect on exogenously photosensitised E.coli 77—90849
laser action, possible head surgery appl. of Ar laser 79—8529
laser applications for discotheque light effects, safety considerations with respect to output power and exposure time, regulations and recommendations *(German)* 80—101224
laser applications in medicine and biology, bibliography, 1963-74 77—25539
laser beam operation in surgery and treatment, safety 78—35903
laser biomedical research in USSR 78—48858
laser damage, fast pulses 78—48827
laser fusion research, safety aspects, control measures and protective eye-wear 77—40711
laser hazards calc., for various viewing conditions 79—39447
laser interactions rel. to medical and biological uses 77—77961
laser IR pulse irrad. of human eye, max. permissible exposure for safety 77—37009
laser iridectomy, energy required, hazards and techniques 78—11713
laser irradiated tissue, significance of blood flow in temp. calcs. 80—55993
laser irradiated tissue, significance of blood flow in temp. calcs. 80—104563
laser irradiated white rats, temp. changes dynamics 79—57594
laser irradiation of biological tissue, temp. distrib., thermodynamic analysis 79—29562
laser low-level prolonged exposure effects on visual function 80—3714
laser medicine in Japan, current status *(German)* 80—98059
laser pulses and generation of acoustic transients in biological material 78—48830
laser safety considerations 77—77940
laser scanned visual displays, pulsed light data extrapolation 80—3713
laser-induced retinal morphological and functional changes and safe energy levels 80—3712
laser-irradiated biological tissue, moving phase transitions, tissue heating 79—83848
laser-stimulated wound-healing; clinical results and action mechanism 77—9299
lasers, effect on lining tissue and applics. in surgery 77—90871
lasers, therapeutic appl. *(French)* 80—108996
late effects on population exposed to accidental radioactivity release to environment 78—15861

biological effects of radiation continued
- lethal diseases from ionising radiation, new index of risks 80—94294
- leukemia incidence in atomic bomb survivors of Hiroshima, Nagasaki 79—57722
- LF electric current stimulation of auditory and visual sensations 78—40261
- light, epileptic subjects, background illumination effect obs., intermittent stimulation 80—98009
- light, non-photosynthetic action, control of plant respiration 77—44717
- light cycle, cockroach locomotor activity circadian rhythm, strong phase response curve 78—11630
- living system biophysical interaction mechanism with RF and microwave radiation 79—79602
- low dose effects, implications for radiological protection 78—15867
- low dose responses, symposium, San Francisco, USA (June 1976) 78—15862
- low frequency electromagnetic fields, assessment *(German)* 77—86529
- low-level, current estimates of hazards to human populations, review 78—57043
- lung, radiation dose-response curves after radioisotope inhalation, beagle obs. 79—66556
- lung cancer, U miners, rel. to radiation exposure time distrib. 79—79605
- lung cancer induction, meas. of ^{210}Po activity in Indian tobacco 77—9224
- lung cancer rel. to Rn in dwellings 80—89870
- LWR, occupational radiation exposure problems 77—18711
- magnetic fields, cooperative phenomena 80—94247
- magnetic fields, magnetoelectrets as possible mech. 80—93157
- magnetophosphenes, quantitative determ. of thresholds 80—61620
- man-made EM fields and georadiations, effect on man and protection from *(Polish)* 80—67258
- mandible, radiation necrosis, dental factors, radiotherapy complication 80—98021
- mandible, radiation necrosis, factors influencing onset, radiotherapy complication 80—98020
- marine animals, influence of sunlight polarisation and intensity 77—56648
- meat, biochemical procedure for detect. of radiation treatment 78—65075
- medical physics conference, Ottawa, Canada (Jul. 1976) 77—16897
- microdosimetry, conf., Brussels, Belgium (May 1978) 80—4472
- microorganism interaction, dye laser spectroscopy 77—86444
- migrating bird response to Project Seafarer's EM field 77—44718
- millimeter range of wavelengths, personnel safety 79—92391
- mosquitofish population fitness after exposure to chronic low-level environmental radiation 77—64096
- mouse foetal body weight effects of 148 MHz irradiation 80—3726
- multilateral EM exposure, corner-reflector applicators for CW irrad. 80—36213
- neuroelectric transmembrane pots., EM radiation effects, possible model of mechanisms 80—26259
- neutron bombs, effects *(German)* 78—814
- NMR imaging, physiological effect threshold for RF and mag. fields 79—66484
- non-ionising EM radiation, biological response research perspectives 79—48289
- non-ionising radiation, hazards in the laboratory 79—57708
- non-ionizing, physiological effects and max. levels *(Italian)* 79—74717
- nonionising electromagnetic radiation bioeffects research and related occupational health aspects 78—73172
- nonthermal laser effects, phys. model 78—35885
- nuclear energy effects on tradescantia, indicator for ecological effects *(Dutch)* 80—45967
- nuclear facility workers, mortality anal. 80—45981
- nuclear power, effect on the environment, general radiation level and waste product disposal 79—18051
- nuclear radiation, public health aspects 77—75003
- nuclear reactor accident, human exposure to radiation, biological consequences 78—7407
- nuclear reactor fission product release, evaluation of population hazards 77—14250
- nuclear research emulsion supralinearity, mimicking response of biological systems 78—20233
- nuclear waste ponds and streams, Hanford, ecological search for radiation effects 80—89804
- ocular hazard of short pulse Ar laser irradiation, primates 79—25030
- ocular rivalry suppression, effect of 9 Hz flashing light 79—34566
- ophthalmic hazards associated with laser endoscopy 79—79598
- optical, finsen and viton meas., using lux-meter *(Hungarian)* 78—28002
- optical, hazards assessment of IR, visible and UV ranges 79—20580
- optical radiation composition and effects and usage in plant experiments *(Hungarian)* 80—109076
- optical radiation influences on plants and animals, appls. *(Japanese)* 78—44556
- optical radiations, effects on men, directives and unit derivation *(Hungarian)* 78—57040
- orchids, photoperiodism effects on growth and flowering 80—89797
- osteosarcomogenic effectiveness of ^{224}Ra and ^{226}Ra in mice 77—86560
- pancreatic cancer, low-level radiation link 80—89803
- para-aortic irradiation, late effects in carcinoma of uterine cervix and endometrium 80—108979
- phage T7, inactivation by visible laser light *(German)* 80—98010
- phospholipid bilayer containing chlorophyll a, photo-oxidation of water 77—16917
- phospholipid membranes, conductivity changes on exposure to HF EM field 79—79483
- photobiological process relative quantum yield determ. using light of different spectral composition 78—65154
- photophobic accumulations model, blue-green algae in light traps 79—11965
- phototaxis in walking fly, water balance and phototactic response 79—20577
- phototherapy, effect of prolonged illum. on luteinising hormone concs. in human infants 78—69138
- pion$^-$ beam stopping distrib. determ. by charge collector 78—53513
- plant biophysics, book 77—60180
- plant leaves, spectral transmission coeff. changes, nonlinear optical effect 79—57707
- plasma lipoprotein lipase in rabbit irrad. by 25 MeV photons, action of corticoids *(French)* 77—90859

biological effects of radiation continued
- plutonium, biologically important physicochemical props. and methods of human contamination *(French)* 80—98004
- portable radio operator exposure eval. at 30 MHz 79—62297
- power line elec. field effect on communication line maintenance personnel 78—40353
- power line ground gradient simulation for biological effect exam. 77—86731
- protection standards, implicit built-in safety factors 77—73596
- public health aspects of radiation 78—35895
- pulmonary clearance of S. aureus after inhalation of ^{144}CeO$_2$ or ^{139}PuO$_2$, mouse expt. 80—36013
- pulmonary effects of radionuclide and chemical pollutants *(French)* 80—8102
- pulmonary gas exchange following irrad. of cervical, mediastinal, hilar and axillary nodes 77—73542
- quality factor, proposal for revision 78—28091
- radiation exposure and other hazards, comparison of relative risks 79—2111
- radiation protection standards, quantitative risk 80—61708
- radiation sensitivity, conf., Rome, Italy (Sept. 1978) 80—62368
- radiation therapy, biologic effect ratios for parallel opposing fields 79—62299
- radiation worker health registry for AECL employees 79—88201
- radioactive releases from nuclear installations, eval. of accidental atmos. discharges 79—39529
- radiogenic cancer, estimate of life shortening per rem absorbed dose 79—11967
- radioisotope applications in agriculture, hydrology, medicine industry etc., booklet 78—35947
- radiolysis of heterogeneous inanimate systems, radiobiology appl. 80—66824
- radiopathology, clinical problems in diagnosis and treatment of radiation damage *(French)* 78—48845
- radioprotection, medical regulations and standards in France *(French)* 78—48897
- radiotherapeutic agents, props., dosimetry and radiobiologic considerations 80—36106
- radiotherapy dose-response relationships, appl. of logistic regression model 78—11724
- radiotherapy electron accelerator neutron production, conf., Gaithersburg, USA (Apr. 1979) 80—46730
- radiowave energy absorption in tissue prolate spheroids, calc. by point matching method 78—44612
- reactor technology, sources, phys. units and biological factors *(German)* 78—46180
- red light, white spruce female cone prod. inhibition obs. 80—30766
- retina, light-induced transient thermal response 78—7340
- retina, primate, temp. rise and tissue damage due to Ar laser irrad. 78—44559
- retina thermal injury following laser irrad., asymptotic rate process calcs. 78—80916
- retinal damage from a white-light laser, thresholds and mechanisms, rhesus monkey obs. 80—108955
- retinal degeneration in dystrophic rats, light-induced, action spectrum 80—41118
- retinal ganglioside synthesis, chick, light stimulation 77—9189
- retinal injury, permanent, due to over-exposure 79—62295
- retinal injury, thermally-induced, due to high optical-radiation doses 80—3710
- retinal injury mechanics, laser exposure limits 79—66485
- RF, average specific absorpt. rate in ellipsoidal conductor and dielec. models of humans and monkeys 78—40349
- RF, suspicion of harmful effects 77—77939
- RF and ionising radiation effects on personnel working with high power electronic systems *(Italian)* 77—21561
- RF EM fields, review of effects and dosimetric data, safety standards development 80—67154
- RF EM fields (300 KHz-100 GHz), human exposure safety level 80—89869
- RF EM waves, part-body and multibody effects after absorpt., animals and man models 80—56124
- RF energy absorpt. of simulated body material using portable transmitters 78—44614
- RF fields hazards, legislation proposals for workers' protection 80—56223
- RF heating for solid tumour destruction, animal expts. 80—61637
- RF power absorption in biological specimens, meas., 10-100 MHz 77—90916
- RF radiation and EM fields, induction of focal hyperthermia in tumour and body models 78—40244
- RF radiation dosimetry handbook, descriptive summary 78—40347
- RF radiation effects and hazards 80—3709
- RF radiation effects on chick brain, induction of Ca^{2+} efflux obs. 80—56127
- RF radiation exposed chicks, behavioural obs. 80—61633
- RF radiation hazards, engineering status review 77—9220
- RF radiation safety guidelines *(French)* 80—30761
- RF telemetry exposure, EM fields and biosystems interaction 77—86533
- RF waves, effects of repeated exposure on growth and haematology of mice 80—61625
- RF-field interactions with biological systems, elec. props. and biophys. mechanisms 80—35957
- rhabdomere transmittance decrease due to blue light; rel. to desensitisation of peripheral photoreceptors 78—64993
- rhythms in animals, role of light, bibliography 77—48986
- safety, permissible dose estimation based on biological risk 78—40352
- safety estimation methods, problems *(French)* 80—98003
- small-bowel damage, prediction by dose-response curve anal. 80—98036
- solar flare, dose at Earth's surface 79—25109
- solar flare particles, possible cause of ancient climatic and biological catastrophes 77—78587
- solar radiation monitoring system, precision 77—52839
- solar receiver radiative loss and eye hazard evaluation by Net-Radiometer 80—89673
- space colonies, radiation effects and protection 77—86651
- space research, biology and medicine 80—41265
- space-related radiobiological studies 80—41266
- spectral luminous efficacy maximum, definition *(German)* 78—54333
- spinach chloroplasts, laser photoinduced changes in high freq. dielectric constant 80—85449

biological effects of radiation continued
- sterilisation of biomedical equipment, polypropylene stability 77—60245
- stomach tissue, canine, temp. increase comparison for Ar and Nd:YAG laser irrad. 79—92290
- stomach tissues, canine, Ar and Nd laser damage 78—48831
- surface charge density variation of excitable nerve membrane exposed to optical radiation 79—34542
- technologically enhanced natural radiation, chemical problems, human exposure 79—96346
- teeth, human, laser interactions 77—52840
- teeth, human, thermal stress effects and surface cracking assoc. with laser use 78—80915
- teeth, rel. to laser appl. of durable dental sealants 78—48868
- temperature increase and skin sensation under strong lighting *(Japanese)* 78—44557
- temperature increase model for exposure to nonionising radiation 79—57706
- teratological study of rat, IR vs. microwaves 78—40255
- Three Mile Island reactor accident, radiological consequences 80—27771
- thymic region shielding in radiobiology expts., dosimetry in irrad. mouse cadavers 78—61257
- thyroid tumours, human, radiation and host factors following thymus irrad. 80—89800
- tissue, temp. distrib. during laser irradiation 79—39449
- tissue heating by laser radiation, temp. profile and scatt. determ. *(German)* 79—2099
- tissue IR absorption, photoacoustic spectroscopy obs. 79—79604
- tissue penetration depth, spectral depend., 0.35 to 1 μ 78—11714
- transmission line AC EM fields, health effects regulation 80—94286
- tumour induction experiments, math. models 77—9221
- tumours, biological effect of 27.12 MHz SW diathermy 79—2102
- UHV, transmission line, effects on animals and plants obs. 80—17003
- UV as initiator of cancer 79—79600
- vagina, rats, delay of constant light-induced persistent oestrus by 24-hour time cues 80—12182
- vaginal mucosa, radiation tolerance obs. 80—104666
- VHF, UHF and microwave radiation effect on human body 80—8101
- VHF and UHF energy 77—73541
- VHF electromagnetic fields and power deposition in body-of-revolution models of man 79—53189
- VHF portable transceivers, heating by induction field, expt. using phantoms 78—57039
- whole-body irradiation, effects on different tissues, rat expts. 80—72216
- wound treatment by RF EM radiation, rabbit expts. 80—61639
- ^{241}Am III retention and distrib. in neonatal beagle 78—28094
- ^{144}CeO$_2$, effects of repeated inhalation exposure, mouse obs. 80—104676
- ^{144}CeO$_2$, inhalation exposed mice, toxicity, dosimetry and ^{144}Ce retention 80—89874
- ^{137}Cs-irradiation, response of pig skin, various schedules of irrad. 80—72237
- ^{144}e inhalation effect of influenza virus infection on pulmonary retention and mouse survival 78—85340
- Fe metabolism disturbance, math. model of migration of ^{59}Fe as citrate, in rats 77—32942
- ^{3}H, chronic HTO exposure of rats, age effect 77—5044
- I radioactive isotopes, nuclear fuel cycle radiation safety problem, *(Russian)* 80—18560
- ^{A}I, A=131-2, comparative effects in rat thyroid glands 80—104670
- ^{131}I, age-related radiosensitivity obs. of guinea pig thyroid glands 80—104671
- ^{131}I therapy for toxic diffuse goitre, incidence of hypothyroidism within 1 year 78—65116
- ^{131}I treatment of hyperthyroidism, carcinogenesis, comparison with surgery 78—85374
- ^{177}Lu organ distribution in mouse 78—48879
- ^{32}P-diphosphonate dose determ. in patients with bone metastases from prostatic carcinoma 78—61251
- Pu(NO$_3$)$_4$, long-term effects of inhalation, influence of inhaled Ca-DTPA 77—66861
- PuO$_2$ aerosol, acute inhalation, predictive model of early mortality 80—36028
- ^{238}PuO$_2$ high-fired particles, inhalation carcinogenesis in rats 78—28009
- ^{239}Pu acute inhalation, early mortality and morbidity estimate 78—96079
- ^{239}Pu, lymphoid tumours and leukaemia induced in mice by bone-seeking radionuclides 78—69141
- ^{239}Pu, use in weapons and energy prod., radiological hazards, security 77—10492
- ^{239}PuO$_2$, inhaled by baboons and dogs, comparison of early mortality 80—108977
- ^{239}PuO$_2$ high-fired particles, inhalation carcinogenesis in rats 77—21576
- ^{239}PuO$_2$ inhaled by rhesus monkeys, cytogenetic and other biological effects 80—108968
- ^{241}Pu bone distribution, high resolution autoradiography 78—7399
- ^{226}Ra, lymphoid tumours and leukaemia induced in mice by bone-seeking radionuclides 78—69141
- ^{226}Ra-burdened dog skeleton, Rn retention rel. to age and dosage 78—65092
- ^{90}Sr, lymphoid tumours and leukaemia induced in mice by bone-seeking radionuclides 78—69141
- U, miners Rn daughter inhalation and pulmonary cancer incidence 78—96080
- U mining in Canada, health hazards associated with Rn daughter inhalation 79—88140
- UO$_2$ inhaled particle distrib. and clearance on first bifurcation and trachea of rats 78—73267

biological effects of ultraviolet radiation
- *see also biomolecular effects of radiation; cellular effects of radiation*
- N-acetyl-DL-valine, single cryst., paramag. centre form. by UV photolysis, room temp. 77—21480
- N-acetylglucosamide, substrate-inhibitor of lysozyme, localisation of unpaired electrons 78—68992
- acid amide+H$_2$O$_2$, aq. solns., photolysis, EPR study of spin-trapped radicals formed during photolysis 78—68996
- albumin, pulsed laser study of adsorbed aromatic mol. excited states 77—86448
- alga, filamentous blue-green, effects of high and low UV fluences 79—48294
- aliphatic amino acids, N-acetyl substituted, photolytic production of methyl radicals 79—96622

biological effects of ultraviolet radiation continued
- amides, substituted, aqueous solns., EPR and spin-trapping study of free radicals 79—16154
- amino acid photodegradation in presence of TiO$_2$ 78—11531
- Anacystis nidulans, unstable protein mediated UV light resist. 77—86536
- bacteriophage ϕ29 in B. subtilis host, effects of temp. and UV irrad 77—86539
- bacteriophage T1, killing by irrad. in dry state with 122 nm and 254 nm light 80—101234
- bacteriophages, T7 and MS2, effect of UV light *(Hungarian)* 79—16153
- bacteriorphage λ, inactivation by combined X-ray and UV light exposure 80—3732
- biopolymers, deform. under uniaxial stretching during UV irrad. 80—108935
- Bloom's syndrome fibroblasts, UV sensitivity and delayed DNA chain maturation 77—29185
- blue-green alga, UV dose modifying effects of acriflavine 79—43963
- blue-green bacterium Anacystis nidulans, resist. to UV in dark phase 77—16957
- caudal fin regeneration in mosquito fish, in vivo exptl. system 77—52844
- cell, surface photoelectron micrographs and quantum yields 78—61148
- cell killing, UV and X-ray damage interaction in Chinese hamster cells 79—11977
- cell lines of Chinese hamster with different repair activity, UV induced chromated aberrations 79—57711
- cell membrane of Herpetomonas samuelpessoai, concanavalin A binding 78—48835
- cell morphologic transformation by UV, effect of X-irrad. and chem. carcinogens 77—1981
- cell repair competency changes after 5-bromodeoxyuridine pulse labelling and near UV light 79—83854
- cell sterilisation modes, cell killing and early differentiation 78—65093
- cells, Chinese hamster, additive action of ionising and non-ionising radiations throughout cell cycle 77—48845
- cells, Chinese hamster, postreplication repair enhancement 78—92678
- Chinese hamster cells, X- and UV-irradiation obs. 79—96627
- chromatin, solubilized, calf thymus, changes in circular dichroic spectrum 79—100678
- chromosome inactivation in UV irrad. E. coli during growth 77—86551
- chymotrypsin-like proteins, γ-irrad. rel. to UV irrad., unfolding obs. 80—35984
- coral reef epifauna, susceptibility to UV irrad. 80—98037
- corneal damage induced by near-UV laser, cumulative effects 80—85448
- cytochrome c, effects of UV and temp. on optical props. and enzymatic activity 80—81648
- cytochrome c-serotonin soln., UV effect on optical props. 80—30663
- dermatology, photobiologic phenomena 78—35909
- dielectric transient response of some biomolecules following UV irrad. 80—51166
- dihydro-6-methyl uracil single cryst., electron and UV irrad., free radicals, EPR 77—29100
- dihydropyrimidine bases in aq. soln., spin-trapped OH radical reactions, EPR obs. 79—88053
- dipeptides, aliphatic, EPR studies of direct photolysis 78—48678
- diploid fibroblasts, human, nondividing, effect on RNA and protein synthesis 79—92291
- diploid fibroblasts human, correls. after potentially lethal damage 80—21493
- DNA, damage from ionising radiation 79—11987
- DNA, damaged by UV or N-acetoxy-2-acetylaminofluorene, rate-limiting steps in excision repair 77—90865
- DNA, properties changes caused by UV- and γ-irrad., electrochem. anal. 80—72271
- DNA, pyrimidine dimers non-random distrib. 79—96628
- DNA, transforming, shape of UV inactivation curve 77—66797
- DNA, UV and gamma-ray damaged, defective repair in Fanconi's anaemia 77—44725
- DNA and post-replication repair, mouse neuroblastoma cells 77—5027
- DNA base damage detection method, UV induced pyrimidine dimers in human cells 79—44067
- DNA degradation in Escherichia coli 78—48841
- DNA from mouse tissue, UV irrad. studies, UV absorpt. spectra 78—11702
- DNA methylation in HeLa cells 77—12979
- dNA repair and longevity assurance in Paramecium tetraurelia 80—3741
- DNA replication and repair in human melanoma cell-line resist. to UV irrad. 77—44721
- DNA replication fork struct. in UV irradiated human cells 79—88117
- DNA strand breaking and rejoining in UV irrad. normal human and xeroderma pigmentation cells 77—4986
- DNA synthesis, nucl., in yeast, UV and gamma-ray effects 77—56428
- λDNA transcription in vitro 77—66827
- DNA unscheduled synthesis, chromosomal localisation 77—25520
- DNA unscheduled synthesis in UV irrad. spleen lymphocytes after X-irrad., rat 78—69156
- dosimeter, for natural radiation meas. in study of photodermatoses and drug photosensitivity 78—40339
- E. coli, DNA double-strand breaks from single photochemical events 79—16151
- E. coli, DNA single-strand breakds and alkali-labile bonds 79—16152
- E. coli, photoreactivation of ionising radiation induced damage 80—3734
- E. coli, relative rates of repair of single-strand breaks and postirradiation DNA degradation 79—16149
- E. coli, repairability of chromosomal and cytoplasmic DNA after γ and UV irrad. 80—30796
- E. coli, UV-induced recovery of γ-irrad. bacteriophage DNA 80—72214
- E coli B/r, UV sensitivity rel. to DNA content obs. 80—108960
- E. coli inactivation, 365 and 254 nm radiation synergism 79—25044
- E. coli K-12 cells, inhibition of X-ray induced UV resistance by nitrofurantoin 78—85342
- E. coli strains, two with lambda lysogens, induced radioresist. 78—69140
- E-coli, enzymatic activities in UV-induced DNA degradation 80—36011
- E.coli, lethality by 365 nm radiation under various conditions 80—61624
- E.coli, radiation response of thymine-starved bacteria 79—11981
- E.coli, respiration cessation obs. after far UV irrad. 80—76799
- embryos of mouse, one-cell and two-cell, in vitro development 77—12967
- erythemic curve for ermeter-dosimeter ERMD-1, UV intensity and dose meas. *(Russian)* 80—12261
- erythropoietic activity in rabbits and rats 77—32940

biological effects of ultraviolet radiation continued
Escherichia coli radiation-damage inducible system, rel. to UV light mutagenesis 78—53458
ethenoadenosine, influence of pH and metal complexion on fluorescence parameter 79—34483
Euglena gracilis, chloroplastic survival after irradiation 79—79606
eye, 300 to 400 nm, literature review 78—57042
eye, lens pigmentation in humans rel. to UV light exposure 78—65100
eye, review 78—80917
eye lens fluorescence due to UV stimulation, appl. to pupillary response meas. 78—64977
eyes, effects and safety measures *(Japanese)* 78—35881
face, solar dosimetry, natural UV exposure rel. to basal cell carcinoma localisation 79—92382
fatty acids, unsaturated, containing peroxide oxidation products, free radicals formed on UV irrad. 80—51165
ferricytochrome, photoreduction in presence and absence of electron donor 78—53337
fetal fibroblasts, UV induced chromosomal abnormalities, New Zealand Black mice 79—43836
fibroblasts, human, UV-irrad., effects of radioactive labelled DNA on excision repair 80—94289
fibroblasts, mouse embryo, clonogenic survival 79—74722
flavins, photoemission of electrons in polar media 79—29507
fluoresceindiacetate hydrolysis and transport in mammalian cells 77—56333
germ cell determinant UV effect, rel. to germ cell form. in Xenopus embryo 77—70503
germicidal, Brown, Boveri irradiation unit, for surface sterilisation, foodstuffs and pharmaceutical industries appl. 79—62302
germicidal, water sterilisation unit design and appl. 79—57713
hazards and protection standards 77—81588
hazards assessment 79—20580
HeLa cell chromosome, UV induced repair pattern 79—57611
herpes simplex virus in carcinogen-pretreated cells, enhanced survival after UV irrad. 78—35894
hybrid X-ray resistant cell line, response to X-irrad., UV, actinomycin D and cordycepin 77—86541
hypotaurine oxidation to taurine by UV irradiation 79—96617
lens pigmentation, human, in vivo, independ. of UV light exposure 77—60202
lipid bilayer electrical strength fall after UV irrad. 78—69002
lipid free radical oxidation, UV effect on lipid-protein complexes and membranes 77—36874
lipid peroxide oxidation fluorescing products, effect of UV on formation 79—57585
lipids of membranes, free radical formation 80—81647
liposomal membrane, oxidation 78—40271
liposome proton permeability increase on peroxide photo-oxidation of lipids 78—69024
lysozyme, electron acceptor props. in photosensitized electron transfer, EPR study 79—79469
mammal gonads, radiation induced morphological and endocrinological changes *(Russian)* 78—77090
mammalian cell line sensitivities to hyperthermia, γ-rays and UV 77—66800
mammalian cells, DNA repair kinetics 79—20513
mammalian cells, laser radiation effects obs. using optical waveguide evanescent fields 80—12183
marine organisms, ecological significance of solar UV 80—45974
measurement of UV in biological appl. 80—35963
measurement techniques 78—37954
medical uses of lamp radiation 79—66504
8-methoxypsoralen, photosensitising agent, detect. in ocular lens rel. to psoriasis treatment 78—15937
micro-organisms, radiation injury, repair and sensitisation, review 78—11700
microorganisms, effects of laser and ordinary UV irradiation 79—70586
Moss cells, regeneration and photoreactivation after UV irradiation 79—88120
nearby supernova, climatic and biological impact 78—28297
nematode, Rhabditidae tokai, killing effects of UV light and X-rays 80—101235
neuroblast, mitotic effects rel. to cell cycle, nucl. membrane breakdown 77—12972
neuroblast, mitotic effects rel. to cell cycle, nucl. membrane breakdown 77—12973
nucleic acid, multiphoton photoreactions of aq. soln., picosec. UV pulse 79—34487
oncogenic transformation of mouse 10T1/2 cell line in vitro 77—12971
orthopedic surgery, prevention of deep wound infection 79—16265
osteosarcoma, human, in vitro, evidence for unusual cellular repair activity 77—48847
phage T7, action spectra for UV and visible light inactivation 80—21498
phosphatidyl choline, oxidised, free radical formation 80—76790
photochemotherapy of psoriasis vulgaris and mycosis fungoides 78—35908
photosynthetic reactions of leaf discs and chloroplast preps. of crop species, 298 nm radiation effects 78—61220
pine pollen, localisation of site of action of tube growth stimulation by micro UV-irrad. 77—56445
pine pollen growing tubes, effects of low and sublethal doses 80—36002
plasmid molecular weight determ. from UV sensitivities 78—44458
Pollen, Pinus Silvestris, effect of X, UV irradiation on NAD(P), NAD(P)H, hydroxyproline levels 79—20582
pollen tube, pine, growth stimulation by low doses of radiation 79—100677
pollen tube growth stimulation, effects of antibiotics 78—28022
postreplication repair enhancements in UV-irrad. Chinese hamster cells by irrad. in G_2- or S-phase 78—77085
postreplication repair in mammalian cells, model 78—80918
potato virus S on Chenopodium quinoa 'Valdivia' leaves, local lesion development obs. 80—81654
preimplantation mouse embryo sensitivity to UV irrad. in vitro, postreplication repair 78—20224
protein, radical limiting conc. on UV irrad. at 77K, effect of luminesc. quenchers 80—30662
protein aggregates, limiting conc. of paramag. centres 78—24029
protein synthesis control studies, exptl. probe using psoralen and near UV light 77—66881
proteins, luminesc. quenching 78—15768

biological effects of ultraviolet radiation continued
proteins, paramag. centre accumulation, kinetic eqn. 77—21476
pyrimidine dimers, excision repair of UV damage in monkey kidney cells 78—53332
pyrimidines, substituted, UV irrad. in aq. solns., EPR of free radicals 78—40115
retinal autofluorescence in land snails 79—53103
retinal damage by 325 nm He-Cd laser radiation 78—69136
ribonucleotide reductase of E.coli, in vivo photoinactivation by near-UV 77—52841
RNA, heterogeneous nucl., effects of UV irrad. and postirrad. incubation on size in murine cells 78—69139
RNA, low molecular weight, synthesis sensitivity to UV irradiation 79—57591
skin, effects and safety measures *(Japanese)* 78—35882
skin and UV radiation physics, review 80—81661
skin cancer, evidence 80—35962
skin cancer incidence modelling 78—77091
skin cells, human herpes virus production as repair marker 80—30783
skin disease therapy 80—36057
skin Na entry site irreversible inhibition by photosensitive amiloride analogue, in frog 78—69030
solar UV meas. and physics 80—41784
solar UV radiation, changes at Earth surface due to stratospheric O_3 reductions 80—94577
soybean suspension cultures, thymine dimer and glyceollin accumulation 80—104646
sub-lethal damage accumulation site, evidence for location in Chlamydomonas 78—7390
synchronised cultured human liver cell survival 77—56439
thymine dimer excision from DNA of UV-irrad. plant seedlings 78—61221
thymine dimer excision kinetics in UV-irrad. human cells 78—53331
thymine dimer induction by UV as function of cell stage 79—57715
trypsin, photoluminescence after UV irradiation *(German)* 79—92137
tyrosinase in buffer soln., UV effect on biological activity 80—30791
UV radiation from lamps, harmful effects *(Swedish)* 80—35996
UV radiation level measurement problems 78—37057
vibrios UV inactivation kinetics 77—90854
VUV, broad-band synchrotron radiation, effects on wet yeast cells 80—108972
wallaby cells, absence of effect of photoreactivation on sub-lethal damage accumulation 79—11970
wound healing promotion by UV burners, rat expts. 79—62310
yeast, inducible enyzme synthesis, UV effects on regulation and activity per cell 78—69157
yeast, UV-inactivation kinetics and division delay during different growth phases 77—25517
yeast Candida guilliermondii, photoprotection and reversible inactivation by 313 nm light 77—25509
yeast cell, caffeine inhibition of liquid-holding recovery from UV induced budding delay 79—11985
yeast cell suspensions, vac. UV irrad., 163 nm, lethal and genetic damage 77—21573
yeast cells, alpha-irrad., UV-induced reactivation 78—80920
Yoshida sensitive and resistant cells, dimer form., excision and DNA strand growth after UV irrad. 77—90858
H_2O_2, UV prod. of OH radicals, reactions with peptides in aq. soln., EPR 78—68993
HeLa cells, synchronised, DNA damage from UV irradiation 79—25034
O_3 depletion is stratosphere, effects of prolonged exposure to intensified UV radiation 77—91256

biological effects of X-rays
see also biomolecular effects of radiation; cellular effects of radiation
abdominal epidermis histogenesis and age depend. of X-ray sensitivity in flesh fly metamorphosis 78—65084
N-acetyl-L-cysteine, ^{33}S nucl. coupling and nature of free radicals 77—52743
N-acetylglycine, X-irrad., stable radical electronic and mol. struct., ENDOR and ESR 80—80637
acid phosphatase activity following hyperthermia of mouse spleen, rel. to heat potentiation of X-ray damage 78—48842
adoptive antibody responses in DBA/2 and BALB/c mice, differential effects of preirrad. 78—80926
L-alanine:Cr^{3+}, X-irrad., thermoluminesc., ESR, UV photobleaching 77—9104
alveolar macrophages, mouse obs. 80—98024
amino acid absorption by rat intestinal prep., effect of supralethal X-irrad. 77—56444
amino acid utilisation in cultured insect cells 77—5043
amino acids, EPR determ. of radical yields 79—34491
amobarbital, radiation-prod. free radicals in pyrimidines, EPR 77—25374
anaesthesia effects on hypoxia in normal tissues 78—28007
aneuploidy in mouse fetuses after paternal exposure to X-rays 79—79607
arterial wall damage, fast neutrons vs. X-rays 77—29183
bacterial spores, breaking survival curves and O_2 removal times obs. 80—81658
bacteriophage T1 radiosensitivity on various host strain mutants of E. coli 78—20228
bacteriorphage λ, inactivation by combined X-ray and UV light exposure 80—3732
benign tumours, spontaneous and radiation-induced, in parabiont rats 79—88133
binucleate cell formation induced by X-irradiation 80—17015
biochemical indicators of radiation injury 79—34607
blood, alterations in toad erythrocytes and aq. solns. of haemoglobin 78—11699
blood, gas valves, anal. in mice following pulmonary irrad. 80—104673
blood cell permeability to K^+, Na^+ repair after X-ray, fast-neutron damage 79—57615
blood vessels, radiation induced damage, mouse, dose-effect time relationship 79—34603
bone, appl. of EPR spectra of quasirandomly oriented centres 77—21667
bone, changes in ^{99m}Tc pyrophosphate imaging after X-irrad. 80—72239
bone, histopathological and physiological changes, rabbit expts. 80—51171
bone, mouse, rel. between ^{239}Pu deposition in bone and ^{59}Fe uptake in marrow 78—85395
bone, radiation induced osteosarcomas, rabbits, scintigraphic and radiographic detect. 80—101231

biological effects of X-rays continued
bone marrow, mouse, late effects of X-irrad on ability to support haematopoiesis 77—70496
bone marrow cell-culture, RBE of different-energy neutrons 79—34508
bone marrow erythrocytes of mice, X-ray induced micronuclei 78—77088
bone marrow erythropoiesis, abscopal suppression obs. on mice 80—17020
bone marrow regeneration from cortex after segmental fractionated irrad. 77—70495
brain, late changes in biochem. and blood flow, rate expts. 80—72218
brain, monkeys, delayed damage from therapeutic range irrad. 80—76801
brain tumour cells, rat, anal. of interaction of 2 nitrosourea compounds and X-radiation 80—72230
brain tumour cells, rat, BCNU-modification of in vitro X-ray response 77—70498
brain tumour cells, Z-ray-BCNU interactions in vitro, isobologram anal., rats 80—81662
brain vasculature, late functional changes after local irradiation, rat 80—30774
breast dose and cancer risk due to fluoroscopic chest exams. of women with tuberculosis 78—65128
5-bromodeoxyuridine, single cryst., X-irrad. at 77K, $C_{5'}$-centred deoxyribose radical 78—20032
cancer X-ray sensitivity increased by 434 MHz EM irradiation 78—24180
cancers, genetic defects, resulting from use of various energy sources 79—16259
carbohydrate absorption in vivo in rats with gastro-intestinal radiation syndrome 77—70494
carcinogenesis, influence of chronic environmental stress 77—25516
carcinogenic effects of different mammographic techniques 79—70617
cartilage, baby rat tails, hyperthermia and X-irradiation, O_2 enhancement ratio 79—57712
cataract development in micr irrad. at different ages 78—20232
cell killing, UV and X-ray damage interaction in Chinese hamster cells 79—11977
cell killing and the sequencing of hyperthermia and radiation 79—100673
cell membrane permeability changes after X-irradiation 79—39370
cell membrane potential changes on X-irradiation 79—39369
cell morphologic transformation by UV, effect of X-irrad. and chem. carcinogens 77—1981
cell neoplastic transformation and dose fractionation, role of damage repair 80—72242
cell radiation effects and hyperthermia, effect of post-exposure incubation conditions 78—40273
cell radiosensitivity mammalian anal. using radio-sensitive and radio-resist. clones in vitro 77—9226
cell sterilisation modes, cell killing and early differentiation 78—65093
cell survival, hyperthermia interactions with radiations of different LET, C ions and X-rays 77—48846
cell survival, mol. theory anal. of synergistic interaction with Pt complex 77—21565
cell survival after hypoxic irradiation 79—74719
cells, ^{125}IUdR-labelled and X-irrad., 4.2K and above 80—72211
cells, Chinese hamster, additive action of ionising and non-ionising radiations throughout cell cycle 77—48845
cells, nuclear lesions induced by X-irradiation of Chinese hamster cells, ultrastruct. anal. 80—21494
cells, phosphoresc. microscopy 78—3454
cells, viable hybrids of lethally irrad. hamster cells and unirrad. mouse cells. 77—5034
cellular chromosome condensation and X-induced G_2 arrest 79—34510
cerebral capillaries, increased radiosensitivity in neonatal Gunn rats rel. to Sprague-Dawley rats 80—17006
cervical carcinoma, external small-field X-irradiation 79—16269
cheek pouch epithelium, tumour-bearing, radiation-induced vascular alterations, Syrian hamster 80—17016
Chinese hamster cell, repair of potentially lethal damage after X- and α-irrad. 78—28014
Chinese hamster cell sublethal damage repair after fast neutron irrad. with or without X-irrad. 78—20218
Chinese hamster cell survival and sublethal repair, ultra-high dose rate electron irrad. compared with X-rays 78—40272
Chinese hamster cells, combined effects of hyperthermia and X-rays 80—45977
Chinese hamster cells, DNA replication after X-irradiation 79—11986
Chinese hamster cells, hyperthermic radiosensitisation to X-rays 80—21450
Chinese hamster cells, pot. lethal damage rel. to sublethal damage 80—36012
Chinese hamster cells, X- and UV-irradiation obs. 79—96627
Chinese hamster ovary cell X-ray induced division delay, effect of hydroxyurea 78—31865
Chinese hamster ovary cells, changes in cellular heat and/or radiation sensitivity obs. 79—74727
Chinese hamster ovary cells, X-ray response during latter part of G_2 80—30775
Chlamydomonas reinhardi, dividing, X-ray and proton-induced ultrastruct. changes 78—65085
Chlorella pyrenoidosa, clonal survival after irradiation 79—79606
Chlorella pyrenoidosa synchronised cultures, effect of extremely low doses of secondary radiation from ^{32}P 78—73176
5-chlorodeoxyuridine, single cryst., X-irrad. at 77K, $C_{5'}$-centred deoxyribose radical 78—20032
CHO cells, alterations in radiosensitivity by anisotonic treatments 80—72251
CHO cells, asynchronous, fractionation of combined heat and radiation, cell-cycle redistrib. 80—76807
CHO cells, cyclic AMP levels rel. to X-ray induced mitotic delay 80—51170
CHO cells, effects of X-irrad. and hyperthermia on SCE freq. 80—36021
chromatid breaks induced in Chinese hamster cells rel. to pion$^-$ irradiation 80—26270
chromosome aberration specificity, X-irrad. human T-cell line 78—80921
chromosome aberrations, alteration in freqs. of different classes throughout first cell cycle after irrad. 80—104672
chromosome aberrations in spermatogenesis of mature monkeys, single and fractional dosage *(Chinese)* 79—39451

biological effects of X-rays continued
chromosome aberrations in vivo effect of US alone and in combination with X-rays 78—20210
chromosome aberrations induced by low doses of X-rays in human lymphocytes in vitro 80—72235
chromosome aberrations of peripheral lymphocytes in rabbits exposed to whole body X-irradiation 79—43834
chromosome recombination during oogenesis in silk worm 77—2030
chromosomes, interaction of X-ray induced primary breaks in form. of dicentrics 77—12963
chromosomes of human female lymphocytes, distrib. of X-irrad. induced lesions, dose-effect relation 80—51175
collagen, rat tail, radiation damage during X-ray small angle scattering using energy dispersive methods 79—12051
colon crypt survival after whole- or partial-body irrad. of mouse 77—56427
colon crypts, mouse, induction of radioresistance by X-rays 80—45970
colonic epithelium, compensatory proliferative response to multi-fraction irradiation 79—88128
computerised tomography, health risks due to radiation exposure 80—61654
creatine biogenesis, effects of whole-body X-irrad., rat 78—3559
Crepis seed, influence of post irradition moisture alteration on biological after-effect 79—20581
Crepis seeds, heat rel. to storage in X-ray injury modification 79—88118
cumbu seeds, effects on R_1 and R_2 progenies 79—29571
cyclic nucleotide changes in X-irradiated synchronized Tetrahymena 79—25046
3'-cytidylic acid, stable radical in ribose moiety, compared with cytidine 77—25375
cytochromes ratio in radiation-induced leukemia cells, mouse 80—21500
cytophotometry, multiparametric pulse technique for cell and radiation research *(German)* 77—78060
cytosine monohydrate single cryst., OH addition radical and decay product 77—86447
cytosine.H_2O crystals, radical form. by X-irrad. at 77 and 300K 77—12886
cytotoxicity of X-rays rel. to ^{238}Pu 4.4 MeV α-particles 80—72265
delta-electrons prod. in water by high-energy electrons and X-rays 77—29178
diagnostic X-rays, effects, risks and protection, review 78—3591
dicentric chromosome induction in human lymphocytes by 30 kV X-rays, RBE 78—3563
dimethyl sulphoxide radioprotection of mammalian cells, exposed to X-rays, heavy charged-particle beams 79—79609
diploid cell culture, human, neoplastic transformation 80—51172
diploid cell populations, human, acute and late effects of single exposure 80—98029
diploid yeast, O_2 effect in killing by photon irrads. of different energies 80—36018
diploid yeast, split dose and liq.-holding recovery after X-irrad., growth phase depend. 77—64088
diploid yeast, split-dose and liq.-holding recovery, depend. on cellular protein metabolism 77—86547
diploid yeast cell ribosomal RNA gene inactivation curves and cross-sections 80—26297
DNA, damage from ionising radiation 79—11987
DNA, high mol. wt., sedimentation data, radiation-induced single-strand breakage, additives effect 80—30667
DNA, mammalian, organisation of repeated nucleotide sequences in replicons 77—73506
DNA, single-strand break repair after X-irradiation, cultured insect and mammalian cells 79—74725
DNA, single-strand breaks, yield and repair, E. coli cells 77—9173
DNA, subchromosomal synthesis in X-irradited V-79 cells 80—41141
DNA, thymine damage production and excision, mammalian cells, high-LET irrad. obs. 80—72261
DNA, transforming, X-ray sensitivity rel. to presence of free radicals 78—68995
DNA, triplet state excited by X-rays 77—9174
DNA, X-irradiation production of alkali-labile lesions 79—43820
DNA, X-ray induced damage in rat cerebellar neurons and brain tumour cells 78—80922
DNA and chromosomal proteins syntheses in rat thymus after whole body irradiation 79—34492
DNA damage of Chinese hamster ovary cells on X-irradiation after preheating 79—34493
DNA films, luminesc. and optical absorpt., rel. to γ-induced free radicals 77—5033
DNA lesion production, role of radicals, E. coli X-ray endonuclease specificity 77—52745
DNA non-rejoining break induction by high LET radiation, rel. to cell death 77—44596
DNA replication kinetics in X-irrad. Chinese hamster ovary cells 78—20226
DNA synthesis in chick embryonic Mullerian ducts, X-ray dose response obs. 79—88130
DNA synthesis in X-irrad. HeLa cells, depend. on dose and time after exposure 77—37025
DNA synthesis inhibition in vitamin-E-depleted lymphosarcoma cells by X-rays and cytostatics 77—56429
DNA unscheduled synthesis in diploid yeast after X-irrad. in different phases of cell cycle 77—44722
DNA unscheduled synthesis in UV irrad. spleen lymphocytes after X-irrad., rat 78—69156
dosimetry intercomparisons for evaluation of X-irradiation late effects 79—62361
Drosophila, induced mutations rel. to X-ray dose 77—32944
E. coli, photoreactivation of ionising radiation induced damage 80—3734
E. coli, repairability of chromosomal and cytoplasmic DNA after γ and UV irrad. 80—30796
E. coli, value of photoreactivable component after exposure to ionising radiation 80—72224
E. coli ^{125}I and X-ray damage, effect of cell DNA content 78—28006
E. coli K-12 cells, influence of uvrD mutation on survival and repair 77—86540
E. coli K-12 cells, inhibition of X-ray induced UV resistance by nitrofurantoin 78—85342
E. coli strains, two with lambda lysogens, induced radioresist. 78—69140
ear, mouse, effect of prior heat treatment on thermal enhancement of radiation damage 79—48291

biological effects of X-rays continued
- ear chamber microvasculature, rabbit, radiation damage and subendothelial repair 77—52847
- ear skin, mouse, fractionation effects in response to combined heat and X-rays 80—76805
- E.coli, radiation response of thymine-starved bacteria 79—11981
- Ehrlich ascites carcinoma cell fluoresc. after X-irrad. 78—69143
- Ehrlich ascites carcinoma cells, effects of pions$^-$ rel. to electrons and X-rays 80—26267
- Ehrlich ascites tumour cell, thymidine transport kinetics and DNA synthesis 78—20215
- Ehrlich ascites tumour cell membranes damaged by X-rays, biochem. interaction of heparin 78—31864
- Ehrlich ascites tumour cells, influence of O_2 tension of X-ray-induced fall in anodic mobility 79—34526
- embryo of 2 cells, mouse, cell cycle-dependent radiosensitivity obs. 80—104669
- embryo pronuclear zygote stage, mouse, X-ray rel. to π^- effects 80—26274
- embryonic cell viability and survival in mouse, preimplantation X-irradiation effects 79—88137
- embryos of mouse, one-cell and two-cell, in vitro development 77—12967
- EMT6 tumour cell response to single fractions of X-rays and cyclotron neutrons 78—20230
- EMT-6 cells in vitro, potentially lethal damage recovery following X-ray or neutron irrad. 79—62308
- endothelial cells, human, replication in culture, X-ray induced inhibition 77—21571
- energy transfer in biological model structs. *(German)* 78—15906
- enzyme induction in X-irrad. E. coli B and B/r 78—28005
- epidermal cells, mouse dorsal skin, regeneration and dose-response characts. 77—5031
- epidermal mitotic activity during mouse skin wound healing 77—56436
- epidermal mitotic activity during wound healing in adrenalectomised mice, effect of head irrad. 78—20220
- epidermia, enzymatic behaviour rel. to age and lesion location 77—64089
- epidermis, ultrastruct. stereology after X-irrad., rat tail expts. 80—36003
- epithelial stem cell survival parameters, considerations in use of mouse foot system 80—36017
- epithelium of hamster cheek pouch, enhancement of DMBA tumour genesis by repeated low-level exposures 78—53456
- erythrocyte membrane, X-ray induced structural changes, fluorescent probe obs. 79—88129
- erythrocyte membrane struct., intrinsic fluorescence obs. 79—74724
- erythrocyte membranes, fluidity change after X-irrad., pyrene excimer fluoresc. obs. 80—72262
- erythrocyte surface charge decrease, target of X-irrad. and dislocation of sialic acid 77—52853
- erythropoietin action, identification of two components by irrad. in vitro 78—65094
- evoked potentials, averaged, long-term changes after X-irrad., rabbit 78—11704
- ferredoxin of adrenal cortex, destruction of chromophore centre on exposure to X-irrad. 78—76993
- ferric haemoglobin, EPR studies before and after irradiation 79—29503
- feto-placental tissues, irrad. effects after treatment of material genital carcinoma 80—45964
- fibroblast L-929F, mouse, radiosensitivity and recovery during cell cycle, 200 kVp X-irrad. 78—28019
- fibrosarcoma, mouse, therapeutic advantage of combined heat and X-rays 78—44562
- fibrosis rel. to early inflammatory response in rats 78—48839
- fluoroscopy, organ dose per unit exposure, estimation method for artificial pneumothorax 78—96097
- free plant cell, suspension-cultivated, survival after X-ray and fission neutron irrad. 79—92296
- generation times in two successive generations of X-irrad. FM3A cells 78—31872
- germ cell and embryo development effects after X-irradiation, toad 80—8107
- giant cell formation, influence of conditions enhancing potentially lethal damage repair 77—25519
- gliosarcoma 9L cells, response to hyperthermia and X-irrad. 80—36030
- granulocyte growth enhancement on peritoneal cell-coated membranes following irradiation 80—21504
- growth of inbred mice irradiated at different ages 78—44566
- haematopoiesis progenitor and effector cells, expt. murine system, whole body irrad. obs. 80—98034
- haemopoietic repopulation and stromal cell viability in X-irrad. mice 78—15872
- haemopoietic stem cells, mouse, proliferative and differentiative ability, ^{226}Ra and X-irrad. effects 79—79611
- haemopoietic stem cells of shielded bone marrow, role of migration 77—9225
- haemopoietic system of mice, X-irrad., damage repair modification by microwaves 78—24096
- head irradiation by fast neutrons and X-rays, pathological effects on rabbits 78—31860
- heart, dog expts. 80—104679
- Hela cells, recovery from sub-lethal damage when irradiated at ultra high dose rates 79—79608
- heritable lesions, radiation induced, in proliferating mammalian cells, review 79—20602
- hybrid X-ray resistant cell line, response to X-irrad., UV, actinomycin D and cordycepin 77—86541
- 15-hydroxy prostaglandin dehydrogenase activity in tissues of mice 80—51169
- hyperthermia, US induced in previously X-irradiated sites 79—62315
- hyperthermia and radiation effects on tumours and production of disseminated disease 80—40967
- hyperthermia and X-ray combined effects on CHO cells, rel. to temp. and order of appl. 78—65088
- hyperthermia combined with radiotherapy, normal and cancer cell effects obs. 80—45972
- hyperthermia combined with X-irrad., fractionation studies 80—56138
- hyperthermia effect on nonhistone proteins isolated with DNA 78—80843
- hyperthermia modification of X-ray damage in Chinese hamster ovary cells, 40 and 45°C 77—86557
- hyperthermia/radiation interaction, temp. coeff. of interaction 78—11617

biological effects of X-rays continued
- hyperthermia/X-ray survival response of plateau-phase V-79 cells, effect of delay 78—3555
- hyperthermia/X-rays, combined effect, response of skin, intestine and cartilage 77—16955
- hypoxic cells, rel. to O prod. in anaerobic water by X-rays 77—25514
- hypoxic tumour cells, hyperthermia effect in vivo 77—70499
- ileum, guinea-pig, immediate X-ray induced contractions, localisation of effect by drugs 77—56443
- ilium, exteriorised upper segment in rat, glucose, proline uptake 79—11984
- immune capacity suppression, mice to intestinal cestode, comparison of fast neutrons to X-rays 79—16257
- in vitro transformation, conf., Toronto, Canada (May 78) 80—67931
- intenstinal crypt cells, extreme sensitivity to X- and γ-irrad. 77—90864
- intestinal cell sublethal damage after mixed treatment with X-rays and fast neutrons, mouse 77—64086
- intestinal epithelium of rat, fine-struct. effects of 1200R abdominal X-irrad. 78—3561
- intestine, mouse, hyperthermic sensitisation, effect of sequence and temporal separation of treatment 78—44561
- intestine, small, acute and late damage following fractionated neutron and X-irrad. mouse 78—11706
- irradiation doses, effects and sources of ionising radiations *(French)* 79—66494
- keratinocytes, dose-dependent vol. changes after X-irrad. 80—61652
- kidney, degenerative and age related changes, rat 79—57723
- kidney, mouse, late effects of unilateral irradiation 80—21505
- kidney, X-irradiation and induced autoallergic glomerulonephritis effects, rat obs. 80—76793
- kidney radiation injury, mouse, light microscopy 78—35891
- lactate dehydrogenase, O_2 effect in radiolysis obs. 80—72223
- leaf, Saintpaula, dose-effect curve shape rel. to radiation-stimulated repair 80—26291
- lethal doses, repair of radiation damage, mammals 78—11703
- leukaemia cell radiosensitisation by hyperthermia and nitroimidazoles, rel. to hypoxia 77—86555
- leukaemic cell line, mouse, radioprotection by procaine 78—65080
- leukemias, nonlymphatic, rel. to adult exposure to diagnostic X-rays 80—67158
- life shortening of mice exposed to fractionated X-irrad., repair and biochem. protection 78—69153
- limb, mouse, early and late response to multifractionated X-irradiation 79—88123
- lipid membrane models, dose-rate and O_2 effects, linoleic acid 77—48841
- liposomal membrane permeability, radioresist. 78—80919
- liver, guinea pig, X-irrad. induced changes in glycogen, phosphorylase and glucose-6-phosphatase activity 80—51173
- liver, in vivo repair of injury leading to interphase death, rat 77—52850
- liver, mouse, irrad. effect on tyrosine aminotransferase activity circadian rhythm 80—41121
- liver cell proliferation, rat, failure of X-ray hepatoma production 79—25050
- liver membrane alternations after X-irrad., normal and vitamin E deficient ducklings 80—41139
- liver membranes, mouse, dose-rate effects 80—94293
- long-term effects on female mice, rel. to π^- 80—26273
- low dose/dose rate RBE of ^{3}H β-rays and other low LET radiations 80—12190
- low-dose RBE and quality factor for X-rays and gamma-rays 78—73175
- lung, late biochem. changes after hemithoracic irrad. of rat 77—5053
- lung, late biochem. changes after whole body irrad., rat 77—56432
- lung, pathological changes following single and multi-fraction irrad. 78—3553
- lung, single dose, sequence of histological changes, mouse obs. 80—98019
- lung, specific early fine struct. changes 78—31859
- lung cancer in histoculture, continuous isotopic X-irrad. 77—73550
- lung carcinoma treatment by local irrad. and Corynebacterium parvum, mice 78—65091
- lung damage, mouse, plethysmographic method for pulmonary function meas. 79—20721
- lung early radiation dose-response, ultrastruct., dog 78—35890
- lung epithelial cells, type 2, proliferative response after X-rays and fission neutrons 80—108974
- lung irradiation for pulmonary metastases prevention, expt. with model system 77—37021
- lung tumour induction in RFM mice after localised X- or neutron irrad. 80—72260
- lungs, alveolar macrophage number and index of effect 78—31869
- lymph nodes, calf, study of interaction between histone F2b and DNA 78—85346
- lymphatic metastasis from primary tumour growing in foot, localised preinoculation X-irrad. influence 80—45976
- lymphocyte chromosome aberrations, influence of blood storage after X-irrad. 77—66828
- lymphocyte chromosome aberrations, irrad. in vitro and in vivo, monkeys 77—37012
- lymphocyte chromosome aberrations and the Poisson distrib. 79—100675
- lymphocyte chromosome aberrations in humans induced by photon and electron irrad., sublesion interaction model 80—26279
- lymphocyte death and transform., effects of X-ray and neutrons 78—69144
- lymphocyte dicentric yield on X-irradiation, human and feline blood 79—96624
- lymphocyte homing patterns, radiation induced alterations 80—17014
- lymphocytes, acentric fragments formation, anal. of primary processes 80—72272
- Lymphocytes, human, effect of irrad. on hexose monophosphate shunt pathway 80—76798
- lymphocytes, human, homogeneous sensitivity to radiation-induced chromosome damage 79—53197
- lymphocytes, human, lethally-irrad., ultrastruct. events in cytoplasmic death 77—48842
- lymphocytes, human, prediction of dose-rate effects for dicentric production by X- and γ-rays 80—72226
- lymphocytes, human, variation in neutron RBE values compared to X-rays 80—101229
- lymphocytes, human peripheral, chromosome sensitivity to various X-ray doses and subsequent storage 80—17011
- lymphocytes, mouse thymus, X-irradiation effects on UV fluorescence 79—66491

biological effects of X-rays continued
lymphocytes, of equine peripheral blood, stimulated with phytohaemagglutinin 77—5032
lymphocytes, survival of T- and B-cells after X-irrad. in vitro 77—12969
lymphoma cell line, murine, inverse split-dose effect 80—17008
lymphoma cell survival after X-irrad., effect of vitamin E 78—92677
lymphoma cells, mouse, of differential sensitivity to X-rays, expt. obs. 80—72221
lymphoma cells, Murine L5178Y, production of radioresistant mutants 80—76809
α_2-macroglobulin values in serum of X-ray workers 78—28020
malignant melanoma, relationship between total dose, fraction number, fraction size 79—5341
mammal gonads, radiation induced morphological and endocrinological changes *(Russian)* 78—77090
mammalian cell, survival of normal and hybrid X-ray resist. lines exposed to X-rays and protons 78—80929
mammalian cell hybridization ability rel. to X-ray dose 79—88138
mammalian cell mutation and activation by radiations of differing LET 77—56431
mammalian cell survival in vitro, average vs. viable cell multiplicity 79—92304
mammalian cells, cultered, effectiveness of 0.3 keV C X-rays in inactivation and mutation 80—35979
mammalian cells, effect of low dose rate radiation on cell growth kinetics 80—8103
mammalian cells, enhancement of potentially lethal damage by low temp. storage 77—37010
mammalian cells, influence of radiation quality on effectiveness of small doses 80—30785
mammalian cells, lack of correlation between heat and radiation sensitivity 79—20599
mammalian cells, premature chromosome condensation following X-irrad. 80—45984
mammalian cells, replicon sizes estimated by X-ray plus bromodeoxyuridine photolysis method 79—16353
mammalian cells in culture, continuous and fractionated irrad., growth rate effect 79—66493
mammalian cells in vitro, 300 keV X-ray, 14 MeV neutron and pion$^-$ effects 78—69155
mammalian chromosomal DNA, single-strand breakage, sensitive detect. by sedimentation anomaly appl. 80—104825
mammalian cultured cell survival after US exposure, synergism with X-ray effects 78—11693
mammary adenocarcinoma, combined hyperthermia and X-ray effect, mouse expt. 77—90852
mammary cell survival following irrad. in vivo, single dose-survival curve 78—31870
mammary gland cells, rat, survival after X-irradiation under different endocrinological conditions 79—34513
mammary tumours, mouse, cytokinetic basis for efficacious radiotherapy protocols design 79—88124
marrow dose estimation by ^{59}Fe uptake in normal and splenectomised rats, 1000 kVp X-irrad. 78—15894
membrane permeability, sheep erythrocytes, O_2 effects 77—5039
membranes, vitamin E deficiency and lipid peroxidation, mouse obs. 80—72263
1-methyl cytosine: 5-fluorouracil X-irrad. at 300K, EPR 78—64941
micro-organisms, effect on colony-forming ability 79—11969
microdosimetry, energy deposition distrib. patterns 79—20600
microvasculature in rabbit ear chamber, electron microscope obs. 77—64092
mitochondria, rat liver, vitamin E deficient, effect of X-irradiation on proteins 79—34511
mitochondria isolated from bean, respiration and cation accumulation effects of X-irrad. 80—56141
mitochondrial protein synthesis in rat liver after whole-body X-irrad. 78—80925
mitotic crossover increase in Nicotiana tabacum after 150 kVp X-irrad. 78—61219
monkey mortality, X-ray and neutron exposure, effect of autologous bone marrow transplantation 79—29572
mouse ovaries, X-ray effect on population of granulosa cells *(Russian)* 78—73177
murine L5178Y cells, correl. of cell cycle parameters with radiation sensitivity 80—98016
murine leukemic lymphoblasts, deficient repair and degradation of DNA after irrad. 80—72249
murine leukemic lymphoblasts, deficient repair and degradation of DNA 80—72253
mutagenicity of X-rays rel. to ^{238}Pu 4.4 MeV α-particles 80—72265
mutations, DNA and target theory 77—5040
mutations, specific locus, re-anal. of mouse data 77—21570
myeloid leukaemia induction in CBA mice 78—44564
necrosis of mouse tails, tolerance after repeated X-ray irrad. 78—96067
necrosis of normal tissue, mouse tail expt. 78—40270
nematode, Rhabditidae tokai, killing effects of UV light and X-rays 80—101235
neonatal duck and chicken radiosensitivity, Conf., Tokyo, Japan (May 1979) 80—31411
neoplastic transformation in vitro induced by neutrons and X-rays, rel. to radiation quality and repair 80—51178
neoplastic transformation of hamster embryo cells irrad. in utero and assayed in vitro 77—32941
nephropathy, glomerular and juxta-glomerular lesions 77—9233
neuronal DNA damage accumulation rel. to death after whole-brain irrad., rats 80—76804
p-nitroacetophenone charge transfer reaction with triplet state of guanine for radiosensitisation 79—92146
nuclear peripheral DNA critical site for radiation-induced reproductive death 79—88131
nucleosides and nucleotides, alkoxy radical and free radical product 77—90623
oncogenic transformations in cultured mouse embryo cells rel. to X-ray dose fractionation 78—35893
one-hit chromosome exchanges 78—3566
oocyte nondisjunction rel. to preconception X-ray exposure, mouse expt. 77—16958
oocytes of Drosophila melanogaster, class B, repair of X-ray induced sublethal damage 80—35987

biological effects of X-rays continued
oocytes of Drosophila melanogaster, Elkind-type recovery from X-ray induced damage 80—35988
oral epithelium, rat, ultrastruct. effects 77—56434
osteosarcoma, human, in vitro, evidence for unusual cellular repair activity 77—48847
ovarian tumour genesis, effect of normal ovarian tissue 78—53452
ovarian tumour types and incidence in mice after whole-body exposure 79—57724
ovariectomy effect on survival and diseases in female mice given 300 R of X-rays 77—52849
ovary cells, Chinese hamster, heat killing and thermal radiosensitization at 42°C 80—45860
ovary development in bonnet monkey after fractionated X-irrad. 78—20227
oxidative phosphorylation in cauliflower mitochondria, radiation inactivation 78—48844
parabiont rat pairs, late effects of successive massive radiation doses 79—29573
parabiont rats, leukaemmia and lymphoma 78—53457
parotid gland, rat, radioprotection by WR-2721 chemoprotector 79—92300
pathologic effects of neutron and photon exposures of lung and spinal cord, rabbit expts. 80—41126
pelvic irradiation in gynaecological malignancy, effect on bile acids absorpt. 80—67160
L-phenylalanine.HCl, X-ray induced radical form. 78—48755
phosphenes, mech. of formation, electrophysiological obs. on albino rats 80—104675
pine pollen grains, tube growth stimulation, site of action localisation 80—45982
pine pollen growing tubes, effects of low and sublethal doses 80—36002
planarian, regeneration of epidermis and basement membrane after total-body X-irrad. 80—36022
plasma kallikrein activity in tumour-bearing rats, effect of focal irrad. 78—35892
plateau phase cells, hyperthermia and radiation response, potentiation and repair 77—64099
pollen, Petunia, post irradiation effects in vitro and in vivo 79—29569
Pollen, Pinus Silvestris, effect of X, UV irradiation on NAD(P), NAD(P)H, hydroxyproline levels 79—20582
pollen mother cells, tradescantia, meiotic chromosomes, stage sensitivity and dose response 80—104648
pollen tube, pine, growth stimulation by low doses of radiation 79—100677
polymorphonuclear granulocytes and FL-cells, effect of X-rays on membrane pot. and electrophoretic mobility *(German)* 77—56442
pre-implantation embryos and implantation reaction in mouse, acute X-irrad. effects 78—69154
prenatal examination frequency and radiation risks in Japan 77—5070
protein-DNA cross linking mediated by X-rays 78—27898
protoplast response to X-irradiation and a chemical mutagen 79—88121
public health aspects of radiation 79—88141
rabbits with staphylococcal B enterotoxemia, X-irradiation effect on survival 80—21503
radiation response modified by degradable star microspheres, rat 79—62298
radiation safety, diffraction and fluorescence anal. equipment 79—12017
radiography, foetal vs. parenteral radiosensitivity 80—51271
radiography, stochastic late effects after partial body irrad. 78—69152
radioprotective and radiosensitising drugs combined use in exptl. radiotherapy 77—86559
radiosensitivity of CHO cells, negative pions rel. to X-rays at various cell stages 80—17021
radiosensitivity of neonatal ducks and chickens, comparative study 80—35997
radiotherapy with multiple daily sessions with ^{60}Co and 250 kV X-rays, clinical experience 78—53475
RBE of megavoltage photon and electron beams for tail necrosis in mice 78—35886
RBE of mouse skin damage, pions$^-$ rel. to X-rays 80—26272
repair of potentially lethal and sublethal X-ray damage, effect of hypoxia and glucose, mammalian cells 78—7404
repair of potentially lethal X-ray damage, effect of hyperthermia 77—5054
repair of sub-lethal and potentially lethal damage in plateau-phase hamster cells 77—21567
reproductive ability of female beagles surviving single midlethal whole-body exposure 77—21577
retina, albino rabbit SEM obs. 80—104674
rhabdomyosarcoma tumours, rat, regrowth rate, morphological characts. and transplantation props. 80—17010
rice, excised mature embryos, effect of 6.5 to 20 kR X-rays 78—85347
RNA of Novikoff Hepatoma ascites cells, effects of sparsely-ionising radiation after in vivo labelling 78—7389
RNA specific activity, Novikoff Hepatoma ascites cells 78—3560
root meristem cells, Vicia faba, micronuclei induction, X-ray rel. to US exposure 79—96633
root meristems, Vicia faba, X- and neutron-induced cell progression delay 77—56437
sarcoma, dose fractionation studies on mice breathing air or O_2+CO_2 78—35889
sarcoma in vivo response, effect of pre-irrad. breathing times of O_2 and CO_2+O_2, mouse 78—35888
seeds, wild papilionaceous, germination obs. 79—74728
serum albumin solns., X-ray induced chemiluminesc. intensification by dye addition 79—79470
sister chromatid exchanges, cultured mammalian cells 79—43832
skin, human, heavily irrad., tolerance to re-irrad. 77—73544
skin, mech. and struct. response 80—35994
skin, mouse, effect of dose rate on prod. of early and late X-ray damage 77—70497
skin, pig, blood flow clearance changes after single X-ray doses 79—29567
skin, pig, combined effects of X-irrad. and microwave heating 80—94290
skin, pig, response to combined X-irrad. and microwave heating 80—61653
skin, rodent, relationship between early and late damage 77—25511
skin, swine, response to single acute exposures, epidermal cell changes quantification 80—72245
skin, visual appearance and mech. props., mouse 77—12960

biological effects of X-rays continued
skin, X-ray and fast neutron damage, relationship between OER, RBE and no. of fractions 80—35978
skin blood volume pulse in humans 77—5029
skin fibroblasts from retinoblastoma patients, survival curves 77—48848
skin growth regulation, mouse, possible role of chalones 79—16168
skin mechanical properties, effects of split dose radiations 77—52842
skin nodules, comparative effects of pion and X-irradiation 79—20659
skin response in guinea-pig, single and fractionated doses 77—21566
skin response to combined hyperthermia and X-rays 77—90857
skin response to fractionated heat and X-rays 78—35887
skin response to heat alone or with X-rays, mouse ear 78—27902
slow repair after X-rays and fast neutrons, mouse lung 77—73547
small intestinal cryptogenic cells in W/W^{v} mutant mice, survival curves 79—11980
small intestine, rat, crypt survival under conditions of radioprotection 79—11979
small-bowel adenocarcinoma, rat, circulating blocking factors of lymphoid cell cytotoxicity 80—72257
soft X-rays, RBE, rel. to ^{125}I therapy 78—7405
somatic cell hybrid, intraspecific, radiation response obs. 80—72246
somatic cell hybrids, X-ray sensitivity 77—21574
somatic dose index, human, typical beam quantities and exposures 79—16306
sperm count reduction and abnormal sperm increase after X-irrad. or ^{22}Na injection, mouse 80—108961
spermatogenesis cell population kinetics under longterm fractionated irrad., mice *(Russian)* 77—48849
spermatogonia of fish, Oryzias latipes 77—5045
spermatogonial stem cell survival in mouse, split dose neutron and X-irrad. 78—28012
spinal cord, rat, effect of single and fractionated doses 78—65076
spinal cord, rat, neuroglial cell population changes after local irradiation 79—100671
spinal cord of adult mouse, combined effect of hyperthermia and X-rays 78—31863
spleen, dihydrofolate reductase activity, whole body irrad., mice 77—37013
splenic cells, rat, enhanced cytotoxic reactivity after X-irrad. 78—85343
splenocyte locomotion, X-ray inhibition and bacterial protection 79—25047
squamous-cell carcinoma, spontaneous, in mice, comparison of neutron- and X-irrad. effects 80—98033
subcutaneous vasculature histological changes in mouse after single 250 kV X-ray doses 77—73549
sublethal damage repair in multi-cell spheroids, fast neutrons vs. X-rays 77—25512
survival increase in mice by postirrad. injections of splenic extract 77—90861
synchronous HeLa cells exposed to low LET radiation, OER 77—37019
tadpole survival and erythropoiesis, effects of whole-body irrad. 77—52845
tail, rat, response to combined heat and X-rays 77—73545
tail, rat, single dose radiation and hyperthrermeia rel. to growth 80—108963
tail necrosis, mouse, multifraction X-irrad., dose-incidence curve steepness anal. 80—98035
tail re-irradiation to necrosis six months after tolerance X-ray or neutron dose, rat 77—73543
testes, mice, comparative effects of various radiations on weight loss and spermatogenic stem-cell survival 80—108976
testis, interstitial cell tumour induction 77—90860
testis, mouse, effects of hyperthermia and X-irradiation, weight loss assay 80—16907
testis damage by ^{125}I in partially blocked thyroid of rats 78—3565
testis mass loss obs., mouse 80—67156
testis radiosensitivity, rel. to alternating rhythm of cellular mitoses 78—3557
testis weight loss, mouse, RBE for fast neutrons rel. to X-rays 78—7396
therapy for gynaecological cancer, extended field irrad., tolerance and early complications 77—21564
thoracic tissues, attenuation coeffs., comparison with tissue substitutes 79—16307
thymic region, neonatal Swiss mice, X-irradiation effects 80—35990
thymine damage in chromatin from heated cells after X-irrad., excision obs. 80—45980
thymocytes, negative surface charge reduction and thymic phagocytosis 80—81663
thymocytes, rat, reduction of interphase death by hyperthermia 80—108970
thyroid, mouse, cellular and tissue changes after local X-ray irrad. 77—66826
thyroid hormone kinetic and serum levels, rats, effects of whole-body irrad. 80—104662
thyroid radiobiological response, sheep cells, single X- and γ-doses 80—41122
thyroid tumours in infant rats 78—65096
Tradescantia clone 02, dose-response curve for pink somatic mutations 77—16959
Triturus cristatus carnifex Laur., X-ray irradiated homotransplanted skin survival time *(Italian)* 78—85335
L-tryptophan-HCl radical form. 78—64940
tumour, effect of vascular occlusion on thermal sensitization and X-irradiation in mouse 79—16253
tumour, murine, cure, cell survival and tumour growth delay 77—48840
tumour and skin, mouse, effect of heating order on radiation response 80—3738
tumour blood flow rel. to radiation and drug response 80—67114
tumour cell in vitro radiosensitivity and recovery, effect of 1400 gauss mag. field 77—44723
tumour cell survival with fractionated doses, pitfalls in use of in vitro survival curves 78—77084
tumour cells, acutely hypoxic, recovery from sublethal damage 79—88116
tumour cells, explanted, reproductive survival after exposure to nitrogen mustard or X-irrad. 77—37023
tumour cells, human, effect of irrad. feeder cells on X-ray survival curve shape 80—98032
tumour cells, human, X-ray sensitivity in vitro 80—104665
tumour cells, interaction of hyperthermia with fast neutrons or X-rays on local tumour response 77—9230

biological effects of X-rays continued
tumour model, potentiation of radiation lethality by hyperthermia 79—25037
tumour oncolysis, mouse, local HF hyperthermia, X-irradiation and apathogenic clostridia 79—100662
tumour regrowth after irradiation in rat hepatoma 79—92292
tumour response, mouse, effect of chronic reduction of arterial partial O$_2$ pressure 79—16252
tumour response to combined heat and X-rays in the mouse 79—48290
tumour response to fractionated fast neutron irrad. rel. to X-rays 77—12974
tumour X-irrad. in vivo, enhanced lymphocyte-mediated killing of tumour cells 78—77086
tumour X-radiation response after prior exposure to reduced O$_2$ environment 79—88127
tumour X-ray response rel. to growth characts. 78—53454
ultrasoft X-ray microdosimetry and biological effectiveness comparison 80—26277
vascular permeability in rat ears after X-irradiation 79—5330
visual phosphenes, mech. of formation, photochem. investigations 80—108877
vitamin C radioprotective effects obs. in Chinese hamster ovary cells 77—73546
vitamin E distribution among tissues and subcellular fractions in sublethally irrad. mice 77—64098
water, X- and γ-irrad., electron slowing-down spectra and photon RBE 80—12197
wheat cultivars, water relations, growth and yield of tall and short cultivars 80—56144
X-ray, cell survival at low O$_2$ tension and dose build-up in Ar 80—72220
yeast, diploid, OER rel. to exposure temp., hyperthermia 77—5036
yeast, haploid, sulphydryl content var. rel. to radiosensitivity 78—7394
yeast cell electrophoretic mobility 78—31868
yeast cells, budding, genetic control of X-ray resist. 77—37024
yeast cells, reparable and irreparable damage induced by sparsely ionising radiation 80—51167
Al ultrasoft X-rays, mammalian cell inactivation and mutation, theory of dual radiation action 77—86548
Al ultrasoft X-rays, phys. props. and Chinese hamster cell expts. 77—86542
Al ultrasoft X-rays vs. different LET radiations, response of Chinese hamster and human diploid cells 77—86543
Ca^{2+} effect on rat cell electrophoretic mobility after X-irrad. 79—92293
HeLa cells, changes in sensitivity after split doses of X-rays 79—74726
O$_2$ effect throughout cell-cycle of human cell line NHIK 3025 cultivated in vitro 77—44724
O$_2^-$ superoxide ion as cause of O$_2$ effect, X-ray induced cell lethality 77—25513
Pt complex potentiation, of X-irrad. lethal effects, rodent cells 78—85345

biological fluid dynamics
see also biorheology; haemodynamics
action potential correlates of pressure-induced changes in cardiac conduction 80—81572
animal joints, mechanics, book contrib., review 80—21488
annual review of fluid dynamic, book 80—94927
aquatic animals with a caudal fin, hydrodynamics *(Russian)* 80—41060
aqueous humor flow rate determination by fluorescein tracer model 79—43943
arterial collapse after subjection to an external press. band 80—94271
articular cartilage, load-displacement-time characts., rel. to fluid flow in matrix 77—48820
bacterial aerosol, deposition and round-nose wedge in interception region 77—81520
bile, Newtonian behaviour obs. 80—35940
bile flow in dogs, empirical relationships 80—3693
bile fluid, system for meas. small flow velocities *(German)* 79—39534
bio-fluid peristaltic transport, peripheral layer viscosity effects 80—61600
bioengineering, international conf., Cape Town, S.Africa (April 1977) 79—20695
bird flight, wake behind finch 80—81629
body fluid distribution, flowing-mixing compartmental hybrid model 77—44582
body fluid pressure meas., Medicor electromanometry 77—90943
body temperature humidification, effect on patient thermal regulation 78—85295
bone, transport mechanism between blood supply and osteocytes in long bones 77—86472
botany, transpiration from plant leaf, simulation expts. 79—48279
capillary counter-current system hydrodynamic effects 77—40695
cardiopulmonary monitoring in respiratory intensive care unit 78—20306
cardiovascular and respiratory system dynamics *(French)* 79—34585
carrier mediated transport theory, survey of applications 77—89113
cartilage, model for surface flow 80—85431
cartilage deformation and interstitial fluid flow, nonlinear interaction 77—32931
catheter, multi-transducer, for intraluminal press. recording in vivo 80—89879
cell flow characteristics, appl. of laser Doppler spectroscopy 79—66598
cerebral spinal fluid pressure elevation, pulmonary haemodynamic responses, dog 79—88108
cerebrospinal fluid, superior sagittal sinus and central venous press. rel. to angular body position 77—56412
cerebrospinal fluid flow meas. 80—17165
cerebrospinal fluid pressure meas. and controlled withdrawal 79—39538
cerebrospinal fluid system models, rel. to third intracranial ventricle dynamic displacement detection 78—57035
cerebrospinal fluid system models for rat, dog, man, intracranial pressure regulation 79—88111
Chaplygin profile oscillating longitudinally, local secondary stationary flows *(Russian)* 77—32920
chest radiology, introduction to physiological aspects 79—25071
CHO fibroblast, press., inhibited thermal killing obs. 80—81564
cilia, fluid transport between parallel plates 78—69123
cilia motion, appl. of Stokes flow due to a Stokeslet in a pipe 78—67268
cochlea, disc model rel. to hydrodynamics in gap between cover membrane and organ of Corti *(German)* 77—86505
cochlea, mammalian, fluid flow permeability through hair cell cilia 79—53157
cochlea mechanics, modes and waves 79—92232
cochlear fluid, two dimensional model 77—32906

biological fluid dynamics continued
cochlear fluid mechanics, flows on a cusp catastrophe 77—77903
cochlear fluid mechanics, kinetic theory 78—53440
cochlear fluid mechanics, signal anal. by Hopf bifurcation 80—26241
cochlear hydrodynamics model, digital simulation 78—31821
collapsible duct, flow properties study *(French)* 79—34587
counter-current system with capillary-size vessels, fluid movements due to hydrodynamic forces 77—5024
craniospinal mechanical fluid systems, dynfunctoning as revealed by stress/strain diagrams 79—25024
decompression model for deep sea diving 77—44709
diffused substance kinetics in biological systems 78—53312
diuresis, medullary Na depletion, digital computer simulation 77—60226
dolphin, hydrodynamic swimming characteristics *(Russian)* 77—32922
dolphin boundary layer pulsations, results of spectral anal. *(Russian)* 80—41063
dolphin floating motion, hydrodynamic characts. *(Russian)* 80—41061
dolphin in channel, swimming kinetics *(Russian)* 77—64068
dolphins and pinnipeds, echolocation system acoustics and hydrodynamics 77—36963
duodenum, fluid mechanics, review, book contrib. 80—97994
electromechanical vessel occlusion device, implantable, remote controllable 78—40446
endolymph, math. model of caloric nystagmus 77—73525
endolymph flow in the semicircular canals 79—92258
epidural intracranial-pressure transducer with reduced tissue stress interference 80—41290
epithelia, pathways for hydraulically and osmotically-induced water flows 77—29112
eye, hydrodynamic model of aqueous flow in posterior chamber 78—69122
fibrinogen, liq. cryst., layer, shear orientation 77—27807
fish (bonito), cutaneous mantle structure rel. to boundary layer control *(Russian)* 77—64171
fish olfactory organ nares, laser velocimeter flow vel. meas. *(German)* 78—69262
flagellar propulsion hydrodynamics, helical waves 79—92185
flagellated microorganisms, hydrodynamic theory of swimming 77—90820
flexible elastic tubes cross-sectional area for varying transmural pressures 79—48276
flow absorption system, reaction vel. parameters rel. to absorbed solutes conc. profile *(Japanese)* 79—74710
flow measurement, NMR spin echo difference method appl. to plant stem 78—14110
flow rate measurement by indicator dil. methods 77—65825
flow-reaction-absorption systems, digital simulation *(Japanese)* 77—86525
fluid flow in semicircular canals, utricle effect 77—86517
fluid-particle separation, chainlike form. of particle deposits 77—77813
haemodialysis treatment model for metabolic waste conc. dynamics and cerebrospinal fluid pressure 77—60305
helical flagella, hydrodynamic props., Oseen-Burgers' theory *(Japanese)* 78—11685
Henle's short loop, microperfused, of rates, computer simulation of flow-depend. absorpt. 79—83820
high-pressure convolutions in rodents, associated heart rate changes 80—67124
hip joints, human, study of synovial fluid, friction and lubrication 79—11956
hydrobionic deforming ellipsoids, calc. of non-stationary boundary layer *(Russian)* 77—64070
intra-articular pressures during joint use, changes with disease, pathological consequences 80—94252
intra-osseous circulation, human and animal, investigation method *(French)* 79—34593
intracellular pressure measurement system 80—109084
intracranial pressure dynamics modelling 79—25026
intracranial pressure estimation, use of visually evoked pots. 80—26398
intracranial pressure regulation, nonlinear parametric feedback model 79—96599
intraocular fluid dynamics meas. by minicomputer-based system 78—24130
intraocular pressure survey, pediatric patient emphasis 80—30712
Japanese black pine, Pinus Thunbergii Parl., water potential and growth stress *(Japanese)* 80—3701
kidney, countercurrent transport, book contrib. 79—5307
kidney, rat, functional model 79—62282
kidney, six-tube vasa recta model as test problem 80—104610
kidney counter current mass transport spatially discrete models 79—39442
kidney filtration fraction, noninvasive determ. by dual tracer technique 77—86596
kidney model, numerical soln. by multiple shooting 80—104609
kidney model transient behaviour 78—65065
kidney modelling, numerical continuation method 79—43944
kidney physiopathology concepts from ^{197}Hg fixation test *(French)* 77—70518
kidney process modelling 78—44524
kidney solute concentration, control core model, input-output studies 77—56405
kidney solute concentration, renal medulla model and limit cases 77—52821
kidney tubule fluid reabsorpt., online meas. 79—92442
labyrinth caloric test, estimation of stimulus strength 78—40210
lunate tail swimming propulsion, hydromechanics 77—29163
lung, zone I, transvascular fluid shifts, rabbit obs. 80—101198
lung lymph transport increase without heart failure after coronary ligation in sheep 80—67122
lung model alveolus, particle deposition by Brownian diffusion during breathing 79—53173
lymphatic vessel network, similarity anal. of design 80—101212
macromolecules, rigid, modelling approaches of hydrodynamic props. 80—61613
micro-organism propulsion, cilia and flagella, fluid mechanics, book contrib. 77—48833
microgravity environments 80—1720
microhydrodynamics, characteristic effects, developments 77—68681
microorganisms, lack of intracellular bubble formation at very high gas supersaturations 80—81562
micturition hydrodynamic model and test results *(Slovene)* 78—44520

biological fluid dynamics continued
milk flow, human, Doppler US flow meas. transducer 79—53200
monoflipper, wave propellant for fast dolphin-like swimming *(Russian)* 80—46102
motile solid particles in fluid, two dimens., convection numerical study 77—56399
myxomycetes plasmodium protoplasmic flow, laser Doppler anemometry obs. 79—57681
nasal airflow resistance, effect of exercise in normal subjects 80—8088
nephron operating model 79—48283
neuron hydrodynamics, numerical methods for creeping flow investigation 77—5019
ocular tonometry through sonic excitation and laser Doppler velocimetry 80—56152
oesophageal manometry by liquid-filled catheters 80—85514
oral reading, breath volume and flow modification 79—57672
ovum transport in oviduct, mechs. 78—80905
oxygenator/haemodialyser combined system, development and feasibility study 79—84024
pathological synovial fluids, viscoelastic props. at different shear rates 79—32430
Penrose tube, water filled, fluid velocity/wavespeed ratio, supercritical-subcritical transition 79—81975
peribronchial fluid pressure rel. to vascular and airway press. and interstitial oedema 80—97971
peristaltic flow, efficiency 77—2018
peristaltic transport, asymptotic method 80—87805
permeable tube mass transport simulation using perfectly mixed compartments 77—40696
physiological compartment tracer flow modelling and digital imaging 80—101257
plants, flow and transport, book contrib. 77—48832
plethysmograph with servo-control of hydrostatic press. 77—5118
pneumodynamics, short-life radionuclides and regional lung function, review 79—53211
pneumodynamics, venous return curves from Valsalva maneuvers 79—53174
pulmonary fluid dynamics, book contrib. 77—52829
pulmonary interstitial fluid space compliance, estimation in isolated perfused rabbit lung 80—104605
pulmonary oedema fluid transport, hybrid computer simulation 78—27915
radionuclide mean clearance time transverse section imaging 78—73222
random effects in tracer and cell cycle kinetics 78—44445
renal countercurrent mechanism, transient and steady state simulation 77—36967
renal countercurrent model eqns., numerical soln. 77—40698
renal counterflow, differential eqn. soln. by sparse matrix techniques 77—21545
renal counterflow system transient soln. computation 77—40699
renal counterflow systems, numerical solution of differential equations 78—92662
renal counterflow systems differential equation, soln. by numerical method 78—24082
renal function rhythms study using Na tracer telemetric detection 77—86586
renal function studies, combined in vitro-in vivo radionuclide procedure, technical aspects 77—90884
renal functions, mathematical modelling 79—83841
renal medulla, human, math. model 78—24081
renal medulla, multinephron models, canonical mass balance eqn. 77—12941
renal medulla, osmotic equilibration by descending limbs of Henle's loop 77—40701
renal medulla single loop solute cycling model, transient behaviour 78—73167
renal medulla solute cycling model soln. by Laplace transforms 77—40694
renal network flow eqns. anal. 79—11961
renal network flows, a priori bounds 77—40693
renal network flows, comparison of numerical methods 77—16945
renal perfusion dynamics during preservation 79—25006
renal solute and water movement models and soln. 77—40692
renal tubule model injection transient response calc. 77—40700
respiration, computer-assisted PaO$_2$ management during veno-arterial bypass and mech. ventilation 77—44838
respiration function testing using ^{133}Xe radio-spirometric meas. system 77—90889
respiratory control, human, input stimulus design for model discrimination 79—53183
review, theory, meas. and appls. 78—35874
saturation dive, 17-day 18.6 ATA exposure effects 79—92256
sea creatures, hydrodynamic mechanisms associated with cutaneous mantle structures *(Russian)* 77—32917
semicircular canal primary afferents, impulse weight functions, frog 78—69116
semicircular canals, unsteady fluid dynamic response, math. model 77—9216
semiconductor pressure transducer *(Japanese)* 80—94394
sessile organism flagellar motions, feeding current generation, optimum motion 79—92184
small intestine, fluid mechs. of longitudinal contracts 80—56098
spatially constricted flow meas. using laser Doppler velocimeter 78—71409
squeeze forces in contact lenses with a steep base curve radius 80—108926
steady flow in collapsible tubes 78—57033
streaming potential measurements of biosurfaces 77—2074
susceptance tympanograms, asymmetry obs. 80—41051
sweating rate, local, effect of skin temp. change rate 80—35848
swimming birds, hydrodynamic indicators of body shape and propulsive mechanism *(Russian)* 77—64069
swordfish, ampoules in skin rel. to boundary layer control *(Russian)* 77—64072
synovial fluid, pathological, rheological props. *(German)* 78—57032
synovial fluid boundary lubrication model, structuring of boundary water 80—35950
synovial fluid polar model, with reference to human joints 79—53169
synovial joints, rheology of synovial fluid, synthetic lubricants for degenerate joints 79—11955

biological fluid dynamics continued
synovial joints, three layer model, incompressible fluid+linear elastic solid, natural lubrication 77—70490
tear turnover meas. by improved slit-lamp fluorophotometer 79—92326
thick layer above an active ciliated surface, fluid transport 80—85425
thorax impedance finite element model for cardiovascular and respiration meas. 77—40887
tracheobronchial clearance of inhaled particles in man 80—8080
transdiaphragmatic pressure measurement using a single gastric-oesophageal probe 80—56248
transducer for intraluminal press. recording 80—17152
tree growth rel. to transpirational flow and air humidity *(Russian)* 78—65066
two-dimensional fluid motions induced by motile particles, convection field and geotactic components 77—55080
underwater body of changing shape, vortex-free flow due to arbitrary motion *(Russian)* 77—32916
unsteady flow in contracting or expanding pipe 77—86523
upper airways in newborn and infants, X-ray physiological exam. using Orbiskop 80—8130
ureteral catheterisation manometry and urodynamics *(Slovene)* 78—44668
urethra, female, tissue elasticity and flow dynamics 77—81522
urethral resistance and mural tension meas. using programmable modules 77—2067
urinary flow rate meas. device 77—48906
urine flow curves of healthy males, math. model 79—88110
urine flow regulation rel. to baroreceptor Na sensitivity 77—48818
urodynamic parameter meas. systems 79—96690
urodynamics, mechs. and hydrodynamics of the lower urinary tract, book 80—98768
US Doppler velocimetry, experimental appls. *(French)* 79—34610
US volume flowmeter, in vivo validation 79—83872
vestibular apparatus, transform. of angular accels. by system of semicircular canals 77—16943
viscoelastic lubricants in human joints 79—57699
water excretion control by antidiuretic hormone, modelling 78—31830
water organism, exptl. simulation of oscillatory motion by flexible plate *(Russian)* 77—32923
water vapour circulation in human organism, model *(Russian)* 79—2093
CO_2, circulation in human organism, model *(Russian)* 79—2093
N_2 circulation in human organism, model *(Russian)* 79—2093
O_2, circulation in human organism, model *(Russian)* 79—2093
O_2 molecule reduction flow probe for cerebrospinal fluid 79—100777
O_2 transport system, multivariate anal. of blood and air flow data from dogs 77—44706
O_2-CO_2 transport real-time and interactive control in mechanically ventilated patients in ICU 79—62404

biological macromolecules *see macromolecules; molecular biophysics*

biological sciences *see biology*

biological specimen preparation
acetylcholine receptor protein structure 80—85339
algae, Lugol preserved, rapid preparation technique for SEM 79—39620
aortic elastin, freeze-dried, SEM 78—65160
aphid neurones, differential sensitivity to sucrose 80—98195
articular cartilage controlled impact test instrum. and procedure 78—28130
ashing, low temp., elemental retention, activation anal. meas. 78—11785
autoradiograms of diffusible intracellular constituent using freeze-dried frozen sections of mammalian intestinal epithelium 79—84039
autoradiograms of serial sections, preparation for electron microscopy 80—67312
baceteriophages, freeze drying method for electron microscopy 80—104826
bacterial growth obs. using SEM 78—15933
biopolymers, epitaxial sandwiching, electron microscopy specimen prep. 78—36080
blood cell exam. by scanning electron microscopy 79—74812
blood cells, red, human, frozen section prep. for electron probe anal., fracturing or cutting 79—39625
bone, technique for studying collagen fibres and ground substance 78—57150
bone biopsies, undecalcified human bone prep. for electron microscopic investigation 78—20332
cardiac fibre isolation method 80—30955
cell cultures, equipment used in a modern labroatory 78—85457
cell cultures, particulate contamination problems rel. to ultrathin sectioning techniques 77—60315
cell cycle and topography in nonsynchronised monolayers, autoradiography and time-lapse use for rigorous SEM obs. 78—24212
cell drying, critical point drying alternatives 78—24210
cerebral slices from rat brain, effects of embedding or freezing an area 79—25166
Cherenkov counting of plants for β-emitter radioassay 78—81088
chick embryos, cross-section preparation and handling, for SEM 80—21588
cool diode sputter coater for heat-sensitive SEM specimens 78—24204
critical point dryer, low-cost, with continuous flow dehydration attachment, for electron microscopy 78—53595
critical point drying for SEM 79—17406
critical point drying of hydrated specimens, principles and procedures 80—76882
critical point drying theory, practice and artifacts, review 78—24211
cryo-ultramicrotomy and myofibrillar fine struct., review 78—53592
cryobiology, freezing and cryofixation 78—28136
cryobiology, struct. and functional aspects of freezing techniques 78—28137
cryofixation, fast freezing device 78—28138
cryofixation of tissue specimens studied by cooling rate measurements and scanning electron microscopy 80—94430
cryomicrotomy of thick sections, cutting work 78—28139
cryopreparation, for biological X-ray microanalysis 80—41349
cryopreservation of cells and biological samples using electronically programmed freezer 79—62420
cryosectioning for X-ray microanal. 79—39626
cryostat for freezing biological materials 78—40437
cryoultramicrotomy, prep. of thin sections for electron probe anal. of calcifying cartilage 78—31988
culture substratum on stainless steel, preparation for SEM studies 78—20328

biological specimen preparation continued
cultured cell preparation for electron microscopy, ethanol and chem. dehydration methods comparison 78—24208
cultured cells preparation for SEM by air drying from org. solvents 77—48965
cuvette for freezing biological preparations 79—92436
dermal elastic fibres, for SEM visualization 79—84036
dispersion staining, in IR and UV 80—76874
DNA, spreading of large associations, dark field electron microscopy 80—85563
DNA and chromatin molecule preparation for electron microscopy 79—25171
DNA electron microscopic preparation on uncharged C films 80—12320
egg shells, electron microscope embedding medium for pore studies 80—98194
electron beam X-ray microanal. of frozen hydrated bulk specimens 78—57142
electron microscope, JEOL JEM 100C, low temperature specimen stage and transfer system 78—32945
electron microscopy, gentle bounce-free assembly for quick-freezing tissues 80—67316
electron microscopy, light microscope attachment for isolating small specific areas from slide embedded monolayers 78—53596
electron microscopy, quarter-micron serial sectioning and stereoscopy 80—72384
electron microscopy, recent applications to biology 80—41347
electron microscopy, staining and X-ray microanal., book 78—4739
electron microscopy conference, Toledo, USA (Sep 1978) 79—100796
electron probe microanalysis, review 77—86730
electron probe X-ray microanal. of frozen-hydrated biological specimens 77—56552
embedding with GMA and Quetol 523 for electron microscopic obs. on semi-thin sections for light microscopy 78—53588
enzyme supports, method for determ. amino and isothiocyanate groups on surface 79—61920
epitaxially sandwiched macromolecules, contrast in TEM 80—85565
EPR, prep. of packed cell samples 78—28145
erythrocytes, technique for observing 3D dim. struct. with a cryo-SEM 78—92765
euglenoid flagellates, sputter and vacuum evap. coating, comparative effects on delicate features 78—24205
Feulgen type staining with Hoffmann's violet-SO_2 under UV exposure 80—12319
fissured biological object prep. for SEM, vacuum deposition and cathode sputtering comparison 80—72390
free cells, preparation technique for electron microscopy using conical glass tube for centrifugation 79—34711
freeze drying technique for SEM 80—104828
freeze etching SEM with glycerinated biological tissues 77—64157
freeze fracture replicas, removal of lipid contamination using chloroform 79—5426
freeze substitution, plant tissue preparation for ion localisation studies 77—9309
freeze substitution for preservation of ciliated surfaces for scanning electron microscopy 79—74805
freeze-dried fresh frozen sections use for electron microscope autoradiography and X-ray microanalysis of diffusible substances 77—60314
freeze-drying apparatus for electron microscopy, appl. to adenovirus particles 80—21578
freeze-drying of articular cartilage 80—26433
freeze-drying process obs. by SEM 78—28142
freeze-drying systems, information systems models 79—58727
freeze-drying technique for chem. unfixed tissue for electron microscopy 78—65164
freeze-drying technique using modified freeze-etching device, for viruses and phages 77—70572
freeze-etching, membrane ultrastruct. rel. to function review 78—15785
freeze-etching improvement using evaporated film 80—85558
freeze-etching of dispersions without contamination of the fracture faces 79—79704
freeze-etching results interpretation 78—28141
freeze-fracture electron microscopy freezing method evaluation by low temp. X-ray diff. 78—57145
freeze-fracture preparation for SEM 78—61290
freeze-fracture replication, in biological research, review 78—40444
freeze-fracture specimen temp. changes during rapid quenching in liq. coolants 78—57140
freeze-fracture technique, appl. to study of animal plasma membranes 80—104842
freeze-fracture techniques and appls. in struct. anal. of mammalian plasma membranes, book contrib. 80—30960
freeze-fracturing effects on membrane struct. 78—28140
freeze-fracturing of biological material with a new specimen table 79—5425
freeze-fracturing of capillary layers of cells, membranes, viruses, new hinged device 78—20327
freeze-fracturing preparation technique, methods and results, review 78—24776
freeze-substitution of plant and animal tissue, for electron probe microanal. 77—37115
freezer fracture autoradiography, red blood cell plasma membrane, electron microscopy 80—98192
freezing, fracturing and coating system for low-temperature SEM 80—76883
freezing and thermal history of cells 79—62419
Freon-TF freeze drying method for SEM sample 79—74802
frozen hydrated specimens, instrumentation for direct obs. in TEM 79—92454
frozen hydrated tissue section prep. for X-ray microanalysis using satellite vacuum coating and transfer system 78—24200
glycol methacrylate embedded chick embryonic tissue, histologic investigation 79—84038
glycoprotein extraction from liver tissue during processing for TEM 79—25167
GMA-Quetol 523, ultraviolet polymerisation in embedding procedure for semithin sections prod. 78—92767
grid handling, of semi-thin sections of GMA-Quetol 523 embedded tissue, with reference to O_5O_4 78—92766
haematopoietic malignancy diagnosis, significance of SEM 80—85529
hard tissue matrix internal space study by SEM, dentine appl. 78—77169

biological specimen preparation continued
  heart cultured cells, rat, temp. control system 79−57830
  histological and cytological reflection contrast microscopy 80−72389
  histology, small object processing device for electron microscopy 80−3887
  human lung tissue, with asbestos exposure, particulate analysis, aspects of specimen prep. and a limitations of precision by SEM and TEM 79−17574
  hydrated, bulk-frozen, prep. for X-ray microanal. 79−39629
  illumination of early chick embryos in ovo using glass rod as light guide 79−84042
  ion beam analysis, few MeV range 77−81768
  ion beam sputtering, application to high resolution electron microscopy 78−32925
  laser microbeam for tissue sampling in biochemistry *(German)* 78−69175
  laser-apparatus for preparation and manipulation of biological microsamples *(German)* 80−56307
  lipid bodies, saturated, in organ pipe cactus visualisation by cytochem. technique 80−76873
  liver sections, comparison of chemically prepared and freeze dried specimens for ion microscopy 80−95189
  low temp. techniques for SEM, X-ray microanal. 79−39627
  low temperature method, using biochamber for X-ray microanal. 79−39628
  low-temperature biological SEM and X-ray microanalysis 79−74818
  lung, rapidly frozen under controlled physiological conditions, electron microscopy prep. technique 79−39619
  lymphocyte surface morphology, human, SEM obs., review 78−53599
  lyophilisation, effect on free radical states of animal cells 77−25391
  macromolecules, 3D struct., electron microscopical anal. 80−35836
  macromolecules, high-resolution metal replication for electron microscopy 77−25621
  melamine resin, as water containing embedding medium for electron microscopy 78−92764
  membrane preparatory procedures, for electron microscopic anal., at mol. level resoln. 80−104843
  membrane thin sectioning development for electron microscopy 79−74819
  microdissection of tissues for real-time stereo SEM 79−80724
  micromanipulator using microscope focus, appl. to yeast asci single spare isolation 78−61292
  microscopical stain colour rendition by dyes produced in reversal colour films *(German)* 80−12318
  microspecimen holder for processing and critical point drying 79−74822
  microspecimen suspensions, simple magnetic holders for critical point drying 77−52946
  microtome modification for improved ultra-thin sectioning 80−17207
  microtoming long specimens of small width/depth, freezing technique 78−3695
  myocardial cells, cats, improved techniques for studying surface topography by SEM 79−34712
  myocardial tissue, shock-frozen, preservation as shown by cryo-ultramicrotomy and freeze-fracture studies 78−53593
  myoepithelial cells, SEM examination 79−34713
  neural structure histological exam., Epon block sectioning technique 79−74814
  neurones, Co- and Ni-filled, differential staining using rubeanic acid 79−84035
  neurons, section embedding technique for sequential light and electron microscopic exam. 80−67317
  optic tract of self-respiring fish, method for obtaining single cell response 77−56545
  orchard leaves, reference sample on membrane filters for X-ray fluoresc. spectrometer 77−60176
  Parlodion coating of highly fragile freeze-fracture replicas 80−8231
  perfusion fixation for electron microscopy, press. controlled device 77−44866
  phosphatidylcholine vesicle sizing by TEM 79−70722
  photosynthetic membranes, supramolecular organisation model based on freeze-fracture electron microscopy 77−29106
  physiological support medium+NaCl+cryoprotective agent, equilib. and nonequilib. behaviour 77−16561
  PIXE anal., review of target backings and specimen preparation 77−48979
  PIXE anal. of biological samples 77−48972
  PIXE anal. of thick and thin targets of biological materials 77−48723
  PIXE analysis of thick biological samples, elimination of charging 78−88775
  plant material, cryofracturing and low temp. SEM 78−24207
  plant root transport studies using ion localisation, freeze substitution method 80−85569
  plasma ashing technique for energy dispersive X-ray analysis of biological specimens in SEM 78−24199
  plasma incineration, O, of epon sections, for X-ray microanal. 79−17584
  plasma membrane, unfixed, ultrathin frozen sections, ultrastructure 78−65161
  plasma membrane vesiculation, new technique for isolation of membranes 77−52950
  polycationic substance layer for preparing suspended biological materials for SEM 77−64156
  polymeric cryoprotectants in preservation of biological ultrastruct., aq. soln. low temp. states 78−65157
  polymeric cryoprotectants in preservation of biological ultrastructure, physiological effects 78−65158
  polymeric cryoprotectants in preservation of biological ultrastructure, morphological aspects 78−65159
  postcontamination avoidance using room with controlled microclimate, for electron microscopy 78−54350
  preservation, effect on attenuation coeff., computerised tomography of in vitro abdominal organs 77−56449
  protein film method, basic, in electron microscopy of nucleic acids 80−104844
  protozoan cell preparation for SEM, freeze-drying technique 79−20724
  radioimmunoassay, instrumentation developments 77−86614
  rapid freezing device for use under controlled and reproducible conditions 78−57139
  red blood cell etching by ion beam sputtering for SEM 80−85554
  refrigerated moving-object technique and accessories *(French)* 77−29235

biological specimen preparation continued
  replication at −150°C with improved freeze-fracture apparatus 80−85560
  resin removal solutions for use on 1 μm thick epoxy sections 78−65165
  resin-embedded unicellular organism preparation for ultrathin sectioning 79−70724
  scanning proton elemental microanal., biological and medical specimens 80−56311
  secretory granule membrane, particle clustering induced by centrifugation, freeze-fracture anal. 80−85559
  SEM, biological applications, state of art of specimen preparation 79−17581
  SEM, comparison of nature and mode of appl. of surface coatings 79−5421
  SEM, efficient processing methods 77−60317
  SEM, metallic deposition in specimens presenting cavities using sputter coater 78−77171
  SEM, non-conductive specimens, determ. of thickness and grain size of deposited films by TEM 78−77170
  SEM, prep. of squid giant axon for obs. of membrane inner surface struct. 77−70579
  SEM, removal of epoxy resins from tissue 79−5424
  SEM chamber attachment for fracturing and coating frozen biological samples 78−69260
  SEM specimen cleaning by puncture perfusion 78−57149
  SEM specimens, effects of preparation on preservation of surface associated microorganisms 80−21582
  semithin large epoxy sections resectioning for electron microscopy 80−8233
  separation in space environment, electrokinetic phenomena and electrophoresis 79−48351
  skeletal muscle preparation for SEM 80−94431
  soft specimens for electron microscopic analysis 80−98190
  specimen-conductivity problem in electron microscopy, review 78−24206
  spray freezing method, size determination of sonicated vesicles, freeze fracture electron microscopy 80−98188
  spray-freezing unit for prep. of specimens for freeze-etching 77−41581
  sputter coating for SEM sample prep. conversion of vacuum coating units 77−34058
  stained biological section, quantitative anal. of contrast 79−66596
  STEM, contrast and radiation damage 79−66592
  structure determination, electron microscopy, optical and digital anal. *(French)* 79−66594
  TEM, methods for image processing, review 79−17405
  TEM, resin slide technique for selection of fixed embedded cells 77−60316
  TEM, specimen damage and dehydration, struct. retrieval, instrumental limitations in biological struct. anal. 79−20735
  TEM specimen freeze drier, all-glass design 80−82854
  tissue blocks, LKB Pyramitome and Target Marker modifications 77−60313
  tissue dimensional changes during SEM specimen prep. 78−24209
  tissue dispersions, unglycerinated, freeze-etching by appl. of oil emulsion technique 78−53594
  tissue element position fixing during processing for electron microscopy 79−25168
  tissue embedding in low viscosity epoxy resin Quetol 651 for electron microscopy, rapid method 78−20322
  tissue section lifting for electron microscopy 79−74823
  tissue surfaces cryofixation for electron microscopy 79−53294
  tooth enamel, SEM study of organic phase 77−52952
  trace metals determination, microwave oven-based wet digestion technique 78−92542
  ultrathin frozen section supported by polyethylene glycol for electron microscopy 78−20337
  ultrathin section mounting on supported grid, wrinkleless, double grid method 79−34714
  vegetation ashing for ^{131}I determ. 78−15930
  virus negative staining technique, applications in electron microscopy 80−41348
  whole-body sections, ^{14}C and ^{3}H determ. by liq. scintillation counting *(German)* 77−5114
  wood, clean cut surface preparation for SEM studies 78−15935
  X-ray microanalysis, graphite grids 80−8232
  X-ray microanalysis, review 78−24214
  X-ray microanalysis 80−73566
  X-ray microanalysis of diffusible elements, methods of drying ultrathin cryosections 78−77166
  X-ray microanalysis of diffusible elements, rapid freezing and ultrathin section prep. 78−77165
  ^{14}C labelled plant material, growth in simply constructed cabinet 79−84044
  Pt shadowing of freeze-fractured or freeze-etched specimens using electron beam gun 78−20329

biological techniques and instruments
  see also biological specimen preparation; biomedical equipment; biomedical measurement; microelectrodes; specimen preparation
  3-D reconstructions of squid statocyst cavity using plastic sheet and modelling clay 79−84037
  40 Hz activity in sigmoid gyrus, nucleus accumbens and amygdala, cross correl. anal. 80−76730
  abdominal CCD camera for continuous video recording of sheep ovary images during reproductive cycle 78−40442
  absorption spectroscopy for blood with red cells using integrated optics 77−29232
  accelerator, compact, characts. and appl. to mouse behavioural stages classification 80−56309
  acoustic holographic in medicine and biology, state of art and future 80−67175
  acoustic levitation technique appl. 79−44906
  acoustic microscope, scanning laser, biomedical research and materials science appls. 78−46878
  acoustic microscope appl., using piezoelectric transducers 80−1387
  acoustic microscopy, principles and appls. 78−18133
  acoustic microscopy, subcellular detail resolution 80−56313
  acoustic microscopy, tissue characterisation 77−64123
  acoustic microscopy for muscle mechanics obs. 78−48952
  acoustic microscopy review, historical development 78−46877
  acoustic parameter frequency depend. meas. 77−40718

biological techniques and instruments continued
acoustic reflex threshold temporal integration, instrumental effects 77—77910
acoustic scanning microscope, operation and appl. 77—84095
acoustic size measurement for sound scatterers in water 80—38199
acoustic wave interferometer, for sound speed meas. in biological liquids 77—50844
action potential clamp to probe effectiveness of space clamp in axons 78—40441
adiabatic calorimetry, thermodynamic props. of biopolymers in helical and coiled state, 4 to 400K 78—20140
aerosol, electrostatically charged, particle deposition in hollow cast of human larynx-tracheobronchial tree 79—43953
aerosol mass distribution, meas. using centrifuge with quartz oscills. *(German)* 79—92004
agargel electrophoresis, protein transport, stochastic model 77—77769
agarose gel immunoelectrophoretic determination of molecular weights of tubulin antigens 80—67313
air-bath cryostat for enzymology at subzero temps. 78—48949
airflow measurement in speech using mask-type wire screen pneumotachograph 77—52808
airway geometry determ. by anal. of acoustic pulse response meas. 78—28026
algae recognition by coherent spatial filtering with simulated input 79—79696
algae sample analysis using coherent optical processing 80—98205
Alopex process: Visual receptive fields by response feedback 80—61546
alpha counting and spectrometry by liq. scintillation, appl. to bone and tissue samples 77—25617
amino acid linear sequence form., cryo-sublimation of frozen aqueous solns. 78—95993
amplifier, head-mounted 24-channel evoked potential preamp. using low noise op. amp. 77—40807
amplifier, special purpose, for insect taste cell spike train recording 80—72394
anaerobic environment integrated system 78—80987
analogue analyser for on-line eye movement detection 79—79699
analogue differential preamplifier for mechanical recording 78—40447
analytical density gradient equilib. centrifugation, appl. to human transferrin 77—64160
analytical density gradient equilib. centrifugation determ. of macromolecules buoyant density 80—17217
analytical electrophoresis, book contrib. 80—12322
analytical instrumentation, status reports, appls. 77—25570
analytical ultracentrifugation technique for direct meas. of DNA sedimentation consts. *(French)* 80—8004
anatomical surface shape meas. method 80—3882
anechoic chamber, miniature, for chronic exposure of small animals to plane-wave microwave fields 80—67304
anemometer, hot-film, appl. to blood flow velocity meas. *(Japanese)* 79—29678
animal biotelemetry studies, historical perspectives and recent applications 78—69266
animal carcinogenicity expts. low-dose-rate data extrapolation 77—56327
animal communication, INFO program using information theory for anal. 77—90712
animal movement monitoring in enclosure, photocell sensing devices, chart recording 77—81765
animal organs, small samples, simple apparatus to evaluate mechanical props. 79—12055
animals, small, nose-only inhalation exposures to $^{106}RuO_4$, system 80—41346
antibiotic concentration assay, computer-aided method *(German)* 79—5414
antibody-selective membrane electrodes 79—84058
aortic valve study, by holographic interferometry and shadow Moire methods 80—104613
apatite powder samples, peak positions determ. from step-scanned X-ray powder diffr. data 80—103217
aperture sources for deep heating by EM energy, design 80—46105
aquatic eyes, retinoscopy, refractive error considerations 80—61750
arterial blood pressure measurement in rats using modified non-invasive method 79—96722
arterial diameter meas. using US transit-time micrometer 78—7410
arterial haemodynamics evaluation using venous US catheter-tip technique 77—44730
arterial O_2 tension, generation of variable amplitude sinusoidal changes for freq. response anal. 77—56563
arteries, small, isolated, perfused, method for simultaneous elec. and mech. recording 80—101300
artery length-force and vol.-press. relations, meas. and empirical formulae 78—65072
articular cartilage controlled impact test instrum. and procedure 78—28130
articular cartilage in uniaxial tension, nonhomogeneous directional mech. props. meas. 77—29167
artifact-free electrodes for recording biopotentials in strong EM fields 78—40452
artificial heart circulatory physiology appl., meas. of resistance to venous return in calves 77—52941
atomic absorpt. spectrometry and thermal neutron activation analysis, Se determ. in human tissue 79—88218
atomic absorption photometer for human serum anal. 79—34417
atomic absorption spectrometry of solid samples 79—74795
atomic beam scattering, for surface struct. determ. 78—53584
ATP content meas. in single red blood cell, using firefly bioluminescent reaction with optical instrument 79—79695
ATP determination, extracellular, in native platelet-rich plasma 77—25615
ATP measurement in single red blood cells using firefly biolum. reaction 78—48951
atrial and/or arterial blood pressure servo control in expt. animals 78—31986
audio dual channel monitor for distinguishing action pots. from two different sources 78—61293
audiometry, pure tone, comparison of ascending and bracketing methods 80—56323
auditory cortex of unanaesthetised monkey, vertical stereotaxic approach to elec. recording 80—72383
auditory evoked potential data acquisition, dual-processor system 79—79712

biological techniques and instruments continued
auditory evoked pots., technique for separating endogenous from exogenous pots. 79—100794
auditory evoked response research on animals, exptl. design 77—78068
auditory temporal summation experiments, procedure and evaluation of results 77—29157
auditory time shift evoked potentials, generation technique 79—16354
auditory-evoked response methodology in animals 80—46103
autodensitometer, flatbed, for biophys. appl., error analysis 77—52937
autoionography of beta-emitting radionuclides distrib. on thin-layer chromatograms 78—20126
automated electrodic potentiometry of respiratory components in E. coli membrane fragments 78—35736
automatic balance, for animal and organ weighing *(Japanese)* 79—25173
automatic biochemical analyser, microcomputer appl. 79—54192
automatic identification equipment for cattle *(Czech)* 80—109073
automatic image analysis, standard field area frame 77—52947
automatic parameterization of vocal cord motion from ultra high speed films 80—85419
automatic sampling apparatus, features 78—7550
automatic sprayer with programmable dose for serial expts. *(Hungarian)* 80—104822
automatic structure analyser, EPIQUANT, linear anal. of histologic preparations 78—40443
autopsy tissues, proton induced X-ray emission anal., calibration, correction methods 77—56466
autoradiographic visualisation of rat brain dopaminergic nerve endings, test of technique 80—61742
autoradiography, coating of slides with nuclear emulsions, new semiautomatic device 77—70574
autoradiography, criterion for classifying radioactive cells 77—37041
autoradiography, direct deposition method, radioactivity detect. 78—77167
autoradiography, double radionuclide methods for tissue sections or cell smears, using light microscopy 77—5113
autoradiography, high-sensitivity α detect. technique for bronchial epithelium tissue 80—17210
autoradiography, increasing detect. power of type M nucl. emulsion gel 78—20269
autoradiography and soft laser scanning in radioisotope work, appl. to metabolic studies 78—3576
autoradiography of serial sections, method for holding electron microscope grids 78—20331
averaged multiple unit activity as estimate of local neuronal activity changes, vol. conducted pots. 80—89917
avian heart rate meas. using autocorrel. techniques 78—31989
backscattered electron images of biological specimens 80—104827
bacteria in H_2O, detection by resonance Raman spectra 80—94418
bacteria species identification and conc. estimation by light scatt. 77—56564
bacterial cells, tethered, rot. rate and direction detect. apparatus 77—73620
bacterial growth detection by impedance meas., electrode characts. 77—60325
bacterial growth meas. using conductivity changes 78—61288
bacterial movement tracking using one-dimens. fringe system 78—73299
bacteriochlorophyll, photooxidation, picosecond absorption spectroscopy investig. 78—82053
bacteriorhodopsin proton pump, elec. demonstration of rapid light-induced conform. changes 77—44597
basilar membrane model, nonlinear, meas. apparatus and circuits *(Japanese)* 78—35868
beta-ray attenuation, inhomogeneous medium density determ., calcs. and meas. 80—98182
bilayer membranes, permeation of water mols. meas. using fluoresc. quantum yield solvent-isotope effect 79—34710
binocular flicker stimulator using polarisers 78—24075
binocular synchronism monitoring, prolonged monolateral occlusion, electro-oculographic response 79—20543
bio-selective membrane electrode using tissue slices 79—48387
bioanalytical systems using mass spectrometry with atmospheric press. ionisation 78—88680
biochemical research using sonicator processor 79—18639
biochemical sensor devices, review *(Japanese)* 79—12050
biocompatibility testing, cell culture and animal test correlation 77—81655
bioelectric potentials, hybrid system for on-line anal. of composite pots. 77—9313
bioelectrochemical sensor using immobilised enzyme electrodes *(Japanese)* 80—109071
bioelectronic research fields *(German)* 80—17211
biofeedback thermometer, low-cost research-oriented, with digital readout 79—29673
biological effects of EM radiation expt. techniques 80—8239
biological research, electron microscopy, megavolt, advantages 77—70580
biological safety cabinet design, testing 79—16362
biological signal conditioning for system identification 77—44578
biological signal processing, minicomputer, rat experiments example 77—37119
biological tissue samples, normal and diseased, elemental comp., PIXE anal. 79—5364
bioluminescence sensor, moving linear, for ocean light field meas. 79—20732
biomagnetic fields, meas. and anal. 79—11952
biomagnetic information, and its meas. *(Japanese)* 80—30735
biomass determ. in immobilised cell biocatalyst by luminol assay for haem 79—66590
biomechanical force measuring platform *(Polish)* 80—36212
biomechanical impact data, digital filtering 77—78070
biomembrane, apparatus for meas. of fluoresc. polarisation *(French)* 77—9307
biomembrane, distance meas. by radiationless energy transfer, transition probabilities 78—24187
biomembrane phospholipid topological asymm., review 77—90736
biomembranes, excited, automatic meas. of ionic current electrophysiological characts. *(Russian)* 80—76865
biomembranes, low noise amplification of voltage and current fluctuations 78—44741
biomembranes and macromolecules, contrast enhancement by single sideband phase contrast interference 77—45920

biological techniques and instruments continued
biomolecules, Fe-containing, appl. of spectroscopy 79—24956
Biophysical Society, 23rd annual meeting, conf., Atlanta, USA (Feb. 1979) 79—34468
biophysics and cell biology, new techniques, book 77—56556
biopolymer time-resolved reson. Raman spectroscopy 78—76999
biopotential recording interference and motion artifact sources and suppression 77—81634
biotelemetry antenna and propagation requirements for appl. for fresh water fish 77—78074
biotelemetry interference minimisation techniques *(Russian)* 79—29685
biovegetation anal., remote sensing technology appls. 77—5349
birefringence, detect. of cell excitation *(Japanese)* 77—66876
birefringence analysis in biological materials 78—56954
blind mobility aid, computerised instrumentation system for simulation and evaluation 79—12045
blood, stored, microaggregation direct meas., effects of micro-filtration *(German)* 79—2168
blood alcohol determ., spectrophotometric method *(German)* 79—5415
blood cell, red, Fe content anal. by electron microprobe and scanning electron microscopy 79—53065
blood cell aggregation, conductometric meas. 77—25614
blood cell computerised counting and sizing system 78—31932
blood cell leukocytes, automatic recognition and classification systems *(Italian)* 80—81780
blood cell profile direct meas. using SEM beam reference lines 78—81094
blood cell suspensions, deep-freezing improvements by thermal history automatic detect *(German)* 79—88215
blood cells, computerised spectral meas. 79—25058
blood corpuscle settling rate automatic fast meas. *(German)* 79—5413
blood erythrocyte count and haemoglobin determ. by mobile miniphotometer *(German)* 79—5416
blood flow meas. using implantable pulsed Doppler flowmeter, dogs 77—90966
blood flow sensing in conscious rats, multichannel pulsed Doppler technique 78—44577
blood flow telemetering system using implantable CW Doppler US flowmeter, IC appls. 78—11749
blood flowmeter, design considerations 80—23853
blood flowmeter, implantable bidirectional device, micropower ICs 77—13038
blood flowmeter, implantable bidirectional pulsed Doppler, for animal research 78—44749
blood gas analysis data processing system *(German)* 79—5419
blood gas sampler, for gas chromatography, design, construction and characteristics *(Japanese)* 78—85458
blood gases, meas. of O_2 and CO_2 concs. using P electrodes 79—20725
blood mech. transfer function, modifications by some biological factors and study method 80—16969
blood plasma, X-ray emission anal. by proton excitation 79—84054
blood plasma filtration, stagnant 77—48948
blood pressure automated control in dogs using microprocessor 80—81797
blood pressure mean, indirect meas. in pony using oscillometric method 78—36085
blood pressure measurement in baboons, direct vs. indirect methods 77—29233
blood pressure noninvasive meas. techniques for rhesus monkeys and beagle dogs 77—44871
blood pressure or flow control system for unanaesthetised animal 77—48983
blood pressure recording transducer, arterial and venous 79—34708
blood pulse measuring by computer *(German)* 80—104823
blood sampling system, remote radio controlled, for unrestrained monkeys 77—90967
blood sedimentation, at controlled shear rates 77—66877
blood sedimentation, three-component anal. by method of characts. 77—70577
blood sedimentation rate free from gravity influence, rapid determ. from density meas. *(German)* 78—81085
blood serum, neutron activation determ. of Zn, Se, Rb, and Fe concs. 78—20252
blood serum, trace element anal. of thick samples, photon excited X-ray fluoresc. 78—3423
blood serum Fe determination using AAS 1 at. absorpt. spectrophotometer 77—48706
blood temperature monitoring transducer, during extracorporeal circulation 78—44639
blood vessel rheological props. and haemodynamic parameters meas. *(French)* 79—66587
blood vessel wall composition analysis with selective histologic staining 79—84067
blood white cells classification, automation using computer, expt. 78—3663
blood-brain barrier, problems in quantifying effects, comparison of methods 80—61643
blue adaption, use in study of Drosophila behaviour and visual receptor mechanisms 80—8224
body joints, centres and angles of rotation meas., errors and optimisation study 80—61604
body surface potential mapping, exptl. study of isochaemia in dogs 78—44750
body temp. regulation method for hyperthermia and hypothermia study 78—15778
bone, cow femur, mineral comp., neutron activation anal. 78—27859
bone, marrow and leucocyte preservative freezing apparatus 79—39617
bone, whole tubular, rigidity comparison technique 80—3881
bone accelerometer package attachment method 79—70717
bone density and cortical thickness, meas. by photon absorptiometry 79—8535
bone healing, use of anodised Ta electrode, meas. of electrochem. reactions 78—95931
bone loading method, controlled and time-varying 79—70566
bone mineral elemental anal. by α-particle backscattering 79—92449
bone strain in-vivo telemetry in monkeys, method 78—3697
bone strain telemetry system, in vivo, monkey 77—86720
bone strains of canine radius and ulna, in vivo meas. and anal. 80—67130
bone tissue preservation, effect of treatment on chemilum., rel. to bone fragment transplantation 77—86709

biological techniques and instruments continued
bone transverse elastic coeff. determ. 78—27985
borosilicate glass, cleaning for biological appl. 77—29234
brain, instrumental neutron activation anal. of trace element distrib., rel to blood serum conc. 80—17215
brain autoradiographs, rapid semiautomatic quantification, microprocessor appl. 80—41332
brain enzymes inactivation in rats, comparison of microwave radiation at 986 vs. 2450 MHz 79—53188
brain fixation, rat, microwave device 77—81761
brain impedance meas., spatial resolution of 4 electrode array 79—84033
brain potential comparison, average evoked, on spectral and coherency function basis 77—2072
brain pressure, epidural, implantable LC cct. transducer, cat exp. results 77—32962
brain reflectance, mapping technique using optical fibres 80—72381
brain tissue, microwave fixation, neurochemical technique, review 78—20323
brain tissue specific-impedance meas. four electrode method 78—3647
brain unit and slow-wave field activity, telemetry with FM pulse subcarrier 77—25625
bremsstrahlung X-ray spectra, lightly filtered, generated at 200 to 300 kV 80—72397
Brownian motion and NMR spin relax., book 78—15054
Brumberg, Y.E., biographical note 79—75309
C-filter: a method for filtering of biomedical specimens 79—20736
calorimeter, AC, high-resolution, for organic- and biological-material melting study 79—6127
calorimetric instrumentation for studies of biopolymer model compounds 80—61746
calorimetric measurements of microwave energy absorption. of mice, equipment and obs. 80—55996
calorimetry, use of high heating rates in study of thermal denaturation of proteins 77—81470
cancer, appls. of EPR and NMR, review 78—69173
cancer cell cycle kinetics, flow microfluorometric DNA distribution representation 77—21669
canine aorta Young's modulus, 10 MHz US meas. 79—57836
capacitance-dynamic electrode for bioelectric potentials 79—57782
capsular organ observation, technique for direct SEM observation, based on epoxy removal 79—20728
captured nerve fibre multiple single-unit recording by tubular electrode array 77—60321
carbocyanine dyes, fluoresc. probes, effect on Ca-depend. K efflux 77—12896
cardiac circumferential fibre shortening vel. determ. from meas. left ventricular dimensions 77—48867
cardiac fibrillation thresholds for 60 Hz currents and voltages directly applied to heart 80—101301
cardiac intracellular transmembrane action pots., automated anal. 79—70729
cardiac muscle isolated preparation, determ. of segment length by mag. induction 77—48982
cardiac output calculations by N_2O technique, corrections for press. and temp. 77—16948
cardiac output thermodilution meas., thermistor probe construction for use in small animals 77—64161
cardiac strength interval curve rapid generation, computer system 78—40456
cardiac tachometer, instantaneous, with extendable range 79—20700
cardiovascular flow visualisation methods for in vitro studies 77—56409
cardiovascular neurography: cardiac-rhythm based neurosignal distribution display 80—41351
cartilage, articular, meas. of surface microgeometry 80—3880
cartilage proteoglycan simultaneous localisation by light and electron microscopy 80—85571
cataract microstructure meas., picosecond range-gated light scatt. technique 79—8584
cataractous lenses, PIXE elemental anal. 80—21468
cathodoluminescence detection of Giemsa stain and its appls. 80—67323
cathodoluminescent microscopy of biological materials, improved resolution 77—56549
cathodoluminescent mode obs. of wet objects in raster electron microscope 78—11782
cationic dye interaction with mitochondria, absorpt. spectra 77—52752
cattle feed utilisation exam., microscopic samples molecular analysis, with Raman microprobe 80—57391
cattle insemination, optimum time determ. by vaginal impedance meas., proposed instrumentation 80—36210
cell analysis, fast feature extraction for medical image structural analysis *(German)* 79—5393
cell analysis, high speed light scattering system 79—12042
cell analysis in flow systems, geometry for orienting flat cells 78—77161
cell analysis in haematology, LARC system overview 78—31931
cell average size and shape meas. light scatt. photometry compared with microscopy 79—84030
cell counter, electronic, model 927-TC for cell culture laboratories 79—39616
cell deposition system for deposition at predefined locations on microscopic slide 80—76876
cell discrimination, paraxial anal. of light scatt. in flow system 79—11907
cell discrimination by US Gaussian resonator and lens 77—21587
cell electro-orientation and dielectrophoresis meas. devices *(Russian)* 80—51300
cell electrophoretic mobility meas. using new automatic method 80—67322
cell element observations in same sections by light microscopy, TEM and/or SEM 80—85556
cell freeze conservation control unit *(German)* 79—5410
cell handling, leucocytes, differential counts, comparison between light and electron microscopic results 79—5429
cell high-speed analysis, laser absorpt. and scatt. meas. *(German)* 78—92687
cell image analysis on PDP-12, software system for information from scanning microphotometer *(German)* 78—20333
cell marking and relocating method for electron microscopy 79—74808
cell medically relevant class determ., scatt. light cluster anal., cervical smear tests *(German)* 78—92686
cell membrane diffusion coeffs. meas. 77—48962

biological techniques and instruments continued
cell membrane particle diameters meas. by computer from electron micrographs 80—101307
cell membrane particles diameter meas. via picture processing 79—84065
cell microsurgery using UV laser beam *(German)* 77—60235
cell migration, sample changer for foil chambers in time lapse cinemicrography *(German)* 77—44857
cell mobility, meas. via alternating field microelectrophoresis apparatus 77—29237
cell morphological parameters extraction from diffr. pattern, Fourier optical approach 78—92749
cell nuclei staining parameters, evaluation regarding reproducibility of fluorescence measurements 80—21590
cell observation, interference effects 79—84055
cell separation, local conc. gradient determ. by conductivity meas. *(German)* 79—5411
cell separator with mechanical sorting operation 80—41355
cell size meas., laser flowthrough microphotometer, double-beam technique, internal calibrated 79—17391
cell size meas. by static light scatt. Fourier transform 80—81793
cell sorting, automated, with flow systems, review, book contrib. 79—5435
cell structure and function investigation by laser microirradiation 79—66599
cell study, optical device for time lapse recording in vitro *(German)* 79—74813
cell surface receptor marking by Au 79—74806
cell suspension six-channel aggregometer 78—81001
cell water permeability during freezing and thawing, cryomicroscope multiple nonlinear regression analysis 79—92197
cells growth research, non-thermal effects, BWO appl. *(German)* 80—105684
cells laser Doppler meas., scattering characts. of intersecting beams *(Russian)* 80—3874
cellular elastomer selection for use in biomechanical capacitive force transducers, measuring device *(German)* 80—85545
cellular fluorescence polarisation measurements in flow systems, epi-illumination optical design 80—89908
cellular identification of free cells by light microscopy and SEM 78—53589
cellular image segmentation using multispectral information 79—88224
cellular images, detection by segmentation method using colour information *(Japanese)* 78—11783
cellular mechanical and chemical analysis, recommendations of workshop on future of biomedical instrum. 80—81776
cellular microsurgery, microscope vertical illuminator adaptation by laser microbeam 79—20727
cellular protein two-dimensional analytical electrophoresis 79—96528
centrifugal method for bacteriological testing of medical grade papers 79—84045
centrifugal technique for evaluating human erythrocyte deform. 78—27976
centrifuges, gas, liquid, appls., review 79—53289
cerebral blood flow, tissue pO_2 and pCO_2, continuous and simultaneous meas. 79—57829
cerebral blood flow determination, computer assisted method for multiexponential curve fitting 78—20246
cerebral blood flow meas. in animals using ^{14}C-ethanol 80—41205
cerebral blood flow system using H_2 clearance method 78—40457
cerebral cortial blood flow transients in cat. meas. technique using tissue heat transfer 79—92457
cerebral cortical microfluorometry at isosbestic wavelengths for correction of vascular artifact 80—56322
cerebrovascular permeability, quantitative method for meas. of alterations 80—61748
chamber for microscopical obs. of biophysical effects of US 77—13039
charged particle activation anal., determ. of Pb distrib. in human teeth 80—101303
charged particle detection by photographic recording systems, appls. 78—17527
chemical analysis, electron energy loss spectroscopy anal. appl. 79—39269
chemical ionisation mass spectrometry, therapeutic drugs in blood analysis 79—57317
chemical ionisation mass spectrometry for amino acids isotopic enrichment determ. 79—79694
chemical relaxation spectrometry, new electric field methods 79—8586
chemiluminescence of aldehyde-preserved plant tissues on exposure to salts of heavy metals 78—77160
chlorella, delayed fluoresc., ns laser pulse excited, fast phase kinetic anal. 79—24951
chlorobenzenes determination by gas chromatography with photoionis. detection 80—35809
chlorophyll a phosphorescence in cellulose triacetate polymer matrix 77—36867
chloroplast membrane proton gradient and osmotic vol. determ. 78—28143
chloroplast membranes, electron microscopy, electron optical artifacts 78—15934
chromatin structure of cell nuclei using scanning microphotometry and TV image anal. 79—34720
chromatogram, thin layer, computer controlled photometer for quantitative anal. 77—60326
chromatograms, two-dimensional, quantitative evaluation 79—84064
chromatographic purification of rhodopsin into three isochromic forms 77—52951
chromatography, detect. of indolic compounds in pigmentary retinal epithelium of trout *(French)* 79—53115
chromatography, gas, for drug determ. in biological samples 79—34388
chromatography, reversed liq. phase, biochem. application, review 79—34371
chromatography, reversed-phase liquid, hydrophobic effect 79—34385
chromatography and mass spectrometry, conference, Carlsbad, Czechoslovakia (April 79) 80—73097
chromatography for amino acid composition determ. of proteins 79—44070
chromatography refractive index detector for monitoring model dialysis expts. 79—96724
chromosome analysis, automatic, specialised image treatment equipment *(French)* 77—37111

biological techniques and instruments continued
chromosome analysis by automatic image recognition *(French)* 77—37110
chromosome band online linear scanning, human, BANDSCAN computer program 78—92758
chromosome banding pattern technique, human, automatic classifying system 79—84062
chromosome classification system, banding technique 80—67320
chromosome classifying system based on banding technique 79—84060
chromosome identification, mammals, banding technique developments 77—56561
chromosome metaphase spread, automatic finding, prep. and eval. of object spectra 80—98168
chromosome model reconstruction from electron microscopic projections 80—8235
chromosome spread automated detect. and classification 77—60328
chromosome-classification system based on banding technique 80—36199
chromosomes, irradiated, identification by pattern classification system 77—37114
chronobiological movement transducer *(Spanish)* 80—89902
Cibacron Blue F3GA affinity chromatography 77—78061
ciliary activity obs. by laser light-scatt. spectroscopy 78—36076
cinematography, high-speed, appl. to laser damaged flagella of microscopic organisms 80—81785
cinemicrographs, time lapse, of cultured cells, computer-aided analysis 78—92756
circular dichroism of phototransients, meas. apparatus using modulation excitation 77—46656
citrinin distribution in tissues and serum protein, radioactive chem. anal. 79—53292
clonogenic cell assay, for radiosensitivity of human tumour cells from pancreatic carcinoma xenograft 77—5041
cloud chamber, low-press. to study spatial distrib. of ionization 77—34513
cochlear nerve fibres, hysteresis of tuning curves 77—52806
code generator to identify time, date, and events in physiologic event recording 77—86674
coherent radiation scattering, calc. of diameter distrib. function of long hollow cylinders 77—70569
collagen fibre electrode for peripheral neural activity recording *(Japanese)* 77—66879
collagen investigations, expt. confirmation technique for calc. phases and electron density profile 79—62408
colon signal multistage decimation and filtering, multiple-input algorithmic processing 77—78069
colonic contractile activity meas., pharmacological tests in dogs appl. 80—109068
colorimetric analysis, automatic, biological fluids, contamination study 77—25564
colour vision physiological measurement facility, monkey detected responses *(Japanese)* 78—92752
computer control of isolated heart preparation for biomedical research 78—53603
computer graphics for red cell anal. 80—21597
computer-assisted mapping with the light microscope 80—67308
computer-controlled double-beam scanning microspectrophotometry for rapid microscopic image reconstructions 80—18008
computerised EEG signal averager, flexible and low cost 79—43998
computerised multiple response parameters meas. 78—57136
computerised technique for rapid eye movements detect. during paradoxical sleep 80—76870
computerized GCMS solid state magnet control, metabolic disorder study appl. 79—12879
conductometric cytometer for blood cells conc. meas. 79—92437
cone, computer-driven hardware model, response obs. 80—72402
confinement device for determ. of whole-body radionuclide concs. in live ducks 80—67299
confocal scanning light microscopy, imaging modes 80—86401
confocal scanning light microscopy with high aperture optics 80—86400
constant pressure resevoir for organ perfusion 80—94437
contact microscope for medical laboratory use 80—85540
continuous flow analysis, cell for use with O_2 membrane electrode, appls. 80—61736
continuous relaxation spectra, direct anal. 80—104831
contraction recorders for animal nictitating membrane and skeletal muscle 77—48969
contrast and radiation damage in biological specimens, conf., Nancy, France (May 1978) 79—66591
contrast enhancing filter for banded chromosomes 78—92755
convective heat loss assessment from humans in cold water 78—81093
coral growth form, light control, computer simulation 77—2076
cornea light scatt. meas. apparatus 77—5123
coronary perfusion pressure programmable control circuit 79—92278
coronary regional intravascular resist. determ. 78—31853
correlative SEM-TEM of primate infundibular recess 78—20336
Couette viscometer for short time shearing of blood 80—98179
Coulter Counter, design and construction of RF interference enclosure 79—96721
Coulter electrical sizing principle, appl. to new multiparameter system 80—89911
cowpea chlorotic mottle virus packing in crystalline monolayers, electron microscopy 80—89922
cryostat, multi-purpose, for freezing biological material 78—15940
cryoultramicrotome sections, reproducible spreading device 80—21585
crystallography, packing anal. appl. to cyclic hexapeptide 77—2070
culture device for cell growth, quantitative microscopy and autoradiography 78—65163
cultured cell obs., SEM STEM comparison 79—74801
current injector for Coulomb titration of chloride 79—29684
current pulse-induced voltage variations in bilayer membranes, apparatus 80—94420
cutaneous receptors, on-line receptive field mapping technique 79—74797
CW Doppler flowmeters, implanted, for renal/iliac bloodflow telemetering from exercising dogs 77—90822
cyanine fluorescent dye membrane probe effects on cell props., rel. to bacterial chemotaxis 78—35815
α-cyclodextrin and α,β-D-xylose, absorption mode spin-echo spectra appl. 80—78634
cylindrical cell with time-variant membrane resist., passive parameter meas. 77—29113

biological techniques and instruments continued
cytochemical leucocyte differentiation and radioimmune assay *(German)* 79—5412
Cytocomputer biomedical image analysis 79—92419
cytofluorometer, imaging system for correlating fluoresc. cell meas. in flow 78—61240
cytofluorometric measurements by fluorescence extinction through a diaphragmed objective 80—67319
cytogenetics, applications of photomicrography 80—21577
cytogenetics microscope for automatic metaphase spread finding 77—56550
cytological cell feature extraction using optical moments 80—98206
cytological preparation evaluation, optical preliminary data reduction *(German)* 79—5392
cytological preparation image processing, filter construction *(German)* 78—36026
cytometry, fast flow-through, pattern recognition by light scatter meas. 79—88228
cytometry, hydrodynamic orientation of sperm heads in flow systems 78—77162
cytomorphological contour classification for mass cancer screening 79—79682
cytopherometer, reproducibility improvement 77—52954
cytophotometer, automatic 2-wave, with a calculator 80—104820
cytophotometric and autoradiographic simultaneous anal. device 78—77172
cytophotometric histogram, computer aided analysis of cell-cycle phase 78—92759
cytophotometry, multiparametric pulse technique for cell and radiation research *(German)* 77—78060
cytospectrofluorometric installation, scanning attachment to dual-prism monochromator 80—101837
dark field electron micrographs, image array filtering in reciprocal space 77—74557
data collection systems, rapid, for time resolved X-ray scatt. expts. in mol. biology 80—61740
DC proportional heater/cooler temperature controller for physiological research 78—7553
deconvolution nomogram for single exponential fluoresc. decays 80—67290
deep body temperature measurement in rodents, inexpensive telemetry system 78—24185
deep body temperature measurement using piezoelectric transducer, sampled data system, unrestrained domestic fowl appl. 78—57152
deep-sea animals trapping, pressure vessel with simply actuated closure 78—3821
deoxyhaemoglobin, proton NMR, modified DEFT technique for obs. hyperfine shifted line, T_1 values meas. 80—76871
depolarised dynamic light scattering, determ. of rotational diffusion coeff. of bacteriophages T4B and T7 80—85549
dermal-resistance meter with high resolution *(German)* 79—84031
determination in organic cpds. and biological samples by combustion method with isotope exchange 79—57333
dextran T-10 and α-cyclodextrin, absorption mode spin-echo spectra appl. 80—78634
dialysis device, high-speed 80—17205
diaphragm muscle, canine, in vivo stiffness props., obs. and meas. system 80—97988
diathermy applicator for irrad. of rat brain 80—94425
diatom photography characterisation by Fourier transform differences 79—79697
diatom recognition, using coherent optical processor with interference contrast microscope input 80—43281
diatom recognition and counting, matched-filter and statistical method 80—101304
dielectric meas. of biological liquids, reflection meas. of complex dielectric const. 80—101309
dielectric properties meas. technique using an in vivo probe, VHF to microwave freqs. 80—85542
dielectric properties of living tissue, 10 MHz to 6 GHz meas. 77—78071
dielectric props. meas at RF and microwave freq. by coaxial line reflection methods 80—109065
dielectric props. of biological substances, physical meas. 80—94417
dielectric relaxation in biological model systems, time-range meas. method *(German)* 80—71308
dielectric spherical radiator, horn-fed, near field characteristics for microwave exposure expts. 77—56543
dielectrophoretic force, theory expt. 80—72403
differential emissivity calorimeter, use in thermal stress energy studies of small mammals 78—40118
differential scanning calorimetery for enzyme-substrate reactions, digital simulation 79—74794
differentiating circuit for LF signals 79—12044
diffractometric method for meas. of cellular deformability 80—98187
digital gas chromatography/mass spectroscopy system for cancer research 80—22469
digital image registration with automatic microscope, appl. to cell analysis 77—29239
digital readout instrument for use in ion transport studies 79—74815
digital-analogue hybrid 3-channel sequential stimulator 79—92445
dipalmitoyl phosphatidylcholine monodomain samples with varying concs. of water and other ingredients, prep. 78—15780
directional Doppler flowmeter, implantable, pulmonary artery flow meas. after lung homograft in dogs 77—90823
discharges electrophotographic obs., high-frequency *(German)* 80—17216
disperse system, electro-optical effect, use of two-phase Rc field 79—55060
displays, three dimens., in biostereometrics 78—81010
diving physiology research facility 80—82106
DNA, γ-irradiated, N-formamido group formed in place of thymine fragment, evaluation method 80—30790
DNA base damage detection method, UV induced pyrimidine dimers in human cells 79—44067
DNA derivate melting curves, automatic recorder using real time processing *(French)* 80—104833
DNA distributions automatic processing and interpretation 78—92757
DNA double helix unwinding obs. technique 79—70512
DNA electron damage repair in E. coli mutants, appl. of rapid lysis techniques 78—31775
DNA entrapment mechanism at air-water interface 77—60181

biological techniques and instruments continued
DNA helix destabilising protein cryst., electron microscopy 80—85338
DNA histograms from flow cytometry, program for anal. 80—41337
DNA hybrid molecule construction and cloning 77—56559
DNA strand breaking and rejoining in UV irrad. normal human and xeroderma pigmentation cells 77—4986
Doppler flowmeters, directional, totally implantable, for animal research 80—67293
double wavelength rapid scanning spectrophotometry of intact mitochondria 78—4699
double-barrel ion-sensitive microelectrodes, extra thin tip diameters, intracellular meas. appl. 80—101298
double-sucrose-gap voltage-clamp method, mathematical model 79—96539
drug analysis, by chemical ionisation and electron impact mass spectrometry 79—57316
dye indicators of membrane pot., review 80—21594
dye laser photodermatological uses, erythema production, psoriasis treatment, tumour destruction *(German)* 80—56164
dynamic wind-tunnel balance, two-component, for mounted flying insects 80—22350
ear canal temperature meas. in cattle, telemetry 77—86714
earthworm locomotor behaviour pattern meas. 78—88772
ECG telemetry, totally implantable multichannel system 78—44746
echocardiography, noninvasive meas. of ventricular dimensions in awake dog 77—44863
education, Bernoulli's eqn. and Hagen-Poiseuille's law, capillary bed representation 80—57039
education, course on biological instrumentation, physical principles 78—40436
EEG, event-related, sequential freq. anal., hybrid method 77—81759
EEG activity chronic recording in conscious dogs using implantable Ag electrode 77—13042
EEG activity telemetering from isolated olfactory bulb of rabbits 77—86516
EEG band analysis, correl. with neuroendocrine phenomena during human sleep 77—9314
EEG biotelemetry, multielectrode, for remote monitoring and stimulation of ambulatory monkeys 79—5386
EEG evoked frequency response polygons, computer anal. technique 77—40961
EEG telemetry system for monitoring olfactory bulb of salmon 77—86718
electric field exposure of miniature swine, vertical 60 Hz fields 78—53587
electric field probe, dielec. insulated, for field meas. in finite heterogeneous biological bodies 79—2170
electric-field probes, effect of material interface on probing internal field 79—53204
electrical discharges from biological objects, charge image method 80—8238
electrical evoked response recording, 7-electrode totally-implanted stimulus-monitor unit 78—31996
electrical excitation of liver cells, DC 77—56565
electrical heart stimulator, versatile, wide-range, for animal expts. 80—89912
electrical stimulation remote control device for studying neural mechanism of monkey 77—86719
electrical threshold continuous monitoring method for single intraspinal nerve fibres 80—46104
electrochemical cell for determ. of O_2 partial press. in biological fluids 78—85420
electrode, implantable, for recording nerve signals in awake animals 77—5119
electrode, implantable stress-resist. design for biotelemetry 78—44629
electrode, self-correcting spherical design 77—32960
electrode for pN_2O and pO_2 anal. in blood and gas 79—62412
electrode pair, implantable, for recording from intact small nerves 80—36204
electrodes, C-loaded teflon, for chronic EEG recordings in microwave research 80—67305
electrodes, glassy C, meas. in saline 77—81764
electrodes, laminated, for nerve biopotential recording 78—92760
electrodes, polished Pt, linear AC electrode polarisation impedance anal. 77—40806
electrodes, Pt, elec. props., impedance meas. and time-domain anal. 78—40360
electrodic potentiometry system, automated, for chem. anal. 78—35735
electroejaculation, intestinal-prostatic impedance in bulls 78—40458
electrofocusing, current major appls. 80—101306
electroglottograph application experience 77—78062
electromechanical vessel occlusion device, implantable, remote controllable 78—40446
electromechanical viscometer with digital readout, biological fluid meas. appl. 78—28131
electromyographic electrodes, small-size, meas. of uptake area 79—74799
electron diffraction, cryst. bending and high resolution protein struct. determ. 78—53325
electron diffraction, low dose, of wet protein cryst. 80—85550
electron micrograph image processing and synthesis 79—25180
electron micrograph images, determ. of structs. relative orientation 79—70714
electron micrograph processing computer programs 79—57835
electron micrographs, bright field 77—73621
electron micrographs preprocessing of nucleic acid molecules for automatic computer anal. 79—70711
electron microprobe anal. of thin sections, use of pure C specimen holders 77—56555
electron microscope, fluoro-autoradiography, improvement of efficiency 78—65162
electron microscope, Siemens EM-101, modified specimen airlock *(German)* 80—9076
electron microscope autoradiographs, iterative anal., sample sizes and confidence limits 79—35896
electron microscope autoradiographs, iterative anal. method 79—35895
electron microscope autoradiography, soln. of reverse problem 80—94419
electron microscope autoradiography and X-ray microanalysis of diffusable substances using ultrathin frozen sections 77—60314
electron microscope autoradiography of isolated mols. 80—85564
electron microscope exam. of new cryst. form of catalase, Fourier transform. method 77—11447

biological techniques and instruments continued
  electron microscope examination of alveolar brush cells of rats 79−34517
  electron microscope film, image reversal process 79−2892
  electron microscope image real-time processing 79−25181
  electron microscope image texture discrimination and automated meas., pituitary tissue appl. 78−57099
  electron microscope imaging with superconducting lenses 80−73553
  electron microscope phase contrast properties, incoherent illumination method appl. 79−57820
  electron microscope superconducting lens system for reduction of radiation damage 79−34718
  electron microscope visualisation of chromatin, DNA-protein complexes, book contrib. 79−5434
  electron microscope wet technique for study of living materials 80−12317
  electron microscope with electrostatic decelerator *(German)* 79−30620
  electron microscopic examination of Birbeck granule-containing cells of mice, occurrence of cored tubule 79−34515
  electron microscopic investigation using tilting technique, for ribosomal particles 79−34514
  electron microscopy, 3-dimens., appl. to yeast fatty acid synthetase 77−12883
  electron microscopy, 3-dimens. computer graphics, computational morphology appl. 78−28132
  electron microscopy, application in modern science, review 79−26182
  electron microscopy, computer anal. of cell ultrastructure 80−85555
  electron microscopy, conf., Toronto, Canada (Aug. 1978) 80−82579
  electron microscopy, detection and resolution of atom images *(French)* 79−66595
  electron microscopy, high resolution, mol. struct. determ. 80−21595
  electron microscopy, high-resolution imaging of biological specimens, radiation damage, review 79−5331
  electron microscopy, HV, design features of photographic film 78−8478
  electron microscopy, HV, in biology and medicine *(German)* 79−57834
  electron microscopy, image contrast from carbonaceous material 77−10142
  electron microscopy, image processing, optical diffraction and filtering, fast Fourier transforms 80−30956
  electron microscopy, image reconstruction of low and high dose micrographs of neg. stained glutamine synthetase 80−85551
  electron microscopy, LV, biological appls. 79−6223
  electron microscopy, LV 77−37118
  electron microscopy, microdensitometer−computer correlation analysis of ultrastructural periodicity 80−85553
  electron microscopy, origin of contrast in images *(French)* 79−66593
  electron microscopy, phase problem, review 80−33862
  electron microscopy, quarter-micron serial sectioning and stereoscopy 80−72384
  electron microscopy, real-space filtering of images from optical autocorrel. patterns 78−8479
  electron microscopy, recent applications to biology 80−41347
  electron microscopy, staining and X-ray microanal., book 78−4739
  electron microscopy, three dimensional, minimal dose technique 80−86526
  electron microscopy, very high resolution, in biology *(French)* 78−28144
  electron microscopy, with hollow cone illumination, transfer functions *(French)* 79−63327
  electron microscopy conference, Pretoria, South Africa (Dec. 1978) 79−71576
  electron microscopy conference, Toledo, USA (Sep 1978) 79−100796
  electron microscopy freeze-fracture image enhancement by reversal processing of sheet film 78−62267
  electron microscopy of biological objects, 3-dimens. image, computer simulation 77−13046
  electron microscopy of biomacromolecules, image analysis *(Czech)* 78−31983
  electron microscopy of frozen hydrated crystalline specimens, meas. and reduction of damage 80−85552
  electron microscopy of guinea pig keratinocytes and melanocytes 80−21583
  electron microscopy study of tissue, Sephadex spheres used for localising specific regions 79−5428
  electron photomicrography of marine microorganisms on submerged surfaces 78−85454
  electron probe analysis, effects of electron irrad. of sample 79−43969
  electron probe analysis, ZAF-correction procedures 79−44073
  electron probe microanalyser cold stage 78−31746
  electron probe microanalysis, charging effect in electron-irrad. ice 78−57141
  electron probe microanalysis, review 77−86730
  electron probe microanalysis of biological thin sections, quantitative methods 77−25620
  electron probe microanalysis of biological thin sections, STEM meas. of local mass thickness 79−62416
  electron probe X-ray microanal. determ. of distrib. in bullfrog skin 79−79707
  electron probe X-ray microanalysis, quantitative investigation of thin specimens 80−101068
  electron probe X-ray microanalysis for calcification studies of bone and cartilage 80−76885
  electron-probe X-ray microanal., ion distrib. in fluid transporting epithelium 77−4991
  electronic circuits implanted in freely moving animals, wireless power supply 79−29682
  electronic feature extractor for action potential parameters 79−84047
  electronic method for determ. of footfall patterns of animals during treadmill locomotion 80−72386
  electronic metronome with luminous and audible signals *(Spanish)* 80−89885
  electronic speckle pattern interferometry, small vibr. detection and meas. 77−72253
  electronic speckle pattern interferometry, vibrating object meas., use of chopped laser light 79−85165
  electronic speckle pattern interferometry in vivo 80−109083
  electrooculargram recording, single channel method for vertical and lateral eye movements 79−16205
  electrophoresis, cells, appls., techniques and Zeiss rectangular chamber cytopherometer 77−13034
  electrophoresis, deflected-lamina, biological materials fractionation in space 78−85397

biological techniques and instruments continued
  electrophoretic analysis of cell suspension, Doppler spectra line shape smoothing 79−84053
  electrophoretic measuring microscope, PARMOQUANT, biological appl. 79−79700
  electrophoretic measuring microscope, test results with PARMOQUANT 79−79701
  electrophoretic mobility measurement using wide-angle, crossed-beam laser Doppler scattering configuration 80−33011
  electrophoretic separator, continuous flow, for biological materials on sounding rocket 78−85398
  Electrophysiological Data Interface 79−79677
  electrophysiological instrument calibrator 77−48970
  electrophysiological measuring, unity gain follower with buffer 79−12048
  electrophysiological recording from behaving animals, 10-channel commutator 79−84050
  electrophysiological stimulator, microprocessor based 78−44748
  electrophysiologoal techniques for exam., of visual function in man, review 78−35843
  electroretinography, human, psychophysical appl., review 78−35859
  electrostimulators, new Russian devices 78−85353
  element anal., proton-induced X-ray emission method *(Russian)* 77−40939
  elemental anal. of biological specimens by proton excitation by charact. of X-ray emission 79−1976
  elemental analysis, quantitative, using energy-dispersive X-ray spectrometer 80−104840
  ellipsometric monitoring of mol. and cellular biological processes in vitro 77−48852
  ellipsometric protein adsorption expt., film thickness estimation 78−44740
  ellipsometry, kinetics of protein adsorpt. and immunological reactions at liq./solid interface 77−52948
  EM, electron exposure-dependent contrast transfer 80−104837
  EM control of cell functions 80−85535
  EM field cell culture exposure under controlled temp. and field strength conditions 78−40449
  EM field probe, implantable design for finite biological body 77−21670
  EM method for noninvasive analysis of cell suspension physiology and induced pathophysiology 79−2125
  EM method for stretching muscles of chronically implanted animals 80−56308
  EM microelectrode holder for pulsating penetration of brain tissue 80−98199
  EM radiation biological effects, conf., Amherst, USA (Oct. 1976) 78−40243
  EM wave exposure facilities for bioeffects research, survey 78−73174
  EMG, multichannel data acquisition system for the survey of intercostal muscle activity 80−81790
  EMG, rel. to skeletal joint torques, for prosthesis control 77−48953
  EMG data synchronised with cine records by LED display device, rats appl. 77−81754
  EMG electrode array for single muscle fibre activity measurement *(Swedish)* 78−24193
  EMG jitter, single fibre electronic meas. device 77−40832
  EMG of muscular exterior carpi radialis, form recognition by freq. spectrum 78−15939
  emission photometer for human serum anal. 79−34417
  emulsion scintillation counting of ^{222}Rn and ^{226}Ra 78−81089
  endocardium motion during contraction, anal. method 80−109072
  endocrine research, continuous blood sampling and time series anal. 78−77130
  endogastric probe for telemetric pH meas. *(German)* 78−85452
  endopelvic fascia, human, stress/strain history relations in simple elongation 78−44539
  energy dispersive X-ray analysis of thin sections, detection limits 78−24215
  energy loss spectrometry microanal. using field emission STEM 78−53286
  energy-dispersive X-ray fluoresc. anal. of trace elements, mass determ. by scatt. 77−48971
  environmental particulate exposure in humans, documentation using SEM and energy-dispersive X-ray analysis 80−76886
  environmental samples, X-ray fluoresc. anal. absorpt. corrections 77−60169
  enzymatic activity meas., electrical method 77−12863
  enzyme activity, kinetic assay, progress curve algorithm for spectrophotometric meas. 78−20083
  enzyme electrode, for species-selective electrochem. sensors, in book, for teachers 78−8200
  enzyme reaction rate determ. by capacitance meas. 78−31997
  enzyme reactions in tissue sections, quantitative microscopy using microdensitometry 77−86728
  enzyme-linked immunosorbent assay, apparatus for meas. light absorbance of small vols. of liquids 80−72387
  enzymolysis technique for study of aortic mechanics 79−43941
  epicardial and body surface pot. meas. in intact dog, transfer coeffs. calc. 78−92614
  epidemiological monitoring of human hair, neutron activation trace element anal. 80−17212
  epidermal imprinting by celloidine 79−25170
  epiphyseal plate, method for evaluation and control of growth activity 80−81789
  epithelioid fibre system decoration by sera, immunofluorescence microscopy visualisation 78−15801
  EPR, detect. of Cr-tissue complexes 77−9310
  EPR, rat liver and hepatoma mitochondrial lipids, stochastic anal. 78−76984
  EPR and saturation transfer EPR, fast computation, master supermatrix eqn. soln. 78−62213
  EPR and saturation transfer EPR, fast computation, perturbation approach 78−62212
  EPR and saturation transfer EPR, fast computation, perturbation approx. extension for overmodulation 78−82754
  EPR and saturation transfer EPR spectra at high microwave field intensities 79−34488
  EPR and ST-EPR spectra of nitroxide spin labels in rigid-lattice limit, rapid computer simulation 79−93189
  EPR applications in agriculture 80−56298

biological techniques and instruments continued
EPR spectra of quasirandomly oriented centres, appl. to radiation damage centres in bone 77–21667
EPR studies of metalloproteins 78–64936
EPR studies of radiation damage to biomols. using aqueous LiCl glass as neutral matrix 79–96632
ERG photostimulus calibration by standard photometer and photodiode 80–8222
ergometer for small-animal research 80–101295
ermeter-dosimeter ERMD-1, UV intensity and dose meas. *(Russian)* 80–12261
erythrocyte deformability, viscometric flow and laser diffractometric technique 78–35879
erythrocyte filtration through polycarbonate filter determ. method *(German)* 79–79708
erythrocyte high gradient magnetic separation 78–53585
erythrocytes of human blood, diameter meas. by specific elec. cond. 78–53353
Euglena gracilis, motion parameters meas. by laser light scatt. 79–16173
eukaryotic cells, improved method to detect small amounts of DNA radiation damage 80–36205
evaporative water loss meas. from small animals by dew-point hygrometry 78–20326
event counter, with selectable time gate, for neurophysiological applic. 77–40944
event-related desynchronisation, graphical display and statistical evaluation 78–24192
evoked potential analysis, on-line signal optimisation using minicomputer 77–5112
evoked potential estimation, method for evaluation of Wiener filtering method 78–24190
evoked potentials, recording and evaluation procedure for neurophysiology and medical diagnostics *(German)* 80–26404
evoked potentials, visual and auditory, interlab. vs. intralab. and intersession vs. intrasession variability 77–70570
evoked potentials steady state, recording and appls., review 78–35823
evoked response averaging for schistosome activity monitoring 79–34613
evoked responses, statistical detect., evaluation of Woody's adaptive filter 77–81757
evoked responses, Wiener filtration vs. averaging 78–3689
experiments, RF losses in elec. conducting samples 80–21580
extensometer for in vivo meas. of human skin biomech. props. 77–44704
extracellular action potential recording, interference suppression 78–61294
extracorporeal irradiation method for blood in rats 80–72396
extracorporeal multichannel telemetry system for physiological meas. of small animals 77–86715
eye, intact bovine lens protein, Raman spectroscopy with intensified Vidicon detectors 79–29525
eye, subjective meas. of monochromatic aberrations 78–35837
eye blink elicitation and measurement, human infant appl. 80–56293
eye injury potential of propelled objects, assessment system 80–21591
eye lens, vertebrate, as system for study of mol. processes 77–90770
eye movement control during single unit recording in pigmented rat 77–81767
eye movement meas. using ocular mag. search coil 79–74798
eye movement recorders, problems, use in laboratory 80–41331
eye movement research, data collection using on-line computers 80–41329
eye movement tracking and regulation test station *(German)* 79–16321
eye tracking raster graphics device, picture processing computer appls. 80–41330
eyetracker, accurate three-dimens. system 78–48944
fast neutron facilities for radiobiological irrad. 80–109064
fast neutron fields produced by Kyoto University Cyclotron for radiobiological expts. 80–27840
femoral cortical bone tensile props. instrumentation system 77–60025
ferritin particle visibility in SEM with field emission gun 79–25174
ferromagnetic contact ring for two-dimensional eye movement meas. 79–5387
fibre optic heterodyne interferometer for vibr. meas. in biological systems 78–77101
fibre optic micro-spectrophotofluorimeter for in vivo animals studies 77–60327
fibre optic pH sensor, miniature, for physiological use 80–109074
fibre-optic force transducer for isometric muscle contraction meas. 79–79715
fibre-optic microfluorimeter for animal haemodynamic and pharmacokinetic meas. 79–92455
field desorption mass spectrometry, appl. to biochemistry, medicine, and environmental science 80–35592
field effect potentiometric sensor 78–44644
field-desorption mass spectrometry, principle and technique, appl. to corrins and vitamin B_{12} 78–80821
film analysis, minicomputer-based interactive graphics system 78–44744
filtering method for biomedical specimens, C-calculus appl. 79–84061
filters as selective electrodes for synthetic penetrating ions 80–104821
finger-tip transducer for meas. digital vol. pulse, skin-resist. response and ECG 77–86729
fingerprints, phys. props. and detect. methods 78–78056
fingerprints, radiographic and physicochem. techniques, for detect. 78–78055
fish stock discrimination, X-ray fluoresc. tissue anal., pattern recognition technique 77–60330
fish surgery, low-cost audible heart rate monitor 77–70575
flameless atomic absorption spectrometer, modification for background correction 78–11581
flameless atomic absorption spectrometry, Be determ. *(Japanese)* 80–26428
flash photolysis, appl. to biological systems, review 78–11530
flavins, meas. of sub ns fluoresc. decay by time-correl. photon counting and Ar laser 80–94429
flow cytometer, high-resolution, based on net flow configuration 80–8223
flow cytometric data, computerised display and anal., review, book contrib. 80–109082
flow cytometry, fluoresc. polarisation meas., appl. to fluorescein in mammalian cells 77–52942
flow measurement, NMR spin echo difference method appl. to plant stem 78–14110

biological techniques and instruments continued
flow microcalorimeter, meas. of heat prod. from human lymphocyte cultures 77–81473
flow microcalorimetry, bioassay and enumeration, drug biopotency meas. 80–95100
flow through measurements, K selective disc electrode, PVC matrix, valinomycin in diphenyl ether, low drift potential 77–29229
flow velocity determination with pulsed NMR, appl. to plants 78–83506
flow velocity meas. at olfactory organ nares of fishes, laser velocimetry *(German)* 78–69262
fluid density measurement techniques, biological macromolecules in solution appl. 78–92751
fluid mixing and bottling unit improvement 78–61291
fluorescence and fluorescent probes, appls. 78–15932
fluorescence decay of biomembranes, apparatus for direct meas. *(French)* 77–5116
fluorescence depolarisation, E-type delayed, rotational motion probe technique 80–36207
fluorescence immunoassays, review 79–79693
fluorescence marker concentration dynamics, as probe of mobility 77–9303
fluorescence microscopy, water pollution abatement, self-cleaning capacity of epipelic bicenoses 79–79702
fluorescence microscopy of living cells, low level, appls. of image intensification 80–94432
fluorescence photobleaching recovery experiments, criticality of beam alignment 80–56296
fluorescence photobleaching recovery for meas. of mol. motion, cell surface heating 77–48956
fluorescence photobleaching recovery method, bleaching light effect on membrane diffusion meas. 80–94434
fluorescence photomacrography, bone growth and remodelling exam. 78–31982
fluorescence polarimeter for flow cytometry 78–73191
fluorescence polarisation microscope for cell membrane fluidity screening 77–44855
fluorescence spectroscopic investigations of the dynamic properties of proteins, membranes and nucleic acids 80–101148
fluorescence spectroscopy, in study of biochem. processes, review 78–11784
fluorescence spectroscopy applied to biopolymer dynamics and struct. 77–60329
fluorescence spectroscopy technique, appl. to study of proteins at interfaces 80–12315
Fluorescent EXAFS data using solid state detector, for metals in dilute biological systems 78–66595
fluorescent excitation anal. of stable Rb, erythrocyte survival determ., rabbits 80–81788
fluorescent microscopical technique in diagnostic microbiology 78–20339
fluorescent probe binding to proteins error in interpretation of double-reciprocal plot and Scatchard plot 78–24021
fluorescent tagged reagents, for chem. or biological analyses 77–21440
fluorescently labelled molecules as probes of living cells struct. and function, review 80–67321
fluorocarbon detection by gas chromatography *(German)* 78–96117
fluorometry, nanosec. system, appl. to biological samples at cell and tissue levels 77–17010
FM telemetry, short-range, for skeletal muscle O_2 conc. meas., rabbit 77–86722
FM transmitter for heart rate/respiratory freq. changes of ducks during submersion 77–86717
food samples, determ. of fluorine conc. using $^{19}F(p,p'\gamma)$ 79–5218
footfall pattern transduction by foot or shoe cover 79–57799
force plate, mech. design, construct. details and calibration 80–85544
force/tension transducer for small muscle meas. 80–41281
fossil dating by ESR technique 80–95209
Fourier transform. IR obs. of complex systems 78–68945
Fourier transform IR spectroscopy of polymer systems 78–58870
Fourier transform IR transmission spectroscopy, appl. to natural and model membrane study 80–17218
free radical EPR saturation corrections 77–48963
free-moving mouse EEG recording and drug infusion technique 79–57831
freeze fracture autoradiography, red blood cell plasma membrane, electron microscopy 80–98192
freeze-drying techniques; mass transfer, appl. of calorimetric instrumentation 77–25628
freeze-etch unit for rotary shadowing and low temp. freeze-fracturing 79–5423
freeze-fracture techniques and appls. in struct. anal. of mammalian plasma membranes, book contrib. 80–30960
frequency response measurement technique for press., vol. and flow transducers 80–41344
functional residual capacity meas. instrumentation for neonates and small animals 78–53590
gait recording technique, digital 79–70725
galvanic electrode, tissue O_2 tension meas. in rabbits 77–13040
gamma camera in rat renal function studies, appl. to radiation effects monitoring 77–56454
gas chromatography-mass spectrometry, integrated analytical systems, applics. in biomed. and related sciences, review 80–36200
gastro-intestinal electrical rhythms, freq. estimation using auto-correlation and auto-regressive modelling 77–44875
gastrointestinal motility, extraluminal meas., FM telemetric system 77–13043
gastrointestinal signals, quantitative analysis 80–41339
Gaussian-beam launcher for microwave exposure studies, dielectric hemisphere-loaded scalar horn 80–12206
gel electrophoresis, 2-dimens., in study of somatic cell differentiation 80–46114
gel permeation chromatography of interacting multicomponent systems, protein isomerisation study 78–68950
gel permeation chromatography of interacting multicomponent systems, protein isomerisation kinetic consts. determ. 78–68951
gel scanner for location of proteins separated by isoelec. focusing 80–30953
glass electrode impaled into single cells, meas. of membrane and electrode elec. props. 80–89916
glass microelectrodes, Na^+ and K^+ selective, electrochemical props. 79–91957
glass micropipette, mechanics of pulling 80–56295

biological techniques and instruments continued

- glass micropipettes, comparative calibration by optical microscopy and SEM *(German)* 80—98201
- glucoregulation in blood of diabetic dog 77—86652
- glutamine synthetase reconstruction from electron micrographs using computer averaging 79—92452
- goniometry, for total knee motion determ. 77—52902
- gradiometer, balancing, system of adjustable superconducting plates, biomag. signal meas. 79—25162
- graphical analysis of nonideal monomer self-associating systems by equilibrium ultracentrifugation 80—41335
- grid-gated photomultiplier photometer with subnanosecond time response, for fluorescence photobleaching recovery expts. 80—37071
- gross surgical specimen photography, centimetre rule/elevator rod technique 78—61287
- haematocrit determination in dog using radionuclides 79—62411
- haeme disorder characterisation in haeme proteins, PMR method 79—92152
- haemocoagulometer 79—39541
- haemodynamic parietal friction meas. by pulse type Doppler velocimeter 80—17206
- haemodynamic resistance long. distrib. in organ, meas. using saline injection 77—36996
- haemolysis kinetics, US differential absorption meas. 77—77877
- haemorheology in near zero gravity environment 80—3661
- hair, human, multielement neutron activation anal. of trace element concs., Tokyo area 80—45602
- hair, human, PIXE analysis, correction factor, rel. to pollution monitoring 80—61743
- hand position and forces during manual work, documentation method 79—74803
- head holder, orientable, for use in visual research 79—2171
- heart beat rate monitoring in animals, range 0.01 to 10 Hz, VLF meas. cct. *(German)* 79—34709
- heart electrical and mechanical monitoring on extensometer 80—45944
- heart muscle cells, paraffin-embedded, cryofracture, SEM and TEM obs. 78—57148
- heart muscle contractility calc. using analogue computer *(German)* 78—7378
- heart rate module, implantable, with AGC, for animal use 78—44753
- heart rate radio telemetry for rats, nonobtrusive system 77—90964
- heat flux/temp. data telemetering for energy flow study of peccary 77—86716
- heat loss measurement apparatus, evaporative and radiative, man in normal working mode 79—25178
- heavy ion induced X-ray emission anal. 77—48727
- heavy ion microlithography, obs. of submicroscopic structs. 80—51227
- helical structure reconstruction from projections, phage tail appl. 80—8237
- heparin assay in animal model of Pseudomonas sepsis, rheological approach 77—52953
- heterodyne interferometer, light scatt., for vibr. meas. in auditory organs 77—2073
- high resolution time lapse cinemicrography, use of improved air stream incubator 80—98196
- high voltage electron microscope autoradiography, HeLa cells 78—36077
- high-pressure chamber for electrophysiological meas. 80—98185
- high-speed autoradiography, evaluation of effectiveness 80—47100
- histological and cytological reflection contrast microscopy 80—72389
- histological data quantitative anal. using optical-mark-recognition computer cards 77—81612
- histological marking with multiple thin-film electrode probe for intracortical recording 80—67297
- hole-burning spectroscopy, electron phototransfer in reaction centres of Chlorella photosystem I 80—81561
- holocamera for 3-D micrography of the alert human eye 80—98057
- holographic interferometry meas. of eye deform. due to intraocular press. changes 79—20720
- holographic interferometry set-up for seed studies 80—67325
- holographic interferometry with optical fibres, hearing mechanism obs. 80—76879
- holographic microscope, theory and appls., review 78—45690
- holographic microscopy, image plane holograms of test target, blood cells and hair 78—58944
- holographic models of neural structs., optical system *(Russian)* 80—76878
- holographic motion pictures of microscopic plankton 78—48946
- holographic refractometer, for refractive index increments for macromolecules in soln. 79—27205
- holography, autocorrelation of diatoms as a function of depth of focus [holography in biology] 80—67324
- holography, conf., Munster, Germany (Mar. 1979) 80—62390
- holography in biology and medicine 79—8528
- horse's hoof movement/load relationship camera and multicomponent force meas. panel *(German)* 79—16352
- HPLC, base line drift correction circuit 80—45604
- human metaphase chromosomes, specimen preparation and SEM examination 79—84034
- human platelets, air-dried, topography and thickness measured by correlative TEM and SEM 79—84041
- hydraulic microdrive for recording single nerve cell activity 79—70727
- hydraulic transport of fragile nonspherical solids, algae aqueous suspensions 77—73618
- hydrodynamic generator for blood flow simulation 79—79706
- hydrodynamics of flexible plate, exptl. simulation of water organisms oscillatory motion *(Russian)* 77—32923
- hyperthermia of expt. mouse cancers using 2450 MHz microwaves 79—2119
- hyperthermia producing heating system for expt. tumours in unanaesthetised mice 80—56316
- hyperthermia production technique using UHF currents in superficial rat tumours 80—30947
- hypoxic cell fraction determ. in transplantable murine sarcoma 77—64164
- IC control unit for generating random and nonrandom events 80—36202
- IC implantable systems for animal expts. 80—76887
- image analysing computer, Quantimet, device for automatic scanning of irregular areas 77—5906
- image analysis system, 2D TAS Leitz, compact bone substance porosity determ. *(German)* 78—92753
- image convertors, for HVEM 80—104839

biological techniques and instruments continued

- image intensification of X-ray diffr. patterns 77—66878
- image intensifier TV X-ray detector, high sensitivity, biological structure diffr. study appl. 78—89609
- image optical differential operation processor 77—52911
- image processing algorithm for distortion anal. 79—88229
- image processing applications at IBM Madrid Scientific Center 80—102657
- image processing for identification of human chromosomes 79—62418
- image restoration and enhancement, conf., London, England (Dec. 1978) 79—25101
- immobilised enzyme systems, optimisation of porous glasses 77—12891
- immunoassay, differential pulse polarography method 79—79709
- immunochemical analysis, standardisation of light scatt. meas. 78—36081
- immunochemical analysis, standardisation of light scattering meas. 77—56548
- immunoelectronmicroscopy in detect. of antibodies to rabies virus 80—85567
- immunoelectrophoresis, fluorography of ^{3}H-labelled proteins 80—17220
- immunofluorescence diagnosis using AR laser *(German)* 79—5335
- immunoglobulin G, enzyme immunoassay, electrochem. determ. with antibody-bound membrane 79—53293
- immunology, Ni plated slides, effect of metallic shield on cosmic radiation effects 80—56317
- immunology slide, darkening, Mie scatt., Maxwell Garnett theory 77—9315
- immunonephelometric assays 79—84046
- implantable biotelemetry, multichannel, for recording physiological data of monkey 77—86660
- implantable stimulators for studying functional adaptation in skeletal muscle of rabbit 77—86721
- incubator, closed chambered, use in enzyme and immunoperoxidase histochemistry techniques 80—98191
- inelastic electron tunnelling spectroscopy appls. 78—92770
- inelastic electron tunnelling spectroscopy appls. 78—92771
- inert-gas clearance method for blood coronary disease and myocardial infarctions investigation 77—5121
- infrasonic test chamber for research into effects on man *(German)* 80—67147
- infrasound and pressure waveform generator, compact, for small cavity appls., animal research 80—104830
- infusion pump, portable, electrolytically driven, laboratory appl. 78—31987
- inhalation exposure system, microprocessor-controlled for repeated exposure of animals to aerosols 79—70726
- insect optical cells anal. using microcomputer *(German)* 77—86724
- integrated circuit approach to totally implantable telemetry systems 80—67291
- integrated FET micro ion sensor, for pH and pNa monitoring 78—44641
- integrated micro multi-ion sensor using IGFET 78—40439
- integrator with automatic reset, for respiratory activity obs. in expt. animals 79—29683
- intelligent microscopes, recent and near-future advances 80—98166
- interactive film anal. system 80—3876
- interactive image scanner, high resolution 80—94423
- interference microscopy, for plant cell wall and cytoplasm refr. index determ. 78—57151
- interference reflection microscopy, image interpretation theory and appl. to cells 79—80677
- interference refractometer obs. of phosphatidylcholine dispersion phase transitions 78—44459
- internal reflection spectroscopy of biological samples *(German)* 79—5417
- intestinal absorption of Ca and P in rat, simultaneous in vivo determ. using ^{47}Ca and ^{32}P 78—48882
- intracavity resonance Raman amplification, appl. to cytochrome c 77—66794
- intracellular conductivity meas., indirect method 77—40950
- intracellular potential amplifier input capacitance determ. errors 77—60320
- intracellular pressure measurement system 80—109084
- intracellular recording from pulsating cerebral cortex 77—48960
- intracortical recording of field pots., 16-fold semi-microelectrode 80—67298
- intramembrane potential jump meas. by potentiodynamic method 80—81778
- intraorbital microcirculatory studies, ultramicrospectrophotometry techniques 80—21589
- intravascular thrombus induction in vivo using localised hydrodynamic shear stresses 80—97997
- inverse scattering problem, soln. in Rayleigh-Debye approx. for assemblies of long cylinders 77—48693
- inverse scattering problem, soln. in Rayleigh-Debye approx. for thin spherical shells 77—48694
- inverted camera microscopes, IM 35 and ICM 405, for biology, medicine and metallography 79—30540
- inverted microscope, differential interference contrast, appl. to study of in vitro perfused nephron 80—51303
- ion beam anal. in few MeV range, review 77—81768
- ion electron-loss microscopy, high-energy, signal-to-damage ratio 79—25175
- ion exchange membrane selectivity w.r.t. dialysis prospects 80—45560
- ion microradiography, of hydrated cells with SEM imaging 79—16360
- ion scanning high resolution probes, appl. to physics and biology 80—47156
- ion sensitive FET, mechanism 77—48741
- ion sensitive FET's development review, biological applications *(French)* 77—70578
- ion sensitive FET micro pH sensor 78—44643
- ionic channel formation in living cell membrane, microelectrode obs. 78—53372
- ionisation mass spectrometer, with dedicated minicomputer, biological appls. 78—53586
- ionophore A23187, use to meas. and control free and bound cytoplasmic Mg in intact red cells 77—52755
- ionselective multi-disc electrode *(German)* 78—3687
- iontophoresis, gated HV system with accurate current monitoring 78—69259
- iontophoresis circuit isolated current monitor for cell membrane studies 77—60311
- iontophoretic isolated current monitor for cell membranes 77—25626

biological techniques and instruments continued
iontophoretic pipettes, theoretical physics of drug release 80—67311
IR laser absorpt. spectroscopy with ATR prism 79—98480
IR noninvasive monitoring of cerebral and myocardial O_2 sufficiency and circulatory parameters 78—44583
IR photography, principles and appls., book 78—82068
IR thermometry, appl. to remote detect. of biological stresses in plants 80—61749
IR-ATR spectroscopy, appl. to struct. investigation of biological material in aq. environment 80—61735
irradiation chamber and sample changer for biological samples 80—56198
irradiator, for project ZEUS field studies of small mammal populations 77—5126
isobaric contraction system for left ventricular performance analysis *(Japanese)* 79—29677
isoelectric focusing method for human globin chain separation 80—17219
isopycnic centrifugation method for rapid separation of murine thymocytes 80—104832
isotonic capacitive transducer 79—66585
isotopic continuous X-irrad. and monitoring of human lung cancer in histoculture 77—73550
karyotyping automatic image processor *(French)* 77—40953
kinetic IR spectroscopy IR, appl. to biochem. systems 80—98178
kinetic resonance Raman spectroscopy, bacteriorhodopsin Schiff base deprotonation dynamics 77—48981
kinetics of drugs and tracers, simulation of biological systems 77—40956
lactate concentration meas., enzymatic and electrochem. methods *(German)* 79—2169
LAMPF, medium energy particle beams, biomedical appl. 79—53216
laser absorption spectroscopy with ATR plates for biomed. use *(German)* 78—36084
laser application in medical and biological fields 77—77961
laser applications in biology and medicine *(Japanese)* 80—3752
laser applications in medical research, biophysical aspects 80—51201
laser applications in medicine and biology, bibliography, 1963-74 77—25539
laser desorpt.- mass spectrometry, polar nonvolatile bio-organic mol. anal. appl. 78—92534
laser differential scattering system for red cell shape monitoring 77—90873
laser diffractometer for rapid anal. of microparticles and biological cells 79—66589
laser Doppler anemometer, directionally sensitive two-component, velocity meas. in artery casts 80—75004
laser Doppler microscope for blood velocity meas. 79—62329
laser Doppler microscopes for flow vel. meas. 78—37052
laser Doppler spectroscopy, biology appls. 79—66598
laser Doppler velocimeter, blood cell speed absolute meas. in retinal vessels 79—83884
laser Doppler velocimeter, blood flow meas. in fish *(Japanese)* 79—84052
laser electrophoretic light scattering observation of biological surfaces 80—41359
laser exposure of mammalian cells using evanescent fields created in optical waveguides 78—73298
laser flash absorption change kinetics spectroscopy at 820 nm, photosynthesis study appl. 78—92769
laser inelastic scatt. from enzymes, e.m. mol. electronic reson. phenomenon 77—9166
laser interferometer meas. of axon diameter changes concurrent with action pot., crayfish 77—64029
laser microbeam microscope, neuronal cell culture appl. *(German)* 78—3694
laser microfluorometer for fluorescence decay meas. 79—66449
laser microirradiation for biological tissue exam. 80—26422
laser microphotometry with laminar hydrodynamic focusing 77—37965
laser microprobe mass analyser, achievements and appls. 80—73536
laser microprobe mass analyser, development for biological specimens 79—17554
laser microprobe mass analyser, for biomedical appls. 79—39630
laser photo-CIDNP as surface probe for proteins in soln. 78—73138
laser probe in biomedical research 77—9298
laser projection microscope, with brightness amplifier for biology and medicine 80—76875
laser radiation effects on mammalian cells, obs. using optical waveguide evanescent fields 80—12183
laser Raman spectroscopy, appls. 77—52940
laser Raman spectroscopy for living cell metabolism obs. *(German)* 79—29577
laser remote probing of photosynthesising organisms, fluoresc. technique 79—66434
laser spectroscopy of primary energy conversion in photosynthesis 79—66461
laser sterometry light-scattering technique, cardiac images 80—56310
laser systems for on-line meas. of muscle sarcomere length 79—48383
laser techniques for biophys. studies, review 77—90975
laser-apparatus for preparation and manipulation of biological microsamples *(German)* 80—56307
laser-Raman microprobe studies of mineralizing tissues 80—76884
lasers, influence in biological and medical research, review 80—26318
latency meter, digital, for evoked pots. 77—60322
leaf temp. meas., infrared thermometer method in connection with plant physiology *(Japanese)* 78—31993
leukaemia cells locomotion analysis 80—40983
leukocyte uptake of radiolabelled compounds in whole blood, liq. scintillation method 77—90882
leukocytes of human blood, gravity sedimentation anal. 80—98197
LF 4-probe impedance meas. system 78—7554
LF dielectric measurements using time-domain technique, 20 Hz to 10 kHz 80—57329
lichen indicator appl. in PIXE and NRA environmental studies 80—61744
light absorption and orientation of absorpt. momenta in biological structs. 78—53326
light flash intensity meas. for neurophysiological research 79—49270
light microscopic stereoscopy, tilt stage 80—21587
light scattering, low-angle, from cell model, eikonal approx. 78—44466
light scattering, quasi-elastic, from moving bacteria 77—23617
light scattering from cells, model, anomalous diffr. approx. 77—25396

biological techniques and instruments continued
light scattering measurement with photodiode array, for biological cell anal. 78—28146
light scattering photometer, meas. of structural change dynamics in biological particles 79—39615
light scattering spectrometer, power spectrum analyser, for quasielastic scatt. *(German)* 80—12314
light single particle scattering, asphericity effects 79—7069
light transmission microscope, object diffr. evaluation, object and field stop spectrum separation *(German)* 78—92685
linear filter appl. to evoked pot. data 79—84032
lipid bilayer, planar, light guide effect, bilayer spectrosc. appls. 79—29509
lipid bilayer hydrophobic ion interactions, inner volt. clamping method 78—28129
lipid bilayer nonlinear electric effects studied by harmonic anal. 78—24188
lipid bilayers, bacteriorhodopsin containing, photoelectric activity investigation 79—16148
lipid bilayers, solvent-depleted membrane prep. from conc. lipid solns. 78—53347
liposome-cell interaction, transfer and intracellular release of trapped fluoresc. marker 77—36901
liquid scintillation counting of ^{3}H or ^{14}C amino acids, optimisation factors 80—30951
liquid scintillation counting of ^{45}Ca in plant and soil material 77—44536
liquid-crystal optical fibre temp. probe rel. to thermometry and dosimetry of heat 80—98204
lithography, heavy ion, tool for object investigation and replication 80—90931
liver tissue mech. props. exam. using rheological method *(German)* 78—7377
LKB Multiphor, universal system for electrofocusing, electrophoresis, immunoelectrophoresis and isotachophoresis 80—7888
load measurements on artificial muscle system in animals 77—44852
locomotion studies, technique for correlating film and EMG 78—24186
low-temperature biological SEM and X-ray microanalysis 79—74818
low-temperature biology, appls. to medicine *(Japanese)* 77—44870
lung, canine input impedance meas. by transient forced oscillations 79—16359
lung, mechanical response at high frequencies, input impedance computation method 79—16239
lung, specific airway resistance changes meas. technique 80—8228
lung burdens of low-energy photon-emitters, interlaboratory comparison of meas. techniques 79—20671
lung compliance loop recovery eliminating cardiac interference by digital filter 79—20570
lung degassing, evaluation of 2 methods 80—101294
lung histological sections, techniques for studying radionuclides 80—56315
lung irradiation for pulmonary metastases prevention, expt. with model system 77—37021
lung sound transmission meas. 78—28149
lung translation, rot. and strain calc. from roentgen-videographically recorded marker displacements 78—31843
lung volume estimation method, constant inflation pressure 80—67306
lymphocyte carbohydrate metabolism in response to mitogens, liq. scintillation vial for radiometric assay 78—61248
lymphocytes, human, radioactive labelling with ^{111}In 79—5354
lyophilised solutions, electron probe anal., calibration curve linearity limits 79—44075
lysozyme, absorption mode spin-echo spectra appl. 80—78634
macromolecular crystallography, method for preventing cryst. slippage 77—76258
macromolecule electron density map, low-resolution phase extension using matrix direct methods 77—66875
macromolecule observation using CTEM and STEM with negative staining 80—85561
macromolecule structure studies, neutron scattering from soln. of biological particles 77—16906
macromolecules, nonlinear laser photomodification, radiation damage 80—61120
macrophotography, simple flash equipment 79—17513
magnetic alignment of macromolecules and membranes, high fields 77—64163
magnetic circular dichroism of biological molecules, review, book contrib. 80—109080
magnetic focus generation for NMR biological meas. *(Japanese)* 79—12041
magnetic micro-rheometer evolution and theory 80—92099
magnetic micromixer attachment for SPECORD UV VIS spectrophotometer for immobilised cytochrome C investigs. 80—56302
magnetic recording, one-channel, direct and reversible synchronisation unit 78—3620
magnetic recording of central nervous system, book contrib. 79—5304
magnetic relaxation study of micro-struct. of water-protein layer of spin-labelled lysozyme preps. 78—76980
magnetic search coils for eye position meas., implantation method 80—85548
magnetic susceptibility instrument, supercond., automatic, biological appl. 78—57153
magnetic susceptibility measurement, living rats 80—72391
magnetometer, induction type, for biomag. fields *(German)* 79—88207
maize mutation distinguishment by EPR 79—57580
mammalian cells, heavy ion effects, irrad. facilities and methods 80—35981
mammalian cells, replicon sizes estimated by X-ray plus bromodeoxyuridine photolysis method 79—16353
mammalian chromosomal DNA, single-strand breakage, sensitive detect. by sedimentation anomaly appl. 80—104825
mammography techniques, appl. to bird skull struct. anal. 80—36209
marine life forms recording, using CCD colour TV camera 80—51301
marine organism conc. of superheavy element 116, proposed anal. techniques 77—3503
marine pollution bioassay using fertilised mollusc eggs *(Japanese)* 79—52969
mass fragmentography with glass capillary columns, trace anal. of pesticides in biological extracts 77—9312
mass spectrometry applications in study of porphyrins and related tetrapyrroles 80—51306

biological techniques and instruments continued
mass spectrometry appls. in struct. studies of bioactive compounds 80—51305
mass spectrometry in steroid research 80—51308
mass spectrometry instrumentation for chemists and biologists 80—42297
mass thickness of biological sections, determ. from electron micrographs 77—70573
mass-analysed ion kinetic energy spectrometry, appl. to intact DNA modified bases characterisation 80—3591
mast cell automatic counting using image analysing computer Quantimet 720 78—20335
material identification of soft tissue using membrane inflation 80—41345
mean caliper diameter of lung nuclei determ. 80—98189
mean electrical axis of heart trace on CRT, electronic technique, teaching aid 77—13022
measured value preprocessing and direct sample identification *(German)* 79—5418
meat, biochemical procedure for detect. of radiation treatment 78—65075
mechanical prestressing, compensation of isolated muscle specimens *(German)* 80—36201
mechanical properties of soft animal tissue, in vitro testing, apparatus review 78—31985
mechanostimulator, physiological appl. 78—92762
melanoma therapy regime study using athymic nude mice 77—48839
membrane, molecular motion determ. using periodic pattern photobleaching 79—34719
membrane architecture obs. by electron energy loss spectroscopy 79—25177
membrane electron density profiles, determ. method on an absolute scale 79—16358
membrane energy transduction probes, review 77—21666
membrane fluorescence test, rapid modification base on Microtiter system 78—20334
membrane fracture faces obtained by freeze fracturing, complementary struct., digital image processing 79—62205
membrane multilayer arrays, surface-induced lamellar orientation, theory and method 80—89724
membrane noise analysis by integral spectrum procedure 77—48958
membrane noise spectral density measurement, use of octave filters 77—48957
membrane optical thickness meas. using Fabry-Perot interferometer 77—71367
membrane permeabilities, dynamic, meas. under non-equilib. conditions, appls. 80—46107
membrane potentials meas. using the dye safranine 79—48386
membrane potentials tracing system, using amplifier for voltage clamping *(German)* 78—61285
membrane responsiveness curve automated on-line determ. 78—92761
membrane studies in transmitted polarised light, interpretation of results 77—37113
membrane surface charge visualisation using SEM 80—85566
membranes, synthetic, use in biophys. research 77—70418
metabolite mapping by ^{31}P NMR in whole animals, diagnosis appl. 80—36211
metacarpophalangeal joint, motion meas. technique for 6 degrees of freedom 77—56418
metal electrodes, impedance props., chronic recording from mammalian nerves 79—12043
metal ions, in complexes and biological systems, preliminary vibr. assignment method 78—62953
metalloenzymes, ^{113}Cd as NMR active site probe 78—68999
metalloprotein solns., use of Faraday magnetic balance 78—70170
methionine sulfoxide in protein, ^{13}C NMR anal., method and expt. obs. 80—56305
method for gaining access to auditory nerve of guinea pig 78—85455
8-methoxypsoralen detection in ocular lens, rel. to psoriasis treatment with photosensitising agent 78—15937
micro projection attachment with integrating plate, histological meas. of thyroid 77—78067
micro-light guide photometry of biological tissues 80—46005
micro-object geometric feature determination, TV set 80—85538
micro-organism electrical characteristics meas., elec. cond. and dielec. props. *(Italian)* 78—3684
micro-organism enzymic activity indicator 79—57819
MICRO-VIDEOMAT, use in light microscopic liver diagnosis 77—78013
microalgae, correl. of light scatt. patterns from pure and mixed asynchronous cultures 78—44737
microanalysis biological tissue using Raman laser microprobe 78—88773
microbe thermistor for metabolite anal. 77—78063
microbeam anal., conf., Ann Arbor, MI, USA (June 1978) 79—39258
microbiology, US appls., status and problems of methods used 80—21592
microbiology applications of pattern recognition 78—81084
microcalorimetry of isolated cells of mammalian brown adipose tissue 77—56343
microcinematographic analysis of cytotic processes of unicellular organisms 79—100800
microcircuit electrodes, extracellular, recording of action pots. from cultured neurons 80—72382
microcolony technique, regeneration and dose-response characts. of irrad. mouse epidermal cells 77—5031
microcomputer-based system for rat locomotor activities meas. 79—20722
microdensitometer for X-ray crystallography use in molecular biology lab. 77—35438
microdrive assembly, subminiature, for electrophysiological recording from freely moving rats 80—61737
microelectorde system for simultaneous recording of neuron single-unit pots. *(Japanese)* 79—57826
microelectrode, chronically stable, reproducible, with parylene insulation 77—40942
microelectrode, glass, with piezoelectric drive for cell membrane penetration 79—5420
microelectrode, liquid ion exchanger, appl. to meas. of large extracellular Na transients 77—52949
microelectrode, metal-filled, reproducible manufacture 78—69263
microelectrode, Pt, potentials and small-signal impedances 79—34716
microelectrode, W, potential and small-signal impedances 79—34715
microelectrode current and voltage clamp cct. for central nervous system neurons 78—24191
microelectrode geometry determ., indirect method 77—40949
microelectrode puller for reproducibility 77—48967

biological techniques and instruments continued
microelectrode tip fabrication method 77—81758
microelectrodes, KCl filled, boiled and not boiled, potential and resistance comparison 77—81760
microelectrodes, Na-selective liquid ion-exchanger, for intracellular meas. 80—3888
microelectrodes, open tip glass, influence of diffusion, double layer, and glass conduction on elec. resistance 80—67300
microelectrodes, vibrating, excursion in tissue 80—104829
microelectrodes for tissue measurements of local PO$_2$, local flow and local ion activity 80—51287
microelectrophoresis, intracellular, contrib. of volumetric charge to mobility of nuclei 77—86710
microfluorimeter design for medical-biological research 79—57818
microfluorometric measurements of DNA dye complex using cryostat 80—17949
microinterferometry and microfluorometry determ. of oxirane-acrylic bead radical conc. gradient *(German)* 79—100799
microiontophoresis apparatus, circuit to automatically supply current balance 80—41341
microkymography, and related techniques 80—36215
microkymography, flow vel. meas. in microvascular bed after exdotoxin administration *(German)* 78—77173
micromanipulator, hydraulic, versatile remote control and economic construction 79—25163
micromanipulator for use in closed system 80—37013
microphotometer, automatic fluoresc., using image dissector tube, quantitative cytochem. appl. 79—97413
microphotometer, multipurpose integrated digital, type TsIMF-2 80—4753
microphotometry, compensation for fluctuations in illumination 80—73413
microphotometry of biological materials, digital picture analysis 80—17991
micropipettes of very low resistance for intracellular meas., production method 80—61738
microprocessor—based unit data acquisition and reducing system 80—21598
microprocessor based data acquisition and exptl. control system 78—36086
microprocessor based telemetry demodulation system 79—20738
microscope, laser-scanning, high resolution and depth of field 79—26118
microscope, phase-locked interf., design and construction 78—49894
microscope, phase-locked interferometric, design and construction 78—45687
microscope automatic image analyser, performance, appls. *(German)* 78—4691
microscope bidirectional illumination and viewing, living cells 80—51304
microscope photometer/semiautomatic image anal. instrument system for morphometric and photometric value meas. 80—82815
microscope-photometer for visible region absorpt. of single living cell *(German)* 79—66588
microscopic cell image scene segmentation technique 77—78073
microscopic cell images classification by feature extraction 79—88225
microscopic equipment, methods, appls. and related topics, bibliography 80—94941
microscopic equipment, methods, appls. and related topics, bibliography 80—105450
microscopic equipment, methods, appls. and related topics, publications 79—75566
microscopic image anal. system, cell cycle, cancerous blood and bone marrow cells appls. 79—88223
microscopic image processing *(Japanese)* 80—81784
microscopic image semi-automatic anal. device 79—79705
microscopic images of biological specimens, partially coherent illum. 77—610
microscopical image analysis, problems and approaches 79—80725
microscopy, argentaffin cells, correlative light microscopy, SEM and TEM 80—85557
microscopy, spatial freq. filtering appls. 77—79760
microscopy, system for automatically tracking white blood cells 77—78064
microscopy instruments and appl. techniques, Zeiss equipment 77—74497
microscopy of living single cells and other particles, circumfusion chamber *(German)* 77—44865
microscopy using ultrasoft X-rays, potential operating region for biological materials 77—90972
microspectrofluorometry of biogenic amines, automatic correction of excitation spectra, on-line system 77—9308
microspectrophotometer, rapid scanning, rhodopsin photoproduct kinetics in frog retinas 78—92763
microspectroscopy, using electrodynamic moving-condenser scanning unit 77—5903
microstrip microwave biological exposure system 80—89924
microstructure fabrication, using STEM and X-ray lithography and reactive ion etching, appl. 79—15844
microthin film chromatogram evaluation by scanning fluorimetry and digital image analysis *(German)* 79—5188
microwave, exposure system for marine animals, dosimetry and reflectometric obs. 80—56319
microwave appl., bio-clutter interference effects 79—11992
microwave backscattering for respiration meas. 77—5058
microwave compatible MIC temperature electrode for use in biological dielectrics 79—88216
microwave complex permittivity meas., noninvasive selective exposure 79—20729
microwave device, for murine brain rapid thermal fixation 78—92689
microwave enzyme inactivation system, electronic control to reduce dose variability 78—40285
microwave enzyme inactivation system with electronic dose control 77—81762
microwave exposure, densitometry and dosimetry techniques in bioeffects research 77—78072
microwave exposure array device for uniform irrad. of multiple animals 77—40941
microwave exposure of animals, perturbation by dielectric restraining materials 77—21665
microwave exposure source, compact light-weight Gaussian-beam launcher 78—96119
microwave exposure system for primates 78—40451

biological techniques and instruments continued
microwave exposure system for study of effects on isolated nerve and muscle preps. 78—53443
microwave Gaussian beam launcher, focal region field aberrations 78—44580
microwave Gaussian-beam launcher for producing focused exposure field 77—40728
microwave generator for induced hyperthermia in small animals 79—2118
microwave heating system for improving temperature uniformity in heated tissue 79—100795
microwave imagery of isolated canine kidney, use of orthogonal polarisations 80—81783
microwave imaging, scatt. parameters, homogeneous, heterogeneous dielectric targets 79—20608
microwave imaging, time delay spectroscopy 79—20609
microwave imaging using water immersed microwave antennas 79—34623
microwave irradiation, long-term, methodology and evaluation of ocular and physiologic effects, rabbits 80—101225
microwave permittivity measurement of thin samples and plant leaves, method 79—57825
microwave radiators for biological effects research, waveguide slot array with const. intensity 78—40450
microwave radiometry, natural emission detection, experimental results 77—32949
microwave radiometry applications 77—81770
microwave spot-size controlled Gaussian-beam launcher for microwave exposure studies 80—89920
microwave system for controlled production of local tumour hyperthermia in animals 79—34624
microwave temperature-jump apparatus, with spectrophotometric detection 79—20733
microwave time delay spectroscopic imagery of isolated canine kidney 80—46109
microwaves, direct-contact heating of dielec. encapsulated mouse tumour using dual-beam TEM applicator 78—40245
mineral fibre characterisation using energy dispersive X-ray spectrometry in TEM *(French)* 80—82857
miniature endplate potential amplitude online meas., programmable calculator conversion 79—84051
minicomputer-based scheme for turbulence measurements with pulsed Doppler ultrasound 80—26435
minimum depth electron probe X-ray microanalysis for determining S content of human hair surface 80—22500
mitochondria, giant, elec. props. study by double impalement technique 79—92446
model sampling/identification, input signal anal. 78—69267
moire contourography, computer-aided replication of human anatomy 80—67189
moire depth contouring of moving biological objects, snail propag. meas. *(German)* 79—74816
moire fringe biostereometry using parallel light beam 79—100701
molecular biology, use of MWPC 79—5433
molecular biophysics, protein crystallography, interdisciplinary course 77—33720
molecular microprobe, microscope system 78—45686
molecular modelling, design of computing systems 77—18814
molecular models, semiautomatic coordinate meas. device using laser beams 79—37573
molecular spectroscopy, conference, Wroclaw, Poland (Sept. 1977) 78—62951
molecular weight determ. by fluctuation spectroscopy 77—10800
molecular weight determination by STEM 79—92451
monoflipper, wave propellant for fast dolphin-like swimming *(Russian)* 80—46102
monopole immersed in lossy medium, elec. props. of in vivo tissues 80—12205
morphometric cytology pictorial pattern recognition 80—81796
morphometric cytology pictorial pattern recognition appl. 79—25179
MOSFET preamplifier bioelectric measurements including intracellular potentials 77—40855
Mossbauer measurements at very low temp. 78—24909
Mossbauer spectroscopy 77—13047
motion online detection in digital video images, mice identification in labyrinth expts. *(German)* 78—92754
motion transducer for use in intact in vitro human lumbar spine 78—57155
motor unit recruitment and firing freq. control in elec. stimulated muscles of cat 78—81092
motor unit sequential stimulation in cats through peripheral motor nerves 79—57635
mouse head immobilisation apparatus 80—41352
moving cell microelectrode puller 80—67309
moving-coil microelectrode puller 80—30964
multi-microelectrode system characts., neuron single-unit pots. recording appl. *(Japanese)* 80—21581
multi-microelectrode system for simultaneous recording of closely spaced neurons *(Japanese)* 78—61284
multi-microelectrode system with independent penetration and structural reinforcement by mag. coupling, characts. *(Japanese)* 79—66586
multichannel analyser spectroscopy using XRF, minicomputer appls. 78—20106
multidimensional space and time signal processing in biology and medicine 80—85493
multielectrode for intracortical recordings prod. by thin-film technology 77—48959
multilateral EM exposure, corner-reflector applicators for CW irrad. 80—36213
multimode time-varying enclosures for exposure and dosimetry in bioelectromagnetic experiments 80—85497
multiple incubators, temp. drift elimination, for biological expts. 78—3696
multiple internal reflectance-IR spectroscopy for quantitative study of leucocyte adhesion 77—56562
multiple internal reflection IR spectroscopy, for eye tissue examination 77—9304
multiplexing system for measuring physiological responses 80—56292
multispike signal detection and sorting hardware 79—79711
multispike train, anal. techniques 77—44868

biological techniques and instruments continued
muscle, mech. pulse propag. vel. meas. using piezoelectric crystals, elastic moduli 78—92668
muscle, skeletal, deriving viscoelastic modulus from transient pulse propag. 78—77077
muscle, smooth, intestinal cell, voltage clamp studies of hyperpolarising inactivation 78—80847
muscle, vertebrate striated, camera for low angle diffraction expts. with synchrotron radiation 77—87888
muscle cell force development meas., isometric contractile props. 77—29137
muscle contraction, single, high-time resolution X-ray investigation method 80—81777
muscle contraction, time resolved studies using small angle X-ray diffr., design of data collection system 79—12052
muscle contraction, time-resolved X-ray diffr., data-collection system *(Japanese)* 80—46108
muscle contraction kinetics obs., time-resolved X-ray diffr. appl., with aid of computer *(Japanese)* 80—56291
muscle contraction process, 10 ms time resolution X-ray diffr. 80—61741
muscle fibre tension fluctuation meas. during contraction 78—20153
muscle isometrical contraction maximum and standby tension, additional equipment *(Hungarian)* 80—41342
muscle single fibres, Rb$^+$, Cs$^+$ and Na$^+$ localisation, autoradiographic demonstration at 77K 79—96726
muscle viscoelasticity dynamic meas. 77—86667
mycoplasma contamination detect., SEM sensitivity 80—85568
myelinated axon identification, SEM technique 80—85570
myocardial excitability evaluation, strength-interval curves generation under computer control 80—41336
myocardial regional function and coronary blood flow study during ischaemia in baboons, telemetry system 78—44752
myocardial transmural heat gradient instantaneous meas. 78—44661
nanosecond flash photolysis, techniques and biological appls. 78—68905
negative staining of freeze-fractured envelopes of Escherichia coli K$_{12}$ 79—39622
nerve axon automatic counting 78—31994
nerve bundle conduction velocity distrib. meas. and transfer function anal. 77—44867
nerve fibre automatic counting using an array processor in a multi-mini computer system 79—79710
nerve signal optimal filtering 77—73616
nerve spike trains, interleaved, in a noisy channel, separation system 80—94424
nerve tissue magnetic stimulation, capacitive stimulatory effect 79—2116
nervous activity monitoring in Drosophila by [^{3}H]deoxyglucose 80—56024
neural excitation detection by real-time detect. of small birefringence change *(Japanese)* 78—15938
neural histological section, computer-assisted mapping with the light microscope 80—30963
neural multiunit signals, educable waveform recognition system for sorting unit discharges 80—51312
neural network observation methods, US and optical data processing 80—8234
neural signal recording using implantable electrode and telemetry system, awake animals *(Japanese)* 80—94427
neural signals, non-stationary, pattern trajectory anal. 78—36082
neural single unit activity from foetal pig brains, recording method 80—67315
neural single unit activity recording with photoetched Au multimicroelectrode surface 79—57824
neural spike window discriminator confirmation by analogue delay cct. 77—21664
neural stimulator, in vitro phrenic nerve diaphragm 79—25161
neural system sensitivity anal. by receiver operating characts. 77—44629
neurological coaxial depth electrode development 79—29687
neurological coaxial microelectrode, W-Re core, CVD coatings, elec. cond. and bending props. 78—11752
neurological multichannel depth probe fabricated using electron-beam lithography 79—57822
neuron firing rate meas. by freq.-to-voltage converter 79—70715
neuron soma model with high reliability and low power consumption 80—72392
neuronal average firing frequencies, digital display 77—5117
neuronal interconnection meas., semiautomatic system design 78—44742
neuronal membrane DC resting pot., automatic offset cct. 77—40940
neuronal population density estimation, robust distance method 79—70721
neuronal response analyser with microprocessor *(French)* 79—20730
neuronal spike activity discriminator 77—48966
neuronal spike train sampling, implementation of French-Holden algorithm 78—40440
neuronal spike train separation by improved time amplitude window discriminator 77—86726
neurone activity, simultaneous recording from several neurones in invertebrate central nervous system 77—66880
neurone potentials, 2 pulse series anal., histogram of recurrence time intervals 77—60196
neurons, single, rapid killing by irrad. of intracellularly injected dye 80—81795
neurophysiological data semiautomatic processing, computer program for data reduction 77—44861
neurophysiological experiments, fast data acquisition and processing system, minicomputer appl. *(Japanese)* 80—85536
neurophysiological spike unit data acquisition and reduction system 79—79713
neurophysiology, computer assisted unit data acquisition/reduction 78—61266
neurophysiology, real-time display techniques 77—2071
neurosecretory cell IR photomicrography 80—30959
neurostimulation automatic triggering as function of several EEG parameters, apparatus 80—98203
neutron activation anal., optimal conditions, blood appl. *(Bulgarian)* 78—85280
neutron activation anal., rapid method for milk minerals determ. 79—96717
neutron activation anal., using standard reference materials as multielement irrad. standards 78—80815
neutron activation anal. of biological samples, device for opening quartz ampoules 78—61121

biological techniques and instruments continued

- neutron activation analysis, appl. to microelement depend. of cotton plant wilt disease 77—64165
- neutron activation analysis, cyclic activation and short-lived isotopes meas. 79—88217
- neutron activation analysis, determ. of As and Hg in biological materials 80—36216
- neutron activation analysis, determ. of organically-bound chlorine and bromine in biological samples 80—21593
- neutron activation analysis, gamma-ray spectra prediction, detection limits, computational procedure 78—85242
- neutron activation analysis, sample contamination due to quartz container 77—48980
- neutron activation analysis, trace element determ. in human and animal muscle 78—27869
- neutron activation analysis, trace elements in biological samples 79—12058
- neutron activation analysis, transportable system for determ. of P in sheep bone 80—109066
- neutron activation analysis for trace elements 79—57827
- neutron activation analysis in vivo, rats 78—73115
- neutron activation analysis of biological materials by the monostandard method 80—72398
- neutron activation analysis of biosamples, ^{32}P radioactive interference 79—12059
- neutron activation analysis of Sn at nanogram level by ^{121}Sn liq. scintillation counting 78—3693
- neutron activation analysis using coincidence counting, biological and soot samples *(Japanese)* 80—97750
- neutron activation analysis using thermal neutrons, Br determ. in human tissue 79—88219
- neutron capture γ-ray analysis with prompt. neutrons, in vivo N meas., body H use as internal standard 79—92441
- neutron data acquisition system, low angle, for molecular biology 79—12053
- neutron diffraction, book, with emphasis on technical aspects 79—60225
- neutron diffraction appl. to biological problems, book contrib. 79—62417
- neutron diffractive study of bone 77—40952
- neutron radiography of extended objects *(German)* 78—15880
- neutron scatt. anal. of biological structs. 77—29238
- neutron scattering, meas. of protein locations and radii of gyration in E. coli ribosomes 79—11892
- neutron scattering, small-angle, using time of flight method, spectrometer, appl. 79—1371
- neutron scattering spectroscopy, recent advances, biology and chem. phys. appls. 77—35445
- neutron-induced autoradiography, visualisation of fissionable radionuclides in rat lung 78—28055
- NMR, ^{1}H and ^{13}C, appl. for lipid mobility and lipid metabolism studies 80—40965
- NMR, AsF$_6^-$ as probe for protein anion binding sites 78—48748
- NMR, high-resolution studies of double helical polynucleotides, review 77—86450
- NMR, human whole-body line-scan imaging 79—5334
- NMR, noninvasive meas. of biological information, magnetic focus generation *(Japanese)* 78—85355
- NMR, pulsed, agriculture appls. 80—56297
- NMR, simultaneous multinucl., by alternate scan recording of ^{31}P and ^{13}C spectra 80—26426
- NMR, two-dimens., state-of-the-art 78—74044
- NMR, zeugmatographic expt. sensitivity 80—21579
- NMR and molecular biology research *(Chinese)* 79—39459
- NMR applications to cells, ^{31}P and ^{13}C studies 80—46110
- NMR applications to phosphoryl transfer enzymes and metal nuclei of metalloproteins, review, book contrib. 80—109081
- NMR determination of phys. and biological struct. *(Rumanian)* 78—49874
- NMR flat crossed-coil detector for blood flow meas. 79—83880
- NMR for biological and medical imaging 78—69172
- NMR Fourier transform spectroscopy, high-field, of biological systems 79—39457
- NMR imaging, and biomedical appls. 80—46006
- NMR imaging, biological and medical appls. 80—26319
- NMR imaging, display of cross-sectional anatomy 78—44579
- NMR imaging, multiple sensitive point technique 79—11993
- NMR imaging by multisensitive point method, appl. to $\sim$10 cm biological systems 77—86581
- NMR imaging of biological objects, sensitivity, performance time 79—96718
- NMR imaging of living organisms *(Polish)* 78—77098
- NMR in biochemistry using supercond. magnets 79—74811
- NMR medical imaging, resolution and S/N ratios 80—26406
- NMR of ^{31}P for anal. of living tissue 77—37117
- NMR of living tissue, biological and medical appls. 77—77959
- NMR of perfused working rat hearts, using ^{31}P 77—29236
- NMR of proteins, ^{13}C, review 77—86449
- NMR spectroscopy, instruments and techniques 78—28148
- NMR spin echo image formation 77—22588
- NMR spin echo pulsed gradient, cell struct. size determ. from water diffusion 78—77159
- NMR studies of ion binding in biological and model systems, quadrupole effects 79—39357
- NMR studies of water in biological systems 80—3886
- NMR study of lipid organisation in Acholeplasma laidlawii membranes, using ^{2}H 77—86456
- NMR study of molecular conform. in soln., use of La ion probe 77—60324
- NMR zeugmatographic imaging 80—51203
- noise analysis for differentiation between equilib. and nonequilib. kinetic systems 78—44439
- noise generator for auditory neurophysiological and psychophysical experiments 79—29676
- non-invasive meas. survey *(Japanese)* 77—25567
- nondestructive proton and neutron activation analysis comparison 78—3691
- noninvasive beam-wave reflectometer for complex permittivity meas. at microwave freqs. 78—74030
- noninvasive beam-wave spectrometric instrumentation for measuring dielectric constant at microwave frequencies 79—70728
- nonlinear filtering technique for identification of biological signals 78—40438

biological techniques and instruments continued

- nuclear Overhauser effect, truncated driven, in presence of spin diffusion 80—1095
- nuclear Overhauser effect in ^{1}H spectra of proteins, appl. to lysozyme 79—43823
- nuclear physics appl. to life sciences 78—15882
- nucleic acid optical measurements in presence of phenol and protein impurities 77—56546
- ocean biological instrumentation requirements, review 79—12049
- ocean surface chlorophyll concentration obs. from high altitude 77—4976
- oculomotor control system, expt. set-up for clinical investigation, visual, acoustic, vestibular stimulations 78—80990
- oculomotor system parameter identification, strabismus appl. 78—3478
- oesophageal accelerometer evaluation for cardiac function noninvasive meas. 79—92458
- oesophageal geometry changes in swallowing, transduction, for animal grazing studies 80—76888
- online measurement of fluid reabsorption in renal tubules 79—92442
- oocytes, salamander, free and bound intracellular solutes, reference phase anal. 79—24966
- optical analysis system for agar-cultured micro-organism colonies, microcomputer-based 80—56304
- optical confocal scanning microscope, image form. 80—68249
- optical detection of cell-surface changes associated with malignant transformations 79—79703
- optical instruments for medicine and biology 80—21517
- optical irradiance modulation, for sound-radiating cuticular motion meas. in insects 79—84057
- optical large format display, generation of generalised psychophysical stimuli 79—44072
- optical microscope, focusing technique for digital image anal. system 80—68250
- optical microscope, scanning, resolution, contrast and depth of focus improvements 78—29155
- optical microscopes, scanning and reflection scanning 79—21809
- optical microscopy, online difference image method *(German)* 78—92688
- optical microscopy of single molecules, fluoresc. tagging, appl. to γ-globulin 77—21662
- optical mixing method, for periodic conversions obs. in biological system solns. 78—96029
- optical processor, real-time, for pattern recognition of biological specimens 78—40454
- optical radiation composition and effects and usage in plant experiments *(Hungarian)* 80—109076
- optical rotating spiral scanner for frog muscle contraction meas. 78—96120
- optical rotatory dispersion and circular dichroism of biopolymers, review 77—3497
- optical rotatory dispersion meas. method for macromol. conformation, press. effects 77—48984
- optical stimulator for vision expts., microcomputer-controlled 80—26423
- optical teaching microscope for investigation of transparent biological objects 80—82622
- optics in medicine and biology, conf., San Diego, California (1977) 77—44876
- optokinetic nystagmus, evaluation of a simple study device 80—56299
- oral force monitoring, piezoelectric transducer, with thin bite element 77—48888
- organ blood flow determ. using radioactive microsphere technique, PDP-11 interactive program 78—20247
- oscillation camera data, processing and post-refinement 80—24316
- osmotic pump for drug delivery, design and operating principles 77—56544
- ovum movement measurement in rabbit oviduct using radioactive surrogate and CdTe detector 78—36087
- oxidative phosphorylation mechanism, nature of residual current 78—20151
- oximeter, noninvasive tissue reflectance, development and evaluation 79—20703
- oxytocin radioimmunoassay, human plasma 79—5353
- pancreatic cell moving granules anal. by digital moving image processing 79—84063
- papillary muscle selection and testing, some mech. considerations 80—89919
- paramagnetic metal ions as structural probes for NMR investigation of inorganic and bioinorganic compounds 78—62828
- particle counting and vol. determ. in suspensions, optical-electronic device 78—57894
- particle dimension distributions calc., general analytic method using scattering data 79—10753
- particle etch track technique determ. of U trace content in normal human blood 80—89910
- passive dynamic characteristics of man in lying posture, testing apparatus 78—80893
- passive telemetry, by modulated backscattered incident CW RF carrier beam, cattle temp. meas. appl. 77—90968
- pattern recognition, rotational matched spatial filter 80—76866
- pattern recognition of biological specimens via matched spatial filtering 78—69261
- patterns, drifting contrast, electronic device for generation 80—26421
- PC implant, Ni-Fe microelectrode array probe for electrophysiology 79—84049
- pCM telemetry for physiological data 80—36059
- peak discriminator controlled sampling of multiunit spike trains 79—34717
- peak-detecting window discriminator for neuronal spikes 77—60323
- peptide analysis by field desorption mass spectrometry using pretreated Si emitter 80—55751
- peptide and glycopeptide research methods 80—51307
- peripheral nerve, generation of unidirectionally propagated action pots. by brief stimuli 80—85546
- peripheral nerve, single unit detection by real time correlation 79—12047
- peripheral nerve conduction velocities distribution estimation 77—90757
- permittivity meas. for lossy high dielec. constant materials, method 78—93732
- permittivity meas. using resonator terminated by infinite sample 79—21777
- permittivity measurement for human sera and erythrocytes at microwave freqs. 80—26424

biological techniques and instruments continued
  permittivity measurement method for RF and microwave freqs. 80—52275
  perturbed gamma-ray angular correlations 78—44739
  pesticide uptake into membranes meas. by fluoresc. quenching 78—7323
  Petri dish autoradiographed cell counter 79—70723
  phase contrast microscopic identification of cat neuron cytoplasmic laminar bodies 79—48385
  phase microscopy techniques 78—45684
  phase-lock interference microscopy, real-time, design, appls. 79—17480
  phase-shift fluorometer using laser and transverse electrooptic modulator for sub-nsec lifetime meas. 78—20319
  phospholipid bilayers, use of nitroxide free radical spin label EPR spectra, determ. of rot. correl. time and HFS coupling 80—74260
  phospholipid transmembrane asymm. studied by NMR spectroscopy with displacing reagents 78—31984
  phosphorescence microscopy of cells 78—3454
  photo-electron-microscope pictures of organic samples on metal supports 80—26431
  photoacoustic spectrometry of macroporous haemoglobin particles 80—85543
  photoacoustic spectroscopy, biological and medical appls., book contrib. 80—109078
  photoacoustic spectroscopy, blood and proflavine obs. *(French)* 80—101845
  photoacoustic spectroscopy, theory, techniques and appls., book contrib. 80—9050
  photoacoustic spectroscopy appls. to dermatology research 79—57823
  photoaffinity labelling of tetraethylammonium binding sites in crayfish axon membranes 77—64026
  photobiological process relative quantum yield determ. using light of different spectral composition 78—65154
  photocounting pulse fluorimetry, mol. rot. correl. times determ., statistical accuracy 77—61777
  photodiode camera improvement of shading correction 80—56325
  photoelastic substrate technique for dynamic measurements of forces exerted by moving organisms 79—39621
  photoelectric colorimeter reconditioning methods 79—39618
  photoelectric concentration meter, acceptable error determ. for automatic biochemical anal. 79—92435
  photoelectric haemoglobinometer type GF-3 79—92438
  photoelectrode for recording intracerebral Ca^{2+} transients 80—30961
  photoelectrode for recording intracerebral cellular Ca^{2+} transients 80—67307
  photoelectron microscopy, bacteriochlorophyll monolayer quantum yield and image contrast 78—44453
  photoelectron microscopy of surfaces power requirements for high magnification 77—40963
  photoelectron spectroscopy, impact on biology 78—65156
  photoelectron spectroscopy, review 77—56558
  photographic immunogram recording apparatus, self-contained, modified version using Polaroid film 80—17209
  photographic technique for anal. of neural unit activity rel. to movement 80—67310
  photography, future development 79—71551
  photography of fluorescent human chromosomes, improved method and system 77—60318
  photokinetic microassay of adenylate kinase using the firefly luciferase reaction 80—56306
  photometer, differential light scatt., for rapid analysis of particles in flow, appl. to biological cells 80—77834
  photometric device for arterial thrombosis investigations 78—85456
  photometric phase-contrast microscopy, lamellarity determ. of artificial phospholipid membranes 79—39368
  photomicrography, elimination of dust 77—70576
  photomicrography with colour films, colour reproduction *(German)* 78—20338
  photon correl. spectroscopy, macromolecular soln. dynamics, review 79—59603
  photon correlation, obs. of calf thymus DNA dynamics 77—40631
  photon correlation spectroscopy, automatic processing device, microprocessor, laboratory appl. *(German)* 77—40938
  photon correlation spectroscopy, biomedical appls. 78—3575
  photon correlation spectroscopy, determ. of particle size distribs. in lipid vesicle suspensions 77—86711
  photon correlation spectroscopy, motility evaluation of bull spermatozoa 77—48964
  photon correlation spectroscopy for spermatozoa motility eval. 79—92440
  photon correlation spectroscopy meas. of bacterial translation 78—44738
  photon correlation spectroscopy of light scattered from microscopic regions 79—44933
  photon counting and fluctuation of molecular movement 79—29686
  photon counting microspectrophotometer for study of single vertebrate photoreceptor cells 80—12323
  photon irradiance sensor for determ. of energy available for photosynthesis in sea 78—32843
  photon-correlation spectrsocopy in near UV, large flexible macromol. internal modes obs. 79—75621
  photoreceptor membranes, incorporation into a multilamellar film 80—89907
  photoreceptor spectral sensitivity on-line computation using programmable pocket calculator 78—69264
  photostimulator, LED fibre optic, for research on visual nervous integration 80—67302
  photostimulator for visual electrophysiology 78—35846
  photosynthesis, picosec. spectroscopic investig. 78—68964
  photosynthesis, picosecond spectroscopy appls. 78—53601
  photosynthesis, primary, selectively excited by tunable ps parametric oscillator 79—48163
  photosynthesis measurements in wheat using IR analyser and Geiger counter *(German)* 77—70436
  photosynthetic reaction centre functional reconstitution in planar lipid bilayers 80—97881
  photosynthetic systems, computer assisted scanning and kinetic spectrophotometry 78—68963
  photosynthetic systems, computer-assisted scanning and kinetic spectrophotometry 78—48950
  physiological data recorder, microprocessor-based hybrid system 77—44872
  physiological light-emitting diode photocell monitor 79—92444

biological techniques and instruments continued
  physiological signal pre-forming system for automatic freq. anal. 78—3621
  physiological stimulator, programmable, real-time numerical simulation appl. to laboratory instrumentation 77—44873
  physiological stimulator, rabbit heart stimulator, variable frequency/width and amplitude oscillator 78—31991
  physiological system anal. using swept sine wave 78—28133
  picosecond fluorescence spectroscopy, competing events 78—58051
  picosecond lasers, appl. to study of photosynthesis 77—81480
  picosecond phase shift measurements at 358 MHz using synchrotron radiation 79—44949
  picosecond phenomena in photolabile species, appl. to emission lifetime of bacteriorhodopsin 77—17009
  picosecond relaxation measurements book contrib. 77—64166
  picosecond spectroscopy, appl. to chem. and biological reactions 79—80697
  picosecond spectroscopy, probe for ultrafast biological process inc. vision 79—8507
  picosecond spectroscopy of biological systems, exptl. system and rhodopsin example 80—56312
  picosecond spectroscopy using ultrashort laser pulses, appls. 79—54195
  piezoelectric measurement transducers 80—19205
  PIXE, analytical applications 79—48008
  PIXE, appl. to bioenvironmental anal. 77—48976
  PIXE, appl. to primate trace element retention 80—81792
  PIXE, biological material anal. precision, accuracy and appl. to cancer tissues 80—56199
  PIXE, biomedical and biophysical appls. 80—61691
  PIXE, external beam elemental anal. method, sensitivity obs. for biological samples 79—5227
  PIXE, synaptic vesicle ion content determ. 78—61166
  PIXE, trace element determ. in bovine retina rod outer segments and disc membranes 79—48012
  PIXE anal. of elemental variations in mouse blood following gamma-ray injury 77—48973
  PIXE anal. of protein quality of leguminous plants 77—48978
  PIXE anal. of S content of plant materials 77—48977
  PIXE anal. of trace elements in ashed human tissues, correl. with diseases 77—48866
  PIXE anal. of trace elements in rat liver 77—48975
  PIXE anal. of trace elements on liquids 77—48732
  PIXE applications, conf. 77—48715
  placental villi, human, average diameter estimation by stereologic method 80—67318
  planimeter for use with mechanical digital counters 78—40448
  plankton animal groupings pattern recognition, average similarities of Fourier spectra 80—104818
  plant photosynthesis, signal II, electron spin-echo method 78—96118
  plant trace element anal. by X-ray fluoresc. for environmental pollution study 78—3690
  plant uptake of transuranics, techniques for long term field studies 79—57821
  plant water content meas. using high-sensitive impedance meter *(Japanese)* 77—5125
  plasma fractionation, development of automatic continuous process 77—52955
  plasma protein interaction with polyion complex studied by circular dichroism and UV spectroscopy *(Japanese)* 80—12316
  plethysmograph and pneumatic differentiator, static and dynamic testing 78—28150
  plethysmograph for long-term ventilation meas. in unrestrained animals 79—62413
  plethysmograph with servo-control of hydrostatic press. 77—5118
  Plexiglas animal holders, effect on microwave energy absorpt. 78—92674
  PMR, Fourier transform, in aq. soln., exchange and relax. rate meas. 78—15049
  PMR, nuclear Overhauser enhancement difference spectroscopy, for macromolecules 78—81091
  pneumotachograph, for flow and vol. meas. in normal and dense atm. 77—5120
  point processes in biological signals, detect. and anal. 77—44770
  polyacrylamide gel, automated scanning of ^{14}C 80—17221
  polymer, bioabsorbable, standards for in vitro and in vivo comparison and qualification 78—3677
  polymer biocompatibility evaluation by cell culture method *(Japanese)* 80—12301
  polypeptide hormones fragmentation anal. by chromatography 79—92448
  polyphase envelope detection for physiological signals *(Korean)* 79—66565
  porphyrins, determ. in blood by phosphoresc. of porphinatocopper(II) 78—11574
  portable microcomputer system, associated movement study 80—51299
  position sensitive, X-ray detectors, linear, circular, two-dimens. 78—62281
  positron annihilation lifetime technique, appl. to phospholipid vesicle phase transition 79—88061
  positron camera system, ring detector, brain research, computed transaxial tomography 80—61739
  positron imaging instrumentation for physiological functions 78—24196
  preamplifier, non-blocking AC type, for tip recording from insect taste hairs 77—90971
  precision rate calibrator 79—20731
  preparative scale thin-film dialysis apparatus 80—101296
  pressure jump method for fast kinetics using optical rotation and circular dichroism 78—77175
  pressure meter, up to 40 kPa and 4 kPa, temperature and time stability 79—84059
  pressure sensing SAW resonator 77—23850
  pressure transducer, local press. meas. in cadaveric human hip joint 78—40445
  pressure transducers, differential, air-filled, dynamic characts. 80—3879
  pressure-diameter characteristics of tubular organs, in vivo vs. in vitro characts. 77—36982
  primate restraint device, for microwave biological research 77—40945
  programmable PRP 8 computer photometer, design, uses 77—74483
  projection system with brightness amplifier, laser appl., for medicine and biology 80—36060
  prosthetics, in vivo method for evaluation of effects of materials on arterial thrombosis 78—81071

biological techniques and instruments continued
  protein adsorbed layers on field-emitter tips, removal by UV radiation 80−104836
  protein analysis using $^{14}N(p,n)^{14}O$ reaction 77−81769
  protein crystallography, min.-variance Fourier coeffs. from isomorphous replacement method by least squares anal. 77−52938
  protein crystallography, MWPC as area detector 78−65166
  protein crystallography, synchrotron radiation appl. 77−52936
  protein data measured on oscillation camera, collection and reduction method 79−29672
  protein iodination, protection from volatilisation using plexiglas iodination box 77−56484
  protein molecular weight and ultrastruct. determ. in STEM 80−85562
  protein molecule, simulation of single mol. images combining computer and electron micrograph analysis 78−37781
  protein molecules, new representation for mapping chain-folding 77−44588
  protein NMR spectra, comparison of convolution and pulse methods for line narrowing 78−78729
  protein sequencing, solid-phase techniques 77−56557
  protein structure, mol. replacement method for rennin and pepsin rel. mol. orient. 77−36866
  protein structure factors from electron density, test on model crystal 78−47204
  protein structure factors from electron density distrib., theoretical foundations 78−47203
  protein structure least squares refinement technique based on fast Fourier transform algorithm 78−91197
  protein supramolecular structure, ordered, electron micrographs, image processing 80−89923
  protein synthesis 77−32965
  protein synthesis control studies, exptl. probe using psoralen and near UV light 77−66881
  protein titrations by NMR, pH depend. of internal reference 77−86727
  protein X-ray crystallography, book contrib., review 77−40958
  protein-ligand binding parameters estimation from continuous ultrafiltration results 77−12878
  proteins, mol. wt. determ. by monolayer surface press. meas. technique 80−89526
  proteins, X-ray scattering data, Soule-Porod plots 77−51273
  proton beam trace element anal. at atmospheric press. 77−81454
  proton correlation NMR spectroscopy of living cells, appl. to E. coli anaerobic metabolism 79−43978
  proton induced X-ray chem. anal., Fe and minor elements concs. in biological material 78−23989
  proton induced X-ray emission anal., trace element levels rel. to human disease 77−56467
  proton induced X-ray fluoresc., anal. of lateral distrib. of trace elements in biological samples using microbeam scanner 79−5431
  proton induced X-ray spectroscopy, for tracer anal. of tumour 77−5122
  proton microbeam analysis in air 77−9311
  proton microprobe elemental anal. in air 77−37116
  proton microprobe for nondestructive trace element analysis 78−64911
  proton scattering, appl. to ^{15}N anal. 79−61926
  proton-induced X-ray emission anal. of single human hair roots 77−90973
  proton-induced X-ray emission and nuclear reactions for determ. of protein quality in cereal and grain legumes 78−20321
  Pseudemys scripta hemibladder $^{36}Cl^-$ transport meas. system 79−96529
  pseudo-cyclic instrumental neutron activation anal. of trace multielement conc. 80−17214
  psychophysics as method of meas. of biosystems *(Japanese)* 78−53591
  Pulfrich effect study device, versatile, multi-input 80−8221
  pulmonary capillary blood flow atraumatic meas. in dogs 78−7552
  pulmonary function, plethysmographic meas. method to assess X-irradiation damage in mouse 79−20721
  pulmonary function parameter meas. system for small animals 80−8227
  pulmonary oedema of intact dogs, meas. by transthoracic γ-ray attenuation 80−81787
  pulmonary vascular response to hypoxia, online impedance analysis system 77−52943
  pulse height analyser for Coulter counter particle size distribs. display 79−70716
  pulse radiolysis appl. to biomolecule reactions and struct., review 78−61145
  pulsed magnetic field gradient programme, meas. of water diffusion adsorbed on protein mols. 79−21794
  pyronin dye, use as fluorescent indicator of energetic state of mitochondria 77−66790
  quadrupole mass spectrometry applics., book contrib. 77−25622
  quantitative microscopy, object delineation program 80−41338
  quartz resonator determ. of water content of nucleic acid nitrogenous bases 79−92439
  quasi-white random signals optimal use in biological system identification 77−73502
  quasi-white random signals optimal use in biological system identification 77−73528
  rabbit ear chamber for continuous microscopy of implanted biomaterials 77−81755
  radial nerve potential recording at wrist in man *(French)* 77−81756
  radiation biology conf., Sapporo, Japan (Sept. 1978) 80−8105
  radiation induced free radicals in amino acids, lyoluminesc. techniques 77−29230
  radiation response assay systems, for cells of artificial pulmonary metastases 77−12977
  radiation-damage artefacts in biological electron microscopy, technique for visualisation 79−20726
  radio-liquid chromatograph system, determ. of ^{14}C-labelled amino acids *(Japanese)* 80−104834
  radioacetylation of whole cells in culture 80−26348
  radioactive aerosol, human inhalation administration technique, deposition/clearance expts. 77−60312
  radioactive material location technique, rat small intestine 80−8226
  radioactive microsphere prep. and props. for localised irrad. of lung tissue 78−53445
  radioactivity, absolute measurement technique using a gamma camera and a computer 79−25087
  radioactivity of bone and muscle, separation by dermestid ingestion 80−30949
  radiochemical determination of short-lived radionuclides in neutron-activated biological samples 80−109067

biological techniques and instruments continued
  radiochromatographic scanning procedure for ^{32}P-labelled compounds 77−9151
  radioimmunoassay, automated on-line system, Gammaflow 77−9247
  radioimmunoassay, fitting of general form of fundamental physical model 80−94150
  radioimmunoassay, probe for fine struct. of biological systems, review 78−73217
  radioimmunoassay 79−43982
  radioimmunoassay and competitive protein binding, automatic treatment of assay data 77−13037
  radioimmunoassay detection limit 79−79318
  radioimmunoassay for anti-HBs by AUSAB procedure, computer anal. 77−13036
  radioimmunoassay for thromboxane B_2 with thromboxane B_2-^{125}I-tyramide 79−88222
  radioimmunoassay of insulin receptor, receptor structure and function 79−88164
  radioimmunoassay techniques development 78−88743
  radioisotope counting techniques for analytical appls. in biology and medicine, review 80−81794
  radioisotope X-ray fluoresc. analysis of trace elements in biological specimens 80−12240
  radiolabelled microspheres, use in meas. of regional blood flows during $+G_z$ stress 80−81786
  radiolabelling of T gas, by microwave discharge, for amino acid sequence determ. of proteins 79−12057
  radiometric estimation of bacteria replication time in culture using $^{14}CO_2$ 79−16170
  radiometric microbiologic assay for biologically active forms of niacin 80−17208
  radiotelemetry system for avian ECG meas. 80−98202
  radiotelemetry transmitter, for temp. meas. from unrestrained subjects 79−16356
  Raman difference spectroscopy in study of reactions of biological mols. 78−44368
  Raman spectroscopy, recent advances, reivew 78−41359
  Raman spectroscopy of biomolecules 77−52939
  Raman studies of biomembranes, phospholipid-d, as nonperturbing components 78−53330
  random pulse generators 78−24189
  random pulse train inputs, use of digital filters *(Japanese)* 78−53547
  Random-Access Memory-Interval Timer and buffered storage system 79−84066
  ratio analogue pulse height module for fluorescence activated cell sorter 79−20734
  reading addition determination, comparison of 3 methods 80−36198
  real time online data processing system for EEG and body movement, mouse 79−92443
  red blood cell aggregation detect. during blood flow by US 79−84068
  red blood cell sizing, evaluation of automated Electrozone Celloscope in haemolysis study 78−40455
  reference electrode, internally charged PdH_2, stability rel. to charging current density 79−57251
  reference electrode liquid junction, press.- and flow-insensitive 77−4906
  reference electrodes for in vivo meas. 79−52687
  reference ion sensitive FET for compensation, biomedical appl. 78−44642
  reflectance spectrophotometer, non-contact for biometric meas. *(German)* 79−12865
  reflected-light fluorescence microscope, LABOVAL 2a.fl, for routine and research 80−56300
  refractometer laser detector for anal. of liquids 80−101830
  refrigerated moving-object technique and accessories *(French)* 77−29235
  regional myocardial perfusion determ. from H_2 washout curve 79−92459
  relative humidity indirect meas. in electron microscope side entry environmental stage 78−8480
  relaxation spectrometry, injected white noise as soln. of phase problem 78−76830
  remote sensing applications in agriculture 80−56329
  renal tubulus, digital picture anal. 79−70712
  repeated random sequence generator for white noise anal., coherence improvement 80−36203
  replicon autoradiograms, computer-assisted measurement 78−92692
  resistance strain gauge-meas. techniques in biomech. expts. *(German)* 80−104819
  resistance strain gauges bonded to bone surface in vivo, post-mortem calibration 78−28135
  resonance neutron activation analysis technique 78−3692
  resonance Raman effect, appl to β-carotin, haeme proteins and rhodopsin *(Hungarian)* 78−74666
  resonance Raman kinetic spectroscopy of bacteriorhodopsin on μsec time scale 78−20320
  resonance Raman spectra of biomols., review 77−90976
  resonance Raman spectroscopy appl. to visual excitation study 77−56378
  resonance Raman studies of visual pigments 77−90729
  respirator, servo-controlled, constructed from positive-press. ventilator 77−13041
  respiratory monitor and histogram computer for rodent studies 77−52944
  respiratory muscle EMG anal. by digital computer technique 78−28102
  respiratory process parameters determ., air flow consumption meas., using electric model *(Bulgarian)* 80−76867
  respiratory system, freq. characts. determ. 77−5093
  respirometer process appl. of Kalman filter *(French)* 79−5408
  respirometry with flow-through mask, meas. of VO_2, VCO_2 and evaporative water loss 77−48961
  retinal feature mapping in freely moving eye with precise control of retinal stimulus position 80−12097
  retinal ganglion cell activity induced by ELF mag. fields, method for study 80−56321
  retinal light responses, simultaneous recording by extra- and intracellular electrodes in crayfish 78−69055
  retinal neurones, differential labelling by ^{3}H-2-deoxyglucose 79−92447
  retinal neurons studies, appl. of white noise anal. *(Japanese)* 79−66471
  retino-tectal mapping using microprocessor controller 78−31995
  reversing rectangular pulse generator for transient electric birefringence 78−45657
  review of biophysics and bioengineering, book 80−105437
  RF powered cage system for implant telemetry 78−44745

biological techniques and instruments continued
  RF powered cage system for implanted biotelemetry 79—20737
  RF telemetry for pressure/temp. monitoring of free swimming freshwater fish 77—90965
  RF wave applicator for investigating effects on mammalian cells 79—100802
  RF-powered cage system for implant biotelemetry 80—94422
  rheometer, analytical, optical sliding contact, for flow visualisation at articular surface 80—104847
  ribosome subparticle fine struct. investigation by optical filtration of electron microscope images 80—81779
  RNA nucleotide sequence, determ using computer 79—29500
  rod outer segment membrane current, light-induced fluctuations recorded in single toad rod 77—86493
  roentgen stereophotogrammetric methods for human knee joint evaluation 80—30952
  room temperature phosphorimetry, anal. technique, review, methodology, instrumentation, appls. 78—95972
  rotating wedge spatial filter, pattern recognition of biological speciemens (algae) 78—33837
  sampling of aerosol inhaled, exhaled, for dust deposition investigs. 79—96719
  saturation transfer EPR, appl. to mol. rot. diffusion obs. 77—8387
  scalp hair as monitor of population exposure to environmental pollutants, nucl. activation analysis 78—3940
  scanning Auger microscopy for analysis of biological material 80—73535
  scanning electron microscopy at macromolecular resolution in low energy mode on biological specimens coated with ultra thin metal films 80—72401
  scanning laser acoustic microscope, principles and analytical capabilities 79—18655
  scanning laser acoustic microscope for US vel. meas. of mammalian collagen threads 79—43972
  scanning microcalorimeters for studying macromolecules 80—61747
  scanning microscope, depth of field rel. to thick biological slice obs. 78—86328
  scanning microscope photometric image analysis, appl. to chromatin packings *(German)* 79—5409
  scanning proton elemental microanal., biological and medical specimens 80—56311
  scanning transmission microscopy, proton vs. electron, ratio of elastic to inelastic cross-sections 77—22625
  Schottky barrier chemical sensor, for H_2 detect. 78—44646
  scintigram improvement by computer processing 79—16296
  scintillation counting method for $^{14}CO_2$ in carbohydrate metabolism studies 79—62410
  scintillation counting using polyethylene mini-vials, construction of permanent standards 77—38550
  seawater transparency meter, for biological activity, photocell device 80—8442
  secondary ion microanalysis, of Co ions, epilepsy study *(French)* 79—62414
  sector scanning sonar, use in fish heart rate telemetry 80—8225
  sedimentation process for biological isotope separation 79—44066
  seed germination enhancement, effects of microwave energy on Acacia longifolia 79—53190
  selective laser excitation of atoms and mols., photophys., photochem. processes, appls. 77—54630
  SEM, human erythrocyte surface area and vol. calcs. from micrographs 79—5259
  SEM, image interpretation 78—53597
  SEM, in situ ion etching facility, description and appl. 77—54020
  SEM, mitochondria in rat liver and monkey cardiac muscle 79—34516
  SEM, moist environment ambient temp. scanning, for untreated fresh biological specimens 79—100797
  SEM, photographic densitometry, appl. to chromosomes 78—77168
  SEM, real-time stereo, techniques used in microdissection of biological tissues 79—80724
  SEM, reflected, viewing specimens in air 80—82853
  SEM, shielded specimen holder for X-ray microanalysis 77—49816
  SEM, surface struct. of leukocytes in motion 77—29116
  SEM, wet, live and frozen objects, review 79—26183
  SEM and human lymphocyte surface morphology, review 78—53599
  SEM and X-ray microanalysis of biological material 79—39627
  SEM cathodoluminescence appls. 80—72400
  SEM cathodoluminescence detection system for transmission optical fluorescence analysis 78—23999
  SEM cathodoluminescence microscopy, mirror detector system 78—24000
  SEM cathodoluminescence probing of biomol. species at 100 Å resolution or below 78—24197
  SEM cold stage microscopy, thin frozen hydrated specimens, temp. rise and sublimation of water 78—24198
  SEM energy dispersive X-ray imaging techniques and appls. 78—48740
  SEM examination of myoepithelial cells 79—34713
  SEM fundamentals for biologists, bibliography 78—24213
  SEM laboratory, health and safety hazards 78—21295
  SEM of cell organelles, thick sections etched by O plasma 80—21584
  SEM visualization method for concanavalin A receptors on lymphoid cells 79—74800
  SEM/STEM cold stage thick specimen heating model 78—61289
  semiconductor force transducer suitable for use with small muscles 80—72395
  separation method, flow field-flow fractionation 77—960
  serial section models of human lung endothelial cell nuclei, estimation of mean caliper diameter 79—29679
  serial section models of rat lung cell nuclei, estimation of mean caliper diameter 79—25165
  serum, trace element anal. by PIXE 79—48008
  serum analysis using high performance liquid chromatography 79—79334
  shock scrambler, IC 78—48898
  shoulder contact areas, canine, in vivo determ. method and obs. 80—56324
  sickle cell anaemia sickling kinetics, multiangle laser scatt. spectrophotometer 79—79494
  signal detection, including speech and α-activity *(Czech)* 77—5124
  silastic strain gauge as in vivo muscle force transducer 79—29680
  silhouette photography, high-speed, of small biological subjects 78—44743
  silicone rubber substrata, appl. to study of cell locomotion 80—104835

biological techniques and instruments continued
  SIMS, histological section, high mass resolution by ionic analyser *(French)* 80—109069
  SIMS anal. appl. to biological specimens 79—44074
  SIMS apparatus for investigation of monolayers 79—89038
  simulated microbes, suspension, size determ., teaching expts. 79—71178
  sinew dynamic elasticity modulus meas. apparatus *(German)* 79—2167
  single cell quantitative anal. and sorting 78—28147
  single unit activity, computer program for generating on-line raster dot displays 78—57087
  sinoatrial node activity, intracardiac recording by prememorised averaging 77—81621
  skeletal Ca, facility for regional in vivo neutron activation anal. 79—25088
  skeletal muscle bulk specimen, quantitative X-ray microanal. of diffusible ions 78—57143
  skin electrical quantities, frog, method for in situ meas. 80—36208
  skin humidity meas. using bridge cct. and digitally steered logic cct. 77—13018
  skin water exchange measurement 77—81763
  sleep automated analysis, rat appl. 77—90969
  sleep telemetry in rat, automatic identification and recording of vigilance states 78—48948
  sleep telemetry in rat, miniaturised FM-AM transmitter for EEG and EMG 78—48947
  slide sync tape recorder, sensory modality matching tests 80—41334
  slow flash photolysis using conventional spectrophotometer, visual pigment appl. 78—68904
  small liquid biological sample microwave complex permittivity meas. 80—17222
  small-animal microwave induced hyperthermia development system 78—11715
  soft tissue covering bony prominences, techniques for derm. mech. props. 79—62415
  soft X-ray microscopy, high resolution 77—87889
  solar radiation monitoring system 77—52839
  solution X-ray scattering, review of recent developments, book contrib. 80—109077
  space research, biology and medicine 80—41265
  spacelab instruments, costs, safety 80—41267
  spatially constricted flow meas. using laser Doppler velocimeter 78—71409
  specimen carrier for freeze fracturing 79—74810
  specimen recognition with partially matched spatial filter 80—46113
  specimens, quantitative electron probe microanal., analysed spot ρX value 79—25169
  spectral analysis method in photon correl. study of spermatozoa motility 80—12063
  spectrochemical analysis of biological solns. using wall stabilised arc source 80—41343
  spectrophotometer method for rat molar surface enamel Ca content determ. 80—56303
  spectrophotometer/fluorimeter for university biochem. courses 77—33807
  spectrophotometer/fluorometer, dual-wavelength, high-performance 80—98198
  spectrophotometers used in analysis of structural colours of beetles, reflectance measurements 80—18023
  spectropolarimeter for analysis of scattering objects *(Russian)* 79—26110
  spectroscopic measurement of energy electron transfer through macromol. in soln. 77—38766
  spectroscopic/electrochemical cell for protein studies 78—76832
  spectroscopy, wide-band multichannel picosecond absorpt., bacterial photosynthesis obs. 79—66462
  spectroscopy of biomolecules, DNA-dye complex fluoresc. 77—86444
  speech, fast continuous meas. of lip-opening area 78—3520
  spermatozoa, bull, swimming speed distribs. determined by quasi-elastic light scatt. 78—44478
  spermatozoa, human, motility evaluation, photon correlation meas. 80—61745
  spermatozoa mobility meas. by laser light scatt. *(French)* 78—36083
  spermatozoa motility meas. by laser light scatt. *(German)* 79—12056
  sphere population overall mean caliper diameter estimation 79—70719
  spin labelling in biophysics, NO radicals 77—44860
  spin labels, appl. to study of assoc. of adenosine, AMP, ADP and ATP 78—81086
  spin labels, water soluble, factors restricting diffusion, rel. to biological use 77—86436
  spin labels and biomembranes, review 78—69265
  spin probe investigation of adsorpt. of non-paramag. compounds on proteins 78—65153
  spinal cord conduction velocity, indirect estimation in intact man 77—25616
  spiral biological object indexing, use of optical diffractometer 78—96121
  spongy bone, dynamic elastic props., determ. techniques 80—56326
  spot scan TEM technique 80—82846
  SQUID, appl. to monitoring visually evoked magnetic response of human brain 77—29231
  SQUID instrumentation for biomagnetic meas. in unshielded and noisy environments 80—104710
  SQUID magnetometer with selective pickup loop to biomagnetic meas. 79—63286
  STEM, computer driven, image registration 80—104838
  STEM, contrast and radiation damage 79—66592
  STEM, low-dose, using digital data processing system 78—24203
  STEM, obs. of single heavy atoms, in frozen biological specimens 80—89921
  STEM , on-line data processing system 78—24202
  STEM and CTEM comparison, image contrast, radiation damage 77—49811
  STEM and FE-TEM obs. of human low density lipoproteins 79—100566
  STEM coupling to small computer 79—54235
  STEM dark-field mode capabilities 79—74821
  STEM examination of Bacillus subtilis cell wall struct., S/N enhancement by interactive computation 79—5427
  STEM methods for mass measurement 80—73537
  STEM of thick objects, influence of detector geometry on image props. 77—56554
  STEM of unstained biological sections 78—31990
  STEM use for two-dimensional molecular assemblies construction 78—24201

biological techniques and instruments continued

- STEM/SEM cold storage specimens, electron beam heating temp. profiles 79—5422
- stepping motor presettable digital control for neurophysiological microelectrode drive 78—36079
- stereo electron micrographs restitution, approximate soln. 79—26189
- stereo-fibrescope with magnetic interlens bridge for laryngeal observation 79—44068
- stereological method for estimating relative membrane surface area 77—64158
- stereological method for rapid volume ratio estimation 79—80571
- stereological methods in neurobiology, recognition and classification of struct. 77—64159
- stereology, determ. of preferred orientations of cancellous bone 77—36987
- stereology conference, Salzburg, Austria (Sep. 1979) 80—22134
- stereology of parallel straight circular cylinders, for appl. to intestinal crypts 77—13044
- stereophonic equalisation of artificial heads without exact replication of eardrum impedance 80—81614
- stereoscopic instrumentation, kinematic and kinetic analysis of human wrist 80—16999
- stereoscopic method of viewing internal structures in resin-embedded biological specimens 80—21586
- stereotaxic electrode placement in the neonatal rat 80—30962
- sterotaxic method for recording from single neurons in the cat eye 80—89913
- stimulating electrodes of different materials implanted in cat skeletal muscles, threshold meas. 80—101297
- stimulator, programming unit for prolonged cyclic stimulation 78—3685
- stimulator for electrophysiological expts., constant-current device 77—21663
- stimulus artifact suppression, sample and hold amplifier system 78—77163
- stimulus generator for evoked response studies 78—57011
- stopped flow kinetic studies, problems concerning mixers and detectors 79—8585
- strain gauge application on compact bone 80—3883
- strain gauge transduction of lip and jaw motion in midsagittal plane 79—44069
- streaming potential measurements of biosurfaces 77—2074
- Streptococcus mutans 10449, size determ. by laser light scatt. 80—109062
- stress analysis of aortic valve leaflets, using smoothed geometrical data 77—52815
- stress-strain behaviour of living human skin, in plane method of 2-dimens. meas. 77—37120
- structural determinations using synchrotron X-rays 80—46112
- subcellular motions in Nitella flexilis, photon correl. spectroscopy 79—66465
- subcellular particle membrane pot. difference, compensation meas. method 77—56547
- subnanosecond single photon counting fluorescence spectroscopy using tunable dye laser excitation 78—86355
- substrate core sampler, lightweight low-friction, ecological survey appls. 80—95090
- suction capillary for holding moving cells during intracellular elec. recording 79—100793
- superconducting susceptometer, automatic, sensitivity calibration, biological appl. 78—57154
- supralinear photographic emulsions, radiobiological aspects 80—26290
- surface dynamic representation by TV moire topography *(German)* 78—89430
- surface labelling techniques for eukaryotic cells 77—56560
- swept-freq. magnitude method for dielectric characterisation of chemical and biological systems 80—104824
- swimming parameters of aqueous organisms, determination by cine recording and computer processing *(Russian)* 77—32921
- synchrotron radiation low angular scatter in biopolymer solns., use of proportional chambers 78—65155
- tail structure of temperate phage no.1 of Bacillus megaterium, electron micrograph 3-D reconstruction 80—35831
- tape recorder ZK-246 appl. to 4 channel recording of physiological phenomena 78—24154
- tape recording, low freq. FM, of nerve action potentials 79—57832
- technobiology, advanced, conf., Paris, France (June to July 1978) 80—41945
- telemetered cardiovascular changes with free-ranging and treadmill exercise in dogs 77—90821
- telemetered neurophysiological activity in olfactory system of rabbits, and pheromones 77—90816
- telemetric complex implantation into dolphin skin *(Russian)* 77—64155
- telemetry, embedded bare and insulated receiving antennas, for animal identification 77—40947
- telemetry, implantable transmitter, for monitoring diving duck heart rate and respiratory freq. 77—44858
- telemetry, implantable transmitter for 6 differential signals 77—48968
- telemetry, low power PAM/FM system for ventricular press. and cardiac dimension meas. 78—44747
- telemetry, micropowered multichannel PAM/FM system for brain research 77—25618
- telemetry, multichannel, quality criteria and meas. methods 77—48887
- telemetry, system for continuous meas. of metabolism and energy balance in unrestrained rats 77—86712
- telemetry, totally implantable, integrated power controllers and RF data transmitters 80—67295
- telemetry, unrestrained dogs, renal haemodynamics appl. of implanted system 77—32927
- telemetry for ureteral elec. activity in unrestrained dogs study 77—86664
- telemetry of body temp./heat rate of hibernating/normothermic ground squirrels 78—3688
- telemetry radio receiver 77—48892
- telemetry system, implantable, multichannel, for physiological research 80—67292
- telemetry system, implantable, multichannel, IC, for animal physiological data recording 77—86661
- telemetry system, implantable, multichannel, inductively powered, for animal cardiovascular data recording 77—86662
- telemetry system, inductively powered, for animal monitoring 79—74796
- telemetry system, totally implantable, for dimensions meas., animal physiological research 80—67294

biological techniques and instruments continued

- telemetry system for wild animal heart rate activity monitoring 77—86713
- telemetry systems, totally implantable, appls. to chronic medical research 80—67296
- telemetry techniques for studies of brain elec. activity 77—60310
- telestimulation and telemetry, use in study of cardiac freq. regulation in animals 77—44859
- TEM, digital image enhancement 80—82852
- TEM, electronic prod. of hollow cone illum. 77—54026
- TEM, high resolution, low-noise B supports 80—8236
- TEM, high resolution obs. by incoherent illum. method 77—70571
- TEM, instrumentation for direct obs. of frozen hydrated specimens 79—92454
- TEM, low-temp., radiation damage, review 78—57147
- TEM, low-temp., struct. determ. of frozen, hydrated, cryst. biological specimens 78—57146
- TEM, thin section uniform region quantitative meas. 78—58097
- temperature and humidity monitor for biological exposure chambers, microprocessor-controlled 79—49239
- temperature biotelemetry system for free-swimming fish 77—25624
- temperature control system for small biological preparations, fast heating and cooling capability 77—40948
- temperature regulation cct. for laboratory use 77—45836
- temperature stabilisation of biological media, electronic device 80—85539
- temperature telemetry system for small animals, miniature CMOS 4-channel PWM design 78—44751
- temperature telemetry system with interference suppression, implantable, long-life, animal expts. appl. 80—101302
- temperature telemetry transmitter, crystal-controlled, surgically implantable, for animal expts. 80—72393
- tensile testing of small animal ligaments, gripping device 80—81791
- test serums quality determ. by microscopic-fluorometric method 79—53290
- thawing of cryogenically preserved canine kidneys using microwaves and HF EM waves 77—5059
- thermal blooming spectroscopy for enzymatic anal. 80—86441
- thermal imaging, fast response system with 50 element detector 78—18064
- thermal properties of tissue, thermistor meas., influence of blood vessels using simulation model 77—40962
- thermistor probe, implantable, for continuous core temp. in rats 78—3686
- thermistor probe use to meas. energy distrib. in US fields 80—109075
- thermocouple, nonmetallic, differential-temp. probe for use in microwave fields 80—56320
- thermocouple probe, heated, for perfusion meas., two-regime model 77—5110
- thermocouple probe, spherical heated, for perfusion meas. 79—92456
- thermoelectric needle probe for medical and biological temp. meas. 80—101299
- thermographic system model parameter calc. 79—79477
- thick-section parallel membrane separation estimation 79—70718
- thin section quantitative analysis and mapping by EELS 79—74820
- three dimensional optical microscope, tracking of bacterial dispersal 80—30965
- thyroid cells in culture as radiobiological model, sheep, culturing method 80—41327
- thyroid epithelial cell, methodology of thickness determ. 78—20330
- tibosomal RNA interacting sequences, expt. determ., method and results 80—3586
- time resolved EPR spectroscopy, stopped flow EPR apparatus for biological appl. 80—36206
- time series concatenation and homogeneity 77—40627
- time-resolved X-ray diffraction data collection by position sensitive detector 77—51269
- time-resolved X-ray scatt. method for molecular biophysics 79—62409
- timer compatible with transistor logic and auxiliary equipment 77—67420
- tissue, trace element anal. by PIXE 79—48008
- tissue analysis by IR microinterferometer 79—79714
- tissue biopsies, sampling, storage and anal., evaluation by neutron activation anal. 78—11595
- tissue change detection in rabbit urinary bladder, holographic laser interferometry appl. *(German)* 79—34625
- tissue element position fixing during processing for electron microscopy 79—25168
- tissue fluorochrome meas. with He-Cd UV laser 77—77962
- tissue impedance meas. by phase-sensitive voltage and current detection 78—53602
- tissue lipid content analysis by photon absorpt. using ^{153}Gd 78—28041
- tissue metal detection, histochemical method 79—29681
- tissue mimicking materials for ultrasound phantoms 79—5333
- tissue O_2 uptake continuous meas., high-sensitivity device 78—20324
- tissue sections, electron probe anal., improvement of peak/background ratios 79—39631
- tissue substitutes, comparison of X-ray attenuation with thoracic tissues for phantom calibration purposes 79—16307
- tissue substitutes in experimental radiation physics 79—20680
- tissues, soft, apparatus for mechanical testing 79—44064
- tissues thin sections obs., Raman laser microprobe analysis appl. 80—57390
- TLD in medicine and biology 79—74762
- tobacco mosaic virus, solutions, Rayleigh scatt., elec. induced variations, spectral width and intensity meas. 78—48187
- tomogram reconstruction in desired plane 80—41340
- tone detection and choice reacion times, cat, behavioural system and apparatus 78—20187
- total body in vivo activation analysis, sealed tube neutron generator system, 14 MeV 79—88162
- toxicity experiments, processing of automatic analyser data using trace reader and computer 78—24195
- toxicity studies, TOXIPAC-300 data processing system *(Japanese)* 79—25172
- trace element characterisation, by instrumental neutron activation anal. 78—73116
- trace element determ. in dry biological samples by neutron activation anal. and collection of active C 80—17213
- trace element determination, using DC plasma echelle spectrometer, automated 78—53277

biological techniques and instruments continued
- tracer identification of time varying parameters in compartmental biosystems 77—40960
- tracheal ciliary beat, improved device for freq. recording 80—109070
- tracheal mucociliary transport, bronchoscopic evaluation 77—60270
- tracking microscope, design and operation 80—36214
- transducer for recording elec. and mech. chronic intestinal activity 77—44862
- transient circular dichroism meas. in chiral biomolecules 78—5372
- transient recorder/digitiser for time-varying analogue voltage signals 77—40943
- translation motion probe, fluorescence energy transfer in the rapid-diffusion limit 79—92151
- transmission microscopy of unmodified material, radiation dose with electrons vs. ultrasoft X-ray 78—11788
- transmitter-specific retrograde labelling in the striato- and raphe-nigral pathways 80—51309
- transponder dipole antennas in and near three-layered body 80—98181
- transuranium oxides, uniformly dense aerosols prod. by gas phase neutralisation of acidic droplets, for inhalation obs. 80—26427
- tris(hydroxymethyl)methylamine buffer effect on acetylcholine responses in Aplysia neurons 77—64020
- tumour localisation, animal tumour models for evaluation of radioactive agents, review 77—9249
- tunnelling spectroscopy, appls., review 78—92588
- turbidity spectrum method for erythrocyte relative refractive index, dimensions and conc. meas. 79—79698
- TV-computer interface system for human body sway study 77—81526
- ultrasound, diagnostic uses in medicine and biology, bibliography 80—36795
- uniaxial testing of soft human tissues, in vitro apparatus 78—61295
- US effects, review 79—66498
- US equipment, selection of material for concentrator-instrument section 80—21242
- US evaluation of cardiovascular changes assoc. with age in dogs 77—25504
- US generator, general purpose broad-band, for biological object handling 79—48381
- US imaging, overview of principles and instrumentation 79—66579
- US implantable IC CW Doppler flowmeter 78—31877
- US meas. of larynx height and vocal fold vibratory pattern 80—98184
- US observation of haemodynamic props. of beagle puppies, growth effects 77—25505
- US surface waves for studying props. of human tibia 77—25619
- US surgery, severing corpus callosum in rats 80—26306
- US synchronized pulsed Doppler blood flow and dimension meas. in conscious dogs 79—62318
- US system for quantification of bubbles formed during decompression of animals and man 80—76869
- US tissue model, liq. mixture component selection aid 77—78066
- US transducer, shear-wave vel. meas., bone elastic moduli determ. 78—83201
- US velocimeter, differential, for meas. of dilute suspensions 77—78065
- US velocity measurement of elastic moduli in bone 77—25623
- US velocity-of-propagation meter, based on interferometer 80—79084
- US/EMG transducer for biodynamic research, speech appl. 78—77164
- Ussing miniature chamber for obs. of size and shape of lateral intercellular spaces in living epithelium 78—77032
- USSR metrological-provision programme 79—96700
- USSR research 79—96703
- uterine cancer cells automatic classification via cellular differentiation 79—88226
- uterine cytology, automated, adenocarcinoma recognition 79—88227
- UV irradiated human strain cells, herpes virus production as repair marker 80—30783
- UV meas. in biological appl. 80—35963
- vector impedance meter for biological tissue 78—57138
- velocity sedimentation separation of mammalian cells 80—101293
- ventilators for animals, automatic sigh feature 80—98186
- ventricular myocardium plastic cast global Young's mod., calc. from angiograms 77—48827
- ventricular volume determ. from indicator dilution curves, dog expts. 79—57696
- vertebrate cornea, transparent layered structure thickness monitor 78—92737
- vertical plane serial sectioning of identified tissue culture cells 79—74807
- VERTIVAL microscope with interference contrast equipment after NOMARSKI for gonorrhoea types classification 80—56301
- vesicle visualisation in semi-thin sections by heat removal of epoxy resins 78—24194
- vesicles, large, anal. of adhesion to surfaces, expt. procedure 80—109063
- vestibular research, rotating room acceleration and damping 79—84048
- VHF/UHF complex relative permittivity meas., lumped capacitance technique 77—74460
- vibro-interference, for 3-dimens. imaging of biospecimens using holography 78—53584
- Vickers M85/M86 microdensitometer, film holder 79—21832
- video fluorimetry and microscopy at low light levels 77—44874
- video-tracking of micro-circulation, appl. of bit-slice processors *(German)* 78—88749
- vidicon Raman spectrometer, appl. to heme protein study 80—94428
- vidicon television camera, movement meas. appl. 80—41333
- virology laboratory minicomputer appls. 77—44856
- virometer, real time of viruses in biological fluids 78—48869
- virometer, real time virus detect. and identification in biological fluids 78—7555
- virus negative staining technique, applications in electron microscopy 80—41348
- virus size measurement using optical microscope, Virometer design 78—61296
- viscoelastic constants, meas. method for gel-like cylinder immersed in silicone oil 77—73619
- viscoelastic shear, indentation test appl. to rabbit articular cartilage 77—36973
- vision, annular artificial pupils, props. 80—41356
- vision, Macular pigment, role in polarised light detect., meas. technique 80—61560
- vision experiments, rapid cycling dual shutter control system [for vision research] 80—41358
- visual adaptation, technique for estimating the contrib. of photomech. responses 80—85547

biological techniques and instruments continued
- visual cell stimulation in insect eyes, using blue SiC LED *(German)* 79—39623
- visual evoked cortical potential, contrast sensitivity meas. of 6 month old infant 77—12913
- visual evoked cortical potential, removal of alpha by selective averaging 77—81766
- visual evoked cortical potentials, transient response, techniques review 78—35844
- visual evoked potential, steady state latency determ. 77—21516
- visual evoked potential recording in high-noise environment, biphasic 60 Hz synchroniser cct. 78—24155
- visual evoked potentials, cortical extracted pattern response with bipolar and monopolar recordings 77—12919
- visual evoked potentials, transient, real-time filtering 78—31940
- visual evoked scalp potentials, spatiotemporal mapping for human 78—35845
- visual field testing, three-channel optical system *(Spanish)* 79—24993
- visual physiology and psychophysics polar coordinate data 78—56988
- visual pigment regeneration studies, use of $[15^3$-H]all-trans-retinal tracer 80—41357
- visual stimulator, computer-controlled, for electrophysiology expts. 78—69230
- visual stimulator for eye movement and visual evoked pots. study, microcomputer-controlled 80—41350
- visual stimuli generation for psychology experiments, Z-80 based system 80—41328
- visual stimulus deflector, three-dimens. 78—48945
- visual stimulus generator, electronically controlled 79—74817
- visual system neuron response to light stimulus, computer monitored method 77—86725
- visual system simulator, human *(Russian)* 80—76877
- visually evoked brain potentials, meas. of signal components 77—40946
- vital microscopy, electronic thermostatic system 80—85537
- vocal tract, computer representation of geometrical configuration *(Russian)* 80—46111
- voltage clamp, single electrode, design for neuroresearch 80—72385
- voltage clamp of multicellular preps. 77—40955
- voltage clamping of multicellular myocardial preps. 79—84056
- voltage sensitive dyes, appls. for cell voltage meas. 79—57833
- volume reproduction by foreshortening roentgenograms, compound hologram method 79—57748
- water bath, temperature-controlled, for organ perfusion apparatus 79—96723
- waveguide system for chronic exposure of small animals to microwaves 80—56318
- white blood cell images boundary finding 79—12021
- white blood cells classification and feature extraction 78—3655
- whole body autoradiography of bumetanide-^{14}C in dogs by round saw method 80—72399
- whole organs, sampling, storage and anal., evaluation by neutron activation anal. 78—11595
- whole-body counter for meas. of radionuclides in large dogs 78—11786
- wholebody autoradiography, B-radioluminescence method for tritium detection 77—52945
- wildlife biotelemetry, reviews 80—30966
- wood boring insects larvae study, acoustic amplifiers, activity integrator 79—16357
- X-ray absorption analysis of heavy elements in organic substances 77—2075
- X-ray absorption spectroscopy of biological molecules, book contrib. 79—5436
- X-ray absorption spectroscopy using synchrotron radiation, appl. to metalloproteins 78—64938
- X-ray analysis, appls., conf., Denver, USA (Aug 1975) 77—56307
- X-ray crystallography for symm. cryst., absorption-correction technique for arbitrary orientation 77—65932
- X-ray crystallography for symm. cryst., semi-empirical absorption-correction technique 77—65931
- X-ray diffraction, time-resolved, using position sensitive counter 77—13831
- X-ray diffraction data acquisition using position-sensitive counter *(Japanese)* 78—88774
- X-ray diffraction pattern of biological mols., improved method for solvent contrib. calc. 79—16355
- X-ray diffraction patterns, nanosec. technique 80—26429
- x-ray diffraction studies of the heart, review, book contrib. 80—109079
- X-ray diffraction study of biological structs. in native form, selection of radiation 78—81087
- X-ray diffraction with synchrotron radiation, absorpt. factor, CsDNA appl. 78—76988
- X-ray diffuse scattering, large angle, conformation change obs. of proteins in soln. 79—12054
- X-ray energy spectroscopy, use in monitoring trace elements of mussel 80—30954
- X-ray films, selected, response to ^{14}C-β-radiation 80—90937
- X-ray fluoresc. anal. system for small medical samples, computerised target changer 77—60249
- X-ray fluorescence anal., importance to geometry 79—5430
- X-ray fluorescence spectroscopy for trace element anal. human blood 78—20248
- X-ray kinetic diffr., position sensitive counter 78—62283
- X-ray laser holography, possible appl. to crystal and biological microstructure 78—55322
- X-ray low angle diffractometry of specimens with semiconductor spectrometer SERP-1(M) 79—53288
- X-ray microanal. of cultured skeletal muscle cells, calibration 79—100798
- X-ray microanal. of epon sections after O plasma incineration 79—17584
- X-ray microanalysis, in TEM at high accelerating voltages 78—36078
- X-ray microanalysis, iso-atomic droplets as models 78—53598
- X-ray microanalysis 80—41349
- X-ray microanalysis of thin biological specimens, quantitation problems 79—25164
- X-ray microscope, using holographically made zone plates and gratings 78—37855
- X-ray microscopy and X-ray lithography, techniques, appls. 77—34059
- X-ray microscopy of biological specimens, flash X-ray method 80—51310
- X-ray microtomography in SEM 80—101308
- X-ray non-isotropic small-angle scatt. curves from lamellar systems, collimation correction 79—10755

biological techniques and instruments continued
- X-ray photography of biological objects, using soft X-ray emission of laser plasma mirror 79—43983
- X-ray powder diffraction camera, absorpt. attachment, appl. to gallstone study 77—41744
- X-ray scattering, large-angle diffuse, rel. to globular protein struct. anal. in soln. 77—86723
- X-ray scattering, small-angle, of biological structures 79—11889
- X-ray scattering method for determ. of membrane struct. parameters 80—30948
- X-ray small angle scattering, employing synchrotron radiation and energy dispersive techniques, proteins in solution anal. 79—12051
- X-ray small-angle data processing for planar multilayered structures, theory 79—37582
- X-ray small-angle scatt., appl. to erythrocytes *(German)* 78—35812
- X-ray small-angle scattering from lamellar structures, deconvolution method 79—10756
- X-ray spectrometry, energy dispersive, ultramicroanalysis of biological fluids 78—92768
- X-ray stereography, method of precision position determ. 80—56314
- X-ray structural study of biopolymers using synchrotron radiation and multichannel detector 78—47210
- X-ray techniques for anal. of environmental particulates in tissue, blood 77—56322
- XPS source area minimisation, appl. to 30μm trachelomonas cell surface anal. 79—48037
- yeast cells in suspension, vacuole detect. by transmittance radiometry 80—26418
- zeaxanthin ([3R,3′R]-β,β-carotene-3-3′diol) as optical probe of membrane struct. 79—92124
- zeugmatography, state of the art 78—74043
- zeugmatography of ^{31}P metabolites 80—76872
- zoology, instrument development 79—96720
- ^{133} Xe custom trapping and holding system for animal research, design and evaluation 80—30950
- Al shielded room for biomag. meas. 80—104846
- Al, thick-walled conducting shield in biomag. expts. 80—104845
- Am determination in biological samples by solvent extraction and liquid scintillation counting 79—53260
- Ba, determ., in biological materials, by thermal NAA 78—27854
- C-fibre microelectrodes, neurophysiology appl. 80—67314
- CO_2 electrode, dynamic response 79—92025
- CO_2-^{14}C animal exhalation meas. by liquid scintillation counting *(French)* 79—48384
- ^{13}C NMR spectroscopy, 270 and 90 MHz, ^{1}H noise decoupling field heating effects 79—38389
- ^{14}C and ^{3}H determination in whole-body sections by liq. scintillation counting *(German)* 77—5114
- ^{14}C fallout from nucl. weapons testing, use as biological tracer 77—64162
- ^{14}C-labelled compound analysis, continuous radio-scanning method for chromatograms and electrophoretograms 77—70367
- Ca, whole-body, determ. method for rats using neutron activation anal. 80—51302
- Cd determ. in whole blood by atomic absorpt. spectroscopy 79—44071
- Cf determination in biological samples by solvent extraction and liquid scintillation counting 79—53260
- Cl^- ion selective electrodes, appl. to biological materials 77—90974
- Cm determination in biological samples by solvent extraction and liquid scintillation counting 79—53260
- Co staining technique modification for cut axons, single optic nerve fibres in Limulus brain 79—53096
- Cr, determ., in biological materials, by NAA 78—27855
- Cu determination in serum/tissue specimens using flameless atomic absorption spectroscopy, effects of sample prep. and matrix 80—98200
- D NMR, appls. for physics, chemistry and biology 77—87801
- Dy^{3+}, free-radical relax. agent in biological tissues 78—81090
- ^{18}F, prep. with an electron linear accelerator, medical and biological appls. 80—98136
- Fe utilisation studies by stable tracer ^{58}Fe technique 80—61734
- Ga melting-point apparatus for thermometer calibration, enzymologic appl. 78—85460
- H_2^+, 6 MeV, PIXE anal. of organic materials 80—26087
- ^{3}H labelled biologically active compounds obtained using at. ^{3}H bundles, appls. 80—30888
- HeNe laser light determ. of erythrocyte distrib. profiles during sedimentation 80—81563
- ^{3}He cryostat, continuously operating for Mossbauer investigation of biological samples 79—96725
- I determination in biological materials by neutron activation anal. 79—57828
- I, stable tissue content, meas. by coherently and Compton scatt. photons 79—88220
- ^{131}I in milk, rapid method of detect. 80—46106
- ^{113m}In-labelled transferrin, use in meas. of blood vols. in rat, rabbit 80—3878
- K channel blocking agent, 3,4-diaminopyridine 78—69028
- ^{6}Li, quantitative microlocation in the brain by a (n,α) nuclear reaction 80—41353
- N depth distribution in barley seeds, use of ^{14}N(d,p_0)^{15}N 79—5221
- ^{13}N-labelled NH_3 and NO_3 ions, prod. for biol. expts. using 3 MV Van de Graaff accelerator 80—26349
- ^{15}N(p,$\alpha\gamma$)^{12}C, anal. of protein quality of leguminous plants 77—48978
- Na^+ multicompartment flow model of frog skin epidermis, experimental verification 78—92607
- NaI opposed detector/turntable γ counter for voluminous samples 79—100706
- Na^{125}I tracer telemetric detection for biological rhythms in renal study 77—86586
- ^{63}Ni applications in biological research 80—12321
- O_2 concentration meas. in tissue, pulse-mode method, equipment 78—7551
- O_2 partial pressure and bioelectric potential simultaneous meas. in living tissue *(German)* 78—85453
- O_2 sensing electrode stability 77—60268
- O_2, singlet product. detect. by EPR 79—66597
- O_2 uptake on-line meas., analogue approach 78—28134
- ^{31}P NMR analysis of intact tissue, review 80—26432
- ^{31}P NMR investigation of heart physiology 78—69018
- ^{31}P NMR studies of isolated rat liver cells 78—61150

biological techniques and instruments continued
- ^{32}P and ^{45}Ca determination by Cherenkov and liq. scintillation counting 80—98183
- Pb, determ. in aqueous solns. by Delves Cup technique and flameless atomic absorpt. spectrometry 78—68973
- Pb poisoning in human teeth, determ. using alpha-sensitive plastic track detector 80—94433
- Pb stain artefacts in electron microscopy, technique for minimizing occurrence 79—84040
- Pb traces in human blood plasma, atomic absorpt. anal., nonspecific absorpt. correction using Zeeman effect 80—76881
- PdO-Pd miniature pH electrode description and use 80—89886
- Pt microelectrodes for O_2 sensing, operation 79—84043
- Pu skeletal level estimation based on DTPA induced excretion in faeces 78—85390
- ^{239}Pu localisation in bone using neutron-induced autoradiography 77—40773
- ^{81}Rb, prod. and characts. for myocardial imaging studies 79—29628
- ^{103}Ru in determination of rate of passage of food through gut of captive wild birds 80—26425
- Sb determ. in biological and environmental samples by neutron activation anal. 79—53008
- Si force transducer, extraluminal meas. of oviduct contractile activity 77—40805
- Si-SiO_2 interface as electrode for electrical and ellipsometric meas. of adsorbed organic molecules 80—15366
- T determination in samples, field instrument 77—9306
- Ta-Al_2O_3 microelectrode array, design and fabrication 80—76868
- U abundance in Himalayan plants, fission track determ. 80—101305
- U atomic motion on thin C substrate, low-temp. obs., biomolecule marking appl. 79—25176
- U stain artefacts in electron microscopy, technique for minimizing occurrence 79—84040
- ^{238}U/^{226}Ra dating of quaternary corals by γ-spectrometry 79—88221
- ^{133}Xe clearance, meas. of pig cerebral blood flow 80—94421
- ^{133}Xe radio-spirometric measuring system for regional respiration function testing 77—90889

biology
- *see also biological fluid dynamics; biological techniques and instruments; biophysics; blood; cardiology; ecology; evolution (biological); medicine; physiology; zoology*
- algal density in Iowa lakes, rel. to water transparency 79—2308
- N.American trees, cellulose D/H ratios rel. to palaeoclimatology (9500-22000 BP) 77—60462
- Antarctic Ocean, interdisciplinary studies 78—11915
- aquatic ecosystems, acid precipitation effects, review 77—37257
- aquatic life, protocols for evaluating effects of chemical substances 78—53604
- Arrhenius equation and accel. testing 78—53182
- Central Atlantic Ocean, biological characts. rel. to irradiance meas. *(Russian)* 78—77257
- S.Atlantic Ocean, sea water plankton content rel. to hydroptic struct. variability *(Russian)* 78—77262
- atmospheric ice nuclei, bacterial sources 77—5292
- atmospheric ice nuclei, terrestrial and marine sources 77—5291
- bacteria as natural ice nucleants at −1°C 77—53221
- baikal grayling, oxygen debt and swimming efficiency *(Russian)* 77—64168
- S.Benguela Current, upwelling site nutrients, zooplankton and phytoplankton 80—104987
- biocenoses, use of statistical mechs. 77—21467
- biochemical reactions, stratification *(Russian)* 78—57884
- biochemical systems stability anal., practical guide 78—73135
- biochemistry and biophysics horizons, book 78—7315
- biochemistry and biophysics horizons, book 78—68977
- bioclimatic coefficients, change with respect to climatic zones *(Russian)* 77—53169
- biogenic lipids and marine environment from aeolian transport 77—64327
- biological system modelling, optimal control theory appl. 77—40628
- biosatellite Cosmos-782, biological expts. 80—61710
- biosphere and active solar processes link, role of Earth's natural electromag. field 78—61211
- catastrophe theory, elementary approach 79—11881
- catastrophe theory application, claims and accomplishments 78—29
- cathodoluminescence, bibliography of papers till 1977 79—21482
- chronobiology in plants 80—56328
- circadian rhythms in humans, role of light, bibliography 77—48985
- compartmental models with delays, phys. realisability 78—53313
- coniferous forest canopy, vertical air motion in underlying stratified ground layer *(Russian)* 78—96266
- cosmology, physics and biology in an open universe 79—97119
- cotton plant wilt disease, microelement depend. by neutron activation anal. 77—64165
- dissipative systems, dynamical field theory, hierarchical struct. of field thermodynamics 78—73132
- dolphin acoustorespiratory system, morphology and function *(Russian)* 77—64060
- epidemic in discrete time, threshold theorem 80—61504
- fish, acoustic estimation of oceanic scatt. layer comp. 77—86909
- fish, effect of acidification of Canadian lakes 77—37259
- fish, in Irish Sea and other United Kingdom fishing grounds, Hg content 78—36204
- fish, skeletal muscle ultrastructure rel. to swimming efficiency *(Russian)* 77—64169
- fish metabolism rel. to swimming velocity *(Russian)* 77—64170
- forest canopy of mountain watershed with ski basin, influence on heavy metals pollution 79—20903
- freshwater ecosystems in Norway, acid precipitation effects 77—37258
- glasses as bioactive materials, review 78—3698
- HV electron microscopy, recent progress, book contrib. 79—67442
- Indian Ocean, ecologic and palaeoclimatic implications of vars. of O. universa 77—9445
- Indian Ocean middle latitudes, Subtropical Convergence fluctuations and Quaternary climates 77—13087
- information in biological systems 77—29090
- interdisciplinary course, physical theory in biology 79—58462
- JOINT-I expedition of Coastal Upwelling Ecosystems Analysis program 77—60470

biology continued
Laccadive Sea, chemical oceanography and biological productivity 80—104995
larval bivalves, shell morphometry as palaeoclimatic tool 79—53510
leaves of African crop plants, optical props. rel. to photosynthesis 77—25629
lichenometry in central Asia, appl. to earthquakes age determ. 79—92505
life, thermodynamic and informational aspects, model 77—1974
life support system with autonomous control employing plant photosynthesis 77—25563
long range coherence in biological systems 78—20137
marine organisms around Marshall Islands nucl. test site, $^{113}Cd^{m}$ conc. 80—109174
marine plankton, C isotope ratio rel. to surface water masses 79—29783
Mars, possible surface reactions, Viking biology expts. simulation 78—7904
mathematical biology meeting, Philadelphia, USA, (Aug. 1976) 78—53311
metallic pollutants, study of movement in environment and biological chains *(French)* 77—41162
microbial activity in Recent Texas continental shelf and slope sediments, rel. to light hydrocarbons distrib. 79—2213
microbial degradation of organic molecules in lake sediment 79—84331
minimum mixing principle as method of choosing form of dynamic model 77—36857
morphogenesis and biological differentiation, computer simulation 80—30691
multistable self-wave media 80—86094
Murray-Darling river system, Australia, symposium (Melbourne, 13 October 1977) 79—92556
network analysis of biological systems, review 80—30635
nitrifying soil microorganisms and soil N_2O emission, effects of acetylene and water content 79—83672
ocean, biogenic agent as source of Cu bearing aerosol particles 79—58050
ocean, trace metal enhancement in estuarine tidal front biotic component 79—2265
ocean biological characteristics, statistical relationships with transparency field *(Russian)* 79—88361
ocean deserts and ocean oases 79—5500
oceanic benthic communities, carbonate shells, $^{18}O/^{16}O$ vars. in East Pacific Rise hydrothermal field 80—109173
S.E.Pacific Ocean, consequences of 1975 El Nino 77—41063
E.Pacific Rise, benthic communities of hot springs areas 80—101360
pathogenic bacteria as air pollutants from municipal wastewater plants, monitoring 79—80050
photosynthesis in British coastal waters, inhibition by Zn pollution 79—24921
plankton in Massachusetts Bay, vertical displacements by tidally generated internal wave packets 79—44190
plant growth, effects of drought, appls. to agriculture 77—56707
plants, submerged, in Derwent Reservoir N.England, Zn, Cd and Pb contents 79—25286
pollen record for past 150000 years in N.Pacific sediments, palaeoclimate marine-continental correl. 79—80008
pollen record in N.America NW. coast region, appl. to Quaternary temps. and precipt. determ. 80—98438
porous solid with below-freezing pt. adsorbate, isothermal adsorption and dimensional changes obs. 78—75925
radioactive waste disposal and deep sea biology 79—29638
radioactivity waste, low-level, shallow land disposal, microbiological aspects 79—85630
rhythms in animals, role of light, bibliography 77—48986
roadside soil and plants in Alexandria district, Egypt, contamination with Cd, Ni, Pb and Zn 78—81171
self-organisation, origin of information 77—32868
sharks, red muscle structure rel. to swimming velocity *(Russian)* 77—64172
space research, biology and medicine 80—41265
Spacelab, biological and medical appls. 77—45281
stochastic and deterministic time delays in living systems 80—30636
tooth enamel crystallites, contrast effects in TEM 80—85572
tree rings, climatic information from $^{18}O/^{16}O$ in cellulose, lignin and whole wood 78—24355
tropical rain forests, exploitation causing destruction *(German)* 80—101137
vegetation, hydrocarbon emissions oxidation as atmospheric CO and H_2 source 78—88881
vegetation, release of particles containing metals into atm. 77—41135
vegetation layer, effect on ground surface temp. and moisture content 78—73373
water quality system, biological process models 79—5540
wheat, as source of S in rain 77—56698
wheat endosperm, radiometric determ. of Cd conc. following Cd addition to soil *(German)* 77—25631
zero gravity expts. on Cosmos 782 satellite, results 78—85818

biology computing
see also computerised instrumentation; computerised signal processing
40 Hz activity in sigmoid gyrus, nucleus accumbens and amygdala, cross correl. anal. 80—76730
Alopex process: Visual receptive fields by response feedback, trigger features 80—61546
aortic dynamics in man, analogue simulation model 78—80903
arterial dynamics, model of multilayered shell with fluid flow 77—29171
articulatory-to-acoustic transformation in vocal tract, inversion by computer sorting 78—69110
auditory neuron, characts. of digital model 78—3516
auditory system from middle ear to primary auditory nerve, analogue and computer model 77—29158
bacterial cell wall structure study 79—5427
BANDSCAN, program for online linear scanning of human banded chromosomes 78—92758
binaural hearing digital model, stimulus-response characts. 78—20192
binocular depth perception, model suggested by neurophysiological evidence 77—21527
biochemical pathway enzymes kinetics, simulation *(German)* 77—5102
biological macromolecules, computer simulation of solvent struct. 78—40113
biophysics, physiology, pharmacology CAI 77—25

biology computing continued
biophysics, teaching appls. of analogue computers 79—84890
bladder smooth muscle impulse propag., math. anal. *(Japanese)* 78—53359
blood flow, finite element soln. 80—94269
blood pressure automated control in dogs using microprocessor 80—81797
bone resonance, effects of geometrical parameters, shear and rot. inertia, finite element model 77—29165
bones, long, struct. anal., appl. to human tibia 77—21551
brain cortices large-scale simulation via BOSS system 79—2039
brain O_2 transport, nonlinear Monte Carlo simulation, hybrid computer implementation 78—40131
brain potential comparison, average evoked, on spectral and coherency function basis 77—2072
brainstem respiratory activity, math. model of computer-simulated neurons 77—44637
cancer cell cycle kinetics, flow microfluorometric DNA distribution representation 77—21669
cardiac and torso models for ECG forward and inverse problems 77—40837
cardiac electromechanical field model and computation, inverse problems 79—39400
cardiac output flow wave calculator *(Japanese)* 77—70489
cardiac performance mechanics from computer anal. of circumferential fibre shortening vel. 77—37095
cardiograms, image processing, cardiac function meas. *(Japanese)* 80—94354
cardiovascular research database system 78—53549
cat superior colliculus, neuronal network characts. 78—31808
cell population survival kinetic parameters derived by computer simulation of radiobiological data 77—56433
cellular kinetics, random walk model 77—44606
cerebral blood flow determination, computer assisted method for multi-exponential curve fitting 78—20246
cerebral collateral circulation, simulated on computer model 77—36995
chromosome density profiles, description and classification 79—43830
cochlear micromechanics, mechanism for transforming mech. to neural tuning within cochlea 78—11666
colonic contractile activity meas., pharmacological tests in dogs appl. 80—109068
compartmental systems controllability, observability and structural identifiability analysis 77—40625
coral growth form, light control, computer simulation 77—2076
cortical surface interacting neural net model 77—21512
coupled biological oscillators simulation, interactive modules 78—35792
cytophotometric histogram, computer aided analysis of cell-cycle phase 78—92759
data processing, radioimmunoassay and bioassay, logistic curve fitting routine adapted to desk top computer 77—37059
digital image registration with automatic microscope, appl. to cell analysis 77—29239
disease prognosis, appl. to haemorrhagic shock, nonlinear dynamical model 79—83838
disturbed cell renewal systems simulation via microprocessor system 79—48227
diuresis, medullary Na depletion, digital computer simulation 77—60226
DNA, hydrodynamic shearing simulation 80—16895
DNA, polymorphism, X-ray diffr. and computerised model building study 78—27894
DNA distributions automatic processing and interpretation 78—92757
DNA histograms from flow cytometry, program for anal. 80—41337
DNA hydrodynamic shearing model 79—39337
DNA thermal transition midpoint, CAA 79—74593
dosimetry calculations due to radionuclides in aquatic food chains, NEPTUN interactive code in FORTRAN 80—109039
DOTS, program for generating on-line raster dot displays of single unit activity 78—57087
electron microscopy of biological objects, 3-dimens. image, computer simulation 77—13046
electron probe microanalysis of biological thin sections, quantitative methods 77—25620
EMG signal generation, quantification using automata theory 77—29132
enzyme mechanisms, multiple pathway, analysis and modelling 77—81388
epileptic activity modelled as chain reaction within system of interconnecting cells 77—48787
ergometric test, computer interpretation of heart-rate var., anal. of cardiac control in exercise 78—85430
excitation spread equation boundary conditions for undistorted impulse movement pattern 77—56365
eye movements, vergence and version, reciprocal innervation model 77—48798
eye readaptation after dazzle, multidimensional functional model *(German)* 79—16208
flagella bend propagation, derivation of eqns. of motion and simulation 78—77074
flow cytometric data, computerised display and anal., review, book contrib. 80—109082
fluorescence marker concentration dynamics as probe of mobility 77—9303
gait kinematics, human, computer generation program 79—74703
gastrointestinal electrical rhythm frequency estimation by autoregressive modelling 78—56948
glutamine synthetase reconstruction from electron micrographs using computer averaging 79—92452
dGMP γ-irrad. in frozen soln., free radical form., computer EPR spectra anal. 78—31774
haemodynamics, pulsatile viscous flow through diseased coronary arteries of man 77—90835
haemoglobin, sickle cells, 3-dimens. reconstruction of fibres 78—44452
head injury model with viscoelastic brain tissue, mech. response 78—69117
heart muscle contractility calc. using analogue computer *(German)* 78—7378
human body planar motion in free fall, interactive computer graphics 78—40221
image processing, boundary trace transform: an edge and region enhancement transform 79—70713
insect optical cells anal. using microcomputer *(German)* 77—86724
interactive film anal. system 80—3876

biology computing continued
Interactive Simulation Language application to nerve cell kinetics 77—21507
intestinal electrical activity, motility, computer anal. of electrophysiological study on dogs 78—80851
intracardiac electrograms processing 80—21553
joint centre analysis using stored program calculator 77—29166
kidney modelling, numerical continuation method 79—43944
knee flexion, computerised instant centres of rot. 77—44710
left ventricle stress and power, computer simulation 77—56406
leg joint moments during walking, humans 77—56396
leucine aminopeptidase crystalline aggregates, interpretation of electron microscope images 78—68988
ligand distribution among multiple binding sites on different proteins in plasma 77—12877
lumbar spine, human, dynamic 3D modelling, computer code 80—108948
lung, apical and basal regions, asynchronism in non-sequential ventilation 78—48820
lung pressure-volume characts., curve-fitting anal. using programmable calculator 77—48821
lung structure and elasticity, 3-dimens. modelling 77—36992
macromolecular structure, interactive model building program 77—52738
macromolecular structure factor, FFT calc. 77—51268
macromolecule conformations, computer graphics 77—36865
mandible, human, in vitro, math. model 77—52816
mathematical modelling in biological research, role of computers *(Chinese)* 79—1996
McCollough effect, synaptic modification associative learning model 77—21531
membrane dynamic equation solving, practical algorithm 78—77038
mesenteric artery Na kinetics, digital simulation of 3 compartment model 77—44616
mesh generation-optimisation, for partitioning of intricate biological struct. for 3-D finite element anal. 77—40630
microcirculation autoregulation mechanistic theories, computer simulation 78—27995
microprocessors in bioscience, review 80—21557
microscopic image processing *(Japanese)* 80—81784
microscopy cell distributions topographical size analysis, TOGA interactive program *(German)* 77—40951
middle ear systems simulation from physiological data 78—44514
minicomputer-based interactive graphics biology film anal. system 78—44744
models of complex systems, based on network thermodynamics 78—20955
molecular graphics appl. to struct. determ. of snake venom neurotoxin 78—27892
molecule vibrational analysis, comparison of algorithms for soln. of secular eqns. *(French)* 79—100565
morphogenesis model 79—83722
multicompartment systems, analytical techniques 79—83689
multimodal probability density functions fitting, FORTRAN program 77—37748
muscle, skeletal, bond graph simulation of glucose metabolism 77—36894
muscle coordination in cat hindlimb during maximal vertical jump, computer model 77—40662
musculoskeletal complex shape cross-sectional props., interactive graphics software package 79—79595
musculoskeletal system modelling, interactive computing and graphical display techniques 77—40685
myelinated axon impulse cond. simulation, sensitivity to nodal and internodal parameters 78—35831
myocardial electrical activity modelling, dialogue mode *(Russian)* 79—2021
myocardial excitability evaluation, strength-interval curves generation under computer control 80—41336
myocardial infarction dimension model and FORTRAN program *(Russian)* 79—2038
myoelectric single motor unit potential generation model 77—29131
nerve fibre automatic counting using an array processor in a multi-mini computer system 79—79710
neural multiunit signals, educable waveform recognition system for sorting unit discharges 80—51312
neural nets, frequency response characteristics analysis, interactive model implementation 78—44487
neuron and neuronal assembly 3D computer reconstruction 80—21596
neuron hydrodynamics, numerical methods for creeping flow investigation 77—5019
neuronal membrane process field potentials anal. and synthesis, computer system 80—85374
neuronal populations, diffusely-connected, computer simulation 78—53384
neurophysiological experiments, fast data acquisition and processing system, minicomputer appl. *(Japanese)* 80—85536
nonlinear describing function for biological data 77—13045
nonlinear system analysis by Wiener kernel estimation in freq. domain 77—1973
organ blood flow determ. using radioactive microsphere technique, PDP-11 interactive program 78—20247
otolith membrane, finite element model, computer soln. of differential eqns. 77—40636
papillary muscle Na kinetics, diffusional and compartmental models 77—44617
pattern recognition in microbiology 78—81084
pericardial potential simulation and mapping in dog 79—39399
peripheral nervous system multichannel data anal., frog sartorius muscle mechanoreceptor transducer characts. *(Japanese)* 80—3656
photoreceptor spectral sensitivity on-line computation using programmable pocket calculator 78—69264
point processes in biological signals, detect. and anal. 77—44770
protein data measured on oscillation camera, collection and reduction method 79—29672
protein structure least squares refinement technique based on fast Fourier transform algorithm 78—91197
protein transport across endothelial membrane 80—3601
protein-ligand binding parameters estimation from continuous ultrafiltration results 77—12878
proteins, conform. anal., algorithms and data structs. for array processing 80—83530
proteins, globular, prediction of β-turns by computer 79—83698

biology computing continued
psychoacoustical aspects of synthesized vertical local cues, computer synthesis 78—61198
pulmonary gas exchange function model *(Russian)* 79—2092
pulmonary gas transfer, on-line digital integration 78—20325
pulmonary mechanics computation algorithms on programmable calculator 78—7382
pulmonary oedema fluid transport 78—27915
pulsatile flow of blood through tube containing rigid and distensible sections, num. soln. technique 77—56419
quantitative microscopy, object delineation program 80—41338
radioisotopes in tissue, specific energies of ^{239}Pu and ^{131}I, crit. cell concept 77—2031
radionuclide accumulation in marine organisms, computer kinetic modelling 79—53261
radionuclide concentrations in food products, FOOD II interactive code calc. 79—48348
radionuclide intake by man through terrestrial pathways, TERMOD II interactive code analysis 79—48349
rapid eye movement analysis during sleep 80—76870
ray-tracing for physiological optics 77—25420
renal autoregulation, math. model of transient adjustments 77—90842
renal countercurrent mechanism, transient and steady state simulation 77—36967
renal counterflow systems, numerical solution of differential equations 78—92662
renal medulla, human, math. model 78—24081
renal network flows, comparison of numerical methods 77—16945
replicon autoradiograms, computer-assisted measurement 78—92692
retinal information processing, computer model 77—66814
RNA nucleotide sequence, determ using computer 79—29500
scanning eye movement target point selection, computer model 78—24066
sekeletal muscle dynamics, isometric and isotonic contraction model 78—31807
sensory neuron, second order, summation of excitation and inhibition by computer simulation 80—76769
serial section alignment by serial filtering 79—20723
serial section models of human lung endothelial cell nuclei, estimation of mean caliper diameter 79—29679
serum samples, trace element anal., automatic data acquisition, on-line method 78—48726
shape differences comparison, between two-dimensional irregular forms, computer program 77—87639
single ligand binding constant computation, regulatory enzyme exponential model 79—79454
sinus node and AV junction, automaticity model based on weakly coupled relax. oscillators 78—24017
skeletal muscle mechanical props. and model, contractile force depend. *(Japanese)* 80—56091
skin of frog, radioactive Na washout rate anal., numerical simulation 78—3456
slow motor nerve cond. meas. by blocking technique, simulation 78—36027
sound analysis, reversible computer method adapted to bioacoustical expts. 78—57137
space-filling molecular models constructed by computer 77—40633
spermatozoa, bull, motility evaluation by photon correl. spectroscopy 77—48964
statistical mechanics, ensemble methods 79—66437
Steinbuch's Lernmatrix appl. in assessment of airborne Pb effects on children 77—44878
STEM, low-dose, using digital data processing system 78—24203
STEM, on-line data processing system 78—24202
structure-function relationships of biologically active molecules, programs *(Russian)* 79—16137
swimming parameters of aqueous organisms, determination by cine recording and computer processing *(Russian)* 77—32921
TC-chromatograms online analysis by scanning system 77—40599
temperature biotelemetry system for free-swimming fish 77—25624
thermoregulatory system simulation, rat 80—3594
thylakoid membrane of green plants, simulation of electron transport in primary photosynthesis reaction, in PL/1 *(German)* 77—86468
thyroid junction assay digital simulation 77—44778
tooth-jaw system, mech. anal. 77—40703
transcapillary water movement resulting from non-oncotic osmotic forces 78—44548
ventilatory phonetics, analogic 80—51131
ventricular function computer simulation, development of model and parameter estimation 78—53439
ventricular myocardium plastic cast global Young's mod., calc. from angiograms 77—48827
vertebral model, computer-aided technique for 3-D finite element model generation 78—92591
visual cortex neurones, rabbit, organisation of background activity 78—69044
visual cortical neurone reaction patterns to const. illum. 78—80871
visual foveation system, afferent part, computer simulation model 77—25437
voice production, analysis synthesis, computer appl. *(Dutch)* 77—12938
voltage clamp of multicellular preps., sucrose gap method simulation 77—40955
weightlessness, haematological response, math. and exptl. simulation 80—61714
Wiener kernels, first- and second-order, real-time estimates 79—12046
X-ray diffraction, time-resolved, using position sensitive counter 77—13831
^{3}H biological half-life estimation in man 79—20689
Na exchange in tissue, incorporating diffusion effects into multicompartment models using digital simulation 80—3611
Na$^+$ multicompartment flow model of frog skin epidermis, experimental verification 78—92607

biomagnetism
60 Hz high intensity electric fields, behavioural and biological effects in living organisms 80—89740
AC fields, human response 77—77923
agricultural soil and plant improvement by ferromagnetic additives *(Russian)* 77—66882
albumin, Reanal serum, mag. field effect on photoinduced reactions 79—92154

biomagnetism continued
- alternating field effects on tetrahymena pyriformis 79—83814
- arogenesis correlation with geomagnetic field reversals *(Russian)* 78—36089
- auditory magnetic evoked fields, human 79—16212
- baceterial photosynthesis, mechanism of mag. field effects 79—83810
- bacteria, freshwater magnetotactic, identification of magnetite, Mossbauer obs. 80—3657
- bacteria, magnetotactic, navigational compass 80—72183
- bacteria magnetotaxis, Mossbauer study 80—41056
- barley growth in very weak magnetic field *(Russian)* 78—20200
- bean and corn seed growth effects of constant mag. field *(Russian)* 79—83811
- behavioural sensitivity of a domestic bird to 60-Hz AC and to DC mag. fields 80—61622
- biologically active magnetic field strength meter calibration, 0.1 to 10.MHz, 2 to 250 A/m *(Polish)* 80—51311
- biomagnetic fields, meas. and anal. 79—11952
- biomolecules, electric and mag. props. 77—44584
- bird migration and homing, physicochem. mechanism for mag. field detect. 77—52811
- blood cells, electrokinetic props. on exposure to phys. factors 77—70431
- blood plasma ^{1}H NMR relax. rates, cancer-induced decrease obs. 80—56075
- bone apatite, Hall coefficient dependence on mag. field, obs. 79—92248
- bone stress wave detection using piezoelec. effect, non-invasive technique 78—31948
- brain, appl. of expressions for magnetic fields of dipole in volume conductor shapes 77—81514
- brain, human, mag. fields 80—72182
- brain, human, neural generator localisation underlying auditory evoked mag. fields 80—104703
- brain, human, somatically evoked mag. fields 78—48818
- brain, mag. evoked field mapping 80—104705
- brain, magnetoencephalogram power spectrum estimation 80—104704
- brain magnetic response to visual stimulus monitoring using SQUID 77—29231
- cancer cause, nature and cure, possible effects of static mag. fields 77—32914
- cardiac bloodflow mag. meas. 78—44517
- cardiac cycle P-R segment non-invasive information, clinical pot. of elec. and mag. methods 80—36182
- cardiac electrical activity, mag. detect. *(Japanese)* 77—81515
- cardiac mechanical activity, noninvasive mag. detect., instrumentation 80—89820
- cardiac mechanical activity, noninvasive mag. detect., theory 80—89819
- cardiomagnetism, high resolution 80—104698
- cardiovascular measurements, conf., Bellingham, USA (Sept. '78) 80—31419
- cell growth, effects of weak mag. field on tissue culture 79—62271
- cells, magnetic sensitivity test of 3 different biological systems 79—92247
- cellular current flow and biomag. fields 80—101192
- central nervous system, magnetic phenomena, book contrib. 79—5304
- cerebral magnetic field meas. and personnel selection 79—2026
- chloroplast, mag. relax. of water protons and state of water photodissociation system 80—51133
- chloroplasts, spin glass type structs., mag. anisotropy obs. 79—79490
- cooperative phenomena, rel. to biological effects of mag. fields 80—94247
- current dipole models of biological sources, mag. field distribs. 78—7375
- cytochrome c_3, haeme-haeme mag. interaction obs. 80—108836
- deoxyhaemoglobin, high mag. field Mossbauer spectra, electronic states 80—35845
- deoxymyoglobin, high mag. field Mossbauer spectra, electronic states 80—35845
- diamine oxidase solutions, proton mag. relax. dispersion obs. 80—51136
- dipalmitoylphosphatidylcholine, changes in vol. mag. susceptibility at the phase transition 80—76770
- direct and indirect action of constant magnetic field on biological subjects 79—34580
- E. coli cells, iron-storage protein, Mossbauer spectra obs. 80—8022
- EEG, magnetoencephalogram, current dipole model, central nervous system disease diagnosis applications 79—48238
- egg lecithin membranes, magnetic anisotropy obs. 79—20520
- erythrocyte high gradient magnetic separation 78—53585
- experimental investigations, review *(Croatian)* 79—53164
- eye, retina injuries, magnetoretinographic meas. using SQUID magnetometer 80—104702
- ferredoxin, from Clostridium pasteurianum, Mossbauer effect, ESR, and mag. susceptibility meas. 80—40961
- ferredoxin synthetic analogues, $[Fe_4S_4(SR)_4]^{3-}$ clusters, Mossbauer effect, EPR, and mag. props. 80—41057
- ferric myoglobin compounds, single crysts., Mossbauer spectrum in small mag. field 79—100571
- field detection by invertebrates Tenebrio and Talitrus, distinct from light detect. 78—77073
- fish, lorenzinian ampullae detect. of geomag. variations 79—39381
- fluorescence polarisation of chlorella cells and pea chloroplasts orientated in a mag. field 80—51055
- frequency/depth-penetration considerations in hyperthermia by magnetically induced currents 80—63887
- genetic and physiological process control by magnetic methods *(Russian)* 79—2088
- geomagnetic field sensitivity in animals, ferromag. coupling to muscle receptors as basis 80—72185
- geomagnetic fluctuations effects on road accidents 78—15958
- gradiometer, balancing, system of adjustable superconducting plates, biomag. signal meas. 79—25162
- gradiometer for human heat magnetic field study 78—48914
- Gribble Limnoria tripinctata, reaction to intensity gradient of mag. fields *(German)* 80—56074
- guppy life cycle, effect continuous static mag. field 80—21481
- heart, human, elec. and mag. events, phase and amplitude relationship recording 80—104695
- heart attack as biological effect of geomag. fluctuation 79—83812
- heart attacks, no correl. with geomag. activity 80—21482
- heart attacks correl. with geomag. activity 79—39424
- heart vector components, simultaneous meas. with unipositional lead system 80—104697
- heart vector meas. in humans 78—35873
- His-Purkinje conduction system, human, mag. study 80—89818

biomagnetism continued
- homing pigeon sensitivity to Earth-strength mag. field, 0.5 gauss 77—52812
- human brain, neuromagnetic fields evoked by sensory stimuli 79—83813
- human perception tests, 60 Hz moderate strength magnetic fields 79—11951
- HV lines to 800 kV, elec. and mag. field effects on human beings *(French, English)* 80—72209
- hyperthermia by magnetically induced currents, freq.-depth-penetration, comments and reply 80—108991
- instrumentation and meas. 80—36181
- intracellular water, effect of paramag. impurities on proton spin-lattice relax. 80—51134
- LF biomag. meas. using thick-walled Al enclosure 80—62698
- lung, mag. field meas., comparison between two methods 80—104712
- lungs, freeze-dried, localised-field magnetopneumographic meas. 80—104714
- lymphocytes, living and dead, mag. props. and mag. sedimentation 80—35925
- lysozyme, electric and mag. props. 77—44584
- macromolecules, effects of permanent mag. field 77—25364
- macromolecules and membranes, struct. in high mag. field 77—64163
- magnetic auditory evoked response using SQUID 78—80889
- magnetic susceptibility applications, review of literature 1975-1977 78—82006
- magnetocardiogram, effect of torso geometry 77—60222
- magnetocardiogram and cardiac output meas. with integrated system 80—104709
- magnetocardiogram enhancement by applied mag. field 80—104701
- magnetocardiogram meas. first order gradiometer and DC-thin film SQUID 80—89877
- magnetocardiogram recording on normal subjects, morphological and multipole analysis 79—39426
- magnetocardiogram study using computer model 78—3528
- magnetocardiograms from normal hearts, interpretation *(Japanese)* 78—53433
- magnetocardiograms of normal and abnormal subjects, anal. using 2D displaying method *(Japanese)* 80—67177
- magnetocardiography, appl. of Nb SQUID 77—22583
- magnetocardiography, clinical appls., instrumentation and methods 80—35927
- magnetocardiography, field meas. techniques *(French)* 77—37073
- magnetocardiography and ECG, R and T waves 80—104699
- magnetocardiography in hospital environment, normal aspects 79—39550
- magnetocardiography in weak DC ambient magnetic fields 79—79567
- magnetocardiography overview 79—92246
- magnetocardiography recording, props. of ideal system, appl. of ECG theory 80—104700
- magnetoelectrets, possible mech. of mag. field effects 80—93157
- magnetoelectric dipole structure hypothesis, biological and cosmic appls. 80—91124
- magnetoencephalogram and electroencephalogram, comparison of spatial response 80—26245
- magnetoencephalogram genesis mechanisms 78—53432
- magnetoencephalography, correl. with EEG for normals and patients 78 -65062
- magnetoencephalography, distrib. of detector sensitivity, reciprocity appl. 80—72278
- magnetoencephalography, sensitivity distrib. 80—101246
- magnetometer, induction type, for biomag. fields *(German)* 79—88207
- magnetometry of human heart in small ferromag. enclosure, using SQUID 78—92726
- magnetophosphenes, quantitative anal. of thresholds 80—72184
- magnetophosphenes, quantitative determ. of thresholds 80—61620
- magnetopneumographic measurement of particle conc. and clearance in the lung 80—21514
- magnetopneumography, analytic methods 80—104713
- magnetopneumography, evaluation for assessing thoracic accumulation of welding fume particulate 80—101247
- magnetotherapeutic apparatus and application statistics *(German)* 79—16340
- mammalian cell growth and genetics under constant mag. field exposure 79—34520
- mammalian tissue mitotic activity inhibition by strong mag. fields 79—34519
- mammary tumours, paramagnetic changes during development in rat 79—39425
- MCG, PR segment theory rel. to current sources within heart 80—101191
- measurement and significance *(Japanese)* 80—30735
- measurement facility installation in hospital environment, design criteria and procedure 80—104707
- measurements in unshielded and noisy environments 80—104710
- median nerve, transient responses to elec. stimulation, SQUID appl. to somatically evoked field meas. 80—104706
- membranes, electric and magnetic props. in smectic liquid crystal state *(Russian)* 77—60190
- metabolite mapping by ^{31}P NMR in whole animals, diagnosis appl. 80—36211
- metallo-proteins and model systems, susceptibility and struct., SQUID magnetometer uses 79—53036
- microcirculatory phenomena, effect of const. mag. field 77—32935
- molecules, mag. circular dichroism, review, book contrib. 80—109080
- moving cells, mag. force 77—70486
- muscle, mouse, NMR multiwindow anal. and proton local fields and magnetisation distrib. 80—21444
- muscle water, frog, varied mag. field, multiple-pulse and magic-angle spinning ^{1}H NMR obs. 80—51135
- muscle water, mouse, ^{1}H NMR anal. above and below freezing 80—56073
- nerve bundle magnetic stimulation, capacitive coupling effect 79—48242
- nerve conduction velocity, biomagnetic response of lobster circumesophageal connective 78—92619
- nerve membrane potential, effect of constant mag. field 79—57679
- nerve stimulation, contactless, electromagnetic induction technique 77—52779
- nerve tissue magnetic stimulation, capacitive stimulatory effect 79—2116
- neuromagnetic fields sources location, using SQUID system, comparison with electrical method 80—101190
- neuromagnetic response latency of human visual cortex 78—40151
- neuroradiography by NMR imaging 80—51197

biomagnetism continued
NMR imaging, physiological effect threshold for RF and mag. fields 79—66484
NMR of living tissue, biological and medical appls. 77—77959
nocturnally migrating bird orientation rel. to geomag. disturbance 77—66820
nucleic acids, discontinuous mag. field effects, room temp. superconductivity 79—62195
orientation of organisms in mag. fields, evidence from particles suspended in electrolytes 78—48657
oxyhaemoglobin, mag. susceptibility of frozen aq. soln., 25 to 250K 78—6507
parametric biostimulation, mag. field calcs. 80—36054
photosynthetic reaction centres, triplet population, mag. field and g-factor differences effect 80—97879
photosynthetic systems, magnetoorientated, fluorescence polarisation theory 79—16165
physiological aqueous solution, possibility of hydromag. wave excitation 80—94246
physiological saline, movement of dissolved O_2 in mag. field 79—57678
pigeon homing performance, correlation with magnetic storm due to sunspots 79—2087
pigeon magnetic field sensing capability 80—56076
pigmented biomembranes, photoelec. and magneto-orientation effects, review 77—48766
red blood cell, human, axial trajectory meas. in high-gradient magnetic separation 79—53165
remanent magnetization as evidence for room temp. superconduction in biological materials 80—35926
retinal ganglion cell activity induced by ELF mag. fields, method for study 80—56321
retinal rod external segment mag. anisotropy decrease after total photolysis 77—52838
RF SQUID, use in magnetocardiography *(Dutch)* 79—79670
rhodopsin, visual pigment, mag. anisotropy estimation 80—51137
sensory apparatus for weak EM radiation detect. in humans, anatomical localisation 80—8075
somatosensory cerebral evoked potential changes under constant mag. field 79—39383
spirostomum, mag. field effects on drug induced contractility and mortality 79—74607
SQUID applications in biophysics 79—29640
SQUID arrays, for mag. field meas., geophysical, biomedical appls. 78—32830
SQUID detector appl., techniques 78—96061
SQUID fluxgate magnetometers, magnetopneumographic meas. 80—104711
SQUID gradiometer, second-derivative, magnetocardiogram meas. 80—104696
SQUID instruments and shielding for low level mag. meas. 77—40840
SQUID magnetometer with selective pickup loop to biomagnetic meas. 79—63286
static and LF mag. field biological effects and hazards 79—34579
static and low frequency magnetic fields, biological effects review *(Slovak)* 78—88722
steady current-produced fields in human body 80—94248
superconductive helmet with SQUID for magnetoencephalography 80—104708
susceptibility measurement, living rats 80—72391
susceptiblity instrument, supercond., automatic, biological appl. 78—57153
synovial fluid analysis by ferrography 80—101242
trace element conc. factors, mag. field effects 77—70438
tumour cell in vitro radiosensitivity and recovery, effect of 1400 gauss mag. field 77—44723
vector magnetocardiogram meas. using supercond. magnetometer 77—29213
vector magnetocardiography, practical lead system 77—44698
virus orientation by high mag. fields 80—13110
visually evoked elec. and mag. response simultaneous recording for diagnosis 78—53558
volume conductor electrical source information from elec. and mag. surface data 79—83727
water in biological systems, pulsed NMR obs. 80—35930
water mobility in blood plasma, NMR determ., viscosity correl. to $1/T_2$ 80—67176
water molecules in biological systems, relax. rel. to vol., pulse NMR obs. 80—40960
Al shielded room for biomag. meas. 80—104846
Al, thick-walled conducting shield in biomag. expts. 80—104845
Ca ions activity change due to magnetisation as possible mechanism of biological effect *(Russian)* 79—39423

biomechanics
see also biological fluid dynamics; biorheology
abdominal aorta, human, mech. characts. w.r.t. atherosclerosis 79—20571
abdominal aorta wall, human, after endarterectomy, deform. and strength 77—25497
abdominal wound strength, meas. method for expt. animals 79—44003
above-knee prosthesis, polycentric knee-ankle mechanism 79—48379
acceleration effects in women after 15 days bed rest, fluid and electrolyte shifts 77—48881
acceleration effects on thermoregulatory responses of unanaesthetised rats 77—48882
accelerator, compact, characts. and appl. to mouse behavioural stages classification 80—56309
acoustic diagnostic technique for prosthetic fixation evaluation 80—21510
acrylic bone cement spinal fixation, mech. props. 78—81072
actomyosin from a non-muscle system, tension generation 80—76781
adaptive control mechanisms for complex motor systems 80—81573
adaptive stiffness control in human movement 80—108947
airway smooth muscle, contracted, hysteresis, dog expts. 80—81634
ambulation, energy expenditure in disabled subjects vs. normals 77—44712
anatomical surface shape meas. method 80—3882
aneurysm of ascending aorta, stress/strain characts. and elastic moduli 77—37001
angular momentum of human body, computational technique 77—56403
animal joints, mechanics, book contrib., review 80—21488
animal motion, nonstationary mode near air-water interface *(Russian)* 77—32869

biomechanics continued
animal organs, small samples, simple apparatus to evaluate mechanical props. 79—12055
ankle compliance, human, dependence on joint angle 79—11959
ankle joint, human, compliance 78—57034
antagonistic muscles, functional elec. stimulation optimisation, math. modelling, joint motion 80—61730
aorta, canine, mech. props. following hypercholesterolemia 80—104620
aorta, canine, mech. props. following hypercholesterolemia 80—108938
aorta, human, morphological and functional aspects of study of mech. props. 77—25499
aorta, root of, functional anatomy and deform. props. 80—67136
aorta, strength variation with age in humans 78—48823
aortic compliance in living dogs measured by elec. admittance plethysmography *(Japanese)* 80—3748
aortic compliance meas. from transthoracic admittance plethysmogram, dog expt. 78—31925
aortic mechanics, canine, interaction of smooth muscle cells and collagen 79—43941
aortic stiffness noninvasive determ. methodology, echocardiographic recording 79—83875
aortic tissue failure props., effect of age 78—31839
aortic valve, expansible nature of base, rel. to prosthetic design 78—40232
aortic valve, finite element stress anal., human data 77—44699
aortic valve histology rel. to mechs., porcine expts. 80—85430
aortic valve leaflet stress anal., pig 79—53168
aortic valve leaflets, stress anal. with smoothed geometrical data 77—52815
aortic valve mechanics, anal. in diastole 80—35928
aortic valve mechanics, material props. of natural porcine valves 79—39440
aortic valve prostheses, hydrodynamic losses eval. 80—72378
aortic valve study, by holographic interferometry and shadow Moire methods 80—104613
aortic valve tissue, porcine, glutaraldehyde-treated, mech. fatigue study 80—67112
aortic-iliac junction, geometry and elastic response 80—16977
apexcardiogram, math. model of endogenous thoracic forces 78—31849
arbitrary movements control theory 79—74641
arm, lower part, statics and equilib., for 1st yr. medics 79—35505
arm and forearm exercise joint force musculoskeletal model 79—92272
arm mobility, human, struct. and functional features 80—35946
arm movements controlled by peripheral feedback, in humans, simulation 78—80891
arm posture control, spring model and equivalent neural network 80—101196
arm swing in human locomotion, mathematical model, electromyographic recordings 79—39434
arterial collapse after subjection to an external press. band 80—94271
arterial grafts, in vivo mech. props., biological vs. synthetic grafts 77—37002
arterial grafts, synthetic, mech. props. 80—17192
arterial segment loading-unloading simulation and analysis 79—83844
arterial segments, canine, nonlinear anisotropic viscoelastic props. 78—20205
arterial smooth muscle, pig, estimates of cellular mechanics 79—16229
arterial vessels, small, critical changes in lumen 80—61615
arterial wall, role of stress conc. in atherogenesis 80—16970
arterial wall axial deform. and anisotropy *(Japanese)* 78—53437
arterial wall axial deformation and anisotropy obs. 79—83833
arterial wall empirical linear response models 77—90831
arterial wall mechanics, regional, species and age related vars. 80—3665
arterial walls, human coronary, optical density determ. 80—12173
arteries, human, intracranial and extracranial, stiffness and elastic behaviour 80—85436
arteries, small, pulmonary, elasticity in the cat 80—108942
arteriograft, fracture phenomena, of bovine, swine 78—92746
artery, finite deform. elastic model, large amplitude oscills. 77—37000
artery, mechs. of corrugated collagen fibrils 77—48823
artery length-force and vol.-press. relations, meas. and empirical formulae 78—65072
articular cartilage, asymptotic theory for thin layers with appl. to knee joint 78—44537
articular cartilage, electromechanical props. during compression and stress relaxation 78—92667
articular cartilage, energy absorbing ability during impact 79—92254
articular cartilage, function of collagen fibril ultrastruct. 79—34597
articular cartilage, in vitro studies of wear against stainless steel 79—74714
articular cartilage, load-displacement-time characts., rel. to fluid flow in matrix 77—48820
articular cartilage, mech. stiffness in confined oscillating compression 79—74697
articular cartilage, mechanical behaviour, ionic environment effects 80—41085
articular cartilage in uniaxial tension, large deform. nonhomogeneous and directional props. 80—3696
articular cartilage in uniaxial tension, nonhomogeneous directional mech. props. meas. 77—29167
articular cartilage under compressive stress, elastic behaviour 77—73536
articular surfaces, math. representation of positron 80—3685
articulated total body model, generation of child data sets from anthropometric data, for crashes 78—80912
articulating joint motion description 78—27988
articulation mechanical properties and physical aspects of lubrication *(French)* 79—34591
articulations lubrication, global anal. *(French)* 79—34592
artificial heart valves, dynamics 80—72379
artificial hip joint biomechanical test procedures *(German)* 79—8577
artificial hip joint construction compatible with femoral natural stress distrib. *(German)* 79—8576
artificial knees, mobility, stability and stress 79—12032
associated movement study, portable micro-system 80—51299
astronaut body, rotational motion during weightlessness 78—15914
back strength, correl. of clinical and Cybex isokinetic and isometric assessment 78—40230
back strength, torso muscular capacity assessment by isokinetic analysis 79—96606
baikal grayling, oxygen debt and swimming efficiency *(Russian)* 77—64168

biomechanics continued
Baikal grayling, swimming efficiency and optimum velocity *(Russian)* 77—32924
ballistic walking, math. model of swing phase 80—67131
ballistocardiograms, statistical pattern recognition 80—26408
basilar membrane, anisotropic rigidity components evaluation 79—79569
binocular retinal image motion during active head rotation 80—72158
biodynamic subminiature piezoresistive accelerometer performance evaluation 78—20340
bioengineering, international conf., Cape Town, S.Africa (April 1977) 79—20695
bioengineering advances conference, San Francisco, USA (Dec. 1978) 79—92416
biomedical engineering textbook for undergraduates 80—8750
biopolymer materials, review of mechanics of tissue 78—69131
biopolymers, deform. under uniaxial stretching during UV irrad. 80—108935
biotelemetry, conf., Garmisch-Partenkirchen, W.Germany (May, June 1978) 79—43980
biped and quadruped locomotion energetics 80—30755
biped dynamics, feedback on-off model 80—30709
biped locomotion control, digital simulation 78—80904
biped locomotion dynamics, control theoretic study *(Japanese)* 79—11963
bipedal hopping in small mammals, energetic cost obs. 80—108936
bipedal locomotion, simple model of step control 79—11958
bladder distensibility and contractility characterisation indices 79—92265
blood, US backscattering, haematocrit and erythrocyte aggregation depend. 80—45961
blood vessel coagulative commissures, influence of high amplitude elec. impulses on strength 80—104600
blood vessel compliance, theoretical investigation 80—41091
blood vessel dynamic strain tolerance at different post mortem conditions 80—16988
blood vessel wall mech. props. *(Japanese)* 80—56092
blood vessel wall rheological properties, continuum-mechanical analysis *(Hungarian)* 78—35875
blood vessel walls, dynamic test apparatus 80—41354
blood vessels, exam. of mech. props 80—12175
blood vessels, medium sized, mech. characts. 80—41101
body motion, quantitative meas. by Schottky barrier Si photodiode and laser beam 80—12207
body motion computer-aided tracking using CCD image sensor 78—61269
body shape and movement meas. using the vector stereograph 80—17148
bone, anisotropy of Young's modulus, fibre-reinforced composite model 80—35944
bone, anisotropy of Young's modulus, US meas. 78—11687
bone, appl. of stress-wave detection of an edge crack to healing rate 78—30236
bone, attempts to stimulate longitudinal growth in dogs by mech. vibration 80—81638
bone, cancellous, of knee and ankle joints, preferred orientations, determ. and significance 77—36987
bone, compact, deform. and strength 78—24087
bone, compact, fatigue damage, residual strength and stiffness 77—90834
bone, compact, human, microscopic struct. rel. to fractures 80—56106
bone, compact, long-term torsional creep obs. 80--104619
bone, comparison of electromech. effects in wet and dry bone 80—97985
bone, crack velocity depend. of longitudinal fracture, bovine tibia 80—97965
bone, deformation capacity of compact tissue of human tibia subjected to torsion, age effect 77—52827
bone, demineralised dense human, strength props. nonuniformity 80—104611
bone, elastic and damping props. of human femur in bending 77—25489
bone, elastic characts. of compact bone tissue of human tibia, differences and correls. 77—25490
bone, foetal mouse, stress effects in vitro, including ectopic ossification 77—36989
bone, fresh and preserved by freezing, bending strength 77—25488
bone, Haversian plate in man, microhardness 78—48825
bone, human, acoustic emission in restressing 80—3704
bone, human, demineralized, deform. props. on stretching 80—3703
bone, human cortical, local piezoelec. polarisation as function of stress freq. 77—32933
bone, human cortical, US properties and microtexture 80—51144
bone, human vertebral, compressive strength and elastic mod. depend. on age and density 77—36985
bone, hydroxyapatite nucleation energetics 78—40127
bone, impact energy absorpt. changes with age 80—3698
bone, impact loading, anisotropy of compact bone tissue 77—25491
bone, internal remodeling induced by medullary pin 79—29552
bone, mammalian, acoustic emission testing 80—76783
bone, mech. props., normal vs. pathological cancellous bone *(Japanese)* 77—25480
bone, mechanical properties rel. to density and mineral phase orientation and particle size 80—16989
bone, mechanical props. of deer's antler, cow's femur and fin whale's tympanic bulla 80—3686
bone, moduli of elasticity and rupture, rel. to composition 78—31835
bone, orthogonal machining, forces and energies 79—29559
bone, piezoelectric effect on exposure to US, effect of sample rot. 78—80913
bone, radius remodelling, sheep, rel. to functional stress and strain 80—35939
bone, strain-related potentials, freq. depend., effect of meas. system parameters 80—16991
bone, stress distrib. in long bone due to prosthesis positioning 77—36984
bone, stress generated potentials at osteon level 78—31837
bone, stress generated pots., linear piezoelec. model 80—3688
bone, tensile strength rel. to strain rate, microstruct. and density 77—44703
bone, tibia, human, physical stress effect on state, US meas. 78—24088
bone, US velocity rel. to mineral content 80—45962
bone, vibr. propag. through human femur 77—25494
bone, vibrational motion meas. by skin-mounted accelerometers, soft tissue effect 80—35954
bone, whole tubular, rigidity comparison technique 80—3881
bone accelerometer package attachment method 79—70717
bone bending stiffness determ. by LF impedance probe 79—96695

biomechanics continued
bone callus, dynamic characts. determ. by induced vibr. method 79—62284
bone compressive strength, rel. to density and strain rate 77—36976
bone compressive strength quantitation and effects on bone remodelling 78—31836
bone dynamic mechanical props., postmortem transition 77—21554
bone elastic modulus meas., US transducer fabrication 78—83201
bone fracture callus mech. props., intramedullary nailing rel. to plating 80—85438
bone fracture fixation anal., Oxford fixator 80—17188
bone fracture healing determ. by US propag. 78—24105
bone from Cu deficient chicks, viscoelastic props. 79—79578
bone loading method, controlled and time-varying 79—70566
bone material, compact, destruction, anisotropy in 80—12174
bone mechanical properties characterisation by dynamic response 80—76782
bone mechanical properties determ. in vivo, noncontacting EM device 78—77133
bone morphology and fracture, exam. 78—57036
bone piezoelectric effect, theoretical anal. 79—70567
bone piezoelectric response obs., freq. depend. 79—92287
bone remodelling, adaptive elasticity theory 79—25016
bone remodelling, quantification of stresses 80—85437
bone remodelling, small strain adaptive elasticity 77—16949
bone remodelling beneath internal fixation plates of varying stiffness, parametric study 80—16990
bone resonance, effects of geometrical parameters, shear and rot. inertia, finite element model 77—29165
bone section geometrical props. determ. by laminography and phys. section 78—20202
bone strains of canine radius and ulna, in vivo meas. and anal. 80—67130
bone strength, rel. to mineral supplemental diet in young rabbits 77—36986
bone stress distrib., apatite crystal orientation 79—39431
bone stress wave detection using piezoelec. effect, non-invasive technique 78—31948
bone surface remodelling, math. theory 78—31847
bone tissue, compact, destruction 80—67135
bone tissue, compact, fracture 80—12178
bone tissue, dry, piezoelectric model 79—25015
bone tissue, human, nonlinear creep on stretching 80—3702
bone tissue, human, subjected to longit. extension, acoustic emission 77—25495
bone tissue crystals, effect of compression 77—25492
bone transverse elastic coeff. determ. 78—27985
bone-pin connections, anchoring characts. rel. to pin diameter 78—44698
bone/porous polyethylene interface, tensile strength 80—30737
bony tissue, compact, from human tibia, creep under tension 77—25487
bony tissue, human, mechanoluminesc. during rupture 79—20572
bovine hip bone, compression tests, effect of specimen shape and size on mech. props. and fracture mode 78—69132
bowel anastomosis dynamic strength testing device, electronically controlled *(German)* 80—36160
brain, experimental oedema, serial meas. of specific gravity and computerised tomography attenuation 80—98005
brain injury, pulse loading effect 78—57029
brain injury and instabilities 80—45943
brain retraction pressure monitoring, meas. system for surgical procedures 80—21563
brain tissue, human, creep and relaxation props. 79—92263
brain tissue, human, nonlinear constitutive relations 78—80910
brain tissue elastic response props. in vivo 78—31840
breathing movement dynamics, human fetus 80—3707
burn-scarred human skin rheological props. in vivo meas. 78—31935
buttock deformations and stresses, sitting person, finite element anal. 79—16241
car accidents, correl. of field injuries and GM Hybrid III dummy responses 80—108939
cardiac, left ventricular mural force changes rel. to myocardial pump performance 80—8092
cardiac adaptation and hypertrophy, ventricle model *(Japanese)* 78—31828
cardiac aneurysms, possibility of blow out 79—88100
cardiac arteries, human, effect of age on mech. props. and biochem. composition 80—8091
cardiac chemical power, appl. of power, work and efficiency eqns. to left ventricular energetics in man 80—16912
cardiac chemical power, derivation of chem. power eqn. and determ. of eqn. consts. 80—16911
cardiac contractile filament and series elastic work and power, mathematical model 80—16981
cardiac contractile filament and series elastic work and power, clinical correls. 80—16982
cardiac contraction dynamics study 78—44523
cardiac disc mitral valve in left ventricle, computer model of motion 80—8214
cardiac energy density function encompassing elastic and contractile props. 79—62279
cardiac function modification by synchronised oscill. accel. 80—56089
cardiac left ventricle, contractile filament stress rel. to wall stress 80—56096
cardiac mechanical activity, noninvasive mag. detect., instrumentation 80—89820
cardiac mechanical activity, noninvasive mag. detect., theory 80—89819
cardiac mechanical function assess., left ventricular wall stress and strain anal. *(Japanese)* 79—96589
cardiac mechanical function assessment methods *(Japanese)* 79—2148
cardiac muscle, mathematical contractile model *(Japanese)* 79—57632
cardiac muscle *(Japanese)* 80—72201
cardiac muscle fibre, stresses in left ventricular wall, biaxial stress-strain relations 79—29558
cardiac muscle force-velocity relation, anal. in time domain 80—35943
cardiac muscle series elasticity, effects of mech. history and time in twitch 77—37004
cardiac muscle stress/strain relationship determ. by computerised tomography 79—92262
cardiac Purkinje fibres, intracellular Na^+ activity rel. to tension, sheep obs. 80—51060

biomechanics continued
- cardiac responses of dogs to nonsynchronous and heart synchronous whole-body vibration 80—3675
- cardiac wall motion and regional ejection fraction, comparison at rest and during isometric exercise 80—30857
- cardiovascular system contractility characterisation by programmed premature contractions 79—88113
- carotid arteries of dog, longitudinal stretch effect on dynamic elastic props. 78—27977
- carotid arteris, human, strength props., changes with age 80—16993
- carotid artery, human, shear modulus determ. 80—26253
- carpal tunnel syndrome, some biomech. aspects 80—16983
- cartilage, articular, meas. of surface microgeometry 80—3880
- cartilage deformation and interstitial fluid flow, nonlinear interaction 77—32931
- cartilage/bone plugs, impact stress/strain data 79—43950
- cat eardrum model as thin shell using finite element method 78—65036
- cell membrane interaction theory of molecular level mechanics 79—92174
- cell membrane nuclear hydrodynamic shear, non-equil. Ising model, master eqn. 78—61146
- cellular deformability, diffractometric method for meas. 80—98187
- cellular elastomer selection for use in biomechanical capacitive force transducers, measuring device *(German)* 80—85545
- centrifugation stress, effects on pituitary-gonadal function in male rats 80—98149
- cerebro-spinal specific elastance in cats, in vivo determ. 78—40236
- cervical spine, human, stability under tension 79—16236
- cervix, force-dilatation characts. math. model, expt. results 77—81523
- cetaceans, drag reduction and self regulation of skin damping while swimming *(Russian)* 77—32918
- child, normal, locomotion kinematics, TV data study 79—70561
- chitin, in lobster shell and apodeme, piezoelec. rel. to remodelling 78—64929
- chronobiological movement transducer *(Spanish)* 80—89902
- cilia and flagella, displacement and sliding of twisted filaments 77—32929
- cilia of mollusc, gill, effective stroke bending process 80—30756
- ciliated microorganism locomotion, porous prolate-spheroidal model, swimming rel. to sedimenting 77—48822
- circadian oscillators, two-dimensional limit model for constant light 79—92255
- claw hand optimal surgical correction, finger biomechanical model 79—92268
- cochlea, 3-dim. model, point-impedance charact. of basilar membrane 78—57009
- cochlea, two dimensional model, method for computing motion 78—65037
- cochlea mechanics, modes and waves 79—92232
- cochlear mechanics freq. sensitivity anal. 78—24078
- cochlear model vibration mode visualisation by holographic interferometry 79—2083
- collagen, 3-dimens. struct., rel. to props. of connective tissue 80—67038
- collagen, tendinous, highly ordered maromolecular composite, mech. props.-ultrastruct. relation 77—52826
- collagen fibres, mech. props., role of struct. organisation 80—72207
- collagen fibres, of dermis, structural and mech. charact. and natural interweaving 78—48824
- collagen membrane H^+ diffusion-limited binding electromechanics 79—79489
- collagenous tissues, flat, struct. theory for homogeneous biaxial stress-strain rels. 80—3695
- compact bone, empirical strength theory, biaxial stress characts. 78—77081
- cone and bone prostheses, strain gauge meas. on loaded femur 77—60228
- conference, Ankara, Turkey (July 1978) 80—51953
- conference, Ann Arbor, USA (Oct. 1978) 80—31408
- conference, Pennsylvania, USA (Oct.1979) 80—82567
- corneal pressures due to soft contact lenses and corneal asymmetry 80—104621
- corneal wound holographic stress testing in postoperative patients, specular illum. arrangement 78—65102
- coronary arteries, human, mech. prop. changes with age 78—65068
- cortical bone, anisotropic anal. of strain rosette information 79—16237
- cortical bone, bovine, fatigue strength, stress freq. influence 80—16997
- cranial bone, fetal, elastic modulus obs., appl. to fetal head moulding biomechanics 80—67128
- creeping locomotion kinematic modes, ideally elastic model 78—15853
- critical light reflection at a plastic/glass interface and appl. to foot press. meas. 80—81681
- cruciate ligament cross-section evaluation, press. depend. of area micrometer method 80—56101
- crutch walking, lower-limb vertical ground-reaction forces 78—77079
- deformations of bioconstructs. at different stages of morphogenesis 80—51140
- deltoid muscle, myoelectric signal rel. to physiological props. 79—70539
- dental implant fixation, electrically mediated process, interfacial strength 79—16348
- dental implants, stress anal; effect of elastic parameters and geometry 80—30930
- dental implants, stress anal., effect of root-length and pseudo periodontal ligament incorporation 80—30931
- denture base acrylic tensile testing 80—16621
- diaphragm mechanics, dog 77—12947
- diaphragm muscle, canine, in vivo stiffness props., obs. and meas. system 80—97988
- diastolic semilunar valve vibrations, heart sounds, one-dimensional model 79—79580
- disabled human operator, new approaches to modelling 79—92253
- dolphin, hydrodynamic swimming characteristics *(Russian)* 77—32922
- dolphin fins, controllable hydroelastic effect *(Russian)* 80—41062
- dolphin swimming, leaping for efficiency at high speed 80—61619
- eardrum vibration meas. using electronic speckle pattern interferometry 80—67209
- education, Newtonian mechanics, estimates of human body mechanical performance 78—40211
- ejection fraction rel. to ventricular vol., computer anal. 80—104599
- elastic modulus, incremental, for orthotropic incompressible arteries 80—30751
- elastic strain energy storage in muscle and other tissue 77—16950

biomechanics continued
- elastometer probe system for localised in vivo compliance meas. 78—31960
- elbow angular vel. in horizontal flexion rel. to integrated EMG 80—3620
- elbow flexion at maximal vel., power prod. 79—57691
- elbow flexion-extension and forearm pronation-supination for elbow endoprosthesis design 80—3682
- elbow joint, human, mech. anal. 80—104626
- elbow joint, moments transmission, isometric tests 80—41083
- elbow joint forces derivation and rel. to prosthesis design 79—96591
- elbow three-dimensional rotation 78—69129
- electromechanical model for human articular cartilage 80—104631
- EMG, weighted sum rel. to total torque, human triceps surae 78—20203
- EMG period-amplitude analysis, cat locomotion and jumping obs. 80—67057
- EMG silent period and muscle mechanics in human soleus muscle 80—67060
- endocardium motion during contraction, anal. method 80—109072
- endopelvic fascia, human, stress/strain history relations in simple elongation 78—44539
- engineering and medical, conf., Riga, USSR (Oct. 1975) 77—25481
- epiphyseal plate, method for evaluation and control of growth activity 80—81789
- epithelium of small intestine, mech. props. of intercellular contacts 78—53351
- equation of motion of a cyclist 80—30748
- equine long bone forces and moments, in vivo and anal. studies 78—40216
- ergometer for small-animal research 80—101295
- erythrocyte, rheological models *(French)* 78—24083
- erythrocyte, sectioned, generalised theory of geometrical shape 78—65071
- erythrocyte deformability, viscometric flow and laser diffractometric technique 78—35879
- erythrocyte deformation in centrifugal field 78—27976
- erythrocyte flexibility, pharmacological effects, aging model *(German)* 79—79583
- erythrocyte membrane, viscoelastic props., theoretical and expt. studies 79—16157
- erythrocyte osmotic fragility curve, statistical synthesis 78—65070
- erythrocytes, surface area calc. method in elastic deform. 79—70571
- extraocular eye muscle force duction tests after administration of succinylcholine or pancuronium 80—26255
- extraocular muscle system mechs. model for clinical ophthalmology 78—40155
- extraocular muscles, relative tensions 79—34554
- eye, astigmatism induced by pterygium 78—40139
- eye, direction of gaze, determ. method using Listing's law 79—34677
- eye, elasticity of sclera and choroid in humans, rel. to scleral rigidity and accommodation 78—80907
- eye injury potential of propelled objects, assessment system 80—21591
- eye lens, human, microwave-induced hazardous non linear thermoelastic vibrs. 79—83853
- eye lens thermoelastic stresses due to microwaves 78—80914
- eye level acceleration forces experienced with rotation on the horizontal bar 80—45937
- eye movement detect., on-line analogue analyser 79—79699
- eye movements, additivity of fusional vergence and pursuit eye movements 80—35884
- eye position measurement, method for implantation of mag. search coils 80—85548
- eyeblink, human, dynamics model 78—61167
- facial skeleton strain distrib. arising from orthodontic appliance activity, holographic interferometry 80—67143
- femora, bovine, fracture toughness, critical crack length, plastic zone size 79—43948
- femoral bone, bovine, slow fracture propagation obs. 79—79592
- femoral components, probability model for fracture taking into account patient's age 80—41070
- femoral fracture brace, biomech. study of function during stance 80—97990
- femoral head replacement prosthetic, transmission of load actions 80—56284
- femoral necks, fracture fixation by Muller screws, mech. investigation 80—72377
- femoral shaft, human, age and sex-related changes in struct. and strength 77—56401
- femoral shaft fractures, early weight-bearing treatment using cast-brace 80—16985
- femoral stress and strain calc., finite element method *(German)* 79—2089
- femoral subtrochanteric fracture stress anal. 79—79591
- femur, bovine, crack vel. and fracture mech. 79—57690
- femur, canine, in-depth mech. props. anal. 80—16979
- femur, dog, work to fracture meas. 79—57687
- femur, flexural coupling to hip-prosthesis stem, theoretical anal. method 79—39428
- femur, human, finite-element plane stress model 79—79590
- femur, human, with implanted Charnley prosthesis, stress anal. 78—20314
- femur, rat, influence of hypergravity on compressive strength 80—3690
- femur compact bone, adult human, relation between torsional props. and histology 79—16234
- femur intracondylar cancellous bone, compressive strength rel. to loading rate 78—40219
- femur strength, rat, rel. to growth, bone-length, gravity 80—16978
- femur stress analysis, three-dimensional, using finite element method 78—7379
- femur with proximal prosthesis, 3-dimens. anisotropic stress anal. and failure prediction 78—40424
- femurs, human, elastic constants determ. 80—35951
- fetal head moulding, finite element model investigation 80—67129
- fetal membrane tissue, human, elastic parameters determ. 79—66481
- fibrosarcoma cells, buoyant density, effect of hypoxic growth conditions in vitro 80—104601
- fibula, direct meas. of load bearing function 80—104624
- film data reduction and anal. using PLATO system 79—35873
- finger prosthesis, elastomeric bearing as internal joint 79—92429
- finger tendons, functional anal. of role 80—35936
- finite element analysis as an aid to implant design 80—30932
- fish, endoepithermal secretions rel. to swimming speed *(Russian)* 77—32967

biomechanics continued

fish, fast swimming, drag reduction by slimy secretions into boundary layer *(Russian)* 77−32915
flagella bend propagation, derivation of eqns. of motion and simulation 78−77074
flagella bend propagation, dynein cross-bridge kinetics 79−43942
flapping wing propulsive efficiency for plane parallel flow (bionics) *(Russian)* 77−32919
floor reaction, meas. and medical appl. *(Japanese)* 80−12291
fly wing mechanism, model for teaching 77−33799
foetal membrane rupture, human, mechanics, superempirical mathematical model 79−83843
foot function assessment system, normal and pathological feet, computerised system 79−100760
foot load dynamic distrib., quantification system 80−94388
foot load static distrib., quantification using the PET computer 80−94387
foot load-bearing duration meas. technique 80−17149
foot pressure distributions, technique for display 80−85508
foot static weight distrib., meas. of lower extremity disability 80−41289
foot vertical force during walking, continuous meas. device *(Japanese)* 78−73273
foot-pressure measurements, static and dynamic, in clinical orthopaedics 80−98163
foot/floor contact temporal patterns during walking, automated on-line meas. system 78−77128
footfall pattern transduction by foot or shoe cover 79−57799
footfall patterns of animals during treadmill locomotion, electronic method for determ. 80−72386
force measuring platform *(Polish)* 80−36212
force plate, mech. design, construct. details and calibration 80−85544
force platform centre of pressure paths, averaging technique 79−57692
force-line visualisation system for artificial legs and lower-limb orthoses 80−17200
forces applied to a bicycle during normal cycling 80−16980
forces exerted in walking and running, Fourier anal. 80−94266
forces in animal joints 80−94251
forearm musculature, quantitative anal. 77−36981
form and engineering design mechanical aspects *(Japanese)* 78−24089
fracture healing in rabbits, temporal changes in phys. props. 78−40215
fractured femur fixation device, optimum design using finite element anal. 78−36050
gait, automatic 3D anal. using a Selspot centred system 80−108998
gait, EMG investigations 80−8198
gait, human, limb segment inertia influence on joint loading 79−92270
gait, representation by 4 dimens. vectors *(German)* 78−88723
gait abnormality index for locomotion efficiency evaluation 80−56100
gait analog tracings and computerized analysis through a PDP-11/45 79−29643
gait analyser/trainer instrumentation system 80−17150
gait analysis and the CARS-UBC electrogoniometer 80−56263
gait analysis in humans using pattern recognition 78−40374
gait analysis of bipedal locomotion 80−56104
gait analysis subsystem for smoothing and differentiation of human motion data 80−35953
gait assessment using components of the ground reaction force vector 80−101284
gait consistency test based on the impulse-momentum theorem 80−17166
gait instrumentation for foot/ground interaction meas. and display 79−96696
gait joint torque and energy patterns in normal humans 78−80897
gait kinematics, human, computer generation program 79−74703
gait measuring system for treatment evaluation, microprocessor controlled 80−61731
gait of cerebral palsied children, EMG investigations 80−72186
gait quality indication by temporal asymmetry 80−98164
gait recording technique, digital 79−70725
gait studies, planar control in multi-camera photogrammetric calibration for 3-D studies 80−67194
gastropod locomotion, role of pedal mucus 80−76780
geometric properties of paired human tibiae 80−67127
glass-ceramic implants, loaded, expt. studies on anchoring in the femur *(German)* 80−81624
glenohumeral joint biomechanics, mathematical treatment 79−43956
gravicentre oscillation frequency spectra in healthy human subjects 77−56413
ground reaction forces during ambulation, real time video vector display system 79−96688
ground reaction forces in distance running 80−97983
hair cells of organ of Corti, thermal noise 78−15845
hand, human, normative model for biomech. anal. 78−40227
hand, normative model for biomechanical analysis 80−41086
hand function, normal finger functional strength meas. 79−92276
hand motion in grasping, mechanical model 79−57694
hand position and forces during manual work, documentation method 79−74803
hand-arm system, distributed-parameter dynamic model 78−92663
hand-arm system, vibrational responses of hand 78−7380
hand-arm vibration, analytical model of hand vibr. response characts. 77−64074
hand-arm vibration, subjective response characts. to hand-induced vibr. 77−64062
hand-arm vibration, vibr. transmission characts. including meas. technqiue 77−64075
Haversian bone, exam. of mechanical failure at microstructural level 78−77080
head, spheroidal model, effect of bending on axisymm. vibrs. 77−29168
head impact, tolerance level for bridging vein disruption, math. model 80−16987
head impact injuries to children, biomech. anal. 80−56097
head injury model with viscoelastic brain tissue, mech. response 78−69117
head movements of mealworm beetle, props. and role 80−76772
head movements of mealworm beetle, responses to rotating panoramas 80−76773
head response to impact loading, parametric study by finite element modelling 77−48826
head viscoelastic model, impact response 78−40234
head-neck impact response using realistic human model 78−80909
heart, beating, kinematics theory 80−76777

biomechanics continued

heart, elastic props., forces, stresses and press. *(Dutch)* 78−73170
heart, ellipsoidal model, appl. to left ventricular contractions study 80−104608
heart, intact, relationship between velocity, muscle length, force and contractile state 78−44543
heart, isolated, grass-snake, motor reactivity obs. 80−67100
heart, mech. model, role of pericardium 80−35938
heart contractility, muscle tissue quality and sliding filament micromechanism *(Dutch)* 78−73171
heart contraction mechanism, modelling 80−72204
heart electrical and mechanical monitoring on extensometer 80−45944
heart left ventricle, finite element stress analysis 77−86518
heart motion kinetic anal., force-displacement relation 78−40222
heart muscle, behaviour of myosin projections during staircase phenomenon 78−53362
heart muscle, contraction variable preload and afterload independence, thermodynamic and clinical consequences 79−79576
heart muscle contraction force, rhythm influence modelling, intracellular pool Ca 79−79568
heart muscle excitation contraction coupling, mathematical model 79−96542
heart valve tissue, glutaraldehyde preserved, stress/strain and fatigue behaviour 78−40217
heart valves, crescent-shaped aorta, deform. props. by holographic interferometry 80−61616
heart valves, fluid-mechanical study 79−53171
heart valves, natural and prosthetic, simple stress estimation method 80−8210
heart velocity-strain loop in normal and abnormal left ventricular function 78−31850
heart vibration quantitative characterisation by multipolar acoustic heart model, minicomputer method 78−85429
hepatocytes, adhesive strength of ultrastructural elements 79−57682
Hill equation, fitting to expt. data 80−89777
hind-limb reflex movements, chelonian, simulation 79−74642
hip, human, kinematics and kinetics 78−69130
hip bone stress analysis using finite element model 78−44518
hip disarticulation amputee locomotion 78−44696
hip guidance articulations, principles and practice 80−3873
hip joint, maximum force analytical determ. by biomechanical model *(German)* 79−88099
hip joint local pressures in human cadaver, press. transducer direct meas. 78−40445
hip joint movements, electrogoniometer for meas. and anal. 79−74766
hip prostheses, Charnley, expt. anal. of surface stresses 80−17191
hip prostheses femoral component biomechanics, bone cement stress 80−56285
hip prosthesis design, femoral stem 78−36058
hip prosthesis stem loosening in human femur, biomechanical causes investigation 80−85435
holographic interferometry, rigid body motion compensation 80−67213
horse's hoof movement/load relationship camera and multicomponent force meas. panel *(German)* 79−16352
human body angular momentum about three orthogonal axes through centre of gravity 79−29551
human body mechanics review, book contrib. 80−12176
human body planar motion in free fall, interactive computer graphics 78−40221
human motion 3-dimens. monitoring by optoelectronic means, calibration and meas. 78−31913
human motion and force sensory mechanism model 80−8094
human skull, stresses due to pulse loading 79−48280
hyperbaric hyperreflexia, tendon-jerk and Hoffman reflexes in Man, soleus muscle 80−61530
IEEE 7th Northeast Bioengineering Conference, Troy (1979) 79−79672
iliac arteries, human, strength props., changes with age 80−16993
impact of human head against wall, expt. anal. of package cushioning 77−21555
inductive sonde, large bloodvessel movement, transcutaneous meas., design and realisation *(Italian)* 79−70602
insect fibrillar muscle fibres, stiffness and tension obs. during and after sudden length changes 80−56078
internal carotid artery, canine, under const. load regime, mech. props. 77−90843
intervertebral disc, pressure distribution determ. using intervertebral pressure transducer 80−41089
intervertebral disc response to shear stress 79−92261
intervertebral discs, effects of fluid injection on mech. props. 80−3697
intervertebral discs, statics and dynamics 80−104612
intervertebral disk of Rhesus monkey, response to P-A shear stress 80−104617
intervertebral joint, systems identification for material props. 78−69125
intestinal motor activity, math. model 78−77078
intestine, small, effect of pH on permeability and mech. props. of intercellular contacts 79−57613
intracellular membrane microviscosity, rat liver and hepatoma 27 80−30675
intracranial pressure meas. in newborns, new non-invasive technique 80−67272
isometric muscle contraction meas., fibre-optic force transducer 79−79715
isopycnic centrifugation method for rapid separation of murine thymocytes 80−104832
Japanese black pine, Pinus Thunbergii Parl., water potential and growth stress *(Japanese)* 80−3701
jaw, growth anal. in human using kinematic fundamentals 79−16243
jaw action of lizard, mechanical significance of streptostyly 80−51143
jaw muscle, electromyographic activity and mandible static loading 79−43951
joint centre analysis using stored program calculator 77−29166
joint differential mobility meas., periodontal ligament and temporomandibular joint 80−8093
joint displacements, finger and wrist, relationship with extrinsic finger flexor tendons 79−8520
joint hyperextensometer for laxity quantification 79−100761
joint instantaneous centre and angle of rotation, minimum error optimisation 79−96605
joint instantaneous centre of rotation, least square analysis 79−29555
joint kinematics and pathokinematics, study of instant axis concept 79−70565

biomechanics continued
joint lubrication model, nonporous compliant bearing, effects of cartilage stiffness and lubricant viscosity 80–3692
joint moment charting in functional elec. stimulation of the upper limb 80–41310
joint motion meas. by triaxial electrogoniometer, for human prosthesis design 78–11781
joint performance rel. to articular cartilage roughness 80–89782
joint position descriptive coordinate system 79–92269
joint replacements, mech. factors 80–56286
joint rotation, human, meas. by triaxial goniometer 79–92417
joints, cartilage swelling, congruity of regularly curved joints 79–8523
joints, centres and angles of rotation meas., errors and optimisation study 80–61604
joints, human, elastohydrodynamic lubrication 78–44522
joints, major articulating, human, review of biomechanics 80–56105
juvenile T-wave pattern incidence rel. to age and QRS transition zones 79–43849
kinematic gait, system for simple meas. 80–85509
knee, human, ligament primary and coupled load transmission meas. 79–92271
knee, human, nonlinear coupled stiffness characts. 77–36974
knee, human, torsional characts. and passive elements, simulated anatomical conditions 80–104628
knee, human in-vitro, varus-valgus and torsional load-displacement characts. 80–17000
knee arthrograph for study of stiffness 79–12022
knee biomechanics, review of some basic assumptions 80–94265
knee flexion, computerised instant centres of rot. 77–44710
knee impedance testing machine 80–21555
knee joint, anatomy, menisci load carrying capacity, expts. using four-spring model 80–41067
knee joint, appl. of anthropometric scaling method 77–52817
knee joint, human, torsional load-displacement characts. in vitro 78–40235
knee joint, menisci load carrying capacity 80–41068
knee joint, method for locating optimal fixed axis of rotation 79–62286
knee joint dynamics, appl. to artificial joint design *(German)* 77–56516
knee joint forces on rising from chairs 79–74698
knee joint impact response, comparison of normal and osteoarthritic joints 78–31848
knee joint kinematics accuracy 78–27987
knee joint movement during walking, meas. method using photographic records 80–17048
knee joint static force transmission obs., humans 77–86519
knee ligament disorder diagnosis, radiological meas. of laxity *(French)* 80–8136
knee ligaments, load transmission characts. during axial tibial rotations 80–104629
knee motion in gait and stair activities, normative data 78–40229
knee movement measurement with variable axis electrogoniometer 79–44012
knee osteo-arthritis, evolution of max. stress 77–48825
knee prosthesis, influence of cyclic loading on loosening of cement bone interface 79–44056
knee prosthesis, sliding meniscus, design concepts, biomechanical techniques for movement study 80–41315
knee prosthesis tibial component fixations compared 79–92431
knee-joint forces, routine clinical assessment method 79–83831
lap-shoulder belt restraint, correl. of field injuries and GM Hybrid III dummy responses 80–108946
larger head-neck motion analysis 79–79579
lateral tibial plateau, axisymm. finite element anal. 78–69127
lecithin membrane, depend. of Young's modulus in plane of membrane on deform. 78–80894
left ventricle, math. model of mechs. 80–101195
left ventricle, model study of isovolumic and non-isovolumic contracts 80–85428
left ventricle active model deform., nonlinear finite element anal. 78–35877
left ventricular diastole mechanics 80–94261
left ventricular function, correlation with myocardium deformation 79–16244
left ventricular function, normal and abnormal, vel.-strain relationship 78–69119
left ventricular mech. behaviour, orthotropic elastic moduli 79–57695
left ventricular wall finite element stress analysis, humans 77–64079
left ventricular wall force, comparison of models used in calc. 80–56093
leg, human dynamic nonlinear finite element model 80–35949
leg, lower, external compression effect on venous blood vol. 80–97989
leg joint moments during walking, humans 77–56396
leg lengthening, tension/stretch ratio, method and clinical results *(German)* 78–36031
leg loading components correlation in snow skiing 79–96608
leg loading in snow skiing, computer anals. 80–101208
leg muscle EMG pattern variability on stairs and in level walking 79–53175
leg muscle forces, normal human walking, optimisation methods 79–16240
leg-foot, complex, in conditions of lesion and reconstruction, holography 80–67142
lethicin, bilayer membrane, elastic props., in direction perpendicular to membrane plane 79–57602
leucocyte β-glucoronidase release on exposure to shear stress 78–40125
ligament length calculation technique, appl. to human knee joint 79–43949
ligaments, medial collateral, compliance changes under cyclic loading 79–92284
limb muscle dynamic force meas. by surface EMG 79–34689
limb tremor, normal and alcohol withdrawal, nature and etiology 79–29544
limbs motion analysis appl., prosthesis microcomputer control 80–51138
lipid bilayer elastic modulus freq. depend. 78–48762
lipid bilayers, curvature elasticity 79–48222
lipid bilayers, effect of oxidation and hydrolysis on elastic props. 79–92165
lipid bilayers, elastic props. changes on exposure to different agents, elec. and chem. 80–81548
living tissue mechanical props., boundary value problems 77–70491
locomotion, analogue simulation of swing phase 78–31827
locomotion, clinical assessment of normal and abnormal foot 80–17168

biomechanics continued
locomotion, human, multi-link chain model anal. 79–8518
locomotion dynamics, human, math. model 80–97981
locomotion in normal humans 80–3705
locomotion of a stomatopod, backward somersaulting obs. 80–21487
locomotor system analysis in humans by holographic interferometry *(Croatian)* 78–44519
long bone mechanics study under microprocessor control 80–76851
long jump take off, angular momentum considerations 78–20204
low back mobility and activity levels, EMG obs. 80–41059
lower oesophageal sphincter, press.-diameter characts., in vivo vs. in vitro characts. 77–36982
lumbar spin motion segments, mech. props. in humans 79–96597
lumbar spine, human, dynamic 3D modelling, computer code 80–108948
lumbar spine, human, modelling and simulation 79–83840
lumbar spine, lateral flexion, radiographic studies 79–8522
lumbar spine, mech. and kinematic anal., orthogonal radiography 79–74708
lumbar spine, mech. props. 79–100645
lumbar spine, moments transmission, isometric tests 80–41083
lumbar spine curvature in sagittal plane, meas. and modelling 79–96607
lumbar spine loads, anal. and meas. 80–104622
lumbar spine loads during work at a table 80–101210
lumbar spine motion segments, mech. props. in humans 79–96596
lumbar spine motion transducer for use in intact in vitro preps. 78–57155
lumbar vertebra cortical surface strain distribution tests 78–11692
lumbo-vertebral facet forces and injuries 77–56395
lung, canine, strain variations in excised lobe, finite element anal. 79–8517
lung, distributed response of complex branching duct networks 78–57027
lung, finite element model for macroscopic deform. 80–108945
lung, gravitational deformation, excised canine lungs, linear elasticity soln. 80–30747
lung, macroscopic deformation, finite element model 80–89781
lung, shear modulus and pleural membrane tension, improved meas. 80–30746
lung, static mech. behaviour 77–36993
lung airway smooth muscle mech. alterations in canine asthmatic model 79–100648
lung compliance loop recovery eliminating cardiac interference by digital filter 79–20570
lung deflation, large-deform. anals. of strains in excised lobes, dog 80–3689
lung elasticity in regional and diffuse pulmonary fibrosis 80–30742
lung lobes, parenchymal deformation analysis using rotationally corrected strains 80–41087
lung parenchyma, elastic props., pressure-volume hysteresis effect on large blood vessels 80–41084
lung parenchyma, math. model 80–108940
lung parenchyma anisotropic props. 78–31842
lung sound transmission meas. 78–28149
lung structure and elasticity, 3-dimens. modelling 77–36992
lung tissue elasticity, constitutive eqn. 79–96595
lung translation, rot. and strain calc. from roentgen-videographically recorded marker displacements 78–31843
mammal locomotion, role of joint receptors in limb control *(Russian)* 79–43938
mammalian tendon, struct.-strength relations 79–16230
mammalian tendon stress/strain relations obs. and structural model 79–29554
mandible, human, in vitro, math. model 77–52816
mandible opening force rel. to EMG of digastric muscles 79–74619
mandibular bone, compressive strength rel. to microstruct. and strain rate 79–57689
material identification of soft tissue using membrane inflation 80–41345
mathematical function fitting to exptl. data 79–48278
mechanical calorimetry of red cell membranes 80–45854
mechanical efficiency of fast- and slow-twitch muscle fibres during cycling 80–41074
mechanical impedance of human soft tissue in vivo 77–40705
mechanomyocardiography, left ventricular, technique for detect. of diseased myocardial elements and states 80–72363
mechanoreceptor hair motion in fluid environments, mathematical model 79–88092
mechanosensitive ionic channel, model of reception and macromolecular rearrangement, effect of deform. 79–79564
medullary implants with porous coating, stress distrib. 78–69256
membrane distortion near ionic channel formed by gramicidin A 79–92164
membrane elasto-viscous properties determined from bilayer meas. 80–30671
membrane flexural fluctuations and non-equilib. noise 80–76712
membrane mechanics and thermodynamics, review 80–45863
membrane mechanics and thermodynamics, review 80–51052
metacarpi, equine, fracture toughness 80–3694
metacarpophalangeal joint, biomechs. 77–52820
metacarpophalangeal joint, human, kinematic investigation 79–8519
metacarpophalangeal joint, motion meas. technique for 6 degrees of freedom 77–56418
metacarpophalangeal joint compressive strength rel. to subchondral bone density, prosthetic development 79–92286
metacarpus-phalangeal joint movement modelling 79–88112
microbiomechanics, crystal defect theory approach 80–3687
mitral valve leaflets, mathematical anal. 79–39435
mitral valve replacement, prediction of postoperative systolic left ventricular wall stress 78–40427
mitral valve vibration anal. to detect first heart sound freq. 78–40233
motion analysis, human, 3D coordinate data processing 80–56260
motion data derivatives and Fourier coeffs., calc. using spline functions 79–70564
motion studies and tissues and fluids characterisation *(French)* 80–89778
motor output response to applied torque perturbations in man, nonlinearities evaluation 80–76771
motor systems, eye and hand, optimal response in pointing at visual target 80–56079
movement data smoothing, use of spline functions 80–3699
movement dynamics, human, investigation using a computer 80–51284
movements of humans, computer modelling 77–21544

biomechanics continued
- mucus mechanical props. rel. to mucociliary transport, effect of pharmacologic interventions 80—3663
- muscle, active frog skeletal, isometric tension, slow stretch effect, X-ray diffr. study 78—80906
- muscle, anatomical model, internal pressure effects 80—67103
- muscle, contractile element behaviour as force and shortening generator, Hill's model 80—3681
- muscle, elastic and viscous props. of resting frog skeletal muscle 77—44700
- muscle, elec. stimulated, closed-loop control of force 80—76728
- muscle, flexibility of thin filaments, dynamic light-scatt. evidence 80—41064
- muscle, frog, vacuolation and subcellular comp. in fatigue, electron probe anal. 79—24963
- muscle, frog skeletal, time resolved X-ray diffr. obs. during isotonic twitch 79—83836
- muscle, glycerol-extracted fibrillar fibres, cross-bridge slippage induced by AMP-PNP and stretch 78—77075
- muscle, human, physiological and metabolic studies in health and disease 79—39443
- muscle, human skeletal, mech. simulation 78—35878
- muscle, in computational model of cerebellar cortex and peripheral muscle 78—11629
- muscle, kinetic model of single contraction 79—57629
- muscle, mech. pulse propag. vel. meas. using piezoelectric crystals, elastic moduli 78—92668
- muscle, mechanochem. contractile system as thermodynamic machine 78—20201
- muscle, myosin regulated, changes in crossbridge attachment 78—53361
- muscle, opposite end mech. transients in single isolated fibres 78—44541
- muscle, red and pale, human skeletal, force rel. to fatigability, EMG obs. 80—8076
- muscle, skeletal, deriving viscoelastic modulus from transient pulse propag. 78—77077
- muscle, skeletal, dynamic behaviour modelled as unidimens. viscoelastic medium 77—25484
- muscle, skeletal, exptl. results and modelling of biomech. props. 77—25486
- muscle, skeletal, tension development, F-actin subunits struct. non-equiv. model 78—64959
- muscle, striated, analytical soln. to isometric mechanogram of Hill's model 78—73168
- muscle, striated, mol. basis of force development 78—40126
- muscle, striated, reversible loss of Ca control of tension assoc. with removal of regulatory light chains, scallop 78—53360
- muscle, upper extremity, eccentric-concentric contract. study 80—85432
- muscle actions, model for semi-quantitative studies 80—61605
- muscle activity prediction, optimisation method adaptation 79—92273
- muscle contractile force in unskinned rat heart fibre 80—30955
- muscle contraction, elementary catastrophe theory model, reliability anal. 78—44471
- muscle contraction, time-resolved X-ray diffr., data-collection system *(Japanese)* 80—46108
- muscle contraction kinetics obs., time-resolved X-ray diffr. appl., with aid of computer *(Japanese)* 80—56291
- muscle dynamic stiffness rel. to crossbridge action 78—48819
- muscle electromagnetic stretch, sensorimotor cortex neurons in behaving primates 79—88073
- muscle fibre bundle tension development, action of regulatory light chains 80—94270
- muscle fibre tension fluctuation meas. during contraction 78—20153
- muscle fibres, Ca^{2+}-activated, effect of MgATP on stiffness meas. at 5 and 100 Hz 78—48822
- muscle fibres, fibrillar, tension transients affected by stretch-dependent binding of AMP-PNP 79—20562
- muscle fibres, rabbit psoas, stiffness and tension after sudden length changes 79—25007
- muscle fibres, relaxed, skinned, stretch and radial compression obs., frog 80—30736
- muscle fibres of Lethocerus maximus, temp. dependance of cross bridge parameters 80—61598
- muscle force development, filament spacing effect on axial forces 80—61597
- muscle force development, geometrical factors influencing radial forces 80—67102
- muscle force prediction, use of optimisation techniques 79—16242
- muscle force rel. to EMG 78—40231
- muscle force transducer, in vivo meas. using silastic strain gauge 79—29680
- muscle isometric contraction force rel. to surface integral electromyogram 79—74618
- muscle mechanics in isometric contraction, linear approx. 77—73535
- muscle mechanics obs. by acoustic microscopy 78—48952
- muscle mechanics thermodynamic model 78—80908
- muscle stiffness in hypertonic solns. 80—67140
- muscle strength and movement speed rel. to age and morphology 80—3672
- muscle strength gain, neural factors rel. to hypertrophy 80—12168
- muscle strengths and musculo-skeletal geometry of the upper limb 79—74699
- muscle stretch reflex system, math. model *(Japanese)* 80—67067
- muscle system, contractile system, sliding motion anal. 80—67104
- muscle tension of quadriceps femoris during knee extension and straight leg raises 80—8038
- muscle tissue, math. models 77—25358
- muscle tone study by meas. of muscle density, bridge instrument 80—3833
- muscle transfer function online evaluation by impulse response transformation, rehabilitation test appl. 79—57637
- muscle viscoelastic props. determ., appl. of forced longit.-vibr. of elastic rod on viscoelastic half-space 78—44538
- muscle-tendon junction strength, ultrastruct. elements 77—25485
- muscles, stretched fibres, mechanical activation and voltage-depend. charge movement 80—3630
- muscular activity in pasture maintenance, control mechanisms study via spectral anal. 79—5306
- muscular contraction, sequential 77—48824
- muscular fatigue, EMG meas. and analogue model *(Japanese)* 79—8498
- muscular organ mechanics 77—90836

biomechanics continued
- muscular strength, relationship with muscle energy sources, Wistar rat 79—11904
- musculo-skeletal shock absorption, relative contribs. of bone and soft tissues 79—29549
- musculo-skeletal system, human, complete set of control eqns. 78—40223
- musculoskeletal complex shape cross-sectional props., interactive graphics software package 79—79595
- musculoskeletal joint systems, graphical interpretation of redundant problem solution 79—29561
- myelin swelling and meas. of forces between membranes 79—62204
- myocardial activity determ. at surgery using shrinking stress meas. 78—31966
- myocardial excitability evaluation, strength-interval curves generation under computer control 80—41336
- myocardial inhomogeneity effect on left ventricular circumferential stress distrib. 79—92267
- myocardial local tension, strain gauge transducer 79—48357
- myocardium, mechanical recording using analogue differential preamplifier 78—40447
- myocardium, quiescent, anal. of some theological and mech. props., rat 79—74709
- myocardium of human left ventricle, stiffness distrib. rel. to shape change in diastole 80—41095
- myofibrils, contracting, tension fluctuations and their interpretation 80—41065
- myosin heads movement during a heart beat 79—48207
- navicular bone, morphological features in functional adaptation of the foot *(Croatian)* 80—108944
- nematode oesophagus pumping mechanism 78—69121
- neointimas developing on flocked surfaces of left ventricular assist device, mech. anal. 78—40431
- ocular contusion injury from propelled objects, evaluation model 79—43955
- oesophageal accelerometer, cardiovascular function indication 80—104798
- oesophageal geometry changes in swallowing, transduction, for animal grazing studies 80—76888
- opto-electronic target tracker for limb movement meas. and anal. 80—56166
- orofacial posture and movement, photo-elec. recording method 80—108995
- orthopaedic applications of holography 80—67196
- orthopaedic biomechanics *(Japanese)* 80—67133
- orthopaedic load meas. using strain gauges 80—56262
- orthopaedics, exptl., quantitative eval. of holographic deform. investigations 80—67197
- osteons with crossed lamellae, micromech. study 77—25493
- osteosynthesis, internal, deform. of bone *(Croatian)* 80—108943
- paediatric intertrochanteric osteotomy fixation of modified Kuntscher's nail *(Croatian)* 78—44675
- papillary muscle selection and testing, some mech. considerations 80—89919
- papillary muscles, macroscopic inhomogeneities in mech. response 79—79571
- passive dynamic characteristics of man in lying posture, testing apparatus 78—80893
- patella, human, biomechs. and implications for chondromalacia 77—90839
- patella stress analysis, rel. to patellar articular cartilage lesions 80—35942
- patellar tracking patterns meas. by analytical X-ray photogrammetry 80—30864
- patellofemoral joint, anal. model 80—104625
- patellofemoral joint forces, exptl. determ. 77—36988
- pathological gait clinical assessment, data processing of vertical foot-forces *(Japanese)* 80—21554
- patient equilib. function study using servo-controlled force plate *(Japanese)* 79—74775
- pelvic forces, math. model 77—52818
- periodonal ligament, in vitro rupture obs. 80—97982
- peristalsis, review of functions and waveforms, book contrib. 79—16245
- peristaltic reflex dynamics model 80—56080
- peristaltic transport, influence of wave form *(German)* 79—79570
- photogrammetric method for estimating biomechanical props. of three body types 79—43947
- photographic technique for anal. of neural unit activity rel. to movement 80—67310
- physicomechanical properties of biotissues, rel. to selecting alloprosthetic material 77—25596
- pinch action of thumb and index finger, musculoskeletal anal. 78—40225
- planar biped finite state control, appl. to walking and sitting 80—16986
- plant fibres, fracture mechanism 80—35931
- plastic surgery, biomechanical aspects 80—56103
- polyethylene implant-bone composite interfacial strength, porous high density polyethylene 78—31979
- post-operative human gait, EMG mes., pattern recognition appl. 79—34599
- posterior knee joint capsule, cat, receptor neuronal response to stress 79—92212
- postural equilibrium, role of kinematic mobility of human cervical spine 77—52837
- postural equilibrium automatic meas. and real-time evaluation in man, instrumentation system 78—77127
- posture control system response to random accel. disturbances *(Japanese)* 80—72200
- posture-control system, responses to pseudorandom accel. disturbances 80—81640
- pressure distribution under the foot during static activities 80—97964
- pressure-induced tissue breakdown, fundamental problems 78—31838
- propulsor, flexible, slender, large-amplitude unsteady motion 79—53172
- prostheses articulating surfaces, contact area and wear meas. using holographic interferometry 78—40415
- prosthesis mechanical efficacy determ. by holographic strain meas. *(German)* 79—8573
- prosthetic, heart valves, load cell for meas. of dynamic forces 80—104815
- prosthetic, joint function restoration, biomech. operating principles 78—69257
- prosthetic above-knee sockets, total surface bearing, self suspending 80—51294

biomechanics continued
prosthetic deformation measurements using holographic interferometry *(German)* 78—35911
prosthetic fitted below-knee amputees, pylon transducer signal variability anal. 79—74715
prosthetic heart valves, rigid leaflet and caged-ball types, diastolic ventricular mechs. 78—81079
prosthetic knee, control by biofeedback training 79—34700
proteins, plastic deformation during freeze-cleavage, review 78—14400
pulmonary mechanics and perfusion rel. to meas. gas concs. at mouth, simulation 78—31845
pulmonary mechanics vector scope meas., error anal. 78—40358
pulmonary vascular interdependence in isolated dog lobes, continuum mechs. anal. 80—3671
pulse wave propagation in arteries, initial stresses and muscle activity effects 80—12172
pupil noise amplitude control, interaction of sensory and motor mechanisms 78—64998
quadriceps femoris, function under maximal concentric and eccentric contractions 80—97963
quadriceps tendon/infrapatellar ligament tension ratio calc. and obs. 77—86520
rapid eye movements, computerised anal. method, REM sleep period appl. *(Japanese)* 80—41273
red blood cells, equilib. shapes in osmotic swelling 80—85368
red blood cells, minimum energy anal. of membrane deform. 80—72141
red cell membrane elastic area compressibility meas., osmotic correction 78—20147
red cell membrane thermoelasticity obs. 79—57684
reflex stiffness of man's anti-gravity muscles during kneebends while carrying extra weights 80—61601
regeneration of soft biological tissue, mech. conditions 80—104615
regressive osteometric scaling appls. to mirror symmetry and statistical coordinate models 80—104627
resistance strain gauge-meas. techniques in biomech. expts. *(German)* 80—104819
resistance strain gauges bonded to bone surface in vivo, post-mortem calibration 78—28135
retina detachment, math. model 78—44536
retinal image stabilisation quality during small body rotations in man 79—100595
rib cage deformation during static inspiratory efforts 80—45933
rigid body motion calculated from spatial co-ordinates of markers 80—94267
rigidity increase of material of bioconstructs. during morphogenesis 80—94249
roentgen stereophotogrammetric methods for human knee joint evaluation 80—30952
role of stress-gradient effects 80—67113
runner's forward motion, effects of wind assistance and resistance 80—101204
running, influence of track compliance, model and expts. 80—61602
salmon in spawning migration, swimming velocity and efficiency *(Russian)* 77—32925
scaling model, for biological systems 77—60875
scoliosis correction, by lateral surface elec. stimulation of muscles 78—44717
scope and recent trends *(Japanese)* 80—16984
semiconductor force transducer suitable for use with small muscles 80—72395
semilunar valvular motion vibr. model during early diastole, rel. to second heart sound 78—44533
semilunar valvular vibration in early diastole, rel. to second heart sound 78—44544
shearing forces on the sole of the foot, meas. system 80—72342
short-below-knee-stump, simplified model 78—27986
shoulder complex in arm elevation, mechanism approach 79—29547
shoulder contact areas, canine, in vivo determ. method and obs. 80—56324
shoulder movements, EMG analysis of levator scapulae and rhomboideus major muscles 80—3627
silk, spider, tensile, fracture strength, elongation and ageing effects 80—41072
sinew dynamic elasticity modulus meas. apparatus *(German)* 79—2167
skeletal muscle, excitation-contraction coupling, blockade by high extracellular concs. of Ca buffers 79—20528
skeletal muscle, freq. response characteristics evaluation 79—96594
skeletal muscle, frog, active tension changes during and after mech. stimulation 80—94262
skeletal muscle mech. props. from in vitro studies of biopsies 80—41098
skeletal muscle mechanical props. and model, contractile force depend. *(Japanese)* 80—56091
skeletal muscle rhythmic contractions, temp. distrib. study 79—11901
skeletal muscles, attachment and composition rel. to function 80—41092
skeletal muscles, cat, force-vel. and fatiguability obs. 80—81637
skeletal muscles, contracting, simulation studies of mech. stretch 80—94263
skin, human, reconstructive surgery, in-plane compressive strain limits prediction 80—41069
skin, human abdominal, volume compressibility 79—16238
skin, living, human, constant strain rate, hysteresis and stress relax. behaviour 78—40237
skin, mech. and struct. response to X-irradiation 80—35994
skin and subcutaneous tissue, human, influence of strain rate on mech. props. 79—20575
skin components, rheological props. under compressive load 80—35945
skin elasticity of living dolphins *(Russian)* 80—45926
skin mechanics, effects of some clinical treatments 79—100644
skin recoil characteristics, human, in vivo meas. apparatus 79—57698
skin stress-strain curves, step phenomenon 79—70569
skin stress-strain relation, model calcs. 79—74705
skin undulation propagation rate, dolphin expts. *(Russian)* 80—45927
skin wrinkling, human, using model of thin elastic shell on continuum foundation 77—52819
skull, holographic interferometric NDT 80—41162
skull, human, deformation, model of cupola with flat base 77—36966
skull, macerated, human, orthodontic forces induced bone displacement obs. 80—61603
skull and auditory ossicle vibr. anal., human preps., using holographic interferometry 80—67210

biomechanics continued
skull-brain system, human, prolate spheroidal viscoelastic shell containing viscoelastic fluid, axisymm. vibrs. 78—80901
slender body propulsion by boundary layer deform. in viscous fluid *(French)* 77—42798
soft animal tissue mech. props. in vitro testing, apparatus review 78—31985
soft biological materials, nonlinear behaviour, numerical modelling 79—100642
soft connective tissues, biomechanical behaviour 80—56102
soft tissue, living, stress/strain relationship, mathematical, model 77—29170
soft tissue covering bony prominences, techniques for derm. mech. props. 79—62415
soft tissue nonlinear viscoelastic behaviour 78—69128
soft tissues, elastic stress/strain relation based on a struct. model 80—101205
soft tissues, finite elastic deformation anal. 77—90845
soft tissues, human, rheological props. from local cyclic loading method 80—108932
soft tissues, human, rheological props. investigation using elastography 80—108933
soft tissues, inversion of class of nonlinear stress-strain relationships 79—96593
soft tissues, tension field theories 78—65064
soleus muscle, human, stretch and Hoffmann reflexes during phasic voluntary contractions 79—16193
spatial motion, data collection method using sonic digitiser 79—39441
spatial movement of man, biodynamic characts. model 77—16944
sperm flagella equation of motion 78—80895
spinal column, human, strength of construction 80—67137
spinal cord, dog, in vivo dynamic material props. 77—40706
spinal ligaments, human, mech. implications of collagen fibre crimping 79—100646
spine, human, finite element model for in vivo freq. response anal. 80—104623
spongy bone, dynamic elastic props., determ. techniques 80—56326
sports activities, velocity meas., stroboscopic photography, teaching appl. 79—44679
stabilograms, influence of platform geometry 78—81038
stabilometric test, subject optimal feet positions 78—44540
static charge sensitive bed, method for recording body movements during sleep 80—3840
statistical biomechanics, regularity 77—25483
step length measurement apparatus 80—67271
strain gauge application on compact bone 80—3883
strain measurement in elastic thin membranes, moire interferometry method, appl. to human skin 80—30828
strain-energy function for soft tissues, large deform. anal. 77—5018
striated muscle contraction, intracellular control of force development 79—48228
student laboratory expts. using a crane boom 78—81759
surface EMG, computer anal. during isometric exercise, muscle tension quantification 80—85505
suture line stress in end-to-side anastomosis, math. assess. in pulsatile flow 80—97986
suture line stress in the end-to-side anastomosis, math. assessment 80—61606
swimming efficiency of fish, calc. *(Russian)* 77—64071
swing-through crutch gait, kinematics and energy variations 80—35937
synovial joints, immobility effects, pathomechs. of joint contracture 80—97954
systemic muscular arterial wall medial smooth muscle orientation obs. 79—70572
teeth and mandibles, deforms. due to occlusal forces, holographic interferometry 80—67205
teleost fish, max. speed paradox resolution 80—67138
tendon, digital, human, viscoelastic deform. activation, energy, creep T-jump expt. 79—37264
tendon, rat tail, creep failure obs. 79—62289
tendon, rat tail, struct. and mech. props. 80—97953
tendon mechanics, discrete nonlinear viscoelastic model *(German)* 78—44525
tendons preserved by different means, strength and morphological struct. 80—72208
tensile stress of human soft tissue at const. elongation, temp. effects 77—32938
tensile testing of small animal ligaments, gripping device 80—81791
tenuissimus muscle, cat dynamic properties 80—8041
thoracoabdominal mechanics during relaxed and forced vital capacity 80—30740
thumb functions in normal and pathological state, biomech. eval. 77—40708
thumb joints, mech. anal. 80—94264
thumb trapeziometacarpal joint motion kinematic anal. 78—40226
tibia, human, natural freq. anal. 80—85433
tibia, human, simplified method of radiographic anal. of its cross-section, anthropometric correls. 80—89827
tibia flexural wave propagation, discontinuous model and in vitro study 77—29169
tibial bone reaction to hydromech. implant dynamic loading *(German)* 79—8574
tibial bones, of highly trained athletes phys. stress effect type as measured by US techniques 80—16992
tibial fractures, treatment with plaster casts, biomech. study 79—74696
tibial shaft internal fixation, biomech. study 78—20313
tibialis anterior muscle stiffness meas. during voluntary contraction, human *(Japanese)* 80—56090
tissue breakdown prevention, material design criteria 78—31964
tissue damage and death rel. to mech. props., US interaction 80—51151
tissue pressure, continuous monitoring instrument 79—100762
tissue properties, skin and other soft connective tissues 78—44521
tissue response to retraction during open-heart surgery 80—26254
tissues, soft, apparatus for mechanical testing 79—44064
tongue and jaw point movements in connnected sounds of Japanese, articulatory characts. 80—26243
tooth intrusion for different loading rates 79—57686
tooth support, model of periodontal vasculature 80—85434
tooth-jaw system, mech. anal. 77—40703
torque-velocity relationships and muscle fibre composition, elite female athletes 80—41080

biomechanics continued
- trabecular bone from human vertebral body, elastomech. props. 80—67141
- trabecular bone-porous coating-hip prosthesis interface, mechanical behaviour 79—39436
- trachealis muscle, dog, spontaneous mech. activities in vivo 80—101203
- tractor drivers, minimisation of vertical vibration responses 80—81626
- tractor vibrations, response of human body, vibration minimisation 80—101213
- two-body and massless leg model for human level walking 79—83839
- tympanic membrane investigations in living man using holographic interferometry 80—67207
- tympanic membrane vibr. studies in living man using holographic interferometry 80—67208
- ulna bending stiffness, microprocessor-automated noninvasive meas. 79—92275
- uniaxial testing of soft human tissues, in vitro apparatus 78—61295
- upper extremity multifunctional isometric strength tester 78—44658
- upright posture maintenance, static forces in normals and hemiplegics 78—40228
- urease shear inactivation, metal ion effect, rel. to shear deform. effects in enzyme catalysis 78—76982
- urethra, female, elastic length, initial obs. 80—81642
- urinary bladder, pig, active mech. props. of smooth muscle 79—92252
- urinary bladder interferometry, holography of bladder deforms. in vitro, rabbit expt. 80—67201
- urinary bladder interferometry, tumour and lesion detect. by holography 80—67202
- urinary bladder passive props., collection phase model 79—34596
- US shear velocity of muscle tissues, mech. props. determ. 80—108930
- uterine contraction promotion and bleeding suppression cryocoagulator 79—39591
- uterine muscle, passive mech. props. in vitro 79—16235
- uterine muscle penetration by flexible IUCD shield 79—29556
- valve vibrations, aortic and mitral, anal. and role in heart sound production 80—101214
- vascular compliance interaction with const. vascular taper 77—36999
- vascular smooth muscle, undamped and damped series elastic components 79—83819
- vascular tonus model 77—25482
- vascular walls, effect of prostheses pumping 78—40429
- vascular walls, physical theory of permeability rel. to atherogenesis, mech. effects 80—16908
- veins, simulation of collapse 78—44535
- venous oscillations, ultrasonic Doppler study 80—108931
- ventricle, left, human, geometric modelling using biplane cineangiograms 80—35955
- ventricular aneurysms, mechanical behaviour, mathematical model 79—11953
- ventricular function computer simulation, development of model and parameter estimation 78—53439
- ventricular function quantitative meas. by torque ballistocardiography 78—44660
- ventricular myocardium plastic cast global Young's mod., calc. from angiograms 77—48827
- ventricular wall dynamics and obs. on blood flow 78—80896
- vertebra, dynamical response analysis 80—3684
- vertebrae, human, deflected US wave propag. tests 80—61617
- vertebrae, human, mech. props. 80—72206
- vertebrae, human, strength under sagittal compression 80—61618
- vertebral column, appl. of natural freqs. of composite cylinders 79—83830
- vertebral response to laminectomy, finite element model 80—41090
- vesicular lipid membranes, vol.-elastic props. determ., US obs. 80—45861
- vibration duration effects on human comfort and task proficiency 80—26247
- vibrations, sinusoidal and random whole-body, subjective equivalence 77—13050
- vidicon television camera, movement meas. appl. 80—41333
- virus solid, low density, yield stress model 78—88725
- visceral smooth muscles in vertebrates, viscoelastic and plastic props. 78—73169
- viscoelastic lubricants reln. to human joints 79—39430
- vocal cord vibration, computer model of air vol. displacement 78—69111
- voluntary movement, electromyographic silent period *(Japanese)* 79—74622
- voluntary movements in man, force gradation and motor unit activity 80—97887
- walking, 5 body-3D dynamic anal. 80—97987
- walking, computer animation of gait 79—11957
- walking, energy-information performance criteria 79—53181
- walking, nervous command study 79—53184
- walking, normal, with different footwear, skeletal transients on heel strike 80—101207
- walking, synchronisation of optical press. distrib. and 3-dimens. force meas. under sole human foot *(German)* 78—35975
- walking cycle stance phase, dynamic load line considerations *(German)* 80—81625
- walking insect, Carausius morosus, coordination of force oscills. and leg movement 80—76775
- walking insect, Carausius morosus, oscillations of force in standing legs 80—76774
- wheelchair cushion effect on skin temperature, heat flux, and relative humidity 79—83707
- wheelchair locomotion, power output requirements for manual operation 80—94416
- whitefly, meas. of highest contraction freqs. yet recorded in non-fibrillar flight muscles 79—83835
- whole-body low-frequency vibrations, subjective freq. doubling expts. 77—64063
- work done in human movement, new definition 79—88107
- work-effort ratio of a large muscle group, theoretical model 80—108949
- wound healing, var. of mech. props. in different areas 78—27984
- wrist, human, kinematic and kinetic analysis by stereoscopic instrumentation 79—92274
- wrist, human, kinematic and kinetic analysis by stereoscopic instrumentation 80—16999
- wrist kinematics investigation, analytical development 80—35941
- wrist kinematics investigation 79—70570
- wrist motion, human, muscular activity model and expt. 79—92285
- wrist position that facilitates max. power grip strength 80—101209

biomedical applications of computing *see medical computing*

biomedical electronics
- *see also electrocardiography; electroencephalography; microelectrodes; patient monitoring; patient treatment; prosthetics; sensory aids*
- 15-channel analogue selector, for intensive care 77—40898
- acceleration sensor for heart implantation, heart attack warning *(German)* 79—57802
- acoustic microscope appl., using piezoelectric transducers 80—1387
- active attenuator, for US pulse-echo system 77—40835
- AGC system for biomedical instrumentation, digitally controlled 77—56493
- amplifier, input, 43dB, biofeedback appl. *(Dutch)* 77—37100
- amplifier-electrode hybrid module for surface EMG pots. meas. 80—41294
- analogue divider for heart ratemeter 78—40368
- analogue multiplexer for FM tape recording 79—34691
- angiohaemodynamical catheterisation lab., electromedical devices 80—85515
- artifical vision machine for blind people *(Korean)* 79—66583
- artificial blood circulation system electrical control *(Spanish)* 78—3680
- artificial eye for blind people, implementation through the optical nerve *(Croatian)* 80—109060
- artificial heart operation and monitoring system *(German)* 79—8583
- artificial sight and hearing, appl. of microcircuits 78—20311
- audiometer, Bekesy-type, for clinical use 78—3499
- automatic recording device, for lung isopressure-flow-volume curves 78—40382
- auxiliary blood circulation pump, electronic control circuit 77—78050
- bicycle ergometer for cardiovascular medical diagnosis, model AM 368 *(Italian)* 80—30918
- bioelectrode methods *(Japanese)* 80—30919
- bioelectronics symposium, Ahmedabad, India, (Dec 1975) 77—40808
- biofeedback controlled parameter determ. circuits, Medicor diagnostic bag 79—100775
- biotelemetry and radiotracking receiver 77—48892
- blind aids, Spanish electronic devices *(Spanish)* 79—39613
- blind person's rocking motion sensor and recorder 77—52921
- blind persons' aids, review 77—29227
- blood cell counter, abnormal erythrocytes detection *(Japanese)* 77—44869
- blood pressure Hg manometer contactless readout and recording cct. 77—81603
- blood pressure monitor, semiautomatic, using electronic sphygmomanometer 78—20300
- blood pressure monitoring systems simulator 79—83963
- blood-pressure meter, IC, using pressure transducer microprocessor controlled 79—35709
- body temp. meas. via implantable miniature transmitter *(Dutch)* 78—48908
- brain α-activity detection *(Czech)* 77—5124
- breath amplitude meas. optoelectronic displacement sensor 77—66868
- breathing ratemeter for neonatal intensive care 80—41311
- calibrator for ECG/respiration monitor 80—98159
- cancer treatment by local microwave hyperthermia system 79—83893
- cardiac arrhythmia monitor, solid state delay unit 79—25126
- cardiac arrhythmias management, automated feedback control of drug therapy 80—41307
- cardiac output measurement, continuous electronic thermodilution meas. 77—40859
- cardiac system pressure pulse LF wave synthesizers, mammalian cardiac system 77—9301
- cardiotachometer, digital device using sliding averages 77—56503
- cardiotachometers, comparison of 4 designs 79—92412
- cell deposition system for deposition at predefined locations on microscopic slide 80—76876
- cerebral activity monitor, using biofeedback rhythms inducing cct. *(Spanish)* 80—72359
- cerebral blood flow automated analyser for ^{133}Xe studies 77—86597
- checkerboard pattern generator for vision research 77—40801
- chronically implantable instrumentation for medical research animals 80—30834
- cineangiography, physiological event marking using ECG R-wave triggering 77—52873
- circuit breaker, recording and stimulation from same electrode 79—34680
- coherent line-frequency noise in evoked pot. recordings, cancellation 80—98161
- communication interface for non-vocal physically handicapped using 3-electrode EOG 77—25603
- computed tomographic rotating fan-beam scanner, exptl. bench design 80—51230
- computer interface for a linear accelerator 80—51226
- computerised tomography, X-ray photography appl. 78—44588
- conference on medicine and techniques, Zagreb, Yugoslavia, 1979 80 101667
- contact lens pupillography electronics, pupillary reflex recording of noncollaborating subjects 78—40381
- contourograph using ICs for quasi-periodic and nonidentical physiological signals 77—44791
- contributions to medical electronics by NPL 80—36169
- data averager/printer, 7-channel, for cardiovascular and other physiological signals 78—40366
- DC micromotor controlling feed rates in syringe pumps, appl. to drug administration 78—48923
- deep-body pressure transducers, monolithic capacitive struct., pulse-period output 80—67274
- detector array for 4-dimens. reconstruction of radioisotopic activity in brain 78—11732
- developments review 77—13017
- diagnostic ultrasonic instrumentation, effect of integrated electronics technology 80—17029
- diagnostics, monitoring and therapy, 1979 development trends w.r.t. Czechoslovak instrumentation *(Czech)* 79—70689
- digital detector, FM, multichannel, EEG appl. *(Danish)* 78—35980
- digital filtering, high efficiency freq. anal. and data compression 78—31939
- digital frequency-to-temp. convertor for use in radio telemetry systems 80—8119
- digital processing of biomedical pictures, enchancement techniques 77—40815

biomedical electronics continued
- digital socially acceptable monitoring instrument, for heart beat counting 78−40367
- digital techniques for signal and image processing *(Croatian)* 78−44623
- digital thermometer, precision, for 35 to 40°C, operation *(German)* 77−56499
- digital thermometer, simple, inexpensive design 80−36178
- discharges electrophotographic obs., high-frequency *(German)* 80−17216
- display stabilising circuit, for systolic-diastolic blood-pressure monitors 78−40364
- ECG atrioventricaulr transmission intervals, automatic recording and processing 77−25568
- ECG electrode motion artifact reduction, electronic method 77−40872
- ECG multichannel recording using TDM 80−101283
- ECG signal recognition and anal. *(Slovenian)* 79−83958
- ECG-gated scintigraphy, appl. to studies of heart 78−7440
- ECG-telemetry apparatus, single-channel, PLL demodulator appl. *(German)* 78−57097
- echocardiographic tracking, digital range-gating 79−16260
- education, position in Hungary 79−67127
- educational course, BSc level option, Lanchester Polytechnic, England 79−17158
- EEG electronic recording and display systems *(French)* 77−13025
- EEG recorder with interference suppression for open heart surgery 79−100784
- eEG transient detection by matched inverse digital filtering 80−85506
- electro-optics appl., 1980 development trends 80−85464
- electrode amplifier, fast recovery, for electrophysiology 79−70654
- electrode process research instruments, biological appls. 78−21174
- electroglottograph application experience 77−78062
- electromanometric system frequency response visualisation device 77−48890
- electromedical equipment, computer controlled systems *(German)* 79−62421
- electromedical instruments, charact. and appl. 78−3642
- electromedical instruments manufactured by the Electronics Corporation of India Ltd. 80−36168
- electromyogram, muscle electrical impulses provide audible or visual indication using biofeedback 80−81782
- electronic instrument production 79−96675
- electronic meas. application areas 78−57094
- electronics appl., conf., Portland, Ore., USA, May, 1977 77−81598
- electrophrenic respiration, feedback control of tidal vol. *(Japanese)* 80−41316
- electrophysiological average transients computer, 200 point 80−12284
- Electrophysiological Data Interface 79−79677
- electroplethysmograph for regional lung function evaluation 77−21647
- electroretinogram, photopic, freq. response characts. meas. with synchronous detect. 77−48796
- electrostimulator for percutaneous nerve stimulation, chronic pain treatment *(German)* 79−16342
- electrostimulator three-mode control unit 79−20693
- EM radiation probes, implantable, design factors 78−73258
- EMC standard for medical electronic devices 77−81597
- EMG, filter bank analyser for automatic anal. 80−98162
- EMG, surface-recorded, stabilisation of isoelec. line using high-pass filter 78−31917
- EMG amplifier, wideband isolated, cct. 78−57089
- EMG biofeedback device 79−96706
- EMG jitter, single fibre electronic meas. device 77−40832
- engineering in medicine and biology, conf. Atlanta, USA (Oct. 1978) 79−39332
- enuresis alarm for mentally sub-normal children, low-cost and portable 79−53266
- equipment development, production, conf., Madras, India, 1978 July 79−96674
- equipment development in India, noninvasive diagnostic techniques appl. 79−96698
- event counter, with selectable time gate, for neurophysiological applic. 77−40944
- evoked potential preamplifier, head-mounted 24-channel type 77−40807
- eye, retinal photoreceptor model, FET cct. realisation 80−56027
- eyeglass lipreading aid system 77−25602
- Farnsworth-Munsell 100-hue test, electronically scored instrumentation 77−52895
- FET transducer, H^+, Ca^{++} and K^+-sensitive, features, appls. 78−28117
- FET transducer research and development for biomedical appl. 78−44640
- field effect potentiometric sensor 78−44644
- functional electrical stimulation of extremities 77−40926
- functional electrical stimulators, multisite appls. extremity stimulation 77−48936
- galvanic skin response meter cct. using bipolar transistors 80−72380
- gamma camera/computer pulse-stretching interface 78−40380
- gamma-camera images of liver, improvement using physiological gating mechanism 80−98065
- haemodynamic variables analysis, using HYDRA, hybrid analyser, sequential transcoder appl. *(Czech)* 77−21668
- hand opening by proportionally controlled electrical stimulator *(Croatian)* 78−44693
- health care and instrumentation, Indian scene 77−40813
- health care expansion aided by integrated electronics 78−11751
- hearing loss detection using electronic aids needing no patient feedback 78−11760
- heart, human, elec. and mag. events, phase and amplitude relationship recording 80−104695
- heart beat counter, versatile digital SAMI 80−85510
- heart rate measurement system using phaselock loop device 77−52906
- heart rate recorder 80−41288
- heart-rate variability meas., integral pulse freq. modulator spectral props. 77−90951
- HF current surgery, instruments and problems *(Hungarian)* 80−98172
- high-speed digital image processing 78−12680
- hospital equipment maintenance 79−100771
- hypertension treatment, elgctrosleep apparatus with rotating polarisation current 77−21655
- hyperthermia generator digital readout device 79−70697
- IC, generalised, Kitchip, for biotelemetry system design 77−86665
- IC differential amplifiers 77−48891
- IC four-channel EEG amplifier 79−39535

biomedical electronics continued
- IC implantable systems for animal expts. 80−76887
- image optical differential operation processor 77−52911
- implantable biomedical pressure transducer 77−73606
- implantable biotelemetry transmitter for 6 differential signals 77−48968
- implantable electronic pancreas and blood glucose monitor 78−88767
- implantable multichannel neural stimulator, custom IC fabrication 80−85534
- implanted hearing stimulators 79−79561
- in India, report on the prevailing level of medical electronics 77−40810
- instrumentation, development in Serbia, Croatia and Slovenia *(Slovene)* 77−21636
- instrumentation, review *(French)* 80−89884
- instrumentation elements, electrophysiology appl., review, book contrib. 80−12293
- instruments review *(Japanese)* 77−56494
- integrated circuit technology in MBE *(Japanese)* 79−44014
- integrated electron devices in medicine 78−40372
- integrated FET micro ion sensor, for pH and pNa monitoring 78−44641
- intensive care instrumentation 78−53559
- intracranial pressure telemetric monitoring system 79−74736
- intravascular O_2 measurement, current-to-voltage convertor 79−34684
- ion sensitive FET, reference, for compensation 78−44642
- ion sensitive FET micro pH sensor 78−44643
- ion-specific electrode output volt. linearisation 78−35991
- IR telemetry system for surgical patient monitoring 80−30836
- isotope digital densitometer exponential curve lineariser *(Polish)* 78−24160
- LED true checkerboard pattern reversal stimulator for visually evoked pots. study 80−61658
- leg-load alarm system for partial-weight-bearing walking exercise *(Japanese)* 79−29658
- LF direct meas. cct. for heart beat disturbances anal. *(German)* 79−96671
- LF interference current therapeutic apparatus *(Bulgarian)* 80−26314
- LF meter used for measuring period between pulses 79−85128
- LF meter with instantaneous response 79−40539
- low light level device applications, conference, Reston, USA (1976) 77−39091
- maintenance training programmes 79−96681
- manipulator, computer controlled, for use as remotely controlled arm 78−81083
- manufacture of medical electronic equipment, India 79−96676
- measurement of temp., press. and flow, for teaching 78−49621
- medical electronics equipment, maintenance and repair organisation 77−40814
- microelectronics revolution, appl. in telecommunications, medicine, education 80−31446
- micropowered IC modulator for implantable biomedical telemetry 77−78000
- microprocessor applications and costs 79−44011
- microprocessor applications to biomedical systems 78−57095
- microprocessor appls., sensory aids and diagnostic imaging developments 80−51285
- microprocessor based telemetry demodulation system 79−20738
- microprocessor use for routine cardiac assessment 79−83962
- microprocessors appl., development trends *(Italian)* 80−17173
- microstrip antennas for biomedical applications of microwaves 80−3762
- MIDCON conference, Dallas, USA, Dec. 1978 79−87939
- millivoltmeter, instantaneous peak value response, biomedical appls. 80−42208
- mobility aid for blind, passive optical system 77−25604
- moire topograms, real-time, video electronic generation 80−67198
- MOSFET, Pd gate, to monitor H_2, H_2S and NH_3 78−44645
- MOSFET preamplifier, bioelectric measurements including intracellular potentials 77−40855
- multichannel functional electrostimulator design for paretic gait correction 79−57810
- multichannel implantable stimulator *(Slovenian)* 80−81773
- muscle conduction velocity, meas. and recording methods 79−100688
- muscle potential monitor, using battery-operated IC, for electroconvulsive therapy 77−40899
- myoelectric control of an artificial hand, sequential movement, tropical climate 80−41323
- myofeedback control system, design 80−51296
- myofeedback control system trainer 80−51297
- nerve trunk multifibre activity quantitation 80−76853
- nervous system, electrical stimulation, laboratory research *(Norwegian)* 78−77096
- neural spike window discriminator confirmation by analogue delay cct. 77−21664
- neurology, biomedical engineering 79−96678
- neuromuscular motor structures, programmed multichannel electrostimulation apparatus 77−25585
- neuromuscular system electrical stimulator using biopotential amplifier 79−48315
- neurostimulator, with improved rectangular pulse cct. *(Rumanian)* 77−21637
- NMR whole-body imaging system design 80−98064
- noise generator for auditory neurophysiological and psychophysical experiments 79−29676
- noise generator for masking click stimuli 80−108980
- nonimplantable electrostimulator advances for urinary incontinence correction 79−57817
- nonlinear filtering technique for identification of biological signals 78−40438
- nystagmus analysis, microprocessor based instrum. 77−44799
- obstetrics, microprocessor based system for studying kinematics of labour 77−44769
- ocular pulse measurement, electronic/US system for carotid occlusion diagnosis 77−37081
- otology application of medical electronics *(Japanese)* 80−67268
- oximeter, noninvasive tissue reflectance, development and evaluation 79−20703
- oximeter, red/IR, catheter tip mounted 77−40836
- oxyhaemoglobin dissociation curve analyser, devel. and improvement 77−13019
- pain relief via pulse generator implantation in human body 78−96112
- pallaesthesiometer automatic signalling and signal fixation unit, vibr. sensibility threshold meas. 79−57784

biomedical electronics continued
- paralysed leg stimulation, programmed six-channel stimulator for walking *(Slovene)* 77—40923
- partial weight-bearing walk, limb load alarm system 79—29661
- particle simulation unit for counter circuitry testing 78—81002
- parylene (vacuum deposited polymeric coating) appl. 80—108607
- patient's surface contour measuring device 80—104717
- pattern rotation system for a visual stimulator 80—98061
- pCM telemetry for physiological data 80—36059
- peak discriminator controlled sampling of multiunit spike trains 79—34717
- perfusion blood temp. monitoring, zero-heat-flow transducer 80—8201
- petit mal epilepsy treatment, unobtrusive wearable device 77—25592
- phase locked loop device for sleep spindles automatic detection 79—16316
- phase-lock techniques, for gastric elec. signal analysis from surface electrodes 79—34688
- phase-lock techniques, for gastric elec. signal analysis from surface electrodes 79—34687
- phase-lock-loop principles appl. foetal breathing movement electronic anal. 79—2152
- phonocardiograph modulator design trends 78—24171
- piezoelectric insulin pump and valves for diabetes patients 78—53565
- platelet estimation in whole blood by electronic particle size anal. 78—28104
- polyphase envelope detection for physiological signals *(Korean)* 79—66565
- power sources, implantable, radioisotope thermoelectric generators appls., high reliability contacts using local heat pulses 79—52952
- preamplifier, isolated, electrophysiology appl., cct. 78—31922
- precision testing technique for intensive care instrumentation 79—70687
- pressure sensor, monolithic, capacitive, with pulse-period output, microminiature and implantable 80—81752
- problems of computer applications *(German)* 79—20696
- prosthetic larynx, Polish developed, design and operation 80—46098
- pulmonary parameter identification adaptive analogue tracker 77—48911
- pulse rate monitor, digital, IR absorpt. detect. 80—26322
- pulsed integrator for EMG analysis 80—61719
- quality health care and cost containment, conf., Washington, USA (Mar.-Apr. 1978) 79—39333
- radio pressure pills for back stress monitoring 77—73604
- radiocardiograph equipment TESLA NRG 724, description 78—28062
- radioisotope image magnifier/rotator for enhanced visualisation 78—15889
- radioisotope rectilinear scanning, direct recording of images on 4×5 in. film 77—5066
- radionuclide cardiac motion study, computer-processed, ECG gating device 78—73210
- radiotelemetry transmitter, for temp. meas. from unrestrained subjects 79—16356
- reaction timer cct., using bipolar transistors and LEDs 80—81781
- rectal potential difference meas. instrument, mineralocorticoid activity determ. 77—17002
- renography with electronically assisted kidney localisation 78—11716
- respiration, artificial, servo control of end-tidal CO_2 in paralysed animals 79—39607
- respiration rate automatic meas. device *(German)* 79—2146
- respiratory flow integrator with improved stability 79—16331
- respiratory flow-volume integrator 77—48914
- respiratory impedance measurement instrumentation 77—37079
- respiratory phase detector system, battery operated cct., air temp. change meas. 79—100770
- respiratory total compliance non-invasive meas. in free-breathing rabbits 78—28123
- review of the emerging field of biomedical engineering 80—36167
- rheography, integral method and electrode for exertion function tests 77—77995
- roller pumps, automatic safety shutdown 78—44720
- safety on health care facilities, recommendations for Spanish hospitals *(Spanish)* 80—72350
- sample/long term hold digital circuit, for physiological signal monitoring 77—40803
- Schottky barrier chemical sensor, Pd-Si, for H_2 detect. 78—44646
- Schottky barrier diode/laser beam system for quantitative meas. of body motion 80—12207
- scintigraphic image motion blurring, centroid following circuit 79—39493
- scintigraphy of human organs, digital image anal. 78—20251
- scintillation probe pulse multiplexing device 79—92347
- service, repair facilities in hospitals 79—96682
- signal conditioning CCD transversal filter 77—52901
- signal source ccts., galvanic separation *(Dutch)* 77—90939
- simulated inductors, large voltage swing, used for oscillator and floating coupling cct. 78—69227
- skin conductance meas. IC operational amplifier cct. 77—25566
- skin humidity meas. using bridge cct. and digitally steered logic cct. 77—13018
- skin impedance simulation w.r.t. Cole-Cole circular arc law 77—5101
- solid state delayed auditory feedback system for speech therapy 77—13028
- speech formant extraction, tracking loop filters 78—65051
- sphygmanometer, Omron's 77 model, accurate meas. 79—74773
- sphygmomanometer, direct and indirect methods for blood pressure meas. 79—25125
- spinal-cord stimulation in multiple sclerosis, electronic aspects 80—41313
- SQUID gradiometer, second-derivative, magnetocardiogram meas. 80—104696
- state of art, seminary, Brno, Czechoslovakia (Sept. 1976) *(Czech)* 77—17001
- stimulator, implantable RF powered dual channel device for hip stabilisation 77—40930
- stimulator for electrophysiological expts., constant-current device 77—21663
- strain gauge pressure transducer, signal simulator, for physiological monitoring applic. 77—40804
- synchronised clock pulses used for measurement of physical function *(Korean)* 77—56502
- systalic blood pressure monitor, type SCS-501 *(Japanese)* 77—70565
- technological developments, 1977 trends 78—48902
- technological transfer for medical electronic equipment development 79—96679
- technology transfer from development to manufacture 79—96680

biomedical electronics continued
- telemetry system, portable, multi-sensor, for rural health network 80—30835
- telemetry systems for chronically instrumented animal model for electrophysiological research 80—26323
- teletherapy machine electronic dual timer 78—85358
- temperature stabilisation of biological media, electronic device 80—85539
- terminology and future problems for the industry 80—36170
- thermistor simple device for mean skin temp. meas. 79—2151
- thermometer, electronic digital, for long-term patient monitoring 80—90849
- thermometer with digital display 79—25129
- timer, for use with Farmer dosimeter type 2502/3, in radiotherapy units 79—25114
- timer for plasma viscosity measurement 79—20690
- training for engineers in India 79—80390
- transducer, noncontact, for blood temp. monitoring during extracorporeal circulation 80—85513
- transient recorder, with digitised O/P, for biomedical applic. 77—40943
- transition of bio-electronics from the research laboratory to the clinic 77—40809
- tympanic contactless membrane thermometer 79—34692
- US computerised tomography, data acquisition system 80—26310
- US Doppler blood velocimeters, max. freq. detector 79—53201
- US Doppler signals, real-time spectrum analyser, haemodynamic appls. 80—36040
- US imaging techniques *(French)* 80—26304
- US tomography, signal processing for improved directivity 77—44729
- US tracking focusing annular array transducer *(French)* 80—26301
- US transducers for imaging, modelling *(French)* 80—26302
- venous pressure clamp for heart-lung machine, automatic controller, photoelectric sensor 77—78053
- vibrotactile speech training deaf aid, frequency analysis system 77—29214
- video radiographical images, enhancement 80—94353
- vital microscopy, electronic thermostatic system 80—85537
- voice controlled system for the disabled 79—5407
- walking, synchronisation of optical press. distrib. and 3-dimens. force meas. under sole human foot *(German)* 78—35975
- worlwide inequalities and development prospects *(French)* 79—70660
- X-ray image intensifier noise evaluation, digital method 80—98097
- CO_2 analysis, amplifier and lineariser for Beckman LB-1 analyser 77—29215
- Si miniature biomedical piezoresistive pressure transducer *(German)* 80—37016
- Si(Li) detector probe with RFT radiation meas. unit for diagnosis of intraocular tumours *(German, English)* 78—20265

biomedical engineering
- *see also biomedical electronics; biomedical equipment; orthotics; patient treatment; prosthetics; sensory aids*
- advances in bioengineering, conference, San Francisco, USA (Dec. 1978) 79—92416
- amputee-appliance system, lower extremity, functional status analysis and evaluation, integrated approach 77—13032
- antenna two-element array, insulated, in relatively dense medium 77—25794
- anticipatory display, for communication by severely disabled nonverbal person 77—78002
- appropriate technology appl. 78—44634
- audiometric facility at West Middlesex Hospital, London for standardised hearing tests 80—76858
- bioengineer's role in modern medicine 77—86673
- biomagnetic measurement facility installation in hospital environment, design criteria and procedure 80—104707
- blood pulsative flow digital simulation by finite element method 78—92670
- Canadian biomedical engineering research for handicapped persons, review 79—29662
- cardiac computing conf., Geneva, Switzerland, (Sept. 1979) 80—82582
- clinical engineering, university based shared service, history of N.New England programme 77—44776
- clinical engineering and health care in nonaffluent underdeveloped nations 78—80991
- clinical engineering internship at Ohio State University 77—41432
- clinical engineers' acceptability to hospital administrators 77—21640
- clinical physics, the lessons of history, review 80—62447
- clinical support surfaces, mech. compliance evaluation 80—92053
- communications conf., EUROCON, Venice, 1977, May 78—53552
- Communications Technology Satellite biomedical communications expt., selection of Earth terminal parameters 77—48898
- communications using pre-existing statewide microwave network 77—48899
- component quality control system 77—48884
- computer applications, review *(Japanese)* 80—12289
- conference, Boston, USA (Nov. 1976) 77—25573
- conference, engineering in medicine and biology, Atlanta, USA (Oct. 1978) 79—39332
- conference, Jerusalem, Israel (Aug. 1979) 80—98758
- conference, Los Angeles, U.S.A., (Nov. 1977) 78—28105
- conference, New York, USA (Dec. 1979) 80—104561
- conference, Stockholm, Sweden (Dec. 1979) 80—31410
- conference, Stuttgart, Germany, (May-June 1978) 78—80988
- conference, Washington, USA (Oct. 1979) 80—51956
- conference on medicine and techniques, Zagreb, Yugoslavia, 1979 80—101667
- cooperation requirement between countries at various stages of development 80—94382
- curriculum enhancement through collaboration in rehabilitation medicine 77—81596
- dental materials, uses and props., review 78—53548
- developing countries, problems and their solution in Nigeria 78—31938
- developing countries, Yugoslavia and Egypt 78—28882
- developing country, prod. of practical engineer 78—28884
- dialysis, ultrafiltration, meas. and control using differential flowmeter 77—21657
- doctor degree course for physicians at Federal Institute of Technology, W.Germany *(German)* 78—3627
- Dutch development of medical physics *(Dutch)* 80—3877
- education, advantages of cooperative education between hospital and college 78—28879

biomedical engineering continued
education, clinical engineering introductory course 78—28880
education, position in Hungary 79—67127
education, professional society emphasis areas 80—27069
education and certification of biomedical engineers in Canada 79—80389
education and professional training in W.Germany 78—41106
education in France 78—73807
education in Sweden and other Nordic countries 77—71169
education program in medical radiological physics based on nucl. engineering 80—31448
education to continue the clinical engineer's career 80—17733
educational programs, accreditation 80—27070
electrical safety, one-day seminar for nurses 77—37701
electrical safety programme on low budget, with offline inventory control 77—40821
electromedical instruments, charact. and appl. 78—3642
employment information sources 79—92918
equipment technician certification, status and trends 77—37683
gas supply to hospitals 77—90942
head protective devices design, military 78—11793
health care role fostered by hospital based student training 77—41433
holographic display of medical images 77—29193
holography in dentistry, review 78—48859
hospital buildings, harnessing of solar energy 79—79383
hospital engineering, conf., Lisbon Portugal (May, June 1978) 79—79667
hospital engineering education in the USA 79—79668
human factor studies, conf., San Francisco, USA (Oct. 1977) 78—48742
IEEE 7th Northeast Bioengineering Conference, Troy (1979) 79—79672
image processing, state of art *(Japanese)* 80—56251
implant material, hydroxylapatite synthesis and characterisation 77—4749
India, health care problems and trends 77—48897
in India, report on the prevailing level of medical electronics 77—40810
instruction, microprocessor-based instrumentation system 77—22361
instrumentation, review *(French)* 80—89884
instrumentation teaching, using guided design format 78—28881
interdisciplinary aspects 78—8214
interdisciplinary aspects and problems 78—53553
internships in community hospitals, cost effective program 79—97132
Japanese medical technology, development and future problems *(Japanese)* 80—12287
laboratory course, clinical engineering practicum 78—28878
laminar air flow room and clean room microbiology in treatment of bone marrow transplant patients 80—26411
laser applications, book 78—48857
laser applications in biology and medicine *(Japanese)* 80—3752
Massachusetts General Hospital, Boston, clinical engineering *(German)* 78—35976
materials for orthopaedic implants, review 80—76862
microwaves, medical applications and biological effects *(Spanish)* 80—26260
motion analysis, human, 3D coordinate data processing 80—56260
motorized orthotic shoe for submaximal assist 80—56289
Nigeria, 3 years' experience of practical problems 79—2147
NIGMS evaluation workshop recommendations for research, inc. physiology 79—12018
occupational physiology and psychology laboratory 77—48885
operating theatre safety fundamentals *(Japanese)* 79—2149
patient electrical safety in crit. care areas using isolated patient environment 77—40914
peristaltic pumping by a lateral bending wave 80—53862
photoacoustic spectroscopy, biological and medical appls., book contrib. 80—109078
physics aspects *(German)* 78—92735
picture communication systems 78—57104
PIGMI, linear pion generator, mechanical technologies 79—72008
PIGMI prototype, linear pion generator, initial performance 79—72007
polycarbonate purification for medical use 78—84759
polymeric biomaterials for blood-contacting appls., problems and new dimensions 78—85423
quality health care and cost containment, conf., Washington, USA (Mar.-Apr. 1978) 79—39333
R&D programmes in Norway *(Norwegian)* 78—48909
radiation processing of new materials 77—70542
radiation therapy, automatic checking system for treatment parameters *(Japanese)* 77—73614
recent advances, conf., London, England (Mar. 1980) 80—94924
regional health care distribution systems, systems approach 77—48896
rehabilitation medicine, potential research areas 77—40913
remote medical care technology 77—48895
renal tubulus, digital picture anal. 79—70712
review of biophysics and bioengineering, book 80—105437
review of developments and facilities 80—12292
review of nucl. medicine 1977 78—85459
review of present state 80—17023
review of the emerging field of biomedical engineering 80—36167
rural health care delivery system model 78—44633
rural hospital grouping for resource sharing 79—83978
safety design, probabilistic approach, use of basic n-element configurations for safety education 77—57137
safety design, probabilistic approach by appl. of Markov chains to n-element environments 77—37106
signal modelling and recognition, system identification approach 80—51286
signal processing and telemetry, digital bandpass analysis 78—57107
Spanish and foreign professional and educative trends *(Spanish)* 79—83964
standards development, as educational and design review process 78—44647
state of art, seminary, Brno, Czechoslovakia (Sept. 1976) *(Czech)* 77 17001
systems approach 77—5094
teaching, philosophy of new methods 78—28883
technobiology, advanced, conf., Paris, France (June to July 1978) 80—41945
technological advances, rigorous assessments of benefits and costs 80—17163
technology assessment, interdisciplinary approach to policy formulation and decisionmaking 77—48900
technology impact on health care productivity 80—17171
terminology and future problems for the industry 80—36170

biomedical engineering continued
terminology and tasks survey *(Hungarian)* 78—35983
textbook for undergraduates 80—8750
thermoregulatory system, human, engineering models, review 77—81471
tissue substitute materials formulation, effective atomic numbers 80—17169
TLD in medicine and biology 79—74762
trained personnel requirement in W.Germany *(German)* 78—3626
training biomedical engineers and technicians in developing countries 80—62408
training experience at Ecole National Superieure des Telecommunications *(French)* 77—40817
training for engineers in India 79—80390
undergraduate degree program, state university approach 78—77646
undergraduate programmes in USA, career prospects 78—28877
USA nationwide survey of present use of clinical engineering in hospitals 80—36177
USSR development of equipment and instruments 79—96699
X-ray intensifier, CCTV viewing system 77—9251
Yugoslav university training 79—35442
Ni-Ti shape memory alloy processing and medical applications *(German)* 80—17203
Ti, physical props., implant surgery appl. 77—73615

biomedical equipment
see also biomedical electronics; biomedical measurement; orthotics; prosthetics; radiography; radioisotope scanning and imaging; sensory aids
4-channel cassette recorder for 24-hour epileptic patient EEG monitoring 78—3639
21-channel EEG monitor with real-time result colour display 80—72364
60 Hz harmonic eliminator 78—77124
70 mm photographic camera, for scintillation camera, with roll film *(Japanese)* 77—70546
A/D conversion, multichannel, without timing skew, for LF biological signals 78—61271
Aberdeen phased array, real-time US scanner with dynamic focus 80—72276
accelerator leakage measurements 80—89839
accelerators, international standards 80—51272
acoustic impedance meter, principle aspects of development 79—24999
acoustic microscopy using scanning laser beam as remote sensing microphone 77—81382
acoustic scanning microscope, operation and appl. 77—84095
acoustically evoked potentials in EEG, meas. by adaptive matched filters *(German)* 78—88755
active human muscle visco-elasticity dynamic meas. 77—86667
activity meter for nuclear medicine, ionisation chamber characts. 79—66558
adaptive correlation ratemeter for Doppler foetal heart rate meas. 78—88732
AGC system for biomedical instrumentation, digitally controlled 77—56493
air compressor used in system for treatment of decubitus ulcers, noise reduction 80—48513
air filters, portable electrostatic devices 80—36158
air sampling pump, personal, for hospital operating staff 79—12019
airway resistance measurement in infants, heated rebreathing system 78—7471
ambulatory activity monitor with solid-state digital memory 77—52894
amputee monitoring system for rehabilitation programmes, assessment 80—17167
anaerobic environment integrated system 78—80987
anaesthesia delivery system, microprocessor controlled 77—44832
anaesthesia stage indicator, signal divider 80—3858
anaesthesiology, characts. of elec. currents 80—46093
analogue instrument for living tissue stimulation energy threshold meas. 79—57745
analogue tape recorder, low cost using hi-fi cassette player 80—41282
analysis instrumentation in clinical enzymology 78—88675
analytical instrumentation, status reports, appls. 77—25570
aneasthesia delivery system, closed loop design 78—40402
anemometer, const.-temp. hot-wire, for respiratory gas flow meas. 79—83967
Anger, Hal O., work at the Donner Lab. 80—42027
Anger camera field-uniformity correct., effect of spatial distortion 79—100721
Anger camera/computer system using seven pinhole collimator for myocardial perfusion tomography 80—61663
Anger rectilinear tomographic scanner 78—20257
Anger scintillation camera, development since 1958 80—12234
Anger scintillation cameras, state-of-the-art in suitable photomultiplier tubes 78—40304
Anger-type bar cameras, positron imaging 80—61687
angio-tomographic device, posterior fossa midline visualisation 79—34642
angiography, free arc, with film changer and image intensifier mounted on U-arm 77—86601
angiography, standardised general and cerebral under automatic exposure control 78—24121
angiography installation, first experiences 80—17080
Angioskop multidirectional examination unit for advanced radiographic examinations 78—28039
angiotomography in the diagnosis of intracranial tumours 79—48333
anomaloscope, portable filter type, for colour vision genetics study 77—5004
anthropomorphic phantom, assess. of bulk element lacks by neutron activation anal. 79—39497
anthropomorphic torso section phantom for US imaging 80—45987
apnoea monitor, computerised, for premature infant respiratory pattern monitoring 77—81635
applanation tonometer correlations for intraocular press. meas. 78—77047
arrhythmia ambulatory anal. in real-time with minicomputer 80—85523
arrhythmia detection, edit and recall system, microprocessor-based 80—89891
arrhythmia detection using a low-power, CMOS processor 78—73276
arrhythmia detection with a multi-microprocessor system for distributed and parallel processing 80—85524
arterial blood pressure preprocessor 79—83979
arterial O tension servocontrol in preterm infants 80—17183

biomedical equipment continued
arterial pO$_2$ intravascular monitoring using catheter-tip polarographic electrode *(German)* 78—85408
arterial pressure automatic indirect monitor 80—56231
arterial pressure modulator for perfusion circuit of isolated organ *(French)* 78—81004
arterial tonometer, microprocessor based 78—31955
arterial US scanner, colour coded differential velocity display 79—34617
arthrographic equipment for double contrast knee exam. 79—48320
articulated support system, appl. to Ganzfeld ophthalmological stimulator 79—83970
artificial blood circulation system, thermoelectric heat exchanger control unit 79—25149
ATP-12M infrared imaging system (USSR), body temperature meas. 80—67280
audio dual channel monitor for distinguishing action pots. from two different sources 78—61293
audiometer, pure-tone and speech, computerised *(Japanese)* 79—74774
audiometer, screening, and real-time computer techniques 78—81009
audiometers, principles, appls. and commercial models 78—44669
audiometers produced by Medicor Works 79—62384
audiometric earphones influence of cushion dimensions on output 79—41547
audiometry using cortical evoked response, use of portable programmable tape recorder 77—60279
auditory and visual impairment simulator development project 79—83982
auditory ipsilateral acoustic reflex stimuli calibration 80—17170
Auger camera performance, effects of a reduction in crystal thickness 80—41187
auscultation, portable clinical electronic device for simultaneous multiple auscultation 77—56507
auscultation instruments, evaluation of acoustic props. 77—81601
automata and automatic meas. appl. in medical engineering 79—62381
automated procedures and equipment development, laboratory medicine trends *(Japanese)* 77—44766
automatic radioisotope production devices adapted to a medical cyclotron 80—12260
automatic test system for implanted pacemaker performance assessment 78—11778
autotransfusion, variable speed pump head control 77—52918
autotransfusion, variable-speed pump head control 78—57121
Autoweigh system, electronic weighing device for premature infants 78—44632
averager for neuroelec. response meas., operation mode *(German)* 77—77887
axial tomography of skull, modified technique 77—86600
betatron bremsstrahlung field shaping apparatus for teletherapy 78—57062
betatron redundant solid-state controller 79—88163
Bevalac Minibeam facility, biomedical heavy-ion beam 77—83359
Bioconverter for upper extremity rehabilitation 79—48364
bioelectric signal measurement and processing instrument trends *(Croatian)* 78—44665
bioelectrode motion artefact model and artefact reduction by amplifier input stage design 80—56261
bioengineering advances conference, San Francisco, USA (Dec. 1978) 79—92416
biofeedback devices for control of unconscious physiological processes 78—35992
biofeedback diagnosis system, physiological parameter meas. considering psychic effects 79—100774
biofeedback training device for speech therapy, portable, microprocessor-based 80—104808
biofocal diverging collimator for equilibrium radionuclide ventriculography 80—72310
biomagnetic instrumentation and meas. 80—36181
biomagnetic measurements in unshielded and noisy environments 80—104710
biomaterial compatibility for cardiovascular appls., biological evaluation 78—36056
biomedical engineering textbook for undergraduates 80—8750
biotelemetry, conf., Garmisch-Partenkirchen, W.Germany (May, June 1978) 79—43980
biotelemetry, conf., Pacific Grove, Calif., USA, May 1976 77—86653
bipolar suction electrode catheter for intracavitary ECG 79—44018
blood, filter evaluation 78—69250
blood, pressure and pulse rate, system for determ. long term variations 79—57792
blood cell computerised counting and sizing system 78—31932
blood cell differential counter, ADC 500, pattern recognition based image processing system 78—73282
blood cell electrophoretic mobility study, semi-automatic system 80—3851
blood clotting timer, automatic 77—52896
blood flow detection in human heart, US pulsed Doppler flowmeter system, microcomputer based 80—104690
blood flow measurement by US Doppler method, computer-aided determ. of angles *(German)* 78—80931
blood flowmeter, cylindrical crossed-coil NMR, for noninvasive measurement 79—62328
blood gas analyser, microprocessor based 78—40356
blood gas analysers, review 78—69238
blood gas catheter, fast-responding, flow-independent, for O$_2$ meas. 80—101277
blood gas catheters, flow-dependent, in vivo calibration 79—16330
blood gas continuous monitoring, current trends 80—56237
blood gas microanalyser, calomel electrode efficiency restoration 77 25575
blood gas monitor for extracorporeal procedures 79—100756
blood glucose sensor for implantable artificial β-cell 79—83973
blood microfilter materials and designs 79—48352
blood pressure ambulatory recordings, minicomputer processing 80—89887
blood pressure automatic monitoring, long-term, minicomputer system 80—101276
blood pressure continuous recording system for ambulant hypertensives 79—62390
blood pressure cuff control unit, automatic multi-function device 78—36013
blood pressure electric sensor for extracorporeal circulations *(German)* 78—92721

biomedical equipment continued
blood pressure instruments, direct systolic/diastolic meas., review 78—69234
blood pressure instruments, noninvasive arterial meas. using US Doppler effect 78—69167
blood pressure long-term recordings, fast data reduction, hybrid system 80—41278
blood pressure meas. instrument for newborn infants 79—92406
blood pressure monitor/conditioner, noninvasive cuff device 77—73605
blood pressure recording transducer, arterial and venous 79—34708
blood pressure transducer for student use, using hybrid IC 78—8186
blood pressure transducers, technical evaluation 79—44002
blood pressure transistor device, high sensitivity, quasi-digital 79—79675
blood pulse wave velocity, digital meter *(Japanese)* 79—39546
blood pump, biventricular, brushless DC motor powered, development and in vivo evaluation 79—53285
blood temperature monitoring transducer, during extracorporeal circulation 78—44639
blood viscometer, capillary type 77—40844
blood viscometers and anticoagulants compared 79—83834
blood viscosity and red cell aggregation at zero and 1G, instrumentation for Space Lab 3 80—61716
body motion computer-aided tracking using CCD image sensor 78—61269
body radioactivity measurement, SABRE 3 computer system 78—85425
body scanning using nuclear magnetic resonance method 79—53274
body surface potential mapping, microcomputer processing system *(Japanese)* 80—72347
bone conduction vibrators, calibration force levels 78—65046
bone healing in humans, appl. of pulsed mag. field to stimulation 78—28029
bone mechanical properties determ. in vivo, noncontacting EM device 78—77133
bone mineral analyser, microcomputer based 79—53218
bowel anastomosis dynamic strength testing device, electronically controlled *(German)* 80—36160
brain imager, transverse-section, for single-gamma emitters 80—3794
brain impedance scanner principles and exptl. results 79—57804
brain impedograph, computerised 78—77139
brain isotope distribution reconstruction, error anal. for instrument design 80—3772
brain reflexes meas., using Sredetz device *(Bulgarian)* 80—30909
brain retraction pressure monitoring, meas. system for surgical procedures 80—21563
Brattle Physiological Synchroniser, simulator for testing respiratory gating function 80—109055
breast thermography, use of liq. cryst. sheets 80—41166
breathing ratemeter for neonatal intensive care 80—41311
breathing state tester, portable *(French)* 80—51288
bronchoscopic tumour localisation, small radiation detector probes, scintillation and semiconductor detectors 80—61676
cameras, multi-, planar control in photogrammetric calibration for 3-D gait studies 80—67194
Canadian biomedical engineering research for handicapped persons, review 79—29662
Canadian hospitals, equipment maintenance, questionnaire answers 79—53263
cancer prescreening, automated cell image analysing system *(German)* 79—83892
cancer therapy, invasive microwave system localised hyperthermia 79—100700
cancer therapy facility, microprocessor based control system 78—40398
canopy ventilation monitor for quantitative meas. of ventilation during sleep 80—104792
capacitance-dynamic electrode for bioelectric potentials 79—57782
capacitor discharge mobile X-ray apparatus *(Japanese)* 79—88165
capillary viscometer for blood flow meas. 79—79671
cardiac activity signal simulator 80—56230
cardiac arrhythmia monitors, review 78—69233
cardiac arrhythmia simulator 79—100755
cardiac mechanical activity, noninvasive mag. detect., instrumentation 80—89820
cardiac monitor, heart rate meter and alarm eval., proposed standard test tapes 80—89899
cardiac noise, automatic segment anal. *(German)* 78—88759
cardiac nuclear medicine instrumentation, review, book contrib. 80—101260
cardiac output analysers, equipment, maintenance and ccts., review 78—69239
cardiac output measurement, in vitro comparison of six commercially available thermodilution systems 78—77135
cardiac probe, microprocessor-based, for gated equilib. and beat-by-beat left ventricle function 79—62396
cardiac rate meter, based on analogue low-frequency meter *(Czech)* 77—37084
cardiac resuscitator, automatic, emergency treatment of cardiac arrest 79—88147
cardiac scintigraphic image handling using microprocessor system 80—85489
cardiac sound frequency shifting stethoscope 79—29647
cardiac stimulator power supply battery selection 77—48931
cardiac synchronised augmented pulsation pressure concept, prototype 77—78058
cardiac tachometer, instantaneous, with extendable range 79—20700
cardiac valve prosthesis simulator, role in prosthesis design 79—12033
cardiological data processing in real time by hybrid computer, optical link 77—86677
cardiology, development progress 78—3646
cardiology data processing system, computer 80—56236
cardiopulmonary function automated testing system 79—70673
cardiopulmonary noninvasive noncontacting monitor using coherent microwave interferometer 78—40290
cardiotachometer calibration, precision pulse generator, cct. 77—86682
cardiotachometer histogram indicator, prototype 80—41268
cardiotachygram, anal. of recurring beat sequences *(German)* 78—88753
cardiovascular computerised monitoring in medical intensive care unit 78—20304
cardiovascular dynamics instrumentation evolution (1940-80) 79—83983
cardiovascular monitoring, single freq. RF powered implantable multichannel telemetry system 77—52897

biomedical equipment continued
cardiovascular nuclear medicine, instrumentation and data processing, ventricular function evaluation 80—85481
Carshalton halo-pelvic traction apparatus, design improvements 79—39594
cassette recorder, portable, for continuous ECG monitoring on commercial pilots 77—86659
catheter, conductive, reduced risk of cardiac fibrillation 78—35972
catheter, multi-transducer, for intraluminal press. recording in vivo 80—89879
catheter flow probe for left ventricular source parameters meas. 79—92324
catheter for female bladder aseptic catheterisation 79—79674
catheter systems for respiratory intra-oesophageal pressure meas., selection, testing 77—90937
catheter tip device incorporating CO_2 and O_2 sensors 79—100783
catheter tip pH electrodes for continuous intravascular recording 80—81755
catheter-tip electrode for continuous pO_2 and pCO_2 meas. 79—34693
catheterisable sensors, PO_2 probes, press. transducer and photometers 80—46080
catheters, intravenous, eval. of polymers, tissue response 77—37065
catheters and guides sterilising/storing device 78—7455
Cathetron, high intensity Co, gynaecological cancer therapy 80—72300
cathetron for cervical cancer treatment, description for teaching 78—49617
Cathetron linkages, safer coupling collar 77—73612
cell analysis in haematology, LARC system overview 78—31931
cell electrophoretic mobility meas. using new automatic method 80—67322
cell freeze conservation control unit *(German)* 79—5410
cell high-speed sorter, data acquisition and display 78—44622
cell recognition and counting using adaptive coherent optical processor 78—77120
cell suspension six-channel aggregometer 78—81001
cephalostat for speech physiology research 78—65140
cerebral activity monitor, using biofeedback rhythms inducing cct. *(Spanish)* 80—72359
cerebral angiography, evaluation of Contrac injector 78—40293
cerebral angiography routine enlargement system, Poly Diagnost N 77—86602
cerebral blood flow computer for use in angiogram theatres 78—73227
cerebrospinal fluid pressure meas. by passive telemetry, improved instrument 78—31927
cervical cytological sample screening, coherent optical processing, via Fourier transforms 78—36006
cervical cytological sample screening, coherent optical processing via Fourier transforms 78—36007
cervical cytological sample screening, coherent optical processing via Fourier transforms 78—36008
cervical dilation measurement in human parturition using Hall effect 77—48851
cervical mucus spinability automatic meas. device 78—31928
chart recorders, simple test for phase characteristics quantification 79—92409
chemical analyser, customer serviceability design 78—44653
chest radiograph nodule detection system 80—8140
chest X-ray automated screening, texture anal. of lung fields 80—41228
choledochoscope, rigid optical-fibre, KhVS-1, bile duct inspection, surgical appl. 77—37071
chronic sphenoidal electrodes, material improvement 79—16328
chronically implantable instrumentation for medical research animals 80—30834
cineangiocardiograms, automatic anal. using TV system on line with minicomputer 78—92699
circulatory system expt. model for heart valve testing 77—52932
Cleon imager, clinical evaluation 78—24128
clinical chemistry temperature standard, Ga melting-point 78—80997
clinical laboratory technology, new developments, diagnostic immunology and microbiology 78—81037
clinical paediatric gait biotelemetry 78—3652
code generator to identify time, date, and events in physiologic event recording 77—86674
coils for RF powered implant telemetry, design 78—31926
cold finger, for cryosurgery, heat transfer characts. *(Russian)* 77—22556
cold urticaria diagnosis and treatment assessment, stable low temp. source 78—61276
colonic contractile activity meas., pharmacological tests in dogs appl. 80—109068
colorimetric analysis, automatic, biological fluids, contamination study 77—25564
colour TV, single tube SICOLOR, appl. to endoscopy *(German)* 78—88758
combined microwave heating and radiometry methods 80—85465
communication device for mute paralytic 78—40420
communication prothetics, adaptive, microprocessor-based, for persons with severe motor handicaps 78—48941
communication/control systems for motor impaired people, standardisation 80—17198
computed tomographic rotating fan-beam scanner, exptl. bench design 80—51230
computed tomography, scanner evaluation and selection 80—46065
computed tomography image display system 80—46039
computed tomography scanner, fourth-generation, performance evaluation 80—46035
computed tomography scanner geometry optimisation 80—46037
computer assisted ring detector positron camera system for brain reconstruction tomography 78—40306
computer graphic optokinetic stimulus pattern for study of optokinetic nystagmus 79—44008
computer tomography detector vibr. sensitivity 78—35955
computer tomography head scanner, translate-rotate type with Xe detectors, performance characts. 80—46036
computer-aided diagnosis of medical images, conf., Coronado, USA, (Nov. 1976) 77—78018
computer-aided intensive care in paediatrics *(German)* 78—88754
computer-controlled stimulator for ventricular myocardial function analysis 77—60267
computerised EEG signal averager, flexible and low cost 79—43998
computerised tomographic head unit, Siretom 2000, operation 78—28037

biomedical equipment continued
computerised tomographic scanner acceptance testing 77—73569
computerised tomographic scanner image quality evaluation phantom 77—73573
computerised tomographic scanner slice thickness meas. *(Japanese)* 79—92353
computerised tomographic scanning, engineering status 77—73571
computerised tomography, basic physics, mathematics and data reconstruction 78—73218
computerised tomography, dynamic 3D imaging system for cardiac structures and functions 78—44600
computerised tomography, dynamic spatial reconstructor, high temporal resolution scanner 80—51235
computerised tomography, EMI CT5005 scanner aids, radiation therapy treatment planning 79—100704
computerised tomography, EMI first generation scanner, dose rel. to collimator geometry 79—74760
computerised tomography, expt. dual Xe detectors for quantitative CT and spectral artifact correct. 80—76825
computerised tomography, image construction, restoration and enhancement 77—44743
computerised tomography, operating principles, image construction, appls. 78—28047
computerised tomography, positron emission, crystal size optimisation 80—61681
computerised tomography, positron emission CT device with continuously rotating detector ring 80—81697
computerised tomography, scanner for early detect. and evaluation of heart disease 79—66521
computerised tomography, scanners, status in 1979 79—66536
computerised tomography, Shimadzu scanner SCT-100N, development *(Japanese)* 78—61277
computerised tomography, single-photon emission, imaging capabilities of Ge camera 80—61668
computerised tomography, Siretom 2000 initial clinical experience 78—28038
computerised tomography, software balancing of multiple detectors during CT scanning 80—46026
computerised tomography, Somatom fast whole body tomograph with direct image reproduction 78—28036
computerised tomography 80—89832
computerised tomography body scanners, comparison of translate-rotate, pure rotary types 78—69211
computerised tomography equipment, for intracranial diagnosis 78—31884
computerised tomography image processing and evaluation using PDP-10 computer 78—44587
computerised tomography nuclear imaging system, initial performance of SPRINT 79—66523
computerised tomography performance phantom optimisation 78—48892
computerised tomography scanner commissioning 77—73570
computerised tomography scanner resolution, geometrical limitations 78—73237
computerised tomography scanner X-ray tubes 79—66537
computerised tomography scanners, effect of X-ray source filtration on dose and image perform. 80—30865
computerised tomography scanners, survey of noise, dose and contrast detectability and resolution 80—104750
computerised tomography scanning, review of technical aspects 79—34635
computerised tomography system, high speed heart imaging 79—66544
computerised tomography system for circulatory system visualisation, 250 simultaneous scans 79—79625
computerised tomography tilting unit, advantages in skull diagnosis *(German)* 80—94351
computerised tomography with X-ray transmission pencil beam scanner 77—44741
concentric disc electrode for bladder urine vol. determ. *(Japanese)* 78—31921
conference, Denver, USA (Apr. 1979) 80—73100
conference on nuclear power systems, Washington, USA (1978) 79—41045
constant current supply for percutaneous electrophoresis of amino acids and urea 78—61237
contact microscope for medical laboratory use 80—85540
contourograph using ICs for quasi-periodic and nonidentical physiological signals 77—44791
contributions to medical electronics by NPL 80—36169
controlled filter for bioelec. pots. 78—40357
coordination therapy electronic aid using pattern recognition methodology 80—56276
cornea light scatt. meas. apparatus 77—5123
corona ion generator for removing dust and aerosol particles in rooms *(Finnish)* 77—66883
coronary arteriography, current techniques and equipment 78—35940
coronary care unit equipment failure finding and prediction 78—44648
corrosion resistance and mechanical performance in medical instruments 79—39537
couch-cover, heatable, use in X-ray exams. *(German)* 80—104751
Coulter S blood analyser and IBM 1800 computer, minimum-interrupt digital interface 80—3849
critical care unit instrumentation care and servicing, book 78—69231
cryocatheter tourniquet, appl. 78—7521
cryocoagulator for uterine contraction promotion and bleeding suppression 79—39591
cryogenic equipment for freezing and in-transit temp. control 79—58714
cryoprobe, clinical appl. 80—12295
cryoprobe, for medical surgery 80—56274
cryosurgery, self-contained apparatus 80—56271
cryosurgical apparatus coolant supply system 77—81637
cryosurgical applicator, temp. distrib. reproducibility 79—39589
cryosurgical instrument for proctological and gynaecological operations for malignant tumours 79—70699
cryosurgical instruments, open and closed circuit supplies compared 79—39592
cryosurgical probe, heat transfer coeff. within cavity formed by tip 80—36188
cryoultrasonic surgical instrument 77—78027
cutaneous blood flow meas. instrument, laser beam Doppler shift method 78—28030
CW FM sonar with aural displays, improvements 78—87221

biomedical equipment continued
cyclotron for radioisotope and labelled compound prod. 79—53245
cyclotrons, production of radionuclides and radiopharmaceuticals using proton and deuteron accelerators 79—53240
cyclotrons for fast neutron radiotherapy and radioisotope prod. 79—53244
cyclotrons for radionuclide prod. 79—53238
cytofluorometer, imaging system for correlating fluoresc. cell meas. in flow 78—61240
cytopherometer, reproducibility improvement 77—52954
dark adaptometer, normative and clinical data 80—41019
data collection station, based on autonomous CAMAC crate 80—61689
data evaluation system, for use with gamma cameras in nuclear medicine 78—92732
DC micromotor controlling feed rates in syringe pumps, appl. to drug administration 78—48923
deaf-blind communication, electromech. hand 78—48943
deformable electronic components for biomedical meas. *(French)* 77—70564
dental instrument noise studies, canine evoked response audiometry system 77—29226
dental suction system, at Guy's Hospital, London 79—8556
dental unit US 10/100 78—36040
dermatological photobiology, fibre optic light guides for phototesting 78—53472
diabetes mellitus, devices for control of continuous insulin infusion 80—17184
diadynamic current therapy apparatus Tonus-1 78—7523
Diagnost 73 P, universal diagnostic system for paediatric radiology 79—48334
Diagnost C, localisation of intracavity Rn applicators 79—48331
Diagnost C for gastro-enterological X-ray diagnosis 77—86599
diagnostic image systems, image analysis, structural methods 77—86564
diagnostic imaging systems, image quality assessments 77—90890
diagnostic imaging systems, non-silver halide, recent developments and pot. 80—41223
diagnostic picture-display systems, developments and limitations *(German)* 79—100705
diagnostic system, portable, for regional and district doctors 77—5104
diagnostic system, portable, operational experiences 77—5105
diagnostic system, portable, principle and appl. 77—5103
diagnostic ultrasonics, electronic techniques, present applications and future developments *(German)* 79—100683
diagnostic X-ray tubes, meas. of focal spot size 80—89831
dialysis equipment elec. hazards and safety 79—84010
diathermy indifferent electrodes, performance electrodes. 80—72367
dielectric spectrometer, in vivo, for tissue dielec. loss and permittivity meas. 79—57743
digital automatic blood pressure recorder *(Japanese)* 78—24168
digital cardiac defibrillator tester 80—41286
digital ECG systems testing 80—81756
digital filtering and edge detection 80—58065
digital memory recorder, electromyography and nerve conduction appls. 79—43999
digital moving target indicator system for detection of intracranial arterial echoes 80—17035
digital pulse counter for cardiovascular monitoring 78—35978
digital US gauge for ventricular dimension meas. 78—20238
direct coupled electrocardiograph *(Japanese)* 78—24166
disabled children's therapeutic aid using myoelectric feedback 78—36048
display board for non-vocal communication encoded as eye movements 77—52927
display system perceived dynamic range evaluation from receiver operating charact. curves 78—44662
displays, three dimens., in biostereometrics 78—81010
Dopper echocardiography sample vol. tracking unit 79—57730
Doppler flowmeter average frequency processor 79—83873
Doppler signal centre freq. estimation using quadrature zero-crossing counter, US blood flowmeters 78—31879
Doppler US flow transducer for human milk flow meas. 79—53200
dose compensation filter design using megavoltage radiography 80—3785
dosimeter system, transit type, for ^{60}Co rot. therapy, electronic modification 77—2053
drip feed unit microprocessor control development 78—53563
drug assessment system, elec. interf. and bubble free induction of thrombi 79—44017
drug injection device for cavernous tuberculosis treatment 78—7520
dye laser photodermatological uses, erythema production, psoriasis treatment, tumour destruction *(German)* 80—56164
dynamic focusing transducer design for diagnostic image quality improvement 80—41155
dynamic motion simulator for testing plastic ligaments and tendons *(German)* 78—81070
dynamic phantom for radionuclide cardiology 80—12232
dynamometer DE 1, digital, mass diagnosis locomotor and nervous system disorder appl. 77—40854
ear characteristics meas., acoustic impedance meas. instrument *(Hungarian)* 78—36012
early equipment review *(German)* 77—77994
earphone shielding effectiveness for artifact control, auditory evoked pots. meas. 79—57790
ECG, ambulatory, computer processing system 80—89897
ECG, cordless electrocardiograph and heart rate meter *(Japanese)* 78—80984
ECG, EK1T Malyshch equipment, operational errors 80—61717
ECG, interactive analysis techniques with Random Access Mass Storage ECG Analysis System 78—81034
ECG, long-term continuous recorder *(Japanese)* 77—66871
ECG, long-term recordings, rapid computer analysis system Argus/H 78—36002
ECG, microprocessor based ambulatory monitor 77—48918
ECG, QRS detector/delineator devel. and eval. 80—89892
ECG 24 hr recording, anal. using operator-controlled computer system 80—89888
ECG amplifier with automatic lead switching 78—28106
ECG amplifiers, instruments and maintenance, review 78—69232
ECG analysis system, long term recordings, quantitative evaluation of rhythm disturbances *(German)* 80—76847
ECG arrhythmia simulator for monitor testing 78—61270
ECG automated monitoring, new electrode system 80—89898
ECG capacitive electrodes for burn appls. 80—41279

biomedical equipment continued
ECG cassette recording and automatic processing microprocessor system 78—36021
ECG data-acquisition module, low-power, for microprocessor systems 80—41292
ECG diagnostic interactive minicomputer system 78—36022
ECG equipment and physiological basis *(German)* 79—100757
ECG gated acquisition cardiac imaging, quantification of left ventricular function 79—70638
ECG gated radionuclide cardiac imaging system 79—70639
ECG instrument requirements, examination methods, recording, computer interface unit 80—41303
ECG monitor, non-fade, battery-powered, emergency/surgery appl. 78—7528
ECG potential distribution mapping instrumentation 80—21561
ECG quasiperiodical signal changes evaluation, automatic *(Czech)* 78—40371
ECG real-time analyser with digital readout, portable device 80—56234
ECG recorder, with statistical pulse train interval digital analyser *(German)* 77—78007
ECG S-T segment elevation meas. instrument, programmable 78—31956
ECG signal-averaging system, flexible, computerised 80—67270
ECG slow wave real-time anal., hardware implementation of selective Bouilland transform. 80—56233
ECG surface potential recording electrodes 79—100779
ECG-gated radiography, interlaced system for improved chest X-rays 80—26344
ECG-triggered scintigraphy of intracardiac space 78—28033
echo distribution evaluation *(German)* 78—80934
echo-oculometer, accurate meas. of eye length 77—37030
echocardiogram, M-mode, automatic computer anal. *(Japanese)* 80—72274
echocardiogram computer-assisted interactive interpretation 78—80938
echocardiographic and systolic time interval processor 79—83869
echocardiographic images, video recorded, interactive segmentation 80—89817
echocardiography, automatic range gate tracker 79—83868
echocardiography, bidirectional, for detect. of cardiac cycle 78—15877
echocardiography, binocular stereoscopic display system 79—48297
echocardiophone, CW swept freq. US echo location system 77—70514
echoencephaloscope, two-probe three-mode design 78—44567
Echophthalmograph-21, appl. to cardiovascular disease diagnosis *(Russian)* 79—39456
Echosimulator, function generator for meas. of US diagnostic equipment characts. *(German)* 80—104685
echosonography, real-time, computer controlled bidirectional phasing 79—12023
echotomographic system, ultrafast, using optical processing of US signals 77—52855
education, position in Hungary 79—67127
EEG, automatic nocturnal sleep sampling 78—31916
EEG biotelemetry, multielectrode, for remote monitoring and stimulation of ambulatory subject 79—5386
EEG cassette recording system, portable four-channel 77—56498
EEG data acquisition and data processing system, peripheral equipment 80—41270
EEG device in equipment system used for complex examination of nervous system 80—41302
EEG digital recording system for epileptic event observation 78—3641
EEG frequency analyser, real-time, microprocessor monitored 78—57092
EEG period and amplitude anal. system, microcomputer-based 80—72353
EEG potential measuring equipment *(French)* 80—85516
EEG recording system, portable pulse-interval modulation telemetry/multiplexing system, home use 80—67261
EEG signals, analyser-integrator model ANIEG-8 for frequency analysis 80—41295
EEG spectrum analyser using digitally controlled band-pass filter 77—44792
EEG sphenoidal electrode assembly for long-term monitoring of ictal or interictal EEG 77—48907
EEG telemetry, including PWM multichannel system 78—31914
EEG telemetry time-multiplex unit, ambulatory patients 79—44007
elastometer probe system for localised in vivo compliance meas. 78—31960
electric admittance blood flow monitor, clinical evaluation 80—81759
electric field control electrode for stimulation of peripheral nerve 80—21515
electric impedance meas. using 4-terminal instrumentation system for oedema detect. 78—48853
electrical, international standardisation, current problems 77—73603
electrical equipment, safety problems 80—56228
and electrical safety, for nurses, book 78—57100
electrical transducers for skin pressure meas., accuracy obs. 79—83959
electrically rechargeable hand held device for painful subjective sensation prod. in teeth, pulpa vitality *(German)* 78—80944
electro oculography, computerised diagnostic system 80—21566
electro-medical apparatus, guideline for provisional safety standard *(Japanese)* 78—73274
electro-medical servicing, quality maintenance 78—77126
electro-optics, conference, Utrecht, Netherlands (Oct. 1978) 80—31420
electro-osmotic valve, implantable, for controlled drug administration 78—40399
electroacoustic impedance instruments, meas. of temporal characts. and filter response 78—3512
electrocardiographs, portable, Phillips Cardiopan 531, clinical/electronic evaluation 78—11757
electrocardioscopes, appl. and designs 80—41304
electrochemical cell for determ. of O_2 partial press. in biological fluids 78—85420
electrochemical sensor for continuous transcutaneous meas. of PCO_2 77—13020
electrochemical sensors for partial press. meas. in blood 80—67303
electroconvulsive therapy, servo-controlled volt. machine 78—77148
electroconvulsive therapy pulse instrument 78—53562
electrocutaneous information transmission system using stimulus energy control device *(Japanese)* 80—101280
electrode, C-fibre, elec. props. and EEG appls. 80—72355
electrode, implantable, for pH meas., thick film hybrid fabrication *(German)* 78—40369
electrode, implantable stress-resist. design for biotelemetry 78—44629

biomedical equipment continued
electrode, self-correcting spherical design 77—32960
electrode with SiO_2 film *(Japanese)* 80—3848
electrodes, Ag/AgCl, properties, production, problems in biomedical appl. 77—40959
electrodes, ECG, EEG, interfering signals arising by cable motion 80—41296
electrodes, glassy C, meas. in saline 77—81764
electrodes, glassy-C, elec. props. 80—17157
electrodes, miniature, dry, for infant heart rate determ., clinical evaluation 77—56505
electrodes, polished Pt, linear AC electrode polarisation impedance anal. 77—40806
electrodes, Pt, elec. props., impedance meas. and time-domain anal. 78—40360
electrodes, stainless steel, cathodic protection against corrosion 77—90923
electrodynamic earphone, mag. field probe 79—34690
electrogoniometer, variable axis, for knee movement meas. 79—44012
electrogoniometer for meas. and anal. of hip joint movements 79—74766
electromanometry, Medicor equipment for meas. of blood and body fluid press. 77—90943
electromechanical scanner for microwave scattering parameter imagery of isolated canine kidney 80—3755
electromechanical system for diagnosis of spinal abnormalities 78—73286
electromechanical viscometer with digital readout, biological fluid meas. appl. 78—28131
electromedical equipment, computer controlled systems *(German)* 79—62421
electromedical equipment, safety by monitoring leakage currents *(German)* 80—81749
electromedical instruments, charact. and appl. 78—3642
electromedical instruments manufactured by the Electronics Corporation of India Ltd. 80—36168
electromyographic analyser and recorder 79—57785
electromyographic device development 77—40852
electron accelerators, energy calibration method based on Cherenkov effect in gases 80—18721
electron beam applicator, variable field, dosimetry evaluation 80—76839
electron collimation system for use with electron cones of Varian Clinac 18 accelerator 78—11725
electron linear accelerator, 10 MeV, standing wave triperiodic structure 77—10498
electron linear accelerator, radioactive and toxic gas production 80—94378
electron microscopy, wide-field, appls. in biology and medicine 77—56553
electronic communicator for disabled, Fingercom 80—17199
electronic diagnostic apparatus, input earth isolation 77—48905
electronic equipment, service and repair facilities in hospitals 79—96682
electronic equipment in India, noninvasive diagnostic techniques appl. 79—96698
electronic instrumentation, development in Serbia, Croatia and Slovenia *(Slovene)* 77—21636
electronic linear-scanning US diagnostic equipment, high resolution 80—30813
electronic metronome with luminous and audible signals *(Spanish)* 80—89885
electronic radiography, computerised, for early detect. of vacular disease 80—41226
electronic system for leg prostheses axial load meas. *(German)* 79—84006
electronystagmography system for vestibular testing, microprocessor-based 4-channel 80—41293
electrooculographic system for detect. of oculomotor abornormalities in neurological disorders 80—108888
electrophoretic radiographic device 80—22501
electrophotetic X-ray imager, self-contained instant display erasable 80—22491
electrophysiology application, elements of instrumentation, review, book contrib. 80—12293
electroradiographic image laser readout 80—41225
electrospinal stimulation system for scoliosis treatment 77—40908
electrospinal stimulation system for scoliosis treatment 77—40909
electrostatic airborne particle repulsion system for surgical room contamination protection 78—28125
electrostatic X-ray imaging, book contrib. 80—36112
electrostimulation, external, solid-state therapeutical equipment *(Spanish)* 77—78038
electrostimulator, portable, for transcutaneous analgesia 78—36032
electrostimulator for leg muscles to correct defective walking 78—36051
electrostimulator for muscles, Stimul-1 78—36035
electrostimulators, new Russian devices 78—85353
electrosurgery, tissue coagulation, effects of HF current parameters 80—3746
electrosurgery system using HF surgery unit Radiotom 704 78—73292
electrosurgical dispersive electrodes, thermal performance evaluation method 79—74735
electrosurgical dispersive electrodes metal-foil, dry thermal props., skin temp. rises 80—98171
electrosurgical instrumentation review 78—44680
electrosurgical load-independ. const. current generator 78—44684
electrosurgical passive grounded electrode/patient equivalent circuit analysis 77—78025
EM flowmeters for blood flow and vel. meas. 77—78008
EM strip transmission line energy coupler, for medical diagnostic appls. 80—17045
EM syringe for injecting energy into deep-lying tissues 78—53545
EM vibrator for denture prosthetics 80—104716
EMG, instrumentation requirements 80—41301
EMG, miniature skin-mounted preamplifier for surface meas. 78—35990
EMG, myographs design and technical requirements 80—40996
EMG, surface, system for meas., recording and digital anal. *(German)* 80—76848
EMG potential sensing electrodes, types, selection criteria 77—90953
EMG quantitative analysis instrument 78—81041
EMG results from a study of nerve-muscle disorders 77—40811
EMG silent period measurement, automated system 80—89883
EMI brain and body scanners, patient radiation dose 79—48341
emission tomography, comparison of scanner and camera systems 79—66529

biomedical equipment continued
emission tomography, improved coded-aperture system 79—66534
endoholoscope, urinary bladder interferometry, holography of bladder deforms. in vitro, rabbit expt. 80—67201
endoholoscope, urinary bladder interferometry, tumour and lesion detect. by holography 80—67202
endoscope for holographic diagnosis and laser therapy *(German)* 79—96645
endoscope with rigid to flexible imaging multifibre coupling, MTF 79—23052
endoscopes, equipment for checking optical and illum. characts. 80—56157
endoscopes, flexible optical fibre, comparative study 77—37068
endoscopes, flexible optical fibre, gastrointestinal investigation appl. 77—37070
endoscopes, rod shaped elements improve luminosity 77—37069
endoscopic Ar ion laser photocoagulator for bleeding digestive lesions 78—40287
endoscopic carrier, design having complete directional control 80—101248
endoscopic carrier, directional control using magnetic clutches 77—2066
endoscopic coagulation of mucous membrane lesions using HF elec. current *(German)* 78—80945
endoscopic laser coagulator with recirculating gas-jet assist 78—48867
endoscopic laser photocoagulation, use of gas jet appositional pressurisation 78—53468
endoscopic manometry in gastroenterology 78—92730
endoscopic miniature camera with fibre-optic faceplate 80—77896
endoscopic roentgenography appliance users' experience 77—25544
endoscopic system advances 78—57096
engineering in medicine and biology, conf. Atlanta, USA (Oct. 1978) 79—39332
epicardial mapping, computerised display system *(Japanese)* 80—101279
epicardial mapping, DC, during exptl. coronary occlusion, digital data acquisition system 80—85527
epicardial signal recording probe, hand-held 80—12286
epidural intracranial press. monitoring with press.-sensitive on-off type switch sensor 78—44626
epidural intracranial pressure meas. by piezoresist. transducer *(German)* 78—85404
epidural intracranial-pressure transducer with reduced tissue stress interference 80—41290
equipment safety in diagnostic X-ray departments 79—48346
esophageal multiprobe for temp. ECG and heart and lung sounds meas. 79—57791
esophagogastroscope, flexible fibre optic instrument, experience of use of 79—34622
evaluation and preventative maintenance of medical devices 77—44777
evoked-response data acquisition system, specification and design 80—56165
exercise body plethysmograph, head-out, for extrathoracic airways investigation 80—81754
exercise cardiopulmonary response analysis, breath-by-breath computer system 78—35995
exercise therapy, walking simulator 80—81770
extensometer for in vivo meas. of human skin biomech. props. 77—44704
extracellular action potential recording, interference suppression 78—61294
extracorporeal blood oxygenator safety and efficacy, review 78—77153
extrasystole monitor using FIFO 80—72360
eye, internal pressure meas., early diagnosis of glaucoma 79—25140
eye contrast sensitivity testing instrument 78—73275
eye examination, computer-assisted, evaluation of Refractor III system for subjective exam. 78—3622
eye fine movement recording through closed eyelid, piezoelec. transducer 78—35988
eye movement recording system for clinical appl. 78—3623
eye refractor, automatic, optical system 78—61274
eye testing using screen image divider 78—57114
eye-movement monitors, compensation for distortion 80—56244
eyetracker, accurate three-dimens. system 78—48944
face mask, mouldable for infant respiratory assistance 77—52914
fan-beam scanners, circular artefacts reduction 78—35924
fast freq. meter for voice freq. meas. *(German)* 78—3518
fast plastic scintillators for medical applications 77—44744
femur fractures, reduction apparatus 79—16343
ferrite pot core pressure transducer development and compensation 79—75519
ferromagnetic contact ring for two-dimensional eye movement meas. 79—5387
fetal breathing movements, US meas. device 79—34616
fever alarm device using telemetry 80—21556
fibre endoscope, image quality improvement 78—71219
fibre endoscope one-component objective dimensional design *(Russian)* 78—69228
fibre optic, catheter transducer, side hole type, for intracardiac press. meas. *(Japanese)* 78—73272
fibre optic catheter, for intravascular press. and sound meas. 78—44638
fibre optic catheter oximeter system, solid-state, using three single optical fibres 78—44637
fibre optic catheter tip pressure transducer, for intracardiac press. meas. 79—2150
fibre optic catheter-tip micromanometer as intracardiac press. transducer *(Japanese)* 78—73270
fibre optic endoscope, incoherent optical power launching limits 78—63193
fibre optic endoscope, SVO-1 sigmoidoscope USSR 77—37067
fibre optic probe for neonatal oximetry and dye curves 79—70603
fibre optics applications, review 77—48901
fibre optics in medicine, diagnostic and therapeutic appls. 79—39466
fibrescopes using leached fibre image bundles, manufacture 80—83670
fibrous microfilter for blood, disposable 78—7527
film projection system, eye movement monitoring of cerebral palsied children 79—16329
films for nuclear medicine, sensitometry 80—72292
finger electrode system, tetrapolar elec. impedance plethysmography meas. 77—81608
finger tremor amplitude and freq. artefact reduced routine meas., portable equipment *(German)* 78—85407
finger-tip transducer for meas. digital vol. pulse, skin-resist. response and ECG 77—86729

biomedical equipment continued
flowmeter, bidirectional fluidic, respiratory meas. appl., tests 78—35993
flowmeter, differential, for ultrafiltration dialysis meas. and control 77—21657
flowmeter, EM blood, comparison of dynamic calibration methods 78—40362
flowmeter, implantable Doppler design with phase-locked loop 78—31873
flowmeters, digital 2D full range Doppler velocity meter for cardiovascular diagnosis 78—88731
fluorescein angiography of the ocular fundus 80—67185
fluorescence angiography, colour and black and white, use of interference filters 78—48856
fluorescence angiography, of vascularised cornea, using camera slit lamp 78—48855
fluorescence bronchoscope for lung tumour localisation 77—60277
fluorescence polarimeter for flow cytometry 78—73191
fluorescent decay thermometer for cancer treatment dosimetry 80—86306
fluorescent X-ray intensifying screen efficiency determ., standard method 78—69198
fluorimeter for medical sample anal. 79—92323
fluorography with image intensifier, apparatus for mass stomach survey *(Japanese)* 77—73575
fluorophotometer, slit lamp type, for tear measurements 77—2064
fluoroscopic examinations, multi-image camera for spot radiography 80—109020
fluoroscopic image recording using multiformat camera 80—51234
fluoroscopic installations with undertable X-ray tubes, survey form and techniques 77—73597
fluoroscopic spot film system image quality evaluation and optimisation 78—69205
fluoroscopic system, alignment checking device 77—86604
fluoroscopic unit, variable aperture, reduced patient exposure 79—92368
fluoroscopy, kVp variable, with automatic brightness stabilisation, X-ray tube pot. var. 78—69202
FM electronics system for biomedical data recording 79—44010
FM freq. convertor for bioelec. process mag. recording 78—7469
foetal breathing monitor for humans in utero, US pulsed Doppler instrument 78—69164
foetal movement monitors, detecting asymm. abdomen shape changes and wall impulses 77—52904
foot function assessment system, normal and pathological feet, computerised system 79—100760
foot scale plantar pressures, meas. device 79—44004
foot vertical force during walking, continuous meas. device *(Japanese)* 78—73273
foot/floor contact temporal patterns during walking, automated on-line meas. system 78—77128
footfall pattern transduction by foot or shoe cover 79—57799
force measurements during operative correction of spinal deformities 80—76861
force-line visualisation system for artificial legs and lower-limb orthoses 80—17200
force/tension transducer for small muscle meas. 80—41281
foreign-body detector for intraoperative localisation of stones in biliary tract 78—3657
frame recording method for intermittent X-ray TV to reduce exposure dose in fluoroscopy *(Japanese)* 78—89607
frequency-time domain signal processing system 80—81760
Fresnel zone plate aperture for γ-ray imaging system, digital modelling 78—7442
Friedmann quantitative analyser for study of posterior pole disease *(Italian)* 80—17172
fundus photography in optometric practice 80—67183
gait analyser/trainer instrumentation system 80—17150
gait analysis and the CARS-UBC electrogoniometer 80—56263
gait analysis automated accelerometry system 77—90934
gait measuring system for treatment evaluation, microprocessor controlled 80—61731
gait trainer for hemiplegic patients with lower limb sensory loss 78—48940
gamma camera, 3-D particle track chamber using Compton interactions 77—86622
gamma camera, computer controlled, nuclear cardiology appl. 80—61682
gamma camera, electronically collimated, for single gamma emission computed tomography 78—44603
gamma camera, influence of digital representation on image quality *(German)* 78—88738
gamma camera, line spread function meas., practical considerations 79—17585
gamma camera, multidetector Ge 79—49353
gamma camera imaging, recent advances 80—17127
Gamma Camera ON 110, physical properties, clinical applications 77—44739
gamma camera oscillosocpe display, performance meas., computer simulation 78—7425
gamma camera performance comparison 78—44595
gamma camera systems, methods for MTF meas. 80—94324
gamma camera using CdTe detectors, medical appls. 79—49351
gamma camera visual outcome units comparison, use of MTF 80—94323
gamma camera with brightness amplifier *(French)* 77—37036
gamma cameras, appl. of orthogonal light propag. 77—16979
gamma cameras, performances under high counting rates 79—16277
gamma cameras, state of art 80—3802
gamma computerised camera for medical diagnosis *(Swedish)* 79—70607
gamma detector, gaseous, good low-energy resolution for ≤ 50 keV imaging 80—3795
gamma ray image intensifier camera, using Si posn. sensitive strip detector 77—81565
gamma spectrometer, single-channel, transform. into computer controlled multichannel analyser 79—57765
gamma teletherapy unit, radiation head, temp. distrib. 79—72790
gamma topograph, GSG-2 twin-sensor, functional and clinical qualities 80—56172
gamma-camera adaptive gating device for heart synchronisation 78—31898
gamma-camera for gated caroliovascular imaging 79—5367
gamma-camera image information prob., methods of checking *(German)* 78—88734
gamma-camera used in nuclear medical examinations, developments in photographic recording *(German)* 78—88733

biomedical equipment continued
gamma-ray cameras of Anger type, optimisation *(French)* 80—26328
gamma-ray total-body counter 79—100728
Gammatron S80 telecobalt unit, reduction of electron contamination in beam 79—92330
gas analyzer, response time, incorporation in gas exchange computations 80—72344
gas chromatography-mass spectrometry, integrated analytical systems, applics. in biomed. and related sciences, review 80—36200
gas-filled channel convertor for fast coincidence cameras 77—60276
gastrointestinal tract electrostimulator, Endoton-1 78—36033
Gevamatic 240 developing machine, constancy testing by test film strips in a radiological practice *(German)* 80—95206
Gipospast-1, thermoelec. apparatus for local hypothermia 80—104807
Glossynograph system for presenting printed text synchronously with speech for hearing-impaired persons 80—56153
glottiscope in investigation of ventilatory phonetory conflict 80—51145
goniometer, electromech., for total motion knee goniometry 77—52902
goniometer, triaxial, for human joint rotation meas., theoretical justification 79—92417
goniophotography in optometry 80—67182
gonioscopy, foot-operated camera trip for Nikon photo slit lamp 78—80986
gradiometer for human heat magnetic field study 78—48914
grey-scale image recording systems, comparison of 9 different types 79—16319
grey-scale to colour convertor for foot pressure distrib. pattern meas. 79—20691
GT-2 gamma scanner, improvement, neurosurgery appl. 78—11719
guarded double insulation, reduction of shock hazard of grounded elec. systems in hospitals 77—56497
gynaecological cryogenic treatment apparatus 79—57807
gynaecological endoscopic photography, increased mobility using articulated lens 77—48928
gynecological cryosurgical apparatus using N_2O as coolant 78—7525
gyroscopic X-ray television apparatus for clinical studies 78—15883
haematofluorometer, for testing Pb poisoning 78—53554
haemocoagulometer 79—39541
haemodynamic and cineangiographic data treatment, computer system SYSCORMORAM 78—81030
haemodynamic parameters monitoring by SOLO, an interactive minicomputer based bedside monitor 80—26392
haemoglobin-O_2 equilibrium curve, instrument for determ. based on membrane diffusion 80—81761
haemoperfusion, using activated C cloth 77—37105
haemoperfusion device comparative evaluations 78—44690
handicapped persons technical aids, R&D in Sweden *(Japanese)* 78—48934
haploscope, automated miniaturised device for testing binocular visual function 77—2004
hardware unit for evaluation of psychophysical stress from long term ECG recording *(German)* 80—26388
head holder for treatment of head and neck cancers 80—94333
headlight, light-operated remote-control device for handicapped persons 78—53571
hearing aid measurement system comparison 78—65151
heart assist energy convertors, using fluid controls logic 79—53286
heart monitor, using IR transducer, design and construction 79—83891
heart or respiration rate calculator 78—35987
heart rate analyser for long-term continuous ECG recordings *(German)* 78—3649
heart rate control device, appl. for cardiac rehabilitation 79—83995
heart rate module, implantable, with AGC, for animal use 78—44753
heart rate recorder 80—41288
heart ratemeter based on analogue divider 78—40368
heart-rate digital meter, instantaneous, precision 77—86681
heart-rate store, PLL circuit, portable *(German)* 78—65139
heat exchanger for heating/cooling blood, thermal design, equipment and blood props. considerations, appls. 78—92744
heavy ion facility for radiation therapy 77—86588
HF current surgery, instruments and problems *(Hungarian)* 80—98172
high density proportional counter, medical imaging of e^+ radioisotope distrib. 79—5399
high technology medical equipment, Angioscan, Cardiac Output Computer, Medishield Analyser, Tomographic Scanner 80—36171
holocamera, clinically useful, for 3-D microscopy of unanaesthetised eye 78—48863
holocamera for 3-D micrography of the alert human eye 80—98057
holographic stress testing of corneal wounds in postoperative patients, specular illum. arrangement 78—65102
holography applications in ophthalmology 80—67200
hot-film shear probes, position sensitivity 80—101286
hot-film wall shear probes, miniature, for biomedical appls., method for alignment 79—53262
Humphrey Vision Analyser, reliability and validity of refr. error meas. 78—61265
hybrid MWPC gamma ray detecting system for applications in nuclear medicine 79—5397
hybrid neural stimulator for chronic expts. 78—28124
hydrocephalus surgical treatment, valve system design *(Japanese)* 78—31963
hydroelastic wave oscillator for treatment of human body tubular diseases *(Chinese)* 79—39588
hydrophone, miniaturised for internal use, calibration apparatus *(Japanese)* 77—64144
hygrometer electronic for respiration meas. and diagnostics *(French)* 77—70564
hyperthermia cancer treatment procedure, monitoring instrumentation 79—96716
hyperthermia induction apparatus for neoplasia treatment 79—44048
hypodermic needle Po_2 electrode 80—98156
IEEE 488-1975 interface bus, high speed ADC and addressable trigger generation 80—41283
IEEE conf., scintillation and semiconductor counters and nucl. power systems 77—54389
IL 282 CO-Oximeter for measurements on whole blood 80—56159
for ill new born infants care appl. 77—32963
image amplifier, 14 inch, clinical appls. *(Japanese)* 79—92355
image amplifiers, high performance for clinical use *(Japanese)* 77—73579

biomedical equipment continued
- image analyser, semiautomatic, use in investigation of muscle biopsies 80—85466
- image analysis, opto-manual semiautomatic quantitative system 77—56551
- image enhancemdnt using 2-dimens. digital filters *(Italian)* 78—53539
- image intensifier fluorography, low-dose studies of infant hip dysplasia 79—48343
- image intensifier fluorography in paediatric radiology 80—41201
- image intensifier fluorography with fast exposure technique 78—31900
- image intensifier fluorography X-ray installation, appl. to abdominal surgery 79—92340
- image intensifier fluoroscopy, surgical treatment of renal and ureteral calculi 79—92342
- image intensifier with 14 inch input field, clinical experience 78—31899
- image quality descriptor relationships using signal detect. theory 78—71050
- imaging system evaluation using contrast-detail-dose anal. 80—98108
- imaging systems, information capacity considerations 80—98090
- imaging techniques, book 80—12861
- imaging techniques implemented on pipeline minis and array processor, nerve fibre counting appl. 80—98165
- immunological reaction monitor using laser light scatt. 80—85463
- impedance automatic recording system 78—44625
- impedance camera for spatially specific meas. of thorax 78—53464
- impedance cardio-telemeter *(Japanese)* 77—44790
- impedance meter, AC, battery-operated, for contact resist. determ. before patient monitoring 78—81006
- incubator, portable, with radiant heating system and fine O_2 control 77—56511
- incubators, portable, improvements 78—81055
- induction receivers, for articulatory activities meas., computer control 77—56391
- inductive sonde, large bloodvessel movement, transcutaneous meas., design and realisation *(Italian)* 79—70602
- infusion pump control by labour and foetal heart rate *(German)* 78—85415
- inhalation apparatus, technique of continuous and intermittent working 78—36038
- instruction in biomedical instrumentation, modular laboratory equipment development 78—89283
- instruction using modularised signal processor 78—41131
- instrument maintenance, inspection, hospitals appl. 79—96684
- instrumentation development, separation science and mass spectrometry, current status and future trends 80—55665
- instrumentation requirements, appl. of system design 77—48894
- instruments, problems and prospects 77—40812
- integrated electron devices in medicine 78—40372
- intelligent microscopes, recent and near-future advances 80—98166
- intensive care, instrumentation and control, conf., London, England (May 1979) 79—70702
- intensive care instrumentation 78—53559
- intensive care unit, use and acceptance of automated monitoring systems 78—81057
- intensive care unit/coronary care unit safety 78—69252
- intensive care ventilator, microcomputer-controlled 80—51292
- intensive monitoring computer system, SOLO, one-patient multiparameter bedside monitor 78—81053
- intracorneal adhesion of human skin, piezoelectric transducer, skin disease diagnosis, appl. 77—48819
- intracranial pressure and temp. two-channel telemetry system 77—81619
- intracranial pressure noninvasive monitor for infants, fontogram 78—40373
- intracranial pressure telemetric meas. *(German)* 78—85403
- intracranial pressure telemetric monitoring system 79—74736
- intravascular O_2 continuous monitoring, electrochem. sensor 80—56238
- intravascular PO_2 probe routine appl., practical experience 80—56239
- intravenous angiography, digital video subtraction system 80—98089
- intravenous catheters, comparative study of polymers in animals and man 78—7459
- ion selective electrodes, appl. 79—44022
- ion sensitive FET theory based on membrane electrodes 80—41280
- ion-selective disc electrodes with neutral cation-carriers for automated electroanal. of serum *(German)* 78—73269
- ion-selective electrodes for blood serum anal. 78—3645
- ionization-chamber-dependent factors for calibration of megavoltage X-ray and electron beam therapy machines 80—18704
- ionselective multi-disc electrode description *(German)* 78—3687
- iontophoresis, gated HV system with accurate current monitoring 78—69259
- iontophoresis device for safe elec. administration of ionised drugs 78—31965
- IR back-scattered from vaginal tissue, self-stabilising meas. system 80—72281
- IR electropupillometer design, using closed-cct. TV *(Japanese)* 77—66870
- IR optometer for studying accommodation microfluctuations in humans 80—12124
- isocentric fast neutron therapy facility at Edinburgh 80—30842
- isotope generators, comparison of weekly and biweekly systems rel. to radiation safety 77—2049
- Japan, devel. of computerised tomography and US technology 80—30879
- Japanese developments 78—24164
- jet injector, compressor operation mode 78—7524
- jittermeter, microcomputer based, for single fibre EMG 80—46078
- joint hyperextensometer for laxity quantification 79—100761
- kinematic gait, system for simple meas. 80—85509
- knee analyser for mediolateral stability determ. 78—7475
- knee arthrograph for study of stiffness 79—12022
- knee impedance testing machine 80—21555
- knee joint loading machine with aligning device 80—41067
- kymography, motion picture apparatus 80—30851
- laboratory instrument to computer coupler 80—41271
- laboratory test interpretation using computer 79—74770
- labour meter with tape recorder for ambulatory patients *(German)* 78—85413
- LAMPF biomedical channel, beam shaping section tuning 77—86591
- laparoscopic sterilisation techniques, preclinical and clinical testing 77—48929
- laparoscopic surgery, bipolar sterilising forceps and uterine manipulator 77—48926

biomedical equipment continued
- laparoscopic tubal sterilisation instrumentation 77—48927
- large field scintillation gamma cameras, performance characts. 78—7441
- laryngeal cinematography, high speed, optical/lighting system 80—17055
- laser applications in medical research, biophysical aspects 80—51201
- laser applications in ophthalmology 77—90869
- laser back pointer for ^{60}Co radiotherapy unit 77—86583
- laser beam applications in medicine and surgery, review *(French)* 79—34626
- laser beam appls. *(French)* 80—41165
- laser correlation spectrometer for virology and immunology 80—56158
- laser Doppler anomemeter for velocity fields meas. near prosthetic heart valves 79—57814
- laser Doppler velocimeter, blood cell speed absolute meas. in retinal vessels 79—83884
- laser endoscope, coagulation in gastrointestinal haemorrhages *(German)* 78—69178
- laser endoscopic photocoagulation of bleeding lesions, using Ar laser *(French)* 79—34627
- laser fibre optic bronchoscope for optical fluoresc. localisation of early lung cancer 78—48921
- laser fluorescence bronchoscope for occult lung tumor localisation 80—30832
- laser image printer for X-ray tomographs *(French)* 80—72119
- laser instrumentation system for simultaneous meas. of transcutaneous O_2 and skin blood flow 80—26321
- laser interferometer, for sensing of respiratory sounds 77—90872
- laser medicine in Japan, current status *(German)* 80—98059
- laser microprobe mass analyser 80—98060
- laser possibilities, limits and prospects *(Italian)* 80—56156
- laser pupillometer, especially suitable for anesthetised cats 79—48317
- laser retinoscope using He-Ne laser light source 80—41159
- laser scalpel and micromanipulator for neurosurgery, CO_2 laser system *(German)* 80—3753
- laser stethoscope, non-contact high sensitivity, using interferometer technique *(German)* 78—69176
- laser stethoscope for respiratory sounds meas., comparison with acoustical method *(German)* 80—98058
- laser surgery, flexible fibre-optic beam-guiding system, oto-rhino-laryngology appls. *(German)* 79—83886
- laser surgical unit for clinical rhinology *(German)* 78—69177
- laser video recorder 80—36065
- lasers, influence in biological and medical research, review 80—26318
- lasers in medicine, appls. and equipment development 78—48862
- latency time meter LT-1, nerve conduction velocity measurement appl. 77—40853
- leakage currents from mains transformers, safety measures *(German)* 78—3625
- leg lengthening, tension/stretch ratio, method and clinical results *(German)* 78—36031
- lens mounting, apparatus for longit. spherical aberration meas. of soft contact lenses 79—79684
- Lexiscope, portable pocket size X-ray imaging system for medical/dental radiography 78—92701
- light beating spectroscopic instrument for continuous meas. of tissue blood flow 80—41160
- light sequence bar, electronically controlled, for EOG study of eye pursuit movements *(German)* 80—36058
- line isolation monitor with adjustable alarm level for hospital elec. systems 77—56496
- linear accelerator, 4 MV, use for whole-body irrad. 80—109001
- linear accelerator, computer interface 80—51226
- linear accelerator, field separation between lateral and anterior fields, dose distrib. 80—94336
- linear accelerator, SL 75-20, clinical results with 79—48332
- linear accelerator, Varian Clinac 18/10, use of polystyrene filters for electron energy modification 80—56168
- linear accelerator beam profile scanner 80—101267
- linear accelerator calibration monitor with a memory 80—3821
- linear accelerator dosimetry control system, solid state 80—94371
- linear accelerator primary and leakage radiation attenuation in concrete 79—63823
- linear accelerator servo system for shifting range of pion beams 77—83358
- linear accelerators, neutron dose equivalent rate obs. 79—70643
- linear accelerators, source definition for head shielding requirements, effect on room shielding design 80—46068
- lingual tactile sensory system, automated instrumentation for research 80—8205
- liquid scintillation detector module for bulk-sample and whole-body counters 77—3216
- liquid scintillation vial system, new container geometry for better sensitivity 80—46021
- liquid-scintillation vial system, biphasic, for radiometry, modifications 80—101253
- liver Cd, transportable in vivo meas. system 79—39496
- load cell for meas. of prosthetic heart valves dynamic forces 80—104815
- locomotion evaluation equipment, computerised, clinical practice appl. 77—86676
- long bone mechanics study under microprocessor control 80—76851
- Luer lock afterloading device for ^{192}Ir brachytherapy 80—104735
- lung, mag. field meas., comparison between two methods 80—104712
- lung function meas. system, mobile, computer aided *(German)* 78—3630
- lung function testing, area under max. expiratory flow-vol. curve, meas. using analogue device 80—41284
- lung gas analysis using redox gas sensors *(German)* 78—85440
- lung phantom, dynamic, use as educational tool 80—8757
- lung scintiphotography with dry aerosol, generation and delivery system 78—24126
- lung tissue characterisation by US, instrumentation, model and results, book 78—44575
- lung ventilation device for newborns, especially during incubation 79—100786
- lung ventilator, development, engineering appraisal 78—3673
- lung volume, online calc. by digital computer 80—72351
- LV electromedical equipment and radiological apparatus, standardisation *(French)* 77—73602
- macroradiographic X-ray diagnostic table *(Japanese)* 79—88166
- magnetic heart vector components, simultaneous meas. with unipositional lead system 80—104697

biomedical equipment continued
- magnetic recording, one-channel, direct and reversible synchronisation unit 78—3620
- magnetiser for psychosomatic complaint treatment 78—15878
- magnetocardiogram and cardiac output meas. with integrated system 80—104709
- magnetocardiogram meas. first order gradiometer and DC-thin film SQUID 80—89877
- magnetocardiography, clinical appls., instrumentation and methods 80—35927
- magnetocardiography recording, props. of ideal system, appl. of ECG theory 80—104700
- magnetometer, induction type, for biomag. fields *(German)* 79—88207
- magnetometer, superconducting, appl. to vector magnetocardiogram meas. 77—29213
- magnetometers, use to vol.-reference flow-vol. curves 80—104694
- magnification skeletal radiography, imaging parameters and clinical relevance 78—69185
- maintenance in forward military hospitals 79—96683
- maintenance programme for electronic communications systems and biomedical equipment 79—5385
- mammographic equipment system, use for early cancer diagnosis 79—100724
- mammographic film and film/screen combinations, quantitative evaluation 79—88151
- mammographic image quality comparison phantom 78—85357
- mammographic imaging, historical review in terms of image quality and reduced radiation dose 80—41229
- mammographic screen-film systems, comparison of laboratory and clinical evaluations 78—69187
- mammographs, high quality low-radiation, tone reproduction system 80—41198
- mammography, detective quantum efficiency anal. of electrostatic imaging and screen-film imaging 80—41232
- mammography, exposure timing by use of film/screen systems 80—17059
- mammography, method for reducing radiation exposure and improving image quality 78—31901
- mammography, test object for assessing image quality 80—56171
- mammography, utility of modelling 78—69188
- mammography techniques comparison, in vitro studies of breast microcalcification detectability 80—41230
- mammography with magnification and grids: detail visibility and dose measurements 80—41231
- mandibular movements diagnosis, system for meas. and processing *(Japanese)* 80—101249
- manipulation unit equipment for radiotherapy depts. 80—30903
- manometer system, cerebrospinal fluid pressure meas. and controlled withdrawal 79—39538
- manufacture of medical electronic equipment, India 79—96676
- mass production of medical instruments, quality control *(Hungarian)* 79—48354
- mass spectrometer, blood gas anal., silicone rubber catheter operating mechanism *(Japanese)* 78—61273
- mass spectrometer for respiratory, blood and tissue gas anal. *(Japanese)* 77—70566
- MDS computer systems, improvement of pulse-mode photographic images 80—30862
- mechanical action resistance testing, method standardisation 79—92403
- mechanical and chemical analysis at cellular level, recommendations of workshop on future of biomedical instrum. 80—81776
- mechanical pointer for communication with handicapped children 79—84013
- mechanostimulator, physiological appl. 78—92762
- median nerve, transient responses to elec. stimulation, SQUID appl. to somatically evoked field meas. 80—104706
- medical CRT displays, review 78—69240
- medical devices, safety and efficacy, legislation 77—2062
- medical diagnostic imaging, photographic film 77—78023
- medical electronics equipment, maintenance and repair organisation 77—40814
- medical ion accelerator, cyclotron and synchrotron design studies 79—54661
- Medicor diagnostic bag assembly for out-of-hospital use 78—36014
- membrane hydrophone for 0.5 to 15 MHz range, press. meas. in US fields 80—108987
- meson beam line at Rutherford Lab. using SNS 79—74758
- Mevatron 60, X-ray linear accelerator 80—21530
- micro projection attachment with integrating plate, histological meas. of thyroid 77—78067
- micro-light guide photometry of biological tissues 80—46005
- micro-object geometric feature determination, TV set 80—85538
- MICRO-VIDEOMAT, use in light microscopic liver diagnosis 77—78013
- microcapillary system, staged, tortuous, for haemodialysis and ultrafiltration 77—37107
- microchannel plate image intensifier, quantum detection efficiency 77—83462
- microcirculation semiquantitative demonstration using US noninvasive meas. method *(German)* 78—85348
- microcomputer based biomedical signal processor 80—26390
- microcomputer based digital filter for electroencephalogram processing 78—73278
- microcomputer scanning system for respiratory mass spectrometer 78—88756
- microcomputer system for on-line analysis of electroencephalographic data 78—73277
- microcomputer system for urethral pressure profiles meas. *(Slovenian)* 79—2154
- microcomputer-based data acquisition and anal. system for CO$_2$ rebreathing studies 78—36005
- microcomputer-based data acquisition and analysis system for CO$_2$ rebreathing studies 80—36161
- microcomputer-based neurophysiological stimulator, design of and impact on clinical procedures 80—26393
- microcomputer-based pulmonary wedge pressure measurements 80—26391
- microcomputers for bedside monitoring of patients *(German)* 78—88751
- microcomputers in biomedical and clinical applications 78—73283
- microelectrode, chronically stable, reproducible, with parylene insulation 77—40942
- microelectrode, Pt, potentials and small-signal impedances 79—34716

biomedical equipment continued
- microelectrode, W, potential and small-signal impedances 79—34715
- microelectrode puller with high temp. heating element 77—61059
- microelectrodes, metal, noise characts. *(Japanese)* 80—3846
- microelectrodes, surface applied, quantification of motion artifacts *(German)* 80—3829
- microelectrodes for tissue measurements of local PO$_2$, local flow and local ion activity 80—51287
- microneurology, appl. of colour TV as surgery teaching aid 78—40396
- microphotometer, automatic fluoresc., using image dissector tube, quantitative cytochem. appl. 79—97413
- microprocessor based instrument, Dinamap, for arterial press. automatic determ. 78—96108
- microprocessor based respiratory function analyser 79—25131
- microprocessor based system for monitoring human long bone healing 80—21511
- microprocessor equipment to analyse eye movements during radiograph scanning 79—25130
- microprocessor systems for data acquisition, image processing, RIA anal., patient data retrieval 80—61670
- microprocessor-based instrumentation, present and future trends 80—26405
- microprocessor-based instruments 80—21559
- microprocessor-based system for studying average evoked potentials 80—56150
- microprocessor-based tilting bed for blood pressure control 80—26412
- microprocessor-controlled cardiac output meter 80—36162
- microscope, quantitative for diagnostic appls. 77—60273
- microscope, scanning mirror, with optical sectioning characts., ophthalmology appls. 80—85461
- microscopic image processing system, subclassification of acute leukaemia by automated morphological anal. 77—81620
- microscopy instruments and appl. techniques, Zeiss equipment 77—74497
- microstrip antenna for biomedical applications 80—89826
- microstrip slot radiator for medical appls. 80—108994
- microwave, Gaussian beam launcher, for selective partial body exposure of biological substances 79—29578
- microwave antenna, invasive, for locally-induced hyperthermia for cancer therapy 80—67193
- microwave apparatus for cancer treatment by controlled local heating, 915 MHz or 2450 MHz 80—76860
- microwave applicator, broad band, for heating tumours 80—30830
- microwave applicator for localised heat treatment of prostate, dog expts. 79—100698
- microwave applicators, comparison of stray radiation patterns 80—61660
- microwave applicators for localised hyperthermia treatment of malignant tumours 80—89824
- microwave diathermy applicator with choke, 2450 MHz, slab-loaded, direct contact 80—89825
- microwave diathermy direct-contact applicators, comparative heating patterns 78—40286
- microwave enzyme inactivation system with electronic dose control 77—81762
- microwave hyperthermia, localised, biomedical devices 80—104724
- microwave hyperthermia treatment and thermometry system 80—72280
- microwave induced hyperthermia in cancer treatment, apparatus and preliminary results 79—62296
- microwave probe for linear meas. of human skin stratum corneum water content 80—21518
- microwave respiration monitor 79—96646
- microwave scanner for soft tissue tumour detect. 80—17054
- microwave system, dual mode, to enhance early detect. of cancer 80—89823
- microwave tissue heating system for hyperthermia research 80—30829
- micturition reflex elec. restoration, sequential stimulator 78—53567
- Mingograph in clinical electroretinography 78—92731
- miniature pH-sensitive polymer membrane electrode 79—100781
- minicomputer system, automatic visual stimuli, hand and eye movement monitoring *(French)* 79—34682
- mirror, new design for hemianopia detect. 80—108992
- mirror positioner, tip/tilt, high performance 79—59795
- mitral valve prosthesis in vitro tester, unique design 78—40426
- mobile gamma camera with remote image processing computer system, for nuclear medicine 78—92700
- mobile X-ray unit, Mobil XR 78—24122
- Moire topography camera, simulator mounted, for constructing compensating filters 80—46024
- Monitor DKS4T-01 system, surveillance of severely ill patients 79—34679
- monitor using Walsh transform on standard microprocessor 80—26399
- monitoring instrument for continuous tissue pressure meas. 79—100762
- MORPHOQUANT automatic microscope image analyser, universal program system 80—56160
- motion phantom for ECG-gated cardiac computerised tomography 80—98115
- motor nerve conduction velocity measurement, neuromuscular disorder diagnosis using semiautomatic meter 77—48909
- multi-channel EEG wave analyser, design and development 80—56254
- multi-channel telemetry system for tissue O$_2$ tension meas. 77—56506
- multichannel analyser, microprocessor-controlled, transfer of blood pressures and neural activities for computer anal. 80—72356
- multichannel audio monitor for detecting electrical signals, neurophysiological expt. appl. 79—20694
- multicrystal detection system for localisation and meas. of photon emitters without external collimation 77—32959
- multiformat imager modification, cardiac blood pool imaging over complete cycle 77—40737
- multimicrocomputer system with dynamic variable hierarchy for real-time data acquisition 78—44654
- multimode square waveguide applicator, for microwave therapy 79—34630
- multiparameter clinical diagnostic miniature transducers, colloquium, London, England (May 1979) 79—100776
- multiple electrochemical analyser for flowing liquids and gases, features *(German)* 78—27846
- multiple microprocessors for continuous patient monitoring 80—26389
- multiple-electrode measurement system for ECG evaluation of acute myocardial infarction *(German)* 80—26386
- multiple-input algorithmic processor for multistage decimation and filtering 77—78069

biomedical equipment continued
  multiplexing system for multichannel signal averaging of visually evoked responses 80—36165
  multipoint electrode for biological pot. recording 80—104784
  multiwire proportional chambers, adaptions and appls. 77—86618
  muscle conduction velocity, meas. and recording methods 79—100688
  muscle spindle afferent activity and tone meas. in man, apparatus generating controlled ramp movements 78—77121
  muscle tone study by meas. of muscle density, bridge instrument 80—3833
  MWPC, appl. to radiation localisation problems in medicine and biology, review 79—5432
  MWPC positron camera, two detector, appl. medical imaging 79—5398
  myelographic device based on concentric principle 79—92369
  myocardial infarct scintigraphy, inexpensive rib phantom 77—56461
  myocardial transmural heat gradient instantaneous meas. 78—44661
  myointegrator for EMG signal analysis 80—40997
  myophone, appl. to functional rehabilitation *(Spanish)* 78—48924
  myoscope MG 23, two channel, ocular muscle measurement, myasthenia gravis diagnosis appl. 77—37085
  nasal air emission in speech disorders, electrodynamometric evaluation 78—77134
  nasal catheter for alveolar CO_2 meas. in infants 79—66564
  nasal flowmeter for preterm infants, self-retaining 80—98158
  nasal tract filter efficiency measurement, for exclusion of air-borne particles 77—56492
  neonatal oxiconsumeter for dynamic meas. of O_2 consumption in neonates 78—44631
  neonatal peripheral circulation, human, characterisation by US pulsed Doppler technique 80—76815
  neonate cardiorespiratory monitoring, automatic system with microprocessor 80—94399
  neonatological care, intensive therapeutical and monitoring system 79—100785
  nerve stimulation apparatus and electrodes 78—36034
  nervous system electrostimulation, stainless steel electrode corrosion control 78—7464
  neural pulse wave analysis, microprocessor-based instrument 80—104791
  neurological coaxial depth electrode development 79—29687
  neurological coaxial microelectrode, W-Re core, elec. cond. and bending props., CVD coatings 78—11752
  neurological function tracking-task instrument, portable, features 77—86678
  neurology monitoring system for stroke patients 80—26394
  neuromuscular block indicator, model INMB-1, EMG amplitude meas. 80—104785
  neuromuscular blockade monitoring device, twitch box 78—77132
  neuromuscular miniature endplate potential online acquisition microcomputer system 78—36015
  neurophysiology, computer assisted unit data acquisition/reduction 78—61266
  Neuroscope, for multiprojectional isocentric fluoroscopy and angiography 78—40292
  neurosurgical cryoprobe, self-contained, with replaceable flask, features 78—7526
  neurosurgical intraoperative X-ray equipment use 79—92344
  neutron 14 MeV generator therapy facility 77—81568
  neutron activation in vivo total body anal. using 14 MeV neutrons, calibration and evaluation of system 78—53490
  neutron activation system for in vivo meas. of Cd 80—67224
  neutron beam for cancer radiotherapy 77—81567
  neutron radiotherapy facility at Fermilab 77—86590
  neutron source for radiotherapy, gas target, energy spectra, flux, dose rates 78—92698
  NMR, field-focusing, formation of chemical scans in man 78—85354
  NMR computerised tomography, human whole-body line scan imaging system 79—66502
  NMR flat crossed-coil detector, for blood flow meas. 78—40284
  NMR flat crossed-coil detector for blood flow meas. 79—83880
  NMR imaging by multisensitive point method, appl. to ~10 cm biological systems 77—86581
  non-invasive technology assessment, multiple endpoints 80—17179
  noncontact microprocessor-based ocular pulse monitoring system 80—46089
  noninvasive diagnostic technology, history and necessity 78—36029
  nuclear instrumentation manufacture in India 79—96653
  nuclear medical instrumentation, mobile, review 80—101262
  nuclear medicine, bolus-injection system for dynamic time-function studies 80—41194
  nuclear medicine, camera aperture for data collection optimisation 80—67221
  nuclear medicine, clinical and parametric evaluation of three large-field-of-view cameras 80—76823
  nuclear medicine, coded-aperture imaging of the heart, improved aperture 80—98072
  nuclear medicine, computer systems, buyer's guide to current performance and future promise 78—48883
  nuclear medicine, digital data collection system, portable, cost-effective 80—41195
  nuclear medicine, image processing, measure of quality 77—86626
  nuclear medicine, image processing system 80—41174
  nuclear medicine, phantom for clinical evaluation of total system resolution 80—41197
  nuclear medicine, photomultiplier tube balance assessment 80—41196
  nuclear medicine display systems 79—16298
  nuclear medicine hard-copy image display systems comparison 79—74744
  nuclear medicine imaging system for computerised longitudinal tomography 80—61666
  nuclear medicine instrumentation, recent developments 80—81692
  nuclear medicine instrumentation trends 78—44594
  nuclear medicine instruments and radiopharmaceutical production, review *(French)* 80—17056
  nuclear medicine instruments maintenance, IAEA programme in Southeast Asia 80—46082
  nuclear-medicine image display system, dynamic physiological function visualisation 79—5396
  nystagmus analysis system using microprocessor 77—48917
  obstetric computer-aided monitoring system *(German)* 80—41300
  ocular cinema photography 80—67186
  ocular photodocumentation, conf., Birmingham, USA (Dec. 1977) 80—62362

biomedical equipment continued
  ocular photography, accessory fill-in flash for the Nikon photo-slit lamp 80—36056
  ocular photography, new instrumentation and techniques 80—67187
  ocular tilt aftereffect, clinical assessment apparatus and obs. 79—83954
  oesophageal accelerometer, cardiovascular function indication 80—104798
  oesophageal accelerometer evaluation for cardiac function noninvasive meas. 79—92458
  oesophageal motility study in humans, circumferentially-sensitive miniature press. sensor 78—77131
  oesophageal multiprobe for temp., ECG and heart and lung sound meas. 78—77146
  oesophageal temperature probe position verification by ECG 80—56250
  olfactometry, smell intensity meas. *(French)* 80—8073
  online vectorcardiographic analysis microprocessors and instrumentation 78—36020
  operating table with interchangeable top 78—36042
  operating theatre patient monitoring problems and trends 79—92422
  operating theatre X-ray installation planning 79—92339
  Ophthalmetron, refractive error meas. cycloplegia effect 80—41002
  ophthalmic photography, external 80—67180
  ophthalmic photography instrumentation, survey of clinical impressions 80—67188
  ophthalmic US B-scanner 80—30804
  ophthalmological instrument design and construction, for eye diagnosis 78—15918
  ophthalmological instrument manufacture, development trends 78—48903
  ophthalmological instruments and eye models in teaching, training and education 80—51993
  ophthalmolscopic and vision function meas. instruments 79—96689
  ophthalmoscope, for interior and refraction error of eye exams. 77—81606
  ophthalmoscope, hand-type, supplementary unit for photoelectric measurements 78—48907
  optical fibre applications, review *(Italian)* 78—53540
  optical fibre endoscope type OD-20Eh, internal surface inspection 79—79216
  optical instrument for visual fusional power and reserve determ. 79—88148
  optical instrumentation appl. in medicine, conf., Boston, USA (Sept. 1977) 78—69184
  optical instrumentation in medicine, conf., Toronto, Canada, (Mar. '79) 80—36777
  optical instruments for medicine and biology 80—21517
  optical monofibres for medical practice, appls. *(French)* 79—39462
  optical scan system for encoding and tabulation of visually scored sleep data 80—8197
  optical scanner, automated, for blood agglutination reactions 77—52861
  optical stimulator for vision expts., microcomputer-controlled 80—26423
  optical system for automatic eye refractor 79—25127
  optical waveguides for endoscopic laser photocoagulation *(German)* 77—78037
  opto-electronic appls. for reducing electrical shock hazards with ECGs 79—44016
  opto-electronic target tracker for limb movement meas. and anal. 80—56166
  optokinetic stimulation device, expt. and clinical appls. 80—3844
  optometer, automated subjective meas. of eye refraction 78—35971
  optometer, IR, highly sensitive, for accommodation microfluctuation dynamics study 80—81580
  optometer, refractive error correction optical system with continuously variable spherocylindrical power 79—62385
  optometer recorder of human eye microfluctuations, IR *(French)* 78—7463
  optometry, dark adaptometer for student use and optometric practice 78—48912
  oral neoplasm geometry stomatoscopic apparatus 79—39539
  oral sensori-motor disorder treatment appliances 78—36030
  organ cryopreservation apparatus 77—37060
  organ transport system, portable, const. temp. maintained by solid-liq. phase equilib. 77—40921
  oscilloscope with digital storage for elec. signal obs. and storage 80—104786
  OTF of radiographic imaging systems 80—17085
  oximeter calibration, humans exposed to centrifugation 78—92734
  oximeter for spectrophotometric monitoring of arterial O_2 saturation in the fingertip 80—41161
  oxygen electrode, catheter tip assembly, intravascular blood oxygen tension recording appl. 77—29218
  pacemaker interference test signal generator, operation and cct. *(Spanish)* 78—20315
  pacemaker patient simulator 80—41322
  pacemaker patient surveillance by automatic pacemaker function analyser 78—3679
  pacemaker power supplies, biogalvanic, biofuel cells, implant in dogs, exp. results 77—52935
  paediatric chest stand, working procedure and radiation exposure 79—48337
  paediatric X-ray examination equipment assessment, point system 77—21603
  parametric echoscanner for medical diagnosis 80—36041
  parodontosis treatment portable vacuum apparatus 79—39593
  passive dynamic characteristics of man in lying posture, testing apparatus 78—80893
  patient monitoring during surgery, 4-channel telemetry system 78—31961
  patient topology, optical process for three dimensional assessment 79—20692
  patient-contouring, electronic device, for radiotherapy treatment planning 77—13029
  pattern reversal generator for visually evoked responses studies 80—46004
  pencil chamber for direct beam CT meas., evaluation 80—46056
  penetrameter cassette, multiple exposure, for meas. of effective kilovoltage of diagnostic X-ray beams 80—61662
  penetrameter for measuring peak kilovoltage of dental X-ray sets 80—41171
  perfusion and intraaortic balloon pumping system, Biopul's-3 78—7536
  perfusion pump, low-compliance, for oesophageal manometry 79—53272
  perfusion pump EM drive, features 78—7532
  perimeter localising, for visual field study and retinal tear location 78—85442

biomedical equipment continued
permanent magnets, semifinished, columnar structure castings 79—54157
petit mal epilepsy, portable detect. device 79—83984
pH multichannel measurement apparatus for upper gastrointestinal tract 79—57781
phantom, perspex, for assessment of nuclear medicine imaging equipment 79—25089
phantom for imaging biological fluids by US and computerised tomography scanning 80—104692
phased array echosonographic systems for medical diagnosis 77—81543
phasic signal integrator with automatic drift correction 78—35985
phoneme recognition system based on human audition, psychophysical expts. 78—69115
phonocardiographic microphones, air cavity characteristics, effect of vibrations, room noise 77—81611
phonocardiography, Fonokard type instruments 80—56229
photocoagulating scalpel for laser surgery 78—48866
photoelectric concentration meter, acceptable error determ. for automatic biochemical anal. 79—92435
photoelectric haemoglobinometer type GF-3 79—92438
photofluorographic camera with electro-optical image intensifier 80—36128
photographic cassette, 10×10 cm, for photographic recording from oscilloscope screen 77—25574
photographic immunogram recording apparatus, self-contained, modified version using Polaroid film 80—17209
photokeratoscopic technique for corneal image study 77—1993
photoluminescent thermometer probes, temp. meas. in microwave fields 80—104721
photometer, computer-controlled, for quantitative anal. of thin layer chromatograms 77—60326
photomultiplier and TV camera tubes for nuclear medicine 77—44787
photomultiplier tube instability, consequences for radioactivity meas. accuracy 79—76272
photon beam characts. of 20 MV accelerator for radiation therapy appls. 80—26430
photon correlation velocimetry of blood flow in retina 77—90828
photophonic relaxer for neuropsychic relax. 80—3832
photoplethysmograph for capillary blood volume flow determ., Hemorheograph 78—31934
photoplethysmography, audio-visual heart monitor based on light transmission through skin 79—53206
photoscanner, computer driven, for prod. of hard copies of medical images 78—40370
physical activity determination, analogue/digital data output equipment appl. 77—70560
physically handicapped persons' apparatus, recent status of R&D *(Japanese)* 78—44703
physically handicapped persons' apparatus standardisation *(Japanese)* 78—44699
physiological signal pre-forming system for automatic freq. anal. 78—3621
physiotherapy apparatus as sources of air ionisation in rooms 77—78035
piezoceramic cardiovascular acceleration transducer 79—39536
piezoelectric earphones, usefulness in recording brain stem auditory evoked pots. 80—94389
piezoelectric strain gauge transducer, for clinical recording of ocular microtremor 78—96109
PIGMI, 250 kV proton injector system 79—45467
PIGMI, accelerator control system 79—45475
PIGMI, linear proton accelerator, mechanical description 79—45474
PIGMI program at LASL, proton linac development for medical appl. 79—45471
pilot function and working capacity medical and physiological investigation apparatus 78—85399
pinhole camera, hole size required for no distortion 80—46028
pion$^-$ biomedical beam line, CAMAC control 77—90886
pion factories, biomedical appls. 78—21791
pion radiotherapy facility at TRIUMF, dosimetry and radiobiology 77—70526
pion range shifter for clinical therapy 77—32953
planimeter for use with mechanical digital counters 78—40448
plasma fractionation, development of automatic continuous process 77—52955
plastic optical fibres, multiwavelength laser illuminators 77—58435
plastic scintillation filament detector system for $^{14}CO_2$ breath anal. tests 78—65122
platform for visual presentation of centre of press. for prosthetic alignment and postural control 77—56535
plethysmograph, automatic venous occlusion device 80—17176
plethysmograph, body, vol.-displacement using large flowmeter without press. compensation 80—72345
plethysmograph, calibration-free Hg strain-gauge device 80—17161
plethysmography system for brain blood flow meas. in the cat 79—83887
plettysmography system, simultaneous multifinger meas. 80—21516
plotting instrument for close-range photogrammetry 78—77137
Pneuma-Tonometer, evaluation of for intraocular pressure meas. 79—34678
pneumothorax diagnosis in deep-sea divers, using Sonicaid portable instrument 78—85351
polarised polyvinylidene fluoride film, piezoelectric transducer 80—75993
polyacrylamide gel block electrophoresis instrument 78—7549
polygraph for simultaneous recording of diagnostic parameters 78—36011
polypropylene-covered galvanic cell, O_2 consumption anal. 78—31923
portable low-dose X-ray imaging system 78—85375
positive pressure respirator, electronic control *(Spanish)* 77—29224
positron annihilation detectors ring, wobbling mathematics 79—63867
positron camera, 3-D imaging, noise anal. 78—85445
positron camera, 3-dimens., for nucl. medicine 78—73225
positron camera, $Bi_4Ge_3O_{12}$ as potential scintillation detector 78—3586
positron camera, circular ring transverse axial, performance and evaluation 77—64124
positron camera, cylindrical, multilayer hybrid computed tomographic system, $Bi_4Ge_3O_{12}$ scintillation crysts. 78—48876
positron camera proportional chamber, Fourier deconvolution technique 78—40297
positron camera using ring detector system, for emission tomography of brain 80—30880
positron camera-computer system for various section images 79—66528
positron circular ring cameras for computerised tomography, trends and prospects 79—66524

biomedical equipment continued
positron computerised tomography, system design considerations 79—66525
positron emission computed tomograph, POSITOLOGICA 80—104753
positron emission detector system for computerised tomography 79—66522
positron emission transaxial tomograph, PETT IV and computer system 78—80959
positron emission transaxial tomography, ring detector, attenuation, scatt. radiation and random coincidences 80—61684
positron emission transverse tomograph, PETT IV 78—40299
positron emission-computed tomography, multi-slice, design criteria, shielding 80—61673
positron imaging device for dynamic brain studies 79—48327
positron imaging instrumentation 77—44745
positron imaging system using annihilation coincidence detection, model, design, performance 78—40303
positron ring, 280-crystal, design and construction for 3D imaging 78—28063
positron ring cameras for emission computed tomography 77—44742
positron tomography, Donner 280-crystal high resolution system 79—66533
postural equilibrium automatic meas. and real-time evaluation in man, instrumentation system 78—77127
potential intervals meas. device, electromechanical, with semiautomatic processing of results 77—5115
power sources for wheelchair, artificial arms and communication devices, development 78—15917
power supplies, energy conversion Conf., San Diego, CA, USA (Aug 1978) 79—48038
preamplifier for muscle spindle afferents identification during in vivo recordings in man 80—98155
precision testing technique for intensive care instrumentation 79—70687
pressure cuffs, hazards in single-stage regulation 80—98160
pressure integrating transducer for oesophageal manometry 79—88208
pressure monitoring device design infection control considerations 77—21641
pressure recording apparatus for hydrostatic press. changes during dowel-retained prostheses cementation 80—67287
pressure regulator for proportional regulation of two gas pressures, anaesthetic appl. 78—53560
pressure transducer, miniature implantable, biomedical appl. IC fabrication techniques 80—76849
pressure transducer design, CAI for biomedical instrumentation students 77—45656
pressure transducer performance, effect of zero offset changes 80—56255
pressure transducers, information exchange and humanisation *(German)* 79—88204
pressure transducers in clinical use 79—96692
presterilisation treatment of instruments to lower sterilising gamma dose 77—81558
production efficiency and quality improvement 80—3830
programmable calculator system for human energy expenditure meas. 79—92415
projection system with brightness amplifier, laser appl., for medicine and biology 80—36060
proportional chamber, multiwire, low energy radionuclide distrib. 80—61679
proportional multidetector for lung function study *(French)* 77—37035
proton pion generator for medical applications, beam dynamics 77—38475
proton pion generators for Medical Applications 77—38474
proton-pion generator for medical irradiations, mechanical fabrication 77—38496
pulmonary filtering capability measuring instrument 79—100729
pulmonary function test automated apparatus for use on Space Shuttle 78—31912
pulmonary measurement system, HP model 47804A 80—36163
pulmonary volume calculator, automatic analogue device, performance in hospitals *(French)* 78—31930
pulsatile blood pump development and characteristics 77—81659
pulse rate meter for heart monitoring 78—31915
pulse rate monitor, digital, IR absorpt. detect. 80—26322
pulse/phono pick-up appls. in ambulant cardiological practice 78—40377
pulsed Doppler blood velocity meter readout 78—69158
pulsed Doppler flowmeter, development and cardiac appls. *(Japanese)* 80—36037
pulsilogium of Sanctorius for pulse rate meas. 79—71215
pumps for pulsed insulin delivery, modification 80—101290
pupil responses, human, instrumentation for automated study 80—36164
pupillometer, objective device using counter-rot. perspex blocks 78—81000
pupilometry, instrumentation for stimulating and monitoring human pupil 78—48911
pupilometry equipment, pupil response as indicator of visual function 78—40154
pyroelectric vidicon, medical diagnostic appls. 77—65635
quality health care and cost containment, conf., Washington, USA (Mar.-Apr. 1978) 79—39333
R&D programmes in Norway *(Norwegian)* 78—48909
radiation balance microwave thermograph, simultaneous independent temp. and emissivity measurements 79—100692
radiation balance microwave thermograph 80—26315
radiation detectors, Ge rel. to Na(Tl), imaging efficiency and scatter rejection 79—83915
radiation sterilisation ^{60}Co plant design for developing countries 77—60246
radiation sterilisation facilities, for medical products 77—70543
radiation sterilization of medical products using electron accelerators and gamma sources 79—49870
radiation therapy, thin Pb sheets as tissue compensators for larger field irrad. 80—104736
radiation therapy afterloading system for oesophagus tumours 79—74742
radiation therapy applicator, self-adjusting, cervical cancer appl. 80—51208
radiation therapy electron accelerator target, depth-dose obs. 79—70618
radiation therapy using proton and pion beams *(Czech)* 77—44738
radioactive aerosol, human inhalation administration technique, deposition/clearance expts. 77—60312
radioactivity checking instrument for shielded syringes 80—94325
radioaerosol delivery, US nebuliser system 77—2050

biomedical equipment continued

- radiographic $CaWO_4$ intensifying screen, meas. of X-ray induced light photons emitted 80—41218
- radiographic contrast improvement using fore-and-aft rotating aperture wheel device 80—41227
- radiographic equipment, computer-assisted quality assurance 80—89838
- radiographic equipment acceptance testing, systems approach 78—69203
- radiographic equipment servicing by hospital-based group 78—69247
- radiographic film/screen combinations and patient exposure, Nationwide Survey of X-ray Trends 78—73233
- radiographic image quality comparison for different screen/film combinations by subjective judgments 78—73229
- radiographic image-forming systems, reciprocity-law failure 79—53229
- radiographic imaging, digital video acquisition system for extraction of subvisual information 78—69208
- radiographic intensifying screen information content and contrast, comparison of rare earth with $CaWO_4$ 78—73232
- radiographic phantoms for testing X-ray imaging performance 80—51229
- radiographic proximity X-ray image intensifier tube 78—69206
- radiographic screen-film system, determination of charact. curve and its gradient 79—5362
- radiographic screen-film system evaluation, intensity vs. time scale sensitometry 80—41219
- radiographic screen-film system evaluation, sensitometric method 80—41220
- radiographic table, remote-controlled, clinical experiences 79—43987
- radiographic tomography, comparative survey of multi-directional units 78—61242
- radiographic transmission wedge for anatomical localisation, prior to radiopharmaceutical injection 79—16333
- radiographic X-ray image intensifier video system, design characts. 78—69209
- radiographic X-ray image intensifier video system, psychophys. evaluation rel. to system measures 78—73234
- radiographic X-ray tube current, effect of electron evaporation 78—69204
- radiographical apparatus for mech. and kinematic anal. of lumbar spine 79—74708
- radiographical equipment and layout in up-to-date working places 79—62352
- radiographical scanning multiple slit assembly, design and performance 79—70616
- radiographical subtraction device for daily practice and vascular procedures 80—36090
- radiography, anal. of making, reading and reporting films, rel. to equipment design 80—17123
- radiography, cerebral angiography in stereoscopic magnification *(Japanese)* 77—73574
- radiography, computed, low-dose X-ray imaging system 80—98092
- radiography, computerised tomography using video techniques 77—73568
- radiography, diagnostic, X-ray spectra determ., high intensity 80—41217
- radiography, dynamic, automatic control system design 77—60244
- radiography, equipment needs for radiology department, math. model 78—65107
- radiography, falling load technique, performance evaluation 78—69201
- radiography, held radiograph technique and radiation protection 78—73199
- radiography, holographic 3-D synthesis of X-ray pictures 80—67245
- radiography, low dose, intensified minification camera 78—20262
- radiography, metal screen-film detector MTF at megavoltage X-ray energies 80—30868
- radiography, micro-dose system 80—51233
- radiography, motor-tilted diagnostic examination device Model UV-5B 80—85479
- radiography, panoramic tomograph users' experience in exam. of teeth and jaws 77—21605
- radiography, principles of design of assemblies 78—57065
- radiography, rare-earth screens, effect of P X-rays 80—30867
- radiography, scanning grid for novel and effective Bucky movement 80—104754
- radiography, stereoscopic image evaluating device, Medicor Model SZRK 80—85478
- radiography, systems approach to scale of equipment 78—57064
- radiography, test objects for systems performance evaluation 80—46022
- radiography, test phantom for meas. of phys. parameters *(German)* 78—57068
- radiography, working places incorporating Medicor equipment 78—35942
- radiography equipment, idealised, for routine chest exams., specifications and requirements 80—46034
- radiography grid for elimination of scatter, zig-zag design 78—3598
- radiography of breast, recent techniques *(French)* 77—81564
- radiography screen-film combination selection 80—46047
- radioimmunoassay, automated on-line system, Gammaflow 77—9247
- radioimmunoassay, automatic reservoir for serial pipetting 79—100723
- radioimmunoassay, instrumentation developments 77—86614
- radioimmunoassay, plasma renin activity estimation, microprocessor controlled 80—46023
- radioimmunoassay appls. of Philips gamma counter PW 4800 and scintillation counter PW 4700 80—56173
- radioisotope diagnosis, equipment and methods *(French)* 78—48888
- radioisotope hybrid scanner, design of detector and collimators 78—7423
- radioisotope image magnifier/rotator for enhanced visualisation 78—15889
- radioisotope imaging, eight-sensor low-energy γ topograph *(Russian)* 78—35932
- radioisotope imaging, optimal collimator design parameters for dynamic spatial resolution 80—17087
- radioisotope imaging device assessment, psychophysical approach 77—86625
- radioisotope scanner performance improvement, subtraction of Compton scattering 79—16273
- radioisotope tomography, time modulated apertures 77—64127
- radioisotope tomoscanner, low cost 78—40313
- radioisotope whole-body imaging methods and devices, comparison 78—44597
- radioisotopic sources containing ^{238}Pu, ^{241}Am, and ^{252}Cf 77—26915
- radiological diagnostic equipment, ergonomic design problems *(German)* 79—74729
- radiological imaging instruments comparison for dogs with liver hepatomas 80—17074

biomedical equipment continued

- radiological-endoscopic combined setups for gastrointestinal organ exam., experience 77—90947
- radiology, diagnostic, analytical stereo system 80—67231
- radiology, new industrial contributions, review 78—31924
- radionuclide emission tomography of head with ^{99m}Tc and scintillation camera 77—52866
- radionuclide tomography, 3-dimens., with circular ring positron camera 77—73566
- radiotelemetry, transmitter for small animal temp. meas. 79—83888
- radiotelemetry pill for biomedical meas. of ionising radiation using HgI_2 detector 78—40318
- radiotherapy, high-energy accelerators, mixed photon-neutron field meas. 80—51267
- radiotherapy, linear accelerator neutron sources and characts. 80—51239
- radiotherapy, Mevatron 20, compact high-output linear accelerator 78—28035
- radiotherapy, missing tissue compensator 80—3784
- radiotherapy, purpose and technology, radiotherapy department planning 78—28034
- radiotherapy, vertical couch extender 80—3783
- radiotherapy accelerator neutron leakage survey 80—51269
- radiotherapy accelerator primary beam neutron contamination 80—51268
- radiotherapy afterloading applicator, dose distrib. around 79—53249
- radiotherapy Clinac-18, satellite digital display 78—3599
- radiotherapy compensation filter for chest portals 78—31887
- radiotherapy electron accelerator neutron prod. 80—51240
- radiotherapy electron accelerator neutron production, conf., Gaithersburg, USA (Apr. 1979) 80—46730
- radiotherapy electron accelerator photoneutron prod., survey of European meas. 80—51241
- radiotherapy hard X-ray machine, RT 305, phys. aspects and appl. 80—81709
- radiotherapy high energy X-ray machines, effect on tumour cure rate 80—36067
- radiotherapy high-energy linear accelerator photon beam exit design for neutron prod. minimisation 80—51242
- radiotherapy neutron leakage characts. rel. to room shielding 80—51273
- radiotherapy sidelight using laser cross-hair image 78—35939
- radiotherapy simulator accessory for lateral therapy portal placement 79—100710
- radiotherapy tissue compensators, use in improving dose uniformity in total body irrad. 80—104767
- real time phaseless filter with delay circuit, ECG appl. *(Japanese)* 80—56253
- real-time data acquisition system design 78—35994
- recorders, direct-writing analogue type, biomedical appls., techniques and maintenance, review 78—69241
- rectilinear scanner, large crystal, improved focused uptake probe 78—28053
- rectilinear scanner, multichannel analyser interface 80—101254
- rectilinear scanner, multiple window, for nuclear imaging, modification of 79—70620
- rectoscopes, optical fibre, unified design for adults and children 77—40827
- red blood cell freezing, cryopreservation and refrigeration 80—67262
- red/IR oximeter operating cct. 78—28101
- reference microelectrode sterilizable with ethylene oxide 80—17153
- reflex hammer with peizoelec. cryst. for accurate reflex latency meas. 80—3839
- reflexotron, 25 MeV, tested in medical therapy config. 77—83139
- refractometer for eye refr. error meas. 80—81583
- refractometers, IRF-454 and IRF-456 models 80—104715
- refractor, for vision defect anal., remote subjective device using sphere-cylinder corrections 77—1992
- Refractor III system, computer-assisted eye examination 79—34698
- reliability requirement determ. and assessment method 77—5091
- REM detecting machine, portable 79—92410
- renal dialysis membrane leak detector 77—60294
- reoentgenokymographic unit, physical and operational characts., plate thickness optimisation 79—57747
- respiration calorimetry determination of O_2-calorie equivalence of thyroid patients and normal subjects *(German)* 78—85412
- respiration electrical stimulation, appls. and equipment 78—36054
- respiration mass spectrometer, delay and response time measurement *(Hungarian)* 77—73617
- respiration monitor, microwave Michelson interferometer 79—8557
- respiration monitor for premature infants, non-contacting device using air-transmitted US 77—52915
- respiration rate meter, corona discharge identification and ionisation current control *(French)* 79—92411
- respiration rate meter tester 80—81758
- respirator based on jet-flow vortex-type components *(Russian)* 79—79683
- respiratory flowmeter, hot-wire, evaluation for clinical appls. 80—72346
- respiratory flowmeter switching device incorporating delay for synchronisation with mass spectrometer 80—17160
- respiratory gas monitoring instrument using microprocessor *(Japanese)* 80—72358
- respiratory jacket for ventilatory measurements in children 79—62379
- respiratory mass-spectrometer appls. 79—62383
- respiratory mass-spectrometer model QGA-11 79—62382
- respiratory measuring equipment, flow and vol. calibrator 79—96687
- respiratory monitors, instrumentation and maintenance, review 78—69236
- respiratory rate and ventilation digital recorder 78—81005
- respiratory rate monitor using microphone pickup 79—79617
- respiratory support system, portable, for vehicular patient transport 77—52917
- respiratory test performance indicator for subject motivation 79—57797
- respiratory total resistance meas. in pre-school children using modification of forced oscill. technique 78—77129
- respirometer, flowmeter-polarographic electrode sensor, for respiratory function telemetering 78—80995
- respirometer, noncommercial respiratory transducer for EEG laboratory 78—65138
- retinal camera with infrared TV obs. *(German)* 79—2145
- retinal image cinematographic recording, accommodation microfluctuation appl. 80—81579
- retinoscopic system, theory including aperture stops 78—85308
- review of developments and facilities 80—12292
- review of the emerging field of biomedical engineering 80—36167

biomedical equipment continued
RF mass spectrometer, MKh 6202, for respiratory gas anal. 78—7468
RF SQUID, use in magnetocardiography *(Dutch)* 79—79670
RF-powered cage system for implant biotelemetry 80—94422
rheocardiography, 4-electrode, in computer-aided cardiac output determ. 80—61718
rheograph, multichannel, with automatic calibration 80—3831
rheograph linear-distortion estimation 80—85502
rheographic electrode system for thyroid gland 79—57783
rheoplethysmograph type RPG-202 79—92405
rhino-rheo-manometer for dynamic and static nasal pressure meas. with capacitance probes 79—83961
rhinomanometer, new-type, and relating test experiences 79—100768
ring pseudorandom aperture for transverse section radioisotope tomography 77—64129
ring-core magnetometer sensor for articulatory meas. of jaw movements 80—101243
Roentgen-video computed tomography for 3D dynamic imaging by heart lungs and circulation 80—17112
roentgenocardiograph with photoelectronic sensors, calibration device 78—57061
ROM based ECG monitor 80—26401
rotating aperture wheel device for radiographic contrast improvement 80—56202
rotating disk device for slit radiography of the chest 80—98116
safe voltage differences, practical equipot. limits 78—44649
safety, micro-electrocution and EM wave effect on human body 77—9295
safety and reliability in medical electronic equipment 80—36172
safety and reliability of electromedical equipment *(Croatian)* 78—48901
safety and technical service centres *(German)* 80—98151
safety aspects, leakage currents meas. and minimising 78—11748
safety standards for electromedical equipment and installations *(Croatian)* 80—104795
scanning cytophotometer controller design method 78—31920
scattered radiation grids, method for testing 80—81717
scholiosis treatment, Electro-Spinal instrumentation 78—48925
Schottky barrier diode/laser beam system for quantitative meas. of body motion 80—12207
scintigrams recorded on X-ray films, simple method for copying and photographic data processing 79—16283
scintigraphic camera systems and their assessment by computer 78—57063
scintigraphic multiplane tomographic scanner, simulated, correct. for out-of-focal-plane blurring 80—51221
scintigraphic TV displays, 4 standard types, comparative study 80—109005
scintigraphy and angiography, equipment for quant. evaluation and off-line operation *(German)* 78—88736
scintillation analyser for aerosol particles size meas., inhalation technique development *(Slovak)* 79—74750
scintillation camera, multidetector design with 254 channels 77—40739
scintillation camera, with 2 mm intrinsic resolution 77—70525
scintillation camera based on image intensifier tubes, for nucl. medicine appls. 77—5069
scintillation camera collimator image form. 80—89844
scintillation camera dead time with and without computer 80—3777
scintillation camera device for labelling film with patient identification number 77—60242
scintillation camera electronics capable of high processing rates, clinical significance 77—40740
scintillation camera field uniformity, global and local, statistical features 80—61677
scintillation camera single-photon computed tomography, optimised collimator 78—77106
scintillation camera transaxial tomograph, Humongotron 77—52867
scintillation camera upgrading, comparative study 80—12236
scintillation camera whole-body single-photon emission computerised tomography system 80—17086
scintillation camera/high energy collimator system, misleading results with a bar phantom image 80—12237
scintillation cameras, deadtime meas., scatter conditions simulating nuclear cardiography 79—16276
scintillation cameras, effect of photon energy on field uniformity tests 79—16278
scintillation cameras, large-field-of-view 78—44596
scintillation cameras for radioisotope imaging *(Spanish)* 78—7428
scintillation cameras using liq. and solid Xe detectors *(French)* 77—37034
scintillation chamber, operating model 80—30848
scintillation counter, liq. Xe, for imaging of positron emitters 77—2042
scintillation-camera simulator for remote-data acquisition testing 80—46020
Searle Pho/Con tomographic multiplane scanner, tomographic plane separation and detector distance determ. 78—20258
semiconductor disc memory, high speed, for storing body surface pot. maps 77—78014
semiconductor gamma-cameras in nuclear medicine 80—81693
sensors for diagnostic instruments, classification scheme 79—53267
sensors produced by Medicor Works 79—100769
servo-controlled force plate for patient equilib. function study *(Japanese)* 79—74775
shadowgraph for finger clubbing meas. 80—21519
Sharplan 791 CO_2 laser for clinical surgery 78—35904
shearing forces on the sole of the foot, meas. system 80—72342
Shimadzu medical equipment manufacture trend *(Japanese)* 79—88209
signal processing system for high counting rate spectrom. 77—44788
single cell quantitative anal. and sorting 78—28147
skeletal maturity determination system *(French)* 80—41209
skeletal muscle motor units, system for rapid acquisition of surface pot. maps 80—46077
skeletal radiographic imaging, computer/scanner approach 77—77989
skin evaporimeter, anal. of performance 80—56256
skin impedance dynamic meas. system 79—57744
skin recoil characteristics, human, in vivo meas. apparatus 79—57698
skin sensitivy meas., instrumentation for 79—74767
slit lamp, hand-held, with lid opener for ocular exam. 80—67179
slit lamp photodocumentation of ocular structure 80—67181
slow scan SIT detector for X-ray diffraction studies using synchrotron radiation 79—48382
smoking pattern recorder, portable 80—94385

biomedical equipment continued
solid state track recorders in nuclear medicine 79—26830
SOLO monitor, microcomputer bedside monitor 80—94404
sonic anaesthesia during tooth hard tissue operations, BN-1 apparatus 78—85350
sonic digitiser method for biomechanical spatial data collection 79—39441
sonic digitizer, 2-sensor, accuracy obs., radiation therapy appls. 80—30806
Sono Diagnost R multi-element scanner, use for upper abdomen US diagnostics 80—17028
SonoChromascope, US B-scan image acquisition, display and recording 80—30818
sorbent haemoperfusion systems, characterisation of solute removal 78—44689
Soviet requirements, X-ray diagnosis, radiotherapy, short lived isotopes in diagnosis, review 77—37032
spectral reflectance photography of the ocular fundus 80—67184
spectrophotometric standards, glass filter SRM 930 by NBS, clinical laboratory appl. 78—54331
spectroscopic system, noninvasive method for in vivo blood anal. 77—60234
speech synthesis, portable equipment *(French)* 80—51291
speech trainer, correction of vowel articulation *(Japanese)* 77—25473
speech trainer for correction of intonation for hard of hearing children *(Japanese)* 77—25472
speech trainers, with visual display system, systematic use for hard of hearing children *(Japanese)* 79—39596
speech trainers using visual display system, for hard of hearing children *(Japanese)* 79—39595
sphygmomanometer, random-zero design with variable height reservoir 78—35986
sphygmomanometer control valve, improved design 77—60266
spine and forearm Ca changes, meas. apparatus using ^{252}Cf neutron activation anal. 79—39490
spot scanning system for proton radiotherapy 80—89836
SQUID, appl. to human brain mag. response monitoring 77—29231
SQUID, fabrication and LF and HF appls. including magnetocardiography 77—22583
SQUID, for magnetic field and spatial gradient meas., design and advantages 77—26369
SQUID, medical application *(Japanese)* 80—12290
SQUID applications in biophysics 79—29640
SQUID arrays, for mag. field meas., geophysical, biomedical appls. 78—32830
SQUID detection, low temp., NMR imaging improvement towards mol. kinetic meas. 80—104723
SQUID fluxgate magnetometers, magnetopneumographic meas. 80—104711
SQUID gradiometer, second-derivative, magnetocardiogram meas. 80—104696
SQUID instruments and shielding for low level mag. meas. 77—40840
SQUID magnetometry, low-level, of human heart in small ferromag. enclosure 78—92726
stammerer fluency aid using delayed auditory feedback, body-worn aid 80—56283
standardisation and maintenance, role of Indian Central Scientific Instruments Organisation 79—74778
standing aids for physically handicapped assessment of 4 types 79—12026
static charge sensitive bed, method for recording body movements during sleep 80—3840
step length measurement apparatus 80—67271
stereo-ophthalmoscope 110, for viewing of fundus oculi 78—48905
stereo-ophthalmoscope 110, stereophotography of fundus 78—48906
stereophotography, using camera slit lamp, ophthalmic applications 78—48904
stereopsis clinical test 80—61566
stereoscopic X-ray unit for medical diagnostic sets 80—85467
stereovision techniques for diagnosis *(Japanese)* 80—67279
sterilisers, ethylene oxide, evaluation of effectiveness and hazards 77—60269
stethophonendoscopes, design and production 80—104686
still-shade-temperature meter for use in assessing personnel cold stress 80—81764
stimulated Raman scatt. Dewar cell 80—99799
stimulation electrode, implantable standardisation problems 77—64151
stimulator encapsulation for implantation, biomaterials 78—40416
stimulus generator for evoked response studies 78—57011
stomach double-contrast exam. using Orbiskop 78—73200
stomatology, needle holder for intraosseous infusion 80—3859
strain gauge, Hg-in-rubber, for plethysmography, temp. drift error and compensation 77—52900
strain gauge plethysmograph, automated 2-channel 79—29648
strain gauge transducer for jaw force meas. 77—86669
strain gauge transducer for myocardial stimulation, local tension meas. 79—48357
strain-gauge pressure transducers 79—100778
strength tester, multifunctional isometric device for upper extremity 78—44658
stress exercise facility automation using microcomputer system 79—70682
stress/duress automated detect. system 80—76852
strobe-sequenced device to facilitate 3D viewing of cross-sectional images 80—104720
Subjective Refraction System, American Optical SR III, phoropter comparison 79—83953
superconductive helmet with SQUID for magnetoencephalography 80—104708
supraventricular arrhythmia rapid anal. from long-term oesophageal recordings, drug assessment 80—89904
supraventricular tachycardia, diagnosis and management, instrumentation and therapeutic techniques, review 79—39598
surgery, microprocessor-based patient monitoring system 78—44681
surgical aspiration automatic control device for cardiac surgery *(French)* 78—61282
surgical diathermy units, selection guidelines 77—73613
surgical equipment, crest factor definition 80—56273
surgical lasers, effect on lining tissue and applics. 77—90871
surgical microscope, model 310, photographic documentation in eye operations 80—56161

biomedical equipment continued
surgical wound preoperative force meas., transducer device 78—36041
sweat test equipment safety improvement 79—29649
switch valve, lightweight, remotely actuated, for rebreathing exercise studies 80—101278
Synthalyzer, three dimens. synthesis and analysis by optical dissection 78—81011
systolic time interval meas. microprocessor system for heart malfunction detect 79—79681
tachometer, digital, for heart rate measurement 80—17162
tachystoscope, computer-controlled, for eye accommodation time and rest position meas. *(German)* 79—2143
tape recorder three-channel modulation scheme for biological signals 78—61272
tape recorders, correction of timing errors due to tape speed variation 80—72354
target, water-cooled pion-production, remote exam. and disassembly 80—25975
teaching, using guided design format 78—28881
teaching laboratory, efficient use of animal expts. 77—37700
technical servicing, determ. of quality 80—3834
technical servicing, determ. of range of preventive maintenance 78—85421
technological transfer for medical electronic equipment development 79—96679
telemetric system, with external storage, for detect. of radionuclide tracers in humans 77—12995
telemetry, transmission and reception with embedded antennae 78—77125
telemetry demodulation system, microprocessor based 78—44627
telemetry device, chronically implanted, controlled transcutaneous powering 80—98152
telemetry system synchronisation, with time division of channels 80—94386
telemetry unit for noninvasive determ. of anterior spinal fusion following corrective surgery 77—44851
teletherapy machine electronic dual timer 78—85358
television data compression, for cytology and chromosome anal. 77—86683
television ophthalmoscope image processor/graphics system 77—81633
temperature biotelemeter, modular, expandable, implantable 80—67191
temperature probe design, exptl. calibration results and numerical model predictions 80—56258
tendon reflex stimulation threshold meas. device for man 78—7467
test instruments, scientific and medical instrumentation capability 78—69242
tethered float radiometer for US therapy equipment output power meas. 80—104691
text-to-speech synthesizer for blind and handicapped 80—96142
TGM-1 multidirectional tomograph, operating characts. 80—104726
Therac 6 linear accelerator, computer controlled evaluation for X-ray therapy 79—5363
Therac 6 linear accelerator, field elongation effects on depth-dose curves, central-axis output of X-rays 79—5361
therapy/measuring combined unit for pacemaker implantation *(German)* 78—7519
thermal convertor component for artificial heart, R&D 78—20318
thermal entrainment device for cardiovascular investigation 80—104793
thermal oscillating pump for nuclear powered artificial heart 78—20317
thermistor stability, ageing in constant temp. baths 79—21745
thermistor-respiratory flow sensor, shunted, characts. *(German)* 78—28097
thermographic diagnosis, high resolution dynamic method, detector system 80—41167
thermometers, electronic, review 78—69235
thoracic electrical impedance camera for chest fluid meas. 77—40889
thoracic impedance of humans, meas. using automatic recording device on defibrillator 78—61239
three dimensional imaging, conf., San Diego, USA (Aug. 1977) 78—78971
thyroid fluorescent scanning system of concentric source-detector design 77—40738
tissue characterisation by computer-aided US method *(German)* 78—80932
tissue microelectrode design for skin pH meas. 79—100780
tissue reflectance oximeter, noninvasive solid-state device 78—35919
tissue-equivalent compensators for 4-MV X-rays, basic data 80—98069
tissue-equivalent liquid bolus, physiologically compatable, for microwave tissue heating 79—39465
TOMAX autostereoscopic display, three-dimens. viewing of tomographic data 78—85446
tomofluorographic camera with lens objective and angular tube 79—57750
tomography, computerised, principles and development 78—31945
tomography, single photon emission, camera configs., performance anal. 80—61686
tomography equipment and reconstructive methods, review 80—30849
tomography equipment for intracranial diagnosis, Japan 77—53877
tomography machine uses radioisotopes for patient diagnosis 77—56464
tomography simulator, emission computed, design 80—61672
tongue movement observation using dynamic palatography 78—44687
tongue movement study using dynamic palatography 77—29160
tonometer, applanation, for intraocular pressure meas. 80—30833
tonometer, non-contact, for intra-ocular press. meas., status report 77—2063
toxic compounds, enzymatic sensor for continuous determ. *(French)* 78—73099
track detector direct dosimetry in fast neutron beams 78—20277
transducer, non-invasive, for continuous meas. of arterial blood press. 77—44817
transducer and perfusion system, ambulatory blood pressure recording in man 79—53271
transducer design *(Hungarian)* 79—92408
transducer for intraluminal press. recording 80—17152
transducer for non-invasive intracranial pressure meas. in newborns 80—67272
transmit/receive 2D ceramic piezoelectric arrays, construction and performance, medical, NDT appls. 78—87223
transmitting antennas, body-mounted, telemetry appl., design 77—90927
transthoracic intramyocardial pacing wire for emergencies 78—69254
transverse axial film tomography with a therapy simulator 80—81716

biomedical equipment continued
triaxial vector accelerometry for quantifying tremor and ataxia 78—28116
trichometer for hair growth rate assess. 79—92325
TRIUMF biomedical negative pion beam line, tuning 78—96113
TRIUMF meson factory, biomedical appls. 78—21792
tuned loop receiving antennas, 100 MHz, for indoor telemetry 77—90925
TV communication aid for disabled, Telecad 80—17197
TV installation for projection of high-resolution X-ray images *(German)* 79—57751
TV pupillometer, anal. of dynamic performance *(Japanese)* 79—39545
ultrasonotomography with electronic sector scanning, cardiac diagnosis appl., features 77—66829
Unibed patient monitoring system based on microcomputer and LSI technology 78—20305
unification of instruments 80—3835
uniplanar force meas. system for orthodontic appliances 78—31970
ureter recordings, electroureterograph and dynamoureterograph 80—56235
urine glucose analyser with audible output 77—52909
urodynamic parameter meas. systems 79—96690
urology, universal room using Uro Diagnost 78—31902
US apparatus for blood bubbles detect. and meas. *(Japanese)* 80—1712
US B-scan imaging with automated water-delay system 80—98041
US bladder volume sensor, pocket-size 80—36034
US blood flowmeter *(Japanese)* 78—31875
US blood flowmeters, early history 77—77946
US camera for patient diagnosis *(French)* 77—37028
US computed tomography of breast, progress 80—51196
US diagnosis, 1977 state of art and developments 78—48847
US diagnosis, human abdominal tissue phantom 80—51152
US diagnosis, tissue simulators 80—51153
US diagnosis, transmission tomography by reconstruction compared with pulse-echo imaging, tissue-equiv. test objects 80—51154
US diagnostic equipment, operation principles and constructional features, advantages *(German)* 79—100684
US diagnostic equipment, portable radiation-force balance 78—69163
US diagnostic equipment, power meas. via acousto-optic method 77—832
US diagnostic equipment, US power and intensities produced 78—69162
US diagnostic equipment development *(Japanese)* 78—44572
US diagnostic instrument performance evaluation, work of USA AAPM and AIUM 78—69170
US diagnostic instruments, output meas., irrad. effects *(Japanese)* 78—80936
US digitiser/processor for extraction of clinical parameters from Doppler-shift waveforms 80—36042
US Doppler spectragrams refreshed display and haemodynamic parameter meas. 80—41152
US Doppler velocimetry for 3D blood flow meas. 78—88730
US dynamically focused electronic sector scanner based on CCDs 80—98042
US echo probes, flexible, and prospects for use in oncology 80—56147
US echo-ranging FM-CW system, distance resolution 80—36043
US echographic time-distance recorder for foetal breathing movement meas. 78—24109
US echolocating blind mobility aid, interpretation of stereophonic output 80—108989
US echotomography for intrahepatic vessel and duct structure diagnosis 77—90868
US equipment for intra-rectal prostate imaging 79—48296
US equipment quality control, tissue phantom *(German)* 78—3567
US field focusing upon transmission using annular transducer 78—44574
US flowmeter for measuring rapidly changing gas flows, freq. range, excitation and signal processing *(German)* 78—83502
US FM blood vol. flowmeter processing technique 78—31878
US grey scale display on storage oscilloscope system 78—3569
US grey scale scanner dynamic range testing 78—69169
US high-resolution 3-dimens. real-time imaging system 77—86575
US imaging equipment, quality control problems 78—69171
US imaging systems, high-resolution, real-time 78—69160
US implantable CW Doppler blood flowmeter, optimal system design 78—53460
US implantable IC CW Doppler flowmeter 78—31877
US instrum., patient diagnosis appl., bibliography 78—7417
US instrumentation standardisation, physician's need 78—69168
US instruments with elec. controlled directivity patterns, design 77—838
US mean frequency Doppler modulator performance, blood flow meas. appl. 80—45991
US monitor for fetus cardiac pre-ejection period continuous meas. 79—74732
US ophthalmological transducer, with controlled weight, eye axial length meas. appl. 78—20239
US ophthalmoscope, eye axial distances meas. 80—36032
US phantoms, water-based gels 80—81671
US probes, power meas. by use of semiconductor strain gauges 80—87679
US pulse-Doppler device linked to grey scale B-scan equipment, clinical evaluation 79—92311
US pulse-echo diagnostic equipment performance meas. methods 77—77957
US pulse-echo equipment, tissue equiv. test objects for routine performance checks 78—73182
US Pulse-echo transducer standardization 78—73181
US pulsed Doppler flowmeter, vel. accuracy and range resolution 77—77945
US real-time diagnostic system 80—30819
US real-time diagnostic system for dynamic and still images, wireless echovision 78—65101
US real-time scanner with pulsed Doppler and T-M facilities, obstetrical appls. 80—67172
US scanner, real-time rotating transducer, for heat and abdomen exams. 79—20603
US system for blood press. anal. during treadmill stress testing 80—81674
US system for left ventricular function quantitative evaluation 80—85457
US therapy device surveys, performance standard drafting 79—79613
US tissue analysis, comprehensive system 80—51189
US tomography for umbilical cord complications diagnosis 77—90867
US transceivers, gain transfer characts. 80—30814
US transducer, air coupled, for non-contact transduction of kinetocardiogram 77—86568

biomedical equipment continued
US transducer, high resolution, with toroidal acoustic lens 77—65656
US transducer, US energy meas. for echography 80—36044
US transducer, wideband, for tissue characterisation, 1 to 10 MHz 79—16262
US transducer design rel. to vibration geometrical effects 79—83871
US transducers, low-loss wideband for noninvasive appls., characts. 78—48846
US transmission/reception system with single crystal, principle *(Japanese)* 77—84093
USSR development of equipment and instruments 79—96699
USSR measuring equipment state testing system 79—96701
USSR metrological servicing procedures 79—96702
USSR metrological-provision programme 79—96700
uterine contraction waveform online digital processing system 78—15916
vaccine atomiser for liquid aerosol immunisation 77—81638
vaginal photoplethysmographic transducer, blood vol. change monitoring in menstruation 78—92733
vascular clamps, endothelial lesions in cardiovascular surgery 79—53278
vascular interface system for automation of haemodynamic monitoring and therapy 78—81054
vascular laboratory instrum. management using computer 78—7460
vascular pressure measurement systems, calibration 79—96691
vector cardiograph for pacemaker pulse display 80—41325
vectorcardiographic microprocessor system *(Bulgarian)* 80—61722
vectorstabilograph, for investigation of man's stability of stance 77—44772
venous infusion drop-rate calibrator 79—96705
venous pressure clamp for heart-lung machine, automatic controller, photoelectric sensor 77—78053
venous system visualisation combined with press. meas., technique and equipment 80—36094
ventricle volume characts., nuclear medical determ., appl. of computer system *(German)* 78—88737
ventricular arrhythmia detector, arrhythmia data base of American Heart Association 79—62391
ventricular arrhythmia on-line study, computer system 78—81060
ventricular arrhythmias, intraoperative mapping system 80—56242
ventricular function monitor, ambulatory, CdTe detector, cardiac ejection fraction meas. 80—61680
ventricular functionanalyser, microprocessor-based 80—26402
ventricular septal defect plastic repairing instrument 78—7522
vergence accommodation meas., dynamic optometer 78—35852
vertebrate cornea, transparent layered structure thickness monitor 78—92737
vestibular postural control evaluation in humans using computer-TV interface system 77—44773
Victoreen 555 integral and rate exposuremeter, digital display plug-in module 77—405
video camera 10 μm, human body surface visualisation 79—94326
video cassette recorder for analogue data 79—44009
video correlating system for blood flow vel. meas. in microvessels 78—53543
video display system for observing ground reaction forces during ambulation 79—96688
video patient monitoring system for clinical seizures, long term time-lapse, EEG synchronisation 79—39461
video processor for computer calc. of press.-vol. indices from left ventriculograms 78—53495
video-tracking of micro-circulation, appl. of bit-slice processors *(German)* 78—88749
vidicon tube for low level X-ray and γ-ray imaging 77—81561
vision testing instrument, determ. of visual acuity and depth perception threshold 78—81007
visual acuity screens, reflectance obs. 80—67178
visual behaviour monitoring system, EMG triggered photographic technique 78—31919
visual evoked human-scalp EEG data monitoring, processing and displaying system 77—90936
visual evoked potentials, transient, real-time filtering 78—31940
visual evoked response meas. using versatile pattern-reversal stimulator 80—17177
visual perception, computer-based testing system for expts. 79—74769
visual spectral sensitivity, direct readout system for clinical and research purposes 78—3488
visual speech vocoder as teaching aid for deaf 78—36069
visual stimulation apparatus, stepper-motor shutter drive using monostables 78—35860
visual stimulator, computer-controlled, for electrophysiology expts. 78—69230
visual stimulator for flicker fusion expt. 78—96053
visual stimulus deflector, three-dimens. 78—48945
visual stimulus device for characterizing temporal MTFs in man 80—51204
visually evoked response test goggle system using liquid crystal shutters 79—79676
vitreous surgery via pars plana, instrument design 78—81056
vocal synthesiser using programmable filter *(French)* 80—48524
voice controlled system for the disabled 79—5407
voltage measuring equipment, leakage current protective measures *(German)* 78—3629
walking appliance for paraplegic adult, design 77—60299
wax phantom simulating flat tumour with diffuse edges for subtraction radiography 77—70536
weight monitoring, continual in-bed method 78—48910
wheelchair, Emory detachable elec. powered drive 77—25606
wheelchair, power reclined back 79—12027
wheelchair cushion effect on skin temperature, heat flux, and relative humidity 79—83707
wheelchairs, electric, PWM control DC motors drive system *(German)* 77—56491
whole body counting systems, parametrisation of operational conditions *(German)* 77—9284
whole-body counter, 4 π, at Hamburg, performance parameters 77—16975
whole-body counter, shadow-shielded, for detection, identification, and localisation of incorporated radionuclides *(German, English)* 78—20266
whole-body counter based on liq. scintillation detector modules 77—48883
whole-body NMR imaging machine 80—101285

biomedical equipment continued
Wirbelrespirometer dynamic response improvements *(German)* 78—28099
Wisconsin mammographic kVp cassettes, evaluation of spectral response 80—81715
workshop on status and future of biomedical instrumentation 80—46081
writing aid for motor handicapped, microprocessor-based device, LOGOS 78—81077
X-ray apparatus, practical aspects in cardiac work 79—96659
X-ray apparatus electrical circuit fault classification 77—21604
X-ray apparatus optimal operating conditions 80—30847
X-ray area exposure product monitor, DQ-20 *(Japanese)* 77—73578
X-ray beam characteristic time vars. meas. using solid state devices 80—46048
X-ray collimators, semi-automatic and automatic, manufactured by Medicor Works 80—85475
X-ray colour TV system with soft X-ray preferred display 80—56186
X-ray diagnostic equipment, method and algorithm for adjusting 80—30852
X-ray diagnostic sets, operation of optical centreing systems 80—30831
X-ray diagnostic system compatible with DHEW standards 78—7445
X-ray diagnostic table, computer controlled, multidirectional, CASSETTE-LESS spotfilm device *(Japanese)* 78—61278
X-ray equipment, physical characts. of radiation 80—26334
X-ray equipment, state of the art 80—81688
X-ray equipment, STATUS X, for canine teeth localisation 77—90881
X-ray equipment selection for intensive care unit 79—92346
X-ray equipment survey in hospital and preventive medicine establishments 77—21602
X-ray film, reversal-developed, image quality with reference to density 79—100713
X-ray film with reduced crossover, evaluation 79—70621
X-ray films sensitive to green light, reciprocity law failure 78—69199
X-ray fluorescence analysis system for small samples 77—60249
X-ray fluorescence in vitro, medical applications, automated system 77—5063
X-ray generation for time cutting in ECG synchronised computerised tomography 79—66538
X-ray high potential generator, PD150L, standardisation of exposure factors *(Japanese)* 77—73577
X-ray high tension unit, HD150G-40 *(Japanese)* 77—73576
X-ray image convertor with video signal output 80—36125
X-ray image intensifier closed circuit TV system 80—3775
X-ray image intensifier freq.-contrast charact. curves determ. 78—7427
X-ray image intensifier noise evaluation, digital method 80—98097
X-ray image intensifier performance, image quality, and development trends 80—36124
X-ray image intensifier tube, 14 in 79—16285
X-ray image intensifiers, appls. and limitations 79—79644
X-ray image intensifiers, design and future possibilities 79—74756
X-ray image intensifiers, quantum noise meas. 80—46033
X-ray image quality, MTF anal. of influencing factors *(Japanese)* 77—73580
X-ray image storing equipment of Medicor Works 80—85476
X-ray image transmission systems of Medicor Works 79—100725
X-ray imaging gas scintiliating proportional counters, performance in medical appl. 79—2153
X-ray imaging MWPC, spatial resolution improvement by pulse height selection 77—18744
X-ray intensifying screen, role of reflective layer 80—62816
X-ray intraoperative diagnostic equipment for orthopaedic surgery 79—92341
X-ray locator for transthoracic punch biopsy 79—92331
X-ray machines, pulsating pot., filter method for peak volt. and inherent filtration meas. 78—73201
X-ray machines output rating, equivalent DC power standard *(German)* 78—3650
X-ray picture digital transmission over voice-grade telephone channels, laser scanning system 78—80953
X-ray RUM-20 apparatus, obs. on improving roentgenogram quality 80—30850
X-ray scanners, fast, incomplete scan geometries 80—26330
X-ray scanning system, fast 3D, using limited tilting angle 77—73556
X-ray screen-film processing sensitometry standard developed by ANSI 78—69196
X-ray shielding device, Pb glass, for use with ceiling mounted tube 79—92397
X-ray source, high intensity, polarised, for fluorescent excitation anal. 77—60238
X-ray spot-camera of Medicor Works 80—85477
X-ray tube, focal spot size determ. from pinhole camera images 79—79627
X-ray tube, grid control type, diagnostic, quality improvements 78—11733
X-ray tube, new type, Super Rotalix Ceramic 80—104749
X-ray tube focus, MTF rel. to current *(Japanese)* 77—70545
X-ray tube operation, guide 79—49350
X-ray tube single- and three-phase generator performance comparison *(Japanese)* 79—92354
X-ray tube thermal monitoring system, LOADIX, features 78—3658
X-ray tubes, target angle and inferential kilovoltage meas. 80—30843
X-ray TV, high-resolution system and video recorder 78—24120
X-ray TV chain MTF and image quality determ. factors 80—36126
X-ray TV display system, transmission characts. *(German)* 79—53215
X-ray XX 80—98091
Ag filter for surface dose reduction in ^{60}Co teletherapy 79—79641
Ag/AgCl highly stable electrode 78—35989
Ar$^+$ laser application in clinical otorhinolaryngology 77—90870
CO$_2$ partial pressure in blood, meas. by rapid response electrode system *(German)* 78—85409
CSF detector, positron emission tomography 80—61688
CdTe detectors, portable miniature scanner, bone mineral meas. using ^{125}I X-rays 77—44750
CdTe detectors, props. 77—61658
CdTe detectors, small, props. uses in biotelemetry 77—44747
CdTe detectors in nuclear medicine, capabilities, limitations, X-ray transmission tomography appl. 77—44748
CdTe low-cost portable detector, 3D lung densitometer, diagnosis and evaluation 77—44749
CdTe matrix γ-camera 80—76827

biomedical equipment continued
- CdTe semiconductor detector system, ^{133}Xe clearance meas., muscle blood flow in man 78—40305
- CdTe sensors, review of medical appl. 77—64147
- ^{252}Cf source projector for plesiocurietherapy 77—29197
- Cl^- ion selective electrodes, appl. to biological materials 77—90974
- CsF scintillator, pot. advantages for a time-of-flight positron camera 80—81706
- ^{137}Cs-^{137m}Ba generator, for nucl. medicine, preparation by ion exchange chromatography 78—28071
- Ge camera, 2-detector, 512 element high purity prototype 78—40301
- Ge detectors array, collimated, computer-driven scanning bed, clinical appls., tomography 78—40309
- Ge planar detector array for Pu detect. in lungs 77—17004
- HgI_2 detectors for X-ray 80—89837
- HgI_2, energy response to ^{137}Cs photons, appl. to medical imaging 78—44592
- HgI_2 in vivo medical probe, DC and pulse counting meas. 78—44593
- HgI_2 miniature probes for in-vivo medical appls., fabrication, spectroscopic evaluation 78—40308
- HgI_2 nuclear detectors, bulk homogeneity, spectral response, performance 78—37524
- HgI_2 probe with charge sensitive preamplifier 79—66555
- ^{131}I waste in urine, filter system 77—60319
- ^{81}Kr^m, new type generator using cellulose chromatography paper, for hospital use 79—8541
- Li cells appl., 1979 state of art *(Spanish)* 79—96432
- NaI crystals, used in nuclear medicine, determ. of cause of breakage 80—98077
- NaI opposed detector/turntable γ counter for voluminous samples 79—100706
- NaI(Tl) scintillation cameras, image artifacts and counting losses 80—94345
- Na(Tl), circular ring transaxial positron camera, coinc. electronics 78—31953
- Nd:glass laser with freq. doubling compatibility, for glaucoma surgery 78—40403
- O_2 analyser instrumentation and operation 78—69237
- O_2 consumption, monitoring instrumentation using replenishment technique 79—39547
- O_2 consumption and CO_2 prod. continuous meas. for men in hyperbaric chambers 78—81008
- O_2 consumption continuous measurement, under N_2O anaesthesia during surgery 77—81640
- O_2 electrode, membrane-covered catheter-tip system, construction and performance 78—81003
- O_2 molecule reduction flow probe for cerebrospinal fluid 79—100777
- O_2 monitoring, combined system for transcutaneous and intravascular determ. of partial press. 80—56241
- O_2 partial pressure measurement with thin-layer polarographic probe, intracortical appl. *(German)* 78—85410
- O_2 sensing electrode stability 77—60268
- O_2 therapy equipment improvements 78—36039
- PdO-Pd miniature pH electrode for blood and extracellular fluid pH meas. 80—89886
- Ra storage safe, design, safety, ease of use 78—92736
- Sb-Sb_2O_3 pH electrode improvement 79—53270
- Si diaphragm pressure sensor, integrated signal conditioning 80—76859
- Si pressure transducer, miniature, implantable, features 77—86666
- Si(Li) detector probe with RFT radiation meas. unit for diagnosis of intraocular tumours *(German, English)* 78—20265
- ^{82}Sr-^{82}Rb generator improvement using inorganic exchangers 80—17135
- Ti alloys, props. appl. 78—7456
- ^{127}Xe, handling and dispensing technique 78—85378
- ^{127}Xe, simple device for efficient transfer and unit dose packaging 78—85377
- ^{133}Xe charcoal traps, simple leak tests, nuclear medicine appl. 80—104734
- ^{133}Xe trapping and re-use system for nucl. medicine 78—28051

biomedical measurement
- *see also biological techniques and instruments; biomedical equipment; electrocardiography; electroencephalography; radiography; X-ray apparatus*
- 400 kV substation electric fields, long-term exposure, epidemiologic investigation *(French, English)* 80—21599
- abdominal foetal ECG and VCG recording/processing systems 78—31947
- abdominal wound strength, meas. method for expt. animals 79—44003
- absorption-edge fluoroscopy, spectral considerations 77—21618
- acceleration sensor for heart implantation, heart attack warning *(German)* 79—57802
- Achilles tendon reflex measurement by photocell signal analogue computer evaluation *(German)* 78—7465
- acoustic impedance meter, principle aspects of development 79—24999
- acoustic reflex, meas. of temporal characts. and filter response of electroacoustic impedance instruments 78—3512
- acoustic reflex, statistically based measure and relation to stimulus loudness 77—32907
- acoustic reflex threshold, variability of measurements 77—16938
- active human muscle visco-elasticity dynamic meas. 77—86667
- acupuncture point location using elec. impedance meas., statistical anal. 78—44628
- aerosol particle size meas. by scintillation counting, inhalation technique development *(Slovak)* 79—74750
- airflow measurement in speech using mask-type wire screen pneumotachograph 77—52808
- airway resistance measurement in infants, heated rebreathing system 78—7471
- alveolar CO_2, technique for meas. in infants 79—66564
- ambulatory blood pressure recording in man, transducer and perfusion system 79—53271
- amplifier-electrode hybrid module for surface EMG pots. meas. 80—41294
- anatomic deadspace meas. in mechanically ventilated patients, using N_2 washout 79—96694
- angiographic computerised evaluation of left ventricular wall motion 79—70634
- antibiotic concentration assay, computer-aided method *(German)* 79—5414
- aortic blood pressure, harmonic signal anal. by computer 77—52899

biomedical measurement continued
- aortic compliance in living dogs measured by elec. admittance plethysmography *(Japanese)* 80—3748
- aortic compliance meas. from transthoracic admittance plethysmogram, dog expt. 78—31925
- aortic haemodynamics meas. in humans using US pulsed Doppler transoesophageal method 80—30808
- aortic pressure meas. using intact unmodified intra-aortic balloon 78—31844
- aortic regurgitation rel. to thoracic impedance cardiogram, dog expt. 77—40890
- aortic valve prosthesis water hammer pulse effect *(Japanese)* 78—3676
- aortic valve replacement, computerised simultaneous press./vol. anal. before and after 80—85531
- arterial blood pressure, indirect noninvasive automatic meas. device 77—44771
- arterial blood pressure, non-invasive transducer for continuous meas. 77—44817
- arterial blood pressure noninvasive monitoring by US imaging and phono cuff-sphygmomanometry 80—36180
- arterial diameter meas. using US transit-time micrometer 78—7410
- arterial elasticity measurement in vivo using transit-time US micrometer 77—40719
- arterial flow velocity, Doppler US vascular diagnostic system 77—29190
- arterial haemodynamics evaluation using venous US catheter-tip technique 77—44730
- arterial impedance plethysmographic signal quantitative interpretation 79—57742
- arterial physio/pathological data from transcutaneous CW Doppler-shifted US 77—44731
- arterial pressure automatic determ., using microprocessor based instrument, Dinamap 78—96108
- arterial pulse wave vel. meas. by Doppler shifted US and EM flowmetry 78—69229
- arterial stenosis detection by transcutaneous pulsed Doppler method 77—44732
- arterial wall motion determ. using Doppler US system 78—15876
- arteriovenous O_2 difference, noninvasive meas. method *(German)* 78—85441
- articulatory activities measurement, computer-controlled method 77—56391
- artificial heart, non-invasive determ. of instantaneous cardiac output and dynamic performance 77—44845
- artificial muscle, load meas. in animals 77—44852
- astigmatism in infants meas. by photorefraction 79—62242
- ATP measurement in single red blood cells using firefly biolum. reaction 78—48951
- atrial septal defect assessment by echocardiography 79—70600
- auditory evoked cortical potential online detector 78—31952
- auditory multifrequential impedance meas. 80—17031
- auditory system evoked potential, human, automated recording and analysing complex 79—57780
- auditory thresholds in children, forced-choice adaptive procedure 79—29644
- automatic measurements and automata appl. in medical engineering 79—62381
- averager for neuroelec. response meas., operation mode *(German)* 77—77887
- back strength, correl. of clinical and Cybex isokinetic and isometric assessment 78—40230
- bacteria counts, light scatt. pattern anal. 78—80946
- bacteria species identification and conc. estimation by light scatt. 77—56564
- bacterial growth detection by impedance meas., electrode characts. 77—60325
- bicycle ergometer for cardiovascular medical diagnosis, model AM 368 *(Italian)* 80—30918
- bile fluid, system for meas. small flow velocities *(German)* 79—39534
- binocular oculomotor problems, phoria, vergence and fixation disparity 78—35835
- bioacoustic tissue property determ. by US pulse echo anal. *(German)* 78—85349
- bioelectric process mag. recording, FM freq. convertor 78—7469
- bioelectric signal recording using surface electrodes, methods of reducing movement interference *(German)* 78—85405
- bioengineering advances conference, San Francisco, USA (Dec. 1978) 79—92416
- bioengineering and medical instrumentation, symposium, Laramie, USA, (May '76) 77—25571
- biofeedback diagnosis system, physiological parameter meas. considering psychic effects 79—100774
- biofeedback thermometer, low-cost research-oriented, with digital readout 79—29673
- biological tissue samples, normal and diseased, elemental comp., PIXE anal. 79—5364
- biomagnetic fields, meas. and anal. 79—11952
- biomagnetic information, and its meas. *(Japanese)* 80—30735
- biomagnetic instrumentation and meas. 80—36181
- biomagnetic measurement facility installation in hospital environment, design criteria and procedure 80—104707
- biomagnetic measurements in unshielded and noisy environments 80—104710
- biomagnetic signal, adjustable supercond. plates for gradiometer balancing 79—25162
- biomechanical spatial motion, data collection method using sonic digitiser 79—39441
- biopotential recording, skin pot. artifact reduction 77—40873
- biopotential recording interference and motion artifact sources and suppression 77—81634
- biostereometrics, automatic iconics meas. system 80—67214
- biotelemetering, industrial product survey *(German)* 77—29220
- biotelemetry, conf., Garmisch-Partenkirchen, W.Germany (May, June 1978) 79—43980
- biotelemetry, literature survey 78—80996
- bladder pressure noninvasive determ. from micturition cinecystourethrogram 79—92370
- bladder urine volume determ. with concentric disc electrode *(Japanese)* 78—31921
- bleomycin radioimmunoassay 77—37050
- blood, abnormal erythrocytes detection *(Japanese)* 77—44869
- blood, agglutination reactions, automated optical scanner 77—52861

biomedical measurement continued
blood, light back-scattering theory 78—77099
blood, mean arterial pressure, noninvasive automatic determ. 79—57796
blood, normal and pathologic, NMR T_2 relax. time studies 80—81682
blood, O_2 saturation meas. in nonhaemolized sample, by laser light *(German)* 77—44735
blood, Pb content, PIXE determination 80—51228
blood, pressure and pulse rate, system for determ. long term variations 79—57792
blood, pressure waves, forward and backward, total-occlusion method for anal. 80—56257
blood, quantitative flow meas. by constant infusion of short-lived isotopes 80—17088
blood, stored, microaggregation direct meas., effects of micro-filtration *(German)* 79—2168
blood, viable cells, automated differential cell counting 79—74777
blood, X-ray fluorescence spectroscopy for trace element anal. 78—20248
blood ^{59}Fe/^{51}Cr activity, simultaneous measurement by liq. scintillation counting 77—29195
blood alcohol determ., spectrophotometric method *(German)* 79—5415
blood analysis in vivo, noninvasive spectroscopic method 77—60234
blood and body fluid pressure meas., Medicor electromanometry 77—90943
blood bubbles detect. and meas. by US apparatus *(Japanese)* 80—1712
blood cell motion dynamics tracking and quantification, automatic picture processing method 79—53074
blood cell neutrophil automated classification, feature selection 78—73281
blood cell speed absolute meas. in retinal vessels, using laser Doppler velocimeter 79—83884
blood clotting timer, automatic 77—52896
blood coagulation parameter selection for automatic digital recording 77—21543
blood coagulation time, US meas. 79—83870
blood electric impedance, effects of pulsatile flow *(Japanese)* 80—21513
blood erythrocyte count and haemoglobin determ. by mobile miniphotometer *(German)* 79—5416
blood flow, capillary, frog web, laser Doppler microscope 77—36964
blood flow, comparison of methods of meas. from digital angiograms *(German)* 79—39468
blood flow, EM flowmeters 77—78008
blood flow, future appls. and prospects 77—78010
blood flow, in objective determ. of human $+G_z$ accel. tolerance, ultrasonic method 78—3619
blood flow, multiple noncritical stenoses, fluid dynamics expt. 77—90844
blood flow, peripheral, meas. by elec. impedance technique 79—70601
blood flow, radiotracer meas., automatic bolus injector 77—9238
blood flow, real-time US carotid arteriography system 78—24108
blood flow, regional, assessment by intravenous injection of ^{99m}Tc pertechnetate 80—104732
blood flow, transcutaneous EM flowmetry meas. using steady mag. fields 80—41158
blood flow, true volumetric US technique 77—90824
blood flow, using Hg-in rubber strain gauge, temp. drift error and compensation 77—52900
blood flow and cardiac output, using indocyanine green and microspheres 77—77925
blood flow calc. by indicator dilution, pulsatile error analysis 77—60225
blood flow detection in human heart, US pulsed Doppler flowmeter system, microcomputer based 80—104690
blood flow disturbance detect. using pulsed US Doppler method 77—40724
blood flow echography using Doppler techniques *(French)* 80—26303
blood flow meas., cerebral, using NMR 77—40730
blood flow meas. by laser Doppler system *(Swedish)* 80—51199
blood flow meas. from US Doppler signals, on-line computer system decoding 78—3570
blood flow measurement, finite diff. soln. of forced convection from hot-film probe 80—12177
blood flow measurement, UDP-30 arterial US pulse Doppler flowmeter 80—104805
blood flow measurement by CW Doppler technique using implanted transducers, accuracy 77—25537
blood flow measurement from freq. analysed US Doppler signal 78—44573
blood flow measurement in dynamic phantom using ^{81}Rb-^{81m}Kr and NaI detector 77—66843
blood flow measurement using NMR and flat crossed-coil detector 78—40284
blood flow measurement using NMR flat crossed-coil detector 79—83880
blood flow measurements by NMR of the intact body 80—81680
blood flow speed and quantity determ. from digital angiograms *(German)* 78—92690
blood flow telemetering using implantable CW Doppler US vel. meter, IC 77—86565
blood flow values in iliac artery, angiocinedensitometry meas. in conscious humans 79—25022
blood flow vel. meas. in microvessels using video correl. system 78—53543
blood flow velocity profiles, US MTI meas. 80—36033
blood flow velocity waveform freq. anal., invasive and noninvasive meas. near stenosis 77—56417
blood flow-velocity meas. by US techniques, Kalman filter appls. 79—100686
blood flow/pressure relationships, when to meas. flow or hold flow const. 77—77926
blood flowmeter, cylindrical crossed-coil NMR, for noninvasive measurement 79—62328
blood flowmeter, noninvasive US Doppler device 77—44733
blood flowmetry, noninvasive, in upper limbs of patients with arteriovenous dialysis fistulas 80—21562
blood flows and vols. in patients with transposition of great vessels, indicator-dilution meas. 78—61209
blood gas analyser, microprocessor based 78—40356
blood gas analysers, review 78—69238
blood gas analysis data processing system *(German)* 79—5419
blood gas analysis in vivo using gas chromatography 78—40355
blood gas and acid-base calculations, electronic data computing 79—25139
blood gas chromatographic analysis, in vitro evaluation 77—81604

biomedical measurement continued
blood gas microanalyser, calomel electrode efficiency restoration 77—25575
blood gas sampler, for gas chromatography, design, construction and characteristics *(Japanese)* 78—85458
blood gases in artery and vein, quantitative continuous meas. of pO_2, pCO_2 78—40363
blood glucose sensor for implantable artificial β-cell 79—83973
blood indicator dye microconcentration meas. instrument 79—39565
blood intravascular mean vel. meas. using crosscorrel. technique 80—81763
blood K^+, Ca^{2+} concs. in rat, technique for continuous vivo meas. *(German)* 79—39533
blood O_2, meas. by fast-responding flow-independent blood gas catheter 80—101277
blood O_2 affinity variability, automated meas. method 79—39544
blood O_2 level, optical continuous noninvasive method 77—2068
blood O_2 partial pressure meas. with membrane covered probe, signal non-linearity 79—53264
blood O_2 saturation measurement, analogue electronic calculator 77—81614
blood oxygen saturation, catheter tip mounted red/IR oximeter 77—40836
blood perfusion rate estimation from diffusible indicator meas., sensitivity anal. 80--104803
blood plasma, vol. meas. in man using ^{99m}Tc, ^{131}I labeled serum albumin 79—29602
blood plasma, X-ray emission anal. by proton excitation 79—84054
blood pO_2 meas. polarographic technique 79—100782
blood pressure, automatic indirect sphygmomanometry methods, equipment 77—81616
blood pressure, blood gas anal., silicone rubber catheter operating mechanism *(Japanese)* 78—61273
blood pressure, cuff method errors, Korotkov and impedance plethysmography techniques 77—40886
blood pressure, digital automatic device *(Japanese)* 78—24168
blood pressure, human, noninvasive meas. *(Japanese)* 80—94395
blood pressure, indirect meas., meaning of max. oscills. point in cuff press. 80—94396
blood pressure, using electronic sphygmomanometer 79—25125
blood pressure continuous recording system for ambulant hypertensives 79—62390
blood pressure cuff control unit, automatic multi-function device 78—36013
blood pressure direct measurement for intensive care and operations, computerised correction system 78—44635
blood pressure for extracorporeal circulations, elec. sensor *(German)* 78—92721
blood pressure Hg manometer contactless readout and recording cct. 77—81603
blood pressure in brachial artery, monitoring by modified phonosphygmomanometry procedure 77—2065
blood pressure indirect meas., occluding cuff design criteria 77—64146
blood pressure instruments, direct systolic/diastolic meas., review 78—69234
blood pressure instruments, noninvasive arterial meas. using US Doppler effect 78—69167
blood pressure meas. instrument for newborn infants 79—92406
blood pressure measurement, new air release valve design for sphygmomanometers 77—60266
blood pressure measurement, noninvasive techniques 80—41298
blood pressure measurement in baboons, direct vs. indirect methods 77—29233
blood pressure measurement with portable systems using Korotkov sounds, meas. accuracy 80—76855
blood pressure monitor, semiautomatic, using electronic sphygmomanometer 78—20300
blood pressure of neonate, noninvasive technique 77—48916
blood pressure recording, simple method for fidelity improvement, Korotkoff sounds 80—76811
blood pressure transducer for student use, using hybrid IC 78—8186
blood pressure transistor device, high sensitivity, quasi-digital 79—79675
blood pulse wave vel. meas. in man, effect of arterial tree anatomical struct. 79—53180
blood red cell shape, laser differential scatt. system for continuous monitoring 77—90873
blood sedimentation rate free from gravity influence, rapid determ. from density meas. *(German)* 78—81085
blood serum, neutron activation determ. of Zn, Se, Rb, and Fe concs. 78—20252
blood serum analysis, ion-selective electrodes 78—3645
blood turbulent flow measurement with pulsed Doppler US 77—40871
blood velocimeters, US transesophageal meas. of human haemodynamic parameters 80—41146
blood velocity, catheter meas., cross correl. technique 78—80943
blood velocity analysis during pulsed Doppler US imaging of carotid artery disease 77—29189
blood velocity in abdominal aorta and common iliac artery of man 80—16972
blood velocity in brain capillaries, microkinematic obs. *(Russian)* 79—5366
blood velocity meas., absolute, US Doppler method *(Japanese)* 79—43974
blood velocity meas., real time multichannel US Doppler signal analyser 77—73551
blood velocity measurement using laser Doppler microscope 79—62329
blood velocity measurements in vicinity of aortic prostheses 79—74706
blood velocity noninvasive meas. in large vessels, broadband pulsed Doppler US system 78—61224
blood velocity waveform display by spectrum analysers, direction Doppler signal preprocessing 79—34611
blood viscometers and anticoagulants compared 79—83834
blood volume flow quantitative estimation with transcutaneous Doppler US 80—36052
blood white cells classification, automation using computer, expt. 78—3663
blood-flow velocity estimation, Kalman filters for Doppler ultrasonic meas. 79—62325
body components, anal. by X-rays, developments 80—3810
body elemental composition meas., feasibility study 79—70615
body Fe stores meas. technique, nuclear resonant scatt. 79—83914

biomedical measurement continued
body fluids meas. by basal thoracic elec. impedance 78−48852
body motion, quantitative meas. by Schottky barrier Si photodiode and laser beam 80−12207
body movements, using microwave interferometers *(French)* 78−53469
body N meas. by anal. of prompt γs from neutron capture 80−51220
body shape and movement meas. using the vector stereograph 80−17148
body temp. meas. via implantable miniature transmitter *(Dutch)* 78−48908
body temperature, current status of microwave thermography 79−66503
bone, elastic props. of cortical bone of female human femurs, noninvasive meas. 77−21552
bone, human hand, CC Ca anal. by local neutron activation 79−83902
bone, mineral content, coherent scatt. of photons 80−67238
bone, vibrational motion meas. by skin-mounted accelerometers, soft tissue effect 80−35954
bone, X-ray fluorescence technique for in vivo determ. of Pb conc. 79−25084
bone bending stiffness determ. by LF impedance probe 79−96695
bone biopsy, automatic image anal., var. in rib architecture 78−61253
bone blood flow, meas. with a ^{133}Xe washout method 80−72288
bone blood flow determ., comparative study of ^{99m}TcO$_4$ and ^{131}I-iodoantipyrine 78−28046
bone C partial-body determ. by proton activation anal. 77−86605
bone Ca activation anal., prod. of uniform ^{38}K yield using range modulator 77−40735
bone Ca level meas. using computerised tomography, correl. with ACTA numbers 77−40756
bone density, osteoporosis early detection by Compton gamma-ray spectroscoopy 78−11729
bone density and irregularity meas. in normal hands by radiography 80−30839
bone density determination in vivo, computed tomography vs. mineral analyser 77−73567
bone density measurement by ^{125}I photon absorptiometric anal., dialysis patients 80−36075
bone distribution profile from radiographs, healing process obs. appl. 78−15890
bone elemental analysis by prompt γ-ray spectra due to ^{252}Cf neutron irrad. 80−17065
bone F measurement by neutron activation anal. 77−86592
bone in vivo properties determ., effect of soft tissue on wave propag. and vibr. tests 78−3660
bone marrow haemopoietic activity assessment in normal subjects 80−36073
bone mass measurement, effect of rot. on radiographic dimens. 77−5062
bone mass measurement using Xe-filled multiwire proportional counter as detector 78−15884
bone mechanical properties characterisation by dynamic response 80−76782
bone mechanical properties determ. in vivo, noncontacting EM device 78−77133
bone mineral, evaluation of ^{159}Dy 77−48861
bone mineral, photon absorptiometry after successful renal transplantation 77−48854
bone mineral, using ^{125}I X-rays and CdTe scanner 77−44750
bone mineral analyser, microcomputer based 79−53218
bone mineral concentration estimation by beta-ray backscatt. *(German)* 78−69179
bone mineral content meas. using gamma-ray attenuation by pair prod. 77−44740
bone mineral mass and width meas. using the Cameron-Sorenson technique 79−62345
bone mineral measurement using EMI scanner vs. densitometry 78−24119
bone mineral measurement using polychromatic X-rays, correls. 78−53478
bone mineral measurement using X-ray (low energy γ-ray) transmission, positioning errors 78−96084
bone movements, accel. transmission from iliac crest to sensor on body surface *(German)* 77−21542
bone strength prediction, long, from bending stiffness and bone mineral content meas. 78−11787
bone stress wave detection using piezoelec. effect, non-invasive technique 78−31948
bone-seeking radionuclide skeletal burden determ. from in vivo scintillation meas. of head 78−15915
bowel anastomosis dynamic strength testing device, electronically controlled *(German)* 80−36160
brain, mag. evoked field mapping 80−104705
brain, magnetoencephalogram power spectrum estimation 80−104704
brain, radioisotopic activity, 4-dimens. reconstruction using 200-element detector array of Ge 78−11732
brain blood flow meas. in the cat 79−83887
brain impedance, computerised system 78−77139
brain magnetic response to visual stimulus monitoring using SQUID 77−29231
brain reflexes meas., using Sredetz device *(Bulgarian)* 80−30909
brain retraction pressure monitoring, meas. system for surgical procedures 80−21563
brain tissue specific-impedance meas. four electrode method 78−3647
breast tissue exam. using neutron activation and electron microscopy 80−21536
breath amplitude meas. optoelectronic displacement sensor 77−66868
breath anal. by gas chromatography, use of relative time programming 78−61268
breath by breath anal. of ventilation and pulmonary gas exchange, minicomputer system 79−62393
breath volume and time components, computer aided meas. using magnetometers 79−16332
breathing parameters, simple testing method *(Hungarian)* 78−31918
broadband communication network combining satellite link and TV broadcast techniques 77−64145
burn-scarred human skin rheological props. in vivo meas. 78−31935
cancellous bone, Compton scatter densitometry meas. 79−39489
cancerous mouse hyperthermia meas., microwave, IR and thermocouple methods *(French)* 80−3768
capacitoplethysmography for heart and lung meas. *(Japanese)* 78−53465
capillary blood flow, dual beam laser velocimeter anal. 80−75015

biomedical measurement continued
capillary blood volume flow determ. by improved photoplethysmograph, Hemorheograph 78−31934
capillary viscometer for blood flow meas. 79−79671
cardiac bidirectional shunt quantification, thermodilution method 80−3837
cardiac blood flow meas., computerised system 80−36051
cardiac bloodflow mag. meas. 78−44517
cardiac catheterisation data analysis programs 78−36017
cardiac circumferential fibre shortening vel. determ. from meas. left ventricular dimensions 77−48867
cardiac contractile filament and series elastic work and power, clinical correls. 80−16982
cardiac cycle P-R segment non-invasive information, clinical pot. of elec. and mag. methods 80−36182
cardiac function, reliability of noninvasive methods for meas. during exercise 79−16231
cardiac hybrid computer for dye-dilution curves 78−40365
cardiac left ventricle blood flow field off-line computation from Doppler US velocimetry 79−62324
cardiac left ventricle function, nucl. medicine equilib. meas. 79−62357
cardiac left ventricle regional wall motion, spatial resolution and correl. between segments 79−62359
cardiac left ventricular efficiency evaluation using pot. energy distrib. 77−40757
cardiac left ventricular ejection fraction meas., scintigraphic count-volume and geometric methods compared 79−83896
cardiac left ventricular wall motion assessment from computer-processed fluoroscopy 79−62358
cardiac mechanical activity, noninvasive mag. detect., instrumentation 80−89820
cardiac mechanical activity, noninvasive mag. detect., theory 80−89819
cardiac output, rel. to recirculation maths. 77−56404
cardiac output analysers, equipment, maintenance and ccts., review 78−69239
cardiac output and right ventricular residual fraction determ. with rapidly responding pH sensor 77−40860
cardiac output and shunt calc. from dye dilution curves using automated catheterisation system 78−81023
cardiac output and shunts, automatic computation from indicator dilution curves 79−48359
cardiac output automatic determ. by indicator dilution in computerised monitoring system 78−81022
cardiac output determ. by Stewart-Hamilton method, computer algorithm 77−86691
cardiac output estimated by impedance cardiography 79−57741
cardiac output estimation by N$_2$O rebreathing method in adults and children 77−12953
cardiac output estimation during exercise by rebreathing technique, automated system 77−37090
cardiac output meas. by US transoesophageal probe 79−92315
cardiac output meas. method evaluation by impedance cardiography *(Japanese)* 77−90948
cardiac output measurement, continuous electronic thermodilution meas. 77−40859
cardiac output measurement, in vitro comparison of six commercially available thermodilution systems 78−77135
cardiac output measurement, tracer transport model accounting for recirculation 77−36978
cardiac output measurement error due to nonuniform dye distrib. 77−36979
cardiac output on-line determ. by thermodilution in coronary care unit 78−81021
cardiac parameter extraction from 2-dimens. US images 77−25533
cardiac performance mechanics from computer anal. of circumferential fibre shortening vel. 77−37095
cardiac pressure measurement, by US resonant scatt. from bubbles 77−37029
cardiac pressure noninvasive US measurement, scatt. from encapsulated bubbles 80−36048
cardiac rate meter, based on analogue low-frequency meter *(Czech)* 77−37084
cardiac scintigraphy-radiocardiography left ventricular ejection fraction and regurgitation meas. *(French)* 77−29194
cardiac stroke volume meas. from impedance, rel. to aortic flow waveform 77−86522
cardiac tissue intramural resistivity, canine obs. 79−92319
cardiac V$_{max}$ determination from intraventricular press., on-line digital computation 77−40866
cardiocirculatory measurement, noninvasive RF EM transcutaneous meas. technique *(Italian)* 78−85352
cardiology, computer aided pressure meas. anal. *(Swedish)* 77−44779
cardiology, radioisotope sequential meas. of ventricular vols. and cardiac output 80−94319
cardiomagnetism, high resolution 80−104698
cardiopulmonary analysis, computerised data reduction 77−44814
cardiopulmonary stress test data acquisition and control systems 79−79673
cardiopulmonary stress testing in children 80−30911
cardiotachometer calibration, precision pulse generator, cct. 77−86682
cardiotocography, Partecust equipment, effect of technical recording conditions 77−44783
cardiovascular changes associated with age, US obs. in dogs 77−25504
cardiovascular flow disturbance detection by pulsed US Doppler velocimeter autocorrelograms 77−25526
cardiovascular measurements, conf., Bellingham, USA (Sept. '78) 80−31419
cardiovascular parameters correl. with freq. components of oesophageal phonocardiogram 77−52836
cardiovascular response to dynamic/static exercise monitoring, four-channel radiotelemetry 78−3633
carotid arterial disease evaluation using noninvasive photoplethysmography 78−40390
carotid artery pressure, noise-resistant trigger cct. 77−48889
carotid back pressures in conjunction with cerebral angiography 80−98119
carotid-vertebral circulation exam. by variable range-gated directional Doppler technique 77−29188
cartilage generated noise, computer-aided acoustical correl. 78−40391
cataractous lenses, PIXE elemental anal. 80−21468

biomedical measurement continued
- catheter pressure meas., transducer smearing correction using microprocessor based discrete deconvolution 80—67275
- catheter systems for respiratory intra-oesophageal pressure meas., selection, testing 77—90937
- catheter tip device incorporating CO_2 and O_2 sensors 79—100783
- cell medically relevant class determ., scatt. light cluster anal., cervical smear tests *(German)* 78—92686
- cell membrane particle diameters meas. by computer from electron micrographs 80—101307
- central venous-, pulmonary artery end-diastolic- and pulmonary capillary wedge-pressure 77—90955
- cerebral blood flow, atraumatic meas. by ^{133}Xe *(French)* 77—37039
- cerebral blood flow, confidence limits with positron emission 79—11994
- cerebral blood flow automated analyser for ^{133}Xe studies 77—86597
- cerebral blood flow computer for use in angiogram theatres 78—73227
- cerebral blood flow determination, computer assisted method for multi-exponential curve fitting 78—20246
- cerebral blood flow estimation in newborn infant, noninvasive technique 77—90949
- cerebral blood flow meas., lateral counting corrections 79—8536
- cerebral blood flow meas., regional, computer program description 77—5098
- cerebral blood flow meas. by radioisotope clearance, radiation scattering effect 78—3600
- cerebral blood flow noninvasive meas., analytical problems 80—41208
- cerebral blood flow regional meas., cyclotron prod. of ^{77}Kr 77—56468
- cerebral blood volume meas. by ^{11}C-labelled carboxyhaemoglobin 80—8134
- cerebral echo-pulsation curve and plethysmograms anal. of cardiac arrhythmia 78—7413
- cerebral magnetic field meas. and personnel selection 79—2026
- cerebral regional blood flow and vol. meas., intravenous isotope method 77—86610
- cerebral regional blood flow assessment by continuous carotid infusion of ^{81m}Kr 78—20254
- cerebral regional blood flow meas., ^{133}Xe inhalation method with on-line computer 77—40734
- cerebral regional blood flow meas. by ^{133}Xe clearance 79—83912
- cerebral regional blood flow meas. by ^{133}Xe inhalation, anal. method comparison 78—44604
- cerebral regional blood flow meas. with ^{133}Xe, functional landscapes in brain 78—85356
- cerebral regional blood volume, meas. with EMI 1010 scanner 79—53212
- cerebral regional blood volume, variations meas. by computerised axial tomography 79—29583
- cerebral tissue perfusion rate determ. from ^{15}O activity decay after photon activation 80—26341
- cerebrospinal fluid flow meas. 80—17165
- cerebrospinal fluid pressure meas. and controlled withdrawal 79—39538
- cerebrospinal fluid pressure meas. by passive telemetry, improved instrument 78—31927
- cervical dilation measurement in human parturition using Hall effect 77—48851
- cervical mucus spinability automatic meas. device 78—31928
- chemical analysis by activation methods, review, book contrib. 80—11995
- chest motion due to heart action, imaging by holographic interferometry 79—20699
- chest wall compliance meas. with biofeedback using 2-electrode oesophageal-balloon catheter 77—52905
- chopping pyrometer for remote meas. below 200°C *(German)* 80—86313
- choroidal blood flow, non-invasive meas. 77—40704
- choroidal blood flow meas., theoretical basis using radioactive inert gas 79—92349
- chromatic visual perception of humans, colour picture signal transmission system model, math. treatment 77—25441
- chromoretinoscopy and its instrumentation 80—94201
- chromosome size meas., fast karyotype approach 78—61153
- cineangiocardiograms, automatic anal. using TV system on line with minicomputer 78—92699
- cineangiography, left ventricular contour segmentation from anatomical landmark trajectories and its application to wall motion analysis 80—94363
- circulatory variables, power spectra of spontaneous variations 79—29538
- clinical chemical anal. using OLLI 4000 KLS microcomputer *(Swedish)* 77—44764
- clinical perimetry, glossary of basic information *(Italian)* 79—39413
- composite signal anal., by cepstral inverse filtering, biomedical appl. 78—69243
- Compton scatter densitometry, geometrical considerations 80—30869
- compton scatter densitometry determ. of bone density in living patients 80—17102
- Compton scatter tissue densitometry, calc. of single and multiple scatter photon fluences 78—28048
- computed tomography, electron density and at. no. determ. 77—81553
- computerised tomography, effective photon energy and linearity meas. 80—30841
- conference on pattern recognition and signal processing, Paris, France (June/July 1978) 79—59864
- contact lens radii and thickness meas. by interferometry 80—8118
- contact lenses, soft, apparatus for longit. spherical aberration meas. 79—79684
- contour plotter, computer-compatible, for use in radiotherapy treatment planning 77—70567
- controllable force supply for human muscle voluntary reactions meas., design features 79—100801
- cornea O_2 flux, meas. when covered by soft contact lens 79—34705
- cornea thickness, human, topographic pachometry meas. 79—11921
- corneal curvature meas., simple photokeratoscope 78—3624
- corneal topography using moire contour fringes 80—26316
- corneal wound holographic stress testing in postoperative patients, specular illum. arrangement 78—65102
- coronary artery blood flow thermographic visualisation during by-pass surgery 79—53265
- coronary artery quantitation using digital image processing techniques 80—85517
- coronary blood flow, calc. from myocardial clearance of systemically administered ^{133}Xe 77—16967
- coronary blood flow meas., precordial counting collimator 77—77967

biomedical measurement continued
- coronary haemodynamic parameter estimation using elec. analogue 77—37092
- coronary heart disease screening, direct-writing ECG recorder ST segment distortion assessment *(German)* 77—90945
- coronary regional intravascular resist. determ. 78—31853
- coronary sinus blood flow on-line computerised assessment by thermodilution 78—81024
- cortical bone diameter meas., manual and computer-aided methods comparison 78—85376
- critical light reflection at a plastic/glass interface and appl. to foot press. meas. 80—81681
- cruciate ligament cross-section evaluation, press. depend. of area micrometer method 80—56101
- crythropoiesis, combined use of ^{52}Fe and contaminant ^{55}Fe in bone marrow studies 77—56447
- cutaneous blood flow, laser beam Doppler shift method, instrument 78—28030
- cutaneous temperature of living human body 79—83976
- CW Doppler bloodflow meas., perivascular transducer effect on accuracy 77—90825
- data analysis in biomedical research, statistical techniques 80—42046
- deep body thermometer testing and modelling 77—40816
- deep-body venous and arterial press. meas., monolithic capacitive transducers 80—67274
- deformation behaviour of human vertebrae using holographic interferometry *(German)* 77—77924
- dental enamel, SnF_2 treated, depth profiling by ESCA 78—53298
- dental enamel F concentration, proton activation anal. 79—70608
- dermal-resistance meter with high resolution *(German)* 79—84031
- dermatological appls. of photoacoustic spectroscopy, water content meas. and drug detect. 78—31883
- dialysis, ultrafiltration, meas. and control using differential flowmeter 77—21657
- dielectric props. of biological substances, physical meas. 80—94417
- dielectrography methods and apparatus, recording capacitance changes due to blood vol. fluctuations 78—57046
- digital memory recorder, electromyography and nerve conduction appls. 79—43999
- digital pulse counter for cardiovascular monitoring 78—35978
- digital US gauge for ventricular dimension meas. 78—20238
- display system using data compression, differential diagnosis hand tremor, artificial limb tracking appl. 77—86697
- distance resolution with the FM-CW ultrasonic echo-ranging system 80—36043
- dolorimetry, cerebral response to noxious CO_2 laser stimulation 78—31882
- Doppler sonographic flow meas. over small cross-sections in vitro and in vivo *(German)* 78—88729
- Doppler US flowmeters, optimum vel. resolution 77—957
- drug radioreceptor analysis applications 80—94315
- dual-beam tissue absorptiometry, iterative method for K_β filter elimination 77—70533
- Dutch development of medical physics *(Dutch)* 80—3877
- dynamic telemetry noise reduction methods 77—86672
- ear characteristics meas., acoustic impedance meas. instrument *(Hungarian)* 78—36012
- ear drum, human, vibr. meas. using electronic speckle pattern interferometry 79—53205
- ear impedance, interactions among tympanometric variables 78—27964
- ear impedance, tympanometric asymmetry 78—27963
- ear internal sound pressure, monitoring for noise exposure meas. 77—52799
- ear static acoustic-immittance measurements 80—76758
- ECG automatic analysis, of cardiac rhythm histograph *(German)* 78—28114
- ECG R-R interval measurement by statistical-difference conversion 80—56232
- echocardiography and pulsed Doppler, off-line data processing of left ventricle performance 79—62323
- education, applied science CNAA degree course at Kingston Polytechnic 79—35454
- EEG alpha detection and meas. method 80—21552
- EEG audiometry, objective anal. 79—100632
- EEG cable telemetry seizure-monitoring system 78—3640
- EEG multichannel radiotelemetry for epileptogenic focus localisation 78—3653
- EEG physiological data teletransmission system 77—86687
- EEG telemetering, FM/PWM, multichannel, from unrestrained psychiatric patients 78—3636
- eight-channel computer controlled scanning electromyograph 79—29674
- ejection fraction determ. from left ventricular time-activity curves, noise effects 77—40741
- elastometer probe system for localised in vivo compliance meas. 78—31960
- electrical conductivity and permittivity imaging, computed tomography technique 80—98055
- electrical impedance of physiological tissues, guard ring appl., critique 78—7462
- electrical impedance pulse in limbs, origins, separation of blood vol. and resist. change 77—40891
- electrical resistance of human body *(German)* 78—53541
- electro-medical measuring equipment, leakage current protective measures *(German)* 78—3629
- electro-oculographic response, diagnostic tool for principal ocular disorders *(Italian)* 79—5391
- electro-oculographic response, recording and interpretation review *(Italian)* 78—73156
- electrocutaneous stimulation, information transmission characts. *(Japanese)* 80—35872
- electromyogram, muscle electrical impulses provide audible or visual indication using biofeedback 80—81782
- electromyogram envelope spectral anal., muscular control study 78—92750
- electronic instrument production 79—96675
- electronic meas. application areas 78—57094
- electronic speckle pattern interferometry used to meas. eardrum vibrs. and other biol. movements 80—67209
- electronics of temp., press. and flow meas., for teaching 78—49621
- electronystagmography signal processing *(French)* 77—37078

biomedical measurement continued
electrophonocardiographic systolic time intervals, influences on 79—34681
electrophysiological signal degradation reduction, patient virtual earth and electrical interference monitor 79—57800
electroretinogram, automatic meas. of b-wave amplitude and peak latency *(German)* 78—80993
electroureterogram telemetric registration using implantable Nikrothal LX electrode 77—86668
ELF magnetic field effect on personal vegetative status meas. by elec. resist. between hands 77—81533
ellipsometric monitoring of mol. and cellular biological processes in vitro 77—48852
EM methods for medical diagnosis, review 80—36063
EM radiation probes, implantable, design factors 78—73258
emergency medical telemetry standard development and implementation 78—3635
EMG, abdominal, for uterus activity recording *(German)* 78—92712
EMG activity in extraocular muscles, visual display 77—40834
EMG and temporal information during gait, clinical telemetry 78—80994
EMG electrode array for single muscle fibre activity measurement *(Swedish)* 78—24193
EMG filtered signal in isometric muscle contraction, S/N ratio anal. *(German)* 77—81490
EMG index for localised muscle fatigue 78—57093
EMG muscle activity of spastic gait monitoring, wideband telemetry system 77—90924
EMG results from a study of nerve-muscle disorders 77—40811
EMG signal onset and termination establishment method 79—83761
EMG silent period measurement, automated system 80—89883
EMG surface power density spectral bandwidth rel. to electrode parameters 79—29517
EMG technique for percutaneous lateral pterygoid muscle 80—3841
endocrine research, continuous blood sampling and time series anal. 78—77130
energy expenditure in man, simple apparatus for meas. 79—92415
engineering in medicine and biology, conf. Atlanta, USA (Oct. 1978) 79—39332
enzyme-radioimmunoassay for meas. of dopamine in human plasma and urine 79—53231
epidemiologic monitoring, neutron activation anal. of trace elements in human skin lesions 80—17100
epidemiologic monitoring, neutron activation analysis of blood and blood components 80—17099
epidural intracranial pressure meas. by piezoresist. transducer *(German)* 78—85404
EPR investigation of high-spin Fe III in cancer 78—53466
erythrocytes, ^{51}Cr-labelled, simplified technique for survival estimation 80—51217
esophageal multiprobe for temp. ECG and heart and lung sounds meas. 79—57791
essential hypertension statistical analysis 78—89309
evoked potential optimal filtering in sequential range *(German)* 78—85401
exchange parameters in compartmental models, identification, biomedical appls. *(French)* 80—42044
exercise cardiopulmonary response analysis, breath-by-breath computer system 78—35995
eye, direction of gaze, determ. method using Listing's law 79—34677
eye, intact bovine lens protein, Raman spectroscopy with intensified Vidicon detectors 79—29525
eye, internal pressure meas., early diagnosis of glaucoma 79—25140
eye, refractive state, optical system for autorefractor 79—25127
eye, retina injuries, magnetoretinographic meas. using SQUID magnetometer 80—104702
eye accommodation time and rest position, computer-controlled tachystoscope meas. *(German)* 79—2143
eye axial distances meas. using US ophthalmoscope 80—36032
eye axial length, meas. by ultrasonography, obs. on Hirschberg test 79—34551
eye axial length, using controlled weight direct contact US ophthalmological transducer 78—20239
eye chromatic aberration meas. with chromoretinoscopy 80—81581
eye chromatic aberration rel. to accommodation, meas. using dynamic laser speckle pattern 80—81582
eye deformation due to intraocular press. changes, holographic interferometry meas. 79—20720
eye fine movement recording through closed eyelid, piezoelec. transducer 78—35988
eye fundus photographs, automatic assembly using blood vessel structure 79—83991
eye length, accurate meas. by US echo-oculometer 77—37030
eye movement, minicomputer processing of dual Purkinje image eyetracker data 79—29645
eye movement during radiograph scanning, microprocessor equipment for analysis 79—25130
eye movement evaluation in target tracking using EOG 80—109057
eye movement meas. using elliptical projection 78—15931
eye movement meas. using ocular mag. search coil 79—74798
eye movement measurement, IR technique *(French)* 77—36916
eye movement measurement, laser Doppler technique 79—92322
eye movement phase planes, antiaircraft tracking operator performance anal. 78—15825
eye movement recording using non-contacting US transducer system 78—7414
eye optic disc topography, by laser contour angiography, error model 77—60236
eye position measurement from surface-recorded ERG 80—26400
eye refraction measurement, automated subjective optometer 78—35971
eye refractive error, AO SR III Subjective Refraction System compared with phoropter 79—83953
eye refractive error, meas. using modified Foucault knife-edge test 77 4999
eye refractive error, simplified anal. of meridional refr. data 78—65149
eye refractive error measurement by Ophthalmetron, cycloplegia effect 80—41002
eye refractive error measurement using Humphrey Vision Analyser, reliability and validity 78—61265
eye surface point distance to needle tip within eye, geometric meas. method 79—53273

biomedical measurement continued
eye two-dimensional movement meas. with ferromag. contact ring 79—5387
facial skeleton strain distrib. arising from orthodontic appliance activity, holographic interferometry 80—67143
faecal samples, Ca determ. method using instrumental fast neutron activation anal. 80—104733
Farnsworth-Munsell 100-hue test, electronically scored instrumentation 77—52895
femoral neck fractures, meas. of fissure, X-ray picture anal. *(Croatian)* 80—109023
femur, human, pulse-echo technique for US vel. meas. in vivo 80—89812
femurs, human, elastic constants determ. 80—35951
ferritin, iron core particle size distrib., Mossbauer determ. 78—92696
fetal breathing movements, US meas. device 79—34616
fibre optic, catheter transducer, side hole type, for intracardiac press. meas. *(Japanese)* 78—73272
fibre optic catheter-tip micromanometer as intracardiac press. transducer *(Japanese)* 78—73270
fibre optic CRT recorder appl. 79—27389
field desorption mass spectrometry, appl. to biochemistry, medicine, and environmental science 80—35592
finger clubbing meas. by modern shadowgraph 80—21519
finger instantaneous arterial press. meas. method 80—56245
finger length meas. by ferroelectric wedge thermal transducer 77—78001
finger tremor amplitude and freq. artefact reduced routine meas., portable equipment *(German)* 78—85407
floor reaction, medical appl. *(Japanese)* 80—12291
flow parameters in curved tubes and branching networks, indicator dil. meas. 77—66824
flow rate measurement by indicator dil. methods 77—65825
flowmeter, bidirectional fluidic, respiratory meas. appl., tests 78—35993
flowmeter, directional Doppler, carotid artery stenosis diagnosis, stroke prevention appl. 77—52823
flowmeters, digital 2D full range Doppler velocity meter for cardiovascular diagnosis 78—88731
fluid viscosity, using electromech. viscometer with digital readout 78—28131
fluorescent excitation anal., high intensity source of polarised X-rays 77—60238
foetal breathing movement electronic anal., phase-lock-loop principles appl. 79—2152
foetal breathing movement meas. using US echographic time-distance recorder 78—24109
foetal diameter, assessment of gestational age 78—7415
foetal ECG and heart rate radiotelemetry monitoring 78—3651
foetal heart rate, real-time ECG detect. using near-orthogonal basis functions 77—21638
foetal heart rate, US time-position mode scanning, heart model 78—24111
foetal heart rate recording, interference due to infusion pump *(German)* 78—85414
foetal respiratory movements, US imaging and differential meas. system 80—41154
foetal ventricular ejection time, registration and clinical significance 78—85417
foot and ankle vol. meas. system 79—70659
foot function assessment system, normal and pathological feet, computerised system 79—100760
foot load dynamic distrib., quantification system 80—94388
foot load static distrib., quantification using the PET computer 80—94387
foot load-bearing duration meas. technique 80—17149
foot pressure distribution pattern, using grey-scale to colour convertor 79—20691
foot pressure distributions, technique for display 80—85508
foot scale plantar pressures, meas. device 79—44004
foot vertical force during walking, continuous meas. device *(Japanese)* 78—73273
foot-pressure measurements, static and dynamic, in clinical orthopaedics 80—98163
footfall pattern transduction by foot or shoe cover 79—57799
force, portable meas. device, instrumented shoes 77—29217
force distribution under human foot, online meas. system 78—96110
force measurements during operative correction of spinal deformities 80—76861
functional residual capacity meas. in neonates with endotracheal tubes 78—53556
functional residual capacity meas. instrumentation for neonates and small animals 78—53590
gait, abnormal and normal, meas. using walking speed as basis 77—56402
gait, automatic 3D anal. using a Selspot centred system 80—108998
gait, human, limb segment inertia influence on joint loading 79—92270
gait analog tracings and computerized analysis through a PDP-11/45 79—29643
gait analysis, temporal/distance factors, meas. system 77—13016
gait analysis in humans using pattern recognition 78—40374
gait analysis system 77—44774
gait assessment using components of the ground reaction force vector 80—101284
gait consistency test based on the impulse-momentum theorem 80—17166
gait evaluation technique for normal and abnormal subjects 78—11682
gait instrumentation for foot/ground interaction meas. and display 79—96696
gait measuring system for treatment evaluation, microprocessor controlled 80—61731
gait patterns, normalised, using computer anal. of EMG and fast-fall patterns 77—40819
gall bladder stones, human, X-ray anal. 80—36081
gallstone vol. meas. system, computerised 79—62348
galvanic skin response meter cct. using bipolar transistors 80—72380
gamma spectrometry, low-level, in vivo, optimum detector size and position 78—28075
gamma-camera adaptive gating device for heart synchronisation 78—31898
gamma-ray bulk sample assay, equipment specification 78—24158
gas chromatography-mass spectrometry, integrated analytical systems, applics. in biomed. and related sciences, review 80—36200

biomedical measurement continued
gastric emptying measurement by scintigraphy, techniques and errors 78—73206
gastric motility measurement, non-invasive US pulse-echo scanning method 77—64101
gastro-intestinal electrical signals, maximum-entropy correlation and spectral analysis 79—66577
gastroelectric surface signal analysis, phase-lock system design 79—34687
gastroelectric surface signal analysis, phase-lock system performance 79—34688
gastrointestinal pressure measurement using electronic transducer system, diagnosis appl. 77—86695
glioblastoma tumour volume monitoring, autopsy rel. to computerised tomography meas. 80—21526
glomerular filtration rate and renal plasma flow, simultaneous meas. by radioisotope clearance 77—56458
glomerular filtration rate meas., comparison of 4 commercial preps. of ^{99M}Tc(Sn)DTPA 80—81704
glomerular filtration rate telemetry by external detect. of DTPA-(Sn)-^{99m}Tc with CdTe 78—44591
gonioscopic method for grading of the anterior chamber angle 80—108993
gravimetric plethysmography for leg blood flow meas. 80—36176
haematocrit, noninvasive meas. by elec. admittance plethysmography technique 80—56246
haemodynamic properties of beagle puppies, effects of growth, US obs. 77—25505
haemodynamic research, human, physiological signal acquisition and processing 77—44768
haemodynamics, X-ray filming, video techniques, review 77—52822
haemoglobin concentration meas., in whole blood, using IR reflectance 77—52860
haemoglobin-O$_2$ equilibrium curve, instrument for determ. based on membrane diffusion 80—81761
haemoglobin-O$_2$ equilibrium curve determ., semipermeable membrane transport model 79—92418
hair, biopsy material for trace elements in human body 79—83955
hair growth rate assessment using a simple trichometer 79—92325
hand function, normal finger functional strength meas. 79—92276
haploscope, automated miniaturised device for testing binocular visual function 77—2004
hearing, rational determ. of evoked response audiometry thresholds (window-ERA) *(German)* 77—70477
hearing, threshold of octave masking test, interpretative obs. 80—56064
hearing aid assessment and fitting by free field pure tone audiometry 80—108983
hearing aids in situ tests, appl. of acoustic press. field meas. alongside manikin's head 77—90805
hearing loss, electronic aids needing no patient feedback 78—11760
heart, studies by ECG-gated scintigraphy 78—7440
heart congenital defect evaluation from dynamic tracer meas. 78—40378
heart contraction kinetics recording using thorax elec. fields *(Czech)* 78—77138
heart or respiration rate calculator 78—35987
heart rate analyser for long-term continuous ECG recordings *(German)* 78—3649
heart rate measurement system using phaselock loop device 77—52906
heart rate measurement using digital cardiotachometer 77—56503
heart valve element, artificial, visual representation of flow *(Russian)* 77—32926
heart valve prosthesis mean press. gradient meas. under in vitro pulsatile flow 77—56531
heart volume determination by angiography, X-ray magnification estimation 78—73197
heart-rate digital meter, instantaneous, precision 77—86681
heart-rate variability meas., integral pulse freq. modulator spectral props. 77—90951
heart-rate variability measurement, clinical and neural cardiovascular research appl. 77—81610
hepatic Cu measurement in vivo by nucl. reson. scatt. 77—9245
hepatic effective blood flow, meas. by fractional clearance of ^{198}Au-colloids 79—66547
herpes simplex virus radiometric detect. 78—65117
hip dynamic contact force distribution meas. 79—39624
hip joint geometry, human, three-legged micrometer spherometric errors 79—83832
hip joint movements, electrogoniometer for meas. and anal. 79—74766
hip joint prosthesis internal strain, by built-in gauge, calibration and error sources *(French)* 78—44705
hip prosthesis pressure radiotelemetering, design features 78—3671
Hippuran plasma clearance meas. using gamma camera and cardiac background subtraction 77—52870
history *(Japanese)* 80—12288
holographic interferometry, rigid body motion compensation 80—67213
holographic interferometry in dentistry 80—67203
holography, conf., Munster, Germany (Mar. 1979) 80—62390
holography using pulsed lasers 77—25540
hormonal short time series, state-plane anal. 77—44800
human body sway study using TV-computer interface system 77—81526
human limb movement characterisation by accelerometry with FM telemeter 77—86680
human motion three-dimensional monitoring by optoelectronic means, calibration 77—86658
human serum, definitive meas. of constituents 80—93818
human serum and erythrocyte microwave complex permittivity meas. 80—3889
human thorax, mapping of transmitted microwave power 80—3756
humanisation, distance between organ examined and instrum., compromises *(French)* 78—24159
hyperaldosteronism screening test with rectal potential difference probe *(German)* 79—16323
hypernasal speech, oral/nasal intensity ratio meas. 79—83804
immunochemical analysis, standardisation of light scatt. meas. 78—36081
immunology slide, darkening, Mie scatt., Maxwell Garnett theory 77 9315
impedance, four-point probe technique 77—17000
impedance automatic recording system 78—44625
impedance plethysmography, appl. to arterial diagnosis 77—56508
impedance plethysmography, influence of erythrocyte vel. 78—61238
impedance plethysmography and appl. of finite-element method, torso model and elec. potential distrib. 80—30958

biomedical measurement continued
implantable accelerometer for cardiac performance telemetering 77—86670
inductive sonde, large bloodvessel movement, transcutaneous meas., design and realisation *(Italian)* 79—70602
infant heart rate determ., clinical evaluation of miniature dry surface electrode 77—56505
inhaled heavy elements deposited in vivo, external counting, review 80—36152
instrumental neutron activation analysis studies of tissues from patients with pulmonary diseases 80—21535
instruments, problems and prospects 77—40812
insulin, radioimmunoassay, improvement in precision and accuracy of commercial kit 78—48884
intensive care, O$_2$ conc., blood O$_2$, fluid balance, ocular microtremor, for teaching 78—49622
intensive care instrumentation 78—53559
interactive computer program for measurement of data obtained using the extra-stimulus technique during electrode-catheter studies 78—24156
intestinal absorption of Ca and P in rat, simultaneous in vivo determ. using ^{47}Ca and ^{32}P 78—48882
intra-ocular pressure measurement, non-contact tonometer, status report 77—2063
intra-ocular pressure measurement using sonics and coherent optics 77—81548
intracardiac blood flow measurement, noninvasive ultrasonic technique 77—86569
intracardiac pressure measurement, using fibre optic catheter tip press. transducer 79—2150
intracorneal adhesion of human skin, piezoelectric transducer, skin disease diagnosis, appl. 77—48819
intracranial pressure, remote meas. by passive reson. cct. detector *(French)* 77—37074
intracranial pressure and its epidural meas. 80—101282
intracranial pressure and temp. two-channel telemetry system 77—81619
intracranial pressure estimation, use of visually evoked pots. 80—26398
intracranial pressure meas. in newborns, new non-invasive technique 80—67272
intracranial pressure measurement, some considerations 80—17155
intracranial pressure monitoring by passive radiosonde 79—57798
intracranial pressure telemetering, in vivo and in vitro, with capacitance transducer 78—7457
intracranial pressure telemetric monitoring system 79—74736
intracranial pressure temp. monitoring, implantable two-channel telemetry system 78—3637
intraocular fluid dynamics meas. by minicomputer-based system 78—24130
intraocular pressure, evaluation of Pneuma-Tonometer 79—34678
intraocular pressure, importance of tonometry in glaucoma diagnosis and therapy 78—40383
intraocular pressure, telemetry monitoring 78—3632
intraocular pressure measurement, applanation tonometer correls. 78—77047
intraocular pressure measurement, for glaucoma, comparison of Schiotz standard tonometer and applanation tonometer 78—48915
intraocular tumour diagnosis, Si(Li) detector probe with RFT radiation meas. unit *(German, English)* 78—20265
intrauterine pressure measurement during labour, limitations 77—56504
intravascular O$_2$ measurement, current-to-voltage convertor 79—34684
intravascular O$_2$ saturation continuous meas. using fibre optic catheter *(German)* 78—85411
intravascular O$_2$ sensors, Monopolar, in vitro evaluations 79—34683
invisible information imaging techniques 77—5819
ion-selective electrodes for determination of urine-electrolytes *(German)* 80—94384
IR back-scattered from vaginal tissue, self-stabilising meas. system 80—72281
IR photography, principles and appls., book 78—82068
IR spectrometric method for meas. of slight heavy water enrichment in natural water *(French)* 80—104718
jaw force meas. using strain gauge transducer 77—86669
jaw movement meas. using linear position transducer with improved linearity 77—44765
joint angle of limbs in two-dimensional movement, linear RF transducer appl. 77—90938
joint differential mobility meas., periodontal ligament and temporomandibular joint 80—8093
joint motion meas. by triaxial electrogoniometer, for human prosthesis design 78—11781
joint rotation, human, meas. by triaxial goniometer 79—92417
joint wear in humans, ferrography appl. 79—34694
kidney, human, PIXE and neutron activation anal., appl. to cancer tissues 80—56199
kidney filtration fraction, noninvasive determ. by dual tracer technique 77—86596
kidney stones, human, X-ray anal. 80—36081
kinematic gait, system for simple meas. 80—85509
kinetocardiography, non-contact technique using air-coupled US transducer 77—86568
knee, human, ligament primary and coupled load transmission meas. 79—92271
knee analyser for mediolateral stability determ. 78—7475
knee impedance testing machine 80—21555
knee joint movement during walking, meas. method using photographic records 80—17048
knee motion in gait and stair activities, normative data 78—40229
knee movement measurement with variable axis electrogoniometer 79—44012
knee-joint forces, routine clinical assessment method 79—83831
lactate dehydrogenase, H-forms, radioimmunoassay 80—67219
laser absorption spectroscopy with ATR plates for biomed. use *(German)* 78—36084
laser applications, review *(Japanese)* 80—94311
laser applications in medicine and biology, bibliography, 1963-74 77 25539
laser applications in otology, review 78—48860
laser instrumentation system for simultaneous meas. of transcutaneous O$_2$ and skin blood flow 80—26321
laser interferometer for detecting biological signals due to displacement *(Italian)* 78—53467
laser microprobe mass analyser (LAMMA) appl. 80—18041

biomedical measurement continued
- laser pupillometer, especially suitable for anesthetised cats 79—48317
- left venticular ejection fraction meas. in equilib. radionuclide angiography 80—46009
- left ventricle ejection fraction meas., scintillation camera deadtime 79—62355
- left ventricular boundary determ., automated analogue method 77—60281
- left ventricular dimensions and dynamics during coronary occlusion determ. by B-scan US in dog model 78—48849
- left ventricular ejection fraction determ., comparison of three radionuclide techniques with contrast angiography 78—31889
- left ventricular ejection fraction determ. by equilib. radionuclide angiography 80—12227
- left ventricular ejection fraction determ. using multicryst. scintillation camera 78—73213
- left ventricular ejection fraction determ. using radionuclides 78—80962
- left ventricular function evaluation using ECG synchronised scintillation camera 78—65110
- left ventricular pressure volume anal. in eval. of heart diseases 79—70628
- left ventricular regional function anal. from cineangiogram, computer system appl. 78—80963
- left ventricular volume meas. by ECG-gated scintillation probe system 78—31891
- left ventricular wall motion determined by echocardiography in elderly subjects 80—98039
- left-ventricular ejection fractions meas. by equilib. radionuclide angiography 80—12226
- leg electrical impedance freq. characts. *(Japanese)* 80—56252
- leg long bone growth meas. in children from radiogram, error reduction using computer processing 78—77103
- leg prostheses axial load meas., electronic storage system *(German)* 79—84006
- leukocyte uptake of radiolabelled compounds in whole blood, liq. scintillation method 77—90882
- light beating spectroscopic instrument for continuous meas. of tissue blood flow 80—41160
- light level measurement using photographic meters 80—94304
- light sectioning, three-dimensional measurement system in medicine 78—24113
- limb blood flow automated monitoring system using venous occlusion admittance plethysmography 78—31937
- limb blood flow meas. by elec. admittance plethymography, evaluation of theory and accuracy 78—31936
- limb muscle dynamic force meas. by surface EMG 79—34689
- limbs motion analysis appl., prosthesis microcomputer control 80—51138
- lipid malabsorption, study by meas. of expired $^{14}CO_2$ *(French)* 80—94350
- liquid crystal thermometry, optically active binary mixture 79—42952
- liver, bovine, PIXE and neutron activation anal. 80—56199
- liver, radioimmunoassay for carcinoembryonic antigen as adjunct to radioisotope scan 79—100720
- liver Cd, transportable in vivo meas. system 79—39496
- liver fat content determ. by photon scatt. technique 78—24124
- liver functional reserve capacity meas. by organ-reflectance spectrometry *(Japanese)* 80—94313
- liver mass estimation from γ-camera images, computer assisted method 79—83908
- liver volume measurement by emission computerised tomography 80—12230
- living tissue stimulation energy threshold meas. using analogue instrument 79—57745
- locomotion, clinical assessment of normal and abnormal foot 80—17168
- low light level video fluorimetry and microscopy 77—44874
- lower extremity disability meas. using foot static weight distrib. 80—41289
- lower resistance meridian investigation, method discussion *(Chinese)* 79—79716
- lumbar spine curvature in sagittal plane, meas. and modelling 79—96607
- lung, mag. field meas., comparison between two methods 80—104712
- lung, maximum expiratory flow-volume curves, anal. of configuration 79—20565
- lung, precision meas. of anatomic dead space, theory 79—29536
- lung circulation, density dilution method appl. to obs. of fast osmotic fluid shifts 80—104781
- lung closing volume meas. using acoustic He analyser 78—61223
- lung compliance loop recovery eliminating cardiac interference by digital filter 79—20570
- lung densitometer, 3-dimens., for oedema studies, using CdTe detectors 77—44749
- lung density, Compton scatt. meas., multiple photon interactions 80—67146
- lung emptying patterns, multiple breath N_2 washout data 78—92666
- lung function, regional, electroplethysmograph 77—21647
- lung function meas. system, mobile, computer aided *(German)* 78—3630
- lung gas analysis using redox gas sensors *(German)* 78—85440
- lung nuclei, mean caliper diameter, method independent of shape assumptions 80—98189
- lung parameter estimation during artificial ventilation 77—21642
- lung parameter measurement, rebreathing technique for small lung vols. 77—36994
- lung perfusion determination by dilution principle with expiration detection of indicator *(German)* 78—85326
- lung perfusion determination using O isotopes and dilution principle *(German)* 78—85327
- lung regional ventilation and perfusion, dynamic meas. with ^{133}Xe 77—86595
- lung response data area-distance inversion, consequences of wave dispersion and branching asymm. 78—27994
- lung tissue stereological parameter computer anal. 78—73280
- lung ventilation regional and whole, math. model for radioactive tracer studies 78—20249
- lung ventilation studies test for free Br in carrier gas from ^{81}Kr^{m} generator 79—79642
- lung ventilation studies with ^{133}Xe, patient dose 78—24146
- lung volume, online calc. by digital computer 80—72351
- lung volume change estimation from torso hemicircumferences using Whitney gauge transducers 78—65141
- lung volume determination, interactive graphics 77—77985

biomedical measurement continued
- lung volume measurement from supine portable chest radiographs 80—81703
- lungs, freeze-dried, localised-field magnetopneumographic meas. 80—104714
- lymphocyte carbohydrate metabolism in response to mitogens, liq. scintillation vial for radiometric assay 78—61248
- lymphocyte sensitisation meas., electrophoretic mobility test improvements 79—25138
- magnetic heart vector components, simultaneous meas. with unipositional lead system 80—104697
- magnetic heart vector meas. in humans 78—35873
- magnetic recording of central nervous system, book contrib. 79—5304
- magnetic susceptibility measurement via superconducting magnetometer, sample holders modification 77—26367
- magnetocardiogram and cardiac output meas. with integrated system 80—104709
- magnetocardiogram enhancement by applied mag. field 80—104701
- magnetocardiograms from normal hearts, interpretation *(Japanese)* 78—53433
- magnetocardiography, field meas. techniques *(French)* 77—37073
- magnetocardiography, magnetometers for very weak fields 79—30510
- magnetoencephalography, sensitivity distrib. 80—101246
- magnetometry of human heart in small ferromag. enclosure, using SQUID 78—92726
- magnetopneumographic measurement of particle conc. and clearance in the lung 80—21514
- magnetopneumography, analytic methods 80—104713
- magnetopneumography, evaluation for assessing thoracic accumulation of welding fume particulate 80—101247
- mass density distribution of human body, in vivo meas. using ACTA scanner 77—29198
- mass density distribution of human body, in vivo meas. using ACTA scanner 77—29199
- mass density evaluation in vivo from computerised tomographic scans 77—12992
- mass spectrometer for respiratory, blood and tissue gas anal. *(Japanese)* 77—70566
- mass spectroscopy, continuous in vivo meas. *(Japanese)* 80—94309
- mechanical properties, dynamic, of long bones, in vivo determ. 77—40906
- median nerve, transient responses to elec. stimulation, SQUID appl. to somatically evoked field meas. 80—104706
- medical physics conference, Ottawa, Canada (Jul. 1976) 77—16897
- metabolic substrate regional utilisation rate meas. by emission tomography 78—69183
- methods for quantitative meas. and localisation of peripheral arterial occlusive disease 79—96640
- metrological support, state-of-the-art and development 79—16318
- microcomputer-based data acquisition and analysis system for CO_2 rebreathing studies 80—36161
- microcomputer-based pulmonary wedge pressure measurements 80—26391
- microdensitometry applications *(Czech)* 79—30524
- microelectrodes, KCl filled, boiled and not boiled, potential and resistance comparison 77—81760
- microprocessor appl., advantages 79—44065
- microprocessor-controlled cardiac output meter 80—36162
- microprocessor-controlled contrast sensitivity measurements 79—92327
- microprocessors appl., development trends *(Italian)* 80—17173
- microvascular pressure, using micropipet, capacitive modulation of impedance 77—37080
- microwave attenuation measurement in human torso, 1.8-2.7 GHz 77—70517
- microwave complex permittivity meas. using noninvasive beam-wave reflectometric instrumentation 78—74030
- microwave interferometers appl., physiological movements meas. 79—25137
- microwave measurements *(Japanese)* 80—94314
- microwave radiometry applications 77—81770
- microwave scattering parameter imagery of isolated canine kidney 80—3755
- microwave thermography principle and appls. *(French)* 80—30957
- miniature endplate potential amplitude online meas., programmable calculator conversion 79—84051
- mitral valve velocity meas. by digital echocardiographic tracking system 77—21579
- moire contourography, computer-aided replication of human anatomy 80—67189
- moire fringe biostereometry using parallel light beam 79—100701
- moire topography, devel. and present status 80—63960
- moire topography, historical review 80—9024
- Moire topography, theoretical aspects and practical appls. 79—39463
- Moire topography imaging system, evaluation of 79—39464
- Mossbauer spectroscopy of Fe deposits in thalassaemic heart tissue 78—73202
- motile spermatozoa, speed distrib. by light scattering obs. 77—37061
- motion analyser system for 3-dimens. location of body parts 77—40820
- motion analysis, assessment of derivative determining technique 77—90838
- motor nerve conduction vel. and evoked pots. in peripheral nerve lesion localisation 78—31802
- motor nerve conduction velocity determ. in normal subjects 77—60275
- motor nerve conduction velocity measurement, neuromuscular disorder diagnosis using semiautomatic meter 77—48909
- motor unit action potential duration meas. by surface electrode EMG 78—81039
- movement dynamics, human, investigation using a computer 80—51284
- mucociliary tracheal clearance vel., radiological method for determ. 80—104727
- multiple-electrode measurement system for ECG evaluation of acute myocardial infarction *(German)* 80—26386
- muscle, human skeletal, conduction vel. estimation in situ by surface electrodes 80—8196
- muscle conduction velocity, meas. and recording methods 79—100688
- muscle pH percutaneous microsensing during haemorrhagic shock and resuscitation 77—52907
- muscle relaxation in surgical patient indicated by frontalis muscle spontaneous elec. activity 78—44686
- muscle surface pH meas., significance of impedance changes 77—52908

biomedical measurement continued
- muscleforce-freq. curve recording from humans, α excitability evaluation *(Japanese)* 78—3643
- muscular effort monitoring, prototype instrument 77—5092
- mutual impedivity spectrometry 80—17046
- myelinated nerve fibre simultaneous meas. and counting grid 79—39540
- myocardial activity determ. at surgery using shrinking stress meas. 78—31966
- myocardial blood flow, meas. by fractional uptake of ^{84}Rb and microspheres 79—34656
- myocardial contractility, real time meas. by analogue computer with digital displays *(Japanese)* 79—44015
- myocardial dimension measurement system using pulsed Doppler US 80—26313
- myocardial infarct size computerised quantification from ^{201}Tl scintigrams 78—44601
- myocardial infarct sizing, comparison of noninvasive methods, dog expt. 77—66869
- myocardial infarct sizing using computer programming and 3-dimens. model 77—90888
- myocardial local tension, miniature strain gauge transducer 79—48357
- myocardial performance index from left ventricular area ratios 77—56465
- myocardial perfusion index calculator for prediction of subendocardial ischaemia in cardiac surgery 77—40915
- myocardial regional blood flow from dynamic anal. of ^{201}Tl 79—70627
- myocardial transmural heat gradient instantaneous meas. 78—44661
- myocardium, regional wall motion, assessment by radionuclide kymography 79—39478
- nasal air emission in speech disorders, electrodynamometric evaluation 78—77134
- nasal mucociliary transport, mucous velocity meas. using roentgenographic method 79—29600
- neonatal oxiconsumeter for dynamic meas. of O_2 consumption in neonates 78—44631
- nerve action potentials, low-frequency FM tape recording 79—57832
- nerve bundle conduction velocity distrib. meas. and transfer function anal. 77—44867
- nerve conduction velocity distribution based on compound nerve action pot. 78—40138
- nerve conduction velocity variability, effect of averaging and limb warming 77—60274
- nerve fibre conduction vel. distribs., estimation from two compound action pots. 80—8044
- nerve or muscle potentials, using electromechanical device, semiautomatic processing of data 77—5115
- nerve trunks, method for determ. of conduction velocity distribs. 79—48241
- neuromagnetic fields sources location, using SQUID system, comparison with electrical method 80—101190
- neuromuscular junction continuity, freq. sweep anal. of EMG 79—96686
- neutron activation, total body in vivo anal., neutron fluence meas. 77—86613
- neutron activation anal., Cd conc. in kidney and liver, organ depth determ. 80—72321
- neutron activation anal. of bulk and trace elements in bovine liver matrix 78—28050
- neutron activation analysis, in vivo, total body, neutron uniformity 78—40315
- neutron activation analysis in vivo, neutron flux uniformity 77—9246
- neutron activation analysis meas. of O and N 80—46032
- neutron activation in vivo total body anal. using 14 MeV neutrons, calibration and evaluation of system 78—53490
- neutron activation methods and applications, in vitro and in vivo *(French)* 77—66834
- neutron capture γ-ray analysis with prompt, neutrons, in vivo N meas., body H use as internal standard 79—92441
- neutron capture γ-spectroscopy, medical appl., Cd and N meas. in living human subjects 80—67241
- NMR, appl. in medical technology *(Japanese)* 80—51202
- NMR, noninvasive meas. of biological information, magnetic focus generation *(Japanese)* 78—85355
- NMR images using line scanning method, appl. to tumorous rat leg 78—92683
- NMR imaging, biological and medical appls. 80—26319
- NMR imaging, book contrib. 80—36064
- NMR imaging, H tomography and pot. for imaging other body constituents 80—98062
- NMR relaxation time of particular target measured by magnetic focusing method 79—34621
- NMR spin density imaging using line shaped mag. field 78—73190
- NMR spin echo image formation 77—22588
- non-invasive meas. survey *(Japanese)* 77—25567
- nonperturbing dielectric microthermometer probes 78—11743
- nose aerodynamics, proposal for meas. method 79—83956
- nuclear data uses, including neutron activation and photon absorptiometry 77—25553
- nuclear medicine, appl. of midi-maxi computer interaction to renographic data 78—7476
- nuclear medicine measurements, quality assurance 77—40764
- nuclear physics appl. to life sciences 78—15882
- nystagmus, automatic on-line anal. *(German)* 80—76846
- occlusal force by human teeth, using small piezoelec. triaxial cell *(German)* 78—20303
- ocular axial dimensions, development following eyelid suture in cat 79—43870
- ocular fundus reflectometry 78—48861
- ocular microtremor clinical recording, using piezoelec. strain gauge transducer 78—96109
- ocular position determination for communications system, IR system 80—76821
- ocular pulse, electronic/US system for carotid occlusion diagnosis 77—37081
- ocular tilt aftereffect, clinical assessment apparatus and obs. 79—83954
- oedematous tissue quantification by elec. impedance meas. 78—44630
- oesophageal manometry, low-compliance perfusion pump 79—53272
- oesophageal manometry by liquid-filled catheters 80—85514
- oesophageal multiprobe for temp., ECG and heart and lung sound meas. 78—77146
- open-heart surgery, brachial artery blood flow measurement, noninvasive ultrasonic Doppler technique 77—86570

biomedical measurement continued
- ophthalmology and vision research, appl. of lasers, holography 80—12210
- opthalmology, appl. of picosecond optical range gating 77—81549
- optic disc changes meas. using retinal stereophotogrammetry, glaucoma detect. appl. 80—3757
- optical instrumentation in medicine, conf., San Diego, California (1976) 77—44829
- optics in medicine and biology, conf., San Diego, California (1977) 77—44876
- opto-electronic target tracker for limb movement meas. and anal. 80—56166
- oral neoplasm geometry stomatoscopic apparatus 79—39539
- organ blood flow determ. using radioactive microsphere technique, PDP-11 interactive program 78—20247
- organ blood flow measurements, effect of instantaneous partition coeff. of Xe 80—101256
- organ depth estimation by gamma-ray spectral comparison 77—86612
- organ dimensions, using implantable echo ultrasonometer 77—90866
- organ radionuclide uptake, quantitative meas. by a γ-camera 80—51212
- organ volume determination by US scanning 80—17034
- orofacial posture and movement, photo-elec. recording method 80—108995
- orthodontic tooth movement, holographic interferometry determ. of rigid-body motions 79—72527
- orthopaedic applications of holography 80—67196
- orthopaedic load meas. using strain gauges 80—56262
- orthopaedics, exptl., quantitative eval. of holographic deform. investigations 80—67197
- orthopaedics, grating—TV method, image evaluation using moire figures 80—67199
- oviduct contractile activity, extraluminal meas. using Si force transducer 77—40805
- oximeter calibration, humans exposed to centrifugation 78—92734
- oximetry for haemoglobin and O_2 saturation in blood meas., problems 77—90952
- oxyhaemoglobin dissociation curve analyser, devel. and improvement 77—13019
- oxytocin radioimmunoassay, human plasma 79—5353
- pacemaker patient routine monitoring using telephone-telemetry system 77—90957
- pacing, meas. of ohmic electrode-tissue contact resistance and voltage applied to myocardium 80—67284
- paediatric radioluscent bone length meas. 78—48891
- parametric interactions in EEG period analysis 79—29675
- Parkinson tremor, long-term recording and evaluation 77—21639
- patellar tracking patterns meas. by analytical X-ray photogrammetry 80—30864
- pathological gait clinical assessment, data processing of vertical foot-forces *(Japanese)* 80—21554
- pathological samples, mol. microanal. in situ with laser-Raman microprobe 80—81683
- patient's surface contour measuring device 80—104717
- patient contour drawing using US compound B-scanner 79—83865
- patient surface geometry, determ. by stereo-photogrammetry 79—62330
- patient topology, optical process for three dimensional assessment 79—20692
- percutaneous electrophoresis of amino acids and urea 78—61237
- perfusion blood temp. monitoring, zero-heat-flow transducer 80—8201
- perfusion in capillary beds, two-regime model of heated thermocouple probe 77—5110
- perfusion rate measurement by dynamic thermal dilution 77—40883
- perimetry, automated, history, theory and practical application 79—92402
- peripheral circulation evaluation, noninvasive techniques 80—56163
- pH determination, improved Sb-Sb_2O_3 electrodes 79—53270
- pH measurement techniques, equipment 78—77158
- pH of upper gastrointestinal tract, multichannel meas. apparatus 79—57781
- phonothyreogram and phonocardiogram frequency spectrum analysis by minicomputer, ECG reference time signal 79—83966
- photocardiogram contact microphone 77—21634
- photokeratography using moire techniques 77—21590
- photoluminescent thermometer probes, temp. meas. in microwave fields 80—104721
- photon absorptiometry of soft tissue and fluid content, method, precision and accuracy 78—73221
- photon correlation spectroscopy, biomedical appls. 78—3575
- photon sources, low-energy, spectrum shapes, in vivo detection 77—65377
- photoplethysmography, supraorbital, for detect. of carotid artery occlusive disease 77—40731
- physics aspects in medical engineering *(German)* 78—92735
- physiological fluid, human, identification in situ by proton relax. *(French)* 79—48316
- piezoelectric earphones, usefulness in recording brain stem auditory evoked pots. 80—94389
- PIXE, biomedical appls. 80—61691
- placenta, human, detect. of pulsatile flow in situ by impedance meas. 80—104799
- placental blood flow evaluation, comparison of ^{113m}In and ^{133}Xe intravenous injection methods 78—28043
- placental function and foetal development during pregnancy, US diagnosis and chem. anal. 78—35897
- plasma total Fe-binding capacity meas. by EPR 77—17003
- platelet estimation in whole blood by electronic particle size anal. 78—28104
- plethysmogram detection and its clinical usefulness *(Korean)* 79—62380
- plethysmograph and pneumatic differentiator, static and dynamic testing 78—28150
- plethysmography, elec. admittance, blood flow meas., evaluation of theory and accuracy *(Japanese)* 79—43979
- plethysmography, impedance, sampling field in the human calf 79—57740
- plethysmography, respiratory mechanics model 77—90846
- plethysmography, tetrapolar elec. impedance meas. of finger, electrode system 77—81608
- plethysmography over past 30 years 78—31933
- plethysmography using Hg strain gauge, in evaluation of efficacy of nitroglycerine paste 77—40905
- plettysmography system, simultaneous multifinger meas. 80—21516
- pleural liquids in weak fields, PMR relaxation times, medical diagnosis appl. *(French)* 78—73187

biomedical measurement continued
pneumodynamic MEFV curves, smoothing by digital filtering 80—98157
pneumotachograph, for flow and vol. meas. in normal and dense atm. 77—5120
porphyrins, determ. in blood by phosphoresc. of porphinatocopper(II) 78—11574
portable X-ray imaging system for small-format applications 79—21886
positron computerised tomographic scanning, radionuclide conc. determ. 78—3587
positron emission tomography, appl. to meas. of cerebral metabolic rate 80—3799
positron ring, 280-crystal, design and construction for 3D imaging 78—28063
post-operative human gait, EMG mes., pattern recognition appl. 79—34599
potentiophotometric platelet aggregation meas. by turbidity change 80—36061
pressure catheters, resist rel. to applied volt., elec. shock risk 77—40818
pressure inside hollow organs, recording through tubes, nomograms for calc. of system parameters 80—3836
pressure meter, up to 40 kPa and 4 kPa, temperature and time stability 79—84059
pressure recording apparatus for hydrostatic press. changes during dowel-retained prostheses cementation 80—67287
pressure sensor, catheter-tip, with on-chip compensation and signal processing 77—44818
pressure telemetry system using capacity-type transducer 77—86671
pressure transducer design with negative feedback 77—48910
pressure transducers, gas-filled, effects of gas density on freq. response 80—56249
progesterone in crude serum extracts, radioimmunoassay using ^{3}H and ^{125}I labelled tracers 80—56185
prostatic acid phosphatase, human, development of determ. by radioimmunoassay *(Japanese)* 80—98110
prosthesis wear, holographic studies using optical contouring 80—67288
prosthetic internal strain meas. by built-in gauges *(French)* 78—32806
proton induced X-ray emission anal., trace element levels rel. to human disease 77—56467
proton induced X-ray emission anal. of autopsy tissues, calibration, correction methods 77—56466
proton-induced X-ray emission anal. for anal. of blood and liver tissue 79—53291
proton-induced X-ray emission anal. of single human hair roots 77—90973
psychogalvanic reflex curve automatic anal. 78—7332
psychophysical laboratory unit organisation and meas. system for persons with impaired locomotor system *(Croatian)* 78—44667
psychophysics as method of meas. of biosystems *(Japanese)* 78—53591
psychophysiological techniques applied to aircraft design and other operational problems 80—26384
pulmonary and recirculation parameter identifiability following sequential bolus inputs of ^{133}Xe 78—44605
pulmonary arterial hypertension meas., Bubble Ultrasonic Resonance Pressure method 79—92313
pulmonary arterial press. rel. to thoracic baseline impedance, intravascular fluid vol. meas. 77—40888
pulmonary artery press. estimation using pulse wave velocity 80—12203
pulmonary blood flow, method for noninvasive bedside determ. 80—81762
pulmonary blood flow, noninvasive meas. using PDP 12 digital computer 79—70685
pulmonary capillary permeability inferred from lymph and multiple-indicator expts. 77—44604
pulmonary conductance, elastic recoil, computerized meas. 79—16317
pulmonary diffusing capactiy, anatomic dead space meas. 77—25502
pulmonary filtering capability measuring instrument 79—100729
pulmonary function, SI unit system 77—21541
pulmonary function analysis, parameter estimation, lumped-parameter model 77—44815
pulmonary function test automated apparatus for use on Space Shuttle 78—31912
pulmonary function testing, continuous distribution of specific ventilation from N_2 washout 78—92665
pulmonary function testing, training course features 78—24169
pulmonary gas transfer, on-line digital integration 78—20325
pulmonary haemodynamics meas. using US oesophageal probe 78—35902
pulmonary measurement system, HP model 47804A 80—36163
pulmonary mechanics and perfusion rel. to meas. gas concs. at mouth, simulation 78—31845
pulmonary mechanics computation algorithms on programmable calculator 78—7382
pulmonary mechanics parameters, meas. of breath-to-breath vars. 77—36990
pulmonary mechanics vector scope meas., error anal. 78—40358
pulmonary oedema detect. by quantitative elec. impedance plethysmography 78—31951
pulmonary pressure-flow curves measured by a data-averaging circuit 80—61725
pulmonary regional perfusion, comparison of ^{81M}Kr continuous intravenous infusion, ^{99M}Tc macroaggregates 79—39477
pulmonary resistance measurement by forced oscill. technique 77—40877
pulmonary right-to-left shunting, quantitation by double indicator and O_2 techniques 77—12951
pulmonary single-breath N_2 washout rel. to mech. function 77—36991
pulmonary testing equipment, training and application techniques 78—24170
pulmonary venous pressure estimation from routine chest radiographs using hybrid optical-electronic system 78—44657
pulmonary ventilation studies using ^{133}Xe, personnel exposure from unshielded system 78—15899
pulmonary volume calculator, automatic analogue device, performance in hospitals *(French)* 78—31930
pulmonary volume meas. by closed-cct. He mixing method, reproducibility 77—48904
pulse rate, blood press. and rate-press. product automatic meas. during rest and exercise *(German)* 78—35974
pulse rate meas. by pulsilogium of Sanctorius 79—71215
pulse rate recorder providing printed record 78—3644
pulse-wave velocity measurement in humans *(German)* 80—81751
pupil, closed-circuit TV infrared electropupillometer design *(Japanese)* 77—66870

biomedical measurement continued
pupillary near reflex static and dynamic characteristics *(Japanese)* 79—29524
pupillary reflex of noncollaborating subjects, contact lens pupillography electronics 78—40381
pupillary response meas., use of black light stimulation 78—64977
pupillometer, Fick-Broca, modification to overcome problems 79—5276
pupillomotor latent period 77—60200
quality health care and cost containment, conf., Washington, USA (Mar.-Apr. 1978) 79—39333
quantitation of infarct size using radionuclides 80—85492
radial arterial deformation, based on impedance rheography 78—3545
radiation balance microwave thermograph, simultaneous independent temp. and emissivity measurements 79—100692
radiation balance microwave thermograph 80—26315
radiation meas. bibliography (1972-76) *(German)* 80—95510
radioactive depositions, shallow, on body surfaces, meas. using M X-rays 80—67223
radioactive tracer kinetics, compartmental system identification by optimum sampling 77—86615
radioactivity in body, SABRE computer system for assessment 77—77998
radiocardiography, noninvasive meas. in clinical cardiology 77—40754
radiochromatograms, thin-layer, anal. by proportional chamber 78—77174
radiocolloid particles, size and charge distribs. nuclear medicine appls. 80—30853
radioimmunoassay, automated on-line system, Gammaflow 77—9247
radioimmunoassay, automatic reservoir for serial pipetting 79—100723
radioimmunoassay, instrumentation developments 77—86614
radioimmunoassay, plasma renin activity estimation, microprocessor controlled 80—46023
radioimmunoassay, probe for fine struct. of biological systems, review 78—73217
radioimmunoassay, statistical evaluation of normal range data 77—90885
radioimmunoassay and competitive protein binding, automatic treatment of assay data 77—13037
radioimmunoassay appls. of Philips gamma counter PW 4800 and scintillation counter PW 4700 80—56173
radioimmunoassay as aid to diagnosis, review *(French)* 80—21522
radioimmunoassay for anti-HBs by AUSAB procedure, computer anal. 77—13036
radioimmunoassay for biopterin 80—36101
radioimmunoassay of acute myocardial infarction markers 80—3809
radioimmunoassay of free thyroxine with prebound anti-T_4 microcapsules 80—46014
radioimmunoassay of insulin receptor, receptor structure and function 79—88164
radioimmunoassay techniques development 78—88743
Radioimmunoassay Total System *(Japanese)* 79—92356
radioimmunological assay of gentamycine *(French)* 79—96652
radioisotope angiocardiographic image, left ventricular contour extraction and vol. computation *(Japanese)* 80—3798
radioisotope counting techniques for analytical appls. in biology and medicine, review 80—81794
radioisotope production for medical appl. using cyclotron 80—51256
radioisotope production for medical diagnostics using cyclotron 80—51255
radioisotope retention in man, whole-body counting of ^{67}Cu, ^{32}P and ^{51}Cr 79—62378
radiommunoassay, review, book contrib. 80—109021
radionuclide cardiac output determination, automated computer program 80—56196
radionuclide mean clearance time transverse section imaging 78—73222
radionuclide measurement in large samples using liq.-filled Cherenkov counter 78—53491
radionuclide production, UC-Davis program 80—51257
radionuclide tracer telemetry, semicond. memory systems for data storage 77—90877
radiotelemetry with 9-channel accelerometer for head crash impact accel. meas. 77—86655
radius, human, compact bone mineral density meas. 79—74739
random pulse train inputs, use of digital filters *(Japanese)* 78—53547
random summing in multi-detector counting system meas. radionuclide mixtures 80—36097
rapid eye movements, computer analysis 78—48900
reaction timer cct., using bipolar transistors and LEDs 80—81781
reaction times, for functional exploration of sensory, sensory-motor and auditory routes *(French)* 77—37077
reaction timing, digital timer cct., CMOS, LED 78—53600
receptor binding radiotracer preparation 80—51258
rectal potential difference, automatic, mineralocorticoid activity determ. 77—17002
red blood cell diameter meas. from He-Ne laser beam diffr. pattern 77—86582
reflex hammer with peizoelec. cryst. for accurate reflex latency meas. 80—3839
regional ventilatory clearance, estimation by Xe scintigraphy 80—30854
renal blood flow measurement using externally monitored ^{131}I-hippurate uptake 77—2036
renal extraction fraction determ. by double-tracer method 77—37045
renal function measurement with ^{111}In-DTPA in dogs 77—66838
renal function studies, combined in vitro-in vivo radionuclide procedure, technical aspects 77—90884
renal length, from radiograms, importance of renal inclination as meas. by US 78—77092
renal perfusion dynamics during preservation 79—25006
renal uptake measurements using $^{197}HgCl_2$, single tracer method for background subtraction 80—67217
renography using ^{99M}Tc-DTPA and scintillation camera 78—20256
renography with electronically assisted kidney localisation 78—11716
residual latency techniques and related physiological procedures 79—44001
respiration, automated real-time whole-body plethysmographic anal. system 78—28112
respiration, indirect monitoring, ballistocardiography 77—29222
respiration, looped receiver impinging jets flowmeter with circular and rectangular jets 77—40878
respiration calorimetry determination of O_2-calorie equivalence of thyroid patients and normal subjects *(German)* 78—85412

biomedical measurement continued
respiration function testing using ^{133}Xe radio-spirometric meas. system 77–90889
respiration rate automatic meas. device *(German)* 79–2146
respiration remote meas. instruments, appl. to studies in centrifuge 77–77996
respiration using microwave technique 77–5058
respiratory data recording using XY recorder with data storage 78–7474
respiratory flow rate, improved vane respirometer *(German)* 77–40826
respiratory flow telemetering with mag. type flowmeter 77–86654
respiratory flow-volume integrator 77–48914
respiratory function indices, microprocessor based analyser 79–25131
respiratory function telemetering by combined sensor 78–80995
respiratory function telemetering using combined receptor 77–86657
respiratory functional residual capacity, time const. of body-plethysmograph systems 77–40875
respiratory gas analyser utilising glow discharge selective spectral emission, microprocessor based 79–100772
respiratory gas flow meas., constant-temp. hot-wire anemometer evaluation 79–83967
respiratory impedance, by forced oscillations, meas. instrumentation 77–37079
respiratory impedance meas. system for small children 79–92277
respiratory impedance measurement, direct-display oscill. method 80–36174
respiratory mechanics, effect of breathing He-O_2 and SF_6-O_2 78–27992
respiratory mechanics, effect of endotracheal tube turbulence and inertia 77–21549
respiratory parameter meas. using 200 Hz acoustic pneumograph 77–48913
respiratory parameter measurement with mass-spectrometer 79–62382
respiratory process parameters determ., air flow consumption meas., using electric model *(Bulgarian)* 80–76867
respiratory rate and ventilation digital recorder 78–81005
respiratory resistance measurement, modified forced oscill. technique using computer 77–86692
respiratory response to exercise, computer-based anal. 78–7458
respiratory sounds, sensing by laser interferometer 77–90872
respiratory sounds meas., laser vs. acoustical methods *(German)* 80–98058
respiratory system, freq. characts. determ. 77–5093
respiratory system forced perturbation, traditional model 79–83815
respiratory test performance indicator for subject motivation 79–57797
respiratory total compliance non-invasive meas. in free-breathing rabbits 78–28123
respiratory total resistance meas. in pre-school children using modification of forced oscill. technique 78–77129
respiratory tracer gas nonlinear computer anal., non-invasive meas. method 79–62395
respiratory uptake of aerosols, PIXE anal. of elemental composition in particle size fractions 77–48726
respirometric open systems, error anal. *(German)* 80–104782
reticulocyte production rhythm investigation by spectral analysis 78–73279
retina, blood flow, photon correlation velocimetry 77–90828
retinal blood flow, laser Doppler meas. 78–69174
retinal resolving power meas. by laser interferometry 80–36066
retinoscopic and subjective measurements, discrepancy, effect of age 79–34550
rheoencephalogram parameters vs. mech. props. of cerebral artery walls 78–3547
rheoencephalographic curves, bipolar and tetrapolar techniques, comparison *(Croatian)* 80–104796
rheograph linear-distortion estimation 80–85502
rheography, integral method and electrode for exertion function tests 77–77995
rheoplethysmography, for study of artery function *(French)* 77–37075
rheoplethysmography with occlusion, for study of vein function *(French)* 77–37076
rheumatoid arthritic activity quantitative evaluation with ^{99m}Tc-HEDP 78–20255
rhino-manometry measurements, theory of some systematic errors *(German)* 79–83957
right atrial diameter, dynamic/static, using US sonomicrometer technique *(Japanese)* 78–3568
right ventricular wall thickness meas. by echocardiography, comparison with necropsy 78–40277
ring-core magnetometer sensor for articulatory meas. of jaw movements 80–101243
saline conductivity method for measuring cardiac output simplified 79–92318
sandwich holography and applicability biomedical investigations 80–67211
scanning proton elemental microanal., biological and medical specimens 80–56311
scattering media optical meas. for biomedical applications 79–83890
segmental myocardial wall motion velocity during cardiac cycle 77–37094
SEM cathodoluminescence appls. 80–72400
sensing devices, biochemical, review *(Japanese)* 79–12050
sensors for diagnostic instruments, classification scheme 79–53267
sensory nerve conduct. vel. of medial antebrachial cutaneous nerve 80–3654
serum, human, PIXE and neutron activation anal. 80–56199
serum, human, trace elements determ. by proton activation 80–81731
serum, PIXE anal. of trace elements 77–48974
serum automated electroanal. using ion-selective disc electrodes with neutral cation-carriers *(German)* 78–73269
serum density of human, improved mech. oscillator technique *(German)* 78–28098
serum samples, trace element anal., automatic data acquisition, on-line method 78–48726
serum thyroxine, radioimmunoassay by the antibody-coated test tube method *(Japanese)* 80–67237
serum-electrophoresis, quantitative, by digital picture processing *(German)* 80–94306
shearing forces on the sole of the foot, meas. system 80–72342
SI units and legislation in medical measurements *(Croatian)* 80–104797
signal processing, common structure for filters, correlators and Fourier analysers *(German)* 78–88748

biomedical measurement continued
signal processing using microcomputer 78–81012
signal time averaging, digital Wiener filtering and detection statistical aspects 78–35979
simplified constant temperature electrolytic respirometer 79–12040
six-channel extracorporeal telemetry system 77–90931
skeletal Ca, facility for regional in vivo neutron activation anal. 79–25088
skeletal Ca estimation by exhaled ^{37}Ar meas., fast neutron dose requirement 77–16962
skeletal muscle motor unit contractile characts. determ. through twitch characts. 80–17159
skeletal radiographic imaging, computer/scanner approach 77–77989
skin, human, impedance circuit 79–20607
skin blood flow meas. by ^{133}Xe, radiation dose 77–16994
skin conductance meas. IC operational amplifier cct. 77–25566
skin conductivity measurement, electrode materials *(German)* 78–85406
skin electrical impedance, search for elec. located acupuncture points 79–43976
skin electrical resistance, w.r.t. galvanic reaction *(Hungarian)* 78–35982
skin humidity meas. using bridge cct. and digitally steered logic cct. 77–13018
skin impedance, Laplace plane anal. 79–39458
skin impedance dynamic meas. system 79–57744
skin lesion Mn, Cu and Zn conc. meas. by neutron activation 80–17063
skin perfusion, quantitative meas. with ^{133}Xe 80–81707
skin pressure meas., accuracy of elec. transducers 79–83959
skin recoil characteristics, human, in vivo meas. apparatus 79–57698
skin sensitivy meas., instrumentation for 79–74767
skin stratum corneum, human, linear meas. of water content using microwave probe 80–21518
skin temperature, influence of cosmetics and ointments on spectral emissivity 77–9285
skin temperature, mean, simple meas. device using thermistors 79–2151
skin temperature measurements using a disc sensor, effect of press. 80–56259
skin transient impedance between acupuncture stimulation points 79–43977
skin water exchange measurement 77–81763
skull and auditory ossicle vibr. anal., human preps., using holographic interferometry 80–67210
slow motor nerve cond. meas. by blocking technique, computer simulation 78–36027
soft tissue temp. increases due to US Doppler blood flowmeters, thermographic meas. 79–62294
soft tissues, human, rheological props. from local cyclic loading method 80–108932
soft tissues, human, rheological props. investigation using elastography 80–108933
somatosensory evoked potential measurement and analysis on a small laboratory computer 78–92729
Spacelab, biomedical expts. 77–16999
speech analysis, children, improved spectrogram 80–94238
speech disorder evaluation using basilar membrane electronic model 78–40206
speech reception threshold, reliability in the determ., psychometric function 80–61657
spermatozoa motility evaluation by laser scatt. 78–48864
spermatozoa motility meas. by light scatt., appl. to reproduction immunology *(French)* 79–34628
sphygmanometer, Omron's 77 model, accurate meas. 79–74773
sphygmomanometer, random-zero design with variable height reservoir 78–35986
spinal cord conduction velocity, indirect estimation in intact man 77–25616
spine and forearm Ca changes, meas. apparatus using ^{252}Cf neutron activation anal. 79–39490
spirometric data, automatic classification 79–57803
spirometric parameters, interactive on-line computerised computation 78–44656
splenic sequestration measurement by external scanning, calibration methods 77–2043
SQUID detector appl. in biomagnetism, techniques 78–96061
SQUID fluxgate magnetometers, magnetopneumographic meas. 80–104711
SQUID gradiometer, second-derivative, magnetocardiogram meas. 80–104696
stability of human stance, meas. using vectorstabilograph 80–41275
stabilometric test, subject optimal feet positions 78–44540
static campimeter with CRT display 77–90941
step length measurement apparatus 80–67271
stereophotogrammetry, meas. of deforms. in human body *(Croatian)* 80–108997
stereopsis assessment with operant conditioning in young children 79–83783
stimulation threshold noninvasive meas., long-term follow-up 77–81711
stomach surface and serosal elec. activity meas., autoregressive anal. 79–70656
strain measurement in bone and prosthetic materials *(French)* 79–34695
strain measurement in elastic thin membranes, moire interferometry method, appl. to human skin 80–30828
strength, multifunctional isometric strength tester for upper extremity 78–44658
stress distribution of patient sitting immobile, instrumented wheelchair 77–90930
stress-strain behaviour of living human skin, in plane method of 2-dimens. meas. 77–37120
stroke index determination from impedance cardiography 77–25569
stroke volume calc. from transthoracic impedance plethysmogram 78–7381
stroke volume calc. using noninvasive pressure pulse contour method *(German)* 78–3631
structure extraction, search-free technique, appl. to M-mode echocardiogram and chromosome image 78–81025
subcutaneous temperature meas., for thermoregulation obs., using passive microwave sensors 79–34721
superconductive helmet with SQUID for magnetoencephalography 80–104708

biomedical measurement continued
supraorbital Doppler evaluation of blood flow in vascular surgery 79—88144
surface dose, meas. considerations 79—100748
surface EMG bipolar recording, influences of electrode geometry 79—53269
surgical wound preoperative force meas., transducer device 78—36041
susceptometer, Fe stored in human tissue meas., in vivo 80—101245
sweat Na concentration meas. in situ using elec. field, for cystic fibrosis diagnosis 77—73554
sweat Na measurement by elec. field, math. anal. of skin elec. field 77—73553
synchronised clock pulses used for measurement of physical function *(Korean)* 77—56502
synovial fluid analysis by ferrography 80—101242
systalic blood pressure monitor, type SCS-501 *(Japanese)* 77—70565
systolic time interval meas. microprocessor system for heart malfunction detect 79—79681
systolic time intervals from surgical patients, continuous real-time computation and display 77—37098
tactile senses pattern discrimination power meas. 79—83971
tape recorder ZK-246 appl. to 4 channel recording of physiological phenomena 78—24154
tear measurement, slit lamp fluorophotometer 77—2064
tear turnover meas. by improved slit-lamp fluorophotometer 79—92326
teeth and mandibles, deforms. due to occlusal forces, holographic interferometry 80—67205
telemetry, multichannel, quality criteria and meas. methods 77—48887
telemetry, role of SAW oscillators and IR detectors 77—90926
telemetry, TDM, for data trasmission using one carrier freq. 77—90928
telemetry, transmission and reception with embedded antennae 78—77125
telemetry of EMG and temporal data during gait 78—3638
telemetry system, implantable, single-freq., for monitoring body temp., blood pressure and ECG 77—86688
telemetry system, seven-channel fully integrated, patient monitoring appl. 78—3634
temperature, application of electronics, replacement of mercury thermometers 78—7473
temperature, human body-temp. sensor-environment system, analogue model of interaction 80—104783
temperature, thermographic image digitisation and anal. 77—16960
temperature measurement, electrical *(Hungarian)* 80—30910
temperature monitoring system using implantable thick film telemeter 77—40825
temperature probe design, exptl. calibration results and numerical model predictions 80—56258
tendon reflex stimulation threshold meas. device for man 78—7467
therapy/measuring combined unit for pacemaker implantation *(German)* 78—7519
thermal conductivity and thermal diffusivity simultaneous meas. technique 78—57098
thermal injury determination in deep dermal burns, US pulse-echo technique 77—70511
thermal properties of tissue, thermistor meas., influence of blood vessels using simulation model 77—40962
thermistor-respiratory flow sensor, shunted, characts. *(German)* 78—28097
thermoelectric needle probe for medical and biological temp. meas. 80—101299
thermogram enhancement by tissue-condition correction 79—39460
thermograph, use of pyroelectric vidicon camera 79—25060
thermographic meas., three-dimensional signal detection, expt. 78—3662
thermographic system model parameter calc. 79—79477
thermography, clinical, effect of obliquity 77—9286
thermography, colour, environmental physiology appl. 78—58043
thermometer, precision digital device for 35 to 40°C range *(German)* 77—56499
thermometer, using a thermistor bead 79—21741
thermometers, electronic, review 78—69235
thermometery, use of salt-hydrate transition temps. as fixed points 80—104801
thermometry considerations in localised hyperthermia, review 78—53561
thoracic electrical impedance camera for chest fluid meas. 77—40889
thoracic impedance of humans, meas. using automatic recording device on defibrillator 78—61239
thorax impedance finite element model for cardiovascular and respiration meas. 77—40887
three-dimensional cellular tree structure meas. semiautomatic system 79—70720
thrombophlebitis diagnosis, reliability of Doppler and impedance techniques 78—77144
thyroid ^{123}I uptake meas., correction for thyroid depth 78—11728
thyroid ^{131}I uptake determination *(Hungarian)* 80—94339
thyroid ^{99m}TcO$_2$ uptake meas., gamma camera method 78—20244
thyroid function radioimmunoassay, quality control, computer program *(French)* 80—94348
thyroid gland, vol. estimation by US in addition to scintigraphy 79—74730
thyroid gland ^{131,132}I concentration diagnostic counter 77—81557
thyroid I measurement by X-ray fluoresc. scanning, effect of background radiation change 78—73216
thyroid junction assay digital simulation 77—44778
thyroid uptake meas., influence of gland depth, mass and lobe separation 78—61245
thyroxine, free, radioimmunoassay for quantitative meas. of serum conc. 80—94344
tibia, human, simplified method of radiographic anal. of its cross-section, anthropometric correls. 80—89827
tibia bending strength meas. using tibiometer, eval. from postmortem findings 77—37063
tibialis anterior muscle stiffness meas. during voluntary contraction, human *(Japanese)* 80—56090
tissue, mammalian, US attenuation and speed determ. as function of temp. 80—41108
tissue composition measurement by fast neutron activation 77—64131
tissue dielectric loss and permittivity spectrometer 79—57743
tissue elemental composition meas. by computerised tomography 80—3804
tissue lipid content analysis by photon absorpt. using ^{153}Gd 78—28041

biomedical measurement continued
tissue O$_2$ electrode design criteria and perform. characts., recessed cathode 79—39543
tissue O$_2$ tension, O$_2$ consumption of polypropylene-covered galvanic cell 78—31923
tissue O$_2$ tension by multi-channel telemetry 77—56506
tissue pH electrodes for clinical applications 80—36175
tissue reflectance oximeter, noninvasive solid-state device 78—35919
tissue reflectance oximetry, exptl. and theoretical models 79—79624
tissue refractive index spatial distrib. meas. by US computer assisted tomography 78—69161
tissue-reflectance oximetry, simple homogeneous tissue model for calibration 77—40858
tongue motion tracking by optical distance sensing 79—57673
tooth mobility measuring instrum. employing 24 V transducers 80—36187
tooth surface moire topography *(German)* 78—80992
topographical mapping of the human face by Moire photography 80—85462
total body in vivo activation analysis, sealed tube neutron generator system, 14 MeV 79—88162
trace element anal., proton-induced X-ray emission 77—70548
trace element anal. of medical samples, using neutron activation, clinical appl. 80—17101
trace element anal. using PIXE 77—48865
trace element anal. with low power monoenergetic X-ray tube 78—70686
trace element analysis of human tissues, using PIXE correl. with diseases 77—48866
trace element transport meas. during haemodialysis by PIXE 80—36102
trace elements, proton-induced X-ray emission 77—70547
trace elements in rat liver, PIXE anal. 77—48975
tracheal mucociliary transport, bronchoscopic evaluation 77—60270
tracking task measures applicable to normal and pathological subjects 77—44819
transcutaneous blood flow measurements using pseudorandom noise Doppler system 80—36035
transcutaneous pO$_2$ measurement in computer-assisted monitoring of infants 78—85432
transdiaphragmatic pressure measurement using a single gastric-oesophageal probe 80—56248
transducer for intraluminal press. recording 80—17152
transducers and measurements, review *(Japanese)* 80—94393
transuranic element meas. in vivo at CRNL 77—77993
triaxial vector accelerometry for quantifying tremor and ataxia 78—28116
triiodothyronine/thyroxine assay in unextracted serum using double tracer radioimmunoassay 77—37051
tumour blood flow, meas. by photon activation, ^{15}O decay technique 80—104755
tumour electrolyte exchange kinetics, meas. using fast neutrons 77—64125
two way scanning method for total body in vivo neutron activation anal. 78—92697
tympanic membrane investigations in living man using holographic interferometry 80—67207
tympanic membrane vibr. studies in living man using holographic interferometry 80—67208
ulna bending stiffness, microprocessor-automated noninvasive meas. 79—92275
uniplanar force meas. system for orthodontic appliances 78—31970
upper extremity function documentation in athetoid and spastic patients 77—40879
urethral pressure profiles, meas., microcomputer system *(Slovenian)* 79—2154
urethral resistance and mural tension, using programmable modules 77—2067
urinary bladder interferometry, holography of bladder deforms. in vitro, rabbit expt. 80—67201
urinary bladder interferometry, tumour and lesion detect. by holography 80—67202
urinary flow rate meas. device 77—48906
urinary gross α activity determ., radioactive element adsorption on silica gel 79—88155
urinary tract infections, radiorespirometric testing of antibiotic sensitivity 80—81705
urine glucose analyser with audible output 77—52909
urine U analysis by delayed neutrons 80—26331
urine U content, meas. by fluorometry 79—57788
urodynamic parameter meas. systems 79—96690
US attenuation of soft tissues, signal processing of broadband pulsed US 78—77094
US bladder volume sensor, pocket-size 80—36034
US blood flow meas. using random noise, target model and optimal receiver 77—21589
US blood flow spectral anal. using coherent optics 78—53459
US blood flowmeters, early history 77—77946
US crown rump length meas., comparison of methods 80—45992
US Doppler blood flow telemetering using generalised IC Kitchip 77—86665
US Doppler blood flowmeter, geometrical spectrum broadening anal. 77—86567
US Doppler flow measurement, effects of geometrical spectrum broadening 77—40725
US Doppler flowmeter spectra for asymm. transducers 78—31880
US Doppler spectra, transit time and geometrical broadening 78—44576
US Doppler spectragrams refreshed display and haemodynamic parameter meas. 80—41152
US Doppler velocimetry, experimental appls. *(French)* 79—34610
US Doppler-shift arterial flow signals, Fourier anal. 77—29187
US flowmeter data processing, transfer function modelling of arteries 78—61225
US probes for blood stream meas. using Doppler technique *(German)* 79—2113
US pulsed Doppler flowmeter, vel. accuracy and range resolution 77—77945
US pulsed Doppler technique for quantitative blood flow meas. 80—45990
US pulsed Doppler techniques for cardiovascular meas. 77—77947
US range-gated echo Doppler techniques for cardiac output and aortic flow meas. 78—40276

biomedical measurement continued
US renal volumetry in children, accuracy and simplicity of the method 80—98044
US telemetry for monitoring heart/respiration rate and body/skin temp. of scuba divers 77—90929
USSR measuring equipment state testing system 79—96701
USSR metrological-provision programme 79—96700
USSR research 79—96703
uterine activity in induced labour, analogue monitoring 77—13021
uterine activity monitoring, internal and external methods 78—35973
vascular murmurs, model studies of origin and character 77—56398
vascular pressure measurement systems, calibration 79—96691
vector magnetocardiogram meas. using supercond. magnetometer 77—29213
vector magnetocardiography, practical lead system 77—44698
vectorcardiogram, computer treated, discrimination between normals, LBBB with and LBBB without myocardial infarction 78—85448
velopharyngeal orifice area meas. by appl. of aerodynamic forced oscill. principles 77—5017
venous system visualisation combined with press. meas., technique and equipment 80—36094
venous volume measurement, eval. of elec. impedance plethysmography 77—40885
ventilation inhomogeneity identification using minicomputer data processing 77—44816
ventilation regional measurement using ^{81m}Kr, math. lung model 77—86611
ventilation studies, clinical comparison of ^{127}Xe and ^{133}Xe 77—86594
ventilation-perfusion ratio, practical considerations of multiple inert gas elimination technique 77—56411
ventilation-perfusion ratio distrib. determ. from inert gas data with enforced smoothing algorithm 78—61208
ventilation-perfusion ratio distribs., graphical assessment from inert gas elimination data 77—52834
ventilation-perfusion ratio obtained by noninvasive freq. response technique 77—12952
ventilation-perfusion ratio recovery from inert gas data 77—40829
ventilator-patient circuits, long-term monitoring using turbulent air flowmeter 77—64149
ventilatory function testing, appl. of versatile microcomputer 80—41291
ventilatory measurements in children, respiratory jacket for 79—62379
ventricle regional wall motion parameters, angiography vs. echocardiography 79—62392
ventricular, pressure, noninvasive meas. based on Doppler effect 79—5384
ventricular dimensions noninvasive meas. in awake dog by echocardiography 77—44863
ventricular ejection fraction determ. by radionuclide angiocardiography, correction of noisy data 77—48868
ventricular function, left, dual-probe system for rapid bedside assessment using radionuclide 77—2039
ventricular function quantitative meas. by torque ballistocardiography 78—44660
ventricular mean transit time, right, using radiocardiography 77—2040
ventriculography, algorithm for automatic selection of end diastolic and end systolic cine frames 78—88757
vergence accommodation meas., dynamic optometer 78—35852
vertebrate cornea, transparent layered structure thickness monitor 78—92737
vessel wall motion, US Doppler shift meas. 77—25538
vibration detection of living bodyparts, holographic interferometry appl. *(Swedish)* 79—43981
vibration sensibility threshold meas., pallaesthesiometer automatic signalling and signal fixation unit 79—57784
vibration transmission characts. of hand and arm, accelerometer meas. 77—64075
vibration waveform measurement using temporally modulated holography 80—67212
vibrotactile stimulation of blind, using electrical and mechanical stimuli, reading aid appl. 77—5109
video processor for computer calc. of press.-vol. indices from left ventriculograms 78—53495
videodensitometry and image analysis, minimum computer system 79—34664
vision, objective and automatic meas. of dynamic functions 77—1989
visual acuity, amblyopic children, before and after treatment *(Italian)* 79—20540
visual acuity meas. computer-aided system *(German)* 79—2144
visual acuity of amblyopic eyes, meas. reliability 78—65011
visual acuity test letters, with and without serifs, comparitative expts. 79—34564
visual acuity tests, comparison of STYCAR and Lighthouse tests for preschool children 78—35851
visual behaviour monitoring system, EMG triggered photographic technique 78—31919
visual contrast sensitivity function rapid meas. 78—56975
visual evoked cortical potential meas., signal optimisation using Kalman filter *(Japanese)* 80—72348
visual evoked potential recording in high-noise environment, biphasic 60 Hz synchroniser cct. 78—24155
visual evoked potentials, monocular, recording under binocular conditions 78—81035
visual evoked response meas. using computerised rapid random flash 79—83776
visual evoked scalp potentials, spatiotemporal mapping for human 78—35845
visual field, Bausch and Lomb Autoplot tangent screen standardisation 78—64976
visual field investigations, recent developments 79—96552
visual spectral sensitivity, direct readout system for clinical and research purposes 78—3488
visually evoked brain potentials, meas. of signal components 77—40946
visually evoked response, simultaneous recording to flashes at different retinal locations. 80—72279
vitamin B_{12}, ^{57}Co-labelled, meas. using liquid-scintillator whole-body counter 79—96648
vitreous sample, human, viscoelasticity determ. by Weissenberg rheogoniometer 79—92266
vocal fundamental frequency measurement, comparison of contact microphone and electroglottograph 80—109056
voice frequency meas. using fast freq. meter *(German)* 78—3518

biomedical measurement continued
volume estimation algorithm based on polyhedral approx., using US or CT data 80—104790
volume measurement in vivo using computer-based u.s. echography, errors 77—2033
walking, synchronisation of optical press. distrib. and 3-dimens. force meas. under sole human foot *(German)* 78—35975
walking speed meas. methods and characteristics, humans *(Croatian)* 78—44624
Walsh transformation processing, matrix relationship with discrete Fourier transformation *(Russian)* 78—26
weight sensation quantification by EMG meas. 77—90940
wheelchair locomotion, power output requirements for manual operation 80—94416
whole-body counter based on liq. scintillation detector modules 77—48883
whole-body counting, comparison of Buddha posture with other geometries 77—66839
whole-body counting, effects of changes in relative organ position 77—66847
whole-body K content, ^{42}K calibration of whole-body counters 79—25086
X-ray fluorescence for static or dynamic organ studies *(French)* 77—37033
X-rays with spatial modulation, pattern recognition 78—45761
^{10}B concentration in tissue meas. *(Japanese)* 79—83913
^{210}Bi, determ. in human urine by direct extraction by Ni foil 79—100707
CO uptake in respiration, computer aided measuring system *(German)* 80—3875
CO_2 analysis, amplifier and lineariser for Beckman LB-1 analyser 77—29215
PCO_2, continuous transcutaneous meas., electrochem. sensor 77—13020
CO_2 expiratory concentration analysis by computer 78—57106
CO_2 partial pressure in blood, meas. by rapid response electrode system *(German)* 78—85409
CO_2 respiratory output, continuous meas. in man 77—29216
$^{14}CO_2$, respiratory, determ. by $Ba^{14}CO_3$ decomposition in sample oxidiser 79—88153
$^{14}CO_2$ breath analysis tests, plastic scintillation filament detector system 78—65122
Ca and P determination in small bone biopsies by neutron activation 79—88154
Ca, fate of ^{37}Ar prod. by fast neutron exposure 77—5075
Ca in vivo meas. by ^{37}Ar method, effect of recirculating breath collection systems on exhalation rate 78—40316
Ca in vivo measurement by ^{37}Ar method, inert gas elimination in humans 78—61247
Ca kinetics, use of ^{48}Ca stable tracer analysed by proton activation 77—21622
Ca measurement in vivo by neutron activation anal. 79—92350
Ca, system for meas. total amount in human body using $^{40}Ca(n,\alpha)^{37}Ar$ reaction 79—25083
Ca, total-body meas. by neutron activation and ^{37}Ar meas. 78—3589
CaO, coherent/incoherent scatt. cross-sections of 136-278 keV γ-rays 78—70881
Cd levels in kidney and liver, facility for in vivo meas. by neutron capture prompt γ anal. 78—15885
Cd, organ tissue levels, in vivo meas. system using neutron activation 80—67224
Cd trace detection in human liver by neutron activation analysis 79—79632
CdTe detectors, small, props. uses in biotelemetry 77—44747
Cl determination in small samples of healthy and burnt skin 79—5343
Cl^- ion selective electrodes, appl. to biological materials 77—90974
^{137}Cs body burden in Japanese, biological half-life meas. 79—57795
$^{59}Fe/^{55}Fe$ activity ratio of blood, meas. using semicond. detector 80—17062
H ion concentration monitoring, by integrated FET micro ion sensor 78—44641
Hg in human thumbnails, neutron activation anal. 77—64130
I meas. in tissue, separation of bone and water, appl. of filtered bremsstrahlung spectra 79—74747
I, stable, conc. meas. using ^{139}Ce, absorpt.-edge transmission technique 80—56194
I, stable, tissue determ. by X-ray photographic method 77—70540
^{125}I in the thyroid, 2-probe meas. method 80—81718
^{131}I measurement in human thyroid gland, use of NaI(Tl) scintillation survey meter 78—80970
K determination in small samples of healthy and burnt skin 79—5343
K in blood, using catheter-tip selective electrode 77—90935
^{42}K, whole-body content, sex-dependent calibration factor of NaI scintillation counter 79—29593
N human whole body measurement, using neutron activation anal. 79—29594
N in vivo determination using neutron capture gamma anal. and Pu-Be sources 77—86606
N, total body meas. by $^{14}N(n,2n)^{13}N$, interfering reactions and spatial sensitivity 77—60240
N, whole body in vivo meas. by neutron activation, fractional charge collection technique 77—88345
$^{14}N(n,2n)^{13}N$ reaction for clinical total-body N meas. 79—29589
Na determination in small samples of healthy and burnt skin 79—5343
Na ion concentration monitoring, by integrated FET micro ion sensor 78—44641
O whole-body meas. by neutron activation analysis 79—29590
O_2 analyser instrumentation and operation 78—69237
O_2 consumption and CO_2 prod. continuous meas. for men in hyperbaric chambers 78—81008
O_2 consumption during anaesthesia, whole-body meas. 77—37064
O_2 consumption meas. with flow-through system, accuracy assessment 78—65067
O_2 consumption rate determination, dynamic mode of N_2 storage in man 78—27997
O_2 electrode, membrane-covered catheter-tip system, construction and performance 78—81003
O_2 molecule reduction flow probe for cerebrospinal fluid 79—100777
O_2 partial pressure, transcutaneous meas. 79—83965
O_2 partial pressure determ. in biological fluids, electrochem. cell 78—85420
O_2 partial pressure measurement with thin-layer polarographic probe, intracortical appl. *(German)* 78—85410

biomedical measurement continued
O_2 partial pressure on blood sample, polarographic method, error reduction 78−7470
O_2 sensing electrode stability 77−60268
P, in urine, 14 MeV neutron activation method *(French)* 78−61254
Pb content of children's teeth, in situ meas. by X-ray fluoresc. 77−16976
Pb, determ. in aqueous solns. by Delves Cup technique and flameless atomic absorpt. spectrometry 78−68973
Pb exposure, determ. from X-ray fluorescence anal. of children's teeth in situ 77−64128
^{210}Pb, external γ-counting and bioassay meas. on retired U miners 80−26332
^{212}Pb inhaled body burden calibration, general phantom procedure 77−64138
^{147}Pm, in-vivo measurement by phoswich detector 78−28087
^{210}Po, determ. in human urine by direct extraction by Ni foil 79−100707
Pu assay, in vivo methods for humans 79−20674
Pu body burden estimation from urine data influenced by DTPA therapy 78−73259
Pu skeletal level estimation based on DTPA induced excretion in faeces 78−85390
^{226}Ra body burden determ., postprandial changes in exhalation rate of Rn prod. in vivo 78−69224
^{81}Rb/^{81m}Kr ratio as radioactive tracer study of organic bleeding *(Dutch)* 80−3807
$^{106}RuO_4$ in lung, in vivo meas. and dosimetry 78−53515
Se, determ. of quantity in human urine by neutron activation anal. 80−36079
^{99m}Tc-EHDP accumulation in canine tibia, meas. method 78−20245
U conc. in blood meas. by thermal neutron induced fission, chem. etching, conc. rel. to leukaemia 80−21532
U in vivo chest survey confirmation by autopsy specimen anal. 77−66859
U stored in lung, meas. using NaI and solid-state detectors 78−28090
^{133}Xe air contamination, meas. technique 80−41255

biomedical phenomena
see also biomagnetism
aerosols, biomedical influence, conf., Dusseldorf, Germany (Oct. 1979) 80−94915
antibodies, fluorescent, bound to murine EL-4 tumour cells, motion determ. 79−34719
blood compatibility of isolated veins and synthetic biomaterials, surface props. 77−56522
drug-nucleic acid interactions, conformational flexibility at intercalation site 78−96005
erythrocyte membranes, ESR study of abnormalities in Duchenne muscular dystrophy 78−96111
heart attack as biological effect of geomag. fluctuation 79−83812
heart attacks, no correl. with geomag. activity 80−21482
heart attacks correl. with geomag. activity 79−39424
NMR zeugmatographic imaging 80−51203
red cell membrane, Li transport in manic depressives 80−61525
skin burn thermal conditions, review of exptl. results for man and animals 77−48758
space motion sickness medication, biomedical parameters interference 78−53536
thermoregulation, subcutaneous temp. meas. using passive microwave sensors 79−34721

biomedical ultrasonics
3D imaging and vol. from series of arbitrary sector scans 80−8109
3D real time display diagnosis 80−51182
4 MHz range-gated US Doppler flowmeter design and application 78−59527
A-mode echo computer spectral anal. 80−51193
A-mode ultrasonography and oculometry in retrolental fibroplasia 80−89816
A-scan quantitative analysis of normal and cirrhotic livers 77−64109
A-scanners, performance assessment using system transfer functions 79−23169
abdomen, US imaging using contact B-scanners, book contrib. 80−36046
abdominal abscesses detection, role of ^{67}Ga-scintigraphy, ultrasonography and computerised tomography 80−17096
abdominal and pelvic diagnosis, US and computed tomography evaluation 78−61228
abdominal aortic aneurisms, US and X-ray computerised tomography diagnostics *(German)* 79−79616
abdominal aortic aneurysms, comparative study of computerised tomography and ultrasonography 79−29586
abdominal diagnosis, combined, complementary appl. of echoscopy, echotomography and echography 80−21507
abdominal scanners survey, clinician's viewpoint 79−66582
abdominal ultrasonography, clinical appl. 80−30826
Aberdeen phased array, real-time US scanner with dynamic focus 80−72276
absorption in tissue, possible mechanisms 80−45951
acoustical imaging, US visualization and characterization, conf., vol.8, Key Biscayne, FL, USA (May-June 1978) 80−83720
acousto-optic deflector for TV and oscillograph displays 77−39099
anatomical feature or lesion volume estimation algorithm 80−98080
annular array design and logarithmic processing 79−34615
annular array with dynamic focusing 77−32947
anthropomorphic torso section phantom for US imaging 80−45987
antischistosomal drug screening in vitro by multichannel US activity monitor 79−20604
aortic haemodynamics meas. in humans using US pulsed Doppler transoesophageal method 80−30808
aortic stiffness noninvasive determ. methodology, echocardiographic recording 79−83875
applications and new developments, review 78−11712
arterial blood pressure noninvasive monitoring by US imaging and phono cuff-sphygmomanometry 80−36180
arterial diameter meas. using US transit-time micrometer 78−7410
arterial disease obs. using refl. amplitude, study on simulated vessel walls 77−25534
arterial elasticity, transcutaneous assessment by US Doppler flowmeter 77−77948
arterial elasticity determ. and transcutaneous continuous pressure monitoring analysis 79−53179

biomedical ultrasonics continued
arterial elasticity measurement in vivo using transit-time US micrometer 77−40719
arterial flow Doppler-shift signals, Fourier anal. 77−29187
arterial haemodynamic transfer function calc. from Doppler US flowmeter waveforms 78−61235
arterial haemodynamics evaluation using venous US catheter-tip technique 77−44730
arterial physio/pathological data from transcutaneous CW Doppler-shifted US 77−44731
arterial pulse wave vel. meas. by Doppler shifted US and EM flowmetry 78−69229
arterial stenosis detection by transcutaneous pulsed Doppler method 77−44732
arterial US scanner, colour coded differential velocity display 79−34617
artifical heart, stroke vol. and cardiac output meas. by echographic technique 80−41319
aspiration-biopsy transducer development 78−61233
atherosclerosis, simulated, US assess., in-vitro and in-vivo comparisons 79−96639
atrial septal defect assessment by echocardiography 79−70600
attenuation in soft tissue 80−45952
attenuation measurement of soft tissues, signal processing of broadband pulsed US 78−77094
attenuation reconstruction from back-scatt. US 80−30821
attenuation reconstructive tomography 80−30822
attenuation vs. frequency in soft tissue 80−45956
attenuation/backscattering by mammalian organ as function of time after excision 78−7412
automated system for absorption coeff. meas. in tissue using transient thermoelectric techniques 80−76817
B-mode images of human tissue, real-time speckle reduction 80−74634
B-mode scans, speckle reduction 78−22233
B-scan complementary use with radionuclide imaging 77−37043
B-scan echography, real-time, appl. in obstetrics and gynaecology 80−41150
B-scan imaging, pancreas scans of cystic fibrosis sufferers, amplitude anal. 80−94302
B-scan imaging, theory of image formation, technique for restoration 80−94300
B-scan imaging with automated water-delay system 80−98041
B-scan recording on video tape-recorder 78−77095
B-scan US, technical factors influencing the imaging of small anechoic cysts 80−98049
B-scanning, computer simulation 80−81675
B-scanning in medicine, book 78−73180
backscatter analysis, from human tissue, imaging 77−86576
backscattering from human tissue, model 77−40715
bank 80−51969
beam detector, two-dimensional 78−94495
beam transmission through human tissue, focusing and attenuation studies 80−45948
bibliography from 1971 80−98769
bibliography from Jan. 1971 80−86053
bibliography of diagnostic uses of US in medicine and biology 79−96641
bibliography of diagnostic uses of US in medicine and biology 80−41975
bibliography of diagnostic uses of US in medicine and biology 80−62407
biliary ductal system, status demonstating ability of ultrasonography and computerised tomography 79−92310
biliary tract disorders, evaluation by cholescintigraphy, ultrasonography and computerised tomography 80−17093
biliary tree gas appearance in US B-scan 78−80930
biodynamic research, US/EMG transducer, speech appl. 78−77164
biological effects, review 79−96614
biological effects of US, review 79−66498
blind children's CW FM sonar 79−70708
blood, angular depend. of US scatt., rel. to erythrocyte mech. props. determ. 77−81542
blood, canine, US attenuation and speed, rel. to packed cell vol., 37°C 80−41106
blood, Doppler-shift waveforms, physiological interpretation 80−89814
blood, US backscattering, determ. of variation with haematocrit 79−43970
blood, US backscattering, haematocrit and erythrocyte aggregation depend. 80−45961
blood absorption and vel. during tumour development in exptl. animals 77−25524
blood bubbles detect. and meas. *(Japanese)* 80−1712
blood cell banding in US standing wave field 79−62291
blood clotting characterisation by US digital fixed path interferometer 78−44670
blood coagulation time, US meas. 79−83870
blood fat emboli detection by Doppler US flow meter digital signal processing 77−25525
blood flow, true volumetric meas. technique 77−90824
blood flow detection in human heart, US pulsed Doppler flowmeter system, microcomputer based 80−104690
blood flow disturbance detect. using pulsed US Doppler method 77−40724
blood flow echography using Doppler techniques *(French)* 80−26303
blood flow imaging model eqns. and implications 79−48308
blood flow meas. from US Doppler signals, on-line computer system decoding 78−3570
blood flow meas. using random noise, target model and optimal receiver 77−21589
blood flow measurement, future appls. and prospects 77−78010
blood flow measurement, in objective determ. of human +G, accel. tolerance 78−3619
blood flow measurement by CW Doppler technique using implanted transducers, accuracy 77−25537
blood flow measurement by Doppler method, effects of geometrical spectrum broadening 77−40725
blood flow measurement by US Doppler method, computer-aided determ. of angles *(German)* 78−80931
blood flow measurement from freq. analysed US Doppler signal 78−44573
blood flow sensing in conscious rats, multichannel pulsed Doppler technique 78−44577
blood flow spectral anal. using coherent optics 78−53459
blood flow spectrum, coherent optical anal. 77−40722

biomedical ultrasonics continued
blood flow telemetering system using implantable CW Doppler US flowmeter, IC appls. 78—11749
blood flow telemetering using implantable CW Doppler US vel. meter, IC 77—86565
blood flow velocimeter, MTI filter, with inherent A/D 79—16263
blood flow velocity profiles, US MTI meas. 80—36033
blood flow velocity waveform freq. anal., invasive and noninvasive meas. near stenosis 77—56417
blood flow-velocity meas. by US techniques, Kalman filter appls. 79—100686
blood flowmeter, directional Doppler device, transducer design 77—25535
blood flowmeter, implantable bidirectional device, micropower ICs 77—13038
blood flowmeter, implantable bidirectional pulsed Doppler, for animal research 78—44749
blood flowmeter, noninvasive US Doppler device 77—44733
blood flowmeter, pulsed Doppler, vel. accuracy and range resolution 77—77945
blood flowmeter *(Japanese)* 78—31875
blood flowmeters, early history 77—77946
blood pressure analysis system for treadmill stress testing 80—81674
blood pressure instruments, noninvasive arterial meas. using US Doppler effect 78—69167
blood pressure measurement in baboons, direct vs. indirect methods 77—29233
blood turbulent flow measurement with pulsed Doppler US 77—40871
blood velocimeters, US transesophageal meas. of human haemodynamic parameters 80—41146
blood velocity analysis during pulsed Doppler US imaging of carotid artery disease 77—29189
blood velocity meas., absolute, Doppler method *(Japanese)* 79—43974
blood velocity meas., real time multichannel US Doppler signal analyser 77—73551
blood velocity meas., US Doppler velocimetry, experimental appls. *(French)* 79—34610
blood velocity measurement, instantaneous, ultrasonic Doppler system appl. *(Dutch)* 78—31832
blood velocity noninvasive meas. in large vessels, broadband pulsed Doppler US system 78—61224
blood velocity patterns meas., using pulsed Doppler velocity meter 78—15855
blood velocity waveform display by spectrum analysers, direction Doppler signal preprocessing 79—34611
blood vessel bubble detection and flow evaluation 79—34612
blood vessel US localisation for puncturing 77—77956
blood volume flow quantitative estimation with transcutaneous Doppler US 80—36052
blood-flow velocity estimation, Kalman filters for Doppler ultrasonic meas. 79—62325
bone, 2 to 8 MHz US attenuation obs. 79—57701
bone, cancellous, US attenuation and dispersion 80—51149
bone, surface wave propag. 78—44578
bone, US surface waves for studying props. of human tibia 77—25619
bone, US velocity meas. in temp. range of room temp. to 90°C 80—76787
bone acoustic emission diagnosis, soft tissue effects 79—48362
bone fracture, human tibia, ultrasonic propag., surgical manipulation effect 80—3745
bone fracture healing determ. by US propag. 78—24105
bone surface wave vel. rel. to mech. props. 77—32937
bovine femur crack detection by acoustic emission 79—48312
brachial artery blood flow measurement, noninvasive ultrasonic Doppler technique 77—86570
Bragg diffraction imaging for medical use 78—53462
Bragg diffraction scanner for ultrasonic tissue characterisation in vivo 77—77949
Bragg imaging in the reflection mode and designs for improved optics 80—17040
brain, normal and abnormal, attenuation, vel. and impedance 80—45955
brain scanning, 2-dimens., normal anatomy of excised brain 77—77950
brain study, use of anterior fontanelle as US window 80—41144
brain US imaging through skull 80—51185
breast calcifications, tomographic visualization by US scatt. 79—66497
breast cancer connective tissue content correl. with US attenuation 80—45997
breast carcinoma detect. by US Doppler signals 80—8110
breast echography, possibilities, results and indications *(French)* 78—7408
breast examination, grey-scale echoscopy rel. to mammography 79—62313
breast examination by radiography, thermography and US *(French)* 78—7472
breast malignant tumour, freq. depend. US attenuation, fast Fourier transform technique 80—45996
breast tissue characterisation in vivo by US TOF computed tomography 80—51186
breast tumour detection by US Doppler blood-flow signals 80—46001
breast tumour diagnosis, computer aided 3D display system 80—45988
broad-band echo characterization, unified method for diagnostic US 80—104687
broadband US tomography 80—26311
bubble detection in decompression sickness, US imaging method 79—8527
C-CD devices appl. in electronically focused US imaging system 80—56148
camera for patient diagnosis *(French)* 77—37028
cancer thermographic diagnosis enhancement by US irradiation 79—79614
cancer treatment by ultrasound with radiotherapy or chemotherapy 79—48299
canine aorta Young's modulus, 10 MHz US meas. 79—57836
cardiac blood flow meas., computerised system 80—36051
cardiac function and anatomy evaluation, complementary role of echocardiography and radionuclide imaging, book contrib. 80—101241
cardiac left ventricle blood flow field off-line computation from Doppler US velocimetry 79—62324
cardiac output meas. by US transoesophageal probe 79—92315
cardiac parameter extraction from 2-dimens. US images 77—25533
cardiac pressure measurement by US resonance scatt. from bubbles 77—37029

biomedical ultrasonics continued
cardiac pressure noninvasive US measurement, scatt. from encapsulated bubbles 80—36048
cardiac US and nuclear medicine, complementary roles 80—98051
cardiac valve motion obs. CW FM sonar 78—61230
cardiology, analysis of echography and bioecholocation, progress and prospects 80—21509
cardiology, development progress 78—3646
cardiology, pulsed Doppler velocimetry, clinical appls. 80—46003
cardiology diagnosis, real time system for simultaneous image displays 80—41148
cardiotocograph for foetal heart-rate monitoring *(German)* 77—86566
cardiovascular changes associated with age, US obs. in dogs 77—25504
cardiovascular disease diagnosis, US appls. *(Russian)* 79—39456
cardiovascular flow disturbance, US detection 77—60231
cardiovascular flow disturbance detection by pulsed US Doppler velocimeter autocorrelograms 77—25526
cardiovascular measurements, conf., Bellingham, USA (Sept. '78) 80—31419
carotid arteries, high definition imaging using standard commercial US 'B' scanner 79—88142
carotid arteries, normal and stenosed, local Doppler audio spectra 80—30811
carotid arteries, US imaging, using CW, pulsed Doppler and pulse echo techniques, book contrib. 80—36047
carotid arteriography real-time imaging system 78—24108
carotid artery disease, Doppler and pulse-echo detection techniques 79—11989
carotid artery imager, CW Doppler US and spectrum analyser 79 -57731
carotid bifurcation scanner, differential velocity display with colour coding 77—21588
carotid bifurcation tomographic scanner, US Doppler colour coded vel. display 77—25529
carotid-vertebral circulation exam. by variable range-gated directional Doppler technique 77—29188
cell discrimination by US Gaussian resonator and lens 77—21587
cerebral echo-pulsation curve anal. of cardiac arrhythmia 78—7413
cerebral tissue, freq.-dependent US backscatter obs. and correl. 79—79620
cervical dilation during labour, continuous meas. with US device 77—86574
characteristics and appl. patient diagnosis appl. *(German)* 78—1527
chemotherapy enhancement, time/intensity studies using cell suspension and mechlorethamine 77—29175
chronic liver disease, ultrasonic detect. method 79—48295
chronic splenic enlargement diagnosis by digital A-scan analysis 77—64110
cine display of numerous static US images 80—108984
clinical applications of US techniques 79—79619
coherent US data processing in health care systems, possibilities 79—66499
collagen threads, mammalian, US meas. using scanning laser acoustic microscope 79—43972
composite strip piezoceramic US receiving array 78—42511
computed tomography, cancer detect. appl. 80—30820
computed tomography of breast, progress 80—51196
computer analysis of US signals in diffuse liver disease 80—67173
computer-aided tomography and US, conf., Haifa, Israel, (Aug. 78) 80—27035
computerised image processing of US and radiographic images 79 -79195
computerised tomographic reconstruction, breast scans 80—41216
computerised tomography, data acquisition system 80—26310
computerised tomography, improvements in data acquisition and preprocessing 80—26309
computerised tomography, new imaging methods 79—66496
computerised tomography, phase incoherent and other signal processing obs. 80—26312
computerised tomography, refr. index and attenuation images rel. to breast tissue types 80—17036
computerised tomography, var. of acoustic speed with temp. in excised human tissues 80—51150
computerised tomography scanner evaluation 79—48301
computerised tomography using ultrasonic sources, review 80—17083
conference, international congress of radiology, Rio de Janeiro, Brazil (Oct. 1977) 79—16284
conference, Munich (May 1975) 77—32945
contact B-scanners, calibration method 79—23161
contrast agents, aqueous solns. 80—41157
coral skeleton US velocity and Young's modulus anisotropy obs. 79—57837
cortical bone US velocity dispersion obs., 1 to 10 MHz 77—21583
crown rump length meas., comparison of methods 80—45992
cryoultrasonic surgical instrument 77—78027
CW FM sonar with aural displays, improvements 78—87221
CW measurement method for US velocity in small biological tissue specimens 80—76786
cylindrical transducer scatter scanner for medical ultrasonographic imaging 80—96154
cyst liquid of human breast, US absorption obs. 79—62319
data compression 78—77093
data recording method using videotape *(German)* 80—81666
decompression studies using ultrasonic imaging of bubbles 79—11988
delay technique using US phased array imaging system 80—30810
developments review 77—13017
diagnosis, 1977 state of art and developments 78—48847
diagnosis, appls., principles and equipment, review 78—11709
diagnosis, basic principles 80—17037
diagnosis, dynamic focusing improvement, using analogue-switch phase shifters 77—52856
diagnosis, F mode images for any diagnostic plane utilising microcomputer and light pen 80—41147
diagnosis, human abdominal tissue phantom 80—51152
diagnosis, newer clinical imaging appls. 80—30825
diagnosis, numerical information from signals 77—86577
diagnosis, principles, instrumentation and appls. 78—44571
diagnosis, tissue simulators 80—51153
diagnosis principles and tissue characteristic impedances 79—83861
diagnostic devices, power meas. via acousto-optic method 77—832
diagnostic Doppler systems, development in Brazil 79—39455

biomedical ultrasonics continued
- diagnostic equipment, operation principles and constructional features, advantages *(German)* 79−100684
- diagnostic equipment, portable radiation-force balance 78−69163
- diagnostic equipment, US power and intensities produced 78−69162
- diagnostic equipment development *(Japanese)* 78−44572
- diagnostic equipment progress in Japan 79−25053
- diagnostic imaging, digital scan convertors 79−66581
- diagnostic imaging, opto-acoustic transducer, equiv. cct. and simulation 77−60283
- diagnostic imaging, prospects and limitations 80−98040
- diagnostic imaging, transducer field intensity distribution meas., liquid-surface relief method for pulsed transducers 80−95073
- diagnostic imaging systems, methods and terminology 79−66580
- diagnostic imaging techniques, monitoring and therapy appls., review 79−92308
- diagnostic instrument performance evaluation, work of USA AAPM and AIUM 78−69170
- diagnostic instruments, output meas., irrad. effects *(Japanese)* 78−80936
- diagnostic methods, non-invasive, seminary, Brno, Czechoslovakia (Sept. 1976) *(Czech)* 77−17001
- diagnostic methods 78−77145
- diagnostic pulse-echo US, inhomogeneous media model for determination of acoustic parameters in tissues 80−108981
- diagnostic system, real-time, for dynamic and still images, wireless echovision 78−65101
- diagnostic system, real-time, for dynamic and still images 79−92309
- diagnostic techniques, basic principles *(Dutch)* 80−3744
- diagnostic trends and developments 80−30807
- diagnostic ultrasonic instrumentation, effect of integrated electronics technology 80−17029
- diagnostic ultrasonics, electronic techniques, present applications and future developments *(German)* 79−100683
- diagnostic ultrasound techniques, status report in biomedical field 79−43971
- diagnostic ultrasound technology, federal govt. decision making 80−17030
- diagnostic US, review 79−92307
- diagnostic US role of computer 80−8111
- diagnostic uses, bibliography 79−62322
- diagnostic uses in medicine and biology, bibliography 80−36795
- diagnostic uses of US, bibliography 79−34619
- diagnostic uses of US in medicine and biology, bibliography 78−69166
- diagnostic uses of US in medicine and biology 80−4481
- Diasonograph incorporating pulsed Doppler system 77−77955
- diffraction analysis in the investigation of liver desease 80−30803
- diffraction scanner for in vivo tissue characterisation 78−61226
- diffraction tomography, experimental results 80−76818
- digital image focusing in near field of sampled acoustic aperture 77−60232
- digital moving target indicator system for detection of intracranial arterial echoes 80−17035
- digital moving target indicator system for diagnostic use 78−11710
- digital scan convertor for use in medical US scanning 80−30816
- digital US gauge for ventricular dimension meas. 78−20238
- digital US imaging with microprocessor manipulation 78−96082
- digitiser/processor for extraction of clinical parameters from Doppler-shift waveforms 80−36042
- dignosis, transmission tomography by reconstruction compared with pulse-echo imaging, tissue-equiv. test objects 80−51154
- discrete-time Doppler frequency meter for blood flow imaging 79−57704
- distance resolution with the FM-CW ultrasonic echo-ranging system 80−36043
- distortion of ultrasound beams in tissue and tissue-equivalent media 80−45945
- Dopper echocardiography sample vol. tracking unit 79−57730
- Doppler blood flowmeter, geometrical spectrum broadening anal. 77−86567
- Doppler blood flowmeter modulation *(Japanese)* 79−2115
- Doppler blood velocimeters, max. freq. detector 79−53201
- Doppler diagnostic technique of carotid artery disease, objective feature extraction 80−72273
- Doppler flowmeter, new modulation method, blood flow meas. 80−45989
- Doppler flowmeter average frequency processor 79−83873
- Doppler foetal heart detector, plant tissue acoustic microstreaming obs. 79−62292
- Doppler methods for quantitative meas. and localisation of peripheral arterial occlusive disease 79−96640
- Doppler shift signal processing, maximum frequency follower 79−62320
- Doppler signal centre freq. estimation using quadrature zero-crossing counter, US blood flowmeters 78−31879
- Doppler signal LF spectral analysis for blood flow model 79−62312
- Doppler signal processing, swept-frequency transient signal filtering 78−48848
- Doppler signal time-domain frequency analyser, numerical assessment 79−92314
- Doppler signals, real-time spectrum analyser, haemodynamic appls. 80−36040
- Doppler sonographic flow meas. over small cross-sections in vitro and in vivo *(German)* 78−88729
- Doppler spectragrams refreshed display and haemodynamic parameter meas. 80−41152
- Doppler technique, pulsed, clinical usefulness in intracardiac blood flow visualisation *(Japanese)* 79−96638
- Doppler US blood velocity meas., phase-locked loop technique 78−61234
- Doppler US decompression data, divers, spectral anal. of bubble transients 77−70513
- Doppler US equipment design and biological applications *(Spanish)* 78−7409
- Doppler US flow transducer for human milk flow meas. 79−53200
- Doppler US flowmeters, optimum vel. resolution 77−957
- Doppler US system, for internal organs imaging 79−5332
- Doppler US system for arterial wall parameter determ. 78−15876
- Doppler-shift blood-velocity waveforms, real-time spectrum analyser 79−88145
- drug screening using US intravascular mural thrombi formation technique 78−24091
- Dutch development *(Dutch)* 80−3877
- dynamic focusing transducer design for diagnostic image quality improvement 80−41155

biomedical ultrasonics continued
- dynamic imaging, high resolution 80−17042
- dynamically focused electronic sector scanner based on CCDs 80−98042
- dynamically focused US diagnostic phased array 78−61232
- echo and reconstruction imaging via adaptive ray tracing 79−83867
- echo distribution evaluation *(German)* 78−80934
- echo probes, flexible, and prospects for use in oncology 80−56147
- echo ultrasonometer, implantable, for organ dimension meas. 77−90866
- echo-Doppler, range-gated, pulsed, review and evaluation 79−96642
- echo-oculometer, accurate meas. of eye length 77−37030
- echo-shadow method of visualizing foreign bodies 80−3742
- echo-tomographic imaging with SAW processing, ultrafast 80−74639
- echoaortocardiography, Kymo-two-dimensional, aortic root diagnosis appl. 78−24110
- echocardigram, automatic anal. and VTR recording 80−8112
- echocardiogram, M-mode, automatic computer anal. *(Japanese)* 80−72274
- echocardiogram, M-mode, computer-assisted anal. 78−80942
- echocardiogram analysis in a pattern recognition framework 79−83864
- echocardiogram computer-assisted interactive interpretation 78−80938
- echocardiogram Fourier analysis 78−28028
- echocardiogram on-line computer anal. 78−80941
- echocardiogram processing, microprocessor-based system 77−40726
- echocardiograms, 1D and 2D, computer processing *(German)* 80−81665
- echocardiograms, computer assisted left ventricular anal. *(German)* 80−81667
- echocardiograms, M-mode, microcomputer editing for semiautomatic anal. 80−94299
- echocardiograph signals, M-mode, analogue storage using video tape 80−94298
- echocardiographic, graphic representation of 2-dimens. structs. in motion 79−70597
- echocardiographic and systolic time interval processor 79−83869
- echocardiographic images, video recorded, interactive segmentation 80−89817
- echocardiographic images enhancement by lateral filtering 79−70592
- echocardiographic left-ventricular diameter time curve automated analysis 77−21578
- echocardiographic system, two-and three-dimensional, computerised, atrial septal defect detection appl. 78−20237
- echocardiographic tracking, digital range-gating 79−16260
- echocardiographic tracking system, microprocessor-controlled 80−67169
- echocardiography, 2D, transducer beam profile effects on tissue aperture detection 78−73185
- echocardiography, automatic range gate tracker 79−83868
- echocardiography, bidirectional, for detect. of cardiac cycle 78−15877
- echocardiography, binocular stereoscopic display system 79−48297
- echocardiography, clinical appls. of new techniques 80−36050
- echocardiography, clinical significance *(German)* 80−81664
- echocardiography, contrast cross-sectional *(Japanese)* 80−101237
- echocardiography, high-resolution, computerised US signal processing 80−76814
- echocardiography, picture processing of 2-dimens. data 77−77958
- echocardiography, pulsed Doppler, variable sample vol. dimension 80−76816
- echocardiography, safe method for acquiring morphological and functional data *(German)* 79−16261
- echocardiography, two-dimens., wall motion and thickening quantification by computer-aided contouring 78−80937
- echocardiography and pulsed Doppler, off-line data processing of left ventricle performance 79−62323
- echocardiography appl. of pattern recognition 78−35898
- echocardiology, book 77−64103
- echocardiophone, CW swept freq. US echo location system 77−70514
- echoencephalography, US pulsatile, prototype instrument and trial obs. *(Russian)* 80−17174
- echoencephalography applied to brain stem tumours 77−70515
- echoencephaloscope, two-probe three-mode design 78−44567
- echographic analysis of pneumatically actuated artificial heart, air chamber inlet design 77−48943
- echographic and rapid scanning methods, diagnostic appl. *(French)* 79−74734
- echographic diagnosis of lesions of the abdominal aorta and lymph nodes 80−17033
- echographic information related to left ventricle and mitral valve in diastole, anal. by small computer 78−80939
- echographic phased array for medical diagnostics, dynamically focused insonification 80−89813
- echography, in vivo A-scan dynamic autocorrel. anal. 80−51192
- echography, real time, contrib. to diagnosis and management of palpable breast lumps 80−17027
- echography appl. to artificial heart performance studies 78−44728
- echohepatograms in children, computer analysis 79−57728
- echolocating blind mobility aid, interpretation of stereophonic output 80−108989
- echomammography: indications and limitations in tumours with or without calcification *(French)* 80−36039
- echopyelographic visualisation of pacemaker induced contractility in calyceal structs. of human kidney 78−48850
- echoscopic meas., random error sources *(Croatian)* 78−44569
- Echosimulator, function generator for meas. of US diagnostic equipment characts. *(German)* 80−104685
- echosonography, real-time, computer controlled bidirectional phasing 79−12023
- echotomograph, ultrafast, using optical processing of US signals 80−51180
- echotomographic system, ultrafast, using optical processing of US signals 77−52855
- echotomography for intrahepatic vessel and duct structure diagnosis 77−90868
- EHV synchronous generation for US pulse-echo systems 77−78011
- electronic linear-scanning US diagnostic equipment, high resolution 80−30813
- electronic scan US tomography, array transducer, shading function design *(Japanese)* 77−84100
- electronically scanned ultrasonic imaging systems *(Japanese)* 79−25054
- electronically scanned US diagnostic systems, electromechanical coupling coeff. for plank-shaped transducers 80−33383
- engineering in medicine and biology, conf. Atlanta, USA (Oct. 1978) 79−39332

biomedical ultrasonics continued
- equivalent circuit anal. of US rod concentrators for US surgery 78—50997
- erythrocyte aggregation detect. by US scatt. 77—40721
- erythrocyte US scatt. frequency dependence obs. 77—64119
- erythrocyte-rouleaux formation, US detect. by spectral anal. 78—40280
- etched arrays for medical imaging 79—25057
- evoked response averaging for schistosome activity monitoring 79—34613
- excised breast tumour US attenuation meas., 6 to 10 MHz 79—48311
- eye axial length, meas. by ultrasonography, obs. on Hirschberg test 79—34551
- eye movement recording using non-contacting US transducer system 78—7414
- femur, human, pulse-echo technique for US vel. meas. in vivo 80—89812
- femurs, human, elastic constants determ. 80—35951
- fetal breathing, in utero, CW US Doppler method for recording 80—41215
- fetal breathing movements, US meas. device 79—34616
- fibrosarcoma, hamster, absence of metastases following US treatment 80—35960
- film for US imaging 79—88143
- flowmeter, implantable Doppler design with phase-locked loop 78—31873
- flowmeter data processing, transfer function modelling of arteries 78—61225
- flowmeter for measuring rapidly changing gas flows, freq. range, excitation and signal processing *(German)* 78—83502
- fluid characterisation by US and computed tomography 80—98045
- FM blood vol. flowmeter processing technique 78—31878
- focused US for input of auditory information into aural labyrinth 78—40275
- focusing field upon transmission using annular transducer 78—44574
- foetal breathing monitor for humans in utero, US pulsed Doppler instrument 78—69164
- foetal breathing movement computer anal., from real-time US images 78—40375
- foetal breathing movement electronic anal., echoscope connected to time-dist. recorder 79—2152
- foetal breathing movement meas. using echographic time-distance recorder 78—24109
- foetal development and placental function during pregnancy, US diagnosis and chem. anal. 78—35897
- foetal gestational age assessment appl. 78—7415
- foetal growth estimation from US image meas. 80—101239
- foetal head position in late pregnancy, B-scan estimation 77—77952
- foetal heart and uterus diagnostic monitoring and functional mechanics 78—36009
- foetal heart rate recording, interference due to infusion pump *(German)* 78—85414
- foetal respiratory movements, US imaging and differential meas. system 80—41154
- foetal ultrasound image analysis using computer 77—77999
- foetal valve movement, automated detect. using Doppler US 77—40727
- foetal weight estimation using B scanning method 78—3573
- gall-bladder fossa collections after biliary tract surgery, US diagnosis 79—53199
- gall-bladder kinetics, real-time US study method 79—100682
- gallstones, acoustic shadow formation 80—98047
- gas analyser for lung closing vol. meas. 78—61223
- gastric motility measurement, non-invasive US pulse-echo scanning method 77—64101
- grey scale display on storage oscilloscope system 78—3569
- grey scale scanner dynamic range testing 78—69169
- grey scale sonoarterographic imaging 77—25532
- grey tone rapid process films for US imaging 78—96081
- grey-scale image recording systems, comparison of 9 different types 79—16319
- grey-scale US images, local diagnoses and artefacts identification *(German)* 77—86571
- haemodynamic properties of beagle puppies, effects of growth, US obs. 77—25505
- haemolysis kinetics, US differential absorption meas. 77—77877
- heart diagnosis, electronic sector-scanning cross-sectional echocardiograph, model SSH-10A 79—57732
- heart diagnosis, using two dimensional real-time sector scanning facilities 80—81672
- heart rate meas. (foetal), adaptive correlation ratemeter 78—88732
- heart wall motion quantification using computerised US technique 78—40279
- heart-lung machine blood flow line gas bubble US detector 77—77954
- hepatic mass evaluation, relationship of ultrasonography, nuclear medicine and computerised tomography 80—17092
- hepatic metastases, γ-scan accuracy for detect., comparative study with grey scale ultrasonography *(French)* 80—104741
- hepatic metastases detect. by grey-scale US scanning 78—73179
- hepatic tissue characterisation by US reflection, estimator variance reduction 79—48307
- hepatic tissue in vitro acoustic attenuation slope spatial correlation obs. 79—57702
- high-resolution blood flow imaging system using binary phase coded pseudonoise sequences 79—57703
- histopathological information obtained from US tissue signatures and microscopy of biopsy samples 80—51195
- histopathology, A-scan pattern recognition, use in signal processing 77—64108
- holographic in medicine and biology, state of art and future 80—67175
- holographic visualisation *(Slovak)* 79—41527
- holography in biology and medicine 79—8528
- hyperthermia, localised, comparison of EM and US diathermy 80—104725
- hyperthermia, localised, design of heating protocols 80—104693
- hyperthermia, nonintrusive meas. by US temperature tomography 79—53282
- hyperthermia, US induced in previously X-irradiated sites 79—62315
- image coding, mammograms appl. 77—81544
- image data, moving heart surfaces extraction 80—8114
- image digital processing methods *(Chinese)* 80—30805
- image feature enhancement via digital processing 78—73183
- image formation, perception and measurement, conference, Leeds, England (Mar. 1976) 77—86561
- image processing, appl. to film recorded images 77—25531

biomedical ultrasonics continued
- image quality with US arrays for real-time diagnostics, artefacts *(German)* 80—61656
- image reconstruction processing limitations 78—73184
- images corrected for refr. and attenuation, comparison of high resolution methods 80—30817
- imaging, analogue fast Fresnel transform methods 79—46116
- imaging, as aid to cancer radiation therapy treatment planning 77—12982
- imaging, ceramic and PVF$_2$ transducers compared 79—57734
- imaging, clinical information, comparison of two types in detect. of focal intrahepatic lesions 77—64100
- imaging, computerized, digital data acquisition system 79—39454
- imaging, conf., San Diego, USA, (Aug 1978) 80—17025
- imaging, conference, San Diego, USA (Aug. 1979) 80—94919
- imaging, overview of principles and instrumentation 79—66579
- imaging, piezoelectric micro-array technology for improved image quality *(German)* 80—98052
- imaging, single-transducer technology, state of art review 77—843
- imaging, spread energy method, theory 80—14533
- imaging, use of fibre optic recorder 77—5057
- imaging and holography, review *(French)* 77—827
- imaging applications of US and acoustic methods *(Dutch)* 78—27719
- imaging including Doppler techniques, book 80—31426
- imaging modalities for medical appls. 80—81669
- imaging of neoplasms 80—17032
- imaging over view, appls. and future trends 80—48536
- imaging overview 80—98082
- imaging system, 3D, based on serial tomograms, processing system 79—83859
- imaging system, 3rd generation development, high resolution, 3-D 77—86575
- imaging system for chest and other body organs 80—67174
- imaging systems, high-resolution, real-time 78—69160
- imaging techniques, book 80—12861
- imaging techniques, developments, review 80—26324
- imaging techniques, theory and advantages 78—92682
- imaging techniques and appls., for teaching 78—49620
- imaging techniques for diagnosis *(French)* 80—26304
- imaging techniques including use of US scanner 80—72388
- imaging technology status 78—24174
- impedance image reconstruction, reflection and transmission techniques 79—53202
- impedance profiling, analytical and physical model 77—64121
- impediography, deconvolution and processing procedures and corrections 77—64122
- impediography, quantitative characterisation of lesions in vivo 80—17039
- impediography, US propag. theory for stratified media *(French)* 79—11990
- implantable bidirectional pulsed Doppler US blood flowmeter, timing and signal processing ICs 80—76812
- implantable CW Doppler blood flowmeter, optimal system design 78—53460
- implantable IC CW Doppler flowmeter 78—31877
- implantable SAW pressure transducer/transmitter 79—29575
- Indian status in 1979, industry and medicine appl. 80—81668
- inhomogeneous media model for acoustic vel. calc. in tissues 79—43945
- instrument design with elec. controlled directivity patterns 77—838
- instrumentation standardisation, physician's need 78—69168
- intracardiac blood flow measurement, noninvasive ultrasonic technique 77—86569
- intracranial pathology in infants, US evaluation, new technique 80—98046
- intraoesophageal imaging, heart dynamics 80—94303
- Japan, devel. of computerised tomography and US technology 80—30879
- kidney echoes computer anal. 78—35901
- kidney radiology conf., Brussels, Belgium (Oct. 1978) 80—31409
- kidney stone contactless destruction by US shock waves 79—48300
- kidney stone destruction by US shock wave focusing 77—32946
- kinetocardiography, non-contact technique using air-coupled US transducer 77—86568
- larynx height and vocal fold vibratory pattern meas 80—98184
- lateral and range resolution improvement by optical computer 79—53203
- layer-by-layer endography of multiply scattering objects 79—48303
- left ventricular diameter-time curve shape from M-mode echocardiogram, automated anal. 78—80940
- left ventricular dimensions and dynamics during coronary occlusion determ. by B-scan US in dog model 78—48849
- left ventricular function quantitative evaluation by 2D ultrasonography system 80—85457
- left ventricular hypertrophy with bundle branch block, ECG/VCG and echocardiogram correlation 79—44035
- left ventricular potential quantitative assessment rel. to echocardiographic meas. 79—44042
- left ventricular wall motion determined by echocardiography in elderly subjects 80—98039
- lesion production in rabbit liver, kidney and testicle, thresholds, thermal model 77—81527
- LF surgery in practical medicine, refinements in methods and apparatus 80—21508
- linear-filter model for signal transmission process 80—17026
- liquids with very low US propag. velocities for use in biomedical optical computer 80—28392
- liver, comparison of radionuclide imaging, computer tomography and grey-scale US 77—52864
- liver, comparison of scintigraphy, US and computerised tomography scanning 80—17105
- liver, human, scattering structure theoretical modelling 80—89785
- liver, US backscatter from human tissue, depend. of freq. and protein/lipid content 80—45960
- liver cirrhosis detection, accuracy of US diagnosis 80—30802
- liver diagnosis, estimating acoustic attenuation coeff. slope from reflected US signals 80—5876
- liver pathology characterisation, clinical appl. of a US attenuation coeff. estimation technique 80—76813
- liver sector scans, echoes across diaphragm 78—69165
- liver tissue, attenuation coefficient slope statistical estimation from refl. US signals 80—46000
- local circulatory system characterisation by CW Doppler US flow meas 78—57109

biomedical ultrasonics continued

- low-loss wide-band US transducer design for noninvasive medical appls. 79—44021
- lung, US tissue characterisation 77—40717
- lung surface US tissue signature 80—45957
- lung tissue characterisation by US, instrumentation, model and results, book 78—44575
- lymph nodes, pathologically enlarged, Doppler US exam. obs. 79—62311
- lymphocyte cell DNA damage by US diagnosis 80—67148
- mammalian tissues, US vel. and atten. 78—57044
- mammographic US image correlation with histopathologic sections 80—101240
- mammography, remote focus arc scanning 80—89815
- mastodynia and ultrasonography 80—85456
- measurement appls. *(Japanese)* 80—89811
- medical electronics, new forms and techniques 80—3856
- medical physics conference, Ottawa, Canada (Jul. 1976) 77—16897
- membrane hydrophone for 0.5 to 15 MHz range, press. meas. in US fields 80—108987
- merits rel. to computerised tomography and radionuclide imaging 79—48324
- microcirculation semiquantitative demonstration using US noninvasive meas. method *(German)* 78—85348
- microprocessor-controlled digital compound scan system 79—57735
- microscopy, principles and appls. 78—18133
- midline echoencephalography, automatic histogram prod. system 77—64102
- mitral valve velocity meas. by digital echocardiographic tracking system 77—21579
- mobility aid for blind, quantitative depth perceptor 77—25605
- monitor for fetus cardiac pre-ejection period continuous meas. 79—74732
- monolithic cascade CCD ultrasonic lens applications 78—22231
- multidimensional space and time signal processing in biology and medicine 80—85493
- multielement acoustic array characterisation by acousto-optic diffraction 80—99911
- multilayer 3-D display adapter 79—18498
- multiple freq. array for improved diagnostic imaging 79—14170
- multiple pregnancies, problems in US monitoring 80—41145
- multiple section tomogram simultaneous display equipment 78—61227
- multiscan echocardiography *(Chinese)* 79—66495
- Multison 400 linear array scanner, real-time sonography 79—62314
- muscle mechanics obs. by acoustic microscopy 78—48952
- muscle viscoelastic props. determ., appl. of forced longit.-vibr. of elastic rod on viscoelastic half-space 78—44538
- myocardial and hepatic tissue US backscatter comparison 79—48310
- myocardial dimension measurement system using pulsed Doppler US 80—26313
- myocardial dimensioning system, pulsed ultrasound method 79—48298
- myocardial injury, correlation of US and enzymatic indices 77—21581
- myocardial tissue, relationship between collagen and US attenuation 79—43973
- myocardium, acoustic microscopic anal. 80—45995
- myocardium, normal and ischaemic, US attenuation 80—45954
- near-field transient acoustic beamforming with short pulse arrays 79—57738
- nebulized aerosol, droplet size distrib., evaporation effect 78—24084
- neonatal peripheral circulation, human, characterisation by US pulsed Doppler technique 80—76815
- noisy blood flow meas. pulsed US spectral analysis 79—57705
- nonperiodic wave diffr. anal. *(French)* 80—48486
- nucleic acid component pulse sonolysis obs. 79—53186
- obstetric practice, the place of real-time and static B-mode scanning, educational syllabus 80—86057
- obstetrics, microprocessor based system for studying kinematics of labour 77—44769
- obstetrics and gynecology, safety and pot. hazards, review 80—67170
- ocular pulse measurement, electronic/US system for carotid occlusion diagnosis 77—37081
- ophthalmic diagnosis, use of US 80—81673
- ophthalmic tissue signature characterisation by US frequency-domain analysis 77—40857
- ophthalmic US B-scanner 80—30804
- ophthalmological diagnosis, US contact stabilisation method 77—25523
- ophthalmological diagnostics and therapy *(Croatian)* 78—44570
- ophthalmological signal acquisition and image enhancement 78—57045
- ophthalmological tissue differentiation, digitisation of HF US signals 78—80935
- ophthalmological transducer, with controlled weight, eye axial length meas. appl. 78—20239
- ophthalmoscope, eye axial distances meas. 80—36032
- optical instrumentation appl. in medicine, conf., Boston, USA (Sept. 1977) 78—69184
- orbital tissue visualisation by A-scan echography 77—77953
- organ volume determination by US scanning 80—17034
- organ-puncture needles, US wave propag. in needle and tissues 80—96052
- output measurement and calibration 77—39183
- pancreas carcinoma, grey-scale US characts. 79—53198
- pancreatic disease, study by multiple imaging modalities 80—17094
- pancreatic lesion visualisation and documentation by diagnostic US 78—11708
- pancreatic US, systematic approach to scanning technique 79—74731
- parametric echoscanner for medical diagnosis 80—36041
- patient contour drawing using US compound B-scanner 79—83865
- patient diagnosis, experiences in private practice 78—92680
- patient diagnosis, principles and methods 79—74733
- patient diagnosis, review of future developments and applications 79—79615
- patient diagnosis appl., bibliography 78—7417
- phantom for imaging biological fluids by US and computerised tomography scanning 80—104692
- phantoms, water-based gels 80—81671
- phase contrast imaging with electronic scanning 77—31190
- phased array beam steering, phase error grating lobes 79—48313
- phased array diagnostic instrument with microcomputer *(Japanese)* 79—88146
- phased array echosonographic systems for medical diagnosis 77—81543
- phased array sector scanning review 80—36038
- phased array US imaging, real-time digital scan conversion and multidimensional processing 79—48363

biomedical ultrasonics continued

- phased array US imaging with multiscan processing 79—57736
- phased-array US scanners, coarse phase quantisation effects 79—57739
- piezoelectric ceramic plates, expt. data for design of line arrays, medical diagnostics appl. 77—84099
- pneumothorax diagnosis in deep-sea divers, using Sonicaid portable instrument 78—85351
- polarity estimation for reflected echo in ultrasonotomography 80—108986
- porcine skin, acoustic impedance variations at burn-nonburn interfaces, burn depth determ. 79—2114
- porous coated implant removal 79—79618
- power measurement using const.-flow calorimeter, 1.5 to 3 MHz 77—50843
- pressure sensing SAW resonator 77—23850
- probe power meas. by use of semiconductor strain gauges 80—87679
- probes, main parameters and characterisation 79—25056
- problems of computer applications *(German)* 79—20696
- propagation velocity in tissue, meas. device 80—45993
- proptosis diagnosis, contrib. of echography 78—28023
- prostate, intra-rectal US imaging, equipment for 79—48296
- prostate tumour diagnosis by pattern recognition in US sectional pictures 79—83866
- prostate US sectional pictures, pattern recognition for tumour diagnosis 80—51194
- prostatic carcinoma treatment planning, US imaging rel. to computerized tomography 80—3786
- pseudosources, non-surgically implanted in tissue imaging appl. 78—3572
- pulmonary arterial hypertension meas., Bubble Ultrasonic Resonance Pressure method 79—92313
- pulmonary artery press. estimation using pulse wave velocity 80—12203
- pulmonary haemodynamics meas. using US oesophageal probe 78—35902
- pulse echo analysis, bioacoustic tissue prop. determ. *(German)* 78—85349
- pulse echo and Doppler diagnosis, technical and physical aspects *(Croatian)* 78—44568
- pulse echo digital processing 77—32948
- pulse echo system using interaural localization 80—89769
- pulse echo US, intensity meas. errors assess. when using miniature hydrophones 80—3743
- pulse echo US and freq. domeain deconvolution for tissue anal. 77—40720
- pulse echo waveform rel. to acoustic characteristics of continuous medium 80—67145
- pulse-Doppler device linked to grey scale B-scan equipment, clinical evaluation 79—92311
- pulse-echo diagnostic equipment performance meas. methods 77—77957
- pulse-echo equipment, US tissue equiv. test objects for routine performance checks 78—73182
- pulse-echo scanning, echo struct. 77—52857
- pulse-echo system, active attenuator 77—40835
- pulse-echo systems, improved sensitivity using pseudo-random binary-code phase-modulated signals 80—38182
- Pulse-echo transducer standardization 78—73181
- pulsed Doppler blood flow and dimension meas. in conscious dogs 79—62318
- pulsed Doppler blood velocity meter readout 78—69158
- pulsed Doppler flowmeter, development and cardiac appls. *(Japanese)* 80—36037
- pulsed Doppler system, differentiation of bile ducts and blood vessels in liver 79—34618
- pulsed Doppler techniques 77—77947
- pulsed US grating obs. in optical farfield 79—41534
- quality control problems for diagnostic US imaging equipment 78—69171
- quality health care and cost containment, conf., Washington, USA (Mar.-Apr. 1978) 79—39333
- quantitative US attenuation tomography, effects of phase cancellation, reflection and refraction 79—48302
- radiation balance for US power meas. 79—83863
- radiation treatment planning interactive computer/ultrasound system 77—9269
- radiology conference, London, England (Apr. 1979) 80—30838
- radiotherapy renal blocking, use of diagnostic US to determine renal size and position 78—31874
- radiotherapy treatment planning, appl. of US imaging *(German)* 78—53463
- radiotherapy treatment planning and follow-up of superficial tumours, US B-scan appl. 78—11721
- random signal US, transducer limitations 77—25536
- range-gated echo Doppler techniques for cardiac output and aortic flow meas. 78—40276
- raylography, acoustic medium characterisation and imaging, non-biological model expt. 77—25528
- raylography, freq. domain deconvolution technique for pulse echo ultrasonography 77—25527
- real time digital echocardiography using burst analogue sampling 77—9234
- real time imaging with hand-held linear array scanner, clinical experience 79—62317
- real time imaging with hand-held linear array scanner, technical description 79—62316
- real time scanner, performance meas. 77—29191
- real-time B-scan machine attachment for three-dimensional display 78—61229
- real-time diagnostic system 80—30819
- real-time image computerised anal. 79—70598
- real-time real-space US scanning principle 79—70594
- real-time scanner with pulsed Doppler and T-M facilities, obstetrical appls. 80—67172
- real-time US spectroscopy in suspensions, pulse transmission system 77—19495
- realtime echographic imaging system, acoustic field study *(Italian)* 79—96636
- recent advances, review *(Japanese)* 78—35899
- reconstructive tomography and applications to ultrasonics 79—66578
- reconstructive US tomography 78—92681
- renal diagnosis, clinical results 78—28027
- renal imaging with radionuclides, US and computerised tomography 80—17095

biomedical ultrasonics continued
renal inclination measurement, importance in radiographic meas. of renal length 78—77092
renal pelvic dilatation in children after fluid intake demonstration by US scanning 77—77951
renal volumetry in children, accuracy and simplicity of the method 80—98044
resolution improvement techniques and C-mode scan for patient diagnosis 79—25052
respiration monitor for premature infants, non-contacting device using air-transmitted US 77—52915
review, physics and diagnostic, therapeutic and surgical methods 77—66830
review, US mapping and signal processing 77—60282
review of the emerging field of biomedical engineering 80—36167
right atrial diameter meas., dynamic/static, using sonomicrometer technique *(Japanese)* 78—3568
right ventricular wall thickness meas. by echocardiography, comparison with necropsy 78—40277
safety standards, review of BRH, FCC, CPSC, FDA and OSHA regulations 77—57311
scanner, real-time rotating transducer, for heat and abdomen exams. 79—20603
scanners, ceiling suspension 80—30815
scanning diagnosis systems, design fundamentals 80—26308
scanning laser acoustic microscope 79—7263
scattering by heart and liver, quantitative meas. 80—45959
scattering by human tissue, theoretical models 78—7411
scattering by single objects 80—99892
shadowing due to calculi and gas collections, differentiation 80—98048
signal analysis applied to medical imaging 80—17038
signal processing 80—36049
signal processing aspects 78—7418
single-transducer coupler for diagnostic pulsed Doppler or pulse-echo US instrumentation 78—61236
skull bones, human, US flexural wave study 80—72277
small-area ultrasonotomogram magnification and smoothing 77—86572
soft tissue characterisation by US backscatter analysis 77—21586
soft tissue temp. increases due to US Doppler blood flowmeters, thermographic meas. 79—62294
soft tissue US attenuation coefficient slope estimation 77—21582
sonic digitizer, 2-sensor, accuracy obs., radiation therapy appls. 80—30806
Sono Diagnost R multi-element scanner, use for upper abdomen US diagnostics 80—17028
SonoChromascope, US B-scan image acquisition, display and recording 80—30818
sonographic diagnosis of pancreatic diseases 78—7416
sonography, diagnosis of tumours, comparison with other methods *(German)* 79—34614
spectra-colour ultrasonography, instantaneous power spectra, theoretical anal. 80—51190
spectral estimation of a narrow-band Gaussian process 80—51181
spectral estimation technique for high-resolution pulse-echo US 79—57729
spectral information display in colour ultrasonogram 77—21584
spherically curved transducers, anal. of focusing action 80—64332
spleen, grey scale echography 80—30812
spread energy method, use of time gain control 80—108988
spread energy method investigation using Golay code 80—30809
stochastic noise influence on perceived image 80—98053
structure extraction, search-free technique, appl. to M-mode echocardiogram and chromosome image 78—81025
superior vena caval pathway obstruction diagnosis following Mustard's operation, transcutaneous Doppler US 79—70596
supraorbital Doppler evaluation of blood flow in vascular surgery 79—88144
surgical equipment, selection of material for concentrator-instrument section 80—21242
swept-frequency diffraction by cylinders and arrays for tissue characterisation 78—53461
synthetic aperture imaging resolution 77—25530
temperature noninvasive monitoring using temp. depend. of US vel. in tissue 78—40281
tethered float radiometer for US therapy equipment output power meas. 80—104691
therapeutic appls., status and outlook for research on physiological foundations 80—26307
therapy device surveys, performance standard drafting 79—79613
therapy equipment, sonoluminesc. generation in water and blood plasma 77—77930
thermal injury determination in deep dermal burns, US pulse-echo technique 77—70511
Thermo-Acoustic Sensing Technique for noninvasive tissue analysis 77—64117
thermoelastic expansion flexible acoustic probe 80—16618
third intracranial ventricle dynamic displacement detection 78—57035
thrombophlebitis diagnosis, reliability of Doppler and impedance techniques 78—77144
thrombophlebitis patients, venographic, impedance and Doppler US findings 78—48919
thrombosis detection by US, plethysmography and phlebography 78—7435
thyroid gland, vol. estimation by US in addition to scintigraphy 79—74730
time of flight tomography, reconstruction of US vel. distribs. in soft tissue 77—48850
time-position mode scanning in obstetrics, heart model practice aid 78—24111
tissue, mammalian, survey of US vel. and attenuation data 80—46744
tissue, mammalian, US attenuation and speed determ. as function of temp. 80—41108
tissue acoustic parameter characterisation by induced transient thermal gradient 77—64116
tissue acoustic parameters, freq. depend., freshly excised rat tissue 77—86573
tissue analysis, comprehensive system 80—51189
tissue analysis, two-beam thermo-acoustic sensing technique 77—40716
tissue characterisation, challenges and opportunities 77—64105
tissue characterisation, clinical spectrum anal. techniques 80—45998
tissue characterisation, conf., Gaithersburg, USA (Jun. 1977) 80—41940

biomedical ultrasonics continued
tissue characterisation, seminar, Gaithersburg, USA, (May 1975) 77—64104
tissue characterisation, US propag. parameter meas. 80—45953
tissue characterisation, US propag. props. 80—45950
tissue characterisation by acoustic microscopy 77—64123
tissue characterisation by angle scan and freq.-swept scatt. technique 80—45958
tissue characterisation by attenuation, absorption, and velocity 77—64106
tissue characterisation by backscattered field space-time processing 79—48305
tissue characterisation by computer-aided US method *(German)* 78—80932
tissue characterisation by computer-aided US method *(German)* 78—80933
tissue characterisation by scattering 77—64107
tissue characterisation by US backscattering 79—70595
tissue characterisation by US diffraction 77—21585
tissue characterisation by US frequency-dependent attenuation and scatt. 77—66832
tissue characterisation by US scatt. frequency and angular dependence 77—64118
tissue characterisation model selection nomogram 79—62321
tissue characterisation pattern recognition approach 78—73186
tissue characterisation practice and risk 79—48309
tissue characterisation using wideband US transducers, 1 to 10 MHz 79—16262
tissue characteristics, swept freq. meas. of US attenuation and vel. 78—40278
tissue characteristion, static and moving, high spatial resolution US meas. techniques 80—51187
tissue characterization in vivo, broadband integrated backscatter 80—74635
tissue characterization in vivo by differential attenuation measurements 80—45999
tissue damage and death rel. to mech. props., US interaction 80—51151
tissue damaging effects of US 77—21559
tissue identification, conf., London, England (Apr. 1980) 80—98757
tissue identification by colour-coded B-scan display 77—64112
tissue macrostructure determ. by swept-frequency US scatt. 77—64120
tissue mimicking materials for ultrasound phantoms 79—5333
tissue parameter identification by digital processing of real-time US clinical cardiac data 80—51191
tissue parametric stimulation by inductive transducer and US phased array 79—92320
tissue phantom for diagnostic US equipment quality testing *(German)* 78—3567
tissue pulse-echo US absorption estimation model 79—48304
tissue quantitative characterisation, review 80—81670
tissue refractive index and attenuation distrib. reconstruction from time-of-flight and amplitude profile 77—64113
tissue refractive index spatial distrib. meas. by US computer assisted tomography 78—69161
tissue signature analysis, cepstral signal processing 80—46002
tissue structures characterisation, method of obtaining an acoustic impedance profile 80—67171
tissue US absorption thermoelectric meas., beamwidth and thermocouple size effects 79—48306
tissue US attenuation and velocity meas. by direct and phase-contrast imaging 77—64114
tissue US attenuation and velocity meas. by reflection techniques 77—64115
tissue US attenuation and velocity meas. by time delay spectrometry 77—64111
tissue US backscatter and attenuation distrib. mapping, digital reconstruction 80—51188
tissue US parameters, quantitative cross-sectional imaging 79—53277
tissue US signal analysis methods 79—57737
tissues, fixed and unfixed, US propagation, backscattering coeffs. and speech determ. 80—41109
tissues, mammalian, US absorpt. and attenuation determ. by thermoelectric method 80—41110
TOMAX autostereoscopic display, three-dimens. viewing of tomographic data 78—85446
tomography, review 78—31876
tomography, signal processing for improved directivity 77—44729
tomography, time-of-flight, computerised, breast pathology appl. 78—24107
tomography based on perturbation solns. of wave eqn. 79—70593
tomography equipment, electronic sector scanning type, Japan 77—53877
tomography for umbilical cord complications diagnosis 77—90867
tomography in cardiology 80—30824
tomography techniques survey 80—30823
tomography using laser-generated acoustic fan beam 79—83862
tooth blood supply determination, US CW Doppler appl. 80—104684
tracking focusing annular array transducer *(French)* 80—26301
transceivers, gain transfer characts. 80—30814
transcutaneous blood flow measurements using pseudorandom noise Doppler system 80—36035
transducer, high resolution, with toroidal acoustic lens 77—65656
transducer, US energy meas. for echography 80—36044
transducer 2-D array technology, state of art review 77—844
transducer characterization methods at the NBS 79—27481
transducer characterization standards, tissue equivalent testing for hospital use 79—29651
transducer design rel. to vibration geometrical effects 79—83871
transducer evaluation by optical interferometry 77—39184
transducer evaluation for inspection and diagnostic appls. 79—27480
transducer routine eval. methods 79—23173
transducers, design 79—100685
transducers, low-loss wideband for noninvasive appls., characts. 78—48846
transducers arc array with automatic sector scan echo signals presentation system *(Italian)* 79—96637
transducers for imaging, modelling *(French)* 80—26302
transfer functions for describing ultrasound system performance 79—25055
transit-time US volume flowmeter, in vivo validation 79—83872
transkull transmission of axisymm. focused US beams, 0.5 to 1 MHz 80—51184

biomedical ultrasonics continued
- transmission image reconstruction, inverse scatt. and tomography 78—61231
- transmission media for ultrasonography 80—98050
- transmission tomography 80—94301
- transmission tomography by reconstruction, imaging soft tissue through bone 77—70512
- transmission/reception system with single crystal, principle *(Japanese)* 77—84093
- transmitter-receiver matching network for US pulse-echo system 77—78012
- transmitters and receivers for medical ultrasonics 80—76819
- transrectal echographical ultrasound system, prostate, seminal vesicles and bladder exam. 80—41153
- tumour detection by US Doppler blood-flow signals 78—3571
- tumour irradiation, closed-loop energy and temp. control 79—83874
- TV display of colour images tissue disease diagnosis appl. 79—29576
- two dimensional scanning, obstetrics appl. 77—25613
- two-dimensional ECG images, direct conversion 77—60233
- two-dimensional echocardiographic images enhancement by lateral filtering 80—81677
- two-dimensional US attenuation coefficients, computerised tomographic reconstruction 79—57733
- ultrasensitive US system for NDT, medical diagnosis and nonlinear US 78—59224
- ultrasonographers, pot. hazard from previously administered radionuclides 80—98120
- ultrasonography, computer method for axisymmetric transducers with various boundary conditions 80—87591
- ultrasonography of the kidney in 1979 *(French)* 80—56149
- ultrasonography rel. to computerised tomography in upper abdomen and retroperitoneum exam. 80—21506
- ultrasonotomography with electronic sector scanning, cardiac diagnosis appl., features 77—66829
- urological illnesses diagnosis *(Hungarian)* 78—35900
- US bladder volume sensor, pocket-size 80—36034
- US cardiotomography, cardiovascular system diagnosis appl. *(German)* 77—77944
- US Doppler flowmeter spectra for asymm. transducers 78—31880
- US Doppler returns from foetal heart, processing, valvular timing information extraction 80—101238
- US Doppler spectra, transit time and geometrical broadening 78—44576
- US Doppler velocimetry for 3D blood flow meas. 78—88730
- US echography for medical diagnosis *(French)* 80—26305
- US image sequences, logical neighbour operations appl. 80—8113
- US imaging, improvement of sensitivity or reduction of dose 80—74641
- US probes for blood stream meas. using Doppler technique *(German)* 79—2113
- US transducer evaluation and calibration conf., London 1977, May 79—23167
- USA National Science Foundation incentive programme 77—66831
- uterus, mouse, US irradiation at therapeutic intensities in standing wave fields 80—41112
- variable-focus US membrane transducer, medical imaging appls. 77—39185
- vascular access complications, US evaluation 79—92312
- vascular diagnostic system using Doppler vel. detectors 77—29190
- vascular imaging, Doppler method, improvement 78—24106
- vascular laboratory instrum. management using computer 78—7460
- vascular stenosis detection using flow continuity and turbulence, US Doppler method 77—40723
- vascular system, US Doppler imaging, book contrib. 80—36045
- vectorcardiographic P loop correlation with left atrial volume echocardiogram 79—44025
- velocity temperature depend. in soft tissue, rel. to temp. distrib. monitoring 80—45994
- venous flow, mech. oscills., ultrasonic Doppler study 80—108931
- venous flow, US determ. of cross-sectional shape of elastic tubes 77—25506
- ventricle, left, human, 3-D time-varying reconstruct error sources and magnitude estimation 80—85454
- ventricle regional wall motion parameters, angiography vs. echocardiography 79—62392
- ventricular circumferential segmental shortening, from US sector scanning images in ischaemic dogs 79—70599
- ventricular dimensions noninvasive meas. in awake dog by echocardiography 77—44863
- vessel wall motion, US Doppler shift meas. 77—25538
- video photography in computed tomography and US imaging, film selection 80—41224
- Vidoson 735, real time scanner for sonography 78—28024
- volume estimation, computer algorithm 80—98043
- volume estimation algorithm based on polyhedral approx., using US or CT data 80—104790
- volume measurement in vivo using computer-based u.s. echography, errors 77—2033
- wideband general-purpose US generator for biological object handling 79—48381
- PVF_2 polymer probe for mapping pressure field from arrays 80—74669

biomembrane transport
- *see also osmosis*
- acetylcholine receptor electrophoretic movement in embryonic muscle cell membrane 78—85298
- acetylcholine receptor protein, binding kinetics and Ca ions, rel. to membrane cond. changes of acetylcholine 77—40649
- acetylcholine receptor response to rapid photochem. prod. increases in agonist conc. 77—36909
- active transport, rel. to second law of thermodynamics 77—9178
- active transport, review 78—15814
- active transport and energy transformation, quantum mechanism 78—53364
- admittance, integral representation 78—15811
- ^{14}C-alanine transport, photo-depend., into H.halobium cells 77—70439
- albumin flux, differential permeability of endothelial and epithelial barriers, sheep expts. 80—81553
- alga intracellular potential, effect of ionic composition of external medium 78—20157
- amino acid permeability of E. coli K-12 78—77029
- amphipathic apolipoprotein ApoC-III bound to phosphatidylcholine bilayers, lateral mobility 80—97884

biomembrane transport continued
- anterior pituitary cell action pots., stimulation by thyrotropin-releasing hormone 78—48771
- aortic tissue, rabbit, convective and diffusive transport of ^{125}I-serum albumin 78—44482
- aortic wall, albumin transport during acute angiotensin induced hypertension 77—44619
- apical membrane of toad gallbladder, K^+ selective channels 79—2018
- artificial kidney dialysis exchange model reliability tests *(German)* 79—2165
- artificial membranes, excitable and ion-selective, review of axon and bilayer membrane props. 77—86451
- artificial membranes, excitable and ion-selective, review of non-bilayer lipidic membrane props. 77—86452
- artificial membranes, transport regulation by environmental H^+ conc. 80—89725
- asymmetrically permeable membrane channels in cell junction 80—94187
- Na^+, K^+-ATPase, identification of membrane-embedded segment of large polypeptide chain 78—3447
- Na^+,K^+-ATPase preparations, tryptophan fluoresc. 77—21477
- atrial muscle, cyclic GMP rel. to negative isotropic effect of acetylcholine 77—48781
- atrium, bullfrog, mechanisms for positive inotropism of low-K Ringer soln. 77—77884
- atrium of bullfrog, tension components and temp. effects 77—52760
- autorhythmicity and entrainment in excitable membranes 80—108866
- axon, elec. field distrib., ionic selectivity and permeability 79—34532
- axon, giant squid, current fluctuations obs. 79—24973
- axon, squid, Na channel gates, interactions with quaternary lidocaine and tetrodotoxin 79—83745
- axon, squid giant, exponentiated exponential model g Na^+ and K^+ cond. changes 78—44493
- axon, squid giant, poisoned with quaternary strychnine, block of Na conductnace and gating current 79—83746
- axon, squid giant, temp. effects on gating currents 78—96037
- axon, squid giant, transient polarisation currents 77—86477
- axon asymmetry currents and admittance, squid 77—73518
- axon membrane, squid, freq. domain anal. of asymmetry current 80—51064
- axon membrane, squid, null space in Hodgkin-Huxley eqns., critical test 79—83747
- axon membrane freq. domain currents 79—62222
- axon Na conductance and Ca transport, squid, mol. model 78—85305
- axonal K^+ transport, single-file model for squid giant axon 77—73517
- axonal K conductance anal., squid giant axons 79—96543
- axonal membrane of mammals (myelinated fibres), K channel conduction 80—61538
- axonal transport, components, mechanisms and specificity, book contrib. 79—96551
- axons, giant, squid, interaction of Ba^{2+} with K^+ channels 80—85379
- axons, squid, effects of internal and external cations and ATP on Na-Ca and Ca-Ca exchange 77—90745
- bacteria chemotactic behaviour regulation by Ca^{2+} 78—15851
- bacteria motility, proton pump as molecular engine 78—40130
- bacterial flagella, protonmotive driving force 78—48774
- bacterial flagella rotation rel. to ion transport down electrochem. gradient 77—73515
- bacteriorhodopsin, enthalpy changes during photochemical cycle 79—34602
- bacteriorhodopsin, kinetic isotope effects in photochem. cycle 77—44592
- bacteriorhodopsin in model membranes, new component of displacement photocurrent 79—43827
- bacteriorhodopsin in planar membranes, elec. response to light 78—35806
- bacteriorhodopsin proton pump, elec. demonstration of rapid light-induced conform. changes 77—44597
- bacteriorhodopsin-containing membrane fragments, quantum yield of flash-induced proton release 79—34601
- barbiturate-induced slow outward currents in Aplysia neurones 78—80866
- bilayer lipid membranes, dimer mechanism of action of nigericin 78—24048
- bilayer lipid membranes, effect of stress factors on elec. props. 79—92161
- bilayer membrane, galvano-static regime of non-steady process 78—64963
- bilayer membranes, ion transfer parameter calcs. 79—53053
- bilayer membranes, permeation of water mols. meas. using fluoresc. quantum yield solvent-isotope effect 79—34710
- bimolecular lipid membranes, electrophoretic mobility 79—79479
- bioelectrochemistry and bioenergetics (book) 80—8749
- bioenergetics and proton-electron systems 79—57596
- bioenergetics and proton-electron systems of membranes, review 78—96030
- biological membranes, transport props., rel. to synthetic membranes 78—77030
- biological n-compartment model, identification by filtering techniques 79—34507
- Biophysical Society, 23rd annual meeting, conf., Atlanta, USA (Feb. 1979) 79—34468
- black lipid membranes, permeability of cyclic nucleotides 79—39376
- bladder, toad, temp. dependence of ADH-induced water flow and intramembranous particle aggregates 80—61520
- blastocyst, rabbit, amiloride-sensitive rheogenic Na^+ transport 78—15812
- blood cell aggregation, conductometric meas. 77—25614
- blood coagulation and fibrinolysis under influence of direct elec. current 78—48766
- blood vessel wall ion permeability 77—32934
- blood vessel walls, active and passive transport of Na^+ and K^+ 77—44618
- blood-brain barrier permeability obs. after microwave irradiation, rat 79—74718
- brain capillary endothelial cells, Na^+-dependent neutral amino acid transport 79—57616
- brown adipose tissue mitochondria, increased proton cond. pathway rel. to diet-induced thermogenesis 80—89722
- brush border and basolateral membranes, rat duodenum, Ca-stimulated ATPase 79—74613
- brush border of renal proximal tubule and intestinal mucosa, review 78—15815
- bursting pacemaker neurons, Ca^{2+} effects modelling 78—44484
- bursting phenomena in excitable membranes 79—66455

biomembrane transport continued
- capillary counter-current system hydrodynamic effects 77—40695
- capillary permeability determ. from multiple indicator data, effects of finite red cell permeab. 78—44483
- capillary wall filtration 77—32936
- carbohydrate active transport in membrane vesicles of Acholeplasma laidlawii cells 78—64965
- cardiac pacemaking, role of catecholamines 77—70437
- cardiac Purkinje fibre, Na current model 79—43861
- cardiac Purkinje fibres, rabbit, Na channels 79—43828
- cardiac Purkinje fibres, sheep, intercellular clefts effect on elec. props. 79—34522
- carrier-mediated photodiffusion membranes 78—23965
- catalysis, ADP,ATP carriers of mitochondria *(German)* 79—29512
- cell, membrane permeability, review 78—15813
- cell contact region during communication, obs. of gap junction 80—45873
- cell membrane, electrophoresis and diffusion obs. 79—57599
- cell membrane diffusion coeffs. meas. 77—48962
- cell permeability changes after X-irradiation 79—39370
- cell permeability polarity and control by phytochrome, red light irrad. of mass 78—77025
- cell-cell junction membrane form., quantum jumps of cond. 78—73145
- cells without highly permeable cell contacts, elec. connection 77—70440
- cellular testing potential, membrane pot. rel. to ionic diffusion *(French)* 80—94184
- charge transfer in thin membranes, discrete models, nonsteady state, low polarising volts. 77—70420
- charge transfer in thin membranes, discrete models, nonsteady state at high polarising voltages 78—69023
- charge transfer in thin membranes, steady state, discrete models 77—16913
- charged membrane osmotic transport, generalised flux eqns. 78—24050
- chemiosmotic theory of ATP synthesis 78—61151
- chlorotetracycline transport by bacillus megaterium 79—24971
- cholesterol transmembrane movement in human erythrocytes, radioactive tracer expt. 78—3459
- cholinergic channel without const. field, permeab., phase-boundary pot. and conductance 77—60191
- collagen membrane H^{+} diffusion-limited binding electromechanics 79—79489
- colon, turtle, active Na transport via an electrogenic Na-K exchange pump 80—108856
- colon Na transport in vitro, rabbit, amiloride effect blocked and reversed by p-chloromercuribenzene sulphonate 78—44479
- composite membrane, anion exchanger-urease, coupling of transport and enzymic reaction 79—83510
- conductance channels, current-induced coupling, multi-channel interaction and mean field cond. 80—67063
- conductance fluctuations and ionic pores, review 77—90752
- conductance fluctuations in cultured spinal neurones induced by γ-aminobutyric acid 78—80867
- cone ionic channel closure, turtle 78—15830
- cone outer segments, light-induced changes in membrane current, tiger salamander and turtle 80—108899
- corneal hydration endothelial control theory 78—35841
- cortical spreading depression, math. model 78—80857
- cortical tissue membranes, benzodiazepine receptor coupling to chloride anion channel 79—79486
- counterion condensation, soln. of Poisson-Boltzmann eqn. for two parallel charged plates 79—87849
- crosslinked collagen membranes, transport props., physical props. effects 78—77028
- current noise parameters in embryonic heart cell aggregates 80—21459
- current separation using Paramecium mutant 77—66806
- current-voltage relations, Nernst-Planck anal. 79—83715
- dendrite membrane, steady voltage-current characteristic 79—92203
- dendritic membranes, active vs. passive effects on simulated neuron transfer properties 79—24976
- diffusing membrane channels, mechanism by 1/f noise 78—27911
- diffusion measurement by fluorescence photobleaching recovery method, bleaching light effect 80—94434
- digital readout instrument for use in ion transport studies 79—74815
- digitalis inotropy rel. to enhanced slow inward Ca current 78—61155
- digitalis receptor binding, Na^{+},K^{+}-ATPase as model 78—40111
- double-sucrose-gap voltage-clamp method, mathematical model 79—96539
- dynamic interfacial electrochem. phenomena, toad urinary bladder membrane system 78—27912
- dynamics of a membrane-moderated controlled release 79—2016
- eel electroplaque, temp. dependence of four ionic processes of spike electrogenesis 77—36899
- egg cell membranes, starfish, inward rectification blocking model 80—61523
- electrical breakthrough of bilayer lipid membranes 79—70531
- electrical conductivity mechanisms of membranes with TTFB 77—52746
- electrical relaxation, time-depend. rectification, cellulose acetate model 77—90731
- electrically excitable membrane, phys. model, voltage-current characts. 77—25382
- electrodiffusion, steady-state, scaling, exact. soln. and phase plane 77—25403
- electrogenic ion transport along oligomer channels capable of conformational transitions 80—108854
- electrogenic Na pump, role in slow synaptic inhibition 77—48780
- electrokinetic model of transport through biological barriers 80—45871
- electrolyte transport across a simple epithelium 79—88063
- electrolyte-membrane-electrolyte, freq. depend. of capacitance and cond., model 77—21488
- electromotor system of Torpedo, as model cholinergic system 78—53388
- electron and proton transport 80—67052
- electron flow, photosynthetic and respiratory, in dual functional bacterial membrane 80—16914
- electrons, advantage to low mobility in biological systems 79—39346
- electroosmotic model of longitudinal transport 80—45870
- electrophoresis along cell membranes 77—25405
- electrophoresis of concanavalin A receptors along embryonic muscle cell membrane 77—29121
- electrostriction and/or cooperativity as membrane excitability models 79—79487
- end plate current quantitative description and reconstruction 77—52770

biomembrane transport continued
- endocytosis, review 78—15816
- endplate acetylcholine-induced channels and transmitter release, humans 78—24063
- endplate channel lifetime and cond. alteration by permeant cations 78—3467
- enniatin B, Rb^{+} complex of LDLLDL analog, verification of ion transport through membrane by conformation investigation 79—60348
- enteric bacteria, transport functions of the outer membrane, book contrib. 79—16179
- enzymatic active transport model 80—51049
- enzymatic charge transfer across oil-water interface, effect of dielec. const. 77—70419
- enzymes, monosubstrate inhibited, conc. response, multiplicity and memory 80—30679
- epithelia, pathways for hydraulically and osmotically-induced water flows 77—29112
- epithelial cell, phospholipase A and mechanism of aldosterone action 78—24053
- epithelial cells, of unpoisoned non-depolarised frog skin, intercellular junctions 77—12897
- epithelial K active transport system of insect midgut, pump-mediated efflux 78—80846
- epithelial membrane conductance rel. to extracellular shunting, rabbit salivary duct 77—77881
- epithelium, fluid-transportin, tight junctions in an insect 80—3613
- epithelium, fluid-transporting, ion distrib. determ. by electron-probe X-ray microanal. 77—4991
- epithelium, leaky, effect of plant cytokinins on microfilaments and tight junction permeab. 77—12899
- epithelium, small intestine, asymm. behaviour under influence of osmotic press. 77—52747
- epithelium intercellular contacts, small intestine, permeab. and mech. props. regulation by Ca ions 77—81482
- epithelium membrane permeability, effect of intracellular Na conc. 77—32882
- erythrocyte, human, chloride distrib. and transport, cell membrane struct. 77—1983
- erythrocyte Ca transport in myotonic muscular dystrophy patients 78—80849
- erythrocyte $H^{32}PO_4^{-2}$ transport, inhibition by high press. 77—12900
- erythrocyte integral membrane protein lateral mobility, human cells 77—66805
- erythrocyte membrane, pulse NMR meas. of water exchange 79—43826
- erythrocyte membrane hydraulic cond. determ. 79—34528
- erythrocyte membrane permeability, sheep, O_2 effects with X-ray and neutron irrad. 77—5039
- erythrocyte membrane thermal transitions identified from ANS permeability 79—53055
- erythrocyte membrane water permeability defect in human epilepsy, NMR 77—29122
- erythrocyte membranes, human, elec. cond. characts., ghosts and lipid bimol. membranes 77—9180
- erythrocyte suspension, laser-induced fluoresc. of intact human membrane cell 77—90733
- erythrocyte suspensions, human, HCO_3^-, Cl^- exchange 79—8487
- erythrocytes, avian, US effects on transport 79—96613
- erythrocytes, frozen human cells, conc. polarisation effect 78—3460
- erythrocytes, human, effect of hydration on water content 77—16921
- erythrocytes, human Li efflux through Na/K pump 78—48775
- erythrocytes, rabbit, increased passive efflux of ^{22}Na and ^{86}Rb on microwave irrad. 80—108957
- excitability, review 78—15786
- excitable fibre, steady speeds of spread of stable and unstable impulses, depend. on membrane ionic currents 78—53382
- excitable membrane, rapid transient changes in Na ion conductivity 77—44613
- excitable membrane, with asymm. behaviour of inner and outer sides, oligomeric transport model *(Japanese)* 77—44611
- excitable membrane K^{+} conductance temp. dependence *(Japanese)* 78—24051
- excitable membranes, nonstationary ion fluxes 77—44599
- extra-retinal photoreceptor model for Aplysia californica 78—44506
- fixed charge membrane modules, pot. controlled transient gating mechanism, book contrib. 80—12067
- flexural fluctuations and non-equilib. noise 80—76712
- flow equations for membrane transport, nonelectrolyte solute plus water case 80—26205
- fluoresceindiacetate hydrolysis and transport in mammalian cells after UV and gamma irrad. 77—56333
- fusion rosettes in Paramecium, possible function as Ca^{2+} gates 78—56958
- GABA uptake or exchange by synaptosomal fractions 77—12907
- gallbladder epithelial cells, compartmental anal. of osmotically induced permeability changes 78—3455
- gallbladder epithelium Na^{+} pump site distribs., frog 78—27914
- gas exchange system, mathematical model 77—12870
- gastro-intestinal electrical activity model, frequency entrainment of oscillators 77—81489
- gastrointestinal electrical activity, Hodgkin-Huxley type electronic modelling 78—61165
- gating charge immobilisation by inactivation-simulating substance 78—61154
- gating currents, role of nonlinear capacitive currents of electrostrictive origin 77—48771
- glial-neural interaction demonstrated by Na^{+} and Li^{+} injection into cortical glia 77—36905
- gliovascular interphase in irrad. brain tissue, horseradish peroxidase transport 80—41119
- global flow eqns. from local eqns. of motion, nonelectrolyte solutes plus water 79—34525
- glomerular permeability in foetal rabbit 80—85372
- glucose transport in human red cell ghosts, effect of chlorpromazine and temp. 78—77026
- glucose transport system from pig small intestine, reconstitution in phospholipid vesicles 77—29111
- glutamate Na-stimulated uptake in membrane vesicles of E. coli, role of ion gradients 78—48776
- glycolipids, regional synthesis, axonal transport, in neuron of Aplysia californica 79—83755

biomembrane transport continued

- gramicidin A channel cation permeation interactions and anion binding 78—53370
- gramicidin A channel struct., elec. meas. with lipid bilayer membranes 78—15783
- gramicidin A ion channel kinetic behaviour, electrostatic calcs. 78—53368
- gramicidin channels, interaction of countercurrent cation fluxes 79—70528
- gramicidin ion pore, potential variation 79—34506
- gramicidin single-channel currents, rate theory calc. using NMR-derived rate consts. 80—94186
- growth, self-reproduction and autoregulation model, anal. of reactions with stretchable semi-perm. walls 77—81460
- guard cells, anion, light-sensitive membrane pots. 78—11622
- haemoglobin-O_2 equilibrium curve determ., semipermeable membrane transport model 79—92418
- hair cell receptor pot., ionic basis in vertebrates, bullfrog obs. 80—26239
- Halobacterium halobium R_1 cells, photogeneration of two-vector transmembrane gradient of protons 78—80845
- Halobacterium species, passive elec. props., membrane ionic flow 79—24970
- heart activity characteristics in terms of membrane potentials *(Dutch)* 80—8034
- heart muscle cells, Na current, electrophysiological studies, rat 79—43838
- Henle's loop, transport equations for permeable elastic tubules 79—20519
- hydrophilic side groups, linear H-bonded systems, proton conduction, across biomembranes 80—40973
- 5-hydroxytryptamine receptors on visceral primary afferent neurones in rabbit nodose ganglion 77—56364
- ileal mucosa, human, theophylline-induced changes in ion transport and cond. 77—64017
- inhalation anaesthetics, effect on conductivity and time of adhesion 79—53070
- integral proteins, mobility increase in spherocytic erythrocytes obs. 80—81569
- intercellular contact high permeab. 78—48773
- intercellular oedema resulting from reduced efficiency of cellular membranes at low body- temp. 77—29225
- internodal cell, Nitella, mebrane pot. instability 79—92204
- intervesicular lipid transfer, direct fusion of phospholipid vesicles, kinetic basis comparison 78—96034
- intestinal epithelium, effect of Ca ions and pH on osmotic pot. 78—20156
- intestinal membrane transport of oligopeptides, intracellular study of underlying ionic events 80—104572
- intestine, small, effect of pH on permeability and mech. props. of intercellular contacts 79—57613
- ion channel, energy and pot. profiles and interactions between ions 78—53367
- ion channel formation in artificial lipid bilayer membranes by synthetic peptides 77—90750
- ion exchange membrane, unstirred layer effects on pot. difference calcs. 77—48680
- ion specificity, determ. criterion 79—57597
- ion transport and chem. reactions in brown adipose tissue, network thermodynamics 78—92606
- ion transport in thin non-uniform membrane, jump vs. electrodiffusion description, volt. clamp 77—36897
- ion transport model, intracellular osmoregulation mechanism 77—25400
- ionic channel formation in living cell membrane, microelectrode obs. 78—53372
- ionic channel formed by gramicidin A, membrane distortion 79—92164
- ionic channels, dipole cooperative model 79—53054
- ionic channels and gating currents in excitable membranes, review 77—90764
- ionic channels dipole cooperative model, excitable membranes 79—79480
- ionic channels in excitable membranes, current problems and biophysical approaches 78—53369
- ionic current in excited membrane, automated meas. of electrophysiological characts. *(Russian)* 80—76865
- ionic mechanisms of excitation in Paramecium, review 80—21458
- ionic transport in thin membrane, jump vs. electrodiffusion description, volt. clamp 77—36896
- ionic transport in thin membranes, jump vs. electrodiffusion description, for steady transfer 77—36895
- ionophoretic model for Na-Ca counter transport 79—2017
- ions, active transport through membranes, elec. events, book contrib. 80—12068
- iontophoretic isolated current monitor for cell membranes 77—25626
- junctional membrane channels, size limit of permeating mols. 77—36900
- K channels, influence of Coulomb effects on interaction of unilateral fluxes 78—24047
- Kedem-Katchalsky equations for fluid flux, flow limits 77—1979
- kidney, isolated, perfused in vitro, sugar reabsorpt. rel. to Na transport, rabbit 78—20155
- kidney preservation, analogue model of perfusion dynamic changes 79—83724
- kidney solute concentration, control core model, input-output studies 77—56405
- kidney solute concentration, renal medulla model and limit cases 77—52821
- Krogh tissue cylinder, transient convective mass transfer 80—3598
- lateral diffusion calcs. for membranes containing cholesterol 80—85356
- lateral diffusion on a spherical surface, normal mode anal. 80—61518
- lecithin bilayer force meas. and modification 77—56346
- light irradiation of fluorescent concanavalin A, membrane damage 80—56123
- light response and kinetics in Aplysia giant neuron 78—53381
- Light-regulated body ion balance in marine slug Elysia virdis (Montagu) 78—73146
- lipid bilayer, 1 MHz US effects on cond. and capacitance 78—77082
- lipid bilayer, elec. cond. in presence of proteolytic enzymes and substrates 78—15779
- lipid bilayer, flat, permeab. in presence of vesicles of sarcoplasmic reticulum 77—21490
- lipid bilayer, hydrophobic ion current noise, autocorrel. anal. 80—30676
- lipid bilayer diffusion transport modelled by dimeric β-cyclodextrin complexes, cryst. struct. anal. 78—80838
- lipid bilayer electrical strength fall after UV irrad. 78—69002

biomembrane transport continued

- lipid bilayer gramicidin A channel cation flux interaction 78—56957
- lipid bilayer membrane permeability modification by drugs 78—69026
- lipid bilayer membranes, ionic displacement current 79—34503
- lipid bilayer membranes, spectrophotometric and elec. correls. of cyanine-dye adsorpt. 80—85358
- lipid bilayer membranes, steady-state permeability behaviours induced by cyanine dyes 80—85357
- lipid bilayer properties in presence of tetra-alkylammonium salts, effect of surface charge 77—21489
- lipid bilayers, Ca^{2+} transport system of rat liver mitochondria 78—64966
- lipid bilayers, evidence against channel form. by nystatin 77—44598
- lipid bilayers, ion transport modification by 2,4-dichlorophenoxyacetic acid 79—83710
- lipid bilayers, K^+ transport modification by 2,4-dichlorophenoxyacetic acid 79—83709
- lipid bilayers, limiting stages of induced ion transport 77—36878
- lipid bilayers, piezo-effect, background conductivity and filtration coeffs. 79—57598
- lipid bilayers, static, dynamic current response effect of local anaesthetic 77—52750
- lipid bilayers containing gangliosides, cholera toxin effect, formation of ion transport channels 78—88702
- lipid membrane, black, adsorpt. of phloretin 79—34504
- lipid phase transition, cluster model, appl. to bilayer mol. passive permeation and struct. relax. 78—53346
- lipid planar bilayers, lateral diffusion meas. using fluoresc. correl. spectroscopy 77—36884
- lipid requirement of membrane-bound enzymes 79—20521
- lipid transport through water, exchange mechanism 79—62203
- lipid-bilayer-aqueous soln. interface with surface-active ions, double elec. layer 77—36872
- lipid-water smectic phase, water and thermal diffusivity, light scatt. meas. 78—96031
- liposomal membrane permeability, radioresist. 78—80919
- liposome, photoinduced electron transport across phospholipid wall using methylene blue 79—74614
- liposome proton permeability increase on peroxide photo-oxidation of lipids 78—69024
- liposome suspension, coupled transport of K^+, Cl^-, H^+ and OH^- ions 79—53069
- liver, distributed model for transcapillary exchange and solute removal 79—34524
- liver cells, regenerating, specific resist. and electrophoretic mobility, effect of RNase and neuraminidase 77—25402
- liver membrane potential in situ, effect of blood flow changes 78—48772
- lung, duck, O_2 and CO_2 exchange and cardiopulmonary control interaction model 80—3600
- lung, intrapulmonary haematocrit maldistrib., effect on O_2, CO_2, inert gas exchange 80—8033
- lung alveolar membrane, dog, role of bulk fluid flow in protein permeability 77—52814
- lung gas concentrations during air breathing, influence of gas exchange 77—12942
- lung transport and metabolic processes, indicator-dilution study 77—44711
- lymphocyte stimulation rel. to early Ca flux 77—52758
- mammal cell junction, permeability of cell-to-cell membrane channel 80—51061
- mechanosensitive ionic channel, model of reception and macromolecular rearrangement, effect of deform. 79—79564
- membrane charge transfer, possible role of α-helical proteins 80—81524
- membrane excitability mechanisms, book contrib. 80—12062
- methotrexate effects, cellular response simulation 77—40647
- microwave effects of membrane level, athermal electrophysiological mechanisms and experimental test 79—2108
- mitochondria and submitochondrial particle membrane pot. generation in anaerobic conditions 78—69015
- mitochondria and submitochondrial particle phosphate transport, influence of thiol oxidation 78—27913
- mitochondria membrane Ca^{2+} interaction, influence of oestrogens 78—53349
- mitochondrial Ca^{2+} transport, effect of cations on temp. sensitivity, compared with liposome spermine uptake 78—11621
- mitochondrial Ca^{2+} transport, inhibition by antibodies directed to Ca^{2+}-binding glycoprotein 77—4990
- mitochondrial Ca^{2+} transport, rat liver, effect of Mg^{2+} and spermine 77—64015
- mitochondrial membrane monovalent Tl^+ ion transport 78—31787
- mitochondrial membrane pot., respiratory chain study by method of penetrating ions 78—64951
- mitochondrial outer membrane, permeability pathway obs. 79—74602
- mitochondrial proton pump coupled to cytochrome c oxidase 77—25406
- mitochondrial regulators, membrane-active 77—25397
- modular gating channel and the Cole-Moore effect 80—30708
- molecular motion determ. using periodic pattern photobleaching 79—34719
- molecular transport across biological membranes, quantum mech. theory 79—8489
- monosynaptic potentials onset and propagation, discrete-dynamic equations 78—77040
- motor nerve endings, hyperosmotic neurosecretion rel. to internal Ca conc. 77—56368
- motor nerve impulse, conventional Ca^{2+} channel mediating asynchronous acetylcholine release 78—11638
- motor nerve terminals, cyclic nucleotide-mediated Ca flux 77—73524
- moving semipermeable boundary, diffusion transport in liquid solution 77—80639
- mucous membrane of dolphin tongue, neural struct. and function of taste receptors *(Russian)* 79—43937
- muscle, cross-striated, effect of uncouplers of oxidative phosphorylation on conc. of ATP 78—20149
- muscle, excitation and contraction processes, book contrib. 79—5262
- muscle, K^+ concentration effect on Na^+ efflux rate obs. 79—79495
- muscle, locust, pot.-depend. transition temp. of ionic channels induced by glutamate 77—77882
- muscle, single ionic channels obs. in tissue cultures 80—30699
- muscle, single postsynaptic channel currents in tissue cultures 80—30700
- muscle, skeletal, Na:K rel. to Na:Na exchange by Na pump 77—66807
- muscle, skeletal, permeab. of stretched membrane rel. to EMF *(Japanese)* 77—36886

biomembrane transport continued
- muscle, skeletal fibres, intramembrane charge movement and Ca transients 79—66453
- muscle, smooth, depolarised, tone change due to hyperpolarising current 77—86471
- muscle, smooth, depolarised in hyper K medium, spontaneous relax. 77—86470
- muscle, smooth, effect of hyperosmolar soln. on elec. connections between cells 78—69027
- muscle, smooth, intestinal cell, voltage clamp studies of hyperpolarising inactivation 78—80847
- muscle, striated, charge movement in membrane, book contrib. 79—5263
- muscle, striated, possible gating signal for K channel 77—64018
- muscle cell osmotic state and membrane permselectivity repeated microwave irrad. effects quantitation 80—56131
- muscle cells in tissue culture, acetylcholine-induced current fluctuations 77—29119
- muscle contraction activation, membrane mechanisms, guinea-pig 79—53071
- muscle endplate, desensitisation rel. to selective alteration of Na$^+$ channels 77—77890
- muscle fibre end-plate current pot. depend., effect of phenylalkylamines, frog 78—31799
- muscle fibre membrane pot., effect of eserine, frog 77—56345
- muscle fibre post-synaptic membrane, ionophore-mediated Ca influx effects 78—11637
- muscle fibre resting pot. in cricket, influence of ions 78—24046
- muscle fibres, skeletal, resting, Cs$^+$ rel. to volt. depend. block of inward K currents 77—52756
- muscle membrane, insect, permeation of Mn, Cd, Zn and Be through Ca channels 77—56357
- muscle Na channel use-depend. block by local anaesthetic, pH effect, frog 78—20160
- myelin swelling and meas. of forces between membranes 79—62204
- myelin vesiculation simulated by nerve exposure to Ca ionophore 77—29128
- myoblast membrane lateral transport of lipid probe and labelled protein 77—40646
- myocardial fibre accommodation, role of incoming currents 77—36898
- myocardial fibre excitation and contraction uncoupling on slow Na-Ca channel block 78—15810
- myocardial fibres, ionic nature of repeated responses 77—70441
- myocardium contraction amplitude depend. on freq. of elec. stimulation, frog 78—77027
- myocardium of frog, temp. effects on membrane currents 77—52759
- myotonia, Ca induced, computer simulation 79—57633
- myotonia and Ca permeab., math. model 78—11620
- myotubes, human, cultured, acetylcholine-induced conductance fluctuations 78—61157
- Myxicola axons, Na tail currents compared with membrane asymm. currents 77—66808
- nephron functioning, diffusion and selective osmosis *(French)* 80—45864
- Nernst-Planck analog equations and stationary state membrane electric potentials 79—92196
- nerve axon, phys. model, ionic distrib., pot. profile and resting pot. 77—12901
- nerve axon adsorption model, action pot. and excitation currents, volt. clamp test 80—56018
- nerve cell membrane, flow of Na$^+$ and K$^+$ through ion channels 79—74644
- nerve excitability, interactions between intrinsic membrane protein and elec. field 78—53377
- nerve excitation, gating currents and dipole transitions 80—67056
- nerve fibre membrane analogue-code conversion, ionic mechanisms 80—81575
- nerve fibre membrane Na permeab. reversible blockage by increase in temp. of medium above 45°C 80—81576
- nerve fibres, myelinated, diffusion of ions 79—24965
- nerve impulse, physical mechs., ion transport through membranes, review 78—85306
- nerve impulse electro-diffusion model 79—53078
- nerve impulse equation, dynamic responses of impulse 78—64972
- nerve impulse propagation, subthreshold solns. of Hodgkin-Huxley eqns. 78—77044
- nerve impulse stability theory, Hodgkin-Huxley eqns. appl. 78—48782
- nerve ionic permeability of K, Na and Cl, regulation by fixed charges and pH, crayfish 77—66809
- nerve membrane, excitatbility, genetic alteration, temp.-sensitive paralytic Drosophila mutants 80—97895
- nerve membrane, steady-state finite cable model, complementary variational principles 79—34545
- nerve membrane permeability changes, fluctuation anal. 78—11636
- nerve membranes, protein channels for Na and K ions, mol. mechanisms 77—4994
- nerve signals, dipole theory of interactions 80—81574
- nervous tissues, Ca dependent K activation, book contrib. 79—5266
- network thermodynamic two-port element, representation of salt, current coupled flow 79—34505
- neural membrane depolarisation, possible role in work of molecular computer 79—53075
- neural nets, dynamic charact. of encoders in receptors and neurons *(German)* 77—36914
- neural repetitive firing, Hodgkin-Huxley axon modification suggested by crustacean axon results 77—48776
- neuro-secretion, role of Ca in control mechanism 77—64028
- neuroblastoma cells, quiescent, rapid ionic conductance changes, serum induced 79—74612
- neuroblastoma cultured cells, membrane currents under volt. clamp 77—60193
- neuroelectric transmembrane pots., EM radiation effects, possible model of mechanisms 80—26259
- neuromuscular blockade by amantadine by suppression of acetylcholine receptor ionic cond. 78—64975
- neuromuscular junction, crustacean, ethanol effect on excitatory postsynaptic current duration 77—48777
- neuromuscular junction, frog, Ca-depend. presynaptic action 77—52773
- neuromuscular junction, frog, volt.-depend. effect of curare 77—52775
- neuromuscular junction, snake, synaptic channel gating differences at twitch and slow junctions 78—80868
- neuromuscular junction channel, in frog, endplate current fluctuations 77—25416

biomembrane transport continued
- neuromuscular synapse, response to acetylcholine 77—40660
- neuron, dorid giant, K activation associated with intraneuronal free Ca 79—8494
- neuron adaptation model allowing for Ca influence on membrane K permeability 79—79508
- neuron input current, Helix pomatia, rel. to membrane pot. and extracellular Sr and Ca ion concs. 80—81577
- neuron late outward current, Ca-dependent depression, snail 78—7335
- neuron membrane, design of a single electrode voltage clamp 80—72385
- neuron membrane Ca channels, displacement currents assoc. with activation of gating mechanism 77—81486
- neuron membrane inward Ca current, blocking effect of Cd^{2+} ions 77—81485
- neuron model of burst generation, FET analogue 77—44630
- neuronal adaptation to osmotic stress and facultative blood-brain barrier in marine osmoconformer 77—29127
- neurone Ca conduction units, Helix aspersa 78—77041
- neurone membrane, asymm. displacement currents and effect of internal F anions 77—48773
- neurones of large horse-leech, electrophysiological characts. rel. to intracellular Na$^+$ conc. 78—53374
- neurons, phenylethanolamine as putative neurotransmitter in Aplysia 77—48783
- nexus, evidence for fixed charge, permeability, obs. 80—94193
- node of Ranvier, crit. pot. of repeat responses 79—70538
- noise, 1/f, empirical relations and theories 79—24969
- noise in channels with open-closed kinetics 79—100579
- nonlinear electrotonus problem exact soln. 77—70446
- nonspiking neurones, pharmacological evidence for fast Na channels 78—73151
- opercular epithelium of killifish, isolated, membrane rich in Cl$^-$ cells, active Cl$^-$ transport 77—36882
- osmotic pressure effect on contacts and surface of liver cells 77—56354
- ouabain resistance, contact-mediated resist. in mammalian cells in culture 77—77883
- oxidative phosphorylation mechanism, role of closed condition of mitochondrial membranes 78—77013
- pancreatic acinar cell basolateral membrane, α-amylase transport 78—44481
- pancreatic islet glucose-sensitive Ca pools, rel. to secretion 77—32883
- Paramecium, artificial deciliation causes loss of Ca-depend. responses 77—2017
- Paramecium excitation, model anal. 80—61524
- passive transport of neutral solute and solvent 79—83717
- permeabilities, dynamic, meas. under non-equilib. conditions, appls. 80—46107
- permeability coefficient of the wall of a villous membrane 79—16177
- permeability of membrane system, basic property *(French)* 79—16175
- permeable tube mass transport simulation using perfectly mixed compartments 77—40696
- pesticide uptake into membranes meas. by fluoresc. quenching 78—7323
- phase change determination methods *(Czech)* 80—3599
- phospholipid artificial membrane phase state and passive permeab. for Ca ions, effect of valinomycin 78—80836
- phospholipid bilayer melting transition, thermodynamic fluctuations, ion permeability, statistical mechanics model 78—73140
- phospholipid bilayer membrane modified by valinomycin, volt. fluctuations 78—31777
- phospholipid bilayer membranes, voltage depend. channel form. by colicin K 79—8490
- phospholipid membrane, 4-dimethylaminochalcone fluoresc. probe of H_2O mol. surface mobility 79—79450
- phospholipid membranes, conductivity changes on exposure to HF EM field 79—79483
- phospholipid plane membranes, interaction of soluble brain Na$^+$, K$^+$-ATPase 80—35851
- phospholipid vesicles, NMR determs. of maleic acid permeation coeffs. 79—83711
- phospholipids, exchange between membranes, book contrib. 80—30695
- phospholipids, synthetic, ionic permeability in region of phasic transition 79—53052
- photoinduced electron transport across protein-containing membranes 80—30768
- photoreceptor, barnacle, upper limit on translational diffusion of visual pigment 80—8053
- photoreceptor rod cells, vertebrate, visual transduction, book contrib. 79—96561
- photosensory membrane of Limulus ventral nerve photoreceptor, effect of extracellular Ca/Na ratio 78—69067
- photosynthesis, electron path across membrane rel. to chlorophyll 77—44607
- photosynthesising membrane, hydrophobic pocket near photosystem II 80—55999
- photosynthetic electron transfer by radical pair mechanism, electron spin polarisation 79—34471
- physico-chemical aspects 77—29107
- physiology, flow problem, one tube 80—89703
- picrate anion active transport through organic liq. membrane 78—11556
- pituitary cell, Na and Ca action potential 77—48770
- placenta models, heat, O_2 and CO_2 transport, construct. and usefulness of models 80—3604
- plant sieve tube sucrose loading, role of pH gradient and membrane ATPase 77—52757
- plants, transfer cells and their roles in transport of solutes 78—73148
- plasma membrane H$^+$ and K$^+$ circulation, role in bacterial growth 77—90751
- plasma membrane of mouse egg, effect of fertilisation on lateral diffusion of lipids and proteins 78—44480
- plasmalemma of Nitella flexilis, selective centres of excitable channels of early ionic current 80—81568
- polarised spherical cell, ionic conc. profiles and charge distrib. 78—73144
- poly-L-lysine, membrane phase, transport processes, helix-coil transition 78—77031
- ^{125}I-polyvinylpyrrolidone, pluridisperse soln., permeab. of artificial membranes 77—12890
- Porphyra osmoregulation, struct. aspects 80—85370
- portal currents rel. to intramembrane charge displacement, one-dimens. approx. 78—31789
- postsynaptic conductance charge, quantal event at nicotine synapses, numerical reconstruction 79—83748

biomembrane transport continued
  potassium p-nitrophenoxide transport across carbohydrate membrane, cyclodextrin induced ionic equilibria perturbation 79—96523
  potential and active transport, information theory approach 80—35855
  presynaptic Ca^{2+} current rel. to synaptic transmission, in squid giant synapse 77—16926
  protein kinases, cAMP-depend., membrane-localised, and regulation, of slow inward current, frog heart 80—81567
  protein membranes, immobilised, H^{+} ion transport, assoc.-dissoc. timescale factor 79—34529
  protein secretion by pancreas, accounted for by diffusion-like process 80—21457
  protein transfer across microsomal membranes reassembled from separated membrane components 78—69029
  protein transport across endothelial membrane 80—3601
  proteins, immobilised, intrinsic electric fields and proton diffusion 79—24964
  proteins involved in active membrane transport, struct. review, book contrib. 80—108844
  proton transfer from water to octane coupled with ATP hydrolysis by chloroplast ATPase 77—36876
  proton transport, mol. mechanisms 78—96035
  proton transport across charged membrane and pH oscillations 80—61516
  Pseudemys scripta hemibladder ^{36}Cl^{-} transport meas. system 79—96529
  pulmonary capillary permeability inferred from lymph and multiple-indicator expts. 77—44604
  pulsing elastic alveoles, gas transport, conc. depolarisation *(French)* 78—85328
  Purkinje fibres, calf, role of intracellular Ca in transient outward current 77—90748
  purple membrane light-driven proton pump mechanism in Halobacterium halobium 78—35820
  purple membrane of Halobacterium halobium, quantum efficiency of proton pumping 80—72140
  purple membrane protein chromophore photoisomerisation rel. to proton pump 78—35804
  purple membrane suspensions, light-induced conductivity changes, pH and temp. effects 80—51157
  pyrene, migration between lipid vesicles in aq. soln., fluoresc. stopped-flow obs. 80—85360
  quantum-chemical investigation of cation motion mech. in membrane model 80—30678
  radionuclides, sediment-bound, absorpt. through digestive tract of marine demersal fish 79—92400
  Ranvier nodes exposed to DDT, asymm. currents and Na currents 77—48778
  reaction-diffusion problem, nth order, asymptotic anal. 79—11764
  red blood cell plasma membrane, Ca^{2+} transport stimulation by calmodulin 80—12066
  red cell, human, increased passive permeability below 12°C 80—94185
  red cell ghosts, human, Ca-depend. K efflux, effect of carbocyanine dyes 77—12896
  red cell ghosts active transport, cytoplasmic contamination, electron microscopic obs. 80—45874
  red cell membrane, Li transport in manic depressives 80—61525
  red cells in dilute suspensions, turbulent flow and effect on O$_2$ uptake kinetics 77—60223
  renal brushborder membrane vesicle, proline and glycine uptake 77—44614
  renal countercurrent model eqns., numerical soln. 77—40698
  renal counterflow system transient soln. computation 77—40699
  renal medulla, osmotic equilibration by descending limbs of Henle's loop 77—40701
  renal medulla solute cycling model soln. by Laplace transforms 77—40694
  renal network flows, a priori bounds 77—40693
  renal solute and water movement models and soln. 77—40692
  renal tubule model injection transient response calc. 77—40700
  reptile epidermis, water permeability rel. to lipid content 80—97875
  respiration model analytical soln. 79—48282
  responsiveness curve automated on-line determ. 78—92761
  retardation currents in excitable membranes and models of flicker noise 78—92618
  retinal rod, localisation of Na^{+}, K^{+}-ATPase and Ca^{2+}-activated Mg^{2+}-depend. ATPase 77—44652
  retinol-binding proteins in retinal pigment epithelium 79—20525
  rhodopsin-containing bilayer membranes, light-induced transmembrane channel form. 77—52784
  rod, Ca-depend. regenerative responses 78—3480
  rod disc membrane ion transport props. 78—15829
  rod disc membrane phosphodiesterase control 79—79527
  rod external segment fragment suspension, Ca^{2+} activity rel. to illum. 77—36918
  rod external segment surface membrane, lateral diffusion of rhodopsin 78—15828
  rod outer segment adaptation anal. based on a simple equiv. cct. 78—73157
  rod outer segments membrane current fluctuations 79—79530
  rod outer segments membrane current obs. 79—79529
  rod photoreceptor membrane, pot. regulation by cyclic GMP 79—74654
  salivary gland cell junction, Ca^{2+} produces graded changes in membrane channel permeab. 77—64016
  salt gland, avian, significance of extensive leaky cell junctions 77—77880
  sarcolemmal permeability changes during early myocardial anoxia 80—85371
  sarcoplasmic Ca pump, efficient ion translocating system 77—90746
  sarcoplasmic reticulum, fragmented, voltage-dependent Cs^{+} blockage of K^{+} channel 79—96524
  sarcoplasmic reticulum Ca^{2+},Mg^{2+}-ATPase transient kinetics obs. by fluoresc. 78—61156
  sarcoplasmic reticulum membrane rearrangements on peroxide oxidation of lipids 78—69025
  sarcoplasmic reticulum membranes, temp.-dependent functional changes 80—81550
  sarcoplasmic reticulum vesicle permeability, light scatt. meas. 77—12889
  Schwann cell layer of squid axon, diffusion models 80—40985
  serotonergic excitation, unconventional response in Aplysia 77—86484
  sinatorial node of rabbit heart, vagal stimulation, K^{+} permeability and extracellular transients 78—92608
  single-file ionic transport theory, reduced flow diagrams 78—69022

biomembrane transport continued
  single-file model of ion transport, predicted current rel. to internal state transitions 80—85359
  single-ion channels in unmodified membrane at phase transition temp. 80—45559
  skeletal muscle of frog, displacement currents, K cond. channel contrib. 79—39409
  skin, human, permeation of scopolamine in vitro 77—21487
  skin, role of diffusion during transport of radioactive substances 78—20158
  skin, transport of radioactive substances, diffusion model 77—81483
  skin Na entry site irreversible inhibition by photosensitive amiloride analogue, in frog 78—69030
  skin of frog, radioactive Na washout rate anal., numerical simulation 78—3456
  soleus muscle, rat, electrogenic Na^{+}-K^{+} transport obs. 80—21456
  solute transport, review of current ideas 77—32878
  spectrin-actin monolayer, adsorbed at Hg-H$_2$O interface, ionic permeability 80—12064
  sphingomyelin bilayer systems, monolayer coupling, choline methyl proton line width 78—35807
  spinal motoneurones refractoriness accumulation and secondary range firing model 77—1985
  squid giant axons, oscillatory subthreshold responses and pot. fluctuation obs. 78—27918
  stomatal function, blue light-stimulated swelling of guard cell protoplasts 77—77885
  stratum corneum of rat, surfactant diffusion and sorption phenomena, model for human skin 78—77007
  subcellular particle membrane pot. diff., proton channels in oxidative phosphorylation 78—64964
  subcellular particle membrane pot. difference, compensation meas. method 77—56547
  subcellular particle pot. difference, chemiosmotic and chemielec. generation mechanism 77—52751
  substrate exchange between vascular and extravascular compartments, saturation kinetics 80—104571
  sugar transport system dependent regulation of adenylate cyclase, review 78—69031
  sweat secretion, role of Ca, in vitro meas. 78—40129
  synaptic action of pentylenetetrazole, selectivity for Cl cond. 78—7336
  synaptic and ephaptic transmission, quantum mech. tunnelling model 77—52772
  synaptic conductivity effect on conditions of spike appearance 79—79507
  synaptic terminal, choline transport obs. 79—70544
  synaptic transmission, long-lasting potentiation by postsynaptic mechanism 77—32885
  synaptosomal preparation, depolarisation-induced ATP release, direct detect. 77—48779
  synthetic voltage-dependent cation-selective transmembrane channel characterisation 78—77009
  taste reception, physicochem. mechanism and chem. sensors development *(Japanese)* 80—85423
  teaching, single-file diffusion 78—54127
  tetraethylammonium binding sites in crayfish axon membranes 77—64026
  tetrodotoxin, volt.-depend. action 77—44620
  thylakoid membrane of green plants, simulation of electron transport in primary photosynthesis reaction, in PL/1 *(German)* 77—86468
  thymocyte membrane props. modification by hyperthermia and gamma-rays 78—69017
  tissues, excitable, dipole flip-flop theory for excitation and conduction 80—101153
  tonoplast ionic channels in charophyte algae cell, role of Ca ions in excitation 77—81481
  trabecula membrane of frog auricle, electrophysiological characts. from ionic currents on pot. clamping 78—24049
  tracheal ephithelium, effect of Ca on ion transport and elec. props. 79—34527
  tracheal epithelium, dog, interdependence of Na^{+} and Cl^{-}transport 80—61519
  tracheal mucosa, canine, interaction between Na^{2+} and Cl^{-} transport 79—88060
  transcapillary water movement resulting from non-oncotic osmotic forces 78—44548
  transepithelial current-voltage relationships of toad urinary bladder and colon 79—92195
  transepithelial electrical parameters in midgut of Lepidoptera larvae 78—20154
  transepithelial ion transport endogenous regulation, implications of ouabain-like activity in toad skin 78—73147
  translational dynamics, fluorescence redistrib. after photobleaching obs. 80—21491
  transmitter kinetics model computer simulation results 78—92617
  unmyelinated nerve Na channels optimum density, analytic treatment 78—24061
  urophysis, transport across isolated skin of a marine teleost 79—74617
  vascular walls, physical theory of permeability rel. to atherogenesis, mech. effects 80—16908
  ventricular action potential, mammalian, analysis 79—62227
  ventricular muscle, mammalian, slow inward current depression by acetylcholine 79—92210
  vesicle membrane, large unilamellar, ^{1}H NMR study of acetic acid permeation 80—8031
  viral infection, membrane leakiness, rel. to development of antiviral agents 78—53371
  visual cell, proposed role of cyclic GMP 78—64997
  visual cell membrane cond. control, arthropod 78—15831
  visual cell microvilli membrane fragment protonic and ionic processes, cephalopod 78—73159
  volumetric charge effects on membrane and near-membrane transport processes 78—53366
  water, self diffusion in frog muscle 80—8037
  water diffusion meas. by pulsed gradient NMR, cell struct. size determ. 78—77159
  water diffusion through narrow pores, ^{1}H NMR obs. 79—92194
  water transport, NMR methods *(Rumanian)* 80—94435
  yeast cell membrane, water transport study, pulse NMR obs. 80—40981
  Ca conductance, inactivation without facilitation in Cs-loaded Aplysia neurones 78—56965
  Ca pump driven by ATP in squid giant axons 78—77043

biomembrane transport continued
Ca spike enhancement during neurite in tissue culture 79—70545
Ca, transport in intestinal epithelium, extracellular route *(Russian)* 78—40128
Ca^{2+} conductance of acetylcholine-induced endplate channels 79—70546
Ca^{2+} current in Paramecium, inactivation of Ca channel 79—79488
Ca^{2+} incoming current obs. in trabeculae of frog atrium 79—79497
Ca^{2+}, passive and active fluxes across membranes, review 80—97886
Ca^{2+} voltage-depend. facilitated entry into voltage-clamped aequorin injected molluscan neurons 77—90763
Ca-Na channel of cell, reconstruction in lipid bilayer 77—25404
Cl^- active transport inhibition by piretanide, in teleost intestine cell 78—64967
Cl^-, role of Ca^{2+}-dependent regulator protein in intestinal secretion 79—66454
^{137}Cs, study of absorpt. by Lemna minor 80—30677
H^+ channels and mol. electrostatic generators 77—21501
K channel blocking agent, 3,4-diaminopyridine 78—69028
K channel ionic interactions, squid giant axon 78—3458
K current components in node of Ranvier membrane frog Rana ridibunda 78—31800
K ion noise currents and inactivation in voltage-clamped node of Ranvier 77—16924
K^+ currents in squid axons, single channel recordings 80—76721
K^+ ion flux through membrane channels, nerve impulses, random walk anal. 78—77045
K^+ ion transport inducing compound identification in mitochondria and bilayer lipid membranes 78—31788
K^+ permeability of E. coli, membrane lipid role in radiation damage 78—48834
K^+ permeability of mitochondrial and artificial bilayer membranes 78—53365
K^+ permeability of pancreatic islet cells, effect of Ca^{2+}, glucose 79—74615
K^+ transport of squid axon membrane, internal pH effects 79—62221
K-like channel passage of ions, physical model 77—56356
Li^+ ion entry through Na channel in cultured mouse neuroblastoma cells, biochem. obs. 77—81487
^{15}N-NH_4, absorpt. and transfer to amino-N, rat small intestinal sac 80—16909
Na^+,K^+-ATPase generation of pot. jump at octane-water interface 77—81484
Na channel, fully coupled excited state model, conductance in volt. clamped case 78—85297
Na channel, fully coupled transient excited state model, action potential generation, threshold, accommodation and repetitive firing 79—57634
Na channel, graph of states 77—25383
Na channel density in myelinated nerve fibres and nature of axonal membrane 77—52777
Na channel fluctuations, phys. nature, microscopic model 80—35869
Na channels, inactivation delay in biological membranes 80—45872
Na channels, one-to-one binding of purified scorpion toxin, tunicate egg membrane 77—32877
Na channels in nerve, evidence for two conductance states 78—11634
Na channels in squid giant axons, n-alkanol potentiation 79—83744
Na permeability inactivation in squid giant nerve fibres, review of exptl. work 78—73154
Na pump, electrogenesis in model of boundary transfer 77—25401
Na pump activation by external cations in squid axon, effect of ATP levels 78—35818
Na pump in red blood cells, cholesterol interactions 77—12898
Na transport mediation by ionophore A23187 in absence of divalent cations 78—11623
Na^+ intracellular activity rel. to Na^+ transport across a tight epithelium 80—67051
Na^+ multicompartment flow model of frog skin epidermis, experimental verification 78—92607
Na^+ pump, unphosphorylated, occlusion of K ions 79—88065
Na^+ pump rel. to increasing thermogenesis in cold acclimation in rats 78—7326
Na^+ saturation kinetics in frog skin, compartmental aspects 80—67050
Na-channel gating current carriers, electronic model 79—70542
Na-K pump reversal and apparent affinity for intracellular K 77—86473
Na-like channel passage of ions, physical model 77—56355
Na-specific membrane channels of frog skin, pore mechanism, current fluctuation obs. 77—36883
^{99m}Tc-labelled radiopharmaceuticals, brain uptake by passive membrane transport 80—51053
^{133}Xe diffusion through frog skin, toad bladder and water boundary layer 77—66803
Zn^+, transport in cation-exchange membranes 78—96033

biomembranes
see also biomembrane transport; lipid bilayers
9.712 GHz irradiation effect on vagal heat membrane bound acetylcholinesterase 80—3593
Acetabularia cell electrical parameters and equiv. cct. 77—56350
acetylcholine receptor from Torpedo Californica, struct. anal., low-angle neutron scatt. obs. 80—30651
acetylcholine receptor phosphorylation by membrane protein kinase in receptor-enriched T.californica membrane 77—56370
acetylcholine receptor phosphorylation in vitro, E. electricus membrane fragments 77—56371
acetylcholinesterase, membrane bound, activity rel. to struct. changes induced by cAMP 80—30674
active transport, variational-Lagrangian thermodynamic theory 78—41255
adenylyl cyclases, stimulation by hormones and regulation by nucleotides, review 78—15760
adhesion of artificial membranes, bivalent cations effect 78—64946
adsorbed monolayers of lecithin and cholesterol on aerosil, as model membranes, IR spectra 78—15753
adsorption isotherm for study of interfacial and biological phenomena 77—59207
ageing process, role of cell membranes, review 78—15809
aggregation in membranes, fluctuation-induced interactions in liquid crystals 77—90732
n-alkanes, adsorption into bimolecular lipid layers 80—88435
anaesthetic effects, struct. rearrangements 77—36873
1,8-anilinonaphthalene sulphonate in bacterial suspension, fluoresc. spectra 79—88052

biomembranes continued
animal plasma membranes, study using freeze-fracture technique 80—104842
antibody binding and complement interactions at the cell surface, dynamics, book contrib. 80—30689
antibody-bound membrane for electrochem. determ. of immunoglobulin G 79—53293
antigenic nature of mammalian cell surfaces, review 78—15805
architecture obs. by electron energy loss spectroscopy 79—25177
artificial membranes, excitable and ion-selective, review of axon and bilayer membrane props. 77—86451
artificial membranes, excitable and ion-selective, review of non-bilayer lipidic membrane props. 77—86452
asymmetry, review 77—48768
ATPase, Ca^{2+}-activated, of sarcoplasmic reticulum, rot. motion and evidence for oligomeric structs. 80—72124
Na, K-ATPase membrane prep. struct. characts. studied by paramag. probes 78—64930
ATPase of A-laidlawii membrane, Arrhenius plot artifacts due to temp. depend. of substrate-binding affinity 78—64949
atrial trabecula membrane, frog, accommodation, repeat responses and anode-breaking excitation 78—64956
atrioventricular region of rabbit heart, passive elec. props. rel. to intercellular link 78—48767
atrium trabecula membrane, changes in elec. props. due to elec. stimulus 77—36891
axon, squid giant, compensation of potential changes produced by Er ion with applied potentials 79—16181
axon membrane admittance change during action pots., squid 79—57621
axon membrane asymm. current, squid, freq. domain anal. 78—44494
axon membrane white noise, stimulation, strength-freq. relationship, squid 78—3466
bacillus megaterium membrane lateral phase separations and chlorotetracycline transport 79—24971
bacterial cell wall, surface charge and morphogenesis of regular arrays of macromols. 80—85366
bacterial chemotaxis, cyanine fluorescent dye membrane probe effects on cell props. 78—35815
bacterial chemotaxis in Escherichia coli, membrane pot. changes 77—44695
bacterial membrane, light-induced generation of elec. pot. difference 78—28001
bacterial radiation survival, E. coli, effect of membrane fluidity 77—21568
bacterial sensory electrophysiology, motility depend. on membrane pot. and chemotaxis 78—53373
bacteriochlorophyll monolayer quantum yield and image contrast in photoelectron microscopy 78—44453
bacteriorhodopsin, photoelec. conversion in charged synthetic membranes 80—108954
bacteriorhodopsin Br570, bathochromic shift of absorpt. band in external elec. field 80—35838
bacteriorhodopsin membrane preps. associated with lipid-water interface, form. of elec. pot. diff. 80—81551
bacteriorhodopsin orientation in Halobacterium halobium, selective proteolysis investig. 78—77010
barnacle photoreceptors, lateral vs. median, elec. props. and early receptor pots. 77—44651
basilar membrane, 2-dimens. model of cochlear fluid 77—32906
basilar membrane, anisotropic rigidity components evaluation 79—79569
basilar membrane, auditory system pitch detection mechanism model 77—90811
basilar membrane, gerbil and guinea pig ear, sound transmission and cochlear microphonic characts. 77—32909
basilar membrane, mechanism for transforming mech. to neural tuning within cochlea 78—11666
basilar membrane, nonlinear electric circuit model, distortion 77—25459
basilar membrane, nonlinear model rel. to two-tone suppression 77—48811
basilar membrane, two-stage lateral inhibition for auditory selectivity 77—56382
basilar membrane displacement, electronic model 77—29159
basilar membrane electronic model for evaluation of speech disorders 78—40206
basilar membrane model, nonlinear, meas. apparatus and circuits *(Japanese)* 78—35868
basilar membrane model using digital filter for voice features extraction 78—77069
basilar membrane motion linear and nonlinear models 77—90800
basilar membrane nonlinear model assessment, spatial differentiation as auditory second filter 77—36949
basilar membrane nonlinearity 77—25461
basilar membrane point-impedance charact. in cochlear mechs. 78—57009
bilayers quasitwo dimens., theoretical models 80—76713
bilipid vesicles, theoretical shapes under conditions of increasing membrane area 79—24960
bimolecular lecithin membranes, artificial, rheological and viscoelasic props. 80—26252
bimolecular membranes, interaction with liposomes, elec. resistance obs. 80—81549
bio-selective membrane electrode using tissue slices 79—48387
biochemical reactions, fast, in solns. membranes and cells, conf., Airlie, USA (Apr. 1978) 79—8485
bioenergetics and proton-electron systems of membranes, review 78—96030
biomembranes, lipid-protein interactions, flexoelectric effects 78—92600
birefringence, interpretation of results of studies in transmitted polarised light 77—37113
birefringence analysis in biological materials 78—56954
black lipid membranes and bilayer vesicles in solution, thermodynamic stable states anal. 80—45856
blood, red cells as fluid droplets, erythrocyte membrane dynamics in shear flow 79—74711
blood cell damage in extracorporeal circulation, haemorheological effects of mech. factors 79—62280
blood cell membrane phospholipid asymm. rel. to coagulation 77—73511
blood oxygenation simulation in stirred membrane cell 78—40421
bone, microscopy cell distributions topographical size analysis, TOGA interactive program *(German)* 77—40951
brain rhythmic activity generation models *(Dutch)* 78—73150

biomembranes continued
- brush border of renal proximal tubule and intestinal mucosa, review 78−15815
- burst-generating neuron model, field effect transistor analogue 77−25411
- cardiac cell membrane electrogenesis, selective adaption 79−57617
- cardiac intracellular transmembrane action pots., automated anal. 79−70729
- carrier mediated transport theory, survey of applications 77−89113
- cell adhesion, review 78−15803
- cell adhesion models, reaction kinetics and forces 78−80844
- cell binding, role of surface carbohydrates 78−15804
- cell cycle regulation by membrane, mathematical model 79−92180
- cell division, model relating cell deformation to elastic props. of cell membrane 80−3606
- cell electric circuit model, alternating signal interaction 78−77011
- cell electric circuit model, alternating signal interaction 78−77012
- cell growth in vitro, rel. to cell surface, review 78−15808
- cell membrane fluidity screening using fluoresc. polarisation microscope 77−44855
- cell membrane interaction theory of molecular level mechanics 79−92174
- cell membrane nuclear hydrodynamic shear, non-equil. Ising model, master eqn. 78−61146
- cell membrane organisation dynamics, book contrib. 80−30687
- cell membrane particle diameters meas. by computer from electron micrographs 80−101307
- cell membrane particles, max. density of random placing 79−44862
- cell membrane particles diameter meas. via picture processing 79−84065
- cell membrane potential changes on X-irradiation 79−39369
- cell membrane potential levels in Acetabularia 77−70427
- cell membrane radiobiology, impact on radiation protection 79−70585
- cell membranes, at mol. resoln., introduction 80−104841
- cell membranes, effects of hydrostatic pressure, review 78−15790
- cell membranes, ionising and UV radiation effects, review 78−15875
- cell motility and adhesion measures, Markov chain model 77−66804
- cell surface immunoglobulins, characts., mobility and role in immune phenomena, review 78−15806
- cell surface organisation, dynamic aspects, book 80−27047
- cell surface receptors, molecular movements 80−45866
- cell suspension physiology and induced pathophysiology, noninvasive analysis using EM method 79−2125
- cell wall, Acetabularia, deform. rel. to genetic and geometric factors 77−56348
- cell wall deform. and morphogenesis, local control of viscoelastic deform., Acetabularia 77−56349
- cerebral tissue, Ca^{2+} binding rel. to weak oscill. elec. fields 77−1984
- chemical reaction kinetics, modelling non-enzymatic influence of membranes 78−64945
- chlorophyll black lipid membranes in dil. electrolyte solns., bifacial tension meas. 79−16162
- chloroplast membrane proton gradient and osmotic vol. determ. 78−28143
- chloroplast membranes, effect of protons and cations visualised by bound ANS fluoresc. 78−24034
- chloroplast millisecond afterglow, activation and suppression 78−96025
- chloroplasts, isolated, broken, fluoresc. changes and involvement of elec. double layer 78−44464
- chloroplasts and subchloroplast fractions, linear dichroism 77−90744
- cholesterol in erythrocyte membranes and models, interaction of lucensomycin, spectral parameters 77−9177
- chromaffin granule electrophoretic mobility meas. by light scatt., effect of Ca^{2+} and Mg^{2+} 78−53357
- chromatophores, oriented, of photosynthetic bacterium Chromatium minutissimum, linear dichroism 80−35841
- chromophore orientation in micellar, liposome solns., liq. cryst. phases, dichroism, NMR 79−53059
- chromophore transverse location, determ. by fluorescence energy transfer in the rapid-diffusion limit 79−92151
- chromophores in membrane suspensions, determ. of orientational order, intensity depend. of flash-induced anisotropy 80−94177
- cochlea, disc model rel. to hydrodynamics in gap between cover membrane and organ of Corti *(German)* 77−86505
- cochlear LF variable geometry model for morphological disorder compensation 78−40182
- coloured membranes, unsymmetric, rectification and current oscillation *(Japanese)* 77−36871
- concanavalin A binding to cell membrane of Herpetomonas samuelpessoai, UV effect 78−48835
- corneal stroma, small angle X-ray and neutron diffr. study 79−11923
- current pulse-induced voltage variations in bilayer membranes, apparatus 80−94420
- cylindrical cell with time-variant membrane resist., passive parameter meas. 77−29113
- cytochrome *a* interaction with mitochondrial matrix H$^+$ ions 79−43806
- cytoplasm spherical drop with effective surface tension influenced by oscillating enzymatic reactions 80−108862
- cytoplasmic membranes in somatic cell interaction and hybridisation, review 78−15792
- DECHEMA symposium, Tutzing, Germany, (Mar. 1978) 80−62373
- Deiter's cells of organ of Corti, well developed gap junctions 77−29155
- dimyristoyl lecithin lipid vesicles, sonicated, ^{13}C relax. times model for gauche-trans isomerisation 78−33520
- dioleoyl-phosphatidylcholine/dipalmitoyl-phosphatidylcholine bilayer membranes, phase transitions 79−39367
- dipalmitoyl phosphatidyl choline vesicle damage by picosecond laser pulses 79−79599
- dipalmitoyl phosphatidylcholine containing CaCl$_2$, monodomain sample phase behaviour birefr. obs. 79−83712
- dipalmitoyl phosphatidylcholine vesicles, appl. of depolarised light scatt. theory from hollow spherical particles 80−45946
- discrete charge effect, dipicrylamine anions surface absorption 79−16159
- distance measurement by radiationless energy transfer, transition probabilities 78−24187
- DNA synthesis by DNA-membrane complexes from electron irradiated E. coli 79−16167
- drug tolerance, spin label study of ethanol effects 77−66799
- dye indicators of membrane pot., review 80−21594
- dynamic aspects, review 78−69005
- dynamic receptor pattern generation model 79−62207
- dynamical mechanical spectroscopy, mol. interactions 77−29109

biomembranes continued
- E. coli, membrane struct. rearrangements in presence Ca^{2+} induced by heating 79−79482
- E. coli fatty acid auxotroph, factors influencing survival after γ-irradiation 80−17007
- eardrum vibration meas. using electronic speckle pattern interferometry 80−67209
- E.coli, radiation killing, role of membrane fluidity, hypothermia and local anaesthetics 80−104653
- EEG potential in model of thin cerebral membranes, tangentially orientated dipoles 78−15818
- EEG potentials in model of thin membranes of brain, multilayered spherical cable model 77−25408
- egg cell membrane elec. props 80−21455
- egg lecithin, magnetic anisotropy obs. 79−20520
- egg lecithin+myelin protein (N-2), X-ray diffr. anal. 79−57600
- egg lecithin+myelin protein (N-2), X-ray scatt. obs. 79−57601
- Ehrlich ascites tumour cell membranes damaged by X-rays, biochem. interaction of heparin 78−31864
- Ehrlich ascites tumour cells, influence of O$_2$ tension of X-ray-induced fall in anodic mobility 79−34526
- elastic and viscoelastic monolayers, dynamic surface potentials 80−3603
- elasto-viscous properties determined from bilayer meas. 80−30671
- electric and magnetic props. in smectic liquid crystal state *(Russian)* 77−60190
- electric properties measurement method using glass electrode impaled into single cell 80−89916
- electrical capacity of membrane-covered cubes in cubic array at high conc., analogue soln. 77−40642
- electrical double layer theory, through Born-Green-Yvon eqn. 80−35539
- electrically excitable membrane, phys. model, excitation mechanism 77−36902
- electrically excitable membrane, phys. model, voltage-current characts. 77−25382
- electrically excited, nonlinear dynamic models for simulation 80−94178
- electron density profiles, determ. method on an absolute scale 79−16358
- electron microscope contrast enhancement of negatively stained macromols. and biomembranes by single sideband phase contrast interference 77−45920
- electron microscopic analysis at mol. level resolution, prep. procedures 80−104843
- electronic neuron model incorporating both active and passive responses 80−8040
- embryonic skeletal muscle differentiation, electrophysiological and biochem. membrane props. 78−53363
- energetics, conf., Bloomfields Hills, USA (Jul. 1979) 80−94923
- energy control, review 78−15807
- energy transduction, mol. probes, review 77−21666
- energy transformation, intracellular, phys. aspects 77−86462
- enzymes, membrane bound, influence of membrane fluidity on activity, book contrib. 80−30688
- enzymes, membrane-bound, activity on exposure to 2450-MHz microwave radiation 80−56126
- epithelial cells of Hydra, mechanically dissociated, spontaneous and evoked pots. 77−21499
- epithelium, living, size and shapes of lateral intercellular spaces 78−77032
- epithelium, tight, impedance anal. using distributed resistance model 79−62201
- epithelium mucociliary activity during exposure to ionising radiation, temp. effect 77−70493
- epithelium of small intestine, mech. props. of intercellular contacts 78−53351
- erythocyte membranes, complement proteins interaction, ESR 79−100584
- erythrocyte, human, chloride distrib. and transport, cell membrane struct. 77−1983
- erythrocyte, human, dynamic osmotic haemolysis and ghost repair, resistive pulse spectra 79−62208
- erythrocyte, rheological models *(French)* 78−24083
- erythrocyte electrophoretic mobility, effect of UHF EM radiation 78−53442
- erythrocyte ghost IR spectra in region of amide I and II bands on microwave irrad. 77−86531
- erythrocyte ghost membrane, collimation correction for non-isotropic small-angle X-ray scattering curves 79−10755
- erythrocyte ghost membrane, deconvolution method for evaluating small angle X-ray scattering 79−10756
- erythrocyte ghost membrane, human, electron density, small-angle X-ray diffr. 77−73510
- erythrocyte ghost membrane struct. effects of fusogenic agent, fusion mechanism 78−31782
- erythrocyte ghosts, human, fusion promoted by Ca^{2+} and PO$_4$ ions 77−4987
- erythrocyte membrane, appl. of nanosecond fluorometric system 77−17010
- erythrocyte membrane, carbocyanine dye orientation, microscopic fluorescence polarisation obs. 79−83694
- erythrocyte membrane, cooperative pH-sensitive state transition, Raman spectroscopy 77−36881
- erythrocyte membrane, phys. state of lipids, X-ray diffr. 78−80835
- erythrocyte membrane, spin-label study of γ-irrad. effect 80−51168
- erythrocyte membrane, viscoelastic props., theoretical and expt. studies 79−16157
- erythrocyte membrane, X-ray induced structural changes, fluorescent probe obs. 79−88129
- erythrocyte membrane alterations, rheological technique evaluation 80−61611
- erythrocyte membrane fluidity, adult and neonatal human cells 77−36885
- erythrocyte membrane lattices, partially disordered, X-ray scatt., anal. method applied 78−91196
- erythrocyte membrane protein alterations in Huntington's disease, EPR 77−56347
- erythrocyte membrane struct., radiation effects, intrinsic fluorescence obs. 79−74724
- erythrocyte membrane struct. changes due to cAMP, spin-probe study 78−31779
- erythrocyte membrane viscoelastic props., area and vol. of cells entering micropipette 77−29114

biomembranes continued
erythrocyte membrane-haemoglobin interaction, γ-ray effects, EPR 78—7402
erythrocyte membranes, ESR study of abnormalities in Duchenne muscular dystrophy 78—96111
erythrocyte membranes, fluidity change after X-irrad., pyrene excimer fluoresc. obs. 80—72262
erythrocyte membranes, human, elec. cond. characts., ghosts and lipid bimol. membranes 77—9180
erythrocyte membranes, US absorpt. in 12 to 68 MHz range 80—89727
erythrocyte surface charge decrease, target of X-irrad. and dislocation of sialic acid 77—52853
erythrocytes, human, glycophorin and concanavalin A receptor 78—48764
erythrocytes, membrane protein vertical displacement, rel. to microviscosity changes 77—44608
erythrocytes of human blood, diameter meas. by specific elec. cond. 78—53353
excitability, review 78—15786
excitable, statistical theory, nonlinear force-flux reln. and fluctuation 77—9179
excitable, surface-charge density when exposed to optical radiation 77—29176
excitable biomembrane electronic cct. model utilising time variant negative res. 78—88696
excitable cell model, numerical method 78—53376
excitable medium model with existence of several stable pulses of different duration 78—77036
excitable membrane analysis, computer calcs. 80—56004
excitable membrane phenomena, mathematical analysis 79—74635
excitable nerve membrane exposed to optical radiation, surface-charge density variation, comment 79—8524
fatty acid auxotroph, membrane fluidity, EPR study 79—70574
fatty acid composition effect on E. coli K-1060 radiosensitivity 79—92306
ferredoxin-like centres, membrane bound, in photosystem I of blue-green algae, Mossbauer and EPR study 80—40974
fetal membrane tissue, human, elastic parameters determ. 79—66481
Fitzhugh nerve conduction equations, appl. of higher order Hopf bifurcation formula 77—86483
FitzHugh-Nagumo equations, perturbation anal. of slow periodic wave soln. 78—24060
fluid disturbances, compartmental anal. *(Japanese)* 80—3607
fluidity modification, mechanism of hyperthermic cell killing and therapy appl. 80—104569
fluorescence and fluorescent probes, appls. 78—15932
fluorescence decay, direct meas. apparatus *(French)* 77—5116
fluorescence polarisation, meas. apparatus *(French)* 77—9307
fluorescence polarisation decay theory 78—20138
fluorescence spectroscopic investigations of the dynamic properties of proteins, membranes and nucleic acids 80—101148
fluorescence test, rapid modification base on Microtiter system 78—20334
fluorescent probe binding to proteins error in interpretation of double-reciprocal plot and Scatchard plot 78—24021
fluorescent probe interaction with surface structs. of E. coli 78—69007
foetal membrane rupture, human, mechanics, superempirical mathematical model 79—83843
Forster energy transfer problem in 2D, analytic soln. 80—26195
Fourier transform IR transmission spectroscopy, appl. to natural and model membrane study 80—17218
fracture faces obtained by freeze fracturing, complementary struct., digital image processing 79—62205
freeze-etching results interpretation 78—28141
freeze-fracture replication, in biological research, review 78—40444
freeze-fracture techniques and appls. in struct. anal. of mammalian plasma membranes, book contrib. 80—30960
freeze-fracturing effects on membrane struct. 78—28140
freeze-fracturing of capillary layers of cells, membranes, viruses, new hinged device 78—20327
freezing injuries, membrane destabilisation of egg yolk membrane *(French)* 79—48221
frog node, Cole-Moore effect 79—92170
functions and molecular properties *(Japanese)* 77—70422
gap junction structure and cell coupling, Ca^{2+} effects 78—31786
gastrointestinal electrical rhythm simulation, differential quadrature method 77—44634
giant axon, inner surface struct. obs. by SEM 77—70579
gramicidin A in biomembrane channel, IR spectroscopic obs. 80—16901
green-rod outer segment membrane of frog, photoproduct orientation 77—25433
H. halobium, light-induced surface pot. changes in purple membranes and bacteriorhodopsin liposomes 80—98015
Halobacterium halobium membrane microstruct. 77—25386
Halobacterium halofium, photo-products spectral conversions, purple membrane formation 79—57605
hearing mechanism, tympanic membrane vibr. anal., holographic interferometry obs. 80—76879
n-hexadecyltrimethylammonium bromide micelles, ^{13}C relax. times model, for gauche-trans isomerisation 78—33520
Hodgkin-Huxley equations for nerve membrane elec. activity, crit. topological test 78—35826
Hodgkin-Huxley reduced model, speed of spread of excitation, integral differential eqn. 77—21509
host cell membranes in animal virus reproduction, review 78—15791
human red cell membranes, surface adsorpt. of dextrans 78—15799
hydrophobic effect, organisation of living matter 79—11887
hyperthermic cell death, influence of membrane lipid composition and procaine 78—27907
immobilised enzyme membrane oscillations and pH fronts 77—25387
immobilised enzyme systems, optimisation of porous glasses 77—12891
immune cell membrane receptors, rel. to memory *(German)* 77—66811
immunoresponsive membrane, pot. associated with immunochem. reaction between membrane-bound antigen and free antibody 77—86453
intercellular communications and membrane electrical noise in embryonic heart cells 77—44612
interdigital membrane of frog, const. mag. field effect on microcirculation 77—32935
intervesicular lipid transfer, direct fusion of phospholipid vesicles, kinetic basis comparison 78—96034

biomembranes continued
intestinal smooth muscle cells, non-cholinergic excitatory transmission 77—77891
intracellular membrane microviscosity, rat liver and hepatoma 27 80—30675
iontophoresis circuit isolated current monitor for cell membrane studies 77—60311
IR-ATR spectroscopy, appl. to struct. investigation of biological material in aq. environment 80—61735
kidney membrane conformational changes anal. after renal ischemia 78—73142
lechithin-cholesterol interaction, effect of lecithin struct. 78—64922
lecithin, inelastic light scattering at second micellar formation 77—21492
lecithin bilayers, spontaneous form. at air-water surface 79—74603
lecithin liposomes, binding sites for Fe(CN)$_6^{3-}$ ions, PMR obs. 79—79481
lecithin membrane, depend. of Young's modulus in plane of membrane on deform. 78—80894
lecithin membranes, mag. susceptibility anisotropy, phase contrast microscope obs. 78—92601
lecithin monolayer model, equilib. and metastable states 77—60188
L$_\alpha$-lecithin multilayers, shear-induced biaxiality near solid surfaces 78—24035
lecithin vesicle shapes, rot. symmetric, opt. microscopy 77—64011
lecithin-water system, structural changes 78—96023
lethicin, bilayer, elastic props., in direction perpendicular to membrane plane 79—57602
librational motion effects on fluoresc. depolarisation and NMR relax. in macromols. and membranes 80—85324
light irradiation of fluorescent concanavalin A, membrane damage 80—56123
light scattering from biological cells, backscatter depend. on membrane thickness and refr. index 79—48225
lipid bilayer, of dipalmitoyl-lecithin, NMR dispersion of layers dispersed in D$_2$O 79—48223
lipid bilayer chromophore energy transfer 79—62200
lipid bilayer couple, cation-phospholipid-induced shape changes 80—108855
lipid bilayer head group, orientational order and rotational diffusion, NMR obs. 80—21451
lipid bilayer membrane incremental resistance unaffected by anaesthetics 79—83718
lipid bilayer phase transition, semiphenomenological model 77—35670
lipid bilayer structure, X-ray refl. phases from oriented model membrane systems 78—96022
lipid bilayer vesicles and liposomes, conc. quenching of chlorophyll fluoresc. 77—4985
lipid bilayers, cytochrome b$_5$ rotational diffusion, influence of lipid physical state 79—83693
lipid bilayers, effect of oxidation and hydrolysis on elastic props. 79—92165
lipid bilayers, elastic props. changes on exposure to different agents, elec. and chem. 80—81548
lipid bilayers, spin probes EPR partitioning between lipid and aq. phases 79—79455
lipid cell membranes, thermal structural rearrangements 79—92163
lipid free radical oxidation, UV effect on lipid-protein complexes and membranes 77—36874
lipid function in excitable membranes 80—12095
lipid hydrocarbon chain, biomembrane, rot. motion and fluidity 80—76714
lipid layers and membranes, dynamic molecular organization 79—39364
lipid membrane models, dose-rate and O$_2$ effects, linoleic acid 77—48841
lipid mobility and organisation, using D-NMR and spin label EPR as probes 77—44600
lipid monolayer, statistical mech. theory 78—73141
lipid monolayer phase transitions, model 78—2338
lipid monolayers and bilayers, phase transitions, model 78—44460
lipid organisation in Acholeplasma laidlawii membranes, ^{2}H NMR 77—86456
lipid thermotropic clustering in Tetrahymena endoplasmic reticulum membranes 80—85363
lipid-protein interaction in membrane bound Na$^+$, K$^+$-ATPase, spin label anal. 79—11902
lipids, buried charges, virial expansion 79—16158
lipids, free radical formation on UV irrad. 80—81647
liposomal membrane UV effects 78—40271
liposome phasic transitions, use of hydrophobic fluoresc. probes 78—96021
liposome structural lability, fluoresc. anal. 78—24033
liposomes, nanosecond relax. processes 79—8477
liquid crystal, lyotropic, form. in biological systems 77—86454
liquid crystal biomembranes, struct. and energy characts. and appl. *(Chinese)* 79—16163
liquid crystal physics appl. to functions of biological membranes 79—53051
liquid crystal technological appls., role in biological systems *(Croatian)* 79—10788
liquid crystals in living and dying systems, review 77—44602
liver biomembranes of gamma-irrad. animals, postradiation recovery 80—35976
liver membrane alternations after X-irrad., normal and vitamin E deficient ducklings 80—41139
liver membranes, mouse, X-irrad., dose-rate effects 80—94293
low noise amplification of voltage and current fluctuations 78—44741
lung membrane indentation anal. on elastic half space 79—20522
lymphocyte B and T cell membrane receptors, human effects of ^{60}Co gamma-rays 77—21575
lymphocyte plasma membrane components, distrib. and mobility, book contrib. 80—30690
lymphocytes, human, lethally-irrad., ultrastruct. events in cytoplasmic death 77—48842
macromolecular membrane, statistical mechanics 79—66456
macromolecular systems, statistical thermodynamic analysis, heat capacity function 80—61514
macromolecule adsorption to charged surface, rel. to cell metabolism 77—19118
malignant transformations, optical detect. of cell-surface changes 79—79703
mammalian cell membranes, plasma membrane responses, book 78—15787

biomembranes continued
mammalian cell membranes and cellular functions, book 78—15784
mammalian surface membrane turnover, review 78—15788
material identification of soft tissue using membrane inflation 80—41345
mechanical calorimetry of red cell membranes 80—45854
mechanics and thermodynamics, review 80—45863
mechanics and thermodynamics, review 80—51052
mechanoreception, Millipore-DOPH model membrane showing excitation with press. stimulus *(Japanese)* 78—3526
mechanoreceptors, energy transform. problem 78—96058
megakaryocytes, guinea pig, membrane elec. responses 78—44472
membrane dynamic equation solving, practical algorithm 78—77038
membrane noise analysis by integral spectrum procedure 77—48958
membrane noise spectral density measurement, use of octave filters 77—48957
meninges, US propag., influence of subarachnoid struct., rel. to brain lesion prod. 77—16952
mesomorphic monolayers, quasitwo dimens., theoretical models 80—76713
N-methyl acetamide, Na$^+$, Mg^{2+} binding to carbonyl O, lipid membrane permeation mechanisms 79—16134
microbial cell vibratory spectra, interpretation 77—70425
microviscosity measurement, light scatt. effects 79—39365
milk fat globule membrane, cryst. struct. 80—85364
Millipore-dioleylphosphate model membrane potential oscillation mechanism 79—57603
miniature endplate current decay, effects of extracellular Ca^{2+} and Mg^{2+} 78—24064
mitchondrial complex III membranes preps., cryst. struct. 80—85365
mitochondria, giant, elec. props. study by double impalement technique 79—92446
mitochondria, interaction of cationic dyes, absorpt. spectra 77—52752
mitochondria and submitochondrial fragments by high resolution NMR 77—16918
mitochondria and submitochondrial particle membrane pot. generation in anaerobic conditions 78—69015
mitochondria membrane Ca^{2+} interaction, influence of oestrogens 78—53349
mitochondrial inner membrane, ribbon struct. 78—11618
mitochondrial membrane charging by cytochrome oxidase, role of protons 79—43807
mitochondrial membrane potential meas. with microelectrodes 77—48769
mitochondrial membranes, effect of temp. on struct. state of lipids 77—36879
mitochondrial permeability, transport and energy-coupling processes, effect of fatty acids and acyl-CoA 77—21498
mitochondrial regulators, membrane-active 77—25397
mixed protein phospholipid films, viscoelastic behaviour and Marangoni effect 80—3602
mobility, mol. and struct., using fluoresc. marker conc. dynamics 77—9303
molecular forces between and within lipid membranes 80—51051
moving cells, mag. force 77—70486
multilayer arrays, surface-induced lamellar orientation, theory and method 80—89724
multiple steady states and solution of irreversible phase transitions with enzyme controlled membranes 80—108857
muscle, Ca transients in frog slow muscle fibres 77—77892
muscle, cell surface, heterogeneity of acetylcholine receptor molecules 80—16910
muscle, skeletal, birefringence signals rel. to Ca transients 78—24041
muscle, skeletal, K-contractures and membrane pot., rat 77—29117
muscle, smooth, cell plasma membrane, inhomogenous distrib. of filipin-sterol complexes 79—83720
muscle, translocation of intracellularly stored Ca during contraction-relax. cycle 77—86474
muscle cell membrane fluidity rel. to fusion 77—77873
muscle fibres, slow and twitch type, of frog, contractile activation 77—32884
muscle membrane, skeletal, lanthanide ionic radius selecting 78—24042
muscle-tendon junction strength, ultrastruct. elements 77—25485
myelin, frog nerve, comments on the paracrystalline nature 79—16161
myelin, paracrystalline nature 77—52748
myelin membrane, frog, with paracrystalline lattice distortions, X-ray determ. of electron-density profile 79—11903
myelin sheath, thickness irregularities distrib., paracryst. struct. 77—12892
myenteric plexus, mediation of slow synaptic excitation by substance P 78—73153
myocardial cell transmembrane potential QRS-T wave simulation *(Japanese)* 77—90740
myocardium mitochondria lipid composition and phase transitions rel. to depth of hypothermia, rats and dogs 78—53350
nematode oesophagus pumping mechanism 78—69121
nerve, cell excitation detect. using birefringency changes *(Japanese)* 77—66876
nerve, model for flicker noise 77—29125
nerve action potential, molecular events and energy changes 78—44497
nerve and muscle elliptical fibres, physico-math. anal. 78—11639
nerve cell membrane detection of HF EM fields, possibility discussion *(Russian)* 80—76785
nerve excitable membrane, EM wave effect on surface charge density 78—85334
nerve fibres, mammalian, demyelinated, continuous cond. 77—4995
nerve impulse encoding, elec. processes 80—76718
nerve membrane, excitable, charge density due to optical irrad. 79—8526
nerve membrane potential, effect of constant mag. field 79—57679
nerve membrane response due to time depend. stimulus 79—24974
nerve-muscle anisotropic syncytia, electrotonic membrane pot. distrib. 78—64971
nerves, electrochem. theory, steady and transient pots., in book, for teaching 78—8202
nerves, microwave reception by brain 77—12958
neural membrane two-factor two-mode model 78—7330
neural modelling and identification, state variable approach 78—35825
neuroblast nuclear membrane breakdown, mitotic UV effects rel. to cell cycle 77—12972
neuroblast nuclear membrane breakdown, mitotic UV effects rel. to cell cycle 77—12973
neuromuscular junction, membrane surface pot. changes effect on drug interactions 80—3631

biomembranes continued
neuromuscular junction of crab, in vitro action of anaesthetic and convulsant ethers 77—29140
neuromuscular miniature endplate potential online acquisition microcomputer system 78—36015
neuron membrane, electrostatic plasma probe physical analogue 80—79573
neuron model as universal element of self-learning network 77—44621
neuron multi-input model diffusion approx. 77—29135
neuronal membrane DC resting pot., automatic offset cct. 77—40940
neuronal membranes, organisation book contrib. 79—2032
neurone compartmental chain model membrane voltage changes 77—29124
neurone electrical activity modulation by cholesterol, Aplysia 78—7329
neurones A and B of mollusc, effect of acetylcholine chloride and chlorocholine chloride on resting pot. and membrane resist. 78—53375
neurones light stimulation of ganglioside synthesis, chick retina model 77—9189
neutrophils rabbit, chemotactic factor-induced release of membrane Ca 79—88095
nictitating membrane, devices for recording contractions 77—48969
Nitella, fluctuation and instability in membrane pot. near threshold 80—89723
NMR Fourier transform spectroscopy, high-field, of biological systems 79—39457
nonpolar molecules, adsorption into lipid bilayer membranes 80—61517
nuclear peripheral DNA critical site for radiation-induced reproductive death 79—88131
oocyte membrane, existence of acetylcholine receptor 78—24040
optical thickness meas. using Fabry-Perot interferometer 77—71367
organ of Corti, guinea-pig, rectangular arrays of intramembranous. particles at zonula adherens 77—70480
organised molecular systems, monomolecular layers, micellar and bilayer membranes, conf., Elmau, W.Germany (April 1978) 79—39188
oscillatory membrane reactions, focal nucleation size 79—92171
otolith membrane, finite element model, computer soln. of differential eqns. 77—40636
otolith membrane, variable gravity model 80—85573
pacemaker transmembrane potential generation in fish heart sinoatrial cells 79—39395
pancreatic acinar cell stimulus-secretion coupling, fluoresc. probe detect. of cell Ca redistrib. 77—77872
pancreatic acinar cells, acetylcholine null pot., mouse 77—4988
pancreatic acinar cells, acetylcholine-like effects of intracellular Ca^{2+} appl. 77—66801
papillary muscle fibres, rabbit, effect of preliminary stimulation on repeat responses 78—48768
Paramecium membrane potential changes during chemokinesis 80—26209
parchment-supported, thermodynamic parameters, membrane and bi-ionic pot. theories testing 79—92168
parodontosis treatment portable vacuum apparatus 79—39593
phase changes and determination methods *(Czech)* 80—3599
phase transition studies by positron annihilation energy spectroscopy 80—35854
phase transitions in cell membranes 78—35808
pheophytin containing monolayers, phase separation and domain interaction, surface press. and fluoresc. meas. 79—100580
phosphatidylcholine bilayers, fluidity changes and phase transitions, intramol. excimer fluoresc. obs. 80—85342
phosphatidylcholine dispersion, phase transitions obs. with interference refractometer 78—44459
phosphatidylcholine monolayer vesicles, US irradiation formation, quasielastic laser light scatt., dynamics 77—48764
phosphatidylserine vesicles, sonicated, Ca-induced fusion, temp. depend. 79—92172
phospholipid, orientational order and integral protein struct. 80—45862
phospholipid, struct. in high mag. field 77—64163
phospholipid artificial membrane phase state and passive permeab. for Ca ions, effect of valinomycin 78—80836
phospholipid bilayers, carbonyl groups dynamics, ^{13}C chem. shift anisotropy obs. 80—85326
phospholipid crystallography rel. to lipid-lipid and lipid-protein interactions 77—44590
phospholipid inter-and intra-molecular interactions, PCILOCC and pot. function calc. 80—3570
phospholipid lateral diffusion in membranes, photochem. method 79—100583
phospholipid membrane, 4-dimethylaminochalcone fluoresc. probe of H$_2$O mol. surface mobility 79—79450
phospholipid membrane, polar head motion, NMR and EPR linewidth study using TCNQ$^-$ ion-radical *(French)* 80—45865
phospholipid membrane solubilisation by human plasma high density lipoprotein 77—16916
phospholipid mixtures, phase transition anal. by high sensitivity differential scanning calorimetry 77—40637
phospholipid plane membranes, interaction of soluble brain Na$^+$, K$^+$-ATPase 80—35851
phospholipid topological asymm., review 77—90736
phospholipid transmembrane asymm. studied by NMR spectroscopy with displacing reagents 78—31984
phospholipid vesicle phase transition probed by positron annihilation lifetime technique 79—88061
phospholipid vesicles, Ca^{2+}-induced aggregation 79—62202
phospholipid vesicles, surface charge equilib. distrib., calc. method 78—96019
phospholipid vesicles, surface charge equilib. distrib., calc. results 78—96020
phospholipid vesicles, synthetic, phase transitions, dynamic light scatt. obs. 79—53058
photoreceptor, Drosophila mutant with phototransduction defect 77—90777
photoreceptor cell disk membrane, photoinduction of pot. 79—70548
photoreceptor function, rel. to prolonged depolarising afterpot. 78—15832
photoreceptor membrane, lipid free radical oxidation kinetics rel. to lipid composition 78—80872
photoreceptor membrane, protein-lipid interactions on peroxide oxidation of lipids 77—21522
photoreceptor membrane, squid rhodopsin thermal stability 77—32893
photoreceptor membrane fragment modified artificial lipid membranes, effect of light 77—77898
photoreceptor membrane interfacial pots., light-induced 80—72161

biomembranes continued
photoreceptor membrane lipid-rhodopsin interactions 80—12094
photoreceptor membrane photostable pigments and possible role 78—15837
photoreceptor membrane potential reconstruction from simultaneous intra- and extracellular recordings, S. atlantica 77—86494
photoreceptor membrane rhodopsin orientation model 77—90775
photoreceptor membrane viscosity and component dynamics, recombination kinetics method 79—39366
photoreceptor membranes, dynamic aspects of molecular texture 79—79519
photoreceptor membranes, incorporation into a multilamellar film 80—89907
photoreceptors, vertebrate, light-activated GTPase 78—3481
photosynthesis, interaction of paramag. probe I (12,3) with bean chloroplast membranes 78—77015
photosynthetic, electron microcopy 80—26210
photosynthetic, exciton dynamics, picosecond pulse train study 79—8483
photosynthetic membrane, optical and electrochromic props., chloroplast chlorophyll orientation 77—48763
photosynthetic membrane model, electron transfer and charge separation in photoexcited chlorophyll aggregates 77—81468
photosynthetic membranes, anal. of laser-induced fluorescence with Pauli master eqn. 79—39350
photosynthetic membranes, functional processes, polarisation effects 80—67045
photosynthetic membranes, supramolecular organisation model based on freeze-fracture electron microscopy 77—29106
photosynthetic processes, electron conformation interactions 80—94183
photosynthetic systems, magnetoorientated, fluorescence polarisation theory 79—16165
photovoltaic effect in pigment films in contact with electrolyte, phthalocyanin model system 77—16907
Physarum polycephalum, true slime mold, surface membrane simulation using liquid ion-exchange membrane *(Japanese)* 78—31781
pigmented, photoelec. and magneto-orientation effects, review 77—48766
pigments, visual and purple membrane, charge stabilisation mechanism 79—34500
planarian, regeneration of epidermis and basement membrane after total-body X-irrad. 80—36022
plant lipids and their role in membrane function 79—83716
plant protoplast membrane, osmotically induced changes in elec. props. 78—27910
plasma membrane, unfixed, ultrathin frozen sections, ultrastructure 78—65161
plasma membrane lipids of M. angiospora, orderly crystallisation revealed by freeze-fracturing 77—36880
plasma membrane vesiculation, new technique for isolation of membranes 77—52950
platelets, human blood, adenine nucleotide content and release reaction after ^{60}Co γ-irrad. 78—28021
pleural membrane tension and shear modulus of the lung, improved meas. 80—30746
poly (N$^{\alpha}$,N$^{\epsilon}$-terephthaloyl-L-lysine) membrane for artificial red blood cells, interaction with serum proteins *(Japanese)* 80—12061
polyelectrolyte membranes, persistent polarisation in aq. environment, neural model 78—48763
polymorphonuclear granulocytes and FL-cells, effect of X-rays on membrane pot. and electrophoretic mobility *(German)* 77—56442
potential generation by submitochondrial particles, direct meas. 80—35852
potentials, meas. in ionic environment, biological membrane simulation 80—3412
potentials meas. using the dye safranine 79—48386
presynaptic electrical coupling in Aplysia, effects on postsynaptic chem. transmission 77—48782
protein, double layer mediated energy conversion using imposed freq. and wavelength 78—88695
protein, structure determination, electron microscopy, optical and digital anal. *(French)* 79—66594
protein concentration 79—83714
protein membrane multilayers, thickness depend. of props. 80—89726
protein-lipid complexes, spatial organisation obs. 79—70529
protein-lipid interaction, appl. of surface tension meas. 79—24940
protein-lipid interactions, ^{2}H NMR investig. 78—80826
protein-lipid interactions, in bilayer membranes 79—5254
protein-lipid interactions, review 77—90719
proteins, props. rel. to membrane functions, review 77—44601
purple membrane, anomalous amide I IR absorpt. 80—12058
purple membrane, bacteriorhodopsin chromophore mobility 77—25366
purple membrane, bacteriorhodopsin reorientation due to elec. field 77—66789
purple membrane, effect of illum. on thermogenesis of growing culture of halophilic bacteria 77—86530
purple membrane, electron microscopy of frozen hydrated crystalline specimens, meas. and reduction of damage 80—85552
purple membrane, new intermediates in bacteriorhodopsin photochem. conversion 78—96010
purple membrane, of Halobacterium halobium chromophore excitonic interaction, protein location 77—21497
purple membrane, orthorhombic 2D crystal form 80—85362
purple membrane, photocycle and light adaptation of dark-adapted bacteriorhodopsin 77—73508
purple membrane, polarized IR spectroscopic struct. study 79—43809
purple membrane asymm. struct., X-ray diffr. data anal. 77—73512
purple membrane films, absorpt. and circular dichroic spectra 79—83708
purple membrane fragment suspensions, elec. dichroism obs., trimer model interpret. 80—89728
purple membrane fragments, Debye rot. relax. times, modulation excitation spectrophotometric obs. 79—3532
purple membrane fragments, proteolysis and flash photolysis obs. of bacteriorhodopsin 79—62185
purple membrane light energy transduction, bacteriorhodopsin photoreactions 77—90726
purple membrane of halobacterium halobium, aggregate optical spectra, moment anal. 79—2007
purple membrane of Halobacterium halobium, energy transfer 78—44467
purple membrane of Halobacterium holobium, review 77—86457
purple membrane of halophil cells, homogeneity based on IR spectra 78—69003
purple membrane of H.halobium, bacteriorhodopsin luminesc. 77—36890

biomembranes continued
purple membrane of H.halobium, effect of 560$\rightleftarrows$570 transition and blue light on photochem. 80—30673
purple membrane particles, freeze-fractured, protein content 77—90735
purple membrane protein, quantum efficiency for photochem. conversion 77—29099
purple membrane protein chromophore, fluoresc. 78—44454
purple membrane protein synthetic pigment analogues 77—73504
purple membrane rhodopsin, H exchange 77—29096
purple membrane struct., Halobacterium halobium 78—15782
purple membrane structure, effects of bleaching and regeneration, H-halobium 77—86532
purple membrane suspensions, light-induced conductivity changes, pH and temp. effects 80—51157
purple membrane thin layers, hydration effects on bacteriorhodopsin photocycle 78—7320
purple membrane topography of Halobacterium halobium 79—48211
purple membranes from Halobacterium halobium, spectral transitions 80—12056
quantum chemistry, biology, and pharmacology, conference, Kiev, USSR (Sept. 1978) 79—96499
R. sphaeroides, polarisation of photosynthetic membranes and reaction centres in elec. field 80—94277
radial autocorrelation, function, significance in X-ray diffr. patterns 80—51048
radiation biology conf., Sapporo, Japan (Sept. 1978) 80—8105
red blood cell elastic deforms. 77—56400
red blood cell ghosts, light scatt., ang. depend. struct. 77—81475
red blood cells, minimum energy anal. of membrane deform. 80—72141
red cell extensional recovery, determ. of membrane viscosity 79—57683
red cell membrane, human, surface elasticity and viscosity 80—61608
red cell membrane, temp. dependence of viscoelastic recovery 80—40979
red cell membrane elastic area compressibility meas., osmotic correction 78—20147
red cell membrane protein monolayers, viscoelastic props. 79—48224
red cell membrane thermoelasticity obs. 79—57684
Renshaw spinal interneuron repetitive firing, model 77—90760
reptile epidermis, water permeability rel. to lipid content 80—97875
retina, light-adapted, of carp, intercellular junctions between pigmentary epithelium and cones *(French)* 77—12911
retina of turtle, horizontal cells influence on bipolar cells' membrane pot. 78—88708
retina photoreceptor membrane, light and GTP-regulated GTPase interaction 80—45897
retina receptor layer current spatial distribution, frog, electrical model 77—40666
retinal damage by visible light, role of singlet O 78—15858
retinal disc membrane, frog, isorhodopsin chromophore conform. and orientation 78—64980
retinal horizontal cell reaction to non-uniform illum., model 77—56375
retinal horizontal cells, amplification of graded pots. 77—32889
retinal pigment epithelium, identification of membrane protein binding retinol 77—21515
retinal pigment epithelium, variations in phagosome content rel. to cyclic lighting 77—90772
retinal rod discs, intradiscal surface, photoreceptor membrane carbohydrate 77—4998
retinal rod external segment mag. anisotropy decrease after total photolysis 77—52838
retinal rod outer segment membranes and liposomes of extracted phospholipids, proton spin-lattice relax. rates 77—90782
retinal rod photoreceptor membrane orientation in intact eye, X-ray diffr. 77—48790
retinal-entrapped membrane, photo-induced potential 78—20148
retinular cells, arthropod, light-induced membrane cond. change rel. to membrane pot. 77—5001
review, plastic deformation during freeze-cleavage 78—14400
RF and microwave field nonthermal effects 77—86534
rhabdomere transmittance decrease due to blue light, rel. to desensitisation of peripheral photoreceptors 78—64993
rhodopsin in model membranes, charge displacements in interfacial layers 77—52785
rhodopsin membrane at oil-water interface, effect of illumination, rel. to cephalopod visual cells 77—44646
rhodopsin thermal stability in photoreceptor membrane, role of lipids, PMR spectroscopy 80—35874
rhythmic heart-cell clusters, fluctuations in interbeat interval, membrane voltage noise role 80—30705
rigidity increase of material of bioconstructs. during morphogenesis 80—94249
rod external segment membrane, phospholipid auto-oxidation during conform. changes 77—21523
rod outer segment membrane, bovine rhodopsin conform. 77—44587
rod outer segment membrane current, light-induced fluctuations recorded in single toad rod 77—86493
rod outer segment shedding, intraocular initiation 78—85309
rod outer segments, accel. membrane renewal after light exposure 77—64035
rod photoreceptor disc membrane, cooperative conform. change induced by bleaching 77—81499
rod photoreceptor model sensitivity, depend. on level of background light intensity 78—20179
sarcoplasmic reticulum, temp. dependent struct. rearrangements 79—53056
sarcoplasmic reticulum hydrated oriented multilayers, lamellar X-ray diffr. 78—11614
sarcoplasmic reticulum membrane rearrangements on peroxide oxidation of lipids 78—69025
sarcoplasmic reticulum membranes, small angle X-ray data processing 80—81536
secretory granule membrane, particle clustering induced by centrifugation, freeze-fracture anal. 80—85559
semilunar valvular motion vibr. model during early diastole, rel. to second heart sound 78—44533
sensory fibres, amphibian, spike freq. adaptation due to slow K channels 79—2025
single ligand binding constant computation, regulatory enzyme exponential model 79—79454
sinus node of rabbit heart, intercellular coupling 78—20159
skin, extensometer for in vivo meas. of human skin biomech. props. 77—44704

biomembranes continued

- solute environment influence on membrane struct. and function, review 78-15789
- spherical three-layer particles as cell models, light scatt. and attenuation, shell effect 78-82913
- spin labels applications, review 78-69265
- spin probe distribution between water and membrane in different conditions 77-21491
- spin-labelled fatty acid derivatives, interaction with biomembrane lipid and protein components 77-70421
- squid joint axon membrane potential fluctuations, cross-correlations 78-92616
- stereological method for estimating relative membrane surface area 77-64158
- Streptococcus, effect of ionising radiation on transmembrane pot. 80-36019
- structural constitution and function *(German)* 79-5256
- structural lability, albumin-unsaturated fatty acid binding kinetics, fluoresc. anal. 78-15755
- structural lability, complexing between albumin and fatty acids, fluoresc. anal. 77-25381
- structural order of lipids and proteins, fluoresc. anisotropy data eval. 80-97873
- structure, review of current ideas 77-32878
- structure determination of asymmetric membrane profiles, iterative Fourier method 79-43810
- structures and phase transitions *(Japanese)* 77-70423
- submitochondrial particle membranes, interaction with paramagnetic probes 79-57604
- surface charge density variation of excitable nerve membrane exposed to optical radiation 79-34542
- surface charge distributions, discrete, fluctuations near individual channels 79-16160
- surface charge visualisation using SEM 80-85566
- surface conditions simulation, relative compatibility of amino acid residues at interface 80-71951
- surface labelling techniques for eukaryotic cells 77-56560
- suspensions of conducting spheres covered with thin nonconducting membrane, dielectric behaviour 80-45563
- synaptic membrane, acetylcholine-activated, interaction of fluoresc. probe 77-90762
- synaptic transmission modulation and information processing model 77-29142
- synaptic vescles and synaptosomal membranes, electrokinetic props. 80-67055
- synaptosomal membranes of brain, temp. induced struct. rearrangements 77-36877
- syncytium, passive three-dimens. and anisotropic, modelled as continuous medium 77-16898
- synthetic, use in biophys. research 77-70418
- teaching demonstration using molecular membrane model 77-57117
- thermal fluctuations, surface tension, rel. to 2-D phase transformation 77-1980
- thermal fluctuations and mechanoreception problem 79-53057
- thick-section parallel membrane separation estimation 79-70718
- thickness distrib. determ. from orthogonal intercepts 79-74804
- thin sectioning development for electron microscopy 79-74819
- thylakoid, light collection and exciton dynamics 79-48215
- thylakoid membranes, pulsed NMR, photosynthesis appl. 78-80839
- thylakoid membranes of wheat chloroplasts, proton spin-lattice relax. time, −8°C phase transition 80-108853
- thymocyte membrane props. modification by hyperthermia and gamma-rays 78-69017
- transmembrane potential rel. to surface pot., ionic permeab. 80-35853
- transport coeff. meas., laser interferrometric technique 78-15936
- tumour cells, differences in fluidity between bilayer halves of plasma membranes 79-16164
- tympanic membrane, tympanometry in normal neonates 80-3651
- tympanic membrane acoustic admittance in aging ear 79-100630
- tympanic membrane investigations in living man using holographic interferometry 80-67207
- tympanic membrane perforations, expt. induced, in cats, middle ear transmission loss 77-32908
- tympanic membrane vibr. studies in living man using holographic interferometry 80-67208
- tympanic membrane vibration study, phase sensitive holographic technique *(German)* 78-3513
- tympanic membrane vibrs. in human temporal bones, double pulsed holographic anal. 78-40289
- ultrastructure rel. to function, review 78-15785
- unilamellar lipid vesicles, Ca^{2+} initiation of fusion or lysis 79-2008
- unilamellar lipid vesicles, in vivo breakdown, gamma-ray PAC study 78-53348
- US perturbation obs. at cellular level 78-61214
- vaginal mucosa, radiation tolerance obs. 80-104666
- valinomycin monolayers, struct., area and compressibility determ. 78-44461
- valinomycin-cholesterol (stearic acid) monolayers, struct., area and compressibility determ. 78-44461
- vesicles, large, anal. of adhesion to surfaces, expt. procedure 80-109063
- vesicles containing chlorophyll, energy transfer and fluorescence quenching 79-39349
- vesicular artificial membrane struct., effect of protein-lipid interaction 77 -25385
- vesicular bilayer membranes, gangliosides orientation, ^{1}H NMR, viscometric and ultracentrifugation obs. 79-92162
- vesicular closed systems, mechano-chemistry 77-60189
- vesicular lipid membranes, vol.-elastic props. determ., US obs. 80-45861
- vesicular phospholipid membranes dispersion, luminescence spectra of Eu complexes 79-79478
- virus envelopes, plasma membranes, review, book contrib. 79-5257
- virus-cell interactions, early molecular events, fluorescence and radioactivity obs. 79-100561
- virus-cell interactions, early molecular events, kinetic study 79-100562
- visual cells, daily rhythms and vision research 78-61176
- voltage clamp of multicellular preps. 77-40955
- volume-conductor fields of isolated axon, linear filtering problem 78-3463
- water, lyotropic phase orientation, ^{17}O and ^{2}H NMR study 78-27905
- X-irradiation, vitamin E deficiency and lipid peroxidation, mouse obs. 80-72263

biomembranes continued

- X-ray scattering method for determ. of struct. parameters 80-30948
- yeast cell electrophoretic mobility, X-ray effect 78-31868
- yeast cell IR spectrum, effect of membrane components 77-70433
- zeaxanthin ([3R,3′R]-β,β-carotene-3-3′diol) as optical probe of membrane struct. 79-92124
- ^{125}I toxicity in cultured mammalian cell, primary site for division delay 77-52851

biomolecular effects of radiation

see also biological effects of .... (type of radiation)
see also photosynthesis

- 9.712 GHz irradiation effect on vagal heat membrane bound acetylcholinesterase 80-3593
- 50 Hz EM fields, mechanism of effect *(Russian)* 80-51158
- N-acetyl-L-cysteine, X-irrad., ^{33}S nucl. coupling and nature of free radicals 77-52743
- acetylcholine, dielectric transient response following UV-irradiation 80-51166
- N-acetylglucosamide, substrate-inhibitor of lysozyme, localisation of unpaired electrons 78-68992
- N-acetylglycine, X-irrad., stable radical electronic and mol. struct., ENDOR and ESR 80-80637
- acid amide + H$_2$O$_2$, aq. solns., photolysis, EPR study of spin-trapped radicals formed during photolysis 78-68996
- adenine, nucleic acid component, selective action by ps light pulses 80-72213
- adenovirus, decreased repair after γ-irrad. when infecting Xeroderma pigmentosum fibroblasts 80-61650
- albumin, human serum, kinetics of eosin-sensitised photochemilum. of solns. 78-68991
- albumin, pulsed laser study of adsorbed aromatic mol. excited states 77-86448
- alcohol dehydrogenases, yeast and horse-liver, radiation chem. evidence for differences in amino acid composition 78-40116
- aliphatic amino acids, N-acetyl substituted, photolytic production of methyl radicals 79-96622
- alkaline endonuclease activity in thymus and spleen of irrad. mice 78-28004
- allophycocyanin solutions from F-diplosiphon, photoreversible absorbance changes 80-97862
- amides, substituted, aqueous solns. UV-irradiated, EPR and spin-trapping study of free radicals 79-16154
- amino acid, in polycryst., γ-irrad. induced radical pair form., 77K, EPR obs. 78-85292
- D-amino acid oxidase, crit. residues, pulse radiolysis and inactivation study 78-27897
- amino acid photodegradation in presence of TiO$_2$ 78-11531
- amino acid photoresolution, rel. to origin of optical activity in life 77-40634
- amino acid sequence threadlike cryst. growth, light irrad., polycondensation 78-96009
- amino acid transport in rat liver after whole-body gamma irrad. 77-9232
- α-amino acids, γ-irradiated, primary oxidation products, ESR and ENDOR 77-48754
- amino acids, aq. solns. EPR of spin-trapped radicals, hydrated electron reactions 78-27796
- amino acids, He(I) photoelectron spectra 79-34499
- amino acids, high energy radiation effects and chemical evolution 77-63937
- amino acids, technique for study of radiation in induced free radicals using lyoluminesc. 77-29230
- amino acids, X-irradiated, EPR determ. of radical yields 79-34491
- amobarbital, radiation-prod. free radicals in pyrimidines, EPR 77-25374
- dAMP.dTMP costacking complexes, γ-irrad., charge migration, computer-assisted EPR 77-86446
- amphipathic apolipoprotein ApoC-III bound to phosphatidylcholine bilayers, lateral mobility 80-97884
- aspartate transcarbamylase, solid, enzyme activity and allosteric characts. after gamma irrad. 78-53341
- aspartate transcarbamylase, solid, sedimentation and subunit interactions, after gamma irrad. 78-53342
- ATP formation, quantum efficiency of photosynthetic energy conversion 78-44473
- bacteria, E. coli B, microwave radiation effects on colony formation and mol. struct. 78-24097
- bacterial photosynthesis, and model systems, electron transfer, ps studies 79-48214
- bacterial photosynthesis, light collection and harvesting processes investig. on psec. time scale 77-90743
- bacterial photosynthetic reaction centre, fast electron transfer processes 79-8479
- bacteriochlorophyll, photochem. oxidised, kinetics of dark reduction, R. rubrum chromatophores 77-25390
- bacteriochlorophyll, R. rubrum reaction centres, selective ps laser excitation in condensed phases 79-48217
- bacteriochlorophyll a, bacterial photosynthesis primary electron transfer processes, psec. dynamics 78-80841
- bacteriochlorophyll-800, implication in picosec. electron transfer to bacteriopheophytin in R.rubrum reaction centres 80-35844
- bacteriophage, gamma-ray induced cross linkage of DNA and protein 77-21485
- bacteriophage DNA and protein cross-linkage by ^{60}Co gamma-rays 78-77002
- bacteriophage S13, lethal effect of ^{33}P transmutation, mech. of DNA double helix rupture *(French)* 80-98018
- bacteriophage T1, killing by irrad. in dry state with 122 nm and 254 nm light 80-101234
- bacteriophage T1 radiosensitivity on various host strain mutants of E. coli 78-20228
- bacteriophage T7, radiation inactivation 78-65083
- bacteriophages, T7 and MS2, effect of UV light *(Hungarian)* 79-16153
- bacteriopheophytin, bacterial photosynthesis primary electron transfer processes, psec. dynamics 78-80841
- bacteriorhodopsin, 13-cis and trans isomers, photochem. and dark equilib. 77-90798
- bacteriorhodopsin, dark-adapted, photocycle and light adaptation 77-73508

biomolecular effects of radiation continued
- bacteriorhodopsin, excited state energy surface to explain photochemistry 79−48218
- bacteriorhodopsin, kinetic isotope effects in photochem. cycle 77−44592
- bacteriorhodopsin, new intermediates in photochem. conversions 78−96010
- bacteriorhodopsin, photoreactions, purple membrane light energy transduction 77−90726
- bacteriorhodopsin, photosensory mechanism for Halobacterium, rel. to visual photoreception 77−90738
- bacteriorhodopsin, primary intermediates in photochem. cycle 78−96011
- bacteriorhodopsin, ps flash-photolysis obs., room and low temps. 79−57581
- bacteriorhodopsin, purple membrane of H.halobium, effect of $560 \rightleftharpoons 570$ transition and blue light on photochem. 80−30673
- bacteriorhodopsin, reson. Raman kinetic spectroscopy on μsec time scale 78−20320
- bacteriorhodopsin, selective ps laser excitation in condensed phases 79−48217
- bacteriorhodopsin, subpicosecond spectroscopy, photochemical formation of bathobacteriorhodopsin 79−16156
- bacteriorhodopsin 580 nm ultrafast transient, psec kinetics 78−44455
- bacteriorhodopsin chromophore, light-induced isomerisation 80−108956
- bacteriorhodopsin chromophore photoisomerisation rel. to purple membrane proton pump 78−35804
- bacteriorhodopsin in planar membranes, elec. response to light 78−35806
- bacteriorhodopsin in purple membrane fragments, proteolysis and flash photolysis obs. 79−62185
- bacteriorhodopsin of purple membrane, quantum efficiency for photochem. conversion 77−29099
- bacteriorhodopsin photoconversion products, EPR and low temp. spectrophotometry 78−15769
- bacteriorhodopsin photocycle hydration effects, in thin purple membrane layers 78−7320
- bacteriorhodopsin photocycle quantum efficiency 77−29098
- bacteriorhodopsin phototransients, circular dichroism meas., comment 78−21954
- bacteriorhodopsin proton pump, elec. demonstration of rapid light-induced conform. changes 77−44597
- bacterioviridin, photochem. oxidation mechanism 77−25370
- bacterioviridine photo-oxidation in monomer and aggregated states, free radical form., EPR 78−76994
- beta-decay, chem. and biological consequences 78−28018
- beta-decay in labelled molecule, chem. and biological consequences 78−11541
- bilirubin, aq. soln., pulse radiolysis 78−48761
- biomembrane architecture obs. 79−25177
- Bose condensation, and time threshold for biological effects 79−100664
- Bowman-Birk soybean proteinase inhibitor, gamma irrad. 78−53343
- 5-bromodeoxyuridine, single cryst., X-irrad. at 77K, $C_{5'}$-centred deoxyribose radical 78−20032
- carotenoids related to visual chromophore, electronic struct., band shape model 78−20142
- catalase, glucose embedded, measurement and reduction of radiation damage in frozen hydrated crystalline specimens 80−89810
- catalase, solid state, electron microscopy radiation damage, amino acid composition 77−25377
- cell surface anisotropic molecular motion, photobleaching 80−97883
- cell survival, mol. theory anal. of synergistic interaction with Pt complex 77−21565
- cerebral macromolecules, long-range order models, RF field effects 80−56132
- chirality, origin via natural beta-dacay 77−86445
- 5-chlorodeoxyuridine, single cryst., X-irrad. at 77K, $C_{5'}$-centred deoxyribose radical 78−20032
- chlorophyll, photosynthesis mechanism, upconversion, EPR and O_2 evolution data anal. 78−35811
- chlorophyll a, photo-oxidation obs. using pulse photoconductivity 79−79447
- chlorophyll a fluorescence duration in chloroplasts rel. to ferricyanide and vitamin K_3 conc. 77−25393
- chlorophyll a of photosystem II, fluoresc. when electron transport on acceptor side is blocked 78−7324
- chlorophyll analogues, mechanism of activation of photosensitising action 79−57583
- chlorophyll and analogues, role of O_2 in regeneration of photoreduced pigments in soln. 78−68980
- chlorophyll excited stated, redox pots. 77−25372
- chlorophyll fluorescence changes in isolated broken chloroplasts and involvement of elec. double layer 78−44464
- chlorophyll photo-oxidation, role of singlet-excited and triplet states 80−51156
- chlorophyll photo-oxidation, spectral detect. of exciplex in triplet state 77−25368
- chlorophyll photo-oxidation by quinones, cation-radical yield 77−86442
- chlorophyll photo-oxidation mechanism, effect of spectral composition of light 77−25369
- chlorophyll photochemical activity, rel. to microviscosity of detergent micelles 77−21478
- chlorophyll photoexcited aggregates, pigment-pigment electron transfer and charge separation 77−81468
- chlorophyll solutions, photopotential rel. to EPR signal 79−53045
- chlorophyll-a, microcryst., trapped-electron doping in photovoltaic sandwich cells 78−53334
- chlorophyll-acceptor and chlorophyll+protein-acceptor lamellar systems, steady photocond. 78−53328
- chlorophyll-duroquinone photochemical interaction, photopot. 77−16903
- chlorophyllide fluorescence quantum yield during photochlorophyllide reduction in etiolated leaves 80−81542
- chlorophylls a and b, photo-oxidation primary processes 79−79468
- cholesterol, dielectric transient response following UV-irradiation 80−51166
- cholic acid, dielectric transient response following UV-irradiation 80−51166
- cholinesterase, microwave radiation interaction studies 79−39363
- chondromucoprotein, effects of ^{60}Co γ-irrad. 78−7400
- chromatin, solubilized, calf thymus, changes in circular dichroic spectrum by UV irradiation 79−100678
- chromatin extracted from cultured mammalian cells, gamma radiolysis, DNA alkali-labile strand damage 78−77003

biomolecular effects of radiation continued
- chromatin from cultured mammalian cells, radiolysis, DNA-protein cross-links formation 80−81655
- chromosomal proteins and DNA syntheses in rat thymus after whole-body X-irradiation 79−34492
- chromosomal proteins from Yoshida ascites tumour chromatin, γ-irradiation effects 79−96626
- chromosome aberration form. by gamma irrad. in lymphocytes, protection by free radical scavenging 78−20216
- chymotrypsin-like proteins, γ-irrad. rel. to UV irrad., unfolding obs. 80−35984
- chymotrypsin-like proteins, gamma irrad. induced struct. changes 77−44594
- chymotrypsin-like proteins, gamma-irrad., inactivation rel. to struct. changes 77−56341
- concanavalin A-carbohydrate interactions, implication of protein aromatic amino acids, radiolysis 78−40110
- conference, Rotterdam, Netherlands (Aug. 1980) 80−105425
- creatine monohydrate, single cryst., radiation damage, ENDOR obs. 78−96016
- cytidine-5′-monophosphate, γ-irrad. aq. soln., spin-trapped radicals, liq. chromatography and EPR spectroscopy 78−53340
- 3'-cytidylic acid, X-irrad., stable radical in ribose moiety, compared with cytidine 77−25375
- cytochrome c, γ-irradiation, electron reactions at −196°C 79−62194
- cytochrome c, effects of UV and temp. on optical props. and enzymatic activity 80−81648
- cytochrome c and related metalloproteins, fast electron transfer processes 79−8478
- cytochrome c conformationally-nonequilibrium state reactivity obs. by pulse radiolysis 79−43816
- cytochrome c-Fe(CN)$_6$ electron transfer, vibronically coupled tunnelling description 77−52737
- cytochrome c-serotonin soln., UV effect on optical props. 80−30663
- cytosine, cryst., electron damage, electron microscope study 78−22762
- cytosine derivatives, photosensitised induction by H-addition radicals in frozen aqueous soln. 78−20146
- cytosine monohydrate, single cryst., γ-irrad., ion radical recomb., EPR 78−15776
- cytosine monohydrate single cryst., X-irrad., OH addition radical and decay product 77−86447
- cytosine.H_2O crystals, radical form. by X-irrad. at 77 and 300K 77−12886
- damage model in cells, radiation chemistry approach for direct and indirect effects 79−11974
- 11-cis-13-demethylretinal, photoisomerisation, high quantum yield 79−57253
- deoxyribonuclease I in aq. soln., inactivation by thermal neutrons 80−104664
- deoxyribonucleoprotein, gamma-ray protein damage 78−53338
- dihydro-6-methyl uracil single cryst., electron and UV irrad., free radicals, EPR 77−29100
- dihydrouracil, EPR study of light- and temp.-induced free radical conversions 80−35824
- dipeptides, aliphatic, EPR studies of direct photolysis 78−48678
- diploid fibroblasts, human, nondividing, effect on RNA and protein synthesis 79−92291
- DNA, γ-irrad., 2-deoxy-D-erythro-pentonic acid isolation from alkali-labile site 78−20144
- DNA, γ-irrad. at 77K, effect of visible light, EPR 77−52744
- DNA, γ-irradiated, N-formamido group formed in place of thymine fragment, evaluation method 80−30790
- DNA, additive action of ionising and non-ionising radiations in Chinese hamster cells 77−48845
- DNA, alkali-stable, lesion excision repair by γ-endonuclease Y enzyme 79−92145
- DNA, calf-thymus and superhelical PM2 aq. solns., electro-optic obs. of γ-irrad. damage 80−85452
- DNA, combined effects of thermal neutrons and agents which interact with DNA, amoeba 78−20219
- DNA, cytosine ^{14}C-2 labelled, gamma radiolysis products from N-glycosidic bond rupture 77−9171
- DNA, double strand breaks, protein cross-links, induced by fast neutrons, γ-rays 79−66446
- DNA, double strand breaks, recombination, formation of chromosomal rearrangements 78−85289
- DNA, free radical induction due to proflavine and light treatment, influence of DNA struct. 79−100573
- DNA, gamma irradiated biologically active double stranded, alkali labile sites, post irradiation effects 80−35991
- DNA, gamma-irradiated, enzymatic digestion, separation by ion exchange chromatography 78−85290
- DNA, gamma-ray effects on hydration, PMR of frozen and liq. solns. 78−27900
- DNA, high mol. wt., sedimentation data, radiation-induced single-strand breakage, additives effect 80−30667
- DNA, mammalian, organisation of repeated nucleotide sequences in replicons 77−73506
- DNA, properties changes caused by UV- and γ-irrad., electrochem. anal. 80−72271
- DNA, radiation induced mol. size change, electron irradiated, effect of p-nitroacetophenone 80−89807
- DNA, radiation-induced strand breaks in deoxygenated aq. solns. 80−61649
- DNA, single-strand break repair after X-irradiation, cultured insect and mammalian cells 79−74725
- DNA, single-stranded, alkali-labile sites and post-irrad. effects induced by H radicals 78−68994
- DNA, single-stranded, in aq. soln., gamma-ray induced alkali-labile sites 77−9170
- DNA, thymine base damage release, γ-irrad. Tetrahymena pyriformis 80−72268
- DNA, transforming, shape of UV inactivation curve 77−66797
- DNA, transforming, X-ray sensitivity rel. to presence of free radicals 78−68995
- DNA, triplet state excited by X-rays 77−9174
- DNA, UV and gamma-ray damaged, defective repair in Fanconi's anaemia 77−44725
- DNA, UV irrad. of mammalian cells, postreplication repair model 78−80918

biomolecular effects of radiation continued
DNA, X-irrad. E. coli, influence of uvrD mutation on survival and repair 77—86540
DNA, X-irradiation production of alkali-labile lesions 79—43820
DNA, X-ray induced damage in rat cerebellar neurons and brain tumour cells 78—80922
DNA, X-ray induced mutations and target theory 77—5040
DNA, X-ray induced single-strand breaks, yield and repair, E. coli cells 77—9173
DNA and polynucleotide hydration, γ-irrad effects, NMR of frozen H_2O and D_2O solns. 77—21484
DNA base damage detection method, UV induced pyrimidine dimers in human cells 79—44067
DNA bases, selective ps laser excitation in condensed phases 79—48217
DNA break rejoining capacity rel. to mouse age 78—69148
DNA breaks in E. coli and superinfecting phage λ, repair rel. to buffer. 77—25376
DNA chain growth in vivo in intestinal crypt cells, effect of ^{60} gamma and hydroxyurea 77—66795
DNA costacking nucleotides, γ-irrad., charge-migration phenomena, EPR obs. 80—36015
DNA damage and repair in γ-irrad. rat brain tumour, detect. by S_1 nuclease 78—48838
DNA damage of Chinese hamster ovary cells on X-irradiation after preheating 79—34493
DNA degradation in Escherichia coli after UV irrad. 78—48841
DNA double-strand break induction by binding with ^{125}I-iodoproflavine 78—20145
DNA double-strand breaks, gamma-ray induced, temporal local denaturation 78—48754
DNA double-strand breaks during γ-irrad. of Micrococcus radiodurans, O_2 effects 78—7393
DNA double-strand breaks in irradiated yeast cells, survival and yield, O_2 influence 80—35992
DNA electron damage repair in E. coli mutants, appl. of rapid lysis techniques 78—31775
DNA end group characterisation after low dose γ-irrad. of thymocytes 78—11613
DNA films, X-ray induced luminesc. and optical absorpt. rel. to γ-induced free radicals 77—5033
DNA from mouse tissue, UV irrad. studies, UV absorpt. spectra 78—11702
DNA hydration characts. in H_2O/D_2O frozen solns., γ irrad. effects, PMR 78—31772
DNA inactivation by γ-rays in vitro, O_2 effect in presence of metalloporphyrins 79—92303
DNA interaction with nucl. non-histone proteins, γ-ray effects 78—7401
DNA kinetics in soln., electron pulse radiolysis using light scatt. detect. 77—16910
DNA lesion production, role of radicals, E. coli X-ray endonuclease specificity 77—52745
DNA light induced diffusion in solutions due to laser cutting *(Russian)* 80—81646
DNA methylation after UV irrad., of HeLa cells 77—12979
DNA non-rejoining break induction by high LET radiation, rel. to cell death 77—44596
DNA pyrimidine dimers non-random distrib. after UV irradiation 79—96628
DNA radiation-induced damage in Chinese hamster V79 spheroids and monolayers 80—41130
DNA repair after γ-irradiation, action of hyperthermia in HeLa cells 79—100577
DNA repair competency changes after 5-bromodeoxyuridine pulse labelling and near UV light 79—83854
DNA replication and repair in human melanoma cell-line resist. to UV irrad. 77—44721
DNA replication fork struct. in UV irradiated human cells 79—88117
DNA replication kinetics in X-irrad. Chinese hamster ovary cells 78—20226
DNA single and double strand radiation damage comparison 79—92153
DNA single-strand breaks in preheated cells irrad. under N_2 and N_2O saturation 78—28017
DNA single-strand breaks in rat thymocytes due to irrad. histidine and γ-rays 77—56438
DNA strand breakage, prod. of monophosphate end groups 77—32873
DNA strand breaks, lymphoma cells, detected by hydroxyapatite chromatographic technique 79—43819
DNA strand breaks, radiobiological effects theories 77—77943
DNA strand breaks in ^{60}Co γ-irrad. thymocytes 78—7395
DNA strand breaks in developing rat brain and their repair 80—30786
DNA strand-break repair in chick embryo Mullerian ducts 80—36020
DNA synthesis, nucl., in yeast, UV and gamma-ray effects 77—56428
DNA synthesis in chick embryonic Mullerian ducts, X-ray dose response obs. 79—88130
DNA synthesis inhibition in vitamin-E-depleted lymphosarcoma cells by X-rays and cytostatics 77—56429
λDNA transcription, effect of UV irrad. 77—66827
DNA unscheduled synthesis in diploid yeast after X-irrad. in different phases of cell cycle 77—44722
DNA-acridine orange complexes, energy transfer after dye laser excitation 79—2005
dye proflavine bound to synthetic polynucleotides, selective laser photodamage 80—99525
E. coli, DNA repair in radiation resistant and radiation sensitive strains 79—34489
E. coli, relative rates of repair of single-strand breaks and postirradiation DNA degradation 79—16149
E. coli, UV-irradiated, DNA double-strand breaks from single photochemical events 79—16151
E. coli, UV-irradiated, DNA single-strand breakds and alkali-labile bonds 79—16152
E. coli ^{125}I and X-ray damage, effect of cell DNA content 78—28006
E. coli B irrad. with 0.8 MeV electrons in oxygenated and anoxic states, mol. alterations 78—24031
electron microscope superconducting lens system for reduction of radiation damage 79—34718
electron microscopy of frozen hydrated crystalline specimens, meas. and reduction of damage 80—85552
endotoxin of S. typhimurium, radiation-induced alterations 78—7391
enzyme activity rate reduction by EM fields *(Russian)* 78—61142
EPR studies using aqueous LiCl glass as neutral matrix 79—96632

biomolecular effects of radiation continued
erythrocyte membrane, intrinsic fluorescence obs., radiation effects on struct. 79—74724
ethenoadenosine, influence of pH and metal complexion on fluorescence parameter 79—34483
fatty acids, unsaturated, containing peroxide oxidation products, free radicals formed on UV irrad. 80—51165
ferredoxin of adrenal cortex, destruction of chromophore centre on exposure to X-irrad. 78—76993
ferric haemoglobin, EPR studies before and after irradiation 79—29503
ferricytochrome, photoreduction in presence and absence of electron donor 78—53337
ferricytochrome c photoreduction, transient absorpts. in indole aq. solns., 600 to 800 nm 78—53228
fetal fibroblasts, UV induced chromosomal abnormalities, New Zealand Black mice 79—43836
fibrinogen, bovine, high energy-induced aggregation, time resolved spectra 80—61655
fibrinogen solution, effect of scavengers on radiation-susceptible sites 78—11701
flavins, photoemission of electrons in polar media 79—29507
fluoresceindiacetate hydrolysis and transport in mammalian cells after UV and gamma irrad. 77—56333
fluorescent light induced DNA crosslinkage and chromatid breaks, mouse cells 79—96615
5-fluorocytosine, electron beam damage assessed by EELS 80—89809
food components, ESR studies of free radicals 79—52699
β-galactosidase induction in X-irrad. E. coli B and B/r 78—28005
genetic material, mol. conformation and struct., ESR, NMR and optical meas. 80—26201
glyceraldehyde-3-phosphate dehydrogenase radiolysis, active-site and SH loss 78—77000
glycine, electron-irrad. polycrysts., stable products obs. by ^{13}C NMR 78—15775
dGMP γ-irrad. in frozen soln., free radical form., computer EPR spectra anal. 78—31774
green-rod pigment of frog, Rana temporaria, long-lived photoproducts 77—25433
greening bean leaf low-temp. fluorescence induction obs. 79—39354
haemoglobin, aq. soln., X-ray induced changes 78—11699
haemoglobin, bovine type A, γ-induced changes obs. 79—43811
haemoglobin, dielectric transient response following UV-irradiation 80—51166
haemoglobin+CO reaction kinetics, using various regimes of photolytic illum. 78—48753
haemoglobin-CO reaction kinetics, relax. meas. on photolytic illum. 77—70405
haemoglobin-erythrocyte membrane interaction, γ-ray effects, EPR 78—7402
immunoglobulin, human, high energy-induced aggregation, time resolved spectra 80—61655
indole, aq. solns., flash photolysis, transient absorpts., 600 to 800 nm 78—53228
invertase, S-containing glycoprotein, gamma-irrad., secondary radical reactions, EPR 77—9175
^{125}I-iododeoxyuridine, effect of ^{125}I-decay, mol. consequences of Auger effect 77—4982
o-iodotyrosine, intramol. effects of ^{125}I decay 80—108973
3-iodotyrosine, intramolecular effects of ^{131}I decay 77—36870
ion electron-loss microscopy, high-energy, signal-to-damage ratio 79—25175
lactate dehydrogenase+free radicals, reactions, pulse radiolysis 78—7214
laser irradiation, selective photochemical mechanisms 79—66450
laser selective photophysics and photochemistry, book contrib. 79—79273
lecithin bilayers, reaction kinetics of radicals, OH, e_{aq}^- 79—11886
DL-leucine degradation with longitudinally polarised electrons 79—79474
lipid, peroxide photo-oxidation, increase in liposome proton permeab. 78—69024
lipid bilayers, bacteriorhodopsin containing, photoelectric activity investigation 79—16148
lipid peroxide oxidation fluorescing products, effect of UV on formation 79—57585
living system biophysical interaction mechanism with RF and microwave radiation 79—79602
lumirhodopsin, photoconversion at 77K, quantum efficiency estimation 80—67081
lysine vasopressin, amide H exchange rates in aq. soln., ^{1}H NMR effects 79—83692
lysozyme, 0.01% soln., mag. and radiofreq. effects on activity 78—61136
lysozyme, dye-sensitized photoinactivation rate constant studies 79—79476
lysozyme, light-induced riboflavin binding 78—27899
macromolecular synthesis in root meristem cells, 2 MHz US effects, Pisum sativum 77—9218
malic dehydrogenase isoenzymes in wheat shoots and chloroplasts, effect of light 78—11696
malignancy analysis based on somatic mutation 78—69147
mammalian cells, replicon sizes estimated by X-ray plus bromodeoxyuridine photolysis method 79—16353
mammalian cells, UV-irradiated, DNA repair kinetics 79—20513
mammalian cellular DNA; breaks induced by accelerated heavy ions, impaired repair capacity 80—41129
metarhodopsin I-II transition obs. by absorpt. changes of eriochromblack T 77—44593
metarhodopsin transitions rel. to visual response in barnacle photoreceptor 78—69050
1-methyl cytosine: 5-fluorouracil X-irrad. at 300K, EPR 78—64941
11-cis-14-methylretinal, photoisomerisation, high quantum yield 79—57253
micro-organisms, radiation injury, repair and sensitisation, review 78—11700
microorganisms, effects of laser and ordinary UV irradiation 79—70586
microorganisms, photobehaviour, review, book contrib. 79—5329
microtubule polymerisation in vitro, effects of ^{60}Co gamma irrad. 78—20222
microwave cellular, subcellular and molecular effects *(Russian)* 79—16249
microwave effect observation prerequisite conditions 80—3592
myoglobin conformationally-nonequilibrium state reactivity obs. by pulse radiolysis 79—39353
myoglobins, kinetics studied by picosecond spectroscopy 79—43804

biomolecular effects of radiation continued
nanosecond flash photolysis, techniques and biological appls. 78−68905
natural fats, effects on fatty acid composition and lipid peroxide formation 79−96623
p-nitroacetophenone charge transfer reaction with triplet state of guanine for radiosensitisation 79−92146
nucleic acid, multiphoton photoreactions of aq. soln., picosec. UV pulse 79−34487
nucleic acid component pulse sonolysis obs. 79−53186
nucleic acid components, low-intensity US effects 77−32874
nucleosides and nucleotides, X-irrad., alkoxy radical and free radical product 77−90623
optical asymmetry correl. with parity violating weak interaction 78−69000
optically active molecules and polarised bremsstrahlung 77−63938
oxytocin, amide H exchange rates in aq. soln., ^{1}H NMR effects 79−83692
papain inactivated by OH radicals and H_2O_2, optical density, amino acid composition and fluoresc. 78−53344
peptide aqueous solution, EPR of spin-trapped radicals, OH radical reactions 78−68993
peroxidase, low-temperature radioreduction, MCD and absorpt. spectra 78−31763
peroxidase, photo-induced reduction, reaction with indole acetic acid 79−79452
L-phenylalanine.HCl, X-ray induced radical form. 78−48755
pheophytin a, photo-oxidation primary processes 79−79468
pheophytin reduction obs. in higher plant photosystem II 79−43817
pheophytin-a, photochem. generation of cation-radical, spectral-kinetic characts. 78−96008
photo-induced charge transfer, mechanism and range 77−60182
photochemical formation of self-sustaining coacervates, rel. to origin of life, review 78−11611
photodermatological uses of dye lasers, erythema production, psoriasis treatment, tumour destruction *(German)* 80−56164
photoreceptor membrane viscosity and component dynamics, recombination kinetics method 79−39366
photosensory retinal pigments in Halobacterium halobium 80−97860
photosynthesis, Blinks effect rel. to two-photosystem hypothesis 79−57590
photosynthesis, electron spin polarisation and mechanism of electron transfer in photosystem I 78−40122
photosynthesis, energy and electron transfer speed, time resolution meas. *(Russian)* 80−94161
photosynthesis, energy upconversion and minimum quantum requirement 77−29115
photosynthesis, fluoresc. and energy transfer, time resolved obs. 79−48216
photosynthesis, fluoresc. induction modelling by elec. diagram 79−57589
photosynthesis, in vitro models 78−77023
photosynthesis, picosecond fluorometry in primary events 79−8476
photosynthesis, primary, selectively excited by tunable ps parametric oscillator 79−48163
photosynthesis of green plants, tripartite model for photochem. apparatus 78−44474
photosynthetic membrane, in vivo, light collection and exciton dynamics 79−48215
photosynthetic membranes, anal. of laser-induced fluorescence with Pauli master eqn. 79−39350
photosynthetic membranes, exciton dynamics, picosecond pulse train study 79−8483
photosynthetic reaction centre, chlorophyll function, review, book contrib. 79−5251
photosynthetic reaction centre spectroscopy by tunable picosec. parametric oscillators 80−61513
photosynthetic reaction centres, primary electron transfer rate 79−8481
photosynthetic solar energy conversion, biometric analogue 79−52914
photosynthetic systems, temperature dependence of excitation transfer 78−92598
phthalocyanine, cryst., electron damage, electron microscope study 78−22762
phthoralocyanin porous films, Becquerel photovoltaic effect 77−16907
physical, molecular, cellular and macrocolony level obs. 80−12193
phytochrome, role of light in regulating plant growth and development, review 78−11695
picosecond flash photolysis in biology and biophysics, book contrib. 79−5328
pigment reversible changes due to illumination of leaves 79−43818
pigment spectral forms of Rhodospirillum rubrum, picosecond energy transfer 79−92182
plasmid molecular weight determ. from UV sensitivities 78−44458
polynucleotide hydration characts. in H_2O/D_2O frozen solns., γ irrad. effects, PMR 78−31772
polynucleotide solution, elec. field induced orientation and effects 80−85348
polynucleotides, gamma-ray effects on hydration, PMR of frozen and liq. solns. 78−27900
polynucleotides, single-stranded, reaction of O_2 with radiation-induced free radicals 78−48759
polynucleotides poly(A+U), double-stranded, radiolysis in presence of O_2 78−48760
porphyrin, reduced, photoregeneration mechanism in the presence of O_2 79−57582
porphyrins, effects of ultrasound on biosynthesis links 79−62184
prelumirhodopsin, psec. kinetics, primary photochem. event in vision, proton translocation 78−44508
protein, electron radiation damage on primary and secondary struct. level 80−89808
protein, radical limiting conc. on UV irrad. at 77K, effect of luminesc. quenchers 80−30662
protein aggregates exposed to UV radiation, limiting conc. of paramag. centres 78−24029
protein synthesis control studies, exptl. probe using psoralen and near UV light 77−66881
protein-containing membranes, photoinduced electron transport 80−30768
protein-DNA cross linking mediated by X-rays 78−27898
proteins, UV irrad., paramag. centre accumulation, kinetic eqn. 77−21476
proteins, UV irradiated, luminesc. quenching, EPR and absorpt. spectra 78−15768

biomolecular effects of radiation continued
pulse radiolysis appl. to biomolecule reactions and struct., review 78−61145
purine, powder, γ-irrad., dose-response curves 78−7215
purine and pyrimidine, γ-irrad. investig. by diffuse refl. spectrophotometry 77−48756
purple membrane of Halobacterium halobium, energy transfer 78−44467
purple membrane protein chromophore, fluoresc. 78−44454
purple membrane protein retinal chromophore, role of protein in photochem. 78−15772
purple membrane structure, effects of bleaching and regeneration, H-halobium 77−86532
purple membranes from Halobacterium halobium, spectral transitions 80−12056
purple photosynthetic bacteria, in vitro duplication of primary light-induced charge separation 79−39361
pyrimidine dimers, excision repair of UV damage in monkey kidney cells 78−53332
pyrimidine powder, γ-irrad., dose-response curves 78−7215
pyrimidines, substituted, UV irrad. in aq. solns., EPR of free radicals 78−40115
quinacrine mustard, 2-step laser-induced photodamage 80−85198
quinacrine mustard-DNA complex molecule, laser-induced fluorescence 77−60187
radiation biology conf., Sapporo, Japan (Sept. 1978) 80−8105
radiolysis of DNA and other bipolymers 80−67163
retinal, highly polar excited electronic states, electron transfer 78−48757
retinal isomers, dark equilib. and photochem. 78−15771
retinal photoisomerisation mechanism for light-driven proton pump in H. halobium 78−35820
retinal Schiff bases in lipid bilayer membranes, photoelec. effects *(Japanese)* 78−7322
retinal-entrapped membrane, photo-induced potential 78−20148
retinals, prod. and quenching of singlet oxidation 80−35840
rhodopseudomonas sphaeroides, reaction centre triplet state fluoresc. mag. field depend. 78−53358
rhodopsin, bathorhodopsin and isorhodopsin, mech. of photoconversion 78−53336
rhodopsin, bovine, photochem. cis-trans isomerisation at liq. He temps. 78−64939
rhodopsin, cis-trans isomerisation on psec time scale 77−86498
rhodopsin, conformeric states, spectrophotometry 77−90725
rhodopsin, excited state energy surface to explain photochemistry 79−48218
rhodopsin, isorhodopsin, photochem. on picosecond time scale, bathorhodopsin form. 79−83706
rhodopsin, isorhodopsin and bacteriorhodopsin, and photoproducts, temp. and wavelength effects on photochem. 78−11612
rhodopsin, photo- and thermo-bleaching rel. to heterogeneity problem 80−41114
rhodopsin, primary photophys. and photochem. processes in visual excitation 78−15773
rhodopsin, solubilised, photoinduced conform. changes, spin-label method 77−81496
rhodopsin, transient light-induced conform. changes 78−15774
rhodopsin and thermal intermediates, fast struct. fluctuations in protein component 80−72137
rhodopsin bleaching, cooperative conform. change in rod photoreceptor disc membrane 77−81499
rhodopsin flash photolysis, rabbit retina 78−76996
rhodopsin in model membranes, charge displacements in interfacial layers 77−52785
rhodopsin phosphorylation as possible mechanism of visual adaptation 78−15836
rhodopsin photochemistry, relevance of Halobacterium photosensory mechanism 77−90738
rhodopsin photolysis, retinal rod external segment mag. anisotropy decrease 77−52838
rhodopsin stability in rods and dark noise in retinal bipolar cells 78−11644
rhodopsin-containing bilayer membranes, light induced transmembrane channel form. 77−52784
ribonuclease inactivation cross-sections for slow heavy ions 80−26286
ribonucleotide reductase of E.coli, in vivo photoinactivation by near-UV 77−52841
ribosomes, E. coli, form. of covalent linkages between RNA and proteins due to gamma irrad. *(French)* 77−56340
RNA, heterogeneous nucl., effects of UV irrad. and postirrad. incubation on size in murine cells 78−69139
RNA, low molecular weight, synthesis sensitivity to UV irradiation 79−57591
RNA, messenger, synthesis in rat livers, ionising radiation and partial hepatectomy effects 79−92144
RNA of Novikoff Hepatoma ascites cells, effects of sparsely-ionising radiation after in vivo labelling 78−7389
RNA specific activity, Novikoff Hepatoma ascites cells 78−3560
RNA synthesis in regenerating liver of irrad. adrenalectomised rats 77−64087
RNA synthesis in slime-mould, effects of electrons and neutrons, caffeine modification 77−12962
RNA synthesis in vitro, thiopyronine-sensitised photodynamic inactivation 77−29177
RNase, damage and energy deposition by low-energy ions 77−9172
RNase inactivation due to elastic nucl. collisions 78−28008
serium albumin, bovine, high energy-induced aggregation, time resolved spectra 80−61655
serum albumin, human, mechanism of eosin-sensitised photochemiluminescence 79−53044
serum albumin solns., X-ray induced chemiluminesc. intensification by dye addition 79−79470
synergism of radiation and other DNA damaging agents 80−26299
testosterone, dielectric transient response following UV-irradiation 80−51166
thiamine, radiolysis, one electron redox pot. 79−53048
thymidine, frozen aq. solns., final products of gamma radiolysis 78−77001
thymidine monophosphate aqeous solution, gamma irrad. effect on base damage, phosphate release 80−89806
thymidine-5-monophosphate, γ-irrad. aq. soln., spin-trapped radicals, liq chromatography and EPR spectroscopy 78−53340

biomolecular effects of radiation continued
thymine, γ-irradiated, EPR study of post-radiolysis growth of spin-trapped radicals 79−16155
thymine dimer excision from DNA of UV-irrad. plant seedlings 78−61221
thymine dimer excision kinetics in UV-irrad. human cells 78−53331
thymine dimer induction by UV as function of cell stage 79−57715
thymine fragment damage retained in DNA polynucleotide chain after γ irrad. in aerated soln. 78−31773
time effects in molecular radiation biology 80−72269
5-trifluoromethyluracyl, electron beam damage assessed by EELS 80−89809
trypsin, in suspension, radical form. and inactivation after Γ-irrad. 78−3564
trypsin, photoluminescence after UV irradiation *(German)* 79−92137
trypsin, study by pulse radiolysis 79−8480
L-tryptophan-HCl radical form. after X-irrad. 78−64940
tryptophanase induction in X-irrad. E. coli B and B/r 78−28005
L-tryptophan.HCl, irradiated single crystals at 295K, EPR study 79−11900
tryptophyl peptides, pulse radiolysis, hydrated electron reaction 78−48679
tunable lasers and applications, conference, Loen (1976) 77−54720
tyrosinase in buffer soln., UV effect on biological activity 80−30791
ubiquinone-Fe complex, bacterial photosynthesis primary electron transfer processes, psec. dynamics 78−80841
UDPG-dehydrogenage, rat liver, struct. alterations and functional vars. due to γ radiation 78−15873
uracil, nucleic acid component, selective action by ps light pulses 80−72213
uracil derivatives, photosensitised induction by H-addition radicals in frozen aqueous soln. 78−20146
uridine 5′-phosphate (Na salt), EPR study of PO_4^{2-} radical 79−57592
uridine-5′-monophosphate gamma-irrad. solutions, short-lived radical detect. by spin-trapping method 77−21479
uridine-5′-phosphate.2Na$^+$ single crysts., radiation damage, ESR obs. 80−108964
UV, correls. in human diploid fibroblasts after potentially lethal damage 80−21493
UV, dNA repair and longevity assurance in Paramecium tetraurelia 80−3741
l-valine, cryst., electron damage, electron microscope study 78−22762
valyl-tRNA synthetase from chick embryo brain, effect of ^{60}Co γ-radiation 79−34490
visual pigment chromophores, models, spectroscopic and photochemical studies 80−30723
visual pigment reactions, coupling of charge stabilisation, torsion and bond alternation 78−64999
visual pigment retinal chromophore, role of protein in photochem. 78−15772
visual pigment solutions, flash photolysis, time resolved difference spectra, temp. var. 77−25434
visual pigments, slow flash photolysis using conventional spectrophotometer 78−68904
visual pigments in solution, flash photolysis kinetics, effect of prep. 77−32892
vitamins, B group, γ-irrad. resist. 78−76890
water photo-oxidation in presence of porphyrins adsorbed on octane-water interface 78−64933
X-ray fluorescence anal., importance to geometry 79−5430
zinc-porphyrins, photodestruction in E. coli in presence of O_2 79−79601
CO-haemoprotein photolysis, transient Raman study, quantum yield origin 80−67155
O_2 radiobiological effect, molecular and cellular basis 80−26211
O_2^- superoxide ion as cause of O_2 effect, X-ray induced cell lethality 77−25513

biomolecules *see macromolecules; molecular biophysics*

bionics *see biocybernetics*

biophysics
see also biological fluid dynamics; biomechanics; cardiology; cellular biophysics; haemodynamics; hearing; molecular biophysics; speech; vision
air ions, biological impact 77−1972
analogue computers, teaching appls. with biological examples 79−84890
animal navigation; rel. to motional EMF 77−60879
antennular chemosensitivity in spiny lobster, amino acids as feeding stimuli 78−53431
aortic wall stress-strain characts. after sequential enzymolysis 78−3530
arterial vasa vasorum deformation/hydraulic resist. study *(Japanese)* 78−3544
biochemical systems, temporal and spatial patterns 80−3340
biochemistry and biophysics horizons, book 78−68977
biochemistry and biotechnology, conf., Helsinki, Finland, 27-31 Aug. 1979 80−57001
biological systems, entropy of fluctuations, time evolution, NMR obs. 79−53017
bioluminescence of firefly larva, circular polarisation 80−94441
biomass system studies, review *(Japanese)* 80−26436
biomaterial growth phenomena and behaviour, math. theory 77−81458
biometeorology, plants, animals, human beings, weather change effects *(French)* 80−17360
blood, preserved, oxidative pot. 77−81771
body temp. regulation method for hyperthermia and hypothermia study 78−15778
bone, compact, fracture mechs., effects of density and specimen thickness 78−3534
bone, deformation under unloading and repeated loading 78−3546
bone, human, ulnar bending stiffness, mineral content, geometry and strength 78−3537
bone, osteonic lamellae, evidence for state of initial stress 78−3536
bone density determination, effective attenuation coeff. of soft tissue, Compton scatt. 80−101220
book, horizons in biochem. and biophys. 78−7315
book, inc. bioengineering, annual review 79−5246
book, physics for applied biologists 78−53310
botany, transpiration from plant leaf, simulation expts. 79−48279
brain, pulsations of third ventricle, mathematical description 77−64081
calcified tissue, role of collagen in elastic props. 78−3539
calcium phosphates, seeded growth, effect of solid/soln. ratio, calcification 78−15303
biophysics continued
cardiac muscle, resting, activation monitored by intensity fluctuation spectroscopy 80−108953
β-carotene glass, photoconductivity mechanism 79−28368
catalytic reaction model, instability and spread of excitation waves, nontrivial modes 78−20161
catastrophe theory, statistical biophysics applications 79−39334
cerebral artery walls, rheoencephalogram parameters vs. mech. props. 78−3547
coherent mode excitations, bose condensation-like, Frohlich vibr. model, Boltzmann eqn. approach 79−39336
colloidal particles, in a flowing solution, SAXS 80−61163
comb filter, use for describing time-varying biological rhythmicities 80−97852
constrained systems, statistical mechanics, generalized canonical approach 78−48743
convective heat loss assessment from humans in cold water 78−81093
cryosurgery, freezing patterns of normal and diseased tissues 78−44685
cryosurgery, math. and biophys. foundation 77−40920
cutaneous pressure sensitivity, effect of skin surface temp. on localisation error and two-point threshold 78−77072
cutaneous system energy depend. in conditions of simultaneous, residual and reverse masking, humans 78−20196
deconvolution of exponential response functions 80−16894
desert plants' temperatures, adaptability of leaf size 79−24957
diffused substance kinetics in biological systems 78−53312
dissipative structures, formation and stability 80−108950
dissipative systems, dynamical field theory, hierarchical struct. of field thermodynamics 78−73132
distributed systems, stability of spatially inhomogeneous states 80−30629
ear, mouse, induced thermal resistance 79−48220
ecosystems, biophys. of living organisms communities in natural state 77−73503
electrocutaneous stimulus magnitude sensation, effect of pulse height and width *(Japanese)* 78−31998
EM energy deposition in inhomogeneous block model of man for near-field irradiation conditions 80−89788
EM energy deposition in man models with grounding and reflector effects, numerical calcs. 80−56114
energy expenditure of man, anal. determ. from external respiration parameters 78−69268
energy fluence rel. to energy incident on, emitted by or imparted to a body 80−17002
energy spectra of δ-rays produced due to high energy particles with biological systems 80−108951
excitable medium, 1-dimens., non-steady processes, division of arrested excitation front 77−70401
excitable medium, auto-oscillatory, 1-dimens., stability complex regimes 78−15752
forearm carrying angle variation study during elbow flexion 78−3532
Frohlich steady state model, asymptotic solns. 80−21435
growth and patterns of spatial organisation 80−81287
growth of scientific knowledge 79−71219
Hamiltonian content of biodynamics 80−89704
head protective devices design, military 78−11793
heart tissue, thalassaemic, Mossbauer spectra of Fe deposits 78−73202
history in USSR 78−93506
horizons in biochemistry and biophysics, book 79−16118
human skin and subcutaneous tissue, unsteady state heat transfer, similarity transformations 78−95990
hyperthermia, dynamic temp. distribs. in normal and neoplastic tissues during diathermy 78−31776
hyperthermia in dogs, rel. to post surgical rewarming by thoracic flush 78−80834
hyperthermia research, importance of good thermal dosimetry 78−64942
introductory biophysics, personalised system of instruction course 79−5929
lake monsters, prod. by image distortion due to atmospheric refr. 80−46259
laser scattering in biological samples 79−79596
leaf optical system modelled as stochastic process 77−44877
light absorption by leaves and pigment containing cells 77−75416
light penetration depth in tissue, spectral depend., 0.35 to 1 μm 78−11714
living and lifeless matter, complementarity 79−66436
locomotion of human leg, swing phase anal., analogue simulation 78−3531
luminescence, cryptic, midwater shrimp 80−3890
lung, beta-emitting particles, fraction of energy absorbed, rat obs. 80−104641
magnetic field detection by invertebrates Tenebrio and Talitrus, distinct from light detect. 78−77073
magnetoelectric dipole gas as explanation of biocosmic phenomena, summary of phenomena 80−8241
magnetoelectric dipole gas as explanation of biocosmic phenomena, theoretical concepts 80−8242
magnetoelectric dipole gas as explanation of biocosmic phenomena, theory development 80−8243
man's size in terms of fundamental constants 80−105489
manual control operator performance, gain and vibration effects interaction 78−44756
marine green alga, Ulva fenestrata, afterglow in the ms and ds intervals of attenuation 80−104636
mathematical biology meeting, Philadelphia, USA, (Aug. 1976) 78−53311
medical physicists, training, survey of program directors 79−17159
metabolism, energy conservation 77−81459
metacarpo-phalangeal joint, 3-dimens. biomech. anal. 78−3533
microwave power absorption differences between normal and malignant tissue 80−104640
molecular computer, biophys. rel. to phys. of real world 80−30630
Monte-Carlo simulation of photon transport in a heterogeneous phantom 80−26257
multirhythm system, transition in causal dynamics 78−4580
muscle contraction, simulation of thermophysical processes 78−96063
myocardial tissue, US attenuation depend. on time after excision and temp. 78−11711
nautiloid growth, rel. to Earth-Moon system palaeodynamics 80−41713
negative superionisation, biological effects, investigation *(French)* 78−3946
network structures of a system coded by groups 80−81286

biophysics continued
neutron cross-sections and kerma values for C, N and O from 20 to 50 MeV 80—101217
neutron scattering techniques in applied research, medium-flux research reactors 79—13514
noise analysis for differentiation between equilib. and nonequilib. kinetic systems 78—44439
nonlinear analysis for shaping and threshold actions 77—12871
nonlinear system analysis by Wiener kernel estimation in freq. domain 77—1973
nonlinear systems, mode-locking, computer simulation 77—12872
nuclear and atomic data sources 79—25081
nucleus growth, spatial kinetic systems, multi-stationary state transitions, Langevin stochastic approach 78—73136
ocean, seawater biomass content distrib. rel. to hydrochemical characts. and transparency 80—31057
optical constants and dispersion eqns. of lecithin, cholesterol, fucose and chloroform 80—30762
osteon system piezoelec. polarisation model 78—3540
otolith sensitivity assoc. with habituation to linear accels. capable of inducing motion sickness 78—44621
oyster shell, IR and atomic mineral anal. 78—61116
phase boundaries and multiphase systems, conf., Tokyo, Japan (Sept. 1977) 79—29415
phase transition in system with diffusion, noise-induced 79—100560
phase transitions in physics and biology 79—43803
photon interactions, calc. of average energy absorbed 80—45947
physical and biological science, conf., Japan (Jan. 1979) 80—8734
plant biophysics, book 77—60180
plant leaves, microwave photoconductivity obs. 80—104637
plant leaves, spectra of nonlinear optical effects *(Russian)* 78—48829
plasma in biological solids, resonant interactions with microwaves 80—101222
prolate spheroidal models of humans in near field of short electric dipole, irrad. 80—104639
proteoglycans, swelling pressures at the concs. found in cartilaginous tissues 80—67327
pyroelectricity, anomalous behaviour of leaf epidermis of palm-like plant Encephalartos Villosus 78—44755
radioactive contamination in aquatic organisms, evaluation by statistical and information theory 78—53535
respiratory tract, human, model, aerosol particle deposition meas. 78—24086
respiratory tract, human, polydisperse aerosol deposition models 78—24085
review of biophysics and bioengineering, book 77—86433
review of biophysics and bioengineering, book 80—105437
reviews of biophysics and bioengineering, book 80—17723
RF EM plane wave incident on a man model, energy absorpt. by and fields in calcs. 80—56115
RF higher-frequency energy absorpt. by biological models, geometrical optics calcs. 80—56116
sea chlorophyll concentration, estimation from outgoing radiation spectrum meas. from helicopter 80—36333
Seebeck coefficient in solid biopolymers, meas. apparatus 78—21172
skeletal muscle fibre orientation, US attenuation meas. 80—30763
skin, in vivo, light absorpt. and scatt., theoretical and expt. study 80—101219
skin response to fractionated heat and X-rays 78—35887
smell meas., status *(Japanese)* 78—92661
space biophysics, Soviet research programme *(Russian)* 78—40354
space motion sickness 80—61712
spaceflight factors combined effects on man 78—53537
statistical mechanics of biophysical systems, ensemble theory 79—96502
student laboratory apparatus, electronic, modules by Thornton 79—71206
tachyon magnetoelectric monopoles, polymerised, delocalised clouds as possible cause of auras 80—41362
tendon composite, structural hierarchies and interactions 77—86526
thermal insulation of animal coats and human clothing, review 78—73139
thermal stress energy studies of small mammals, use of differential emissivity calorimeter 78—40118
thorax, human, elastic finite element anal. models 78—3542
tissue, perfused, macroscopic temp. distrib. 78—64944
tissue, rabbit, comparison of NMR water proton T_1 relax. times 80—101221
tissue model, two-layer, theoretical anal. of diffuse reflectance 80—35956
tree rings, ^{13}C vars. in N.hemisphere trees during last 150 years 80—17363
tree-ring analysis in palaeoclimatology, preliminary survey and scope for Indian region 80—90212
trees, use as local climatic wind indicator 80—82007
US scattering by human tissue, theoretical models 78—7411
vibration effects on continuous manual control 78—61169
vibrations of seated subjects, effect of position of axis of rot. on discomfort 78—85461
vitalism, nonlinear transforms in Hilbert space 78—73133
water loss, evaporative, by man in a gravity-free environment 79—57779
weightlessness and man, sled programme, Spacelab 80—94381
Br^{6+}, 42 MeV, stopping power and radial dose distrib. obs. in tissue-equivalent gas 80—101218
^{58}Co-cyanocobalamin, whole-body retention in rats, age effect 77—70559
^{60}CoCl$_2$, whole-body retention in rats, age effect 77—70559
^{137}Cs whole-body content in a normal New Mexico population 1956-1977 80—26382
FeS$_2$, acid bacterial leaching, lixiviant alteration by fungal absorpt. of Fe 80—108617
^{129}I in bovine thyroid glands, activation anal. obs. 80—94380
^{133}Xe solubility coefficients in water, saline, dog blood and organs 80—56331

biorheology
aorta, human, morphological and functional aspects of study of mech. props. 77—25499
arterial stenoses, fluid mechanics 80—35948
articular cartilage, drag-induced compression during a permeation expt. 80—97955
articular cartilage, normal, quasi-linear viscoelastic props. 80—108937
articular cartilage, viscoelastic properties *(Japanese)* 80—101215
articular cartilage biphasic rheological model 79—92264

biorheology continued
articular cartilage in compression, biphasic creep and stress relax., theory and expts. 80—94275
articular cartilage matrix, flow-independent viscoelastic props. 79—43952
articular cartilage of normal rabbit, viscoelastic shear behaviour 77—36973
articular cartilage single layer model, flow fields created by a sliding load 80—104630
atherogenesis, haemorheology-fluid dynamical factor *(Japanese)* 80—12171
atherosclerosis, rheological aspects *(Japanese)* 80—94268
bimolecular lecithin membranes, artificial, rheological and viscoelasic props. 80—26252
biosystems under stress, prerupture behaviour 79—39437
blood, adhesion of platelets and granulocytes in stagnant blood, effects of gravity and erythrocytes 80—3662
blood, couple stress fluid flow through narrow tubes 80—67105
blood, Fahraeus effect and cell screening rel. to dextran-induced aggregation 79—62273
blood, Fahraeus effect and cell screening rel. to volume flow rate 79—62272
blood, heparin assay in animal model of Pseudomonas sepsis 77—52953
blood, pulsatile viscous flow through diseased coronary arteries of man 77—90835
blood, red cell flexibility, effect on blood flow through tubes of 30-500 µm 80—67111
blood, red cell flexibility, whole blood filtration technique using 5 µm pores *(German)* 78—57030
blood, red cells, rheological props. meas. by Couette viscometer 80—97992
blood, red cells as fluid droplets, erythrocyte membrane dynamics in shear flow 79—74711
blood, rheological behaviour, viscoelastic model *(French)* 80—76779
blood, rheological characts., heat transfer rel. to myocardial infarcts 79—79573
blood, rheological hysteresis at low shear rate 80—97962
blood, rheological parameters for viscosity, viscoelasticity and thixotropy 80—16963
blood, rheological properties in transient flow at low shear rate *(French)* 80—41103
blood, rheological props. in transient regime to low velocity shear flow 79—79582
blood, thermophysical and rheological props., physicochem. composition depend. 78—80902
blood, viscoelastic properties, transient flow obs. 80—97980
blood cell damage in extracorporeal circulation, haemorheological effects of mech. factors 79—62280
blood cells, stored, rheological behaviour obs. *(French)* 80—67110
blood clotting timer, automatic 77—52896
blood droplet deformation in Courette flow suspension, expt. *(German)* 79—16227
blood flow, US Doppler signal LF spectral analysis 79—62312
blood flow in artery, stenosis effects on non-Newtonian flow 80—89775
blood flow mechanics 80—76778
blood flow model, hydrodynamic study with simulant fluid 79—25023
blood flow through narrow capillaries, rheological mechs. 80—97961
blood mech. transfer function, modifications by some biological factors and study method 80—16969
blood mixtures, artificial and whole 80—45928
blood oscillatory flow, Fahraeus-Lindqvist effect 80—3668
blood perfusion prediction from meas. of phase shift between heat flux and temp. 80—104804
blood perfusion rate estimation from diffusible indicator meas., sensitivity anal. 80—104803
blood plasma, normal and haemophilic, coagulation kinetics study 80—67107
blood plasma, reduced viscosity in joggers rel. to non-joggers 80—16967
blood plasma and serum temp.-viscosity relationship studies 79—20564
blood plasma viscosity in sickle-cell anaemia 80—94250
blood rheology, clinical changes in peripheral vascular disease and smokers 80—16965
blood rheology, erythrocyte rigidity effects on viscoelastic dilatancy 80—61610
blood rheology effect on haematocrit distrib. in pulmonary sheet flow 79—79572
blood velocity measurement using laser Doppler microscope 79—62329
blood vessel rheological props. and haemodynamic parameters meas. *(French)* 79—66587
blood vessel wall rheological properties, continuum-mechanical analysis *(Hungarian)* 78—35875
blood viscoelasticity, haematocrit dependence and interdonor difference compensation 79—62277
blood viscometers and anticoagulants compared 79—83834
blood viscosity and red cell aggregation at zero and 1G, instrumentation for Space Lab 3 80—61716
blood viscosity and red cell aggregation changes after haemodilution 80—97952
blood viscosity and red cell aggregation under near-zero gravity 80—3660
blood viscosity at low shear rate, capillary viscometer and obs. 80—98180
blood viscosity factors and functions, clinical appls. 80—3664
blood viscosity factors in severe nondiabetic and diabetic retinopathy 78—65069
blood viscosity variations associated with hyperlipoproteinaemia, rel. to cardiovascular risk factors *(German)* 78—57031
blood volume regulation, effects of space flight, review 80—3826
bone, cement line motion due to torsional load 79—74712
bone viscoelastic behaviour, anal. on basis of microstruct. 80—85429
brain tissue, human, nonlinear constitutive relations 78—80910
brain tissue, nonlinear constitutive relations 77—40707
bronchial elasticity and air flow, mathematical anal. 80—45942
burn-scarred human skin rheological props. in vivo meas. 78—31935
capillary blood viscometer for clinical use 77—40844
capillary viscometer for blood flow meas. 79—79671
cardiac muscle, passive, viscoelastic theory and obs. 80—94273
cell suspensions, stability to small disturbances in circular Couette flow 80—56099
cellulose, mech. relaxation at low temps. rel. to adsorbed H$_2$O 77—43277
cervical mucus spinability automatic meas. device 78—31928

biorheology continued
  colloidal dispersions, microrheology, chains of spheres in shear flow 77—7354
  colloidal dispersions, microrheology, pairs of interacting spheres in shear flow 77—7352
  colloidal dispersions, primary and secondary doublets of spheres in shear flow 77—7353
  conference, Osaka, Japan (June-July 1979) 80—62364
  cortical bone, wet, non-linear constitutive eqn. of viscoelastic props. 80—30754
  cortical bone, wet, torsional and biaxial viscoelastic props. obs. 80—30752
  cortical bone, wet, viscoelastic props., relax. mechs. 80—30753
  Couette viscometer for short time shearing of blood 80—98179
  couple stress fluid pulsatile flow through circular tubes 79—62275
  DNA ios-ionic solutions, anti-thixotropic props. 79—57680
  electromechanical viscometer with digital readout, operating principles 78—28131
  epithelial mucus, rheology and mol. organisation 80—97959
  erythrocyte, flow resistance into pores 80—61609
  erythrocyte, human, dynamic osmotic haemolysis and ghost repair, resistive pulse spectra 79—62208
  erythrocyte, rheological models *(French)* 78—24083
  erythrocyte, sectioned, generalised theory of geometrical shape 78—65071
  erythrocyte membrane, viscoelastic props., theoretical and expt. studies 79—16157
  erythrocyte membrane alterations, rheological technique evaluation 80—61611
  erythrocyte membranes, fluidity change after X-irrad., pyrene excimer fluoresc. obs. 80—72262
  erythrocyte osmotic fragility curve, statistical synthesis 78—65070
  erythrocytes, human, cholesterol-loaded, rheological and kinetic dysfunctions 80—45867
  erythrocytes, motion and deform. in the microcirculation 79—29513
  eye lens, bovine, rheological analysis 77—90767
  fibrinolysis and coagulation, dynamic rheological studies 80—61614
  fish slime in aqueous soln., rheological characts. *(Russian)* 77—64067
  gelatin gels, in water and glycerol/water mixtures, dynamic viscoelastic props. 80—64508
  haemolytic secondary effects in cone-plate viscometers 79—62281
  haemorheology, lecture *(Japanese)* 80—98752
  haemorheology and diseases, conf., Nancy, France (Oct. 1979) 80—56991
  haemorheology in near zero gravity environment 80—3661
  haemorheology related to blood cells, conf., Hamburg, Germany (Aug. 1979) 80—62365
  heart, muscle preparations, viscoelastic props. anal., meas. and model *(German)* 79—83817
  hip joints, human, study of synovial fluid, friction and lubrication 79—11956
  intervertebral disc, small solute diffusion, in vivo obs. 79—62276
  intervertebral disc material, human, viscoelastic response obs. 80—51141
  joint lubrication model, nonporous compliant bearing, effects of cartilage stiffness and lubricant viscosity 80—3692
  knee semilunar cartilage, viscoelastic props. 79—70568
  lecithin, rheology and structure in conc. solns. and liquid crystalline state 77—64007
  lecithin-water system, lamellar phase, rheology 80—89779
  ligament, canine anterior cruciate constitutive nonlinear viscoelastic behaviour eqn. 79—96592
  lubrication mechanism model for knee joint replacement 79—74790
  lung, rheological properties of excised rabbit lung stiffened by repeated hyperinflation 80—41078
  magnetic micro-rheometer evolution and theory 80—92099
  mammalian DNA, viscoelastic behaviour, rat obs. 80—8078
  membrane fluidity, influence on activity of bound enzymes, book contrib. 80—30688
  membrane fluidity of fatty acid auxotroph, EPR study 79—70574
  mesentery tissue, burn induced alterations of interstitial diffusion 80—104634
  micropolar fluid model for blood flow through narrow tubes 80—67109
  morphogenesis, growth, elastic and non-elastic deforms. 80—108928
  muco-ciliary transport mechs. 80—97956
  mucociliary flow mechanics, channel model obs. 80—97957
  mucus mechanical props. rel. to mucociliary transport, effect of pharmacologic interventions 80—3663
  muscle, skeletal, exptl. results and modelling of biomech. props. 77—25486
  muscle, three-element model with viscoelastic passive elements 77—32930
  myocardium, quiescent, anal. of some theological and mech. props., rat 79—74709
  oscillatory tube flows of viscoelastic fluids 79—77252
  pathological synovial fluids, viscoelastic studies *(German)* 79—79585
  phosphatidylcholine bilayers, fluidity changes and phase transitions, intramol. excimer fluoresc. obs. 80—85342
  plant cell walls, viscoelastic props., hysteresis loop in the stress-strain curve 79—25009
  plant cell walls, viscoelastic props., mathematical formulation for stress relax. 79—25008
  plant cell walls, viscoelastic props., pre-extension rate effect on stress relax 79—29542
  plastic deformation during freeze-cleavage, review 78—14400
  plasticity of the neuronal network *(Japanese)* 79—57693
  platelet diffusivity estimation in flowing blood 79—25010
  platelet interaction with vessel surface, blood rheological factor influences 80—61612
  platelets, shear-induced activation 79—74704
  protein film, at liq. interfaces, shear rheologica props. 80—94256
  protein network formation dynamics, review, book contrib. 80—97995
  proteins, stress-induced struct. and activity changes 79—43812
  pulmonary surfactant film, surface dilatational viscosity obs. 79—62278
  rectal wall, mathematical anal. of passive viscoelastic props. *(French)* 77—66822
  red blood cell, human, rheologic effects of shape transform. 79—62216
  red blood cell ADP release at high shear stresses 80—98002
  red blood cell micromechanics in viscometric flow 80—98000
  red blood cells, viscoelastic study of aggregation 80—97960
  red cell extensional recovery, determ. of membrane viscosity 79—57683
  red cell membrane, human, surface elasticity and viscosity 80—61608
  red cell membrane, temp. dependence of viscoelastic recovery 80—40979
  respiration model analytical soln. 79—48282

biorheology continued
  rheoencephalographic curves, bipolar and tetrapolar techniques, comparison *(Croatian)* 80—104796
  rheometer, analytical, optical sliding contact, for flow visualisation at articular surface 80—104847
  sickle-cell blood, flow in capillaries 80—41066
  skin, human forearm, thixotropic props., rotary displacement obs. 79—39438
  skin components, rheological props. under compressive load 80—35945
  skin rheological behaviour, expt. results and struct. model 80—16968
  soft tissues, human, rheological props. from local cyclic loading method 80—108932
  soft tissues, human, rheological props. investigation using elastography 80—108933
  space experiments at microgravity 80—3659
  sperm, human, flagellar propulsion in cervical mucus, interaction hydrodynamics model 80—97878
  spermatozoa swimming in cervix, effects of dynamical interaction and peripheral layer viscosity 78—69126
  sputum viscoelasticity, meas. using conventional dynamic and raised cosine pulse methods *(Japanese)* 80—67132
  synovial fluid, normal and pathological, viscoelasticity 80—16966
  synovial fluid, pathological, rheological props. *(German)* 78—57032
  synovial fluid, pressure-viscosity characts. 79—25012
  synovial fluid, rheological eqns. 79—62285
  synovial fluid boundary lubrication model, structuring of boundary water 80—35950
  synovial fluids and models, rheological exam. *(German)* 79—79584
  synovial joints, rheology of synovial fluid, synthetic lubricants for degenerate joints 79—11955
  tendon, viscoelastic deform. obs. 80—101211
  Third International Congress of Biorheology, La Jolla, USA (Aug 1978) 79—74695
  thrombosis, rheological aspects *(Japanese)* 80—94268
  tracheal muco-ciliary transport, theoretical and expt. study 80—97958
  tracheal mucus gel props., changes induced by divalent cations 80—51142
  uterine muscle, isotropy and anisotropy during labour contract. 80—94257
  vascular system, haemorheology and two-phase flow *(French)* 79—34586
  vein, normals rel. to varicose conditions, human great saphenous vein 77—25498
  vein, rheological props. of human great saphenous vein, normals rel. to varicose conditions 77—25498
  visco-diffractometric techniques and erythrocyte deformability 78—35879
  viscoelastic biological tube dynamic rheology 79—62274
  viscoelastic lubricants, behaviour rel. to human joints 79—39430
  viscoelastic tube, pulsatile flow, non-Newtonian effects *(French)* 80—59113
  vitreous humour, human, viscoelasticity, in vivo obs. 80—56077
  vitreous sample, human, viscoelasticity determ. by Weissenberg rheogoniometer 79—92266
  water mobility in blood plasma, NMR determ., viscosity correl. to $1/T_2$ 80—67176

Biot-Savart law *see electromagnetism*

biothermics
  9 GHz radiometry of tumours *(French)* 80—3767
  acceleration response in man, heart and acute dehydration effects 80—30907
  acoustic speed temp. var. in excised human tissue, US computerised tomography 80—51150
  adenocarcinoma cells, mouse, MADCAP 37, hyperthermia and irradiation response 80—40971
  albumin denaturation, investigation by PMR 80—3582
  algal host cells, kinetics, mechanism and thermodynamics of cyanophage A-1 absorpt. 79—57614
  anaesthetised human subject temperature change model 79—92160
  anthers from cultured barley, effects of light and temp. environments 80—56119
  aortic wall, canine, speed of 10 MHz sound, effects of temp., storage, formalin soaking 80—56112
  applicator, 915-Mhz direct-contact, for therapeutic heating of tissues, development 79—2120
  aqueous temperature stabilisation, expt. evidence and related models 77—40713
  asymptotic rate process calcs. of thermal injury to the retina following laser irrad. 78—80916
  Bacillus subtilis spores, interdependence of thermal and EM effects in response to microwave exposure 78—15860
  bacteriophage Φ29, effects of temp. and UV irrad. on multiplication 77—86539
  bee, thermoregulation by evaporative cooling of head (honeybee) 80—61515
  behavioural alterations of rats, interaction of ambient temp. and microwave irrad. 80—67153
  benthic animals, colonies assoc. with deep-sea hydrothermal site on strike-slip fault 80—21710
  biological effects of EM radiation expt. techniques 80—8239
  biomedical thermal entrainment device for cardiovascular investigation 80—104793
  biometeorology, plants, animals, human beings, weather change effects *(French)* 80—17360
  biopolymer soln. heat capacity, conformational props. temp. depend. 80—8009
  black coat of desert goat, to save metabolic energy? 80—51047
  black lipid membranes and bilayer vesicles in solution, thermodynamic stable states anal. 80—45856
  bladder, toad, temp. dependence of ADH-induced water flow and intramembranous particle aggregates 80—61520
  blood and its constituents, coeff. of thermal expansion *(German)* 80—104556
  blood cell suspensions, deep-freezing improvements by thermal history automatic detect *(German)* 79—88215
  blood cells preservation at low temps., certain charact. features 78—24043
  blood flow, influence on temp. distrib. in exteriorised mouse intestine 79—48219
  blood flow in human skin, modelling thermal effects 79—24959
  blood flow measurement, finite diff. soln. of forced convection from hot-film probe 80—12177

biothermics continued
- blood heating or cooling, thermal design of a heat exchanger 78–92744
- blood perfusion, meas. by heated thermocouple probes' temp. transients anal. 79–96598
- blood perfusion prediction from meas. of phase shift between heat flux and temp. 80–104804
- blood perfusion rate determ. from temp. perturbation, unbiased minimum variance linear estimator 79–92283
- blood rheology thermal factors rel. to myocardial infarcts 79–79573
- blood temperature monitoring during extracorporeal circulation, noncontact transducer 80–85513
- blood vessel heat transfer 80–108851
- blood-brain barrier, effects of microwave-induced hyperthermia, rat 80–61642
- body temperature humidification, effect on thermal regulation 78–85295
- body temperature regulation, the set-point *(Japanese)* 78–24032
- brain hyperthermia, reversible, during audiogenic seizures, rat 80–8098
- brain lesion induction thermocoagulation, Ni-Pd-Mn alloy as thermoseed implant *(Japanese)* 79–61114
- brain tissues pot. temp. rise induced by EM field 79–29564
- breast cancer 30 GHz and 68 GHz telethermography *(French)* 80–3765
- breast cancers, microwave irradiation, EM energy and temp. distrib., numerical calculations 79–100697
- brown adipose tissue, mitochondria implicated in diet-induced thermogenesis 80–89722
- burn-induced leakage of macromolecules in living tissue, meas. method and obs. 79–29514
- burnt skin, heat and water losses 78–31790
- caloric nystagmus, mathematical model 77–73525
- caloric nystagnus, air and water, math. model 79–24983
- calorimetric instrumentation applied to the study of mass transfer in freeze-drying techniques 77–25628
- calorimetric instrumentation for studies of biopolymer model compounds 80–61746
- calorimetric investigation of the growth of luminescent bacteria 77–25378
- calorimetric measurements of microwave energy absorption. of mice, equipment and obs. 80–55996
- cancer therapy, invasive microwave system localised hyperthermia 79–100700
- cancer therapy, microwave hyperthermia, design of implantable radiators 80–41164
- cancer therapy, physical hyperthermic techniques, EM coupling modalities 80–41163
- cancer treatment appl. of microwave arrays for localised tumour heating 80–94308
- cancer treatment by hyperthermia *(French)* 80–17024
- cancer treatment by local microwave hyperthermia system 79–83893
- cardio-pulmonary system, heat and mass transfer of thermal indicator, modelling 79–25017
- catalase crystals and solns., calorimetric investigation 79–70526
- cell killing and the sequencing of hyperthermia and radiation 79–100673
- cell mechanisms of fever and pasteurisation at supra-optimal temps. 79–62211
- cell membrane Na pump as mechanism for increasing thermogenesis during cold acclimation, rats 78–7326
- cell organelles, deep cooling, change in lipid anti-radical activity 77–70426
- cell proliferation and viability, normal and malignant human cells, temp. effects 80–21449
- cell thermal injury, kinetics 78–56955
- cells, mouse embryo, innocuous freezing during warming 80–94175
- cells, volumetric changes during freezing and thawing, thermodynamic model 80–108863
- cellular radiation effects and hyperthermia, diploid yeast obs. 77–5036
- cellular radiation effects and hyperthermia, influence of post-exposure incubation conditions 78–40273
- cerebral cortial blood flow transients in cat. meas. technique using tissue heat transfer 79–92457
- cerebron, thermotropic and lyotropic mesomorphism 80–76703
- Chinese hamster cells, hyperthermic radiosensitisation to X-rays 80–21450
- Chinese hamster ovary cells, changes in cellular heat and/or radiation sensitivity obs. 79–74727
- chlorella cells, effects of light and low temp. on chlorophyll content and metabolism 80–56118
- chloroplasts, isolated, effect of temp. on photo-induced pH gradient 80–81566
- CHO cells, asynchronous, fractionation of combined heat and radiation, radiation sensitivity obs. 80–76806
- CHO cells, asynchronous, fractionation of combined heat and radiation, cell-cycle redistrib. 80–76807
- CHO cells, comparative effects of water-bath- and microwave-induced hyperthermia on survival 80–55997
- CHO cells, effects of X-irrad. and hyperthermia on SCE freq. 80–36021
- CHO cells, modification of radiation damage by hyperthermia at 40 and 45° C 77–86557
- CHO cells exposed to hyperthermia, radiosensitivity and recovery from radiation damage 80–72250
- CHO fibroblast, press., inhibited thermal killing obs. 80–81564
- chromatin, factors affecting the heat-induced increase in protein content 80–97832
- chromatin protein, increase kinetics for heated cells, possible role in cell killing 80–40980
- ciliated cells activity during ionising irrad., effect of temp. 77–70493
- circadian rhythm related to human body temp. 79–70525
- climatic stress on man, parameter recording and processing, math. method *(German)* 80–82047
- clothing of Bedouins in hot deserts, why black robes? 80–40969
- cold adaption by repeated immersions, dogs, catecholamines 79–100575
- cold exposure, mild, increased survival obs. in rats with medial preoptic lesions 80–101151
- cold urticaria, stable low temp. source for testing 78–61276
- cold water accidental immersion, aircrew survival and protection 79–88058
- collagen, hydration and intramolecular fusion, NMR and calorimetry obs., dynamic model 79–79451
- computer tomographic thermography, numerical simulation 79–83889
- conference, New York, USA (Dec. 1979) 80–104561

biothermics continued
- conformal applicators, therapeutic potential for hyperthermia induction 79–100696
- convective heat loss from a horizontal cylinder in different hyperbaric environments 77–48760
- convective heat loss from humans in cold water, assessment 78–81093
- convective heat loss from the human body 77–48759
- corneal curvature alterations by elec. heating 77–40665
- corneal temperature range, implications in prediction of laser thermal damage 80–108848
- corneal temperatures, normal and laser-injured corneas in the dutch belted rabbit 79–11919
- cortical evoked potentials, math. model for source localisation, somatosensory stimulation 80–89774
- cranial structure exposed to RF radiation, thermal response model 80–94285
- Crepis seeds, heat rel. to storage in X-ray injury modification 79–88118
- cryobiology, appls. of H_2O-NaCl phase diagram 78–15777
- cryogenic instruments, choice of working temps. for local destruction of tissue 78–36036
- cryogenically preserved canine kidneys, simultaneous microwave and HF thawing 77–5059
- cryoprobe, for medical surgery 80–56274
- cryosurgery, clinical appl. 80–12295
- cryosurgery, interrelations with physical props. of tissue 78–44685
- cryosurgery, mathematical and biophysical foundations 77–40920
- cryosurgery applicator, temp. distrib. reproducibility 79–39589
- cryosurgery instruments, effects of heat-transfer material on working parameters 78–36037
- cryosurgical probe, heat transfer coeff. within cavity formed by tip 80–36188
- current field heating, localised, as an adjunct to radiation therapy 80–98056
- cutaneous human tumours, selective heating at 27.12 Mhz 79–2123
- cutaneous receptors, on-line receptive field mapping technique 79–74797
- cytochrome c_3, anhydrous film, elec. cond., temp. and ambient press. depend. 80–85327
- cytochrome c, effects of UV and temp. on optical props. and enzymatic activity 80–81648
- D-leucine, exchange diffusion in mouse Ehrlich ascites tumour cells, temp. reduction effect 80–67053
- deep body temp. meas. technique, non-invasive, assessment 77–40816
- denaturing of tissues and cell nuclei, cooperative charact. of process 79–57593
- desert plant temperatures, leaf size adaptability perspective 79–24957
- diathermic heating, 27.12 MHz short-wave effect in exp. tumours 79–2102
- diathermy, prediction of dynamic temp. distrib. in normal and neoplastic tissues 78–31776
- diathermy, shortwave and microwave, for deep-tissue heating 80–17050
- diathermy, temp. distribs. obtained with a phantom 80–17051
- diathermy applicator for irrad. of rat brain 80–94425
- diathermy interference with cardiac pacemakers, simulation models 79–84007
- differential emissivity calorimeter in small mammalian thermal stress energy studies 78--40118
- digital frequency-to-temp. convertor for use in radio telemetry systems 80–8119
- digital readout biofeedback thermometer, low-cont. research-orientated 79–29673
- digital thermometer, simple, inexpensive design 80–36178
- digital thermometer 79–21741
- dihydrouracil, EPR study of light- and temp.-induced free radical conversions 80–35824
- 1,2-dimyristoyl-sn-glycero-3-phosphoserine multilayers, phase transitions, temp. depend., ellipsometric study 80–108846
- 1,2-dipalmitoyl-sn-glycero-3-phosphocholine multilayers, phase transitions, temp. depend., ellipsometric study 80–108846
- DNA, sorption and desorption of water, thermal-stimulated press. and thermogravimetric anal. 80–8008
- DNA and polydeoxyribonucleotides thermal props. wide range of concentrations of the ions of neutral salts and of polymer 78–80833
- DNA derivate melting curves, automatic recorder using real time processing *(French)* 80–104833
- DNA in water-ethanol solns., B-A transition, enthalpy evaluation 77–70412
- DNA melting, local stability correl. with environmental conditions 79–88048
- DNA of preheated cells, production and excision of dihydroxydihydrothymine type products 79–34493
- DNA repair after γ-irradiation, action of hyperthermia in HeLa cells 79–100577
- DNA thermal transition midpoint, CAA 79–74593
- DNA water salt solns., microcalorimetric investigation of phase transition and eutectic fusion 79–79448
- DNA-type macromolecule, melting, low mol. wt. impurity effect 80–12050
- E. coli, membrane struct. rearrangements in presence Ca^{2+} induced by heating 79–79482
- ear, mouse, induced thermal resistance 79–48220
- ear, mouse, response to heat applied alone or combined with X-rays 78–27902
- ear labyrinth caloric test, estimation of the stimulus produced 78–40210
- ear skin, mouse, fractionation effects in response to combined heat and X-rays 80–76805
- E.coli, radiation killing, role of membrane fluidity, hypothermia and local anaesthetics 80–104653
- ectothermia in small mammals, drug-induced 78–40350
- education, human body, live, thermodynamics of cooling for treatment purposes 80–73128
- effective temperature and the hot spell of June-July 1976 in British Isles 77–53166
- effective temperature criterion for exercise heat stress prescription 79 92159
- electrical skin burns caused by defibrillator ground-loop current 77–78039
- electro-surgical dispersive electrode sites, temp. distrib. meas. 79–96519
- electrocoagulation, monoactive, controlled destruction and temp. distribs. 80–94176
- electrosurgical dispersive electrode site temp. and current density distrib. model 79–92424

biothermics continued
electrosurgical dispersive electrodes, thermal performance evaluation method 79—74735
EM deep heating, design of aperture sources 80—46105
EM irradiation, temp. distrib. in simulated living tissues 80—85354
EM wave heating effects, radiowaves and microwaves 80—98011
embryo early development, chickens, microwave irrad. and body temp. effects 80—56135
endometrial cryosurgery of perfused human uterus, investigation of temp. field produced 80—55995
energy conservation in metabolism 77—81459
energy deposition in simulated human operators of 800-Mhz portable transmitters 79—8525
enthalpies of assembly of protein supramolecular structures 77—90717
environmental conditions and handling influence on rat temp. rhythm 80—35847
environmental temperature and microwave radiation effects on mouse O_2 consumption 80—51161
enzyme-catalysed reactions, network thermodynamic modelling 80—89463
erythrocyte membrane thermal transitions, identification from ANS permeability 79—53055
erythrocyte nucleosomes, chicken, temp. dependence of ^{31}P-NMR spectra 80—94280
erythrocyte thermal fragility, expt. obs. 79—62198
erythrocytes, human, slowly frozen, physical-chemical basis of protection by glycerol 78—77020
erythrocytes, human, slowly frozen in various glycerol concs., temp. dependence of survival 78—77019
erythrocytes, investigation of thermal and athermal effects of microwave irradiation 79—70581
esophageal multiprobe for temp. ECG and heart and lung sounds meas. 79—57791
evoked potentials, use in monitoring residual function of injured spinal cords 80—81747
exercise thermoregulation after 14 days of bed rest 80—97865
extravascular lung thermal vol., reappraisal as meas. of pulmonary oedema 80—97867
eye lens, human, microwave-induced hazardous non linear thermoelastic vibrs. 79—83853
face cooling in man, bradycardia, possible production by selective brain cooling 80—30670
femoral implant, numerical simulation of acrylic grout curing 80—40968
fibrin molecule formation, thermodynamic model 79—70527
fibrosarcoma, hamster, US treatment, tissue temp. elevation 80—35960
fibrosarcoma, mouse, therapeutic advantage of combined heat and X-rays 78—44562
fibrosarcoma, para-7, hamster, local thermal conductivity obs. 80—104562
flow equations for membrane transport, nonelectrolyte solute plus water case 80—26205
focal hyperthermia as induced by RE radiation and EN fields 78—40244
freezing, numerical calcs., 3rd kind of boundary condition 77—84891
freezing and cryofixation 78—28136
freezing injuries to biomembranes, expt. evidence *(French)* 79—48221
freezing phase transition and mol. dynamics in tissues, proton spin relax. obs. 78—68983
freezing techniques, struct. and functional aspects 78—28137
freezing temperature of finger skin 77—21486
frequency/depth-penetration considerations in hyperthermia by magnetically induced currents 80—63887
frozen cells, struct. and function of freezing patterns and post-thaw survival 78—64960
fundus oculi tissue, thermal effects on exposure to laser radiation 80—26261
glioma cells, cultured, influence of microwave irradiation 79—100661
gliosarcoma 9L cells, response to hyperthermia and X-irrad. 80—36030
glucose-deprived hypoxic cell killing with moderate hyperthermia 79—92157
γ-glycine, effects of temp. on cryst. struct., obs. at 83K and 298K 80—35825
gynaecological cryogenic treatment apparatus 79—57807
hand pathology, role of thermography 80—8120
hand temperature self-regulation, assessment technique 80—16906
head heating by EM waves, human and infrahuman models 80—56125
heart, frog, possible altered trophic influences during cold acclimation 79—83754
heat capacity function, of macromolecular systems, statistical thermodynamic analysis 80—61514
heat content control, human, method and appl. 78—15778
heat potential distribution in model of cranial struct. exposed to microwaves 79—2105
heat survival curves of normal and thermotolerant CHO cells, Arrhenius anal. 80—35849
heat transfer, transient, analytical solns. for living tissue 79—62197
heat transfer equations for model of clothed man, development and evaluation 79—24958
heat transfer in biological tissue 77—40635
heat transport phenomena in laminar blood flow 78—92669
heat-dissipation rate of mice after microwave irradiation 77—81472
HeLa cell nuclei protein content, effect of hyperthermia 80—40972
HeLa cells, hypothermic potentiation of radiation lethality 80—45978
hypercapnia, influence of aspects of heat exchange, rabbit obs. 80—97863
hyperthermia, apparatus for localised induction, neoplasia treatment 79—44048
hyperthermia, biological research, time-temp. conversions 80—104560
hyperthermia, combined heat and X-ray response of rat tail 77—73545
hyperthermia, deep local, induction by US and EM fields, problems and choices 80—94283
hyperthermia, digital readout of feedback control temp. 79—70697
hyperthermia, effect on nonhistone proteins isolated with DNA 78—80843
hyperthermia, effects on protein-to-DNA ratio of isolated HeLa cell chromatin 79—11905
hyperthermia, effects on radiation response of mouse jejunum 79—25039
hyperthermia, local, theoretical and expt. study, nonperfused phantom *(French)* 80—104559
hyperthermia, localised, comparison of EM and US diathermy 80—104725
hyperthermia, localised, effect on mouse mammary tumour 79—57716

biothermics continued
hyperthermia, localised, in the patient, clinical requirements 80—98173
hyperthermia, microwave radiation and L-ascorbic acid effects on Ehrlich ascites carcinoma cell metabolism 79—2104
hyperthermia, role of blood flow 80—3596
hyperthermia, role of thermal conduction 80—104558
hyperthermia and ionising radiation, interaction kinetics in Tribolium confusum 78—31867
hyperthermia and OER for damage to baby rat cartilage 79—57712
hyperthermia and radiation, selective thermal effect on chronically hypoxic tumour cells in vivo 77—70499
hyperthermia and radiation, the survival surface 78—11616
hyperthermia and radiation effects on tumours and production of disseminated disease 80—40967
hyperthermia and radiation interaction, temp. coeff. of interaction 78—11617
hyperthermia and X-rays, combined effects on Chinese hamster cells 80—45977
hyperthermia at 42°C, whole-body, temp. gradients in pigs 80—67043
hyperthermia by local EM heating and local conductivity change 77—86578
hyperthermia by magnetically induced currents, freq.-depth-penetration, comments and reply 80—108991
hyperthermia combined with radiotherapy, normal and cancer cell effects obs. 80—45972
hyperthermia due to exercise, effects on breathing pattern 80—72196
hyperthermia in tissue-like substances, EM and US induction 80—98012
hyperthermia interaction with fast neutrons or X-rays in local tumour response 77—9230
hyperthermia interaction with radiations of different LETs 77—48846
hyperthermia modification and inhibition of repair of potentially lethal X-ray damage 77—5054
hyperthermia phantom for point by point temp. mapping 79—70698
hyperthermia producing heating system for expt. tumours in unanaesthetised mice 80—56316
hyperthermia production technique using UHF currents in superficial rat tumours 80—30947
hyperthermia research with dual-beam microwave applicator 80—17052
hyperthermia response of rat tail 77—73509
hyperthermia therapy, temperature distrib. in human body 77—16911
hyperthermia-induced sensitisation of tumour cells to antibody-complement cytotoxicity 80—104570
hyperthermic death of cells, influence of membrane lipid composition and procaine 78—27907
hyperthermic effect on exponential and plateau ascites tumour cells 77—86465
hyperthermic sensitisation of mouse intestine to damage by X-rays 78—44561
hyperthermic treatment of cancer by microwaves 77—52859
hyperthermic treatment of tissue, biological effectiveness estimation, minimum inactivated cell ratio 79—100574
hyperthermic tumour-cell devitalisation in vivo 77—70424
hypothalamic temperatures, rat, effects of low power density microwaves 79—96619
hypothermia, acute, dependence of myocardial mitochondria lipids composition and phasic transitions on depth 78—53350
hypothermia, local, Gipospast-1, thermoelec. apparatus 80—104807
hypothermia in dogs, expt. and theoretical investigation 78—80834
hypothermia production, effects of inhalate thermal conductivity and high O_2 80—30669
hypoxic tumour cell radiosensitisation by simultaneous administration of hyperthermia and nitroimidazoles 77—86555
immersion in various liquids, anal. of dynamic cold sensation *(Japanese)* 80—21448
immune system, RF induced alterations due to hyperthermia, mouse obs. 80—35975
inhalation rewarming from hypothermia, provision of thermal increment 80—45858
instrumentation for measurement of heat loss rates from man in normal working mode 79—25178
intestinal crypt cells, mouse, effect of local hyperthermia 79—88054
intestinal transport of hexoses in the rat following chronic heat exposure 80—30668
intracranial heating by metal powder, medical appl. *(German)* 79—16337
intratumour temperature in a heated superficial tumour, calc. 77—32876
intratumour temperature in heated superficial tumour 77—32876
IR technology industrial and civil appls. 78—58042
IR thermography in medicine 78—61279
IR thermometry, appl. to remote detect. of biological stresses in plants 80—61749
kinetic proofreading in biosynthetic pathways, thermodynamic constraints 80—108861
labelled microspheres, localised embedding by microwave heating of tissues of hypothermic dogs 80—61640
laser irradiated tissue, significance of blood flow in temp. calcs. 80—55993
laser irradiated tissue, significance of blood flow in temp. calcs. 80—104563
laser irradiated white rats, temp. changes dynamics 79—57594
laser radiation to heat conversion in biological tissues, effect of optical scatt. *(German)* 79—2099
laser use on human teeth, thermal stress effects and surface cracking obs. 78—80915
laser-irradiated biological tissue, moving phase transitions, tissue heating 79—83848
leaf temperature, meas. by means of IR thermometer in connection with plant physiological information *(Japanese)* 78—31993
leaves of Encephalartos villosus, anomalous pyroelec. behaviour 78—44755
leg, human, elevated temps. induced by microwave diathermy with surface cooling 80—61638
leghaemoglobin, thermal denaturing in cryst. and soln. 80—108849
light-induced transient thermal response of the retina, prediction 78—7340
Limulus retina, temp. dependence of the dynamic response 79—43866
lipid cell membranes, thermal structural rearrangements 79—92163
lipid membrane melting, field effects 78—92602
lipids and lipid mixtures phase transitions investigation 77—40637
lipoprotein, low density, human, size and surface effects rel. to phase transitions 78—3446

biothermics continued
  liver cytochromes, concs. at different stages of adaption to cold 79−62196
  living cell volumetric changes in freezing and thawing, thermodynamic model and expt. 79−92192
  lumbo-sacral motoneuron pools, human, response patterns to distant somatosensory stimuli 80−108924
  lymphocyte cultures, human, heat production obs. 77−81473
  lymphocyte in vivo migration modulation by whole-body hyperthermic RF irradiation, mouse 79−100668
  lymphocytes, human, effects of heat and radiation 80−97864
  lymphocytes exposed to temps. of 37-45°C, two types of interface death 80−104566
  lysosomal hyperthermic response rel. to heat-induced thermal resistance 79−57595
  lysozyme, cryst., dynamic sp. ht. capacity meas. 80−21447
  lysozyme, sorption and desorption of water, thermal-stimulated press. and thermogravimetric anal. 80−8008
  macromolecualr thermodynamics and its possible relevance in physiology 80−53176
  macromolecules, conformation studied by calorimetry, review 80−97870
  malignant melanomas, value of IR thermography 80−36062
  mammal, brain-cooling system 80−3597
  mammalian cell culture, thermal sensitivity rel. to cholesterol level 80−51058
  mammalian cell thermal sensitivity, comparative evaluation 78−15802
  mammalian cells, in vitro US irrad. at hyperthermic temps. 80−94282
  mammalian cells, lethality due to hyperthermia under oxic and hypoxic conditions 78−40124
  mammalian cells, thermal enhancement of γ-radiation effectiveness in reproductive death induction 79−34509
  mammalian cells lack of correl. between heat and radiation sensitivity 79−20599
  mammary adenocarcinoma, mouse, combined hyperthermia and radiation treatment 77−90852
  man, wind chill distrib. in lowland Britain 79−66782
  maxillary gum trigeminal evoked pots. in humans 80−97948
  mechanical calorimetry of red cell membranes 80−45854
  median nerve, transient responses to elec. stimulation, SQUID appl. to somatically evoked field meas. 80−104706
  medical temperature measurement, electrical *(Hungarian)* 80−30910
  medical thermography, quantitative 78−61280
  melanoma, B16, in mice, effect of hyperthermia alone and in combination with ^{60}Co radiation 80−72138
  membrane, parchment-supported, thermodynamic parameters, membrane and bi-ionic pot. theories testing 79−92168
  membrane fluidity modification, mechanism of hyperthermic cell killing and therapy appl. 80−104569
  membrane mechanics and thermodynamics, review 80−45863
  membrane mechanics and thermodynamics, review 80−51052
  membrane phase transition studied by positron annihilation energy spectrometry 80−35854
  membrane thermal fluctuations and the problem of mechanoreception 79−53057
  memory, retrograde amnesia for old memory, hypothermic obs. 79−83735
  mesentery tissue, burn induced alterations of interstitial diffusion 80−104634
  metabolic and thermoregulatory effects of acute ^{60}Co γ-radiation in myomorph rodents 79−88134
  microbe thermistor 77−78063
  microcalorimetric investigations of the metabolism of yeasts 78−3451
  microcalorimetry of isolated mammalian cells 77−56343
  microstrip slot radiator for medical appls. 80−108994
  microwave and temperature effects on the murine ocular lens in-vitro 80−89798
  microwave antenna, invasive, for locally-induced hyperthermia for cancer therapy 80−67193
  microwave applicator, broad band, for heating tumours 80−30830
  microwave applicator for effective deep-tissue heating in humans, evaluation 79−2121
  microwave applicators for localised hyperthermia treatment of malignant tumours 80−89824
  microwave compatible MIC temperature electrode for use in biological dielectrics 79−88216
  microwave diathermy, performance of a new direct contact applicator 79−2122
  microwave diathermy comparative heating-pattern study of direct-contact applicators 78−40286
  microwave diathermy direct-contact circular aperture applicator with corrugated flange, design 80−67190
  microwave dosimetry, thermographic comparison of temp. probes 79−96521
  microwave enhancement of tumour thermographic visibility 78−73193
  microwave heating combined with radiation therapy, skin and tumor thermal enhancement ratios 80−67192
  microwave heating of tissue, effect of surface cooling and blood flow 78−57038
  microwave heating patterns in simple tissue models 77−86537
  microwave heating system for improving temperature uniformity in heated tissue 79−100795
  microwave hyperthermia, localised, biomedical devices 80−104724
  microwave hyperthermia, microwave leakage during treatment 80−76820
  microwave hyperthermia applicators, development 79−25059
  microwave hyperthermia of a model mouse carcinoma, uniform and replicable, induction techniques 79−2119
  microwave hyperthermia to cancer treatment *(Spanish)* 80−89795
  microwave hyperthermia treatment and thermometry system 80−72280
  microwave induced hyperthermia in cancer treatment, apparatus and preliminary results 79−62296
  microwave irradiation of rats, protacted, thermal and endocrinological effects 78−40249
  microwave radiation, use in surgery and cancer therapy 79−5336
  microwave radiation at resonant and nonresonant wavelengths, behavioural and thermal effects 78−40262
  microwave system for controlled production of local tumour hyperthermia in animals 79−34624
  microwave thermography: principles, methods and clinical applications 79−100691
  microwave thermography, appl. in cancer diagnosis *(Spanish)* 80−67195

biothermics continued
  microwave thermography, current status for medical appls. 79−66503
  microwave thermography and local heating by same system, clinical applications 79−100695
  microwave tissue heating, physiologically compatable tissue-equivalent liquid bolus 79−39465
  microwave tissue heating system for hyperthermia research 80−30829
  microwave-diathermy, pulsed, expt. obs. 79−83849
  microwave-enhanced thermographic tumour detection, investigation of sweep-freq. illumination 78−73194
  microwave-exposed rats temp. and corticosterone relationships 78−92676
  microwave-induced chronotropic effects in the isolated rat heart 78−69137
  microwave-induced hazardous thermal stresses in the human eye lens 78−80914
  microwave-induced hyperthermia, dose definition 79−2135
  microwave-induced hyperthermia, rats, classical conditioning obs. 80−61629
  microwave-induced hyperthermia, rel. to visually evoked electrocortical response, guinea pig 80−61627
  microwave-induced hyperthermia in small animals, system for developing 79−2118
  microwaves, medical applications and biological effects *(Spanish)* 80−26260
  mm-wave thermography, application to breast cancer 79−100693
  motor reactivity, isolated heart of grass snake, pH and temp. effects 80−26219
  multicell spheroid cycling, noncycling, and hypoxic cell response to hyperthermia 79−92156
  murine brain, new microwave device for rapid thermal fixation 78−92689
  muscle, thermodynamic cycles problem 79−53049
  muscle contraction thermophysical processes, simulation 78−96063
  muscle fibres, frog, transition temp. of excitation-contraction coupling 79−83751
  muscle fibres of Lethocerus maximus, temp. dependance of cross bridge parameters 80−61598
  muscle water, mouse, ^{1}H NMR anal. above and below freezing 80−56073
  myocardial heat gradients, transmural, instantaneous meas. technique 78−44661
  myosin helical fragments, stepwise pattern of thermal denaturing 80−40966
  neck node metastases, effectiveness of microwave hyperthermia combined with ionising radiation 80−94307
  nerve membrane, excitatbility, genetic alteration, temp.-sensitive paralytic Drosophila mutants 80−97895
  nerve Na conductance, anomalous temp. dependence of rabbit rel. to frog 79−62235
  neural conduction times, central and peripheral, in multiple sclerosis, somatosensory obs. 80−89773
  neural organisation and evolution of thermal regulation in mammals 79−20535
  nonequilibrium linear behaviour, enzyme-mediated multidimensional inflection points 80−72122
  oesophageal temperature probe position verification by ECG 80−56250
  optically active binary liquid crystal thermometry 79−42952
  ovary cells, Chinese hamster, heat killing and thermal radiosensitization at 42°C 80−45860
  Peracarida, burrowing, temp. effects on emergence rhythms *(French)* 80−94174
  perfusion blood temp. monitoring, zero-heat-flow transducer 80−8201
  perfusion measuring heated thermocouple probe, 2 regime model 77−5110
  perspiration mass transfer coefficients and clothing models 79−92158
  phospholipid bilayer, hydrated, monoclinic (ripple) phase, thermodynamic model 79−70532
  phospholipid bilayer, one- and two-component, main phase transition, Landau phenomenological theory 80−97872
  photoluminescent thermometer probes, temp. meas. in microwave fields 80−104721
  photosynthesis, electron transfer reactions in carrier mol. complexes, kinetics and thermodynamics 80−108859
  physical and biological sciences, conf., Japan (Mar. 1979) 80−17714
  physicochemical changes on cooling baterial suspensions 77−86458
  physiological thermoregulation, math. model 80−94173
  placenta models, heat, O_2 and CO_2 transport, construct. and usefulness of models 80−3604
  plant fibre temperature stability investigation, rotary diffusion, spin label obs. 80−81529
  plasma water shifts during thermal dehydration 80−67044
  plateau phase V-79 cells, effect of dealy between heat and X-irrad. on survival response 78−3555
  populations exposed to supraphysiological temp., haemolysis time history 80−35850
  postburn cooling, therapeutic effects 79−29663
  prostate, dog, microwave localised heat treatment, new applicator 79−100698
  protein crystal lattice, thermal stability 77−25380
  protein crystal physical state, microcalcrimetric obs. 77−70413
  protein crystal physical state, thermal heating curves struct. 77−70409
  protein thermal desaturation studies, use of high heating rates 77−81470
  proteins at liquid interfaces, adsorpt. isotherms 79−79461
  purple membrane suspensions, light-induced conductivity changes, pH and temp. effects 80−51157
  pyroelectric vidicon camera as a medical thermograph 79−25060
  pyroelectricity and induced pyroelec. polarisation in leaves of palmlike plant Encephalartos villosus 77−77876
  radiation balance microwave thermograph, medical appls. 80−26315
  radiation balance microwave thermograph, simultaneous independent temp. and emissivity measurements 79−100692
  radiation damage thermal enhancement, mouse ear, effect of prior heat treatment 79−48291
  radiation lethality potentiation by hyperthermia in a tumour model 79−25037
  radioresistant malignant tumours, HF hyperthermia and γ-rays therapy results 79−100699
  radiotelemetry, transmitter for small animal temp. meas. 79−83888
  radiotelemetry transmitter, μA, for unrestrained subjects' temp. meas. 79−16356

biothermics continued
- rat thermoregulatory behaviour when subject to microwave irrad. 80—81547
- rectal and testis temp. obs. in conscious mice, direct heating effects 80—55994
- rectal temperature and operant behaviour during 2.45-GHz microwave irrad., squirrel monkey obs. 80—61630
- red cell, human, increased passive permeability below 12°C 80—94185
- red cell membrane, temp. dependence of viscoelastic recovery 80—40979
- red cell membrane thermoelasticity obs. 79—57684
- regional perfusion rate determ. by dynamic thermal dilution 77—40883
- reproductive capacity of Drosophila, effects of microwave radiation rel. to conventional heating 80—21492
- respiration calorimetry determination of the O_2-calorie equivalence of thyroid diseases patients and normals *(German)* 78—85412
- respiratory heat exchange analysis, during inspiration, under environmental conditions of deep diving 78—15856
- respiratory phase detector system, battery operated cct., air temp. change meas. 79—100770
- retinal injury, thermally-induced, due to high optical-radiation doses 80—3710
- retinal laser photocoagulation, dynamic meas. of temp. and bleaching *(German)* 79—2098
- retinal rods, thermal activation of visual transduction mechanism 79—74651
- RF EM fields, review of effects and dosimetric data, safety standards development 80—67154
- rheymatology, quantitative thermology *(German)* 78—92684
- rhodopsin, photo- and thermo-bleaching rel. to heterogeneity problem 80—41114
- Salmonella typhimurium LT2 mutants, effects of microwave radiation and heat 80—108958
- salt-hydrate transition temps., use as fixed pointed in biomedical thermometry 80—104801
- sarcoma, rate, temp. effect on microvascular haemodynamics during early growth 80—72188
- sarcoplasmic reticulum membranes, temp.-dependent functional changes 80—81550
- scanning microcalorimeters for studying macromolecules 80—61747
- serum low density lipoprotein, human, anomalous permittivity behaviour 80—81540
- skeletal muscle undergoing rhythmic contracts.,theoretical study of temp. distrib. 79—11901
- skin, mouse, response to combined hyperthermia and X-rays 77—90857
- skin, normal, heat and H_2O migration, unsteady state 79—92155
- skin, pig, combined effects of X-irrad. and microwave heating 80—94290
- skin, pig, response to combined X-irrad. and microwave heating 80—61653
- skin, response to fractionated heat and X-rays 78—35887
- skin, simple device for measuring mean temp. 79—2151
- skin, thermal recovery after cooling 79—53050
- skin blood flow, reflex control by skin temp., role of core temp. 80—85427
- skin burns, thermal conditions which cause 77—48758
- skin IR radiation, spectral anal. 79—88057
- skin temperature as an indicator of stress in soft tissue 77—48923
- skin temperature change rate effect on local sweating rate 80—35848
- skin temperature estimation during sweating 77—48757
- skin temperature increase as a result of lighting *(Japanese)* 78—44557
- skin temperature measurements using a disc sensor, effect of press. 80—56259
- skin temperature probe design, exptl. calibration results and numerical model predictions 80—56258
- skin temperature rises, thermal props. of dry metal-foil dispersive electrosurgical electrodes 80—98171
- skin veins temperature increase due to subcutaneous perpendicular to surface 80—40970
- small intestine, mouse, transient heat-induced thermal resistance, crypt survival assay 80—108850
- soft tissue temp. increases due to US Doppler blood flowmeters, thermographic meas. 79—62294
- solar and thermal radiative heat loads in the energy balance of man 77—48761
- solar radiation utilisation by homopolar homeothermic species, optical model for pelts 80—51045
- somatosensory evoked potentials, abnormalities due to brainstem lesions 80—56070
- somatosensory evoked potentials, reduction during movement, cat extralemniscal pathways recordings 80—85421
- somatosensory evoked potentials, review of acquisition and anal. 80—101281
- somatosensory evoked potentials, short latency, in man following median nerve stimulation 80—94243
- somatosensory pathways, assessment of central conduction 80—97949
- somatosensory potentials following electroconvulsive therapy 80—97947
- space suit cooling, automatic control of human thermal comfort 80—109046
- species diversity and palaeotemp., parallel changes in the lower miocene 79—39866
- spinal cord, mouse, combined effects of hperthermia and ionising radiation 78—31863
- spleen hyperthermia, mouse, acid phosphatase activity 78—48842
- still-shade-temperature meter for use in assessing personnel cold stress 80—81764
- stomach tissue, canine, temp. increase comparison for Ar and Nd:YAG laser irrad. 79—92290
- stomatal response to microwave induced thermal stresses 77—2021
- surface EMG and fatigue, muscle temp. and blood flow 80—94199
- surface thermodynamics, equilib. and nonequilib. processes, review 77—44505
- surface tissue, two-phase theory for circulatory influence on heat transfer 80—104564
- surgical diathermy indifferent electrodes, performance electrodes. 80—72367
- sweating responses during heat acclimation and moderate conditioning 79—100576
- tail, rat, single dose radiation and hyperthrermeia rel. to growth 80—108963
- telemetering system for mammalian energy flow studies, heat flux and temp. data 77—86716

biothermics continued
- telemetry system with interference suppression, implantable, long-life, animal expts. appl. 80—101302
- telemetry transmitter, crystal-controlled, surgically implantable, for animal expts. 80—72393
- TEM applicator, dual-beam, for direct-contact heating of dielectrically encapsulated malignant mouse tumour 78—40245
- temperature biotelemeter, modular, expandable, implantable 80—67191
- temperature distrib. in microwave-irradiated cylinders simulating living tissues 80—3760
- temperature distribution in the human body, dependence on how hyperthermia is induced 77—16911
- temperature measurement, human body-temp. sensor-environment system, analogue model of interaction 80—104783
- temperature of denaturing of collagen as a linear function of the amino acid composition 79—57571
- temperature regulation in man, development of a new concept 78—35805
- testis, mouse, effects of hyperthermia and X-irradiation, weight loss assay 80—16907
- thawing of frozen cells, mechs. of dehydration 77—81478
- thermal burn depth early diagnosis, appl. of multispectral photographic anal. 78—3648
- thermal conductivithermal diffusivity of biomaterials, a simultaneous meas. technique 78—57098
- thermal conductivity and diffusivity of neuroblastoma tumour 79—5252
- thermal dosimetry, need for accuracy in hyperthermia research 78—64942
- thermal energy, balance in leaves, crops, hot and cold blooded animals 77—32875
- thermal resistance induction, heating time rel. to temp 80—3595
- thermal sensation evaluation, comfort chart *(Japanese)* 80—81545
- thermal stress of humans in Australia, climatic classification 80—31115
- thermocouple, nonmetallic, differential-temp. probe for use in microwave fields 80—56320
- thermocouple probe, spherical heated, for perfusion meas. 79—92456
- thermodynamic analysis of laser irrad. of biological tissue 79—29562
- thermodynamic network anal analysis of biological systems 77—86435
- thermodynamic process applied to biological systems 80—45855
- thermodynamic values of collagen, helical and coiled states, at temps. of 77—25379
- thermodynamics of biological controls-cooperative phenomena in haemoglobin 77—44577
- thermoelectric method, US absorpt. and attenuation determ. in mammalian tissues 80—41110
- thermoelectric needle probe for medical and biological temp. meas. 80—101299
- thermogenesis control in cold-exposed rabbits, variable open-loop gain 80—97868
- thermogenic control during exercise in a cold environment 80—72139
- thermogram enhancement by tissue-condition correct. 79—39460
- thermographic and behavioural studies of rats in the near field of 918-MHz radiations 78—7386
- thermographic system model parameter calc. 79—79477
- thermographic tumour detection enhancement using microwave heating 79—2124
- thermography, cm and mm wave, tumour detect. survey 79—100690
- thermography, mm-wave, head and neck diseases, preliminary findings 79—100694
- thermography and environmental physiology 78—58043
- thermography as a means of blood perfusion measurement 80—56167
- thermometry and dosimetry of heat rel. to liquid-crystal optical fibre temp. probe 80—98204
- thermometry considerations in localised hyperthermia 78—53561
- thermophysical and rheological props. of certain biological fluids 78—80902
- thermoregulation in rhesus monkey, thermal balance study 80—8029
- thermoregulation in swimmers and runners 80—45859
- thermoregulation in unrestrained rats during and after exposure to 1.5-4 G 80—45857
- thermoregulation investigation, passive sub-cutaneous temp. meas. 79—34721
- thermoregulation mechanism model, human 80—8028
- thermoregulation of rabbit head, facial vein myogenic mech. 80—97869
- thermoregulatory responses, men rel. to women 79—88055
- thermoregulatory responses of unanesthetised rats, effects of acceleration 77—48882
- thermoregulatory system, human, engineering models 77—81471
- thermoregulatory system, human, mathematical treatment of struct. and function 77—12888
- thermoregulatory system simulation, rat 80—3594
- thermorestoration of mutagenic radiation damage in bacterial spores 79—20524
- thermotropic properties of phospholipid membranes, effects of bivalent cations and prteins 77—48765
- thymine damage in chromatin from heated cells after X-irrad., excision obs. 80—45980
- thymocyte membrane, rat, props. modification by hyperthermia and ionising radiation 78—69017
- thymocytes, rat, reduction of interphase death by hyperthermia 80—108970
- thyroid scan with ^{99m}Tc-bleomycin, evaluation of cold areas 80—56183
- tissue, soft, temp. distrib. monitoring by temp. depend. of US vel. 80—45994
- tissue heat balance, relationship between blood perfusion, metabolism and temp. 80—108852
- tissue heating by induction field of VHF portable radio transmitters 78—57039
- tissue macroscopic temp. distrib. 78—64944
- tissue perfusion measurements made with thermal diffusion probe, effect of probe geometry 80—104802
- tissue response to combined hyperthermia and X-rays 77—16955
- tissue sphere temp. profiles due to EM heating 79—100578
- tissue temperature distribution during laser irrad. 79—39449
- tissue temperature simulation in cryosurgery 80—85355
- tissue thermal props. meas., influence of blood vessels, simulation model 77—40962
- tissue-equivalent medium, heating patterns produced by 434 MHz Erbotherm UHF^{69} 80—98013
- tissue-equivalent plastic, A-150, thermal diffusivity, sp. ht., thermal cond. obs. 80—34258

biothermics continued
tissues exposed to nonionising radiation, dimensionless model for temp. increase calc. 79—57706
transient temperature distribs. in an infinite perfused medium 79—96520
Tribolium confusum interaction between 2450-MHz microwaves and ionising radiation 79—2103
tryptophan residue in horse liver alcohol dehydrogenase, room-temp. phosphoresc., temp. and enzymic complex form. effects 80—61512
tumor irradiation using focused microwave array system, feasibility 79—100689
tumors, effect of inhomogeneities, finite boundaries on temp. distribs. 79—62199
tumour cells, thermotolerant, hyperthermic radiosensitisation 79—74600
tumour detection, computer processing of microwave enhanced thermographic images 80—8125
tumour growth inhibition in mice by microwave hyperthermia, streptolysin S and colcemide 78—40254
tumour growth inhibition in mice by microwave hyperthermia, polyriboinosinic-polyribocytidylic, and mouse interferon 79—2101
tumour heating by microwaves, temp.-controlled 77—77963
tumour response to combined heat and X-irrad., mouse, therapy implications 79—48290
tumour thermal sensitisation, mouse, effect of vascular occlusion 79—16253
tumours, solid, destruction by RF heating 80—61637
tumours, spontaneous, in dogs and cats, treatment by ultrasound-induced hyperthermia 79—62290
turtle, sex determination during embryo development, temp. depend. 80—81546
tympanic thermometer, noncontact 79—34692
unsteady state heat migration problems, appl. of similarity transformation 78—95990
US attenuation in tissue, temp. and freq. dependence 80—45949
US hyperthermia, localised, design of heating protocols 80—104693
US induced hyperthermia in previously X-irradiated sites 79—62315
US irradiated cells, temp. distrib. calcs. 80—61623
US tumour irradiation, closed-loop energy and temp. control 79—83874
vasodilation, peripheral, induced in squirrel monkeys by microwaves 80—104682
vasomotor thresholds, squirrel monkey, central and peripheral temp. effects 80—97866
vegetation thermal IR emissivity, ecological variations 80—104557
viscosity-temperature relationship of human plasma and serum 79—20564
visual evoked potentials during hyperthermia and prolonged circulatory arrest 79—16204
voluntary temperature control and cold stress tolerance, effects of feedback 80—16905
warm-blooded animals, model of body surface temp. distrib. 78—64943
water sorbed on DNA, temp. anomaly, IR spectroscopic obs. 80—51046
whale biothermal mathematical model 80—12059
wheelchair cushion effect on skin temperature, heat flux, and relative humidity 79—83707
wheelchair sent evaluation by time-lapse and quantitative thermography of skin after sitting 80—51205
whole-body hyperthermia, core body temp. regulation by oesophageal temp. feedback 80—72371
whole-body hyperthermia with oesophageal temp. feedback control 79—92423
wind speed limits to work under hot environments for clothed men 80—8030
X-irradiation combined with hyperthermia, fractionation studies 80—56138
X-irradiation response of mouse tumour and skin, effect of heating order 80—3738
yeast, hyperthermic inactivation and interaction of hyperthermic and γ-irradiation damage 79—96518
yeast cell suspension in salt soln., dynamic effects of freezing 79—70533
yeast cells, determ. of thermal equivalent to MM microwaves 80—67151
yeast cells, elevated temp. effect on radiation sensitivity 79—79610
CO_2 responses of conscious rabbits at ambient temps. of 5, 20 and 35°C 80—56085
H^+-ATPase, soluble mitochondrial, thermal stability obs. 80—55992

biotite *see mica*

biotransport
see also biodiffusion; biological fluid dynamics; biomembrane transport; cellular transport and dynamics; neurophysiology
actinide industrial dusts, lung clearance studies at NRPB 78—65137
aerosol deposition/clearance, radioactive particle administration technique 77—60312
aerosol transport into blood and retention, rel. to alveolar microenvironment 77—25630
agargel electrophoresis, protein transport, stochastic model 77—77769
albumin, bovine serum, solutions, fluctuation transport theory 78—70057
albumin transport kinetics in renal cortical interstitium, heterogeneity model 80—30632
alveolar epithelium transport of albumin and sucrose, conc. diff. effect 80—67329
alveoli albumin clearance, tissue permeation vs. airway displacement 78 -27979
arterial flow lipid transport model 78—44552
arteries with longit. ridges, flow field and mass transport anal. 77—44702
artery avascular region O transport analysis 77—40691
bile acid hepatobilary kinetics, compartmental model validity 80—30971
blood O_2 uptake during flow in rectangular channels 77—81516
blood-brain barrier, reversal of microwave-induced permeability 80—61641
blood-organ transfer kinetics of radioisotopes 80—109044
body fluid distribution, flowing-mixing compartmental hybrid model 77—44582
bone, transport mechanism between blood supply and osteocytes in long bones 77—86472
bone imaging radiopharmaceutical local accumulation model 78—24127
brain O_2 transport, nonlinear Monte Carlo simulation, hybrid computer implementation 78—40131
carbohydrate absorption in vivo in rats with gastro-intestinal radiation syndrome 77—70494
carrier-facilitated steady-state diffusion problems 80—41360

biotransport continued
cartilage deformation and interstitial fluid flow, nonlinear interaction 77—32931
cerebrovascular permeability, quantitative method for meas. of alterations 80—61748
chemotactic bacteria, struct. of steadily propagating rings 77—44693
compartment systems, almost closed, generalisation of results 80—30633
compartmental models with delays, physical realisability 80—7998
compartmental system analysis: state of the art 80—35815
dialysis efficiency prediction using convective field theory 77—48945
diuresis, medullary Na depletion, digital computer simulation 77—60226
Douglas fir, evapotranspiration determ. using weighing lysimeter 77—64353
drugs and tracers distribution determ. by biological system simulation 77—40956
electron transport and energy migration in higher plant photosynthesis 80—40976
electron transport over large distance in biol. systems, medium as mediator 80—35820
epithelial mucus, rheology and mol. organisation 80—97959
extracorporeal processing devices, review, book contrib. 80—12308
eye centrifugal fibres in nonavian vertebrate, source revealed by horseradish peroxidase transport 77—36921
flow reaction-absorption systems, digital simulation *(Japanese)* 77—86525
food rate of passage through gut of captive wild birds, determ. using ^{103}Ru 80—26425
gas exchange in normal and abnormal lungs, effects of inspiratory flow pattern 80—45936
gas exchange kinetics determinants during exercise, dog expts. 80—45932
granuloma pouch Na exchanges during initial and final stages of inflammatory process 77—77886
haemoglobin as a transducer for O_2 transport in fish 79—96505
haemopoietic stem cells of shielded bone marrow, X-ray effects, role of migration 77—9225
heat and H_2O migration through normal skin, unsteady state 79—92155
heat conduction in cryosurgery 77—40920
heat transfer in tissue, Pennes model vs. Wulff model 77—40635
hepatic elimination, statistical mechanics 79—96503
hygroscopic particle size, air humidity depend., applic. to lung dynamics 77—90841
IEEE 7th Northeast Bioengineering Conference, Troy (1979) 79—79672
inert gas, exhange in living organs, stochastic description 80—81520
inert gas absorption, closed lung system study 80—30969
inert gas dynamics in subcutaneous gas pockets 77—44707
inert gas transport in the microcirculation, isobaric supersaturation risk 80—45939
intestinal transport of hexoses in the rat following chronic heat exposure 80—30668
kidney process modelling 78—44524
lipids, albumin-fatty acid complexing kinetics using fluoresc. probes 77 25381
lung gas transport model, derived from human anatomical data 77—5020
mass transport to walls of stenosed arteries rel. to Reynolds number and blood flow separation 80—41093
maternal-placental blood flow model with vel.-depend. permeability 78—40224
mesenteric artery Na distrib. in early salt-induced hypertension 78—27999
mesenteric artery Na kinetics, digital simulation of 3 compartment model 77—44616
microcirculation autoregulation mechanistic theories, computer simulation 78 27995
mitochondrial permeability, transport and energy-coupling processes, effect of fatty acids and acyl-CoA 77—21498
mobility, mol. and struct., using fluoresc. marker conc. dynamics 77 -9303
muco-ciliary transport mechs. 80—97956
muco-ciliary transport monitoring method using ^{99m}TcS colloid, bronchiectatic patient appl. 80—30840
mucociliary flow mechanics, channel model obs. 80—97957
mucociliary tracheal clearance vel., radiological method for determ. 80—104727
multiple indicator-dilution study of saturable uptake of metabolised substance in dispersing organ 78—27998
mutlicompartment analysis, direct estimation of parameters, appl. to drug conc. 77—44580
nasal mucociliary transport, mucous velocity meas. using roentgenographic method 79—29600
nephron functioning model *(French)* 80—36218
octane-water interface, electron transfer in presence of chlorophyll 77—81474
ovum transport in oviduct, mechs. 78—80905
oxygenator efficiency prediction using convective field theory 77—48945
oxyhaemoglobin dissociation curve direct obs. in man in vivo, computer investigation 78—85433
peristaltic transport, influence of wave form *(German)* 79—79570
photosynthesis, redox conversion kinetics in the electron transport chain 80—40950
placental function and foetal development during pregnancy, US diagnosis and chem. anal. 78 -35897
protein synthesis, stochastic eqns., ribosome translation along mRNA and tRNA selection processes 79—66440
pulmonary air emboli, effect of ventilation with different gas mixtures 78—27991
pulmonary fluid dynamics and mass transport, book contrib. 77—52829
pulmonary function analysis, parameter estimation, lumped-parameter model 77—44815
pulmonary gas exchange in man, effect of increased gas density 77--16947
pulmonary oedema fluid transport, hybrid computer simulation 78—27915
radiation transport calcs., pions, neutrons, protons, α-particles, ions 77 25555
radionuclide concentration by marine organisms, temp. effect 77—90920
radionuclide transfer in terrestrial animals 78—24152
radiopalmitate kinetics in rats, reliability range of model parameters 79—96500
renal countercurrent mechanism, transient and steady state simulation 77—36967

biotransport continued
- renal counterflow systems differential equation, soln. by numerical method 78—24082
- renal medulla, human, math. model 78—24081
- renal medulla, multinephron models, canonical mass balance eqn. 77—12941
- respiration, human, managment of artificially ventilated patients 79—70576
- salivary gland electron transport, Lone Star tick 80—72144
- skeletal muscle, canine, blood flow and O_2 uptake obs. in acute anaemia 80—45930
- skeletal muscle O_2 and lactic acid transport, effet of reactive hyperaemia 78—35817
- skin water exchange measurement 77—81763
- soybean plants, radiation-stressed, photosynthesis and photophosphorylation rel. to photoassimilate export 80—56140
- spinal cord conduction velocity, indirect estimation in intact man 77—25616
- statistical mechanics, ensemble methods 79—66437
- tissue microwave dielectric props. rel. to rot. mobility of tissue water 77—29092
- trace element transport meas. during haemodialysis by PIXE 80—36102
- tracer transport in blood, model accounting for recirculation, rel. to cardiac output meas. 77—36978
- tracheal muco-ciliary transport, theoretical and expt. study 80—97958
- tracheal mucociliary transport, bronchoscopic evaluation 77—60270
- transendothelial albumin transport in steady state pipe flow at high shear rates 77—32939
- transuranics biological availability, influence of DTPA at soil-plant and plant-animal interfaces 78—73264
- tree rings, ^{14}C radial flow and chemical pretreatment for ^{14}C meas. 78—28346
- 3,3′,5′-triiodothyronine plasma to tissue transport rate estimation from 3-compartment model 78—31792
- water exchange dynamics of body in normal and pathological conditions 78—64914
- water in plants, transport during droughts, agricultural aspects 77—56707
- ^{241}Am III retention and distrib. in neonatal beagle 78—28094
- Ba isotopes, uptake and retention of ^{133}Ba and ^{140}Ba-^{140}La in mouse tissues, eye and skeleton doses 77—9276
- ^{14}C fallout from nucl. weapons testing, use as biological tracer 77—64162
- ^{144}Ce gastrointestinal absorpt. and distrib. in suckling pig 78—15942
- ^{252}CfCl$_3$, metabolism in rat and effect of in vivo DTPA chelation therapy 78—85387
- ^{244}CmO$_2$, mobility in bronchially intubated rat 80—30967
- ^{60}Co retention in mouse, rat, monkey and dog, at tracer levels 77—9271
- Fe loss from asbestos fibres in pulmonary tissue, obs. 79—74825
- ^{57}Fe transport and storage compounds 77—12875
- ^{203}Hg-methyl mercury chloride retention in man after inhalation 77—9277
- ^{131}I$_2$ transport via pasture-cow-milk pathway, stat. anal., thyroid dose uncertainty 79—83950
- K^{14}CN, rat metabolism and internal dose 77—44754
- ^{79}Kr, kinetics after inhalation in man, rel. to internal dosimetry calcs. 78—28073
- ^{79}Kr, kinetics of total body retention and clearance after inhalation 77—37121
- ^{28}Mg, intestinal absorpt. obs. in man 80—36217
- N_2 storage in man, dynamic model 78—27997
- ^{95}Nb inhalation in beagle dogs, deposition and retention, dosimetry 78—35959
- O_2 biomolecular transport proteins and metabolism 79—24946
- O_2, haemorrhagic shock, effect of anemia 80—67330
- O_2, haemorrhagic shock, effect of increased blood-O_2 affinity on O_2 transport 80—67331
- O_2 mass transport and regulation, microelectrode and math. modelling study 78—44534
- O_2 supply to porous implants in bone analysis 79—70707
- O_2 transport from pulsatile viscous blood flow to diseased coronary arteries of man 78—40220
- O_2 transport system, functional state, math. model 80—104548
- O_2 transport system, multivariate anal. of blood and air flow data from dogs 77—44706
- ^{203}Pb-acetate, tissue distrib., comparison with ^{67}Ga citrate as abscess-localising agent 77—5064
- ^{212}Pb ion clearance from rabbit bronchial epithelium to blood 77—86641
- Pu body burden estimation from urine data influenced by DTPA therapy 78—73259
- Pu IV citrate, monomeric, containing ^{237}Pu and ^{239}Pu, early retention in mice 78—80983
- Pu translocation from simulated wound sites in rat 78—77117
- ^{239}PuO$_2$, in vivo solubility in rat lung 78—28093
- ^{239}Pu uptake by pea plants 77—9282
- ^{226}Ra long-term retention in contaminated dial painters 77—90917
- Sr isotope excretion in man, comparison of stable Sr, ^{85}Sr and ^{90}Sr 78—24153
- ^{89}Sr distribution between bound and free forms, in vitro meas. of rat soft tissue 78—28095
- ^{201}Tl distribution in stressed rats, imaging, organ uptake and myocardial kinetics 78—65114
- ^{201}Tl, human distrib. and phys. imaging props. 77—37042
- ^{187}W, absorpt., distrib. and milk secretion by dairy cow 77—9281
- ^{127}Xe, kinetics of total body retention and clearance after inhalation 77—37121
- ^{127}Xe whole-hody retention for dosimetry calcs. 77—60257

bipolar integrated circuits
- camera control IC, single chip 78—21234
- collector diffusion isolation bipolar technology, assessment of radiation tolerance 79—45430
- flowmeter, direction sensitive 77—7484
- function testing with stroboscopic microcomputer-controlled SEM 80—68294
- implantable bidirectional blood flowmeter, micropower ICs 77—13038
- integrated light-sensor device with broad operating range and enhanced-blue spectral response 80—13140
- junction isolated, ionising radiation performance, black box modelling 77—83467
- Kitchip, generalised, for biotelemetry system design 77—86665

bipolar integrated circuits continued
- p-n homojunction integrated tandem solar cell performance 80—3521
- parallel optical fibre channels, pulse skew model 77—68279
- phototransistor static characteristics, effect of insulating p-n junction *(Russian)* 78—52069
- temperature transducer, intrinsic bandgap voltage as reference, Fahrenheit, Celsius or arbitrary scale operation 80—82761
- temperature transducer, LX 5700 A, for −100 to +150 degree C temps., operation *(French)* 77—67431
- temperature transducer, two-terminal, operation and characts. 77—10021
- thermometer with K° output, using AD 590 IC transducer 79—80615
- BN glass transfer process appl. 80—107459
- GaAs-GaAlAs bipolar transistor and heterostruct. laser, monolithic integration 80—102858

bipolar transistor circuits
- *Used for general papers and papers where use of bipolar transistors is significant*
- avalanche transistor switchout, high performance, for external pulse selection at 1.06 μm 79—7158
- dynamic load line construction amplifiers, tutorial 80—67963
- electronic thermometer with adjustable alarm setting *(French)* 79—63209
- environmental thermometer, using ICs and Si transistor 79—67300
- injection laser temperature-compensating drive circuit 79—45971
- logarithmic converters and amplifiers, principle and appl. *(German)* 79—9233
- op amp, type 108, radiation hardening by modified processing, failure anal. 77—18751
- photodetector with automatically adjustable threshold level, design considerations 80—62724
- pulse generator for image convertor shutter control 78—4653
- reaction timer, using LEDs 80—81781
- temperature regulator circuits, using thyristors and triacs *(Spanish)* 79—6115
- temperature regulators using Darlington cct. as sensor and controller *(German)* 79—30467
- thermometer, for 0 to 100°C *(German)* 79—6122
- thermometer, using Motorola MTS 102 transistor temperature transducer and LM 10 IC op amp *(French)* 80—86298

bipolar transistors
- *see also bipolar integrated circuits*
- burst noise, physical sources 79—24033
- carrier-domain magnetometer, novel Si mag. field sensor 79—9224
- current gain β, common-emitter, measurement of low values 79—63268
- defects, dislocation propagation and emitter edge defects in Si wafer 77—1128
- development, decisions and attitudes 78—12524
- dislocations, TEM/SEM observations comparing diffr., elec. and luminesc. contrast 78—38714
- emitter-push effect, TEM analysis of isolated dislocation helices 80—70203
- emitter/collector pipes obs., use of electron-beam-induced current mode of SEM 79—82665
- Gaussian graded p-n junction under high forward bias, depletion region width calc. 79—47157
- heavily doped semiconductor devices, review 79—47039
- heavily doped shallow-emitter p-n junction solar cells, diodes and transistors, Auger recombination 79—96445
- heavily doped transparent-emitter devices, analytical treatment 79—96444
- identification, Si or Ge 77—17744
- III-V semiconductor, low temperature, high mobility transistor materials 78—87970
- interstitial supersaturation near P-diffused emitter zones 79—65541
- junction breakdown voltage, temp. effects 79—7882
- lifetime profile measurements in heavily doped emitter structures using electron beams 80—15538
- magentic field sensor using carrier domain rotation, operation and performance 77—2671
- magnetic field sensor using carrier domain rotation, proposed device design 77—2670
- magnetotransistor, lateral with two meas. collectors, characts. 79—7887
- material parameter determ., appl. of normal modes of p-n junction devices 77—4426
- MNOS struct. with complementary tunnelling emitter bipolar transistors, current transport characterization 79—91146
- n-p-i structure, exclusion effects on I-V characts. 77—15945
- n-p-n heterojunction transitor 80—6959
- neutron damage by fast burst reactor neutrons, Pb, paraffin shields 77—23172
- noise figure, measurement by connecting source resistance between input and output *(French)* 80—68214
- p-i-p structure, two-dimensional carrier transport at high injection rate 79—15213
- pnp switching transistors, anomalous breakdown regions, laser scanning obs. 80—34854
- sequentially diffused, Ga and As profiles, radiotracer obs. 78—10073
- STEM characterisation 78—34893
- surface recombination effect, dynamic relationships 79—82664
- thermometer sensor, precision, −50 to +125 deg. C at ±0.1 deg. C 78—21134
- BP-Si junctions epitaxial growth and device appls. 78—48333
- GaAlAs/GaAs, n-p-n heterojunction transistor, elec. props. 79—87149
- GaAs-GaAlAs bipolar transistor and heterostruct. laser, monolithic integration 80—102858
- Si, defect obs. using stroboscopic SEM 79—9261
- Si epitaxial stacking fault nucleation site identification, annihilation, and suppression 77—76705
- Si, heavily doped, excess intrinisic carrier density, deionisation of impurities as explanation, bipolar transistor/solar cell models 80—96864
- Si single-junction magnetotransistor, characts. 79—24066
- Si transistor damage characts. by neutron displacement cross section 79—42118
- Si:Al lamellar devices, surge protector, solar cell, HV diode and negative resistor appls. 78—10068
- Si:P, quantitative model for diffusion of P and emitter dip effect 77—76611

bipolar transistors continued
  Si/Si$_3$N$_4$ substrate/film system, implantation effects on substrate hardening and film stress reduction 78—71748
  Si-SiO$_2$ interface, elec. props. and influence on service performance and stability 78—23171

bipoles *see network analysis; network synthesis*

birefringence
  see also flow birefringence; Kerr electro-optical effect; light polarisation; magneto-optical effects; mechanical birefringence; optical constants; optical rotation
  4-octyl-4-cyano-biphenyl, nematic to smectic A phase transition texture changes, thermoelectrooptic effect 80—49098
  absorbing anisotropic and gyrotropic slab between crossed polarisers, transmitted intensity patterns 80—78762
  AC Kerr effect meas. in conducting liquids 78—23431
  acousto-optical diffraction, multifrequency, in optically birefringent media 80—74300
  adsorbed polymer layer, on particles in suspension, thickness meas. by mag. birefringence 80—42191
  alkali halide:CN$^-$, Kerr effect and birefringence from paraelectric CN$^-$ defects 78—43838
  alkali metal fluo-perovskites, weakly discontinuous phase transition, linear birefringence obs. 80—11362
  alkoxy-cyanobiphenyls, isotropic phase, Cotton-Mouton effect 80—16013
  p,p′-n-alkoxyazoxybenzene homologous compounds, nematic, DC Kerr constants 78—27185
  p-alkoxybenzylidene-p-n-butylanilines, optical and mag. anisotropies in liq. cryst. phase, thermal variations of order parameter *(French)* 79—82149
  alkyl ammonium manganese chloride, birefringence, two-dimens. mag. behaviour, magneto-optical meas. 78—31175
  alkyl-cyanobiphenyl homologues, isotropic-nematic phase, optical Kerr effect 80—91866
  alkyl-cyanobiphenyls, isotropic phase, Cotton-Mouton effect 80—16013
  p-alkyl-p′-cyanocyclohexylcyclohexanes, thermotropic nematics with positive dielectric and negative diamag. anisotropy 78—34435
  di-alkylammonium copper tetrachloride, weakly discontinuous phase transition, linear birefringence obs. 80—11362
  trans-4-alkylcyclohexane carboxylic acids, visible and UV spectroscopy transparent matrix 80—45102
  analogue birefringent element built from polarising wide field Michelson interferometer 80—91895
  anisotropic crystal, induced birefringence, systematic errors elimination 79—99848
  anisotropic dielectric crystal, EM fluctuations 79—19857
  anisotropic material elements in optical systems, point and line image intensity distribs. *(German)* 79—55058
  anisotropic objects, path-difference measurement 80—4758
  anthracene, birefr. changes due to thermal expansion 78—52468
  antiferromagnetic crystal, birefringence, optical class lowering induced by longitudinal mag. field *(Russian)* 79—8127
  atomic degenerate system, Doppler-free laser-induced dichroism and birefringence 78—82711
  atomic resonant lines, ang. momentum depend. of laser-induced birefr. and dichroism 79—10367
  atoms interacting with polarised light, resonant Voigt effect, analysis 79—76390
  azobenzenes, p-acryloyl- and p-methacryloyl-oxy-p′-substituted, monomers and polymers, liq. cryst. props. 79—99065
  azoxy compound, liquid cryst. mixture, nematic, elec., optical and viscoelastic props. 79—55803
  azoxybenzenes, nematic, refr. index, birefringence, internal field 78—34427
  azoxybenzenes, p-acryloyl- and p-methacryloyl-oxy-p′-substituted, monomers and polymers, liq. cryst. props. 79—99065
  beam splitter, birefringent, polarisation-independent 80—5814
  bending wave propag. in transversely struck plate, birefringence obs. *(German)* 78—48582
  benzene, orientational correlation parameter for liquid 79—73090
  benzene, quadrupole moments, elec. field-gradient birefringence method 80—95746
  benzil, optical activity and circular dichroism 79—61328
  benzyl crystal, determ. of linear birefringence in absorpt. band 79—56761
  biaxial crystal, light perpendicular to axis 79—8117
  biaxial crystal, phase matched directions in SHG 77—34909
  biaxial crystal plate, refl. and trans. wave amplitude 78—95573
  biological material, birefr. analysis 78—56954
  birefringent plates, cracks, stress intensity factors, refl. caustics method 80—93718
  boracites, spontaneous birefr., meas. and appl. 79—15434
  borosilicate, anisotropic glasses, birefringence and microstruct. 77—8541
  borosilicate glass, birefringent, X-ray small-angle scatt. study 80—103937
  borosilicate glass single-polarisation single-mode fibres 80—64205
  borosilicate microporous glasses, structural anisotropy and birefringence 79—8114
  Brewster cases, generalised interface with uniaxial media, dispersion rels. *(German)* 80—5682
  N-(p-butoxybenzylidene)-p-pentylaniline, refr. index and density in nematic and isotropic phases 79—90538
  N-p-butoxybenzylidene-p-n-octylaniline, smectic A-B transition, birefringence pretransitional behaviour 80—15226
  calcite, polished sphere as teaching aid 77—71172
  carbazole, birefr. meas., 20 to 190°C, crystal-to-crystal phase transform. 80—45031
  cartilage proteoglycan, association with hyaluronic acid, elec. birefringence obs. 80—85332
  ceramics, Rochelle-type, controllable transparency *(Russian)* 77—630
  chain light filters theory, fund. formulae *(Russian)* 77—50772
  chalcogenide glass, stress-induced birefringence meas., 1-12 μm 77—24818
  chalcopyrite crystals, refractive index, temp. depend., appl. to nonlinear devices 80—60555
  chalcopyrites, refr. index dispersion 80—55057
  chiral smectic liquid crystal, A-C phase change, electroclinic effect 79—42224
  chiral substances, electro-optical responses, Jones matrix, meas. sytem for rot. anisotropy 80—84723
  cholesteric, Grandjean lines, optical study *(French)* 79—46560

birefringence continued
  cholesteric liq. cryst., helical sense and pitch from birefringence meas. 78—59744
  cholesteric liquid crystal, molecular polarisability, arrangement order calc. *(Polish)* 80—10495
  cholesteric liquid crystal coatings, superimposed left- and right-handed, peak refl. and colour gamut 80—74472
  cholesteric liquid crystals, orientational order determ. using birefringence 79—94902
  coherent birefringent optical pulse compression 80—106437
  collagen, polarisation, contribution of permanent and induced dipole moments, elec. birefringence 80—85351
  colloid, electro-optical characterisation methods 77—24821
  colloid patterns interference colours associated with mag. domains 80—2598
  colloid submicron particle size measurement, ultrasonically induced birefringence technique 80—30290
  colloidal dispersions, birefringence in Rayleigh and anomalous diffr. approximations 80—29710
  colloidal particles, intrinsic optical anisotropy, anomalous diffr. approx. 80—53213
  colloids, macromolecules, particle size distribution, reduced electric dipole moments, polarisabilities using electric birefringence 78—95958
  colloids, rigid, size distributions, transient electric birefringence 80—85223
  compensator with adjustable birefr. dispersion 78—82017
  composite flat-belt-drive materials, testing of birefringent coatings 77—77652
  condensed phases, picosec. relax. polarisation spectrosc. meas. 78—68530
  copper acetate monohydrate, ESR in resonant cavity, meas. of Cotton-Mouton-Voigt effect *(French)* 78—89514
  corundum, growth of large crystals of high opt. quality 77—34916
  cotton, otpical anisotropy, multiple-beam interferometric obs. 79—8115
  Cotton-Mouton effect in Jupiter ionosphere and magnetosphere, rel. to decametre radio emission modulation 80—67643
  crystal, internal conical refraction 80—1126
  crystal faces, birefringent, meas. method of growth and dissoln. rates 80—79719
  crystal wafers, orientation anisotropy determ. method 78—31167
  crystalline optical material props., symmetries and tensorial relationships 80—108174
  cubic crystal, electrobirefringence from paraelectric defects 78—39529
  cubic ionic crystal, photoelastic shear consts. 79—86833
  4-cyano-4'-octyloxybiphenyl, nematic-smetic-A transition, optical birefr. temp. coeff. 78—47505
  cyano-biphenyls, nematic liq. crysts., director fluctuation quenching by mag. field *(French)* 78—87613
  4-cyanophenyl esters, of 4′-n-alkylcinnamic acids, birefringence 79—64991
  p-cyanophenyl p-n-alkylobenzoates, nematic, birefringence, polarisability and order parameter 80—100642
  defect crystal structure determination, light interference, diffraction and scattering 80—103316
  definition brightness in optical systems, birefr. tolerance *(German)* 77—75429
  demonstrations with polarised light 77—45657
  detection system for polarisation opt. props. meas. 77—57385
  p,p′-di-n-alkoxy-azoxybenzenes, homologous cpds., nematic, refr. indices and opt. anisotropy, temp. depend., order parameters 77—16278
  diammonium layer compound, $(CH_2)_2(ND_3)_2MnCl_4$, mag. and optical props. 79—51760
  diammonium layer compound, $(CH_2)_n(NH_3)_2CuCl_4$, mag. and optical props. 79—51760
  diammonium layer compound, ND_3-$(CH_2)_2$-ND_3CuCl_4, antiferromag., magneto-optical meas. birefringence 78—68483
  diamond, elasto-optical constants, determ. from piezobirefringence 79—73899
  diamond, natural type IB, thermal conductivity anomaly, defects obs. 77—85003
  diamond, synchrotron electron beam damage, study by optical, cathodoluminesc. and X-ray topography 80—39155
  2,2-dichloropropane, polymorphism obs. 78—18571
  dipalmitoyl phosphatidylcholine containing CaCl$_2$, monodomain sample phase behaviour birefr. obs. 79—83712
  dipalmitoyl phosphatidylcholine monodomain samples with varying concs. of water and other ingredients, prep. 78—15780
  disperse system, dilute, orientationally induced conservative dichroism 80—102623
  dispersion of opt. characts. in amplification range, freq. spectrum of stimulated emission, calcs. *(Russian)* 77—54757
  DNA, calf thymus, flexible polyelectrolyte, elec. birefr. meas. 79—16126
  DNA, calf-thymus and superhelical PM2 aq. solns., electro-optic obs. of γ-irrad. damage 80—85452
  DNA, dye labelled elec. dichroism and birefringence, comparison with mol. props. from polarised fluoresc. 80—84785
  DNA, induced birefringence, conformation and struct. 80—26201
  DNA solution, elec. birefringence, stabilised induced dipole behaviour 80—85349
  DOBAMBC, smectic A to C transform., birefringence and optical rotary power 78—75812
  domain lattice of transparent crystal regular birefr. regions, optical wave diffr. divergence 80—102616
  doubly refracting crysts., appl. in quantitative schlieren technique 77—11040
  dye laser tuning by birefringent Fabry-Perot etalons *(Japanese)* 77—7125
  dye solution, induced birefringence as result of illumination dichroism 79—28709
  EBBA, nematic-isotropic transition, birefringence anomaly at clearing pt. 79—46788
  electro-optical cryst., birefringence in electrically excited Z sections 80—55067
  electrogyration rel. to birefr. 78—27190
  electronic polarizabilities of ions in doubly refracting crystals 78—79551
  ellipsoids, intrinsic, shape and configurational birefringence 80—9805
  EM propagation, birefringent layered media 79—76582
  EM wave propag., birefringence in moving anisotropic media 79—80432
  EM wave propag. in birefringence medium, geometrical optics approx. *(Russian)* 77—68167
  estar base reconnaissance film, in optical correlator 77—74538

birefringence continued
- ethidium bromide E-DNA, intercalated birefringent fibres, microspectrophotometric investig. *(German)* 80—57392
- trans-4-ethoxy-4′-alkanoyloxyazobenzenes, nematogenic liquid crysts., birefr., order parameters, vol. changes during nematic-isotropic transitions 78—59742
- exciton luminescence, macroscopic characts., high reabsorption conditions in uniaxial cryst. 78—19545
- Faraday rotators in fibre Raman lasers 80—58775
- ferroelectric, large-gap type, vibronic theory and opt. props., anomalous bulk photovoltaic effect 80—103939
- ferrofluid, mag. birefringence pulsed field meas. 79—82943
- ferrofluid birefringence, construction of mag. fields *(Russian)* 77—65553
- ferrofluid constitution examination by rotating test tube method 80—33693
- ferromagnet, linear mag. birefr. *(Russian)* 80—93284
- ferromagnetic sol, relaxation of mag. birefr. and dichroism 79—57301
- ferromagnetic suspension, birefringence in mag. field *(Russian)* 77—43979
- fibre, liquid core, polarisation props., bending effect 77—58440
- fibre, single-mode evolution and polarisation 78—9432
- fibre interferometric secondary light source 80—105702
- fibre optical polarisation rotator, single mode 79—76808
- fibre ring interferometer optical gyro, reciprocity of birefr. single-mode fibres 79—81513
- fibre-ring interferometer, rotation-sensing, polarisation analysis 79—64333
- fibres, birefringent single-mode, linear polarisation 79—10382
- filter, alternate partial polariser, design 77—7188
- filter, birefringent, field of view effects 80—14428
- filter, birefringent, transmission expression derivation 79—18522
- filter, birefringent tunable, theoretical anal. 77—88906
- flat glass, commercial, birefr. due to laminar inhomogeneities 78—39731
- fluorene, mol. polarisabilities and opt. props. of cryst. 79—24285
- fluorene, optical birefr., temp. depend., 25 to 90°C 79—82944
- Freon-11, liq., elec. birefringence *(French)* 78—88278
- Fresnel's classical papers, history and present appls. *(French)* 78—37800
- garnet. mag. domain structure obs. by birefringence of mag. colloid 79—51809
- garnet thin film waveguide, magneto-optical effects 77—54802
- gels, non-linear behaviour under strong deform. 78—7240
- glass, phase separated, opt. props. of elongated phases 78—27179
- glass fibre preforms, elastic stresses 79—64343
- glass fibre reinforced polyester, photoelasticity, optical characts. 79—18709
- glass narrow sandwich seal, correction factor for thermal expansion mismatch 78—75110
- glass plate with nonuniform temper, mottled pattern obs. 79—61750
- gravitational waves, new detector 79—97291
- 4′-n-heptyl-4-cyanobiphenyl, nematic, mag. field depend. of birefringence and order parameter 77—76534
- 4′-n-heptyloxy-4-cyanobiphenyl, 70CB, anomalous mag. field induced birefr. in isotropic phase 78—56461
- hexafluorobenzene, quadrupole moments, elec. field-gradient birefringence method 80—95746
- hexamethylbenzene, quadrupole moments, elec. field-gradient birefringence method 80—95746
- N-p-hexyloxybenzylidene-p-toluidine, optical props., density, and order parameter in liq. cryst. phases 79—55657
- HOAB-cholesteryl benzoate mixture, twisted smectic-C and twisted nematic phases, optical and X-ray investig. 77—84634
- HOAB-d_{30}, biaxial liq. cryst., NMR of spinning sample 79—64987
- HOBHA, smectic A to C transition, crit. biaxiality *(French)* 77—4039
- holographic data storage and processing, photosensitive electro-optical materials *(French)* 77—31077
- holographic storage of information using birefringent electrooptic crystals 79—98322
- hybrid field-effect liquid-crystal light valve, optical data processing performance 80—99860
- Iceland spar double refracting prism, rotated e-ray 77—769
- image difference detection using the Weigert effect 79—81376
- induced, electro-optical anisotropy in plane of light wave-front 79—8121
- induced birefringence, meas. using photoelec. polariscope quartet 78—21204
- inhomogeneous birefringent optically active medium, polarisation evolution 78—9328
- inhomogeneous optically anisotropic media, parameters by photoelec. polarimeter 77—74486
- integrated retardation technique, rotationally symmetrical bodies, thermal stress 80—38362
- interface of uniaxial crysts., EM wave refl. and refr. laws, tensor derivation 78—71029
- internal conical refraction of bounded light beams in biaxial crystals 79—28708
- internal conical refraction theory 77—603
- interstellar birefringence, determ. from polarisation obs. of Cygnus OB2 association 77—33577
- IR to visible AC Kerr efficient switches using liquid O_2 and liquid CS_2 80—19078
- isoclinics and isochromatics in birefr. slice, speckle pattern visualization 77—2687
- isopachics measurement of birefr. object, using immersion method polarisation holography 80—99672
- isopropyl ammonium chloroplatinate and chlorostannate, ferroelastic transition, thermal, optical, and elastic meas. 79—28096
- isotropic solid, electrostrictive birefr. induced by high-intensity laser radiation 79—27340
- kaolinite, aq. suspension, mag. and optical props., Fe_2O_3 impure particles 78—76933
- Kerr electro-optical effect, weakly ionised gases, in presence of mag. field 77—35313
- large optical components for high-power lasers, coating birefr. meas. 79—44927
- large-molecule system, field-induced birefringence theory 78—76421
- laser active materials, ruby and garnet, crystal defects influence obs., on energetic effectiveness *(Czech)* 78—79022
- laser materials with inclusions, thermal stresses 77—729
- laser mirror birefringence, ellipsometric meas. using stabilised two-frequency laser 80—101820

birefringence continued
- laser optical component props. depend. on material flow props. *(Russian)* 80—38047
- laser reflector, uniaxial cryst., optic axis orientation determ. by polarisation meas. 77—3598
- laser technology, parallel plate, polarisation problems obs. and solution 80—1225
- $LiNbO_3$, stoichiometry effects 77—59549
- lipid liquid crystals, parabolic focal conics and polygonal defect arrays 79—37618
- liquic crystals, orientational order parameter, optical birefr. meas., polarisation field problems 80—79688
- liquid, electro-optical parameter meas. agreement with calc. values using exact local field expression and ellipsoidal model *(French)* 77—8545
- liquid, optically induced birefringence in elec. field 79—78648
- liquid, US-induced birefringence, Brillouin scatt. linewidth, sound absorption coeff. 78—27180
- liquid crystal, isotropic phase, surface induced ordering, birefringence obs. 80—14998
- liquid crystal, nematic, boundary aligning forces, studied by wall-induced pretransitional birefringence 79—73096
- liquid crystal, positive, dielec., Kerr effect and orientational relax. 77—77171
- liquid crystal and solns. laser and pulsed electric field Kerr effect 77—40210
- liquid crystal cell, colour generation, special electrodes 77—68911
- liquid crystal cells, twisted, mol. orientation, refr. index and birefringence meas. 77—27818
- liquid crystal cpds. incorporating trans-1,4-substituted cyclohexane ring system, synthesis and phys. props. 79—90543
- liquid crystal optical birefringence determ. from interference meas. 77—72551
- liquid crystals, cholesteric, Bragg diffraction, light Pendellosung fringes, theory 77—27830
- liquid crystals, cylindrically aligned, optical characts., interferometric analysis 79—73897
- liquid crystals, high resolution birefr. meas. 79—2803
- liquid crystals, internal field anisotropy changes during phase transformations, optical parameter determ. 79—86711
- liquid crystals, refractive index meas. by cylindrical cell method 80—11358
- liquid crystals close to nematic-isotropic transition, Cotton-Mouton effect meas. 79—99302
- liquid laser and pulsed electric field Kerr effect 77—40210
- liquid short chain molecules, optical investig. of mol. motions 80—40123
- liquids, anisotropic, light propag., intermol. correlation technique for mol. susceptibility tensor 77—58251
- liquids, Cotton-Mouton effect 79—47417
- liquids, US induced, temp. depend. study by optical farfield method 78—16826
- lithium formate biaxial crystal, nonlinear conical refr. obs. in harmonic generation 80—23745
- macromolecular, solutions, mol. orientation, time-depend. torque, rot. diffusion eqn. 78—68471
- macromolecular soln., birefringence kinetics 79—99847
- macromolecular soln., electro-optical characterisation methods 77—24821
- macromolecular solution, rot. diffusion coeff. calc. method w.r.t. mol. struct., elec. birefringence relax. time data interpret. 80—85331
- macromolecular solution, transient elec. birefringence in reversing fields of arbitrary strength and duration 80—84719
- macromolecule, dynamic birefringence and volume effects, rigidity determ. *(Russian)* 77—42456
- magnetic colloids, birefringence and dichroism, magnetically-induced, sign inversion 80—60548
- magnetic crystals, intrinsic magneto-optical effects, phenomenological anal. 79—33679
- magnetic fluids, mag., optical, and hydrodynamic props.,, expt. study, review 80—60376
- magnetic fluids, optical birefr. and dichroism in mag. field 80—60547
- magnetic materials, transparent, optical studies of phase transitions 77—66481
- magnetically induced linear optical birefringence and dichroism in colloidal dispersions 78—8431
- magneto-nonlocal fluids, optical properties 77—58840
- magneto-optic current sensing with birefringent fibres 79—75544
- magnetoelectric susceptibilities, phenomenological rules for computation 80—55068
- MBBA, elec. field effect on optical indicatrix orientation 77—36202
- MBBA, isotropic, surface-induced ordering 80—108176
- MBBA, isotropic-nematic transition, birefringence for tricrit. exponents 79—37816
- MBBA, liq. cryst., light scatt. and birefr. 78—22646
- MBBA, nematic, birefringence determ. by new simple method 78—79526
- MBBA, nematic liq. cryst., transverse electrooptic effect 79—94897
- MBBA, nematic-isotropic transition, birefringence anomaly at clearing pt. 79—46788
- MBBA film, nematic liq. cryst., visible interaction of low-intensity US waves 78—10126
- MBBA-BBCA mixture, field-induced distortion of mol. orientation 79—99060
- membrane studies in transmitted polarised light, interpretation of results 77—37113
- metals, elastic-plastic boundary, photoelastic determ., birefringent coatings 79—81739
- 2-methyl-4-nitroaniline, nonlinear cryst., large optical second-harmonic coeff. meas. 79—76750
- microwave at gyrotropic boundary by inclined plane wave *(Slovak)* 78—55281
- mixed crystals, of equimol. conc. with NaCl struct., piezo-optic birefringence theory 80—100643
- modulator devices for sensitive polarisation determ. 78—8437
- molecular anisotropy from molar Cotton-Mouton and Kerr constants 77—46652
- molecular crystal symmetry props. from optical activity and gyrotropic birefringence calc. *(French)* 78—42941
- muscle, skeletal, birefringence signals rel. to Ca transients 78—24041
- myosin rod, and subfragments, flexibility, birefringence relax. in soln. 78—53320
- near IR transparent material, birefringence meas. polarimeter 79—44925
- nematic cell, twisted, Leslie threshold field verification 77—84638

birefringence continued
nematic liquid cryst., birefringence determ. by new simple method 78—79526
nematic liquid crystal, acousto-optical effect obs., model 77—55767
nematic liquid crystal, colour effects using birefringent films and pleochroic dyes 80—24353
nematic liquid crystal, optical anisotropy, determ. from NMR and birefringence data *(German)* 77—40205
nematic liquid crystal, oriented, transient behaviour of field induced reorientation 78—30536
nematic liquid crystal, pretransitional effects, mol. statistical calc. 77—27990
nematic liquid crystal, S-effect, growth and decay times 78—2824
nematic liquid crystal, US induced birefringence and opacity 77—28544
nematic liquid crystal, ZLI-207, electro-opt. props. *(Russian)* 77—43967
nematic liquid crystalline mixture, orientational order parameter calc. 77—24259
nematic liquid crystals, acoustically induced birefringence 78—38126
nematic liquid crystals, appl. as acoustic image detectors 79—41537
nematic liquid crystals, light transmission exam., positive and negative dielectric anisotropy 77—43141
nematic liquid crystals, orientation fluctuations in high mag. field, quenching, birefringence effects 80—64892
nematic liquid crystals, refractive index and birefringence by interference method 80—96440
nematic liquid crysts. of mols. containing nitrile groups, dipole moments determ. 77—19872
nematic oriented film, birefringent stripe pattern generation by ultrasonic waves 77—76301
nematic-isotropic transition, correlation functions, Cotton-Mouton coeffs. 80—15228
nerve membranes, cell excitation detect. using birefringence changes *(Japanese)* 77—66876
nitrobenzene, boundary phase in 5-layered light guide, birefr.. and equilib. thickness determ. 79—28711
nondipolar liquids, axially-symm., diamag. mols., Kerr effect and Cotton-Mouton effect meas. 78—39524
nonlinear crystals for frequency conversion of optical radiation, review *(Russian)* 80—38068
nonlinear optical uniaxial crystals, review and summary of data 77—75615
nonmutual optical effects, in an external mag. field 80—40097
nonpolar molecule solutions, birefr. kinetics 80—100648
nucleosomes and nucleosomal DNA, electro-optical props., relax. times and chain struct. 80—85350
numerical calculation using optics 80—95832
numerical optical data processor, representation and implementation 78—78947
Nylon 6,6 fibres, birefringence determination, using backscattered light intensity distrib. 79—42939
trans-p-n-octyloxy-α-methyl-p′-cyanophenyl cinnamate, mag. and elec. birefr. in isotropic phase 80—80744
N-p-octyloxybenzylidene-p-toluidine, optical props., density, and order parameter in liq. cryst. phases 79—55657
optical ceramics, dispersion, double refraction and storage effects, material appls. *(German)* 80—69471
optical fibre, current measurement appl. 80—96015
optical fibre, highly birefringent, Faraday rotation 80—58672
optical fibre, single-mode, single-polarisation, with refractive-index pits on both sides of core 80—99846
optical fibre sensors, single-mode, polarisation effects 80—43426
optical fibres, automated measurement system 79—64352
optical fibres, characterisation of polarisation using automatic birefringence measurement system 79—93205
optical fibres, in limit of weak guidance and slight ellipticity 80—1309
optical fibres, single mode, polarisation and magnetooptic props., expt. meas. 78—33830
optical fibres, single-mode, birefringence due to core ellipticity 79—68442
optical fibres, single-mode low birefr., prep. and polarisation characts. 79—7195
optical fibres, slightly elliptical 80—106602
optical fibres with elliptical cross-section 79—59816
optical systems containing birefringence elements, generalisation of pupil function 78—55310
optically active crystals, light diffraction by US waves 77—43965
organic bases, biologically important, and derivatives, optical crystallograhpic props. 78—3449
Orientational optic effects from above Rayleigh particles 80—106453
orthorhombic crystal, birefr. and refr. index determ., refl. method 80—86380
orthotropic composite model materials, photoelastic calibration 80—87715
parametric transformation of light polarisation in crystals 78—1153
pentyl cyanobiphenyl, laser and electric field induced Kerr effect 80—84061
4-n-pentylbenzenethio-4′-n-alkoxybenzoates, birefr., crit. behaviour near smectic A-C transition 80—80745
pentylcyanobiphenyl, liquid crystal, isotropic phase, surface induced ordering, birefringence obs. 80—14998
4-n-pentylphenylthiol-4-n′-octyloxybenzoate, birefringence, crit. suppression 78—76422
perfluorobenzene, orientational correlation parameter for liquid 79—73090
periodic magnetic structure, light propag., paramagnetic interaction 77—55774
periodic stratified medium, birefr., phase matching, X-ray lasers 77—65566
PET, amorphous, intrinsic birefringence calc. from wide angle X-ray scatt. 80—108178
PET, intrinsic briefringence 80—29711
PET fibres, amorphous, exam. of birefringence 80—11360
phase difference and axis of birefr. medium, point by point determ. *(French)* 77—762
phase transitions, obs. of crit. indices of primary and secondary order parameters 77—28541
phase-rotating plate, smooth transverse intensity distrib. form. in light beam 79—59837
phenanthrene birefr. changes due to thermal expansion 78—52468
photoanisotropic materials for polarisational holographic recording 77—75443

birefringence continued
photochromic glasses, anisotropic recording of optical data *(Russian)* 77—1651
photographic emulsion coated on birefr. substrate, construction of multicapacity matched filters 80—74478
photomicrography of submicrometer birefringent contaminants in C black dispersions in polymer particles 80—62757
photoreceptor membrane rhodopsin orientation model 77—90775
plasma, shearing, field-free, birefringence effects rel. to pulsar microstruct. 80—17483
plastic birefringent filters, design, construction and system appls. 78—50943
plastic dielecs. with general work-hardening, birefringence, representation by index tensor 79—8113
plates, birefringent rot., as modulated optical filters, polarised light meas. appl. *(French)* 77—67490
PLZT, optically induced birefr. change 78—43832
PMMA, birefringence in elec. field 80—88962
PMMA, modified with dibutyl phthalate, mech. and optical props. *(Polish)* 77—52423
polarisation 80—9573
polarised beams selective interference in crysts. with isotropic pt. 79—72484
polarised light in materials research, birefr., electro-, magneto-, elasto- and acousto-optics 77—48143
poly(p-phenylene terephthalamide) fibres, optical anisotropy determ. 79—4786
poly(vinylcarbazole), stress-induced crystn. from melt, optical studies 80—84113
poly(vinylidene fluoride) orientation, solid state deformation by coextrusion 80—40394
poly-4-vinylpyridine, electro-optic study of conformational changes induced by heavy metal ions 80—84725
poly-γ-benzyl-L-glutamate, preliq. cryst. mol. alignment, space charge effect, electro-optical obs. 77—40206
poly-γ-benzyl-L-glutamate-dichloroethane in conc. soln., mol. assoc., electro-opt. investig. 78—1973
polyalkyl methacrylates, oriented stretched membrane, gas diffusion, entropy correl. theory 79—69291
polyamide, directionally solidified, morphology 79—10808
polyamide, directionally solidified, X-ray diffr. 79—10809
1,4-polybutadiene, stress-induced crystn. from melt, optical studies 80—84113
polybutene-1 film, deform. mechanism, rheo-optical meas. 80—21041
polybutene-1 film, tubular-extended, anal. of orientational and form birefringence 80—29712
polycaproamide, oriented filaments, mech. props. 80—66550
polycarbonate, bisphenol A, birefringent plates, cracks, stress intensity factors, refl. caustics method 80—93718
polycarbonate fibre, highly-oriented, drawing behaviour and mech. props. 78—76708
polydisperse dilute suspensions, of rod-like particles, anisotropy of electric polarisability 80—85224
polydisperse discs, particle size distrib., transient elec. birefr. data, two-parameter distrib. functions 78—40083
polydisperse ellipsoids, particle size distrib., transient elec. birefr. data, two-parameter distrib. functions 78—40084
polydisperse rod suspension, elec. birefringence relax. 78—23430
polydisperse system, rotatory diffusion const., electro- optic decay curve, size distrib. 78—20079
polyester fibres, orientation in drawn fibres, birefringence meas. 78—35344
polyethylene, crosslinked networks, stress-induced crystallisation, theory 77—24277
polyethylene, extended chain, prep. and study of separated single crystals 78—42924
polyethylene, low density, α mgch. dispersion in relation to spherulite deform. mech. 80—25781
polyethylene, stretched, birefringence rel. to struct. changes 80—84714
polyethylene fibres, high density, ultra oriented, physical, mech. props. 80—25649
polyethylene terephthalate, birefringence of solid 79—69805
polyethylene terephthalate, mech. props., influence of cryst. arrangement and noncryst. region struct. 78—76707
polyethylene terephthalate, uni- and biaxially drawn films, preferred planar orientation 78—80590
polyethylene terephthalate fibres, interdependence between struct. and thermal contraction *(Rumanian)* 78—91259
polymer, amorphous, bulk, structure models and exptl. methods, review 78—22671
polymer, birefringent, stress intensity factor determ. 80—14633
polymer, uniaxial, fluoresc. polarisation, orientation and mol. dynamics effects 78—76516
polymer film, melt grown, birefr. effect on polarised light scatt., phase limitation 78—10867
polymer films, rod-like superstruct., small-angle light scatt., vol. fraction, orient. effects 79—1795
polymer films and sheets 78—80590
polymer foil, optical props. study by photoelasticity in const. and oscillating mech. fields *(German)* 78—31168
polymer gels, with liq. cryst. solvents, theory 80—11963
polymeric films, solvent cast, optical anisotropy origin 80—20610
polymers, birefringence coeff., polarisation-spectral method *(Russian)* 78—52470
polymers, crosslinked networks, stress-induced, crystallisation, theory 77—24277
polymethacrylic acid, swollen networks, viscoelastic photoelastic behaviour 80—59366
polynucleotide solution, elec. birefringence, stabilised induced dipole behaviour 80—85349
polypeptide, conformational change induced by strong elec. field 80—85336
polypeptide in conc. soln., mol. assoc., electro-opt. investig. 78—1973
polypeptides, ionic and non-ionic, electro-optical studies of conformation 80—71379
polyphenylenesilsesquioxane, cast film, correlation between optical and mech. anisotropy 78—95000
polyribonucleotide complexes, mag. field orientation of nematic liq. cryst. solns., light scatt. and birefr. meas. 79—82152
polystyrene, atactic, uniaxially oriented, Fourier transform IR spectroscopic exam. 80—25360

birefringence continued
polystyrene filament, melt spun, struct. and mech. props., effect of drawing, twisting, annealing, untwisting 80—45331
polystyrene-polyisoprene copolymers, macromol. chain conform. in lamellar phase *(French)* 80—2720
polyvinylidene fluoride, birefr. change induced by elec. field 80—55065
polyvinylidene fluoride film, stretched, struct. and elec. props. 79—90572
porcelain glaze, stress meas., by using quartz optical wedge and polarising microscope *(Japanese)* 78—31537
potassium palmitate-water bilayer, lamellar liq. cryst. polymorphism, NMR and birefringence 79—60270
prism couplers, birefringent, for thin film optical waveguides 78—55468
prism cut from anisotropic media, ray refr., appl. to atm. optics haloes 80—63916
projection dyadic treatment, for teaching 77—33789
N-(p-propoxybenzylidene)-p-pentylaniline, refr. index and density in nematic and isotropic phases 79—90538
PT asymmetry and four-fold EM degeneracy lifting, appl. to ring laser mode splitting, optical prop. effects 80—23606
pulsating X-ray sources, radiation polarisation and beaming, vacuum birefringence effect in mag. field *(Russian)* 78—93476
PVC, filled, drawn, mol. orientation study by Raman spectroscopy 79—73919
pyroelectric, uniaxial, spontaneous polarisation, calc. from results of optical meas. 78—27162
quartz, birefr. and opt. rot. near structural phase transition points 78—75823
quartz, cryst., birefringence, temp. depend., intracavity method meas. 80—78931
quartz, electro-optical props. near phase transition 80—80756
quartz, far IR ordinary-ray optical constants 80—45025
quartz, normalised dispersion 79—28713
quartz, synthetic, lattice distortions, optical inhomogeneities by X-ray topography and optical birefringence meas. 78—55887
quartz plate, z-cut, light transmission, linear polarisation conversion 77—8542
quasi-homogeneous magneto-optically active media, Muller and Jones matrices 79—8126
radar vertical probing of glaciers, signal depolarisation 77—9557
radiation induced transmission loss in optical materials 79—94306
radiowave propagation and polarisation in birefringent medium such as ice sheet 77—56755
Raman spectrum birefringence effect in crystal not cut parallel to principal axes 79—69836
random copolymer solution, electrooptics of crystal-like mols. *(Russian)* 77—63396
rare earth compounds, paramagnetic, Faraday and Cotton-Mouton effects for acoustic phonons 78—52476
reactor amplitude determ. for single axis optical crystal systems *(German)* 79—55059
retardation plate matrix representation 79—22894
reversing rectangular pulse generator for transient electric birefringence 78—45657
ring laser, nonreciprocal effects on appl. of transverse mag. field to active medium 80—53341
rod outer segment, Rana pipiens, birefringence meas. of struct. inhomogeneities 78—77048
rod outer segment birefringence changes following intense light flashes, frog 77—90789
rod outer segment birefringence gradient, struct. interpretation, 3-dielectric layer model 79—83771
semiconductor, induced birefr. in presence of electroabsorpt. 77—32351
semiconductor, two photon spectra, quantitative investigation, polarisation depend. 80—50373
semiconductor defect birefringence detection by polarisation IR microscopy 79—83405
semiconductor dislocation Burgers vector exam., birefringence method 78—30626
semiconductor iso-index coupled-wave electrooptic filter 80—1324
sepiolite, electric polarisability, anisotropy, length depend. of ionic contrib. 80—85224
sepiolite, size distributions, transient electric birefringence 80—85223
servo-polarimeter utilizing rotating plastic film 79—71509
silicate glasses, stabilised, exam. of stress relaxation and deformation 78—92292
single mode fibres, noncircular core influence on polarisation performance 78—37973
single-mode fibre birefringence and optical activity obs. 78—1394
small area change real-time detection using photodetectors *(Japanese)* 78—15938
small retardation measurement, modified Babinet compensator using interference-colour method 78—16827
smectic A-nematic phase transform., liq. cryst. binary mixture, birefringence study 80—59638
smectic liquid crystal, chiral, electroclinic effect at A-C phase transition 77—39668
sodium bentonite, Wyoming suspension, comparison of optico-optical scattering and birefringence 80—85226
sodium octyl benzene sulphonate, micellar aq. soln., Cotton-Mouton effect in mag. field 79—16047
Solc birefringent filter, transmission spectrum calc. 79—55052
spatially incoherent light depolaris. by birefringent cryst. 79—98273
speckle interferometry, S/N ratio improvement, image subtraction method 79—86144
speckle pattern props., appl. to three-dimensional photoelasticity *(French)* 77—23920
spectroscopy, high-resolution polarisation, in 10 μm region 79—6196
squaric acid, antiferroelec., struct. phase transition mechanism 80—75969
squaric acid, two-dimens. antiferroelec., temp. depend. of order parameter, birefr. obs. 80—11351
Stokes parameters, of light beam, polarisation modulation meas. 79—21803
stress-induced crystn. from melt, optical studies 80—84113
stressed state in reactor pressure vessels, model studies by polarised optics 78—78454
styrene-butadiene copolymer, birefringence and stress relaxation 78—44158
surface waves, interface with uniaxial media, dispersion rels. *(German)* 80—5682
suspension of absorbing particles, simultaneous meas. of dichroism and birefringence in elec. field., photocurrent signal obs. 80—82801

birefringence continued
suspension of rod-like molecular particles, rot. diffusion coeff. from decay rate of birefr. 79—38520
symmetric slab waveguide in birefr. media, coplanar optical axis slab, modes 79—32053
tanane, crit. behaviour near ferroelec.-ferroelastic transition 78—52459
three-stage birefringent filter, tuning over visible region 80—58667
time-dependent birefringence, linear dichroism, and optical rotation resulting from rigid-body rotational diffusion 79—47411
transient Kerr effect relaxation, in strong unidirectional elec. field 79—69811
transparent medium, linear birefringence meas. turning birefr. method *(French)* 79—8112
s-triazine, molar Cotton-Mouton const., Kerr const., 298K, 633 nm 77—16286
2,4,6-trichloro-s-triazine, molar Cotton-Mouton const., Kerr const., 298K, 633 nm 77—16286
1,1,1-trichloroethane, polymorphism obs. 78—18571
1,3,5-trifluorobenzene, quadrupole moments, elec. field-gradient birefringence method 80—95746
1,3,5-trimethylbenzene, quadrupole moments, elec. field-gradient birefringence method 80—95746
triphenylphosphite, acoustically induced birefringence 80—93274
tunable birefringent filter, 4500 to 7000 Å 77—46806
tuning filters without secondary peaks 78—29994
twisted anisotropic media, light propag., appl. to photoreceptors 78—63004
twisted single-mode fibres, polarisation optics 79—81524
uniaxial and biaxial optical crysts., thermal strain 78—46733
uniaxial crystal plate, transmission of light in case of inclined incidence 78—1152
uniaxial crystals, refl. ellipsometry nonlinear eqn. inversion 80—95120
uniaxial media, reflection (refraction) in directions of vanishing double refraction *(German)* 79—13894
unified approach to optical constitutive relations 79—59631
US stress birefringence, visualisation using LED as short duration stroboscope 77—14863
UV microscope for polarised light, determ. of birefringence, linear dichroism and optical rotary dispersion *(German)* 78—29152
vacuum birefringence, magnetic field induced, expt. detection method 79—85252
vanadyl bisacetylacetonate, polarised X-ray absorption and double refraction 80—50459
viologen films, on transparent oxide electrodes, morphology, electro-optical obs. 80—100703
vitamin B_{12}, circular dichroism and birefringence, polarisation modulation meas. 79—21803
Voigt effect, reson. absorpt. description 80—30302
volume holograms in electrooptic birefr. crysts., light diffr. 79—55084
waveguide, symm. slab, with optical axis not in slab plane, modes 79—996
wire grid polarisers, new optical model 79—902
Ag halide bleached photographic plate, uniaxial medium generation 79—2848
Ag halide thin-film optical recording medium 80—102786
Ag-AgCl emulsion, anisotropy induced by two coherent perpendicular light vibrs. 79—55196
Ag-containing glasses, colour adaptation, photoinduced optical anisotropy 79—61331
AgCl emulsion, spatial differentiation, of intensity distrib., using Weigert effect 79—81377
$AgGa(Se_{1-x}S_x)_2$, crystal growth, phase studies, optical props. 78—48305
AlAs-GaAs monolayered periodic cryst., optical props. 77—81079
$Al_xGa_{1-x}As$-GaAs multilayer heterostructures, optical birefringence 78—64422
As-S chalcogenide glassy semiconductors, induced anisotropy 79—32013
As_2S_3, electron beam deposited film, photoinduced birefringence and dichroism *(Russian)* 78—2934
Au sols, acoustically induced birefringence 80—93274
B_2O_3-SiO_2 optical fibres, exposed cladding technique, birefr. and polarization props. 79—14094
$BaCa_2Mg[SiO_4]_2$, synthesis and struct. characterization 78—22698
$BaMnF_4$, struct. phase transition, optical parameters obs. 80—100328
$Ba_2NaNb_5O_{15}$, birefr. material, thermal cond. determ. by optical method 78—18851
$Ba_2NaNb_5O_{15}$, cryst. comp. effect on low temp. phase transition 80—71346
$Ba_2NaNb_5O_{15}$, low temp. ferroelectric transitions, birefr. and dielec. meas. 79—38499
$Ba_{0.39}Sr_{0.61}Nb_2O_6$, electro-optical props. 80—2728
$Ba_2TiGe_2O_8$-$Ba_2TiSi_2O_8$, pseudobinary system, pyroelectricity and related props. 78—95553
$BaTiO_3$, cubic-tetragonal phase transition, birefringence meas., surface distortion effects 78—95564
$BaTiO_3$, dielec. and optical props. using shell model 79—33654
$BaTiO_3$ type vibronic ferroelectric, light induced refractive index change *(Russian)* 79—91399
$BaTiO_3$, vibronic ferroelec., spontaneous birefringence calc. 78—68473
$BaTiO_3$, vibronic theory and opt. props. 80—103939
$Ba_2TiSi_2O_8$, fresnoite, unsuitability for phase matched SHG 78—46721
$Bi_{12}SiO_{20}$ in insulator-semicond.-insulator struct., induced birefr., influence of kinetics of transient processes 79—24294
$BiVO_4$, ferroelastic phase transition, birefringence meas. using rotating-analyser method 80—80742
$BiVO_4$, ferroelastic phase transition, birefringence meas. at simultaneous high pressure and temp. 80—80743
CO, boundary layer birefringence of rarefied heat conducting gas 77—80265
CS_2 optical shutter, time resolution rel. to birefr. relax. time 77—58452
CS_2, orientational correlation parameter for liquid 79—73090
$CaCO_3$, aragonite, conical intensity distrib. 79—1747
$CaCO_3$, birefr. and electronic polarisabilities of constituent ions 80—7322
$CaCO_3$, calcite, picosecond pulse stacking 79—61330
$CaCO_3$ calcite linear polarizer, role in laser technology 80—64165
$CaCO_3$, Iceland spar, polarizing prism, struct. defects effect 78—18065
$CaCO_3$, point-dipole theory and optical birefringence 79—73896
$Cd_{1-x}Fe_xCr_2S_4$ series of magnetic semiconductors, magneto-optical effects, expt. *(Japanese)* 77—40212
$CdGe(As_{1-x}P_x)_2$, crystal growth, phase studies, optical props. 78—48305
CdP_2, birefringence and optical activity 78—15143
CdS, deposited anthraquinone, decoration patters 77—1137

birefringence continued
CdS film, ellipsometry of natural boundaries *(Russian)* 79—4866
CdS, temp. coeffs. meas. of refr. index and birefr. 77—55762
CdS, thermoreflectance spectra, additional boundary conditions in terms of optical constants 79—15478
$CdSiP_2$, birefringence meas. 78—56455
$CdSiP_2$, effects on hydrostatic pressure and temp. 80—45033
$CdSiP_2$, optical activity near isotropic point, absorpt. spectra 79—69804
$CdSiP_2$, pseudodirect bandgap semiconductor, natural birefringence 79—65834
CdTe, hexagonal film, effective birefringence 80—16004
Co film, linear mag. birefr. dispersion 77—69807
$CoCO_3$, birefringence of light *(Russian)* 78—56456
$CoCO_3$, linear magneto-optical effect, birefr. 80—66155
CoF_2, 180-degree antiferromag. domain obs. by new magnetooptical effect 80—44855
CoF_2, linear and quadratic mag. birefr. 80—16005
CoF_2, linear magneto-optical effect, birefr. 80—66155
$CoFe_2O_4$ film, Faraday rot., birefr. 77—1663
copper phthalocyanine, size distributions, transient electric birefringence 80—85223
$Cr(CO)_6$, linear dichroism, distortion and local field contribs. 79—87415
CrO_2 acicular particle suspensions, mag. props., optical meas. 80—44874
$CsCaCl_3$, birefringence, twinning and structural phase transitions 79—38480
$CsCuCl_3$, birefr. and opt. rot. near structural phase transition points 78—75823
CsH_2PO_4, lattice consts., temp. depend. of dielec. const. and birefringence, high temp. phase transitions 79—56746
$CsMnCl_3.2H_2O$, Heisenberg antiferromag., linear mag. birefringence meas. 77—16277
$Cs_2NaM^{3+}Cl_6$, (M=Bi,Nd,Pr), struct. transitions, polarisation optical expts. 79—99318
$CsPbCl_3$, birefringence, twinning and structural phase transitions 79—38480
$CsPbCl_3$, refr. index and birefr., struct. transition effects 77—90126
$CsSrCl_3$, birefringence, twinning and structural phase transitions 79—38480
$CsSrCl_3$, refr. index and birefr., struct. transition effects 77—90126
CuF_2, stress-induced birefringence meas., 1-12 μm 77—24818
$CuF_2.2H_2O$, powder, Cotton-Mouton-Voigt effect and EPR in Q-band *(French)* 79—8045
$CuF_2.2H_2O$, X-band ESR powder spectrum and related magneto-microwave effects 79—24214
$Dy_3Al_5O_{12}$, antiferromag., optical birefringence in fields along [111] meas. 77—28540
$DyAsO_4$, cooperative Jahn-Teller transition, optical study 80—15240
$DyVO_4$, cooperative Jahn-Teller transition, optical study 80—15240
$DyVO_4$, cooperative Jahn-Teller phase transition, linear birefr. meas. 80—88960
Eu-Fe garnet, light mag. linear birefringence and dichroism near absorption band *(Russian)* 80—55063
Fe film, evaporated at oblique incidence, optical and mag. anisotropies 80—7134
Fe film, linear mag. birefr. dispersion 77—69807
$FeBO_3$, photoinduced linear birefringence *(Russian)* 78—52469
Fe_3BO_6, Faraday rotation and birefringence 80—100650
Fe_3BO_6, orthorhombic cryst., birefr. and refr. index determ., refl. method 80—86380
α-Fe_2C_3, anisotropic linear mag. birefr., light modulation 77—8548
α-Fe_2O_3 and α-Fe_2O_3:Mn, linear mag. birefringence near Morin transition 77—52052
α-Fe_2O_3, haematite, birefr. under uniaxial stress in mag. field *(Russian)* 78—88285
α-Fe_2O_3, haematite, linear mag. birefr., Morin transition 77—8309
Fe_2O_3, haematite, optical indicatrix deform. and rot. during field induced phase transition 78—68482
α-Fe_2O_3, pure and Mn doped, characts. of Morin phase transition, linear mag. birefringence meas. 77—69560
γ-Fe_2O_3:Cr, pure and doped, acicular particle suspensions, mag. props., optical meas. 80—44874
Fe_3O_4 ferrofluid suspension, mag. props., stability 79—87293
Fe_3O_4 in suspension, ferromagnetic colloid, optical meas. 78—10906
$Fe_xZn_{1-x}F_2$, Neel point and short range order, dilution effects, mag. birefr. obs. 80—71019
GaAs, birefringence in presence of electroabsorpt. 77—32351
GaAs, electrooptic effect, birefr. harmonics, permittivity dispersion 77—52044
GaAs, refr. index and induced birefringence dispersion 80—2717
GaAs, temp. coeff. of induced birefringence 80—93277
GaP, large cryst., optical birefr. images of dislocations 78—30627
GaP single crystal, direct obs. of dislocations by birefringence 79—14810
GaP, temp. coeff. of induced birefringence 80—93277
GaS(Se), birefringent layer cryst., indices of refraction 77—20815
GaSe, optical orientation and free exciton alignment on reson. excitation *(Russian)* 77—69812
$GdCrO_3$, Faraday rot. and linear birefr. meas., 0.8 to 2 μm 77—77180
$Gd_3Ga_5O_{12}$, optical birefringence images of edge dislocations 77—1129
$Gd_2(MoO_4)_3$, electro-optical properties 78—88281
$Gd_2(MoO_4)_3$, ferroelec. temp. depend. of spontaneous biref. and electrooptic reponse 79—33662
$Gd_2(MoO_4)_3$, spontaneous birefringence, pulsed field switching, compression effect, domain movement 78—27187
$Gd_2(MoO_4)_3$, spontaneous electrooptic effect, role of induced birefringence 78—68480
Ge, strain-confined electron-hole liq. 77—47738
H_2I_2, crysts., growth, optical props. *(German)* 77—77167
α-HIO_3, optically active biaxial crystal, conical diffr. intensity patterns 79—4785
αHIO_3, second harmonic conical refraction 77—46758
Hg_2Br_2, crysts., growth, optical props. *(German)* 77—77167
Hg_2Cl_2, calomel, birefractive cryst., light spreading *(German)* 77—77168
Hg_2Cl_2, cryst., birefringence and dichroism, 200-500 nm and far IR 78—27257
InSb-GaSb solid solution ingots, orientation, twinning and orientation depend. reflectance 79—28001
KAg_4I_5, superionic phase transition, dynamical and crit. pt. props. 80—107535
$K_2Ba(NO_2)_4$, temp. depend. of birefringence 79—55887
KBr-KCl, birefringence, annealing effects, photoelasticity 78—72483

birefringence continued
KCN, multidomain birefr. solid, light scatt. and IR transmission spike 80—60587
$KCaF_3$, struct. phase transitions, DSC, birefr., and neutron powder diffr. obs. 80—70149
$KCdF_3$, structural phase transitions using linear birefringence studies 78—76424
KCl birefringence, annealing effects, photoelasticity 78—72483
KCl, diffr. by M-centres, thick plane wave hologram recording 77—7021
$KCl{:}Pb^{2+}(Cu^{+})$ 80—34890
KCl-KBr, with equimol. conc., piezo-optic birefringence theory 80—100643
KCl-KBr mixed crystals, sign reversal of piezo-optic birefringence 79—99849
KCl(Br)(I), stress-induced birefringence meas., 1-12 μm 77—24818
K_2CoF_4, two-dimens. Ising antiferromag., nearest neighbour correl. function, birefr. expts. 80—71386
K_2CoF_4, two-dimensional Ising-like antiferromag. birefringence, short-range order effect 77—81081
$KCuF_2$, linear chain Heisenberg antiferromag., nearest neighbour correl. function, birefr. expts. 80—71386
$KCuF_3$, one-dimensional S=1/2 Heisenberg antiferromag., mag. energy, optical birefringence meas. 78—52467
K_2CuF_4, 2-D ferromagnet, optical and magneto-optical props. 77—52062
KD_2PO_4 monocrystal, electrooptical props. in paraelectric phase *(Polish)* 80—11368
KD_2PO_4 photo-spatial light modulator, optical data processing 80—102839
$KD_3(SeO_3)_2$, optical and dielec. props. near ferroelastic phase transition 79—38518
$KFe(MoO_4)_2$, phase transitions at 312 and 139K 80—70396
KH_2PO_4, and isomorphs, dielec. props. and birefr., simultaneous obs. 78—15130
$K^2H_2PO_4$ electro-optic shutter natural birefringence compensation by β-$LiIO_3$ monocrystal 79—55247
$KH_3(SeO_3)_2$, optical and dielec. props. near ferroelastic phase transition 79—38518
$KLiSO_4$:(Cr), uniaxial crysts., circular dichroism and optical activity 80—45029
$KMgF_3{:}Ni^{2+}$, acoustic Faraday and Cotton-Mouton effects, theory 80—65987
$KMnF_3$, birefr. and opt. rot. near structural phase transition points 78—75823
$K_2Mn_2(SO_4)_3$, optical and dielectric props. 79—11403
$KNbO_3$, dielec. and optical props. using shell model 79—33654
$K_5Nd(MoO_4)_4$, dielec. and optical props. 79—33590
K_2NiF_4, obs. of short range order by optical birefringence 79—11318
$KTa_{1-x}Nb_xO_3$, local polarisability in quantum paraelec. and quantum ferroelec. phases 78—64325
$KTaO_3$, crit. dielec. and optical props. and storage, 4K 77—24805
$(La,Nd)P_5O_{14}$, optical props., ferroelastic phase transition induced 79 95731
$LaBO_3$, single cryst., not cut parallel to principal axes, Raman spectra birefringence effect 79—69837
$Li_{0.5}Fe_{2.5}O_4$, domain struct. in (110) and (111) plates, Faraday effect meas. 79—61180
$LiGd_3(MoO_4)_5$, single crysts., cryst. growth, optical props. 80—60763
$Li_2Gd_4(MoO_4)_7$, Czochralski growth, struct. and optical props. 78—27397
Li_2GeO_3 monocrystal conoscopic figure in polarised white light 79—15433
LiH_2PO_3, nonlinear and linear optical props. 80—48330
$LiNH_4SO_4$, phase transitions, temp. depend. of NMR, spontaneous polarisation, birefringence and SHG 78—10191
$LiN_2H_5SO_4$, single cryst., refr. indices, birefringence, optic axes orientation 77—90125
$LiNbO_3$ birefringent crysts., holographic writing, image polarisation characts. storage 77—61926
$LiNbO_3$, hologram, light diffr. with electro-optical rot. *(Russian)* 78—1190
$LiNbO_3$, laser induced optical inhomogeneity in external electric field 79—95730
$LiNbO_3$, photoinduced birefringence obs. 78—15144
$LiNbO_3$, photorefractive effect sensitivity 78—43833
$LiNbO_3$, vol. hologram recording and reconstruction 78—9349
$LiNbO_3$:Fe, induced optical inhomogeneity, refr. index and short-circuit photocurrent meas. 79—69806
$LiNbO_3$:Fe, local photodeform. and photorefraction 80—16003
$LiNbO_3$:Fe, photoinduced refractive index discontinuities at surface 80—75999
$LiNbO_3$:Fe, photorefr., surface recombination 79—56759
$LiNbO_3$:Fe crystal conductivity and photoinduced birefringence obs. *(Russian)* 78—60151
$LiNb_{1-y}Ta_yO_3$, Czochralski grown, refr. index, 5893-10600 Å, and zero birefr. 78—31166
$LiNd(PO_3)_4$, crystallisation from $LiPO_3$ flux, exam. of optical props. *(German)* 79—11401
$LiTaO_3$, multidomain cryst., birefringence, Tyndall cone struct. 77—4618
$LiTaO_3$ optical waveguide, Ag-Li ion exchange 80—91888
$LiTaO_3$ platelet, electro-optical tunable filter, birefr. electro-optic cryst., light energy coupling 79—59804
$MgCO_3$, point-dipole theory and optical birefringence 79—73896
MgF_2, stress-induced birefringence meas., 1-12 μm 77—24818
MnAs in suspension, ferromagnetic colloid, optical meas. 78—10906
$MnCO_3$, point-dipole theory and optical birefringence 79—73896
MnF_2, piezo-optical effect, birefringence variation on uniaxial compression *(Russian)* 80—34887
MnO, linear optical anisotropy meas. at antiferromag. transition 77—36205
$Mn_{1-c}Zn_cF_2$. Heisenberg antiferromag., linear mag. birefringence meas. 77—16277
$Mn_{1-x}Zn_xF_2$, linear mag. birefr., crit. behaviour 77—52061
$Mn_xZn_{1-x}F_2$, Neel point and short range order, dilution effects, mag. birefr. obs. 80—71019
$Mo(CO)_6$, in nematic matrix, linear dichroism, distortion and local field contribs. 79—87415
N_2, boundary layer birefringence of rarefied heat conducting gas 77—80265
$(NH_4,Cs)Cl$, negative isotope effect on II-III phase transition *(German)* 78—95155

birefringence continued
$NH_4Ag_4I_5$, superionic phase transition, dynamical and crit. pt. props. 80—107535
NH_4B_r, birefr. and opt. rot. near structural phase transition points 78—75823
$(NH_4)_2BeF_4$ crystals, incommensurate-commensurate phase transitions, optical props. 79—95733
NH_4Cl, order parameter, electro-optic measurement 78—88280
NH_4FeF_4, Mossbauer and optical evidence for crystallographic transition 79—14931
α-NH_4HgCl_3. Raman study of phase transition *(French)* 80—11378
$(NH_4)_{1-x}M_xX$, and $(ND_4)_{1-x}M_xX$ M=Tl, Rb, Cs, X=Cl, Br, phase diagrams birefringence obs. *(German)* 79—83185
$(NH_4Rb)Cl$, negative isotope effect on II-III phase transition *(German)* 78—95155
Na vapour, Zeeman coherence, transient and stationary, polarisation spectroscopy 80—58212
NaCN, multidomain birefr. solid, light scatt. and IR transmission spike 80—60587
Na_2CO_3, phys. props. related to phase transitions 80—96643
NaCl, stress-induced birefringence meas., 1-12 μm 77—24818
NaCl, uniform deformation and birefringence in nonuniform elec. field *(Russian)* 79—87396
$NaNbO_3$, birefr., temp. depend., behaviour at $P\rightleftarrows N$ struct. transition 78—64331
Na_2O-B_2O_3-SiO_2, two-phase, stresses arising during leaching 80—81086
Na_xWO_3 bronzes $(0.4<x<1)$, domain, surface and substrate structs. 80—34281
Nd:glass laser rod, pumped, thermal relaxation 80—69397
Nd:YAG laser, influence of birefraction and cooling on output characteristics *(Italian)* 79—50299
Nd^{3+}:YAG laser, high repetition rate electrooptic Q-switching, birefringence 80—69430
$NdGa_5O_{12}$ wafer, dislocations, etch pits and birefr. obs. 78—83818
Ne gas, laser induced birefr., polarised light interf. obs. 77—19368
Ne, two and three level systems, laser induced dichroism and birefr. 78—79065
Ni film, linear mag. birefr. dispersion 77—69807
NiO, linear birefringence in S-domains near antiferromag. phase transition 80—60261
NiO, temp. depend. 78—10664
$NiSO_4.6H_2O$, uniaxial crysts., circular dichroism and optical activity 80—45029
O_2, heat-flow birefringence 77—84395
O_2 solid film, optical and structural props. 78—56052
PLZT ceramic birefringence props., transverse electro-optical meas. 78—72487
PLZT ceramics, electro-optic characts., w.r.t. future instrument applics. *(German)* 78—33792
PLZT ceramics, transparent ferroelec., photorefraction and photocond. study 79—42581
PLZT, controlled light scatt. 78—10909
PLZT, phase transitions, permittivity, birefr. and light scatt. meas. 77—81074
PLZT slim-loop and linear ceramics, longit. electrooptic effects, display appl. 80—80751
PLZT transparent ceramics, electro-optical anisotropy due to hot pressing 77—12720
PLZT type ceramics, variation of light scatt. during field induced $AF\rightarrow F$ transition *(French)* 77—90158
PLZT, with broad phase transition, birefr., electro-optic and dielec. props. 77—16280
PLZT-based polarised ceramic, electro-opt. props. 77—52041
(PLZT)(PLZN) system, ferroelec. transparent, prep. and study 79—42911
$PbGeO_3$, cryst. struct., dielec. and optical props. 77—1118
Pb_3GeO_5, cryst. struct. dielec. and optical props. 77—1118
$PbHPO_4$, optical props. near ferroelec. transition 79—33663
$PbHPO_4$, single cryst., growth, optical props., ferroelec. transition 78—35285
$PbMg_{1/3}Nb_{2/3}O_3$, photoinduced change in birefr. 77—24590
$Pb_3MgNb_2O_9$, birefringence, pulse response of electro-optical effect 79—87417
$Pb_3(PO_4)_2$ ferroelastic, dielec. consts. and birefringence meas. 78—2793
$Pb_3(PO_4)_2$-$Pb_3(VO_4)_2$, direct obs. of ferroelasticity 77—21203
$PbTiO_3$, optical birefringence in low temp. region 80—93276
$PbTiO_3$, single crysts., lattice parameters and birefringence as function of temp. 79—38517
$PbTiO_3$, vibronic theory and opt. props. 80—103939
$Pb_3(VO_4)_2$-$Pb_3(PO_4)_3$ solid solutions, ferroelastic, dielec. consts. and birefringence meas. 78—2793
$Pb_3(VO_4)_3$, ferroelastic, dielec. consts. and birefringence meas. 78—2793
$RbAg_4I_5$, 208K phase transition, Jahn-Teller-like model 77—35694
$RbAg_4I_5$, struct. transition at 209K, Ising like behaviour 78—14460
$RbAg_4I_5$, superionic phase transition, dynamical and crit. pt. props. 80—107535
$RbCdCl_3$, birefringence, twinning and structural phase transitions 79—38480
$RbFeF_4$, Mossbauer and optical evidence for crystallographic transition 79—14931
RbH_2PO_4, ferroelec. phase transition, birefringence studies 80—108162
$Rb_xK_{1-x}MnF_3$, struct. transitions, NMR and birefr. expts., 60-300K 77—47577
$RbMnCl_3$, birefringence, twinning and structural phase transitions 79—38480
$RbMnCl_3$ crystal, structural phase transition, birefringence, elastic moduli and Raman spectra 80—15243
$RbMnCl_3$, structural phase transition 78—91442
$RbMnCl_4$, changes in birefr. due to spin flopping 79—73910
Rb_3MnCl_4, quasi-2D-antiferromag., linear birefr. and optical absorpt. spectra 80—71385
Sb_5O_7I, polytypes 2MC and 2MA, photoferroelastic phenomena 79—95447
SbSBr, single crystals, birefringence meas., ferroelec. transition obs. 80—88933
SbSI, birefr. and phase transitions 78—60405
SbSI, ferroelec., phase transitions, birefringence meas. 78—56440
SbSI, paraelectric phase, nonlinear optical props. 78—10870
SbSI, photoelectric current, modulated due to light intensity 79—19626
SbSI, photoinduced birefringence, effect of elec. field 77—52037

birefringence continued
Sb_2Se_3 single crysts., phys. prop. anomalies, 400-450K *(German)* 79—38072
Si, birefringence of dislocation lines in (111) wafers 79—61332
Si film, optical characterisation from guided wave optics 78—48245
n-Si, nonlinear birefr. and dichroism at microwave freqs. and intervalley scatt. 79—19602
n-SiC (6H), doping effect on birefingence dispersion, effective electron mass 79—69807
SiC, polytypes, birefr. meas. 77—43963
SiO_2-Al_2O_3-B_2O_3-MgO-CaO-Na_2O, strengthened by ion exchange, exam. of internal stresses using polarising microscope 78—88549
$SmFeO_3$, orthoferrite, anisotropy of Faraday rotation 79—61341
SmI, Zeeman coherence, transient and stationary, polarisation spectroscopy 80—58212
$Sm_{0.55}Tb_{0.45}FeO_3$ orthoferrite, optical and magneto-optical props. 79—61396
$Sm_xTb_{1-x}FeO_3$, gyrotropic props. and birefringence, in spin reorientation range 80—7324
$Sm_xTb_{1-x}FeO_3$ orthoferrites, crystallo-optical props. 79—42027
$Sr_{0.61}Ba_{0.39}Nb_2D_6$, photoinduced birefr. 80—7325
$Sr_xBa_{1-x}Nb_2O_6$, domain struct. influence on electrooptical props. 80—93283
SrF_2, stress-induced birefringence meas., 1-12 μm 77—24818
$SrTiO_3$, crit. dielec. and optical props. and storage, 4K 77—24805
$Ta_2O_5N_x$, sputtered birefr. film, deposition conditions effect on refr. index 77—39118
$Tb_3Fe_5O_{12}$, weak field mag. transition, magneto-optical and magnetisation meas. 77—69551
$Tb_cGd_{1-c}VO_4$, cooperative Jahn-Teller effect, linear birefringence 77—76550
TbIG, [111] magnetoelastic props., rel. to Cotton-Mouton birefringence, 90-500K 80—103876
TbIG, anisotropic linear mag. birefr., light modulation 77—8548
TbIG, mag. birefringence rel. to sublattices 79—28723
TbIG, refr. index, higher-order anisotropic mag. contrib. 77—69808
$TbPO_4$, linear optical birefr. meas. near bicritical point 80—15719
$TbVO_4$, cooperative Jahn-Teller effect, linear birefringence 77—76550
TeO_2 shear wave acousto-optical device with polarisation filtering 80—106619
$TlCdF_3$, weakly discontinuous phase transition, linear birefringence obs. 80—11362
$TlGaSe_2$, electrooptic effect and refr. index anisotropy 77—16281
TlI, on KCl, epitaxial growth habit rel. to optical scatt. 77—50738
$TlMnCl_3$, birefringence, twinning and structural phase transitions 79—38480
$TlMnCl_3$, refr. index and birefr., struct. transition effects 77—90126
$TlSbS_2$, single cryst., spectral transmission distrib., polaris. effect, refractivity, dispersion 77—59551
$W(CO)_6$, in nematic matrix, linear dichroism, distortion and local field contribs. 79—87415
YAG crystals, dislocations and inclusions, birefringence topography obs. 80—107248
YAG rods, thermally induced birefringence in (001) direction, transmission loss *(Chinese)* 77—77166
YAG:Nd crystal, orientation influence on thermally induced birefringence *(Chinese)* 80—88958
$YFe_{1-x}Co_{x/2}Ti_{x/2}O_3$, orthoferrite, anisotropy of Faraday rotation 79—61341
YIG, and Ga-substituted YIG, mag. birefringence rel. to sublattices 79—28723
YIG, anisotropic linear mag. birefr., light modulation 77—8548
YIG, refr. index, isotropic exchange and higher-order anisotropic mag. contribs. 77—69808
$ZnGeP_2$, effects on hydrostatic pressure and temp. 80—45033
$ZnGeP_2$, pseudodirect bandgap semiconductor, natural birefringence 79—65834
ZnP_2, birefringence, circ. dichroism, temp. depend. *(Russian)* 79—1748
ZnP_2, birefringence and optical activity, dispersion 78—2821
ZnP_2, birefringence dispersion *(Russian)* 77—85686
ZnS, deposited anthraquinone, decoration patterns 77—1137
ZnS, microregions disorientation degree anal. by birefringence, ESK and decoration methods 79—60389
ZnS, natural and stress induced birefringence dispersion 78—6651
ZnS striated platelets, SEM studies of local variations in cathodolum. and birefringence 78—15232
ZnS(Se), stress-induced birefringence meas., 1-12 μm 77—24818
ZnSe, cubic cryst., optical birefringence obs. 77—4616
ZnSe in insulator-semicond.-insulator struct., induced birefr., influence of kinetics of transient processes 79—24294
ZnSe, optical axes for birefringence *(French)* 77—20819
ZnSe, parasitic birefringence dispersion induced by lattice plane defects 77—4617
ZnSe, resonant Brillouin scatt. by injected acoustic waves 77—12394
ZnSe single crystals, birefringence due to native defects and electro-optic effect *(French)* 79—24293
ZnSe, twinning effect on electro-optical props. 78—68478
$ZnSiAs_2$, effects on hydrostatic pressure and temp. 80—45033
$ZnSiAs_2$, pseudodirect bandgap semiconductor, natural birefringence 79—65834
$ZnSiP_2$, effects on hydrostatic pressure and temp. 80—45033
$ZnSiP_2$, pseudodirect bandgap semiconductor, natural birefringence 79—65834

bismuth
see also nuclei with ......
acoustic cyclotron reson., sound interaction with cyclotron waves *(Russian)* 77—35959
acoustic plasma wave excitation 78—10520
acoustic plasmon excitation 77—89793
acoustic wave drag, acousto-elec.-mag. effects *(Russian)* 79—19638
acoustic waves, giant quantum attenuation at high mag. fields, angular depend. *(Japanese)* 79—4585
adsorption, and condensation on W 79—73394
adsorption of organic cpds. 80—20038
AES and characteristic energy loss spectra, expt. and interpretation 78—27354
Alfven wave dispersion, non-local, freq. and relax. time depend. effects 80—29429
Alfven wave mode mixing 77—4381
Alfven-like waves, new branch obs. at 300 GHz 80—49794

bismuth continued
amorphous, microbridge prep. and transition from superconducting to normal state 78—34933
amorphous, superconductivity and the very strong electron-phonon interaction *(Japanese)* 79—95552
amorphous film, supercond. fluctuation effects in resist. transition 78—10609
amorphous films, supercond. fluctuation effects in perpendicular mag. fields 79—60980
amorphous metal films, crystallisation with and without mag. field 80—70570
anisotropic crystal, dislocation wall stress field and strain energy 80—100233
anodic oxide film capacity in various soln. 80—104320
anodisation, electric breakdown 79—20377
atom, $6p_J^3$-$6p_J^3$, search for optical rot. induced by weak neutral currents 78—82710
atom, α-particle impact K-shell ionisation, 40 to 110 MeV 78—17752
atom, electron config. mixing and parity nonconservation 78—13439
atom, electron impact, relativistic, L-shell ionis., $L\beta/L\alpha$ branching ratio energy depend. 79—98228
atom, electron impact ionisation, characteristic X-radiation ang. distrib. obs. 80—1069
atom, electron impact M-shell ionisation, 60-600 keV, absolute cross sections meas. 80—83493
atom, excited configs., mag. hyperfine splitting factors, interferometric determ. near 200 nm 80—32852
atom, Faraday effect and magnetic circular dichroism 80—83399
atom, hyperfine structure 79—3375
atom, K-shell electrons, γ-ray inelastic scatt. cross-sections 77—14395
atom, keV electron impact, L X-ray prod. cross section 79—18293
atom, L-shell X-ray photoelectric cross sections, fluorescence spectra 78—58636
atom, L-subshell ionisation cross-section ratio by ion beam impact, projectile charge and vel. depend. 77—6920
atom, metastable states collisional quenching, temp. depend. 77—88526
atom, neutral current-induced parity nonconserving optical rot., Dirac-HF calcs. 80—47948
atom, nuclear K-X-ray satellites, $Z=50$-83, by α-bombard., 17.5-22.5 MeV 80—42984
atom, optical activity, search for parity nonconservation 79—36574
atom, optical activity and HFS, neutral weak currents *(Russian)* 79—13660
atom, optical activity of vapour as indication of electron-nucleon weak interaction *(Russian)* 77—10618
atom, optical transitions, struct. of weak neutral currents *(Russian)* 77—88420
atom, outer electron shielding, parity non-conserving optical rot. 79—18153
atom, parity non-conserving E1 matrix elements, many body calcs. 80—47924
atom, parity non-conserving optical rot., Weinberg-Salam relativistic central field theory vs. obs. 78—953
atom, parity non-conserving optical rotation search 77—10642
atom, parity nonconservation in heavy atoms, weak electron-electron interaction *(Russian)* 78—55132
atom, parity nonconserving optical rot. upper limit, obs. vs. Weinberg-Salam theory 78—952
atom, parity-nonconserving optical rotation 79—63968
atom, search for parity nonconservation 79—36593
atom, UV absorption spectrum, flash photolysis method 78—90105
atomic, parity violation in M1 transition 79—85927
atomic beam excited passing discharge region, new light source of forbidden lines 78—90112
atomic electron collision cross sections 77—42410
atomic polarisability, oscillator strength and radial integral, Dirac eqn. calc. 79—22620
atomic spectroscopy, search for parity-violating weak interaction of electrons with nuclei 79—36571
atomic-transition lasers based on two-photon dissociation of metal-triiodide vapors 80—23679
attenuation coefficient of sound, effect of impurity on gas-liq. type phase transition 78—39167
Auger $N_{6,7}O_{4,5}O_{4,5}$ spectra, X-ray excited 77—85886
Azbel-Kaner type cyclotron reson. obs. 78—56379
band structure, empirical pseudopot., temp. and press. depend. 78—18955
band structure, hydrostatic press. effect, thermoelec. power meas. 79—69406
band structure model parameters, deformation theory *(Russian)* 78—56067
Bernstein waves, electrostatic wave dispersion relation in mag. field 80—34471
carrier spectrum, deform. model, holes 79—60680
charge carrier drift velocity *(Russian)* 78—84208
charge carrier interaction with twinning planes in strong transverse mag. fields *(Russian)* 80—88577
chemical bonding in group V and VI elements and compounds with tetradymite structure 80—15036
chemical shift of X-ray L-absorption edge 79—52044
chemisorption of O_2 on (0001) surface, LEED, AES and electron loss meas. 79—77908
clusters, 2 to 500 atoms, nucleation, mass spectra 80—102596
coadsorbed with Pb on Cu (100), Bi, LEED and AES meas. 79—15017
concentration in gas, determ. by analytical photon catalysis 77—52685
cooling element for radiation detector, shape effect on heat removal efficiency 78—12691
core-level line shape in liq. and solid phases, high-resolution XPS meas. 77—59668
crystal growth from melt, impurity distrib. control by electrotransfer method *(Russian)* 80—66418
current states, symmetry and self-oscills., macroscopic mag. moment by RF irradiation *(Russian)* 79—19749
cylindrical thin crystal, size effect oscills. in longit. magnetoresist. *(Russian)* 77—69357
DC Bi:Te, elastic consts., electronic contrib. 77—84826
Debye-Waller factors and thermal expansion 78—43089
defects, quenching and annealing, resist. meas. 78—87973
deformation calculations, band struct. variation, electron phase transitions due to deform. *(Russian)* 80—65137
deformation theory of the charge carrier spectrum from Shubnikov-de-Haas data *(German)* 78—84235

bismuth continued
degenerate electron liquid, skipping orbit cyclotron resonance, surface state transitions 80—103889
determination, in complex alloy, by at. absorpt. 77—40582
dielectric anomalies, electronic relax. times at far IR frequencies 77—24513
diffusion in Cu, diffusion coefficient temp. depend. *(Russian)* 77—84987
diffusion in liquid Cu *(Japanese)* 78—59962
diffusion size effects 79—60824
diffusion thermoelectric power in mag. field, calcs. 78—56167
dislocation internal friction, HF, rel. to temp., freq., amplitude *(Russian)* 78—26574
elastic moduli, calc. from interatomic forces 79—95071
electrical conductivity and thermal EMF at press. up to 12 kbar 77—47806
electrical resist., thermal cond. and thermopower, low temp. transport props. 80—49708
electrical resistivity, electron-hole scatt. 77—4331
electrical resistivity due to electron-phonon scatt. on small cylindrical Fermi surface 79—4562
electrical resistivity measurement, 1.1 to 100K 77—69321
electromechanical polishing method 78—53073
electron band models, simultaneous meas. of giant quantum oscills. and diamag. reson. 78—14653
electron Fermi surface, energy dispersion, deform. model and k.p. calcs. 79—51469
electron gas heating at low temp. 78—60133
electron heating due to acoustic phonon scatt. *(Russian)* 80—10991
electron irradiated, displacement threshold energy *(French)* 79—23649
electron isoenergetic surface, variation of connectivity under press. *(Russian)* 78—60050
electron isoenergic surface coherence var. under press. *(Russian)* 77—55476
electron mean free path, stopping and straggling 78—91367
electron properties, carrier spectrum, review 78—84137
electron scattering rates, mag. field depend., de Haas-van Alphen meas. 78—10436
electron specular refl. by binary plane, ang. depend., focusing by transverse mag. field *(Russian)* 77—80798
electron tunnelling and band struct., mag. field effect 79—37979
electronic properties, review 77—15742
ellipsoidal model of textured specimens with uniaxial symm. *(Russian)* 80—80100
EM wave dispersion and damping, Voigt configuration, non-local calcs. 80—100475
EM wave excitation *(Russian)* 77—32093
energy band model, resolution of theoretical discrepancy 77—11849
energy band model for electrons 77—35849
energy bands, longitudinal magnetoacoustic effects 77—28095
energy spectrum changes under strong uniaxial compression, Shubnikov-de Haas effect 77—28098
energy spectrum variation under strong uniaxial tension 79—73432
enstatite chondrite, Bi and Pb microdistribution obs. 80—62085
entropy of fusion, vibr. contrib. 77—47601
epitaxial film, magnetoresist., EM meas. in mag. fields up to 85 kG 77—32095
epitaxial film, twinning, electron diffr. 77—35838
epitaxial films, grain boundary struct., electron microscopy obs. *(Russian)* 79—46671
epitaxial films, size effect in elec. props. 80—54813
epitaxial growth, decoration of Sb surface 79—28227
evaporated film, internal friction 77—7998
excitonic phase in strong mag. field, sound absorption 77—20243
failure under hydrostatic press., kinetics 78—52944
Faraday effect, in vapour, P-invariance in M1 transitions, calc. 78—82805
Fermi energy, quantum variations, freq. mixing of de Haas-van Alphen oscills. 77—80721
Fermi surface, $2^1/_2$ order electron phase transition under extension *(Russian)* 78—75981
Fermi surface, change in connectivity under press. 79—73431
Fermi surface changes due to strong elastic tensile strains *(Russian)* 77—85133
filament, size-quantized, magnetoresist. oscills. 78—19062
film, adatom surface diffusion at low temps., elec. resist. study *(French)* 80—65376
film, amorphous, temp. dependence of SAW attenuation 80—75679
film, automatic fabrication and simultaneous computer-controlled measurement equipment 79—69984
film, carrier conc. and mobility, resist., galvanomag. and thermoelec. meas. 78—52111
film, charge carrier scatt. *(Russian)* 78—80079
film, cryst., orientation dependence on substrate struct. 77—1335
film, deposition props. on specially prepared substrate, desorption energy and surface diffusion 79—90917
film, elec. cond., obs. of epitaxial growth mechanism *(French)* 78—84329
film, ellipsometric obs. of optical props. 79—78776
film, evaporated, elect. and elastoresistance props. 79—33367
film, evaporated, lattice distortion spectrum, elec. resistance temp. variation 80—54806
film, evaporated, nuclei size distrib. 77—11802
film, evaporated on W, work function obs. by field emission method 78—6834
film, granular, enhancement of laser machining and ageing characts., using $Mg_{0.25}In_{0.75}$ sensitising layer 77—62020
film, Hall effect, magnetoresist., resist. and TCR 78—2589
film, high density direct read after write recording 77—38818
film, high-mobility, quantum size effects, struct. and kinetic characts. improvement 79—91174
film, in mag. field up to 40 kOe, microwave skin effect 77—12032
film, influence of target texture on backscatt. yield of 2 MeV ^4He particles 79—4875
film, initial stages of growth and orienation, TEM study 79—28237
film, kinetic props. of electrons, resist., cond., magnetoresist., Hall effect 77—63011
film, laser beam hole machining 80—30207
film, on Sb_2Te_3, mean scatt. length of low energy electrons meas. 77—36370
film, on Si(111) substrate, MBE deposition kinetics 80—10817
film, optical, magneto-optical and struct. props. 77—1664

bismuth continued
film, optical props., inverse problem of phenomenological theory 79−43053
film, optical props. as function of wavelength *(Russian)* 78−52591
film, orientation on mica, effect of deposition parameters 77−28085
film, oxidation, UPS, valence band, cond. band and 5d core states 77−20995
film, oxidation kinetics and interfacial bonding using final states 77−56127
film, oxidation process rel. to X-ray diffraction *(Japanese)* 79−29273
film, polycrystalline, elec. resistivity, thickness depend., temp. coeff. 78−14839
film, quantum size effect, electric field effect, Thomas-Fermi approx. energy surfaces, cond. 78−47890
film, quantum size effect and band struct. Bi-dielec.-metal system 80−54811
film, quench-condensed, disorder effect on optical cond. and band struct. 77−1746
film, refractive index determ. using Rayleigh-Lowe refractometer 80−7427
film, resistivity, rel. to thickness 80−107928
film, single layer and multilayer systems, thickness determ. by X-ray fluoresc. 80−68180
film, size effect of carrier heating, surface scatt. *(Russian)* 80−100474
film, size effect on electrical cond. 78−84331
film, structural evolution 8 to 573K, supercooling effects *(French)* 79−90921
film, structure and elec. props. 77−1339
film, structure and electronic props. 80−70562
film, supercooling, exam. by electron diffr. and electron microscopy *(French)* 78−14636
film, surface defects and struct., electron microscopy and elec. props. *(French)* 80−15415
film, thermoelec. power in transverse mag. field *(French)* 78−23183
film, transparency meas. in mag. field, electronic isoenergetic surface cross section *(Russian)* 79−47532
film, transverse mag. field depend. of thermoelec. power *(French)* 78−2587
film, ultrathin, crit. mag. fields *(Russian)* 78−23214
film, vap. deposited, effect of deposition parameters and substrate condition on crystallinity 78−10290
film, X-ray diffr. anal., {001} textured growth 78−72016
film A1-type supercond. vapour-quenched transition temp., A7-type phase transition 78−52145
film deposition by vacuum evaporation on $NaNO_3$ single cryst. cleavage 80−35091
film photopot detector characteristics for adaptive optical systems 79−59741
films, resistance changes due to bombardment by N, C, or Ar ions 80−103670
foil, splat quenched, preferred orientation 80−40381
foil, traversed by $H^+(He^+)$, energy loss and straggling meas. 78−95100
foil pressure transducer, determ. normal stress components in solid state high pressure test cell 80−73378
fused, solubility of GaP, thermodynamics, rel. to epitaxial growth 78−34721
fusion reactor molten-salt blanket, effect of Pb and Bi neutron multiplication zones on the fission rates of ^{232}Th and ^{235}U 80−99272
galvanomagnetic wave propag. obs. *(Russian)* 79−33301
galvanothermomagnetic instability 80−49785
galvanothermomagnetic refrigerating element, cooling mechanism *(Russian)* 77−26308
gas-liquid type transform. and sound attenuation in strong mag. fields, electron-hole correl. effects 80−88598
germanate glass:Bi^{3+}, time-resolved spectra, radiative and nonradiative processes 79−47501
germanate glass:Bi^{3+},Eu^{3+}, time resolved spectra for Bi-Eu energy transfer 79−33748
giant negative phonon drag thermopower, pure sample 77−76851
giant quantum attenuation anomalies of sound waves at high mag. field, temp. and freq. depend. 80−70587
giant quantum attenuation of sound, anomalous temp. depend. 77−76728
giant quantum attenuation of sound due to electronic phase transitions 79−60718
giant quantum attnuation anomalies of sound waves at high mag. field, extra attenuation peaks 80−70588
grain boundary scattering effect on temp. depend. of electroresistivity, galvanomagnetic effect *(Russian)* 78−56148
growth of single cryst. wires with high resistivity ratios 78−68622
Gruneisen parameter, high press. phase transitions 79−60467
Hall effect and helicon resonance at high magnetic fields 79−60861
helical wave instability, spatial amplification regime 77−24580
HF EM wave propagation in Voigt configuration 78−68045
hole pocket, far-IR magnetospectroscopy, electron-electron interaction effects 77−77211
hole relaxation time, temp. depend. 79−47108
impurity, effect on morphology and growth mechanism of vapour grown crysts. 79−23546
impurity content, neutron activation anal. by short lived isotopes *(Russian)* 77−40616
impurity diffusion of Rb, Sr, Ba, Cs 79−77819
impurity distribution in Si, planar oscills. effects, low angle backscatt. obs. 78−34534
impurity dopant incorporation and diffusion during MPE growth of IV-VI semiconductors 79−66012
interface with He I, transient heat transfer 77−85123
interlattice displacement and second-order elastic consts. 80−34121
intervalley scatt. influence on mobilities, thermopower calc. 78−26866
intervalley scattering processes, surface struct., transverse electron focusing study *(Russian)* 80−84352
intravalley electron-phonon scatt. non parabolicity, thermoelectric power 79−99539
ion scattering, low energy $^4He^+$ scatt. yield, ang. and energy depend. 78−27361
island films, effect of surface press. on lattice spacings 79−11045
Landau level spin splitting factor, US exam. 77−20281
laser, pulse stimulated emission of 472.2 nm line 78−17920
laser, pulsed, stimulated emission mechanism at 472.2 nm 80−19022
lightly doped, superconductivity, resist. obs. 78−64160
liquid, collective motions, cold neutron scatt. obs. 78−67639

bismuth continued
liquid, coordination numbers, calc. in microinhomogeneous struct. model *(Russian)* 80−38902
liquid, diffusion of Sb, 713-853K *(Russian)* 77−15611
liquid, elec. cond. and assoc. optical scattering 78−76040
liquid, electrical resistivity with spin-orbit scatt. 78−64018
liquid, electron component of entropy *(Russian)* 79−23747
liquid, environment for wear resistance testing of carbon steels and Armco iron *(Russian)* 77−59941
liquid, eqn. of state parameters rel. to Earth core energetics 77−15536
liquid, field ion source emission characts. 80−74059
liquid, in fused alkali chloride binary mixtures, electrocapillary phenomena 77−40553
liquid, in fused KCl-KBr mixtures, electrocapillary phenomena 77−40554
liquid, interference functions by double hard sphere model 80−49090
liquid, pure, surface tension meas. *(German)* 77−35799
liquid, struct. factor, interat. interaction pot., X-ray diffr. obs., 280-800°C *(Russian)* 78−14270
liquid, structure factor shoulders and interatomic pot. rel. to electron theory 77−7658
liquid, US vel. and thermophysical props. meas., 500-1000K 78−38778
liquid and solid, UPS, optical densities of states 80−2924
liquid effect on short time strength of Nb based alloy *(Russian)* 77−25186
longitudinal thermomagnetic amplifier 77−47838
magnetic field dependent electron and hole scatt., quantum limit 77−15878
magneto-quantum oscillations obs., new method 77−62946
magneto-thermopower, weak-field, implication for scatt. mech. 80−49790
magnetoacoustic attenuation, line shape anal. 80−2429
magnetoacoustic attenuation, tilt effect 79−91106
magnetoacoustic attenuation peak at low temp. 79−91105
magnetoplasma effects at 300 GHz in Voigt configuration 80−39619
magnetoplasma waves, freq. doubling in propag. 79−28367
magnetoplasma waves at 9 to 100 GHz microwave freqs. 79−78127
magnetoplasma waves in strong mag. fields at 300 GHz 79−38116
magnetoreflectance, L-pt. band parameters 80−25344
magnetoreflection of circularly polarised IR radiation, band struct. 77−52094
magnetoreflection spectra, reson. Landau level transitions 77−52096
magnetoreflectivity in high fields under press., energy band parameters 79−61346
magnetoresistance, high temp. oscills, props. *(Russian)* 80−65606
magnetoresistance high-temp. oscills. rel. to Fermi surface *(Russian)* 77−24570
magnetoresistance in high mag. fields *(Japanese)* 80−54720
magnetoresistance under phonon generation conditions 77−11940
magnetothermal EMF, twinned layer effect 80−49784
magnetotransport props. in quantising mag. fields 77−20340
melt-grown single crystal from Bridgman's method, triangular facet formation 80−28933
melting curve, effect by asymmetrical friction in piston-cylinder device 80−86292
metal cluster generator for gas-phase electron diffr., variation of microcryst. with size 78−63645
microcontact, resistivity at low temp. *(Russian)* 78−80054
microwave field induced instability 78−19076
microwave frequency shift associated with magnetosonic electric effect 79−60865
microwave magneto-absorption, NENP Cohen model 77−39766
molecular clusters, laser fluoresc. spectrosc. 80−95755
molecular laser, optically pumped, review 80−58519
molecule, radiative lifetime and self-quenching cross sections meas. from laser induced fluorescence expt. 80−69189
molten, density, surface tension, temp. depend. 77−69147
$muon^+$ diffusion, spin relax. temp. depend. *(Russian)* 77−48115
muonic Knight shift, temp. and mag. field depend. 79−91331
Nernst amplifier, feasibility with heat sink and magnet winding at liq. N_2 temp. 77−53932
neutron activation anal., mapping using ^{210}Po α-particle tracks 78−20129
neutron activation anal. of Hg and Au 79−57336
neutron radiation defects 78−47430
nonequilibrium phonons, negative differential cond., life time oscills. *(Russian)* 78−76117
nonlinear cyclotron resonance on EM wave irrad. *(Russian)* 79−73815
nonlinear properties under sound generation conditions 79−60845
optical phonon anharmonicity and melting, light scatt. study 80−60621
optical phonon temp. depend., Raman scatt. meas. 77−76509
oscillations with short periods of collector voltage for transverse focusing of electrons *(Russian)* 77−47837
overlayer on 2-dimens. $Bi_xSb_{2-x}Te_3$ cryst. interface props., UPS obs. 78−34881
oxidation, charge transfer obs. from final state changes 77−51703
oxidation kinetics 80−25914
oxide glasses with Bi or Se granules, elec. props. and microstructure 78−2490
parity non-conservation effect 80−68395
parity nonconservation, light polarisation plane deflection by components of ultrafine splitting *(Russian)* 78−46456
parity nonconservation effect *(Russian)* 80−77985
phase diagram, low-temp., using diamond anvil pressure cell and X-ray diffr. 78−1951
phase transformation due to high press. and shear stress 80−75357
phase transformation in high-press. chamber *(Russian)* 77−76544
phase transitions under high press. 80−96641
phonon density of states by neutron scatt., sp. ht. and Debye temp. 80−2132
phonon generation rate, nonreciprocity of current-voltage curve *(Russian)* 77−89776
phonon scattering by lattice defects, thermal cond. calc. for deformed cryst. 78−22802
phonon-drag low temperature thermoelectric refrigeration 80−22366
photodetector, fast-response thin-film, employing charge carrier photon entrainment 80−73462
photoionisation cross section of d-core level synchrotron radiation study of spin-orbit branching ratio 79−74057
photon drag of carriers, longit. EMF, 77.3-300K *(Russian)* 77−32048
pinch effect in solid-state plasma, review 77−1441

bismuth continued
- plasma echo for elliptic Fermi surface, echo coordinates *(Russian)* 80−44633
- plastic deformation, and stored energy of cold work of polycrystn. samples 79−43348
- plasticity at low temp., temp. effect on strain hardening, slip *(Russian)* 77−31713
- polymorphic transition up to 30 kbar, neutron diffr. investigation 79−14723
- positive muon diffusion mechanisms, zero field spin relax. studies as probe 80−34840
- positron annihilation parameters, temp. depend. 78−76553
- positron annihilation rates, electron-electron and electron-positron correl. effects 78−76548
- powder, sintering in air, glycerol or vacuum 79−91604
- powdered, mag. resistance *(German)* 79−28358
- powders, fine, precipitation on passivated electrodes 80−2977
- pressure measurement, I-II transition at 25°C, equipment 79−21763
- pulsed Ettingshausen cooling 78−91670
- quadrupole interaction of ^{69}Ge, TDPAD expts. 78−48089
- quantum photomagnetoelectric effect 77−72883
- quantum-EM excitations 80−88471
- quasimol, KX-ray spectra, Doppler shift 77−19044
- quench-condensed films, superconducting transition temp., elastic stress and strain effects 80−70883
- radioelectric effect in far IR 80−24967
- radiography, ^{209}Bi spatial distrib. on microscopic scale, ^{4}He 30 MeV ion beam 77−12859
- Raman conversion of XeCl-laser radiation in metal vapours, up to 40% efficient 79−23025
- recrystallisation, effect of Sb, Sn and Pb 78−52841
- resistivity at ultralow temp., high precision meas., scatt. mechanisms 77−80776
- rhombohedral crystals, slip dislocations and slip systems 79−23617
- semimetal-semiconductor transition in high mag. fields *(Japanese)* 80−50192
- shock loading and unloading, 293 and 473K 77−84840
- Shubnikov-de Haas effect *(Russian)* 79−7840
- Shubnikov-de Haas effect 79−28361
- Shubnikov-de Haas effect and Fermi surface under strong uniaxial deform. 77−43474
- Shubnikov-de Haas effect in high mag. fields 80−2404
- skipping electrons cyclotron resonance, electron-electron interaction parameter determ. 80−34351
- slip systems, crit. resolved shear stress 80−59470
- solid and liquid, positron annihilation temp. depend. 80−108296
- spheres, mean inner pot., elec. biprism and interf. electron microscopy 80−49063
- spin splitting factors of electrons for heavy mass directions 77−31935
- static skin effect 78−56177
- static skin effect *(Japanese)* 80−15555
- stationary I-U curve, falling portion under phonon generation conditions 79−15195
- strain hardening curve correlation with slip band nucleation stress spectra 80−70217
- substrate, epitaxial growth of Sb 78−95246
- superconducting amorphous film, Kosterlitz-Thouless transition 80−88699
- superconducting microbridge, high-resistance, with Bi crosspiece 80−93050
- superconducting modification obtained by impact compression *(Russian)* 80−93020
- superconducting transition temp., two-band model 80−25034
- superconducting ultrathin film, metastable, supercond. props. *(Russian)* 79−7917
- superconductor, A1-type, critical mag. field 79−69638
- superconductor, strong coupling, LF EM response function 78−10605
- superconduting film, critical temp., thermal equilibrium *(Russian)* 80−80438
- surface, (111) plane, chem. and thermal etch pit orientation, reactivity depend. 77−35559
- surface, anodic oxide film nucleation and growth 77−59966
- surface, laser irrad., press. pulse 79−24392
- surface detection of high mass cluster ions by SIMS and XPS surface monitoring 77−16442
- surface impedance change, reflected RF EM wave interaction *(Russian)* 80−49867
- surface potential under high mag. fields 78−26887
- texture of deformed polycryst. 77−59809
- thermal conductivity at ultralow temp. 79−1532
- thermal conductivity under plastic deform., phonon scatt. by dislocations and twin boundaries 77−11746
- thermal diffusivity by laser flash technique 78−6189
- thermal EMF giant quantum oscills. *(Russian)* 80−59960
- thermal neutron cross sections, in single crysts. 80−19672
- thermoelectric power, electronic thermal cond., in mag. field 80−60015
- thermoelectric power, influence of mag. field reversal, drift vel. method 77−69363
- thermomagnetic wave dispersion, propagation *(Russian)* 80−49696
- thermomagnetic waves obs. *(Russian)* 78−80008
- thermopower meas., 9K-40 mK 78−91673
- thin cylindrical monocrystal, dimens. oscills. of longitudinal magnetoresist. *(Russian)* 77−8124
- thin film, 1/f noise, boundary scatt. effect 80−49836
- thin single-crystal filaments in glass insulation 77−44147
- thin wire, resist. anomaly, possibility of one-dimensional quantum size effect 80−54809
- trace quantity determ. by atomic absorption spectroscopy with heated graphite atomizer 78−15749
- transport of spatially inhomogeneous current under mag. fields, dynamical props. 79−87082
- transverse magnetoresistance, field depend., static skin effect 79−11149
- trigonal, weak field thermomagnetic coefficients 77−72874
- twin shape variation under long period loads *(Russian)* 80−65007
- twinning dynamics of single crystal 77−4115
- US attenuation, annealed sample, 0.6 kbar, 25-120°C 78−47474
- US attenuation in strong mag. fields, electron-hole correlation effects 80−11049
- US propagation anomalies, under hydrostatic press. *(Russian)* 78−83884
- US velocity, renormalisation in mag. field 77−59246

bismuth continued
- US vibrations, damping under high hydrostatic press. 77−55324
- vacancy concentration, equilib., thermal expansion meas. 77−59007
- vacuum deposited film on LiF, surface failure induced by laser impulse *(Russian)* 77−35585
- vacuum deposited metal film, elec. field effect on residual struct. 78−51836
- valence bands in solid and liq. phases, XPS meas. 77−32504
- vapour, optical activity, Faraday effect, parity nonconservation, mag. transitions *(Russian)* 80−55070
- vapour, optical rot., parity nonconservation 80−23353
- vapour, optical rot., parity nonconservation expts. 80−23354
- vapour, parity violation in optical activity 79−26938
- vapour deposited on NaCl cleavages, crystallinity depend. on deposition parameters 78−63955
- vapour pressure calc. from transpiration expts. on Mg-Bi and Pb-Bi alloys 77−76571
- weak charge, SU(2)×U(1) model anal. 79−26281
- whiskers, de Haas van Alphen oscills, 4.2K, meas. using magnetometer 79−63284
- whiskers, elec. resist. under strain *(Russian)* 79−91164
- whiskers, electron transition on simple extension, elec. resist. and magnetoresist. meas. *(Russian)* 80−29422
- whiskers, excess 1/f noise, 50 to 350K 80−92951
- whiskers, hardness, elec. props. *(Russian)* 78−51874
- whiskers, persistent metallic behaviour, elec. resist. meas. 80−75544
- whiskers, thermopower, temp. depend., 77 to 300K phonon drag effect 79−82615
- wire, elastically bent, elec. resist. in mag. field 80−44568
- wire, field effect and magnetoresist., surface scatt. 77−43570
- X-ray absorption, discontinuities and limits, chem. combination effects 80−93435
- X-ray M_5 absorpt. limits 78−6812
- X-ray production by 9.5 to 41.8 MeV Fl ions, total L-shell cross-sections 77−85847
- XPS, electronic struct. 80−7464
- Young's modulus and internal friction, 20°C to melting point *(Russian)* 80−89278
- zone centre phonons and elastic consts., hydrostatic press. depend. 78−59905
- Al:Bi, anodic oxidation, mobility of foreign atoms 77−90494
- Al-Pb:Bi, tunnel-junction relax. oscillator, appl. to thermometry 79−85138
- AlSb-Bi system, molten, enthalpy change due to mixing *(German)* 79−86892
- As_2Se_3:Bi, annealing kinetics, cond. activation energy and density 79−73503
- BaS:Bi phosphors, polycrystalline, effect of grain size on thermolum. 79−61446
- Bi, $6p^3(^2D_{3/2}{}^0)$ and $6p^3(^2D_{5/2}{}^0)$, collisional deactivation 77−61702
- Bi (0001) surface, angle resolved UV photoemission spectra 77−66578
- Bi film, carrier conc., mobility and 1/f noise 80−44748
- Bi I, hyperfine struct. determ. 78−935
- Bi I, transition probabilities in 195-600 nm range 79−6898
- Bi II homologous ions series, Stark broadening trends 80−105157
- Bi II ion, relativistic effects in hyperfine splitting of second spectrum 80−23344
- Bi III, 4809.1 Å multipole line, hyperfine struct. splitting factor 77−68004
- Bi, radiative lifetimes of excited states 79−3410
- Bi V, relativistic oscill. strengths 77−14388
- Bi^-, photodetachment cross-section meas., crossed beam expt. 77−61723
- Bi^+, radiative lifetimes of excited states 79−3410
- Bi^{3+} activated phosphors, luminesc. characts. 80−2849
- Bi^{3+} desorption, Au (111) surface, struct. changes kinetics 80−54500
- Bi^{3+}, in soln., luminesc., halide ion effects 78−35187
- Bi^{3+} monolayers on Ag(111), two-dimens. phase formation, desorption obs. 77−15680
- Bi:garnet thick layers, regular domain structure, magnetooptical diffr. of light 80−108188
- Bi:N film, ion-implanted, struct., X-ray obs. 77−76692
- Bi:Sb, solid soln. struct., growth rate effects 77−52246
- Bi:Sn,Te, and undoped sample, low-temp. transport meas., electron scatt. 77−24551
- Bi:Sn(Pb), carrier dispersion law, Shubnikov-de Haas meas. 77−20345
- Bi:Sn(Pb)(Sb)(Te) polycrystal elastic constants for US velocity obs. 79−69180
- Bi:Te neutron radiation defects 78−47430
- Bi:Te(Sn,Sb,Pn), US attenuation meas. 80−92614
- Bi:Te(Sn) , elec. resist., 1.8 to 77K, electron-phonon scatt. mechanism 79−15144
- Bi:Tl(Sn)(Pb)(Ag), microhardness anisotropy 80−21079
- Bi/H_2O interface, halide ion adsorption parameters, zero charge pot. conc. depend. 80−40706
- Bi-barium stearate-Bi structs., internal voltage work function meas. 79−82684
- Bi-$Bi_{0.5}Sb_{1.5}Te$ system, stratified medium with artificial anisotropy, transverse cooling effect 79−28364
- Bi-Bi_2S_3 superlattice, elec. props. 78−10558
- Bi-$BiBr_3$ liquid system, miscibility gap, elec. cond. meas. 79−90790
- Bi-$BiCl_3(Br_3)(I_3)$ molten solution, US velocity and compressibility 77−84845
- Bi-BiI_3 mixture, molten, NMR meas. 77−51976
- Bi-$BiI_3(BiBr_3)$ liquid binary mixtures, phase separation under press. 80−34183
- Bi-BiO_2O_3 black layer, on polyvinylidene fluoride film, thermal diffusivity pyroelec. camera tube for IR imaging 80−57369
- Bi-MnBi, directionally solidified composite, processing parameter role on mag. props. 80−35352
- Bi-NbO_2-Bi system, Schottky barrier effects in transport and dielec. props. 80−29486
- Bi-Sb, bicrystal rearrangement of grid of nonconformity dislocations on (111) interface during heating 79−28215
- Bi-Sb film thermopiles for radiation pyrometry 78−214
- Bi-Sb interface, film, thermoelectricity, ageing differential efficiency *(German)* 78−60146
- Bi-SiO_2 cermet films, elec. and optical props. 79−78775
- Bi-Sn, superconductive microsegregations, 3.7K resist. drop 79−69646
- Bi-Te, combination freq. in Shubnikov-de Haas and surface impedance oscillations *(Russian)* 78−10476
- Bi-Te multilayer thin film struct. thermoelec. props. 80−92964

bismuth continued
Bi-YIG layer struct., Landau electron absorpt. mechanism, spin wave amplification 78−72344
Bi-Zn, light ion large angle scatt. in weakly screened Rutherford region 80−84823
Bi+H^{+}, L X-ray production cross sections, 0.3-1.8 MeV, expt. rel. to PWBA prediction 80−53115
Bi+H^{+}, L-shell ionis., 0.5-3.5 MeV, X-ray emission obs. 77−54528
Bi+Kr^{n+}, K-L level matching, X-ray obs. 79−63948
Bi+N, BiN form., IR matrix spectra, comparison with group V nitrenes 80−18853
Bi+NF, near-resonant electronic energy transfer, surface-hopping model 79−86030
Bi+NF(a$^{1}\Delta$), near-reson. electronic energy transfer, rate const. and cross-section meas. 79−18273
Bi$_2$, in Ar matrix, electronic states, vis. and near IR absorption spectra 78−5213
Bi$_2$, optically pumped CW dimer lasers 80−14322
Bi$_2$, optically pumped continuous laser oscill. 79−933
Bi$_2$, three photon excitation, Bi Rydberg series 80−106280
Bi$_2$, vap., optically pumped, laser action 78−71081
Bi$_4$, relativistically parameterized extended Huckel theory 79−49924
BiI, multiconfiguration Dirac-Fock calc. of 6p^{3}, 6p^{2}7s, and 6s6p^{4} configurations 79−3374
Bi$_2$O$_3$/Bi^{+}/electrolyte system, field and temp. depend. of electronic current 80−66814
^{207}Bi optical HFS intensity profile for nuclear spin determ. 77−54619
^{209}Bi, hyperfine struct., relativistic matrix element determ. 77−42251
^{209}Bi I, tunable CW dye laser spectroscopy, energy levels, lifetimes and hyperfine struct. 79−6905
^{209}Bi, pionic 4f→3d transition, pionic 3d state strong interaction level shift and width 79−98251
^{209}Bi, transitions, parity nonconservation due to neutral weak currents 77−13913
^{209}Bi+^{209}Bi collisions, 1 GeV, mol. orbital X-rays 79−49978
^{209}Bi→Pb, electron capture decay, LL-vacancy production by KLl Auger transitions 77−18832
^{210}Bi, determ. in human urine by direct extraction by Ni foil 79−100707
^{210}Bi, separation from ^{210}Pb, radiochem. determ. 77−56266
^{210}Bi, separation from ^{210}Pb, using silica gel ion exchanger 78−86961
^{210}Bi→^{210}Po→^{206}Pb, decay chain, L-shell ionisation investig., X-ray emission during β, α decay 77−18891
Bi(6^{4}S$_{3/2}$)+acetylene(ethylene), absolute rate consts., time-resolved reson. fluoresc. meas. 78−27731
CaLaGaO$_4$:Bi^{3+}, luminesc. of α- and β-phases 77−90186
CaLaGaO$_4$:Eu^{3+},Bi^{3+}, luminesc. influenced by struct. transition 78−6773
CaO:Bi surface, O$_2$ chemisorpt., positive ion emission determ. 80−92785
CaO:Bi^{3+}, impurity centres vibronic spectra, lattice dynamics and electron-phonon interactions 80−7396
Ca$_2$O:Bi, positive ion nonequilibrium emission in heterogeneous chemical reaction, mass spectra 80−55277
CaO(S):Bi^{3+}, luminesc. 77−73166
CaS:Bi, Tm, phosphor sensitisation mechanism, energy transfer 78−60507
CaS:Bi,Dy phosphors, thermoluminesc. 77−69921
CaS:Bi as UV dosimeter 80−34991
CaS:Bi phosphors, UV dosimetry by thermolum. 80−55199
CaS:Bi^{3+}, Pd^{2+}, phosphor, electroluminesc., brightness and mechanism 77−48248
CaS:Bl^{3+},Na^{+}(Li^{+}) phosphors, luminescence of associated centres *(French)* 80−40155
CaS-Bi, Mn, phosphors, thermoluminesc., phosphoresc. 78−2928
CaSO$_4$:Bi, cryst. growth, luminesc. props. 77−58993
CdI$_2$:Bi^{3+}, luminesc. *(Russian)* 78−2913
CdP$_2$:Bi,Zn, photolum. and photocurrent stationary characts. 78−27317
CdS:Bi film, implantation and post annealing, superlinearity 78−52028
CdS:Bi film, spectral response characts. 78−2512
CdS:N, P, As, Sb, Bi photoluminescence obs. 78−10965
Cs-Bi vapour saturated semiconducting film on collector, thermo-emission characts. *(Russian)* 78−23577
Cs$_2$NaYCl$_6$:Bi^{3+}, luminesc., cryst. growth, Stockberger method 79−8174
Cs$_2$NaYCl$_6$:Bi^{3+}, luminescence props., emission and excitation spectra 80−108262
Cs$_2$O-B$_2$O$_3$:Bi^{3+} glass, optical basicity, variation with probe ion and comp. 80−2800
Fe:Bi, impurity site distrib., channelling and nucl. orientation obs. 77−15447
Fe$_2$(MoO$_4$)$_3$:Bi, chemical, struct. and catalytic modifications 77−86362
GaP:Bi, gap vibrs. and impurity conc. determ. 79−69869
GaP:Bi, luminesc. decay kinetics 79−38646
GaP:Bi,N, photoluminesc., electroluminesc., 4.2 to 300K, excitons and hole traps 80−108275
GaSb-Bi system, molten, enthalpy change due to mixing *(German)* 79−86892
GdBO$_3$:Bi^{3+},Eu^{3+}, vacuum UV excitation spectra and quantum efficiencies 79−28811
GdB$_3$O$_6$:Bi^{3+}, Tb^{3+}, energy transfer from sensitiser to activator, intermediate role of Gd^{3+} 80−50389
GdPO$_4$:Bi^{3+}, Dy^{3+}, energy transfer from sensitiser to activator, intermediate role of Gd^{3+} 80−50389
Ge:Bi, donor bound exciton luminesc. and absorpt. 80−29777
Ge:Bi, γ-irrad., carrier trapping and recomb. at point radiation defects 80−107810
n-Ge:Bi, irradiated with fast electrons at 77K, investigation of 300K annealing stage 79−51155
n-Ge:Bi,O, plastically deformed, dislocation scatt. anisotropy, effect of state of O in Cottrell atm. 78−19028
H, and He, stopping powers meas. 80−42904
HCl:Bi^{3+} solution, characts. of luminesc. spectra, 82 to 130K *(Russian)* 79−28835
HCl:Bi^{3+} solution, kinetics and struct. of luminesc. spectra *(Russian)* 77−77290
HCl-Bi^{3+} soln., luminesc., quantum yield and lifetime *(Russian)* 79−33834
In$_{1-x}$Al$_x$P:Bi, radiative recombination at isoelectronic centres 79−52027
In$_{1-x}$Ga$_x$P:Bi, radiative recombination at isoelectronic centres 79−52027
InP:Bi, isoelectronic impurity states, emission and absorpt. obs. 79−42491
InP:Bi, uniaxial stress effect on free and Bi-bound excitons 79−56854
InSb-Bi, thermodynamic props. *(German)* 78−75847

bismuth continued
InSb-Bi system, molten, enthalpy change due to mixing *(German)* 79−86892
K$_2$O-BaO-GeO$_2$:Bi^{3+}, Nd^{3+}, absorpt. and excitation spectra, fluoresc. 77−90183
LaPO$_4$:Bi, fluoresc. props., blue emission mechanism 79−52002
Li$_2$O-B$_2$O$_3$:Bi^{3+} glass, optical basicity, variation with probe ion and comp. 80−2800
LiScO$_2$:Bi^{3+}, luminesc., vibr. struct. 79−33790
LiTiZn ferrites, elec. resist., mag. props., effect of Bi addition 78−95474
NaCl:Bi^{3+}, complex form. in soln., absorpt. spectra 77−28591
NaLnO$_2$:Bi^{3+}, (Ln=La, Gd, Sc), luminesc., vibr. struct. 79−33790
Ni:Bi, impurity site distrib., channelling and nucl. orientation obs. 77−15447
Pb:Bi, type II superconducting film, penetration depth meas. 77−28285
Pb/PbF$_2$/BiF$_3$/Bi thin solid film reversible galvanic cell 79−52928
Pb$_{1-x}$Sn$_x$Te:Bi film, polycryst., struct., elec., optical props. 79−42542
PbTe:Bi, thermoelec. props., thermal and elec. cond. 79−82616
n-PbTe:Bi thermoelectric props., 300-750K 78−34851
PbTe:Bi-PbSmTe-PbTe, epitaxial laser struct., growth, p-n junction position and lasing region 79−89908
Se-Bi bilayers chemical reactions, differential scanning calorimetry technique and obs. results 78−2398
Si:B standards, ion implanted, absolute Rutherford backscatt. yields, accuracy 79−47572
Si:Bi, dopant solubility limit, laser irrad. effects 80−84295
Si:Bi, high resolution study of group V impurities absorption 80−7388
Si:Bi, ion implantation and pulsed laser annealing, supersat. alloy form. 80−54267
Si:Bi, ion implanted, annealing of heavy ion cascade damage, channelling meas. 80−89255
Si:Bi, ion implanted, channelling obs. of pulsed Q-switched ruby laser annealing 80−59542
Si:Bi, ion-implanted, solid phase epitaxial growth during annealing, supersaturated solid soln. form. 80−103384
Si:Bi, luminescence associated with transitions from bound exciton excited states 78−23534
Si:Bi(,As), optical polarisation of ^{29}Si nuclei, nucl. relax. due to optical pumping 80−2665
Si:Mn,Bi, standard, doubly implanted, Rutherford backscattering meas. at MeV energies, screening corrections 80−88204
Si(Bi), elimination of He^{+} beam effect on channelling dips 80−54292
SrO:Bi^{3+}, impurity centres vibronic spectra, lattice dynamics and electron-phonon interactions 80−7396
Te:Bi, impurity spectroscopy 80−65499
Te:Bi, photoconductivity in strong mag. fields, doping effects, impurity levels 80−75602
Te-Bi, thin film system, stress-relief appearance conditions 80−65416
Xe+Bi, Bi Kα X-ray lines, Doppler broadening 78−62759
^{136}Xe+Bi, 625 MeV, probability of forming 1sσ vacancies 78−25681
YAl$_3$B$_4$O$_{12}$:Bi^{3+}, luminesc., vibr. struct., energy transfer 79−38584
YBO$_3$:Bi^{3+},Eu^{3+}, vacuum UV excitation spectra and quantum efficiencies 79−28811
YVO$_4$:Bi^{3+}, absorpt. and emission props., excitons 79−38592
ZnTe:Bi, laser annealing, channelling, reflectivity spectra 80−66215

bismuth alloys
see also bismuth compounds
Bi-Ni base alloys, heterogeneous, supercond., magnetisation meas. *(French)* 78−6477
bounded semimetals, phonon two-stage drag of electrons, thermoelectric power, scatt. mechanism 80−92919
electron scattering rates, mag. field depend., de Haas-van Alphen meas. 78−10436
liquid amalgams mixing, excess entropy, vibr. contrib. *(Russian)* 79−51263
rare earth monobismuthides, LCAO calc., electronic struct. *(Russian)* 77−39777
semicond. alloy, spin splitting and effective g-factor of T-holes *(Russian)* 77−51643
Wood's alloy, liq. enthalpy effects when solute is added 80−39314
Ag-Bi, dil., elec. quadrupole interactions on ^{111}Cd probe nuclei, time differential PAC meas. 78−15066
Ag-Bi, discrete eutectic form. mechanism *(Russian)* 77−66634
Ag-Bi, liq. alloys, thermodynamic investigation 80−70428
Ag-Bi, liquid alloy, thermoelectric power and magnetic susceptibility 77−8076
Ag-Bi, melt, crystal growth of Ag, conditions for transition from round to face forms *(Russian)* 79−28906
Ag-Bi, metastable phases *(German)* 77−16543
Ag-Bi (0.2 at.%), grain boundary energy and struct., solute atom effects 77−47465
Ag-Bi-Tl, system calculated from optimised binary boundary systems *(German)* 77−16545
Al-Al-PbBi double tunnel junction structs., quasiparticle relax. times, energy and temp. depend. 79−56412
Al-Bi, containing low melting point inclusions, impact props., temp. depend. 78−60792
Al-Bi, monotectic system, rapid cooling from melt, effect on struct. *(Russian)* 79−70053
Al-Bi, rapid quenching, struct. and decomp. 80−76244
Al-Bi liquid alloy, surface tension and surface adsorpt. determ. *(French)* 79−69325
Al-Bi-(Fe), directionally solidified monotectic, growth parameters for aligned microstructs. 79−43236
Al-Bi(Cd)(Pb)-Ti, containing low-melting pt. inclusions, mech. props. 80−93632
Al-Mg-Bi -Na, Bi additions to prevent Na embrittlement 77−86153
Al-PbBi superconducting tunnel junction as phonon spectrometer 78−47477
AlBi, X-ray fluorescence analysis *(Japanese)* 78−88663
Au-Bi, elec. resist. in liquid and solid state *(Russian)* 79−51549
Au-Bi, liq. alloys, Bi activities, ht. of mixing 77−4921
Bi:Sb, semimetallic alloy, microwave spectroscopy 78−87908
Bi-Cd, liq., Hall coeffs. 78−14711
Bi-Cd, solidification in mag. field, crystallite obs. *(Russian)* 77−4770
Bi-Cd eutectic alloy, directionally solidified, contact melting kinetics, mass transfer during solidification *(Russian)* 77−52310
Bi-Cd-Sb, calc. of phase equilibria using thermodynamic values from different models 78−60646
Bi-Cd(Sn), eutectic, contact melting kinetics *(Russian)* 80−70377

bismuth alloys continued
- Bi-Cd(Zn) *(Russian)* 80—39561
- Bi-Cu, liquid, interstitial index, definition and variation with temp. *(French)* 80—2011
- Bi-Cu, molten, struct., cold neutron scatt. in region of small momentum transfer 77—39527
- Bi-Cu, molten, struct., thermal neutron diffr. meas. 77—39526
- Bi-Cu melts, struct., neutron scatt., conc. of segregated regions calc. 77—39528
- Bi-Gd(Th) systems, heats of form. 80—89517
- Bi-In, dilute, oxidation kinetics 80—25914
- Bi-In, liq., Hall coeffs. 78—14711
- Bi-Mn, dil. liq. alloy, static and dynamic props. of localised Mn moments 79—82755
- Bi-MnBi, directionally solidified composite, processing parameter role on mag. props. 80—35352
- Bi-MnBi, mag. props. singularities, electron microscope exam. *(Russian)* 78—39363
- Bi-MnBi directionally solidified eutectic alloys, struct. and mag. props. 79—51815
- Bi-MnBi eutectic, directional crystallisation and microstruct. *(Russian)* 77—55915
- Bi-MnBi eutectic composites, microstructure and mag. props., annealing effect 79—82827
- Bi-MnBi eutectic region, of Bi-Mn phase diagram 80—81034
- Bi-Pb, complex-regular eutectics, structural modification 78—23695
- Bi-Pb, dilute, electrical cond. and thermal EMF at press. up to 12 kbar 77—47806
- Bi-Pb, dilute, oxidation kinetics 80—25914
- Bi-Pb, supercond. crit. temp., effects of press. up to 30 kbar. *(Russian)* 77—20484
- Bi-Pb amorphous alloys, superconductivity and the very strong electron-phonon interaction *(Japanese)* 79—95552
- Bi-Pb-Hg, liquid, surface tension and density *(Russian)* 77—55418
- Bi-Pb-Sn, eutectic alloys, struct. instability and absence of superplasticity *(Russian)* 77—8882
- Bi-Pb-Sn, molten metallic system, contribution to sign inversion of effective charge *(Czech)* 78—60656
- Bi-Sb, conditions for dendritic crystallisation, accompanying rapid cooling *(Russian)* 79—34020
- Bi-Sb, crack appearance in diffusion zones *(Russian)* 78—76727
- Bi-Sb, cryst., hopper growth 78—18564
- Bi-Sb, crystallisation temp., overcooling temp. *(Russian)* 80—97472
- Bi-Sb, dil., mag. field depend. electron scatt. rates, de Haas-van Alphen meas. 78—10436
- Bi-Sb, dil., magnetothermal oscillation and spin splitting of electrons 78—43362
- Bi-Sb, dilute, oxidation kinetics 80—25914
- Bi-Sb, film, elec. resist., magnetoresist., Hall coeff., 4.2K, conc. depend., anomalous size effect *(Russian)* 77—89884
- Bi-Sb, magnetic susceptibility, 4.2 to 270K, field and band parameter depend. 77—36051
- Bi-Sb, magnetoplasma waves in strong mag. fields at 300 GHz 79—38116
- Bi-Sb, magnetoresist. in high mag. fields *(Japanese)* 80—54720
- Bi-Sb, melts, interdiffusion, long capillary method and electron probe obs. 77—89563
- Bi-Sb, semiconducting, lattice dielec. const., comp. depend. 80—39516
- Bi-Sb, semiconductor-semimetal transition under pressure 78—34870
- Bi-Sb, semimetallic, magnetoplasma effects at 300 GHz in Voigt configuration 80—39619
- Bi-Sb, semimetallic alloy, cyclotron reson. and quantum oscillations 77—28096
- Bi-Sb, Shubnikov-de Haas effect and semimetal-semicond. transition in high mag. fields 80—44674
- Bi-Sb, single cryst., role of complexing agents on etching characts. 80—54238
- Bi-Sb, single cryst., semimetal-semicond. transition. cond. 77—1459
- Bi-Sb, solid solns., thermoEMF in transverse mag. field 77—47841
- Bi-Sb, solidification, predicted vol. change 77—28802
- Bi-Sb, thermal EMF giant quantum oscills. *(Russian)* 80—59960
- Bi-Sb, thermoelectric figure of merit, direct meas. in transverse mag. field 78—10485
- Bi-Sb (0 to 6 at.%), semimetal, magnetoplasma waves at 9 to 100 GHz microwave freqs. 79—78127
- Bi-Sb (1 at.%) alloy single cryst. growth solid-liq. interface study 80—107073
- Bi-Sb (12 at.%), cryst. growth from melt, impurity distrib. control by electrotransfer method *(Russian)* 80—66418
- Bi-Sb (1.2-7 at.%) solid solns., microhardness of single crystals 77—28886
- Bi-Sb (5-12 at.%), single cryst. cleavage plane, microhardness parameters depend. 78—35486
- Bi-Sb (6 at.%) whiskers, persistent metallic behaviour, elec. resist. meas. 80—75544
- Bi-Sb alloy, magnetothermoelec. quality factor of single crystals 77—51771
- Bi-Sb alloy film, elec. props. *(Russian)* 79—11245
- Bi-Sb alloy films, quantum size effect *(Russian)* 77—85351
- Bi-Sb alloys, electron work function determ., contact pot. difference method 77—39920
- Bi-Sb alloys, magnetoacoustic attenuation, tilt effect 79—91106
- Bi-Sb alloys, metal-semimetal point contacts, volt-ampere characteristics *(Russian)* 80—65683
- Bi-Sb alloys, thermomagnetic quality factor 77—15882
- Bi-Sb film, amorphous nature, AC and DC cond. and Hall coeff. obs. 80—11114
- Bi-Sb film, tunnel conductivity, proximity effect *(Russian)* 79—51726
- Bi-Sb mixed cryst., zone melting crystn. parameters *(German)* 79—43140
- Bi-Sb solid soln., crystallisation in capillaries *(Russian)* 78—44006
- Bi-Sb solid soln., thermoelectric props., 80 to 300K *(Russian)* 78—43425
- Bi-Sb-Sn, Sn and Sb partition coeffs. during crystallisation 77—48394
- Bi-Sb-Te melt, Sb and Te distribution coeffs. during crystallisation *(Russian)* 80—93472
- Bi-Sb-Te system, epitaxial film prep. in closed-crucible 77—52230
- Bi-Sb(-As), band struct., effects of Sb and As, mag. susceptibility meas. *(Russian)* 80—65775
- γ-Bi-Se phase, electronic props. 77—43493
- Bi-Se system, high-temp. calorimetry *(French)* 77—44501

bismuth alloys continued
- Bi-Si, dil., mag. field depend. electron scatt. rates, de Haas-van Alphen meas. 78—10436
- Bi-Sn, complex-regular eutectics, structural modification 78—23695
- Bi-Sn, dil., superconductivity, resist. obs. 78—64160
- Bi-Sn, dilute, electrical cond. and thermal EMF at press. up to 12 kbar 77—47806
- Bi-Sn, dilute, oxidation kinetics 80—25914
- Bi-Sn, hydrostatic press. effect on band struct., thermoelec. power meas. 79—69406
- Bi-Sn, liq., Hall coeffs. 78—14711
- Bi-Sn, maximum diamagnetism rel. to electron density 80—54865
- Bi-Sn, thermoelec. props. from 2 to 300K 80—24872
- Bi-Sn, thermopower from 50 mK to 25K 80—24880
- Bi-Sn melt structure, radial distrib. function of atoms, anal. *(Russian)* 80—14995
- Bi-Sn(Pb), liq., conc. and temp. depend. nucl. relax. rates meas. 78—19357
- Bi-Te, dil., superconductivity, resist. obs. 78—64160
- Bi-Te, dil. alloy, elec. cond. depend. on Te conc. *(Russian)* 78—76042
- Bi-Te, dilute, oxidation kinetics 80—25914
- Bi-Te, electron isoenergetic surface, variation of connectivity under press. *(Russian)* 78—60050
- Bi-Te(Se), liq., diamag. susceptibility, semicond./metal behaviour 78—14927
- Bi-Tl, complex-regular eutectics, structural modification 78—23695
- Bi-Tl, dilute, oxidation kinetics 80—25914
- Bi-Tl, thermal cond., 1.5 to 50K, temp. depend. 78—26990
- Bi-Tl film, superconductivity and phonon spectrum *(Russian)* 79—91190
- Bi-Zn, liquid, interstitial index, definition and variation with temp. *(French)* 80—2011
- $BiIn_2$, dHvA effect, Fermi surface determ., free-electron model 77—15744
- BiMn, ferromag., nucl. orientation of Bi isotopes 78—13010
- BiMn, with ferromag. inclusions, magnetisation changes by US pulses 80—34732
- $Bi_{0.96}Mn_{0.04}$, powder particles, magnetisation 77—48014
- $Bi_{95.6}Mn_{4.4}$, magnetisation of ferromag. precipitates, effect of ultrasonic pulses 80—2121
- $Bi_{1-x}Pr_x$-Al oxide-Al tunnel junction, cryst. field struct. obs. in conductance 78—84358
- BiSb (>20 wt.%), electronic band struct. 80—107698
- BiSb, alloys, semimetallic, camera, dispersion relations 80—59854
- p-$Bi_{0.9}Sb_{0.1}$, Fermi surface anisotropy var. on press. induced transition to gapless state *(Russian)* 77—43483
- $Bi_{0.91}Sb_{0.09}$, magnetoresistance anisotropy in strong magnetic field 79—82613
- $Bi_{0.91}Sb_{0.09}$, thermomag. power in strong mag. field, temp. and field depend. 78—43421
- $Bi_{0.924}Sb_{0.076}$, doped, optical, oscillation and galvanometric effects *(Russian)* 77—85247
- $Bi_{0.925}Sb_{0.075}$, semiconductor-semimetal transition under tensile strain, Shubnikov-de Haas oscills. obs. 80—44678
- $Bi_{1-x}Sb_x$ alloy films, quantum resistance oscills. at low temps., surface band distortion *(Russian)* 80—11110
- $Bi_{1-x}Sb_x$, combination freq. in Shubnikov-de Haas and surface impedance oscillations *(Russian)* 78—10476
- $Bi_{1-x}Sb_x$, crystalline, vibrational, spectra, second order Raman scattering 79—47455
- $Bi_{1-x}Sb_x$, deformation calculations, band struct. variation, electron phase transitions due to deform. *(Russian)* 80—65137
- n-$Bi_{1-x}Sb_x$, determ. carrier dispersion relation parameters 79—38107
- $Bi_{1-x}Sb_x$ epitaxial layers, effect of film thickness on elec. props. *(Russian)* 79—11244
- $Bi_{1-x}Sb_x$ epitaxial thin films, galvanomag. props. in semimetal and semicond. regions 79—11254
- $Bi_{1-x}Sb_x$, far IR transmittance meas. *(Russian)* 77—44006
- $Bi_{1-x}Sb_x$ film, evaporated, cross-sectional struct., electron microscopy and replica technique study *(German)* 78—22977
- $Bi_{1-x}Sb_x$, growth by horizontal zone refining, low charge carrier conc. 77—21020
- $Bi_{1-x}Sb_x$, lattice dielec. const. from helicon wave propag. 77—47756
- $Bi_{1-x}Sb_x$, magnetoacoustic attenuation 80—2428
- $Bi_{1-x}Sb_x$, magnetoacoustic attenuation, line shape anal. 80—2429
- $Bi_{1-x}Sb_x$, magnetoresist., mag. field and ang. depend. 78—19063
- $Bi_{1-x}Sb_x$, reson. Landau level transitions, magnetorefl. 77—52096
- $Bi_{1-x}Sb_x$, semicond. alloy, mag. freeze-out effect, superlow temps. *(Russian)* 77—89775
- $Bi_{1-x}Sb_x$, semicond. alloy, EM wave propag. in direction perpendicular to mag. field 79—60687
- $Bi_{1-x}Sb_x$, semicond.-semimetal transition, temp. and press. depend. of transport props. 78—76120
- $Bi_{1-x}Sb_x$ semiconducting alloy, band struct. study, Shubnikov-de Haas effect *(Russian)* 80—80181
- $Bi_{1-x}Sb_x$, semimetallic, plasma effects, submm. wave expts. 77—35881
- $Bi_{1-x}Sb_x$, Shubnikov-de Haas effect, Abrikosov-Falkovskii treatment of Fermi surface anisotropy *(Russian)* 78—43285
- $Bi_{1-x}Sb_x$, sputtered thin films, first order Raman scatt. 79—69831
- $Bi_{1-x}Sb_x$, supercond. transition temp., press. depend., 30-80 kbar 77—8223
- $Bi_{1-x}Sb_x$, thin film, elec. props., composition variations *(Russian)* 79—7841
- $Bi_{1-x}Sb_x$ thin films, elec. props., 4.2-300K *(Russian)* 79—24087
- $Bi_{1-x}Sb_x$:Te(Sn), band struct., plasma refl. spectra and galvanomag. tensor 77—16315
- $Bi_{1-x}Sb_x$:Te(Sn), dispersion law of charge carriers *(Russian)* 79—87114
- $Bi_{100-x}Sb_x$, lattice dielec. const. meas. 78—10490
- $Bi_{100-x}Sb_x$, chem. microhomogeneities, topographical and electron beam microanalysis obs. 79—65206
- $Bi_{88}Sb_{12}$-Sn, current carrier energy spectrum *(Russian)* 78—60139
- $Bi_3Sr_{1-x}Eu_x$, supercond. and mag. ordering 78—56252
- Bi_2Te_3 alloy thermocouples for solar thermoelectric conversion 80—94095
- $Br_{1-x}Sb_x$, alloy wire, magnetoresistance in high longitudinal fields *(Russian)* 79—87113
- Cd-Bi, liq., US vel. and thermophysical props. meas., 500-1000K 78—38778
- Cd-Bi, molten, EMF meas. of liquid separation 78—39747
- Cd-Bi alloys, electron work function determ., contact pot. difference method 77—39920
- (Cd-Bi)-Sn, eutectic alloy, directionally solidified, contact melting kinetics, mass transfer during solidification *(Russian)* 77—52310

bismuth alloys continued
- Cd-Pb-Bi melt, enthalpies of form. *(Russian)* 79—51277
- Cd-Pb-Bi-Sn system, ternary liq. alloys, thermodynamic props. 78—51701
- Cd-Sn-Bi, appl. of computational techniques for treatment of thermodynamic data, phase diagram calc. 78—10172
- Ce-Bi, heat of formation, calorimetric meas. 78—44392
- Ce-Bi, liquid, solubility and thermodynamic props. *(Russian)* 78—19717
- CeBi, anisotropic mag. ordering and mag. structural transitions 79—78324
- CeBi, lattice distortion modes and mag. structural transitions 79—78325
- $Ce_x(La_{0.76}Y_{0.24})_{1-x}Bi$, mag. phase diagrams 79—56535
- $CeMn_2(Si_xGe_{1-x})_2$, $Ce(Mn_{1-x}B_x)_2Si_2$, (B=Fe, Cu) mag. props. 80—25134
- $Co_{80}B_{20}$, amorphous metal ribbon, stresses, magnetoelastic anisotropy and zero-field mag. domain struct. 80—44896
- Cu-Bi, embrittled grain boundary obs. using STEM, Cu-SiO_2 comparison 78—38730
- Cu-Bi, grain boundary struct. intergranular fracture, segregation role 80—66648
- Cu-Bi, grain boundary thickness obs. using electron diffr. techniques 80—79811
- Cu-Bi (0.0115 wt.%), embrittled, grain boundary faceting, TEM study 79—27998
- Cu-Bi (0.02 wt.%), intergranular fracture, Kossel X-ray diffr. in SEM obs. 80—108579
- Cu-Bi alloys, grain boundaries, electron microscopy 77—12694
- Cu-Bi alloys, grain boundary segregation 79—61596
- Cu-Bi foil, electron diffr. effects and images from inclined grain boundaries 79—82241
- Cu-Bi-Fe, Fe effects on embrittlement 77—28900
- Cu-Bi-(O)(S), evaporation of Bi in vacuum induction melting 77—28742
- Cu-Bi(Bi-O), stirred at different speeds under press., evaporation of Bi 77—47555
- Dy-Bi, heat of formation 77—86349
- Fe, cast, fused metal solidification enhancement using Bi and Te *(Italian)* 80—7540
- Fe, cast, Mg, despheroidising effect of Bi, Sn on graphite in alloy 78—56670
- Fe, cast, nodular graphite form. by Bi and Pb additions *(Japanese)* 77—63693
- $Fe_{81.5}B_{14.5}Si_4$, amorphous metal ribbon, stresses, magnetoelastic anisotropy and zero-field mag. domain struct. 80—44896
- $Fe_{4.7}Co_{70.3}Si_{15}B_{10}$, amorphous ferromag., roll mag. anisotropy 79—51773
- $Fe_5Co_{70}Si_{10}B_{15}$ amorphous magnetic alloy, decrease of permeability after demagnetisation, disaccommodation 80—39814
- $(Fe_{1-x}Ni_x)_{77}Si_{10}B_{13}$ amorphous alloy system, saturation mag. moment, Curie temp., mag. susceptibility 80—39753
- Ga-Bi, liquid binary alloys, magnetic susceptibility *(Russian)* 77—24671
- Ga-Bi liquid binary mixtures, phase separation under press. 80—34183
- GdFeBi, amorphous ferrimag. films, magneto-optical props., optical spectra 80—76008
- $(Gd_{1-x}Fe_x)_{1-y}Bi_y$ amorphous films, saturation magnetisation, Kerr and Faraday rotation 80—40093
- Hg-Bi, liquid dilute amalgams, elec. cond. and thermoelec. power 78—51976
- Hg-In-Bi, liquid alloy, elec. resist. *(Russian)* 79—51544
- In-Bi, dil., supercond., ideal superheating and supercooling limits 77—4465
- In-Bi, dil., supercond. penetration depth field depend. meas. 77—4464
- In-Bi, liq., PAC of ^{111}Cd 77—4584
- In-Bi, liq., spreading kinetics on Cu surface 80—10742
- In-Bi, mixed state, pinning centre distrib. statistics, I-V characts. *(Russian)* 80—100571
- In-Bi, single crystal, vacuum UV optical props. 77—1697
- In-Bi, single spheres, supercond. props. 79—73617
- In-Bi, small κ supercond., phase transitions higher than second order 80—88668
- In-Bi, supercond. crit. RF mag. field, rel. to superheating 78—2632
- In-Bi (2 at.%), supercond. film, thermal cond. in perpendicular mag. field 77—8229
- In-Bi (2-33.3 at.%), phase diagram DTA, X-ray diffr. and supercond. T_c meas. 79—38795
- In-Bi (22 at.%), directionally grown eutectic two phase superconductors, magnetisation behaviour 77—28293
- In-Bi (2.5 at.%), supercond. foils, transport current effect on magnetisation 79—56379
- In-Bi alloy system at high press. and temp. 78—92238
- InBi, anisotropy of temp. depend. elec. resist., 4.2-293K 78—43354
- InBi, Knight shift and quadrupole interaction of ^{115}In 77—55717
- InBi, quadrupole interaction precession frequency of ^{111}Cd, TDPAC meas. 77—16224
- In_2Bi, cryst. struct. and density *(German)* 80—24407
- In_2Bi, de Haas-van Alphen effect 78—91594
- In_2Bi, magnetisation curve, interpretation using boson formulation of supercond. 78—2619
- In_2Bi, pre-melting absorption of sound 80—88277
- In_2Bi, press.-induced supercond. phase transform. 79—24099
- In_2Bi, quadrupole interaction precession frequency of ^{111}Cd, TDPAC meas. 77—16224
- In_2Bi-In, thin lamellar eutectic strips, unidirectionally solidified, morphologic and crystallographic study *(French)* 77—55264
- In_2Bi-In(Bi) laminar eutectic alloy, SNS struct., Josephson behaviour *(French)* 78—26996
- InSb-Bi, metallic soln., quasibinary alloy, association 78—15373
- La-Bi, phase diagram, struct. of intermetallic compounds 77—44214
- Li-Bi, liq. semicond., electronic struct., resist. and thermoelec. power meas. 77—47712
- Li-Bi, liquid alloys, calorimetry study *(German)* 80—25664
- Li-Bi, molten, sorption of tritium, appl. as thermonuclear reactor material 77—1301
- Li-Bi, thermodynamic props., 355-600°C 78—34634
- Mg-Bi, liq., far IR reflectivity meas. 77—52105
- Mg-Bi, thermodynamic study vapour pressure measurement by transpiration 78—44395
- Mg-Bi (30 at.%), molten, short range order and partial struct. factor, neutron and X-ray diffr. 78—9941
- Mg-Bi alloy, liq., far IR reflectivity rel. to possible transport processes 78—2827
- Mg-Bi melt; X-ray and neutron diffr., conc. depend., correl. number and nearest neighbours 80—49091

bismuth alloys continued
- Mn-Bi, low-field magnetoresistance and domain drag 78—68014
- Mn-Bi, magnetically uniaxial, strongly uniaxial, discontinuous mag. reversal singularities *(Russian)* 77—48010
- Mn-Bi alloy, melting and solidification under microgravity, mag. props. *(German)* 80—45296
- Mn-Bi alloys, mag. props. improvement study *(Japanese)* 78—43617
- Mn-Bi eutectic alloy, mag. anisotropy 78—68220
- Mn-Bi film, amorphous, form. and crystn. 79—28923
- Mn-Bi film, negative transverse magnetoresist. in c-plane, domain wall effects 77—20465
- Mn-Bi film, with perpendicular anisotropy, galvanomag. props., hysteresis loops 77—20464
- Mn-Bi magneto-optic memory system 77—85511
- Mn-Bi mictomagnetic alloy, mag., elec. and elastic props. *(Russian)* 80—108028
- Mn-Cu-Bi ternary cpd. thin films for magneto-optic memory applic. *(Japanese)* 77—63238
- Mn-Cu-Ni-Bi, magneto-optic film for storage appl. 77—12165
- MnBi, domain boundaries shift, mag. reversal processes 79—87286
- MnBi, domain boundary inertia during mag. reversals *(Russian)* 80—88776
- MnBi film, electrical props., in situ annealing effect 80—65708
- MnBi film, ferromag., diffr. efficiency of mag. holograms, Faraday effect 77—32355
- MnBi film, hologram form. at 2.76 μm, using CaF_2:Er^{3+} crystal laser 79—10270
- MnBi film, magnetic hologram recording appl. *(Russian)* 77—1573
- MnBi film, magnetic reversal mechanism, hysteresis loops for polycryst. and single cryst. specimens *(Russian)* 78—60318
- MnBi film, on Al_2O_3, quantitative electron microprobe analysis 77—9150
- MnBi film, optical, magneto-optical and struct. props. 77—1664
- MnBi film, optical radiation spectral conversion 79—64344
- MnBi film anisotropy field intensity meas. by Faraday rotation *(Russian)* 77—12162
- MnBi film for recording optical information, analogue characts. *(Russian)* 78—50716
- MnBi films, prep. by ionised-cluster beam deposition technique, magnetooptical props. 80—100790
- MnBi films, stability of magneto-optical props. on pulse heating *(Russian)* 78—88282
- MnBi, ionized-cluster beam and reactive ionized-cluster beam deposition 80—16202
- MnBi, Kerr effect and TEM obs. of mag. domains 77—89974
- MnBi, mictomag. alloys, elastic props. *(Russian)* 80—7141
- MnBi particles, demagnetised, coercivity, remanence and magnetisation reversal 78—19281
- MnBi particles, effect of grinding on coercivity 77—36098
- MnBi, thin film, fine mag. domains, SEM obs. 79—24202
- MnBi, thin film, struct. and mag. props. 79—47315
- MnBi, two-phase coercive force for domain wall motion, mag. reversal nucleation mechanism *(Russian)* 77—48009
- MnBi-Bi garnet film structure, thermomag. information recording appls. *(Russian)* 78—23305
- MnBi-Bi garnet film struct., thermomagnetic recording 80—100588
- MnCuBi film, coated with SiO layer Kerr readout characts. 77—85509
- MnCuBi film, for mag. storage appl., prep. by RF sputtering, and props. 77—8369
- MnCuBi film, optical and magneto-optical props. 77—4695
- $MnCu_{1-x}Dy_xBi_{0.86}$ film, mag. and magneto-optic props., appl. as storage medium 77—8550
- Mn_2Sb, Bi-modified, mag. first order phase transition 79—51777
- $Mn_2Sb_{1-x}Bi_x$ $(0 \leq x \leq 0.175)$, mag. transition, thermal expansion, thermomag. effects and lattice constant changes *(Japanese)* 79—78375
- $Mn_{0.75}Ti_{0.25}Bi$ films as magnetooptic storage medium, mag. interferogram recording 78—19288
- Mo-Bi amorphous films, supercond. transition temp. and residual elec. resist. *(Russian)* 79—19680
- $Na_{1-x}Bi_x$ liq. alloys, metal-nonmetal transition, mag. susceptibility meas. 79—82525
- Ni-Bi dil., impurity effects on grain boundary mobility *(Polish)* 79—96073
- Pb/Bi-I-Al tunnel injected nonequilibrium supercond. struct., diffusive quasiparticle instability, multiple gap states 80—50005
- Pb-Bi, annular superconductor, field replication and flux shielding 77—28286
- Pb-Bi, creep, low-temp., thermal heating and quantum mechanisms, supercond. transition effects 80—79868
- Pb-Bi, dirty strong-coupling supercond., Ginzburg-Landau parameters, type II behaviour deviations 77—8249
- Pb-Bi, elastic moduli, internal friction from US velocity meas. 79—15717
- Pb-Bi, liq. calc. of electromigration forces and resist. 79—82572
- Pb-Bi, liquid alloy, chemical and intrinsic diffusion coeffs., exam. *(German)* 78—83987
- Pb-Bi, peritectic reaction, microstruct. changes 78—52753
- Pb-Bi, splat quenched, solubility limit, vacancy conc. and supercond. transition temp. 77—12046
- Pb-Bi, strength loss in supercond. transition, nonmag. and paramag. impurities influence *(Russian)* 80—70875
- Pb-Bi, strong coupling superconductor, LF EM response function 78—10605
- Pb-Bi, supercond., anomalous thermal cond., transition induced creep *(Russian)* 77—36020
- Pb-Bi, supercond., crit. mag. fields, influence of parameters 80—75691
- Pb-Bi, supercond. alloys, microwave surface resist., mag. field depend. *(French)* 77—24647
- Pb-Bi, supercond. T_c evaluation, from ab initio band struct. calcs. on Pb 80—75502
- Pb-Bi, supercond. tunnelling, effect of phase composition and press. 79—15261
- Pb-Bi, temp. regime of crystn. on rapid cooling *(Russian)* 80—66495
- Pb-Bi, thermodynamic props. 77—59743
- Pb-Bi, vacuum deposited supercond. films, T_c chem. comp. depend. *(Russian)* 78—19174
- Pb-Bi, X- and γ-ray attenuation obs. 79—61457
- Pb-Bi (12 at.%), Sn fibre reinforced type II superconductor, flux pinning *(German)* 77—85397
- Pb-Bi (4.1 at.%) solid soln., tetragonal distortion field for substitutional Bi atoms, neutron scatt. 78—51568
- Pb-Bi alloy, fine powder electrodeposition and X-ray struct. obs. 78—11163

bismuth alloys continued
Pb-Bi alloy, liq., thermal cond. and elec. resistance up to 900°C 77−47785
Pb-Bi alloy, vapour press., meas. using transpiration method, thermodynamic props. determ. 78−3365
Pb-Bi alloys, phonon-electron interaction, normal and supercond. state thermal cond. and elec. resist. meas. 79−60460
Pb-Bi amorphous films, supercond. transition temp. and residual elec. resist. *(Russian)* 79−19680
Pb-Bi counterelectrode Pb alloy Josephson junctions 80−65743
Pb-Bi eutectic alloy flow rate meas. apparatus 77−79412
Pb-Bi eutectic melt, in contact with Cu, mutual indentation *(Russian)* 77−59853
Pb-Bi film, amorphous and polycrystalline, specific heat meas. 77−80715
Pb-Bi liquid alloy, Pb and Bi diffusivities, temp. and conc. depend. *(German)* 80−84311
Pb-Bi molten alloys, density, surface tension, temp. depend. 77−69147
Pb-Bi-Tl, supercond., crit. mag. fields, influence of parameters 80−75691
Pb-Si superconducting solutions, effect of hydrostatic compression on tunnelling *(Russian)* 80−65746
Pb-Sn-Bi-Cd low melting point alloy block for organ shielding in radiotherapy *(Korean)* 80−36154
Pb-Sn(Bi) alloys, dil., impurity effects on softening at T_c *(Russian)* 78−23220
Pb-Tl-Bi-In, localised phonons studies by supercond. tunnelling 79−87210
PbBI-Al superconducting tunnel junctions, optically illuminated, quasiparticle energy distribution 80−75688
PbBi-AlO_x-Al tunnel junction, quasiparticle energy distrib. in nonequilib. supercond. 77−80881
$Pb_{0.9}Bi_{0.1}$, strong-coupled superconductor, quasiparticle recombination time 79−15259
$Pb_{0.98}Bi_{0.02}$-Cd, superconductor-normal-metal boundary resist., mag. field depend. 80−44772
$Pb_{0.99}Bi_{0.01}$, superconducting-normal interface, boundary resist. 80−50006
$Pb_{1-c}Bi_c$, liquid alloys, local fluctuations and quadrupolar relaxation 80−66060
$Pb_{55}Bi_{45}$ film, amorphous, supercond. energy gap and transition temp. 78−14866
Pb_xBi_{1-x}, quench-condensed films, superconducting transition temp., elastic stress and strain effects 80−70883
Pd-Pb-Bi supercond. alloy, X-ray, microscopic, thermographic anal. *(Russian)* 77−32106
PdBi, rhombic, cryst. struct. determ. *(German)* 79−77556
Pd_5Bi_2, cryst. struct. *(German)* 79−51053
Pd_2PbBi, and Pd_4PbBi_3, cryst. struct. *(German)* 79−94963
PtBi, XPS, electronic struct. 80−7464
$PtBi_2.h_3$, cryst. struct. *(German)* 80−107113
$PtPb_{0.7}Bi_{1.3}$, crystal structure *(German)* 80−84139
$PtPb_3Bi$, cryst. struct. *(German)* 78−59783
Pt_4PbBi_7, cryst. struct. *(German)* 80−107113
Sb-Bi, melting kinetics of solid soln. during high heating rates, superheating *(Russian)* 78−15358
Sb-Bi, X-ray diffr. investig. of high-press. polymorphism 77−43324
Sb-Bi (2%), medium-oriented, plastic deformation *(German)* 77−70109
Sb-Te-Bi, miscibility limits, computer study 78−79773
$Sb_{1-x}Bi_x$ alloys, Shubnikov-de Haas *(Russian)* 78−23007
Sb_2Te_3-Bi_2Te_3, low-temp. thermoelectric mats., growth of microhomogeneous crysts. 77−48337
Se-Bi, liquid alloys, vapour phase effect on activity determ. *(German)* 79−43210
Sn-Bi, atomic self-motions *(Rumanian)* 78−47226
Sn-Bi, crystal struct. and superconductivity after appl. of high press. and quenching 80−10531
Sn-Bi, crystallisation temp., overcooling temp. *(Russian)* 80−97472
Sn-Bi, eutectic, superplastic anisotropy *(German)* 80−25808
Sn-Bi, liq., US vel. and thermophysical props. meas., 500-1000K 78−38778
Sn-Bi, small κ supercond., phase transitions higher than second order 80−88668
Sn-Bi, supercooled, dendritic growth rates *(Russian)* 78−80533
Sn-Bi, temp. regime of crystn. on rapid cooling *(Russian)* 80−66495
Sn-Bi, thermal analysis in non-faceted/faceted eutectic systems 80−71637
Sn-Bi (up to 2.2 at.%) whisker, supercond. crit. temp., stress depend. 77−39988
Sn-Bi alloy, splat-quenched, energy dispersive X-ray diffr. 78−23728
Sn-Bi dilute alloys, thermo EMF *(Russian)* 79−33285
Sn-Bi fine alloy powder, electrodeposition, electrolyte comp. effect 80−7519
Sn-Pb-Bi, microduplex eutectic, cavitation during superplastic flow 78−48457
Sn-Pb-Bi-(Cd) infiltrated Ti base composite sintered bearing material, antifriction props. 80−60981
TbBi, mag. transitions, quadrupolar interaction effects 80−80512
Th-Bi-H, hydride form. and supercond. 77−36007
Ti-Bi, eutectoid decomposition 79−24491
Tl-Bi, liq., mag. susceptibility, MP to 1000°C, anomalies due to electron-ion interaction 77−20546
Tl-Bi system, phase transitions near Tl_3Bi, elec. props. meas. 80−35181
Tl-Bi-Hg alloys, phase diagrams and equilib. *(Russian)* 79−52166
Tl-Bi-Pb, phonon anomaly near Fermi surface topological transition, phonon softening at X point 78−95120
Tl-Pb-Bi, critical field and specific heat 79−73631
Tl-Pb-Bi, supercond., electronic density of states from heat capacity meas. 79−56383
Tl-Sn-Bi, liquid alloy, thermodynamic props. *(Russian)* 79−10968
$TlBi_2$, cryst. struct. and density *(German)* 80−24407
Zn-Bi, discrete eutectic formation mechanism *(Russian)* 77−66634
Zn-Bi, liquid, inconsistent conjugated liquidus 80−76232
Zn-Bi, liquid, surface tension, size effect *(French)* 80−15341
Zn-Bi, specific elec. resist., temp. and conc. depend., 20-800°C 79−82571
Zn-Bi liquid alloy, surface tension and surface adsorpt. determ. *(French)* 79−69325
Zn-Cd-Bi, appl. of computational techniques for treatment of thermodynamic data, phase diagram calc. 78−10172

bismuth alloys continued
Zn-Cd-Bi-Sn phase diagram with liquid-liquid immiscibility, computer calc. 77−36463
Zn-Sn-Bi, ternary phase diagrams, interactive computer program 80−71629

bismuth compounds
see also bismuth alloys
$AgBi(CrO_4)_2$, synthesis, thermolysis, crystallography *(French)* 80−33946
n- $(Bi_{1-x}Sb_x)_2Te_3$, magnetoresist. in quantising mag. field 80−24953
$Bi_{1-x}Sb_x$ narrow band gap semiconductors, galvanomagnetic, optical and photoelectric props. 80−15544
$Bi_7Ni_4NbO_{21}$, crystal point group determ. by high resolution electron microscope image 79−51036
chemical bonding in group V and VI elements and compounds with tetradymite structure 80−15036
electron spin echo envelope modulation, 2-dimens. Fourier transform 80−63680
halides, X-ray L_{III}-absorption edges 78−82750
molybdates, on SiO_2, EPR rel. to surface processes *(French)* 78−64271
oxide film, struct. by electron diffr. and TEM obs. 80−6678
oxides, antiferroelec. and ferroelec., pyrochlore struct., struct. and dielec. props. 79−38488
oxides containing perovskite layers, ferroelec. cryst., electron microscopy, dislocation and domain boundaries 77−52030
phosphates, X-ray electron spectra 77−36352
tellurites, acousto-optical criterion estimation 79−82945
Fe_2O_3-Bi_2O_3 sintered material, elec. switching effects due to thermal ionic breakdown *(Korean)* 80−70776
AgI-BiI_3, phase equilib. study *(French)* 79−66047
$Ag_2S(Se)(Te)$-Bi, temp.-comp. diagram 78−44105
$AlBr_3.BiBr_3$, CT complex, NQR 77−20747
As_2-Se_3-Bi_x amorphous system, elec. and photocond. props. 79−51574
As_2Se_3-Bi_2Se_3, semiconducting crystallized glasses, elec. conductivity mechanism 77−39843
$AsSe_{1.5}Bi_{0.05}$ glasses, soln. rate in alkali solns. 80−16531
$AsTeBi_x$, chalcogenide glass, thin film crystallisation 79−7758
$B_{12}GeO_{20}$, cryst. powder, phonon electroacoustic echo signal storage 78−68055
Ba_2BiRuO_6, perovskites, prep., struct., emission control catalysts 77−68957
$BaBi_6Ti_3Nb_2O_{21}$, cryst. struct. 77−47428
$BaBi_4Ti_4O_{15}$, SHG, temp. depend. ferroelec.-ferroelec. transition 78−15121
$BaBi_8Ti_7O_{27}$, cryst. struct. 77−47428
BaO-Nd_2O_3-TiO_2-Bi_2O_3 system ceramics, high stability low loss dielectric preparation 80−81008
$BaPb_{1-x}Bi_xO_3$, supercond. T_c and crit. fields, comp. depend. 79−73623
$BaTiO_3$-$BiFeO_3$ solid solns., ferroelec.-antiferromag., magnetoelectric effect at ferroelec. transition 80−100637
$Be_4Ti_2O_{12}$ grain oriented ferroelectric ceramic, prep. by molten salt synthesis-tape casting method 80−40296
$(Bi,Sb)_2$ $(Te,Se)_3$, thermoelectric alloys, phase diagrams, and imperfection chemistry 80−108422
$(Bi, Sb)_2Te_3$ solid soln., semiconductor film, oxidation, electrophysical props. 80−45407
$(Bi_{2/3},Sr)TiO_3$, ferroelec. solid solution, dielec. nonlinearity in nonpolar phase *(Russian)* 77−32317
Bi complex, $BiCl_7^{4-}$ in HCl aq. soln., photolum. excitation spectral characts. by stroking method *(Russian)* 79−78753
Bi complexes, Bi(III) halide complexes, Raman spectra in aq. soln. 80−25354
Bi garnet-MnBi film structure, thermomag. information recording appls. *(Russian)* 78−23305
Bi-$Bi_{0.5}Sb_{1.5}Te$ system, stratified medium with artificial anisotropy, transverse cooling effect 79−28364
Bi-Bi_2S_3 superlattice, elec. props. 78−10558
Bi-$BiBr_3$ liquid system, miscibility gap, elec. cond. meas. 79−90790
Bi-BiI_3 mixture, molten, NMR meas. 77−51976
Bi-$BiI_3(BiBr_3)$ liquid binary mixtures, phase separation under press. 80−34183
Bi-BiO_2O_3 black layer, on polyvinylidene fluoride film, thermal diffusivity pyroelec. camera tube for IR imaging 80−57369
Bi-layered compounds, stability in rel. to structural mismatch 80−39040
Bi-O system, phase equilib., diagram *(German)* 80−55380
Bi-S liquid soln., S activities meas. by EMF method *(Japanese)* 80−70425
Bi-Sb, semiconduct., e.m. wave propag. perpendicular to mag. field 79−82517
Bi-Sb, semiconducting solid solution, forbidden band width Sb-conc. depend. 77−66117
Bi-Sb narrow gap semiconductor, EM wave propagation in direction parallel to mag. field 78−80014
Bi-Sb-O-I glasses, acousto-optic props. 77−31121
Bi-Sb-S-I system glasses, vitrification and volt-ampere characts. 77−31756
Bi-Se, fused, mag. susceptibility, temp. and conc. depend. 77−36052
Bi-Te, fused, mag. susceptibility, temp. and conc. depend. 77−36052
Bi-Te(Se), liq., diamag. susceptibility, semicond./metal behaviour 78−14927
Bi-Te(Se), liq. chalcogenides, elec. cond. and mag. susceptibility 79−51578
Bi^{3+}-HCl solution, metal cation influence on spectra and luminescence kinetics *(Russian)* 80−78627
$BiAMTeO_6$, A=Ba, Pb, Sr, M=Li, Na, antiferroelectric, synthesis and charact. 77−55758
$Bi_2Al(Ga)_4O_9$, fluoresc. and X-ray data 78−80403
$Bi_2Al_4O_9$, luminesc. expts. 80−60656
$Bi_3B_5O_{12}$, crystal growth from melt, exam. of growth kinetics 78−72717
$Bi_2B'_xB''_{2-x}O_7$, pyrochlore-structured compounds, diffuse transition 77−36182
$Bi_2Bi_4Fe_2Ti_3O_8$, dielec. and magnetoelec. props. 78−95562
$BiBi_4Ti_3FeO_{15}$, perovskite-like layer-type ferroelec. magnetic cpd., Mossbauer expts., 80-1200K 78−64329
BiBr, $A^3(0^+)$ and X^3Sigma$^-(0^+)$ states, pot. energy functions comparison 80−43133
BiBr, empirical pot. energy curves for $A^3\pi(0^+)$ and $X^3\Sigma^-(0^+)$ states 79−22617
$BiBr_3$-Bi molten solution, US velocity and compressibility 77−84845

bismuth compounds continued
$BiBr_3$-$HgBr_2$(-$CdBr_2$), molten, elec. cond., 500-870K, composition depend. 78-55965
$Bi_{3-2x}Ca_{2x}$ $Fe_{5-x-y}In_yV_xO_{12}$, growth and mag. props. of single crystals *(Chinese)* 77-40056
$Bi_{3-2x}Ca_{2x}Fe_{3-x}V_xO_{12}$, crystallization in $Bi_{0.7}Ca_{2.3}Fe_{3.85}V_{1.15}O_{12}$-$Bi_2O_3$-PbO 77-48330
$Bi_2CaNa_{n-2}Nb_nO_{3n+3}$, intergrowth, IMV high-resolution electron microscopy 80-107436
$BiCaVFe_5O_{12}$, magneto-optical near UV reflection-spectra, meridional and polar intensity effects *(Russian)* 78-39572
BiCl, form., microwave spectrum, hyperfine struct., mol. rot. vibr. consts., bonding 77-14418
$BiCl_3$, nuclear electric hexadecapole interactions of ^{209}Bi 79-1722
$BiCl_3$, Raman scatt. spectrum, librational and translational vibr. *(Russian)* 77-54562
$BiCl_3$-Bi molten solution, US velocity and compressibility 77-84845
$BiCl_6^{3-}$, model force fields and vibr. amplitudes calcs. 78-62780
$Bi_4Cl_2S_5$, X-ray single cryst. struct. determ. 79-19199
$BiCl_3.GaCl_3$ complex, NQR of ^{209}Bi, $^{69,71}Ga$ and $^{35,37}Cl$ 78-25569
$BiCl_3$.nitrile complex, NQR spectra changes during complex form. 77-12242
$BiCo_{1-x}Fe_xO_3$, $x \leq 0.7$, ferromag., X-ray powder diffr. data, configuration 79-64956
$BiCoO_3$, X-ray powder diffr. data, configuration 79-64956
$Bi_{24}CoO_{37}$, in Bi_2O_3-CoO system, X-ray diffr., thermal anal. and metallography obs. 80-24598
BiF, fine-structure in C_1-X and C_2-X systems 79-810
BiF, mm spectrum, HFS struct., HFS, vibr. and rot. consts. and equilib. distance 77-79604
BiF, spectrum, 5800-6600 Å, vibr. anal., electronic transition assignment 80-992
BiF_3 coating materials for IR laser components 80-33105
BiF_3 thin films, optical props. 79-32005
BiF_6^{2-}, prod. in gamma irrad. $CsAsF_6$:BiF_6^-, EPR 78-19329
$^{209}BiF_6^{2-}$, radical, prep. and EPR comparison with other hexafluoride radicals 78-68381
$BiF_3(I_3)$, new coating materials for IR laser optical components 79-65821
$BiF_2Si_2O_8OH$, crystal struct., space groups by RHEED 78-47297
$BiFeO_3$, ferroelec., antiferromag., cryst. and mag. struct., neutron diffr. study 80-65786
$BiFeO_3$, pyroelectric-antiferromag., magnetoelectric effect *(Russian)* 78-43625
$BiFeO_3$-$LaFeO_3$, solid solns., antiferroelec.-antiferromag., magnetoelectric effect at antiferroelec. transition 80-100637
$BiFeO_3$-$Pb(Fe_{0.5}Nb_{0.5})O_3$, ferroelec., magnetoelec. obs. temp. and conc. depend. 80-50156
$Bi_{12}FeO_{20}$, longitudinally vibrated bars, reson. freq., DC elec. field effects, elastic coupling polarising correction terms 80-60503
$Bi_2Fe_4O_9$, antiferromag., mag. glass props. *(Russian)* 77-4519
$Bi_2Fe_4O_9$, mag. struct., neutron diffr., transition 78-52217
$Bi_2Fe_4O_9$, mag. struct., neutron diffr. meas. 78-91844
$Bi_2Ga_2O_{63}$ electro-optic and electrogyratory coefficient meas. 77-43974
$BiGeO_{20}$, photocurrent oscills. in pulsed illumination rel. to piezoelec. props. 80-80325
$Bi_{12}GeO_{20}$, acoustic vel., absorpt. coeff. and photoelastic consts. rel. to acoustooptical parameters 79-56762
$Bi_{12}GeO_{20}$, cryst. chirality and optical rotation sense 79-61327
$Bi_{12}GeO_{20}$, crystal gyrotropy, meas. in IR region 80-88957
$Bi_{12}GeO_{20}$ crystals, principal carriers obs., in dark and under laser illumination *(Russian)* 80-80312
$Bi_{12}GeO_{20}$, Czochralski single crystal growth 79-1823
$Bi_{12}GeO_{20}$, elastic and piezoelectric consts., thermal expsn. 78-31157
$Bi_{12}GeO_{20}$, elastic wave leakage across gap between piezoelectrics 78-6204
$Bi_{12}GeO_{20}$, electroacoustic interaction obs. 77-11966
$Bi_{12}GeO_{20}$, electromech. props. 79-38455
$Bi_{12}GeO_{20}$, electron beam recording 79-32075
$Bi_{12}GeO_{20}$, electrophys., props. determ. *(Russian)* 78-51987
$Bi_{12}GeO_{20}$, finite amplitude SAW distorted rippling profiles, optical probing obs. 80-34287
$Bi_{12}GeO_{20}$, high sensitivity read write vol. holographic storage 77-7026
$Bi_{12}GeO_{20}$, holographic recording and photoinduced refractive index change exam. 78-37851
$Bi_{12}GeO_{20}$, hopping cond., carrier mobility and density 78-19040
$Bi_{12}GeO_{20}$, IR reflection spectra studies of lattice vibrations 79-99879
$Bi_{12}GeO_{20}$, laevorotatory, cryst. struct. redeterm. 80-15065
$Bi_{12}GeO_{20}$, light polarisation, elec. field effect *(Russian)* 77-66480
$Bi_{12}GeO_{20}$, mechanism of creation of internal fields and photoelectret effect 80-25290
$Bi_{12}GeO_{20}$, monocrystal, space-time optical modulator appl. *(Russian)* 77 1652
$Bi_{12}GeO_{20}$ monocrystal optical homogeneity requirement for light beam control 79-82952
$Bi_{12}GeO_{20}$, optical phonon freq. in vicinity of Brillouin zone, linear wave-vector depend. 79-19892
$Bi_{12}GeO_{20}$, photocond. spectra, current-voltage charact., photoelectret effect 79-69552
$Bi_{12}GeO_{20}$, photoelectret state 80-11315
$Bi_{12}GeO_{20}$, photoelectretic states in real time spatial light modulators, photorefractive effect 80-80676
$Bi_{12}GeO_{20}$, piezo- and thermo-optical props., dispersion theories and models 79-56764
$Bi_{12}GeO_{20}$, piezoelec. resonator, electroelastic coeffs. 77-52020
$Bi_{12}GeO_{20}$, piezoelectric, secondary electron emission yield 79-91546
$Bi_{12}GeO_{20}$ plate cut along (110) axis, torsional thickness oscillations calc. *(Czech)* 77-55754
$Bi_{12}GeO_{20}$, pulse photocond., V-I characts., 0.35-0.55 μm *(Russian)* 78-68048
$Bi_{12}GeO_{20}$, reflection of Gulyaeb-Bluestein waves from end of acoustic channel 77-84852
$Bi_{12}GeO_{20}$, reflectivity spectrum and band struct. 79-47474
$Bi_{12}GeO_{20}$, selective dislocation etching in nonaq. Br_2 solns. 79-77601
$Bi_{12}GeO_{20}$, single cryst., electro-optical and photocond. props., image recording *(Russian)* 77-73129
$Bi_{12}GeO_{20}$, single crysts. optical homogeneity depend. on growth conditions 78-95007
$Bi_{12}GeO_{20}$, spatial-temporal electrooptic modulator, UV image conversion 77-3680
$Bi_{12}GeO_{20}$ substrate, for interdigital transducer *(Czech)* 80-19201

bismuth compounds continued
$Bi_{12}GeO_{20}$ substrate material for SAW devices, book contrib. 79-50522
$Bi_{12}GeO_{20}$, thermal cond. and absorptivity 80-70480
$Bi_{12}GeO_{20}$, third-order elastic moduli determ. 80-65121
$Bi_{12}GeO_{20}$ vacuum-deposited film elec. and photoelec. props. *(Russian)* 78-60237
$Bi_{12}GeO_{20}$, vol. hologram recording, charge transfer process 78-5437
$Bi_{12}GeO_{20}$ wide-zone dielectric injection contact characteristics *(Russian)* 78-60236
$Bi_{12}GeO_{20}$, X-ray sensitive ceramic, sintering 80-25621
$Bi_{12}GeO_{20}$:Cr^{3+}, level distrib. of Cr^{3+} ion, spectroscopic parameters, spin Hamiltonian, EPR spectrum 78-48030
$Bi_{12}GeO_{20}$:Dy(Ho)(Er), luminesc., emission and excitation spectra 80-103975
$Bi_{12}GeO_{20}$:Ga,Ca, photocond. suppression by simultaneous Ga and Ca doping, and appl. to electro-optic light valve 79-78134
$Bi_{12}GeO_{20}$:Mn, Cr, reversible photochromic effects, absorpt. spectra before and after illum. 79-91471
$Bi_{12}GeO_{20}$-CdS, air gap coupled system, SAW energy transfer 77-11774
$Bi_4Ge_3O_{12}$, 38 mm scintillator, γ-ray response 80-58048
$Bi_4Ge_3O_{12}$ as potential scintillation detector in positron cameras 78-3586
$Bi_4Ge_3O_{12}$ crystals, doped with Dy^{3+}, Ho^{3+}, Er^{3+}, Tm^{3+}, Yb^{3+}, growth, spectral and laser props. 80-45115
$Bi_4Ge_3O_{12}$, low-temp. scintillation props. and appl. to high-energy γ-imaging devices 80-55191
$Bi_4Ge_3O_{12}$, temp. depend. luminesc. meas. 77-20910
$Bi_4Ge_3O_{12}$:Er^{3+}, host-sensitised energy transfer, laser time resolved spectroscopy 79-83013
$Bi_4Ge_3O_{12}$:Nd^{3+} cryst., absorpt. and luminesc. spectra, 4.2-300K 80-34957
Bi_3GeVO_9, dielec. props. and twin struct. 77-12350
$Bi_6(H_2O)(NO_3)O_4(OH_4)[(NO_3)_5]$, X-ray cryst. struct. determ. and refinement 79-32958
$BiH(PO_3)_4$, condensed, thermal behaviour and IR spectra 80-19912
BiI_3, absorpt. spectra, role of impurities *(Russian)* 79-51994
BiI_3, band struct., empirical pseudopotential calc. 77-15766
BiI_3, characts. of low-temp. photoluminesc. 77-8646
BiI_3 coating materials for IR laser components 80-33105
BiI_3, doped, IR photolum. and EPR spectra 78-19558
BiI_3, enthalpy, entropy of melting 78-34598
BiI_3, excitonic shifts of quasiatomic optical core to cond. band transitions, UPS obs. 78-11079
BiI_3 film, exciton peaks, temp. depend. 90-270K, and press. depend. up to 3500 atm. 77-36265
BiI_3 film, exciton-phonon interaction, optical consts., Faraday effect., permitt. 80-59884
BiI_3, lamellar single cryst., absorpt. spectra and Urbach rule *(Russian)* 77-28606
BiI_3, layered compound, exciton spectra, surface and stacking fault effects 80-40134
BiI_3, layered semicond., valence bands UPS and XPS obs. 78-11078
BiI_3, layered single crystal, band-edge excitons, optical constant meas. *(Russian)* 77-90171
BiI_3, molten, electrical cond., press. effect, 0-1 kbar 78-55963
BiI_3, octahedrally coordinated, layer cpd., electronic struct. using synchrotron-radiation photoemission spectroscopy 79-74058
BiI_3, photoacoustic spectroscopy 79-42992
BiI_3 photographic film, photochem. decomposition kinetics *(Russian)* 80-93782
BiI_3, photopolarisation, photoelectret state, electron-hole transitions 77-12300
BiI_3 photosensitive layers, optical and thermal development *(Russian)* 80-73512
BiI_3 single crystals, refl., absorpt. and photoluminesc. spectra, exciton transitions 77-52164
BiI_3, structure, exciton states and physicochem. characteristics *(Russian)* 80-100435
BiI_3, UV reflectivity meas. 78-72545
BiI_3:Cr^{3+}, ESR, spin-lattice relax., temp. depend. 78-88178
BiI_3:Mn^{2+}, ESR, spin-lattice relax., temp. depend. 78-88178
BiI_3-Bi molten solution, US velocity and compressibility 77-84845
BiI_3-Bi_2Te_3, p-T-x phase diag. 77-36477
BiI_3-CdI_2, molten, elec. cond., temp. depend. 77-89562
BiI_3-$Sb(As)I_3$, phase diags. 78-6905
BiIG, transparent, domain struct. realignment in external mag. field 78-10739
$Bi_3In_5S_{12}$, X-ray cryst. struct. determ. 80-107126
$Bi_{2-x}La_xWO_6$, synthesis and crystallography 80-66459
BiLi, gas phase thermodynamics, Knudsen effusion mass spectrosc. 80 -100057
Bi_2MoO_6 ceramic, permittivity, ferroelec. T_c and hysteresis 79-82932
Bi_2MoO_6, superplasticity during phase transitions 80-108498
$Bi_2Mo_2O_9$, thermal decomp. rel. to catalytic oxidation 80-35520
BiN, form., IR matrix spectra, comparison with group V nitrenes 80-18853
$Bi^+(NH_3)_n$, gas phase clusters, relative bond strengths, thermodynamic props. 78-35649
BiNbS(Se), struct., X-ray powder diffr. meas 80-44175
BiO, dissoc. energy calcs. 77-3486
BiO_2-Li-containing ferrite, phase diagrams and sintering conditions 79-52141
Bi_2O_3, AES and characteristic energy loss spectra, expt. and interpretation 78-27354
Bi_2O_3 additions in Fe_2O_3-BaO-CoO system, effect on phase comp. and mag. props. 79-29032
Bi_2O_3 admixture, effect on props. of $Co_{3-x}Mn_xO_4$ and $MnCo_2O_4$ spinel cpds., thermistor appl. 78-15325
Bi_2O_3 and sillenite struct. derivatives, $MO_x.6Bi_2O_3$, IR and Raman spectra, vibr. anal. 78-76464
Bi_2O_3, anharmonicity effect, Debye temp. determ. from Mossbauer spectra 77-63335
Bi_2O_3, anodic film, dielec. props. 77-20794
Bi_2O_3 anodic film form. on Bi, electric breakdown 79-20377
Bi_2O_3 anodic films, struct. and electronic props., photoeffects 80-44749
Bi_2O_3, doped, secondary ion emission, at. and mol. processes 78-68588
Bi_2O_3, elec. props. of α, β, γ and δ phases 79-23771
Bi_2O_3, electronic struct., X-ray emission, XPS, UPS obs. 78-52638
Bi_2O_3, energies of formation, solid-state electrochemical techniques 80-6527

bismuth compounds continued
Bi_2O_3 film, dielec. meas. 80−2696
Bi_2O_3, film, resist. and current controlled negative resist. 78−39238
Bi_2O_3 film, thermally grown, I-V characts., current controlled neg. resist. 80−15637
Bi_2O_3, ionic crystal, possible high-temp. thermometer using elec. cond. changes 80−52203
Bi_2O_3 layer thermally grown on Bi film, thickness meas. by capacitance method 79−1554
Bi_2O_3, low-melting additive to $Li_{0.5}Fe_{2.5}O_4$ 77−85494
Bi_2O_3, molecular versus atomic secondary ion emission, rel. to quantitative analysis 79−61481
Bi_2O_3, molten, reaction with water, reactor fuel-coolant interaction simulation 78−58363
Bi_2O_3, oxide film on polycrystalline Bi, exam. of oxide film growth rate using XPS *(German)* 79−11041
Bi_2O_3, polymorphic transformation and elec. resistivity *(Japanese)* 80−93555
Bi_2O_3, powder diffr. patterns and struct. 79−27961
α-Bi_2O_3, single cryst. growth and refractive indices 77−21018
Bi_2O_3, smoke particles prep. by burning metal in Ar-O_2 gas, electron microscope obs. 77−52238
Bi_2O_3, thermally-grown capacitor-film, dielec. props. 80−2480
Bi_2O_3, thermoelec. props., 500-1500K 80−29423
δ-Bi_2O_3, thermoelectric power, heat of transport of O^{2-} ions 80−92713
δ-Bi_2O_3, thermoelectric power rel. to fast ionic conduction 80−107549
Bi_2O_3, thin film, oxidation of Bi rel. to X-ray diffraction *(Japanese)* 79−29273
Bi_2O_3, thin film, struct. and dielec. meas. 79−78622
Bi_2O_3, thin film capacitor elec. props. under reduced press. 80−80397
Bi_2O_3, transmission spectra of thin films 78−76440
Bi_2O_3 vacuum deposited films, dielec. props., 90 to 298K, freq. range 0.1 to 10 kHz, ageing effect 80−55036
Bi_2O_3, X-ray absorption, discontinuities and limits, chem. combination effects 80−93435
Bi_2O_3, X-ray photoelectron spectra and electronic struct. 77−32493
Bi_2O_3:MoO_3 sintered, oxide ion conduction 77−80646
Bi_2O_3/Bi^+/electrolyte system, field and temp. depend. of electronic current 80−66814
Bi_2O_3-$AlPO_4$, phase equilib. 80−35168
Bi_2O_3-B_2O_3 melt, solubility of rare earth iron borates and their crystallisation 80−19736
Bi_2O_3-BaO, ion cond. and oxide ion vacancy 79−28139
Bi_2O_3-based glass, in ZnO-glass-ZnO struct., current-voltage characts. and TSC *(Russian)* 77−69404
Bi_2O_3-CdO system, phase diagram 77−25032
Bi_2O_3-CoO system, X-ray diffr., thermal anal. and metallography obs. 80−24598
Bi_2O_3-$M_2O_5(M_2O_3)$ (where M=V,Nb,Ta,Y,Gd) ion cond. and oxide ion vacancy 79−28139
Bi_2O_3-$M2O_5$, sintered, (M=V, Nb, Ta), high oxide ion cond. 78−14503
Bi_2O_3-MoO_3, ion cond. and oxide ion vacancy 79−28139
Bi_2O_3-$Mo(W)O_3$ melts, electrophys. props. 77−89817
Bi_2O_3-$Mo(W)O_3$ system, elec. cond. and dielec. const. obs. 77−89816
Bi_2O_3-PbO, glass, cond. meas. using complex impedance anal. *(French)* 80−92707
Bi_2O_3-Si-O, general features of reaction 79−11819
Bi_2O_3-$SiO_2(GeO_2)$, melt struct. model 80−33870
Bi_2O_3-$SiO_2(GeO_2)$, metastable phases form., crystn. conditions, melt viscosity and density effects 80−35167
Bi_2O_3-$Si(Ge)O_2$ melts, phys. props. 77−89566
Bi_2O_3-Sm_2O_3 eutectoid system, isothermal deformation 77−63625
Bi_2O_3-SrO, ion cond. and oxide ion vacancy 79−28139
Bi_2O_3-SrO, solid state phase diagram, thermal and high temp. X-ray anal. *(French)* 79−65190
Bi_2O_3-SrO system, stoichiometric cpds., cryst. data *(French)* 79−99153
Bi_2O_3-TiO_2-Nb_2O_3, subsolidus phase equilibria 77−55954
Bi_2O_3-WO_3, catalyst, X-ray diffraction studies 78−38677
Bi_2O_3-WO_3, ion cond. and oxide ion vacancy 79−28139
Bi_2O_3-ZnO, phase diag. 77−40416
Bi_2O_3-ZnO(CdO), elec. cond., dielec. const., mag. susceptibility meas., effect of melting transition 77−7849
α-Bi_2O_3+KCl, quantitative anal. of multocomponent powders, full-profile refinement of Guinier-Hagg X-ray film data 79−39249
BiOBr, tetragonal, lattice coupling with cubic and hexagonal ZnS and ZnSe, heterojunctions 79−60919
BiOCL, nuclear electric hexadecapole interactions of ^{208}Bi 79−1722
BiOCl ($BiCl_3$), nuclear electric hexadecapole interactions 80−65513
BiOCl, cryst. growth, Raman and IR spectra *(German)* 77−21012
BiOCl, exam. of crystal structure and morphology, as function of growth conditions, using electron microscopy 79−52103
BiOCl film, crystalline, growth 77−40364
BiOCl, tetragonal, lattice coupling with cubic and hexagonal ZnS and ZnSe, heterojunctions 79−60919
BiOCl-ZnS electroluminesc. heterojunction phys. props. 77−66198
BiOCl-ZnSe, electroluminesc. heterojunction phys. props. 77−66198
$Bi_{12}O_{15}Cl_6$, struct. derivation from $Bi_6X_{7+n}Cl_3$ by chem. twinning 77−35520
$Bi_6O_7FCl_3$, struct. derivation from $Bi_6X_{7+n}Cl_3$ by chem. twinning 77−35520
BiOI, synthesis, thermal decomposition in dry O_2 *(French)* 78−53205
BiOI, UV reflectivity meas. 78−72545
$Bi_6O_5(OH)_3(NO_3)_5.3H_2O$, cryst. struct. determ. and refinement, X-ray anal. 79−7586
δ-$(Bi_2O_3)_{1-x}(Y_2O_3)_x$, thermoelectric power rel. to fast ionic conduction 80−107549
$6Bi_2O_3.GeO_2$, single crysts., selective etching in HNO_3, Bi_2 and H_2O_2 solns. 79−99201
25 $Bi_2O_3.P_2O_5$, hydrothermal growth, vib. spectrum 77−63555
$6Bi_2O_3.SiO_2$, stable γ-phase cryst. form. from supercooled melt, metastable δ-phase precip., surface contamination role 79−91635
$3Bi_2O_3.5B_2O_3$, viscosity, molar volume of melt and enthalpy of fusion 79−10924
BiP_5O_{14}, condensed, thermal behaviour and IR spectra 80−19912
$Bi_{12}RO_{20}$, R=Ge, Si, photoinduced birefringence, dynamic transparency prod. 78−90472
$BiReO_4$, prep. and cryst. struct. 80−28991
Bi_2S_3, electrodeposition, using nonaqueous solvents 80−76200
Bi_2S_3 film, evaporated on W, work function obs. by field emission method 78−6834

bismuth compounds continued
Bi_2S_3, photostimulated electron emission, cryst. growth conditions depend. 77−44135
Bi_2S_3, superheavy element search using neutron multiplicity counter 80−4011
Bi_2S_3-Bi_2Se_3 and Bi_2Te_3-Bi_2Se_3 systems, thermal cond. change during phase transitions 80−100368
Bi_2S_3-$CuPbBi_5S_9$, solid solution, semiconductor and dielectric props. 79−69511
Bi_2S_3-$CuPbBiS_3$ series, ordered chem. twinning 79−55717
BiSBr, optical B_u modes of paraelectric phase, simple model 78−75747
$Bi_2(SO_4)_3$ thermochem. cycle, process engng. design for H prod. 80−30599
$Bi_2S(Se)(Te)_3$, X-ray photoelectron spectra and electronic struct. 77−32493
BiSb, Azbel-Kaner type cyclotron reson. obs. 78−56379
n-BiSb, cyclotron mass meas., high hydrostatic press. 79−77991
BiSb, dendritic growth, transverse striations photomicrograph 77−4277
BiSb, hybrid resonance in a quantising magnetic field 78−67933
$Bi_{0.88}Sb_{0.12}$, semiconducting transport props., 2 to 100K 80−59989
$Bi_{0.89}Sb_{0.11}$, effect of band structure on the dispersion of magnetoplasma waves 77−47845
$Bi_{0.9}Sb_{0.1}$, epitaxial film, defect struct. and galvanomagnetic props. 77−89889
$Bi_{0.9}Sb_{0.1}$, magnetophonon effect on hot electrons *(Russian)* 80−107814
n-$Bi_{0.924}Sb_{0.076}$, energy spectrum variation under strong uniaxial tension 79−73432
n-$Bi_{0.924}Sb_{0.076}$, one-ellipsoid to two-ellipsoid fermi surface transition in extended cryst. *(Russian)* 78−14657
$Bi_{1-x}Sb_x$, band inversion under press., Fermi surface anisotropy, galvanomag. meas. 77−51637
$Bi_{1-x}Sb_x$, EM wave propag. for rot. of mag. field from Faraday to Voigt config. 80−84419
$Bi_{1-x}Sb_x$, elec. resist., 1.8 to 77K, electron-phonon scatt. mechanism 79−15144
$Bi_{1-x}Sb_x$, far IR magnetoabsorption, band struct. study 80−50351
$Bi_{1-x}Sb_x$ film, low temp. anomalies of elec. props. and quantum size oscillations 79−65571
$Bi_{1-x}Sb_x$, galvanomag. props., energy spectrum *(Russian)* 79−56248
n-$Bi_{1-x}Sb_x$, Hall effect in strong mag. fields 79−69532
$Bi_{1-x}Sb_x$, narrow band gap semicond., photocond. and photomagnetic effect 79−51630
$Bi_{1-x}Sb_x$, non-ellipsoidal Fermi surface, cyclotron reson. meas. at 35 and 70 GHz 77−62804
$Bi_{1-x}Sb_x$, semicond., photoconductivity *(Russian)* 79−7857
$Bi_{1-x}Sb_x$, semiconductor, anomalous conductance in strong electric and longit. quantised mag. field *(Russian)* 78−76084
$Bi_{1-x}Sb_x$, semiconductor film, X-ray diffraction in thin cryst. with linear variation of lattice period 78−26373
$Bi_{1-x}Sb_x$, solid soln., temp. depend. of weak-field galvanomag. coeffs. *(Russian)* 80−70724
$Bi_{1-x}Sb_x$:Pb $(0.08 \leq x \leq 0.13)$ Seebeck, magneto-Seebeck coeff., longitudinal Nernst coeffs. 78−56168
$Bi_{86}Sb_{14}$:Te, single crystal, dispersion of magnetoplasma waves *(Russian)* 80−70739
$BiSbO_4$, synthesis, struct. and m.p. 77−84714
$Bi_xSb_{1-x}SI$, atomic substitution and ferroelec. phase transition 78−68464
$Bi_xSb_{1-x}SI$, low freq. Raman spectroscopy 78−15162
$(Bi_{0.25}Sb_{0.75})_2Te_3$, opt. props. of bulk and films 78−27206
$Bi_{0.5}Sb_{1.5}Te_3$ film, effect of struct. on thermal cond. 79−28257
$Bi_{0.52}Sb_{1.48}Te_3$, microstructure rel. to thermoelec. props. 77−85249
$Bi_{0.52}Sb_{1.48}Te_3$ thermoelec. solid soln., homogeneity, effects of prep. method 78−52698
$Bi_{0.52}Sb_{1.48}Te_3$-Te, phase-equilibrium boundary, Hall coeff. meas. 78−44094
$(Bi_{1-x}Sb_x)_2Te_3$, highest valence band struct., Shubnikov-de Haas effect 78−14661
n-$(Bi_{1-x}Sb_x)_2Te_3$, magneto-Seebeck and Shubnikov-de Haas effect 79−42568
$Bi_{2-x}Sb_xTe_3$, solid soln. film on mica substrate, effect of stresses on elec. cond. 78−51859
$Bi_{88}Sb_{12}Te_{0.05}$, helicon dispersion, effect of slope of electron ellipsoids 79−28365
$Bi_xSb_{2-x}Te_3$, 2-dimens. cryst. interface props. of Bi overlayer UPS obs. 78−34881
$Bi_{2-x}Sb_xTe_{3-y}Se_y$, elec. cond. and thermoelec. props., neutral defects influence 80−60017
$Bi_{2-x}Sb_xTe_{3-y}Se_y$ solid solution, density-of-states effective mass, carrier mobility temp. depend. 80−24931
BiSe, reflection spectra 77−16325
ρ-BiSe, single crystal, synthesis and elec. props. 77−16490
p-Bi_2Se cryst. growth, elec. props. 77−8748
Bi_2Se_3, amorphous thin film, charge transport at high fields *(Rumanian)* 79−60841
n-Bi_2Se_3, cryst. nonparabolic cond. band., IR refl. and Hall voltage meas. 77−31940
Bi_2Se_3 film, partly oriented, electron diffr. dynamic effects 77−7996
Bi_2Se_3, mechano-caloric energy conversion 80−10962
n-Bi_2Se_3, nonparabolicity of cond. band and anisotropy of electron effective mass 79−60692
Bi_2Se_3, Raman spectra, Raman and IR-active modes 79−56776
n-Bi_2Se_3, single cryst., new aspect of carrier scatt. 80−49707
Bi_2Se_3:Hg point defects in crystal lattice, Hall coefficient and IR spectra determ. 80−55129
Bi_2Se_3:Sn(Pb), dopant influence on elec. cond. 79−51569
Bi_2Se_3-Bi_2Te_3, liquid, mixture enthalpies *(German)* 79−77770
BiSeBr, optical B_u modes of paraelectric phase, simple model 78−75747
BiSeI film, growth, effect of artificial nucleation centres 79−11032
BiSeI, optical B_u modes of paraelectric phase, simple model 78−75747
BiSeI, sublimation, vapour pressure 77−11686
$Bi_2(SeO_4)_3$, single cryst. growth in silica gels, X-ray diffr., IR and emission spectroscopy study 79−74075
n-$Bi_2(Se_xTe_{1-x})_3$, Shubnikov-de Haas oscills., 1.7-4.2K 77−15874
Bi_2Si_3, cryst., RI anisotropy obs., polarised light effects 77−12354
$Bi_{12}SiO_2$ Pockels readout optical modulator, X-ray response 79−64313
$Bi_{12}SiO_{20}$, acoustic vel., absorpt. coeff. and photoelastic consts. rel. to acoustooptical parameters 79−56762
$Bi_{12}SiO_{20}$, cryst. chirality and optical rotation sense 79−61327
$Bi_{12}SiO_{20}$ crystal, for programmable optical guided-wave device 79−23069

bismuth compounds continued
$Bi_{12}SiO_{20}$ crystal, programmable optical integrated circuit, exam. 78—38078
$Bi_{12}SiO_{20}$ crystal, real-time holographic recording 79—72540
$Bi_{12}SiO_{20}$ crystals, for real-time coherent object edge reconstruction 78—90372
$Bi_{12}SiO_{20}$ crystals, phase-conjugate wavefront generation via real-time holography 79—27213
$Bi_{12}SiO_{20}$ electrooptic crystals, vol. phase holograms, light diffr. and non-linear image processing 80—37972
$Bi_{12}SiO_{20}$, electrooptic photorefractive crysts. for optical information processing 80—74313
$Bi_{12}SiO_{20}$ film, photoelectric props. obs., UV illumination effects *(Russian)* 80—80313
$Bi_{12}SiO_{20}$, film and single cryst., optical absorpt. edge and optical transitions 79—33730
$Bi_{12}SiO_{20}$, for real-time double-exposure holographic interferometry 77—71951
$Bi_{12}SiO_{20}$, growth of single cryst. thin plates by EFG method 80—97423
$Bi_{12}SiO_{20}$, high sensitivity read write vol. holographic storage 77—7026
$Bi_{12}SiO_{20}$, holographic recording and photoinduced refractive index change exam. 78—37851
$Bi_{12}SiO_{20}$, IR reflection spectra studies of lattice vibrations 79—99879
$Bi_{12}SiO_{20}$, image recording possibility 79—27432
$Bi_{12}SiO_{20}$ in insulator-semicond.-insulator struct., induced birefr., influence of kinetics of transient processes 79—24294
$Bi_{12}SiO_{20}$, laevorotatory, cryst. struct., absolute piezoelec. d_{14} coeff. 79—94974
$Bi_{12}SiO_{20}$, light polarisation, elec. field effect *(Russian)* 77—66480
$Bi_{12}SiO_{20}$, mechanism of creation of internal fields and photoelectret effect 80—25290
$Bi_{12}SiO_{20}$, monocrystal, space-time optical modulator appl. *(Russian)* 77—1652
$Bi_{12}SiO_{20}$ monocrystal optical homogeneity requirement for light beam control 79—82952
$Bi_{12}SiO_{20}$, optical information recording, PROM device resolution 79—41443
$Bi_{12}SiO_{20}$, optical quality, Czochralski growth 78—31324
$Bi_{12}SiO_{20}$, optical sensor for measurement of high electric field intensity 80—69509
$Bi_{12}SiO_{20}$, optically active photorefractive cryst., light diffr. by vol. holograms 79—64185
$Bi_{12}SiO_{20}$, optically controlled multimode planar switch 78—42476
$Bi_{12}SiO_{20}$ PROM device, image recording and erasure mechanism 80—74490
$Bi_{12}SiO_{20}$, phase-conjugate wavefront refl. depend. on dynamic hologram spatial freq. 80—53358
$Bi_{12}SiO_{20}$ photoconductive electrooptic crysts. for time average holographic interferometry 78—25813
$Bi_{12}SiO_{20}$ photoelectret, in optical processing and X, γ ray imaging 80—23764
$Bi_{12}SiO_{20}$, photoelectretic states in real time spatial light modulators, photorefractive effect 80—80676
$Bi_{12}SiO_{20}$, photorefractive, vibr. struct. mode pattern visualisation, phase conjugation and dynamic holography 80—95938
$Bi_{12}SiO_{20}$, photorefractive medium, real-time image processing via four-wave mixing 80—95944
$Bi_{12}SiO_{20}$ photosensitive electro-optical materials for holographic data storage *(French)* 77—31077
$Bi_{12}SiO_{20}$, pulling large crystals 79—11507
$Bi_{12}SiO_{20}$, stationary current obs. on polarised light illum., photogalvanic effects *(Russian)* 79—91095
$Bi_{12}SiO_{20}$ surface and pseudosurface wave props. 79—46908
$Bi_{12}SiO_{20}$, third-order elastic moduli determ. 80—65121
$Bi_{12}SiO_{20}$, use in incoherent-to-coherent optical image convertor of transmission type 79—94340
$Bi_{12}SiO_{20}$, visible and UV refl. and absorpt. spectra 80—34950
$Bi_{12}SiO_{20}$, vol. hologram recording, charge transfer process 78—5437
$Bi_{12}SiO_{20}$, volume hologram polarisation props. and appls. 78—74859
$Bi_{12}SiO_{20}$:Mn, Cr, reversible photochromic effects, absorpt. spectra before and after illum. 79—91471
$Bi_{12}SiO_{20}$:Nd, light absorpt. and transmission spectra, photoluminescence spectrum, optical absorpt. coeff. 79—74001
$Bi_{12}SiO_{20}$:Nd, single cryst., photoluminesc. meas. *(Russian)* 78—23519
$Bi_{22}SiO_{20}$, Pockels readout modulation struct., information registration *(Russian)* 77—10990
$Bi_4Si_3O_{12}$, eulytine, change in band structure on transition to amorphous state 79—15081
$Bi_4Si_3O_{12}$:Nd^{3+} cryst., absorpt. and luminesc. spectra, 4.2-300K 80—34957
$Bi_{72}SiO_{20}$:Sn(Mo), Raman scatt. spectra, impurity effect 80—80795
$Bi_xSi_yO_z$ films on Si, form. kinetics and props. 80—35358
$Bi_2Sn_2O_7$, polymorphic phase transition, X-ray, DSC, SHG, dielec. and optical obs. 80—44163
$Bi_2Sn_2O_7$, prep., stability, and crystallographic exam. *(French)* 78—51510
$Bi_{1-x}Sr_xO_{1.5-x/2}$ vacancy-type solid soln., anionic cond. *(French)* 80—49407
$Bi_2TE_{3-x}Se_x$, solid solution films, prep. and props. 78—44013
$Bi_8T_7S_5$, thin crystal, optical consts. from transmissivity spectra, classical oscillator anal. 77—1748
$BiTaO_4$, cryst. growth. hydrothermal method 77—8736
$BiTaO_4$, X-ray and ESR study of phase changes 78—72476
BiTaS(Se), struct., X-ray powder diffr. meas 80—44175
$Bi_2(Te,S)_3$, thin crystal, min. metallic conductivity 79—1610
n-$Bi_2(Te,Se)_3$ semiconducting solid solns., plastic deform. during hot extrusion 79—20143
BiTe, reflection spectra 77—16325
BiTe, X-ray powder cryst. struct. determ. and refinement 79—19203
BiTe-In(Gn,Sn)Te system, physicochemical anal., eutectic type phase diagram with solid soln. region 77—16556
Bi_2Te_3, anodic film form., in situ ellipsometric study 80—104318
Bi_2Te_3, anodic oxide films, two-dimens. nucleation and growth 80—11807
Bi_2Te_3, Bi_2Se_3, $Bi_2(Te_{1-x}Se_x)_3$, Raman and far infrared investigation of phonons 78—23453
Bi_2Te_3, bulk n- and p-type samples, thermoelec. power meas. 77—79092
Bi_2Te_3, chemical bonding models, correctness test using mag. susceptibility, and chemical substitution 78—67680
Bi_2Te_3, constant current anodisation, representation of layer periodicity 80—3218

bismuth compounds continued
Bi_2Te_3, crystallisation in constant electric field, thermoelectric parameters 77—44146
Bi_2Te_3 film, effect of struct. on thermal cond. 79—28257
Bi_2Te_3, galvanothermomag. props. up to 14 kbar 77—47829
n-Bi_2Te_3, galvonomagnetic props., influence of hydrostatic press. 79—73536
Bi_2Te_3, lattice vibrs. coherent inelastic neutron scatt. meas. 78—34576
Bi_2Te_3, layered semiconductor, angle resolved photoemission 79—28893
Bi_2Te_3, liq. semicond., thermal cond. meas., resistive probe method 77—15636
n-Bi_2Te_3, magnetoresist. under uniaxial stress 77—35956
Bi_2Te_3, mechano-caloric energy conversion 80—10962
Bi_2Te_3, p- and n-type, free charge carrier mag. susceptibility, 90-650K 78—10643
Bi_2Te_3, Raman spectra, Raman and IR-active modes 79—56776
Bi_2Te_3, Shubnikov-de Haas effect, high press. effect on band struct. 77—51767
Bi_2Te_3 single crystal, thermoelec. power anisotropy 77—55554
Bi_2Te_3 single crystals, melt grown, structural perfection 80—15101
Bi_2Te_3, surface prep. by etching for electroplating elec. contacts 80—108647
Bi_2Te_3, thermoelectric coolers with high current pulse and finite cold junction, fast transient behaviour 80—27290
Bi_2Te_3, thermoelectric p-n junction, pulse refrigeration 78—23156
Bi_2Te_3/Hastelloy C-276 contacts, elevated temp. compatibility, appl. to radioisotopically powered thermoelec. generator 79—49680
Bi_2Te_3-based solid solns., decomp. kinetics under flux layer 77—81205
Bi_2Te_3-Bi_2Se_3, thermoelectric materials, physico-chemical study 78—30945
Bi_2Te_3-Bi_2Se_3 solid solns., bladed cryst. growth, electrophysical props. 78—43387
Bi_2Te_3-Bi_2Se_3 solid solns., single cryst. growth and thermocouple construct. 80—104056
Bi_2Te_3-Bi_2Se_3 thermoelectric alloys, diffusion and evaporation of volatile component during prep. 80—35118
Bi_2Te_3-Bi_2Se_3-Sb_2Te_3, solid solution, single crystal, elec. cond., thermoelectric props. 80—88550
Bi_2Te_3-BiI_3, phase diagram, and BiTeI cryst. struct. 77—28788
Bi_2Te_3-InTe, thermoelec. props. 77—85250
Bi_2Te_3-Sb_2Te_3, Bi:Sb=1:2, 2:1, solid soln. deviation from stoichiometric cross section 79—43221
Bi_2Te_3-Sb_2Te_3, plastically deformed by hot extrusion, diffusion meas. using micro-X-ray spectrum anal. 79—14954
Bi_2Te_3-Sb_2Te_3 composite billet, diffusion during plastic deformation *(Russian)* 79—23767
Bi_2Te_3-Sb_2Te_3 film, cond., galvanomag. Seebeck and Nernst-Ettingshausen effects under press., band model 77—47907
Bi_2Te_3-Sb_2Te_3 film, residual cond. 78—52110
p-Bi_2Te_3-Sb_2Te_3 semiconducting solid solns., plastic deform. during hot extrusion 79—20143
Bi_2Te_3-Sb_2Te_3 solid soln., deviation from stoichiometric cross section 78—35362
Bi_2Te_3-Sb_2Te_3 solid solns., powders, particle shapes determ., device 78—60899
Bi_2Te_3-Sb_2Te_3:Cu, electrical cond. and thermopower, disorder effects *(German)* 77—1422
Bi_2Te_3-$SbTe_3$, ordered structure formation, heat treatment effect on thermal cond. 80—54448
Bi_4Te_3, X-ray powder cryst. struct. determ. and refinement 79—19203
BiTeI, cryst. struct., Bi_2Te_3-BeI_3 phase diagram 77—28788
BiTeI crystals, eutectic decomp. in transmission electron microscope 79—20024
BiTeI, elec. props., crysts. grown from melt in excess iodine 79—4907
BiTeI, influence of lamination effects on mag. suscept. *(Russian)* 78—80125
BiTeI, layered cryst., anisotropy and temp. depend. of mag. susceptibility 79—73673
BiTeI, melt and vapour grown, optical props. 80—84746
BiTeI-SbTeI, solid solns., phase diagrams, photocond., elec. props. 79—38125
BiTeI-SbTeI solid solns., form., crystn., elec., thermal props. 78—44003
$Bi_{1-x}Te_xO_{3/2+x/2}$, solid solutions, phase transformations, dielectric and differential microcalorimetry *(French)* 79—55886
$Bi_{2/3}Te_{1-x}S_x$, single cryst. film, field effect mobility, peaked struct. 77—66207
$Bi_2(Te_{1-x}S_x)_3$ film, optical consts. meas., Shamir-Graff method evaluation 80—11489
$Bi_2(Te_{1-x}S_x)_3$, low field magnetocond. meas. 79—87117
$Bi_2(Te_{1-x}S_x)_3$, quasi 2-D cryst., I-V and magnetocond. meas. 77—85360
$Bi_2(Te_{1-x}S_x)_3$, thin cryst. two-dimens. system, electronic props. 78—60181
$Bi_8Te_7S_5$, anisotropic dielec. const., oblique incidence reflectivity data 77—73124
$(Bi_2Te_3)_{0.9}(Sb_2Te_3)_{0.5}(Sb_2Se_3)_{0.05}$ n-type alloy for thermogenerators, thermo-EMF, elec. cond. and thermoelec. efficiency factor, 300-600K 80—70735
$Bi_2Te_{2.7}Se_{0.3}$, magnetoresistance and Hall EMF meas., using AM method 80—52278
n-$Bi_2Te_{2.88}Se_{0.12}$, extrusion deformed, powder dispersion degree influence on thermal and elec. props. *(Russian)* 80—39366
$Bi_2Te_{2.88}Se_{0.12}$, solid soln., single cryst. growth and doping, thermoelec. efficiency and Hall coeff. 79—33921
$Bi_2Te_{3-x}Se_x$ films, surface band struct. and scatt. mechanism 80—34535
$Bi_2Te_{3-x}Se_x$ films, thermal cond. depend. on grain size, phonon-boundary scatt. 79—69304
$Bi_2Te_{3-x}Se_x$, microstructure rel. to thermoelec. props. 77—85249
$Bi_2Te_{3-x}Se_x$ solid solution, Hall effect anisotropy parameter, thermoelectric power, depend. on carrier density 79—69536
$Bi_2Te_{3-x}Se_x$, thermoelec. mat., prep. effects on inhomogeneities 78—51576
$Bi_9Ti_3Fe_5O_{27}$, combined hyperfine interaction 79—28663
$BiTiNbO_6$, cryst. struct. determ. *(German)* 78—79570
$Bi_7Ti_4NbO_{21}$, mixed-layer cryst. struct. determ. by super-high-resolution electron microscopy 77—84703
$Bi_5TiNbWO_{15}$, cryst. struct. 77—47428
$BiTiO_3$, ferroelec., repolarisation in SEM 79—15424
$Bi_{12}TiO\ {}_0$ electro-optic and electrogyratory coefficient meas. 77—43974
$Bi_{12}TiO_{20}$ electro-optic and electrogyratory coefficient meas. 77—43974
$Bi_{12}TiO_{20}$, RF sputtered epitaxial film on $Bi_{12}GeO_{20}$, for optical waveguiding 78—9462

bismuth compounds continued
$Bi_2Ti_4O_{11}$, anomalous temp. depend. of phonon modes, Raman spectra 78−10893
$Bi_2Ti_4O_{11}$:PbO, anomalous temp. depend. of phonon modes, Raman spectra 78−10893
$Bi_4Ti_3O_{12}$, $Bi_2Ti_2O_7$, $Bi_2Ti_4O_{11}$, crystal growth from melts in Bi_2O_3-V_2O_5-TiO_2 system 78−19659
$Bi_4Ti_3O_{12}$ ceramics, ferroelectric, hot-forged, grain orientation and dielectric props. 80−40076
$Bi_4Ti_3O_{12}$, coaxial magnetron sputtering technique 79−83123
$Bi_4Ti_3O_{12}$, elec. characts., phase transition obs. 80−60517
$Bi_4Ti_3O_{12}$, ferroelec. film, on Si substrate, polarisation reversal and film struct. 79−91392
$Bi_4Ti_3O_{12}$, IR refl. spectrum, 60-2000 cm^{-1} 77−69843
$Bi_4Ti_3O_{12}$ stoichiometric thin film prep. by DC sputtering with powder target 77−90273
$Bi_4Ti_3O_{12}$, thick single cryst. growth from Bi_2O_3-B_2O_3-TiO_2 77−8746
$Bi_4Ti_3O_{12}$-CdS optical storage plane 77−39006
$Bi_xTi_yO_z$, poling method 77−59544
$Bi_2TiO_4F_2$, one-layer perovskite-like ferroelec., dielec. study 79−38486
$Bi_2(Ti_{1-x}S_x)_3$, thin crysts., adsorpt. effects on elec. cond. 78−19034
$Bi_7Ti_{2.5}Sn_{0.5}Fe_3O_{21}$, layered ferroelec. antiferromag., superparamagnetism, Mossbauer spectra obs. 77−51999
$Bi_7Ti_4TaO_{21}$, cryst. struct. 77−47428
BiTm ferrite garnet coating on $LiNbO_3$:Ti optical waveguide *(Russian)* 77−42623
$(BiTm)_3(FeGa)_5O_{12}$ ion implanted epitaxial garnet film, bubble domains, cryst. struct. disorder 80−93150
$(BiTm)_3(FeGa)_5O_{12}$, monocrystalline films, mag. anisotropy 80−2609
$(BiTm)_3(FeGaTm)_3O_{12}$, layer separation of domain struct. 80−44857
$BiVO_4$, cryst. growth and struct. 80−35078
$BiVO_4$, ferroelastic, observation of soft optical phonon 78−2856
$BiVO_4$, ferroelastic domains, electron microscopy and electron diffr. obs. 80−100254
$BiVO_4$, ferroelastic phase transition, birefringence meas. using rotating-analyser method 80−80742
$BiVO_4$, ferroelastic phase transition, birefringence meas. at simultaneous high pressure and temp. 80−80743
$BiVO_4$, ferroelastic transition, soft optical phonon mechanism 79−51230
$BiVO_4$, linear coupling between soft optical and ferroelastic acoustic modes 78−79716
$BiVO_4$, NQR spectra of ^{209}Bi 79−82891
$BiVO_4$, struct. and ferroelastic phase transition 80−29004
Bi_2WO_6, ferroelectric, dielectric props., elec. cond. and relaxation phenomena obs. 80−80692
Bi_2WO_6 film, RF sputtering, possible piezoelec., pyroelec. and photolithography appl. 77−15705
Bi_2WO_6 grain oriented ferroelectric ceramic, prep. by molten salt synthesis-tape casting method 80−40296
Bi_2WO_6, hydrothermal and flux growth 80−76166
Bi_2WO_6, ionic cond. and relaxation polarisation, capacitance, losses 80−24657
Bi_2WO_6, layer-like ferroelec., cryst. growth 78−23598
Bi_2WO_6 layered ferroelectric, anomalous photovoltaic effect, photovoltaic current 80−75603
Bi_2WO_6 single crystal, growth from flux in Bi_2WO_6-Na_2WO_4, below transformation temperature 78−72713
Bi_2WO_6, superplasticity during phase transitions 80−108498
$Bi_2W_2O_9$, energy transfer and luminesc. props. 80−55177
$Bi_2W_2O_9$, layered struct., 1 MV high-resolution electron microscopy obs. 79−27955
$Bi_2W_2O_9$, struct., dielec. props., melting character and thermal stability 79−23572
$Bi_2W_2O_9$:Mo(Eu), energy transfer and luminesc. props. 80−55177
$Bi_2W_2O_9$-$BiVO_4$, solid soln., X-ray diffr. study 80−2001
$Bi_xYb_{3-x}Fe_5O_{12}$ LPE film, phase grating integrated optic coupler-modulator 77−11048
BsSI, optical B_u modes of paraelectric phase, simple model 78−75747
$Ca_{2x}Bi_{3-2x}Fe_{5-x-y}V_xIn_yO_{12}$, ferromagnetic relax. meas., 4.2-300K 80−44923
$Ca_{2x}Bi_{3-2x}V_xFe_{5-x}O_{12}$ ferrogarnet, magnetis. distrib., correl. with morphological habit 79−42802
CaO-Ga_2O_3-Bi_2O_3, vitrification regions 77−15557
CdO-Bi_2O_3-Al_2O_3, glass formation and IR transmission *(Japanese)* 80−54146
$Ce_{1.25}Bi_{3.78}S_8$, cryst. struct. determ. *(French)* 77−80467
$CsBi(MoO_4)_2$, low temp. phase transition, permittivity meas. 79−28698
$Cs_5Bi(MoO_4)_4$, synthesis, X-ray and thermal investigations 77−36390
$Cs_3BiSbBr_9(Cl_9)$, ^{121}Sb Mossbauer chem. shifts, optical reflectance spectra, solid state band populations 77−40162
$Cs_2NaBiCl_6$, struct. transitions, polarisation optical expts. 79−99318
$(Cu,Ag)_2Se/(Bi, Sb)_2Te_3$, P type selenide segmented element fabrication, thermoelectric props. 80−107835
$Cu_3Bi_5S_9$, modulated struct. 79−99147
$(ErBi)_3Fe_{5-x}Ga_xO_{12}$ film, ferrimag., splitting of domains into layers 77−28420
$EuBi_2Te_4$, elec. cond., Hall, thermo-EMF coeffs. determ., 300-1100K 78−43386
Fe garnet, Bi-substituted, film, domain boundary transform. into canted phase at compensation point 77−24724
Fe_2O_3-Bi_2O_3 sintered material, elec. switching effects for temp. range 700-850°C *(Korean)* 80−70775
Fe_2O_3-Bi_2O_3 system, mag. props., hyperfine parameters, Mossbauer spectrum 77−69746
GaS:Bi_2S_3, photocond. and optical obsorpt. 79−51634
$(Gd, Bi)_2$ $(Fe, Ga)_5O_{12}$ magneto-optic LPE garnet films, high-energy heavy ion irrad., props. 80−71390
$(Gd,Bi)_3$,$(Fe,Al,Ga)_50_{12}$ LPE film, 180° Bloch wall pinning at etched nucl. tracks 78−39376
$(Gd,Bi)_3(Fe,Ga)_5O_{12}$ magneto-optic film, ion irrad. effect on storage props. 78−52324
$(Gd,Bi)_3(Fe,Ga)_5O_{12}$, LPE film, coercivity, influence of nuclear tracks 79−51829
$(Gd,Bi)_3(Fe,Ga)_5O_{12}$ epitaxial garnet film, nucl. tracks effect on mag. props. 80−11234
$(GdPrBi)_3(FeGaIn)_5O_{12}$, pure and In^{3+} doped, near IR absorpt. and Faraday rot. 78−95580
Ge-Bi-S system, semicond., elec. cond., glass transition temp. and optical absorption meas. 77−16329
Ge-Bi-S system glasses, opt. props. and glass transition temp. 77−77224
N-Ge-Bi-Se glass, elec. and optical props. 80−65550

bismuth compounds continued
Ge-Bi-Te system, thermal cond. change during phase transitions 80−100368
Ge-Pb-Bi-O glass, photoelasticity, glass transition limits 79−33670
n-$Ge_{20}Bi_{10}Se_{70}$ glass, preparation and elec. props. 79−74126
$Ge_{20}Bi_xSe_{70-x}Te_{10}$, n-type semiconducting glasses, resistivity and thermoelectric power meas. 80−54695
$GeBi_2Te_4$, Hall const., thermoelec. power, and elec. cond. 80−29407
GeTe-Bi_2Te_3, thermoelectric materials, physico-chemical study 78−30945
HgI_2-BiI_3, molten, elec. cond., temp. depend. 77−89562
In-Sb-Bi system, solid solns., solubility limits, microhardness, microstruct. investig. 78−35368
$K_{1.14}Bi^{III}_{0.64}Bi^{V}_{1.73}O_{5.85}(H_2O)_{0.97}$, cryst. struct. *(French)* 77−72596
$K_2BiNb_5O_{15}$ substrate for $K_3Li_2Nb_5O_{15}$ film for optical waveguide, cryst. struct., dielectric props. 80−79016
$K_5Bi_{1-x}Nd_x(MoO_4)_4$ solid soln., growth, spectroscopic and laser props. 78−2901
$KBi(PO_3)_4$, cryst. struct. 77−43188
$(K_{3/4}Bi_{1/4})(Zn_{1/6}Nb_{5/6})O_3$, cation disordered perovskite, elastic consts. and thermal expansion 80−96587
KCl:$BiCl_3$, electrical cond. as a function of temp., charge transport mechanism 78−83996
$LiBi(MoO_4)_2$, acoustooptic characteristics 79−8118
$LiBi_xNd_{1-x}P_4O_{12}$ waveguide laser layer epitaxially grown on $LiNdP_4O_{12}$ substrate 80−23709
$Li_2Bi_2O_3$ quenched glasses, crystn. and ionic cond. 80−33899
$Li_{0.5}Fe_{2.5}O_4$-$Bi_2O_3(V_2O_5)$ systems, phase diagrams, sintering conditions 78−35366
Li_2O-Bi_2O_3, rapidly quenched glasses, Li ion cond., elec. cond. 80−100346
$(Lu,Bi)Fe_5O_{12}$, magneto-optic colour effects 78−23308
$(MnTe)_{1-x}(Bi_2Te_3)_x$ $(x \leq 0.05)$ solid solution, electrophys. props. 80−24925
$NaBiMTeO_6$, M=Mg, Co, Cd, Ca, antiferroelectric, synthesis and charact. 77−55758
$NaBi(MoO_4)_2$, electrically induced optical activity 79−82942
$NaBi(MoO_4)_2$, low-temp. paraelectric, permittivity meas., 4.2-400K 79−95702
$NaBi(MoO_4)_2$, photoelastic props., acousto-optical figure of merit meas. 78−60420
$Na_{0.5}Bi_{4.5}Nb_2WO_{15}$, cryst. struct. 77−47428
$Na_{0.5}Bi_{0.5}TiO_3$, dielectric const. thermal hysteresis, ferroelectric-antiferroelectric transitions 80−50281
$Na_{0.5}Bi_{0.5}TiO_3$, phase transition, hysteretic behaviour 80−71330
Na_2O-B_2O_3-Bi_2O_3, glass with metallic Bi granules, elec. cond. 80−84493
Na_2O-B_2O_e3-Bi_2O_3-SiO_2, heterophase glass, diffusion and elec. cond. 78−67858
Na_2O-Bi_2O_3-TiO_2, subsolidus phase equilibrium at 1000 degrees C 78−48384
$Pb/PbF_2/BiF_3/Bi$ thin solid film reversible galvanic cell 79−52928
$Pb_{1-x}Bi_xF_{2+x}$, fast ionic conduction of F^- ions 79−99360
$Pb_{1-x}Bi_xF_{2+x}$, solid anionic conducting electrolytes, struct., elec. props. 77−84977
$Pb_{1-x}Bi_xF_{2+x}$, solid soln., struct. and ionic cond. correl., neutron diffr. study *(French)* 80−84324
$(Pb_{1-x}Bi_x)_5Ge_3O_{11}$, spontaneous and induced electrogyration 79−42946
$PbBi_2Nb_2O_9$ ceramic, grain oriented, dielectric and piezoelectric props. 79−42896
$PbBi_2Nb_2O_9$, hot-forged ferroelec. ceramic with layer struct. 79−43175
$PbBi_4Ti_4O_{15}$ ceramic, dielec. props., temp. depend. 78−95561
$PbBi_4Ti_4O_{15}$, hot-forged ferroelec. ceramic with layer struct. 79−43175
$PbBi_8Ti_7O_{27}$, cryst. struct. 77−47428
$Pb_2Bi_4Ti_5O_{13}$, hot-forged ferroelec. ceramic with layer struct. 79−43175
$PbMg_{1/3}Nb_{2/3}O_3$-$BiMg_{2/3}Nb_{1/3}O_3$, dielectric polarisation of solid solutions 78−43776
$Pb(Mg_{0.5}W_{0.5})O_3$-$BiFeO_3$, dielec. props., cryst. struct. 78−84534
PbO-B_2O_3-Bi_2O_3, glass with metallic Bi granules, elec. cond. 80−84493
PbO-B_2O_3-SiO_2-Al_2O_3-ZnO-CuO-Bi_2O_3 solder glass, crystallisation prevention by Cu addition 80−11654
PbO-Bi_2O_3, thermodynamic props. 77−59743
PbO-Bi_2O_3-Al_2O_3, glass formation and IR transmission *(Japanese)* 80−54146
PbO-Bi_2O_3-GeO_2, exam. of glass forming and liquid phase separation regions, and optical props. 78−88453
15PbO.3B_2O_3.2WO_3, struct. and electrophys. characts. 77−84716
PbTe-Bi_2Te_3 system cpds., powder pattern calcs. 77−43185
$PdBi_2O_4$, cryst. struct. *(French)* 78−51516
$RiRe_2O_6$, prep. and cryst. struct. 80−28991
$(Sb,Bi)_2(Se,Te)_3$ profiled crystalline ingot continuous elongation 79−69975
Sb-Te-Bi, computer study of miscibility limits, 273 to 300K 78−52781
$Sb_{1-x}Bi_xSI$, mixed cryst., ferroelec. phase transition 79−33629
$Sb_{1-x}Bi_xSI$, SHG at microwave freqs. 79−55188
$(Sb_{1-x}Bi_x)_2Te_3$, δ phase, equilib. state, electrophysical props. 79−52178
p-$Sb_{1.48}Bi_{0.52}Te_3$, extrusion deformed, powder dispersion degree influence on thermal and elec. props. *(Russian)* 80−39366
$Sb_{1.48}Bi_{0.52}Te_3$, obtained by zone crystallisation, effect of extrusion and annealing on elec. props. 79−96038
$Sb_{1.5}Bi_{0.5}Te_3$ solid solution, electrical, thermoelectric and thermal properties, temp. influence obs. *(Slovak)* 78−30946
p-$Sb_xBi_{2-x}Te_3$ *(German)* 79−51618
SbSI-BiSI, solid solns., phase diagrams, photocond., elec. props. 79−38125
Sb_2Se_3-Bi_2Se_3, liq. semicond., thermal cond. meas., resistive probe method 77−15636
$(Sb_2Se_3)_x$-$(Bi_2S_3)_{1-x}$ single crystals, elec. and photoelec. props., stoichiometry deviations influence 79−60870
$(Sb_2Se_3)_{0.7}(Bi_3Se_3)_{0.3}$, solid soln., prep. and elec. properties of layered crystals 80−70762
Sb_2Te_3-Bi_2Te_3, thermoelectric materials, physico-chemical study 78−30945
Sb_2Te_3-Bi_2Te_3 solid solns., bladed cryst. growth, electrophysical props. 78−43387
Sb_2Te_3-Bi_2Te_3 solid solns., single cryst. growth and thermocouple construct. 80−104056
Sb_2Te_3-Bi_2Te_3 system, thermal cond. change during phase transitions 80−100368
Sc_2O_3-Bi_2O_3-SiO_2, three-layer antirefl. coatings, form. and props. 77−58420
Se-Bi-I, amorphous, high sensitivity visible-near IR photoconductor development and characterisation 78−39153

bismuth compounds continued
SnTe-Bi_2Te_3 system, phase diagram 77−36474
Sr_2BiRuO_6, perovskites, prep., struct., emission control catalysts 77−68957
$SrBi_2Ta_2O_9$, SHG, temp. depend. ferroelec.-ferroelec. transition 78−15121
$SrBi_6Ti_3Nb_2O_{21}$, cryst. struct. 77−47428
$Sr_x(Na_{0.5}Bi_{0.5})_{1-x}$ solid solutions, piezoelec. and ferroelec. props. *(French)* 80−108158
$Sr_x(Na_{0.5}Bi_{0.5})_{1-x}TiO_3$ ferroelec. ceramic, hot pressing, numerical simulation *(French)* 80−76220
SrO-Ga_2O_3-Bi_2O_3, vitrification regions 77−15557
$SrTiO_3$-$Bi_2Ti_2O_7$-$CaTiO_3$ system, solid solns., elec., optical props. 79−11375
Te-$(Bi_xSb_{1-x})_2Te_3$ eutectic, electrophys. props., directed crystn. conditions influence and comp. depend. 80−107827
Te-Bi_2Te_3 and Te-$(Bi_{0.1}Sb_{0.9})_2Te_3$ system eutectics, crystn. rate effect on electrophys. props. mutual solubility effect 80−60774
Te-Bi_2Te_3 oriented eutectic, microhardness, influence of size of phases *(Russian)* 78−92322
Te-Bi-Sb ternary system, phase drag. calc. 77−27980
$Te_{80}Ge_{20-x}Bi_x$, DSC studies of struct. phase transformation 80−66505
Tl-Bi-Sb-Te system, peritectic reactions in $TlBiTe_2$-$TlSbTe_2$ cross section, crystn. character 80−108406
$Tl_4Bi_2S_5$, X-ray cryst. struct. determ. *(French)* 79−69063
$Tm_{2.2}Bi_{0.8}Fe_{3.5}Ga_{1.5}O_{12}$ epitaxial film, Faraday effect and domain struct. near compensation point 77−20838
$Tm_{2.7}Bi_{0.3}Ga_{0.3}Co_xFe_{4.7-x}O_{12}$, Co ion concentration effect on mag. props. close to mag. compensation point *(Russian)* 79−73788
$(Y,Gd,Yb,Bi)_3(Fe,Al,Ga)_5O_{12}$ films, magnetic bubble domains, domain wall motion examined 78−19294
$(Y,Gd,Yb,Bi)_3(Fe,Al)_5O_{12}$ film, nonreciprocal effects in domain boundary motion in inhomogeneous field 77−24726
$(Y, Gd, Yb, Bi)_3(Fe, Al)_5O_{12}$ epitaxial film, domain wall motion and oscill. 80−2616
$(Y,Gd,Yb,Bi)_3(Ga,Al,Fe)_5O_{12}$, bubble conversion to anomalous behaviour 78−23309
$(Y,Gd,Yb)_{3-x}Bi_x(Fe,Al)_5O_{12}$, LPE, for magneto-optical appls. 78−48341
$Y_{1.6}Bi_{1.0}Ca_{0.4}Fe_{4.4}In_{0.4}V_{0.2}O_{12}$, cation distrib. 79−19211
$(YBi)_3Fe_{5-x}Ga_xO_{12}$ film, ferrimag., splitting of domains into layers 77−28420
$Y_2BiFe_{3.8}Ga_{1.2}O_{12}$ film, colour contrast between different domains 77−12166
$Y_2BiFe_{3.8}Ga_{1.2}O_{12}$ film, magnetooptic interference of light 77−32458
$Y_2BiFe_{3.8}Ga_{1.2}O_{12}$, film, dynamics of domain walls 78−27065
$Y_{3-x}Bi_xFe_{5-y}Ga_yO_{12}$, epitaxial film, domain wall dynamics *(Russian)* 78−2718
$Y_{3-x}Bi_xFe_{5-y}Ga_yO_{12}$-PbO-$B_2O_3$-$Bi_2O_3$ system, crystn. fields 78−43996
$Y_{3-x}Bi_xFe_5O_{12}$, ferrite-garnet formation 78−52737
$(YBiSmCa)_3(FeGe)_5O_{12}$ epitaxial layer, growth kinetics and struct. as functions of cryst. lattice parameter mismatch 80−6677
$(YBi)_3.(FeGa)_5O_{12}$ film, interaction between Bloch walls and dislocations *(Russian)* 79−61196
$(YCdYbBi)_3(FeAl)_5O_{12}$, cylindrical domain wall vel. anisotropy *(Russian)* 77−59440
$Y_{1.4}Gd_{0.6}BiFe_{3.8}Ga_{1.2}O_{12}$ film, bistable bubble domains, static, dynamic and optical props. 79−28574
$(YGdYbBi)_3$ $(FeAl)_5O_{12}$ epitaxial film, diffuse domain wall, bubble domain expansion 80−25170
$(YGdYbBi)_3(FeAlGa)_5O_{12}$ film, motion of mag. bubble domains in inhomogeneous pulsed mag. field 78−27064
$(YGdYbBi)_3(FeAl)_5O_{12}$, epitaxial garnet film, with mag. compensation point, behaviour of 'compromise' phase boundary 78−60321
$(YGdYbBi)_3(FeAl)_5O_{12}$, garnet, epitaxial film, interior domains 79−91268
$(YGdYbBi)_3(FeAl)_5O_{12}$ ferrite-garnet films, effect of in-plane field on dynamics of domain walls 80−65979
$(YGdYbBi)_3(FeAl)_5O_{12}$ epitaxial garnet film, uniaxial ferromagnet domain struct., phase transition *(Russian)* 80−108044
$(YGdYbBi)_3.(FeAl)_5O_{12}$ films, substrate orientation influence on max. vel. of domain boundaries 79−15330
YIG, Bi-substituted, LPE, domain wall reson. 80−60387
$(YLaBi)_3(FeGa)_5O_{12}$, pure and In^{3+} doped, near IR absorpt. and Faraday rot. 78−95580
YRBiFe garnets, epitaxial films, R=Gd+Yb, Faraday effect and phys. props. 77−69928
$(YRBi)_3(FeAl)_5O_{12}$ films, R=Gd, Yb, Faraday effect in transverse mag. field, orientation depend. 80−88971
YbPrBiIG, wave props. of domain wall 78−48011
ZnO-Bi_2O_3, ceramic semiconductor, injection currents 79−11141
ZnO-Bi_2O_3, heterojunction, current-voltage characts. 79−56291
ZnO-Bi_2O_3 varistor, grain boundary segregation, STEM study 79−78980
ZnO-Bi_2O_3-CoO-MnO-Sb_2O_3 (97.5, 0.5, 0.5, 1.0 mole%), exam. of elec. props. at different annealing temps. 80−3099
ZnO-Bi_2O_3-Sb_2O_3-Co_2O_3-MnO_2-Cr_2O_3, nonohmic ceramic, microstruct. exam. 78−47292
ZnO-Bi_2O_3-ZnO structure, injection currents, SCL and TSC obs. *(Russian)* 77−32068

bistable multivibrators *see flip-flops*

Bitter patterns *see magnetic domains*

bitumen *see materials*

BL Lacertae-type objects
1 mm continuum emission, obs. 78−36720
0406+121, optical spectra 4950-7950 Å 80−51895
1308+32, rapid optical outburst, 1980 June to July 80−98733
1309−216, probable BL Lacertae object with absorpt. red shift 1.49, optical spectrum 80−67856
1418+54, new violently variable BL Lacertae object, historical light curve 78−93410
2A 1219+305, high latit. X-ray source identification with BL Lacertae object 79−48960
absorption spectra, effects of intervening galaxies 78−16561
absorption spectra 78−86036
absorption spectra origin, intervening galaxy hypothesis 79−5894
AO0235+164, model of outburst rel. to variability 77−26061
AO 0235+16.4, another source exceeding the speed limit 77−2482
AO 0235+164, nature of associated nebulosity 78−28778
AO 0235+164, nonthermal emission spectral break development 77−57092
AO 0235+164, optical and radio absorption line systems 78−16520

BL Lacertae-type objects continued
AO 0235+164, optical outburst obs. 80−56924
AO 0235+164, radio halo obs. 78−4386
AO 0235+164, radio polarisation, evidence for rot. in variable radiosource 79−48917
AO 0235+164, radio study of z=0.524 absorpt. system 78−65680
AO 0235+164, relativistic blast-wave model for rapid flux vars. 79−9017
AO 0235+164, search for X-ray emission 79−17106
AO 0235+164, UBVI photographic magnitude obs. during flare 79−25724
AO 0235+164, VBLI obs. of redshifted H I absorpt. 80−46658
B2 1101+38, UBV photometry 78−8114
B2 1101+38, UV spectrum from International Ultraviolet Explorer (IUE) obs. 78−96540
B2 1101+38 (Markarian 421=2A 1102+384), soft X-ray flux discovery 79−25721
B2 1308+326, optical and IR variability during 1978 outburst 80−51888
B2 1308+326, photometry and polarization during 1978 outburst 79−25718
B2 1308+32 (CSVS 6997, OP 313), common identification 78−8128
B2 1523+29, optical variability from archival plates 77−26056
blue stellar objects, from MC2 and MC3 catalogue, polarisation obs., BL Lacertae objects 79−48918
brightness fluctuations, source size limits 77−45585
brightness rapid variability, search in eight quasars and BL Lacertae objects 80−90567
BZ 1652+39, photoelectric intraday photometric obs. 78−36681
4C 03.59, radio halo obs. 78−4386
3C 371, photoelectric intraday photometric obs. 78−36681
3C 66 A, photoelectric intraday photometric obs. 78−36681
catalogue, optical revised 80−105177
classification of galaxies with active nuclei 79−97071
compact radio sources, relativistic jets model 80−4448
compact radiosources, flux density and linear polarisation at 3.7 and 11.1 cm wavelength 77−49490
diffuse gamma-ray emission from active galaxies 80−12806
distance determination, from correl. anal. of radio luminosity features and optical light curve *(Russian)* 80−51880
distances, statistical upper limits determ. from absence of redshifted C IV absorpt. lines 80−62267
emission lines, broadening and displacement during nonlinear transfer in turbulent plasma *(Russian)* 77−91418
extended radiosource 1400+162, in group of galaxies 78−4339
extragalactic nature *(Russian)* 78−69888
galactic nuclei, rotating supermassive magnetized disc model 79−84849
galaxies, flat spectrum, in 5 GHz S4 survey, Westerbork obs. and identification as BL Lacertae objects 79−58435
H 2155−304, highly luminous BL Lacertae object, spectral obs. 80−4459
H 2156−304, intense high-latit. soft X-ray source and possible new BL Lacertae object 79−92891
HIA 2344+094, new source near quasar (PKS 2344+09) 77−37659
highly polarised objects detection device *(Japanese)* 80−82209
BL Lacertae, coordinated obs. 1979 September 19-25 period 79−80354
BL Lacertae, existence of periodic components in light vars. *(Russian)* 79−101205
BL Lacertae, flat-spectrum radio source, variability at 962 MHz 77−82317
BL Lacertae, major radio outburst, (1980 April 17 to May 6) 80−73043
BL Lacertae, optical monitoring by three-colour photographic photometry 78−16525
BL Lacertae, periodic light vars. *(Russian)* 77−57096
BL Lacertae, photoelectric intraday photometric obs. 78−36681
BL Lacertae, polarisation and flux density data, prolonged particle generation at single location 79−35376
BL Lacertae, polarisation at visible and IR wavelengths 77−9803
BL Lacertae, radiowave dispersion by plasma ejected from core 80−82516
BL Lacertae, spectrum and magnitude of associated galaxy 78−24552
BL Lacertae, spectrum and redshift 77−26055
BL Lacertae, submillimetre photometry 78−4353
BL Lacertae, very high resolution radio obs. 77−33663
AP Librae, emission line obs. in (1976) 77−29932
AP Librae, extended source obs. by photoelectric photometry 78−4348
AP Librae, polarisation at 2.2 μm, nonthermal emission 79−2566
linear optical polarisation, obs. *(Russian)* 78−57640
local space density, of BL Lacertae objects, galaxies active nuclei and quasars 78−57676
luminosity function, implications for X-ray background 80−8682
M87 jet knots, optical and radio props. similarity with BL Lacertae objects 80−12817
Markarian 011, radio continuum obs. at 1410, 2380 and 5000 MHz 80−46668
Markarian 180 and 421, spectra of stellar population 78−54047
Markarian 421, optical and radio obs., identification with 2A 1102+384 X-ray source 79−5899
Markarian 421, radio variability 77−49483
Markarian 421, X-ray spectrum change 79−101196
Markarian 421 (2A 1102+384), low-energy X-rays detect. 78−54083
Markarian 421 and 501, polarisation data 78−93406
Markarian 421 and 501, X-ray obs. in 2-60 keV band 79−17094
Markarian 501, identification with 4U 1651+39 by HEAO 1 modulation collimator 79−5918
Markarian 501, large-z object, electronographic obs. 77−91624
Markarian 501, UV and X-ray obs. of BL Lacertae-type object 80−36717
MC2 1210+121 and 1620+103, radio-quiet objects 80−101641
MC5 1307+121, radio spectrum shape, VHF and SHF obs. 80−67866
millimetre temps. of planets, galactic and extragalactic sources 78−28556
millimetre wave emission, rapid variability obs. *(Russian)* 80−90559
millimetre-wave emission, 90 GHz obs. 78−16548
Mk 421, optical counterpart of 2A 1102+384, X-ray emission detect. 78−57698
MRK 80, optical variability from archival plates 77−26056
multiaperture UBV photometry, of peculiar extragalactic sources 78−28772
nature and radiation source 78−8127
nebulosity around non-stellar type objects 78−57648

BL Lacertae-type objects continued
NGC 1275, possibly BL Lacertae object 78–45406
OA 33, variability of optical counterpart 78–45421
OE 110, optical variability from archival plates 77–26056
Ohio radio sources, optical identification using radio and optical positions meas. by Texas interferometers 78–28808
OI090.4 and OJ–131, discovery from polarisation survey 78–4359
OI 090.4, photometric history 80–77491
OJ287, photographic photometry, comparison star variability determ. 80–26882
OJ–131, photometric history 80–77491
OJ 287, case for synchronous optical-radio outbursts 80–8679
OJ 287, colour variability during flare-ups 79–9021
OJ 287, periodicity investigation at 21 cm 80–82529
OJ 287, radiowave dispersion by plasma ejected from core 80–82516
ON325, photographic photometry, comparison star variability determ. 80–26882
ON 325, extragalactic nature *(Russian)* 78–69888
optical polarisation model, synchrotron radiation 77–2479
Penrose pair production as power source 79–44352
photometry, comparison stars photoelectric UBV sequences 77–5562
physical problems 78–57649
PKS 0521–36, radio and optical props. 79–84854
PKS 0548–322, X-ray spectrum 80–17654
PKS 0548–322 (H0548–32), X-ray obs. in 2-60 keV band 79–17094
PKS 0548-322, possible BL Lacertae object, low-energy X-rays detect. 78–89270
PKS 0548-322, surface photometry of X-ray emitting object 80–22069
PKS 0735+178, B mag. brightening (1977, March) 77–37654
PKS 0735+178, brightening and linear polarisation obs. 77–22318
PKS 0735+178, flat radio spectrum as component synchrotron radiation 80–94880
PKS 0735+178, flat spectrum radio source struct. 78–16549
PKS 0735+178, low absorption line redshift object, search for nearby faint galaxies 79–17121
PKS 0735+178, search for redshifted H I 21 cm absorpt. line 77–49478
PKS 0735+178 spectrum, multiple components in $z=0.424$ absorpt. system 79–25707
PKS 1144–379, radio, IR and optical obs. 80–4451
PKS 2155, UV flux meas. by IUE 80–12833
PKS 2155–304, rapid X-ray variability obs. 80–73035
PKS 2155–304, spectral slope from far UV obs. 80–82509
PKS 2155-304 (H2155–304), newly discovered BL Lacertae object, optical and X-ray props. 80–36702
PKS 2201+04, compact galaxy, optical variability 77–26051
polarisation, visual and IR photometry and polarimetry of 10 objects 80–77480
polarisation at cm., mm., IR and visual wavelengths 79–5913
radio emission, variable, temporal characts. *(Russian)* 80–62307
radio structure and spectral index, reviews 80–46672
radiosource 0109+22, optical and radio props. 78–32567
radiowave dispersion by plasma ejected from core 80–82516
review, characts. and relation to QSOs and normal galaxies 78–89259
review (up to September 1975) 77–26069
southern BL Lacertae type objects, optical monitoring 80–56969
spectral flux distributions from 0.36 to 3.5 micrometers of seven BL Lacertae objects 77–45537
variable quasi-stellar sources, IR and visible polarimetry and photometry 78–16528
0846+51W1, eruptive BL Lae object with high z, visible and radio obs. 79–62899
white holes, appearance rel. to quasars and BL Lacertae objects 78–81650
X-ray emission, high-energy obs. 80–31353
X-ray emitting BL Lacertae objects, location by HEAO 1 scanning modulation collimator expt. 79–48921
I Zw 1727+5015, redshift and spectra 78–41044
H I and Mg II absorpt. lines obs. 78–28838
OJ 287, periodic light vars. *(Russian)* 77–57096

black holes
see also gravitational collapse
Abelian Higgs and Goldstone models, no-hair theorems for black holes 79–17016
accreting black holes, contrib. to background radiation density 80–4461
accreting compact object in binary system, magnetosphere theory, X-ray sources 80–46394
accreting massive black holes, energy source and time variation of quasars and Seyfert galaxies 79–40214
accreting matter, nuclear γ-ray line emission 78–4403
accretion, disc temp. around black hole near Eddington luminosity 77–45479
accretion disc, selfgravitating, model 79–25466
accretion disc surrounding black hole, effect of pressure gradient force 78–45355
accretion discs, boundary-layer behaviour of flow at disc inner edge 80–46598
accretion discs, Lightman-Eardley instabilities rel. to disc thickening 80–31324
accretion discs, thick discs models rel. to supercritical luminosities 80–101614
accretion disk model, gas flow above alpha disk 80–62161
accretion disk models 80–36659
accretion disks around massive black holes: persistent emission spectra 78–93296
accretion environment, photon pair prod. in transrelativistic plasma 78–20632
accretion of large mass flows including matter-radiation interaction 77–41389
accretion on massive black holes in galactic nuclei 79–80335
accretion onto rapidly moving gravitating centre, self-similar soln. 80–17609
accretion process giving rise to X-ray emission 80–90459
active galactic nuclei, conference, Cambridge, (England 1977) 79–75281
active galaxy nuclei energy sources, choice between, magnetoid, black hole and compact star cluster *(Russian)* 77–78885
adiabatic accretion onto Schwarzschild black hole 80–77445
analytic models of supernovae and black holes, Einstein eqn. solns. 78–4258

black holes continued
angular momentum in general relativity, defn., asymptotic behaviour 77–49650
angular momentum reduction in dense stellar system 77–29874
anticorrelated spectral var. in black hole candidate and other X-ray sources 77–53709
KR Aurigae, irregular variable as black hole candidate 79–58362
KR Aurigae, peculiar variable star, possible black hole *(Russian)* 77–87420
axially symmetric stationary black hole states of Einstein gravitational theory 77–37614
axially symmetry gravit. vacuum configs., theorem *(French)* 77–67341
axisymmetric accretion discs and flows, thickening 78–40989
axisymmetric accretion flows very near black holes and Rosen-collapsed objects 80–12778
axisymmetric accretion two-dimensional gas-dynamic theory 77–33334
binary stars with single optical component, ellipsoidality effect on light vars. 79–92806
binary X-ray sources, review 77–17631
binary X-ray systems, accretion flows 78–12432
black holes, reversible and irreversible transforms in Torimatsu Sato space times 79–2554
blackbody radiation from incipient black hole 77–9767
Bogoliubov transformations, propagators, and the Hawking effect 79–2698
boson field in external potential, instability, Klein paradox, particle creation 77–6017
C-metric black hole solution to vac. Einstein field eqns. 78–89216
Cassiopeia A, identification as black hole 79–75244
characteristics and evolution, from radio, X-ray, and γ-ray obs. 77–37611
charge black hole, Reissner-Nordstrom metric 78–12277
charged, evolution of scalar perturbations near Cauchy horizon 79–35608
charged, perihelion precession for two body problem in general relativity 77–78626
charged, rotating, mag. trapping equilib. conditions 79–48845
charged, rotating evaporating, stress-energy tensor 77–71126
charged black hole, motion in EM field, EM and gravitational perturb. of Reissner-Nordstrom space time 80–82407
charged black hole, plasma horizons 78–12282
charged black hole, QED effects, Cauchy horizon *(Russian)* 80–51803
charged black hole interaction with EM waves, decoupled eqns. for Debye potentials 77–22261
charged black holes, total charge, energy and size relationship, cosmic censorship validity 80–113
charged fluid sphere, gravitational collapse 80–31637
charged particle motion in an electromagnetic field on Kerr background geometry 79–9167
charged particle self-interaction in black hole gravitational field 79–97275
charged particle trajectories in mag. field in Schwarzschild geometry 77–41296
charged particle trajectories in static Ernst space-time 79–17291
charged rotating black hole, mag. torque effects 79–17010
charged sphere, freq. shift of radiation from moving surface 77–57260
Christodoulou-Ruffini mass formula 78–40990
Circinus X-1, black hole candidate, position meas. 78–93459
Circinus X-1, ms X-ray bursts, possible black hole 78–4404
circular orbits, existence and stability in a Schwarzschild field with non-vanishing cosmological constant 79–92660
close binary systems, circumstellar gas motion 77–17628
close binary systems, neutron stars tidal disruption by black holes 77–13387
in closed universes 78–16454
in clusters of galaxies rel. to elliptical galaxies form. by tidal interactions 77–78865
cold black holes, fields and particles surrounding hole, motion in elec. field 78–20850
collapsing magnetized rotating spheroid, mag. dipole radiation 79–35106
collapsing relativistic stars, linearised odd-parity radiation 78–93297
collapsing shell, Schwarzschild-de Sitter space-time, thermodynamics and radiation, black hole emission and Rindler effect interplay 80–17607
collisions, generation of gravitational radiation 77–13663
collisions, time-asymmetric initial data from nonsingular vacuum Cauchy hypersurfaces 80–82408
collisions and scatt., gravit. radiation, zero frequency limit 77–64980
coloured cosmological black holes, soln. of Einstein-Yang-Mills system 79–12492
compact X-ray sources, time-depend. spherically symmetric accretion 79–21462
conformal invariance in general relativity, black hole nonexistance 79–25929
conformally invariant gravit. theory, astrophysical appl. 77–82428
conservation equations and the gravitational symplectic form 79–2679
coordinate covariant second quantisation, quantum processes in black hole evaporation 77–82670
cosmic censorship, black holes, and particle orbits 79–44802
cosmic censorship and test particles, black hole destruction 80–105552
cosmic exploration by X-rays, 1978 Bakerian lecture 79–48964
cosmological density 78–77573
cosmology, quantum effects, black and white holes 78–12441
counter-rotating relativistic disks 79–16822
Cygnus A model, radio source powered by M87 type knots 78–57661
Cygnus X-1, accretion disk round black hole, temp. var. 80–109561
Cygnus X-1, bimodal behaviour of accretion disc 77–60850
Cygnus X-1, black hole candidate, review 78–16577
Cygnus X-1, compact X-ray source, mass 78–12430
Cygnus X-1, evidence for new variabilty in hard X-ray emission 80–27011
Cygnus X-1, extended-bandwidth X-ray obs. 80–17689
Cygnus X-1, hard X-ray spectrum 79–71156
Cygnus X-1, line blending effects rel. to black hole candidacy 77–64878
Cygnus X-1, physical reality of millisecond bursts questioned, shot noise effects 78–45429
Cygnus X-1, possible black hole, astronomical background to speculations *(French)* 78–77624
Cygnus X-1, rotating black hole existence, obs. test 77–33699
Cygnus X-1, status report 78–77618
Cygnus X-1, X-ray flux time variability struct. *(Russian)* 80–51921

black holes continued
Cygnus X-1 (HDE 226868), 78.4 day period search in X-rays and optical polarisation 79—75297
Cygnus X-1 (HDE 226868), accretion disk size 80—51910
Cygnus X-1 (V1357 Cygni), optical light curve vars. rel. to X-ray vars. 80—109560
Cygnus X-1 possible existence of black hole in binary system 78—16457
Cygnus X-3, gamma-ray emission from mag. accretion disc 77—78894
decoupling of fields from escaping sources in a de Sitter universe 79—12698
definition 79—2555
definition for any causal space-time 80—31620
degenerate accretion disc model 79—25467
dense stellar systems, collapse to massive black hole 79—25652
density matrix in quantum electrodynamics, equivalence principle and Hawking effect 78—66060
Derrick's theorem in curved space 79—12658
dipole field in charged black hole electrostatics 80—112
Dirac eqn. in Kerr-Newman space of black hole, class of solns. 77—49828
Dirac equation generalized total ang. momentum operator in curved space time 79—49128
Dirac quanta detection in Rindler and black hole space times, ξ quantisation scheme 80—31651
disc accretion onto black hole at subcritical luminosity 77—64791
disc accretion onto magnetised compact objects, theory *(Russian)* 79—44467
dissipative test EM fields in black hole background 79—25627
distributional geometry, appl. to black holes in general relativity 79—93006
domains of stationary communications in space-time 78—62133
Dopplers, Hα line freq. depend. general relativistic formula, appl. to (SS 433) 79—97010
dust, thin spherical shell, around black hole, dynamics, Russner-Nordstrom geometry 78—77481
dyons, possible non-explosion 77—78817
early speculation by John Michell (1770s) 79—44691
early universe, thermal radiation during quantum era rel. to relic radiation origin *(Russian)* 78—81717
Einstein black hole, existence, local instantaneous symm. of space-time, variable vel. *(Chinese)* 77—13381
Einstein eqn. spherically symm. solution in presence of conformally invariant scalar field 80—17846
Einstein vacuum field eqns. solns. using local symm., rotating body neutrics 78—54257
Einstein-Yang-Mills pseudoparticles and electric charge quantization of dyon black hole 79—12703
elastic spacetime rel. to black holes and gravitational waves 78—73625
electrified, with accretion discs, positron and photon beams 77—13383
electrodynamics and Carter tetrad 77—49426
electrodynamics in curved space, theory 80—90465
electron pair production by photons in constant electromagnetic field in general relativity 78—8568
electron-positron pair production in hot unsaturated Compton accretion models, rel. to X-ray sources 80—36658
elliptical galaxies, massive central objects rel. to halo formation 78—4366
EM energy extraction through charged tachyons 79—17013
EM field of external sources for observer near nonrotating black hole *(Russian)* 78—8040
EM generalisation of Robinson's identity, Kerr uniqueness theorem 78—81649
EM radiation near black holes and neutron stars 78—53978
energy emission, Heisenberg's uncertainty principle 80—105454
energy release mechanisms 79—75242
energy sources in quasars and nuclei of galaxies 77—60849
energy states, classical and quantum 78—12285
entropy on horizon, sense or not 80—52092
equilibrium in radiation filled cavity 80—52093
equilibrium with radiation field, canonical ensemble 80—52121
ergoregion instability of rotating stars, eigenfrequency calc. 79—8835
ergosphere instability to scalar and EM perturbations 79—12489
ergosphere of massive Kerr black hole, energy mechanism, Penrose photoproduction processes 80—31365
evaporation, Higgs particles producing Hawking particles 79—2553
evaporation, implications of pair prod. in intense mag. fields 77—13505
evaporation, inevitability of associated naked singularity 80—36924
evaporation, particle origin outside horizon 77—33550
evaporation, predictability, CPT invariant superscatt. operator and S-matrix 80—46600
evaporation back reaction problem, conserved energy flux 80—85972
evaporation black holes, observational consequences of positron prod. 80—46599
evaporation effects, criticism of analysis 77—67031
evaporation of primordial objects and search for associated γ-rays 78—36633
event horizons, thermodynamic quantities and props. 79—97113
existence, event horizon theory confirmation *(Russian)* 77—60792
existence in cosmic rays discussed *(Russian)* 77—29875
exploding, instantaneous Cauchy surfaces topological change 78—12087
exploding, radio pulse spectrum calc. 78—12271
exploding, search using atm. Cherenkov method 78—49473
exploding black holes, upper limit for radio pulse emission rate 77—87469
explosions, detect. method, search for powerful radio bursts 77—37613
explosions, theory of optical and radio detect. 77—53622
explosions rel. to universal origin 78—8178
exponential amplification in gravitational field of ultrarelativistic rotating body 78—93594
extragalactic radio sources models, internal dynamics and brightness distribs. 77—22323
falling through black hole into another universe, theory 78—32748
five-dimensional theory, conditions of existence of horizons 78—73907
formation, effect on radiation-matter flat universe 80—94900
formation, entropy, temperature and radiation, review *(Norwegian)* 79—40211
formation, generation of pairs by collapsing body *(Russian)* 77—13234
formation, gravothermal catastrophe of finite amplitude 79—2476
formation by collapsing cloud of quantal particles 79—2552
formation following stellar collapse and explosion, massive star core hydrodynamics 79—16995

black holes continued
formation in cold early universe, influence on galaxy form. 78—16585
formation of neutron stars and black holes *(Swedish)* 78—69823
free falling body in field of black hole, superluminal speeds, tachyons 77—78816
galactic active centre, relativistic astrophys. *(Russian)* 77—13233
galactic centre, distrib. of stars and dust, black hole hypothesis 78—86010
galactic centre, tidal disruption of stars and massive black hole evolution *(Russian)* 78—12371
galactic centre object 80—22089
galactic centres, possibility of existence in M31 77—26025
galactic mass compact objects, rel. to quasar image doubling assoc. with absorpt. systems 80—22112
galactic nuclei, black hole model and quasar/galaxy relations 78—32582
in galactic nucleus, black hole sustenance rel. to quasars power source 78—57632
in galactic nucleus, recurrent outbursts explained 79—21423
galactic nucleus, tidally disrupted star gas debris accretion and radiation spectrum 80—90467
galaxies active nuclei, irradiated stars mass loss rel. to black hole feeding rate 80—56949
galaxies active nuclei, massive black hole binaries model 80—109546
galaxies active nuclei, massive black hole model and Monte Carlo simulation of relativistic Comptonisation 80—90566
galaxies active X-ray sources, hard X-ray emission mechanism 79—97080
gamma rays, emission from accreting black holes 78—32504
gamma rays from accretion onto rotating holes 79—48841
gamma-ray binaries, emission during spherically symmetric accretion onto black hole 80—17608
gamma-ray burst production near rapidly rotating accreting black holes 77—49422
gamma-ray bursts from primordial black holes 79—30085
general relativistic plasma MHD conservation laws, black hole rot. energy 79—2685
general relativity conference, Trieste, Italy, 1975, July 78—8285
geodesic equation, rel. to Hawking's black hole area theorem 80—90468
geodesics in black hole space-times 80—4602
giant black holes mass-density diagram *(French)* 80—94828
Gibbs-Duhem relation from Weinholds geometric approach 80—57153
globular cluster black holes rel. to gamma- and X-ray bursts *(Russian)* 77—17721
globular cluster X-ray source, evolution of 100 M⊙ black hole in binary 78—61932
globular cluster X-ray source formation by collisions of compact and normal stars 78—28854
in globular clusters, close binary systems rel. to black hole form. 79—44530
globular clusters with massive black holes, dynamical evolution 78—4302
globular clusters with massive black holes, stellar density cusp 78—4303
golbular cluster NGC 5824, assoc. with bright transient X-ray source Centaurus XR-4 78—12420
grand unified theories, baryon production through primordial black holes 80—101970
gravitation, charges, cosmology and coherence, elementary particles and Dirac large numbers 79—2477
gravitational aspects *(Hungarian)* 80—46894
gravitational collapse, bimetric general relativity theory 80—85853
gravitational collapse of stellar core, secondary indications 80—62177
gravitational collapse with charge and small asymmetries, interacting EM and gravitational perturbation 80—105274
gravitational cyclotron instability, mechanism for cosmic radio emission 78—65724
gravitational effects on polarised radiation from vicinity of black hole 77—82440
gravitational field, existence outside black holes 79—9158
gravitational inertial field and critical systems, free motion 78—93484
gravitational lens effect, EM wave diffr. in Schwarzschild space-time 80—90750
gravitational lens effect, focusing by slowly rotating relativistic spherical mass 80—105155
gravitational lens effect and pregalactic halo objects 80—17484
gravitational lens effect of moving black hole 77—33549
gravitational Michelson-Morley expt., proposed, experimental and Schwarzchild metrics, black holes 79—97289
gravitational mirror effect, appl. in black hole detect. technique *(Russian)* 78—40987
gravitational radiation, collapsed objects and exact solns., Einstein Centenary Summer School, Perth, Australia, 1979 January 80—105434
gravitational to EM conversion on charged black holes, low-freq.-limit cross-section 77—25935
gravitational wave detection, astrophysical sources, resonant mass, laser interferometer and Doppler ranging methods 80—68122
gravitational waves, emission, from trajectories plunging into nonrotating black hole 80—4246
gravitational waves and limiting stability of self excited oscillators *(Russian)* 78—45540
gravitational waves emission, theory and astronomical appls. 79—92664
gravitational waves radiation, reson. freqs. of rotating black holes free oscills. 80—105271
gravitational-inertial field of Universe, crit. systems struct. 80—8720
growth in dense stellar systems with evaporation of stars 80—62178
GX 339—4, black hole candidate 79—48962
GX 339—4 (4U 1658—48), possible black hole binary, optical studies 79—101220
Hawkin's exploding black holes, Arnowitt-Deser-Misner quantisation of metrics with two parameter isometry groups 77—45779
Hawking's effect, quantum field theory applied in curved space-time 78—12268
Hawking effect, temp. relativity, axiomatic field theory 80—109456
Hawking effect, thermal nature of the density matrix for black hole particle prod. *(Russian)* 78—89644
Hawking effect and Euclidean QFT 78—73732
Hawking emission, simple theory 77—82338
Hawking mini black-holes origin and cold early Universe 78—93298
Hawking radiation and 'vacuum polarization' near black hole 77—67030
Hawking radiation and strong gravity black holes 79—67213
Hawking radiation of scalar and Dirac quanta from a Kerr black hole 79—30334
HD 152667=OAO 1653—40, black hole candidate 79—17021

black holes continued

- HD 152667 (V861 Scorpii), eclipsing binary X-ray source, possible black hole 79—53858
- HD 152667 (V861 Scorpii), phys. props. and orbital parameters, supergiant star with black hole companion model 79—71067
- HD 152 667 companion 79—48848
- HD 49798, strange composite sdO star, possible existence of collapsed companion 78—49435
- HD 72 754 companion 79—48848
- hot accretion disks in galactic nuclei, pair production and gamma-ray luminosities 80—56930
- hot corona around black hole accretion disc and Cygnus X-1 model *(Russian)* 77—22265
- hot universe with primordial black holes, neutrino radiation kinetics *(Russian)* 78—93485
- hydrodynamic evaporation *(Russian)* 79—48846
- instability of black hole inner horizons 78—12276
- interactions, gravitational wave emission 79—125
- interior Kerr metrics, tests 78—28666
- international school proc. (Varenna, Italy, 1975 July 14-26) 79—80334
- inverted black holes, anisotropic collapse, static vacuum, electrovacuum field struct. 80—67776
- ion viscosity in hot accretion disc around black hole 79—62813
- irreducible mass for the Tomimatsu-Sato space-times 79—49133
- irreversible thermodynamics, fluctuation-dissipation theorem 77—60791
- Israel's theorem, uniqueness of Schwarzschild black hole 78—4097
- KdV eqn., particular N-soliton soln. 80—31971
- Kerr, Dirac eqn., anomalous Zeeman splitting of energy level 77—74081
- Kerr, EM fields of stationary sources in vicinity 77—49424
- Kerr black hole, EM extraction of energy and ang. momentum 77—53621
- Kerr black hole, gravit. perturbations in spin coeffs and Weyl tensor components 78—12273
- Kerr black hole, gravit. perturbations of quantities finite in stationary state 78—12274
- Kerr black hole, gravitational perturbations 79—44819
- Kerr black hole, high-freq. radiation from falling particle 78—16452
- Kerr black hole, irreducible mass, unincreasable angular momentum, isoareal transforms. 78—32503
- Kerr black hole, low-freq. radiation from infalling particle 80—62176
- Kerr black hole, massive fermion superradiance 79—25948
- Kerr black hole, neutrino wave reflection and transmission 77—9765
- Kerr black hole, orbiting fluid discs analytic theory 78—36631
- Kerr black hole, orbits of spinning particles 80—31326
- Kerr black hole, spin thermodynamics 79—93015
- Kerr black hole, tidal interactions and gravit. radiation 78—4276
- Kerr black hole, weak EM field of point charge on symm. axis 77—53624
- Kerr black hole in thermal equilibrium and the ν vacuum 79—97022
- Kerr black hole symmetries, Petrov type D Einstein Maxwell fields 78—12269
- Kerr black hole with tilted accretion disc, mag. alignment 77—60789
- Kerr black holes, charged current loop field and pot. 78—40988
- Kerr black holes, energetics, reversible transformations 78—85968
- Kerr black holes, stable circular orbits of test particles moving in equatorial plane 80—85970
- Kerr gravitational field effect on optical images 77—45480
- Kerr hole, elec. and mag. cond. 79—25625
- Kerr metric, geometrical optics appls. to light propag., analytical results 77—29637
- Kerr metric, null trajectories 79—25925
- Kerr metric, test particle motion *(Russian)* 77—45752
- Kerr metric and stationary axisymm. gravit. fields 78—12272
- Kerr metric effect on EM wave plane of polarization 80—94827
- Kerr metric in cosmological background, event horizon radius 77—74082
- Kerr naked singularities, accretion disks 79—30084
- Kerr naked singularity, classical instability 78—57834
- Kerr naked singularity evolution surrounded by accreting disc of matter 79—75245
- Kerr Newman black hole, Dirac electron eqn. separation 77—2583
- Kerr source, energy extraction by tachyon injection 79—48844
- Kerr-Newman, scalar and electric charge at rest *(French)* 77—67108
- Kerr-Newman background space, nonstatic nuclear forces, meson field at black hole event horizon 78—61880
- Kerr-Newman black hole, massive spin-1/2 wave, non-allowed superradiant scatt. 77—61002
- Kerr-Newman black holes, isoareal transformations 78—36630
- Kerr-Newman black-hole interior, quantised massless field, instability 80—82409
- Kerr-Newman geom., equatorial circular geodesics 78—4533
- Kerr-Newmann black hole, spontaneous discharge 78—12288
- Kerr-type particle, uniformly accelerating and rotating, Schwarzschild, Rindler and Kerr surfaces 80—85855
- Killing horizon as event horizon, a necessary condition in general relativity 78—8295
- Killing horizons around a uniformly accelerating and rotating particle emitting gravitational radiation 80—105557
- Klein paradox and vacuum polarization 78—8329
- Klein-Gordon equation for massive scalar meson field, Kerr-Newman metric 77—22262
- Kron 3, globular cluster, identification with 4U 0026—73 rel. to central black hole 79—5919
- lifetime and cosmic censorship 77—13384
- light propagation, observer in accretion disc of rotating black hole, sky appearance 80—17605
- light propagation near rotating black hole and accretion disc, sky appearance 80—17606
- linearized Einstein theory, twistors, plane fronted impulse wave backgrounds 79—30329
- M15, globular cluster, dynamical models without black hole 78—32536
- M87, anisotropic stellar vels. distrib. rel. to supermassive black hole model 80—82500
- M87, central regions luminosity distrib., isothermal core, point source or black hole models 79—71110
- M87, dynamical evidence for central mass concentration 78—49529
- M87, evidence for supermassive object in galaxy nucleus from SIT and CCD area photometry 78—49528
- M87, giant elliptical galaxy, appl. of black hole theory *(French)* 79—92866
- M87, spectroscopic evidence for large central mass 80—94873
- magnetic, black holes 78—12283

black holes continued

- magnetosphere, charge particle trapping 78—57573
- magnetospheres existence, theory 77—64792
- magnetostatics, general multipole solns. 77—33913
- Mansouri-Chang gravitation theory, no hair theorem for black holes 79—49145
- marginally bound dust collapse, time functions in numerical relativity 79—71321
- mass positivity for black hole space-times 80—8880
- massive, rotating, charged, phenomena based on Schwarzschild and Kerr-Newman metric solns. 79—71064
- massive black hole ejection from galaxies, quasar-galaxy association 77—22263
- massive black hole in globular cluster, star distrib. for unequal star masses 78—8062
- massive black holes, existence in galaxies nuclei and quasars 79—25713
- massive black holes spherical accretion, thermal limit rel. to X-ray bursts 78—45430
- massive extreme Kerr black holes, Penrose pair production 79—21322
- massive particle finite motion in Kerr and Schwarzschild fields *(Russian)* 79—8833
- massive vector fields and black holes 78—96499
- massless quantum fields in curved asymptotically flat space-time, particle creation near black hole *(Russian)* 78—57846
- massless scalar field in a de Sitter universe and its thermal flux 79—127
- massless Thirring model is curved space, black holes, thermal states, conformal anomaly 79—26221
- materials motion around a source whose luminosity changes 79—12394
- matter-antimatter accounting, thermodynamics, and black-hole radiation 79—49136
- maximal surfaces in closed and open spacetimes 78—8294
- maximons, maximon swarm hypothesis *(Russian)* 79—48847
- MHD near a black hole 78—12281
- MHD processes near compact superdense objects 79—40206
- MHD relativistic processes, in black hole fields 78—12280
- mini black holes, formation in condensed stellar mass object core 77—49425
- mini black holes fast explosive evaporation in plasma and solar flares, analogy, energy conversion processes 78—96388
- miniblack holes, general props. and theories 77—41388
- minicompact objects according to the bimetric theory of gravitation 79—49140
- missing mass in galaxies, role of brown dwarfs and black holes 78—61879
- multiply-connected space-time, black holes and tachyons 79—30315
- in N-body stellar systems, two-body tidal dissipation rel. to form. 78—93329
- N-particle distrib. functions, space- and time-depend., possible appl. to black holes 77—26237
- naked singularities, event horizons, and charged particles, test particle motion in Reissner-Nordstrom field 79—71684
- naked singularities in Kerr metric, relationship to black hole 79—21600
- naked singularity in scalar-tensor gravit. theory 79—8826
- naked singularity solutions, gravit. collapse with axial symm., geodesics, particle orbits 78—41215
- nearly collisionless spherical accretion, theory 78—12090
- neutrino fluxes from rotating black holes and thermal radiation, parity violating effects 80—22034
- neutron stars mass upper limit for stability against black hole form. 78—96498
- Newman-Penrose formalism and its application in general relativity, review *(Russian)* 79—21595
- NGC 4151, Seyfert galaxy, massive collapsed object accretion model for repeated X-ray flaring 80—90534
- NGC 4151, X-ray flares in Seyfert, thermal model and central black hole 78—93407
- NGC 6251, radio galaxy, evidence for central supermassive object from CCD photometry 80—26966
- in NGC 6624, globular cluster, X-ray, optical and IR obs. 77—45498
- NGC 741, 1316, 7626, radio galaxies, central dense star clusters luminosities rel. to accreting black holes 80—94871
- no-hair theorem for Abelian-Higgs model 80—46601
- non-linear wave equations in a curved background space 78—65827
- nonequatorial tachyon trajectories in Kerr spacetime, and second law of black hole phys. 79—71244
- nonrotating black hole, distant stars distrib. seen by freely falling observer *(Polish)* 80—26897
- nonsymmetric disc accretion onto rotating black hole *(Russian)* 80—36661
- Novikov-Thorne accretion disc models, boundary condition modification and vel. matching at inner edge 77—13380
- nuclear forces near massive, charged slowly rot. black hole 77—60999
- null surface quantization and quantum field theory in asymptotically flat space-time *(German)* 79—25959
- observational status 79—97019
- observational traits of black holes in the optical band 80—67777
- optical appearance of collapsing star 80—4391
- pair production by gravitational waves in field of black hole 77—22474
- parity nonconservation and rotating black holes 79—12491
- particle capture from plunge orbits, spin and charge evolution 77—25936
- particle creation due to Casimir effect 79—35607
- particle creation in curved space-time, back reaction effect 77—49645
- particle creation in gravit. collapse, absorpt. effect 77—91420
- particle creations in the pseudoparticle gravitational fields 79—2704
- particle detectors and black holes 78—12287
- particle emission and critical mass, Kessler model, comment and reply 79—71190
- particle emission from rot. black hole 77—26024
- particle emission in the de Sitter universe for massless fields with spin 79—40434
- particle emission model, for teachers 78—62018
- particle emission process, high energy limit 77—5544
- particle emission rates from nonrotating black hole 78—24718
- particles in stationary spherically symmetric gravit. field 77—41293
- Penrose pair production in massive Kerr black hole, power source for active nuclei 79—44352
- Penrose powered black holes in Centaurus A, 3C 273 and NGC 4151, gamma rays emission 80—56925
- perturbation due to a rotating, enclosing spherical shell of matter 78—81648
- photon orbit charts for teaching 77—33783

black holes continued
- plane EM wave diffraction by spherical gravit. lens, Poynting vector calc. 79—25945
- plasma processes, space-time curvature 79—84873
- point source spherical model, Schwarzschild coord. frame, nature of interior universe 77—67107
- pregalactic black holes, constraint an abundance 80—12777
- pregalactic black holes in Galaxy, accretion of interstellar matter 78—8039
- primordial, formation 80—12776
- primordial, possibility of cold cosmological singularity *(Russian)* 77—22266
- primordial, role in galaxy form. in chaotic cosmology 77—57112
- primordial, search for high energy gamma ray bursts 78—54084
- primordial, search for radio pulses 79—25626
- primordial, self-similar growth, stiff eqn. of state 78—36629
- primordial, small mass black holes and fundamental length *(Russian)* 77—22264
- primordial, statistical clustering 77—49423
- primordial, upper bound on number density calc., big bang nucleosynthesis 78—65649
- primordial black hole development 78—93299
- primordial black hole evaporation, baryon prod. and excess 80—41852
- primordial black hole evaporation rel. to D origin *(Russian)* 77—74172
- primordial black hole explosions, search for optical pulses 77—57006
- primordial black holes, as Universe antimatter content hiding place 80—22126
- primordial black holes, baryons generation 80—98750
- primordial black holes, evaporating, rel. to galactic positrons primary source and fates 80—109319
- primordial black holes, evaporation, effects on background EM radiation spectrum 79—88695
- primordial black holes, form. in anisotropic universe 78—32507
- primordial black holes, form. in stiff universe *(Russian)* 80—51802
- primordial black holes, form. in tepid early universe 78—20919
- primordial black holes, influence on galactic radio spectrum 80—62179
- primordial black holes, prod. and decay rel. to Universe lepton number 80—8730
- primordial black holes, radiation accretion in early Universe 80—67918
- primordial black holes, self-similar growth for general sound speed case 79—5856
- primordial black holes and big bang nucleosynthesis *(Russian)* 79—17151
- primordial black holes evaporation, cosmological implications 79—21325
- primordial black holes explosions, limits on microsecond cosmic radio bursts 79—17119
- primordial black holes form. and accretion of matter 80—36660
- primordial black holes formation, hydrodynamics 79—21324
- primordial explosions, gamma-ray bursts rate upper limit 77—29873
- primordial low mass black holes, effect on H recomb. kinetics *(Russian)* 79—17152
- primordial low mass black holes evaporation and H recomb. kinetics *(Russian)* 78—61943
- primordial mini black holes explosion rate, upper limit from gamma-ray bursts search 80—67911
- primordial singularity in uniform Friedmannian universe 80—101656
- primordial small mass black holes evaporation, obs. consequences *(Russian)* 77—78818
- production of massive objects in active galactic nuclei unlikely 78—89261
- properties and possible existence, review 79—48842
- QSO black tide model, destruction of stars in isothermal sphere 77—78884
- QSOs, accretion disc model 77—64872
- QSOs, black flash model 78—57673
- QSOs model, stellar tidal disruption by black hole 77—33674
- quantum evaporation, baryon asymmetry of the Universe *(Russian)* 80—109577
- quantum evaporation, vacuum definition in external grav. field 79—21642
- quantum evaporation in projective relativity 79—17014
- quantum field coupled to Schwarzschild-de Sitter metric, vacuum energy-momentum tensor 80—52091
- quantum gravitational fluctuations, energy dissipation mechanism 78—57572
- quantum gravity, semiclassical theory, appl. book contrib. 80—22268
- quantum gravity, unpredictability 78—54277
- quantum gravity action integrals and partition functions, Kerr-Newman and de Sitter examples 77—64984
- quantum gravity and path integrals, supersymmetric theory, virtual Planck-mass black holes 79—2706
- quantum linearization instabilities 79—44835
- quantum mechanical evaporation, predictability breakdown, principle of ignorance 77—17356
- quantum mechanical particle prod., black hole radiance 78—81647
- quantum mechanics, particle escape by tunnelling 77—82272
- quantum particle creation of Hawking effect in nonstationary black holes 78—4278
- quantum processes, especially Hawking thermodynamic emission process near black holes 78—12284
- quantum processes, review 77—17614
- quark confinement, event horizons around a particle surrounded by a static confinement potential 78—66075
- quasar, black hole model *(Japanese)* 80—22114
- quasar energy source models and cosmological evolution 80—27002
- quasar energy sources, choice between, magnetoid, black hole and compact star cluster *(Russian)* 77—78885
- quasar-like objects, black hole model for IR and optical emission 78—20905
- quasars, accreting black holes model 78—57678
- quasars, accretion discs thermal continuum as optical emission source 78—54075
- quasars, black hole model 78—32582
- quasars, gravit. and Doppler redshifts, interpreted as massive black holes ejected from galaxies 80—46695
- quasars, massive black hole model and Monte Carlo simulation of relativistic Comptonisation 80—90566
- quasars and active galactic nuclei, magnetic flare model, magnetised accretion disc around massive black hole 80—22113
- quasars and galaxy nuclei, black hole gravity power model 78—57667
- quasars and related objects, stellar debris clouds in black hole model 78—32597

black holes continued
- quasi-isotropic Tolman solution for black hole form. and accretion *(Russian)* 77—91561
- radiance, Planck spectrum local calc. 78—45354
- radiant energy from hot black holes *(Norwegian)* 79—40212
- radiation accretion by primordial black holes in the early Universe 79—44519
- radiation from moving mirrors and from black holes 77—67372
- radiation from particles moving near black hole in external mag. *(Russian)* 78—49474
- radiation hydrodynamics of high-luminosity accretion 78—77571
- radiation pressure effects on spherical accretion 78—61725
- radiation spectrum fluctuations from spherical symmetric black hole 77—25937
- radiation-dominated non-relativistic gas, Bondi accretion problem 78—77575
- radio galaxies, relativistic jets and beams 78—96541
- recoil velocities due to gravitational radiation reaction 80—85969
- Reissner Nordstrom background geometry, gravitational and EM perturbation functions 78—49472
- Reissner Nordstrom charged black hole, EM and gravit. waves propag. 77—87470
- Reissner-Nordstrom, construction of metric and vector pot. perturbations 80—8647
- Reissner-Nordstrom, coupled gravit.-EM perturbation anal. 77—26022
- Reissner-Nordstrom, coupled gravitational and EM perturbs., scatt. matrix, energy conversion, quasi-normal modes 80—67775
- Reissner-Nordstrom, electrostatics, Maxwell's eqns. multipole solns., field of point test charge 77—17613
- Reissner-Nordstrom, Green's function anal. of odd-parity perturbations, normal modes 77—17612
- Reissner-Nordstrom, scalar perturbations inside the event horizon 79—2556
- Reissner-Nordstrom, theories of interacting perturbations 79—97021
- Reissner-Nordstrom and Schwarzschild black holes, perturbations, potential barriers with equal reflection and transmission coefficients 80—27191
- Reissner-Nordstrom black hole, force free fields 78—77572
- Reissner-Nordstrom black hole, metric perturbations 79—71319
- Reissner-Nordstrom black hole, perturbation treatment using Newman-Penrose formalism 79—44820
- Reissner-Nordstrom black hole, stationary interacting fields 78—24710
- Reissner-Nordstrom black holes, instability of the Cauchy horizon 79—67201
- Reissner-Nordstrom naked singularity as quantum mech. scatterer 77—57267
- Reissner-Nordstrom-de Sitter metric, the third law, and cosmic censorship 79—35609
- Reissner-Norstrom black hole, interior final state evolution 80—8648
- relativistic accreting discs, hydrodynamic struct. 78—36632
- relativistic arguments against existence 79—75243
- relativistic fluid accretion discs with constant ang. momentum per baryon, equilib. struct. 77—78815
- relativistic particle falling into black hole, EM and gravitational radiation *(Russian)* 80—52097
- relativistic particle radiation near a black hole in an external mag. field 80—22035
- relativistic star, rotating shell model 79—88650
- review 77—17610
- Robertson-Walker universe, pair-creation of particles 80—22265
- Rosen's bimetric theory of gravity, orbital topoography and other astrophysical consequences 78—54274
- rotating, electromagnetic perturbations 78—12279
- rotating, gravit. waves emitted by particles in circular orbits 79—17009
- rotating, neutrino emission ang. depend. 79—88696
- rotating, stationary axially symmetric perturbations 77—17611
- rotating, weak EM field of point charge on symmetry axis 78—20852
- rotating (kerr) black hole perturbations, spin weighted spheroidal harmonics 78—4277
- rotating black hole, interaction with weak mag. field, ang. momentum changes 77—74080
- rotating black hole, Kerr metric, spontaneous creation of massive spin 1/2 particles 78—89217
- rotating black hole energy loss, Penrose conversion, upper bounds 78—16455
- rotating black hole formation by dust cloud gravitational collapse 79—2557
- rotating black hole in mag. field, particle creation 77—2452
- rotating black hole perturbations, ang. momentum 77—53623
- rotating black hole reson. oscills., gravit. radiation 77—9766
- rotating black holes, instabilities of massive scalar perturbations 79—54026
- rotating black holes, superradiance, spin thermodynamic explanation 80—86179
- rotating neutron stars, general relativity, exact solns. for slow rot. 79—75239
- rotation, spin-up by thick accretion discs 80—105273
- scalar charge, instability under monopole perturbations 78—77576
- scalar fields around charged rot. black holes 78—32505
- scalar quanta emission rate, effect of static scalar field solns. in Schwarzschild metric 77—45765
- scalar waves in Schwarzschild metric, approx. scheme 79—54025
- Schwarzchild black hole, gas accretion 80—56871
- Schwarzschild, elastic scatt. and absorption of waves 79—5857
- Schwarzschild, in ext. mag. field, radiation emitted by relativistic particles 78—96501
- Schwarzschild, perturbations, transformations between governing eqns. 77—60790
- Schwarzschild, scalar and electric charge at rest *(French)* 77—67108
- Schwarzschild, stress tensor trace anomalies, Hawking effect 77—67110
- Schwarzschild black hole, $\gamma > 5/3$ gas accretion 79—17011
- Schwarzschild black hole, absorpt. and emission spectra, computational methods, cross sections 79—2558
- Schwarzschild black hole, focusing gravit. mirror effect 80—46602
- Schwarzschild black hole, master differential eqn. for perturbations 77—26214
- Schwarzschild black hole, plane EM wave diffraction, Poynting vector near horizon 80—22250
- Schwarzschild black hole, prob. distrib. of incoming radiation 78—8300
- Schwarzschild black hole, props. of polarised radiation from point source comparison 77—67109

black holes continued
- Schwarzschild black hole, scatt. of gravit. waves, low freq. limit 78−16456
- Schwarzschild black hole, stationary source fields, general solns. 77−29864
- Schwarzschild black hole, wave scatt. and adsorpt. cross-section 78−8283
- Schwarzschild black hole perturbations, zero rest mass fields in algebraically special curved space-time 77−74078
- Schwarzschild black hole stationary spherical accretion, stability 80−51800
- Schwarzschild electrodynamics, rel. to black holes and neutron stars 78−77480
- Schwarzschild gravitational field, partially polarised EM radiation *(Russian)* 80−51801
- Schwarzschild hole in radiation heat bath, stochastic evolution 80−85971
- Schwarzschild metric, tachyons from free falling body 77−53625
- Schwarzschild metric and tachyon production inside horizon 78−36635
- Schwarzschild space-time, electrostatics, electric fields and black holes *(French)* 79−40432
- Schwarzschild space-time, radial wave functions, global prop., irregular singular point 77−2567
- Schwarzschild space-time, vacuum polarisation induced by gravitation 80−82410
- V861 Scorpii=OAO 1653−40, black hold candidate 79−17021
- V861 Scorpii, IR obs. of black hole candidate 79−44538
- V861 Scorpii (HD 152667), X-ray binary, behaviour of Hα 79−101171
- second law of black hole physics and tachyons 79−49117
- self-consistent spherical accretion and X-ray emission 79−53936
- self-similar relativistic disks in rotation 79−16823
- selfgravitating accretion disc with hot corona, model of active galactic nucleus 79−62812
- Seyfert nuclei, black flash model 78−57673
- Seyferts and quasars, broad line emission from black hole accretion disc 77−60819
- shear hell holes and anisotropic universes 80−95011
- singularities in general relativity theory 79−35591
- slowly rotating nonhomogeneous bodies, quasistationary gravit. collapse in general relativity 77−49289
- slowly rotating weakly charged black hole, space-time and physical fields perturbs. *(Russian)* 78−36634
- small, quantum mechanical approach 78−16453
- small black hole absorpt. cross section for Dirac and scalar particles 77−26023
- small mass, spin effects on formation in Einstein-Cartan theory 77−71125
- solar companion star, black hole in hyperbolic orbit 78−12198
- solitons and hadronic temperature 77−26498
- sources of gravitational radiation, conf. proceedings (Seattle, 24 July-4 Aug. 1978) 80−36778
- spacelike geodesics in the Nordstrom geometry 79−88852
- spacetime singularities 78−8291
- spherical black hole with thin accretion disc, image 79−67049
- spherical stellar system, distrib. of stars around massive central black hole 78−65660
- spherically accreting, radiation near Eddington limit 79−48843
- spherically symmetric, perturbations, linearised Einstein-Maxwell eqns. 80−72992
- spherically symmetric accretion with self-gravitation, criteria for enhanced accretion 79−71098
- spin entropy of a rotating black hole 79−75246
- spinning charged test particles near black hole, cosmic censorship hypothesis 79−62866
- spontaneous particle creation in strong gravitational field, semiclassical theory 78−54281
- spontaneous particle creation leading to black hole evaporation 78−40986
- SS 433, accreting black hole model 80−85958
- SS 433, circumstellar ring model rel. to weak lines pair wavelength vars. 79−67023
- SS 433, emission regions and black hole accretion disk 80−67746
- SS 433, mass loss rates and lifetime from W50 optical filaments 80−12804
- SS 433, massive black hole and pulsar models rel. to precessional motion origin of 164^d period 80−62138
- SS 433, precessing ring model, test by spectral line obs. 79−101152
- SS 433, ultra-close black hole-degenerate dwarf binary system model 80−4384
- star clusters containing massive central black holes, Monte Carlo simulations 79−8955
- star clusters massive central black holes, self-consistent potentials for dynamical simulations 80−26915
- star distribution in vicinity of massive black hole *(Russian)* 77−74083
- stars near massive compact body, steady state distrib. *(Russian)* 78−16481
- static plasma polarisation in Schwartzschild gravitation field *(Russian)* 79−16825
- static stars, mathematical curiosities in Newtonian and general relativistic aspects 77−74045
- stationary, uniqueness theorems 78−96500
- stationary accretion disc, numerical anal. of struct. 79−17015
- stationary accretion disk structure, assuming vertical distribution given by a polytrope 78−20851
- steady state universe, hawking process and cosmic microwave background 79−80380
- stellar cluster around massive black hole, stationary state *(Russian)* 80−67806
- stellar collapse, neutrino radiation for black hole form. rel. to envelope outburst problem 78−45350
- stellar collapse and the black hole limit from a dynamical view 79−30081
- stellar collapse to neutron stars and black holes, computer generation of spherical spacetimes 80−46385
- stellar collisions near Kerr black hole, compact extragalactic source model 79−12490
- stellar consumption rate in N-body system *(Russian)* 77−91562
- stellar distrib. around black hole in cluster, Fokker-Planck eqn. 79−21364
- stellar distribution and consumption rate around massive collapsed object 77−45497
- stellar flares caused by tidal action *(Russian)* 79−30086

black holes continued
- Stephen Hawking and black hole studies 78−8042
- Stephenson-Sanduleak 433, anomalous emission lines, gas around central massive black hole 79−53831
- Stephenson-Sanduleak 433, massive black hole hypothesis 79−71057
- Stephenson-Sanduleak 433, model, precessing ring around massive black hole 79−88678
- stimulated emission, superradiance, Einstein A and B coefficients 77−67111
- stress-energy tensor for two-dimens. evaporating black hole 78−24706
- of , strong gravity, identification with elementary particles 78−16973
- strong gravity and Dirac numbers 78−21372
- subcritically accreting, model for X-ray sources in globular cluster cores and X-ray burster sources 80−12779
- Sun possible companion, mass, vel., and luminosity 79−2490
- superadditivity and concavity, black hole systems 80−98867
- supercritical accretion discs around black holes, models 80−105272
- supercritical accretion discs winds struct. and appearance, numerical models 80−21984
- supercritical disc accretion rel. to quasars and type 1 Seyferts 80−41850
- superluminal frames and tachyons, introductory view, book contrib. 79−44719
- superluminal particles motion in gravit. field of nonrot. black hole *(Russian)* 78−93103
- supermassive, rel. to galactic nuclei and quasars energy source 79−40213
- supermassive black holes, unsaturated Compton accretion discs models for hard X-ray spectra 80−22033
- supermassive black holes and exploding galaxies, review 79−80355
- supermassive compact objects, accel. by emission of asymmetric radiation 77−45481
- supermassive objects rel. to radiogalaxies 78−61882
- supermassive star, expanding, and contracting dust shell, Einstein's theory of gravit., black hole formation 78−12088
- supermassive star collapse to black hole, Einstein eqns., numerical soln. 80−41851
- supermassive stars and black holes, work of Johann Georg Soldner (1776-1834) 78−81787
- supersymmetric, in supergravity, spin 3/2 perturbation of Schwarzschild black hole 78−93300
- surface geometry of a black hole in a magnetic field 80−52095
- surface thermodynamics *(Russian)* 78−12270
- symmetry of charged rotating body metrics 78−77776
- tachyon detection 79−17012
- tachyonic scalar waves in Schwarzschild space-time 78−45558
- tachyons interaction with gravity, rel. to cosmology and black holes 79−25839
- Terzan 2, globular cluster, identification with XB 1724−31 rel. to central black hole 79−5919
- test particle motion in crossing Schwarzschild surface, book contrib. 79−44816
- theory and observational methods *(Hungarian)* 78−77574
- theory for holes with accretion disks 79−97024
- thermal equilibrium between black hole and heat bath, thermal Green functions 78−12275
- thermal particle prod. spectra in Taub-Nut spacetime 77−13382
- thermal propagators and accelerated frames of reference 79−67211
- thermally evaporating, Raychaudhuri eqn. 80−109457
- thermodynamic behaviour of charged black holes, phase transitions 77−74079
- thermodynamic mechanisms, review 78−93301
- thermodynamic theory, phase transition, specific heat, stability criteria 77−33548
- thermodynamics, cosmological event horizons and particle creation 77−67152
- thermodynamics, general review 80−31696
- thermodynamics, rel. to time asymmetry 77−2451
- thermodynamics, second order phase transitions 80−46897
- thermodynamics and entropy 80−4613
- thermodynamics and space-time distortion 78−8041
- thin spherical time like shells, eqn. of motion from Lanczos eqns. 79−67199
- third law for black hole mechanics, counterexample 79−88855
- tidal disruption by a massive black hole and collisions in galactic nuclei 78−77597
- tidal disruption by massive black hole in dense star cluster, fate of debris 79−67069
- tidal fields, d'Alembert's principle and test rigid rod 78−40812
- tidal gravitational radiation from body in field of black hole 78−4540
- time symmetric gravitational waves evolution, initial data, apparent horizon 78−12626
- toroidal singularities in general relativity 79−97023
- trace anomalies in a two-dimensional de Sitter metric and black-body radiation 78−65841
- turbulent accretion onto massive black holes 79−62865
- two-body restricted problem, almost circular orbits in general relativity *(Ukrainian)* 79−101056
- 3U 1820−30 in globular cluster NGC 6624, binary star model for recurrent X-ray bursts 77−33701
- ultrarelativistic black-hole encounters 79−30330
- unification of gravitation and matter, crossing terms in Einstein's eqns., singularity 78−21039
- unified gravit. and electromag. field theory of black-hole evaporation 78−53979
- Universe and microcosm, gravitational-inertial field theory 80−8721
- vacuum, empty, fields and quanta, strong gravity, particle-antiparticle annihilations 80−68400
- vacuum black holes, gravit. radiation scatt. 78−65648
- vacuum uniqueness theorem and generalisations 78−12278
- variable quasars and active galactic nuclei, strong gravity effect on light curve 79−16812
- variable rest masses, black hole solutions and neutron star models 79−30162
- wave front near black hole 78−8282
- white holes, angular appearance 78−45352
- white holes, appearance rel. to quasars and BL Lacertae objects 78−81650
- white holes, local big bang inhomogeneities and observability 78−45353
- white holes, nonexistence, anal. of star bursting Schwarzschild barrier 78−32506
- white holes, optical appearance 79−21323

black holes continued
white holes present appearance 78-61881
white holes spectral features in Nordstrom and Kerr-Newman metrics 77-29967
X-ray backgound, produced by pregalactic black holes? 80-56978
X-ray binaries, variable optical polarization rel. to black hole secondary component 78-20910
X-ray binary stars, observational evidence for black holes 77-57007
X-ray burst sources, accreting compact objects models 78-12427
X-ray burst sources, black hole accretion models 78-49566
X-ray luminosity of massive black holes 77-33547
X-ray radiation, polarisation features 80-46700
X-ray source, intensities from stellar wind flow past compact object 80-22116
X-ray source candidates *(Czech)* 80-31325
X-ray sources, high-freq. EM waves propag. through magnetised plasma in curved space time 80-48894
X-ray sources, rapid variability and dying pulse trains rel. to black hole candidacy 80-56872
X-ray sources in galactic bulge, disk model 80-17691
X-ray sources in globular clusters, central massive black hole model 78-12428
X-ray sources of galactic bulge, highly compact binary model 79-35430
X-ray spectrum, from disc accretion onto massive black holes 78-40985
X-ray stars in globular clusters 78-20916
Yang-Mills field source 78-8280
zero point fluctuations 78-12286
^{2}H production, by neutrino-induced nucleosynthesis 77-87582

blast waves *see shock waves*

blending
irregularly shaped particles 77-77441
nuclear fuel preparation, moderation control in large-capacity process unit 77-65316
polymer property-molecular weight distribution relation, non uniqueness, blending expts. 77-36445
polystyrene-mineral oil mixture, viscosity and normal stress coeff. 80-44349
solar collector material selection and blending guidelines 79-62060
U enrichment plant criticality analysis *(Japanese)* 78-46156

Bloch walls *see magnetic domain walls*

blood
see also haemodynamics
abdominal fluid accumulation meas. using electric impedance 77-48912
acceleration effects in women after 15 days bed rest, fluid and electrolyte shifts 77-48881
acrylonitrile-dimethylaminoethyl methacrylate copolymer structure and blood compatibility 77-81656
acute lymphocytic leukaemia patient data analysis system CLINFO 77-66823
adenylate energy charge changes of lymphocytes, platelets, erythrocytes after γ-irradiation 79-57718
adhesion of platelets and granulocytes in stagnant blood, effects of gravity and erythrocytes 80-3662
aerosol transport into blood and retention, rel. to alveolar microenvironment 77-25630
agglutination reactions, automated optical scanner 77-52861
albumin, human serum, adsorption studies, feasibility of radiolabelling 78-85359
alcohol determ., spectrophotometric method *(German)* 79-5415
amino acids, isotopic enrichment determ. by chem. ionis. mass spectra 79-79694
analysis, using differential pulse anodic stripping voltammetry 78-20089
angiographic images, simulated, blood vessel detection, evaluation of observer performance 79-5357
antithrombotic polymeric materials for artificial heart and devices for assisted blood circulation 78-36052
aorta, dog, simulation via adaptive model 79-11964
arterial O_2 partial pressure, chronic reduction, effect on radiation response of tumour in mice 79-16252
arterial O_2 tension, generation of variable amplitude sinusoidal changes for freq. response anal. 77-56563
arterial pO_2 intravascular monitoring using catheter-tip polarographic electrode *(German)* 78-85408
arterial thrombosis, in vivo method for evaluation of effects of materials 78-81071
arterial vessels, small, critical changes in lumen 80-61615
arteriovenous O_2 difference, noninvasive meas. method *(German)* 78-85441
artificial β-cell glucose sensor 79-83973
artificial and whole blood mixtures 80-45928
artificial blood substitutes, surface energetics anal. 80-41321
artificial liver support, protein-bound metabolite adsorbent equilibrium props. 79-20709
artificial liver support, protein-bound substance removal kinetics 79-20710
atherosclerosis, rheological aspects *(Japanese)* 80-94268
ATP content meas. in single red blood cell, using firefly bioluminescent reaction with optical instrument 79-79695
ATP measurement in single red blood cells using firefly biolum. reaction 78-48951
auto-immunity, math. model of cell dynamics 77-16900
biomaterial compatibility for cardiovascular appls., biological evaluation 78-36056
biomaterial evaluation considering species-related haematological differences 77-60291
blood analysis, optimal conditions *(Bulgarian)* 78-85280
body fluid volume changes induced by spaceflight 80-61715
bombardment of human blood cells, morphological detail of radiation damage 77-60230
bone marrow ^{32}P effects during postnatal development of Swiss albino mice 78-53450
bone marrow colony-forming units in beagles, response to whole-body γ irrad. 79-25043
bone marrow haemopoietic activity assessment in normal subjects 80-36073
bone tumours, human, scintigraphic assessment of ^{99m}Tc-diphosphonate 79-20613
brain-blood barrier, effects of microwave-induced hyperthermia, rat 80-61642

blood continued
brain-blood barrier, neutral amino acid transport into isolated brain capillaries 79-57616
brain-blood barrier, problems in quantifying effects, comparison of methods 80-61643
brain-blood barrier, reversal of microwave-induced permeability 80-61641
brain-blood barrier permeability obs. after microwave irradiation, rat 79-74718
bubble detection in decompression sickness, US imaging method 79-8527
bubble oxygenator, O_2 transfer controlling factors 78-53568
bubbles, spectral anal. of Doppler US decompression data 77-70513
C1q of human complement, neutron scatt. obs., conformational calcs. 80-81537
capillary permeability determ. from multiple indicator data, effects of finite red cell permeab. 78-44483
capillary tracer exchange, 4-phase model 80-101152
capillary viscometer for blood flow meas. 79-79671
cardiac blood pool, ECG-gated emission computerised tomography 80-98117
cardiac chamber imaging, comparison of red blood cells labelled with ^{99}Tc^{m} in vitro and in vivo 78-65109
cardiac output estimated by impedance cardiography 79-57741
cardiac pool, dynamic radio-isotopic images, time-motion display 79-5347
cell aggregation, conductometric meas. 77-25614
cell anal., weighted chi-squared test 80-30925
cell banding in US standing wave field 79-62291
cell computerised counting and sizing system 78-31932
cell counter, electrical meas. of suspended particles *(Japanese)* 77-44869
cell differential counter, ADC 500, pattern recognition based image processing system 78-73282
cell electrokinetic props. on exposure to phys. factors 77-70431
cell electrophoretic mobility meas. using new automatic method 80-67322
cell electrophoretic mobility study, semi-automatic system 80-3851
cell exam. by scanning electron microscopy 79-74812
cell freeze conservation control unit *(German)* 79-5410
cell high-speed analysis, laser absorpt. and scatt. meas. *(German)* 78-92687
cell K^{+} ion X-ray absorpt. edge fine struct., frog 79-66459
cell motion dynamics tracking and quantification, automatic picture processing method 79-53074
cell separation, local conc. gradient determ. by conductivity meas. *(German)* 79-5411
cell smear pathology differentiation by optical transform method 78-69248
cell suspensions, deep-freezing improvements by thermal history automatic detect *(German)* 79-88215
cell suspensions, stability to small disturbances in circular Couette flow 80-56099
cells, computerised spectral meas. 79-25058
cells conc. meas. by conductometric cytometer 79-92437
cellular radiation dose of labeled neutrophils and platelets 79-100749
cerebral regional blood volume, meas. with EMI 1010 scanner 79-53212
cerebrovascular permeability, quantitative method for meas. of alterations 80-61748
characterisation by US and computed tomography 80-98045
chlorobenzenes determination by gas chromatography with photoionis. detection 80-35809
chromosome aberration form. by gamma irrad. in lymphocytes, protection by free radical scavenging 78-20216
chromosome aberrations, dose-effect relationship, population exposed to increased natural radioactivity 80-72254
chromosome aberrations induced by low doses of X-rays in human lymphocytes in vitro 80-72235
chromosome aberrations of peripheral lymphocytes in rabbits exposed to whole body X-irradiation 79-43834
chromosomes of human female lymphocytes, distrib. of X-irrad. induced lesions, dose-effect relation 80-51175
circulation simulation development 77-66825
circulation system model 77-90848
circulatory regulation by artificial heart *(Japanese)* 77-36971
clinical oximetry for haemoglobin and O_2 saturation meas., problems 77-90952
clotting characterisation by US digital fixed path interferometer 78-44670
clotting of rabbit blood, Fourier transform. IR obs. 78-68945
clotting time measurement by automatic photometric system, digital display *(Danish)* 77-90826
clotting timer, automatic 77-52896
coagulation, effect of polyurethane morphology 79-39610
coagulation, rel. to membrane phospholipid asymm. 77-73511
coagulation and fibrinolysis under influence of direct elec. current 78-48766
coagulation in gastrointestinal haemorrhages, using laser endoscope *(German)* 78-69178
coagulation kinetics of normal and haemophilic plasma, rheological study 80-67107
coagulation parameter selection for automatic digital recording 77-21543
coagulation time, US meas. 79-83870
computerised high-speed blood cell anal. software system 78-44671
coronary disease and myocardial infarctions investigation using inert-gas clearance method 77-5121
corpuscle settling rate automatic fast meas. *(German)* 79-5413
Couette viscometer for short time shearing of blood 80-98179
couple stress fluid flow through narrow tubes 80-67105
criticality accidents, dosimetry using activations of blood and hair 80-89857
cryocoagulator for uterine contraction promotion and bleeding suppression 79-39591
crythropoiesis, combined use of ^{52}Fe and contaminant ^{55}Fe in bone marrow studies 77-56447
cytochemical leucocyte differentiation and radioimmune assay *(German)* 79-5412
cytoskeletal proteins of human erythrocyte, in vitro complex formation 79-96514
damage, technological problems of implantable artificial heart 77-44839

blood continued
damage by artificial part-hearts and pumps, dwell minimisation model *(German)* 79—16345
decompression studies using ultrasonic imaging of bubbles 79—11988
deoxygenated sickle cell and haemoglobin S solution acoustical props. 78—3453
deoxyhaemoglobin, ferrous heme of high-spin type, MCD spectra in Soret, visible and near IR regions 80—94156
deoxyhaemoglobin, proton NMR, modified DEFT technique for obs. hyperfine shifted line, T_1 values meas. 80—76871
diafiltration, with capillary membranes *(German)* 77—48921
diafiltration process, technical aspects *(German)* 77—48920
dialysis and simultaneous diafiltration for blood purification *(German)* 78—31967
dialysis therapy, single compartment model appl. to urea and creatinine kinetics 78—48931
dialysis without circulating dialysate, approach to portable artificial kidney 77—48949
disturbed cell renewal control system modelling and simulation 79—29510
dosimetry in ^{131}I therapy 77—48869
droplet deformation in Courette flow suspension, expt. *(German)* 79—16227
electrode for pN_2O and pO_2 anal. in blood and gas 79—62412
electrophoretic waveform analysis for blood serum protein composition determ. 78—64928
elemental variations following gamma ray injury of mice, PIXE anal. 77—48973
endocrine research, continuous blood sampling and time series anal. 78—77130
energy metabolism of blood morphotic elements, ionising radiation effects 80—61645
epidemiologic monitoring, neutron activation analysis of blood and blood components 80—17099
erythrocyte, flow resistance into pores 80—61609
erythrocyte, human, chloride distrib. and transport, cell membrane struct. 77—1983
erythrocyte, human, dynamic osmotic haemolysis and ghost repair, resistive pulse spectra 79—62208
erythrocyte, human, steady rate of glycolysis rel. to ATP conc., quantitative model 78—53354
erythrocyte, rheological models *(French)* 78—24083
erythrocyte, sectioned, generalised theory of geometrical shape 78—65071
erythrocyte, surface area and vol. calcs. from scanning electron micrographs 79—5259
erythrocyte aggregation detect. by US scatt. 77—40721
erythrocyte aging, model for pharmacological effects on erythrocyte flexibility *(German)* 79—79583
erythrocyte bulk lysis prod. by pulsatile blood pump, in vitro eval. 77—44840
erythrocyte Ca transport in myotonic muscular dystrophy patients 78—80849
erythrocyte count and haemoglobin determ. by mobile miniphotometer *(German)* 79—5416
erythrocyte deformability, viscometric flow and laser diffractometric technique 78—35879
erythrocyte deformation in centrifugal field 78—27976
erythrocyte distribution profiles during sedimentation as determ. by HeNe laser light 80—81563
erythrocyte electrophoretic mobility, effect of UHF EM radiation 78—53442
erythrocyte ghost IR spectra in region of amide I and II bands on microwave irrad. 77—86531
erythrocyte ghost membrane, human, electron density, small-angle X-ray diffr. 77—73510
erythrocyte ghost membrane struct. effects of fusogenic agent, fusion mechanism 78—31782
erythrocyte ghosts, human, fusion promoted by Ca^{2+} and PO_4 ions 77—4987
erythrocyte $H^{32}PO_4{}^{-2}$ transport, inhibition by high press. 77—12900
erythrocyte haemolysis, human, thermodynamic and kinetic model 79—92191
erythrocyte high gradient magnetic separation 78—53585
erythrocyte integral membrane protein lateral mobility, human cells 77—66805
erythrocyte membrane, appl. of nanosecond fluorometric system 77—17010
erythrocyte membrane, carbocyanine dye orientation, microscopic fluorescence polarisation obs. 79—83694
erythrocyte membrane, cooperative pH-sensitive state transition, Raman spectroscopy 77—36881
erythrocyte membrane, phys. state of lipids, X-ray diffr. 78—80835
erythrocyte membrane, pulse NMR meas. of water exchange 79—43826
erythrocyte membrane, spin-label study of γ-irrad. effect 80—51168
erythrocyte membrane, viscoelastic props., theoretical and expt. studies 79—16157
erythrocyte membrane, X-ray induced structural changes, fluorescent probe obs. 79—88129
erythrocyte membrane alterations, rheological technique evaluation 80—61611
erythrocyte membrane fluidity, adult and neonatal human cells 77—36885
erythrocyte membrane hydraulic cond. determ. 79—34528
erythrocyte membrane lattices, partially disordered, X-ray scatt., anal. method applied 78—91196
erythrocyte membrane permeability, sheep, O_2 effects with X-ray and neutron irrad. 77—5039
erythrocyte membrane protein alterations in Huntington's disease, EPR 77—56347
erythrocyte membrane struct., radiation effects, intrinsic fluorescence obs. 79—74724
erythrocyte membrane thermal transitions identified from ANS permeability 79—53055
erythrocyte membrane water permeability defect in human epilepsy, NMR 77—29122
erythrocyte membrane-bound acetylcholinesterase, activity rel. to struct. changes induced by cAMP 80—30674
erythrocyte membrane-haemoglobin interaction, γ-ray effects, EPR 78—7402
erythrocyte membranes, ESR study of abnormalities in Duchenne muscular dystrophy 78—96111

blood continued
erythrocyte membranes, fluidity change after X-irrad., pyrene excimer fluoresc. obs. 80—72262
erythrocyte membranes, human, elec. cond. characts. 77—9180
erythrocyte membranes of rabbit, dog, man, microwave irrad. effects obs. 80—56130
erythrocyte nucleosomes, chicken, temp. dependence of ^{31}P-NMR spectra 80—94280
erythrocyte osmotic fragility curve, statistical synthesis 78—65070
erythrocyte radiosensitivity for cells with increased level of superoxide dismutase 77—44726
erythrocyte sedimentation rate in inclined tubes 80—67048
erythrocyte surface charge decrease, target of X-irrad. and dislocation of sialic acid 77—52853
erythrocyte survival after slow freezing in glycerol, temp. depend., human cells 78—77019
erythrocyte survival in mice, effects of polymeric ^{239}Pu 77—9227
erythrocyte survival in mice, effects of polymeric ^{239}Pu 80—45973
erythrocyte suspension, laser-induced fluoresc. of intact human membrane cell 77—90733
erythrocyte suspensions, human, $HCO_3{}^-$, Cl^- exchange 79—8487
erythrocyte thermal fragility, expt. obs. 79—62198
erythrocyte transmembrane cholesterol movement, human cells 78—3459
erythrocyte US scatt. frequency dependence obs. 77—64119
erythrocyte-rouleaux formation, US detect. by spectral anal. 78—40280
erythrocytes, ^{51}Cr-labelled, simplified technique for survival estimation 80—51217
erythrocytes, ^{99m}Tc-labelled, spleen scanning in humans 80—67230
erythrocytes, avian, US effects on transport 79—96613
erythrocytes, determ. of relative refractive index, dimensions and conc. from turbidity spectrum 79—79698
erythrocytes, frozen human cells, conc. polarisation effect 78—3460
erythrocytes, gas reactions, shape changes microspectrophotometry obs. 79—8488
erythrocytes, haemolysing action of u.s. 77—2019
erythrocytes, human, cholesterol-loaded, rheological and kinetic dysfunctions 80—45867
erythrocytes, human, effect of hydration on water content 77—16921
erythrocytes, human, haemoglobin's suspending medium, dielec. props. obs. 80—76716
erythrocytes, human Li efflux through Na/K pump 78—48775
erythrocytes, investigation of thermal and athermal effects of microwave irradiation 79—70581
erythrocytes, motion and deform. in the microcirculation 79—29513
erythrocytes, rabbit, increased passive efflux of ^{22}Na and ^{86}Rb on microwave irrad. 80—108957
erythrocytes, rat, ^{99m}Tc labelled, factors affecting splenic deposition of heat damaged cells 79—29596
erythrocytes, slowly frozen human cells, phys.-chem. basis of protection by glycerol 78—77020
^{51}Cr-erythrocytes, splenic sequestration meas. by external scanning, calibration methods 77—2043
erythrocytes, surface area calc. method in elastic deform. 79—70571
erythrocytes, technique for observing 3D dim. struct. with a cryo-SEM 78—92765
erythrocytes, X-ray small-angle scatt. *(German)* 78—35812
erythrocytes labelled with stable Rb, survival determ. by fluoresc. excitation anal., rabbits 80—81788
erythrocytes of human blood, diameter meas. by specific elec. cond. 78—53353
erythropoiesis and survival of tadpole after whole-body X-irrad. 77—52845
erythropoietic activity clinical assess., distrib. model of Fe kinetics 79—100587
erythropoietic differences in mice after whole-body irradiation 79—25045
extracorporeal heart-lung bypass, mechanical support of circulation *(Japanese)* 77—40690
extracorporeal irradiation method for rats 80—72396
extracorporeal irradiation of blood and lymph, in adrenalectomised calves 77—5055
extracorporeal irradiation with ^{137}Cs, expt. research and clinical appl. *(German)* 78—69149
ferric haemoglobin, EPR studies before and after irradiation 79—29503
fibre optic probe for neonatal oximetry and dye curves 79—70603
fibrin molecule formation, thermodynamic model 79—70527
fibrinolysis and coagulation, dynamic rheological studies 80—61614
fibrous microfilter, disposable 78—7527
filter evaluation 78—69250
filtration during transapical left ventricular bypass 77—48940
flow measurement, UDP-30 arterial US pulse Doppler flowmeter 80—104805
flow model, hydrodynamic study with blood simulant 79—25023
flow plethysmograph microprocessor control 79—62402
flow through narrow capillaries, rheological mechs. 80—97961
flowmeter, implantable bidirectional device, micropower ICs 77—13038
frozen red cell structure and function, freezing patterns and post-thaw survival 78—64960
gas analysers, review 78—69238
gas analysis data processing system *(German)* 79—5419
gas analysis in vivo using gas chromatography 78—40355
gas analysis using mass spectrometer *(Japanese)* 77—70566
gas and acid-base calculations, electronic data computing 79—25139
gas bubble motion, behaviour 79—10605
gas catheters, flow-dependent, in vivo calibration 79—16330
gas chromatographic analysis, in vitro evaluation 77—81604
gas microanalyser, calomel electrode efficiency restoration 77—25575
gas sampler, for gas chromatograph, design, construction and characteristics *(Japanese)* 78—85458
gas valves, anal. in mice following pulmonary irrad. 80—104673
gases, meas. of O_2 and CO_2 concs. using P electrodes 79—20725
gated blood pool scan, radioisotope evaluation of ventricular performance 80—85483
globin genes, human fetal, charact. of deletions of DNA 79—70519
glow-discharge polymer surface blood compatibility, Lindholm coagulation tests 77—81658
glucoregulation in blood of diabetic dog, computer controlled system 77—86652
glucose monitoring technique for appl. in artificial endocrine pancreas 78—36062
glucose regulation parameter estimation, optimal inputs 78—64920
granulocytes, human, spatial trajectories in isotropic medium 79—34523

blood continued
haematocrit, noninvasive meas. by elec. admittance plethysmography technique 80—56246
haematocrit determination in dog using radionuclides 79—62411
haematofluorometer, for testing Pb poisoning 78—53554
haematologic disorders, radionuclide therapy 80—36109
haematological findings significance for medical exam. of radiation employee *(Japanese)* 79—11971
haematopoiesis progenitor and effector cells, expt. murine system, whole body irrad. obs. 80—98034
haematopoietic malignancy diagnosis, significance of SEM 80—85529
haematopoietic microenvironment, progenitor cells radiosensitivity, mouse expts. 80—45983
haeme-liganded sickle cell haemoglobin, spin label detection of intermolecular interactions 79—16122
haemocoagulometer 79—39541
haemodialysers, hollow fibre type, haemofiltration and thrombus formation effects 78—3672
haemodialysis, effects of blood and dialysing soln. flow rates on efficiency 78—36053
haemodialysis cellulosic films and hollow fibres, diffusive and hydraulic permeabilities 78—28128
haemodialysis membranes, for disposable dialysers, comparison of cuprophane and cellophane 77—78049
haemodialysis rel. to EEG, spectral anal., Hjorth's descriptors, blood variables and psychological data 78—31968
haemodialysis technique with dialysate regeneration by absorpt. and ion exchange *(German)* 77—48919
haemodilution effects on viscosity and red cell aggregation 80—97952
haemofiltration, appls. and limitations in clinical use *(German)* 80—21568
haemofiltration as alternative to conventional chronic dialysis *(German)* 80—21569
haemofiltration control system *(German)* 79—5403
haemofiltration experiments and application limits *(German)* 79—5402
haemofiltration treatment, chronically intermittent, principles and results *(German)* 79—5404
haemoglobin, conformational change, relation with CO binding 79—8473
haemoglobin, dielec. transient response following UV irrad. 80—51166
haemoglobin, effect of adsorpt. on struct. and props. 79—92121
haemoglobin, human, maleimide spin labeled, proton ENDOR spectra obs. 80—89719
haemoglobin, O_2 linked Cl binding sites, pH dependence 79—62174
haemoglobin, quaternary struct., hydration and self-association, ^{1}H NMR obs. 80—67040
haemoglobin aqueous solutions, γ-irrad. in air and Ar 80—41135
haemoglobin as a transducer for O_2 transport in fish 79—96505
haemoglobin concentration meas., in whole blood, using IR reflectance 77—52860
haemoglobin haem structure after photo-deligation, Raman spectra 80—61510
haemoglobin in solution, conc. depend. of diffusion coeff. 79—29546
haemoglobin-O_2 equilibrium curve, instrument for determ. based on membrane diffusion 80—81761
haemoglobin-O_2 equilibrium curve determ., semipermeable membrane transport model 79—92418
haemolysis due to intra-aortic balloon pumping, model expts. 77—81664
haemolysis due to ventricle type blood pump 78—44707
haemolysis kinetics, US differential absorption meas. 77—77877
haemolytic characteristics of polydimethylsiloxanes 77—60290
haemolytic secondary effects in cone-plate viscometers 79—62281
haemoperfusion, large agarose beads, prep., props. and appls. 79—16349
haemoperfusion device comparative evaluations 78—44690
haemopoiesis, kinetic basis for compensation during continuous irrad. with low doses 80—36010
haemopoietic stem cell population and proliferation model 77—44610
haemopoietic stem cells of shielded bone marrow, X-ray effects, role of migration 77—9225
haemopoietic system of mice, X-irrad., damage repair modification by microwaves 78—24096
haemorheology, lecture *(Japanese)* 80—98752
haemorheology and diseases, conf., Nancy, France (Oct. 1979) 80—56991
haemorheology in near zero gravity environment 80—3661
haemorheology related to blood cells, conf., Hamburg, Germany (Aug. 1979) 80—62365
haemorrhagic shock, effect of anemia on O_2 transport 80—67330
haemorrhagic shock, effect of increased blood-O_2 affinity on O_2 transport 80—67331
heart valves, implanted, cause of thrombus form. 77—78047
heat exchanger for heating/cooling blood, thermal design, equipment and blood props. considerations, appls. 78—92744
heparin assay in animal model of Pseudomonas sepsis, rheological approach 77—52953
Hippuran clearance, rel. to deconvolution anal. of scintillation camera renogram 77—21599
Hippuran plasma clearance meas. using gamma camera and cardiac background subtraction 77—52870
homeostasis, bioimpedance rel. to tissue distrib. in living tissues 77—32879
human, proton-induced X-ray emission anal. for Cu, Zn and Fe 79—53291
human red cell membranes, surface adsorpt. of dextrans 78—15799
IC pressure meter using pressure transducer, microprocessor controlled 79—35709
IL 282 CO-Oximeter for measurements on whole blood 80—56159
immunological processes after laser irrad. of exptl. tumours *(German)* 78—40242
implantable electronic pancreas and blood glucose monitor 78—88767
indicator dye microconcentration meas. instrument 79—39565
indocyanine green fluoresc. spectrum in blood and other solvents, rel. to angiography 78—28057
instrumental neutron activation analysis studies of tissues from patients with pulmonary diseases 80—21535
insulin receptors on human platelets, ^{125}I-insulin binding meas. 79—92245
intra-osseous circulation, human and animal, investigation method *(French)* 79—34593
intracerebral spontaneous haematoma diagnosis and prognosis by computed tomography 78—73195

blood continued
intravascular mural thrombi formation by in vivo US streaming 78—24091
intravascular O_2 saturation continuous meas. using fibre optic catheter *(German)* 78—85411
ion-selective electrodes for serum anal. 78—3645
isoelectric focusing method for human globin chain separation 80—17219
kidney microporous membrane plasma filtration efficiency 78—48926
Krogh tissue cylinder, transient convective mass transfer 80—3598
laminar blood flow, gas and heat transport, platelet and protein diffusion 78—92669
laser irradiation, selective photochemical mechanisms 79—66450
laser photocoagulation in diabetic retinopathy therapy 79—79622
leucocyte, human, fluorochromed with acridine orange, spectral characts. 78—96024
leucocyte β-glucoronidase release on exposure to shear stress 78—40125
leucocyte adhesion studied quantitatively by multiple internal reflectance-IR spectroscopy 77—56562
leucocyte classification by parametric and nonparametric analysis 77—78016
leucocytes, differential counts, comparison between light and electron microscopic results 79—5429
leucocytes, human, US effects, sister chromatid exchange anal. 79—96612
leucocytes, microsonation effect, cell destruction critical threshold determ. 78—20212
leucocytes, radioactive-labelled, appl. for proof of inflammations 80—67218
leukaemia in children associated with nuclear weapon test fallout 80—12186
leukocyte migratory patterns, use of ^{99m}Tc as radioactive label for study 80—51222
leukocyte motility and chemotaxis parameters meas., quantitative anal. of under agarose migration assay 79—96525
leukocyte uptake of radiolabelled compounds in whole blood, liq. scintillation method 77—90882
leukocytes, automatic recognition and classification systems *(Italian)* 80—81780
leukocytes automatic anal., nuclear texture parameters appl. 78—77136
leukocytes in motion, surface struct., SEM 77—29116
leukocytes of human blood, gravity sedimentation anal. 80—98197
light back-scattering, multipole expansion of integral photon density expressions 78—77099
liposomal membrane permeability, radioresist. 78—80919
liver assist, improved haemoperfusion sorbents and plasma filtration system 78—48939
liver support, artificial, detoxifying enzymes bound to artificial carriers, extracorporeal application 79—25160
lung numerical modelling, human 78—80911
lung tissue simulation, O_2 exchange in silicon rubber capillaries 79—44060
lymphocyte, hog, energy metabolism effect of ionising radiation 79—92301
lymphocyte, human, dicentric yield, γ dose rate dependence calc. 79—92294
lymphocyte B and T cell membrane receptors, human effects of ^{60}Co gamma-rays 77—21575
lymphocyte chromosomal aberrations of people exposed to ^{226}Ra and ^{3}H paints 77—37011
lymphocyte chromosomal localisation of UV induced unscheduled DNA synthesis 77—25520
lymphocyte chromosome aberrations, influence of blood storage after X-irrad. 77—66828
lymphocyte chromosome aberrations, irrad. in vitro and in vivo, monkeys 77—37012
lymphocyte chromosome aberrations, pion^{-} peak expansion to range of depths useful in radiotherapy 78—20243
lymphocyte chromosome aberrations as biological dose-response indicator 80—17019
lymphocyte chromosomes, interaction of X-ray induced primary breaks in form. of dicentrics 77—12963
lymphocyte cultures, human, heat prod. meas. with flow microcalorimeter 77—81473
lymphocyte death and transform., effects of X-ray and neutrons 78—69144
lymphocyte dicentric yield on X-irradiation, human and feline blood 79—96624
lymphocyte function evaluation after 2450 MHz CW microwave exposure, mouse 79—100667
lymphocyte homing patterns, radiation induced alterations 80—17014
lymphocyte in vivo migration modulation by whole-body hyperthermic RF irradiation, mouse 79—100668
lymphocyte levels, RF induced alterations due to hyperthermia, mouse obs. 80—35975
lymphocyte metaphase spread finding using automatic microscope 77—56550
lymphocyte morphology and chromosomes, effect of 2450 MHz microwaves 78—40252
lymphocyte plasma membrane components, distrib. and mobility, book contrib. 80—30690
lymphocyte radiosensitivity, compared with thymocytes 77—37026
lymphocytes, chromosome aberrations rel. to radiation dose, A-bomb survivors 79—43835
lymphocytes, human, chromosome aberration yields due to 15 MeV electrons 77—48843
lymphocytes, human, chromosome aberrations induced by ^{252}Cf neutron radiation 79—16169
Lymphocytes, human, effect of irrad. on hexose monophosphate shunt pathway 80—76798
lymphocytes, human, effects of heat and radiation 80—97864
lymphocytes, human, effects of low-dose radiation on repair processes 80—98023
lymphocytes, human, effects of US irradiation 79—96609
lymphocytes, human, homogeneous sensitivity to radiation-induced chromosome damage 79—53197
lymphocytes, human, lethally-irrad., ultrastruct. events in cytoplasmic death 77—48842
lymphocytes, human, RBE for d(42 MeV)-Be neutrons based on chromosome-type aberrations 80—104663
lymphocytes, human, sister chromatid exchanges obs. after γ-irrad. 80—41140

blood continued
  lymphocytes, human, variation in neutron RBE values compared to X-rays 80—101229
  lymphocytes, human peripheral, chromosome sensitivity to various X-ray doses and subsequent storage 80—17011
  lymphocytes, human peripheral blood grown in γ-irrad. medium, sister chromatid exchanges 80—104658
  lymphocytes, in vitro ^{60}Co gamma-ray response of leucoagglutinin stimulated human cells 78—57041
  lymphocytes, living and dead, mag. props. and mag. sedimentation 80—35925
  lymphocytes, of equine peripheral blood, stimulated with phytohaemagglutinin, X-irrad. 77—5032
  lymphocytes, perinatal rats, effects of 2450-MHz CW microwave irrad. 80—56133
  lymphocytes, peripheral, chromosome aberrations due to ^{222}Rn rich water 79—70587
  lymphocytes, peripheral, population changes following radiation therapy to limited and extended fields 80—72236
  lymphocytes, radiation induced chromosome aberrations and the Poisson distrib. 79—100675
  lymphocytes, stimulated, cell cycle progression perturb. by tritiated thymidine radiation 79—57726
  lymphocytes, survival of T- and B-cells after X-irrad. in vitro 77—12969
  lymphocytes exposed to temps. of 37-45°C, two types of interface death 80—104566
  lymphocytes irrad. in vitro, effect of radiotherapy on mitogenic response to phytohaemagglutinin 78—24100
  lymphocytes of man, rabbit and swine, chromosome aberrations induced by ^{60}Co gamma rays 80—56146
  α_2-macroglobulin values in serum of X-ray workers 78—28020
  magnetic relax. time of H_2O protons 79—11898
  maintenance haemodialysis, circulation study *(Japanese)* 77—40689
  mechanical calorimetry of red cell membranes 80—45854
  mechanical transfer function, modifications by some biological factors and study method 80—16969
  mechanics of blood flow 80—76778
  membrane oxygenator, CO_2 transfer 79—25154
  membrane oxygenator effectiveness 79—48365
  mesenteric blood vessels, response to β-irrad., mouse expts. 80—36009
  mesentery tissue, burn induced alterations of interstitial diffusion 80—104634
  metabolites, dynamics of depend. sorption by C sorbents 77—70487
  microcirculation regulation study *(Japanese)* 77—36972
  microfilter materials and designs 79—48352
  micropolar fluid model for blood flow through narrow tubes 80—67109
  microprocessor-based blood gas analyser computational algorithms 79—57805
  microprocessor-based gas analyser 78—40356
  microwave effects on blood-brain barrer, review 80—56121
  microwave effects on Japanese quail embryo, 2.45 GHz exposure during development 78—20214
  microwave effects on plasma corticosterone, repeated exposures 78—40246
  microwave long-term effects on haematologic profiles of rats 78—40267
  monitoring of blood vol. change in menstruation, vaginal photoplethysmographic transducer 78—92733
  monitoring technique in late pregnancy toxaemia 77—81602
  monocyte function rel. to irrad. in breast cancer patients 80—72238
  morphologic alterations in brain-blood barrier of hamster after microwave radiation 77—77935
  myocardial ^{99m}Tc scintigraphy, use of blood-pool imaging 80—12228
  neutrophil automated classification, feature selection 78—73281
  neutrophils, rabbit, chemotactic factor-induced release of membrane Ca 79—88095
  NMR T_2 relaxation time studies in normal and pathologic blood 80—81682
  nuclear-dockyard workers, radiation-induced chromosome aberrations 79—34606
  optical properties, high-resolution 77—36869
  organ transfer kinetics of radioisotopes 80—109044
  oscillatory tube flows of viscoelastic fluids 79—77252
  oxidative potential in preserved blood 77—81771
  oximeter, noninvasive tissue reflectance, development and evaluation 79—20703
  oximeter calibration, humans exposed to centrifugation 78—92734
  oximetry, tissue-refl. method, simple homogeneous tissue model for calibration 77—40858
  oxygen saturation meas., catheter tip mounted red/IR oximeter 77—40836
  oxygenation, extracorporeal, in treatment of acute pulmonary failure 78—7539
  oxygenation, membrane oxygenator design with tubes wound in woven patterns 79—84020
  oxygenation simulation in stirred membrane cell 78—40421
  oxygenator, artificial membrane lung 77—78051
  oxygenator, biocompatibility of continuously generated and collapsed blood-fluorocarbon interface 77—48944
  oxygenator, bubble, blood damage test standardisation *(German)* 79—2158
  oxygenator, capillary membrane, semiautomatic fabrication 79—20711
  oxygenator, convective-diffusion model 78—44711
  oxygenator, membrane envelope type, capacity improvement *(German)* 79—2157
  oxygenator, membrane type 79—84023
  oxygenator, rotating disc design 78—44710
  oxygenator gas transfer performance test standardisation *(German)* 79—2159
  oxygenator membrane blood compatibility, correl. of IR spectroscopy with platelet morphology 79—53279
  oxygenator using microchannel membrane, transport and flow phenomena 78—69253
  oxygenators, progress and problems 78—36064
  oxyhaemoglobin dissociation curve analyser, devel. and improvement 77—13019
  oxyhaemoglobin dissociation curve direct obs. in man in vivo, computer investigation 78—85433
  partial pressure of gases meas., in vitro electrochemical sensors 80—67303
  particle etch track technique determ. of U trace content in normal human blood 80—89910

blood continued
  perfusion, using activated C cloth 77—37105
  perfusion blood temp. monitoring, zero-heat-flow transducer 80—8201
  perfusion prediction from meas. of phase shift between heat flux and temp. 80—104804
  perfusion rate estimation from diffusible indicator meas., sensitivity anal. 80—104803
  peripheral polymorphonuclear leucocyte system model, humans 78—56956
  peripheral reticulocyte count as biologic dosimetry of ionising radiation, mouse expts. 80—46051
  pH determination, improved Sb-Sb_2O_3 electrodes 79—53270
  photodiode camera improvement of shading correction 80—56325
  photoelectric haemoglobinometer type GF-3 79—92438
  placenta, human, rational modelling 79—11962
  plasma, constituents rel. to O_2 diffusivity 79—92460
  plasma, reduced viscosity in joggers rel. to non-joggers 80—16967
  plasma, vol. meas. in man using ^{99m}Tc, ^{131}I labeled serum albumin 79—29602
  plasma, X-ray emission anal. by proton excitation 79—84054
  plasma ^{1}H NMR relax. rates, cancer-induced decrease obs. 80—56075
  plasma antiheparin activity changes after irradiation 79—57717
  plasma filtration, stagnant 77—48948
  plasma filtration from whole blood, effect of various parameters 78—48826
  plasma filtration through microporous membranes 77—48947
  plasma fractionation, development of automatic continuous process 77—52955
  plasma high density lipoprotein solubilisation of phospholipid membranes 77—16916
  plasma kallikrein activity in tumour-bearing rats, effect of focal irrad. 78—35892
  plasma proteins, high energy-induced aggregation, time resolved spectra 80—61655
  plasma proteins, ligand distrib. among multiple binding sites, computer program 77—12877
  plasma sonoluminescence generation by US therapy equipment 77—77930
  plasma steroid levels in male rats, microwave effects 77—81530
  plasma total Fe-binding capacity meas. by EPR 77—17003
  plasma viscosity in sickle-cell anaemia 80—94250
  plasma with red cells, absorption spectroscopy using integrated optics 77—29232
  platelet adhesion to solid surfaces, effects of plasma proteins and substrate wettability 78—35814
  platelet aggregation induced by US under specialised conditions in vitro 80—45963
  platelet aggregation studies using TEXAC whole picture analysis 79—25133
  platelet diffusivity estimation in flowing blood 79—25010
  platelet estimation in whole blood by electronic particle size anal. 78—28104
  platelet interaction with vessel surface, blood rheological factor influences 80—61612
  platelet morphology and function modification by US exposure 77—77929
  platelet transport between blood and artificial filtering surfaces 78—40423
  platelet-rich plasma, determ. of extracellular ATP 77—25615
  platelets, human blood, adenine nucleotide content and release reaction after ^{60}Co γ-irrad. 78—28021
  platelets, shear-induced activation 79—74704
  PMR relaxation times in peripheral blood of cancer patients 77—86579
  pO_2 meas. polarographic technique 79—100782
  Poiseuille flow viscosity of a couple stress fluid 79—25011
  poly (N^{α},N^{ϵ}-terephthaloyl-L-lysine) membrane for artificial red blood cells, interaction with serum proteins *(Japanese)* 80—12061
  polymer modification and blood compatibility 79—39609
  polymeric biomaterials for blood-contacting appls., problems and new dimensions 78—85423
  populations exposed to supraphysiological temp., haemolysis time history 80—35850
  positron-emitting blood pool imaging agents compared 80—12213
  preservation at low temps. 78—24043
  pressure, industrial noise effects on man, cardiovascular disease risk factors 79—5321
  pressure, volume, heart rate and cardiac function regulation *(Japanese)* 77—40688
  pressure control model 77—21557
  pressure control system dynamic behaviour identification 79—2097
  pressure meas. using digital sphygmomanometer *(Spanish)* 77—40846
  protein-polymer interfacial behaviour, influence of hydrophilic-hydrophobic type of microphase separated struct. *(Japanese)* 80—12051
  proton induced X-ray chem. anal., Fe and minor elements concs. in biological material 78—23989
  pulmonary arterial circulation process nonlinearity 77—12944
  pulmonary thromboembolism treatment and prophylaxis by percutaneous caval filter 77—48925
  pulsatile blood pump development and characteristics 77—81659
  pulse diffusion in densely distributed scatterers, whole blood 79—3632
  pump, pressure servovalve control, moving coil system *(German)* 78—24182
  purification methods and portable kidney machines *(German)* 79—5405
  radioimmunoassay for thromboxane B_2 with thromboxane B_2-^{125}I-tyramide 79—88222
  radionuclide therapy, pot. future appl. 80—36031
  radiopharmaceuticals, γ-emitting, in rat blood, continuous monitoring technique 79—2129
  red blood cell, human, axial trajectory meas. in high-gradient magnetic separation 79—53165
  red blood cell, human, rheologic effects of shape transform. 79—62216
  red blood cell aggregation detect. during blood flow by US 79—84068
  red blood cell damage in extracorporeal circulation, haemorheological effects of mech. factors 79—62280
  red blood cell freezing, cryopreservation and refrigeration 80—67262
  red blood cell plasma membrane, Ca^{2+} transport stimulation by calmodulin 80—12066
  red blood cell profile direct meas. using SEM beam reference lines 78—81094
  red blood cell shape, optimality, O_2 diffusion approach 80—30693

blood continued
- red blood cell sizing, evaluation of automated Electrozone Celloscope in haemolysis study 78—40455
- red blood cells, equilib. shapes in osmotic swelling 80—85368
- red blood cells, in vivo labelling with ^{99m}Tc with stannous pyridoxylideneaminates 80—46049
- red blood cells, minimum energy anal. of membrane deform. 80—72141
- red blood cells, rheological props. meas. by Couette viscometer 80—97992
- red blood cells, type O, using optical system for light scatt. expts. 79—76786
- red blood cells, viscoelastic study of aggregation 80—97960
- red blood cells labelled with ^{99m}Tc, evaluation of gastrointestinal hleeding 80—51219
- red cell, human, increased passive permeability below 12°C 80—94185
- red cell Ca pump, ATP regulation 79—29511
- red cell diameter meas. from He-Ne laser beam diffr. pattern 77—86582
- red cell effect on blood flow velocity profiles in small tubes 79—25014
- red cell elastic deforms. 77—56400
- red cell etching by ion beam sputtering for SEM 80—85554
- red cell extensional recovery, determ. of membrane viscosity 79—57683
- red cell flexibility, effect on blood flow through tubes of 30-500 μm 80—67111
- red cell ghosts, human, Ca-depend. K efflux, effect of carbocyanine dyes 77—12896
- red cell ghosts, light scatt., ang. depend. struct. 77—81475
- red cell ghosts active transport, cytoplasmic contamination, electron microscopic obs. 80—45874
- red cell haemolysis rates in subsec. to sec. range, normal human cells 78—15796
- red cell in vivo labelling with ^{99m}Tc for blood pool imaging 77—37052
- red cell membrane, human, surface elasticity and viscosity 80—61608
- red cell membrane, Li transport in manic depressives 80—61525
- red cell membrane, temp. dependence of viscoelastic recovery 80—40979
- red cell membrane elastic area compressibility meas., osmotic correction 78—20147
- red cell membrane protein monolayers, viscoelastic props. 79—48224
- red cell membrane thermoelasticity obs. 79—57684
- red cell Na-K pump reversal and apparent affinity for intracellular K 77—86473
- red cell permeability to K^+, Na^+ repair after X-ray, fast-neutron damage 79—57615
- red cell shape, laser differential scatt. system for continuous monitoring 77—90873
- red cell suspensions, backscatt. of light 80—41107
- red cell suspensions, haemoglobin NMR relax., T_1 and T_2 meas. 78—80832
- red cell-hydrocarbon surface long-range attraction 77—77874
- red cells, ^{99m}Tc labelling 80—41236
- red cells, Ca stimulated increase in K permeability, dog 79—62218
- red cells, human, frozen section prep. for electron probe anal., fracturing or cutting 79—39625
- red cells, intact, use of ionophore A23187 to meas. and control free and bound cytoplasmic Mg 77—52755
- red cells, interactions, of cholesterol with Na pump 77—12898
- red cells as fluid droplets, erythrocyte membrane dynamics in shear flow 79—74711
- red cells of thalassemia, sickle-cell anaemia, and haemoglobin Hammersmith, ferritin-like Fe, Mossbauer study 80—8018
- red cells separation in vivo, transfusion therapy appl. 79—92190
- red/IR oximeter operating cct. 78—28101
- renograms, single injection technique for subtraction of blood background 79—29581
- reticulocyte blood count data analysis by maximum entropy spectral estimate 77—78017
- reticulocyte production rhythm investigation by spectral analysis 78—73279
- reticuloendothelial system, granulopectic activity modification in mice exposed to 1 to 10 GHz fields *(French)* 77—21560
- RF radiation effects on inflammation, white cell counts 78—40253
- RF waves, effects of repeated exposure on growth and haematology of mice 80—61625
- rheological and thermophysical fluid props., physicochem. composition depend. 78—80902
- rheological behaviour, viscoelastic model *(French)* 80—76779
- rheological behaviour of stored blood cells *(French)* 80—67110
- rheological characts., heat transfer rel. to myocardial infarcts 79—79573
- rheological hysteresis at low shear rate 80—97962
- rheological parameters for viscosity, viscoelasticity and thixotropy 80—16963
- rheological properties in transient flow at low shear rate *(French)* 80—41103
- rheological props. in transient regime to low velocity shear flow 79—79582
- rheology, clinical changes in peripheral vascular disease and smokers 80—16965
- rheology, erythrocyte rigidity effects on viscoelastic dilatancy 80—61610
- rheology conference, Osaka, Japan (June-July 1979) 80—62364
- rheology effect on haematocrit distrib. in pulmonary sheet flow 79—79572
- sampling system, remote radio controlled, for unrestrained monkeys 77—90967
- SCF-LCAO-ASMO and CI calcs. of low-lying multiplets and excited states 80—94155
- sedimentation, at controlled shear rates 77—66877
- sedimentation, three-component anal. by method of characts. 77—70577
- sedimentation rate free from gravity influence, rapid determ. from density meas. *(German)* 78—81085
- serous triglyceride evolution in mice exposed to 2 to 10 GHz radiation *(French)* 77—64083
- serum, Fe determ. method using AAS 1 at. absoprt. spectrophotometer 77—48706
- serum, human, PIXE and neutron activation anal. 80—56199
- serum, human, trace elements determ. by proton activation 80—81731
- serum, neutron activation anal., sample contamination by quartz container 77—48980
- serum, neutron activation determ. of Zn, Se, Rb, and Fe concs. 78—20252
- serum, PIXE anal. of trace elements 77—48974
- serum, rapid anal. by mass spectrometry/mass spectrometry 80—61173

blood continued
- serum, trace element anal. of thick samples, photon excited X-ray fluoresc. 78—3423
- serum automated electroanal. using ion-selective disc electrodes with neutral cation-carriers *(German)* 78—73269
- serum concentration, rel. to trace element distrib. of brain 80—17215
- serum Fe after whole-body ^{60}Co irrad., rel. to ^{67}Ga tumour uptake 78—65081
- Shroud of Turin, blood presence identification, spectroscopic and chem. tests 80—102875
- sickle cell, effect of deoxygenation on US absorpt. coeff. 78—44477
- sickle cell, in capillaries, flow resistance, O_2 consumption effect model 78—48821
- sickle cell anaemia sickling kinetics, multiangle laser scatt. spectrophotometer 79—79494
- sickle cell disease, capillary diffusion and transport compensation 79—92198
- sickle-cell blood, flow in capillaries 80—41066
- skeletal muscle O_2 and lactic acid transport, effet of reactive hyperaemia 78—35817
- solubility and partition coefficients for gases in rabbit brain and blood 80—46116
- sorbent haemoperfusion systems, characterisation of solute removal 78—44689
- spectrochemical analysis of biological solns. using wall stabilised arc source 80—41343
- steady state diffusion in red blood cell and model supspension 77—40644
- stenosis effects on non-Newtonian flow in artery 80—89775
- stored blood, microaggregation direct meas., effects of micro-filtration *(German)* 79—2168
- strain gauge blood pressure transducer, chopper preamplifier cct. 78—3659
- supersaturation by counterperfusion and diffusion of inert gases 77—90829
- suppressor cells, non-specific, appearance after local irradiation of breast carcinoma 79—20597
- surgical aspiration automatic control device for cardiac surgery *(French)* 78—61282
- synthetic substitutes, review 79—62405
- temperature monitoring during extracorporeal circulation, noncontact transducer 80—85513
- thermal expansion coeff. of blood and its constituents *(German)* 80—104556
- thrombi, induced, for drug assessment system 79—44017
- thrombogenesis and corrosion of cardiovascular prostheses 77—9300
- thrombogenicity of radiation grafted polymers, meas. by vena cava ring test 79—44062
- thrombosis, deep-vein, comparative imaging of ^{111}In platelets and ^{131}I fibrinogen 79—29607
- thrombosis, rheological aspects *(Japanese)* 80—94268
- thrombosis diagnosis in deep veins with Na^{99m}TcO$_4$ 77—16971
- thrombus formation, effect of contacting polymer surface roughness 79—48369
- thyroid substances levels in blood serum of rats exposed to 0.2, 0.6 and 1 W/cm^2 of US energy 78—69134
- tissue of new, proton spin-lattice relax. time study, blood, liver and tail samples 79—20515
- tissue reflectance oximeter, noninvasive solid-state device 78—35919
- toxicity studies, TOXIPAC-300 data processing system *(Japanese)* 79—25172
- transfusion filters, comparison of methods for microaggregate removal evaluation 80—46097
- transport in biomembrane, NME determ. methods *(Rumanian)* 80—94435
- transport of catecholamines from adrenomedullary cells 79—66464
- trauma in extracorporeal oxygenation, conf., Stolberg, Germany (Nov. 1978) 80—94922
- 3,3′,5′-triiodothyronine plasma to tissue transport rate estimation from 3-compartment model 78—31792
- ultrafilter-adsorber system in interaction with uraemic patient model 78—48937
- US absorption and vel. during tumour development in exptl. animals 77—25524
- US apparatus for blood bubbles detect. and meas. *(Japanese)* 80—1712
- US attenuation and speed, rel. to packed cell vol., 37°C, canine blood 80—41106
- US backscattering, determ. of variation with haematocrit 79—43970
- US backscattering, haematocrit and erythrocyte aggregation depend. 80—45961
- US flowmeter, design considerations 80—23853
- US propagation, effects of red cell shape and orientation 78—24104
- US scattering, angular dependence 77—81542
- US scattering, theoretical study 80—51147
- UV effect on erythropoietic activity in rabbits and rats 77—32940
- vascular occlusion, effect on thermal sensitization and X-irradiation of mouse tumour 79—16253
- vascular system, haemorheology and two-phase flow *(French)* 79—34586
- venous gas bubble prod. by transient deep isobaric counterdiffusion of He against N_2 78—11790
- venous thrombosis, deep, detection by ^{125}I fibrinogen testing 79—16282
- vessel replacement, compatibility of isolated veins and synthetic biomaterials, surface props. 77—56522
- vessel walls, dynamic test apparatus 80—41354
- vessels, medium sized, mech. characts. 80—41101
- viable cells, automated differential cell counting 79—74777
- viscoelastic properties, transient flow obs. 80—97980
- viscoelastic tube, pulsatile flow, non-Newtonian effects *(French)* 80—59113
- viscoelasticity, haematocrit dependence and interdonor difference compensation 79—62277
- viscometers and anticoagulants compared 79—83834
- viscosity and red cell aggregation at zero and 1G, instrumentation for Space Lab 3 80—61716
- viscosity and red cell aggregation under near-zero gravity 80—3660
- viscosity at low shear rate, capillary viscometer and obs. 80—98180
- viscosity factors and functions, clinical appls. 80—3664
- viscosity factors in severe nondiabetic and diabetic retinopathy 78—65069
- viscosity measurement, clinical capillary viscometer 77—40844
- viscosity variations associated with hyperlipoproteinaemia *(German)* 78—57031

blood continued
volume regulation, effects of space flight, review 80—3826
water mobility in blood plasma, NMR determ., viscosity correl. to $1/T_2$ 80—67176
weightlessness, haematological response, math. and exptl. simulation 80—61714
whale biothermal mathematical model 80—12059
white blood cell images boundary finding 79—12021
white blood cells classification and feature extraction 78—3655
white cells, automatic tracking system 77—78064
white cells classification, automation using computer, expt. 78—3663
X-ray fluorescence spectroscopy for trace element anal. of human blood 78—20248
X-ray induced alterations in toad erythrocytes and aq. solns. of haemoglobin 78—11699
CO diffusion in dog lungs, effect of static or slowing flowing blood 80—30970
CO-haemoprotein photolysis, transient Raman study, quantum yield origin 80—67155
PCO_2, continuous transcutaneous meas., electrochem. sensor 77—13020
CO_2 level in artery and vein, quantitative continuous meas. 78—40363
CO_2 partial pressure in blood, meas. by rapid response electrode system *(German)* 78—85409
Ca^{2+}, concs. in rat, technique for continuous vivo meas. *(German)* 79—39533
Cd determ. in whole blood by atomic absorpt. spectroscopy 79—44071
^{144}Ce, intravenous injection, wound site absorption, comparison of metabolic behaviours in rats 79—8545
Fe content anal. by electron microprobe and scanning electron microscopy 79—53065
Fe III, high-spin, in cancer, EPR 78—53466
^{59}Fe/^{51}Cr activity, simultaneous measurement by liq. scintillation counting 77—29195
^{59}Fe/^{55}Fe activity ratio of blood, meas. using semicond. detector 80—17062
^{111}In 8-hydroxyquinoline labelling of human platelets 80—12259
^{111}In labelled human platelets, dose obs. 80—94370
K level meas. using catheter-tip selective electrode 77—90935
K^+, concs. in rat, technique for continuous vivo meas. *(German)* 79—39533
O_2 affinity variability, automated meas. method 79—39544
O_2 level, optical continuous noninvasive meas. 77—2068
O_2 level in artery and vein, quantitative continuous meas. 78—40363
O_2, meas. by fast-responding flow independent blood gas catheter 80—101277
O_2 measurement, catheter oximeter system, solid-state, using three single optical fibres 78—44637
O_2 partial pressure meas., polarographic method, error reduction 78—7470
O_2 partial pressure meas. with membrane covered probe, signal nonlinearity 79—53264
O_2 saturation meas. in nonhaemolized blood by laser light *(German)* 77—44735
O_2 saturation measurement, analogue electronic calculator 77—81614
Pb content in blood, PIXE determination 80—51228
^{99m}Tc labelled red blood cells, ultrafiltration labelling technique 80—51243
^{99m}Tc-labelled red blood cells, kit preparations 79—11999
U conc. in blood meas. by thermal neutron induced fission, chem. etching, conc. rel. to leukaemia 80—21532
^{133}Xe solubility coefficients in water, saline, dog blood and organs 80—56331

blood circulation *see haemodynamics*

blood dynamics *see haemodynamics*

blood flow *see haemodynamics*

blood platelets *see blood*

blue brittleness *see brittleness*

Bode diagrams
see also frequency response
condensation in tube, appl. to dynamic model of reboiler 77—7298
dominant noise process slope intersections, time/frequency-domain conversion 79—54107
heart rate control in man, system anal. 77—25478
heat conduction in tube wall, transfer functions determ. 77—7287

boilers
100 MW fluidised bed combustion district heating plant burning high S content residual oils 80—108777
200 MW atmospheric fluidised-bed combustion steam generator, comparison of three designs 80—108776
1200 MwE FBR, nuclear steam boiler system Super Phenix 79—93816
1200 MWe FBR steam generators, Creys-Malville in France, manufacture 80—27797
AGR helical coil boilers, analogue 77—58763
AGR steam generators, materials specifications 80—42772
air pollution reduction measures, 1974-76 results for Zagreb *(Croatian)* 77—37362
air to water heat pump and solar water heating, dual purpose installations for family house *(German)* 79—87969
atmospheric fluidised-bed combustion boiler development facility, first year of operation 80—108775
Babcock & Wilcox steam supply system, operating experience 78—21752
BN-350 fast reactor, operating experience (1972-77) *(Russian)* 79—97868
brown coal combustion product recirculation, in combustion chamber of a steam generator, 200 MW *(Czech)* 78—27759
burner with diffusive control, intermixing of gas streams with transverse swirled air flow 78—87418
BWR, boilers and pressure vessels, in-service inspection, General Electric's code 77—3152
BWR pipe assemblies, stress corrosion cracking avoidance by improved welding methods 80—42838
BWR steam turbine, blast cleaning to remove radioactive deposits 80—18554
carbon steel water tubes in alkali loaded solvents, corrosion speed investigation *(Hungarian)* 78—48559
convective heating surface fouling with ash, NO_x formation dependence 79—83678
corrosion protective coatings for reliable operation 78—11424
CRBR steam generator design 79—97790

boilers continued
creep life of boiler tubes, in service inspection, techniques assessment *(Japanese)* 77—81356
Creys-Malville station, nuclear boiler studies and construction, Super Phenix 1 *(French)* 79—36301
density wave instability in once-through boiling flow system, distrib. parameter model 79—67815
drum boilers, working at 11.0 to 15.5 MPa, pH control by addition of caustic soda *(Russian)* 80—89420
dryout, premature in conventional and nuclear power station evaporators, model 78—94120
dynamic simulation of the Gentilly-1 reboiler system 78—82439
EBR-II steam generator duplex tubing, US inspection 80—32379
EBR-II steam generator tube bore side inspection probe and drive 79—9850
elastic creep fatigue rules fo ASME B&PV code case 1592 78—44211
evaporating surfaces, boiling heat transfer aspects 77—89011
fast breeder reactor boiler tubes, eddy current probe insertion for in service inspection, method development *(Japanese)* 80—822
FBR power stations, development of modular steam generators 79—76058
feedwater pH meas. apparatus improvements 79—79341
feedwater redox potential meas. by Pt thin-layer electrodes 80—89578
finned steam generating tubes, heat transfer enhancement, optimum geometry 80—48551
flow dynamics stability in once-through steam generator *(Czech)* 77—38386
fluidised bed, energy conversion, Conf., San Diego, CA, USA (Aug 1978) 79—48038
fluidised-bed steam generating system to supply 100000 lb/h of saturated steam burning high S coal 80—108778
forced-convection boiling upflow system, instabilities in parallel channel, nonlinear model 77—57724
fuel, sawdust waste of timber mills *(German)* 80—40805
fusion reactor blanket concept, 1500 to 2000K Li boiler for process heat/electric power generation 80—37633
gas cooled fast breeder reactor steam generators, development programmes 77—18648
GCFR steam generator cavity closure plug, smearing in axisymm. finite element anal. 77—14222
heat and pressure chamber for steam turbine clearance meas. transducer testing 77—53881
heat exchange intensification fission reactor tubular fuel elements 77—61497
heat transfer crisis location under conditions of nonuniform heat release 80—64534
heat transfer in vertical steam generating tube, at low pressures and moderate mass velocities of flow, post-dryout coeff. calc. 78—67257
high pressure, in-service scavenging by intermittent dosing with chelating agent 80—89485
HTGCR, downstream water flow steam generator 80—5223
HTGR steam generator, construction and development *(German)* 77—369
HTGR steam generator or heat exchanger materials, compatibility with coolant circuit media 77—57721
HTGR steam power plant, nonlinear dynamic model, digital simulation 78—78437
HWR reboiler hybrid computer dynamic simulation 78—8949
Incoloy 800, design problems in steam generators of high temp. reactors 79—45352
inlet temps. and corrosion product deposits, water chemistry effects 80—89528
LMFBR, Creys-Malville boiler construction and features *(French)* 80—47542
LMFBR, H burden from steam side corrosion in Na heated steam generators 78—58355
LMFBR, leak detection by acoustic spectra meas. *(Czech)* 78—54849
LMFBR, modular steam generators, breakdown protection 79—76059
LMFBR, Na-H_2O steam generators, safety problems and their solution in the USSR 80—63318
LMFBR, selection of steam conditions 80—18404
LMFBR, water leaks in secondary cooling circuit boilers 78—86572
LMFBR diagnosis, electrochemical and physical methods 79—97787
LMFBR evaporator tube, critical heat flux meas. 80—591
LMFBR modular steam generator tube plates, stress anal. 79—71883
LMFBR modular steam generators, heat transfer intensification using helically-ribbed tubes *(Czech)* 80—560
LMFBR Na-heated steam generator, flow instability detection by noise anal. 79—97854
LMFBR secondary cct. components 79—97793
LMFBR secondary Na ccts., design, construction and operating experience *(French)* 79—97789
LMFBR steam cycle selection 80—18403
LMFBR steam cycles comparison, PLBR design 80—18405
LMFBR steam generator, small leak detection by surface oscillation meas. during Na-water reaction 77—67789
LMFBR steam generator, small-leak Na+water reaction, dissolution rate of hydrogen 78—29545
LMFBR steam generator heat exchange doublex tube element, design and development 79—71882
LMFBR steam generator leak, meas. of sound produced during steam injection into Na 79—93782
LMFBR steam generator rupture disks, dynamic instability anal. 79—85662
LMFBR steam generator tube thermal oscillation obs. 79—9672
LMFBR steam generators, behaviour of heat exchange tubes in Na-water contact 80—13670
LMFBR steam generators, flow induced vibr., review 77—23240
LMFBR steam generators, leak detection of steam or water into sodium 79—13434
LMFBR steam generators, leak detection of water into sodium, magnetic flowmeter bubble noise monitor 80—9000
LMFBR steam generators, mass transfer props. of steel, test *(Japanese)* 77—348
LMFBR steam generators, reliability considerations 79—22437
LMFBR steam generators, safety alarm system, water leakage detection *(Czech)* 78—33268
LMFBR steam generators, use of alloy 800 77—3108
LMFBR-type steam generator, consequences of intentional steam tube failure 79—54544

boilers continued
LOCA, experimental and theoretical study of the blowdown of the secondary side of a steam generator 80—761
local heat transfer in tubes with heat flux constant over length and variable over perimeter 78—30163
LWR fossil fired superheater technical and economic assessments 78—8966
LWR steam generator behaviour during core blowdown tests 80—772
Monju heat transport system design and related R & D work 79—97791
multifuel fluidised bed combustion packaged boiler to supply 10000 lb/h saturated steam at 100 psig 80—108779
multiphase processes, density-wave oscillations, linear stability anal. 80—48775
nuclear, linearised transient anal. 80—18378
nuclear electric plants, vertical steam generator tubes, forced convection heat transfer *(French)* 79—98729
nuclear LMFBR steam generator, Cr-Mo low alloy steels comparison 78—54834
nuclear power plant steam generator reliability, Canadian practice 79—22451
nuclear power reactor, austenitic stainless steel, appl. 77—3102
nuclear power station steam generators, Na-water type, design 77—50215
nuclear power stations, steam generator inspection by photographic and visual methods 79—54557
nuclear power stations, Turkey Point steam generator repair and influence of water chemistry 79—54556
nuclear steam generator life evaluation, safety features in stress anal. for some accidents 79—54560
nuclear steam generator tubes testing and evaluation, using CIS/DASIO system *(Czech)* 80—63301
nuclear steam supply system, design developments of Combustion Engineering System 80 79—97755
nuclear steam supply system, German licensing conditions 77—46340
oil-fired, opacimeter use possibilities *(Rumanian)* 80—87483
oil-fired boilers, noise reduction by casing *(Hungarian)* 80—106663
once through steam generator, Na-heated, stability anal. nuclear reactor systems model 80—91218
once-through high press. boiler feedwater solutes behaviour 80—63233
once-through nuclear boiler at 14.5 MPa hydrothermal and chemical conditions 80—63232
once-through steam generator, modelling 77—88271
P-67 type, operational efficiency increase, air-water heat exchanger application 79—68710
Palisades Plant steam generator operation rel. to water chemistry 79—9854
PHWR, forced circulation steam generator selection criteria *(Rumanian)* 79—3232
plant efficiency at Beaver Valley power station number 1, anal. of generating capability deficiency 79—67828
plate restriction two-phase flow hydraulic resistance calc. 78—1734
pollution detection and control, SO_2 emission reduction by limestone-additive process *(German)* 78—53724
power plant dynamics and control, conf. Hyderabad, India (Feb. 1979) 80—91215
pressurized fluidized bed combustor/steam generator design evaluation for combustion of high-S coals 80—30346
pulverised coal combustion, in combustion chambers of steam generators *(German)* 78—27758
PWR, forced circulation steam generator selection criteria *(Rumanian)* 79—3232
PWR, German, U-tube steam generators, inspection findings 79—9849
PWR, heat transfer equations for boiler tubes *(Rumanian)* 79—3189
PWR, Oconee station, steam generator availability 80—22921
PWR, steam generators, design, subcooled and bulk boiling correls. 79—611
PWR, tube local corrosion causes and preventive methods *(French)* 78—8963
PWR boiler tubes, corrosion risk reduction methods 79—39045
PWR boiler tubes, denting type corrosion, control by use of neutralisers 80—106109
PWR development in France *(French)* 78—8962
PWR heat rate improvements, controllable loss system 79—67827
PWR LOCA, effect of steam generator tube rupture, computer simulation 80—23006
PWR modular steam generator, application possibilities 79—76057
PWR natural circulation U-tube steam generator, digital code UTSG 78—50242
PWR occupational radiation exposure reduction techniques 79—9901
PWR once-through steam generators, operating reliability 80—13558
PWR power station secondary water chemistry study, progress report 80—106108
PWR steam generator, γ-dose rate distrib. meas. 80—5382
PWR steam generator, design and development 80—9335
PWR steam generator, integral economiser U-tube, mathematical model 77—74911
PWR steam generator blowdown review of international handling procedures 80—690
PWR steam generator chemical cleaning 79—93819
PWR steam generator corrosion problems and design implications 79—93812
PWR steam generator degradation, operating experience, regulatory considerations 79—93817
PWR steam generator eddy-current inspection results 79—9855
PWR steam generator force anal. during LOCA 80—13666
PWR steam generator operations, Westinghouse, benefits of contaminant control 79—93818
PWR steam generator repair options 80—22923
PWR steam generator tube rupture, probability distrib. for releases of ^{131}I and ^{133}Xe 80—13668
PWR steam generator tube rupture accident, radio-I behaviour 79—59230
PWR steam generator tubing, corrosion problems 79—24683
PWR steam generators, remote controlled TV for detection of leaking tubes *(French)* 80—791
PWR twin header bore welded steam generator design 79—93813
PWR with straight tube steam generator, 1300 MW, characts. *(German)* 78—50292
PWRs in Framatome plants, manufacturing phases, quality assurance 77—38323

boilers continued
radiant heat flux portable direct reading measuring device, CERL flux-probe features 78—45633
radiation heat exchanger, temp. distribution, model 77—39210
radioactive corrosion product accumulation in nuclear steam generators 80—13579
reactor steam generator tube perform. anal., corrosion failure 79—59178
SNR 300 LMFBR steam generators 79—97792
SNR-300 LMFBR steam generator transients, computer simulation 80—23012
solar, water heater, low-temp., tubular heat receiver, temp. distribution, heat-balance differential equation solution 79—94464
solar energy, two-phase flow in two parallel horizontal tubes in solar collector receiver tubes, fluctuations *(Japanese)* 79—79377
solar energy collectors, cylinder-parabolic, with envelope pipe, steam generation efficiency calculation model *(German)* 80—33112
solar power station, tower-type, heliostat field solar energy collection, achievements and projections *(French)* 79—100490
solar water heaters, aluminium alloy rolled-welded heating panels production and use 79—96421
stability of boiling channels, nonlinear math. model calc. of coolant-vel. perturbations 79—89353
stationary spherical solar collector design 79—62107
steam, hydraulic calc., mathematical model computer applications 79—68816
steam, in nuclear plant with water-cooled water-moderated reactor cooling system faults, hybrid simulation *(Russian)* 78—5008
steam generating tube, with ribbon like dry-out patch, temp. distrib. calcs. 79—1085
steam generator, accumulation type, using NaOh as thermal storage material *(French)* 80—40914
steam generator, flow distribution anal., computer code 79—49653
steam generator, heat transfer, surface ash and internal pipe deposit resistance calcs. 79—1089
steam generator, modular, liquid Na heated, pressure and temp. loading in breakdown situation *(Czech)* 78—50264
steam generator, multiple tube rupture, radiological consequences 78—74452
steam generator, Na-heated, local heat exchange characts. 80—23867
steam generator design life, probabilistic approach 77—46395
steam generator leakage in the AVR nuclear power station 80--596
steam generator TP-87 with bottom burners NO_x formation *(Russian)* 77—83072
steam generators, steady 2-dimens. two-phase flow and heat transfer calc. 79—1237
steam generators of water cooled nuclear power plants, corrosion phenomena, Review 80—558
steam-generating channels with cosine law heat liberation, mass exchange conditions 79—81710
steam-generating pipe with internal ribbing, heat exchange 78—4979
steam-generating tube, bubble/plug flow boiling regimes, elevated press., drift vel. and void fraction determs. 78—87379
steel, AGR boilers, gas side corrosion, breakaway oxidisation treatment 78—48558
steel, Cr-Mo, annealed, microstructural effects on creep-rupture behaviour 79—57120
steel fatigue crack propagation test results *(Hungarian)* 79—83293
steel tubes, Cr-Ni-Mo, austenisation conditions effect obs., on structure and mechanical props. 80—3151
Super Phenix reactor vessel research and development *(French)* 79—30947
supercritical steam generators, flow instability conditions determination 78—46936
superheated steam, control system using an adaptive regulator, synthesis *(Polish)* 79—75518
superheaters, flue-gas temp. difference influencing pressure loss calculation programme *(German)* 80—38225
SuperPhenix nuclear boiler, design and construction 79—97761
thermally expandable fluid transients, finite difference method 77—79418
thermionic topped steam power plant, conceptual design 79—48156
TPP 210 A steam generator, radiant heat flux distrib., light model simulation 78—94567
tube, serpentine geometry at high press., two phase heat transfer 78—94077
tube corrosion investigation using gamma-ray transmission meas. technique 77—9011
tube failures at water cooled nuclear plants, world experience in 1975 77—38394
tube inspection, new acoustic device characteristics 77—68343
Turkey Point nuclear power plant operation, steam generator tube denting effects 79—9852
U-tube steam generator transient simulation using extend implicit continuous-fluid Eulerian method 79—89356
vapour generator for K, heat transfer with drop motion in tube in supercrit. region 80—23880
vibration analysis of heat exchanger and steam generator designs 78—66333
volumetric steam content determ. by noncontact neutron sensor 79—30904
volumetric steam content determ. of steam generating channels by slow neutron method 79—30903
wall thickness US measuring equipment *(German)* 78—18136
water conditions, chemical monitoring development in UK *(Russian)* 77—88217
water flow instability in Na heated once through steam generators 80—27737
Westinghouse steam generator experience with all volatile treatment 79—9853
Westinghouse steam generators, operations update 78—21683
Westinghouse steam generators, operations update 78—21751
Zion Generating Station steam generator operating experience 79—9851
CO_2 supercritical boilers, forced flow, frictional pressure drop 80—14689
NO_x formation study during combustion 78—3434
Na heated steam generator, flow instability 77—46214
Na heated steam generators, tube degradation induced by dryout instability 77—46213
Na/water steam generator problems, soln. in USSR *(Russian)* 79—97876
Na-cooled fast reactors, tube material corrosion problems 79—36328

boilers continued
- Na-H_2O reaction jets, material wastage experimental data anal. 80—27705
- Na-H_2O reaction jets, metal wastage production prediction 80—27704

boiling
- *see also boiling point*
- acetone, heat emission in crit. region, press. and heating surface temp. effects *(Russian)* 80—69634
- acoustic emission from boiling water in annular channel *(Russian)* 77—54302
- Alad'ev wall superheat correl., expt. validity test 78—83393
- alloy, vapour bubble growth dynamics, electron-beam vol. heat source 77—47565
- annuli, (non)-uniformly heated, pressure drop during boiling, expt. results 79—81971
- annuli, concentric (eccentric), with turbulence promoters, boiling crisis 78—55639
- annuli with different lengthwise heat flux distrib., boiling crisis 79—1057
- annuli with turbulence promotors, heated, lengthwise-uniform and non-uniform heat release, boiling crisis 80—48703
- aqueous solution boiling, heat transfer coeff. calc. *(Rumanian)* 79—81693
- bed space of boiling layer, laser radiation probe 77—15115
- benzene, nucleate boiling heat transfer, press. factor 77—69080
- benzil-benzene, dil. soln., thermodynamic equilib., ebulliometric investig. 78—18752
- binary and ternary mixtures boiling, heat transfer and heat flux density *(German)* 79—68559
- binary film boiling, theory 77—84912
- binary liquid drops, nucleate boiling evaporation on heated surface 77—27531
- binary mixture, boiling, liq.-vapour equilib. data, circulation apparatus determ. *(German)* 77—24375
- bubbel nucleation in oscill. press. field 79—32216
- bubble, contact of internally heated bodies, temperature increase obs. *(German)* 77—35019
- bubble boiling, calc. of initial microlayer thickness 77—11248
- bubble boiling in large volume at cylindrical and spherical surfaces, max. crit. heat flux 77—11188
- bubble departure, diameter and frequency 80—38481
- bubble departure frequency, effect of superheat and cavity size 77—80610
- bubble detachment and dispersion, heater vibration effects 77—55355
- bubble detachment size during quasistatic growth on heater surface 77—84120
- bubble growth and condensation in pure and binary systems 79—23191
- bubble growth at superheated horizontal wall, pure liq. and binary mixtures 79—41719
- bubble growth in slow formation regime of nucleate pool boiling 78—90687
- bubble growth in variable press. fields 79—32215
- bubble growth modulus at BP, arbitrary radius time depend., theoretical expression 77—46894
- bubble growth on heating surfaces in pool boiling, conservation eqns. soln. *(German)* 80—74715
- bubble population prediction in flow boiling, from gas bubble nucleation 78—90696
- bubbles, active nucleation site spatial distrib., bubble flow density 78—71267
- bubbles, evaporating, of low-boiling liq., surface condensation of high-boiling mixture vapours 80—59021
- bubbles, growth and breakoff, two-dimensional and axisymmetric problem 80—48783
- burnout, for heaters cooled by liquid jets 79—59979
- BWR, coupled vibrations of a structure and fluid excited by pressure shocks 80—13546
- BWR, method for detecting bypass coolant boiling 80—571
- BWR boiling loop in low-pressure operation, stability anal. 78—8894
- BWR boiling noise, local and global component obs. and calc. 78—94066
- capillary and porous surfaces, liquid boiling and evap. heat transfer 78—94526
- capillary porous bodies, boiling heat transfer to liquid N_2 or He 80—1575
- capillary-porous structs., heat transfer and max. heat flux with boiling 80—33600
- capillary-porous submerged coating, boiling model 77—65792
- carbon tetrachloride-acetone (chloroform) mixtures, film boiling on elec. heated horizontal wire, atm. press. 77—20061
- channel, rectangular, forced flow boiling and burnout 78—94530
- channel flow, thermally induced two-phase flow instabilities, thermal nonequilib. 78—51240
- channel with nonuniform heat emission, crit. heat flux density determ. *(Russian)* 79—64489
- channels, transient boiling flow, two-phase two-fluid approach 79—41756
- channels with boiling and flow parallel to rod bundles, press. drop 79—1059
- circuit system, effect of intense electric field *(Russian)* 78—46887
- collective heterogeneous boiling nuclei formation, statistical dynamic model using wettability 77—89531
- colligative properties of simple solns. 77—21466
- convective, of refrigerants in horiz. tube, statistical anal. of heat transfer data 79—7283
- convective flow, forced, transition boiling boundaries meas. 79—27499
- cooling, by liq. boiling in capillary porous layer, statistical model 77—89196
- critical boiling heat fluxes to liquids at subatmospheric pressures 80—64345
- critical heat flux, forced convection boiling in vert. annular channel, generalised correlations 79—46171
- critical heat flux for forced convection boiling in heated round tubes, generalised correlation 79—68697
- critical heat flux for liquids in free motion conditions *(Russian)* 77—24400
- critical heat flux in annuli, general correlation 80—43705
- critical heat flux in boiling channels, BURN-2 computer program 77—54863
- critical heat flux of saturated natural convection boiling with heating from below 80—10114
- critical heat flux prediction in uniformly heated vert. tube, generalised graphical method 79—46313

boiling continued
- critical heat flux variation, very nonuniform annular heat release 78—51043
- critical heat transfer to flowing cooling water 77—74910
- cryogenic and ordinary liquids on vertical surface, film boiling heat transfer 80—48555
- cryogenic binary mixtures (Ar, N_2), nucleate pool boiling 79—60495
- cryogenic fluid, boiling, vapour bubble growth rate 77—24397
- cryogenic fluid, boiling, vapour bubble growth rate 77—24398
- cryogenic fluid boiling in capillary tubes, heat transfer 79—59915
- cryogenic fluids, nucleate boiling, heat transfer rate 77—39199
- cryogenic liquid, boiling, heat transfer coeffs. 78—9539
- cryogenic liquid, bubble population density meas. on immersed heated surface 77—30169
- cryogenic liquid, critical heat fluxes, effect of cylindrical heater dimensions 79—35756
- cryogenic liquid, heat transfer during transition boiling 77—35017
- cryogenic liquid, pool boiling heat transfer, vapour bubble dynamics 77—31765
- cryogenic liquid pool boiling, crises and heat transfer 80—1576
- cryogenic liquids, boiling, crit. heat flux, heating surface props. effects 78—90662
- cryogenic liquids, boiling in capillary-porous bodies, heat transfer 80—48552
- cryogenic liquids, investigations on heat transfer 79—60494
- cryogenic liquids, nucleate boiling, influence of thermal props. of heating surface material 77—46888
- cryogenic liquids, transition boiling 79—65182
- cryogenic liquids on flat horizontal surfaces, film boiling heat transfer 80—48553
- cylindrical specimens in underheated media, calc. of heat transfer during quenching *(Russian)* 78—39821
- density wave oscillation in boiling channels *(Japanese)* 79—14400
- depressurised subcooled liquid, boiling boundary phase-change front transient propag. 80—43768
- dielectric fluid, on porous coating *(Russian)* 79—72788
- dielectric fluid at porous surface, heat transfer crisis *(Russian)* 79—50575
- dielectric liquids, boiling process in narrow horizontal channels due to action of elec. field *(Russian)* 80—74707
- diphenyl-benzene, dil. soln., thermodynamic equilib., ebulliometric investig. 78—18752
- distilled water, transition boiling curve on Inconel surface under forced convective conditions 80—10653
- ditolylmethane, boiling in circuit system, effect of intense electric field *(Russian)* 78—46887
- downward-facing flat plate, stable film boiling heat transfer 77—23954
- drinking-straw honeycomb flat plate solar collector expts. 79—62086
- drop, gradient explosion, under conditions of bulk heat release 78—83226
- dryout heat fluxes in debris beds cooled at the bottom and having subcooled liquid at the top 80—13652
- dryout in an SGHWR rod bundle, exptl. and calc. comparison 79—3192
- EHD coupled minimum film boiling in dielec liqs. 77—42921
- electrolyte aq. soln., boiling, heat transfer coeff. 78—9532
- ethane, heat transfer during boiling in tube *(Russian)* 77—68589
- ethane, pool boiling heat transfer 79—1058
- ethanol, aq. subcooled soln., acoustic phenomena during nucleate boiling 78—10181
- ethanol, boiling, crit. heat flux in low press. region 78—90663
- ethanol, boiling at subatmospheric press., heat transfer rate, heating surface effects 80—69630
- ethanol, boiling in large enclosure, critical heat flux 79—18685
- ethanol, nucleate boiling heat transfer, press. factor 77—69080
- ethanol-water mixture, saturated, min. film boiling temp. on horiz. stainless steel and Cu surfaces 78—90692
- ethylene, heat transfer during boiling in tube *(Russian)* 77—68589
- ethylene, pool boiling heat transfer 79—1058
- ethylene glycol solution, flow boiling and pool boiling critical heat flux, effect of flow passage geometry 77—62250
- ethylene-ethane mixtures, boiling heat transfer 78—9535
- evaporating surfaces, heat transfer aspects 77—89011
- expanding vapour bubble, anal. of reactive forces exerted by evaporating molecules 78—1548
- explosive boiling in free contacting mode, spontaneous nucleation model 79—81700
- explosive flashing in pools of liquids 80—92024
- extended liquid masses, film boiling heat transfer, partial evaporation method 78—90668
- falling film rewetting 78—75906
- fast reactor safety, TREAT tests, statistical model to identify boiling inception 79—93779
- ferromagnetic layer boiling, mag. characteristics meas. 78—59499
- film, boiling, laminar, with chem. react. on catalyst surface, model 80—45553
- film, instability, during quenching in subcooled water *(French)* 79—46167
- film boiling, bubble nucleation and venting 78—30153
- film boiling, conduction and radiation from flat plate *(German)* 79—72789
- film boiling, contact heat transfer meas. 77—42037
- film boiling, heat-exchange intensification, nitrogen in pipes 79—81876
- film boiling, hot sphere in subcooled liq. press. excursion of vap. film 79—14231
- film boiling, minimum heat flux anal. 78—90665
- film boiling and vapour explosions from small spheres 80—18543
- film boiling crisis, surface material thermophys. props. influence, data correl. 80—5923
- film boiling destabilisation, liq. drop falling onto hot liq. surface 78—94588
- film boiling from cylindrical surfaces, organic compounds 79—23194
- film boiling instability at high temp. *(French)* 79—86322
- film boiling mode, disperse, of cryogenic liqs., heat transfer and modified Reynolds model 80—5924
- film boiling on small wires, prediction of elec. field effects on most unstable wavelength 78—87239
- film boiling on sphere, in forced convection 79—32211
- film boiling under natural convection conditions, heat transfer 78—83231
- film region flow boiling dynamics 79—59145
- film- and transition-boiling heat transfer to cryogenic fluids 80—92026
- films of thickness of mm range, critical thickness for destruction *(Russian)* 77—80611

boiling continued
  fin in boiling water, convection and heat transfer coeffs. 80—19219
  fission energy generation in vol. boiling pool systems, microwave heating simulation 80—18386
  fission reactor nine-rod cluster, film boiling behaviour 79—89444
  fission reactors, flow boiling dynamics in film region 80—83142
  flow boiling, critical heat flux, review 79—4074
  flow boiling crisis in horizontal tubes, fluid-to-fluid modelling, water and Freon-12 80—48785
  flow film boiling, void fraction meas. 80—92207
  flow instabilities in sustained and transient boiling, inlet subcooling effect 78—94809
  flow structure for critical discharge conditions of boiling water through cyl. channels 80—83145
  fluid bed boilers, temp. profiles 79—32663
  fluidised bed, boiling layer, axial mixing of solid phase *(Russian)* 78—47035
  fluidised bed, heat transfer from transverse streamlined cylinder during surface boiling 80—43708
  fluidised bed, two-dimensional, with transverse gas supply, fluid dynamics obs. *(German)* 78—34192
  fluorocarbon refrigerant, film boiling heat transfer from heated plate 79—55380
  forced convection boiling, critical heat flux, Fe_2O_3 scale effects 80—64344
  forced convection boiling, heat transfer correlations *(German)* 80—53781
  forced convection boiling heat transfer, Dengler and Addoms concept 78—1546
  forced convection film boiling on plate with varying heat flux 78—5737
  forced convection quench data rel. to steady-state nucleate boiling data 78—90995
  forced convective film boiling, math. model 79—18686
  forced convective transition boiling, prediction methods, literature review 77—3825
  forced-convection boiling upflow system, instabilities in parallel channel, nonlinear model 77—57724
  free convection boiling, critical heat fluxes generalised eqn. 77—62138
  free convective heat transfer from horizontal tube to refrigerants near crit. state *(German)* 77—11192
  Freon F-113, boiling on porous Cu coating *(Russian)* 79—72788
  Freon-113, boiling and heat transfer on horizontal pipes with annular fins 80—74855
  Freon-113, pure and mixed with methanol, EHD coupled minimum film boiling, surface wave model 78—87240
  Freon-114, Leidenfrost phenomena, crit. press. obs. 78—90667
  Freon-11, forced convection boiling heat transfer in vertical annular passage 79—32509
  Freon-11, pool-boiling, heat transfer from inclined plate 78—51046
  Freon-12 in heated tube, flow boiling dryout, transient heat transfer investigation, reactor LOCA 80—32359
  gas and vapour bubble nucleation on brass surface in water 78—71845
  gas-liquid flow, hydrodynamics and transport processes, electrodiffusion modelling method 79—90309
  gassy two-liq. pool., hollow sphere formation, LMFBR simulation 77—61518
  glass fibre reinforced epoxy resin, destruction by freezing or boiling of phase separated water 78—48512
  heat and mass transfer in boiling in capillary gaps 78—46885
  heat exchange, nonstationary, with phase transformations, delayed boiling influence *(Russian)* 78—83235
  heat generating and transmitting elements, thermal dynamics anal. 78—9548
  heat transfer, bubbling and boiling, under conditions of free and forced convection 78—90637
  heat transfer, heating surface material effect 77—42704
  heat transfer, surface roughness effect 78—9534
  heat transfer channels, annular, hydraulic resist. rel. to boiling *(Russian)* 77—80143
  heat transfer coefficients, heater plate thickness effects 78—34124
  heat transfer conference, Aug. 78, Toronto, Canada 78—90624
  heat transfer crisis detect., sensitivity of bridge and thermocouple methods 77—61064
  heat transfer crisis in annular channel containing unheated sections 77—23945
  heat transfer during boiling on circumferential fins 78—59272
  heat transfer enhancement 78—9530
  heat transfer in narrow channels and capillaries 78—9543
  heat transfer in two-phase thermosyphons 78—90686
  heat transfer rates, Rohsenow's pool boiling correlation eqn. 77—80052
  heat transfer under reduced gravity conditions 77—4192
  heat-emitted pipe, with surface boiling, temp. fluctuations *(Russian)* 80—102962
  heated disc with impinging jet, saturated forced convection boiling, CHF upper limit 79—81891
  heated tubes, alternate dry and rewet, flow boiling, obstruction effects 79—1181
  heated wires, liquid surrounded, surface thermal state under boiling, from large applied heat flux 79—81690
  heating element, heat exchange, effects of nonstationary liberation of power *(Russian)* 80—69636
  heating surface during boiling, temp. distrib. for a sudden increase in power *(Russian)* 77—84114
  n-heptane, pseudoboiling mechanism, improved heat transfer 78—6152
  n-hexane and mixtures with n-pentane, nucleate boiling from tube arrays 78—22251
  horizontal coiled tube banks, two-phase flow boiling heat transfer and hydrodynamics 80—48708
  horizontal cylinder, local boiling heat flux density, saturated, subcooled conditions 78—90659
  horizontal heated surface, post-nucleate boiling and crit. heat flux models 78—90664
  horizontal multitube bundles, boiling heat transfer 80—10122
  horizontal tube transition and flow boiling heat transfer, bubble flow 78—18292
  horizontal tubes, saturated flow boiling, non-uniform heat flux effects *(German)* 80—74716
  hot surface quenching rate, countercurrent single- and two-phase flow effects 78—59451
  hydrocarbons, boiling heat transfer 78—9535

boiling continued
  hydrocarbons, pool boiling, heat transfer, surface roughness effect 80—48705
  hydrothermal flows in permeable media, boiling rel. to two-phase flow struct. 80—85693
  incipient boiling, transition to film boiling 78—90660
  incipient boiling characteristics at atmospheric and subatmospheric pressures 78—90688
  increased gravitation, heat exchange mechanism bubble form., review 77—46895
  injection bubbling and boiling in liqs., heat transfer 77—68672
  instability of gradient explosion 78—83917
  internal boiling and superheating in vaporizing multicomponent droplets 79—3906
  isopropanol, nucleate pool boiling, bubble freq. model, surface effects 78—90651
  jet, forced-convection boiling system, burnout 78—38378
  laminar film boiling heat transfer, thermal conductivity and convection effects 80—74864
  laminar film boiling of binary liquid mixture, heat transfer rates *(German)* 77—7398
  laminar vapour flow in film boiling, stability limits 78—90832
  law of metastability, appl. to effect of mag. field on boiling liqs. 78—79199
  Leidenfrost effect, demonstrations 78—81744
  limiting vapour qualities in second boiling crisis 79—81970
  liquefied natural gas, boil rate composition depend. 79—69235
  liquid, forced channel flow with surface boiling, analogies between heat and momentum transfer 77—47014
  liquid, superheated, gas content effect on boil-up and cooling 79—1061
  liquid, underheated, boiling, sonic pulses generation, time and spectral characteristics 80—107373
  liquid boiling on surface of annular rib, heat cond. anal. 79—55315
  liquid boiling wave processes at heat releasing surfaces 79—90773
  liquid film, nucleate boiling suppression 78—75055
  liquid film, with nucleate boiling, heat transfer and film breakdown 78—34122
  liquid film flow, preheated to boiling 77—62244
  liquid films, boiling, heat transfer peculiarities 78—90656
  liquid films on horizontal tubes, combined boiling and evaporation 79—81882
  liquid in granular bed, heat transfer enhancement 78—9533
  liquid jet, burnout in nucleate boiling 78—90991
  liquid layers, superposed, boiling, convection heat transfer 78—30159
  liquid metal boiling, mag. field effect on bubble growth 79—32217
  liquid metal film boiling, thermodynamic superheat limit rel. to Leidenfrost temp. 79—55325
  liquid metal fragmentation following reactor core meltdown accident, contribution of collapsing vapour bubbles 80—755
  liquid metals, incipient boiling press. signal and evaporation coeff. meas. 79—77734
  liquid metals, incipient boiling superheats, heat flux effects 80—74697
  liquid microlayer form. and stability in pool boiling, dry area growth 79—18683
  liquid pools, vol. heated, transient boiling, convex flux relations, fission reactor safety 77—31340
  liquid pools, vol. heated, transient boiling non-convex flux relations, fission reactor safety 77—31341
  liquid refrigerants, heat transfer enhancement during boiling at low heat fluxes 78—9529
  liquid thin film rupture, heat-transfer surface state effect 78—55552
  liquid-gas bubbles system, phase transition kinetics and kinetic eqns. 78—83933
  liquid-liquid interface, nucleate boiling 78—2342
  liquids, saturated, boundaries of region of existence of nucleate boiling, thin film breakdown 80—48695
  LMFBR, acoustic anal. from Na boiling tests using THORS bundle 6A 79—31033
  LMFBR, boiling pools with internal heat generation, void distrib. 78—21626
  LMFBR, bubble collapse reactivity increases in boiling fuel/steel pools 79—31025
  LMFBR, coolant start of boiling detection by acoustic method 78—86646
  LMFBR, local boiling calculations in subchannel geometry, feasibility study using CLAYMORE code 78—25280
  LMFBR, Na incipient boiling under forced convection in seven pin bundle 79—22401
  LMFBR, transient boiling of Na in 7-pin fuel bundle under loss-of-flow conditions 79—41007
  LMFBR, transient boiling of sodium in seven-pin bundle under transient overpower conditions 79—76056
  LMFBR 19-pin simulated fuel assembly, dynamic boiling tests 79—31029
  LMFBR boiling acoustic detection sensitivity, PFR commissioning expts. 79—13452
  LMFBR carbide fuel and steel, boiling flow regimes 79—85617
  LMFBR core disruptive accidents, flow regime obs. in two-phase volume heated boiling pools 79—31014
  LMFBR core meltdown accidents, void distribution in volume-heated boiling pools 77—46318
  LMFBR fuel subassembly, approach for treating two-dimensional coolant boiling 79—31030
  LMFBR fuel subassembly, effect of bundle insulation degradation on boiling stability tests 79—54548
  LMFBR LOCA, use of temperature variance to detect sodium boiling 79—54527
  LMFBR Na boiling, two-phase flow calculations in low-pressure systems 80—103068
  LMFBR Na heated steam generator tubes, transition boiling characts. 79—81006
  LMFBR Na-cooled 7-rod bundle acoustic and temp. noise obs. 79—13391
  LMFBR safety anal., sAS-3D evaluation of boiling at decay-heat levels in FFTF 80—47634
  LMFBR subassembly local boiling detection by outlet temp. fluctuation analysis 79—13390
  LMFBR unprotected loss-of-flow accidents, boiling incoherency effects 79—31007
  LMFBR wire-wrapped subassemblies, Na boiling behaviour 79—31031

boiling continued
  LOCA, counter-current flow limiting phenomena with vapour condensation, model 77—61519
  low quality flow boiling, turbulent forced convection and nucleate boiling heat transfer 80—14696
  LWR, boiling heat transfer anal. 80—27724
  LWR, stationary boiling front in liquid film cooling of a vertical heated rod 79—45341
  LWR fuel rod quenching, two-dimensional heat conduction model 79—93815
  mass force field boiling crisis, critical heat flux for swirling tube flow 79—90248
  maximum heat fluxes under special conditions 78—9547
  mechanism model based on rotating vortex model with spatial heating 80—14694
  metal-polar fluid boundary, double electric layer effect on boiling 78—59274
  metastable flows of water, spontaneous boiling 80—106709
  methane, boiling on water, initial water temp. effect 77—19606
  methane(-ethane)(-N_2), heat transfer in nucleate boiling of liquified gases and binary mixtures *(German)* 79—18687
  methanol, boiling, on Cu surface, rel. to H_2O 78—90654
  microlayer, formation and evaporation, theory 78—9536
  mixture, binary, nucleate boiling heat transfer, conc. depend. 78—87249
  mixtures, heat transfer 78—9538
  modelling by bubbly liquid press. variation 79—1060
  molten metal-reactor coolant interaction, vapour film collapse expts. 79—13474
  mushroom shaped heating surface, computational errors and heat losses 80—64347
  narrow spaces, heat transfer mechanism with boiling, interferometry obs. 78—94527
  natural convection boiling, heat-transfer coeff. 80—33421
  natural convection film boiling, from spheres to saturated liquids, integral calcs. 78—34129
  non-flowing boiling water films, critical breakup thicknesses 79—94468
  non-stationary heat transfer crisis *(Russian)* 77—24401
  nonequilibrium transient flow boiling, method of characts. soln. 80—14789
  nonisothermal two-phase flow in vertical channel, rel. to natural convection boiling 77—24013
  nonvolatile liquid, nucleation eqn. in phase space 79—27495
  nuclear fuel assembly boiling and voiding, THARC-S code 80—13646
  nuclear reaction flow boiling nucleate region, dynamics 77—88205
  nuclear reactor, BWR, bypass flow distrib. 77—42017
  nuclear reactor flow boiling anal., numerical standards 77—79448
  nuclear reactor fuel, Leidenfrost temperature for spherical fuel particles, rel. to FCI anal. 78—17371
  nuclear reactor safety and performance, boiling crisis, state of the art review 80—63312
  nuclear reactor spherical element surface boiling dynamics 80—27736
  nuclear reactor system, subcooled nucleate pool boiling, intensity and power spectral density of acoustic emission 78—17282
  nuclear reactors, BWR and PWR, boiling mixing studies in water loops 79—26502
  nucleate, heat transfer mechanism 77—75785
  nucleate, subcooled, latent heat transport contrib. 78—75046
  nucleate, superheating, heterogeneous nucleation theory calc. 79—46170
  nucleate, surface topography 78—90653
  nucleate boiling, active sites role 77—15569
  nucleate boiling, anal. of microlayer thicness 79—77234
  nucleate boiling, binary mixture, bubble growth, saturation press.-temp. relation 77—46892
  nucleate boiling, conservative nature of heat transfer laws 77—24395
  nucleate boiling, heat transfer model 78—75056
  nucleate boiling, self-similarity region boundary in terms of heating wall thickness 79—90245
  nucleate boiling, single bubble growth at wall, shape and departure 78—90647
  nucleate boiling, vapour flow in liquid enclosure with temp. distrib. 77—15083
  nucleate boiling at surface near peak heat flux, mechanism 77—75780
  nucleate boiling bubble dynamics, calc. 78—90648
  nucleate boiling heat transfer, bubble population density correl. 77—27525
  nucleate boiling heat transfer, nucleation factor 77—69079
  nucleate boiling in horizontal tube, heat-transfer correl. for refrigerants 79—59911
  nucleate boiling of liq. Ar, N_2, in centrifugal accel. field, heat transfer and flux 78—94538
  nucleate pool boiling, bubble freq. model, surface effects 78—90651
  nucleate pool boiling, influence of surface conditions, bubble flux density 79—55379
  nucleate pool boiling, meas. of void frequency distribs. and profiles using neutron beams 80—27691
  nucleate pool boiling, Mikic-Rohsenow correlation for heat flux 79—55324
  nucleate pool boiling 78—38174
  nucleate pool boiling heat transfer including microlayer evap., model development 77—42833
  nucleate to film boiling transition collective phenomena, Nukiyama curve 78—9531
  nucleate type, boiling acoustic emission and bubble dynamics 77—46893
  nucleation at wall, influence of dissolved gases 77—76537
  nucleation centres interaction, obs. technique 78—14065
  nucleation of boiling and cavitation 77—89008
  nucleation sites, possible mean no. 77—62628
  n-octane, low-press. boiling on Cu surface, accel. heat transfer due to porous Ni layer 77—85056
  oil-water emulsions, pool boiling heat transfer 79—55378
  once-though boiling flow system, density wave instability 79—22367
  organic fluids, natural convection and boiling heat transfer, electric field freq. effects 80—1560
  organic heat carriers, charact. *(German)* 78—79198
  oscillatory turbulent subcooled flow, transient radial heat transport effects 77—42834
  parallel channel forced convection boiling upflow system, instabilities 80—9327
  parallel channel of forced convection boiling upflow system, instabilities 77—61494
  partial nucleate boiling, eval. of Kutateladze's eqn. 80—79298

boiling continued
  peak heat flux in pool boiling, hydrodynamic and surface effects 78—90661
  peak heat fluxes as determined by steady state and transient expts. 80—14549
  n-pentane and mixtures with n-hexane, nucleate boiling from tube arrays 78—22251
  n-pentane-water interface, nucleate boiling 78—2342
  phase-change front propagation during reactor transients, appl. to LOCA in PWR 79—631
  polynary mixtures, natural convection boiling, heat transfer 78—90658
  pool boiling, heat transfer stability prediction, finite disturbances 78—75044
  pool boiling, Rohsenow eqn. 79—59910
  pool boiling burnout, prediction with mechanical energy stability criterion 79—81699
  pool boiling expt., computer controlled temp.-controlled operation 79—14238
  pool boiling heat transfer from horizontal plates *(Japanese)* 78—67016
  pool boiling in very low gravity, proposed spacelab expt. 78—63849
  pool-boiling and bubbling heat transfer, freely convecting liq. 79—32212
  pool-boiling of horizontal cylinders, effect of heater diameter on critical heat flux 77—39281
  porous coated surfaces, thermally nonconductive, boiling features 79—76946
  post-dryout heat transfer, review 79—1094
  power reactor, water cooled and moderated, tube film boiling heat transfer coeffs. 80—73877
  pressure fluctuations in heat transfer channels with surface boiling *(Russian)* 78—14088
  pressurised pipe guides, nonstationary discharge of boiling liq. in thermodynamic equil. approx. 79—81711
  pure liquid and binary soln. superheat, convective heat transfer from thin wire 80—92139
  pure liquid vapour pressure determination apparatus 78—41274
  PWR, new design procedure for DNB limits 80—573
  PWR, rod bowed to contact departure from nucleate boiling tests in cold-wall thimble cell geometry 79—30892
  PWR core thermal hydraulic calculation *(Hungarian)* 78—25282
  PWR fuel rod failure during film boiling, power cooling mismatch test 79—89445
  PWR neutronic calcs., subcooled boiling and open channel effects 80—23053
  quenching rates on hot surfaces, wetting of outer tube walls by water 77—82996
  quenching temperature, 0.03-1.3 MPa, base material thermal props. depend. 78—94587
  reactor coolant flow boiling crisis, tube diameter effect 79—85603
  refrigerants, nucleate boiling, oil impurity effects 78—90657
  rewetting, boiling heat transfer, one-dimens. cond. model 79—598
  rewetting model using generalised boiling curve 79—9675
  Reynolds analogy for boiling, heat transfer 78—59277
  rod bundle dryout, liq. film, droplet entrainment and deposition 78—13204
  rod bundles, boiling crisis and press. drop, heat transfer enhancement devices 78—55638
  rod-bundle in nuclear fuel element, mathematical model for transient subchannel analysis 77—79430
  rotating heat exchanger, frictionless two-phase tube flow, centrifugal accel., choked flow 80—48792
  saturated liquid, boiling onset, film boiling transition, crit. heat flux densities *(Russian)* 78—83234
  shock boiling, liq. discharge through short nozzles, flow blocking 79—86491
  simultaneous boiling and forced convection heat transfer from horizontal cylinder to water in crossflow 77—15018
  sphere in saturated liquid, transient film boiling, liq. heat conduction effects on press. 77—84118
  spheres in vertical flow, transient transition boiling heat fluxes 78—90994
  steady-state flow boiling curve, meas. using temp. controllers 79—32720
  steam generating channel, nonuniform heat release, heat transfer crisis location 80—64534
  steam generating channels, boiling crisis, critical heat loads 79—90247
  steam generating pipe with Fe oxide deposits on wall, steam bubble growth 79—76947
  steam generating tubes, burnout mechanism 78—90984
  steam-generating channels with cosine law heat liberation, mass exchange conditions 79—81710
  steam-generating tube, bubble/plug flow boiling regimes, elevated press., drift vel. and void fraction determs. 78—87379
  structured surfaces to liquid nitrogen, boiling heat transfer *(German)* 80—99919
  subcooled boiling flow, flow quality and void fraction for channel 79—90249
  subcooled boiling flow, vapour bubble growth and recondensation 79—93692
  subcooled film boiling heat transfer from spheres 78—51047
  subcooled forced convection boiling heat transfer at subatmospheric pressure 78—94525
  subcooled forced convection film boiling in forward stagnation region 80—43702
  subcooled liquid boiling in duct, vapour voids size distrib. 78—5783
  subcooled nucleate boiling, mechanistic model 78—90697
  subcooled two-phase water flow, boiling mechanism during burnout 78—94529
  sugar solution, boiling, natural convection mechanisms on horizontal tube 77—24396
  supercritical boiler, algorithm for numerical determ. of transient heat transfer processes 77—23944
  supercritical water, transient loads and flow, tube hot spots, nucleate boiling departure 80—64349
  superheat in heterogeneous nucleation on rough Cu surface 79—37146
  superheated binary solns., flashing kinetics, nucleation and critical bubble 80—92035
  superheated droplets, flash boiling, undergraduate student expt. 78—81748
  superheated drops, boiling in immiscible liq. 77—31368
  superheated liquid, elec. field induced nucleation, pre-nucleation relax. phenomenon 77—51489

boiling continued
superheated liquid, growth of spherical bubbles, anal., numerical calcs. 77—24399
superheated water, flashing kinetics, γ-radiation effects 80—92025
surface, in closed containers, similarity approach *(German)* 77—11684
surface boiling in tube, heat transfer model 78—9551
surface coated with porous structure, transport mechanism of nonvolatile impurities 78—2365
surface roughness influence on boiling heat exchange of light hydrocarbons and N_2 *(Russian)* 79—68562
surface-boiling flow in pipe, high-frequency pressure oscillations 77—35239
surfaces covered with capillary-porous structures, heat transfer with boiling, approximate theory 78—94537
surfactant, aq. subcooled soln., acoustic phenomena during nucleate boiling 78—10181
swirled flow of water in pipes, boiling crisis 79—90241
teaching demonstration, boiling phenomena when red-hot balls enter water of different temps. 78—24627
teaching demonstration of freezing by boiling, using low capacity pump without acid 78—8192
thermal hydrodynamic instability, heating condition effect 78—18288
thermoacoustic vibrations of subcritical press., vibrs. onset mechanism 77—47026
thermodynamic nondimensional parameters *(Italian)* 79—76959
thermosiphons, boiling heat transfer 78—9537
thermosiphons, two-phase heat exchange in supply zone, anal. 80—19387
thick capillary-porous structure, mass exchange during boiling 80—19503
thin film evaporator grooves, fluid evaporation and boiling heat transfer 80—38227
thin liquid film flows, boiling crisis models 80—74710
transient, bubble nucleation and growth instabilities 78—90649
transient (film) boiling on surface of small Cu drop in water 77—1219
transient boiling heat transfer crisis 77—62137
transient boiling heat transfer in vertical flow 77—354
transient effects, leading up to nucleate boiling 78—90650
transient flow boiling in duct, dynamics 78—94528
transient pool boiling heat transfer, incipient boiling superheat 78—30157
transient pool boiling water transfer, burnout 78—30158
transient superheat on vertical surfaces in subcooled boiling 79—7282
transition boiling curves from quenching expts., two-dimens. model with axial conduction 79—19360
transition boiling heat transfer in vertical flow, boiling curve determ. 77—7394
transition boiling heat transfer with forced convection, composite test section, steady state method 79—19361
transition flow boiling heat transfer to water in verticle annulus, BWR LOFA appl. 77—23182
trifluorotrichloroethane, influence of porous coating of heating surface on rate of heat transfer on boiling *(Russian)* 79—10452
tube, vert., uniformly heated, forced convection boiling, crit. heat flux 79—27498
tube, vertical, steam generating annular flow, dry-out position prediction, computer model 78—59447
tube wall temperatures of an eccentrically located horizontal tube within a narrow annulus 79—32201
tubes, horizontal and vertical cooled, boiling crisis and critical heat flux 80—48712
tubes, nucleate pool boiling, critical heat flux, ferric oxide scale effects 80—64343
tubes, straight and coiled, boiling heat transfer with low pressure water flows 80—74856
tubes, temp. and heat transfer coeff. variation upon boiling mode changes 80—69629
two-phase boundary layer, temp. fluctuations 78—51222
two-phase flow, boundary vapour contents for critical state of heat transfer of second kind 78—1722
two-phase flow, nonequil., true mass steam content meas. by diffusion indicator method 79—86538
two-phase systems, thermally induced flow oscillations investig. 77—42907
underheated liquid, lift height of vapour bubble for boiling on vertical wall 77—15104
unstable heat transfer conditions, free convection-film boiling transition 78—14006
unsteady critical heat flux during boiling 77—23946
unsteady heat transfer with phase transition, boiling delay 80—48690
vaporisation sites, number variation with fluid layer height 78—59273
vapour bubble, behaviour during growth at subatmospheric pressures 78—9678
vapour bubble in saturated liq. free convection boiling, growth rate and detachment diameter 80—103057
vertical tubes with zero inlet subcooling, forced convection boiling, critical heat flux 80—64549
vertical uniformly heated tubes, forced convection boiling, critical heat flux, inlet subcooling 80—19374
void fraction and phase distrib. meas. in transient flow boiling by neutron scatt. 78—94870
volatile liquid, statistical thermodynamics of new phase form. *(Russian)* 78—18739
volatile liquid droplets, impaction on hot liquid surfaces 77—39330
water, boiling, heat transfer around single nucleation site 77—24394
water, boiling, natural convection mechanisms on horizontal tube 77—24396
water, boiling and heat transfer on horizontal pipes with annular fins 80—74855
water, boiling at subatmospheric press., heat transfer rate, heating surface effects 80—69630
water, boiling critical heat flux density, free motion conditions, 1-205 bar *(Russian)* 79—68560
water, boiling curves, subcooled and forced convective conditions 79—14230
water, boiling on finned surface, heat transfer crisis 78—9540
water, crit. outflow, compressibility effect on hydrodynamics, resistance coeff. 78—55684
water, free-convection boiling, critical heat flux density 80—48691
water, heat transfer for boiling of liquid at finned wall 77—42817
water, heat transfer from high temp. quenched solid *(French)* 77—62136
water, maximum boiling superheat, of drop submerged under immiscible liquid layer 80—79928

boiling continued
water, nucleate and transient boiling in narrow space between disks 77—84115
water, nucleate boiling heat transfer, press. factor 77—69080
water, on Cu surface, natural boiling site cavities, SEM obs. 77—31763
water, pool boiling, produced by distrib. internal heat sources, in homogeneous nucl. reactor 78—90685
water, subcooled, boiling in vertical channel 78—9544
water, subcooled and low quality flow film boiling, at atmospheric pressure 80—32324
water, surface boiling in tubes, heat transfer 78—9541
water, temp. field for surface boiling in round tube 77—42818
water, transition boiling under forced convective conditions, reactor accident condition 78—89961
water, transmittance in laser radiation field, effect of thermal defocusing *(Russian)* 79—1745
water, vibr. effect on heat transfer crisis 80—33423
water boiling in annuli under forced convection, boiling noise 79—1062
water boiling in tube, critical heat flux 78—83232
water droplet evaporation, heat transfer characts., on heated surfaces 78—59269
water droplets react. with molten Na 78—71263
water film on Teflon surface, boiling heat transfer 79—90124
water flow instability in Na heated once through steam generators 80—27737
water in cylindrical cavity in copper block, quenching data and heat loss, boiling curve 77—84119
water in Laval nozzles, discharge and dynamic characteristics 80—19470
water jet impinging on horizontal heated surface, single-phase convection and nucleate boiling regions *(Japanese)* 80—48761
water jet impinging on hot surface, boiling heat transfer 78—90993
water steam, boiling and nonboiling vertical two phase flow in tube, void fraction correl. 77—55073
water subcooled nucleate flow boiling, void fraction, incipient boiling pt. 77—39203
water-fuel emulsion drop, microexplosive boiling of metastable overheated water, microblast *(Russian)* 80—74930
water-in-oil emulsion, boiling, bubble formation, cinemicrophotography 80—74961
wedge, forced-convection film boiling, boundary layer flow 79—46366
wetting front propagation, solid quenching in subcooled water *(French)* 79—77108
BF_3, boiling/condensation heat transfer props., cryogenic appls. 78—79192
CO, boiling/condensation heat transfer props., cryogenic appls. 78—79192
CO_2, nucleate boiling, heat transfer rate 77—39199
Cu, horizontal plate, pool-boiling heat transfer, nucleation centre size, surface roughness 78—90652
Cu wire, transient current pulsed heating, explosive inhomogeneous boiling explosive 78—38562
Fe_2O_3, haematite, effect of boiling on the mass transfer of corrosion products in high temperature, high pressure water circuits 80—71766
H_2, internal characts. 77—89529
H_2, liq., bubble growth consts. calc. at heated wall during boiling 77—35680
H_2, pool boiling, heat transfer coeffs. determ. 78—30165
H_2-N_2-Ar, two-phase flow film boiling, in vap. generator, heat transfer 78—75190
H_2O, boiling, crit. heat flux in low press. region 78—90663
H_2O, boiling, on Cu surface, rel. to methanol 78—90654
H_2O, nucleate pool boiling, bubble freq. model, surface effects 78—90651
H_2O, pressurised, circulating, vaporisation in tube immersed in NaOH thermal storage material *(French)* 80—40914
H_2O, squeezed boiling, internal characts. 78—90655
He, boiling in tubes, heat transfer, cryogenic stabilisation 78—30162
He, boiling on surfaces, heat transfer coeff. 78—9545
He boiling tube hydraulic resistance and burnout expt. 80—24085
He, bubble boiling, heat exchange regimes 80—23879
He, bubble-type boiling crisis on various surfaces 77—11682
He II film boiling, heat transfer prediction 80—33424
He, liq., bubble growth consts. calc. at heated wall during boiling 77—35680
He, liq., flow boiling in vertical channels, visualisation 77—42938
He, liq., ht. transfer in centrifugal acceleration fields, free convection and boiling regimes 77—89604
He, liq., sat., nucleate and film pool boiling heat transfer 78—18854
He, liquid, heat transfer from heated plate 79—63235
He liquid, transient heat transfer, static coolant 78—75049
He, liquid film, transient heat transfer, film boiling regime 78—83219
He, nucleate pool boiling, heat transfer 77—31823
He, nucleate pool boiling, heat flux and press. effect on heat transfer 79—14235
He pool boiling, charact. curve 77—46887
He, superfluid, anal. of film boiling 80—10716
He, vapour formation and heat transfer in supercond. magnet cooling channels 79—32197
He-I in capillary channels, forced convection boiling heat transfer 80—48707
^{4}He, heat transfer crises 79—94466
^{4}He, liq., nucleate boiling crisis in supercond. magnet cooling channels 79—32196
^{4}He, superfluid, liquid film, subcooled, film boiling Kapitza resistance of Al 79—23794
^{4}He, superfluid, on electron-hole drops in Ge, threshold phenomena *(Russian)* 79—42462
^{4}He, superfluid, saturated, size and orientation effects on free convection film boiling from flat surfaces 79—60577
^{4}He, superfluid, transient heat transport 80—10715
^{4}He, superfluid saturated liq., recovery heat flux from silent and noisy film boiling states 79—72784
Hg, droplets, film boiling 78—14453
Hg, pool boiling heat transfer in mag. field 80—33584
K, boiling, expt. study of outflow from accelerating two-phase nozzle 78—1721
K channel flow, incipient boiling superheats 80—74709
K, in tubes, superheat and instability 77—35136
K, stagnant, mag. field infuence on boiling 77—47096
N_2, boiling, press. effect on internal characts., bubble growth 77—15568
N_2, boiling curve, unsteady-state quenching method 79—14232

boiling continued

- N_2, boiling in tubes, heat transfer, cryogenic stabilisation 78−30162
- N_2, boiling on water, initial water temp. effect 77−19606
- N_2, cooling internal surface of cold finger, heat transfer *(Russian)* 77−22556
- N_2, evaporating in horizontal tube, local heat transfer coeff. 77−23959
- N_2, heat transfer during boiling in field of centrifugal forces 79−60493
- N_2, heat transfer during nucleate boiling, heating wall and metallic coating thicknesses depend. 79−32210
- N_2, heat transfer in boiling on surface of vertical cylindrical rod 80−48706
- N_2, liq., boiling, cryogenic, heat transfer rel. to sinusoidal elec. field 77−72135
- N_2, liq., infuence of electric field on heat transfer 80−53770
- N_2, liq., nucleate boiling heat transfer from PTFE coated surface 78−34000
- N_2, liquid, film boiling heat transfer coeff. for vertical surfaces 80−48556
- N_2, liquid, heat transfer from heated plate 79−63235
- N_2, liquid, nucleate boiling heat transfer at reduced pressures 80−48557
- N_2, liquid film boiling heat transfer, orientation effect 80−48554
- N_2, pool boiling, heat transfer, surface roughness effect 80−48705
- N_2 pool boiling in high centrifugal accel. fields, peak nucleate boiling heat flux 79−59907
- N_2, transient pool boiling, premature transition to stable film boiling 79−81709
- NH_3, superheated liq., boiling kinetics 80−15231
- NO, boiling/condensation heat transfer props., cryogenic appls. 78−79192
- N_2O_4, dissociating in vertical tube, boiling heat transfer 80−1568
- Na boiling acoustic emission burst detection in parasitic noise 79−3214
- Na boiling detection technique tests, FFTF capabilities 79−13395
- Na boiling expts. ref. to fast reactor safety *(Italian)* 79−9764
- Na boiling in LMFBR, acoustic detection using pulsed system 79−97839
- Na boiling in tubes, heat transfer and pressure drop 80−28408
- Na boiling under low heat flux condition during loss-of-heat sink accident in LMFBR 80−47636
- Na, fast reactor coolant, boiling in circular pipe, single-bubble model 77−10466
- Na in 7-pin bundle, LMFBR safety, KNK II driver zone 77−88246
- Na, incipient boiling in the presence of a mag. field 79−37411
- Na, LMFBR coolant, SAS-3D analysis of natural-convection boiling behavior in the sodium boiling test facility 80−47635
- Na, LMFBR safety, flow rundown expts. in seven pin bundle 77−88240
- Na, LMFBR safety, seven pin bundle expts., flow patterns, two-phase press. drop 77−88241
- Na, liq., boiling hazard in LMFBRs *(French)* 80−78402
- Na, liq., in vert. pipe, hydraulic resistance under boiling conditions 78−90968
- Na, liq., incipient superheat meas., expt. and physical parameter effects 78−18289
- Na, liquid, local boiling behind local flow blockage, simulated LMFBR fuel subassembly 78−54842
- Na, pool boiling heat transfer, liq. head effects 78−89951
- Na, superheated, LMFBR safety, formation of critical boiling nuclei 77−88242
- Na test loop boiling, acoustic detection expts. 79−13487
- Na transient boiling in single-pin annular channel under loss of flow 78−89933
- Na-UO_2 interaction, dropping experiments and subassembly test 78−82460
- O_2, boiling, press. effect on internal characts., bubble growth 77−15568
- O_2, liquid, pool boiling in inhomogeneous mag. field 77−31766
- O_2, superheated liq., spontaneous boiling and life-time, press. variation *(Russian)* 78−22839
- Pt, nucleate and film boiling in travelling wave regime 80−19231
- Sb, vaporisation behaviour, transpiration and boiling temp. studies 80−29161
- Sb-S, saturated vap. press. 78−43116
- UO_2, boundary heat transfer from volumetrically boiling pools following LMFBR HCDA 80−47654
- UO_2, closed boiling system, effect of condensation on dispersion following LMFBR HCDA 78−8936
- UO_2 fuel-coolant interaction, film boiling and vapor explosion phenomena 80−95363
- UO_2 volume boiling pools, meas. and calc. of average void fraction for LMFBR HCDA anal. 80−47653

boiling point

- *see also boiling; heat of vaporisation*
- alkali halides, boiling, melting points rel. to mol. wt. 79−46785
- alkanes, latent heat of vaporisation calc. at normal boiling pt. by group contrib. method 79−77737
- bubble point calc., iteration scheme 79−19359
- classical fluid, elementary molecular theory 77−19859
- ethane, viscosity and thermal cond. of liquid and gas, correl. eqns. 78−26715
- gas solubilities near solvent critical point 79−51258
- halomethanes, vap. press. and boiling point data tables 79−77736
- heteroazeotropic system, thermodynamics in Gibbs pot. metrics *(Russian)* 79−96355
- inert gas liquid independent structure model, critical point, liquid-vapour equilib., second virial coeff. *(Spanish)* 77−4031
- latent heat of vaporisation prediction at normal boiling pt., correl. 79−86881
- liquids, nonpolar, b.p. calc. as function of mol. polarisability, ionisation energy, and size 79−95148
- measurement via thermistor ebullioscopes, sensitivity uncertainty 78−12695
- melting and boiling points vs. Coulomb pot., parabolic behaviour 80−70375
- organic compounds, crit. temps. correl. with boiling pts. 78−91421
- organic liquids, electric field effect 77−15566
- petroleum fractions from USSR fields, isobaric integral heats of condensation *(Russian)* 79−65181
- phase change derivation, phys. chem. textbook assumption removal 80−17772
- polarity parameters correlation with compressibilities at boiling point 79−19305
- saturated densities of liqs. and mixtures, new correlation method 80−15174

boiling point continued

- solutions, dilute, colligative props., kinetic derivation from elastic collision processes 78−91048
- solutions with large conc. gradient, in capillary, diffusion near crit. point *(Russian)* 77−84958
- sulphonyl compounds, H-bonding by methyl groups, Raman spectra obs. 79−24320
- ternary system, bubble pt. equilib. compositions determ. from dew pt. meas. 79−77733
- vapour-liquid crit. props. for pure liqs. and mixtures 80−65213
- vapour-liquid equilibrium, T-x meas. by semi-micro method 78−87782
- Ar, rel. to IPTS reference pt. 77−104
- H_2, thermometric fixed points determ. 77−82511
- H_2 triple, boiling and 17K equilib. points realization, cryostat and method 80−27314
- ^4He, P-ρ-T data near vaporisation crit. point *(Russian)* 80−88373
- HgS, melting point and vapour pressure 77−15549
- Ne, normal boiling point reproducibility, cryostat appl. 78−79757
- O_2, realisation rel. to IPTS 77−105
- O_2, rel. to IPTS reference pt. 77−104
- Sn-S system, use of boiling points to investigate vapour pressure 80−54361
- $TlNO_3$, boiling and melting pts., heats of transformation, solid-solid transformation 78−91441
- UF_4, vaporisation behaviour 80−84283
- Xe, suitability as temperature fixed point 78−77838

bolometers

- 100 GHz bolometer mount efficiency meas. calorimeter *(Japanese)* 78−54460
- amplifier, power supply ccts., IR spectrometer for Meteor artificial satellites *(German)* 78−28484
- astronomical bolometers, liq. He-cooled MOSFET preamplifier 77−61123
- astronomical far IR balloon telescope with composite bolometers 78−45228
- astronomical far IR bolometric and photoconductive detectors 77−41305
- atmospheric transmittance meter, absolute filter device 80−51584
- autobalancing radiometer, electrical compensation 78−86067
- composite superconducting transition edge bolometer 77−71371
- cone absorption calorimeter for pulsed laser meas. 80−98980
- contactless temperature meas. methods *(Dutch)* 77−67433
- cryostat using ^3He for space appls. 77−22077
- differentiated structure low heat capacity ^3He cooled bolometer, performance 79−30544
- energy capacitor discharge from RC network, RF power, energy measurement appl. *(Russian)* 77−37940
- far IR polarimeter for balloon astronomy 79−35094
- ferromagnetic resonance absorpt. lineshape 24 GHz microwave transmission apparatus 77−49755
- figure of merit for comparison of types of thermal detectors *(German)* 78−57954
- film thermal device appl. 78−70189
- foil, fast, large-signal, free-standing, for measuring ultrasoft X-ray burst fluence 80−4770
- frequency characteristic correction, calculations and design of a correcting amplifier 80−52305
- heat filters for bolometers cooled to very low temperatures 80−52315
- heat-pulse technique for radiationless relax. meas. in solids 77−36277
- immersion thermistor bolometer use in radiometer 78−70188
- IR detection by microbolometer with Bi film 79−75594
- IR detector/preamplifier systems at cryogenic temps. 78−45710
- IR spectrophotometry, device description, noise levels, and spectral and freq. characts. 79−6195
- lag correction network ccts. 78−288
- laser beam energy distribution reconstruction using data from grid of bolometers 80−53350
- laser calorimeter types and techniques 80−69441
- laser emission convertors, thin wire, EM energy absorption, thermal processes *(Russian)* 77−18094
- laser narrow pulse recording appl. *(German)* 78−4692
- laser power meter, sensitive meas. IR to vacuum UV spectral range 78−82031
- light intensity meas. 79−49295
- microwave, self-balancing DC-substitution RF power meter 77−18012
- microwave power measurement *(Hungarian)* 77−18091
- millimetre-wave bolometer mount for waveguide power meas. at 100 GHz 77−71372
- molecular beam detector using fast supercond. bolometer 78−86383
- mount, effective efficiency meas., computerised calorimeter system 78−86272
- multipurpose, large thermal vacuum chambers, Johnson Space Centre 80−31875
- radiation laws and practical instruments *(German)* 77−5844
- sensitivity stabilization, electronic cct. 80−52306
- solar energy meas., photometric and bolometric methods 78−12470
- submillimetre wavelength composite bolometer 78−65964
- submillimetric composite bolometers with metal film absorbers 77−37997
- submillimetric-wave negative-feedback-loop thermistor bolometer 79−44931
- superconducting, effect of LF noise on threshold sensitivity 79−89005
- superconducting, free floating, sensitive heat pulse detection 77−79149
- superconducting, high-speed, based on Ag-Sn double films 80−57368
- superconducting, space appl. 80−85836
- superconducting bolometers, mm wave superconducting devices, present status 79−26119
- superconducting double multivibrator used as near- and medium-infrared radiation detector *(German)* 80−90892
- superconducting normal electron tunnel elements, interaction with 0.6-40 μm EM radn., radn. detection appl. *(German)* 79−24103
- superconductive bolometers for submillimetre waves 78−37063
- superconductive FIR detectors, Josephson-junction direct devices and transition edge bolometers, review 80−77865
- surface temperature contactless meas. instrument 78−57946
- TGS, capacitive bolometer effect in paraelectric phase 77−57389
- thermistor type, reliability anal. 78−24795
- thin absorbing films, EM plane-wave interaction 80−95767
- thin film, CW CO_2 laser power meter appl. *(Russian)* 77−37992
- thin film, in liq. He, freq. characts. *(Russian)* 78−32874
- thin film structures, characts. *(German)* 78−62226

bolometers continued
  Tokamak energy loss determ., fast time resolution bolometer *(Russian)* 77—76193
  type BN (USSR), construction and characts. 80—57372
  Al granular superconducting bolometer as mol. beam detector 80—73524
  C film bolometer detection system with <0.1 μs response time 79—63226
  C resistor, characts. in field modulation studies 77—37882
  CO, rot. distrib. in supersonic beam, IR bolometry using tunable diode laser 80—63869
  Ge and Ge-diamond bolometers operated at 4.2, 2.0, 1.2, 0.3, 0.1K, design and construction 80—77868
  Ge bolometer, cooled low-noise preamplifier 78—4698
  Ge cryogenic bolometer, for 20 to 500 μm spectral region 78—70187
  Ge film bolometer, radiation loss from JFT-2 Tokamak, meas. 80—95141
  Ge, low-temperature bolometer, characts. 79—30561
  Ge surface ion implanted far IR composite bolometers 79—30549
  Ge:B, ion implantation and depletion at low temps., radiation and DC characts. 79—60392
  Ge:Ga,Sb, compensated, low temp. props. rel. to appl. in bolometry 80—31867
  Ge:Sb, bolometer element, absorpt. spectra, bias depend. 79—30553
  n-$Hg_{0.8}Cd_{0.2}Te$, microwave bolometer heterodyne receiver based on magnetic field induced phase transition 80—13135
  n-InSb electronic bolometer, appl. in system for millimetre and submillimetre wave detection 78—24860
  Ni film, for measurement channels of actiometric apparatus of Meteor Earth satellite 79—35828
  Si low-temperature far and middle IR bolometers 79—71529
  n-Si:P, etched, high sensitivity temperature sensor, 1-10K 77—13757
  p-Tl_xSe_y, IR bolometer detector performance 78—24856

Boltzmann equation
  see also transport processes
  abstract averaging theorem 77—2510
  accommodation coefficients, effects on evaporation and condensation *(Japanese)* 78—81933
  aerosol, spherical, binary gas mixture thermal slip along surface 78—34168
  alloy, dil., thermoelectric coeff., vertex and other electron-phonon corrections to impurity scatt. 79—95390
  anisotropic media transport theory, particle scatt., Boltzmann eqn. 79—26004
  approach to equilibrium for spatially homogeneous solutions 79—26007
  atomic beam, highly expanded free jet, quantum and intermol. pot. effects 77—61823
  atomic momentum distrib. modification by travelling wave reson. light field 79—72280
  attenuated gas flow round plate, Monte Carlo soln. of Boltzmann eqn. 79—68754
  average force field caused by anisotropic momentum, changes, applic. to neutron and gas transport 77—13714
  BBGKY hierarchy, scaling method of kinetic eqn. derivation 78—54286
  BBGKY hierarchy derivation of Boltzmann eqn., Boltzmann gases 79—93080
  bilinear functionals, upper-bound estimations 77—67796
  binary gas mixture, isothermal creep along flat surface, half-space moments method 77—42873
  biological system, coherent mode excitations, bose condensation-like, Frohlich vibr. model, Boltzmann eqn. approach 79—39336
  Boltzmann's theorem 79—40459
  Boltzmann H-theorem for gases in thermostat *(Russian)* 77—17927
  Boltzmann-Enskog equation, nonlinear, acoustical approx. for elastic sphere system 78—41252
  boundary conditions, and heat transfer between parallel plates 77—67390
  boundary conditions, general reciprocity postulate 77—65012
  boundary layer effect on transport phenomena in MHD generators, Boltzmann transfer eqn. 79—23463
  Brownian fluid affected by potential, Maxwell-Boltzmann distrib. in infinite-time limit 80—105573
  Carleman model, increase of entropy 79—80558
  carrier transport, temp. dependent energy levels effect 77—89743
  linear Chapman-Enskog procedure, evolution equations of hydrodynamic variables 80—49075
  charge carrier mobility, field depend. collision terms 77—51714
  charge imbalance relaxation freq. depend. near superconducting T_c 80—93030
  classical Boltzmann kinetic theory justification using Liouville theory 80—87838
  clean superconductor, effect of impurity scatt. on thermally induced charge imbalance 80—60135
  collision integral, relax. problem soln. 79—64706
  collision integrals, rigorous soln. of relaxation phase *(Russian)* 78—8231
  collision operators as generators of Markov processes and their spectra 79—63150
  colloid, spherical particle, diffuse double layer, modified nonlinearised Poisson-Boltzmann equation 79—79305
  counting gas mixtures, calc. of electron transport coeffs. 79—32727
  DC resistivity as functional of generalised dynamical susceptibilities, solid state model 79—28330
  degenerate polar semiconductor, asymptotic soln. to Boltzmann transport equation 77—4332
  degenerate semiconductors and metals, cond. current and generalised Einstein rel. 77—15810
  dense matter, transport props., neutron stars appl. 79—67236
  diffusion of test particle, in conservative field, integral Boltzmann eqn. solns. 79—97324
  dilute gas, kinetic perturbation theory 80—100051
  dilute monatomic gas flow round macroscopic object, kinetic theory 77—965
  dilute simple gas, transport coeff. determ. 78—38439
  dipole relaxation in electric field, teaching 80—90625
  discrete kinetic theory, maths. and numerical aspects, Couette flow appls. 80—19413
  discrete model, lattice limit and non-Maxwellian gases 80—52139
  Doppler-shift attenuation, γ-rays from slowing down of excited particles 77—26945
  dynamic conductivity in metals, generalised linear Boltzmann eqn. perturbation soln. 78—34818

Boltzmann equation continued
  early Universe, baryon number generation due to CP- and B-violating interactions 80—109571
  eigenvalue precision, influence of boundary conditions 80—27689
  eigenvalue precision, influence of boundary conditions 80—27690
  eigenvalues of the stationary and time-dependent Boltzmann equation in its integro-differential and integral forms 79—80549
  elastic media, dissipative, relativistic electrodynamics 80—73219
  electrical double layer theory, generalised Poisson-Boltzmann eqn., numerical method for soln. 78—48667
  electrical double layer theory, Poisson-Boltzmann eqn. including hydration forces 78—48668
  electrical resistivity with spin-orbit scatt. 78—64018
  electrolyte solutions, interionic radial distrib. function approx. scheme 77—32796
  electromigration, driving force, bootstrap arguments 77—20107
  electron avalanches parallel and perpendicular to electric field, Boltzmann eqn. anal. 78—30502
  electron backscattering, X-ray prod., transport eqn. soln. 79—38698
  electron backscattering transport theory, SEM and EPMA appl. 80—57439
  electron diffusion in high electric fields 77—51757
  electron diffusion to absorbing electrodes, Monte Carlo and Boltzmann calc. comparison 80—6204
  electron diffusion to anode, Monte Carlo and Boltzmann calcs. comparison 80—38519
  electron energy distrib. functions in weakly ionised gas under high E/N 80—53916
  electron ensemble, weak turbulence, diffusion and collisions in elec. and mag. fields *(German)* 78—83564
  electron probe analysis, spatial distrib. of electrons in homogeneous, isotropic target 79—43687
  electron reflection from solid, elastic secondary electrons 79—43078
  electron scattering by impurities in mag. field 80—44559
  electron swarm with anisotropic vel. distrib. function 80—38520
  electron swarms in electrostatic fields in gases, inelastic collisions effect on diffusion coeffs. 77—76022
  electron swarms in gases with large inelastic cross sections, accuracy of numerical solns. of Boltzmann's eqn. 79—94756
  electron transmission, secondary electron emission *(French)* 80—20740
  electron transport, continuous-slowing-down approx., adjoint Monte Carlo model 80—49269
  electron-electron scatt. and elec. resistivity of metals 79—95396
  electron-neutral collisions, calc. with respect to momentum transfer, new approach to Boltzmann collision integral 80—92255
  electronic multiple-band systems, dielec. function in generalised relax.-time approx. 80—103637
  electronic transport coeff., soln. between Mori-Green-Kubo formulae and Boltzmann approx. 78—79971
  electrons, field-accelerated, in dry air and pure O_2, macroscopic props. comparison *(French)* 80—59161
  energy deposition, transport eqn. for point anisotropic source in infinite homogeneous medium 80—88228
  energy transfer to electrons by fast atoms 77—35613
  equilibrium birefringence for weakly ionised molecular gas in strong mag. field 80—83881
  equilibrium continuous nonnegative soln., nonexistence of zero pt. 78—41250
  exact transport eqn. for randomly perturbed focusing medium 79—81344
  exactly soluble, with persistent scatt. 80—46997
  fast-electron transfer in lamellar materials 78—86230
  Fermi liquid, transverse sound, soln. to dispersion eqn., with nonzero Landau F_2 77—20150
  film, thermomagnetic effects in mag. field or arbitrary magnitude 78—47885
  film, transport equation treatment of transmitted electrons *(French)* 77—80558
  fluctuating Boltzmann gas, stochastic theory of hydrodynamic systems 79—75476
  fluctuations of low density gas in μ-space 77—17929
  fluid, infinite, non-uniform, validity of Boltzmann integrodifferential eqn. 79—7434
  fluid dynamical approx. at level of Navier-Stokes eqn. 80—22308
  Fokker-Planck model, transport equation renormalisation 80—82732
  forward and backward Boltzmann eqns., use in radiation damage calcs. 79—17360
  free electron storage ring laser, Boltzmann simulation 79—72547
  free electrons in mag. field, gauge-independent statistical mechanics 78—47754
  friction const. of Brownian particle density expansion 77—87694
  Galerkin type methods for approx. soln. 77—87706
  gas, Boltzmann collision operator with cut-off for intermolecular potentials 78—42697
  gas, dense, thermal electron drift, Boltzmann eqn. soln. 80—1734
  gas, electron and hole transport theory, free-path method, orders of approx. 80—62598
  gas, electron collision and vel. distrib. in elec. field, Boltzmann eqn. 77—30115
  gas, moderately dense, Bhatnagar, Gross and Krook model from Chapman-Enskog equations 80—106864
  gas, slowing down of fast atoms, nonlinear Boltzmann eqn. 79—98196
  gas, two dimensional, initial value problem for model Boltzmann eqn. 79—44885
  gas, weakly ionised, electron distrib. function, isotropic component, collision source 80—62599
  gas, weakly ionised, electron transport quantities, divergences 80—57222
  gas, weakly ionised, ionis. and attachment effects on electron swarm parameters 78—5845
  gas dynamics eqn. boundary conditions in Chapman-Enskog Boltzmann eqn. soln. 80—96284
  gas flows, entropy prod. determ. using Boltzmann's H-theorem, Knudsen effusion 80—106867
  gas governed by Boltzmann eqn., approach to Maxwellian distrib. 79—58622
  gas mixture, Boltzmann collision operator matrix elements 79—86545
  gas mixture, multivel. multitemp., gasdynamic eqns. 79—77052
  gas mixture, reacting, Boltzmann kinetic eqns., Chapman-Enskog method 78—15656
  gas mixture in electric field, electron distrib., transport coeff., vibr. excitation rates, Fortran program BOLTZ 77—11304
  gas mixture in Knudsen layer, transport eqns. 77—47045

Boltzmann equation continued
  gas model of rigid spheres, Boltzmann eqn., eigenvalues eigenfunctions of Hilbert operator 77-26250
  gas-particle mixture, shock wave structs., particle specific heat effect 78-14072
  gas-particle mixtures, effect of thermal radiation on shock wave 78-91032
  gas-radiating particle mixture, shock wave struct. numerical investigation 80-10298
  gas-solid suspension, kinetic eqn. for gas phase from Boltzmann eqn. *(Russian)* 79-85059
  gasdynamic equations, multiatomic gases with different elastic and inelastic rates 79-81993
  gaseous mixture, Boltzmann kinetic equations, soln. methods 78-83511
  gases, electron motion, Boltzmann eqn. soln. two-term approx., validity 77-35309
  Gauss-Hermite quadrature procedures comparison for soln. of nonlinear BGK eqn. 77-49692
  general nonlinear eqn. for electrons and phonons 77-28151
  general relativistic statistical mechanics, BBGKY hierarchy and Boltzmann eqn. 79-63127
  generalised kinetic eqn. of Boltzmann type, eikonal approx. *(Russian)* 77-35297
  global solutions, bounded convex domain 78-57876
  global solutions on a lattice 79-80536
  glow discharge cathode region microscopic model 78-67524
  H-space fluctuations, Boltzmann eqn., master eqn. for drift motion 79-146
  Hagedorn early universe dissipation, Boltzmann kinetic eqn. soln. 80-8723
  hard sphere fluid mixture, density fluctuations 77-19657
  hard sphere gas, H-theorem for Enskog kinetic eqn. 77-68905
  hard sphere gas mixture, vel. autocorrelation function calc. 80-75019
  hard sphere system, kinetic eqns., Boltzmann and modified Enskog eqns. 80-130
  hard spheres in thermal eqn., time correlation functions in low-density limit 80-64859
  heat conduction, instantaneous propagation paradox 80-10109
  heavy ions in light gases in electric field, limits of Kihara distrib. 80-87837
  heterogeneous media, energy deposition of slowing down particles 80-88230
  Hilbert asymptotic expansion method for evolution equations in Banach spaces 79-17368
  hot atom+mol. reaction, steady state vel. distrib., Boltzmann eqn. with BGK elastic collision model 80-66856
  hot atom chemistry, general variational principles 80-11941
  hot atom reactions, nonequilib. time-depend. theory, model calcs. 80-61125
  hot electron phenomena, calc., review 78-26870
  hot neutron star matter, neutrino transport, opacity 79-75238
  hydrodynamic fluctuations, reduction of Boltzmann eqn. 78-8245
  inhomogeneous systems, stochastic version of Boltzmann eqn. 79-55442
  initial boundary value problem of the linearized Boltzmann equation in an exterior domain 80-90797
  initial value problems, global soln. 79-44883
  internal state, similarity solutions 80-86231
  internal stationary boundary value problem, soln. *(Russian)* 79-85100
  invariant solution 77-71282
  ion+neutral reaction, ion speed effects in flow-drift tubes, statistical mechanical theory 77-56220
  ion velocity distributions for polarisation collision model 77-45241
  ionised gas, macroscopic props. of field accelerated electrons, soln. of Boltzmann eqn. 80-61118
  itinerant electron magnet, low temp. resist., collective excitations 77-72851
  Kapitza resistance, metal-liquid He interface, theory of thermal boundary resist. 77-62730
  kinetic eqn., influence of stochastic sources 77-2627
  kinetic theory, Boltzmann eqn. generalisations for relatively dense systems 79-98851
  kinetic theory of dense fluids, derivation, transport coeffs., soln. of kinetic eqn. by moment method 79-54032
  kinetic theory of gases, asymptotic soln. 80-33720
  kinetic theory of one-dimensional evaporation and condensation problem *(Japanese)* 78-81932
  Knudsen flow under external pot. field 77-3848
  Knudsen layers, by linearised Boltzmann eqn. 79-98759
  Krook-Wu conjecture, and Tjon phenomenon 80-13009
  Krook-Wu model solutions, distribution function *(French)* 80-17898
  Kubo formula derivation of Boltzmann equation, resolvent method 78-95277
  Landau-Lifshitz hydrodynamic fluctuations in nonequilib. systems, Boltzmann eqn. reduction 78-81929
  lasing, in glow discharge, excitation freq. calc., electron upflux, book contrib. 77-50648
  lattice model, convergence 79-97314
  lattice thermal conductivity, general transport theory, phonon Boltzmann eqn. 80-54446
  linear, Pade approximants, appl. to spherical geometry 80-52143
  linear, scatt. operator existence 77-65009
  linear, scattering matrix 77-18643
  linear, spatial homogeneous eqn. with soft potential 80-77730
  linear Boltzmann eqn. with external EM forces 78-93630
  linear Boltzmann equation, transport and scatt. props. and solns. 78-93628
  linear Boltzmann system, appl. of parabolic diffusion equation 77-82468
  linear Boltzmann system, stochastic model of spatially heterogeneous fluctuations *(Russian)* 77-22497
  linear Boltzmann system, theory of fluctuations, Tolubinskii's method *(Russian)* 77-22495
  linear rarefied gas dynamics, integral transport equation functional anal. 79-50756
  linear response theory, master eqn. approach 80-31663
  linear transport operator spectrum, semi-infinite medium 77-2626
  linearised, constructive soln. using vector BGK model, temp. density eqn. 79-93081
  linearised, half-space anal. 77-74337
  linearised, uniqueness theorem 78-32774
  linearised Boltzmann eqn., constructive soln., scalar BGK model eqn. 79-161

Boltzmann equation continued
  linearised eqn. with long range pots., numerical anal. 77-35168
  linearised non-steady eqn., stationary boundary reflexion conditions *(French)* 77-17925
  linearised plane Couette flow, rarefied gas with infinite range molecular interactions, asymptotic anal. 79-23340
  linearized Boltzmann equation for semicond. plasma, carrier wave phase vel. 77-43634
  Liouville problem, quasi-particle dynamics from a given kinetic eqn., inverse 80-101749
  Lorentz electron gas, long time behaviour in const. uniform elec. field 80-42140
  Lorentz gas, Fourier's law of heat cond. 79-58620
  Lorentz model, hydrodynamic kinetic stages asymptotic equivalence 79-55438
  low ionised anisothermal plasma, ionising electron collision kinetics *(German)* 80-33730
  low-pressure discharge electron kinetics 78-75483
  magnon gas of Heisenberg ferromag., transport eqn. 77-12112
  many-body distrib. function, dilute system generalised Boltzmann equation 79-30351
  many-valley semiconductors, conduct. in heating electromag. wave 80-84483
  Maxwell models, exact soln. of non-linear Boltzmann eqn. 79-35646
  Maxwell models, similarity solutions 80-86231
  Maxwellian distribution, numerical aspects 79-54034
  Maxwellian thermonuclear plasma, quantum mechanical slowing in distrib. of energetic charged particles 79-86588
  metal, electron Boltzmann eqn. solns., energy depend. 80-88537
  metal, influence of phonon drag on thermoelec. coeffs. *(German)* 77-80766
  metal, linearized Boltzmann eqn. soln., resist. and deviation from Matthiessen's rule 80-65523
  metal, new method for solving Boltzmann equation for electron 78-72127
  metal, quasi-one-dimensional, elec. resist. due to electron-electron scatt. 79-4549
  metal anisotropic normal metal, linearised Boltzman eqn., Hall effect coeffs. 79-1595
  metal electrons, kinetic eqn., iteration soln. 77-43564
  metal film, Hall coeff. and cond. using Boltzmann transport eqn. 79-11240
  metal-liquid He interface, electron-phonon interaction, thermal boundary resistance 78-67899
  metallic film, oscill. kinetic effects, boundary electron scatt. *(Russian)* 78-52104
  metals, acoustic attenuation in collision regime, variational principle 79-82648
  metals, elec. cond., band mixing generalisation 79-38060
  metals, energy depend. relax. times in electronic transport props. 79-60804
  metals, magnetoresistance of localized impurities, multiple scatt. theory 78-43360
  metals, nearly-free-electron, holelike Fermi surface, Hall coeff. and magnetocond. tensor 79-4547
  metals, surface positronium formation, stopping distance, positron-phonon interactions 80-96582
  Milne-problem for isotropic scatt. with backward leak 78-8870
  mixtures of reacting gases, extension of Chapman Enskog method *(Russian)* 78-57878
  monatomic homogeneous gas, relax. anal. *(Russian)* 77-35298
  Monte Carlo method, stochastic models 78-21618
  multitemperature gas-mixture, linearised Boltzmann operator, matrix elements 78-47085
  N-component gas, exact solns. 77-47131
  neutral particle transport in 2-D, appl. of space angle synthesis 77-83107
  neutron Boltzmann eqn., P_1 and diffusion eqn. asymptotic equivalence 80-95334
  neutron diffusion across absorpt. discontinuity in water assemblies 78-21620
  neutron energy deposition calc. using adjoint Boltzmann eqn. 79-6723
  neutron gas system in stationary power reactor with decoupling thermodynamics and distrib. function 80-86950
  neutron moderation, linear Boltzmann operator, in various geometries, contributions to spectral theory *(Rumanian)* 78-46128
  neutron moderator energy deposition calc., role of adjoint Boltzmann eqn. 78-4974
  neutron slowing down and transport in medium of const. cross-section 78-33235
  neutron transport, eigenvalue defn. and use 77-54275
  neutron transport, finite element diffusion and P_1 eqns. soln. by iteration 77-50188
  neutron transport, ZEPHYR code for general two-dimensional geoms. 77-65249
  neutron transport eqn. cylindrical and spherical geometrics, characteristics formulation in CHART program 80-5197
  neutron transport in parallelepiped, functional methods use 77-57701
  neutron transport space-energy-angle depend. theory 77-14204
  neutron transport theory, slabs and spheres, criticality problems 80-57817
  noble metal, thermal resistivity temp. depend., free electron approx., phonon spectrum 77-66152
  non-linear transport equations: Properties deduced through transformation groups 80-4680
  nonequilibrium particle distribs., finite energy intervals *(Russian)* 80-77736
  nonequilibrium superconductor, effect of pair breaking on branch relax. 79 78257
  nonequilibrium superconductors, microscopic and Boltzmann eqn. approach 80-15649
  nonequilibrium thermodynamics, statistical formulation by general Onsager Machlup formula 79-54089
  nonisotropic binary collision cross sections inversely proportional to relative speed, Boltzmann eqn. soln. 80-13010
  nonlinear, Abel transformation 79-85097
  nonlinear, classes of exact solns. 78-49779
  nonlinear, diffuse binary scattering in microcanonical ensemble, similarity solutions 80-86231
  nonlinear, exact solns. for one-component gas 78-12656
  nonlinear, generalised Pade resummation of soln. 80-169

Boltzmann equation continued
nonlinear, Krook-Wu conjecture and Tjon phenomenon 79—97319
nonlinear, soln. of Cauchy problem 79—40497
nonlinear, with analytic solns. 78—29066
nonlinear, with soft potential, spatially periodic problems 80—77731
nonlinear Boltzmann eqn., rarefied gas, fluid dynamical limit 78—79336
nonlinear Boltzmann equation, for internal state and Maxwell models 80—77733
nonlinear Boltzmann equation, hierarchy kinetic model 79—98758
nonlinear Boltzmann equation, solns. of Krook-Tjon-Wu model, Laguerre expansion of distrib. function 80—68157
nonlinear Boltzmann-Enskog equation and asympotic behaviour of the time autocorrelation functions 78—70079
nonlinear electrical conductivity theory based on integral Boltzmann eqn. 78—72125
nonlinear electron and ion transport in thermionic diode 77—13717
nonlinear equation, Bobylev approach, relaxation equilibrium 80—17897
nonlinear equations, exact class of solns. 79—54075
nonlinear evolution eqn., family of H-theorems 80—31685
nonstationary, direct case, linear and nonlinear problems, Cauchy problem 80—36954
nuclear one-body dissipation formula derivation from Boltzmann eqn. 79—67686
numerical method of soln., weakly ionised heterogeneous gas 77—49693
numerical solution, local Green's function method 79—97327
one group, integral transport eqn. for homogeneous sphere, neutron scatt., classical diffusion, anal. 78—62589
one-component gas, relativistic Burnett eqns. and sound propag. 77—15150
one-dimens. hard rods, linear Boltzmann eqn. exact soln., vel.- and Van Hove self-correl. function *(French)* 78—38441
open systems, S-matrix and density matrix formalism 79—88872
optical properties, temp. depend., transport eqn. 78—23421
Pade approximants for linear eqn. 80—551
phonon and electron transport in bounded systems 80—39545
phonon transport, Peierls-Boltzmann nonlinear eqn., soln. struct. and stability 77—84878
phonon-electron interaction, kinetic equation for dynamic system *(Russian)* 80—54619
Planck thermal radiation spectrum in quantum theory, relativistic free particle Boltzmann distrib. inconsistency 79—85001
plasma, fission fragments generated, electron distrib. function 77—19731
plasma, high-temperature, elec. cond. in uniform mag. field 79—4112
plasma, non-isothermal, low-ionised, influence of HF elec. field on electron ensemble *(German)* 79—77383
plasma, of glow discharge, electron velocity distribution function relax., periodic behaviour in highly modulated elec. field 79—64935
plasma, relativistic Boltzmann theory, reduction of collision integrals 80—79560
plasma column, of electrons, transport across mag. field to thermal equilib. 79—37531
Poisson Boltzmann equation, counterion condensation for two parallel charged plates 79—87849
Poisson-Boltzmann equation, appl. to polyelectrolytes 79—77483
polar semiconductor, HF mobility in longitudinal quantising mag. field 79—51619
positive solution for spatially homogeneous situation 79—17369
quantised linear eqn. as contracted form of second quantised neutron diffusion eqn. 77—17926
quantum Boltzmann eqn., Hartree Fock configuration-space analogue 78—49780
quantum form, one-particle Γ_s-distrib. function 78—45579
quantum neutron diffusion eqn., Boltzmann eqn. classical limit 80—13524
radiation damage calcs., role of Boltzmann transport eqn. 79—77653
radiation damage cascade, time-energy distrib. of atoms determ. 77—1159
radiative heat transfer, integral theory with anisotropic scatt. and general boundary conditions 78—32339
randomly-packed spherical particle bed, coord.-no. distrib., effective thermal cond., stat. thermodynamic theory 78—75028
rarefied gas, solns. of linearised modeled Boltzmann equation 80—53912
rarefied gas, steady-state solns. 77—35172
rarefied gas between parallel surfaces, collisional models of heat transfer 79—86464
rarefied gas flow, intermolecular interaction, Boltzmann eqn., Monte Carlo simulation *(German)* 78—34165
rarefied hypersonic flow past flat-plate, numerical simulation 77—19626
reacting systems, transport processes, rate coeffs. 77—86284
reactor dynamics, localised, P, approx. to Boltzmann eqn. 80—78347
reactor shielding materials, Pb, and steel, γ leakage spectra, numerical integration of Boltzmann eqn. 78—58350
relativistic, series convergence 78—36949
relativistic Boltzmann eqn. and MHD eqns. with radiative reaction 80—36956
relativistic Boltzmann equation 79—17367
relativistic Boltzmann equation and macroscopic eqns. of conservation 79—17359
relativistic Boltzmann kinetic eqn. derivation 80—68161
relativistic gas, one-component, transport eqns. 77—966
relaxation time approximation 78—65888
resistivity formula rel. to Boltzmann eqn. 77—47784
resistor, metallic, nonlinear current fluctuations, microscopic calc., heating, perturbation theory 79—69484
resolution of transport equation, by linearisation *(French)* 78—79989
S_N method of soln., exponential supplementary eqns., one-dimens. case 77—50189
Saturn's rings, vel. dispersion calc. 78—61795
scaling, time inversion, linear mono-energetic eqn. 77—2630
scattering medium, with quasistatic fluctuations, average field weakening calc. 79—71367
Schottkey barrier, high freq. rectification, transport theory 79—82660
self-diffusion of hard sphere gas, scaled Boltzmann theory of correl. functions 79—68894
semiconductor, ambipolar diffusion, electron-hole scatt. effect 80—59976
semiconductor, carrier distribution function 78—26856
semiconductor, cubic, bulk hot-electron props., soln. of Boltzmann eqn. 79—99553
semiconductor, doped photoemission, calc. of escape probability of electrons *(Russian)* 79—24408

Boltzmann equation continued
semiconductor, electron and hole transport theory, free-path method, orders of approx. 80—62598
semiconductor, homogeneous, nondegenerate, single-level Schockley-Read-Hall recomb. centres, flicker noise 80—70779
semiconductor, rel. to nonlinear current density 78—56149
semiconductor, two-layer nondegenerate, dimens. depend. of elec. cond. *(Russian)* 77—51804
semiconductor junctions, quantum statistical theory in thermal equilibrium 78—39197
semiconductor superlattice, nonlinear HF conductivity 77—15889
semiconductor with energy-dependent relax. time, acoustoelectric absorpt. 79—56268
semiconductors, energy-balance eqn. for hot electrons 79—73521
semiconductors, generalised transport equations 79—95398
semiconductors, kinetic fluctuations, global estimation 78—43376
sensitivity theory, general nonlinear algebraic equations with constraints 78—21086
separation of inhomogeneous kinetic operator 77—74333
shock formation in piston problem, kinetic description 77—31334
simple gases, relativistic shock wave struct., Boltzmann eqn. soln. 80—1644
slowing down particles, spatial depend. of energy spectrum 79—65129
soft X-ray photoemission, electron transport method development 78—31296
soluble-model Boltzmann equations for spatially uniform systems, written in form of stochastic equation 80—95046
solute transport in a saturated-unsaturated porous medium 79—23362
solution, for small Knudsen nos. *(Russian)* 77—61033
solution for electron-LO phonon scatt. in a static elec. field 79—19586
solution for small Knudsen numbers 79—81924
solution for small Knudsen numbers 79—81925
solution for small Knudsen numbers 79—81926
solutions on lattice, existance and uniqueness 79—80537
spatially inhomogeneous Boltzmann eqn., soln. continuity from existence and uniqueness theories 80—105592
sphere, drag in low velocity rarefied gas flow 80—48752
spinodal decomposition, phase separation kinetics, Boltzmann's transport eqn. calcs. 80—79952
stability anal. by Lyapunov functionals 78—29069
stationary Boltzmann equation for straight and semi-straight conditions *(French)* 80—8933
statistical mechanics, foundations 80—22271
steady state one dimensional transport in prism with partially absorptive walls and fixed scatt. centres 78—41248
steel, liquid, Stokes coagulation model, particle motion according to Boltzmann eqn. *(German)* 80—40357
stochastic Boltzmann equation, hydrodynamic fluctuations 80—68158
stochastic phase spaces and master Liouville spaces in quantum statistical mechanics 79—85076
sunlight transmission through uniform waterdrop atmosphere, appl. 78—36244
superconducting weak links, order parameter and quasiparticle dynamic props. 80—100555
superconductor, kinetic eqn., scatt. by paramag. impurities *(Russian)* 77—36015
superconductors, nonequilibrium, T^* model of quasiparticle and phonon distribs. 80—25039
superconductors, nonequilibrium, BCS-Boltzmann and Ginzburg-Landau descriptions 79—65589
superconductors, relax. and collective motion, two-fluid model 79—56369
superconductors, relaxation and collective motion two-fluid theory 79—73625
swarm transport coefficients, iterative method calcs. 80—96336
teaching, transport processes in gases, relax. approx. to Boltzmann eqn. approach 78—73804
test particle diffusion under conservative field, integral Boltzmann eqn. soln. 79—97325
test particle slowing down, rarefied gas added to host, with external conservative force 79—97326
thermal conductivity of semiconductors calc. using numerical soln. of Boltzmann eqn. 80—44373
thermohydrodynamics equations, derivation from Boltzmann eqns. 77—75875
time depend. linear Boltzmann operator as semi-group generator 77—87651
time-dependent boundary-value problem soln., half-range, orthogonality relations 79—14508
TOKAMAK and other fusion reactor realisation, plasma beam control, Boltzmann eqn. 79—97903
Townsend discharge, macroscopic quantities, Boltzmann eqn. and Monte Carlo calcs. 80—38848
transport eqn., unsteady convective diffusive, upwind finite element scheme 79—97320
turbulence, dynamic methods appl. 78—1640
turbulent scalar fields, transport eqn. for probability density function, closure 80—1585
two component Boltzmann gas, fluctuating kinetic eqn. 80—171
two-vector, analytical solns. in nonplanar geom. 77—65246
uniqueness and local existence of spatially non-homogeneous Boltzmann eqn. 78—29065
urn problem of P. and T. Ehrenfest, Boltzmann theory of gases 79—71384
velocity distrib. function of light ions in heavy gas in elec. field 78—83526
Venus atmosphere, photoelectrons energy deposition 77—9687
water assemblies, poisoned, thermal neutron diffusion calc., absorption discontinuity effect 78—13191
weakly interacting systems, S-matrix, density matrix, Pauli and Boltzmann eqns. 79—88871
weakly ionised gas, Boltzmann kinetic eqn. 77—57288
weakly ionised gas, kinetic theory of electron component 77—47132
Wigner distribution function, transport eqns. 80—32907
(π,γ), cross sections from Boltzmann eqn. 79—89330
$(\pi^{+},\pi^{+\mathrm{or}0})$ inelastic reactions, cross sections from Boltzmann eqn. 79—89330
Al, photoemission spectrum for exploding wire radiator source, Boltzmann eqn. soln. 79—26949
Al, secondary electron emission by reflection, Boltzmann eqn. resolution method 80—45178
Ar, elec. discharge, electron energy distrib. function 79—50911

Boltzmann equation continued

- Ar, electron avalanche development, exact Boltzmann eqn. anal. 80−59318
- Ar, electron avalanches at high E/N values, Boltzmann eqn. anal. 77−35311
- Ar, electron avalanches parallel and perpendicular to electric field, Boltzmann eqn. anal. 78−30502
- Ar, electron ionisation and excitation coeffs. in low E/N region 80−48090
- Ar, nonequilibrium discharge radial characts., two-temp. model 79−94833
- Au, photoemission spectrum for exploding wire radiator source, Boltzmann eqn. soln. 79−26949
- Au, secondary electron emission *(French)* 80−55238
- CO discharge plasma, electron energy distrib. and kinetic coeffs., ground-state mols. 80−43867
- CO_2, low energy electron scatt. cross sections, vibr. excitation, Boltzmann eqn. 80−18942
- CO_2-N_2-He, vol. discharge, negative ions effect 80−14956
- CO_2-N_2-He laser mixtures, electron swarm parameters, Boltzmann eqn. anal. 79−18396
- Cl_2, electron-attachment rate const., room temp. and 250°C, in $Ar(N_2)$ discharges 79−45841
- Cu, secondary electron emission *(French)* 80−55238
- Cu-superfluid ^{4}He interface, exponentially damped surface solutions generated by heat flow 79−55980
- GaAs, optical cond. of free carriers 78−19436
- GaAs, temp. depend. of intervalley gap from Schottky diodes meas., thermionic emission theory generalization 79−73586
- GaAs-$Al_xGa_{1-x}As$ heterostructures, real-space electron transfer by thermionic emission, analytical model 80−100512
- H_2, elec. discharge, non-equilib. ionisation rate calcs. 80−59319
- H_2, electron swarm transport coeffs. determ. by Boltzmann and Monte Carlo methods 79−90359
- H_2, interstellar, departure from translational equilib. 78−8081
- H_2 plasma, electron transport coeffs. at high E/N values 79−94835
- H_2-H mixture positive column, static electric charact. 78−67500
- HB rot. relaxation, diffusion theory 80−106313
- HCl, in nonequilib. plasma, electron energy distrib. function and dissoc. kinetics 80−11882
- HCl, rot. relaxation, diffusion theory 80−106313
- HF+HF, momentum exchange rate, Boltzmann eqn. predictions 78−78781
- ^{3}He, normal phase, spin-zero-sound solns. of the quasi-particle Boltzmann equation 79−77856
- ^{3}He, superfluid, B-phase, transport processes at low temp. 77−55412
- ^{3}He, superfluid, transport and relax. processes close to transition temp. 77−55411
- ^{3}He, superfluid B-phase, shear viscosity, s-p-d wave approximation 80−96715
- ^{4}He, electron localisation, mobility in dense low temp. gas 80−92247
- ^{4}He, liq., cyclotron reson. of hot electrons 80−88377
- ^{4}He, superfluid, Boltzmann transport equation, search for exponentially damped surface solns. 78−67878
- Hg positive column, electron energy distrib., numerical soln. of Boltzmann eqn. 80−87982
- Hg Townsend discharge, electron swarm props. Boltzmann eqn. anal. 80−19648
- InP, free carriers, freq. depend. relax. time 80−2385
- InSb, polar semicond. longit. magneto-Seebeck coeff., effect of polar-optical-phonon scatt., iterative soln. of Boltzmann eqn. 79−56250
- n-InSb, stationary energy transport velocity of light scattered from bunched solid-state plasma 79−95720
- K, ideally pure, anisotropy correction to elec. resist. 77−4317
- Kr, electron ionisation and excitation coeffs. in low E/N region 80−48090
- Li, elec. resist., soln. of Boltzmann transport eqn. 78−39090
- Li-Mg, Mathiessen's rule, elec. and thermal deviations, impurity scatt. 80−88536
- N, electron swarm development, Boltzmann eqn. method 80−43832
- N_2, diffusion approx. for slow electrons 79−82044
- N_2, electron energy distrib. and transport coeffs. in E×B fields 78−51277
- N_2, electron swarm develop., Boltzmann eqn. anal. 78−79487
- N_2 plasma, electron transport coeffs. at high E/N values 79−94836
- N_2 plasma, electronic excitation levels in gas-discharge 80−24280
- N_2 positive column, superelastic collisions and electron distrib. function 80−1858
- N_2, weakly ionised, electron transport coeffs., Boltzmann eqn. anal. *(Japanese)* 80−59183
- Na, Hall coefficient, quasiclassical Boltzmann eqn. calcs. 80−103678
- Nb, high temp. elec. resist., supposed failure of Boltzmann eqn. 77−72849
- Nb, high-temperature nonlinear electrical resistivity, supposed failure of Boltzmann eqn. 78−91664
- Nb, nonlinear resistivity, failure of Boltzmann equation 77−11893
- Ne discharge, Boltzmann eqn., numerical study 77−35424
- Ne discharge, numerical study 79−32838
- Ne, elec. discharge, electron energy distrib. function 79−50911
- Ne, low ionised anisothermal plasma, ionising electron collision kinetics *(German)* 80−33731
- Ne plasma, electron collision ionisation, electron kinetic behaviour during elec. field perturbation *(German)* 80−64676
- Ne-Cu pulsed discharge, electron energy distrib., ionis. rate 78−51387
- O_2 discharge, electron gas, transport coeff. and energy distrib. function calcs. 77−68742
- O_2, dissociative attachment coeff. calc. 77−19100
- O_2, weakly ionised, electron transport coeffs., Boltzmann eqn. anal. *(Japanese)* 80−59183
- SF_6, electron swarm development, Boltzmann eqn. anal. 80−6205
- SF_6-N_2 mixture, electron swarm development, Boltzman eqn. anal. 80−87841
- n-Si (100) inversion layer mobility depend. on intersubband scatt. at low temps. 79−95506
- Si, two-dimensional inversion layer on surface, minigap and conductivities 80−20267
- SiO_2, amorphous electron transport and breakdown at high elec. fields 79−78108
- Xe, electron ionisation and excitation coeffs. in low E/N region 80−48090
- Xe, Townsend discharge, electron energy distrib. functions 79−4198

Boltzmann-Vlasov equation *see Vlasov equation*

bond angles

- (3×3) order systems, force constant calcs. using isotopic freqs., parametric method 78−21907
- S,S′-dimethyldithiocarbonate, pot. for rot. about $C(sp^2)$-S bonds, electron diffr. obs. 80−23572
- adamantane, derivatives in solution, mol. motion and methyl group rot. barriers from ^{13}C NMR relax. times 80−74179
- aluminates, interdepend. between tetrahedral d(T-O) bond lengths, non-bonded d(T...T) separations and TOT angles (T=Al,Si,P), using regression anal. 79−19182
- benzene-d_0,-d_6, $^1B_{2u}$ excited states, high resolution two-photon spectra 77−506
- benzenoid-o-quinoidal systems, valence isomerisation, EHT calcs. 77−77757
- benzyl fluoride, mol. struct., NMR and gas electron diffraction obs., ab initio and mol. mechanics calcs. 80−23574
- benzyl radical trapped in X-irrad. potassium hydrogen bisphenylacetate, ENDOR 77−10695
- bis(diethylamino)dithiaboretane, cryst. struct., bond lengths and angs. X-ray diffr. obs. 78−18628
- bond bending, bond orbitals rel. to nucl. motion 80−95513
- bridging bond angle variations in siloxanes, silicates, Si nitrides and sulphides, mol. orbital calc. on model systems 78−55125
- bromochlorofluoromethane, struct., vibr. amplitudes, gas phase electron diffr. obs. 79−31690
- 4-bromophenoxyacetyl-4-ethylbenzene, single crystal, X-ray struct. determ. 79−1426
- 3-bromopropene, ^{79,81}Br, microwave spectrum, mol. struct., nucl. quadrupole coupling consts., rot. consts. 77−6767
- bromtrinitromethane, electron diffr. study of gas phase mol. struct., rot. isomerism 78−1080
- cis- and trans-2-butene, proton-proton coupling consts., valence angle depend. 77−23508
- t-butylphosphine, microwave spectrum, meas., determ. 78−58675
- carbenes, bond angles, inversion barriers, singlet-triplet energy differences, struct. fragments method 77−10782
- carbonyl halogen substituted cpds., geometric and electronic struct., LCAO-SCF calc. 79−89603
- carboxyl groups, $-COO^-$, $-COOH$, $-COOCH_3$, bond lengths and angles relations 80−53158
- carboxyl groups, H_2 bonded, C-O vs. O-H length correlation using neutron diffr. data 79−54987
- 2-chloro-3-fluoro-1-propene, struct. and conformers, force field and vibr. amplitudes 78−25747
- chloroethane diradical, MINDO/3 for optimised geometry and heat of form. 78−78830
- chloromethylene radical, MINDO/3 for optimised geometry and heat of form. 78−78830
- chlorotrinitromethane, electron diffr. study of gas phase mol. struct., rot. isomerism 78−1080
- covalent semiconductors, displacement correlations, adiabatic bond charge model 80−70350
- cyclic 4-ring rotation-puckering, use of spherical coords. 80−58193
- cyclopentadienyl cobalt dicarbonyl, mol. stuct., gas phase electron diffr. obs. 79−31688
- N,N′-diacetyl-1,2,1′,1′-tetrahydro-1,1′-diisoquinoline, cryst. and mol. struct. 78−2106
- 2,5- diamino-1,4-benzoquinone, interpretation of bond lengths and angles 79−13836
- o-dibromobenzene, r_α-struct. determ. from PMR with ^{13}C satellites, bond lengths and angles 78−25560
- o-dichlorobenzene, r_α-struct. determ. from PMR with ^{13}C satellites, bond lengths and angles 78−25560
- 1,2-dichloroethane, enclathrated, conform., reorientation, PMR line shape anal. 79−91300
- dichloromethylene radical, MINDO/3 for optimised geometry and heat of form. 78−78830
- 1,1−difluoroethylene, mol. struct., gas phase electron diffr. and microwave data 77−65542
- 2,5-dihydroxy-1,4-benzoquinones, interpretation of bond lengths and angles 79−13836
- o-diiodobenzene, r_α-struct. determ. from PMR with ^{13}C satellites, bond lengths and angles 78−25560
- 9,10-cis-endo-dimethyltricyclo$[4,2,2,0^{2,5}]$dec-7-ene, substituted, crystal and molecular struct. 79−86785
- effective hamiltonians, pseudopotentials and applics. 77 −30754
- ethane, nuclear spin-spin coupling consts., vicinal proton-proton coupling calcs. 80−32737
- ethanol, conformational anal., barriers of internal rotation, electronic structure 79−63916
- ethylene, mol. geometry, ab initio calcs., basis set depend. 78−82636
- ethylene, molecular geometry optimisation, variable metric method, internal geometry 80−95744
- ethylene, proton-proton coupling consts., valence angle depend. 77−23508
- ethylene ozonide-d_4, isotopic species, microwave rot. spectrum assignments, struct. 77−57982
- fatty alcohol solid monolayers in H_2O, interface struct., model 80−54505
- cis-formic acid (-d_2,d_2), and isotopic forms, bond lengths and angs., microwave spectrum obs. 78−55169
- formyl fluoride, and isotopic forms, mol. struct., from electron diffr. and microwave data 80−23570
- furan-2-aldehyde, mol. struct., electron diffr. and IR spectroscopic examination 79−10106
- group frequencies study of bond ang. change 79−98057
- hydrides of 1st three row elements, pseudopotential calcs., PSIBMOL algorithm 77−26963
- hydrocarbons, unsaturated, empirical potential model EPEN/2 parameterisation, testing 79−50103
- icosahedral cage, symmetry coords. and vibration freq. 80−47966
- intramolecular potentials, quantum chemical calc. 78−13436
- Kevlar 49 fibre, poly p-phenylene terephthalate, Raman spectroscopy, heat, stress, radiation effects 79−65871
- maleic anhydride, struct., DRM microwave spectra, isotope shifts 78−21918
- metal surface, chemisorbed water molecule struct., interband angle 80−59787
- methane, $1B_1(1T_2)$ state, photodissoc., extended basis calcs. 78−9093

bond angles continued
methanol, conformational anal., barriers of internal rotation, electronic structure 79—63916
methanol, molecular geometry optimisation, variable metric method, internal geometry 80—95744
methyl meristotropate, mol. and cryst. struct. 78—95047
methyl vinyl sulphide, syn-gauche equilib., force field and ab initio calcs., microwave and Raman spectra 80—23573
methylene, optimised geometry, CI calcs. using partitioning theory 77—38616
methylmercury nitrate, in nematic and lyotropic liq. crysts., r_α-struct. and anisotropy of Hg-C coupling const. 80—43071
model of bond geometry, lone pair stereoactivity 79—45649
molecular geometry, vibr. anharmonicity effects 79—50159
molecules, bridge angle, vibr. behaviour, simplified and accurate calcs. 80—95735
α-monochloroacetic acid, hydrogen-bond motifs 77—11529
β-monochloroacetic acid, hydrogen-bond motifs 77—15397
Ni complex, di-(trichloroacetate).4n-para-anidine crystal struct. 79—86774
n-nitro-n′-methylbenzylidene-aniline, triclinic, cryst. and mol. struct. 77—43205
nonlinear molecules, bending vibrs., correlated bender theory 78—37627
norbornane, derivatives in solution, mol. motion and methyl group rot. barriers from ^{13}C NMR relax. times 80—74179
organic molecules, saturated, empirical potential model EPEN/2, parameterisation testing 79—54933
organosilicon polymers, ladder-type, local conforms. *(Russian)* 77—19121
oxirane cation, struct. rearrangement following vertical ionisation, ab initio CI calc. 80—58191
peptide, NMR spectroscopy study 78—88694
phenanthrenoid compounds, abnormal bond lengths, MO calculations 77—31020
phenols, ^{13}C and D substituted, microwave spectra, substitution struct. and absolute dipole moment 79—31511
phenyl cation, singlet, triplet state mol. geometries, energies, ab initio UHF STO calcs. 77—6672
phosphates, interdepend. between tetrahedral d(T-O) bond lengths, nonbonded d(T...T) separations and TOT angles (T=Al,Si,P), using regression anal. 79—19182
polyacetylene:I, NMR investigation of struct. 80—39011
polyatomic mol. gas phase spectra, struct., review and tabulation 80—14136
polycapromide, fracture, interatomic bonds deform. 79—57107
polyethylene, deformation, Hartree-Fock SCF calcs. 80—18949
polyethylene terephthalate, fracture, interatomic bonds deform. 79—57107
polymer, deformation of interatomic bonds, IR spectral meas. 79—38918
polymer chains 80—3116
polypropylene, fracture, interatomic bonds deform. 79—57107
polypyromelliteimide, fracture, interatomic bonds deform. 79—57107
potassium oxalate monohydrate, cryst., O-H bond lengths, H-O-H angles, corrections 79—32945
p-propoxysalicylidene-p′-butylaniline cryst. and mol. struct., intramolecular bonding 80—44197
propylene, proton-proton coupling consts., valence angle depend. 77—23508
protein, NMR spectroscopy study 78—88694
pyramidal XY_3 molecules, mol. geometry calcs. using centrifugal distortion const. 80—18841
pyromellitic N,N′-dimethyldiimide-anthracene, cryst. struct. determ. 78—2107
qauche NMR effect in ^{13}C, ^{19}F and ^{31}P chem. shifts and directly bonded coupling consts., bond angle effects 77—68056
quartz, low, cell parameter variations between 94 and 298K 80—96497
quinazolines, enzyme inhibitory, structure-activity quantitative study 80—78540
second-row hydrides, equilib. geometry, FSGO model pot. calcs. 77—50347
selenoacetaldehyde, microwave spectrum, struct. internal rot. barrier, CCSe bond 78—74645
selenoketene, microwave spectra, 26.5-40 GHz, mol. config., bond angle and length 78—46322
silica, and silicate minerals, interdepend. between tetrahedral d(T-O) bond lengths, nonbonded d(T...T) separations and TOT angles (T=Al,Si,P), using regression anal. 79—19182
sodalites, aluminogermanate- and aluminate-, IR spectra rel. to T-O bond length and T-O-T ang. 79—91445
spirohydrocarbons, strained, bond angles, interatomic distances, semiempirical and ab initio calcs. 80—95533
TCNQ, semiempirical CNDO calcs. of electronic struct. and absorpt. spectra 78—995
TCNQ complex with 5-phenyl-[1-thiol]-3-selenol-2-thione, charge-transfer salt, cryst. and mol. struct. 80—33986
tetrafluoro-p-benzoquinone, mol. struct., gas phase electron diffr. obs. 80—58386
1,1,1,2-tetrafluoroethane, mol. struct. studied by gas-phase electron diffr., vibr. amplitudes, bond angles and lengths calc. 80—95740
thermal-motion correction for bond angles, harmonic approx. 78—55777
thiocarbonates, mol. struct., S-substitution effect *(French)* 80—23335
thiocarbonyl halogen substituted cpds., geometric and electronic struct., LCAO-SCF calc. 79—89603
thioformamide(-d_2), photoelectron and absorption spectra, vibr. struct., excited state configs. 77—6847
thionitrates, mol. struct., S-substitution effect *(French)* 80—23335
toluene, mol. struct., ab initio calcs. 80—106262
trans-propargyl amine, microwave spectra, dipole moments and struct., isotopic species 78—974
transition metal bonds with H, C and P, angles, lengths and numbers 78—42947
triatomic dihydride molecules, Walsh's rules and small bond angle states 80—106255
1,2,3-trichlorobenzene, oriented mols., ^{13}C satellites use in proton spectra, r_α-structure 80—18872
1,1,2-trifluoroethane, mol. struct., gas phase electron diffraction, rotamer abundance 79—76514
trifluoromethyl sulphonyl chloride, mol. struct., electron diffr. obs. 79—7016
trimethylphosphine, chem. shift anisotropy, struct., liq. cryst. NMR 77—61768

bond angles continued
trimethylphosphonium oxide (sulphide) (selenide), chem. shift anisotropy, struct., liq. cryst. NMR 77—61768
trinitromehtane, electron diffr. study of gas phase mol. struct., rot. isomerism 78—1080
triphenyl-(triphenylgermanylperoxy)silane, cryst. and mol. struct. 80—39066
tris(dimethylamino)phosphorus, ^{15}N and ^{31}P NMR aligned in liq. cryst., geom. struct. 78—82751
DL-tryptophan, polycryst., amino group rot., reorientation, mol. struct., 77-555K, PMR obs. 78—35047
vinyl bromide, mol. struct., from gas-phase electron diffr. and microwave data 80—23571
vinylchloride, mol. struct., gas-phase electron diffraction and microwave spectra, vibr. amplitudes 79—76421
vinylfluoride, gas phase electron diffr. and microwave spectra, rot. consts., struct., isotope shifts 79—31686
water, liq., H bond distrib., Monte Carlo simulation calcs. 80—54106
$AlBr_3.NH_3$, mol. struct., vap. phase electron diffr. obs. 77—65541
$Al(PO_3)_3$, vitreous struct. 78—26443
$AsCl_3$, 100 to 200 GHz spectra, mol. struct., harmonic force field 78—42042
AsF_3, millimetre rot. spectra, vibr. excited states, anharmonic force field 78—33502
AsF_3, mol. geometry calcs. using centrifugal distortion const. 80—18841
As_2O_3 crystalline and amorphous, EXAFS study of struct. 80—19776
$BClF_2$, microwave spectrum, struct., quadrupole coupling consts. 77—57986
B_2F_4, molecular structure, barrier to internal rotation, temperature effects 78—13625
BH_2, Walsh's rules and small bond angle states 80—106255
$Ba(ClO_3)_2.H_2O$, cryst., O-H bond lengths, H-O-H angles, corrections 79—32945
$Ba(ClO_3)_2.2H_2{}^{17}O$, fine struct. in quad. reson. of ^{17}O, DNMR 77—8453
BeO_4 tetrahedra, variabilities in interatomic distances and angles 79—46594
BrF_5, gas phase electron diffraction and microwave rot. consts. data anal., mol. struct. 79—76363
$Br(H_2O)_n^-$, geometric and electronic struct., CNDO/2 calcs. 77—79542
C-CH_2-C fragments, bond angles 77—14601
C_3, $\bar{A}\,^1\Pi_u$ state, orbital angular momentum 80—78514
CH_2, FSGO LCAO calc., bond angles 77—34557
CH_2^+, Walsh's rules and small bond angle states 80—106255
$COCl_2$, microwave spectra, 24-154 GHz, rot. and centrifugal distortion consts. 78—46324
$CaCO_3$:Li, CO_3^{3-}-Li^+ centre, irradiated synthetic single crystal, bond angle and wave function 77—81006
CdX_2, (X=Br, Cl), spectroscopic parameters of mols. from vibr. isotopic effects 78—74798
CdXY, (X, Y=Cl, Br, I), spectroscopic parameters of mols. from vibr. isotopic effects 78—74798
ClF_4 radical, geom., ab initio MO calcs. 79—89610
ClF_5, microwave spectrum, rot. transitions, dipole moment, struct., nuclear quadrupole coupling consts. 77—14423
$Co(CO)_3$, bond angles, hybrid bond orbital calcs. 78—94188
$Cr(CO)_3$, bond angles, hybrid bond orbital calcs. 78—94188
$Cs_{11}O_3$, ionic clusters in alkali metal suboxide cryst., struct., vibr. freqs., Raman spectra 79—37772
Cs_2Te_3, synthesis and cryst. struct. 80—88115
Cu complex, [Cu(1,4,7,10-tetrabenzyl-1,4,7-10-tetraazacyclododecane)Cl]NO_3, cryst., struct. 80—64966
DO_2, IR spectra, config. of $^2A'$ and $^2A''$ states 79—36636
D_2O_2, equilib. geometry, O-D bond length and angle 77—75326
N,N-dimethyloxamide, conform. anal., CNDO/2 energy optimisation, mol. props. 77—75328
Fe complex, nitrile nonacarbonyl, cryst., mol. structs. 80—64967
Fe complex, nitrile nonacarbonyl cryst., mol. struct. 80—64968
$Fe(CO)_3$, bond angles, hybrid bond orbital calcs. 78—94188
GaAs, (110) surface, bond angle and lengths of rearranged As and Ga atoms 78—71918
$GaBr_3.NH_3$, mol. struct., vap. phase electron diffr. obs. 77—65541
$GeCl_2$, combined electron diffr. and mass spectra mol. struct. determ. 79—89783
H_3^+, ab initio calcs. of vibr. spectrum 77—6753
HCN, SCF ab initio ground state pot. energy surface, geometry, rel. to HCN^- 78—78646
HCN^-, SCF ab initio ground state pot. energy surface, geometry, rel. to HCN 78—78646
HCN^+, $^2\Sigma^+$ and $^2\Pi$ states, SCF and CI calcs. for determ. optimum linear geometries, bond angles calc. 80—74114
$H_2CN^+H_2 \rightarrow HCN^+H + H_2$, ab initio GO SCF pot. energy surface, saddle point, reaction path 77—50379
HCl, mol. cryst., angles of H-bonded mols., ab initio calcs. 78—6037
$HCo(CO)_4$, mol. struct., gas phase electron diffr. expt. 78—13623
HF-ClF complex, and isotopic forms., mol. beam elec. reson. spectra, config., bonding, spectroscopic consts. 77—30860
$H_2Fe(CO)_4$, mol. struct., gas phase electron diffr. expt. 78—13623
$HMn(CO)_5$, mol. struct., gas phase electron diffr. expt. 78—13623
HNC^+, $^2\Sigma^+$ and $^2\Pi$ states, SCF and CI calcs. for determ. optimum linear geometries, bond angles calc. 80—74114
HO-H...OHX, X=H, CH_3, NH_2, OH, F, H-bonds, electron donor substituted, mol. orbital calc. 78—13422
H_2O, excited states, pot. energy curves w.r.t. bond ang., one-centre expansion approx. 79—6886
H_2O, ground state, energy, bond parameters, diagrammatic perturbation theory calcs. 78—25414
H_2O, ground state correlation energy, diagrammatic perturbation theory 80—18774
H_2O, inelastic electron scatt., geometrical parameters determ. 77—88585
H_2O, pot. energy surface by MS $X\alpha$ method 79—13656
H_2O, rot.-vibr. Schrodinger eqn. soln., bond lengths and angles, force consts. 79—41151
H_2O, roto-vibrational structure, correlated bender theory 78—37627
H_2O, valence shell electron pair interactions, VSEPR theory test 79—31393
H_2O^+, in X(0,0,0) level 77—473
H_2O_2, equilib. geometry, O-H bond length and angle 77—75326
H_2O_2, structural parameters of vibr. ground state 80—28116
HOO radical, lowest doublet electronic states, rel. to photodissoc. 79—93914

bond angles continued

- H_2O...HF complex, force field, vibr. freqs., equilib. geometry bond energy, ab initio calc. 77—65450
- H_2S, valence shell electron pair interactions, VSEPR theory test 79—31393
- $HeNO_2$, molecular geometry and stability, ab initio calcs. 78—90075
- HgX_2, (X=Cl, Br), spectroscopic parameters of mols. from vibr. isotopic effects 78—74798
- HgXY, (X, Y=Cl, Br, I), spectroscopic parameters of mols. from vibr. isotopic effects 78—74798
- I-containing molecules, geom. struct. and dipole moments, CNDO/2 calc. 79—94103
- IF_5, gas phase electron diffr. and B_0 rot. const., struct. determ. 79—89782
- $I(H_2O)_n^-$, geometric and electronic struct., CNDO/2 calcs. 77—79542
- $Li+O_2$, semiempirical pot. surfaces, dynamical considerations 79—11766
- Li_2O_2, ab initio geometry, vibr. freqs., ionis. pots., and force consts. 77—65421
- $Mn(CO)_3$, bond angles, hybrid bond orbital calcs. 78—94188
- NH_2, X^2B_1, A^2A_1 and B^2B_2 states, ab initio SCF CI calcs. 78—29746
- NH_3, lowest triplet state geometry, SCF and CEPA-PNO calc. 80—914
- NH_3, pot. energy surface by MS $X\alpha$ method 79—13656
- $(NH_4)_3Sc(SeO_4)_3$, cryst. struct. 79—99122
- $Na_3H(SO_4)_2$, cryst. struct. refinement, short asymmetrical H bond, S-OH vs. O-H...O correlation 79—37663
- Ni complex, cis-dichloro-bis(1,2,cyclohexadionedioxime) cryst. and mol. struct. 80—44198
- NiF_2+CO, Ar matrix isolated, ab initio MO calcs. 78—92458
- O_3, MC SCF and MC CI calc., open and closed form mols. 78—78831
- $OH+H_2$, pot. energy surface, barrier heights and transition state geometry, POL-CI calc. 80—55649
- ONBr, force constant calcs. using isotopic freqs., parametric method 78—21907
- ONCl, force constant calcs. using isotopic freqs., parametric method 78—21907
- ONF, force constant calcs. using isotopic freqs., parametric method 78—21907
- OPF_3, distortion moment microwave obs., rot. consts., mol. config. 77—50426
- Os complexes, N-1-adamantylimido OsO_3, bis(N-tert-butylimido) OsO_2, cryst. struct., bonding, ligands π-donor capability 80—64969
- P, black allotrope, orthorhombic bonding, up to 26.6 kbar, neutron diffr. obs. 79—99106
- PD_3, forbidden rot. spectra, spectal consts., bond lengths and angles 77—83581
- PF_3, mol. geometry calcs. using centrifugal distortion const. 80—18841
- PH_2 radial, pot. energy curves. config., ab initio SCF-MO calcs. 77—50419
- PH_3, forbidden rot. spectra, spectal consts., bond lengths and angles 77—83581
- $P_2O_4(OH)_4^{2-}$ group, electronic struct. calcs. 78—67971
- PSF_3, in orienting smectic solvent, ^{19}F and ^{31}P mag. shielding anisotropies, F-P-F bond angle 77—18942
- $RbBO_2$, mean geometrical config., vapour phase electron diffr. 77—46651
- Rb_9O_2, ionic clusters in alkali metal suboxide cryst., struct., vibr. freqs., Raman spectra 79—37772
- Rb_2Te_3, synthesis and cryst. struct. 80—88115
- $^{32}SF_2$, $^{34}Sf_2$, matrix IR spectra, vibr. and force fields, bond angle *(German)* 78—74662
- S_2N_2, $(SN)_x$, (x=2 or 3), minimal STO-3G basis HF ab initio LCAO SCF MOC, geometry 78—903
- SO_2, $X \rightarrow A$ electronic absorpt. band system, non Condon effects study 80—18837
- $ScH(SeO_4)_2.2H_2O$, $Sc(HSeO_3)_3$, cryst. struct. 79—99122
- $Sc_2(SeO_4)_3(.5H_2O)$ cryst. struct. 79—99122
- Si_2H_6, tetrahedral edge sharing, distortions, MO calcs. 77—14380
- SiH_3NCO, geometric struct., ab initio MO calc. 79—13834
- Si_2H_6O, geom. and electronic struct., ab initio MO calc. 79—97972
- SiO_2, chem. bond and rel. props. 77—43199
- SiO_2, vitreous, III-V analogues and bonding topology 79—73102
- Si_2O_2, tetrahedral edge sharing, distortions, MO calcs. 77—14380
- $Si_2O_6(OH)_2^{6-}$ group, electronic struct. calcs. 78—67971
- Si_2S_2, tetrahedral edge sharing, distortions, MO calcs. 77—14380
- Sn(IV)-, Sn(II) halide mols., rare gas matrix-isolated ^{119} Sn spectra 77—48097
- ThV_2O_7, V-O-V bridge stretching freq. correl. with bond angle 78—74636
- TiF_4, equilib. config., force field, Coriolis consts., vibr. freqs. and amplitudes 80—32835
- $(UO)_2V_2O_7$, V-O-V bridge stretching freq. correl. with bond angle 78—74636
- W (100), adsorbed H-induced lattice reconstruction, surface vibr. obs. 79—19445
- ZnX_2, (X=Cl, Br, I), spectroscopic parameters of mols. from vibr. isotopic effects 78—74798
- ZnXY, (X, Y=Cl, Br, I), spectroscopic parameters of mols. from vibr. isotopic effects 78—74798

bond lengths

- S,S′-dimethyldithiocarbonate, pot. for rot. about $C(sp^2)$-S bonds, electron diffr. obs. 80—23572
- ab initio effective core pot. method appl. to F_2, Cl_2 and LiCl 80—32625
- N-acetyl-valine, NMR of solid, ^{14}N-^1H dipolar spectra, NH bond length 78—48055
- acetylene, chemisorbed on W(100), geometry distortion 77—30919
- acetylene, chemisorption on Pt (111), ethylidyne group form., LEED and ELS obs. 78—73075
- acetylene, vibr. fine struct. accompanying core ionis., STO calcs. 78—62844
- alkali hydroxides, dissoc. energies and bond lengths, ion props. depend. 78—86801
- alkali metaborates, dissoc. energies and bond lengths, ion props. depend. 78—86801
- alkali metal monoxides, bond distance, dissoc. energy and vibr. freq., electron gas model 77—30846
- alkali metal nitrates, Raman spectra, interionic interactions effect on bond lengths, dissoc. energies and vibr. 79—36653
- allyl radical, restricted ab initio SCF LCAO solns., doublet stability 77—79539

bond lengths continued

- aluminates, interdepend. between tetrahedral d(T-O) bond lengths, non-bonded d(T...T) separations and TOT angles (T=Al,Si,P), using regression anal. 79—19182
- 18-annulene, geometrical parameters, STO-3G ab initio calc. 80—52867
- asymmetric top molecules, R_S-struct., bond length mass depend. 78—94230
- AX_n molecules, vibrationally-hot, bond lengths, simple treatment 79—68202
- basis set effect, and approx. natural orbitals, SCF CI GTO calcs. 78—76904
- benzene, unlabelled and ^{13}C labelled PMR, oriented in liq. crysts., r_α struct., solvent effects 79—94017
- benzene-d_0,-d_6, $^1B_{2u}$ excited states, high resolution two-photon spectra 77—506
- benzenes, disubstituted, monosubstituted, effect of bonding electrons on molecular dimensions as determ. by X-rays 79—7595
- benzonitrile, excited single state B_1, electron-vibr. spectra and electronic struct. 79—26904
- bicyclo[3.1.0]hexane, zero-point average struct., microwave spectra and electron diffraction 78—25738
- bis(diethylamino)dithiaboretane, cryst. struct., bond lengths and angs. X-ray diffr. obs. 78—18628
- bis(fluoroxy)difluoromethane, ab initio MO calcs. of geometry, torsional barriers 78—90313
- bond order, maximum principle, LCAO formalism 78—29728
- bone powder and ash, PMR and IR spectra, chem. anal., bond lengths 78—3414
- boranes, nido and arachno, bond length-bases bond enthalpies 80—30265
- bromoacetylene, microwave spectrum, r_5-struct., dipole moment, quadrupole coupling consts., vibr. excited states 77—79606
- bromochlorofluoromethane, struct., vibr. amplitudes, gas phase electron diffr. obs. 79—31690
- 4-bromophenoxyacetyl-4-ethylbenzene, single crystal, X-ray struct. determ. 79—1426
- 3-bromopropene, $^{79,81}Br$, microwave spectrum, mol. struct., nucl. quadrupole coupling consts., rot. consts. 77—6767
- bromotrifluoromethane, mol. struct., electron diffr., microwave spectra, CNDO/2 calcs. 78—37766
- bromtrinitromethane, electron diffr. study of gas phase mol. struct., rot. isomerism 78—1080
- butadiene, J_{C-H} spin-spin coupling const., bond length depend. 78—37660
- t-butyl bromide, bond lengths, nucl. quadrupole coupling, microwave spectrum 79—31512
- carbon tetrachloride, internucl. parameters meas. using total scatt. of fast electrons 80—32857
- carbon tetrachloride, low-energy X-ray emission spectra, MO anal., ionis. pot., rel. to CH_4 and $CHCl_3$ 79—85975
- carbonyl groups, intermol. interactions in H_2CO-H_2CO system, quantum chem., classical calcs. 78—86932
- carbonyl halogen substituted cpds., geometric and electronic struct., LCAO-SCF calc. 79—89603
- carboxyl groups, $-COO^-$, $-COOH$, $-COOCH_3$, bond lengths and angles relations 80—53158
- carboxyl groups, H_2 bonded, C-O vs. O-H length correlation using neutron diffr. data 79—54987
- cellulose trinitrate, in soln., gel-like aggregate form. rel. to configuration 77—31036
- 2-chloro-3-fluoro-1-propene, struct. and conformers, force field and vibr. amplitudes 78—25747
- chlorobenzene-d_5, and isotopic forms, microwave spectrum, rot. consts. 78—58667
- chloroethane diradical, MINDO/3 for optimised geometry and heat of form. 78—78830
- chloromethylene radical, MINDO/3 for optimised geometry and heat of form. 78—78830
- chloroperoxidase, ferric form, X-ray absorpt. fine struct., Fe-N and Fe-S lengths 79—48213
- chlorotrifluoromethane, mol. struct., electron diffr., microwave spectra, CNDO/2 calcs. 78—37766
- chlorotrinitromethane, electron diffr. study of gas phase mol. struct., rot. isomerism 78—1080
- core hole state, anharmonicity in Franck-Condon analysis 79—41186
- covalent semiconductors, displacement correlations, adiabatic bond charge model 80—70350
- crystal structural fragment, automatic construction, taking account of attainable chem. bond lengths 80—92419
- cyclobutadiene, π face bonding with CO, HCN, benzene 79—98180
- cyclopentadienyl cobalt dicarbonyl, mol. stuct., gas phase electron diffr. obs. 79—31688
- cyclopropane, J_{C-H} spin-spin coupling const., bond length depend. 78—37660
- cytochrome P-450, ferric form, X-ray absorpt. fine struct., Fe-N and Fe-S lengths 79—48213
- N,N′-diacetyl-1,2,1′,1′-tetrahydro-1,1′-diisoquinoline, cryst. and mol. struct. 78—2106
- diammonium oxalate monohydrate, NMR spectra, ^{13}C-^{13}C interaction, chemical shift effects 78—29800
- diamond, ab initio calcs. of struct. using FSGO method 77—80753
- diatomic, molecules, interat. distances calc. from zero, second-order energy, modified PCILO method 79—36533
- diatomic isovalent systems, pot. curves, ab initio MRD-CI method 80—83293
- diatomic mol., Hellman pseudopot. calcs., dissoc. energy, ionis. pot., bond length 77—10577
- diatomic molecules, inner-shell ionisation, relax. effects calcs. 77—42351
- diatomic mols., 2nd row, STO and HF calcs., bond length, dipole moment 77—23431
- diatomic systems, reln. between internuclear distances and force constants 80—43205
- o-dibromobenzene, r_α-struct. determ. from PMR with ^{13}C satellites, bond lengths and angles 78—25560
- o-dichlorobenzene, r_α-struct. determ. from PMR with ^{13}C satellites, bond lengths and angles 78—25560
- dichlorodinitromethane, mol. struct., electron diffr. investig. 78—86950
- dichloromethylene radical, MINDO/3 for optimised geometry and heat of form. 78—78830
- 1,1—difluoroethylene, mol. struct., gas phase electron diffr. and microwave data 77—65542
- o-diiodobenzene, r_α-struct. determ. from PMR with ^{13}C satellites, bond lengths and angles 78—25560

bond lengths continued
- 9,10-cis-endo-dimethyltricyclo[4,2,2,$0^{2,5}$]dec-7-ene, substituted, crystal and molecular struct. 79—86785
- 2,4-dinitrophenol, cryst. and mol. struct. 77—15394
- effective hamiltonians, pseudopotentials and applics. 77—30754
- EHT method, population analysis and bond lengths forecasting 80—18800
- electronegativity equalisation in atom-atom reactions 79—66272
- ethane, $^{13}CH_3{}^{12}CD_3$, $^{12}CH_3{}^{13}CD_3$, microwave spectra, Stark effect, C-C bond length and mol. consts. 77—50428
- ethane, nuclear spin-spin coupling consts., vicinal proton-proton coupling calcs. 80—32737
- ethane-d_n, IR spectra, r_0, r_z and r_e structs. 79—59453
- ethyldifluoroborane, microwave, Raman, IR spectra, conform., dipole moments, vibr. assignment 78—90155
- ethylene, chemisorbed on W(100), geometry distortion 77—30919
- ethylene, chemisorption on Pt (111), ethylidyne group form., LEED and ELS obs. 78—73075
- ethylene, diatomics-in-mols., semiempirical valence bond π-electron theory 80—99461
- ethylene, electron affinities, pi* anion, bond lengths, electron transmission spectroscopy study 80—18925
- ethylene, mol. geometry, ab initio calcs., basis set depend. 78—82636
- ethylene, molecular geometry optimisation, variable metric method, internal geometry 80—95744
- ethylene ozonide-d_4, isotopic species, microwave rot. spectrum assignments, struct. 77—57982
- ferrocene, metal to ring distance, ab initio MO SCF calcs. 80—47870
- 9H-fluorene, soln., correl. times from ^{13}C relax. 80—23438
- fluoroethylenes, electron affinities, pi* anions, bond lengths, electron transmission spectroscopy study 80—18925
- fluoroxyperoxytrifluoromethane, ab initio MO calcs. of geometry, torsional barriers 78—90313
- formic acid, dimerisation energy, non-empirical MO SCF calc. 79—37656
- cis-formic acid (-d_2,d_2), and isotopic forms, bond lengths and angs., microwave spectrum obs. 78—55169
- formyl fluoride, and isotopic forms, mol. struct., from electron diffr. and microwave data 80—23570
- furan-2-aldehyde, mol. struct., electron diffr. and IR spectroscopic examination 79—10106
- graphite layers, C-C bond length increase on intercalation by metals *(French)* 77—28994
- graphite-Br_2 intercalation cpds., EXAFS study 80—71515
- graphite-HSO_3F intercalation compound, Raman spectral study *(French)* 80—60581
- graphitised viscose fibre, fluorination, change in struct. 80—88039
- group IV elements, ^{57}Fe isomer shift, quadrupole coupling and interat. distance correl. 78—52408
- halogen molecule, orbitals calc., correlation effects, force const., dissoc. energy, bond length 77—26964
- halogen molecule negative ion, $Cl_2{}^-$, $Br_2{}^-$, $I_2{}^-$, $ClBr^-$, ClI^-, pot. curve calc. 77—10596
- Hartree Fock Slater method, transition state method 78—9075
- heavy metal diatomic halides, Wasastjerna pot. function, force consts. internulcear separations and binding energies 80—14187
- heterocyclic compounds, bond lengths, fifth overtone of C-H stretching vibrs. obs. 80—91528
- homonuclear diatomic ions, static polarisabilities, internuclear separation effects 80—5494
- hydrides, MH^+, MH_2, M=alkaline earths: Zn, Cd, Hg, Yb, No, relativistic (non-relativistic) HF one-centre expansion calcs. 80—52908
- hydrides of 1st three row elements, pseudopotential calcs., PSIBMOL algorithm 77—26963
- hydrocarbons, cyclic, non alternant, nonsingle instabilities of HF solns. 80—58164
- ice, press. effects on Raman spectrum 78—95582
- inorganic crystal, bond lengths prediction 77—47371
- intermolecular interactions, PCILO method for fixed wavefunctions 78—17571
- internuclear element-H distance, rel. to vibr. amplitude 77—88444
- internuclear parameters measurement method using total scatt. of fast electrons 80—32857
- iodotrifluoromethane, mol. struct., electron diffr., microwave spectra, CNDO/2 calcs. 78—37766
- isotypic compounds, relationship between cell vol., mean bond length and effective ionic radius 78—26483
- lipid extract from lung surfactant, IR spectra, H-bond lengths 79—24941
- maleic anhydride, struct., DRM microwave spectra, isotope shifts 78—21918
- metal halides, bond distances and cohesive energies calcs. 80—18783
- methane, $1B_1(1T_2)$ state, photodissoc., extended basis calcs. 78—9093
- methane, excited states, photochem., ab initio calcs. 77—14371
- methane, low-energy X-ray emission spectra, MO anal., ionis. pot., rel. to CCl_4 and $CHCl_3$ 79—85975
- methane(-d_4), force field representation, equilib. struct. 78—42238
- methanediol, bond length distortions and torsion pots., ab initio calcs. 79—6836
- methanol, molecular geometry optimisation, variable metric method, internal geometry 80—95744
- methanol glass solvated electrons, EPR, ^1H spin flip satellites, geometrical model 80—7146
- methanol-water, assoc. mixture, rot. barrier solvent effect, CNDO/2 calc. 78—29861
- methyl cpds., MeP, MeS, isolated CH stretching freq., bond strength, bond length 78—90167
- methyl isocyanide-d_2, IR spectrum, rovibr., ground state struct. 78—25537
- methyl meristotropate, mol. and cryst. struct. 78—95047
- methyl vinyl sulphide, syn-gauche equilib., force field and ab initio calcs., microwave and Raman spectra 80—23573
- methyldiborane, microwave spectra, bond lengths, dipole moments, rot. consts. 77—83579
- methylene, optimised geometry, CI calcs. using partitioning theory 77—38616
- methylmercury nitrate, in nematic and lyotropic liq. crysts., r_α-struct. and anisotropy of Hg-C coupling const. 80—43071
- N-methylthioacetamide(-d_1), reson. Raman spectra obs. and mechanism 78—17672
- mineral, rel. to photoelectron spectra *(French)* 77—36364

bond lengths continued
- MO calc. methods, correl. with experimental values, teaching appl. 77—29974
- molecular complex, bond lengths and heat of form., INDO calc. 79—54783
- molecular geometry, vibr. anharmonicity effects 79—50159
- molecule, changes on ionisation 77—34573
- molecules of rows 1-3, equilib. geometries, orbital energies, ab initio rel. to pseudopot. calcs. 78—82613
- α-monochloroacetic acid, hydrogen-bond motifs 77—11529
- β-monochloroacetic acid, hydrogen-bond motifs 77—15397
- naphthalene, X-ray diffr. anal. of cryst. and mol. struct. at −150°C 77—7707
- naphtho[1,8-cd:4,5-c′d′]bis[1,2,6]thiadiazine, mol., electronic, cryst. struct. 80—64984
- NH_4 halides, halides, simple, complex, polycryst., hydrogen bonding, NH_3D^+ probe ion IR spectra 79—82966
- nonlinear molecules, bending vibrs., correlated bender theory 78—37627
- optical fibres, material dispersion 79—27377
- oxalic acid dihydrate, NMR spectra, ^{13}C-^{13}C interaction, chemical shift effects 78—29800
- oxides with spinel struct., interionic distances calc. 80—39057
- periodic table of diatomic molecules, internuclear separation 79—45859
- phenanthrenoid compounds, abnormal bond lengths, MO calculations 77—31020
- phenols, ^{13}C and D substituted, microwave spectra, substitution struct. and absolute dipole moment 79—31511
- phenyl cation, singlet, triplet state mol. geometries, energies, ab initio UHF STO calcs. 77—6672
- phenylacetylene, excited single state B_1, electron-vibr. spectra and electronic struct. 79—26904
- phenylcarbene, singlet and triplet ground states, rearrangement to cycloheptatrienacarbene, MINDO/3 calc. 78—13430
- phosphate glass, electron-irradiated, charge accumulation, comp. depend. 78—2159
- phosphates, interdepend. between tetrahedral d(T-O) bond lengths, nonbonded d(T...T) separations and TOT angles (T=Al,Si,P), using regression anal. 79—19182
- phospholipid, 1,2-dilauroyl-DL-phosphatidylethanolamine, X-ray diffr. anal., crystallogrpahy, bond lengths 77—44590
- polyacetylene:I, NMR investigation of struct. 80—39011
- polyatomic mol. gas phase spectra, struct., review and tabulation 80—14136
- polycapromide, fracture, interatomic bonds deform. 79—57107
- polydiacetylenes, electronic structure, bond length variations effect, Xα SCF calc. 78—5378
- polyene, deformed excited state, bond length rel. to bond order 77—75071
- polyethylene, deformation, Hartree-Fock SCF calcs. 80—18949
- polyethylene terephthalate, fracture, interatomic bonds deform. 79—57107
- polymer, deformation of interatomic bonds, IR spectral meas. 79—38918
- polymer chains 80—3116
- polymethine coupling effect, long distance bonds between sp^2 hybridized C atoms 79—13836
- polypropylene, fracture, interatomic bonds deform. 79—57107
- polypyromelliteimide, fracture, interatomic bonds deform. 79—57107
- porphins, reson. Raman spectra, selection rules, normal coord. treatment 80—53175
- potassium oxalate monohydrate, cryst., O-H bond lengths, H-O-H angles, corrections 79—32945
- p-propoxysalicylidene-p′-butylaniline cryst. and mol. struct., intramolecular bonding 80—44197
- pyramidal XY_3 molecules, mol. geometry calcs. using centrifugal distortion const. 80—18841
- pyridine-H_2O, bonding, double quadrupole reson. obs. 80—32749
- pyromellitic N,N′-dimethyldiimide-anthracene, cryst. struct. determ. 78—2107
- quinazolines, enzyme inhibitory, structure-activity quantitative study 80—78540
- rare earth metal orbital radii, quantum-mech. calcs. rel. to inner series contraction 77—83514
- rare earth vanadites, X-ray fluoresc., IR and UV spectra 77—77206
- resonance Raman spectra intensity distribs. in soln. 79—22763
- second-row hydrides, equilib. geometry, FSGO model pot. calcs. 77—50347
- selenoacetaldehyde, microwave spectrum, struct. internal rot. barrier, C=Se bond 78—74645
- selenoketene, microwave spectra, 26.5-40 GHz, mol. config., bond angle and length 78—46322
- silica, and silicate minerals, interdepend. between tetrahedral d(T-O) bond lengths, nonbonded d(T...T) separations and TOT angles (T=Al,Si,P), using regression anal. 79—19182
- sodalites, aluminogermanate- and aluminate-, IR spectra rel. to T-O bond length and T-O-T ang. 79—91445
- spirohydrocarbons, strained, bond angles, interatomic distances, semiempirical and ab initio calcs. 80—95533
- sulphones, group electronegativities, empirically estimated from geometrical and vibr. data 79—81300
- TCNQ, semiempirical CNDO calcs. of electronic struct. and absorpt. spectra 78—995
- TCNQ complex with 5-phenyl-[1-thiol]-3-selenol-2-thione, charge-transfer salt, cryst. and mol. struct. 80—33986
- TCNQ salt, HMTTF-TCNQ, Madelung energy, intermol. charge transfer, 1-dimens. disorder 79—7572
- tertiarybutylisocyanide-borane, vibr., rot. consts., moment of inertia, microwave spectra obs. 80—32706
- 1,1,1,2-tetrafluoroethane, mol. struct. studied by gas-phase electron diffr., vibr. amplitudes, bond angles and lengths calc. 80—95740
- tetrafluoromethane, $\nu_2+\nu_4$ band, high resolution diode laser spectra 80—69138
- tetrafluoromethane, bond length and chemical shielding, NMR lineshape anal. of multispin system 80—32741
- tetrakis(trifluoromethyl)germane, gas phase electron diffr. struct., torsional force consts., CNDO/2 calc. 79—31687
- thiocarbonates, mol. struct., S-substitution effect *(French)* 80—23335
- thiocarbonyl halogen substituted cpds., geometric and electronic struct., LCAO-SCF calc. 79—89603
- thioformamide(-d_2), photoelectron and absorption spectra, vibr. struct., excited state configs. 77—6847
- thionitrates, mol. struct., S-substitution effect *(French)* 80—23335

bond lengths continued

toluene, mol. geometry, electron diffraction obs. 78−9270

toluene, mol. struct., ab initio calcs. 80−106262

toluene, mol. struct., electron diffr. obs. 77−88559

transition metal bonds with H, C and P, angles, lengths and numbers 78−42947

tri-O-ethylamylose-solvent complexes, cryst. struct., chain conforms. 79−65067

1,2,3-trichlorobenzene, oriented mols., ^{13}C satellites use in proton spectra, r_α-structure 80−18872

trichloromethane, low-energy X-ray emission spectra, MO anal., ionis. pot., rel. to CCl_4 and CH_4 79−85975

trifluoroacetic acid, ab initio MO calcs. of geometry, torsional barriers 78−90313

1,1,2-trifluoroethane, mol. struct., gas phase electron diffraction, rotamer abundance 79−76514

trifluoromethyl bromide, microwave spectra, mol. rot., isotopic variation in bond lengths, Stark meas., dipole moments determ. 80−74165

trifluoromethyl iodide, microwave spectra, mol. rot., isotopic variation in bond lengths, Stark meas., dipole moments determ. 80−74165

trifluoromethyl sulphonyl chloride, mol. struct., electron diffr. obs. 79−7016

trihalide anions, VB pseudopot. calcs. on electronic states 77−26984

trimethylphosphine, chem. shift anisotropy, struct., liq. cryst. NMR 77−61768

trimethylphosphonium oxide (sulphide) (selenide), chem. shift anisotropy, struct., liq. cryst. NMR 77−61768

trinitromehtane, electron diffr. study of gas phase mol. struct., rot. isomerism 78−1080

triphenyl-(triphenylgermanylperoxy)silane, cryst. and mol. struct. 80−39066

triptycene, soln., correl. times from ^{13}C relax. 80−23438

DL-tryptophan, polycryst., amino group rot., reorientation, mol. struct., 77-555K, PMR obs. 78−35047

uranyl complexes, IR spectra, complexation effects on force consts. and bond lengths 78−980

uranyl complexes, IR spectra and bond distances 80−74167

urea molecule, bond-length corrections for external and internal vibrs. 80−106402

valence states and binding energies 77−30757

vinyl bromide, mol. struct., from gas-phase electron diffr. and microwave data 80−23571

vinylchloride, mol. struct., gas-phase electron diffraction and microwave spectra, vibr. amplitudes 79−76421

vinylfluoride, gas phase electron diffr. and microwave spectra, rot. consts., struct., isotope shifts 79−31686

$Z=114$, Dirac-Fock one-centre calcs., tetravlent hydride prediction 77−34551

Ag_2, AgAu, AgCu, AgH, AgLi, VB calcs. 77−57883

Al, chemisorption of H_2, calc. of bond lengths vibr. freq. and activation energy 79−46953

Al, chemisorption of O, O-Al and O-O bond lengths, surface extended X-ray absorpt. fine struct. 80−29267

$AlBr_3.NH_3$, mol. struct., vap. phase electron diffr. obs. 77−65541

$ArBF_3$, microwave spectrum and struct. 79−76420

ArF, Ar_2F, electronic struct., pot. energy curves, radiative transition probability calcs. 77−57879

ArF^+, selected valence-electron split-shell MO calc., ground state props. 79−22585

ArH^+, $^1\Sigma^+$ ground state, molecular consts. calc. from pot. curves 80−9680

$AsCl_3$, 100 to 200 GHz spectra, mol. struct., harmonic force field 78−42042

AsF_3, millimetre rot. spectra, vibr. excited states, anharmonic force field 78−33502

AsF_3, mol. geometry calcs. using centrifugal distortion const. 80−18841

As_2O_3 crystalline and amorphous, EXAFS study of struct. 80−19776

Au_2, AgAu, AuCu, AuH, AuLi, VB calcs. 77−57883

AuF_3, ^{19}F NMR chemical shift, crystal chemistry 78−87645

AuH, AuCl, relativistic effective core potentials, ab initio calcs. 78−86767

α-B, rhombohedral, surface energy calc. 77−85048

$BClF_2$, microwave spectrum, struct., quadrupole coupling consts. 77−57986

B_2F_4, molecular structure, barrier to internal rotation, temperature effects 78−13625

BF_3CO, microwave spectrum and struct. 79−76420

BH, mol. spectroscopic consts., FSGO calcs. 77−6758

BH_3, electronic wave function determ., genealogical technique using Clebsch-Gordan coeff. 80−95529

B_2H_6, cryst., mol. charge distrib. anal., using struct. factors from mol. densities 80−15068

$B_nH_n^{2-}$ anions, bond enthalpies 80−30266

BH_2NH_2, microwave spectra, rot. consts., dipole moment, mol. struct. 79−85957

BH_3NH_3, complexation energies and interatomic distances, SCF and CEPA calcs. 78−25446

$Ba(ClO_3)_2.H_2O$, cryst., O-H bond lengths, H-O-H angles, corrections 79−32945

$Ba(ClO_3)_2.2H_2{}^{17}O$, fine struct. in quad. reson. of ^{17}O, DNMR 77−8453

$BaNpO_2(H_3C_2O_2)_3.2H_2O$, structure and bonding study 77−27868

$BaSO_4$, barite, crystal struct. and sulphate force consts. 78−83784

BeO_4 tetrahedra, variabilities in interatomic distances and angles 79−46594

BiF, mm spectrum, HFS struct., HFS, vibr. and rot. consts. and equilib. distance 77−79604

Br_2 in Ar, solvent effects on equilibrium props. 80−61128

Br_2, liq. struct. factor by neutron diffr., wavelength depend. 77−89370

BrCN, ICN, and isotopic forms, force field calc., freqs., rot. consts. 79−22693

BrF_5, gas phase electron diffraction and microwave rot. consts. data anal., mol. struct. 79−76363

$Br(H_2O)_n^-$, geometric and electronic struct., CNDO/2 calcs. 77−79542

C-C, C-H, vibr. amplitudes-internucl. distance relation validity, Badger's rule 77−68028

C-C, diamond clusters and corresponding saturated hydrocarbon ab-initio HF and PCILO calcs. 78−42951

C-C bond length electron difference density depend., approx. HF calc. *(German)* 78−5127

C-H bond containing molecules, correls. among bond lengths, stretching freqs. and bond order matrix elements 77−58192

bond lengths continued

C_2, pot. curves, binding and ionisation energies and config. variational cellular method 80−32597

$C_2(C_2^-)$ pot. energy curves calc. using SCF, MCSCF and CI methods, dissoc. energies, bond lengths, electron affinity 80−95523

CF, electronic Rydberg states, dissoc. energy, multiconfig. HF calcs. 79−59360

CF, low-lying electronic valence states, dissoc. energy, multiconfig. HF calcs. 79−59359

CO, ^{13}C chem. shielding, temp. and internuclear distance depend. 77−75068

CO, carbonyl group stretching freq. force const., CNDO/2 and localised orbitals calc. 77−30784

CO, chemisorbed, CNDO calcs. of mol. struct. *(German)* 79−96368

CO, chemisorption on Pt (111) and Ni (100), (111), C-O bond lengths, electronic struct. 78−6210

CO, core pseudopot. valence electron calc., orbital energy and bond length 79−72233

CO, electronic struct., binding energy and interatomic distance, SCF variational cellular calc. 80−9498

CO, inner-shell ionisation, relax. effects calcs. 77−42351

CO, inner-shell ionisation, vibr. struct., sudden approx. calcs. 79−50002

CO, polarisability derivatives, bond length depend., SCF and CI calcs. 80−58162

CO, pot. curves, binding and ionisation energies and config. variational cellular method 80−32597

CO_2, static polarisabilities, ab initio SCF HF calcs., internucl. separation depend. 78−9073

C_2O_3, liq., mol. conform. and orientation correlation 79−32877

$COCl_2$, microwave spectra, 24-154 GHz, rot. and centrifugal distortion consts. 78−46324

CS, core pseudopot. valence electron calc., orbital energy and bond length 79−72233

C*O, core hole species at equilibrium, soft X-ray spectra examination 79−41186

$Ca_2HPO_4SO_4.4H_2O$, synthetic, cryst. struct. and relation to brushite and gypsum 78−83785

CaI_2, mol. struct. parameters and geom. config., gaseous electron diffr. obs. 80−37883

$CaK_2As_2O_7$, cryst. struct., bond lengths 77−31639

Cd, effective core potentials calcs. rel. to bond lengths and energies 78−66464

$CdK_2P_2O_7$, cryst. struct., bond lengths 77−31639

ClCN, and isotopic species, force field calc., freqs., rot. consts. 79−22692

ClF, ^{19}F chem. shielding, temp. and internuclear distance depend. 77−75068

ClF_2, CNDO/2 calcs., mol. struct. and props. 77−79543

ClF_4 radical, geom., ab initio MO calcs. 79−89610

ClO, dissoc. energy and bond length, CI calcs., bond function effects 80−102450

ClO, rot. spectrum, mol. parameters in $\nu=0$, $\nu=1$ states 78−70821

^{35}ClO, microwave spectrum in excited vibr. state, centrifugal distortion const. 77−83580

ClO($X^2\Pi_i$) radical, first ionis. pot., photoelectron spectrosc., vibr. struct., bond length 77−14495

$^{35}Cl^{35}Cl$, $B^3\Pi(0^+)\rightarrow X^1\Sigma^+$, 6300 to 9900 Å, rot. anal., mol. consts., equilib. internuclear separation 78−42082

$^{35}Cl^{37}Cl$, $B^3\Pi(0^+)\rightarrow X^1\Sigma^+$, 6300 to 9900 Å, rot. anal., mol. consts., equilib. internuclear separation 78−42082

$^{37}Cl_2$, pure rot. Raman spectrum 78−94252

Co complexes, EXAFS obs. 80−998

Co-Al, X-ray K-absorption spectrum 80−97378

β-CrOOH(D), crystal struct., isotope effects on bond lengths 77−15371

α-CrOOH(D), isotope effects in bond lengths 77−80488

Cs_2, fluoresc at 6270 Å, rot. consts. 79−45744

$Cs_{11}O_3$, ionic clusters in alkali metal suboxide cryst., struct., vibr. freqs., Raman spectra 79−37772

Cs_2Te_3, synthesis and cryst. struct. 80−88115

Cu, at. cluster, EXAFS study of bond length and binding energy 79−81317

Cu complex, [Cu(1;4,7,10-tetrabenzyl-1,4,7-10-tetraazacyclododecane)Cl]NO_3, cryst., struct. 80−64966

Cu complexes, EXAFS obs. 80−998

Cu-Br, EXAFS study, in $CuBr_2$ 78−52593

Cu-N, EXAFS study, in $[Cu(NH_3)_4]^{2+}$ 78−52593

Cu-O, EXAFS study, in CuO, Cu_2O, $CuSO_4.5H_2O$, $Cu(OH)_2$ and $Cu(NO_3)_2.3H_2O$ 78−52593

Cu_2, AgCu, AuCu, CuH, CuLi, VB calcs. 77−57883

$CuM_2X_4.2D_2O$, MX=alkali or ammonium halide, quadrupolar interaction, 4-300K, reorientation 79−73848

$Cu(NO_3)_2$(pyrazine), single cryst. PMR 78−2761

CuO, ab initio HF-MC-SCF with GTO basis set, dissoc. energy and bond length 80−47890

DO_2, IR spectra, config. of $^2A'$ and $^2A''$ states 79−36636

D_2O_2, equilib. geometry, O-D bond length and angle 77−75326

N,N-dimethyloxamide, conform. anal., CNDO/2 energy optimisation, mol. props. 77−75328

F_2, ^{19}F chem. shielding, temp. and internuclear distance depend. 77−75068

F_2, pot. curves, binding and ionisation energies and config. variational cellular method 80−32597

FBO, electronic struct. calcs. 77−30772

FCN, and isotopic forms, force field calc., freqs., rot. consts. 79−22691

FO free radical, detection by CO_2 laser mag. reson. 80−45594

FSO_2OF, wide-line NMR anal. of mol. struct., chem. shielding tensor 77−83622

Fe complex, nitrile nonacarbonyl, cryst., mol. structs. 80−64967

Fe complex, nitrile nonacarbonyl cryst., mol. struct. 80−64968

GaAs, (110) surface, bond angle and lengths of rearranged As and Ga atoms 78−71918

$GaBr_3.NH_3$, mol. struct., vap. phase electron diffr. obs. 77−65541

Ge-Ni, amorphous, struct., EXAFS study 80−49110

Ge-O cpds., bond lengths rel. to force consts. 77−46653

$GeCl_2$, combined electron diffr. and mass spectra mol. struct. determ. 79−89783

GeTe, liq., neutron diffraction study 79−77485

H bond length and vibr. freq., deuteration effect 79−26911

H bond two-dimensional model dynamics, vibrs. freq. rel. to equil. interatomic distances 79−26910

bond lengths continued

- H + methane, abstraction and exchange reaction, barrier height calc. using POL-CI wave functions 80—81304
- H_2, ${}^3\Sigma_g{}^+$ state, improved adiabatic energy, dissoc. energy 79—10011
- H_2, pot. curves, binding and ionisation energies and config. variational cellular method 80—32597
- H_2, total energy, HF SCF approx. formula, internucl. distance depend. 78—21837
- $H_2{}^+$, ground state energy inverse power expansion of two proton distances 79—97976
- $H_2{}^+$, high (10^9 G) mag. fields, dissoc. energy, electron binding energy and equilib. separation 80—52910
- $H_2{}^+$, ionisation energy, internucl. separation in intense mag. fields, var. calcs. 77—57898
- $H_2{}^+$, ionisation energy in strong mag. field, variational calcs., equilib. internucl. separation 77—46654
- $H_2{}^+$, mol. props. in intense mag. fields 79—81169
- $H_2{}^+$, SCF multiple scatt. calc. 80—916
- $(HBr)_2$, intermol. distances, dipole moments, MINDO/3 and IR intensities and shifts calcs. 78—46335
- HCN, SCF ab initio ground state pot. energy surface, geometry, rel. to HCN^- 78—78646
- HCN, vibr. fine struct. accompanying core ionis., STO calcs. 78—62844
- HCN^-, SCF ab initio ground state pot. energy surface, geometry, rel. to HCN 78—78646
- HCN^+, A and B ${}^2\Sigma^+$ states, pot. surfaces, ab initio SCF calcs. 80—27959
- $HC^{14,15}N$ dimer, and $(DCN)_2$, microwave rot. spectrum identification and struct. 77—50427
- $H_2CN^+H_2 \rightarrow HCN^+H + H_2$, ab initio GO SCF pot. energy surface, saddle point, reaction path 77—50379
- HCl, bond dependence of dipole polarisabilities 78—74573
- $(HCl)_2$, intermol. distances, dipole moments, MINDO/3 and IR intensities and shifts calcs. 78—46335
- $HCo(CO)_4$, mol. struct., gas phase electron diffr. expt. 78—13623
- HDO molecules in solid hydrates, D quadrupole coupling consts., O-H and O-D stretching freqs., H bond distances 78—29773
- HF, Auger transition energy calcs. 77—34704
- HF, bond dependence of dipole polarisabilities 78—74573
- HF, spectroscopic consts., FSGO calcs. 77—6758
- HF-ClF complex, and isotopic forms., mol. beam elec. reson. spectra, config., bonding, spectroscopic consts. 77—30860
- $(HF)_2$, energy decomp. anal. of H-bonding, ab initio SCF MO calcs. 77—57868
- $(HF)_n$, $n=1$-∞, ab initio hydrogen bond and electronic parameters, phonons 77—14342
- $H_2Fe(CO)_4$, mol. struct., gas phase electron diffr. expt. 78—13623
- $HMn(CO)_5$, mol. struct., gas phase electron diffr. expt. 78—13623
- H_3N-HF, energy decomp. anal. of H-bonding, ab initio SCF MO calcs. 77—57868
- HNC (DNC), anharmonic force field, equilib. struct., rot. consts. and bond lengths 78—90147
- HNSO, centrifugal distortion anal. 79—59438
- HO-H...OHX, X=H, CH_3, NH_2, OH, F, H-bonds, electron donor substituted, mol. orbital calc. 78—13422
- H_2O, ground state, energy, bond parameters, diagrammatic perturbation theory calcs. 78—25414
- H_2O, inelastic electron scatt., geometrical parameters determ. 77—88585
- H_2O, molecule, shape as function of O-H separation 80—43203
- H_2O, pot. energy surface by MS Xα method 79—13656
- H_2O, rot.-vibr. Schrodinger eqn. soln., bond lengths and angles, force consts. 79—41151
- H_2O, roto-vibrational structure, correlated bender theory 78—37627
- H_2O^+, in X(0,0,0) level 77—473
- H_2O^+, spin and rot. fine struct., orbital angular momentum 80—83247
- $(H_2O)_2$, energy decomp. anal. of H-bonding, ab initio MO calcs. 77—57868
- H_2O_2, equilib. geometry, O-H bond length and angle 77—75326
- H_2O_2, r_0- and r_e-structs. 79—59594
- $(H_2O)_2$, struct. from mol. beam elec. reson. spectra 77—54555
- H_2O_2, structural parameters of vibr. ground state 80—28116
- $H_5O_2{}^+$, aq. soln., IR continua with polarisable H-bonds 79—26979
- HOO radical, lowest doublet electronic states, rel. to photodissoc. 79—93914
- H_2O...HF complex, force field, vibr. freqs., equilib. geometry bond energy, ab initio calc. 77—65450
- HSO radical, ground and excited first states, ab initio SCF and CI calcs. 77—30776
- HSiN-HNSi isomers, MRD-CI calcs. of struct. and stability 78—82635
- ${}^1H^3H$ and ${}^2H^3H$, pure rot. and vibr.-rot. Raman spectra 80—14145
- HeI_2, rot. fluoresc. spectra, nonlinear equilib. struct. 78—37672
- $HeNO_2$, molecular geometry and stability, ab initio calcs. 78—90075
- HfF_4, mol. struct. and vibr. freqs., gaseous electron diffr. obs. 80—32836
- Hg, effective core potentials calcs. rel. to bond lengths and energies 78—66464
- HgH, $HgCl_2$, relativistic effective core potentials, ab initio calcs. 78—86767
- HgXe, excited molecule formation 77—23519
- I-containing molecules, geom. struct. and dipole moments, CNDO/2 calc. 79—94103
- I_2, adsorption on Ag(111), adsorbate-substrate bond length X-ray anal. 78—84679
- I_2, Phillips-Kleinmann pot. derivation, pseudopot. for ground state orbitals bond length, vibr. freq. 77—65418
- IF_5, gas phase electron diffr. and B_0 rot. const., struct. determ. 79—89782
- $I(H_2O)_n{}^-$, geometric and electronic struct., CNDO/2 calcs. 77—79542
- Ir (111), $(\sqrt{3}\times\sqrt{3})30°$ S overlayer struct., LEED obs. 80—15365
- KDF_2, deuteron mag. reson., quadrupole coupling consts., F-D distance 77—63313
- $K_2HgCl_4.H_2O$, cryst., IR spectra, water mol. struct., H-bonding 77—81089
- $KMnO_4$, cryst., bond lengths and coordination numbers, EXAFS meas. 79—51043
- $K_4NpO_2(CO_3)_3$, structure and bonding study 77—27868
- KOH, MHD plasma mol., pot. energy curves and dipole moment, bond lengths 78—71462
- KrF^+, selected valence-electron split-shell MO calc., ground state props. 79—22585
- Kr_2F, semi-empirical VB calcs. of hyperfine interactions and struct. 79—85902

bond lengths continued

- Li sites, determ. in cryst. structs. using method based on bond-strength calcs. 79—7514
- Li_2, ab initio pseudopotential for FSGO calcs., bond length 77—75043
- $Li_3{}^-$, ab initio pseudopotential for FSGO calcs., bond length 77—75043
- $Li_3{}^+$, ab initio pseudopotential for FSGO calcs., bond length 77—75043
- $LiBeF_3$, pot. energy surface, struct., stability and internuclear distances, ab initio calc. 80—58147
- LiBr, pair pot., dipole moment, polarisability tensor, bond length depend., finite field SCF calcs. 80—58127
- LiCl, polarisability bond length depend. 77—23422
- LiF-NH_2 adduct, mol. consts., ab initio SCF LCAO MO calcs. *(French)* 78—13423
- Li_2F_2, struct., internuclear-distances and mean amplitude of vibr. determ. by electron diffr. 80—69252
- LiH, ab initio pseudopotential for FSGO calcs., bond length 77—75043
- LiH, finite-field method calcs., dipole moment gradients, polarisability gradients and elec. field effects 77—88589
- LiH, LiH^-, pot. energy curves, electron affinity, spectroscopic consts. 78—5129
- $LiH_2{}^+$, ab initio pseudopotential for FSGO calcs., bond length 77—75043
- Li_2H^+, ab initio pseudopotential for FSGO calcs., bond length 77—75043
- Li_2O_2, ab initio geometry, vibr. freqs., ionis. pots., and force consts. 77—65421
- $(Li_2SiO_3)_x$, bond length variations, mol. orbital study 78—26500
- Mg, chemisorption of H_2, calc. of bond lengths, vibr. freq. and activation energy 79—46953
- $MgCl_2$, mol. struct. parameters, average values, geom. config., gaseous electron diffr. obs. 80—37904
- MgF_2, cryst., atomic vibrs., anisotropy parameters, bonding 80—54195
- $MnO_4{}^-$, bond lengths and coordination numbers, EXAFS meas. 79—51043
- Mo-Mo bonds, review 77—76352
- Mo-N, bond-strength bond-length relationships 80—91702
- N-H bond containing molecules, correls. among bond lengths, stretching freqs. and bond order matrix elements 77—58192
- N_2, electronic struct., binding energy and interatomic distance, SCF variational cellular calc. 80—9498
- N_2, inner-shell ionisation, relax. effects calcs. 77—42351
- N_2, pot. curves, binding and ionisation energies and config. variational cellular method 80—32597
- N_2, static polarisabilities, ab initio SCF HF calcs., internucl. separation depend. 78—9073
- N_2BF_3, microwave spectrum and struct. 79—76420
- NH, mol. spectroscopic consts., FSGO calcs. 77—6758
- NH_2, spin and rot. fine struct., orbital angular momentum 80—83247
- NH_2, X^2B_1, A^2A_1 and B^2B_2 states, ab initio SCF CI calcs. 78—29746
- NH_3, lowest triplet state geometry, SCF and CEPA-PNO calc. 80—914
- NH_3, pot. energy surface by MS Xα method 79—13656
- NH_3-lithium halide complex, ab initio calcs., Li bond rel. to H bond 77—14343
- NH(D) radical, and isotopic species, laser mag. reson., hyperfine parameters 77—10694
- $(NH_4)_2M(SO_4)_2.6H_2O$, Tutton's salts, IR spectra, correl. of vibr. freq. and N...O distance for NH_3D^+ 78—92066
- $(NH_4)_3Sc(SeO_4)_3$, cryst. struct. 79—99122
- $NO_2{}^+$, gas phase equilib. geometry, force consts., vibr. freq., dipole moment function MCSCF/CI calcs. 80—78520
- $N_2{}^*$, core hole species at equilibrium, soft X-ray spectra examination 79—41186
- Na, chemisorption of H_2, calc. of bond lengths, vibr. freq. and activation energy 79—46953
- $Na_4NpO_2(O_2)_3.9H_2O$, structure and bonding study 77—27868
- Na_2O-GeO_2 glasses, neutronographic study of Ge^{4+} struct. state 80—19711
- $Na_4UO_2(O_2)_3.9H_2O$, structure and bonding study 77—27868
- $NbCl_5$, mol. struct., vibr. assignments, barries to pseudorotation 78—29858
- $NbSe_2$ intercalated with Rb, EXAFS 80—2897
- $NbSe_2$, intercalated with Rb, EXAFS meas. 80—40185
- Ni (001), chemisorpt. of O_2, MSXα total energy calcs. with non-muffin-tin corrections 77—72795
- Ni (100), chemisorption of O, S and Se, struct. and energy levels calc. 77—47663
- Ni, at. cluster, EXAFS study of bond length and binding energy 79—81317
- Ni surface, adsorption, chemisorption of at., mol. H_2, semi-empirical CNDO MO calcs. *(German)* 79—95465
- Ni_2 and $Ni_2{}^+$, lowest electronic states, GVB and POL-CI calcs. 79—31409
- $NiCl_2$, aq. soln., Ni^{2+} coordination from extended X-ray absorption fine struct. 80—1913
- O-H...F H bonds in metal fluoride hydrates, geometry 78—34458
- O_2 isotopes, ${}^{17}O_2$, ${}^{16}O^{17}O$, ${}^{17}O^{18}O$, pure rot. Raman spectra, bond lengths 78—42071
- O_3, analytical potentials from spectroscopic data, vibr., bond length, dissoc. 77—10613
- O_3, MC SCF and MC CI calc., open and closed form mols. 78—78831
- $O_5{}^{2-}$, hypothetical, mol. self-consistent study, possible prep. method *(French)* 80—91717
- OCSe, isotopic species, microwave and IR spectra 77—38658
- OH, band oscill. strength, rot. excitation effects 80—23460
- $OH + H_2$, pot. energy surface, barrier heights and transition state geometry, POL-CI calc. 80—55649
- $OH^- + CO_2 \rightarrow HCO_3{}^-$ react., MO-LCAO-SCF calcs., energy barrier 78—76846
- OHO bonds, O-H vs. O...O distance correlation and geometric isotope effect 78—75615
- OHO H-bond, IR spectra, stochastic model 77—27060
- OPF_3, distortion moment microwave obs., rot. consts., mol. config. 77—50426
- Os complexes, N-1-adamantylimido OsO_3, bis(N-tert-butylimido) OsO_2, cryst. struct., bonding, ligands π-donor capability 80—64969
- P, black allotrope, orthorhombic bonding, up to 26.6 kbar, neutron diffr. obs. 79—99106
- P-O cpds., bond lengths rel. to force consts. 77—46653
- PD_3, forbidden rot. spectra, spectal consts., bond lengths and angles 77—83581
- PF_3, mol. geometry calcs. using centrifugal distortion const. 80—18841

bond lengths continued

- PH_2 radial, pot. energy curves. config., ab initio SCF-MO calcs. 77—50419
- PH_3, forbidden rot. spectra, spectal consts., bond lengths and angles 77—83581
- $PbSO_4$, anglesite, crystal struct. and sulphate force consts. 78—83784
- $RbCaF_3$, cubic to tetragonal phase transition, neutron diffr. obs. 79—23730
- $RbCaF_3$, cubic to tetragonal phase transform., X-ray, neutron, Mossbauer diffr. study 80—49360
- Rb_9O_2, ionic clusters in alkali metal suboxide cryst., struct., vibr. freqs., Raman spectra 79—37772
- Rb_2Te_3, synthesis and cryst. struct. 80—88115
- S atom, van der Waals radius, mean statistical value 77—83515
- S_2, at. force consts. and internuclear distance 77—42439
- SCl_2, microwave spectrum, quadratic pot. function, average struct. 77—65456
- SF_6, hot, vibr. anharmonicity, electron diffr. study, 298-10^3K 79—68316
- SF_6, struct. by electron diffr. 78—29859
- SH^+, bond lengths derived from UPS in VUV region 79—98153
- SN, electronic states, ab initio, SCF, and CI calcs. 77—75053
- S_2N_2, $(SN)_x$, (x=2 or 3), minimal STO-3G basis HF ab initio LCAO SCF MOC, geometry 78—903
- SO_3, rotational Raman spectrum, rot. consts. and bond lengths 79—18195
- $ScH(SeO_4)_2.2H_2O$, $Sc(HSeO_3)_3$, cryst. struct. 79—99122
- $Sc_2(SeO_4)_3(.5H_2O)$ cryst. struct. 79—99122
- SeO_3, rotational Raman spectrum, rot. consts. and bond lengths 79—18196
- Si, (111) surface, EXAFS of oxidation stage, O-Si bond length 79—95876
- Si-H bond containing molecules, correls. among bond lengths, stretching freqs. and bond order matrix elements 77—58192
- Si-O cpds., bond lengths rel. to force consts. 77—46653
- Si_2, SCF Xα calcs. using pseudopots. and PW basis set 77—34558
- Si_2H_6, bond lengths, photoelectron spectrum, mol. orbitals calcs. 78—5132
- SiH_3NCS, microwave spectrum, mol. consts., isotope effects 77—46559
- Si_2H_6O, geom. and electronic struct., ab initio MO calc. 79—97972
- Si_3N_4, CVD on Si (111), EXAFS 79—95876
- SiO, core pseudopot. valence electron calc., orbital energy and bond length 79—72233
- SiO_2, on Si (111), EXAFS 79—95876
- SiO_4 tetrahedra, mean Si-O bond lengths var. 78—63699
- SiO_6 octahedra, var. of mean Si-O bond lengths 78—18577
- SiS, core pseudopot. valence electron calc., orbital energy and bond length 79—72233
- SrI_2 mol. struct. parameters and geom. config., gaseous electron diffr. obs. 80—37883
- $SrSO_4$, celestite, crystal struct. and sulphate force consts. 78—83784
- $^3T_2$, pure rot. and rot.-vibr. Raman spectrum 78—94253
- $TaBr_5$, gaseous, electron diffr. obs. of vibr. assignment, mol. struct. and barrier to pseudorot. 79—81293
- $TaCl_5$, mol. struct., vibr. assignments, barries to pseudorotation 78—29858
- Te_4^{2+}, pseudopot. SCF-MO calcs., spectrum assignments 80—83269
- $TiCl_4$-$SiCl_4$($SnCl_4$), liq., beat effects, neutron diffr. studies 80—38897
- TiF_4, equilib. config., force field, Coriolis consts., vibr. freqs. and amplitudes 80—32835
- UF_4, 5f element fluoride bond length-strength anal. 80—54166
- $V_{0.985}Al_{0.015}O_2$, insulating T-phase cation disproportionation and V-V pairing 77—62825
- VO_4^{3-}, charge transfer transition, bond length effects calcs. 77—83721
- VSe_2, 1T, band struct. calc. 79—95324
- V_xSe_2 (x=1.04,1.13,1.15), crystallographic parameters correlation to heats of formation and reduced length 79—27963
- XeF^+, selected valence-electron split-shell MO calc., ground state props. 79—22585
- XeF_2, pure rot. Raman spectrum 78—94254
- XeO, $d^1\Sigma^+ \rightarrow a^1\Sigma^+(b^2\Pi)$, green band emission spectroscopic anal., RKR pot. curves, bond lengths and dissoc. energies 79—41181
- $Y_2[Pt(CN)_4]_3.21H_2O$, first order phase transform., spectroscopic and thermodynamic anal. 78—38829
- ZrF_4, mol. struct. and vibr. freqs., gaseous electron diffr. obs. 80—32836
- $Zr_2F_8(H_2O)_6$, cryst. struct. refinement 78—18592

bonds (adhesive) *see adhesion*

bonds (chemical)

- *see also binding energy; bond angles; bond lengths; crystal binding; hydrogen bonds; intermolecular forces; lattice energy*
- π-binding energy and bond orders relation *(German)* 79—76346
- A_2B_{2N} mols. and ions, strengths of A-A single bonds symmetries 78—74790
- ABS polymers, deposited in internal magnet magnetron sputtering system, adhesion of Cu films 79—83121
- acetate crystal hydrates, bonding determ. from IR spectra 77—42321
- acetones, halogen substituted, photoelectron spectra 77—14490
- acetonitrile, adsorption on MgO, IR and TPD study 80—70528
- acetylene, adsorbed on Ni (111), vibr. spectra from electron energy loss *(French)* 78—34696
- acetylene, and -d_2, integrated IR intensities, effective charges 77—18921
- acetylene, and -d_2, integrated IR intensity, meas. and interpretation 78—66551
- acetylene, and cation, SCF MOGO calc. of electronic struct. 77—34556
- acetylene, chemisorbed on Pt and Pd (111), surface complex form., UPS spectra 77—12826
- acetylene, chemisorbed on W(110), rehybridization 78—31289
- acetylene, photoionisation cross section at distance from threshold, chemical bond influence 80—69196
- acetylene chemisorbed on Pd (100) and Ru (0001) surfaces, substrate effects on bonding, electronic spectrum 78—63933
- actinide (V) dioxocation containing compounds, coordinating props. 77—27869
- actinide compounds, band structure and bonding calcs. 80—10871
- actinide compounds, bond lengths in oxygen and halogen compounds of d and f elements 79—37653
- actinide compounds, electronic configurations correlation 80—6385
- actinide cpds., ESCA spectra, intense shake-up satellites, model 78—50589
- actinide oxides, chem. bonding, mol. cluster theory 80—10526
- actinide oxides, electronic props., review 77—28115

bonds continued

- actinides, band structure and bonding calcs. 80—10871
- additivity approximation extension, elec. tensor props. trend for struct. related mols. 78—5111
- adenine, UV photoelectron spectra, valence electronic struct. 77—16905
- adsorbed diatomic molecule, coupled-harmonic-oscillator model for vibr modes 79—82461
- adsorbed layers, bonding determ. by desorption 77—62746
- AES, chemical-state effects 78—92566
- albumin, human serum, AsF_3^- NMR probe for anion binding sites 78—48748
- albumin-unsaturated fatty acid binding kinetics, fluoresc. anal., rel. to struct. lability of biomembranes 78—15755
- aliphatic ketones, freq.-topology-milieu relation, IR study, struct. and solvent effect *(French)* 80—95623
- alkali bromides, photofragment spectra, 266 nm, bond energies and excited state symmetries 80—53072
- alkali halide:VO^{2+}, impurity behaviour, elec. cond. and IR absorpt. obs. 77—8607
- alkali halide, strain polarisability parameter, evaluation 77—35617
- alkali halides, bond order correl. with dissoc. energy 80—32596
- alkali halides, diamagnetic susceptibility, interatomic charge transfer effect 78—50660
- alkali iodides, photofragment spectra, bond energies and excited state symmetries 80—5589
- alkali ionic conductors with sheet structures, ion mobility and influences 80—107522
- alkali metal, chemisorpt. on Re surface, bond, valence energy level broadening *(French)* 79—33176
- alkali metal chlorides, photofragment spectra, bond energies and excited state symmetries 80—87190
- alkali metal dimers, $^1\Sigma_g^+$ ground state, density functional theory 78—37573
- alkali metal halides, zero point Compton profile anisotropies and bond polarities, correl. 80—78659
- alkali metal intercalation compounds, ionicity, struct., size, intercalation amount, ion mobility anal. 80—39041
- alkali metal tetrafluoroborates, intramol. force fields and mean vibr. amplitudes 80—2743
- alkali metal uranyl nitrates, IR spectra, force constants, bond orders 77—30873
- alkali suboxides, structure and bonding, book contrib. 80—972
- alkaline earth phosphate (MO-Al_2O_3-P_2O_5) irradiated electret glasses, relax. of external field intensity on heating 80—25282
- alkane+He, scattering at high velocities, short-range pot. determ. 77—27143
- alkane+He, scattering at high velocities, short-range pots. determ. 77—27142
- alkanes, and cycloalkanes, saturated hydrocarbon chains PMR characterisation *(Portuguese)* 80—5562
- alkanes, bonding, optical anisotropy and polarisability 79—22713
- alkanes, electron density, bond order, hydrogen suppressed graphs, extended Huckel theory 78—90088
- alkanes, mol. electro-optical props. 79—50162
- alkenes, π bond dissoc. energies, derivation from isomerisation kinetics, for teaching 79—58498
- alkenes, bonding, optical anisotropy and polarisability 79—22713
- alkyl chlorides, mol. electro-optical props. 79—50162
- alkyl halide+K potentially reactive collisions, electronic excitation 80—74239
- alkyl halides, conform. energy calcs., polar bonds and polarisability, polaris. model appl. 80—58188
- alkyl metal carbonyls, phosphine monosubstituted, LF vibrs., IR and Raman spectra 80—95585
- alkylbenzenes, electronic struct.. photoelectron spectra rel. to semiempirical CNDO/S CI calcs. 79—54770
- allene-d_4, high resolution IR spectra 80—83365
- alternant hydrocarbons, polarisabilities rel. to bond orders using Huckel's method *(French)* 79—31405
- aluminate glasses, new families, light transmission, 0.4 to 6 μm 77—24843
- amide C-N bond character, metal ion bonding effects 77—6801
- amino acid residues, contacting, ligand binding rate dependence on specific microdynamics 80—51031
- 2-amino-4-chlorophenol in solutions, IR absorpt. spectra 80—69135
- 2-amino-p-cresol in solutions, IR absorpt. spectra 80—69135
- aminoacetaldehyde, conformation calcs. rel. to protein struct. and bonding 80—74273
- aminoarsines, NQR freq. of ^{14}N, ^{75}As, ^{35}Cl, N-As bonds 78—25566
- aminoboranes, NQR freq. of ^{14}N, ^{75}As, ^{35}Cl, N-B bonds 78—25566
- amorphous semiconductor, localised gap states, hopping cond. and chem. bonding 78—23052
- amorphous semiconductor, stereochemistry, shape of disorder 79—64994
- amorphous semiconductor alloy, bonding and transport properties 79—90950
- amorphous tetrahedrally coord. solids, bond charge model 80—49108
- amorphous thin film on crystalline substrate, computer simulation 79—15045
- angle-resolved photoemission, review 80—45214
- anthracene, harmonic force fields, bond orders, normal coord. anal. 78—25418
- anthracene, structural changes induced by UV irradiation *(German)* 79—42100
- aromatic hydrocarbons, proton chem. shifts with ring currents, π-bond model 79—81215
- aromatic hydrocarbons, proton chemical shifts, localised π-bond model calcs. 80—43070
- arsenates, $M^{II}M^{IV}(AsO_4)_2$, (M^{II}=Ba,Sr; M^{IV}=Ge,Ti,Sn,Zr,Hf), vibr. spectra, cryst. struct., bonding 77—36225
- atomic and molecular negative ions, quantum chemical calcs. 78—62703
- atomic chemisorption on simple metals, chem. trends, core-hole relax. 78—14586
- atomic cluster on metallic surface, density functional calculations 80—44699
- atomic d orbitals, symmetry considerations 77—79536
- atomic orbital cross-sections, bonding interactions, spring model, teaching aid 78—93503
- BEBO method calculations 77—19007
- benzaldehyde derivatives, Raman intensities obs., phenyl ring-carbonyl group conjugation 78—29792

bonds continued
  benzene, trifluoromethyl derivatives, first ionis. pots., CF_3 group nature 79—27110
  benzene-I_2, π-σ charge-transfer complex, frozen soln., Mossbauer spectra obs. 80—91655
  benzenes, 1,4-disubstituted, ^{13}C NMR spectra, chem. shift, substituent effects 77—14456
  benzenes, substituted, optical bond anisotropies, by depolarised Rayleigh scatt. 78—90171
  benzenetricarbonylchromium, neutron inelastic scatt. spectrum and valence force field 80—48096
  benzocondensed five-membered heterocycles continuing S and O, optical anisotropy, depolarised Rayleigh scatt. obs. *(French)* 79—31533
  benzyl bromide and chloride, bond orders estimation, bond polarisability derivative 80—32594
  benzyl chloride, mol. polarisability, bond polarisability derivatives 78—74793
  beryllocene, gas phase struct., ab initio LCAO SCF calc. 78—41942
  binary crystals, electrical conductivity versus interatomic bond character 80—59948
  biological and model systems, ion binding, from NMR quadrupole effects 79—39357
  biphenylene, harmonic force fields, bond orders, normal coord. anal. 78—25418
  black chrome, electroplated layer, field ion microscopy study 79—28246
  bond bending, bond orbitals rel. to nucl. motion 80—95513
  bond charge parameters from integrated IR absorption intensities 77—6853
  bond energies estimation from Mulliken overlap populations 78—13405
  bond order, max. principle rel. to choice of basis orbitals and wavefunctions 79—36498
  bond order orbitals and eigenvalues 79—41088
  bond-order, vector projection weighting procedure 80—9504
  bonds in reactions, form, and breaking, partitioning anal. of electron reorganisation 80—104419
  boranes, nido and arachno, bond length-bases bond enthalpies 80—30265
  boranes, polyhedral, bonding topology, graph-theoretical interpretation 78—33408
  borides, electronic struct., review, book contrib. 78—47700
  borides, nature of chem. bond, book contrib. 78—47276
  borides, proposed classification 80—19741
  borides, ternary, struct. classification, props., book contrib. 78—47309
  bound diatomic molecules, covalent bonding concept in undergrad. chem. courses 80—22177
  bromobenzene, mol. polarisability, bond polarisability derivatives 78—74793
  4-bromobenzoyloxymethyl-trifluorosilane, cryst. struct., X-ray study 80—70187
  α-bromofluoro alkyl pi-radical, signs of hyperfine and quadrupole couplings, ESR determ. 80—97141
  bromomethane, ^{79}Br, ^{81}Br quadrupole bond magnitude ratio *(Russian)* 79—76452
  bromomethane-$d_{0,1,2,3}$, IR spectra intensities, dipole moment, bond charge, force consts. 77—83588
  4-bromophenoxyacetyl-4-ethylbenzene, single crystal, X-ray struct. determ. 79—1426
  t-butanol and -d_1, deuteration effect on self-assoc., dielectric polaris meas. 79—28672
  carbenes, heterosubstituted, singlet-triplet splitting depend. on heteroatom electronegativity and conform. 80—63553
  carbonyl frequency correlation of aromatic derivatives with nonaromatic analogues 79—22709
  carboranes, bonding topology, graph-theoretical interpretation 78—33408
  carboxylic acid-fluoride system, H---F bond, ab initio MO study 79—76528
  cellulose acetate fibre and film, stabilisation, post UV-irrad. mech. strength *(Russian)* 79—24778
  chain mols., conformational transition kinetics 80—83339
  charge distribution in ions and mols., inductive effect 80—47837
  charge distributions and chemical effects, mol. energy formula 79—89585
  chemical bonding, antisymmetrised geminal power and simple correlated wave function 80—102423
  chemically-assisted fracture, atomic modelling at crack tips 80—106754
  chemisorption, charge-density maps 79—19453
  chemisorption of H_2 on graphite, substrate relax. effects 77—7962
  chemisorption of H on large cluster, bonding energy, HF calc. 79—39204
  chemisorptive bonding on metal surface, PES 80—10791
  Chevrel phase compounds, bonding and phys. props. rel. to struct., book contrib. 80—49209
  6-chloro 2,4-dimethoxypyrimidine, ^{35}Cl NQR, Zeeman effect 80—18874
  m-chloroacetanilide, cryst., ^{35}Cl NQR, Zeeman effect 77—8443
  chloroform-d in soln., vibr. and reorientational relax., Raman study 80—63636
  chloromethanes, elec. bond moments calcs. *(French)* 79—36562
  p-chloronitrobenzene, struct. determ. by electron diffr., influence of NO_2 group on C-Cl bond 80—69251
  cholesterogens, non-sterol, odd-even effect in helix 80—19701
  chromocene, mag. suscept., zero-field splitting, ligand field, 1-303K 77—89924
  cis-3,5-dibromo-4-oxo-2,2,6,6-tetramethylpiperidin-1-yloxy, cryst. struct., secondary and multi-centre bonding 78—63751
  cobalt dimethyl glyoximate, molecular struct., cryst. structure 80—79769
  complex disordered systems, IR absorption spectra, chem. bond. *(Russian)* 77—90155
  conjugated molecule, charge distrib. calcs., refinement by exptl. quadrupole moments 77—3258
  conjugated molecule, $H_3C-NC_5H_4-CH-CH-C_6H_4-O$, large second-order polarisability, resonance struct. 78—66683
  conjugated polymers, effect of long-range coulombic repulsion of electrons on ground state 77—68147
  conjugated systems, symmetry-depend. rules 79—89592
  coordination compounds, ligands studied by XPS 78—62842
  coreless pseudopots. for atoms K through Zn 78—55121
  Coulson and Pauling bond orders, rel., for alternant topologies 78—37534
  covalent amorphous semiconductors, local struct., bonding and electronic props. 78—51882
  covalent bonding from superposition of one-centre charge densities 80—37722

bonds continued
  covalent crystal, brittle-ductile transition *(Russian)* 77—56071
  covalent elements, cohesion in condensed phases, corrections to simple Huckel approx. 78—59779
  covalent elements, cohesion of σ and π bonds in condensed phases, simple Huckel approx. 78—59778
  covalent semiconductor, structural props. using electron-ion Hamiltonian using density-fundamental methods 79—82177
  crystal symmetry, implications in charge density studies 78—71694
  crystalline materials, magnetisation density distrib. determ. by polarised neutron beam technique 79—77456
  crystals, modern theories of chemical bonding 78—2064
  cyanide, on Ag, at electrolyte interface, enhanced Raman effect 79—28767
  cyanogen azide, electron-density maps of bent bonds 80—1084
  2-cyanoguanidine, electron-density maps of bent bonds 80—1084
  1,2,6-cyclononatriene, mol. struct. and conformation, gas phase electron diffr. 80—106400
  cyclopropanone, electronic struct., UV photoelectron spectrum 78—33428
  d-orbital participation in bonding, positron ang. correlation 79—97979
  delta function equation, bond order rel. to bond polarisability 77—61693
  density distribution of bonding electrons, simple refinement, method 78—18573
  density distribution of bonding electrons, simple refinement, applic. to diborane 78—18574
  density matrix perturbation theory, bond order matrix differentiation, in nonorthogonal basis 78—887
  deoxyhaemoglobin, Fe(II)-N_ϵ(His-F8) stretching freq. rel. to quaternary struct. 80—94160
  determ. of glass phases, phys. props. meas. 79—23526
  diamond, C-C bonding, Compton profile calcs. 77—75232
  diamond, synthetic, transition metal impurity effect on IR absorpt. 79—82980
  diamond and zinc blende struct. bonding charges 77—76356
  diamond with local-field correction, dielec. const. calc. 80—11312
  diatom., binding and excitation energy 79—50160
  diatomic bonding energy, changes due to Van der Waals interactions with other atoms 78—95012
  diatomic bound molecules with zero bond order, excited biexcitons 78—9049
  diatomic molecule, hetero- or homonucl., empirical rel. for vibr. freqs. 79—81197
  diatomic molecule, homonuclear, modified simple bond charge model 79—89595
  diatomic molecule polarity, nucl. charge depend., empirical formula 79—26870
  diatomic mols., electronegativity, bond charge and chemical pot. approach 80—91703
  diatomic orbitals, bonding criteria 78—46254
  diatomic system, pair polarisability curve shape, rel. to chem. bonding 80—42930
  diborane, density distribution of bonding electrons, simple refinement 78—18574
  2,4-dibromo-1,5-diphenylpenta-3-one, cryst. struct., secondary and multi-centre bonding 78—63751
  2,6-dichloroacetanilide, NQR, cryst. struct., band character 78—6596
  m-dichlorobenzene, nucl. quadrupole coupling consts., hyperfine struct., bonding 77—14422
  4,6-dichloropyrimidine, ^{35}Cl NQR, Zeeman effect 80—18874
  dicyanoketene, and isomeric forms, heat of form., ab initio STO-3G calcs. 80—58190
  diethyl ether, conformational analysis and electronic structure 78—33429
  diethyl tin dihalides, cryst. struct., secondary and multi-centre bonding 78—63751
  dihydromuconic acid, C=C bond, ^{13}C shielding tensor, NMR meas. 78—1005
  diimide, electron-density maps of bent bonds 80—1084
  dilute alloy, surface segregation, bond and strain energy effects, atomic calc. 79—69256
  dimethoxyphenyl-1,1-dicyanomethylene, donor-acceptor systems, fluoresc., through-band interaction 79—13751
  dimethyl aluminium hydride dimer, electron density distrib., electrostatic mol. pot. anal. 80—52885
  dimethyl cadmium, core level ligand field splitting, PES, model for covalent mols. 78—37681
  dimethyl ether, O donor capacity *(Russian)* 77—71741
  dimethyl sulphide, S donor capacity *(Russian)* 77—71741
  dimethyl zinc, core level ligand field splitting, PES, model for covalent mols. 78—37681
  2,5-dimethyl-3-hexyn-2,5-diol-d_{12}, cryst. struct. and electron density distrib., 90K 77—51362
  2,2-dinitropropane-d_0(-d_6), phase polymorphism, vibrational assignments, IR and Raman study 80—16031
  dioxane-$HgCl_2$ complexes, IR and Raman vibr. spectra, inter- and intramol. forces 77—66489
  dipeptide, struct. and bonding, ab initio calcs. 79—53039
  dipeptides, aliphatic, EPR studies of direct photolysis 78—48678
  diphenyl halonium compounds, X-ray struct. anal. and NQR, chem. bonding 77—12232
  distorted one dimensional system with bond disorder, electron density of states, CPA calcs. 80—24778
  dithioferrates (III), electronic struct. and hyperfine interactions, $X\alpha$ calcs. 80—100448
  DMSO-$PdCl_2$ complex semi-empirical INDO calc. of bonding 80—32611
  DNA, cytosine ^{14}C-2 labelled, gamma radiolysis products from N-glycosidic bond rupture 77—9171
  DNA binding to ethidium bromide derivatives, competitive and non-competitive bonds *(German)* 79—79446
  DNA calf thymus binding to cis- and trans-dichlorodiammineplatinum(II) extended X-ray absorpt. spectra 78—85291
  DNA pyrimidines, cryst., lattice dynamics 78—75766
  DNA-adduct systems, binding geometry, determ. by induced circ. dichroism 80—55988
  DNA-protein interaction, effect of cooperativeness on recognition of specific sites 77—81463
  double molecules, with weak reson. bond, quasilinear *(Russian)* 78—74640
  education, H_2^+ bonding and virial theorem 78—49599
  effective atomic charge distribution in mols., multiple scatt. calcs. 80—83244
  effective atomic charge rel. to electronegativity and ionicity 77—24287

bonds continued
electrode surface, covalently bound molecules, redox reactions, steric effects 78—73077
electron charge densities, coherent X-ray and neutron diffr., review 77—76260
electron pair mechanism, non-specialist teaching appl. 78—89279
electron pairs, destiny in chem. reactions 79—52652
electron spectroscopy and surface chemical bonding, book contrib. 80—24992
electron-density maps of bent bonds, in non-cyclic mols., flexible-spring model 80—1084
electronegativity simple bond charge model 78—9050
electronic energies, determ. from exptl. electron densities 79—31365
electronic structure and solid props., rel. to chemical bonding, book 80—86044
element+O bond energy, electrostatic contrib. rel. to water-rock partition coeff. 79—44200
element-halogen bond, NQR freq. field consts. 78—25568
elements, monotonous series based on atomic bond energy, for mech. and phys. props. calc. *(Russian)* 80—19740
energies and distances, Hartree Fock Slater method, transition state method 78—9075
energy partitioning scheme for ab initio SCF calc. interpretation 79—93918
entropy maximisation, chemically organising effects 77—26107
epoxy polymers, dense-network, elastic deform. rel. to props. *(Russian)* 80—40468
ethane, CH bond orbitals, internal rot. barriers, antisymmetrization effects 80—63529
ethane, photoionisation cross section at distance from threshold, chemical bond influence 80—69196
ethane(-d_6,d_3,d_1), electro-optical parameters from IR intensities, least-squares calc. 80—9584
ethane gas, local mode overtone bands 80—83444
ethanol, conformational analysis and electronic structure 78—33429
ethenediol, σ conjugative interactions role in rot. isomerism 79—31443
ethenethiol, σ conjugative interactions role in rot. isomerism 79—31443
ethenol, σ conjugative interactions role in rot. isomerism 79—31443
ethidium bromide E-DNA, intercalated birefringent fibres, microspectrophotometric investig. *(German)* 80—57392
ethyl radical, C-C bond barrier rot., IR spectra 80—76536
ethyl-trimethyl phosphines, $(C_2H_5)_{3-n}P\{E^{IVB}(CH_3)_3\}_n$, ($E^{IVB}$=C;Si;Sn; n=0,1,2,3), (^{1}H, ^{13}C, ^{29}Si, ^{31}P, ^{119}Sn) NMR 80—32744
ethylene, adsorbed on Ni (111), vibr. spectra from electron energy loss *(French)* 78—34696
ethylene, and radical ion, SCF-MO calc., bonding and electronic struct. 77—38610
ethylene, benzene, and fluorinated derivatives, photoelectron ang. distribs. of C-C π electrons 79—10146
ethylene, photoionisation cross section at distance from threshold, chemical bond influence 80—69196
ethylene, planar dissociation, electronic rearrangement, states, bonds, ab initio multiconfigurational SCF calcs. 80—27937
ethylene glycol, conformational anal., photoelectron spect. 80—43107
exotic atoms, utilisation in chem. struct. studies, review 79—79277
f^n-electron system, paramag. principal susceptibilities, calcs. using ang. overlap model 77—32158
ferrocene, bond polarisability, quantum mechanical delta-function potential study 77—23571
ferrous nitrosylhaemoglobin, NO binding, spin distrib., orbital model and mag. props. 80—81534
first row atom-H molecules, ellipsoidal Gaussian basis in MO theory 79—93919
first-row diatomic molecules, bonding, spin density functional theory 78—17558
fluorides, chem. formulae, advances in preparative chem. 79—47915
fluorinated ethylenes, valence bond polar parameters, IR intensities, MO calc. 80—28013
2-fluoro ethanol, Ar matrix, induced conformational isomerisation by IR irrad. 80—101010
fluorophosphate glasses, rare-earth activated, luminesc., bonding 78—64415
formaldehyde, $^3A''$ state, zero-field splitting param., ab initio CI calcs. 80—99454
formaldehyde, atomisation and bond energies, LMO calc., conjugation contrib. 80—9496
formaldehyde, bond polarity effect on other bonds and lone pairs, LMO calc. 80—9495
formic acid, electron-density maps of bent bonds 80—1084
free energies, table for chem. student use 80—22171
furan, trifluoromethyl derivatives, first ionis. pots., CF_3 group nature 79—27110
furane, crystalline, lattice vibr. 78—79694
[2,2](2,5)furanophane, through bond and through space interactions, UPS obs. 78—82786
garnets with Fe^{3+} ions in tetrahedral sublattice, mag. ordering and bond geometry 77—32163
glass, ionicity and coordination, tight binding calcs. 80—49129
glass, irrad. with laser beam, damage accumulation kinetics 79—99991
glass fibre reinforced polyester resin, interfacial bond strength, effect of surface treatment 77—21303
glass systems, electronic props. 79—42495
graphite, adsorbed butane, struct. and dynamics, neutron scatt. study 78—87870
graphite, bonding effects 78—26482
graphite, fibre reinforced Sn-Pb investment castings, tensile strength 77—48487
graphite, irrad., lattice expansion, vacancies and interstitials contrib., bond order role 80—65042
graphite nitrate, charge transfer, ionic salt model 79—11780
graphite ribbon, interlayer interaction effects on diamagnetism London theory 78—52201
Group IA element halides, bond order correl. with dissoc. energy 80—32596
Group IIA hydrides and halides, ionic bonds 80—18789
Group IIIA element halides, bond order correl. with dissoc. energy 80—32596
Group IV tetrabromides, intramol. force fields and mean vibr. amplitudes 80—106316
group IVA tetrahalides, force consts., bond strengths, Urey-Bradley calcs. 77—50558

bonds continued
Gruneisen parameters, bond anharmonicities and press induced freq. shifts 80—107397
haeme proteins and metalloporphytins, redox chem. and oxygen binding 80—3573
halogen compounds, chem. bond, MO LCAO SCF calcs. 79—41104
halogen derivatives of group IV elements, NQR correl. anal. 77—12239
halogen molecular crystal, bond charge model, for lattice dynamics 78—79692
halogenonaphthalenes, bond and mol. polarisability, semi-empirical delta-function 79—31441
halogens, solid, intermolecular bonding influence on nucl. quadrupole interaction tensor 77—62882
heavy elements, covalent bonding relativistic corrections, kappa valence method 80—91461
heteroconjugated molecules, π-electron props., graph theory anal. 79—89586
heterocyclic molecules, ionisation pot. and heat of form., IOC-ω method 79—31733
hexafluoropropane, isolated CH stretching freqs. and bond props. 79—94104
hexagonal layers, lattice distortions, chem. bond model 78—79560
hexamethylbenzene in tetrachloromethane soln., local mode overtone bands 80—83444
hexaoxy ions, octahedral, mol. consts. calcs. 80—106317
HMO calculations, minicourse in HMO theory using small computers 78—25444
homopolymers, ESCA methods, core levels of simple homopolymers 78—88673
hydrationally active phases, electron structs. and props. of anions 77—44574
hydrazine adsorbed on Al, decomp., XPS obs. 80—92783
hydrazoic acid, electron-density maps of bent bonds 80—1084
hydrazones, protonation energy and basic strength 80—37719
hydrides, diatomic, dipole moments, atomic anisotropies effective charges 78—46458
hydrides, localised mol. orbital density, spatial distrib., principal lobe description evaluation 78—888
hydrocarbons, π SC bond orders 77—50349
hydrocarbons, bond polarisation characts. 77—3487
hydrocarbons, CH, bond moments, sense and magnitude 79—45861
hydrocarbons, Compton profiles, deviations from bond additivity, rel. to strain energy 79—81240
hydrocarbons, conjugated, ^{1}H chem. shifts calc. 79—98121
hydrocarbons, liq., Compton profiles, bond additivity 80—93423
hydrocarbons, nobenzoid, ionisation pot. and heat of form., IOC-ω method 79—31733
hydrocarbons, non-alternant, reson. energies 80—106278
hydrocarbons, unsaturated, Penning electron and photoelectron spectra, relative intensities comparison 79—81237
hydrogen embrittlement, model for metallic cohesion reduction mech. 80—7679
ice, O-H and O-D bond stretching vibrs., Raman spectra at atmospheric press. 80—66166
II-IV-V_2 semiconductors, heat of formation from spin-orbit splitting in valence bands 77—31985
II-VI compounds, acceptor state model 80—2059
III-V crystals, ionicities 77—51342
III-V semiconductor effect of covalent bonding on mag. sysceptibility 80—11153
increased valence when octet rule is obeyed 79—76323
inert gas compounds, chem. bond, MO LCAO SCF calcs. 79—41104
inert gas dimer ions, electronic struct., chem. binding 79—31376
inorganic binary iono-covalent compounds, cryst., inorganic static effective charge calcs. *(French)* 80—2331
inorganic complexes, quantum mech. ideas development and use 80—12878
inorganic complexes, quantum mech. ideas development and use 80—12879
inorganic compounds, chemical bonds using $K\alpha_1$ line chem. shifts, Mossbauer isomer shifts 77—27089
inorganic molecules, UV photoelectron spectroscopy, spectral assignment criteria, bonding 78—17717
inorganic molecules with polytopic bonds, motion of nuclei 79—41125
integrated spatial electron populations, evaluations for simple mols. 80—78524
intercalation compounds, synthesis, reaction mechanism, struct. and bonding 80—39047
intermetallic diatomic compounds, with multiple bonds, bond energy, VB calcs. 79—31440
intermetallic molecules, diatomic, enthalpy of form. by model description 79—83497
intermolecular interaction energies, calcs. in terms of local contrib. 77—30755
internal scalar pressure determ. in atom or molecule, density functional theory 80—47857
intramolecular donor-acceptor systems, fluoresc., through-band interaction 79—13751
iodates, complex and simple, effects of bonding on NQR spectra of ^{127}I 77—12234
iodobenzene bis(dichloroacetate), cryst. struct., secondary and multi-centre bonding 78—63751
iodobenzene diacetate 78—63751
ion-molecule equilibria in solvolysis, secondary β ^{2}H isotope effects, hyperconjugation 80—50874
ionic adsorption, quantitative approach 80—49522
ionic bonding, new elements, incomplete orbitals 77—35893
ionic crystal, Compton profile interpretation to give ionic deform. and bonding 77—40301
ionic crystalline materials, radiational stability *(Russian)* 77—80539
ionic lattice $ABCL_3$ systems, covalency parameters estimation from nucl. quadrupole coupling 80—25246
ionic type function ν(XH), non-monotonic freq. variations, effect on Hammett freq. factors *(French)* 79—22690
ionicity and struct., interrelation, appl. to zincblende, rocksalt and wurtzite structs. and amorphous semiconductors 77—1093
IR absorption band integrated intensities, ab initio and LMO studies 80—23458
IR intensities, theory, rel. to mol. moments and vibr. 77—10703
isomerism, directional effects of σ conjugation 78—37769
IV-VI compounds, interaction of internal s states 79—10826

bonds continued
IV-VI compounds, interaction of outer s states 79—10825
ketones, bonding, optical anisotropy and polarisability 79—22713
Kovar, effect of magnetic electrons on atomic interactions 77—43820
Kruszewski's rule, for stability of isomeric polycyclic conjugated cpds., proof 80—106249
β-lactam antibiotics, ab initio SCF-MO-LCAO calcs., amidic bond breaking, methoxy substitution effect 80—78533
lanthanide complex, struct. and equilib. by time resolved Eu(III) spectrosc. 80—78736
lanthanide ion bound to macromol., struct. and equilib. by time resolved Eu(III) spectrosc. 80—78736
large complex systems, mixed electrostatic-quantum chemical approach 79—89605
ligand binding to macromolecules, allosteric and sequential models of cooperativity 80—12870
ligand field distortion parameters 77—46512
linear chain molecules, cooperative ligand binding, teaching approach 77—87610
linear mols., π orbital electron energy contrib. to reaction heat 80—76539
linear momentum operator expectation values calcs. in molecules, for AH and AB bonds (A, B=Li to F) 79—7566
liq., mag. susceptibility meas., electron localisation and chem. bonding 80—60178
liquid alloy, thermodynamic props. rel. to struct. 77—1237
liquid crystals, lyotropic, counterion binding, NMR, ion condensation model 80—1922
lithium acetylene, SCF MOGO calc. of electronic struct. 77—34556
lithium ethylene, SCF-MO calc., bonding and electronic struct. 77—38610
localisation, bonds, physical models of molecular reality 77—30756
localisation approach, applic. to additive props. 77—30752
localisation in ionized and excited states, conf. 77—30750
localisation of orbitals in loges, cf electron pair concept 77—23401
localised mol. orbital struct., octet rule violations, fractionality 78—25445
localised molecular orbital density, spatial distrib., principal lobe description evaluation 78—888
localised orbitals method for describing chem. bonds *(French)* 79—89593
loge theory and chemical reactivity 77—30758
lone pair localised MOs, energy contribs. and second moments in 10-electron hydrides 77—14341
lone pair stereoactivity, bond geometry model 79—45649
long-range interactions, rel. to internal kinetic and pot. energy variations, chem. bond theory 78—1046
lysozyme, light-induced riboflavin binding 78—27899
lysozyme complex with substrate-inhibitors, photosensitised electron transfer, role of Cu^{2+} 80—30638
magnetic rotations, Faraday effect determ. of additive props. 77—30746
malonic acid, and α-alkyl derivatives, photoelectron spectra, lone-pair interactions 80—58315
mass spectra fragments, MO-model calcs. 77—417
maximum bond order principle LCAO formalism 78—29728
rel. to mechanical strength of solids, temp.-time depend. 79—28040
metal, Bloch-Simon struct. index, chem. bond geometry interpretation 77—35508
metal, lattice decohesion due to H_2 78—15533
metal atom cluster compounds, bonding calc. using d-orbital overlap model, SCF-Xα-SW calc. 80—102595
metal borides and carbides, thermal stability 79—8286
metal carbonyls, gaseous, metal-carbon bond, dissoc. energy and enthalpy of form. 78—44393
metal clusters, bonding topology, graph-theoretical interpretation 78—33408
metal complexes, theory of bonds *(Hungarian)* 79—3340
metal phases *(Russian)* 79—73131
metal surface, mol. chemisorption, self-consistent calc. 79—95260
metal-H system, bond energy calcs. 78—51940
metal-ligand, complex anion electronic struct., outer sphere cation effects, X-ray fluoresc. spectra 78—86884
metal-ligand 3-orbital-4-electron, 4-orbital-4-electron bonding, perturbation theory 79—98000
metal-ligand bonds, frequencies, predominantly stretching vibrations 79—41154
metal-metal bonds, unstable, singlet unrestricted HFS model 80—902
metal-rich compounds, pnictides, chalcides and halides, struct. and bonding, review 79—46626
metal-rich compounds, struct. and props. 78—95045
metallic glasses, structure and formation, thermodynamic props., cluster relaxation approx. 80—54143
metallic phase structures, dimensional analysis, bonding information from valency effects appearing as artefacts 80—96471
methacrylates, cross-linked, structure-transformation relations, properties *(German)* 79—55677
methane, bonding, electron pairs, size and shape parameters, Gaussian basis set MO calcs. 80—27935
methane, coord. bond calcs. 80—58129
methane, H-X bond position, correlation with electronegativity 78—9069
methane(-d_1,d_2,d_3), electro-optical parameters from IR intensities, least-squares calc. 80—9584
methanes, halogenated, interacting segment model for elec. tensor props. 78—5111
methanes, halogenated, nonlinear optical polarisability, bond-bond interaction role 78—18010
methanol, coord. bond calcs. 80—58129
methotrexate-dihydrofolate reductase complex form., conform., laser Raman obs. 80—104553
methyl cpds., MeP, MeS, isolated CH stretching freq., bond strength, bond length 78—90167
methyl fluoride, coord. bond calcs. 80—58129
methyl green-DNA binding, linear dichroism anal. 77—88479
methyl iodide, and -d_1, dissolved in nematic phase, C-H bond orientation, ^{13}C NMR 78—46371
N-methyl m-fluoroaniline, conformational anal., microwave spectra obs. 80—58247
methylamine, coord. bond. calcs. 80—58129
methylated benzene-I_2, π-σ charge transfer complex, frozen soln., Mossbauer spectra obs. 80—91655
(+)-(3R)-methylcyclohexanone, vibr. optical activity, Raman obs. 80—102499

bonds continued
mica, crystal chemistry, review 79—46612
MINDO/3, limitations for unusually bonded mols. 78—25439
MO, LCAO method, chem. bond order, ZDO approx. 79—41102
MO-LCAO scheme for binding energy, correlation correction, physical fragmentation 77—46490
model potential approach to mol. bond orbital model, appl. to Li_2 and LiH 79—49923
modular cast Fe, probability prediction of spheroidisation by parametric diagram of chem. bond *(Chinese)* 80—66543
molecular bond energies from time-of-flight chemiluminesc. 78—40051
molecular charge distrib., quantum topology, bonding theory and molecular structure 80—5463
molecular conformational props., internal rot. barriers, PCILO-CNDO calcs. 77—75056
molecular duplexes, graph construction yields 80—106245
molecular electric field gradient, overlap and ligand contribs. 78—58575
molecular electronic structures comparison, arbitrary electronic state, distance and similarity measures appl. 80—9487
molecular energies partitioning, energy components relationship 80—47838
molecular ions, negative, polar, thermally stable 79—7033
molecular orbitals, localised and delocalised for polyatomic mols., undergraduate course 78—32630
molecular structures, topological code, modified Morgan algorithm 80—58122
molecular topology, branching, distance matrix, information theoretic calcs. 78—25405
molecule, electronic struct. and physicochem. props., modified partial neglect of differential overlap 78—82645
molecule, IR intensity, Mayants-Averbuch theory d-parameters, rel. to valence optical theory 77—34700
molecule, semi-empirical MO calc. of atom-pair interactions 80—915
molecule near metal surface, proximity effects 79—36797
molecules, bond contributions to electronic energies, ab initio STO 3G calcs. 77—6669
molecules, chemical bonding studied using scattering theory concepts 80—103289
molecules, direct CI calcs. with multiconfigurational reference state 80—63506
molecules, Faraday effect measurement in pulsed mag. field 80—80758
muon capture probabilities of elements in ionic solids, chem. struct. factors 77—50550
muscle chemomechanical energy transduction, mol. basis 80—72143
MX_4^n-type ions, modified Urey-Bradley force field 78—21905
myoglobin, Fe-O_2 bonding and oxyhaeme struct. 78—96006
myoglobin, O_2 and CO bonds, flash light photolysis *(Hungarian)* 79—29501
myoglobins, Fe-, Co-substituted, O_2 binding, comparisons, thermodynamic investig. 80—67030
naphthalene, harmonic force fields, bond orders, normal coord. anal. 78—25418
naphthalene, trifluoromethyl derivatives, first ionis. pots., CF_3 group nature 79—27110
nematic-isotropic transition temp. depend. on anisotropy of C-X bond polarisability for terminal substituents 77—20058
neopentane liq., local mode overtone bands 80—83444
niobate based ceramics, synthesis, struct., elec. cond., mag. props. *(Czech)* 80—45259
niobates of divalent metals, bonding characterisation 78—38680
nitrocyclopropane, vibr. spectra struct. and bonding 80—102520
nitromethane, ab initio SCF MO calcs. of geom. and bond energies 79—31381
nitromethyl anion, ab initio SCF ab initio MO calcs. of geom. and bond energies 79—31381
non-polar cpd. semiconductor surfaces, chemisorption of O, π-bonding contrib. 80—6631
nonafluoro-iso-butane, isolated CH stretching freqs. and bond props. 79—94104
noncrystalline solid element, polymorphic bonding and thermal stability 77—31597
noncrystalline solids, bond stiffness rel. to thermodynamic and kinetic props. *(French)* 77—72561
noncyclic molecules, bent bonds, electron density maps 79—49960
NQR, electronics appls. 80—63668
nuclear radiation as a probe of chemical bonding, review of theory and expt. techniques 79—79339
nuclear spin-spin coupling constants, directly bonded C-C and C-H, CDOE/INDO LMO calcs. 80—95546
nucleic acid purine, pyrimidine bases, base pairs, hydration scheme 79—92127
nylon-6 fibre, chain rupture and tensile deform. viscosity-av. mol. wt. obs. 78—76714
octahedral systems, intramolecular force fields and vibr. amplitudes, Wilson's FG matrix method 77—31021
octane, fragmental and molecular orbitals, CNDO/2 approx. calcs. 80—42947
olefins, minimum energy goemetry, torsion of double bond 77—71755
optical harmonic generation in ferroelec. materials 78—76395
orbital interaction, polaris. in chem. reactions 78—31613
orbital interaction and chemical bonds. Exchange repulsion and rehybridization in chemical reactions 78—85142
orbital regions, density anal. *(French)* 79—9989
organic chemistry courses, unified approach to teaching of struct. and bonding 80—17732
organic compound, substituent π-conjugative effects, ab initio calcs. 79—45633
organic compound containing ^{35}Cl, NQR, crystal splitting, bonding effects 77—12221
organic dielectric layered structures quasi two dimensional conductors *(Russian)* 80—33989
organic halides, NQR shift in external elec. field, rel. to bonding 77—12237
organic molecules, bond polarisability, semi-empirical delta-function method 79—31442
organic paramagnetic systems, multiple internal motions, nucl. spin dipolar relax. obs. 80—28037
organic ring compounds, He ion stopping cross sections, ring struct., bond strain and Bragg rule deviations 79—98188
organo tin polymers, glow discharge formed, interface composition and adhesion 79—82467

bonds continued
organolead compounds, aliphatic and aromatic, ^{13}C and ^{207}Pb NMR 79—95657
organolithium cpds., ab initio SCF-MO calcs. of C-Li bond character 77—410
organometallic compounds, EHT method calcs., parametrisation, population anal. *(French)* 80—58157
organometallics, group V, XPS spectra interpretation, pot. model 78—50587
oxides, chem. formulae, advances in preparative chem. 79—47915
oxyfluoride ferroelectrics, chemical bonding, Curie temp., spontaneous polarisation 80—75981
Pauling relation, generation of reaction coordinates 77—25251
pentacoordinated ferrous porphyrins, ^{1}H and ^{19}F NMR, hyperfine shift, π electron binding 78—78719
peptide linkages, H bonding effects, review 77—10783
percolation probability for lattices of bonds and sites 77—63956
percolation problem for lattices of bonds, sites, perforation points, graphical technique 77—63954
percolation problem for lattices of bonds, sites, perforation points, graphical technique 77—63955
perturbation expansions, convergence calcs. 77—6662
perylene, harmonic force fields, bond orders, normal coord. anal., mean amplitudes calcs. 78—25418
PET film interatomic bond determ. by IR transmission and reflection spectroscopy 77—65958
phenol, PMR in absence of intermol. proton exchange, long-range coupling and conformations 77—34660
phenol (-d_1, d_5, d_6), excited A state, normal vibr. freqs, force consts., compliance coeffs. 78—50534
phosphate-H_2O-Na^+ system, interactions 77—30773
phosphates, $M^{II}M^{IV}(PO_4)_2$, (M^{II}=Ba,Sr; M^{IV}=Ge,Ti,Sn,Zr,Hf), vibr. spectra, cryst. struct., bonding 77—36225
phosphides of Cu,Ag,Zn,Cd,Ga,In, d-electron participation in chem. bonds 77—28682
photoelectron spectroscopy, charact. of vapours oven heated inorganic solids 80—52239
photoelectron spectroscopy of solids, review 80—55263
piperidine-$MnBr_2$ complexes, substituted, excitation spectra, ligand field theory 77—27103
PMMA, amorphous, structural cause of orientation modification, exam. 78—67664
polar semiconductor, conduction states, pseudopot. and tight-binding calcs. 80—24785
polar tensors, compact formulation on bond moment hypothesis 80—58108
polarity parameters, IR intensities, molecular orbital study 79—63914
poly(dimethylsiloxane) rubber, filled with modified silica, cross-linking 79—95990
poly(p-phenylene), electronic struct., one-electron band theory 80—65450
polyacetylene, electronic struct., one-electron band theory 80—65450
polyacetylene film, anisotropy of dielec. const. 80—108146
polyamides, molecular breaking under load, hydrolysis 78—11519
polyarylate-polyethylene oxide block-copolymers and mixtures, phase separation, DSC obs. *(Russian)* 79—55895
polyatomic molecule, crit. consts. evaluation from intermol. force consts. 80—37844
polyatomic molecules, bond distribution functions, anharmonicity effects of electron diffr. pattern 80—69234
polyatomic molecules, bond polarisability, semi-empirical delta-function method 79—31442
polyatomic molecules, cyclopropane, selective bond breaking by multiple IR photon absorption 80—66834
polyatomic molecules, electron density, generalised Berlin diagram appl. to H_2O internal modes 79—98001
polycyclic aromatic ring systems, localised MOs and wave functions 79—31398
polydiacetylene, monocrystal, vibr. freq. stress depend., Raman obs. 77—50574
polydiacetylene cryst., electronic struct. change at phase transition, Raman spectra 78—2833
polyelectrolyte complexes, nonstoichiometric, solubility in water *(Russian)* 80—55674
polyelectrolyte complexes, nonstoichiometric water-soluble structure *(Russian)* 80—54112
polyelectrolyte ion binding, Poisson-Boltzmann eqn. 80—45511
polyenes, highly branched, large networks, abnormal bond orders 79—59610
polyesters, aromatic, structural variation rel. to low temp. relax. 79—66096
polyethylene, correlation between valence energies and low temp. flexibility 80—25815
polyethylene, filled, linear, struct., strength 79—29149
polyethylene, high-density, damage accumulation kinetics under creep during prolonged loading 80—40447
polyethylene, nonoriented partially cryst., kinetic damage accumulation cure 80—71753
polyethylene film, chain rupture and tensile deform., viscosity-av. mol. wt. obs. 78—76714
polyethylene films, lifetime under small loads 79—95301
polyethylene molecule, fractured, local electron level calc. 80—14263
polyethylene terephthalate, chain rupture and tensile deform., viscosity-av. mol. wt. obs. 78—76714
polyethylene terephthalate, fatigue failure under cyclic loading, overstress in chem. bonds 79—57106
polyethylene terephthalate, simultaneous mech. loading, UV rad. effects on overstrained chem. bonds 79—52706
polymer, ESCA investigations on selected systems, struct. and bonding obs. 78—14302
polymer crystal, conformational energy calcs., appl. to defect props. 80—54154
polymer film, supermolecular structure and mech. stress distrib. among chem. bonds 78—75562
polymer matrix composites, component interaction mass spectrometry investigation *(Russian)* 80—35511
polymer surface, struct., bonding and reactivity, ESCA meas. 79—52073
polymer surfaces, appl. of ESCA to struct. and bonding 79—57344
polymeric, liq., spike-strain test relevance for network connectivity destruction by deformation 80—6001
polymers, breaking down of anharmonic chain, computer calc. 80—106410

bonds continued
polymers, crosslinked, specific characts. *(German)* 78—75585
polymers, decomposition by hydrolytic mechanisms 79—55016
polymers, ESCA investigation of struct., reactivity and bonding, O_2 (inert gas) surface modification 78—3438
polymers, linear, melt crystallisation, intrachain trans double bonds influence 79—14701
polymers, struct., bonding, reactivity by ESCA 78—53299
polypropylene, film and fibre, chain rupture and tensile deform., viscosity-av. mol. wt. obs. 78—76714
polypyrrole, electronic struct., one-electron band theory 80—65450
polysiloxene, irrad., linear, IR and solubility obs. 80—93775
polystyrene, amorphous, structural cause of orientation modification, exam. 78—67664
polyurethane, elastic fibres, cross link density effect on mech. props. 77—70023
praseodymium β-ketoesters, Pr^{3+}, visible spectrum, interaction, intensity and bonding parameters 80—993
n-propanol, preferred conformers, PCILO study 80—95542
propiolyl chloride(-d), 357-333 nm absorpt. system 80—69161
propiolyl fluoride(-d), 290 nm absorpt. system 80—87142
propion-aldehyde ion, fragment/mol. ion current ratio, field ionis. mass spectrum, CNDO/BW calc. 77—65544
n-propyl alcohol-α-picoline, donor-acceptor complex form., solvent effects, IR spectra 77—38660
protein, structure and bonding, quantum theory, ab initio calcs. 80—61509
protein-ligand equilibrium binding, mathematical models 78—48688
protein-lipid interaction effect on struct. of artificial vesicular membranes 77—25385
proteins, structure and bonding, modelling using aminoacetaldehyde 80—74273
proteins, thermal denaturation, use of high heating rates to separate denaturation and aggregation 77—81470
protohaeme-CO binding dynamics, flash photolysis, activation energy, entropy 77—21472
pulsed opto-acoustic spectroscopy 80—62743
purines, biological, UV photoelectron spectra, valence electronic struct. 77—16905
pyramidal molecules and ions, bond polarisability and force constants 80—69260
pyrazine, triplet-triplet absorpt. related to state splitting 80—47917
pyridazine, π bond order calc. using U(3) basis algebra 80—18810
pyridine, π-electronic structs., ab initio VB calcs. 78—70749
pyridine intercalation cmpd. of layered transition metal dichalcogenide, ionic bonding model 79—65052
pyridine-I_2, n-σ charge-transfer complex, frozen soln., Mossbauer spectra obs. 80—91655
pyridine-$MnBr_2$ complexes, substituted, excitation spectra, ligand field theory 77—27103
pyrrole, 6-electron 5-centre bonding units, increased valence theory calcs. 77—46500
quantum topology of mol. charge distribs., mol. struct. and its change 79—68175
quartz, $\alpha \rightarrow \beta$ transition obs. from nonlinear optics and bond polarisability model 77—15336
quartz, low, CC Si-O bond characteristics 80—84132
quartz, low, ionicity of Si-O bond 80—84133
quartz glasses, viscosity rel. to crystallisation 77—24386
p-quaterphenyl, mol., charge density and bond orders, polynomial matrix method 78—74808
radical radiation formation in solid organic compounds 80—85201
Raman spectroscopy, in high temp. chem., review 80—52234
rare earth alloys, RCd_2, bonding props. 77—58969
rare earth alloys, RCo_5, X-ray absorpt. spectra, electronic struct. 80—16122
rare earth arsenides and bismuthides, chemical bonding and structural features, coherent alloying theory 80—107101
rare earth compounds, bond lengths in oxygen and halogen compounds of d and f elements 79—37653
rare earth cpds., ESCA spectra, intense shake-up satellites, model 78—50589
rare earth germanides, X-ray emission, absorption and photoelectron spectra *(Russian)* 80—11509
rare earth intermetallics, RGa_2, AlB_2-type struct., electron transfer, bonding, heat of form. theory 78—92499
rare earth metals, electronic structure rel. to valence, chem. bonding 80—54601
rare earth monobismuthides, thermal expansion, thermal cond., 300-900K 78—91453
rare earth orthovanadates, covalency, chemical bonding and opt. spectra 77—80442
rare earth oxides, electronic structure rel. to valence, chem. bonding 80—54601
rare earth phosphates:Eu, electronic-vibr. spectra rel. to struct. 79—56850
rare earth sesquioxides, cubic covalency, overlap integrals calc. 77—89401
rare earth tellurides, electron density distrib. from Mossbauer spectra 78—23374
rare earth theoretical chemistry, book contrib. 80—42919
rare earth-B, RB_2, thermochemistry and stability 80—97723
rare-earth tetraborides, electronic structure and bonding determ. from X-ray spectra 77—59646
refractory metal compounds, electronic structure and chem. bonding 79—27948
relativistically parameterized extended Huckel theory 79—49924
9-cis retinal, visual pigment chromophore, twisting mechanism 80—58333
11-cis retinal visual pigment chromophore, twisting mechanism 80—58333
rhodamine C and 6G, strong base solns., electronic spectra, temp. depend. 79—85987
RPA calculation of ground state correlation energies 80—47847
sandwich compounds, orbitally degenerate, EPR 78—86893
saturated organic molecule, photolysis, primary step prediction using Rydberg and valence-shell transitions 77—21404
Schottky barrier heights, semi-empirical tight-binding calc. 79—28408
semi-empirical calc. methods 77—57880
semiconductor, amorphous, diamagnetic susceptibility enhancement 79—65640
semiconductor, diamagnetism rel. to chem. bonds 77—59380

bonds continued
semiconductor, electronic properties, rel. to chem. bonding and lattice dynamics 80−44169
semiconductor-electrolyte contact, electrolytic decomposition and photodecomposition 78−95357
semiconductor-metal boundary, Schottky barrier form., chem. mechanisms 80−49869
semiconductor-metal Schottky barrier interfaces in pairing model, covalent-ionic trend 78−95367
semiconductors, amorphous, electronic structure, chem. bond approach 79−65374
semiconductors, multiply doped, donor-acceptor complexes and interactions, physicochem. nature 80−15472
semiconductors, photoelectron spectra and band struct., book contrib. 80−16155
shock waves, starvation kinetics 78−64841
silane coupling agent deposited on E-glass fibre, hydrolysis and drying effect on siloxane bonds 80−85072
silicate binary glasses, $SiK\alpha$ and $SiK\beta$ X-ray emission spectra 77−24272
silicate glasses, model of struct. element, calc. of physicochem. props. 79−69016
silicate glasses, polyalkali effect 77−24270
silicates, Si-O-Si configurations 78−26484
small molecules, localised charge densities calcs., bond length effects 80−83256
sodium cholate-decanol, soln., aggregate form., comp. and dynamics 80−45575
sodium oxalate:Cu^{2+}, anhydrous spin Hamiltonian and bonding parameters and orbital-reduction factors 80−60408
solid, mol. and complex ion intramolecular configs., nucl. quadrupole double reson. obs. intramolecular configs., nucl. quadrupole double reson. obs. 80−34821
solid-state theory, introduction, book 79−33215
solids, chemical bonding studied using scattering theory concepts 80−103289
spin polarisation analysis using intermolecular interactions theory, chemical polarisation, exchange repulsion 80−76510
spinless fermion systems, Coulomb repulsion, bond alternation, Peierls distortion, HF approx. 80−44524
steel, H_2 embrittlement, effect on band strength 80−104293
structure and bonding, book 80−972
sulphide compounds of Si, Ge and Sn, struct. and chem. bonding *(French)* 78−30580
sulphides, d-orbital participation in bonding, positron ang. correlation 79−97979
sulphides, of Cu,Ag,Zn,Cd,Ga,In, d-electron participation in chem. bonds 77−28682
sulphones, d-orbital participitation in bonding, positron ang. correlation 79−97979
superconducting alloy, meas. and interpretation of electron distrib. 79−1572
surface segregation and bond strength-atomic size representation 80−20940
surface structure and bonding, review 77−4252
surface theory, aims and recent accomplishments 80−75413
surfaces, electron spectroscopy, review 78−92169
synthetic metals, anisotropy of elec. props. rel. to chem. bond struct. 80−24888
tautomerism and alternating bonds, representation, Chemical Abstracts Systems 80−63851
$(TCNQ)_2$, dimeric interactions, MO calcs., applicability to crystal struct. 80−75215
TCNQ salts, charge transfer and ionic bonding 77−39558
TCNQ salts, vibr. and electronic spectra 79−45704
ternary semiconductors, defect tetrahedral crystals, band structure 77−11850
tetracyanoplatinates, quasi 1d anion deficient, elec. and struct. props. 80−103683
tetracyclo[4,2,2,$O^{2,5}$,$O^{3,7}$] decane-10-carboxylic acid, lactone substituted, molecular, crystal struct. 79−90640
tetramethylbutane in hexachlorobutadiene soln., local mode overtone bands 80−83444
tetraselenotetracene, electronic structure, conductivity studied by ESCA 79−4889
tetrathionaphthalene, electronic structure, conductivity studied by ESCA 79−4889
tetrathiotetracene, electronic structure, conductivity studied by ESCA 79−4889
tetrazine-Ar, van der Waals bond, nonstatistical vibr. energy distrib., photochemical reaction effects 80−30255
tetrohydrofuran-$HgBr_2$ complexes, IR and Raman vibr. spectra, inter- and intramol. forces 77−66489
TGSe:Cu^{2+}, EPR ang. depend., coord. of Cu^{2+}, Cu-ligand bond obs. and ferroelec. transition anomaly 80−7156
thermal energy storage feasibility 79−57495
[2,2](2,5)thiophenophane, through bond and through space interactions, UPS obs. 78−82786
thiophosphoryl compounds, bond ionisation energies, mol. struct. from UV photoelectron spectra 78−82782
l-thioproline single cryst., X-irrad., ESR and ENDOR study of radicals 80−45528
thioureas, alkyl and phenyl groups trisubstituted, conformation, steric and stacking interaction 80−95587
three open shell configs., inter electron repulsion integrals 77−55499
three-electron bonds, stability and dissoc. energies 77−78935
three-electron bonds, strengths, ab initio LCAO MO CI calcs. 80−87046
topological props. of bond order 77−75041
topological resonance energy, appl. to benzene and cyclobutadiene 80−5462
topology of molecular bonds 78−46253
transferability, group or loge functions 78−41939
transition metal, 4d BCC, electron-phonon interactions 79−95107
transition metal, dichalcogenide layer cpds., bonding and phase transitions 80−34186
transition metal borides, XPS meas. and chem. bond 80−20761
transition metal carbides, APW bands and bonding, cohesion energy and valence bandwidth 77−59245
transition metal cluster, local densities of states and bonding props. 77−20401
transition metal clusters, bonding capabilities, MO calcs. 79−22589
transition metal clusters, chemisorption, alloying effects, model calc. 77−62751
transition metal complex, linear chain type, synthesis 78−6047
transition metal complexes, ligand field spectroscopy, selection rules, intensity enhancement of forbidden transitions 80−45049
transition metal complexes, proton NMR chem. shift, covalency parameters calcs. 78−42098
transition metal compound form., Miedema's empirical theory, microscopic basis 80−45541
transition metal compounds, bond lengths in oxygen and halogen compounds of d and f elements 79−37653
transition metal compounds, localisation of electrons, review 80−49650
transition metal compounds, phonon anomalies due to d-band effects, electron-phonon matrix elements 78−30720
transition metal compounds, phonon anomalies rel. to superconductivity 77−12055
transition metal cpds., ESCA spectra, intense shake-up satellites, model 78−50589
transition metal cpds., rock salt struct., surface energy bands, Shockley surface states, bonding 80−92956
transition metal diborides, heats of formation derived from theoretical bonding model 79−65027
transition metal dichalcogenides, optical phonon modes and localised effective charges, reflection spectra 78−76453
transition metal diiodides, (V, Cr, Mn, Fe, Co, Ni, Cd), Mossbauer spectrum, electronic and mag. props. 77−32302
transition metal germanides, X-ray emission, absorption and photoelectron spectra *(Russian)* 80−11509
transition metal ion pairs, simply reducible symmetry group crystal fields, kinetic exchange theory 80−39541
transition metal nitrides, APW bands and bonding, cohesion energy and valence bandwidth 77−59245
transition metal nitrides, liquid interactions, ab initio LCAO MO SCF calcs. 79−18256
transition metal oxides, APW bands and bonding, cohesion energy and valence bandwidth 77−59245
transition metal pentachlorides, photoelectron spectra 79−821
transition metal systems, ESR studies, polarised absorption, ligand field model, group theory applications 80−43077
transition metal-carbonyl cluster molecules, electronic struct., localised orbital pseudopot. method 80−39653
transition metal-O bond energy in O_2 glow discharge, mass spectrometry obs. 80−64808
transition point of random Ising model with bond dilution 79−93060
transiton metal hydrate complexes, struct., bond energies, CNDO cals. 79−41111
transplutonium element symposium, Baden-Baden, Germany (September 1975) 77−28974
tri-t-butylstannyl hydroxide, Mossbauer spectrum, tin coordination *(German)* 80−32716
trialkylthioureas, N-H stretching vibrs. and conformation 80−95586
triatomic mol. bond-bond interaction force consts., simple MO theory 78−50452
triatomic systems, compliance const., L matrix approx. method 78−74797
trichloroanilines in solutions, IR absorpt. spectra 80−69136
tridymite, low, synthetic, struct. refinement, Si-O bond lengths and Si-O-Si bridging angles 77−80456
triethylamine-I_2, n-σ charge-tranfer complex, frozen soln., Mossbauer spectra obs. 80−91655
trifluoroethane, isolated CH stretching freqs. and bond props. 79−94104
trifluoroformamide, thermal dissoc., shock wave study 79−34284
trigonal and triatomic molecules, orbital valency force field const. calcs. 80−78516
trimers, 3-body interactions in binding, semiclassical approx. calcs. 78−21994
trimethylbromosilane, microwave spectra, struct., chemical bonding 80−95602
1,3,5-trinitro 1,3,5,-triazacyclohexane, shock-induced intramol. bond breaking, XPS and EPR study 80−76512
trinitrotoluene, shock-induced intramol. bond breaking, XPS and EPR study 80−76512
tris(trimethylstannyl)amine, gas phase electron diffraction 80−106401
$(TTF)_2$, dimeric interactions, MO calcs., applicability to crystal struct. 80−75215
TTF-TCNQ, dimeric interactions, MO calcs., applicability to crystal struct. 80−75215
tungstates:Eu, electronic-vibr. spectra rel. to struct. 79−56850
two and three-centre molecules, periodicity and internal torsional conformers around single bond, symmetry analysis 80−69250
two-centre integrals calculation in semi-empirical INDO method 80−32611
two-centred bonds, CNDO calcs. of electrostatic energy components, complexing effects 77−18791
two-electron bond, energy expectation values from density matrix partitionings 77−75059
U(3) symmetric matrices algebra applic. to π bond order calc. 80−18810
UHFS model, CI, CC, and MBPT approaches, appl. to weak δ-δ bonds and δ-δ^* excitation 80−32585
uranyl pentafluoride complexes, normal coordinate anal. 79−22596
urea, bond electron density distrib., 123K, simple refinement 78−55857
urea adducts, crystn., geometry of urea-cation bonding 80−39061
ureas, alkyl and phenyl groups trisubstituted, conformation, steric and stacking interaction 80−95587
valence electron distribution, in crysts., diffr. data processing 80−92418
valence states and binding energies 77−30757
valence-nonbonded H atoms interaction and two-centre contrib. to total energy of mol. 80−32624
valency concept development, reln. to chemical bonds, teaching approach *(Hungarian)* 79−756
Van der Waals complex, PCILO calc. of dispersion energy and geom. conf. 79−63930
vanadium hexacarbonyl, EPR in frozen glasses, optical spectra in soln., solid, assoc., bonding 77−6807
vinyl fluoride based polymer stabilisers, thermal degradation, post UV-irrad. mech. strength *(Russian)* 79−24778
vinyl sulphides, divalent S linking with multiple bonds, spectrosc. obs. *(Russian)* 78−21929

bonds continued
- virial partitioning of mol. charge distrib., defn. of bond paths and directions 78—886
- visual pigment unprotonated chromophore-protein bond, ^{13}C NMR spectra 78—11607
- wheat germ agglutinin, struct. of binding sites, ligands with heavy atoms 79—24947
- X-ray photoelectron spectra of solids, satellite lines *(French)* 77—36363
- X-ray spectroscopy, book 80—2899
- XX H-X band, proton mag. shielding, linear electric field depend. 77—79545
- zeolite surfaces, bonding of Cu^{2+}, Cr^{3+}, Co^{2+} ions, EPR, optical spectroscopy investig. *(German)* 79—95266
- zero-gap semiconductors, lattice defects and chemical bonds *(Japanese)* 79—73161
- zinc blende type crystals, internal displacements 80—34127
- SnTe-PbTe-GeTe, alloy semiconductor, phase transition *(Japanese)* 78—91443
- AF_n^{x-} compounds, A-F nucl. spin-spin coupling, ligand influence 77—14454
- Ag (111) surface, adsorbed I, geometry and bond length, surface EXAFS 78—71952
- Ag chalcogenide melts, changes in short-range order struct. during heating 79—50973
- Ag halide bonding LCAO-MO treatment 79—23561
- Ag, matrix isolated, fluoresc. spectra. excimeric bond effects 78—50498
- $AgClO_3$, ClO_2 spin Hamiltonian 78—60326
- AgF(AgI,AgBr,AgCl), NMR chemical shifts 80—74180
- $AgGaSe_2$, and Ag_9GaSe_6, XPS, Auger and direct electron spectra 78—52620
- AgM (M=Mg, Ca, Sr, Ba, Zn, Hg) intermetallic mols., Ar matrix isolated, ESR investig. 79—811
- $Ag_xMo_3S_4$, chevrel phase, charge transfer and valence electron conc. 78—6029
- Ag_2Te, liq., elec. cond. at high temps. and pressures 79—11119
- Al, adsorption of O_2 and CO, interatomic Auger transition spectroscopy 80—11521
- Al complex of glycine, XPS study of glycine binding 79—41196
- Al-Ga(Sn), ab initio calcs. of partial enthalpy and result for enthalpy of mixing 79—43197
- Al-Pd, preferred sputtering on surface, mass difference and chemical bonding difference effects, AES obs. 79—83078
- Al-Pd(Si) film, preferred sputtering on surface, mass and bonding difference effects, AES obs. 79—87552
- Al-Si, preferred sputtering on surface, mass difference and chemical bonding difference effects, AES obs. 79—83078
- Al-vitreous C composite, microchem. inhomogeneity of transition zone 77—24985
- $Al_{.20}As_{.40}Te_{.40}$, amorphous alloy, radial distribution function anal., X-ray diffr. *(Spanish)* 80—28915
- AlB_2 electronic struct. calcs. 78—2417
- AlB_2, thermochemistry and stability 80—97723
- Al_2H_6, electron density distrib., reaction channels and bonding characts., electrostatic mol. pot. CNDO/2 calc. 80—23309
- β-Al_2O_3-D_2O, anhydrous, prep. and struct. of $DAl_{11}O_{17}$ 80—107187
- β''-Al_2O_3-$H_3O^+(Na_2O)$, struct. basis for superionic cond. 80—107498
- Al_2O_3-Nb composites, influence of gas impurities on solid-state bonding on annealing 80—11739
- Al_2O_3-W cermet, phase bonding 78—52745
- Al_2SiO_5, andalusite, phonon spectra and rigid-ion model calcs. 80—11391
- AmO, and AmO_2, electronic struct. and chem. bonding and XPS line shape calcs. 79—33264
- aminoarsines containing As-NH group, IR spectrometry, configuration isomers and hybridization state of N *(French)* 77—23495
- ArHBr, bond energy, IR spectra determ. 77—58000
- As, black phosphorous struct., Raman vibr. spectra and bonding 80—11411
- As, pulsed NQR, bonding, bond angle distrib. obs. in different phases 80—54984
- As-O, single bond stretching force consts. and bond orders 77—26994
- As-S, amorphous, glass transition and specific heat, intermolecular bond saturation 80—15011
- As-Se, amorphous, glass transition and specific heat, intermolecular bond saturation 80—15011
- As-Se glass film, rel. to photoinduced absorpt. changes 79—87519
- As-Se-Sb, crystallised glasses, struct. from Mossbauer spectra 80—64917
- As-Se-Te glasses, glass form., charact. temp., density, thermal expansion and dynamical viscosity, struct. model 78—26672
- As-Te-Ga, glass, elec. cond., 190-300K *(Russian)* 80—54702
- $AsO_{3/2}$-$BO_{3/2}$, glass, props. and struct. *(Japanese)* 77—27836
- $As_{1-x}S_x$ glasses, building blocks and bonds 80—54141
- As_2S_3, amorphous semicond., photo-induced optical and structural changes *(Japanese)* 78—47244
- As_2S_3, cryst. and vitreous, struct. determ. by electron spectroscopy 79—65979
- $As_xS_{100\ x}$ amorphous films, optical props. and photoinduced changes 80—60700
- AsSI, cryst. and vitreous, struct. determ. by electron spectroscopy 79—65979
- $As_2S_3(Se_3)$ evaporated films, struct. and thermally induced effects 79—41963
- $As_2S_3(Se_3)$ evaporated films, optical absorpt. and thermally induced effects 79—42989
- As_2Se_3, cryst. and vitreous, struct. determ. by electron spectroscopy 79—65979
- As_2Se_3, liquid, strong covalent bonding between unlike atoms 79—23514
- As_2Se_3, monoclinic, chem. bonds rel. to electronic and vibr. states 80—64951
- AsSeI, cryst. and vitreous, struct. determ. by electron spectroscopy 79—65979
- As_2Te_3, cryst. and vitreous, struct. determ. by electron spectroscopy 79—65979
- $As_4Te_5I_2$, cryst. and vitreous, struct. determ. by electron spectroscopy 79—65979
- Au-O bond energy glow discharge, mass spectrometry obs. 80—64808
- $Au+Al_2O_3$, solid-state reaction, bonding, temp. depend. 78—48695
- AuH, AuCl, relativistic effective core potentials, ab initio calcs. 78—86767
- B hydrides, relaxation time meas., ^{11}B NMR spectroscopy 77—32276
- B-O(S)(Se)(Te)(Po) compounds, prep. and struct., book contrib. 78—47306

bonds continued
- $B_{13}C_2$, chem. bonding nature, static deform. densities and pictorial representation 80—92489
- $B_{13}C_2$, crystal struct. refinement, X-ray diffr. 79—55702
- $B_{13}C_2$, dynamic deformation densities and valence densities 80—1971
- $B_{13}C_2$, infinite network struct., X-ray diffr. meas. 80—15070
- $B_{13}C_2$, structural anal., electron density and bonding 80—15071
- BCl_2NCO, soln., force fields and normal modes, vibr. spectra, IR and Raman obs. *(French)* 80—58266
- BF_2 radical, thermomechanical studies by mass spectrometry, enthalpy of form. and ionisation pot. determ., chem. bonds 80—81382
- BF_3, dissoc. pathways and mol. vibr., compliance consts. and min. energy coords. 78—35661
- BH_4 , CNDO/2 calc. of chemical bonding 79—76345
- B_2H_6, APSG method as a localised process 78—33415
- B_2H_6 and $B_2H_5NH_2$, electronic struct. and bonding, comparative calcs. 79—31397
- B_4H_4, B_4H_{10}, APSG method as a localised process 78—33415
- B_5H_9, B_5H_{11}, APSG method as a localised process 78—33415
- B_6H_{10}, APSG method as a localised process 78—33415
- $B_nH_n^{2-}$ anions, bond enthalpies 80—30266
- $B_nH_n^{2-}$, n=5-12, localised orbitals, bonding, PRDDO calcs. 78—13431
- BH_3CO, vibrational spectra in Ne matrices, pot. consts., bond strengths 79—45696
- BH_3F^-, B-F bond, interference density and kinetic energy 78—74566
- BH_3F^-, CNDO/2 calc. of chemical bonding 79—76345
- $(BH_2H)^-$ ion adduct, form., kinetic energy, interference charge density changes, CNDO/2 calc. 79—57211
- BN, chem. bonding and electronic struct., AES and SIMS meas. 80—50512
- BN, cubic, ab initio SCF calcs., band struct., ground state props. 78—51891
- B_2O_3, chem. bonding, electronic struct., ESCA, Auger, and SIMS spectra 80—50512
- B_2O_3, vibrational force consts. and B-O bonding, Green's function method 77—14406
- B_2O_3, vitreous, struct. and bonding determ., NMR obs. 77—39545
- $BX_2{}^{14}NCS$ (X=Cl, Br, I), soln., force fields and normal modes, vibr. spectra, IR and Raman obs. *(French)* 80—58266
- Ba, oxidation, SXAPS 77—73189
- $Ba+Br_2(I_2) \rightarrow BaBr(BaI)+Br(I)$, time-of-flight chemiluminesc., mol. bond energies determ. 78—40051
- BaO-B_2O_3-V_2O_5 glass, oxidation-reduction of V, thermodynamics 80—85169
- $BaTiO_3$, displacive ferroelectric, effective charge determ. 80—97212
- $BaTiO_3$, electronic props., SCF-MS-Xα calc. 80—54607
- Be compounds, electronic structure, configs., energy, bonding, of small mols. and complexes 78—13420
- Be, electron density and bonding, Fourier method study 78—26481
- Be, HCP metals, K-emission valence bands, structure and bonding 80—7438
- Be_3, 3-body interactions in binding, semiclassical approx. calcs. 78—21994
- $BeAr^+$, long range pot., pot. inversion method 78—21992
- BeO_2, and anion, dimerisation energy and binding of electron, ab initio calc. 79—45628
- Bi phosphates, X-ray electron spectra 77—36352
- BiCl, form., microwave spectrum, hyperfine struct., mol. rot. vibr. consts., bonding 77—14418
- $BiCl_3$.nitrile complex, NQR spectra changes during complex form. 77—12242
- $Bi_{1-x}Sb_x$, crystalline, vibrational, spectra, second order Raman scattering 79—47455
- Bi_2Te_3, chemical bonding models, correctness test using mag. susceptibility, and chemical substitution 78—67680
- $BiVO_4$, NQR spectra of ^{209}Bi 79—82891
- BkO, and BkO_2, electronic struct. and chem. bonding and XPS line shape calcs. 79—33264
- BrF_2^--, $BrFCl^-$-, $BrCl_2$, inert gas cpds., localised MOs and bonding nature 78—9061
- C, amorphous, diffraction intensities, chem. bonding effects 77—72557
- C, amorphous, X-ray and electron diffr. intensities, model struct. 78—26441
- C, amorphous film, spin resonance, IR spectra, microhardness 80—71157
- C polymeric chains, reduced from poly(tetrafluoroethylene), reactivity 80—89488
- C-C bonds, single, double, triple, electron density distrib., X-ray diffr. data accuracy rel. to ab initio calcs. 79—89805
- C-C σ bonds, mag. suscept., refined variational calc. 77—68136
- C-H, H chemisorption on graphite, regular phase, CO-NDO approx. 77 15681
- C-H bond containing molecules, correls. among bond lengths, stretching freqs. and bond order matrix elements 77—58192
- C-H bonds, mag. suscept., vector pot. variational calc. 77—68137
- C-N bond in methylamine, nucl. mag. isoscreening line diagrams 80—78555
- C_2, bond order values, ab initio calcs. and basis set depend. 80—32605
- $C_2B_{n-2}H_n$, n=5-12, localised orbitals, bonding, PRDDO calcs. 78—13431
- CF_3, CF_3^-, and CF_3^+, optimised struct. and bonding, ab initio SCF MO calc. 80—23334
- CF_3O , bonding, ab initio calcs. 77—50350
- CH bond dipole calcs. 80—69067
- C_2H_3 species formed in chemisorption of ethylene on Pt, vibr. anal. 80—61150
- C_2N_2, $2\nu_4$ band overtones, Raman intensities, bond polarisability theory 80—63639
- CO, adsorbed on Pd (210), inclined bonding config., electron stimulated desorption and LEED obs. 80—39430
- CO and $(CO)_6$, electronic struct. and bonding, SCF-Xα-MSW calcs. 78 25431
- CO, coadsorbed with hydrocarbons on Ni (111) and Pt (111), C$\equiv$O bond weakening 79—90863
- CO molecular adsorbed on Mo (110) surface, electronic states, photoemission spectra 80—65363
- CO-myoglobin, mol. tunnelling, isotope effect, time resolved IR Fourier transform obs. 80—72126
- CO_2, chemisorption ZnO nonpolar surface, covalent bonding 79—65321
- CO_2, stretch-stretch interaction force const., electron correlation influence, ab initio CI study 80—58161

bonds continued
$COCl_2$, phosgene, Cl_2 nuclear quadrupole coupling tensor, microwave spectra 80−52982
CS_2, high resolution X-ray emission, valence electron struct. and chemical bonding 79−31545
^{13}C-^{13}C spin-spin coupling const. and stretching force consts., single and double bonds 80−63867
^{13}C-^{15}N spin-spin coupling consts. calcs., lone pair contribs. 77−480
C=C bond, ^{13}C shielding tensor, NMR meas. 78−1005
C=N, CNDO calcs. of electrostatic energy components, complexing effects 77−18791
C=O, CNDO calcs. of electrostatic energy components, complexing effects 77−18791
Ca, oxidation, SXAPS 77−73189
Ca-water interactions, in crystalline hydrates, geometry 80−39024
$CaBaFe_4O_8$, overlap contribution to $^{57}Fe^{3+}$ isomer shifts, nuclear size change 80−39903
CaCl, $X^2\Sigma$ pot. energy curves, polarisability and dissoc. 80−91629
$CaFe_2O_4$, overlap contribution to $^{57}Fe^{3+}$ isomer shifts, nuclear size change 80−39903
$Ca_3SbSnFe_3O_{12}$, mag. ordering and bond geometry rel. to tetrahedral Fe^{3+} 77−32163
$CaWO_4$:Er, spectroscopic parameters calcs. 80−50379
$Ca_3ZrSbFe_3O_{12}$, mag. ordering and bond geometry rel. to tetrahedral Fe^{3+} 77−32163
Cd, effective core potentials calcs. rel. to bond lengths and energies 78−66464
Cd-P compounds, X-ray emission bands intensity distrib., influence of chem. bonds 77−28658
$CdAs_2$, cryst. struct. and vitrification capacity 80−88126
$CdAs_2$ glasses, covalently bonded, energy gap correl. with average atomisation enthalpy 77−76740
Cd_3As_2 and $CdAs_2$, molten, thermal expansion and atomic bond strength parameters 80−65257
CdHg(Mg), Ar matrix absorpt. spectra, vibronic spacing and bonding 79−3453
$CdIn_2S_4$ cubic spinel, electronic band struct. and chem. bonds 78−34768
CdO, ionicity, X-ray powder diffraction meas. 78−18616
Cd(S, Se) film grown on InP substrate, mismatch dislocations and lattice distortion, dangling bond density 80−84406
CdS-Al(Au) interfaces, bonding and interdiffusion, XPS obs. 80−80000
CdSb, energy spectrum, influence of chem. bonds, LCAO calc. 80−34356
$CeFe_2Si_2$, charge state of 3d shell, state of Fe atoms, atomic bonds *(Russian)* 80−47884
CeO_2, X-ray absorpt. spectrum, 4d absorpt. edge region, chem. binding effects 77−12467
CeO_2:Yb^{3+}, ENDOR, evidence for covalency 78−80247
Ce_2O_2S, free energy of formation and nonstoichiometry of CeO_2 79−83498
Ce_2S_3, 4d absorpt. edge region, chem. binding effects 77−12467
Cl overlayer on Cu (100), adatom bonding effects, photoemission study 80−104044
Cl^- hydration complexes, gas phase, electrostatic calcs. 80−100055
Cl-containing molecules, hybridisation, bonding orbitals effects 79−36510
$(Cl_2)_2$, binding, dispersion energy predominance 78−25421
ClF_n-, $ClF_n{}^+$-, $ClF_n{}^-$-, inert gas cpds., n=1-6, localised MOs and bonding nature 78−9061
$ClO_n{}^+$, ClO_n and $ClO_n{}^-$ (n=1 to 3), ab initio calcs., localised MO and nature of Cl-O bond 80−69070
CmO, and CmO_2, electronic struct. and chem. bonding and XPS line shape calcs. 79−33264
Co complex, Co-thiourea compounds, X-ray K-absorpt. edge, effective nuclear charge 80−35006
Co complex, $Co(NO_2)_6{}^{4-}$, bond. props. and Jahn-Teller distortion, INDO-LCAO-MO calcs. 80−75532
Co complex, metal-metal bond, correl. effects, SCF calc. 77−65425
Co complex, O_2CoCl_4 and $O_2CoCl_4NH_3{}^{2-}$, struct. and bonding model, CNDO-UHF calcs. 80−95541
Co complex, with p-amino salicylic acid, X-ray K-absorpt. discontinuity, shape, chem. shifts 79−47545
Co compounds, X-ray K-absorpt. edge, effective nuclear charge 80−35006
Co, orientated mol., (e,2e) spectra, electron momentum density 79−98236
CoAl, bonding, self-consistent energy bands 78−91610
Co(II) Schiff base complexes, structure and bonding, book contrib. 80−972
CoIII salen complexes, O binding, reson. Raman obs. 80−58267
trans-Cr $(III)(NH_3)_4XY$ complexes, d-d irradiation preferential labilisation, Adamson's rules, ang. method overlap 77−40557
Cr, oxidation, Cr-O bonding, characterisation by high resolution AES *(French)* 79−100468
Cr-Ge system, XPS, X-ray and neutron diffr. and mag. meas. to study chem. bonding and electronic struct. 80−60749
Cr_3C_2, bond energy and ionization efficiencies from SIMS 79−24400
$Cr(CO)_6$, bonding, IR intensity anal. 78−25526
$Cr(CO)_6$, electronic struct. and bonding, SCF-Xα-MSW calcs. 78−25431
$CrCl_4$, ligand field states, multiple scatt. Xalpha calcs. 80−47891
$Cr(NO)_4$, bonding, shake-up intensities and shake-up energies, SCF Xα multiple scatt. calc. 80−74121
$Cr(NO)_4$, XPS and UV photoelectron spectra, compared to NO data 80−58317
Cr_3Si, charge distrib. X-ray diffr., rel. to supercond. V_3Si 77−68944
Cs-Au(Sb), liq. alloys., mag. susceptibility and electronic struct. 77−1537
$CsCoCl_3$, covalency parameters estimation from nucl. quadrupole coupling 80−25246
CsI crystals, relation of struct. and bond type to slip geometry 80−88165
$Cs_2KTmBr_6(Cl_6)(F_6)$, Cs_2NaTmF_6 and Cs_2RbTmF_6, mag. behaviour 2.9 to 251.3K, cryst. field levels, ang. overlap model *(German)* 80−29520
Cs_2O-MgO-SiO_2 system, glasses, crystn. prods., composition, props. 79−41961
$Cs_2O.4SiO_2$, glass, behaviour of VO^{2+} as spectroscopic probe 79−78510
$Cs_9(XeO_3Cl_2)_4Cl$, neutron and X-ray diffr. struct. determ., Xe-Cl bonding 78−30591
Cu (100), chemisorption of CO, vibr. excitations and struct., EELS and LEED study 80−39437

bonds continued
Cu (110), adsorption of pyridine, angle-resolved photoemission, selection rules 80−40231
Cu, cluster and bulk, struct. and electronic props. 78−95592
Cu complex, $(Cu[H_2O]_6)^{2+}$ in $MgSO_4.7H_2O$, EPR and optical spectra anal. 79−38377
Cu complex, bis-L-tyrosinato copper(II) complex, electronic spectra and dichroism 79−41183
Cu complex, bis(N,N-diethyl-N′-benzoylthioureato)Cu(II), ESR 77−8393
Cu complex, bis(1,1-diisobutyl-3-benzoyl-selenoureato)Cu(II), single cryst. ESR, ^{77}Se hyperfine struct., bonding 77−77086
Cu complex, catena-μ-isothiocyanato-(N′-pyridylmethylene-N″-salicyloylhydrazinato-NN′O) copper (II), EPR and visible spectra 80−5566
Cu complex, Cu(II) impurity in α-glycine crysts., ligand ENDOR spectra 79−65765
Cu complex, Cu(II)-L-asparagin complexes, ESR spectra, mag. and bonding parameters 78−23326
Cu complex, $Cu(NO_2)_6{}^{4-}$, bond. props. and Jahn-Teller distortion, INDO-LCAO-MO calcs. 80−75532
Cu complex, N,N′-ethylenebis (salicylaldiminato) copper (II)-thiourea, in solns., bond strength and hyperfine linewidth, EPR 80−74186
Cu complex, N,N′-o-phenylenebis (salicylaldiminato) copper (II)-thiourea, in solns., bond strength and hyperfine linewidth, EPR 80−74186
Cu complex, with acetylene, Ar matrix-isolated EPR obs., bonding 78−50564
Cu complexes, N ligands, X-ray K-absorpt. edge, expt. 80−89084
Cu complexes, of polyamines, ESR in soln., coordination around Cu(II) ions 78−5254
Cu complexes, with L-glutamic acid and DL-aspartic acid, EPR, bonding and hyperfine linewidth 78−25572
Cu-Co heterobinuclear complex, cryst., mag. susceptibility of Cu-$Co(fsa)_2$ en, $3H_2O$ 80−2556
Cu-Te system, cryst. chem., Mossbauer investig. 77−16220
CuCl, bonding, ab initio pseudopot. calcs. 79−6857
Cu(I) olfactory binding site 78−96060
Cu(II)-DL-proline complex, ESR, magnetic susceptibility and optical absorption 80−93167
Cu(II)-nucleic acid base interaction, MO calcs. 79−10013
$Cu_xMo_3S_4$, chevrel phase, charge transfer and valence electron conc. 78−6029
Cu(100), N chemisorption, bonding, MO theory 77−76659
$D_5O_2{}^+$, isotope effects, easily polarisable H and D bonds 78−94231
D_2SO_4, pure, IR and Raman spectra in liq. state, assignments and cryst. spectra comparison *(French)* 79−33699
Dy, bidirectional orbital interpretation of L_{III} absorption discontinuity shape 77−16423
Er, bidirectional orbital interpretation of L_{III} absorption discontinuity shape 77−16423
Eu complex, Eu(III) β-diketonates, Mossbauer studies 79−61286
Eu pyrochlores, $Eu_2Z_2O_7$, (Z=Ti, Ru, Ir, Mo, Sn, Zr, Pb, Pt and Hf), elec. field gradient, Mossbauer expt. 79−8077
$F+N^{4+}$, bonding effect on Kα satellite struct. 79−59392
F_2, charge distrib. anal. rel. to Berlin's binding and antibonding regions 79−6875
FNO, four electron three centre bonding units, ab initio valence bond calcs. four electron three centre bonding units, ab initio valence bond calcs. 80−27949
$(Fe,Cr)_3C$, reln. between bond energy and X-ray emission line shifts 78−50555
Fe (110), complexes with PF_3, CO and cyanomethane, UV photoelectron obs. 78−19629
Fe complexes, 1-(2-pyridylazo)-2-naphthol and 1-(2-pyridylazo)-2-phenanthrol, back co-ordination, Mossbauer study 80−20572
Fe complexes, Fe (III) bis(dithiocarbamato) iodides, transferred hyperfine interactions and mag. ordering 77−20759
Fe-Co, compositional diffusionally bonded alloy, mass transfer investigation *(Russian)* 80−39342
Fe-Mn-C, atomic interaction structure in carbides 78−42955
FeAl, bonding, self-consistent energy bands 78−91610
FeB and Fe_2B, ESCA and mag. spin data, electronic struct., isomer shifts, valence bands and chemical bonding 80−75489
$FeCl_3$, intramolecular force fields, compliance consts. and vibr. amplitudes 80−58234
FeF_3, overlap contribution to $^{57}Fe^{3+}$ isomer shifts, nuclear size change 80−39903
FeO_2, matrix isolated IR spectra, cyclic complex struct. 77−88449
FeS, structural chem., influence of itinerant 3d electrons and valence-band holes 79−23563
α-FeSe, site symm. and bonding mechanism 79−24239
GaAs (110), oxidation, 3d core level binding energy, multiple bonds 78−35543
GaAs (110), oxidation, 3d core level binding energy, single bonds 78−35544
GaAs (110) surface, atomic geometry from elastic LEED intensities 77−20170
GaAs (110) surface, chemisorption of O_2, electronic struct. theory, oxidation, electron spectra interpretation 79−42376
GaAs, (110) surface structure, rotational relaxation, cluster model *(Chinese)* 80−107621
GaAs, lattice dynamics, phonon freq., bond bending force model calcs. 80−70335
GaAs, modulation X-ray diffr. obs. 80−96464
GaAs, X-ray K absorpt. edge, effective ionic charge and bonding schemes 80−29827
GaAs-Au interface, atomic modulation of interdiffusion, effect of reactive Al monolayers 80−49432
$GaCl_3(Br_3)(I_3)$, intramolecular force fields, compliance consts. and vibr. amplitudes 80−58234
GaI, rot. spectrum, EHF spectra obs. 80−58245
$Ga_{1-x}In_xSe$, magnetic susceptibility anisotropy, chemical bonds, electron density distribution *(Russian)* 80−50073
GaSb, lattice dynamics, phonon freq., bond bending force model calcs. 80−70335
$GaSe_{1-x}S_x$, magnetic susceptibility anisotropy, chemical bonds, electron density distribution *(Russian)* 80−50073
Gd, bidirectional orbital interpretation of L_{III} absorption discontinuity shape 77−16423
$GdF_3(Br_3)$, chem. binding, 4d X-ray spectra obs. 79−69910
$Gd_3Ga_5O_{12}$, chem. binding, 4d X-ray spectra obs. 79−69910

bonds continued

Gd_2O_3, chem. binding, 4d X-ray spectra obs. 79–69910
Ge (100), dimer reconstruction, photoemission obs. 80–80939
Ge, amorphous film, persistent photoconductivity, dangling bonds 80–84487
Ge, lattice stability, pseudopotential theory and problem of covalent bonding 77–55490
Ge, self-diffusion mechanism 79–90824
N-Ge-Bi-Se glass, elec. and optical props. 80–65550
Ge-Ce liquid alloys, enthalpies of mixing, exothermal effects *(Russian)* 80–34192
Ge-rare earth alloys, nature of chemical interaction, X-ray emission, absorpt. and photoelectron study *(Russian)* 80–55261
Ge-Se glass film, rel. to photoinduced absorpt. changes 79–87519
Ge-Te, As-Te, Ge-As-Te molten systems, metal-semicond. transition, cond. obs. *(German)* 77–1457
Ge-Te alloy, liq., magnetic susceptibility 79–87232
Ge-Te and Ge-Te-As system glasses, local struct., ^{119}Sn Mossbauer obs. 79–41968
GeO_2, electronic struct. and densities of states, tight-binding calcs. 80–15447
$GeO_2{:}Mn^{2+}$, EPR, struct. of vitreous and crystn. states 77–48039
GeP, thermodynamic characts. 10-300K, interatomic bond elasticity 80–59677
GeS_x, neutron irrad., thermal and elec. conductivity and heat capacity 78–2165
$Ge_{1-x}S_x$ glasses, building blocks and bonds 80–54141
$Ge_{42}S_{58}{:}Cu(Ag)(I)$, glass, impurity effect on e.p.r., dangling bonds 77–4553
$GeSe_2$ evaporated films, struct. and thermally induced effects 79–41963
$GeSe_2$ evaporated films, optical absorpt. and thermally induced effects 79–42989
$GeSe_2$, liquid, strong covalent bonding between unlike atoms 79–23514
H atom transfer reactions, activation energies from bond energies 78–40037
H chemisorption on Ni, Pd, and Pt, bond nature 80–34297
H chemisorption on Pd(111) bonding, photoemission spectra, SCF electronic struct. 79–33320
H_2 and H_2^+, covalent bonding and classical charge density 80–37722
H_2, channel coupling theory of covalent bonding, dissoc. energy 78–13419
H_2 chemisorbed on jellium, contraction of mol. band 79–28202
H_2, electron correlation, dynamic description using boson Hamiltonian 79–26897
H_2, fluid, Raman meas., 0.2-630 kbar, at room temp. 80–58269
H_2, many electron systems, chem. binding, local stresses and force densities 80–27920
H_2, semiempirical model for polarisation of s-type AOs, pot. curve and surfaces determ. 77–88400
H_2, two-electron bond, energy expectation values from density matrix partitionings 77–75059
H_2^+, mol. electron density distrib., binding/antibinding anal. 80–95534
H_2^+, semiempirical model for polarisation of s-type AOs, pot. curve and surfaces determ. 77–88400
H_2^{2+}, two-electron bond, energy expectation values from density matrix partitionings 77–75059
H_2-like molecules, change of binding type and dissoc. in strong mag. field 78–62744
$H_2+D_2 \rightleftharpoons 2HD$ catalysis, MgO surface, SCF UHF calc. 77–9120
H_3, semiempirical model for polarisation of s-type AOs, pot. curve and surfaces determ. 77–88400
H_3^+, two-electron bond, energy expectation values from density matrix partitionings 77–75059
H_3BO_3, chem. bonding, electronic struct., ESCA, Auger, and SIMS spectra 80–50512
HF, H-X bond position, correlation with electronegativity 78–9069
HF_2^-, four electron three centre bonding units, ab initio valence bond calcs. 80–27949
HNO, four electron three centre bonding units, ab initio valence bond calcs. 80–27949
HNO, isomerism, low lying electronic states, ab initio MRD-CI calcs. 80–83291
HNO_2, and protonated forms, electrostatic pot. predictions, basis set depend. 78–74786
H_2O, affinity for $Li^+(Na^+)(K^+)$, ab initio SCF calcs. 80–58125
H_2O, bonding electron pairs, size and shape parameters, Gaussian basis set MO calcs. 80–27935
H_2O, excited stretching vibrs., quantum mechanics. 80–91535
H_2O, H-X bond position, correlation with electronegativity 78–9069
H_2O, localised MO, basis set depend. 79–36525
H_2O, Raman and IR spectrum in overtone OH stretching region 80–58263
H_2O-(HF)(F_2) complexes, CNDO/2 calcs. for electronic struct. and props. 78–25442
H_2SO hypothetical molecule, nonempirical STO calc. of chem. bonds 80–23307
H_2SO_4, pure, IR and Raman spectra in liq. state, assignments and cryst. spectra comparison *(French)* 79–33699
He_2^+, bond strength ab initio LCAO MO CI calcs. 80–87046
HeH, bond strength ab initio LCAO MO CI calcs. 80–87046
HeH^+, bond energy calcs., using density matrix partitioning 78–46417
HeI_2, Van der Waals mol. vibr. predissoc. anharmonicity effects 80–52971
HfC, bond energy and ionization efficiencies from SIMS 79–24400
HfC, pressing regime influence on high-temp. creep *(Russian)* 80–100852
HfC, quasi-self-consistent energy band structures using relativistic KKR calcs. chemical bonding 79–51484
HfN, electronic struct., relativistic energy band struct. calc. 80–34354
$HfS_3(Se_3)$, phonon study of chemical bonding 80–20645
HfX_4, (X=Cl,Br,I), He I and He II photoelectron spectra, ionis. energy, chem. bonding 78–46394
Hg, effective core potentials calcs. rel. to bond lengths and energies 78–66464
HgH, $HgCl_2$, relativistic effective core potentials, ab initio calcs. 78–86767
HgI_2, Raman spectrum 114 cm^{-1} line, differential analysis using covalence bonds modulation 79–24315
$Hg_2{}^{129}I_2$, Mossbauer effect, bonding, quadrupole coupling const., comparison with $Hg^{129}I_2$ 78–2774

bonds continued

HgZn(Cd), Ar matrix absorpt. spectra, vibronic spacing and bonding 79–3453
Ho, bidirectional orbital interpretation of L_{III} absorption discontinuity shape 77–16423
$HoCl_3$, white line struct. in X-ray L_{III} absorption edge 79–15560
Ho_2O_3, white line struct. in X-ray L_{III} absorption edge 79–15560
I compounds, XPS, binding energies and bond orders 77–18976
I^- hydration complexes, gas phase, electrostatic calcs. 80–100055
$I_2{}^*He$, vibrational predissociation, van der Waals molecules, vibration-translation scaling theory 80–43135
In, oxidised surface, bonding of Cd arachidate monolayers, XPS 79–15011
In-Se(Te), liq., mag. susceptibility meas., electron localisation and chem. bonding 80–60178
$InCl_3$, intramolecular force fields, compliance consts. and vibr. amplitudes 80–58234
$In_xMo_3S_4$, chevrel phase, charge transfer and valence electron conc. 78–6029
InS(Se)(Te), fused, charge transfer nature 77–89757
InSb (110) surface, LEED intensity dynamical anal. 80–88412
InSe, energy band structure, chem. bond polarity, photoemission, semiempirical tight binding method 80–44504
KAl_2Br_7, NQR double-reson., $Al_2Br_7^-$ ion in cryst. 78–91993
$K_xAl_xTi_{8-x}O_{16}$, ionic cond., K mobility rel. to struct. and bonding *(French)* 77–76594
$K_xAl_xTi_{8-x}O_{16}$, ionic cond., rel. to struct. and chemical bonding *(French)* 78–18824
$KBrO_2F_2$, struct. data, vibr. spectra 77–39563
K_2Cs, Laves phase, electronic charge density pseudopotential calcs. 79–77549
K_7Cs_6, μ-phase variant, electronic charge density pseudopotential calcs. 79–77549
$KFeO_2$, overlap contribution to $^{57}Fe^{3+}$ isomer shifts, nuclear size change 80–39903
KM_gF_3, bond energy, equilib. distances and compressibility calcs. 80–70159
$K_xMg_{x/2}Ti_{8-x/2}O_{16}$, ionic cond., K mobility rel. to struct. and bonding *(French)* 77–76594
$K_xMg_{x/2}Ti_{8-x/2}O_{16}$, ionic cond., rel. to struct. and chemical bonding *(French)* 78–18824
$KNbO_3$, displacive ferroelectric, effective charge determ. 80–97212
$KNbO_3$, electronic props., SCF-MS-Xα calc. 80–54607
K_2O-AlF_3-B_2O_3 glass, Al atom bonding mode, optical absorption of VO^{2+} and AlK_α spectrum *(Japanese)* 78–11023
K_2O-TiO_2-SiO_2 glass, Si-O bonding, SiKβ X-ray fluorescence and IR spectra 80–10500
$K_2O.4SiO_2$, glass, behaviour of VO^{2+} as spectroscopic probe 79–78510
$KTaO_3$, electronic props., SCF-MS-Xα calc. 80–54607
K_2UF_6, X-ray photoelectron spectra 77–32491
$K_xZn_{x/2}Ti_{8-x/2}O_{16}$, ionic cond., K mobility rel. to struct. and bonding *(French)* 77–76594
$K_xZn_{x/2}Ti_{8-x/2}O_{16}$, ionic cond., rel. to struct. and chemical bonding *(French)* 78–18824
Kr-F_2, energy, photoionisation mass spectrometric study 79–45772
KrF_2, Mossbauer spectra, quadrupole coupling strengths, isomer shift and bonding 77–50458
$KrF_2.AsF_5(SbF_5)$, Mossbauer spectra, quadrupole coupling strengths, isomer shift and bonding 77–50458
KrHCl, van der Waals complexes, struct., RF and microwave spectra, isotope effects 80–37806
La-Au liq.-quenched alloys, Mossbauer spectra, struct. 80–15841
LaB_6, metallic, energy bands and bonding 77–43486
LaB_6, Shockley surface states, angle-resolved photoemission 79–56278
LaB_6, synthesis and props. *(Japanese)* 80–40255
$LaNi_4Al$, solubility and sorption props. of H_2, effect of Al 80–103482
La_2O_3-Y_2O_3-Al_2O_3-SiO_2, coloration by transition metal oxides, absorpt. bands *(Japanese)* 80–55148
Li compounds, electronic structure, configs., energy, bonding, of small mols. and complexes 78–13420
Li projectiles, electronic stopping cross section meas., intermolecular interactions 80–75279
Li/H_2O, ten atom models of binding sites on nonreconstructed Li surfaces 79–69359
Li^+ +He collisions, K-shell vacancy sharing, ab initio LCAO-SCF, CI calcs. 77–19054
Li_n, equilibrium struct., effect of p-functions *(German)* 79–89823
$LiAlH_4$, $LiBH_4$, ab initio calc. of geom. struct., charge distrib., bonding and pot. energy surfaces 80–18796
$Li_{4+x}B_7O_{12+x/2}$ Cl, solid solns., ionic cond. rel. to struct. and chemical bonding *(French)* 78–2295
$Li_{4+x}B_7O_{12+x/2}Br$, solid. solns., ionic cond. rel. to struct. and chemical bonding *(French)* 78–2295
LiBe(Mg)(Ca), $^2\Sigma^+$ and $^2\Pi$ states, mol. binding energy curves 80–58189
LiBr, Compton profile anisotropies 79–27044
LiF, Compton profile interpretation to give ionic deform. and bonding 77–40301
LiF crystals, relation of struct. and bond type to slip geometry 80–88165
LiF, elastic electron scatt. intensity, rel. to electron density distrib. 78–1079
LiF, electron elastic scattering, by highly polar mols., chem. bond effects 78–9248
LiF-ethylene complex, ab initio calcs. of bonding 78–29745
LiH, cryst., Compton profile, position space anal. 79–47536
LiH, directional Compton profiles 79–4867
LiH, electron elastic scattering, by highly polar mols., chem. bond effects 78–9248
LiH-NH_3(ethylene)(acetylene), struct. and props., SCF ab initio calcs. 80–106250
LiH_2PO_3, P-H bond dipole direction, nonlinear optical coeffs. meas. 80–69253
$Li^{129}I$, Ar matrix isolated and cryst., Mossbauer verification of distortion overlap 77–63325
LiNC, mols. with polytopical bond, spatial distrib. and motion of Li 78–66533
LiNC type molecules, Born-Oppenheimer approx. applicability 80–32603
$LiNH_3^+$, $LiNH_2$, Li_2NH, localised orbital anal., bond props. 77–6676

bonds continued

- LiNO, four electron three centre bonding units, ab initio valence bond calcs. 80—27949
- LiO_2-Al_2O_3-SiO_2, bonding of Si-O exam. by X-ray emission spectra 78—52594
- Li_2O, elastic electron scatt. intensity, rel. to electron density distrib. 78—1079
- Li_2O, electron elastic scattering, by highly polar mols., chem. bond effects 78—9248
- Li_2O-GeO_2 glass, synthesis, Ge coordination state 77—24271
- LiON, four electron three centre bonding units, ab initio valence bond calcs. 80—27949
- $LiTaO_3$, displacive ferroelectric, effective charge determ. 80—97212
- LuF, $^1\Pi$ hyperfine struct. parameters, bonding 77—58036
- Mg, HCP metals, K-emission valence bands, structure and bonding 80—7438
- MgF_2, electronic struct. and densities of states, tight-binding calcs. 80—15447
- MgO, bonding, pressure effects in lower mantle 80—72491
- $Mg(PO_4)_2.xH_2O$, $x=8$, 22, dehydration and water bonding 77—44456
- MgZn(Cd), Ar matrix absorpt. spectra, vibronic spacing and bonding 79—3453
- $Mg^{2+}.nH_2O+PO_4H_2^-$, binding mechanisms, SCF ab initio calcs. 79—22586
- Mn compounds, simple and complex, X-ray absorption near edge structs. 80—104013
- Mn-C_2H_2 and Mn-C_2H_4, π-bonded, pot. energy curves, SCF calc. 78—5136
- MnO, SCF CI calcs., ground and first excited states, bonding mechanism 77—14347
- $MnO_3F(Cl)$, He (I) photoelectron spectra, metal-ligand bonding, EHMO calc. 78—9193
- Mo, chemical binding to dinitrogen and dinitrogen hydrides 77—86368
- Mo complex, [triply bridged binuclear Mo (V) cation]$[MoOCl_4(H_2O)]^-$ struct. 77—76371
- Mo complex, halogenoxomolybdenum (V), cryst. and electronic struct., reactivity 77—76369
- Mo complex, hexadimethylamino molybdenum, electronic description of triple bonds and verification by photoelectron spectroscopy 78—41949
- Mo complex, metal-metal bond, correl. effects, SCF calc. 77—65425
- Mo complexes, dinuclear, chem. and spectroscopic props. 77—77239
- Mo complexes, electron-rich bis(phosphine) dicarbonyl, chemistry and props. 77—77754
- Mo complexes, monomeric Mo(V) and Mo(IV) species 77—77803
- Mo complexes, μ-oxo, di-μ-oxo, di-μ-oxo-μ-carboxylato bridged oxodimolybdates (v), structures 77—76370
- Mo complexes, organic derivs. of heteropolymolybdates 77—79701
- Mo complexes, oxo-bridged dimers, ^{16}O and ^{18}O-substituted synthesis, IR spectra 77—77188
- Mo complexes derived from electron-rich olefins, cryst. chem. 77—76372
- Mo complexes with poly(iminoethylene)-dithiocarbamate polymer, synthesis and spectra 77—77189
- Mo complexes with thousands and L-cystein, formation and Ir-spectra 77—81096
- Mo cpds, chemistry and uses, conf., Oxford, Eng., Sep (1976) 77—77749
- Mo nitrido complex, with multiple Mo-N bonds, prep., struct. and reactivity 77—83758
- Mo-Mo bonds, review 77—76352
- Mo-N, bond-strength bond-length relationships 80—91702
- Mo-Ni (40 at.%), exam. of ion transfer *(Russian)* 79—28127
- $Mo_2Br_8^{4-}$, electronic and reson. Raman spectra, Mo-Mo band 78—82745
- Mo_2C, bond energy and ionization efficiencies from SIMS 79—24400
- Mo_3C_2, pressing regime influence on high-temp. creep *(Russian)* 80—100852
- $Mo_2(CH_2)_2P(CH_3)_2$, δ-$\delta^*(^1A_{2u}$-$^1A_{1g})$ transition, vibr. struct. anal. 80—53006
- $Mo(CO)_6$, bonding, IR intensity anal. 78—25526
- $Mo(CO)_5Kr$, dispersion energy, stabilisation energy, Mo-Kr separation 79—98241
- $Mo_2Cl_8^{3-}(Mo_2Cl_9^{3-})$, electronic struct. and metal-metal bonding, HMO calcs. *(Russian)* 78—1118
- $Mo_2(NH_2)_6$, electronic description of triple bonds and verification by photoelectron spectroscopy 78—41949
- $Mo_2(OH)_6$, electronic description of triple bonds and verification by photoelectron spectroscopy 78—41949
- Mo(100), adsorbed H_2, photoemission rel. to surface resonances and surface reconstruction 80—44417
- N compounds, influence of chemical bond on relative muonic capture rates in elements 78—58874
- N-H bond containing molecules, correls. among bond lengths, stretching freqs. and bond order matrix elements 77—58192
- N-H bond in methylamine, nucl. mag. isoscreening line diagrams 80—78555
- N_2 adsorbed on W(100), vibr. spectra, bonding struct., LEED study 80—84387
- N_2, bond order values, ab initio calcs. and basis set depend. 80—32605
- N_2, orientated mol., (e,2e) spectra, electron momentum density 79—98236
- NF_3, NF_3^-, and NF_3^+, optimised struct. and bonding, ab initio SCF MO calc. 80—23334
- NH_3, 35 keV electron elastic differential cross section, bond formation, independent atom model 79—31683
- NH_3, adsorption of Al surface, NH_3 decomp., XPS obs. 80—92783
- NH_3, affinity for $Li^+(Na^+)(K^+)$, ab initio SCF calcs. 80—58125
- NH_3, bonding electron pairs, size and shape parameters, Gaussian basis set MO calcs. 80—27935
- NH_3, H-X bond position, correlation with electronegativity 78—9069
- NH_3, vibr. excitation in soft X-ray emission and core ESCA spectra 80—69163
- NH_3-^{57}Fe, solid, Mossbauer study of iron bonding to solid ammonia and its photofragments 80—15833
- NH_3-$(HF)(F_2)$ complexes, CNDO/2 calcs. for electronic struct. and props. 78—25442
- NH_3-lithium halide complex, ab initio calcs., Li bond rel. to H bond 77—14343
- $(NH_4)_2BeF_4$, X-ray cryst. struct. determ., hydrogen bonds 79—69072
- $(NH_3)_nBi^+(Rb^+)(K^+)$, gas phase clusters, relative bond strengths, thermodynamic props. 78—35649
- NH_4F, electron distribution and charge transfer in NH_4^+ ion 78—91291

bonds continued

- NH_4NO_3, shock-induced intramol. bond breaking, XPS and EPR study 80—76512
- $(NH_4)_2SO_4$, ESR study of NH_3^+ radicals 79—38367
- $(NH_4)_2SO_4$-K_2SO_4 mixed crystal, ESR study of NH_3^+ radicals 79—38367
- $NH_4UO_2(NO_3)_3$, IR spectra, force consts., bond orders 77—30873
- NO dimer, asymmetric, characterisation, Raman, IR spectroscopy 79—41176
- NO_2, peroxy isomer, stability, ab initio SCF calcs., bond strength 77—14605
- $(NO_2)_2$, struct. and force fields of isomers, ab initio calcs. 77—18783
- NO_3^-, geometry in crystals *(French)* 79—65045
- NOH isomerism, low lying electronic states, ab initio MRD-CI calcs. 80—83291
- $NO^+.N_2$, rate const., enthalpy and bond strength 77—16809
- $N=N$, CNDO calcs. of electrostatic energy components, complexing effects 77—18791
- Na^+, interaction with purine and pyrimidine bases of nucleic acids, ab initio study 77—64005
- Na-Co strip-chain silicates, structural-composition inhomogeneities 80—88122
- $Na+O_2$, semiempirical pot. surfaces, dynamical considerations 79—11766
- Na_3, EPR spectrum, Ar matrix, bonding models 77—14462
- $NaAlH_4$, $NaBH_4$, ab initio calc. of geom. struct., charge distrib., bonding and pot. energy surfaces 80—18796
- NaBr, Compton profile anisotropies 79—27044
- $NaCa_2Sb_2Fe_3O_{12}$, mag. ordering and bond geometty rel. to tetrahedral Fe^{3+} 77—32163
- Na_2O-CaO-P_2O_5:Co glass, bonding, symmetry meas. 79—46572
- Na_2O-P_2O_5 glass, XPS quantitative struct. anal. 80—2917
- Na_2O-SiO_2 glasses, Na_2O effect on Si-O bonds *(Japanese)* 78—42918
- Na_2O-TiO_2-SiO_2 glass, Si-O bonding, SiKβ X-ray fluorescence and IR spectra 80—10500
- $Na_2O.4SiO_2$, glass, behaviour of VO^{2+} as spectroscopic probe 79—78510
- $Na_2S_2O_6.2H_2(D_2)O$, bonding in $[S_2O_6]^{2-}$, X-ray diffr. refinement and pictorial representation 80—54177
- Na_2SbF_5, linear and nonlinear optical props., hyperpolarisability 78—30010
- $Na_{4-x}(Si_{1-x}P_x)O_4$, $(O\leq x\leq 0.25)$, exam. of Na ion conductivity by impedance meas. *(French)* 78—51731
- $Na_3Te_2Fe_3O_{12}$, mag. ordering and bond geometry rel. to tetrahedral Fe^{3+} 77—32163
- $Na_3UO_2F_5$, IR and Raman spectra, struct. *(French)* 79—11409
- Na_xWO_3, band struct. calcs. 77—62824
- Na_xWO_3, bronze, composition-dependent microhardness, rel. to bonding 79—24606
- $Na^+.nH_2O+PO_4H_2^-$, binding mechanisms, SCF ab initio calcs. 79—22586
- Nb chalcogenides and chalcogenide halides, geometrical struct. and metal-metal bonding 80—80172
- Nb complex, $NbCl_5$ complex with O- and S-containing ligands, prep., and characterisation 79—14729
- NbC, bond energy and ionization efficiencies from SIMS 79—24400
- NbC, chemical bonding and X-ray emission spectral analysis 77—44088
- NbC, pressing regime influence on high-temp. creep *(Russian)* 80—100852
- NbC, rock salt struct., surface energy bands, Shockley surface states, bonding 80—92956
- $NbC_{0.86}$, single crystal work function, thermionic emission and contact pot., microhardness and binding 79—19649
- $Nb_2Cl_9^{3-}$, electronic struct. and metal-metal bonding, HMO calcs. *(Russian)* 78—1118
- $NbH_{0.76}$, protonic model, Compton profile anisotropy 77—73182
- NbN, chemical bonding and X-ray emission spectral analysis 77—44088
- NbO chemical bonding and X-ray emission spectral analysis 77—44088
- NbO_2, rutile phase, energy levels, momentum density, and Compton profile, embedded cluster model 80—50453
- $NbSe_3$ and related cpds. bands, bonds and charge density waves 79—95327
- $NbSe_3$, chemical bonding and dimensionality 78—75992
- $NbSe_3$, phonon study of chemical bonding 80—20645
- Nb_3Sn, anisotropic thermal parameters of Nb 79—99282
- Nb_3Sn, atomic displacements induced by radiation damage, X-ray study 80—2085
- $Nb0_2F$, strain energy due to {001} crystallographic shear planes 79—99223
- Nd complex, with ortho-phenanthroline and $\alpha\alpha'$-dipyridyl tris-trifluoroacetate, absorption spectra 79—98113
- Ne_3, 3-body interactions in binding, semiclassical approx. calcs. 78—21994
- Ni (001), chemisorption of CO, back donation in chemisorption bond, UPS study 80—107642
- Ni (001) surface, chemisorbed O_2, electronic struct. and overlayer struct. theory 79—28391
- Ni (100) surface, model, bonding of S 78—56027
- Ni (111), chemisorption bonding of H, UPS obs. 77—76671
- Ni (111) surface, with O_2, Se, S and Te adsorbed layers, bonding geometry and electronic struct. 79—77909
- Ni, adsorbed S(Se) surface bonding mechanism for ang. resolved photoemission 79—69360
- Ni, CO adsorbed mols. on (100), bonding struct., vibr. excitations 77—15687
- Ni catalyst, chemisorption of ethylene-(d), Raman and vibr. spectra 80 108747
- Ni, chemisorptive binding of O, CNDO calc. of potential energy curves *(German)* 80—44431
- Ni cluster-H, electronic struct. calc., H-metal bonding 77—89823
- Ni complex, nickel di-(trichloroacetate).4n-toluidene complex, crystal struct., bond angles 79—82189
- Ni complex, nickel di-(trichloroacetate).(aniline)4 complex, crystal struct., bond angles 79—82190
- Ni complex, nickel-bis-dithiolene, pseudopot. MCSCF and limited CI calcs. 80—83292
- Ni complexes, $Ni(PX_3)_4$ $(X=F, OCH_3, Cl, CH_3, H)$, CNDO/2 calc. of magneto-optical props. and electronic content of metal-ligand bonds 77—23430
- Ni, electroplated layer, field ion microscope study 79—28246
- Ni-Pd-P, Ni-Pt-P, amorphous and electronic structs., NMR Knight shifts and linewidths meas. 78—68400

bonds continued
Ni_2 and Ni_2^+, lowest electronic states, GVB and POL-CI calcs. 79−31409
NiAl, bonding, self-consistent energy bands 78−91610
NiAl, vapour phase mass spectra, correl. between bond strengths in liq. and gas phases 77−35466
NiCO, liquid interactions, ab initio LCAO MO SCF calcs. 79−18256
$Ni(CO)_4$, back donation, multiple scatt. Xalpha calc. 79−63913
$Ni(CO)_4$, bonding, IR intensity anal. 78−25526
$Ni(CO)_4$, bonding, shakeup energies, and shakeup intensities for photoelectron spectra 80−50528
NiCu molecule, electronic states determ. by ab initio HF and CI methods 80−69087
NiO:Fe, estimation of 4s covalent bonding of Fe^{2+} and Fe^{3+} ions, Mossbauer spectra 78−72441
NiO_2, $Ni(O_2)_2$, coordination of mol. O_2 with Ni, EHT calcs. 77−18795
Ni(111), chemisorption of H_2, geometry, LEED anal. 79−28200
Np, ternary oxides, electronic and structural props., ^{237}Np Mossbauer spectroscopy 79−33570
NpO, and NpO_2, electronic struct. and chem. bonding and XPS line shape calcs. 79−33264
O, overlayer on Ni (001) bonding overlap of O orbital with Ni 4s4p states 79−65319
O-containing anions of d-elements forming hydration-active phases, electron structs. and props. 79−42005
O_2, I and I′ resonance series, vibr. level populations in autoionisation, photoelectron spectra, bond length determ. 80−91612
$O_2F(Cl)(Br)$ radicals, matrix IR spectra, bonding 78−90160
P, black phosphorous struct., Raman vibr. spectra and bonding 80−11411
P, bulk red amorphous, Raman scatt. and IR absorption 79−24323
P compounds, solid, ^{31}P NMR and π bond 79−4732
P-O bond parachors 80−14247
P-S, amorphous, glass transition and specific heat, intermolecular bond saturation 80−15011
P-Se, amorphous, glass transition and specific heat, intermolecular bond saturation 80−15011
P-Se system glasses, magnetochem. investig. 77−51325
Pb_2, low-lying states, energy curves, bonding 79−76367
$Pb_{1-x}Ge_xTe$, Raman scatt. from soft TO-phonon modes 79−95773
$PbO-B_2O_3(SiO_2)$ glasses, absorpt. spectra of Cu^{2+} ions and interpret. 78−27276
$PbO-GeO_2$ glass, synthesis, Ge coordination state 77−24271
$PbO-SiO_2$ and $PbO-SO_3-SiO_2$ system glasses, struct. and IR absorpt. spectra 79−41967
$PbO-SiO_2$ glasses, absorpt. spectra of Nd^{3+} ions and interpret. 78−27277
PbO_2, electronic struct. and densities of states, tight-binding calcs. 80−15447
$12PbO.6SiO_2.PbSO_4$, crystn. from $2PbO-SiO_2-xSO_3$ melts, struct. and vibr. spectra 80−59400
PbS, crystals, relation of struct. and bond type to slip geometry 80−88165
PbS, mol. diamag. susceptibility, bonding types 78−31046
$Pb_{1-x}Sn_xTe$, correlation between elec. props. and crystalline environment 77−80773
Pd (111), chemisorption bonding of H, UPS obs. 77−76671
Pd and Pt mixed valance complex, $[Pd(ethylenediamine)_2Pt(ethylenediamine)_2Cl_2](ClO_4)_4$, Raman spectra 80−84734
Pd cluster-H, electronic struct. calc., H-metal bonding 77−89823
Pd complex, $Pd^IPt^I(CNCH_3)_6(PF_6)_2$, vibr. spectra, M-M bonds. *(French)* 80−47997
Pd/Si, Schottky-barrier type devices, chemical and polarisation characteristics, comparative study 79−78173
$Pd/SiO_x/Si$, Schottky-barrier type devices, chemical and polarisation characteristics, comparative study 79−78173
Pd-H, nature of the 50K anomaly, residual resist. 79−7818
Pd-Si-Fe amorphous alloy, Mossbauer spectra, struct. and bonding 80−7224
Pd-Zr alloy, activity coeff. rel. to electronic props. *(German)* 77−20084
$Pd^{2+}-L-Cl^-$, model fragment ($L=Cl^-$, F^-, OH^-, H_2O, NH_3) bond strengths, EHT calcs. 77−23434
$Pd(CO)_4$, ab initio LCAO MO SCF results invalidate pseudopot. calc. 77−6675
$PdH_{0.72}$, Compton profile, electronic struct. *(German)* 78−92140
Pr complex, with ortho-phenanthroline and $\alpha\alpha'$-dipyridyl tris-trifluoroacetate, absorption spectra 79−98113
l-proline monohydrate single cryst., X-irrad., ESR and ENDOR study of radicals 80−45528
Pt (100) surface, chemisorption of acetylene and benzene, AES, UPS, LEED and flash dehydrogenation 77−59216
Pt (111), chemisorption bonding of H, UPS obs. 77−76671
Pt (111) surface, surface struct. and bonding of (2×2) acetylene overlayers, LEED analysis 77−85067
Pt cluster-H, electronic struct. calc., H-metal bonding 77−89823
Pt complex, $Pt^{II}(CNCH_3)_4(PF_6)_2$, $Pt_2^I(CNCH_3)_6(PF_6)_2$, and $Pt^IPd^I(CNCH_3)_6(PF_6)_2$, vibr. spectra, M-M bonds. *(French)* 80−47997
Pt compounds, L X-ray spectra and X-ray electron spectra, influence of chem. bonds 77−28656
Pt-Zr alloy, activity coeffs. rel. to electronic props. *(German)* 77−20084
$Pt^{2+}-L-Cl^-$, model fragment ($L=CL^-$, F^-, OH^-, H_2O, NH_3), bond strengths, EHT calcs. 77−23434
Pt(O)-Pt(O) dimers, bounding in a $d^{10}-d^{10}$ system 78−74579
$Pt(diethylenetriamine)(guanosine)(ClO_4)_2$, crystal and molecular struct. 79−73157
δ-Pu alloys, struct. rel. to anomalous props. 77−19910
PuO, and PuO_2, electronic struct. and chem. bonding and XPS line shape calcs. 79−33264
Rb compounds, X-ray K absorption edge, fine struct. 77−77319
$RbICl_4$, ^{35}Cl NQR spectra, press. cond. temp. depend 80−20501
$Rb_9(XeO_3Cl_2)_4Cl$, neutron and X-ray diffr. struct. determ., Xe-Cl bonding 78−30591
Re (0001), chemisorption of CO, role of d-orbitals, angular resolved UPS and thermal desorption meas. 80−40232
$Re_2Cl_8^{2-}$, $Re_2Cl_8^{3-}$, ab initio calcs. of metal-metal bond 78−82633
$Re_2Cl_8^{2-}$, spectral assignment, metal-metal bonds, SCF Xα SW calcs., relativistic corrections 80−53006
Re_3Cl_9 metal cluster complexes, He(I) photoelectron spectrum, SCC DV Xα calcs., $Re_2Cl_8^{2-}$ comparison 80−28063
$Re_3Cl_9^-$, electronic struct. and metal-metal bonding, HMO calcs. *(Russian)* 78−1118

bonds continued
ReO_3, Fermi surface, pressure induced anomaly 79−19505
Rh, oxidised surface, bonding of Cd arachidate monolayers, XPS 79−15011
$RhBr_3$, bond distances exam. by EXAFS 78−26525
$Rh_4(CO)_{12}$, bond energy terms from thermochem. data 78−62967
$Rh_6(CO)_{16}$, bond energy terms from thermochem. data 78−62967
Ru complex, HF calc., electron densities and Mossbauer isomer shift, chemical binding 78−50470
S compounds, influence of chemical bond on relative muonic capture rates in elements 78−58874
S cpds., electronic struct. of some 2-and 4-valence states *(French)* 77−10591
S-S bond chirality, biomolecule struct. and activity depend., review 78−27889
S-Se(Te)(Tl), liq. semicond., bonding energies and entropies, mag. susceptibility meas. 80−49082
S_8^{2+}, electronic struct. and localised MOs, bonding nature and geom. struct. 80−18798
SBr_2, transient species, He(I) photoelectron spectroscopy, discrete variational HFS calc. 79−31594
$(SCN)_2^-$, and $(SCN)_2$, vibr. anal., bond strengths 80−9582
SCl_2, microwave spectrum, quadratic pot. function, average struct. 77−65456
$(SN)_x$, electronic struct., one-electron band theory 80−65450
$(SN)_x$, π-bonding, increased valence theory calcs. 77−46500
S_2N_2, $(SN)_x$, (x=2 or 3), minimal STO-3G basis HF ab initio LCAO SCF MOC, geometry 78−903
S_2N_2, π-bonding, increased valence theory calcs. 77−46500
$S_4N_2^+$, π-bonding, increased valence theory calcs. 77−46500
S_4N_4, 6-electron 5-centre bonding units, increased valence theory calcs. 77−46500
SO_3, dissoc. pathways and mol. vibr., compliance consts. and min. energy coords. 78−35661
Sb-containing glasses, ^{121}Sb Mossbauer spectra 77−20764
$SbBr_x^{-y}(I_x^{-y})$, low freq. Raman and IR spectra, force consts. 80−55097
$SbF_3.(NH_2)_2CS$ and $SbF_3.[(NH_2)_2CS]_2$, X-ray cryst. struct., IR spectrum *(French)* 78−87643
SbI_3, intermolecular bonding study using ^{129}I Mossbauer effect 78−72438
$SbO_{3/2}-BO_{3/2}$, glass, props. and struct. *(Japanese)* 77−27836
$Sb_2S_3(Se_3)$, IR spectra rel. to bonding, amorphous film and cryst. 77−16410
Se, bonding coordination defects 80−59927
Se compounds, influence of chemical bond on relative muonic capture rates in elements 78−58874
Se, electronic struct. of cryst. phases and hydrostatic press. effects 80−59865
Se, mol. structure, local atomic arrangement at intrinsic bonding defects 80−59374
Se, trigonal, Raman scatt. at very high press. 80−60566
Se:Cd dilute liquid, perturbed ang.-correl. meas. of motional-correl. time 79−41930
Se-Ge, chalcogenide glass, Raman scatt. and bond struct. 79−95772
Se_8^{2+}, electronic struct. and localised MOs, bonding nature and geom. struct. 80−18798
$SeMoOCl_7$, prep., cryst. struct., characterisation *(French)* 78−63722
$SeOCl_2:Pr^{3+}(Nd^{3+})(Er^{3+})$, $SbCl_5$ acidified, Racah and Judd-Ofelt parameters in laser liqs. 80−106516
SeTe liquid alloy, effect of branched chain polymers on bond equilib. 80−24348
Se_xTe_{1-x} system melts, bonding system change obs. using density meas. 77−11456
Sf_6, high resolution X-ray emission, valence electron struct. and chemical bonding, LCAO comparison 79−31545
Si (100), dimer reconstruction, photoemission obs. 80−80939
Si (111), chemisorbed O_2 bonding geometry, electron yield EXAFS meas. 80−50461
Si (111), intermediate oxidation state, core photoelectron absorpt. vs. chemical shifts 80−81220
Si (111) 7×7 surface, H_2S interaction, LEED and AES 78−38966
Si (111) surface, Al overlayers, theoretical study 78−95366
Si, (111) surface, oxide formation, AES and EELS meas. 80−3232
Si (111) surface, surface energy bands and atomic position of chemisorbed Cl 78−56041
Si, amorphous, control of dihydride bond density using RF sputtering 80−34327
Si amorphous, diffraction intensities, chem. bonding effects 77−72557
Si, amorphous, hydrogenated, electronic density of states determ. from Schottky diode meas. 80−49907
Si, amorphous, spin-pairing at defect centres, mechanism in terms of chem. bonding 79−23928
Si amorphous film, glow-discharge, optically detected mag. reson., annealing and substrate temp. effects 80−20519
Si, amorphous film, RF plasma deposition from $SiCl_4-H_2$, characterisation 80−66435
Si, atomic displacements damped by chemical bonds, computer calc. 78−47370
Si, charge disturbance around neutral defect, simple new method, appl. to ideal vacancy 79−82554
Si, chemically etched, model of structural transforms. during thermal oxidation 78−79557
Si, chemisorption of H on (111) 77−62743
Si, electronic properties, rel. to chem. bonding and lattice dynamics 80−44169
Si, enhanced conductivity in plasma hydrogenated films, thermionic emission 80−70692
Si, H chemisorbed, relation of Si-H vibr. freq. to surface bonding geometry 80−49502
Si, hydrogenated amorphous film, XPS and UPS 78−19636
Si, impurity states, localised orbital approach 80−92851
Si, lattice stability, pseudopotential theory and problem of covalent bonding 77−55490
Si, oxidised surface, bonding of cadmium arachidate monolayers XPS 79−15011
Si, self-diffusion mechanism 79−90824
Si, structural props. using electron-ion Hamiltonian using density-fundamental methods 79−82177
Si, total energy calcs. by r-space method, Wannier functions 80−88503
Si, van der Waals electron correlation energy 78−95013

bonds continued
Si:F(,H), amorphous, electronic struct., orthogonalised LCAO calc. 80—44486
Si:H, amorphous, 2p level shift, XPS obs. 80—97401
a-Si:H, electronic states and bonding config. 80—64900
Si:H amorphous films, ESR, optical gap and elec. cond. meas. 80—75842
Si:H amorphous films, reactively sputtered, prep. and characterisation 80—100785
Si/Al interfaces, chemical bonding states, low energy AES 80—6985
Si-Al-O-N systems, behavioural diagrams 79—24507
Si-H, amorphous, energy gap negative-U states, Si-H-Si three centre bond model 78—91606
Si-H (up to 15 at.%), amorphous, ion implanted, laser annealing obs. 79—69133
Si-H amorphous film, reactively sputtered, prep. and props. 79—78889
Si-H bond containing molecules, correls. among bond lengths, stretching freqs. and bond order matrix elements 77—58192
Si-O bonds, cryst. chem. at high press., rel. to Earth mantle mineralogy 79—48470
Si-Pd, preferred sputtering on surface, mass difference and chemical bonding difference effects, AES obs. 79—83078
Si-Pd film, preferred sputtering on surface, mass and bonding difference effects, AES obs. 79—87552
Si-SiO_2, bonding at (111) interface, stoichiometry and kinetics, synchrotron radiation photoemission spectroscopy 80—24744
Si-SiO_2-Si_3N_4 MNOS structure, chem. comp. and electronic states, Auger and energy loss spectra obs. 80—92999
Si-Te system glasses, local struct., ^{119}Sn Mossbauer obs. 79—41968
Si_2, electronic struct. and bonding, atomic effective pot. appl. 80—95745
$SiAs_2$, electron charge density calc., nature of bonding determ. 77—1098
Si_xAs_{1-x}:H, amorphous system, struct. and defects, Raman and EPR meas. 80—49103
SiC, chem. stability, mech. and thermal props. rel. to appls. 80—21103
Si_xC_{1-x}:H reactive sputtering deposition, compositional and structural props. 79—99077
$Si_xC_{1-x}H_z$ amorphous films, IR absorpt. bands 80—100705
SiF_4, photoelectron spectra, bonding, MS Xα calcs. 79—18116
SiH_4, photoelectron spectra, bonding, MS Xα calcs. 79—18116
Si_2H_4, Si-Si double bond, ab initio GO calc. 78—94187
$SiH_{4-n}F_n$ (n=1 to 3), photoelectron spectra, bonding, MS Xα calcs. 79—18116
SiH_3X (X=H, F, NH_2, OH), coord. bond calcs. 80—58129
SiN_x film, plasma deposited, comp. and characterisation, optical and elec. props. 80—15401
Si_3N_4, amorphous, CVD prep., struct. characts. by pulsed neutron diffr. 80—33891
Si_3N_4 amorphous film, CVD, core and valence electron excitations, low energy electron loss spectroscopy and AES 80—2365
Si_3N_4, CVD, chem. bond nature, Compton scatt. expts. 80—49539
Si_3N_4, film, H_2 concentration profile, chem. bonding 79—33205
Si_3N_4 film in MNOS memory struct., distrib. and role of N-H and Si-H bonds 79—33358
Si_3N_4:H, amorphous, ion induced H transfer from N to Si, band passivation, elec. props. 78—47439
SiO, alumina surface deposited film, SiH bond form., inelastic electron tunnelling spectra 79—69375
SiO-B_2O_3 composite dielec. films, EPR, dangling bonds and dielec. loss 80—11246
SiO_2, amorphous, phonons, cluster-Bethe lattice approach 78—10150
SiO_2, amorphous, struct. and chem. bonding 78—51422
SiO_2, amorphous and cryst., neutron irrad. and unirrad., intrinsic defect photolum. 80—50401
SiO_2, amorphous estimate valence alternation pairs 80—54132
SiO_2 amorphous film, thermal, core and valence electron excitations, low energy electron loss spectroscopy and AES 80—2365
SiO_2, chem. bond and rel. props. 77—43199
SiO_2, chemical bond and related props. 77—43171
SiO_2 film on Si, irradiation behaviour anal. 78—26957
SiO_2, freq. and wavenumber depend. dielec. function, bond-charge approx. 79—56155
SiO_2, fused, broken bond defect generation mechanisms 80—88044
SiO_2, pseudopotential study of bonding and structure 78—75622
SiO_2 surfaces, bonding of Cu^{2+}, Cr^{3+}, Co^{2+} ions, EPR, optical spectroscopy investig. *(German)* 79—95266
SiO_2 vitreous film on Si, defect struct. comparison with crystalline SiO_2 and Si-O bond nature 80—54557
SiO_2, vitreous films on Si, channel and network defects 80—54142
SiO_2:TiO_2, prep., amorphous struct., effect of roasting, bonds 78—44061
SiO_2-Al_2O_3-CaO-Na_2O:Fe^{3+}, optical absorpt. due to Fe^{3+} ligand field and charge transfer 80—89020
SiO_2-GeO_2, synthetic, struct, IR spectra 79—42993
SiO_2-Na_2O(Li_2O) glasses, bonding of Si-O exam. by X-ray emission spectra 78—52594
SiO_4 tetrahedra, semi-empirical molecular orbital model, radiation compaction application 79—73433
SiO_x, amorphous film, dispersion of refr. index and chem. comp. 80—7429
SiO_x, core level shifts, nature of bonding 77—84698
SiO_x, electronic struct., mixed-crystal and random-bonding models 79—65029
SiO_x, electronic struct., random bonding model 79—82175
SiO_x, freq. and wavenumber depend. dielec. function, bond-charge approx. 79—56155
SiO_xN_y, low temp. films, comp., chem. bonding and contamination 78—47676
SiP, thermodynamic characts. 10-300K, interatomic bond elasticity 80—59677
SiP_2, electron charge density calc., nature of bonding determ. 77—1098
Sm complex, with ortho-phenanthroline and $\alpha\alpha'$-dipyridyl tris-trifluoroacetate, absorption spectra 79—98113
$SmCo_5$, X-ray K absorpt., chem. shift 79—91531
$SmCu_5$, X-ray K absorpt., chem. shift 79—91531
α-Sn, ion implanted, defect struct., Mossbauer spectra 80—80214
α-Sn, lattice stability, pseudopotential theory and problem of covalent bonding 77—55490
Sn, oxidised surface, bonding of cadmium arachidate monolayers, XPS 79—15011
Sn-Se(Te), liq., mag. susceptibility meas., electron localisation and chem. bonding 80—60178
Sn-Te alloy, liq., magnetic susceptibility 79—87232

bonds continued
Sn_2, low-lying states, energy curves, bonding 79—76367
$SnCl_2.1.5H_2O$ single cryst., ^{35}Cl NQR, cryst. struct. 80—60449
Sn(IV)-, Sn(II) halide mols., rare gas matrix-isolated ^{119} Sn spectra 77—48097
$Sn_xMo_3S_4$, chevrel phase, charge transfer and valence electron conc. 78—6029
SnO_2, electronic struct. and densities of states, tight-binding calcs. 80—15447
SnTe, Raman scatt. from soft TO-phonon modes 79—95773
$^{119}Sn^{i}$, total mass absorpt. coeff. of gamma quanta, chem. binding influence, determ. using Mossbauer effect 80—99467
Sr, oxidation, SXAPS 77—73189
Sr^{+}, hydration, gas phase clustering mass spectra, thermodynamics, bonding 77—16814
Ta complex, $TaCl_5$ complex with O- and S-containing ligands, prep., and characterisation 79—14729
TaC, bond energy and ionization efficiencies from SIMS 79—24400
TaC, pressing regime influence on high-temp. creep *(Russian)* 80—100852
TaC, quasi-self-consistent energy band structures using relativistic KKR calcs. chemical bonding 79—51484
TaN, electronic struct., relativistic energy band struct. calc. 80—34354
TaS_2 (1T) and (2H), bonding and charge density wave phase transitions 80—44282
TaS_2 (2H) intercalated with pyridine, ionic bonding model 79—65052
TaS_2/pyridine intercalated, struct. and bonding 78—91323
$TaSe_3$, phonon study of chemical bonding 80—20645
Tb, bidirectional orbital interpretation of L_{III} absorption discontinuity shape 77—16423
$TcCl_8^{3-}$, metal-cluster, EHT calcs. of electronic struct., metal-metal bonding *(Russian)* 77—61687
Te compounds, X-ray photoemission, core level binding energy shifts rel. to Mossbauer isomer shifts 78—2984
Te, electronic struct. of cryst. phases and hydrostatic press. effects 80—59865
Te, trigonal, Raman scatt. at very high press. 80—60566
TeO_2, electronic struct. and densities of states, tight-binding calcs. 80—15447
Te_xS_{1-x}, chemical bonding from ^{129}I and ^{125}Te Mossbauer spectra 79—73867
$TeSe_{20}$, vitreous alloy, elec. and thermal cond. during crystallisation 79—7550
Te_xSe_{1-x}, chemical bonding from ^{129}I and ^{125}Te Mossbauer spectra 79—73867
$^{124}Te^{M}$, internal conversion in valence shell for M1 and M4 transitions, effect of chemical environment 78—33149
Ti (III) halides, bonding, struct., ligand field splitting, electron gas calcs. 78—17557
Ti complex, bis cyclopentadienyl Ti:N_2, liquid interactions, ab initio LCAO MO SCF calcs. 79—18256
Ti:C, molecular cluster approach to electronic struct. and bonding mech. for impurity C 77—20270
Ti_2, electronic structure of five and ten atom chains SCF-Xα-SW calcs. 80—5483
TiC, bond energy and ionization efficiencies from SIMS 79—24400
TiC, Shockley surface states and bonding 78—91739
TiC, TiN and VC, charge distrib. and bond ionicity 78—63961
TiC, X-ray emission spectra and chem. bonding 77—20958
TiC-TiN, hardness var. charact. in homogeneity field 80—3192
TiC_xO_y, elastic characts. 77—80568
$TiCl_4$, $t_1 \rightarrow 2e(^1A_1 \rightarrow {}^1T_2)$ transition, bond props. and LCAO MO calcs. 80—18889
Ti_xGe_y, interrelationship of X-ray charact. with physical props. *(Russian)* 77—1765
TiH, electronic structure of five and ten atom chains SCF-Xα-SW calcs. 80—5483
TiN, X-ray emission spectra and chem. bonding 77—20958
TiN-MnN, solid solns., electrophys. props. 77—35914
TiN_x, film, non-stoichiometry rel. to optical characts. 77—12456
TiN_7O_y, cubic, thermal expansion coeffs., Ti-Ti bond screening 79—10970
TiO, X-ray emission spectra and chem. bonding 77—20958
TiO_2, K^{+} implantation, extended defects and precipitates 80—49251
Ti_2O_3:Sc_2O_3(Al_2O_3), struct. changes on Sc(Al) substitution 77—55276
$TiSe_2$ (1T), phonons and CDWs, inelastic neutron scatt. meas. 79—28059
TiX_4, (X=Cl,Br,I), He I and He II photoelectron spectra, ionis. energy, chem. bonding 78—46394
Tl-Te alloy, liq., bond equilib. theory for electronic props., thermochemistry 77—89365
TlI, mol. beam photodissoc., bond order and state symm. 77—34706
Tl(III) organocompounds, XPS study *(French)* 79—64047
Tl_2Se-As_2Se_3-SnSe system alloys, covalent component of chem. bond effect in vitrification processes, Mossbauer obs. 77—36156
Tl_xSe_{1-x}, liquid semiconductor, diamagnetism and paramagnetism, dangling bond paramag. centres, mag. susceptibility obs. 80—44797
Tl_xTe_{1-x}, amorphous, bonding and electrical conduction 79—90951
$TmCo_5$, covalent electron number, from chem. shift of Co X-ray absorption spectra 77—59641
TmSe, nonstoichiometry, high temp. chem. and valence instability *(German)* 79—23743
γ-U alloys, struct. rel. to anomalous props. 77—19910
U complex, $[UO_2(CO_3)_3]^{4-}$, vibr. and low-temp. optical spectra, rel. to U recovery from oceans 79—73939
U compounds, equatorial bonds, MO calcs. 78—82621
UB_2, thermochemistry and stability 80—97723
UC, quasi-self-consistent energy band structures using relativistic KKR calcs. chemical bonding 79—51484
UF_4, X-ray photoelectron spectra 77—32491
UGe_3, induced magnetisation density and f-d bonding, polarised neutron diffr. study 80—50063
UN, electronic struct., relativistic energy band struct. calc. 80—34354
UO_2 and U_4O_9 single crysts., optical props. rel. to chem. bonding 77—28598
UO_2, U_2O_5, U_3O_8, and UO_3, bonding and valence obs. by ESCA and EPR 77—28696
UO_2, uranyl cpds., X-ray photoemission spectra obs. of electronic struct. 77—28695
UO_2^{2+}, electronic struct. theory, applied to solid phase $Cs_2UO_2Cl_4$ and $CsUO_2(NO_3)_3$ 79—73476

bonds continued

- $UO_2(NO_3)_2$ complexes, IR spectra, normal coordinate anal., vibr. assignments, force consts. and ligation effects 80—9608
- V, and $VD_{0.68}$, anisotropic Compton profiles 80—97368
- V^{4+}, cryst. field effect on ESR parameters 77—36116
- V^{4+}, doped in single crysts. bonding character and g-factor interpretation 77—55704
- V-O coordination complexes, CNDO calcs. of stability and bonding *(German)* 79—31404
- V_2, formation, spectra, electronic struct. 77—54642
- VC, bond energy and ionization efficiencies from SIMS 79—24400
- VC, TiC and TiN, charge distrib. and bond ionicity 78—63961
- $VD_{0.77}$, Compton profile, electronic struct. *(German)* 78—92140
- VH, electronic struct. and X-ray emission spectra 77—52201
- $VH_{0.71}$, Compton profile, electronic struct. *(German)* 78—92140
- VN-Mn, solid solns., electrophys. props. 77—35914
- VO^{2+}+alkyl dinitriles, reaction, CN stretching freqs., bonding effects 77—16820
- V_2O_3-Al_2O_3 solid soln., interactions between V atoms, comp. and temp. depend. of mag. susceptibility 77—8056
- V_2O_5, energy band structure, bonding props., projected density of states anal. 80—70603
- V_3Si, electron charge distrib., martensitically transforming single cryst., X-ray diffr. meas. 78—75631
- W (100), adsorbed H-induced lattice reconstruction, surface vibr. obs. 79—19445
- W (100), chemisorption of H, struct. determ. by surface vibr. modes anal., EELS obs. 80—39435
- W, (100), with ordered C overlayer, adsorption of O_2 and CO, UPS meas. 79—77907
- W complex, $Li_4W_2(CH_3)_{8-x}Cl_x$.4THF, quadrupole bond stability, crystallographic investig. 77—58193
- W:K-Al-Si, state of bonding, distribution of impurities 78—92212
- WC, bond energy and ionization efficiencies from SIMS 79—24400
- $W(CO)_6$, bonding, IR intensity anal. 78—25526
- WO_3-$N6_2O_5$ system, strain energy due to {001} crystallographic shear planes 79—99223
- Xe compounds, Xe chemical and isomer shifts, electron valence struct. *(Russian)* 80—53056
- Xe_2, near metal surface, proximity effects 79—36797
- $XeCl^-$, well depth of mol., $Xe+Cl^-$ elastic cross-section expt. 79—86027
- XeF,(Cl)(Br) matrix isolated, absorpt. and emission spectra 77—14446
- XeF, in Ar and Ne matrices, reson. fluoresc., ground $X^2\Sigma^+$ state pot. well 77—14482
- XeF^-, well depth of mol., $Xe+F^-$ elastic cross section expt. 79—86027
- XeF_2, stereochem. of structs. and valence bonds 79—69066
- XeF_4, stereochem. of structs. and valence bonds 79—69066
- $Xe_2F_3{}^+$, 6-electron 5-centre bonding units, increased valence theory calcs. 77—46500
- Xe(II, IV, VI and VIII) compounds, Mossbauer study 79—65772
- XeO_3, stereochem. of structs. and valence bonds 79—69066
- YB_6, metallic, energy bands and bonding 77—43486
- $YCa_3Zr_2Fe_{2.75}Ga_{0.25}O_{12}$, mag. ordering and bond geometry rel. to tetrahedral Fe^{3+} 77—32163
- YCo_5, covalent electron number, from chem. shift of Co X-ray absorption spectra 77—59641
- YSi_n, electronic struct., calc. and X-ray obs. *(Russian)* 79—13634
- YVO_4:Eu, cluster electron struct., X-alpha calc., emission spectra 78—2898
- YbH(YbD), and isotopic forms, optical and EPR matrix isolated spectra, HFS, bonding 77—83613
- Zn, HCP metals, K-emission valence bands, structure and bonding 80—7438
- Zn_3As_2 and $ZnAs_2$, molten, thermal expansion and atomic bond strength parameters 80—65257
- Zn_3As_2, determ. of ionicity by X-ray absorption method 78—31278
- ZnHg(Mg), Ar matrix absorpt. spectra, vibronic spacing and bonding 79—3453
- $ZnIn_2S_4$, electronic props. of polytypic forms, pseudopot. calc. 80—38997
- $ZnIn_2S_4$, valence band photoemission spectroscopy 78—56569
- ZnO $(10\bar{1}0)$ and $(11\bar{2}0)$ surface, atomic geometry from elastic LEED intensities 77—20170
- ZnO, chemisorpt. of pyridine, acetone, dimethyl sulphoxide, UPS, mol. orbitals effect on bonding 78—72699
- Zn_3P_2, determ. of ionicity by X-ray absorption method 78—31278
- Zn_3P_2, evaporated metal contact barrier heights 80—80375
- ZnS, lattice dynamics, phonon freq., bond bending force model calcs. 80—70335
- Zr complex of glycine, XPS study of glycine binding 79—41196
- Zr-H alloy, soft X-ray emission spectra, electronic struct. 79—65959
- ZrB_2, self-consistent band struct., XPS, reflectance, NQR, Hall effect and density of states meas. 80—107689
- ZrC, bond energy and ionization efficiencies from SIMS 79—24400
- $ZrC_{0.84}$, single crystal work function, thermionic emission and contact pot., microhardness and binding 79—19649
- ZrF_4-BaF_2-MF_n (M=Na, Ca, Ln, Th, n=1, 2, 3, 4), vitreous phases, network formers, modifiers and stabilisers *(French)* 80—64909
- ZrO_2:Cu, point defects, electrochem. characterisation 80—35599
- ZrS, electronic struct., bonding effects, photoelectron spectroscopic and low temp. heat capacity cal. 80—96780
- $ZrS_3(Se_3)(Te_3)$, phonon study of chemical bonding 80—20645
- ZrX_4, (X=Cl,Br,I), He I and He II photoelectron spectra, ionis. energy, chem. bonding 78—46394

bone

- 2 to 8 MHz US attenuation obs. 79—57701
- accelerometer package attachment method 79—70717
- acoustic emission diagnosis, soft tissue effects 79—48362
- acoustic emission in human bone tissue subjected to longit. extension 77—25495
- acoustic emission of fresh mammalian bones 80—76783
- acoustic method for monitoring healing of human long bones 80—21511
- acrylic bone cement containing second phase dispersions, strength 77—81663
- acrylic bone cement viscosity characterisation 79—79690
- acrylic bone cement-stainless steel interface, shear strength 77—86706
- acrylic bone cements, for fixation of orthopaedic implants 79—84000
- alumina-acrylic composite bone cement 79—79689
- anelastic deform. and friction stress 78—19871

bone continued

- aneurysmal cyst response to low doses of ^{60}Co gamma radiation with prolonged treatment 78—73196
- ankle compliance, human, dependence on joint angle 79—11959
- apatite, Hall coefficient dependence on mag. field, obs. 79—92248
- apatite crystal growth in skeletal tissues 80—94181
- apatite crystal orientation, and growth, X-ray and neutron diffr. meas., effect of chem. and heat treatment 79—39431
- apatite crystals, neutron diffr. study, possible determ. of load-bearing function 77—40952
- apatite powder samples, peak positions determ. from step-scanned X-ray powder diffr. data 80—103217
- archaeological, Al determ. using neutron activation anal. 79—52847
- archaeological, characterisation by neutron activation anal. 78—353
- arm and forearm exercise joint force musculoskeletal model 79—92272
- articular cartilage biphasic rheological model 79—92264
- articular cartilage controlled impact test instrum. and procedure 78—28130
- articular surfaces, math. representation of positron 80—3685
- artificial hip joint, noncemented, with bone development stimulator *(German)* 79—8575
- artificial knees, mobility, stability and stress 79—12032
- bending, elastic and damping props. of human femur 77—25489
- bending strength prediction, from bending stiffness and bone mineral content meas. 78—11787
- benign diseases, the particular usefulness of radioisotope methods 80—51209
- bioceramic implants, surface structure *(German)* 79—44057
- bioceramics in orthopaedic surgery, internal struct. of inorganic parts in bones *(Polish)* 79—20714
- biocompatible implants, developed for bone fracture prevention, development research criteria 78—77155
- biomaterial microwave complex permittivity meas., noninvasive selective exposure 79—20729
- biopsies, undecalcified human bone prep. for electron microscopic investigation 78—20332
- biopsy, automatic image anal., var. in rib architecture 78—61253
- blood flow, meas. with a ^{133}Xe washout method 80—72288
- blood flow and tracer uptake in normal and abnormal canine bone 80—17072
- blood flow determ., comparative study of $^{99m}TcO_4$ and ^{131}I-iodo-antipyrine 78—28046
- bone-cement interface bond enhancement technique 78—31980
- bovine bone, degraded, ESR study 79—39432
- bovine femur crack detection by acoustic emission 79—48312
- bovine hip bone, compression tests, effect of specimen shape and size on mech. props. and fracture mode 78—69132
- calcification studies using electron probe X-ray microanalysis 80—76885
- calcified tissue, role of collagen in elastic props. 78—3539
- callus, dynamic characts. determ. by induced vibr. method 79—62284
- cancellous, Compton scatter densitometry meas. 79—39489
- cancellous, human femoral head, mech. props., normal vs. pathological *(Japanese)* 77—25480
- cancellous, of knee and ankle joints, preferred orientations, determ. and significance 77—36987
- cancer induction by α radiation 78—15871
- cartilage/bone plugs, impact stress/strain data 79—43950
- cement, fretting corrosion of orthopaedic implant materials 80—104813
- cement line motion due to torsional load 79—74712
- cement used to grout hip prosthesis, stress distrib. obs. 80—104816
- cervical spine, human, stability under tension 79—16236
- collagen structures, piezoelec. effect, in rel. to mol. struct. 80—41100
- compact, deform. and strength 78—24087
- compact, empirical strength theory, biaxial stress characts. 78—77081
- compact, fracture mechs., effects of density and specimen thickness 78—3534
- compact, human, microscopic struct. rel. to fractures 80—56106
- compact, long-term torsional creep obs. 80—104619
- compact bone fatigue damage, residual strength and stiffness 77—90834
- compression effects on bone tissue crysts. 77—25492
- compressive strength, rel. to density and strain rate 77—36976
- compressive strength quantitation and effects on bone remodelling 78—31836
- computerised tomography spectral artifact correction 78—35953
- conduction mechanism rel. to hearing, holographic interferometry with optical fibres 80—76879
- cortical, anisotropic anal. of strain rosette information 79—16237
- cortical, human, local piezoelec. polarisation as function of stress freq. 77—32933
- cortical bone, bovine, fatigue strength, stress freq. influence 80—16997
- cortical bone, wet, non-linear constitutive eqn. of viscoelastic props. 80—30754
- cortical bone, wet, torsional and biaxial viscoelastic props. obs. 80—30752
- cortical bone, wet, viscoelastic props., relax. mechs. 80—30753
- cortical bone diameter meas., manual and computer-aided methods comparison 78—85376
- cortical bone microstrucutre model for dosimetry using ionising particle path lengths 77—40774
- cortical bone US velocity dispersion obs., 1 to 10 MHz 77—21583
- cow femur, mineral comp., neutron activation anal. 78—27859
- crack velocity depend. of longitudinal fracture, bovine tibia 80—97965
- cranial bone, fetal, elastic modulus obs., appl. to fetal head moulding biomechanics 80—67128
- cranial computerised tomography scans, picture processing, image anal. and computer graphics appls. 80—8183
- creep, nonlinear, on stretching human bone tissue 80—3702
- creep of compact human bony tissue under tension 77—25487
- deformation and strength, change dynamics at early stages of form. 78—7383
- deformation capacity of compact tissue of human tibia subjected to torsion, age effect 77—52827
- deformation in vivo telemetering in monkey, Si strain gauge 77—86720
- deformation under unloading and repeated loading 78—3546
- demineralised dense human, strength props. nonuniformity 80—104611
- density and irregularity meas. in normal hands by radiography 80—30839
- density determination, effective attenuation coeff. of soft tissue, Compton scatt. 80—101220
- density determination in vivo, computed tomography vs. mineral analyser 77—73567

bone continued
density measurement by ^{125}I photon absorptiometric anal., dialysis patients 80—36075
dental implant fixation, electrically mediated process, interfacial strength 79—16348
destruction of compact bone material, anisotropy in 80—12174
destruction of compact tissue 80—67135
dielectric relaxation in cortical bone 77—40964
disease diagnosis, automatic texture anal. methods 80—8156
diseases, pot. use of stimulated positron emission in detect. and monitoring 80—81712
distribution profile from radiographs, healing process obs. appl. 78—15890
dose distribution calculation method for bone- and lung-equivalent material, diagnostic X-rays *(German)* 80—61704
dose factors for radiosensitive tissues in bone irrad. by surface-deposited radionuclides 78—53512
dosimetry, meas. of LiF powder packing density in trabecular bone cavities by radiography 77—66855
dosimetry, radial scanning of trabecular bone, path length probability distribs. 77—66854
dosimetry, thermal neutron distrib. in bone in paraffin phantom irrad. with 14 MeV neutrons 78—3616
dosimetry model, surface and volume distribution of ^{239}Pu 79—8550
dosimetry of alpha-emitting radionuclides, particularly ^{226}Ra and ^{239}Pu 77—16993
dosimetry of beta-emitting volume-seeking radionuclides in human bone, mean skeletal dose factors 78—77115
dosimetry of bone-seeking radionuclides, comparative study in man, rhesus monkey, beagle and miniature pig 80—72338
dosimetry of irradiated rat, bone marrow electronic cell sizing and counting 79—100744
dynamic mechanical props., postmortem transition 77—21554
elastic characteristics of compact bone tissue of human tibia, differences and correls. 77—25490
elastic moduli determ., US transducer, shear-wave vel. meas. 78—83201
elastic properties of cortical bone of female human femurs, noninvasive meas. 77—21552
elbow flexion-extension and forearm pronation-supination for elbow endoprosthesis design 80—3682
electrical properties, AC and DC, moisture effects 77—2077
electrical stimulation and callus *(Japanese)* 80—12204
electrical stimulation effects on healing of exptl. model for non-union in canine bone 77—60287
electrical stimulation of growth in treatment of non-union, review 80—17043
electrical stimulation of growth treatment of non-union and delayed fractures problems 80—17044
electrode-induced growth, function of implanted cathodes 80—41312
electromechanical effects, comparison in wet and dry bone 80—97985
elemental analysis by prompt γ-ray spectra due to ^{252}Cf neutron irrad. 80—17065
embryonic bone and cartilage, effects of in vitro gamma irrad. 78—65089
endosteal implants, alveolar bone growth enhancement by elec. stimulation, dog expts. 80—26413
epiphyseal plate, method for evaluation and control of growth activity 80—81789
equine long bone forces and moments, in vivo and anal. studies 78—40216
erythropoietic marrow, recovery of Fe uptake following large field radiation therapy 79—20616
Ewing's sarcoma, place of bone scanning 80—72308
exoskeletons of Magicicada sp., detect. of thermolum., possible use as TLDs 80—30896
facial bone scanning by emission tomography 78—31892
femora, bovine, fracture toughness, critical crack length, plastic zone size 79—43948
femora, dog, tissue ingrowth in porous sucrose filled acrylic cement 79—39611
femoral bone, bovine, slow fracture propagation obs. 79—79592
femoral cortical bone tensile props. instrumentation system 77—60025
femoral head activity in Perthes' disease ^{99m}Tc tracer uptake estimation 79—29606
femoral head disease radionuclide uptake patterns 78—28042
femoral neck fractures, meas. of fissure, X-ray picture anal. *(Croatian)* 80—109023
femoral necks, fracture fixation by Muller screws, mech. investigation 80—72377
femoral shaft, human, age and sex-related changes in struct. and strength 77—56401
femoral stem size and design effects on cement extrusion pressure, hip replacement 79—79692
femoral stress and strain calc., finite element method *(German)* 79—2089
femoral subtrochanteric fracture stress anal. 79—79591
femur, bovine, crack vel. and fracture mech. 79—57690
femur, canine, in-depth mech. props. anal. 80—16979
femur, dog, work to fracture meas. 79—57687
femur, expt. studies on anchoring of loaded glass-ceramic implants *(German)* 80—81624
femur, flexural coupling to hip-prosthesis stem, theoretical anal. method 79—39428
femur, human, finite-element plane stress model 79—79590
femur, human, pulse-echo technique for US vel. meas. in vivo 80—89812
femur, human, with implanted Charnley prosthesis, stress anal. 78—20314
femur, loaded, intact and with prostheses, strain gauge meas. 77—60228
femur, rat, density and cortical thickness, meas. by photon absorptiometry 79—8535
femur, rat, influence of hypergravity on compressive strength 80—3690
femur compact, adult human, relation between torsional props. and histology 79—16234
femur fractures, reduction apparatus 79—16343
femur intracondylar cancellous bone, compressive strength rel. to loading rate 78—40219
femur strength, rat, rel. to growth, bone-length, gravity 80—16978
femur with proximal prosthesis, 3-dimens. anisotropic stress anal. and failure prediction 78—40424
femurs, human, elastic constants determ. 80—35951
fetal head moulding, finite element model investigation 80—67129

bone continued
fibula, direct meas. of load bearing function 80—104624
fixation plate, laminated polymer-metal, fabrication 79—79685
fixing pins, stainless steel, strength, ultrasound effect 80—71710
fluid-saturated, dielec. props. obs. 80—51316
fluorescence photomacrography, bone growth and remodelling exam. 78—31982
fossil, age determination, nondestructive neutron activation anal. 78—15743
fossil bones from N. Greece, conc. of U and daughter prods., γ-spectroscopy, activation anal. 77—60161
fossil dating by ESR technique 80—95209
fracture, evaluation of finite element and exptl. models of internal fixation plates 77—48934
fracture, human tibia, ultrasonic assessment, surgical manipulations effect 80—3745
fracture callus mech. props., intramedullary nailing rel. to plating 80—85438
fracture fixation, oblique, mechs. using finite element model 77—52922
fracture fixation anal., Oxford fixator 80—17188
fracture healing, radionuclide imaging evaluation, rabbit obs. 79—70613
fracture healing, significance of scintigraphy *(German)* 80—76833
fracture healing, sonic diagnosis 77—21580
fracture healing in rabbits, temporal changes in phys. props. 78—40215
fracture of compact bone tissue 80—12178
fractured femur fixation device, optimum design using finite element anal. 78—36050
functional adaptation model and thermodynamic consideration *(Japanese)* 78—7316
geometric properties of paired human tibiae 80—67127
geometrical properties of sections, determ. by laminography and phys. section 78—20202
glass-ceramic/bone histological and mechanical bonding *(German)* 79—8569
growth stimulation attempts in dogs using mech. vibration 80—81638
hand CC Ca anal. by local neutron activation 79—83902
hand radiographs, congenital abnormalities classification 80—30870
Haversian bone, exam. of mechanical failure at microstructural level 78—77080
Haversian plate in man, microhardness 78—48825
healing, use of anodised Ta electrode, meas. of electrochem. reactions 78—95931
healing augmentation by electric currents and fields 80—8116
healing electrostimulation, clinical aspects 79—83879
healing enhancement by elec. stimuli, effect of stimulation modality 77—40907
healing fracture, blood flow rel. to ^{85}Sr uptake 80—72187
healing in humans, appl. of pulsed mag. field to stimulation 78—28029
hip bone stress analysis using finite element model 78—44518
hip joints, human, study of synovial fluid, friction and lubrication 79—11956
hip prosthesis stem loosening in human femur, biomechanical causes investigation 80—85435
human, acoustic emission in restressing 80—3704
human, demineralized, deform. props. on stretching 80—3703
human compact, longit. shear, constituents and failure mech. 77—81518
human intervertebral discs, strength changes under compression 78—11690
hydrazine deproteinated, rat, UV induced thermolum. flow peak obs. 80—29814
hydroxyapatite nucleation energetics 78—40127
imaging radiopharmaceutical local accumulation model 78—24127
impact energy absorpt. changes with age 80—3698
impact loading, anisotropy of compact bone tissue 77—25491
implant/bone interface, tensile strength and bone form., effect of elec. stimulation 77—5108
intervertebral disc, small solute diffusion, in vivo obs. 79—62276
intervertebral disc response to shear stress 79—92261
jaw, growth anal. in human using kinematic fundamentals 79—16243
joint differential mobility meas., periodontal ligament and temporomandibular joint 80—8093
joint displacements, finger and wrist, relationship with extrinsic finger flexor tendons 79—8520
joint position descriptive coordinate system 79—92269
joint rotation, human, meas. by triaxial goniometer 79—92417
joint wear in humans, ferrography appl. 79—34694
joints, cartilage swelling, congruity of regularly curved joints 79—8523
knee arthrograph for study of stiffness 79—12022
knee joint impact response, comparison of normal and osteoarthritic joints 78—31848
lateral tibial plateau, axisymm. finite element anal. 78—69127
leg long bone growth meas. in children from radiogram, error reduction using computer processing 78—77103
lesions in CBA mice from nanocurie amounts of ^{239}Pu 80—81657
loading method, controlled and time-varying 79—70566
long bone, bent, distrib. of induced elec. activity 78—3541
long bone bending stiffness determ. by LF impedance probe 79—96695
long bone mechanics study under microprocessor control 80—76851
long bones, canine, elastic and strength props. 77—64080
lumbar spine, lateral flexion, radiographic studies 79—8522
lumbar spine, mech. and kinematic anal., orthogonal radiography 79—74708
lumbar spine, mech. props. 79—100645
lumbar vertebra cortical surface strain distribution tests 78—11692
machining, orthogonally, mechanics of, forces and energies 79—29559
mandible, compressive strength rel. to microstruct. and strain rate 79—57689
mandible static loading and jaw muscle electromyographic activity 79—43951
mandible X-ray image changes, desmodontal gap evaluation with data-processing system 79—62337
mandibular bone graft fate determ., quantitative radionuclide imaging 80—3792
marrow, effect of a 600 MeV neutron beam, mouse 79—96630
marrow, haematopoietic stem cells, γ-irradiation, mouse 79—100674
marrow, mouse, late effects of X-irrad. on ability to support haematopoiesis 77—70496
marrow and leucocyte preservative freezing apparatus 79—39617
marrow cell-culture, RBE of different-energy neutrons 79—34508
marrow cells, SEM and optical microscope correlation before and after culture 79—74605

bone continued

- marrow colony-forming units, dose-dependence of the split-dose response 80—61701
- marrow colony-forming units in beagles, response to whole-body γ irrad. 79—25043
- marrow erythropoiesis, abscopal suppression after X-irradiation of mice 80—17020
- marrow haemopoietic activity assessment in normal subjects 80—36073
- marrow of Indian desert gerbil, effects of ^{45}Ca 80—45971
- marrow regeneration from cortex after segmental fractionated irrad. 77—70495
- marrow scanning in pediatric oncology, evaluation of ^{99M}TcS colloid 80—17067
- marrow stem cells of C$_3$H mice, long term radiation effects 80—30787
- marrow transplantation, autologous, effect on monkey mortality after X-ray and neutron exposure 79—29572
- marrow-engrafted mice, survival after γ-irrad. 80—104681
- mass measurement using Xe-filled multiwire proportional counter as detector 78—15884
- materials for orthopaedic implants, review 80—76862
- maxillary lesion evaluation by bone-conducted vowel spectral estimation *(Japanese)* 79—5395
- mechanical model with appl. to human upper tibia, porous material, deform. *(Japanese)* 78—88724
- mechanical properties, dynamic, of long bones, in vivo determ. 77—40906
- mechanical properties, in vivo determ., effect of soft tissue on wave propag. and vibr. tests 78—3660
- mechanical properties and functional adaptation *(Japanese)* 77—25479
- mechanical properties characterisation by dynamic response 80—76782
- mechanical properties determ. in vivo, noncontacting EM device 78—77133
- mechanical properties of human vertebral bone, depend. on age and density 77—36985
- mechanical properties rel. to composition 78—31835
- mechanical properties rel. to density and mineral phase orientation and particle size 80—16989
- mechanical props. of deer's antler, cow's femur and fin whale's tympanic bulla 80—3686
- medullary implants with porous coating, stress distrib. 78—69256
- medullary pin, induced internal bone remodeling 79—29552
- metabolic bone disease diagnosis using whole-body retention of ^{99}Tc^{m}-diphosphonate 78—73208
- metabolic bone diseases in childhood, X-ray diagnosis *(German)* 80—17091
- metacarpi, equine, fracture toughness 80—3694
- metacarpophalangeal joint, human, kinematic investigation 79—8519
- metacarpophalangeal joint compressive strength rel. to subchondral bone density, prosthetic development 79—92286
- metacarpus-phalangeal joint movement modelling 79—88112
- metastases detect., clinical comparison of ^{99m}Tc HEDP and ^{99m}Tc MDP 79—83904
- metastases of prostatic gland carcinoma, ^{89}Sr therapy 80—36076
- metastatic calcification, role of bone scanning 79—92366
- microwave absorbed dose rate distrib. in phantom heads irrad. by aperture source 77—73581
- microwave in vitro effects on granulocyte and macrophage precursor cells, mouse obs. 80—76789
- mineral concentration estimation by beta-ray backscatt. *(German)* 78—69179
- mineral content, coherent scatt. of photons 80—67238
- mineral content, photon absorptiometry 77—25553
- mineral content meas. using gamma-ray attenuation by pair prod. 77—44740
- mineral elemental anal. by α-particle backscattering 79—92449
- mineral mass and width meas. using the Cameron-Sorenson technique 79—62345
- mineral measurement using ^{125}I X-rays and portable miniature CdTe scanner 77—44750
- mineral measurement using EMI scanner vs. densitometry 78—24119
- mineral measurement using polychromatic X-rays, correls. 78—53478
- mineralisation, obs. using ^{125}I-7-iodo-6-demethyl-6-deoxytetracycline HCl 80—12214
- morphology and fracture, exam. 78—57036
- musculo-skeletal shock absorption, relative contribs. of bone and soft tissues 79—29549
- navicular bone, morphological features in functional adaptation of the foot *(Croatian)* 80—108944
- nuclear medicine, value of whole body bone scan in breast carcinoma pre-operative assessment 80—51210
- nuclear medicine conference, Karlovy Vary, Czechoslovakia (May, 1979) 80—12840
- orthopaedics, exptl., quantitative eval. of holographic deform. investigations 80—67197
- orthotic plate, variable-stiffness, absorbable 79—79691
- osteomyelitis, suspected, in children, value of radioisotope bone scanning 80—67216
- osteon system piezoelec. polarisation model 78—3540
- osteonic lamellae, evidence for state of initial stress 78—3536
- osteons with crossed lamellae, micromech. study 77—25493
- osteoporosis early detection by Compton gamma-ray spectroscopy 78—11729
- osteosynthesis, holographic interferometry appl. 79—88213
- osteosynthesis, internal, deform. of bone *(Croatian)* 80—108943
- paediatric intertrochanteric osteotomy fixation of modified Kuntscher's nail *(Croatian)* 78—44675
- patella, human, biomechs. and implications for chondromalacia 77—90839
- patella stress analysis, rel. to patellar articular cartilage lesions 80—35942
- patellofemoral joint, anal. model 80—104625
- photon absorptiometry after successful renal transplantation 77—48854
- piezoelectric, dielectric and elastic constants, rel. to temp. and hydration 77—16946
- piezoelectric effect, theoretical anal. 79—70567
- piezoelectric effect distribution in bent long bone, anal. model 77—36983
- piezoelectric effect on exposure to US, effect of sample rot. 78—80913
- piezoelectric model for dry bone tissue 79—25015
- piezoelectric response obs., freq. depend. 79—92287
- piezoelectricity, role of stress-gradient effects 80—67113
- pin-bone connections, mech. behaviour 78—44698

bone continued

- PMMA bone cement, free radical EPR, feasibility study 80—94318
- PMMA femoral cement compactor for total hip replacement 79—79688
- PMR and IR spectra, chem. anal., bond lengths, human bone powder and ash 78—3414
- polychrome fluorescence labelling and photomicrography 80—89821
- polyethylene implant-bone composite interfacial strength, porous high density polyethylene 78—31979
- porosity of compact bone substance, TAS Leitz 2D image analysis system *(German)* 78—92753
- porous coated implant removal by ultrasound 79—79618
- preservation, effect of treatment on chemilum., rel. to bone fragment transplantation 77—86709
- prosthetic material-bone composites, fracture toughness 77—37108
- pyrogenic infection treatment by non-invasive EM technique 78—48854
- radiation biology conference, Rotterdam, Netherlands (Aug. 1980) 80—105425
- radiation damage centres, appl. of EPR spectra of quasirandomly oriented centres 77—21667
- radioactivity of bone and muscle, separation by dermestid ingestion 80—30949
- radiocarbon dating, inclusions as source of error 78—346
- radiography, skeletal diagnostics, direct magnification, exposure technique and timing 80—104747
- radioisotope scanning, improved quantitative method 78—24125
- radioisotope scanning of bone, historical survey 80—42029
- radioisotope scans, appearance following fractures 80—56189
- radioisotope therapy in bone and joint disease 80—36111
- radioisotope uptake, rel. between ^{239}Pu deposition in bone and ^{59}Fe uptake in marrow 78—85395
- radioisotope uptake of bone-seeking radioisotopes in normal bone rel. to blood flow 80—94320
- radionuclide imaging in infants and children, review 78—77107
- radionuclide skeletal burden determ. from in vivo scintillation meas. of head 78—15915
- radionuclides, short-lived, gamma-ray spectrometry, correction for dead-time losses 80—42312
- radius, human, compact bone mineral density meas. 79—74739
- radius remodelling, sheep, rel. to functional stress and strain 80—35939
- rare earth bone uptake, Mossbauer study 80—8019
- rectilinear scanning, differentiation between metastases and degenerative spinal disease 78—44585
- regeneration, morphology, effect of US 80—41111
- remodeling of bone surface due to force-fitted meduallary pin 80—3683
- remodelling, adaptive elasticity theory 79—25016
- remodelling, quantification of stresses 80—85437
- remodelling, small strain adaptive elasticity 77—16949
- remodelling beneath internal fixation plates of varying stiffness, parametric study 80—16990
- remodelling of long bone, effect of internal fixation plate 77—48935
- resonance, effects of geometrical parameters, shear and rot. inertia, finite element model 77—29165
- revascularisation processes study method, local blood flow dynamic anal. using ^{85}Sr 80—81684
- scintigraphic investigations in neuroradiology *(German)* 80—12242
- scintigraphy, importance in pretherapeutic development of mammary neoplasms *(French)* 80—8135
- scintigraphy as detect. method for bone and bone marrow involvement in malignant lymphoma 80—36086
- scintigraphy clinical comparison of ^{99}Tc^{m}-diphosphonate and -pyrophosphate 78—65112
- scintigraphy in osteomalacia 78—73204
- scintigraphy in renal osteodystrophy 79—70611
- SEM, technique for studying collagen fibres and ground substance 78—57150
- silicate glass bonding to bone rel. to Ca$_3$(PO$_4$)$_2$ surface film form. 80—85212
- skeletal blood flow, implications for bone-scan interpretation 80—72199
- skeletal Ca, facility for regional in vivo neutron activation anal. 79—25088
- skeletal Ca estimation by exhaled ^{37}Ar meas., fast neutron dose requirement 77—16962
- skeletal demineralisation osteopathy, quantitative diagnosis, review *(German)* 80—30872
- skeletal disease, profile scanning, ^{47}Ca rel. to ^{32}P 80—51218
- skeletal maturity determination system *(French)* 80—41209
- skeletal scintigraphy benefits in metastatic and primary bone tumor patients 79—88168
- skeletal system computerised tomography examination 78—88740
- skeletal system V incorporation mechanism 79—82341
- skeletal tracer kinetics, ^{18}F in rats, evaluation of model 80—56188
- skeletal tracer kinetics, ^{99m}Tc(Sn)methylenediphosphonate uptake in canine tibia rel. to blood flow 80—56192
- skeleton, mouse, distribution of ^{239}Pu 79—12002
- skeleton, uptake of ^{95m}Tc, ^{96}Tc pyrophosphate evaluated by autoradiography 79—29608
- skull, acoustic characteristics 79—96730
- skull, birds, struct. anal. using mammography techniques 80—36209
- skull, frontal diagnostics of injuries *(German)* 80—36104
- skull, holographic interferometric NDT 80—41162
- skull, human, deformation, model of cupola with flat base 77—36966
- skull, macerated, human, orthodontic forces induced bone displacement obs. 80—61603
- skull, struct. changes due to Recklinghausen's disease, X-ray and nuclear medicine diagnosis *(German)* 80—76831
- skull bones, human, US flexural wave study 80—72277
- space flight, bone formation inhibition in rat 79—48350
- spinal column, human, strength of construction 80—67137
- spinal fixation using acrylic bone cement, mech. props. 78—81072
- spine, double exposure technique in computerised tomography 80—21524
- spine, upper cervical, pathology evaluation using computerised tomography 79—29585
- spine and forearm Ca changes, meas. apparatus using ^{252}Cf neutron activation anal. 79—39490
- spongy, dynamic elastic props., determ. techniques 80—56326
- stimulation, EM fields in capacitative and inductive devices 78—40283
- stimulation devices, anal. of sinusoidal EM fields 80—108990
- strain gauge application on compact bone 80—3883
- strain in-vivo telemetry in monkeys, method 78—3697
- strain measurement, in-vivo *(French)* 79—34695

bone continued
  strain-related potentials, freq. depend., effect of meas. system parameters 80—16991
  strains of canine radius and ulna, in vivo meas. and anal. 80—67130
  strength, rel. to mineral supplemental diet in young rabbits 77—36986
  strength of fresh bone and bone preserved by freezing 77—25488
  stress analysis of human femur, three-dimensional, using finite element method 78—7379
  stress distribution in long bone due to prosthesis positioning 77—36984
  stress effects in vitro, including ectopic ossification, foetal mouse bone 77—36989
  stress estimation, analytical 79—92250
  stress generated potentials at osteon level 78—31837
  stress generated potentials rel. to collagen piezoelectricity 77—32932
  stress generated pots., linear piezoelec. model 80—3688
  stress wave detection using piezoelec. effect, non-invasive technique 78—31948
  stress-wave detection of an edge crack, appl. to healing rate 78—30236
  structural analysis of long bones, appl. to human tibia 77—21551
  structure, anal. by X-ray pictures *(German)* 80—89828
  substitute materials, sintered hydroxylapatite as bioceramic 79—12036
  surface remodelling, math. theory 78—31847
  synovial joints, rheology of synovial fluid, synthetic lubricants for degenerate joints 79—11955
  tensile strength of interface with porous polyethylene 80—30737
  tensile strength rel. to strain rate, microstruct. and density 77—44703
  thick inhomogeneity effects on charged particle beams 79—25041
  tibia, human, natural freq. anal. 80—85433
  tibia, human, physical stress effect on state, US meas. 78—24088
  tibia, human, simplified method of radiographic anal. of its cross-section, anthropometric correls. 80—89827
  tibia fractures, ^{99m}Tc-pyrophosphate scans, algorithm for automatic computer anal. 79—88171
  tibial bone reaction to hydromech. implant dynamic loading *(German)* 79—8574
  tibial bones, of highly trained athletes phys. stress effect type as measured by US techniques 80—16992
  tibial fractures, treatment with plaster casts, biomech. study 79—74696
  tibial plateau fixation, biomech. factors 77—56534
  tibial shaft internal fixation, biomech. study 78—20313
  tissue inclusions, close from photon emitters in bone 80—36149
  tissue interface, dose distrib. due to anisotropic electron emission 80—36144
  tissue interface, fast neutron dosimetry 79—25113
  tissue regeneration process, investigation of elec. characts. 80—51313
  trabecular, density and other parameters, normal values in adults and children using computerised tomography 79—20611
  trabecular bone from human vertebral body, elastomech. props. 80—67141
  trabecular bone mineral analyser, microcomputer based 79—53218
  trabecular bone-porous coating-hip prosthesis interface, mechanical behaviour 79—39436
  trabecular density, increased in children with chronic renal failure, computerised tomography expts. 79—20612
  transport mechanism between blood supply and osteocytes in long bones 77—86472
  transverse elastic coeff. determ. 78—27985
  tubular, whole, rigidity comparison technique 80—3881
  tumour evaluation, contribution of computerised tomography 79—66552
  tumours, human, scintigraphic assessment of ^{99m}Tc-diphosphonate 79—20613
  ulna, mineral meas. using X-ray (low energy γ-ray) transmission, positioning errors 78—96084
  ulna bending stiffness, microprocessor-automated noninvasive meas. 79—92275
  ulnar bending stiffness, mineral content, geometry and strength, human bone 78—3537
  US attenuation and dispersion in cancellous bone 80—51149
  US longitudinal and shear wave velocity meas. for elastic moduli 77—25623
  US propag., rel. to fracture healing 78—24105
  US properties and microtexture of human cortical bone 80—51144
  US surface wave propag. 78—44578
  US surface wave vel. rel. to mech. props. 77—32937
  US velocity meas. in temp. range of room temp. to 90°C 80—76787
  US velocity rel. to mineral content 80—45962
  vertebra, dynamical response analysis 80—3684
  vertebrae, abnormal accumulations found in the bone scintigram of cancer patients 80—67233
  vertebrae, human, deflected US wave propag. tests 80—61617
  vertebrae, human, mech. props. 80—72206
  vertebrae, human, strength under sagittal compression 80—61618
  vertebral response to laminectomy, finite element model 80—41090
  vibration propagation through human femur 77—25494
  vibrational motion meas. by skin-mounted accelerometers, soft tissue effect 80—35954
  viscoelastic behaviour, anal. on basis of microstruct. 80—85429
  viscoelastic properties of Cu deficient chick bones 79—79578
  X-irrad., histopathological and physiological changes, rabbit expts. 80—51171
  X-irradiated, changes in ^{99m}Tc pyrophosphate imaging 80—72239
  X-ray induced osteosarcomas, rabbits, scintigraphic and radiographic detect. 80—101231
  xeroradiography of frontal skull and nasopharynx *(German)* 80—30873
  Young's modulus, anisotropy, fibre-reinforced composite model 80—35944
  Young's modulus anisotropy, US meas. 78—11687
  Ca activation analysis, prod. of uniform ^{38}K yield using range modulator 77—40735
  Ca and P determination in small bone biopsies by neutron activation 79—88154
  Ca levels correlated with ACTA numbers from computerised tomography 77—40756
  Ca partial-body determ. by proton activation anal. 77—86605
  Ca salts, biological mineralization mechanism 78—31764
  F content measurement by neutron activation anal. 77—86592
  I meas. in tissue, separation of bone and water, appl. of filtered bremsstrahlung spectra 79—74747
  ^{113m}In-tripolyphosphate, new radiopharmaceutical for bone scanning 80—67247
  O_2 supply to porous implants in bone analysis 79—70707

bone continued
  P, sheep, transportable system for neutron activation anal. determ. of P 80—109066
  Pb, X-ray fluorescence technique for in vivo determ. of Pb conc. 79—25084
  Pu dose to lung and bone from contaminated soils, statistical uncertainties 80—109028
  ^{239}Pu, bone model for calc. of annual limits of intake in man 79—53252
  ^{239}Pu localisation using neutron-induced autoradiography 77—40773
  ^{241}Pu bone distribution, high resolution autoradiography 78—7399
  ^{241}Pu in reindeer cortical bone from Swedish lichens 78—15912
  ^{226}Ra in Taiwan buffalo bone and environmental samples of N. Taiwan power reactor site 77—64142
  ^{226}Ra-burdened dog skeleton, Rn retention rel. to age and dosage 78—65092
  ^{90}Sr concentrations in pronghorn antelope bones near a nuclear fuel reprocessing plant 80—89875
  ^{99m}Tc radiopharmaceuticals, As for P substitution, bone-seeking agent analogues 80—51250
  ^{99m}Tc scintigraphy, use in uremic pulmonary calcification detect. 80—3788
  ^{99m}Tc-EHDP accumulation in canine tibia, meas. method 78—20245
  ^{99m}Tc-MDP scans in investigation of diffuse alterations, quantitative assessment 80—72287

Boolean algebra
  see also Boolean functions; formal logic
  antifreezing circuit design appl. *(German)* 77—64914
  axiomatisation of set of formulae of intuitionistic logic 78—57730
  Boole's search for universal analysis method influence on creation of algebraic logic 77—57144
  Boolean systems, atomicity and determinism 79—35518
  Boolean-valued models and independence proofs in axiomatic set theory, book 78—32649
  decidability of theory of Boolean algebras with cardinality quantifiers 77—67183
  digital m-of-n system with error indicating components reliability calc. *(German)* 78—41133
  formulae and transforms for automobile technicians *(French)* 80—94946
  mass spectra data identification, text search system based on Boolean logic 79—20480
  multielement, representation of multigradation images 77—31071

Boolean functions
  digital optical processing, optical parallel logic device and half-adder cct. 79—94364
  formulae and transforms for automobile technicians *(French)* 80—94946
  optical binary discrete deflector with deflection angle degeneracy 79—55239
  power system work-capability anal. *(Russian)* 77—49550
  quantum mechanics, meas. problem 80—12948
  significant variables determ., minimum number of checks 80—22187

Boolean lattices *see Boolean algebra*

bootstrap models *see bootstrapping*

bootstrap theory *see bootstrapping*

bootstrapping
  1/N dual unitarisation, triple bare pomeron parameters of Gribov's Lagrangian 78—74232
  baryon and baryonium states with string junctions in dual unitarisation scheme 78—25021
  baryon models and the planar bootstrap condition 79—3005
  baryonium mass spectrum in planar bootstrap model 78—25020
  cascade models, bootstrap eqn. and diffusion eqn. 78—29317
  cluster expansion in the truncated bootstrap model and linear graphs theory 80—102029
  conformal invariant field theory solns. *(Russian)* 78—58142
  conformal-invariant field theory, anomalous dimensions, coupling consts. 80—4870
  coupling strength of particle production, Ball-Zachariasen model of diffractive scattering 80—9158
  critical indices, conformally invariant bootstrap method 79—12955
  cumulative hadron production, statistical bootstrap model with strangeness *(Russian)* 80—62948
  dimensionality in the statistical bootstrap model 79—97606
  dual bootstrap model size of σ_{el}/σ_T anal. 77—22706
  dual bootstrap models, solns. satisfying Lee-Veneziano relation 79—71729
  dual bootstrapping and Reggeon phases 77—34132
  dual multiperipheral model, Pade approx. 77—30347
  dual multiperipheral model planar bootstrap 78—4837
  dual topological unitarisation, review of S-matrix developments for hadron bootstrap theory 78—62381
  Dual Topological Unitarisation scheme, flavour symmetry breaking 80—102030
  dual unitarisation scheme, planar amplitudes, Regge cut cancellation 77—87954
  dual unitarity scheme, single particle distrib., bootstrap eqn. 78—17002
  dual unitarization scheme with several trajectories, diffractive scatt. predictions 79—89133
  Eastern mystical philosophy, quantum mechanics and the bootstrap-quark controversy 79—84883
  fireball decay, internal symmetry structure of statistical bootstrap models 77—57501
  fireball decay in statistical-bootstrap theory 78—436
  fireball mass spectrum, bootstrap condition, J-depend. 77—67626
  gamma-ray multiplicity meas., fast converging bootstrap method for data anal. 78—70730
  hadronic eqn. of state in statistical bootstrap model and linear graph theory 77—22704
  hadronic matter, critical point exponents 79—58944
  hadronic matter, statistical bootstrap model and critical behaviour 80—42430
  hadronic matter governed by statistical bootstrap eqn. of state, hydrodynamical flow 77—22705
  Hagedorn's bootstrap model of early Universe, dense matter eqn. of state, external mag. field 78—86044
  Hagedorn Frautschi statistical bootstrap model, modification for baryon charge and strangeness conservation *(Russian)* 80—27489
  internal quantum numbers for quarks and leptons in bootstrap approach 80—95254
  internal symmetry, unitarity constraints 77—41825

bootstrapping continued
J-dependence of statistical bootstrap mass spectrum, S-matrix and semiclassical formalism comparison 78–86448
leptons, geometrical approach 80–95258
leptons, topological bootstrap approach, rishon model 80–78046
level density formula in hadron physics 77–13938
low mass diffractive dissociation in a simple t-depend. dual bootstrap model 79–13089
low mass diffractive dissociation in a simple t-dependent dual bootstrap model 79–36042
low multiplicity diffractive dissociation, 1/N dual unitarisation scheme 79–75753
mass degeneracy at fixed particle number, differential eqn. for bootstrap degeneracy 78–24732
meson mass spectrum, planar bootstrap, and Regge approach 80–22581
meson spectrum in simple planar bootstrap model 78–8618
mesons, unnatural parity, in dual unitarization scheme 77–87951
multiple scatt. in 1-D 79–44754
multipomeron bootstrap and rising cross sections *(Russian)* 77–46029
nucleon-nucleus collisions, cumulative pion prod., inelastic rescatt. contrib., statistical bootstrap model *(Russian)* 78–54766
planar bootstrap, Regge cuts cancellation, asymptotic terms 78–54619
planar bootstrap eqns. and symm. breaking 77–13939
planar bootstrap model calcs., $Q\bar{Q}$ and QQQ mass spectra 78–89685
planar pole bootstrap, and existence of good finite mass sum rules 78–16948
Pomeron t-depend. bootstrap eqn., cylinder discontinuity 79–85282
pp collisions, high energy, fireball mass, rapidity, spin distribs. 80–57645
quantum field scatt. theory of hadrons on Regge trajectory, bootstrap and quark interpretation 77–54046
quantum gas, ideal relativistic, cluster decomposition appl., statistical bootstrap eqn. 77–30095
quark confinement bootstrap model harmonic oscill. pot. 77–49912
quarks, bootstrap theory 79–49451
quarks and leptons, topological bootstrap approach, rishon model 80–78047
quarks and leptons in bootstrap topological approach 80–95253
Reggeon vertices and finite mass sum rule, bootstrap eqn., dual resonance model 80–13292
relativistic four dimensional field theoretical model of strong interactions based on statistical bootstrap 78–29315
S-matrix, planar, building of cylinder correction in topological expansion or dual unitarisation 78–62321
simultaneous bootstrap of mesonic and baryonic trajectories in dual topological unitarisation 80–42429
soliton conservation laws, S-matrix bootstrapping approach *(German)* 79–9274
soliton field theory, construction of Green's functions from an exact S matrix 79–71629
statistical bootstrap duality in inelastic scatt. 77–18239
statistical bootstrap model, hadronic mass spectrum, pion condensation, boson gas 78–70345
statistical bootstrap model for hadronic matter and multiparticle reactions 77–57502
statistical bootstrap model with spin, large transverse momenta distribs. 77–65141
statistical bootstrap with Bose statistics, cluster decomp. soln. 77–82714
statistical mechanics, relativistic formulation, appl. of bootstrap theory to thermodynamics and cosmology 79–40452
strong interaction spontaneous symmetry breakdown and finite struct. const. calc. 77–22707
strong interaction symmetry, calc. of fine struct. const. α 77–41788
tachyons, relativistically invariant hadron bootstrap, book contrib. 79–44721
thermodynamical quark bootstrap, hadron prod. 77–30336
topological bootstrap prediction for three coloured, eight flavoured quarks 80–86694
topological colour and disc mating unitarity as the source of zero triality 79–49492
topological dual bootstrap model and hadron collisions 77–22708
uncorrelated jet model with Bose-Einstein statistics, statistical bootstrap model 78–86445
vertex bootstrap conditions in dual unitarisation scheme 77–38135
vertex bootstraps conditions in dual unitarisation 77–74660
$\bar{N}N$ annihilations, statistical bootstrap model anal. 78–37224
$N\bar{N}\rightarrow$pions, direct channel scheme based on statistical bootstrap, low-energy region 78–12924
$p\bar{p}$ annihilations, multipion distrib., statistical bootstrap model 80–68472
pp interactions, cluster mass spectrum 80–37307
π cumulative prod. probability in high energy nuclear collisions *(Russian)* 77–46028
$\pi^{\pm}p$, 2-9 GeV/c, large angle elastic scatt. cross sections, parton and bootstrap model test 78–78209
$\pi^{\pm}p$ elastic scatt., 1.9-9.5 GeV, test of parton and statistical bootstrap models 78–89728

bootstraps *see bootstrapping*

borate glasses
absorption spectrum of Nd^{3+} ion, chem. composition effects, group IV element effects *(Polish)* 78–10932
alkali, ^{77}Se isotope containing, ESR of SeO_2^- and SeO_3^- radicals 79–65740
alkali, borate glass:S, blue and green coloration, absorpt. spectra 79–87470
alkali, Li^+ motion, ^7Li NMR spectra, nucl. relax. 80–34804
alkali, mech. and dielec. relaxs. and interpet. 78–27159
alkali borate, γ-irrad., paramag. SO_3^- radicals 79–42838
alkali borate, ionic motion, ^7Li NMR obs. 78–27107
alkali borate, Mossbauer effect 78–39476
alkali borate, Mossbauer expts. 85-500K 78–80260
alkali borate binary glass, energy storage behaviour studied by thermoluminesc. 80–50432
alkali borate glass networks, π-electron distrib. SCF INDO LCAO-MO calc., O basicity 78–79924
alkali borate glasses, phase separation 79–41965
alkali borate glasses, Raman study at high temps. 80–93306
alkali borate glasses, single and mixed, viscosities 80–92701
alkali boroaluminosilicate system, self-focusing fibres with aperture of 0.18 80–87548

borate glasses continued
aluminoborate glass, Fe and Cr ion interaction, mag. and spectral props. 80–103883
biased spectral decomposition in glass, ^{11}B NMR spectroscopy 78–88198
borate glass: Ni, absorption spectra, mag. props., coordination behaviour *(German)* 80–40147
borate glass:Er^{3+}, $^4I_{13/2}$ level relax. 79–87476
boric acid content, differential-photometric determ. using SPEKOL spectrocolorimeter 78–23984
boric oxide-alkali oxide glasses, use of optical spectral lines of Nd,Co,Ce as struct. changes *(Polish)* 77–68926
borosilicate optical waveguide glass, B content determ. using nuclear track counting 80–95969
boroxyl ring breakdown in vitreous B_2O_3, Raman intensity investig. 80–45058
borozirconia glazes, low-melting, struct. and liq.-phase separation 79–60282
calibo glass:Eu^{3+}, Ho^{3+}, energy transfer 78–76510
critical stress intensity factor and fracture surface energy *(French)* 77–76487
electron trap centres in borate glass containing Ag_2O, ESR obs. 77–20697
electronic structure of linear polyborates, borate clusters and transition metal doped glasses 78–10347
fibre, elongation, force depend., deviations from linearity 80–45334
fusion buttons with unknown sample/flux ratio, X-ray fluoresc. analysis 79–24851
glass:CuO, band-pass characts. improvement by doping 77–54797
heat treated, thin foil prep. for TEM obs. 78–7154
laser glass cladding composition and design criteria 79–18450
laser glasses, Cl^- coordinated, Tl^+, Mn^{2+} and Nd^{3+} impurities, absorpt. and X-ray obs. 79–38575
lead borate glasses, struct. 77–35485
mechanical relaxation in transition range 78–80575
melts, struct. determ. using graph theory 79–64980
mixed alkali borate glass, IR absorption spectra and structure 79–8148
mixed-alkali borate-glasses with high-alkali content, densities *(Japanese)* 77–7794
NMR of ^{11}B, fast stable analysis technique 78–6585
NMR of B, spectral analysis, singular-value decomposition 77–36141
nuclear spin lattice relax. in amorphous state, review 79–11354
phase separated, EPR rel. to struct., elec. and opt. props. 78–23333
radioactive waste management, French research program for solidification and disposal in borosilicate glass 80–95377
Raman scattering, low-freq., 6-700K, excess scatt. 78–23473
secondary and tertiary coordination number of Co^{2+} and chem. composition *(Polish)* 78–9960
sodium tetraborate glass, melt, temp. depend. of high viscosity property *(Russian)* 80–39336
specific heat at low temp. depend. on thermal treatment 80–54401
thermoluminescence, additives effect 78–27337
volatility of B_2O_3, effect of batch composition of liquating glass 77–27995
wetting and reactions on Pt, effect of C and water 77–7951
XPS, chemical shift *(Japanese)* 79–34416
Ag halide photochromic glasses, optical properties, effect of Cu ions 80–93364
$(AgI)_x(Ag_2O\ B_2O_3)_{1-x}$, amorphous superionic compound, ^{11}B lineshape and relaxation 80–108107
$(AgI)_x(Ag_2O.B_2O_3)_{1-x}$ glass, ionic cond. and disorder modes 80–39344
Ag_2O-B_2O_3 glasses, electrical props. and dielectric relaxation *(Japanese)* 80–20199
Ag_2O-Na_2O-B_2O_3 mixed cation glasses, electric conduction *(Japanese)* 77–24432
Ag_2O-Tl_2O-B_2O_3, mixed-cation glass, electrical cond. 79–95210
Ag_2O-Tl_2O-B_2O_3 mixed cation glasses, elec. cond. 77–80644
Al^+ ion coordination study by $AlK_{\alpha 1,2}$ X-ray fluorescence spectra *(Japanese)* 78–7308
Al_2O_3-B_2O_3-P_2O_5 glasses, formation and props. 78–83737
Al_2O_3-B_2O_3-P_2O_5 system, glass formation by laser melting 78–44074
Al_2O_3-B_2O_3-RO, glass, (R=Ba,Ca,Cd,Mg,Sr,Zn), ionic and DC cond., comp. effects 77–31804
$AsO_{3/2}$-$BO_{3/2}$, glass, props. and struct. *(Japanese)* 77–27836
B_2O_3 glass, nonlinear structural relaxation model for glassy state 78–26448
B_2O_3 glass, struct. and phonon spectra 80–50324
B_2O_3, glassy, influence of annealing on transition region 80–44145
B_2O_3 thermal conductivity, 1.5 to 30K *(French)* 77–39704
B_2O_3, vitreous, struct. and bonding determ., NMR obs. 77–39545
B_2O_3, vitreous, struct. obs. using small-angle X-ray scatt. 79–41966
B_2O_3, vitreous, torsional deform., above T_g under low stresses, temp. effect 80–21052
B_2O_3, vitreous, torsional deform. above Tg under low stresses 80–25804
B_2O_3-BaO, liquid immiscibility region, equilibration and quenching expts. 80–45288
B_2O_3-CaO-Fe_2O_3 glasses, semicond., cond. models, electronic props., 77-800K 80–54688
B_2O_3-Fe_2O_3, Fe_2O_3 crystallite formation, Mossbauer obs. 78–68429
B_2O_3-GeO_2 system melts evaporation coeffs. 79–65180
B_2O_3-K_2O-Na_2O-Rb_2O-Cs_2O glass, small angle X-ray scatt. exam. of struct. 80–38922
B_2O_3-Li_2O-Fe_2O_3, prep. by quenching methods, exam. of microcrystalline precipitates of Li_2O-Fe_2O_3 *(French)* 79–20019
B_2O_3-Li_2O-Li Cl(F)(I)(Br), vitreous, ionic cond. of Li *(French)* 79–90823
B_2O_3-Li_2O-LiCl, ionic conductor, IR refl. Raman study 80–66173
B_2O_3-Li_2O-LiCl, X-ray irradiation, EPR of Cl_2^- colour centres *(French)* 79–47333
B_2O_3-Li_2O-LiCl glass system, exam. of ionic conductivity of Li *(French)* 78–51730
B_2O_3-Li_2O-LiCl glasses, solid electrolyte, NMR meas. 80–29208
B_2O_3-M_2O:S_2 glass, (M=Li, K, Na), absorpt. spectra of S_2 mols. 79–24337
B_2O_3-Na_2O-BaO glass, rare earth doped, nonradiative decay and multiphonon relax. 77–85802
B_2O_3-Na_2O-Fe glass, mag. susceptibility 79–42733
B_2O_3-NaF-$NaBF_4$, crystalline compounds and glasses 78–11210
B_2O_3-NaKO glass, dielectric relaxation at low temp. 79–11384
B_2O_3-PbO glass-ceramic-cement composites, review 79–38783
B_2O_3-PbO-GeO_2-Fe_2O_3 glass, Mossbauer exam. of Fe valence states 79–78597

borate glasses continued

- B_2O_3-PbO-GeO_2-Fe_2O_3 glasses, mag. props. and Mossbauer spectra, speromag. order at low temps. 80−80530
- B_2O_3-TeO_2 glass, TEM obs. 78−9958
- B_2O_3-V_2O_5-P_2O_5, glass, mech. and elec. props 80−84228
- $[(100\text{-}x)B_2O_3.xLi_2O]_{98}.2CdO$, glass, X-ray irrad., EPR study of Cd^+ centres *(French)* 78−43638
- BaB_2O_4-RF_2, R=Mg, Ca, Sr, Ba, glass form., struct. and props. 80−84077
- BaO-Al_2O_3-B_2O_3:Ce^{3+}, EPR spectra, before and after X-irrad. 78−19320
- BaO-Al_2O_3-B_2O_3:Ag, X-ray irrad., atomic centre interactions, EPR spectra 80−25207
- BaO-Al_2O_3-B_2O_3-V_2O_5, spectra, oxidation-reduction behaviour, DC cond. 77−76814
- BaO-B_2O_3, composition effects on mean dispersion 78−80313
- BaO-B_2O_3, refraction, refractive index from 0.365 to 2.50 μm 80−88953
- BaO-B_2O_3 glass, $Mn^{2+} \to Nd^{3+}$ energy transfer, fluoresc. obs. 77−8621
- BaO-B_2O_3 melt, Fe_2O_3-Fe_3O_4 equilibrium, ferrite prep. 77−36428
- BaO-B_2O_3: UO_2^{2+}, Eu^{3+} glass, nonradiative energy transfer 77−59602
- BaO-B_2O_3:UO_2^{2+}, Nd^{3+} glass, radiative and nonradiative energy transfer 78−60508
- BaO-B_2O_3:$UO_2^{2+} \to Er^{3+}$ glass, energy transfer 78−2895
- BaO-B_2O_3-Al_2O_3:$Mn^{2+}(Cu^{2+})(Fe^{3+})$, EPR spectra 77−8394
- BaO-B_2O_3-GeO_2, exam. of glass formation and physicochemical props. 79−4959
- BaO-B_2O_3-V_2O_5 glasses, polaron hopping cond., optical absorpt. and ESR spectra 79−23966
- BaO-B_2O_3-V_2O_5 glass, oxidation-reduction of V, thermodynamics 80−85169
- BaO-B_2O_3-$V_2O_5(Fe_2O_3)(Cu_2O)$, glass, resist. and activation energy, reduced valency 77−51749
- BaO-Fe_2O_3-B_2O_3 glass system, mag. struct., Mossbauer study 78−39485
- BaO-Fe_2O_3-B_2O_3 glass, Mossbauer study of struct. and mag. props. 79−47369
- BaO-Fe_2O_3-B_2O_3 glass, struct. and mag. props., Mossbauer spectra 80−7226
- BaO-Fe_2O_3-B_2O_3 glass, splat cooled, low temp. micromagnetism 80−34660
- BaO-Fe_2O_3-B_2O_3 glasses, high Fe_2O_3 content, mictomagnetic props. 80−65916
- BaO-La_2O_3-B_2O_3, refraction, refractive index from 0.365 to 2.50 μm 80−88953
- BaO-M_xO_y-B_2O_3, UV absorpt., inherent absorpt. wavelength and oscill. strength, cation effects 78−80374
- $BaPO_3F$-Al_2O_3-B_2O_3 glasses, phys. props. 78−63676
- $BaPO_3F$-Al_2O_3-B_2O_3 glasses, viscosity in the softening region and crystn. range 80−29105
- $BaPO_3F$-Al_2O_3-B_2O_3 system, liq. phase separation, IR spectra, microstruct. 80−29940
- CaO-B_2O_3-Al_2O_3:$Mn^{2+}(Cu^{2+})(Fe^{3+})$, EPR spectra 77−8394
- CaO-B_2O_3-Al_2O_3-V_2O_5, cond. mechanism, current carriers, V_2O_5 conc. effects 77−62668
- CaO-B_2O_3-Fe_2O_3, dielec. relax., AC and DC cond., dielec. const. and loss 78−23393
- CaO-B_2O_3-Fe_2O_3 glass, electronic and dielec. props. meas. 77−24574
- CaO-B_2O_3-Fe_2O_3 glasses, effect of heat treatment on electronic props. 78−2480
- CaO-B_2O_3-GeO_2 system, physicochem. props., alkaline earth oxides effect 79−65827
- CaO-Fe_2O_3-B_2O_3, phys. props. rel. to struct. and comp. 78−23331
- CaO-Li_2O-B_2O_3, calibo glass, $Dy^{3+} \to Ho^{3+}$ non-radiative energy transfer, diffusion limited relaxation 79−65925
- CaO-Li_2O-B_2O_3 calibo glass, diffusion limited energy transfer from $Tb^{3+} \to Ho^{3+}$ 78−31235
- CaO-Li_2O-B_2O_3:Dy^{3+} glass, optical excitation energy transfer from $Dy^{3+} \to Nd^{3+}$ 79−15515
- CaO-Li_2O-B_2O_3:Er, Tb, calibo glass, nonradiative energy transfer 78−19541
- CaO-Na_2O-B_2O_3, Raman scatt. studies of glass struct. 77−90147
- CdO-B_2O_3-GeO_2 system, phase equilibria at 800°C, X-ray powder diffr. anal. 79−4956
- Cr complexes, ESR study of effect of glass composition on symmetry 80−88052
- Cs_2O-B_2O_3:$Tl^+(Pb^{2+})(Bi^{3+})$, optical basicity, variation with probe ion and comp. 80−2800
- Cu^{2+} impurity near IR electronic spectra, effect of alkali contents 78−27267
- xFe_2O_3-$(1-x)PbO$-$3B_2O_3$ glass, Mossbauer study of Fe cations 79−91325
- Fe_2O_3-B_2O_3-PbO glass, semicond., elec. resist. meas. 78−95300
- Fe_2O_3-$B2O_3$-PbO glasses, visible and UV optical props. *(Rumanian)* 78−48196
- Fe_2O_3-BaO-B_2O_3, magnetic props. of Fe-rich amorphous oxide *(French)* 80−80511
- Fe_2O_3-BaO-B_2O_3 glass, Mossbauer spectra, ^{57}Fe hyperfine interactions 80−39969
- Fe_2O_3-Dy_2O_3-Na_2O-B_2O_3 glass, AC mag. susceptibility, antiferromag. interactions 77−32179
- Fe_2O_3-PbO-B_2O_3 glass, X-ray and electron microscope studies, mag. and Mossbauer effect meas. 80−28919
- $(Fe_2O_3)_x$-$(3B_2O_3.PbO)_{1-x}$ glass, thermal cond. and diffusivity obs. 79−60561
- $xFe_2O_3(1-x)[PbO.3B_2O_3]$ glasses, mag. props. 77−73012
- $(Fe_2O_3)_x(3B_2O_3.PbO)_{1-x}$ glass, X-ray diffr. struct. obs. 79−32915
- $xFe_2O_3.(1-x)[3B_2O_3.PbO]$ glasses, diffuse refl. spectra 79−51982
- $20Fe_2O_3.80[3B_2O_3.(1-x)PbO.xGeO_2]$ glass, phys. props. 80−49119
- K_2O-Al_2O_3-B_2O_3, subsolidus compatibility relations determ. *(Japanese)* 79−4957
- K_2O-Al_2O_3-B_2O_3:Fe_2O_3, glasses, liq.-liq. phase separation, Fe^{3+} ions rel. to mag., optical props. 77−15322
- K_2O-AlF_3-B_2O_3 glass, Al atom bonding mode, optical absorption of VO^{2+} and AlK_α spectrum *(Japanese)* 78−11023
- K_2O-B_2O_3, γ- and UV-irrad., thermodecolorisation and thermolum. 80−20721
- K_2O-B_2O_3, laser decolorisation of colour centres 79−43008
- K_2O-B_2O_3 glass, PbO-activated, luminesc. and excitation spectra *(Russian)* 78−10979
- K_2O-B_2O_3:Cu II, glass, O basicity, ESR study 78−80199
- K_2O-B_2O_3:Mn^{2+}, fine struct. parameter distribs., EPR meas. 80−11256
- K_2O-B_2O_3-Fe_2O_3, γ-irrad., Mossbauer spectroscopic study 80−108132

borate glasses continued

- K_2O-B_2O_3-Fe_2O_3 glasses, nonbridging O formation, Mossbauer spectroscopy 80−55001
- K_2O-B_2O_3-P_2O_5 glass struct. studies using NMR 79−24221
- K_2O-B_2O_3-SiO_2, glass crystallisation range *(German)* 80−38934
- K_2O-BaO-B_2O_3 glasses, ESR detection of immiscibility rel. to Cu II ions 80−20916
- K_2O-CaO-B_2O_3:CuII, immiscibility, ESR detect. 78−80200
- K_2O-CaO-BaO-B_2O_3, calc. of network refraction and exam. of glass structure 79−4783
- K_2O-CaO-BaO-B_2O_3, refraction, refractive index from 0.365 to 2.50 μm 80−88953
- K_2O-MgO-B_2O_3:Cu^{2+}, micro-inhomogeneities, EPR and Raman study 80−84080
- $K_2O.nB_2O_3$ (n=6, 4, 3), heat of soln. *(Japanese)* 77−77802
- Li^+-rich, high elec. cond. 78−84000
- Li^+-rich borate glasses, ionic cond. and activation energy 80−107561
- $Li_2B_2O_4$-$LiFe_5O_8$, mag. props. of Fe^{3+} cations 80−100599
- $Li_2B_2O_5$ glass, phase separation 79−41965
- $Li_2B_4O_7$, ferroelectric glass, phase transition, permittivity, electrochromism, photochromism 80−80719
- $Li_2B_4O_7$, melt-crystal interface temp. meas. during crystallization of melts 79−44908
- $(Li_2B_4O_7)_{1-x}(WO_3)_x$ dipolar glass, space charge injection, thermally stimulated depolarisation currents 80−66103
- $Li_2B_4O_7.xWO_3$ (x=0 to 1 mol.) glass, random elec. dipole, cooperative phenomena 79−28693
- Li_2O-B_2O_3, crystalline and glassy, thermolum. meas. 77−16406
- Li_2O-B_2O_3, low Li_2O content, ^7Li NMR study 80−84657
- Li_2O-B_2O_3 glass, conductivity, permittivity, and dielectric loss obs., mixed isotope effect 78−95182
- Li_2O-B_2O_3 glass struct. study using ^{10}B NMR 80−84658
- Li_2O-B_2O_3 glass system, 4-coordinated B atomic fraction determ. 78−94999
- Li_2O-B_2O_3 glasses, fast ion transport 80−107470
- Li_2O-B_2O_3:Cr^{3+}, absorpt. spectra, Fano antireson. and vibronic Lamb shift 80−71458
- Li_2O-B_2O_3:Eu^{3+} glass, laser induced fluoresc. line narrowing, struct. 79−38613
- Li_2O-B_2O_3:Mn^{2+}, fine struct. parameter distribs., EPR meas. 80−11256
- Li_2O-B_2O_3:$Tl^+(Pb^{2+})(Bi^{3+})$, optical basicity, variation with probe ion and comp. 80−2800
- Li_2O-B_2O_3-P_2O_5, glass, mech. and elec. props 80−84228
- Li_2O-B_2O_3-WO_3 glass, photochromic and electrochromic props. 79−28787
- Li_2O-Li_2SO_4-B_2O_3 vitreous electrolytes, ionic cond. and Raman spectra *(French)* 80−24656
- Li_2O-LiCl-B_2O_3 system, new solid electrolytes, conductivities and activation energies 79−28137
- Li_2O-LiCl-B_2O_3 system, fast Li^+ ion vitreous superconductors, EPR study *(French)* 80−11269
- Li_2O-LiF-B_2O_3 glasses, fast Li^+ conduction 80−79984
- Li_2O-LiF-B_2O_3-Li_2SO_4 glasses, DC cond. and secondary struct. relax. 80−107469
- Li_2O-LiX-B_2O_3 glass, X=halogen, high anionic cond. of new solid electrolytes 80−107546
- $Li_2O.nB_2O_3$ (n=6, 4, 3), heat of soln. *(Japanese)* 77−77802
- M_2O-MnO-B_2O_3 glasses, M=Li, Na, K, glass-forming region and physicochem. props. 78−63678
- MgO-B_2O_3 system, glass and cryst. compd. struct. determ. by ^{11}B NMR 79−94905
- MgO-Na_2O-B_2O_3, Raman scatt. studies of glass struct. 77−90147
- $y(Mn_xFe_{3-x}O_4)$-$(1\text{-}y)B_2O_3$ glasses, elec. and struct. props., 400-1000K 79−51575
- Na borate glass, nonradiative energy transfer from $Sm^{3+} \to Nd^{3+}$ 78−80394
- Na_2-B_2O_3 glass, pulsed EPR study of Cu 78−84479
- $2NaBO_2$-B_2O_3 melt, thermodynamic props., mass spectra 80−65252
- $Na_2B_4O_7$, melt-crystal interface temp. meas. during crystallization of melts 79−44908
- NaO_2-B_2O_3 melts, fluctuations 79−94865
- Na_2O-$2B_2O_3$ glass, numerical optimisation of ESR V^{4+} spectra 79−38370
- Na_2O-$2B_2O_3$ molten glass, reactions with conducting materials 80−85186
- Na_2O-Ag_2O-B_2O_3 glass, Ag^+ ion distrib., X-ray diffr. study 80−84076
- Na_2O-Al_2O_3-B_2O_3, kinetic study of Cu^+-Cu^{2+} equilib. 79−8448
- Na_2O-B_2O_3, covered with PbO film, deep penetration of Pb^{2+} ions 78−79535
- Na_2O-B_2O_3, enthalpy of form., calorimetric study 80−66861
- Na_2O-B_2O_3, $Eu^{3+} \to Nd^{3+}$ diffusion-limited energy transfer, quantum efficiency 78−31238
- Na_2O-B_2O_3, ferroelectric glass, phase transition, permittivity, electrochromism, photochromism 80−80719
- Na_2O-B_2O_3, mag. susceptibility, annealing and base comp. effect 79−91811
- Na_2O-B_2O_3, microhardness and boric oxide anomaly 77−36624
- Na_2O-B_2O_3 glass, absorptivity of OH determ. 79−52763
- Na_2O-B_2O_3 glass, γ- or UV-irrad., laser and thermal bleaching of colour centre, absorpt. spectra 79−33744
- Na_2O-B_2O_3 glass, Na and Ag diffusion, elec. cond. 79−51300
- Na_2O-B_2O_3 glass, negative thermal expansion, LF Guneisen parameter, numerical analysis 77−11707
- Na_2O-B_2O_3 glass, PbO interdiffusion layer form. 79−51318
- Na_2O-B_2O_3 glass, struct. interpretation of ^{10}B and ^{11}B NMR spectra 78−80241
- Na_2O-B_2O_3 glass, wetting and adherence on Au 80−24714
- Na_2O-B_2O_3 glass struct. study using ^{10}B NMR 80−84658
- Na_2O-B_2O_3 glass-forming melts, thermodynamic functions 80−25673
- Na_2O-B_2O_3 glasses, electrical props. and dielectric relaxation *(Japanese)* 80−20199
- Na_2O-B_2O_3 melt, crystallisation of $Na_2B_8O_{13}$ 78−59763
- Na_2O-B_2O_3:Au glasses, Au solubility, oxidation state and opt. absorpt. 80−44321
- Na_2O-B_2O_3:Ce (III) and (IV), u.v. absorpt. 77−4658
- Na_2O-B_2O_3:Cu^{2+}, glasses, ESR and optical absorpt. 80−34760
- Na_2O-B_2O_3:Cu^{2+}, Mn^{2+} glasses, Cu^{2+}-Mn^{2+} interaction studied by ESR 80−93166
- Na_2O-B_2O_3:Fe_2O_3 glass, $Fe^{2+(3)}$ impurity ions struct.-chem. state, Mossbauer data 80−40028
- Na_2O-B_2O_3:Mn^{2+}, fine struct. parameter distribs., EPR meas. 80−11256

borate glasses continued
- Na_2O-B_2O_3:$PbBr_2$ glasses luminescence damping kinetics *(Russian)* 77—16393
- Na_2O-B_2O_3:Se, EPR, γ-ray effects *(Russian)* 78—31109
- Na_2O-B_2O_3-B_2O_3, glass with metallic Bi granules, elec. cond. 80—84493
- Na_2O-B_2O_3-CoO, Co^{2+} ions activated, magneto-opt. study 79—65844
- Na_2O-B_2O_3-Cr_2O_3, Raman spectra obs. of Cr^{VI} 77—52076
- Na_2O-B_2O_3-CuO, γ-irrad., CuO effects on EPR 80—84645
- Na_2O-B_2O_3-GeO_2 glass-forming melts, thermodynamic props. and vaporisation processes, mass spectrometric study 80—79926
- Na_2O-B_2O_3-GeO_2 system glass-forming melts, mass spectrometry obs. of thermodynamic props. 80—97468
- Na_2O-B_2O_3-Na_2SO_4, glass, exam. of chemical differentiation, using Cu ion segregation 78—87625
- Na_2O-B_2O_3-P_2O_5 glass, mech. and elec. props 80—84228
- Na_2O-B_2O_3-SiO_2, torsional deform. above Tg under low stresses 80—25804
- Na_2O-B_2O_3-SiO_2, two-phase, stresses arising during leaching 80—81086
- Na_2O-B_2O_3-SiO_2:Fe_2O_3, effect of liquid phase separated structure on transparency in near UV and visible regions 79—4823
- Na_2O-Li_2O-B_2O_3:Fe_2O_3, Mossbauer spectra, isomer shift and quadrupole splitting *(Korean)* 79—51889
- Na_2O-MgO-B_2O_3:Cu^{2+}, micro-inhomogeneities, EPR and Raman study 80—84080
- Na_2O-NaF-B_2O_3 glass, nature of conductivity 78—63876
- Na_2O-Tl_2O-B_2O_3, mixed-cation glass, electrical cond. 79—95210
- $Na_2O.2B_2O_3$-Fe_2O_3, Fe_2O_3 crystallite formation, Mossbauer obs. 78—68429
- $Na_2O.3B_2O_3$, effect of Fe_2O_3 conc. and temp. on UV absorption 77—16340
- $Na_2O.nB_2O_3$ (n=6, 4 or 3), heats of soln. *(Japanese)* 77—77802
- $Na_2S.9H_2O$-NaOH-H_3BO_3, glass, IR and Raman spectra of boro-ultramarine, exam. of S_3^- presence 78—68502
- $Na_20.3B_2O_3.xFe_2O_3$, borate glass, Fe^{3+} spin state and distrib. meas. 80—39966
- PbO-$2B_2O_3$-Fe_2O_3 glass, Mossbauer study, struct., crystallite formation, broadened quadrupole doublet 78—59761
- PbO-Al_2O_3-B_2O_3 vitreous system with relaxation structure, spinodal decomposition 78—75553
- PbO-B_2O_3, absorpt. spectra of Cu^{2+} ions and interpret. 78—27276
- PbO-B_2O_3, glass exam. of Raman spectra *(Japanese)* 79—19894
- PbO-B_2O_3, solder glass, thermal reduction of Cu^{2+} and Cu^+:Cu^{2+} effect on thermal props. 78—15350
- PbO-B_2O_3, structure toughness-composition relationship 80—104257
- PbO-B_2O_3, X-ray emission spectra of Fe and Cu 77—44089
- PbO-B_2O_3 glass-forming melt, specific volume and viscosity, temp. depend. 80—84073
- PbO-B_2O_3 glasses, microhardness 80—66612
- PbO-B_2O_3 phase-separated glass, fracture toughness, Vickers indentation method 80—85023
- PbO-B_2O_3:Cu^{2+}, glasses, ESR and optical absorpt. 80—34760
- PbO-B_2O_3-Al_2O_3 glass, spinodal decomp. during continuous cooling, theoretical anal. 80—1935
- PbO-B_2O_3-Al_2O_3 system melts and glasses, viscosity, phase separation, and supercritical fluctuations effects 79—65235
- PbO-B_2O_3-Bi_2O_3, glass with metallic Bi granules, elec. cond. 80—84493
- PbO-B_2O_3-Fe_2O_3-CuO glass, electric cond. and struct. *(Japanese)* 78—23093
- PbO-B_2O_3-SiO_2, molten mixture, microprobe state anal. by X-ray OK and BK emission band spectra *(Japanese)* 78—19606
- PbO-B_2O_3-ZnO solder glass, with admixtures, crystallisation and thermal expansion 80—24364
- PbO-ZnO-B_2O_3, Corning 7575 seal glass, devitrification 78—79532
- PbO-ZnO-B_2O_3, glass ceramic cements, crystallisation kinetics and character 77—85982
- PbO-ZnO-B_2O_3:TiO_2 glass, circuit corrosion protection on alumina substrates 79—29236
- $PbO.B_2O_3$ glass, additional IR absorpt. *(Russian)* 77—85730
- $PbO.2B_2O_3$, vitreous, structural aspects studied by Raman scattering 77—8575
- $(PbO.2B_2O_3)_{1-x}(Fe_2O_3)_x$ glass, mag. resonance studies 79—78509
- $PbO.3B_2O_3$:Fe_2O_3, EPR of Fe^{3+} ions 78—72400
- $xPb0.(1-x)B_2O_3$:Fe_2O_3, Mossbauer spectra 79—87338
- S-doped, (boro-ultramarine), blue chromophore identification 77—20888
- Sb-containing glasses, ^{121}Sb Mossbauer spectra 77—20764
- $SbO_{3/2}$-$BO_{3/2}$, glass, struct. and props. *(Japanese)* 77—27836
- SiO_2-Al_2O_3-CaO-MgO-B_2O_3, E-glass, acid resist. studies 80—60991
- SiO_2-B_2O_3, Brillouin scattering meas. of attenuation and vel. of hypersounds 80—100309
- SiO_2-B_2O_3, struct. and phonon spectra 80—50324
- SiO_2-B_2O_3 glass system, gel hot pressing synthesis and characterisation *(French)* 80—66468
- SiO_2-B_2O_3-Na_2O-K_2O glass, strengthening by partial leaching 80—60993
- SiO_2-BPO_4, glasses and devitrificates prep., IR spectra *(Polish)* 80—71624
- SiO_2-CaO-ZnO-B_2O_3-Na_2O-S, SrO effect on crystallisation 80—54135
- Sn borate glasses, IR and ^{119}Sn Mossbauer spectra 78—60438
- SrO-B_2O_3-GeO_2 system, physicochem. props., alkaline earth oxides effect 79—65827
- Tl_2O-B_2O_3, glass, ^{205}Tl NMR 77—59470
- Tm^{3+}, in oxide glasses, multiphonon relax. rates and fluoresc. lifetimes 77—77266
- $UO_2^{2+} \rightarrow Ho^{3+}$, energy transfer processes 78—10969
- V_2O_5-ZnO-B_2O_3 glass, sputtered, optical absorpt., band gap and Urbach tail 77—8597
- WO_3-B_2O_3-ZnO semiconducting glasses, DC cond. and optical absorpt. 80 -107783
- ZnB_2O_4-MF_2 (M=Mg, Ca, Sr, Ba) glass system, physicochem. props. 80—34877
- ZnB_2O_4-RF_2, R=Mg, Ca, Sr, Ba, glass form., struct. and props. 80—84077
- ZnO-B_2O_3, glass, ESR exam. of paramagnetic centres formed during mech. destruction by grinding 78—88188
- ZnO-B_2O_3, refraction, refractive index from 0.365 to 2.50 μm 80—88953
- ZnO-B_2O_3, structure toughness-composition relationship 80—104257
- ZnO-B_2O_3:Cu^{2+}, glasses, ESR and optical absorpt. 80—34760
- ZnO-La_2O_3-B_2O_3, refraction, refractive index from 0.365 to 2.50 μm 80—88953

Bordoni effect
- dislocation motion, thermally activated, kinetics in periodic pot. 79—99193
- FCC high purity metals, Double Kink Generation model 80—79873
- relaxation modes, internal friction and microdeformation rel. to dislocations *(French)* 79—37758
- thermally activated double kink form. model without approximations 78—63805
- Ag, Bordoni effect during recrystallisation 77—90388
- Ag, internal friction vibr. reed technique 78—43276
- Al, Bordoni relaxation, microdeform. 80—104204
- Al dilute alloys, cold worked, internal friction peaks 80—97520
- Al, lattice resistance stress, Bordoni relax., microdeform. and US attenuation results 80—25747
- Al, microdeformation associated with double kink formation *(French)* 77—28873
- Al, pure, Bordoni effect during recrystallisation 77—90388
- Al, pure, cold worked, internal friction peaks 80—97520
- Au, polycrystn., dislocation relaxation under high pressure 79—77605
- Au-Cu(Ag)(Pt), cold worked, impurity conc. rel. to internal friction Bordoni peak, solid soln. hardening mech. 80—16363
- Cu, elastic modulus and internal friction during plastic deform., dislocation props. determ. 80—35244
- Cu, electron irradiated, dislocation defect dragging, 4.2 to 350K 78—43027
- Cu single crysts., Bordoni peak, 10.2 and 30.6 MHz 80—66566
- Cu-Au(Ni)(Zn), elastic modulus and internal friction during plastic deform., dislocation props. determ. 80—35244
- Cu-Ni(Au), elastic modulus and internal friction during plastic deform., dislocation props. determ. 80—35244
- Fe, magnetic disaccommodation, low temp. in neutron-irrad. sample, Bordoni relax. 77—4542
- Mg, pure, Bordoni relax. behaviour after plastic deformation 80—20997
- Ni, cold-worked, Bordoni peaks activation parameters 79—82282
- Pb, activation energy and primary characts. of Bordoni relax. peak 77—69040
- Pb, high purity, polycrystalline, Bordoni relaxation peak high vacuum annealing effect 78—39828
- Ta, polycrystn., dislocation relaxation under high pressure 79—77605
- Ti, irradiated and cold worked, internal friction pdaks 77—86074

boron
- *see also nuclei with ......*
- abrasive props. of β-B 77—63808
- abundance determ. in rocks, soils, plants, waters and fertilisers 78—85559
- abundance in meteorites rel. to interstellar grain synthesis 79—16894
- abundance in solar system 77—49318
- abundances in α Lyrae (Vega) and α Canis Majoris (Sirius) 77—53585
- addition to C fibres, effect on struct. and physical props. 78—68715
- adsorption on W, with La, field emission meas. 78—47662
- amorphous, crystn., α-rhombohedral B prep., book contrib. 78—48295
- amorphous, hopping cond., book contrib. 78—47797
- amorphous, microimpurities determ. using hollow cathode discharge 80—85247
- amorphous, prep. methods, review, book contrib. 78—48358
- amorphous, X-ray Raman edge extended modulation for struct. study 80—49111
- amorphous, X-ray Raman scatt. 78—48157
- amorphous film, elec. cond. in strong elec. field 77—11928
- amorphous film, interference enhanced Raman scatt. 80—50326
- amorphous film, Raman scatt. exam. 78—39545
- atom, and 1st row ats., Compton profiles, momentum distribs., correlation effects 77—88429
- atom, beam-foil populations, charge state distribs., independent electron model 77—19035
- atom, electron affinity, modified variational approx. 78—66679
- atom, electron impact ionisation, in RF ion source, effective cross-sections 78—22034
- atom, ground state energy, HF calc., second-order correction 78—86784
- atom, ground state static polarisability and hyperpolarisability, numerical SCF method 79—36567
- atom, ground state wave function, 2s-2p electron promotion effect 78—86779
- atom, ground state wavefunction, SCF HF calc. 78—90070
- atom, K-shell ionis., double and single, cross section meas. by ion bombardment 78—50629
- atom, min. basis of Slater-transform-Preuss functions 79—59343
- atom, model pots., STO calcs. 77—408
- atom, muonic X-ray intensities in low-Z elements and their hydrides 80—9761
- atom, optimised one-electron wave functions 77—38598
- atom, oscill. strength distribs., Stieltjes imaging determ. 77—6731
- atom, s-shell spin polarisation calcs. 77—75318
- atom, SCF electron-gas local-spin-density model including correlation 80—9488
- atom, spectra and energy level data tables 79—59386
- atom, X-ray spectra, chemical bonding and multiple ionis. effects 78—50630
- atom, X-ray spectral line broadening in solid and gas targets 77--6713
- atomic correlation energies, perturbations and near degeneracy 79—3371
- atoms and ions, excited in single gas collisions, high-resolution Auger spectra 80—9717
- atoms and ions, regularities within Stark widths of reson. lines 78—78662
- Auger and energy loss spectra *(French)* 78—23565
- bare nucleus+He, electron capture to excited states, X-ray cross-sections 77—71814
- book 78—48292
- boriding of high purity Fe with cryst. B powder 80—84951
- boriding W and Mo, Cu influence 80—21165
- boronising, titanium alloys, effect on wear 78—19903
- boronizing Ti-Mo alloys, reaction kinetics 79—61797
- borosilicate optical waveguide glass, B content determ. using nuclear track counting 80—95969
- BR3 reactor, instrumentation for continuous monitoring of primary water B content *(French)* 80—32408
- burnable poison in reactor fuel side plates, identification by neutron radiography 79—54492
- carbonaceous chondrites, B concs. 79—16897
- channelled ions, meas. of stopping power in Si:Th 79—28025

boron continued
- chemical anal. in complex matrices by charged particle track registration in plastic detectors 79—18080
- chemical properties, reacts., review, book contrib. 78—48653
- chemical transport with I_2, BI_3 synthesis 78—52682
- coadsorption with La on W, field emission and field ion microscopy 80—104049
- coating on mild steel, sliding and abrasive wear, corrosion resist. 78—11428
- coating on steel 45, effect of abrasive particle size on wear 78—44225
- coatings on graphite, fusion reactor appl. 80—23147
- concentration determ. in atm. and rainwater in Vizcaya, Spain *(Spanish)* 78—57264
- concentration profiling in solids by neutron TOF using $^{11}B(p,n)^{11}C$ 79–51131
- conference, Varna, Bulgaria (Oct. 1978) 80—12842
- CVD, closed system, deposition rate, models for interpretation 80—97438
- CVD, closed system, deposition rate and rate-limiting steps 80—93492
- CVD, deposition rate, in closed system, influence of HCl 80—84855
- CVD, deposition rate and supersaturation relationship using combined flux model 80—84856
- CVD, morphologies, influencing factors, temp. range 1390-1640K 80—89154
- CVD, structure of deposits-process relations 78—27410
- CVD from BBr_3-H_2, thermodynamic anal. mixtures 79—47634
- CVD from BCl_3-H_2 and BBr_3-H_2 gas mixtures onto inert substrate, thermodynamic approach *(French)* 78—44020
- CVD from BCl_3-H_2 mixture, on metallic substrate, thermodynamic exam. *(French)* 78—27412
- CVD from impinging jets, mass transfer, equilib. and kinetics 78—27409
- CVD on inert and metal substrates, Gibbs free energy minimisation 80—16201
- deep diffusion into Si, expt. results 80—54437
- determ. by atomic absorption, using low temp. flames 80—30307
- determination, in Al, spark-source mass spectrometric method 79—74479
- determination, in Si, by AES *(Japanese)* 78—91356
- determination by activation anal. (α,n), (α,p) reacts. investig. 80—61206
- determination in high purity Al 77—90707
- determination in non-oxidising austenitic steel by secondary ion emission and X-ray microanal. *(French)* 80—11985
- determination in nuclear power station waters, flame photometer method 78—45672
- determination in optical waveguide glass by DC plasma emission spectroscopy 80—87446
- diamond: B, doping by diffusion at high temp. and press. 79—19273
- diamond: B, natural, sub PPM determ. of B, identification of acceptor centre 77—59035
- diamond:B, B conc. and impurity-to-band activation energy 79—56165
- diamond:B, electron irradiated, defects at low temps., elec. resist. meas. 77—11593
- diamond:B, electron irradiated, threshold energy for atomic displacement, elec. cond. meas. 77—11594
- diamond:B, electronic struct. of deep levels, LCAO, SCF method 79—82555
- diamond:B, epitaxial layer, charge transfer and acceptor state 78—19169
- diamond:B, photoconductivity and electroabsorpt. spectra 77—4647
- diamond:B, substitutional impurities 79—87056
- diamond:B, synthetic, current-voltage characteristics, temp. depend. *(Russian)* 79—7825
- diamond:B, synthetic semicond., thermostimulated conductivity *(Russian)* 79—7834
- diamond:B, thermoluminesc., TSC, correlation meas. 78—88369
- diamond:B, variable-range hopping cond., effect of electron irrad. induced compensating centres 77—43599
- diamond:B hopping conductivity in range 12 to 1300K 78—51994
- diffusion, stress-enhanced, in Si, using SiO_2 diffusion masks, photodiode fabrication 78—67865
- diffusion in Si, distrib. of B in thin diffusion layers 77—7753
- diffusion in Si, implantation damage effects 78—55988
- diffusion in Si, in oxidised atmosphere, minicomputer model *(Rumanian)* 79—82247
- diffusion in Si, influence of dislocations 78—18840
- diffusion in Si, proton enhanced diffusion and vacancy migration 78—67747
- diffusion in Si, radn. enhanced 80—29216
- diffusion in Si, separation factor estimation 79—86926
- diffusion in SiC, elec. cond. meas. 80—96696
- diffusion in Sic, polytype struct. effect 78—59983
- diffusion in solids, double, gettering of impurities 80—75383
- diffusion in X-ray interferometer analyser, effect on moire pattern *(Russian)* 79—44994
- diffusion in ZnO based ceramic, effect on electrophys. and structural props. *(Russian)* 80—49423
- diffusion into Co base alloys, boride coating formation, microstruct. and mech. props. 78—11427
- diffusion into Si, SiO_2 from sputtered borosilicate glass film 80—29040
- diffusion into Si from CVD BN covered with Si_3N_4, appl. to master slice p-MOS IC 80—107564
- diffusion into steel, boride coating formation, pack cementation process, microstruct. and mech. props. 78—15592
- diffusion layer, multicomponent, formation on Ni *(Russian)* 77—44400
- diffusion layer formation on Ni *(Russian)* 77—48570
- diffusivity, in Si:P, versus Si oxidation rate 77—15436
- dispersed fractionated powder, struct. obs. 80—19703
- effect on grain refinement in Al 78—52828
- electrical conductivity, influence of impurities in β-rhombohedral phase 77—4345
- electron beam deposition, rotatable support for ulta high vacuum system 79—40586
- electron beam non-crucible zone remelting prep., anal. of gaseous impurities 80—20785
- electron beam zone melting growth, crystn. and defect form. 80—15020
- electron beam zone refining of β-phase, crucibleless, crystn. front shape 79—78871
- electron microprobe local anal. of light elements, ultrasoft X-ray spectroscopy 80—99027
- electron structure study by positron annihilation 80—16117
- electronic structure, X-ray emission spectra *(Russian)* 79—33865
- epoxy laminate, notched, fatigue damage 78—3215
- evaporated, electronic struct., XPS, SXS and isochromat investig. 80—76143

boron continued
- fibre, fracture, Griffith criterion appl. 77—12684
- fibre, metallisation by continuous casting in Al and Al alloys *(Russian)* 78—35538
- fibre, plasticizing and wettability-enhancing coatings 79—29252
- fibre, prep. by closed CVD system, mech. props. and surface defects 79—52311
- fibre, prep. in closed CVD system 79—83129
- fibre, proximate void origin and initial growth stages 77—80498
- fibre, reinforced Al and SiC coated reinforced Al-V-Ti, tensile and compressive strength, prior thermal treatment effect 78—11264
- fibre, surface energy meas. from Griffith cracks 77—77563
- fibre, US inspection, immersion method 80—66757
- fibre addition to graphite reinforced epoxy, radiographic inspection aid 78—95880
- fibre prep. 79—28983
- fibre reinforced 6061 Al alloy, fracture 80—11773
- fibre reinforced Al, crack tip damage and fracture toughness 79—57093
- fibre reinforced Al, elastic props., 300-4K 77—86066
- fibre reinforced Al, fracture 79—57092
- fibre reinforced Al, fracture mechanical study, unidirectional composites 78—88520
- fibre reinforced Al, fracture propag. 78—23823
- fibre reinforced Al, fracture toughness 77—70157
- fibre reinforced Al, hot pressed forged, plasma sputtered *(Russian)* 78—35330
- fibre reinforced Al, hot reverse moulding of tubes, calc. of process optimum parameters *(Russian)* 78—15344
- fibre reinforced Al, impact behaviour under fatigue 80—7661
- fibre reinforced Al, impact damage tolerance and reliability 80—81177
- fibre reinforced Al, interaction between fibre and matrix 80—10712
- fibre reinforced Al, orthotropic elastic stiffness consts., US vel. meas. 80—49289
- fibre reinforced Al, prep. by reaction sintering 79—38769
- fibre reinforced Al, residual stress, internal friction anal. 80—45339
- fibre reinforced Al, strength of fibre-matrix interface and tensile strength *(Russian)* 80—21005
- fibre reinforced Al, stress redistrib. anal., upon brittle fibre breakage 78—48527
- fibre reinforced Al, stress redistribution in fibre elastic deformation failure *(Russian)* 79—47740
- fibre reinforced Al, stressed state nondestructive testing method *(Russian)* 80—40631
- fibre reinforced Al, tensile strength and brittle fracture 80—11707
- fibre reinforced Al, thermal degradation of tensile strength, due to fibre strength degradation 78—39861
- fibre reinforced Al, thermal expansion 77—51525
- fibre reinforced Al, thermophys. props. 80—59745
- fibre reinforced Al, unidirectional, K-calibration and compliance curves 78—88518
- fibre reinforced Al, with imperfect separation boundary, material stability *(Russian)* 80—54307
- fibre reinforced Al, X-ray investigation of internal stresses *(Russian)* 77—73290
- fibre reinforced Al alloy, corrosion resistance, electrochemistry 80—11806
- fibre reinforced Al alloy, influence of bond strength on failure *(Russian)* 79—43387
- fibre reinforced Al alloy 6061, cross plied laminate, tension-compression fatigue 79—38940
- fibre reinforced Al alloy D16T, sheet reinforced by Ti alloy butt straps, fatigue 79—100262
- fibre reinforced Al alloys, hot compression moulding, optimum parameter calc. by pipe piercing *(Russian)* 79—66027
- fibre reinforced Al composite, transverse creep, comparison with laminated Al 77—36587
- fibre reinforced Al composites, corrosion, electrochem. behaviour 79—20225
- fibre reinforced Al laminate, effect of ply by-up sequence on fracture toughness 78—35492
- fibre reinforced Al laminate, unidirectional, interlaminar shear strength exam. 78—35434
- fibre reinforced Al matrix, matrix-fibre interaction depend. on metallic dopants *(Russian)* 80—76479
- fibre reinforced Al strength determ. procedure in annular specimens *(Russian)* 78—95864
- fibre reinforced Al VKA-1 composite, fibre/matrix interface reaction during prep. 80—25619
- fibre reinforced Al-Cr(Mg)(Mn)(Si), calc. of thermodynamic interaction potential between B fibre and matrix 80—11627
- fibre reinforced Al-Mg, heat treatment effect on struct., tensile strength 80—55487
- fibre reinforced Al-Zn-Mg composite, packet rolling, thermodeform. process parameters *(Russian)* 80—55433
- fibre reinforced epoxy, fracture mechanical study, unidirectional composites 78—88520
- fibre reinforced epoxy, fracture mechanics 80—35294
- fibre reinforced epoxy, laminate, stress anal. finite element modelling 79—59924
- fibre reinforced epoxy, tensile anal. of edge notch 77—70159
- fibre reinforced epoxy angle-ply laminate wave propag. during transverse impaction 79—83295
- fibre reinforced epoxy composites, notched, tensile strength and failure modes 80—81205
- fibre reinforced epoxy resin laminate, fatigue damage, stiffness/strength comparison 77—90451
- fibre reinforced Mg, exam. of fatigue props. and corrosion 80—11751
- fibre reinforced Mg, fibre-matrix interfacial reactions 80—20043
- fibre reinforced W double coaxial composition rod, waveguide, normal mode US propag. 79—100317
- fibre reinforcement of thermoplastics, creep resist. and elastic moduli 80—55458
- fibre-reinforced epoxy and Al, cryogenic tensile, compressive and shear props. 78—6983
- fibres, amplitude depend. of internal friction 80—20990
- fibres, prod. and phys. props. *(French)* 78—23647
- fibres, quality evaluation from morphological and fractographic characteristics *(Russian)* 79—70150
- fibres, radial cracks 78—15505
- fibres, surface morphologies rel. to mech. props. 80—11749

boron continued
  fibres of various diameters, tensile strength, elasticity, elongation 78−3189
  fibres with brittle coatings, critical thickness and strength *(Russian)* 80−40426
  filament, light emission during fracture 77−28896
  filament, uncoated and SiC coated, high temp. physicomech. props. 79−20140
  filament CVD technology, book contrib. 78−48352
  filaments, CVD prep., elec. resist. 80−15523
  filled elastomer mould, surface coating for wear prevention in mould 78−64728
  film, electric field effect on struct. 80−20050
  film, prep. by H reduction of BCl$_3$, struct. and hardness 80−54543
  film, vacuum deposited, as first wall material, sputtering yield meas. *(Japanese)* 80−25513
  film growth by phys. vapour deposition 80−16200
  films, amorphous, prep., struct., props., review, book contrib. 78−48321
  fumarole B isotope composition, Satsuma Iwo-Jima, Japan 80−67358
  fusion reactor He embrittlement simulation, splat cooling in development of B doping 80−30072
  galactic B abundance, rel. to cosmic-ray nucleosynthesis and extragalactic matter infall rate 79−17084
  graphite, pyrolytic doped with B^{11}, neutron irrad. damage at 60°C 79−90702
  HTGR pebble bed core, initial heterogeneous poisoning by B and HF 80−22981
  ignition and burning *(Russian)* 80−45502
  implantation distribution in Si, determ. using ion bombardment 80−44230
  implanted ions in n-type Si, high-temp. treatment effect on distrib. profile *(Russian)* 77−89454
  impurity in Al nuclear reactor fuel tubes, proton activation determ. 80−27741
  impurity in Cr-Mo-V low-alloy steel, effect on prior austenite grain boundary embrittlement 80−66657
  impurity migration from doped Si sources in epitaxial layers *(Russian)* 80−107570
  inorganic B, in St. Lawrence Estuary, determ. *(French)* 78−77274
  interstellar abundance and depletion models 80−46630
  interstellar B, detect. in front of κ Orionis 80−51841
  interstitials, in transition metals, electronic structure 79−1583
  ion, equilib. charge state distrib. in C foil and doubly excited states *(French)* 77−27171
  ion beam prod. and ionisation 78−843
  ion implantation in laminar Si-SiO$_2$ systems struct. change investig. by MSSI *(Russian)* 80−107918
  ion implantation in Si, damage obs. by X-ray double refl. 77−15463
  ion implantation in Si, processing parameters for diffusion redistribution 79−10871
  ion implantation into Si, ranges of implanted B$^+$ and B^{2+} 77−31687
  ion implanted MOS struct., form. and annealing of radiation damage 79−56321
  ion implanted MOS structure, radiation defects and impurity activation 80−103757
  ion sputter source 79−93857
  ions, beam-foil excitation, relative initial populations, lifetime curves 80−14210
  IR-active phonons, reflectivity and absorption spectra 79−82294
  isoelectronic sequence, ionization equilib. balance, solar and stellar atms. appl. 79−36587
  isoelectronic series, dipole oscill. strengths, multiconfigurational Hartree-Fock calcs. 77−83540
  isotope separation, laser photochem., method, using Ti catalyst 77−61612
  isotope separation, microwave reson., triplet state photochem. technique 77−32818
  isotopic analysis, by AAS, using Ne-filled discharge lamp source 78−20097
  laser, X-ray range, inner-shell photoionis. pumped, practicability 77−58319
  lateral diffusion in polycryst. Si, influence on submicron MOST fabrication 78−26588
  liquid, thermoelastic props. near melting point 80−19862
  main-sequence stars, Li, Be and B abundances rel. to envelopes hydrodynamical instabilities 78−93202
  meteorites, B isotopic anomalies rel. to protosolar cosmic ray fluxes 80−4462
  microalloyed Cu, elec. cond. and strength props. *(Polish)* 80−89285
  multidionate acceptors for electrophotography 79−19632
  muonic X-ray transitions, nuclear charge radii 80−99589
  neutron capture therapy of brain tumours, simultaneous flux monitoring system 79−92352
  neutron irradiated, quantitive anal. using cellulose nitrate solid state track detectors 78−56937
  nuclear appls., review, book contrib. 78−46154
  nuclear target, self supporting film production 80−18747
  ohmic contacts from Ni and Pd electrodeposition 77−44177
  Pacific Ocean bottom sediments, interstitial waters B content 80−36289
  pellets preparation from powder, for X-ray materials testing under pressure 80−50569
  photoemission of β-rhombohedral B, photon energy depend. of work function 78−19637
  piezoconductivity of β-rhombohedral phase 78−39110
  plasma, efficient heating by superelastic laser energy conversion 80−96372
  poisoned ^{235}U-H$_2$O solns., subcritical limits calc. 79−85723
  polymorphic modifications, struct. changes on Zn incorporation 78−79596
  polymorphism, cryst. chem., struct., growth, book contrib. 78−47278
  polymorphism rel. to CVD mechanics and deposit structs. 80−15403
  powders, modifications, exam. of physical props. and electron structure 79−94954
  preparation and purification, physical characterisation *(French)* 80−16189
  preparation by vacuum decomposition of purified BI$_3$, purity 79−91589
  properties of α- and β-rhombohedral, and tetragonal B, review 79−42532
  protective coatings, in situ prep. for controlled nuclear fusion devices 79−3238

boron continued
  protective coatings for first wall, prep. by means of low press. plasma CVD 80−35103
  proton activiation analysis of B and Li local levels in minerals, rocks and ores 79−74477
  proton induced X-rays as source for mass absorption coeff. meas. 78−2942
  purity evaluation by elec. meas. 78−59822
  PWR, critical B concs. and cycle lifetime predictions 80−9365
  PWR, on-line meas. of B concentration in water using neutron absorption method *(French)* 80−32409
  pyrocarbon:B, g-factor anisotropy *(Russian)* 79−47001
  pyrolitic, CVD 77−12536
  quartz glass, Ge and B dopants, OH impurities, preform material and fibre optic waveguide struct. 80−64173
  reinforced Al laminates, applic. of linear elastic fracture mechanics 77−28893
  residual photoconductivity in single crysts. 80−20241
  β-rhombohedral, appl. in abrasive pastes 80−21114
  β-rhombohedral, C-doped, EPR meas. partly resolved absorpt. spectra 80−20449
  β-rhombohedral, containing Sc, X-ray diffr. indicating ScB$_{28}$ 78−34464
  β-rhombohedral, containing Zr, X-ray obs. of ZrB$_{\sim 51}$ 79−23574
  β-rhombohedral, dielectric loss temp. depend., −196 to 350°C 80−20585
  rhombohedral, elec. cond., thermoelec. power, and Hall coeff. 80−6843
  β- rhombohedral, elec. props. at high temps. and in strong elec. fields, thermistor appls. 80−92903
  β-rhombohedral, EPR, book contrib. 78−48041
  β-rhombohedral, high field elec. cond., single voltage pulse meas. 80−20201
  β-rhombohedral, hopping cond., book contrib. 78−47797
  β-rhombohedral, Knoop hardness and room temp. resist., rel. to purity 80−21084
  β-rhombohedral, localised states charact., review, book contrib. 78−47728
  α-rhombohedral, mag. susceptibility temp. depend. 80−34585
  α-rhombohedral, magnetic props. and ESR spectra 80−20452
  β-rhombohedral, optical absorpt. band, temp. depend., anomalies *(Russian)* 79−28772
  β-rhombohedral, optical absorption band in 8 μm region, anomaly of temp. dependence 80−29735
  α-rhombohedral, prep. methods, book contrib. 78−48295
  β-rhombohedral, purification by electron beam melting and CVD 80−20781
  β-rhombohedral, single cryst. growth, modified Verneuil method *(French)* 78−44005
  αrhombohedral, surface energy calc. 77−85048
  β-rhombohedral, thermally activated hopping, 140-300K 80−20189
  β-rhombohedral form, field effect on hopping cond. 79−82589
  β-rhombohedral structure, accurate refinement 77−58973
  in seashells, B loss during weathering rel. to palaeosalinity determ. 77−78204
  seawater, bulk viscosity and l.f. sound attenuation, Be and B influence 77−3696
  segregation in alloy steels, assessment 77−63627
  semiconductive, diffusion of Au, Ag and W, temp. depend. of coeffs. mechanism 77−7898
  semiconductor doping, diffusion process using water vapour press. to control B-glass vapour press. 77−7749
  semiconductor properties and use for making devices, review 78−60131
  n-Si:B, ion implanted, rapid identification of faulted loops 79−19254
  Si:B, isolated A$^+$ states under high compressive stress, long wavelength photocond. spectra 79−60765
  sintering, isothermal, surface area reduction 77−8779
  skarns, B distrib. as mineralisation test, (n,α) radiography 77−17091
  solid solution, in Si, equilib. with B$_2$H$_6$ 80−97721
  sputtering yields on light ion bombardment 79−38702
  stainless steel determination of 0.001 to 0.01% by extraction and photometry 77−56275
  steel:B, brittle rupture, (n,α) radiography method *(Russian)* 78−48491
  steel, B concentration and solubility depend. on introduction of rare earth metals *(Russian)* 80−65226
  steel, hardenability, role of B and P segregation 80−97486
  steel cladding, B distrib. after Na exposure and high-temp. 77−57719
  sublimation of β-rhombohedral form, 1823 to 2253K, torsion-effusion and mass spectroscopic meas. 77−39673
  tetragonal, cryst. struct. 80−15045
  tetragonal, phase I, prep. and struct., book contrib. 78−47277
  tetragonal, X-ray diffr. and C doping obs. *(French)* 79−14731
  β-tetragonal form, cryst. struct. related to α-AlB$_{12}$ 79−77551
  transport and lattice parameter change during sintering of β-SiC 80−108370
  wires, thin fatigue limit and tensile strength 80−25834
  X-ray Kα spectra rel. to structure of rare earth tetraborides 77−59646
  zone melting, solar energy appl., struct. and elec. props. 77−16492
  zone-refined effect of Ni doping on conductivity type, microhardness and metallographic obs. 77−31682
  Al:^{12}B, relax. mechanism for polarised implant 78−87693
  Al-B fibre-D16 alloy welded composites, structure, strength and fracture props. *(Russian)* 80−108524
  Al-SiO$_2$-Si structs., implanted B$^+$ ions, high-freq. CV characts. *(Russian)* 78−80056
  Al-SiO$_2$-Si:B ions, annealing effect on energy spectrum of radiation defects *(Russian)* 78−88488
  Am-B, neutron fluence-to-dose conversion factors 79−6771
  B fibre reinforced Al, dynamic Young's modulus and internal friction 80−25754
  B fibre reinforced epoxy, dynamic Young's modulus and internal friction 80−25754
  B fibre reinforced epoxy resin, anisotropic laminate, effective modulus of elasticity 77−4802
  B fibre/Al laminates, use in neutron collimators 79−45506
  B I, spectra calcs., fine struct., transition energies 77−42260
  B I, weighted oscillator strengths for elec. dipole and forbidden transitions, data tables 80−37779
  B I and II, high spin and mixed states 77−61709
  B I isoelectronic sequence, forbidden transition probabilities for ground terms 77−2376
  B II, electron-impact excitation calcs. 79−81286

boron continued
B II, oscill. strengths for $2s^2$, $2p^2$, $2s3s(^1S)$-$2s2p(^1P)$ transitions 77—46533
B II, Stark shift, shock tube meas. 77—50403
B III, IV, laser produced plasma, satellite spectra 78—5165
B III, optical oscillator strengths for excitations from $1s^2 2s(^2S)$ ground state 79—98044
B IV, doubly-excited states, energy levels, calc. and expt. *(French)* 78—41971
B IV, ionisation rate coeff. in θ-pinch plasma, spectral meas. 77—6911
B IV, V, beam-foil meas. of mean lives below 450 Å 78—90120
B V, and isoelectronic series, in laser-produced plasma, Balmer fine struct. (broadening) 80—48860
B$^-$, metastable, electron affinity calcs. 79—31439
B$^-$, photodetachment cross-sections, crossed beam meas. *(German)* 77—42298
B$^+$, beam-foil excitation, absolute Auger yield meas. 80—14203
B$^+$, beam-foil excitation; absolute Auger yield meas. 79—45685
B$^+$, dynamic multipole polarisability, coupled Hartree-Fock 78—82858
B$^+$ fraction from Freeman type high current source for implantation appl. 78—66005
B$^+$, Hund's first rule, new interpretation 78—78620
B$^+$ ions, beam foil excitation, L-Auger decays, autoionisation 77—14569
B$^+$, reson. line regularities in plasma Stark widths and shifts 80—43881
B^{2-}, parameters for analytical radial orbitals, total and binding energies 77—6668
B^{2+}, ^2S, $^2P^0$ and ^2D autoionising states, positions and widths 79—26944
B^{2+}, $1s3s3p\ ^4p^0$ state, Hartree-Fock function, third-order energy 78—37569
B^{2+}, multipole polarizabilities and shielding factors, calcs. on open shell ions 78—46263
B^{3+}, electron impact excitation, cross-sections, modified Oppenheimer approx. 78—82843
B^{3+}, few-parameter two-electron wavefunction of ground state 77—75051
B^{4+}, resonant coherent excitation of channeled ions 79—51178
B:C,H amorphous film, IR absorpt. spectra 77—77312
B:H amorphous CVD films, IR, visible, and near UV optical props. 80—50442
B:H amorphous films, optical band gap, thermal treatment effect 80—93415
B/Na ratio in coastal N. Florida rainfall 77—21838
B-Al cast braid, crystallisation and structuring of Al matrix *(Russian)* 78—52725
B-C system, electron probe microanalysis and destructive chem. methods of study *(French)* 80—11982
B-epoxy-Al sandwich laminate. influence of residual stresses on tensile strength 78—60703
B-H, possibility of thermonuclear fuel in relativistic plasma *(Russian)* 80—37573
B-like ions, autoionisation states calcs. 80—43006
B-like ions, highly ionised, up to Fe XXII, Breit-Pauli approximation 78—53810
B-p fusion reactor advanced fuel development and confinement 79—13516
B-Ti composite material, for loudspeaker's diaphragm, preparation by physical vapour deposition *(Japanese)* 80—58883
^{10}B-loaded liquid scintillator with pulse-shape discrimination 79—59309
B+Ar(Kr)(Xe), B emission line broadening in glow discharge lamp 77—3304
B+C^{2+}(N^{2+})(O^{2+}), K Auger electron spectra 79—89758
B+C(N)(O) ions, 10-40 MeV, soft X-ray spectra 77—75089
B+CsF(RbF)(KF)(NaF), gas phase chemiluminescence reaction 77—29013
B+H$^+$(He$^+$), double K-shell ionis., projectile Z depend. 78—25680
B+He (methane), B atom K-shell binding energy by Auger spectra 78—50525
B+He (methane), collisional excitation, prompt decay line energy, projectile Auger spectrosc. 79—85941
B+He(Ne)(Ar), ground and excited states interaction, B spectral line breadth 77—68092
B+N$_2$O, chemiluminesc. reaction, vibr. state distribs. 79—20354
B+O$_2$, chemiluminesc. reaction, vibr. state distribs. 79—20354
B+O$_2$(NO$_2$)(N$_2$O)(O$_3$)(ClO$_2$), chemiluminesc. metal oxide formation 80—35509
B+O$_2$(SO$_2$)(CO$_2$)(N$_2$O), gas phase rate consts., 300K, at. absorption obs. 79—83445
B+Ti, self-propagating, high-temp. synthesis wave, radiating power 79—100377
B+Xe(Kr), reson. radn. quenching 77—30820
B$^+$+CH$_4$, 200 keV, Auger spectra, single and double K-vacancy states 77—83706
B$^+$+inert gas atom, pot. interactions 78—55219
B$^+$+methane, single collision, time delayed autoionisation spectra 78—1067
B^{2+}+H, electron capture by slow ions, pseudo-crossing 80—43176
B^{3+}+H, charge transfer cross sections, ab initio potential energy curves 78—37741
B^{3+}+He, charge-exchange total cross-sections 77—79691
B^{4+}+H, excitation distrib. following electron capture 79—36763
B^{5+}+He(C)(Ne), K-shell charge transfer cross sections, Bates-Born formalisms 79—45834
B^{n+}+H, charge transfer cross sections, oscillatory behaviour in low-energy collisions 80—63806
B^{n+}+H, electron capture cross-sections, Li- and He-like ions 79—59559
B^{n+}+H$_2$, electron capture cross-sections, Li- and He-like ions 79—59559
B^{q+}+Ar(He)(H$_2$), keV electron capture cross section 80—14229
B$_2$, bonding, spin density functional theory 78—17558
B$_2$, canonical exchange energy modulation parameters, MTXα calc. 79—97997
B$_2$, ground state, multiconfig. SCF CI calcs. 78—58590
B$_2$, total Xα energy, LCAO calc., rel. to local density models 80—32607
B^{n+} H(H$_2$), one electron capture and loss 80—18921
B$^+$(^{3}P$_u$)+D$_2$, reactive scatt., 1-40 eV, ion products ang. and energy distrib. 79—98214
^{10}B concentration in tissue meas. *(Japanese)* 79—83913
^{10}B enriched coatings, neutron collimators, comparison with Gd$_2$O$_3$ coatings 78—82564
^{10}B enrichment by low-temp. exchange in BF$_3$.SO$_2$ system *(Japanese)* 78—55251
^{10}B self supporting target preparation up to 500 μg/cm^2 80—18745

boron continued
^{10}B separation using anion exchange resin, isotopic plateau holding displacement chromatography *(Japanese)* 78—56886
^{11}B, ground state, two-determinant numerical self-consistent at. orbitals appl. 79—93937
^{11}B ion implantation in SiO$_2$ microresistor, followed by inert gas ion implantation 77—15432
^{11}B, neutrino-induced prod. in stellar C layer 80—82337
^{11}B self supporting target preparation up to 500 μg/cm^2 80—18745
$_5^{10}$B^{n+}+Cu to Rb, 4-38 MeV, K-shell ionis., X-ray obs. 79—59549
β^{3+} quantum defects, rel. to angular momentum, nuclear charge, Coulomb-Born approx. method *(Japanese)* 77—50534
β-epoxy composite, intermittently bonded, water and ice effects 77—12685
C:H,B film, amorphous elec. props., chem. modifications by doping with B 80—84523
Cd$_{0.2}$Hg$_{0.8}$Te:B, ion implanted, B range and range straggling 80—54273
Cr-C facing alloys, effect of B on phase composition and facings props. during abrasive wear 80—21117
Cu:B, two site occupation by implanted ^{12}B 78—6077
Cu-Cr-Zr-Ti-B alloy system, solidification cracks formed during welding, reduction by microalloying with B 79—96148
α-Fe:B, valency effect of interstitials 80—65502
Fe-C-Mn-Si (4, 2, 1.5 wt.%), cast wire, influence of B addition on struct. and elec. cond. *(Russian)* 80—55391
(FeNi)PB amorphous wires, surface oxidation and annealing influence on induced anisotropy 80—100957
GaAs:^{11}B, physicochem. and resistivity meas. 80—24933
GaAs:B, deep levels, optically stimulated transient current method *(French)* 80—59919
GaAs:B, electron or neutron irradiated, low symmetry interstitial B centre 78—79605
GaAs:B, impurity conc. profile by glow-discharge optical spectroscopy 80—49258
GaAs:B, incorporation of B during growth 80—93471
n-GaAs:Si, B, IR absorpt. spectra, reson. and localised modes 80—66172
n-GaAs:Si, B, LEC crystal, carrier conc., B acceptor centres 78—6717
Ge, high-purity, with Al, B and P, residual impurities, photothermal cond. 80—24965
Ge:B, epitaxial film, exam. of doping during chemical deposition from gas phase 79—1446
Ge:B, impurity ground state levels from photo-thermal cond. in mag. field 77—51699
Ge:B, ion implantation and depletion at low temps., radiation and DC characts. 79—60392
Ge:B, ion implanted, laser-induced regrowth 79—69130
Ge:B, shallow acceptor spectral line intensities 80—88517
Ge:B, single crystals, grown by Czochralski method, exam. of B distribution ratio and diffusion coeff. 79—95042
Ge:B, uniaxially stressed, photoionisation of acceptors, impurity photocond. meas. 78—10509
H+B^{q+}(C^{q+})(N^{q+})(O^{q+}), ($2 \leq q \leq 4$, 5), cross sections at keV energies 80—78705
H+H$^+$(Arq^+)(Kr^{q+})(B^{q+})(C^{q+})(N^{q+})(O^{q+}) charge transfer and impact ionis. cross sections calcs. 77—88555
H+Li^{3+}(Be^{4+})(B^{5+})(C^{6+}), charge transfer cross sections, distorted wave Born approx. 79—72415
He+B^{3+}(C^{4+})(N^{5+})(O^{6+}), electron transfer 78—13598
Ni:B, hyperfine interactions, recoil-implanted β-NMR method *(Japanese)* 79—51865
Ni:B, impurity electronic struct. calc., ^{12}B NMR data anal., magnetisation decrease 79—47046
Pd-Ag, Fermi energy influence on soln. behaviour of H, B and C *(German)* 80—44323
β-rhombohedral, AC cond. meas., 150 to 300K, hopping cond. mechanisms 80—15521
β-rhombohedral, EPR anisotropy 80—25183
Si, B, ion implanted, enhanced annealing behaviour, p-n junction formation 77—43233
Si diffusion profiles, P and B diffusion determ. *(Rumanian)* 79—77615
Si:^{11}B, amorphous, calc. of implanted-ion range and energy-deposition distrib. 77—7748
Si:B, amorphous, annealing effect on cond. *(Korean)* 79—15142
Si:B, amorphous, ESR-linewidth temp. depend. meas. 80—20459
Si:B, amorphous, laser effects 79—69921
Si:B, amorphous, negative magnetoresist., localised mag. states 80—70731
Si:B, amorphous, photo- and dark conductivity 77—28216
Si:B, annealing mechanism of radiation change and dopants in pulsed laser irrad. ion implanted layers 79—46691
Si:B, anomalous B profiles prod. by BF$_2$ implantation 80—75252
Si:B, antiferromagnetic ordering of holes, recombination radiation polarisation *(Russian)* 80—45121
Si:B, appl. of ion implantation systems, high throughput 80—34029
Si:B, As, first and second order Raman scatt. by pair modes 79—65869
Si:B, autodoping during epitaxial growth from SiH$_4$ 77—47476
Si:B, binding energy, excited state spectra, photolum., semi-empirical short range pot. 80—44534
Si:B, bound many-exciton complexes, luminescence spectra, mag. props. 80—103994
Si:B, bound multiexciton complexes, work function thermodynamic determ. 78—72078
Si:B, bound multiexciton luminesc., recomb. kinetics 79—38591
Si:B, conc. depend. of B diffusion coeff. 80—39353
Si:B, conc. profile of implanted cryst., by ^{11}B(p,α) chem. anal., annealing *(German)* 78—83843
Si:B, conc. profiles of ions and recoiled N after implantation through Si$_3$N$_4$ films 79—55764
Si:B, deep diffusion at solid solubility limits for p-channel MOS IC 78—10070
p-Si:B, defect energy levels with 1 MeV electron irrad. and annealing, transient capacitance spectra 77—62860
Si:B, deform. coeff. due to impurity diffusion 78—18671
Si:B, detection of atomic plane displacement in near-surface layers, ang. depend. of photoemission during X-ray Bragg diffr. 78—47207
Si:B, diffusion for very shallow defect free p$^+$-n junc. for solar cells 79—15218
Si:B, diffusion from BN source with H$_2$ injection, AES study 80—19986
Si:B, diffusion induced imperfections, laser annealing, rel. to junction characts. 78—75678
Si:B, diffusion length, SEM-EBIC/Schottky diode 79—82605

boron continued
Si:B, diffusion of As atoms from ion implanted layers, conc. profiles 77—43376
Si:B, diffusion of B atoms and growth kinetics of oxidation induced stacking faults, correlation 79—37720
Si:B, diffusion of B from B_2H_6-CO_2 system, lower temp. limit of 775°C 77—43232
Si:B, diffusion of randomly implanted ions during high temp. processing 77—24439
Si:B, diffusion with BN, expt. *(Bulgarian)* 78—59824
Si:B, diffusional impurity redistrib., elastic stress field effect *(Russian)* 77—72719
Si:B, dislocated crystals, DC conductivity, Hall effect, energy spectrum 78—10400
Si:B, dislocated crysts. microwave cond., localised electron energy spectrum 78—14694
Si:B, dislocation net form. during annealing 77—51385
Si:B, dislocations under high stress, stacking fault energies, TEM study 80—70202
Si:B, distrib. profiles, high temp. treatment effects 79—69150
Si:B, dopant density and temp. depend. of hole mobility and resistivity 79—38075
Si:B, dopant density determ. by nucl. track technique 78—55886
Si:B, dopant profile changes induced by laser irrad. using SIM and backscatt. meas. 79—69148
Si:B, doping, new paint-on diffusion source 77—4118
Si:B, doping, pyrolytic BN wafer as diffusion source characterisation 78—91352
Si:B, ESR at zero and small external stress, interpreted in spin Hamiltonians 78—43641
Si:B, ESR at zero and small external stress, elastic strengths for point defects 79—19764
Si:B, effect of impurities on solar cell performance 80—55848
n-Si:B, elec. cond. oscills., electron instability effects due to dislocations 80—103704
Si:B, electron excited, recomb. radiation, high resolution investigation 78—15233
p-Si:B, Fe, 0.45 eV majority carrier trapping level after quenching 78—18990
Si:B, Ge(P), impurity-pair diffusion, influence of elastic stresses 78—87824
Si:B, glow discharge deposited amorphous film, UV absorpt. spectra 80—25420
a-Si:B, Hall effect and impurity cond. 77—72871
Si:B, He$^+$ irradiation-induced diffuiion, effect on impurity distrib. 80—70470
Si:B, heat treatment centres changes, EPR obs. 80—29601
Si:B, heavily diffusion-doped layers, Co diffusion 78—59982
Si:B, heavily doped, form of occurrence of acceptor impurities 77—11581
Si:B, heavily doped, paramagnetic props., anomalous hole spin susceptibility *(Russian)* 80—54861
Si:B, heavily implanted wafers, secondary defect generation suppression by HCl oxidation 78—10069
Si:B, heavy-doping effects and impurity segregation during high-press. oxidation 80—65014
Si:B, high conc. effects in ion implantation 80—75245
p-Si:B, high temp. treatment, effects on ion implanted impurity distrib. profile 78—79625
Si:B, highly-doped polycryst. thin film, growth kinetics and properties 78—44016
Si:B, hole mobility calc. for dopant density and temp. var., resistivity meas., effective mass calcs. 80—54703
Si:B, hole trapping by B atoms at low temps. 79—7837
Si:B, hot-carrier scatt. and recomb. characts. 79—91069
Si:B, IR spectra of acceptor levels 80—34953
Si:B, implantation energy, rel. to dose, Szabo-Bogancs effect 78—38740
Si:B, implanted, effectiveness of charged vacancies in diffusion 80—34239
Si:B, implanted, free carrier conc. and impurity location, Raman scatt. obs. 77—55295
Si:B, implanted, laser-annealed, lattice dilatation 79—46690
Si:B, implanted, oxidation induced precipitate defects, TEM 78—31556
Si:B, implanted, oxidation-induced stacking faults, EBIC and TEM expts. 78—39923
Si:B, implanted, shrinkage of rod shaped defects 78—6061
Si:B, implanted CW laser annealing, elec. props., cryst. struct. and limitations 80—39131
Si:B, implanted laser annealed, lattice strain, X-ray study 80—96554
Si:B, implanted layers as strain sensors 77—35098
Si:B, implemented laser annealed samples, unidirectional contraction 78—71747
Si:B, impurity conc. from photoluminesc. anal. 78—63785
Si:B, impurity content characterisation, exciton luminesc. 80—60653
Si:B, impurity diffusion from implanted layer, influence of radiation damage 77—76621
Si:B, impurity excited state lifetimes 78—60083
Si:B, impurity range distrib. determ. by ^{10}B(n,α)^{7}Li reaction 78—11585
Si:B, impurity-peak form. during proton-enhanced diffusion 79—55772
Si:B, influence of proton beam irrad. on concentration profiles *(French)* 77—51402
Si:B, inhomogeneous surface layer, diffusion and implanted, X-ray rocking curves 80—6603
Si:B, interstitial Si atom formation by light ion bombardment 78—47406
Si:B, ion implantation, 20-2800 keV, obs. of X-rays produced 78—14367
Si:B, ion implantation, anal. of disordered regions in crystal with Promiss protonograph 80—19823
Si:B, ion implantation, channelling and random distrib. of B ions meas. 77—47473
Si:B, ion implantation, channelled, through metal silicide film 80—70231
Si:B, ion implantation using B_2O_3-B mixture, Auger spectra, channelling anal. 79—4317
Si:B, ion implanted, comparison of range and range straggling 77—55293
Si:B, ion implanted, depth and lateral profiles of B atoms, Monte Carlo simulation 77—55297
Si:B, ion implanted, doping profile, pulsed laser annealing effects 80—88197
Si:B, ion implanted, electroreflection spectra 79—51983
Si:B, ion implanted, ellipsometric study for low doses, cryst. damage parameter 79—65105
Si:B, ion implanted, laser annealing 78—34525

boron continued
Si:B, ion implanted, laser and thermal annealing compared, TEM obs. 78—75681
Si:B, ion implanted, laser annealed, elec. characterization 79—69137
Si:B, ion implanted, laser annealed, thermal annealing effect 79—73191
Si:B, ion implanted, laser annealed, IR and Raman spectra 79—73914
Si:B, ion implanted, laser annealed, Raman scatt., Fano interactions, lattice damage 79—78711
Si:B, ion implanted, localised defects, TEM study 78—87699
Si:B, ion implanted, polycryst., annealing characts. 77—24324
Si:B, ion implanted, pulsed laser annealing appl. to device fabrication 79—73180
Si:B, ion implanted, radiation defect accumulation and annealing, X-ray diffr. obs. 79—37726
Si:B, ion implanted, redistrib. of dopants by pulsed laser annealing 79—7620
Si:B, ion implanted, SOS device struct., nonlinear impurity redistrib. 79—1625
Si:B, ion implanted, struct. of rod defects, TEM obs. 78—71744
Si:B, ion implanted, structure defects formation and behaviour under annealing in various ambients 80—65033
Si:B, ion implanted crystalline and amorphous, laser annealing 80—97509
Si:B, ion implanted film, elec. prop. impurity depend. 80—24467
Si:B, ion implanted layers, carrier distrib. meas. precision 77—43603
Si:B, ion-implantation doped, influence of radiation dose on diffusion processes 77—1141
Si:B, ion-implanted, annealing by incoherent light source 79—19267
Si:B, ion-implanted, dislocation climb, TEM obs. 78—6062
Si:B, ion-implanted, influence of US waves on charged particle channelling 79—23668
Si:B, ion-implanted, rod-like defects, TEM obs. 77—68975
Si:B, ion-implanted, scanned laser and electron beam annealing 79—73182
n-Si:B, ion-implanted damage, positron annihilation and sheet resist. meas. 80—35003
Si:B, ion-implanted polycrystalline films, laser annealing 79—73181
Si:B, ionisation-assisted annealing 79—23628
Si:B, irrad. with fast neutrons true profiles of impurity photocond. bands from piezodichroisms 79—91103
Si:B, lateral effect of oxidation on B diffusion 80—29217
Si:B, lattice location of implanted ions after laser annealing 78—30660
Si:B, layer resist. depend. on implanting and annealing conditions *(German)* 80—96551
Si:B, low conc. B diffusion using doped-oxide film 77—76431
Si:B, low noise avalanche photodiode fabrication by channelling implantation 79—35827
Si:B, MBE, on n$^+$ Si, with wide range doping control 78—27402
Si:B, many-body exciton-impurity complexes, stress depend. of photolum. meas. 79—28833
Si:B, mean square dynamic displacement of atoms, effect of electron-phonon interactions *(Russian)* 78—10145
Si:B, microdefect formation depend. on doping, Cu decoration, X-ray transmission topography, preferential etching 79—69120
Si:B, minority carrier diffusion coeffs. 79—99559
Si:B, multiparticle impurity complexes *(Russian)* 78—72601
Si:B, multiple-particle exciton-impurity complex form. *(Russian)* 78—43925
Si:B, N-implanted junction capacitance meas., appl. of dynamic lateral photovoltaic effect 77—85304
Si:B, near intrinsic ⟨100⟩ and ⟨111⟩ samples, inert and oxidising ambients, diffusion, segregation 78—75882
Si:B, nonequilibrium solid solutions obtained by heavy ion implantation and laser annealing 80—92544
Si:B, P, first and second order Raman scatt. by pair modes 79—65869
Si:B, P, high temp. diffusion, effects of laser irrad. on diffused layer 79—14834
Si:B, P, long range enhancement of B diffusivity by P diffusion 80—103386
Si:B, p$^+$-n junction form., ion implantation damage, leakage current 77—24334
Si:B, p-n junction diodes, scanning-electron-beam annealing, elec. characts. 79—79128
Si:B, p-n junction form. by B deposition and laser-induced diffusion 78—87690
Si:B, photocond. spectra of H$^-$-H$^+$-type complexes 79—95451
Si:B, photoconductivity, impact neutralisation of H$^-$-like centres 77—69377
Si:B, photolum. of heavily doped p- and n-type 80—20708
Si:B, piezospectroscopic studies of bound multiexciton complexes 80—16006
Si:B, piezothermoelec. power 78—56173
Si:B, plastic deform. and formation of dislocation loops, effect of Au atoms 79—69184
Si:B, polarisation of recombination radiation from multiparticle exciton-impurity complexes, induced by uniaxial deform. *(Russian)* 79—78754
Si:B, polycryst., effect of laser annealing on struct. and elec. props. 79—11243
Si:B, polycryst., N_2 heat treated, anomalous resist. change due to Bn form. 78—2591
Si:B, polycryst. film, piezoresistive gauge factor 77—12029
Si:B, polycrystalline, depth profiles of implanted B atoms, meas. by secondary ion mass spec. *(Japanese)* 78—67734
Si:B, polycrystalline, ion implanted, AES analysis 77—31690
Si:B, positron annihilation in 100 and 111 orientation 77—44083
Si:B, predeposition of B using BBr_3 78—55882
Si:B, proton enhanced diffusion, vacancies diffusion length 80—29226
Si:B, proton-irrad., impurity uphill diffusion, vacancy mechanism 80—92719
Si:B, proton-irrad.-enhanced diffusion 80—29227
Si:B, RF glow discharge sputtering damage centres, barrier formation 79—33329
Si:B, recombination spectra of bound multiexciton complexes, Zeeman splitting *(Russian)* 79—38526
Si:B, redistrib. of B during thermal oxidation, numerical and analytical calcs. 80—49259
Si:B, resonant scattering of phonons by bound holes in temp. range 1 to 5K 80—75393
Si:B, SEM obs. of dislocations using Schottky barrier EBIC technique 78—79614
Si:B, selective etching by NaOH soln. 79—70189

boron continued
Si:B, self-interstitials location by Rutherford backscatt. of channelled ions 80—2101
Si:B, single cryst., transmission characts. for IR optical components 77—27325
Si:B, single crysts., oxidation investigations, 780°-1150°C 79—5068
Si:B, solubility and precip., and supersat. resulting by thermal predeposition 78—11232
Si:B, spreading resist. calibration for Si:Al, Si:Ga 80—103690
Si:B, sputtering influence on distrib. profile of ion-implanted impurities 79—42091
Si:B, TEM study of stacking fault form. and annealing 78—51566
p-Si:B, thermoelec. power, 20-300K 78—19067
p-Si:B, total piezoresist. tensor, 20 to 300K 78—19037
p-Si:B, trace determ. of U impurity by fission track method 79—79354
P-Si:B, US spectroscopy, energy splitting of acceptor ground state 79—33260
Si:B, uniaxially stressed, impurity-assisted intervalley scatt., photoluminesc. obs. 80—34979
Si:B, use of BN source to achieve high surface concentration of B *(Russian)* 80—107639
Si:B, using oxidised BN dopant source, sheet resist., rel. to temp. and deposition time 77—43231
Si:B, with insulating coating, mechanical stress influence on B diffusion, strained surface layers 80—29224
Si:B,As selective area simultaneous doping 80—34015
Si:B,In, sharp line series in near-band-edge photolum. 80—16092
Si:B,P, anomalous diffusion 80—29229
Si:B,P, diffusion patterns obs., for SiO_2 deposited by means of centrifuge *(Bulgarian)* 77—76429
Si:B,P, double implanted layer, n-p-n struct., single pulse laser annealing 80—49247
Si:B,P, high conc. diffusion without disloc. generation 78—10072
n-Si:B,P, radiative recombination at thermal defects, luminescence centre electron struct. 79—91496
Si:B,P, simultaneous diffusion, radioactivation techniques 77—76622
Si:B (0.2 wt.%) ion implanted, B atom displacement due to low temp. irrad. 80—88234
Si:B amorphous film, CVD prep., EPR, elec. and optical props. 79—4558
Si:B deposition diffusion from B_2H_6, AES analysis 78—6085
Si:B device, anal. using SEM-AES-IMA combination with SIM spectrometer *(Japanese)* 78—85249
Si:B diffusion at Si-SiO_2 interface, Auger spectra, Rutherford backscattering 80—70471
Si:B doping from BN sources, impurity transfer considerations 77—76441
Si:B effect of dopants on grain growth 80—54575
Si:B effect of elec. field on carrier capture by attractive centres. 79—11145
Si:B epitaxial layer, B diffusion coeff. 79—99372
Si:B film, amorphous, doping and transport props. *(French)* 78—47403
Si:B film, electronic props. 78—84330
Si:B film, polycrystalline, deposition on Si wafer, doping effect on bending 79—95276
Si:B film, sputter-deposited, elec. props., struct., SEM and TEM obs. 79—95298
Si:B high temp. impurity diffusion via vacancies and self-interstitials 80—24667
Si:B high-temp. diffusion, glass layer formation obs. 78—7069
Si:B implanted wafers, ionis. assisted annealing and effects 80—100257
Si:B impurity conc. profile determ. by anodic oxidation 79—28010
Si:B ion implanted, strain profiles from X-ray rocking curves 80—107290
Si:B ion implanted, X-ray topographical images at different absorption conditions 80—2052
Si:B ion implanted grating-type solar cells, var. of junction depth, collection efficiencies 80—93934
Si:B ion implanted layers, light refl. and transmission coeffs., computer program 80—66316
Si:B ion ion implanted, channelling and random equivalent depth distrib. 80—100293
Si:B MOS structures, implanted laser beam irrad. effects on interface electrophys. props. 79—1627
Si:B material for space solar cell 80—94007
Si:B photodiode front region collection efficiency models 80—96899
Si:B polycrystalline thin film, plasma annealing, effect on elec. props. 80—7005
Si:B radiation damage and minority carrier lifetime, SEM-EBIC obs. 80—96573
Si:B recombination emission polarisation of bonded multiple-exciton complexes in mag. field *(Russian)* 78—2905
Si:B sputtering by Ar^+, computer simulation of sputter broadening in impurity depth profiling 80—2908
Si:B wafers, anal. by combined ion beam techniques and X-ray microanal. 79—5238
p-Si:B-SiO_2 interface in MOS structures, carrier mobility and impurity distrib. 78—34902
Si:B^+, ion implanted, lateral spread of B^+ ions through SiO_2 mask 79—51130
Si:B^+, recrystallisation of implanted amorphous layers, elec. props. 79—55762
Si:B^+, TEM of lateral implantation effects near mask edges in wafers 79—37724
Si:B(Ga), even-parity acceptor excited states, bound exciton two hole transitions 77—85793
Si:Fe, B, Fe reaction with ion implanted B 79—77620
Si:Fe, B thermally activated Fe interstitial, elec. and kinetics props. *(German)* 80—34035
Si:Ge B, strain compensation, X-ray Bragg reflexion 80—39137
Si:H,B, amorphous, field effect and thermoelec. power 80—96924
Si:In, neutron irrad. to compensate for residual B, photocond., IR focal plane array 78—67727
Si:P,B, amorphous, localised level density 79—56168
Si:P,B, wafer, long range enhancement of B diffusivity induced by high surface conc. P diffusion 79—46687
Si:Se,B, diffusion of Se, solubility and ionization levels, Hall effect and photocond. meas. 79—42486
Si-B, diffusion-free annealing, use of scanning CW Kr laser 78—91345
Si-B, exam. of two stage diffusion of B, under a gas phase oxide film 79—95044
Si-B, P diffusion and activity after Ar ion bombardment 78—95192

boron continued
Si-B crystal, Bond method, of meas. lattice parameters, asymmetric Bragg reflections appl. 80—38861
Si-Ge:B, hot-pressed alloy, thermoelec. props. 78—91711
Si-H,B, in situ prepared amorphous film, photoemission studies 80—35060
Si-SiO_2 interface, ^{11}B implantation effects on charge density 79—10865
Si-SiO_2:B, ion-implanted, shallow trap energy spectra 80—80392
SiC:B, 4H-, 6H- and 3C-polytypes, melt growth and photoluminesc. 77—24885
β-SiC:B, diffused structures, current-voltage characts. 78—47865
SiC:B, dislocation induced deceleration of impurity diffusion 77—28043
SiC:B, electroabsorption, 0.35-0.45 eV, under UV illumination 79—4831
SiC:B, impurity distribution determ. by neutron activation anal. 77—76452
SiC:B, ionisation energy of deep centres from absorpt. spectra, electron-phonon coupling 77—4663
SiC:B, p-n junction, LED with new low-temp. alloy 79—73582
α-SiC:B, piezoresist. rel. to acceptor levels 78—60129
SiC:B, struct. of spectrum of excitons bound to neutral B atoms 78—19523
4H-SiC:B, very slow decays of luminesc., 2-300K 77—1718
p-SiC:B (4H), absorption spectra of bound excitons 78—88338
SiC:B (6H) LEDs, fabrication by rotation dipping technique, electrolum. mechanisms 80—50426
β-SiC:B p-n junction, IR electroluminesc. spectrum 77—44067
SiC-B, hot pressing, role of grain boundaries 77—24999
$Si_{1-x}H_x$:B film, amorphous, RF sputtered, optical consts. 79—95866
SiO_2:B, B segregation during dry, nearly dry and wet O_2 oxidation 79—66178
SiO_2:B, ion implanted, props. 79—65106
SiO_2:B film, high temp. deposition and evaluation 79—69989
SiO_2:B film, implanted, electronic cond. mechanism in MOS struct. 77—15983
SiO_2:B film, on Si, AES meas. 77—39951
SiO_2:B implanted, thin films, props. *(Polish)* 80—39692
SiO_3:B, P films doped by pyrolisis and ion implantation, IR absorpt. obs. of impurity conc. 77—72802
$Si0_2$:Ge, B, P, optical fibre, radiation induced optical absorpt. spectra, 0.4 to 1.7 μm region 80—58761
$SrTiO_3$:B layers, ion implanted, conductive props. Hall mobility, defect energy levels 79—82693
VO_2, thin films, doping by ions of Ar, B, P 77—84781
W:La, B coadsorption and work function, FEM and FIM obs. 79—52087
W-ThO_2-B, thermocathodes diffusion mobility, based on deboronation kinetics 80—39349
(W-Au)-SiO_2-Si:B MOS transistor, ion implantation effect on threshold voltage 78—34903
YIG:B,Pb, IR spectrum, localised modes, rel. to impurities and O vacancies 80—50377
ZnS:B, new luminesc. centre 79—38635
ZnSe:B(F), ion implantation, photocond. and cathodoluminesc. meas. 78—26586
ZnTe:B^+ native and implant-created defects 77—76446

boron alloys
see also boron compounds
alkaline earth platinum borides, $M_{0\ 67}Pt_3B_2$, cryst. struct. and supercond. props. 79—38231
amorphous ribbon, saturation magnetostriction, and electronically controllable delay line 79—1700
austenitic solid solution, chem. evaluation of B and its correlations with hardenability and hardness *(German)* 79—39230
Colmonoy, self-weldability in high temp Na *(Japanese)* 80—89392
Colmonoy hardfacing materials, friction characts. in high temp. Na *(Japanese)* 80—89356
conference, Varna, Bulgaria (Oct. 1978) 80—12842
$Fe_{40}Ni_{40}P_{14}B_6$, amorphous, tape wound core, fluctuations of driving field 78—10726
$Fe_{40}Ni_{40}P_{14}B_6$, $Fe_{32}Ni_{36}Cr_{14}P_{12}B_6$, amorphous Hall effect, press. and temp. depends. 77—66155
Hayes alloy no.716, Fe-Cr-Ni-Co-W-Mo-Si-C-B (26, 22, 12, 3.5, 3, 1.2, 1.1, 0.4 wt.%), hardfacing alloy 80—100802
low-temp. resistivity in mag. field 78—91667
metal-boron systems, correlation of phase equilibria, with boride crystal chemistry 79—11562
Metglas 2605, and 2605 A, transport props., resist. and magnetoresist. 79—1590
Metglas 2605 ribbon, saturation magnetostriction meas. by small-angle magnetisation rot. 80—60391
Nimonic alloy, effect of annealing on hardness, carbide phase strengthening *(Russian)* 79—34137
rare earth-B, RB_2, thermochemistry and stability 80—97723
steel, austenitic, high-temp. crack resist., B and Mo influence *(Russian)* 80—16435
steel, austenitic stainless, B effect on corrosion resistance 78—35569
steel, austenitic stainless, Cr-Ni-Mo (21,6,9 wt.%), N_2-strengthened, surface segregation of B, Auger and XPS spectra 79—90854
steel, austenitic stainless B-containing, decomp. of solid solns., effect of cooling conditions 77—44256
steel, B-Si, grain-oriented, high induction, Cu impurity effects 80—89366
steel, Cr-Mo (1.25, 0.5 wt.%), creep, fracture, Ti and Ti+B effects 77—36603
steel, Cr-Ni-Ti-B, grain size effect on mech. and struct. props. *(French)* 80—45361
steel, ferrite nucleation, appl. to B hardenability 78—27505
steel, medium C 80—11752
steel, medium Cr, B effects on struct. and toughness 77—21265
steel, Mn-Ti-B-rare earth, distrib. of B *(Chinese)* 78—84811
steel, Ni-B, B effect on temperability and microstructure 79—15710
steel, stainless, liquid boronizing, wear resistant coating *(Korean)* 79—43475
steel, stainless, Ti stabilised, creep props. rel. to B conc. *(French)* 79—20132
steel, stainless austenitic, low alloy 316, high temp. plasticity, B addition effects *(Russian)* 77—28852
steel, stainless complex alloy, hot ductility, B effect 80—30038
thermoelectric materials, B_4C_x and $(B,Si)_4C_x$ P-type LaS_x N-type alloys, fabrication and thermoelectric props. 80—107771
transition metal-boron, $M_{1-x}B_x$ amorphous film, crystn., TEM obs. 79—87019

boron alloys continued
- transition metal-Si-B ternary and quaternary amorphous alloys, effect of comp. on crystn. *(Japanese)* 79—94910
- Al-B, dil., diffusion of ^{12}B 79—60541
- Al-B, enthalpies and free energies, effusion and mass spectra, phase diagram 78—23665
- Al-B, manufacture, use of $NaBF_4$, transfer of B 78—27453
- Al-B_4C, neutron shielding materials, long term radiation effects 80—9413
- Al-Ti-B, liquidus surface at Al corner *(Japanese)* 77—55948
- Al-Ti-B alloys, phase comp. and distrib. of components, X-ray obs. *(Russian)* 79—52164
- Al-Ti-B alloys, segregation of Ti, electron microscope exam. 78—52820
- Al-TiB_2-Si, Si effect on grain refinement *(German)* 79—91656
- AlB_2, thermochemistry and stability 80—97723
- $Al_{1.1}Be_{0.6}B_{22}$, metal distrib., X-ray diffr. study 80—75204
- B fibre reinforced AlB_2, fibre coating effect on strength *(Russian)* 80—40426
- B-C alloys, prep., struct., phys., chem. props., appls., review, book contrib. 78—48388
- B-Cr(Si), diffusion coatings on alloy steel U8, wear resistance 78—56823
- B-Cu(Al) coating on steel 45, effect of abrasive particle size on wear 78—44225
- B-Fe (16 at.%), magnetisation in high mag. field, Arrott-Noakes plot 80—54919
- B-Ni, form by Ni doping of zone-refined B, elec. conductivity 77—31682
- B-Si, (0 to 14.3 at.%), phase charact., regions of existence *(French)* 80—104117
- B-Si alloys, B-rich, prep., anal. and cryst. growth *(French)* 80—104091
- B-Si alloys prep., struct., phys., chem. props., appls., review, book contrib. 78—48388
- B-transition metal, amorphous thin film, crystallisation, TEM obs. 79—19483
- B-transition metal thin films, amorphous to cryst. transformation 80—7563
- B_4C, piston, commencement of yielding, in high-press. anvils 79—54150
- B_4C-Ti(V)(Cr), contact reaction with liq. Ni 80—55707
- BMn, ferromag., ^{55}Mn magnon-induced pseudoquadrupole processes 79—19802
- Be-B, ion implanted surface hardened layer on Be 80—16604
- Cd-B particulate composite, dispersion hardening, grain size and texture strengthening 77—8840
- $Ce_2Co_5B_2$, crystal struct. *(Ukrainian)* 79—51050
- $(Co,Fe,M)_{78}Si_8B_{14}$ amorphous alloys (M = V,Nb,Ta,Cr,Mo,W,Mn or Ni), zero magnetostriction and low field mag. props. 80—34741
- $(Co,Fe)_{80}B_{20}$ glass, induced anisotropy and time changes of permeability 80—75815
- Co-B, amorphous alloys, phase diagram 79—96002
- Co-B (6.6 at.%), columnar alloys, metallographic obs. of eutectic struct. *(Russian)* 78—27469
- Co-B alloys, amorphous, mag. moment and exchange stiffness constant 79—1662
- Co-B alloys, amorphous, saturation magnetisation, mag. moments, X-ray diffr. obs. 79—4704
- Co-B glass, X-ray obs. of struct. 79—1399
- Co-B-Mo-Cr, amorphous, Mo and Cr addition effect on corrosion behaviour 80—16568
- Co-B-Si, mag. props. different in amorphous and cryst. phases 77—69617
- Co-B-Si amorphous alloy, liq. quenched, elec. resist. and cyclic deform. 80—59949
- Co-B-Si ternary system, partial phase diagram, Co rich region 77—52293
- Co-B(-Cr) thin film glasses, mag. props. and corrosion resist. 80—80576
- Co-Fe-B, amorphous, crystn. and thermal stability 80—107057
- Co-Fe-B films, amorphous, mag. annealing behaviour 79—73782
- Co-Fe-B sputtered amorphous films, mag. props. and corrosion resist. 79—28567
- Co-Fe-Ni-Si-B glasses, soft mag. props. 79—73774
- Co-Fe-Si-B, amorphous alloys, substitution effect on mag. props. 79—69695
- Co-Fe-Si-B, decomp. of amorphous state during annealing below recryst. temp., electron microscope study *(Russian)* 80—75164
- Co-Fe-Si-B, ferromag., magneto-optical spectra in amorphous and cryst. states *(Russian)* 80—84749
- Co-Fe-Si-B amorphous alloys, mag. props. 77—16055
- Co-Ga-B, phase diagram, metallographic, X-ray and electron probe anal. 78—92241
- Co-Gd-B, rules of cmpd. form. in related systems 79—34010
- Co-Mn-Ni-Fe-Si-B amorphous alloys, mag. props., low magnetostriction 80—75832
- Co-Mo-B metallic glass ribbons, tensile strength, crystn. temp. 80—89173
- Co-Ni-Cr-B, centrifugally cast metallurgical coatings for wear resistance in plastics molding machines 79—29285
- Co-Ni-Cr-B, X-306 centrifugally cast cylinder lining alloy, compatibility with hardfacing alloys 77—32726
- Co-Ni-Fe-B, amorphous ribbon, magnetostriction meas. 80—15778
- Co-Si-B, amorphous ribbon, saturation magnetostriction meas. by small-angle magnetisation rot. 80—60391
- Co-Si-B, embrittlement by crystallisation *(Japanese)* 78—48513
- Co-Si-B amorphous alloys with metalloid elements, embrittlement/crystn. relationship *(Japanese)* 79—96134
- Co-Si-B-Fe alloy magnet, Al_2O_3 particle embedded surface, amorphous mag. anal. using electron diffr. 79—56568
- CoB and Co_2B, electrochem. behaviour in H_2SO_4 79—39030
- $Co_{1-x}B_x$, polycrystalline and amorphous sputtered films, Brillouin spectra 80—2775
- $Co_{100-x}B_x$, amorphous, mag. struct., mag. susceptibility meas. 80—80485
- $Co_{100-x}B_x$, amorphous alloys, saturation magnetostriction and annealing behaviour 80—34739
- $Co_{100-x}B_x$ glassy alloys, mag. props. 79—73689
- Co_3B, crystalline, photoemission and electronic struct. 80—2926
- Co_3B, glassy and cryst., hyperfine field distrib., ^{59}Co spin echo spectra 80—80635
- $(Co_{1-x}Fe_x)$-B-Si, amorphous mag. props. *(Japanese)* 77—85433
- $Co_{74}Fe_6B_{20}$, metallic glass, zero magnetostriction, magnetisation characts. 77—12158
- $Co_{79}Fe_{6.5}B_{14.5}$ amorphous thin films, zero magnetostriction, high magnetisation 80—34708

boron alloys continued
- $(CoFeB)_{100-x}Cr_x$ thin films, magnetic props. and corrosion resist. 80—34709
- $(Co_{0.93}Fe_{0.07})_{75-x}Cr_xSi_{15}B_{10}$ amorphous alloy, thermal stability, Cr conc. effects, DTA expts. 80—59395
- $(Co_{0.89}Fe_{0.11})_{72}Mo_3Si_{15}B_{10}$, metallic glass, strain- and field-induced mag. anisotropy 80—108004
- $Co_{57}Fe_5Ni_{10}(Si,B)_{28}$, amorphous, soft mag. props., switched-mode power supply appls. 80—88850
- $(Co_{1-x}Fe_xNi_y)_{80}(Si_{1-z}B_z)_{20}$, amorphous films, spin wave spectra 80—34777
- $Co_{70}Fe_5Si_{15}B_{10}$, amorphous, crystn. and thermal stability 80—107057
- $Co_{70.4}Fe_{4.6}Si_{15}B_{10}$, amorphous, mag. aftereffect spectra and annealing props. 80—88831
- $Co_{75-x}Fe_xSi_{15}B_{10}$, quenched ferromag. ribbon, Brillouin spectra 80—2776
- $(Co_{1-x}M_x)B$, M = Mn or Fe, paramag., spin echo NMR spectra, ferromag. transition, spin-lattice relax. 80—29645
- $(Co_{1-x}M_x)B$, M = Mn or Fe, ferromag., internal fields meas. by NMR spin echo 80—29646
- $(Co_{1-x}Mn_x)_2B$, magnetocrystalline anisotropy meas., 4.2-300K 80—71006
- $Co_{73}Mo_2Si_{15}B_{10}$, metallic glass, strain- and field-induced mag. anisotropy 80—108004
- CoNiB, corrosion-resistant amorphous mag. thin films 80—54923
- $Co_{40}Ni_{40}B_{20}$, magnetostriction, temp. depend. 78—91921
- $Co_{40}Ni_{40}B_{20}$, spontaneous Hall effect and resistivity 79—19576
- $Co_{50}Ni_{20}Fe_6Si_{12}B_{12}$, amorphous, mag. props., effects mech. deform. 80—39840
- $(Co_{1-x}Ni_x)_{75}(PBAl)_{25}$, amorphous, high-field magnetoresist. meas. 80—34423
- $Co_{78}P_{14}B_8$, amorphous, photoemission and electronic struct. 80—2926
- $Co_{74}Si_{10}B_{16}$ amorphous toroidal core, switching characts. and domain structs. 78—95477
- $Co_{74}Si_{10}B_{16}$, amorphous ferromagnetic alloy, isothermal annealing effect on static magnetic props. *(Japanese)* 79—52398
- $Co_{75}Si_{15}B_{10}$, amorphous, crystn. and thermal stability 80—107057
- $Co_{75}Si_{25-x}B_x$ glass, mag. moment, Curie temp., and microhardness, metalloid comp. depend. 77—55665
- Cr, and Cr alloys, cast, B additions effect on struct. and props. *(Russian)* 78—19891
- Cr-B system, phase diagram, CrB_6 synthesis 79—78931
- Cu-B, microvoid form., gaseous impurity atom effects, positron annihilation study 80—49275
- Cu-BN composite electromachining tools, dynamic hot pressing 80—84889
- $(Er_{65}Fe_{35})_{100-x}B_x$ glasses, mag. props. 79—73693
- $Er_{1-x}Ho_xRh_4B_4$, mag. and supercond. transitions, cryst. field effects 80—107950
- $ErRh_4B_4$, reentrant supercond., mag ordering, neutron diffr. obs. 78—14879
- $ErRh_4B_4$, supercond., electronic props. of Er^{3+} using Mossbauer effect in ^{166}Sr 79 56651
- $ErRh_4B_4$, supercond. and mag. props. 79—4631
- $ErRh_4B_4$, supercond. and mag. props., influence of mag. fields 79—56374
- $Er_{1-x}Tm_xRh_4B_4$, mag. and supercond. transitions, cryst. field effects 80—107950
- (Fe,Co,Ni)-B, amorphous alloys, magnetostriction rel. to soft mag. props. 80—84633
- $(Fe,Co)_{0.8}B_{0.2}$ alloy amorphous thin films, anisotropic mag. and microstruct. props. 78—95487
- (Fe,Co)PBAl, metallic glass, viscous flow, alloying effect 78—79793
- $(Fe,Mo)_{80}B_{20}$, glassy alloy, Curie temp. and crystn. temp., Mo additions effect, Mossbauer spectra 78—68428
- (Fe, Ni, Co)-Si-B, amorphous, compositional effect on struct. changes, after heating up to 700°C, exam. *(Japanese)* 78—48433
- $(Fe,Ni)_{83}B_{15}C_2$, amorphous alloy, mag. props., possible appl. to power transformers 79—28558
- $(Fe,Ni)_{80}(P,B)_{20}$, quenched alloy ribbon, mag. moments, Curie temp. 77—40041
- $(Fe,Ni)_{80}P_{14}B_6$ amorphous alloy, mag. props., possible appl. to power transformers 79—28558
- Fe, cast, white, high Cr, phase composition, B effect 80—104172
- Fe-(Co)-B, amorphous, crystn. 80—79704
- Fe-B, (16.3 at.%) amorphous, coercive force temp. depend. 80—25158
- Fe-B, amorphous, anomalous thermal expansion, ΔE effect, Invar and Elinvar characts., delay time 80—80589
- Fe-B, amorphous, crystn., metal or metalloid exchange influence 80—75172
- Fe-B, amorphous, elec. resist., temp. depend. 80—44563
- Fe-B, amorphous, induced anisotropy, development by mag. annealing and under applied mech. stress 80—65868
- Fe-B, amorphous, induced anisotropy by heat treatment in mag. field and under applied mech. stress 80—75758
- Fe-B, amorphous, Invar-type alloy, mag. moment and high field susceptibility 78—34965
- Fe-B, amorphous, mag. aftereffect, initial susceptibility time depend. 80—88829
- Fe-B, amorphous, short-range order, Mossbauer meas. 80—44986
- Fe-B, amorphous alloy, mag. props. 80—84618
- Fe-B, amorphous alloys, compositional study on short-range struct. 80—84095
- Fe-B, amorphous alloys, phase diagram 79—96002
- Fe-B, amorphous ferromag., temp. depend. of resist., appl. of extended Ziman theory 80—59950
- Fe-B, amorphous metallic glasses, high-temp. mag. anal. 78—91258
- Fe-B, amorphous paramag. alloys, hyperfine field distrib., Mossbauer study 80—39958
- Fe-B, amorphous phase form. by rapid quenching from melt *(Russian)* 77—66664
- Fe-B, binary alloys, giant ΔE effect and Elinvar characts. 78—76291
- Fe-B, columnar alloys, metallographic obs. of eutectic struct. *(Russian)* 78—27469
- Fe-B, eutectic, crystallisation *(Russian)* 79—70087
- Fe-B, for infiltration of Fe compacts 80—60806
- Fe-B, liq., mag. susceptibility meas. 80—75740
- Fe-B, metallic glass, Mossbauer investigation of electronic struct. 78—92009
- Fe-B, metallic glass, theoretical studies on structural models 79—37633
- Fe-B, metallic glasses and vapour deposited films, amorphous to cryst transition 80—88048
- Fe-B, method of revealing structural components 80—21228

boron alloys continued
Fe-B, rapidly quenched, metastable phases 80−76234
Fe-B, rapidly quenched metastable solid solns., prop. and mag. props. 78−92218
Fe-B, rapidly solidified, metastable phases *(German)* 79−29045
Fe-B, sputtered amorphous film, strong stripe domains, Kerr effect obs. and theory 79−91265
Fe-B (14-25 at.%), amorphous, saturation magnetisation, temp. and comp. depend. 77−85430
Fe-B (15-25 at.%) glass, quasicryst. struct. Mossbauer expts. 79−4255
Fe-B amorphous, crystallisation, activation energy conc. depend., DTA calcs. 79−60284
Fe-B amorphous alloy, annealed, microstruct. and mag. domain changes 80−75790
Fe-B amorphous alloy, crystallisation kinetics 78−83736
Fe-B amorphous alloy, fast neutron and ^{235}U fission fragment irrad. 80−100288
Fe-B amorphous alloy, Invar effects, mag. props. meas. 79−56594
Fe-B amorphous alloy, mag. anisotropy temp. depend. 80−15846
Fe-B amorphous alloys, mag. aftereffect 80−65970
Fe-B amorphous alloys, Mossbauer spectra, soft ferromag. props. 80−11302
Fe-B amorphous alloys, Mossbauer spectra, struct. 80−15840
Fe-B amorphous alloys, Mossbauer spectra, mag. moment conc. depend. 80−15847
Fe-B amorphous alloys, valence band spectrum, XPS study 80−50534
Fe-B amorphous Invar alloy, elastic props., Elinvar characts. and ΔE effect 79−56595
Fe-B amorphous ribbons formation, high-speed photography investigation 80−76216
Fe-B based alloys, amorphous, amorphous, thermopower meas., Nordheim-Gorter relations 79−99535
Fe-B ferromag. film, props. 79−4709
Fe-B films, amorphous, mag. annealing behaviour 79−73782
Fe-B glass, crystallisation kinetics, elec. resist. meas. 78−83741
Fe-B glass, crystallisation kinetics, elec. resist. meas. 79−4254
Fe-B glass, X-ray obs. of struct. 79−1399
Fe-B metallic glass, hardness, elastic moduli, density, cryst. temp., mech. props., for flywheel appl. *(Dutch)* 78−52878
Fe-B metallic glass, role of Fe_3B in crystn., mag. and Mossbauer expts. 78−94997
Fe-B metallic glass, struct. and crystallisation, Mossbauer spectra, calorimetry and magnetisation meas. 79−23528
Fe-B metallic glass, X-ray diffr. meas., semi-empirical struct. model 80−107059
Fe-B metallic glasses, crystn. kinetics by differential scanning calorimetry 78−91257
Fe-B metallic glasses, density, mech. and thermal props. 78−31432
Fe-B metallic glasses, diffusion coeffs. from primary crystn. data 80−100345
Fe-B metallic glasses, short-range orders 79−65002
Fe-B metallic glasses, short range order 79−77528
Fe-B metallic glasses, struct., stability and crystn. 80−75173
Fe-B metallic ribbons, correl. between quenching temp. and mech. and mag. props. 80−89373
Fe-B metastable alloys, Mossbauer spectroscopy and electron microscopy 79−28653
Fe-B phase ferromag. amorphous alloys, stiffening below Curie temp., pole effect *(Japanese)* 80−84632
Fe-B ribbon, microhardness, and static coercive force, melt overheating effect 80−84978
Fe-B_4C powder mixtures, phase changes and struct. of sintered materials *(Russian)* 78−6872
Fe-B_4C sintered material, mech. props. and struct. characts. 79−100084
Fe-B-C, amorphous, effects of replacement of B by C on mag. props. 80−84621
Fe-B-C, method of revealing structural components 80−21228
Fe-B-C alloys, amorphous, temp. depend. of magnetisation 79−73690
Fe-B-C amorphous alloy, formation, mag. props., thermal stability and density 80−75796
Fe-B-C amorphous alloys, room-temp. saturation induction over 17.5 kG 79−47300
Fe-B-C amorphous alloys, atomic struct., energy dispersive X-ray diffr. meas. 79−73100
Fe-B-C amorphous alloys, effect of Si addition on mag. props. 80−34694
Fe-B-C amorphous alloys for use in power transformers 80−88808
Fe-B-C amorphous alloys with high saturation induction 80−84617
Fe-B-C system, phase composition, morphology after heat treatments, $Fe_{23}B_5C$ struct. 77−28779
Fe-B-Cr(Mo), metallic glasses, mag., struct., and elec. props. 80−88751
Fe-B-Cr(Si) thin film glasses, mag. props. and corrosion resist. 80−80576
Fe-B-Mo-Cr, amorphous, Mo and Cr addition effect on corrosion behaviour 80−16568
Fe-B-Si, amorphous ferromag. alloys, mag. struct., Mossbauer study 80−39746
Fe-B-Si amorphous alloy, liq. quenched, elec. resist. and cyclic deform. 80−59949
Fe-B-Si amorphous alloys, crystallisation temp., Curie temps., saturation magnetisation 79−82820
Fe-B-Si amorphous ribbon, strain induced anisotropy, and toroid diam. effect on mag. props. 80−34623
Fe-B-Si amorphous ribbons, effect of annealing conditions on magnetomechanical props. 80−34740
Fe-B-Si-C amorphous alloys, prep. and props. 80−88748
Fe-B(-Co), two amorphous phases form. and crystallisation 79−27924
Fe-B(-Si), glassy, field-induced mag. anisotropy near eutectic comp. 80−93110
Fe-B(-Si) alloy filaments produced by glass-coated melt spinning 80−76213
Fe-B(-Si)(-Ni), amorphous alloy, anelastic relaxation 79−4997
Fe-B(−Ni), chemical ordering, crystallisation and glass transition temp. 79−90563
Fe-C-B, amorphous, room-temp. saturation induction 78−95476
Fe-C-B, exam. of phase diagram using neutron autoradiography 79−8279
Fe-C-B, splat cooled, formation of metastable crystalline phases and glasses 78−88461
Fe-C-Mo-Nb-Al-Ti-B (0.015, 5.75, .7, 1.6, 2.5, 0.1 wt.%), TZM sheet, wear resistance, effect of surface hardening 77−59985

boron alloys continued
Fe-Co-B, metallic glass, Mossbauer investigation of electronic struct. 78−92009
Fe-Co-B powders, synthesis and mag. props., appl. to mag. recording 80−20432
Fe-Co-C-B, amorphous, room-temp. saturation induction 78−95476
Fe-Co-Ni-Si-B amorphous alloy, magnetostriction and permeability, effect of annealing 79−1701
Fe-Co-Si-B, amorphous, rapidly quenched, mag. heads appl. *(Japanese)* 80−54922
Fe-Co-Si-B, amorphous soft ferromagnet with high mag. induction 80−84619
Fe-Co-Si-B, zero magnetostrictive amorphous alloy with high saturation induction, mag. annealing 80−60362
Fe-Co-Si-B sputtered amorphous thin film, coercivity, galvanomagnetic props., resistivity 80−29578
Fe-Co-Si(B), amorphous ferromagnet, mag. after effect on soft mag. props. 80−84626
Fe-Cr-B, amorphous, Elinvar and Invar charact. *(Japanese)* 80−11832
Fe-Cr-B, B inhibition of oxidation, AES study 79−61785
Fe-Cr-B amorphous alloys, corrosion resistance, Invar and Elinvar characts. *(Japanese)* 79−96213
Fe-Cr-b amorphous Invar alloy, elastic props., Elinvar characts. and ΔE effect 79−56595
Fe-Mn-B, B effect on intergranular embrittlement 80−108555
Fe-Mn-P-B-Al metallic glass, exchange anisotropy 77−16068
Fe-Mn-PBAl, amorphous mixed mag. system, resist. minima 79−60784
Fe-Mo-B metallic glass ribbons, tensile strength, crystn. temp. 80−89173
Fe-Ni-B, amorphous, crystn. 80−79704
Fe-Ni-B, metallic glass, Mossbauer investigation of electronic struct. 78−92009
Fe-Ni-B and Fe-Ni-B metallic glasses, Curie pt. anomalies 80−60256
Fe-Ni-B glassy ribbons melt spinning, gas boundary layer effects 80−76217
Fe-Ni-B metallic glass, X-ray diffr. meas., semi-empirical struct. model 80−107059
Fe-Ni-B-Mo, crystn. temp. and elec. cond. correl., Mo effect 80−75179
Fe-Ni-B-Si, amorphous, mag. props., heat treatment effects 80−89370
Fe-Ni-B(-P), ferromag., magneto-optical spectra in amorphous and cryst. states *(Russian)* 80−84749
Fe-Ni-B(-P) amorphous alloys, mag. annealing mechanism, induced anisotropy 78−95484
Fe-Ni-C-B, and Fe-Ni-Co-B-C-Si, amorphous, room-temp. saturation induction 78−95476
Fe-Ni-Cr (35, 15 wt.%) superalloy, stress rupture and tensile props., C and B additions effect *(Chinese)* 80−104244
Fe-Ni-Cr-B, X-101 centrifugally cast cylinder lining alloy, compatibility with hardfacing alloys 77−32726
Fe-Ni-Cr-P-B, Metglas 2826A, hardness, elastic moduli, density, cryst. temp., mech. props., for flywheel appl. *(Dutch)* 78−52878
Fe-Ni-Cr-P-B amorphous alloy, localized corrosion 80−16559
Fe-Ni-P-B, amorphous, crystn. and struct. 80−75175
Fe-Ni-P-B, amorphous, magnetically induced anisotropy 77−89948
Fe-Ni-P-B, amorphous alloy, anelastic relaxation 79−4997
Fe-Ni-P-B, amorphous ferromag. alloys, mag. struct., Mossbauer study 80−39746
Fe-Ni-P-B, amorphous paramag. alloys, hyperfine field distrib., Mossbauer study 80−39958
Fe-Ni-P-B, metallic glasses, struct. relax., annealing effects on mag. props. 80−89261
Fe-Ni-P-B amorphous ribbons, form. by melt spin technique 80−76215
Fe-Ni-P-B metallic glass, crystallisation temperature values from isothermal transformation times 80−59397
Fe-Ni-Si-B, amorphous paramag. alloys, hyperfine field distrib., Mossbauer study 80−39958
Fe-P-B, amorphous alloy, anelastic relaxation 79−4997
Fe-P-B, amorphous alloy, Mossbauer effect and short-range order 80−2675
Fe-P-B, amorphous alloys, mag. props., conc. depend. 77−8314
Fe-P-B-Al, amorphous, magnetostriction as function of glass formers 78−19299
Fe-Si (3 wt.%), containing B, grain boundary segregation, AES evidence 77−86046
Fe-Si-B, embrittlement by crystallisation *(Japanese)* 78−48513
Fe-Si-B, high induction, hot rolling treatment 80−89266
Fe-Si-B, high induction alloy, improving mag. props. by adding B to coating 79−83338
Fe-Si-B, magnetic metallic glasses, mag. props. 80−84620
Fe-Si-B, melt C content effect on grain growth and induction 80−35351
Fe-Si-B, surface tension, density, and oxidation kinetics 80−20028
Fe-Si-B amorphous alloys, metalloid content effects on Curie temp. and mag. moments 78−14956
Fe-Si-B amorphous alloys, Mossbauer spectroscopy *(French)* 80−80653
Fe-Si-B amorphous alloys with metalloid elements, embrittlement/crystn. relationship *(Japanese)* 79−96134
Fe-Si-B amorphous films, mag. props. 80−34710
Fe-Si-B amorphous powder, production by spark erosion, and mag. props. 77−90290
Fe-Si-B ferromagnetic amorphous alloys, Young's modulus and delay time characts. *(Japanese)* 77−85543
Fe-Si-B glassy alloys, mag. props., comp. effects 80−88752
Fe-Si-B magnetic powder, amorphous, prep. by atomisation technique 78−92213
Fe-Si-B metallic glass, magnetisation meas. 78−23252
Fe-Si-B metallic glasses, crystn., differential scanning calorimetry obs. 79−82160
Fe-Si-B sputtered amorphous films, mag. props. and corrosion resist. 79−28567
Fe-Si-B-S, grain-oriented, high induction, B and S addition effect on magnetic props. *(Slovak)* 79−4697
Fe-TiB_2, phase composition, secondary ion-ion emission study *(Russian)* 80−20896
$(Fe\text{-}Co\text{-}Ni)_{78}Si_8B_{14}$, amorphous, low coercivity and zero magnetostriction 78−23299
$(Fe\text{-}Ni\text{-}Mo)_{80}(P\text{-}B)_{20}$, amorphous, mag. aftereffects and struct. instabilities 80−88833
FeB and Fe_2B, multiplet splitting of ESCA Fe 3s core levels 80−29847
$Fe_{1-x}B_x$, amorphous, hyperfine fields and local mag. moments, Mossbauer study 80−75895
$Fe_{1-x}B_x$ amorphous films, mag. props. and thermal stability 79−78446

boron alloys continued
$Fe_{1-x}B_x$ film, optical and magneto-optical characts., mag. preps. 79—82956
$Fe_{1-x}B_x$ metallic glasses, struct. and cryst., Mossbauer spectra, DSC, and magnetisation meas. 79—94906
$Fe_{1-x}B_x$, polycrystalline and amorphous sputtered films, Brillouin spectra 80—2775
$Fe_{100-x}B_x$ $(11.5 \leq x \leq 22)$, magneto-volume effect 78—91922
$Fe_{100-x}B_x$, amorphous, effect of metalloids on mag. props. 79—11304
$Fe_{100-x}B_x$, amorphous, mag. saturation, spin wave stiffness, temp. depend. 80—75741
$Fe_{100-x}B_x$, amorphous, mag. struct., mag. susceptibility meas. 80—80485
$Fe_{100-x}B_x$ amorphous alloys, magnetostriction meas. 79—19760
$Fe_{100-x}B_x$, amorphous alloys, saturation magnetostriction and annealing behaviour 80—34739
$Fe_{100-x}B_x$, crystalline and glassy, low temp. magnetisation study 79—95608
$Fe_{100-x}B_x$ glass, magnetostriction meas., temp. depend. 79—73792
$Fe_{100-x}B_x$, mag. and struct. props., comp. depend. 78—60314
$Fe_{100-x}B_x$ metallic glass, magnetisation meas. 78—80134
$Fe_{100-x}B_x$, quenched ferromag. ribbon, Brillouin spectra 80—2776
$Fe_{100-x}B_x$ ribbon, magnetostriction exam. 79—73794
Fe_3B, distinctness of magnetic hyperfine fields associated with structurally unique Fe sites 77—63330
Fe_3B, mag. props., ^{57}Fe Mossbauer spectra meas. 79—95693
$Fe_{75}B_{25}$ metallic glass, nonisothermal meas. evaluation, non-existence of dynamic correction term 80—107406
$Fe_{80}B_{20}$, absolute thermoelectric power between 300 and 1000K 79—19579
$Fe_{80}B_{20}$, amorphous, Brillouin scatt. from magnons, ferromag. reson. 80—65844
$Fe_{80}B_{20}$, amorphous, cold neutron scatt., local and extended defects 80—84089
$Fe_{80}B_{20}$, amorphous, crystallization 78—42917
$Fe_{80}B_{20}$, amorphous, crystn. temp. under press. 79—23523
$Fe_{80}B_{20}$, amorphous, crystn. 80—75187
$Fe_{80}B_{20}$, amorphous, deform. and annealing effects on mag. and mech. props. 77—12717
$Fe_{80}B_{20}$, amorphous, elec. and mag. hyperfine field distribs., Mossbauer study 80—39964
$Fe_{80}B_{20}$, amorphous, evaluation of complex Mossbauer spectra 78—43755
$Fe_{80}B_{20}$, amorphous, fast neutron and fission fragment irrad., effect on elec. resist. 80—19846
$Fe_{80}B_{20}$, amorphous, mag. permeability aftereffect during annealing 80—88834
$Fe_{80}B_{20}$, amorphous, transverse magnetoresist., stress effect 80—15501
$Fe_{80}B_{20}$ amorphous alloy, low field magnetic props. 77—55690
$Fe_{80}B_{20}$ amorphous alloys, domain struct. exam., magneto-optic Kerr effect 79—28550
$Fe_{80}B_{20}$, amorphous ferromag., temp. depend. of hyperfine field distrib. 78—43756
$Fe_{80}B_{20}$, amorphous ferromag. metallic glass, stress-induced rot. of magnetisation, Mossbauer study 80—20445
$Fe_{80}B_{20}$, amorphous ferromagnet, Mossbauer hyperfine fields, mag. struct. 80—75894
$Fe_{80}B_{20}$ amorphous ribbons, magnetomechanical coupling constant and Young's modulus, mag. annealing 79—15333
$Fe_{80}B_{20}$ amorphous ribbon, initial susceptibility time lag 80—100579
$Fe_{80}B_{20}$, amorphous struct., Mossbauer spectroscopy investigation 80—84677
$Fe_{80}B_{20}$, amorphous to cryst. transorm. 80—34188
$Fe_{80}B_{20}$ amorphous wire, crystn. by annealing at 780°C 80—100177
$Fe_{80}B_{20}$, crystallisation of amorphous alloys, TEM and X-ray diffr. exam. of struct., growth characts. 78—79539
$Fe_{80}B_{20}$, elastic, magnetoelastic and thermal props. 79—19759
$Fe_{80}B_{20}$, evaluation of complex Mossbauer spectra 78—60370
$Fe_{80}B_{20}$, $Fe_{78}Mo_2B_{20}$ glasses, internal friction and shear modulus 79—52287
$Fe_{80}B_{20}$, ferromagnetic metallic glasses, Brillouin scattering 78—92085
$Fe_{80}B_{20}$ film, amorphous metallic, standing spin waves, Brillouin scatt. obs. 80—97291
$Fe_{80}B_{20}$ glass, low-field mag. props. 77—8380
$Fe_{80}B_{20}$ glass, magnetisation reorientation, Mossbauer effect 80—66092
$Fe_{80}B_{20}$, glassy, ferromag. anisotropy of resistivity 79—23939
$Fe_{80}B_{20}$, hardness, elec. cond., photo emission, and mag. props. *(Norwegian)* 79—32909
$Fe_{80}B_{20}$, METGLAS 2605, mag. anisotropy and electronic struct., Mossbauer meas. 77—28384
$Fe_{80}B_{20}$, magnetostriction, temp. depend. 78—91921
$Fe_{80}B_{20}$, metallic glass, ferromag. props. 77—16107
$Fe_{80}B_{20}$, metallic glass, elec. resist., 78 to 1000K, probe of crystn. process 77—76787
$Fe_{80}B_{20}$, metallic glass, Mossbauer spectroscopy 78—60365
$Fe_{80}B_{20}$ metallic glass, spin texture determ. 80—15842
$Fe_{80}B_{20}$, metallic glass, high-resolution XPS study, electronic state struct. 80—29846
$Fe_{80}B_{20}$, metallic glass, low temp. specific heat, metalloid effects 80—34654
$Fe_{80}B_{20}$, metallic glass, triplet correlation, field-ion microscopy study 80—38921
$Fe_{80}B_{20}$, metallic glass, Doppler broadening of positron annihilation γ-radiation and elec. resist. 80—66321
$Fe_{80}B_{20}$ metallic glass, crystn. and struct. relax., Mossbauer effect study 80—75182
$Fe_{80}B_{20}$ metallic glass, crystn. kinetics 80—84083
$Fe_{80}B_{20}$ metallic glasses, stability and transforms. 80—75174
$Fe_{80}B_{20}$, Metglas 2605, amorphous ferromag., resistivity down to 60 mK 79—60783
$Fe_{80}B_{20}$, Metglas 2605, amorphous ribbon, power loss variation with freq. and applied stress 80—88849
$Fe_{80}B_{20}$, Metglas 2605, Young's modulus meas. using piezoelectric US composite oscillator technique 80—108656
$Fe_{80}B_{20}$ Metglass, Mossbauer spectra line broadening 78—52400
$Fe_{81}B_{19}$ amorphous alloy, mag. anisotropy temp. depend. 78—14953
$Fe_{83}B_{17}$ metallic glass, struct. from neutron diffr. study 80—6363
$Fe_{83.4}B_{16.6}$, amorphous, mag. props. and microstruct., cooling rate and melt overheating effects 80—65965
$Fe_{83.4}B_{16.6}$ amorphous, mag. props., melt overheating and cooling rate effects 80—89371
$Fe_{84}B_{16}$, amorphous, struct., X-ray diffr. meas. 79—4252
$Fe_{84}B_{16}$, metallic glass, electrical resistivity and crystallisation 80—88526

boron alloys continued
$Fe_{84}B_{16}$, metallic glass, ion implanted, UPS meas. 80—97411
Fe_xB_{100-x}, amorphous, mag. props., ^{57}Fe Mossbauer spectra and magnetisation meas. 79—95693
Fe_xB_{100-x}, amorphous, stress relax. after annealing 80—55447
$Fe_{80}(B_yC_{1-y})_{20}$, amorphous, saturation magnetostriction, comp. effects 80—34735
$Fe_{84}B_{16-x}C_x$, amorphous, hyperfine interaction and Curie temps., Mossbauer meas. 79—73858
$Fe_{84}B_{16-x}C_x$, amorphous, mag. saturation, spin wave stiffness, temp. depend. 80—75741
$Fe_{84}B_{16-x}C_x$, amorphous alloys, short range order, Mossbauer and DSC study 80—39960
$Fe_{80}B_{20-x}Ge_x$, amorphous, mag. saturation, spin wave stiffness, temp. depend. 80—75741
$Fe_{80}B_{20-x}M_x$ (X=Al, Si, Ge, C, P) and $(FeCo)_{80}B_{20}$ glass, magnetisation, Curie and crystn. temps. 79—87289
$Fe_{80}(B_{1-x}P_x)_{20}$ amorphous alloys, isothermal crystallisation kinetics 80—33895
$Fe_{40}B_{40}P_{14}B_6$, Metglas 2826, amorphous ribbon, power loss variation with freq. and applied stress 80—88849
$Fe_{78}B_{12}Si_{10}$, amorphous, continuous versus discrete hyperfine field distrib., Mossbauer spectra 79—33583
$Fe_{78}B_{12}Si_{10}$, amorphous, Mossbauer study of hyperfine interaction and mag. anisotropy 80—40027
$Fe_{78}B_{12}Si_{10}$, amorphous ferromagnet, long and short range exchange interactions, Mossbauer spectra and interpretation 79—56526
$Fe_{80}B_{15}Si_5$ metallic glass, large uniaxial magnetostrictive anisotropy, magnetisation reversal 80—34736
$Fe_{80}B_{20-x}Si_x$, amorphous, mag. saturation, spin wave stiffness, temp. depend. 80—75741
$Fe_{80}B_{20-x}Si_x$, metallic glass, mech. and mag. props., depend. on metalloid content 79—91213
$Fe_{80}(B_ySi_{1-y})_{20}$, amorphous, saturation magnetostriction, comp. effects 80—34735
$Fe_{82}B_{15}Si_3$, metallic glass, low temp. specific heat, metalloid effects 80—34654
$Fe_{82}B_{18-x}Si_x$ glasses, soft mag. props. 79—73774
$Fe_{83}B_{16.5}Si_{0.5}$, amorphous, spin waves, inelastic neutron scatt. meas. 79—73701
$Fe_{84}B_{13}Si_2$, metallic glass, electrical resistivity and crystallisation 80—88526
$Fe_{100-x}Be_x$, amorphous ribbon, saturation magnetostriction, and electronically controllable delay line 79—1700
$Fe_{80}(C_{1-x}B_x)_{20}$ amorphous alloy, α-Fe crystn., morphology 80—70129
$(Fe_{0.06}Co_{0.94})$-B, amorphous, ferromag., mag. instability rel. to struct. 79—99729
FeCoB, corrosion-resistant amorphous mag. thin films 80—54923
$(FeCo)_{80}B_{20}$, glass, elastic consts. 79—83249
$(Fe_{0.5}Co_{0.5})_{1-x}B_x$, amorphous, hyperfine fields and local mag. moments, Mossbauer study 80—75895
$Fe_{0.65}Co_{0.35}B$, crystalline disordered, evaluation of complex Mossbauer spectra 78—60370
$Fe_5Co_{75}B_{20}$, amorphous, magnetisation reversal and domain boundary configs. 80—88809
$Fe_{71}Co_9B_{20}$, glassy ribbon, magnetostatic effects 79—73790
$Fe_{80-x}Co_xB_{20}$, ferromag. metallic glass saturation magnetostriction meas. 77 - 36108
$Fe_{80-x}Co_xB_{20}$, spontaneous Hall effect and resistivity 79—19576
$Fe_xCo_{80-x}B_{20}$, amorphous, mag. after-effect 79—61189
$Fe_{35}Co_{32}B_{20}Si_{10}Al_3$, stress-induced variation in magnetisation and dynamic magnetostrictive charact. 80—88855
$(Fe_{0.07}Co_{0.93})_{75-x}Cr_xSi_{15}B_{10}$, amorphous, disaccommodation of mag. permeability and induced anisotropy 80—88741
$(FeCoNi)_8B_{20}$, glass, evidence supporting split-band model from magnetostriction 78--95509
$(Fe_{100-x}Co_x)_{79}P_{13}B_8$, amorphous, hyperfine field distrib., ^{59}Co NMR spin-echo meas. 80—34818
$(Fe_{0.05}Co_{0.95})_{78}Si_8B_{14}$ amorphous ribbon, anomalous mag. aftereffect 80—100602
$(Fe_{0.9}Co_{0.1})_xSi_yB_2$, $(Fe_{1-x}Co_x)_{78}Si_8B_{14}$ amorphous ribbons, magnetomech. coupling and saturation magnetostriction 78—68353
$(Fe_{1-x}Co_x)_{77}Si_{10}B_{13}$ alloys, amorphous, induced mag. anisotropy by mag. annealing 79—4671
$(Fe_{1-x}Co_x)_{77}Si_{10}B_{13}$, amorphous, mag. moments at 0K, Curie temp., mag. interactions 79—4670
$(Fe_{1-x}Co_x)_{77}Si_{10}B_{13}$, amorphous magnetic alloys, density meas. 80—1934
$(Fe_{1-x}Co_x)_{78}Si_{10}B_{12}$, amorphous, Hall effect and magnetoresist. *(Japanese)* 77—85199
$(Fe_{1-x}Co_x)_{78}Si_{10}B_{12}$, amorphous alloys, magnetic anisotropy meas. 80—2570
$(Fe_{1-x}Co_x)_{78}Si_{10}B_{12}$, amorphous, roll mag. anisotropy 80—75757
$(Fe_{1-x}Co_x)_{78}Si_8B_{14}$ ribbon, magnetostriction exam. 79—73794
$Fe_5Co_{70}Si_{15}B_{10}$, amorphous ribbon, zero magnetostriction, low residual mag. loss 77—12157
$Fe_5Co_{70}Si_{15}B_{10}$, amorphous ribbon, HF mag. characts., magnetostriction role 77—66408
$Fe_5Co_{70}Si_{15}B_{10}$, amorphous, change of mag. props. by low temp. annealing 78—27058
$Fe_5Co_{70}Si_{15}B_{10}$, amorphous toroidal core, switching characts. and domain structs. 78—95477
$Fe_5Co_{70}Si_{15}B_{10}$, amorphous ferromagnetic alloy, isothermal annealing effect on static magnetic props. *(Japanese)* 79—52398
$Fe_5Co_{70}Si_{15}B_{10}$, amorphous, crystn. effect on mag. props. *(Russian)* 80—44858
$(Fe_xCo_{1-x})_{100-y}(Si_{0.4}B_{0.6})_y$ amorphous alloy zero magnetostrictive, mag. props. 79—99743
$(Fe_xCo_{1-x})_{78}Si_8B_{14}$, amorphous, saturation magnetostriction, strain modulated FMR obs. 80—75863
$(Fe_xCo_{100-x})_{100-(y+z)}Si_yB_z$ amorphous ribbon, mag. moment and Curie temp., comp. depend. 78—95421
$Fe_{85-x}Cr_xB_{15}$ metallic glass, Curie temp., crystn. temp. and room temp. elec. resist., Cr content effect 79—91229
$Fe_{36}Cr_{32}Ni_{14}B_{12}B_6$, amorphous X-ray absorpt. spectra, effective coordination charges 80—84805
$Fe_{83-x}M_xB_{17}$ and $Fe_{78-x}M_xSi_{10}B_{12}$ (M=refractory metal), glass form. and thermal stability 80—79703
$(Fe_xMn_{1-x})_{75}P_{16}B_6Al_3$, amorphous, mag. ordering temp., hyperfine field distrib., elec. resist. 80—34633
$Fe_{76}Mo_4B_{20}$, quenched ferromag. ribbon, Brillouin spectra 80—2776

boron alloys continued
$Fe_{78}Mo_2B_{20}$, amorphous, transverse magnetoresist., stress effect 80–15501
$Fe_{78}Mo_2B_{20}$, amorphous, fast neutron and fission fragment irrad., effect on elec. resist. 80–19846
$Fe_{78}Mo_2B_{20}$, amorphous ferromag., $T^{3/2}$ depend. of hyperfine field 78–39474
$Fe_{78}Mo_2B_{20}$, amorphous ferromag., mag. props. 79–38309
$Fe_{78}Mo_2B_{20}$ amorphous ribbons, magnetoelastic effects in as-quenched and stress-relieved states 80–80588
$Fe_{78}Mo_2B_{20}$, Elinvar-type behaviour 79–66091
$Fe_{78}Mo_2B_{20}$, exam. of mag. props. between 300 and 900K 78–85010
$Fe_{78}Mo_2B_{20}$ glass, thermal expansion, glass transform. and crystn. temps. 80–2183
$Fe_{78}Mo_2B_{20}$, glassy, ferromag. anisotropy of resistivity 79–23939
$Fe_{78}Mo_2B_{20}$, metallic glass, elec. resist., 78 to 1000K, probe of crystn. process 77–76787
$Fe_{78}Mo_2B_{20}$, metallic glass, triplet correlation, field-ion microscopy study 80–38921
$Fe_{78}Mo_2B_{20}$, metallic glass, Doppler broadening of positron annihilation γ-radiation and elec. resist. 80–66321
$Fe_{78}Mo_2B_{20}$, Metglas 2605 A, amorphous ferromag., resistivity down to 60 mK 79–60783
$Fe_{80-x}Mo_xB_{20}$ metallic glasses, Curie temp., crystn. temp., elec. cond. as function of composition 79–60285
$(Fe_{93}Mo_7)_{80}B_{10}P_{10}$, amorphous, neutron scatt. investig. of spin waves, magnetisation 77–47984
$(Fe_xMo_{1-x})_{75}P_{16}B_6Al_3$, amorphous, effects of Mo on mag. props., Mossbauer meas. 79–73859
$Fe_{40}Ni_{38}$-Mo_4B_{18} amorphous alloys, compatibility of DC and AC mag. props. 80–34695
FeNiB, amorphous alloy, high resolution imaging by electron microscopy 79–99039
$(FeNi)_{80}B_{20}$, glass, elastic consts. 79–83249
$(Fe_{0.6}Ni_{0.4})_{100-x}B_x$ and $(Fe_{100-x}Ni_x)_{80}B_{20}$ amorphous alloys, X-ray diffr. struct. determ. 80–64906
$(Fe_{1-x}Ni_x)_{75}B_{25}$, amorphous and cryst., short range order, Mossbauer study 80–39961
$(Fe_{1-x}Ni_x)_{83}B_{17}$, amorphous alloys ferromagnetic resonance 80–108080
$(Fe_{100-x}Ni_x)_{100-y}B_y$, metallic glass, embrittlement and crystn. 80–7685
$(Fe_{100-x}Ni_x)_{83}B_{17}$, amorphous, crystn. 80–75176
$Fe_{38}Ni_{38}B_{24}$, amorphous, magnetisation and FMR expts. 79–95607
$Fe_{40}Ni_{40}B_{20}$ alloys, crystalline and amorphous, resistivity minimum, X-ray, Mossbauer studies 79–73489
$Fe_{40}Ni_{40}B_{20}$, amorphous, induced mag. anisotropy, reorientation kinetics 77–43829
$Fe_{40}Ni_{40}B_{20}$, amorphous, hyperfine field distrib., Mossbauer effect meas. 79–4755
$Fe_{40}Ni_{40}B_{20}$, amorphous, hyperfine field distrib., Mossbauer study 79–28657
$Fe_{40}Ni_{40}B_{20}$, amorphous, anomalous thermal dilatation 79–55668
$Fe_{40}Ni_{40}B_{20}$, amorphous, resist. min. disappearance on annealing 79–60786
$Fe_{40}Ni_{40}B_{20}$, amorphous, processing conditions effect on mag. props. 79–73775
$Fe_{40}Ni_{40}B_{20}$, amorphous, mag. loss meas. 79–73776
$Fe_{40}Ni_{40}B_{20}$, amorphous, high-field magnetisation curve, spin wave spectrum and microstructural inhomogeneities 80–15702
$Fe_{40}Ni_{40}B_{20}$, amorphous, mag. props., effects mech. deform. 80–39840
$Fe_{40}Ni_{40}B_{20}$, amorphous, phase transforms., resistometric anal. 80–75538
$Fe_{40}Ni_{40}B_{20}$, amorphous, RF annealing effects 80–108037
$Fe_{40}Ni_{40}B_{20}$, amorphous ribbon prod., apparatus parameters effect on dimens. 77–12570
$Fe_{40}Ni_{40}B_{20}$, amorphous ferromag., resist. and galvanomagnetic props., rel. to magnetisation 78–14712
$Fe_{40}Ni_{40}B_{20}$, amorphous and crystalline, resist. minimum 79–47079
$Fe_{40}Ni_{40}B_{20}$, amorphous ferromag., resistivity down to 60 mK 79–60783
$Fe_{40}Ni_{40}B_{20}$, amorphous ribbon, anal. of casting conditions 79–95965
$Fe_{40}Ni_{40}B_{20}$, amorphous ribbon, power loss variation with freq. and applied stress 80–88849
$Fe_{40}Ni_{40}B_{20}$ and $Fe_{40}Ni_{40}P_{14}B_6$, amorphous, mag. aftereffect spectra and annealing props. 80–88831
$Fe_{40}Ni_{40}B_{20}$ glass, ^{10}B self-diffusion, meas. by SIMS 80–49406
$Fe_{40}Ni_{40}B_{20}$, metallic glass, embrittlement kinetics and crystn., quenching influence 78–68766
$Fe_{40}Ni_{40}B_{20}$, metallic glass, low temp. specific heat, metalloid effects 80–34654
$Fe_{40}Ni_{40}B_{20}$, molten, jet streaming, planar and cylindrical, instabilities rel. to glassy alloy casting 80–35129
$Fe_{50}Ni_{30}B_{20}$, crystallisation of amorphous alloys, TEM and X-ray diffr. exam. of struct., growth characts. 78–79539
$Fe_{80-x}Ni_xB_{20}$ and $Fe_{80-x}Ni_xP_{14}B_6$ amorphous alloys, microhardness correl. with mag. props. 80–88826
$Fe_{80-x}Ni_xB_{20}$, $Fe_{80-x}Ni_xP_{14}B_6$, amorphous, microhardness meas., dependence on mag. props. *(Croatian)* 79–11688
$Fe_{80-x}Ni_xB_{20}$, ferromag. metallic glass, saturation magnetostriction meas. 77–36108
$Fe_{80-x}Ni_xB_{20}$, spontaneous Hall effect and resistivity 79–19576
$(Fe_xNi_{1-x})_{80}B_{20}$, $(Fe_xNi_{1-x})_{80}P_{14}B_6$, new soft amorphous ferromagnetic glasses *(Croatian)* 79–11298
$(Fe_xNi_{1-x})_{80}B_{20}$, amorphous alloys, engineering mag. props. 79–51832
$(Fe_xNi_{1-x})_{80}B_{20}$, amorphous, Mossbauer spectra, mag. props. 80–15843
$(Fe_xNi_{100-x})_{80}B_{20}$, glassy, elec. resist. at elevated temp. 79–73484
$Fe_xNi_{80-x}B_{20}$, amorphous ferromag., low temp. resistivity 79–56181
$Fe_xNi_{80-x}B_{20}$ and $Fe_xNi_{80-x}P_{14}B_6$ metallic glasses, low temp. resist. and galvanomag. effects, mag. state influence 80–84461
$Fe_xNi_{80-x}B_{20}$, $Fe_xNi_{80-x}P_{14}B_4$, amorphous Hall effect voltage meas. *(Croatian)* 79–11102
$Fe_xNi_{80-x}B_{20}$, $Fe_xNi_{80-x}P_{14}B_6$, amorphous ferromag., galvanomag. props. 79–56196
$Fe_xNi_{80-x}B_{20}$ glass, resist., magnetoresist., and thermoelec. power 80–70681
$Fe_xNi_{80-x}B_{20}$, quenched ferromag. ribbon, Brillouin spectra 80–2776
$(Fe_yNi_{1-y})_{80}B_{20}$, mag. anneal anisotropy in amorphous alloys 77–16069
$(Fe_{1-y}Ni_y)_{0.8}B_{0.2-x}P_x$, amorphous, hyperfine fields and local mag. moments, Mossbauer study 80–75895
$Fe_{1.6}Ni_{78.4}B_{10}P_{10}$ metallic glass, superparamag. behaviour, chem. inhomogeneities role 80–84625
$Fe_{20}Ni_{60}B_{19}P_1$, amorphous, spin waves, inelastic neutron scatt. meas. 79–73701

boron alloys continued
$Fe_{40}Ni_{40}B_{20-x}P_x$, amorphous, mag. saturation, spin wave stiffness, temp. depend. 80–75741
$Fe_{40}Ni_{40}B_{20-x}P_x$ metallic glasses, local struct. and dynamic disorder of Fe and Ni, EXAFS obs. 80–89088
$Fe_{80-x}Ni_xB_{20-y}P_y$, amorphous, Rayleigh region and coercive force 80–88806
$(FeNi)_{80}Bi_{17.5}Al_2Si_{0.5}$, stress-induced variation in magnetisation and dynamic magnetostrictive charact. 80–88855
$Fe_{32}Ni_{36}Cr_{14}P_{12}B_6$, Metglas 2826A, Hall resistivity, effect of thermal cycling and annealing 78–56125
$Fe_{32}Ni_{36}Cr_{14}P_{12}B_6$, shear band form. 78–68756
$Fe_{32}Ni_{36}Cr_{14}P_{12}B_6$, elastic, magnetoelastic and thermal props. 79–19759
$Fe_{32}Ni_{36}Cr_{14}P_{12}B_6$, glassy, ferromag. anisotropy of resistivity 79–23939
$Fe_{32}Ni_{36}Cr_{14}P_{12}B_6$, METGLAS 2826A, metastable crystallization phases, TEM obs. 79–55671
$Fe_{32}Ni_{36}Cr_{14}P_{12}B_6$, amorphous ferromagnet, long and short range exchange interactions, Mossbauer spectra and interpretation 79–56526
$Fe_{32}Ni_{36}Cr_{14}P_{12}B_6$, amorphous mag. solids, Mossbauer exam. 79–61281
$Fe_{32}Ni_{36}Cr_{14}P_{12}B_6$, Metglass 2826A, mag. props. under high press., Mossbauer meas. 79–73860
$Fe_{32}Ni_{36}Cr_{14}P_{12}B_6$ glass, thermal expansion, glass transform. and crystn. temps. 80–2183
$Fe_{32}Ni_{36}Cr_{14}P_{12}B_6$, metallic glass, Doppler broadening of positron annihilation γ-radiation and elec. resist. 80–66321
$Fe_{32}Ni_{36}Cr_{14}P_{12}B_6$ metallic glass, crystn. kinetics by TEM 80–75186
$Fe_{32}Ni_{36}Cr_{14}P_{12}B_6$, Metglas 2826A, EPR at 20 GHz 80–75848
$Fe_{40}Ni_{40}(Mo,Si,B)_{20}$, amorphous, soft mag. props., switched-mode power supply appls. 80–88850
$Fe_{40}Ni_{38}Mo_4\ B_{18}$ amorphous ribbons, magnetoelastic effects in as-quenched and stress-relieved states 80–80588
$Fe_{40}Ni_{38}Mo_4B_{18}$, amorphous, crystallization, heat treatment and irradiation effects *(French)* 79–90558
$Fe_{40}Ni_{38}Mo_4B_{18}$, amorphous, mag. anisotropy, Mossbauer study 80–65864
$Fe_{40}Ni_{38}Mo_4B_{18}$, amorphous, reversible enhancement of mag. directional ordering rate 80–103829
$Fe_{40}Ni_{38}Mo_4B_{18}$ glassy alloy, high permeability, low field mag. characts. 78–68301
$Fe_{40}Ni_{38}Mo_4B_{18}$ metallic glass, reorientation kinetics of magnetization 79–24155
$Fe_{40}Ni_{38}Mo_4B_{18}$, metallic glass, mag. and transport props. 80–39752
$Fe_{40}Ni_{38}Mo_4B_{18}$ ribbon, magnetic characterisation 80–34680
$(Fe_{0.04}Ni_{0.96})_{80}P_{10}B_{10}$, amorphous, mictomagnetic to ferromag. transition 78–34981
$(Fe_{0.04}Ni_{0.96})_{80}P_{10}B_{10}$, amorphous magnetisation, field and temp. depend. 80–39755
$(Fe_{1-x}Ni_x)_{80}P_{10}B_{10}$, amorphous, magnetostriction meas. by ferromag. reson., induced anisotropy 77–32232
$Fe_{20}Ni_{60}P_{14}B_6$, $Fe_{30}Ni_{50}P_{14}B_6$, amorphous ferromags., thermoelec. power and resistivity near Curie temp. 79–56200
$Fe_{27}Ni_{53}P_{14}B_6$, amorphous, Hall resist. and mag. props., short range order effects 80–34422
$Fe_{40}Ni_{40}P_{14}B_{06}$, amorphous, strip domains, anisotropy const. effects 80–29571
$Fe_{40}Ni_{40}P_{14}B_{20}$, Metglas 2826, amorphous ferromag., resistivity down to 60 mK 79–60783
$Fe_{40}Ni_{40}P_{14}B_6$, amorhpous ribbon, influence of torsion on mag. props. 80–7138
$Fe_{40}Ni_{40}P_{14}B_6$, amorphous ribbon, cold rolling, annealing mag. props. 77–8958
$Fe_{40}Ni_{40}P_{14}B_6$, amorphous, deform. and annealing effects on mag. and mech. props. 77–12717
$Fe_{40}Ni_{40}P_{14}B_6$, amorphous, magnetoelastic props. 77–16136
$Fe_{40}Ni_{40}P_{14}B_6$, amorphous alloy, small angle X-ray scattering 77–65953
$Fe_{40}Ni_{40}P_{14}B_6$, amorphous, domain struct. 78–10719
$Fe_{40}Ni_{40}P_{14}B_6$, amorphous tape wound cores, mag. props. *(German)* 78–10727
$Fe_{40}Ni_{40}P_{14}B_6$, amorphous, mag. props. 78–10728
$Fe_{40}Ni_{40}P_{14}B_6$ amorphous ribbon, mag. anisotropy distrib. near surface 78–95430
$Fe_{40}Ni_{40}P_{14}B_6$, amorphous toroidal core, switching characts. and domain structs. 78–95477
$Fe_{40}Ni_{40}P_{14}B_6$, amorphous ferromagnet, domain struct., Rayleigh region and coercive field 79–28559
$Fe_{40}Ni_{40}P_{14}B_6$, amorphous, stress-induced mag. easy axis 79–33516
$Fe_{40}Ni_{40}P_{14}B_6$, amorphous, continuous versus discrete hyperfine field distrib., Mossbauer spectra 79–33583
$Fe_{40}Ni_{40}P_{14}B_6$, amorphous, transverse magnetoresist., stress effect 80–15501
$Fe_{40}Ni_{40}P_{14}B_6$, amorphous, mag. props., effects mech. deform. 80–39840
$Fe_{40}Ni_{40}P_{14}B_6$, amorphous, resistometric study of short-range ordering rel. to heat treatment 80–70140
$Fe_{40}Ni_{40}P_{14}B_6$, amorphous ferromagnet, Mossbauer hyperfine fields, mag. struct. 80–75894
$Fe_{40}Ni_{40}P_{14}B_6$ amorphous alloy, temper embrittlement 80–76295
$Fe_{40}Ni_{40}P_{14}B_6$, amorphous, mag. polarisation in approach to ferromag. saturation 80–80560
$Fe_{40}Ni_{40}P_{14}B_6$, amorphous, steady-state creep rate, cryst. effect 80–81102
$Fe_{40}Ni_{40}P_{14}B_6$, amorphous, mag. permeability aftereffect during annealing 80–88834
$Fe_{40}Ni_{40}P_{14}B_6$, amorphous ferromag., spin wave excitations 80–97079
$Fe_{40}Ni_{40}P_{14}B_6$ amorphous ribbon, mag. domains and anisotropy distrib. 80–108029
$Fe_{40}Ni_{40}P_{14}B_6$, elastic, magnetoelastic and thermal props. 79–19759
$Fe_{40}Ni_{40}P_{14}B_6$, $Fe_{29}Ni_{49}P_{14}B_6Si_2$ glasses, internal friction and shear modulus 79–52287
$Fe_{40}Ni_{40}P_{14}B_6$, $Fe_{35}Ni_{32}Cr_{15}P_{12}B_6$, amorphous ferromagnets, Barkhausen noise and core losses 77–69618
$Fe_{40}Ni_{40}P_{14}B_6$, ferromagnetic metallic glasses, Brillouin scattering 78–92085
$Fe_{40}Ni_{40}P_{14}B_6$ glass, low temp. heat capacity meas., electronic, phonon contributions exam. 78–10689
$Fe_{40}Ni_{40}P_{14}B_6$ glass, crystn. kinetics, DSC expts. 78–26444
$Fe_{40}Ni_{40}P_{14}B_6$ glass, struct. relax., ferromag. reson. and X-ray scatt. 79–90566
$Fe_{40}Ni_{40}P_{14}B_6$ glass, thermal expansion, glass transform. and crystn. temps. 80–2183
$Fe_{40}Ni_{40}P_{14}B_6$ glass, viscosity near T_g, using rapid heating, and fusion characts. 80–70438

boron alloys continued

- $Fe_{40}Ni_{40}P_{14}B_6$, glassy metal fabric for mag. shield 77—8347
- $Fe_{40}Ni_{40}P_{14}B_6$, glassy, mag. props. and hyperfine interactions, Mossbauer obs., 4.2-1000K 78—10812
- $Fe_{40}Ni_{40}P_{14}B_6$, glassy, ferromag. anisotropy of resistivity 79—23939
- $Fe_{40}Ni_{40}P_{14}B_6$, hardness, elec. cond., photo emission, and mag. props. *(Norwegian)* 79—32909
- $Fe_{40}Ni_{40}P_{14}B_6$, high-field suscept. and spin wave spectrum 78—10662
- $Fe_{40}Ni_{40}P_{14}B_6$, induced anisotropy energy and saturation magnetisation temp. depend., torque magnetometer meas. 78—10680
- $Fe_{40}Ni_{40}P_{14}B_6$, metallic glass, acoustic emission generated during viscous flow 78—39853
- $Fe_{40}Ni_{40}P_{14}B_6$ metallic glass, dynamic mechanical props. 79—10894
- $Fe_{40}Ni_{40}P_{14}B_6$, metallic glass, cryst., isothermal annealing behaviour 80—6367
- $Fe_{40}Ni_{40}P_{14}B_6$ metallic glass, ferromag. reson., spin waves, thermal ageing and long-range order effects 80—25214
- $Fe_{40}Ni_{40}P_{14}B_6$ metallic glass, isothermal viscosity and crystn. 80—49395
- $Fe_{40}Ni_{40}P_{14}B_6$ metallic glass, crystn. 80—70127
- $Fe_{40}Ni_{40}P_{14}B_6$, Metglas 2826, ferromag. antireson. transmission at 24 GHz, 26 to 270°C 77—69696
- $Fe_{40}Ni_{40}P_{14}B_6$, Metglas 2826, magnetising processes 78—10725
- $Fe_{40}Ni_{40}P_{14}B_6$, Metglas 2826, acoustic emission during viscous flow 78—42915
- $Fe_{40}Ni_{40}P_{14}B_6$, Metglas 2826, amorphous ribbon core, appl. in force transducer 78—93669
- $Fe_{40}Ni_{40}P_{14}B_6$, metglas 2826, amorphous, Hall resistivity, thermal cycling and annealing effects 79—38050
- $Fe_{40}Ni_{40}P_{14}B_6$, Metglas 2826, hot forming 80—84980
- $Fe_{40}Ni_{40}P_{14}B_6$, Metglas 2826, amorphous ribbon under tension, mag. domain walls and pulsed magnetisation reversal 80—88825
- $Fe_{40}Ni_{40}P_{14}B_6$, quenched amorphous, high field susceptibility and microstructure 77—69506
- $Fe_{40}Ni_{40}P_{16}B_6$, amorphous, kinetics of induced mag. directional order 80—44824
- $Fe_{40}Ni_{40}P_yB_{20-y}$, amorphous, mag. props. effect of metalloid elements 79—28658
- $Fe_{46}Ni_{40}P_{16}B_6$, ferromagnetic amorphous alloy, even magneto-optic effects 77—55776
- $Fe_cNi_{80-c}P_{14}B_6$, amorphous, annealing effects on mag. props. 79—78383
- $Fe_xNi_{1-x}P_{14}B_6$, amorphous, spin-glass regime, magnetoresist. meas. 80—34418
- $(Fe_xNi_{1-x})_{80}P_{10}B_{10}$, amorphous, weak itinerant ferromag., Arrott plots 77—73007
- $(Fe_xNi_{1-x})_{80}P_{10}B_{10}$, amorphous, magnetisation reversal and domain boundary configs. 80—88809
- $(Fe_xNi_{1-x})_{80}P_{14}B_6$, Mossbauer spectroscopy, mag. hyperfine interaction, Curie temps. 78—6617
- $(Fe_xNi_{100-x})_{80}P_{10}B_{10}$, amorphous, elec. resist., 2 to 300K, composition depend. 80—44562
- $Fe_xNi_{80-x}P_{14}B_6$ (x=0, 20, 40, 60, 80), metallic glass, low temp. sp. ht. 80—2588
- $Fe_xNi_{80-x}P_{14}B_6$, amorphous, sp. ht. and susceptibility meas., spin glass and mictomag. props. 78—68274
- $Fe_xNi_{80-x}P_{14}B_6$, amorphous ferromag., resistivity, mag. contrib., 1.5-50K 79—56182
- $Fe_xNi_{80-x}P_{14}B_6$, amorphous ferromag., T^2 saturation in resist. below 0.3K 79—60785
- $Fe_xNi_{80-x}P_{14}B_6$, and $Fe_xNi_{80\ x}B_{20}$ glass, microhardness, correl. with mag. props. 79—57085
- $Fe_xNi_{80-x}P_{14}B_6$ glass, resist., magnetoresist., and thermoelec. power 80—70681
- $Fe_xNi_{80\ x}P_{14}B_6$ metallic glasses, low temp. resistivities 78—91659
- $Fe_xNi_{80-x}P_{14}B_6$, metallic glass, low temp. sp. ht. for spin-glass and spin-cluster-glass regime 80—71071
- $(Fe_yNi_{100-y})_{79}P_{13}B_8$, metallic glass, low temp. sp. ht. for spin-glass and spin-cluster-glass regime 80—71071
- $(Fe_{0.3}Ni_{0.7})_{0.75}P_{0.16}B_{0.06}Al_{0\ 03}$, amorphous, spin wave spectrum, neutron scatt. 77—16064
- $(Fe_{0.5}Ni_{0.5})_{75}P_{16}B_6Al_3$ glass, struct. relax. as origin of Curie temp. ageing 78—84418
- $(Fe_{1-x}Ni_x)_{75}(PBAl)_{25}$, amorphous, high-field magnetoresist. meas. 80—34423
- $(Fe_{1-x}Ni_x)_{75}P_{16}B_6Al_3$, amorphous alloy, low temp. elec. resist. saturation 78—68005
- $(Fe_{65}Ni_{35})_{75}P_{16}B_6Al_3$, amorphous ferromag., high temp. spin dynamics 78—47965
- $(Fe_{65}Ni_{35})_{75}P_{16}B_6Al_3$, amorphous ferromagnet, mag. excitations 79—7984
- $(Fe_{65}Ni_{35})_{75}P_{16}B_6Al_3$, amorphous, crystn. temp., press. and heating rate depend. 80—70132
- $(Fe_xNi_{1-x})_{0.75}P_{0.16}B_{0.06}Al_{0.03}$, metallic glass, thermal expansion 78—43151
- $(Fe_xNi_{1-x})_{75}P_{16}B_6Al_3$, amorphous, spin wave excitations and low temp. magnetisation 79—33468
- $(Fe_xNi_{1-x})_{75}P_{16}B_6Al_3$, magnetisation temp. depend., spin wave theory 80—44927
- $Fe_{29}Ni_{49}P_{14}B_6Si_{12}$, Metglas fibre reinforced mortar, fracture props. 79—70159
- $Fe_{29}Ni_{49}P_{14}B_6Si_2$ glass, crystn. kinetics, DSC expts. 78—26444
- $Fe_{29}Ni_{49}P_{14}B_6Si_2$, Metglas 2826B, Hall, elec. resist., magnetisation and heat capacity meas. 78—68019
- $(Fe_{1-x}Ni_x)_{80}PyB_{20-y}$, local struct. disorder and crystallisation, Mossbauer exam. 79—1728
- $(Fe_{1-x}Ni_x)_{77}Si_{10}B_{13}$, amorphous magnetic alloys, density meas. 80—1934
- $(Fe_{1-x}Ni_x)_{77}Si_{10}B_{13}$, amorphous, Landau-Ginzburg theory, magnetisation and Curie temp. 80—75700
- $(Fe_{1-x}Ni_x)_{78}Si_{10}B_{12}$, amorphous, Hall effect and magnetoresist. *(Japanese)* 77—85199
- $(Fe_{1-x}Ni_x)_{78}Si_{10}B_{12}$ amorphous alloys, cold rolled and as-quenched, mag. anisotropy 80—97089
- $Fe_{62.4}Ni_{15.6}Si_7B_{15}$ amorphous ferromagnetic alloy, anomalous magnetisation possible reasons, Mossbauer spectra *(Russian)* 79—78441
- $Fe_{1-x}(P,B)_x$, amorphous and crystalline, photoemission and band structure 80—60754
- $Fe_{79}P_{13}B_8$ amorphous alloys, splat cooled, Mn, Cr and V substituted, mag. and transport props. 80—84593
- $Fe_{80}P_{14}B_6$ glass, ferromag., low temp. heat capacity meas., electronic, phonon contributions exam. 78—10689
- $Fe_{75}P_{16}B_6Al_3$, aged metallic glass, Mossbauer effect 79—91318
- $Fe_{80}P_{16}B_1C_3$, ferromag. metallic glass, Mossbauer spectra, crystn. 77—12276

boron alloys continued

- $Fe_{80}(P_{13}C_7)_{20-y}B_y$, density, microhardness, and crystn. temp., comp depend. 80—84093
- Fe_5SiB_2, Mossbauer spectra, 140-784K, spin rotation 78—52409
- $Fe_{75}(Si_{0.5}B_{0.5})_{25}$ film, amorphous, sputtered, ferromag., thermal stability 78—76280
- $Fe_{75}Si_{15}B_{10}$, amorphous ferromagnetic alloy, isothermal annealing effect on static magnetic props. *(Japanese)* 79—52398
- $Fe_{75}Si_{15}B_{10}$, duplex ferromag. alloy, thermoremanent magnetization 79—73778
- $Fe_{75}Si_{15}B_{10}$, mag. behaviour rel. to magnetostatic interactions 80—11224
- $Fe_{78}Si_{10}B_{12}$, amorphous toroidal core, switching characts. and domain structs. 78—95477
- $Fe_{78}Si_{10}B_{12}$ amorphous ribbons, magnetomechanical coupling constant and Young's modulus, mag. annealing 79—15333
- $Fe_{79.5}Si_{1.5}B_{19}$, evaluation of hyperfine parameter distribs. from overlapped Mossbauer spectra at room temp. 79—99804
- $Fe_{80}Si_5B_{15}$, amorphous, soft mag. props. and potential uses 80—88807
- $(Fe_{1-x}Si_x)_{1-y}By$, metallic glass, mag. props., crystallisation 80—65885
- FeTiB, corrosion-resistant amorphous mag. thin films 80—54923
- $Fe_{80}b_{20-x}C_x(Si_x)(Ge_x)$, amorphous, size effect of metalloids on mag. props. 80—84594
- Gd-Co-B system, phase composition, struct., phase equilibria 78—35355
- Gd-Fe-B ternary systems, phase equilibria and cryst. struct. *(Ukrainian)* 80—11626
- $Gd_xEr_{1-x}Rh_4B_4$, effects of Gd ion on supercond. transition temp., mag. transition temp. and upper crit. field 79—56392
- $Gd_xEr_{1-x}Rh_4B_4$, ferromag. and structural transitions, low temp. calorimetric meas. 79—55888
- $(Gd_{65}Fe_{35})_{100-x}B_x$ glasses, mag. props. 79—73693
- $(Gd_{65}Fe_{35})_{90}B_{10}$, amorphous, mag. props., Mossbauer study 80—93093
- $(Ge,Si)_{1-x}B_x$, amorphous struct., kinetically determined topological model 79—55666
- Hf-B, abrasive props. 80—16489
- Hf-Ge-B system, phase equilibria 78—35356
- $HfC-HfB_2$, wear in vacuum, role of boride phase 80—21113
- $HfC-HfBr_2$, preparation and high temp. antifriction props. 79—1918
- $(La,Ce)B_6$ dil. alloy, Kondo effect, impurity-impurity interaction, mag. susceptibility, mag. to non mag. transition 78—47948
- $(La,Gd)B_6$, dil. alloy, spin glass behaviour, 4.2 to 200K AC mag. susceptibility, RKKY calcs. 78—47994
- La-B, amorphous, B-rich, low freq. modes, Raman scatt. obs. 80—108202
- La-B, phase and thermodynamic props., vaporisation 78—51660
- La-Re-B, annealed and quenched, X-ray structural and phase anal. 78—11207
- LaB_6 cathode gun from transmission electron microscope appls. 80—18048
- LaB_6, de Haas-van Alphen effect and Fermi surface 77—15743
- LaB_6-Cu, form. by wetting of LaB_6 with Cu 80—100813
- $LaNi_{4.4}B_{0\ 6}$, H_2 absorpt. props. 80—88432
- Li-B (0-60 at.%), density, elec. resist. and Hall coeff. 78—39089
- Li-B alloys, Li extraction and determ. using potentiometric titration 79—48016
- Li_5B_4 form., thermodynamic considerations 79—56959
- Li_5B_4, molecular and electronic struct. 80—20107
- MO-B, B effects, rolled, segregation of implanted elements, Auger spectroscopy exam. *(Russian)* 78—35389
- $(Mn_{1-x}Cr_x(Fe_x))B$, Invar charact. 77—15602
- $Mn_{0.6}Ni_{0\ 4}B_{0.02}$, liqs., enthalpy of formation of B_4C at 1320K 79—11814
- Mo-B, electron beam melted, alloying addition effects on brittleness and ductility 79—61728
- Mo-B, Mo-B-Fe(Ni), microalloying influence on mechanical props., cold rolling, plasticity *(Russian)* 80—40502
- Mo-B alloys, B distrib. in welds, nuclear track autoradiography study 79—43282
- Mo-B-Al-C, alloy TsM-10 rolled, recrystallised, deformed system, behaviour under cyclic loading 79—91795
- Mo-B-Al-C, stress cycling at room temp. *(Russian)* 77—25148
- Mo-C-Zr-B (0.004, 0.12, 0.002 wt.%) effect of grain size, cellular dislocation structure, on mech. props. *(Russian)* 79—34105
- Mo-Ge-B, phase diag., struct. of $Mo_{1.7}Ge_{0\ 3}B$ 77—52285
- Mo-Zr-B, neutron irrad. at 780-1080°C, porosity, hardening and embrittlement *(Russian)* 80—29062
- Mo-Zr-B, porosity and mech. props. after neutron bombard., 780-1080°C *(Russian)* 80—24502
- Mo-Zr-B-C, dil. alloy, struct. changes under prolonged high temp. annealing *(Russian)* 78—6944
- Mo-Zr-C-B, dilute, electron microscope obs. of planar defect diffr. contrast patterns 77—43227
- Mo_2B_5-based alloys, mech. props., rel. to appl. as electrodes in electrospark machining 80—21174
- $Mo_{70}B_{30}$, amorphous, local symmetry around glass-former sites, elec. quadrupole effects, NMR 80—80618
- $Mo_{80}P_{10}B_{10}$, amorphous supercond. high-κ, upper and lower crit. fields 79—4629
- $(Mo_{0.6}Ru_{0.4})_{0.8}B_{0.2}$-Fe amorphous supercond., upper crit. field as function of temp. 79—73646
- $(Mo_{0.6}Ru_{0.4})_{82}B_{18}$, supercond. metallic glass, neutron irrad. effects 80—29060
- $Mo_{48}Ru_{32}B_{20}$, amorphous, local symmetry around glass-former sites, elec. quadrupole effects, NMR 80—80618
- $(Mo_{0.6}Ru_{0.4})_{80}Si_{10}B_{10}$, amorphous supercond. matrix, flux pinning by MoRu precips. 80—65756
- $Mo_{70}Si_{20}B_{10}$, amorphous alloys obtained by liq. quenching, superconductivity 80—75670
- Nb-B, atomic order, stability, supercond. *(French)* 80—50021
- Nb-Si-B, ductile amorphous, superconductivity 80—60131
- $Nb_{40}Fe_{40}P_{14}B_6$, metallic glass, explosive compaction, mech. props. 80—89176
- Nd-Fe-B ternary systems, phase equilibria and cryst. struct. *(Ukrainian)* 80—11626
- Ni-B, amorphous alloys, phase diagram 79—96002
- Ni-B, film crystallisation on C fibres and sapphire crystals *(Russian)* 80—75455
- Ni-B, grain boundary internal friction, B solid solubility as function of grain size 80—60903
- Ni-B, hydrogen embrittlement, effect of B additions *(Japanese)* 78—84973
- Ni-b, hyperfine interactions from 6 to 730K, ^{12}B NMR 80—29372

boron alloys continued
- Ni-B (3 at.%), columnar alloys, metallographic obs. of eutectic struct. *(Russian)* 78−27469
- Ni-B alloy film, magnetisation-temp. characts., order-disorder transform. *(Japanese)* 78−76279
- Ni-B alloys, amorphous, thermal anal. and X-ray diffr., solidification struct. development *(French)* 78−91253
- Ni-B amorphous alloy film, atomic and electronic transport *(French)* 78−84325
- Ni-B amorphous films, electronic transport and crystn. activation energies *(French)* 80−6807
- Ni-B electroless-plated amorphous films, anomalous mag. temp. characts. 80−96757
- Ni-B glass, X-ray obs. of struct. 79−1399
- Ni-B thin film glasses, mag. props. and corrosion resist. 80−80576
- Ni-B-Cr, composite, wear resistant coating on steel 45 78−11420
- Ni-Cr-B-Si, hard faced with WC, exam. of abrasion and wear props. 79−34202
- Ni-Cr-B-Si-Fe alloy, Cr content by X-ray fluoresc. 79−43654
- Ni-Cr-Fe-Si-B wear-resist. and corrosion-resist. coatings by furnace melting 80−35428
- Ni-Mo-B metallic glass ribbons, tensile strength, crystn. temp. 80−89173
- Ni-Si-B, amorphous, thermal stability of ductility 80−76327
- Ni-Si-B, embrittlement by crystallisation *(Japanese)* 78−48513
- Ni-Si-B amorphous alloys with metalloid elements, embrittlement/crystn. relationship *(Japanese)* 79−96134
- Ni-Si-B powder, oxidation at 850°C, SEM, ESCA, and elec. cond. meas. 80−7717
- Ni-W-B, superalloy, M_5B_3 type boride 78−44131
- Ni-ZrB_2 powders, densification by hot pressing 80−25604
- Ni_3Al-B, $L1_2$ type intermetallic cpd. room temp. ductility improvement by B addition *(Japanese)* 80−35263
- $Ni_{100-x}B_x$, amorphous, mag. struct., mag. susceptibility meas. 80−80485
- $Ni_{100-x}B_x$, rapidly quenched, mag. moment, temp. and comp. depend. 78−47957
- $Ni_{66}B_{34}$, morphological, structural and phys. props. *(French)* 80−44444
- $(Ni_{1-c}Co_c)_{0.78}P_{0.14}B_{0.08}$, amorphous, mag. props., local environment model 77−12119
- $Ni_{40}Fe_{40}B_{20}$ glass alloy, rapidly quenched, explosive welding to A516-70 steel and to itself 78−39954
- $Ni_{50}Fe_{30}B_{20}$, magnetostriction, temp. depend. 78−91921
- $Ni_{35}Fe_{30}Cr_{15}P_{14}B_6$, amorphous, anodic polarisation and localised corrosion 77−21310
- $Ni_{36}Fe_{32}Cr_{14}P_{12}B_6$, metallic glass, crystallisation 79−77520
- $Ni_{36}Fe_{32}Cr_{14}P_{12}B_6$, amorphous, electrochem. corrosion in chloride solns. 80−50763
- $Ni_{36}Fe_{32}Cr_{14}P_{12}B_6$ metallic glass, mech. props. and thermal stability 80−76362
- $(Ni_{100-x}Fe_x)_{79}P_{13}B_8$, amorphous dil. alloys, spin glasses, magnetisation meas. 79−61178
- $Ni_{80-x}Fe_xP_{14}B_6$, amorphous alloy, resistivity variations near critical temp. 79−73488
- $(Ni_xFe_{1-x})_{80}P_{10}B_{10}$, amorphous, Curie temp., press. effect 80−75833
- $Ni_{78-x}M_xSi_{10}B_{12}$ (M=refractory metal), glass form. and thermal stability 80−79703
- $(Ni_{0.75}Mn_{0.25})_{82}Si_{10}B_8$, amorphous, exchange anisotropy, mag. susceptibility meas., 4.2K to room temp. 80−11186
- NiPB amorphous alloys, ^{31}P and ^{11}B NMR near paramag.-ferromag. transition 79−33558
- $Ni_{78}P_{14}B_8$, amorphous, local symmetry around glass-former sites, elec. quadrupole effects, NMR 80−80618
- $Ni_{78}P_{14}B_8$, $Ni_{80}P_{12}B_8$, amorphous mag. clusters, sp. ht. meas. 78−68274
- $Ni_{80}P_{14}B_6$ glass, low temp. heat capacity meas., electronic, phonon contributions exam. 78−10689
- NiPBAl, metallic glass, viscous flow, alloying effect 78−79793
- $Ni_{78}Si_{10}B_{12}$, amorphous, struct. factor temp. depend., X-ray diffr. study *(Japanese)* 79−51005
- PdB_xH_c, superconducting transition temp. conc. var. 77−8221
- $(Pd_{86}Si_{15})_{61}/(Fe_{85}B_{15})_{39}$, compositionally modulated amorphous film, diffusion, struct. relax. 80−103518
- Si-B amorphous film, plasma deposited, characterization 79−69828
- Si-B based CVD coating for gas turbine blading, props. 80−40615
- $Si_{1-x}B_x$:H, amorphous films, thermopower and cond. for mixed band and broad tail state cond. 80−49786
- SiC-B eutectic alloys, struct. of crystallising graphite 79−38829
- Sm-Fe-B ternary systems, phase equilibria and cryst. struct. *(Ukrainian)* 80−11626
- $(Ti,Cr)B_2$, sintering kinetics and props. 80−100811
- α-Ti alloys, plastic deforms ands rupture mechanisms, depend on B additives *(Russian)* 79−61650
- Ti-Al-V-Be-B, melt-extracted polycryst., mech. props. 80−76360
- Ti-B, abrasive props. 80−16489
- Ti-B, binary inclusions, interaction with diamond in polycryst. diamond sintering *(Chinese)* 78−80484
- Ti-B-Mo system, phase equilibria at 1400°C 78−35354
- Ti-B-W(Mo), annealed at 1400°C, exam. of phase diagram, using X-ray phase and metallographic analysis 79−1847
- Ti-Cr-B system, self-propagating high temp. synthesis, crystallochemical and mech. props. 80−20861
- TiB_2, electrode, hot pressed, erosion resistance, struct. and porosity effects 78−3228
- TiB_2 high temp. hardness of single crystals *(Japanese)* 77−48522
- TiB_2, low temp. radiation damage, calorimetric investigation 77−27916
- TiB_2-(Ni) (20 wt.%), initial stage sintering under high press., lattice strain 77−55905
- TiC-TiB_2, preparation and high temp. antifriction props. 79−1918
- TiC-TiB_2, wear in vacuum, role of boride phase 80−21113
- TiC-TiB_2 alloys, composition effect on surface layer rupture at various temps. 80−25879
- $Ti_{70}Co_{20}B_{10}$, amorphous alloys, crystn. behaviour, TEM study *(Japanese)* 80−84087
- $Ti_{70}Fe_{20}B_{10}$, amorphous alloys, crystn. behaviour, TEM study *(Japanese)* 80−84087
- $Ti_{70}Ni_{20}B_{10}$, amorphous alloys, crystn. behaviour, TEM study *(Japanese)* 80−84087
- Ti(Zr,Hf)-Gd-B system, phase equilib. 80−11629
- $TmRh_4B_4$, mag. and supercond. props., mag. susceptibility and sp. ht. meas. 79−78344
- U-Fe(Ni)(Co)-B, isothermal section of phase diagram, X-ray obs. 79−52157
- UB_2, thermochemistry and stability 80−97723

boron alloys continued
- W-Ge-B, phase diag. 77−52285
- W-Ru-B, W-Ru-Al-B and W-Ru-Si-B glasses, struct. obs. 80−1938
- W_2B_5-based alloys, mech. props., rel. to appl. as electrodes in electrospark machining 80−21174
- WCuB prep. by infiltration of W skeleton by CuB, hardness meas. *(German)* 78−64508
- $W_{70}Si_{20}B_{10}$, amorphous alloys obtained by liq. quenching, superconductivity 80−75670
- Y-B, amorphous, B-rich, low freq. modes, Raman scatt. obs. 80−108202
- Y-Ni-B, X-ray and microstruct. anal., phase composition 77−16539
- Y-Re-B, annealed, and quenched X-ray structural and phase anal. 78−11207
- $(Y_{65}Fe_{35})_{100-x}B_x$ glasses, mag. props. 79−73693
- Zr-B, abrasive props. 80−16489
- Zr-B (1.3 wt.%), investigation of swelling due to neutron irrad. *(Russian)* 79−60404
- Zr-Cr-B system, self-propagating high temp. synthesis, crystallochemical and mech. props. 80−20861
- Zr-Ge-B system, phase equilibria 78−35356
- ZrB_2-Nb, reactions between components 80−100812
- ZrC-ZrB_2, preparation and high temp. antifriction props. 79−1918
- ZrC-ZrB_2, wear in vacuum, role of boride phase 80−21113

boron compounds
- *see also boron alloys*
- acetylacetonatobutyl halides, equilib. reacts. redistribution of −F, −Cl monofunctional groups *(French)* 78−64816
- appl. *(German)* 77−42006
- in aqueous solution, determ. via azomethine H colorimetric method 79−92115
- B_4C, Auger and energy loss spectra *(French)* 78−23565
- BO_3^{-3} triangle, perfect trigonal symm. *(Korean)* 78−19367
- boracite, single cryst. prep. and phys. props. 80−100763
- boracites, spontaneous birefr., meas. and appl. 79−15434
- boracites, trigonal, spontaneous polarisation behaviour 77−43945
- boral, reactivity worths of fixed neutron absorbers 78−21654
- boral shielding material, neutron transmission calc. 80−854
- boranes, $B_9H_{12}OCH_3S(CH_3)_2$, $C_2B_{10}H_{10}Br_2$, $B_{18}C_4H_{22}$, cryst. struct. *(Czech)* 78−87649
- boranes, nido and arachno, bond length-bases bond enthalpies 80−30265
- boranes, $OCH_3(B_9C_2H_{10})_2Co$ and $(C_2H_5)_2Co_2CB_9H_{10}^-$, cryst. struct. *(Czech)* 78−87649
- boranes, polyhedral, bonding topology, graph-theoretical interpretation 78−33408
- borate inhibitors, for high-temp. oxidation of Fe-Cr alloys 80−66705
- borazines, substituted, Urey Bradley force field, pot. energy consts. 80−78588
- boride coatings, diffusion-deposited on WC-Co, elemental and phase comp. 80−15402
- boride coatings, technology, props., book contrib. 78−48574
- boride coatings on steel effect of Cu impurities in reaction mixture on brittleness, acoustic emission meas. 80−16581
- boride diffusion coatings on steel, fractographic exam. of struct. 78−44270
- borides, B_{12}, cryst. chem. classification, book contrib. 78−47302
- borides, B rich, protective coatings, in situ prep. for controlled nuclear fusion devices 79−3238
- borides, B-rich, cryst. chem., struct., review, book contrib. 78−47278
- borides, book 78−48292
- borides, electronic struct., review, book contrib. 78−47700
- borides, hexa- and di-, electronic structs., elec. props., book contrib. 78−47701
- borides, hexa- and tetra-, prep., struct., elec., mag. props., book contrib. 78−47303
- borides, lightweight ceramic armour appls., ballistic tests, computer simulation, book contrib. 78−48556
- borides, metallic, sintering, review, book contrib. 78−48359
- borides, nature of chem. bond, book contrib. 78−47276
- borides, nuclear appls., review, book contrib. 78−46154
- borides, proposed classification 80−19741
- borides, refractory compounds, classification 79−94985
- borides, spatial correls. of valence and external core electrons 80−10523
- borides, ternary, struct. classification, props., book contrib. 78−47309
- borides containing B_{12} polyhedral units, tetraborides, structural determinants, book contrib. 78−47301
- borides of group VIb elements, prep. and struct., book contrib. 78−47306
- borophosphate glasses, effect of F on props. 78−67657
- borosilicate cladding compatibility *(Russian)* 77−66741
- borosilicate glass film, vapour-deposited, structural model, IR spectra meas. 77−1084
- borsic fibre reinforced Al, hot pressed forged, plasma sputtered *(Russian)* 78−35330
- borsic fibre reinforced Ti, unidirectional, K-calibration and compliance curves 78−88518
- borsic fibres, fibre, metallisation by continuous casting in Al and Al alloys *(Russian)* 78−35538
- 9-bromo-meta-carborane, mol. reorientation, ^1H and ^{11}B NMR 77−16185
- cabal glass:$SiO_2(TiO_2)$, microheterogeneity, and elec. cond. 78−83997
- carborane anion, ^{11}B NMR 78−90190
- ceramic, B content by emission spectrosc. with high freq. plasma excitation *(French)* 80−76477
- conference, Varna, Bulgaria (Oct. 1978) 80−12842
- core electron expansion, kinetic energy in Compton profiles 78−72628
- cutting tool coating by cubic BN reactive vapour deposition 80−40545
- diamond: B_4C, doping by diffusion at high temp. and press. 79−19273
- diborides of light metals, X-ray emission spectra and transition probability calcs. *(Russian)* 77−52203
- ESCA shifts and effective charges 80−78648
- fluoroborates in non-aq. solns., ^{19}F-^{11}B spin-spin coupling 77−23512
- GCFR core-catcher crucible, material compatibility for UO_2-316 stainless steel BN system 79−59171
- graphite-BC body, hot pressing, props. *(Japanese)* 79−78923
- halide+metal halide, vapour deposition of Mo, W, Nb, and Ta borides *(French)* 77−36406
- halides, diatomic isovalent sequence, free-mol. electronic transition intensity consts., systematics 78−42137
- hydrides, doubly isotopic, in 2-step nucl. fusion dissipative confinement, using inert gas hydride laser 78−82506

boron compounds continued
hydrides, relaxation time meas., ^{11}B NMR spectroscopy 77–32276
hydrides and related cpds., cryst. struct., secondary and multi-centre bonding 78–63751
isotope exchange reactions, equilib. consts. 78–19999
materials for thermoelectric conversion of solar energy *(French)* 80–89660
methane-BCl_3, single-photon absorption reaction chemistry in solid state 77–73454
molecule, ground state MNDO calcs. 77–88391
molecules involving B and C atoms, self-consistent charge calcs. of core-electron binding energy shifts 80–69084
optical fibres, GeO_2-$B_2O_3SiO_2$, ageing effects of moisture on fatigue and tensile strength 80–66539
optical fibres, ultratrace impurities determ., and behaviour during production by CVD process *(Japanese)* 80–87505
organoarsinoboranes, ^{11}B NMR 78–90190
orthoborates, dolomite type, vibr. spectra, vibr. coupling effects *(French)* 77–65464
phosphides, gas phase deposition from B-P-U-H systems, thermodynamics 79–11518
polycrystalline cubic BN plunger chamber for high-pressure Mossbauer meas. 80–31786
rare earth metal-B systems, phase equilibria, phase diagrams, book contrib. 78–48389
salt toxic effect on activated sludge micro-organisms *(Chinese)* 79–24919
semiconductors, props. review 79–42532
steel, low C, electroboronising by superimposed cyclic current, Na_2CO_3, B_4C, NaCl, NaOH activator studies 80–85081
synthesis, struct. and mag. props. 77–89934
ternary metal borides, struct. chem. 79–14769
trihalides, mol. force field using parametric represent. method 80–27991
trihalides, quadratic potential functions, Coriolis consts. calcs. 79–72239
trimethylamino borane, ^{11}B NMR 78–90190
Ag_2O-Na_2O-B_2O_3 mixed cation glasses, electric conduction *(Japanese)* 77–24432
Al/SiO-B_2O_3/Au *(French)* 80–39681
Al-B(-C) system, synthesis and struct. of boride phases 80–45282
AlB_{12}, α- and β-forms, elec. props. at high temps. and in strong elec. fields, thermistor appls. 80–92903
γ-AlB_{12}, struct. rel. to isohedral B framework 78–2086
Al_2O_3-B_2O_3 system, phase comp. and sorption props., Al salts chem. nature influence 79–51426
Al_2O_3-B_2O_3-P_2O_5 system, glass formation by laser melting 78–44074
Al_2O_3-B_2O_3-RO, glass, (R=Ba,Ca,Cd,Mg,Sr,Zn), ionic and DC cond., comp. effects 77–31804
Al_2O_3-B_2O_3-SiO_2 system, liq. phase calc. for commercial quartzite powders 80–25671
Al_2O_3-SiO_2-CaO-B_2O_3(1,1,1 wt.%) chemical analysis by photocolorimetry and titration 79–20483
Al_2O_3-SiO_2-MnO-Cr_2O_3-B_2O_3 system, additive in sintering of high-alumina ceramic 79–61544
B C powders, effect of C on sintering 80–40312
B-B_4C materials, hot-pressed, elastic modulus and flexural strength rel. to grain size and porosity 79–79018
B-C, B-C-Ti, B-C-Cr, paramagnetic centre struct. and defect form. 80–66034
B-C system, free C determ. 79–87907
B-C system, region of existence of B_4C phase 78–76636
B-C system, struct. of paramag. centres 80–20460
B-C(Si) systems, phase diagrams, review, book contrib. 78–48388
B-Mg-N system, precipitation mech. of BN 79–70068
B-S compounds, relative antiwear efficiency 78–35532
β-B-Sc solid soln., rhombohedral, X-ray diffr. indicating ScB_{28} 78–34464
B-Si compounds, thermoelec. material, prep. by pyrolysis of BBr_3-$SiBr_4$ mixture 80–20862
B-Zn solid soln., struct. changes on Zn incorporation into α- and β-rhombohedral B 78–79596
β-$B_{12}Al$, prep. and electrothermal props. 80–20863
$B_{14}AlMg$, prep. and electrothermal props. 80–20863
$B_{12}Al(Mn)(W)$, growth from melt and phys. props. 80–20782
BAs and B_6As, sp. ht., 55 to 310K, thermodynamic functions 77–24414
BAs, chem. transport equilib. with I_2 in gaseous phase *(French)* 77–55876
B_6As, single crysts., prep. by chem. transport reactions 79–100032
$BAsO_4$, XPS of cryst., inner shell binding energies of elements 79–43092
BBR_3, quadratic potential functions, Coriolis consts. calcs. 79–72239
$(B_{12})_4B_2Ti_{1.3-2.0}$, tetragonal, cryst. struct. 77–15360
BBr_3-H_2 mixtures, B CVD, thermodynamic anal. 79–47634
BBr_3-PCl_3-H_2, gas phase equilib. comp. 80–35166
BC boronising sintering of porous stainless steel 78–60594
BC, EPR, book contrib. intensity correl. with elec. cond., Hall coeff., book contrib. 78–48041
BC, fine powder prod. *(German)* 77–32549
BC, ion bombarded, chemical effects on secondary photon and ion emission 78–95637
BC, physical and chemical interaction with energetic T 79–97902
BC, sintered, struct. and props. 80–104181
BC, sintered and hot pressed, friction and wear, 20 to 1500°C 78–60844
BC, specimen preparation for TEM by ion beam thinning *(German, English)* 80–11861
BC_4 gas-suspended, cooling of D-D fusion blanket, neutronics calc. 80–834
BC_x, IR-active phonons, reflectivity and absorption spectra 79–82294
BC_x X-ray scatt., polarised radiation excitation source for X-ray fluoresc. anal. 78–7314
$B_{12}C_3$, sintering and subsequent high temp. annealing, struct. and props. 80–20858
$B_{12}C_x$, phonon energies and electronic props., x depend., refl. spectra and thermoelec. power meas. 80–16052
$B_{13}C_2$, chem. bonding nature, static deform. densities and pictorial representation 80–92489
$B_{13}C_2$, crystal struct. refinement, X-ray diffr. 79–55702
$B_{13}C_2$, dynamic deformation densities and valence densities 80–1971
$B_{13}C_2$, infinite network struct., X-ray diffr. meas. 80–15070
$B_{13}C_2$, structural anal., electron density and bonding 80–15071
B_4C, absorber material for fast reactor control appl. 78–8919

boron compounds continued
B_4C absorber pin in-reactor rupture test 79–93701
B_4C absorber rods, nondestructive exam. with dual-energy gamma gauge and multigauge scanners 79–93721
B_4C, behaviour as control rod in commercial reactor 78–8918
B_4C brittle coating for B fibres, critical thickness effect on strength *(Russian)* 80–40426
B_4C coating, erosion rates under H^+ ion bombard., fusion reactor appls. 80–39179
B_4C, coating for oxidation resistance 77–32704
B_4C, densification kinetics during hot pressing, 1800-2200°C 80–60817
B_4C, determ. of H_2O, Hz content by hot extraction methods *(German)* 79–49808
B_4C, effect of fast neutron irradiation on struct. 78–26597
B_4C, enthalpy of formation, 1320K, appl. of high-temp. solution calorimetry 79–11814
B_4C, FBR control rod elements, neutron damage and post-irrad. annealing 80–13581
B_4C fibres, yarn prep. from C fibres, mech., chem. props., struct., book contrib. 78–48365
B_4C filtering of FBR spectra for generation of neutron reference source 80–42884
B_4C, first-wall coating for Tokamak, H retention and release 80–18620
B_4C fission reactor material, behaviour in spent fuel storage pools 80–42771
B_4C, fusion reactor material, low energy ion erosion expts., Kaufman source appl. 80–68942
B_4C, gas suspended, coolant for catalysed D fusion reactor blanket 78–58400
B_4C, He release correlation during fast-neutron irradiation in fast reactor 78–8965
B_4C, kinetics of high temp. oxidation in oxygen, chromatography method 77–21305
B_4C, LMFBR control material, integral capture cross section meas. in CFRMF 77–26760
B_4C, meas. of T retention of fast-neutron-irradiated absorber elements 78–8903
B_4C, mech. and thermal props. 80–21083
B_4C, melting and phase homogeneity range 80–20911
B_4C, metallography and Knoop microhardness *(French)* 78–76730
B_4C, morphology and struct. of vap. grown crysts. 79–7562
B_4C neutron absorber for EBR-II, He release, in-reactor meas. 80–73951
B_4C, neutron absorber material for FBR, in-reactor performance meas. 80–18429
B_4C, quantitative electron microanalysis *(French)* 78–76948
B_4C, reaction kinetics with liq. Al, Si, Ni and Fe 80–84344
B_4C reflector-shield concept for fusion reactor designs 80–102293
B_4C rings, Al bonded, exam. of fabrication techniques 78–72748
B_4C, solid-state ^{13}C NMR spectra 79–24220
B_4C, sputtering, low energy, H, D and He ions 80–100734
B_4C, sputtering yield, use as first wall material 78–95629
B_4C, synthesis in HF EM field 80–20864
B_4C, TEM investigation using C replicas 80–61034
B_4C, thermal cond., nonstoichiometry effect 78–63887
B_4C, thermophysical props. and neutron absorpt. 80–103488
B_4C, used as control rods in FBR, irradiation effects 78–67742
B_4C-304 stainless steel cermet for nuclear shielding appls. 80–102352
B_4C-Al composite moderator rods, production and props. *(Russian)* 79–18006
B_4C-Al(silicone)(graphite), neutron shielding materials, long term radiation effects 80–9413
B_4C-Cu cermet fabrication for neutron shielding appls. 80–102354
B_4C-graphite, irradiation-induced dimens. changes, rel. to HTGR conditions 78–8905
B_4C-phenolic fibre reinforced composite for nuclear shielding appls. 80–102353
$B_{50}C_x$, x=1 to 2, prep. and struct., book contrib. 78–47277
B_xC_y, desorption of D, activation energies 79–65330
B_xC_y, pure and technical, sintering behaviour 77–63611
$(B_{12})_4C_2Ti_{1.86}$, X-ray cryst. struct. determ. *(German)* 80–54188
$(B_{12})_4C_2V_{1.29}$, X-ray cryst. struct. determ. *(German)* 80–54188
BCl_3, endothermic reduction in H_2 thermal plasma and nonequil. H_2 plasma discharge 78–15671
BCl_3, frozen, selective evaporation of $^{10}BCl_3$ and $^{11}BCl_3$ by CO_2 laser irrad. *(Russian)* 77–3422
BCl_3, gas, isotope separation, laser stimulation-filtering diffusion method *(Russian)* 77–555
BCl_3 gaseous phototropic shutter control of CO_2 laser PRF 78–50833
BCl_3, high-resolution IR Ar matrix-isolation spectra, 10K 80–32708
BCl_3, high-resolution polarisation spectroscopy in 10 μm region 79–6196
BCl_3, IR active mols., homogeneous excitation by laser pulses 78–9202
BCl_3, in solid Ar, Kr, high resolution IR absorpt. spectra, isotopic splitting 80–87109
BCl_3, in tetrachloroethylene trimerisation IR laser-specific reaction 77–12809
BCl_3, intense IR radiation absorption singularities 79–76432
BCl_3, interaction with evaporated metal films, adsorpt. 78–75945
BCl_3, isotope enrichment, heterogeneous condensation in prescence of CO_2 laser irrad. 78–70953
BCl_3, ν_3 vibr. level, fine struct., nonlinear reson. 77–6783
BCl_3, optoacoustic laser spectroscopy of excited vibr. molecular states 77–19106
BCl_3, photochemical reaction, chirping laser induced, calc. of optimal detuning rate 77–38902
BCl_3, quadratic potential functions, Coriolis consts. calcs. 79–72239
BCl_3, sensitiser, in tetrachloroethylene trimerisation IR laser-specific reaction 77–12809
BCl_3, strong IR CO_2 laser field, isotopically selective dissociation 79–18245
BCl_3, vibr. excited states distrib. in reson. radiation, photodissoc. rate 78–50603
BCl_3, visible fluoresc., IR laser induced, acousto-optical effects *(Chinese)* 79–78733
BCl_3, visible fluorescence dynamics due to IR laser irrad. *(Chinese)* 80 102534
BCl_3-$COCl_2$, impurity removal by laser irrad., IR spectra meas 78–15686
BCl_3-H_2, photochem. with Ti, Pb catalysts, isotopic excitation by laser 78–64882

boron compounds continued
BCl$_3$-N$_2$ mixtures, thermodiffusion props., effect of resonant excitation of mol. vibr. by laser, isotope separation 80−100047
BCl$_3$ + H$_2$ laser induced chemistry, theory 78−76884
BCl$_3$ + methane reaction, laser-induced, vibr. excitation influence on reactivity, isotope selectivity 80−11921
BCl$_3$ + N(CH$_3$)$_3$ $\rightarrow$ BCl$_3$N(CH$_3$)$_3$, complex formation, reaction product isotopic composition change *(Russian)* 80−81316
BClF$_2$, microwave spectrum, struct., quadrupole coupling consts. 77−57986
BCl$_2$F, in solid Ar, Kr, high resolution IR absorpt. spectra, isotopic splitting 80−87109
BCl$_2$NCO, soln., force fields and normal modes, vibr. spectra, IR and Raman obs. *(French)* 80−58266
BCl$_2$SH, BCl$_2$SD, Raman and IR spectra, barrier to internal rot. 78−5223
B$_x$Cy, metal-insulator transition, elec. cond. and thermoelec. power, 80 to 700K 80−44673
B$_x$Cy, protective coatings for first wall, prep. by means of low press. plasma CVD 80−35103
BF, bonding, spin density functional theory 78−17558
BF, diagrammatic perturbation theory, using universal even-tempered basis set 80−58131
BF, isoelectronic sequence, Rydberg transitions, term value-ionisation pot. correl. 80−58276
BF, matrix HF calcs. using universal basis sets 79−59354
BF, mol., nucl. spin-spin coupling, diamag. contrib. 79−36665
BF, quadratic vibr. force const., from X-ray scatt. factors 79−45864
BF, vibrational structure in X-ray spectra, calcs. 77−30884
BF, X$^1\Sigma^+$ state, many-body effects, HF STO calcs., diagrammatic perturbation theory 77−50355
BF, X-ray and high-energy elastic electron scatt., vibr. averages 79−81279
BF$_2$ radical, thermomechanical studies by mass spectrometry, enthalpy of form. and ionisation pot. determ., chem. bonds 80−81382
BF$_2$$^+$ ion implantation in Si:P, anomalous carrier profiles 80−2048
^{49}BF$_2$, ionised mols., implanted in n-type Si, layers of p-type resistivity 78−31003
BF$_3$, ^{11}B NMR chem. shift., temp. depend., virial coeffs. 78−58722
BF$_3$, ^{19}F chem. shielding, depend. on internal coords. 78−5249
BF$_3$, ^{19}F NMR, chem. shielding, intermol. interactions and rovibr. motion effects 78−9171
BF$_3$, boiling/condensation heat transfer props., cryogenic appls. 78−79192
BF$_3$, bond order and Raman intensity, delta function eqn. 77−61693
BF$_3$, dissoc. pathways and mol. vibr., compliance consts. and min. energy coords. 78−35661
BF$_3$, IR intensity anal. 77−58081
BF$_3$, mass spectrometry, additional memory effect *(Japanese)* 79−29432
BF$_3$, mean amplitude of mol. vibration, approx. calc. method 79−13697
BF$_3$, molecular charge density contours for cryst. struct. 78−38645
BF$_3$, molecular effects in F K-shell ionisation by 0.5 to 1.5 MeV protons 77−50515
BF$_3$, optoacoustic laser spectroscopy of excited vibr. molecular states 77−19106
BF$_3$ proportional counter, high press. *(Japanese)* 78−66453
BF$_3$, pure rot. spectra of ground vibronic state, calc. 79−63975
BF$_3$, quadratic potential functions, Coriolis consts. calcs. 79−72239
BF$_3$, threshold photoelectron, photoionisation and coincidence ion-threshold photoelectron spectra 79−820
BF$_3$, X-ray fluorescence, electronic struct. determ. 78−86887
BF$_3$, geometric struct. of ground state, ab initio calc. 78−5130
BF$_3$. radical, struct., EPR spectrum 77−8406
BF$_3$-BF$_3$.SO$_2$, gas-liq., multistage ^{10}B isotope exchange, low temp. *(Japanese)* 78−33636
BF$_3$-CO$_2$ mixtures, ang. neutron flux distribs. meas. 77−54276
BF$_3$-H$_2$O mixtures, vapour density and dissociation, 150-400°C 77−7491
BF$_3$ + BF$_3$(D$_2$) (inert gas), US dispersion meas. 78−17758
BF$_4$, bond order and Raman intensity, delta function eqn. 77−61693
B$_2$F$_4$, mol. force consts. and vibr. amplitude, force field study 79−31729
B$_2$F$_4$, molecular structure, barrier to internal rotation, temperature effects 78−13625
BF$_2$CH$_3$, nonrigid, symmetry group calcs. 80−106254
BF$_3$CO, core ionisaton phenomena, nonempirical LCAO MO SCF investig. 80−37906
BF$_3$CO, microwave spectrum and struct. 79−76420
BF$_2$H$_4$$^+$, AB$_6$, non-transition element complexes, shapes and other props. 78−82647
BFHOH, transient mol. form., microwave spectroscopic obs. 78−74643
BF(OH)$_2$, identification, rot. and centrifugal consts., mol. struct., microwave spectra obs. 80−32705
BF$_3$.BrF$_3$ complex, F NMR 78−37658
BF$_3$.SO$_2$, ^{10}B enrichment by low-temp. exchange *(Japanese)* 78−55251
BH, $^1\Sigma^+$ ground state, mag. susceptibility, paramag. contrib., large config. interaction wave function calcs. 80−47899
BH, A$^1\Pi$ state, fluoresc. decay radiative lifetime meas. 79−13771
BH, ab initio spin-projected EHF method pot. curve calcs. 79−10054
BH, CI wavefunction, terms selection for pot. energy surface 77−88401
BH, correlation energy, many-body Rayleigh-Schrodinger perturbation theory calc. 78−894
BH, correlation energy, perturbation calc. using Gaussian-type geminals 79−10042
BH, correlation energy, quadruply excited configs. effects 79−54773
BH, elec. polarisabilities and dipole moments, var. perturbation obs. 80−63527
BH, electron density, basis set, electron correl. effects 78−74581
BH, electron density and localizability partitioning calcs. 78−21847
BH, electronic distribution functions and correl. holes, theory 78−17562
BH, electronic structure, SCEP theory calcs. 77−10579
BH, force const. evaluated in first order of perturbation theory 77−34781
BH, Franck-Condon factors, rot. quantum number effect 79−31613
BH, localisability in MO calcs., measured by absolute overlap and 2nd moment dispersions 78−74557
BH, mag. field depend. susceptibility, gauge invariant GO calc. 78−1100
BH mag. susceptibility calc., coupled Hartree-Fock perturbation approach 79−868
BH, mol. electronic momentum distrib. functions and correl. holes in **p**-space 79−97978
BH, multipole expansion of diatomic overlap, MEDO calcs. 78−46264

boron compounds continued
BH, one electron props., SCF-Xalpha scattered wave method 80−83279
BH, PE curve, spectroscopic consts., perturbation theory appl. 80−23341
BH plasma, hot, proton and deuteron transport calc., moment method 78−22458
BH, pot. curve, one-config. Hartree-Fock-Roothaam calc. for force consts. 78−82627
BH, SCF and CI wavefunctions for electronic struct. and one-electron props. 77−67978
BH, spectroscopic consts., FSGO calcs. 77−6758
BH, spin-coupled theory of mol. wavefunctions, mol. struct. and props. 77−50337
BH, susceptibility and mag. screening calcs. 77−57861
BH, variation-perturbation minimal Gaussian geminal basis sets correl. energy calc. 78−78629
BH, X$^1\Sigma^+$ states, many body effects, diagrammatic perturbation theory 77−79547
BH$^+$, PNO-CI and CEPA calcs. of electron correl. effects 77−34561
BH^{5+}, spurious avoided-crossings, variationally calc., perturbation theory approach 78−5295
BH$_2$, potential energy surface, DIM method 79−18110
BH$_2$, Walsh's rules and small bond angle states 80−106255
BH$_2$$^+$, BH$_3$, force consts., ab initio calcs. with differentiated estimation of integrals 77−67974
(BH$_2$)$_n$, energy band structure 80−5478
BH$_3$, electron correl. quadrupole excitation in correl. energy theories 79−36538
BH$_3$, electronic wave function determ., genealogical technique using Clebsch-Gordan coeff. 80−95529
BH$_3$, localisability in MO calcs., measured by absolute overlap and 2nd moment dispersions 78−74557
BH$_3$, multipole expansion of diatomic overlap, MEDO calcs. 78−46264
BH$_3$, variationally deorthogonalised localised molecular orbitals, electronic struct. 79−97968
BH$_4$$^-$, BD$_4$$^-$, intramol. force fields, F$_2$ vibrs., isotope shifts 77−3336
BH$_4$$^-$, CNDO/2 calc. of chemical bonding 79−76345
BH$_4$$^-$, electron momentum distribution and Compton profiles, FSGO calcs. 80−87032
BH$_4$$^-$ motion in solids, nucl. spin-lattice relax. exam. 78−56388
BH$_4$$^-$, pot. energy surfaces and mol. deform. induced by external cation 80−106285
BH$_4$$^-$, reduction of IrCl$_6$ by hydrolysis products 78−76854
BH$_x$, photoluminesc. spectra 80−2815
B$_{10}$H$_{14}$, cryst. struct. *(Czech)* 78−87649
B$_{10}$H$_{14}$, LiBH$_4$, muonic X-ray intensities in low-Z elements and their hydrides 80−9761
B$_{10}$H$_{14}$, molecular charge distrib. 78−26513
B$_{12}$H$_{12}$$^{2-}$, icosahedral cage, symmetry coords. and vibration freq. 80−47966
B$_2$H$_5$$^+$, FSGO ab initio calc. of geometry, CNDO/2 calc. 78−41943
B$_2$H$_6$, APSG method as a localised process 78−33415
B$_2$H$_6$ and B$_2$H$_5$NH$_2$, electronic struct. and bonding, comparative calcs. 79−31397
B$_2$H$_6$, appl. to boriding 80−30159
B$_2$H$_6$, cryst., mol. charge distrib. anal., using struct. factors from mol. densities 80−15068
B$_2$H$_6$, electron momentum distribution and Compton profiles, FSGO calcs. 80−87032
B$_2$H$_6$, equilib. with solid soln. of B in Si 80−97721
B$_2$H$_6$, ground state props., coupled cluster and MBPT methods appl. 80−47881
B$_2$H$_6$, LMO population calc. method appl., from given SCF eigenvector matrix 80−14063
B$_2$H$_6$, localisation of MOs using density matrix formalism *(Russian)* 79−93911
B$_2$H$_6$, mol., static electron densities 78−79552
B$_2$H$_6$, molecular charge distrib., quantum topology, bonding theory and molecular structure 80−5463
B$_2$H$_6$, quadratic valence force field, rel. to ethene 79−3382
B$_2$H$_6$, variationally deorthogonalised localised molecular orbitals, electronic struct. 79−97968
B$_2$H$_n$, struct., ab initio SCF calcs. *(French)* 79−22598
B$_3$H$_8$$^-$ anisotropic motion in powdered tetramethylaminoborane, ^{11}B NMR 77−90045
B$_3$H$_8$$^-$, electron momentum distribution and Compton profiles, FSGO calcs. 80−87032
B$_3$H$_n$, struct., ab initio SCF calcs. *(French)* 79−22598
B$_4$H$_{10}$, ^{11}B NMR line broadening, B-B coupling 78−62826
B$_4$H$_{10}$, electron momentum distribution and Compton profiles, FSGO calcs. 80−87032
B$_4$H$_4$, B$_4$H$_{10}$, APSG method as a localised process 78−33415
B$_5$H$_9$, ^{11}B NMR line broadening, B-B coupling 78−62826
B$_5$H$_9$, B$_5$H$_{11}$, APSG method as a localised process 78−33415
$^{10:11}$B$_5$H$_9$ gas (liq.) phase, vibr. dephasing and Raman spectra 80−48101
B$_6$H$_{10}$, APSG method as a localised process 78−33415
B$_{n+3}$H$_{n+8}$, n=1-7, ab initio 6-3G and 3G/MODPOT LCAO-MO-SCF calcs. 79−10026
B$_n$H$_n$$^{2-}$ anions, bond enthalpies 80−30266
B$_n$H$_n$$^{2-}$, n=5-12, localised orbitals, bonding, PRDDO calcs. 78−13431
B$_x$H$_y$ compounds, doubly-isotopic, laser driven nuclear fusion, energy release 78−78499
B$_{10}$H$_{12}$As$^-$, ^{11}B NMR 78−90190
BHBr$_2$, and isotopic forms, mol. pot. consts., amplitudes, Coriolis coupling, centrifugal distortion 78−50662
BH$_3$CO, core ionisaton phenomena, nonempirical LCAO MO SCF investig. 80−37906
BH$_3$CO, struct., quadrupole coupling consts., dipole moment, microwave spectra 77−54557
BH$_3$CO, vibrational spectra in Ne matrices, pot. consts., bond strengths 79−45696
BHCl$_2$, and isotopic forms, mol. pot. consts., amplitudes, Coriolis coupling, centrifugal distortion 78−50662
BHF$_2$, and isotopic forms, mol. pot. consts., amplitudes, Coriolis coupling, centrifugal distortion 78−50662
BH$_3$F , B-F bond, interference density and kinetic energy 78−74566
BH$_3$F$^-$, CNDO/2 calc. of chemical bonding 79−76345
(BH$_2$H)$^-$ ion adduct, form., kinetic energy, interference charge density changes, CNDO/2 calc. 79−57211
(BHNH)$_n$, band structure, ab initio calcs. 79−23895
BH$_2$NH$_2$, microwave spectra, rot. consts., dipole moment, mol. struct. 79−85957

boron compounds continued
$(BH_2NH_2)_n$, band structure, ab initio calcs. 79—23895
BH_3NH_3, complexation energies and interatomic distances, SCF and CEPA calcs. 78—25446
$(B_{10}H_{12})_2Ni^{2-}$, high resolution ^{11}B NMR 79—31553
$BH(OH)_2$, transient mol. form., microwave spectroscopic obs. 78—74643
$B_{10}H_{12}S$, ^{11}B NMR 78—90190
$B_{10}H_{12}Se$, ^{11}B NMR 78—90190
$B_{10}H_{12}Te$, ^{11}B NMR 78—90190
B(I) hydrides, ab initio calcs., proton and hydride affinities 79—10029
BI_3, appl. to prep. of B, effect of purification treatments on product purity 79—91589
BI_3, direct synthesis, chem. transport of B with I_2 78—52682
BI_3, mol. force field using parametric represent. method 80—27991
BI_3, quadratic potential functions, Coriolis consts. calcs. 79—72239
BN, ^{15}N zero point vibr. energy from nuclear photon scattering 80—59593
BN adsorpt. of Ar, thermodynamic values calc. from pot. parameters *(German)* 79—95268
BN, adsorption of methane in first monolayer domain, thermodynamic props. *(French)* 80—29275
BN, adsorption of NO, crit. and triple point temps. of first adsorbed layer 78—91548
BN, artificial production of growth twins 78—30641
BN, Auger and energy loss spectra *(French)* 78—23565
BN brittle coating for B fibres, critical thickness effect on strength *(Russian)* 80—40426
BN, cathode, production of D ion beam impurities 79—86592
BN ceramic with organosilicon polymer additions, strength and oxidation resistance 80—20880
BN ceramics, sintered, oxidation kinetics 79—96171
BN, channel for CO_2 waveguide laser 77—14743
BN, chem. bonding and electronic struct., AES and SIMS meas. 80—50512
BN composites, polymer impregnated 80—7526
BN, contact reactions with Ti and WC-Co at high pressures 80—61029
BN, conversion of wurtzite into cubic form, stress state effect 80—64943
BN, crystal structure stability, P-T diagrams 78—51886
BN, cubic, ab initio SCF calcs., band struct., ground state props. 78—51891
BN, cubic, cryst. growth in systems containing H_2 80—55279
BN, cubic, energy band and piezoelec. calcs. 78—72071
BN, cubic, growth pressure-temp. region in system BN-Mg 79—66053
BN, cubic, high press. synthesis using H_2O, H_3BO_3 and urea catalysts 79—83160
BN, cubic, high pressure synthesis, solvent effects 80—40310
BN, cubic, press. and temp. stability region in presence of ammonium borate 77—85922
BN, cubic, sintering technology and cutting performance of tools 80—29919
BN, cubic, water catalysed form. 78—53199
BN, cubic single crysts., dislocations and other defects, X-ray topography study 79—99207
BN, cubic struct. form. from hexagonal struct. at high press., catalytic effects *(Japanese)* 77—90308
BN cutter contact plates, struct. and phase changes on working steel *(Russian)* 80—108433
BN, degree of conversion from cubic to hexagonal, determ. method 79—15887
BN, deposition of wurtzite type layers, by reactive pulse plasma crystallisation 79—28953
BN diffusion semiconductor technology appl. *(Bulgarian)* 78—59824
BN, dislocation struct., single crystals, positron annihilation study 78—11016
BN, dislocation tilt boundaries, Laue photograph exam. 77—11562
BN, EPR, book contrib. 78—48041
BN, electron energy loss spectra, core edges, orientation depend. 79—61478
BN, electron spectra, regularisation method *(Russian)* 79—41215
BN, electronic energy band struct., X-ray spectra, pseudopotential calcs. 79—78008
BN, electronic struct., exact exchange HF calcs. 80—65438
BN, epitaxial, refl. spectra, 5-12.5 eV 79—99967
BN external crystal morphology, SEM obs. 79—73078
BN fabricated CO_2 CW capillary waveguide laser for optically pumping D_2O 80—48278
BN fibres, prep., struct., thermal, mech. and elec. props., appls., book contrib. 78—48360
BN film, high temp. reactive plasma deposition, struct., resist., and dielec. const. meas. 77—7988
BN, film, stability, high temp. and electron irrad. effects 77—39747
BN film, undoped and P-doped, effect of CVD parameters on props. 80—25571
BN films, elastic stiffness and thermal expansion 80—49559
BN films, elec. resist., depend. on relative humidity 79—4609
BN films, humidity sensitive elec. props. and switching characts. 80—107938
BN films, optical and electrophysical props. *(Russian)* 77—20941
BN glass transfer process 80—107459
BN, graphite-like, twinning and shear 77—4114
BN, ground state of electron subsystem, quasimolecular model 79—69055
BN, hardness rel. to temp., phase compositions 78—60752
BN, hexagonal, anisotropic emission of the X-ray K-emission band 78—23557
BN, hexagonal, electronic struct. from X-ray emission and XPS 79—47009
BN, hexagonal, long optical vibrs., elastic consts. from valence force consts. 78—51621
BN, hexagonal, low freq. Raman active vibr. 78—43880
BN, hexagonal, parallel to basal planes, thermal conductivity 78—22907
BN, hexagonal, prod., props., uses *(German)* 79—74120
BN, hexagonal, prod. from CaB_6 *(German)* 79—74121
BN, high pressure synthesis, exam. of relationship between synthesis condition, and crystal shape, size *(Japanese)* 79—20018
BN, high temp. compatibility with insulating oxides 77—24995
BN, high-temp. plasmochem. synthesis, control of props. 80—55333
BN, in Ag-BN-Si-Al sandwich, humidity sensitive threshold switching 78—88046
BN in contact with W, barrier layers for good high-temp. stability 79—70194

boron compounds continued
BN, interatomic interactions from XPS 80—49171
BN, lattice dynamics, X-ray characts. *(Russian)* 77—80593
BN, lattice dynamics of cubic cryst. 79—77694
BN, low-Z material, outgassing expts. 79—209
BN, martensitic character of transition from wurtzite-type to graphitelike modification 79—43248
BN, O content depend. on heat treatment temp., neutron activation analysis 80—16356
BN on Si substrate, elec. characts. of BN-Si interface, expt. 77—20459
BN particle, microanal. by energy loss spectrometry using field emission STEM 78—53286
BN, phosphided, luminescence spectra of products 77—12418
BN, polycryst. cubic, props. 80—21013
BN, polycrystalline cubic, compressive strength and thermal stability 78—44170
BN, polymorphic modifications form. under low and high press. 79—15597
BN powder, shock wave compression prior to sintering 77—66615
BN powder, wurtzite sphalerite struct. phase transition, effect on substruct. 80—25690
BN powder particles coated by Ti or Mn, thermal stresses generated in vac. deposition 77—40455
BN, powder-cushion gripping to promote good alignment in tensile testing 78—92418
BN prep. by water solvent, electron microscope charact. 78—47253
BN preparation technology, powder, thin film and volume crystals *(Czech)* 78—3037
BN production, powdered, in arc plasma *(Chinese)* 79—98999
BN, production kinetics of gasification of organosilicon binders 78—60635
BN, pyrolytic, diffusion source for Si 78—91352
BN, pyrolytic, in contact with various metals, friction and transfer behaviour 78—88535
BN, Raman scatt. exam. of high press. effects on force const. anisotropy 79—38542
BN, resonance energy neutron radiography using dynamitron accelerator 79—52480
BN, self focusing high current relativistic electron beam for structural and chemical transformations *(Russian)* 80—15190
BN, semicond. film, chemical deposition 80—71596
BN, shock compression, polymorphic transform. kinetics 79—86838
BN, shock synthesis *(Japanese)* 80—29918
BN, shock-compressed pyrolytic and hot-pressed, phase transitions to 120 GPa 77—70048
BN, solubility product in Fe-Si (3.1 wt.%) 79—10955
BN, sphalerite to graphite-like transform. in the 1100-1700°C range *(Russian)* 77—16572
BN, sphalerite transform., simple direct mechanism *(Russian)* 77—21135
β-BN, struct. of twin seam obs. by opticalmicroscopy 77—39596
BN, structural changes at high pressures and temps. 80—40345
BN, structural changes occurring during shock compression in presence of H_2O 80—16301
BN structure after high temp. shock compression 80—39220
BN surface spark discharge, channel spreading and substrate vaporisation 77—89336
BN, TEM investigation using C replicas 80—61034
BN tetrahedrally bonded valence crystals, SCF perturbation theory appl. 79—37658
BN thermal diffusivity meas. using ruby laser beam *(Spanish)* 79—90835
BN thick film, crystn. and semicrystn. CVD on C steel substrate 79—87586
BN, thin film prep. and I-V characts. of Al-BN-Au device *(Japanese)* 77—73230
BN, toughening by stress-induced phase transforms. 78—80635
BN, turbostatic, hot pressing, struct. rearrangement, temp., residence time effects 77—8789
BN, use to obtain Si layers with high surface concentration of B *(Russian)* 80—107639
BN, Wannier functions and density matrix determ. in terms of localised orbitals 78—2408
BN, wave-vector depend. of electron energy losses 77—51688
BN, wurtzite, chem. comp. and processing props. in prep. of Geksanit-R sinterings 80—25632
BN, wurtzite type, effect of TiB_2 and B additions, on transformation to zinc blende type 78—80542
BN, wurtzite type, phase and struct. changes at high temps. 77—12618
BN wurtzite-sphalerite phase transition, stacking fault role 80—6418
BN, wurtzite-type, lattice distortions 77—11636
BN, wurtzite-type, prepared by static compression, struct. 77—35539
BN, wurtzitic, temp. characts. of thermodynamic props., 5-320K 77—55361
BN, X-ray spectra, chemical bonding and multiple ionis. effects 78—50630
BN:C, hardening by doping, p-T diagram, cryst. struct. *(Russian)* 77—77491
BN/BN composites, prep., mech. props. 77—21080
BN-AlB, cubic phase solid soln., crystallographic and metallographic study, thermal resist. *(Russian)* 78—30599
BN-based coatings, fabrication and wear resist. 80—40576
$BN\text{-}SiO_2$ composites, sintered, oxidation kinetics 79—96171
BN_3, adsorpt. of Ar, Kr and Xe 79—73395
BN_3, adsorption of Xe and Kr, first layer study 79—73397
BN_3, hexagonal, intercalation cpds. with metal fluorides, prep. and props. 80—40686
BN_x refractories, thermal cond. determ. using IR laser heating 79—94479
$B_{50}N_x$, $x=1$ to 2, prep. and struct., book contrib. 78—47277
$BNC \rightleftharpoons BCN$, isomerisation energy/barrier correlation, rel. to HNC(LiNC) 80—50840
$B_3N_3H_6$, allowed character of 1900 Å band, two-photon spectra 78—74719
$B_3N_3H_6$, electronic struct., mag. susceptibilities, ab initio calcs. 78—74571
$B_3N_3H_6$, isotopic variants, pure rot. Raman spectra 77—71803
$B_xN_xH_{x+3}$, energy levels and wave functions, π-electron approx. 77—38608
BO, Franck-Condon factors, rot. quantum number effect 79—31613
BO, radiative lifetime, first excited state 78—62848

boron compounds continued
  BO, spectroscopic properties, PNO-CI and CEPA calcs. 78—41961
  BO, transition moment of diatom., ρ-evaluation 79—31612
  BO , ionisation pot. calcs. 77—75076
  BO_2, $A^2\Pi_u$-state, Hanle effect, press. and Zeeman broadening 79—18239
  BO_2, Doppler free spectra, backscatter fluoresc. line narrowing, theory and obs. 80—53034
  BO_2, fluoresc. excitation spectra, vibronic level fluoresc., Fermi reson., force field 77—79643
  BO_2, gas, optically detected mag. reson. spectrum, $X^2\Pi$ rovibronic sublevels 78—82756
  BO_2, intermodulated fluoresc. spectra using stabilised dye laser 79—27020
  BO_2, laser excited fluoresc. spectra assignments, vibronic and electronic states 77—46590
  BO_2, laser saturation spatial spectroscopy of diffusion coeff., interaction pot. 77—75341
  BO_2, photoexcitation and fluoresc. spectra, rot. transitions, assignment and deconvolution 79—27003
  BO_2, Π vibronic states, laser induced fluoresc. obs. 80—58301
  BO_2, radiative lifetime, first excited state 78—62848
  BO_2, reson. fluoresc. assignment of vibr. and vibronic transitions 78—17663
  $BO_3{}^{3-}$, X-ray fluorescence, electronic struct. determ. 78—86887
  B_2O_2, thermochem. evidence rel. to mol. structure 77—38738
  B_2O_3, amorphous, acoustic props. at 20 GHz, Brillouin scatt., 3-300K 80—24536
  B_2O_3, bipyramidal struct., stability, ab initio SCF-MO calcs. 80—99446
  B_2O_3, chem. bonding, electronic struct., ESCA, Auger, and SIMS spectra 80—50512
  B_2O_3, effect of conc. on mag. props. and defects of YSmLuCaGeIG films grown in PbO-B_2O_3 solvents 78—68321
  B_2O_3, effect on elec. cond. of fused CaF_2 78—43157
  B_2O_3, effect on high temp. creep of MgO 78—48450
  B_2O_3, effect on props. of PbO containing cryst. glass 80—24637
  B_2O_3, effect on sintering and stability of ZrO_2-based solid solns. 77—40410
  B_2O_3 encapsulant in GaAs single cryst. growth by Czochralski technique 80—11554
  B_2O_3 glasses, Raman study at high temps. 80—93306
  B_2O_3 laser-produced plasmas, isotopic enhancement 80—92349
  B_2O_3, microprobe state anal. by X-ray OK and BK emission band spectra *(Japanese)* 78—19606
  B_2O_3, molten, BO_3 triangles in boroxyl rings and random networks, Raman intensity investig. 80—45058
  B_2O_3, molten, growth and dissolution of air, N_2, O_2 gas bubbles 77—20070
  B_2O_3, molten, reaction with water, reactor fuel-coolant interaction simulation 78—58363
  B_2O_3, spray coated, reaction with Si, IR investig. 79—39197
  B_2O_3, struct. determ., continuous random network approach 78—67693
  B_2O_3, thermal conductivity, 1.5-30K *(French)* 77—39704
  B_2O_3, vibrational force consts. and B-O bonding, Green's function method 77—14406
  B_2O_3, vitreous, Raman cross sections, rel. to appl. in fibre Raman lasers 78—31176
  B_2O_3, vitreous, struct. and bonding determ., NMR obs. 77—39545
  B_2O_3, vitreous, struct. study using small-angle X-ray scatt. 80—84071
  B_2O_3, vitreous, struct. study using ^{10}B NMR 80—84658
  B_2O_3, vitreous and crystalline, Raman spectra exam. 77—66491
  B_2O_3 vitreous and liq., ^{11}B NMR line shape and spin-lattice relax. meas. 77 4575
  B_2O_3, volatility, effect of batch composition of liquating glass 77—27995
  B_2O_3-BaO, liquid immiscibility region, equilibration and quenching expts. 80—45288
  B_2O_3-containing ceramic glaze, neutron probe anal. for control of prep. process *(Polish)* 80—97751
  B_2O_3-Li_2O-Fe_2O_3, prep. by quenching methods, exam. of microcrystalline precipitates of Li_2O-Fe_2O_3 *(French)* 79—20019
  B_2O_3-Na_2O-SiO_2-Al_2O_3, effect of alumina dispersions on the thermal cond./diffusivity/stress resist. 80—39368
  B_2O_3-$Na_2O(K_2O)(V_2O_5)$, thermal cond. of melt in region 900 to 1100°C, effect of convection 78—2309
  B_2O_3-NaKO glass, dielectric relaxation at low temp. 79—11384
  B_2O_3-Nb_2O_5 complexes, phase equilib. high resolution TEM obs. 78—35378
  B_2O_3-Nb_2O_5 system, phase equil. and phase struct. obs. by high resolution TEM 80—108419
  B_2O_3-SiO_2 optical fibres, exposed cladding technique, birefr. and polarization props. 79—14094
  $(B_2O_3)_x$-$(SiO_2)_{1-x}$, spontaneous Raman scattering *(French)* 79—78674
  BOH→HBO system, heterovalent isomerism, ab initio calc. of pot. surfaces and min. energy paths, geom. parameters 80—32622
  $B(OH)_3$, $^1H/^2H$ quadrupole reson. freqs. detected by double reson. with level crossing 78—84497
  $B(OH)_3$, sea water relaxation and sound absorption 79—68466
  $(B(OH)_3)_2$, hydrogen bond, ab initio MO calcs. 78—58588
  $B_2O_3.Fe_2O_3.nMO$ (M=Fe, Co, Ni, Cu, Mg), synthesis and mag. props. 80—20384
  $B_2O_3.Fe_2O_3.nMO$, (n=2 or 4, M=Mg, Co, Ni, Cu), mag. props., transitions 80—75763
  BP coatings, on Mo by CVD and their composition and microhardness 79—28942
  BP, cryst. growth from Cu-fluxed melt, and characterisation 77—85920
  BP, epitaxial, CVD on Si substrate, cryst. imperfections 78—10294
  BP epitaxial film, hardness meas. 77—11629
  BP, epitaxial growth on Si substrate, Si impurity profile, ion microanal. 78—87886
  BP, epitaxial growth using B_2H_6-PH_3-H_2 system 79—28937
  BP, etching by HCl gas, temp. and HCl conc. effects 77—86205
  BP film, high temp. thermoelec. power, scattering processes 80—80305
  BP, ground state of electron subsystem, quasimolecular model 79—69055
  BP, semicond., ^{31}P nuclear mag. shielding 79—33549
  BP, sp. ht., Debye temp., compressibility and Gruneisen coeff. meas. 78—63865
  BP, VPE, diffused layers formed in Si substrates, device appls. 78—56585
  BP wafers, epitaxial growth by thermal decomp. of $B_2H_6+PH_3$, struct. imperfections 77—62774
  BP:Ni pillar crystal growth from vapour 80—60758

boron compounds continued
  BP:Zn(Se)(Cd), epitaxial layers, ion implantation, defects and lattic locations, channelling obs. 80—88179
  BP-BAs, quasi-binary system, X-ray emission and electron spectra of solid soln. *(Russian)* 77—1764
  BP-BAs solid solns., electronic struct. of valence bands and nature of interatomic interaction 78—34764
  BP-Si junctions epitaxial growth and device appls. 78—4 333
  $BP+N_2(NH)_3$, dissoc. reacts. 79—43627
  $B_{13}P_2$, epitaxial, micro-Vickers hardness number 77—40444
  BP_xAs_{1-x} system, electron struct. and interatomic interactions, X-ray spectroscopy 80—20736
  BPO_4 crystal, P K-band X-ray emission spectra, state anal. 80—40190
  BPO_4, XPS of cryst., inner shell binding energies of elements 79—43092
  BPO_4-$AlPO_4$, non-equil. phase diagram, electron microscope obs. 79—43225
  $B_xP_yO_4$, temperature programmed desorption, depend. on P/B ratio 79—23828
  BS, and isotopic forms, two new emission bands, mol. consts. 77—18960
  B_2S_3-Tl_2S system, phase diagram and verification 80—35165
  B_2Se_3-Tl_2Se_3 system, phase diagram 80—35165
  $B_{14}Si$, β rhombohedral, conduction mechanism, thermoelectric props. 80—24932
  $B_{14}Si$ elec. props., medium range disorder model 80—15522
  $B_{14}Si$ refractory thermoelectric material CVD and application 77—77411
  $B_{14}Si$, switching and high field effects, cond. mechanism 78—64048
  BX_3, X=F, Cl, Br, I, mol. force consts., parametric representation method 78—25503
  $BX_2{}^{14}NCS$ (X=Cl, Br, I), soln., force fields and normal modes, vibr. spectra, IR and Raman obs. *(French)* 80—58266
  BaF_2+BCl_3, crossed beam metathesis, total cross sections 77—21354
  BaO-B_2O_3 melt, Fe_2O_3-Fe_3O_4 equilibrium, ferrite prep. 77—36428
  BaO-B_2O_3-V_2O_5 glasses, polaron hopping cond., optical absorpt. and ESR spectra 79—23966
  BaO-Mn_2O_3-B_2O_3, amorphous mag. oxide, field-cooling effect *(Japanese)* 80—84615
  $BaTiO_3$-PbO-B_2O_3, liquid phase sintering, effect on props. *(German)* 79—33980
  $Bf(^1\Sigma^+)$, diatomic molecular form factors, vibr. average, study of convolution approx. 79—50926
  Bi_2O_3-B_2O_3 melt, solubility of rare earth iron borates and their crystallisation 80—19736
  $3Bi_2O_3.5B_2O_3$, viscosity, molar volume of melt and enthalpy of fusion 79—10924
  Bn, cubic, formation from hexagonal BN using Cao and Li_3N catalysts *(Japanese)* 80—54374
  2,4-$C_2B_5H_7$, polyhedral, spin coupled ^{11}B-^1H systems, 2-dimens. correl. NMR 80—69166
  ^{13}C NMR spectroscopy 79—89691
  CaB_6-SmB_6 system complex borides, prep. and props. 78—52703
  CaO-B_2O_3-SiO_2 glass-forming additive, effect on Al_2O_3 ceramics sintering 80—89187
  $CaO.3B_2O_3$, form. by dehydration of hydrated calcium borates *(Japanese)* 79—74378
  ClBS, form., photoelectron and microwave spectra 78—90214
  CsB_3H_8, IR, Raman and inelastic neutron scatt. spectra 79—42966
  Cu-SiO/B_2O_3-Cu thin film, amorphous, conductance and capacitance, effect of electroforming 80—34537
  CuB_{24}, elec. props. at high temps. and in strong elec. fields, thermistor appls. 80—92903
  $Eu_3B_2O_6$, synthesis, struct. and mag. props. 77—89934
  FBO, electronic struct. calcs. 77—30772
  Fe-Cr-SiC-B_4C powder mixture, compressibility and elec. cond. in cold pressing under low press. 78—60609
  $FeBMO_4$, M=Mg, Cu, Co, Ni, mag. props. meas. 80—34607
  G_2-B_2O_3 melt, thermodynamic props. from mass spectroscopy 80—39318
  Gd_2O_3-Fe_2O_3-PbO-B_2O_3, primary crystallisation regions 77—12604
  H_3BO_3-$B(OH)_4{}^-$ relaxation in ocean, rel. to pH depend. of low-freq. sound absorpt. 77—49072
  H_3BPF_3 and D_3BPF_3, laser augmented decomposition 79—52713
  H_3N-BH_3, cryst., electronic struct., ab initio, MO calcs., fractional charge model 77—34547
  $KI:BH_4{}^-$, far IR absorption in phonon gap 77—12406
  K_2O-AlF_3-B_2O_3 glass, Al atom bonding mode, optical absorption of VO^{2+} and AlK_α spectrum *(Japanese)* 78—11023
  $100(Li_2O.2SiO_2).3B_2O_3$, directionally solidified, thermal and mech. props. *(Japanese)* 80—16295
  $MgO:CaO(SiO_2)(B_2O_3)(Cr_2O_3)$, effective of impurities on high temp. creep 80—40455
  MnO-B_2O_3, polycryst. cpds., mag. susceptibility and ^{11}B NMR 79—8056
  Mo-Y(La)(Ce)-B, X-ray diffr., reciprocal lattice, crystal struct., phase equilibria 77—21122
  $Mo_5(B,Si)_3$, stability of heatproof coating 77—86201
  NH_3BF_3 and d_3, polycryst., for IR spectra, lattice vibrs., cryst. and mol. struct. interpret. 80—2771
  $Na_2B_4O_7$, nuclear spin lattice relax. in amorphous state, review 79—11354
  $Na_3B_5O_8(OH)_2.H_2O$, synthetic, cryst. struct. 78—18591
  Na_2O-B_2O_3 glass, negative thermal expansion, LF Guneisen parameter, numerical analysis 77—11707
  Na_2O-B_2O_3-GeO_2 vitreous melts, thermodynamic props. from mass spectra 80—65253
  Na_2O-B_2O_3-NiO melts, NiO activity and solubility meas. by EMF method *(Japanese)* 80—92677
  Na_2O-B_2O_3-SiO_2 glass, fracture toughness, effect of microheterogeneous struct. 80—104256
  $Na_2O.3B_2O_3$, effect of Fe_2O_3 conc. and temp. on UV absorption 77—16340
  $Nb_5(B,Si)_3$, stability of heatproof coating 77—86201
  Nd-Cr-B system, phase equil. at 800°C, boride lattice parameters *(Russian)* 78—31388
  Ni-Ca-B, Ni-B side of ternary diagram 77—59766
  OBF, band strengths, shock tube IR spectrosc. meas. 80—106358
  $PbO/PbF_2/B_2O_3$ solvent system, density, surface tension and expansivity data, effect of B_2O_3 conc. 79—19985
  PbO-B_2O_3 glasses, microhardness 80—66612
  PbO-B_2O_3 melt, activity of PbO 77—11708
  PbO-B_2O_3-$Li_2O(Na_2O)(K_2O)$ melt, activity of PbO 77—11708
  PbO-ZnO-B_2O_3, glass ceramic cements, crystallisation kinetics and character 77—85982

boron compounds continued
- $(PbTiO_3)_{0.9}(B_2O_3)_{0.1}$, amorphous ribbons, prep., electron and X-ray diffr. obs., dielec. const. temp. depend. 79—50993
- Pr-Cr-B system, phase equil. at 800°C, boride lattice parameters *(Russian)* 78—31388
- n-propylboranes, ^{11}B NMR 78—90190
- $Si:B_2O_3$, analytic study of Si-B phase formed 79—19269
- $Si:BF_2$, p^+-n junction form., ion implantation damage, leakage current 77—24334
- $Si:BF_2^+$, anomalous migration of F and electrical activity of B 78—34654
- $Si:BF_2^+$, ion implantation appl. in semicond. device production 80—103383
- $Si:BF_2^+$, ion implanted, arc annealing by flash lamp 80—44223
- $Si:BF_2^+$, recrystallisation of implanted amorphous layers, elec. props. 79—55762
- $Si:BF_2^+$, recrystallisation of implanted amorphous layers, F migration 79—55763
- $Si:BF_2^+$ implanted, low-temp. annealing characts. 79—55759
- $Si:Bf_2^+$ layers, ion-implanted, anomalous carrier tail generation mechanism 80—19819
- Si-Al-B-O-N, calc. of phase diagrams from data set 80—55362
- Si-B system, DTA, X-ray diffr. and metallographic study *(German)* 80—66484
- Si-B system, liq., surface tension, density, and oxidation kinetics, 1410-1700°C 80—20011
- Si-B-O film, electron probe microanal., Monte Carlo calcs. 79—83533
- Si_xB_{1-x} films, anal. of H ratios and profiling using nucl. techniques and Rutherford backscatt. 80—61202
- α-SiC, sintered, influence of B, C additives on microstructure, SEM exam. 79—8262
- SiC-B_4C, hot pressing, role of grain boundaries 77—24999
- SiC-B_4C (B+1 wt.% C), sintering 77—36432
- SiC-B_4C eutectic, directional solidification, growth and mech. props. 79—91638
- SiC-Bn composite, polymorphic transforms. 77—81259
- $SiCl_4$-$GeCl_4$-BCl_4 particulate layers consolidation, in fabrication of optical fibre preforms 80—60787
- SiO-B_2O_3, amorphous composite dielec. film, AC conductivity 79—51703
- SiO-B_2O_3 composite dielec. films, EPR, dangling bonds and dielec. loss 80—11246
- $SiO_2:B_2O_3$ doped, IR spectra 79—78664
- $SiO_2:BF_2$, ion implanted, F influence on oxidation-induced stacking faults 80—65011
- SiO_2-Al_2O_3-CaO-BaO-SrO-ZnO-Na_2O-K_2O-B_2O_3, glaze effect of P_2O_5 additions 80—60824
- SiO_2-Al_2O_3-CaO-MgO-NaO-K_2O-B_2O_3-ZrO_2, glaze, exam. of zircon crystallisation 79—19155
- SiO_2-Al_2O_3-Fe_2O_3-CaO-MgO-Na_2O-B_2O_3-SO_3, exam. of white flaky inclusions, causes and formation time 79—29237
- Sm-Cr-B system, phase equil. at 800°C, boride lattice parameters *(Russian)* 78—31388
- $Sm_{1-x}B_xS$, valence transition induced by alloying 80—96829
- Ti-B-C system, complex carbide phase synthesis by crystallisation from gas phase 77—16526
- Tl-B-Se system, vitrification region, primary crystallisation fields 77—15321
- V_2O_5-B_2O_3-ZnO semiconductivity glasses, optical and modulated absorpt. spectra in band gap region 77—48189
- W-Y(La)(Ce)-B, phase equilib., struct. of crysts. 77—21122
- $W_5(B,Si)_3$, stability of heatproof coating 77—86201
- $Y_{3-x}Bi_xFe_{5-y}Ga_yO_{12}$-$PbO$-$B_2O_3$-$Bi_2O_3$ system, crystn. fields 78—43996
- Y_2O_3-Fe_2O_3-Ga_2O_3-PbO-P_2O_3, primary crystallisation regions 77—44222
- Y_2O_3-Lu_2O_3-Eu_2O_3-CaO-GeO_2-Fe_2O_3-PbO-B_2O_3 system, garnet crystn. fields 78—43995
- ZnO-GeO_2-MnO-B_2O_3 wideband cathodoluminescent phosphor 80—55196
- ZnO-PbO-B_2O_3, exam. of glass formation and its props. 79—8283

borosilicate glasses
- absorption spectra, influence of Ti on spectra of transition metals in glass 77—12403
- alkali, phase separation, observation using SEM-EDX technique 80—76224
- aluminoborosilicate, working props. during microfibre and ultrafine fibre prod. 79—24486
- alumoborosilicate glass for mirror of large azimuthal telescope 77—62025
- anisotropic glasses, birefringence and microstruct. 77—8541
- antireflection films, on alkali-borosilicate glasses produced by chem. treatment 80—66677
- assignment of IR reflection spectra *(Japanese)* 78—10902
- at temp. below annealing range *(Czech)* 79—43305
- ball mill grinding, rate constant determination *(Japanese)* 78—95828
- ball mill grinding, wet, dry, rate constant determination *(Japanese)* 78—95827
- birefringent, X-ray small-angle scatt. study 80—103937
- boroaluminosilicate glasses, alkali free, density calc. *(Chinese)* 78—14396
- ceramic form., fixation of long-lived fission products 77—61558
- chemical acceptance tests for use as neutron absorbers in nuclear reactors 79—22446
- cladding, for optical fibres of phosphate glasses, transparent in UV region 78—87113
- cleaning for biological appl. 77—29234
- crack growth, phase separation effects 80—89336
- crown glass-pyrex adhesively bonded interface, Stoneley wave study 80—49530
- dielectric constant down to 5 mK, new behaviour 77—63354
- diffusion strengthening technique 78—31418
- dynamic compression and unloading K-8 glass 77—9029
- electrical relax., Debye-Falkenhagen theory 80—108155
- EM and elastic wave interactions, at low temps. 77—31724
- EM wave effects on acoustic absorpt. at low temp. 77—47866
- fibre inhomogeneous dispersion, direct meas. method 78—1400
- field-induced electron emission into ultra-high vacuum 80—104048
- film, props., rel. to deposition conditions, appl. in semicond. devices 78—23612
- film, SiO_2 rich, prepared by modified CVD, refr. index behaviour 78—60526
- film, vapour-deposited, structural model, IR spectra meas. 77—1084

borosilicate glasses continued
- fission product waste solidification, high-level, for final storage *(German)* 80—22958
- fixation of radioactive waste in high-SiO_2 glasses 79—49708
- fluxing material, effect on oxidation of graphite crucibles *(Japanese)* 78—84755
- fusion reactor material, chem. interaction with H plasma discharge impurity ions 77—35357
- gamma irradiation effect on density, refractive index, thermal expansion 80—79838
- gem stones, synthetic prep. X-ray studies for optimum conditions of heat treatment 80—45263
- glass-Ag composite, elec. cond. 80—10970
- high activity waste immobilisation, potential solidification material properties 79—49790
- holograms, photoinduced anisotropic recording media 79—41354
- impact of microparticles, on brittle solids, high speed photography obs. 78—44223
- interface with Si, B impurity diffusion, separation factor estimation 79—86926
- IR reflection spectra resulting from phase separation *(Japanese)* 78—39542
- layer, high-rate electron-beam evaporation 78—35310
- leach rates of high activity waste from borosilicate glass 79—36358
- lead borosilicate glass, phase separated, components distrib. by electron probe microanal. *(Japanese)* 79—52844
- liquids, viscosity meas. up to 1840°C *(French)* 80—79969
- machinable glass ceramic, elastic moduli, press. and temp. derivatives 78—52873
- magnetic and spectral properties, Fe and Cr ion interaction 80—103883
- microporous, structural anisotropy and birefringence 79—8114
- multimode fibres, cladding influence on light attenuation 79—76855
- NMR of B, spectral analysis, singular-value decomposition 77—36141
- optical fibre, elliptically clad borosilicate single-mode, strain birefringence 80—33148
- optical fibre, low-loss, production with high numerical aperture 80—48450
- optical fibre, low-loss graded index, produced by double crucible technique 80—48449
- optical fibre fracture stress and mirror size obs. 79—37020
- optical fibres, GeO_2-$B_2O_3SiO_2$, ageing effects of moisture on fatigue and tensile strength 80—66539
- optical fibres, graded-index, manufacture, double-crucible method 80—83688
- optical fibres, low-loss single mode, design, fabrication and transmission characts. 78—71199
- optical fibres, prepared by modified CVD, reproducibility 78—90531
- optical fibres, refr. index and comp. data 77—79950
- optical filter glasses with band-pass characts. for red spectral region 78—25936
- optical grade, refractive index-density relationship changes assoc. with reannealing 78—27175
- optical waveguide fibre cladding composition effect on stress corrosion and fatigue 77—3664
- phase separated, DC cond. and elec. breakdown 78—23400
- phase separated, depolarised light scatt. in terms of Rayleigh-Gans theory 79—87452
- phase separated, EPR rel. to struct., elec. and opt. props. 78—23333
- phase separation effect on HF etch rate 78—11208
- phase-separated, refr. index. and density changes 77—66025
- photochromic glass, darkening effect due to γ-irrad. 80—96566
- photochromic glasses, photosensitivity rel. to AgCl particle shape 78 31223
- porous, IR spectroscopic obs. of coordination state of B atoms 77—24268
- porous, surface area change with acid treatment, adsorption of N_2 and H_2O *(Japanese)* 78—44244
- powder, sintering, foaming by chemical reactions 80—81017
- pyrex, fission fragment track detector, neutron dosimetric meas. 78—13347
- Pyrex, fracture initiation, influence of temperature and composition 79—100246
- quartz glass, boron-containing, struct. investig. using ESR spectra 77 7673
- radiation and thermal effects on props. 77—61557
- radioactive high level waste management 80—5271
- radioactive waste, high-level, evaluation of products for solidification 77—61555
- radioactive waste, Magnox, development and radiation stability of glasses for vitrification 77—61554
- radioactive waste confinement, stability characts. *(French)* 77—61556
- rain erosion mechanisms 79—34154
- refractive index freq. depend., dispersion eqn. calc. 80—40083
- residual stresses, comparison of optical and fractographic meas. rods, compressively clad 80—108539
- Simax, tensile and impact strength, effect of surface damaging and annealing *(Czech)* 79—74227
- Simax glass, internal and surface temp. during heating *(Czech)* 79—42285
- simulated high level radioactive wastes in borosilicate glasses, characterisation *(Japanese)* 79—93745
- single mode fibres, noncircular core influence on polarisation performance 78—37973
- single-mode optical fibres with different B_2O_3-SiO_2 compositions 78—1392
- sintering 77—85980
- sodium-alumoborosilicate photochromic glasses, Weigert effect *(Russian)* 77—68250
- sputtered film, phys. and chem. props., B diffusion into Si, SiO_2 80—29040
- strontium alumoborosilicate glass, effect of vaporous and liq. Cs 77—44509
- surface, adsorption of Au, AES study, electron bombardment effects 80—65380
- surface, damage due to impact of small glass and steel spheres 78—52994
- surface conductivity at solid/liq. interface 79—78152
- surface flattening kinetics by sinusoidal profile decay method *(Japanese)* 80—34284
- surface mass transport mechanisms at high temperatures *(Japanese)* 80—54479
- surface struct. rel. to HF etching and stressed state 79—100276

borosilicate glasses continued

- tensile and impact strength, effect of surface damaging and annealing *(Czech)* 79−74227
- thermal conductivity meas. by laser flash method *(Japanese)* 77−69124
- US attenuation saturation by microwaves, low-temp. obs. 77−36114
- US attenuation temp. dependence rel. to γ irrad. 79−46755
- vacuum-deposited intermediate layer, stable structure formation 80−80979
- Van de Graaff accelerator, construction of stack insulators accelerator tubes, using borosilicate glass 78−33317
- Van der Waals interaction between two samples, influence of optical absorpt. 79−95273
- viscoelastic characterisation using harmonic dispersion of longit. reson., for KG-33 Kimax 79−10538
- Vycor glass, manufacture, struct., physical and chem. props. 80−7527
- X-ray scattering at small angles study 80−84071
- Ag halide photochromic glass, darkening mechanisms under pulsed laser excitation 78−25938
- Al_2O_3-B_2O_3-SiO_2, alkali glasses, granulating mechanism for medical use 80−40315
- Al_2O_3-B_2O_3-SiO_2 glasses, elec. cond. study, 700-1900°C 79−65487
- Al_2O_3-B_2O_3-SiO_2 sheet glass, solar energy appl., optical and mech. props. 80−87447
- Al_2O_3-B_2O_3-SiO_2 system, metastable liq.-liq. phase separation 79−42263
- Al_2O_3-CaO-B_2O_3-SiO_2(-Na_2O) composite glasses, high strength, prod. by overlayering 80−89193
- Al_2O_3-glass seals, diffusion of Al, electron microprobe study 80−107577
- Al_2O_3-SiO_2 clad with B_2O_3-SiO_2 effect of drawing tension on residual stresses 78−64554
- B_2O_3-Na_2O-SiO_2-Al_2O_3, effect of alumina dispersions on the thermal cond./diffusivity/stress resist. 80−39368
- B_2O_3-SiO_2, glass synthesis by hot pressing of gels 79−15637
- B_2O_3-SiO_2 (95.5 wt.%) glass, dielec. relaxation 79−78620
- B_2O_3-SiO_2 glass film, CVD, differential IR studies 80−55213
- B_2O_3-SiO_2:Ce glasses, radiation resistance mechanism, optical absorpt. and luminesc. obs. *(Polish)* 79−86825
- B_2O_3-SiO_2-Na_2O phase-separated glass, creep fracture morphology 80−81151
- BPO_4-SiO_2 system, new data to prevent B_2O_3 or P_2O_5 loss at elevated temp. 80−20914
- BaO-B_2O_3-SiO_2 system glass, electronic cond. of Ti ions 78−23095
- BaO-B_2O_3-SiO_2:Ti^{3+}, elec. cond., struct. 78−72148
- BaO-B_2O_3-SiO_2:Ti^{3+}, optical absorpt. spectra 78−72564
- BaO-B_2O_3-SiO_2:Ti^{3+}, Ti^{4+}, glass EPR spectra, variation of g-factor with temp. 79−99757
- BaO-GeO_2-Na_2O borosilicate core glasses for high numerical aperture fibres 80−69534
- CaO-Al_2O_3-B_2O_3-SiO_2-FeO, glass, IR spectra at room and melt temp. 80−88986
- CdO-B_2O_3-SiO_2, glass, dielec.-relax. currents 78−52004
- CdO-B_2O_3-SiO_2, phase equilibria at 800°C, photoelectric effects 78−68675
- Fe_2O_3-NiO-Na_2O-Li_2O-B_2O_3-SiO_2 glass, EPR meas. of exchange interactions 77−32243
- GeO_2-B_2O_3-SiO_2, glass fibre, pulse transmission meas. of zero material dispersion 77−88937
- GeO_2-B_2O_3-SiO_2 optical fibres, optical transmission loss as function of drawing conditions 79−32038
- GeO_2-Na_2O borosilicate glass fibre prod. by phase separation and leaching 80−69558
- $GeO_2.B_2O_3.SiO_2$ glasses, material and mode dispersion 77−19415
- $K_2(F,O)$-B_2O_3-SiO_2, effect of replacing B_2O_3 by Al_2O_3 or Ga_2O_3 78−63677
- K_2O-Al_2O_3-B_2O_3-SiO_2, glass, ESR exam. of paramagnetic centres formed during mech. destruction by grinding 78−88188
- K_2O-B_2O_3-SiO_2 system glasses, hypersound propag., 77 to 300K, Brillouin scatt. obs. 77−84850
- K_2O-PbO-ZnO-B_2O_3-SiO_2, corrosion and microhardness, effect of detergents 80−16518
- Li_2O-B_2O_3-SiO_2 glass systems, phase separation effect on the diffusion processes 78−26734
- Li_2O-Na_2O-B_2O_3-Al_2O_3-SiO_2 glass, Young's modulus and density, ion exchange effects 80−84982
- Li_2O-Na_2O-B_2O_3-SiO_3, exam. of metastable phase separation region 78−88450
- Na borosilicate glass microsphere material, sintering, struct., strength props. *(Russian)* 80−108383
- NaO-B_2O_3-SiO_2, phase separated glass, viscosity and microstruct., heat treatment effect 79−99343
- $20Na_2O$-$(80\text{-}x)B_2O_3$-$xSiO_2$ system, structure toughness-composition relationship 80−104257
- Na_2O-Al_2O_3-B_2O_3-SiO_2:Ag, photochromic glass, EPR of Ag^0 and $Ag_2{}^+$ centres 77−24741
- Na_2O-Al_2O_3-B_2O_3-SiO_2 photochromic glass, $AgCl_{1-x}Br_x$ activated, comp. optimisation by Box-Wilson method 77−50741
- Na_2O-Al_2O_3-B_2O_3-SiO_2, glass, ESR exam. of paramagnetic centres formed during mech. destruction by grinding 78−88188
- Na_2O-Al_2O_3-B_2O_3-SiO_2-$AgBr(Cl)$, photochromic glass, exam. of role of O and Cu ions, using luminescence spectra 79−4849
- Na_2O-Al_2O_3-B_2O_3-SiO_2, CuCl crystal activated photochromic glasses, absorpt. spectra 79−27353
- Na_2O-Al_2O_3-B_2O_3-SiO_2-$AgCl(Br)$, photochromic glass, kinetics of thermal decolorisation 80−103931
- Na_2O-Al_2O_3-CaO-B_2O_3-SiO_2, used in solidification of radioactive waste *(Russian)* 77−61560
- Na_2O-B_2O_3-SiO_2, ^{11}B NMR obs. of struct. 78−38625
- Na_2O-B_2O_3-SiO_2, containing halogens glass formation 80−103254
- Na_2O-B_2O_3-SiO_2, optical waveguide glass, molar absorptivity of water 80−80066
- Na_2O-B_2O_3-SiO_2 glass, type DB-1, exam. of distrib. of rare earth activators, by absorption study 79−4832
- Na_2O-B_2O_3-SiO_2 glass, phase separated, HCl leaching rate and microstruct. 79−29242
- Na_2O-B_2O_3-SiO_2 glass fibre, prep. with low loss 79−59850
- Na_2O-B_2O_3-SiO_2 glass, phase-separated, leaching 79−66394
- Na_2O-B_2O_3-SiO_2 glass, NMR, struct. 79−87325
- Na_2O-B_2O_3-SiO_2 glass, Rayleigh scattering losses 79−99893
- Na_2O-B_2O_3-SiO_2 glass fibre, plastic coating influence on strength 80−58697
- Na_2O-B_2O_3-SiO_2 glass fibre, plastic-coated, liq. N_2 strength 80−58707

borosilicate glasses continued

- Na_2O-B_2O_3-SiO_2 glass, low-loss GRIN fibres, double-crucible prod., loss and bandwidth meas. 80−69559
- Na_2O-B_2O_3-SiO_2 glass-Ni compact, indented, strength and fracture toughness 80−93636
- Na_2O-B_2O_3-SiO_2 glasses, phase-separated, leaching rate 80−104131
- Na_2O-B_2O_3-SiO_2 glass, fracture toughness, effect of microheterogeneous struct. 80−104256
- Na_2O-B_2O_3-SiO_2 low-loss optical fibre prep. by double crucible technique *(German)* 78−33929
- Na_2O-B_2O_3-SiO_2:GeO_2 medium-loss graded-index preform fabrication by phase separation and leaching *(German)* 78−33930
- Na_2O-B_2O_3-SiO_2:Yb(Tb), luminesc. cooperative processes, glass struct. and comp. effect 80−16101
- Na_2O-B_2O_3-SiO_2/$AgNO_3$, thermodynamic characteristics of ion exchange process 79−8452
- Na_2O-B_2O_3-SiO_2/$AgNO_3$ exam. of ion exchange equilibria 79−5178
- Na_2O-B_2O_3-SiO_2-$As_2O_3(As_2O_5)$ glasses, DC and AC resist., bipolaronic hopping cond. 80−88558
- Na_2O-B_2O_3-SiO_2-Fe glass, near IR optical absorption of Fe (II) 78−84616
- Na_2O-B_2O_3-SiO_2-MoO_3 glass containing high level radioactive waste, phase separation 80−25683
- Na_2O-B_2O_c3-Bi_2O_3-SiO_2, heterophase glass, diffusion and elec. cond. 78−67858
- Na_2O-B_2O-SiO_2, high temp. mech. relax. 79−96071
- Na_2O-B_20_3-SiO_2, mechanical strength and swelling in liq. 80−85024
- Na_2O-BaO-SiO_2, metastable two liquid tie line calc. 78−92246
- Na_2O-CaO-Al_2O_3-SiO_2-F-B_2O_3-ZrO_2 glaze, crystallisation, MgO, ZnO, BaO and SrO effects 79−60279
- Na_2O-Li_2O-NiO-Fe_2O_3-B_2O_3-SiO_2 glasses, thermally stimulated cond. studies of trapping centres 79−78113
- Na_2O-PbO-B_2O_3-SiO_2, homogeneous melt formation rate, exam. 78−64520
- Na_2O-SiO_2, crack front shape corrections for crack velocities in double torsion specimens 79−91778
- Na_2O-SiO_2-B_2O_3 glasses, phase separation meas. by optical absorption spectra of VO^{2+} *(Japanese)* 79−70414
- Na_2O-SiO_2-B_2O_3-Al_2O_3, comp. changes as evidence for spinodal decomposition 79−11549
- Na_2O-SiO_2-Ga_2O_3-Al_2O_3-B_2O_3-SnO_2, ion exchange reactions with $NaNO_3$ and KNO_3 melts 80−16673
- Na_2O_3-B_2O_3-SiO_2, glass, effect of composition on mech. props. 78−48435
- $Na_2O^{-}K_2O$-B_2O_3-SiO_2, character of elec. cond. 80−103516
- PbO-B_2O_3-SiO_2, glass enamel, heat treated, exam. of microstructure and chemical durability 79−29254
- PbO-B_2O_3-SiO_2-Al_2O_3-ZnO-CuO-Bi_2O_3 solder glass, crystallisation prevention by Cu addition 80−11654
- PbO-B_2O_3-SiO_2-Li_2O-$MgO(CaO)(ZnO)(Al_2O_3)(TiO_2)(ZrO_2)$, glass enamel, heat treated, chemical durability, MgO, CaO, ZnO, Al_2O_3, TiO_2, ZrO_2 addition effects 79−29255
- PbO-B_2O_3-SiO_2-Li_2O-ZrO_2-$CdO(CoO)(CuO)$, glass enamel, chemical durability, microstruct., CuO, CdO and CoO addition effects 79−29256
- Sb_2O_3-Na_2O-B_2O_3-SiO_2, elec. cond. meas., −160 to 200°C 80−20190
- Si-borosilicate glass, Van der Waals interaction meas., influence of optical absorpt. 79−95273
- Si-Na-B-O-N glass, synthesis and characterisation 80−108381
- SiO_2 fabric, prep. from E-glass, structural stability rel. to brittleness, X-ray diffr. and IR spectrosc. studies 80−96634
- SiO_2:B_2O_3 glass, sintering kinetics 80−84898
- SiO_2:B_2O_3/SiO_2 glass fibre waveguide, γ-radiation optical stability 80−23799
- SiO_2-Al_2O_3-B_2O_3, glass fibre, water and acid resistance 80−11799
- SiO_2-Al_2O_3-B_2O_3 glass mech. strength increased by etching 80−97609
- SiO_2-Al_2O_3-B_2O_3-LiO_2 ($LiO_2.Na_2O$) (Na_2O) glass exam. of optical props. 78−88277
- SiO_2-Al_2O_3-B_2O_3-CaO-Na_2O-K_2O system glasses, relax. of struct. stresses rel. to forming process 79−34088
- SiO_2-B_2O_3, optical fibre, wavelength dispersive props. and comp. 78−33793
- SiO_2-B_2O_3 used for fabrication of tubing and optical fibres 79−50462
- SiO_2-B_2O_3-Al_2O_3-$Na_2O(K_2O)$ glasses, Ag interdiffusion, optical and NMR studies 80−24683
- SiO_2-B_2O_3-GeO_2, optical fibres, UV radiation-induced losses 80−87517
- SiO_2-B_2O_3-Li_2O-Al_2O_3 (28, 2, 1 wt.%) glass, dielec. const. at 3 GHz 80−93233
- SiO_2-B_2O_3-Na_2O, high silica, conductivity behaviour, Na ion dependence 80−24652
- SiO_2-B_2O_3-Na_2O-K_2O system glass, phase separated, loss of oxides during acid leaching, atomic absorpt. anal. 79−11716
- SiO_2-GeO_2-B_2O_3, prepared by modified CVD, refr. index behaviour 78−60526
- SiO_2-GeO_2-B_2O_5-P_2O_5, optical waveguide glass, comp. determ., plasma emission spectra 80−87446
- SiO_2-P_2O_3, optical attenuation in IR region 77−75665
- SiO_2-PbO-B_2O_3-Al_2O_3-CaO-Na_2O-K_2-O glaze, interaction with aluminosilicate glass-ceramics 80−84398
- $SiO_2B_2O_3$-K_2O-Al_2O_3-As_2O_3 glass fibres containing metallic granules, tensile strength, Young's modulus, DC conductivity 80−30023
- $SiO_2.B_2O_3.(Al_2O_3)$ film, formation mechanism on Si, X-ray spectral anal. 79−87008
- SrO-Al_2O_3-B_2O_3-SiO_2, glass, corrosion by Cs vapour or liq. 77−16706
- ZnO-B_2O_3-SiO_2 glass-ceramic-cement composites, review 79−38783

Borrmann effect *see X-ray crystallography; X-ray diffraction*

Bose-Einstein statistics *see quantum statistical mechanics*

Bose gas *see boson systems*

boson fluids *see boson systems*

boson systems

- *see also liquid helium-4; quantum statistical mechanics*
- ^4He, superfluid, one phonon excitation spectrum and interaction pot. 80−54455
- λ-transition, renormalisation-group theory 80−143
- λ-transition, time development of coherent and superfluid props. 79−4439
- adsorbed Bose liquid, ground-state energy calc. 77−20157
- algebraic approach, equilib. states and hierarchy of stability 77−22491
- alpha matter, abnormal boson occupation 79−26387
- anharmonic oscillators, divergence of perturbation theory 79−75393
- bilinear Hamiltonian, diagonalisation methods 78−32716

boson systems continued
binary, variational calc. of ground state props., appl. to dil. ^{3}He-superfluid ^{4}He mixtures 79—73372
binary boson mixtures, thermodynamics ground state 79—35630
binary mixtures, ground state configs. 80—105570
biological Bose condensation, and time threshold for biological effects 79—100664
biological system, Bose condensation, microscopic approach to Frohlich's theory 78—24022
biological system, Bose condensation of phonons, Frohlich model 77—16904
biological system, coherent mode excitations, bose condensation-like, Frohlich vibr. model, Boltzmann eqn. approach 79—39336
Bogoliubov boson transformation, matrix elements estimated 77—17907
Bogoliubov boson transformations, simple derivation of closed formula 77—49672
Bogoliubov inequality for unbounded operators in Bose gas 77—2605
Bose 1-D gas with point interaction 78—49762
Bose condensate, bounds in dimensions $\nu\geq 3$ 78—54294
Bose condensate in dimensions $\nu\geq 3$, bounds 79—54051
Bose condensation, kinetics 79—63139
Bose condensation into a state with finite momentum 79—97300
Bose description of fermions, model 77—53833
Bose description of fermions 78—89402
Bose electron-hole liquid, existence of states with superfluid flow, Ginzburg-Landau theory *(Russian)* 78—72085
Bose expansion for general spin, exact 80—31662
Bose fluid, structure factor determ. 78—34667
Bose fluids, normal, conserving evaluation of dynamic struct. factor 79—14975
Bose gas, ideal, virial series 80—42139
Bose gas, one dimensional, long wave asymptotic multi particle Green functions *(Russian)* 80—77700
Bose gas, spatially inhomogeneous, kinetics in presence of condensate 78—16730
Bose gas, temp. depend. of quasiparticle sound velocity 77—69128
Bose gas, weakly interacting in restricted geometries, low-temp. thermodynamics 80—34261
Bose lattice gas, statistical systems with well defined entropy 79—30395
Bose modes, spin-1/2 approx. in quantum theory 79—6047
Bose partition functions, functional integral representations and inequalities 80—31667
Bose system functional formulation, renormalisation group approach 78—66026
Bose-Einstein condensate, theory of relaxation time 77—13694
Bose-Einstein condensate dynamics, two-fluid hydrodynamics, Mori theory 77—28061
Bose-Einstein condensation in an Einstein universe 78—77797
Bose-Einstein condensation in confined ideal systems, onset criteria 77—37812
Bose-Einstein condensation in Einstein universe 80—46959
Bose-Einstein condensation of a relativistic gas in d dimensions 80—8902
Bose-Einstein condensation of ideal gas 80—22272
boson expansions, convergence of various methods 79—93037
boson field in neighbourhood of classical solution, quantisation by appl. of Bogolyubov's method 78—8566
boson linear coupling systems, general props. 80—2124
boson operators, exponential ordering of quadratic forms 78—77800
boson operators, transform. between normal and antinormal expansions 79—97295
boson scattering, variational method 79—255
boson-fermion interacting system, coherent states on Lie groups and evolution operator 78—36932
boson-fermion system, semiclassical anal. approach 80—27401
bosonization in positive definite Hilbert space 78—49974
bound state of three identical bosons, pair-pot. in two-dimens. 79—58632
bound states, pulsating soliton solns. *(Russian)* 77—74267
bound states near limit of lower continuum 77—49885
canonical formalism, tensor product composition of algebras 77—71177
charged Bose condensates in supercritical external fields, relativistic field theory 78—8766
charged Bose gas, ground state energy *(Russian)* 77—26240
charged Bose gas, optimal BDJ-type ground state props. 78—54295
charged Bose gas at high density, momentum distrib. 80—31665
charged Bose gas in uniform mag. field, zero-temp. dielec. response 77—5758
charged boson interactions in random potential, extended states 80—86202
charged boson system, long range order, extended boson matter density matrices 80—22731
classical equipartition theory nonvalidity 80—139
cluster expansion formalism, independ. pair correlations 78—73922
coherent states in quantum field theory and statistical mechanics 77—17911
collective motion in many boson system, collective coords. theory 77—57277
collective variable approach to many-boson high-density systems 77—49676
condensate, dynamic eqn. functional formulation, many body theory 80—84334
condensates and Bose-Einstein correlations, quantum optics formalism 79—59028
condensation, finite geometry, condensate fraction growth and spatial correls. 77—22489
condensation, momentum, correlation function 80—46966
condensation, polar modes with elastic restoring forces, metastable ferroelec. state 77—81464
condensation, solvable quantum field theoretic model 77—57447
condensed, canonical ensemble approach 78—89400
condensed, crit. behaviour, renormalisation group approach 78—41231
condensed Bose fluid, chaotic phenomena and statistical physics, review of the contributions made by J. Schwinger 79—63135
condensed Bose system, roton spectrum 79—63133
condensed Boson hard-sphere system, Jastrow wave function 78—84018
condensed phase of the imperfect Bose gas 80—86201
condensed systems, functional integrals exact formulation 80—4638
continuous boson system, entropy density of quasifree states 79—142
core-hole processes, electronic Hamiltonian, many-body theory 80—91443
correlation function, variational calcs., hard-sphere, Coulomb, ^{4}He, nucl. Yukawa fluids 77—76638

boson systems continued
cosmic coherent avalanche catastrophies, gamma-freq. graviton radiation 78—85844
created boson multiplicity distribs., method of combinants 78—81917
critical exponent, η and z to second order in $\varepsilon=2-d$ at $T=0$ 80—77696
crystal, ground-state lattice vacancies and Bose-Einstein condensation 77—7943
damping superoperator eigenvalue problem, direct soln. for boson field 80—57180
degenerate Bose fluid, Lee and Yang formulation extension 78—45563
degenerate Bose fluid, very low temps., equilib. props. 78—45564
degenerate Bose systems, condensate theory versus pairing theory 79—67224
degenerated, superfluid ground state theory 77—20141
dense hard sphere Bose liquid, vel. of sound 79—69308
density and current correlation functions *(Japanese)* 79—54046
density matrix, coherent-state basis 78—21060
density matrix of impenetrable Bose gas, Painleve-type eqn. 80—62576
density of states of the Tomonaga-Luttinger model 80—57182
density operator function space, boson fluid, uniform many particle system description 80—73260
Dicke model with classical spins, phase operator and phase transition 77—82448
diffusion equation for semiclassical bosons and fermions 79—40446
dilute hard-sphere Bose-gas model, low-density atomic H gas property-calc. 80—87194
dynamical plane rotator model, dynamical correl. functions in mol. field approx. 80—88758
dyonium model, space reflection operator and boson fermion puzzle 79—36118
Dyson-Lenard lower energy bound for boson matter, proofs, two-point correl. function 77—22488
eigenvalue spectra widths, symmetry, Wigner coeffs. 80—18213
electron gas, proton, electron liq. in collective description 80—10895
elementary excitation spectrum of a strongly coupled charged Bose gas 79—58631
elementary-excitation dispersion relation, He-like excitations 77—31816
energy spectrum determ. from thermodynamic functions *(Russian)* 79—35631
equilibrium states, wavepocket representation 79—75451
Euclidean fermion-boson systems on lattice, appl. to field theory 78—45559
Euler-Lagrange equations and hypernetted chain calculations of boson matter 79—40871
even-even nuclei with $A\approx 150$, excited states calculation, phenomenological models: band-mixing, vibrational-rotational and interacting-boson model 80—22653
excitation interactions, Bogoliubov-Zubarev formalism 77—43401
excitation spectrum of system of interacting bosons 78—71897
exciton superfluid, Bose condensation, DLRO and ODLRO 77—43515
excitonic molecule, Bose condensation, optical response 77—43512
excitons, Bose condensed long range order, superfluidity 77—43514
Fermi-Bose similarity, parafermi and parabose algebras 77—30091
ferromagnets, crit. temp. region, transform. to antiferromag. phase 77—51911
Feshbach-Villars transformation, bosons, fermions 77—87647
FHNC equations, derivation 79—54048
finite Bose system, condensate fraction growth, boundary condition effects 77—74318
fluid, pairing function, cluster anal. 79—4441
fluid, Wigner representation, Fourier transform., replacement by series *(French)* 79—9181
fluid surface density variation, Bose hard-sphere fluid model 77—20163
Fokker-Planck equation, generalised for three interacting fields 79—3663
Fokker-Planck equation, generalised for three interacting fields 79—3664
free boson gas in weak external pot. 80—86203
Frenkel exciton spectrum under the condition of Bose condensation 79—56133
generator coordinate method and the theory of metals 79—28299
Goldstone systems, effective medium theory 80—19890
gravitational gas, one dimens., ground state energy 77—5757
Green function for Bose liq. near lambda point 77—87689
ground state, mean energy, binary distrib. function calc. 79—40456
ground state energies of N-boson systems, upper band formula 79—58629
ground state energy, coherent-state representation, high density limit 77—37813
ground state of interacting boson system 79—58630
Hamiltonian approx., with Bose-Fermi and Fermi-Fermi cross interactions 79—85062
hard disc Bose gas, ground state energy 78—95196
hard disc Bose gas, integral solns. 79—44856
hard sphere Bose gas, low temp., distrib. function calc. 78—136
hard-spheres, analytical treatment of hypernetted-chain and Percus-Yevick eqns. 79—30359
Hartree approx., time dependent, 1-D system of bosons with attractive δ-function interactions 78—16728
Hartree approximation, time-dependent, 1-D boson system with δ-function interactions 79—9184
Heisenberg eqns. on C^* algebra of quasilocal observables, boson and fermion systems 78—57854
Heisenberg-Ising chain, bosonisation, spin wave vel. calc. 80—54905
helicity modulus at low temperatures 78—70052
helicity modulus for ideal Bose fluid 77—71267
high density Bose model, Bogolubov approx. as spectral density method 2nd order approx. 80—8901
high density Bose model, low temp. thermodynamic props. 79—80502
high-density Bose model, validity of Bogoliubov approx. 79—30355
hole recoil, vibrational shake-up and photoelectron lineshapes, in mols. and solids 80—55265
hydrodynamic equations in external fields 80—36944
hydrodynamics, description of rot. flow 77—49675
hypernetted chain generalised eqn. optimal solns. 80—75396
hypernetted chain var. calc. 77—64997
ideal Bose gas, approach to equilibrium 77—41553
ideal Bose-Einstein gas, review 77—87692
impenetrable bose gas, density matrix, fifth Painleve transcendent 80—77701
imperfect Bose gas, quasiparticle sound velocity, temp. depend. 78—51761
imperfect gas, condensed state, limit Gibbs state 80—52124

boson systems continued
impulse approx. inadequacy for hard core potl. 77—15646
integrals of motion for δ-function interaction pot. *(Russian)* 78—21069
interacting, microscopic theory, ground state and excitation energies, second-order corrections 77—2607
interacting, sp. ht. at low temps. 77—15651
interacting Bose fluid, renormalisation group approach 78—45562
interacting Bose gas, T=0K, self-consistent description 80—80015
interacting Bose system, off-diagonal long-range behaviour 77—37816
interacting boson problem, appl. to diffusion constant of Brownian particles 79—164
interacting bosons, second and third virial coeffs. calc. 77—26264
interacting bosons, statistical mechanics, temp. depend. energy levels 77—59163
interacting gas, approx. equilib. states 80—46962
interacting many boson system, self consistent theory without anomalous propagators 77—33942
invariants, exact and approx. 79—85063
IR divergence in field theory of Bose system with condensate *(Russian)* 79—2944
irreducible cluster expansion for the logarithm of the s-particle density matrix of a many-boson system 79—21657
Jahn-Teller systems as displaced para-Bose oscillators 80—77695
Jastrow theory, momentum distrib. of boson and fermion systems 78—45561
Jastrow wavefunction, hypernetted chain method applied to Fermi and Bose systems 80—17866
Josephson junctions, inelastic tunnelling, pair-quasiparticle interference current 80—84566
K-flows quasi-free reversible, generalised 78—54297
Kirkwood-Salzburg integral eqn. solns. for boson and fermion systems *(Ukrainian)* 79—93036
lattice, soln. of Bloch eqn. for many-particle lattice systems 77—12078
lattice sums, Poisson's summation formula, Walfisz's formula, ideal boson system 80—8903
Lie group Sp(8,R), Lorentz subgroup anal. and null plane boson realisation 78—62116
liquid-gas transition, zero temp. 77—39710
low-dimensional systems, infrared problems and phase transitions of continuous order 78—6286
magnetised Bose gas, confinement effects 79—54050
magnetised ideal gas, effect of confinement, anal. 80—12987
magnetism, Bose operator expansions of tensor operators 77—63061
magnon gas of Heisenberg ferromag., transport eqn. 77—12112
many boson non-relativistic systems, classical field limit of scatt. theory 79—80501
many boson system, excitation modes and interactions 79—71362
many boson systems, excitation modds and interactions 79—71361
many boson systems, representation of coherent states 79—30363
many particle, radial distribution function, functional derivative 78—137
many-body problem, two-dimens., for low-density hard-disc Bose gas 78—95195
many-body scattering processes in one-dimens. boson system, nonrelativistic $|\phi|^4$ theory 77—30093
many-boson absorption, nonreson. maximum 78—8343
many-boson model, spontaneous symmetry breakdown and restoration 80—52123
massless boson collision theory in local field theory 77—18155
momentum distrib., binary cluster term evaluation, 3D Lennard Jones gas, 1D hard rod gas 77—37808
multicomponent, transport coeffs., crit. behaviour, kinetic theory 77—2611
multimode quadratic expression in boson operators, ordering or exponential 77—45728
multiparticle system interacting with boson field, calc. of quasimeans 77—13695
N-body generalised entropy, time derivatives calcs. 77—5781
N-level systems in contact with singular Bose reservoir 77—22487
N-particle distrib. functions, space- and time-depend., possible appl. to black holes 77—26237
negative bosons interacting with positive particles via Coulomb forces, $N^{5/3}$ law 79—44792
nonideal Bose gas, calc. of correlation functions by method of collective variables 77—30098
nonlinear Bose systems, Dyson-Wick expansions 78—73921
nonrelativistic many boson systems, scatt. theory, classical field limit 79—49103
normal forms for classical and boson systems annihilation and creation operator, linear canonical transformations 80—22275
normal quantum fluid, kinetic theory, transport props. 78—77799
nuclear many body problem, boson-fermion descript. *(Chinese)* 78—82297
nuclear shell-model basis of interacting boson model, correspondence between fermion and boson states and operators 80—52593
nuclei, deformed even-even, boson expansions for vibr. anharmonicities 78—527
one dimensional continuous quantum systems, limit Gibbs state 78—93599
one particle distributions, entropy bounds 80—62607
one particle reduced density matrix, one-dimens. impenetrable bosons, zero temp. 79—17336
one particle reduced density matrix of impenetrable bosons in one dimension at zero temperature 80—17863
one-dimensional many boson system, ground-state props., SCF approx. 78—49761
Ornstein-Uhlenbeck process, devrivation from fluctuation quanta model, boson fields 80—12988
$P(\phi)_2$ Euclidean field theory, boundary conditions rel. to ferromagnetic spin systems 77—54036
pairing equations for bosons in one-dimensional model, exact soln. 77—17904
para-Bose algebra representations using single Bose field 79—49157
para-Bose coherent states 79—96
para-Bose operator, explicit representations 79—85064
para-Bose operators, simplified description 80—86200
paramagnet and ferromagnet, multibeam spin wave representation 79—4664
Peierls phase transition, in one-dimens. conductor 79—60806
phase transition in an exactly solvable nonpolynomial model 79—40455
phase transition kinetics, ideal and weakly interacting systems 77—35775

boson systems continued
phase transitions, sp. ht. and excitons in system with anisotropic dispersion laws *(Russian)* 77—4229
photon Bose condensation theory in nonequilib. systems, semiconductor laser analogy 80—23689
pion gas, relativistic, kinetic props., non-equilib. statistical operator method 79—30718
pion gas, thermodynamical functions 77—64995
pion relativistic quantum gas, crit. temps., Bose-Einstein clustering 77—54084
plane rotator model, Hamiltonian and mol. dynamics 80—52122
polarons, energy eigenvalue, systematic calculation procedure 80—84439
polymer expansion for quantum many-body problem 80—57181
potentials, attractive discreteness of ground state 80—46957
quadratic boson Hamiltonian, diagonalisation 78—93600
quadratic Hamiltonian diagonalisation 80—82719
quantised rotator, classical correspondence of Schwinger boson representation 79—9492
quantum crystal, soln. of Fermi-Bose quasiparticle 79—28173
quantum crystals, appl. of method of quasiaverages 80—10737
quantum crystals, approx. second quantisation method 79—23804
quantum magnetic hamiltonians with remarkable spectral properties 80—82717
quantum spin systems, exact boson representation and crit. behaviour 79—78423
quantum theory, boson expansion method, appls. 78—36884
quantum thermodynamical system in one space dimension, high-order perturbation expansion 80—4636
quantum vortices, dynamics 80—59758
quark liberation in (1+1)-dimensions 79—324
quasi-one-dimensional electron gas with strong on site interactions 77—4306
quasi-particles in lattice system *(Russian)* 79—75462
radiation field in flat parallelepiped, ideal photon gas eigenvalue spectrum 78—8344
rare-earth, mag. supercond., appl. of boson theory to mixed state 80—7050
relativistic charged Bose gas, excitation spectrum 79—17334
relativistic Fermi-Bose system quantisation, by compensated functional method *(Russian)* 80—42142
relativistic quantum ideal gas of massive particles, eqns. of state 79—2721
renormalisation group transformation, scaling equation of state for boson system 78—12643
restricted geometry, coherent states, suppression of Bose-Einstein condensation 79—46854
return to equilibrium states 78—29044
rigorous second-order cumulant expansion 79—44853
S-matrix, probability struct. in Euclidean domain 79—89071
S-matrix for interacting extended boson fields, scatt. amplitude, self energy 78—66047
Schwinger boson representation, quantised rotator 80—18164
Schwinger boson representation for the quantized rotator 78—93602
Schwinger representation of SU(2), coupling of ang. momenta 78—41196
second quantisation, in weak external EM field, as one-particle problem 78—12462
Segal-Weinless approach to linear Bose fields, uniqueness result 80—98
self-interacting boson field, interaction with classical current, S-matrix elements 79—21963
series expansion; spin 1/2 operators, coeffs. 79—30358
single particle aspects in collective formalism 77—2608
single particle occupation probability and one body density matrix, of quantum fluids 77—4233
SO(2N+1) algebra, time-dependent Hartree-Bogoliubov theory, quantisation 80—62575
spatial Bose-Einstein condensation, teaching examples 79—71176
spatial correlations and elementary excitations in many-body systems 80—22730
spectral distrib. method for approximated level densities, validity in boson space 79—462
spectral distribution method in space of M-bosons 77—49673
spin glass, marginal fluctuations 80—2586
spin operators, arbitrary, coeffs. in Boson series expansions 79—80507
spin operators, general spin values, multi-boson expansion coeffs. 80—42141
spin-1 system, lattice of verifiable propositions 77—45789
spin-phonon system, transition to self-trapping 80—10606
spurion boson model in solvable regularised quantum field theory 77—54047
stability and stratification of quantum liq. mixture 80—59754
stability properties of equilibrium states, free Bose gas 78—8368
statistical bootstrap model, hadronic mass spectrum, pion condensation, boson gas 78—70345
statistical mechanics of bosons with attractive interaction 79—12717
strong coupling asymptotic behaviour for solvable field theory 77—54048
strongly coupled charged Bose gas, ground state energy calcs. 79—6050
structure factor and sound vel., first and second sound 78—34668
structure factors, static and dynamic, quantum conserving approx., normal ^{4}He liq. appl. 79—51321
superconducting systems, electrodynamics and quantum theory 80—60134
superconductivity, complete Lagrangian formulation 77—89897
superconductivity and elementary particles theory, review 80—4911
superconductor, type II, cubic, flux-line lattice anisotropy, boson method calc. 80—2536
superfluid, hydrodynamical action functional *(Russian)* 77—47639
superfluid, pot. depend. of pairing soln. 79—55977
superfluid as a source of all interactions 79—21620
superfluid Bose liquid, hydrodynamics allowing for dissipative processes 79—23796
superfluid flow rel. to local gauge invariance 80—54450
superfluid system, LF asymptotics of self energy parts at T=O *(Russian)* 79—95230
superfluid viscous liq., hydrodynamics and transport coeffs. 77—69134
superfluidity, model Hamiltonian 80—44377
superfluidity of two weakly interacting Bose gases at finite temp. 79—19411
superspace with Fermi and Bose coords., appl. to graded Lie bundles and supergravity 77—26143
three identical bosons, props. in low energy range *(Russian)* 78—36933

boson systems continued
three-particle structure function, convolution approx. for ground state 78—26746
time depend. Hartree eqn. quantisation, boson expansion, particle hole excitations 79—13230
time dependent Hartree eqn. quantisation, finite and infinite boson expansions 79—13231
time evolution of Bose system passing through crit. point 77—37815
trimer ground states, quantum exchange effects 78—1117
two-body density matrix of Bose fluids 79—40875
two-dimensional charged Bose gas in zero mag. field, dielec. response, RPA 80—142
two-dimensional gas, energy spectrum and specific heat 77—15656
two-dimensional nonideal Bose gas, ground state, theory 78—93601
two-dimensional quantum systems at zero temp., liquid to gas phase transitions 78—77798
vacuum spontaneously broken symmetry of Higgs field and Bose condensation 80—82912
vortices in infinite free Bose systems in condensation region 80—73259
wave mechanical representation of one-dimens. Bose-like oscillator, Wigner commutation relations 78—36872
weakly coupled non equilibrium systems, time asymptotics and reversibility 79—54049
Weyl, normal, and antinormal ordered forms of exponential of quadratic in boson operators 77—45727
Weyl quantization of classical spin systems quantum spins and Fermi systems 80—31585
Yukawa Bose fluids, Jastrow wave function, Monte Carlo computation 79—73375
Yukawa potential-ground state boson interaction, Monte Carlo study 78—51768
π condensation, vacuum instability in external fields 78—50114
H, Bose condensed spin-aligned, superfluid, elementary excitations 77—72729
H, condensed, spin-aligned, props. from variational calcs. 80—4637
H, spin-aligned, ground state and elementary excitations 79—54047
H, spin-aligned Bose gas, Born-Oppenheimer approximation 80—46958
H, spin-polarised, Bose condensation, phenomenological description 80—77699
H, spin-polarised, Bose-Einstein condensation 80—77698
H_2, electron correlation, dynamic description using boson Hamiltonian 79—26897
^{3}He, superfluid, Bose spectra stability, phonon branches, dispersion coeff. *(Russian)* 80—49452
^{3}He superfluid, Bose spectrum nonphonon branches *(Russian)* 80—92750
^{4}He atomic Bose system, equilibrium superradiance 78—55994
π phase transition and multiplicity distrib. in Feynman gas model with Bose statistics *(Russian)* 78—89683

bosons
see also alpha particles; boson systems; deuterons; gravitons; intermediate bosons; meson resonances; mesons; photons
axions, possible evidence from existing expts. 79—436
Bogolyubov-boson transform., coherent states 78—32715
conformal relativity, classification of metric bosons 78—93803
extended objects from Goldstone bosons in relativistic quantum field theory 79—285
fermion field operators for constructing boson field operators 80—27416
leptoquark bosons, confinement in SU_4 theory 79—45052
monopole boson, pairing rotations and quadrupole modes in transitional nuclei 80—18165
$O(5)\supset O(3)\times O(3)$, basis states using modified boson operators 78—4554
pseudoscalar boson arising from colour gauge theory of strong interactions 78—37153
pseudoscalar bosons rule in astrophysics *(French)* 79—44361
QED of charged bosons in Lorentz gauge 77—49884
quantum field theory, fermion-boson correspondence, spinor field quantisation 78—8496
quantum soliton and classical soliton 80—12986
Regge trajectories, asymptotic behaviour *(Russian)* 77—38103
sine-Gordon model, boson-soliton scatt. amplitudes 80—9109
sound information quantum, in quantum mechnical treatment of structural information theory 77—14822
spinor Bethe Salpeter and Goldstein eqns., fermion-boson coupling, numerical soln. 78—86400
strong external fields, fermion and boson interactions 78—49987
three-boson stimulated scatt., quantum mechanics *(Russian)* 78—78115
unification of fermions and bosons, interacting model 79—21629
unification of fermions and bosons, math. structures and phys. questions 79—21630
unification of fermions and bosons, physical foundations of local (algebraic) approach 79—21628
vector boson elast. scatt., Lorentz covariant scatt. amplitude and Compton scatt. 77—2776
Young's double beam interference experiment with spinor and vector waves 78—89363
χ, suggested J^P values, is $\chi(3505)$ a vector boson? 78—62473
$\mu \rightarrow \bar{\nu}_\mu x^+$, hypothetical, search for scalar charged boson, apparatus and theoretical aspects 78—58177
NN interaction,, neutral scalar, pseudoscalar and neutral vector boson radiative corrections, explicit formulae 78—70372
X, $\bar{X}$ bosons evaporation by black holes, rel. to primordial baryon generation 80—98750

boundaries *see boundary layers; boundary value problems; grain boundaries; metal-insulator boundaries; semiconductor-insulator boundaries; semiconductor-metal boundaries*

boundary layer flow *see boundary layers*

boundary layer turbulence
see also atmospheric boundary layer
α-effect turbulent dynamo, consistency 79—72954
ablating plane (axisymmetric) body, turbulent boundary layer with neg. press. gradient 78—79389
abruptly rotated cylinder, turbulent boundary layers, numerical anal. 80—43716
accelerated flow, at permeable graphite burning surface, turbulent heat/mass transfer 78—38417
accelerated fully rough turbulent boundary layer, stability conditions 77—84240
acoustic liner, interaction 79—81857

boundary layer turbulence continued
acoustic noise aerodynamically generated, refl. at solid boundary, boundary layer turbulence *(French)* 80—43694
acoustic orifice under turbulent boundary layer 77—23838
adiabatic layer with nonunity Prandtl number, vel.-temp. rels. 77—62241
aerodynamic drag on heated spheres and cylinders, effective Reynolds no 77—89090
aerodynamic effects 78—1680
aerodynamically heated body, stable shape during ablation *(Russian)* 78—75162
aerofoil, stall props. meas. with acoustic flow control 80—23991
aeronautics, infinite swept attachment line boundary layer, turbulence 80—74840
aerosol deposition on plate in turbulent flow 78—87380
aft-loaded airfoil, boundary layer displacement effect and wake near trailing edge 78—22366
agitated vessel, flow behaviour and transport phenomena, correlation eqns. *(Japanese)* 78—38300
air, compressible, approx. local anal. 77—75895
air, turbulent flow in circular pipe, temp., velocity profiles, heat transfer, flow resist. 79—55370
air and combustion products *(Russian)* 78—5732
air entrainment at solid/liquid/gas interface 77—1276
air flow, with slot-injected He, vel. profiles, mass fractions and densities meas. 77—42808
air flow above water waves, numerical model 77—81912
air flow in vertical annular channel with rot. inner cylinder, heat transfer 77—58679
air flow over heated tank of liquid *(Russian)* 77—68577
air flow over rearward facing step, flow separation meas. 80—69885
air in heated channel, turbulent flow, velocity and temp. pulsation characteristics 80—14820
air scoops at supersonic and hypersonic vels., throttling, separation and central body cooling 80—14739
air turbulent flow in heated channel, effect of gravitational field 80—64533
air wall-jet immersed in uniform flow, aerodynamic forces on circular cylinder 77—62287
air-H_2O turbulent-turbulent stratified flow in circular tube 79—90307
air-water film flow, transport phenomena, wary interface motion 77—35213
air-water interface, turbulent heat and mass transfer 79—68551
aircraft interiors, turbulent boundary layer noise 77—11087
airflow above waves, numerical simulation *(Russian)* 80—4076
airflow in pipe at low Reynolds numbers, effect of flow laminarisation on heat transfer 77—23942
airfoil, leading-edge separation bubbles, shear layer and transitional reattaching flow 77—27580
airfoil, wave drag in transonic flow, shear interferometry obs. 79—77165
annular diffusers, straight core, flow and boundary layer development, finite difference and marching integration 80—53760
annular pipe, heat transfer for turbulent flow of liq. with const. thermophysical props. 78—1657
annular turbulent flow with rot. core tube, numerical predictions 77—55010
annulus, turbulent flow, experimental study *(Italian)* 79—81977
anodic dissolution of metal turbulent stream of electrolyte, laws *(Russian)* 79—39156
aortic stenosis, turbulent wall press. meas. in exptl. model 78—3538
approximation errors for boundary layer equations *(German)* 79—86416
arc in channel bearing turbulent gas flow, arc parameters calc. 80—6298
aromatic hydrocarbons, heat transfer to ascending (descending) streams, near-crit. press. 77—65742
atmoshere, eddy momentum fluxes within maize canopy 77—91203
atmosphere, above ocean waves, scaling laws for optically relevant turbulent parameter C_T^2 78—85677
atmosphere, acoustic sounder for remote probing 77—17243
atmosphere, acoustic sounder return interpretation 77—37417
atmosphere, air pollution statistical anal. rel. to meteorological conditions 77—37379
atmosphere, and air-sea interactions 78—92953
atmosphere, around Rock of Gibraltar, wind tunnel simulation 78—28284
atmosphere, book contrib. 77—60459
atmosphere, buoyantly interactive boundary layer with entrainment, similarity theory 77—49116
atmosphere, canopy flow, higher order closure model 78—44944
atmosphere, convective boundary layer turbulence struct. 77—49117
atmosphere, cotton canopy aerodynamic features 77—45105
atmosphere, daytime, turbulent energy budget parameterisation 77—56674
atmosphere, diffusion modelling, Gaussian plume and spectral solns. 78—24328
atmosphere, dissipation effects on parallel shear instability near ground 78—69406
atmosphere, drag coeff. rel. to intermittent convection 78—44898
atmosphere, dynamic modelling *(Russian)* 77—13097
atmosphere, effect of coherent structures on temp. struct. functions 77—64361
atmosphere, energetics of entrainment across density interface 77—5283
atmosphere, flow over wavy boundary, water waves 77—73792
atmosphere, fluxes and turbulence, in unstable surface layer over land 77—66962
atmosphere, heat and humidity exchange laws, model approach 77—66948
atmosphere, horizontal vel. spectra in unstable surface layer 78—73427
atmosphere, horizontal wind coherence statistics 77—91201
atmosphere, hot-wire meas. of wind and temp. on S.W. Kansas, Denmark 77—9458
atmosphere, influence of built-up area on turbulence in lower boundary layer *(Russian)* 78—44925
atmosphere, Kolmogorov-von Karman relationship generalisation 77—78299
atmosphere, Lagrange characts. of turbulent diffusion 77—33131
atmosphere, maize canopy, turbulent transport 77—33129
atmosphere, marine turbulent boundary layers disturbance by wind waves, dynamical eqns. *(Russian)* 78—44840
atmosphere, meas. using computerised instrumentation system 77—56761
atmosphere, micrometeorological statistical tests 78—3866
atmosphere, mixed layer depth model based on turbulent energetics 77—5284

boundary layer turbulence continued
atmosphere, mixed layer diffusion, use of Taylor's translation hypothesis 77—17193
atmosphere, model scale factor in wind tunnel simulations 78—28285
atmosphere, modified flow propag. downstream from surface roughness change 77—17200
atmosphere, moist layer struct. with higher order turbulence closure model 77—78310
atmosphere, momentum and heat flux profile relations above tall vegetation 78—49115
atmosphere, momentum flux-angle distrib. from propeller anemometer meas. 77—17190
atmosphere, momentum transfer during abrupt laminar-turbulent transition 78—65365
atmosphere, multi-component linear digital simulation 78—61513
atmosphere, neutral wind profile following surface roughness change, calc. 78—73483
atmosphere, numerical modelling 79—84396
atmosphere, pollutant dispersion in horizontally-homogeneous boundary layer 78—36263
atmosphere, pollutants turbulent diffusion in Ekman boundary layer 77—73783
atmosphere, Reynolds shear stress and heat flux fluctuations over rough surface 78—44902
atmosphere, shear instability in airflow near ground 77—87004
atmosphere, small-scale struct., airborne hot-film meas. during GATE 77—29373
atmosphere, SO_2 turbulent diffusion above and within forest 77—45055
atmosphere, stratified baroclinic, method for determ. coeffs. of horizontal turbulent diffusion 78—32135
atmosphere, stratified surface layer, turbulence and diffusion, basic Lagrange characts. 78—81270
atmosphere, surface layer, producing wavefront random deform., statistical anal. *(French)* 77—87074
atmosphere, surface layer parametrisation, turbulence covariances 77—70758
atmosphere, surface turbulent fluxes modelling in stable conditions 78—61482
atmosphere, Taylor's hypothesis and high-frequency turbulence spectra 77—87005
atmosphere, temp. diurnal vars. in surface layer *(Russian)* 77—13100
atmosphere, thermal plumes and turbulence spectra 77—73793
atmosphere, three dimensional turbulent flow anal. 78—69395
atmosphere, three vel. component modelling 78—28252
atmosphere, turbulence and internal waves spectra in stably stratified boundary layer *(Russian)* 78—81297
atmosphere, turbulence characts. near neutral stability 77—29369
atmosphere, turbulence energy modulation by longit. rolls 77—2202
atmosphere, turbulent and radiative transport interaction in development of fog and low-level stratus 78—81313
atmosphere, turbulent convection in nondiffusional approx. *(Russian)* 77—73803
atmosphere, turbulent diffusion in surface layer 77—66950
atmosphere, turbulent diffusion of pollutants 77—41113
atmosphere, turbulent interface layers theory 78—71323
atmosphere, turbulent vel. components in surface layer under convective conditions 77—78297
atmosphere, vel. struct. functions and energy dissipation rates, acoustic Doppler meas. 77—66966
atmosphere, vertical turbulent exchange in surface layer, nonlocal parameterization 78—3902
atmosphere, wind speed and turbulence characts. near ground over escarpments 78—44897
atmosphere and ocean boundary layer similarity rel. to turbulent transport 77—17131
atmosphere boundary layer, turbulent flow under influence of strong wind, engineering model *(Russian)* 77—5280
atmosphere surface layer, calc. of mean velocity and temp. profiles *(Russian)* 80—8415
atmosphere-ocean, penetrative convection regime, entrainment rate *(Russian)* 78—69401
atmosphere-ocean layer, meas. distortion caused by rolling ship 78—3805
atmospheric turbulence characts. determ. method 78—7815
attached supersonic turbulent boundary-layer/flap interaction pressures, correlation technique 80—48683
auto-correlation measurements and integral time scales in three-dimensional turbulent boundary layers 80—33570
averaged velocity field from universal power law *(Russian)* 80—79276
axial compressor with unshrouded blades, cald. method 79—98702
axial flow compressor stator blade, anal. by ensemble-averaging technique 79—4002
axial flow under pressure gradient, turbulent boundary layer on rot. cylinder 77—62256
axial turbomachine, cascade and through-flow theories as inner and outer expansions 78—75148
axisymmetric, weak and strong disturbances effect on skin friction, mean. vel. and shear stress 78—90857
axisymmetric afterbodies, separated turbulent flows, wakes, exhaust plume effects 80—74885
axisymmetric bluff body flows, near wake props. 77—58694
axisymmetric body, pot. flow/boundary layer interaction models 80—1546
axisymmetric body, skin friction, injection, surface roughness 78—9630
axisymmetric cylinder-flare body, turbulent boundary layer response to lateral divergence 79—90236
axisymmetric field flow around obstacle, effect on heat transfer *(Russian)* 78—83385
axisymmetric slow viscous flow past a symmetric tumbler-shaped body *(Korean)* 79—23308
axisymmetric supersonic turbulent base pressures 78—94764
axisymmetric transonic turbulent base pressures 80—19425
axisymmetric turbulent boundary layers, low-freq. pressure fluctuations 80—59014
axisymmetric turbulent boundary-layer flow, noise generation 77—47001
balance eqns. in unstable atmos. boundary layer 77—73787
base pressure correlation technique, turbulent supersonic flow, conical bodies 77—89146
binary mist flow, heat and mass transfer anal. *(Japanese)* 79—14467
bluff bodies immersed in turbulent boundary layers, flow patterns, press. forces acting on inclined plates 77—58662
bluff bodies in rough wall layers 78—46953

boundary layer turbulence continued
bluff body, laminar incompressible flow, separation, reattachment, eddies, drag 79—59964
bluff body, turbulence scale rel. to mean drag 77—27518
bluff body, two-dimens., mean vel. profile characts. 79—37301
blunt flat plates, air flow, 2-D, thermal boundary layer characteristics, nose shape effects 80—92121
blunt nosed body, arbitrary shape, surface heat transfer and curvature effects, numerical soln. 79—1173
blunt-based axisymmetric body, subsonic turbulent near-wake 78—94740
blunt-body boundary layers, three dimensional, surface curvature effects 80—1520
body force effect on turbulent transport near surface 78—26116
body of revolution, flow interaction near tail, iterative procedure 77—35128
body of revolution, iterative soln. for flow within and exterior to boundary layer and wake 77—35129
body of revolution, low-drag, thick axisymmetric turbulent boundary layer and near wake 80—19352
body of revolution, turbulent wake and asymm. hydrodynamics 77—89127
body of rotation in supersonic turbulent flow, base press. 79—86455
boiling crisis at concentric (eccentric) annuli with turbulence promoters 78—55639
boiling crisis in swirled flow of water in pipes 79—90241
boiling of liquid at finned wall, heat transfer simulation 77—42817
boundary layer shear stress distribution calc. 79—98701
boundary layer transition, two-equation model, mean velocity profiles *(French)* 77—65736
bubbly flow, wall press. fluctuations in turbulent boundary layer 77—58776
buoyancy and extra strain effects, mathematical modelling 78—94674
buoyancy effects in a wind tunnel simulation of the atmospheric boundary layer 79—68687
buoyancy effects in entraining turbulent boundary layers: a second-order closure study 80—21815
buoyant plumes behaviour on release at ground level, lab. wind tunnel obs. 80—30624
buoyant surface jet, entrainment intermittancy props. at stratified interface *(Japanese)* 79—81940
burst cycle and drag reduction 77—15003
bursting, spanwise struct. obs., in turbulent channel wall region 78—90855
bursting phenomenon in open channel flow, space-time correlations structure *(Japanese)* 80—96311
bursting phenomenon near the wall in open-channel flows and its simple mathematical model *(Japanese)* 79—81974
bursts in turbulent shear flow 77—11178
BWR, air clearing in H_2O-type press. suppression systems, scaling laws 79—54563
BWR, air clearing in H_2O-type press. suppression systems, scaling laws 79—54564
calculation, on spinning and curved surfaces 77—65737
calculation methods, book contrib. 77—58655
cascaded blade surface, appl. turbulent boundary layer with suction or injection 77—31377
cascaded blades with injection or suction, boundary layer theory and cascade tests 79—18878
catalyst granular bed, static, flow transfer processes 80—45554
cavitation onset on cylinder, effect of dil. aqueous polymer solns. 77—68645
Cebeci-Smith eddy viscosity model 79—10553
centre plane boundary in sq. duct, side walls effect 78—79311
channel, 2-dimens. rectangular, vel. profiles and fluctuations, laser Doppler anemometry 80—53864
channel, axisymmetric, with axial press. gradient injection, turbulent boundary layer characts. 79—37304
channel, corrugated wall 77—80157
channel, nonequilib. merged boundary layer 78—5734
channel, temp. field 79—4005
channel, two-dimens., turbulent flow with separation 80—19356
channel, with stepwise change in wall roughness, relax. processes 78—90861
channel and pipe flow, turbulence calcs. *(Russian)* 80—6152
channel bottom, kinematic characts. of nonuniform flow, limiting stability, erosion 80—94547
channel flow, mixing length from max. stability principle 80—53859
channel flow, smooth-rough surface discontinuity with zero press. gradient 77—51121
channel flow, turbulent vel., press., and temp. fields, direct numerical simulation 80—19361
channel flow, velocity and eddy viscosity distribs. for turbulent shear flow 77—89104
channel flow, velocity correl. function truncation *(Russian)* 78—75124
channel flow transport, inequalities, variational principles 79—60063
channel flow with temperature-dependent viscosity and internal viscous dissipation 79—94721
channel flows, severe nonsymmetric constriction, curving or cornering, separation 80—92222
channel liquid flows, nonsteady convective heat transfer 80—59023
channel with one moving wall, turbulent flows near steps 77—68693
channel with parallel walls, turbulence studies 80—38493
channels, constricted or dilated, pulsatile flow at high Reynolds number 80—74985
characterisation by velocity and temperature profiles *(Russian)* 78—34115
characteristics induced by two-dimens. bluff bodies 80—64525
circular cylinder, local heat transfer by turbulence of free-stream flow of viscous liquid, theoretical determ. of influence *(Russian)* 80—96252
circular cylinder flows, coherence function method 80—96068
circular cylinder near wake in turbulent crossflow, expt. techniques 80—14705
circular cylinders, surface-roughness effects on mean flow, turbulent boundary layers 80—92128
circular impinging jet, heat transfer characts., stagnation point, boundary layers 80—79303
clay aqueous suspension turbulent flow, average velocity profile and functional loss in pipe 80—48778
closure models comparison 77—84236
coaxial cyclone flow, heat transfer from a cylinder 80—48698

boundary layer turbulence continued
- cocurrent flow, jet initial zone, boundary mixing layer turbulisation, fluctuations 80—1657
- coherent motion mechanism in turbulent shear flow wall region 78—90854
- coherent motions in outer layer, eddies 78—22337
- coherent structure meas., minicomputer appl. 80—10338
- cohesionless bottom sediments, limiting stability in turbulent channel flow, erosion 80—94546
- combined laminar and turbulent flow, over a rotating disc 77—3809
- compliant membranes, appl. of tension 77—31287
- compliant wall drag reduction 78—26193
- compressible, data compilation 78—14035
- compressible, two-point finite difference method 77—19617
- compressible flow near oscillating porous plate 77—84268
- compressible fluid, turbulent boundary layer on permeable plate 79—1169
- compressible gas with heat transfer, surface roughness 78—90931
- compressible layer, Reynolds number effects on turbulence field 80—19434
- compressible nonadiabatic gas flow in tube, eqns. system numerical integration *(Russian)* 78—83427
- compressible supersonic turbulent boundary layers, compressible press. gradient effects 79—60001
- compressible turbulent boundary layer, extended mixing length appls. 78—94655
- compressible turbulent boundary layer, improved Van Driest skin-friction formula 77—58712
- compressible turbulent boundary layer flow on insulated flat plate, anal. 77—51045
- compressible turbulent boundary layer with injection, eddy viscosity and turbulence energy methods 77—62267
- compressible turbulent shear layers, reviews, book contrib. 77—47034
- computational modelling by finite elements 79—1163
- concentration interface in turbulent mixing layer, visual growth 80—38392
- condensation in circ. tube, turbulence model, boundary layer with suction approx. *(Russian)* 79—59971
- conditional sampling, detection and data signal phase relation, turbulent boundary layer appl. 78—24772
- cone, rotating, flow and heat transfer obs., disc theories applicability 77—58673
- cones at incidence, high Reynolds no., similarity soln. 77—89103
- cones at incidence, supersonic viscous flow 80—38439
- conference, Niagara Falls, NY, USA (June 1979) 80—1542
- conical diffuser, oscillating turbulent flow characts. 77—51047
- conical flow, Pohlhausen method appl. to 3-D boundary layers 77—65746
- conical surface, boundary layer due to swirling flow with throughflow 77—47024
- contrary wall jet, interaction with supersonic flow on plate with turbulent boundary layer *(Russian)* 78—22398
- convection, integral approach 79—55390
- convection, nonlinear double-diffusive, low Prandtl number, boundary layer method 80—69816
- convection in fluid layer with internal and external heating, reactor safety anal. 79—32514
- convection in vertical boundary layer 79—32501
- convection in vertical layer 78—42599
- convective heat transfer from flat plate 77—7387
- convective turbulent heat transfer from rough surfaces 79—27638
- convergent and divergent flows, turbulent boundary layer with press. gradient, Reynolds analogy 78—83382
- cooling efficiency in flow around wall, initial turbulence effects 80—79315
- corner, right dihedral interaction between turbulent boundary layer 79—86414
- corner and junction flow, complete aircraft aerodynamics, lecture 78 -22325
- corner boundary layer, press. gradient and leading edge effects 80—14652
- corner flow at intersecting plates 77—47000
- corner interaction of boundary layer and shock wave, flow separation 80—96287
- corner separation, empirical criteria for 90° corner 78—18278
- corrugated wall, exptl. study of flow *(French)* 78—90844
- Couette flow, statistical linear algebraic model 78—47002
- critical flow separation, modified Stratford method 77—15000
- crossflow developing in boundary layer during longit. flow around right dihedral angle 80—59049
- curtain cooling, behind permeable surface section, effect of injected gas flow distrib. 78—42657
- curved duct, boundary layer collision, entry and core flow 80—74984
- curved surface, mean flow meas. in turbulent boundary layer 77—58661
- curved surfaces, turbulence meas. 78—79310
- curved surfaces, turbulent boundary layer heat transfer 80—6056
- curved wall, turbulent boundary layer detachment by perpendicular compressive thrust *(German)* 78—94661
- curved wall flow turbulence, integral method calc. *(French)* 77—54984
- curved wall with vertical compression shock, separation onset criterion *(German)* 79—14431
- curvilinear surface, integral method, velocity profiles and Stanton numbers 79—81861
- cylinder, transverse curvature and turbulence effects on axisymmetric liquid flow *(Russian)* 80—59015
- cylinder based bodies, turbulent boundary layers, three dimens., soln. method 79—1167
- cylinder disturbance 78—67188
- cylinder in cross flow, turbulence effect on heat transfer 79—1075
- cylinder in cross flow in turbulent pipe flow, heat transfer 78—90874
- cylinder in flow close to plane boundary, boundary turbulence and vortex shedding 79—32484
- cylinder in turbulent or pulsed flow, heat transfer improvement *(French)* 77—42824
- cylinder in viscous fluid, circular oscillations 79—14387
- cylinders, aerodynamic noise vs. drag relationships 79—32550
- cylinders, rot., intervening turbulent flow struct., model eqns. calc. 78 90852
- cylindrical annuli, concentric, eccentric horizontal, natural convection heat transfer 79—55382
- cylindrical heated pipe, suction effects on time derivs. of vel. fluctuations and temp. *(French)* 77—51116

boundary layer turbulence continued
- cylindrical shells containing turbulent flowing fluid, numerical anal 77—72291
- decaying vortex core, boundary layer dynamics, atmospheric appl. 79—55394
- decelerating boundary layer turbulence in the region of applicability of half-power law 79—90237
- deceleration rate parameter, algebraic prediction 77—84244
- detached flow around wing in ideal fluid, vortex sheet break-up 77—11200
- detonation wave, turbulent, boundary-layer treatment 80—106791
- developed, response to local transverse surface motion 77—35127
- developing turbulent boundary layer, in bounded flow, props. 79—46298
- development with fluctuating mainstream, integral method for calculation 79—94597
- difference method, for turbulence calc. *(Ukrainian)* 79—37303
- diffuser, conical, tangential boundary layer blowing, flow struct. and efficiency 77—47033
- diffusers, conical, injection for boundary layer control 78—90864
- diffusers, optimum press. recovery 80—1539
- diffusion 78—38305
- diffusion boundary layers, with surface reactions, laminar or turbulent regimes, thermal simulation method 77—75912
- diffusion flame in turbulent boundary layer on liq. propellant surface behind shock wave 80—53763
- diffusion of polymer additives 77—35176
- dilute polymer solns., turbulent boundary layers, turbulence simulation 79—98767
- dimensionless temperature profiles downstream from heat line source in boundary layer *(French)* 77—15008
- disc, rotating, convective mass transfer 80—43707
- disc normal to wall, turbulence intensities and local mean vels., separated flow 80—64531
- discontinuous flow struct. in wall region 78—18280
- disperse systems, coagulation, slow, turbulent 78—53259
- dispersed particles steady-state radial distrib., in turbulent vertical gas flow 78—55680
- dissipation in incompressible fluid 78—1647
- dissipation integral calculation method *(German)* 79—86418
- downstream of step change in surface temp. 79—81862
- drag of three-dimensional body in hypersonic Newtonian flow *(Russian)* 78—22369
- drag on bodies of revolution, effect of distributed boundary layer suction 77—46998
- drag reduction, compliant wall motion 78—22336
- drag reduction, diffusion of polymer soln. introduced via slit 79—68685
- drag reduction, Polyox coagulant effects on turbulent boundary layer 78—26165
- drag reduction by compliant wall, numerical simulation of turbulent boundary layer 78—26114
- drag reduction mechanism 78—26107
- drag reduction polymer molecule turbulent diffusion and degradation for boundary layer 80—1686
- drag reduction with compliant coatings, review 78—26115
- duct, annular, turbulent flow and heat transfer over backward facing step, finite difference soln. 79—1175
- duct, curved transition type, three-dimens. turbulent subsonic flow calc. 80—38498
- duct, square, developing turbulent flow 80—19351
- duct, square, developing turbulent flow computation 80—1554
- duct, variable density fluids, vel. profile axial development due to heat transfer 80—74987
- duct flow, two-dimens., large and small scale motions 80—83847
- duct flow near suction tube, turbulence intensities 80—64627
- duct with heated parallel plates, turbulent flow and heat transfer in entrance region, num. prediction 77—42830
- duct with rough walls, turbulent shear flow, stability anal. 80—38496
- ducts, 3-dimens. viscous compressible flow, inviscid flow considerations for 90° elbow 80—64639
- ducts, steady 2-dimens. axisymmetrical turbulent boundary layer, compressible fluid *(Chinese)* 80—59109
- eddy diffusivity, near open channel free surface, heat transfer expt. 78—5798
- eddy viscosity, reorientation and stretching of vortex elements 77—31289
- eddy viscosity model dynamics 77—54981
- eddy viscosity relations, three dimensions 77—84237
- elastic shells, excitation and stress field in compressible fluid 78—51183
- elastic surface, turbulent boundary layer, hydraulic drag reduction 80—33572
- electrochemical measurement of mass transfer, turbulent pipe flow 78—5830
- electrodiffusion method for turbulent boundary layers in adverse pressure gradients 80—10321
- electrolytic method of mass transfer meas., advantages and disadvantages 79—68827
- emitting-absorbing-scattering layer, radiative transfer anal. using effective absorptivity 78—5827
- end-wall boundary layer flow in vortex chamber 77—7403
- energy dissipation, preferential spectral transport by irrotational straining 80—1551
- entrainment in turbulent jets and plumes 78—94781
- entrainment mechanism 78—1649
- equilibrium, in asymptotic theory framework 78—30273
- ethyl alcohol, free fluid surface, thermo-capillary forces on transport process, turbulent gravitational heat convection 77—75920
- ethylene glycol solution, flow boiling and pool boiling critical heat flux, effect of flow passage geometry 77—62250
- expansion corner effect on shock-wave and boundary layer interactions 80—14737
- external flow, book contrib. 77—58653
- external supersonic flow, turbulent boundary layer interaction on concave corner and spherical intake 77—55032
- external turbulent shear flow 77—3817
- ferromagnetic suspensions, convective heat transfer and thermophysical props., mag. field effects 79—77264
- film condensation of vapour on rough surface, heat transfer 77—39285
- film cooling, by injection from porous section 77—51041
- film cooling, from single hole and hole row, free stream turbulence effect 79—46310
- film cooling effectiveness of tube wall, axially and radially flowing coolant 79—1186

boundary layer turbulence continued
film flow down rough surface, kinematic features *(Russian)* 80—79277
final self preserving state of disturbed large 2-dimens. shear layer 78—90851
finite amplitude wave propagation in nearly parallel flow 80—74899
finite-difference/Galerkin finite element soln. for turbulent boundary layer 78—26104
finned plate surface, convective heat transfer, vortex flow and turbulence intensity 77—72296
flame, atm. press., ion sampling aerodynamic disturbance by sampling system 77—60142
flame, atm. press., supersonic sampling, boundary layer cooling 77—60143
flame gases, effect of EHD boundary layer on heat transfer 77—80228
flame holders, two-, three-dimensional, wake struct. 80—53786
flame jet, premixed, impinging on plane surface, turbulent heat transfer 79—4054
flat bodies with blunt tail sections, subsonic flow and wake obs. 77—68616
flat plate, adiabatically densified fluid film, turbulent two-substance boundary layer *(German)* 78—90845
flat plate, with and without mass transfer, differential methods and finite-difference methods comparison 78—18279
flat plate boundary layer, particle cloud concentration profile 77—24016
flat plate in air flow, heat transfer at inner boundary layer 78—94715
flat plate in electrostatic field, flow pattern, induction curtains, heat dissipation *(Korean)* 77—27619
flat plate skin friction meas. by splitter plate method 80—38385
flat rectangular channel turbulent water flow, free stream and viscous sublayer temp. fluctuations 78—83369
flate plate, turbulent boundary layer calc. by straight line method *(Russian)* 79—90234
flow acoustic interaction near a plane heat conducting compliant boundary 80—69809
flow around plate with elastic surface *(Russian)* 77—54982
flow around rotating cones and discs, momentum, heat and mass transfer 79—1203
flow distribution on continuously moving flat plate, Navier-Stokes solns. *(German)* 79—86417
flow effects on structures, conf., New York, USA, (Dec. 1976) 78—46927
flow over backward step with nonzero plate inclination 77—89107
flow over body, Fredholm integral eqn., spline fit approx. 79—37302
flow separation in transonic turbulent boundary layer, shock wave causing separation *(French)* 79—77186
flow separation suppression by sequential wall jets 77—31354
flow stability between concentric cylinders, WKB approx. 77—51120
flow stability mechanical model using Orr-Sommerfeld eqn. 79—81856
flow structure in immediate vicinity of wall 79—1215
flow visualisation in shock tube, book contrib. 80—1715
fluctuating boundary layer in a rotating fluid with variable suction 79—50718
fluctuating flows near walls, turbulence intensity distrib. Thompson's velocity profiles 78—67189
fluctuations in shear stress of turbulent flow near wall *(German)* 80—19345
fluctuations in viscous wall region for Newtonian and drag reducing fluids 78—26160
fluid eddy viscosity and thermal diffusivity model *(Russian)* 78—46957
fluid meter discharge coefficient based on boundary layer values 80—48828
fluid-elastically coupled coaxial cylindrical shells, response to external flow 77—89063
fluidised bed wall-to-liquid mass transfer, local particle influence 79—94713
fluidised fine particles, ascending gas flow in cylindrical channel, review 78—42643
forced convection along vertical cylinder with uniform surface heat flux, buoyancy effects 77—15026
forced convection heat transfer from cylinder in cross flow, turbulence intensities 79—1190
forced convective heat transfer, wall capacity and resistance effects 79—1192
forced-convection heat transfer from irregular melting wavy boundaries 80—38389
forward facing step, neutrally stable atmospheric flow, shear layer, separation, vortices 80—48685
free, calc. of mean and fluctuating characteristics 79—72885
free and surface-mounted obstacles, topology, flow visualization 78—51157
free coaxial jets with independent air supply to nozzles *(Bulgarian)* 78—59436
free connection heat transfer from isothermal spheroids, thick boundary layer and turbulence effects 77—15022
free convection, vel. profile 78—94693
free convection from rough surface, heat transfer 79—55388
free convection in fresh and salt water, characts., visualisation 79—18888
free oscillation of liquids through a tube with abrupt changes in flow sections, damping ratio calc. 79—77149
free shear layer, Reynolds stress closures systematic modelling rules 80—1552
free shear layer behavior in rotating systems 80—1545
free stream turbulence and shear effects on boundary layer and wake structs. 78—26112
free stream turbulence effect on skin friction and heat transfer from bluff body 79—86413
free-stream turbulence, effect on large struct. in turbulent rising layers 78—46949
free-stream turbulence near plane moving boundary 78—26105
freely flowing liquid film, cooling, heat transfer, turbulent transport model calcs. 80—64560
freestream turbulence effects on boundary layer development 80—48684
freezing in steady state turbulent flow between parallel plates 77—58680
frequency-wave-vector spectrum determ. of turbulent pressure fluctuations using acoustic transducer 78—38430
friction factor in pipe, explicit eqn. 80—19508
fully developed turbulent channel flow, perturbation propag. in viscous sublayer and wall region 80—19513
fully developed turbulent flow, between parallel plates, heat transfer in entrance region 78—1658

boundary layer turbulence continued
fully developed turbulent pipe flow, low Mach number wall turbulence—sound interaction 80—6148
fully turbulent environment with transitional boundary layer spot 78—26110
gas, reson. oscills. in channel, local heat transfer coeffs. 78—1659
gas, turbulent boundary layer vel. distrib., probabilistic statistical approach, vortices 80—92123
gas, with variable physical props., pipe flow, turbulent momentum and heat transfer calc. 78—90869
gas bubble boundary surfaces in turbulent liq. flow, equivalence of photographic, chem. determs. *(German)* 79—32630
gas dispersion turbulent flow in tubes, nonisothermicity rel. to deposit form., heat transfer 79—55409
gas flow around thermally insulated porous surface, optimal suction from boundary layer 77—35123
gas flow in duct with fin, heat transfer, drag 77—62253
gas flow in rectangular channel with single fin, heat exchange and pressure drop *(Russian)* 77—23957
gas flow through pipes, inside wall liquid film effects *(Russian)* 79—41755
gas jet, wall impact model, subsonic 78—34176
gas jet blowing into supersonic flow without 3-dimens. boundary layer separation, nozzle shape 80—100009
gas screen, subsonic turbulent boundary layer, friction behind permeable section 80—92127
gas-liquid upward flow, effect of tube size on liq. side mass transfer 78—9682
gas-solid interactions, rel. to reduction of aerodynamic friction and aerothermal heating 79—95896
gas-solid particle suspension, turbulent flow in curvilinear channel, local heat exchange 78—63484
gas-solid turbulent flow, press. drop, Reynolds eqn. 77—31370
gas-solid turbulent flow, press. drop, solids phase momentum eqns. 77—31371
gas-solid turbulent shear channel flow, particulate motion, numerical simulation 80—53863
gasdynamic laser nozzle wake, flowfield props. boundary layers 80—24027
geophysical flow, turbulent bursting phenomenon, sedimentological implications 77—13093
Gortler stability at rigid and elastic plane plates *(Russian)* 80—79261
Gortler vortex type perturbation profiles in boundary layers problem on curved surface *(Russian)* 80—74834
gradient sublayer turbulence of two dimensional boundary layers undergoing turbulence 80—87763
granular materials, flow around heated cylinder, thermal wake and separation point 77—31302
gravity current head dynamics when advancing over no-slip horizontal surface 80—6036
grid flows and boundary layers, with (without) press. gradient, turbulence fine struct. 77—51040
grid turbulence decay, near moving wall 77—84239
growth of turbulent layer of fluid, lab. study 79—1170
Hassid-Poreh energy model anal., inc. accel. and surface heat transfer step change 78—51158
heart valves, blood flow, vortex-grid method 80—41105
heat and mass transfer, at turbulent boundary layer, diffusion model 78—94544
heat and mass transfer and friction under complex thermogasdynamic conditions 79—1209
heat and mass transfer from wall with roughness ridges 77—39286
heat and mass transfer in abruptly changing wall boundary conditions 78—94545
heat and mass transfer with condensation from turbulent nonuniform boundary layer, analysis 77—89124
heat and momentum transfer to axisymmetric bodies 77—11216
heat flux equation, turbulent boundary layer, local similarity model 78—75142
heat flux transport eqn. for equilibrium retarded turbulent layer 80—19380
heat pipe, with header and single or two-phase artery systems 78—90981
heat source driven turbulent convection between 2 rigid plates at arbitrary Prandtl number 80—69829
heat transfer, effect of conduction error on hot wire meas. in turbulent flow near wall 79—7423
heat transfer, effect of free-stream turbulence 79—55385
heat transfer, flow between parallel plates, asymptotic expansion calcs. 77—47008
heat transfer, flow between parallel plates, wall cond. effects 77—47007
heat transfer, highly cooled supersonic flow 78—9652
heat transfer, in tube with circumferentially varying wall heat flux 77—65738
heat transfer, turbulent water film, different initial flow conditions, high temp. gradients 78—90862
heat transfer across boundary layer, external flow turbulence effect 78—94713
heat transfer across boundary layer, free-stream turbulence effects 78—94714
heat transfer and rough wall, variable wall temp. and blowing 78—38308
heat transfer at permeable plate with shock wave interaction 79—81922
heat transfer behaviour, turbulent boundary layer on rough surface with blowing 78—71334
heat transfer behind hydrodynamic starting length, analytical method *(German)* 79—72892
heat transfer between two moving fluids separated by wall containing heat sources 77—23948
heat transfer case, integral method soln. 79—72890
heat transfer coeff. meas. by dilatometry 78—83388
heat transfer coefficients using two-zone model 77—89119
heat transfer from single sphere, turbulent air stream 78—22342
heat transfer improvement in coeff. using turbulence promoter 77—72297
heat transfer in gaseous screen with longitudinal press. gradient 80—23998
heat transfer in liq. metal flow near wall 77—35142
heat transfer in rough pipes, mixing length method 77—7450
heat transfer in thermal boundary layer 77—42821
heat transfer measurements in axisymmetric external separated and reattached flow 80—10234
heat transfer of cylinder in longitudinal flow, artificial boundary layer turbulence effect *(Russian)* 78—14008

boundary layer turbulence continued
heat transfer to axisymmetric bodies, super- and hypersonic freestream turbulence effects 77—75916
heat transfer to isothermal flat plate 77—89121
heated and cooled, local anisotropy 77—3820
heated flat plate, turbulent boundary layer, wall suction effects *(French)* 77—58666
heated flat plate in water, critical Reynolds number, heat transfer 80—69766
heated horizontal pipe flow, temp. and vel. fluctuations obs. 77—75894
heated pounds, turbulent boundary layer of stratified airflow, surface waves 80—92133
heated wall experiments, turbulent field from temp. fluctuations 78—94667
high favourable pressure gradients, method of analysis 77—58664
high free stream turbulence, turbulent boundary layer characts., fluctuations 80—14674
high Reynolds no. flow past rough walled circ. cylinder 78—46952
high Reynolds number supersonic flow, compression corner flowfields, turbulent boundary layer separation 80—14735
high subsonic Mach number boundary layer, turbulence effects on artificial thickening 77—27545
high subsonic speed, coherent structures 80—19422
high-temperature turbulent air flow in round tube, friction resistance, cooling *(Russian)* 78—75135
highly accelerating flow near smooth wall, prediction method 80—1550
holonomic formulation of boundary layer eqns., use of tensors 79—1153
homogeneous and inhomogeneous gases, turbulent boundary layers, phenomenological model appl. 79—98696
hot wire readings, wall proximity effects heat transfer 80—48822
hot wire signal conditional sampling techniques for transition intermittency studies *(French)* 79—77066
hot-wire anemometer, static and total press. probes turbulence effects 78—34240
hot-wire measurements, wall proximity corrections 80—74841
hydrofoil cavitation noise and inception, boundary layer development 77—55057
hydrofoil profile for accelerating cascade, surface press. distribs. 78—18321
hydrofoils, tail-loaded, fully cavitating, avoidance of turbulent separation 78—94659
hydrofoils, two-dimens., with massive turbulent separation, press. distrib. prediction 77—7377
hypersonic blunt-slender cones, artificially induced boundary layer transition 80—28496
hypersonic boundary layer over slender sharp cone, turbulent shear stresses, heat transfer 77—23989
hypersonic transitional/turbulent boundary layer, wall cooling effect 78—26149
hypersonic turbulent compression corner flow, numerical simulation 77—62276
hypersonic turbulent flow measurements, electron beam fluoresc. method 77—35282
ice-water interface, wave formation, heat transfer in presence of turbulent flow 80—103015
ideal fluid flow round body with formation of tangential separation *(Russian)* 77—35124
imcompressible fluid, asymptotic expansion anal. 80—33573
impulse equation treatment *(German)* 77—14996
impulse response to short regions of high surface curvature 79—90235
impurity diffusion in boundary layer 77—89110
inclinable pipe, suspension in turbulent flow, Markovian model, eddies 80—48790
inclined rectangular plate, heat transfer and fluid flow, finite width effects 79—81884
inclined turbulent jet exhausting from flat plate into turbulent subsonic crosswind 77—42885
incompressible fluid, retarding boundary layers, analysis from similarity consideration 78—18283
incompressible fluid flow vorticity-streamfunction computation 77—47018
incompressible gradient flow before separation and on rough surface, turbulent viscosity 78—87338
incompressible layer thickness change in presence of longitudinal pressure gradient 80—92126
incompressible liquid, gradient turbulent flow, heat transfer of nonisothermic surfaces in wide range of Pr and Re numbers 77—35135
incompressible Newtonian fluid, flow past wall with small particle injection *(French)* 79—46384
incompressible turbulence mixing length in diaphragm flow pipe region *(French)* 80—69775
incompressible turbulent boundary layer flow on flat plate, anal. 77—51044
inertial wave and flow struct. for disturbances at low Rossby number 78—22360
infinite vertical limiting surface with suction, Stokes free convection effects 80—19364
inhomogeneous wall flow, turbulence integral scale, expt. determ. 80—38386
instabilities, Mach number 7 77—65760
integral method for turbulent boundary layer with separated flow 80—1547
integral momentum eqn. for flows with entropy gradients across inviscid streamlines 77—11214
interaction of turbulent spot with turbulent boundary layer, flow struct. obs. 78—90858
interface layers turbulent flow, appl. to air/sea boundary layer 78—71323
interfacial boundary layer in water tank, heat transport, thermal struct. 78—9638
interference between two circular cylinders, discontinuities 78—9633
intermittancy in transition zone of boundary layer *(French)* 77—72274
internally finned helical coil, fluid flow and heat transfer 77—62249
irrotational strain dissipation eqn. sensitisation 80—106794
isotope separation by gaseous diffusion, aerodynamic effects 78—59469
jet, 3-dimens., at wall, two-point statistical props. 79—1223
jet, conical annulus, turbulent exit vel. calc. method 77—55069
jet, liquid, falling in gaseous atmosphere, laminar and turbulent flow boundary layers *(German)* 77—7427
jet, liquid, turbulent, gas absorpt. *(Japanese)* 80—38473
jet, mixing layer, axisymmetric, influence of initial and boundary conditions 79—94689

boundary layer turbulence continued
jet, plane turbulent, in incompressible liquid *(Russian)* 77—55060
jet, turbulent, plane, impinging on plane surface, RMS boundary press pulsations 78—59438
jet, turbulent, plane, impinging on solid wall, spectral characts. of pulsations 78—9668
jet, turbulent wall type, self-preserving flow 78—79352
jet, two-dimensional turbulent, in moving stream, preferential entrainment 80—1660
jet, upstream influence on near field 77—89181
jet curved surface impingement 78—14051
jet flow past ellipsoid of revolution 79—81937
jet in concurrent stream at permeable surface 77—7444
jet mixing, effect of nozzle wall boundary-layer state 77—27568
jet stagnation point heat transfer on plate, turbulence effects, liquid crystal meas. 78—18327
jets, flat and axisymmetric, submerged in incompressible fluid, calc. using turbulent energy balance eqn. 77—47051
jets, radial turbulent, flow, attachment to disc plate, flow patterns, nozzle dimension effects 78—83443
journal bearings, performance, turbulent lubrication theory using frictional law appl. 79—98695
k-ε turbulence model, three dimens. finite difference anal. 78—51154
kurtosis of velocity field, prediction method 80—23990
Lake Baikal, ice covered, statistical props. of velocity and temp. profiles *(Russian)* 77—78269
Lake Ontario, north shore coastal boundary layer response to storm 78—24322
Lake Ontario atmosphere turbulence, vel. and scalar statistics 77—33128
laminar boundary layer, turbulent 'spot' 77—19587
laminar pipe gas flow, fluid-wall mass transfer, sonic oscills. enhancement 77—910
laminar source flow between parallel porous discs with equal suction and injection, in mag. field 77—84331
laminar sublayer on permeable surface with injection 79—64645
large eddies in wake and turbulent boundary layer, vel. fluctuations 80—24036
large free stream to wall temp. ratio turbulent boundary layers *(German)* 80—1540
large organised struct., bursting phenomena 78—26109
large scale eddy destruction effects on skin friction and Clauser shape factor 78—90860
large scale structure, turbulent spots model, bursts 78—90847
Large structure in turbulent boundary layer, comments, correct angle of backs 80—6037
large-scale structure, temp. contamination investigation 79—32483
large-scale turbulence modes obs. using mesh screen and heat wake 78—90859
laser, elec. discharge type, flow generated by an array of eccentric porous tubes 79—965
law of the wall, appl. to turbulent boundary layer calc. with injection or suction 78—67187
leading edge bubble formation, peaky airfoil *(French)* 80—64524
lifting-surface theory of straight cascades of swept blades 77—19596
limiting relative law of heat and mass transfer and friction, permeability parameter effect 80—23999
linear shear flow and around cylinder, velocity gradient effects *(Japanese)* 79—23305
liquid, forced channel flow with surface boiling, analogies between heat and momentum transfer 77—47014
liquid film, gas absorpt. 79—50714
liquid film, heat transfer, friction factor 77—42819
liquid film, heat transfer predictions for nonsheared and sheared films 77—15024
liquid film, in vertical tube with turbulent gas flow, friction coeff., press. losses 77—89189
liquid film, subcooled, heat transfer and film breakdown 78—34121
liquid film flow, preheated to boiling 77—62244
liquid film flow affected by streaming turbulent gas *(Russian)* 79—14386
liquid film on rotating surface, hydrodynamics and heat exchange, entrance section influence, interface frictional forces 79—86433
liquid film stability adjacent to supersonic boundary layer 77—930
liquid flow in viscoelastic pipeline, dynamic charact. 77—35126
liquid flows in channels with porous walls, turbulence development *(Russian)* 77—27590
liquid fuel film, combustion behind shock wave, heat and mass transfer in turbulent boundary layer *(Russian)* 78—71401
liquid layer, flowing on pipe wall, gas absorption rates 79—94696
liquid metal, film, turbulent flow down vertical wall under gravity, heat transfer 78—59396
liquid metal heat transfer in regular fuel element arrays, Nusselt no. calc. 78—89932
liquid system, turbulent flow, drag reduction, neutral stability 77—7380
liquid-gas mixer, perforated disc stirring cascade type, power dissipation, mechanism and correlation 79—1238
liquid-metal-H_2O stratified flow, horizontal co-current, interface heat transfer, turbulence model 80—92131
longitudinal blunt circular cylinder, axisymmetric separated and reattached flow, turbulence 80—79285
longitudinal surface curvature effects calc. 80—19337
longitudinally ribbed surfaces, turbulent boundary layer drag and heat transfer characts. 80—14684
losses in channels for increased turbulence 77—75899
low eddy friction polymer soln. hydrodynamics 80—53818
low Mach number duct flows, combustion noise generation by chemical inhomogeneities 80—92237
low Reynolds number flow, rel. to porous plate data 77—31288
low-Reynolds-number turbulent boundary layers 80—1556
lubrication, turbulent, eqn. derivation using friction law 79—98694
Mach 6 turbulent boundary layer, surface roughness effects 80—19338
Mach waves, kinematics inside and outside supersonic jets, book contrib. 80—1640
magnetic convection, nonlinear, mean field approx., boundary layer method 80—69930
magnetic field as a tool for investigating transition and turbulence 80—1696
marine bottom layer and atm. surface layer, turbulence spectra similarity scaling 78—44860
mass and momentum transfer at a wall, turbulence promoter effects 78—9631

boundary layer turbulence continued
mass exchange for spherical particle in flow at high Peclet numbers and $Re \leq 100$ 77—54988
mass transfer, near-wall liq., coherent struct.-caused, numerical computation 78—59379
mass transfer in turbulent falling film with or without chem. reaction 79—41766
mass transfer in viscous sublayer, statistical method *(Russian)* 80—87764
mass transfer in viscous sublayer by electrochemical method, expt. 78—83368
mass transfer to wall, fluctuations, Schmidt no. effect 77—58659
mean heat of emission and hydraulic resist. of banks of tubes *(Russian)* 80—96262
measurement of microstructure with hot and cold wires 80—24109
MHD convertor, diagonal channel, conversion efficiency optimisation by sliding descent method, turbulence *(Russian)* 78—75226
MHD flow over flat plate, boundary layer function 79—27696
MHD forces, effect on turbulent boundary flow 77—24026
MHD generator, combustion-driven, boundary-layer profile meas. 77—24194
MHD generators, technique for boundary layer voltage loss determ. 77—72507
MHD in rot. circ. vessel, drag 80—33697
MHD of flow at porous surface, crossed inhomogeneous fields 79—77274
MHD steady state turbulent flow, flow near wall, heat emission theory *(Russian)* 78—5810
MHD turbulent heat and momentum transfer in 2-dimens. channel with transverse mag. field 78—94848
mildly curved surface, turbulence struct. 78—38303
mixing, in two-dimens. turbulent layer, initial conditions effect 78—90848
mixing layer, free, axisymmetric, turbulent spot, data processing 80—79280
mixing layer, free, axisymmetric, turbulent spot, vorticity and Reynolds stress 80—79281
mixing layer at high R_e, large struct. dynamics and entrainment 77—15001
mixing layer growth from turbulent and nonturbulent boundary layer 79—68686
mixing length determination, from turbulence characts. meas., in tubes and boundary layers *(Russian)* 78—83371
mixing length in pipes on basis of measured turbulence characts. 80—38494
mixing length in wall region 77—62242
mixing lengths, outer layer 78—13999
model applicability and expt. verification 77—3821
model development expts. with numerical simulations 77—27551
modelling, coeffs. and parameters calc. *(Dutch)* 79—55365
modelling of wavevector-frequency spectrum, turbulent boundary layer wall pressure 80—106793
momentum, heat and mass transfer during flow around a sphere, free stream turbulence effects *(German)* 79—41677
momentum, heat and mass transfer during flow around a sphere, free stream turbulence effects, mathematical model *(German)* 79—41678
momentum exchange by coherent motions in turbulent wall boundary layer, quantitative model 79—7372
moving equilibrium turbulent boundary layers, in adverse press. gradient, dimensional anal. 79—32486
moving surface, integral and numerical methods 78—63421
moving surface layer, flow structure in front *(German)* 78—1712
multicomponent chemically reacting flows, turbulent boundary layer at flat plate 79—98822
multilayered stratified flow investigation using water tunnel *(Russian)* 80—1703
multiphase flows, drag coeff. changes due to saturation *(German)* 77—15109
natural convection, vertical isothermal surface, K-ε turbulence model 77—58683
natural convection boundary layer turbulence next to heated vertical surfaces 79—68684
Navier-Stokes equations for turbulent and transition flows, num. soln. methods 77—54979
near-wake for slender cone, Mach number depend. of laminar transition 77—62277
Newtonian and non-Newtonian pipe flow, LF turbulent press. similarity 78—5772
noise generation, role of tornado-like vortices 80—69811
nominally planar turbulent boundary layer, spanwise nonuniformity and vortices 80—53762
nominally steady, two-dimens., vel. and temp. profile prediction method 80—1624
nominally two-dimensional boundary layer, spanwise nonuniformity, uniformalisation 77—72283
non-Newtonian flow, in coiled tubes, anal. and exptl. verification 77—55052
non-Newtonian turbulent boundary layer flow of power law fluid, mass transfer 77—31339
nonequilibrium adverse pressure gradient flow, turbulence model 77—58660
nonequilibrium turbulent flows near wall, matching problem 80—96250
nonisothermal laminar and turbulent plane free jets with buoyancy effect, boundary layer theory *(German)* 80—53830
nonisothermal turbulent suction-controlled boundary layer, heat and mass transfer coeffs. at chemically-reactive surface 79—77102
nonlifting airfoil, response to streamwise gusts 77—65753
nonlinear interaction of two waves in boundary-layer flows 80—59016
nonseparated turbulent flow, along solid wavy wall, amplitude effects 77—75896
nonstationary layer with longitudinal press. gradient, friction law *(Russian)* 80—74842
nozzle, convective heat transfer, turbulent boundary layer regime 78—9670
nozzle, convergent-divergent, compressible turbulent boundary-layer heat transfer *(German)* 78—22399
nozzle, subsonic and supersonic, turbulent boundary layer heat transfer 79—1229
nozzle of rocket, compressible turbulent boundary layers, heat transfer and skin-friction 79—14451
nozzles, flat and axisymmetric, supersonic flow calc. method for arbitrary inlet gas props. 77—68657

boundary layer turbulence continued
nuclear reactor pin bundle, two-phase flow, eqns. of motion 78—86570
numerical method, fourth-order 79—1174
numerical simulation of turbulent mixing layers via vortex dynamics 80—19362
ocean, eddy diffusion effects on western coast boundary layer struct. 77—17142
ocean, turbulent interface layers theory 78—71323
ocean, wind mixed layer deepening theory *(Russian)* 79—8638
ocean bottom boundary layer turbulent struct. in tidal current 79—84284
ocean bottom layer beneath waves, residual flow and boundary shear stress 78—24300
ocean mass transport by waves in turbulent bottom boundary layer 78—3797
ocean stratified layer under ice, turbulence calc. 77—49077
ocean surface, turbulent layer self-similar development in homogeneous fluid 79—44196
ocean surface layer, 2-parameter turbulence models *(Russian)* 80—79275
ocean surface mixed layer dynamics 78—44855
ocean surface pattern morphogenesis and catastrophe theory 77—5217
ocean surface wind wave related turbulence meas. by impellor current meter array 80—46301
ocean turbulent boundary layer under pack ice 77—17130
ocean upper layer, turbulence coeff. calc. 77—49076
oceanic bottom boundary layer, struct. and dynamics 79—20842
oceanic upper layer, modelling 79—84292
ogive cylinder, mag. suspended, subsonic flow, reverse Magnus flow, turbulent boundary layer 78—51153
one-dimensional turbulent flow at rough wall, heat transfer and hydraulic resist., effect of viscosity variation 77—42816
one-equation turbulence model, finite element anal. 79—7371
one-layer theory of stationary turbulent flows, equilib. boundary layers *(Russian)* 77—35131
open channel flow, turbulent intensity modelling 79—1172
oscillating airfoil drag in fluctuating free stream, laminar and turbulent boundary layer anal. 80—53746
oscillatory flow, expt. anal. of turbulent boundary layers 77—11177
oscillatory MHD boundary layer flow, free convection effects 78—91018
outer flow turbulence, influence on boundary layer friction law 79—46300
packed bed wall-to-liquid mass transfer, local particle influence 79—94714
particle transverse motion in turbulent boundary layer 78—79358
particles in a fluid, convective diffusion and mass transfer, wakes, chemical reactions 80—38394
passage, arbitrary cross-section, fully developed flow prediction method 79—1254
PBR core, coolant flow predictions using PEBBLE computer code 79—54474
perforated flat plate over porous medium, turbulence penetration, eddies, mass transfer 80—64528
periodic intermittent model for wall region 78—87336
permeable plate, numerical anal. of turbulent boundary layers 78—67186
permeable plate, turbulent boundary layer at different free stream turbulence levels, injection 80—10233
permeable plate, with injection, heat transfer 79—1247
permeable plate boundary flow, with strong injection 79—81963
permeable plate gas screen region, heat transfer and friction laws 79—1250
permeable surface, turbulent boundary layer, in crossed elec. and mag. fields *(Russian)* 78—94836
permeable surface with intensive blowing 77—84241
permeable tube with wall injection, transient turbulent boundary layer 78—83486
pipe, annular two-phase flow, downtake turbulent film and gas flows, pressure drop 80—92218
pipe, asymmetrically heated, turbulent transport and thermal diffusivities 80—64636
pipe, axially rot., turbulent flow patterns and hydraulic resistance 80—106850
pipe, heated, vertical, gas buoyancy effect on downward flow and heat transfer 78—74427
pipe, mean temp. and conc. profiles in turbulent liquid flow 77—47011
pipe, mean temp. and conc. profiles in turbulent liquid flow 77—47012
pipe, porous, uniform air outflow, turbulent momentum flow and friction coeffs. formula 78—1737
pipe, struct. similarity in radial correlations and spectra of longitudinal vel. fluctuations 79—32482
pipe, turbulent aerosol flows at high wall temps., heat transfer 80—74862
pipe, turbulent vel. components during ejections and sweeps *(French)* 79—1166
pipe, turbulent velocity profiles from stability criteria 79—50717
pipe, unstable phase following turbulent flow past sudden enlargement *(French)* 79—1157
pipe entrance region, mean vel. fluctuation 80—64526
pipe entrance region boundary layer, turbulent temp. and vel. fluctuations *(Japanese)* 78—38301
pipe flow, depend. of particle deposition velocity on particle inertia 77—35219
pipe flow, eddy viscosity decay, phenomenological theory 79—98700
pipe flow, finite element wall model for high Reynolds number flow 80—28565
pipe flow, response to change in roughness 78—47040
pipe flow, Reynolds shear stress, roughness effects 78—22426
pipe flow, turbulent, large Schmidt number mass transfer 79—90230
pipe flow, turbulent, past rectangular roughness element 80—1555
pipe flow, turbulent, perturbed by sudden enlargement 80—19354
pipe flow, turbulent, temp.-depend. viscosity effect on convective heat transfer 78—90884
pipe flow, wall and shear turbulence during bursting periods 78—1743
pipe flow with suction or injection, high Prandtl no. heat and mass transfer 80—74857
pipe flow with uniform internal heat generation, turbulent heat transfer *(German)* 79—72893
pipe inlets, turbulent local mass and heat transfer, swirling effects 80—64542
pipe outflow, turbulent, with wall suction, dynamic and thermal fields *(French)* 79—4082
pipe wall, temp. distrib. 79—32668

boundary layer turbulence continued
- piped fluids in motion, turbulent flow, direct analytical soln. 78−87393
- pipes, heat transfer to low Prandtl number turbulent fluids, numerical prediction 80−69833
- pipes and bends, structure-borne sound behind a jet nozzle *(German)* 80−87804
- pipes with buoyancy effects, turbulent flow and heat transfer 79−90253
- plane channel with one or two rough walls, turbulent flow 80−79278
- plane converging duct, separation zone for turbulent boundary layer and oblique shock interaction 80−14759
- plane isothermal jet propagation in bounded secondary stream 77−24008
- plane mixing layer analysis in homogeneous incompressible fluid 77−46999
- plane plate with roughness element, nonsteady flow, numerical calc. *(German)* 78−94663
- plane turbulent Couette-Poiseuille flow, asymptotic anal. 80−33674
- plane turbulent jet, interface crossing freq. as self-preserving flow variable 80−38472
- plane-parallel channel, convection in turbulent liquid flow for Pai vel. profile 77−47013
- planetary boundary layer model with variable eddy viscosity coeff. 77−9482
- plant canopy, model, turbulent flow 77−60443
- plasma, MHD flow in channel, wall friction 78−14092
- plate, flat, attached subsonic and transonic turbulent boundary layers, press. fluctuations effect 79−94642
- plate, flat, turbulent boundary layer, mainstream turbulence, vorticity effects 78−83408
- plate, flat, two-dimensional turbulent boundary layers 79−32478
- plate, flat, with suction, boundary layer eddy viscosity, mixing length, Von Karman's constant 80−1680
- plate, flat, with suction, boundary layer turbulence and momentum props. 80−1679
- plate, mean temp. and conc. profiles in turbulent liquid flow 77−47011
- plate, mean temp. and conc. profiles in turbulent liquid flow 77−47012
- plate, rotating, 3-D boundary layer turbulence, effects of rotating radial end-plates 80−69843
- plate, thick, parallel flow, with separation and reattachment, local and average mass transfer *(German)* 78−22339
- plate, thin, in gradient current flow, coupled heat exchange *(Russian)* 78−83398
- plate, yawed, flat, leading edge vortex induced 3-dimens. turbulent boundary layer 78−90856
- plate at angle to flow, heat loss meas. for boundary turbulence and separation 78−90846
- plate oscillation effect on horizontal free convection flow 77−75904
- plate surface with mass blowing and suction, heat transfer in turbulent boundary layer 80−64559
- plate to high turbulence air flow heat transfer 80−79292
- plate type heat exchangers, with hemispherical projections, heat transfer and drag 80−48560
- plate with cylinder in turbulent boundary layer, forced convection heat transfer 80−64540
- plate with simultaneous injection and suction, turbulent layer friction and vel. profile 78−83469
- plates roughened by wires, flow resistance, press. distrib. meas. 77−51046
- plume, turbulent, thermal, along vert. wall, struct. and heat transfer 78−90880
- plumes, vertical, round, diffusion, flow props. 80−43755
- polyacrylamide weak soln., wall turbulent flow 80−38450
- polymer additives for drag reduction, plane 2-D channels and circular pipes 78−26167
- polymer containing liquid, turbulent pipe wall flows, friction and heat transfer 79−98802
- polymer soln., diffusion in boundary layer 78−87368
- polymer soln. turbulent flow over plate, drag reduction 78−5768
- polymer solns., turbulent boundary layer in pipe flow 78−67256
- polymer solns., weak, turbulence near walls *(German)* 77−15109
- polymer solution, boundary layer having laminar, transitional and turbulent flow zones *(Russian)* 77−80185
- polymer solution, drag reduction in turbulent flows, book contrib. 78−59432
- polymer solution, logarithmic equations fo resistance of turbulent friction 77−51042
- polymer solution, mass transfer between solid surfaces and drag-reducing fluids 78−79339
- polymer solution, power laws of reduced turbulent friction for pipe flow 77−15068
- polymer solution, turbulent boundary layer, drag reduction 78−22414
- polymer solution, turbulent boundary layers 78−18317
- polymer solution, turbulent wall flow model 78−18316
- polymer solutions, turbulent, mass transfer rate, frictional force *(French)* 79−37357
- polyox solution, turbulent flow in tube with large surface roughness 78−1651
- Polyox-701 aq. soln., turbulent press. suppression, spectral effects in pipe flow 78−5771
- polystyrene solution, drag reduction, mean vel. profile 78−22384
- polystyrenes, toluene soln., turbulent drag reduction, mol. wt. and struct. influence 79−7373
- porous plate, heat transfer in turbulent boundary layers 79−98714
- porous plate, suction, turbulent field anisotropy effect *(French)* 78−51156
- porous plate boundary layer, vel. and friction stress distribs. 77−84243
- porous plate skin friction, injection or removal from boundary layer due to turbulent wall jet 78−47029
- porous tube array, flowfield struct., turbulence and vorticity distribs. 77−27589
- porous tube entrance segment, heat transfer anal. with initial flow swirl and transverse injection 77−24025
- power laws for turbulent jets wakes and shear layers, marginal instability 79−32458
- power-law fluid, free convection around thin bodies of revolution under second kind boundary conditions 77−7422
- prandtl's mixing length hypothesis and the spectrum of turbulent compression stress *(German)* 79−10554
- precipitation of aerosol particles on an evaporating droplet in a turbulent gas flow 80−7870
- pressure correlation functions 80−83792
- pressure fluctuation meas. by optical interferometry 78−26222

boundary layer turbulence continued
- pressure fluctuation source, model of turbulent boundary layer 77−27515
- pressure fluctuation spectrum, elastic boundary compliance effect 78−63422
- pressure gradient velocity correlations 80−64530
- pressure gradients, parametric method for turbulent boundary layer eqn. solns. 80−10232
- pressure-fluctuation spectra, reasons for roughness 77−58665
- pressure-head Couette flow of capsule pipeline transportation system 77−35125
- Preston tube calibration in transpired turbulent boundary layer 78−79397
- pulsating flow of turbulent boundary layer on wall of subsonic wind tunnel *(French)* 77−27517
- pulsating turbulent flow onto elastic surface, boundary-value problem *(Russian)* 78−75153
- pulsating turbulent pipe flow, press. and vel. distribs. 77−24023
- pulsating turbulent pipe flow, velocity field and press. gradients 80−64641
- radially rotating pipe, heat transfer coeffs. in various flow regimes 78−1668
- rarefied flow, low-speed flow over sphere, convergence of integral methods 78−22375
- Rayleigh-Benard system, turbulence near onset of convection 80−48686
- re-entry vehicle acoustic/vibration environment expt. 78−20620
- rearward facing step, turbulent incompressible reattaching flow, adverse press. gradient effects 80−69773
- reattaching laminar and turbulent separated flow, three-dimens. heat and mass transfer 77−65759
- recirculating flow, numerical prediction 79−1152
- recirculating flow behind backward-facing step, mean vel. and Reynolds stresses meas. 80−19355
- recovery tube, turbulent boundary layer effect on press. variation 77−84238
- rectangular cavity with porous filling, steady convection and boundary layers 80−79309
- rectangular cylinders, 2-dimens., drag coeff., correction method comparison 80−64568
- rectangular elbow, 3-dimens. turbulent compressible duct flow, stagnation pressure losses, vortices 80−64640
- rectilinear channels, incompressible liquid turbulent flows from turbulent exchange 79−98805
- research problems *(French)* 77−31285
- reservoir, surface layer turbulence and water masses dynamic stability *(Russian)* 77−33107
- response to random fluctuations in external stream 77−3818
- response to step change in heat flux 77−39291
- retarded turbulent boundary layer, expt. study of turbulence energy balance components 79−86415
- Reynold's stress tensors, rot. probe meas., in 3-dimens. boundary layer 78−94656
- Reynolds mean uw shear stress gradient meas., press. driven boundary layer 77−54986
- Reynolds shear stress, turbulent flow over a periodic rough surface 78−71326
- Reynolds stress model, appl. channel flow and boundary layer flow over square cavity 77−39280
- Reynolds stress tensor components in turbulent boundary layer subjected to sudden transverse strain 80−19339
- Reynolds stress tensor in curved duct expt., single rotating slanting hot wire technique 80−75006
- Reynolds stresses meas. 77−42807
- rotating bodies in axial flows, laminar and turbulent boundary layers *(Japanese)* 79−77127
- rotating cone-cylinder body, boundary-layer flow in uniform stream 77−23965
- rotating cylinder, exptl. anal. of boundary layers stability, transition and growth 77−31309
- rotating cylinder, turbulent transport 77−7402
- rotating disc, local heat transfer, Prandtl's mixing length hypothesis 77−27540
- rotating disc, local heat transfer, two-eqn. model of turbulent flow 77−58690
- rotating disc, particle migration in turbulent boundary layer 78−22333
- rotating disc in polymer solutions under a turbulent regime 80−33634
- rotating inner cylinder annular flow computation 80−1544
- rotating metal disc electrode, mass transfer under turbulent conditions, suspended particle effects 78−27772
- rotating radial convergent duct, air flow heat transfer boundary conditions, turbulent and transition flow 78−83476
- rotational flow between rot. and static discs, with radial flow, numerical method 78−59403
- rotor blade at high Mach nos., heat transfer 79−72887
- rough permeable surface, compressible boundary layer with heat transfer 79−1176
- rough pipe, gas-liq. flow pattern transition model 78−14084
- rough pipes, variable property turbulent friction and heat transfer 80−6153
- rough surface, Reynolds analogy extension 78−51159
- rough surface heat transfer in turbulent boundary layer, mixing length hypothesis 78−83378
- rough surface turbulent flow heat and mass transfer, Reynolds analogy deviations 78−83380
- rough tube, effect of Prandtl number on heat transfer 77−35139
- rough wall, incompressible boundary layer with adverse press. gradient *(Japanese)* 77−72289
- rough wall incompressible boundary layer flows calc. 80−1537
- rough wall with blowing and heat transfer, boundary layer struct. 79−81863
- rough-wall incompressible boundary layer, calc. model 79−1165
- round tubes, non-Newtonian fluid transition and turbulent flow regions *(Russian)* 80−59077
- seawater-clay suspension, turbulent boundary layer 79−20858
- second moment turbulence closure to heat and mass transport in two-dimens. thin shear flow 80−24010
- second order fluid, unsteady motion between parallel plates 78−30321
- secondary flow prediction , three-dimens. turbulent boundary layers, skin-friction 78−22341
- segmented-conic body, flow structure close to lateral surface and formation of breakaway zones 77−58727

boundary layer turbulence continued
semiempirical calc. using arbitrary free stream press. gradient 78—94640
semiopen channel vel. distrib. 77—54303
separated boundary layer flow, vel. characts. and recirculation 80—38456
separated flow behind double step at duct entrance, turbulent fluctuations and heat transfer 77—42829
separated flow types over slotted wings 80—38458
separated flows, three-dimens., with vortex filaments, num. simulation 77—58706
separated flows around circular cylinder, numerical solns. 77—3815
separated high Reynolds number flow past a corner, numerical solns. 79—81855
separated incompressible boundary layer prediction, including viscous-inviscid interaction 80—1548
separated internal flow computation using coupled boundary layer-inviscid core, elliptic representation 80—1549
separating boundary layer, subsonic, integral prediction method 80—1623
separating flow 79—98703
separating layer with airfoil-type press. distrib. 77—31290
separating turbulent shear layers, flow field prediction 78—71321
separation, incipient, viscous interaction, laminar and turbulent boundary layers, similitude props. 77—72325
separation, review 80—1543
separation, transverse surface curvature effect 79—64644
separation at curved wall with shock 79—46343
separation criterion for axially symm. flow at tail of body of revolution 78—22340
separation near step 79—64646
separation of flow, and displacement 79—4001
separation of subsonic and supersonic flows, ultra-short duration visualisation *(French)* 78—75128
separation point, turbulent boundary layer numerical prediction, heat transfer *(French)* 78—94657
separation point boundary layers, with adverse press. gradients and injection 77—72287
separation prediction for turbulent boundary layer *(Chinese)* 80—6035
separation region, oscillatory flow effects 78—75127
separation region near wall, turbulent energy power law *(German)* 77—31293
separation zone behaviour 78—71320
shallow flows, turbulence in depth-limited boundary layer 80—12406
shallow water basin, wind-driven current, eddy viscosity, bottom friction 78—65319
sharp variations in boundary conditions, numerical anal. 79—98697
shear, interacting, in duct 77—19597
shear boundary layer in stratified medium 79—64736
shear layer, axisymmetric and plane jet, initial condition effect 78—90850
shear layer attachment near Mach 6, peak heating 78—26153
shear stress generation models, three-dimens. boundary layers 80—19360
shear turbulence, vorticity transfer theory *(Russian)* 79—50719
shear-stress transport, hyperbolic system of eqns., Keller-Cebeci 'box' scheme 80—79274
ship hulls, three-dimens. turbulent boundary layer eqn. soln., exact integral method *(Japanese)* 77—54985
ship model, hydrodynamic resistance, analytic calc. *(Russian)* 78—75123
shock interaction with turbulent boundary layer, heat transfer 77—23994
shock separated turbulent boundary layer at compression corner, mean flow meas. 77—42867
shock tube driver gas flow with fluctuations 80—96282
shock tube wall boundary layer instability, transition evolution 79—64642
shock wave interaction in turbulent boundary layer 79—41711
shock wave interaction with turbulent boundary layer disturbed by injection 80—74916
shock wave interactions, Reynolds no. effect 78—1689
shock wave turbulent boundary layer interaction, numerical simulation, Navier-Stokes eqns. soln. 77—31332
shock-boundary layer interaction flows, multieqn. turbulence modes for duct and channel 80—24093
shock-separated flows, turbulence models 78—71365
shock-wave boundary-layer interaction, wall shear stress meas. 79—1212
shock-wave interaction, sweep effect on separation conditions 77—62280
short crested waves, boundary layer vels. and mass transport 80—92169
short plane diffuser, wall turbulence meas. 80—38384
sill fjord, vertical diffusion driven by internal waves 77—2178
silt suspension turbulent boundary layer, steady state model 78—28242
simple law of wall formulation for Newtonian fluid, unified time mean velocity profile model 80—103017
skewed layers, near-wall collateral flow 78—26103
skin friction, heat transfer, free-stream turbulence effect 78—30276
skin friction and surface pressure meas. by total head/static probe 77—62311
skin friction coeff. determ. 77—84242
skin friction in supersonic laminar and turbulent flows 79—98751
skin friction meas. techniques 78—1770
skin friction measurement, comparison of viscosity balance and Preston tube methods 77—55109
skin-friction balance measurement, error sources 77—65828
slender bodies of revolution, subsonic normal force, centre of pressure, boundary layer method 80—48735
slender conical flow, separation from smooth surface 79—32479
slit suction effects in turbulent boundary layer 79—81859
slot injection of He, Favre averages 80—83791
smoke flow visualisation combined with hot-wire anemometry, technique, appl. to turbulent boundary layer 78—91044
smooth circular pipe, turbulent wall flows, velocity fluctuation probability distrib. 79—98804
smooth pipe flow, location of eddy viscosity maximum 79—81860
smooth wall velocity distrib., explicit expression 80—14669
solid propellant erosive burning, reacting turbulent boundary layer approach 79—32703
solid wavy wall, amplitude effects on separated turbulent flow 79—50715
sonic boundary layer counterjet interaction with supersonic flow 79—64728
sound emission by turbulent layer over inhomogeneous boundary 77—68297
space-time correlations, external zone *(French)* 78—42593
space-time vel. correl., liq. flow over rough surface *(Russian)* 77—31292

boundary layer turbulence continued
spherical shell, constrained fluid-loaded, vibrations and noise associated with response to turbulent boundary layer excitation 79—90239
spheroid at incidence, flow separation, laminar separation lines, turbulent separation 79—72878
spinning disc causing laminar and turbulent flow, mass transfer 79—41691
square cavities, laminar and turbulent incompressible flows 80—10307
square cylinders, smooth/turbulent lift, drag, vortex shedding 77—89109
square duct, developing turbulent flow and heat transfer, computational procedure 80—69926
square duct, developing turbulent flow and heat transfer, numerical prediction 80—74986
square prism in uniform flow, wall press. of separation-reattachment flow 78—26123
square prism separation-reattachment wall press. 79—98704
square prisms, interaction in two flow fields 78—9632
stability of flow between two rotating cylinders, effect of thermal diffusion 78—18308
stable atmos. conditions, turbulence spectra 77—73786
staggered radial tube bundle in viscous liquid crossflow, flow, forces and drag 80—38387
staggered tube bundle, pressure and friction drag, mass transfer effects 80—38388
stagnating thermal turbulent boundary layer mean and fluctuating characts., divergent flow heat transfer 78—83370
stagnation boundary layer response to change in external velocity 79—64648
stagnation region heat transfer in hypersonic particle environments 77—31325
steady flows, fully stalled, flow computation in two dimens. passages 78—94826
steady two-dimens. viscous boundary layer, transport physics and math. characts. 80—14673
steam condensation on turbulent water surface 79—64748
steam-generating tube, bubble/plug flow boiling regimes, elevated press., drift vel. and void fraction determs. 78—87379
steam-generating tubes, rough (smooth), post-dryout, heat transfer 78—55678
step, rearward-facing, downstream turbulent flow 78—59380
Stokes flow between two spheres, flow separation 77—11176
Stokes layer stability in dusty gas 80—19493
stratified flow, vel. profile *(Russian)* 79—10601
stratified fluid, turbulent layer development *(Russian)* 78—63477
streamflow turbulence effect on bottom topography 79—39780
streamline curvature effects, anal. 78—59382
streamline curvature effects 78—13998
streamline pattern in confined vortex flow 77—51063
streamwise bar of rectangular cross section on flat plate, boundary layer development 77—72284
streamwise vortices in nominally two-dimens. turbulent boundary layer, spanwise nonuniformity 77—23964
stress on wall in contact with Rivlin-Ericksen fluid, viscometric flow *(French)* 77—72210
structural response to turbulent forcing field, decomposition calc. method 77—72282
structure and development in oscill. external flow 80—19353
structure at smooth solid wall *(Russian)* 77—58667
structure of boundary layer turbulence with low external flow turbulence *(Russian)* 79—68689
structure of plane turb. boundary layer rel. to external flow *(Russian)* 78—38331
structures and mechanisms of turbulence, conference, Berlin, Germany (Aug. 1977) 78—94647
subcooled forced convection boiling heat transfer at subatmospheric pressure 78—94525
subcritical steady plane flow past profile with sharp trailing edge, smoothness and circulation *(French)* 78—18312
subsonic streamwise corner, laminar-turbulent transition 77—62269
subsonic turbulent boundary-layer flow, compressibility effects 77—62268
subsonic turbulent flow past a downstream facing annular step, flow separation 80—43696
subsonic turbulent flow past a planar fence, separation bubbles 80—53807
suction or blowing flows through openings in the wall of a boundary layer *(French)* 79—18947
suction under nonisothermal conditions, heat and mass transfer 80—92125
suction-induced asymptotic boundary layers, exptl. and predicted props. 80—1553
sudden enlargement in circular pipe, downstream flow reorganisation, spatio-temporal study *(French)* 80—38497
supercavitating blocked flow, finite cavity, anal. for wake displacement thickness 78—18322
supercavitating hydrofoils with pseudo Kirchhoff noses, drag, nose press. 77—27566
supercritical HeI, heat transfer to turbulent pipe flow 80—64348
supercritical jet flapped airfoil, relax. soln. for transonic flow 77—23984
superimposed miscible liquids, dynamic stabilization, turbulent transport through diffuse boundary layer 80—74844
supersonic, flare-induced separation 77—3843
supersonic, on nonadiabatic surface, solution to equations 77—89148
supersonic, turbulent boundary-shock wave interaction, aerodynamic heating 78—26155
supersonic, wall temp. effect 78—94765
supersonic and hypersonic flow, turbulent boundary layer separation and reattachment on flat plate with ramp 77—23990
supersonic boundary layer, laser Doppler velocimeter meas. 77—35273
supersonic boundary layer, prediction by hybrid marching integration procedure 77—65761
supersonic boundary layers interacting with cooling wall jets, turbulent and optical characteristics 80—106792
supersonic compressed boundary layer on two-dimens. plate, unstable localised disturbance characts. 77—55031
supersonic diffuser with surface cooling, flow and heat transfer meas. in pseudo-shock region 77—42868
supersonic equilib. dissoc. and ionised gas 77—47039
supersonic flow, self-induced oscills. 78—67215
supersonic flow, separated, self-excitation of acoustic oscillations 77—7411

boundary layer turbulence continued
  supersonic flow along wavy wall including boundary layer effects *(German)* 77—84274
  supersonic flow of turbulent boundary layer over wavy wall 79—55366
  supersonic Mach 6 hydrodynamic flow past permeable wedge, holographic interferometry meas. *(Russian)* 78—14108
  supersonic separated turbulent boundary layer, laser velocimetry meas. 77—35274
  supersonic separation flow, 2- and 3-dimens., turbulent boundary layer and shock wave 80—100017
  supersonic shock-wave boundary-layer interaction, appl. laser anemometer 77—35275
  supersonic shock-wave-turbulent boundary layer interaction, appl. photon correlation anemometry 77—35277
  supersonic turbulent boundary layers, separation ahead of protuberances 78—14040
  supersonic turbulent compression corner flow, numerical simulation 77—62276
  supersonic turbulent surface flow around yawed cone 79—4037
  surface cooling, Mach 7 flow, multiple slot injection 78—9653
  surface friction in turbulent boundary layer, meas. using plane Pitot tube 80—79284
  surface roughness and injection 78—94654
  surface shear stress fluctuations, role in generation of 80—23994
  surface-mounted cube in uniform and turbulent streams 77—27535
  surfaces with porous section 79—86412
  swirled turbulent flow in cylindrical channels, heat and momentum transport, local props. 80—14819
  swirling annular capillary jet flow *(Russian)* 78—75180
  swirling jets, confined, axisymmetric viscous incompressible flow, numerical prediction 77—84286
  swirling viscous flow with applied mag. field, differential eqns. for boundary layer 78—22428
  symmetrical airfoil, transonic flow, inviscid and turbulent flow props., wake 80—48736
  tangential injection boundary layer control, vel. profiles, prediction method comparison 80—14671
  tangential slot injection, effects on turbulent boundary layer 80—33578
  Taylor column for hemisphere, nonlinear effects 77—11199
  Taylor-Gortler instability in turbulent shear flows and boundary layer transitions 78—90836
  temperature and velocity fluctuations, spectral analogy 77—7376
  temperature dissipation fluctuation component simultaneous meas. 78—26113
  temperature dissipation fluctuations, in turbulent boundary layer, meas. technique and errors 77—84255
  temperature dissipation log normality 78—34135
  temperature field, dispersion meas. 78—38322
  temperature fluctuation space correlation coeff. in turbulent core *(Russian)* 78—14001
  temperature fluctuations, correlations and probabilities 79—46303
  temperature fluctuations, local isotropy 79—1191
  temperature fluctuations, turbulent diffusion *(French)* 77—62248
  temperature fluctuations 77—75898
  temperature fluctuations downstream of heat source *(French)* 77—911
  temperature profile and Reynolds analogy expressions 78—87337
  temperature ramps in surface layer of atmosphere 79—88434
  temperature spatial derivatives, skewness 80—28497
  tensorial volume of turbulence 80—59012
  thermal, on rough surface, temp. distrib. 78—30279
  thermal and dynamic fields analogy, with wall suction *(French)* 79—1249
  thermal characteristics of a turbulent boundary layer with an inversion of wall heat flux 80—19350
  thermal energy storage by latent heat of fusion *(French)* 79—3893
  thermal layers on flat plates 79—23307
  thick axisymmetric turbulent boundary layer on a circular cylinder, similarity laws 80—64529
  thick water film in turbulent flow over impermeable slope, erosion and sedimentation *(French)* 80—43692
  thin-wall cylinder method for heat transfer studies in tubes and channels 77—24045
  three dimens., on side wall of curved rectangular duct 78—18282
  three dimens. turbulent boundary layer, fourth order Mehrstellen integration 77—3816
  three dimensional separated turbulent flows at supersonic speeds 80—19435
  three dimensional turbulent boundary layers, modelling heuristic approach 79—81864
  three dimensional turbulent boundary layers, turbulence meas. c.f. shear stress hypothesis *(German)* 78—94664
  three-dimensional, in turbomachinery rotor, experimental study 79—32490
  three-dimensional compressible mixing and reacting ducted flows, modelling 77—27621
  three-dimensional flow, in orthogonal curvilinear coordinates 77—23940
  three-dimensional flow along enclosed rot. disc, roughness effects 79—94628
  three-dimensional flow around bodies of arbitrary shapes, soln. method 78—79312
  three-dimensional flow in highly-loaded axial turbomachine, vorticity effects 78—26130
  three-dimensional flow structure in circular cylinder *(French)* 77—23941
  three-dimensional layers, peak of Johnston's triangular model 77—35130
  three-dimensional model of turbulent transfer in rectilinear channel 77—35138
  tidal flow in channel, modelling using turbulence energy closure scheme 79—79859
  Tollmien-Schlichting waves, characteristic structures in timefunctions from turbulent wall pressure fluctuations 80—92130
  tornado-like boundary layer flow, two-eqn. simulation 77—35151
  torque suppression in mech. stirred liqs. and multiphase systems, additives 77—3864
  trailing-edge turbulent flow noise, incident surface pressure field effect 78—90865
  transition from laminar to turbulent boundary layer, results of photographic expt. *(Russian)* 77—62243
  transition to hypersonic turbulent flow, boundary layer acoustic monitor 78—34237
  transitional turbulent pulsatile flow in channel 77—46993
  transonic, shock penetration 78—14044

boundary layer turbulence continued
  transonic flow, meas. by hot-wire anemometer 78—14103
  transonic flow, shock wave interaction *(French)* 78—34163
  transonic flow, shock wave interaction with turbulent boundary layer, pressure distrib. 80—74918
  transonic flow, shock wave interaction with turbulent boundary layer, wall shear stress 80—74919
  transonic flow, unsteady, turbulence modelling, compression waves developing into shock wave 80—74909
  transonic flow about lifting aerofoil 79—4032
  transonic flow over airfoil, steady and unsteady, shock-induced separation 79—59999
  transonic flow past airfoil section, boundary layer, laser velocimetry meas. 77—35274
  transonic flow with pressure gradients static pressure hole meas. errors 79—94645
  transonic nonseparating normal shock-turbulent boundary layer interaction, approx. anal. theory 77—23992
  transonic normal shock-turbulent boundary layer interaction, Reynolds no. and mass transfer effects 79—37353
  transonic shock wave-boundary layer interaction, dual-scatter laser velocimeter meas. 77—39376
  transonic shock wave-turbulent boundary layer interaction, integral computation method 79—1213
  transonic shock/boundary-layer interaction subject to large pressure fluctuations 80—38433
  transonic turbulent boundary layer, Mach 0.8, skin friction reduction by slot injection 77—39309
  transonic two-phase vapour-drop flow in channel, stability singular point 77—55078
  transonic vel. profiles, local skin friction coeff. 78—67214
  transparent turbulent gas flow past radiating plate, heat transfer anal. 77—35257
  transport eqns. soln. by accurate numerical method 80—28498
  transport processes, model 77—58663
  tube, annular high Prandtl no. flow, turbulent heat transfer, surface rejuvenation model 78—71333
  tube, cylindrical, sudden expansion, turbulent flow meas. by laser Doppler velocimeter 80—75003
  tube, vertical, laminar and turbulent heat transfer, air and Ar 78—71332
  tube arrays in cross-flow, flow induced vibrs. 78—46984
  tube bank, heat transfer and flow around second cylinder of three cylinders in cross flow 77—15025
  tube bank, in-line, acoustic reson. generation mech. 78—46958
  tube banks, heat transfer, viscous flow, numerical anal. 79—55375
  tube banks in turbulent flow, heat transfer prediction 79—1080
  tube bundle in turbulent water crossflow, bent tube vibrations 80—92124
  tube bundles, high Re crossflow, hydraulic drag and flow patterns, boundary layers 80—92122
  tube flow, gel-walled 79—90334
  tube flow, longitudinal turbulent dispersion of dye pulse, asymptotic stage, Taylor conditions 77—51050
  tube flow, velocity correl. function truncation *(Russian)* 78—75124
  tube flow, with spiral blades, heat transfer, drag resistance 78—1672
  tube flow initiated by expansion wave, viscous effects 78—26192
  tube wall, gas film-cooled, turbulent heat exchange, coolant turbulence intensity influence *(German)* 79—18895
  tubes, viscous liquid turbulent unsteady flow, pressure drop in transition region 80—74978
  turbine blade, calcs. 79—64647
  turbulence characteristics, in separated, reattached, and redeveloped regions of 2-d flow over flat-plate 78—94660
  turbulence characteristics in 3D layer 79—46297
  turbulence generators in combination with barriers and/or roughness, characts. 79—94598
  turbulent boundary layer with separation, calc. using integral method 79—77087
  turbulent boundary layers in oscillating flow with a mean adverse pressure gradient *(French)* 79—77085
  turbulent compressible boundary layer with heat-transfer effects on conditions at the sublayer 80—14672
  turbulent core of boundary layer 79—1168
  turbulent energy and length scale eqn., mean vel., similar solns. 77—89102
  turbulent flow relaminarisation, flow visualisation 78—75244
  turbulent gas flows in channels with high freq. press. oscillations, heat transfer 80—24024
  turbulent heat transfer from flat plates, facing curved wall effects *(Japanese)* 80—83799
  turbulent horseshoe vortex 80—103016
  turbulent liquid flow, at wall, physical model 77—27514
  turbulent natural convection boundary layer, space-time correl. meas. 78—71322
  turbulent pipe flow, segmented blockage, downstream flow and pressure characts. 80—43778
  turbulent Prandtl number behaviour near a wall 80—79279
  turbulent pulsating tube flow, friction resistance and energy losses *(Russian)* 77—51039
  turbulent shear flow using hot-wire probe, effects of orientation 79—27722
  turbulent shear stresses in compressible boundary layers 80—14736
  turbulent skin friction at subsonic and supersonic speeds, wake component influence 80—19340
  two circular discs in tandem, drag reduction, wakes 80—106795
  two dimensional shockwave—turbulent boundary layer interaction, flow separation 80—14758
  two tandem circular cylinders, flow at very high Reynolds numbers 80—19341
  two-dimensional fence flows, wall constraint 78—59381
  two-dimensional supersonic viscous in reactions near walls, prediction method 77—58726
  two-dimensional turbulence on the surface of a sphere 78—73447
  two-phase flow, and droplet entrainment and deposition at boundary 77—62299
  two-phase flow, boundary vapour contents for critical state of heat transfer of second kind 78—1722
  two-phase flow, turbulent boundary layer, drag reduction 78—22414
  two-phase flow, unstratified, in permeable tube, hydraulic resistance 77—35205
  two-phase flow between parallel corotating discs, laminar or turbulent throughflow, bulk-parameter anal. 77—39336

boundary layer turbulence continued
- Uchinskii reservoir, ice covered, statistical props. of velocity and temp. profiles *(Russian)* 77—78269
- underground cable system, convectively cooled, vel. distribs., press. drop correlations 78—71330
- underwater sound, cancellation of turbulent boundary-layer press. fluctuations 77—88978
- unified similarity theory, turbulent convection at vertical surface 78—90890
- universal velocity profile 78—1639
- unsteady, near separation, oscill. press. gradient effect struct. features 78—75126
- unsteady boundary layers, separated and attached, review 78—71313
- unsteady boundary layers, separated and attached, review 79—77086
- unsteady boundary layers with reversal and separation 78—75163
- unsteady convective heat transfer in heating liq. in pipe 77—89117
- unsteady flow past semi-infinite porous flat plate with suction, velocity profiles 80—92129
- unsteady heat transfer from rotating disc or cone with large suction 77—47025
- unsteady laminar boundary layers behind blast waves, num. soln. 80—69776
- unsteady symmetric channel high Reynolds no. flow 80—24096
- unsteady transitional and turbulent boundary layers, expt. and calc. methods *(French)* 78—75125
- unsteady transonic flow about oscillating airfoil, perturbation soln. 77—23985
- unsteady turbulent boundary layer developing in oscillatory external flow *(French)* 77—72288
- unsteady two-dimens. boundary layers, fluctuations in external vel. 77—51043
- upstream perturbation propagation, supersonic flow, self-induced press. boundary layer on moving surface 80—74914
- upward turbulent free convection, adjacent to horizontal surfaces 79—59977
- vaporisation channels, rough and smooth, heat transfer in post dry-out region 80—96255
- velocity, complete profile formula including wake deficit and inner layer function 77—51048
- velocity distrib., wall friction in rotational turbulent laminar boundary flow *(German)* 80—1526
- velocity distrib. and eddy current model *(Russian)* 80—33574
- velocity distribution in cylindrical pipes 79—37299
- velocity measurement by single-beam laser time-of-flight method 79—77298
- velocity profile calc. by Du Fort Frankel scheme 79—94600
- velocity profiles over smooth surface 78—67183
- vertical plate boundary layers, affected by liq. surface waves 79—72884
- viscoelastic fluid, turbulent flow, frictional drag reduction 78—1696
- viscoelastic fluid, turbulent wall motion 77—55047
- viscoelastic liquid, boundary layer anal. of oscillating cylinder flows 77—65771
- viscous drag of two-dimensional contours moving in a weak polymer solution 80—100014
- viscous drag reduction by polymer injection at high Reynolds number *(Chinese)* 79—32582
- viscous flow, between concentric rot. spheres, visualisation and meas. 77—15038
- viscous flow near edge of rotating disc *(Russian)* 77—72303
- viscous liquid, logarithmic equations for resistance of turbulent friction 77—51042
- viscous sublayer and near wall turbulence struct., stroboscopic visualisation 80—19349
- viscous sublayer interaction with fully developed turbulent region, instability 78—1652
- viscous sublayer temp. fluctuation spatial correlations *(Russian)* 78—34114
- viscous sublayer turbulent Prandtl no., wall heat cond. influence 79—94616
- viscous two-dimens. incomp. flow with separation at cascade inlet edge, num. calc 79—90232
- viscous wall region representation by regular eddy pattern 80—23992
- viscous-inviscid flow interaction method, using blowing and suction flows 79—1154
- vortex chamber, friction losses on end walls, Kantorovich method 77—47021
- vortex flow, atmospheric, two-eqn. modelling, predictor-corrector multiple iteration 77—91237
- vortex shedding from smooth and roughened cylinders in crossflow near plane surface 79—81911
- vortex-array representations, interaction, of free-stream turbulence near semiinfinite flat plate 78—90842
- vortices, two-dimens., in bounded container, statistical mechanics 77—3831
- vortices in end-wall boundary layers, numerical anal. 77—80168
- wake, for turbulent shear layers, modified law 77—35146
- wake, heated, interface statistics 79—27645
- wake flow behind, cone placed on flat plate, separation and vortex form. 77—72302
- wake of circular cylinder with boundary layer suction 80—53785
- wall, turbulent struct. 78—26106
- wall boundary layer, induced turbulence influence from jet and vortex generator *(Russian)* 79—59970
- wall flows, constant press. and press. gradient flows, book contrib., review 80—19347
- wall flows, struct. 78—18281
- wall flux, down-stream from linear heat source in turbulent boundary layer *(French)* 79—32489
- wall interference effects of static pressure probes 78—1762
- wall jet, 3-dimens., surface layer props., computation 80—1667
- wall jet, algebraic Reynolds stress model calc. 80—1668
- wall jet, radial, temp. field and heat transfer meas. 77—72341
- wall jet, three-dimens., press. and vel. meas. 80—19456
- wall jet on flat smooth plate, mean vel., turbulence and press. distribs. 77—62288
- wall jet over convex surface, turbulent flow characts., Reynolds shear stress 77—42890
- wall jet turbulence, cylindrical streamwise surface curvature 77—55066
- wall pressure meas. using rectangular membrane as spatial filter 77—72107

boundary layer turbulence continued
- wall region heat and mass transfer in turbulent Newtonian and viscoelastic flow 80—14680
- wall region of relaxing flow 78—34113
- wall shear stress, small amplitude perturbations 78—14000
- wall shear stress meas. in shock wave-boundary layer interaction, comments 80—14670
- wall shear stress meas. with hot film device in var. temp. flow 77—51142
- wall shear stress prediction in three-dimensional turbulent boundary layers 78—67184
- wall suction and heating, inner region anal. *(French)* 77—19595
- wall turbulence, single harmonic theory, second moments closed theory 79—98699
- wall turbulence, turbulent correlation equations 78—94673
- wall turbulence and bursts, surface rejuvenation model, u^+ and T^+ inner laws 80—96251
- wall turbulence in drag-reducing pipe flow 77—68578
- wall turbulence struct., adverse pressure gradients effects, fluctuations and separation 80—10231
- wall turbulent flows with drag reduction, Reynolds stress model 80—43695
- wall-pressure spectrum in turbulent boundary layer, rel. to noise generation by boundary layer-surface interactions 80—69810
- water, flowing, eddy patterns rel. to wall scallops and ripples sizes 79—27628
- water, turbulence rel. to fine struct. of thermal boundary layer near air-water interface *(Russian)* 78—22332
- water, turbulent flow, effect of polymeric additives 79—1216
- water adjacent to vertical uniform flux surface, buoyancy driven flow, transition and transport 79—27631
- water film flow behaviour and effect on cocurrent air flow, press. distrib. along rigid wavy structures 77—55029
- water jet appearance, nozzle shape and polymer additive effects, boundary layers 80—53828
- water surface, free, roughness determ., from air flow struct. anal. 78—63441
- water turbulent heat transfer downstream of unsymmetric blockage in tube 79—55377
- water vapour, wet, boundary layer in compressible flow 80—10295
- water-air interface, overall heat transfer coeffs., humidity and density profiles, turbulent pulsations *(Russian)* 78—22349
- wave generation on elastic surfaces, expt. study 80—74843
- weak polymer solution in smooth pipes, turbulent wall motions 80—14823
- weak polymer solutions, wall region turbulence models *(Russian)* 79—14440
- weakly-separated zones, numerical prediction *(French)* 77—72276
- wedge-shaped leading edge of plate, local air (water) flow heat transfer 78—1660
- wedges, high Reynolds number flow, base pressure in near wake 80—59038
- wind generated wave damping in medium with natural turbulence *(Russian)* 77—41058
- wind simulation, air jets perpendicular to wind-tunnel stream 77—56691
- wind tunnel, roughness element geometry anal. 78—47079
- wind tunnel study of roughness effects of multiple windbreaks 77—72285
- wind tunnels, turbulent boundary layers on rough surfaces, simple roughness elements, natural wind simulation 80—69774
- wind-driven water waves, numerical model calcs. 77—922
- wind-wave interaction, two-layer flow, numerical simulation 78—92823
- wing, 3-dimens. boundary layer calc. method 80—1622
- wing, swept, 3-dimens. turbulent boundary layer, numerical anal. 80—1621
- yawed flat plate at incidence, three-dimens. boundary layer turbulence meas. 78—51160
- CO_2 absorption in H_2O, aq. solns. with interfacial turbulence due to microstirrers 80—64527
- CO_2, turbulent cooling tube flow, at supercrit. press. 78—14005
- Co_2 flow in heated tubes, with near critical parameters, turbulent flow, heat transfer 80—59022
- H_2 gas launcher, boundary layer closure, heat transfer 79—55387
- H_2-O_2 reaction, numerical anal. *(German)* 77—35253
- H_2O channel flow, heat transfer from cylinder oscill. in cross flow 79—55386
- H_2O flow in heated tubes, with near critical parameters, turbulent flow, heat transfer 80—59022
- He, near-critical, friction factors for flow in curved tubes 78—83367
- He, supercritical, turbulent pipe flow, heat transfer by Melik-Pashayev technique 80—74860
- NH_3, flow in steel tubes, wall heat transfer with catalytic dissoc. 78—14099
- N_2O_4, dissociating, turbulent pipe flow, heat transfer, resistance 78—91026
- N_2O_4 dissociating gas flow in channel, turbulent boundary layer *(Russian)* 79—60067
- N_2O_4, dissociating turbulent convection on horizontal plate *(Russian)* 80—1587
- N_2O_4, turbulent dissoc. flow, along heated tubes, heat transfer 80—63225

boundary layer turbulent flow *see boundary layer turbulence*

boundary layers
- *see also atmospheric boundary layer; boundary layer turbulence*
- ablating body shape, numerical soln. method *(Russian)* 78—75134
- ablating boundaries, algorithm for automatic tracking 79—32240
- ablation, transient, with time-depend. heat flux, integral solns. 79—60088
- absorbing-emitting, natural convection boundary layer flow 77—58808
- absorbing-scattering semitransparent planar layer, flat temp. waves 78—90683
- acoustic, enclosure, thermoviscous dissipation at walls, normal mode theory 78—83171
- acoustic field effect on compressible liquid flow in laminar boundary layer *(Russian)* 77—68617
- acoustic impedance influence of a cylindrical wall cavity 80—69784
- acoustic streaming in boundary layer of viscous heat cond. medium 79—86544
- adaptive-wall wind tunnel, iterative anal. of subsonic flow 78—22364
- admixtures, convective-diffusive transfer in cylindrical channel, soln. 77—7391
- aeolotropic elasticity, semi-infinite medium, axisymmetric problem solns. *(French)* 80—8795

boundary layers continued
aerodynamic ablation of melting bodies, effect of temp.-depend. heat capacity 79—37431
aerodynamic ablation of spinning steel shells, side force 79—37347
aerodynamic drag on heated spheres and cylinders, effective Reynolds no. 77—89090
aerodynamic flow round wing section with two vortex sources, calc. *(Russian)* 77—31318
aerodynamic laminar boundary layer on curvilinear thermally conducting surface, optimum suction *(Russian)* 77—54968
aerodynamically heated body, stable shape during ablation *(Russian)* 78—75162
aeroelasticity of unsteady aerodynamics, force calc. methods *(French)* 78—75095
aerofoil, dynamic forces acting, subsonic instabilities *(French)* 78—67213
aerofoil, thin, windward surface shock layer, hypersonic flow 78—34158
aerofoil, two-dimens., in incompressible flow, unsteady motion 78—67171
aerofoil in oscillating flow, vel. field, surface press. 78—75164
aerofoil in unsteady airstream, two-dimens. viscous flow, numerical predictions 78—75166
aerofoil in unsteady viscous flow, numerical soln. procedures 78—75165
aerosol, interaction with surfaces past which they flow 77—80198
aerosol, simultaneous diffusion and sedimentation in rectang. tube 77—11266
aerosol enclosures under convective stirring conditions, quiescent boundary layer thickness 79—66364
aerosol particles in flow type chamber, coagulation, deposition 80—69908
aerosols, particle-droplet inertial collisions 79—47989
aft bodies, two-dimensional, min. pressure drag in supersonic flow 77—27555
agitated vessel, flow behaviour and transport phenomena, correlation eqns. *(Japanese)* 78—38300
agitated vessels, heat transfer models, thermal boundary layer 80—79288
Agulhas Current, topographically induced changes in struct. of inertial coastal jet 80—72545
air, dissociated, hypersonic flow over blunt axisymmetric body, nonsteady heat exchange 79—37319
air bubbles, rising in glycerine-water mixture, boundary surface velocity *(German)* 79—32631
air flow between rotating discs, exptl. obs. and theory *(Russian)* 77—55009
air flow over water surface instability 79—46290
air flow separation over water waves 77—11208
air layer near water surface, diurnal characts., equatorial region, GATE meas. 78—61527
air scoops at supersonic and hypersonic vels., throttling, separation and central body cooling 80—14739
air-atomised water mixture, high temp. surface impact, heat transfer *(French)* 79—4015
air-sea interaction, surface drift current speed and direction calc., geostrophic wind factor 78—61422
air-sea interface, oceanic variability obs. during Project BOMEX 78—69362
air-solid flow in pipe bends, circ. and elliptical, press. drops 79—32642
air-vapour flow in channel, laminar, with wall vapour-ice transition 79—94617
air-water interface, aqueous sublayer thickness determ. 77—60395
air-water mixture, vertical flow, temp. influence on boundary lines between flow regimes 80—43764
air-water two-phase flow in vertical pipe, heat transfer *(Japanese)* 77—24011
airborne dusts collection by bluff bodies 79—4065
airfoil, oscillating, unsteady leading edge separation bubble calc., using finite difference procedure 77—72317
airfoil, thin, pulsating, HF subsonic flow 79—59998
airfoil trailing edge, incident acoustic wave diffr., flow depend. 78—26143
airfoil with oscillating jet flap, press. distrib. meas. 77—23976
airfoils and cascades, unsteady wakes meas., rel. to predictions 77—72300
airfoils placed near ground or in tunnels, flow with separation *(German)* 79—37345
airfoils with oscill. jet flaps, quasisteady theory 78—63467
algebraic decay, solns. of boundary layer eqns. 79—37280
alkali metal vapour condensation from gas flow (He,Ar,N_2) heat and mass transfer 78—75192
angular perturbations, stability and convergence 78—90827
annual review of fluid dynamic, book 80—94927
annular climbing film flow dispersion models 78—83473
annular conduit, wall suction, turbulent flow *(French)* 78—18343
annular gap turbulent flow calcs. 79—55417
annular gap with axial flow and rot. inner cylinder, heat transfer coeffs. 79—27489
annular rib cooled by boiling liq. on surface, heat cond. anal. 79—55315
annuli, laminar flow, pressure drop and heat transfer with dissipation allowance 80—74858
annulus, spherical, rot., forced thermal convection of viscous fluid 79—27634
annulus laminar flow of Newtonian fluids, kinetic energy correction factor 77—31271
annulus with rotating inner cylinder, momentum integral soln. of developing flow 77—35149
arbitrary body, unsteady separated inviscid incompressible flow, numerical soln. 80—28509
arc, boundary layer cooling of atmospheric arcs, arc interruption by moving rod 78—87545
arterial bifurcation, steady convective diffusion model 77—21546
asymmetric flow past wings, nonlinear-discrete vortex method 78—71351
asymptotic drag formulas for rapidly rotating radial channels of rectangular cross section 80—6065
asymptotic free convection from an insulated vertical flat plate at high Prandtl number 80—24014
atmosphere, large scale flow, quasigeostrophic approx., Ekman layer effects 79—2355
atmosphere, molecular boundary layer struct. over sea *(German)* 77—86989
AURORA machine studies of air chem., cond. and boundary layer 78—32144
average Nusselt numbers for external flows 80—38412

boundary layers continued
axial flow between cylinders, stability to asymmetric disturbances 78—38294
axially symmetric laminar boundary layer, on finite disc, vel. profile *(Russian)* 77—84219
axisymmetric boundary layer flow between wall and paraboloid *(Russian)* 78—75121
axisymmetric channel, laminar boundary layer in presence of external stream swirls 80—64631
axisymmetric channels of different configuration, heat transfer, gradient method appl. 80—24098
axisymmetric channels of slowly varying cross section, 3-dimens. acoustic disturbance propag. 79—90266
axisymmetric duct design for incompressible flow 77—47090
axisymmetric flow past pointed body of revolution *(Russian)* 77—55034
axisymmetric free shear layer, effects of initial momentum thickness 78—71325
axisymmetric laminar boundary layer, swirling flow through conical hydrocyclone, heat transfer 79—98733
axisymmetric Laval nozzles, numerical flow study including overexpansion and breakaway 79—90304
axisymmetric rotating round nosed bodies, flow and heat transfer, buoyancy effects 80—79306
axisymmetric stagnation flow on circ. cyl. 78—79298
axisymmetric viscous flow near vertex of body 77—19586
axisymmetry jet, inblow parameter effect on separation, boundary layers and heat transfer *(Russian)* 80—24064
backflow appearance conditions for rot. fluid in channel, stability *(Russian)* 79—86439
bacterial aerosol, deposition and round-nose wedge in interception region 77—81520
baroclinic two-layer flow in channel, instability, geophys. appl. 79—55420
base flow at supersonic vel., rockets and re-entry vehicles appl. 78—67243
beams, slender tapered with internal or external axial flow, dynamics theory 79—64499
beams, slender tapered with internal or external axial flow, dynamics experiment 79—64500
Benard convection in a finite box, secondary and imperfect bifurcations 79—50725
beneath potential vortex, finite-difference schemes 77—14982
bidimensional flow past symmetric profile 77—60942
binary boundary layer with press. pulsations, friction and heat and mass transfer 80—14653
binary fluid layer, heated from below or above, stability anal. 80—33563
binary mixture vapour condensation, forced-free convection, finite difference treatment 78—5741
biological cell saturation density, evidence against diffusion-limited process 78—48770
black hole accretion discs, boundary-layer behaviour of flow at disc inner edge 80—46598
blades in transonic flow, shocks and boundary layers, time marching method 79—4036
Blasius boundary layer, non-parallel flow stability 79—41668
Blasius boundary layer, Orr-Sommerfeld eqn., temporal eigenvalue spectrum 78—42589
Blasius boundary layer, sound and Tollmien-Schlichting waves 79—10578
Blasius eqn., generalised, boundary value problem 79—35567
Blasius flow, horizontal, heated from below, longitudinal vortices onset 78—71342
Blasius flow, Orr-Sommerfeld eqn., spectral props. 77—89097
Blasius profile, eigenvalues determ. using Riccati transform. method 77—65731
Blasius type boundary layer subject to blowing or suction, transition behaviour 79—18869
blockage effects in layer with mass transfer 78—26096
blood flow in branching vessels, visualisation using water model 77—25477
blood oxygenation using coiled tubes 78—40422
bluff bodies, cavitating, constrained flow, drag and vortex shedding 78—47006
bluff bodies in confined flow, free-streamline model 78—46931
bluff body, boundary layer separation, control method 79—72881
bluff body, two-dimens., drag and wake *(Japanese)* 78—55647
bluff body configuration and its effect on flame stabilization 79—94719
blunt axisymmetric bodies, supersonic flow modelling, drag and entropy layer 80—48740
blunt biconic at incidence, laminar viscous shock layer, supersonic/hypersonic flow 78—30313
blunt body, boundary and wake, supersonic viscous gas flow, numerical soln. 80—38441
blunt body, unsteady supersonic flow, grid characteristic method 80—38442
blunt body problem in nonuniform flow fields 78—5748
blunt circ. cylinder, separated, reattached, redeveloped air flow, heat transfer characts. 77—58692
blunt nosed body, laminar or turbulent flow, heat transfer and curvature effects, numerical soln. 79—1173
blunt obstacles in channels, MHD with inertia 77—84330
body of revolution, slender, nonlinear normal forces, Reynolds no. influence *(German)* 78—51191
body of revolution with heating and cooling, boundary layer transition and separation 80—64518
body shape optimisation at small Reynolds number 79—41659
boiling, non-stationary heat transfer crisis *(Russian)* 77—24401
boiling, nucleate, superheating, heterogeneous nucleation theory calc. 79—46170
boiling, nucleation centres interaction, obs. technique 78—14065
boiling, transition type, in forced convective flow, boundaries meas. 79—27499
boiling, two-phase boundary layer, temp. fluctuations 78—51222
boiling and bubbling heat transfer under the conditions of free and forced convection 78—90637
boiling burnout, for heaters cooled by liquid jets 79—59979
boiling mechanism during burnout phenomena in subcooled two-phase water flows 78—94529
boundary layer on conical body with gas injection *(Japanese)* 78—59417
Brownian particles, reversible adsorption and reversible coagulation, kinetic eqns. 79—16045
bubble, of vap., with microlayer, universal growth relations 78—71266

boundary layers continued

- bubble, rising, hydrodynamic interaction with suspended solid particle 78—51221
- bubble boundary layer formation over inclined porous plate 80—19504
- bubble collapse and jet formation in vicinity of wall, effect of polymer additives 79—81956
- bubble columns, large diameter, liq. phase duration *(German)* 79—32632
- bubble growth in combined gravitational and non-uniform temp. fields 78—22249
- bubble growth in superheated liquid, thin thermal boundary layer 78—38391
- bubble of gas rising in fluid filled tube, wall effects *(French)* 79—7399
- bubble oxygenator, O_2 transfer controlling factors 78—53568
- bubble population prediction, in flow boiling, from gas bubble nucleation expts. 78—90696
- bubbles, active nucleation site spatial distrib., bubble flow density 78—71267
- buoyancy boundary layer, supercritical solns. 79—55384
- buoyancy cross-flow effects on longitudinal boundary layer flow 77—58687
- buoyancy driven flows originating from heated cylinders submerged in a finite water layer 80—59024
- buoyancy effects, heat transfer and flow over semiinfinite plate 77—80152
- buoyancy induced flow over inclined heated porous surface, vortex instability 80—33601
- buoyant cylinder within rapidly rotating horizontal cylindrical container, steady flow 79—86441
- BWR Channel, two-phase flow fluctuations and continuity 80—14786
- camphene-coated surface, convective local mass-transfer coeffs., holographic interferometry method 78—75234
- canal, converging, unsteady 2-D compressible boundary layer flow 79—20885
- capillary condensation and adsorption, adsorptive pot. boundary layer approx. 78—2366
- carbon tetrachloride drops falling through H_2O, surfactants rel. to deform., oscill. *(French)* 80—66880
- carboxymethylcellulose, aq. soln., hydrodynamics of falling liquid film *(Russian)* 79—64715
- carboxymethylcellulose, aq. soln., real flow curve determ., with wall effects, in rotation viscosimeters *(Russian)* 79—64714
- Cartesian model, viscous boundary layer flow over topography 78—92904
- cascade, high-deflection, transonic two-dimens. flow *(French)* 79—27664
- cascade flow problem reduction of part channel of varying width to plane cascade problem 80—83844
- cascade flow problem reduction of part-channel of varying width 80—83843
- cascade with slender profiles, transonic flow, numerical soln. 80—38436
- catalyst surface, laminar film boiling with chem. react., model 80—45553
- catalytic reactive flow, normal velocity in laminar boundary layer *(French)* 77—75988
- catalytic surface boundary layer struct., kinetic, diffusion reaction phases 80—33706
- cathodic diffusion boundary layer, free convective flow obs. with shadow Schlieren method 78—68894
- Cauchy-Poisson problem on sphere *(Russian)* 77—35156
- cavitating plates, boundary layer and drag *(Russian)* 77—27504
- cavitation erosion, non-spherical bubble collapse near a solid wall, analytical soln. using matched asymptotic expansions 80—106824
- cavitational oscill. in blade pump, linear math. model 77—35187
- cavity, cylindrical in compressible liq., dynamics, underwater explosion appl. 79—7385
- cavity, horizontal, laminar natural convection heat transfer 79—55383
- cavity flow at high Reynolds numbers 77—31276
- cavity flows, two and three dimens., multistep technique with implicit difference schemes 79—37398
- channel, annular, with vortex generators, and uniform (nonuniform) heat injection length, crit. heat flux *(Russian)* 78—83397
- channel, axisymmetric, appl. of clipping approx. for inhomogeneous turbulence simulation 80—19331
- channel, constant depth, wave field from uniform movement bidimensional source *(French)* 80—79332
- channel, curved (straight), entry flow, slender channel approx. 78—47042
- channel, curved rectangular, secondary flow, Taylor-Gortler vortex pattern 80—106849
- channel, cylindrical, arbitrary cross section, nonlinearly viscous medium motion 80—69928
- channel, friction, with a pseudoshock 77—27546
- channel, horizontal, eccentric annular free convection in laminar flow 78—38310
- channel, laminar boundary layer, Gortler vortices 80—64572
- channel, rectangular, laminar forced convective heat transfer for 3rd kind temp. boundary conditions 78—87341
- channel, shock wave stationary motion for axial blowing and two-layer detonation 80—92177
- channel, vertical, round, in nonuniform mag. field, steady-state MHD convection 80—33696
- channel, with diverging walls, blood streaming viscous-convected inertia effect 77—52828
- channel and tube flow with mass transfer and vel. slip 77—84322
- channel bounded by confocal porous elliptic walls, steady viscous incompressible flow 80—43776
- channel bounded by two hyperbolas, steady laminar flow, vel. distrib. 77—68565
- channel flow, laminar to turbulent alternating transition, crit. Reynolds no. 78—46935
- channel flow, nonerodible porous lining thickness effects 77—58788
- channel flow, variable viscosity, with high heat generation 78—9717
- channel flow stability, influence of nonparallelism 80—83845
- channel flow with longitudinal press. gradient, friction meas. 77—58792
- channel flow with rough walls, drag 79—86512
- channel laminar flow, thermal entrance zone, heat transfer, optically thin gas layer effects 80—74861
- channel thermal inlet zone, heat transfer in laminar boundary layer 79—1178
- channel two phase flows, threshold steam qualities and cutoff heat fluxes 79—90242
- channel with blocked branch, laminar flow, nonregular domain transformation into rectangular domain 80—64635

boundary layers continued

- channel with falling liq. film and two-phase flow, heat transfer 78—30337
- channel with porous walls, convective diffusion and mass transfer *(French)* 80—79305
- channel with sloping bottom, heavy perfect fluid flow 80—96309
- channels, buoyancy induced flow, general correl. eqn. 77—58790
- channels with lengthwise nonuniform heat release, critical heat flux density 80—69824
- channels with unequal wall temps., low Peclet no. heat transfer 77—42813
- chemical boundary layer theory, similarity soln. 78—30369
- chemical laser nozzle, effect of geometry and boundary layers on flowfield 77—27622
- chemical reactor, falling-film gas-liq. type, mathematical model 79—86526
- chemical shock tube flow, laminar to turbulent boundary layer transitions 77—48642
- chemically frozen multicomponent boundary layer, thermal diffusion effects behind strong shock 80—53772
- chemically reactive, nonequilibrium boundary layer flow, exact and approx. solns. 80—79409
- chemically reactive boundary layer problems with relaxation processes, Enskog-Chapman method modification *(Russian)* 80—19523
- cholesteric liquid crystal, flow between two parallel plates 78—18539
- circular cone, axisymmetric laminar boundary layer, exact similar soln. 80—14650
- circular cylinder, non-Newtonian fluid flow boundary layer eqn. approx. soln. 80—14752
- circular cylinder in laminar incompressible viscous flow, finite element anal. 77—84216
- circular cylinder moving in stationary fluid, skin friction and heat transfer 79—50701
- circular cylinders and spheres, fluid flow and convective heat transfer *(German)* 79—94624
- circular plane parallel flow around cylinder *(Russian)* 77—68618
- circular tube, non-Newtonian fluid linear flow, heat transfer 79—98810
- circular tube laminar flow, heat transfer with temp. depend. heat generation 77—68582
- circular tube thermal entrance region, laminar droplet flow convective heat transfer 80—6049
- circular tube under centrifugal accel. field, condensation heat transfer 80—74713
- circulation flows near wall, ideal liq., two-dimens. anal. in Cartesian coords. 78—51173
- circulatory viscous incompressible liquid flow, momentum eqn. anal. *(Russian)* 79—59992
- closed torus in Stokes flow, eddy-type motion and vortices 77—42850
- coaxial circular discs, hydrodynamical problem 80—24032
- coiled tubes, laminar flow and heat transfer, efficient numerical procedure 80—64633
- collapsible tube subjected to external pressure or body forces, unsteady flow 80—14822
- combination of potential and vortex flows, boundary value problem for incompressible liquid *(Russian)* 77—68595
- combined convection flow along vertical surface, fluctuating boundary layers 80—96254
- combined convective flow through circular pipe, viscous dissipation effects 79—68803
- combined convective laminar boundary flow, vertical cylinder in horizontal flow, finite difference approx. 78—90893
- combined forced and free convection in horizontal tubes with temp. depend. viscosity 77—15023
- combustion gas flow, spectroscopic temp. meas., cold boundary layer effects 77—31399
- combustion in laminar diffusion gas jets, computation of diffusion flare 80—10276
- complex aerofoils, compressible flows, isoparametric Hermite cubic element 80—1617
- compound lifting surfaces at high supersonic flight speeds 77—19622
- compressible, refractive index meas. by light refl. 78—8438
- compressible and incompressible flows, recent theoretical and expt. developments, book 80—1620
- compressible boundary layer flows, curvature near separation 78—55661
- compressible flow, Navier-Stokes eqns. similarity solns. for large Prandtl number 77—3801
- compressible flow around expanding cylinder and sphere 77—35158
- compressible flow in rot. cylinder, linearsed anal., appl. to gas centrifuges 78—71345
- compressible flow past profile set between permeable walls 79—46335
- compressible fluid flow past degenerate star-red giant interacting binary stars 80—67779
- compressible fluid flow through annular orifices, computer-aided numerical anal. 80—87806
- compressible laminar, at large Prandtl numbers, pressure gradient effects 80—19321
- compressible laminar, stagnation point flow with continuous moving surfaces 77—15054
- compressible laminar boundary layer with large acceleration and cooling 77—11213
- compressible laminar boundary-layer, 2D eqn., near separation, numerical soln. 77—46989
- compressible Navier-Stokes equations, mixed explicit-implicit splitting method 77—58715
- compressible oscill., numerical anal. 77—89140
- compressible stagnation point, discontinuous solns. for three-dimens. flow 77—42856
- compressible stagnation pt. boundary layers for laser heated flows 77—89141
- computational fluid mechanics, book 80—1517
- concentration distribution on models during erosion by air flow 78—67172
- condensate film flow on finned surfaces, heat transfer, heat exchanger design 78—75038
- condensation, flow of vap. over cylinder, two-phase boundary layer eqns. 79—46306
- condensation of laminar film on helical elliptical cylinders, governing eqns. soln. 78—9689
- condensed medium, semitransparent, plane layer radiative-conductive heat transfer 80—43590

boundary layers continued
condenser system, submerged, buble pumped augmented natural convection 78—94535
conducting flow over oscillating plate with suction or intermediate layer 77—47098
conducting fluid film drainage over permeable wall in transverse mag. field 79—41761
conduction-controlled rewetting of hot surface, two-parameter relation 77—19605
conduit, speed of disturbance waves conveying aerated water 77—27581
conduit with lateral outlet, two-dimens. flow past barrier 80—64642
conduit with variable gradient, rapidly flowing incompressible liquid, short waves 80—92219
conduits, two-dimens., suddenly expanding, laminar flow patterns, temp. influence 80—19505
cone, convective mass transfer, in nonlinear viscous field, rel. to heterogeneous reaction kinetics 77—55103
cone in transition Reynolds no. domain, tangential injection effect on heat transfer 79—64654
cone revolving in tube, finite cavity flow, drag force coeffs., cavitation 80—33641
cone with arbitrary surface deviations in supersonic gas flow, aerodynamic characts. 77—19620
confined perfect gas, thermal disturbance response, slow transients 79—81976
confined thermal convection driven by non-uniform heating from below, boundary layers 80—87769
conical body laminar boundary layer with heat transfer *(Japanese)* 78—30257
conical diffuser, with suction, compressible boundary layer swirling flow 78—38360
conical nozzle and diffuser, laminar compressible boundary layer swirling flow 80—48768
conical surface, boundary layer due to swirling flow with throughflow 77—47024
conservation relations with heat/mass transfer and vel. slip 77—62246
constrained and unconstrained flow about pitching foil 78—26137
continental shelf sediment transport, turning effect in bottom boundary layers 77—37235
convection, forced, laminar, wedge flow with separation 80—1523
convection, forced, over rot. bodies with non-uniform surface temp. 79—23315
convection, free, and radiative transfer, at vertical plane surface 78—55645
convection, free, in saturated porous medium boundary layer with lateral mass flux 79—27689
convection, free, in vert. rectangular enclosure, Gill's soln. consts. determ. 79—50728
convection, free, laminar, three-dimens., about surface, numerical anal., visualisation *(French)* 78—87343
convection, free laminar flow, between two parallel vertical walls 77—47010
convection, laminar assisting forced and free, comprehensive correlating equation 77—51051
convection, laminar mixed forced/free, about sphere, buoyancy effects 77—75907
convection, mixed, about sphere with uniform surface heat flux 79—32519
convection, mixed forced/free, from horizontal plate, in porous medium 77—75908
convection, mixed free/forced, about inclined surfaces in porous medium 77—75973
convection, natural, from vert. DC current-heated plate, linear stability anal. 78—90873
convection, natural, in porous medium, singular perturbation problem 79—94715
convection, natural, in presence of transverse mag. field similarity soln. 78—67197
convection, natural, in spherical layer of viscous compressible gas 78—9640
convection, natural, laminar, enclosure with heat source and sink on horiz. boundary 78—90882
convection, natural, laminar, in open vertical channel, numerical soln. method 78—5799
convection, natural, on vertical heated surface, expt. *(Japanese)* 80—5912
convection, natural, over uniform heat flux vertical surface, higher-order approx. 78—59388
convection, past hot porous circ. cylinders, of 2nd-order liq. 79—14476
convection along plate, MHD boundary layer eqns. soln. 77—11276
convection in channel downstream of constriction, local transfer coeffs. augmentation 78—5800
convection in vibr. layer of fluid heated from above 79—86424
convection of vertical layer, flow stability, boundary thermal props. effect 78—55644
convection on vertical flat plate in infinite fluid 78—22345
convection problems approx., using finite element analysis 77—89115
convective diffusion to drop, large Peclet no., finite Reynolds no., asymptotic soln. 79—41742
convective diffusion to surfaces of poorly streamlined bodies 80—6041
convective heat and moisture transfers with const. heat flux *(French)* 80—33582
convective heat transfer, with conjugate boundary conditions *(Russian)* 77—23956
convective heat transfer augocentation thermal entrance regions using thermal instability 79—81887
convective heat transfer in coaxial horizontal channel, influence of electroviscous effects 79—77100
convex wall jet, characterisation of external boundary, indentation lengths and velocities at interface *(French)* 78—1705
cooled pipe, droplets from vapour condensation, size distrib., laminar flow 80—79111
cooling efficiency, axisymmetric air flow past rot. cylinder, main flow swirl effect 78—75132
corrugated plates, Stokes flow phase shift transverse to corrugations 80—48802
Couette flow, permeable wall layer, heat transfer and temp. distrib. 78—51165
Couette flow, plane, past permeable bed, buoyancy effect 80—92215
Couette flow, striated boundary effect on viscous drag 78—59367
Couette flow along surface, isothermal slip 78—67220

boundary layers continued
Couette flow analogy to slip flows 80—1508
Couette flow and heat transfer in rot. system 77—75878
Couette flow stability, transformation of perturbation eqns. 77—7474
counter-current two-phase flow, annuli, rod bundles, liq. film behaviour, flooding 78—59452
countercurrently flowing fluids separated by thin wall, heat transfer 77—23949
creeping flow about sphere, general soln. of linear Navier-Stokes eqn. 78—71307
cross flow effects in oscillating boundary layers 77—42802
cross-flow effects in unsteady flow past yawed infinite cylinder 78—30258
crossflow developing in boundary layer during longit. flow around right dihedral angle 80—59049
curly-viscous fluids, free convection under boundary conditions of second kind 77—75942
curly-viscous fluids, three-dimens. free convection about slender bodies of revolution 77—75943
curvature and displacement effects on separation of accelerated flow past cylinder 80—10272
curvature effects on hydraulically driven inertial boundary currents 80—33676
curved duct, boundary layer collision, entry and core flow 80—74984
curved semicircular sectors, fully developed viscous flow and heat transfer, Navier-Stokes soln. 80—14814
curved tube, wall shear rates in entry region, vortex struct. 79—81972
curved tubes, fully developed laminar flow and heat transfer 80—79308
curved wall power fluidics characts. 80—103053
CW supersonic chemical laser, porous nozzle, chemically reacting boundary layer 80—100022
cyclone flow, boundary layer on cylindrical insert surface 80—10251
cylinder, axisymmetric stagnation flow, steady state heat transfer, boundary layer solns. 77—31296
cylinder, circ., impulsively started from rest, heat transfer, numerical anal. 80—10248
cylinder, circ., separated wake stagnation pt., 2nd order boundary-layer soln. 78—63432
cylinder, circular, with slit, flow characts., control, patterns, wake flow, vortices 78—83404
cylinder, in viscous fluid impulsive translation, numerical computation method 78—5727
cylinder, permeable, in viscous fluid, friction coeff. 79—46385
cylinder, rot., with inner cylinder eccentric torque-free rot., viscous flow 78—34144
cylinder, rotating, 3D boundary layer eqn. expansion 77—84259
cylinder array, 2-dimens. viscous laminar flow field, finite difference method 78—42585
cylinder array, convective mass transfer with surface reaction 78—79369
cylinder array in cross-flow, potential flow interactions 77—51029
cylinder drag, low Reynolds number flow transverse to axis, wall effects 79—64624
cylinder drawn from aperture in presence of heat transfer *(Russian)* 79—77062
cylinder in cross flow, skin friction and vortex shedding freqs. 78—94758
cylinder in inviscid conducting fluid flow, non-aligned mag. field distortion 77—27597
cylinder in near-critical flow, influence of acoustic surface vibrs. on drag 78—5729
cylinder on β-plane, prograde and retrograde rot. flows, boundary layer separation 80—92189
cylinder rotation in stream of viscous fluid, numerical soln. *(Russian)* 77—58704
cylinders, circ., various arrangements, flow interference, review 78—46985
cylinders, eccentric rot., Newtonian flow inertial effects 77—919
cylinders, square cross section, oscills., vortex shedding freq. 78—46983
cylinders and cooling tower models, wind tunnel walls effect on flow 78—46930
cylindric flow in tubes, temp. distrib. *(German)* 77—31391
cylindrical capillary, mass transfer kinetics during evaporation, BGK eqn. basis 77—47044
cylindrical channel, sudden expansion of supersonic jet 80—48800
cylindrical channel walls, adsorption from fluid in Poiseuille flow 78—84048
cylindrical slab of fluid, in weightlessness condition, surface-tension driven convection *(Russian)* 78—90872
cylindrical tube, free vibration in viscous incompressible liquid *(Russian)* 78—55636
cylindrical tube rows downstream flow, complex struct. 79—64812
Czochralski bulk flow in the growth of garnet crystals 80—38979
deep ocean, bottom boundary layer short-term variability 79—2269
deformable body moving in pot. flow, hydrodynamic moment 79—64626
deformable tubes, unsteady flow of incompressible fluids 80—1682
deformation section in flow in constricting devices 78—75206
delta wing, oscillating, with attached shock wave, flowfield theory 77—84276
detonation cell model, geometry, kinematics, mixture kinetics 79—66296
developed flow in curved channels, vortex formation *(German)* 80—1689
diamagnetic boundary layers, kinetic theory, rel. to solar wind 77—9642
dielectric organic liquid, concentric annuli, heat and momentum transfer, electric field effects 80—96315
difference schemes for aerodynamics 77—35160
diffusers, 2-dimens., with suction through porous parallel side walls, characts. *(Japanese)* 78—83492
diffusers, curved, performance, separation in subsonic, transonic channels *(French)* 78—94818
diffusion battery anal. for ultrafine aerosol particle size determ. 79—92010
diffusion boundary layers, with surface reactions, laminar or turbulent regimes, thermal simulation method 77—75912
diffusion flow on interacting surfaces, laminar and turbulent, in Newtonian or nonNewtonian fluids *(French)* 77—27516
diffusively induced boundary layers in tilted square cavity, finite difference method 77—7385
dilatant liquid, plane laminar boundary layer 79—64712
dilute monatomic gas flow round macroscopic object, kinetic theory 77—965
dilute suspension, boundary layer in presence of electric field *(Russian)* 78—63503

boundary layers continued
- dimensionless slippage coefficient of flow over wall, meas. method *(Japanese)* 79—94582
- disc, rotating, convective mass transfer 80—43707
- disc in electrically conducting fluid, hydromagnetic flow due to torsional oscillations about non-zero mean 80—74992
- disc rotating in fluid with surfactant surface layer 80—10284
- disc rotating in jacket in presence of transitional boundary layer, local heat transfer 79—94608
- disc-halo galaxies gaseous components, boundary layer circulation 78—57627
- disk, fluctuating flow induced by periodic suction 77—68592
- disperse system, flotation of fine particles by group of bubbles, kinetics 78—53261
- dispersed drop-vap. flow, heat transfer, wall deposition and boiling 77—75965
- dissociated high enthalpy hypersonic laminar air flow, heat transfer to flat plate 80—69828
- dissociating air, non-equilibrium laminar boundary-layer 77—952
- dissolving sphere, mass exchange with elec. currents carrying liq. 77—11274
- divergent duct, vortex flow breakdown, group vel. criterion 80—87807
- dolphin boundary layer pulsations, results of spectral anal. *(Russian)* 80—41063
- double boundary layers in standing interfacial waves, mass transport velocity 77—3835
- double boundary layers on an electrically conducting plane surface in a rotating environment 79—46397
- double boundary-layer model of mass transport in progressive interfacial waves 79—10573
- double pipe heat exchangers, calc. of overall heat transfer coeff. 79—77109
- double-boundary vessels, flow calcs. using finite-difference transforms 78—44526
- double-diffuse convection, diffuse interface model, high Rayleigh nos. 78—90963
- downstream development of velocity-profiles behind flat plates 79—18870
- downward-facing flat plate, stable film boiling heat transfer 77—23954
- drag, on circular cylinder low Reynolds number 77—84218
- drag for fluids of grade three 80—33635
- drag force on sphere moving in medium with variable viscosity 78—67173
- drag in Stokes' couple stress fluids 79—14379
- drag minimised bodies, given length and base, Newtonian theory calcs. 77—84267
- drag on a sphere moving axially in a long rotating container 79—50734
- drag on group of cylinders 77—58703
- drag on sphere accelerating rectilinearly in elastico-viscous fluid, Fourier transform technique 78—51145
- drag prediction, of bodies of revolution, importance of near wake 77—23962
- drainage, withdrawal and postwithdrawal drainage with inertial effects, unified treatment 77—23932
- draining film off plate rim, drop form. 78—46926
- driven polar cross section cavity, laminar incompressible recirc. flow 78—46988
- drop, centrally-located with thin jet in infinite viscous fluid 79—32614
- drop, in electric field, transient heat and mass transfer 77—80226
- drop formation hydrodynamics, macroencapsulation 80—64603
- drop interaction with boundary layer on rot. disc 78—47020
- droplets, vaporising, in gas stream in channel laminar entry region 78—30347
- drops, column, vertical, approaching interface, shape 79—32725
- duct, circ., laminar convective MHD heat transfer for 3rd kind temp. boundary conditions 78—87342
- duct, curved, laminar incompressible viscous flow 78—46932
- duct, narrow, plane, temp. distrib., heat flow to dense blown layer *(Russian)* 78—83402
- duct, nonconducting walls, MHD volumetric flow rate under uniform mag. field 80—1691
- duct, rectangular, laminar non-Newtonian flow, vel. profiles 80—92217
- duct, rectangular, MHD flow under uniform transverse mag. field at high Hartmann no. 77—55094
- duct, supersonic flow downstream oscillations from abrupt cross section increase, nozzles 80—74976
- duct, thermal entrance region, laminar forced convection, finite-element soln. 80—10118
- duct entrance region, laminar heat transfer, finite element method 80—69836
- duct flow, compressible laminar flow, superimposed sound field effect 77—75933
- duct flow development, step-by-step anal. for laminar flow 80—64634
- duct flow with oscill. plate, numerical soln. 79—50794
- duct of arbitrary cross section, const. rate heat transfer 77—62304
- duct wall cavities, heated bottom surface, forced convection heat transfer 80—6048
- duct with varying cross section and viscous mean flow, acoustic wave propag. 80—96267
- ducts, non-circular, forced convection heat transfer problems 80—64557
- ducts, noncircular straight, steady and unsteady flow 77—65795
- ducts, one-dimensional models for transient gas-liquid flows 80—64614
- ducts, rapidly rot., variable area, rectangular, steady flow, inertial perturbations for small divergences 80—59112
- ducts, spanwise-periodic and corrrugated, heat transfer and laminar flow 80—64547
- ducts with porous walls, Navier-Stokes exact eqns. 78—67266
- dust-liquid channel flow, with varying inlet temp., transient forced convection soln. 78—87375
- dusty fluid, laminar boundary layer flow, 2-D stagnation point near oscillating plate 80—64606
- dusty fluid, motion induced by impulsive plane boundary motion and cylinder motion 78—79362
- dusty fluid flow past plate, small amplitude oscillations 80—14792
- dusty gas, unsteady flow in channel with annular sector cross section 79—77247
- dusty viscous flow through a cylinder of elliptic section under time-dependent pressure gradient 79—77248
- dwarf novae accretion discs, soft X-ray emission form boundary layer 77—45457
- dynamic heat transfer meas. at Mach 8, digital Fourier anal., boundary layer transition 80—14682

boundary layers continued
- Earth core, effect of boundary irregularities on fluid speed and geomag. field 78—73333
- Earth core-mantle interface, topographic coupling 78—44794
- Earth crust, thermal boundary layer/topography coupling rel. to thermoelastic strains and tilts 78—20346
- Earth magnetotail, obs. of hot tenuous plasmas, fireballs and boundary layers 77—29588
- edge waves over trench-ridge topography adjoining straight coastline 78—44838
- EHD, liq. dielectrics interface equilib. and instability, curved wall effects *(Russian)* 78—5807
- EHD, lubricating layer *(Russian)* 78—47061
- Ekman and Hartman layers on plate with variable suction or blowing 78—38416
- Ekman boundary layer, incompressible, nonlinear stability, numerical soln. 80—38378
- Ekman layer, mechanically induced unsteady compressible, theory 80—24033
- Ekman layer, suspended particles effect 78—24349
- elastic liquid flow past porous plate 77—15078
- elastic tube conveying compressible flow, 2-dimens. model nonlinear stability anal. 79—64547
- elastico-viscous flow around oscillating cylinder 77—35177
- elasticoviscous flow along plane wall with periodic suction 79—10594
- elastohydrodynamic point contact, mathematical model for lubricating film thickness *(German)* 78—63464
- elbow primary flow field, 2-dimens. laminar flow 80—43779
- electric current induced flow past a cone *(Russian)* 77—24030
- electrical discharge, in supersonic boundary layer, density distrib., gas laser appl. 77—84544
- electrically conducting fluid, laminar flow mass transfer at high Peclet numbers 80—43784
- electroconvective instabilities overstable 79—27706
- electrodes, kinetic behaviour for quinone electrochem. reduction in packed, fluidised beds 79—57235
- electrodialysis desalination plant, boundary layer thickness, effect on plant perform. and design 79—26725
- electrodiffusion method for convective heat transfer characts. in various liquids 79—94746
- electrolyser, rotating, flow field 79—52682
- electrolyte layer, convection onset condition 79—14492
- electrostatic boundary layer in stationary liqs. 78—15682
- electrostatic precipitator, re-entrainment, particle trajectories and gas flow 78—13642
- ellipsoid in inviscid flow, surface pressure distrib. 80—48831
- elliptic flows calc., EMIT numerical procedure 80—79255
- elliptical disc in viscous liquid, slow broad-side motion anal. 77—58635
- elutriator, inclined tubular, for spherical particles, collection efficiency 79—90354
- emulsion, films, thinning vel. and lifetime, surfactant in continuous and dispersion phases 77—84306
- emulsion, relative drop-drop and drop-wall motions, slow 79—32641
- emulsion films, thinning vel., surfactant in continuous and disperse phases 77—84305
- entrance region of straight channel with uniform heat flux, heat transfer 77—58688
- entry laminar flow in curved parallel plate channel 77—31386
- ethane, flow continuity in arterial capillary systems in cryogenic heat pipes 80—64536
- evanescent waves in total reflection, Raman scatt. direct recording, boundary layer obs. 80—52317
- evaporation with natural convection, simultaneous heat and mass transfer in laminar boundary layer, numerical anal. *(French)* 80—53778
- evapotranspiration calc. using planetary boundary layer theory 77—25716
- exit region central source flow, between finite close parallel rot. discs 77—42849
- explosion, spherical, Rayleigh-Taylor instability, boundary between products and surrounding atm. *(Russian)* 78—26135
- extended Graetz problem, approx. soln. by orthogonal collocation 77—89118
- extended Graetz problem with Dirichlet wall boundary conditions 80—74706
- exterior linear elliptic problem, numerical method, appl. to 2-dimens. wave resistance 80—28485
- external condensation problem, with suction (blowing), self-similar soln. 79—94705
- external disturbance transformation into boundary layer waves 80—28523
- Eyring model fluid, dispersion in laminar falling film 77—89167
- Falkner Skan eqn., exact soln. 79—98680
- Falkner-Skan boundary layer eqn., non-monotonic solns. 80—6023
- Falkner-Skan boundary layer problem, asymptotic solns. 79—18860
- falling film, finite amplitude equilib. surface waves 77—19614
- falling film, linear stability theory, applicability 77—23938
- falling film flow, equivalence of spatial and temporal formulations for linear stability 77—19589
- falling films, nonisothermal flow *(German)* 78—83439
- ferrofluid droplet, interphase boundary hydrostatic characts. in uniform mag. field 80—33692
- ferroliquid in annular channel, hydromag. stability, thermomagnetic effect 79—94593
- ferromagnetic fluid rotating about vertical axis, convective instability of layer 79—27698
- film, liq., flowing down inclined plane with heat transfer, interfacial shear, stability 79—37290
- film coating of flat wall, effect of coolant supply injection angle 77—23951
- film condensation, along vertical plate in enclosed chamber, effect of non-condensable gas 77—80703
- film condensation inside pipes, heat transfer, general correlation 79—46312
- film condensation of moving vapour on horizontal cylinder, exptl. dependences 80—58892
- film cooling, comparison with combined and external cooling of flat plate 77—23950
- film cooling, leading edge effectiveness 79—1185
- film cooling, with upstream injection and intermediate panel temp. 79—1184
- film cooling at separated zone 79—1187

boundary layers continued
film cooling in subsonic boundary layers, tangential slot injection 77—3839
film cooling with density difference between mainstream and secondary fluid, heat-mass transfer analogy 78—30293
film flow down vertical cylinder, linear hydrodynamic stability 77—19588
film flow of an inviscid liquid 79—68675
film heating in axisymmetric flow around cylinder, bulk flow twist effect on efficiency 77—23952
fin array, shrouded, with, without tip clearance, laminar heat transfer 79—55376
finite amplitude stability, perturbative and iterative methods 78—38293
finite depth stratified flow over topography on a beta-plane 80—6128
finite difference approx., boundary layer flow 78—51155
finite difference methods, nonuniform grid generation 80—83780
finite difference numerical solns 78—9661
finite element method 77—80135
finite length plate in supersonic low density flow, surface pressures and corrections 80—14741
finite shrouded disc, laminar boundary layer in rot. compressible isothermal flow 80—43727
fish, fast swimming, drag reduction by slimy secretions into boundary layer *(Russian)* 77—32915
fish (bonito), cutaneous mantle structure rel. to boundary layer control *(Russian)* 77—64171
fixed porous beds under isothermal conditions, velocity distrib. flow model *(German)* 79—77242
flame, laminar mixed-mode forced-free diffusion type, on vert. burning fuel slab 78—91033
flame jet, premixed, impinging on plane surface, turbulent heat transfer 79—4054
flame propagation through stratified charge combustion channel, model 79—64795
flame spread over PMMA sheets in laminar forced oxidising gas flow 80—35535
flat duct, inlet zone turbulence under differing boundary layers, heat transfer, expt. 78—83481
flat insulated plate, supersonic laminar boundary layer stability 79—98749
flat plate, gradual acceleration in variable viscosity fluid 78—30281
flat plate boundary layer flow model and spherical particle drag expt. 79—18871
flat plate boundary layer in porous medium, free convection, similarity solns. 78—75199
flat plate trailing edge in rarefied supersonic airflow, boundary layer 80—24046
flat plates, transitions considered as cascade of instabilities 79—41676
flat porous plate with suction, unsteady heat transfer, boundary layers 79—77105
flat vertical plate, transient natural convection in air 80—64556
flexible cylinder in axial flow, flow-induced motions 79—98679
flexible cylinders, dynamics in axisymmetrically confined axial flow, two-phase flow 79—64757
floating heat layer interaction with solid wall, computation, book contrib. 80—1642
flow, slotted test sections, inviscid theory of wall interference 78—9665
flow, through a surface 78—38341
flow about arbitrary 2-dimens. boundary, implicit finite difference simulation 78—94628
flow around elastic damping surface, disturbing motion in laminary boundary layer *(Russian)* 77—31273
flow between coaxial rotating cones, frictional moment coeff. determ. *(Japanese)* 77—39299
flow between rotating spheres, frictional moment 78—79301
flow between two oscillating discs 77—39355
flow effects on structures, conf., New York, USA, (Dec. 1976) 78—46927
flow from a channel with a flexible barrier 80—69922
flow in base region of body, surface thermal conditions effect 78—42603
flow in narrow annular channel, heat exchange, hydraulic resistance *(Russian)* 77—72299
flow near wall and dividing streamline intersection 79—3994
flow on continuous axisymmetric elastic surface *(Ukrainian)* 79—37285
flow over cone, dual-plate holographic interferometry 78—63512
flow past an arbitrary body, extended variational principle, local pot. method 77—89089
flow past axially uniform viscous vortex, tornado mathematical model 78—59405
flow past circular cascade of arbitrary profiles 77—39303
flow past circular disc, appl. of Hess' surface source model 77—11167
flow past cone with large wall injection velocity, model 79—32561
flow past nonuniformly heated plate, construction of upper and lower solns. 77—75915
flow separation in diffuser 77—84221
flowing viscoelastic fluid, bubble and solid particle separation through apertures *(German)* 79—37389
flowmeter, flux distortion, tests using analogue rig to simulate flow with boundary layer 78—38420
flows from fixed to moving surfaces, gap effects 79—14377
flows on sphere surfaces, comparison of spectral methods 79—72877
fluctuating boundary layer, at horizontal plate, free and forced convection 78—30277
fluctuating boundary layer on a heated horizontal plate 79—4004
fluctuating flow, mass transfer near front stagnation point of axisymmetric body 80—48675
fluctuating flow of viscous fluid through a porous medium bounded by a porous plate 80—24088
fluctuating flow past a cylinder at high frequencies 80—1518
fluctuating flow past an infinite plate with suction and constant heat flux, heat transfer analysis 79—50724
fluctuating free convection flow on horizontally magnetised plate 80—33683
fluid, convective heat transfer with alternating circulation, mathematical model *(Rumanian)* 79—14208
fluid flow along heated inclined wall, double diffusive instability 79—55405
fluid layer between co-axial cylinders, instability of natural convection 80—64558
fluid layer overlying layer of porous medium, convection 77—68587
fluid mechanics, mathematical introduction, book 80—66

boundary layers continued
fluid motion in open basin, free boundary problem *(Italian)* 79—18868
fluid-solid interface, sliding friction coeff., calc. method 77—14987
fluidised bed, heat transfer from transverse streamlined cylinder during surface boiling 80—43708
fluidised beds, heat transfer to horizontal tube *(German)* 78—59387
fluorocarbon refrigerant, film boiling heat transfer from heated plate 79—55380
forced and free convection in laminar flow over plate 80—24005
forced and free convective flow past a semi-infinite vertical plate 79—37286
forced and free convective heat and mass transfer *(French)* 80—48689
forced convection, over horizontal plate, buoyancy-induced streamwise press. gradient effects 77—58681
forced convection heat transfer at inclined plates, solar collector appl. 78—30285
forced convection heat transfer in horizontal layers, buoyancy effects 78—90901
forced standing wave instability in viscous stratified fluid, stratosphere quasibiennial oscill. simulation 79—55396
forced- and free convection joint flow past flat plate 77—47002
forces on cylinders, Morison eqn. coefficient determ. 77—54962
forest canopy layers, numerical studies of two-dimens. flow 77—37290
form drag of in-line tube banks in water cross-flow *(Russian)* 79—7412
free atmospheric convection, rigorous formulation using matched asymptotic expansions *(French)* 77—65740
free boundary problems of the steady water cone in the well of a petroleum reservoir *(Chinese)* 79—50699
free convection, fluctuating boundary layer flow 77—11183
free convection between horizontal concentric cylinders in a slightly-thermally stratified fluid 79—59972
free convection boundary layer flow and heat transfer, variational technique 80—106796
free convection boundary layer on arbitrary shaped bodies in saturated porous media 80—24009
free convection boundary layer on flat plate due to small temp. fluctuations 79—64663
free convection boundary layers on cylinders of elliptic cross section 78—90877
free convection effects in flow past accelerated plate in dissipative liquid 80—10246
free convection effects on MHD accel. flow past vertical porous limiting surface 80—23996
free convection effects on the Stokes problem for an infinite vertical plate 78—90879
free convection flow over plate induced by chemical diffusion and reaction 78—18358
free convection flow past vertical porous plate set in impulsive motion 80—69818
free convection heat transfer from vertical thin wire to air, laminar-turbulent transitions *(Japanese)* 80—92152
free convection in an enclosure 77—80162
free convection in laminar boundary layer along rot. plate, nonsimilarity solns. 77—31307
free convection in Stokes' problem for infinite vertical limiting surface, mass transfer effects 80—28501
free convection mass transfer from horizontal surface, electrochemical and holographic interferometric obs. 78—87344
free convection past circular cylinder, curvature effects 77—31308
free convection suppression, inclined air honeycomb, radiative coupling 77—58684
free convective flow around cylinders near rigid walls, finite difference soln. 77—51053
free convective heat tranfser at a vertical semiinfinite plate 78—79318
free convective heat transfer from horizontal tube to fluid near critical state *(German)* 77—7397
free convective heat transfer from horizontal tube to refrigerants near crit. state *(German)* 77—11192
free convective heat transfer in fluid confined by wavy wall 78—55642
free convective laminar flow, non-uniform gravity effects, finite difference soln. 80—33604
free interaction with supersonic flow, dispersion eqn. solutions 80—69867
free laminar convection for liquid in ribbed slot 80—96261
free liquid surface over solid surface *(Russian)* 77—35116
free molecular flow fields near plate leading and trailing edges 79—86463
free overflow, inviscid soln. for gravitational effects and open channels 79—64773
free shear, channel and turbulent flows, finite element anal. 79—68808
free surface flows from nozzle at low Reynolds number 80—43758
free surface flows under gravity, exact selfsimilar solns. 80—48725
free surface on simple fluid between cylinders undergoing torsional oscills. 77—35152
free-convection boundary layer on an isothermal horizontal cylinder 79—41688
free-forced convection from a heated cone, cross flow transition, similarity soln. 78—90892
free-forced convection from a heated longitudinal horizontal cylinder 80—10244
free-molecule flow, through circular tube with sudden enlargement or contraction 78—14047
freely interacting laminar boundary layers in channels 79—81981
freestream turbulence statistical characts., convective heat transfer calc., boundary layer eddy viscosity 78—83366
freon-114 boundary layer, stability, press. gradient and heating effects 79—18891
Freon-12, annular mist flow in tube, wall film mass flow rate 80—69905
friction in ducts of non-circular cross section 78—18342
frictional force and torque in anisotropic spatially inhomogeneous viscosity fluid, variational principle 79—37367
frustum of cone, laminar natural convection flow 80—53768
fuel, condensed, combustion and extinction in stagnation pt. boundary layer 79—29356
fuel-vapour gas-phase diffusion flame ignition, stagnation point boundary layer 77—58803
fundamental convective heat transfer, entropy generation 80—38411
fundamental problems in general fluid dynamics and hydromag. dynamo theory, book contrib. 77—84213
furrowed channels with pulsatile flow, Navier-Stokes soln. flow patterns, separation 80—33672

boundary layers continued
- furrowed channels with pulsatile flow, observed flow patterns, separation and vortices 80−33673
- fusion reactor, gas blanket confinement, drift mode instabilities 78−18403
- Galerkin finite element-finite difference soln. of laminar boundary layer flows 78−42586
- Galerkin-finite element formulation in viscous flow 79−14367
- gas, conducting, stream flow in orthogonal mag. and mass forces fields *(Russian)* 77−27618
- gas, diatomic, flow around a sphere, using kinetic eqns. 77−906
- gas, low-viscosity, incompressible flow in perforated tube *(Russian)* 77−39351
- gas, oscills. in tubes at reson. freq., shock wave heating *(Russian)* 79−32570
- gas, perfect, vortex sheet, separation from smooth body at large Reynolds number *(French)* 80−74908
- gas bubble motion in power-law fluid, heat and mass transfer with chemical reaction 79−77227
- gas carrying ducts in plate type heat exchanges, heat transfer and pressure drop 80−79291
- gas centrifuge with insulated end walls, Stewartson layer struct., temp. distrib. 78−46973
- gas centrifuge with insulated side wall, Stewartson layer struct., linearised eqns. 78−46974
- gas filled tube, radial resonances excitation, boundary layer considerations 79−98808
- gas flow, high-temp., heating of graphite body, numerical soln. 79−37318
- gas flow, in tubes, effect of cross-sectional shape 79−64710
- gas flow behind supersonic spheres *(Russian)* 79−14423
- gas flow in ducts, global solns. for quasilinear hyperbolic system 79−86511
- gas flow in plane-parallel channel, irreversible thermodynamics *(Russian)* 77−84382
- gas flow over semiinfinite plate with heat sources, unsteady conjugate heat exchange 77−75918
- gas flow regime choice in pipes with max. temp. at outlet 80−19396
- gas flow round porous axisymm. body with injection, vorticity *(Ukrainian)* 77−75923
- gas ignition in boundary layer on heated plate 79−64798
- gas in closed tube, resonant oscills., Chester's eqn. soln. 77−3869
- gas mixture, binary, condensation in boundary layer flow, numerical method 79−1236
- gas mixture separation by membranes *(Japanese)* 78−48691
- gas particulate flow on flat plate, laminar boundary layer, finite difference method 80−43688
- gas-liquid boundary layer, droplet precipitation enhancement 78−1735
- gas-liquid flow, mass transfer in laminar streams with circulation in wet-walled columns 79−94698
- gas-liquid mixture, entrained downward flow in vert. channel 79−94704
- gas-liquid moving interface diffusion 78−22404
- gas-liquid reacting flow, interfacial area and liq.-side mass transfer 79−37420
- gas-liquid transient flow in horizontal pipes, flow pattern transitions 79−32629
- gas-liquid turbulent flow, friction, velocity and gas content profiles 80−14793
- gas-particle mixtures, supersonic flow past wedge, shock wave *(Japanese)* 77−47070
- gas-particulate laminar boundary layer on a flat plate 79−77068
- gas-solid horizontal pipe flow, vertical concentration distrib. *(French)* 80−14824
- gas-streamlined liquid film, quasiharmonic motion development in vertical flow 77−55014
- gaseous microbubble growth in laminar separation bubbles 80−106821
- gentle curvilinear topography with sudden change in surface roughness 77−45110
- geophysical fluid dynamics theory, book 80−105443
- geostrophic flows in rapidly rot. gases, thermally insulating boundaries, Ekman and Stewartson layers 80−14711
- glassy material, destruction at critical point in radiative gas stream *(Russian)* 79−32910
- Goertler functions for steady boundary flows *(German)* 79−86401
- Gortler vortices, high value eigenstates, stability diagrams, book contrib. 80−1606
- Gortler vortices in the nonlinear region, book contrib. 80−1607
- gradually varying channel, solitary wave evolution, KdV eqn. soln. 80−24040
- gravity wave, internal, propag. in shear layer, discontinuity form. 79−32543
- gravity waves propag. over permeable bed *(Polish)* 78−38353
- grey bodies system, closed combined radiation convection heat transfer, two-layer gas model 78−75052
- groove and tongue flow in ground layer *(Ukrainian)* 80−6144
- grooved horizontal conduit, film mass transfer enhancement 79−72947
- ground effect wings, minimum induced drag 77−7367
- groundwater adjacent to horizontal impermeable surfaces, similarity solns. for convection 78−11940
- groundwater singly dispersive convection, finite-difference simulation 77−37265
- growth at rear stagnation point 77−46988
- growth in 3-dimens. with aligned mag. field 79−64790
- growth of boundary layer on parabolic cylinder at angle of attack 77−68568
- growth on spinning sphere, screw motion 77−31315
- Gyarmati principle appl. 79−3993
- haemodynamics, 3-dimens. problem numerical solns. 78−40238
- Hagen-Poiseuille flow, natural transition freq. 79−32459
- harmonically oscillating visco-elastic boundary layer flow 79−55401
- Hartmann layer control of spin-up of stratified, conducting fluid 77−42923
- heat and moisture flux in stratified atmosphere 77−21867
- heat budget of upper ocean under light winds 77−41055
- heat conduction, at freezing/melting boundary, model for approx. calcs. 78−5630
- heat exchange, radiant plate, diametrical Ar gas flow *(Russian)* 78−94565
- heat exchange in dense layer at large Biot no. *(Russian)* 78−83400
- heat exchanger tube banks, flow-induced vibrs. 78−46929

boundary layers continued
- heat exchangers, high temp. thermal storage using latent heat method *(French)* 80−40912
- heat flux transducers for local heat exchange meas. of air flow in tube *(Russian)* 78−83509
- heat loss of internally heated body, to peripheral flow, oblique derivative boundary conditions 79−72778
- heat pipe, evaporator section, evap. and vap. flow between parallel planes 80−10115
- heat pipe, heat transfer agent flowrate through porous wick, approx. calc. method 78−75197
- heat transfer, laminar periodic flow regime in channel, appl. heat exchanger 77−58678
- heat transfer, large Prandtl numbers, second order effects 77−35140
- heat transfer, through convective boundary layer, nonisothermal surface 78−46965
- heat transfer across low aspect enclosure, solute layering effect 77−75776
- heat transfer and drag on moving bodies 78−9706
- heat transfer and film breakdown in falling film with nucleate boiling 78−34122
- heat transfer augmentation, convective, effect of mech.-produced unsteady boundary layer flow 78−71261
- heat transfer bibliography, Japanese works 79−23317
- heat transfer bibliography 78−63425
- heat transfer coefficient, interpolating eqns. between two limiting cases for flow along vertical plate 79−37309
- heat transfer dynamics in channel, anal., impulse function method 79−37317
- heat transfer from blunt plate, separated and reattached flow 79−32500
- heat transfer from cylinder to air cross flow, surface roughness effect 77−39287
- heat transfer in a second-order fluid for flow around a circular cylinder 79−41683
- heat transfer in boundary layers, variational description 77−68581
- heat transfer in circular tubes and annular passages 77−72133
- heat transfer in laminar freely convecting boundary layer, series soln. predictive capability 78−71335
- heat transfer meas. using local heat flux sensor, appl. to heat transfer in supersonic flow 79−82015
- heat transfer to laminar flow with internal heat source in channel 80−64532
- heat transfer with flow reversal 79−37313
- heat transmission, dimensional analysis *(Spanish)* 79−59906
- heated flat plate in water, critical Reynolds number, heat transfer 80−69766
- heated water laminar boundary layer props., approx. methods 79−64628
- heavy liquid, soln. existence and uniqueness 80−1511
- helical flow in simple fluid, uniqueness 78−14017
- helically rib-roughened tubes, forced convection heat transfer and friction characts. 80−96258
- high loading ratio slurries, pressure flow, pressure drop calcs. in pipes 80−92202
- high Reynolds no. flow past rough walled circ. cylinder 78−46952
- high temperature boundary layer mass transfer, nonequilib. ionisation effects 78−93634
- highly attenuated gas flow around body, surface interactions, free molecular conditions 79−90285
- history, book contrib. 77−46992
- hollow vortex enclosed in cylindrical vessel, internal disturbances 79−77122
- holography for cavitation and flow research 78−38436
- holonomic formulation of boundary layer eqns., use of tensors 79−1153
- homogeneous rotating fluid, topography/shear flow interaction 79−55354
- horizontal buoyancy effects on the pressure distribution of a body in a duct 80−19515
- horizontal channel with differentially heated ends, forced and free convection heat transfer 80−6045
- horizontal circular cylinder, mixed convection, boundary layer effects 77−15011
- horizontal cylinder, laminar free convective heat transfer 78−75130
- horizontal cylinder with different end temps., natural convection, jets 80−99996
- horizontal cylindrical surface, free convection, local nonsimilarity anal. 78−75120
- horizontal parallel plates, unsteady laminar flow of viscous fluid, Navier-Stokes eqn. solns. 80−1683
- horizontal pipe subjected to external convection and radiation, laminar forced convection 80−79307
- horizontal pipelines, two-phase flow patterns, pipe dia. and fluid prop. effects 80−48791
- horizontal surface, flowing vapour laminar film condensation 77−15661
- horizontal tube, heat transfer with filmwise condensation, vapour vel. influence 80−33598
- horizontal wavy channels, heat transfer and flow 80−69921
- hot film in reversing shear flow, heat transfer 77−15014
- hot film probe in reversing flow, forced convection, finite difference soln. 80−14702
- hot surface quenching rate, countercurrent single- and two-phase flow effects 78−59451
- hot wall with impinging liq. droplet, transient temp. profile 78−75050
- hot-film probe, in reversing flow, forced convection, finite difference soln. 80−12177
- hot-wire measurement errors in shear flows 77−55119
- hydraulic anal. of flow in complex networks of gas pipelines *(Russian)* 77−947
- hydraulic drag on banks of profiled twisted tubes in cross-flow of gas *(Russian)* 79−7381
- hydraulic loss, flow patterns in pipes with two bends, effect of bend curvature and wall roughness 78−14081
- hydrobionic deforming ellipsoids, calc. of non-stationary boundary layer *(Russian)* 77−64070
- hydrodynamic control of increase of diffusional boundary layer upon plate immersed in Ostwald fluid *(French)* 78−87329
- hydrodynamic lubrication, free boundary problem, variational inequalities 80−62475
- hydrodynamic thermal explosion in power-law fluid flow 79−77158
- hydrodynamics at finite visible contact angles, interface motion, drop spreading, solns. *(Russian)* 77−27640
- hydrofoils, porous surface producing suction, triparametric calc. of laminar boundary layer *(Russian)* 77−54967

boundary layers continued
hydromagnetic flow, suction effect near accelerated plate 80—92232
hydromagnetic free convection flow, similarity solutions 79—27639
hydromagnetic free jet boundary layer equations, similar soln. 79—50811
hydromagnetic thermal instability of rotating fluid layer, Hall current effects 79—27699
hydroplaning of a rotating cylinder on water 78—63522
hydroplaning plate, lift, drag 78—63523
hypersonic aerodynamics, limiting shock layer *(Russian)* 78—30316
hypersonic boundary layer eqns. including chemical reactions, numerical error control, book contrib. 80—1699
hypersonic conical nozzle, boundary layer separation from compression shock 80—48766
hypersonic flow, nonequilibrium gas mixtures past blunt bodies, Navier-Stokes equation *(Russian)* 79—18909
hypersonic flow, separation behind aerofoil 77—42864
hypersonic flow about yawed blunted cone, similar boundary layer anal. for lee-surface heating 77—27553
hypersonic flow around blunt bodies, surface friction, physiochemical processes in shock layer 78—46997
hypersonic flow around three-dimensional wing 77—19621
hypersonic flow field behind blunt body, approx. calc. and electron density in wakes *(Russian)* 79—86461
hypersonic flow over blunt body, viscous shock-layer eqns. 79—60002
hypersonic flow past blunt axisymmetric body, shock layer 78—9654
hypersonic flow past blunted cones, shock waves 78—1684
hypersonic flow with attached shock waves over plane delta wings 77—27556
hypersonic gas flow, radiant heat and evaporative cooling 78—91028
hypersonic laminar, nonequil. ionis. problem 80—59129
hypersonic laminar, stagnation pt., slip, mass transfer 77—19625
hypersonic laminar boundary layer, shock wave interactions 77—89151
hypersonic laminar boundary-layer flow over expansion corner 77—65758
hypersonic laminar heat transfer to cones at angle of attack 79—1211
hypersonic shock layer, screening of selective heat radiation in boundary layer *(Russian)* 79—32497
hypersonic slender-body theory, parallel-source correspondence 78—26151
hypersonic stagnation point boundary layers with massive blowing in presence of mag. field 79—94649
hypersonic transitional/turbulent boundary layer, wall cooling effect 78—26149
hypersonic viscous flows over sphere cones at high angles of attack 79—98746
hypersonic viscous shock layer, three-dimens., numerical calc. on sharp cone at incidence 77—47041
hypersonic viscous state stability of sharp cone at incidence 77—23987
ice growth in laminar flow through a channel with two parallel flat walls 79—3908
ideal fluid with free surface, laminar flow instability, reson. surface wave buildup 78—34106
ideal fluid within three-dimens. toroidal geom., stagnation pts. existence 77—51020
ideal gas in plane asymmetric nozzles, calcs. in overexpanded flow regimes 79—41730
ideal plastic material, film flow along oscillating wall 79—81927
ignition of gas near heated plate *(Russian)* 78—9725
immersed bodies in buoyant fluid, steady state oscills. 77—15052
immiscible fluids interface, conditions for viscous displacement in homogeneous porous medium 80—10301
immiscible liquid horizontal layer, convective stability 77—7392
immiscible liquid-liquid system, laminar jet, vel. profiles and form 79—64752
impactor performance, effect of boundary layers 77—60133
imploding rotating liquid cylinder, viscous boundary layer formation on free surface 79—81894
impringement flow, skin friction and heat transfer meas., hot and cold-film sensors 77—27629
impulsive stagnation flow, unsteady thermal boundary layer 77—75914
impulsively started circular cylinder, initial flow, separation, vortices, wakes and boundary layers 80—19401
impulsively started vertical plate, mass transfer and free convection currents 80—64567
inclined flat plate, vapour boundary layer eqns. for water and steam 79—50700
inclined surface, natural convection flow, transition, vortex system, meas. method 79—27632
incompressible, around arbitrary profile 77—39272
incompressible boundary layer separation, review, book contrib. 77—51033
incompressible fluid, between infinitely long circular cylinders 79—50711
incompressible fluid, past flat plate, least square and Galerkin finite element soln. 77—13615
incompressible fluid laminar boundary layer, Gortler function existence problem *(German)* 80—64516
incompressible fluid MHD flow over flat plate, press. gradient, fluid injection effects 77—68698
incompressible Kramers problem, direct simulation 79—94666
incompressible laminar boundary layer, three-dimensional, hyperbolicity of integral equations of momentum 77—27505
incompressible laminar planar flow between parallel plates, ang. vorticity formulation 80—64643
incompressible separated boundary layers including viscous-inviscid interaction, transition bubble 80—64515
incompressible temp. boundary layer, von Mises variables, explicit finite difference method 79—80448
incompressible viscous fluid through straight two dimens. channel, induced by prescribed injection 80—38491
inertial waves, produced by obstacle in deep rotating container 79—59993
infinite elements in fluid-struct. interactions 77—35132
infinite oscillating plate in viscoelast. fluid 79—27670
infinite porous plate, heat and mass transfer 78—30352
initial-value problem for boundary layer flows, behaviour of small velocity perturb. 79—94588
injection effects of viscoelastic liquid flowing into channel 80—53823
inlet flow with slip, laminar in incompressible Newtonian fluid 79—94659
instabilities, Mach number 7 77—65760
insulated plate thermometer, incompressible boundary layer flow 78—55626
integral spline method, boundary layer eqns. 79—32450

boundary layers continued
interacting boundary layers in high Reynolds number laminar separated flow 77—42865
interaction with induced sound, flow past a square plate in a duct 80—69783
internal solitary waves prod. by tidal flow over three-dimens. ridge, ocean appl. 79—46332
inviscid flow over elastic medium, surface waves generation 77—49603
inviscid flow with vorticity, boundary layer form. 78—14022
ion beam, intense, adiabatic wall focusing for thermonuclear microexplosion ignition 77—61611
ion wind enhancement of evaporation into a laminar air stream 80—53773
ionising Ar flows, shock wave and laminar boundary layer coupled interaction 80—59071
irregular viscous fluid between rot. cylinders, temp. and press. distribs. 77—65769
irregular wavy flow of a liquid film down a vertical plane 80—106808
irrotational flow, heating by rigid walls 79—98730
isothermal circular cylinder, unsteady combined convection in viscous incompressible flow 79—55391
isothermal continuous cylinder, thermal laminar boundary layer 78—22321
isothermal expansion of a two-phase fluid in a magnetohydrodynamic generator duct 80—1695
isothermal flat plate, boundary layer flow with transpiration, heat and mass transfer 79—94613
isothermal horizontal circular cylinder, laminar free convection, thick boundary layer 80—64566
jet, adiabatic, interaction with inclined barrier 79—94694
jet, cross stream injection boundary layer, flow and temp. field 79—1225
jet, heavy, flowing into nonmixing medium 78—51212
jet, laminar, in liq.-liq. system, vel. profile, numerical analysis 80—28545
jet, mixing layer, axisymmetric, influence of initial and boundary conditions 79—94689
jet, subsonic, flow and heat near blunt body stagnation point 77—65774
jet, supersonic, flowing onto infinite perpendicular barrier, limiting expansion ratio 78—59439
jet, supersonic, two-dimens., impingement on flat plate, shock-interference heating 79—94688
jet flow, appl. of Meksyn's method 80—96292
jet flow, numerical modelling of boundary layer 78—22397
jet impact system with unilateral outlet, air flow, heat exchange *(Russian)* 78—83449
jet impingement heat transfer to melting ice surface 78—22394
jet impinging on liq. pool, submerged biphasic region 77—31350
jet impinging wall, heat and momentum transfer, approx. solns. 79—60041
jet noise, external boundary-layer flow effect in flight 77—75901
jet stagnation point heat transfer on plate, turbulence effects, liquid crystal meas. 78—18327
jet-like, separation from wall, nature of reversed flow 77—75956
jets, adiabatic, spatial form 79—46284
jets, micropolar fluid, impinging normally on flat plate, thermal boundary layer 80—28536
jets, open and immersed, instability induction by corona discharge, use in automatic systems *(Russian)* 77—11269
Jupiter, atmosphere, subliming boundary layer flow, simulation 78—65545
kerosene drops in crystallising $MgCl_2$ brine, direct contact cooling 79—1053
kinematic models of dry convective layer with dual-Doppler radar wind obs. 77—37292
laminar, acceleration on partially moving surface *(Russian)* 77—51032
laminar, along concave wall, vortex instability analysis 77—55000
laminar, approx. soln. of Von Mises eqn. 77—27503
laminar, behaviour on continuous accelerating surfaces 78—22320
laminar, calculation of characteristics 77—35114
laminar, characteristics during increased turbulence in bulk stream *(Russian)* 77—23937
laminar, circular cylinder, axisymmetric flow 78—9623
laminar, compressible, two-point finite difference method 77—19617
laminar, compressible, with adverse press. gradient, development and separation 78—26144
laminar, convection in flow between coaxial cylinders *(French)* 78—38314
laminar, convective diffusion due to incident turbulent jet 78—67242
laminar, experimental wing profile surface pressure, spine function, single-parameter method 80—33556
laminar, extraction through slots of finite width *(Russian)* 79—27692
laminar, finite amplitude high frequency oscillations 80—6024
laminar, flow stagnation with suction 79—68676
laminar, fourth-order numerical method 79—1174
laminar, heat transfer, mass transfer and friction coeffs. *(German)* 80—74881
laminar, heat transfer along static and moving cylinders 80—79316
laminar, heated, stability 78—38332
laminar, hydrodynamic stability over flexible surface with constant suction 79—77070
laminar, in elevated-free stream turbulence 77—80139
laminar, in viscoelastic fluids, stability *(German)* 77—72335
laminar, integral eqn. finite element soln. 80—10127
laminar, local self-similarity method 79—32453
laminar, local wall deform. effect on evol. of natural instabilities *(French)* 78—30263
laminar, longit. surface curvature effects calc. 80—19337
laminar, nonsimilar incompressible heat transfer analysis using method of strained coords. 77—42811
laminar, on concave curved walls, heating effect on stability 77—65745
laminar, regular separation free from Goldstein singularity *(Italian)* 79—41657
laminar, semiempirical calc. using arbitrary free stream press. gradient 78—94640
laminar, separating, incompressible over smooth step of small height 80—19325
laminar, separation, transverse surface curvature effect 79—64644
laminar, separation at angular inflection on solid surface 78—67169
laminar, separation in water, heating and suction, comments 79—14378
laminar, sharp press. gradient, calc. method 78—1628
laminar, similarity method with universal eqn. 79—90215
laminar, skin friction, determ. with small Pitot probe 78—18269

boundary layers continued
  laminar, small amplitude oscillation development, stability characts. 80—48674
  laminar, small temp. factor, high Mach no. 78—34156
  laminar, solution of the Falkner-Skan equation by quasilinearization 79—1156
  laminar, stability, Navier-Stokes eqns., finite difference model 77—14991
  laminar, transient convective heat transfer 78—30286
  laminar, turbulent 'spot' 77—19587
  laminar, universal eqn. in differential form 78—46925
  laminar, velocity measurement by single-beam laser time-of-flight method 79—77298
  laminar, vorticity genesis 78—1630
  laminar, with press. fluctuations heat transfer, friction *(Russian)* 77—89114
  laminar, with suction or injection, parametric calc. method 78—22323
  laminar boundary alyer flow, heat transfer, rel. to vel. fluctuations 78—94710
  laminar boundary flow over spinning blunt body of revolution, Magnus forces 78—94745
  laminar boundary layer, along a heated horizontal hollow cylinder, buoyancy and variable viscosity 78—46964
  laminar boundary layer, elongational viscosity and secondary instability 77—23997
  laminar boundary layer, heated, stability 78—9626
  laminar boundary layer, heated, with nonuniform surface temp. distrib., stability 78—67175
  laminar boundary layer, on permeable surface, in crossed elec. and mag. fields *(Russian)* 78—75118
  laminar boundary layer, optimal control, group theoretic approach 79—32452
  laminar boundary layer, optimal control by wall suction or blowing 79—1242
  laminar boundary layer, subsonic, strong slot injection, triple deck theory 80—74831
  laminar boundary layer development under continuous incipient separation conditions 78—63415
  laminar boundary layer eqns. soln. by inverse series method 79—41662
  laminar boundary layer flow, Gortler functions, uniqueness *(German)* 80—52034
  laminar boundary layer flow along vaporising liq. layer *(German)* 78—83403
  laminar boundary layer flow past two dimens. slot 78—5724
  laminar boundary layer flow with suction (blowing) and pressure gradient, finite element anal. 79—18866
  laminar boundary layer heat transfer over rot. bodies 79—32517
  laminar boundary layer induced wake behind cylinder attached to plate 80—43712
  laminar boundary layer mass transfer with thermal diffusion 80—19323
  laminar boundary layer on a circular cylinder started impulsively from rest 79—64627
  laminar boundary layer on heated plate, numerical results 79—10545
  laminar boundary layer on moving surface under combined action of free and forced convection *(Ukrainian)* 79—50695
  laminar boundary layer on rot. disc in counter-rot. fluid 77—35113
  laminar boundary layer on rot. sphere 79—27648
  laminar boundary layer on rotating sphere in still fluid *(Japanese)* 77—35112
  laminar boundary layer over porous flat plate, recovery factor, general soln. 77—46987
  laminar boundary layer reattachment in supersonic flow, num. soln. 80—53809
  laminar boundary layer solns. on moving surfaces, series method 79—32455
  laminar boundary layer swirling flow with heat and mass transfer in conical nozzles and diffusers 79—81842
  laminar boundary layer with press. fluctuations, friction and heat transfer 79—64652
  laminar boundary layer with separated bubble 77—23935
  laminar boundary layer with separation and reattachment, unsteady 79—59963
  laminar boundary layers, compressible, Prandtl=0.72, sharp pressure rise effect 80—83782
  laminar boundary layers in incompressible micropolar fluids 77—80140
  laminar boundary layers in three dimens., integral relation method 77—31277
  laminar boundary on surface of circular cylinder moving in fluid, flow pattern and heat transfer 80—28487
  laminar boundary-layer flows with swirl and large suction 80—1519
  laminar boundary-layer reattachment in supersonic flow 79—46342
  laminar bubble separation, stalling. lecture 78—22325
  laminar channel flow, heat transfer in entrance region 79—32518
  laminar channel flow, symmetrical, with wall suction 77—31389
  laminar chemically nonequilibrium mixture flow, characts. of combined heat and mass transfer *(Russian)* 79—59965
  laminar combined free and forced convection across horizontal cylinder, flow and heat transfer characts. 77—84245
  laminar compressible, on rot. sphere with heat transfer, buoyancy and viscous dissipation effects 77—15053
  laminar compressible, with hard suction 78—26097
  laminar compressible boundary layer, with vectored mass transfer 77—23974
  laminar compressible boundary layer flow at stagnation pt., vectored mass transfer 79—27661
  laminar compressible boundary layer flow at stagnation pt. 79—10583
  laminar compressible boundary layer swirling flow in nozzle, flow and heat tranfer 78—94795
  laminar compressible boundary layers, radiative interactions 79—50812
  laminar compressible boundary layers, Taylor-Gortler instability 78—26140
  laminar compressible MHD boundary layer flow, effect on heat transfer 79—14489
  laminar condensation heat and mass transfer at stagnation point of droplet in ternary mixture 79—14227
  laminar convection, heated vertical surface, boundary-layer thickness and Prandtl number 78—51161
  laminar convection, in vertical cylinder const. heat flux 79—46307
  laminar convection anal. by integral and characts. methods 78—34137
  laminar convection from upward-facing inclined flat plate 77—7395
  laminar Couette flow between parallel plates, heat transfer 77—31299

boundary layers continued
  laminar dispersion in rectangular conduits, side wall effects, convection 78—94636
  laminar equalising flow in Couette-type channel flow *(German)* 78—51239
  laminar film, convective coupled heat transfer, Nusselt no. computation 78—59398
  laminar film, mass transfer with dissolution 78—26098
  laminar film boiling of binary liquid mixture, heat transfer rates *(German)* 77—7398
  laminar film condensation from moving vapour, with suction 78—59459
  laminar flow, direct finite difference calc. of through separated regions 77—35115
  laminar flow, entry region and numerical soln. for square channel 77—84325
  laminar flow, of fluid with free surface, in triangular-shaped open channel *(Russian)* 77—51028
  laminar flow, steady heat transfer between parallel plates, with conduction in wall 77—47003
  laminar flow, three-dimens., soln. using method of integral relations 77—58645
  laminar flow along porous vertical wall 78—90825
  laminar flow around free and surface-mounted obstacles, topology, flow visualization 78—51157
  laminar flow at three-dimensional stagnation point with large injection rates 77—23934
  laminar flow between parallel plates, reactant injection effects 78—34208
  laminar flow between porous plates, heat transfer 79—68708
  laminar flow in bifurcating, blocked or constricted tubes, entry flow effects 77—19636
  laminar flow in curved annulus, heat transfer effects 77—42820
  laminar flow in planar (quasiplanar) channel with variable cross section, heat transfer 78—1661
  laminar flow instability, nonlinear theory 78—63416
  laminar flow on a flat plate 79—68677
  laminar flow on rot. cylinder 77—89130
  laminar flow over parabola, second approx. 78—63414
  laminar flow over periodic wavy surface, nonlinear anal. 78—90826
  laminar flow over plate, convective heat transfer 77—39290
  laminar flow over porous flexible boundary, oscillatory flow 80—92107
  laminar flow over shallow cavities, oscills. 77—89091
  laminar flow past sphere, unsteady mass transfer, heterogeneous chemical reaction 77—55102
  laminar flow pattern, press., enthalpy, vel. from point source of heat 78—79316
  laminar flow with injection in straight duct, vel. distrib. and press. drop 77—11263
  laminar forced convection between concentric spheres, num. soln. 77—42831
  laminar forced convection to turbulent free convection transition over heated plate 79—32516
  laminar free convection, boundary layers, similar solns. 77—27524
  laminar free convection past heated vertical plate, leading and trailing edge and discontinuous temp. effects 77—15028
  laminar free convection with uniform heat flux on vertical plate *(French)* 77—39292
  laminar free convective flow, three-dimens., num. soln. 77—42826
  laminar free convention boundary-layer in three-dimensional systems 80—33587
  laminar heat exchange in thermally initial portion of tube with variable wall temp., asymptotic soln. 77—58675
  laminar heat transfer for boundary layers with mass injection and chemical reactions *(Chinese)* 80—59020
  laminar hot wire readings, wall proximity effects heat transfer 80—48822
  laminar hypersonic flow over insulated accelerating slender wedge 78—1685
  laminar incompressible boundary layer eqns. finite element soln. 78—79304
  laminar incompressible flow past rot. elliptic cylinders 77—27538
  laminar jet at wall, heat transfer 79—41725
  laminar liquid film, falling, O_2 adsorpt. with zero order react. in entrance region 80—64652
  laminar liquid film in vertical flow down solid surface, coherence *(German)* 78—22322
  laminar liquid film moving along sloping surface, hydrodynamics 77—7365
  laminar liquid flow around plate, boundary-value problem soln. for generalised diffusion eqn. 77—7366
  laminar natural convection along cylinder, stability 78—1663
  laminar natural convection boundary layers on horizontal circular discs 79—77067
  laminar natural convection boundary layers on horizontal heated plates 77—7396
  laminar natural convection over a slender vertical frustum of a cone *(German)* 79—77116
  laminar non-Newtonian falling liquid films, dynamics 79—7393
  laminar non-Newtonian fluid jet, swirling, impinging on normal plane 77—42889
  laminar pipe flow heat transfer, simultaneous wall and fluid axial conduction 80—74870
  laminar semi-infinite jet on porous surface, initial part calc. *(Russian)* 79—77203
  laminar separated flow between periodically varied walls, num. simulation using perturbated primitive variables method 77—54971
  laminar separation, from upstream-moving wall 78—13989
  laminar separation of incompressible fluid streaming past smooth surface 77—75897
  laminar shear layer on oscill. plate 79—32454
  laminar stagnation point, surface curvature effect on heat transfer 78—38316
  laminar stationary 2D viscous duct flow, generalised Prandtl eqns., soln. methods 78—5726
  laminar supersonic, separated bubble induced by wall depression 78—9651
  laminar symmetric sink flow between parallel plates 80—1524
  laminar to turbulent boundary layer shear flow, three-dimens., stability eqns. 78—38284
  laminar to turbulent boundary layer transition, nonlinear wave interaction, numerical calc. 78—38281
  laminar to turbulent boundary layer transition, Orr-Sommerfeld eqn. eigenvalues, series representation 78—38280

boundary layers continued
laminar to turbulent boundary layer transition, outer-stream turbulence effect 77–75881
laminar to turbulent boundary layer transition prediction, linear stability theory 78–38279
laminar to turbulent boundary layer transitions, numerical simulation 78–38286
laminar to turbulent flow boundary, sound field radiated by Tollmien-Schlichting wave 78–18090
laminar to turbulent transition, IR emission meas. 78–38438
laminar to turbulent transition, layer with press. grad. and suction 78–38282
laminar to turbulent transition, natural convection instabilities effect *(French)* 78–38333
laminar to turbulent transition, numerical method *(French)* 78–38289
laminar to turbulent transition, stability theory 78–38274
laminar to turbulent transition, Tollmien Schlichting wave development *(French)* 78–38285
laminar to turbulent transition, transport eqns. *(French)* 77–62234
laminar to turbulent transition, wall heating effect 78–38334
laminar to turbulent transition in oscillating layer *(French)* 78–38288
laminar to turbulent transition on cone at Mach 5 78–38368
laminar to turbulent transition on cone at Mach 5 78–38369
laminar to turbulent transitions, conference, Lyngby, Denmark (May 1977) 78–38278
laminar to turbulent transitions, temp. factor effect 78–63417
laminar trailing edge stall, triple-deck eqns. num. soln. 77–55020
laminar tube flow, gravitational deposition of growing aerosol particles 80–59099
laminar unsteady flow past flat plate, finite difference method 79–18864
laminar unsteady free convection flow past vertical flat plate, effects of suction 78–18296
laminar unsteady viscous plane stagnation flows, incompressible boundary layer, heat transfer 80–1584
laminar vapour flow between parallel disks with asymmetric sublimation 79–18865
laminar vapour flow in film boiling, stability limits 78–90832
laminar viscoelastic boundary layers, role of fluid relaxation time 79–81829
laminar wall plume in transverse mag. field 79–86398
laminar water boundary layer on heated cones, variable viscosity effect, heat transfer, shear stress 79–32520
laminar wing flow, tip vortex stability 77–19611
laminar/turbulent intermittent transition, local skin friction 78–30260
large Reynolds number, 2-D hydrodynamic lubricating theory *(Russian)* 78–59368
larunar, low free stream perturbations influence, hydrodynamic waves 79–98738
laser heated nozzle flow with swirl, axisymmetric comp. boundary layer 80–14775
laser-Doppler technique, local size and vel. probability distrib., two-phase suspension flow 78–59517
latex suspension liquid film flow, local thickness meas. 79–4070
Laval nozzle, surface burning in two-phase flow, boundary layer interaction, Rakhmatulin model 78–83452
leading edge effect on free-convection heat transfer 78–79319
leading edge signal on flat plate in uniform shear 78–30259
Leidenfrost layer, liq. drop falling onto hot liq. surface, boiling instability 78–94588
lift correction to transonic equivalence rule 77–62273
lifting boundary in low Mach number flow, sound scatt. anal. 77–42648
lifting surface, varying thickness shear layer, soln. using kernel function 77–89137
lifting surface in unsteady motion in inviscid fluid 78–14036
limiting relative law of heat and mass transfer and friction, permeability parameter effect 80–23999
linear stability of flat Stokes layers 78–13994
linear supersonic flow round a yawed elliptic cone *(German)* 77–65762
linear vortex over plane with projecting edge, sound radiation 77–811
linearised boundary layer equations with self-induced pressure, anal. for $M_\infty=1$ case 79–86458
liquid, stratified, internal waves generated by local disturbances 79–86485
liquid, with temp.-depend. thermophysical props., flow over nonisothermal surface *(Russian)* 79–64661
liquid continuous film flow, range of existence 77–39273
liquid coolant, porous evaporative cooling for subcritical, critical, supercritical coolant parameters 79–55372
liquid falling film, surfactant effects 77–89093
liquid film, absorption with chem. reaction 77–42929
liquid film, falling, laminar, evaporation model 79–46305
liquid film, falling, laminar, transport augmentation by surface waves 78–71343
liquid film, falling, theory of mass transfer 79–65309
liquid film, flow over horiz. smooth tubes 78–38273
liquid film, influence of waves on mass transfer *(Russian)* 79–64677
liquid film, subcooled, heat transfer and film breakdown 78–34121
liquid film breakdown, numerical anal. 79–46285
liquid film condensation on vertical wall, linearised stability anal. 79–55381
liquid film flow, cellular convection 77–68588
liquid film flow down inclined plane, deflection toward underside 79–18867
liquid film flow down inclined plane, stability, anal. quadrature by differentiation method 79–90219
liquid film flow on vertical wall 77–62237
liquid film flow regimes, on rot. disc 78–1671
liquid film flowing down polymer surface, heat transfer 78–30278
liquid film on vertical plane, hydrodynamic stabilisation *(Russian)* 77–35117
liquid film on vertical surface, viscous lifting and drainage 78–18348
liquid films, heated horizontal channel, heat transfer and dry patch formation 80–64554
liquid flow, incompressible, electro-hydrodynamic analogy, design 77–27627
liquid flow around a self-propelled body 79–86399
liquid flow around cylinder, thermophys. charact. rel. to friction and heat transfer *(Russian)* 78–38328
liquid flow in viscoelastic tube, wave propag. 78–9714
liquid flow past plate, boundary layer heat transfer rel. to external flow *(Russian)* 78–38329

boundary layers continued
liquid fuel droplet heating with internal circulation 78–75194
liquid in pipes, continuity determ., gamma-ray appl. 79–94748
liquid jet air wake boundary layer eqns. 77–75954
liquid layer appl. using rubber roller, nip flow operations anal. 78–71310
liquid layer creeping over surface, angle of contact, viscous liq. 78–51149
liquid layer flow down plane, stability *(Russian)* 78–9627
liquid layer flowing down inclined plane, heating and cooling effects on stability 80–79254
liquid layer on inclined plane, stability 79–64631
liquid layer on rot. Archimedes spiral, mass transfer 79–14413
liquid layer on rot. surface, heat transfer, gas flow interaction 78–22347
liquid metal, laminar convective heat transfer along cylinder 77–914
liquid metal MHD generator, wall-jet gas injection 80–28830
liquid metal second-order thermal boundary layer 79–77106
liquid metal-gas two-phase MHD generator, pot. loss mechanisms, rel. to fluid dynamic processes 77–39359
liquid metals laminar flow in curved channels, transversely applied mag. field, flow anal. 80–59116
liquid metals with variable thermal cond. and capacity, forced convection 79–37310
liquid slip inside channel exit 79–10612
liquid thin film, evaporation and breakdown driven by shear stresses 80–38410
liquid vertical layers, convective flows with spatially modulated temp. distrib. at boundaries *(Russian)* 79–32496
liquid with temp. dependent thermophysical props., boundary layer eqn. *(Russian)* 77–84220
liquid-phase motion in filling of cylindrical channel, Navier-Stokes eqn. 77–58791
liquid-vapour flow, heat transfer crisis, wall shear stress 78–90986
liquids, immiscible, convection at interface induced by coupling between chem. reacts., hydrodynamics *(French)* 79–41682
liquids, throttling, temp. field near boundary 80–43757
LMFBR beam-type core components separated by thin fluid layers, transverse impulsive motion, Timoshenko beam anal. 77–88203
LMFBR triangular rod array, flow resistance wall shear stress in interior subchannel 80–63244
local heat transfer coeffs. for flow around sphere, semi-empirical method 80–24026
local heat transfer from inline tube bank to air crossflow *(Russian)* 78–5746
local mass/heat transfer distribution on surfaces roughened with small square ribs 80–19506
local supersonic zone near wing profile of infinite span flow calcs. 79–32565
longitudinal and cross flow around heat exchanger tube bundles comparison, heat transfer efficiency aspects 78–94687
longitudinal counterrotating vortices, wall boundary layer of flow with ang. momentum *(German)* 77–75922
longitudinal gas flow in cylindrical channel, heat transfer with elec. arc 77–11189
low Mach number duct flows, combustion noise generation by chemical inhomogeneities 80–92237
low Reynolds-number flow in the vicinity of axisymmetric constrictions 80–6147
low speed flow up a step 78–79303
low velocity vertical steam-water flow, void fraction in pipes 80–74964
lubrication, boundary conds. and cavity-fluid interface, review 77–55058
lubrication, cavity-fluid interface, wavy interface anal. 77–55059
lubrication, hydrodynamic, free boundary problem including surface tension 80–19542
LWR safety, critical flow of two-phase one-component mixtures *(Italian)* 79–71880
Mach reflection transition, steady (unsteady) flow, with (without) relax. 79–50752
macroparameters in relaxing boundary layer *(Russian)* 80–33557
magnetic field, flow stability of thin layer *(Russian)* 78–9721
magnetic field as a tool for investigating transition and turbulence 80–1696
magnetic fluid (cable coolant), natural convection heat transfer 78–94846
magnetic fluid boundary layer, flow stability 79–64782
magnetic fluid layer, thermocapillary instability with thermally insulated boundary 80–33595
magnetic liquid film flow in mag. field, laminar regime 78–34203
magnetisable liquid layer, with solid boundaries, convective stability 79–94592
magnetoelectrolysis in steady Hartmann flow cells, hydrodynamics, mass transport 77–36759
magnetopause, compressible field reconnection model and plasma boundary layer flow 77–37485
magnetosphere, frontside boundary layer obs. and reconnection problem 78–89010
magnetosphere, plasma, energy and momentum transfer from magnetosheath 77–22008
magnetotail, hot tenuous plasmas, fireballs and boundary layers rel. to substorm processes 78–32300
magnetotail, hot tenuous plasmas, fireballs and boundary layers 78–77438
mainstream acceleration effect on heat transfer and wall temp. downstream of gas injection 79–1251
marine boundary layer microwave sensing, estimation techniques 79–74993
Mars, saltation threshold, interparticle force, surface roughness and low atm. density effects 77–5478
Mars, wind speed requirements for particle motion 77–5479
mass force field boiling crisis, critical heat flux for swirling tube flow 79–90248
mass transfer in laminar flow between two plane parallel plates 79–37321
mass transfer rates at spheres, moving on circular path 77–3890
mass transfer with chem. surface reaction on flat plate in flow *(German)* 79–72961
mass transport in boundary layer second approx. 77–15049
mass transport velocity in progressive gravity waves, double boundary layer model 77–78217
matched asymptotic expansions method, asymptotic matching principle for higher approx., boundary layer problems appl. 78–94642

boundary layers continued
- matter-antimatter boundary layers, theory 77—49284
- matter-antimatter boundary layers with mag. neutral sheet, model 78—53807
- Maxwell fluid, unsteady flow past flat plate, transform technique 78—59428
- Maxwell viscoelastic liquid, drag on circular cylinder with transient vel. 78—18270
- MBBA, nematic phase, effect of elec. field on flow alignment angle 79—10792
- melting at horizontal boundary, steady-state convection, interface corrugations 78—26118
- melting heat transfer in steady laminar flow over flat plate 77—15027
- melting surface, air bubble evolution effect on boundary layer separation 78—67015
- melting/freezing interface, annular region, perturbation soln. 78—59286
- membranes with low porosity, diffusional boundary layer resistance 77—58778
- metal, laminar flow thermal boundary layers, variable thermal cond. 79—59962
- metallic heat carrier in loops, phase transition process, temp. field 79—55867
- metastable flows of water, spontaneous boiling 80—106709
- MHD, gas boundary layer swirling nozzle and diffuser flows with mag. field 80—1693
- MHD, gas outflows and inflows with viscous, ohmic and thermal dissipation between inclined walls 77—11278
- MHD, in container, induced by rapidly alternating or rot. mag. field 79—64785
- MHD, nonsimilar incompressible laminar boundary layers, finite-difference scheme 78—79386
- MHD, sink flow with transverse mag. field, boundary layer thickness 80—69940
- MHD, Stokes problem, boundary layers and skin friction 80—14837
- MHD, unsteady free convection flow past vertical porous plate 78—30361
- MHD, viscous flow between two rotating porous cylinders, in axial mag. field 77—72364
- MHD boundary layer flow, on flat plate, effects of varying velocity 78—67275
- MHD boundary layers, laminar, control problem *(German)* 78—91024
- MHD boundary layers, unsteady on porous plate in rot. system 77—24027
- MHD boundary-layer control, effects of free-stream vel. and press. gradients 79—55423
- MHD channel and boundary layer flows, rel. to energy sources, review 79—37403
- MHD channel flow, entry region, in axial mag. field 77—47097
- MHD channel flow heat transfer, third-kind temp. boundary conditions 77—47095
- MHD channels, voltage losses near electrodes 80—103079
- MHD convection, free, near plane and axisymmetric bodies 79—94728
- MHD convection in boundary layer, overplane and axisymm. bodies, theory 79—77270
- MHD convection in rapidly rot. fluid layer, stability, rel. to geomagnetism 79—50808
- MHD duct flow, boundary value problem, dual extremum principles, operators and bounding functionals 79—64791
- MHD Ekman layer, near accelerated porous media, flow anal. 77—75987
- MHD Ekman layer on free convection past infinite porous flat plate 80—14830
- MHD flow, impulsively started plate, Hall effect 78—1747
- MHD flow, past porous flat plate, Hall effects 78—14093
- MHD flow and heat transfer over semi-infinite plate under transverse mag. field 77—80225
- MHD flow between parallel plates, temp. field, vel. field, skin friction, heat transfer 77—68700
- MHD flow between rotating parallel porous walls 79—64779
- MHD flow in annular and linear channels, boundary layer conditions *(Chinese)* 79—37404
- MHD flow in rot. channel, wall conductances effect on heat transfer 78—51245
- MHD flow near a time-varying accelerated porous plate 79—23372
- MHD flow on flat plate, effect of transpiration 77—24028
- MHD flow over flat plate, boundary layer function, asymptotic behaviour 79—46393
- MHD flow over oscillating porous plate, Hall current and rot. effects 78—5803
- MHD flow over porous plate, Hall effect 78—51246
- mHD flow past a semi-infinite flat plate with heat transfer, exact numerical solns. of boundary layer similarity eqns. 80—83861
- MHD flow past circular cylinder 77—51126
- MHD flow past moving plate with const. suction 77—11268
- MHD flow past plate with suction 77—68697
- MHD flow past vertical plate, similarity solutions 77—65803
- MHD flows in the presence of a transverse magnetic field 79—55425
- MHD forced convection, with transverse mag. field, surface curvature effect 77—35245
- MHD forced convection in channel bounded by plate and permeable bed, Hall effects 80—69934
- MHD free convection about semi-infinite plate in strong cross field, skin friction, heat transfer 77—15134
- MHD free convection effects on oscill. flow of viscous incompressible fluid past porous limiting surface 79—81985
- MHD generator, compressible laminar boundary layer separation from segmented electrode wall 77—27598
- MHD generator, electrothermal instability in the seeded combustion gas boundary layer near cold electrodes 78—71547
- MHD generator, non-equilibrium, ionisation instability, finite boundary layer effect calc. 79—19098
- MHD generator, open cycle, with shaped magnetic induction, theory of nonuniform electrical conduction 80—28831
- MHD generator, plasma, conductivity rel. to boundary layer during internal cooling *(Russian)* 78—38557
- MHD generators, channel subsonic flow, gas dynamic, elec. parameters 79—55567
- MHD laminar boundary layer with variable elec. cond., nonstationary flow *(French)* 77—39356
- MHD laminar flow, in entrance region of flat duct 78—30367
- MHD laminar flow down vertical wall 77—11270

boundary layers continued
- MHD laminar flow in parallel-plate channel with unequal wall temperature, thermal entry heat transfer 77—42927
- MHD laminar plane-wall jet flow 79—55424
- MHD oscillatory flow past semi-infinite plate 78—14091
- MHD plasma diagnostics, by holographic interferometry and Fourier filter correlation 80—48965
- MHD radial flow between planes *(Russian)* 77—7465
- MHD shift flow, in strong field, of viscous fluid 80—28576
- MHD stability of laminar boundary layer flow along flat plate with transverse mag. field 79—27709
- MHD stratified flow between oscillating disks, boundary layers 80—28570
- MHD thermal boundary layer flow near oscill. limiting surface, stellar atm. appl. 78—94831
- MHD unsteady free convection flow, past hot vertical plate, calcs. 77—75986
- MHD unsteady free convection past a hot vertical plate 78—87396
- MHD unsteady thermal boundary layer flow 77—7460
- MHD unsteady thermal boundary layer flow with zero heat transfer, astrophys. appl. 77—87250
- MHD viscoelastic free convection boundary layer flow past porous plate 80—10317
- micro-polar fluid, on flat surface, effect of couple stresses on unsteady drainage 77—14985
- micropolar fluid, heat transfer in boundary layer flow, past curved surface 79—46316
- micropolar fluid, heat transfer in stagnation point flow 80—79356
- micropolar fluid, laminar boundary layer, longitudinal surface curvature effects 80—48669
- micropolar fluid, laminar flow through slot 80—10313
- micropolar fluid, nonsimilar incompressible laminar boundary-layer flow 77—35184
- micropolar fluid, thermal boundary layer at stagnation point 80—53820
- micropolar fluid boundary layer flow past circular cylinder 79—41658
- micropolar fluid flow, circular cylinder asymptotic boundary layer 79—18916
- micropolar fluid flow between concentric cylinders 78—5767
- micropolar fluid flow due to an oscillating plane subject to rotation 79—98763
- micropolar fluid flow on arbitrary surface, three-dimens. boundary layer eqns. 77—68633
- micropolar fluid jet normal impingement on curved surface, flow near stagnation point 78—90949
- micropolar fluid on circular cylinder, thermal boundary layer 78—75174
- micropolar fluid through constricted channel 78—9715
- Mises' equation, first order perturbation by finite differences method 77—39271
- mist flow over heated cylinder, particle size and temp. difference effects 80—38409
- mixed convection on vertical plate with unheated starting length, num. soln. 77—42827
- mixed layer growth, penetrative convection in stratified fluid 78—44908
- mixing layer growth from turbulent and nonturbulent boundary layer 79—68686
- moderate density gas, isothermal creep along planar surface 79—82022
- molecular gas radiation in the thermal entrance region of a duct 80—6051
- molecular hydrodynamics of inhomogeneous systems, slip boundary conditions 77—89165
- molecular shield for Shuttle Orbiter, effect of expts. on density distrib., model 78—22374
- momentum and mass transfer in moving-wall channel 77—39344
- momentum transfer in curved pipes 79—68814
- monatomic gas, between parallel plates, higher kinetic moments, differential eqns., boundary conditions 77—75921
- moving contact line, slip boundary condition 77—11168
- moving fluid interface, force singularity removal by slip flow 77—31275
- moving fluid interface on rough surface, slip coeffs. 77—3806
- moving horizontal flat plate, laminar boundary layer, buoyancy effects 80—74877
- moving surface, free liquid layer, laminar and turbulent flow, Navier-Stokes anal. 79—94589
- moving surface, thermal laminar boundary layer under forced and free convection *(Russian)* 79—46286
- moving wall, boundary layer separation, use of integral theory 77—58640
- moving wall, use of integral theory 77—23933
- multi-layered liquid films, instability 79—1158
- multibody flow problems, boundary-fitted coords. for accurate numerical soln. 79—37289
- multicomponent, in models undergoing breakdown 78—42588
- multicomponent nonequilibrium chemically reacting boundary layers, transport coupling theory 79—77294
- multicomponent viscous gas flow, diffusion, boundary layer eqn. soln. *(Russian)* 77—7493
- multiconnected airfoil systems, inverse problem, book contrib. 80—1515
- multiperforate laminae, mass transfer of chem. species by diffusion, plate and associated boundary layer case 80—40736
- multiphase flow in annulus, incompressible immiscible fluids, velocity profile 77—62298
- multiplane, steady, plane and inviscid flow 77—23980
- multiplanes, design theory 79—37284
- n-incompressible and immiscible rarefied gases, pulsating flow between two plates 80—10306
- narrow curved channels, vels. and flow rate, intrinsic coordinates formulation 80—79406
- natural convection, heat and mass transfer interaction, around vertical flat plate 77—58669
- natural convection air flows, vel. meas. using laser velocimeter 79—82016
- natural convection boundary layer, laminar to turbulent transition, critical values for air *(Japanese)* 80—14657
- natural convection flow, nonisothermal flat plate, numerical soln. 78—67194
- natural convection flow adjacent to vertical surface, leading edge effect 79—55389
- natural convection heat transfer, nonuniform alternating electric field influence 77—50860
- natural convection heating of liqs. in closed containers 77—15006
- natural convection mass transfer along porous vertical plate 78—90876
- natural convection of air over a heated plate with forward-facing step 78—90875

boundary layers continued
natural convective wall plume, boundary layer eqns., higher order anal. 80—64550
natural laminar convection, side wall effects on heat transfer through vertical air layer 80—19377
natural laminar convection about isothermal cylinder, Navier-Stokes eqn. soln. 80—92143
natural laminar convection over cone with const. wall heat flux *(German)* 80—38414
Navier-Stokes eqns., bluff body aerodynamics, numerical simulation methods 78—75115
Navier-Stokes equation, limiting form at high Reynolds number *(French)* 80—74823
Navier-Stokes equations, linearised, numerical soln., effect of cell Reynolds number 80—106780
Navier-Stokes equations, numerical soln. appl. to viscous flow around cylinder *(French)* 77—75869
Navier-Stokes stationary 2-D eqns. in parabolic form, optimal control *(French)* 77—72321
nematic liquid crystal flow in flat channel, heat transfer anal. *(Russian)* 77—72397
Newtonian die swell eval. for axisymm. tube exits using finite element anal. 78—1741
Newtonian fluids, momentum transfer in curved pipes 79—68813
Newtonian liquid, coating on to rotating roll 79—41692
Newtonian viscous fluid, flow through thin pipe, with thin linear elastic wall 78—42664
non Newtonian fluid, mass transfer due to rot. disc 79—41717
non-isothermal disc rot. in quiescent compressible gas, heat transfer 80—14704
Non-Newtonian falling film, hydrodynamic entrance length 77—58743
non-Newtonian falling film, Taylor diffusion of solute 77—39317
non-Newtonian flow about rotating sphere 78—30323
non-Newtonian flow along thin needle, vel. profile, skin friction 78—67229
non-Newtonian flow in entrance region of tubes, press. drop 77—27563
non-Newtonian fluid, forced convection, on circular cylinder, suction and slip velocity effects 78—34169
non-Newtonian fluid, in convergent channel, eqn. derivation by perturbation method 78—30322
non-Newtonian fluid, laminar boundary layer, surface heat transfer rate 80—24055
non-Newtonian fluid, laminar pipe flow, nonisothermal, heat transfer, with internal heat sources 79—68763
non-Newtonian fluid, pseudoplastic, nonlinear singular boundary value problem 80—79362
non-Newtonian fluid, purely viscous, Rayleigh problem, pseudosimilarity soln. *(German)* 79—37364
non-Newtonian fluid, rot. liq. film, free surface instability 79—37294
non-Newtonian fluid, secondary flow in noncircular pipe 77—15075
non-Newtonian fluid, unsteady laminar incompressible boundary layer eqns., flow, heat and mass transfer, similarity solns. 79—32590
non-Newtonian fluid, viscoelastic boundary-layer flow past a parabola and a paraboloid 80—83817
non-Newtonian fluid film flow along vertical oscillating plate *(German)* 78—59431
non-Newtonian fluid in cylindrical annulus, axial flow iterative calc. *(German)* 77—11225
non-Newtonian fluid solution, film flow over soluble wall, solvent layer form 78—42634
non-Newtonian fluids, boundary layer theory 80—83818
non-Newtonian fluids, lubrication, elastohydrodynamic, between two rot. cylinders 78—83435
non-Newtonian fluids in jacketed agitated vessel, heat transfer, viscosity correl. 78—75143
non-Newtonian laminar boundary layer flow, mass transfer 77—27562
non-Newtonian laminar flow through parallel plates, kinetic energy correction factor 77—31271
non-Newtonian liq.-air annular flow, film thickness rel. to rate 77—3860
non-Newtonian liquid, heat flux from nonisothermal surfaces to gradient flows *(Russian)* 79—68767
non-Newtonian liquid, isothermal Couette flow in slowly converging channel with complex shear 77—15069
non-Newtonian non-similar laminar boundary layers, rapid calc. procedure 78—90943
non-Newtonian pulsatile laminar pipe flows, multiviscous approx. 77—3871
non-Newtonian unsteady flow between parallel walls, velocity and temp. fields 77—39314
non-steady boundary layer, turbulence development 78—90829
non-uniform pipe gas flow simulation model 80—33682
nonequilibrium flow past thin profile 77—84344
nonequilibrium ionised boundary-layer flow, numerical anal. 77—11324
nonequilibrium ionised radiating gas flow over blunt bodies 78—9727
nonequilibrium reactive flow over solid body, conjugate heat and mass exchange 77—42931
nonideal plasma generation, by electrolyte impulse diaphragmic discharge 78—71506
nonisothermal boundary layer, laminar flow of dilute particle suspension, self similar soln. 77—65785
nonisothermal flow of viscous or non-Newtonian fluids over rotors of centrifugal heat exchangers 79—77097
nonisothermal laminar and turbulent plane free jets with buoyancy effect, boundary layer theory *(German)* 80—53830
nonlinear convection in a layer with nearly insulating boundaries 80—33592
nonlinear flow, boundary value problems, solvability for analytic functions 79—98677
nonlinear stability of boundary layers for disturbances of various sizes 80—6025
nonlinear wave development during laminar to turbulent transition *(Russian)* 77—80173
nonlinearly viscous non-Newtonian media, boundary layer theory 79—90289
nonparallel stability of two-dimensional nonuniformly heated boundary-layer flows 80—38401
nonsimilar axisymmetric stagnation flow on a moving cylinder 78—79297
nonsimilar laminar free convection flow along a nonisothermal vertical plate, finite difference method 78—75119
nonsimilar moving wall boundary layer problem 77—27508
nonslender body, minimal drag determ. 77—39306

boundary layers continued
nonstationarity near cylinder in air cross-flow *(Russian)* 79—7382
nonstationary boundary layer with self-induced press. 78—34164
nonstationary boundary layer with self-induced press. at transonic external stream vels. 78—83428
nonstationary boundary layers, higher order approx., parametric treatment *(French)* 79—86419
nonsteady flow in one-dimens. pipe systems, boundary condition based anal. 80—1685
nonsteady flow of dropping compressible liquid in pipes, effect of friction laws 77—55091
nonsteady gas flow through ramified pipelines, asymptotic anal. 77—72358
nonsteady MHD thermal boundary layer, in incompressible laminar flow with variable elec. cond., approx. soln. 78—91022
nonsteady plane stagnation point flow with hard blowing 80—33579
nonuniform grids in finite difference approximations, application to fluid flow problems 80—105507
nonuniform parallel stream, slender wing theory, flow and lift 80—74830
nose separation for laminar boundary layers on body of revolution 80—59091
nose surface, press. distrib. of bodies of revolution, $\alpha=0$ to 10° 77—27549
nozzle, chemical laser, laminar boundary layer 77—42529
nozzle, critical air flow, heat transfer, numerical study 79—98778
nozzle, heat transfer of transonic air flow 79—1230
nozzle and diffuser flow, laser heated, laminar compressible boundary layers 80—53831
nozzle boundary layer, hypersonic, static press. variation and Reynolds stress 77—84294
nozzle boundary layer equations for laser heated flow, similarity soln. 77—31355
nozzle discharge coefficients, boundary layer soln. 79—32626
nozzle flows with boundary layer, CO_2-N_2-He, gain coefficients 80—14312
nozzle in different jet regimes, internal and external flows, separation and wakes 80—100023
nozzle wall laminar boundary layer, effect on jet turbulence 77—55065
nozzles, supersonic, thermal protection by gas curtain, vel. gradient 78—51215
nucleate boiling, anal. of microlayer thicness 79—77234
numerical methods, book contrib. 78—59369
numerical soln. of boundary layer problems *(Russian)* 77—68569
numerical solution of problems in unbounded regions, use of coord. transforms 78—8219
oblating heat shield, Jupiter probe, C vaporisation into nonequilib. stagnation point boundary layer 79—1264
ocean, abyssal shear zone obs. 78—73386
ocean, air-water interface, effects on gravity waves 79—57947
ocean, boundary layers parametrisations rel. to vertical eddy viscosity effects on Rossby and Eady waves 80—51404
ocean, hydrodynamic friction layer instability rel. to Langmuir circulation 78—92840
ocean, low temp. skin-layer model *(Russian)* 78—36180
ocean, topographically bound vortices theory 79—57956
ocean, two-layer, stable wind-driven equatorial currents theory *(Russian)* 78 61427
ocean, vel. fluctuations scaling in surface mixed layer 77—45009
ocean, wave-induced mass transport in stratified bottom boundary layer 79-2282
ocean baroclinic Rossby waves generation by meteorological forces 77—86916
ocean benthic boundary layer, diffusion-controlled model for deep-sea Mn nodules growth 79—2212
ocean bottom, density stratification over continental margins 77—86931
ocean bottom boundary layer, mass transport by gravity waves *(Russian)* 78—16036
ocean boundary current flow along continental margin, effect of localised topographic irregularity 80—72539
ocean boundary-forced planetary waves, model mid-ocean response to strong current variability 80—72541
ocean deep-water channel flow, rotating hydraulics theory 80—94539
ocean dynamic response to atm. disturbances 77—13084
ocean eddies and islands, effects on mixing 78—85572
ocean gyre, boundary layer circulation effect on poleward heat flux 80—85668
ocean surface currents mapping, HF radar system appl. 80—94626
ocean surface mixed layer, climatological numerical model, comments 77—86927
ocean upper layer temperature, influence of mesoscale eddies *(Russian)* 78—81191
ocean warm wavy surface, lab. study of evaporation 77—86924
ocean-atmosphere heat balance over northern hemisphere, annual cycle 77—41040
ocean-atmosphere interface, coupled energy transfer, turbulent and radiative 79—2290
ocean-atmosphere sensible heat flux in extratropical synoptic-scale systems 77—78223
oceanic fronts, circulation due to cabbeling and double diffusion 79—2263
oil and polyisobutylene-oil, laminar plane stagnation flow kinematics, laser Doppler anemometry 78—38374
oil-cooling baffled shell-and-tube heat exchanger expt. 78—83395
Oldroyd B-fluid flow between porous plates with fluctuating vel. 78—26168
Oldroyd liquid, unsteady flow between two porous walls 78—63452
one dimensional two phase flow, critical flowrate in channel calc. 80—10292
opaque gas medium movement, deformation of temp. fields 77—51132
open cavity heat and mass transfer 78—55640
open cycle MHD generator, channel metal surfaces, elec. characts. of boundary layer 77—39473
open pipe exits, flow during acoustic resonance, vortices and boundary layers 80—92224
optically thick horizontal fluid layer heated below, heat transfer 80—99993
optimal coordinate theory, appl. to physical problems 77—71211
optimal coords. for 3-D incompressible laminar boundary layers 77—72273
optimal nodal point distribution for improved accuracy in computational fluid dynamics 80—48670

boundary layers continued
- optimally controlled boundary layer eqns., group fibering 79—41663
- Orr-Sommerfeld eqn., continuous spectrum and eigenfunctions 78—67176
- Orr-Sommerfeld eqn., eigenvalue series representation 79—7364
- oscillating airfoil drag in fluctuating free stream, laminar and turbulent boundary layer anal. 80—53746
- oscillating body, three dimens. unsteady laminar boundary layer flow 77—27507
- oscillating flow past flat plate, heat transfer, viscous dissipation effect 77—80151
- oscillating porous flat plate boundary layer, hydromagnetic flow 78—51250
- oscillating radial flow between two parallel rotating disks 79—55393
- oscillating source flow of ducting fluid between parallel discs 80—99986
- oscillating three-dimens. flow around cylinder 78—34104
- oscillating viscous flow around cylinder *(French)* 77—905
- oscillatory boundary layer, on bed beneath gravity waves, laser Doppler anemometry 78—90929
- oscillatory convective flow, double boundary layers 79—81874
- oscillatory flow around the edge of a flat plate 79—72879
- oscillatory flow in U-tube manometers, effect of drag reducing polymer additives 80—64584
- oscillatory flow past infinite, porous plate, free convection current effects 78—14079
- oscillatory flow past infinite vertical plate with variable suction and constant heat flux 78—38324
- oscillatory flow past porous bed, boundary layer characts. 80—48797
- oscillatory flow past vertical porous plate with constant suction, free convection effect, correction to earlier paper 77—27594
- Oseen, unsteady three dimens., applied conc. force 78—67167
- Oseen flow, unsteady, around flat-plate airfoil 78—5723
- Pacific Ocean, barotropic and baroclinic tides over continental slope and shelf off Oregon 80—72543
- Pacific Ocean boundary flow forcing rel. to oceanic circulation around New Zealand 80—72538
- parabolic marching problems, edge-corrected linearisation technique 77—89081
- parallel channels with short flow constriction, laminar transport phenomena 79—81886
- parallel fixed planes, incompressible viscous flow *(French)* 77—72269
- parallel flow between concentric cylinders, stability, heat transfer 77—11190
- parallel flow between parallel plates, substruct. distrib. and apparent viscosity 78—13983
- parallel flow stability, numerical calc. 79—32460
- parallel plate channel, combined forced and free convective laminar flow, solute disperison 79—98801
- parallel plate channel, convective-radiative interaction, air-operated solar collectors appl. 80—96259
- parallel plates, longitudinal dispersion in laminar flows homogeneous in streamwise direction 79—98811
- parallel streams with interfacial mass transfer, laminar boundary-layer anal. 77—31272
- parallel tube banks in transverse viscous flow, heat transfer and hydraulic drag *(Russian)* 79—10450
- parallel-plate channel, convectively-cooled, liq. solidification 77—68666
- particle convective diffusion to rot. disc surface 78—18334
- particle impacting wall diffusion layer, enhancement of mass transfer *(French)* 79—60050
- particle-vapour subliming boundary-layer flow, local nonsimilar solns. 77—80206
- passage, arbitrary cross-section, fully developed flow prediction method 79—1254
- paste-like composite with polymer binding, rheological props., wall effect 77—47072
- Penrose tube, water filled, fluid velocity/wavespeed ratio, supercritical-subcritical transition 79—81975
- periodic, with large Strouhal number, parametric method 77—51030
- periodic laminar boundary layers, theory 80—79257
- periodic wavy surface, laminar boundary layer, nonlinear anal. for long waves, separation 80—87759
- periodically interrupted surface, developing and fully developed heat transfer coeffs. 79—81885
- permeable bed boundary layer flow, temp. distrib. and Nusselt no. 78—51166
- permeable boundaries in multidimensional unsteady flow 80—38490
- permeable boundary, stability of flow, velocity slip effects 77—68571
- perturbations, three freq. wave resonance *(Russian)* 79—32538
- Petrov-Galerkin finite element method, boundary value problem 78—69989
- phase interfaces, balance eqns. and struct. models 78—59453
- pipe, heated, straight, free-forced convection in entry region 78—90883
- pipe, horizontal, straight, heated, entry flow 79—32675
- pipe, laminar friction factor and heat transfer, finite-element technique 80—10247
- pipe, particulate suspension flow, sticking probability and erosion, data correlations 79—41744
- pipe, smooth, entrance regions, laminar flow 79—50696
- pipe, swirled flow, friction law and form parameters 79—37329
- pipe, swirled flow, integral calc. method 79—37402
- pipe entrance, unsteady effects of fluctuating main flow on laminar boundary layer thickness 77—39274
- pipe flow, disturbed flow conditions, effect on orifice plate discharge coeff. 80—19510
- pipe flow, drag reduction polymer molecule turbulent diffusion and degradation 80—1686
- pipe flow, laminar with nonlinear wall heat fluxes, axial cond. 79—27636
- pipe flow, spatial cavitation-nuclei-measurements by means of laser velocimeter 80—64593
- pipe fluid flow, solid particle impurity propag. 80—64630
- pipe subjected to circumferentially varying external heat transfer coeff., laminar heat transfer 80—10242
- pipe with laminar flow in boundary layer and const. wall temp., initial section heat exchange 79—86432
- pipeline systems, nonstationary flow distrib. modes simulation, computer-aided methods 79—94717
- pipes, hydraulic, with nonlinear boundaries, transient waves 80—43722
- pipes, turbulence and heat exchange 80—24094
- pipes with regular artificial wall roughness, laminar flow stability, turbulence 79—98803
- plane flow of second grade fluid through contraction 77—3870

boundary layers continued
- plane jet, stability and autooscillations from channel anal. 80—100018
- plane jet propagation in incompressible liquids, numerical solution *(Russian)* 80—43753
- plane laminar relaxing gas jets, mixing with radiation accounted for, boundary layer eqns. 79—90349
- plane Poiseuille flow, instability caused by nonlinear, nonperiodic and three-dimensional disturbance 78—38291
- plane Poiseuille flow in channel, stability, orthogonal expansion method *(Russian)* 78—5730
- plane stagnation point flow in the presence of transverse magnetic field 80—14834
- plane thermal boundary layer, temp. distrib. determ. by var. formulation 77—23947
- plane-parallel flow instability with coordinate depend. viscosity *(Russian)* 78—22328
- planetary, at Tarama Island, wind structure, balloon obs. 77—45052
- plasma, magnetised, cold-banket systems, boundary layer analysis 80—28605
- plasma, radial boundary layers, diffusing toroidal equilibria 77—89285
- plasma, shock heated, Al-seeded, boundary layer influence on Al I reson. line profiles 80—43876
- plasma impurity diversion through ambient boundary layer flow 80—19603
- plastic disperse systems, generalised flow theory with account of wall effect 78—87320
- plate, downward-facing, flat, heat transfer augmentation by nonuniform elec. field corona 78—94873
- plate, flat, normal to oncoming stream, 2-D boundary layer, extended series expansions 80—83781
- plate, flat, optically thin boundary layer, of grey medium near leading edge, radiative-convective heat transfer 78—91027
- plate, flat, with uniformly distributed vectored surface mass transfer, flow and heat transfer analysis 77—42838
- plate, heat transfer from high enthalpy hypersonic air boundary layer 78—34210
- plate, heated, semiinfinite, vertical, with heat sources and sinks natural convection 80—59035
- plate, laminated composite, under tension, interlaminar stresses around circ. cutout 78—34010
- plate, thin, in gradient current flow, coupled heat exchange *(Russian)* 78—83398
- plate, vertical, free convection boundary layers and heat transfer 80—59002
- plate, vertical, with time depend. temp. or heat flux, unsteady natural convection 77—75777
- plate, with suction, three-dimens. fluctuating flow, heat transfer, skin friction 78—87389
- plate, with temp. and vel. profile nonuniformities, laminar flow and heat transfer 77—75913
- plate and laminar slug flow with periodically changing temp., transient heat transfer 80—74872
- plate at angle to flow, heat loss meas. for boundary turbulence and separation 78—90846
- plate in nonhomogeneous fluid 78—94639
- plate kinematics in oscillatory bending, particle trajectories *(Russian)* 79—37209
- plate leeside, viscous hypersonic flowfield boundary layer separation 80—48743
- plate temp. oscillations, response of horizontal free convection boundary layer 78—59391
- plate with circular cylinder, boundary layer control 79—77060
- plate with nonsteady temp. on lower surface, laminar flow, conjugate heat transfer 80—74879
- plate with periodic suction and injections in supersonic region, boundary layers *(German)* 80—59069
- plate with steady state thermal boundary layer flow, appl. of governing principle of dissipative processes 79—50722
- plates, collinear, interrupted, flow-aligned, heat transfer and press. drop 78—87232
- plates, flat, rotating stratified flow, boundary layers 80—53793
- plates, vertical and inclined, mixed convection combined, heat and mass transfer 80—64552
- plume, above vert. heated plate, development of wall and free types 78—90881
- PMMA, struct. of boundary layers on solid substrate determ. by total internal reflection *(Russian)* 79—32922
- pneumatic transmission line transient response anal. by characteristic curve method 79—77244
- pneumatic transmission lines with and without steady flow, freq. characts. 79—77245
- Poiseuille channel flow, finite amplitude, instability shear layer parallel flow, cellular motion 80—1601
- Poiseuille flow, plane, horiz., rot., stability, effect of Coriolis force 78—67203
- Poiseuille flow in pipe, bifurcation from infinity, nonlinear differential eqn. 79—98806
- Poiseuille flow with flexible boundaries, MHD stability 77—11277
- Poisseuille pipe flow transitional behaviour, effect of inlet flow disturbances 79—90216
- polyatomic gas, plane Couette flow in Knudsen regime, wall induced polarisation 80—19443
- polyethylene, high-density, polymer melt, shear stress at wall 80—19450
- polymer flow on inclined plane, edge effects 80—19451
- polymer sheet, stretching, with suction and blowing, heat and mass transfer 78—34033
- polymer solns., dilute, extensional and sink flow in channel 80—74925
- polymer solns., laminar-turbulent transition 78—9663
- polymer solution, boundary layer having laminar, transitional and turbulent flow zones *(Russian)* 77—80185
- polymer solution, flow visualization near rot. disc 79—72914
- polymer solution, vortex inhibition, velocity profile meas. 77—19628
- polymer solutions, viscoelastic, tubular entry flow, vortex characts. in stable flow 79—32428
- porous boundary with blowing, numerical exponential box scheme 79—1240
- porous channel inlet region, second order fluid flow, injection effects 79—68804
- porous cylinder, rot., lift, torque, appl. to wind power generation 78—46987

boundary layers continued
  porous insulation filled cavity wall, forced and free convective heat loss 77—75909
  porous media filled enclosure, convective heat transfer, boundary layer 79—59908
  porous medium, saturated, mixed convection boundary layer flow on vertical surface 80—106798
  porous plate, gas injection, squeezing out of liq. 80—64622
  porous plate, wall shear stress with mass transfer 78—47032
  porous plate, with time-varying motion, surrounding liq. MHD flow 78—51251
  porous plate with suction and blowing, hydrodynamic and MHD flow 78—34201
  porous solid boundary layer flow catalytic reaction, model 78—31684
  porous straight channel, MHD flow 80—69932
  porous surface, heat exchange optimal control 79—32661
  porous vertical wall, laminar flow integral approach to flow 79—77059
  positive column, metastable atom radial transport, effect of wall boundary conditions 78—67493
  post shock expansion behind normal shock on curved wall, flow separation, book contrib. *(German)* 80—1628
  potential flow, approx. numerical solns. 78—79293
  potential flow 2-D bodies synthesis with limited interactive graphics 77—11166
  potential flow about bodies of revolution, general analytic method 78—1629
  potential flow about boundary shape, method of singularity with spline fit distrib. 78—22324
  potential flow around axisymmetric bodies 78—63412
  potential flow around axisymmetric bodies 79—41656
  potential flow in region with sharp boundary change 79—55352
  potential flow over bodies, convective heat transfer 78—59395
  potential flow over wing with free vortex 78—63444
  powder flow over inclined surfaces 78—63488
  power law fluid, approx. soln. of two-dimens. laminar boundary layer flow *(Japanese)* 77—72337
  power law fluids, mass transfer into boundary layers 79—32588
  power law liquid, comparison of 2-D and axisymmetric jet flows 78—79351
  power law non-Newtonian liquid, stability of laminar boundary layer 77—55048
  power-law fluid, fluctuating flow past porous flat plate 77—68639
  power-law fluid, nonsteady heat exchange during steady flow in initial thermal section of tube 77—47046
  power-law fluid, two-stream mixing along flat plate, variational solns. 80—53817
  power-law non-Newtonian conducting fluid, laminar boundary layer in transverse mag. field 80—33694
  power-law non-Newtonian fluids, laminar flow in concentric annuli, vol. flow, press loss. calcs. 79—94681
  Prandtl's equations for stationary boundary layer, method of linear soln., existence, convergence *(German)* 77—58642
  probe, elec. highly negative, in flowing continuum plasma, ion sheath 77—72493
  pseudo-periodic flow in U-shaped tube, stability anal. 79—98809
  pseudoplastic fluid, flowing upward in vert. heated tube, variable physical props. 78—90945
  pseudoplastic liquid film, wave motion 79—32583
  pseudoplastic liquid flow in planar laminar boundary layer 79—86470
  pulmonary resistance, lower, effect of gas phys. props. and flow 77—12945
  pulsating laminar compressible flow in cylindrical pipe with through flow 77—80216
  pulsating laminar-boundary layer, heat transfer and skin friction 78—94711
  pulsating stars asymptotic theory, boundary layer method 80—82389
  PVC, emulsion, melts, slip, visual observations 79—4047
  PVC cpds., rigid, plasticised, capillary flow 79—4046
  qualitative analysis of unsteady heat and mass transfer modes in a boundary layer with chemical reactions and intensive injections 80—69819
  quench front motion, heat transfer coeff., surface approx. using boundary layer anal. 79—45342
  radial source flow between parallel disks, vorticity transport eqn. 78—42615
  radial wall jet, circular jump characts., boundary layer form. 77—24005
  radiating laminar boundary flow over flat plate at large free stream Mach no. 79—1270
  radiation-flow field interactions with injection of absorbing gas 78—5826
  radiative boundary shock wave struct. 80—10264
  radiative gas, boundary shock waves 79—64694
  radiative heat transfer, two-dimensional, in planar layer bounded by nonisothermal walls 80—1413
  radiative transfer in expanding homogeneous sphere *(Russian)* 78—73945
  radiative viscous-shock-layer analysis for equilib. flow about blunt axisymm. body, effect of coupled ablation injection 77—24033
  radiative-convective heat transfer, numerical methods 78—94577
  rapid surface vaporisation with back pressure, Knudsen layer, flow Mach number 79—77168
  rarefied flat plate flow, direct simulation and expt. 79—94667
  rarefied flow, boundary conditions for gasdynamic eqns. in presence of evap., condensation and chem. reactions 77—47042
  rarefied flow, visco-magnetic heat flux, in Burnett regime 79—98844
  rarefied flow over body with small accomodation coeff. 79—90286
  rarefied flow over plane wall, slip coeffs. 79—90287
  rarefied gas, laminar flow with swirl, slip regime 77—31336
  rarefied gas flow in rectangular groove facing moving wall, eqns. derivation and soln. 77—42874
  rarefied gas flow induced by thermal stress, imperfect accommodation at boundary 78—87362
  rarefied hypersonic flow on wedge, numerical anal. *(Japanese)* 79—32580
  rarefied hypersonic flow over blunt wedge, cooling 77—35169
  rarefied hypersonic flow past flat-plate, numerical simulation 77—19626
  rarefied polyatomic gases, ang. momentum polarisations, boundary layer behaviour 78—51200
  rarefied transition flow, past bluff faced cylinder, Monte Carlo calcs. 79—94670
  Rayleigh-Benard convection, induced, pretransitional 79—55374
  Rayleigh-Benard convection, wave number selection, sidewalls effect 80—106799

boundary layers continued
  Rayleigh-Stokes problem for a corner *(German)* 80—28483
  re-entry vehicle flight tests, boundary layer acoustic meas. 78—16275
  reacting particle in fluid, convective diffusion, nonlinear surface reaction kinetics 80—106854
  real gas laminar boundary-layer separation prediction methodology 80—19322
  recirculating flow, numerical prediction 79—1152
  rectangular body, laminar flow, separation bubble and stagnation line 80—64514
  rectangular canal, added mass of rectangular cylinder 77—51118
  rectangular cavities, end effects, vortex flow and wall jet 80—10309
  rectangular cavity walls, shear stress by electrodiffusion method 80—10308
  rectangular channels, turbulent forced convection, momentum and heat transfer, secondary flows *(German)* 79—77259
  rectangular ducts, fully developed laminar forced convection, general inequality theorem 80—43780
  rectilinear flow, pressure error upper and lower bounds with pressure gradient 80—6010
  reflection, of obliquely incident waves, at permeable quaywall with reservoir *(Japanese)* 79—32546
  regenerators with hygrostatic materials, combined heat and mass transfer 79—81689
  reinterpretation of entrainment process in laboratory expts. 80—51405
  relaxing wakes behind surface-mounted obstacles in rough wall boundary layers 79—94625
  resonant gas oscillations in open pipes due to moving piston 79—68805
  riffle formation model 78—63482
  rigid wall-hot gas stream interaction, heat cond. eqns. soln. 78—79194
  ripple and dune formation on erodible bed by low Froude number flow 80—106784
  ripple formation, growth and decay in oscillatory flow *(Polish)* 79—25227
  ripple induced bed roughness, effect on surface waves attenuation *(Polish)* 79—25262
  rising core, at centre of vortex, analysis for laminar flow 78—1666
  rivulets, flowing down vertical solid surface, contact angles, roughness effect 79—27731
  roll of slender wings at incidence in separated flow 77—3840
  roll-wave stability on thin laminar flow down inclined plane wall 80—28488
  rolling motion of sphere on plane boundary in oscillatory flow 77—3834
  Rossby small amplitude wave stability in channel 77—56684
  rotating bodies in axial flows, laminar and turbulent boundary layers *(Japanese)* 79—77127
  rotating body, axisymmetric, arbitrary surface temp. distrib., thermal boundary layer, exact solns. 78—75133
  rotating body in Ostwald fluid, rate distrib. near wall, electrochem. methods *(French)* 77—42847
  rotating channel flow, hydraulic control theory 77—56642
  rotating cone-cylinder body, boundary-layer flow in uniform stream 77—23965
  rotating cylinders, stagnation flow-based profiles 77—89096
  rotating cylindrical annulus, transition to Taylor vortices, Ekman layers 80—87776
  rotating disc, heat exchange into unbounded rotating fluid, thermal and hydrodynamic boundary layers 80—59050
  rotating disc, laminar boundary layer heat transfer, Prandtl no. effects calcs. 77—31306
  rotating disc, laminar to turbulent boundary layer stability 78—38283
  rotating disc apparatus, thin-film, minimum irrigation density determ. 77—47125
  rotating disc boundary layer transition regime, spiral vortices 80—59040
  rotating disc with suction and stationary disc, flow between 78—46975
  rotating disk with sink flow, heat and mass transfer 80—19402
  rotating flow, nonstationary eqns. soln., appl. to flow between discs 80—28516
  rotating fluid, boundary layer modification by axial vel. imposition 79—77133
  rotating fluid, driven by periodic flows, viscous boundary layers 77—3804
  rotating fluid, waves due to sources and internal boundaries 79—37323
  rotating gas, vertical boundary layers 77—19609
  rotating heat exchanger, frictionless two-phase tube flow, centrifugal accel., choked flow 80—48792
  rotating sphere, small yaw ang., laminar boundary layer *(Japanese)* 78—38272
  rough cylinder in critical Re water crossflow, heat transfer 80—1571
  rough interface between two fluids, coherent acoustic scatter 80—96074
  rough plate, drag and heat transfer at various Pr numbers 79—94610
  rough subliming surface, laminar boundary layer, anal. 78—51148
  rough surface boundary layer calculation methods 80—1595
  rough wall with blowing and heat transfer, boundary layer struct. 79—81863
  round tube flow, laminar dispersion 80—64638
  saturated liquid, boiling onset, film boiling transition, crit. heat flux densities *(Russian)* 78—83234
  saturated porous medium, free convection boundary layers, lateral mass flux effects 77—27592
  SAW, phase velocities on solid-liquid boundary 78—83151
  scattering index from rough surface, meas. in high speed molecular flow 79—94653
  sea surface temperature deviation at very low wind speeds 77—78224
  sea-air heat and moisture exchange, zonally averaged model *(Russian)* 77—17161
  sea-air interface fluxes of sensible heat and moisture, parameterization 77—41041
  seawater during evaporation, optical interferometry *(Russian)* 80—61919
  second order fluid, oscillatory convection flow from vertical plate 77—7423
  second-order boundary-layer effects for large injection or suction, book contrib. 80—1531
  second-order fluid, flow separation at straight edge 77—15079
  second-order fluid, plane flow past submerged boundaries 77—75945
  second-order fluid forced flow against rot. disc with uniform high suction 77—27564
  second-order unsteady stagnation pt. solns. 77—89092
  secondary flow beside cylinder in complex sound field 79—14376
  secondary flow effects on decaying torsional oscills. of sphere and plane 77—3808

boundary layers continued
secondary flows in curved ducts of rectangular cross-section 77—84323
secondary flows in lee of porous shelterbelts 78—3852
secondary vorticity in internal waves 79—72899
selective radiative heat exchange screening in shock boundary layer 79—90283
semi-bounded slow viscous flow past cylinder 79—41660
separated flow, heat transfer 78—79315
separated flow and freestream, simultaneous numerical anal. 78—38271
separated flow with laminar mixing region, heat and mass transfer, math. simulation 78—59397
separated supersonic boundary layer, moderate injection with reattachment, shear layer 79—32562
separated unsteady flows around bodies, streamline and steakline photographs 78—1634
separating boundary-layer flow calculations 79—68678
separating laminar boundary layer, horsehoe vortex 80—19405
separation, variational methods, book contrib. 79—32456
separation of flow along line of regular surface *(French)* 79—41661
separation of laminar boundary layer in water, heating and suction effects 78—9625
separator intertray space, development of liq. laminar flow 79—81893
shallow water eqns., errors arising from irregular boundaries in ADI solns. 79—64765
shallow-water slender-ship flow past slowly varying bottom 78—1742
sharp cone, symmetry plane viscous layer 77—58639
sharp-edged disc, semiempirical anal. of cavitation in wake 77—35188
shear flow past cylinder with elliptic limacon cross-section, stagnation points 80—23984
shear flow separation past cylinder and plane 77—68567
shear layer, impingement upon corner or cavity edge, organised nature 79—81840
shell deformation by supersonic gas flow, drag 80—96279
ship boundary layers, book contrib., review 80—19346
ship hydrodynamics, drag on displacement ships, hydrofoils, hovercrafts 78—63423
shock capturing application of the finite element method 79—27665
shock layer, hypersonic, vibr. nonequilib., near stagnation streamline, low Reynolds no. flow 78—87417
shock layers, flow over blunted cone, finite difference scheme 79—32435
shock separated boundary layer, suction effects, compressible Navier-Stokes eqn. solns. 80—24050
shock tube, unsteady boundary layer 77—23995
shock tube flows, unsteady non-equilibrium, discretisation of boundary layer terms 80—14742
shock wave, laminar to turbulent boundary layer transition, effect on current flow 79—41709
shock wave boundary layers, eqns. of motion 77—42857
shock wave generation, liq.-liq. interface with temp. discontinuity 78—51197
shock wave interactions, oblique incidence *(Japanese)* 78—55662
shock wave interactions with boundary layers, review, book contrib. 80—96283
shock wave reflection, regular to Mach transition, Monte Carlo simulation 77—75936
shock wave structure close to wall, book contrib. 80—1650
short crested waves, boundary layer vels. and mass transport 80—92169
short cylindrical channel, laminar axisymmetric nonstationary viscous gas flow, oscillations 80—38495
shpere between plane parallel boundaries, creeping parallel motion, strong interaction theory 80—103075
similarity problems, unified approach 79—10543
single point jet injection on boundary layer over flat plate, direct calc. method 79—68772
singular nonlinear differential eqns., boundary layer flow 78—63413
singularities in unsteady boundary layers 80—14651
singularity near pt. of separation, integral method *(French)* 77—62235
sink flow in a rotating basin, Ekman layer 79—94629
skewed boundary layers in duct with streamwise press. grad. variation 78—79302
skin friction in supersonic laminar and turbulent flows 79—98751
skin friction variation with Reynolds number, viscosity balance meas. compared with Preston tubes 77—72377
slender body oblique entry into incompressible fluid 79—64625
slender body potential flow between closely spaced walls 77—89095
slender body propulsion by boundary layer deform. in viscous fluid *(French)* 77—42798
slender cones, drag meas. in hypersonic flow using mag. suspension and balance 79—4039
slender delta wing with leading edge vortices, thickness effect synthesis 79—98734
slender streams for incompressible inviscid heavy liquids, jets, wall and channel flows 79—77205
slender torus, hydromechanics in low Reynolds number flow 80—19324
sliding interfaces and impact, numerical treatment 79—41631
slightly rarefied flow over specularly reflecting body, sphere and thermophoresis 77—55040
slightly rarefied gas, unsteady motion about rotating cylinder, slip effects 77—39312
slip boundary condition, rough sphere ang. vel. correlations, hydrodynamic anal. 77—51286
slip flow, developing, vel. distrib. and press. drop, Navier-Stokes analysis 77—55039
slip flow, MHD, over porous plate, with variable suction, heat transfer 78—79337
slip flow over surface due to temp. difference 77—932
slip flow with suction or injection, Rayleigh problem 77—19627
slow viscous flow due to motion of sphere on axis of circular cone 80 14654
slow viscous flows over flat plate with mixed boundary conditions 78—1632
small body in nonuniform flow, stability 79—18873
small channels, gas flow, graph and nomograph for anal. eval. 80—106848
smectic-A liquid crystal, permeative flow around obstacle, extended boundary layers 78—67644
solar chromosphere, boundary layers in shock heating problem 77—29745
solar wind flow past planets, axisymm. implicit blunt body computation technique 78—96370

boundary layers continued
solid dielectric particle dilute suspension in flat duct, electric field effect 80—53868
solid particle systems, high Reynolds number, momentum trasfer. Karman-Pohlhausen method 80—74947
solid reacting particles, ordered system at high Peclet numbers, mass transfer, convection 80—69830
sonoprobe survey, automatic recognition of submarine sediments *(Japanese)* 79—39985
sound absorptive boundaries, model scaling laws 77—75727
sound generation near infinite compliant wall 80—53766
Soyuz spacecraft, modelling of boundary layer flow by reactive streams of controlling motors of Apollo spacecraft *(Russian)* 77—82098
spacecraft atmospheric entry, body shape for minimal radiative heat inflow *(Russian)* 78—77457
sphere, conducting, proous in uniformly conducting fluid flow 78—34204
sphere, external laminar boundary layer vel. profile, photographic-tracer film anal. 79—50698
sphere between plane parallel boundaries, creeping perpendicular motion, strong interaction theory 80—100035
sphere drag coefficient in transonic flow at high Reynolds number 77—31323
sphere in gas slip flow, vel. field, heat exchange, friction dissipation *(German)* 78—34138
sphere in unsteady motion in liq., drag. calc. 78—67170
sphere in viscous incompressible fluid, surface force density calc. 77—7368
sphere moving in incompressible fluid, surface force density 77—7369
sphere rotating in viscous fluid, induced flow 77—15036
sphere surface viscoelastic Prandtl boundary layer flow, separation point 78—63460
sphere towing expts. in water tank *(Russian)* 77—68573
sphere with fluid source at centre, heat transfer to fluid stream 79—18887
spheres, concentric, cooling by forced convection, at low Reynolds no. 79—1183
spheres, deformable contiguous, in incompressible inviscid fluid, hydrodynamics 78—1727
spherical gas bubble in unsteady viscous flow, unsteady boundary layer 79—55357
spherical particle in circular tube flows, lateral migration 80—92221
spheroid at incidence, flow separation, laminar separation lines, turbulent separation 79—72878
spheroid in electrically conducting fluid, induced flow 77—75984
spheroids, harmonically oscillating, unsteady airload prediction, analytical soln. 78—51184
spillway surfaces, flow around three dimens. projections, cavitation 78—67232
spinning disc causing laminar and turbulent flow, mass transfer 79—41691
spinning yawed axisymmetric body, three-dimens. flow 80—38422
square cavities, laminar and turbulent incompressible flows 80—10307
square cylinders, smooth/turbulent lift, drag, vortex shedding 77—89109
square duct entrance region, Laminar flow and heat transfer to non-Newtonian fluid 80—10243
square prisms, interaction in two flow fields 78—9632
squeeze-films, elastico viscous, torsional balance rheometer meas. 77—3851
squeeze-films, elastico-viscous, superimposed rotation 77—3850
stability, neutral, Taylor-series expansion of dispersion relation 80—53744
stability, nonlinear effects 78—1636
stability of catalytically recombining gas 79—41768
stability of convective motion in two-dimens. vertical fluid layer with permeable boundaries 77—55086
stability rel. to transverse curvature for laminar flow with disturbances *(Russian)* 77—62233
stability theory, Blasius boundary layer, high viscous eigenstates 77—907
stably and neutrally stratified flow over three dimens. hill 80—48770
stably stratified shear flow in channel, internal gravity wave packet mean flow 79—98740
stagnation counterflow, interface perturbations growth and decay 78—30264
stagnation flow, nonlinear stability 78—90831
stagnation flow, stability to three-dimens. disturbances 78—30265
stagnation flow at a heated curved wall, ignition condition 80—96242
stagnation point 3D compressible layer, large injection rate 77—89139
stagnation point boundary layer flow with radiation 80—79258
stagnation point boundary layer on subliming surface with roughness elements 78—94635
stagnation point boundary layers, unsteady, three dimensional, compressible, numerical soln. 79—37335
stagnation point flow, least square finite element soln. 77—14981
stagnation point flow impinging obliquely on wall 79—27617
stagnation points on cycloidal boundary in flow with const. shear 80—87755
stagnation-point boundary layer with hot wall, mag. field effect 77—72359
standing surface waves, double boundary layers 77—25694
static pressure probe, laminar limiting boundary layer *(French)* 77—31402
stationary boundary layer flow, plane heat balance eqn. asymptotic soln. *(German)* 78—63430
stationary Ekman flow, bifurcation into stable periodic flow 79—32449
stationary flows in channels, Hagen-Poiseuille law generalisation, technical appls. 79—81980
stationary temperature boundary layers generation by surface waves *(Russian)* 80—1611
steady flow close to rotating disc, numerical soln. of boundary layer problem *(Russian)* 77—54969
steady flow over finite obstacle on horizontal bottom, Neumann-Kelvin problem *(French)* 77—72267
steady laminar interacting boundary layers *(German)* 80—14655
steady low Reynolds number flow, past circular cylinder, soln. and drag calc. 79—37287
steady motion through branching tube, high Reynolds no. 77—51119
steady rotating flow over topography, steady β-plane channel, quasi-linear theory 80—92159
steady separation from curved surfaces 77—75879
steady transonic flow past aerofoil, viscous effects, prediction model 80—14732

boundary layers continued
  steady viscous flow past circular cylinder, numerical study, vortices and separation 80—92108
  steady vortex driven by heat line source, math. anal. 79—23329
  steam, horizontal flow on cylinder, condensation 78—94550
  steam condensation heat transfer on below-freezing pt. surface 78—75042
  steam generating channel, nonuniform heat release, heat transfer crisis location 80—64534
  steam generating channels, boiling crisis, critical heat loads 79—90247
  steam generating channels, heat exchange intensification by surface roughness in transcritical region 79—55371
  steam generator tubes, forced and natural circulation, inception condition correlations 80—74868
  steam-generating channel hydraulic characts., two phase flow instability effects 79—90333
  steam-generating tube, bubble/plug flow boiling regimes, elevated press., drift vel. and void fraction determs. 78—87379
  steam-liquid, annular-dispersed flow, hydrodynamic characts. 78—94806
  steam-water, flow characts. at high press. 78—94805
  steam-water mixture, with high vap. content, annular flow, heat transfer, press. loss 78—75193
  steel, stainless, cylinder, in thermal aerodynamic tube, nonsteady heat transfer method 79—37147
  steel target-supersonic plasma impact effect, boundary layer role 79—32780
  stellar atmospheres, free convection effects on unsteady laminar boundary-layer flow 79—35237
  stellar atmospheres, hydromagnetic flow near oscillating porous limiting surface 78—12200
  sticking condition for fluid at solid boundary, entropy change 78—83359
  stochastic model of fluctuations 78—90818
  Stokes' problem for vertical infinite plate with variable temp. 79—23301
  Stokes flow, asymm. streaming, past spherical cap, wakes, drag, torque 77—15032
  Stokes flow, axisymmetric, about body of revolution whose section is cardioid 78—55629
  Stokes flow, eddy structure between two spheres with relative vel. 79—27647
  Stokes flow, Faxen relations generalisation 79—32438
  Stokes flow, in wedge-shaped trench, separation of variables theory 77—47093
  Stokes flow, past spherical caps, visualisation of separation 79—60076
  Stokes flow, round smooth body with attached vortex 77—14984
  Stokes flow, separation, appl. of bipolar coordinates to two-dimensional creeping motion of liquid 79—14375
  Stokes flow, slender body theory for viscous incompressible fluid 80—92160
  stokes flow due to circular scraping 79—46329
  Stokes flow ellipsoid of min. drag, limited by cylindrical front *(French)* 79—53982
  Stokes flow in a trench between concentric cylinders 78—83360
  Stokes flow past circ. arc, separation 79—90214
  Stokes flow past plane with cylindrical ridge or trough, separation 78—55653
  Stokes flow past radially deforming sphere at small Reynolds number 78—67174
  Stokes flow past slender body of revolution 77—14986
  Stokes flow past smooth cylinder 78—55627
  Stokes flow separation, local boundary geometry depend. 77—54949
  Stokes flow through channel and tubes with sinusoidal boundaries as model for porous media 78—18337
  Stokes layer, centrifugal instability and asymmetric disturbances 79—98686
  Stokes layer centrifugal instability, nonlinear theory 77—31280
  Stokes problem, effects of free convection on oscillatory flow past infinite porous vertical limiting surface 80—109348
  Stokes problem for infinite vert. plate, hydromagnetic free convection effects 80—10318
  Stokes problem of motion of Cassinian cylinder in viscous fluid 78—71312
  Stokes series, computed extension, circular boundary flow 78—42583
  straight ducts of arbitrary cross section, oscillatory and steady flow 80—48801
  straight wing in circular cross section in wind tunnel, induced drag 77—15055
  stratification effects in boundary layer flow over hills 78—53707
  stratified boundary layers, stability calc., numerical integration *(German)* 80—53834
  stratified flow, Coriolis force blocking attenuation, wakes, baroclinic vorticity and boundary layers 80—6129
  stratified flow over two-dimensional obstacle, upstream influence and Long's model 77—75962
  stratified fluid, Boussinesq eqn. for infinite wall 78—30336
  stratified fluid, duct, equilibrium breakdown, thermosiphon work *(French)* 80—59114
  stratified fluid confined between horizontal planes, flow due to object motion 77—51097
  stratified inlet, anal. of wind influence on surface layer 77—41051
  stratified inlet, obs. of wind influence on surface layer 77—41050
  stratified liquid flow around submerged body, wave motion *(Russian)* 79—14453
  stratified nondiffusive flow, over horizontal flat plate, boundary layers and wakes 77—47058
  stratified water surface layers, unsteady energy transfer 77—41092
  stream distribution in channel with porous wall, energy eqn. soln. 77—7445
  stream swirling, effect on laminar flow struct., heat exchange in round tube 77—11265
  streaming, of vel. and temp., in oscill. boundary layers 78—83358
  streaming, past axisymmetric bluff bodies, approx. theory 77—84217
  streaming, uniform, past fixed semicirc. infinite strip 79—23299
  streaming Stokes flow, free eddies 79—77065
  stress near rigid boundaries 77—80200
  stress-driven entrainment expts. scaling in stratified flow 79—50768
  strong interaction of boundary layer and hypersonic flow, boundary conditions local perturbation 80—14738
  subcooled boiling flow, flow quality and void fraction for channel 79—90249
  subcooled forced convection film boiling in forward stagnation region 80—43702

boundary layers continued
  subcritical flows past lifting profile *(French)* 77—72322
  subcritical steady flow past swept semi-infinite elliptic cylinder 77—62275
  submarines, aero/hydrodynamic forces and moments 77—89094
  submerged cylinders, forced oscills. test in water 78—5728
  submerged moving bodies, free surface and surface tension effects 80—1522
  submersion of a body into a fluid *(Ukrainian)* 80—33610
  subsonic, three dimensional flow transverse to circular cylinder 77—58719
  subsonic compressible flow, past symmetric profile, num. soln. method *(French)* 77—58720
  subsonic flow around delta wing, vortex breakdown pt. stabilisation 77—39305
  subsonic flow past pulsating airfoil 78—71348
  subsonic flowfield, three dimensional geometrics, correction for viscous effects 79—98744
  subsonic high-angle-of-attack flow 78—38358
  suction controlled boundary layer flow, perturbation caused stability loss 77—75886
  suction effects on shock wave-boundary layer interaction, numerical Navier-Stokes soln. 79—1243
  suction or blowing flows through openings in the wall of a boundary layer *(French)* 79—18947
  suction-induced asymptotic boundary layers, exptl. and predicted props. 80—1553
  supercavity hydrofoil, wall effects, nose rounding 80—64594
  supercritical flow of an ideal fluid over a spillway 78—94638
  supercritical water flow in curved channels, heat transfer and drag 79—90246
  superheating-convective instability, effect of boundaries 77—35137
  superposed fluids, Taylor instability nonlinear theory for wavenumbers near linear cutoff value 79—55355
  supersonic, external acoustic perturbations *(Russian)* 78—34152
  supersonic, laminar to turbulent transition 78—38437
  supersonic, leeside flowfields of planar delta wings, Reynolds number 79—60003
  supersonic blown off, reattachment by injection cut off 77—3844
  supersonic blunt body flow of viscous perfect gas and nonequilib. gas mixture 80—28578
  supersonic boundary layer, prediction by hybrid marching integration procedure 77—65761
  supersonic boundary layer flow about cones, method of integral relations 79—10589
  supersonic boundary layer in external acoustic field 79—68740
  supersonic boundary layer on plate with leading edge blunting, stability 79—64688
  supersonic combustion past a conical body with normal surface blowing 79—41770
  supersonic corner flow, boundary region 79—32559
  supersonic corner flow, viscous-inviscid interaction 79—32563
  supersonic flow, inviscid, over external axial corner, shock wave and vertical singularities 77—42866
  supersonic flow, jet injection, separation zone, boundary layer thickness and transverse curvature effects 80—48745
  supersonic flow, nonstationary separation of laminar boundary layer, numerical method *(Russian)* 79—14425
  supersonic flow, self-induced oscills. 78—67215
  supersonic flow, viscous, past corner, energy eqn., asymptotic solns., heat transfer 79—32564
  supersonic flow along wavy wall including boundary layer effects *(German)* 77—84274
  supersonic flow around blunt bodies with combined cross sections, num. comput. 77—58728
  supersonic flow around wings with attached shock wave on leading edge, num. soln. 77—51080
  supersonic flow of inverted population gas flow round blunt bodies, amplification factor 78—5828
  supersonic flow of nonstationary boundary layer with self-induced pressure near vibrating wall 79—86459
  supersonic flow over compression ramp, laminar separation, second order asymptotic soln. 80—83828
  supersonic flow over deep cavity, flow disturbances, laser appl. 79—98748
  supersonic flow past blunt body, radn. effect on flow field and heat flux 77—47113
  supersonic flow past flat faced cylinders, second order shock capturing finite difference method *(Japanese)* 79—4038
  supersonic flow past slender body, wave system 77—31327
  supersonic flow past slender cone at high incidence 78—90932
  supersonic flow past solids of revolution, small perturbation theory 79—68742
  supersonic flow past thin sharp bodies with intensive blow *(Russian)* 77—31329
  supersonic flow through cascade, linearised theory *(French)* 78—94766
  supersonic jet flow over obstacle, discrete tones generation 78—1708
  supersonic laminar, response to oblique slot blowing 77—11220
  supersonic laminar boundary layer separations, quasi-3-dimens. 78—46995
  supersonic laminar boundary layer with conjugated heat transfer 79—64687
  supersonic laminar boundary layers, strong slot injection, flow separation 80—48738
  supersonic laminar boundary-layer separation by slot injection 79—98747
  supersonic laminar flow over backward facing step, numerical soln. at high Reynolds number 77—47040
  supersonic laminar viscous flow, partial differential eqns., separation 80—24062
  supersonic lifting surface, finite element anal. and collocation method 78—1687
  supersonic separated flow changes, caused by throttling in round duct 78—63446
  supersonic stream, laminar separation, Reynolds no. effect 80—19432
  supersonic thermal boundary layer, effect of wall hollow-induced separated bubble *(French)* 78—5784
  supersonic viscous flows, interactive numerical calc. procedure 77—31326
  supersonic wave drag of planar singularity distributions 78—83430
  supersonic wings with subsonic leading edges, minimum drag *(German)* 77—15058

boundary layers continued
  - surface friction dependence on compressible fluid injection and removal by suction from wall jet 77—47052
  - surface heat flux, rel. to boundary conditions, modified integral method calcs. 79—59978
  - surface mass transfer interaction with transverse curvature in natural convection boundary layers 80—24008
  - surface mounted obstacles, effects on flow, Navier-Stokes eqns., 3-dimens. integration 79—59960
  - surface reacting layer, thermodynamic coupling theory 77—72369
  - surface reactions and mass transport, in Leveque's approx. 78—76907
  - surface streamlines, governing eqns. 78—71309
  - surface wave generation of stationary flow *(Russian)* 79—39731
  - surface with sharp boundary condition change, laminar flow, concentration distrib., convective diffusion *(Russian)* 79—94590
  - surface-mounted cube in uniform and turbulent streams 77—27535
  - suspended particles, influence on turbulence struct. in tube flow 77—75969
  - suspension, laminar Poiseuille flow, particle lateral migration, tubular pinch effect 79—98783
  - suspension, parallel flows with boundary layer characts. 77—15093
  - suspension bearing flow, turbulent energy balance in pressure pipe flow 80—48777
  - suspensions of charged particles, laminar tube flow, entrance deposition 80—59100
  - swirling convective boundary layer, vorticity dynamics 80—59048
  - swirling flow, fluid between rotating discs, nonmonotonicity of solns. 78—59404
  - swordfish, ampoules in skin rel. to boundary layer control *(Russian)* 77—64072
  - symmetrical flow past double wedge at subsonic Mach nos. 78—51182
  - T-junction laminar flow, partially elliptic flow numerical calcs., recirculation 80—64632
  - T-tube plasma, influence of boundary layer on H_γ line 80—48862
  - tapered tubes, flow of closely fitting spheres and cones 80—48789
  - Taylor column for hemisphere, nonlinear effects 77—11199
  - Taylor instability of two fluids in EM field *(Russian)* 77—27602
  - Taylor-Gortler instability of boundary layer with suction and blowing 77—27512
  - temperature boundary layer on rotating curved surface, constant wall temp. case 79—81903
  - ternary gas mixture, natural convection, naphthalene sublimation appl. 80—6511
  - thermal, dissociation effects anal. by numerical anal. *(Japanese)* 78—5733
  - thermal, in gradient flow around nonisothermal surfaces, temp. depend. of fluid thermophys. props. influence *(Ukrainian)* 77—51054
  - thermal, second-order layer on blunted wedge 77—7379
  - thermal, separation from wall, nature of reversed flow 77—75956
  - thermal, singular parabolic partial differential eqns., impulsive motion appl. 78—38326
  - thermal, thickness for Poiseuille flow past permeable bed 79—46299
  - thermal accommodation coefficients from heat transfer data for low-density gases 77—35167
  - thermal blooming in axial pipe flow: comment [and reply] 80—95966
  - thermal boundary layer in water near air-water interface, fine struct. *(Russian)* 78—22332
  - thermal boundary layer interactions in shock tube sampling for kinetic obs. 80—104420
  - thermal convection, between nonuniformly heated plates, stability 77—58668
  - thermal creep for gas flow in flat channel, accommodation coeff. 77—11264
  - thermal layer plane shock interaction flow props. and temp. profiles 77—58735
  - thermal mixing layer development over water and heated land, lab. simulation 78—73449
  - thermal response behaviour, laminar flow 78—75136
  - thermal-ignition analysis in boundary-layer flows 79—64800
  - thermoacoustic vibration generation, in heated channel laminar flow 78—14029
  - thermocapillary convection, unevenly heated liq. stream near gas bubble 78—59460
  - thermoconvective waves in horizontal gas layer 77—7407
  - thermocouple hot-wire anemometer for boundary layer meas. with free convection in liquids *(German)* 80—10329
  - thermoelectric MHD, pipe end problem, boundary layers and rotation 80—69942
  - thick wing, two-dimens. aerofoil, boundary conditions 77—62274
  - thin body moving in shallow water 77—11169
  - thin cylindrical body acceleration in viscous fluid 79—10571
  - thin laminar flow down inclined plane wall, roll wave form. 80—48673
  - thin pipe with thin linear elastic wall, viscous fluid motion model 79—64769
  - thin profile near interface of two heavy fluids, steady motion 77—58633
  - three dimensional boundary layer, streamline coords., similarity transforms 78—90816
  - three dimensional free convection flow and heat transfer along a porous vertical plate 78—90866
  - three dimensional growing boundary layers, linear stability 80—74833
  - three dimensional incompressible boundary layer flow, temporal and spatial stability relation 80—14659
  - three dimensional layer theory, using shell geometrical concepts 78—90815
  - three dimensional parallel shear flows, stability and transition for rot. disc 80—74887
  - three-component system transport coefficient determ. 78—21082
  - three-dimens. flow over blunt bodies 78—79296
  - three-dimens. low Reynolds no. flows with free surface 77—49600
  - three-dimensional boundary layer eqns. 80—96241
  - three-dimensional boundary-layer separation 80—92188
  - three-dimensional flow, in tube bundles, theory 78—34198
  - three-dimensional flow in orthogonal curvilinear coordinates 77—23940
  - three-dimensional flow over wings with leading-edge vortex separation 80—74927
  - three-dimensional incompressible flow, with mag. neutral points 79—64788
  - three-dimensional laminar incompressible internal flow, general computation method 77—42803
  - three-dimensional laminar stream tube network, convective mixing 80—14815

boundary layers continued
  - three-wave resonance interaction of disturbances in a boundary layer 79—90264
  - Tokamak, neutral injection system, cold gas flow pattern evaluation 78—66397
  - Tollmien Schlichting secondary instability, in boundary layer flows 79—64632
  - Tollmien Schlichting wave, two-dimens., flat plate downstream flow field 78—38357
  - Tollmien-Schlichting wave packet produced by turbulent spot in laminar boundary layer 79—68733
  - Tolman-Schlichting waves in boundary layer effected by external perturbation 79—90265
  - topographically induced vorticity in homogeneous rot. flow, free surface effect 78—42612
  - toroidal thermosyphon flow with ang. displacement of heated and cooled sections 80—33680
  - tracer dispersion in annular climbing film flow 79—64751
  - transient and periodic flows through cascades, blade oscillation 78—22318
  - transient boundary layer on porous plate, coolant injection, laminar flow stability and heat transfer 78—83389
  - transient boundary layers between porous plates 77—46990
  - transient free convection from an isothermal horizontal circular cylinder *(German)* 79—77115
  - transient freezing of liquids in turbulent flow inside tubes 80—6494
  - transient gas flow in channel of cylindrical solid with free movement between end chambers 77—15120
  - transient natural convection in curly viscous fluids, boundary layer approx. 79—77096
  - transient natural convection in horizontal cylinder with constant cooling rate 77—42841
  - transient temperature field approx. in cylindrical and spherical bodies *(Polish)* 79—32192
  - transition, detection using holography 78—14101
  - transition from laminar to turbulent boundary layer, results of photographic expt. *(Russian)* 77—62243
  - transition in the infinite swept attachment line boundary layer 80—19326
  - transition region extension, initial turbulence effects *(Russian)* 79—90233
  - transition research at AEDC, review 78—38290
  - transitional, engineering predictions 78—38275
  - transitional, oscills., stability waves, vortices 78—38287
  - transitional, second-order closure model 78—38276
  - translational friction, for arbitrary shaped objects, modified Oseen tensor calcs. 78—71311
  - transonic boundary layer, fluctuation anal. from hot-wire anemometry data 77—65817
  - transonic boundary layers, freely interacting, compressive and expansive flow 77—89145
  - transonic channel flow, unsteady, with shock waves 77—23991
  - transonic flow, unsteady inviscid, local linearisation soln. for pitching bodies of revolution, $M_\infty=1$, stability anal. 77—31322
  - transonic flow, viscous effects, Navier-Stokes eqns. soln. method 77—55023
  - transonic flow, wind tunnel wall and viscous effects, numerical simulation 77—27552
  - transonic flow around airfoil, finite-difference calc., computer code 78—26147
  - transonic flow around bodies of revolution, flow boundary effects 79—90275
  - transonic flow around bodies of rotation *(Russian)* 78—87357
  - transonic flow around lifting round-nosed airfoil, extended integral eqn. method 77—62271
  - transonic flow around quasi axially symmetric bodies, series expansion and parabolic method 77—15057
  - transonic flow around slender bodies, unsteady linearized formulation 77—89143
  - transonic flow around spheres, orthogonal collocation soln. 77—39307
  - transonic flow over body of revolution, perturbation theory and numerical body 79—60000
  - transonic flow past nonaxisymmetric slender shapes, classical equivalence rule assessment 80—6079
  - transonic laminar boundary layer flow near convex corners 79—64686
  - transonic nonseparating normal shock-laminar boundary layer interaction, approx. anal. theory 77—23992
  - transonic potential flow, axisymmetric inlets and bodies at angle of attack 78—9648
  - transonic potential flows past cascades, in nozzles and channels, pseudo-unsteady method 80—14727
  - transonic profile flow with shock, supercritical flow 77—15056
  - transonic shock-boundary layer interaction, shock obliquity effect 78—90933
  - transonic similarity parameter, simple waves 77—23982
  - transonic steady potential flow 77—72324
  - transonic unsteady flows calc. using integral eqn. method, aerodynamics 79—32554
  - transonic viscous flow around 3D wings 79—37346
  - transonic wind tunnel laser velocimeter meas. interpretation 77—31324
  - transverse curvature, consistent integral thickness utilization 78—13990
  - trench flow, square section, viscous liquid, laminar and turbulent conditions obs. 77—75981
  - trench with radiative wall conditions, free convection 80—79324
  - tube, elliptical, laminar liq. flow, nonsteady heat transfer 78—42598
  - tube, horizontal, laminar combined convection, circumferentially nonuniform heating effect 78—71331
  - tube, severely-contricted, symmetric, separating flow 79—50697
  - tube, vert., uniformly heated, forced convection boiling, crit. heat flux 79—27498
  - tube, vert., uniformly-heated, crit. heat flux prediction, generalised graphical method 79—46313
  - tube, vertical, laminar and turbulent heat transfer, air and Ar 78—71332
  - tube, vertical, steam generating annular flow, dry-out position prediction, computer model 78—59447
  - tube, with heated inner eccentric rod, steady convective laminar heat transfer 78—38311
  - tube bank heat transfer in air crossflow at high Reynolds nos. *(Russian)* 78—14010
  - tube bank streamlining in critical flow regime with heat transfer *(Russian)* 78—14009

boundary layers continued
tube banks, in-line, with pyramidal roughness, flow and heat transfer 78—18152
tube banks in air crossflow, hydrodynamic vibration models *(Russian)* 78—46981
tube entrance laminar flow, influence of film condensation *(German)* 79—77260
tube flow, charged particle suspension deposition 79—37416
tube outlet section gas flow at supercritical pressure differentials 80—28569
tube rows and arrays, fluid elastic whirling 78—46928
tube with two hyperbola bounded cross section, steady laminar flow 79—94723
tube with variable boundary conditions, heat transfer, Laplace transform appl. 80—74859
tubes, heat transfer laws, longitudinal turbulent diffusion influence 80—33597
tubes, horizontal and vertical cooled, boiling crisis and critical heat flux 80—48712
tubes, nonstationary thermal processes, heat transfer coeff. quasistationary value applicability 80—64562
tubes, straight and coiled, boiling heat transfer with low pressure water flows 80—74856
tunnels with continuous and perforated walls, cavity size 80—92193
turbomachine airfoil cascades, variational and dual extremum principles for aerodynamic problems *(Chinese)* 80—43729
turbomachines, boundary layer charact., influence of external flow turbulence 80—87811
turbulence, of viscous fluid flowing along wall 77—912
turbulence models for heat transfer, review 79—4017
turbulent boundary layer generation in unsteady flow 78—90828
turbulent channel flow wall region, fluctuating vel. components 79—77250
turbulent heated wake, interface statistics 79—27645
turbulent jet mixing layers, exptl. investig. of large scale structs. *(French)* 79—41728
turbulent shear flow with streamline curvature, algebraic stress-heat flux model 79—27625
two dimensional boundary layer encountering three dimens. hump 78—5725
two dimensional Laval micronozzles, laminar boundary layer approx. calcs. 80—24070
two flat plates, fluid flow anal. for fluid control meas. *(Chinese)* 79—81997
two infinite parallel plates, non-Newtonian fluid linear flow, heat transfer 79—98810
two parallel infinite plates, Couette flow of dusty gas 80—1681
two-component fluid, laminar boundary layer, temp. and conc. field calcs. *(German)* 78—71386
two-dimensional Hartmann flows, for fluid with cross-stream dependent elec. cond. 79—64771
two-dimensional laminar boundary layers, perturbation development, secondary flows 80—1521
two-dimensional laminar flow between porous walls 79—14477
two-dimensional viscous flow accompanied by stagnation point on plane wall 80—6021
two-dimensional viscous flow past circular cylinder, rapidly convergent series soln. 80—96244
two-layer film flow stability down inclined plane 79—90222
two-parameter skin friction formula for adiabatic compressible flow, shocked relaxing boundary layer 78—51188
two-phase boundary layer, successive approx. method 79—32647
two-phase flow, an.. of induced vibral in horizontal piping system 77—80215
two-phase flow, disc straddling interface 78—90971
two-phase flow, nonstratified, adiabatic, hydraulic resistance calc. 77—7440
two-phase flow, transient, interfacial heat and mass transfer, surface renewal model 79—27683
two-phase flow instability in parallel channels 78—94810
two-phase flow through variable cross section channels, critical flow rate 79—55410
two-phase laminar boundary layer, forced convection condensation *(Japanese)* 78—34191
two-phase laminar channel flow, forced convection energy eqns. 77—55090
two-phase liquid film flow, hydrodynamic and heat transfer in downward annular motion 77—89190
two-phase medium,, laminar boundary layer eqns. 80—38476
two-phase mixture flow in rotary mixer, optimal dimensions 78—63485
two-phase nonequilibrium flow, spectral characts. 78—94854
two-phase pressure driven stratified laminar pipe flow 80—64609
two-phase vertical adiabatic flow in tubes, actual gas content determ. 77—11245
underground cable system, convectively cooled, temp. distribs., heat transfer correlations 78—71262
underwater acoustics, virtual modes and surface boundary condition 77—31160
underwater axisymmetric boundary layer on deforming body of rotation *(Russian)* 77—32916
unstable boundary layer, streamwise vorticity growth 77—58700
unstable flow past cavities, shear layer oscill. freqs. 77—84228
unstable heat transfer conditions, free convection-film boiling transition 78—14006
unstable laminar boundary layer, response to acoustic excitation 79—98681
unstable laminar boundary layers, nonlinear evolution and breakdown 80—92109
unsteady, analysis of self-similarity and fibering of equations by Lie group theory 77—89108
unsteady, in shock tube, behind moving shock wave, expt. 78—46998
unsteady, through pipes, modelling and simulation *(German)* 80—64637
unsteady, transitional and turbulent, expt. and calc. methods *(French)* 78—75125
unsteady airfoil stall in laminar boundary layer, water tunnel visualisations 80—53745
unsteady boundary layer, similarity problems 78—1633
unsteady boundary layer coupled to non-uniform flow, num. determ., shock tube appl. *(French)* 77—65752
unsteady boundary layer flow, past suddenly cooled vertical plate 79—32480

boundary layers continued
unsteady boundary layer of a plate with a time-interrupted suction *(Russian)* 80—23988
unsteady boundary layer on a two dimensional or axisymmetric body with higher order effects 80—92106
unsteady boundary layer on infinite yawed wedge 77—42800
unsteady boundary layer over an impulsively started flat plate using finite elements 79—14366
unsteady boundary layer separation, mathematical criterion 80—69884
unsteady boundary layers, separated and attached, review 78—71313
unsteady boundary layers with reversal and separation 78—75163
unsteady comp. laminar boundary layer flow, num. anal. 79—94586
unsteady compressible 3-D boundary layer flow, near axisymmetric stagnation point 80—103011
unsteady compressible boundary layer equations, generalised soln. 79—32463
unsteady eqns., asymptotic soln. 77—72275
unsteady flow analysis in duct with junction, FLIC method 78—18340
unsteady flow damping by compliant boundaries 77—31274
unsteady flow of viscous fluid through elastic tube with outward suction 77—68690
unsteady flow past wavelike bulge on flat plate, num. soln. of Navier-Stokes eqns. 77—58644
unsteady forced convection heat transfer from impulsively started circ. cylinder 79—27633
unsteady free convection flow past a vertical porous plate with variable suction and transverse magnetic field 79—32691
unsteady free convection flow past an infinite plate with constant suction and heat sources 79—81868
unsteady heat transfer effect on boundary layer growth at forward stagnation point 79—10555
unsteady hydromagnetic thermal boundary layer problem, numerical treatment 80—92227
unsteady imcompressible laminar boundary layers around impulsively started cylinders *(French)* 79—72876
unsteady incompressible laminar boundary layer, eqn. soln. for 2-dimens. flow 80—48672
unsteady laminar boundary layer, approx. solns. 77—23936
unsteady laminar boundary layer flows induced by impulsive accelerating motion *(Japanese)* 80—69765
unsteady laminar boundary layers, collision at equator of rotating sphere 79—72896
unsteady laminar boundary layers at incompressible 3-dimens. stagnation point, heat transfer 79—64659
unsteady laminar boundary layers in an incompressible three-dimensional stagnation flow 79—81848
unsteady laminar boundary layers in an incompressible three-dimensional stagnation flow, book contrib. 80—1525
unsteady laminar viscous incompressible fluid flow through channels 77—68566
unsteady local linearization solution for pulsating bodies in transonic flow 77—11219
unsteady MHD flow between two coaxial cylinders 77—68701
unsteady pipe flows, finite difference scheme 80—6146
unsteady rotating boundary layer flows between porous plates 77—47112
unsteady stagnation-point flow impinging obliquely on oscillating flat plate 80—6020
unsteady thermal boundary layer, parametric method appl. 77—11170
unsteady three dimens. laminar boundary layer separation, anal. 79—32451
unsteady two-dimensional and axisymmetric compressible boundary layers 79—27616
unsteady viscous separated laminar flow, numerical modelling 78—46933
upstream adiabatic zone, subsonic, supersonic downstream boundary layer heat transfer effects 78—83379
US flowmeters, thermal boundary layers, diffraction effects on sound transit time 80—14858
vaporising liquid layer at nonadiabatic evaporation, binary laminar boundary layer flow *(German)* 80—1588
vapour generator, two-phase flow dynamics 78—94808
vapour-liquid two-phase flashing flow, isentropic streamtube model 79—55412
vapour-noncondensible gas mixture, body force convection condensation *(Japanese)* 79—50574
variable resistance boundary layers, frictional resist. effects on motion of bodies 80—96243
velocity gradient factor, use as pressure gradient parameter 77—27506
velocity profile for boundary layer flow along a rectangular corner *(Japanese)* 80—74832
vertical circular channel, convective stability relative to periodical disturbances *(Russian)* 80—43711
vertical coplanar Y-junctions, two-phase steam-water flow 80—38478
vertical flat plate, wave instability of liminar mixed convection flow 80—10245
vertical internally heated annulus entry region, mixed convection in water 80—24015
vertical layer with space-modulated temp. distrib. on boundaries, convective motions 79—90240
vertical plane turbulent buoyant jet in confined depth channel, stability and mixing 79—90302
vertical plate with uniform blowing, laminar combined forced and free convection 80—74876
vertical tube, pressure loss coeff. in two-phase flows 77—27582
vertical tube with liq. flow, free and forced oscills. 77—7457
vertical water entry into cone, partial cell marker and cell method 77—42801
virtual mass of sphere in axisymm. potential flow near plane wall 77—68560
visco-elastic liquid, flow past hot porous circular cylinder, free and forced convection 78—83386
viscocapillary flows, interface shape and evolution eqns. 80—19507
viscoelastic and inelastic fluid flow past sphere, creeping and boundary layer flows, drag coeff. 77—51090
viscoelastic boundary layer flow, second order, at stagnation point, heat transfer 80—103025
viscoelastic conducting fluid on oscill. plate in mag. field 77—72365
viscoelastic Ekman layer on porous plate 77—72336
viscoelastic flow, channel entrance, heat transfer at low Deborah numbers, rheological effects 80—19445
viscoelastic flow at stagnation point over moving wall 78—18319
viscoelastic flow past stationary and rotating cylinders 80—43744

boundary layers continued
viscoelastic fluid, axial laminar flow, force exerted on wall *(German)* 77—68643
viscoelastic fluid, creeping flow through tapered contraction 77—55050
viscoelastic fluid, MHD flow past porous plate in slip flow 79—4084
viscoelastic fluid, suddenly started in circular pipe entrance region, momentum, thermal boundary layers 78—9658
viscoelastic fluid, thermal boundary layer on porous plate 77—84283
viscoelastic fluid, unsteady flow through long circular ducts 79—77249
viscoelastic fluid film, flow along conical rotor 78—1697
viscoelastic fluid flow in annulus entrance region, boundary layer anal. 78—63459
viscoelastic fluid fluctuating flow past infinite porous wall in slip flow regime 79—18917
viscoelastic fluid in channel entrance, hydrodynamic and thermal boundary layers 79—18915
viscoelastic fluid layer, convective instability, boundary thermal cond. independence 78—9659
viscoelastic fluid layer, thermal instability, lift and thermocapillary forces effect 79—86434
viscoelastic fluid unsteady flow through pipes under different press. gradient conditions 78—75172
viscoelastic free convection boundary layer flow past infinite plate with constant suction 78—90936
viscoelastic laminar flow round spherical obstacle, finite boundaries effect 77—15076
viscoelastic layer, flow down inclined plane, finite amplitude long wave stability 79—37365
viscoelastic liq., motion of slender rod falling near vertical wall 80—43743
viscoelastic liquid, boundary-layer flow past symmetric wedge or right circular cone 80—64513
viscoelastic Maxwell liquid, torsional transient motion between concentric spheres 77—62283
viscoelastic pipes, press. transients 80—64644
viscoelastic radial flow between parallel discs 78—67223
viscoelastic reacting fluids flowing over flat plate, boundary layer anal. of surface deposition 78—42675
viscoelastic Rivlin-Ericksen flow past stretching plate, skin friction, heat transfer calc. 77—72272
viscoelastic squeeze films, effect of normal oscill. and fluid inertia 78—67224
viscometer, high pressure, non-isothermal flow, thermal boundary conditions *(German)* 78—67292
viscoplastic liquid film on vertical vibr. wall, with slip, shaking loose 78—59371
viscous boundary layer, hybrid random choice method, internal combustion engine appl. 80—38461
viscous conducting fluid, laminar flow, boundary effect in helical induction machine *(Russian)* 77—47105
viscous dissipation effect on heat transfer, circ. cylinder axisymmetric stagnation flow 78—51164
viscous dissipation effects on combined forced and free convection 77—54995
viscous drag computation for axisymmetric bodies at high Reynolds numbers 80—19343
viscous drag reduction by polymer injection at high Reynolds number *(Chinese)* 79—32582
viscous drainage, over naturally permeable wall, steady-state film profile 77—27509
viscous drainage, over permeable wall, Navier-Stokes eqn. 77—31278
viscous film, nonlinear stability w.r.t. side-band disturbances 77—75887
viscous flow, downstream boundary layers finite-difference and Chebyshev approx. 80—33555
viscous flow, non-Navier Stokes computations, parabolic and thin layer approx. 80—48666
viscous flow, numerical boundary conditions 77—23929
viscous flow, past thin obstacle, iteration method *(Japanese)* 79—94599
viscous flow calcs., polynomial interpolation methods 77—65729
viscous flow due to motion of cylinder on wedge centre-line 79—77063
viscous flow field inside locally constricted cylindrical duct *(French)* 77—51115
viscous flow in curved tube of triangular cross-section 77—7458
viscous flow in oscillatory spherical annuli 79—32542
viscous flow induced by wavy motion of wall 77—14983
viscous flow induced by wavy motion of wall 77—62236
viscous flow of stably stratified fluid over barrier 77—75961
viscous flow over flat plate, comput. method developments 77—54970
viscous flow past circular cylinder, two coord. systems description 77—58643
viscous flow past multiple planar arrays of small spheres 79—37288
viscous flow past solid body at large Reynolds number, spiral form. 77—42799
viscous flow past two-dimensional bluff body, new approx. theory 77—918
viscous flow through rough wall cracks, friction factor formula *(Rumanian)* 80—69925
viscous fluid, plane squeezing flow, invariance group 80—79252
viscous fluid, variable thermal conductivity, variational calc. of vel. profile and temp. in laminar boundary layer *(French)* 78—55625
viscous fluid flow through slot between fixed and rotating surfaces of revolution *(Polish)* 78—79300
viscous fluid in rotating channel pulsatile flow 80—10311
viscous fluid in straight porous tube, annular effect 79—77240
viscous fluid magnetic throughflow in slot, inertia effect 79—37418
viscous fluid motion, between concentric spheres, non-linear analysis *(Russian)* 78—42587
viscous fluid squeezing between two plates 77—46991
viscous fluid steady flow, lift and drag of body 77—51027
viscous fluid with free surface, three-dimens. flow 79—86400
viscous heat conducting fluid, acoustic boundary layer 80—107377
viscous impressible fluid bounded by cylindrical boundaries, slow motion of small sphere 77—14978
viscous incompressible flow, past porous sucking vertical plate, free convection 78—30283
viscous incompressible liquid between two coaxial cylinders, exponential rate of heat addition, temp. distrib. 77—68586
viscous incompressible Newtonian fluid, hyperbolic flow 77—46983
viscous liquid, linear radial flow between parallel infinite discs 77—904
viscous liquid, three-dimensional flow and convective diffusion toward particle, nonlinear kinetics 80—19397

boundary layers continued
viscous liquid, transverse flow around cylinder, heat exchange *(Russian)* 78—46971
viscous liquid, unsteady laminar flow between parallel plates 80—10310
viscous liquid boundary layer, nonlinear wave growth in perturbed flow, stability 78—34107
viscous liquid laminar flow in gap, nonstationary Reynolds differential eqn. *(German)* 77—58641
viscous liquid unsteady flow in annular channel 78—75205
viscous mixing at trailing edge 78—1635
viscous radiating gas, hypersonic flow over blunted cones 77—51131
viscous sheet flow over sloping dry bed 77—72270
viscous transonic cascade flows around airfoil, coord. system for numerical calcs. 78—42627
viscous-inviscid flow interaction method, using blowing and suction flows 79—1154
viscous-inviscid flow matching, separation, shock waves *(French)* 78—34105
viscous-inviscid supersonic (transonic) flow matching, two-dimens., numerical method *(French)* 78—79334
von Mises' eqn., finite element solution to eqns. of laminar boundary layer *(French)* 77—72268
vortex shedding behind circular cylinder, wake 78—75149
vortex shedding from smooth and roughened cylinders in crossflow near plane surface 79—81911
vortex sheet approx. for incompressible boundary layers 78—67201
vortex-edge interaction, low frequency component generation mechanisms 80—53795
vorticity of free stream adjusting to flat plate, Laplace eqn. soln. 78—59406
wake of step, with pulsating jet, thermal convection *(French)* 80—10240
wall, plane, nonsteady heat transfer, conjugate problem soln. 79—37128
wall jet negotiating a trailing edge 79—41726
wall shear layer of infinite duct, acoustic field generated by single line source 78—1455
wall temperature distributions, in regions of deteriorated heat transfer 78—83377
walls, permeable, cooling characts., heat exchange, rad. emitter design 80—64535
water, annular mist flow in tube, wall film mass flow rate 80—69905
water, cooling, boundary layer thermal state during transition from free to forced convection *(Russian)* 78—81192
water, hot, film, wavy laminar flow down vertical plate at high surface tension numbers 79—94587
water, internal circulation in falling drops, boundary layer theory 77—66964
water, nondimensional heat transfer law for a slanted hot film 80—74853
water, Tollmien-Schlichting waves and transition 79—81845
water, vertical boundary layer convection, salinity and press. depends. 79—37316
water adjacent to vertical uniform flux surface, buoyancy driven flow, transition and transport 79—27631
water bodies, cooling from surface under free and forced convection regimes *(Russian)* 78—36179
water boundary layer along heated cylinder, buoyancy and variable viscosity effects 80—79256
water evaporative cooling, convection and mass transfer, fog formation in boundary layers 80—79293
water evaporative cooling, heat and mass transfer coeffs., fog formation effects 80—79294
water film flow over cylinder, laminar to turbulent transition, heat transfer rates 77—58691
water flow vel. meas. in oscillating pipe 77—68691
water jet, round, impinging, heat transfer in interference zone of film flow along wall 77—58750
water pulsating flow in heat exchanger effect of pulsations on heat transfer 79—94614
water vapour, 2-D laminar boundary layer 80—19492
water vapour, condensation from moist air in curved channels, mass and heat transfer 79—90251
water vapour, wet, boundary layer in compressible flow 80—10295
water viscosity changes close to quartz surface, fine capillary calcs. 80—54422
water viscosity changes effect on electrokinetic phenomena in capillaries 80—53867
water wave damping, effect of large grooves 77—11209
water waves, oscillatory boundary layer meas. using laser Doppler anemometry 79—27719
water-entrained gas flow, force on moving body 78—63480
wave drag, rel. to momentum and pseudomomentum fluxes 79—37332
waves, two-dimensional, growth on flat plate boundary layer 77—84263
wavy fluid film, instantaneous vel. profile meas. 78—79299
wavy wall, Rayleigh problem 77—3807
weak shock wave and sound wave refl. at shallow incidence, boundary layer effects 78—22373
weakly-separated zones, numerical prediction *(French)* 77—72276
Wedemeyer spin up model, Ekman compatibility conditions, Navier-Stokes eqns. 80—83802
wedge, forced-convection film boiling, boundary layer flow 79—46366
wedge flow, parabolic series method, drag coeff., press. distrib. 77—89142
wedge impulsively set into motion, boundary layer development 80—79259
wetting of a vertical plate by a liquid, model 78—22319
wind flow over complex terrain, wind tunnel simulation 80—76596
wind shear fluctuations downwind of surface roughness elements 78—92918
wind tunnel, wall interference, two-dimens., correction method, examples *(French)* 78—67293
wind tunnel contraction section, smoothly varying nozzle construction method 78—47081
wind turbines, flow vel. to compact shrouds 77—72373
wing, 3-dimens. boundary layer calc. method 80—1622
wing, leading edge transition 78—38361
wing, permeable, moving through a stationary liquid, flow calcs. *(Russian)* 80—38377
wing, rectangular, with tip clearance in channel, aerodynamic characts. 78—59415
wing section theory of Kutta and Zhukovski, book contrib. 80—1514
wing-body configurations, boundary layer induced secondary flows 80—48671

boundary layers continued
wire, in longitudinal laminar air stream, heat exchange *(Russian)* 78—83401
wire gauzes resistance coefficient measurement at low air velocity *(Japanese)* 80—106843
yawed cone, anal. of compressible laminar boundary layer 77—23973
yawed wedge, local heat transfer 78—18295
Ar atom populations in partially ionised flat plate boundary layer 77—65847
Ar ionised gas flow, quasi-steady laminar boundary layers 79—10544
Ar, ionising boundary layer in shock-tube side-wall flow 79—60144
Ar plasma electrostatic probe meas. *(Japanese)* 78—5933
Ar, shock-tube end-wall boundary layer 80—79348
C particle combustion, diffusion and reaction in stagnant boundary layer 77—68705
CO, boundary layer birefringence of rarefied heat conducting gas 77—80265
CO_2 gas flow impinging on heating surface, heat transfer radiation 80—43710
CO_2, laminar free convection at supercrit. press. under cooling conditions, heat transfer analysis 79—86428
Fe-Ni-B glassy ribbons melt spinning, gas boundary layer effects 80—76217
GaAs, VPE layer props. control using boundary layer characts. 80—50561
H, dissociated, heat transfer to catalytic surfaces, shock tube investigation 80—64551
H_2-O_2 gas mixture in chem. equilib., elemental diffusional separation in nonisothermal flow 79—55429
H_2O foams, shock wave propagation 79—64737
He, film, Brownian motion, boundary layers and quantised vortex prod. 80—6579
He, flowing, pressure and temp. oscillations near critical states 79—58744
He, supercritical, laminar free convection heat transfer, analytical study 79—23311
^{4}He film, vortex pair prod., boundary layer problem 79—99378
InP, VPE layer props. control using boundary layer characts. 80—50561
K channel flow, incipient boiling superheats 80—74709
Li, liquid, transverse flow around tube bundle, heat transfer 80—64537
MHD flow and heat transfer, porous disc eccentric rotations at infinity 79—18965
$MnCl_2$, aq. soln., thermomagnetic convection, in transverse flow round cylinder *(Russian)* 77—47100
N_2, boundary layer birefringence of rarefied heat conducting gas 77—80265
N_2, cryogenic, shock wave-boundary layer interaction *(German)* 78—71370
N_2 molecular beam generation, parameters rel. to stream perturbation before skimmer 79—86468
N_2 vapour columns, cryogenic, complex flow 78—34119
N_2O_4 corroded annular channels, heat transfer and pressure drop 80—1569
N_2O_4, dissoc. flow in tube, heat transfer and drag 78—71402
N_2O_4, dissociating, nonsteady flow in steam-generating channel 79—37422
N_2O_4 flowing in axisymmetric channels, mass and heat transfer calcs. 80—1570
$N_2 \rightleftharpoons 2N$ layer, hydrodynamic stability anal. 77—75993
Na, liq., in vert. pipe, hydraulic resistance under boiling conditions 78—90968
Na liquid metal boundary layer attenuation of temp. oscillations, appl. to LMFBR 77—83013
Si horizontal epitaxial reactor transport expt. and model 77—77399
Si, VPE layer props. control using boundary layer characts. 80—50561
^{133}Xe diffusion through frog skin, toad bladder and water boundary layer 77—66803

boundary-value problems
see also initial value problems
$\varepsilon grad^2 u = \delta u/\delta y$, $0<\varepsilon\ll 1$, over rectangle, asymptotic soln., MHD appl. 77—9863
$\lambda\phi_2^4$, Glimm-Jaffe-Spencer expansion for classical boundary conditions and phase coexistence 79—54245
a mixed boundary value problem in elasticity 79—23274
absorbing boundary conditions for num. simulation of waves 77—87638
acoustic plane wave diffr. by semicircular infinite soft strip 77—84025
acoustic reflection from liquid surface, influence of condensation and evaporation 79—46097
acoustic resonant frequencies in an eccentric spherical cavity 78—90548
acoustic scattering at rough boundary to inhomogeneous ocean 79—7247
acoustic transmission, gas with porous medium obstacle, scalar Helmholtz eqn. 80—74552
acoustic wave reflection from flat boundary in micropolar half space, graphical method 77—11060
acoustic wave reflection from reactive impedance boundary, Cagniard's method modification 77—11064
acoustic waveguides, Holmholtz eqns., radiation conditions for boundary value problems 79—14134
acoustic waveguides, sound pressure field variation as function of refractive index 78—94464
acoustic waves, axisymm. emission, locally distributed boundary of a half-space 78—42485
addition formulae for two-point boundary systems 79—71235
aerodynamics, discrete vortices method and multidimensional singular integral eqns. theory 80—19421
aerodynamics, initial-boundary value problems 77—65750
air, in wall cavity, slot filtration, temp. distrib. 77—65662
air flow over irregular surface, three dimens. finite difference model, terrain following coord. transform 77—60452
air pollution, diffusion-deposition-resuspension problem, formulation and soln. 77—2229
airfoil, oscillating, unsteady leading edge separation bubble calc., using finite difference procedure 77—72317
analytic function theory, plane/parallel fields and boundary problems in piecewise inhomogeneous anisotropic media *(Russian)* 79—62996
anisotropic crystal, additional light waves and boundary conditions 77 73121
annular flow of gases with varying physical props., turbulent, heat transfer in two-sided heating 80—48702
annular pressurised crack in transversely isotropic slab 77—72236

boundary-value problems continued
antenna, null field approach, computational method 79—13877
antenna-potential approx. of EM field 80—68060
anti-vibration systems, Fick boundary value problem soln. *(Russian)* 79—35540
antisymmetric stresses in plane elastostatics, rel. to displacements and stress functions *(German)* 77—35038
applied mechanics, collocation least square method 77—74225
approximate solution, boundary value problem for linear partial differential eqns. *(Russian)* 77—57170
approximate solution using patched variational principles, appl. to elliptic and mixed elliptic and hyperbolic problems 77—89144
arc, cathode region, easily ionised admixture effects calcs. 79—14633
astrodynamics, perturbed boundary-value problems, variational formulae 79—21161
asymptotic results for model eqn. for low Reynolds no. flow 79—14371
asymptotic solution of a class of singularly perturbed nonlinear boundary value problems via differential inequalities 79—5970
atmosphere, boundary layer structure of axisymm. vortex, lower boundary condition effect 79—25298
atmosphere, quasigeostrophic models, horizontal boundary condition 79—5576
atmosphere, source disturbances simulating orographic effects, upstream boundary values *(German)* 78—65375
atom-surface scattering from corrugated hard wall, boundary conditions 79—74040
atomic beam, highly expanded free jet, quantum and intermol. pot. effects 77—61823
attenuation of solns. to eqns *(Russian)* 78—65753
automatic piecewise linear approximation of yield function in ideal plasticity 77—46929
axisymmetric elastic problems, stress function solns. *(Japanese)* 80—64371
axisymmetric transducers, with various boundary conditions, single integral computer method for Green's function 80—87591
Banach algebra, Hilbert boundary problems, associated abstract singular integral eqn. *(Russian)* 77—22370
bar, curved, in-plane vibrs., shear deform. and rotatory inertia effects 80—43646
bar, rectangular elastic-plastic, necking in plane tension, boundary value problem 79—50608
bar magnet field, analogue simulation by electrostatic field, boundary conditions 77—61892
beam, elastic, on elastic half-space support, forced flexural vibr. 78—63353
beam, homogeneous, initial boundary value problem of transverse vibr. 79—40367
beam, homogeneous, initial boundary value problem of transverse vibr. 79—41601
beam, nonuniform, sectionalization and averaging method for calc. natural freq. and normal modes *(Chinese)* 80—43643
beam, with attached concentrated mass, nonlinear vibrs. 77—19557
beam and circular plate with compliant boundaries, vibr. response 78—13952
beams, finite, curved, stress anal. under general equilib. loading 79—14258
Beltrami-Michell and Beltrami-Michell type eqns. in static and dynamic elasticity 77—53782
Benard convection, initial and boundary condition effects, book contrib. 80—1591
bifurcation numerical method *(French)* 80—24129
bifurcations, singular perturbations 78—16626
biomechanics, living tissue mechanical props., boundary value problems 77—70491
Blasius eqn., generalised 79—35567
boiling, pool-type, heat transfer stability prediction, finite disturbances 78—75044
Boltzmann eqn., boundary conditions, general reciprocity postulate 77—65012
Boltzmann equation, global solutions, bounded convex domain 78—57876
Boltzmann equation, internal stationary boundary value problem, soln. *(Russian)* 79—85100
Boltzmann equation, two-vector, analytical solns. in nonplanar geom. 77—65246
Boltzmann linearised non-steady eqn., stationary boundary reflexion conditions *(French)* 77—17925
bonded sector plates, stress anal., soln. of elastostatic boundary value problems 80—1425
book, mathematical methods for physics 77—45670
boson system, ideal, lattice sums, Poisson's summation formula and Walfisz's formula 80—8903
bound formula for determining the fundamental frequency 79—81790
boundary layer flow past circular cylinder, rapidly convergent series soln. 80—96244
boundary-integral equation method, stress anal. fracture mechs., computer calcs. 77—80111
boundedness, definiteness of functional eqn. for nonconforming trial functions, finite element method, variational principle 79—2608
Brownian motion with adsorbing boundary, joint position-vel. distribution determ. 80—62581
bubble growth, noncondensing gas-vap. injected into liquid 78—55553
bubbly, two-phase mixtures, numerical anal. of press. transients by explicit-implicit method 78—34185
buckling of elastic bar with varying stiffness, coupled boundary conditions 77—31231
buried convective heat source, in semiinfinite solid, steady temp. distrib., surface temp. 77—58534
buried cylindrical heat source, transient temp. distrib., upper and lower bounds 78—75048
cantilever (Timoshenko), elastically restrained, with attached masses, follower force stability 78—63347
cantilever follower force problem, non-conservative load, boundary conditions and stability 77—46956
cantilevers, joined by a rigid connector nat. freq. determ. 78—83298
capillary surface problems with prescribed contact angle, max. and min. principles 79—37907
capillary-porous body, nonlinear heat/mass transfer problem, soln. using invariant groups 78—55688
cascade flow, transonic anal., by conformal mapping and relax. techniques 77—75934
cascade with slender profiles, transonic flow, numerical soln. 80—38436

boundary-value problems continued
Cauchy problem for system of linear partial differential eqns. with constant coeffs. 77—67215
cavitation, acoustic, threshold conditions for onset 78—59433
celestial mechanics, uniform soln. of Lambert problem 77—49275
channel, annular, long, free-mol. and radiative transport, approx. analytical soln. 80—6165
charge redistribution in system of conductors in relative motion *(Russian)* 79—41267
charged particle in box, nonlinear integrodifferential eqns. with delay, soln. existence 79—27124
chemically reactive flow, stiff boundary valued problems in kinetics and diffusion, numerical methods 79—86525
Cholesky factorisation method for mixed boundary conditions and discontinuous material prop. problems 79—81715
circular cylinders with longitudinal slots, rigorous solution of excitation problem *(Russian)* 79—18340
circular plates resting on viscoelastic half space, dynamic response 79—18801
classical Yang-Mills eqns., multimeron solns., existence theorem 79—92960
Clausius-Mossotti problem for cubic arrays of spheres 78—52422
complex coord. method, error bounds 78—49705
composite, layered, Love wave diffr. by stress-free crack in plane interface 80—33501
composite media with complex geometry, pot. field problems 78—16663
compressible elastic solids, finite plane strain problems, analytic soln., volume changes 77—68452
compressible vortex flow, boundary-value problem 78—26139
concentric domains, two dimensional heat equation general solution *(German)* 80—99918
concentric shock wave self-similarity exponent approximation 78—75169
concentric shock waves in inhomogeneous medium, self-similarity exponent 78—75168
conducting fluid, heated below, stability in parallel mag. and gravit. fields 77—7472
conducting spherical shell, approx. static EM field penetration 80—28146
conductor skin effect calc. by Leontovitch boundary condition *(Russian)* 78—2508
cone, floating on incompressible liquid, vel. field after vertical impact *(Russian)* 79—90193
cone/plate system in fluid, friction heating and convection 78—87238
conic section bounded by straight line, torsion problem, St. Venant semi-inverse method 80—54
conjugate domains, eqns. of math. phys., soln. 78—20967
contact friction stress problems, soln. using superposition principle 79—32394
continuity eqn., boundary conditions for integration 78—3342
continuous heat source, sphere, boundary conditions of second kind, temp. field 77—23851
convection in porous cavity, Darcy medium, 2-dimens. solns. 78—91007
convective diffusion to drop, large Peclet no., finite Reynolds no., asymptotic soln. 79—41742
convergence of perturbation method and boundary conditions at noncanonical surfaces *(Russian)* 78—77696
convergent shock wave in ideal elastic nonhomogeneous medium 77—55036
convex nonlinear boundary value problems, iterative bounds for stable solns. 78—54167
coplanar parallel charged strips, electrostatic problems 79—31765
coplanar parallel strips, electrostatic problems 79—31766
Couette flow, half-range expansions soln., for arbitrary Knudsen nos. 77—51088
coupled radiative plus conductive heat transfer, absorption coeff. temp. depend. allowance 80—74698
cracked composite full-planes, stress singularities 78—34077
cracks, Griffith, at interface of two bonded dissimilar elastic wedges, stress field, inverse Mellin transforms 80—53718
creep mechanics, rational approach to soln. 77—58560
creeping flow in closed cylindrical cavity, numerical calculation 80—16976
crystal growth from melt, thermal conditions effect on stability 77—76343
crystal optics with spatial dispersion 78—92040
crystal-vacuum interface, light reflection and transmission coeffs., additional boundary conditions 80—34870
cubic crystals, elastic strip, moving stress sources, boundary-value problem soln. *(German)* 78—38702
cylinder, elastic, equilib. difference scheme, deformation tensor approx. 79—41583
cylinder, hollow, with external crack, axially symmetric torsion problem soln. 80—14614
cylinder, hollow with internal circular crack, axially symmetric torsion determ., numerical results for boundary value anal. 80—64456
cylinder, in viscous fluid impulsive translation, numerical computation method 78—5727
cylinder in hot gas cross-flow, steady state temp. distrib. 78—30160
cylinder with internal hole, dynamic excitation 79—18712
cylinders, axially compressed, comparative study of elasticity, shell and boundary layer solns. 77—89029
cylindrical elastic shell, fluid-filled, excitation and propagation of normal modes 79—64385
cylindrical pulse diffr. by metallic half plane, boundary value problem, direct transform technique 80—69573
cylindrical punch, three-dimensional stress field, photoelastic studies 80—93272
cylindrical shell mixed boundary value problem, heat cond. and crack torsion 77—35
decomposition approach 80—4557
deformable solids with rough surface, stochastic problem of heat conduction and thermoelasticity *(Russian)* 78—38169
degenerate oblique derivative problem with interior boundary conditions, unique solvability theorem 77—67188
demagnetising field, calc. by FFT 79—38355
dielectric, spatially dispersive, boundary conditions for polarisation waves 79—61296
dielectric ellipsoid or elliptic cylinder, Laplace eqn. soln. to electrostatic boundary value problem 80—63884
dielectric solid, resorption current calc., boundary conditions using method of joint characts. 80—40055
dielectric solid, resorption current due to space charges 80—40053

boundary-value problems continued
dielectric solid, space-charge behaviour, effect of relax. processes 80—40057
dielectrics, elastic, stress tensor, polarisation vector, electric tensor 80—55018
difference approx. for singular perturbation problems 77—33850
differential equations, second-order degenerative, asymptotic expansion *(German)* 80—32
differential equations numerical solution *(German)* 80—35
diffracted wave calculation, potential vector singular over closed curves in surface *(Spanish)* 80—12911
diffraction, Kirchhoff's unique solution, points situated outside the diffraction screen *(Spanish)* 79—59628
diffraction of plane EM wave by grating at interface 79—27139
diffraction theory, integral transform associated with Helmoltz eqn. 77—67300
diffraction waves on arbitrary surface, Gaussian functional integral method 79—76902
diffused substance kinetics in biological systems 78—53312
diffuser, self-similar MHD flows with induced mag. fields 78—34205
diffusion, in critical region, appl. of E.V. Tolubinskii's integral method *(Russian)* 77—24378
diffusion eqn., multi-dimensional parabolic free surface problems, alternating direction method 77—37826
diffusion equation, nonlinear, invariance props., Lie-Backlund groups 80—62596
diffusion for regions with moving boundaries and particle conservation 77—49696
diffusion problem, nonlinear, soln. with const. flux boundary conditions 77—75782
diffusion problems, two dimens., nuclear reactor structs., singularities in finite element approx. 77—6496
diffusion processes satisfying Ventcel's boundary conditions, existence *(French)* 77—71182
diffusion-convection equations, finite difference scheme 78—42596
diffusion-reaction equations systems, existence, stability 79—20365
diffusional boundary value problems, approx. analytical soln. 78—36947
dipole antenna in warm isotropic plasma, multiple water bag model 78—91115
Dirichlet problem, Fourier transform technique for boundary condition of infinitely long strip 77—45679
Dirichlet problem, response function method for fast soln. of Laplace eqn. 78—86119
Dirichlet problem response function method solution 80—27106
Dirichlet-Neumann boundary-value problems, variational principles and hypercircle 78—57749
Dirichlet-Neumann mixed boundary value problem for harmonic functions, integral eqn. method 77—67223
Dirichlet-type time like boundary, discontinuous condition *(French)* 77—49559
disc with variable thickness, cross-section warping and corres. stress quantities *(German)* 78—18206
discontinuous deformation gradients near crack tip in finite anti-plane shear 80—58973
dislocations, elastic theory, book 80—36784
disordered system, one-dimens., density of states and wavefunction shape, periodic boundary condition influence 80—80223
displacement excitation of continuous systems 77—39254
domain monotonicity of first eigenvalue of boundary value problem 77—5638
domain with conical point, elliptic boundary value problem, asymptotic behaviour of soln. 79—17195
domains of possible motions with boundary, geom. *(Russian)* 78—28942
domains without classical symm., possible appl. of group representations 77—13571
domains without classical symm., second and third type, group representations 77—13572
domains without classical symmetry, appl. of group representations 77—13580
drift-diffusion problem with special boundary conditions, numerical soln. by integral eqns. 77—76591
droplet, vaporising, internal temp. field 78—51042
dual extremum principles for heat eqn. 78—70077
Earth interior density distrib., determ. from gravity logging data *(Russian)* 78—92999
eccentric spheres, interior and exterior boundary-value wave problems 77—75384
ECG forward problem, relationships among Green's theorem, Helmholtz theorem and integral eqn. methods 78—57090
echelette grating scatt., smoothing process for mode-matching soln. 78—1134
eddy flow attachment ideal fluid, partial differential eqn. soln. method 78—5752
edge stresses in multilayer laminates, calc. by substructuring 78—34022
elastic and acoustic wave equations, absorbing boundary conditions 78—59320
elastic beam, short rectangular, bidimensional anal. of longitudinal vibration *(French)* 77—7328
elastic body stability under isotropic uniform compression 80—4531
elastic cubic crystals, Dirichlet problem soln. uniqueness 79—75345
elastic dielectric, EM wave effect on displacement field of crack 78—30231
elastic dielectrics with polarisation gradient, boundary value problem exact soln. 80—58898
elastic elliptic stamp, stress and displacement anal., mixed boundary value problem 79—75342
elastic fracture mechanics, boundary integral eqn. anal. 80—14622
elastic half spaces, parametric model of loose bonding 77—11061
elastic half-bounded medium, unidimensional deformation under vibr. loading *(Ukrainian)* 80—5933
elastic incompressible isotropic solids, plane deformations 78—38194
elastic inextensible material, uniqueness of displacement boundary-value problem 78—54195
elastic inhomogeneous strip, resonance props., boundary value problem formulation 80—31513
elastic linear, material of hexagonal symm., half-space, indentation by circular punch 78—34020
elastic membrane dynamic response to expanding ring load 77—46957
elastic modulus in non-homogeneous stratum, hyperbolic variation 77—868

boundary-value problems continued
elastic plastic spherical body, instability under uniform loading 80—58946
elastic plate, infinite, concentrated load, stress. anal., numerical method *(Japanese)* 78—22273
elastic plates and shells with random loading, solution methods *(Russian)* 77—57197
elastic point source problems, differential transform technique in operational form 77—33865
elastic prismatic bar, with rigid ends, lower and upper bounds for torsional rigidity 80—48568
elastic problems for cracks, seepage problems, by direct variational method 78—83331
elastic rectangular plate interaction with ideal incompressible fluid, classical boundary value problems *(Russian)* 77—68556
elastic spatial problems in 1-D 79—30236
elastic strip, Griffith crack interactions, mixed boundary value problem 80—58969
elastic strip with one-sided constraint under moving load 77—7305
elastic wave propag., boundary friction effects 79—46242
elastic waves at frictional boundary, transmission (reflection), approx. anal. method 78—63371
elastic wedge, mixed boundary value problem, use of Mellin transforms 80—23884
elastic wedge, mixed boundary value problem 78—28952
elastic-plastic body, min. principles and strain uniqueness, stress fields 77—3734
elastic-plastic body, strain and stress fields, min. principles 77—3735
elastic-plastic damaged body, unknown boundary value problem explicit solution *(French)* 80—79166
elastic-plastic solid, operator method for variational principles *(Polish)* 77—54898
elastic-plastic torsion, nonlinear boundary value problem 77—89043
elastic-viscoplastic boundary value problem, stress anal. variational method 77—35051
elastically bent crystal, dynamical Bragg diffr. of X-rays 79—14639
elastically clamped variable-stiffness annular plate, thermostability 77—89052
elasticity, mixed boundary value problems, numerical scheme 78—26038
elasticity, mixed boundary-value problems, orthogonal polynomial solns. 78—54193
elasticity, nonlinear boundary-value and evolution problems, Galerkin approx. 77—33870
elasticity, nonlinear two-point boundary-value problems 78—9566
elasticity, pot.-type singular integral approx. algorithm 80—27132
elasticity, soln. with ad hoc assumptions 77—75808
elasticity of multilayered slab, boundary value problems 77—35047
elasticity plane mixed boundary value problem, Legendre polynomials soln. 78—4487
elasticity plane problem formulation using dislocation layers, contact and crack problems 79—64507
elasticity theory, book 78—20969
elasticity theory, index of integrated operator *(German)* 80—5945
elasticity theory, mixed periodic problems, quadrature solution 80—86088
elasticity theory spacial problems, appl. of theory of two complex variables *(Russian)* 77—57194
elasticity with thermodiffusion, vibr. boundary value problems 78—41164
elastodynamic diffraction, by periodic rough surface (stress-free boundary) 78—13826
elastodynamic diffraction, two-dimens., by cracks, matched asymptotic expansions 80—1468
elastodynamic equations of motion 77—42766
elastodynamics, numerical boundary integral eqn. method 79—63036
elastodynamics, time harmonic, pointwise variational principle for mixed boundary value problems 80—31510
elastohydrodynamic contact optimisation 78—79288
elastoplastic coupled boundary-value problems, rock mech. appl. 77—14918
elastoplastic cylindrical bar, with linear hardening, simultaneous torsion and tension 80—53658
elastoplastic fracturing structures, boundary value rate problem, extremum theorems 80—48596
elastoplastic thin vertical columns, postbuckled, deflections 80—87728
elastoplasticity, velocity discontinuities, variational formulation of boundary-value problems *(French)* 79—32284
elastostatics, combination of boundary and finite elements 79—92941
elastostatics, linear, boundary-integral approach for mixed problems 79—64508
elastostatics, nonlinear, boundary value problem of space and traction, error energy, and error norm 80—53631
electric and magnetic fields, 2D open boundary problems, finite element anal. 78—94354
electric arc, steady-state, energy eqn. soln., boundary value problem 80—79601
electric arc parameters, math.-phys. model *(Russian)* 77—51249
electric field, asymptotic behaviour near singular points of conductor surface 78—13641
electric probe in weakly ionised and rarefied plasma *(Russian)* 80—24252
electrochemical diffusion, boundary value problems, orthogonal collocation calcs. 78—40053
electrochemical pit growth, convective diffusion in pits, ionic components conc. calc. 80—45409
electrode surface, partially covered, eqns. for chronopotentiometry 78—85236
electrodynamic boundary problem solution for complex shape regions 80—69300
electroelasticity for piezoelectric medium with cuts, 2-D boundary value problems 80—71319
electromagnet pole-piece design, air gap field computation 79—41295
electromagnetic scatt., time depend., boundary value formulation, integro-differential eqns. 78—66726
electromagnetism, stationary boundary value problems, finite element analysis *(Polish)* 79—98258
electron beam, relativistic, radially inhomogeneous, unneutralised, linear theory 79—50201
electron propagator, Dyson-Schwinger eqn. solns. 78—24984
electron transport in anhomogeneous anisotropically scatt. medium, medium Green's function 80—27244
electron waves in plane periodic system, linear theory 80—48130

boundary-value problems continued
electrostatic, boundary value problem of four strips inside grounded cylinder 79—13862
electrostatic field, axisymmetric, of cond. torus and spherical sector 79—55023
electrostatic mixed boundary value problems 78—42254
electrostatic problems in presence of linear and isotropic quadrupole matter *(German)* 80—37924
electrostatics of conductors and linear isotropic dielectrics, conformal transformation appl. *(Russian)* 80—53183
elliptic, asymptotics of spectrum, with solvable connections *(Russian)* 77—5673
elliptic, local mesh refinement with finite elements 79—9091
elliptic, second order, weak hybrid finite element methods, appl. to Dirichlet problem 78—73835
elliptic boundary problems, reduction to elliptic systems of pseudodifferential eqns. *(Russian)* 79—12573
elliptic boundary-value problem asymptotic solutions, domain varied close to conical points 80—86075
elliptic equation, self-adjoint, with complementary boundary conditions *(Chinese)* 79—35526
elliptic equations, second order, three dimens. boundary-value problems solns. *(Russian)* 77—60904
elliptic equations and systems, free-boundary problem solution method 80—69941
elliptic interior layer problem asymptotic soln. 78—12535
elliptic partial differential equations, nonlinear, approx. soln. by mesh refinement and local inversion 77—26160
elliptic porous slider, fluid dynamics 79—18952
elliptic problem solution, hydrodynamics appl. 79—90210
elliptic problems, representations of first variations, appl. to optimisation and sensitivity anal. 78—77674
elliptic type equations, num. soln. of mixed boundary-value problem *(Russian)* 77—67243
elliptical disc in viscous liquid, slow broad-side motion anal. 77—58635
elliptical tunnel with contained axial conductor, radio transmission 79—55030
EM eccentric spherical cavity, resonant frequencies 79—72457
EM field, in cylindrical conductor, AC excited, with circumferential electrodes, boundary-value problem 79—7055
EM field above two-dimensional inhomogeneous struct., boundary conditions 80—85595
EM field of a homogeneous sphere in an infinite medium, mode decomposition 78—81864
EM field of rotating perfectly conducting sphere, boundary value soln. 77—23597
EM field problem with a non-linear condition 79—18326
EM fields, approx. method for numerical studies of boundary-value problems 80—5658
EM response of anisotropic conducting cylinder to external source 79—7059
EM scatt. integral eqn. resonant solution elimination 79—45895
EM stationary rotationally symm. field representation by superimposing circular aperture and ring fields *(German)* 78—55277
EM wave diffraction in inhomogeneous media, lattice method using approximate boundary conditions *(Russian)* 78—1159
EM wave half-plane diffraction under mixed boundary conditions 79—86116
EM wave propag., nonlinear media, integral eqns. 77—58375
EM wave scattering, from cylinder loaded by active continuously variable surface impedance 78—22068
EM waves diffraction at surfaces with inhomogeneous admittance 80—69296
EM waves scattering, in nonlinear medium with one-dimensional random nonuniformities, statistical analysis 80—106421
Emden-Fowler eqns., nonlinear boundary and eigenvalue problems by group methods 79—71224
engine, internal-combustion, heat exchange, b.c.s of 1st kind determ. from b.c.s of 2nd kind, numerical method *(Russian)* 79—68554
equivalence of direct and indirect boundary element methods 78—81814
estimation of parameters for a beam on an elastic foundation with large deflections and built in at both ends 79—27520
estuary, Jamaica Bay, New York, dissolved O modelling 77—17146
Euler equations, solid-body boundary conditions, numerical implementation 78—90814
Eulerian computation technique for domains with moving boundaries 77—53779
evolving shells, postcritical deformations *(Ukrainian)* 79—32310
extended field method for analysis of free vibration of thin vibrating plates, solns. 80—38311
extended field method for analysis of vibrating thin plates, numerical results 80—36833
exterior Dirichlet boundary-value problem with rot. symm., Fourier-Bessel series soln. 80—1103
exterior Neumann problem for reduced wave eqn. in spherically symm. medium, constructive methods of soln. 77—50799
exterior problems of acoustics, integral eqns. soln. 79—27455
exterior regions containing moving conductors, finite element models 79—41291
external physical fields of sources investigation, modelling devices construction 80—17817
extremum principles for linear initial and mixed boundary value problems of math. phys. 78—49637
Feller eqn., generalised, boundary condition solns. 78—62167
fibre reinforced composite, stress boundary value problem for finite plane deform. 80—48583
fibre-reinforced composite, quasi-one-dimens. thermal diffusion, mixture theory 78—71271
field problem structure, equilibrium, eigenvalue and propagation problems *(Rumanian)* 78—45520
filtration theory problem soln. *(Russian)* 80—74970
finite depth water with immersed vertical boundaries, surface waves 79—77151
finite difference approx. of boundary conditions along irregular boundaries 78—36804
finite difference calc., campylotropic coords. for boundary value problems 78—65757
finite difference methods for nonlinear two point boundary value problems 77—33849
finite elasticity, compatible perturbation method, traction boundary value problem 79—63043

boundary-value problems continued
finite element method, elastic half-space treatment 77—75793
finite element moving boundary computation with an adaptive mesh 79—35536
finite elements construction for natural boundary conditions satisfaction 79—2610
finite hyperelastostatics, continuous dependence result for mixed boundary value problem 79—68574
finitely conducting cross grating theory 80—106635
first boundary value problem for singularly perturbed semilinear parabolic eqns. 77—67221
first-order hyperbolic differential equations, with split boundary conditions, numerical soln. 77—87634
fission reactor fuel rod geometry changes, mech. interactions calcs. 79—40993
fission reactor loss-of-coolant accident, 3-dimens. flow with multiple interfaces 79—41024
flagellar propulsion, hydrodynamic anal. 79—53072
flat elliptical crack, in infinite solid, mixed boundary value problems 78—9602
flow, creeping, about sphere, general soln. of linear Navier-Stokes eqn. 78—71307
flow, oscill., forced, of gas (liq.), in tube, linearised treatment 79—50744
flow, potential type, surface source and vorticity panel method 79—46278
flow, spatial free-boundary 79—46279
flow, three-dimensional region elliptic transformation 78—55624
flow, transversely sheared, unsteady motion scatt. and distortion 79—59997
flow, unsteady, transversely sheared, gusts 78—26142
flow between concentric rot. spheres, nonlinear, axisymmetric 80—19412
flow between rotating discs, finite element anal. using exponentially weighted basis functions 78—16655
flow birefringence and hydrodynamic boundary conditions for ellipsoid particles and Rytov dip 80—45030
flow in circular boundary, computed Stokes series extension 78—42583
flow of shear-thinned fluid, laminar heat transfer and drag 79—68764
flow through porous media, finite element anal., book contrib. 79—32665
flow-duct acoustics, adjointness props. for differential systems with eigenvalue-depend. boundary conditions 77—50787
fluctuating flow, mass transfer near front stagnation point of axisymmetric body 80—48675
fluid bidimensional flow past symmetric profile 77—60942
fluid dynamic problems solution, blast loading on three-dimensional structures, computational simulation 77—68624
fluid dynamics, boundary conditions imposed by stratified fluid 79—55404
fluid dynamics, initial boundary-value problems for partial differential equations 79—30256
fluid dynamics, micropolar, potentials and Green's functions 80—96286
fluid dynamics, pseudoplastic non-Newtonian fluid, nonlinear singular boundary value problem 80—79362
fluid flow analysis, in plasma centrifuges, third-order differential equation solution *(Japanese)* 80—53949
fluid mechanics, boundary element methods versus finite elements 78—73860
fluid mechanics, num. methods and associated problems, book contrib. 77—89087
fluid motion in open basin, free boundary problem *(Italian)* 79—18868
fluid-structure coupling problem soln. using boundary-integral eqn. method 77—54920
fluids with dipolar interactions, boundary conditions for numerical simulation, book contrib. 79—60247
Fokker-Planck equation, numerical soln., Chebyshev polynomial approx., first passage time probability density functions 77—37744
force-free fields, Neumann's type boundary-value problem soln. 78—12585
forward Monte Carlo heat conduction, known-temp. boundary condition treatment 79—158
foundation dynamic interaction with viscoelastic half-space *(German)* 78—79228
Fourier analysis of difference schemes for Laplace eqn. in rot. symm. system 78—77677
fracture analysis, 2D linear, elastic, finite element anal. vs. the edge function method 80—99963
fracture mechanics, conformal mappings to delete singularities, finite element anal. 77—72251
free atmospheric convection, rigorous formulation using matched asymptotic expansions *(French)* 77—65740
free boundary problems with radiation boundary conditions 79—71386
free edge stress fields, in composite laminates 78—67039
freezing, multidimensional problems in arbitrary domains, numerical method 78—90693
fuel element transient heat transfer, temp. distrib. 78—17280
gas, rotating, convective instability in gravitational field 79—27642
gas diffusion eqn., recoil/sticking probabilities at wall 77—51149
gas flow regime choice in pipes with max. temp. at outlet 80—19396
gas flow round porous axisymm. body with injection, vorticity *(Ukrainian)* 77—75923
gas kinetic boundary value problem, non-equilibrium thermodynamics 80—19544
gas nonisothermal stationary motion in pipe anal., solution by iterative method 77—89086
Gaussian beam, equal phase, self-focusing effect calcs. 77—23722
general relativistic stellar evolution code 79—58317
generalised biharmonic eqn., appl. to hydrodynamic stability using homogeneous boundary conditions 78—90834
geodesy, boundary value problem from telluroid definition 78—65171
geodesy, deflections of the vertical determ. 78—3702
geodesy, linear boundary value problem and three-dimensional geodesic mapping eqns. *(German)* 78—73304
geodesy, Molodensky's problem in gravity space, existence and uniqueness of soln. by Newton's method 79—12061
geodesy, results from Molodensky's problem in gravity space 78—65173
geodesy, three dimensional, datum problem rel. to boundary value problem 78—61310
geodesy, uniqueness of free boundary value problem 80—30973
geodesy boundary value problem 80—30975
geodetic boundary value problem, soln. 79—62424
geodetic boundary-value problem, variational formulation 78—92772

boundary-value problems continued
geomagnetic field computation, accuracy of construction of external Dirichlet problem boundary condition 78—44766
geophysical elastodynamics, group theoretical formulation, seismic sources 77—78126
geophysical prospecting, instability of finite difference schemes due to boundary conditions 77—21912
graded-index slab waveguide TE mode analysis 77—72087
graded-index slab waveguide TE modes, exact soln. 79—81568
gravitational wave EM detector, anal. as perturbed boundary-value problem 77—13677
gravity waves, two-dimensional, initial boundary value problem in terms of stream function 77—7409
gravity waves on stratified liquid, linear initial-boundary value problems 77—39301
Green's function methods for linear second order systems 79—12578
Green's functions and boundary value problems, book 80—28
grid generation, automatic mesh-point clustering elliptic partial differential eqns, grid generation, automatic mesh-point clustering 80—31487
Griffith crack in infinite elastic solid, stress distrib. 77—80107
groundwater two-dimensional unconfined saturated flow, boundary integral solns. 78—77291
gyrotropic absorbing crystals, nonorthogonal eigenwave refl. 80—99624
Hadamard's theorem, appl. to thin elastic plates 78—16650
Hadamard conditions in nonlinear elasticity theory *(Russian)* 79—46207
half-space, plane Stefan problem soln., degenerate hypergeometric transformations method 79—86332
half-space, singularities in elementary soln. of boundary value problems for Maxwell's system and elasticity *(French)* 77—71218
harmonic oscillators, relativistic two-body interaction, exactly soluble system 78—16955
heat and electrical transfer differential eqns. 78—67004
heat and mass transfer, mixed and oblique derivative boundary conditions 80—69820
heat and mass transfer in porous bodies, two-dimensional isoparametric finite element method 77—42708
heat cond., mixed boundary value problem, analytic soln. 80—5909
heat conduction, anisotropic medium homogeneous in cylindrical regions, steady-state anal. 77—58526
heat conduction, at freezing/melting boundary, model for approx. calcs. 78—5630
heat conduction, error analysis of determined thermophysical characteristics 79—81687
heat conduction, in monoclinic anisotropic system, various boundary conditions, temp. field soln. 77—58525
heat conduction, inverse nonlinear problems, simulation methods 78—94513
heat conduction, inverse problem, Fourier eqn. Runge-Kutta integration 78—89417
heat conduction, inverse problem, integral eqns. calcs. 80—74695
heat conduction, inverse problems, similarity solns. 77—42688
heat conduction, inverse problems 77—42685
heat conduction, linear boundary inverse problems, soln. method 79—72777
heat conduction, nonhomogeneous transient boundary-value problem 77—42697
heat conduction, quasilinear equations, approx. Galerkin method 80—33416
heat conduction, soln. 80—79106
heat conduction, Sommerfeld problem generalisation for one-dimens. ring 80—5908
heat conduction, steady-state mixed problem, 3rd kind boundary conditions 77—65660
heat conduction, third boundary-value problem, variational soln. 77—7282
heat conduction, transient, one dimensional, early time, method of characts. numerical soln. 77—58524
heat conduction eqn., inverse, boundary conditions recovery, using Cauchy soln. and regularising algorithms 78—26016
heat conduction eqn., isotropic body with fading memory and high cond. 78—1545
heat conduction equation with radiation boundary condition, implicit iterative soln. 78—5635
heat conduction explosive boundary condition problems, accuracy of approx. solutions *(Russian)* 80—99912
heat conduction in cylindrical regions with noncircular boundaries 77—89000
heat conduction in half-space with cutting, Green's functions of boundary-value problem *(Russian)* 78—18145
heat conduction in inhomogeneous slabs 77—39204
heat conduction in nonuniform media, boundary-value problems 78—63266
heat conduction in rectangular domain with variable heat-transfer coeff. 77—7281
heat conduction in region with moving boundaries, analytical soln. methods, review 77—75768
heat conduction in region with moving boundary, asymptotic soln. of first boundary-value problem 77—46884
heat conduction in uniform layer with rectangular cut-out 77—39194
heat conduction inverse boundary problems, soln. using splines 79—90112
heat conduction inverse boundary-value problems, finite difference method 78—63263
heat conduction nonstationary nonlinear problem in absence of heat sources and sinks 80—19211
heat conduction problem, with heat generation in two-dimens. plane 79—68545
heat conduction problems, approx. soln. method 80—33415
heat conduction solution, using generalised differential equations *(Hungarian)* 79—14202
heat conduction solutions in orthotropic circular cylinders 80—10110
heat conduction transient, two-dimens., crit. time step for finite element solns. 78—71260
heat conductivity eqns., soln. of boundary value problems by Green's function method *(Russian)* 78—63267
heat conductors with randomly varying boundaries, Green's functions *(German)* 79—32188
heat diffusion process parabolic control problem numerical treatment 77—847
heat eqn., solvability of boundary value problem *(Ukrainian)* 77—67204
heat equation, time depend. reachable states in boundary control systems 79—44886

boundary-value problems continued
heat equation involving moving phase boundaries, analytic soln. 78—90694
heat equation solution regularity for non-rectangular plane domain *(French)* 77—67199
heat exchange in complex domains, new soln. techniques 78—94509
heat exchanging bodies, inverse heat cond. problem, boundary conditions identification methods 79—37115
heat flow in ring-shaped thin conductor, difference eqn. soln. for periodic problems 79—94460
heat loss of internally heated body to peripheral flow, oblique derivative boundary conditions 79—72778
heat pipe, high temp., subsonic vapour flux, heat exchange and friction 77—75779
heat propagation, finite vel. problem, kinetic theory anal. 77—46881
heat transfer, finite element method of calculation *(Japanese)* 78—89414
heat transfer, laminar, convective, in rectangular channel, for 3rd kind temp. boundary conditions 78—87341
heat transfer, nonstationary, finite element calcs. 80—83795
heat transfer, periodically varying coeff., 1D boundary-value problem, steady-state soln. 77—84125
heat transfer, three-dimensional anisotropic solid of arbitrary shape 77—58527
heat transfer, turbulent, behind hydrodynamic starting length, analytical method *(German)* 79—72892
heat transfer across low aspect enclosure, solute layering effect 77—75776
heat transfer between bodies in gas-filled contact, integral equation numerical solution 79—37130
heat transfer calcs., finite element anal., HEATRAN, diffusion eqn. soln. 77—3710
heat transfer dynamics in channel, anal., impulse function method 79—37317
heat transfer in composite solids with heat generation 79—76949
heat transfer in domains with sources having variable power, soln. 79—72891
Helmholtz equation for region with corners, boundary distribution soln. method 79—58532
Helmholtz equation for two dimens. polygonal regions, numerical soln. method 79—63005
heterogeneous reactor, neutron distrib. determ. by 1-D multiregion cylindrical cell 79—26488
higher order panel method for general analysis and design appl. in subsonic flow 77—55022
hologram grating, boundary conditions for diffracted EM fields 79—3660
hybrid finite element methods 77—49581
hydrodynamic stability problems with time-depend. boundary conditions, numerical simulation methods, review 80—19411
hydrodynamics basic eqn. soln. with large and small Bouguer number 77—68708
hyperbolic conservation laws; initial and initial-boundary value problems, large-time behaviour 77—74233
hyperbolic partial differential equations linear system, numerical soln., boundary methods accuracy 77—67245
hyperelastic, dual extremum principles and global error bounds 79—30253
hypersonic flow, shock wave shape round delta wing, mixed boundary value problem solns. *(Russian)* 79—90279
ice accretion calc. 79—29799
ice growth in laminar flow through a channel with two parallel flat walls 79—3908
immiscible fluids in one dimensional porous medium, regularity and asymptotic behaviour 79—72936
inclined derivative type boundary value problem, geometric criteria for Fredholm case *(Russian)* 77—49566
incompatible basis functions in boundary value problems, limitations of simplified variational principles 80—48587
incompletely parabolic problems in fluid dynamics 79—44749
index of problem with boundary condition containing derivatives *(Russian)* 79—9079
inelastic deform., time-depend. anal. using constitutive relations 77—39237
inelastic deformation, stiff constitutive models, numerical integration 80—96208
infinite depth water with immersed vertical boundaries, surface waves 79—77150
infinite elliptical cylindrical radiators array with mixed boundary conditions, sound field 78—1538
infinite hollow cylinder with external crack, boundary value problem 78—90712
infinite solid, elliptical crack under shear 78—75096
infinite wedge, first boundary value problem *(French)* 77—35041
inflows, density currents, and fronts 79—10542
ingot, hollow cylindrical, temp. field and crystallisation front calc. *(Russian)* 78—63690
inhomogeneous elastic layer, torsion investigation by approx. methods 80—98799
inhomogeneous liquid, diffusion model, correctness of boundary value problems 78—30774
inhomogeneous strip, boundary value problem spectra props. in elasticity theory 80—31512
initial approximations, exact matching of boundary conditions, semiquantitative soln. characts. incorporation 78—28
insulated water layer, combined heat transfer, stratified layer, energy eqn., boundary value problem 80—79290
integral eqns., appl. of method of singularities 77—67254
integral eqns., boundary-values with shift, approx. 77—17795
integral eqns., numerical soln. to multi-part mixed problems 78—62056
integral eqns. in which boundary values and solns. defined on different curves 77—68428
integral equations for three-dimensional fields, isoparametric finite element, variational solution 77—87635
integral equations solution, using weighted residual techniques potential problems and engineering appl. 78—36803
intensive air flow round thin and sharp axially symmetric bodies *(Russian)* 79—37330
interacting finite amplitude waves, reflection and distortion, initial boundary value problem 80—53699
internal waves at surface between two fluids, velocity potentials for singularities 78—90926

boundary-value problems continued
interpolation to boundary data in tetrahedra, appl. to finite elements 77—5645
inverse problem for the heat equation, Neumann and Dirichlet data correl. 79—23184
inverse scattering method for nonlinear evolution eqns. under nonvanishing conditions 78—57808
inviscid conical flowfield structure about external axial corners 79—94646
ionosphere Alfven waves, boundary condition 79—53611
iosperimetric inequality for first eigenvalue of boundary value problem 77—67220
irregular cavity acoustic impedance, finite element analysis 78—42483
isotropic inhomogeneous moving plasma column, cross polarisation of scatt. EM waves 79—98917
isotropic isoceles right-angled triangular plate on elastic foundation, thermal-shock induced vibr. 77—35070
isotropic thin shells with circular hole, stress state, numerical investigation 80—48586
iterated waves, singularities of elementary soln. of limit problems in half-space *(French)* 77—60944
iterative method for second order problems 78—32660
iterative refinement method solving sparse matrix 77—2521
jet, liq., breakup, 3rd perturbation Cosserat soln. 79—32615
jet efflux from channel, asymmetric two dimensional, conformal mapping soln. 77—39319
Josephson junction, in inhomogeneous field *(Russian)* 78—84350
kidney counter current mass transport spatially discrete models 79—39442
kidney model, numerical soln. by multiple shooting 80—104609
Kirchhoff plates, matrix displacement method with parameter transformation by additional compatibility postulation *(German)* 78—79202
Knudsen layers, by linearised Boltzmann eqn. 79—98759
Korteweg-de Vries eqn. and 2nd Painleve transcendent, boundary value problem in plasma theory 80—69971
Kustaanheimo-Stiefel two-point boundary-value problems 77—25927
L-plasticity, boundary value problems for plane strain or stress 80—58926
Lambert's problem, recursive formulation for enhanced computation time 77—89016
Lame eqns. of elasticity, mixed problem in R_+^3, explicit soln. 77—60937
lamina, porous, generalised boundary conditions, heat and moisture transfer Prudnikov problem soln. 78—1551
laminar boundary layer, solution of the Falkner-Skan equation by quasilinearization 79—1156
laminar duct entrance flow, 2nd order numerical method 78—38407
laminar liquid flow around plate, boundary-value problem soln. for generalised diffusion eqn. 77—7366
Laplace equations in thin regions, mixed boundary-value problem 77—35016
Laplace operator on spherical domain, fundamental eigenvalue numerical determ. 77—87628
large field problem soln. by extended Kinzel sectioning method 77—27228
least capacitance region, free boundary optimisation problem 79—13864
least capacitance regions, free boundary optimisation problem 79—13865
Lee waves classical theory, asymptotic approx., upper boundary condition role 80—12472
LF fields in linear media, two-dimensional finite element analysis 79—41297
lifting three-dimensional wings in transonic flow 80—19428
light diffraction, formulae 79—59632
lightpipe, curved const. cross section, steady state and transient transport solns. 77—62068
lightpipe, cylindrical, steady and transient radiation transport, exact soln. 77—27365
lightpipe, helical, const. cross section, varying refr. index, radiation transport 77—65640
linear degenerative parabolic eqns., first boundary problem *(Russian)* 77—22374
linear differential eqns., fourth order, finite difference formulae for boundary value problems 78—73856
linear differential eqns. with separated boundary conditions, Riccati transformations for eigenvalues 77—38
linear elastic micropolar half space, uniqueness of soln. of mixed boundary value problems *(Polish)* 79—63041
linear elliptic and parabolic partial differential eqns. with boundary singularities, numerical soln. 78—41142
linear elliptic PDE, numerical soln. 79—97187
linear hyperbolic mixed boundary value problem, soln. existence, uniqueness, hydraulics appl. *(German)* 78—93514
linear isotropic elasticity, boundary problems, book contrib. 80—39092
linear partial differential eqns. describing transport phenomena, soln. technique 80—13004
linear second order equations with periodic coefficients *(Russian)* 79—58528
linear transport eqn., asymptotic theory for small mean free paths 78—70078
linear transport operator spectrum, semi-infinite medium 77—2626
linear two-point, with non-separable boundary conditions, reduction to Cauchy systems 78—54158
linearised boundary layer equations with self-induced pressure, anal. for $M_\infty=1$ case 79—86458
liquid flow in rot. pipe, fully developed heat transfer 77—58689
Love waves, hypoelastic stratified solid with material boundary 78—30225
lubrication, hydrodynamic, free boundary problem including surface tension 80—19542
macroparameters in relaxing boundary layer *(Russian)* 80—33557
magnetic field calc., two-dimens., boundary integral eqn. method 78—94355
magnetic field in superconducor, calculation method from boundary conditions *(Ukrainian)* 80—34545
magnetic fields, finite element and finite difference anal. 78—94353
magnetic lens design, finite element program improvement 80—69316
magneto-elastic plates under mixed boundary conditions 79—7328
magneto-elasto dynamics, mixed initial and boundary value problems, vibr. circular plate in mag. field 78—67034
magneto-elastodynamics, boundary-value problems 79—49046
magnetoelastic bodies, homogeneous isotropic with couple stresses, spherical inclusions, boundary value problems 77—46917

boundary-value problems continued
- magnetoelastic/piezoelectric composite media, SH-type guided elastic waves, transmission line model 78—27069
- magnetoelasticity, two-dimens. boundary value problems 77—19525
- magnetoelastodynamics problem with mixed boundary conditions 80—1466
- magnetosphere, two-dimens. model, eigenvalues, magnetotail currents 79—53662
- materials testing, strip with semicircular notches, tensile load conditions at end, interf. effects obs. 80—64455
- materials with memory, linear theory of heat cond., final value problem, existence, uniqueness theorems 78—59266
- matrix methods in potential theory and EM scatt. 79—94133
- maximal variational principle for transport theory 78—62166
- Maxwell's eqns., Ewald-Oseen extinction theorem 78—62974
- Maxwell's eqns., homogeneous initial boundary value problem 79—75372
- Maxwell's eqns., time-independent, with boundary condition $n.\varepsilon E=n.\mu H=0$ *(German)* 77—57205
- Maxwell equations, boundary value approx. using finite element anal. *(German)* 80—91718
- Maxwell equations, time-harmonic, exterior boundary-value problem of EM reflection 80—28148
- media with double diffusivity, diffusion theory, boundary value problems 80—75378
- melted ice layer, onset of free convection criterion 77—58685
- melting/freezing interface, annular region, perturbation soln. 78—59286
- metal, compensated, transport of spatially inhomogeneous current under mag. fields, pot. and current distribs. 79—87081
- metal, effects of large scale voids on thermal magnetoresist. 80—10946
- metallic media, varying loads, elevated temp. inelastic anal. using state variable theories 78—83264
- metals, metallic deformation, improved boundary-integral eqn. calc. method 80—28437
- meteorological fields variational adjustment 79—39837
- MHD between coaxial cylinders, difference eqn. soln., Dean's problem 79—94731
- MHD channel, EM field eqns. averaging, at finite mag. Reynolds no. 79—77282
- MHD convection, forced horizontal flow between moving porous walls 77—68695
- MHD duct flow, boundary value problem, dual extremum principles, operators and bounding functionals 79—64791
- MHD electrical potentials, uniqueness of solns. to extended class of elliptic boundary value problems 80—69937
- MHD equilibria, by secondary bifurcation, rectangular boundary conditions 78—42673
- MHD equilibria numerical analysis *(Japanese)* 79—41760
- MHD flow over infinite rotating disc with suction, existence of soln. 78—30366
- MHD generator, simplest physical model 78—71548
- MHD laminar convective heat transfer in circ. duct, for 3rd kind temp. boundary conditions 78—87342
- MHD vortex flow generation, viscous fluid with spherical boundary, by AC EM field 78—5804
- MHD waves, vertically propagating, in isothermal atm. with horizontal mag. field 80—6162
- micropolar elasticity theory, uniqueness of 2-D boundary value problems 78—54192
- micropolar fluid with stretch, convection, appl. to Earth mantle 78—51202
- micropolar thermoelasticity, axial symmetric problems, stationary vibrations 79—68572
- micropolar thermoelasticity, three dimens. theory, pot. method 77—68414
- microstrip anisotropic electrostatic field problems, Green's function technique 78—70998
- MIT bag model, first order formalism for scalar fields 78—16986
- mixed, appl. of direct variational method 77—67252
- mixed boundary conditions in half-space, stochastic resolution *(French)* 77—9866
- mixed boundary value problems for Helmholtz eqn., integral eqn. method 78—57751
- mixed type, arising in kinetic theory of gases 79—55440
- mixture, binary, time-depend. solidification, series soln. 78—75058
- model nonlinear problem with continuous locus of singular points, limiting values 79—12577
- moist porous material subject to sudden heating, mass transfer, press. rise 77—58787
- molar molecule heat and mass transfer phenomena, generalised variational principle 80—79104
- monotony properties and inequalities for Green's functions for multipoint boundary value problems 79—30202
- Monte Carlo heat conduction using transport eqn. approximation 79—159
- moving boundary problems, weak soln. 80—179
- moving interfacial cracks, dynamic stresses, finite difference approx., iterative process 77—46966
- moving load on elastic strip on elastic half plane, steady soln. 80—10215
- multi-part mixed boundary value problems, numerical solns. 77—68430
- multicircuit shells of revolution, computer anal. by field method 77—3729
- multiconnected shell, closure conditions for surface deformations *(French)* 77—23887
- multidimensional diffusion equation, class of general boundary conditions 80—90796
- multidimensional singular integral eqns., numerical methods, anal. of elastic solids 77—17818
- multilayer foundations of complex struct., method of flexibility functions *(Ukrainian)* 79—76969
- multimode cylindrical surface wave excitation, multiple impedance boundary condition simulation 78—26000
- multiphase heat conduction problem, finite-element free boundary formulation 77—62133
- multipoint boundary-value problem, maximisation of Green's function 77—37733
- multiwedge corner, singular stress field, boundary value problem elasticity solns. 79—37174
- Navier-Stokes eqn. boundary problem, soln. via successive approximations 80—36865
- Navier-Stokes eqns., a priori estimates *(Russian)* 78—28957
- Navier-Stokes eqns. in domains with non-compact boundaries *(Russian)* 78—30255

boundary-value problems continued
- Navier-Stokes equation soln. method, finite element anal., 2D unsteady viscous flow 77—89088
- Navier-Stokes equations, numerical soln. appl. to viscous flow around cylinder *(French)* 77—75869
- nematic liquid crysts., surface-aligned and bounded by two parallel substrates, orientational order 79—32885
- neutron diffusion equation, Fourier expansion for xyz-geometry 80—9326
- neutron flux optimum control during nuclear station load following 79—9761
- neutron multigroup diffusion theory, optimum boundary condition 78—41801
- neutron second order transport eqn., variational formulation and projectional methods 80—164
- neutron transport, monoenergetic, periodic boundary conditions 77—343
- neutron transport, two-group transport transforms, comput. merit in finite nonplanar media 77—65247
- neutron transport theory, three dimens. integral monoenergetic, initial value problem 77—344
- Newman's numerical technique for solns. 79—40352
- non-associated plasticity and elastoplasticity, rate boundary value problems, variational principles 80—87726
- non-homogeneous elastic shells transient displacement and stress 77—65684
- non-Newtonian fluid, free convection, heat and mass transfer 79—68765
- non-Newtonian incompressible fluid flow through curved pipe, asymptotic theory *(German)* 77—24000
- non-self-adjoint problems and essential boundary conditions 79—44732
- non-sloping circular arc, large deflections, parametric extension *(Russian)* 80—1429
- nondivergent elliptic equations boundary value problems, bifurcation of solns., critical point index *(Russian)* 77—57159
- nonhomogeneous elastic layer bonded to nonhomogeneous half-space, torsion by circular die 78—87263
- nonlinear, equilibrium of plasma in Tokamak machine 79—19080
- nonlinear boundary-value problem, incremental var. formulation, rel. to elasticity *(German)* 77—33866
- nonlinear diffusion problem, dual extremum principles 77—67218
- nonlinear elasticity, boundary value problems, finite element anal., recent developments 79—44737
- nonlinear elasticity, boundary value problems, numerical anal. 79—92945
- nonlinear elasticity, convexity conditions and existence theorems 77—58550
- nonlinear elasticity, integral estimates for displacement and strain energy, body force 77—54882
- nonlinear elasticity, two-point boundary-value problem 77—75804
- nonlinear elasticity strain energy, integral bound for displacement boundary value problem 79—37171
- nonlinear flow, boundary value problems, solvability for analytic functions 79—98677
- nonlinear free boundary eigenvalue problem in plasma confinement *(French)* 77—67200
- nonlinear heat conduction problems, soln. construction procedure, Kantorovich method 78—59264
- nonlinear heat transfer on boundary, difference method of solving conjugate nonstationary convection problem 80—92020
- nonlinear hyperelasticity, finite deformations in constructive method *(German)* 77—41486
- nonlinear integral equation in creep theory of metals, existence and approx. solns. 78—13931
- nonlinear Maxwell eqns., uniqueness-theorems *(French)* 77—38777
- nonlinear near-sonic potential flow with viscosity, solns. *(German)* 80—1646
- nonlinear parabolic eqn. in noncylindrical domain, existence of weak solns. 77—67208
- nonlinear physical media, boundary valve problem soln. by finite element anal. 79—17214
- nonlinear reaction-diffusion models for interacting populations 78—65886
- nonlinear shell theory, boundary value problem solutions 80—57094
- nonlinear simultaneous transport processes, complimentary form of variational principle *(Russian)* 79—54076
- nonlinear simultaneous transport processes, variational principle *(Russian)* 79—58653
- nonlinear singular perturb. problems, asymptotic equiv. 77—9875
- nonlinear singular perturbation problem on a semi-infinite interval 78—94631
- nonlinear thermal conductivity boundary-values qualitative anal. 77—14879
- nonlinear two-point, numerical solution by Newton method with mesh refinements 78—36809
- nonlinear wave eqns. in n-dimensional space, periodic solns. 78—93540
- nonlinear waves in dissipative or dispersive media 78—49672
- nonlocal elastic half space, boundary forces in solvable integral model 79—35558
- nonreflecting boundary conditions for nonlinear hyperbolic systems 79—50748
- nonreflecting outflow boundary condition for subsonic Navier-Stokes calculations 80—74828
- nonstationary temperature field determination, in a crystal on a substrate *(Russian)* 78—18158
- nonsteady flow in one-dimens. pipe systems, boundary condition based anal. 80—1685
- nuclear reactor Xe oscillation control problem 80—674
- numerical anal. 77—67257
- numerical anal. in applied engineering science (conf. May 1977) 77—67249
- numerical soln. through integral eqns., review 78—81808
- numerical solutions of problems in quantum mechanics and quantum field theory 77—2526
- numerical treatment of boundary integral eqns., three-dimens. elastostatic anal., fracture mechs. appls. 77—46909
- ocean bottom roughness effects on LF propag. 79—41501
- ocean long waves scatt. at mouth of estuaries bordered by continental shelf 77—9442
- ocean wave propagation over flat porous bed, radiation-type boundary condition 78—44851
- oceanic trapped edge waves in a presence of irregular coastline 78—44853
- off-energy-shell generalisation, physical, regular and standing wave boundary conditions 80—18257

boundary-value problems continued
one dimensional diffusion system, boundary control problem, exact soln. *(German)* 79—85101
one-dimensional system, Bose-Einstein condensation at const. press. 80—22276
one-dimensonal heat equation with nonlinear time-dependent boundary conditions, global attraction 78—16754
Onsager model, time-depend. quantum efficiency 79—11194
open resonator with cylindrical confocal mirrors, plane EM wave excitation *(Ukrainian)* 78—55280
optical systems, electronic analogy, systems concepts from communications theory *(German)* 77—3542
ordinary differential eqns., comparison and existence theorems 77—9857
orthogonal polynomial solns. to mixed boundary-value problems in elasticity 77—75857
p-n junction boundary conditions 80—20295
parabolic boundary value problem 78—28925
parabolic boundary value problem optimal control, heating process 78—67021
parabolic eqn. boundary value problems, differential, difference method *(Russian)* 79—58534
parabolic equations, majorising solution boundary conditions, solution comparison 80—68023
parabolic free boundary problem, numerical soln. via Newton's method 80—69632
parabolic free boundary problems, 1-D 77—23856
parabolic operators method for determ. unknown coeffs. 79—30209
parabolic procedure for three-dimens. compressible viscous flow prediction in ducts of arbitrary cross section 79—94716
parallel plate condenser, mixed boundary value problem of electrostatic field 77—58222
patch test for nonconforming finite elements, conditions for piecewise polynomial functions 78—77697
penetration gas cooling, porous wall with external heat appl., stability determ. 79—64761
periodic fluctuations in nonuniform media, mathematical conditions for existence 77—13617
periodic solutions of semilinear elliptic equations in a strip 79—17196
periodic structures, asymptotic anal., book 79—25851
periodic surface scatt., existence theorems *(Russian)* 78—73890
peristaltic transport, asymptotic method 80—87805
permanent magnetic interpolar space uniform region conformal mapping *(Russian)* 77—53960
perpendicular wire grids over conducting half space, e.m. scatt. 77—582
Petrov-Galerkin finite element method, boundary layer behaviour 78—69989
phase change problem, with temp. dependent thermal conductivity, noniterative soln. 79—27493
physiological excitation spread equation boundary conditions for undistorted impulse movement pattern 77—56365
physiology, flow problem, one tube 80—89703
piezoceramic plate, electroelastic equilibrium *(Russian)* 78—43795
piezoelectricity, linear transversely isotropic media, normal mode response, boundary effects 78—52441
pile, numerical soln. of beam eqn. with nonuniform foundation coeff. 80—64361
planar body, with circ. boundary and thermally insulated cracks, temp. distrib. 78—67002
plane elastic wave diffraction by wedge, three dimensional nonstationary problem 80—69723
plane elasticity theory, use of automorphic functions *(Russian)* 79—35563
plane elastostatic boundary value problems, formulation as integral eqns. by singularity method 79—35556
plane elastostatic boundary value problems, integral operators, eigenvalue num. calc. 80—36848
plane elastostatic boundary value problems, Rizzo's integral and Kupradze's functional eqns. 80—57093
plane elastostatics, boundary value problems, spectra of integral operators 78—57782
plane elastostatics, functional eqn. for static boundary value problem 79—80446
plane elastostatics, integral equations for mixed boundary value problem 80—79143
plane elastostatics, numerical props. of integral eqns. describing boundary value problems 78—34013
plane entry flows and energy estimates for Navier-Stokes eqns. 79—37278
plane harmonic Dirichlet problems, soln. for canonical domains 79—21548
plane problems of elastic half-spaces, Somigliana's method 77—13611
plane shear flow, exterior Dirichlet problem for quasilinear elliptic boundary value problem 78—22317
plane stratified media, mixed problems for wave eqn., singularities of Riemann functions 77—30017
plane stratified media, mixed problems for wave eqn., singularities of Riemann functions 77—30018
plasma, centrifuge, boundary-value problem at arbitrary mag. Reynolds no. 77—68760
plasma, hot and bounded, anamalous skin-effect 80—24173
plasma, inhomogeneous, Alfven and ion-Bernstein waves, mode conversion and tunnelling 78—34300
plasma, ion-ion diffusion, 2D problem, multiple mirror expt. 77—84411
plasma, Maxwell-Vlasov system 79—19001
plasma, MHD turbulence, three-dimens. soln. in cylindrical geometry 78—67351
plasma confinement, boundary condition for computational MHD 78—1811
plasma mag. neutral sheet, EM instability threshold 78—38500
plasma transport in collisional divertor scrape-off layer in Tokamak 80—28614
plasma two-stream instability, thin layer, wave modes 77—62361
plasma-filled waveguide, two-stream instability nonlinear evolution, numerical simulation 80—43938
plasmatron melting arc in Ar and CO_2 atmosphere, performance characts., MHD calcs. *(Russian)* 80—38573
plasmonic mode boundary conditions, spatially dispersive metal 80—15549
plastic and viscous hardening of materials, steady and cyclic loading 77—4793
plastic drawing through die, global soln. of boundary problem 77—84157

boundary-value problems continued
plastic flow, plane strain and axially symm. problems 78—51089
plastic flow theory, spatial problems 78—51088
plasticity, boundary value problem in general theory *(Russian)* 80—28441
plasticity, dual extremum principles in rate boundary value problems 79—25845
plasticity, rate-independ. theory for multimode plastic straining, unifying concepts 78—42545
plasticity problem soln. by symbolic computer processing of formulae 80—17803
plate, beam-reinforced, edge support influence on admittance 78—1497
plate, circ., thin, elastic, containing Griffith crack, in infinite elastic medium, stress distrib. 79—32374
plate, circular, elastically supported, free axisymm. vibr. 77—14942
plate, completely free, rectangular, free vibr. analysis by method of superposition 78—83300
plate, elastic, infinite, thick, fixed, subject to axially symmetric load, numerical stress anal. *(Japanese)* 79—50600
plate, elastic rectangular randomly inhomogeneous, free vibrs. 77—84180
plate, finite rectangular, superposition of boundary conditions in temp. distrib. eval. 77—14883
plate, infinite, with circular disc, tensile and compressive stress problems 80—38255
plate, linear elastic, classical boundary value problem 79—14261
plate, orthotropic rectangular, nonlinear fluxural vibrs. 77—84179
plate, polygonal, clamped, free vibrs. analysis 79—94523
plate, rectangular, dynamic stability, periodic compressive forces 77—23910
plate, rectangular, variable thickness, stability and vibr. anal., finite element method 77—54918
plate, semi-infinite with crack on end of stiffened edge, uniform tension 79—68659
plate, thick, containing eccentric spherical cavity, transverse bending stresses 78—63288
plate, thick infinite, transversely isotropic, containing circ. hole, end effects 79—27510
plate, thin circular elastic material, Poisson's ratio effect on natural freqs. 77—84181
plate, with discrete energy source, stationary temp. field, approx. soln. 77—46879
plate and shell theory, generalised two-dimens. theories generation 78—12569
plate clamped along contour, vibr. problem, exact soln. 78—18228
plate deflection theory, discrete methods for boundary value problems 79—49045
plate theory, virtual work principle *(French)* 77—17817
plate-cylinder intersection, elastic, three-dimensional anal. by boundary-point-least-squares technique 77—58558
plates, appl. of improved collocation techniques 77—68434
plates, orthotropic, reduction method for vibr. problems 77—14940
plates, rectangular thin, effect of different edge flexibility coeffs. on transverse vibrs. 78—83294
Plexiglas, spark energy balance 79—23474
point controlled distributed parameter system multiple shooting and sweep algorithm 77—25728
point heat source, natural convection in rotating environment 79—10445
Poiseuille flow, at large Reynolds numbers, Navier-Stokes eqn. soln. *(Russian)* 78—59364
Poiseuille flow, compound matrix method 80—57096
Poisson's equation, finite difference form, numerical soln., unconditionally stable scheme 79—50
Poisson eqn. on surface of sphere, shooting method for finite-difference soln. 77—2527
Poisson equation over complex domain, finite difference method, Neumann boundary conditions 78—79189
polycrystalline metals, effect of grain boundary sliding on steady creep 80—96590
polymers dissolution kinematics, numerical solution and expt. verification 78—26687
polytropic media, shock waves formation processes, boundary condition effects 79—46347
polytropic star, equilib. poloidal mag. field, finite difference-finite expansion method, Fortran program 77—13322
porous catalyst pellets, singular perturbation anal. of boundary value problems modelling reactions 78—76906
porous elastic media, boundary-layer analysis of propagating mode II cracks 78—5696
potential approach appl. 77—68429
potential problem, numerical soln. by integral eqns. without Green's functions 77—26162
potential problems, numerical solution, integral equations without Green's function 78—20950
potential problems, two-dimens., numerical soln. by boundary integral eqn. method 79—58533
Prandtl's equations for stationary boundary layer, method of linear soln., existence, convergence *(German)* 77—58642
preconditioning of indefinite problems by regularization 79—46214
pressure vessels, creep bounds and brittle damage estimates 80—23908
pulsar magnetosphere numerical modelling 77—29871
pulsating turbulent flow onto elastic surface, finite difference method *(Russian)* 78—75153
punch on elastic layer overlying elastic foundation 77—39228
QSO clouds, Rayleigh-Taylor stability of radiation-supported surfaces and slabs 77—53697
quantum elasticity theory, natural vibrations of rectangular parallelepiped and plate 77—27483
quantum statistical mechanics *(Rumanian)* 78—86219
quasi-geostrophic equation, stationary solns. with nonlinear boundary conditions 79—48529
quasigeostrophic flow, horizontal boundary conditions and stability 79—53446
quasisteady primitive equations with associated upper boundary conditions, appl. to large scale atmospheric flow 79—62563
radar scattering from turbulent cylindrical plasma, model 78—22512
radiant heat exchange modelling in rectangular chamber with attenuating medium 80—33433
radiant-convective heat exchange problems, nonstationary, analytical soln. method 80—33432
radiation problem simplified boundary elements 78—86226

boundary-value problems continued

- radiative heat exchange in black body system, conduction, radiation, scatt. and absorpt. 80—38239
- radiative transfer, two-dimens. expansions, for isotropic scatt. semiinfinite medium 78—42522
- radio transmission in Earth-ionosphere waveguide, concise theory 79—48616
- radionuclide geospheric transport eqn., boundary conditions 80—47611
- random walk on lattice, correl. of successive steps, absorbing walls 79—44863
- randomly loaded elastic body dynamics, probability characts., of solns. to boundary-value problems *(Russian)* 77—41490
- rarefied gas dynamics, phase shift formulation 78—1694
- Rayleigh waves scatt. by thin surface strip 77—11773
- reaction of continuous dynamic systems with complex form under time-space random fields 78—65767
- reaction-diffusion system with one degree of freedom, stability anal. of dissipative structs. 79—87826
- reactor theory, method of imbedded elements, construction of coordinate functions 79—59128
- rectangular MHD channels, nonuniform conducting flow calcs. *(Russian)* 77—27613
- rectangular plate vibration, time-dependent boundary conditions 79—68625
- rectangular plates, elastically supported orthotropic, natural freqs. 77—31243
- rectilinear flow, pressure error upper and lower bounds with pressure gradient 80—6010
- reduced wave equation on sphere, mixed boundary value problem 77—64927
- reinforcement material distrib. for specified stress field criteria, plane elasticity hybrid problem 80—64376
- relativistic gas-dynamic eqns., solns. with singularities for initial value problems *(Russian)* 77—58809
- Riemann boundary value problems, partial wave mixing in S-matrix, Jost matrix evaluation 79—89072
- rigid wall-hot gas stream interaction, heat cond. eqns. soln. 78—79194
- ring cavity, dressed mode dynamics of optical bistability 80—19013
- ring plates, stability under compressive stresses *(Russian)* 77—54873
- rivers, pollutant dispersion, boundary conditions effect 78—85611
- rock massif, nonstationary heat conduction near horizontal mine *(Russian)* 77—56620
- rod, current-carrying, steady-state heat conduction, perturbation soln. 78—5629
- rod, expanding, conductive heat transfer computation, fast numerical technique 78—75029
- rod, twisted axially loaded, nonlinear anal. 79—72811
- rod with nonlinear curvature, dynamic stability theory, lateral bending problem under torsion *(German)* 78—54
- rosette cylinder, elastic response under axisymmetric loading 77—58549
- rotating binary mixture over infinite rotating disk, species distrib., existence and uniqueness of solns. 77—15044
- rotating cylinders, Taylor vortex form. and spectral props. of boundary value problems 79—90262
- rotating disc with axisymmetric surface heat source distrib., in laminar flow, heat transfer 79—46314
- rotating disk, in liquid surface with adsorbed film, torque 78—32685
- rotating flexible rods, unstable vibration and buckling 78—79242
- rotating strings, elastic, heavy, nonlinear eigenvalue problems, bifurcating branches of solns. 80—73174
- rotational flow, steady and unsteady, fluid in finite cylindrical container 80—14708
- rotationally symmetric periodic electrostatic focusing system field distrib. 79—76574
- Saint-Venant torsion problem, classical, integral and functional eqns. 78—57780
- Samarsky's boundary conditions for second-order parabolic eqn., soln. uniqueness *(Russian)* 77—17779
- sandwich beam with central mass, free vibr., freq. relations 77—31252
- saturated porous medium, completely confined, onset of thermal convection 78—83387
- scalar wave transmission, through small apertures, appl. of isoperimetric inequalities 79—32109
- scattering from obstacles with impedance boundary condition *(French)* 77—577
- scattering properties of arbitrarily shaped lossy dielectric bodies of revolution 78—22072
- scattering theory for domains with non-smooth boundaries 79—30293
- scattering wave function construction using analytical continuation of bound state 77—74258
- Schrodinger operator, minimal, self-adjointness 80—17836
- Schrodinger operator spectrum with damped oscill. pots. 78—77748
- Schwinger-DeWitt expansion, boundary terms, flat space results 78—77815
- second boundary value problem, soln. in form of Fredholm regular eqn. *(French)* 77—57152
- second order, finite element soln., variational Green's function 77—71193
- second order differential eqns., undirect boundary problem on finite interval *(Russian)* 77—22375
- second-order eqns., boundary points regularity *(Russian)* 77—9960
- seepage flow variational inequalities by finite element method 77—68688
- seismic inversion for boundary shape between two layer stacks 79—16684
- seismic waves diffraction by finite crack, appl. to location of magma lens 79—16416
- semiconductor, nonlinear equation, asymptotics of spectral boundary-value problem 80—6851
- semiconductor slab with disc electrode, spreading resistance treated as mixed boundary value problem 79—87154
- semiinfinite bar, heat conduction problem, hyperbolic eqn. soln. 80—19210
- semiinfinite plate, penetration into incompressible liquid, boundary value problem *(Russian)* 79—88804
- semilinear wave equation, bifurcation of periodic solns. 79—80449
- semishadow field diffraction, boundary wave uniform asymptotics *(Ukrainian)* 78—89350
- sethlets, generalised singular points 79—46
- SH-surface waves, scatt. and excitation in mass-loaded elastic half-space 77—14933
- SH-waves refl. and refr. in presence of slip and friction 79—46243
- shell, spherical, with conical nozzle, thermal stress anal. 78—79204

boundary-value problems continued

- shell of revolution, Green's function of steady heat cond. operator 79—86319
- shells, two-dimensional eqn. system *(Ukrainian)* 78—89342
- shells of revolution, thin-walled, heated, temp. field, thermostatic control 78—67003
- shells of revolution, variable thickness, stress state determ. 80—38275
- shells of variable thickness, eqns. of motion *(Russian)* 77—39226
- shields, thin, boundary conditions, electrodynamic soln., monochromatic external field 77—54647
- shock formation and decay for conservation law in several dimens. 77—53788
- shock layer, hypersonic, vibr. nonequilib., near stagnation streamline, low Reynolds no. flow 78—87417
- shock tube boundary-value problem global soln. *(French)* 78—63449
- Signorini's perturbation procedure in elasticity, branching of solutions 80—27134
- Signorini's problems, reciprocal variational inequalities soln. 79—41585
- simple body melting time with convection boundary condition 80—99914
- simple fluid, Coleman-Noll eqn., appl. hereditary partial differential eqn. 77—35454
- simple fluid, energy stability method 79—27629
- simultaneous Wiener-Hopf equations, solvability in boundary condition case 79—44750
- sine-Gordon eqn., Goursat and Cauchy problems 78—77682
- singular boundary points, behaviour of eigenfunctions of BEP and HEP 80—4920
- singular nonlinear differential eqns., boundary layer flow 78—63413
- singular perturbation of elliptic equation *(Chinese)* 79—35525
- singular potentials, inhomogeneous boundary value problem, eigenvalue equation 79—58530
- singularity methods in math. phys., boundary value problems appl. 77—74198
- singularly perturbed boundary value problem with turning point 79—5972
- singularly perturbed nonlinear boundary value problems with turning points 79—5971
- slip boundary condition, rough sphere ang. vel. correlations, hydrodynamic anal. 77—51286
- slip theory, boundary value problems soln. *(Ukrainian)* 79—41588
- slotted boundary machine field soln., conformal transformation and integral methods 79—41272
- slow viscous flows over flat plate with mixed boundary conditions 78—1632
- Sobolev equations for nonlinear dispersive systems 79—21528
- solar cell analysis, appl. of superposition principle 80—76631
- solar coronal mag. field determ., fixed mesh soln. to Laplace's eqn. 77—2392
- solar coronal magnetic fields, Laplace's eqn. direct soln. using line-of-sight boundary conditions 80—12742
- solar evolving force-free magnetic fields, preflare stage development 77—29739
- solar evolving force-free magnetic fields; variational formulation 78—93182
- solar force-free mag. field calc. with constant α, exact solns. 77—33438
- solar heating of buildings calc., transient thermal flux model 79—62144
- solar magnetograph data, boundary-value problem for force-free mag. fields determ. 79—12445
- solar storage tank, buried, hemispherical, heat cond. to environment, series soln. 79—3891
- solid, crystalline, finite strain, uniqueness criteria and minimum principles 78—51086
- solidification, semiinfinite slab with const. boundary heat flux, transient interface position and temp. field 79—94481
- solids, uniqueness and stability under config. depend. loading 78—30194
- soliton gas, turbulence due to weak dispersion, stochastisation of soliton motion 78—41169
- solution using net method *(Ukrainian)* 79—35524
- spatial dispersion exponential model, boundary conditions *(Russian)* 80—75994
- spatial problems of rigid plastic equilib. 78—55569
- spatially dispersive media, optical boundary value problem 80—45024
- spectral resolution of boundary value problems in half space for partial differential matrix operators 79—25825
- spherical nozzles of high-temperature heaters, heat transfer calcs. 80—103022
- spheroid turn in conducting media, EM field calc. *(Russian)* 78—46481
- spray, numerical computation, appl. to engines 79—37378
- spreading resistance calculations, role of source boundary conditions 78—89499
- stability and convergence 78—90827
- stability evidence 77—84167
- stack of parallelograms, thin partition walls, steady temp. distrib. and heat flux 77—58535
- stagnation point flow, least square finite element soln. 77—14981
- star shaped membranes, new bounds of Poincare const. *(French)* 79—25860
- stars, uniformly rot. polytropes, boundary eqn. 77—74040
- static field and eddy current problems, computational methods for soln. via Fredholm eqns. 79—68344
- stationary flow between water reservoirs separated by non-homogeneous dam, free boundary problem 79—10606
- stationary vibrations in 2-dimensional micropolar thermoelasticity 80—74793
- steady-state heat diffusion equation, alternate general solution 80—79103
- steel, mild, ductile fracture of cracked plates, nonlinear boundary-value problem 77—81318
- Stefan and dam problems, free boundary convexity 78—83356
- Stefan problem, new expansion procedure 77—92
- Stefan problem, one-dimens., third order accurate discontinuous finite element method calc. 79—81701
- Stefan problem of melting in annular duct with nonlinear outer boundary conditions 79—86329
- Stefan problem simulation and control, associated variational inequality 78—67009
- Stefan problems, two-dimensional, approx. of integro-differential eqn. 77—80050
- Stekloff type, Green's functions, asymptotic formulae *(Russian)* 77—22379
- Steklov consts., bounds 79—25861
- stenosed tube, numerical solns. of Navier Stokes problems 80—16975

boundary-value problems continued
stochastic, solns. using digital simulation of space-random fields 79—41510
stochastically inhomogeneous solid with opening, plane deform. problem 79—86337
Stokes problem, second-order difference scheme 80—90678
stratified shear flow, with nonlinear crit. layer, approx. soln. 78—79357
streaming, uniform, past fixed semicirc. infinite strip 79—23299
stress analysis, connection between finite element and integral equation methods *(French)* 77—87649
stress and displacement fields, continuous, algorithm for finite element anal. 78—30178
stress concentrations round cylindrical cavity in half-plane under tension, effect of couple-stresses 77—19524
string with time-variable length, free and forced vibrs. 79—92953
string with variable mass, nonlinear dynamics *(Polish)* 78—12553
strongly irregular boundary value problems 79—63000
structural anal., soln. by orthogonal collocation 78—51063
structural panel, rectangular, with elastic edge constraints, dynamic response, Bolotin's asymptotic method 78—75091
Sturm-Liouville, error estimation 78—81818
Sturm-Liouville nonlinear problem, asymptotic linearity 77—67186
superfluid wave propagation, variational and reciprocity principles 77—72727
supersonic laminar boundary layer separations, quasi-3-dimens. 78—46995
supersonic plane flow past a curved wedge, quasi-linear hyperbolic systems *(French)* 80—10261
supersonic wave drag of planar singularity distributions 78—83430
surface field calc., floating random walk method 79—41273
surface Green's function matching, physical and physicochem. appls., review 77—78954
surface wave, scattering, by submerged sphere 78—34145
surface waves, Hamilton's principle 78—5759
suspended sediment transport theory, elliptic boundary value problem 79—14466
suspension, Brownian rotational-translational particles, at finite conc., dynamics and hydrodynamics 79—7401
symmetrical branches at end of crack, effects on growth 80—103003
Takagi-Taupin equations, boundary conditions in numerical integration, appl. to Bragg and Laue cases 80—1886
temperature field, heat transfer problems, linear algebraic soln. method 78—59281
temperature field analysis application using finite element anal. *(Polish)* 79—94448
thermal conductivity, nonlinear problems, temp. fields with variable thermophys. props., calc. method 79—86324
thermal conductivity infinite and finite integral transforms solution 77—75773
thermal problems, nonhomogeneous, and Stefan single-phase problem in arbitrary domains 80—79102
thermal reistance minimisation, solid with heat-exchanging surfaces, variational method 78—94512
thermal stresses in cylindrical shell with circular hole or rigid inclusion 77—19518
thermionic convertor characts., effect of cathode serration development *(Russian)* 77—81193
thermo-piezoelectricity, of polarised annular disc, deformation due to prescribed temp. distrib. 80—2699
thermoelastic half-space transient response 79—32253
thermoelastic laminated media, aggregate response modelling 77—50897
thermoelastic response of infinite flat slab 80—92052
thermoelasticity, 2-D exterior boundary value problems *(French)* 80—79144
thermoelasticity, linear, energy arguments 78—51067
thermoelasticity, one-dimensional direct approach anal. 80—8797
thermoelasticity, stress-flux initial boundary value problem 80—61
thermoelasticity, uniqueness theorem of stress temp. eqns. 80—4528
thermoelasticity and electrostatics, mixed boundary value problems 80—55
thermoelasticity problem with finite heat propag. vel., acoustic vibr. anal. 77—42770
thermoelasticity with microstruct., existence and uniqueness theorems 80—60
thermoelastodynamics mixed boundary value problem, algorithm *(French)* 77—50979
thermoelectric element, arbitrary shape, cooling efficency 78—67010
thermophysical dynamic characts. of thermal receivers, nonlinear eqn. soln. with 3rd kind boundary conditions 77—43395
thermophysics, numerical solutions *(Russian)* 78—55545
thick infinite plate with circular hole, axisymmetric stress and displacement boundary value problems 79—27511
thick plate elastodynamics, soln. of 3-D axisymmetrical boundary value problem *(Ukrainian)* 80—10140
thick walled sphere, nonsteady hydroelastic oscills. 78—18227
thin circular insulating annulus on conducting half-space, steady heat flow 79—59981
thin circular quadrant, singularly loaded, with clamped radial edges and free circular edge 78—63300
Thomas-Fermi eqn., iterative soln., nonlinear eigenvalue problem technique 78—909
Thomas-Fermi eqn. solns., iterative method 79—9185
three-dimensional neutron transport eqn., boundary value problem 79—67809
three-point, solutions existence and uniqueness 78—32655
tides, shallow water, three-dimens. nonlinear model *(Chinese)* 78—24309
time-dependent boundary-value problem soln., half-range, orthogonality relations 79—14508
time-dependent equations, multistep finite difference methods, boundary conditions 78—36829
Timoshenko beams, eigensolns. for coupled thermoelastic vibrations 79—64577
Tokamak machines, Vlasov plasmas, geometrical optics approach, Tokamak appl. 80—14902
torsion of nonlinear bar with multiply connected cross-section 77—50890
torsion of rectangular bars, appl. of improved collocation techniques 77—68434
torsion of truncated elastic core, mixed boundary value problem 77—46908
torsion problem for elastic cylinder with holes, integral eqn. method soln. 80—36849

boundary-value problems continued
torsional wave propagation in elastic inhomogeneous cylinders 77—80104
traction problem, strain energy bound in finite elasticity with nonzero surface data 80—58909
trajectory, optimal, for lunar mass catcher 79—16844
transformation operators and wave propagation in a spherically stratified medium 79—18569
transient radiation-conductive heat transfer in selectively-absorbing media 78—94572
transmission line modelling of diffusion 79—26011
transonic axisymmetric pot. flow around inlets, Cartesian mesh soln. 77—72323
transonic flow, Euler eqn. soln., Lagrangian method 80—38435
transonic flow, far-field boundary conditions solution 77—55024
transonic flow, similar solns. 78—94762
transonic free jet, overexpanded two-dimens., eqns. formulation and soln. method 80—6109
transparent stagnation point shock layers, non-iterative solution of energy eqn. 79—18911
transport problem stationary, generalised, Laplace operator eigenfunction series soln. *(Russian)* 78—81931
transport process optimal control adaptive criterion study 77—17931
transport-equation, with anisotropic scatt. in finite slab geometry 79—17364
transversally isotropic layer, soln. of three-dimens. problem of theory of elasticity 79—40372
transversely isotropic half-space indented by a flat annular rigid stamp 79—55347
transversely isotropic medium with closed conical cavity, stressed state *(Russian)* 80—43616
tropical cyclone surge model, finite difference method 79—12132
tube, circ., entrance region, mass transfer, asymptotic expansion soln. 78—87392
tubes and flexible hoses carrying moving liquid excited in transverse vibrations, nonconservative boundary-value conditions 79—63056
turbulent boundary layer, complete vel. profile, wake deficit and inner layer terms 77—51048
turbulent flow, similar solutions, computation method 77—89102
two dimensional electrostatic boundary-value problem for two strips and grounded cylinder 79—72452
two or three electrons, interacting with localised mag. moment, wave function determ. *(French)* 79—12636
two-dimensional, conformal transformations combined with numerical techniques, with applications to coupled-bar problems 80—83538
two-dimensional, of small amplitude waves in finite water depth, num. analysis method 77—9444
two-dimensional crystal boundary, oscill. propag. 78—63924
two-dimensional Gauss-Markov field, pinned Karhunen-Loeve transform 77—83827
two-dimensional isoparametric Hermitian element for field problem soln. 77—60914
two-dimensional nonstationary Euler eqn. solution in time-dependent bounded domain *(Italian)* 78—69986
two-point, accurate finite difference method 79—88795
two-point, statistical variant using Einstein-Fokker-Planck eqn. *(Russian)* 78—81924
two-point, statistical version anal. 79—63154
two-point boundary-value problems with eigenvalue parameter in boundary conditions 78—73830
two-point problems, soln. bivariational bounds 77—5646
unbounded linear transformation arising in kinetic theory of gases, spectral representation 79—55441
unclosed shells of revolution with inhomogeneous boundary conditions, two-dimensional statics *(Ukrainian)* 78—89341
unconstrained variational statements 78—93518
unconstrained variational statements for initial and boundary value problems. comment and reply 79—75327
unconstrained variational statements for initial and boundary-value problems 79—92927
underwater sound, acoustically relevant statistics for stochastic internal-wave models 77—46854
unhomogeneous bars, normal mode response, stress anal. by boundary operator method 80—19239
unilateral contact problem, structures with nonquadratic strain energy density 77—31209
unilateral elasticity, two-sided estimates 77—45698
Unimoment method, simplified matrix element representation 77—74207
uniqueness of Dirichlet, Neumann and mixed boundary value problems for Laplace's and Poisson's equations for a rectangle 79—9076
unsteady diffusion in wedge-shaped region with inhomogeneous boundary conditions, appl. of Sommerfeld-Malyuzhinets integral 77—89111
unsteady heat transfer, between dense disperse material and internal object, 4th kind boundary conditions 77—42707
upwindings of high order Galerkin methods in conduction-convection problems 79—3886
variable-thickness elastic orthotropic annular plate nonlinear oscillations 79—68630
variational with constraints, solution by direct method 77—22386
vertical jet under gravity, Riemann-Hilbert problem, numerical soln. 80—36858
vibrating rod, solved by Fourier anal. 77—39258
vibrating systems with mixed boundary conditions, nonorthogonal eigenfunctions 77—14941
vibrosource, characts. in liq. layer 79—81905
viscoelastic fluid, flow induced by elliptic harmonic oscills. of disc 79—4044
viscoelastic fluid flow, die swell problems with free surface, collocation and Galerkin finite element 80—14751
viscoelastic fluid flow in fixed geometry, collocation and Galerkin finite element methods 80—14750
viscoelastic half-space, analytic solns. to boundary-value problems 77—75816
viscoelastic liquid, pulsatile flow in elliptic cross-section channel 79—7392
viscoelastic liquid channel flow, boundary-initial value problem 79—4045
viscoelasticity, linear, exterior problem 78—71283
viscoelasticity, non-homogeneous, Lagrange equations and Galerkin method, boundary value problems 80—53654
viscoelasticity, nonlinear, bifurcation and uniqueness, Hadamard stability 80—43621

boundary-value problems continued
viscoplasticity, min. principle in stress field boundary-value problem 77−46927
viscoplasticity anal., boundary integral eqn. method *(French)* 78−90728
viscoplasticity with singular yield surfaces, side and corner flow rules, finite element applications 80−48594
viscous dissipation effect on heat transfer, circ. cylinder axisymmetric stagnation flow 78−51164
viscous flow computations, boundary approx. and accuracy 79−64621
viscous flow past two-dimensional bluff body, new approx. theory 77−918
viscous fluid, squeezing between elliptic plates 80−28478
viscous impressible fluid bounded by cylindrical boundaries, slow motion of small sphere 77−14978
von Mises' eqn., finite element solution to eqns. of laminar boundary layer *(French)* 77−72268
vortex motion of a compressible liquid *(Russian)* 79−77124
vortex ring, passage through circ. aperture, max. dimensions 77−84262
wall, with cylindrical cooling channels, steady-state temp. distrib. 77−65663
water, boundary conditions for numerical simulation, book contrib. 79−60247
water, thermally-stratified, cooled from above, free convection 79−46315
wave equation in domain with moving boundaries, difference schemes on non-uniform grid *(Russian)* 77−22380
wave equation mixed problem, method of potentials 79−40381
wave equation with extended stability range, explicit difference method 80−4538
wave propagation in random media, oceanic appls. 79−5987
wave supporting system, lossless, distributed parameters from boundary meas. 78−16658
waveguide diffraction application of minimum autonomous block method 79−68362
waves above level bottom, three-dimensional problem periodic solutions 80−57099
weakly disturbed unharmonic operator, spectral function *(Russian)* 77−22378
wedge, 3-dimens., functional equations of static elasticity theory *(Russian)* 79−46203
wedge field, composite truncated, Dirichlet problem, point source appl. 77−5676
wind-driven lake circulation models, boundary conditions 80−85688
x^4 potential, associated ground state wavefunction, sum rules 79−45036
Yang-Mills equation, bounded solutions 80−105764
^{4}He, superfluid, boundary-value problem for confined He 77−39707
^{4}He, superfluid, spatial distribution of order parameter, spectral approach of inverse problem *(Russian)* 77−80659
Si:B, ion implanted, SOS device struct., nonlinear impurity redistrib. 79−1625

bowing *see bending*

brain
see also neurophysiology
40 Hz activity in sigmoid gyrus, nucleus accumbens and amygdala, cross correl. anal. 80−76730
abscess, electroencephalographic computerised tomographic correls. 79−83899
accessory optic projections upon oculomotor nuclei and vestibulocerebellum 80−3643
accessory optic system in the rat 80−21470
acoustic properties of normal and abnormal brain 80−45955
acoustically dependent latency shifts of brain stem evoked response in man 78−85318
afferent visual systems of cat and rhesus monkey, responses to wavelength contrast 80−56030
Alopex process: Visual receptive fields by response feedback 80−61546
alpha activity detection, above-threshold *(Czech)* 77−5124
alpha frequency rel. to head size, implications for brain wave model 78−69035
alpha wave amplitude and frequency control, feedback learning system *(Japanese)* 77−44626
angioscintigraphy in posterior view, clinical value 80−72290
Arnold-Chiari malformation: diagnosis by iodo-myelo-tonsillography with tomography 80−36088
associative noise-like coding memory, algebraic model 80−76720
audiogenic seizures, reversible hyperthermia, rat 80−8098
audiological diagnosis, use of click-evoked elec. brainstem responses 79−92237
auditory brain stem responses in patients with acoustic neuromas 79−92235
auditory cortex of moustache bat, processing const. freq.-FM sonar signals 77−12940
auditory cortex of unanaesthetised monkey, vertical stereotaxic approach to elec. recording 80−72383
auditory cortex unit response to synthesized formants, cat 80−67098
auditory evoked potentials, simultaneous recording of brain stem and freq.-following responses to LF tone 78−11665
auditory evoked potentials in human brainstem, effect of stimulus parameters 77−12935
auditory evoked response, hemispheric differences 77−90801
auditory information, anatomical and physiological basis 79−11944
auditory nerve response and brain stem transmission time 80−45917
auditory receptive fields, centre-surround organisation, owl 79−66476
auditory space neural map, owl 79−8514
autoradiographic visualisation of rat brain dopaminergic nerve endings, test of technique 80−61742
autoradiographs, rapid semiautomatic quantification, microprocessor appl. 80−41332
benzodiazepine receptors in brains of humans and animals, autoradiographic localisation 79−83752
bifurcations geometry, human, effect of static distending press. 80−94259
biomagnetic measurements in unshielded and noisy environments 80−104710
blood flow, linear computer model 79−92288
blood flow, meas. in pig by ^{133}Xe clearance technique 80−94421
blood flow, regional distrib. during exercise in dogs 80−101197
blood flow, tissue pO_2 and pCO_2, continuous and simultaneous meas. 79−57829
blood flow, total and regional, effect of cerebral extracellular fluid acidity 80−67123

brain continued
blood flow display on colour TV using computerised picture processing technique *(Swedish)* 77−44780
blood flow meas., regional, computer program description 77−5098
blood flow meas. in the cat 79−83887
blood velocity in brain capillaries, microkinematic obs. *(Russian)* 79−5366
blood-brain barrier, effects of microwave-induced hyperthermia, rat 80−61642
blood-brain barrier, neutral amino acid transport into isolated brain capillaries 79−57616
blood-brain barrier, problems in quantifying effects, comparison of methods 80−61643
blood-brain barrier, reversal of microwave-induced permeability 80−61641
blood-brain barrier permeability obs. after microwave irradiation, rat 79−74718
bolus material of shredded-gel for use with EMI CT 1010 brain scanner 80−41173
brainstem auditory evoked pots., influence of nonpathologic factors 79−88079
brainstem population responses, inhibitory influence 80−104595
breach rhythm, EEG rel. to skull defects 80−35862
callosal neurones selection, effect of visual experience, cat 79−79524
carotid arteries, US imaging, using CW, pulsed Doppler and pulse echo techniques, book contrib. 80−36047
cat, subdural structure resonance phenomena 77−16923
caudate nucleus, neutotransmitter activity transient alterations after electron irrad., rat expts. 80−72267
cell assemblies in the cerebral cortex 79−2033
cerebellar cortical current appl. rel. to underlying cellular activity 77−60195
cerebellar stimulation and eye movement in cats 80−30719
cerebellum, neuronal organisation, informational capacity of Purkinje cell and climbing nuclear unit 77−25409
cerebral, O_2 sufficiency, noninvasive IR monitoring 78−44583
cerebral angiography, brain O_2 tension response, using animal model 77−52872
cerebral angiography, cortical pO_2 and K^+ dynamics rel. to contrast agent neurotoxicity 78−35954
cerebral angiography, evaluation of Contrac injector 78−40293
cerebral angiography in stereoscopic magnification *(Japanese)* 77−73574
cerebral artery walls, rheoencephalogram parameters vs. mech. props. 78−3547
cerebral blindness recovery, evoked pot. and psychophys. meas. 77−40668
cerebral blood flow, atraumatic meas. by ^{133}Xe *(French)* 77−37039
cerebral blood flow, colour functional imaging 77−5067
cerebral blood flow, radiotracer meas., automatic bolus injector 77−9238
cerebral blood flow automated analyser for ^{133}Xe studies 77−86597
cerebral blood flow computer for use in angiogram theatres 78−73227
cerebral blood flow control in hypercapnia, model 79−100641
cerebral blood flow determination, computer assisted method for multi-exponential curve fitting 78−20246
cerebral blood flow dynamic characts. in sinusoidal hypoxia, goat 79−100652
cerebral blood flow dynamics, computer model 79−83837
cerebral blood flow estimation in newborn infant, noninvasive technique 77−90949
cerebral blood flow meas., lateral counting corrections 79−8536
cerebral blood flow meas. by radioisotope clearance, radiation scattering effect 78−3600
cerebral blood flow meas. in animals using ^{14}C-ethanol 80−41205
cerebral blood flow meas. using NMR 77−40730
cerebral blood flow noninvasive meas., analytical problems 80−41208
cerebral blood flow noninvasive regional meas. and computer analysis 78−35948
cerebral blood flow parameterisation, scintiangiography meas. 79−25025
cerebral blood flow regional meas., cyclotron prod. of ^{77}Kr 77−56468
cerebral blood flow system using H_2 clearance method 78−40457
cerebral blood volume meas. by ^{11}C-labelled carboxyhaemoglobin 80−8134
cerebral capillaries, increased radiosensitivity in neonatal Gunn rats rel. to Sprague-Dawley rats 80−17006
cerebral cortex, cat, partial O_2 pressure meas. 79−83826
cerebral cortex evoked pots. in cat, as electrode safety model 78−31797
cerebral cortex function, rel. to blood flow 79−43988
cerebral cortex rabbit, contribs. of each layer to EEG 79−57618
cerebral cortial blood flow transients in cat. meas. technique using tissue heat transfer 79−92457
cerebral cortical microfluorometry at isosbestic wavelengths for correction of vascular artifact 80−56322
cerebral gas exchange, perfusion and diffusion limitations 80−45940
cerebral hemispheres, right and left, EEG activity comparison during language, non-language tasks 80−45922
cerebral perfusion image processing, minicomputer system 77−29200
cerebral potential impulse response, EEG method *(Japanese)* 78−3661
cerebral potentials preceding unilateral and simultaneous bilateral finger movements 80−26217
cerebral radiographic scintillation detection unit fixture 79−57749
cerebral regional blood flow, computerised monitoring system for stroke patients 79−79626
cerebral regional blood flow and vol. meas., intravenous isotope method 77−86610
cerebral regional blood flow assessment by continuous carotid infusion of ^{81m}Kr 78−20254
cerebral regional blood flow meas., ^{133}Xe inhalation method with on-line computer 77−40734
cerebral regional blood flow meas. by ^{133}Xe inhalation, anal. method comparison 78−44604
cerebral regional blood flow meas. with ^{133}Xe, functional landscapes in brain 78−85356
cerebral regional blood volume, meas. with EMI 1010 scanner 79−53212
cerebral regional O_2 distrib. model during continuous inhalation of $^{15}O_2$, $C^{15}O$ and $C^{15}O_2$ 78−65108
cerebral tissue, Ca^{2+} binding rel. to weak oscill. elec. fields 77−1984
cerebral vascular disease, experience with radionuclide imaging and computed tomography 77−77977
cerebral ventricle, intact, site for allografted mature superior cervical ganglion fragments in rats 79−8493

brain continued
cerebro-spinal specific elastance in cats, in vivo determ. 78—40236
cerebrovascular autoregulation for hypoxia, using variable amplitude sinusoidal PO_2 generator 77—56563
cerebrovascular disorders, computerised tomographic diagnosis, review 79—34638
cerebrovascular permeability, quantitative method for meas. of alterations 80—61748
cingulate cortex, monkey, anterior and posterior differentation by afferents 79—66468
circadian clock in Limulus brain, response increase and noise decrease of retinal photoreceptors 80—94210
circadian pacemaker, transplantation in Drosophila 79—62234
cisternography, transverse section radionuclide scanning 77—2038
clinical applications of US techniques 79—79619
cognitive processing, hemispheric differences probed by auditory evoked pots. 78—15847
complex visual stimuli representation 78—88709
computed tomography of the visual pathways 80—56178
computer assisted ring detector positron camera system for brain reconstruction tomography 78—40306
computer tomograms, shape anal. in isodence lesion characterisation 80—8152
computerised tomography, anatomic and pathologic correls. 79—34636
computerised tomography, clinical interest of coronal and sagittal sections 79—29587
computerised tomography, dose to thyroid and eye 79—92389
computerised tomography, neurodiagnostic studies and head injury management 79—39470
computerised tomography, role and relation compared to radionuclide imaging 79—34637
computerised tomography images, automated anal. 80—8151
computerised tomography of brain and spine, clinical appl. 80—30886
computerised tomography scanning, traumatic and emergency patients 79—34639
contingent negative variation and accuracy of time estimation. A study on cats 80—26216
contingent negative variations, rel. to distraction-arousal hypothesis 77—5002
contrast dose for enhancement of computed tomograms 79—88193
cooling, selective, possible cause of bradycardia during face cooling 80—30670
corpus callosum, cat, effect of sectioning on binocularity of vision 80—97922
corpus callosum, effect of neonatal section on depth perception, young cats 80—61572
cortical event-related potential waveform, effect of stimulus sequence 77—2011
cortical pattern evoked visual pots., estimation of rat eye refr. 77—70455
cortical periodic complex cells, cat, spatial freq. selectivity 78—69057
cortical plasticity in monocularly deprived immobilized kittens, eye movement dependence 80—81588
cortical potentials associated with detect. of visual events 77—52782
cortical projections of area 18 in owl monkeys 77—60207
cortical receptive field binocular differences in kittens after rotationally disparate binocular experience 77—90784
cortical response to callosal stimulation, model for determ. of safe and efficient stimulus parameters 80—3614
cortical visual evoked potential, normal humans, bibliography of research 79—5278
cranial CT, valve and limitations in spreading process diagnosis *(German)* 80—36105
cranial scintigraphy, value of adding emission CT sections to conventional pertechnetate images 80—56187
craniocerebral computer tomography in the neonate, review 79—34640
craniospinal mechanical fluid systems, dynfunctoning as revealed by stress/strain diagrams 79—25024
creep and relaxation props. of human brain tissue 79—92263
diagnosis, clinical efficacy and cost anal. of cranial computed tomography and radionuclide brain scan 77—77974
diagnosis, complementary role of computerised axial transmission tomography and radionuclide imaging 77—77975
diagnostic technologies, comparative study of radionuclides and computerised tomography 80—72320
diathermy applicator for irrad. of rat brain 80—94425
DNA strand breaks in developing rat and their repair 80—30786
dolorimetry, cerebral response to noxious CO_2 laser stimulation 78—31882
echoencephalography, US pulsatile, prototype instrument and trial obs. *(Russian)* 80—17174
echoencephaloscope, two-probe three-mode design 78—44567
EEG, cat, computed unit-EEG correls. and laminar profiles of spindle waves 78—11625
EEG, dominant freq., correl. with cerebral O_2 uptake and blood flow 77—5095
EEG, impulse responses of cat brain obs. 79—79502
EEG, magnetoencephalogram, current dipole model, central nervous system disease diagnosis applications 79—48238
EEG, pathological delta waves, cortical electromicrophysiology, cat 78—11626
EEG, pattern-evoked potentials and nerve conduction vel. in family with adrenoleucodystrophy 80—45875
EEG, real time detection of evoked response, expt. 77—44793
EEG alpha rhythm blocking, absence in visuobehavioural deprivation 78—27944
EEG anal. using Parcor coeffs. 78—35822
EEG and volume conduction in brain, influence of elec. spread on linear relationship of activity 77—90933
EEG potential in model of thin cerebral membranes, tangentially orientated dipoles 78—15818
EEG potentials in model of thin membranes of brain, multilayered spherical cable model 77—25408
elastic response in vivo, influence of methylmethacrylate 77—90818
electric stimulation, awakening thresholds in 5 sleep-waking stages, cat expts. 80—85377
electrical activity restoration, transmission problem *(French)* 80—45876
electrical activity study, telemetric technique development 77—60310
electrical response, rel. to brain functioning in health and neurological disease 80—40998
electrical sources, human, 3D localisation, quantitative evaluation 78—92613

brain continued
electrical stimulation of grasshopper brain, elicitation of singing and courtship movements 79—83731
electroconvulsive shock treatment decreases β-adrenergic receptor sensitivity in rat brain 79—79512
EM microelectrode holder for pulsating penetration of brain tissue 80—98199
EM nonionising weak-field interaction with brain tissue, freq. and power windows 80—35974
EMI brain and body scanners, patient radiation dose 79—48341
encephalic exploration, clinical value of single photon emission CT 80—51216
encephalic receptors, photostimulation in sparrows, induction of Zugunruhe 79—24985
enzyme inactivation in rodents using high-intensity microwave irrad. 80—41116
epidural intracranial pressure meas. by piezoresist. transducer *(German)* 78—85404
epilepsy, photosensitive, role of pattern in TV viewing 80—26214
event-related cortical desynchronisation detected by power meas. of scalp EEG 77—81494
evoked frequency stabilisation in cat brain electrical activity 79—34533
evoked potentials, averaged, comparison on basis of spectral and coherency functions 77—2072
evoked potentials, averaged, long-term changes after X-irrad., rabbit 78—11704
evoked potentials, processing, computer techniques 78—92728
evoked potentials, rel. to perception mechanisms 78—11627
evoked potentials, visual and auditory, comparison of signal components 78—44513
evoked potentials and EEG freq. in patients undergoing haemodialysis and kidney transplantation 78—61160
experience neural correlates in single units of cat visual and somatosensory cortex 80—12120
external geniculate body, cat, geometric props. of space of description of images 80—94203
eye movement control in cephalopods, cerebellar-type system 77—12914
eye removal at birth, producing excessive bilateral branching in rat, Co filling method 77—21520
fluorescent retrograde double labelling, axonal branching in ascending raphe and nigrad projections 79—79504
Frohlich's brain wave model, limit cycle stability 77—73520
gamma-angio-encephalographs, enhancement, reduction of statistical fluctuations *(French)* 79—5345
geniculate neurone spatial resolution, impaired by monocular deprivation in kittens 77—21518
geniculocortical system role in form vision, behavioral anal., cat 80—12137
glial-neural interaction demonstrated by Na^+ and Li^+ injection into cortical glia 77—36905
glioblastoma tumour volume monitoring, autopsy rel. to computerised tomography meas. 80—21526
gliomas, malignant, anal. of dose-effect relationship 80—72331
gliomas, malignant, high dose radiation therapy 80—67254
gliovascular interphase in irrad. brain tissue, horseradish peroxidase transport 80—41119
gliovascular interphase in irrad. brain tissue, phosphatases location 80—41120
glucose utilisation meas. by emission tomography 78—69183
grey matter calcification secondary to radiation therapy, computerised tomography evidence 77—56424
haptic perception, cerebral lateralisation, interaction of responses to braille and music 78—7374
head injury model with viscoelastic brain tissue, mech. response 78—69117
head trauma and the EEG, review 80—46076
hemispheric differential activation during complex visuomotor performance 79—16183
higher cortical functions, EEG correlates 79—100591
hippocampal afterdischarges in rats, activity spread by ^{14}C method 80—26221
hippocampal burst-firing neurons, slow inward current, voltage clamp obs. 80—94194
hippocampus, model of temporal sequence memory, simulation studies 77—9181
hippocampus pyramidal cells, somatostatin as excitatory transmitter 78—64973
human, electrical signals systems analysis 77—21504
human brain functions and foundations of science 80—27103
human brain functions rel. to foundations of physics, science and technology 78—73823
hydrocephalus, role of computed cranial tomography and radionuclide cisternography 77—77978
hypothalamic neurone spontaneous firing over narrow temp. interval 78—56961
hypothalamic temperatures, rat, effects of low power density microwaves 79—96619
imager, transverse-section, for single-gamma emitters 80—3794
imaging, comparative study with γ-camera, single-photon emission CT, and transmission CT 80—109004
imaging, using positron camera *(Swedish)* 78—28032
impact response of viscoelastic head model 78—40234
impedance meas., spatial resolution of 4 electrode array 79—84033
impedance scanner principles and exptl. results 79—57804
impedograph, computerised 78—77139
infarction, abnormality of Xe brain/blood partition coeff. and blood flow 80—97993
inferior colliculus neurons, cat, response to binaural beat stimuli obs. 80—72179
inferior colliculus neurons of unanaesthetised bats, echo detect. characts. 77—70484
inferotemporal cortex, role in visual selective attention, monkey obs. 79—100616
injury and instabilities 80—45943
instrumental neutron activation anal. of trace element distrib., rel to blood serum conc. 80—17215
intellectual activity, classification of normal and anomalous forms, quantised-wave theory of coherent brain appl. *(Russian)* 80—76722
intellectual activity, psychoheuristic relationship of psychotism structs. and giftedness structs. introduction, quantised wave theory of coherent brain appl. *(Russian)* 80—76723

brain continued
interconnected neurons system order development 79—53083
interlimb coordination, human, expt. obs., two handed movements 79—57636
intracellular recording from pulsating cerebral cortex 77—48960
intracephalic implants of embryonic neural tissue in rats, neuronal interactions study technique 80—30702
intracerebral currents, contribs. to EEG and evoked potentials 78—92611
intracerebral spontaneous haematoma diagnosis and prognosis by computed tomography 78—73195
intracranial cystic abnormalities, children, computerised tomography diagnosis, review 79—34641
intracranial disorder diagnosis by cerebral sequence scintigraphy 79—92335
intracranial mass lesion detection, computerised cranial tomography and radionuclide imaging 77—77976
intracranial meningioma diagnosis, use computerised tomography 80—17058
intracranial pressure measurement, some considerations 80—17155
intracranial pressure monitoring in neurotraumatology 80—17156
intracranial pressure telemetric meas. *(German)* 78—85403
intracranial tumours, diagnosis by angiotomography 79—48333
intracranial vascular malformations, use of computerised tomography in diagnosis 80—21525
ipsilateral vibrissae in adult rodents, projections on cortical somatic I barrel subfield 80—8074
irradiated, quantitative assess. by computerised tomography scan anal. 80—72306
irradiation, low dose elective, in small cell lung caricinoma 80—67253
irradiation with C ions, recovery from pot. lethal damage, rat expts. 80—72234
isotope distribution reconstruction, error anal. for instrument design 80—3772
juxtasellar tumour radiotherapeutic management, value of computed tomography 77—56450
lateral geniculate body, types of receptive fields and freq. characts. 77—25424
lateral geniculate cells, functional organisation after visual cortex removal in newborn kittens 80—81587
lateral geniculate nucleus, monkey, cell size changes in undeprived laminae after monocular closure 80—16927
lateral geniculate nucleus in cat, struct. of identified X and Y cells 80—26231
lateral geniculate nucleus in dark-reared cats, Y cell loss without cell size changes 80—3644
lateral geniculate nucleus neutron classes, morphological effects of monocular deprivation 77—52781
lateral geniculate nucleus of cat, periodic stimulation, neural activity transient persistence 80—56021
lateral geniculate nucleus postnatal development in humans 80—12114
lateralisation of function, detect. by alpha-contingent visual stimulation 80—94190
laterality effect in isometric and isotonic labial tracking 79—57625
lateralization, induced by infantile stimulation in rat 79—48239
lesion localisation, EEG abnormality obs., computer display system *(Japanese)* 77—5100
limbic spindles, cerebral activity or artifact 78—48778
locus coeruleus neurons, impulse activity in awake rats and monkeys 80—104581
magnetic evoked field mapping 80—104705
magnetic field meas. and personnel selection 79—2026
magnetic fields 80—72182
magnetic fields of dipole in vol. conductor shapes 77—81514
magnetic fields of human brain, somatically evoked 78—48818
magnetic phenomena, central nervous system, book contrib. 79—5304
magnetic response to visual stimulus, monitoring using SQUID 77—29231
magnetoencephalogram genesis mechanisms 78—53432
magnetoencephalogram power spectrum estimation 80—104704
magnetoencephalography, correl. with EEG for normals and patients 78—65062
magnetoencephalography, distrib. of detector sensitivity, reciprocity appl. 80—72278
magnetoencephalography, sensitivity distrib. 80—101246
magnetoencephalography, superconductive helmet with SQUID 80—104708
mammal, brain-cooling system 80—3597
mammalian neuron connectivity estimate 78—77039
mechanism studies using evoked pots. *(German)* 80—61535
medial preoptic lesioned rats, increased survival in mild cold exposure 80—101151
medullary respiratory neuron activity, rel. to tonic and phasic REM sleep 80—97891
memory, retrograde amnesia for old memory, hypothermic obs. 79—83735
memory, short-term, human brain responses, storage component and recall 79—79503
memory retrieval task, event related potentials in young and old adults 80—40992
meningioma irradiation, prototype circumscribed tumour for planning high-dose brain irrad. 78—35925
meningioma scintigraphy, correl. with angiography and pathology 77—56453
metastasis, clinical symptomatology and computerised tomography 79—29584
microtubule solns., calf, dynamic laser light scattering 79—16150
microwave absorbed dose rate distrib. in phantom heads irrad. by aperture source 77—73581
microwave auditory phenomenon, microwave pulse irrad. of animal brain matter 80—35968
microwave effects on blood-brain barrer, review 80—56121
microwave induced hyperthermia and neurochemical correlates, orientation effects 78—24098
microwave irrad. effects on blood-brain barrier function, overview 80—35967
microwave long-term effects on cerebral cortex ultrastruct. of rats, 2.45 GHz 78—40267
microwave rapid fixation device for inactivation of enzymes in rat brain 77—81761
microwave reception, interaction with nerves 77—12958

brain continued
midbrain, similarities between overlapping visual and tactile maps in mammals and reptiles 80—61550
midbrain reticular stimulation, brightness detect., Rhesus monkey 79—43919
midline echoencephalography, automatic histogram prod. system 77—64102
mind and brain relationship, a fundamental theory 79—100592
mitochondria, mechanism of oxidative phosphorylation 79—53068
mixed-system brain dynamics: neural memory as a macroscopic ordered state 79—57622
morphologic alterations in brain-blood barrier of hamster after microwave radiation 77—77935
mouse, effect of high-LET ^{20}Ne on brain, eye and other head structs. 79—66489
mu rhythm detect. from human scalp, functional topography 78—48777
murine brain rapid thermal fixation using microwave device 78—92689
nerve cell communication and second messengers role 78—7337
nerve net theories, tentative contributions of neuroanatomy 79—74625
neural diseases, quantitative EOG and CT obs. 80—36070
neural generator localisation underlying auditory evoked mag. fields, human brain 80—104703
neural lateralisation of species-specific vocalisations by Japanese macaques 79—62268
neurobiology, recognition and classification of struct. by stereology 77—64159
neuromagnetic fields evoked by sensory stimuli 79—83813
neuromagnetic response latency of human visual cortex 78—40151
neuronal DNA damage accumulation rel. to death after whole-brain irrad., rats 80—76804
neuronal membrane process field potentials anal. and synthesis, computer system 80—85374
neuroradiography by NMR imaging 80—51197
neuroradiology, radiation dose to critical organs of staff and patients 80—8184
nonlinear constitutive relations for human brain tissue 77—40707
nonlinear constitutive relations for human brain tissue 78—80910
nuclear medicine, combined static and circulation imaging 80—51211
nuclear medicine conference, Karlovy Vary, Czechoslovakia (May, 1979) 80—12840
nuclear medicine hard-copy image display systems comparison 79—74744
nuclear medicine studies, automated interpretation 80—8164
occipital evoked potential meas. of contrast sensitivity and acuity of conscious cat 78—48803
occipital potentials, pattern and movement detect. in man and rabbit 78—48805
octopus, Eledone cirrhosa, electrophysiology of isolated central nervous system 80—104577
ocular dominance shift failure after monocular occlusion in kittens, brain catecholamines 77—1998
oedema, experimental, serial meas. of specific gravity and 80—98005
olfactory bulb and cortex, spatial props. of EEG event 79—16223
olfactory cortex of guinea pig maintained in vitro, effects of cooling 78—3525
opiate, receptor, synaptosome, EPR study of stereospecific binding of spin labelled morphine 77—9215
optic tectum, goldfish, fine struct. 80—85396
optic tectum, IR and visual integration in rattlesnakes 78—69054
optic tectum movement detecting cell response to change of wavelength, pigeon 78—7348
optic tract and lateral geniculate neurons, spectral responsiveness and temporal freq. response 77—36923
optic tract fibres, physiologically characterised, projection patterns, cat obs. 80—101167
optokinetic responses in brain lesions, EEG and electro-oculographic correlative study 80—8055
parametric stimulation by inductive transducer and US phased array 79—92320
parastriate cortex, cat, rabbit, selective response of single units 79—74624
Parkinson tremor generation, linear modelling of possible mechanisms 80—3615
pattern recognition of human brain electrical potentials 80—109051
pattern separability in random neural net with inhibitory connections 80—76726
perfusion fixation for electron microscopy, press. controlled device 77—44866
pesticide exposure effects on deep brain structures, filtered EEG spike obs. 77—44806
phonocephalography, passive noninvasive technique, normal tracing 77—81618
photic sensitivity of macaque monkey and pulvinar neurons 80—12106
photoelectrode for recording intracerebral cellular Ca^{2+} transients 80—67307
pineal region tumours, radiation therapy treatment results 80—12219
pineal unitary response to light stimulation in frog central nervous system 77—52780
plasticity, effect of early avoidance training on brain development in kittens 79—83734
positron camera using ring detector system, for emission tomography of brain 80—30880
positron emission tomography, appl. to meas. of cerebral metabolic rate 80—3799
positron imaging device for dynamic studies 79—48327
posterior fossa, device for midline angio-tomography 79—34642
posterior fossa tumours of childhood, use of computerised tomography 79—100702
postsynaptic effects of multiaction gaint interneurone on identified snail neurones 77—70448
prenatal brain development, effects of chronic ingestion of ^{3}HOH, rat expts. 80—36004
pretectum organisation, cat 80—12107
primary visual cortex, orientation selectivity development models, normally and dark reared kittens 80—41007
primary visual cortex orientation selectivity development kinetics, normally and dark reared kittens 80—41006
pulsations of third ventricle, mathematical description 77—64081
radiation therapy, appls. of nuclear reactors *(Japanese)* 79—83913
radiography, computerised transverse axial tomography, contrast 77—86608

brain continued

- radioisotope activity concentration after administration of ^{11}C-α-p-iodoanilinophenylacetonitrile 80—3776
- radioisotope imaging, artifact in supine posterior projection 79—34661
- radioisotopic activity, 4-dimens. reconstruction using 200-element detector array of Ge 78—11732
- radionuclide imaging techniques, book contrib. 80—36113
- rat brain ATP, ADP and AMP levels after 2.45 GHz whole-body irradiation 80—3718
- reflectance, mapping technique using optical fibres 80—72381
- reflexes meas., using Sredetz device *(Bulgarian)* 80—30909
- resonance phenomena in the electrical activity of the brain 79—74627
- retina origin from both sides of embryonic brain, optic chiasma crossing problem 79—62250
- retinal ganglion cell functional pathways, book contrib. 79—96559
- retinal ganglion cells, displaced, projection on accessory optic system, pigeon 77—90781
- retino-suprachiasmatic tract, evidence for in the rat 80—21471
- retinocortical projection abnormality of human albinos, vision defects 80—94208
- retinotectal pathway, uncrossed, development rel. to plasticity studies, rat 80—56025
- retinotectal projection development, Gierer-Meinhardt eqns. appl. 80—56022
- retinotectal projection development, mathematical model *(Japanese)* 80—21467
- retinotectal projection in goldfish to an inappropriate region with a reversal in polarity 80—72153
- retinotectal projection orderly compression following partial tectal ablation, newborn hamster 79—74656
- retraction pressure monitoring, meas. system for surgical procedures 80—21563
- RF modulated energy effect on EEG of mammalian brains, acute and chronic irradiations 79—79603
- RF radiation effects on chick brain, induction of Ca^{2+} efflux obs. 80—56127
- rheoencephalographic curves, bipolar and tetrapolar techniques, comparison *(Croatian)* 80—104796
- scintigraphic investigations in neuroradiology *(German)* 80—12242
- seizure discharge autorhythmicity, spike, discharge freq. regulation in focal epilepsy 78—40133
- sella and parasella lesions, sagittal and coronal reconstructs. using computerised tomography 79—39471
- sensual information, problems in matching to brain 80—51114
- short-term recall, phonological interference effect 79—96537
- single optic nerve fibres in Limulus brain, innervation patterns, modified Co staining technique 79—53096
- single unit activity from foetal pig brains, recording method 80—67315
- skull-brain system, human, prolate spheroidal viscoelastic shell containing viscoelastic fluid, axisymm. vibrs. 78—80901
- sleep-waking process, role of anterior raphe and area postrema 77—36906
- solubility and partition coefficients for gases in rabbit brain and blood 80—46116
- somatosensory cerebral evoked potential changes under constant mag. field 79—39383
- somatosensory evoked potentials, elec. stimulation of fingers in random stimulation 78—11628
- somatosensory system afferent signals, modulatory effect of prior input 77—90758
- speech perception, hemispheric specialisation, acoustic change rate, expt. obs. 80—104594
- stimulation and thalamocortical excitability, index of anticonvulsant effect 80—21461
- striate cortex, cat, differential responses of ‘simple’ and ‘complex’ cells during saccades 80—85394
- striate cortex, cat, inhibitory sidebands of complex receptive fields 80—67079
- striate cortex, cat, movement direction detect. and contrast reversal effects, cell response obs. 80—72155
- striate cortex, spatial mapping approach to perceptual coding 80—101168
- striate cortex single cell response, effects of interacting visual patterns, cat 78—7346
- striate neurons in area 17 of Siamese cats, response props. 80—12116
- striate visual cortex, spatial freq. rows 77—32888
- striato-nigral fibres, feedback loop vs. output pathway 77—29136
- superior colliculus, eye movement pots. in awake cats 77—60208
- superior colliculus and frontal eye field ablations, effects on eye movement control 80—72154
- superior colliculus directional selectivity in hamster rel. to strobe-rearing and dark-rearing 78—69052
- supraoptic neurons, rat hypothalamus, osmosensitivity obs. 80—104578
- synaptic plasticity 79—74643
- synaptic proteins after electroconvulsive stimulation 80—56011
- synaptic vesicle ion content determ. by PIXE 78—61166
- synaptosomal membranes, temp. induced struct. rearrangements 77—36877
- T content in organs, and DNA of rat liver cells, after doses of tritiated food, protein or water 80—56226
- tactile information transfer between hemispheres in normal young children 79—83809
- tectal cells, frog, intracellular recordings 79—79525
- telemetry, micropowered multichannel PAM/FM system 77—25618
- thalamocortical non-specific system, auto-oscillatory processes 77—70443
- thalamus anatomical and functional mapping using computer, for stereotaxic surgery 77—37097
- Thermo-Acoustic Sensing Technique for noninvasive tissue analysis 77—64117
- thermocoagulation of brain lesions, Ni-Pd-Mn alloy as thermoseed implant *(Japanese)* 79—61114
- tissue, dog, dielectric props. between 0.01 and 10 GHz 80—16915
- tissue, freq.-dependent US backscatter obs. and correl. 79—79620
- tissue, microscopy cell distributions topographical size analysis, TOGA interactive program *(German)* 77—40951
- tissue elastic response props. in vivo 78—31840
- tissue perfusion rate determ. from ^{15}O activity decay after photon activation 80—26341
- tissue specific-impedance meas. four electrode method 78—3647
- tomography, computer assisted axial, equipment and technique *(Danish)* 77—52862

brain continued

- tomography, transaxial, ring detector positron camera system for research 80—61739
- transverse axial emission tomography, clinical results 77—73557
- tumour, rat, RBE of cyclotron fast neutrons rel. to ^{60}Co γ-rays 80—76797
- tumour cells, rat, anal. of interaction of 2 nitrosourea compounds and X-radiation 80—72230
- tumour cells, Z-ray-BCNU interactions in vitro, isobologram anal., rats 80—81662
- tumour destruction by 8 MHz implanted metal powder eddy currents *(German)* 79—16337
- tumour detection using ^{99m}Tc-glucoheptonate radiotracer 78—20253
- tumour therapy by RF field controlled temp. gradients 77—25522
- tumours contribs. of histograms to computer tomographic study 79—66548
- US 2-dimensional scanning of excised brain, normal anatomy 77—77950
- US diagnosis, use of anterior fontanelle as US window 80—41144
- US evaluation of intracranial pathology in infants, new technique 80—98046
- US imaging through skull 80—51185
- US propagation across meninges, influence of subarachnoid struct., rel. to brain lesion prod. 77—16952
- vagus nerve cortical projection area, discharge pattern of neuronal units during hypoxia 77—25407
- valyl-h-tRNA synthetase of chick embryo brain, ^{60}Co γ-irrad. obs. 80—72222
- vascular permeability, effect of π^- irradiation in neonatal rats 80—26275
- vasculature, late functional changes after local X-irradiation, rat 80—30774
- video biofeedback for alpha monitor 78—20299
- vision, bioelectric recording from human retina and cortex 80—12111
- vision, human recognition system with thinking, model 80—76744
- vision, right hemispheric sensitivity for McCollough effect 77—16934
- vision binocularity affected by sectioning of corpus callosum, of cat 80—97922
- vision of partially visually deprived cats, cortical orientation selectivity 80—26230
- vision suppression by brain 80—97909
- vision with moving eyes, microelectrode studies of single neurons *(German)* 78—53397
- visual areas of mammalian cerebral cortex, book contrib. 79—96560
- visual centres, habituation, dishabituation, and generalisation induced by colour flashes 77—12918
- visual cortex, altered connections in Siamese cat 80—12091
- visual cortex, cat, functionally characterised neurones morphology and intracortical projections 79—74655
- visual cortex, cat, neurons selectively sensitive to changing size 79—100608
- visual cortex, cat, selectivity for spatial freq. and bar width 78—40152
- visual cortex, circuitry changes gated by postsynaptic activity, kitten 79—74652
- visual cortex, critical period interaction, kitten 78—56972
- visual cortex, geometry of orientation columns 79—100601
- visual cortex, neuron specificity acquisition and loss theory 79—83772
- visual cortex, optic nerve, tracts diseases, ophthalmic literature review 79—83762
- visual cortex, optic nerve and tracts, annual review of ophthalmic literature 78—3475
- visual cortex afferent geometry and neuronal trigger features generation, primates 78—35842
- visual cortex area 19 cells, cat, classification by connectivity and photic responsiveness 80—35886
- visual cortex binocularity and binocular summation, cat expt. 80—16946
- visual cortex cat, effects of alternating monocular occlusion 80—16932
- visual cortex changes in uncrossed retinotectal projection after one eye removed at birth 79—57650
- visual cortex development, kitten, monocular astigmatism effects 78—7345
- visual cortex development model for mammals 77—44672
- visual cortex functional specialisation of rhesus monkey 78—80873
- visual cortex local spectral anal., image description model 78—40143
- visual cortex magnification factor rel. to photopic contrast sensitivity of peripheral vision 78—24071
- visual cortex muscarinic acetylcholine receptor and acetylcholinesterase increase on exposure of dark-reared rats to light 78—24069
- visual cortex neurons, cat, mechanisms underlying receptive field props. 79—74662
- visual cortex of cat, neural mechanisms underlying stereoscopic depth perception 80—12147
- visual cortex of cat, spectral characts. of stimuli and responses of complex receptive field 77—16927
- visual cortex pattern evoked pots. and single unit responses, cat 78—27947
- visual cortex receptive field organisation and spatial freq. characts. 78—69068
- visual cortex receptive field spatial freq. characts. rel. to stimulus speed, cat 78—20174
- visual cortex simple cells, spatial resolution and nonlinearities, cat 77—9187
- visual cortical area 19 of cat, periodic complex cells 78—56974
- visual cortical effects of early visual experience 80—12119
- visual cortical neurone orientational prop. recovery and ocular motility in dark-reared kittens 78—53396
- visual cortical neurone reaction patterns to const. illum. 78—80871
- visual cortical neurons, optimality of bar and grating stimuli 80—85391
- visual cortical plasticity rel. to local perfusion of noradrenaline 78—35847
- visual evoked cortical potential, contrast sensitivity meas. of 6 month old infant 77—12913
- visual evoked cortical potential, rel. to dark adaptation, human 77—9192
- visual evoked cortical potentials in men during compression and saturation in $He\text{-}O_2$ 78—61173
- visual evoked potential augmentation/reduction by cortical mechanisms, cat 78—27945
- visual evoked potential distribution, half-field pattern-reversal and pattern-onset stimuli 77—12912
- visual evoked potential evidence of adaptation to spatial Fourier components in humans 78—69051

brain continued
- visual evoked potential to search in short-term memory, late components 78–61172
- visual evoked potentials, cortical extracted pattern response with bipolar and monopolar recordings 77–12919
- visual evoked potentials from occipital and precentral cortex in visually deprived humans 78–3479
- visual evoked response shape self-regulation in man 78–31809
- visual illusion, cortical simple receptive field neurons, spatial freq. response approximating Fourier analyser 79–53089
- visual information processing in brain damage patients, 'extinguished field' 80–30728
- visual mechanisms of the cortex 79–96557
- visual pattern-evoked occipital pots. in blind boy with visual assoc. cortex destruction, pattern-evoked occipital pots. 78–40145
- visual perception and cerebral dominance 78–7372
- visual responses in geniculo-striate and pulvino-extrastriate systems, squirrel monkeys 77–40667
- visual space, neural representation 77–40670
- visual system, primate, subdivisions and interconnections 80–12110
- visual system, signal processing in brain *(German)* 78–48792
- visual system development in cat, role of binocular interactions 80–12117
- visual thalamus, mammalian, neuronal organisation 78–27948
- visual Wulst, barn owl, neurons selective for orientation and binocular disparity 77–1996
- visual Wulst, owl, effect of monocular deprivation on binocular neurones 77–16929
- visual-vestibular interactions, model of cerebellar influence 78–40156
- visually evoked brain potentials, meas. of signal components 77–40946
- visually evoked cortical potentials in renal failure, latency changes 79–16200
- X-irradiation, late changes in biochem. and blood flow, rate expts. 80–72218
- X-irradiation in the therapeutic range, monkeys, delayed damage 80–76801
- B neutron capture therapy of brain tumours, simultaneous flux monitoring system 79–92352
- ^{11}C-flunitrazepam displacement visualisation in live baboon brains 79–83730
- Ca^{2+} intracerebral transients, photoelectrode for recording 80–30961
- Co induced chronic epilepsy, secondary ion microanalysis *(French)* 79–62414
- Li, quantitative location in brain tissue using nuclear Track Etch techniques 80–98133
- ^{6}Li, quantitative microlocation in the brain by a (n,α) nuclear reaction 80–41353
- O$_2$ partial pressure measurement with thin-layer polarographic probe, intracortical appl. *(German)* 78–85410
- T radiation dose absorbed in rat organs, after feeding with organically bound T 80–51262
- ^{99m}Tc labelled DTPA and MDP, compensative value on brain lesion *(Japanese)* 80–67235
- ^{99m}Tc scintigraphy, early and delayed image evaluation 80–3790
- ^{99m}Tc-labelled radiopharmaceuticals, brain uptake by passive membrane transport 80–51053
- Xe regional kinetics meas., imaging methods in transmission computerised tomography 80–98131

brain models
- *see also learning systems; neural nets*
- amygdaloid kindling phenomenon extended first approx. model 78–53378
- bioelectric activity organisation under nembutal narcosis *(Russian)* 78–31795
- brainstem respiratory activity, math. model of computer-simulated neurons 77–44637
- cerebellar cortex associative memory model 77–21506
- cerebellar function, molecular information processing model 78–31759
- cerebellar Golgi-granular system simulation *(Japanese)* 79–29522
- cerebellar model, spatial freq. characts. *(Japanese)* 80–67068
- cerebellum three-layer random neural net with inhibitory connections, pattern separability 78–44498
- cerebral dynamics model, correlation between brain lesion and loss of function *(Spanish)* 79–92205
- cerebral dynamics model, information sources *(Spanish)* 79–29520
- cerebral macromolecules, long-range order models, RF field effects 80–56132
- cognitive neurological functional pattern description *(French)* 77–9186
- cognitron, feedback-type, self-organising neural network with associative memory 78–56962
- communication and control in brain 77–70451
- computational cerebellar cortex model, cat appl. 78–11629
- cortical neurons interactions model, neural net temporal oscillations 80–3636
- cortical spreading depression, math. model 78–80857
- cortical surface interacting neural net model 77–21512
- cortices large-scale simulation via BOSS system 79–2039
- creativity model, alternating intuitive and rational critical phases *(French)* 77–9159
- developing neurons, optimal stimulus distrib. model 77–25419
- distributed type associative memory model with quantised Hadamard transform 80–108867
- EEG potential in model of thin cerebral meninges, radial dipoles and double layers 77–86476
- EEG potential model with thin meninges, multilayer flat cable model 77–36903
- EEG potential source in model with thin meninges 77–56359
- electrical activity patterns detection and anal. using deconvolution and power spectral density methods 78–40386
- electroluminescent, short-lived memory and time param. *(Russian)* 77–52768
- epileptic seizure spatiotemporal patterns, neuronal network model 77–64019
- evoked responses, electrogenesis, models methodology and wavefront reconstruction 77–44627
- Frohlich brain wave model, limit cycle stability, enzyme-substrate reaction 78–44490
- Frolich's brain wave model, limit cycle collapse and travelling wave onset 78–48780
- hemispheric speech organisation in left- and right-handed, test of models 80–8071
- hippocampus CA$_3$ field model, phasic transition, transfer of spikes in statistical neurone ensembles 78–48781
- holographic, for associative memory chains 77–90753
- holographic brain model for associative memory 79–74640
- information theory appl. to large information systems 77–56325
- injury, pulse loading effect 78–57029
- intracortical EEG relationship model *(German)* 79–16180
- large network models using the brain organisation simulation system 79–8496
- lateral-inhibitory neural fields, excitation pattern dynamics 79–5270
- limit cycle model for brain waves 78–3464
- M-cells, logic cct. model to account for CNS inhibition features 78–64917
- magnetoencephalogram and electroencephalogram, comparison of spatial response 80–26245
- McCollough effect neural network model 77–16928
- memory, as process of information transmission, neuronal organisation 77–21503
- memory geometric-dynamic model in four-dimensional pseudoRiemannian space *(Russian)* 78–27923
- memory model, optimal associative recall by an incomplete key 78–96039
- memory neuron, synapse microchem. for memory component of neuroconnective brain model 80–104579
- Morishita neurons, modelling networks, cerebellum appl. 80–30703
- motion after-effect theory, perception mechanism 78–35862
- movement functional hierarchies representation 77–56362
- music pattern recognition, MACSIM neural network 78–7373
- nervous system perceptual mapping and bionic modelling *(Russian)* 78–27921
- neural circuits, math. models of parallel and sequential processes 77–48785
- neural net discrete-time model and applications *(Russian)* 79–2020
- neural nets, double-layer, analysis and simulation with mutually inhibiting interconnections 77–12905
- neural network, aggregation simplifying simulation 79–8497
- neural theory of association and concept-formation 77–52763
- neuron, frequency response characteristics, interactive model implementation and simulation expt. 78–44487
- neuron ensemble distribution patterns in cortex functional states 77–48774
- neuronal models, spike trains, and the inverse problem 77–52764
- neuronal systems synthesis of fragmented data, computer model of cerebellum 79–74645
- normal and anomalous intellectual activity classification, coherent quantum-wave brain model *(Russian)* 78–27922
- ocularity domains and growth behaviour of axon terminals 79–48249
- olfactory bulb, gain mediating cortical stimulus-response relations, nonlinear 80–12165
- olfactory bulb model, spatial and temporal charact. freqs. of interactive neural masses 77–25476
- optic tectum model of various vertebrates *(Spanish)* 78–40144
- pattern separability and the effect of the number of connections in a random neural net with inhibitory connections 79–20532
- planning and problem solving mechanisms 80–45877
- recall and recognition in class of adaptive networks 79–48234
- rhythmic activity generation models *(Dutch)* 78–73150
- scalp potentials, dipole layer model 78–77035
- self-excited wave medium with memory 78–77034
- self-organising nerve nets, fundamental theory, developmental plasticity anal. 80–67062
- sensori-motor spatial development, analytical theory 78–44488
- sensory information processing, parallel and sequential *(French)* 77–12873
- storage system, associative, capabilities comparison with brain function *(German)* 77–29123
- synapse development, selective stabilisation as network specification mechanism 77–16925
- synchronous and asynchronous brain potentials volume model *(Russian)* 77–40652
- synchronous and asynchronous potential, sets structure *(Russian)* 77–36904
- synchronous and asynchronous potentials, space-time organisation formal anal. *(Russian)* 77–52767
- synchronous brain activities, spatio-temporal filter approach 80–61503
- synchronous oscillation in idealised neuronal circuit with recurrent inhibition *(Japanese)* 80–101164
- system functional organisation, methodical approach *(Russian)* 78–35824
- temperature rise induced by EM field 79–29564
- temporal pattern generation in coupled oscillators, Tritonia mollusc trigger group model 79–96538
- temporal sequence memory design based on dentate gyrus anatomy 77–21508
- thalamocortical interaction model for petit mal seizure pathogenesis 79–83759
- third intracranial ventricle dynamic displacement detection 78–57035
- threshold models of reaction latency, properties 78–44440
- vestibular nuclei neurons in goldfish, model with ocular proprioception 78–40142
- vision, cooperative algorithm for computation of stereo disparity 77–5005
- vision, relative motion extraction 78–48794
- visual cortex development model, mammal 78–3483
- visual cortex direction selectivity development model 79–48251
- visual cortex neural circuitry model for orientation sensitivity 79–11927
- visual cortex neurones, rabbit, organisation of background activity 78–69044
- O$_2$ and CO$_2$ tension dynamics, math. model 77–36965
- O$_2$ transport, nonlinear Monte Carlo simulation, hybrid computer implementation 78–40131

brakes
- disc brakes, location of squeaking noise, using laser holography *(German)* 78–37834
- wheel temperature in railroad service, effect of brake shoes 80–93660

braking
see also regenerative braking
EM field of moving wire calc., parallel to infinite conducting slab 80—18959
linear induction MHD machine, elec. cond. body motion in mag. field *(Russian)* 77—7468
spacecraft braking problem in Jupiter atmosphere, ballistic and navigation aspects 80—61981

brass
α and β phases, Hume-Rothery rules for phase stability 79—99292
α-β phase transformation caused by friction 80—76378
γ-phase region, X-ray and electron diffr. obs. 79—61562
abrasive wear, critical grit size effect *(Japanese)* 80—11783
acoustic emission rel. to stacking fault energy 78—14365
acoustic emission signals in plastic deform., amplitude distrib. *(Japanese)* 78—6978
acoustic harmonic generation by long-range dislocation motion 79—42150
admiralty, stress corrosion cracking, in nonammoniacal sulphate solns. 78—27592
admiralty brass, dezincification conditions in fresh or seawater, thermogalvanic method 80—16548
admiralty brass, stress corrosion cracking, aqueous $CuSO_4$ 77—59961
adsorption of Hg, effect on mech. strength, creep, fatigue, embrittlement *(Russian)* 79—29267
anisotropic bend ductility in single phase alloys 78—60726
anneal hardening, of polycrysts. deformed in tension or rolling *(Japanese)* 80—93564
Auger spectral anal. of oxide corrosion films, quantitative methods 78—35557
B2 structure, appl. of Green's temp. function in atomic ordering *(Russian)* 79—51051
Bauschinger AE peak detection of back stress component in flow stress *(Japanese)* 78—6977
bicrystal, α-β two-phase, interface sliding 80—54248
bicrystal, α-β two-phase, plastic deform. and fracture 78—84898
α/β bicrystal, dynamic obs. of fracture phenomena 79—5040
α-bicrystal, grain boundary fracture at intermediate temp. *(Japanese)* 79—15774
bicrystal, two phase α/β, transgranular slip and fracture across an interface 80—81150
bicrystal, two-phase, α-β phase, deform. and fracture at 450K 80—16409
bicrystal, two-phase α/β, diffusion induced twins in α-phase 79—46967
bicrystal, two-phase α/β, morphology and crystallographic relationships between phases 79—46966
bicrystal, two-phase (α/β), interphase boundary sliding at high temps. 80—88164
bicrystals, α-β two-phase interface struct., made by solid state diffusion couple method 79—28214
binding and cryst. struct., valence arguments 80—88081
bonding to rubber, XPS appl. 78—15648
α-brass, $(211)[\bar{1}11]$ single crystal, rolling deform. 77—21174
β-brass, bicrystal and tricrystal stress strain behaviour 77—36607
α-β brass, cold-rolled, energy dispersive X-ray diffr. studies 80—40379
α-brass, concentrated single crystal, yield region investigation, CRSS, slip 77—48478
β-brass, cryst. struct., elastic consts., central force model 78—51637
α-β brass, interface segregation 80—89231
α-brass, recrystallisation texture, rel. to rolling temp. 80—11664
α-brass, single crystal, obstacle strength variation during stress relaxation 78—68723
β-brass, spinodal decomposition, electron microscope and diffr. study 79—78930
α-brass, strength differential effect, temp. and strain rate sensitivity in saturation cycling 79—66094
α-brass, stress corrosion cracking in 15N ammonia solns., fractographic aspects 80—16547
α-β-brass, two phase bicrysts., deform. and fracture at 150K 80—16388
β-brass, uniaxial tension and compression, cyclic stress-strain behaviour 80—97551
β-brass (40 to 50 at.% Zn), elastic shear consts., comp. depend., pseudo-pot. calc. *(Russian)* 80—24525
β-brass bicrystals, shear-incompatible, grain boundary contrib. to Bauschinger effect 80—97550
α/β-brass bicrystals, two-phase, with nearly uniform and thermodynamic equilib. concs. 80—65383
α-brass steels, earing, R-values and 3-D orientation distrib. functions, comparisons 79—91702
α-β-brass two-phase bicrystals, operative slip systems at 150K 79—70119
γ-brass type alloys, faulted defects, nature determ. by image matching technique 78—63777
brass-SiO_2 codeposited film, optical, elec., mechanical and corrosion props. 77—32708
brittle metal, ductility under tension or compression *(Japanese)* 78—35617
brittle to ductile transition under high hydrostatic pressure and high temp. in gamma phase *(Japanese)* 80—35305
burst acoustic emission during Bauschinger effect 77—48475
calorimetric investigation of thermodynamic props. 79—52172
cavitation during superplastic deform. 79—5011
chemical composition in stacking fault tetrahedron in quenched α-phase 77—21183
circular plate perforation and deformation by square section punch 79—34100
coated steel wire, surface composition oxidation, sulphidation, study by XPS 78—11423
coating, vacuum deposition 77—59693
cold rolled, optical, X-ray and TEM exam. of deformation struct., and textures 78—88500
cold rolling, inhomogeneous texture 80—89251
cold worked, or heat treated, or recrystallised wire specimen, damping behaviour *(German)* 78—88489
cold worked, surface composition anal. oxidation, sulphidation by X-ray photoelectron spectroscopy 78—11423
cold worked β-phase, atomic diffusion kinetics to stacking faults 80—19977
condenser tubes of steam turbine, multipositional apparatus of durability determ. *(Russian)* 77—70247
constitutional vacancies in brass like alloys 80—84168

brass continued
contact resistance against metals, for high compressive stress and high current density 77—59324
corrosion, galvanic, anal., coplanar electrodes with radial symm 79—52416
corrosion and dezincification in water 77—16740
corrosion by HNO_3 vap., holographic interferometry 79—3658
corrosion fatigue and stess corrosion cracking in ammoniacal soln. 78—64757
corrosion fatigue in $CuSo_4$-$(Nh_4)_2$ So_4-NH_4OH *(Japanese)* 77—52543
corrosion in acetic acid soln., inhibitive action of thioureas 79—87759
corrosion in HCl, HNO_3 and NaOH, p-thiocresol inhibitor effectiveness 79—57147
corrosion inhibitors, triazole, benzotriazole, naphthotriazole 77—25182
corrosion pretreatment effect on corrosion inhibition 79—100280
corrosion resistance of L68, LMsh68, MNZH 5-1 to scale-removing solns. *(Russian)* 77—59971
crack initiation at high strain rates, uniaxial and biaxial tests 80—85141
crack opening displacement, rel. to flow stress 78—68810
crack propagation properties in rotating bending fatigue tests 77—32669
creep, cyclic, constitutive eqn. under increasing stress condition 80—93593
creep fracture of α-β phase, tensile tests 78—88531
creep of β and β' phases, influence of order *(French)* 79—38921
crystal structure and morphology of thin needle-like martensite 78—31425
cyclic creep and fracture under stress-controlled cyclic conditions 79—74232
cyclic strain induced creep, relation between modes of stress and strain superposition 78—60733
cylindrical shells, thickness determ. by inductive meas. 79—12760
defect removal, obs. by positron annihilation 78—84677
deformation, tension, torsion compression test exam. *(Russian)* 78—31455
deformation and ductility of α-phase single crystal at elev. temps. *(Japanese)* 79—5012
deformation localisation in tension, determ. in type L 80 79—87790
deformation mode during rolling in α-phase *(Japanese)* 79—79001
deformation texture, orientation distrib. function transformation, rel. between recrystn. texture 79—83222
deformed, texture development 79—87653
delamination effects during grinding 79—52470
dezincification testing in laboratory 79—34226
diffused coating on steel from vapour-gas phase *(Russian)* 79—5080
dislocation etchant, $(NH_4)_2S_2O_8$-HCl-H_2O 80—65004
dislocation structure, α-phase, deform. test *(Polish)* 80—24454
dislocation structure around crack tips in early stage of fatigue 78—60830
disordering under γ-irrad., elec. resist. meas., β-phase *(Russian)* 77—48429
drawability correlation with sheet metal texture 78—60683
duplex, α-β, pole figures 79—87818
effect of original grain size on struct. and props., after deformation and annealing 78—44178
elastic constants, third order, from US velocity meas. 78—76687
elastic free energy meas., rel. to localised soft mode theory for martensitic transforms. 78—10159
elastic modulus and internal friction during plastic deform., dislocation props. determ. 80—35244
electrical resistivity due to crit. fluctuations near order-disorder temp. theory 77—40071
electrode, electrical breakdown of water in μs region 80—103917
electrode, in high repetition rate spark switches, surface ageing 80—106997
electroforming, study of process variables in the electromagnetic bulging of tubes 78—80582
electron irradiated, defect production and interdiffusion 78—67739
electron irradiated, positron annihilation, defect recovery 79—74018
electron irradiated, vacancy migration props., effect on enhanced atomic mobility 79—46829
electronic momentum densities by two-dimensional angular correlation of annihilation radiation 78—91605
β' eutectoid, microstruct. obs. 77—36553
failure obs. with optical microscope 78—11472
fatigue, high temp., effect of mean stress 79—20153
fatigue crack growth, stage I, effect of liquid environment fretting fatigue 77—86164
fatigue crack growth micromechanisms at low stress intensities in α-phase 80—108570
fatigue crack propag., role of dislocation substruct., for α-brass 80—60963
fatigue crack propagation, effect of stacking fault energy as deduced from dislocation patterns, TEM study 79—61719
fatigue hardening and high cycle fatigue under reversed bending 79—20180
fatigue of two phase bicrystal 80—108520
FCC, rolling texture development 79—87657
FCC rolling texture origin with rolling plane parallel to $\{111\}$ 79—91674
fission fragment irrad., simulation of reactor first wall enhanced diffusion 79—63810
flat plate, yield surface, biaxial testing machine *(Japanese)* 77—70268
formation by diffusion in multilayer Cu-Zn condensates 78—43186
fractographic obs. of cracks in early stages of fatigue *(Japanese)* 78—7023
fractographic study of early stage fatigue cracks in vacuum in α-phase *(Japanese)* 79—61781
fracture initiation and propagation during strip drawing 78—64663
fracture under influence of high power US waves *(Russian)* 79—5034
free cutting, machinability and mech. props., cooling rate effects *(Korean)* 77—63695
frictional wear, effect of alloying and metal oxide compounds *(Russian)* 78—31541
grain boundary sliding and intergranular cavitation during superplastic deformation in α/β phase 79—5009
grain nucleation, in alpha 70:30 cold worked annealed samples 80—29998
Gruneisen parameter determ. using thermoelastic effect 79—28068
heat treatment of type LMtsSKA 58-2-2-1-1, struct. and props. 79—83239
hot ductility and torsional deformation *(Japanese)* 79—57069

brass continued
- hot stamping type, resistant to dezincification 79—70208
- hydroextrusion, effect of longitudinal US oscills. *(Russian)* 79—34071
- in-depth profiles, non-destructive determ. 80—93836
- inface segregation in α/β two phase bicrystal and polycrystal *(Japanese)* 79—15675
- insert, cast into Pb-Sn alloy, tensile flow and fracture 78—11290
- interface boundaries, TEM procedures for struct. 80—19814
- internal friction and elastic constants in α phase, reson. vibrs. of metal spheres 78—15443
- interphase boundaries, struct. 80—19813
- intracrystalline slip bands in high temp. creep, single crystal, comparison with polycrystalline Cu *(Czech)* 79—77604
- intrinsic stacking fault energy, effect on cyclic hardening 79—11638
- inversion antiphase domain boundaries, in γ-phase 78—6071
- ion beam-produced surface Cu accumulation, ESCA obs. 78—52612
- isotropic plate, noncollinear three phonon interaction 78—66970
- kinetic friction re-examination using modified pin and disc machine 80—55547
- leaded, effect of Al, Sn, Fe on solidification, differential thermal analysis exam. *(Russian)* 79—29041
- leaded brass, mechanical damping in terms of Granato-Lucke theory, comparison with unleaded brass and Cu_3Au 78—95772
- liquid, thermodynamic props. *(German)* 80—66482
- liquid impact erosion and cavitation erosion comparison 80—104302
- liquid metal embrittlement, eval. by quasistatic crack propag. technique 79—29262
- magnetoabrasive machining, optimum conditions 80—30172
- martensite form. and shape memory effect mech. in single crystals 78—19744
- martensite form. in cyclic transform., reproducibilities 77—16582
- martensite stability 79—91650
- martensitic, β, transform hardening and energy dissipation 77—21141
- martensitic transform., short range order effect 79—61586
- massive transform. in presence and absence of special orientation relationships, nucleation kinetics 77—28808
- mechanical damping in leaded and Pb-free, alpha phase 77—63705
- mechanical damping in terms of Granato-Lucke theory, comparison with Cu_3Au and leaded brass 78—95772
- mechanical ratcheting, plastic theory 78—76702
- microscopy of α-brass voiding during high temp. creep 80—16449
- misfit dislocation struct. in interphase boundaries, electron microscope obs. 78—18649
- morphological stability of α/β phase interface, interface moving direction effect 77—15700
- multiphase binary diffusion couple, layer growth rate of intermediate phase, numerical calc. *(Japanese)* 78—14513
- neutron irradiated, α-phase, effect of voids on positron annihilation 79—15553
- Nimonic alloy reinforced laminate composites, low-temp creep singularities, structural defect changes *(Russian)* 80—11696
- nonradial diffuse streaks and complex diffuse scatt. patterns of electrons 79—7527
- order-disorder transformation temperature effect on quench hardening 78—95745
- order-disorder transition, β-brass crit. temps. and exponents rel. to composition 77—8818
- orientation change in (211) [$\bar{1}$11] single crystals during rolling *(Japanese)* 78—60712
- orientation distribution, texturised materials, Ghost effect demonstration 80—70080
- orientation distribution function anal. by superposition of Gauss type scattering functions 79—86735
- oxidation of α- and β-phases, prompt. nucl. reactions and reson. alpha scatt. study 80—66690
- α-phase, fracture behaviour, effect of deform. temp. and alloying content *(Japanese)* 79—20159
- phonon spectra pseudo potential calcs. rel. to long range order and composition *(Russian)* 79—99279
- photocorrosion in $CuCl_2$ and $FeCl_3$ aq. solns. 79—57145
- plane shock wave loading, microdistortion X-ray anal. *(Russian)* 77—52399
- plane stress ductile fracture, prestrain effects in α-phase 80—108532
- plastic, anisotropic hardening pot., stress/strain relation under combined axial load/torsion 78—52896
- plastic anisotropy, thin sheet, α-phase 77—63683
- plastic deform., stress-strain relation of integral type 80—74754
- plastic deform. under complex loading 79—38890
- plastic flow, rate controlling mech. at high temps. 77—81308
- plastic props., room temp. to recrystallisation temp., stress-strain relations, computer program 77—1865
- plastically deformed, phase transforms. and diffusion phenomena *(Russian)* 79—20115
- plastically deformed $\alpha+\beta$ brass, recovery and recrystn., positron annihilation 79—57003
- plate, spreadability of Cd *(Japanese)* 80—29252
- Portevin-LeChatelier effect in α-phase *(Japanese)* 80—11724
- positron annihilation expts., electronic struct. and Fermi surface studies 80—54594
- positron annihilation in α and $\alpha+\beta$ phase, short-range order, clustering and lattice defects influence 79—29107
- prismatic glide, dislocation speed determ., α-crystals 77—59867
- prow formation processes, sliding against mild steel *(Japanese)* 80—35336
- pseudoelastic effects in single crystals 79—47739
- quenched, secondary defect form. during ageing, TEM obs. for α-brass 78—88482
- quenched single crystal, deform. and slip in β-phase 79—79026
- recovery and recrystallisation of plastically deformed α-phase, comparison of positron annihilation, elec. resist. and microhardness 79—52240
- recrystallisation annealing vacuum induction apparatus for tubes 79—57021
- recrystallisation textures, and deformation formed by dry sliding against steel 79—91698
- recrystallization during induction heating 80—97511
- repeated friction contact, form. of thick hardened surface layer 79—39056
- reversible shape memory effect in β_1-phase containing α-precipitates *(Japanese)* 78—60711
- rolling and recrystallization texture as function of Zn-content 79—91676

brass continued
- rolling texture development, dependent on relative stacking fault energy for α-brass 79—52237
- rolling texture development and deform. struct., shear bands effect *(Japanese)* 80—84952
- rubber-brass interface, adhesion failure, XPS study 80—40671
- rubbing of mild steel, magnetic field effect on diffusive wear of cutting tools 80—60985
- serrated yielding, tensile tests and TEM obs. in α-phase 79—34110
- shape memory effect, two-way, and other training phenomena in single crystals 77—48505
- shape memory effect and martensitic transform. depend. on heating-cooling cycles *(Russian)* 80—97482
- shear band, twinning, development during rolling *(Japanese)* 78—39849
- shear bands and recrystallisation in α-phase sheet 79—91680
- shear mode of ductile fracture of material with few inclusions 77—36652
- sheet, in-plane stretching, limit strain meas. 78—80573
- sheet, steel core/steel tube duplex reinforced, fatigue crack growth 77—28894
- sheet metal, texture heterogeneity, numerical simulation *(French)* 78—92274
- signature response, for friction and wear 80—40541
- simulation of rolling and shear texture, using an adapted Taylor theory 78—52835
- sliding contact in magnetic field, model for cross diffusion 79—79121
- slip band growth, thermally activated 80—40457
- solid soln., ductility, comp. effect *(Japanese)* 79—43334
- α-solid soln., intermediate temp. embrittlement *(Japanese)* 79—20158
- solid solution hardening, theory 78—19771
- solid solution range of existence in LANKMts 77—12653
- spark gaps with brass, parallel plane electrodes, erosion characts. 80—70076
- sphere, dissolution in H_2SO_4 in elec. field *(Russian)* 77—4867
- spinodally decomposed, morphology and characts. 80—60863
- spring alloys, microplastic deform. and endurance limit 80—81197
- steel, austenitic stainless, FCC, fractographic obs. of SCC 78—64786
- steel/brass, explosively bonded and roll bonded clad plate, fatigue crack growth *(Japanese)* 79—61706
- steel/brass couple, wear results from talysurf traces 79—52392
- strain at high-speeds, effect on struct. and props. *(Russian)* 77—59855
- strain tempering by rapid heating and cooling of cold drawn wires *(Japanese)* 78—84863
- stress corrosion cracking, effect of strain rate 79—20257
- stress corrosion cracking, in ammoniacal atmosphere, surface stress change and crack growth *(Japanese)* 77—59986
- stress corrosion cracking, intergranular 78—15597
- stress corrosion cracking at low stress intensity factors 77—73362
- stress corrosion cracking at low stress intensity factors 79—29264
- stress corrosion cracking constitution of Pourbaix diagrams for ternary systems by digital computer 78—35595
- stress corrosion cracking in 15 N ammoniacal soln. of 2-phase 79—47802
- stress corrosion cracking in ammoniacal soln., strain rate effect in α-phase 79—91830
- stress corrosion cracking in Mattsson's soln., benzotriazole inhibitive effect in α-phase 80—16554
- stress corrosion cracking in neutral ammoniacal soln., tarnish film role in α-phase 79—96183
- stress corrosion cracking in nontarnishing ammoniacal environment, fractography, chemical anal. 77—40466
- stress corrosion cracking of α-brass single and bicrystals 77—4866
- stress corrosion cracking of α-phase, initiation and propag. stages 77—73361
- stress corrosion cracking of α-phase, X-ray study *(Czech)* 78—85043
- stress corrosion fracture surface anal. by AES 80—104321
- stress corrosion in ammoniacal solns., mechanically assisted dezincification of α-phase 80—3243
- substrate for Al electroplate from $AlCl_3/NaCl$ melt 77—77434
- superplastic deform. rate rel. to flow stress, determ. methods 78—60709
- superstructures and defect obs. in alloys with γ-brass struct. 80—107284
- surface, contact angs. meas., aq. ethanol (glycerine) solns., 20-70°C 78—56025
- surface, heated, water droplet evaporation, heat transfer characts. 78—59269
- surface, Leidenfrost pt. of drops of water (Freons) (carbon tetrachloride) (chloroform), press. effect 78—87784
- surface hardening by electrohydraulic forming *(Japanese)* 80—16571
- surface microstruct. changes on immersion in $CuSO_4+H_2SO_4+HI$ soln. 78—19945
- surface pretreatment effect on joint bond strength by cyanoacrylate adhesive Kanokonlit-E *(German)* 79—57202
- surface reddening during strip reduction process 79—43490
- tensile curve and specific value of anisotropy coeff. *(French)* 77—28867
- tensile tests, -196 to $+20$°C 79—61692
- texture, recrystallised orientation distrib. function comparison with 40°⟨111⟩ rolling texture 80—25723
- texture development, and nucleation in cold rolled 70:30 80—45320
- textured thin specimens, fracture 78—60816
- thermal and elec. cond., 4 to 300K, Zn conc. depend. 80—29379
- thermal conductivity, 80 to 280K, depend. on Zn conc. 77—1405
- thermal conductivity, effect of material on working parameters of cryosurgery instruments 78—36037
- thermal conductivity, electronic and lattice components, separation methods 80—29380
- thermal conductivity, lattice component, 30 to 300K, microscopic mechanisms 80—107758
- thermal conductivity, lattice component, 4.2 to 30K, microscopic mechanisms 80—107757
- thermodynamic anal. *(German)* 80—25663
- two-phase, acoustic emission from β' plastic flow and γ cracking 80—16452
- two-phase superplastic alloy, hydrodynamical behaviour, constitutive law 80—40452
- US attenuation, crit., in β-phase 79—99272
- US velocity, meas. method for isotropic nondispersive solids 80—69616
- vacancy form., ordering effect, positron annihilation obs. 80—93427
- vacancy form. enthalpy, determ. from threshold temp. for positron trapping in vacancies 78—80433
- vacancy formation energies in mixed $\alpha+\beta'$ phase 80—59456
- vacancy formation enthalpy, composition depend., positron annihilation obs. in Cu rich phase 79—95872
- vacuum coating deposition by vaporisation *(Russian)* 79—74093

brass continued
water/brass interface leaky Rayleigh wave reflectivity loss meas. 78—59187
wear, cyclic, on steel 79—52380
wear, rubbing on mild steel, mag. field influence 80—60982
wear and cutting surface against acrylic, epoxy and polyamide resins *(Japanese)* 78—56779
whisker growth in Zn reduction, morphological change to dendrites 79—28261
Whittemore gauge length meas., reliability 77—36669
Widmanstatten α-precipitates, edgewise growth 77—77481
wire, US inspection, immersion method 80—66757
workhardened thin specimens, fracture, anisotropy coeff. role *(French)* 80—104276
yield stress and operative slip systems, orientation depend. β-CuZn 77—48498
yield stress decrease in compression, rel. to previous elongation for brass M63 *(Polish)* 80—50665
yielding behaviour, rel. to low temp. annealing treatment *(Japanese)* 80—93582
yielding of α-β brass two-phase bicrysts., activated slip systems 78—84911
Young's modulus, effective, in isoaxial bi- and tri-crystals 77—90391
AL bearing, alpha phase, high temp. relief cavitation SEM, STEM, TEM, SIMS and EDX anal. 79—5039
Al brass condenser tubes, XPS study of protective layers 80—35383
Al/brass/Al bimetal, three layers, formed by cold rolling, exam. of formation of intermetallic phases at interface 78—56658
Al-brass, clad sheet metal, optimum combination of composing sheets for deep drawing 77—81241
Al-brass tubes, passivation treatment for atmospheric corrosion protection during storage and transport 80—85079
β-brass, nonisoaxial bicrystal, simultaneous hardening and softening 77—36606
Cr-brass bilayer system, optical mechanical and corrosion properties 77—32707
β-Cu Zn, cross slip 78—26576
Cu-brass system, realisation of selective transport mode with friction, effects of normal stresses 79—87735
CuCl$_2$-brass, chemically deposited photosensitive cells, photovoltaic characts. 79—39303
β(CuNi)Zn alloys, effect of normal stress on $\{112\}$ $\langle 111 \rangle$ slip 79—47760
β-(CuNi)Zn, cross slip 78—26576
γCu$_5$Zn$_8$, high pressure effect on brass struct. 80—107108
β-Cu(ZnMn), slip geometry, anomalous strengthening 78—10056
CuZn32 bands, mechanical props. anisotropy after annealing at variable heating rates 77—90364
electrical resistivity, relax. time near order-disorder transition 78—87788
H$_2$ permeability in α-phase 77—62675
Pb effects on plastic deform. 77—44310
Sn-α brass interface, heat flux rectification, rectification coefficient 78—76048
Sn-brass, couple in souring substances, corrosion 79—87760
Ti-brass bilayer system, optical mechanical and corrosion properties 77—32707

Bravais lattice *see crystal atomic structure*

braze bonding *see brazing*

brazing
see also soldering
ceramic ring assemblies, brazing techniques for TFTR injector and pumping ports 80—32476
electron probe microanalysis for high-temp. applic. *(French)* 77—29074
filler metal, deformation mechanism at brazed joint 78—80616
fusion reactor, TFTR, large section water cooled Cu conductor, brazing joints 80—91260
glow discharge as welding heat source, appls. 79—73051
high-temperature, kinetics of filling capillary gaps obs., by X-ray cinematography 77—5954
JET Tokamak toroidal field coil manufacture 79—31206
materials processing in Spacelab 78—35295
particle beam accelerator grid assemblies, 120 keV, fabrication and brazing 78—66379
permanent joining techniques 80—82782
steel, C, brazed joint, corrosion mechanical strength 79—43491
steel, low-alloy Si-Mn, uphill diffusion of C, at brazed joint with pig Fe 78—44280
steel, stainless, with Ni base filler metals, brazed joint strength *(Japanese)* 80—16636
steel, stainless and plain C, brazed joints used in thermal power plants, corrosion resistance 79—43492
transition metal alloys, binary eutectic, props., thermionic converter appls. 77—90236
Be lightweight optical substrate fabrication 79—23107
Mo alloy VM1 to stainless steel 1Kh18N10T 79—43551
Ni-Cr-Ti-Al/Au-Ni brazed joint, high temp., AE under elev. temp. and loading *(German)* 78—31597
n-Si, *p*-type regrowth layer formed by brazing with metal support disc, diode appl. *(Japanese)* 79—15833
TiB$_2$-Al$_2$O$_3$, thermal stability of composite materials 78—60638
TiB$_2$-CaO, thermal stability of composite materials 78—60638
TiB$_2$-MgO, thermal stability of composite materials 78—60638
TiB$_2$-Y$_2$O$_3$, thermal stability of composite materials 78—60638
ZnS/ZnSe composite window, erosion-resistant, fabriction and evaluation 78—71211

breakage *see fracture*

breakdown (electric) *see electric breakdown*

breakdown (mechanical) *see manufacturing processes*

breakdown diodes *see avalanche diodes; Zener diodes*

breeder reactors *see fission reactors*

bremsstrahlung
see also electron radiation; gamma-ray spectra; gamma-rays; X-ray emission spectra; X-rays
Abell 2256, rich cluster, steep-spectrum radiosource obs. 79—9016
afterglow discharge, electron-atom bremsstrahlung, time decay 78—63620
Alfven wave accelerated particles, bremsstrahlung radiation losses rel. to self-similar soln. for distrib. function 80—56702

bremsstrahlung continued
alloys, effective atomic number from β-ray produced bremsstrahlung meas. 78—22046
Ar plasma jet, emission of electron-neutral atom bremsstrahlung *(French)* 78—26332
Ariel 0620—00, transient X-ray source, continuous spectrum as thermal bremsstrahlung 78—12426
atmosphere bremsstrahlung produced by precipitating electrons, theoretical characts. 79—66862
atom, bremsstrahlung of electrons allowing for polarisability *(Russian)* 77—3475
atom, electron impact, bremsstrahlung orientation and alignment parameters 78—33628
atom, Kβ/Kα ratio anomalies, K-capture rel. to bremsstrahlung excitation 77—18825
atom, scatt. of nonrelativistic electrons, bremsstrahlung cross section *(Russian)* 77—88575
atom electron bremsstrahlung energy spectra above 2 MeV, partial wave interpolation 79—72416
atom-electron collision, atomic electron contrib. to bremsstrahlung *(Russian)* 77—79694
atomic electron scatt., bremsstrahlung spectra *(Russian)* 78—37744
atomic ions, electron impact, 1 to 100 keV, bremsstrahlung emission, theory 78—22005
atomic photoeffect, K-shell, radiative corrections and HF end of bremsstrahlung spectrum 77—23477
Auger peaks, bremsstrahlung-induced, utility in spectroscopy 79—30618
Auger peaks, bremsstrahlung-induced 80—45199
auroral bremsstrahlung X-ray flux comp. 77—60508
auroral X-ray bremsstrahlung rel. to VLF emissions 78—45106
auroral X-rays, balloon obs. in Canada rel. to X-ray illuminating regions determ. 80—31156
auroral X-rays, visible arcs and precip. primary electrons, satellite correlated obs. 79—35029
axion production search in low energy electron bremsstrahlung 79—63401
beta-induced bremsstrahlung spectra and average energies, analytic calc. method 80—22985
betatron, 5 MeV, ang. distrib. and penetrating power 78—70657
betatron bremsstrahlung field shaping apparatus for teletherapy 78—57062
Bethe-Heitler cross section formula, intermediate energy approx. 77—54126
binary collisions, inverse bremsstrahlung absorpt. in strong radiation field 79—89788
binary inelastic collisons, inverse bremsstrahlung absorpt. in large radiation field, Born approx. calcs. 78—42222
biological material photon interactions, calc. of average energy absorbed 80—45947
Brown-Goble soft photon approx. 80—95777
bulk media, shielding study, Monte Carlo anal. of thick target spectra 78—59839
cascade showers, three-dimens., Landau-Pomeranchuk-Migdal effect 78—49993
channelled electrons, characteristic radiation, sharp lines obs. 80—65111
channelling, spontaneous radiation, coherent bremsstrahlung and synchrotron radiation 80—6446
channelling coherent radiation and bremsstrahlung 80—65079
circular polarisation of bremsstrahlung, from longit. polarised electrons in single nonmag. crysts. 78—15242
classical gravitational bremsstrahlung, wave generation 78—93093
classical stimulated bremsstrahlung, electron beam bunching 80—69306
clusters of galaxies, X-ray temps. rel. to bremsstrahlung and emitting gas mass 77—91668
coating thickness measurement using bremsstrahlung radiation from monoenergetic fast electrons 77—77609
coherent bremsstrahlung, energy and momentum spectral function 80—22546
coherent bremsstrahlung from polarised electrons, asymmetry coeff. *(Russian)* 78—92139
coherent EM radiation intensity, produced by modulated electron/ion beams in gas 78—50686
coherent EM radiation of modulated beam of charged particles 77—19149
coherent radiation from modulated electron beam in residual gas 77—594
colliding beams, effect of external field on bremsstrahlung 77—74670
computer program for calc. ang. distrib. of nonrelativistic bremsstrahlung intensity 78—87001
conference on few body systems and nuclear forces, Graz, Austria (Aug. 1978) 79—67567
cosmic ray electrons in closed galaxy model, bremsstrahlung rel. to gamma ray flux 77—13189
Coulomb electron atom scatt. in laser field, asymptotic dynamics 79—94084
Coulomb field, high-energy bremsstrahlung and pair prod. 78—4811
crystal, relativistic electron and positron bremsstrahlung *(Russian)* 79—61459
V1500 Cygni (Nova 1975), continuous energy distrib., IR obs., thermal bremsstrahlung 79—80315
Debye shielding corrections for 1- and 2-photon cross sections 80—106157
deconvolution method for X-ray spectra from hot plasma 80—54030
diamond, low-energy γ-ray anomalous yield produced by 800 MeV electrons, collimation effect 79—91521
diamond crystal, radiation of channelled 800 MeV electrons 79—61274
dielectric trapping, bremsstrahlung shielding meas. 78—78507
dose measurement around 1000 MeV bremsstrahlung beam incident on Pb and W thick targets 77—9265
double bremsstrahlung in e-nucleus Coulomb scatt. *(Russian)* 77—50117
double bremsstrahlung of soft photons *(Russian)* 77—31052
double internal bremsstrahlung in electron capture decay of ^{37}Ar, ang. correl. meas. 78—25157
Drell-Yan formula in QCD, lepton pair prod. 78—33025
elastic scattering and bremsstrahlung theory of fast charged particles in crystals *(Russian)* 79—28853
electron, coherent, on thin diamond monocrystals, polarisation *(Russian)* 77—6603
electron + atom, 1-500 keV, bremsstrahlung ang. distrib. prediction 79—41312

bremsstrahlung continued
electron and photon transport, SANDYL program, statistical accuracy, optimisation 77−8675
electron beam, relativistic, strong mag. field, transverse energy determ. by bremsstrahlung 77−62344
electron bremsstrahlung due to atoms and ions, static approx. calc. *(Russian)* 77−75308
electron bremsstrahlung spectrum, sharp γ-lines present 77−82846
electron bremsstrahlung spectrum in point Coulomb field, classical and nonrelativistic quantum theory 78−65792
electron bunching, scattering and bremsstrahlung in cryst. lattice in strong EM field 80−65113
electron high-energy collisions, mag. field effects *(Russian)* 77−61906
electron neutral inverse bremsstrahlung in electron beam sustained discharge 78−63604
electron probe X-ray microanalysis, quantitative investigation of thin specimens 80−101068
electron scattering by Coulomb potential in Born approx., bremsstrahlung statistics 80−5665
electron scattering from atoms, bremsstrahlung cross-section, near HF limit 79−18288
electron storage ring, vacuum system for synchrotron radiation source 79−63830
electron streams, thick-target, relax. and bremsstrahlung, Legendre expansion, solar X-ray flares appl. 79−70950
electron to positron conversion efficiency, 20 to 70 MeV 77−23335
electron-atom-bremsstrahlung standard radiometric source improvement 78−67484
electron-ion bremsstrahlung with shielding 78−66667
electron-ion collisions, stimulated multiphoton bremsstrahlung 79−19007
electron-ion plasma, stimulated bremsstrahlung light absorption *(Russian)* 78−87438
electron-photon cascade simulation by Monte Carlo programs 79−54330
electron-photon cascades, Monte Carlo simulation of cascade development 79−44322
electron-sheath collision, laser absorpt. inverse bremsstrahlung prod. 77−58877
electronic oscillations in relativistic plasma, hydrohydrodynamic model *(Russian)* 78−79434
energy deposition as function of converter foil thickness 77−23388
energy flux unit, 0.8 to 8 pJ, USSR special standard 77−30730
energy spectra, 1 to 2000 keV, neutral atoms Z=2 to 92 78−62920
fast-pulsed electron beam energy meas. using bremsstrahlung absorption spectroscopy 78−49940
field interface of moving particles in statistically inhomogeneous medium 79−6063
filtered spectra, equivalent half-value thicknesses and mean energies 80−46011
filtered spectral source for radiological studies 77−77969
flare stars, fast electrons nonthermal bremsstrahlung rel. to flare emission spectrum 80−67731
flaw detection systems based on semicond. detectors and scintillation crysts. for hard bremsstrahlung 79−11748
flow detectors, radiation type, electron bremsstrahlung irrad. field dia. calc. 78−56857
free electron laser, collective and single electron interactions, book contrib. 79−27234
free electron lasers, mag. bremsstrahlung, Compton and Cherenkov, types *(Chinese)* 79−31851
free-free photoabsorpt. of electron-atom systems 78−62770
free-free transitions, mutiphoton, energy absorption laser pulse shape-independ. 80−43184
free-free transitions in quantum electronics 80−28183
galactic disc, bremsstrahlung gamma radiation emissivity and local interstellar electron spectrum 79−25417
galactic disc, non-thermal electron bremsstrahlung rel. to gamma-rays prod. 78−24414
galactic disc gamma-ray emission, 80 keV to 8 MeV obs. rel. to bremsstrahlung contrib. 80−82540
galactic electron spectrum below 1000 MeV 79−5718
galaxy clusters, X-ray luminosity function, predictions from thermal bremsstrahlung model 79−101208
galaxy clusters X-ray emission, thermal bremsstrahlung model rel. to intracluster Faraday rot. obs. 79−75285
Galaxy gamma-ray emission, fluxes determ. from cosmic ray electron spectrum 80−62257
gamma, from thin target of betatron 80−86999
gamma quanta and high-energy electron transport in matter, secondary bremsstrahlung *(Russian)* 77−63479
gamma-rays generation by fast electrons travelling through antiferroelectric or antiferromagnetic crystalline structures 78−76545
global structure of space-time, classical bremsstrahlung problem 80−105547
gluon bremsstrahlung and multiperipheral cluster models 79−22082
gravitational bremsstrahlung, from orbiting point masses, post-Newtonian theory 77−13226
gravitational wave generation by stellar encounter, bremsstrahlung formulae 78−4096
gravitationally induced EM bremsstrahlung 78−24991
graviton, improved gravit. coupling of scalar fields 79−49151
hadron multiprod., long-range correl., overlapping independent emission 78−82141
hadron-hadron, e^+e^- pair prod. calc., high energy internal conversion of bremsstrahlung photons 79−420
hadron-nucleus collisions, bremsstrahlung analogy effects for particle prod. 77−14098
Hamilton-Jacobi equation solns. in Coulomb pot. and quasiclassical approx. 80−46765
HB 3, supernova remnant, H thermal bremsstrahlung model for soft X-ray spectrum 80−56915
heavy ion-nucleus reactions, reaction mechanism anal. using γ-ray bremsstrahlung spectra 79−76016
AM Herculis, grey body magnetoemission as source of linear and circular polarisation 78−8053
HF discharge in inert gas, optical diagnostics, bremsstrahlung 78−9871
HF spectral region, radiative corrections 77−58242
Higgs boson, bremsstrahlung prod. with heavy fermion pair in e^-e^+ collisions 78−86449
high current short bremsstrahlung pulse sources 80−5400
high frequency cross section limit for neutral ats. and ions 79−27142
of high-energy particles in EM excited medium 77−19147

bremsstrahlung continued
hydrodynamical models anal. 78−8617
inclusive processes, bremsstrahlung approx. 77−50033
inert gas, HF discharge continuous emission, radiation standard 80−1856
inert gas discharge, moderate press., visible and UV radiation spectrum 77−31533
inert gas glow discharge, origin of visible continuum radiation, bremsstrahlung theory 77−62421
influence on γ dose buildup factors rel. to penetration depth *(Russian)* 79−13542
infrared radiation in potential scattering 80−42098
insulating materials, high energy radiation effects 80−19835
intensity distribution at origin in thick W target by attenuation anal., 60 to 140 kV 77−34060
internal bremsstrahlung in s-electron capture 80−63133
inverse bremsstrahlung, for $\gamma + e_1^- + Ze \to e_2^- + Ze$, Born approx. *(Russian)* 78−13064
inverse bremsstrahlung, high energy, nucl. mag. contribs. 78−74350
inverse bremsstrahlung absorption intensity depend., in inhomogeneous standing wave, laser fusion appls. 78−67382
inverse bremsstrahlung at high energies, coherence effects in crystals 77−48267
inverse magnetic bremsstrahlung around the electron-cyclotron frequency 79−27781
ion+electron collision, resonant electron bremsstrahlung *(Russian)* 80−102580
ion electron scatt., series expsn. for intensity components 78−50648
ion-induced X-rays, review 79−96405
ionosphere, X-ray flux depend. on precipitating electrons energy spectrum 78−40744
ions, electron impact, nonrelativistic bremsstrahlung intensity components 79−72426
isochromat spectroscopy using a modified XPS apparatus 79−35912
JIPP-T-II Tokamak plasma, time resolved spatial profiles of impurities 80−48950
kerma partition to account for energy deposition in matter 79−66482
Langmuir waves, turbulent bremsstrahlung process 80−62009
laser plasma, free-free X-ray bremsstrahlung prod., intensity and polarisation anisotropy 77−89320
laser possibility in soft X-ray region 77−646
laser solenoid radiation test facility 77−83430
laser-gas interaction, neutral atom inverse bremsstrahlung, laser induced electron avalanche *(French)* 78−26309
laser-heated plasma, energy deposition, bremsstrahlung spectra calcs. 77−3968
laser-heated plasma, energy deposition, Gaunt factor calcs. 77−7576
laser-heated plasma, energy deposition, suprathermal electron calcs. 77−7577
laser-induced bremsstrahlung beyond the dipole-approximation 79−3615
laser-produced plasma, X-ray bremsstrahlung and fast ion meas. 78−5936
lepton pair photoproduction, neutral weak current consequences *(Russian)* 78−12899
lepton-hadron inelastic scatt., bremsstrahlung of gluons *(Russian)* 77−2839
lepton-nucleus scattering, bremsstrahlung and neutral currents 80−32268
linear polarisation enhancement of bremsstrahlung in crystals, spin effects 79−11359
low-energy theorem for soft-photon end pt. from elastic scatt. 78−17796
low-frequency approximation for scattering in a laser field 79−92996
lowest-order EM correction in point particle scatt. 77−87978
LW, evaluation of calibration constants of ionisation detector 79−68147
M87 halo, thermal bremsstrahlung contrib. to X-ray emission from Faraday rot. 80−67844
magnetobremsstrahlung and optical polarisation in white dwarfs 77−45417
magnetosphere conjugate electron precipitation, high time resolution riometer and X-ray meas. 80−41666
massive lepton pairs, bremsstrahlung prod. in QCD, gauge invariance effects 77−74650
massive photon magnetic bremsstrahlung *(Russian)* 78−41461
meson resonances in nuclear field *(Russian)* 78−78424
metal surface plasmon light emission due to low energy electron irrad. 80−34997
molecular electron resonance scatt., bremsstrahlung *(Russian)* 78−37752
monochromatic photon beam generation by high energy electron beam *(Japanese)* 78−74821
multiphoton bremsstrahlung process in presence of laser beam, cross-section calcs. 77−34797
multiphoton inverse bremsstrahlung, plasma laser absorpt. coeff., correspondence principle method 79−32749
multiquark systems in Feynman's bremsstrahlung analogy, Regge intercepts 79−97590
muon, cross-section corrections necessitated by target excitation 78−4931
muon, in collisions with nonpointlike nuclei 78−8803
nanosecond pulse electron and bremsstrahlung generator 78−21308
neutral atoms, bremsstrahlung of low-energy electrons, polarisation effects 80−102577
neutral atoms, high freq. limit, effect of resonance scatt. 79−31473
neutral atoms, high freq. limit 79−31472
neutrino and photon pair prod. in strong mag. field 78−407
neutrino bremsstrahlung by degenerate electron gas, neutral current effects, stellar interiors appl. 77−13225
neutrino bremsstrahlung in an intense magnetic field 79−30055
neutrino-bremsstrahlung, neutral current effects in Weinberg model 77−65150
neutron activation anal., self attenuation of neutrons and gammas, Monte Carlo determ. 79−1980
neutron production by electron linear accelerator beam, bremsstrahlung and (γ,n) processes *(Japanese)* 78−78532
neutron secondary spectra prod. by high energy bremsstrahlung in C, N, O and tissue 80−41239
neutron star, neutrino-pair bremsstrahlung in hot plasma, strong mag. field 78−61878
neutron stars, neutrino-pair bremsstrahlung in collisions between neutrons and nuclei 77−74789
nonrelativistic bremsstrahlung, program determ. of ang. distrib., extension to high freq. 79−64162
nuclear excitation and target recoil effects *(Russian)* 77−26677

bremsstrahlung continued
- nuclear fireball model, low energy bremsstrahlung cross-sections in relativistic heavy-ion collisions 77—54253
- nuclear levels, mean life determ. by reson. fluoresc. under bremsstrahlung bombardment *(French)* 77—54179
- nuclear reactions, meas. of reaction time using bremsstrahlung emission *(Russian)* 79—49613
- nucleon-nucleon bremsstrahlung expts. review, comparison of results with theory 78—62447
- p-p bremsstrahlung, forbidden asymmetries and choices of geometry 79—58972
- parity nonconservation due to neutral currents 77—6076
- particle production, comments on Brodsky and Gunion model 79—93362
- particles accelerated by Alfven waves, distrib. function self-similar solns. 79—32757
- pellet, laser irrad., absorpt. and refl. processes 78—30457
- Perseus cluster, hard X-ray obs. 77—13493
- photon-nucleus reactions in nuclei with A=27-238, 450 MeV to 2.2 GeV *(German)* 78—33164
- PIXE anal. of insulating samples, reduction of bremsstrahlung background 79—20489
- PIXE trace element anal., new method to determ. concentrations 78—76966
- plasma, bremsstrahlung of fast particles, collective effects 79—10645
- plasma, collisional absorption of two laser beams, inverse bremsstrahlung 78—26292
- plasma, electron density and temp., spectroscopic diagnostics, book contrib. 77—51242
- plasma, electron energy spectrum, local meas., X-ray method 78—9842
- plasma, H_2, underdense, CO_2-laser radiation filamentation 80—14941
- plasma, highly ionised, bremsstrahlung, stimulated, multiphoton, electron-electron collisions effect 77—76039
- plasma, in mag. field, electron distrib. depend. of linear polaris., diagnostics *(Russian)* 77—47158
- plasma, in strong mag. field, bremsstrahlung by relativistic electrons *(Russian)* 77—62393
- plasma, inverse bremsstrahlung, EM fields effect 77—68833
- plasma, inverse bremsstrahlung for intense radn. fields 78—51288
- plasma, inverse-bremsstrahlung absorption rate in an intense laser field 80—24201
- plasma, laser induced, bremsstrahlung emission, X-ray diagnostics, review 77—55176
- plasma, laser-produced, electron energy from continuum X-ray emission 78—22563
- plasma, laser-produced, spherically symmetric absorption (reflection), simulation 78—51285
- plasma, magnetised, bremsstrahlung emission coefficient in the dipole approx. 80—19562
- plasma, nonequilib. weakly ionised, electron-electron bremsstrahlung, time depend. 77—11323
- plasma, turbulent, anomalous EM wave electron radiation 80—43889
- plasma, X-ray bremsstrahlung polarisation and anisotropy, evidence of suprathermal electron fluxes 80—103193
- plasma density plateau effect on inverse bremsstrahlung 80—43894
- plasma diagnostics, using multichannel X-ray spectrometer 80—57445
- plasma electron temp. meas. by soft X-ray energy anal., pulse pileup effects 79—64910
- plasma expanding into vacuum, bremsstrahlung radiation intensity *(Russian)* 79—7448
- plasma heating by laser beam, radial expansion effect, quasistatic model 79—37520
- plasma illuminated by strong optical field, electron stimulated bremsstrahlung 78—59623
- plasma spectrum, mag. field effects 78—67323
- plasma strong field inverse bremsstrahlung, Lorentz model 77—35327
- plasma temperature from recombination continuum, bremsstrahlung emission 79—50887
- plasma-laser inverse bremsstrahlung heating, Coulomb screening effect 79—68940
- polarisation, lepton and photon nuclear interactions, bremsstrahlung, pair production *(Russian)* 77—88104
- polarisation of coherent bremsstrahlung at nonaxial collimation 77—20950
- polarisation-frequency characteristics for monoenergetic electron beam in Coulomb potential 80—95778
- polarised bremsstrahlung and optically active molecules 77—63938
- polarised electron bremsstrahlung γ-quanta from ultrarelativistic electrons in mag. field *(Russian)* 78—46502
- polarised electrons, azimuthal asymmetry due to spin-orbit coupling 80—60705
- polarised superhigh energy electron prod. in magagauss mag. field *(Russian)* 78—42270
- positron bremsstrahlung, anomalous reduction in single cryst. 80—7433
- quantum optics, phase relations, bremsstrahlung struct. *(Russian)* 78—74870
- quark charge meas. from deep inelastic bremsstrahlung *(Russian)* 78—41555
- quasiclassical limit 77—67606
- radiation absorption in magnetoplasma, rel. to laser fusion 80—92273
- radiation from a uniformly accelerated charge 80—31495
- radiative energy loss of electrons in thick layers of material, interpolation formulae 78—21829
- radiative power loss, from plasmas in steady state ionisation balance 79—82063
- radiobiological experiments, lightly filtered X-ray spectra generated at 200 to 300 kV 80—72397
- rare earth metal, 4f levels, obs. by bremsstrahlung isochromat and XPS spectroscopy 79—24411
- rare earth metals, density of 4f states below and above Fermi level, XPS and bremsstrahlung isochromat spectroscopy 80—76140
- rare earth metals, XPS and bremsstrahlung isochromat spectra of f^{n+1}, f^{n-1} states 80—40220
- reactor shielding materials, Pb and steel, 6 MeV γ penetration bremsstrahlung 78—58350
- reflectivity and temp., scaling laws 80—87913
- relativistic electron beam, tightly pinched streak camera obs. of X-ray bremsstrahlung 77—49818
- relativistic electron beam deposition, field-enhanced, bremsstrahlung prod. 78—29677
- relativistic electron beam diode, anode scatt. effects on electron pinch radius 77—68877

bremsstrahlung continued
- relativistic electron bremsstrahlung on nucleus, screened Coulomb potential effect *(Russian)* 78—46050
- relativistic electron collision with heavy ions 78—75376
- relativistic electrons instability in plasma *(Russian)* 78—47103
- relativistic electrons near nucleus in mag. field, soft photon approx. *(Russian)* 77—46676
- relativistic gyratron, coherent microwave mag. bremsstrahlung, general theory of masers *(Russian)* 78—1141
- relativistic high current electron beam parameters from bremsstrahlung yield meas. 79—93861
- relativistic particle beam in crystal, collimation, cooling 80—42885
- relativistic particles, energy loss in solids 80—39188
- relativistic particles motion and radiation in electric and mag. fields, gravitational field effects *(Russian)* 79—97269
- relativistic positron and electron bremsstrahlung under conditions, theory 79—19301
- resonance absorption, in laser-produced plasma, X-ray bremsstrahlung emission obs. 78—59559
- resonant electron-electron bremsstrahlung in EM wave field *(Russian)* 80—52488
- Rochester cross section, bremsstrahlung study, soft photon region 78—62401
- scalar one-loop integrals, soft bremsstrahlung and radiative corrections 79—75682
- scattered gamma ray spectra, bremsstrahlung contribution from low energy electrons 80—78192
- V818 Scorpii (Scorpius X-1), bremsstrahlung, model for UV continuum energy distrib. 80—82541
- secondary bremsstrahlung, contrib. in gamma quanta transport problems 79—40782
- soft auroral bremsstrahlung and K_α line emission 77—87153
- soft photon expansion and theorem, bremsstrahlung cross section 79—17728
- soft-photon anal. of πp bremsstrahlung 78—25076
- solar flare transmission region radioemission, role of thermal bremsstrahlung *(Russian)* 79—48763
- solar flares, polarisation and directivity of hard X-ray bremsstrahlung from thermal source 80—90374
- solar flares fast electrons scatt. in atm., X-ray spectrum 78—77542
- solar flares nonthermal electron beams, reverse currents effects on dynamics and X-ray bremsstrahlung 80—51711
- solar flares X-ray spectra, use of a priori information in derivation of temp. structs. 78—20778
- solar hard X-ray bursts, thermal bremsstrahlung model with collisionless cond. front 79—44427
- solar impulsive X-ray bursts, polarisation, directivity and spectrum of bremsstrahlung radiation 78—4160
- solar microwave bursts, source, energetic electrons *(Russian)* 79—21258
- solar radio emission S-component, local sources struct. 80—46528
- from solitons 77—59240
- source spectra anal. in terms of integral moments, solar hard X-ray burst appl. 79—16810
- spatially resolved suprathermal X-ray emission from laser-fusion targets 80—48984
- spontaneous electron bremsstrahlung in field of intense EM wave *(Russian)* 79—3616
- stars with extended envelopes and mass outflow, radio emission 77—74063
- stellar atmospheres, H_2 and N_2 free free absorpt. rel. to opacity 78—81610
- stimulated bremsstrahlung, high intensity, convergence of approx. 78—16687
- stimulated emission, resonator consideration *(Japanese)* 80—5721
- stimulated linear acceleration bremsstrahlung 79—92658
- stratosphere, energetic radiation belt electron precip. natural depletion mechanism for O_3 77—41134
- substorms, satellite obs. of impulsive bremsstrahlung X-ray events, electron precip. 79—2438
- surface electron state characterisation by X-ray techniques 77—55868
- synchrotron spectral tip calc. refinement, transition rates for mag. bremsstrahlung, computing techniques 79—49430
- thick target, spatial distrib. of energy transfer meas. with miniature dosimeter 78—15897
- thin solid target, proton bombarded, secondary electron bremsstrahlung, directional anisotropy 77—69953
- 4U 1700—37 (HD 153919), high-energy obs. rel. to thermal bremsstrahlung X-ray spectrum 80—86014
- UHF nonequilibrium plasma diagnostics by atomic bremsstrahlung continuum 78—67483
- ultrarelativistic beam quasilinear relativistic plasma relax. in strong mag. field, magnetobremsstrahlung *(Russian)* 80—38669
- ultrarelativistic charge collision with atom or diatomic mol., X-ray emission *(Russian)* 78—70776
- ultrarelativistic charge in absorbing plate, radiation taking into account multiple scattering *(Russian)* 77—41792
- ultrarelativistic electrons in single cryst., accel. by bremsstrahlung photon absorpt. 79—56879
- universality of multiplicity distrib., hadronic bremsstrahlung 78—70419
- vector particle in nucl. field 80—37198
- water, distrib. in water, Al, Fe and Pb, 22 MeV electron bombardment 78—59840
- water and water-iron, 22 MeV electron bombardment, spatial distribs. of bremsstrahlung meas. with activation detectors 77—57754
- X-ray bremsstrahlung from energetic thermal and nonthermal electrons 77—49364
- X-ray emitting gas in clusters of galaxies, bremsstrahlung cooling evolution 79—40266
- X-ray intensity, microfocus source, non-linear rise studies 80—77927
- X-ray spectra computation rel. to Ge(Li) detect. meas. spectra 79—52047
- X-ray spectra stripping up to 300 kVp on desk type computer 79—83846
- X-ray spectral composition following backscatt. from semi-infinite reflectors 77—54028
- X-rays emitted from electron cyclotron reson. plasma, degree of polarisation 80—87944
- XPS Auger lines, generation by bremsstrahlung 80—87174
- yield produced by 4 MeV linear electron accelerator, calc. rel. to hazard in radiolysis 79—76181
- $^{12}C+\pi^-$, 40 GeV/c, leading particle spectrum and bremsstrahlung model *(Russian)* 78—41781

bremsstrahlung continued
- (e,e+axion), bremsstrahlung mechanism for axion prod. *(Russian)* 79−54431
- $e^{+}e \to \pi^{+}\pi^{-}\gamma$, virtual electrons bremsstrahlung photon, Feynman diagrams, Weizsacker-Williams approx. 80−52484
- $e^{+}e^{-} \to e^{+}e^{-}\gamma$, new limit for heavy electron existence 78−8640
- $e^{+}e^{-} \to e^{+}e^{-}\rho$, production of neutral vector mesons 80−5006
- $e^{+}e^{-}a\mu^{+}\mu^{-}\gamma$, virtual electrons bremsstrahlung photon, Feynman diagrams, Weizsacker-Williams approx. 80−52484
- eN high-energy scattering, eikonal approx. corrections, bremsstrahlung 77−215
- $e^{+}p \to e^{+}\gamma X/e^{-}p \to e^{-}\gamma X$, deep inelastic scatt., quark-parton model 77−41846
- $e^{\pm}p \to e^{\pm}\gamma + X$, deep-inelastic bremsstrahlung, quark charges, colour gluon mass 78−74216
- γ circular polarisation, neutral current effect in bremsstrahlung and pair production 80−73655
- $\gamma p \to n\pi^{+}$, pion photoprod. using coherent bremsstrahlung beam and polarised proton target *(Russian)* 79−80830
- $\gamma p \to p\pi^{0}$, pion photoprod. using coherent bremsstrahlung beam and polarised proton target *(Russian)* 79−80830
- N-N soft photon bremsstrahlung in pot. model 77−6381
- NN bremsstrahlung amplitude, sensitivity of observables to short and intermediate distance wavefunctions 78−62449
- $NN \to \gamma X$, off-shell effects in the nucleon-nucleon system 79−80839
- np, effects of nonminimal currents and role of various couplings 78−70394
- np bremsstrahlung, one-pion-exchange current 77−82828
- np bremsstrahlung, struct. depend. of interaction current 79−63510
- np bremsstrahlung at 200 MeV 78−66144
- $p+d \to p+d+\gamma$, 6.3 to 6.9 MeV, bremsstrahlung, cross-sections 78−62429
- pd bremsstrahlung near breakup threshold, initial and final state amplitude interference 79−67588
- pp, bremsstrahlung, field theoretic calc., treatment of OBE external emission processes 78−62451
- pp bremsstrahlung, 1.38 GeV/c, differential cross section meas. 79−40796
- pp bremsstrahlung, bounds on external emission amplitude, cross section values 78−62450
- pp bremsstrahlung, criteria for expt. choice 79−67587
- pp bremsstrahlung, Δ isobar excitation and radiative decay 79−67586
- pp bremsstrahlung, field theory calcs. 79−67584
- pp bremsstrahlung, ω radiative decay contrib. at 158-400 MeV 77−74706
- pp bremsstrahlung, ω radiative decay contrib. 78−70386
- pp bremsstrahlung, review of Low theorem soft photon approach 78−62452
- pp bremsstrahlung cross section, 11 and 13 MeV *(German)* 77−10275
- pp bremsstrahlung with polarised p, soft photon approx. 79−67585
- pp interactions, W-boson prod. through bremsstrahlung 77−61247
- $pp \to pX$, bremsstrahlung model and recoil mass distrib. 78−70418
- $pp \to pp\gamma$, 200 MeV, cross section meas., bremsstrahlung at small angles 78−62446
- $pp \to pp\gamma$, 730 MeV, total and elastic cross sections for bremsstrahlung, Low theorem discussion 78−62448
- $pp \to pp\gamma$, applicability limit of Low theorem for pp bremsstrahlung 79−85323
- $pp \to pp\gamma$ bremsstrahlung, 730 MeV, differential cross section 77−46072
- $pp \to$ virtual gamma + hadrons soft bremsstrahlung, external emission dominance model 78−62430
- $\pi^{\pm}N \to \rho^{\pm}\gamma N$, bremsstrahlung in vector meson prod. at high energy *(Russian)* 79−80851
- $\pi p \to \pi p\gamma$, 298 Mev, non-relativistic calc. 77−71528
- $\pi^{\pm}p$, 269 MeV, 298 MeV, bremsstrahlung cross-section and soft-photon theorem 78−89730
- $\pi^{\pm}p$ near Δ resonance, external emission dominance 77−10280
- $\pi^{\pm}p \to \pi^{\pm}p\gamma$, 269-324 MeV, cross-sections, bremsstrahlung energy and ang. depend. 77−6149
- $\pi^{\pm}p \to \pi^{\pm}p\gamma$, 298 MeV, bremsstrahlung cross sections, model calcs. 77−6150
- $^{16}(\gamma,X)$, bremsstrahlung weighted cross section, two-body correlations effects, linked cluster expansion 80−106047
- Ag, beta-generated external bremsstrahlung spectra 77−57625
- Ag, spectral distrib. of X-ray braking radiation, due to electrons, calc. using Monte Carlo method 78−56538
- Ag, surface and volume plasmon light emission due to low energy electron scatt. 80−40177
- Al, 22 MeV electron bombardment, bremsstrahlung distrib. 78−59840
- Al, beta-generated external bremsstrahlung spectra 77−57625
- Al, bremsstahlung isochromat beyond Duane Hunt limit 77−73188
- Al bremsstrahlung, β generated, spectral shape depend. on target thickness 78−56545
- Al, bremsstrahlung spectra, 10 to 30 keV, thick target expts. 77−8687
- Al, β-ray bremsstrahlung in thick target, 30-1300 keV 79−83049
- Al, electron-bremsstrahlung depth-dose distribs., space-shielding appls. 80−39186
- Al laser plasma, high-Z, temp. meas. from bremsstrahlung emission 80−87914
- Al, proton bombarded, secondary electron bremsstrahlung, directional anisotropy 77−69953
- Al, surface, proton bombarded at 450 keV, X-ray bremsstrahlung, 2.5-8.5 keV 78−80436
- Al, X-ray continua emission, proton and ^{14}N bombard. 78−23559
- Ar, electron scatt., in laser radiation field, free-free cross sections meas. 78−74762
- Ar, electron scatt. in laser radiation field, free-free cross sections, reson. struct. 78−74763
- Ar, electron-atom bremsstrahlung continuum, afterglow decay *(German)* 78−83626
- Ar, free ats. electron bombard., subsequent X-radiation ang. distrib. 80−53144
- Ar plasma radiation obs., line and continuous spectra *(French)* 80−19619
- ^{75}As, level lifetimes, bremsstrahlung, reson. fluoresc. *(French)* 79−13248
- Au, spectral distrib. of X-ray braking radiation, due to electrons, calc. using Monte Carlo method 78−56538
- Au+e, atomic field bremsstrahlung, absolute cross section meas. 77−50529

bremsstrahlung continued
- B, evaporated, electronic struct., XPS, SXS and isochromat investig. 80−76143
- Ba, metallic, bremsstrahlung reson. and APS, near 3d threshold 77−69937
- ^{7}Be decay, radiative capture of orbital electrons, inner bremsstrahlung spectrum, decay energy 79−500
- ^{7}Be, nucl. electron capture, inner bremsstrahlung spectrum, partial decay energy 79−6512
- $^{7}Be \to {}^{7}Li$, total electron capture decay energy from inner bremsstrahlung spectrum, student experiment 78−24611
- Be(γ,p), intermediate energy bremsstrahlung, cross sections 78−13061
- C, beta-generated external bremsstrahlung spectra 77−57625
- CO bremsstrahlung by CO^{-} free-free transitions continuous absorption calc. 79−63978
- ^{12}C(p, p), 1.7-1.89 MeV, bremsstrahlung spectra, soft photon and Feshback-Yennie approx. 79−80937
- ^{12}C(p,p), bremsstrahlung near 1.7 MeV resonance 80−68670
- ^{12}C(p,p)^{12}Cm bremsstrahlung near 1.7 MeV resonance 79−45249
- ^{12}C(p,pγ), bremsstrahlung cross section near 1.7 MeV resonance, Feshbach-Yennie approx. 80−42662
- ^{12}C(p,pγ), meas. of bremsstrahlung spectra to determ. reaction time delays of 10^{-20} sec. 77−6378
- ^{45}Ca, internal bremsstrahlung photon intensity and energy yield 78−86509
- CdS laser radiation under excitation by pulsed bremsstrahlung X-rays 79−91467
- Ce, metallic, bremsstrahlung reson. and APS, near 3d threshold 77−69937
- ^{144}Ce photoneutron sources, determ. of standard neutron yield, influence of bremsstrahlung 79−72177
- ^{36}Cl, internal bremsstrahlung spectra, accompanying second forbidden β-decay 78−8776
- ^{59}Co, mean lifetime meas., 1400 to 1650 keV range, by reson. scatt. of bremsstrahlung *(French)* 79−75905
- ^{137}Cs, beta-decay, internal bremsstrahlung meas. 77−79338
- Cu, beta-generated external bremsstrahlung spectra 77−57625
- Cu bremsstrahlung, β generated, spectral shape depend. on target thickness 78−56545
- Cu, bremsstrahlung spectra, 10 to 30 keV, thick target expts. 77−8687
- Cu, bremsstrahlung yield and distrib. of absorbed energy in electron irradiation 79−99245
- Cu plasma, laser-produced high energy X-ray bremsstrahlung, evidence of reson. absorpt. 78−42776
- Cu, spectral distrib. of X-ray braking radiation, due to electrons, calc. using Monte Carlo method 78−56538
- ^{A}Cu, A=63,65, mean lifetime meas., 1400 to 1650 keV range, by reson. scatt. of bremsstrahlung *(French)* 79−75905
- $e^{-}e^{+}$ pair photoproduction in crystals by circularly polarised γ-quanta 78−17005
- Fe, 22 MeV electron bombardment, bremsstrahlung distrib. 78−59840
- Fe, impurity atoms in hot plasma, radiation energy loss 78−18441
- ^{55}Fe electron-capture decay double internal bremsstrahlung 79−63633
- Ge, bremsstrahlung spectra for 1 GeV electrons and positrons, planar and axial channelling *(Russian)* 77−32465
- Ge, electron and positron bremsstrahlung spectra *(Russian)* 79−91522
- Ge, ion implanted, cond. and valence bands study by X-ray bremsstrahlung and photoelectron spectra 80−2360
- ^{71}Ge, energy release accompanying electron capture 78−17148
- H, electron and positron bremsstrahlung, differential cross sections 79−18294
- H, electron scatt. in EM field, reson. emission and absorpt. of photons 79−27087
- H electron scattering bremsstrahlung cross section, laplace transform method in two-photon spectroscopy theory 79−10084
- H_2-He plasma interface in strong gravit. field, bremsstrahlung, neutron stars and pulsars appl. *(Russian)* 79−67048
- ^{1}H(d,dγ) 6.3-7.1 MeV, bremsstrahlung anomaly near breakup threshold 78−89888
- ^{2}H(p,pγ), elastic cross sections, bremasstrahlung, threshold and Coulomb effects 80−91186
- ^{3}H conc. meas., scintillation detector appl., bremsstrahlung from β-rays 78−55042
- Hg arc, continuum radiation meas. 77−62416
- I meas. in tissue, separation of bone and water, appl. of filtered bremsstrahlung spectra 79−74747
- ^{A}In, A=113,115, mean lifetime meas., 1400 to 1650 keV range, by reson. scatt. of bremsstrahlung *(French)* 79−75905
- ^{A}Ir, A=191,193 photoneutron yield curves, nuclear shape and giant dipole resonances, 8-21 MeV *(Russian)* 79−13268
- Kr, free ats. electron bombard., subsequent X-radiation ang. distrib. 80−53144
- Kr+Ti, 200 MeV, collision, quasimol. bremsstrahlung, semiclassical calcs. 77−88530
- La, metallic, bremsstrahlung reson. and APS, near 3d threshold 77−69937
- LiF film, guided wave excitation by fast electrons 79−24384
- LiF, Kα-satellites of F^{-} *(German)* 79−28864
- ^{7}Li, photodisintegration, cluster model wave function, bremsstrahlung weighted cross section 80−63163
- Mo, bremsstrahlung spectra, 10 to 30 keV, thick target expts. 77−8687
- N, electron bremsstrahlung, configuration interaction 78−13483
- N, electron elastic scatt. resonance, neutral bremsstrahlung 77−46639
- Nb, bremsstrahlung spectra for 1 GeV electrons and positrons, planar and axial channelling *(Russian)* 77−32465
- Ne, electron-atom bremsstrahlung continuum, afterglow decay *(German)* 78−83626
- Ne medium-pressure discharge, electron temp. radial profile meas. by electron-atom bremsstrahlung continuum 78−67497
- Ni, bremsstrahlung isochromat, incident electron energy and final-state symm. effects 79−69909
- Ni, X-ray intensity reson. near 2p threshold 80−60717
- ^{58}Ni, mean lifetime meas., 1400 to 1650 keV range, by reson. scatt. of bremsstrahlung *(French)* 79−75905
- Os(γ,xn), photoneutron cross section, bremsstrahlung yield curves 78−17176
- ^{32}P, half-life, integrated internal bremsstrahlung intensity meas. 77−57629
- Pb, 22 MeV electron bombardment, bremsstrahlung distrib. 78−59840
- Pb, beta-generated external bremsstrahlung spectra 77−57625

bremsstrahlung continued

- Pb, bremsstrahlung, β generated, spectral shape depend. on target thickness 78−56545
- Pb, photon showers produced by 150 MeV electrons 77−10563
- pp bremsstrahlung, intermediate nucleon isobars contrib., relativistic model, nuclear force significance 78−93899
- ^{143}Pr, internal bremsstrahlung 77−82879
- ^{A}Pt, A = 194-8 photoneutron yield curves, nuclear shape and giant dipole resonances, 8-21 MeV *(Russian)* 79−13268
- ^{106}Ru photoneutron sources, determ. of standard neutron yield, influence of bremsstrahlung 79−72177
- ^{35}S, beta-decay, internal bremsstrahlung spectrum meas. 77−50089
- ^{35}S, internal bremsstrahlung photon intensity and energy yield 78−86509
- Si, bremsstrahlung spectra for 1 GeV electrons and positrons, planar and axial channelling *(Russian)* 77−32465
- Si, channelling of relativistic electron beam, anal. of low-energy bremsstrahlung meas. 77−36304
- Si, impurity atoms in hot plasma, radiation energy loss 78−18441
- Si KLL Auger peaks, bremsstrahlung-induced 80−45199
- Si, X-ray continua emission, proton and ^{14}N bombard. 78−23559
- Sm surface, electron spectroscopy of 4f energy shift 80−2925
- ^{145}Sm, electron capture decay, internal bremsstrahlung 78−13035
- Sn, bremsstrahlung, β generated, spectral shape depend. on target thickness 78−56545
- ^{90}Sr photoneutron sources, determ. of standard neutron yield, influence of bremsstrahlung 79−72177
- ^{90}Sr + ^{90}Y bremsstrahlung efficiency for humans, ^{90}Sr body content determ. 77−2061
- Ta, (111) surface, 100 eV electron bombardment, adsorbed mol. luminesc., coherent bremsstrahlung *(Russian)* 78−31290
- Ta, bremsstrahlung emission meas., using vac. UV isochromat spectrometer 77−74521
- Ta, bremsstrahlung yield and distrib. of absorbed energy in electron irradiation 79−99245
- Th, valence and 5f states, XPS and bremsstrahlung isochromat spectroscopy 80−66393
- Ti, X-ray continua emission, proton and ^{14}N bombard. 78−23559
- ^{204}Tl, beta ray generated bremsstrahlung yield consts. 80−42588
- ^{204}Tl β-decay, K-shell autoionisation accompanying internal bremsstrahlung 80−57745
- ^{204}Tl β-particle excitation of external bremsstrahlung spectra from thick targets 80−84797
- U, valence and 5f states, XPS and bremsstrahlung isochromat spectroscopy 80−66393
- UO$_2$, electronic struct. and Coulomb correl. energy, XPS and bremsstrahlung spectra 80−55272
- ^{230}U, production, tracer appls., α-spectra 77−61644
- W, bremsstrahlung spectra, 10 to 30 keV, thick target expts. 77−8687
- Xe, free ats. electron bombard., subsequent X-radiation ang. distrib. 80−53144
- ^{90}Y internal bremsstrahlung, evidence for detour transitions in β-decay processes 78−66247
- ^{91}Y, beta ray generated bremsstrahlung yield consts. 80−42588

brick industry

- calcining of clay, particulate emission removal using electrostatic precipitator 79−24925

bridge circuits

see also bridge instruments

- AC, for ferromagnetic ring complex reluctivity meas. *(Russian)* 78−54412
- AF reactance comparison by transformer bridges 77−82564
- anemometer characts., hot-wire linearised type for turbulence research 77−55118
- capacitive loss-angle resistor meas. bridge, 1 mHz to 100 Hz *(German)* 77−79125
- capacitor tolerance measured using astable multivibrator 78−4628
- coaxial loadless balanced bridge cct. for magnetophonon oscill. separation 78−2499
- data logger for precision meas. of resistance temperature detectors 79−88925
- DC resistance decades, precision, integral verification 78−242
- detector for use with low-temp. capacitance thermometer 79−54132
- dielectric loss tangent meas., microwave resonator bridge method 77−37914
- differential resist. meas., resist. thermometry appl. 77−79126
- differential tunnelling spectroscopy, bridge design 78−5309
- EHV choke coil measuring bridge *(German)* 77−18047
- electrical conductivity, of electrolytic solns., bridge cct. for cond. cell *(German)* 79−9220
- electrical temp. meas. methods and trends *(German)* 78−93681
- electro chemical hygrometer, direct reading *(Spanish)* 78−32254
- electromag. convertor, forming part of unbalanced bridge circuit, exam. of characts. 78−85100
- errors due to changes in resistance thermometer conductor resistance 79−30473
- exposure meter with photoresistor, semi-automatic, methodical error calc. *(Russian)* 77−54008
- four-terminal meas. circuit stray-impedance errors 78−77940
- inductive transducer, parameter anal., appl. 78−45608
- inductor-convertor bridges, for Tokamak supercond. coils active energy transfer rate control 78−13338
- Kelvin bridge, link resistance compensation 78−86292
- linear unbalanced DC bridge 77−79123
- nonlinear for inductive transducers, operation *(German)* 77−10007
- ohm, absolute determ. based on standard capacitors 77−82565
- p-n junctions capacitance meas., using analogue multiplication *(Bulgarian)* 78−57977
- phaser for lock-in null detectors 77−79122
- position sensor, differential, built with magnetic resistances *(Italian)* 79−85155
- psychrometer for relative humidity of air meas., modification *(French)* 77−78451
- RC double-balanced bridge analysis *(Polish)* 78−89498
- resistance thermometer, conductor resistance effect compensation using hexagonal bridge *(German)* 78−77910
- resistance thermometer, precision bridge using single inductive current divider 77−82517
- resistance thermometer appl. *(German)* 77−74394
- resistive thermometric transducer appl. for temp. meas. *(Russian)* 77−33987

bridge circuits continued

- ring core flux-gate thickness transducer with permanent magnet 79−67280
- semiautomatic bridge for high-precision DC resistance measurements on pure metals at low temperatures 79−35788
- semiconductor superlattice microwave/infrared detectors 80−13138
- sensitive temp. meas. with thermo-elements, theory *(German)* 77−71323
- skin humidity meas. using bridge cct. and digitally steered logic cct. 77−13018
- SQUID resistance bridge, ultra high resolution 79−63275
- strain gauge, amplification technique for high meas. accuracy 77−5826
- strain gauge amplifiers, ccts., features *(German)* 77−71311
- strain-gauge dynamometer, effect of temp. on characts. 78−93677
- temperature control system for biological preparations 79−57830
- temperature controller, based on Wheatstone bridge and thermistor, high precision 78−86258
- temperature controller, use of ICs, at cryogenic temps. 80−90856
- temperature measurement, thermistor multivibrator applic. 77−26289
- temperature monitor using thermistor sensor 78−209
- thermal conductivity of fluid meas., automatic Wheatstone bridge, theory 78−65933
- thermistor, laboratory temp. control, modified window air conditioner 80−68192
- thermistor ebullioscope cct., uncertainty in sensitivity 78−12695
- thermistor thermometer bridge network charact. linearisation *(German)* 78−86271
- thermocouple principles, ccts., and instrum. *(Dutch)* 78−198
- thermoelectric thermometer cold junction thermo-EMF compensation, parameter optimisation *(Russian)* 78−86270
- thermometer with automatic balancing, for liquid streams temperature meas. 80−47055
- Tokamak EF coil energy transfer supercond. solenoids and phase-shifting bridge 79−31213
- transformer, for meas. displacement *(Russian)* 80−98884
- unbalanced, anal. of circuits with thermistors and pulsed supplies 79−30474
- US transmission/reception system with single crystal, principle, biomedical appl. *(Japanese)* 77−84093
- voltmeter with offset zero for freq. meas. *(French)* 80−22331
- Wheatstone bridge, optimisation of sensitivity 78−86298
- Wien bridge oscillator, critical phenomena simulation, threshold instabilities 77−1211
- N$_2$, liquid, sensor using domestic incandescent gas lighter element 79−63201

bridge instruments

see also bridge circuits

- 1 Ω to MΩ resistance meas. bridge *(Spanish)* 77−74457
- 1 MN combination load/bending moment transducer *(German)* 77−79080
- AC, with two-freq. modulation of supply, for tunnelling spectroscopy 80−13196
- AC bridge for small resistance meas. at low temps. 79−67347
- AC mutual inductance bridge using operational amplifiers, mag. susceptibility meas. 78−89508
- AC resistance bridge for low resistance meas. 77−26337
- AC thermometry and DC heating circuitry in thermal props. meas. 78−74000
- accelerator ion beam position monitor 79−89040
- admittance bridge, microcomputer controlled, for passive network testing 77−18037
- admittance bridge, modification for large conductances meas. 78−4660
- AF impedance bridge, 4-terminal-pair, 40 Hz to 2 kHz 79−88978
- automatic conductometer, exam. 78−56933
- automatic resistance thermometer bridge 80−98913
- bead thermistor Wheatstone bridge for temperature measurement in meteorology and oceanography *(German)* 77−21920
- biomaterial microwave complex permittivity meas., noninvasive selective exposure 79−20729
- bonded joints, device for automatically recording internal stresses 80−25963
- capacitance detector for ion cyclotron resonance signals 80−62792
- capactiance meas. system for assessment of deep levels in semiconductors 80−105674
- cell and setup for elec. resist. meas. of semicond. ceramics, 300-1400°C 79−30488
- closed Wheatstone bridge for tenso resistor, resistance meas. *(Russian)* 79−12821
- comparator for checking capacitance standard *(Polish)* 78−41331
- complex mutual inductance concept for bioelectric impedance transformer bridge 80−63886
- components of (30-100) Hz and (1-10) kV, Schering bridge amplifier system appl. *(Bulgarian)* 77−61083
- continuous recording apparatus for resist. change during heating and cooling 77−22568
- cross-correlator for broad-band impedance meas. using high-speed CMOS switches 77−26324
- crystal bridge for equivalent electrical parameters meas. of piezoelectric crystals 78−54404
- Curie temperature determ. by AC ccts. 77−49749
- current comparator, for AC, 60 Hz, power meas. 77−18040
- DC, high-resistance wide-range, measurement error 79−75548
- DC resistance strain gauge using integrated operational amplifier 79−75522
- deep level transient spectrometer, automatic calibration cct 80−37067
- dielectric const. meas. using automatic system *(German)* 80−90864
- dielectric loss measurement, Schering bridge appl. *(Portuguese)* 77−67461
- digital meter used to measure L, R, and C 78−12715
- digital Wheatstone bridge, automatically compensated, temperature transducer appl. *(Rumanian)* 80−57287
- DLTS for diodes with large leakage currents 80−34504
- dual resistance wire wavestaff system for laboratory and coastline 80−46324
- electric resistance strain gauge appl. 77−41589
- electrical conductance of concrete meas., automatic instrument 77−77659
- electrometric circuit switching by magnetically controlled contact 77−79108
- electron and ion conductivity meas. of oxidic materials up to 2000°C. 79−96247

bridge instruments continued
electronic potentiometer, attachment for measuring deform. 77−17974
electroplethysmograph for regional lung function evaluation 77−21647
environment protection when siting power station, temp. and humidity meas. methods *(French)* 79−12318
ferrofluids, magnetic material conc. distrib. meas. device 78−16821
FET voltmeter with high input impedance *(Spanish)* 77−37934
four-arm bridge measuring circuits with linearised characteristics *(Russian)* 79−12820
four-probe AC bridge technique for ionic cond. meas. 80−57340
gas analyser, two-bridge, based on voltage ratios meas. 80−50907
high-resolution cryogenic resist. bridge using SQUID null det., construction and performance 79−2792
implantable biomedical pressure transducer 77−73606
industrial resistance thermometers testing using incomplete bridge balancing technique 78−73998
intrinsic inductance, standardisation instruments *(Czech)* 78−32837
Kelvin double bridge, precison, for capacitance meas. up to 1 F, ratio arm adjustment 79−21776
magnetic susceptibility meas., of Fe alloys, temp.-time instability *(Slovak)* 78−57989
manganin resistance gauge for high pressure meas. 77−10036
manometer, membrane, for low pressures meas. 80−31777
Maxwell bridges for meas. of small complex impedances in RF range 80−98931
metal foil gauge, long-term stability of strain meas. 79−17417
microwave, self-balancing DC-substitution RF power meter 77−18012
miniature drag force anemometer 78−14117
multi-bridge device, computerised, for capacitance and loss angle meas. *(Russian)* 78−70159
muscle tone study by meas. of muscle density 80−3833
mutual inductance bridge using operational amplifiers 78−54407
nonlinear bridge circuits, for inductive transducers *(German)* 77−10007
off balance interferometric bridge, using heterodyne detection for recording vibratory phenomena 78−70119
percentage ohmmeter, wide-range, using unbalanced DC resist. bridge 78−239
phase device for low freq. NMR expts. 80−31837
phase-sensitive detector, programmable, for automatic bridge appl. 79−21773
piezoresistive C gauge for low shock pressure meas. 79−1278
plane shearing stress meas. with wired strain gauges *(German)* 78−89471
plethysmograph, calibration-free Hg strain-gauge device 80−17161
pneumatic Wheatstone bridge for roughness measurement, improved version 80−62629
porosimeter, continuous scan mercury type, pore pot. contrib. to hysteresis 80−77928
pressure pick-up with Si column strain-gauge convertor 80−31732
primary standard capacitor design appl. 77−53944
quartz crystal impedance and admittance bridge development 77−37944
RC double-balanced bridge analysis *(Polish)* 78−89498
recording mercury manometer, student apparatus 77−26119
relays inductance measurement to TGL 24961 specification methods for Fe-cored coils *(German)* 80−4736
resistance meas., of quartz resonator, improved accuracy 77−10056
resistive voltage-ratio standard for 10 kV DC meas. 77−5873
RF voltage standard, precision, using thermistor bridge, HF-UHF range 78−89504
RF voltage standard, precision, using thermistor bridge, HF-UHF range 79−21772
RLC bridge, with oscillator and having ten ranges 79−2785
semiconductor integrated bridge strain gauges with diffusion piezoresistors, strain sensitivity *(Polish)* 80−73341
single-ended cavity resonator loaded Q-factor meas. using reflection bridge 78−54405
small active resistance and inductance meas. AC bridge 78−86299
soil pressure meas., using capacitive sensor with polyurethane foam dielectrics *(Slovak)* 80−86281
standards comparison, capacitance-inductance, transformer ratio bridge *(Polish)* 79−80645
strain gauge bridges, automatic multirange calibrator 79−67285
strain gauge transducers temperature compensation methods 77−22541
strain gauges, single shunt calibration to simulate bridge unbalances 77−22542
temp. meas. of rotating object, non-contact method with thermistor and pyrometric voltmeter 79−35742
temperature check, linearisation of bridge measuring circuit *(Russian)* 80−90847
temperature difference meas. by automatic thermistor bridges 77−22547
temperature measuring bridge, using constant-current FET circuits 77−129
temperature measuring potentiometer, thermistor appl. 78−207
tensile test diagram remote recording device 78−7139
tensometer, semicond., with parallel channel, operation principle *(Russian)* 80−73352
thermometer, transistorised, with remote indication, up to 150°C *(German)* 80−73356
thermometric AC bridge for temp. meas., 13.81-273.15K range *(Polish)* 78−93683
thermostat with stability of $\pm 3.5\ \mu$K, using thermistor based AC Wheatstone bridge 78−21132
three-term error-normalising instruments, optimum range and information capacity determ. 77−13732
transducer for recording elec. and mech. chronic intestinal activity 77−44862
transformer, automatic testing resistance thermometer appl. 77−53906
transformer ratio arm, used for measurement of dielectric relaxation of conducting solns. at low freqs. 79−80641
unbalanced resistance bridge with linear charact., appl. to press. meas. using electroresistive gauges or extensometric transducers *(Polish)* 80−73385
US beam power meas. calorimeter bridge for 1 to 15 MHz 77−27446
US transducer loading, effect of US field geometry 80−102950
wattmeter, in-line, for transmitter output power monitoring 77−79103
Wheatstone, unbalanced with magnetodiodes, for measuring magnetic induction 79−80644
Wheatstone bridge, sensitivity optimisation 77−26330
Wheatstone bridge fed from a bilateral constant current source 80−57338

bridge instruments continued
Wheatstone bridge formed by pressure sensor using Ge:Au film strain gauges *(Japanese)* 80−105631
wheatstone bridge technique for magnetostriction measurements 80−57348
Wheatstone bridge using thermistors for temp. meas. in calorimeter, optimisation *(German)* 78−86275
Wien bridge oscillator, for continuous recording of elec. resist. changes 77−53931
Wien oscillator, low-power, for low-temps. ~25 mK 78−93680
Wiltron bridge used for 70 MHz-4 GHz, oscilloscope indicator *(French)* 80−42241
Hg-in-glass thermostat 80−22359
Pt res. thermometer linearisation cct. *(German)* 78−200

Bridgman method *see crystal growth from melt*

brightness
see also sky brightness
0957+561A, B, double quasar, intervening galaxy IR obs. and holometric luminosity 80−73065
1308+32, BL Lacertae object, rapid optical outburst, 1980 June to July 80−98733
1418+54, new violently variable BL Lacertae object, historical light curve 78−93410
1978 SB, asteroid, UBV photometry 78−96422
1978 SB, fast-moving object, discovery positions and magnitudes 78−93142
Abell 1060 galaxy cluster, X-ray surface brightness distrib. from HEAO-2 spectral obs. 80−82518
Abell clusters of galaxies, Westerbork obs. rel. to radio and X-ray luminosity 78−96549
Abell clusters of galaxies, X-ray luminosity function 78−36704
Antarctic glaciers thermal radio emission, theory for random layered media *(Russian)* 77−33106
AO 0235+164, BL Lacertae object, photometric obs. of optical outburst 80−56924
AO 0235+164, BL Lacertae object, relativistic blast-wave model for rapid flux vars. 79−9017
AO 0235+164, BL Lacertae object, UBVI photographic magnitude obs. during flare 79−25724
Arakelian 120, Seyfert 1 galaxy, optical variability 79−40259
asteroid 433 Eros, brightness changes during major opposition 77−67061
asteroids, magnitudes and phase relations compilation 79−88617
asteroids, similarity of opposition effect 80−62064
astrometric instrument index mark optimum brightness calc. 79−53720
astronomical observations, brightness distribs. uniquely related to fringe visibility intensities 79−8842
atmosphere, brightness temps. vars. in H_2O 1.35 cm reson. region *(Russian)* 78−81403
atmosphere thermal radiation, effect of large hailstones on brightness temp. in 0.86 to 17 cm range *(Russian)* 78−36222
atmospheric radiance polarisation and ellipticity of multiply scatt. solar radiation 77−9457
aureole around UV source at finite distance 78−77320
aureole radiance field about point source in scatt.-absorbing medium 78−77319
aurora, atmospheric absorption effects on satellite obs. 80−12538
automatic cameras, exposure error compensation 80−52346
average hemispherical illum. from point source, calc. *(Czech)* 77−46778
barred spiral galaxies in Virgo cluster, surface photometry 77−13453
binary galaxies, late type, mass-to-light ratios from luminosity-weighted averages 78−8113
binary galaxies, luminosity function and colours 80−41900
black hole, massive, radiation spectrum of gas debris from tidally disrupted star 80−90467
black holes accretion discs, thick discs models rel. to supercritical luminosities 80−101614
Broca-Sulzer effect in a Ganzfeld 79−53151
3C 120, radio galaxy, nucleus brightness changes rel. to vars. in optical spectrum *(Russian)* 80−90540
3C 120, Seyfert galaxy, X-ray luminosity 77−78890
3C 288, complex extragalactic radio source, radio brightness distrib. model 80−90558
3 C 31, radio jet brightness and shape rel. to beam and slingshot models 79−25741
CA 0340−538 (3U 0328−52?), southern cluster of galaxies, vel. dispersion and total luminosity 78−36705
camera films, automatic exposure, theoretical anal. 78−86363
capillary discharge, high-current, magnetogasdynamic regime 79−86628
capillary discharge mode selection for IR brightness standard *(Russian)* 79−55198
Cassiopeia A, secular decrease in radio emission flux density at 437 and 510 MHz *(Russian)* 80−8702
Cassiopeia A, supernova remnant, 927 MHz emission secular decrease 79−75255
cataclysmic binaries, accretion disc surface brightness distrib. determ. 80−109492
Centaurus galaxy cluster, X-ray surface brightness distrib. from HEAO-2 spectral obs. 80−82518
centimetric quiet Sun, brightness reinterpretation rel. to coronal long distance arches density 78−28597
chromatic replacement of matched luminance, chromatic stimuli, duration thresholds 79−57657
clinical light level measurement using photographic meters 80−94304
clouds, reflected brightness, effects of cloud size and cloud particles, comments and reply 79−88425
cluster galaxies, luminosity function 78−54058
clusters of galaxies, Bautz-Morgan classes and luminosity function 78−54057
clusters of galaxies, radiation intensity and space distribs. nonrandomness *(Chinese)* 79−17111
clusters of galaxies, X-ray luminosities rel. to intracluster gas evolution 79−40266
colour vision, normal and dichromatic, vector model 80−51099
Coma Cluster galaxies, photometry and luminosity function 78−12381
Coma cluster X-ray source, X-ray brightness distrib. prediction 79−92896
Comet Bennett (1970 II), CN (0-0) band brightness profile obs. rel. to CN prod. 80−82303
Comet Bradfield (1979c), total visual magnitude estimates, (1979 August 4 to 12) 79−88623

brightness continued
Comet Bradfield (1979c), total visual magnitude estimates (1979 August 17 to September 10) 79−92721
Comet Bradfield (1979l), visual obs. (1979 February 8 to 20) 80−46489
Comet Machholz (1978l), visual magnitude estimate (1978, September 19) 78−89126
comet tails, H_2O^+ surface brightness rel. to CO^+ 80−72880
Comet West (1976 VI), CN (0-0) band brightness profile obs. rel. to CN prod. 80−82303
Comet West (1976 VI), Lyman α isophotes 80−46485
Comet West (1976 VI) ionosphere CO^+ brightness profile 80−85896
cometary nuclei, brightness meas. technique 79−84745
comets, brightness prediction 79−75164
comets, brightness variation and nuleus struct. 79−2521
comets, convolution of brightness profiles by circular diaphragms 79−12433
comets, fluctuations rel. to solar activity 77−25983
comets, magnitude distrib. 80−72886
comets, monochromatic brightness var. 78−81590
comets, monochromatic brightness vars. core-mantle model 78−81589
comets, neutral species brightness profiles, average random walk model for mol. photodissociation 80−77351
comets, vaporisation of nuclei rel. to light curves 80−56772
compact galaxies, mean surface brightness and integral brightness relation 78−93412
compact radio sources, brightness distrib. mapping from VLBI data 78−89266
contrast telephotometer, multiwavelength, instrument design, data interpretation, atm. visibility determ. 79−66842
cosmic microwave background, brightness depletion due to Compton scatt. by galaxy clusters gas 78−24575
cosmology, sources luminosity evolution from scale parameter for Friedmann models 80−77527
Crab Nebula, optical and X-ray surface brightness from supernova remnant physical theory supernova 80−51834
Crab Nebula, total intensity mapping at 2.7 GHz with 3.7×10 arcsec ang. resolution 79−40248
cross radiance measurement, computer soln., adjacency effects on imaging 79−100939
cumulus clouds, size and particles effects on satellite-observed reflected brightness 78−73510
Cygnus Loop, 25 MHz brightness distrib. and total flux density 78−54027
Cygnus X H II region, maps of calibrated surface brightness of (Hα+N II) 77−78854
dayside aurora, brightening during magnetospheric substorms 77−87148
Deimos, opposition brightness surge from Viking obriter images 80−72838
DFB laser, limiting spectral characts. 79−64197
diamond, round brilliant cut, statistical assessment of brilliance and fire 78−90361
diamond, round brilliant cut style modifications, brilliance, sparkliness and fire 78−90362
diamond simulants, brilliance, sparkliness and fire 78−90363
diffracted image illuminance distrib. for partially coherent truncated bar targets 79−76609
discharge, hollow-cathode, holographic meas. of radn. coherence props. 79−76784
double radio source structures, brightness distrib. evolution and superluminal expansion 78−8141
double radio sources, brightness effects on ang. size-redshift test 77−57100
Draconid meteors, number and brightness function in (1972) 77−67077
Earth's surface, radiance of natural formations 79−62515
Earth satellite, tumbling, cylindrical, rot. axis location from max. brightness/min. brightness ratio 79−80200
Earth surface, apparent radiance data appl. to groundwater flow pathways remote determ. 79−16522
electron-optical convertor screen luminance, effect on observer's eye pupil diameter 80−35890
elliptical galaxies, correl. between isophotal twisting and flattening 80−41896
elliptical galaxies, surface brightness-axial ratio relation and three-dimensional figures 80−36704
elliptical galaxies, U−R colours synthesis from chemical evolution model 80−67843
elliptical galaxies cores light distrib., effects of seeing 80−12814
182 Elsa, photoelec. light curve and rot. period of asteroid 80−56750
433 Eros, photographic obs. at 1975 opposition 78−49373
247 Eukrate, UBV photometry, light curve and rot. period 80−21942
extragalactic radio sources, flux densities and variability at 2.7 GHz 77−53694
faint quasars from CTIO 4 metre survey, spectroscopy and luminosity function 78−32592
field galaxies, luminosity function 78−16526
field galaxies, luminosity function and space distrib. 79−88731
finite planar sources of arbitrary coherence states, radiance function existence 79−50208
flare stars physical characts. 77−41383
flashbulb integrated radiance meas. rel. to max. permissible exposure 77−79911
fluorescent materials, reflective radiance factor meas. by two-monochromator method *(Japanese)* 80−68237
Fornax cluster, luminosity function determ. by photographic photometry 80−82523
Fornax cluster of galaxies, bright members surface photometry 78−96548
galactic γ-ray sources, number intensity relation rel. to galactic disc emission 80−46702
Galactic central IR surface brightness obs. by balloon *(Japanese)* 78−61925
galactic diffuse IR radiation obs. at 2.4 μ 77−33656
galactic diffuse soft X-ray emission, brightness distrib. 79−53942
galactic H I regions, brightness temp. from 21 cm obs. 80−85987
galaxies, absolute magnitudes and distances determ. from H II regions rel. dispersions 80−31360
galaxies, bright, in Virgo cluster area, standard total magnitudes and mean errors 78−65685
galaxies, bright, nearby, vel. field and luminosity functions for Hubble types and luminosity classes 80−36699

brightness continued
galaxies, brightness distrib. rel. to stellar disc central density min. 80−17663
galaxies, counts to apparent magnitude 25 rel. to luminosity evolution *(Russian)* 80−51879
galaxies, early-type, brightness/dia. relations rel. to sequences and populations 79−58415
galaxies, early-type, in NGC 7331 field, average surface brightnesses rel. to distances 80−4435
galaxies, early-type, luminosity criteria rel. to relative distance moduli 80−22080
galaxies, early-type, photometric determ. of twists in three objects 79−25703
galaxies, early-type, relative luminosities and distances 80−31363
galaxies, elliptical, surface photometry 78−57625
galaxies, extrapolated central surface brightnesses 79−25705
galaxies, faint, number magnitude counts 80−26976
galaxies, interacting, luminosities and diameters 80−17677
galaxies, IR magnitude/H I vel. width relation rel. to distance scale and Universe expansion rate outside Local Supercluster 80−105325
galaxies, low surface brightness, luminosity function, props. 78−96532
galaxies, luminosity enhancement rel. to ang. redshift anisotropy 77−2472
galaxies, luminosity evolution rel. to angular dia. counts 77−91623
galaxies, luminosity functions of elliptical and lenticulars 79−97057
galaxies, mean surface brightness rel. to radio emission *(Russian)* 77−91615
galaxies, normal, X-ray luminosity evolution rel. to contrib. to diffuse X-ray background 79−17141
galaxies, optical surface brightness rel. to density wave induced star formation 80−17649
galaxies, redshift-magnitude bands and evolution from Perseus and A1367 clusters obs. 78−54033
galaxies, surface brightness parameters as tests of evolution 77−13462
galaxies, surface brightness rel. to evolution, cosmological appls. 77−9801
galaxies active nuclei, high-energy neutrino luminosity and detectability 80−4432
galaxies binary systems, luminosity/separation correl. as dynamical friction effect 80−36700
galaxies containing giant H II regions, absolute luminosities 79−8973
galaxies in clusters, luminosity functions and morphology 78−12383
galaxies in compact groups, anomalous luminosity function 80−82520
galaxies in field of Abell 1781, photometric obs. 78−77609
galaxies in small groups, luminosity function 78−12385
galaxies in Virgo area, reduction of magnitudes to standard B_T system 79−92852
Galaxy central region, 2.47 μm surface brightness profile 77−29935
galaxy cluster X-ray sources, luminosity function evolution 80−62314
galaxy clusters, brightness spectrum and cosmic luminosity 78−81696
galaxy clusters, luminosity dispersions of real and spurious clusters 80−101643
galaxy clusters, luminosity of brightest galaxy, statistical model test 77−29938
galaxy clusters, luminosity rel. to self-similar gravitational clustering 80−4447
galaxy clusters, X-ray brightness distrib., gravitational potentials 79−12529
galaxy clusters, X-ray luminosity function, predictions from thermal bremsstrahlung model 79−101208
galaxy clusters X-ray sources, luminosity evolution and redshift depend. 79−17133
galaxy groups, mass-to-light ratios and crossing times 77−45572
gas poor disc galaxies, radio and optical props. 77−22310
Gaussian beams, increase of axial brightness during wave front smoothing *(Russian)* 80−5774
GD 428, extreme dwarf Cepheid, obs. rel. to intrinsic luminosity 77−78798
gegenschein, brightness correl. with Danjon relation *(French)* 79−96968
general optical concentrator, max. radiant power density at receiver 80−102794
generalised radiance propag. through lenses 79−27359
generalised radiance uniqueness theorem 78−94365
geological IR multispectral aircraft scanner data, image processing 80−98454
giant E and cD galaxies, surface photometry rel. to optical extent. 77−45557
giant H II regions, radio maps interpretation 78−85994
glare source position and BCD brightness relationships under uniform field brightness, expt. *(Japanese)* 80−35889
globular clusters, NGC 6440, 6541, 7099, surface brightness, star density and colour profiles 80−12783
globular clusters, southern, surface-brightness profiles rel. to struct. and stellar content 79−71078
globular clusters, structural parameters and integrated magnitudes 80−46623
globular clusters (M3, M5, M13, M15), equidensity curve meas. *(Russian)* 79−97041
globular clusters in Virgo cluster of galaxies, luminosity distrib. 78−12308
globular clusters of Virgo galaxies, luminosity function and Hubble const. new determ. 79−92902
globular star clusters, brightness and density distrib., two parameter generalised isochronous models 80−67807
grating, sine-wave, average-luminance surround effect 80−51092
gravitational lenses, high-intensification regions brightness 79−25463
hazes, information provision on particle size distrib. of brightness and polarisation phase functions *(Russian)* 78−44998
HZ Herculis, eclipsing binary, accretion disc brightness distrib. from optical light curve 78−65658
heterogeneous medium, interactions of laser radiation 80−28765
high-power laser luminance contrast meas. 78−87055
hologram image reconstruction without using reference beam, brightness characts. *(Russian)* 80−69348
holographic head-up display 79−50266
holographic image luminance determ. 79−81394
holography, white light refl., developer compositions compared 80−102669
HVC 132+23−221, small high vel. H I cloud, brightness temp. struct. 78−89241

brightness continued
illuminance, scalar and cylindrical illuminance meas., instrument quality *(German)* 77—10088
illumination, relative, easy calc. 80—63920
illumination and reflection edges, recognition by human visual system 80—94209
illumination engineering, contributions of luminous surfaces *(Rumanian)* 80—4750
image plane irradiance caused by the natural radiation of the objective lens 78—83068
imagery, 2-D sampled, aliasing and blurring effects 80—99635
inhomogeneous cosmic masers, saturation behaviour, intensity and centre-to-limb var. 78—20898
inhomogeneous source radiant intensity, averaged cross-spectral density concept 78—74958
intensity correlations in presence of additive background noise 79—27167
interacting glaxies, radial vels. and luminosities 77—78874
intergalactic optical surface brightness in Coma cluster, photometry 77—87550
interior scenes, optimum photographic representaton of brightness 80—31921
interstellar dark globules, IR surface brightness and emergent spectra 78—53999
inverse problem for scalar planar sources radiometry and coherence, book contrib. 79—31797
Io, 5 micron variability 80—46463
Io, intense transient brightening obs. near 5 micrometres 79—101113
Io, search for colour changes and brightening upon eclipse reappearance 77—91469
IR radiation brightness unit reproduction error anal., USSR standard 78—45699
irradiance distribution parameters fast meas. by image chopping techniques 79—36839
Jupiter, 5 μm brightness temps. and vertical cloud struct. 77—29710
Jupiter, atmosphere optical parameters latit. vars. from 0.6 to 1.1 μ spectrophotometry 80—46468
Jupiter, far IR spectrum and brightness temp. 77—29681
Jupiter, H I 1216 Å brightness and far UV (1200-1900 Å) spectrum 77—25974
Jupiter, phase effect for disc features brightness coeff. 80—98602
Jupiter tropical and temperate belts, 0.6 to 1.1 μm spectrophotometry, brightness distrib. and atmosphere optical parameters 79—92715
BL Lacertae, existence of periodic components in light vars. *(Russian)* 79—101205
BL Lacertae objects, luminosity function and implications for X-ray background 80—8682
BL Lacertae objects, search for rapid brightness variability 80—90567
BL Lacertae objects, X-ray emitting, optical and X-ray flux vars. 79—48921
laser system, high energy, thermally induced optical distortion 80—38051
layered media, radiative transfer theory for scatt. 79—76553
LED, meas. by photometric method *(Japanese)* 77—82584
LED, red, luminance-brightness discrepancy 80—91942
LED luminous intensity ang. distrib. and total light flux meas. device *(Chinese)* 78—82018
light flux brightness meas., EM vacuum fluctuations, quantum noise 80—57361
light flux leaving a hollow cylinder 80—32909
light source, radiance spectral density meas. 79—30527
light source measurement standard photometric system errors 78—58005
light sources, psychophysical luminous efficiency *(Polish)* 80—33110
lightguide transmission, radiance diminution, Hamiltonian ray optics analysis 78—46787
linear light sources appl., direct component of illumination calc. *(Rumanian)* 80—43421
liquid crystal displays, brightness and contrast ang. depend., meas. apparatus 77—7222
luminance contrast effect on perception of chromatic blur, in colour TV images 79—39419
luminance difference thresholds of foveal vision, uniform surrounding luminance effects *(Japanese)* 79—24988
luminance standard using W halogen lamp *(German)* 79—89980
luminous field of circular source, integral characts. comparison *(Czech)* 80—53394
luminous flux distrib. in room, electrical analogy 80—33266
luminous intensity meas., of retroreflectors and retroreflective materials, photometry accuracy assessment *(Dutch)* 79—85159
lunar craters, brightness vars. during eclipses 78—61770
lunar disc, brightness distrib. determ. from light refl. meas. 80—17512
lunar surface brightness fluctuations, photometric and polarimetric obs. 77—78681
M13, globular cluster, Calculated and observed integral magnitudes comparison 79—97043
M31 bulge, triaxial models rel. to surface brightness distrib. 77—45539
M32-1, planetary nebula in M32, forbidden O III 5007 Å luminosity 79—25664
M82, UBV colours and surface brightness distrib. of galaxy 79—9006
M87, luminosity profile and central supermassive object from SIT and CCD area photometry 78—49528
Magellanic Clouds, UV brightness maps and UV spectra 80—85994
Markarian 231, Seyfert 1 galaxy, optical variability 79—40259
Markarian 335, Seyfert galaxy, 0.36 to 3.5 μm luminosity from spectroscopic investigation *(Russian)* 79—101204
Markarian 509, galaxy, brightness variability meas. *(Russian)* 77—17671
Markarian galaxies, luminosity function rel. to nature 78—28781
Markarian galaxies, UV excess rel. to emission line intensities *(Russian)* 77—17672
Mars, atm. optical props. during 1971 dust storm 77—13274
Mars, brightness temp. and albedo mapping during Viking primary mission 78—20683
Mars, far IR spectrum and brightness temp. 77—29681
Mars, integral photometry 78—61780
Mars, isophotes as clue to aerosol characts. 77—29699
Mars, longit. var. of thermal inertia and 2.8 cm brightness temp. 80—105191
Mars, radio brightness longit. depend. confirmation 80—21937
Mars, rot. vars. in radio brightness 77—45340
maximum spectral luminous efficacy determ. *(Chinese)* 78—16831
MCG—6-30-15, type 1 Seyfert galaxy, X-ray luminosity and X-ray/optical luminosity ratio 80—82479

brightness continued
MCG 8-11-11, X-ray Seyfert galaxy, nucleus, brightness and colour vars. 79—25701
meas., cine projection brightness meter *(Russian)* 77—49797
measurement with LaB_6 cathodes 80—68296
meteors, luminous efficiency coeff. from photographic obs. 78—96440
meteors, magnitude errors and magnitude scales of observers in Sweden and Czechoslovakia 78—36533
meteors, optical brightness rel. to ionised trail props. 80—77354
meteors, television photographs photometry and brightness curves 78—96441
9 Metis, UBV photometry, light curve and rot. period 80—21942
Moon, brightness at 2 and 6 cm wavelength, centre to limb var. 78—81572
Moon, brightness of 1975 November 18 total eclipse, obs. in Tadzhikstan 77—67052
Moon, disc brightness distrib. rel. to photometric props. and dimensional scatt. indicatrix 80—101538
Moon, geometric albedo and full Moon magnitude 77—33374
Moon, integral brightness during 1974 November 29 total eclipse, obs. in Ussuriisk 77—67051
Moon, photometric and polarimetric obs., 1976 April to 1977 December 80—51677
multigradation image, representation in Boolean algebra 77—31071
Neptune, albedo and brightness temp., 5 μm IR obs. 80—82300
Neptune, methane and ethane emission brightness temps. 78—16344
Neptune, secular brightness increase, 1972-76 period 78—16346
NGC 1023, SB0 galaxy, surface photometry, brightness distrib. 77—22316
NGC 1275, luminosity profile and spectra 77—33630
NGC 1275, Seyfert galaxy, nucleus, radio brightness distrib. rel. to mag. field struct. *(Russian)* 80—62288
NGC 1435, refl. nebula near Merope, UV surface brightness rel. to interstellar grains phase function 79—97047
NGC 1999, electronographic imaging polarimetry obs. of reflection nebula 80—26964
NGC 253, barred spiral galaxy, three component luminosity model from surface photometry 80—105327
NGC 2742, spiral galaxy, luminosity and mass/light ratio *(French)* 78—89255
NGC 3115, s0 galaxy, photometric obs. 77—29917
NGC 4565, edge-on spiral galaxy, halo luminosity from grid photography 80—62261
NGC 4565, spiral galaxy, minor axis brightness profile rel. to massive halos problem 78—93409
NGC 4565, spiral galaxy, surface brightness of optical halo 78—12364
NGC 5383, barred spiral galaxy, optical surface photometry 79—9000
NGC 5866, edge-on galaxy, luminosity obs., BV photometry 80—82511
NGC 6251, radio jet brightness and shape rel. to beam and slingshot models 79—25741
NGC 6251, very large radio galaxy with exceptional jet, radio luminosity 78—12394
NGC 6946, galaxy, radio continuum brightness distrib. of nonthermal disc. 77—41407
NGC 7023, refl. nebula, far UV brightness rel. to HD 200775 reddening and dust albedo and scatt. 80—51832
ocean, optically thick medium, asymptotic radiance and polarisation 77—21776
ocean underwater irradiances on horizontal surfaces, effects of clouds on diurnal var. 80—72549
OI 090.4, BL Lacertae object, photometric history 80—77491
OJ—131 BL Lacertae object, photometric history 80—77491
OJ 287, BL Lacertae object, case for synchronous optical-radio outbursts 80—8679
opal glass, spectral reflection coeff. and luminanance factor absolute meas. *(German)* 77—87802
optical ceramic, KO-1, IR scatt. and brightness indacatrices meas. 78—71164
optical fibre array, gradient-index, unevenness of illuminance 80—69482
optical radiation power photometry, USSR system of standards 77—30194
optical-TV velocity detector *(Russian)* 80—105695
Orion Nebula, emission lines surface brightnesses from near IR Fourier spectroscopy 77—57071
partially coherent source radiant intensity, theorems and expts. 80—78768
peculiar extragalactic objects, surface brightness distribs. from multiaperture photometry 78—28772
118 Peitho, rot. period and light curve from photoelectric obs. 80—46454
perceived motion condition for temporal facilitation, stroboscopic motion 79—53132
perception, nonlinearities, computer plotted luminance profiles 77—56380
Periodic Comet Ashbrook-Jackson (1977g), total visual magnitude estimates 78—93169
Periodic Comet Comas Sola (1977n), total visual magnitude estimate, (1978, October 8) 78—96435
periodic Comet Comas sola (1977n), total visual magnitude estimate (1978, November 29) 79—16889
Periodic Comet Schwassmann-Wachmann 1, appearance and total magnitude (1979) December 80—36571
Periodic Comet Schwassmann-Wachmann 1, new outburst, total visual magnitude estimates 79—53774
Periodic Comet Schwassmann-Wachmann 1, total visual magnitude estimate, (1979 February 4) 79—30011
Periodic Comet Stephan-Oterma (1980g), total visual magnitudes and coma diameters, (1980 September 7 to 11) 80—109397
Periodic Comet Tempel 2 (1977d), BV photometry, (1979, January 28 and 31) 79—30012
Periodic Comet Wild 2, (1978b) magnitudes, (1978, February 8 to May 11) 78—53885
PHL 1070, quasar, magnitude and spectrum of surrounding halo 78—28771
PHL 957, quasar, upper limits on Lyman α halo 80—51907
Phobos, opposition brightness surge from Viking orbiter images 80—72838
photographic, two-dimensional field, simulation 77—79778
photometric etalons, scatt. matrix and brightness coeffs. of MS-20, MS-14 reflectors 78—82020
photosphere, new determ. of granule/intergranule contrast 78—20797
photosphere fluctuations, two-dimensional spectral anal. of disc centre granulation 77—53520

brightness continued
phototransduction dynamic props. in fly, Phormia regina, light adaptation effect 79—53109
TX Piscium, disc brightness distrib. and envelope obs. from lunar occultation meas. 80—67725
PK 181+1.1, very low surface brightness planetary nebula near galactic anticentre, discovery 79—17049
PKS 2126—15, QSO (z=3.27), bolometric luminosity from JHK obs. 80—94888
PKS 2155, BL Lacertae object, UV flux meas. by IUE 80—12833
PKS 2155-304 (H2155—304), newly discovered BL Lacertae object, optical polarisation, spectrum and variability 80—36702
planar sources generating same radiant intensity distribs., equivalence theorems 79—89843
planetary disc, brightness distrib. determ. from light refl. meas. 80—17512
planetary nebulae, isophote pictures rel. to spatial structure investigation by mathematical modelling *(Russian)* 79—101188
planetary nebulae, optically thin, radius/surface brightness relation rel. to distance scales 80—109521
planetary nebulae, stellar, radio brightness temps. from VLA obs. 80—22056
planetary nebulae spatial distrib. and luminosity function, evidence from obs. in (M31) 80—109520
planetary solids near opposition, laboratory study of limb-darkening 78—36477
planetary surfaces brightness characts. calc. method 79—62754
planets, far IR brightness temps. recalibration 77—9683
planets, solar activity effects 79—75177
planets photometric properties, theory 80—67601
plasma jet, absolute spectral brightness measurement 80—28832
power luminance spectral density unit, USSR state standard, 0.05 to 0.25 micron wavelength range, synchrotron radiation principle 79—2819
790 Pretoria, C-type asteroid, light vars. obs. and rot. period 80—21941
psychometric measures for specifying colour appearance 80—76747
Q0957+561, double quasar, components brightness ratio var. 80—77509
Q 0420—388, QSO (z=3.13), bolometric luminosity from JHK obs. 80—94888
QSOs, optically selected, intrinsic optical luminosity correl. with radio detectability 80—82536
quasars, absolute magnitude-volume diagrams construction and cosmological appls. *(French)* 80—8705
quasars, absolute magnitudes and Hubble plot 77—91662
quasars, colour variability during flare-ups 79—9021
quasars, cyclic depend. of brightness on parameter ln $(1+z)$ 80—105382
quasars, low-red shift, photoelectric UBV photometry *(French)* 80—51904
quasars, luminosity and emission line intensity ratios 80—86011
quasars, luminosity evolution rel. to faint quasars number limits 79—92884
quasars, luminosity function, const. density model with luminosity evolution 77—5586
quasars, luminosity function and density vars. determ. from Hubble diagram statistics 79—97093
quasars, number-magnitude relation rel. to luminosity function and cosmological evolution 80—77507
quasars, optically selected, radio/optical emission ratio distrib. function 78—20904
quasars, radio intensity and polarisation distribs. at three freqs. 78—96560
quasars, search for rapid brightness variability 80—90567
quasars assoc. with compact radio sources, apparent magnitude-redshift relations for resolved and unresolved sources *(Chinese)* 80—105380
quasars of 4C catalogue, radio structs. and model brightness distribs. 79—75293
quasi-stellar objects, luminosity indicators in emission-line spectra 77—57103
quasi-stellar objects, shot-noise interpretation of historical light curves 77—37666
quasisteller objects in $13^{h}+36°$ field, optical variability from blue magnitudes obs. 79—40291
quiet Sun, 1.35 cm radiogranulation brightness correl. with chromospheric network pattern *(Russian)* 78—40897
quiet Sun, brightness distribs. and temps. at metre and decametre wavelengths 78—4184
quiet Sun, radio brightness and extent at <200 MHz, scatt. effects 78—4183
quiet Sun, supergranulation, radio network and limb brightening obs. at 6 cm 80—36601
radiant intensity from planar sources of any state of coherence 79—27163
radiation fields from polygonal sources, Fock method 78—83060
radio brightness temp. of Earth from Kosmos 243 and Nimbus 5, SHF obs. 80—72521
radio galaxies, radio brightness distrib. obs. with RATAN-600 telescope 78—65698
radio sources, 5 GHz, in galactic plane, catalogue, brightness temps. and flux densities 80—4269
radio sources, brightness distrib. investigation via lunar occultations 78—65712
radio sources, brightness distribs. rel. to measured ang. dias. 79—12534
radio sources, extended, extragalactic, relation between radio luminosity and spectrum 80—51894
radio sources, extended internal dynamics and brightness distribs. 77—22323
radio sources, extragalactic, radiation intensity and space distribs. nonrandomness *(Chinese)* 79—17111
radio sources, extragalactic, study of emission variability in millimeter wave range *(Russian)* 80—90559
radio sources, jets brightness and shape rel. to beam and slingshot models 79—25741
radio sources, luminosity evolution rel. to source counts freq. depend. and spectral index distribs. 78—96554
radio sources, luminosity function cosmological evolution from free-form anal. 78—41070
radio sources with short wave radio emission excess, flux densities and variability at 1.35 cm *(Russian)* 78—57666
radioastronomy, flux density meas. of calibration sources at 2295 MHz 77—37663
radiosources, brightness distrib. determ. via phaseless aperture synthesis 78—32353

brightness continued
radiosources, two-dimensional max. entropy reconstruction of radio brightness 78—28534
random arrays of grains, spectral props., jitter model, comment 79—41339
random arrays of grains, spectral props., jitter model 79—45905
random nonGaussian backgrounds, simulation, calc. spatial correl. function 78—79089
reflectance map calc., surface bidirectional refl.-distrib. function 79—75568
reflecting sea surroundings, IR contrasts 77—5211
relief objects on plane, brightness and illumination characts. calc. 79—904
retinal distribution of illuminance, universal mathematical expression *(German)* 79—92214
retinal rivalry and brightness perception models in binocular vision 80—101180
retinal single-photon impulse coding mechanisms *(Russian)* 78—27941
Saturn, 5-8 µm photometry 77—29711
Saturn, A ring spiral struct. explanation for asymm. brightness 77—9705
Saturn, IR brightness scans (1977 to 1978) 80—90363
Saturn, limb darkening and brightness temp., 1.30 cm interferometry obs. 80—82279
Saturn, phase effect for disc centre brightness coeff. 80—98602
Saturn, ring brightness temp. meas. at 8 mm wavelength 78—36502
Saturn's rings, azimuthal brightness vars., obs. at intermediate tilt angle 78—4145
Saturn's rings model for azimuthal brightness variation 80—31251
Saturn A and B rings, surface brightness obs. *(Russian)* 80—72872
Saturn A-ring, azimuthal brightness var. and particles size 78—32391
Saturn and its rings, aperture synthesis study at 3.71 cm wavelength 79—96963
Saturn and its rings, interferometric obs. at 3.71 cm wavelength 79—96962
Saturn E-ring, obs. and brightness distrib. 80—67647
Saturn ring system, brightness enhancements rel. to existence of supposed satellites (1980 S 7 and 23) 80—94749
Saturn rings, azimuthal brightness var. 78—36503
Saturn rings, IR brightness and eclipse cooling obs. 80—56763
Saturn rings azimuthal brightness vars., obs. at tilt angle (B~11.°5) 79—48732
Saturn rings diffuse reflection, mutual shadowing effect classical calc. extensions 79—84666
Sb-type galaxies, luminosity classification rel. to Hubble const. local value 80—62339
scalar wave fields of fluctuating primary planar sources, coherence and radiant intensity 78—90355
sea, light diffusion, radiance distrib. 77—78216
sea ice, low-salinity, UHF and microwave brightness temps. meas. 78—81175
sea outgoing radiation spectrum, meas. appl. to suspended material and chlorophyll conc. estimation 80—36333
Seyfert 1 galaxy nuclei, luminosity function and implications for X-ray background 80—8682
Seyfert galaxies, nearby, discs radial surface brightness distribs. from photographic study 80—82478
Seyfert galaxies, thermal IR emission vars. 80—67865
Seyfert galaxies, type 1, nuclei props., UV emission, colour index *(French)* 79—48923
Seyfert galaxies, X-ray luminosity function and variability time scale 78—57701
Seyfert galaxies X-ray emission, luminosity function from Uhur obs. 78—93392
shape factors determ., luminous flux transfer meas. 77—31147
shock waves brightness, in air with reduced density 80—86371
140 Siwa, C-type asteroid, light vars. obs. 80—21941
small particles, brightness and contrast of holographic images 80—99675
snow, microwave brightness temps. from 3 to 60 mm wavelength radiometry 80—72561
solar 6 cm radio emission, peak brightness temps. of active region and burst sources 80—62096
solar active regions, brightness temp. enhancements at submillimetre wavelengths 78—12177
solar brightness temperature, 85-250 µm, with balloonborne lamellar grating interferometer 77—13308
solar brightness temperature near its minimum, meas. by balloon-borne lamellar-grating interferometer 78—85921
solar chromosphere line brightness fluctuations *(Russian)* 79—21259
solar corona, 1973 June 30, polarised brightness distrib. rel. to N.polar hole density model 80—98627
solar corona, EUV lines brightness rel. to temps. and temp. gradients 77—17506
solar coronal hole, brightness temp. from λ 8-cm radioheliograph obs. 80—4326
solar coronal hole boundary brightness in Fe XV 284 Å radiation 79—84775
solar faculae, mag., vel. and brightness struct. 79—25557
solar far IR brightness temp. minima rel. to sunspot activity 80—62035
solar flares, radio brightness distrib. processing in one-dimensional synthesis *(Italian)* 80—98628
solar flares, search for auroral type brightness motions 77—60744
solar granulation, brightness fluctuations and lifetime from balloon-borne imagery 78—28601
solar granulation, morphological interpretation of spatial power spectrum 78—65581
solar luminosity and sunspot cycle 79—75176
solar luminosity variation, Ca H and K behaviour at solar minimum and cycle 21 onset 79—16907
solar photosphere, granular brightness fluctuations centre to limb var. 79—66971
solar photosphere faculae intensity, centre to limb var. 80—21967
solar thermal sources, microwave brightness temps. and polarisations derivation 77—22172
source coherence and far-field intensity patterns, cross spectral density function determ. 79—55053
spectral lines, hyperfine struct., brightness distrib., form. model verification 77—57928
specular sphere scatt. radiance matrix, refl. standard for polarised beam scatt. meas. 80—74299
spiral galaxies, local mass-to-light ratio radial var. 80—31361

brightness continued
spiral galaxies, luminosity class correl. with number of comparison 80—77481
spiral galaxies, types Sab to Scd, luminosity, freq. distrib. 80—82482
spiral galaxies nuclear bulges, absolute magnitudes correl. with spectra and stellar population 80—56926
spiral galaxies studied at Westerbork, light distribs. from optical surface photometry 80—17655
star image, true brightness distrib. 80—62034
star magnitude simulator, IC device 78—81742
stars in eclipsing binaries, average absolute brightness *(Polish)* 77—17630
steel, stainless, brightness, vacuum heating effect *(Japanese)* 79—61752
Sun, absolute brightness temp. meas. in far IR with balloon-borne interferometer 80—62095
Sun, brightness distrib. at 33 and 37 GHz 77—53524
Sun, brightness distrib. at 8.6 mm, interferometer obs. 80—56800
Sun, brightness temp. at millimetre wavelengths 77—22171
Sun, brightness var. at extreme limb in centimetre radio waves 80—21969
Sun, equatorial brightness distrib. at 2.8 cm, one dimensional aperture synthesis obs. 77—22173
Sun, north-south brightness asymmetry, obs. 78—45303
Sun, photospheric fine structure, no correlation between brightness and radial vels. *(Russian)* 80—17564
Sun, quiet, small-scale brightness struct. obs. at 8 millimetre wavelength 79—40149
Sun, radius at centimetre wavelengths and brightness distrib. across disc 80—21968
Sun companion star, visible or IR brightness prediction rel. to reality 78—57475
sunspot chromosphere, radial vel. and brightness oscills. regimes *(Russian)* 80—51727
sunspot penumbrae, fine struct. of mag. field and brightness 77—22179
supernova remnants, galactic, new catalogue and surface brightness-dia. relation 79—75120
supernova remnants, galactic, radio evolution and population characts. 79—75254
supernova remnants, radio surface brightness-diam. correl. 77—29899
supernova remnants in LMC, SHF obs. 80—67864
surface brightness, meas. by newly developed reflectometer *(German)* 80—42253
surface brightness distributions in elliptical galaxies 79—40268
87 Sylvia, UBV photometry, light curve and rot. period 80—21942
synchronous spot-scanned underwater viewing system 77—21934
target edge sharpness and temporal brightness enhancement 79—53152
Taurus A (Crab Nebula), supernova remnant, 927 MHz emission secular decrease 79—75255
terrestrial luminance field spatial structure 78—49140
thermal source, use of optical parametric converter for brightness determ. 80—98979
thick layers, refl., transmission and brightness coeffs. 80—63918
Titan, light curve during eclipse by Saturn rel. to Saturn upper atmosphere struct. 80—90362
Titan, secular brightness increase, 1972-76 period 78—16346
Titan, suspected near IR variability 80—46469
Titan (Saturn VI), brightness decrease during eclipse (1979 December 20) 80—31250
tropical cloud clusters, submillimetre radiation obs. from Cosmos 669 *(Russian)* 77—49165
TV colour films, usable range *(German)* 80—57408
two-layer atmosphere with anisotropic scatt., brightness coeffs. *(Russian)* 77—17349
underwater light field, scatt. light influence anal. 77—64322
uneven interface of media with different refractive indices, statistical characts. of images 80—87331
upper atmosphere, IR radiation flux meas. in 4 to 6 μm spectral range 80—61929
Uranus, albedo and brightness temp., 5 μm IR obs. 80—82300
Uranus, methane band limb-brightness obs. 79—84742
Uranus, microwave brightness temp. increase 78—93150
Uranus, secular brightness increase, 1972-76 period 78—16346
UV excess object, variable, discovery and UGR photometry 79—40280
vacuum UV energy brightness spectral standard source, 0.05-0.25 μm range 77—79909
Venus, brightness temps. from high spectral resolution obs. in 450 to 1250 cm^{-1} region 77—91456
Venus, disc brightness distrib. from photometry rel. to models 79—40107
Venus, far IR spectrum and brightness temp. 77—29681
Venus, IR brightness temp., daytime minima 80—77309
Venus, IR brightness temp. and thermal asymmetry 77—53447
Venus IR brightness, limb darkening and thermal anomalies obs. 78—85876
Venus surface panoramas, photometric analysis of Venera 9 and 10 obs. 77—78686
visibility measurement, photometric contrast *(German)* 80—95118
vision, apparent brightness rel. to contrast threshold on photopic background 77—9200
vision, apparent contrast of temporal square waves, from light- and dark-phase matching data 77—36939
vision, asymmetry in the brightness and darkness Broca-Sulzer effects 80—101185
vision, binocular and monocular perception, threshold luminance meas. *(Japanese)* 78—40166
vision, brightness enhancement vs. darkness enhancement at borders 78—7366
vision, brightness subjective evaluation rel. to object and adaptation luminances *(Japanese)* 78—44509
vision, Broca-Sulzer effect, combined temporal and spatial unified model 80—35893
vision, Broca-Sulzer effect under scotopic viewing conditions 77—12924
vision, contrib. of cortical colour channels to brightness sensation 78—11657
vision, desaturating blue increases only chromatic brightness 77—44666
vision, effect of stimulus luminance on dichoptic pattern masking 77—44680
vision, foveal and spatial props. of brightness metacontrast 77—40677
vision, luminous efficiency functions determined by successive brightness matching 79—43906
vision, metacontrast masking rel. to luminance transients 77—81506
vision, peripheral, absence of rod activity 77—9194

brightness continued
vision, photopigment depletion effects 78—56977
vision, wavelength-specific brightness contrast as a function of surround luminance 80—61564
visual flicker-induced asymmetries in border enhancement, brightness and darkness perception 80—67083
visual luminance difference threshold, Holladay's principle *(Japanese)* 78—65000
visual system, nonlinear receptive field model 78—27951
visual temporal brightness enhancement determ. by luminance, chromatic stimuli 79—74672
volume-phase reflection hologram, recording medium thickness effect on image luminance 80—58479
VUV spectral irradiance calibrations, method and appl. 80—87452
VV 8, galaxy, rot., mass and surface brightness obs. *(Russian)* 79—48937
water bodies, natural, surface radiance rel. to suspended sediment remote sensing 79—53558
weak radio galaxies, relationship between radio power and enhanced emission regions separation 79—25726
WLM galaxy (A2359), BV photometry rel. to distance and absolute magnitudes 77—82302
X-ray clusters of galaxies, luminosity evolution over cosmological time scales 78—28770
X-ray clusters of galaxies, X-ray line and continuum brightness distrib. 78—8149
X-ray clusters of galaxies, X-ray luminosity correl. with galactic content 78—32585
X-ray galaxy clusters, luminosity function 79—40277
X-ray sources, extragalactic, luminosity evolution rel. to detect. in deep surveys 78—96567
X-ray sources in SMC, max. luminosities from deep survey 79—25702
zodiacal light, brightness depend. on helioecliptic coords. 80—72878
zodiacal light, search at 1550 Å 79—16882
zodiacal light brightness integral inversion, three-dimensional eqn. 79—75155
zodiacal light brightness integral inversion 79—48738
zodiacal light brightness rel. to galaxies apparent magnitudes estimation *(Russian)* 78—93389
zodiacal light photopolarimetry, brightness annual vars. rel. to zodiacal cloud symmetry plane 78—45276
Zwicky galaxies, luminosity function slope 80—36709
Au vapour brightness amplifier at 627.8 nm, for projection microscope 80—83616
Cu, electrolytic coating, brighness and adsorption of surface-active additives 80—100963
Cu, electroplated surface roughness and brightness rel. to periodic reverse current 79—96201
Cu, spherically shaped crysts., surface melting, IR emission obs. 77—20050
H I regions, 21 cm line brightness temp. rel. to galactic shocks 78—54042
H I survey, brightness temp. contour maps, 21 cm obs. 80—85986
H II regions, anisotropic, with axial symmetry, models and brightness distribs. 78—85993
H II regions is IC 1795/1805, IR luminosity compared with exciting star total luminosity 78—96519
H$_2$O maser source in Orion A, radio flux density and line width during outburst *(Russian)* 80—105320
Hα line brightness in solar prominences, radiation diffusion theory 80—67694
Hf, 0.3 wt.% Zr, melting pt. and radiance temp. meas. by pulse heating method 77—53914
KrF* laser, generation of high-spectral-brightness tunable XUV radiation at 83 nm 80—91846
LaB$_5$ gun, optimum brightness problem 78—21298
LaB$_6$ cathodes, mounting methods and operating characts. 80—57437
LaB$_6$ cathodes, single crystal, of <100> and <110> orientations, brightness meas. from 1500 to 1950K 80—62808
Mo, liquid, spectral emissivity and brightness-temp. meas. at MP 77—43356
Nb, liq., spectral emissivity and brightness-temp. meas. at MP 77—43356
Nd:glass laser amplifier with spatial filters, optimal length and operating conditions 80—48323
Nd:glass laser system, beam spatial profile optimization in amplifier channel 80—74407
Nd^{3+}:phosphate glass laser, brightness enhancement by spatial filtering in amplifying channel 80—48321
Ru, liq., spectral emissivity and brightness-temp. meas. at MP 77—43356
SiC cavity radiator, spectral emissivity and radiance 77—83939
SiO$_2$, fused, high-temp. darkening and absorption spectra meas. 77—36258
SnO$_2$-Cu$_x$S-ZnS:Mn,Cu-Al$_2$O$_3$-Al, light-emitting struct., cond. and electrolum., heat treatment 80—97345
Ta, radiance temp. at melting point 77—15603
Ti, liq., spectral emissivity and brightness-temp. meas. at MP 77—43356
V, liq., spectral emissivity and brightness-temp. meas. at MP 77—43356
Xe pulsed arc lamp with adjustable plateau slope 79—68422
Y$_2$O$_3$ capillary discharge plasma, temp., radiation screening elimination 80—64682

Brillouin scattering *see Brillouin spectra*

Brillouin spectra
see also stimulated Brillouin scattering
acetic acid, liq., sp. ht. of 2nd relax. step *(German)* 79—37766
acetic acid, Rayleigh-Brillouin scatt., 20-115°C, viscoelastic theory anal. 79—28774
adsorbed monolayers, acoustic phonons, obs. method using Brillouin scatt. 80—59804
n-alcohols, sound vel. and absorpt. meas. at hypersonic freqs. 78—18708
alkaline nitrates, Raman and Brillouin scattering, temp. influence on freq. of NO$_3^-$ ion *(French)* 79—69833
n-alkanes, liq., hypersonic attenuation, temp. depend. of Brillouin spectra 79—11426
amorphous polymer, Rayleigh-Brillouin spectroscopy 79—38556
Auger lineshape anal. of molecules and solids 80—76113
benzene, Brillouin scatt., cryst. at 0°C, elastic consts. 78—43882
benzene, high press. Brillouin scatt., hypersonic speed 77—48182
benzene, hypersound propagation temp. depend., Mandelshtam-Brillouin spectra meas. 78—31210

Brillouin spectra continued
benzene, single crystals, Brillouin spectra, elastic consts. and intermol. pot. 79—42977
binary mixtures and simple fluids near crit. point, Rayleigh and Brillouin scatt. 77—36256
biphenyl-d$_{10}$, Brillouin scatt. at room temp. 80—71433
bisphenol A-phthallic anhydride epoxy resin, diglycidyl ether, Rayleigh scatt., Brillouin and IR spectra 80—66211
Bragg diffraction by a 3-D Gaussian ellipsoid and diffraction broadening of Mandelshtam-Brillouin scattering lines 80—55114
butanediol-1,3, viscoelastic props., digital correlation Brillouin scatt. 78—2865
carbon tetrabromide, Brillouin scatt., plastic-liquid transition 77—32389
carbon tetrachloride, liq., Brillouin scatt. for vibr. relax. time 79—4806
carbon tetrachloride, polarized light scatt., relaxation processes 80—60615
CBOOA, isotropic, nematic, smectic-A phases, Brillouin scatt. 80—11421
chlorobenzene, polarized light scatt., relaxation processes 80—60615
chloroform, liq. vibr.-translational energy exchange, temp. depend., Brillouin scatt. obs. 79—73959
2-chloronaphthalene, elastic props. exam. by Brillouin scatt., rel. to polymorphism 79—77669
cholesteric liquid crystals, Brillouin scatt. in isotropic phase 78—2867
coesite, elasticity meas. by Brillouin scatt. 77—44978
collagen and muscle elastic moduli rel. to phonons 77—52824
computer-controlled Gabry-Perot interferometer for Brillouin spectroscopy 79—40622
condensed media, optical spectrometer for freq. shift meas. *(Russian)* 78—29180
crystals, book 80—2774
cubic crystal, acoustic waves, Christoffel elastic eqns. and elastic consts., rel. to Brillouin scatt. 79—51205
cyclohexane, plastic phase, Brillouin scatt., elastic consts. determ. 79—24324
cyclohexane-tetrachloromethane, heteromolecular vibr. relax. time, Rayleigh-Brillouin spectra 78—59731
cyclohexanol, orientationally disordered phase, Brillouin scatt. study 80—93351
diamond, Brillouin spectra meas. using Fabry-Perot interferometers with 20 cm^{-1} free spectral range *(Japanese)* 77—87847
dichloromethane-cyclohexane, liq. mixture, intermol. vibrational energy transfer, US study 80—70313
dielectrics, nonlinear phonon-photon interactions, physical basis 77—61998
differential-type Brillouin scattering system, construction *(Japanese)* 78—89562
dipalmitoyl phosphatidylcholine(-cholesterol) aligned multilamella lipids, elastic props., Brillouin spectra 79—5255
entropy and LA fluctuations in solids, polarisation of scattered light 77—81113
ethanol, aq. soln., conc. fluctuations, shear and longit. relax., Brillouin scatt. and pulse techniques 78—71792
ethyl lactate, sound vel. and absorpt. meas. at hypersonic freqs. 78—18708
ethylene glycol, Brillouin scatt. and segmented motion 79—37609
exchange and dipoles coupled ferromags., light scatt. from mag. surfaces, response theory 79—42820
exciton polaritons, Brillouin scatt. and additional boundary conditions 79—95795
exciton-polaritons, reson. Brillouin scatt. theory 80—50353
ferroelectric and ferroelastic phase transitions, dynamical spectroscopy 80—55115
ferromagnet, light scatt. by spin waves 80—45086
ferromagnet, surface, Brillouin light scatt. by spin waves 80—93359
ferromagnetic metallic glasses, Brillouin scattering 78—92085
ferromagnetic slab, finite thickness, magnetostatic theory of response functions, appl. to Brillouin scatt. 79—61083
ferromagnetic thin films, Brillouin scattering from spin waves 80—65843
fibre optical ring interferometer, Sagnac-effect, sensitivity 79—50379
fibre waveguide, Brillouin and Rayleigh scatt. meas. 78—30085
fibres, natural, Brillouin scatt. shifts, comparison with synthetic polypeptide obs. 80—55991
fluid, dense, statistical mech. of stationary state fluctuations 79—54035
fluid fluctuations about hydrodynamic nonequilibrium steady states, Langevin method calcs. 80—53761
fluid in nonequilibrium steady state, light scatt. hydrodynamics theory 80—50354
fluid with stationary temp. gradient, light scatt. 80—45097
fluids with nonuniform velocity fields, light scatt., and pair correl. functions 79—61389
fluorite crystals, Brillouin scatt. and high temp. disorder 78—80365
fluorite crystals, disorder at high temp. 78—2866
fluorobenzene, liq., vibr. relax., Brillouin scatt. obs. 79—51206
fluorobenzene, polarized light scatt., relaxation processes 80—60615
furan-cyclohexane, liq. mixture, intermol. vibrational energy transfer, US study 80—70313
n-GaAs, semidegenerate, acoustoelec. gain and lattice attenuation, X-ray Brillouin scatt. and elec. meas. 79—15193
gas, dilute, kinetic-hydrodynamic transition obs., Brillouin scatt. 77—7508
gas, nonequilibrium, kinetic theory 79—46421
n-Ge, degenerate, Brillouin scatt. by phonon zero sound, in quantising mag. field 77—69847
glass, laser, elastic, elasto-optic consts. and extinction coeffs., Brillouin scatt. meas. 79—11429
glass destruction, by laser radiation, Brillouin-Mandelshtam scatt. influence *(Russian)* 77—72039
glass film on substrate, Brillouin scatt. from surface phonons, SAW vel. and attenuation 78—95587
halobenzenes, liquid, vibr. relaxation, Brillouin spectra 80—108219
heptyloxylbenzoic acid, isotropic phase, light scatt., ultrasonic vel. and absorpt. meas. 78—48189
n-hexadecane-β,β′-dichlordiethyl ether exfoliating mixture, light scatt. and hypersound vel. 77—28586
2,4-hexadiine-1,6-diol-bis(p-toluene sulphonate), cryst., polymerisation, elastic consts., Brillouin scatt. 79—1950
hexanetriol 1,2,6, liq., light scatt. study of struct. relax., viscosity and dielec. relax. 79—86672
high-precision measurements of Brillouin scattering frequencies 80—27349

Brillouin spectra continued
HOBA, isotropic phase, Brillouin scatt. spectra, hypersound data determ. 79—91453
inelastic light scattering conference, Santa Monica, CA, USA (Jan. 1979) 79—95762
inert gas crystal, dielec. const., Brillouin scatt., short-range at. interaction effect 78—43881
inert gas solids, Brillouin scatt. intensity, elastooptical coefficients 78—10907
inert gas solids, self-consistent phonon theory, book contrib. 77—51460
interferential spectrometry in Brillouin scatt. 77—178
intermolecular spectroscopy and dynamical properties of dense systems, conf., Varenna, Italy (1978) 80—82581
ionic solution, light scatt., hydrodynamic theory 78—6692
isotropic metals, theoretical anal. 78—80367
kinematics and dispersion relation for Brillouin scatt. process, wave vector surfaces representation *(German)* 78—19492
laser light reflection enhancement from expanding laser prod. plasma, Brillouin scatt. 77—3963
laser-target interaction expt., backscattered light and harmonic generation, spectral anal. 78—59676
light scattering in fluid far from equilibrium 80—103965
lineshape, theory in opaque material 77—16323
lineshapes, oblique-incidence Brillouin scatt. by acoustic phonons 78—72534
lineshapes for normal-incidence Brillouin scatt. by acoustic phonons 78—31208
liquid, US-induced birefringence, Brillouin scatt. linewidth, sound absorption coeff. 78—27180
liquid crystal, smectic A and isotropic phases, Brillouin scatt. 77—8591
liquid metals, Brillouin scattering from reflections of surface ripples 78—48188
lithium ammonium tartrate, ferroelectric and ferroelastic transitions, Brillouin scatt. meas. 79—33716
lithium ammonium tartrate, piezoelec., proper ferroelastic transition 78—2812
lithium ammonium tartrate monohydrate, in paraelec. phase, Brillouin scatt. 78—64373
Love waves, theory of Brillouin scatt. by 80—66212
lubricant, glass transition, light scattering study 79—29228
magnetised plasma, Brillouin and Raman scatt. by extraordinary mode 80—92269
magnons, thermal and excited, Brillouin-Mandelstam scatt. 80—70980
malononitrile, displacive phase transition, 294.7K, Raman and Brillouin-Rayleigh scatt. obs. 80—16047
Mandelstam-Brillouin scatt., instrumental distortion 79—97442
MBAB, liq. cryst., Brillouin-Mandelshtam light scatt. and refr. index 80—55119
MBBA, Brillouin scatt. in isotropic phase 78—2867
MBBA, hypersonic props., Mandel'shtam-Brillouin spectra obs. 79—4813
MBBA, isotropic phase, Brillouin scatt. spectra, hypersound data determ. 79—91453
MBBA, isotropic phase, light scatt., ultrasonic vel. and absorpt. meas. 78—48189
metal, light scatt. from surface acoustic phonons 78—76484
methane, gas, Rayleigh-Brillouin scatt., hydrodynamic effects calcs. 77—470
methane, liquid, Brillouin scatt. obs., US vel. and absorpt. 80—45085
methane(-d$_4$), liq., Brillouin scatt. and refr. index measurements 80—76035
methyl alcohol, liq., ratio of Brillouin to total light scatt. intensity 78—52515
β-methyl-butyl-methoxybenzylidene amino cinnamate, smectic-B liq. cryst., US attenuation anisotropy 79—55828
3-methylpentane-nitroethane, binary liq. mixture, crit. correlation function, universality 77—7840
molecular crystal, Brillouin scatt. intensity 79—73958
molecular crystal, orientationally disordered, translation-rot. dynamics, soft modes 78—83906
molecular liquid, depolarised Rayleigh-Brillouin spectra, theory 79—69850
molecular solid, depolarised Rayleigh-Brillouin spectra, theory 79—69850
monodisperse polymer solution, thermodynamic fluctuations, light scattering 77—52107
multipass Fabry-Perot Brillouin scatt. spectrometer, optical alignment 79—35854
multipass Fabry-Perot spectroscopy, linewidth correction 77—59583
nematic liquid crystal, isotropic phase, light scatt., ultrasonic vel. and absorpt. meas. 78—48189
nematic liquid crystals, hydrodynamic correlation functions, propagating modes 78—94988
neopentane, Brillouin scatt. near liq.-plastic cryst. transition 78—19495
nonequilibrium stationary states, light scatt., broken time reversal symm. 79—28776
nonlinear estimates of Brillouin scatter in plasma 80—87895
nonlocality effects on optical phenomena in bounded solids, developments 80—93328
4′-n-octyl-4-cyanobiphenyl, interlayer elastic const. meas. close to smectic-A to nematic transitions 77—80606
opaque crystal, Brillouin scatt., photoelastic and surface corrugation contribs. 79—42980
opaque media, Brillouin scatt. theory 79—19895
optical fibres, single-mode, Brillouin spectrum 79—46032
optical glasses, Brillouin scattering meas., sound vels., Pockels coeffs., phonon damping 79—95792
optical materials, elasto-optic coefficient determ. under static loading, by acousto-optic and Brillouin scatt. techniques 79—4787
optical vacuum furnace for Raman and Brillouin spectroscopy 78—58062
optical waveguide, thin film, Brillouin scatt. obs. 78—35153
organic liquids, propag. of hypersonic shear and longitudinal waves, light scatt. meas. 77—51442
PAA, isotropic phase, Brillouin scatt. spectra, hypersound data determ. 79—91453
PAA, isotropic phase, light scatt., ultrasonic vel. and absorpt. meas. 78—48189
paramagnetic crystal, Mandel'shtam-Brillouin light scatt. by hot phonons 77—52110
parametric interaction of EM and acoustic waves in solids, theory 78—60166
particle interactions with infinite and semi-infinite periodic potentials 78—28991

Brillouin spectra continued

- β-picoline-water solution, light scatt. spectra, ultra- and hypersonic absorpt. *(Russian)* 80−93353
- piezoelectric semiconductors, acoustic phonon-conduction electron interaction, Brillouin scatt. theory 77−40255
- plasma, Brillouin backscatt., Langmuir turbulence effect 77−35347
- plasma, Brillouin backscatt., nonlinear three-wave interaction 78−75356
- plasma, laser produced, light scattering 77−11397
- plasma, parametric decay and Brillouin backscatt. instabilities, IR laser induced 77−47187
- plasma, parylene disc irrad. by 1.06 μm laser beam 78−18430
- plasma, Raman and Brillouin backscatt., nonlinear theory 78−47127
- plasma, sidescatter threshold, non-resonant EM pump field modification 78−67362
- plasma laser pulse amplifier using induced Raman or Brillouin processes 80−1279
- plasma slab, homogeneous, convective Brillouin amplification 77−24089
- plasma target, underdense, Brillouin backscatt. saturation 80−14886
- PMMA, Gruneisen const. and thermal props., temp. depend., 4-300K, Brillouin scatt. obs. 80−100662
- PMMA, low-energy excitations and hypersonic props., Brillouin scatt. meas., 1.7 to 15K 77−90160
- PMMA, oriented, hypersound propag., elastic props. 78−75737
- PMMA, shear-wave Brillouin scatt. intensity from photoelastic consts. 79−91454
- poly(4-methyl-1-pentene), semicrystalline, bulk and film, surface effects using Brillouin scatt. 79−42982
- polycarbonate, amorphous US vels. from Brillouin scatt., room temp. to 250°C 79−91454
- polycarbonate, shear-wave Brillouin scatt. intensity from photoelastic consts. 79−91454
- polydimethyl siloxane, Brillouin scatt. and hypersonic relax. 77−55795
- polydimethylsiloxane oligomers, Brillouin scatt. obs. of hypersonic sound speed and loss, mol. wt. depend. 79−91457
- polydimethylsiloxanes, rubbery and liq., hypersonic sound vel., Brillouin spectra meas. 80−75308
- polyethylene glycol, liquid, Brillouin scatt. and segmented motion 79−37609
- polyethylene terephthalate, film, amorphous, Brillouin scatt. and splitting 77−24857
- polyethylmethacrylate, Rayleigh-Brillouin light scatt. study 79−11425
- polyglycine, band struct., ab initio SCF LCAO calcs. 79−22874
- polyisobutylene, Brillouin scatt. and hypersonic relax. 77−55795
- polymer, amorphous, light scatt. and local struct. 77−81111
- polymer, elasticity of bulk and film from multipass Brillouin spectra 78−76485
- polymer, liq., Brillouin scatt. and segmental motion, appl. to polypropylene glycol 78−91217
- polymer films, Brillouin scatt. at transitions 80−70312
- polymer viscoelasticity and strength characterisation, advanced light scatt. techniques 80−11857
- polymers, amorphous, Brillouin scatt., hypersonic relax. 79−4811
- polypropylene, atactic, Brillouin scatt. and hypersonic relax. 77−55795
- polypropylene oxide, solns., mol. relax., dielectric relax. and Brillouin scatt. obs. 77−23590
- polystyrene, atactic, chain length depend. of hypersonic relax., Brillouin spectra 77−55797
- polystyrene, atactic, Rayleigh-Brillouin scatt. 77−4648
- polystyrene, atactic, thermal behaviour above glass-rubber relax. temp. 77−39548
- polystyrene, shear-wave Brillouin scatt. intensity from photoelastic consts. 79−91454
- polystyrene-cyclohexane mixture, Rayleigh and Brillouin scatt. and struct. relaxation 80−63640
- polyvinyl acetate, Brillouin scatt. and hypersonic relax. 77−55795
- population-inverted semiconductors, resonant Brillouin scattering 80−76042
- quartz, fused, longit. phonon lifetimes, thermal Brillouin scatt. obs. 77−36255
- quartz, fused phonon lifetimes at 2.4K 77−62605
- quartz, x-cut, triplepass Brillouin scatt. by induced phonons 77−28588
- range resolved Brillouin scattering using pulsed laser 80−38055
- reflection and transmission modes, rel. to intense acoustic flux, relation linearity test 80−45098
- resonant Brillouin scatt. as form of modulation spectroscopy 79−91456
- resonant light scattering from magnetic excitations, review 80−97290
- resonant scattering, analogy to modulation spectroscopy *(Japanese)* 78−68526
- Rochelle salt, phase transition mechanisms by optical spectroscopy 79−15411
- scattering cell for liquids 80−106694
- semiconducting crystal, opaque, inelastic dynamical light diffraction 80−25399
- semiconductor, excitons, exciton-phonon interaction, review, book contrib. 80−49624
- semiconductor, opaque, light scatt. from surface acoustic phonons 78−76484
- semiconductor, optical non-locality phenomena near exciton reson. 79−95794
- semiconductor, polaritons, two-phonon Brillouin scattering 80−20656
- semiconductor, resonant Brillouin scattering of exciton polaritons 80−93357
- semiconductor, resonant Raman scatt., book contrib. 77−36251
- semiconductor, surface Brillouin scattering from acoustic phonons 80−55113
- semiconductors, optical props. due to phonons, book contrib. 80−80805
- semiconductors, population inverted, resonant Brillouin scatt., photoelastic consts. 80−89015
- short-pulse laser backscatter from gas target 80−79454
- silicate glasses, low-energy excitations and hypersonic props., Brillouin spectra meas., 1.7 to 15K 77−90160
- small spheroids, Mandelshtam-Brillouin scatt., press. fluctuation effects 77−739
- squaric acid, two dimensional antiferroelec., Brillouin scatt. at structural phase transition 80−71430
- stimulated Brillouin backscatter from theta pinch 78−67359
- Stoneley wave scatt., elasto-optic and surface ripple mechanisms 80−71435
- styrene, thermal polymerization, Rayleigh-Brillouin light scatt. study 78−53206
- superheated water, Brillouin scatt., sound velocity meas. 80−95631

Brillouin spectra continued

- superionic conductors, Brillouin scatt. from thermal fluctuation 77−20866
- superionic conductors, light scatt. and IR absorpt. book contrib. 80−25382
- superionics, with fluorite structure, Brillouin scattering and lattice defect energetics 78−80369
- surface ripple scattering by solids, for acoustoelec. amplified bulk acoustic waves 78−39559
- surface scattering, from acoustic phonons, general theory 80−34932
- surface waves, Brillouin scatt., appl. of surface Green's function mapping method 80−40125
- p-terphenyl(-d$_{14}$), Brillouin scatt. at room temp. 80−71433
- tetracosane melt, Brillouin spectroscopy obs. of struct., 65-250°C 79−55642
- TGS, depolarisation field effect 78−15177
- TGS, deuterated, room temp. and near ferroelec. transition temp. 78−15178
- TGS, elastic and dielec. consts. from Brillouin scatt. 77−48180
- TGS, laser light scatt. spectroscopy 78−10156
- TGSe, depolarisation field effect 78−15177
- thermonuclear fusion plasma, laser coupling and implosion 77−43006
- 1,2,5-thiadiazole, liq., light scatt. from orientational and density fluctuations, hypersonic vel. 77−81110
- thin film, absorbing 79−65943
- thin film elastic constants and SAW velocity and attenuation meas. 79−56101
- thin film on substrate, normal Brillouin scatt. by acoustic phonons 80−20648
- thiourea, Brillouin scatt., Debye relax. 79−87453
- thiourea, room temp. photoelastic consts. *(French)* 78−15182
- transition metal dichalcogenides, layered, surface Brillouin scatt. obs., surface ripple and elasto-optic mechanisms 80−16048
- transparent solids, review *(Chinese)* 79−33714
- triiodomethane, polarized light scatt., relaxation processes 80−60615
- trissarcosine calcium chloride, ferroelec. phase transition, Raman and Brillouin scatt. studies 80−71340
- vibrational relaxation of molecules in condensed media, survey, book contrib. 77−36295
- viscoelastic liquids, structural relax., fast and slow relax. limits 79−47465
- water, Brillouin light scatt., temp. gradient induced 80−100663
- water, hypersound phase vel. and damping by high resolution Brillouin spectroscopy 77−69845
- water, liq., ratio of Brillouin to total light scatt. intensity 78−52515
- water, Rayleigh-Brillouin scattering and compressibility 79−91455
- water, supercooled, Brillouin scatt. 78−43884
- water, supercooled, sound vel. dispersion, struct. relax. effect 80−107375
- water, US vel. meas. by Brillouin scatt., supercooled to boiling range 77−15495
- Wigner lattice, three-dimensional, detect. by Brillouin scatt. 77−36254
- $AgNO_3$, molten, Brillouin scatt. meas. 77−8592
- Al, Brillouin spectra, light scatt. cross section for surface ripples 80−71434
- Al_2SiO_5, sillimanite and andalusite, elastic constants, cryst. struct. 79−60422
- Ar, gas, compressed, Rayleigh-Buillouin spectrum, scaling 80−100062
- Ar, gas, compressed, Rayleigh-Brillouin spectrum, hydrodynamic region 80−100063
- As_2S_3, amorphous, acousto-induced struct. change, Brillouin scatt. meas. 79−27928
- As_2S_3, amorphous, US attenuation obs. 79−46756
- As_2S_3, LF inelastic light scatt. meas. 78−15181
- $(As_2S_3)_{1-x}(GeS_2)_x$, LF inelastic light scatt. meas. 78−15181
- As_2Se_3, LF inelastic light scatt. meas. 78−15181
- B_2O_3, amorphous, acoustic props. at 20 GHz, Brillouin scatt., 3-300K 80−24536
- $BaMnF_4$, incommensurate phase, Brillouin spectra 79−42981
- $BaMnF_4$, incommensurate transition, Brillouin scatt. investigation 79−87406
- $BaMnF_4$, phase transitions review 79−78378
- $BaMnF_4$, spectroscopy near ferroelec. transition, dielec. anomalies near mag. ordering temp. 80−75965
- Bi, microwave frequency shift associated with magnetosonic electric effect 79−60865
- CO, liquid, Brillouin scatt. obs., US vel. and absorpt. 80−45085
- β-CO, single cryst., adiabatic elastic consts., at triple pt., Brillouin scatt. obs. 79−47466
- CS_2, liq., ratio of Brillouin to total light scatt. intensity 78−52515
- $CaMgSi_2O_6$, diopside, elasticity, Brillouin scatt. meas. 80−6454
- CdI_2, interlayer interactions estimate from Raman and Brillouin scatt. 79−99884
- $CdIn_2S_4$, Brillouin scatt., elastic and photoelastic consts. determ. 80−60619
- CdS, acoustic noise amplification along c_6 axis, Brillouin scatt. obs. 78−19101
- CdS, acoustic phonon intensity fluctuations after strong nonlinear amplification 78−59909
- CdS, B exciton-polariton, reson. Brillouin scatt. 79−33717
- CdS, Brillouin scatt. of refl. light, surface ripple mechanism 77−73149
- CdS, Brillouin scatt. of forbidden polaritons 79−33722
- CdS, bulk acoustic phonons, light scatt. from phonon-induced surface ripples 78−75924
- CdS, exciton polaritons, Brillouin scatt. efficiency, additional boundary conditions 79−73960
- CdS, intensity fluctuations of nonlinearly amplified phonons, Brillouin scatt. meas. 77−90163
- CdS large- and small-signal lattice attenuation, Brillouin scatt. obs. 79−47130
- CdS, lattice attenuation meas. by US injection method 78−76480
- CdS, mode corrected TA phonons, reson. Brillouin scatt. 78−72535
- CdS, obs. of forbidden Brillouin scatt. near exciton reson. 78−15180
- CdS, reson. Brillouin scatt. near A exciton 77−69846
- CdS, reson. Brillouin scatt. by longitudinal acoustic phonons 79−38555
- CdS, reson. Brillouin scatt., book contrib. 79−42983
- CdS, reson. Brillouin scatt., quasi-static anal. 79−65887
- CdS, reson. Brillouin scatt. of exciton polaritons 80−11418
- CdS, reson. dispersion of Brillouin shift 78−35160
- CdS, reson. forbidden Brillouin scatt. by TA phonon domains 79−56802
- CdS, reson. scatt. of exciton-polaritons by acoustic phonons 78−60482

Brillouin spectra continued
CdS, resonant Brillouin scatt., photoelastic const., imag. part contrib. 80—108218
CdS, thermal equilib. phonon populations, acoustic intensity meas. by Brillouin scatt. intensity obs. 80—45098
CdS, three-branch exciton-polariton dispersion, direct meas. by reson. Brillouin scatt. 80—60620
CdS, two-phonon resonant Brillouin scatt. 78—84597
CdS, virtually excited biexcitons polaritons dispersion, two photon Raman scatt. 80—45067
CdS-ZnTe, acoustoelectric domain injection across interface, reson. Brillouin scatt. 77—51778
CdSe, resonant Brillouin scatt. via free and bound excitons 79—24330
CdSe:Li, pure and doped, reson. Raman and Brillouin scatt., elastic exciton-defect scatt. 80—80788
CdTe, reson. Brillouin scatt., book contrib. 79—42983
Cds, reson. Brillouin scatt. by piezoelectrically inactive TA phonon domains 78—84593
$Co_{1-x}B_x$, polycrystalline and amorphous sputtered films, Brillouin spectra 80—2775
$CoCO_3$, Brillouin-Mandelstam light scatt. obs. of spin wave spectra 80—93358
$CoCO_3$ light scatt. from parametric magnons and phonons *(Russian)* 80—34937
$CoCO_3$, light scatt. from magnons and phonons excited by microwave pumping 80—66213
$CoCO_3$ light scattering on spin waves *(Russian)* 77—4650
$CoCO_3$, spin wave spectra light scatt. expts., review 80—50081
$Co_{75-x}Fe_xSi_{15}B_{10}$, quenched ferromag. ribbon, Brillouin spectra 80—2776
Cr (111) surface, acoustic phonons Brillouin scatt. data 78—95222
CsD_2AsO_4, piezoelec. coupled soft modes, Brillouin scatt. near Curie temp. obs. 77—52109
CsH_2AsO_4, elastic props., photoelasticity near ferroelectric phase transition 80—29107
CsH_2AsO_4, Mandelstam-Brillouin spectra and US vel. meas. near ferroelec. Curie point 79—38553
CsH_2AsO_4, piezoelec. coupled soft mode, Brillouin scatt. near Curie temp. obs. 77—52109
$CsNO_3$, molten, Brillouin spectra, 420-520°C, hypersonic vel. and sound absorption freq. depend. 77—28589
EuO, light scatt. by spin waves 80—45086
EuO, light scatt. from bulk and surface spin waves 78—19497
EuS films, ferromag., optical spectra and light scatt. from spin waves 80—16116
Fe, light scatt. by spin waves 80—45086
Fe, light scatt. from surface and bulk thermal magnons 80—45087
Fe, thermal acoustic magnons, Brillouin scatt. meas. 78—95424
$Fe_{1-x}B_x$, polycrystalline and amorphous sputtered films, Brillouin spectra 80—2775
$Fe_{100-x}B_x$, quenched ferromag. ribbon, Brillouin spectra 80—2776
$Fe_{80}B_{20}$, amorphous, Brillouin scatt. from magnons, ferromag. reson. 80—65844
$Fe_{80}B_{20}$, ferromagnetic metallic glasses, Brillouin scattering 78—92085
$Fe_{80}B_{20}$ film, amorphous metallic, standing spin waves, Brillouin scatt. obs. 80—97291
$FeBO_3$, Brillouin scatt. from parametrically excited phonons 79—73956
$FeBO_3$, spin wave dispersion at small wavevectors, Brillouin scatt. and ferromag. reson. 78—47962
$FeBO_3$, spin waves, Brillouin scatt. studies 79—99696
$FeBO_3$, weak ferromag., FMR instability, parametric excitation of phonons, Brillouin scatt. obs. 79—78529
$FeBO_3$, weak ferromagnet, spin wave band struct. and microwave props. 79—1661
$Fe_{76}Mo_4B_{20}$, quenched ferromag. ribbon, Brillouin spectra 80—2776
$Fe_xNi_{80-x}B_{20}$, quenched ferromag. ribbon, Brillouin spectra 80—2776
$Fe_{40}Ni_{40}P_{14}B_6$, ferromagnetic metallic glasses, Brillouin scattering 78—92085
GAs, population inverted semicond., resonant Brillouin scatt., photoelastic consts. 80—89016
Ga, liq., Brillouin scatt. obs. 77—24858
Ga liquid, Brillouin scattering from reflections of surface ripples 78—48188
GaAs, Al-coated, surface phonon Brillouin spectra 79—78694
GaAs, Brillouin scatt. from surface ripples 79—15472
GaAs, Brillouin scatt. of refl. light, surface ripple mechanism 77—73149
GaAs, Brillouin spectra, light scatt. cross section for surface ripples 80—71434
GaAs, bulk acoustic phonons, light scatt. from phonon-induced surface ripples 78—75924
GaAs, excitonic polariton reson. interaction with LA phonons 78—60481
GaAs, phonon surface density, Brillouin elasto-optic cross section 78—72536
GaAs, reson. Brillouin scatt., book contrib. 79—42983
GaAs, reson. Brillouin scatt. of exciton polaritons 80—11418
GaAs, resonant Brillouin scattering 79—78695
GaAs, surface Brillouin scattering from acoustic phonons 80—55113
GaAs, surface phonons, scatt. expts. 80—10772
GaAs, thermal equilib. phonon populations, acoustic intensity meas. by Brillouin scatt. intensity obs. 80—45098
GaP, reson. Brillouin scatt., near indirect absorpt. edge 80—11423
GaS(Se), Brillouin scatt. by pure transverse phonons 79—78696
GaS(Se), reson. Brillouin scatt. 80—89010
GaSe, layer struct., fine independent elastic const. using Brillouin scatt. 79—19896
Gal, Brillouin spectra, light scatt. cross section for surface ripples 80—71434
GeS_2, glass, structure correlation range, Raman Brillouin light scatt. determ. 77—20857
GeS_2, LF inelastic light scatt. meas. 78—15181
$GeSe_2$, LF inelastic light scatt. meas. 78—15181
H_2, compressed, Rayleigh-Brillouin spectrum rel. to translational hydrodynamics 77—24856
H_2, Rayleigh-Brillouin spectrum at high densities 78—90189
p-H_2, solid, elastic consts., Brillouin scatt. obs. 79—8149
He, gas, compressed, Rayleigh-Buillouin spectrum, scaling 80—100062
He, gas, compressed, Rayleigh-Brillouin spectrum, hydrodynamic region 80—100063
He, superfluid 78—59991
^{4}He, liq., dynamic structure factor near λ temp. 77—66049
^{4}He, liq., dynamical behaviour to λ-line, light scattering review 79—7717
^{4}He, liq., light scattering, near T_λ 80—29238

Brillouin spectra continued
Hg, liq., Brillouin scatt. obs. 77—24858
Hg liquid, Brillouin scattering from reflections of surface ripples 78—48188
Hg_2Br_2, ferroelastic, Brillouin and Raman scatt. spectra 79—95770
Hg_2Br_2, ferroelastic phase, softening of acoustic and optical modes 79—33064
$HgCl_2$, second order phase transition, elastic consts. meas., Brillouin scatt. 78—10908
HgI_2, red anisotropic polariton dispersion, reson. Brillouin scatt. 80—7366
HgO_2-Y_2O_3, solid soln., elastic and photoelastic props., Mendelstam-Brillouin scatt. 78—6693
KBr(I), absolute cross sections of second order Raman scatt. 78—39548
KCN, Brillouin line width of phonons 78—80370
KCN, elastic anomaly at 168K 78—27242
KCN, elastic functions meas. by US pulse-echo method and Brillouin scatt. 77—84829
KCN, order-disorder transition, high-press. Brillouin scatt. exam. 77—44009
KCN, single cryst., orientationally disordered, Brillouin scatt., elastic consts. 77—85732
$K(CN)_{1-x}Cl_x$, elastic functions meas. by US pulse-echo method and Brillouin scatt. 77—84829
$(KCN)_x(KBr)_{1-x}$, Brillouin scatt. of elastic anomaly 79—28779
KCl, liq., Brillouin scatt. determination of hypersonic vel. 79—82288
KCl molten salt, thermodynamic function, Brillouin spectroscopy, hypersonic vel. *(French)* 78—35161
$KCl:CN^-$, phonon-defect interaction, Brillouin scatt. obs. 80—34935
K_2CuF_4, Brillouin scatt. and US meas. of phonons, elastic moduli and Debye temp. calc. 79—87454
KD_2PO_4, acoustic phonon dispersion, elastic stiffness, light scatt. obs. 80—103966
KD_2PO_4, Brillouin spectrum and broad central component, depend. on scatt. wave vector direction 80—34931
KD_2PO_4, soft ferroelec. mode anisotropy 78—14430
$KD_3(SeO_3)_2$, central peak, soft acoustic shear mode, light scatt. study, isotope effects 78—52518
$KFe(MoO_4)_2$, phase transitions at 312 and 139K 80—70396
KH_2AsO_4, soft shear mode, Brillouin scatt. obs. 78—15176
$K(H_{1-x}D_x)_1P_4$, polarised impurity cluster effects in light scatt. expts. 80—71431
$K(H_{1-x}D_x)_3(SeO_3)_2$, Brillouin spectrum central peak, soft acoustic mode 80—2777
KH_2PO_4, anharmonic phonons and central peaks at struct. phase transitions 79—95775
KH_2PO_4, Brillouin-Rayleigh scatt. studies near ferroelec. transition temp. 80—76036
KH_2PO_4, central peak light scatt., scatt. centre props. 77—52108
KH_2PO_4, depolarised light scatt., dynamic central peak 78—10858
KH_2PO_4, dynamic central peak in ferroelectric phase 78—84538
KH_2PO_4, laser light scatt. spectroscopy 78—10156
KH_2PO_4, light scatt. in elec. field, ferroelec.-paraelec. transition 80—2707
KH_2PO_4, soft branch Brillouin specta, quasielastic central peak suppression by annealing 78—95588
$KH_3(SeO_3)_2$, and $KD_3(SeO_3)_2$, anharmonic phonons and central peaks at struct. phase transitions 79—95775
$KH_3(SeO_3)_2$, central peak obs. by light scatt. 77—32390
$KH_3(SeO_3)_2$, slightly deuterated, central peak obs. in Brillouin spectra 78—64374
$KNbO_3$, ferroelectric transition, neutron diffr. obs. 80—25324
K_2O-B_2O_3-SiO_2 system glasses, hypersound propag., 77 to 300K, Brillouin scatt. obs. 77—84850
K_2ReCl_6, elastic constants, softening of acoustic modes, obs. by Brillouin scattering 80—71440
K_2SeO_4, anharmonic phonons and central peaks at struct. phase transitions 79—95775
K_2SeO_4, Brillouin scatt. at paraelectric-incommensurate phase transition, hypersonic waves 79—78690
K_2SeO_4, elastic props. at commensurate-incommensurate transition, Brillouin scatt. and US study 80—93248
K_2SeO_4, hexagonal-orthorhombic transition, Brillouin scatt. study 80—97208
K_2SeO_4, soft modes below incommensurate transition Raman and Brillouin scatt. meas. 79—91387
K_2SnCl_6, elastic constants, softening of acoustic modes, obs. by Brillouin scattering 80—71440
LaP_5O_{14}, continuous ferroelastic transition elastic and mechanical props. 80—92668
LaP_5O_{14}, ferroelastic transition, soft acoustic mode 77—11656
LaP_5O_{14}, ferroelastic phase transition, thermal expansion and elastic consts. tensors 79—42236
LiCl, hypersonic relaxations studied by Brillouin light scatt. techniques, viscoelastic effects obs. 80—83375
$LiNbO_3$, photoelasticity tensor, including piezoelectrooptic interaction correction, Brillouin scatt. 77—24820
$LiNbO_3$:Ti, in-diffused waveguide, acousto-optical meas. of optical field profiles 79—23054
Li_2SO_4, fast ion conductors, X-ray diffr., neutron diffr., and Brillouin scatt. study 80—107170
Li_2SO_4, liq. and plastic crystalline phases, Brillouin scatt. 79—99897
Li_2SO_4, molten, Brillouin spectra, refr. index meas., hypersonic vel. 78—68523
$LiTaO_3$, photoelastic consts., Brillouin scatt. 77—28546
N_2, liquid, Brillouin scatt. obs., US vel. and absorpt. 80—45085
$(NH_4)_2BeF_4$, ferroelectric, Brillouin scattering study 79—15470
$(NH_4)_2BeF_4$, Mandelstam-Brillouin and US exam. of phase transitions 77—12347
NH_4Br, λ-type phase transition, Brillouin scattering 78—79725
NH_4Cl, λ-type phase transition, hypersonic study using Brillouin scatt. 80—34165
NH_4HSO_4, ferroelec. Brillouin shifts and linewidths 77—16322
$(NH_4)_2SO_4$, Brillouin scatt. from room temp. to -70°C 78—52517
$(NH_4)_2SO_4$, phase transition mechanisms by optical spectroscopy 79—15411
$(NH_4)_2SO_4$, pure and Rb doped, ferroelec. transition, light scatt. meas., dielec. and elastic props. 78—43822
$(NH_4)_2SiF_6$, elastic constants, softening of acoustic modes, obs. by Brillouin scattering 80—71440

Brillouin spectra continued

- $(NH_4)_2SnCl_6$, elastic constants, softening of acoustic modes, obs. by Brillouin scattering 80—71440
- NaCN, Brillouin backscatter spectra of (100) LA phonons, elastic consts. determ. 79—65886
- NaCN, disordered, acoustic phonon mode freqs. 77—48181
- NaCN, elastic const. temp. depend., Brillouin and US exam. 77—80572
- NaCN, single cryst., orientationally disordered, Brillouin scatt., elastic consts. 77—85732
- NaCl, liq., Brillouin scatt. determination of hypersonic vel. 79—82288
- NaCl, molten salt, thermodynamic function, Brillouin spectroscopy, hypersonic vel. *(French)* 78—35161
- $NaH_3(SeO_3)_2$, dynamics of α-β transition, Brillouin scatt. meas. 77—8526
- $NaNO_2$, incommensurate antiferroelec. phase, Brillouin scatt. freq. shift 80—93349
- $NaNO_2$, mechanism of order-disorder transition, opt. spectra 78—76403
- Na_2O-P_2O_5 glass, elastic and viscoelastic props. by Brillouin scatt. 79—51972
- Na_xWO_3, elastic consts., composition depend. Brillouin scatt. meas. 79—61388
- Ne, gas, compressed, Rayleigh-Buillouin spectrum, scaling 80—100062
- Ne, gas, compressed, Rayleigh-Brillouin spectrum, hydrodynamic region 80—100063
- Ne, neutron scatt., limits of classical hydrodynamics for collective motion *(German)* 77—24258
- Ni, Brillouin spectra, light scatt. cross section for surface ripples 80—71434
- Ni film, ferromag., light scatt. from surface acoustic spin waves 79—33719
- Ni, light scatt. from surface and bulk thermal magnons 80—45087
- Ni, thermal acoustic magnons, Brillouin scatt. meas. 78—95424
- O_2, liquid, Brillouin scatt. obs., US vel. and absorpt. 80—45085
- $Pb_5Ge_2O_{11}$ acoustic relax. assoc. with phase transition at hypersonic freq. 78—88267
- $Pb_5Ge_3O_1$, anharmonic phonons and central peaks at struct. phase transitions 79—95775
- $Pb_5Ge_3O_{11}$, dynamic central peaks and phonon interactions near structural phase transitions 78—83903
- $Pb_5Ge_3O_{11}$, light scatt. obs. of unresolved central peak 77—4649
- $PbHPO_4$, ferroelec. phase transition, Brillouin and Raman spectra obs. 79—33683
- $Pb_3MgNb_2O_9$ diffuse phase transition, Brillouin scatt. and acoustic phonons 78—76401
- $PbMoO_4$, Brillouin spectra, photoelastic consts. and optical purity 78—60480
- $PbMoO_4$, molecular light scattering 78—72537
- $Pb_3(P_xV_{1-x}O_4)_2$, ferroelastic phase transition, DTA, dilatometric and Brillouin scatt. study 80—70398
- $RbAg_4I_5$, solid electrolyte, Rayleigh-Brillouin and low-frequency Raman spectra 79—33720
- RbCN, cubic phase, temp. depend. of elastic consts., Brillouin spectra obs. 79—56805
- $RbCaF_3$, elastic consts. near phase transition by Brillouin scatt. 78—38844
- ReO_3, elastic stiffness const. determ. by Brillouin scatt. 78—19494
- Sc_2O_3, Mandelshtam-Brillouin spectra, transverse phonon contrib., elastic and photoelastic consts. 77—81115
- Se, trigonal, surface lattice dynamics, mean square displacement spectra in long wavelength limit 80—54498
- Si, Al-coated, surface phonon Brillouin spectra 79—78694
- Si, amorphous, opaque, surface phonon attenuation, Brillouin scatt. 80—80808
- Si film, hydrogenated amorphous, Brillouin scatt. 78—72538
- Si, surface Brillouin scatt. from acoustic phonons 80—55113
- Si:H, amorphous, Brillouin scattering from acoustic bulk and surface waves 80—11425
- SiO_2 colloid, particle size and density depend. 77—32844
- SiO_2, fused, shear-wave Brillouin scatt. intensity from photoelastic consts. 79—91454
- SiO_2, vitreous, hypersound velocity meas. from Brillouin scatt. freq. 80—27349
- SiO_2, vitreous Brillouin scatt., 35 GHz phonon vel. and absorpt. below 1K 80—100664
- SiO_2-B_2O_3 glasses, Brillouin scattering meas. of attenuation and vel. of hypersounds 80—100309
- $SnCl_2.2H_2O$, Brillouin scatt. and thermal expansion 80—97289
- $SnCl_2.2H_2O$, protonic order-disorder transition, inelastic light scatt. obs. 78—68497
- SnTe, light scatt. from soft modes, theory above and below displacive transform. temp. 79—95791
- $SrTiO_3$, absolute cross sections of second order Raman scatt. 78—39548
- $SrTiO_3$, anharmonic phonons and central peaks at struct. phase transitions 79—95775
- $SrTiO_3$, dynamic central peaks and phonon interactions near structural phase transitions 78—83903
- $SrTiO_3$, phonon interactions and the dynamic central peak near structural phase transition 77—81114
- $Tb_2(MoO_4)_3$, mode softening near ferroelec. transition, Raman and Brillouin spectra 79—33685
- Te, trigonal, surface lattice dynamics, mean square displacement spectra in long wavelength limit 80—54498
- $TlCdF_3$, elastic consts. near phase transition by Brillouin scatt. 78—38844
- Xe crystal, elastic consts. determ. by Brillouin scatt., comparison with neutron scatt. data 77—39622
- Xe, single crystal, Pockel coeffs. and short-range-interaction parameters 79—73962
- Xe sound propag., near crit. point, theoretical anal. 77—69046
- YIG bubble films, light scatt. from spin waves, hysteresis meas. by Voigt effect 80—15770
- Y_2O_3, Mandelshtam-Brillouin spectra, transverse phonon contrib., elastic and photoelastic consts. 77—81115
- $Zn_xCd_{1-x}Te$, reson. Brillouin scatt. meas. using injected acoustic domains 78—27243
- $Zn_xCd_{1-x}Te$, reson. Brillouin scatt., acoustic domain injection 79—38557
- $Zn_xCd_{1-x}Te$, resonant Brillouin scattering *(Japanese)* 79—15474
- ZnO, acoustic phonon intensity fluctuations after strong nonlinear amplification 78—59909
- ZnO, intensity fluctuations of nonlinearly amplified phonons, Brillouin scatt. meas. 77—90163

Brillouin spectra continued

- ZnP_2, Brillouin scattering and optical props. meas. 80—76041
- α-ZnP_2, resonant Brillouin scatt. near indirect band gap 80—93350
- ZnS, reson. Brillouin scatt. and piezobirefringence 80—93348
- ZnSe, photoelastic and elastic constants determ. using thermal Brillouin scatt. *(Japanese)* 79—51974
- ZnSe, polaritons, reson. Brillouin scatt., heavy and light excitons 79—99898
- ZnSe, reson. Brillouin scatt., lifetime broadening 79—51971
- ZnSe, reson. Brillouin scatt., dispersion curves, piezobirefringence anal., electronic state lifetime broadening effects 79—61390
- ZnSe, reson. Brillouin scatt., quasi-static anal. 79—65887
- ZnSe, resonant Brillouin scatt. by injected acoustic waves 77—12394
- ZnTe, Brillouin scatt. spectra, elastic and photoelastic consts. 77—59585
- ZnTe, reson. Brillouin scatt., injected acoustic domains obs. 78—19493
- ZnTe, reson. Brillouin scatt., lifetime broadening 79—51971
- ZnTe, reson. Brillouin scatt., quasi-static anal. 79—65887
- ZnTe(S), reson. Brillouin scatt., acoustic domain injection 79—38557
- ZrO_2-Y_2O_3, solid soln., elastic and photoelastic props., Mendelstam-Brillouin scatt. 78—6693

Brillouin zones

see also band structure

- A^4-phonon theory, model S-matrix negative in Brillouin zone 78—41257
- alkali metals, phonon-phonon scattering relax. times, rel. to elec. resist. 77—39813
- alkali metals, thermal properties and Gruneisen parameters, employing model pot. 78—71815
- alloy, HCP, variations in Brillouin zone due to order-disorder phase transform. *(Russian)* 79—51100
- alloys, dil., of polyvalent and noble metals, deviations from Matthiessen rule 80—65525
- anisotropic linear spin chain, two-magnon problem with arbitrary interaction radius 78—72320
- antiferromagnets, magnon parametric generation with impulses at Brillouin zone boundary *(Russian)* 80—29540
- Bloch electrons, weak magnetism, spin and spin-orbit interactions *(Russian)* 79—33443
- chain crystals, interchain correlations and energy spectrum, Davydov splitting 79—28309
- chemisorption on Ni (001), electronic struct., KKR model calcs. 78—56200
- cubic and hexagonal lattices, Brillouin delta function 79—73261
- cubic metal, vol. and temp. depend. of phonon frequencies 77—15514
- decay state interactions, autoionisation bands *(Russian)* 80—75486
- diamond, (100) surface states, SCF extended tight-binding method 77—47881
- diamond, electronic energy bands of diamond-type crysts., appl. of EHT method 78—87907
- p-dibromo-tetrafluorobenzene mol. cryst., in commensurate phase, quasielastic neutron scatt. 80—107386
- displacive regime, lattice phonons in presence of non-linear excitations 80—44283
- double space groups O_h^6 (Fm3c) and O_h^8 (Fd3c), selection rules 80—10518
- electron state density calcs. by linearly analytical tetrahedron method *(Russian)* 79—82507
- elementary excitations damping, theory of many-particle processes *(Russian)* 79—56522
- extended unit cell-contracted Brillouin zone model, group-theoretical anal. 80—107093
- FCC, BCC and SC crysals, electronic struct. tight binding model 78—84123
- FCC lattice, second-neighbour surface magnons 77—28378
- ferroelectric theory and dynamics, optical, acoustic electro-optical props., Brillouin zone struct. 80—11347
- graphite, electronic props., self consistent LCAO calc., point vacancy in 2-dimens. cryst. 78—51932
- graphite, galvanomagnetic effects, trigonal warping of constant energy surfaces 78—87987
- graphite, minority carriers and H-point magnetorefl. spectra 77—63398
- half space layered cryst., vibr. spectrum, Brillouin zone *(Russian)* 80—100313
- HEED, branch points, critical voltage effect, band theory models 78—1961
- holosymmetric double space groups based on body-centred cubic Bravais lattice, selection rules 79—65019
- Hume-Rothery alloys, magnetism 78—95417
- ice, cubic, LCMO calc. of energy bands 77—51656
- III-V semiconductors, effective mass, forbidden bandwidth and lattice constant relation *(Slovak)* 78—51879
- impurity crystal, light absorpt. max. at Brillouin zone boundary 80—55139
- In-Cd-Sn, supercond. transition temp. and electronic props., Brillouin zone effect 79—56345
- infinite crystal, surface states determ. by complex extension of tight binding 78—80032
- Knight shift theory near Fermi surface points with changing topology *(Russian)* 80—34794
- large unit cell semiempirical mol. orbital approach to props. of solids, general theory 79—87029
- lattice dynamical properties, Brillouin zone summations, convergence 78—91384
- lattice dynamics, normal modes vibrations, use of group of neutral elements of crystalline sites 79—37774
- lattices, FCC and BCC, optical transitions, dipole selection rules 80—97409
- leucosapphire, electronic band struct., optical props. 79—95329
- linear Brillouin zone integration method, generalised susceptibility calcs. 80—88462
- linear chain model, symmetry-adapted, layer dynamics of high-symmetry crystals 80—34148
- marcasite structure, space group selection rules 79—99099
- metal, electron-lattice interaction effect on equilib. struct. form. *(Russian)* 80—34380
- metallic crystals, HCP, Brillouin zone representative points 79—33044
- metals, nearly-free-electron, holelike Fermi surface, Hall coeff. and magnetocond. tensor 79—4547
- metals, positron annihilation expts., electronic struct. and Fermi surface studies 80—54594
- molecular crystal, lattice vibr., Raman and IR obs., review 78—43079

Brillouin zones continued
multiplicities for space group representations 79—60291
n-component spin system, anisotropic Brillouin zone, Wilson-Feynman graph technique, universality 77—5764
noncubic lattice, many special point scheme 78—39002
noncubic lattices, Baldereschi points 77—47370
numerical integration over solid angle and vol. of Brillouin zone, any crystal symm. 77—27843
periodic function integration over Brillouin zone 78—6251
periodic function integration over Brillouin zone 78—6252
photoemission, electron energy, distrib. calc. 80—40237
polyglycine chain with hydrated side group, electronic struct., transport props. 79—16146
polymethylene chain, vibr. spectra, CH stretching region, struct. and assignments 78—70991
α-quartz, electronic energy band struct. calc. 79—23894
random alloy, optical absorption and photoemission spectra 80—45216
rare-earth metal, semi-infinite surfaces with mag. struct., density of states calc. 80—10851
semiconductor, elec. field induced optical SHG theory, Brillouin zone integral 80—69457
semiconductor, narrow band gap, ferromagnetism of electrons in filled band *(Russian)* 79—78300
semiconductor, spin-orbit splitting, tight binding calc. 77—85184
semiconductor, superlattice band structure 79—95490
semiconductor alloys, ternary, energy band calc., compositional disorder effect determ. 79—42442
semiconductor heterojunction, band-edge discontinuities and interface pot. step, two-band narrow-gap approach 80—39665
semiconductors, many-valley, magnetic electron fluctuon states spin direct interactions 80—29364
semiconductors junctions, electron-phonon scatt. 80—24997
silicate minerals, heat capacities rel. to simple lattice vibrational models 80—4005
solid, orthogonalised augmented plane wave method, appl. to ZnS 77—66105
special point formulas from Gauss-Chebyshev integration 79—42001
special point generation, large unit cell method *(Russian)* 80—88469
special point generation by large unit cell approach 80—92806
special points in crystals of different crystallographic classes 77—7687
spectral properties, k-space integration 78—15190
superconductors, polyvalent metals, Brillouin zone boundary influence on Coloumb interactions 80—24827
surface properties, two dimens. Brillouin zone and Wigner-Seitz cell integrations, special point formulae generation 80—70783
symmorphic space groups, irreducible representations, multiphonon IR and Raman spectra *(Japanese)* 79—77541
ternary semiconductor, struct. effects on energy band struct. 78—39021
tetrahedron method for evaluating spectral props. of solids 80—10855
transition metals, second series, electronic band Brillouin zone APW calc., electronic config. effects 78—51883
two-parameter dynamical model, appl. to Ag and Al 80—10597
zone axis patterns, depend. on string integrals or number of bound states, HEED 77—84598
zone axis patterns rel. to projected cryst. pot, HEED 77—84597
Al (001), density of surface states in two-dimensional Brillouin zone 79—60894
Al, angle-resolved XPS from valence levels, Brillouin zone averaging 78—48285
Al, K X-ray absorption, K-emission spectrum, band struct. using APW method 80—97380
Al, positron annihilation, angular distrib., Umklapp effects *(French)* 80—50454
As, band structure on Jones zone boundary, pseudopot. calc. 80—54603
Au (100), normal and reconstructed, electronic struct. changes, ang. resolved photoemission obs. 80—25520
Au, angle-resolved XPS from valence levels, Brillouin zone averaging 78—48285
Be, dielectric function from APW calcs. 79—65817
Be, electronic surface states, (001) surface, Brillouin zone 79—24047
$(BeH_2)_x$, polymer, ab initio calcs., cryst. orbital method 79—37659
Bi, band structure model parameters, deformation theory *(Russian)* 78—56067
Bi-type crystal, deformation model of carrier spectrum, holes 79—60680
$Bi_{12}GeO_{20}$, optical phonon freq. in vicinity of Brillouin zone, linear wave-vector depend. 79—19892
BiSb (>20 wt.%), electronic band struct. 80—107698
$Bi_{1-x}Sb_x$, far IR magnetoabsorption, band struct. study 80—50351
$Bi_{1-x}Sb_x$:Te(Sn), dispersion law of charge carriers *(Russian)* 79—87114
$Bi_{86}Sb_{14}$:Te, single crystal, dispersion of magnetoplasma waves *(Russian)* 80—70739
$C_8K(Rb)$, graphite intercalated, phonon dispersion relations and Raman spectra 80—44272
Cd alloys, spin and spin-orbit contribs. to mag. susceptibility *(Russian)* 79—11287
Cd, anisotropy of free-electrons momenta distribution, positron annihilation meas. 77—36309
Cd, electronic surface states, (001) surface, Brillouin zone 79—24047
Cd-Hg, ω-phase, mag. susceptibility *(Russian)* 79—87231
Cd_3As_2 type crystals, symmetry props. of energy bands 80—39500
CdI_2, band struct., tight binding calcs. and photoemission spectra 78—23018
CdI_2-Ni^{2+}, absorption and mag. circular dichroism, spectra, phonon density of states of CdI_2 deduced 79—19913
$Cd_{1-x}Mg_x$, mag. props. and electron spectrum parameters *(Russian)* 79—33453
CdS, photoemission due to direct transition near L- and M-points in Brillouin zone 77—16451
$CdS_{1-x}Se_x$, zone edge phonons 78—76475
n-$CdSnAs_2$, optical absorption rel. to energy spectra *(Russian)* 78—75994
CdTe, far IR absorpt., two-phonon density of states 78—15155
$CoCO_3$, weak ferromagnet, optic study of spin wave spectrum *(Russian)* 79—47263
$Co_{1-p}Mg_pCl_2$, magnetic excitations, antiferromagnetic resonance spectra response simulation 79—99775
Cs, Fermi-surface press. dependence 80—96772
$CsCrCl_3$, α-β phase transition, dynamical aspects and thermodynamic theory 80—70404
CsI(Br)(Cl), electronic struct. anal. by reflectance and thermoreflectance studies 79—69855

Brillouin zones continued
Cs_2SiF_6, low-energy vibronic struct. of crit. points in Brillouin zone, selection rules 79—60449
Cu (001), O_2 chemisorption, Cu3d-O2p interaction study by angular-resolved photoemission using synchrotron radiation 80—84836
Cu, (110) surface, photoemission obs. of new surface state band 79—91121
Cu, angle-resolved photoemission, band struct. 78—95680
Cu, Brillouin zone integration special directions, electronic density of states calcs. application 80—49569
Cu, electronic transport properties, OPW calcs. 77—43553
Cu-Ni, optical absorption and photoemission spectra 80—45216
Cu_3Au, electrical resistivity and LRO, energy gap formation in Fermi surface 80—88533
CuCl (100), obs. of p- and d-like surface states, angle resolved UPS study 80—104045
CuCl, neutron scatt. of TO phonon at 5K 79—60446
Cu_2Ni_{1-c}, solutions of KKR-CPA equations for paramagnetic alloys 78—95256
EuTe, mag. 'Bragg' scatt. obs. through Raman scatt. 80—66179
Fe, photoemission study of (100), (110) and (111) surfaces, ferromag. band struct. 79—38714
Fe-Al(Si), disordered, obs. of Kohn singularities in X-ray diffuse scatt. 79—27874
Fe_3Al, electrical resistivity and LRO, energy gap formation in Fermi surface 80—88533
GaAs, (100) surfaces, reconstructed, ang. resolved photoemission from surface states, adsorption and annealing effects 80—16143
GaAs, surface states, band struct. by discontinuous potential method 80—20276
GaAs-AlAs alternating monolayers, zone folding effects on phonons 78—72510
GaAs-$Ga_{1-x}Al_xAs$ superlattice, Raman scatt., polar phonon anisotropy 80—45052
$Ga_{1-x}In_xP$, zone edge phonons 78—76475
GaSe, lattice dynamics and elastic props., Born-von Karman model study 80—70337
$Gd(Co_xIr_{1-x})_2$, rel. to comp. depend. of struct. and mag. moments 79—86743
Ge, electronic energy bands of diamond-type crysts., appl. of EHT method 78—87907
Ge(100) surface electronic state localisation, layer density of states calcs. 80—6931
Ge(111), dangling-bond surface states 78—43452
H_2, solid, electronic struct., HF calc. using plane wave basis 79—7772
^4He, FCC quantum cryst., lattice dynamics 79—77859
$Hg_2Br(Cl_2)$, paraphase, Raman scatt. spectra, soft mode from Brillouin zone boundary *(Russian)* 78—2851
Hg_2Cl_2, neutron and Raman scatt. studies, ferroelastic transitions 80—76015
Hg_2Cl_2 prototype phase, soft mode, inelastic neutron scattering, Raman effect 78—91411
Hg_2I_2, thermal softening of mode on Brillouin zone boundary in Raman scatt. spectra 79—73948
$Hg_{1-x}Mn_xTe$, 1.7 to 3.5 eV, reflectivity spectra 78—43899
α-HgS, electronic energy level calcs. 80—6718
In alloys, superconducting transitions temp. rel. to electronic struct. 77—80865
In_2Bi, de Haas-van Alphen effect 78—91594
InP, depend. of phonon spectrum on hydrostatic press., Raman spectra 80—93315
InSb, film, E_0, E_1 absorption edge size quantisation, optical and electroreflectance spectra 80—34998
n-InSb, low temp., spin mag. moment in Brillouin zone *(Russian)* 78—56159
InSb, semiconductor, Brillouin zone spin dependent wave functions calcs. 79—56126
InSb-CdTe solid solns., electroreflectance spectra, Brillouin zone transitions 80—7330
In_2Te_5, energy band struct., localisation of interband transitions in Brillouin zone 80—20642
KI, piezo-optical study of excitons 80—16055
$K_{1-x}Rb_xBr$, lattice dynamics on pseudo-crystal model 78—75762
LaB_6, de Haas-van Alphen effect, low-field 80—75497
Li linear chain, ab initio calcs., cryst. orbital method 79—37659
LiC_6, Raman spectrum, rigid band model anal. 79—4800
LiH (D), single crystals, electronic excitations, review *(Russian)* 78—72574
LiH, linear chain, ab initio calcs., cryst. orbital method 79—37659
Mg, anisotropy of free-electrons momenta distribution, positron annihilation meas. 77—36309
Mg, dielectric function from APW calcs. 79—65817
Mg, electronic surface states, (001) surface, Brillouin zone 79—24047
$Mg(NH_3)_6(ClO_4)_2$, phase transition, group theoretical anal. 80—65218
MgO, chemisorption on (100) surface, surface electronic struct. 79—11016
Mo (100), surface resonances, photoemission and field emission meas. 79—4593
Mo(001) surface, atomic displacements and electronic struct. 78—30963
N_2, solid, lattice dynamical calcs., use of anisotropic at.-at. pot. functions, α-γ transition 78—71811
α-N_2, solid, librational motion, theory 77—43303
α-N_2, solid, librational motion, neutron scatt. 77—43304
Na_2CO_3, structural modulation, theory 77—35535
NaCl (100) face, angle-resolved photoemission 78—56567
Nb (001) ideal surface, self-consistent pseudopot. calcs. 77—76894
Nb-Zr, acoustic phonon anomalies and superstructure, neutron inelastic scatt. meas. 80—19892
NbS_2, 2H layer cpd., tight-binding fit to bond struct. 78—39000
$NbSe_2$, 2H layer cpd., tight-binding fit to bond struct. 78—39000
$NbSe_2$ (2H), metallic layer cpd., angle-resolved photoemission spectra 79—47593
$NbSe_3$ and related cpds. bands, bonds and charge density waves 79—95327
Ni (111), with submonolayer of O, H or C_2H_2, surface phonons obs. by EELS 80—39403
Ni, angle-resolved photoemission, band struct. 78—95680
Ni film, ferromagnet (100), surface states above majority-spin d bands 79—1630
Ni, polarisation-dependent angle-resolved photoemission for band structure studies 78—95678

Brillouin zones continued
Ni(NH$_3$)$_8$(BF$_4$)$_2$, phase transition, group theoretical anal. 80—65218
Ni(NH$_3$)$_6$(ClO$_4$)$_2$, phase transition, group theoretical anal. 80—65218
Ni(100) magnetic surface states, photoelectron spectra, surface Brillouin zones 80—6928
Ni(110), mag. exchange splitting of electronic surface states 80—88610
Pb, single and polytextured thin films, band struct., tunnelling spectroscopy 80—80169
PbI$_2$, ionic layer cpd., lattice dynamics, influence of static dipole moments 79—28057
Pb$_3$(P$_{0.95}$V$_{0.05}$O$_4$)$_2$, ferroelastic transition, soft mode, inelastic neutron scatt. study 80—70357
PbTe, magneto-optical transitions and band parameters 79—82961
Pd, g tensor of d holes near X point in Brillouin zone 79—23890
Pd-H, dil., electronic states, de Haas Haas-van Alphen effect meas. 77—47718
Rb, Fermi-surface press. dependence 80—96772
Rb$_2$Co$_c$Mg$_{1-c}$F$_4$, random 2D antiferromag., neutron inelastic scatt. 79—28505
RbCrCl$_3$, α-β phase transition, dynamical aspects and thermodynamic theory 80—70404
Re, Fermi surface hydrostatic press. depend., de Haas-van Alphen phase shift meas. 80—54593
ReB$_2$, electron struct., Fermi energy and surface, bonding 80—20076
ReO$_3$, mag. breakdown above compressibility collapse transition 80—103617
ReO$_3$ type lattice, group-theoretical symmetry anal. of vibr. *(Russian)* 80—10610
(SN)$_x$, polycryst. films, single crysts., UPS, valence band struct. 77—69967
Sb, electronic struct., depend. on hydrostatic pressure 80—80158
Si, (111) surface, electron inversion layers, obs. of sixfold valley degeneracy 79—38176
Si, electronic energy bands of diamond-type crysts., appl. of EHT method 78—87907
Si, high index surface, natural orientational superlattice in 2D electron gas 79—99598
Si, optical critical point structures, symm. anal. by low-field electroreflectance 77—66478
Si, perfect crystal, dispersion surface of X-ray radiation, X-ray acoustic resonance method 79—41908
SiAs, monoclinic, band struct., OPW calc. 77—59255
SiC polytypes, localisation of cond. band minima in Brillouin zone 80—20082
Si(111), dangling-bond surface states 78—43452
SmS, electron-phonon interaction, lattice dynamical model 80—96610
SmS, semicond.-metal transition, cond. band type, deform. pot. determ. 79—69417
α-Sn, electronic energy bands of diamond-type crysts., appl. of EHT method 78—87907
SnSe, electronic band struct. determ. 78—51890
TaS$_2$, 1T, quasi-octahedral layer compound, band struct. and Fermi surfaces 77—76747
TaSe$_2$, 1T, quasi-octahedral layer compound, band struct. and Fermi surface 77—76747
TcB$_2$, electron struct., Fermi energy and surface, bonding 80—20076
Te, trigonal, high energy reflectivity anisotropy anomaly, Brillouin zone transitions 79—65838
Ti alloys, Fermi sphere limiting electronic capacitance, Brillouin zones *(Russian)* 80—92808
TiC, Shockley surface states and bonding 78—91739
TiO$_2$, electronic energy levels, electrorefl. spectra 77—24870
TiS$_2$, electronic struct. and props., self consistent numerical basis set LCAO calc. 77—89698
Tl, mag. breakdown, electron energy spectrum 78—10335
TlCl, phonon difference band absorpt., far IR laser spectroscopy 80—93325
UN, single crystal, electronic props. 77—77061
VC, energy band struct., chem. bonding 78—18958
VI$_2$, mag. 'Bragg' scatt. obs. through Raman scatt. 80—66179
VSe$_2$, 1T, quasi-octahedral layer compound, band struct. and Fermi surface 77—76747
W (001), surface bands dispersion 77—15930
W (100), surface resonances, photoemission and field emission meas. 79—4593
W (100) and (110) surface, theoretical Debye-Waller factors 80—92773
W (110) surface states, characterisation and transferability obs. 79—33319
W, polarisation-dependent angle-resolved photoemission for band structure studies 78—95678
W, XPS, angle-resolved, from valence bands, obs. of strong temp. depend. and direct-transition effects 80—60752
WO$_3$, condensed phonon modes in successive phases 79—46765
W(001), surface states and surface resonances, self-consistent electronic struct. 80—96960
Zn, anisotropy of free-electrons momenta distribution, positron annihilation meas. 77—36309
Zn, electronic surface states, (001) surface, Brillouin zone 79—24047
Zn, Fermi surface-Brillouin zone interaction, XPS obs. 79—52078
Zr, de Haas-van Alphen studies in high mag. fields, Fermi surface model 80—6702
Zr-Hf, mag. susceptibility, elec. cond., Hall conc., thermoEMF conc. depend. *(Russian)* 80—39551
Zr-Ti, alloy, mag. susceptibility, elec. cond., Hall conc. thermoEMF conc. depend. *(Russian)* 80—39551

bristles *see fibres*

brittle fracture
see also ductile-brittle transition; notch brittleness
δ_R criterion for BCC single crysts. *(Russian)* 78—56732
ABS polymer, transparent, fracture of notched tensile specimens 77—63772
acoustic emission associated with brittle tensile fracture of cylindrical and flat specimens 77—62211
acoustic emission in brittle materials, book contrib. 78—11484
acoustic emission simulation by SiC grain brittle fracture and elastic sphere impact, freq. anal. 78—55504
adhered lap-shear and double cantilevered beam specimens, cyclic stress testing 79—15820
alkali halide, brittle fracture of single crysts. and active struct. of cleavage surfaces 79—28039

brittle fracture continued
alkali halide, effect of lattice of point defects on activity and brittle fracture 79—15785
alkaline earth fluorides, crack propag., cryst. props. effects 78—75720
alkaline earth hexaborides, electron fractography 77—8906
alloy, dispersion hardened, particle size effect on fracture 79—43418
alloys, brittle and plastic, energetic strength theories *(Bulgarian)* 80—38296
alumina, polycrystalline, subcritical crack extension and crack resist. 77—8911
amorphous mat., refraction of propagating crack by stress wave 78—92337
angled elliptic notch problem in compression and tension 79—18824
anisotropic media, brittle fracture orientation *(French)* 78—26085
anodic, and free anodic film on Al substrate, deform.-strength props. *(Russian)* 77—69203
asbestos fibre reinforced Portland cement analytical fracture resistance curve expression 78—76756
automotive materials, microfractography appl. to ductile failure, brittle fracture, crack studies 77—56199
beam, Weibull statistical theory 79—81810
beam test results, unit strength concept interpretation 78—48525
beams, multiple fracture under localised impulsive loading 77—80118
biocompatible implants, developed for bone fracture prevention, development research criteria 78—77155
body loading with cracks, energy conditions for brittle failure *(Russian)* 80—96234
bone, human compact, longit. shear, constituents and failure mech. 77—81518
borate glass, crit. stress intensity factor and fracture surface energy *(French)* 77—76487
boride diffusion coatings on steel, fractographic exam. of struct. 78—44270
bovine hip bone, compression tests, effect of specimen shape and size on mech. props. and fracture mode 78—69132
branched cracks, plane strain stress intensity factors 78—1608
α-brass, Al bearing, high temp. relief cavitation, SEM, STEM, TEM, SIMS and EDX anal. 79—5039
brittle fibre reinforced composite, static strength depend. on component separation boundaries *(Russian)* 80—76304
brittle fracture mech., review *(Russian)* 79—34139
brittle material, wear, acoustic emission obs., effect of ion aggregates in Rebinder-Westwood environment 78—48536
brittle materials, diametral compressive stress considering Hertzian contact, fracture and tensile strength meas. *(Japanese)* 78—72946
carbide, effect of mech. props. on erosion resist. under spark machining conditions 78—11421
cement and mortar, strength, fracture mode, statistical props. *(Japanese)* 78—31520
cement paste, direct tensile tests and tied crack model 78—11306
cement paste, direct tensile tests and tied crack model 78—11307
ceramic, cylindrical cavity effect on fracture 79—66144
ceramic, porosity effects *(Polish)* 77—59934
ceramic filled with polymer, ZrO$_2$ stabilised, fracture mechanism *(Russian)* 80—100895
ceramic turbine disc, subjected to centrifugal stresses, failure probability, photoelastic model 79—18816
ceramics, brittle, heat-transfer variables effect as thermal stress resist., meas. by quenching expts. 80—79871
ceramics, crack propagation, cracking velocity-stress intensity factor data *(German)* 78—35469
ceramics, fracture by single pulse 10.6 μm irrad. 79—99988
ceramics, fracture toughness, exam. of methods of enhancing, merits and limitations 78—60771
ceramics, fracture-mirror boundary formation, criteria 80—70297
ceramics, mechanisms interpreted on basis of material mechanics *(German)* 78—35471
ceramics, microstructure and microcrack processes, applicability of fracture mechanical methods *(German)* 78—31500
ceramics, polycrystalline, fracture mirror form. 77—48541
chemically assisted fracture, atomic models of crack growth 80—64466
chemically assisted fracture, general reaction rate theory and thermodynamics 80—64465
chert, prehistoric Hertzian fracture 77—29292
circular disc under impact loading, fracture mech. 78—88514
cleavage crack, associated effective fracture energy 79—19316
cleavage crack extension, discreteness of atomic struct. effect, one dimensional model 77—81314
cleavage crack extension in brittle material, atomic structure discreteness effect 78—79281
cleavage fracture toughness models 80—40515
closed cylindrical shells with longitudinal cracks, limit equilib. criteria *(Ukrainian)* 79—50646
Columbia Resin, CR-39, fracture mirrors, static and impact tests 78—27601
composite, local crack-driving force, elastic and thermal mismatch 78—7017
composite material, brittle failure prediction 77—89072
composite mode cracks, K$_I$-K$_{II}$, brittle fracture study *(Chinese)* 80—55494
composites, single fibre-brittle zone model, fracture behaviour 80—97570
computational models for one and two dimens. wave propag. 77—11628
concrete, plastic-brittle behaviour, hardening and softening constitutive eqns. 77—21270
concrete continuum model for plastic-brittle fracture 79—27584
concrete slab, explosive shock resist., tensile fracture 80—85065
constructional materials, brittle failure resistance, calc. characts., expt. methods 77—77662
covalent crystals, nanosec. electron beam effects, size depend., Ioffe effect 80—88211
crack analysis, concentric circular arc cracks in anti-plane strain, screw dislocation pile-up model 77—54927
crack extension in elastic bodies, review of expt. and theoretical results 77—14958
crack initation, anal. of mechanics and statistics 79—50658
crack propag. rate variation with resistance to crack movement 77—59926
crack propagation, computer simulation 80—38331
crack propagation, computer simulation 80—59573
crack propagation as wave 77—75852

brittle fracture continued

- crack propagation in non-proportionally scaled elastic structures 79—18807
- crack propagation under compression, finite element anal. *(Japanese)* 78—42567
- crack response to impact by caustics 78—56724
- crack system propagation, stability conditions 78—51131
- crack tip elastodynamic fields, stress intensity factors 77—68535
- cracked elastic surface layer bonded to half-space 79—27586
- cracks, stability, propagation, fracture mech. *(Czech)* 78—79257
- critical equilibrium diag. for microheterogeneous brittle bodies *(Russian)* 77—54930
- critical plane crack size *(Russian)* 77—44329
- critical stress characts. in multicracked brittle plates in complex stress state *(Russian)* 77—58601
- critical stress for fracture propag. in brittle materials, crack interaction effects 79—25234
- crystal, catastrophe theory appl. 77—67232
- cylinder, transversely isotropic brittle elastic, stress and failure probability analysis for internal press. and thermal loading 77—50990
- cylindrical shell, stress intensity factor soln. for crotch corner cracks of tee intersections 79—23279
- Dacron, vascular substitute, exam. of tensile fracture behaviour 78—77157
- damage-induced tensile instability 77—4854
- Debonding of circular second phase particles 78—5688
- deformable dielectric, power of fracture using Griffith criterion 78—22301
- deformation instability, soln. to Griffin problem satisfying stability condition 78—63382
- diametral compression tests, tensile strength meas., appl. to biaxial stress fracture *(Japanese)* 78—72840
- diamond, brittle failure due to liq. Si, SiC layer form. in cracks 77—15720
- diamond, optically active centre effect on strength props. 80—40462
- diamond, sintered compact, fracture and fatigue 79—52352
- dielectric material, self-consistent elec. field produced during fracture *(Russian)* 77—63369
- dislocation struct. effect on crack motion 77—86182
- dislocation theory, elastic energy momentum tensor and crack propagation 80—69741
- distribution functions at threshold of brittle rupture in solid body *(Russian)* 77—84192
- ductile material, model and applic. to H embrittlement ductile material, model and applic. to H embrittlement 78—23814
- ductile metals in liquid metal environments, embrittlement and brittle fracture, exam. 78—60766
- dynamic crack propagation, opening mode case analysis 78—22302
- dynamic crack propagation, sliding mode case analysis 78—22303
- dynamic crack propagation and arrest 78—68758
- earthquakes, brittle fracture model rel. to pore fluids and Q 79—39671
- edge failures, influence on fracture data, method of correcting 78—83346
- edge notched brittle plates, virgin waves and boundary reflections at fracture 80—79233
- elastic crack mechanics influence function method computer program 77—75859
- elastic fracture mechanics, of bondline cracking and crack branching, power type singularities analysis, using finite elements 77—80106
- elastic interaction between solute atoms and stress field at tip of cracks and notches 78—34067
- elastic plane, stress-strain state at brittle crack vertex, geometric nonlinearity effects *(Russian)* 80—79221
- elastic singularity anal., boundary integral eqn. 77—68426
- elastic-plastic fracture mechanics, crack separation energy rates 78—46915
- elastic-plastic fracture mechanics for structure design 77—14961
- elastoplastic fracture mechanics, finite element analysis *(German)* 77—54935
- electron irradiated solids *(Russian)* 78—18680
- electronic devices, failure analysis of metal parts using fractography 79—61811
- energy condition for uniform extension *(Russian)* 80—33534
- energy criteria in rupture and fatigue *(French)* 78—90771
- energy of fracture, meas. by modified double cantilever method 77—73387
- energy release rate, equivalent to Rice integral *(French)* 80—64457
- epoxy resin, effect of environment on stability of cracking 78—95807
- epoxy resins, mech. and elec. low temp. props. 80—25814
- epoxy-rubber particulate composite, toughness and fracture mech. 80—71727
- equilibrium and kinetic aspects of brittle fracture 78—79271
- failure beyond linear elastic regime 78—67141
- fatigue crack growth, mechanisms 78—64703
- fibre reinforced alloys, anal. of fracture process and fibre strength, by Monte Carlo simulation *(Japanese)* 78—80634
- fibre reinforced composite, hybrid C and glass fibre, fracture energy 78—95801
- fibre reinforced composite, with additional matrix toughening component, crack growth 77—56076
- fibre reinforced composites, crack interactions 80—65149
- fibre reinforced composites, transverse plane, elastic, failure behaviour *(Japanese)* 78—48510
- fibrous media, crack interactions 80—10203
- finite element fracture mechanics, appl. to nuclear reactor materials 77—42095
- flat glass in vacuum, exam. of temp. dependence of microhardness and microstrength 78—88532
- float glass, commercially produced, thermally toughened and untoughened, surface damage resistances on air and tin side 79—61612
- float glass, exam. of dynamic fatigue 78—80631
- fluorite, use of proton irrad. to reveal growth and deform. features 80—84216
- fracture mechanics, recent theoretical and experimental developments, review 78—60776
- fracture mirrors, fracture mechanics, stress intensity factor calcs. 79—79082
- fracture toughness, influence of structural parameters 79—96133
- fragmentation mechanism of brittle solid by explosion 77—84843
- friction in transition from plastic to brittle contact *(Russian)* 78—53000
- glass, electron bombarded, brittle failure 77—28909
- glass, failure prediction technique derived from fracture mech. 77—7343

brittle fracture continued

- glass, fracture, by impulse loading, splitting method tests strength properties 79—57118
- glass, fracture, grinding and flaw geometry effect 77—56081
- glass, fracture mechanics studies, specimen *(French)* 77—73401
- glass, prestressed plate, contact induced failure 80—3172
- glass, rupture behaviour, long-term strength, thermofluctuation theory *(Russian)* 80—40536
- glass, strength test, biaxial, use of Weibull statistics 78—68798
- glass, stress intensity factors by double torsion method, crack growth *(French)* 77—73345
- glass, surface erosion, produced by meteorite impact 77—90445
- glass, tempered, spontaneous fracture due to NiS inclusions, exam. of behaviour mechanics 78—71294
- glass, tempered, stress meas. in surface, indentation technique 77—44341
- glass, tempered, surface residual stresses from indentation fracture mechanics 77—90439
- glass, theory, nonisothermal conditions 80—21101
- glass, theory under nonisothermal conditions 79—64593
- glass, wear, acoustic emission obs., effect of ion aggregates in Rebinder-Westwood environment 78—48536
- glass beam, brittle bending fracture and emitted stress waves 77—73329
- glass containers, exam. of fragmentation 79—20148
- glass fibre, optical, smooth fracture faces manufacture using incandescent wire 78—38098
- glass fibre epoxy cross-ply laminates, multiple transverse cracking 78—95800
- glass fibre reinforced plastic laminate, crack resistance under prolonged loading 77—21276
- glass plate, physically or chemically tempered, contact fracture resist., model 78—19895
- glass plates, effect of localized damage on energy losses, during impact by glass spheres 78—52973
- glass plates, fast crack propagation meas. continuous stress meas., new method 78—73009
- glasses, mech. strength fracture dynamics, behaviour forecasting *(French)* 77—73344
- grain boundary, stress induced drift diffusion, appl. to creep and growth of grain boundary voids 78—72811
- grain boundary decohesion, exchange type soft solute segregation in hard hosts 80—54258
- grain boundary sliding and brittle crack extension failure mechanism 80—97557
- grain size dependence 78—80651
- granite cylinders, failure under impact loading, brittle fracture process 77—86864
- granodiorite, fracture under uniaxial compression, mech. and AE meas. *(Japanese)* 78—56748
- graphite, bending strength, surface roughness effect at high temp. *(Japanese)* 79—70131
- graphite, diametral compressive strength, comparison with uniaxial tensile strength *(Japanese)* 78—72947
- Griffith criterion for brittle fracture in nonlinear thermoelasticity 79—77020
- Griffith energy criterion of fracture for edge cracks 80—5992
- Griffith theory generalisation for brittle fracture, dissipation law of rupture *(French)* 80—14621
- Griffith-Irwin-Orowan cracks, unification theory 79—10529
- growth dynamics, crack vel. meas. using evaporated thin conducting film 78—83347
- Hastealloy X, relations between weld heat affected zone cracking and microstruct., Gleeble test *(Japanese)* 78—52858
- Hastelloy, H_2 embrittlement in H_2S environments, impurity segregation effects 80—71724
- Haversian bone, exam. of mechanical failure at microstructural level 78—77080
- Hertz indentation test and Auerbach's law, computer simulation 78—19967
- Hertzian, wavy, thermally induced 77—56082
- Hertzian cracking, anti-plane elastic solid model, surface energy meas. *(Spanish)* 77—31260
- hexagonal crystals, elastic energy of slit cracks 79—60431
- high-Si corrosion-resistant steel, 02Kh8N20S6, mech. props. and heat treatment 77—56003
- hot-pressed with crystn. grain boundary phases 78—95716
- HTR fuel spheres, ice cleavage and subsequent examinations 79—36319
- ice, rupture mechanism exam. *(German)* 78—52976
- ice, thermal fracture 79—65141
- ice sheet deflection by submerged gas source 77—80120
- impact damage in elastic response regime 78—71785
- impact fracture in elastoplastic regime 78—51133
- Impact response of a finite crack in a finite strip under anti-plane shear 78—5691
- Incipient fracture angle, fracture loci and critical stress for mixed mode loading 78—5686
- Inconel 600, Neutron irradiation using HFIR for evaluation as fusion reactor material 78—13324
- Inconel 706 and 718, relations between weld heat affected zone cracking and microstruct., Gleeble test *(Japanese)* 78—52858
- indentation fracture in brittle rocks and glasses 77—41023
- indentation of hard metals, residual stresses, exptl. verification 77—21249
- initiation by ductile tearing 78—64656
- instrumentation for impact, erosion and fracture studies 77—81383
- interaction between cracks positioned at an angle, anal. 78—83871
- intergranular fracture energy, effects of segregated impurities 79—38928
- ionic crystal, exposed to high-current electron beam pulses, min. size of excited region for crack initiation *(Russian)* 78—84961
- ionic crystals, nanosec. electron beam effects, size depend., Ioffe effect 80—88211
- ionisation wave generation, microbreakdown mechanism 79—33032
- kinetics, one-dimensional stress fields and spherical wave reflection 78—9608
- laminates, fracture, effect of adhesive layers 78—90791
- lifetime prediction rel. to spatial variations in K_{IC} and K_I 77—62209
- lightguide fibre, ensuring mechanical reliability 80—79001
- limiting stresses for brittle body with elliptical hole with edge cracks, diag. construction *(Russian)* 78—55600
- line crack subject to shear 78—79268
- linear elastic, singular isoparametric elements properties 77—13592
- linear elastic, special isoparametric elements 77—14957

brittle fracture continued
- linear elastic and post yield fracture mechs., thermal and residual stresses 77—89066
- linear fracture mechanics using isoparametric finite element 77—22420
- LMFBR hexagonal ducts, cracking, effect on safety and fuel pin failure 78—17318
- load-bearing structures, behaviour prediction of materials degradation 79—34133
- marble, Italian Ondagata, diametral compressive strength, comparison with uniaxial tensile strength *(Japanese)* 78—72947
- material with heterogeneous struct., fracture mechanism 78—67127
- materials testing under biaxial normal stress 78—68869
- metal, brittle fracture, low temp. statistical strength criterion 77—73318
- metal, cleavage plane prediction, Ayres-Stein method 79—29214
- metal, cleavage plane prediction, Ayres-Stein method 79—29213
- metal, high plasticity, fracture nature *(Russian)* 77—25149
- metallic composite materials, stress redistrib. upon breakage of brittle fibres 78—48527
- metals, brittle and plastic, energetic strength theories *(Bulgarian)* 80—38296
- metals, brittle intercrystalline fracture, impurities effect 80—100915
- metals, cryogenic fracturing, appl. to surface layer struct. investig. 77—30219
- metals, ductile, specimen dimensions influence *(Russian)* 79—52345
- metals, liquid metal embrittlement, mechanism 79—43495
- micro and macro fracture mechanics, exam. of brittle fracture and fatigue crack growth 78—60774
- microfracture about scratches in brittle solids 79—59945
- micromechanisms of crack extension, conf., Cambridge, England (March 1980) 80—105421
- mineral wool fibre composites, mech. props., effects of thermally induced phys. and chem. changes 77—59884
- mode I 3-dimens. problems, brittle fracture criteria 79—46267
- model mats., porous and nonporous, strength and struct. 77—4849
- modulus of brittleness, crit. tensile span 78—92318
- monolithic component glasses and rigid sintered fibre-optic elements, microcrack form. during grinding 78—87175
- multibarrier kinetics, subcritical crack velocity stress depend., review 80—23958
- nonlinear lattice theory 78—67138
- notch angle effects obs. *(Japanese)* 80—6459
- notch tip, strain velocity effects on critical crack opening displacement 79—18818
- notched or cracked specimens, fracture criterion based on micro and macro crack mechanisms 80—1476
- notched specimen, brittle fracture characts. under impact bending 78—23810
- nylon, partially crystn., temp. effects on fracture 77—63771
- one-dimensional chain, thermal fluctuation induced rupture, computer simulation 78—91378
- optical fibre end fracture torsion effects 79—76802
- optical fibres, fractographic anal. of fracture surface, after proof stressing, SEM exam. 78—38093
- optical fibres, investigated using fracture mechanics *(Japanese)* 79—59817
- overlapping interacting cracks 78—55593
- penny-shaped crack in infinite viscoelastic medium, stress field anal. 77—31254
- perspex, explosively end-loaded bars with transverse holes or section changes 77—63769
- PET, effect of liquid aliphatic compounds on mech. props. 80—55488
- photoelastic dynamic studies 80—38358
- physical model for crystal with high Peierls relief in brittle failure region *(Russian)* 79—65093
- plaster of Paris, explosively end-loaded bars with transverse holes or section changes 77—63769
- plate containing stochastically distributed rigid rod like inclusions, strength *(Russian)* 77—23917
- plate with initial crack subject to extension, brittle fracture energy conditions *(Russian)* 80—103002
- plates, effect of curvature of front of through slit 80—23953
- PMMA, amorphous, structural cause of orientation modification, exam. 78—67664
- PMMA, brittle fracture initiation characts., under biaxial loading, exam. 78—60803
- PMMA, destructive mech. cracks, electron microscope exam. of generation centres 78—68782
- PMMA, ductile glassy, notch brittleness under plane strain 80—100900
- PMMA, fracture rib spacing, temp. effects 77—77564
- PMMA, fracture toughness under biaxial stress 78—76760
- PMMA, indentation fracture mechanics 78—35490
- PMMA, influence of craze configuration on fracture 78—76758
- PMMA, kinetic theory of quasi-brittle fracture *(German)* 78—84991
- PMMA, light absorption, laser crack development 78—68780
- PMMA, optical interference meas. of critical crack tip displacements 78—84964
- PMMA, oriented, indentation fracture 78—35489
- PMMA, overlapping skew-parallel crack dynamic propag. and arrest meas., method of caustics 78—84962
- PMMA, rain erosion behaviour, exam. 78—53001
- PMMA, stability of cracking, effect of environment 78—95806
- PMMA, stability of cracking, effect of environment 78—95807
- PMMA, strain rate effects on viscoelastic crack bifurcation 78—35473
- PMMA and brittle materials, slow crack propagation anal. thermodynamic model 78—35488
- PMMA based composite (acrylic bone cement), effect of $BaSO_4$ and glass particle dispersions, on fracture behaviour 78—76753
- PMMA based plastics, specific fracture energy depend. on crack growth rate., mol. struct. effect 80—66639
- PMMA/PVC, cracking in layered composites 78—95808
- polycarbonate, brittle fracture of notched ductile polymers *(Japanese)* 80—16448
- polycarbonate, ductile glassy, notch brittleness under plane strain 80—100900
- polycarbonate, glassy, craze and crack growth *(Japanese)* 77—8970
- polycarbonate, impact behaviour, effects of thermal pre-treatment and mol. wt. 78—95798
- polycarbonate, notched specimens, impact fracture behaviour 77—28888
- polyethylene, brittle fracture of notched ductile polymers *(Japanese)* 80—16448

brittle fracture continued
- polyethylene, effect of pressure and environment on fracture and yield 78—76757
- polyethylene, high density, biaxial tension, long-time strength 77—66696
- polyethylene, high density, environmental stress cracking and morphology 78—68834
- polyethylene, mech. and elec. low temp. props. 80—25814
- polyethylene, oriented chain-extended, Young's modulus, fracture and compression behavior 80—11747
- polymer, brittle, in vitreous state, resistance to brittleness and fracture kinetics *(German)* 77—32688
- polymer, fracture and crazing under plain strain *(Japanese)* 80—25850
- polymer, fracture mechanism and surface crazing 77—90446
- polymer, glassy, strength and safe stress calcs. for brittle state *(Russian)* 77—59898
- polymer, principal stress distrib. meas. at running crack tip *(Japanese)* 77—42784
- polymer, rigid, prefractured states study, elastic limit and strength 77—70092
- polymer, toughened glassy, crazing within glassy occlusions in rubber particles, micromech. analysis 79—91824
- polymer, ultimate lifetime at high loads 79—20184
- polymer with macrodefects, fracture mechanism *(Russian)* 78—35500
- polymeric glasses, kinetic theory of brittle fracture 78—48526
- polymers, vitreous, quasibrittle fracture 80—21094
- polyoxymethylene, effect of pressure and environment on fracture and yield 78—76757
- polypropylene, crystalline, morphological aspects of crack growth 78—76761
- polypropylene, effect of pressure and environment on fracture and yield 78—76757
- polypropylene partially crystn., temp. effects on fracture 77—63771
- polystyrene, amorphous, fracture mechanism 77—8949
- polystyrene, amorphous, structural cause of orientation modification, exam. 78—67664
- polystyrene, craze and fracture surface morphology 77—12682
- polystyrene, effect of pressure and environment on fracture and yield 78—76757
- polystyrene, glassy, crazing and brittle fracture on flat die indentation 80—60970
- polystyrene, glassy, fracture surface, formation and struct. of striations 77—28892
- polystyrene, mech. degradation, mass spectroscopic investig. 77—16668
- polystyrene, mol. conform., craze fracture 79—15835
- polystyrene, polymerisation route and internal lubricant effects 77—12683
- polystyrene, rubber-filled, mech. props. *(German)* 80—35320
- polystyrene, rubber-modified, impact-strength analysis 79—38972
- polystyrene, rubber-modified, temp.-effect −120-20°C 77—4838
- polystyrene-polyethylene block copolymer, deformation ratios, Poisson ratio and adhesion, dilatometric obs. 80—60937
- porcelain enamel layers on steel, H_2 induced fracture of layers 78—76752
- porous materials, critical stress and crack size evaluation *(Russian)* 78—35494
- porous materials, US fractography appl., expts. on glass 77—44336
- pressure vessel, strength analysis, by thermal shock 78—68819
- pressure vessels, brittle fracture probability using reactor surveillance capsule data 78—80641
- pressure vessels, creep bounds and brittle damage estimates 80—23908
- pressure vessels, unconditioned probability of brittle fracture 78—78479
- pressure vessels for LWRs, brittle fracture initiation, propagation and arrest, investigation 79—22422
- propagation velocity determ., expt. eval. 79—70236
- PVC, brittle fracture of notched ductile polymers *(Japanese)* 80—16448
- PVC, ductile glassy, notch brittleness under plane strain 80—100900
- PVC, glassy, craze and crack growth *(Japanese)* 77—8970
- PVC, optical interference meas. of critical crack tip displacements 78—84964
- PVC, rigid, craze and yield zones in fracture 80—50701
- PVC, rigid, tensile fracture morphology, rel. to mol. props. 77—59883
- PVC products, initiation by defects or flaws 79—5042
- PVC rigid plate specimens, Charpy impacted, SEM exam. of fracture surface *(Japanese)* 78—52953
- Pyrex, impact of small steel spheres 77—73338
- Pyrex glass, Hertzian fracture under quasi-static loading 79—66142
- quartz, phase transform. in brittle materials, plane stress anal. 77—86024
- quartz bearing rocks, RF EM emission with fracture 77—86863
- quasi-cleavage fracture, characteristic length parameter, correlation with fracture toughness *(Chinese)* 80—104246
- rare earth hexaborides, electron fractography 77—8906
- rare reinforced concrete structures, failure, expt. determ. and calc. methods *(Chinese)* 79—74243
- reactor pressure vessel material, radiation embrittlement, current regulation assessment 78—52966
- reactor pressure vessels, sefeguards, American and German ductility requirements *(German)* 79—41017
- refractory ceramic, heterogeneous, significance of non-elastic deform. in fracture 79—47765
- review 80—29116
- rheonomic viscoelastic materials, under prolonged loading, failure hypothesis 80—3180
- rigid body collisions, spalling, tensile stresses on target, appls. 79—7324
- rock, anisotropic, chip form. 78—61407
- rock, continuum model for plastic-brittle fracture 79—27584
- rock, fracture, role of crack inertia 80—109138
- rock, plastic-brittle behaviour, hardening and softening constitutive eqns. 77—21270
- rock and rock joints, empirical laws of friction and fracture 77—21762
- rock samples with saw cut, fracture and frictional sliding, earthquake prediction appl. *(Chinese)* 79—100825
- rocks, failure processes and AE under compression *(Japanese)* 78—56749
- rocks impulsive fracture, criteria 80—85646
- rod, theory of resistance to failure of technical materials 79—10536
- rotating discs, with radial cracks, appl. of linear-elastic fracture mechanics 77—54929
- rupture of brittle bodies exposed to explosive action *(Russian)* 80—79223
- S glass-Ni sphere composite, exam. of crack shape and fracture toughness 78—72886

brittle fracture continued
sapphire, synthetic arc lamp envelope, basal plane cleavage 79—66146
sapphire, white, brittle fracture, microstruct. depend. 80—16469
sapphire 0°, creep deform., fracture anal. 77—56035
sharp contact cracking, residual stress effects 79—100245
silicate glasses, fused, cone cracks around Vickers indentations 79—29189
silicate glasses, indentation form. and fracture 79—66147
size effects in abrasion of brittle materials 79—34131
soda-lime, impact of small steel spheres 77—73338
soda-lime-silicate glass, dynamics of fracture mirror boundary formation 77—86132
solid materials, cracks and strength relations *(Russian)* 78—18703
stability loss near crack 78—55597
stability loss near crack preceding brittle fracture *(Ukrainian)* 79—77007
stability problem, three-dimensional linearised theory *(Russian)* 78—55606
stainless steel brittle fracture resistance improvement by N content reduction 78—95788
statistical anal., evaluation of a fundamental approach 78—64619
statistical approach 77—62210
statistical theory, dislocation mechanism, crack propagation *(Chinese)* 80—106755
statistical theory, fracture of brittle solids, under multiaxial stresses *(Japanese)* 78—90788
statistical theory for mutual actions between adjacent elements *(Chinese)* 80—43673
statistics in brittle materials with surface shear-sensitive cracks 79—41616
steatite, ceramic, exam. of thermal damage by strength meas. 78—84997
steel:B, brittle rupture, (n,α) radiography method *(Russian)* 78—48491
steel, 10Kh11N20T3R, brittle fracture susceptibility rel. to grain size *(Russian)* 77—59901
steel, 12Kh18N9T-TiB_2, eutectic alloy, high temp. props. 78—84931
steel, 15Cr1Mo1VL, susceptibility to brittle struct. and fracture, influence of props. 80—104298
steel, 18 Kh2N4MA, grain size effect on mech. props. 78—44207
steel, 30N9K4, effects of Mo, V, and N on grain growth, tempering, hardenability, strength and toughness 78—44202
steel, 3Kh2V8F, brittleness depend. on high temp. deform. at high stress. temp. *(Russian)* 80—50698
steel, alloy, austenitic, grain size, tempering effect on brittle fracture susceptibility 80—55534
steel, alloy, Fe-Ni-Cr-Mo-V-C, HY130, effect of H_2 and impurities on brittle fracture, review 78—60765
steel, alloy, high-temp. combined ht. treatment and mech. working, C content effects *(Russian)* 78—52854
steel, alloy, medium and low C, quenched and tempered, fracture resist., nonmartensitic transformation products effect 79—96054
steel, alloy, Ni-Cr-Mn, type 4340 intergranular brittle fracture, exam. by impact testing and Auger spectroscopy 78—52978
steel, austenitic, 30KhGSA, grain size before quenching rel. to mech. props. 79—24553
steel, austenitic, type 70, cold brittleness structural depend., fracture mechanisms *(Russian)* 80—97571
steel, austenitic stainless, cathodically charged, H_2 embrittlement, α' martensite effect 80—71725
steel, austenitic stainless, temper embrittled, type 304, Auger spectroscopic exam. of grain boundary surface phases 78—76741
steel, brittle fracture, J-integral fracture criterion *(Japanese)* 77—48597
steel, brittle fracture of compressor materials under impact loading 77—25137
steel, brittle fracture resist., fractography and grain refinement 77—60024
steel, brittle fracture resistance, welding and heat treatment effects 80—50723
steel, C, bainitic, microstruct. and cleavage resistance 77—52481
steel, C, brittle fracture resistance, C effect 80—3163
steel, C, cavitation erosion, exam. of mechanism and rates 79—5063
steel, C, heterogeneous structure, fracture characts. 79—38961
steel, C, tensile fracture surface in high press. H_2 at room temp. *(Japanese)* 80—108540
steel, C, type 1792AF 79—38966
steel, C and low alloy, structural, ductile and brittle fracture resist. in stable crack growth stage 79—52369
steel, C content influence on brittle and tough fracture, heat treatment *(Russian)* 80—40500
steel, C-Mn-Nb, structural for seamless line pipe tube, brittle fracture resistance *(Czech)* 77—70161
steel, case-carburized, low alloy, rolling contact fatigue 78—35518
steel, cast, tendency to brittle fracture *(Russian)* 78—56735
steel, cast, type 20, exam. of strain characts. in premelting temp. range *(Russian)* 79—29140
steel, CC Cr-Ni, rock-like fracture *(Chinese)* 78—31497
steel, chemicothermal treatment quality control by fractographic method 79—39080
steel, cold drawn wire, anisotropic fracture *(Russian)* 77—1867
steel, constructional, fracture toughness in cyclic loading 78—72860
steel, constructional, impact strength/brittle fracture relationship in ductile-brittle transition zone 78—56740
steel, Cr-ferritic stainless, critical strain rate 80—16399
steel, Cr-Mo-Ni-V, dynamic stress intensity factor meas., possibilities and limits *(German)* 80—93719
steel, Cr-Mo-V, heat treatment and influence of cold plastic deform. 78—72858
steel, Cr-Ni (32.8 wt.%), tensile props. and fracture of two phase Fe alloy austenite and ferrite *(Japanese)* 79—8344
steel, crack growth resistance, J-integral approach, crack line wedge loaded specimen 78—35513
steel, crack propagation stress wave obs. *(German)* 77—56110
steel, Cu, precipitation hardening, struct. and fracture *(German)* 79—61696
steel, deformed, Kh18N10T, ageing under gradually increasing load 77—90383
steel, electroplating and failure assoc. with H-embrittlement, in situ anal. 78—7299
steel, fatigue life, structural parameters and chem. comp. effects, rel. to test parameters 77—59928
steel, ferritic, cleavage fracture toughness, temp. and strain rate depend. 80—85028

brittle fracture continued
steel, ferritic, crack extension, cleavage micromechanisms, review 80—108562
steel, ferritic, strengthened by VC interphase precipitation, cleavage 79—74171
steel, for pressure tanks, yield point influence on brittle fracture, tensile strength *(German)* 80—40539
steel, fracture micromechanisms, fracture toughness, exam. 78—56766
steel, fracture toughness, influence of low-cycle damage 78—72873
steel, grain boundary P segregation, effect after quenching and tempering *(Russian)* 80—81145
steel, heat-treatment furnace trays, in service embrittlement, microstruct. and props. changes 77—63784
steel, high C, quenched and tempered, hydrostatic press. effect on brittle fracture stress 79—61727
steel, high strength, plastic deform. and fracture under tensile stress *(Russian)* 77—70100
steel, high-strength, H distrib. and delayed brittle fracture 80—108577
steel, hypereutectoid, type FS-01, HF-1, brittle fracture, fragmentation due to blast loading 80—50699
steel, impact strength, effect of surface decarburization and carburization of faces and core struct. 78—23811
steel, lamellar pearlite, containing proeutectoid cementite, brittle-fracture study *(Japanese)* 80—93648
steel, lamellar pearlite, containing proeutectoid ferrite, brittle fracture *(Japanese)* 79—66152
steel, lamellar pearlite, containing proeutectoid ferrite, prestrain effect on brittle fracture *(Japanese)* 80—45388
steel, low alloy, blunt-notched, fracture mechanism and failure assessment 80—16450
steel, low alloy, brittle fracture, quenched and tempered 80—11677
steel, low alloy, cleavage fracture, fine scale precipitation dispersion effect, TEM obs. 78—60788
steel, low alloy, cold resistance, effect of nitrides, carbonitrides, carbides, Cu precipitates 77—16594
steel, low alloy, elastoplastic strain evaluation in crack weakened cross sections by fracture mechanics 80—45380
steel, low alloy, medium strength, SEM obs. of fracture surfaces, cleavage fracture model 77—36649
steel, low alloy, type 10KhN1M, heat-treated, struct. and resist. to thermal embrittlement 79—15788
steel, low alloy type 14Kh2GMR, high strength, welded joint, impact toughness, welding thermal cycle and tempering effects 80—3157
steel, low alloys, high strength, stress corrosion cracking in saturated $Ca(OH)_2$ solns., due to Cl^- and SO_4^{2-} additions 78—88567
steel, low C, brittle fracture of notched specimens, ferrite grain size and notch geometry effects 78—19860
steel, low C, brittle fracture susceptibility, low temp. deform. effects 77—56103
steel, low C, dynamic stress intensity factor meas., possibilities and limits *(German)* 80—93719
steel, low c, grain size influence on size of brittle transgranular shear facets 80—35327
steel, low C, martensitic, fracture toughness variations during tempering 78—60812
steel, low C, notched sheet under tensile loading, notch tip opening/contraction, J-integral relationship *(Japanese)* 77—4840
steel, low C, notched specimens, brittle fracture stress, effect of ferrite grain size, notch acuity and notch length 79—20187
steel, low C, specimens with notch and fatigue crack, fracture surface features 79—43417
steel, low C, unnotched specimens, brittle fracture beyond general yielding tensile-torsional stresses 77—56096
steel, low S, ESR and electric arc, notch toughness, interaction between overheating and tempering temp. effects 78—52970
steel, low strength notched specimens, preloading effects on brittle fracture 78—27642
steel, low-alloy, fracture resist. assessment from stable crack length *(Russian)* 79—15765
steel, low-alloy, fracture toughness and brittle fracture, S and rare earth additions effect 79—87720
steel, low-alloy, fracture toughness characts., loading rate effect 80—100897
steel, low-Mn low-C, susceptibility to brittle fracture 80—76340
steel, maraging, plastic deform. effects on ageing kinetics *(Russian)* 77—77508
steel, martensite, brittle fracture resistance, struct. after quenching effects, tempering effects 79—57104
steel, martensitic, Cr (12 wt.%), temper embrittlement 79—87722
steel, martensitic, medium alloy, quenched state, deform. hardened, ageing effects *(Russian)* 77—21179
steel, medium strength plate, quenched and tempered, fracture toughness in ductile-brittle range 78—7036
steel, mild, grain size depend. of cleavage fracture toughness 79—8359
steel, mild, impact velocity effect on fracture surface *(Japanese)* 79—96118
steel, mild, microbehaviour of notch tip during increasing load in brittle fracture beyond general yield 78—35487
steel, mild, microstructure effect on cleavage fracture stress 79—8358
steel, mild, type SM41, brittle fracture initiation characts., under biaxial loading, exam. 78—60803
steel, mild, welded struct., dynamic initiation of brittle fracture, testing 77—36716
steel, Mn, H_2 embrittlement mechanism *(Korean)* 78—68774
steel, Mn-B-V, low alloy, transform. singularities *(Russian)* 80—104116
steel, Mn-Si, St 52-3, cleavage fracture toughness, temperature and notch sharpness influence *(German)* 80—35291
steel, Mn-Si, St 52-3, fracture toughness determ. from yield strength and cleavage fracture strength *(German)* 80—35292
steel, Mn-Te, structural, brittle fracture resistance, Ti addition effect *(Czech)* 80—45392
steel, Ni-Co-Mo, dynamic stress intensity factor meas., possibilities and limits *(German)* 80—93719
steel, Ni-Cr, cast, tempering embrittlement due to impurities, Auger spectroscopy exam. 80—11683
steel, Ni-Cr, Sb doped, solute segregation and brittle fracture 80—85033
steel, Ni-Cr, solute segregation and intergranular brittle fracture 80—108568
steel, Ni-Cr-Mo, cleavage fracture toughness, temperature and notch sharpness influence *(German)* 80—35291

brittle fracture continued
steel, Ni-Cr-Mo, fracture toughness determ. from yield strength and cleavage fracture strength *(German)* 80—35292
steel, nonmetallic inclusions effects on low-temp. fracture *(Russian)* 77—59895
steel, notched specimens, strength parameters and crack growth energy correl. 77—73334
steel, pearlitic, brittle fracture of structures 78—72869
steel, pearlitic eutectoid, cleavage fracture, grain size effect 78—60784
steel, pressure tank, heat-treatment effects and mech. props. *(German)* 80—40409
steel, propagation velocity determ., expt. eval. 79—70236
steel, quasi-cleavage fracture *(Chinese)* 80—21060
steel, quenched and tempered, microstructure effect on cleavage fracture toughness 79—74252
steel, reactor vessel, neutron irrad. effect on brittle fracture characts. *(Slovak)* 78—50254
steel, stainless, ferritic, 18%Cr, stress/strain curve, H_2 charging influence, room temp. *(Japanese)* 78—39884
steel, stainless, ferritic, high CR penny shaped central bursting defect in cold drawing 79—20071
steel, stainless, He ion irrad., fracture behaviour, in-situ HV electron microscopy 80—29089
steel, stainless, type 316, LMFBR and P1 cladding tubes, burst tests 78—44210
steel, stainless type 304 attack morphology of stress corrosion cracking, TEM study *(French)* 79—83368
steel, structural, arrested brittle cracks in Robertson test with temp. gradient 77—56052
steel, structural, brittle fracture, intermediate fracture stress, fracture initiation mode transition 78—60802
steel, structural, brittleness susceptibility rel. to heat treatment 79—24620
steel, structural, conditions for predicting brittle fracture in welded structures *(French)* 80—25867
steel, structural, effect of stressed state nature on ductility and failure 79—57078
steel, structural, rel. between static and dynamic fracture toughness 78—68815
steel, structural, susceptibility to brittle fracture criteria, comparison of notch impact and fracture toughness testing *(German)* 77—70237
steel, structural, unalloyed, brittle fracture, grain size and precipitate thickness effect 78—60786
steel, structural 78—68808
steel, tool, high-strength, mech. props. in compression, tempering temp. effect 79—83240
steel, type 20, critical strain rate 80—16399
steel, type 27KhGSNL, castings, exam. of cracks due to treatment 78—44205
steel, type 30KhGSA, critical strain rate 80—16399
steel, type 316 stainless, Neutron irradiation using HFIR for evaluation as fusion reactor material 78—13324
steel, type 4340, effect of H_2 and impurities on brittle fracture, review 78—60765
steel, unalloyed, brittle fracture, effect of prestrain and ageing *(German)* 78—19857
steel, weldable C and alloy, brittle fracture, metallurgical factor effects, NDT data, impact tests *(French)* 79—5128
steel, welded joint brittle fracture susceptibility test 79—29168
steel 12Kh18N10T, struct. and mech. props. after prolonged working at −183°C 77—55988
steel 14Kh2N3MA, brittle fracture susceptibility, heat treatment effects 77—21190
steel 15G2AFDps, brittle fracture of Fe quantitative electron fractography 77—63804
steel 15G2AFDps, fatigue to brittle fracture transition at low temp., stress raiser effect 77—12696
steel bearings, for gas turbines brittle fracture due to stress combination 78—56771
steel components, safety anal. for loading conditions 78—39979
steel for nuclear reactor press. vessels, criteria for brittle fracture, neutron effects *(German)* 77—34389
steel Kh15N5D2T, and Kh16N4B, cold cracking resistance under continuous multipass welding 78—39911
steel layer types St3+0Kh13, acoustic emission parameters, brittle fracture, crack propagation *(Russian)* 80—93633
steel layers, types St3+Kh18N9T, acoustic emission parameters, brittle fracture, crack propagation *(Russian)* 80—93633
steel plate for nuclear reactor containment 77—3115
steel structural components, flaw assessment based on cleavage fracture hypothesis 78—60804
steel structures, appl. of risk analysis to brittle fracture and fatigue 78—56768
steel tearing rate determ. by elec. resist. meas. method *(German)* 78—15619
steel wire reinforced polymer, crack growth matrix toughening effect of glass fibres 77—56076
steels, cleavage fracture model at low temperatures *(German)* 80—35293
steels, strength reduction by adsorpt., stress corrosion *(Russian)* 79—29265
steels, with yield pt. of about 420 to 720 N/mm^2, correlation between yield pt./tensile strength ratio and toughness *(German)* 80—66615
straight bar bending strength, brittle fracture energy conditions *(Russian)* 80—58974
strain driven thermoelastic instability toward brittle fracture 80—103415
strain energy density fracture criteria, extension to brittle and ductile fracture 78—75102
strain intensity criterion for crack branching in brittle mats. 78—55592
strength guides, materials selection for welding *(German)* 78—15534
strength measurement using hydraulic bursting technique 80—35443
strength of materials, empirical determ., cleavage fracture in plane waves 80—96225
strength of structures and fracture mechanics role 78—34073
structural steel, microstruct. and brittleness, rel. to austenizing and heat treatments 77—56091
structure design, method of calculation 78—72869
styrene-acrylonitrile copolymer, crazing and brittle fracture on flat die indentation 80—60970
styrene-diene triblock copolymer, hexagonal struct., flow props. of melt and fracture 78—76729

brittle fracture continued
surface energy of rupture, determ. in brittle materials 80—21074
tensile tests of short duration, fracture prediction 77—70150
Tetron, vascular substitute, exam. of tensile fracture behaviour 78—77157
thermoplastic, acrylic, hot stretched, aircraft cabin windows, exam. of anisotropic fracture 78—76763
thermoplastics, glassy, embrittlement mech. and inelastic deform. criterion for delayed failure 78—52940
thermoset and coating technology, torsional braid and thermal anal. 80—55622
thin sheet impact strength study *(Czech)* 80—59571
tile, resistance to fracture, Weibull statistics *(German)* 77—7338
time dependence of strength *(Russian)* 78—46912
torsional strength of brittle solids under hydrostatic press., statistical approach 77—84194
transition metal carbides, elastic moduli, scratch geometry, micromech. tests 78—35416
transition metal carbides and nitrides, surface energy for brittle fracture from phonon frequencies 78—67790
transition metal carbides and nitrides, surface energy for brittle fracture from phonon freqs. 79—86837
transparent dielectric, laser induced fracture *(Russian)* 77—51406
transparent dielectric, laser pulse energy absorption, refr. wave form. *(Russian)* 79—55167
uniaxially compressed brittle material, failure mechanism theory 78—26624
uniformly compressed elastic medium, brittle rupture, plane fracture wave *(Russian)* 80—53705
unstable growth of thermally induced interacting cracks in brittle solids 79—23273
Van der Waals interactions between brittle cracks and gaseous environments 77—90440
viscoelastic strip, dynamic crack propagation due to antiplane loading 80—64464
Weibull analysis in biaxial loading system 77—89067
welded pressure vessels, residual stresses determination 78—40014
wood, rupture mechanism exam. *(German)* 78—52976
wood-epoxy bond system, cleavage fracture toughness *(Japanese)* 77—77574
Zircaloy, failure assoc. with H-embrittlement, in situ anal. 78—7299
Zircaloy cladding, embrittlement and failure during reactor power-cooling-mismatch 78—21688
Zircaloy-2, effect of simulated fission products on elongation fractography and metallography 80—649
Zircaloy-2, pressure tube, fragmentation on failure 78—72863
Zircaloy-4, exam. of plastic props. at elevated temps. in air 77—4811
Al alloy, forgings, unhealed porosities and crystalline steps *(Chinese)* 79—74178
Al alloys, fracture micromechanisms, fracture toughness, exam. 78—56766
Al, crack growth resistance, J-integral approach, crack line wedge loaded specimen 78—35513
Al, pseudo-brittle fracture, aspect of impact testing 79—79111
Al-Cu alloy bicrystals, neutron irrad. effects on grain boundaries, intergranular fracture and precip. 77—48520
Al-epoxy adhesive systems, opening and edge-sliding fracture toughness 78—95805
Al-Mg alloy A99, intercrystalline fracture during US treatment 79—15795
Al-Zn-Mg type 7017 and 7018 alloy plate, fractographic study of stress-corrosion crack propag. 79—57158
Al_2O_3, bending strength, surface roughness effect at high temp. *(Japanese)* 79—70131
Al_2O_3 brittle ceramic fracture toughness meas. notch requirements *(German)* 77—59937
Al_2O_3, cutting tools, effect of acid etching on cutting performance 79—96169
Al_2O_3, cylindrical cavity effect on fracture 79—66144
Al_2O_3, evaluation of crack resistance and crack velocity, using controlled fracture experiments 78—72881
Al_2O_3 fracture resistance, exam. 78—76826
Al_2O_3, hot-pressed, crack-growth boundaries, subcritical, fractographic criterion 79—100243
Al_2O_3 on Al, anodic oxide film, effect of interface roughness on cracking 78—76755
Al_2O_3, polycrystalline, stress-strain data up to 1.25 GPa 80—100899
Al_2O_3, single crystal, fracture mirror formation, anisotropy of fracture surface energy and elastic constants 78—68824
Al_2O_3/Nb/Al_2O_3 joint, solid state bonded, exam. of bond fracture strength 78—76826
Al_2O_3-Ca (0.6 to 1.6 at.%), fracture behaviour, Ca segregation effect 80—40504
Al_2O_3-SiO_2 glasses, thermally toughened, residual compressive stresses evaluation 78—31523
Al_2O_3-ZrO_2, dispersion hardened, fracture toughness improvement by induced microcracking *(German)* 78—31501
Al_2O_3+TiC system, elastic and fracture charact. at elev. temp. *(German)* 79—43299
B fibre, Griffith criterion appl., tensile test 77—12684
B fibre, surface energy meas. from Griffith cracks 77—77563
B fibre reinforced Al, stress redistrib. anal., upon brittle fibre breakage 78—48527
B fibre reinforced Al, tensile strength and brittle fracture 80—11707
B fibres, radial cracks 78—15505
B reinforced Al laminates, applic. of linear elastic fracture mechanics 77—28893
Be, hot-extruded, fracture in impact, static tensile and fatigue tests *(Russian)* 77—52458
Be single crystal, failure energy 80—81192
C fibre reinforced Al, interaction between components and compatibility, mech. props. effect 80—11761
C fibres, Al coated, effect of annealing on ultimate tensile strength and fracture 78—56744
Cr, physically vapour deposited, struct., mech. props. 77—36400
Cr-Ni VKh-4 alloy, deformation and fracture mechanism investigation *(Russian)* 80—11738
CrC-Ni-(P), hard alloys, sintered, fracture props., P addition effects 78—60610
Cu alloys, appl. of SEM to brittleness study 78—3214
Cu, appl. of SEM to brittleness study 78—3214

brittle fracture continued
Cu, fracture criterion, expt. verification 78—64648
Cu-Bi (0.02 wt.%) alloy, intergranular fracture, Kossel X-ray diffr. in SEM obs. 80—108579
Cu-Ni-Zn, microduplex, superplastic deform., cavitation and fracture 78—64640
Cu-SiO_2 alloy, fracture at elevated temp. 78—39896
Fe and alloys, quantitative determ. of transcryst. and intercryst. portions by opt. and SEM fractography 77—52464
Fe, Armco, fracture in liq. metals, Rebinder effect *(Russian)* 79—29266
Fe, Armco, microstructure in quasibrittle and plastic fracture 77—1863
Fe based alloys, solute segregation to grain boundaries 78—72780
Fe, brittle fracture mech., review *(Russian)* 79—34139
Fe, cast, grey, fracture kinetics, surface hardening effect 80—76354
Fe, cast, grey pipe, resist. to fracture under hydraulic pressure 79—96124
Fe, cavitation erosion, exam. of mechanism and rates 79—5063
Fe, intergranular brittleness, effect of O and S 77—36650
Fe, polycrystalline, fracture surface singularities under single loading conditions *(Russian)* 80—50696
Fe, pure, mech. props. at low temps. 78—44219
Fe, sintered, porosity estimation by screen image of brittle fracture 77—52585
Fe-Al-Si (6.22, 9.63 wt.%), bending test under high press., high temp. 80—85057
Fe-base amorphous alloys, embrittled by H and heat-treatment 80—55518
Fe-C (0.64 wt.%), quasicleavage during fatigue crack propag., pearlitic microstruct. effect 79—11702
Fe-C-Fe_xO_y, cleavage initiation by ductile tearing 78—64656
Fe-CR (26 wt.%), role of C and N in brittle fracture 80—16456
Fe-C(0.001 to 0.44 wt.%), C effect on low temp. brittleness *(Japanese)* 80—50711
Fe-Co-Cr (27, 0.5 wt.%), internal stress and brittleness in ordered state *(Russian)* 79—61698
σ-Fe-Cr, brittle fracture stresses under high hydrostatic press. and high temp. *(Japanese)* 79—43397
Fe-Cr-Mn (11.5, 3 wt.%), microduplex ferritic-martensitic steel, exam. 78—39862
Fe-Mn alloys, α, ε and γ, brittleness 80—35314
Fe-Mn-Cr-C (20, 4, 0.5 wt.%), hyperquenched and predeformed, mech. props. *(French)* 78—23786
Fe-Ni, brittle transgranular and intergranular fatigue crack growth rate, yield strength effect 78—68786
Fe-Ni-Al (18.2 wt.%) aged, fracture toughness and mode, grain size depend. 77—12700
Fe-Ni-C, lenticular martensitic alloy, fractured at liquid N_2 temps., crack propag. mode *(Japanese)* 77—48524
Fe-Ni-C, martensitic delayed fracture *(Slovak)* 79—43401
Fe-Ni-C-Sb, Sb additions effect on fracture charact. of martensite *(Czech)* 77—70162
Fe-Ni-Cr-Ti, superalloy A286, powder, exam. of microstruct. and mech. properties 78—52979
Fe-Si, dislocation struct. of plastic relax. zone at tip of brittle crack 77—77582
Fe-Si (3 wt.%), breaking stress grain size and grain boundary energy during onset of reversible temper brittleness *(Russian)* 77—32673
Fe-Si (3.12 wt.%), brittle fracture, work hardening effect at notch tip 78—44220
Fe-Si (3wt.%), notched sheet under tensile loading, notch tip opening/contraction, J-integral relationship *(Japanese)* 77—4840
Fe(-Ni)(-Si), BCC, cyclic cleavage crack growth model for fatigue 80—55519
Fe_xO_y-Fe, oxide scale fracture on substrate deform. 78—11407
$Gd_3Ga_5O_{12}$, garnet substrate, surface polishing, damage, abrasion, brittle fracture model *(German)* 77—73357
$Gd_3Ga_5O_{12}$, garnet substrate surfaces, working damage, electron microscope investig. 77—77605
Ge mechanical strength in brittle fracture region, influence of Si and O impurities 79—87682
Ge single crystals, deform. during static indentation 79—87714
InAs single crystals, deform. during static indentation 79—87714
InP single crystals, uniaxial compression deform. characts. 80—84991
Ir, impurity segregation to grain boundary effects 78—64637
Ir-W (0.3 wt.%), polycrystn., brittle fracture TEM study 79—61715
Ir-W (0.3 wt.%): Al(Fe)(Th)(Ni)(Rh), effect of additions on grain boundary composition 79—83309
KCl fracture on electron bombardment, probability distrib. functions 79—86820
KCl, irrad. with intense nanosecond electron beam, super-Rayleigh vel. of brittle fracture front 80—6458
$KD_{2x}H_{2(1-x)}$ PO_4 crystals, plastic deform. and mech. props. 79—79035
KH_2PO_4 crystals, plastic deform. and mech. props. 79—79035
$LiAlSiO_4$ glass-ceramic, fracture phenomena as function of initial flaw size and temp. 78—95797
α-$LiIO_3$, surface defect layer struct. due to mechanical working *(Russian)* 80—100238
$LiNbO_3$ single crystals, deform. during static indentation 79—87714
MgO bicrystal, fracture mechanism obs. 77—44339
MgO, fracture and crack tip plastic zones, in situ obs. 80—108686
$Mn_{46}Co_{54}$, amorphous alloy prep. by high-rate sputtering, struct. and prop. characteris. 79—24462
MnZn ferrites, abrasive wear mechanism *(Japanese)* 78—39917
Mo alloys, intercryst. fracture in ductile-brittle transition region, local internal stresses effect 80—81200
Mo, single cryst., δ_R criterion for brittle fracture *(Russian)* 78—56732
Mo single crystal, crystallographic feature of brittle fracture, AE study 79—43415
Mo-Fe metalloceramic alloy, brittle fracture investigation, segregation, morphology, struct. *(Russian)* 80—55503
Mo-Mn metalloceramic alloy, brittle fracture investigation, segregation, morphology, struct. *(Russian)* 80—55503
$NH_4H_2PO_4$ crystals, plastic deform. and mech. props. 79—79035
NaCl, damage process preceding semi-brittle fracture in depend. on deform. microcrack development 77—44272
NaCl, exposed to high-current electron beam pulses, min. size of excited region for crack initiation *(Russian)* 78—84961
NaCl, mechanoluminesc. peaks, microbreakdown mechanism, generation of ionisation waves 79—33032
Na_2O-Al_2O_3-SiO_2, porous glass, crack shape, US fractography obs. 77—44336

brittle fracture continued
Na_2O-CaO glass tube, fracture by field assisted ion exchange 78—68771
Na_2O-CaO-Si_2O glass, mixed mode fracture 79—79083
Na_2O-CaO-SiO_2, double torsion specimens, compliance and fracture load as crack length function 78—48508
Na_2O-CaO-SiO_2, evaluation of crack resistance and crack velocity, using controlled fracture experiments 78—72881
Na_2O-CaO-SiO_2, fracture mirror form. 77—48541
Na_2O-CaO-SiO_2, lifetime predictions, dependence on crack propag. eqns. 78—72882
Na_2O-CaO-SiO_2, origins of acoustic emission in fracture 78—72889
Na_2O-CaO-SiO_2, plates, exam. of Hertz crack branching 78—72887
Na_2O-CaO-SiO_2 glass, Hertzian fracture characts., comp. influence 78—31522
Na_2O-CaO-SiO_2 glass, crack nucleation around plastic indents 78—92327
Na_2O-CaO-SiO_2 glass, sharp contact cracking, residual stress effects 79—100245
Na_2O-CaO-SiO_2 glass, fractographic anal. of delayed failure 80—45387
Na_2O-CaO-SiO_2 glass, hot erosion plastic flow and fracture 80—89354
Na_2O-CaO-SiO_2 glass rods, prediction of thermal fatigue resist. 78—84955
Na_3O-CaO-SiO_2, fracture initiation, influence of temperature and composition 79—100246
Nb, hydrogen embrittlement, deformation behaviour of Nb-H alloys 79—11687
Nb, neutron irrad., embrittlement, yield stress, fracture stress and strain *(Japanese)* 77—76472
Nb-Fe(Co)(Ni)(Os), alloying element influence on strength, ductility, surface and grain boundary energies *(Russian)* 79—74234
β $NbH_{0.82}$, fracture, TEM obs. 80—108519
Ni spheres in glass matrix, brittle composites, fracture 79—66141
Ni_3Al, ductility in poly- and single crystals, compressive and tensile tests 78—56715
Ni_3Ge single crystal, cleavage fracture 79—61694
α-Pu and δ-stabilised Pu-Ga alloy, strain rate effect on tensile props. 77—21284
RbH_2PO_4 crystals, plastic deform. and mech. props. 79—79035
Si, failure in strong melt grown single crysts. 78—3205
Si, monocrystalline, effect of notch root radius on fracture behaviour 78—76751
Si, single crystal, brittle fracture in axisymmetric bending, study at room temp. 80—81180
Si single crystals, deform. during static indentation 79—87714
Si_5-Al-O-N_7, hot pressed, exam. of fracture mechanisms 78—72879
SiC, appl. of replica electron fractography 79—60237
SiC continuous fibres, mech. props. depend. on testing conditions *(Russian)* 80—35297
SiC, failure prediction technique derived from fracture mech. 77—7343
SiC, hot pressed, brittle fracture and subcritical crack growth 78—72885
SiC, meas. of critical stress intensity factor and subcritical crack propag. rates 78—72880
SiC, microrelief of fracture failures *(Ukrainian)* 77—32729
SiC, reaction-bonded, impact erosion by ang. Al_2O_3 particles 80—89362
SiC, self bonded, exam. of fracture 79—20149
SiC, self-bonded, fracture characts. and rupture strength, temp. effects 79—96136
SiC single crystal, friction and fracture in contact with itself and Ti 80—11780
β-SiC, twinned crystals, fracture characts. 80—3193
Si_3N_4, exam. of fracture resistance 78—76826
Si_3N_4, hot pressed, flawed plate under combined stresses, failure prediction 78—72884
Si_3N_4, hot pressed, high temp. compressive cracking, optical and electron microscopy exam. 78—76733
Si_3N_4, hot pressed, slow crack growth from controlled surface flaws 78—80632
Si_3N_4, meas. of critical stress intensity factor and subcritical crack propag. rates 78—72880
Si_3N_4, room temp. fracture strength data, statistical anal. 78—64619
Si_3N_4, struct. of slow crack interface, light and electron microscope obs. 78—68770
Si_3N_4/Zr joint, solid state bonded, exam. of bond fracture strength 78—76826
Si_3N_4-Al_2O_3, hot-pressed with crystn. grain boundary phases 78—95716
SiO_2, crack propag. and bifurcation 78—72888
SiO_2, fused optical fibre, strength, appl. of Weibull type analysis 77—19418
$Sm_{0.8}Gd_{0.2}S$, single cryst., fracture stresses meas. 77—31718
SmS, single cryst., fracture stresses meas. 77—31718
Sn-Pb-(Bi)(Ag)(Sb) (Cu), microduplex eutectic, cavitation during superplastic flow 78—48457
Ti alloy, brittle fracture of compressor materials under impact loading 77—25137
Ti alloy, crack initiation on planar shear bands, H_2 assisted 80—71749
Ti alloy, crack resistance limit, exam. in rotating discs containing cracks *(Russian)* 79—15766
Ti alloy, disc, rotating notched, strength in quasibrittle fracture 80—55533
Ti alloys, crack growth resistance, J-integral approach, crack line wedge loaded specimen 78—35513
Ti alloys, delayed brittle fracture, H_2 effect 80—100912
Ti alloys, failure assoc. with H-embrittlement, in situ anal. 78—7299
α-Ti sheet, texture dependent stress corrosion cracking in Br_2-methanol soln. 80—71803
Ti-Al, elec. spark Al doping of VT-18, surface struct. and props. *(Russian)* 80—76398
Ti-Al-Sn (5, 2.5 wt.%), electron microscope and X-ray diffr. exam., of basal and near basal hydrides 78—80550
Ti-Al-V-Sn (6, 6, 2 wt.%), fatigue crack growth, cyclic freq. and microstruct. influence 80—55515
Ti-Al-V(6,4 wt.%), environmental fatigue crack propag. 77—36632
Ti-Al-Zr-Mo-Si (6, 5, 0.5, 0.25 wt.%), β-processed, fatigue props., hold time effect 80—60961
Ti-Zr-Mo alloy, effect of O_2 on elec. resistivity, microhardness, mech. props. 77—56092
U, two-dimensional expt. fracture map 78—95803
U-Mo (10 wt.%), gaseous O_2 and hydrogen embrittlement, exam. 78—60811
U-V (0.2 wt.%), mech. and struct. props., effect of internal H *(French)* 77—21253

brittle fracture continued

- UO_2 minimum particle size to survive thermal stress fragmentation by fuel-coolant interaction 79—67886
- UO_2, molten, fragmentation in flowing Na under TOP accident conditions 79—30978
- UO_2, surface energy, determ. by Hertzian indentation 80—93641
- V and V-Mo, mechanical properties, O, N_2 and C addition effects 79—52356
- V-Nb-Ti-N alloy, dispersion hardened, fracture characts. 79—15794
- VC, exam. of brittle fracture props., using Hertzian indentation 79—11686
- $VH_{0.55}$, ultra-high vacuum cleavage, H_2 desorption 80—54514
- W fibre reinforced Ni-Cr alloys, Ni, Co, Co alloys, and Ni alloys, effect of alloying on structural stability, mech. props. 78—56600
- W, sintered, brittle fracture, statistical anal. 80—11744
- W wire, AKS-doped, second phase particle obs. by TEM, SEM and atom probe microanalysis 80—108457
- WC-Co, comparison of indentation crack resistance, and fracture toughness 78—76739
- WC-Co alloys, brittle fracture, precision matching of mating fracture surfaces, by SEM fractographs 78—60807
- WC-Co hard-alloy cermets, strength, fatigue, static tests 79—29314
- Y_2O_3-$2Y_2O_3.Al_2O_3$ two-phase refractory, fracture 80—21080
- Zn, cutting mechanism of large crystals *(Japanese)* 77—48523
- Zn, electrode, single crystal, fracture surface charge density effect 78—68787
- Zn, low-temp. thermal fatigue, causing fracture and plastic deform. 77—28837
- Zn, pure, polycrystalline, cleavage fracture, hydrostatic tension effect 78—52990
- Zn single crystals, fatigue failure at low temp., under low-freq. cyclic loads *(Russian)* 79—61697
- Zn, temp.-time depend. of strength in embrittlement region *(Russian)* 77—25125
- Zn-Hg(Ga) metal/liquid metal, exam. of crack propag. in liquid metal environment 78—60766
- ZnS, hot pressed, water drop impact damage, SEM exam., IR transmission 78—88543
- Zr,Nb (2.5 wt.%), interaction of hydride, stress, and crack growth at 600K, metallographic obs. 77—12695
- Zr-Nb (2.5 wt.%), fractographic aspects of H_2 induced delayed cracking 79—47767
- Zr-Nb (2.5 wt.%), nuclear fuel channels, neutron effects on ultimate fracture strength, 293 to 573K 80—85054
- ZrC, brittle mat. discs, ultimate thermal stresses 77—4210
- ZrC, destruction delay time under laser impact 79—38976
- ZrN, microhardness and resist. to brittle fracture 79—87715
- ZrNb, pressure tube, fragmentation on failure 78—72863
- ZrO_2 microsphere stabilised ceramic, fracture characts., thermal stability *(Russian)* 80—76335

brittle materials *see brittleness*

brittleness

- *see also brittle fracture; embrittlement; hydrogen embrittlement; liquid metal embrittlement; notch brittleness*
- abrasive brittle material, rating capability for elastic deformation 78—56680
- abrasive material, brittleness and contact endurance eval. by cyclic microhardness 79—15890
- alloys, fracture toughness and impact strength, correl. breakdown 80—55523
- amorphous thin films, crack networks of voids 78—2399
- atomically sharp cracks, TEM study 80—71729
- beam test results, unit strength concept interpretation 78—48525
- body loading with cracks, energy conditions for brittle failure *(Russian)* 80—96234
- boride coatings on steel effect of Cu impurities in reaction mixture on brittleness, acoustic emission meas. 80—16581
- borosilicate glass, microparticle impact, high speed photography obs. 78—44223
- brittle circular disc under impact loading, fracture mech. 78—88514
- brittle fibre reinforced composite, brittle reaction zones at interfaces, tensile strength 79—52306
- brittle material, fast crack propagation, computer simulation 80—38331
- brittle plate containing stochastically distributed rigid rod like inclusions, strength *(Russian)* 77—23917
- brittle solids, microfracture resulting from anisotropic shape changes 80—88254
- brittle-plastic phase transform. 77—11630
- carbide, effect of mech. props. on erosion resist. under spark machining conditions 78—11421
- ceramic, brittle, specimen prep. for optical and SEM obs. *(German, English)* 80—35457
- ceramic, tensile strengths, uniaxial and equibiaxial in bending statistical comparison 80—25775
- ceramics, brittle, heat-transfer variables effect as thermal stress resist., meas. by quenching expts. 80—79871
- ceramics, brittle, partially absorbing, thermal stress anal. subjected to symmetric radiation heating 80—59570
- ceramics, fracture by single pulse 10.6 μm irrad. 79—99988
- ceramics, fracture-mirror boundary formation, criteria 80—70297
- ceramics, microcracked brittle, thermal stress resistance anal. 80—40472
- ceramics, structural, state-of-art review and survey of R&D techniques 77—63605
- ceramics and brittle solids, abrasive wear, role of plastic deform. and fracture 80—108594
- chrysotile asbestos fibres, texture rel. to mech. props. 77—81300
- coating technique of stress analysis in glass fibre reinforced plastic 80—35299
- composite materials, fracture, elastic mismatch and interfacial bonding influence 80—40506
- compressive strength of brittle material, statistical and micromech. theory 78—64618
- compressive strength of brittle material 77—44358
- concrete, bituminous, thermal stresses and brittle point, automatic installation for meas. 80—55605
- Cr, strain hardened metal and microalloys, low temp. brittleness 79—96140
- crack energy release rates calc., inverse flexibility method 79—41617
- crack extension from flaws under compressive load 78—95812
- cracks, jump determ. from specific failure and elastic energy 79—87712

brittleness continued

- cracks in brittle solids, unstable growth 80—106756
- critical temperatures, determ., impact toughness test results statistical processing 80—100980
- crystalline rocks, transient creep and semibrittle behaviour 79—16460
- diametral compression test, considering Hertzian contact, fracture and tensile strength meas. *(Japanese)* 78—72946
- dispersed media, shock compressibility, brittle destruction 80—49303
- engineering materials, intergranular fragility index 80—66637
- Fe alloy YuNDK35, magnetic, brittle, strength in three axial stress state 79—66134
- fracture props. meas. by Hertzian indentation of brittle solid 79—11686
- fracture toughness, splitting into elastic and plastic deform. terms. *(German)* 78—35468
- fracture toughness characterisation, of brittle materials under multiaxial loading 80—33530
- glass, flat, dependence of microbrittleness on SO_3 conc. 78—84960
- glass, hardness testing, mechanical property determ. *(German)* 80—40669
- glass, surface flaw density, statistical determ. 78—11310
- glass and glass fibres, microbrittleness and strength depend. on chem. comp. 79—38937
- glass fabric, effect of phosphate binders on properties 78—44075
- glass rod, optimum sample shape for compression testing, failure 80—71756
- grain boundary segregation, T-t dependence of temper brittleness 77—36617
- heat resistance criteria on surface during convective heat exchange of brittle material 77—15642
- impact damage thresholds in brittle materials impacted by water drops 80—81149
- indentation analysis, relation of hardness, toughness and brittleness 79—100249
- intergranular creep crack growth, diffusion controlled theory 78—84950
- lacquer coating, brittle, plasticizer *(Japanese)* 77—52479
- laminated paper, decorative, deform. and internal stresses 79—61671
- material classification by brittleness and stress/deform. relationship 78—15528
- materials under complex loading systems, design parameters 79—38917
- metal, BCC, effect of screw dislocations on mech. props. *(Russian)* 78—60704
- metal, brittle, ductility improvement by plating *(German)* 77—8954
- metal, fatigue fracture-stacking fault energy correlation *(Russian)* 78—15499
- metal, hard, brittle, correlation between wear, crack resistance and stress intensity factor *(German)* 77—36666
- metallic glasses, mats. props. review 77—4043
- metals and alloys, thermal stress cracking, installation for −180 to 1100°C 80—3266
- microcrack initiation in brittle materials, grain size depend. 80—40505
- microfracture about scratches in brittle solids 79—59945
- microinhomogeneous brittle bodies, strength theory *(Russian)* 77—58608
- mirror/flaw-size relations, residual contact stresses effect 80—107363
- modulus of brittleness, crit. tensile span 78—92318
- muscovite, exam. of dislocations and props. using elasticity theory *(German)* 79—10854
- nonuniform triaxial compression of brittle materials, material strength gain, exam. 78—76725
- optical fibre, strengthening by molecular stuffing 80—58830
- optimal structural design 78—79207
- particle compressive strength, size effects *(Japanese)* 79—51196
- particles, small, brittleness rel. to impossibility of comminution by compression 78—52709
- plastics, mechanical strength and brittleness, effect of moisture and notches *(German)* 77—48543
- plate with line crack subject to antiplane shear 80—14618
- PMMA, crack size and effective specific work for failure determ. 80—85108
- polyacetylene films, tensile props. and partial alignment 80—104210
- polymer, activation energies of fracture and deform., comparison *(Russian)* 78—11303
- polymer, brittle photoelastic, use of gelatin gels in prep. for optical polarization stress study 80—40325
- polymers, brittle point determ., new method 77—70260
- polypropylene, neutron irradiation effect on weldability and adhesion *(Japanese)* 79—60405
- polystyrene, particles, critical stress 77—28869
- porcelain, correlation between wear, crack resistance and stress intensity factor *(German)* 77—36666
- powders, brittle, shock wave disintegration test method 80—66744
- pyrocarbon, fuel particle coating, strength and Young's modulus meas., brittle ring test 77—8868
- rare earth hexaborides, obtained by melting, micromech. props., rel. to bonding 80—21082
- Rayleigh waves interaction, with microcracks on brittle solids 80—39214
- refractories, classification according to brittleness and thermal shock resistance determ. 79—83321
- refractory ceramic, heterogeneous, significance of non-elastic deform. in fracture 79—47765
- refractory metal alloy, heat resistance and cold brittleness, achievements and trends 78—95718
- rod, optimum specimen shape for compression tests, gluing technique effects 80—50797
- rod, optimum specimen shape for compression tests, struct. and technological parameters 80—50798
- rotating disk, probability theory appl. to rupture strength 80—43662
- safety guide for material treatment and working *(German)* 78—15534
- secondary nucleation, influence of crystal brittleness and degree of supersaturation using in growth *(Italian)* 78—23836
- sharp contact cracking, residual stress effects 79—100245
- silicate glass, mechanical stress field influence on structural mobility 80—103421
- soda lime glass, microparticle impact, high speed photography obs. 78—44223
- solid projectile damage in elastic and elastic-plastic target response regimes 77—8910
- specimen preparation, for strength determ. 80—40632
- spherical shell of brittle material, structural strength of glued permanent joint 79—94559
- steel, 38KhMYuA, brittleness of nitrided case 77—21418

brittleness continued
steel, 3Kh2V8F, brittleness depend. on high temp. deform. at high stress. temp. *(Russian)* 80—50698
steel, alloy, 30Kh2N2SMK5, temper brittleness of 79—96129
steel, alloy, Cr-Mo-V-P, quenched, temper brittleness in relation to V and P concs. 78—52986
steel, C, hollow pipe body with internal crack pattern, ingot segregation, hot shortness 77—32693
steel, C, weldable, ferrite-pearlite, Widmanstatten structs., resist. to fracture 79—29203
steel, cast, cold resistance determination, quick method 80—100997
steel, complex alloy, exam. of temper brittleness 78—44209
steel, Cr-Mo (2.25, 1 wt.%), SCC and temper brittleness, P grain boundary segregation effect 80—55571
steel, Cr-Mo and Ni-Cr-Mo-V low-alloy, additive remedy for temper brittleness 80—66659
steel, Cr-Ni-Mo, handbook data for type 34KhN1M 79—78960
steel, embrittled N18K8M3TYu, toughness enhancement by double quenching 77—59922
steel, fibre reinforced Al composite, role of brittle layers at elevated temps. 79—96135
steel, fracture toughness and impact strength, correl. breakdown 80—55523
steel, high Cr, V additions effect on brittleness near 475°C *(Russian)* 78—19890
steel, low alloy, Mn-P, temper brittleness, rare earth mischmetal effect *(Chinese)* 80—104249
steel, low alloy 10KhSND, thermal embrittlement when held for long periods at 340 to 450°C 77—70178
steel, low alloy structural, heat treated, impurities effect on embrittlement susceptibility and temper brittleness 79—38955
steel, low C, impact strength and crit. brittleness temp., sample thickness and notch radius influence 80—85018
steel, medium C, cast cylinders fragmentation tests 78—35519
steel, mild, hot shortness mechanism, surface enrichment of residual elements and oxidation *(Chinese)* 79—74230
steel, Mn and Mn-Ti, cryogenic mech. props. and intergranular brittleness *(Korean)* 79—70164
steel, nitride coated, brittleness eval. by AE *(Chinese)* 78—11453
steel, nitriding, mag. field effect 79—57153
steel, prestrained pressure vessel, correl. between dynamical toughness characteristics 78—68816
steel, stainless, radiation damage by 1 MeV electrons, dislocation struct., brittleness *(Russian)* 80—75226
steel, stainless ferritic, 10 to 30 wt.% Cr, ductile-brittle transition temp. 80—30095
steel, structural, effect of rare earth metals on cold temper brittleness 79—29202
steel, type 20 CND 10-10, temper brittleness and intercrystalline segregation *(French)* 77—81316
steel, type Kh12M, rel. between structural inhomogeneity and wear resist. *(Russian)* 80—66672
strain rate depend. effect of specimen vol. on strength 78—90726
strain rate dependent effect of specimen vol. on strength 77—56085
strain-sensitive nontoxic brittle coating production 77—86197
and strength estimation in low-deform. inorg. mats. 77—86131
strength measurement, load-transmitting medium in testing apparatus 80—40652
surface energy determ. from AE, automatic system 79—91899
surface energy of rupture, determ. in brittle materials 80—21074
surface science in metallurgy, review 79—42388
tensile strength determ. of brittle materials, based on radial and compression tests 78—7156
thermal stress resistance parameters when subject to thermal stress fatigue 78—90787
thick-walled vessel, of brittle material, strength under external press. 78—30182
ultimate tensile strength determ. by radial compression testing, of brittle material 78—7132
uniformly compressed elastic medium, brittle rupture, plane fracture wave *(Russian)* 80—53705
vitroceramic-metal composite materials development, Spacelab appl., mech. props. *(French)* 78—92229
Weibull modulus estimation for brittle materials 79—55344
Al alloy, cast AL15V, brittle, strength in three axial stress state 79—66134
Al high-strength alloy constitutive eqns. and high-velocity deformation *(Japanese)* 79—79029
Al, pseudo-brittleness 79—79111
Al/Sn interface, effect of plastic deformation on structure and adhesion strength of interface *(Russian)* 79—28218
Al-Mg-Li alloy, subboundary brittleness due to horophilic Na *(Russian)* 77—21244
Al-Mg-Si, brittleness and heat treatment, statistical design of expts. 77—73349
Al-Si alloy, hot shortness, rheological model *(Russian)* 77—56072
Al_2O_3, compressive stress state strength determ. in brittle material 77—16757
Al_2O_3, fracture toughness determ. using four-point-bend specimens 80—108536
Al_2O_3 sintered, and hard metal alloys, comparison of stress intensity factor depend. on notch base dia. *(German)* 78—35470
Al_2O_3, sintered, correlation between wear, crack resistance and stress intensity factor *(German)* 77—36666
Al_2O_3:Cr_2O_3(Ti_2O_3), dopant influence on struct. and mech. props. 80—24471
Al_20_3, corundum, abrasive, evaluation of brittleness, contact endurance by cyclic microhardness 79—15890
B fibre reinforced AlB_2 and TiB_2 fibre coating effect on strength *(Russian)* 80—40426
Be, brittleness problems, elevated plasticity and superplasticity, temp. depend. *(Russian)* 79—15758
Be, strain hardened metal and microalloys, low temp. brittleness 79—96140
Cr, optimum alloying with rare earth metals, Ti, Zr, Hf, Nb, Ta 78—68651
Cu alloys, appl. of SEM to brittleness study 78—3214
Cu, appl. of SEM to brittleness study 78—3214
Fe, Armco, screw dislocation effect on mech. props. *(Russian)* 78—60704
Fe, cast, grey, brittle, strength in three axial stress state 79—66134

brittleness continued
Fe, pseudo-brittleness 79—79111
α-Fe-(Ni,Mn,Cr,Mo,W)-P (1 wt.%). grain boundary segregation, temper brittleness, AES study *(Japanese)* 79—78981
Fe-C(0.001 to 0.44 wt.%), C effect on low temp. brittleness *(Japanese)* 80—50711
Fe-Co-Cr (27, 0.5 wt.%), internal stress and brittleness in ordered state *(Russian)* 79—61698
Fe-Cr alloy, impact strength, rel. to '475°C brittleness' *(Russian)* 78—92323
Fe-Mn (8.25 wt.%), irreversible temper embrittlement, Mossbauer spectra, impact strength depend. on interstitials *(German)* 79—74235
Fe-Ni alloy, hot shortness *(Japanese)* 78—84998
Fe-Ni-P, segregation kinetics, theory, and temper brittleness 80—11649
Fe-Si (3 wt.%), breaking stress grain size and grain boundary energy during onset of reversible temper brittleness *(Russian)* 77—32673
Fe-Si (3 wt.%), chemical comp. and hot rolling effect on brittleness *(Czech)* 80—50712
Ge single crystals, deform. during static indentation 79—87714
InAs single crystals, deform. during static indentation 79—87714
InAs-CdTe, preparation, microhardness rel. to component interactions 77—24350
Ir-W (0.3 wt.%): Al(Fe)(Th)(Ni)(Rh), effect of additions on grain boundary composition 79—83309
$KD_{2x}H_{2(1-x)}PO_4$ crystals, plastic deform. and mech. props. 79—79035
KH_2PO_4 crystals, plastic deform. and mech. props. 79—79035
K_2O-PbO-SiO_2, glass, mech. and optical props. *(Russian)* 77—20860
$LiNbO_3$ single crystals, deform. during static indentation 79—87714
Mo, fibre, brittle to tough transition, impact strength meas. 80—40527
Mo sheet, 45° brittleness due to partial recrystallisation, 45° crack formation and propagation *(Russian)* 79—100238
Mo, strain hardened metal and microalloys, low temp. brittleness 79—96140
Mo-C(Ti)(B)(Zr)(Ru)(Pt), electron beam melted, alloying addition effects on brittleness and ductility 79—61728
Mo-Zr-C (0.08, 0.02 wt.%), struct. and banding tendency, thermomechanical treatment effects 77—86063
$NH_4H_2PO_4$ crystals, plastic deform. and mech. props. 79—79035
NaCl, single crystal, temp. anisotropy of plasticity and brittleness 78—3198
Na_2O-CaO-SiO_2 glass, crack nucleation around plastic indents 78—92327
Nb alloy, VN2AE, influence of nitriding on heat resist. and brittleness *(Russian)* 79—8380
Nb_xC powders, plastic deform. characts. on vibratory milling 78—11183
Ni-Cr machine steel, austenite grain size effects on mech. props. *(Russian)* 77—44292
Ni-Cr-W-Mo-Al-Ti (15,6,3,2,2, wt.%), wrought, Si effect on transition brittleness *(Chinese)* 80—55491
Pb(Zr,Ti)O_3, effect of spherical pores on strength 77—70103
RbH_2PO_4 crystals, plastic deform. and mech. props. 79—79035
Si single crystals, deform. during static indentation 79—87714
SiC, abrasive, evaluation of brittleness, contact endurance by cyclic microhardness 79—15890
SiC, fuel particle, coating meas. of strength and Young's modulus, brittle ring test 77—8868
Si_3N_4, bending strength, deformability, elastic moduli and brittleness 80—81191
Si_3N_4, hot-pressed, fracture toughness determ. using specimens with chevron and straight through notches 80—108538
SiO_2 fabric, structural stability rel. to brittleness, X-ray diffr. and IR spectrosc. studies 80—96634
TiC-TiB_2, strength and antifriction props. over wider range of concs. 80—50673
W, fibre, brittle to tough transition, impact strength meas. 80—40527
W-WC, activated sintering, mech. props. *(Korean)* 78—60622
YAG brittleness anisotropy, microcrack formation due to surface treatment 80—40526
Y_2O_3 fused single crystals, struct. 80—19804
Zn, internal friction anomalies in temp. initiated brittle-plastic transition *(Russian)* 80—96648
Zn single crystals, fatigue failure at low temp., under low-freq. cyclic loads *(Russian)* 79—61697
ZrC-ZrB_2, strength and antifriction props. over wider range of concs. 80—50673
ZrO_2, porous, sintered stabilised microspheres, strength and fracture studies 80—85019
ZrO_2-Al_2O_3, cooling effects on mech. props. *(Russian)* 79—78999

broadband amplifiers *see wideband amplifiers*

broadcasting
see also radio broadcasting; television broadcasting
educational broadcasting for developing countries, case for use of satellites 80—4485
equipment calibration using standard frequency broadcasts 79—67258
galactic broadcast strategies and source position for advanced civilization 77—91449
microphone techniques, practical and aesthetic 80—5885
satellite, rain scatter interference *(Japanese)* 79—16612
satellite direct broadcasting in Europe, associated European Space Agency programme 80—12638
school radio and TV broadcasts and Finnish educational system *(French)* 79—17171
teaching projects, cost effectiveness evaluation 79—40312

bromine
see also nuclei with ......
^{81}Br isotope enrichment by laser photodissociation of HBr 80—1075
adsorbed layer on zeolites, Raman spectra, aromatic bromination catalysis 80—3408
adsorbed on Au(100), EELS obs. 80—50483
adsorbed on Grafoil, EXAFS investig. 77—51602
adsorbed on Pt(111), $M_{2,3}M_{4,5}V$ and $M_{4,5}VV$ Auger spectra 79—69926
adsorbed on Si single cryst., X-ray standing waves obs. at cryst. surface 80—96417
adsorption, on Au electrode, anisotropy of optical props. 80—60534
adsorption on C from CCl_4 soln. 78—10273
adsorption on Fe (100), AES, LEED, work function, and thermal desorption study 80—15375
adsorption on graphite, EXAFS 77—43430
adsorption on Pt(111), irreversible order-disorder transition 79—69361
adsorption on ZnO, γ-irrad. induced centres 80—54513

bromine continued
air pollution from vehicle exhausts, model for dispersion 77—37367
airborne particulate Br levels rel. to vehicular Pb concs. 77—91254
alkali metal chloride: $F^-(Br^-)(I^-)$, anion impurities substitution, energies of soln., association and migration 78—83831
atmosphere quantitative analysis of aerosols 79—12179
atom, Br, reson. line emission attenuation following Br_2 photodissoc. 79—64059
atom, diffusion coeff. in laminar flames 78—51272
atom, diffusion in Ar at 298K, time resolved mass spectrometric determ. 79—90365
atom, ESCA, lifetime broadening, CI resonances 77—18853
atom, ESR study in N-bromosuccinimide, X-irrad. 80—66037
atom, fluoresc. in Ar^*+Br_2 lamp, Br atom conc. meas. by line absorpt. 78—46466
atom, He (I) PES 78—37609
atom, in $NaBrO_3$, study of 4d excited states 77—26989
atom, L-shell soft X-ray emission spectra, oscillator strengths 80—32651
atom, $O^{2+,3+,4+,5+}$ induced K-shell X-ray production cross section, 7 to 24 MeV 77—61850
atom, photoelectron spectra, photoionisation cross-sections 78—90131
atom, photoionisation cross sections and ang. distribs., outer p subshell 80—9572
atom, stripping in gaseous targets, equilib. charge state distrib., statistical anal. 80—5610
atom+O ion collisions, A=16, 18, K-X-ray production 77—23554
atom K-fluorescence yield determ. using MWPC 79—18140
benzene-Br_2 charge transfer complex, Raman spectra, bending modes, electronic excited states 78—56485
benzene-Br_2 complex, cryst., IR spectrum assignments, site symmetry, rel. to benzene 77—36217
Br_2+As(III) reaction, flow coulometry, with ring-disk electrode 80—71966
chemisorbed on zeolites, Raman spectra 80—93301
chemisorption on clean or Na-covered Ag (111) 78—38944
chemisorption on V, layer struct., Na adsorption effects 80—101039
coadsorption with H_2O, on Cu(100), Helmholtz layer model system 80—92777
colour positive developer comsumption, bromine ion extraction from overflow using ion exchange resins *(Russian)* 80—105733
complex formation with pyrazine, n-σ-type, effect on intensity of intercombination transitions *(Russian)* 77—26980
condensed phases, Raman spectra, spontaneous and stimulated, weak and strong radiation fields 79—3450
desorption from W, field ion microscope exam. 78—35270
determination, in silicate rocks, by epithermal neutron activation anal. 78—35741
determination by high press. liq. chromatography, Br-specific detector *(German)* 79—87920
determination in environmental water samples by neutron activation, isotope exchange 77—44550
diatom dissociation and recombination mechanisms, bound complex and triple collision mechanisms 80—23478
diffusion coeff. in graphite 79—42310
diffusion in KBr, Br_2 penetration depth, obs. using OH^- centre decomp. 77—43378
dissociated, recombination in supersonic expansion in nozzle *(Russian)* 78—1757
dissociating flow in supersonic nozzles, atomic recomb. and vibr. relax. effects 78—42677
dopant, in (SN)x, temp. depend. of elec. cond. 79—65563
elastic scattering amplitudes, for high energy electron scattering, by ionised atoms, numerical calcs. 80—49057
etching, of Si monocryst., by Br, Ar laser beam initiation *(Russian)* 77—73358
EXAFS amplitudes, wave function relaxation and chemical effects 78—46365
flowing afterglow, thermal electron dissoc. attachment rate consts. 77—10773
fluoromethane+Br, isotope selective photobromination, using c.w. CO_2 laser irrad. in excess inert gas 78—76843
fluoromethane+$Br(^2P_{3/2})(^2P_{1/2})$, photobromination 78—11535
formaldehyde+Br reactions, rate consts. by EPR 80—93736
gas, sparking pots., ionisation and electron attachment coeffs. 78—42705
Gaussian basis sets, Ga, Ge, As, Se, Br, and Kr, HF calcs. 77—38611
geochemical behaviour in sediments from Namibian shelf 78—32062
geochemistry, Cl and Br degassing by volcanism along Reykjanes Ridge and Iceland 78—36136
graphite-Br_2, in-plane intercalate lattice modes, Raman scatt. 79—42163
graphite-Br_2 intercalation compound, interband Landau level transitions, magnetorefl. 77—52095
graphite-Br_2 intercalation cpd., Fermi level, far IR magnetorefl. expts. 77—40228
graphite-Br_2 intercalation cpds., EXAFS study 80—71515
graphite-Br intercalation compounds, magnetoreflectivity in high fields under press., energy band parameters 79—61346
graphite-Br system, intercalation threshold, ellipsometric investigation 78—26760
human tissue, Br determ. by thermal neutron activation analysis 79—88219
impurity in Li aluminosilicate glasses, ESR spectra 80—66027
intercalating agent, C fibre struct., props. modification by Br_2 78—44237
intercalation compounds with graphite, ^{13}C NMR spectra 80—66048
intercalation in graphite, oxidation and residual Br effects 79—43565
intercalation in graphitised C fibres and its removal 79—43561
intercalation process with graphite 78—63965
ion+target collisions, K-X-ray yields, 1sσ excitation 77—19051
ion+target collisions, K-X-ray yields, 2pσ excitation 77—23549
ion+target collisions, K-X-ray yields, K-vacancy sharing 77—23548
ion+target collisions, X-ray yields, K-L level matching 77—19052
ion collisions, 12-60 MeV, K-vacancy production, multiple and single collisions in mol. orbital excitation 77—83717
ion-atom collision, K-vacancy prod., mol.-orbital method 77—68095
ions, beam-foil spectra from 20 to 238 MeV energy, 5 to 60 nm, lifetime meas. problems 80—9722
isotope separation, microwave reson., triplet state photochem. technique 77—32818
isotopes in bromomethane, quadrupole bond magnitude ratio *(Russian)* 79—76452
isotopic enrichment in BrI after isotopically selective excitation 77—90581

bromine continued
K shell photoelectric cross section, at 74.409 keV 79—72288
laser, electronic transition chemical, stimulated emission at 3685 cm^{-1} 79—27249
laser atomic, pulsed microwave discharge of Br_2 source gas 80—48233
laser UV transitions of ion, performance and spectroscopy 78—22111
lattice dynamics using simple bond charge model 78—55919
liquid, entropy, computer simulation, Widom method 79—77486
liquid, mol. dynamics of '2-Lennard-Jones centres' pair pot. liq. 79—73082
liquid, muon stopping, diamag. shielding of muon-substituted cpds. 79—57279
liquid, neutron diffr., evaluation of effective pair pot. 78—75527
liquid, struct., theory and computer simulation 78—59734
liquid, struct., X-ray diffr. obs. 78—59733
liquid, struct. factor by neutron diffr., wavelength depend. 77—89370
liquid, thermodynamic and struct. props., pair pots. calcs. 77—58939
lung ventilation studies test for free Br in carrier gas from $^{81}Kr^m$ generator 79—79642
methanol-water soln., etching of GaP 78—68833
molecular crystal, bond charge model, for lattice dynamics 78—79692
molecular optically pumped laser, operation 78—25858
molecular static polarisability, ab initio SCF wave functions 80—74106
molecule, (B-X) band spectrum in laser induced fluorescence 79—47931
molecule, $A^3\Pi_{1u}$-$X^1Sigma^+{}_g$ continuum absorptivity meas. 79—68238
molecule, absorpt. spectrum, laser isotope separation *(Japanese)* 77—34649
molecule, absorpt. spectrum, rel. to laser isotope separation 77—10683
molecule, and isotopic forms, new rot.-vibr. lines, laser reson. fluoresc. obs. 78—991
molecule, $B^2\Pi(O_u{}^+)$ predissoc. rates, analytical interpretation 80—91617
molecule, $B^3\pi o_u{}^+$ state deactivation efficiency, temp. depend. 78—70869
molecule, $B\ ^3\Pi_{0u}{}^+$ Hanle effect 77—75234
molecule, continuum reson. Raman scatt., interference effects 79—6946
molecule, diffusion in NO at 298K, time-resolved mass spectrometric determ. 79—90365
molecule, dissoc. and recomb. rate consts. meas., 1200-3000K, techniques comparison 77—63892
molecule, dissoc. attachment by 0-8 eV electrons 78—74776
molecule, dissociative attachment of electrons 78—62931
molecule, extended X-ray absorption fine struct. amplitude 79—59489
molecule, extended X-ray absorption fine struct. amplitude attenuation, rel. to XPS satellites 80—37821
molecule, fluoresc. obs. in UV laser photochem. of dibromodifluoromethane 80—16703
molecule, in Ar, deactivation and dissoc., microscopic process simulation 78—11511
molecule, kinetics of excited states using laser excitation, radiative lifetimes and collisional deactivation 80—74237
molecule, Kr ion laser-excited fluorescence, predissoc. 80—83414
molecule, laser induced photodissoc. in vis. continuum 79—64059
molecule, model potential SCF calcs. 80—95528
molecule, photodissoc., $Br^*(4^2P_{1/2})$ yield, wavelength depend., collisional release 78—64857
molecule, potential curve calcs. 77—6881
molecule, pseudopotential calcs., dissoc. energy, bond length, force const. 77—26964
molecule, Raman reson. excitation profile, Ar matrix, red shift rel. absorption spectrum 77—14440
molecule, relativistically parameterized extended Huckel theory 79—49924
molecule, reson. Raman scatt. *(German)* 79—26983
molecule, reson. Raman scatt. obs., excited-states interference 77—79618
molecule, reson. Raman spectrum, vibr.-rot. struct. 78—17674
molecule, UV laser transition, vibr. anal. 77—75170
molecule, vac. UV absorpt. cross section 80—91574
molecule, vibrational relaxation and dissoc. behind a shock front, absorpt. spectroscopy *(Russian)* 77—88536
molecule in -Z 80—58262
molecule in liq. Ar, effective intramol. pot. 80—69208
molecules, IR radiation excited, monodisperse porous filter permeability changes *(Russian)* 79—91999
molecules, Q branches of Δn=1 profiles, calcs., rotation effect on scatt. amplitudes 80—63643
neutron activation analysis, in environmental materials, reliability aspects 78—40106
nonaqueous solution for selective etching for GaAs 77—40453
in oceans, Cl and Br origin 78—65342
particulate Br levels for Perth, W.Australia, 1971-6 var. 79—34455
pionic, Auger electron emission *(Russian)* 80—69271
poly(sulphur nitride):Br, electronic model for high cond. 80—24923
polyacetlyene:Br film, Raman scatt. 79—47457
polyacetylene:Br, ion implantation effect on elec. props. 80—65026
polystyrene:Br_2, films, electron-beam induced carrier mobility and elec. breakdown 80—80429
polysulphur nitride:Br mag. susceptibility, linear temp. depend. 80—25114
polysulphur nitride:bromine, struct. and phase transition 80—24382
polythylene:Br_2, films, electron-beam induced carrier mobility and elec. breakdown 80—80429
PVC+$Br_2(I_2)$, reaction in surface-modified film subject to thermal-radiative and photochem. action *(Russian)* 77—21385
pyridine-$I_2(Br_2)$ charge transfer complexes, vibr. spectra, vibronic contrib., intensity enhancement 80—53048
separation processes simulation in H_2SO_4-Br cycle 79—74413
solar energy storage as hydrogen from bromine from hydrogen bromide 79—57470
solid, acoustic wave velocity calc. from phonon curves *(French)* 77—1180
solution in methyl alcohol InP substrate etching and polishing appl. *(Slovak)* 78—56576
stratosphere chemistry of Br cpds., and O_3 depletion 80—98391
UV laser possible pumping by synchrotron radiation, NaCl:I(Br) luminesc. 78—66835
AgCl:Br, EPR of excitons, detected in X-ray excited luminesc. spectra at 4K 77—55732
AgCl:Br^-, EPR of mobile electrons, mechanism for photoinduced decomposition 78—80219
$Ba+Br_2(I_2)\rightarrow BaBr(BaI)+Br(I)$, time-of-flight chemiluminesc., mol. bond energies determ. 78—40051
(Br,Zr) quasi-molecular system, 1 s σ orbital, variational calc. 78—37707

bromine continued
- Br, adsorbed on graphite, continuous order-disorder transitions 80−19910
- Br, and Br_2, luminesc. assignments in excimer laser photolysis of CBr_4 and CF_2Br_2 79−39184
- Br I, isoelectronic sequence, multiconfiguration HF calc. of sp^6-s^2p^4d interaction 78−9072
- Br II, visible spectrum, shock tube time-resolved photographic photometry, transition probabilities 77−23449
- Br II levels, NF values meas. in Ne-Br_2 mixtures 78−62753
- Br matrix isolation ESR 80−106336
- Br V, VI, VII, beam-foil spectra 450 to 1000 Å, radiative lifetime meas. 77−54524
- Br^- adsorpt. on Au electrode, specular reflect. investig. 78−61047
- Br^- diffusion plot in AgBr, anomalous curvature near melting point 79−60548
- Br^-, electron photodetachment cross-section determ., from CsBr dissoc. 77−3330
- Br^-, fluoresc. quenching of organic excited singlet states, rate meas., mechanism 77−38685
- Br^-, free-ion polarisability, empirical values 77−20792
- Br^-, in He, ion reduced zero field mobility and free diffusion coeff. 77−47139
- Br^-, ion mobility in Ar, flow drift tube meas. 77−72405
- Br^-, nuclear quadrupole interaction , second-order Stark effect 78−21879
- Br^-, plasma, broadening of free-bound radiation thresholds 80−53940
- Br^-, Thomas-Fermi-Amaldi eqn., approx. variational soln. 80−52870
- Br^+, ionisation pot., periodic regularities, relativistic corrections calcs. 79−49950
- Br^{6+}, 42 MeV, stopping power and radial dose distrib. obs. in tissue-equivalent gas 80−101218
- Br^{9+}, on Ge target, 55 MeV, K X-ray prod. 79−47547
- Br-Ca-Fe H_2O-decomposition cycles for thermochem. H prod. 80−35784
- $Br+{}_5^{10}B^{n+}$, 4-38 MeV, K-shell ionis., X-ray obs. 79−59549
- Br+Br, relativistic effects in variable-screening model 77−14516
- Br+Br, symmetric collisions, MO-2pσ radiation anisotropy, quasimolecular nature 78−70924
- $Br+Br_2$, atom-exchange, rate and activation energy, trajectory model and pot. energy surface 78−64811
- Br+Br+Ar, photoinduced recombination, numerical simulation 79−16018
- $Br+Br+Ar \rightleftarrows Br_2+Ar$ recombinations rate const. calcs. 80−40685
- $Br+CO_2(HCl)$, quenching of $4^2P_{1/2}$ state, vib. excitation, temp. depend. 78−58792
- Br+DCl(HBr), vibr. relax. times, laser induced fluoresc. 77−27159
- $Br+F_2$, reaction kinetics, mass spectroscopic obs. 77−77743
- $Br+H_2$, laser field interacting with collision dynamics, model system 78−62876
- $Br+H_2$, laser radiation field effects, quantum mechanical close coupled expansion 77−50485
- $Br+H_2$, proximity induced electric dipole moment effect in laser field 80−83456
- $Br+H_2O_2$, rate constant upper limit 80−30216
- $Br+H_2(HCl)$, relax. and chem. reaction, time resolved IR fluoresc. and mass spectrometry obs. 80−69177
- $Br+H^+$, 4 MeV beam-foil X-ray production cross-section 79−7003
- Br+HCN, electronic-vibr. energy transfer, $Br(4^2P_{1/2})$ quenching and HCN (001) deactivation, fluoresc. obs. 77−518
- Br+HCl, IR fluoresc. studies of state-selected energy transfer, photochemistry 77−77768
- Br+HCl, vibr. relaxation and reaction rates determ. 80−108698
- Br+HCl(DCl), relax. rates, vibr. photochem. 79−66290
- Br+HCl(ν′), Br+DCl(ν′), reaction and relax., classical trajectory calcs. 77−48625
- $Br+HI \rightarrow HBr+I$, thermal rate const., 220-400K, H/D isotope effect 79−47906
- Br+K, harpooning mechanism interactions, semiclassical optical model 79−89755
- $Br+K_2(Cs_2)$, ionisation reactions, absolute cross sections 80−99565
- Br+NOBr, primary and secondary photochemistry, vibrationally excited NO, IR fluoresc. obs. 80−48030
- $Br+O_2(NO)$, quencher paramagnetism, deactivation rate const., spin-orbit relax. study 80−21263
- $Br+O_3 \rightarrow BrO+O_2$, rate consts., mass spectrometric obs. 77−63897
- $Br+O_3 \rightarrow BrO+O_2$, reaction rate constant, 200-360K 78−73024
- Br+OClO, reaction rate consts., mass spectrometry meas. 78−3316
- Br+target atom, 12-60 MeV, K-vacancy cross sections, target depend. 77−19026
- $Br^-+H_2(D_2)(O_2)(N_2)(CO)(CO_2)$(methane), total electron detachment cross sections for energies around threshold 80−99550
- Br^-+He, electron detachment, SCF calcs., $BrHe^-$ and BrHe pots. 80−23503
- Br^-+He, term parameters, electron spectra and scatt. cross sections 77−27148
- $Br^-+He(Ne)(Ar)(Kr)$, total electron detachment cross sections, near threshold energies 79−3555
- Br^-+K, differential cross-section, small angle scatt. 79−98186
- Br^-+methane(fluoromethane), excitation functions, reactive scatt., eV region *(German)* 78−35677
- Br^-+O_2, 0.2-100 eV, reaction differential cross sections energy depend. meas. 77−63902
- $Br^-+SF_6 \rightarrow SF_5+F+Br$, electron affinity of SF_5 radical 80−45495
- $Br^{25+}+Br^{25+}$. correlation diagrams, inner-shell vacancy prod., characteristic X-rays 77−83503
- $Br^{x+}+Au$, differential single-scatt. cross sections at MeV energies 78−33570
- Br_2, air pollutant, spectroscopic analysis using scanning tunable dye laser 78−81362
- Br_2, atomic phase shifts calc., appl. of EXAFS 77−48276
- Br_2, $B^3\Pi(O^+)$ and $^1\Pi(1)$ states, reson. Raman spectra 79−59470
- Br_2 in Ar, solvent effects on equilibrium props. 80−61128
- Br_2, laser-induced photodissoc. spectroscopy 77−90614
- Br_2, long-lived $A^3\Pi(1_u)$ state, quantum-resolved dynamics of excited states 80−69178
- Br_2, optically pumped at 532 nm, lasing obs. in visible and near IR 78−63094
- Br_2, organic solvent effects on Raman parameters 79−26998
- Br_2, photolytic cage effect in high-press. gases, laser wavelength depend. 80−11925

bromine continued
- Br_2, resonant fluoresc. at 5145 Å, isotope mols., rot.-vibr. states 77−61782
- Br_2, single rot. states, lifetimes and collisional quenching cross sections determ. by obs. fluoresc. decay 80−91595
- Br_2, UV laser transitions, electronic designation 79−944
- Br_2 vapour, four-wave sum mixing near 177 nm 77−10970
- Br_2^-, pot. curve calc. 77−10596
- Br_2-Ar, positive column at. state densities 80−44007
- Br_2-Ar liquid mixture, vibr. relax., 1-D mol. dynamics study 79−73079
- Br_2-Ar system, mol. rot. effects on V-T energy transfer 80−14195
- Br_2-CO_2 chem. pumped photodissociation laser, output energy increase by WF_6 addition 79−45939
- Br_2-CO_2 IR laser with $Br^* \rightarrow CO_2$ electronic-vibr. energy transfer as pump mechanism 80−53260
- Br_2-graphite intercalation compound, Raman scatt. 77−12390
- Br_2-graphite systems, adsorbed and intercalated, EXAFS 78−72638
- Br_2-pyridines, charge transfer complexes, $\nu_{Br\text{-}Br}$ vibr., Raman intensity obs. 79−36644
- Br_2-Xe, UV transient absorption following flash photolysis 79−61879
- Br_2+acetylene, laser-induced photochemistry 80−45498
- Br_2+Ar, collision de-energisation of highly vibr. excited Br_2, mol. dynamics simulation 77−42378
- Br_2+Ar, effective vibr. pot. of Br_2 in Ar gas, Monte Carlo simulation 79−59526
- Br_2+Ar, ergodic deactivation, anharmonic effects on transfer rate 78−82818
- Br_2+Ar, vibr. excited Br_2, de-energisation in high press. Ar 77−71845
- Br_2+Ar collisions, dissociation reaction, trajectory study by ensemble method 80−66765
- Br_2+Ar^*, producing Br, in Ar^*+Br_2 lamp, Br atom conc. meas. by line absorpt. 78−46466
- $Br_2+Ar \rightarrow 2Br+Ar$, 3500K trajectory anal., rate const. 77−52617
- Br_2+CO_2 mixture, Raman laser optical excitation, electron phototransition theory *(Russian)* 80−99711
- $Br_2+Cu(^2D)$, beam-gas chemiluminesc. reactions 80−85151
- Br_2+Ge, heterogeneous photochem. reaction kinetics, laser radiation intensity effect 79−66326
- Br_2+Ge, surface reaction, rate-limiting step, ellipsometric and photochem. meas. 80−16730
- Br_2+H, classically forbidden vibr. excitation, S-matrix 77−516
- Br_2+H, H* prod., IR chemiluminesc. meas. 79−100336
- Br_2+H, nonreactive scatt., long range anisotropic pot. determ. 78−66626
- Br_2+H reaction Br prod., matrix isolated ESR 80−106336
- $Br_2+H(d) \rightarrow HBr(DBr)+Br$, reactive cross-section, collision energy depend. obs. 79−11784
- $Br_2+I(5^2P_{1/2})$, deactivation kinetics, time-resolved spectrosc. obs. 78−95916
- $Br_2+I(5^2P_{1/2})$, deactivation kinetics, $Br(4^2P_{1/2})$ prod., time-resolved spectrosc. obs. 78−95917
- Br_2+K, inelastic scatt., total cross-sections, trajectory surface hopping calcs. 78−46420
- Br_2+K, nonreactive differential scatt., 0-10 eV, scatt. angle 78−42156
- Br_2+Li, bond stretching effect on charge transfer reaction cross section 78−11507
- Br_2+NH_3, gas phase reaction, $NHBr_2$ identified by ESCA 79−31599
- $Br_2+Na(K)(Cs)$, at. negative ion prod. cross sections 77−531
- Br_2+O_2, reaction with W surface, rate of reaction meas., gas flow experiment 78−92510
- Br_2+OH, hydroxyl radicals reactive scatt. 80−85172
- $Br_2+SiAs(GeAs)$, high temp. Raman spectra, cryst. growth mechanism *(French)* 79−26999
- Br_2+Sn, reactive scatt., ang. distrib. and time-of-flight spectra 78−64842
- Br_2+Xe, excitation functions and rotational polarisation, chemiluminesc., crossed beam study 80−76491
- $(Br_2)_2$, mol. beam. elec. deflection obs. 80−53080
- Br_3^-, BB pseudopot. calcs. on electronic states 77−26984
- $Br_2^-(Br^-)$, formed by electron impact from Sn_4, ionis. efficiency curves 77−61865
- BrF, $B^3\Pi(0^+)$ states, collision-free lifetimes laser fluoresc. obs. 78−94278
- $Br^-(H_2O)_n$, hydration energies, orientation, ab initio-LCAO SCF MO calcs. 80−27944
- BrVI(VII), reson. line oscill. strengths, beam-foil spectra 77−38630
- ^ABr A=84-88, fission products, rapid electrophoretic separation technique 79−54982
- ^{35}Br, L-shell X-ray prod. by H(He) ion bombardment 79−47548
- ^{75}Br, excitation functions for production, pot. nuclear medicine appls. 80−98135
- ^{76}Br, ^{77}Br, production from decay of cyclotron produced ^{76}Kr and ^{77}Kr 80−52799
- ^{77}Br-labelled 5α-dihydrotestosterone, synthesis and distrib. in rats rel. to ^{77}Br-bromide 80−51247
- ^{80}Br-bromohippuric acid preparation 79−88187
- $^{81}Br_2$, visible, vibr.-rot. absorption, fluoresc. decay, predissoc. quantum yield 77−18962
- ^{80m}Br labelling of tyrosine, uracil and cytosine 80−51248
- $Br^*+I_2(Br_2)(Cl_2)(IBr)(ICl)(BrCl)$, deactivation rates of $Br^*(^2P_{1/2})$, collision complex form model 78−42179
- Br^*+N_2O, electronic-vibr. energy transfer, time-resolved fluoresc. obs. 79−89753
- Br_2^* laser, excitation mechanism in Ar-Br_2 system 77−31096
- $Br^*(4^2P_{1/2})$ yield, in $Br_2(IBr)$ photodissoc., wavelength depend., collisional release 78−64857
- $Br(4^2P_{1/2})+{}^{12}CO_2({}^{13}CO_2)$, electronic-vibr. energy transfer, temp. depend. meas. 79−10136
- $Br(4^2P_{1/2})+CO_2(COS)(CS_2)$, electronic to vibrational energy transfer rates 78−29839
- $Br(4^2P_{1/2})+H_2(HD)(D_2)$, electronic-vibr. energy transfer, fluoresc. meas. 79−72347
- $Br(4^2P_{1/2})+HCl$, electronic to vibr. and rot. energy transfer from flash photolysis of HCl-Br_2-Ar 80−48069
- $Br(4^2P_{1/2})+N_2O$, electronic-vibr. energy transfer obs. 78−55220
- CO_2-Br laser, pulsed, electron-vibr. energy exchange from Br* 78−29930
- CO_2-Br_2-He mixture, possible gas lasers with solar excitation 80−99695
- $CO_2(00^01)+Br_2$, vibr. relax. rate consts. 77−6898
- $CO(\nu=1)+Br_2$, vibr. relax. rate consts. 77−6898
- $Cl+Br_2 \rightarrow BrCl+Br$, crossed mol. beam, translational energy depend 78−25693

bromine continued
$Cl_2+2Br^-\rightarrow Br_2+2Cl^-$, aqueous soln., specific rate determ., competition technique 78−44348
CuCl(I):Br, lattice-dynamical study of impurity modes 80−29129
H, thermochemical prod. using S-Br cycle, development of lab.-scale plant 80−35774
H-Br systems, thermokinetic oscillations in flame propagation, stability diagram 79−79253
$H+Br_2$, reaction props. dimensionality depend. 77−9050
$H+Br_2\rightarrow HBr+Br$, HBr ang. momentum alignment, scatt. ang. depend. 78−3323
$H+Br_2\rightarrow HBr+Br$, pot. energy surface, ab initio generalised valence bond calc. 78−73026
H_2-Br_2 cell for energy storage appls. 80−72029
$HCl(\nu=1)+H(D)(Cl)(Br)$ reactions, selective vibr. excitation effects, kinetics *(German)* 77−21364
$Hg(^3P_0)+Br_2\rightarrow HgBr(B)+Br$, crossed mol. beam chemiluminesc., cross section 78−31622
$I^*(^2P_{1/2})+Br_2\rightarrow IBr+Br^*(^2P_{1/2})$, rate const., chemiluminesc. obs. 77−40520
$K+Br_2$, stripping reactions at hyperthermal energies 77−16815
$K+Br_2$ (Cl_2), electron transfer crossed beam reaction, energy and ang. differential cross section 79−20358
$K+I_2(IBr)(Br_2)(ICl)(Cl_2)$, ion-pair form., bond stretching effect on cross sections 78−1064
$K_2+Br_2(Cl_2)$, collisional ionisation reactions 77−50508
$K_2+Cl(Br)\rightarrow KCl(KBr)+K^*$ product electronic state distrib., chemiluminesc. 77−40529
KCl:Br, colouration under two-photon excitation, absorption spectra 78−84618
KCl:Br^-, interstitial atomic H centres, formation kinetics and struct., MO calcs. and EPR studies 80−75854
KCl:Br^-, modes of vibr. due to U-centre and additive anion impurities 80−44280
KCl:Na,Br, EPR of interstitial and diinterstitial $BrCl_2^{2-}$ centres 77−81007
KI:Br^-, lattice relaxation around tetragonal and rhombic defects 79−95110
$Li+Br_2$, product mag. deflection slotted disc velocity analysis 77−16806
$NO^++X^-\rightarrow NO+X$ (X=Cl, Br, I), rate const. determ. in flames 78−48633
$Na_2+Br_2(Cl_2)$, collisional ionisation reactions 77−50508
NaCl:Br, host-sensitized luminesc., energy transfer due to excitons and holes 79−38590
NaCl:Br^-, energy of migration of Br^- 77−43380
Ne-Br_2 mixture, at. state densities of Ne I levels, Nf values of Br II levels 78−62753
Ni:Br, ferromagnetic, hyperfine field and relax. time obs. of impurity heavy nuclei 80−75533
$Rb_2+Br\rightarrow RbBr+Rb^*$, product electronic state distrib., chemiluminesc. 77−40529
RbCl:Br^-, interstitial atomic H centres, formation kinetics and struct., MO calc. and EPR studies 80−75854
$(SN)_x$:Br, IR spectra 79−56781
$(SN)_x$:Br, ion implantation effect on elec. props. 80−65026
$(SN)_x$:Br, X-ray absorpt. meas. of mol. struct., orientation and charge transfer 80−25486
$SO_2/H_2O/X_2$ reactions ($X_2=Br_2$, I_2), appl. to thermochem. H prod. 80−35773
Si-SiO_2 interface state distribution, Br incorporation effects 80−11091
W-Br regenerative cycle of linear quartz lamps, metallic impurity effects, thermochemical interpretation 80−3312
Xe-Br_2 discharge, atomic state density determ. 79−36573
Xe-Br_2 mixtures, low-press. excimer form. and quenching by e-beam excitation 79−50071
$Xe+Br_2\rightarrow XeBr^*+Br$, rot. polaris. in chemiluminesc. 79−8432
$Xe(^3P_{0,2})+Br_2\rightarrow Xe^*+Br$, excitation function 78−40028
ZnS:Cu, Br based electroluminesc. cells, light, const. field effects on electroluminesc. 78−84658
$ZnS_{1-x}Se_x$:Cu,Br ceramic, current oscills. and electrolum. under high elec. fields 79−38677

bromine compounds
ESCA chemical shift, indirect evaluation of Coulombic contribution to ionis. pots. for nonbonding electrons 78−92572
ESCA using Au M_α X-rays (2123 eV) 78−72683
ethylene$+Cl_2(Br_2)$ complex, intermolecular interaction and struct. SCF-MO-LCAO CNDO/2 calc. 78−58763
organic π-σ complexes, low freq. spectra 78−78713
TTT^+Br^-, cryst. and mol. struct., X-ray method 80−107202
$BiCN^+$, fluoresc. quantum yields and lifetimes, meas. method, ion form. 77−6815
BiO_3^-, detect. in subway air 78−36273
Br-graphite, intercalation cpd., magnetothermal oscill. and charge-density waves 80−11199
$Br+H_2$, gas phase H-atom transfer reactions, struct.-reactivity correl., pot. energy surfaces 80−104433
$Br+NO\rightarrow Br+NO_2$, reaction rate const., mass spectrometric determ. 79−34288
Br_2Al-Br-$AlBr_3$, Al_2Br_6, vibr. obs., normal coordinate anal. *(German)* 79−26967
BrCN, ^{14}N quadrupole coupling consts., ab initio calcs. 80−58283
BrCN, general quartic force field, Machina-Overend parameters 78−50532
BrCN, ICN, and isotopic forms, force field calc., freqs., rot. consts. 79−22693
BrCN, photodissoc. energy disposal, electronic branching, vibr. and rot. transfer, $CN(B\rightarrow X)$ fluoresc. 77−42364
BrCN photolysis, IR stimulated emission from CN 79−31888
BrCN, pressure-broadened linewidths in microwave region, temp. depend. 77−34694
BrCN, vacuum UV photodissociation spectroscopy, quantum yield, fluoresc. polarisation 80−32736
BrCN+Ar(N), CN quartet state production, fluoresc. anal. 78−68888
$BrCN+N_2^*$, vibr. energy transfer, α_3 vibr.-rot. const., microwave meas. 77−83578
Br_2CO and Br_2CS, signs of dipole moment derivatives, semiempirical CNDO calcs. 79−26890
BrCl, $^3\pi_0{}^+$ state, time-resolved fluoresc. 77−34679
BrCl, elec. dipole moment, Stark effect meas. 78−90211
BrCl, excited $B^3\Pi(0^+)$ state, excitation spectra and predissoc. 78−66593

bromine compounds continued
BrCl, excited $B^3\Pi(0^+)$ state, laser-induced fluoresc., steady-state kinetics 78−66594
BrCl laser induced fluoresc., quantum resolved level dynamics in $B^3\Pi(O^+)$ state 80−74188
BrCl, photoelectron spectrum, assignments 78−5284
BrCl, time-resolved fluoresc. of $a^3\Pi_0{}^+$ state 78−63093
$BrCl^-$ centre in alkali halides, analysis of spin-Hamiltonian parameters of heteronuclear XY^- defects 80−88509
$BrCl+Br^*$, deactivation rates of $Br^*(^2P_{1/2})$, collision complex form model 78−42179
BrCl+HBr, four-centre reaction, quasiclassical trajectory study 79−57213
$BrCl_2^-$, photodissoc. and photodetachment, pot. curves. 79−64060
$BrCl(H_2O)_n$, mean vibr. amplitudes, Raman spectra, isotope effects 77−58014
BrF, $B^3\Pi(0^+)\leftarrow X^1\Sigma^+$ absorption spectrum, high-resolution anal. 79−59478
BrF, fluoresc. decay lifetimes and quenching cross-sections for excited $B^3\Pi(0^+)$ states 78−1030
BrF, He(I) photoelectron spectra, interpretation 79−13766
BrF, laser excitation spectrum, 4850 to 5200 Å, rot. anal. 77−6840
BrF, laser excited fluoresc. 79−50077
BrF, predissociation in $B^3\Pi(0^+)$ state 78−66591
BrF, stable levels of $B^3\Pi(0^+)$ state 78−66592
^{79}BrF, (^{81}BrF), hyperfine struct., elec. dipole moment, rot. transitions, microwave spectral obs. 80−32695
$BrF+H\rightarrow HF+Br$, reaction product energy distrib. 80−30219
BrF_2^--, $BrFCl^-$-, $BrCl_2^-$, inert gas cpds., localised MOs and bonding nature 78−9061
BrF_3 complexes with BF_3, PF_5 and AsF_5, F NMR, struct. and stability 78−37658
BrF_3, electronic struct. and ionisation pot., SCF DV Xalpha method 80−69057
BrF_5, electronic struct. and ionisation pot., SCF DV Xalpha method 80−69057
BrF_5, excited vibr. states, microwave spectrum, rot. const. determ. 78−94237
BrF_5, gas phase electron diffraction and microwave rot. consts. data anal., mol. struct. 79−76363
BrF_5, IR intensities, fundamental, overtone and combination band calcs. 78−29780
BrF_5, microwave spectrum, Coriolis interaction, A_1-A_2 splitting of kl levels 77−38657
BrF_6, EPR of matrix, isolated radical 79−85977
BrF_6, EPR spectra, 'NMR' transitions, mol. symmetry 77−46580
$^{79}BrF_6$, radical, prep. and EPR comparison with other hexafluoride radicals 78−68381
BrF(Cl), rot. spectra in millimeter wave region, rot. transitions obs., equilib. const. determ. 80−78607
$BrF_3.SbF_5$, NQR anal. of complex ion struct. 77−12238
$BrHCN^-$, $BrDCN^-$, IR spectra, rel. to mol. geom. 79−22702
$Br(H_2O)_n^-$, geometric and electronic struct., CNDO/2 calcs. 77−79542
$Br(H_2O)_n^-$, geometric and electronic struct., CNDO/2 calc. 79−41113
$Br_2(H_2O)_n$, mean vibr. amplitudes, Raman spectra, isotope shifts 77−58014
BrHe, pot. energy curve in Br^-+He electron detachment, SCF calc. 80−23503
BrHe , pot. energy curve, in Br^-+He SCF calc. 80−23503
BrI+K, stripping reactions at hyperthermal energies 77−16815
BrN_3, VPS obs., comparison with ab initio and semi-empirical calcs. 80−53043
BrNCO, VPS obs., comparison with ab initio and semi-empirical calcs. 80−53043
BrO, free radical, Ar matrix absorpt. spectra, mol. vibronic states obs., spectroscopic const. determ. 80−83387
BrO free radical, IR spectra in Ar matrix at 10K 79−89669
BrO^-, electron affinity, formed in Br^-+O_2 reaction 77−63902
BrO^- from ozonation of Br^- in seawater 79−16518
BrO+ClO, reaction rate consts., mass spectrometry meas. 78−3316
BrO+NO, temp. depend. kinetic study, stratospheric Br photochemistry implication 80−50866
$BrO+O\rightarrow Br+O_2$, reaction rate constant, 200-360K 78−73024
BrO_2, detection in oscill. Belousov-Zhabotinskii system *(German)* 79−29351
BrO_3^- in $NaClO_3$, Raman spectra, fundamental vibr. modes 78−78711
$BrO_3^-+H_2SO_4+$gallic acid system, uncatalysed oscillatory chemical reactions 78−61004
BrOBr and BrBrO mols., IR spectra in Ar matrix at 10K 79−89669
$BrONO_2$, stratospheric photolysis, UV and IR spectra 78−53227
$BrO(X^2\Pi_i)$ radical, ionisation potential, photoelectron spectroscopic determ. 78−25612
BrSN, force consts. and mean amplitudes of vibr. calc. 77−30855
Br_2SO, A′-force consts., 4th-order secular eqn., L-matrix approx. vs. HLFS methods 79−36556
CBr_x, graphite intercalated, de Haas-van Alphen effect and cyclotron reson. 80−44479
$CuBr_xI_{1-x}$, disorder-induced TA Raman lines 79−73929
$FBrO_3$, gas-phase electron diffr., mol. struct., force field, vib. amplitudes 77−547
$H'+BrH\rightarrow H'Br+H$, collinear reaction, barrier height, PNO-CEPA cals. 78−3328
KBr, effect of addition on corrosion of Cu in seawater 78−80670
OBrO free radicals, IR spectra in Ar matrix at 10K 79−89669

Brownian motion
see also colloids
absorbing boundary, joint position-velocity distribution function determ. for Brownian particle 80−62581
acetonitrile, liq., Brownian reorientation barriers *(Russian)* 79−27901
acridene yellow, glycerol soln., luminesc. intensity and polaris., temp. and viscosity effects 79−56833
aerosol, Brownian coagulation in transition regime 78−11571
aerosol, photophoretic motion, particles ≪ light wavelength, gas collisional effect 77−90646
aerosol, turbulent coagulation in pipe flow 79−37385
aerosol capture by drops, effect of Brownian, thermo- and diffusiophoretic forces 77−16869
aerosol cylindrical particles, overall drift angle in sedimentation 79−50777
aerosol diffusion and sedimentation in horiz. cylinder 78−3385

Brownian motion continued
  aerosol particle capture by drops, thermodiffusionphoresis and Brownian motion effects *(Russian)* 79—39791
  aerosol particle coagulation by Brownian motion 79—96375
  aerosol particles in flow type chamber, coagulation, deposition 80—69908
  aerosols, diffusion to face of Nucleopore filter 79—88025
  aerosols, humidity effects on gravit. settling and Brownian diffusion 78—32203
  alkanes, liquid, chain reorientation, Brownian dynamics simulation, comparison of models 80—49067
  angular velocity autocorrelation function rel. to viscoelastic and inertial effects 77—27932
  anharmonic Brownian oscillator, canonical correlation function based on projection operator technique 78—55926
  anthracene, electronic vibr. spectra, stochastic description, numerical modeling, comparison with expt. 80—63620
  asymmetric top, rot. Brownian motion 79—54058
  asymmetric top, rotational Brownian motion 78—8349
  asymmetric top molecules, complex polarisabilities, NMR line dipolar broadening 79—54058
  asymmetric top rotational Brownian motion and electric polarisation calc. 80—15949
  atmospheric aerosols, particle size distribs. evolution via Brownian coagulation, num. simulation 80—41513
  bead-spring-type model in nonuniform vel. gradient, dil. soln. kinetic theory results 80—64628
  benzene, liq., Brownian reorientation barriers *(Russian)* 79—27901
  biopolymer Brownian diffusion, fluoresc. correl. spectroscopy 79—62193
  Bogolyubov's method of abbreviated description 79—21669
  book, Brownian motion, Hardy spaces and bounded mean oscillation 77—67180
  Brownian oscillators, non markovian diffusion and Fokker Planck eqn. 77—57285
  Brownian particle diffusion in shear induced convection, Poiseuille flow 80—33591
  Brownian quasiparticle model 80—46976
  Brownian sphere, long time fluctuations 79—85077
  causal unification of relativity, gravitation and quantum mechs. 77—33923
  cell surface receptors, molecular movements 80—45866
  charged particles, Brownian motion, long and short range correls. 78—62155
  chemical reactions, Brownian dynamics simulation in soln. 80—104422
  chemical transition rates, Brownian motion theory 77—36731
  chromatography, hydrodynamic, role of colloidal forces 78—48717
  collision operators as generators of Markov processes and their spectra 79—63150
  colloid, Brownian coagulation, with disintegration of aggregates 80—7864
  colloid stability against coagulation 77—32843
  colloidal dispersion, particle growth rate, effects of convection and Brownian motion 79—52778
  colloidal dispersion dynamics, review 80—71956
  colloidal dispersions, microrheology, Brownian diffusion of doublets of spheres 77—4942
  colloidal particles, interacting Brownian spheres, depolarised light scattering 79—34370
  colloidal systems, dynamical props., correlation and response functions 80—22286
  colloidal systems, stochastic transport eqns. 78—93609
  colloids, hydrophobic, coagulation mechanism 78—40085
  coloured noise approach, Smoluchowski eqn. corrections 80—101755
  complex diffusion processes, transforms., and nonrelativistic quantum mechanics 80—82670
  complex diffusion processes and nonrelativistic quantum mechanics 80—90707
  complex molecular systems, collision phenomena by stochastic model, observables distribs. and information entropy 78—25640
  complex molecules, vibr. spectra, stochastic description, appl. to optically active Brownian oscillator 80—52974
  conditional expectations and Brownian motion, stochastic integration *(French)* 77—13585
  conductivity of Brownian particles in periodic medium 79—49170
  convergence props. of new Monte Carlo simulation method, Brownian dynamics appl. 79—12719
  coupled nonlinear oscillators, Brownian motion, thermalised solitons and nonlinear response 78—29053
  critical fluid, critical long time tail 77—79034
  cylindrical surface, aerosol particle capture, thermophoresis forces 80—103060
  Debye generalised fluid model, dielectric relax., depolarised dynamic light scatt. 80—108156
  decalin, liq. and glass mol. motion, kinematic and electrodynamic solns. 80—25293
  deposition rates of Brownian particles calc., interaction forces lumped into boundary condition 77—9131
  desorption from surface, one-dimensional time-dependent escape problem 80—29278
  developments of theory 79—25990
  diatomic molecule in equilib. medium, Brownian motion in Bogolyubov's abbreviated description method 80—36948
  diatomic-like mol. fluid, with isotropic rot. diffusion quasielastic neutron scatt. 77—47312
  diffractals (wave interaction with fractals) 79—58549
  diffusion, in fluid near its critical point *(Russian)* 77—22496
  diffusion coefficient for Brownian particle in periodic potential 80—4649
  diffusion effects in solns. of Brownian particles, light scatt. theory 77—4939
  diffusion equation, derivation from Fokker Planck equation using perturbation methods 78—54117
  diffusion equation, hyperbolic, effect of finite correlation time 80—86214
  diffusion equation for semiclassical bosons and fermions 79—40446
  diffusion in periodic potentials, dynamic correlation functions 77—59138
  diffusion of Brownian particles, treated as many boson problem 79—164
  diffusion of interacting Brownian particles suspended in fluid 78—54304
  diffusion theory, inertial effects 77—13715
  diffusion with wave fronts, definition *(French)* 77—67386
  diffusive motion in periodic potential, correlation functions, Fokker-Planck eqn. method 79—165
  diffusive motion in periodic potentials, low friction nonlinear mobility 79—35645

Brownian motion continued
  dipolar molecular lattice, dielec. absorpt. of disordered mol. solids, electrodynamic influences 80—40040
  dipolar molecules, zero-THz liq. phase dielec. absorpt. and rot. Langevin eqn. 80—40032
  discovery of phenomena, historical review for teachers 78—86090
  discs and spheres with dipole, orientational autocorrel. functions 78—4557
  dispersive magnetisable media, hydrodynamics including Brownian motion 80—59120
  dissipative spin system, oscills. and fluctuations 80—27224
  distribution function, Fokker-Planck eqn., derivation by multiple time scale method 79—44861
  distribution functions of particles in periodic pot. 79—88881
  DNA, fluorescence depolarisation, twisting and bending, rot. Brownian motion 79—70509
  domain wall Brownian motion and diffusion constants 79—37775
  dynamics of colloidal systems: time-dependent structure factors 80—93803
  education, Brownian motion, melting, surface tension and rubber networks, thermodynamic anal. 80—73132
  Einstein, contribution to development *(Russian)* 79—84933
  Einstein's contribution to development of science *(Russian)* 79—84926
  Einstein's nonrelativistic work *(Czech)* 80—27095
  Einstein's work and effect on atomic physics at the turn of the century *(German)* 80—90648
  Einstein and Brownian motion, student project 80—68000
  electrolyte solution, Brownian dynamics approx., time evolution and transport props. 79—37604
  electrolyte solutions, Brownian dynamics 77—63921
  electron in strong randomly rotating mag. field 78—37163
  embeddings in Brownian motion 80—52126
  energy forms, Hamiltonians and distorted Brownian paths 77—57279
  EPR and saturation transfer EPR, fast computation, perturbation approx. extension for overmodulation 78—82754
  exact solution in shear flow by operator formalism 80—17874
  exit problem, diffusion across pot. barriers, chemical reactions and crystal diffusion 79—80527
  in external field, quantum description, effect of fluctuations 77—49687
  fast variables elimination using time-convolutionless projection operator formalism 80—8913
  ferromagnetic fine particles, thermal fluctuations, Brownian motion theory 80—11226
  ferromagnetic sol, relaxation of mag. birefr. and dichroism 79—57301
  Feyerabend's concept of hidden anomalous fact, nontrivial interpretation 77—78950
  Feynman path integrals, white noise approx., inertialess Brownian system 78—57859
  first-passage theory for Brownian motion with an absorbing boundary 80—86207
  flowing incompressible fluid, diffusional mass flux, eqns. of motion in large friction limit 79—93043
  flowing suspension, memory impairment, Brownian rotation of spheroids 80—79386
  fluctuating hydrodynamics, slip coeff. fluctuation-dissipation theorem 78—8348
  fluctuation-dissipation theorem for contracted descriptions of Markov processes 79—54054
  fluctuation-dissipation theorems from the generalised Langevin equation 79—49167
  fluctuations, nonequilibrium, generalised Einstein theory 80—31672
  fluid near citical point, fluctuation-dissipation theorem 80—4647
  fluid stress tensor fluctuations 78—16738
  Fokker-Planck approach to Brownian rotation 78—62160
  Fokker-Planck approx. for n-dimensional nonMarkovian Langevin eqns. 80—57191
  Fokker-Planck eqn., new method of setting up eqn. 77—26202
  Fokker-Planck eqn. deriv. from generalised kinetic eqns. 78—36936
  Fokker-Planck eqn. for Brownian motion of rotating spherical particles *(Russian)* 77—41539
  Fokker-Planck equation, inhomogeneous, eigentheory 78—29068
  Fokker-Planck equation, systematic soln. for high-friction case 78—49767
  friction coefficeint, freq.-depend., spherical Brownian particle in fluid near crit. pt. 78—73929
  friction const. of Brownian particle density expansion 77—87694
  functionals, analysis 77—33949
  gas, evolution according to minimum free energy principle *(French)* 77—26254
  Gaussian generalised stochastic fields, Markov property 80—22287
  generalised Brownian motion, scalar case, computer simulation 80—77704
  generalized multiple Wiener integrals, anal. of nonlinear Brownian functionals 79—30370
  graphite particles, diamag. levitation, Brownian-motion press. gauge appl. 78—24807
  gravitational interactions in Brownian motion theory of quantum mechanics 79—12699
  Hamilton's principal function, Schrodinger-Langevin eqn. 78—41233
  harmonic lattice, impurity motion, generalised hydrodynamics and microscopic theory of long time tail *(Korean)* 77—49683
  harmonic microwave mixing in periodic potentials, stochastic theory 79—65460
  harmonically bound particle, simulation 80—17751
  heavy impurity in harmonic linear chain, kinetic and hydrodynamic scalings 77—2613
  heavy particle, quantum Brownian motion, adiabatic expansion 78—49768
  higher order parabolic differential eqn., probabilistic soln. from heat eqn., with Brownian motion 79—97322
  humid atmosphere, water droplet vaporis. model with natural convection 78—33999
  Huygens' principle, formulation of quantum and classical mechanics *(French)* 78—36851
  Huygens' principle and Broglian waves *(French)* 79—21545
  intensity fluctuation spectroscopy, of charged Brownian particles, coherent scatt. function 78—17857
  intensity fluctuation spectroscopy applics., review 80—52129
  interacting and noninteracting particles in periodic potential driven by external field 79—2726
  interacting Brownian particles, light multiple scatt. by correlation spectroscopy 80—87313

Brownian motion continued
- ion, near metal surface, friction parameter and Brownian motion 80—15584
- ion trajectories in weak electrolytes, dissociation and recomb. of ions 80—85189
- ionic crystal, Brownian sublattice, microscopic theory 78—79681
- itinerant oscillator model, anal. for dielectric relax. and incoherent neutron scatt. 79—90509
- k-dependence of long-time diffusion 80—5645
- ketones, in soln., IR spectral line halfwidths determ., rot. Brownian motion investig. 77—36248
- kinetic fluctuations of Brownian motion 79—25984
- kinetic molecular theory teaching, expt.-oriented approach 80—12868
- kinetic theory, fluctuation effects 80—150
- kinetics of reacting solns., diffusional barrier crossing processes, trajectory simulation 80—81280
- Kolmogorov eqn., separation of variables, applied to oscill. Brownian motion 80—36945
- Kramer's rate formula 78—83992
- Kramers equation, eigenvalues calc., Fokker-Planck eqn. for Brownian motion in a potential 80—86215
- Kramers rate theory, quantisation using Wigner representation 80—52054
- Langevin equation solution, using Wiener's method *(Korean)* 78—49766
- Langevin theory for correlation, for teachers 79—97133
- laser light scatt., photon time-interval statistics 78—9329
- last exit distributions for n-dimensional Brownian motion 80—82722
- light scattering, correlations for interacting Brownian particles 78—82911
- light scattering, interacting particle system, diffusion coeff., lineshape 77—27254
- linear polar molecule, rotational Brownian motion, spherical harmonics 79—30368
- liquid, symmetric top molecule, angular velocity correlation function, from angular position correlation functions 79—86661
- liquid crystal, uniaxial, polarised fluoresc. emission, orientational distrib. function, rot. Brownian motion 78—80390
- long-time versus short-time behaviour of a system of interacting Brownian particles 80—27219
- luminescent semiconductor electron-hole pair creation and migration 77—77304
- lung model alveolus, particle deposition by Brownian diffusion during breathing 79—53173
- macromolecular configurational entropic force, Brownian motion entropy calc. 77—34791
- macromolecular solns., light scattering, polydispersity and internal modes of motion 80—20651
- macromolecule, simulation of Brownian motion of chains, chain dynamics 79—86099
- macromolecule, simulation of Brownian motion of chains, local motions and chain conformations 79—86098
- macroparticle diffusion, role of inertial effects 80—29196
- macroparticles; charged spherical, dilute soln., Rayleigh scatt. 80—84748
- magnetic Brownian particles, theory of Mossbauer effect *(Russian)* 78—68436
- magnetic liq. birefringence and dichroism kinetics, Brownian diffusion *(Russian)* 78—5806
- magnetic reson. lineshape, with slow mol. motion, asymptotic method, strong collision limit 77—48063
- Markovian diffusion, dynamical theory 79—80515
- martingales, stochastic integral representation 77—67379
- material particles movement, differential equation, numerical solution *(Croatian)* 79—25983
- memory function approach to the dynamics of interacting Brownian particles 79—25979
- metals, liquid, structural micro-inhomogeneity, Brownian motion studies *(Russian)* 80—92426
- microemulsion, elec. cond., stirred percolation model 79—79314
- microhydrodynamics, characteristic effects, developments 77—68681
- Minkowski space and special relativity rel. to Brownian motion *(French)* 77—67377
- mobility in periodic pot. 79—35632
- modern theory development *(German)* 77—49684
- molecular collisions, translational energy distribution, Brownian motion model 77—50483
- molecular excited states, absorption spectrum, diffusion rot. effects *(Russian)* 78—74641
- molecular liqs., Maxwell effect relax. timeand light scatt. line broadening 80—76040
- molecular reorientation, orientational autocorrelation functions, appl. to rot. Brownian motion 78—18520
- molecular rotational motion, effects on nonlinear fluoresc. characts. *(Russian)* 78—5275
- molecule, Brownian rotational motion effect on anisotropic props. of absorpt. and luminesc. from excited states 79—93978
- monodisperse particles, Brownian coagulation and diffusive deposition 78—23967
- moving acceptors, direct energy transfer, decay law 80—89045
- multichain polymer system, simulating dynamic and equilib. props. 80—53179
- multiphase flow diffusion equations 78—94801
- multiple light scattering, Brownian polymer particles in water 78—78912
- multiple light scattering, depolarisation ratio and linewidths 78—78913
- N-particle system, Brownian dynamics with hydrodynamic interactions 78—91209
- Navier-Stokes eqn., derivation from Euler equation with Brownian motion 79—41650
- nematic phase thin slab fluid, return to equilib. eqn. *(French)* 77—27829
- neutron diffusion theory, connection with Brownian motion *(French)* 77—61473
- NMR spin relaxation in Brownian motion systems, book 78—15054
- nonequilibrium thermodynamics, statistical formulation by general Onsager Machlup formula 79—54089
- nonlinear, and formation of macroscopic order, theory of instability 78—89408
- nonlinear filtering, conditional laws, smoothness, stochastic calculus of variations *(French)* 80—68128
- nonlinear oscillators, Brownian motion, projection operator method, double well potential oscillator appl. 79—2723
- nonlinear relaxation processes governed by rotational Smoluchowski eqn. 79—71365

Brownian motion continued
- nonlinear response to external field, in the low-friction limit 80—4652
- nonlinear system with control parameter fluctuations, generalised Fokker-Planck eqn. 79—75456
- nonparametric identification for diffusion processes 79—30374
- nonspherical body, rot. Brownian motion, ang. vel. 77—33860
- nonspherical particles, dil. soln., light-scatt. anticorrels. 80—5693
- nonspherical top, rotational Brownian motion, and its appl. to dielec. relax. theory 78—21071
- nonvolatile liquid, boiling, nucleation eqn. in phase space 79—27495
- nuclear fission rate analysis from point of view of Brownian motion *(Chinese)* 80—52657
- one-dimensional chain of harmonically coupled Brownian particles, Smoluchowski eqn. 80—17878
- one-dimensional diffusion, soluble model potentials 79—35649
- one-dimensional ionic conductors, cooperative diffusion and soliton Brownian motion 78—95177
- one-dimensional problem, with absorbing boundaries 80—27221
- optimal stopping based on capture times 77—22494
- organic liquids, Brownian reorientation barriers *(Russian)* 79—27901
- organic nitriles, in soln., IR spectral line halfwidths determ., rot. Brownian motion investig. 77—36248
- orientation autocorrelation functions of spherical Brownian particle 77—7646
- oscillator, whiteness of quantum noise source 78—75
- particle absorption rates at high cell concs., Monte Carlo simulation 80—94141
- particle escape over dynamic barrier, impurity diffusion in solid 80—107569
- particle in a gas, coeff. of friction, Kirkwood-Kubo method 78—4558
- particle in double well potential, appl. to ionic mobility 77—76607
- particle in velocity-dependent random force 77—22493
- particle motion in pariodic field of force, diffusion coeff. in large friction limit 78—38869
- particle with frequency depend. friction, probability distrib. function 79—17348
- particles near free surface, Brownian motion, desorption from monolayer 80—54503
- path integrals for inertial classical particles, Brownian motion between capacitor plates 78—57858
- path sums for Brownian motion and quantum mechanics 80—36882
- periodic potential, bistability effects 80—68139
- periodic potential, hopping to free conduction transition 79—44860
- periodic potential, in presence of temp. and elec. potential gradients 80—4650
- periodic potentials, nonlinear response to external force 79—63156
- photon correl. spectroscopy, macromolecular soln. dynamics, review 79—59603
- photon correlation study 78—25798
- plate, vibration mode, damping of Brownian motion by cold load 78—13967
- polarisable ion, Brownian motion in periodic pot., polarizability effect on cond. 79—4427
- poly-γ-benzyle-L-glutamate in dioxane solution, relax. mechanisms, light scatt. spectra 80—20659
- polymer, conformational transitions, Brownian dynamics, simulation 79—45873
- polymer, spherical, in soln, long time tail in diffusion 80—88018
- polymer, uniaxial, fluoresc. polarisation, orientation and mol. dynamics effects 78—76516
- polymer chain, of bistable oscillators, Brownian dynamics of transitions 78—86983
- polymer chain dynamics, review of Brownian motion theory 80—23589
- polymer in solution, Brownian motion, fluctuation-dissipation theorem 80—46980
- polymer melts and solns., Brownian motion in equilib. state 79—41645
- polymer mols., theoretical description 77—50575
- polystyrene lattices, electro-flotation, collection efficiency 80—74946
- polythene, across energy barrier for multidimensional transition 79—41256
- potential effect, Maxwell-Boltzmann distrib. in infinite-time limit 80—105573
- process characterisation by method of local specifications *(French)* 80—31597
- quantal master equation for any time scale, Brownian motion 78—24725
- quantum dissipative systems, time evolution of state vector 80—12935
- quantum harmonic oscillator, Brownian motion, random walk, dissipative forces and coherent states 79—63086
- quantum harmonic oscillator, quantum dynamical semigroup formalism 77—30100
- quantum mechanical Brownian particle, tunnelling and transport problems 80—4644
- quantum mechanics, Fokker-Planck and Kramers-Chandrasekhar eqn. 79—9186
- quantum oscillator interacting with quantised radn. field, Brownian motion effects 77—34856
- quantum theory, connection with Brownian motion 80—90786
- quasi-deterministic evolution associated with the Brownian motion *(French)* 79—44857
- quasiparticles in statistical physics 80—17873
- random motion and Brownian rotation, review 80—73266
- regularity of boundary points for second-order eqns. *(Russian)* 77—9960
- relativistic, definition as class of diffusion with wave fronts *(French)* 77—53795
- relativistic Brownian motion and the foundations of quantum mechanics 79—63084
- relativistic space-time approach to quantum mechanics 80—31567
- renormalisation theory 79—54060
- repeated-ring kinetic theory, particle in fluid 78—59729
- reversible adsorption and reversible coagulation of Brownian particles, kinetic eqns. 79—16045
- revolving particles, solution of Fokker-Planck eqn. *(Russian)* 78—77802
- rigid particles, Brownian motion, hydrodynamic after-effects 79—30367
- rod-like macromolecules in conc. soln., basic kinetic eqn. and appl. 78—67637
- rotation in external fields, Fokker-Planck eqn. 79—30372
- rotation of ellipsoid of revolution about axis *(French)* 77—74322
- rotational, appl. of modified Smoluchkowski equation 77—33947
- rotational, Smoluchkowski eqn. soln. 78—41234
- rotational Brownian motion, graphical study 77—13702
- rotational Brownian motion of a symmetrical top 79—54061

Brownian motion continued
rotational Brownian motion of an asymmetric body 79—54062
rotational Brownian motion of nonspherical top, Smoluchowski equation 78—24738
rotational Brownian motion of spherical polar mol., diffusion eqn. study, complex polarisability 77—67381
rotational diffusion in n-fold periodic pot., time correlation functions 79—21668
rough sphere fluid, kinetic theory, matrix elements 77—71262
sapphire single-crystal clocks and frequency standards 78—57915
scavenging, in-cloud, rel. to aerosol particle size, mechanisms 78—16108
Schrodinger eqn. with random potential, behaviour of Wiener integrals as $t\to\infty$ and density of states 79—2720
Schrodinger equation, Brownian motion interpretation challenged 80—94974
seed particle motion, near Benard convective instability 77—11172
in shear flow 78—5786
short-time stochastic electron, modified Brownian particle, Schrodinger eqn. 78—36853
simple shear flow of dilute fluid suspension, orthokinetic collisions of hard spheres 77—35199
sine-Gordon chain, cond., finite damping correction 80—46993
sine-Gordon model, overdamped, Brownian diffusion 80—27223
sintering, liquid phase, microstructural evolution, coarsening 77—70014
sintering, liquid phase, microstructural evolution 77—70013
small low-temperature antenna, meas. by low noise preamplifier for gravit. research 78—243
Smoluchowski equation in presence of hydrodynamic interactions, Chapman-Enskog method 80—46979
solar radiation geometric Brownian distribution, implications for economical solar heating system 79—83571
solute transport in porous media, statistical theory 80—28899
solvated ion dynamics, mol. theory 78—35695
solvent, polar, spherical ion radius and limiting elec. cond. Brownian motion 78—95168
spatially periodic convective flow, stability and fluctuations 80—19394
spherical Brownian particle in flow, hydrodynamic model for attractive pot. self-diffusion 77—11293
spherical Brownian particles, interacting, wave vector dependent mutual diffusion 79—44859
spherical particles in cylindrical pores, diffusive and convective transport models 77—32841
statistical mechanics, response theory for systems nonlinearly displaced from equilibrium, graphical approach 80—22285
stochastic calculus, derivation from path integral expansion of conditional probability density 79—67227
stochastic control system, integral inequalities 79—17341
stochastic diffusion in a periodic potential 80—12994
stochastic integral approximation by Stieltjes-Lebesque integrals *(French)* 79—49162
stochastic linear systems with nonwhite parameter fluctuations, differential anal. 79—85082
stochastic Liouville equation, generalised, nonMarkovian and memoryless master eqns. 78—24737
stochastic particles, relativistic dynamics 80—82639
Stokes-Einstein law for Brownian particle, kinetic theory derivation 77—49686
superconducting surface sheath, Brownian motion 79—19708
superionic conductor, correls. among mobile ions role, microscopic model 80—107534
superionic conductor, interacting Brownian particles and correlations 80—29202
superionic conductor, interacting Brownian particles in periodic medium model 80—59712
superionic conductor, one-dimens., soliton Brownian motion and impurity effects 79—77814
superionic conductors, appl. of Brownian motion in polarisable lattice 77—76603
superionic conductors, dynamic properties 78—79673
surface diffusion on solids, model 78—6214
suspended particle with nonlinear friction 80—146
suspension, averaged size and polydispersivity index meas. using laser light scatt. spectroscopy 80—77754
suspension, Brownian rotational-translational particles, at finite conc., dynamics and hydrodynamics 79—7401
suspension, dilute, arbitrary-shape particles, time-depend. flow, Brownian rot. effect 78—26188
suspension, movement in porous solid interior *(French)* 80—43770
suspension, role of inertia in transport props. 77—32839
suspension, sheared, macroscopic transport props. 77—32840
suspension of spherical particles, Brownian motion effect on bulk stress 78—7246
suspensions, rheology, colloidal forces role, review 80—103063
Syton determination of size distribution of submicron particles in colloidal suspension, FODA 78—61057
TBBA, smectic liq. cryst., polarised Raman spectra, 90-300K, 0-400 cm^{-1} 77—12383
teaching, two-dimens. Brownian motion simulation on micro-computer *(Japanese)* 80—31461
tetrabromomethane, liq. and plastic cryst., rot. Brownian motion, far IR absorpt. 77—36234
theory, integro-differential equation 77—26242
thermal desorption theory for catalyst surfaces 80—26052
threshold phase-transition analogy 79—40471
threshold-phase transition analogy 78—70081
time dependent-correlations in many body systems, theory 77—82460
time-evolution of non-Markov processes 78—54305
toluene, liq., Brownian reorientation barriers *(Russian)* 79—27901
transient nonlinear fluctuations, scaling theory, macroscopic order formation 79—80520
translational motion, appl. to differential cross-section calc., incoherent scattering of slow neutrons 78—75504
transport properties of interacting particles in periodic pot. 79—85083
two component Boltzmann gas, fluctuating kinetic eqn. 80—171
two-phase flow, constitutive eqns. for lift force and Brownian motion 77—937
velocity autocorrelation function, direct meas. for Brownian test particle 80—57195
velocity field, generalised Langevin equation 80—147
velocity-force cross-correlations via Langevin eqn. 77—53834
viscous drag case, Monte Carlo simulation, for teachers 78—61984

Brownian motion continued
viscous drop, almost spherical, Brownian motion and fluctuating hydrodynamics 80—87787
α-AgI, superionic conductor, appl. of Brownian motion in polarisable lattice 77—76603
Be, neutron irradiated, gas porosity, Brownian motion 79—73222
$FeSnO_3$ particles in EBBA liq. cryst., Mossbauer study of Brownian motion 79—95691
He, film, Brownian motion, boundary layers and quantised vortex prod. 80—6579
MnO_2 submicron particle collection, by H_2 bubbles 78—11560
$NiCl_2$ aqueous solutions, autocorrelation spectroscopy, Gaussian diffusion 77—36796
Si single-crystal clocks and frequency standards 78—57915
^{236}U fission as multi-dimensional Brownian motion, Fokker-Planck soln. *(Chinese)* 80—99197

Brownian movement *see Brownian motion*

brush discharges *see brushes; discharges (electric)*

brushes
electrical contacts, for homopolar generators, tests at high surface vels. and current densities 78—54964
homopolar machine, pulse power current collection system, for fusion research 78—54949
magnetic brush xerographic development, image noise 79—17526
Cu-graphite starter brushes, effect of high velocities, current densities on wear, friction 78—88544

brushgear *see brushes*

bubble chambers
automatic centring system for bubble chamber film measuring and premeasuring tables 77—83455
automatic film scanner KAMA using CRT with double deflection scheme 77—38552
automatic track meas. 78—25399
AZ MS IV scanning measuring projector system, calibration methods 80—5449
BEBC, bell jars for research into strong interactions at SPS energies *(Dutch)* 77—46463
BEBC, CERN super proton synchrotron, experiments with light particles *(Dutch)* 77—46433
BEBC, on-line control system for RF separated hadron beams 77—38530
BEBC performance of external muon identifier 79—730
BEBC pictures, automatic anal. using flygin spot digitiser 77—88342
Big European Bubble Chamber, optical system 78—17483
cavitation chambers, for cosmic ray heavy nuclei and multiparticle effects detect. 79—84617
CERN 2m HBC, automatic meas. of 12 GeV/c $\bar{p}p$ interactions 79—36471
charmed particle, short lifetime particle, detection system 78—29716
charmed particles and short lived new particle obs. 79—22543
compact digitiser for bubble chamber pictures 77—83452
elastic events separation, appl. to $\bar{p}p$ interactions at 5.7 GeV/c 78—13379
electromagnetic shower photographs, for teachers 78—65737
event recognition by optical correl. *(German)* 78—70704
Fermilab 15 ft bubble chamber, external muon identifier, proportional chambers 77—6629
film, on-line measuring system with manual digitiser 77—18736
film analysis, semiautomatic measuring system 80—58105
film exposure for meas. by HPD 78—58553
film meas. automisation in Spiral reader system 80—14045
film processing using Hough-Powell digitizer, appl. to Mirabelle chamber in K^+p expt. at 32 GeV/c 80—69040
film scanning and digitising system based on Intel 8080 microprocessor 78—29714
finite spotsize model, theoretic comparison with expt. 80—47824
gamma-particle multiplicity distrib. moments meas., statistical method 77—30712
Gargamelle, neutrino physics history, theory and expt. 78—50027
Gargamelle bubble chamber, neutrino physics, book contrib. 79—30728
geometric reconstruction of events meas. on HPD 79—753
HPD, finite spot size in ionisation meas. 80—27892
hybrid devices, recent developments 78—82584
hybrid liquid-gas chamber, new combined track detector 77—83454
hybrid systems, characteristics, construction and use, book contrib. 78—82591
hyperon bubble chamber 11.7 T solenoid 78—50435
images, SNOOP module CAMAC interface to 168/E microprocessor 80—58103
ionisation data from SAMM, max. likelihood anal. 77—67940
ionisation track density meas. in $\bar{p}p$ with HPD 77—10543
large scale projector with separate movement and optical system for bubble chamber pictures *(Italian)* 79—75567
limitations and recent developments in design 77—14313
Lyudmila chamber, DATABOX device for registering servicing information 78—864
measuring projector for bubble chamber film, minicomputer on-line system 80—27878
MIRABELLE hydrogen bubble chamber, control by minicomputer *(French)* 77—3225
monitoring of 25 valve expansion system of 'Skat' chamber 77—6617
multiparticle nuclear fission expts., apparatus *(Russian)* 77—6640
multiprocessor system for nucl. event picture anal. *(Italian)* 80—69047
MWPC, external muon identifiers at CERN 78—37488
on-line display aid for bubble chamber film automatic meas. 78—5098
online analysis of large bubble chamber pictures, data acquisition system, CDC 1700 computer *(French)* 77—42223
photograph anal., auto-correlations with irregular signals, time series anal. 77—18767
photographic recording feed mechanism 78—78564
photographs analysis with PA-BESM-4 system, exchange apparatus 78—9045
photographs digitising machines, distributed computer system 78—5110
photoproduction experiments, use of laser beams 77—38521
picture digitisation system 79—63871
position sensitive detectors of high spatial resolution 79—76276
projection graphic display for computer aided image anal. 80—27895
propane, charge particle multiplicity and charge exchange at 40 GeV/c *(Russian)* 78—55118
propane, for investig. of inclusive reactions *(Slovak)* 77—42214

bubble chambers continued
  proportional delay line chambers for Fermilab external muon identifiers 78—37489
  rapid on-line spatial reconstruction, book contrib. 79—21890
  scanning machine for film 77—18737
  semi-automatic bubble matching method for tracks prod. in liquid hydrogen chambers 77—67941
  signal-processing procedure for inter-image identification of particle tracks in bubble chambers 78—70727
  SKAT, electromagnet, main parameters and magnetic field meas. 80—69022
  SKAT, for neutrino experiments 77—10535
  SKAT, housing and main structural components of propane-Freon chamber 80—69019
  SKAT, photoregistration system for propane-Freon chamber 80—69020
  SKAT, pressure changing system for propane-Freon chamber 80—69021
  spiral-meter system, automatic measurements of reference crosses on photographs 79—67403
  superconducting magnets appl. 80—68990
  superheated drop detector 79—72201
  target trajectory detection in multi-target environment, pattern recognition approach 79—26865
  track extraction using single vidicon tube 78—82580
  track following, predictor-corrector technique 78—90044
  track gap length distributions by PEPR 80—99420
  track rescue system for bubble chamber film meas. 78—70728
  track sensitive target expts., automatic film meas. 78—55105
  tube detectors, review *(Chinese)* 80—52830
  turbulence in bubble chamber fluid, optical distortion effect 77—3221
  turbulent convection diagnostics, using multiple laser beam probe system 77—27630
  ultrasonic bubble chambers *(Russian)* 77—67937
  zero prong events, geometrical and kinematical reconstruction routine 77—57847
  ZGS, 30" bubble chamber 80—91304
  ZGS, superconducting magnet bubble chambers, history 80—91368
  k^-p interaction in hydrogen bubble chamber, <300 MeV/c track sensitive target 80—13333
  π^-p elastic interactions, methodics of identification in bubble chamber *(Rumanian)* 79—63520
  H, MIRABELLE, monitoring by minicomputer *(French)* 77—10531
  H, two-meter type, Ludmila, for particle interaction investigs. *(Czech)* 77—42215
  H_2 bubble chamber, temp. and press. control 79—85860
  Ne-H_2 mixture, 2 m chamber, H_2 track sensitive target 77—396
  Ne+H_2 filled, with hydrogen track-sensing target 77—6616
  Ne+π^-, 25 and 50 GeV, multiplicity of charged particles 78—62575
bubble nuclei *see nuclear density*
bubble point *see boiling point*
bubble points *see bubbles*
bubbles
  see also foams
  accelerating bubble flow of gas-liquid mixture, phase slip 80—53838
  accelerating liquid, low Reynolds number bubble motion 77—19633
  acoustic counting, review 77—42673
  acoustic LF backscattering by wind-generated air bubbles undersea with large-scale roughness 79—86285
  acoustic vel. and absorpt. in liquids containing gas bubbles, effect of polymer additives 78—38779
  acoustical meas. of gas bubble volumes and gas flow rates 80—62633
  acoustics, insertion loss of a layer on a plate 80—96072
  acoustooptical effects in liquid containing gas bubbles 78—50994
  active nucleation site spatial distrib., bubble flow density 78—71267
  activity in acoustically excited spherical flask, obs. 78—42488
  with adsorbed film, migration in Hele-Shaw cell, rel. to materials processing in space 79—28912
  agarose gels, bubble prod., stabilisation by nonionic surfactants 80—76562
  ageing and bursting in trace-contaminated water, rise speeds 78—26184
  air, capture efficiency of n-decane emulsion drop 80—11956
  air, in water, critical angle scattering of light, physical-optics approx. and obs. 80—9797
  air, production of specified bubble size 78—9676
  air, rel. to water/air surface tension, effect of air diffusion and interface struct. 77—4246
  air bubble, in hydraulic oil, effect of diffusion on diameter change 78—90966
  air bubble, rising behaviour in superposed liquid layers 77—62294
  air bubble entrainment in self-aerated flow, channel or pipe flow 80—106832
  air bubble growth meas. by rectified diffusion at 22.1 kHz 80—96155
  air bubbles, rising in glycerine-water mixture, boundary surface velocity *(German)* 79—32631
  air bubbles entrained in channel flow, isotropic turbulence spectral struct. 78—34112
  air fluidised sand bed, large diameter, local bubble characts. obs. 77—58781
  air-bubble two dimens. plume, anal. 78—1715
  air-water, two-phase mixtures, vertical downward flow, void fraction 77—11235
  air-water bubbly flow struct. through vert. venturi 79—64749
  air-water bubbly mixtures, press. wave propag. *(French)* 78—22402
  air/water vertically downward slug flow distrib., bubble vel. meas. 77—51108
  airfoil, leading-edge separation bubbles, shear layer and transitional reattaching flow 77—27580
  airfoil, oscillating, unsteady leading edge separation bubble calc., using finite difference procedure 77—72317
  alloy, vapour bubble growth dynamics, electron-beam vol. heat source 77—47565
  amino acid-quinone complexes, surface bubble form. during SEM obs. 77—15450
  amino acids, surface bubble form. during SEM obs. 77—15450
  axial piston pump, suction performance 78—8389
  barbotage bubble, liquid flow patterns 77—58770
  binary mixture, nucleate boiling, bubble growth, saturation press.-temp. relation 77—46892
  Bingham fluids, single bubble motion and mass transfer 79—50758
  blister formation in He^+-implanted glass, effects of gas diffusivity 77—35604

bubbles continued
  blistering in Al, Cu, Si, by plasma focus discharge deuterons, plasma diagnostics 77—35351
  blistering of barium aluminosilicate glass coating on NbZr, d and He ion irrad. 77—35605
  blistering of brittle materials by p, d and He ion bombardment 77—35603
  blood, gas bubbles, behaviour when subjected to oscill. press. 80—97984
  blood, spectral anal. of Doppler US decompression data 77—70513
  blood, volume expansion effects, gas cavities 80—67134
  blood oxygenator, O_2 transfer controlling factors 78—53568
  blood supersaturation by counterperfusion and diffusion of inert gases 77—90829
  blood vessel bubble detection and flow evaluation 79—34612
  boiling, bubble departure, diameter and frequency 80—38481
  boiling, bubble departure frequency, effect of superheat and cavity size 77—80610
  boiling, bubble growth at superheated horizontal wall, pure liq. and binary mixtures 79—41719
  boiling, calc. of initial microlayer thickness 77—11248
  boiling, non-stationary heat transfer crisis *(Russian)* 77—24401
  boiling, nucleate, subcooled, latent heat transport contrib. 78—75046
  boiling, nucleate pool, influence of surface conditions, bubble flux density 79—55379
  boiling, nucleate type, boiling acoustic emission and bubble dynamics 77—46893
  boiling, nucleation centres interaction, obs. technique 78—14065
  boiling, of liq. film, bubble nucleation and venting 78—30153
  boiling, Reynolds analogy, heat transfer 78—59277
  boiling, under increased gravitation, heat exchange mechanism, bubble form., review 77—46895
  boiling and bubbling heat transfer under the conditions of free and forced convection 78—90637
  boiling at surface near peak heat flux, mechanism 77—75780
  boiling in large volume at cylindrical and spherical surfaces, max. crit. heat flux 77—11188
  boiling in steam generating pipe with Fe oxide deposits on wall, steam bubble growth 79—76947
  boiling mechanism during burnout phenomena in subcooled two-phase water flows 78—94529
  boiling process, heater vibration effects 77—55355
  boiling under reduced gravity conditions, vapour bubble departure 77—4192
  boundary layer formation over inclined porous plate 80—19504
  brain injury and instabilities 80—45943
  break-up in stagnant fluids 78—75182
  breakdown of liquid insulators 80—71313
  bubble and droplet-type contactors, wake shedding 79—4060
  bubble of gas rising in fluid filled tube, wall effects *(French)* 79—7399
  bubble rising in pipe, upward flowing liq. 79—32676
  bubble swarm behaviour and gas absorption in non-Newtonian fluids in sparged columns 79—4061
  bubbly, droplet and particulate flows, drag coeff. and relative vel. relations 80—24072
  bubbly flow, wall press. fluctuations in turbulent boundary layer 77—58776
  bubbly flows, simultaneous meas. of local liq. vel. and void fraction using gas laser *(Japanese)* 77—42947
  bubbly flows, simultaneous meas. of local liquid vel. and void fraction by gas laser, accuracy *(Japanese)* 78—67295
  bubbly liquids, acoustic wave propag. 79—90067
  bubbly mixtures, shock wave form. by compression wave steepening 78—38390
  buoyant bubble demonstration 79—30180
  butane drops, nucleation in flowing water 79—1099
  BWR, air clearing in H_2O-type press. suppression systems, scaling laws 79—54563
  BWR, air clearing in H_2O-type press. suppression systems, scaling laws 79—54564
  BWR, coupled vibrations of a structure and fluid excited by pressure shocks 80—13546
  BWR, void fraction profile determ. by neutron noise anal. 78—46150
  BWR steam discharge piping, acceleration forces exerted on finite cylinders by an oscillating air bubble 80—18503
  capillary waves, progressive, periodic, finite-amplitude 80—79339
  capillary-gravity waves, exact eqn. numerical soln., closed bubbles 80—14715
  Casson fluid, gas bubble motion, behaviour, appl. to bubble in blood stream 79—10605
  cavitating bubble model, numerical soln. 78—79347
  cavitating orifice under reattached flow conditions, noise and vibration characteristics 80—83829
  cavitation, acoustic, threshold conditions for onset 78—59433
  cavitation, acoustic field generated, review 80—74934
  cavitation, free gas content in liquids *(Italian)* 78—22389
  cavitation, free gas content in water, variations during press. fluctuations *(French)* 78—22390
  cavitation bubble, in magnetisable fluid, mag. field and press. effects on shape *(Russian)* 77—27608
  cavitation bubble collapse, num. simulation 77—58747
  cavitation bubble collapse, shadowgraph study 80—48827
  cavitation bubble collapse in water shock tube 78—67231
  cavitation bubble dynamics recording using laser holocinematography 79—86147
  cavitation bubble in liquids with polymer additives, small pulsations 77—68647
  cavitation bubbles, amplitude distrib. of pulses produced by shock waves 80—64252
  cavitation bubbles, appl. of HF holography with ruby laser *(German)* 77—75437
  cavitation bubbles, forced oscills. rel. to noise subharmonic component 77—14851
  cavitation bubbles, linear stability of growth or collapse, slightly viscous liquid 78—90947
  cavitation bubbles in US field, conc. kinetics 77—15085
  cavitation bubbles in water, elec. pulses production 79—47407
  cavitation cloud development *(French)* 78—22388
  cavitation erosion, non-spherical bubble collapse near a solid wall, analytical soln. using matched asymptotic expansions 80—106824
  cavitation gas bubble in compressible liquid, influence of inhomogeneous sound field on motion 80—6131

bubbles continued
cavitation in inviscid compressible liq. 80—28553
cavitation nuclei, radii determ. by filtering gelatin 79—81612
cavitation nuclei stabilization using skins of varying permeability 79—81611
cavitation of deformed ellipsoid bubble near wall, cumulative jet form. 77—934
cavitation shock pressures in venturi, 10 kHz-1 MHz 77—24002
cavitation-produced stress in solid, rel. to erosion and deform 77—24354
chain motion in liquid, terminal velocities 78—9692
chamber-orifice interaction in bubble formation 77—89185
characteristics in three phase fluidised beds 78—9680
charged particle beams in liqs., elastic wave excitation, microscopic bubble acoustic emission 80—43516
cholesteric liquid crystal, bubble domain texture, obs. of forming process 78—26431
cloudy bubble formation in strong nonuniform elec. field 80—53842
coalescence and breakup, in liquids 77—62293
coalescence rate, ambient liq. viscoelasticity effect 78—67248
coalescence time in close-packed dispersion during thin-film drainage 79—86486
collapse and expansion of underwater gas bubbles, surface tension effects 77—42880
collapse and fluid struct. interaction in BWR loss of coolant accidents 80—689
collapse in liq. during laser-induced breakdown 77—89171
collapse in liquid, pressure wave, nonequilib. vapour condensation effects 80—59060
collapsing bubble attached to solid wall 79—68791
collapsing near free surface, cavitation 78—47026
columns, axial dispersion coeffs. rel. to column diameter, gas flow, fluid props. 77—3861
columns, large diameter, liq. phase duration *(German)* 79—32632
compressible liquid, bubble deformation in electric field 80—64618
condensation, in subcooled liquid, high-speed photographic study 78—42654
condenser system, submerged, buble pumped augmented natural convection 78—94535
conical crossflow sonic line, flow patterns and bubble props. 80—69862
contact angle of bubble enclosed between parallel flat horizontal walls *(German)* 77—66071
convective heat and mass exchange, Pe$\leq$1000, in power-law liq. 78—55683
creeping flow, in cloud of round drops of arbitrary size distribution 78—9677
critical two-phase flow, bubble nuclei 80—64615
cryogenic fluid, boiling, vapour bubble growth rate 77—24397
cryogenic fluid, boiling, vapour bubble growth rate 77—24398
cryogenic liquid, bubble population density meas. on immersed heated surface 77—30169
cryogenic liquid, pool boiling heat transfer, vapour bubble dynamics 77—31765
crystal growth, cylindrical pores growth, numerical calcs. 80—92471
decompression of animals and man, quantification of bubbles formed, US system 80—76869
decompression sickness, bubble detection by US imaging 79—8527
decompression studies using ultrasonic imaging of bubbles 79—11988
detachment from wall, zero and negative gravity 77—3863
detachment size during quasistatic growth on heater surface 77—84120
detection in insulating liquid flow, using spiral delay line 80—79415
dielectric liquid, bubble creation in high elec. fields, explained in terms of struct. 79—91370
diffusion coefficient in liquid, determination in bubble column by method of stationary dissolving sample 77—51529
diffusion in turbulent flow 78—22412
diffusion of bubbles in two-phase flow 78—18332
diffusion of rare gases of solar wind origin from lunar fines as bubbles 79—48695
diffusion to chain of bubbles at large Peclet numbers 79—86489
distribution, eruption diam. in fluidised bed with horizontal tube bundle 80—14781
distribution and size of intragranular fission gas bubbles in irrad. UO_2 nuclear fuels 80—57840
drift flux field eqns. for churn turbulent bubble flow 78—94807
ducts, one-dimensional models for transient gas-liquid flows 80—64614
Dynamic fluid interface displacement and prediction of air entrainment 78—2337
dynamic surface tension of solns. measurement, maximal pressure in bubble method 80—10744
dynamic two-phase layer, heat exchange and mass transfer coeffs. of flat element 77—7439
dynamics, book contrib. 77—47050
dynamics and dissolution of bubbles in viscoelastic fluid 78—90970
dynamics in fluid, laser schlieren meas. 79—41773
dynamics in oscillating fluids 80—38483
dynamics of gas and vapour bubbles, review 79—98788
eccentric spherical fluid shell, heat and mass transfer at large Peclet number 77—27520
education, bubble cohesion in foam, binding energy calc. 78—61978
electrostatically charged bubbles for warm fog dispersal 78—20546
ethane, flow continuity in arterial capillary systems in cryogenic heat pipes 80—64536
ethanol, aq. subcooled soln., acoustic phenomena during nucleate boiling 78—10181
ethyl ether, nucleation press. for bubble form., dissolved N_2 effect 77—51486
ethyl ether-N_2, bubble homogeneous nucleation in gas-liq. soln., press., expt. and theory 78—91430
evaporating, surface condensation of vapours of high boiling substance 80—59021
evaporating droplets in immiscible liquid, comments 80—19482
evolving bubble method using crit. size concept. diffusion coeff. meas. of gases in liqs. 80—4828
expanding vapour bubble, anal. of reactive forces exerted by evaporating molecules 78—1548
expansion and collapse, heat conduction moving boundary problems, collocation method using B-splines 77—7288
exploding wire produced, underwater, in closed chamber, air effect *(Japanese)* 78—22596
FBR, energy increase from bubble collapse following recriticality in large molten pools 79—31023

bubbles continued
FBR, void reactivity effects on hypothetical core disruptive accident excursion energy 79—31024
fibre reinforced polymer, soaking, wetting and compounding of materials during production *(German)* 80—93535
fission gas, steady state behaviour in carbide fuels, modelling 78—78469
fission gas, transfer between grain faces and edges in UO_2 78—79815
fission gas behaviour in fast reactor fuel, model, steady state and transient conditions 77—67809
fission gas bubble, equilib. index 78—17368
fission gas bubble, molten fuel mechanism for slow overpower transient 78—17369
fission gas bubble distribs. in mixed oxide fast reactor fuel pin, anal. of TEM obs. 78—58358
fission gas bubble mobility in UO_2 80—91222
fission gas bubbles, model of response to dynamic behaviour of U point defects in $UO_{2\pm x}$ 79—37735
fission gas bubbles, nonequilibrium, relaxation times 77—46239
fission gas bubbles, nonequilibrium intragranular, role during transient heating of fuel 79—6740
fission gas re-solution, comparison of single knock on and complete bubble destruction models 78—82455
fission reactor carbide fuels, effect of burn-up and temp. on appearance of optically visible fission gas bubbles 80—63251
fission reactor mixed oxide fuels, SEM obs. of gas bubble morphology 80—57843
flashing adiabatic flows, calc. taking into account bubble separation freq. variation under forced flow 78—67258
flotation, thin film capillary hydrodynamic theory 79—56038
flotation of fine particles by group of bubbles, kinetics 78—53261
flotation of small particles, capture by bubble, theory 80—11959
flow, gas-liq., hot-film anemometer signal anal. method 79—32639
flow, hydrodynamic eqns. formulation 77—68682
flow, separated incompressible boundary layer prediction, including viscous-inviscid interaction 80—1548
flow boiling bubble population prediction, from gas bubble nucleation expts. 78—90696
flow film boiling, void fraction meas. 80—92207
flow of gas-liquid system accelerating in nozzle, slipping of phases *(Russian)* 77—35202
flow produced by uniform translation along cylinder vertical axis *(French)* 78—90967
flow visualisation in wind tunnel, appl. bubbles around bluff body 77—80238
flow visualisation techniques eval. for liquids 77—58817
flowing viscoelastic fluid, bubble and solid particle separation through apertures *(German)* 79—37389
fluid spheres, touching, motion along line of centres 79—4071
fluid-solid boundary, cavitation by incident P-wave, bubbles 80—6107
fluidisation research review 77—24022
fluidised bed, bubble detection by light probe 78—30376
fluidised bed, bubble size prediction, math. models exam. 80—6135
fluidised bed, conc. profile for mass transfer, appl. Kunii-Levenspiel model 77—11256
fluidised bed, fluidisation uniformity, disturbance criterion with uniform coding medium flow distrib. 80—43772
fluidised bed, gas-fluidised, flow distrib. between phases analysis 80—14804
fluidised bed, heat exchange intensification using bubble motion control 79—86508
fluidised bed, heat transfer from transverse streamlined cylinder during surface boiling 80—43708
fluidised bed, inhomogeneous, gas bubble growth, expt. and model 78—1739
fluidised bed, jet and bubble formation 77—84318
fluidised bed, large scale, gas backmixing, solids movement, bubble activities 78—30349
fluidised bed, low Reynolds number anal. 77—11255
fluidised bed, nonuniform, force on fixed sphere, rising gas bubble force field 78—59476
fluidised bed, three-phase, bubble wake solids content 78—42660
fluidised bed at 20 to 300°C, bubble sizes 77—943
fluidised bed bubble observation using probes and X-rays 80—79379
fluidised bed measurement, optical probe design 79—82000
fluidised bed probing using optical fibres 80—19533
fluidised bed reactors, gas flow, anal. 79—94703
fluidised beds, instability waves and bubble origin, two-fluid eqns. 80—92205
fluidised beds, rise velocities of 2-D and 3-D gas bubbles 80—64610
fluidised beds, screen-packed, bubble props. 77—31372
fluidised beds, theoretical bounding relations, for bubble void fraction 80—96296
foam, interbubble gas diffusion, effect of initial bubble size distribution 79—79304
foam stability relation to structure, criteria derivation w.r.t. drainage stage 80—69904
form in potential flow 79—86490
formation by action of focused laser radiation *(German)* 77—42882
formation during gas injection into liq. through orifice, interfacial area, press. *(German)* 79—18937
formation in flowing liq. 79—64741
free gas concentration in liquids, rapid anal. by acoustic method 78—91041
free motion transition criteria for single bubbles and drops 80—64605
free oscillation of bubble in viscous liquid 77—51105
fusion reactor metals and alloys, microvoid form., gaseous impurity atom effects, positron annihilation study 80—49275
gas, absorption into turbulent liq. jet *(Japanese)* 80—38473
gas, capture by cryst. growing from melt, thermal cond. influence 78—79543
gas, free liquid surface oscills. 80—100025
gas, growth during neutron irradiation, effect of stress 80—49277
gas, growth in solids under irradiation 80—2009
gas, in dielec. liq., dielectrophoresis 77—56233
gas, in ion irradiated Cu, electron microscopy contrast *(German)* 79—99253
gas, in metals, light element implantation, radiation damage review 80—88219
gas, in neutron irradiated Zr-B alloys, swelling study *(Russian)* 79—60404

bubbles continued
- gas, motion in rotating liquid under simulated low and zero gravity 77—55071
- gas, nonlinear response to multi-freq. acoustic excitation 80—38480
- gas, oscillating in liquid, modification by nearby objects, comment 79—90064
- gas, radiation blistering in metals, developments, review 80—44239
- gas *(German)* 79—32630
- gas and vapour bubbles in gas/liquid solutions, growth and collapse *(Italian)* 78—22403
- gas atoms per bubble of inert gas in solid 77—76468
- gas bubble, growth or dissolution, general soln., analyticity 80—10747
- gas bubble, rise and cooling in viscous fluid *(Russian)* 80—74949
- gas bubble adhesion to heat transfer surfaces 79—89375
- gas bubble cloud motion in impulsively accelerated liquid 77—941
- gas bubble collapse in viscoelastic fluid, elongational flow 78—14060
- gas bubble collapse in viscoelastic fluid, elongational flow and viscosity 78—14061
- gas bubble detection recording and measuring system with nanolitre resolution for use in liquid environment 78—31739
- gas bubble diffusion mobility in solids, radius depend. 80—39357
- gas bubble dissolution (growth), convective transport effect 80—87792
- gas bubble dynamics and acoustic props. of gas-bearing sediments 80—87630
- gas bubble dynamics in turbulent jet 79—41741
- gas bubble form. synchronised with AC pot. 80—24080
- gas bubble growth in over-saturated liquid-gas soln. 78—1733
- gas bubble in acoustic field, effect of diffusion on evolution, stability 77—15105
- gas bubble in very low viscosity liquid, terminal velocity *(French)* 80—14795
- gas bubble kinematics under strong acoustic wave press. in liq. *(Russian)* 79—94708
- gas bubble motion in a liquid medium *(French)* 79—98785
- gas bubble motion in power-law fluid, heat and mass transfer with chemical reaction 79—77227
- gas bubble plumes in stratified environments, vertical fluid transport, double plume model 78—47019
- gas bubble suspensions, incompressible nonNewtonian and Newtonian fluids, dilatational props. 78—30343
- gas bubble-liquid system, shock wave refl. 79—81952
- gas bubble-liquid system, struct. of weak shock waves 79—86492
- gas bubble-water mixture with polymer additive, shock wave propag. 78—47021
- gas bubbles, dissolution in liquid, theoretical and expt. obs. 77—15097
- gas bubbles, effect of backscattered acoustic wave on bubble oscillation 79—1021
- gas bubbles, flow and temp. fields, global collocation calcs. 77—47067
- gas bubbles, on liq. surface, bursting, jet and droplet form., math. model *(German)* 77—24012
- gas bubbles, thermal effects and damping mechanisms in forced radial oscills. 77—31375
- gas bubbles at crystallisation front when growing crystals from melt, formation and capture 78—9980
- gas bubbles dissolving in liq. 79—90319
- gas bubbles in fluids, dynamics of acoustic resonance scattering 80—10068
- gas bubbles in liq., controlled vibratory movement under near-zero gravity conditions 78—14119
- gas bubbles in low-viscosity liquids, US attenuation 80—58849
- gas bubbles in metals, trends in modern anal. *(Russian)* 80—15123
- gas bubbles in solids, simultaneous hetero- and homogeneous nucleation model 80—2066
- gas bubbles in vibr. liquid, selective drift in reln. to their size 79—77225
- gas bubbles in vibrating liq., localisation and translational motion *(Russian)* 79—14455
- gas bubbles in vibrating liq., selective bubble drift *(Russian)* 79—14456
- gas bubbling through porous media, liq. repulsion effect 77—58784
- gas emitting from liquid, model *(Russian)* 78—26187
- gas fluidised bed, bubble induced heat transfer 77—7435
- gas fluidised beds, bubble formation 77—39339
- gas holdup, in liq. columns with freely ascending bubbles *(French)* 77—65781
- gas in Ar^+ irradiated Cu foil, electron microscopy study *(German)* 80—2087
- of gas in liquid, unresonance absorpt. of acoustic waves *(Russian)* 78—14404
- gas injection into liquid through porous plate, squeezing out of liq. 80—64622
- gas jet-liquid bath interaction for different degrees of assimilation during blowing 80—43754
- gas sparged devices for viscous liq. systems, design, bubble size 78—83454
- gas-bearing water-saturated sediment, sound vel. as function of bubble distrib. 79—39703
- gas-bubble entrapment in Czochralski-grown oxide crysts., fluid-flow effect 80—84121
- gas-liquid ascending flow, monodispersed, funciton stress on wall, bubble size effect 80—59098
- gas-liquid bed, flow props. and bubble vel. determ. method and instrument 77—72374
- gas-liquid flow, bubble size and density, void fraction, sifting method meas. *(Japanese)* 78—83462
- gas-liquid flow in tubes, bubble rise and liq. holdup 79—4059
- gas-liquid interface of rising bubbles, adsorption rate determ. *(Japanese)* 80—6595
- gas-liquid medium, standing waves 78—9474
- gas-liquid mixture, acoustic disturbance propag. 78—9473
- gas-liquid mixture, bubble mode of flow in vertical pipe 80—24081
- gas-liquid pipe flow, influence of return bends on velocity ratio 80—74962
- gas-liquid systems, vibs. stabilisation of dynamic equilib. and mixing *(Ukrainian)* 80—10291
- gas-liquid two-phase bubbles in immiscible liq. media, configs. 79—4068
- gas-liquid upward flow in granular layer, hydrodynamic conditions 78—34188
- gas-liquid-suspended solid flow, multistage bubble column, residence time 77—84304
- gas-particulate fluidised beds, bubble formation and shock front 79—90318
- gas-solid fluidisation, solid pot. flow around rising bubbles 79—86501

bubbles continued
- gaseous microbubble growth in laminar separation bubbles 80—106821
- gassy two-liq. pool., hollow sphere formation, LMFBR simulation 77—61518
- gel, gas cavitation nuclei, physical props. of surrounding nonionic surfactants 79—100444
- gelatin, bubble formation, model for decompression sickness 77—13051
- generating apparatus for single bubbles, motion in water *(Korean)* 79—23387
- generation at aperture in submerged surface and associated pressure pulses in liquid *(Russian)* 77—68650
- geodetic surveying with bubble levels, apparatus for testing bubble vials 79—29871
- giant monopole resonances in the scattering of waves from gas-filled spherical cavities and bubbles 79—50476
- glacier structure and flow rel. to elongated air bubbles in ice *(Japanese)* 78—88861
- in glass, form., condensate trace quantities determ., spectral anal. techniques *(Russian)* 77—36852
- glass, glass surface, inhomogeneities and defects, detection using microbubbles, implantation technique *(German)* 78—47647
- glass, melt, bubble behaviour during refining, math. model 80—81277
- glass bubble, gas anal. using chromatograph 77—52694
- glass edge cladding-glass laser disc interface, reflection meas. 79—27300
- glass melt, multibubble dissolution 80—81371
- glass microbubbles, method for polishing bubbles into hemispheres 78—95869
- granular layer, bubble coalescence for jet injection under constrained flow conditions 77—89197
- graphite, pyrolytic, numerical discussion of flaking mechanism from ion bombard. 78—52947
- growing bubbles on heated plate, meas. using computerised image anal. system 80—22322
- growth, inertia and diffusion controlled, implosion pure and binary systems 78—1552
- growth, noncondensing gas-vap. injected into liquid 78—55553
- growth and breakoff, two-dimensional and axisymmetric problem 80—48783
- growth and collapse, dilute polymer soln. effects in unbounded and bounded flow 79—81956
- growth and condensation in pure and binary systems 79—23191
- growth and decay, moment and Fokker-Planck eqns. 80—82709
- growth by expansion and dissolution in variable pressure field 78—15723
- growth dynamics, isothermal, gas bubble in liq. 79—14459
- growth in fluidised bed with nonlinear interphase interaction 79—68798
- growth in fluidised beds, due to coalescence, theory 78—26191
- growth in magnetic field 77—7462
- growth in slow formation regime of nucleate pool boiling 78—90687
- growth in variable press. fields 79—32215
- growth modulus at BP, arbitrary radius time depend., theoretical expression 77—46894
- growth of vapour bubble in combined gravitational and non-uniform temp. fields 78—22249
- growth on heating surfaces in pool boiling, conservation eqns. soln. *(German)* 80—74715
- growth rate, during electrolysis in supersaturated liq. 80—61104
- HCDA, radiological consequences, attenuation due to radiative cooling 78—13296
- heart-lung machine blood flow line gas bubble US detector 77—77954
- heat conduction, unsteady, in quarter plane, appl. to bubble growth 78—75045
- heat exchange between bubble and liquid, Nusselt number *(Russian)* 77—35224
- heat transfer between a dispersed system and a vertical heating or cooling surface 79—1069
- heat transfer controlled collapse in isothermal tube 78—90979
- heated air, ascending bubbles, interaction with ambient cold air 79—84362
- Hele Shaw flow with horizontal temp. gradient, slow bubble motion 80—28549
- Hele-Shaw cell, bubble motion, study of 2 phase flows under reduced gravity 79—14457
- hollow drop production by injection of gas bubbles into liquid jet and US excitation 78—1710
- holocinematography, high-speed, of cavitation bubbles 78—37841
- homogeneous nucleation in gas-liq. soln., press., expt. and theory 78—91430
- horizontal tube transition and flow boiling heat transfer, bubble flow 78—18292
- hydrodynamic interaction with suspended solid particle, flotation dynamics 78—51221
- ice crystallisation front movement, water and gas bubble distrib. 78—22830
- ice sheet deflection by submerged gas source 77—80120
- ice-covered lakes (North Slope, Alaska), air bubbles rel. to radar return differences 79—2298
- icicle crystallisation phenomenon, growth mechanism, structure and shape 80—59423
- ideal incompressible liquid, streaming generated by oscillations of a sphere 77—31412
- implosion of cavitation bubble, near solid boundary or free surface *(French)* 77—55056
- incompressible separated boundary layers including viscous-inviscid interaction, transition bubble 80—64515
- induced mass coeff. of single bubble in bubble system 80—53839
- inert gas, in liq. metal, bubble dynamics, simplified model 77—15098
- inhomogeneous fluidised layer in reactor, 2-point boundary value problem, asymptotic anal. 80—33654
- injection bubbling and boiling in liqs., heat transfer 77—68672
- insulating liquid, small air bubble formation, under strong nonuniform electric field 79—46373
- interconnected bubble system, equilib. states, for teachers 79—15
- interphase mass transfer in fluidised bed 79—7405
- inviscid liquid, spherically oscillating, force acting on particle and bubble 77—35222
- ion bombardment, electron microscopical anal. of surface effects and volume defects, review *(Rumanian)* 80—29093
- jet discharge into fluidised bed, bubble form. and growth 77—47084
- jet droplets from bursting bubbles at air/water interface, electrification and size 77—48700

bubbles continued
jet drops from bubbles bursting in seawater, ejection height rel. to organic material 79—39727
jet impinging on liq. pool, submerged biphasic region 77—31350
K_2O-PbO-SnO_2, glass, effect of DC on corrosion of SnO_2 electrodes 80—85075
kinetic energy of particles in fluidised bed rel. to bubbling phenomena, theoretical anal. *(Russian)* 80—74965
Lagrangian hydrodynamics meshes, discrete rezoning algorithm, hot interacting bubbles calcs. 78—42628
laminar boundary layer with separated bubble 77—23935
laminar bubble separation, stalling, lecture 78—22325
laminar separation bubbles, airfoil performance effects, turbulent shear layer reattachment 80—48774
laser breakdown of liquid, dynamics of growth and pulsations 78—51226
laser induced breakdown, high speed holography 78—18360
law of metastability, appl. to effect of mag. field on boiling liqs. 78—79199
leading edge bubble formation, peaky airfoil *(French)* 80—64524
light transmission in bubble swarms 77—79749
liquid, boiling at wall, nucleation, influence of dissolved gases 77—76537
liquid, bubbly, choking phenomena in nozzle flows 77—62300
liquid, bubbly, nozzle flow based on Wijngaarden's model 78—26182
liquid, positronium pick-off annihilation, improved bubble model 80—93424
liquid, spontaneously evaporating, critical discharge from channel 78—59456
liquid and spherical particle permittivity meas. by dielectrophoretic levitation 79—17447
liquid boiling wave processes at heat releasing surfaces 79—90773
liquid cavitation and droplet impact erosion, predictability of prototype machine from lab. tests 78—64723
liquid containing gas bubbles, struct. of supersonic waves and cavitation development 80—33643
liquid crystals, bubble domains *(Japanese)* 78—22413
liquid excited by spherical acoustic radiator, bubble dynamics 77—68679
liquid film, formation and thinning 80—39391
liquid film, hydrodynamics, three-phase contact, perimeter expansion rate, theory 78—22937
liquid layer, gas bubble formation dynamics 80—24083
liquid metal boiling, mag. field effect on bubble growth 79—32217
liquid metal fragmentation following reactor core meltdown accident, contribution of collapsing vapour bubbles 80—755
liquid metal gas inclusions, bubble release dynamics, mag. field effects *(Russian)* 77—3865
liquid with absorbing particles, laser beam illum., refr. index change, bubbles form. 80—25334
liquid with bubbles, small perturbations propag. 78—42651
liquid with gas bubbles, acoustic wave self-transparency effect *(Russian)* 80—14509
liquid with gas bubbles, steady-state perturbations, wave propag. 78—5788
liquid-gas bubble mixtures, shock wave disturbances 78—22411
liquid-gas bubbles system, phase transition kinetics and kinetic eqns. 78—83933
liquid-to-gas surface, dynamic behaviour in near weightlessness *(Russian)* 77—68611
liquid-vapour critical flow, two-fluid model 78—90973
liquid-vapour mixture, acoustic wave propag. 78—90972
liquids with gas bubbles, struct. of pressure pulses 80—38479
LMFBR, boiling pools with internal heat generation, void distrib. 78—21626
LMFBR, bubble collapse reactivity increases in boiling fuel/steel pools 79—31025
LMFBR, condensation from large HCDA vapour-gas bubble onto structures 79—93774
LMFBR, effects on noncondensable gas bubbles on propag. of boiling acoustic noise 77—46364
LMFBR, reactivity variations ass. with randomly distributed bubbles in molten core 77—46331
LMFBR, unified model for fission gas release and Na boiling in reactor coolant channel 78—8921
LMFBR advanced MX-type fuels, low-temp. microscopic swelling, phenomenological model 80—57851
LMFBR core, stochastic void models for bubble worth calcs. 80—22940
LMFBR core disruptive accident, effect of internal circulation vel. and noncondensible gas on vapour condensation from rising bubble 79—31017
LMFBR HCDA, energetics of bubble expansions, potential attenuation mech. 80—83197
LMFBR steam generators, leak detection of water into sodium, magnetic flowmeter bubble noise monitor 80—9000
LMFBR transient fission gas behaviour modelling, bubble equilibration effects FRAS 2 code 79—59168
Loch Ness, bubble clouds in freshwater lake, detect. by acoustic refl. 79—66722
low velocity vertical steam-water flow, void fraction in pipes 80—74964
magnetic flowmeters, bubble noise effects on output signal, Na loop test 78—91038
magnetoelectric composite, growth from melt, gas bubble form. ahead of solidification front 79—29044
marine seismograms, source signatures debubbling 79—16692
mass exchange for spherical particle in flow at high Peclet numbers and $Re \leq 100$ 77—54988
MBBA-cholesteryl chloride mixture, liq. cryst., bubble domain texture, obs. of interference fringes 79—23520
metal, interbubble fracture mech. of blister form., He irrad. 78—6109
metal-Si system, ion implanted, inert-gas-bubble form., TEM and Rutherford backscatt. anal. 79—90682
microorganisms, lack of intracellular bubble formation at very high gas supersaturations 80—81562
microscopic film, with deformable interface, rate of thinning, calcs. 78—43220
microstreaming influence on growth due to rectified diffusion in sound field 78—51232
mixture, binary, nucleate boiling heat transfer, conc. depend. 78—87249
molten metal cavitational bubble collapse and erosion intensity in constant mag. field *(Russian)* 80—60987
motion close to solid wall, surfactant effect 79—81954
motion in a viscous liquid 78—34190

bubbles continued
motion in immiscible liquid, and bubble-droplets, photographic obs. method *(German)* 79—72931
motion in rotating liquid under residual gravity 78—55679
motion in vertical temp. gradient, buoyancy and Marangoni forces 79—46372
motion of bubbles with adsorbed films through a viscous fluid in low-gravity environments 79—18933
motion through liquid under reduced gravity 77—51100
motion under gravity in rotating fluid, differential equations of motion *(German)* 78—90918
multiphase media, dynamic behaviour of bubbles under vibr. in weak gravitational field *(Russian)* 79—77226
negative wake behind bubbles in non-Newtonian liquids 79—64716
Newton black film, line tension, determ. by cnt. bubble method 80—88406
Newton black films, line tension determ. by diminishing bubble method 80—88407
Newtonian medium, change in volume of gas-filled cavity *(Russian)* 77—80199
non-Newtonian fluid, gas bubble form. at single submerged orifice, model 79—32640
non-Newtonian liquid flow from nozzle, bubble form. 79—23356
non-Newtonian liquids, spherical gas inclusion radius change Rayleigh classical equation generalisation 80—19444
non-Newtonian medium, bubble motion and deformation, drag coeffs. 77—89184
nonequilibrium collapse, heat transfer effects 79—98794
nonequilibrium fission bubble behaviour during fast transients in oxide fuel 78—8916
nonhemispherical, attached to solid wall, collapse motion, numerical-variational soln. 77—51103
nonlinear acoustic disturbances in liquid containing gas bubbles 80—59104
nonlinear oscillating gas bubble in compressible liquid, translational motion in an inhomogeneous sound field *(German)* 80—53495
nonNewtonian lubricant, bubble behaviour 78—56786
nonspherical, forced oscillations 80—33663
nonstationary velocity tracking by adaptive cross-correl. algorithm 78—14074
nuclear fuel, gas release and swelling, operational model, grain boundary gas 80—95346
nuclear fuel pin failure, pressure in duct due to gas discharge 78—675
nuclear fuels, fission gas precipitation into intra- and intergranular porosity, theory 80—57849
nuclear oxide fuel element in fast overpower transient, effect of solid fission products and dislocations 80—623
nuclear reactor, LMFBR, HCDA, Eulerian computer code anal., primary system response 77—3127
nuclear reactor fuel, transient fission gas behaviour, exptl. and analytical results 79—59190
nuclear reactor fuel transient heating conditions, mobility of fission gas bubbles 79—59189
nuclear reactor safety analysis, void fraction prediction, depressurization of diabatic systems 77—23222
nuclear reactor transient fuel behaviour, modelling of grain boundary fission gas effects 79—59169
nuclear reactor transit time estimation coolant bubbles appl. 78—94067
nucleate boiling, anal. of microlayer thicness 79—77234
nucleate boiling, single bubble growth at wall, shape and departure 78—90647
nucleate boiling bubble dynamics, calc. 78—90648
nucleate boiling heat transfer, bubble population density correl. 77—27525
nucleate boiling heat transfer, nucleation factor 77—69079
nucleate pool boiling, meas. of void frequency distribs. and profiles using neutron beams 80—27691
nucleate pool boiling 78—38174
nucleation, theoretical experimental review 79—41734
nucleation in oscill. press. field 79—32216
ocean, particular trace metals transport by bubbles 79—57940
ocean and lake waves breaking to form subsurface bubble cloud 80—46185
ocean microbubbles, in situ acoustic meas. 77—37207
ocean upper layer, conc. and size distrib. of wind-produced air bubbles 77—17143
optic cavitation and laser-produced bubbles 80—38463
oscillating gas bubbles, appl. of subharmonic threshold to damping meas. 77—31374
oscillating vapour, evaporation-condensation resonance frequency 80—19488
oscillating vessel with liquid containing compressible sphere, finely disperse inclusion motion 80—74963
oscillations in viscoelastic liq. 77—80202
oscillations of large amplitude for bubbles in fluid of infinite extent 80—96298
oscillations of spherical bubbles damped by acoustic radiation 80—33664
oxide fuel, effect of solid fission products and dislocations on swelling and fission gas release during fast overpower transient 78—8917
oxide nuclear fuel, fission gas release and swelling, simple operational model 80—92565
oxygenator, bubble, blood damage test standardisation *(German)* 79—2158
packed bubble columns, holdup profiles, elec. cond. meas. 77—35201
paraffin drop striking solid plane, microscopic flow regimes, trapped air bubbles obs. 80—53843
plasma bubbles and irregularities in equatorial ionosphere 77—87156
plate, thick, parallel flow, with separation and reattachment, local and average mass transfer *(German)* 78—22339
polybutene oil, rel. to elec. breakdown 79—91360
polymer additive effects on sound propag. in water containing bubbles 77—50810
polymer melts bubbles formation, non-coalescing bubbles theory appl. 78—42640
polymer solns., vap. bubble growth from gas nuclei, viscoelasticity effect 77—89172
polymer solution, bubble collapse calcs. 77—933
polymer solution, bubble elongation dynamics, modelling with viscoelastic constitutive relations 79—37388
polymer solution, Denn model 78—79343

bubbles continued
- polymer solution, dilute, oscillating spherical bubble, natural freq., theoretical study 77—24017
- polymer solution, second-order fluid model 78—79344
- polymer solutions, bubble behaviour in pulsating pressure, natural freqs. 80—64591
- polymeric liquid, viscoelastic, gas bubble pulsations and assoc. dissipation effects 80—59079
- polystyrene lattices, electro-flotation, collection efficiency 80—74946
- pool barbotage, heat transfer coeffs., high-speed cine-photography and oscillography 78—90982
- powders, air fluidisation, bubbling behaviour rel. to particle size 77—31362
- power law fluid, swarm of bubbles motion, mass transfer 79—50759
- power law fluids, single bubble motion and mass transfer 79—50758
- pressure pulses generated by gas released from a breached fuel element 79—26557
- production, pulsation and damping, in dil. polymer solns. 80—69879
- profile and volume, symmetrical about vertical axis, analytical soln. 77—72346
- profile curve of a cylindrical capillary surface *(German)* 79—81983
- pulmonary arterial hypertension meas., Bubble Ultrasonic Resonance Pressure method 79—92313
- pulsating, motion in viscous liquid half-space near boundary with inviscid liquid 80—19494
- pulsating, motion near plane boundary between ideal and viscous incompressible liquids 79—94707
- pulsating, surface oscillations and jet production 80—33640
- pulsating air bubbles in water, stability using optoelectrical method *(German)* 77—27578
- pulsating gas bubbles in acoustic field, thresholds for surface waves 80—33665
- pulsation amplitude threshold for surface waves on oscillating bubbles 79—18900
- radial gas content profiles of rising swarm of bubbles in vertical pipe *(German)* 77—47062
- radiation blistering, fracture model, stress fields around lenticular bubble 79—86823
- radiolytic gas bubble growth in reactor irrad. PMMA 80—65058
- raise rate in nonuniform fluidised bed 78—67263
- reactor suppression pool, acceleration forces generated by an oscillating air bubble 79—54546
- reattachment flow issuing from finite width nozzle, bubble press. parameter 80—10275
- rectangular body, laminar flow, separation bubble and stagnation line 80—64514
- resonant bubbles in standing wave acoustic field, behaviour of stable arrays 77—79988
- resonating gas, model used for deriving eqns. for sound speed and attenuation 80—87670
- Reynolds number effect on heat transfer of forced convection subcooled boiling *(Japanese)* 80—19365
- rotating bubbling beds, heat and mass transfer 78—30351
- rotating thin-ring electrode, bubble nucleation 78—48664
- rotationally symmetric fluid bodies in gravit. field, thermodynamic treatment of capillary phenomena 78—10262
- rupture between two solid walls, effect of drag-reducing polymers on cavitation 80—106822
- saturated liquid, boiling onset, film boiling transition, crit. heat flux densities *(Russian)* 78—83234
- saturated steam-water mixtures, void fraction relationships for upward flow 80—14790
- seawater, bubble populations in coastal waters, photographic analysis 79—100849
- separate-bubble cavitation tests, nucleation meas. by Venturi tube *(French)* 79—55402
- separation mechanism, for bubbles growing slowly on horizontal heater face 77—51104
- shape, fluid flow in Newtonian and non-Newtonian fluids *(French)* 79—46374
- shape description in terms of dimensionless numbers 80—79382
- shape oscillation and static deformation of bubbles driven by modulated acoustic radiation stresses 80—33274
- shape-preserving small gas bubble, motion in rot. liquid, computer study, Runge Kutta Nystrom method 77—47063
- shock augmentation by bubble flow 77—3853
- shock structure in a liquid containing gas bubbles with nonsteady interphase heat transfer 78—83424
- shock wave amplification in nonequilibrium system of liq. and solvent gas bubbles 79—18936
- shock wave breakdown, gas-in-liq. bubble, gas density 78—42653
- shock waves in bubbly liquids *(French)* 78—26183
- shock waves in gas-liquid mixture, nonsteady shock waves 79—68792
- simulation of bubble populations in a gas fluidised bed 78—22415
- single rising, internal mass transfer coeffs. 79—86487
- single-component system, modification of charact. functions by interphase boundary and surface tension 77—90647
- single-phase turbulent flow, bubble and eddy heat diffusivity 80—19477
- size, correction for wall effect in point probe meas. 78—9681
- size and vel. measurements using RF probe 80—6177
- size distribution, changes due to interbubble gas diffusion 78—85204
- size spectra, acoustical determs. 78—9735
- slug in fluidised bed, mass transfer, wall effect 79—4079
- small bubble formation by using strong nonuniform electric field 80—48796
- soap bubbles technique for air flow visualisation *(Japanese)* 78—9737
- soap film in a wedge, expts. for teachers 79—17169
- solidification in space environment, bubbles thermal migration and interaction with solidification interfaces 79—47670
- solidification interface in reduced gravity, bubble interactions 78—84787
- solidification interfaces, bubble departure radii 80—44295
- solitary gas bubble, growth from soln. 80—64617
- soliton interaction in liq. with gas bubbles *(Russian)* 79—14419
- sound pulsation noise damping from small air bubbles in water 80—64253
- sound scattering in liquid, multipole resonances 79—81606
- spectrophotometer dip probe bubble formation prevention 80—13154
- spherical, growth in uniformly ultraheated liquid numerical soln. 78—1550
- spherical, pressure waves produced by collapse *(Japanese)* 80—100027
- spherical bubble impulse press. in viscous compressible liq. 78—26169

bubbles continued
- spherical bubble in finite vol. of liquid, natural freq., numerical calcs. 77—51106
- spherical cap, wake fluid dynamic properties 77—65787
- spherical cap bubble, mass transfer coeff. 80—79383
- spherical cavity gas bubble in compressible liquid, kinematics of free vibrations *(German)* 80—24074
- spherical contaminated bubbles in viscous fluid at arbitrary angle of attack, terminal motion 79—27687
- spherical gas bubble, in nonNewtonian liquids, growth by solute diffusion 78—34677
- spherical gas bubble in compressible liquid, nonlinear free oscillation, asymptotic method *(German)* 80—48773
- spherical gas bubble in liquid at rest, solution accompanied rise 80—10293
- spherical gas bubble in viscous fluid, initial motion 77—65780
- spherical oscillating gas bubbles, nonlinear forced vibrs. in compressible liquid *(German)* 79—98793
- spherical oscillating gas bubbles in fluids, fluid compressibility influence *(German)* 79—37383
- spherical particles, line of centre motion 79—4067
- spherically symmetric flow stability 78—83456
- spheroidal bubble, prolate or oblate, collapse or expansion in incompressible perfect fluid *(French)* 80—74933
- stability of caviton boundary in incompressible liquid 77—80190
- stagnation depth in vertically oscill. liq. column, viscous effect 77—42901
- steam, nonspherical, collapse in suddenly pressurised water *(French)* 78—33997
- steam, superheated, dispersion in saturated water, bubble form., heat transfer 77—47068
- steam, superheated, dispersion in saturated water, bubble form., heat transfer 77—47069
- steam bubbles, condensation, influence of noncondensable gases *(French)* 79—23717
- steam bubbles direct contact condensation in water at high press. 77—39202
- steam mixture of bubble struct., sound velocity, damping decrement 79—55444
- steam-generating tube, bubble/plug flow boiling regimes, elevated press., drift vel. and void fraction determs. 78—87379
- steel, austenitic stainless, tensile stress effect on He bublbe growth 79—87684
- in steel, carbon type, hydrogen press. effect on morphology of hydrogen attack 80—85052
- steel, high-strength low alloy, H_2 attack, 350-510°C 80—97636
- steel, stainless, He ion irrad., fracture behaviour, in-situ HV electron microscopy 80—29089
- subcooled boiling flow, vapour bubble growth and recondensation 79—93692
- submerged gas injection into liquids, flow regimes 80—59101
- submerged jet cone angle from bubble theory 80—79372
- subsonic turbulent flow past a planar fence, separation bubbles 80—53807
- superheated binary liquid mixtures, homogeneous nucleation of bubbles 78—67818
- superheated binary solns., flashing kinetics, nucleation and critical bubble 80—92035
- superheated liquid, growth of spherical bubbles, anal., numerical calcs. 77—24399
- superheated liquid, spinodal, hole thoery 80—19232
- superheated water at reduced pressures, bubble growth, finite difference anal. *(Japanese)* 80—92150
- supersaturated solns. of ethanol and water, bubble nucleation, contact angle effects 79—94702
- supersaturated solns. of nitrogen and water, bubble nucleation, contact angle effects 79—94702
- supersonic thermal boundary layer, effect of wall hollow-induced separated bubble *(French)* 78—5784
- suppression of finite-amplitude primary wave attenuation, parametric acoustic arrays, use of bubbles 80—74563
- surface charge, on small gas bubbles, meas. method 78—21100
- surface tension measurement, student expt. 77—45651
- surface viscosities at high pressure gas-liquid interfaces 78—75907
- surfactant, aq. subcooled soln., acoustic phenomena during nucleate boiling 78—10181
- swarms characteristics in bubble columns 77—42900
- system pressure, thermophysical effects, interfacial area *(German)* 79—41745
- Taylor bubble rise in circular vertical tube 80—64612
- tension pulse, acting on gas bubble in liq., model 79—55406
- thermal, temp. field meas., buoyant vortex bubbles and turbulent thermals 78—34232
- thermal migration, internal heat transport effects in weightless liquids 80—24075
- thermoacoustic vibrations of subcritical press., vibrs. onset mechanism 77—47026
- thermocapillary convection, unevenly heated liq. stream near gas bubble 78—59460
- thermocapillary gas bubble movement, liquid screening 80—19474
- thin liquid film, instability and rupture 80—34279
- transient boiling, bubble nucleation and growth instabilities 78—90649
- transient cavitation-free bubbles, threshold energy 78—75176
- translational motion in a viscoelastic liquid, retarded motion approx. 80—83777
- transparent object, testing for bubbles and light scatt. inclusions 77—88973
- TREAT, fission gas non-equilib. behaviour during fast thermal transients, simulation 78—41831
- turbulent bubbly flow, drift velocity, analytical model of distrib. mechanisms 80—99992
- turbulent bubbly flow, laser meas. of local liquid velocity and void fraction *(Japanese)* 78—9693
- two dimensional cavitation problem, cylindrical bubble, numerical soln. *(German)* 80—14764
- two dimensional void reconstruction, neutron transmission 78—22605
- two-phase bubbly flow, void fraction meas. by laser beam attenuation technique, theory *(Japanese)* 79—50779
- two-phase bubbly flow, void fraction meas. by laser beam attenuation technique, expt. *(Japanese)* 79—50780
- two-phase bubbly flow, void fraction meas. by laser beam attenuation technique, meas. accuracy determ. *(Japanese)* 79—50781

bubbles continued
two-phase dispersion, size distrib. function of bubbles/droplets in thermodynamic equil. 80—7862
two-phase flow patterns, high pressure water in heated four rod bundle 78—89938
two-phase fluid equilibrium, thermodynamic functions and surface tension 78—2262
two-phase mixtures, numerical anal. of press. transients by explicit-implicit method 78—34185
underheated liquid, lift height of vapour bubble for boiling on vertical wall 77—15104
underwater discharge, gas bubble energy 77—19804
underwater explosions as acoustic sources, distrib. of measured bubble pulse periods 79—5495
underwater spark discharge, vapour-gas cavities generation and space-time evolution characts. 80—19650
US absorpt. in liquid containing gas bubbles, investigation using acoustic streaming 80—5863
US detect. and meas. in liquids, blood appls. *(Japanese)* 80—1712
US propag. in liquids with vapour bubbles 80—33661
US wave in cavitating liquids, optical visualisation, nonlinear effects 80—106651
vacuum bubble evaporation and thermodynamics, surface oscill. consideration 80—62608
vapour, analysis of oscillation 80—19487
vapour, in immiscible liquid, collapse 78—94547
vapour bubble, behaviour during growth at subatmospheric pressures 78—9678
vapour bubble, nonsteady behaviour in US field 77—15107
vapour bubble collapse, effect of initial radius and subcooling 77—80196
vapour bubble collapse model for fragmentation of melts in melt/water reactions *(German)* 77—61507
vapour bubble collapse with translatory motion, general and quasi-steady solns. 78—18333
vapour bubble growth in superheated liquid, thin thermal boundary layer 78—38391
vapour bubble growth in uniformly superheated liquid, non-equilibrium effects 80—10294
vapour bubble growth in US field 77—34989
vapour bubble growth in US field 80—87608
vapour bubble in saturated liq. free convection boiling, growth rate and detachment diameter 80—103057
vapour bubble nuclei, stability and nucleation, effect of gases 77—31303
vapour bubble with microlayer, universal growth relations 78—71266
vapour bubble-liquid slug heat transfer, Taylor instability mechanism for LMFBR HCDA 78—8939
vapour bubbled through liquid pool, fractional vapour content 80—106831
vapour bubbles, equilibrium radius from Thomson-Helmholtz eqn. *(German)* 80—53847
vapour bubbles, flow and temp. fields, global collocation calcs. 77—47067
vapour flow in liquid enclosure with temp. distrib. 77—15083
vapour-gas bubble oscillations, heat-transfer and phase-transition effects 80—6133
vapour-gas bubbles removal in arteries of low-temp. heat pipes, anal. 80—19490
vapour-liquid mixture, propagation of acoustic disturbances, model 80—103058
vapour-liquid two-phase flashing flow, isentropic streamtube model 79—55412
velocity in fluidised bed with packing material 78—22416
velocity meas. in two-phase bubble-flow regime laser Doppler anemometry 77—39366
venous gas bubble prod. by transient deep isobaric counterdiffusion of He against N_2 78—11790
vertically vibrated liquid column, surface disintegration, bubbles and drops 80—74943
virtual mass coeff. by Blokh-Ginevskii method *(Russian)* 78—75186
viscoelastic liquid, polymer additives effects on bubble motion and cavitation noise intensity 77—68648
viscous compressible liquid, bubble behaviour analysis by finite method 77—55072
viscous flow in a partially filled rotating horizontal cylinder, effect of speed of rotation on bubble position 79—77125
viscous fluid, bubbling through of air, drop entrainment 80—14787
viscous supersonic flow over external axial corners, shock and bubble generation computation 80—14734
vitreous enamel, bubble struct. and flaw forecasting 78—53118
void fraction meas. by light attenuation technique, derivation of transmission rate reln. *(Japanese)* 80—48795
void swelling, transition from gas bubbles 78—14383
volatile liquid, statistical thermodynamics of new phase form. *(Russian)* 78—18739
vortex ring formation during large air bubble ascent in water 78—83410
wake core recirculation bubbles, adverse press. gradient, wind tunnel visualisation *(French)* 77—54997
water, cavitation, gas supersaturation thresholds under high press. 77—16861
water, cavitation mechanism 120°-250°C, bubble growth 80—14762
water, high-pressure gases effect on stability of liq. film 77—85026
water moderated reactor, local and global effects of gas bubbles 78—17328
water steam, boiling and nonboiling vertical two phase flow in tube, void fraction correl. 77—55073
water-in-oil emulsion, boiling, bubble formation, cinemicrophotography 80—74961
Ag film, He$^+$ ion bombardment, radiation damage, ion entrapment, gas release and bubble formation 78—30679
Al film, deform. under He ion bombardment 80—65073
Al, He bubble behaviour during high plastic deform. 80—29087
Al, He injected, tracing bubble evolution by positron annihilation 77—19992
Al melt, exam. of H_2 bubble origin, using first bubble technique 78—85115
Al-Zn-Mg alloys, H_2 bubbles in embrittlement 78—19868
Ar bubbles injected into Sn, Pb and Cu melts, under laminar flow, characts. 78—38394
Ar in PtSi after 20 to 160 keV sputtering, TEM and backscatt. spectrometry obs. 78—64435

bubbles continued
Ar phase stability boundary, nucleus surface tension rel. to surface radius of curvature 79—60603
B_2O_3, molten, growth and dissolution of air, N_2, O_2 gas bubbles 77—20070
Be, neutron irradiated, annealed, tensile props. and swelling, effect of He bubbles 78—22765
CBr_4, bubble departure radii at solidification interfaces 80—44295
CBr_4, low gravity solidification, bubble behaviour 80—15219
CO bubbles in liq. Fe, homogeneous nucleation 77—60106
CO_2, coalescence time in water 77—42899
Cu, formation of H_2O vapour bubbles, effect as intergranular creep fracture 80—71722
Fe, cast, Mg treated, graphite modularisation by Mg gas bubbles 78—52867
Fe, pig, liquid gas bubble form. at nozzles, acoustic exam. 78—52723
H bubble formation in LMFBR Na coolant loop 77—42042
H bubbles and Li colloids, formation and annihilation in LiH 80—107228
H_2, analysing H_2 with nucl. reactions 78—3422
H_2 bubbles, submicron particle collection 78—11560
H_2 evolution from H_2O electrolysis, nucleate boiling, vapour bubble behaviour, heat and mass diffusion 80—67013
H_2, form. in Al-Zn-Mg after water vapour embrittlement 78—15564
H_2 gas bubble struct. in proton irradiated Cu at 300K 80—92569
H_2, liq., bubble growth consts. calc. 77—35680
H_2O, squeezed boiling, internal characts. 78—90655
H_2S, coalescence time in water 77—42899
He, behaviour in cold worked Al-Li alloys 77—54359
He, behaviour in metals and tritide 79—17981
He blister formation in irrad. Mo, vacancy mutation to divacancies by He trapping 78—51601
He blistering, review 77—43261
He blistering, SiC and C bombardment by 0.6, 3.5 MeV He$^+$, porosity effects 77—35602
He blistering of Al and SAP 930, 300 keV He ion irrad. 77—35601
He blisters on Nb from 5-15 keV He ion bombardment dose rate, temp. effects 77—35595
He blisters on V and VTi alloys during He irrad., temp depend 77—35607
He, bubble boiling, heat exchange regimes 80—23879
He, bubble-type boiling crisis on various surfaces 77—11682
He, bubbles in Cu, volume change calc. from isotropic elasticity theory 78—47445
He, cavity depth distribution in 20 and 500 keV ^{4}He$^+$ irrad. Ni 80—107346
He, depth distrib. in 20 keV ^{4}He$^+$ irradiated Ni foils 79—69166
He, electron and positronium bubbles, density profiles 79—55952
He, embrittlement of austenitic stainless steel irradiated with α-particles 77—69015
He gas, in Al, excited atom lifetime, optical absorption 79—38578
He gas, in neutron irrad. steel, liberation in uniform heating 77—50248
He gas bubble lattice in Cu, Ni and stainless steel, TEM obs. 79—46726
He gas bubbles in Cu and Ni, superlattice struct. 80—2086
He gas re-emission from 20 keV He$^+$ bombarded Al, release mechs., blistering 77—35596
He, growth in Nb-Zr (1 wt.%), α-particle effects 78—67749
He, growth in stainless steel, effect of tensile stress 79—55796
He, growth mech. in α-particle bombarded Al 77—7774
He I, stable microscopic bubbles and evaporation-condensation resonance 78—91381
He, in Al, TEM obs. 77—4132
He, in Al film, He$^+$ irrad., overpressurised bubble obs. 79—51165
He, in α-irrad. Al foils, bubble alignment during deform. 80—107345
He, in ion irrad. FCC metals, eletron diffr. and TEM obs. 79—14858
He, in ion irrad. Ni, cavity depth distrib. determ. 79—51161
He, in Nb-Zr (1%), He bubbles and voids with ringed images, SEM and TEM exam. 78—51529
He in Ni and Nb, stress distrib. from ion beam irrad. 77—35599
He in Ti, 300 keV He$^+$ irrad., exfoliation, flaking, blistering, in-situ SEM obs. 77—35598
He, ion bombardment damage in W, field-ion microscope obs. 77—31701
He, ion implanted in metals, statistical model of low temp. blister formation 78—67754
He ion irradiation of metals, blister form. and bubble growth 80—65072
He irregular bubble growth in implanted Nb-Zr alloy, TEM obs. 80—15164
He, liq., bubble formation mechanism, on surface of deformed crystal *(Russian)* 78—85066
He, liq., bubble growth consts. calc. 77—35680
He, liq., multielectron bubbles *(Russian)* 78—30805
He, liquid, electron bubble tunnelling below surface 79—86945
He, parachute opening flowfield computation, high-speed photography and computer graphics appl. 78—30374
He, pinning of dislocations, high-temp. radiation embrittlement of Ni-Be alloys *(Russian)* 77—44331
He, superfluid, bubblon generation on charged surface, and instability generation *(Russian)* 78—18858
He-assisted, bubble nucleation computer simulation 78—86625
^{3}He, microscopic bubbles in metal tritides 78—30661
^{3}He, superfluid, pair breaking by electron bubbles 79—51352
^{4}He blistering of Be and Al sintered powders by 100 keV ion irrad. 77—35600
^{4}He blistering of V, 80 keV ion irrad., elevated temps. 77—35606
^{4}He, liq., ion bubble surface ^{3}He bound states 78—2329
^{4}He, superfluid, superheating and bubble formation 78—56000
^{4}He, superfluid, tensile strength and visible US cavitation 77—7920
^{4}He$^+$ irradiation of Nb, blister skin thickness, meas.-calcs. correl. 77—35597
He(2^3S) bubble in liq. He, phenomenological model 77—20147
Hg bubble motion with and without mag. field 78—91021
Hg-Ar, two phase flow in vertical tube, transverse mag. field, bubbles and slug flow 77—84303
hydrocarbon-water, emulsions, superheated, bubble nucleation 78—61056
K, motion and growth in incandescent W wires *(Hungarian)* 77—48460
LiNb$_{1-y}$Ta$_y$O$_3$, Czochralski growth and basic props. 77—63556
$Li_2O.2SiO_2$ melt, bubble form. during unidirectional solidification *(Japanese)* 79—70057
Mo, 29 MeV α-particle irrad. in He, micropore and dislocation loops form. 79—14859
N_2, boiling, press. effect on internal characts., bubble growth 77—15568

bubbles continued

- N_2 bubbles coalescence in dil. aq. solns. 79—4062
- N_2 gas jet injection into Hg, interaction at submerged orifice 80—59102
- N_2, liq., elec. breakdown by field induced microbubbles 79—91365
- N_2-Ar-O_2 system, vapour-liq. equilib. 80—54358
- Na boiling in tubes, heat transfer and pressure drop 80—28408
- Na, fast reactor coolant, boiling in circular pipe, single-bubble model 77—10466
- Na, liquid, local boiling behind local flow blockage, simulated LMFBR fuel subassembly 78—54842
- Na pool fuel vapour and aerosol transport in HCDA 79—13455
- Na, superheated flow in pipe, single bubble slug expulsion 78—672
- Na vapour bubble growth in superheated liquid, numerical anal. 78—29576
- Na vapour condensation from rising bubble, effects of internal circulation velocity and noncondensable gas 78—50258
- Na voiding in LMFBR, space time dynamics for localized disturbances 78—21674
- Na_2O-CaO-SiO_2, refining in glassmelting process 78—27467
- Na_2O-SiO_2 glass, bubble gas comp. change 80—79946
- Na_2O-SiO_2 glass melt, dissoln. of O_2 and CO_2 gas bubbles 80—79945
- Nb, blister diameter and blister skin thickness correl. under He ion irrad. SEM obs. 79—82266
- Ni, irradiated, with He^+ bubble depth distrib. meas. by TEM and blister form. mech. 78—95088
- O_2, boiling, press. effect on internal characts., bubble growth 77—15568
- O_2 evolution from H_2O electrolysis, nucleate boiling, vapour bubble behaviour, heat and mass diffusion 80—67013
- O_2, rising in water, dissolution mass transfer coeffs. 79—41737
- Si, laser induced surface deforms. 79—82262
- Si oxidation in HCl-O_2 atms., Si etching and SiO_2 bubble form. 77—63823
- Si-electrolyte interface, incident radiation image form. *(Russian)* 77—7199
- SiO_2, fused, bubble gas comp. rel. to furnace atm. 77—58402
- UO_2, effect of point defects on nonequilibrium bubble behaviour 79—93722
- UO_2, fission gas bubble distrib. from high temp. irradiated SGHWR fuel pins 77—46284
- UO_2, irradiated, intergranular fission gas bubbles 78—21651
- UO_2, irradiated, spacing of intergranular fission gas bubbles 78—66340
- UO_2, irradiated sample, 1000 to 2100K, swelling and fission gas obs. 78—78462
- UO_2, mobility of intragranular bubbles during irradiation 77—6520
- UO_2, relative growth rates of fission-gas bubbles on grain faces 79—6739
- UO_2, resolution of fission gas from grain edge bubbles, porosity effect 79—85607
- UO_2, swelling and gas release at low and intermediate temps. 77—50241
- UO_2 vapour bubble characts. determ. in LMFBR 79—22390
- UO_2 vapour condensation from rising bubble, effects of internal circulation velocity and noncondensable gas 78—50258
- UO_2-PuO_2, mixed oxide fast reactor-fuel pin, fission gas bubble distrib. 78—78459
- UT_3, ^3He distribution from triton decay, NMR meas. 78—19360
- V, ion implanted with 2 MeV He under pulsed conditions, microstructure obs. 80—29088
- V-Ti, and V-Ti-Be(Zr), 4 MeV Ni^{++} irrad., He gas bubble form. 80—29085
- W, annealed wire, analytical determ. of K content of single bubbles 78—64909
- W wires, KSiAl doped cavity formation *(German)* 78—31524
- Xe bonded fission gas, in bubbles and pores, radial distrib. in mixed carbide fuel pins, electron probe anal. 79—36318
- $Y_3Al_3O_{12}$ crystal growth from melt, gas bubble capture theory 80—64941
- Zn single cryst. deform. in liquid N_2, gas bubble form. on growing twins *(Russian)* 79—60378

Buchholz relays *see relay protection*

buckling

- annular plate, algorithm for numerical soln. of critical buckling 78—83275
- annular plate under uniform compression, stability and behaviour 77—42759
- annular plate with axisymmetric initial deflection, thermal buckling 79—32320
- annular plates, nonsymmetric postbuckling behaviour, numerical analysis 80—102968
- annular plates, variable rigidity, post critical stressed and strained state 77—46942
- annular plates under uniform external pressure, Timoshenko's conjecture 77—31226
- arch, uniformly compressed, two-hinged, initial post-buckling behaviour 80—33500
- axial impact buckling of a column with random initial imperfections 79—18762
- axisymmetric buckling of a complete spherical shell under uniform external press. 78—83274
- bar, localised damage region effect on parametric excitation 78—30215
- bar of linearly work hardening material, critical load *(Russian)* 77—89053
- bar on elastic foundation, buckling strength *(German)* 79—64546
- bars, elastic, spatial modes of buckling *(Russian)* 77—885
- beam, axially loaded, resting on nonlinear elastic foundation 78—34042
- beam, buckled, forced oscillations, global bifurcations and chaos 79—27580
- beam, nonuniform, static and dynamic instability analysis 78—13942
- beam, simply supported on nonlinear elastic foundation, equilibrium paths and buckling 79—81747
- beam, stability anal., paradoxical case 79—37200
- beam, stability anal., paradoxical case 79—37201
- beam, unilaterally constrained, Euler critical and buckling load, variational theory 79—37203
- beam boundary conditions vibratory identification 77—27480
- beam or spring connected structures, simple buckling and vibration anal. 79—72843
- beams, buckling loads and fundamental freqs. improved lower bounds 80—64416
- beams, end loaded cantilever, lateral buckling 79—50617
- beams, impact loading, design curve 78—9579
- beams, linearly tapered, transverse vibr. 80—48627

buckling continued

- beams, uniform, slender, effect of principal bending curvature on lateral buckling 77—80089
- beams, uniform elastic, lateral buckling, perturbation methods 80—64417
- Beck problem, tangential buckling load 78—13933
- Beck problem for loaded cantilever column 79—3932
- Bernoulli-Euler beams, maximum stiffness, bending, transverse vibrs., singularities in design 79—81802
- bifurcation, second order, in differentially nonlinear plasticity 79—86362
- bifurcation and limit point instability of dual eigenvalue third order systems 80—87727
- bifurcation and stability of systems derived from a potential, buckling problems *(French)* 79—46240
- bifurcation from rotationally invariant states 78—77671
- bifurcation of non-differentiable operators, appl. to elasticity 77—46945
- bimodular columns, buckling and immediate postbuckling behaviors 79—23232
- box sections, interactive buckling anal. using dynamic relaxation 77—72202
- cantilever column post-buckling, Galerkin finite element analysis 77—54907
- cantilever columns, spring hinged, post-buckling anal. 79—46235
- cantilever cones, buckling under external pressure, exptl. and numerical solns. 78—71287
- cantilever under multiple loads, postbuckling and stability anal. 80—48617
- cap, isotropic and orthotropic shallow spherical with hole, dynamic buckling 80—19258
- catastrophe theory appl. bifurcations in variational problems 80—8789
- ceramics, brittle, phys. props. role in resist. to failure by thermal buckling 79—77673
- ceramics, brittle, post thermal buckling resistance, role of physical props. 78—64585
- channel, straight (buckled), two-dimens. flow, stability anal. 78—59490
- circular annular plates of parabolically varying thickness, buckling and vibrs. 80—69698
- circular arches, lateral-torsional instability with motion-dependent loading 77—89049
- circular cylinder carrying flow, unsteady fluid dynamic forces rel. to stability anal. 78—13936
- circular cylinders, plastic buckling in pure bending 79—90158
- circular plate bending under eccentric loads, elastic buckling eigenfunction method *(Japanese)* 78—22285
- circular plates, elastic buckling 79—27555
- circular ring plates, finite deflections 79—27533
- clamped columns, single and bimodal optimum buckling loads 77—62182
- clamped plate, finite element anal. of secondary buckling, comparison with expt. 79—1120
- column, long, buckling and stability under own weight 79—32307
- column, nonuniform, lower bound buckling load, finite difference scheme 78—18200
- column, stochastically imperfect finite, on nonlinear elastic foundation, buckling 80—48619
- column, tall vertical, optical load, optimal shape, nonlinear differential-integral equation 80—53663
- column buckling criteria determ. using vibr. data 78—34098
- column buckling load problem, constrained minimum weight equivalence 79—7313
- column critical buckling load, approximate eigenvalues 79—64551
- column on nonlinear elastic foundation, buckling imperfection sensitivity, Range-Domain implication *(German)* 80—74786
- column with nonlinear restraints and random initial displacement, buckling 80—79192
- columns, elastoplastic, thin and vertical, postbuckled, deflections 80—87728
- columns, infinitely long with localised imperfections, dynamic buckling 77—27479
- columns, shear deformation effect on post buckling behaviour, iterative analysis 80—38299
- columns and plates, lower bounds to fund. freq. and buckling loads 79—10469
- complex idealised bar, deformation processes, bifurcational elastic eqn. soln., pseudobifurcation *(Russian)* 80—58945
- composite beams, vibration and buckling anal. 79—1123
- composite materials, stratification in regions of compression *(Russian)* 77—36613
- composite plates, postbuckling anal. by exploiting symmetries 77—42756
- composite viscous tube, collapse under external press. and surface tension forces 77—58572
- compound column, shape optimisation for largest critical buckling load 77—46948
- compressed rod with large deflections, optimal design by dynamic programming *(Polish)* 78—22286
- computational methods of treating nonlinear and special linear problems 77—74226
- cone cylinder jointed shell, ring stiffened, external hydrostatic pressure, elastic stability *(Chinese)* 80—64412
- conference, computational methods in nonlinear problems in mechanics and engineering, Austin, Texas, USA (March 1979) 80—51945
- conical shell, buckling in response to shock load 78—5679
- conical shell, skew, truncated, external hydrostatic pressure, elastic stability *(Chinese)* 80—64413
- conical shell subjected to overall external pressure, postbuckling behaviour *(Chinese)* 80—64407
- conical shells, axially compressed with edge constraint, elastic and plastic buckling 78—63341
- continuous beam resting on tensionless elastic foundation, soln. 79—46238
- continuous elastic systems under multiple loads, postbuckling anal., stability theory 80—48616
- creep buckling, effects of small deflexion approximations on predicted behaviour 79—7309
- creep buckling, influence of post buckling characts. 79—7308
- creep buckling of complete spherical shell, perturbation method 77—19552
- creep buckling theory, nonexistence of global solns. for nonlinear eqn. 79—30251
- crumpling of thin tubular struts 79—64544
- curved plane slender bars and frames, geometrically nonlinear behaviour 78—13935

buckling continued
curved plate assemblies under biaxial loading, finite strip buckling anal. 78—18203
curved structural members, large displacement theory, applic. to lateral-torsional buckling anal. of circular arches 80—23924
curved structural members, post-buckling anal. 80—53670
cylinders, approx. of buckling stresses 77—19553
cylinders, circular under end load, post-buckling finite element anal. 79—98640
cylinders, discretely stiffened, buckling under axial compression 80—64408
cylindrical elastic tubes, collapse and buckling under combined bending and pressure loads 78—83277
cylindrical panels, nonlinear buckling and stability 79—72835
cylindrical shell, axially loaded, general random imperfections 78—9580
cylindrical shell, buckling investigation 80—19261
cylindrical shell, creep conditions 80—28447
cylindrical shell and spherical panel, stability, critical loading density 80—53664
cylindrical shell deform., effect of loading history on bifurcation *(Ukrainian)* 78—55578
cylindrical shell of variable wall thickness under radial external press., buckling, expt. study 79—96082
cylindrical shell with circumferential notch under axial compression, stability *(Polish)* 78—79239
cylindrical shell with elliptic cross section, subject to torsion, creep buckling 78—34040
cylindrical shells, correlation between vibration and buckling 80—28463
cylindrical shells, fluid-filled, vibr. and buckling under torsion 78—79253
cylindrical shells, loading history, effect on plastic buckling *(Russian)* 79—14288
cylindrical shells, orthotropic, dynamics under axial impact 79—59936
cylindrical shells of varying thickness, natural freqs. and buckling loads 78—1597
cylindrical shells with small curvature 78—67066
cylindrical shells with various end conditions, buckling under normal pressure 80—69703
cylindrical tanks, ovalization due to foundation settlement 78—18208
cylindrical wound shell with viscoelastic core in axial compression, optimisation 77—4821
deformation of bar elements, derivatives of deformation parameters, appl. to buckling and post buckling anal. 77—89047
developing shells, buckling elastic strain energy 79—86363
diagonal braces in building frame, inelastic stability 78—75083
director rod, elastic instability 78—63292
discs, stationary and rotating, stability under edge load 78—38219
displacement incrementation in nonlinear structural analysis by self-correcting method 77—14932
dynamic buckling of a damped imperfect column on a nonlinear foundation 79—7311
dynamic buckling of axisymmetric spherical caps with initial imperfections 79—3934
dynamic buckling of shells 78—18210
elastic bar with varying stiffness, coupled boundary conditions, buckling 77—31231
elastic beam subjected to nonconservative compressive follower loads, lower bound theorem 77—68459
elastic beams hung at both ends, lateral buckling, variational anal. methods 79—86361
elastic buckling with mode interaction, asymptotic expansion appl. 80—14592
elastic circular cylindrical shells, axially compressed, stable postbuckling equilibria, finite element anal. 78—38224
elastic circular plate subject to nonuniform load, instability 77—62178
elastic lateral torsional buckling of unbraced and braced planar frames 79—46236
elastic members, thin-walled, displacement theories for straight and circ. curved members *(Japanese)* 80—43615
elastic nonlinear, appl. of bifurcation problem left branching soln. 77—67222
elastic plastic spherical body, instability under uniform loading 80—58946
elastic prisms, periodic solns. 80—48582
elastic restrained beam, stability with nonordinary boundary conditions 77—50941
elastic rod, buckling under time-varying load 78—42551
elastic rods subjected to triangular distributed tangential follower forces 77—75826
elastic shells, stable solutions, finite element and Newton-Raphson methods 80—14593
elastic shells of revolution, postbuckling finite-element analysis 77—62185
elastic struct., buckling load, upper limit from Timoshenko coefficients *(French)* 79—68609
elastic structs., stability, buckling and postbuckling 80—1454
elastic structure buckling models for higher order catastrophes 79—1122
elastic structures, buckling and post-buckling behaviour *(Chinese)* 79—72832
elastic thin plate, non-linear theory of dynamic buckling 78—9582
elastic-plastic cylindrical panel, buckling under axial compression 78—1584
elastic-plastic plates and shells, flow rule for lowering buckling stresses *(Japanese)* 80—99949
elastic-plastic spherical shells, internally pressurised, effect of thickness inhomogeneities 77—42761
elastica, buckled at contact, perturbation anal. 79—98646
elastically clamped variable-stiffness annular plate, thermostability 77—89052
elasto-plastic buckling of curved webs, Gauss-Seidel iterative procedure 78—34043
elasto-plastic continua, quasi-bifurcation in dynamics 78—38223
elastoplastic bars, instability modes *(Russian)* 79—10514
elastoplastic buckling of thin torispherical shells 80—5967
elliptic plate, simply supported, under uniform compression 77—42758
elliptical plate, simply supported, under compression 77—17826
epoxy resin parabolic shells, exam. of viscoelastic creep 79—43307
equilibrium and elastic stability problems, appl. of triangular facet shell element method, TRUMP 77—46946
Euler buckling eigensystem for a nonprismatic strut 79—18764
Euler column buckling, imperfect bifurcation in the presence of symmetry 79—72828

buckling continued
eye, detached retinal tears computer localisation for scleral buckling procedure 78—7529
ferromagnetic cantilevered beam plate, magnetoelastic buckling 79—18761
ferromagnetic circular ring, elastic buckling in radial mag. field 78—23314
fibre reinforced composites, metal clad, debonding risk 80—3132
fibre reinforced elastic slab subjected to axial loads, instability and buckling 80—64420
finite element analysis by ASKA program system 79—18753
fission reactor lattices, depend. of material buckling and k_∞ on structure 77—50198
flat plate, simply supported, uniaxial compression, secondary buckling anal. 78—55579
flexural fatigue and surface abrasion 78—15504
flywheel, buckling and vibr. of rotating spoke, anal. 78—71288
forced vibrations of freely supported continuous beam *(Rumanian)* 78—75085
frame, two-bar, with tangential load, snap-through buckling 80—64406
frame corner plane stress distrib. and local buckling *(German)* 78—13940
frame nonlinear postbuckling behaviour, finite element analysis 77—62183
free surface, wrinkling 78—5676
Gauss-Seidel convergence criterion for elastic structural stability 77—53781
GCFR lattice, Monte Carlo and diffusion theory calcs. of steam worth 79—80991
geometrically nonlinear finite element behaviour using buckling mode superposition 80—1449
glass, industrial cylindrical tubular elements under internal and external press., deform. and failure resistance 78—35460
glass fibre reinforced epoxy, unidirectional, buckling 78—44166
glass fibre reinforced plastic, rings, filamentous and layered, outer pressure, stratification *(Russian)* 78—31489
glass fibre reinforced plastic curved panels, expt. snap buckling under lateral loading 77—59849
glass fibre reinforced plastics, cylindrical shells, compressive and flexural strength *(Japanese)* 80—81115
graphite reinforced epoxy laminate with arbitrarily symmetrical struct., stability 79—61649
graphite-epoxy composite, open-section stiffened compression panel, buckling and struct. efficiency 77—35061
graphite-epoxy composites, Thornel 300/Fiberite 1034, effects of thermal spiking on moisture absorpt. characts., tensile strength and buckling modulus 79—43330
H-columns, local and member buckling finite strip method anal. 79—7306
harmonic solid, crack parallel compression, crack plane strain buckling 80—64475
Hauger column critical load in presence of damping *(French)* 79—14291
heavy fabric sheets, fabric folding obs. 79—18756
Hiduminium, shallow spherical cap buckling under uniform external press. 77—23902
honeycomb sandwich beams with laminated faces, flexural wrinkling 80—79183
HY-130 steel, shallow spherical cap buckling under uniform external press. 77—23902
imperfection sensitivity of semisymm. branching, rel. to catastrophe theory, stiffened plate appl. 77—84170
incremental deformations of initially stressed media with couple stresses 78—62077
inelastic critical strength prediction by vibration testing 78—35611
infinite elastoplastic medium, bifurcations at a spherical hole 80—33493
infinite linearly-elastic circular cylinder, wrinkling induced by surface stress 78—26070
infinitely long trapezoidally corrugated plates in shear, elastic buckling 79—32315
initially stressed Mindlin plates, finite strip method, buckling anal. 78—26067
interactive buckling analysis of box sections using dynamic relaxation 79—7304
interbraced parallel structural columns, buckling loads 78—67064
isotropic bodies, stability under all-round compression by dead load *(Russian)* 77—42762
JET vacuum vessel, mechanical reliability in disruptive instability 80—18643
Kevlar-29, flexural fatigue and surface abrasion 78—15504
laminated cylinder, imperfect, buckling under combined loading 80—7620
laminated plate, moderately-thick, biaxial buckling 77—58573
laminated plates, optimum design under shear 80—23925
laminated plates anisotropic anal. and soln. procedure 77—65698
large defection anal., hybrid finite element and finite difference approach 77—72201
lateral, elastic beams analysis, using theory of quadratic operator pencils 80—48607
lateral buckling by bending, and by torsion 77—42763
lattice columns with stochastic imperfections, buckling, Ritz method 79—18757
light gauge steel diaphragms, buckling, bending anal. under concentrated loads 79—23233
linear elastic incompressible solid, stability of void growth under uniaxial tension and shear 79—76972
linearly tapered annular plates, axisymmetric vibrations under in-plane force 79—94537
load-deflection curve, post-buckling behaviour of Hutchinson's plastic buckling model 80—64411
local buckling of twisted double-symmetric rectangular box girders *(German)* 78—13939
magnetoelastic buckling of rectangular plates, edge effect influence 77—80988
magnetoelastic buckling plate in uniform transverse mag. field 79—24208
mechanical stability in creep conditions *(Russian)* 79—18758
metal sheet, strain propag. under non-uniformity distributed load 77—16653
metal structures, inelastic anal. 78—70586
multistorey frames with nonuniform columns, pocket calculator program for buckling 78—1580

buckling continued
  Mylar, shells, conical and cylindrical, high speed photographic exam. of buckling 78—44184
  N-degree-of-freedom system, imperfection sensitivity of compound branching 78—13934
  nearly cylindrical shell of revolution, postbuckling anal. *(Polish)* 77—54911
  noncircular prismatic block between parallel frictional platens, press. distrib. and bulging profiles during compression 78—18207
  nonconservative autonomous and nonautonomous systems, stability, energy approach 78—51097
  nonconservative continuous elastic systems, post-buckling behaviour 79—3931
  nonconservative elastic systems, branching anal. at coincidence buckling loads 77—80090
  nonconservative simple frame, nonlinear divergence buckling, critical load 80—14594
  nonlinear elastic stability problems using a finite difference perturbation method 78—83273
  nonlinear elastic systems, incremental approach to the solution of snapping and buckling problems 79—76975
  nonlinear interactive buckling, sensitivity and optimality 77—80086
  nonlinear plate and shell theory problems soln. 77—53784
  nonlinear post-buckling anal., perturbation approach to imperfect structs. and snap-buckling 78—79244
  nonlinear shell equations, post buckling range, accuracy 78—22290
  nonlinear structural eigenvalue calcs., mode finding 78—51102
  nonlinear sway-buckling of an eccentrically loaded frame of two Timoshenko-bars 79—37204
  nonlinear theory of shells, structural anal. 79—30230
  nonlinear Timoshenko beam, dynamic buckling 80—23928
  nonlinearly elastic plates, buckled states 79—1118
  nonsymmetric structs., static and dynamic imperfection sensitivity, buckling model modification 80—79190
  nonsymmetrical systems, linearised linearised instability analysis instability analysis 77—72195
  nonuniform elastic column, upper and lower bounds on loads 77—72198
  nuclear fuel can designs for Safety Test Facility, structural analysis 77—46310
  nuclear fuel lattice eigenvalue as function of buckling, perturbation theory correction 79—59118
  nuclear power plant components, design rules evaluation 77—3096
  nuclear reactor, coupled cores, calc. of buckling variation and neutron flux, Green's function method 78—74421
  open cylindrical shell, buckling under combined compression and bending stress 77—65697
  open shells, prebuckling state, bending stability, contour deformation effect 79—94519
  optical fibres, due to loose tube packaging 78—25962
  optimal structural design against buckling, complementary energy approach *(French)* 77—68462
  orifice plate buckling in meter, flow meas. errors 77—84371
  orthotropic annular plate, stability *(Polish)* 78—18209
  orthotropic annular plates, general nonsymmetric postbuckling anal. 79—7307
  orthotropic continuous plates, reduction method 77—23906
  orthotropic curved panels under lateral loading, snap-buckling behaviour 77—50939
  orthotropic plate, buckling and postbuckling, stability and stiffness losses 77—27478
  orthotropic skew plates, Fourier series soln. 79—14286
  outstands in stiffened plate 79—98641
  pinched rigid-plastic cylindrical shell, mode of collapse, geometrical parameters 79—10492
  pipe stability and plastic deform. under external couples 80—19259
  pipeline, axially compensated, buckling load determ. *(German)* 78—31456
  plane frame structs., modified pot. energy approach to post-buckling anal. 78—83276
  plane-strain buckling of cracks in incompressible elastic solids 80—79186
  plastic conical shell under axial compression, Al and stainless steel samples 77—72197
  plate, annular circular, thin, of variable thickness, thermal buckling 79—32312
  plate, annular elliptic heated, const. thickness, buckling and stability criterion 80—28443
  plate, buckling, von Karman eqns., generic and nongeneric bifurcation 79—46239
  plate, catastrophe theory appl. 77—67232
  plate, circular, laterally loaded, elastic instability initiation 77—50936
  plate, circular, parabolical tapered, buckling and vibrs. 79—64540
  plate, circular, with annular circle constraints, vibrs. and buckling 79—98652
  plate, heated, vibr. anal., thermal buckling 78—26073
  plate, heated thin annular circular, of variable thickness, buckling, thermoelasticity 78—9581
  plate, increase of first natural freq. and buckling load by optimal fields of initial stresses 78—13945
  plate, multilayer sandwich, stability and buckling analysis by finite strip method 78—26069
  plate, obliquely stiffened, subjected to uniform compression, buckling strength *(Japanese)* 78—67067
  plate, orthotropic, rotationally retrained, buckling under uniaxial compression 77—84169
  plate, simply supported rectangular under axial compression, creep buckling and deformation 79—68605
  plate, thin, elastoplastic, buckling model *(French)* 80—74778
  plate, thin, thermally stressed, vibrations 80—48628
  plate, thin, unilateral buckling, variational techniques *(French)* 80—74780
  plate, thin, unlimited, with noncircular hole, stability problem soln. *(Russian)* 78—18201
  plate, thin elastic, buckling problem, eigenvalue eqn. positive soln. appl. *(German)* 79—68610
  plate, thin elastic, use of Galerkin's method *(French)* 77—72196
  plate, thin stretched, with curvilinear holes, buckling and loss of stability *(Russian)* 79—68607
  plate, with internal crack, in tension, instability of plane solution *(Russian)* 79—50616
  plate and shell structures, review of buckling behaviour 77—72200

buckling continued
  plate boundary conditions and mode jumping, explanation by secondary bifurcation 80—10170
  plate buckling, variational formulation for hybrid finite element method 78—18205
  plate on tridimensional elastic foundation *(French)* 80—79182
  plate structs., buckling under arbitrary loading, finite strip method 79—27556
  plate structs., finite strip method for post-locally buckled anal. 79—30246
  plate with intermediate continuous elastic supports subjected to initial membrane forces 80—106744
  plates, annular, with variable thickness, critical buckling loads 80—106736
  plates, buckling due to nearly homogeneous stresses *(German)* 79—81746
  plates, cracked, buckling under tension, finite element anal. 80—53666
  plates, dynamic instability anal. by finite element method 77—3769
  plates, equil. finite element model 78—5675
  plates, flat, stability of postbuckling behaviour 80—1453
  plates, inelastic buckling including shear effects 79—76984
  plates, perforated, homogenisation and bifurcation 80—53665
  plates, rectangular, stability anal. by complementary energy method 80—48611
  plates, rectangular clamped, elastic buckling 79—68606
  plates, rectangular cross-ply laminated, with nonlinear stress-strain behaviour, buckling 80—64415
  plates, rectangular elastic, secondary buckling states 80—74782
  plates, rectangular isotropic and orthortropic buckling and freq. of flexural vibrs., Rayleigh's method 79—32313
  plates, simply supported, plastic buckling under edge thrusts 79—10510
  plates, thin, harmonic buckling due to constrained thermal expansion 80—48620
  plates and shallow shells, approx. methods for linear and nonlinear anal. 78—51101
  plates at elevated temp., vibr. and buckling, fundamental freq. 80—23935
  plates stiffened, large amplitude flexural vibrs. 78—83307
  plates thin, third order elastic consts., effect on buckling 80—10172
  plates with discontinuous change of thickness 78—38220
  PMMA organic glass shell, circular, cylindrical, under combined twisting moment/axial load buckling 79—100220
  polar orthotropic sector plates, stability 79—18765
  polyester dough moulding compounds, fibre orientation and mech. props. 77—25116
  post-buckling behaviour of flat plates under axial load, secondary buckling values, anal. *(Japanese)* 77—14929
  post-buckling behaviour of flat plates under axial load, secondary buckling values, expt. *(Japanese)* 77—14930
  post-buckling behaviour of structures using a finite element-nonlinear eigenvalue technique 80—92078
  postbuckling analysis of elastic structures by the finite element method 80—96209
  postbuckling at coincident branching points, relation to energy surface umbilic point geometry 80—23926
  postbuckling behavior of thin-walled open cross-section compression members 80—5963
  postbuckling of elastic structs., mode imperfection anal., imperfection sensitivity 77—89048
  postbuckling phenomena, topological classification, bifurcation classification and branching points 79—64541
  pressure loaded rings and shells, finite element method 77—42757
  pressure vessel, cylindrical, thin torispherical ends, expts. on buckling under internal pressure 78—90736
  pressure vessel heads, internally pressurized ellipsoidal and torispherical elastic plastic, nonsymmetric buckling 77—58575
  pressure vessel heads, torispherical, elastic instability and with triangular thin shell finite elements 77—58576
  prismatic beams, element stiffness matrix 78—5653
  prismatic plate assemblies, buckling and vibr. anal. with compact computer program 78—90737
  rapidly increasing compressive forces, critical value, rod, shell and plate buckling 80—33497
  reactor core, uniform infinite lattice eigenvalue as function of buckling 79—609
  rectangular orthotropic plates, buckling strengths stress diagrams *(German)* 79—14289
  rectangular plate, Von Karman eqns., generic bifurcation theory, symmetry props. 79—44748
  rectangular plate static stability soln. with fully conforming element 77—62184
  rectangular plate with central hole, thermal stresses and buckling 77—3755
  rectangular plates, in-plane loaded buckling and vibr. by unified Ritz approach 79—3945
  rectangular plates, orthotropic, buckling determ. using structure smoothing method *(German)* 78—87285
  rectangular plates, supported, (post)secondary buckling behaviour, theoretical anal. 79—81743
  rectangular plates, vibrations and buckling anal. *(Japanese)* 77—80084
  rectangular plates on elastic foundation, approx. large deflection anal. *(French)* 77—68463
  regularly multilayered rectangular elastic plates, post-buckling behaviour 79—98643
  reinforced open cylindrical shells, bending stability 79—41581
  reverse-buckling safety discs, release pressure 78—89489
  ribbed plate single-panel buckling detection, computational procedure *(German)* 78—13941
  rock, folding in simple shear, expt. anal. 78—32077
  rock, strain distrib. across experimental single-layer fold 78—32076
  rocks, fold propagation in viscous layer, finite element model 78—32083
  rod with distributed load, lateral buckling as spatial bifurcation problem, Mathieu eqn. solns. 77—50940
  rods, quasi-bifurcation within axial plastic compressive wave 79—10513
  rotating beam, stability under compressive centrifugal forces 80—23922
  rotating circular cylindrical elastic membranes bifurcation 80—33494
  rotating flexible rods, unstable vibration and buckling 78—79242
  rotating flexible rods at transitional parameter values, vibr. and buckling, off-clampings 80—1464
  rotating neo-Hookean cylinder, stability under large deformation 77—50942

buckling continued
  rotating rods, critical rotation speed, extended Galerkin method 77—35064
  rotational shells, geometric stiffness matrices for finite element anal. *(French)* 77—68464
  rotationally restrained orthotropic plates under uniaxial compression, buckling 78—67065
  round tubes in flexure, critical buckling strains 80—23921
  sandwich panels, nonlinear dynamic buckling 77—19572
  sandwich panels subjected to in-plane shear, short wave wrinkling *(Japanese)* 79—68608
  shallow arch under multiple loads, postbuckling and stability anal. 80—48617
  shallow circular arch, spatial distrib. effect on dynamic snap-through 79—32318
  shallow circular arches, optimal shape against snap-buckling 79—37208
  shallow orthotropic shells, snap through buckling 79—98642
  shallow spherical cap buckling under uniform external press. 77—23902
  shallow spherical shell, parametric anal. of creep buckling by finite element method 77—46938
  shell, axially compressed cylindrical, axisymmetric imperfection effect on plastic buckling 79—64548
  shell, axially compressed orthotropic cylindrical, initial and post buckling 77—31227
  shell, axially loaded isotropic cylindrical, asymmetric imperfections effect on vibrs., buckling 77—31241
  shell, axially stiffened, mode interaction in postbuckling behaviour 77—89046
  shell, circular cylindrical, nonuniform axial compression, thickness effects 77—31230
  shell, circular cylindrical, of anisotropic material, plastic stability under axial compression *(German)* 78—1585
  shell, circular cylindrical with varying wall thickness, creep buckling, variational methods 80—14595
  shell, cylindrical, axially compressed localised diamond-shaped buckling patterns 77—89045
  shell, cylindrical, composite with viscoelastic filler, optimisation w.r.t. long-term stability 79—18760
  shell, cylindrical, creep buckling, perturbation method 77—11134
  shell, cylindrical, elastoplastic plastic buckling in pure bending 80—19257
  shell, cylindrical, inelastic with initial shape imperfections and residual stresses, buckling and carrying capacity *(Ukrainian)* 77—50937
  shell, cylindrical, nonconservative stability performance 77—68466
  shell, cylindrical, nonlinear theory, displacement field definition 77—41484
  shell, cylindrical, nonuniform axial edge load, thermal load, linear buckling 78—63345
  shell, cylindrical, ribbed, with rectangular holes, design for stability in moment precritical state *(Ukrainian)* 77—50938
  shell, cylindrical, under axial shock, unsymmetrical bulging and buckling *(Russian)* 80—33492
  shell, cylindrical, under external press., vibr. and buckling 80—102975
  shell, damped externally pressurised imperfect cylindrical, dynamic buckling 80—48612
  shell, integrally, stringer stiffened circ., cylindrical, buckling under axial compression 78—63346
  shell, multilayer composite, optimisation, buckling under stability and vibr. conditions *(Russian)* 80—53667
  shell, orthogonally stiffened, buckling eqns. 78—26063
  shell, rigidity characts. *(German)* 80—48608
  shell, spherical, existence and stability of axisymm. buckled states 77—58570
  shell, spherical, externally pressurised, axisymmetric and bifurcation creep buckling 80—43637
  shell, spherical, subjected to external pressure, matching conditions 80—1447
  shell, stiffened, buckling under destabilizing loads including torsion 78—26062
  shell and plate, reinforced, viscoelastic and elastic, with transverse shear strain, stability 77—84171
  shell buckling, nonlinear isometric bifurcation 77—68469
  shell buckling under creep conditions, sequential loading method, deformations anisotropy 80—33495
  shell element computation, triangular facet, linear and nonlinear equilibrium and elastic stability appl. 77—68460
  shell of revolution with slightly curved generator, stability under complex load *(Polish)* 77—54910
  shell stability anal., finite element representation and pressure stiffness 79—90160
  shell structure, 10 ft diameter, imperfection survey, buckling load 77—89023
  shell with multiple stiffener sizes, minimum weight design 78—38218
  shells, angle ply laminated circular cylindrical, buckling closed form solutions 79—64552
  shells, axially compressed circular cylindrical, elastoplastic buckling, nonlinear material behaviour 80—48615
  shells, axially compressed cylindrical and conical, post buckling behaviour, large elastic deflections 80—33490
  shells, axisymmetrical, adaptional possibilities anal. after local buckling *(Polish)* 79—64543
  shells, bifurcation and stability 77—54906
  shells, circular cylindrical, creep buckling and post buckling under axial compression 77—46949
  shells, circular cylindrical, in axial compression, axisymmetric creep buckling, isotropic elasticity 80—69704
  shells, circular cylindrical, under compression, postbuckling and imperfection sensitivity 77—68471
  shells, conical and cylindrical, effect of rib stiffness on buckling under external pressure 77—3757
  shells, cylindrical, axially compressed, localised plastic buckling deformation 80—106735
  shells, cylindrical, imperfect, closely-spaced, dynamics and failure criterion for axial impact 78—30207
  shells, cylindrical, large elastic deflections, numerical anal. 79—98613
  shells, cylindricals, composite, buckling and vibrational response to axial compression 80—64423
  shells, determ. of critical loads by nondestructive methods 77—62181
  shells, elastic-plastic circular cylindrical, under internal pressure, bifurcation 80—64421

buckling continued
  shells, flexible shallow elastic-plastic, natural vibrs. and buckling 80—33519
  shells, imperfect circular cylindrical, under torsion, buckling, initial deflection effects 80—64414
  shells, internally pressurised 2:1 ellipsoidal, elastic and elastic-plastic buckling 79—37206
  shells, laminated composite circular cylindrical, prebuckling deformation effects on buckling 80—48609
  shells, large elastic deflections of axially compressed cylindrical and conical structs. *(Polish)* 78—13937
  shells, long cylindrical, plastic buckling under pure bending 80—64409
  shells, nonconservative isometric buckling loads 79—81748
  shells, oval cylinder, orthogonally stiffened, buckling under axial compression 80—74777
  shells, reticulated, nonlinear strain-displacement relationship, overall buckling 77—54908
  shells, shallow spherical, axisymmetric dynamic buckling 80—87729
  shells, shallow spherical, buckling, pole condition significance 80—64418
  shells, stiffened cylindrical under external load, vibration and buckling correlation 79—50629
  shells, thin walled cylindrical, in axial compression, buckling collapse loads 80—48614
  shells, thin walled cylindrical, Yoshimura buckle pattern 80—48613
  shells, truncated conical, thermal buckling, axisymmetric initial deflections 78—79240
  shells, viscoplastic cylindrical, critical velocity for collapse without buckling 77—65673
  shells of arbitrary geometry, finite element anal. 78—34044
  shells with loaded free edges, pressure stiffness matrix symmetricability, buckling pressure 80—92079
  short cylinders, buckling under 79—37207
  short tubes under external press. 79—14292
  simple frame subject to follower force, divergence buckling, limit point instability 79—18763
  skew plate structures, buckling anal. using B-spline functions 80—28446
  skew plates, simply supported, finite element anal. 78—59319
  snap-buckling of orthotropic shallow spherical shells 79—23234
  solid circular rod, generalised displacement function calcs. 79—7289
  space truss analysis in post-buckling range in dual load method 80—38298
  spherical dome, rib-reinforcement arrangement effect on buckling 79—46237
  spherical shell, buckled states, under uniform external pressure, asymptotic methods and Newton's method 80—43635
  spherical shell, laminated 77—65700
  spinning annular plates reinforced with edge beams, vibration and stability 78—38225
  square box sections—experimental behaviour under combined bending and compression 79—61657
  stability, imperfection sensitivity and isoperimetric variational problems 77—42760
  stability predictions through a succession of folds 79—76991
  stayed columns, concise buckling, vibration and static anal. 79—18755
  stayed columns, concise buckling anal. 79—10511
  steel, high strength sheet, absorbed energy during compression and crushing 77—36593
  steel, shell, circ. integrally stringer-stiffened, buckling under axial compression 78—63346
  steel, stainless, ferritic, tensile strain direction and roping phenomena 77—36533
  steel, stainless, type 304, plastic buckling of cylindrical shells under axial compression 80—74785
  steel beams, inelastic, mild, flexural behaviour and lateral buckling anal. under cyclic loads *(Japanese)* 78—87283
  steel column design, I-section, braced multi-storey, torsional buckling at limit state of collapse 78—1586
  steel plate, thin, in compression, initial deflection and postbuckling behaviour analysis 80—50666
  stiffened cylinder, geometrically imperfect, buckling anal. under axial compression 77—62179
  stiffened imperfect cylindrical shell, buckling under axial compression 77—31228
  stiffened plate, model studies of elastic buckling 77—7324
  stiffened plates, tests on interactive buckling 78—71286
  stiffened thin shells, elastoplastic, buckling and stability *(Chinese)* 79—72824
  straight long rod, dynamical buckling under hammering 79—7312
  strength of orthogonally stiffened plates under uniaxial compression 80—5964
  structural anal., soln. by orthogonal collocation 78—51063
  structural elements, high temp. environment, nonlinear effects 77—3756
  structural member, dynamic loading and plastic response, review 80—83756
  structural systems, elastic critical loads 79—18754
  structures, computational method 78—63342
  structures, direct discrete method for buckling and post-buckling analysis 77—68470
  structures with rotational degrees of freedom, large displacement-small strain anal. 78—89310
  strut creep buckling, damage effects 80—102976
  struts, material with yield plateau *(Japanese)* 77—31232
  struts, plain channel section, in compression and bending 77—46947
  superconducting coil, buckling, vibr., lateral constraint and damping effects 78—63344
  superconducting five coil partial torus, buckling and vibrs. 77—79128
  superconducting ring, buckling in toroidal mag. field 79—64550
  superconducting torus, magnetoelastic buckling experiments 79—64549
  symmetric structures, optimal design against postbuckling collapse 78—51100
  tapered cantilever columns, post buckling finite element anal. 79—1119
  TEM bend-contour patterns 79—99040
  tensioned sheet, with central opening, buckling behaviour and parametric reson. investigation 78—90759
  tensioned sheet with edge slot, buckling load, expt. on Al 77—54909
  tensioned sheet with rectangular opening, static and dynamic behaviour 77—27482
  thermal, of heated plates on elastic foundation 77—31229
  thermal buckling of truncated conical shells with various axisymmetric initial deflections, finite-difference anal. 79—90162
  thermal initial post buckling of extensional rod 77—14931

- **buckling** continued
  - thermally buckled finite element panel, flutter anal. 77—11143
  - thick cylinders, static and dynamic instability 80—23923
  - thin elastic bar, impact buckling, Monte Carlo calcs. 79—32317
  - thin elastic plate, birfurcation theory for case of unilateral conditions 78—22283
  - thin elastic plate, dynamic buckling, nonlinear theory 79—37160
  - thin plate elastic-plastic buckling, Hencky effects, von Karman nonlinear strain *(French)* 80—58942
  - thin plates with cracks, local buckling *(Ukrainian)* 77—68461
  - thin-walled beams with initial stresses and initial deformations, lateral buckling 80—1448
  - thin-walled sections, secondary local buckling 79—98644
  - Thornel 300/Fiberite 1034 graphite epoxy composite, elastic moduli, environmental effects 77—86068
  - three hinged circular arch, initial postbuckling 80—64422
  - three-layer plates, circular, stability 80—79188
  - tie column of solid construction, Euler buckling load maximisation 79—23230
  - torispherical vessel heads, elastic-plastic internally pressurized, stresses and buckling 77—58574
  - torispherical vessel heads, internally pressurised, elastic-plastic buckling 78—79241
  - toroidal shell segment subject to external press., stability and postbuckling deform. 79—41595
  - toroidal shell with external press., stability 79—41596
  - toroidal shells and tubes, flexible shell theory and buckling 79—23231
  - truncated conical shells, thermal buckling 77—68467
  - truss struct., accurate nonlinear anal. 79—90159
  - tube, thick walled neo-Hookean, stability under end thrust and external pressure 77—39239
  - tubes, circular cylindrical, critical bending moment 77—68468
  - two-bar frame, dynamic snap-through buckling under suddenly applied load 80—53669
  - two-bar frame, eccentrically loaded, nonlinear stability anal. 78—63343
  - two-mode buckling, asymptotic anal., relation to catastrophe theory 78—34042
  - umbilic catastrophes, buckling mode 78—20945
  - viscida, buckling and stretching, surface tension effects 79—10512
  - visco-plastic approach to plasticity and creep problems, involving geom. nonlinearities 78—26050
  - viscoelastic plate, buckling and stability, convolution var. principle 77—35052
  - viscoelastic plates, buckling 78—13932
  - viscoelastic shell, thick-walled, deform. in post critical stage 77—58566
  - webs, thin, under partial edge loading, stress state obs., influence of longitudinal stiffening determ. 80—79857
  - yielding of plates with hardening and large deformations 78—59311
  - Al alloy 7075-T6, buckling under axial compression on circ. integrally stringer-stiffened shell 78—63346
  - Al alloy cylindrical shells, buckling under combined axial preload, nonuniform heating and torque 80—53662
  - Al, open-section stiffened compression panel, buckling and struct. efficiency 77—35061
  - Al sheet, critical stress intensity factor determ., antibuckling constraint effect 77—40502
  - Al-bronze, input energy, hysteresis, and fracture in low cycle buckling fatigue, superelastic range 78—31527
  - Al-bronze, single crystal rod, energy dissipation, deformed by cyclic buckling in superelastic range 78—31479
  - C fibre, flexural fatigue and surface abrasion 78—15504
  - Fe base superalloy, type A-286, elevated temp. fracture toughness testing of thin section irrad. materials 80—61063
  - Mg-Al cylindrical shells, loading history, effect on plastic buckling *(Russian)* 79—14288
  - PuO_2-UO_2 critical clusters in D_2O, perturbation anal. of buckling 78—29573
  - $(SN)_x$, deform. and defects, lattice strain, fibrillation 80—3139
  - Si thin ribbon grown at high speed, thermal stresses, reduced thermal buckling 80—107078
  - U, natural, lattice param. for rod clusters in D_2O, buckling anal. 77—6484
  - UO_2 critical clusters in D_2O perturbation anal. of buckling 78—29573
- **buffer circuits**
  - asynchronous/synchronous FIFO data buffer *(German)* 77—9996
  - multichannel analyser buffer store, 4096 channel sequential memory, control circuitry 77—57829
  - two-dimensional buffer store based on a multichannel amplitude analyzer 79—26838
  - unity gain follower with buffer for electrophysiological meas. 79—12048
- **buffers (circuits)** *see buffer circuits*
- **building**
  - *see also architecture; civil engineering; erection*
  - air conditioning system using heat storage tank, energy saving control system *(Japanese)* 80—72087
  - architectural acoustics of solid-borne sound, propagation characts., field and model expts. *(Japanese)* 80—64290
  - beams, eqn. of motion of large amplitude vibration of beams *(Japanese)* 80—33511
  - broadcasting studio, 'Deutsche Welle' building construction and meas. *(German)* 80—106668
  - BWR power plant, construction experience 78—86673
  - CANDU plant construction, Bruce nuclear power development, Ontario Hydro 78—86676
  - chimney stacks, prediction transport, dispersion air pollutants, computer program appl. 77—73836
  - codes for seismic zones and earthquake resonant period effects on buildings 77—70602
  - conference, nuclear power plant construction, operation and development, Tokyo, Japan (Sept. 78) 78—86672
  - cooling, solar, in Turkmenian SSR, using open water evaporation, from LiCl solution 79—57463
  - cooling of low-cost houses in Brazil, evaporative and night sky cooling system design and testing 79—62132
  - diffuse reflectance meas. for buildings 80—27334
  - domestic roofing sound insulation, test details, appl. to building industry 80—79058
  - domestic water supply system, hydraulic noise control by energy absorption technique appl. 77—19487
  - earthquake resistant design of offshore building structures 79—12089
- **building** continued
  - embedded foundations, soil-structure interaction problem, spring method 78—79216
  - energy conservation measures obs. and evaluation, Philips expt. house (West German project) 79—61951
  - engineering design to resist earthquake loading 80—81844
  - environmental noise, study re. nuclear power plant construction 78—87194
  - environmental noise controls, new housing sites 80—48505
  - foundation dynamic interaction with viscoelastic half-space *(German)* 78—79228
  - glass application, review 78—3307
  - heat balances of apartment house, in Dutch climate, energy conserving measures 79—61948
  - heat loss meas. using IR TV system 77—45837
  - heat transfer, fundamentals in reln. to heating and cooling load calcs. 78—90628
  - heat transmission of porous walls with air filtration ventilation 79—4016
  - heating, solar, types, construction and thermal and environmental parameters *(French)* 80—85268
  - heating, ventilating and air conditioning, diesel-driven chiller system simulation, with multi-tank thermal storage system 79—48187
  - heating and ventilation, solar and wind energy combination, Danish design 79—57411
  - heating of single family dwellings, heat pump appl., computer-aided analysis 79—43784
  - hospital supply of medical gases, central source, pipelines, O_2, N_2O, compressed air, vacuum appl. 77—90942
  - housing estate heat supply methods comparison *(Hungarian)* 79—2366
  - indoor climate research, anemometers modification and calibration 77—3897
  - insulation, optimal, w.r.t. internal and solar gains, calc. using degree day method 79—62147
  - luminous flux distrib. in room, electrical analogy 80—33266
  - microzonation for safer construction, proceedings of international conf. (San Francisco, 1978 Nov. 26-Dec. 1) 79—88269
  - multistorey buildings, reduction of structure-borne sound levels by floors and walls *(German)* 78—94483
  - noise insulation near airports 78—55508
  - nuclear plant, FUGEN project, Japan, construction and start-up 78—86675
  - nuclear power plant *(Korean)* 78—54819
  - nuclear power plants, construction and engineering problems, layout aspects 78—86702
  - nuclear power stations, construction in the USSR 79—646
  - oxidation and corrosion induced deformation effects 80—3211
  - partially buried, heat flux through soil, calc. *(German)* 78—55554
  - retaining walls, elastic behaviour conoid, cylindrical shells, numerical methods 78—5655
  - solar air heating system, Toshiba Solar House No. 1 performance 79—57458
  - solar cell modules appl., shingle-type mounted on roofs 79—52907
  - solar dwelling independent of servicing networks, digital simulation 79—62149
  - solar energy systems evaluation, passive, use of thermal modelling and 'predicted percentage dissatisfied' 79—62145
  - solar heating, demonstration plant in Athens 79—57410
  - solar heating, of Japanese multi-family housing unit, comparison with expt. results 79—57455
  - solar heating, of North Indian houses, using south walls as collectors, expt. results 79—62152
  - solar heating, transient thermal flux calc. 79—62144
  - solar heating, West German BBC Solar House (Heidelberg) design, operation and performance 79—57405
  - solar heating and air conditioning, financial building (1100 m^2) 79—57465
  - solar heating and cooling, evacuated tubular solar collectors and LiBr absorption system integration 79—62135
  - solar heating and cooling systems performance, US national demonstration program 79—62128
  - solar heating equipment, use of heat tube 79—57412
  - solar heating system, for winter use, technical and economic feasibility 79—62136
  - solar heating/cooling, periodic heat transfer analysis 79—62148
  - solar power utilisation in office complex design, up to 70% energy savings 80—40831
  - solar space heating, with all-air systems, experiences with CSU Solar House II 79—57406
  - solar total energy system, for US Army base buildings, conceptual design and large-scale expt. 79—52899
  - solar total energy system, preliminary design 79—52898
  - stack close to building, necessary height determ. by wind tunnel study 77—2225
  - Taipower, completion of first power plant, construction experience, testing and start-up 78—86674
  - technical meteorology, technical and commercial appls. *(German)* 80—46231
  - thermal energy balance, method for including environmental modulation *(French)* 79—3900
  - thermal environmental control in Northern India, using roof for heat and coolness storage 79—62151
  - thermal insulation, heat conduction in disperse media *(Hungarian)* 79—1056
  - turbulence in atmosphere lower boundary layer, influence of built-up area *(Russian)* 78—44925
  - unsaturated water flow within porous materials, obs. by NMR imaging 79—98840
  - wind and seismic effects, 8th meeting of US-Japan Panel (Gaithersburg, MD, 18-21 May 1976) 77—78395
  - wind effects, engineering model of nonstationary atmosphere boundary layer *(Russian)* 77—5280
  - wind velocity gust factors, analytical approach 78—88897
  - Rn barrier, interior of building structs. foundations built on U mill tailings material 79—2138
  - Rn, diffusion coefficient and exhalation rate from building materials, meas. technique 80—4694
- **bulk density** *see density*
- **bulk diffusion** *see diffusion in solids*
- **bundling** *see packaging*
- **burning** *see combustion*

- **burnout** *see combustion*
- **burst noise** *see random noise*
- **bus conductors (electric)** *see busbars*
- **busbars**
  - EM force dynamic regime of current-carrying bars *(Rumanian)* 79—72455
  - laser fusion reactor, NOVA, pulsed power control system, fibre-optic multi-tapped computer bus 80—95443
- **bushes** *see bushings*
- **bushings**
  - HV, high vacuum, for cryogenic appl. 78—81977
  - Cu-C bushings, powder metallurgically prepared, exam. of friction and wear charact. 79—15813
- **business** *see commerce*
- **BWT** *see backward-wave tubes*
- **C invariance**
  - $\Delta I=1/2$ rule violation of order of charge symmetry breaking 79—93377
  - baryon asymmetry of the Universe, quantum black hole evaporation *(Russian)* 80—109577
  - charmed particles weak decays, generalised charge symm. 78—37184
  - chiral symmetry spontaneous breaking, using vacuum stability condition 79—35986
  - conformal motions coupled to gauge transforms, charge conservation 80—62835
  - Dirac equation, two-component first-order equations for the quantum-relativistic electron 79—17649
  - disconnected gauge groups and the global violation of charge conservation 78—78086
  - Einstein-Maxwell field eqns., and charge conservation 77—5716
  - electric charge conservation *(Russian)* 78—77739
  - Glashow-Iliopoulos-Maiani model, charge symmetry violation 77—18194
  - hadron-hadron 3-jet collisions, charge conjugation asymmetries and trilinear gluon coupling 80—105934
  - heavy nuclei, contrib. of charge-symmetry-breaking nuclear forces to nuclear binding energy 79—75826
  - massive particles with any spin. consistent eqns., Klein-Gordon divisor, review 80—73577
  - metric-torsion gravitational theories, charge conservation 78—45544
  - (non)conservation of isospin, parity, charge conjugation, and time reversal invariance in intermediate energy phys. 79—80772
  - nucleonic form factor, pion exchange, model 80—22608
  - QED, depend. of sign on q^2 79—35974
  - QED, renormalisation group equations, invariant charge function 80—57529
  - quantum field theory, relativistic, discrete symmetries 80—68387
  - relativistic classical nonlinear field theory, PCT violation 77—65081
  - relativistic QFT, spontaneous symmetry violations 80—52411
  - S-matrix theory of overlapping resonances, constraints imposed by analyticity and unitarity 77—22656
  - SU(5), unification of weak, EM and strong interactions, review 80—105814
  - supergravitation, calibration invariance *(Russian)* 78—4548
  - superheavy boson decay, neutrino number and isotropy of Universe in grand unified theories 80—85852
  - tests in strong and electromagnetic interactions 77—57532
  - Weinberg model, spontaneous CP violation 77—26480
  - e decay, lifetime, charge nonconservation, paradoxes 79—6335
  - e^+e^-, weak corrections to three-jet angular distributions 80—22629
  - $e^+e^-\rightarrow F\bar{F}$, with polarised particles, weak asymmetries, unified gauge theory anal. 78—8636
  - eN elastic scatt., polarisation effects, C- and T-invariance perturbation *(Russian)* 77—10256
  - $np\rightarrow d\pi^0$, charge symmetry violation, symmetry breaking mechanism 79—85313
  - $\bar{p}p$, 2.32 GeV/c, cross-sections, C-invariance, π and ρ^0 multiplicities anal. 78—41569
  - $p\bar{p}$ interactions, test of charge-conjugation invariance 78—66145
  - $\bar{p}p\rightarrow K^+K^-\pi^+\pi^-$, 2.32 GeV/c, cross section, C conservation, errors 78—21446
  - $\bar{p}p\rightarrow\pi^+\pi^-$, polarised target, charge parity determ. 77—57567
  - π, photoproduction in $E<450$ MeV region, dispersion relations, CT invariance, review, book contrib. 80—47311
  - $\pi^0\rightarrow 3\gamma$, C-noninvariant decay, branching ratio upper limit 80—47297
  - $\pi^0\rightarrow 3\gamma$, C-noninvariant decay 78—82203
  - $^3H_\Lambda$, charge symm. breaking, Λ separation energy in hypertriton 78—17132
  - $^3H_\Lambda$, charge symm. breaking considerations for hypertriton 78—17133
  - $^{87}Rb\rightarrow{}^{87}Sr+$neutrals, nucleon charge conservation, improved test 80—5098
- **cable insulation**
  - *see also insulating oils*
  - EHD pumping of cable oil 78—87414
  - flame resistant, for nuclear power stations, develop. and qualification tests 79—687
  - flameproof coating for PVC insulated cables, composition, tests *(Russian)* 78—68828
  - high molecular weight polyethylene, characterisation using size exclusion chromatography 80—66897
  - HV cable, PE-insulated, electron beam crosslinking process development 80—66846
  - International wire and cable symposium, Cherry Hill USA (Nov. 1978) 79—37018
  - LAMPF mineral-insulated magnet experience 79—31248
  - liquid dielectrics, thermal performance estimation 80—88582
  - mineral insulated cables in nuclear reactor instrumentation *(German)* 77—6573
  - plastic, of HV and MV cables, dielectric breakdown obs., distribution law parameters estimation *(French)* 77—24794
  - plastics, extrusion props. prediction using capillary rheometer 79—90204
  - polycarbonate, plastic insulation for cryogenic power cable, exam. of dielectric, tensile props. 80—25823
  - polyester (Mylar), plastic insulation for cryogenic power cable, exam. of dielectric, tensile props. 80—25823
  - polyethylene, ageing prediction by isothermal differential scanning calorimetry 78—11485
  - polyethylene, elec. trees free radical ESR study 78—60393
  - polyethylene, low temp. dielec. loss due to antioxidants 79—99822
  - polyethylene, migration and solubility of antioxidants *(French)* 79—46839
- **cable insulation** continued
  - polyethylene, plastic insulation for cryogenic power cable, exam. of dielectric, tensile props. 80—25823
  - polyethylene insulation of HV cables, water-treeing, environmental stress cracking phenomenon of elec. origin 80—40575
  - polyethylene treeing inception voltage, effect of blending and crosslinking 78—43788
  - polymeric cable insulation, radiation modification using electron beams 80—66848
  - polymeric insulating materials, water treeing initiation and growth, effects on cable service life 80—84698
  - polyolefin, cross-linked, insulation system for wire and cable for locomotives 80—66851
  - polyolefin, cross-linked, irradiation appl. to provide improved insulation props. to wires and cables 80—66850
  - polypropylene, plastic insulation for cryogenic power cable, exam. of dielectric, tensile props. 80—25823
  - polysulphone, plastic insulation for cryogenic power cable, exam. of dielectric, tensile props. 80—25823
  - power cables, dry insulation, materials used and characteristics *(Spanish)* 80—81024
  - PVC, cross-linked, irradiation appl. to provide improved insulation props. to wires and cables 80—66850
  - PVC materials, cross-linkable, for wires and cable insulation 80—66849
  - radiation resistance of cable insulating materials for nuclear power stations, expt. 78—59835
  - sheath and insulating materials for wire and cables, crosslinking by irradiation 80—66845
  - solid dielectrics, treeing 78—80285
  - XLPE from HV cables, high-pressure liquid chromatography and differential scanning calorimetry 79—100466
  - Al_2O_3, resistance to high-temp. and intense gamma radiation 78—25332
  - He, liq., elec. discharges at low temps., appl. to elec. insulation for supercond. cables 77—27757
  - He, supercritical, dielec. breakdown 79—65796
  - MgO, resistance to high-temp. and intense gamma radiation 78—25332
- **cable jointing**
  - duplex fibre-optic cable interconnection system 78—46801
  - fibre bundle, termination and polishing using portable tools 77—79977
  - fibre optic connector design eliminating tolerance effects 78—46803
  - fusion reactor, Large Coil Program, low temp. stability, joints, design method 80—106195
  - fusion reactors, Torsatron T-1, demountable resistive joint for high current superconductors 80—106202
  - fusion-welded optical fibre splice loss expts. 79—37023
  - grooved chips, for fibre-optic array splice improvement 77—19456
  - monomode optical fibre dimensions, dispersion, and losses *(German)* 78—33866
  - optical cable splicing, injection-moulded plastic connector 77—11054
  - optical data collection line coupling methods *(German)* 77—62062
  - optical fibre, development and experience 78—9460
  - optical fibre, in-the-field connections 80—69545
  - optical fibre, joint and connector losses *(French)* 78—55464
  - optical fibre and cable splicing and sheath jointing expts. 80—23806
  - optical fibre bandwidth change under production process and splicing *(German)* 78—33858
  - optical fibre cable construction, installation, and testing 78—46797
  - optical fibre cable construction and jointing 77—72075
  - optical fibre cable design, splicing and interconnection system developments 78—42431
  - optical fibre cable splice methods *(Japanese)* 80—58690
  - optical fibre cable structure, jointing procedure *(French)* 78—42459
  - optical fibre connectors, single- and multi-fibre, basic construction *(Japanese)* 80—87509
  - optical fibre cutting tool and automatic splicing machine 80—87575
  - optical fibre demountable connector using injection-moulded thermoplastics 80—53472
  - optical fibre fusing of data highway junctions 77—39097
  - optical fibre fusion splices by discharge heating 78—75007
  - optical fibre jointing by plastic tape wrapping *(German)* 78—38096
  - optical fibre jointing techniques and connections to communication equipment *(Norwegian)* 80—64179
  - optical fibre ribbon splicing with vacuum-assisted injection mould 80—53491
  - optical fibre ribbon-splicing injection-moulded connector with Si chip insert 78—1412
  - optical fibre slicing by collapsed glass sleeve *(German)* 78—38097
  - optical fibre splice delay distortion characteristics, shuttle pulse meas. 77—19457
  - optical fibre splicing, arc fusion, protection and reliability 80—69565
  - optical fibre splicing characteristics and techniques 78—46798
  - optical fibre splicing technique for multifibre cables using slippery fibre holder 79—50471
  - optical fibre splicing techniques 78—79147
  - optical fibre splicing techniques and strategies affecting cable design 78—1408
  - optical fibre splicing techniques for multiple units cable structure *(French)* 77—11021
  - optical fibre splicing using low MP glass solder 79—55252
  - optical fibre systems, effect of system parameters on joint loss 79—50435
  - optical fibres, fabrication and coupling *(French)* 79—68447
  - optical fibres, meas. method of connection loss using steady-state power distrib. 79—46084
  - optical fibres, observation of cascade effect for splices 79—50436
  - optical fibres, single-mode, low-loss detachable connector 79—90022
  - optical fibres, single-mode, splicing method based on discharge fusion 79—90021
  - optical fibres, single-mode, splicing method based on discharge fusion *(Japanese)* 80—28317
  - optical fibres, splicing and connection techniques *(Italian)* 80—38097
  - optical transmission-line cable joining device 79—68433
  - silicone resin clad fibre technology, optical and mech. props. 80—28349
  - single fibre optic cable connector losses 78—46802
  - single-mode fibre low-loss splicing by tapered butt joint method 79—50409
  - underwater electric cable terminations 78—45041
  - Si alignment chips for optical fibre cable connector 78—1411
- **cable laying**
  - 2.1 km optical cable link installation, TV and telephonic transmission expt. *(German)* 78—33890

cable laying continued
- fibre-optic cable design, testing and installation 79—37026
- fibre-optic cable design and installation, environmental considerations 79—94362
- fibre-optic cable manufacture, testing, and installation *(German)* 78—33863
- optical fibre, mechanical performance characterisation methods *(German)* 78—33870
- optical fibre 1.8 km cable, operational, installation underground *(German)* 79—3783
- optical fibre cable construction, installation, and testing 78—46797
- optical fibre cable stress during manufacture and installation 79—37024
- optical fibre cable transmission performance in operational ducts *(German)* 78—33864
- power station fibre-optic system installation 79—37028
- sonar for submarine cable-laying 78—5620
- telephone, underground, seismology appl., rocks location verification 80—72456

cable sheathing
- 9 km fibre-optic telephone transmission system 78—42435
- high-density low-loss optical fibre unit and cable 80—53468
- HV, Rb coverings quality estimation using mechanical tests *(Polish)* 80—97525
- insulating and sheath materials for wire and cable, crosslinking by irradiation 80—66845
- jacketed optical fibre residual stress diagnosis, pulse delay technique 80—53469
- medium-range data transmission optical cables 77—39096
- optical fibre, jacketed and cabled, low-temp. attenuation increase 80—58732
- optical fibre and cable splicing and sheath jointing expts. 80—23806
- optical fibre jacket eccentricity tolerance criteria *(German)* 78—38008
- optical fibre ribbon cable sheath 79—7203
- optical fibres, deformation of cable sheath by bending in plastic range, loss anal. 80—43477
- satellite shielded cables, hardening techniques for reducing X-ray response 79—23642

cable sheaths *see cable sheathing*

cable television
- 2.1 km optical cable link installation, TV and telephonic transmission expt. *(German)* 78—33890
- fibre optic, VSB-FDM system for video trunking, transmission performance 77—62054
- fibre optic Dial-a-Program CATV system, field trial in Holland 79—10262
- fibre-optic directional coupler developments and applications 79—94330
- optical link, experimental loop system field trial 79—72707
- optical two-way TV transmission using single optical fibre and two light sources 79—27419

cables (electric)
- *see also coaxial cables; power cables; submarine cables; superconducting cables; telecommunication cables; underground cables*
- aerial prospecting magnetometer cable length optimisation *(Russian)* 77—73881
- ECG cable continuity tester 77—77997
- flame resistant, for nuclear power stations, develop. and qualification tests 79—687
- flex lead, Ag-Cu corrosion study 80—76406
- International wire and cable symposium, Cherry Hill USA (Nov. 1978) 79—37018
- magnetic fluid (cable coolant), natural convection heat transfer 78—94846
- mineral insulated, radiation induced currents 80—65037
- nuclear power station cables, deterioration test *(Japanese)* 80—27743
- nuclear reactor LOCA environments, damage mechanisms to cables 80—13658
- nuclear reactor power and control cable tests to IEEE standards 80—57884
- oceanographic two-stage mooring design and performance test 77—5365
- optical fibre cables, longitudinal stress in fibres due to twisting in manufacture, anal. 78—30048
- overhead wave solns. of wire dynamics 77—35028
- polyethylene, electric cables, anal. of breaking strength distrib. *(Japanese)* 78—84921
- reactor instrumentation systems 79—76111
- satellite shielded cables, hardening techniques for reducing X-ray response 79—23642
- shielded cables, nonlinearities and multiple exposure anomalies at CASINO, MCCABE code verification 78—58502
- steel ropes, electromagnetic NDT method for cylindrically layered conductors 79—74318
- thermocouple extension leads, universal, geometry of connection 80—57294
- MgO insulated high voltage instrument cables for 650°C, in-vessel breeder reactor service 80—57878

CAD
- *see also architectural CAD; circuit CAD; computer-aided analysis; control system CAD; electric machine CAD; interactive systems; logic CAD; power system CAD*
- 2.6 T supercond. magnet design and manufacture for polarised target 79—31293
- ACCOS V, commercially available optical design and anal. program 79—86230
- ACCOS V program for diffraction evaluation of general optical systems 79—86231
- acoustic design, interior, based on digital meas. techniques *(Polish)* 78—59205
- Adone storage ring transverse wiggler magnet design 79—41054
- air cool transformers for fusion reactors, computer aided design 80—18662
- air pollution density distrib., flow pattern in Tanabe area, Japan, numerical anal. *(Japanese)* 78—96289
- airfoils, lifting, design procedure in transonic flow by integral method *(German)* 77—35163
- alloy design by automatic modelling, CAD system *(Japanese)* 77—52607
- applied mechanics computing, conference, New York (1976) 77—67285
- automatic lens design, pseudo-second-derivative matrix computation 79—14077
- chemical synthesis computer design, interactive strategy 79—91945

CAD continued
- Cherenkov counter using thick liquid H radiators to distinguish pions from kaons 78—37509
- collimator monochromatic MTF computation program 80—14451
- cooled epoxy resin vacuum mould computational simulation of design *(German)* 80—81020
- corrector lens for color television tube 79—86243
- cryogenic refrigeration system, computer design and optimisation 79—71457
- cryogenic refrigeration system, computer design and optimization 79—58750
- curved electron beam system with strong deceleration at collector region, optimisation 78—74106
- deformable mirror design and resonance damping 79—59794
- diffuse system design, optimum conditions, appl. to optical system 78—50886
- disc impedance meas. and US transducer CAD program 79—46157
- dither signals for binary display of images 79—94161
- ECG leads 80—85526
- electromagnet, GFUN program with interactive graphics 77—18053
- electronic systems, analog signal processing, book 80—86047
- electrostatic lens systems, non-rotationally symmetric 77—79740
- engine muffler design, scaling rules using Buckingham's pi principle 79—14152
- engineering design curricula, computer appls. 80—27065
- films, deposition profile with shadow effect, theoretical model 79—82473
- fission reactor pressure vessels, high temperature design system *(Japanese)* 78—673
- flowmeter standard orifice plate calc., for meas. flowrate of liquids, gases and vapours 80—1714
- fluid channels indirect design using global variational method with trial functions 77—27595
- focus determ. for lens tolerancing computer program 79—86240
- forward-looking IR type optical system design programs 79—23047
- Fourier optical evaluation techniques, user oriented 79—86131
- fusion reactor, TNS, electrical design costing 78—55014
- fusion reactor, Tokamak constant tension D-shaped coils, lateral support struct. 78—55013
- gapped pot core and Permalloy foil pressure transducer 79—75520
- graphical designer work station link for ES computers 79—30442
- heat exchanger optimisation 79—3895
- holographic lens design techniques, 488 nm construction, 633 nm read out 79—89866
- holographic optical element design using analogous lens model 78—58955
- holographic spatial filter, optimisation method *(Russian)* 80—28171
- holographic visor helmet-mounted display, optical design 79—86149
- inductive displacement-measuring system synthesis using CAD 78—73982
- infography in automated graphical design *(French)* 77—87747
- instrument CAD considerations *(Hungarian)* 79—93134
- ion beam instrumentation systems 77—13819
- ion extractor electrode CAD *(Japanese)* 78—86680
- IR cryogenic sensors, CAD and evaluation 79—85184
- IR optical systems design, future computer program requirements 79—86260
- IR sensor, spinning cryogenic, integrated thermal/structural/optical evaluations 78—82040
- klystron, high-power, low freq., for LAMPF 77—83174
- large-aperture Pockels cell design 77—19438
- laser galvanometer scanning system, CAD 77—58475
- laser scanning components and techniques, conference, San Diego (1976) 77—58474
- lens, aspheric, stigmatic, for ruby or He-Ne laser *(Czech)* 78—55427
- lens design, automatic, algorithm for accelerating convergence 80—38085
- lens design and ghost focus problem in fusion lasers 79—86247
- lens design computer programs, intercomparison 79—86234
- lens design optimisation, Version 14 program 78—90488
- lens design program 79—86233
- lens first-order design, three-lens zoom system 80—43424
- lens system design with extended depth of focus, Version 14 optimisation program 78—90489
- LMFBR, pool-type, design effect on natural circulation establishment 77—6487
- LMFBR core orificing computer code 79—9681
- magnet design for high-current implanters or small isotope separators 80—68222
- magnet design module, for fusion reactor system 77—23261
- magnetic field computation, conference, Grenoble (1978) 79—41262
- magnetic lens design, finite element program improvement 80—69316
- measuring systems, systematic design 80—95094
- minicomputer optical design and analysis program 79—14075
- MTF tolerancing computer program 80—78934
- multilayer radiation shielding optimisation, conversational procedure 77—14273
- multimode optical fibre optimum refractive index profile 77—14802
- multislit spectrometer for the night airglow observation 78—73542
- Nd:glass 20-beam fusion laser focusing lens design 77—18706
- nuclear reactor, ZOCO VI program appl. *(German)* 78—21668
- optical CAD, conf., San Diego, CA, USA (Aug. 1978) 79—86228
- optical design, contemporary, aspects 80—23766
- optical design, optimisation and interactive graphics improvements 80—78933
- optical design computer programs 79—36977
- optical design techniques, for desk and pocket calculators 78—71181
- optical fibre communication systems, design aids 80—28350
- optical filters, multilayer, thin films, automatic design method 77—58449
- optical multilayer synthesis program, Fourier transform model 79—7196
- optical processing, nonlinear, half-tone screen design methods 79—98294
- optical spectral instrument CAD status and prospects 79—44939
- optical system, k-stage objectives corrected to infinity *(Hungarian)* 79—81502
- optical system design 79—94322
- optical system surfaces *(Russian)* 78—74963
- optical system with annular pupil, orthogonal polynomials, appl. to Fraunhofer diffr. 78—50714
- optical waveguide manufacture appl. *(Italian)* 77—19385
- optical well-baffled axially symmetric system design program GOSBOP 80—78940
- optimised spheric and aspheric optical systems for thermal IR 79—86244
- OTF calculation using gaussian quadrature, rel. to lens system design 78—90383
- paraxial solves in lens design, ACCOS V program style 79—86229

CAD continued
plates, circular, rigid-plastic, optimal design, variational formulation 77—68440
potential flow 2-D bodies synthesis with limited interactive graphics 77—11166
precision-mechanical design, stress distribution of frictional bonds, computing, w.r.t. elastic deformation *(Hungarian)* 79—14275
pressure transducer design, for biomedical instrumentation students 77—45656
pressure vessel, programs and appls. *(Japanese)* 79—21555
prism, Fresnel rhomb, TI 58/59 program 79—32040
prism, rhombic, dimensional design *(Czech)* 80—53431
production cost reduction appl. 79—86239
ray trace program, TI59 calculator 79—32023
ray tracing, generalised, caustic surfaces 79—23043
ray tracing algorithm for programmable pocket calculator 79—81508
reflection conic, obtaining 360 degree panorama 79—86246
reflective and catadioptric systems 79—86242
secondary cells, Pb-acid, cell design analysis computing for optimal electrical performance characterisitics 80—55832
semiconductor device, appl. of parallel computers in University research 79—54114
solar building, using Cal-ERDA programs 79—57456
solar buildings, climatological design assessment interactive CAD techniques 80—61289
solar collectors, passive, window's energy profile determ., using interactive program 79—62146
solar heating and air conditioning system, w.r.t. maximum solar heat gain 79—57466
solar input determination and irradiance maps, analytical model and simulation code 79—34426
sound system design aid, HP 97 program 78—75015
spot diagram automatic computation and plotting program 79—72645
strength of axisymmetric body, optimum shape calc., finite element technique 78—51060
structural dynamics analyser development, microcomputer-based 80—53733
tapered light guide condenser design approach 80—33218
tolerance sensitivities inclusion in merit function for lens optimisation 79—86236
tolerancing procedure based on MTF, lens appl. 79—86237
TRANSPORT, design program for charged particle beam transport systems 80—106220
two-beam laser fusion target illumination system design 77—19292
US Doppler flowmeter spectra for asymm. transducers 78—31880
US transducer thickness mode design, computer simulation using Thevenin equivalent ccts. 78—30143
water quality monitoring system CAD 77—41100
wide field of view high resolution reflecting optics, design techniques 79—86241
zoom and multiconfiguration optimization using the indices of refraction to represent zoom modes 79—86232
CO_2 laser fusion systems, optical design approach for design and assembly 79—86193

cadmium
see also nuclei with ......
absorpt. spectra, line and total absorpt. comparison 80—11991
abundance in sedimentary rocks and stream sediments, geochem. 78—36170
adsorption by Al_2O_3, radioactive waste storage 80—99240
adsorption of Cd on Ge (111), combined RHEED-mol. beam obs. 77—4255
AES, $M_{4,5}N_{4,5}N_{4,5}$, vap. and solid, solid state effects 77—61857
AES and XPS, vapour-metal electron energy shifts 80—16142
AF magnetic field penetration exam. using RF size effect 77—43635
anharmonic interactions, elastic X-ray scatt. 78—75755
anisotropic behaviour of Poisson's ratio, Young's modulus, shear modulus 77—11622
anisotropic thermal expansion 79—23750
atom, $4d^{10}$ subshell photoelectron ang. distrib. 80—14123
atom, $4d^{-1}5p^1P$ autoionising state, electron impact ionisation obs., distortion effects calcs. 80—83491
atom, 5^3P_1 autoionising state, 150 eV electron impact excitation, (e, 2e) ang. distrib. study 80—83495
atom, 5^3P, state, electronic energy transfer to POPOP vap., laser appl. 77—30980
atom, $5,6,7^1D_2 \rightarrow 5^1P_1$ transition probabilities meas. be US pulverisation/flame emission *(French)* 80—42995
atom, 5s5d states, Stark effect *(French)* 80—9543
atom, $5s5p^3P_1$-$5s^2\ ^1S_0$ intercombination line, press. broadening and shift 80—95564
atom, 6^3P_1 level, relax. of alignment and population 78—70795
atom, ^1S, ^3P, ^1P states, dipole polarisabilities from compact variational trial functions 80—63568
atom, (5s7s), (5s6d), (5s7d) configs., triplet state lifetimes *(French)* 77—3326
atom, $(ns\ nd)^1D_2$ states, Hanle effect, alignment destruction by collisions *(French)* 78—5324
atom, absolute photoabsorption. cross section, 40-250 eV 78—58613
atom, absorption spectrum, simultaneous excitation of two electrons 78—58614
atom, Breit-Margenau correction, relativistic calcs. 77—3281
atom, core binding energies, gas phase X-ray photoelectron spectra 78—37611
atom, effective core potentials calcs. rel. to bond lengths and energies 78—66464
atom, electron impact, 6^2D_2 and 7^1P_1 level mixing 80—37889
atom, electron impact, ejected electron spectrum of autoionis. levels 77—27185
atom, electron impact ionisation cross-sections for excited states 80—9742
atom, excitation by slow electrons 79—72428
atom, ground and metastable status, Li^+ electron capture cross sections 10-60 keV 80—48084
atom, ground state correl., photoelectron spectra, multiconfig. Hartree-Fock calcs. 77—50471
atom, inner core neutral binding energies, relaxed orbital relativistic Hartree-Fock-Slater calc. 78—13433
atom, integral Compton scatt. cross sections, of γ-rays from K-shell electrons 78—58643

cadmium continued
atom, integral K-shell Compton scattering, cross-section, for 1250 keV photons 78—90128
atom, $K\beta_3/K\beta_1$ and $K\beta_2/K\beta_1$ relative intensities 77—75088
atom, K-shell photoelectric cross section 79—22676
atom, K-shell X-ray spectra, $K\beta_2/K\beta_1$ determ. 77—23456
atom, $L\alpha$ X-ray spectra, $_{40}Zr$ to $_{48}Cd$, linewidths 79—41131
atom, low energy electron scatt., shape resonances, electron affinity 77—14581
atom, n^1S_0 and n^1D_2 levels lifetimes, time-resolved spectrosc. obs. *(French)* 80—102456
atom, nonadiabatic transitions in two-level system 79—98014
atom, partial photoionis. cross section 78—42022
atom, photoionisation, alignment, linear polarisation 77—83556
atom, photoionisation cross section, many-body perturbation theory, dipole length and vel. calc. 78—78674
atom, quadrupole antishielding factors, Hartree-Fock perturbation theory 78—62723
atom, Stark interaction in $nspz^3P_1$ levels, optical double resonance obs. 79—63941
atom, transition probabilities, 5^1P_2 level lifetime meas. 80—91500
atom, triplet states, hyperfine struct. obs., project expt. 77—33737
atom, UV photoelectron spectra, wavelength depend. of satellite struct. 77—34597
atom, XPS and XES, dynamical effects 80—52924
atomic fluoresc., slow electron excitation 80—938
atomic N-shell vacancy state widths, X-ray photoelectron, Auger spectra 77—18875
atomic resonance fluoresc. of P_1 state in rot. mag. field 77—42271
atomic spectra isotope shifts and hyperfine struct. 77—3316
atomic vibr. and fermion behaviour of HCP metals 80—6474
atomisation, for graphite furnace AAS, using graphite platform 78—32877
atoms, absorpt. spectra in nonreson. biharmonic radiation field 79—3400
atoms, electron binding energy and shift, core level XPS 80—87088
atoms, excited+molecules, collisions 80—58338
Auger electron spectra, electron impact excited, vap. and solid state differences 78—52603
Auger MNV lineshapes, hole-hole interaction 80—45177
Auger spectra, using cylindrical mirror spectrometer 79—63326
background levels in air over S.Norway 79—12239
band structure, density of states and Fermi surface, APW calc. 77—20232
Burgers vector determ. of perfect dislocations obs. by X-ray topography of single cryst. 79—37711
carrier mean free path, temp. depend. 79—7822
cataphoretic laser, transverse separation dynamics 77—38865
cathode erosion components, vac. arc, fusion temp. and charge transfer depend. 77—4010
cathodes arced in vacuum, erosion structs. 80—1872
Cd+molecules collisions 80—58338
chelation with aspartic acid, US study 77—44464
coating, sliding wear resistance 77—12708
coating on steel for watch part finishing, ion plating *(French)* 78—23879
cold rolling texture development 80—25720
compressibilities, temp. depend. *(French)* 79—65135
concentration in a.c. arc, during interruption, time depend. *(Russian)* 78—22597
concentration in snow of Mt. Blanc rel. to air pollution 78—81258
conduction-electron elec. field gradient, probe valence effects 78—47749
contact charge density, press. depend., trends for Ag-Te 78—39077
core level binding energies 80—71564
Cottrell-Stokes law, 4.2 to 300K, forest dislocations and other obstacles 77—43269
cover, effective energy cut-off determ., rel. to neutron flux meas. in high-temp. reactor 78—86573
creep, low-temp., thermal heating and quantum mechanisms 80—79868
creep mechanism at low temps. *(Russian)* 79—11659
critical temp. determ. by exploding wires method, liquid metal enthalpy 78—6149
crystals, concentrated loads, 3-D anisotropic elasticity theory 80—83734
cutoff energies, Monte Carlo calcs. 77—50211
cyclotron reson., data inversion 78—91593
cyclotron resonance of holes, nonlinear surface resist. effects *(Russian)* 77—8010
de Haas-van Alphen effect and mag. breakdown *(Russian)* 77—80722
de Haas-van Alphen effect under press., Fermi surface and pseudopot. form factors 77—43475
deposited layers, on Ti (0001), LEED and AES determ. of struct. 77—72804
deposited layers on Ti (0001), LEED and AES determ. of structure 77—76688
deposition, on metal substrate, pot. sweep, potentiostatic and optical microscopic obs. 77—59967
Derwent Reservoir, N.England, Zn, Cd and Pb in water, sediments and submerged plants 79—25286
detection, using forward scatt. of reson. radiation with Voigt effect 78—23993
determ. in water and organic materials, flameless atomic absorpt. spectrometry with wire loop atomiser 80—45586
determination, by Zeeman effect at. absorpt. spectroscopy 77—32866
determination, in atmosphere, flameless atomic absorpt. in particle size fractionated aerosols 78—69434
determination, in beef extract, by NAA 78—27856
determination, in kidney and liver, in vivo neutron capture prompt γ ray anal. method 78—15885
determination, in plant material, by atomic absorpt. spectroscopy 77—9143
determination, using modified flameless at. absorpt. spectrophotometer 78—82044
determination in blood by atomic absorpt. spectroscopy 79—44071
determination in drinking water by graphite furnace at absorpt. anal. 80—55733
determination in NaCl, serum or urine, AAS, background correction 78—27834
determination in sea and fresh waters, interlaboratory comparison 78—81209
determination in soln. using at. emission anal. with exploding foil excitation 77—12840

cadmium continued
- differential cathode ray polarograph, exam., determination of Cd, Zn 78—56930
- diffusion, in GaAs, from gaseous phase, time depend. 79—46844
- diffusion in InP 79—82246
- diffusion in liq. Te 77—84955
- diffusion in Pb at high press. 77—72721
- diffusion in PbTe and $Pb_{1-x}Sn_xTe$, Hall effect, cond. and solubility meas. 79—69292
- dimethylammonium manganese trichloride:Cd, impurities in quasi-one-dimens. Heisenberg systems, anisotropy effect 80—80502
- discharge, low-press., high current, intensity in middle UV 78—50878
- discharge lamp, electrodeless, microwave excited, SIMPLEX optimisation 78—83061
- dislocation internal friction, orientation depend., for single crysts. 78—52882
- dislocation structure control after prep. low angle boundary decomp. *(Russian)* 78—3142
- dissolution in sulphate solutions, effects of O_2 on mechanism 77—77631
- distribution in Pacific Ocean bottom sediments surface layer 79—20809
- distribution in waters of Yarra River estuary 79—16552
- elastic constants, high press. finite strain theory *(French)* 79—1475
- electric discharge, Paschen pot. and light emission 80—1863
- electric field gradient, magnitude and sign 77—80755
- electric field gradient at nucleus calc. 78—39079
- electric field gradient press. depend., lattice vibrs. effect, PAC expts. 79—61267
- electrical resistivity and anisotropy coeff. at press. up to 80 kbar 77—43554
- electrical resistivity and deviations from Matthiessen's rule of single cryst. 79—23943
- electrocrystallisation on Cu single cryst., asymm. AC influence 78—10292
- electrode, evaporation rate from cathode spot in vacuum arcs 79—37566
- electrodeposition of Zn, from high purity industrial acid sulphate electrolyte, effects on deposit structure 79—56091
- electrodeposition on Cu electrode, conditions for granular growth 80—55310
- electrodeposition on solid Cd or CdHg amalgam, rate, impedance meas. 78—52693
- electrodes plastic bonded, for Ni-Cd accumulators, production methods 80—45659
- electron density at nucleus, press. depend., Hartree SCF calcs. 78—56411
- electron impact ionisation, of autoionising levels, ejected electron spectrum 78—5356
- electron phonon interaction, Azbel'-Kaner high freq. cyclotron reson. meas. 79—11056
- electron probe X-ray microanal. determ. of distrib. in bullfrog skin 79—79707
- electron radiation damage, determ. of threshold displacement energy 78—59837
- electron-electron scatt., RF size effect meas. 79—60821
- electron-phonon interactions, inelastic neutron scatt. meas. 79—99285
- electronic properties depend. on $2^{1}/_{2}$-th order phase transition under high press. *(Russian)* 80—11128
- electronic surface states, (001) surface, Brillouin zone 79—24047
- electroplastic deformation, stress relax. meas. *(Russian)* 79—38894
- epitaxial monolayer, nucleation and growth on Ge (111) 77—7986
- equilibrium between solid and vapour state, quantum statistical mechanics viewpoint *(Croatian)* 79—95154
- evaporation rate, effect of inert gas 80—84285
- faceting of interstitial loops 78—47381
- failure under hydrostatic press., kinetics 78—52944
- Fermi surface, strain depend., from US vel. oscills. 78—84133
- Fermi surface, stress-induced changes 80—96770
- Fermi surface changes under uniaxial compression 78—51876
- Fermi surface press. derivatives, de Haas-van Alphen effect meas. 77—43477
- Fermi surface stress induced changes calcs., principal cross sectional areas 79—60684
- field gradients, temp. depend., electronic and lattice contribs., ab initio study 79—42501
- film, deposition props. on specially prepared substrate, desorption energy and surface diffusion 79—90917
- film, dry lubrication on C steel, tribological behaviour 80—89364
- film, elec. cond., classical size effect 77—89881
- film, freshly deposited, 77K, refl., annealing effect, thickness depend. 77—16413
- film, HCP, crystal struct. changes on ion bombard. 77—69018
- film, nucleation and growth, props. 80—29878
- film, surface RF impedance in strong mag. fields *(Russian)* 80—92920
- film, vacuum deposited, microstruct. exam., X-ray diffr. profile anal. 79—46973
- film, vacuum evaporated, HCP, microstruct., X-ray obs. 80—10827
- films, struct. and props., X-ray diffr. spectra anal. 80—80119
- foil, monocrystalline, anisotropy of size effect 79—38048
- foil, splat quenched, preferred orientation 80—40381
- free-electrons momenta distribution, anisotropy, positron annihilation meas. 77—36309
- gas, refraction, determ. by phase vel. matching method *(Russian)* 78—30406
- gas laser LG-70, specification 78—74889
- geochemistry, chemical speciation in mixed freshwater, seawater and bine solns. 78—20409
- grain growth, and mobility, effect of hydrostatic pressure 79—37717
- grain size effect on acoustic emission generated during plastic deformation 78—80609
- Hall effect and elec. resist., temp. depend. 78—64030
- Hall plasma accelerator, using Cd vap. 78—71553
- Hall resistivity, importance of intersheet scattering 77—76794
- hardening resulting from pyramidal glide 77—48495
- HCP, cryst. dynamics exam. 77—43289
- HCP, phonon dispersion relations, effect of different dielec. functions on model pseudopot. calc. 79—33055
- hexagonal, temp. depend. anisotropy of phonon scatt. resist. 78—51967
- hollow cathode laser, ion laser transitions 80—69366
- Hugoniot curves, elastic anisotropy effect *(French)* 78—18735
- internal friction, cryst. orientation depend. *(Russian)* 77—7730
- ion bombardment, sputtering, re-emitted kinetic energy ang. distrib. 80—2910

cadmium continued
- ion polarisation and point defect resistivity in metals 80—103672
- ions, 300 keV, InSb implantation, dose rate and orientation dependence of radiation damage 77—89482
- isotope enrichment, by refining and pulsed currents 78—3032
- isotopic abundances in 28 meteorites and three terrestrial rocks 78—53891
- isotopic enrichment during zone melting process *(Russian)* 77—10522
- jacket, for shielding of sample from thermal neutrons in reactor 77—63991
- kidney, concentration of Cd, neutron activation anal., organ depth determ. 80—72321
- Knight shift, temp. depend. 80—2655
- L shell prod. cross section of Zr, Mo, Ag, Cd and In for 75 to 150 keV p and e excitation 79—47552
- laser, 441.6 nm, positive column He-Cd discharge, excitation mechanism 78—58983
- laser, white light, hollow cathode, new design concept 80—87405
- laser CW oscillation, Cd^+ transitions in He-$CdBr_2$, He-$CdCl_2$ and He-CdI_2 discharges 78—50765
- laser oscillation at 5378 Å by laser-produced Cd plasma 77—3569
- laser produced plasma evolution, laser possibility 77—80325
- laser produced plasma recombination laser, power output enhancement by plasma confinement 80—63989
- laser radiation absorption in craters on metal targets 80—97386
- lattice defects studied by gamma ray angular correlation 79—51895
- lattice dynamics 77—15513
- Lindemann's rule and X-ray Debye temp., anisotropic single crysts. 79—28076
- liquid, electron component of entropy *(Russian)* 79—23747
- liquid, electron energy states calc. *(Russian)* 79—4506
- liquid, electron transport, nonlocal pseudopot. calc. 77—1404
- liquid, interference function temp. depend. from X-ray diffr., elec. resist. calc. 77—47332
- liquid, isothermal compressibility, harmonic pot. model calc. 79—14870
- liquid, Percus-Yevick eqn., perturbation treatment, struct. factor 77—7641
- liquid, resist. and thermo-electric power using corrected parameters of Shaw model 79—19566
- liquid, small-ang. X-ray scatt., at. microgrouping depend. *(Russian)* 78—14271
- liquid, spin-orbit coupling and resistivity 77—85189
- liquid, thermoelectric power, pseudopotential calc. 80—59959
- liquid, US vel. and thermophysical props. meas., 500-1000K 78—38778
- liquid, viscosity calc. using microinhomogeneous struct. model *(Russian)* 80—15284
- liquid metal, electronic density of states, pseudopotential calcs. 80—70578
- liver, concentration of Cd, neutron activation anal., organ depth determ. 80—72321
- liver Cd, transportable in vivo meas. system 79—39496
- lunar drill sample, neutron activation and radiochemical anal. *(German)* 80—51673
- magnetic susceptibility, temp. depend., electron-phonon interaction effects 79—61046
- magnetoresistance, linear, semiclassical transport theory 77—35925
- marine pollution determ. in Gulf of Fos, NW Mediterranean 79—12141
- metallic precipitates, crystallography dendritic origin of hexagonal prisms 79—66366
- metallographic prep. at room temp. *(German, English)* 77—9026
- microplastic deformation, basal dislocation generation, glide and locking, X-ray topography study 80—88156
- monolayer, epitaxial, nucleation and growth on Ge(111), RHEED and mol. beam study 77—43447
- muscle membrane, insect, permeation of Mn, Cd, Zn and Be through Ca channels 77—56357
- neuron membrane inward Ca current, blocking effect of Cd^{2+} ions 77—81485
- noncubic crystal, temp. depend. of elec. field gradient 79—99515
- nonlinear cyclotron absorption of hole doppleron *(Russian)* 78—10779
- nuclear quadrupole interaction, theory 78—10412
- nuclear quadrupole interaction theory using first-principles pseudopotential 79—73482
- nucleation on Ge (111), struct. and surface coverage, RHEED-mol. beam obs. 77—4265
- organ tissue levels, in vivo meas. system using neutron activation 80—67224
- oscilloscopic polarography determ. in environmental pollution anal. *(Chinese)* 79—53002
- oxidation, chemisorption and oxide regimes, UPS and EELS study 80—81236
- oxidation of (0001) surface, LEED and AES obs. 79—87756
- N.Pacific, trace metal vertical profiles 80—67381
- passivity breakdown breakdown, of high purity metal 80—100947
- phase comparisons for Sondheimer size effect oscills. 78—34823
- phonon density of states calc. from neutron diffr. data 77—24369
- phonon density of states determ. from heat capacity *(Russian)* 80—29131
- phonon dispersion, phenomenological model 79—7660
- phonon dispersion relations, specific heat by modified Cheveau model 78—38792
- phonon spectra and eqn. of state, pseudopot. method *(Russian)* 77—24367
- photoelectric cross sections at 52.4, 60, 72.2 and 84.4 keV 80—69187
- photoelectron spectra, 4d spin-orbit splitting, crystal field and band-broadening effects, CNDO calcs. 78—76577
- photoionisation, 3d subshell absorption spectra 77—10648
- plasma, laser action via recombination process 79—94217
- plasticity study during deformation by twisting *(Russian)* 80—93597
- point contacts, electron-phonon coupling, microcontact spectroscopy investig. *(Russian)* 78—38796
- polarographic determination *(Japanese)* 77—77852
- polycrystalline, effect of strain rate on stress relaxation behaviour 78—72807
- positron annihilation, 4.2-500K, Doppler broadening meas. 78—43957
- positron annihilation, temp. depend. 77—69930
- positron annihilation data anal. by Mijnarends' method 77—20223
- positron annihilation lifetime spectra, low temp. trapping 80—29822
- positron annihilation rates, electron-electron and electron-positron correl. effects 78—76548
- positron lifetime, investigation of temp. effect 78—2940

cadmium continued
- positron lifetime and annihilation lineshape from 4.2K to MP 77—20272
- positron trapping at low temp. lifetime spectra 80—84799
- positron-vacancy interactions, equilib. temp. depend. of positron annihilation 78—76547
- protective coating, on 30KhGSA steel, in Black Sea water 78—19956
- proton-induced L-shell ionisation cross-sections 80—100707
- quadrupole hyperfine interaction of ^{111}Cd, effect of radiation defect annealing 78—43741
- quadrupole interaction for ^{129}I, ^{131}I, and ^{132}I, PAC expts. 78—48087
- quadrupole interaction of ^{107}Cd $11^{-}/2$ states 77—8468
- quadrupole interaction of ^{113}Sn, temp. depend. 77—8469
- recovery, stage III, after α-particle irradiation 77—27924
- resistivity, existence of Einstein type phonon mode 79—42519
- roadside soil and plants in Alexandria district, Egypt, contamination with Cd, Ni, Pb and Zn 78—81171
- shock adiabatics at ultrahigh press. *(Russian)* 77—27941
- single cryst. stress relax. depend. on elec. current, electron plastic effect 79—79021
- single crystal, root-mean-square atom displacement, X-ray meas. 78—75624
- size oscillations in magnetocond. 77—4324
- soil-water system interfacial reactions and heavy metal adsorption 78—3832
- solid metal embrittlement of Ti-Al-V-Sn (6,6,2 wt.%) 80—16551
- solid-photon interaction, energy-power depend. of total and partial process cross sections 77—36305
- solubility and cosolubility in InAs 77—16552
- sorption and accumulation in sediment of Tama River 79—74924
- spin-orbit interac. contrib. to mag. susceptibility of interacting electrons 77—63084
- spreadability on Cu and brass plates *(Japanese)* 80—29252
- sputtered excited states, secondary photon emission, role of transition probability 80—102483
- stopping power nucl., in ferromag. Gd, transient mag. field 78—34555
- substrate for polystyrene film, electrode effect on carrier injection, TSC, I-V characts. 80—34463
- superconducting transition temp., perturbative corrections, direct and indirect ladder diagrams 80—49979
- superconductive fixed points for temperatures above 0.5K 79—63221
- surface, He^{+} ion neutralisation 78—35237
- surface, Hg flow kinetics in temp. grad. *(Russian)* 78—6198
- surface impedance, Gantmakher-Kaner oscills. *(French)* 77—66195
- surface impedance, in mag. field *(Russian)* 78—19079
- surface impedance in mag. field, influence of nature of electron reflection 77—51803
- surface resistance in mag. field, doppleron and Gantmakher-Kaner oscills. *(Russian)* 77—32261
- surface-electron beam interaction, 0.4-5 mA ion beam extraction 77—84456
- tensile properties, texture and grain size depend. of warm-rolled specimens 80—71720
- thermal expansion, temp. depend., vacancy effects 80—79962
- thermo EMF oscills. on mag. breakdown *(Russian)* 79—60801
- thermopower meas. in mag. field, 1.5-4K 80—54675
- thin film, vac.-deposited, X-ray diffr. struct. obs., props. 79—37937
- TMMC:Cd, mag. and non-mag. impurity effects on suscept. and Neel temp. 77—66312
- trace detection in human liver by neutron activation analysis 79—79632
- tree rings, long term environmental pollution histories, neutron activation analysis 79—92107
- tropospheric fallout fluxes in Antarctica and Greenland 79—58007
- twin boundaries, computer simulation 80—39109
- twinning dynamics of single crystal 77—4115
- ultrafine particle, positron annihilation exam. 78—56542
- US attenuation due to conduction electrons 79—46754
- US attenuation of conduction electrons, shear waves calc. 78—91589
- US attenuation of conduction electrons calc. 78—91588
- vapour, excited by electron impact, ejected-electron spectra from autoionising levels 80—37893
- vapour, RF discharge, isotope separation 80—79619
- vapour, VUV harmonic generation 78—42381
- vapour grown crystal, morphology and growth mechanism, Bi impurity effects 79—23546
- vapour laser, operation by dissoc. of metal complex 77—54702
- vapour pressure, over liq. Tl-Cd-Sb alloys and pure metal *(Russian)* 79—51247
- water assemblies, poisoned, thermal neutron diffusion calc., absorption discontinuity effect 78—13191
- wear under reversed friction, temp. effect 80—108588
- wheat endosperm, radiometric determ. of Cd conc. following Cd addition to soil *(German)* 77—25631
- whisker, supercond. crit. temp. stress depend. 77—39989
- work hardening, low temp., in single crystal 78—3138
- XPS and $M_{4,5}N_{4,5}N_{4,5}$ Auger spectra 79—61472
- XPS line intensity ratios for outer electron shells 79—100018
- Young's modulus and internal friction, 20°C to melting point *(Russian)* 80—89278
- Zircaloy-2, Cd metal embrittlement in 300-340°C 77—16747
- AgBr:Cd^{2+}, single cryst., stress-induced migration and aggregation of solute ions, internal friction 79—51200
- $Ag_{0.5}Cd_{0.5}$, Cd 4d band apparent splitting, cryst. field and d-d overlap influence XPS obs. 79—78825
- AgCl:Cd, irradiated, surface defect centres, XPS study 79—28894
- AgCl:Cd, large sheet single cryst. prep. *(German)* 77—32516
- AgCl:Cd^{2+}, EPR of mobile electrons, mechanism for photoinduced decomposition 78—80219
- AgCl:Cd^{2+}, heavily doped, free energy and point defect distrib., integral eqn. method 80—107219
- AgCl:Cd^{2+}, plasticity, impurity hardening effect 78—47466
- AgCl:Cd^{2+}, recombination processes, radioluminescence 78—2915
- AgI:Cd, polycrystalline, thermoelectric power meas. 80—59698
- Al alloys, 7075-T6, H_2 effects and Cd segregation to grain boundaries 78—84764
- (Al-Zn):Cd eutectic system, cellular growth, unidirectional solidification investig. *(Korean)* 77—28805
- BP:Cd, epitaxial layers, ion implantation, defects and lattic locations, channelling obs. 80—88179
- BaF_2:Cd^{2+}, X-irrad., ESR of Cd^{+} centres 77—59459
- CaF_2:Cd^{2+}, X-irrad., ESR of Cd^{+} centres 77—59459

cadmium continued
- Cd, A=110, 116, difference in nuclear charge radius, X-ray isotopic shift meas. 77—18382
- Cd I, 326.1 nm line absorpt. growth curve 79—76375
- Cd I, excited states radiative lifetimes 80—942
- Cd I, II, level crossing in gas laser, at. consts. and collision cross sections determ. 78—50763
- Cd II, $4d^95s^2$ $^2D_{5/2}$, relax. consts. in plasma of ion laser, electron and He collisions 77—19239
- Cd II, A factors of ^{111}Cd and ^{113}Cd isotopes by hyperfine level crossing, stimulated emission 80—9564
- Cd II, Hanle effect, $^2P_{3/2}$ lifetime determ. 77—18852
- Cd II, pulse excitation in discharge *(Russian)* 77—54704
- Cd II ($4d^95s^2$ $^2D_{5/2}$), high order mode-crossing signals, g-factors 79—796
- Cd II lasing action, 441.6 nm, exam. of mechanism for power increase due to I addition, using He-Cd^{+} laser 78—55344
- Cd IV, $4d^9 \rightarrow 4d^85p$ transitions, UV spectra 77—46515
- Cd IV, UV spectral analysis 80—83306
- Cd, influence of source material and shape on sublimation props. 78—80474
- Cd, nuclear quadrupole antishielding effects, ab initio theory 78—34814
- Cd, reactivity worths of fixed neutron absorbers 78—21654
- Cd UV subshell photoionisation cross section, expt. and GIPM theory 78—21887
- Cd^{+} laser in He-halide discharge, CW oscill. 78—17913
- Cd^{+}, lasing in CdI_2-He hollow cathode, discharge 77—10951
- Cd^{+}, polarised emission of light following photoionis, Cooper-Zare model 79—81179
- Cd^{+} trapping in Ag on injection at various temps. 77—76436
- Cd:^{116}Sn, quadrupole interaction, radiation damage effects 78—43752
- Cd:^{11x}Sn, (x=3-6,8), γ-ray spectra, quad. interaction, spin-rot. spectra 77—26571
- Cd:^{67}Ge, elec. quadrupole interaction temp. depend., PAC meas. 79—42877
- Cd:^{67}Ge, quadrupole interaction temp. depend. 77—12264
- Cd:^{67}Zn elec. quadrupole interaction temp. depend., PAC meas. 79—42877
- Cd:^{99}Ru, quadrupole interaction temp. depend., PAC method, electric field gradients 77—73105
- Cd-Ar low-pressure discharge column, energy balance obs. 78—67504
- Cd-barium stearate-Cd structs., internal voltage work function meas. 79—82684
- Cd-$CdCl_2(Br_2)(I_2)$ molten solution, US velocity and compressibility 77—84844
- Cd-$CdCl_2(Br_2)(I_2)$ molten solutions, surface tension 77—85024
- Cd-CdI_2 mixture, molten, nuclear spin relax. 80—88887
- Cd-Cs, vapour, sensitised fluoresc. anisotropy transfer 77—57924
- Cd-Cu-Se, phase diag. 77—52303
- Cd-He hollow-cathode laser, small signal gain 79—31881
- Cd-Hg, sensitised fluoresc., anomalous Hanle effect 79—81186
- Cd-palmitate (arachidate) multilayer struct., hopping rate, direct evaluation 78—88045
- Cd-Sb diffusion couple, layer growth of CdSb phase at high press. 80—2217
- Cd-Sb diffusion couple, layer growth of CdSb phase at high press., elec. meas. 80—2218
- Cd+alkane hydrocarbon, $^3P_{0,1,2}$ state distrib., E to V,R transfer 80—28088
- Cd+Cs, excitation energy transfer in sensitized fluoresc. 79—98210
- $Cd+H_2 \rightarrow CdH+H$, product initial rot. state distrib., pump and probe laser obs. 80—85158
- $Cd+H^{+}(He^{2+})$, L- and M-shell Auger electrons 79—27076
- Cd+He, Penning ionisation cross section of target atom, for $He(2^3S_1)$ 80—63777
- $Cd+He^{+}$, thermal energy charge transfer reaction, ion states, relative yields 79—45840
- $Cd+He^{+}(He_2{}^{+})$ collisions, slow, Cd II excitation 77—83701
- Cd+inert gas, broadening of 5^1P_1 level 80—83479
- Cd+inert gas, transitions between excited Cd states 78—17773
- $Cd+K(+N_2)$, optical excitation, rate consts., collisional energy transfer kinetics 80—32801
- $Cd+N_2$, $A^3\Sigma_u{}^{+}$ state, vibr. excitation 80—1054
- $Cd+N_2$, electronic-vibrational process, state-resolved products distrib. determ. 79—6956
- $Cd+N_2$, vap., creation of inverse population of atomic Cd 6^3S and 5^3P_2 levels 80—58219
- $Cd+Na^{+}$, $Cd(5^3P_1)$ and (5^1P_1) and mag. sublevels, excitation cross-sections 80—9710
- $Cd+O_3$, matrix reactions, IR, Raman and visible spectra in Ar and N_2 matrices 80—87110
- Cd+Te, π^{-} capture, radioactivity meas. 80—47831
- $Cd+Xe^{10+}$ depend. of charge transfer on ionisation pot. of atoms 79—64096
- $^{114}Cd+He$, collisional effects on 326.1 nm line rel. to temp. and conc. 78—5336
- $Cd^{2+}+H$, electron capture by slow ions, pseudo-crossing 80—43176
- Cd_2,(Cd_3), fluoresc. kinetics, optical excitation, energy spacings and equilib. consts. 80—43090
- Cd_2 as 470 nm absorber, multiconfig. SCF calcs. 80—32731
- Cd_2, in Ar and Kr matrices, 10K, UV spectrum, vibr. assignments 77—58038
- Cd_2, matrix isolated, Raman spectra 79—50024
- Cd_2, pot. energy curve of low-lying states, MO theory 79—89624
- Cd_2, quenching and predissociation, possible excimer laser 80—32770
- $Cd_2{}^{+}$, removal using Itaya-zeolite *(Japanese)* 78—95951
- $CdCl_2(Br_2)(I_2)$ polymorphic phase changes of adsorbed NO 77—31900
- Cd(Hg)/$CdSO_4$, aq. electrochem. system, kinetics, impedance *(German)* 77—32807
- ^{113}CdII, hyperfine level crossing, saturation induced in laser 79—18160
- $Cd(^3P_{0,1})+CO(CO_2)(NO)$, absolute quenching cross section, phase-shift method 80—58340
- $Cd(^1P_1)$ excited state quenching by mols., cross sections, chem., phys. exit channels 79—779
- $Cd(^3P_1)$ radiation imprisonment lifetime, inert gas effect, phase-shift method 80—58213
- $Cd(^1P_1)+N_2$(alkanes), laser excitation, absolute quenching cross sections and branching ratios 79—49979
- $Cd(^1P_1)+NO(X^2\Pi) \rightarrow NO(A^2\Sigma^{+}, \nu=0)$ electronic energy transfer react., collisional fluoresc. quenching 77—14548
- $Cd(^3P_J)(^1P_1)+H_2(HD)(D_2)$ reacts., CdH(CdD) yields, quenching cross sections 79—1948

cadmium continued
Cd(^{1}S), dipole polarisability, relativistic effective core pot. calc. 79—76362
CdS:Cd, Cu, single crysts., IR restoration after optical degradation of photosensitivity 79—60867
CdS:Cd, Cu- or defect-compensated, optical ageing rel. to storage cond. 78—84247
CdSe:Cd, Cu, photo-induced changes in absorpt. spectra 78—80382
^{111}Cd impurities in sp metals, elec. field gradient at ^{111}Cd, effects of high press., TDPAC meas. 80—25266
^{111}Cd, KLM- and KLN-Auger transitions 77—18884
^{111}Cd, nucl. orientation coeffs. with axially symm. elec. field gradient 80—97168
^{111}Cd^m bound on DNA, perturbed, γ-γ ang. correlations 79—79457
^{113}Cd, two-level system, absorption spectrum, intense two-photon excitation obs. *(Russian)* 78—33465
^{113}Cd$_2$, two-level system, absorpt. spectrum, subradiative struct. *(Russian)* 80—28008
^{113}Cd^m, in marine organisms and sediment around Marshall Island nucl. test site 80—109174
^{114}Cd λ326.1 nm reson. line, self-broadened, temp. depend. of parameters 79—63964
^{116}Cd/^{106}Cd, isotope fractionation in fractions of H3 chondrites Tieschitz and Brownfield 80—94764
Cd$^*{}_2$, 470 nm absorber, multiconfiguration SCF calcs. 80—27963
Cd$_2$* excimer, fluoresc. band shape, decay rates 78—70866
Cd($5^3P_{0,1}$)+methane (H_2)(D_2)(N_2), absolute quenching cross sections 80—5604
Cd(5^3P_1), (5^1P_1), and mag. sublevels, excitation in Na$^+$+Cd collisions 80—9710
Cd(5^1S_0)+Hg(6^3P_1), spectral width of Cd(5^3P_1) line *(French)* 77—50397
Cu-Cd thin film couples, room temperature interactions 80—96699
Cu+Fe+Cd, nuclear target proparation by evaporation and rolling 80—23224
Cu_2O:Cd, dipolar and quadrupolar bound excitons, absorption spectrum *(Russian)* 78—92099
Cu_2O:Cd, ion-implanted, resonance Raman studies of annealing 79—55765
Cu_2O:Cd^{2+} implanted, reson. Raman scatt., annealing effect 77—24838
Cu_2S:Cd, effects of doping on elec. and optical props. 78—38743
$FeCl_2$:Cd, thermodynamic phase diagram determ., using pulsed dye laser, piezoelectric modulator, and gated amplifier 79—7991
$Fe_{1-x}Cl_2$:Cd$_x$, randomly disordered, tricrit. behaviour, light scatt. 78—68255
Fe_3O_4:Cd^{2+}, Verwey transition 80—6513
p-GaAs:Cd, (110) cleaved surface, defect-induced surface states 80—6925
GaAs:Cd, effect of As vapour press. on etch pit density and junction depth 78—26937
GaAs:Cd, implanted, low temp. photolum. spectra 78—39583
GaAs:Cd, ion implant depth distribs., AES and glow discharge optical spectroscopy meas. 80—65028
GaAs:Cd, lattice defects caused by quenching, elec. cond. 79—56160
GaP:Cd, multiple bound excitons, photoluminesc. obs. 79—95837
GaP:Cd,S, donor-acceptor pair luminesc., excitation spectroscopy 80—25440
GaP:N,Cd, impurity recomb., acceptor binding energies 78—34796
GaSb:Cd, thermal sensitivity, -170 to $+180$°C, resist. meas. 77—39906
GaSb:Te, carrier density dependence on impurity conc., rel. to solubility limit 77—8047
GaSe:Cu(Cd, Sb), photovoltaic spectra 80—20240
Ge:Cd, compensated, complex oscillatory impurity photocond. spectrum 77—43656
p-Ge:Cd,Sb, electron irrad. at 300K, elec. props. 80—6435
p-Ge:Cd$^-$, deep levels, optical-phonon-assisted capture of carriers 79—51597
Hd-Cd hollow cathode laser in mag. field, Cd II stimulated emission 78—79002
He-Cd, afterglow, Cd$^+$ excited state prod. by Penning and charge exchange reactions 77—15252
He-Cd, glow discharge, collision rates calcs. 77—68882
He-Cd, hollow cathode discharge tube, voltage, ion spectral line intensities and metastable states 79—46505
He-Cd, hollow cathode laser, output characts. 77—42525
He-Cd, hollow cathode laser oscillations, cathode temp. effects *(Japanese)* 79—50285
He-Cd, hollow cathode long life laser 77—88769
He-Cd, long life hollow cathode laser 78—29968
He-Cd, metal ion laser, noise props. *(Japanese)* 79—64209
He-Cd, usual glow and hollow-cathode discharges, negative glow, spectroscopic obs. 77—72516
He-Cd, whitelight hollow-cathode type laser design based on cathode fall theory 79—27282
He-Cd bipolar hollow-cathode laser, 441.6, 533.7 and 537.8 nm Cd ion lines 79—50319
He-Cd cataphoretic laser discharge tube, He loss meas. rel. to tube life 79—94252
He-Cd DC discharge, excited at. densities, I-V characts. 78—14230
He-Cd discharge, enhancement of rate of charge exchange collisions 77—83862
He-Cd discharge, principal Cd ionis. mechanism, radial profiles meas. 77—27758
He-Cd extended-life laser characts. 78—46586
He-Cd hollow cathode discharge white light laser *(Chinese)* 79—72555
He-Cd hollow cathode laser, 533.7 and 537.8 nm 77—71976
He-Cd hollow cathode laser, He singlet and triplet metastable number densities 78—29938
He-Cd hollow cathode laser, laterally emitted light 78—66810
He-Cd hollow cathode laser, upper level decay rate, mag. field tuning dip meas. 78—87043
He-Cd hollow cathode laser, axial mag. field effect on oscills. 79—59681
He-Cd hollow-cathode discharge, external cathode type, morphologic study 79—60207
He-Cd hollow-cathode laser tube, description and performance *(Bulgarian)* 79—27279
He-Cd II hollow-cathode laser, 4416 Å pulse oscillation 79—7122
He-Cd II laser, 05378 μm oscill. spectra meas. using scanning interferometer *(Japanese)* 80—9864
He-Cd II laser, power interaction of laser lines 80—9862

cadmium continued
He-Cd II lasers, positive column, hollow cathode types, 4416 Å oscill. characts. *(Japanese)* 78—94392
He-Cd laser, 441.6 nm, low noise, discharge current modulation effects *(German)* 78—22117
He-Cd laser, 442 nm, high order mode crossing signals from Cd II $4d^95s^2$ $^2D_{5/2}$ state 79—796
He-Cd laser, 8067 Å, He metastable atoms effect on power 78—33722
He-Cd laser, drift of Cd$^+$ due to laser field 78—17917
He-Cd laser, freq. self-selection, transverse RF excitation *(Russian)* 77—75490
He-Cd laser, hollow cathode type, quasi-metastable state excitation 78—33721
He-Cd laser, intensity fluctuations meas., comparison with 78—71087
He-Cd laser, intracavity phase modulation, spectral and time characts. 77—61988
He-Cd laser, possible operation using charge-transfer excitation 77—83701
He-Cd low-power low-cost blue lasers 77—19333
He-Cd mixture, Penning ionis. and nonreson. charge exchange in afterglow 79—72414
He-Cd plasma, in discharge tube, excitation mechanism obs. 78—30479
He-Cd positive column laser power, effect of I_2 additive *(Japanese)* 79—7121
He-Cd positive-column laser discharge, excitation mechanisms from radial profiles 77—68205
He-Cd segmental tube laser ageing *(Bulgarian)* 79—18441
He-Cd single-mode laser, linewidth meas. and population calc. 77—14694
He-Cd vapour excitation in hollow cathode discharge 80—64815
He-Cd vapour laser, continuous wave, intensity fluctuations investig. 80—83593
He-Cd$^+$, cataphoretic laser, 441.6 nm line intensity dip due to vapour separation 77—50659
He-Cd$^+$, laser, cataphoretic, power noise meas. 79—36885
He-Cd$^+$, positive column laser, Cd II 441.6 nm line, effect of I_2 77—54697
He-Cd$^+$ cataphoretic laser, freq. fluctuations of 4416, 3250 Å lines 79—72556
He-Cd$^+$ hollow cathode laser, He(2^3S) densities and excitation mechanisms 80—48220
He-Cd$^+$ laser, improved hollow cathode type, design and performance 80—19047
He-Cd$^+$ laser, output radiation, influence of discharge-current fluctuations 79—10289
He-Cd$^+$ laser, population densities of He excited states in positive column discharge 78—58989
He-Cd$^+$ laser, upper and lower laser states population densities, simultaneous determ. 78—87042
He-Cd$^+$ laser discharge, positive column, non-Maxwellian electron energy distrib., electron density determ. 77—84493
He-Cd$^+$ laser output, effects of transverse mag. field 79—86169
He-Cd$^+$ laser plasma, interferometric anal. of spectral lines 77—10892
He-Cd$^+$ positive column laser discharge, ion density 77—68885
He-Cd$^+$ positive column laser, power increase mechanisms by I_2 addition *(Japanese)* 79—98346
Hg-Cd cell, EMF rel. to temp., thermodynamics 77—12805
Hg+Cd, quantum beats under transfer of orientation 79—98206
Hg+Zn(Cd), sensitized fluoresc., orientation and alignment transfers *(French)* 79—13808
$HgCr_2Se_4$:Cd, precipitations during growth by chem. transport method 80—55409
HgSe:Cd, epitaxial growth on CdSe, struct., Cd distrib., and electrophysical props. 77—12540
n-InAs:Cd, p-n junction, photosensitivity spectra depend. on mag. field 79—91137
InAs:Cd,Te, donor-acceptor interaction, elec. cond. and Hall coeff. meas. 80—59988
InAs:Cd,Te interaction between impurities, effect on elec. props., Hall effect. 80—19832
InP:Cd, avalanche photodiode characts., impurity diffusion effects 80—70709
InP:Cd, doping by UV laser photodeposition 80—84191
InP:Cd, p^+-p^--n^- junction form. by diffusion doping 80—84504
p-InP:Cd, single cryst. growth by temp. gradient method 79—28907
p-InP-Cd, ohmic contact formation on InP by laser photochemical doping 80—80369
InSb:Cd, diffusion props. of Cd, modified C-V technique meas. 79—19401
InSb:Cd, heat treatment effects on elec. props. 78—43411
InSb:Cd, ion-irrad., p-n conversion during heat treatment 80—96558
InSb:Cd, thermal conductivity down to 0.38K 80—107582
KBr:Ca, X-ray re-irradiation effects on Z_1 centres 78—75664
KCl:Cd, EPR of anisotropic $Cd_F{}^+$ centres, similarity to Z-centres 77—77101
LiCl:Cd, EPR of anisotropic $Cd_F{}^+$ centres, similarity to Z-centres 77—77101
Li_2O-Al_2O_3-SiO_2:Cd$^+$, glass, ESR study 80—103879
Li_2O-Al_2O_3-SiO_2(P_2O_5):Cd$^+$ glasses, γ-irrad., EPR study 80—84639
Li_2O-P_2O_5:Cd$^+$ glass, γ-irrad., EPR study 80—84639
Li_2SO_4:Cd^{2+}, monoclinic-cubic transform., effect of impurities 79—52744
liquid, polyvalent, electrical resistivity by harmonic model potential 80—54668
$(NH_4)_2SO_4$:Cd$^+$, ferroelec. transition, soft mode contrib., EPR obs. 78—72469
NaCl:Cd, EPR of anisotropic $Cd_F{}^+$ centres, similarity to Z-centres 77—77101
NaCl:Cd^{2+}, dielectric loss following plastic deform. 80—84690
NaCl:Cd^{2+}, superstructure obs. by ionic thermal current meas. 78—39499
NaCl:Cd^{2+}, Z_4-like centre, absorpt. spectra obs. 78—76498
Na_2O_5-P_2O_5:Cd^{2+}, metaphosphate glass, absorpt. spectra of radiation products 78—64865
Ni-Cd, with plastic bonded Ni oxide electrodes, basic electrochemical parameters 80—50951
Ni-Cd accumulators, plastic bonded electrodes, active layer composition influence on galvanostatic and potentiostatic discharge curves 80—55834
Ni-Cd all with MnO_2 doped positive electrodes 79—96439

cadmium continued
Ni-Cd batteries, button and cylinder types, self discharge behaviour during storage *(German)* 80—66960
Ni-Cd cell lifetime prediction, computerised pattern recognition 80—3504
Ni-Cd sealed battery electrode performance meas. 80—66962
Pb-Cd dilute alloys, conc. depend. of Cd diffusivity enhancement 79—73348
Pb-Cd thin films, electron tunnelling study of supercond. proximity effect 80—2525
Pb-Cd-Pb, supercond.—normal-metal—supercond. junction, crit. currents 80—107965
Pb-Cd-Pb junctions, pair pot., mag. field depend., crit. currents meas. 80—84555
Pb^{2+}-Cd^{2+}, solns., differential pulse and anodic stripping voltammetry, in thin-layer cell 77—36812
$Pb_{0.98}Bi_{0.02}$-Cd, superconductor-normal-metal boundary resist., mag. field depend. 80—44772
$Pb_{0.8}Sn_{0.2}Te$:Cd, defect struct., Hall effect and solubility meas. 77—11571
$Pb_{0.8}Sn_{0.2}Te$:Cd, influence of Cd doping on high field magnetoresist. and Hall effect 80—75590
$Pb_{0.82}Sn_{0.18}Te$:Cd, effective distrib. coeff. of Cd *(Russian)* 79—73203
$Pb_{1-x}Sn_xTe$:Cd, Cd diffusion obs. using Hall mobility and Cd solubility expts. 78—26584
$Pb_{1-x}Sn_xTe$:Cd, deep energy level, temp. depend. of elec. cond. 78—18994
$Pb_{1-x}Sn_xTe$:Cd, impurity photocond. spectra 80—6902
$Pb_{1-x}Sn_xTe$:Cd, photocond., photomag. effect, carrier lifetimes 80—44658
$Pb_{1-x}Sn_xTe$:Cd, photoelec. props., surface recomb. effect 80—44659
$Pb_{1-x}Sn_xTe$:Cd, solid solutions, impurity states in photoluminescence spectra *(Russian)* 80—97333
PbTe:Cd, Cd diffusion obs. using Hall mobility and Cd solubility expts. 78—26584
PbTe:Cd, defect struct., Hall effect and solubility meas. 77—11570
$Pb(Zr,Ti)O_3$:Cd,W, electro-optical ferroelec. ceramic, secondary electron emission yield 79—91546
Sb:^{111}Cd,In, elec. field gradient, TDPAC expts. 80—55002
Sb:Cd, electric field gradient temp. depend. for ^{111}Cd 79—51894
Se:Cd dilute liquid, perturbed ang.-correl. meas. of motional-correl. time 79—41930
Si:Cd, n^+-n-n^+ structure, photocond. lifetimes, deep level occupancy in exclusion region 78—72253
Si:Cd n^+-n-n^+ structs., photoresist. props. under exclusion conditions 80—39666
Si/In(-Cd), Si/Cd Schottky contacts, electrochemically deposited 80—88633
SrF_2:Cd^{2+}, X-irrad ESR of Cd^+ centres 77—59459
Te-Se-Cd, sandwich structure, fabrication and characteristics 80—60089
Te-Se-Cd rectifying sandwich structs., elec. forming action, Schottky junction form. 80—80371
Zn, electron radiation damage in HVEM, nature of defect clusters 78—59838
Zn, recovery after 6.1 MeV α-particle irradiation at 4.2K 78—47441
ZnS:Cd, Raman spectra, impurity induced first order transitions 78—88310

cadmium alloys
see also cadmium compounds
ion-selective membrane electrodes development, Ag ion conduction ceramic systems *(Japanese)* 80—61203
liquid amalgams mixing, excess entropy, vibr. contrib. *(Russian)* 79—51263
magnetic susceptibility, spin and spin-orbit contribs. *(Russian)* 79—11287
rare earth alloys, RCd_2, bonding props. 77—58969
rare earth-Cd, dil., elec. field gradient, at ^{111}Cd impurities, temp. depend. 79—28642
rare earth-Cd alloys, existence and cryst. struct. 79—77555
Wood's alloy, liq. enthalpy effects when solute is added 80—39314
Ag-Cd, α and β phase, XPS, effects of atomic order on band struct. 79—42440
Ag-Cd, behaviour of Cd d-bands, comparison with Hg and Au alloys 79—37972
α-Ag-Cd, chemical interdiffusion and Kirkendall shifts 78—87829
Ag-Cd, deviations from Matthiessen's rule 78—10420
Ag-Cd, dil., DPAD meas. on ^{107}Cd and ^{109}Cd, nucl. Larmor precession meas., role of hyperfine interactions 79—47363
Ag-Cd, dil., electron irrad., stage I_E recovery 77—39616
α-Ag-Cd, dil., electronic struct. determ. from thermoreflectance and XPS 78—39011
Ag-Cd, production and annealing of radiation defects 78—47362
Ag-Cd, Zener relaxation, valency and dimensional effects *(Russian)* 78—19802
β′-Ag-Cd (45 at.%), growth kinetics of bainite plates and Widmanstatten needles 77—36551
Ag-Cd (45 at.%), morphology and crystal struct. of stress-induced martensites 78—68693
Ag-Cd (45 at.%), morphology and struct. of bainite plates in β′ phase 79—52213
Ag-Cd (45 at.%) martensite, shape memory mech. and related phenomena 80—30009
Ag-Cd (47 at.%), crystal struct. and internal defects of thermoelastic martensite 77—48438
Ag-Cd (50 at.%), BCC β phase, high temp. creep, existence of master curve 80—55473
Ag-Cd (approx. 50 at.%), disordered hcp to ordered bcc transition, meas. of activation energy 78—72773
Ag-Cd alloys, internally oxidised, thermal stability of CdO, exam. of particle coarsening 78—76789
Ag-Cd dilute alloy, isotope effect and correlation factor for Cd diffusion 78—14501
Ag-Cd dilute α-phase alloys, optical gaps, thermoreflectance meas. 77—66520
Ag-Cd peritectic system, separate crystallisation of phases *(Russian)* 80—66497
Ag-Cd(-Ni), internally oxidised, oxide particle size control *(Japanese)* 80—89480
Ag-Cu-Zn-Cd, solder, UTS, room temp. to 4.2K 79—57064
Ag-Cu-Zn-Cd solid metal lubricant in self lubricating composite steels 78—11340

cadmium alloys continued
AgCd, charge transfer, core-electron binding-energy shift 80—2676
AgCd-AgMg(AgZn), quasibinary alloys, phase relations 79—8273
$Ag_{0.5}Cd_{0.5}$, Cd 4d band apparent splitting, cryst. field and d-d overlap influence XPS obs. 79—78825
Ag_xCd_y, TDPAC meas. of ^{111}Cd 77—28492
Al-Bi(Cd)(Pb)-Ti, containing low-melting pt. inclusions, mech. props. 80—93632
Al-Ca, rapid quenching, struct. and decomp. 80—76244
Al-Cd, containing low melting point inclusions, impact props., temp. depend. 78—60792
Al-Cd hypomonotectic alloy, rapid solidification and decomposition 80—50638
Al-Ni(Cd)(Fe)(Si), cold worked, struct. and props. 80—71666
Au-Ag-Cd, γ-ray PAC of ^{111}Cd, nearest neighbour contrib. to elec. field gradient 77—36161
Au-Ag-Cd, martensitic transformation, preceding struct. anomaly 78—68692
Au-Ag-Cd alloys, martensitic phase transition, elastic anomalies and mode softening 79—91647
Au-Ag-Cd pseudobinary alloys, thermodynamic study of order-disorder and martensitic transform. 78—48399
Au-Cd, behaviour of Cd d-bands, comparison with Hg and Ag alloys 79—37972
Au-Cd, charge-transfer and valence-band behaviour using ^{197}Au Mossbauer and X-ray photoemission spectra 79—60695
Au-Cd, UPS exam. of valence bands 79—19511
Au-Cd (47.5 at.%), effect of cooling rates on stress-strain behaviour 78—76721
Au-Cd (47.5 at.%), modified 2H and 9R martensites 78—14366
Au-Cd (47.5 at.%), single cryst., temp. and press. derivatives of elastic consts. near martensitic phase transform. 77—63667
Au-Cd alloy, α and ζ phase, low temp. sp. ht. 78—18789
Au-Cd system, cryst. struct. of $AuCd_3$ and existence of $AuCd_{\sim 5}$ phase *(German)* 77—25020
$Au_{52.5}Ag_xCd_{47.5}$, pseudoelastic behaviour associated with thermoelastic martensitic transform. 80—16304
Au_3Cd, long-range ordered, periodic antiphase domain boundary struct., X-ray diffr. obs. 79—95028
Au_3Cd, order-disorder phase transform., X-ray diffr. anal. *(Russian)* 80—45297
Au_3Cd, sputtered epitaxial films, order-disorder reaction obs. 78—84092
Au_3Cd_5 and Au_5Ce_8.h, cryst. struct. and binding type *(German)* 79—86742
AuCd.r, cryst. struct. determ. 77—84699
Ba-Cd, variation in interatomic interaction and lattice parameters during ordering, numerical calc. *(Russian)* 77—81255
Ba-Cd system, short-range order calc. *(Russian)* 79—23566
Ba_2Cd, cryst. struct. 77—11505
Bi-Cd, alloy absolute thermoEMF temp. and conc. depend. *(Russian)* 80—39561
Bi-Cd, eutectic, contact melting kinetics *(Russian)* 80—70377
Bi-Cd, liq., Hall coeffs. 78—14711
Bi-Cd, solidification in mag. field, crystallite obs. *(Russian)* 77—4770
Bi-Cd eutectic alloy, directionally solidified, contact melting kinetics, mass transfer during solidification *(Russian)* 77—52310
Bi-Cd-Sb, calc. of phase equilibria using thermodynamic values from different models 78—60646
Ca_3Cd_2, cryst. struct. 77—11505
Cd-Ag, polycryst. quenched foil, the influence of Ag on the recovery spectrum 78—76661
Cd-Ag, polycryst. wire, cold worked, resistivity changes 78—68827
Cd-Ag (0.015 to 0.25 at.%), critical resolved shear stress at low temp. 77—69035
Cd-Ag (3 wt.%), metallographic prep. at room temp. *(German, English)* 77—9026
Cd-Ag-Zn (96, 3, 1 wt.%.) soldering alloy powder, atomised, prod. and appl. 79—100073
Cd-As, liq. alloys, thermodynamic props. and cpd. formation 77—1238
Cd-B particulate composite, dispersion hardening, grain size and texture strengthening 77—8840
Cd-Bi, liq., US vel. and thermophysical props. meas., 500-1000K 78—38778
(Cd-Bi)-Sn, eutectic alloy, directionally solidified, contact melting kinetics, mass transfer during solidification *(Russian)* 77—52310
Cd-Cd_3Ag, peritectic transform. 77—16564
Cd-Cr, dil., estimates of s-d interaction from supercond. transition temp. and mag. susceptibility 78—43561
Cd-Cr, dil., mag. and supercond. props. 79—38237
Cd-$CuCd_3$, off-eutectic alloys, controlled grain growth *(Japanese)* 77—55958
Cd-Fe powders, predetermined comp., electrodeposition 79—70014
Cd-Ge broken lamellar eutectic composite, tensile and compressive props. 80—71694
Cd-Hg, and Cd-Mg-Hg, magnetic susceptibility behaviour *(Russian)* 77—80912
Cd-Hg, dil., anomalously high elec. field gradients below 0.05K 78—72442
Cd-Hg, ω-phase, mag. susceptibility *(Russian)* 79—87231
ω-Cd-Hg alloy, melt-growth, morphology of single crysts. 78—64464
Cd-In diffusion into $Pb_{1-x}Sn_xTe$, changes in elec. props. 78—91348
Cd-In-Sb, liq. alloy, Cd thermodynamic activities, Gibbs free mixing enthalpy *(German)* 80—45279
Cd-In-Sb, liq. alloys, thermodynamic activity of Cd between 833 and 953K *(German)* 80—45278
Cd-Mg, and Cd-Mg-Hg, magnetic susceptibility behaviour *(Russian)* 77—80912
Cd-Mg, dil., elec. resistivity, phonon local mode effect 78—6347
Cd-Mg, dil. alloy, single cryst., electrical resistivity and deviations from Matthiessen's rule 79—23943
Cd-Mg, Fermi surface press. derivatives, de Haas-van Alphen effect meas. 77—43477
Cd-Mg, mag. susceptibility near $2^1/_2$th order electron transition, nonlinear magnetisation anal. *(Russian)* 80—44859
Cd-Mg, selective dissolution, static samples 80—65228
Cd-Mg, selective dissolution, rotating ring disc electrode 80—65229
Cd-Mg, solid solution hardening of Cd single crysts. with Mg 79—87647
Cd-Mg alloys, positron annihilation meas. of Fermi surface 79—56113
Cd-Mg single crystals, exam. of critical resolved shear stress from 77 to 300K *(Czech)* 79—91741
Cd-Mn, dil., lattice state effects on pair breaking 77—8219

cadmium alloys continued
  Cd-Mn, dil., mag. and supercond. props. 79—38237
  Cd-Mn, dil., single cryst., low temp. mag. anisotropy 77—59386
  Cd-Ni, dil., mag. and supercond. props. 79—38237
  Cd-Pb, high pressure effects, eutectic temp. 80—55361
  Cd-Pb-Bi melts, enthalpies of form. *(Russian)* 79—51277
  Cd-Pb-Bi-Sn system, ternary liq. alloys, thermodynamic props. 78—51701
  Cd-Pb-Sn melts, enthalpies of form. *(Russian)* 79—51277
  Cd-Pb(Sn)(Bi) alloy, molten, EMF meas. of liquid separation 78—39747
  Cd-Sb, dil., loss of nucl. alignment of ^{115}Sb by radiation induced defects 78—43344
  Cd-Sb, liq., hard-sphere struct. factors 77—51301
  Cd-Sb, liq., thermoelec. power meas. 79—40591
  Cd-Sb, near CdSb, Hall coeff., resistivity 79—56216
  Cd-Sb alloy condensate film, phase transform. kinetics 77—15721
  Cd-Sb alloys, phase diagram and melts struct., crystn. depend. on heating conditions 79—52155
  Cd-Sb-Sn ternary system, phase equilib. 80—16266
  Cd-Sn, eutectic alloys, struct. instability and absence of superplasticity *(Russian)* 77—8882
  Cd-Sn, spectral determ. of comp. using UHF plasmotron as source 79—52812
  Cd-Sn alloy, superconductivity and microstructure 80—107949
  Cd-Sn binary system, high press. study 80—93539
  Cd-Sn-Bi, appl. of computational techniques for treatment of thermodynamic data, phase diagram calc. 78—10172
  Cd-Sn-Pb composite amalgam electrodes for standard cells 77—5871
  Cd-Sn(-Pb) liquid (0.03 to 0.10 at.% Cd), Cd activity coeffs., interaction parameters, EMF depend. on temp. 80—49383
  Cd-Tl binary alloy system at high press. 80—97461
  Cd-W particulate composite, dispersion hardening, grain size and texture strengthening 77—8840
  Cd-Zn, cryst., internal friction, dislocation interactions 79—87673
  Cd-Zn, directionally solidified lamellar eutectics, specimen prep. for TEM *(German, English)* 78—95885
  Cd-Zn, polycryst. wire, cold worked, resistivity changes 78—68827
  Cd-Zn, solidification in mag. field, crystallite obs. *(Russian)* 77—4770
  Cd-Zn (Ag), annealed, work softened, exam. of crystallographic texture, hardness 78—80559
  Cd-Zn (1.5 wt.%), warm worked, effect of grain size, texture, on mech. props. 79—4988
  Cd-Zn (up to 1.57 at.%), single cryst., precip. hardening, 77-300K 78—60675
  Cd-Zn alloys, splat-quenched, X-ray diffr., SEM and TEM study of struct. 79—66077
  Cd-Zn binary systems, melts, elec. resist., 0-700°C 80—65517
  Cd-Zn eutectic, microstruct. degradation, role of temp. fluctuations 77—4766
  Cd-Zn eutectic and off-eutectic alloys, stability 77—25077
  Cd-Zn eutectics, microstruct. after solidification, heat pipe influence 80—76243
  Cd-Zn single crystal, plasticity, 4 to 50K 79—43362
  Cd-Zn single crystals, crit. resolved shear stress at low temps. 80—3138
  Cd-Zn-Hg, liq., comp. and temp. depend. of Hg VP, activity, free energy and enthalpy *(Russian)* 77—20087
  Cd-Zn(Pb)(Sn), binary metallic melt, deviation from the Kopp law, specific heat *(Russian)* 80—39305
  $Cd_2Fe_4Si_9$ and $CdFeSi_3$, cryst. struct. and mag. suscept., temp. depend. *(Russian)* 78—34957
  $CdGeAs_2$, amorphous, thermal gradient expts., recrystn. 80—55438
  $CdGeAsMn_x$ glass, recrystallisation 80—44133
  CdHg, electric field gradient temp. depend., TDPAD meas. 79—56647
  CdHg, ω phase, mag. susceptibility anisotropy w.r.t. uniform compression *(Russian)* 80—71143
  $Cd_{55}Hg_{45}$, X-ray study of cryst. struct. and thermal expansion 80—24405
  $Cd_{65}Hg_{35}$, X-ray study of cryst. struct. and thermal expansion 80—24405
  CdHg*, metal vapour exciplex laser, stability criteria 78—66802
  $Cd_{1-x}Mg_x$, energy spectrum pseudopotential calcs., mag. props., impurity scatt. *(Russian)* 80—65430
  $Cd_{1-x}Mg_x$, mag. props. and electron spectrum parameters *(Russian)* 79—33453
  $Cd_{1-x}Mg_x$, magnetic susceptibility anisotropy, press. effects, electronic phase transitions *(Russian)* 80—54869
  Cd_xMg_{1-x}, solid-liquid transition 78—6144
  Co-Cd, dil. alloy, impurity hyperfine interactions 78—84416
  Cu-Cd, electron work function, contact pot. difference meas. 78—80041
  Cu-Cd, exam. of diamagnetic susceptibilities *(Russian)* 79—28504
  Cu-Cd, magnetic susceptibility, comp. and temp. depend., melting effects 78—52202
  Cu-Cd, structure, electrolytic deposition on monocrystalline Cu cathodes *(Polish)* 80—44435
  Cu-Cd (0.03 at.%), single cryst., deformed, dislocation arrangement 79—10856
  Cu-Cd (1 wt.%), creep stimulated by interrupted loading 79—74213
  Cu-Cd (1.0 wt.%), yield stress and flow stress 80—97524
  Cu-Cd alloy, CA 162, flat spring, mechanical props. in bending, stress relax. test, 23 to 232°C 78—72806
  Cu-Cd alloy electro deposits on Cu substrate, struct. *(Polish)* 79—51437
  Cu-Cd alloys obtained by electrolysis, struct. 78—91552
  Cu-Cd electrodeposit on Cu, corrosion and its inhibition 79—74287
  Cu-Cd-Cr, precipitation hardened, low temp. elastic props. 77—73299
  Cu-Cd(2.7 wt.%), cellular precipitation kinetics and dissolution *(German)* 80—11651
  Eu-Cd compounds, Mossbauer effect, mag. props. and lattice consts. 77—36164
  Fe-Co-Cd, mag. hyperfine field at Cd site, TDPAC meas. 78—60363
  GaP-Cd, polythermal cross sections 77—52300
  Hg-Cd, behaviour of Cd d-bands, comparison with Au and Ag alloys 79—37972
  Hg-Cd liq. amalgam, elec. cond. and thermoelec. power meas. 77—59273
  Hg-Cd(-Te), partial vapour pressure, determ. for volatile component by static method 80—37150
  In-Cd, dil., elec. field gradient at Cd impurities, press. depend., TDPAC meas. 78—64302
  In-Cd, elastic phase transition, US study 78—6919
  In-Cd, high temp. deviation from Mattheissens rule 77—43560
  In-Cd, shape memory *(Japanese)* 79—43243
  In-Cd, soft mode, latent heats and entropies of fusion 79—46786
  In-Cd alloy crystal, phenomenological study of FCC⇄FCT transform. *(Japanese)* 79—100140

cadmium alloys continued
  In-Cd/p-InP contact evaluation 77—24619
  In-Cd-Sn, supercond. transition temp. depend. on electron conc. and electron mean free path 79—56345
  In-Te-Cd, dil., elec. field gradient, at ^{111}Cd probes, temp. depend. 79—28643
  Li-Cd, phys. props. of liq. phase and LiCd solid cpd. 80—75537
  $Li_2Cd_{2-x}In_x$, optical props., struct., energy bands, interband transitions 78—72539
  $LiCd_{1-x}Tl_x$, intermetallic, X-ray and Knight shift meas. of ^{205}Tl and ^{113}Cd 79—42851
  Mg-Ag-Cd, X-ray diff. exam. of phase fields *(Russian)* 79—56957
  Mg-Cd, anisotropic, dislocation interaction with tetragonal impurity, mobility 77—19953
  Mg-Cd, complex energy band, l-depend. pseudopot. 78—84124
  Mg-Cd, dil., dislocation-point defect interactions in slip systems 78—47417
  Mg-Cd, plasmon loss and plasmon gain, X-ray photoemission and AES 79—23918
  Mg-Cd, single crysts., temp. depend. of crit. resolved shear stress *(Czech)* 80—29112
  Mg-Cd, thermodynamic props., order-disorder transitions based on Helmholtz free energy 79—37853
  Mg-Cd, variation in interatomic interaction and lattice parameters during ordering *(Russian)* 77—81255
  Mg-Cd melts, atomic struct., short range order and melting *(German)* 78—14273
  Mg-Cd single crysts, crit. resolved shear stress, temp. and comp. depend. 79—91659
  Mg-Y-Cd, phase equilibria and mech. props. *(Russian)* 80—20894
  Mg-Y-Zn-Nd-Cd alloys, influence of Zr addition on struct. and mech. props. *(Russian)* 80—40370
  Mg-Zn-Zr-Cd-Nd, Lawes phase separation using acetate electrolyte, Cd and Nd effects 79—70237
  MgCd wire, elongation during disorder-order transform. *(Russian)* 80—104148
  Mg_3Cd, disordering under electron irrad. in electron microscope 78—83849
  Mg_3Cd, effect on order, of compression deformation 78—52924
  Mg_3Cd, lattice imaging of B19 ordering transform. and interfacial struct. 77—36495
  Mg_3Cd, order-disorder transformation kinetics 80—2138
  Mn-Y-Zn-Cd alloy,phase equilibria, plastic deformation, microhardness *(Russian)* 80—40334
  Na-Cd, liq., mag. susceptibility, diamagnetism 78—72326
  Nd-Cd, dil., magnetic susceptibility, impurities effect, free electron gas model 79—91206
  Ni-Cd, dil., ferromagnetic dynamic crit. exponent, hyperfine interaction vs. neutron scatt. expts. 78—84437
  Ni-Co-Cd alloys, electrodeposition from acetate bath 78—68637
  Ni-Fe-Cd, ternary alloy, electrodeposition from acetate bath 79—95950
  Ni-In-Cd, dil., elec. field gradient, at ^{111}Cd probes, temp. depend. 79—28643
  Pb-Cd, supercond. proximity effect, electron tunnelling study 78—10616
  Pb-Cd (1.5 wt.%) discontinuous precipitation, metallographic study *(Japanese)* 77—48440
  Pb-Cd dilute alloys, conc. depend. of Cd diffusivity enhancement 79—73348
  Pb-Cd eutectic composite, mag. flux entry in proximity effect regime 79—33418
  Pb-Cd lamellar eutectic composite, pair potential meas. 79—33396
  Pb-Sn-Bi-Cd low melting point alloy block for organ shielding in radiotherapy *(Korean)* 80—36154
  Pb-Sn-Cd, eutectic and monovariant eutectic, ingot struct. 78—15388
  Pb-Sn-Cd, monovariant eutectic and eutectic alloys, ingot struct. 77—63656
  Pb-Tl-Cd melt, short-range order struct. 80—49088
  Pd-Cd, electronic structure from annihilation quanta ang. distribs. 77—66107
  Pd-Cd alloy, positron annihilation, evidence for microporosity and dislocations 79—78786
  Pd-Cd eutectic, unidirectionally solidified, tensile and compressive props. 78—27567
  Pd-Sn-Cd, non-unique stress/strain rate relations during superplastic flow 77—28855
  γ-Pd_8Cd_{43}, X-ray cryst. struct. determ. 80—54172
  $Pd_2MnIn(Sn)(Sb)$, Cd impurities, hyperfine field meas. 78—15074
  $Pd_2MnSn_{1-y}Sb_y$-Cd, dil., Heusler alloy, hyperfine mag. field on Cd, TDPAC obs. 79—8075
  Pt-Cd, thermodynamic props. 79—43207
  β_1-PtCd, structural parameters 79—27953
  γ-$Pt_8Cd_{40(41)}$, X-ray cryst. struct. determ. 80—54172
  PtMnSn(Sb), Cd impurities, hyperfine field meas. 78—15074
  Si/In(-Cd), Si/Cd Schottky contacts, electrochemically deposited 80—88633
  $Sm_{11}Cd_{45}$, cryst. struct. similarity with γ-brass and α-Mn clusters 78—75625
  Sn-Cd, interface undercooling-growth vel. relationship, horizontal and vertical solidification 79—8294
  Sn-Cd (up to 0.3 at.%) whisker, supercond. crit. temp., stress depend. 77—39988
  Sn-Cd-Pb system, contacting layer struct. and phase composition *(Russian)* 80—66475
  Sn-Pb-Bi-Cd infiltrated Ti base composite sintered bearing material, antifriction props. 80—60981
  Tb-Cd, elec. quadrupole interaction, temp. and press. depend., TDPAC meas. 80—60469
  Tl-Cd, dil., quadrupole interaction, γ-γ ang. correl. meas. 79—56629
  Tl-Cd-Sb, liq., Cd vapour pressure and thermodynamic functions *(Russian)* 79—51247
  TmCd, parastriction, magnetoelastic and quadrupolar exchange coeffs. 79—19758
  TmCd quadrupolar ordering and magnetic interactions 79—73676
  TmCd, quadrupolar phase transitions, magnetoelastic and quadrupolar coupling consts. 80—15744
  TmCd, struct. phase transition driven by quadrupolar pair interaction 79—61583
  Y-Cd, dil., electric field gradient, γ-ray ang. correl. meas. 79—56632
  Zn-Cd, anisotropic, dislocation interaction with tetragonal impurity 77—19953

cadmium alloys continued
Zn-Cd, dil., dislocation-point defect interactions in slip systems 78—47417
Zn-Cd, three-dimensional microstruct. analysis, appl. of basic topological concepts 77—59739
Zn-Cd (1.4 at.%), crystallisation kinetic diagram appl. *(Russian)* 78—15384
Zn-Cd alloys, liq. and solid, ultrasound speed and compressibility meas. 80—102941
Zn-Cd liquid alloy, activity meas. by transportation method *(Japanese)* 78—35358
Zn-Cd liquid/Fe-Ni-Al mag. powder, effective viscosity of composites *(Russian)* 80—54424
Zn-Cd-Bi, appl. of computational techniques for treatment of thermodynamic data, phase diagram calc. 78—10172
Zn-Cd-Bi-Sn phase diagram with liquid-liquid immiscibility, computer calc. 77—36463
Zn-In-Cd, anal. calc. of phase diagram 79—91631
Zn-In-Cd soln., liquid, thermodynamic props. 79—83176

cadmium compounds
see also cadmium alloys
acetate trihydrate, hyperfine forbidden ESR lines of Mn^{2+}, spin Hamiltonians calc. *(French)* 77—28431
alkylammonium cadmium tetrachloride, struct. phase transformation, PMR, spin-lattice relax. time 77—35688
alkylene di-ammonium cadmium tetrachlorides, sp. ht. anomalies at phase transitions 80—70421
alkylene diammonium cadmium tetrachloride, struct. phase transformation, PMR, spin-lattice relax. time 77—35688
arachidate, monolayer, electron mean free path length, XPS obs. 79—74051
arachidate, monolayer transfer from air-water interface to solid, contact angles 77—55424
arachidate monolayer, Ag(Au) substrate, reson. surface plasmon reflection 78—56536
arachidate monolayers, optical props. integrated optics meas. 78—35214
behenate in Langmuir multilayer assembly system, single layer conductance 79—51701
binary, with chalcogenides and pnictides, at. vol. and semicond. props. 77—20089
cadmium formate, γ-irrad., ESR of free radicals 79—65737
cadmium formate, anhydrous, cryst. struct. 80—107195
calcium cadmium acetate hexahydrate, Mn^{2+} doped, EPR 79—65715
cathodoluminescence, bibliography of papers till 1977 79—21482
cation coordination number var. in XO_4 tetrahedral complexes 79—86768
Cd_3As_2, energy band parameter calc., temp. and press. depend. 77—31943
CdS:N, Mn, ion implanted, anomalous enhancement of EPR signal of Mn^{2+} 78—27080
CdS, and CdS:Li 78—10948
CdTe thin polycrystalline film for photoelectrochemical cell 78—23162
chalcogenide spinels, thermal stability, thermochemical, thermodynamic and crystallochemical props. 77—51519
chalcogenides, electronic polarisabilities of ions 78—79559
chalcogenides, film, on NaCl, preferential epitaxy induced by electron bombard. or elec. field 80—10824
chalcogenides, thin films, VPE, needle-like cryst. growth 80—80148
chalcopyrites, refr. index dispersion 80—55057
n-decylammonium cadmium chloride, perovskite-type layer cmpd. n-decylammonium chain dynamics 79—99313
dialkylammonium cadmium chloride, soft modes, phase transitions 78—79723
dicadmium dimethylammonium pentachloride dihydrate, X-ray cryst. struct. 79—77588
diethylammonium cadmium chloride, X-ray study of structural phase transition 78—2055
diethylammonium cadmium tetrachloride, dielec. props., phase transition 80—80675
diethylammonium cadmium tetrachloride, first order phase transition, optical phonon line broadening, spin-phonon coupling model 80—7335
dimethyl ammonium cadmium tetrachloride, dynamics of structural phase transitions 79—73309
dimethyl cadmium, partially oriented in nematic EBBA, mol. geom., PMR obs. 77—71819
dimethylammonium cadmium tetrabromide, room temp. struct. 80—29000
dimethylammonium cadmium tetrachloride, far IR refractive index, extinction coeff. and dichroism obs. 80—66144
ethylammonium cadmium tetrachloride, order-disorder transition, far IR reflectivity obs. 79—65870
ethylenediammonium cadmium chloride, struct. and mag. props., vibr. spectra 79—10842
fluoperovskites, $MCdF_3$, nonlinear elastic behaviour, US velocity, 1 bar-3 kbar 78—59851
graphite/epoxy laminates, with CdO powder filler, stress meas. by X-ray diffr. from fillers 79—43331
halide-CuCl(I) systems, AC elec. cond. rel. to phase diagram 77—72712
halides, CdX_2, positron annihilation ang. correl., bonding depend. 77—20951
halides, Mn activated, electron-phonon interaction, lattice vibr. effective energies *(Russian)* 78—59911
halides-He discharge, CW ion laser oscill. 78—17913
HgCdTe/CdTe, limited diffusion volume photodiode, characterisation 80—75627
inorganic, chemical bonds using $K\alpha_1$ line chem. shifts, Mossbauer isomer shifts 77—27089
Langmuir multilayer films with and without dye-sensitisers, elec. props. 80—97006
nitroprussides, Mossbauer spectra, dehydration effects 79—24237
orthovanadates:rare earth ions, spectroscopic props. 77—16363
oxydiacetate trihydrate, monoclinic, cryst. struct. determ. and refined 77—47438
p-n junction photovoltaic diode, appl. as IR detector 78—86330
perovskite compound combination, Mossbauer spectroscopy study *(Russian)* 80—80666
rare earth-Cd double tungstates, with scheelite structure 78—44103
resist. and magnetoresist. meas., effect of donor impurities 79—19608
solar cells, CdTe, shallow homojunctions, characteristics and surface resistance influences 80—45690

cadmium compounds continued
stearate, multilayer Langmuir films, DC cond., $T^{1/2}$ law 77—12022
stearate based Langmuir films, deposition on p-CdTe, characts. and MIS struct. 80—92998
tetra-ammine cadmium acetate:Cu, EPR dynamical effects 79—61204
TSCD meas. method and applic. 77—43615
wurtzite type materials, optical filters using coupled polarised waves *(French)* 78—33896
zeolites, synthetic, effect of sintering on elec. cond., porosity and microstruct. 79—29009
Ag-CdO cermets, coprecipitated carbonates and hydroxides, physicomech. props. 80—25706
$AgCl:CdCl_2$, point defect model, free energy and radial distrib. functions 80—44201
$AgNO_3$-$TlNO_3$-$Cd(NO_3)_2$-H_2O mixtures, Henry's law, excess free energy 78—68908
$AgPO_3$-CdT_2 glass, elec. cond. and Raman. spectra rel. to struct. *(French)* 79—10979
Al-CdS-Au structure, interfacial phenomena, complex impedance meas. *(French)* 79—42668
Al-CdSe-Ag dry air stabilised struct., elec. cond. mechanism, breakdown phenomena 80—34527
Al-CdTe-Al thin film VLF dielectric props. *(Slovak)* 79—7907
Au-$CdIn_2S_4$ surface-barrier diodes, mech. of current flow 78—56228
Au-CdS junction diodes, chemically etched CdS cryst. surfaces effect on barrier layer 80—44722
Au-CdTe-Au structure, current transport props. 80—80408
$[(100\text{-}x)B_2O_3.xLi_2O]_{98}.2CdO$, glass, X-ray irrad., EPR study of Cd^+ centres *(French)* 78—43638
$BaMoO_4$-CdO and $BaMoO_4$-$CdMoO_4$ systems, phase diagrams 77—25034
$Ba_2Zn_{2-2(x+y)}Cu_{2x}Cd_{2y}Fe_{12}O_{22}$, mag. props. and Mossbauer spectrum 80—75765
BiI_3-CdI_2, molten, elec. cond., temp. depend. 77—89562
Bi_2O_3-CdO, elec. cond., dielec. const., mag. susceptibility meas., effect of melting transition 77—7849
Bi_2O_3-CdO system, phase diagram 77—25032
$Bi_4Ti_3O_{12}$-CdS optical storage plane 77—39006
CEr_2S_4, spinel, crystal struct. *(French)* 78—91326
$(Ca_xCd_{1-x})CO_3$, cryst. struct. and cation isomorphous miscibility 80—33972
$CaF_2:Yb^{3+}$, Er^{3+}, and CdF_2-$CaF_2:Yb^{3+}$, Er^{3+}, IR to visible upconverting system 77—44035
(Cd,Hg)Te epitaxial structures, comp. profile depend. on deposition parameters 80—100795
(Cd,Hg)Te, photoconductive detector, uncooled, for 8-14 μm region 80—31868
(Cd,Tl,Ag),NO_3, mixed aq. solns., vapour press., 98.5°C, Brunauer-Emmett-Teller isotherms 78—51655
Cd complex, $(Cd[SC(CH_3)_2CH_2NH_2]_2CdCl_2)_2.2H_2O$ cryst. and mol. struct. 78—74787
Cd complex, aminoacetate, proton spin-lattice relaxation, temp. depend. 78—31119
Cd complex, aspartic and chelation, US obs. 77—44464
Cd complex, bis(thiosemicarbazide) Cd II sulphate, elec. field gradients, γ-ray PAC spectrosc. 79—65773
Cd complex, Cd (II) halide with 8-aminoquinoline, cryst., photolum. 77—52152
Cd complex, dichlorobis (pyrazole) cadmium:Cu(II), ESR, compressed tetragonal symmetry 78—6568
Cd complexes, Cd(II) mixed halide complex anions, Raman spectra 80—58270
Cd complexes, dithiocyanato(diethylenetriamine) Cd(II) and dithiocyanato(pentamethyldiethylenetriamine) Cd(II), Cu^{2+} doped, ESR 80—108059
Cd etiochlorin complex, visible spectrum, intracomplex electron phototransfer, vibr. effects 79—72330
Cd^{2+} was in electrolyte solns., pulse polarography, polarographic current const. 77—25338
Cd-As system, phase diagram, $CdAs_4$ struct. 79—74138
Cd-As-S chalcogenide glass system, prod. and acoustooptic props. *(Russian)* 78—63158
Cd-B system, interactions, product chem., phase, struct. anal., book contrib. 78—47305
Cd-Bi alloys, electron work function determ., contact pot. difference method 77—39920
Cd-Cu-Se, phase diag. 77—52303
Cd-Ge-As system, quenched samples, phase diagram, DTA after annealing 79—69226
Cd-Hg-Te, phase diagram, computer estimation 80—20903
Cd-P, p-T-x phase diagram, thermodynamic props. 80—88300
Cd-P compounds, X-ray emission bands intensity distrib., influence of chem. bonds 77—28658
Cd-Sb (53-100%), elec. resist. temp. depend. 77—59285
Cd-Sb system, contact fusion in complex metallic systems 78—26664
Cd-Sb system, phase diagram, struct. and stability of phases *(German)* 78—60661
Cd-Sb thin film prep. by vacuum deposition, elec. props. 78—92194
Cd-Sb-S-I, chalcogenide glass film, prep. by laser evaporation, and characterisation 77—12533
Cd-Te-Ge system, CdTe-Ge cross section 77—52298
$Cd_{1-x}Mn_xTe$, exchange interaction, magneto-optical spectra 80—25348
Cd_x-$Hg_{1-x}Te$, cyclotron magneto-optical resons., photoconductivity meas. *(Russian)* 78—23133
$Cd_{1-x}Ag_xCr_2Se$, ferromag., magnetoresistance exam. *(Russian)* 78—84238
$Cd_{1-x}Ag_xCr_2Se_4$, Ag acceptor states effect on exchange interaction 80—20397
$Cd_{1-x}Ag_xCr_2Se_4$, ferromag. semicond., influence of strong elec. field on microwave absorption 77—28207
$CdAl_2O_4$, LWR burnable poison, irradiation and corrosion beahviour *(German)* 79—67846
a-CdAs thin film fabrication for switching applications 78—2415
$CdAs_2$, amorphous, elec. cond. and thermopower 80—49722
$CdAs_2$ based glasses, AC cond. 78—39109
$CdAs_2$ based glasses, cond. and permittivity, freq. depend. 77—76859
$CdAs_2$, cryst. struct. and vitrification capacity 80—88126
$CdAs_2$ glasses, covalently bonded, energy gap correl. with average atomisation enthalpy 77—76740
$CdAs_2$ single crystals, growth from vapour phase 78—88416
$CdAs_2$, synthesis, microstruct., hardness and elec. cond. 79—51268

cadmium compounds continued
$CdAs_2$, thermodynamic functions 79—10961
$CdAs_2$, thermoelec. props., anisotropy 80—34470
Cd_3As, film, amorphous, crystallisation effects 77—35482
Cd_3As_2, amorphous to crystalline transform. 79—77519
Cd_3As_2 and $CdAs_2$, molten, thermal expansion and atomic bond strength parameters 80—65257
Cd_3As_2, anisotropy of electronic g*-factor 80—44483
Cd_3As_2, band struct. and g-factor, Shubnikov-de Haas oscills. meas. 80—49598
Cd_3As_2, band struct. from Shubnikov-de Haas and de Haas-van Alphen effects 80—49597
Cd_3As_2, band structure, Kane model, magneto-Seebeck and Hall data 77—62821
Cd_3As_2, band structure, pressure dependence of galvano- and thermomagnetic effects 80—6722
Cd_3As_2, cryst., gas phase growth, morphology 79—10821
Cd_3As_2, depend. of g-factor on electron conc. at low temps. 77—69218
Cd_3As_2, effect of annealing on elec. transport props. 80—49739
Cd_3As_2, elec. resist. and HF dielec. const. calcs. *(French)* 77—59284
Cd_3As_2, electron conc. temp. depend. heavy hole-cond. band energy gap 79—69410
Cd_3As_2, electron effective mass. temp. depend., Hall effect and thermoelec. power meas. 80—39613
Cd_3As_2, electronic g-factor, effective mass and density of states 79—60691
Cd_3As_2, energy band structure calc. 80—75504
Cd_3As_2 film, crystalline and amorphous films, band structure, optical properties 78—11013
Cd_3As_2 film, optical absorption edge 80—50450
Cd_3As_2 film, size effects, electrical properties 78—2600
n-Cd_3As_2 film, vac. evaporated, Shubnikov-de Haas effect 79—99644
Cd_3As_2 film on NaCl substrate, vacuum deposition, growth morphology, microstructure 80—75479
Cd_3As_2 films, amorphous, elec. resist., Hall mobility, temp. depend., cond. mechanism 77—76982
Cd_3As_2, highly doped, Shubnikov-de Haas type oscills. in optical transmission 79—61352
Cd_3As_2, inverted band struct. 79—90958
Cd_3As_2, ionised-impurity mobility and static dielec. const. at 4.2K 77—32017
Cd_3As_2, low-temp. energy band struct. and depend. of direct gap on press. and temp. 77—62822
Cd_3As_2, phys. props. 78—26527
Cd_3As_2 platelet, single vap.-grown cryst., passive annealing, Fermi energy variation 80—45223
Cd_3As_2, Shubnikov-de Haas effect 80—11020
Cd_3As_2, sp. ht., thermodyn. props. 78—22863
Cd_3As_2, thermal dissoc., 550-850°C 80—35512
Cd_3As_2, thermoelectric power and transverse Nernst Ettingshausen coefficent 79—38104
Cd_3As_2, thermoreflectance spectra 78—6702
Cd_3As_2 type crystals, symmetry props. of energy bands 80—39500
Cd_3As_2, valence band struct., optical absorpt. meas. 80—50293
Cd_3As_2, vapour phase single cryst. growth, X-ray topographic obs. of perfection 78—9976
Cd_2AsCl_2, X-ray cryst. struct. anal. *(French)* 80—64957
Cd_3AsCl_3, X-ray cryst. struct. determ. and refinement *(French)* 80—107119
Cd_2As_3I, X-ray cryst. struct. determ. *(French)* 79—99138
$Cd_5(AsO_4)_3Br$, halogen atom distrib. determ. 78—2078
$Cd_5(AsO_4)_3Br$, X-ray diffr. cryst. struct. exam. and refinement 78—10000
$Cd_3(As_xP_{1-x})_2$, $0\leq x\leq 1.0$, band struct. calc. near Brillouin zone centre 80—107703
$Cd_3(As_xP_{1-x})_3$, thermoelectric power and Hall effect., mag. field depend. 78—10484
$CdB^4C^5{}_2$, chalcopyrite struct., surface energy and compressibility, rel. to glass form. 79—51417
$Cd_2B_2O_5$, basalt atom coordinates isotropic temp. corrections, X-ray study 80—59449
$Cd_3B_7O_{13}Br(Cl)(I)$, boracite, single cryst. prep. and phys. props. 80—100763
$Cd_4(BO_3)_2(OH)_2$, synthetic cryst., structural anal. 79—86764
$Cd_3B_7O_{13}X$, X=Cl or Br, highly insulative, switching obs. 77—51785
$CdBa_3(MO_4)_2$, (M=Ge, Si), cryst. struct., form. 77—19928
$CdBa(PO_3)_4$, $CdSr(PO_3)_4$, struct. from IR spectra 77—47421
$CdBr_2$, cathodoluminescence, 300 and 80K *(Russian)* 79—78760
$CdBr_2$ crystal, transverse and longitudinal lattice mode freq., IR reflection spectra meas. 78—27227
$CdBr_2$, dielec. function and band struct., EELS meas. 80—40195
$CdBr_2$, exciton spectra, temp. and press. effects 77—20881
$CdBr_2$, lattice vibr., IR absorpt. meas. 79—4380
$CdBr_2$, layer cryst., electric field effect on NQR, elec. polarisation mechanism 77—20746
$CdBr_2$, optical refl. spectra, exciton bands obs. around optical gap 78—15192
$CdBr_2$, polytype 12R, cryst. struct. determ. 80—33937
$CdBr_2$, vapour grown crystals, polytype formation, effect of mode and conditions of growth 78—72709
$CdBr_2$, XPS, satellite of Br 4s line 78—56556
$CdBr_2:Ag^{2+}$, strong Jahn-Teller coupling, EPR 79—28605
$CdBr_2:Co$, spectroscopic studies of interactions 80—29769
$CdBr_2:Co^{2+}$, exchange-coupled Co^{2+} pairs, optical absorpt. and Zeeman studies 80—66242
$CdBr_2:Co^{2+}$, ground state g-value, EPR meas. 77—16159
$CdBr_2:Co^{2+}$, polarised IR absorpt. spectra 77—40269
$CdBr_2:Cu^+$, polarised absorption spectra 77—59594
$CdBr_2:Eu^{2+}$, layered, temp. depend. of consts. in ESR Hamiltonian, 16-300K *(Russian)* 77—32254
$CdBr_2:Fe^{2+}(Co^{2+})(Ni^{2+})$, charge transfer near UV spectra, 4.2K, mag. circular dichroism 78—80378
$CdBr_2:I_2$, layered extrinsic cryst., impurity absorpt. band, temp. anomaly *(Russian)* 77—8616
$CdBr_2:Mn^{2+}$, layered, pressure effect of ESR on axial field const. of spin Hamiltonian *(Russian)* 77—32254
$CdBr_2$-$BiBr_3$, molten, elec. cond., 500-870K, composition depend. 78—55965
$CdBr_2$-Cd molten solution, US velocity and compressibility 77—84844
$CdBr_2$-Cd molten solution, surface tension 77—85024

cadmium compounds continued
$CdBr_2(I_2)$, vapour growth crystals, decomposition, electron microscope study 78—92268
$Cd(BrO_3)_2.2H_2O$, cryst. struct. 80—1992
$CdBr_2.4H_2O$, cryst. struct. determ. *(French)* 78—26502
$CdBr_2.4H_2O$, NMR, ^{113}Cd nucl. mag. shielding 78—68395
$CdCO_3$, NMR, ^{113}Cd nucl. mag. shielding 78—68395
$CdCO_3$, thermal expansion temp. depend. 78—18803
$CdCO_3$, three-fold transformation twin in topotactic decompositon 78—44078
$CdCO_3$, topotactic decomp., X-ray diffr. obs. 77—44478
$CdCO_3:Fe^{2+}$, Mossbauer spectra 80—108138
$CdCa_2Cl_6.12H_2O$, X-ray cryst. struct. anal. *(French)* 79—4291
$Cd_xCa_{1-x}MoO_4$, growth and props. 80—71588
$Cd_xCa_{1-x}MoO_4$, intrinsic hole centres EPR study, thermoluminescence and thermal decay 79—99957
$Cd_{1-x}Ca_xS$, solid soln., phase equilib. diagrams 80—108412
$CdCl_2 . 2.5H_2O$, rel. between theoretical and obs. morphology *(French)* 80—70148
$CdCl_2$, adsorption of Ar, two-dimens. condensation of second adlayer 79—99413
$CdCl_2$, aq. soln., Raman spectrum, local order 78—84563
$CdCl_2$, aq. solns., sound absorpt. and relax. phenomena 80—49311
$CdCl_2$, Coulomb energy, pot., field and dipolar moments, selfconsistent calcs. 79—18323
$CdCl_2$ crystal, transverse and longitudinal lattice mode freq., IR reflection spectra meas. 78—27227
$CdCl_2$, deformation densities, relativistic effect 80—42928
$CdCl_2$, dielec. function and band struct., EELS meas. 80—40195
$CdCl_2$, effective core potentials calcs. rel. to bond lengths and energies 78—66464
$CdCl_2$, NMR, ^{113}Cd nucl. mag. shielding 78—68395
$CdCl_2$, optical refl. spectra, exciton bands obs. around optical gap 78—15192
$CdCl_2:Ag^{2+}$, strong Jahn-Teller coupling, EPR 79—28605
$CdCl_2:Co$, spectroscopic studies of interactions 80—29769
$CdCl_2:Co^{2+}$, ground state g-value, EPR meas. 77—16159
$CdCl_2:Co^{2+}$, optical absorpt. spectra, Zeeman study 78—6712
$CdCl_2:Co^{2+}$, polarised IR absorpt. spectra 77—40269
$CdCl_2:Cu$, optical props. 78—43918
$CdCl_2:Cu^+$, polarised absorption spectra 77—59594
$CdCl_2:Cu^{2+}$, meas. of covalency in tetragonal complexes 77—47781
$CdCl_2:Fe^{2+}$, magneto optical study, ferromagnetically coupled Fe(II) pairs 78—6711
$CdCl_2:Fe^{2+}(Co^{2+})(Ni^{2+})$, charge transfer near UV spectra, 4.2K 78—80378
$CdCl_2:Mn^{2+}$, e.s.r. spectra meas. 77—4554
$CdCl_2:Mn^{2+}$, null points in zero-field splitting of mag. impurity levels 79—87066
$CdCl_2:NO_2{}^-$, aqueous solns., luminesc., absorpt. and Raman spectra *(Russian)* 77—36291
$CdCl_2$-Cd molten solution, US velocity and compressibility 77—84844
$CdCl_2$-Cd molten solution, surface tension 77—85024
$CdCl_2$-$CdBr_2$, solid soln., luminesc., optical absorpt. 78—19538
$CdCl_2$-KCl-H_2O, water activity, 0 and 50°C, conc. depend. *(Russian)* 78—31679
$CdCl_2$-NaCl, KCl molten salt mixtures, US velocity and adiabatic compressibility obs. 78—75730
$CdCl_2$-$PbCl_2$, thermodynamic quantity meas. by quantitative thermal anal. of heating process 78—19730
$CdCl_2(Br_2)(I_2)$, adsorption of NO, crit. and triple point temps. of first adsorbed layer 78—91548
$Cd(ClO_3)_2$, irrad., bleaching and annealing expts., EPR and optical absorpt. 79—91476
$Cd(ClO_3)_2$ irradiated single crystal, ESR and annealing, trapped defect centre 80—55141
$Cd(ClO_3)_2$ single crystals, Raman scatt. 80—55106
$Cd(ClO_4)_2$, aq. soln. positronium form., quenching and inhibition 78—15690
$Cd(ClO_4)_2.6H_2O$ and $Cd(ClO_4)_2.6D_2O$, single crystals, EPR study of phase transitions 80—66025
$Cd(ClO_4)_2.6H_2O:Mn^{2+}$, phase transition, EPR of Mn^{2+} meas. 79—56604
$CdCl_2.4H_2O$, cryst. struct. determ. by X-ray diffractometry *(French)* 79—37673
$Cd_{0.75}Co_{0.25}Cr_2S_4$, specific heats 79—11315
$Cd_3Cr_2Ge_3O_{12}$, absorpt. and luminesc. spectra, cryst. field and exchange interactions 77—73154
$Cd_3Cr_2Ge_3O_{12}$, antiferromagnetic ordering of Cd^{3+}, sp. ht. and mag. susceptibility meas. 77—16062
$Cd_3Cr_2Ge_4O_{12}$, antiferromagnetic reson., anisotropy and magnetoelastic interaction effects *(Russian)* 77—69712
$CdCr_2O_4(S_4)(Se_4)$, magnetic exchange interactions 77—24690
$CdCr_2S_4$, $Cd_{1-x}X_xCr_2Se_4$, (X=Zn, Hg), optical and magneto-optical surface effects 79—82953
$CdCr_2S_4$, $CdCr_2Se_4$, variation of elec. props. with chalcogen content of gas phase, 500-700°C 77—20310
$CdCr_2S_4$, EPR line profiles in paramag. and ferromag. phases 79—28602
$CdCr_2S_4$ ferromag. semicond. film, props. 78—76175
$CdCr_2S_4$, ferromag. semicond., band struct., EHT calc. 80—54608
$CdCr_2S_4$, ferromag. semicond., IR refl. spectra, phonon props. and dielec. function 80—66191
$CdCr_2S_4$, ferromagnetic semiconductor films, prep. and props. *(Japanese)* 79—47308
$CdCr_2S_4$, Heisenberg ferromag., obs. of dynamic dipolar crossover, ESR linewidths meas. 79—24209
$CdCr_2S_4$, hot pressed, Faraday effect isolation 10.6 μm, damage tests 77—46750
$CdCr_2S_4$, hot-pressed, optical isolation appl. at 10.6 μm, intrinsic absorpt. props. 78—42368
$CdCr_2S_4$, magnetic semicond., resonance Raman scatt., mag. circular polarisation props. 80—50341
$CdCr_2S_4$ magnetic semiconductor crystal growth, structural defects, physical properties 80—60759
$CdCr_2S_4$, phonon Raman scatt., mag. circular polarization effects 79—8134
$CdCr_2S_4$, photothreshold changes below mag. ordering temp. 80—97406
$CdCr_2S_4$, polycrystalline films, mag. semicond., spinel-type, magneto-optical effects *(Japanese)* 79—47415
$CdCr_2S_4$, pure and Ag doped, electronic struct., mixed valence 80—70612

cadmium compounds continued
p-$CdCr_2S_4$, single cryst., elec. cond. 79—15148
$CdCr_2S_4$, single cryst. prep. and elec. props. 79—38727
$CdCr_2S_4$, single crystal ferromagnetic semiconductor, vapour-liquid transport growth method 77—21013
$CdCr_2S_4$, single crysts., EPR linewidth near Curie point, temp. and susceptibility depend. 77—63272
$CdCr_2S_4$, spin dependent phonon Raman scatt., resonance effects 77—73145
$CdCr_2S_4$, thermodyn. props. 78—51703
$CdCr_2S_4$, thermoreflectance near Curie point 79—78659
$CdCr_2S_4$, thermoreflectance, photoconductance, Raman scattering near magnetic phase transition 80—97298
$CdCr_2S_4$:Ag, mag. semicond., ferromagnet resonance angular and temp. depend. 79—69730
$CdCr_2S_4$:Cu, magnetic microregions caused by s-d exchange 77—77050
$CdCr_2S_4$:Gd, ferromag. reson. and electrical cond. 79—28626
$CdCr_2S_{4-\gamma}$, spinel, anomalies in paramag. susceptibility, Curie pt. *(Russian)* 77—80910
$CdCr_2S_4(Se_4)$, EPR linewidth, 100-300K, spin-lattice relax. 77—51942
$CdCr_2S_4(Se_4)$, electron spectrum, light absorpt. spectrum, calcs. 80—2793
$CdCr_2S_4(Se_4)$, ferromagnetic semiconductors, spinel-type, resonance Raman scattering and electronic structure *(Japanese)* 79—47421
$CdCr_2S_4(Se_4)$, spin depend. phonon Raman scatt., band struct. 78—68491
$CdCr_2S_4(Se_4)$, spontaneous magnetisation temp. depend., nuclear resonance freq. depend. *(French)* 80—80483
$CdCr_2(S_xSe_{1-x})_4$, mag. transition obs. *(Russian)* 77—4517
$CdCr_2S_{4-x}Se_x(O_x)$ X=0, 4, and solid solns., imperfect struct. model from cryst.-chem. investigs. 79—42053
$CdCrSe_4$, ferromag. semiconductor, mag. props. near Curie pt., doping effects 79—1670
$CdCr_2Se$, ferromag. semicond., high field effects, magnon carrier scatt. 78—87981
$CdCr_2Se_3$:Ga, synthesis and photoferromag. effect 77—51936
$CdCr_2Se_4$, crit. behaviour near Curie point 78—31068
$CdCr_2Se_4$, crit. behaviour of optical absorption edge 78—35143
$CdCr_2Se_4$, Crit. relax. processes, mag. reson. expts. 80—60425
$CdCr_2Se_4$, crit. speeding-up of spin-relax. 78—48028
$CdCr_2Se_4$, crystn. from high temp. soln., $CdCr_2Se_4$-$CdCl_2$ phase diagram 78—3009
n-$CdCr_2Se_4$, current- and voltage-controlled negative resist. obs. 78—19041
$CdCr_2Se_4$, deviation from Kittel's mag. resonance formula near T_c 79—87322
$CdCr_2Se_4$, energy band struct calc. by augmented plane wave method 80—103621
$CdCr_2Se_4$, energy structure, magnetooptic effects 80—71394
$CdCr_2Se_4$, evap., mass spectra 78—53238
$CdCr_2Se_4$, excitation of spin waves by current carriers, magnetisation and elec. cond. reduction *(Russian)* 79—7981
$CdCr_2Se_4$, ferromag., localised states on imperfections and red shift of absorpt. edge 77—66527
$CdCr_2Se_4$, ferromag. semicond., P-T phase diagram by annealing expts. between 600 and 964°C 77—63636
$CdCr_2Se_4$, ferromag. semicond., properties and use for making devices, review 78—60131
$CdCr_2Se_4$, ferromag. semiconductor, light scatt. from magnons under strong fields 78—84554
$CdCr_2Se_4$, ferromag. semicond., photoinduced mag. anisotropy 80—50086
$CdCr_2Se_4$, ferromag. semicond., band struct., EHT calc. 80—54608
$CdCr_2Se_4$, ferromag. semicond., conc. anomalies rel. to red shift of absorpt. edge 80—70732
$CdCr_2Se_4$, ferromagnetic semiconductor, P_{Se}-T phase diagram, where $Se=Se_2$, near peritectoid reaction temps. *(Japanese)* 77—52290
$CdCr_2Se_4$, ferromagnetic semiconductor, single cryst. growth *(Japanese)* 79—47612
$CdCr_2Se_4$, ferromagnetic low anisotropy semicond., spontaneous magnetisation RF determ. 80—22396
$CdCr_2Se_4$ film, absorpt. and Faraday effect 78—2936
$CdCr_2Se_4$ film, electron irradiated, struct. 79—15032
$CdCr_2Se_4$ film, ferromag. semicond., prep. by vacuum condensation 77—28724
$CdCr_2Se_4$ film, mag. linear and circular dichroism and Faraday rot. 79—99966
$CdCr_2Se_4$ films, mag. hysteresis, domain struct., mag. viscosity 80—25169
$CdCr_2Se_4$, influence of Co ions on anisotropy and magnetostriction, ferromag. reson. meas. 77—69659
$CdCr_2Se_4$, influence of ferromag. ordering on phonon Raman scatt. 78—2853
$CdCr_2Se_4$, light scatt. by magnons 77—69805
$CdCr_2Se_4$, mag. semicond., threshold and mag. memory switching in single crysts. 77—43672
$CdCr_2Se_4$, mag. semicond., photoinduced binding of domain walls *(Russian)* 78—80174
$CdCr_2Se_4$, mag. semicond., domain struct. by IR Faraday effect 79—95604
$CdCr_2Se_4$, mag. semicond. effect of illum. on domain struct. 79—99726
$CdCr_2Se_4$, magnetic red shift origin, specular reflectivity, band struct. 80—40127
$CdCr_2Se_4$ magnetic semiconductor, photoinduced centre kinetics 80—71110
$CdCr_2Se_4$, magnetisation, study of photoindduced charges 80—80567
$CdCr_2Se_4$, magnon instability, under intense EM field 77—40048
$CdCr_2Se_4$, modulated piezoreflection spectra 80—97237
$CdCr_2Se_4$, Mott ferromagnetic semiconductor, optical absorption edge, critical behaviour 80—97226
$CdCr_2Se_4$, narrow conduction band, crit. behaviour of resistivity 79—78096
$CdCr_2Se_4$, optical absorption due to transitions between bands and local levels 79—38537
$CdCr_2Se_4$, optical reflectivity, dielectric const. by expt. data Kramers-Kronig anal., spinel struct. 79—99903
$CdCr_2Se_4$, photoferromag. effect quenching, photocond. 78—68488
$CdCr_2Se_4$, photoinduced infra-red optical absorption 78—23455
$CdCr_2Se_4$, pure and Ag doped, electronic struct., mixed valence 80—70612
$CdCr_2Se_4$, reactor radiation influence on ferromagnetic phase transform. *(Russian)* 80—75760

cadmium compounds continued
$CdCr_2Se_4$, reflectance magneto-circular dichroism 77—81120
$CdCr_2Se_4$, refr. index variation in strong alternating mag. field 80—23741
p-$CdCr_2Se_4$, resistivity anomalies at mag. transitions, sp.ht. 80—39785
$CdCr_2Se_4$, resonant Raman scatt. 79—4802
$CdCr_2Se_4$ single cryst., photocond. in air, vacuum, mechanism 77—8138
n-$CdCr_2Se_4$, single crystal, transport props. near Curie temp. *(Japanese)* 78—6406
$CdCr_2Se_4$, single crysts., mag. semicond., spinel-type, magneto-optical effects *(Japanese)* 79—47415
$CdCr_2Se_4$, single cryst. growth by chem. transport reactions 80—16163
$CdCr_2Se_4$, spin dependent phonon Raman scat., resonance effects 77—73145
$CdCr_2Se_4$, spin system heating by drifting current carriers, magnon-phonon system energy transfer *(Russian)* 80—29541
$CdCr_2Se_4$, spinel film, struct. SEM study, props. 78—79905
$CdCr_2Se_4$, temp. depend. of resist. and magnetoresist., influence of Se vacancies 78—60130
$CdCr_2Se_4$, thermoreflectance, photoconductance, Raman scattering near magnetic phase transition 80—97298
$CdCr_2Se_4$, velocity-field characts., above T_c 78—64049
p-$CdCr_2Se_4$:Ag, electrical props., 100-300K 80—54692
$CdCr_2Se_4$:Ag, ferromag. reson. meas. 77—8415
$CdCr_2Se_4$:Ag, ferromag. reson. field and linewidth anisotropy, Se vacancy effects 78—60338
$CdCr_2Se_4$:Ag, ferromag. linewidth and eddy current losses 79—33541
$CdCr_2Se_4$:Ag, impurity contrib. to low temp. ferromag. reson. linewidth 79—65743
$CdCr_2Se_4$:Ag, mag. anisotropy, effect of annealing in vacuum 77—80929
$CdCr_2Se_4$:Ag, magneto-electrical props. temp. behaviour depend. on dopant conc. *(Russian)* 80—11006
$CdCr_2Se_4$:Ag, magneto-optical effects in impurity spectral region 80—97313
p-$CdCr_2Se_4$:Ag, oscillatory magnetoresist., temp. and mag. field depend. 78—52011
$CdCr_2Se_4$:Ag(Gd), doping effects on exchange interaction 78—43579
$CdCr_2Se_4$:Cu, elec. props., temp. depend. *(Russian)* 78—72181
$CdCr_2Se_4$:Cu(In), ferromag. semicond., mag. and elec. props. 77—20588
$CdCr_2Se_4$:Ga, sp. elec. resist., temp. and mag. field depends. *(Russian)* 78—26893
$CdCr_2Se_4$:Ga(Ag), and pure, photocond. and photomagnetoresist. spectra 77—80809
$CdCr_2Se_4$:Ga(In), photoconductivity, photomagnetoresistance near Curie point *(Russian)* 80—100485
$CdCr_2Se_4$:In, elec. cond., annealing effect 79—87102
n-$CdCr_2Se_4$:In, electrical props., 93-168K 80—49713
$CdCr_2Se_4$:In, ferromag. semicond., carrier mobility, electron-two magnon scatt. Hall effect 78—51992
$CdCr_2Se_4$:In, influence of Se-deficiency on props. 78—30921
$CdCr_2Se_4$:In, nondegenerate ferromagnetic semiconductor, positive magnetoresistance 78—2505
$CdCr_2Se_4$:In , impurity band, photocond. spectral depend. 78—19088
$CdCr_2Se_4$:In (Ga)(Ag), and undoped, elec. prop., vac. heat treatment effect 80—15518
$CdCr_2Se_4$:In(Ga), elec. resist. and magnetoresist., 2 to 200K 80—96876
$CdCr_2Se_4$:In(Ga), temp. driven metal-semiconductor transition, temp. and mag. field depend. *(Russian)* 78—88003
$CdCr_2Se_4$:In(Ga)(Cu), magnetic microregions caused by s-d exchange 77—77050
$CdCr_2Se_4$:Ir(Cu), mag. props. near Curie temp. *(Russian)* 77—63234
$CdCr_2Se_4$-$ZnCr_2Se_4$, single cryst., mag. props. 79—28526
$CdCr_2Se_{4-x}S_x$, influence of anion substitution on red shift of optical absorption band edge 77—32399
$CdCr_2Se_4(S_4)$, ESR line intensity near Curie point 78—64269
$CdCr_2Si_4$:Ga, negative magnetoresist. effects near Curie temp. 79—11152
$CdCr_2Sr_4$, press. depend. optical aborption edge shift and compressibility 79—28714
$CdCr_2X_4$ (X=S,Se), excess entropy terms 79—86905
$CdCsP_3O_4$, cryst. struct. exam. *(French)* 78—2076
$CdCs_2(SO_4)_2.6H_2O:Mn^{2+}$, EPR, 298K, spin-Hamiltonian parameters, cryst. fields 78—27086
$Cd_{1-x}Cu_xCr_2S_4$, elec. resist., temp. depend., behaviour at Curie point 77—62929
$Cd_{0.96}Cu_{0.04}Cr_2Se_4$, single cryst., galvanomagnetic props. 79—7848
$Cd_{1-x}Cu_xCr_2Se_4$ solid solution, spinel struct., X-ray investigation 79—78940
$CdCu_3Ru_4O_{12}$, synthesis, cryst. struct., mag. and elec. props. *(French)* 80—107151
CdF, mol., ESR spectra in inert gas matrix 79—76455
CdF_2, colour centres, IR absorpt. and photocond. after UV irrad. 80—79784
CdF_2, conversion into semicond. by heating in H_2 atm., resist. meas. 80—20978
CdF_2, dispersion calcs. of cubic nonlinear susceptibility near Raman resonance 79—94292
CdF_2, elastic constants. and Debye temp., 4.2-295K 78—38770
CdF_2, electrical transport limitation by electrodes, polarisation effects 80—96689
CdF_2, electrode polarisation 78—76377
CdF_2, electronic band struct., combined tight-binding and pseudopotential calc. 77—43495
CdF_2, electronic energy bands calc. 78—34762
CdF_2, electronic structure of outermost levels, UPS study 80—7468
CdF_2, high resolution NMR and chem. shifts of ^{111}Cd and ^{113}Cd, double reson. expt. 80—60460
CdF_2, ionic cond., activation vols., freq. depend. cond., press. effects 80—100354
CdF_2, ionic conducting fluoride fluorite, US velocity meas. 80—107381
CdF_2, low temp. heat capacity 78—47490
CdF_2, MnF_2 or rare earth fluoride doped, elec. cond. and electroluminesc. 79—87508
CdF_2, NMR, ^{113}Cd nucl. mag. shielding 78—68395
CdF_2, pure, thin powder layers, electrolum. 79—56865
CdF_2, rare earth doped, multicoloured electroluminesc. 79—78755
CdF_2, rare-earth and transition ion doped, far IR absorption and Zeeman effect 77—40246
CdF_2, UPS and XPS spectra, rel. to optical props. 80—66386
CdF_2, valence band struct. determ. by photoemission meas. 79—47591
CdF_2: rare earth, electronic props., compared to CaF_2 *(French)* 80—49662

cadmium compounds continued
CdF_2: $YF_3(YbF_3)$, photoconversion from insulating to semicond. state, IR absorption and elec. cond. 78—14759
CdF_2:^{241}Am, alpha-decay, ^{237}Np charge state, Mossbauer obs. 79—47367
CdF_2:Co^{2+}, Jahn-Teller split $^4Ag_{2g} \rightarrow {}^4T_{1g}(P)$ absorption band, elec. field effect 78—15202
CdF_2:Co^{2+}, MCD spectra 77—28603
CdF_2:Co^{2+}, parity-forbidden transitions, elec. field effect on electronic-vibr. spectrum 79—65905
CdF_2:$Co^{2+}(Mn^{2+})(Ni^{2+})$, far IR absorpt. spectra peaks 78—27265
CdF_2:Cr^{2+}, orthorhombic Jahn-Teller distortion 78—19007
CdF_2:Cu, paramagnetic centre coordination, g-tensor orientation by anisotropy of ^{19}F ENDOR 80—54993
CdF_2:Er^{3+}, selective monochromatic excitation of $^4S_{1/2}$-$^4I_{15/2}$ transition *(French)* 77—85765
CdF_2:Er^{3+}, Tm^{3+}, evidence for $Er^{3+} \rightleftharpoons Tm^{3+}$ energy transfers, fluoresc. expts. 80—60655
CdF_2:Eu, role of solution and precipitation phenomena on ITC spectra 80—7265
CdF_2:Eu^{2+}, EPR spectra, hydrostatic press. and temp. effects 80—84648
CdF_2:Eu^{3+}, electroluminescence spectra from 400 to 700 nm *(Russian)* 77—69916
CdF_2:Eu^{3+}, luminesc., charge transfer states 79—33799
CdF_2:Eu^{3+}, luminesc. spectra conc. and annealing depend. 79—65917
CdF_2:Eu(Gd), impurity and intrinsic electrolum. 77—36298
CdF_2:Eu(Gd)(Nd), semicond., symmetry of optical centres, optical and elec. props. 77—59592
CdF_2:Gd^{3+}, hydrostatic press. and temp. effects on EPR spectrum 78—76304
CdF_2:Gd^{3+}, investigation of superhyperfine struct. in EPR spectra 79—51851
CdF_2:Gd^{3+}, ligand ENDOR, spin Hamiltonian and hyperfine parameters 77—43903
CdF_2:Ge^{3+}, Ce^{3+}, in semicond. state, elec. cond. and Hall meas. 78—10443
CdF_2:In, evidence for strong impurity-lattice coupling 80—6775
CdF_2:In, shallow versus deep donors 77—85176
CdF_2:Mn, thermolum., recomb. processes 78—15237
CdF_2:Mn, Y, deconversion due to vacuum heat treatment, elec. resist. and electron probe meas. 79—24025
CdF_2:Mn,Y, in MIS struct., blue-green electrolum. 79—52025
CdF_2:Mn films, electroluminesc. meas. *(French)* 79—11471
CdF_2:Mn^{2+},Y^{3+}, thermal stability under vacuum, effect of heat treatment on resist. 79—23969
CdF_2:NaF, formation and reorientation of Na^+-anion vacancy complexes 78—84516
CdF_2:NaF thin films, electroluminescence obs. at 77K *(French)* 80—80866
CdF_2:NaF(AgF), colour centres, IR absorpt. and photocond. after UV irrad. 80—79784
CdF_2:Na(Nd), ionic cond. investigation by complex admittance method 80—100352
CdF_2:R^{3+}, cooperative luminescence influenced by symmetry of centres 78—6791
CdF_2:R^{3+}, far IR Stark and Zeeman splitting 77—48190
CdF_2:Sm^{3+}, photoconverted, thermally stimulated relax. 80—84476
CdF_2:Ti^{2+}, electronic struct. and EPR of Ti^{2+} 78—76034
CdF_2:YbF_3, conversion processes into semiconductor 78—14730
CdF_2-Au metal-semiconductor contact, capacitance and photocurrent, barrier height 77—85321
CdF_2-KF(LiF)(NaF), liquid mixture, enthalpy of mixing 78—48684
CdF_2-metal Schottky diode, photoemission, capacitance and I-V meas. barrier heights 78—26950
CdF_2-YF_3, thermal ionisation energy of monovalent centres 80—80207
CdFCl, CdFBr, existence and vibr. characterisation, IR and Raman matrix isolation obs. 78—78706
CdF_2(FCl)(FBr), matrix isolated IR and Raman spectra, assignments, force consts., isotope effects and thermodynamic props. 80—63631
CdF(OH), X-ray cryst. struct. determ. 79—99134
$CdFe(CO)_4$, IR and Raman spectra, vibr. anal. 78—66553
$Cd_{1-x}Fe_xCr_2S_4$, Fe II electronic struct., Mossbauer spectra 80—15876
$Cd_{1-x}Fe_xCr_2S_4$ series of magnetic semiconductors, magneto-optical effects, expt. *(Japanese)* 77—40212
$Cd_{1-x}Fe_xCr_2S_4$, single cryst., mag. semicond., spinel-type, magneto-optical effects *(Japanese)* 79—47415
$Cd_{1-x}Fe_xCr_2S_4$:Cu, effect of doping on elec. props. and Curie temp. 78—84214
$CdFe_{1/2}Nb_{1/2}O_3$, high temp. X-ray exam. 77—11527
$CdFe_2O_4$, ferrite, synthesis 77—16523
$Cd_{0.010}Fe_{2.990}O_4$, heat capacity investigation of dopant effects on mag. disordering temp. 80—25143
$Cd_xFe_{3-x}O_4$, collective electron states, ^{57}Fe Mossbauer meas. 77—69748
$Cd_xFe_{3-x}O_4$, cond. mechanism, collective electron description 77—4588
$CdFeTi(PO_4)_3$ cryst. struct., and prep., rhombohedral lattice *(French)* 77—27856
$CdGa_2$, excimer visible emission spectra in RF discharge, vibr. struct. 79—18201
$Cd_{1-x}Ga_xCr_2S_3$, spinel, anomalies in paramag. susceptibility, Curie pt. *(Russian)* 77—80910
$CdGaS_2$, single crysts., peculiarities of photocond. in strong elec. field 80—54736
$CdGa_2S_4$, direct excitons, refl. spectra 79—90972
$CdGa_2S_4$ double surface-barrier diodes, current-voltage characts. 80—92972
$CdGa_2S_4$, IR light transmission, IR refl. spectra and cryst. struct. 79—56777
$CdGa_2S_4$, IR refl. spectra 80—60604
$CdGa_2S_4$, interpretation of thermolum. and TSC meas. 78—27336
$CdGa_2S_4$, photoluminesc. and photocond. meas. 78—60159
$CdGa_2S_4$, Raman scatt. anal., optical phonons 79—73951
$CdGa_2S_4$, vibr. spectra, 33-400 cm^{-1}, symm. transform. *(Russian)* 78—23465
$CdGa_2S_4$:Ag(In), photoluminesc. and photocond. meas. 78—60159
$CdGaS_4(Se_4)$, absorption and refl. spectra anisotropy, band struct. 77—69840
$CdGa_2(S_{1-x}Se_x)_4$ solid solns., band struct. behaviour w.r.t. comp. *(French)* 80—107699
$CdGa_2S_4(Se_4)$, band struct., and optical spectra 78—19511
$CdGa_2S_4(Se_4)$, band struct., pseudopot. method 80—92816
$CdGa_2S_4(Se_4)$ film, optical absorpt., and energy gaps 78—11012
$CdGa_2S_{4(1-x)}Se_{4x}$, solid soln., crystallographic studies 78—15301

cadmium compounds continued
$CdGa_2Se_4$, electron traps, energy spectrum, photocurrent decay, TSC temp. depend. *(Russian)* 78—64057
$CdGa_2Se_4$, electrophotographic props. *(Russian)* 78—59100
$CdGa_2Se_4$, IR refl. spectra and cryst. struct. 79—56777
$CdGa_2Se_4$, IR refl. spectra, optical phonon dispersion 80—29746
$CdGa_2Se_4$, linear expansion anisotropy 79—86910
$CdGa_2Se_4$, ordered vacancy compound, Raman scatt. 79—95749
$CdGa_2Se_4$ ordered vacancy compound, Raman scatt. 79—99870
$CdGa_2Se_4$, struct. of valence band, photocond. and reflection spectra meas. 80—6719
$CdGa_2Se_4$, thermoreflectance and visible absorpt. spectra, energy gap, cryst. field splitting 80—34945
$CdGa_2Se_4$-$CdIn_2Se_4$ solid solutions, order-disorder transition 79—19181
$CdGa_2Te_4$ film, effect of thermal annealing on struct., optical absorpt. and photocond. 79—65342
$CdGa_2Te_4$, IR refl. spectra and cryst. struct. 79—56777
$Cd_{0.96}Ga_2Te_{4.1}$, amorphous film crystallisation and conductivity switching 77—4459
$Cd_{0.96}Ga_2Te_{4.1}$ film, switching effect 77—43753
$CdGa_2X_4$, X=S,Se, Fourier IR and Raman spectra, cryst. struct. and symm. *(German)* 79—24313
CdGeAs, vertical Bridgman growth with control of interface shape and orientation 80—66420
$CdGeAs_2$, Ag_3AsS_2, freq. synthesis of 260 THz, 1.15 μm He-Ne laser 79—64263
$CdGeAs_2$, amorphous, SRO 77—84653
$CdGeAs_2$, amorphous and cryst., short-range order, Mossbauer expts. 78—22648
$CdGeAs_2$, cryst. growth and elec. props. *(French)* 77—59682
$CdGeAs_2$ crystals, Bridgman grown, optical props. rel. to O_2 content of starting materials 80—81213
$CdGeAs_2$, develop. of tunable coherent radiation at 16 μm 78—90454
$CdGeAs_2$, elec. and optical props., acceptor levels and energy gap determ. 77—85218
$CdGeAs_2$, electron irradiated, change in electrical props. 79—7829
$CdGeAs_2$, freq. mixing for tunable IR sources 78—59030
$CdGeAs_2$, glassy, structural model 77—35490
$CdGeAs_2$, IR nonlinear material, laser induced surface damage 77—19266
$CdGeAs_2$, optical and elec. props. 79—19590
$CdGeAs_2$, p-n junction form. by heat treatment, photosensitivity 77—28247
$CdGeAs_2$, phase matched fourth harmonic generation, cascade process contrib. 79—76761
$CdGeAs_2$, photosensitivity to linearly polarised radiation 77—55569
$CdGeAs_2$, polarised IR reflectivity, optical modes, optical phonons 77—69836
$CdGeAs_2$, SHG, absorpt. coeffs. and temp. variation of refr. index difference 80—14390
$CdGeAs_2$ tandem crystals, efficient freq. tripling of CO_2 laser radiation 79—45999
$CdGeAs_2$, ternary semiconductor crystals for nonlinear optical applics. 78—33782
n-$CdGeAs_2$:In(Te), resist. and Hall coeff. meas., influence of press. 77—47810
$CdGeAs_2$-$ZnGeAs_2$, and $CdGeAs_2$-$GdGeP_2$, material distrib., possibility of heterostructure *(Russian)* 78—30979
$CdGe_xAs_2$ glass, conductivity and Hall effect for x=0.1 to 0.8, 300 to 600K 77—69347
$Cd_{23}Ge_{12}As_{65}$, amorphous, threshold switching, expt. 80—49830
$Cd_6Ge_3As_{11}$, band gap, DC cond., elastic consts., and glass transition temp., pressure depend. 78—72064
$Cd_6Ge_3As_4$, semiconducting glass, elastic props., US vel. meas. 78—26628
$(CdGeAs_2)_{1-x}D_x$ amorphous films, property control in common target sputtering, elec. cond. 80—7494
$CdGe(As_{1-x}P_x)_2$, crystal growth, phase studies, optical props. 78—48305
$CdGe_{1-x}M_xAs_2$ (M=Si,Sn,Pb), (x=0.0,0.1,0.2), amorphous struct. 78—22651
$CdGe_2O_5$, X-ray crystal struct. determ., comparison with sphene 77—4089
Cd_2GeO_4 anode for H_2O photoelectrolysis 80—108716
n-Cd_2GeO_4, electronic and cond. props. rel. to prep. conditions and defect struct. 80—107787
Cd_2GeO_4, n-type, prep. and photoelectronic props. 80—39628
$Cd_xGe_yO_2$, hydrothermal crystallisation at 300°C 77—52241
$CdGeP_2$, cond. compensation by electron bombardment 79—15151
$CdGeP_2$, crysts., prep. by chem. vapour transport 80—55280
$CdGeP_2$, electronic struct. at cryst./vitreous transition, X-ray K-absorpt. and emission 78—15248
$CdGeP_2$, growth from melt solution in Cd, microhardness 77—44139
$CdGeP_2$, optically anisotropic, orientation, use of polarisation depend. of photo-EMF and photoconductivity 77—89807
$CdGeP_2$, polarisation of luminescence emitted 77—69909
$CdGeP_2$, polarisation of recombination radiation 78—19562
$CdGeP_2$ synthesis and cryst. growth 79—87577
$CdGeP_2$, temp. depend. Sellmeier coeffs. and coherence lengths for chalcopyrite crystals 79—76752
$CdGeP_2$ thermo-optic coefficient, dispersion 80—71396
$CdGeP_2$, u.p. 77—90634
$CdGeP_2$:Cu, impurity behaviour 77—15857
$CdGeP_2$:In, photolum. spectra and kinetic coeffs. 79—19927
$CdGeP_2$:In, polarisation of recombination radiation 78—19562
$CdGeP_2$:In based surface barrier diode, photosensitivity 79—33330
n-$CdGeP_2$-p-$CdGeAs_2$ heterojunction photocells, polarisation-sensitive 80—11075
$CdGe(P_xAs_{1-x})_2$, glass, static current-voltage characteristics *(Russian)* 77—15925
$Cd_{16}Ge_4S_{24}$, SHG obs. 78—46719
$CdGe_{1-x}Sb_xAs_2$ glass, DTA, microhardness meas. *(French)* 77—72564
$CdGe_{1-x}Sb_xAs_2$ system, amorphous and cryst. phases, DTA and microhardness obs. 78—22835
$CdGe_{1-x}Sn_xAs_2$, amorphous, radial distrib. anal. and mag. susceptibility meas. 77—43152
CdH, lifetime, Λ-doubling, hyperfine struct., in $A^2\Pi$ excited states 77—58083
CdH^+, CdH_2, relativistic (non-relativistic) HF one-centre expansion calcs. 80—52908
$CdH_{10}(AsO_4)_4$, X-ray cryst. struct. determ. and refinement *(French)* 80—33941

cadmium compounds continued
$Cd(H_2PO_3)_2.H_2O$, cryst. struct. determ. 78—26507
$CdHfO_3$, electric field gradient temp. depend. 78—39454
CdHg, excimer kinetics and transmission meas. 80—37832
CdHg excimer system, absorpt. meas. 80—48007
CdHg, fluoresc. kinetics, optical excitation, energy spacings and equilib. consts. 80—43090
CdHg, positive gain measurements or 470 nm continuum band 78—66805
$Cd(Hg)/CdSO_4$, aq. electrochem. system, kinetics, impedance *(German)* 77—32807
Cd_xHg_{1-x} Te, elec. characts., impurity effects 80—92890
Cd_xHg_{1-x} Te, photodetectors, recomb. processes, photoconductive decay obs. 79—38129
Cd_xHg_{1-x} Te Ir detectors, props. and manufacture *(German)* 77—2693
Cd_xHg_{1-x}, x=0.2 and 0.26, photomagnetoelectric effect in strongly excited samples 79—47124
$Cd_{1-x}Hg_xCr_2Se_4$, ferromag. semicond. surface magnetism, magneto-optical meas. 77—20831
$Cd_{1-x}Hg_xCr_2Se_4$, photoferromag. effect and photocond. obs. 79—28376
$Cd_{1-x}Hg_xGa_2S_4$ solid solns., band struct. behaviour w.r.t. comp. *(French)* 80—107699
CdHg(Mg), Ar matrix absorpt. spectra, vibronic spacing and bonding 79—3453
$Cd_{0.2}Hg_{0.8}Se$, longitudinal Nernst-Ettingshausen effect, effect of disorder scatt. 78—84240
$Cd_xHg_{1-x}Se$, carrier mobility, 4.2 to 300K, scatt. mechanisms 79—4561
$Cd_xHg_{1-x}Se$, elec. props., 77-400K *(Russian)* 78—2485
$Cd_xHg_{1-x}Se$, Hall coeff. and electron mobility, band parameters 79—73506
$Cd_xHg_{1-x}Se$ mixed cryst., electron mobility and electron scatt. 78—95296
$Cd_xHg_{1-x}Se$, narrow band gap semicond., electron scatt., and transport phenomena 80—49706
$Cd_xHg_{1-x}Se$, phase transition and elastic consts., US vel. study 80—75354
$Cd_xHg_{1-x}Se$ type semiconductor, small-gap, electron scatt. and transport props. 78—95294
$Cd_xHg_{1-x}Se$ type semiconductor, small-gap, electron scatt. and transport props. 78—95295
CdHgTe, anomalous avalanche breakdown 80—80284
CdHgTe detectors, high-performance, for thermal imaging 79—40616
CdHgTe detectors for CO_2 laser appls. 79—40615
CdHgTe, far IR cyclotron emission 79—61226
(CdHg)Te, ion implanted graded gap photodiodes 78—39192
(CdHg)Te photoconductive detector, thermal figure of merit limit 78—89540
(CdHg)Te photoconductive IR detectors, ultimate detectivity 79—58788
CdHgTe photoelectromagnetic detector for 10.6 μm radiation, non-cooled, performance 80—82818
$Cd_{0.1}Hg_{0.9}Te$, polycrystalline thin film, correlation between structure and 1/f noise 78—39234
$Cd_{0.15}Hg_{0.85}Te$, photothermomagnetic effect in mm range 80—92932
$Cd_{0.175}Hg_{0.825}Te$-Au(In) contacts, photo-effect in the 77-300K range, barrier height estimation 80—107850
$Cd_{0.2}Hg_{0.8}Te$, annealing in saturated Hg vapour *(German)* 79—43447
n-$Cd_{0.2}Hg_{0.8}Te$, fundamental absorption edge, influence of temp. 80—20640
$Cd_{0.2}Hg_{0.8}Te$ IR photoresistors/detectors, lateral geometry requirements *(German)* 79—93213
$Cd_{0.2}Hg_{0.8}Te$, ion implantation doping for realisation of IR detectors, responsivity meas., ion range straggling 80—73452
$Cd_{0.2}Hg_{0.8}Te$ recrystallisation for supercooled IR detector production *(German)* 80—86403
$Cd_{0.2}Hg_{0.8}Te$:B, ion implanted, B range and range straggling 80—54273
n-$Cd_{0.21}Hg_{0.79}Te$, excess generation-recombination noise 80—107880
$Cd_{0.24}Hg_{0.76}Te$, mag. quantum oscills. in photovoltaic effect 79—19619
n-$Cd_{0.245}Hg_{0.755}Te$, magnetophonon reson. and quantum oscillations 77—39902
n-$Cd_{0.3}Hg_{0.7}Te$, photoelec. props. at 78K, relax. time, minority carrier extraction 80—107864
n-$Cd_{0.3}Hg_{0.7}Te$, recomb. levels 79—91076
$Cd_{1-x}Hg_xTe$, lattice dynamics of low conc. of Hg atoms, perturbation model impurity description 79—55853
$Cd_xHg_{1-x}Te$ film, vacuum departed, struct. and elec. props. 77—59344
n-$Cd_xHg_{1-x}Te$, action of laser pulses, elec. characts. 79—11212
n-$Cd_xHg_{1-x}Te$ alloys, x=0.19 to 0.21, electron optical heating influence on photoelec. effects 79—11183
$Cd_xHg_{1-x}Te$, Auger effect, temp. depend. of Auger lifetime 79—38097
$Cd_xHg_{1-x}Te$, band struct. and optical props. 80—15450
$Cd_xHg_{1-x}Te$, carrier lifetime, effect of comp. fluctuations and second-phase inclusions 80—80294
$Cd_xHg_{1-x}Te$, cast-recrystallise-anneal growth 79—91578
$Cd_xHg_{1-x}Te$, characts. of low temp. transport props. 78—39160
$Cd_xHg_{1-x}Te$, comp. determ. by electroreflection method 77—52708
$Cd_xHg_{1-x}Te$, comp. in successive layers determ. by chem. polishing etching of surface 77—7868
$Cd_xHg_{1-x}Te$ compressed sintered slabs, Hall coeff. and microstructure obs. *(Russian)* 78—10475
n-$Cd_xHg_{1-x}Te$, conduction band struct., IR refl. spectra obs. 80—39502
n-$Cd_xHg_{1-x}Te$, conductivity inversion under laser radiation *(Russian)* 79—15198
$Cd_xHg_{1-x}Te$, correlation between structural and chemical inhomogeneity *(Russian)* 80—49484
$Cd_xHg_{1-x}Te$, crystallisation from solution in Hg 77—19883
n-$Cd_xHg_{1-x}Te$ crystals, carrier recomb. in extrinsic conduction range 80—70722
$Cd_xHg_{1-x}Te$ crystals, donor compensation, low temp. cond. study 80—75571
$Cd_xHg_{1-x}Te$, current-voltage characts., pinch effect, mag. field effects 80—6858
$Cd_xHg_{1-x}Te$, determ. of slip planes by dislocation etching 79—82220
$Cd_xHg_{1-x}Te$, diffusion and struct. of defects 77—84775
$Cd_xHg_{1-x}Te$, dislocation motion, effect of lattice defects on microhardness *(Russian)* 80—70220
$Cd_xHg_{1-x}Te$, disorder scatt. 78—39137
$Cd_xHg_{1-x}Te$, dopants behaviour and p-n junction formation 80—44225
$Cd_xHg_{1-x}Te$, effects of electron heating at low temps. 80—49823
$Cd_xHg_{1-x}Te$, electron irradiated, elec. and recomb. characts. 78—39113
$Cd_xHg_{1-x}Te$, electron mobility and conc. near gapless state, influence of hydrostatic press. 79—65486

cadmium compounds continued
$Cd_xHg_{1-x}Te$, epitaxial graded-gap layers, elec. transport props. 77—85358
$Cd_xHg_{1-x}Te$ epitaxial graded gap layers, plasma reflection and magnetoreflection 80—71391
$Cd_xHg_{1-x}Te$, epitaxial growth from stoichiometric melt, crystn. and diffusion 80—75475
$Cd_xHg_{1-x}Te$, epitaxial layer p-n junction, current-voltage characteristics of photovoltaic detectors, 1 to 15 μm 80—86407
$Cd_xHg_{1-x}Te$, film, optical props., struct. depend. 77—1751
$Cd_xHg_{1-x}Te$ films, epitaxial growth, optical, elec., and photoelec. props. 79—11512
$Cd_xHg_{1-x}Te$ films, growth by cathodic sputtering in Hg vapour plasma 80—97431
$Cd_xHg_{1-x}Te$, fine-graded gap struct., electrophysical props. *(Russian)* 78—60144
$Cd_xHg_{1-x}Te$, flameless atomic absorpt. anal. using interactive computer processing 79—66380
$Cd_xHg_{1-x}Te$, gap width temp. depend., absorpt. band edge meas. 78—72521
$Cd_xHg_{1-x}Te$, graded gap epitaxial layers, elec. and photoelec. props. 77—85362
$Cd_xHg_{1-x}Te$, graded gap epitaxial layers, spectral characts. of photoelectromagnetic effect 80—60022
$Cd_xHg_{1-x}Te$ graded-gap epitaxial layers, photocond. meas. 0.5 to 6 μm, detector appl. 79—60869
$Cd_xHg_{1-x}Te$, graded-gap layers, galvanomag. props. at low temp. and in weak mag. field 80—75664
p-$Cd_xHg_{1-x}Te$, Hall const. variation with comp. after annealing in Hg vapour 77—15868
$Cd_xHg_{1-x}Te$, high-speed quenching of melt *(German)* 79—65997
$Cd_xHg_{1-x}Te$, homogeneous mixed crysts. with large segregation tendency, Bridgman growth *(German)* 79—33923
$Cd_xHg_{1-x}Te$, IR detector appls., prep., elec. props. *(German)* 78—86332
n-$Cd_xHg_{1-x}Te$, in strong mag. field, current-voltage characts., current instabilities 78—87980
$Cd_xHg_{1-x}Te$, influence of nonparabolicity on transverse magnetoresist. near transition to zero gap 80—20228
$Cd_xHg_{1-x}Te$ inhomogeneous p-n junctions, elec. props. at high hydrostatic press. *(Russian)* 77—80835
$Cd_xHg_{1-x}Te$, inhomogeneous composition effect on carrier lifetime and photosensitivity *(Russian)* 79—73526
$Cd_xHg_{1-x}Te$, intrinsic carriers, Fermi level calc. rel. to conc. 77—55481
$Cd_xHg_{1-x}Te$, isothermal growth of epitaxial layers 78—60577
$Cd_xHg_{1-x}Te$ layers, epitaxial graded-gap, nonlinear elec. effects 80—100468
$Cd_xHg_{1-x}Te$ layers, photoelectromagnetic effect 78—43445
$Cd_xHg_{1-x}Te$, long term stability at 300K, rel. to device appl. 80—59978
$Cd_xHg_{1-x}Te$, low temp. piezoresistance, Hall effect, elec. cond., plastic flow 80—6844
n-$Cd_xHg_{1-x}Te$, magnetophonon oscills. of transverse magnetoresist. 78—72177
$Cd_xHg_{1-x}Te$, magnetoresist. near gapless state, 77-370K 78—2503
$Cd_xHg_{1-x}Te$ magnetoresistor prep. and props. 79—7844
$Cd_xHg_{1-x}Te$, magnetoresistance in range 4.2 to 300K 79—11156
$Cd_xHg_{1-x}Te$ narrow gap semiconductor, charge transfer device for IR detection appl. *(French)* 79—30563
$Cd_xHg_{1-x}Te$, photoconductivity under uniaxial compression, band gap 77—43657
$Cd_xHg_{1-x}Te$ photoconductive detectors, 77 to 300K, normalised thermal figure of merit 80—31878
$Cd_xHg_{1-x}Te$ photodiode, high efficiency, energy level diagram 77—15891
$Cd_xHg_{1-x}Te$ photodiode, IR responsivity and detectivity 78—19139
$Cd_xHg_{1-x}Te$, photoelectric props. at high temp. 77—4403
$Cd_xHg_{1-x}Te$, photomag. and photothermomag. effects *(Russian)* 79—78137
n-$Cd_xHg_{1-x}Te$, photomagnetic effect in the quantum limit under electron heating conditions 79—69553
$Cd_xHg_{1-x}Te$, photomagnetic and galvanomagnetic effects in quantising mag. fields 80—20223
$Cd_xHg_{1-x}Te$, photoresistor, performance at large bias currents *(Russian)* 78—76105
$Cd_xHg_{1-x}Te$, photothermomag. effect and photocond. in millimetre wavelength range 80—44657
$Cd_xHg_{1-x}Te$ polycrystalline films, electrical props., rel. to struct. *(Polish)* 78—31002
$Cd_xHg_{1-x}Te$, precip. 77—90352
n-$Cd_xHg_{1-x}Te$, quantum oscills. of transverse photocond., fields up to 30 kOe, 1.5-4.2K *(Russian)* 77—72885
n-$Cd_xHg_{1-x}Te$, recombination due to surface excitation, photoconductivity, impurity states *(Russian)* 80—60042
$Cd_xHg_{1-x}Te$, resistivity, Hall effect and magnetoresist. in strong elec. field 77—28199
n-$Cd_xHg_{1-x}Te$, semicond. current carrier recombination heating in photoelectric effects *(Russian)* 79—78138
$Cd_xHg_{1-x}Te$, single cryst. homogeneity and molar conc. determ. with electron microprobe *(German)* 78—2109
$Cd_xHg_{1-x}Te$ single crystal, photoconductivity spectral distrib. rel. to surface condition 79—78136
n-$Cd_xHg_{1-x}Te$, single crystal, scattering mechanism on intensity of 1/f noise 80—39642
p-$Cd_xHg_{1-x}Te$ solid soln., thermoelec. effects 79—73538
$Cd_xHg_{1-x}Te$, solid soln., pure and Ag(In) doped, defect struct. model, Hg self-diffusion coeff. 79—95213
$Cd_xHg_{1-x}Te$ solid solns., epitaxial growth under isothermal conditions 77—16504
$Cd_xHg_{1-x}Te$, solid solns., role of stoichiometry defects 77—47813
$Cd_xHg_{1-x}Te$ solid solns., dimensional resonances of HF helicons, band struct. and electron mobility 77—47846
$Cd_xHg_{1-x}Te$, solid solns., solubility in Hg 78—35359
$Cd_xHg_{1-x}Te$, strong elec. field effect on galvanomagnetic effects 79—11159
$Cd_xHg_{1-x}Te$, surface microhardness depend. on surface treatment method 78—15560
$Cd_xHg_{1-x}Te$, temp. shift of energy gap 77—51658
$Cd_xHg_{1-x}Te$, temp. shift of energy gap, contrib. of lattice dilatation 78—51892
$Cd_xHg_{1-x}Te$, thermal cond. in mag. field, thermopower, and Nernst-Ettingshausen effect 77—31814

cadmium compounds continued
n-Cd$_x$Hg$_{1-x}$Te, thermal EMF, in transverse quantised EM field *(Russian)* 79−23993
Cd$_x$Hg$_{1-x}$Te, thermally activated slip, microhardness temp. depend. *(Russian)* 78−34567
Cd$_x$Hg$_{1-x}$Te, tunnelling effect in p-n junctions 80−75630
Cd$_x$Hg$_{1-x}$Te, uniaxially compressed, deform. effects, elec. resist. 78−39114
Cd$_x$Hg$_{1-x}$Te, VPE on CdTe *(Russian)* 78−11129
Cd$_x$Hg$_{1-x}$Te, vac. evap. film struct. rel. to carrier scatt. 77−85116
Cd$_x$Hg$_{1-x}$Te, vacancy electron states, acceptor behaviour, electron mobility 80−70193
Cd$_x$Hg$_{1-x}$Te, vacancy mech. of resorption of Hg droplets 80−39070
Cd$_x$Hg$_{1-x}$Te, variable-gap struct., additional p-n junction in epitaxial film, photosensitivity 77−24588
Cd$_x$Hg$_{1-x}$Te, variable-gap structures, galvanomagnetic effects 80−11014
Cd$_x$Hg$_{1-x}$Te, vertically grown crysts., effects of growth speed on comp. variations 79−55684
Cd$_x$Hg$_{1-x}$Te, X-ray topographic assessment 79−37716
Cd$_x$Hg$_{1-x}$Te, x=0, x=1, effective mass of heavy holes, 4.2 to 300K 77−1353
Cd$_x$Hg$_{1-x}$Te, zero gap semiconductor, interband optical-phonon scattering 80−6846
p-Cd$_x$Hg$_{1-x}$Te-metal contact, negative resist. effects, impact ionisation 77−4440
Cd$_x$Hg$_{1-x}$Te-metal contact, transport mechanism, thermionic and field emission processes 77−20425
Cd$_x$Hg$_{1-x}$Te-metal contacts, schematic energy band diag., transport props. 77−47897
Cd$_x$Hg$_{x-1}$Te, Auger and radiative recombination of acceptor bound excitons 79−47023
Cd$_x$Hg$_{1-x}$Te(:Ag), impurity diffusion, gamma-ray effects 80−54441
CdHg* excimer, kinetic model of sustained discharge excitation 78−66804
CdI$_2$, 2H to 4H structural change, X-ray diffr. study 78−75614
CdI$_2$, 20 layered hexagonal polytypic crysts., struct., transform. 77−7689
CdI$_2$, 6H-based polytypes, transformation characteristics 77−19889
CdI$_2$, activator-induced luminesc. *(Russian)* 78−2913
CdI$_2$, ang. depend. electron energy loss meas. 79−95884
CdI$_2$, aq. soln., isothermal transport props., 298.15K 78−18815
CdI$_2$, aq. soln., transport props., irreversible thermodynamic anal. 78−14490
CdI$_2$, aq. solns., ^{115}Cd isotopic diffusion coeffs. 78−47545
CdI$_2$, band struct., tight binding calcs. and photoemission spectra 78−23018
CdI$_2$, cathodoluminescence, 300 and 80K *(Russian)* 79−78760
CdI$_2$ crystal, method for identification of rhombohedral lattice 77−31637
CdI$_2$ crystal, transverse and longitudinal lattice mode freq., IR reflection spectra meas. 78−27227
CdI$_2$, crystal-solution interfacial tension, from crystn. meas. 79−69045
CdI$_2$ crystals, growth conditions effect on polytypism, X-ray diffr. study 80−28942
CdI$_2$ crystals, photolysis obs. *(Russian)* 80−7833
CdI$_2$, dielec. function and band struct., EELS meas. 80−40195
CdI$_2$, dielec. props. rel. to polytypically modulated structs. 79−94971
CdI$_2$, electronic struct., tight-binding calcs. 80−15446
CdI$_2$, exciton spectra, temp. and press. effects 77−20881
CdI$_2$, faulted 4H structure analysis 77−80447
CdI$_2$, hexagonal to rhombohedral phase transform., SFE 79−91643
CdI$_2$, hexagonal-rhombohedral polytypic transformation, electron diffr. and X-ray diffr. obs. 80−49163
CdI$_2$, interlayer interactions estimate from Raman and Brillouin scatt. 79−99884
CdI$_2$, layered cryst., photoluminesc., and reflection spectra obs. 78−6726
CdI$_2$, luminesc., relaxed excitonic states 79−33758
CdI$_2$, molten, electrical cond., press. effect, 0-1 kbar 78−55963
CdI$_2$, Mossbauer spectrum, electronic and mag. props. 77−32302
CdI$_2$, NMR, ^{113}Cd nucl. mag. shielding 78−68395
CdI$_2$, optical phonon anisotropies and intralayer bonding forces from IR refl. 77−59573
CdI$_2$, photodissoc., spectroscopy and dynamics 79−98169
CdI$_2$, photofragment spectroscopy 79−52718
CdI$_2$ polytypes, centrosymmetric space groups 77−31618
CdI$_2$ polytypes, crystal structure analysis, refinements for structure determination 78−91312
CdI$_2$ polytypes, crystal structures using new refinements for structure determination 78−91313
CdI$_2$ polytypes, defect struct., electron microscopy 79−14809
CdI$_2$, polytypes, dielec. const., periodicity and disorder depend. 77−28506
CdI$_2$ polytypes, vapour growth mechanism 80−84124
CdI$_2$ polytypic crystals, dielectric loss behaviour 80−66108
CdI$_2$, polytypism, phase and growth aspects 78−83764
CdI$_2$, polytypism, review 77−11498
CdI$_2$, polytypism and luminesc. *(Russian)* 78−56520
CdI$_2$ single cryst., EPR of V^{2+}, Mn^{2+}, Co^{2+} 78−68362
CdI$_2$, soln. grown, rotation twinning, arcing and polytypism 78−51557
CdI$_2$, sputtering processes during 6 keV Xe ion bombard. 78−68590
CdI$_2$, sublimed films, preparation, struct. 77−24491
CdI$_2$, thermoluminesc. of traps *(French)* 79−4856
CdI$_2$ type noncubic structures, expansion of Madelung parameters as function of ratio of two lattice parameters 77−84693
CdI$_2$ type structure, Mossbauer line broadening due to diffusion 77−12281
CdI$_2$, UV reflectivity meas., band struct., LCAO calcs. 78−72545
CdI$_2$, valence-band XPS meas. 77−12487
CdI$_2$, vap. growth and cryst. struct. 77−72570
CdI$_2$, vapour, excited by photodissociation, fluoresc. yields 78−55138
CdI$_2$:Fe^{2+}, polarised electronic Raman scatt. 80−29733
CdI$_2$-AgPO$_3$, glasses, ionic conductivity and structure *(French)* 78−67854
CdI$_2$-Cd molten solution, US velocity and compressibility 77−84844
CdI$_2$-Cd molten solution, surface tension 77−85024
CdI$_2$-CdBr$_2$ mixed layer cpds., rigid layer modes and van der Waals interactions, Raman spectra obs. 79−33700
CdI$_2$-Cd(I) mixture, molten, nuclear spin relax. 80−88887
CdI$_2$-He, hollow cathode discharge, simultaneous CW lasing by Cd$^+$ and I$^+$ 77−10951
CdI$_2$-Ni^{2+}, absorption and mag. circular dichroism, spectra, phonon density of states of CdI$_2$ deduced 79−19913

cadmium compounds continued
CdI$_2$-PbI$_2$-NaI, fusion diag. and thermodynamic calc. *(Russian)* 77−48417
CdI$_3$, aq. solns., ^{115}Cd isotopic diffusion coeffs., expt. anal. 78−43160
CdI$_{2-x}$Br$_x$, vapour grown mixed cryst., growth and polytypism 79−69044
Cd(IO$_3$)$_2$, complex salts, phase transitions, cryst. struct. *(Chinese)* 80−70171
Cd(IO$_3$)$_2$, cryst. struct. determ. 78−26523
(CdI$_2$)$_x$(PbI$_2$)$_{1-x}$, layered cryst., photoluminesc., and reflection spectra obs. 78−6726
(CdI$_2$)$_x$(PbI$_2$)$_{1-x}$, reflection and luminesc. spectra obs. 77−8648
CdI$_2$(4H), layer cryst., electric field effect on NQR, elec. polarisation mechanism 77−20746
CdIn$_2$:Cr, photocond. and photoluminesc. spectra 77−28214
Cd$_{1-x}$In$_x$Cr$_2$S$_4$, ferromagnetic spinel, Cr^{3+} exchange interaction mechanism, Cr^{2+} relaxation, EPR line width depend. 79−69715
Cd$_{1-x}$In$_x$Cr$_2$S$_{4-x}$P$_x$, ferromagnetic spinel, Cr^{3+} exchange interaction mechanism, Cr^{2+} relaxation, EPR line width depend. 79−69715
n-Cd$_{1-x}$In$_x$Cr$_2$Se$_4$, effect of doping on elec. cond. and magnetoresist. 78−72174
Cd$_{1-x}$In$_x$Cr$_2$Se$_4$, electric, photoelectric and mag. props., metal-semicond. transition *(Russian)* 80−54738
CdInGaS$_4$, crystal, Raman scattering spectra, polarisation meas. *(Russian)* 80−71410
CdInGaS$_4$, far IR refl. and transmission spectra, lattice vibrs. 79−91439
CdInGaS$_4$, layered structure crystals, refractive index meas. method 80−98966
CdInGaS$_4$ plate in elec. field, photostimulated ocills. 79−65799
CdInGaS$_4$, pure and Cu-doped, electrophotography layers *(Russian)* 80−68282
CdInGaS$_4$, TSC and SCL cond. investig. of electron trap parameters, 120 to 350K 77−69341
CdInGaS$_4$:Au, single crystal, thermostimulated conductivity *(Russian)* 79−11142
CdInGaS$_4$:Er^{3+}, cryst. field parameters, thermal and mag. props. calc. 77−20540
CdIn$_2$O$_4$ anode for H$_2$O photoelectrolysis 80−108716
CdIn$_2$O$_4$, crystal growth from flux, elec. and struct. props. 77−81206
CdIn$_2$S$_4$, band edge study by photovoltaic effect 79−95444
CdIn$_2$S$_4$, Brillouin scatt., elastic and photoelastic consts. determ. 80−60619
CdIn$_2$S$_4$ cubic spinel, electronic band struct. and chem. bonds 78−34768
CdIn$_2$S$_4$, electronic states, sensitivity to cryst. struct., UPS study 80−45209
CdIn$_2$S$_4$ film, vac. deposited, growth, struct., optical and photoelectronic props. 80−10831
CdIn$_2$S$_4$ films, vac. deposited, struct. and photoelec. props. 79−87006
CdIn$_2$S$_4$, fund. reflectivity, 2 to 6 eV, band struct. implications 78−39574
CdIn$_2$S$_4$, fundamental optical constants 78−84549
CdIn$_2$S$_4$, impurity centres, photoluminesc. and photocapacitance data on config.-coordinate diagrams 78−10938
CdIn$_2$S$_4$, partial inverse spinel struct., detection by Fourier transform spectroscopy 80−108197
CdIn$_2$S$_4$, photocond. and trap. distrib. 78−39164
CdIn$_2$S$_4$, photocond. and electron trap distrib. 79−28373
CdIn$_2$S$_4$, photoconducting semiconductors, fundamental absorption edge 80−40130
CdIn$_2$S$_4$, photoluminesc. spectra anal. by method of moments 77−12433
CdIn$_2$S$_4$, photoluminesc., reson. Raman scatt. 78−48179
CdIn$_2$S$_4$, photoluminesc., thermal quenching and recomb. centres 79−24362
CdIn$_2$S$_4$, Raman and IR spectra 78−48181
CdIn$_2$S$_4$, single cryst., oscill. behaviour of photocurrent and luminesc. 78−10501
CdIn$_2$S$_4$ single crystal growth by two-zone horizontal Bridgman technique 78−27400
CdIn$_2$S$_4$ single crystals, recombination process and localised levels 80−93383
CdIn$_2$S$_4$, valence band densities of states, XPS meas. 79−28892
CdIn$_2$S$_4$:CO^{2+}, site symmetry, spectral meas. 79−78729
CdIn$_2$S$_4$:Co, optical absorption meas. 78−64384
CdIn$_2$S$_4$:Cr, absorpt. and photoluminesc. spectra, Cr conc. depend. 79−78712
CdIn$_2$S$_4$:Cr, thermal cond., 1.8 to 200K, phonon scatt. by impurity ions 77−76627
CdIn$_2$S$_4$:Cr^{3+}, ESR and ENDOR 77−20692
CdIn$_2$S$_4$:Er^{3+}, cryst. field parameters, thermal and mag. props. calc. 77−20540
n-CdIn$_2$S$_4$/p-CuInSe$_2$ heterostructure, form. and photovolt. meas. 80−10831
CdIn$_2$S$_4$-HgCr$_2$Se$_4$ heterojunction, prep. and photovoltaic props. *(Japanese)* 78−34889
CdIn$_2$S$_{4-x}$Se$_x$, struct. types anal., X-ray diffr. exam. 79−86756
CdIn$_2$Se$_4$ defect tetrahedral semiconductor, band structure, charge density 77−11850
α-CdIn$_2$Se$_4$, defect zincblende struct., electronic props. 77−15767
CdIn$_2$Se$_4$, defect zincblende semicond., valence band, cryst. struct. effects 78−48278
CdIn$_2$Se$_4$, high resolution electron microscope study of polytypism 80−88119
CdIn$_2$Se$_4$, needle-like cryst. X-ray exam. 79−42031
CdIn$_3$Se$_4$, cryst. growth, photoresponse and optical props. 78−39165
Cd$_2$In$_2$SnTe$_3$, tetrahedral semiconductor, chem. interaction of Sn atoms, Mossbauer study 80−39977
Cd$_2$In$_6$Sn$_3$Te$_5$, tetrahedral semiconductor, chem. interaction of Sn atoms, Mossbauer study 80−39977
Cd$_6$In$_2$SnTe, tetrahedral semiconductor, chem. interaction of Sn atoms, Mossbauer study 80−39977
CdIn$_2$Te$_4$ defect tetrahedral semiconductor, band structure, charge density 77−11850
CdIn$_2$X$_4$, X=S,Se, Fourier IR and Raman spectra, cryst. struct. and symm. *(German)* 79−24313
CdK$_2$(Cr$_2$O$_7$)$_2$.2H$_2$O, X-ray cryst. struct. determ. using MULTAN *(French)* 79−69082
CdK$_2$P$_2$O$_7$, cryst. struct., bond lengths 77−31639
CdK$_4$(P$_3$O$_9$)$_2$.2H$_2$O, cryst. chemistry and cryst. struct. determ. *(French)* 78−26505
CdK$_2$(SO$_4$)$_2$. 6H$_2$O:Mn^{2+}, EPR, 298K, spin-Hamiltonian parameters, cryst. fields 78−27086

cadmium compounds continued
- $CdLi_2(PO_3)_4$, cryst. struct. determ. *(French)* 77—4069
- $CdLn(TiNb)O_7$, Ln=La-Lu, synthesis physicochem. props. 77—43186
- $Cd_xM_{10-x}(PO_4)_6X_2$(M=Ca, Sr, Ba, Pb; X=F, Cl) apatites, IR spectral study *(French)* 80—93316
- $Cd_{1-x}M_xS$ (M=Sr, Ca, Mg, Pb, Sn), solid soln., prep. and semicond. props. 80—2383
- $Cd_2MTa_5O_{15}$ (M=K, Rb, Tl, Cs), relative stability of struct. types, and piezoelec. props. *(French)* 80—49206
- $Cd_2Mg(Co)(Zn)(Mn)(Cd)(Ca)TeO_6$, optical SHG study of acentricity, ferroelec. of low temp. phases 80—71324
- $Cd_{1-x}Mg_xS$, solid soln., phase equilib. diagrams 80—108412
- $Cd_xMg_{1-x}Se$ single crystals, melt grown, struct. and microhardness anisotropy 79—86836
- $Cd_{1-x}Mg_xTe$:Al, donor-acceptor pair and self-activated luminesc. 77—52161
- $Cd_{1-x}Mg_xTe$:P, luminescence centres, photoluminesc. meas. 78—31236
- $Cd_xMn_{1-x}Fe_2O_4$, substitution effect on mag. struct. and exchange interaction *(Russian)* 78—47949
- $Cd_2Mn_3O_8$, mag. props. 79—78339
- $Cd_2Mn_3O_8$, mag. props. and EPR 79—91215
- $(CdMn_2O_4)_{1-x}(MgAl_2O_4)_x$, $0<x<1$, mixed oxide spinels, chemical shifts of Mn K-absorpt. edge 80—29828
- $Cd_{1-x}Mn_xSe$, fundamental optical props. 80—84751
- CdMnTe crystals, exciton binding energy, magnetoabsorption and magnetoreflectivity 79—38523
- CdMnTe, exciton ground state, magnetic field influence 80—54616
- CdMnTe, semimagnetic semiconductor, band structure, optical properties 79—95331
- $Cd_{0.6}Mn_{0.6}Te$ crystals, Mn($3d^5$) band, photoemission evidence 80—11535
- $Cd_{1-x}Mn_xTe$, acceptor photoionisation and light-to-heavy hole absorpt. 79—65908
- $Cd_{1-x}Mn_xTe$, EPR, mag. crit. point 80—39851
- $Cd_{1-x}Mn_xTe$, effect of Mn $3d^5$ states on band struct., exciton refl. struct. in mag. field 79—11094
- $Cd_{1-x}Mn_xTe$, exchange induced ionization of bound excitons, luminesc. meas. 80—97328
- $Cd_{1-x}Mn_xTe$, Faraday rot. meas. up to 150 T 80—29722
- $Cd_{1-x}Mn_xTe$, indirect exchange interaction 80—97087
- $Cd_{1-x}Mn_xTe$, interband Faraday rot., appl. of mixed semicond. calcs. 79—61348
- $Cd_{1-x}Mn_xTe$, magnetic behaviour of Mn 78—14938
- $Cd_{1-x}Mn_xTe$, magneto-optical props. of free excitons rel. Mn^{2+} ions spin alignment 79—47419
- $Cd_{1-x}Mn_xTe$ mixed crystal, fundamental absorption edge 78—10919
- $Cd_{1-x}Mn_xTe$ mixed cryst., giant exciton Faraday rotation 78—27260
- $Cd_{1-x}Mn_xTe$ mixed crystals, excitonic magnetoabsorption 80—40095
- $Cd_{1-x}Mn_xTe$ mixed crystals, Raman spectra 80—103961
- $Cd_{1-x}Mn_xTe$, semimagnetic, exchange interactions between localised and delocalised electrons 80—97245
- $Cd_{1-x}Mn_xTe$, spin-orbit coupled bands, indirect exchange interaction via electrons 80—34407
- $CdMoO_4$, luminesc. efficiency, temp. and high-press. 78—23507
- $CdMoO_4$, refr. index, single crystals having scheelite struct. 78—79082
- $CdMoO_4:Mn^{2+}$, EPR spectrum, temp. depend. of zero field splitting 79—15346
- $CdMoO_4:Mn^{2+}$, zero-field splitting of Mn^{2+}, EPR 80—75531
- $CdMoO_4$-MO, M=Ca,Ba,Sr, phase diag. cross sections and reactions 78—27487
- $Cd(^{15}NH_3)_4{}^{2+}$, IR spectrum, force consts. *(German)* 77—6781
- $Cd(NH_3)_6(BF_4)_2:Ni^{2+}$, EPR of $[Ni(NH_3)_6]^{2+}$, temp. depend. at phase transition 77—20685
- $Cd(NH_3)Br_2$, orientational phase transitions, Raman spectra 80—11382
- $Cd(NH_3)_4Cl_2$:Cu, EPR dynamical effects 79—61204
- $Cd(NH_3)_6Cl_2$, orientational phase transitions, Raman spectra 80—11382
- $Cd(NH_3)_6Cl_2(Br_2)(I_2)$, crit. behaviour of light scatt. intensity at phase transitions 77—90141
- $Cd(NH_4)_2(Cr_2O_7)_2.2H_2O$, chemical prep. and crystal data *(French)* 80—24416
- $Cd(NH_4)_2(Cr_2O_7)_2.2H_2O$, X-ray cryst. struct. determ. *(French)* 80—39012
- $Cd(NH_3)_6I_2$, orientational phase transitions, Raman spectra 80—11382
- $CdNH_4NaP_2O_7.3H_2O$, crystal data and struct. *(French)* 78—14316
- $Cd_2(NH_4)_2(SO_4)_3$, X-ray and optical studies of ferroelec. phase transition 79—38495
- $Cd(NH_4)_2(SO_4)_2.6H_2O:Mn^{2+}$, EPR, 298K, spin-Hamiltonian parameters, cryst. fields 78—27086
- $Cd(NH_4)_2(SeO_4)_2.6H_2O:Mn^{2+}$, EPR of Mn^{2+}, spin-Hamiltonian parameters 79—33528
- $Cd(NO_3)_2$, phase transition, SHG, optical and dielec. meas. 80—71334
- $Cd(NO_3)_2$-XNO_3, (X=Li,Na,K,Tl), molten mixtures, electrical conductance, non-Arrhenian behaviour 78—43158
- CdN_2O_3, vibr. spectra, assignments 77—38670
- $Cd(NO_3)_24.1H_2O$-$CoCl_2$, melt viscosity, equivalent conductivity, glass transition temp. 78—75855
- $Cd(NO_3)_24.1H_2O$-$NiCl_2$, melt viscosity, equivalent conductivity, glass transition temp. 78—75855
- $Cd(NO_3)_2.4H_2O$, high press. phase behaviour, dehydration and congruent melting 79—78947
- $Cd(NO_3)_2.4H_2O:Mn^{2+}$ single cryst., low symm. effects in EPR 77—90020
- $Cd(NO_3)_4.4H_2O$ neutron poison in $UO_2(NO_3)_2$ highly enriched fissile soln., criticality expts. 80—13724
- $Cd_4Na(PO_4)_3$, X-ray cryst. struct. determ. 79—73143
- $CdNa_2(SO_4)_2.2H_2O:Mn^{2+}$, EPR, 300K 79—51848
- $Cd_4Na(VO_4)_3$, X-ray single cryst. struct. determ. and refinement, Patterson synthesis 79—19196
- $CdNb_2O_6$, bonding characterisation 78—38680
- $CdNb_2O_6$, columbite struct., normal coord. anal. 78—964
- $CdNb_2O_6$, columbite struct., IR and Raman spectra *(French)* 78—19485
- $CdNb_2O_6$, force fields rel. to cryst. struct. *(French)* 80—107104
- $CdNb_2O_6$, sp. ht. and Debye temp. meas., 2-25K 79—73319
- $Cd_2Nb_2O_7$, ferroelec., sp. ht. and Debye temp. meas., 2-25K 79—73319
- $Cd_2Nb_2O_7$, Mn^{2+} ESR, hyperfine interaction const., ferroelectric domain orientation 80—54943
- $Cd_2Nb_2O_7$, photolum. and carrier drift mobility at ferroelec. transition 80—71469
- $Cd_2Nb_2O_7$, Raman-scattering investigation of vibrational structure 78—76441

cadmium compounds continued
- $Cd_2Nb_2O_6S$, pyrochlore struct., ferroelec., dielec. and structural study 79—38488
- $Cd_2Nb_{2-2x}Sn_{2x}O_{7-2x}F_x$, solid soln., X-ray diffr. and Mossbauer study *(French)* 78—87659
- $CdNd_4(SiO_4)_3O$, synthesis, cryst. struct. 78—87653
- CdNi ferrite, quadrupole interaction, cation distrib. influence 78—2776
- $Cd_{0.8}Ni_{0.2}Fe_2O_4$ ferrite, Fe spin relaxation Mossbauer study, mag. hyperfine struct. *(Russian)* 80—15932
- $Cd_{1-x}Ni_xFe_2O_4$, solid soln., mag. and structural characterisation 80—103906
- $Cd_xNi_{1-x}Fe_2O_4$, mag. behaviour, Mossbauser meas. 78—52390
- CdO, aqueous-deposited films, struct. and electronic props. for solar cell appls. 80—100797
- CdO, Auger MNV lineshapes, hole-hole interaction 80—45177
- CdO crystallites, formed by $Cd(OH)_2$ decomp., shape determ. *(French)* 78—10194
- CdO, ESCA spectra, Auger effect, initial and final states effect 78—15280
- CdO, effect of compacting pressure on consolidation and elec. cond. 79—29007
- CdO, elec. cond. and IR refl. spectra after sintering and compaction 79—56945
- CdO filled polyvinyl furfural, contact, area filler effect 79—57040
- CdO film, chromatic changes on heat treatment *(Russian)* 77—55843
- CdO films, electrophysical properties *(Russian)* 77—63008
- CdO, influence of initial compacting press. on elec. resis. Hall coeff. 80—20872
- CdO, ionicity, X-ray powder diffraction meas. 78—18616
- CdO, magnetoresistance, temp. depend. of degenerate, narrow and broad samples 78—95306
- CdO, NMR, ^{113}Cd nucl. mag. shielding 78—68395
- CdO, point defect props., band struct., lattice simulation calc. 80—19797
- n-CdO, polycryst., elec. cond. 78—34830
- CdO, spray coated, reaction with Si, IR investig. 79—39197
- CdO thin film conductivity, H_2O and CO adsorption effects 79—56340
- CdO, transparent conducting coatings, book contrib. 78—10587
- CdO, X-ray determ., Debye-Waller factors, Debye temp. and vibration amplitudes 78—55928
- CdO-Al_2O_3-P_2O_5 glass, γ-irrad., EPR study 80—84639
- CdO-B_2O_3-GeO_2 system, phase equilibria at 800°C, X-ray powder diffr. anal. 79—4956
- CdO-B_2O_3-SiO_2, glass, dielec.-relax. currents 78—52004
- CdO-Bi_2O_3-Al_2O_3, glass formation and IR transmission *(Japanese)* 80—54146
- CdO-GeO_2:Tl_2O photochromic glass for optical information retention media 80—33108
- CdO-P_2O_5 glass, ESR of VO^{2+} ions 80—100610
- CdO-P_2O_5 glass, thin film, elec. cond., high and low fields 80—80427
- CdO-P_2O_5 glasses, elec. props. at high elec. fields 80—39573
- CdO-P_2O_5 glasses, prep., density, elec. and optical props. 79—70033
- CdO-P_2O_5-SiO_2 glasses, photoelastic consts. and polarisability 79—65839
- CdO-SiO_2 glasses, photochromism *(Japanese)* 78—15140
- CdO-SnO_2 DC reactively sputtered films, elec. and optical props. 80—103763
- CdO-SnO_2 film, DC reactively sputtered, transparent electrode props., optimum sputtering conditions 80—11116
- CdO-SnO_2 film, DC sputtering prep., visible and near IR transmission, resist. 78—88049
- CdO-SnO_2 film, prep. by RF sputtering, elec. cond. and transparency 80—7492
- CdO-TeO_2, cryst. chem. study, X-ray diffr. powder data *(French)* 80—15080
- CdO-TeO_2 glass, struct. and props. *(Japanese)* 79—32917
- CdO-TeO_2 system, partial phase diagrams 78—84784
- CdO-WO_3, phase rels. and cryst. struct. 80—108410
- CdO-WO_3 phase diagram and prep. of $CdWO_4$ single crysts. 80—29933
- CdO-WO_3-H_2O, interconnection between kinetics of structure formation and chem. reactions 78—53198
- CdO-ZnO-Al_2O_3-Fe_2O_3-SiO_2 system glass, ESR spectra 79—65711
- CdO-ZnO-P_2O_5 glasses, prep., density, elec. and optical props. 79—70033
- CdO_2, catalyst on isopropanol, surface active sites during dehydrogenation 79—43621
- $Cd_3O_2Cl_2$, electrical conductivity 77—43589
- Cd_3OF_4, electrical conductivity temp. quasi-independ., novel semiconductor 77—43589
- $Cd(OH)_2$, adsorption props. of surface, gas-chromatographic investigation 79—66343
- $Cd(OH)_2$ decomposition, martensitic character of struct. transition, CdO crystallite shape determ. *(French)* 78—10194
- $Cd(OH)_2$, decomposition into CdO, crystallite size and shape 79—57219
- $Cd(OH)_2$, highly dispersed precipitate, microstruct. and exchange props. 77—36793
- $Cd(OH)_2$, prep. and growth book contrib. 78—19649
- Cd(OH)Cl, temp. depend. of elec. cond., solid state thermal decomp. 78—19042
- CdOHF (II), polycrystn., X-ray cryst. struct. determ. 79—60344
- β-$Cd_2(OH)_2SO_4$, cryst. struct. *(French)* 77—15353
- γ-$Cd_2(OH)_2SO_4$, cryst. struct. *(French)* 77—15354
- CdP, electron mobility, carrier density depend. calc. 79—56229
- CdP_2, 442 class gyrotropic crysts., self-induced rot. of light polarisation plane 80—99810
- CdP_2, birefringence and optical activity 78—15143
- CdP_2, Cd_3P_2, polymorphic transitions 78—23699
- CdP_2, cryst., tetragonal, 2-phonon IR absorpt. 80—66176
- CdP_2, d-electron participation in chem. bonds 77—28682
- p-CdP_2, Faraday rot., inherent optical activity dispersion *(Russian)* 78—35119
- CdP_2, large tetragonal single cryst. growth from vap. 77—69976
- CdP_2, light polarisation, self-induced optical rotation 79—19860
- CdP_2, polarised spectra of IR absorption and emission of single crysts., oscillatory states *(Russian)* 77—28583
- CdP_2, Raman light scatt. efficiency for He-Ne laser light *(Russian)* 77—52104
- CdP_2, Raman spectra, mode symmetry 79—91441
- CdP_2, reson. interaction of vibr. states, polarised Raman spectra meas. 77—15521
- CdP_2, resonance Raman scatt. singularities *(Russian)* 80—89007
- CdP_2, role of metal d states in valence band formation 79—65380
- CdP_2, surface destruction by ruby laser irrad. *(Russian)* 77—20964

cadmium compounds continued
CdP_2, tetragonal, one and two phonon states using second order Raman spectra 78–43874
CdP_2, two-photon light absorpt. dispersion, allowed-forbidden transition *(Russian)* 78–15193
CdP_2, v.p. 77–90634
CdP_2:Bi,Zn, photolum. and photocurrent stationary characts. 78–27317
CdP_2:Cu, photoluminescence and photocond. characts., interimpurity recomb. of carriers 77–8637
CdP_4, λ-modulated photoemission spectra 79–87565
CdP_4, role of metal d states in valence band formation 79–65380
CdP_4 single crystal growth 80–35065
CdP_4, thermodynamic functions, 55-300K 80–34203
Cd_2P_2, v.p. 77–90634
Cd_2P_3, role of metal d states in valence band formation 79–65380
Cd_3P_2, band struct., D_{4h}^{15} space group symmetry props. 80–34357
Cd_3P_2, band struct., X-ray spectra determ. 78–35225
Cd_3P_2, energy band struct. and electron mobility at low temp. 79–37984
Cd_3P_2, energy band structure for real D_{4h}^{15} symmetry 79–56124
Cd_3P_2, free carrier and interband absorption 78–23446
Cd_3P_2, g-factor of conduction electrons at low temp. 79–56118
Cd_3P_2, high press. phase relns. and cryst. structs. 78–59792
Cd_3P_2, phys. props. 78–26527
Cd_3P_2, role of metal d states in valence band formation 79–65380
Cd_3P_2, sp. ht., thermodyn. props. 78–22863
Cd_3P_2, thermomagnetic transport effects obs. 77–15883
Cd_7P_{10}, cryst. struct., rel. to other Cd-P system structs. 80–33960
$Cd_3P_{2-x}As_x$ solid soln., US wave prop. velocity, composition depend. 77–20013
$Cd_4P_2Br_3$, elec. and photoelec. props. 80–34480
$Cd_4P_2Cl_3$, elec. and photoelec. props. 80–34480
$Cd_4P_2I_3$, elec. and photoelec. props. 80–34480
$Cd_4P_2I_3$, X-ray cryst cryst. struct. determ. and refinement *(French)* 80–107120
β-$Cd(PO_3)_2$, high temp. form, X-ray cryst. struct. anal. *(French)* 79–32953
$Cd(PO_3)_2$, vitreous, microhardness 80–25864
$Cd(PO_3)_2$-$Sr(PO_3)_2$, physicochemical investigation 78–44102
$Cd_5(PO_4)_3Br$, $Cd_5(PO_4)_3Cl$, halogen atom distrib. determ. 78–2078
$Cd_5(PO_4)_3Br$, X-ray diffr. cryst. struct. exam. and refinement 78–10000
$CdPS_3$, layered, organometallic intercalates, X-ray diffr., optical absorpt. and mag. props. 80–45103
$Cd_{14}P_4S_{24}$, SHG obs. 78–46719
$Cd_3(PS_4)_2$, synthesis by roasting, and exam. of props. 79–4926
$Cd_{13}P_4S_{22}I_2$, SHG obs. 78–46719
$Cd_{14-x}P_4S_{24-2x}I_{2x}$, icosahedral structs., synthesis and characts. 77–1107
$Cd_xPb_{1-x}I_2$, photoluminescence comp. and energy depend., band gap 77–44045
$Cd_{1-x}Pb_xSe$, electroless film deposition with variable comp. and polymorphic structs. 79–95952
$Cd_{1.6}Pd_{0.4}Nb_2O_7$, ferroelec., sp. ht. and Debye temp. meas., 2-25K 79–73319
$Cd_{10}(RO_4)_6X_2$(R=As, P, V; X=Cl, Br) apatites, IR spectral study *(French)* 80–93316
CdR_2S_4, (R=Sc, Yb, Tm), IR and Raman spectra, force consts. 78–68503
$CdRbI.H_2O$, cryst. struct., X-ray diffr. 77–19918
$CdRb_2(SO_4)_2.6H_2O:Mn^{2+}$, EPR, 298K, spin-Hamiltonian parameters, cryst. fields 78–27086
$Cd_2Re_2O_7$, specific heats, electronic and lattice contrib. below 20K 80–34200
$Cd_2Ru_2O_7$, specific heats, electronic and lattice contrib. below 20K 80–34200
Cd(S, Se) film grown on InP substrate, mismatch dislocations and lattice distortion, dangling bond density 80–84406
CdS 80–11398
CdS, 200 keV electron induced defects, low temp. annealing 77–80796
CdS, (10$\bar{1}$0) face, deformed zones around microimprints 78–23812
CdS, $A_{n=1}$-exciton, reflectance and thermoreflectance spectra, spatial dispersion and angle of incidence effects 80–25409
CdS, A-exciton-polariton, time depend. optical spectrosc. obs. 78–80376
CdS, absorpt. spectra, 400-650 nm, electron irrad. defects and absorpt. edge shift 78–64382
CdS, acoustic noise amplification along c_6 axis, Brillouin scatt. obs. 78–19101
CdS, acoustic phonon intensity fluctuations after strong nonlinear amplification 78–59909
CdS, acoustic wave attenuation, phonon viscosity and dislocation drag 80–70319
CdS, acoustic-wave-induced increase in cond. 77–59307
CdS, acousto-voltaic effect, asymmetric electron ejection from trap levels *(Russian)* 80–65634
CdS, acoustoelec. interaction, influence of surface pot. 77–1455
CdS, acoustoelectric current fluctuations 79–24020
CdS, acoustoelectric fluctuations 79–7866
CdS, acoustoelectric interaction at wave reflection points 78–2528
CdS, acoustoelectric mobility measurement for X-ray excited carriers 77–15916
CdS, acoustoelectronic current SHG 80–6916
CdS active surface, exciton stimulated emission and superradiance refl. spectra, props. 80–25411
CdS, additional waves and polariton dispersion, reflectivity, transmittivity spectra 80–71443
CdS adsorption of N_2, CO, and O_2, total current spectrum interpretation 77–85857
CdS, ambipolar diffusion meas. using nonlinear transient gratings 78–80000
CdS, amorphous antiferromag., mag. props. of dilute neutral donors 79–78367
CdS and CdSe, for thin film and ceramic solar energy convertors 80–93870
CdS, anomalous behaviour of transient Langmuir dissociation 79–28092
CdS, anti-Stokes excited crystals, luminescence band at 12K 79–19922
CdS, appl. of generalised temp.-factor formulation 78–26383
CdS, application in dynamic holographic correction schemes *(Russian)* 78–55326
CdS, aq. dispersion, O_2^- generation by photolysis, spin trapping detect. 78–11538
CdS, aqueous-deposited films, struct. and electronic props. for solar cell appls. 80–100797

cadmium compounds continued
CdS, attenuation of transmitted light in exciton region, polarisation, coherence, scatt. 77–69852
CdS, Au deposition, Schottky diodes and MIS devices, surface treatment effects, SEM obs. 80–54794
CdS, Auger effects in donor acceptor pair spectra 80–20707
CdS, Auger excitation mech. of 1.6-2.0 micron luminesc. band 79–8184
CdS, Auger interaction between luminescence centres and donor-acceptor pairs 77–63458
CdS, B exciton-polariton, reson. Brillouin scatt. 79–33717
CdS, band structure calcs. by modified orthogonalised plane wave (MOPW) method 80–54609
CdS, biexciton, low intensity nonlinear coherent mixing study 80–49619
CdS, biexciton fluoresc. line shape 77–44059
CdS, biexciton levels, luminescence-assisted two-photon spectra 80–29795
CdS, biexciton luminescence, influence of free excitons on profile 77–4684
CdS, biexcitonic luminesc. for allowed and forbidden polarisation 77–44040
CdS, biexcitonic state existence, 2.5 MeV binding energy *(Russian)* 77–39788
n-CdS, bipolar photocond. and acoustoelectric current 79–19636
CdS, Bleustein-Gulyaev wave transmission characts. at corner 77–59197
CdS, Brillouin scatt. of refl. light, surface ripple mechanism 77–73149
CdS, Brillouin scatt. of forbidden polaritons 79–33722
CdS, bulk acoustic phonons, light scatt. from phonon-induced surface ripples 78–75924
CdS, bulk contact ice nucleation threshold under illum. 77–55343
CdS bulk wave-$LiNbO_3$ SAW piezoelectric coupling 77–23845
CdS, calc. deform. effects on biexcitons, compared to piezoemission meas. 77–52038
CdS, carrier density nonlinearity of interacting acoustic fluxes 77–51781
CdS, cathodolum. in red and exciton regions, surface treatment influence 77–77303
CdS, cathodoluminesc. in SEM, spatial resolution anal. *(Russian)* 77–32448
CdS, CdS_2Se_{1-x}, single cryst. ingot, laser screen for CRT 77–75561
CdS, characts. of interaction of light with dislocations 78–2137
CdS, charge in energy gap caused by acoustic domains 77–20822
CdS, charged dislocations, flow of charge with plastic deform. 80–85010
CdS, charged impurity centres, drift during passage of photocurrent 80–70767
CdS, chem. sprayed film, struct. and morphology 78–72020
CdS, chem. sprayed film growth using centrifugal disc atomiser 78–92189
CdS, chemically precipitated film, optical spectra, annealing effects *(Russian)* 79–11424
CdS, chemically sprayed film, prod. by centrifugal disk atomizer, struct. 79–65343
CdS, clean surface, AES and LEED exam. 80–10762
CdS cleaved in ultrahigh vac., elec. surface props. determ. 77–15926
CdS, coherent interaction of externally generated 35 GHz of sound with light 77–43964
CdS, collision controlled light scatt. by electrons, influence of elec. field *(Russian)* 78–64375
CdS, compensated, characts. of Auger excitation spectra of photoluminesc. and photocurrent 77–90194
CdS, condensation of optically excited carriers, electron-hole-liquid phase diagram 77–31950
CdS, creation of 2P excitons by two photon magneto-absorption 78–2432
CdS, cryst. grown from melt under press., microstruct. 77–59019
CdS, cryst. growth from vapour by one-dimens. nucleation on (110) singular surface, model 78–2048
CdS, cryst. growth from vapour in sealed silica tubes, emission and mass spectra 79–43117
CdS crystal, magnetic field intensity meas. by obs. of Faraday effect 78–93739
CdS crystal, SAW amplification, bulk and acoustic noise 80–39637
CdS, crystal growth from vapour phase, model for interface kinetics 77–76335
CdS crystal growth from vapour, preferential deposition, elec. field effects 80–84122
CdS crystal growth with strong long-lived polarisation echoes 79–43113
CdS crystal with thin photoproduced semiconducting layer, tests of convolver on transverse surface waves 77–42646
CdS, crystallisation and stability in high-temp. alkaline solns. 77–52240
CdS crystals, doped with groups III and VII elements, self-activated emission, modelling *(Japanese)* 78–31247
CdS crystals, electron-hole plasma, carrier optical orientation 80–100689
CdS crystals, one-photon pumping, active layer structure, light amplification 80–78858
CdS crystals, orientational depend. of photoacoustic effect *(Russian)* 80–65167
CdS crystals, radiative recombination, high excitation rates 80–108269
CdS, cubic, ab initio band struct. calcs. within local density functional formalism 78–87910
CdS cylindrical crystal, transverse SAW obs. 78–84042
CdS, cylindrically rounded cryst., Gulyaev-Bluestein wave propag. 77–84852
CdS, d-electron participation in chem. bonds 77–28682
CdS, deep level electron trap characts. 79–78036
CdS, deep level IR luminescence, origin 80–20704
CdS, deep level transient spectroscopy *(French)* 79–11079
CdS, defect struct., dark-field microscopy, anal. of decoration patterns 79–23506
CdS, defect struct. and config. produced by irrad., elastic scatt. expts. 80–84178
CdS, defects formed by laser radiation of subthreshold intensity, bulk photo-EMF investigation 79–91098
CdS, deform. effects on exciton excitation spectra 78–35191
CdS, deformed, dislocation struct., TEM obs. 80–54250
CdS, deposited anthraquinone, decoration patters 77–1137
CdS, desorption of O_2, photostimulated desorption temp. depend. 80–24737
CdS detector, Voyager Sun sensor, evaluation of radiation interference, simulation 79–23644
CdS, dielectric theory of interacting exciton reson., wave-vector polariton dispersion relation 78–14673

cadmium compounds continued
CdS, diffusion of In, 729-1411K 78−22895
CdS, dislocation charges determ. 78−2136
CdS, dislocation effects on radiative recombination processes 79−8186
CdS, dislocation emission, photoluminesc. spectra 80−16084
CdS, dislocation motion, TEM obs. 80−79799
CdS, dislocation structural optical absorpt., plastic deformation *(Russian)* 80−34959
CdS, domain elec. instabilities, elec. field and temp. distribs., optical meas. 79−11405
CdS, donors, EPR and spin-lattice relax., Faraday rot. meas. 80−54939
CdS, doped, amorphous antiferromagnet model, susceptibility and spin-flip Raman scatt. meas. 80−97057
CdS, doped laser mechanism and output study 80−43340
CdS, drift mobility in presence of trapping-recomb. centres 78−19054
CdS, dry process formation from CdO and S *(Spanish)* 78−56607
CdS, EPR of adsorbed oxygen radicals, temp. depend. 80−80612
CdS, edge emission spectra alteration by uniaxial stress *(Russian)* 78−72486
CdS, efficiency of acousto-electrical effects, meas. by bridge method *(Russian)* 77−76881
CdS, elastic, piezoelec. and dielec. props. 80−108157
CdS, elastic, piezoelectric, and dielec. props., 4.2 to 300K 80−60508
CdS, elastic wave propag., in hexagonal piezoelec. crysts. *(Russian)* 77−69777
CdS, elastic wave propag. and interaction with charge carriers, appl. of hardened elastic moduli *(Russian)* 78−35095
CdS, elec. cond., plastic deform. and annealing effects 77−55534
CdS, electro-acoustically active, AC impedance meas. 80−103726
CdS, electroacoustic interaction obs. 77−11966
CdS, electrocrystallisation of films on Cd 78−72014
CdS electrode, in aq. soln., flatband potential, effects of dissolved Cd^{2+} and S^{2-} ions 77−51815
n-CdS electrode, photoelectrochemical behaviour in acetonitrile solns. 78−31644
CdS electrode, photoexcited, charge transfer in electrolyte with Na_2S additive 79−99618
CdS, electroless film deposition with variable comp. and polymorphic structs. 79−95952
CdS, electron and hole trapped centres, EPR, photoluminescence, photoconductivity study 80−108071
CdS, electron beam induced desorption of O_2, AES meas. 79−77921
CdS, electron drift vel. and phonon multiplication 80−6848
CdS, electron micrograph equal thickness fringes, phase angles and absolute struct. pot. 77−76383
CdS, electron traps, admittance spectra on hetero- and Schottky junctions 79−56159
CdS, electron traps, DLTS meas. 80−24949
CdS, electron-beam-pumped laser, basis of scanning optical microscope 80−31864
CdS, electron-exciton elastic scatt. cross sections, central field and exchange approxs. 77−62919
CdS, electron-exciton inelastic collision cross sections 79−90967
CdS, electron-hole condensate, luminesc. obs. *(Russian)* 78−19552
CdS, electron-hole droplet condensation 78−10367
CdS, electron-hole liq., effect of excited electron states lifetime on gain spectra 77−85748
CdS, electron-hole liquid, non-equilib. transmission spectroscopy meas. 77−20883
CdS, electron-hole pairs behaviour in energetic ion tracks 80−65457
CdS, electron-hole plasma phase transition 80−24803
CdS, electron-hole plasma, gain and refl. spectra study 80−66227
CdS, electronic struct. from X-ray emission spectra 77−28661
CdS electronic two- and one-photon Raman scatt. via biexcitons, stimulated config. obs. mag. field shift 80−103963
CdS, emission and transmission spectra, excitonic mols. effect 77−44062
CdS, emission lineshape of excitonic mols., polariton states 77−20918
CdS, energy transfer by normal modes in exciton reson. region 77−89705
CdS, epitaxial film, conductivity control by S vacancy form., light modulation appls. 77−4455
CdS, epitaxial film, structural and electron transport props. 79−82481
CdS epitaxial film, with grain-boundary barriers, field characts. of elec. cond. 77−55626
CdS, epitaxial growth and nucleation, on monocrystn. ZnS, substrate real struct. influence 80−88455
CdS, epitaxial layers on Ge, morphology and six-pointed optic figures obs. 78−2390
CdS, epitaxial layers on (111) Ce, growth and defect struct. 78−18920
CdS, epitaxial layers on Cd single crystal, direct synthesis and struct. 78−68628
CdS epitaxial layers on sapphire, exciton struct. of absorpt., photoluminesc. and photocond. spectra 80−89027
CdS, equivalent gap alteration by light scatt. by acoustic domains 77−85687
CdS, evaporated film, effects of heat treatment on photosensitivity *(Japanese)* 78−39237
CdS evaporated films, growth rate and resist. determ., in situ meas. technique 79−77940
CdS evaporated films, O chemisorpt. kinetics, effects on elec. cond. 78−6464
CdS, even acoustoelec. current due to Lamb waves, freq. depend. 80−20256
CdS, excitation spectroscopy, relation between I_2 bound exciton line and CdS excitonic molecule line 80−40153
CdS, exciton absorpt. at low temps. *(Russian)* 78−48195
CdS, exciton cathodoluminesc. of semicond. with surface pot. barriers 78−88366
CdS, exciton condensation effects on refr. index 77−20818
CdS, exciton condensation, photoluminesc. spectra 80−25448
CdS, exciton droplets, energy condensation *(Russian)* 80−107712
CdS, exciton luminescence, surface recombination, space-charge-layer effects 78−80410
CdS, exciton obs. in thin surface layers, refl. spectrum *(Russian)* 78−2877
CdS, exciton optical and luminescence spectra characts. near dislocation slip bands 80−45111
CdS, exciton polaritons, optical response 77−69792
CdS, exciton polaritons, Brillouin scatt. efficiency, additional boundary conditions 79−73960

cadmium compounds continued
CdS, exciton resonant secondary emission spectrum temporal evolution 79−51499
CdS, exciton spectra anomalies, surface state effects 78−18974
CdS, exciton spectrum of high-density gas of nonequilib. carriers 79−38567
CdS, exciton-LO phonon interactions under high excitation and temp. conditions 77−69899
CdS, exciton-contrib. to reflection spectrum at high excitation intensities 78−43900
CdS, exciton-ionised donor complex, binding energy 78−67949
CdS, exciton-phonon interaction, interpretation of optical absorpt. data 79−14897
CdS, excitonic mol. emission, strain induced splitting 77−44060
CdS, excitonic mol. transitions, optical gain and induced absorpt. spectra 80−11438
CdS, excitonic polariton reflectance, quantitative anal. in spectral range of A-exciton 79−15480
CdS, excitonic polariton reflectance, B-exciton and k-linear term 80−7369
CdS, excitonic region, nonlinear optical meas., 4.2K 78−68531
CdS, explanation for total current spectrum 77−8693
CdS, fast modulator for CO_2 laser, using two-photon magnetoabsorpt. 77−88805
CdS, fast optically controlled modulator using two-photon magnetoabsorpt., for CO_2 laser 78−13736
CdS film, anomalous noise rel. to photomemory effect 77−20374
CdS film, chemical bath deposited, solar energy conversion by photoelectrochem. cells 80−108804
CdS film, chemically deposited, cond. depend. on thickness, grain size, annealing time *(Russian)* 77−8210
CdS film, chemically sprayed, elec. and photocond. props. 78−34913
CdS film, chemically sprayed, carrier conc. and mobility, thermoelec. and photothermoelectric meas. 80−2503
CdS film, cryst. and electronic surface struct., stimulated recrystn. effects 79−78151
CdS film, crystallinity and optical props., effect of cation-anion ratio 77−76689
CdS film, current-field characts. 80−2490
a-CdS film, DC cond. Seebeck data 77−24626
CdS film, dark cond., negative temp. depend. 78−47892
CdS film, doping and recrystn. effect on photocurrent relax. time. 77−4409
CdS film, double-layered polycrystalline, on $LiNbO_3$ substrate, fabrication and props. rel. to SAW appl. 78−64480
CdS film, ellipsometry of natural boundaries *(Russian)* 79−4866
CdS film, exciton exhibiting spatial dispersion, reflectivity, polariton standing-wave struct. 79−4865
CdS film, frozen-in conductivity, nature of recomb. barriers 79−56245
CdS film, growth by chem. bath deposition, photocond. props. 77−59703
CdS film, Hall effect meas. 79−65570
CdS film, high cond., high transmittance, growth by evaporation method, and characterisation 77−77386
CdS film, influence of nonstoichiometric surface layer on props. 78−64148
CdS film, inhomogeneities responsible for residual cond., microinclusions 77−28269
CdS film, non-ohmic elec. cond. 80−2489
CdS film, on Si, structural and transport props. 78−6463
CdS film, polycryst, optical spectra, 0.5-6.5 eV 80−55212
CdS film, polycrystalline, photosensitive, struct., pseudoreplica method, using electron microscopy and microdiffr. 79−15030
CdS film, precipitation from solns., form. characts. 79−11524
CdS film, prep. by hot wall technique, morphology and semicond. props. 79−95292
CdS, film, residual conductivity, effect of transverse electric field 77−4458
CdS film, second harmonic generation by transverse acoustic wave 77−51782
CdS film, spray pyrolysis prep., elec. transport props. 78−2590
CdS film, surface energy levels, thermally stimulated contact pot. difference method 79−99601
CdS film, surface states, surface photovoltage spectroscopy meas. 77−1504
CdS film, surface stoichiometry rel. to CdS-Cu_2S cell performance 78−2956
CdS, film, surface struct. and elec. props. 80−34531
CdS film, temp. depend. of dark and residual cond. 77−55625
n-CdS film, transient photoconductivity effects *(French)* 78−87994
CdS film, vac. condensed, growth and struct., HEED obs. 80−29292
CdS, film, X-ray diffr. and elec. cond. 78−64149
CdS film and heterojunctions, grain boundary and interdiffusion studies, AES and SIMS 79−77842
CdS, film electrolytically deposited, surface and bulk photocond. props. 78−60154
CdS, film for solar cells, struct. and elec. props., thickness depend. 78−72289
CdS film growth, with smooth surfaces through boundary layers 79−28244
CdS film preferred orientation, internal stress, and interface characteristics 78−26795
CdS, film prep. from aqueous soln. of thiourea 77−8767
CdS film SAW two-dimensional image processor 77−39164
CdS film solar cell yield rel. to crystallite column statistics 79−62005
CdS film spray fabrication, physical props., Cu_2S-CdS solar cell applications *(French)* 80−60113
CdS, film with high photocond. and good reproducibility, prep. by chemical deposition 79−66019
CdS films, amorphous and polycrystalline, microinclusion distrib. of high resist. phase and residual cond. 80−7008
CdS films, chem. deposited, growth kinetics and polymorphism 80−75463
CdS films, electrolessly deposited, annealing effect on optical spectra 80−2884
CdS films, electron irrad. effect on electrophys. props., prep. conditions depend. 79−28421
CdS films, from thermal decomp. of organometallics, growth kinetics and struct. 79−78895
CdS films, growth, residual cond., inclusions 78−43492
CdS films, photosensitive, growth by reactive RF sputtering, props. *(French)* 78−35308

cadmium compounds continued
CdS, films, photovoltaic effect in wedge shaped film 79—56331
CdS films, precip. from soln., phase comp. change during annealing in air at 200-600°C 80—15393
CdS films, prep. by reactive pulverisation, chemical, crystallographic and electronic props. *(French)* 80—60112
CdS films, pure and Na doped, chemical bath deposited, photothermoelectric effect 80—6906
CdS films, spray pyrolysis deposition, SEM study, aerodynamics of nozzles 79—68782
CdS films, vac. evaporation from CdS.Cr_2O_3 system, photoelec. props. 78—80074
CdS, fine struct. of two-photon absorption, luminesc. meas. 77—24893
CdS, flexural waves in resonator platelets, synchronous amplification and generation 78—84527
CdS, flux exclusion, superconductivity at high temp. 80—97058
CdS, free-exciton multiphonon luminesc. 78—6741
CdS, GaAs excitons, exciton-phonon interactions, review, book contrib. 80—49624
CdS, gain spectroscopy and plasma recomb. 78—88327
CdS, generation of optical radiation in direction of propag. of streamer 80—69401
CdS, granulated films, optical reson. 79—4863
CdS, green edge luminescence spectrum, temp. depend. 80—108274
CdS, group velocity of light and polaritons, refl. and luminesc. spectra 77—24863
CdS, grown by vac. evaporation on Si 80—25567
CdS, grown from vapour, SEM exam. of dislocation boundaries 80—24456
n-CdS, growth from Te soln., photocond. and cryst. perfection 79—99579
CdS, growth of $CuInSe_2$ on (0001) surface using MBE 79—56936
CdS, growth rate, sublimation rate and etching behaviour along polar axis 80—24387
CdS γ-ray dosimeters with elevated stability under irradiation 80—86995
CdS, heavily doped compensated piezoelectric semiconductor, sound absorpt. coeff. calc. *(Russian)* 79—15194
CdS heteroepitaxial films on ZnS, surface-wave acoustoelectric domain excitation and probing 79—46904
CdS heterojunction solar cells by CVD method 80—45685
CdS, heterojunctions with InP and GaAs, prep. by CdS CVD and etching 78—52062
CdS, high intensity excited, exciton reflection spectra, reflection struct. 80—20692
CdS, high intensity photoexcitation, hot electrons and phonons 78—26905
CdS, high intensity US amplification *(Russian)* 77—28222
CdS, high pressure effects on electrical resistivity and structure 77—15574
CdS, high-energy electron irrad., photoluminescence spectra, course of annealing 77—90198
CdS, highly excited, stimulated emission process at 80K 80—97307
CdS, highly excited cryst., biexciton, impurity transition and electron-hole plasma 79—15092
CdS, highly excited semicond., linear optical response, electron-hole liq. 79—51980
CdS, highly photoexcited, picosec. luminesc. spectrosc. 79—47517
CdS, hole-capture coeff. of deep charged centres, temp. depend., photocurrent meas. 79—7804
CdS, hydrogenlike donor negative ion, ground and excited states, obs. 80—70645
CdS, hydrothermal crystal growth on seeds of various orientations 77—4730
CdS, IR stimulated edge emission 77—59613
CdS, impact ionisation of excitons, photocond. and photolum. meas. 79—56266
CdS, impurity cond., temp. depend. *(Russian)* 78—47829
CdS, in Al-CdS-Au struct., asymm. Poole-Frenkel effect *(French)* 77—76949
n-CdS in DMF solns., electrochem., photoelectrochem., redox. pot. determ. 79—96322
CdS, indirect doping method *(Czech)* 80—24468
p-CdS, indirect doping technique, using short-life radioactive atoms 77—31688
CdS, induced absorption and gain from high density excitons 78—68533
CdS, induced absorption in energy ranges of exciton and exciton-biexciton transitions 78—72548
CdS, influence of Lamb US waves on exciton spectra *(Russian)* 80—7374
CdS, influence of surface states on absorption edge 77—16344
CdS, influence of surface annihilation of excitons on cathodolum. meas. 77—20937
CdS, intensity fluctuations of nonlinearly amplified phonons, Brillouin scatt. meas. 77—90163
CdS, interaction of excitons with charged impurities 78—43906
CdS, intrinsic exciton fine struct., two-photon absorption 77—12397
CdS, ion implantation effect on luminesc. and cryst. damage 78—6758
CdS, ion irrad. damage, obs. using SEM in cathodolumin. mode 79—7633
CdS, irrad. with high doses of fast reactor neutrons, self-healing of radiation damage 79—73221
CdS, kinetics of recomb. radiation 78—31243
CdS, LO phonons, size effect reson., first order forbidden light scatt. 77—44002
CdS, Lamb US wave induced luminesc., green edge radiation *(Russian)* 79—91509
CdS large- and small-signal lattice attenuation, Brillouin scatt. obs. 79—47130
CdS laser, electron beam pumped, catastrophic and gradual degradation 77—61960
CdS laser, electron-beam pumped, excitation of short cavity rhodamine 6G laser 78—25887
CdS, laser, petal shaped cryst., high-temp. spectral characts. *(Russian)* 79—13968
CdS, laser action in dense exciton systems 77—75531
CdS, laser beam spontaneous action *(Russian)* 77—88820
CdS, laser induced transient gratings 78—38020
CdS laser irrad. native defect formation, influence on photoelectric props., IR luminescence *(Russian)* 80—11039
CdS laser radiation under excitation by pulsed bremsstrahlung X-rays 79—91467

cadmium compounds continued
CdS, laser thresholds and stimulated emission, intrinsic recomb. processes 79—15489
CdS, lattice attenuation meas. by US injection method 78—76480
CdS, lattice attenuation meas. by acoustic domains 80—49827
CdS, layer scintillator for backscattered SEM, reflected SEM proposal 78—21291
CdS layers, by vacuum evaporation, formation mechanism of preferred orientation 79—56094
CdS layers, epitaxial, deposited on InP substrates, vapour growth technique 77—21033
CdS layers from $CdS+Cr_2O_3$ system, effect of heat treatment on spectral distrib. of photosensitivity 78—80017
CdS, light scatt. by Bleustein-Gulyaev waves on refl. and transmission 79—24288
CdS, light-induced modulation of absorpt., rise kinetics 77—16342
CdS, linear-circular three-photon dichroism 79—51930
CdS, local cathodolum. of single crysts. under colour contrast conditions in SEM 79—8191
CdS, localised level anal. from generation-recomb. noise spectra 78—14777
CdS, long wavelength lattice vibr. modes 80—49318
CdS, low resist. single cryst., photodeform. mechanism 77—89806
CdS, low temp. IR-induced flash of green edge luminescence 77—63457
CdS, luminesc. and gain spectra of two-photon excited excitons 79—33815
CdS, luminesc. data. statistical anal. *(Russian)* 78—68559
CdS, luminesc. from heavy ion tracks 78—88365
CdS, luminesc. of I_2 bound exciton and excitonic mol. 79—91492
CdS, M_1-M_2 luminesc. band, assignment to exciton-impurity complexes 77—8649
CdS MIS devices surface states 78—72267
CdS, magnetic susceptibility, grinding-induced states 79—61040
CdS, magneto-optical effects in field up to 200 T 77—52059
CdS, magnetoabsorption, explained by D^- centres 79—38019
CdS, magnetooptic study of P line at high excitations, biexciton binding energy values 78—48220
CdS, magnetopolaritons in wurtzite-type crystals 79—78019
CdS, magnetoreflectance spectra of anisotropic II-VI semiconds. by mag. field modulation 77—66519
CdS, magnetoreflectance and magnetoluminesc. of A exciton 78—39597
CdS, mode corrected TA phonons, reson. Brillouin scatt. 78—72535
CdS, model $S={}^1/_2$ amorphous antiferromagnet, spin polarisation 78—52288
CdS, mol. model for exciton-impurity complexes 77—80740
CdS monocrystal petal lasers, single-photon excitation *(Russian)* 80—99736
CdS monocrystalline sputtered X-ray transducer characteristics *(Russian)* 80—47162
CdS, monodisperse particles form. from soln., light scatt. theory use in size estimation 80—76560
CdS, multiphonon reson. Raman scatt. and exciton-phonon luminesc. 77—16319
CdS, multiphoton cross-section determination by means of luminescence experiments 80—93377
CdS, NMR, ^{113}Cd nucl. mag. shielding 78—68395
CdS, neutron and fast electron irrad., local centre form., TSC and photoluminesc. meas. 78—87719
CdS, neutron irradiated, photoelectric props. 77—35962
CdS, neutron irradiated, intrinsic defects 78—51599
n-CdS, new type photoconduction due to magneto-phonon reson. 77—55565
CdS, nonequilibrium electron-hole plasma, optical orientation of carriers *(Russian)* 78—2904
CdS, nonlinear electronic absorption of US waves 79—15196
CdS nonlinear lens, with variable focal length 79—81511
CdS, nonlinear optical suscept., resonant excitonic contrib. 77—3633
CdS, nonlinear refr. index coeffs. meas. by nonlinear refraction method *(Russian)* 78—79066
CdS, nonlinear refr. index meas. by nonlinear lens method *(Russian)* 79—26111
CdS, nonlinear self-action effect and absolute two-photon absorption coeff. 80—83649
CdS, O and CO adsorption effects on surface pot. *(Russian)* 77—47686
CdS, ODMR, bound excitons 78—80253
CdS, obs. of acoustically induced space charge gratings 77—7203
CdS, obs. of forbidden Brillouin scatt. near exciton reson. 78—15180
CdS, obtained from CdS-Cr_2O_3 system, α-Cr_2O_3 effect on props. *(Russian)* 79—65469
CdS, optical activity in exciton spectra region, reflectance spectra 79—28707
CdS, optical axis inversion *(Russian)* 79—24284
CdS, optical detection near absorption band edge 77—749
CdS, optical modulation caused by acoustic domains 77—85689
CdS, optical props., spatial dispersion effect *(Russian)* 79—61404
CdS, optical quenching of noise photooscillations, connection with photoconduction *(Russian)* 77—20363
CdS, optical spectroscopy, absorpt. coeff., lattice vibr. modes, band gap, acoustic approach 77—69822
CdS, optical transform. of biexcitons 77—62844
CdS, optically controlled range of refr. index 78—6650
CdS, optoelectronic devices appl. *(German)* 77—7745
CdS, oriented single cryst. growth method from vapour 77—8734
CdS, parallelicity criteria for Fabry-Perot interf. obs. 78—24850
CdS, parametric action of strong radiation field 78—14752
CdS, parametric interaction of acoustic surface waves *(French)* 77—62083
CdS, phase diagram of electron-hole liqs. in polar semiconds. 77—89706
CdS, phase memory effect and vel. of trap-controlled high-field domains 77—47855
CdS, phonon echoes *(French)* 77—51461
CdS, phonon-coupled photoacoustic spectroscopy 80—54317
CdS phosphor, powdered, in host material, solar cells wavelength shifting 80—85286
CdS, photoanode, flat band pot., depend. on surface ion effects 79—62013
CdS photoanode thin film, for photovoltaic cells, prep. and characts. 78—14818
CdS photoanodes, effect of S substitution, photoelectron spectroscopy obs. 80—2463

cadmium compounds continued
  CdS, photoanodes in sulphide-polysulphide electrolytes, instability 78—80755
  n-CdS, photoanodic behaviour in acetonitrile-iodide solns. 78—47868
  CdS, photocond., acoustoelec. fluctuations 79—24022
  CdS, photocond., spectral depend. at high excitation intensity, exciton effects 80—65619
  CdS, photocond. cryst., stationary and non-stationary temperature-electric instabilities 79—7833
  CdS, photocond. cryst. characterisation of electron-trap responsible for acoustic holographic echoes *(French)* 79—19544
  n-CdS, photocond. film, phase memory effect and deep levels 79—82556
  CdS, photocond. meas. using surface wave acoustoelec. current 77—8131
  CdS, photocond. on supplementary X-irrad. *(Russian)* 77—28212
  CdS, photoconducting, surface acoustic noise amplification by carrier drift 78—72208
  CdS, photoconductive, obs. of high intensity sound self-defocusing 80—24972
  CdS, photoconductive, transverse electric current effect on SAW propagation 79—47127
  CdS photoconductivity, spatial homogeneities exam. using DC and microwave techniques 80—93895
  CdS photoconductor, penetration depth of Bleustein-Gulyaev waves 79—28186
  CdS, photoconductors, spectral sensitisation, role of local centres *(Russian)* 80—90924
  CdS photodetector for integrated optical half adder circuit 79—76877
  CdS, photoelasticity, exchange charge polaris. effect 77—81046
  CdS, photoemission due to direct transition near L- and M-points in Brillouin zone 77—16451
  CdS, photoexcitation, effect of elec. field *(Russian)* 79—1751
  CdS, photoexciton waves, restrictions imposed on nature of additional boundary conditions 79—28789
  CdS, photoinduced sensitisation process, thermal activity *(Russian)* 80—34477
  CdS, photon drag effects 78—23134
  CdS, photophoretic spectroscopy, broadband 80—86469
  CdS, photoplastic effect due to α, β dislocations, spectral depend. 77—90180
  CdS, photoplasticity and photocond., excitation energy conc. near dislocations, hardening 77—24346
  CdS, photopotential changes due to Ar ion bombardment 77—8174
  CdS, photorefl. in exciton region, surface layer influence 78—76489
  CdS, photoreflection exciton spectra *(Russian)* 77—20874
  CdS photoresistor, errors in exposure meter accuracy calc. 77—49773
  CdS photosensitive film production from chelated metallo-organic compounds *(Russian)* 80—49813
  CdS, photosensitivity degradation mechanism due to photocurrent, phtotcarrier lifetime 80—6903
  CdS, photothermal spectroscopy 78—32808
  CdS, piezoelec. polycryst. film layer struct., acoustic harmonic generation 77—89812
  CdS, piezoelec. semicond., piezoresist. of grain boundaries 78—51995
  CdS, piezoelec. semicond., sound absorption 80—60051
  n-CdS, piezoelectric polaron and polaron pinning 77—35872
  CdS, piezoelectric semiconductor, frequency mixing of acoustic waves in oscillatory and DC elec. fields 77—35966
  CdS, piezoelectric semiconductor, space charge distribution at elastic wave propag. *(Russian)* 77—77150
  CdS, piezoelectric semicond., acoustoelectric current of Lamb waves *(Russian)* 77—89815
  CdS plane parallel slab, optical const. determ. methods 80—60531
  CdS, plastically deformed, optical and electronic transport anisotropies 77—8611
  CdS, plastically deformed, photo-EMF rel. to cryst. polarity 77—55581
  CdS, plastically deformed, electronic transport and optical props. 79—73508
  CdS, plastically deformed cryst. with dislocation slip band, residual cond. 80—6839
  CdS plate, amplification of elastic waves by transversely drifting injected carriers 79—7868
  CdS platelet laser, emission spectra, optical coupling between partial resonators 80—69400
  CdS platelet lasers, optically pumped, spatial and spectral distribution of laser emission 80—64032
  CdS plates, noise amplification as function of drift field intensity, conductivity and freq. *(Russian)* 79—73556
  CdS, polar semiconductor, electron-hole liquid, electron-phonon interactions 80—6739
  CdS, polaritons, two-phonon Brillouin scattering 80—20656
  CdS, polaron cyclotron resonance freq. shifts, halfwidths, cumulant expansion method calcs. *(Russian)* 80—88880
  n-CdS, polaron effective mass, DC Hall effect meas. 78—39037
  CdS, polaron IR cyclotron reson. 80—25347
  CdS, polycryst., photoelec. props., pressure time influence *(Russian)* 79—19615
  CdS, polycryst. films, microstruct. and X-ray cond. 79—56336
  CdS, polycrystalline evaporated layers, donor and trap densities 80—20213
  CdS polycrystalline film, pot. barrier at grain boundaries from Hall effect *(Russian)* 77—32094
  CdS polycrystalline films, high strain sensitivity 80—93017
  CdS polycrystalline layers, electron trapping depend. on preparation conditions 79—78232
  CdS polycrystalline thin-film liq. junction photovolt. cell 80—50988
  CdS, polycrystn. films, recrystn. accompanying annealing *(Russian)* 80—20948
  CdS, polycrystn. layers on CdS substrate, electron microscope study of surface struct. 78—22940
  CdS, polytype relative stabilities, entropy contribs. 80—100197
  CdS, porous, dynamic phase transition at high press. 79—23723
  CdS, positron annihilation study 80—60713
  CdS, powder, mechanically induced localised states in energy gap 80—2354
  CdS powder, surface O_2 adsorption, ESR studies 79—65738
  CdS powder layers, surface pot. dark decay, moisture sorption and heat treatment effects 80—18038
  CdS precipitates from acetate solns., crystal structure and photocond. obs. *(Japanese)* 78—10502
  CdS, prepared by ceramic Technol., physical props. 79—60837

cadmium compounds continued
  CdS, press. quenched, mag. moment, semicond.-conducting transition 80—15683
  CdS, props. of shallow acceptors, photocurrent meas. 79—7805
  CdS, ps decay kinetics of luminesc., streak camera obs. 79—78752
  CdS, ps. spectra, high density exciton system 78—19553
  CdS, ps. spectra, high density exciton system 78—19554
  CdS, psec time resolved spectroscopy, electron-hole plasma 79—47500
  CdS pulsed optically detected resonance, time depend. recomb. processor study 79—38411
  CdS, pure and Al doped, vacuum deposited film, photoelectric props., optical absorption 78—60162
  CdS, pure and Cl doped, stimulated emission due to indirect band-band transitions 80—7376
  CdS, pure spin diffusion without charge transport, spin flip Raman scatt. obs. 80—93329
  CdS, quasimonopolar semicond., recombination in near surface space charge region *(Russian)* 80—88574
  CdS, Raman shift dispersion near exciton reson., two-phonon cascade processes 80—11405
  CdS, recomb. radiation of electron-hole liq., quantum oscills. *(Russian)* 77—36293
  CdS, recombination electric domains, production mechanism 80—29433
  CdS, reflectance, transmittance and luminesc. spectra, light group vel. near exciton reson. *(Russian)* 77—69857
  CdS, reson. Brillouin scatt. near A exciton 77—69846
  CdS, reson. Brillouin scatt. by longitudinal acoustic phonons 79—38555
  CdS, reson. Brillouin scatt., book contrib. 79—42983
  CdS, reson. Brillouin scatt., quasi-static anal. 79—65887
  CdS, reson. Brillouin scatt. of exciton polaritons 80—11418
  CdS, reson. dispersion of Brillouin shift 78—35160
  CdS, reson. forbidden Brillouin scatt. by TA phonon domains 79—56802
  n-CdS, reson. obs. in far IR transverse magnetophotoconductivity 78—30949
  CdS, reson. Raman scatt., temp. depend. polarisation, A-exciton 77—12386
  CdS, reson. Raman Scatt. under two-photon excitation of excitonic mols. 78—52486
  CdS, reson. Raman scatt., second-order, theory for case of strong excitonic effects 78—76460
  CdS, reson. scatt. of exciton-polaritons second emission under monochromatic excitation 77—1717
  CdS, reson. scatt. of exciton-polaritons by acoustic phonons 78—60482
  CdS, resonance hyper-Raman light scatt. on optical photons *(Russian)* 80—14396
  CdS, resonant Brillouin scattering and photoelastic consts. in population-inverted material 80—76042
  CdS, resonant Brillouin scatt., photoelastic const., imag. part contrib. 80—108218
  CdS, resonant Raman scattering by LO phonons 78—39551
  CdS, resonant scatt. of exciton polaritons by LO and acoustic phonons 79—95760
  CdS, reversible hardening induced by electron-beam irrad. 77—62580
  CdS, reversible threshold modification of luminesc. spectrum by uniaxial compression 79—38662
  CdS, richardson-Schottky type photoinjection current from photoconductor into insulating liquid 80—15608
  CdS, rock-salt type high-press. phase synthesis using metal sulphide additives 80—104084
  CdS, SAW absorpt., effect of transverse electron drift 77—76879
  CdS SAW convolver, effect of transverse drift of carriers on operation 80—14529
  CdS, SAW meas. of surface elec. props. 77—20387
  CdS SAW monolithic convolver with high resistivity surface layer, non-linear cond. 79—98554
  CdS, SAW superheterodyne amplification 77—55589
  CdS, scanning semiconductor laser with transverse electron-beam pumping 80—9904
  CdS Schottky barrier diode with evaporated Au-Ti blocking contact, rectification props. 77—85319
  CdS Schottky barrier solar cells, spectral distrib. and photocapacitance 80—55864
  CdS Schottky contact, photovoltage 78—95337
  CdS screen, laser electron-beam tube under scanning conditions 79—13983
  CdS screen for laser CRT, stimulated emission with TV type operation 78—59028
  CdS, second order polaritons associated with van Hove singularities, light scatt. expt. 77—90146
  CdS, seeded growth from vapour of large single crystals 78—64449
  CdS, semicond., coexistence of surface and bulk acoustic waves in acoustoelec. domains 80—44404
  n-CdS, semicond. electrode, electrolum. due to hole injection from electrolytes 77—20926
  CdS, semicond. film, contoured anodic photodissolution 79—74277
  n-CdS semicond. liq. junction solar cells, photocurrent spectra, carrier recombination 78—76142
  CdS, semicond. piezoelec. crysts., US investigation of acoustoelectric characts. 77—1456
  CdS semiconducting thin-film optical waveguide polariser 80—33180
  CdS semiconductor laser, longitudinally pumped, electron beam scanning vel. rel. to output parameters 80—9889
  CdS, semiconductor-electrolyte interface, photoelectrochem. processes, hologram recording utilisation 77—88667
  CdS, single cryst., band parameters from optical exciton spectra 79—47021
  CdS, single cryst., bound excitons in surface layers, luminesc. obs. 79—28294
  CdS, single cryst., effects of annealing in Cd or S vapour on photoelectric props. 77—16370
  CdS, single cryst., laser emission following single-photon excitation *(Russian)* 78—37889
  CdS single cryst., lasing action excited by ruby laser picosecond pulses 80—64035
  CdS single cryst., melt growth, improvement of elec. characts. 79—38734
  CdS, single cryst., polar (0001) and $(000\bar{1})$ surfaces, comparison of AES signals 80—16130
  CdS, single cryst., surface treatment effects on photoluminesc., struct. and optical props. *(Russian)* 78—15224
  CdS single cryst., vaporization and form. of negative whiskers 80—92659

cadmium compounds continued
CdS single cryst. Hall effect, temp. depend., 800-1200K *(Russian)* 77—80797
CdS, single cryst. surfaces, diffr. gratings, electrochem. recording of holograms 80—32934
CdS, single crystal, growth by modified Piper-Polich method, props. *(Japanese)* 79—100036
CdS single crystal, laser emission at one-photon excitation *(Russian)* 77—79835
CdS, single crystal, subnanosecond light pulse generation by laser radiation pumping 79—64234
CdS single crystal growth by sublimation *(Japanese)* 78—11093
CdS single crystal laser screen, photolum., determ. of layer depth disturbed by polishing 78—17977
CdS single crystals, depend. of radiative props. on equilib. carrier density 79—19932
n-CdS single crystals, effect of high-temp. annealing on electrical transport props. 79—78098
CdS single crystals, grown from vapour, analysis of static method 79—52092
CdS, single crystals, laser emission from surface diffraction grating 80—95900
CdS single crystals, Roentgenoluminescence, exciton interactions *(Russian)* 80—2853
CdS, single crysts., US luminesc. obs. 80—76092
CdS, single-quantum radiative recomb. of biexcitons due to biexciton-exciton interactions 80—96793
CdS sintered film, photolum. and recomb. photocurrent noise spectra 78—6743
CdS, sintered film, solar cell *(Chinese)* 79—74517
CdS, size effect of dense electron hole systems 80—7413
CdS smoke particle growth, prep. by evaporation in inert gases 77—24938
CdS solar cells, construction, solar photovoltaic systems for remote communications power supply 80—66980
CdS, solar cells, polycrystalline and tandem, for high efficiencies, using compound semiconductors 80—72052
CdS solar photovoltaic panels, deposited by spray pyrolysis, film and junction structure studies 80—45689
CdS, solution growth, using Te solvent 79—65993
CdS, spatial diffusion of excitons under intense excitation 77—44061
CdS, spatial dispersion and surface layer effects on the phase of reflected light *(Russian)* 78—35182
CdS, spatial dispersion effects, exciton decay const. depend. *(Russian)* 78—72086
CdS spatial modulator, 16×18 bit, page composer 77—39050
CdS, spectra of refl. and transmission coeffs. near exciton absorpt. line 80—88951
CdS, spectral anal. of luminesc. of high density excitons 79—11451
CdS, spectroscopic investigation and electron irradiation using He cryostat 77—37899
CdS, spectroscopic study of local centre interaction, change with external illumination 80—80323
CdS, spin flip Raman scatt. linear k term 78—19475
CdS, spin-flip line shape 78—88307
n-CdS, spin-flip Raman echo obs. 77—19370
CdS, spin-polarised electron-hole liquid, theory 78—43307
CdS, spontaneous and stimulated emission from electron-hole plasmas 77—69241
CdS, spontaneous optical activity in exciton spectrum *(Russian)* 78—35167
CdS spray pyrolysis film prep. and characterisation 78—64492
CdS sprayed film, heat treatment effect on props. 79—7916
CdS sprayed film, prep., optical props., struct. and comp. 79—78875
CdS sprayed films, elect. and optical props. 78—39241
CdS sprayed thin films for CdS-Cu_2S heterojunction solar cells 79—61988
CdS, sputter-deposited, electrical and optical props. 79—47181
CdS sputtered film, photocond. props. 78—10586
CdS, sputtered film, Rayleigh wave propag. *(French)* 77—62727
CdS, stimulated and spontaneous emission from degenerate electron-hole plasma at 300K 80—29762
CdS, stimulated emission under N_2 laser excitation 77—14723
CdS, stimulated emission and optical gain in dense exciton system 79—33731
CdS, stimulated Mandelstam-Brillouin scatt. on acoustic phonon amplification *(Russian)* 80—71437
CdS, strain- and electro-gyration, polarised light dispersion curve pseudocrossing 77—36196
CdS streamer laser, generation of ps. light pulses 80—9908
CdS, streamer luminescence 78—6762
CdS, stress-induced photolum. bands, photocond., rel. to dislocation electron states 80—25447
CdS, study of electron dynamics by spin flip Raman scatt. 79—95789
CdS, subMM radiation excitation by N_2 laser pulse 80—60678
CdS, submillimetre laser emission due to transitions between free exciton level 79—27261
CdS, substitutional Ti^{2+} centres, linear electroabsorpt. 77—66525
CdS substrate with Cu_2S sputtered coating for solar cell fabrication 78—39692
CdS substrates, lattice mismatch with ternary chalcopyrite films 79—87012
CdS, superconductor-semicond. device research, future prospects 79—28467
CdS, superluminescence due to pulsed X-rays, 170 and 295K 78—42338
CdS surface, nonequilib. electron effects due to chem. excitation 78—72239
CdS surface, transverse acoustoelec. voltage inversion 77—47885
CdS, surface acoustoelec. current due to Rayleigh wave, ambient medium effects and surface state changes 77—69383
CdS, surface charge and ledge dynamics, point defect annihilation during sublimation 79—90642
CdS, surface elastic wave propag. in piezoelec. plate, elec. screening effect *(Russian)* 79—14999
CdS, surface electronic struct., slow electron reflection, total current spectroscopy *(Russian)* 80—54759
CdS, surface energy evaluation, by a microindentation method 80—16473
CdS, surface energy levels, O(C) adsorpt., AES study *(Japanese)* 78—88008

cadmium compounds continued
CdS, surface energy struct. changes during ion cleaning and thermal annealing 80—92962
CdS, surface layer, photomechanical and photoplastic effects 79—99264
CdS, surface photovoltage transients, surface state, parameters determ. 77—72905
CdS, surface photovoltage in exciton absorpt. range 78—19119
CdS, surface photovoltage, characterisation 80—60033
CdS, surface props., photoreflectance spectra in the exciton region 78—95324
CdS surface spectroscopy using acoustic surface waves, spectral response 77—69402
CdS, surface state meas. by SAW convolver 79—42617
CdS surfce, slow electron refl., 0-6 eV 78—11039
CdS, temp. coeffs. meas. of refr. index and birefr. 77—55762
CdS, temp. depend. of edge emission band shape 77—20934
CdS, theory of photoelastic effect 77—55769
CdS, thermal decomp. kinetics, in vacuo, free electron density depend. 77—59111
CdS, thermal desorption of O_2, photopot. and surface pot. changes 77—11795
CdS, thermal equilib. phonon populations, acoustic intensity meas. by Brillouin scatt. intensity obs. 80—45098
CdS thermo-optic coefficient, dispersion 80—71396
n-CdS, thermodynamic pot. for anodic dissolution, rel. to photoelectrochem. cell efficiency 78—26948
CdS, thermoelec. and photothermoelec. power meas., inhomogeneity effects 80—54728
CdS, thermoemission of positive ions in simple gas atmos. *(Russian)* 77—28676
CdS, thermoreflectance spectra, additional boundary conditions in terms of optical constants 79—15478
CdS, thick acoustoelec. oscillator, time investig. of parametric interactions 77—47867
CdS, thin film, dark- and photo-currents, annealing time effect 79—38199
CdS, thin film, diffusion of Cu, 20 to 200°C *(French)* 80—15424
CdS thin film fabrication processes and conduction mechanism for solar cells, review 79—74522
CdS thin film solar cell fabrication, HCl etching 80—81474
CdS, thin film transducers, electromechanical coupling meas. by light diffr. 77—23840
CdS, thin films, deposition onto hot substances, vapour phase method 78—95694
CdS thin films, growth and evaluation for fabrication of high performance photovoltaic solar cells 80—93501
CdS thin films, slow electron mean free path 79—99998
CdS thin films on brass substrates, nondestructive resistivity meas. tech. 80—93898
CdS thin layers, recryst. from CdS-Cr_2O_3 mixtures, phys. and photoelec. props. 80—96935
CdS, thin plates, piezosemiconductors, second harmonic acoustoelectric current obs. 80—80329
CdS thin-film Lamb wave delay line characteristics and strain effects 77—31185
CdS thin-film polycrystalline solar cell development 79—61993
CdS, third order nonlinear optical difference frequency generation 78—22176
CdS, three-branch exciton-polariton dispersion, direct meas. by reson. Brillouin scatt. 80—60620
CdS, three-photon absorpt. coeff. determ. by nonlinear luminesc. expt. 80—14384
CdS, time-resolved spectra of spontaneous luminesc. from high density electron-hole plasma 80—40156
CdS transducer, US meas. of elastic modulus of Tb 77—11151
CdS, transient phenomena in sublimation 78—30747
CdS, transition metal centres, first-harmonic electromodulation spectra 78—35116
CdS, transmission spectra, region of exciton reson., spatial dispersion effects 79—78704
CdS, transverse acoustoelec. effect, for SAW optical image scanning 77—11001
CdS, transverse acoustoelec. effect rel. to SAW intensity 78—26917
CdS, trapping level parameter determ., limiting current injection *(Russian)* 78—39129
CdS, two photon absorption relative to Raman cross sections 78—87098
CdS, two photon Raman scatt. at high excitation levels *(Russian)* 80—16032
CdS, two photon reson. Raman scatt. by excitons 77—52086
CdS, two-phonon resonant Brillouin scatt. 78—84597
CdS, two-photon absorpt., influence of In and Cu impurities 77—16353
CdS, two-photon absorpt., excitons *(Russian)* 78—39571
CdS, two-photon absorpt. effect on hyper-Raman scatt. 80—74441
CdS, two-photon absorption coefficient rel. to inverse Raman cross section 78—6678
CdS, two-photon excitation of first vibr. state of biexciton, giant oscillator strength calc. 79—7789
CdS, two-photon Raman scatt. via biexcitons, angle- and polarisation depend. 79—87446
CdS, two-photon reson. Raman scatt. by excitons via intermediate excitonic mol., polarisation and polariton effects 78—10880
CdS, two-photon-excitation, tunable laser emission, luminesc. processes 80—55127
CdS type direct semiconductor, high excitation 77—48202
CdS, US dispersion of high intensity waves, nonlinear electron absorpt. *(Russian)* 78—26916
CdS, ultrasonic transducer, multilayer systems, amplitude-freqn. characts. *(Russian)* 77—23843
CdS, ultrasound amplification, hard regime 77—89810
CdS, uncoated and liq. layer coated, vaporisation mechanism, surface morphology 77—35683
CdS, uniaxial pyroelectric, nonlinear optical susceptibility 77—23705
CdS, up-conversion and optical storage, spatially modulated band struct. 78—64397
CdS, vacuum deposited film, orientation axis tilt rel. to vapour angle of incidence 80—88456
CdS, vacuum epitaxial growth on $CuInSe_2$ 78—92193
CdS vacuum evaporated film photoconductivity and In doping effects *(Japanese)* 79—87174
CdS, vap. phase grown cryst., stoichiometry control, elec. cond. 79—100034

cadmium compounds continued
CdS, virtually excited biexcitons polaritons dispersion, two photon Raman scatt. 80—45067
CdS, vol. depend. of refr. index 78—88275
CdS, Wannier exciton and Wannier-exciton-ionised-donor complex, binding energies of lowest excited states 80—34363
CdS, Wannier exciton-ionised donor complex, binding energy 80—44509
CdS, wavelength dependence of pressure coefficients of birefringence 77—20820
CdS, wedge shaped film, photovoltaic effect 77—1454
CdS, wide-gap extrinsic semicond., injection currents, theory 78—19052
CdS with Cu traces, γ-radiation dosimeter, prod. and characts. 78—8999
CdS, with dislocations, optical props. 79—83001
CdS, with electron-hole exchange interaction, energy levels of A and B excitons 79—51494
CdS, with group III or VII dopant, self-activated emission 77—16371
CdS, wurtzite structure, natural optical activity *(Russian)* 79—78647
CdS, X-ray diffr. investig. of high-press. polymorphism 77—43324
CdS, X-ray diffuse scattering 80—14964
CdS, X-ray L-emission spectra of S *(Japanese)* 78—15254
CdS, XPS, secondary illumination effects, band bending, level shifts 80—108324
CdS:Ag, induced impurity photocond. spectrum obs. 77—1447
CdS:Ag, Ni thermographic phosphor luminesc. screen, for IR laser pulse recording 79—64342
CdS:Ag, orange luminesc. at 77K and induced impurity photoconductivity 79—43035
CdS:Ag, vaccuum deposited film, recrystn. by H$_2$S heat treatment 80—34328
CdS:Ag crystals, spectral shifts of induced impurity photocond. bands 80—39633
CdS:Ag phosphor, mechanism of trap ionisation by elec. field, Gudden-Pohl flashes 79—74007
CdS:Bi film, implantation and post annealing, superlinearity 78—52028
CdS:Bi film, spectral response characts. 78—2512
CdS:Cd, Cu, single crysts., IR restoration after optical degradation of photosensitivity 79—60867
CdS:Cd,Cu crystal, formation and bleaching of optically-induced absorption bands 78—31221
CdS:Cd(In), Cu- or defect-compensated, optical ageing rel. to storage cond. 78—84247
CdS:Cl, extrinsic, exciton absorption 78—72569
CdS:Cl, heavily doped, fluoresc. spectrum upper threshold calculated 78—52568
CdS:Cl, resonant Raman scatt. exam. 78—39546
CdS:Cu, C-V curves of MIS diode used to examine trapping levels 80—65697
CdS:Cu, Cd, data storage, optical and photoelec. reading 78—1193
CdS:Cu, Cl films, photocond. growth and decay time 80—60041
CdS:Cu, diffusion doping, photolum. 79—91493
CdS:Cu, dye-sensitised, photocond. and photocurrent decay time obs. 80—6893
CdS:Cu, fast electron irradiated, isochronous annealing of IR photocond. quenching spectra 77—1450
CdS:Cu, Fermi level position, luminesc., and photosensitivity, electron irrad. effects *(Russian)* 78—14652
CdS:Cu, IR photolum. at 10K 79—28824
CdS:Cu, In, Ga, spray deposited film, struct., X-ray obs. 78—71713
CdS:Cu, photocond. under high excitation intensity 78—52033
CdS:Cu, photocurrent, elec. field effect on recombination processes *(Russian)* 80—100484
CdS:Cu, photosensitivity degradation mechanism 80—107851
CdS:Cu, recording holographic medium, exposure characts. *(Russian)* 77—635
n-CdS:Cu, Si, photocond., carrier lifetime, X-ray effects 77—59300
CdS:Cu, spectral sensitisation by cyanine dyes 78—64064
CdS:Cu, US absorpt. in heavily doped piezoelec. semicond. 79—11189
CdS:Cu, V, photoluminescence spectra 79—83027
CdS:Cu,Cl, film, photocond., applied voltage freq. effect on props. 80—39635
CdS:Cu,Cl film, photocond., use in laser-addressed electrolum. display screen 77—51777
CdS:Cu,Pb reflectivity of Ni-salt coated powder, pre-irrad. effect on defect form. 79—27973
CdS:Cu binder layer, photoactive, AC impedance meas. 80—25299
CdS:Cu film, dynamic quenching of photocapacitance, deep levels obs. 77—85175
CdS:Cu films IR quenching of photocapacitance, deep level detection 79—56258
CdS:Cu sintered layers, relaxation photocurrent kinetics *(Russian)* 80—107852
CdS:Cu$_2$S sputtered solar cells, energy anal. of cell fabrication techniques 80—50966
CdS:CuCl$_2$, sintered film, dopant conc. effects on carrier mobility 78—2484
CdS:CuCl$_2$(CdCl$_2$) sintered layer, distrib. of energy levels of local centres 80—15568
CdS:Cu(Ag), charge and transport mechanism of impurities, electrodiffusion doping 80—59725
CdS:Cu(Cl), thin layer, electron pulse induced cond. relax. 80—2501
CdS:Cu(Cl) polycrystalline films with residual conduction, kinetic phenomena *(Russian)* 77—15981
CdS:Cu(Cl) thin films, surface and bulk photoconc. 80—88653
CdS:Cu(In), two-photon and two-step absorption of light 80—7389
CdS:Cu(Se)(Zn), heavily doped, defect struct. 78—22756
CdS:D^{-}, binding energy of D^{-} ion 80—92541
CdS:Er^{3+}, spectra of different emission centres *(Russian)* 77—16356
CdS:F(Cl), shallow donors electronic Raman scatt., reson. enhancement 80—45068
CdS:Ga crystal cathodoluminescence, SEM analysis 80—97349
CdS:Gd^{3+}, mag. susceptibility, cryst. field calc. 78—76035
CdS:I single cryst., I detection by argentometric titration DEP 77—16875
CdS:I$_2$ system, interface kinetics and vapour phase mass transport 80—19732
n-CdS:In, containing excess Cd, effects of In on elec. props. 79—56217
CdS:In, impurity resist., Matsubara-Toyozawa theory extension 80—80264
CdS:In, spin flip Raman scatt., electron dynamics 78—80342
CdS:In, two-photon absorpt. spectra exam. of effects of screening of exciton continuum 79—8166

cadmium compounds continued
CdS:In film, flash evaporated, prep. and elec. props. 80—20792
CdS:In films, vacuum deposited, growth, elec. and optical props. 79—51460
CdS:In whiskers, prep. by vapour deposition 78—75969
CdS:In(Cl) concentration quenching mechanism of luminescence 80—97336
CdS:In(Ga)(Al), cathodolum. on diffusion front 77—32447
CdS:Li, anisotropy of the absorption by impurity centers in hexagonal crystals 78—88343
CdS:Li, complex luminescence centres, recombination-stimulated conversion 80—108268
CdS:Li, donor-acceptor interactions, photochem. reactions *(Russian)* 77—40285
CdS:Li, luminescence bands, photocurrent spectra *(Russian)* 80—60677
CdS:Li, nature of recombination centres responsible for 0.95 μm luminesc. band 77—69908
CdS:Li, photocond. characts., electron and hole traps obs. 77—8140
CdS:Li, pure and doped, green edge luminesc., complex nature of centres 80—60671
CdS:Li, single crystals, anisotropic luminesc. centres 80—80857
CdS:Li, subjected to elec. fields, drift of defects 80—6558
CdS:Li, TSC and optical photocurrent quenching spectra, Auger excitation of recomb. centres 79—33294
CdS:Li, thermochemical changes in microstructure of anisotropic centres, polarisation modulation method meas. 79—38027
CdS:Li chemically deposited filter, elec. props. 80—11113
CdS:Li film, chemical bath deposited, photocond. and optical props. 80—2426
CdS:Li film, optical props. 80—2886
CdS:Li film, photocond., effects of annealing, S vacancies, and O$_2$ adsorption 78—34854
CdS:Li lattice, location of implanted Li atoms 80—6428
CdS:Li^{+}(N^{+})(Ne^{+})(P^{+}), ion-implanted, edge emissions 77—77274
CdS:Li(Cu), pure and doped, electrodiffusion of shallow donors, photocurrent, TSC, and exciton luminesc. meas. 80—79992
CdS:M, M=Zn, Te, doping and solid soln. prep. during VPE 77—85353
CdS:Mn, vacuum deposited film, Mn migration, EPR and X-ray study 80—65411
CdS:Mn gamma-irradiated ESR meas. 79—11342
CdS:Mn^{+}, cryst., X-band ESR 78—2730
CdS:Mn^{2+}, doped, spin-lattice relax. exam. 77—40120
CdS:Mn^{2+}, spin-lattice relax. ang. depend. 79—73807
CdS:Mn^{2+}, temp. depend. of rate of spin-lattice relax. 79—42832
CdS:Mn(Co), intensity and spectral distrib. of luminescence *(Russian)* 77—16392
CdS:N, P, As, Sb, Bi photoluminescence obs. 78—10965
CdS:Na, Hagemark theory, green edge emission line intensity 80—75517
CdS:Na, thin film, dark- and photo-currents, annealing time effect 79—38199
CdS:Na thin film, photoconducting props. 80—39623
CdS:Ni, dark cond. and photoconductivity 78—76110
CdS:Ni, elec., photoelec. and luminesc. props. *(Russian)* 78—84259
CdS:Ni, elec., photoelec. and luminesc. props. 79—95828
CdS:Ni, exciton reflection spectra 78—72557
CdS:Ni, impurity to band electronic transitions, photocond. and dark cond. obs. *(Russian)* 77—8150
CdS:Ni, nonradiative recomb., photocond. spectra 80—70764
CdS:Ni, recomb. parameters, photocond. spectra meas. *(Russian)* 80—49820
CdS:Ni^{2+}, config. interaction and cryst. field theory 77—39811
CdS:Ni^{2+}, Zeeman effect at Ni impurities 80—60633
CdS:P, implanted, photoluminesc. and electroreflection spectra *(Russian)* 78—52544
n-CdS:Te, grown from Te soln., elec. props. 79—65475
CdS:Te-based photoelectrochem. cell, luminesc., thermal manipulation of deactivation processes 80—81479
CdS:Ti^{2+}, superhyperfine interact., ENDOR study at 4.2K 80—80639
CdS/Cu$_{2-x}$S heterostructures, heat treated, capacitance voltage meas. anal. 80—20292
CdS/Cu$_2$S heterojunction solar cells, optimal material props. theory and experimental verification 80—45686
CdS/Cu$_2$S heterojunction solar cells diffusion length determ. using minority carrier SEM 80—61359
CdS/Cu$_2$S solar cell, design and fabrication 80—30481
CdS/Cu$_2$S solar cell fabrication, performance rel. to Cu$_2$S mats. props. 77—77426
CdS/Cu$_2$S solar cells, polycryst. thin film photovoltaic materials, photon loss anal., expt. determ. 80—93888
CdS/Cu$_2$S thin film heterojunctions, photocapacitance meas. of solar cell parameters 80—93897
CdS/Cu$_2$S thin film solar cells, design and fabrication, 9.15% conversion efficiency 80—81438
CdS/Cu$_x$S, sequential evap. for solar cell applic. 80—93902
CdS/InP epitaxial thin films on NaCl, HEED and TEM study 80—88446
CdS/LiNbO$_3$ system SAW convolution signal photoenhancement obs. 77—27431
n-CdS/n-InP/p-InP heteroface solar cell with ultrathin window layer, computer anal. 80—97788
n-CdS/p-ZnIn$_2$Se$_4$ thin film solar cell, photovoltaic props. 80—89628
CdS-Al, ohmic contact stability improved by annealing 78—6443
CdS-Al function formation, coupled interface plasmons, low energy electron energy loss spectra 77—24621
CdS-Al$_2$O$_3$-Al diodes fabricated by MBE, junction characts. 79—65550
CdS-Al(Au) interfaces, bonding and interdiffusion, XPS obs. 80—80000
CdS-Au, Schottky junction, surface defects, photovoltaic, piezoelectric and V-I characteristics *(French)* 80—49898
CdS-Au contacts, electronic states, vacuum UV photoelectron spectra 80—70827
CdS-Au Schottky barrier, piezoelec. effect due to mech. bending 77—69779
CdS-Au structure, work function of {0001} faces of CdS, effect of piezoelec. props. 78—23164
CdS-based phosphor, microstruct. and luminesc. efficiency 78—10959
CdS-based photoelectrochem. cells, characts. 77—25287
CdS-Bi$_{12}$GeO$_{20}$, air gap coupled system, SAW energy transfer 77—11774
CdS-CaS, solid soln., rock salt struct., high press. phase equilibrium study 78—52777

cadmium compounds continued
CdS-CdSe, unactivated film, calc. of induced impurity photocond. due to donor-acceptor pairs 77—43749
n-CdS-CdSe mixed polycryst. electrode for photoelectrochem. cell 78—47867
CdS-CdSe solid solns., bladed crystal prep. from gas phase 77—16478
CdS-CdSe system, overall vapour pressure determ. by Knudsen effusion method 77—28010
CdS-CdTe double layers on various GaAs surfaces, morphology and crystallography 80—34326
CdS-CdTe p-n junction screen printed thin film solar cells 80—72055
CdS-CdTe sintered film, prep. and photocond. props. 77—28220
CdS-CdTe solar cell, prep. by VPE, junction struct. and photovoltaic props. 77—73235
CdS-CdTe solar cells fabrication *(Japanese)* 79—87992
CdS-CdTe thin film photoresistors, optimum photoelec. performance *(German)* 79—60941
CdS-Co^{2+}, IR spectrum, 4.2K, electron-phonon interaction effect on emission spectrum 78—27270
CdS-Cu$_{2-x}$S, chem. formed heterojunction, photosensitivity characts. of Cu$_{2\ x}$S 78—72199
CdS-Cu$_{2-x}$S ceramic solar cells, solar batteries operating characts. 80—93874
CdS-Cu$_{2-x}$S heterojunction, current flow characts. and energy band struct. 77—43709
CdS-Cu$_2$S, thin film heterojunction, dark I-V characts. and heat treatment 79—56294
CdS-Cu$_2$S back illuminated high efficiency thin film solar cells 79—74515
CdS-Cu$_2$S heterojunction, influence of surface recomb. on photoelec. props. 77—43711
CdS-Cu$_2$S heterojunctions, photovoltaic mechanism, model 77—43715
CdS-Cu$_2$S heterojunction, slow relax. of photocurrent 78—26943
CdS-Cu$_2$S heterojunction model 78—39205
CdS-Cu$_2$S heterojunction, elec. and photoelec. characts., effect of etching of CdS 78—80048
CdS-Cu$_2$S heterojunctions, electron trap characterisation by capacitance transient meas. 79—78163
CdS-Cu$_2$S heterojunction solar cell, interface recomb. vel. determ. by capacitance/collection efficiency variation 80—50959
CdS-Cu$_2$S heterojunction, energy-band struct., capacitance-voltage characts., illumination effects 80—96982
CdS-Cu$_2$S heterophotocells based on CdS films of stoichiometric composition, elec. and photoelec. props. 80—93873
CdS-Cu$_2$S junctions, carrier trap density, deep level defects 80—107801
CdS-Cu$_2$S p-i-n structure diode, photoelec. characts. 78—2557
CdS-Cu$_2$S photovoltaic cell, effects of O$_2$ on efficiency 78—14807
CdS-Cu$_2$S single cryst. heterojunction, trap depths in depletion region 78—52064
CdS-Cu$_2$S solar cell, minority carrier generation and transport in emitter 77—43649
CdS-Cu$_2$S solar cells, preparation and stoichiometric control 78—2560
CdS-Cu$_2$S solar cells, design and fabrication, 8.5% conversion efficiency 80—72047
CdS-Cu$_2$S solar cells, microstructural study of heterojunction materials 80—93978
CdS-Cu$_2$S thin film heterojunctions, base doping effect on elec. and photoelec. props. 78—80043
CdS-Cu$_2$S thin-film solar cells, low-cost manufacturing process outline, economic anal. 80—93930
CdS-Cu$_2$S thin-film solar cells, high open-cct. voltage and low refl. losses 80—94088
CdS-Cu$_x$S heterojunctions produced by RF sputtering, for thin film solar cells 79—100053
CdS-Cu$_x$S solar cell, effect on response of thermally induced changes in Cu$_x$S film 77—8181
CdS-Cu$_x$S solar cell, minority carrier diffusion length, SEM determ. 77—72911
CdS-Cu$_x$S solar cell, prep. and characts. *(Croatian)* 80—93876
CdS-Cu$_x$S solar cells, screen printed, prep. and photovoltaic props. 80—40863
CdS-Cu$_x$S solar cells, electron diffusion length determ. using spectral response meas. 80—81475
CdS-CuI film heterojunction photocells, prep., photoelec. props. 78—80044
CdS-CuInS$_2$(Se$_2$)(Te$_2$) photovoltaic heterojunctions, growth and characts. 77—39931
CdS-CuInSe$_2$, solar cell, grain boundary effects on performance 79—83603
CdS-CuInSe$_2$ heterojunction, photovoltaic effect, rel. to optimum conditions for solar cell fabrication 77—51810
CdS-CuInSe$_2$ solar cells, grain boundary and interface recomb. effects 79—39311
CdS-CuInSe$_2$ solar cell, polycrystalline thin film, high photocurrent, characts. 80—61339
CdS-electrolyte, boundaries, photo e.m.f. meas., semicond. energy bands 77—1481
CdS-electrolyte contact, electrolytic decomposition and photodecomposition 78—95357
CdS-GaAs heterojunctions, current transmission mechanism *(Russian)* 77—39924
CdS-GaAs n-n voltage-enhanced photoanode, solar cell efficiency 78—14810
CdS-Ge heterojunction, grown by chemical transport, props. 77—4422
CdS-glass layered system, characts. of phase-velocity dispersion and struct. of surface waves 80—59775
CdS-HgI$_2$ binder layers, surface charge characts. for electrophotography 77—10123
CdS-In, photosensitive granular superconductor 79—78246
CdS-In ohmic contacts, by electrolytic deposition 77—8194
CdS-InP heterostructure formation and elec. evaluation 78—72738
CdS-InP n-p heterodiodes, junction props. using injection electroluminescence 79—82667
CdS-InP photovoltaic heterojunction, growth and characts. 77—39931
CdS-InP solar cell, n-p, fabrication and power conversion efficiency 77—1813
CdS-InP(CdTe)(GaAs)(Ge), solar cell heterojunctions, CVD fabrication, photovoltaic response 80—93878
CdS-Li, hexagonal crystl., orientation degeneracy of anisotropic centres, dichroism of impurity photocond. 79—73981

cadmium compounds continued
CdS-LiNbO$_3$, layered structure, acoustoelectric surface current kinetics 78—43232
CdS-LiNbO$_3$ layer structure, temp. depend. of acoustoelectric current 79—7867
CdS-LiNbO$_3$ monolithic two-dimensional Fourier transformer 79—72516
CdS-LiNbO$_3$ separated medium convolver, illumination effects 77—72766
CdS-LiNbO$_3$ structure, acoustoelectric interaction of surface waves with inhomogeneously distributed free carriers 77—43668
CdS-LiNbO$_3$ structure, transverse acoustoelectric effect 79—69567
CdS-LiNbO$_3$ system, acoustoelectric interaction 78—10516
CdS-LiNbO$_3$ system, expt. investigation of nonlinear Rayleigh wave interaction 80—102946
CdS-metal interface, chemical reactions and local charge redistrib. 79—19661
CdS-metal Schottky barrier form., transition with chemical reactivity 78—30986
CdS-MgS, solid soln., rock salt struct., high press. phase equilibrium study 78—52777
n-CdS-n-SiC heterojunctions, photoelec. and elec. props. 78—80042
CdS-NiCl$_2$ interface, elec. props. using SAW techniques 79—56302
CdS-NiCl$_2$ interface, transverse acoustoelec. voltage spectroscopy 80—49828
CdS-O$_2$, photoactivated O desorption 80—100391
n-CdS-p-CdTe heterojunctions, photovoltaic energy conversion, solar efficiency 77—43700
CdS-PET photoreceptors, air space effects on electrophotographic props. *(Japanese)* 79—44962
CdS-PbS, film production, electrochem. method 77—44180
CdS-PbS heterojunctions, photoresistive props. 80—6970
CdS-PbTe and CdS-Te heterojunctions, electron irrad. effect on electrophys. props., prep. conditions depend. 79—28421
CdS-resin layer on electrophotographic plate with polyvinylcarbazole overlayer 77—61146
CdS-Si n-p heterojunction photodetector, fabrication and characts. 78—52068
CdS-SiO$_2$ layered system, characts. of phase-velocity dispersion and struct. of surface waves 80—59775
CdS-SiO$_2$-Si solar cell, I-V characteristics 80—89621
CdS-SiO$_2$-Si structures, elec. props., role of interface states 79—56286
CdS-SrS, solid soln., rock salt struct., high press. phase equilibrium study 78—52777
CdS-Te, heterostructure, effect of low cond. CdTe interlayer on charact. 80—44721
CdS-Te-Ge heterojunction, prep. photosensitivity, and negative cond., 77K *(German)* 77—20413
CdS-ZnS(CdSe), film, light transmittance spectra, comparison with Schott GG 495 glass filter 78—33838
CdS-ZnTe, acoustoelectric domain injection across interface, reson. Brillouin scatt. 77—51778
CdS+NaCl, roasting processes rel. to flux growth of phosphors 78—23590
Cd$_x$S, electrochemical characterisation and comp. modification at 25°C 77—25272
CdSE, beam splitter coupled optical parametric oscillator 77—88851
3CdSO$_4$.8H$_2$O, cryst., phonon assisted indirect transitions 78—72559
3CdSO$_4$.8H$_2$O:Gd^{3+}, EPR, spin Hamiltonian 79—42833
(CdSO$_4$)$_3$.8H$_2$O:VO^{2+}, polycryst., struct., EPR 78—15014
CdS(PO$_4$)$_3$OH, single crysts., X-ray struct. anal. 78—95019
CdS(Se), electrodeposition, using nonaqueous solvents 80—76200
CdS(Se), excitons bound to ionised donors, binding energy calc. 77—28128
CdS(Se) film, pyroelectric effects, origin 78—88258
CdS(Se), luminesc. due to exciton-electron scatt., calc. 77—16379
CdS(Se), reaction with Sn chalcogenides, thermodynamic anal. 80—40728
CdS(Se)$_3$ excitons and Landau levels meas. by magneto-optical spectroscopy apparatus 77—34032
CdS$_{0.4}$Se$_{0.6}$, reson. excitation of excitons by ultrashort freq.-tunable light pulser 78—46728
CdS$_{0.4}$Se$_{0.6}$, two-photon absorpt., effect of polarisation of laser radiation 77—69856
CdS$_{0.5}$Se$_{0.5}$, picosecond optoelectronic switching 80—54734
CdS$_{0.75}$Se$_{0.25}$, linear electro-optic effect meas., light modulator appl. 78—76434
CdS$_{1-x}$Se$_x$, chem. comp. and luminescence obs. 80—80869
CdS$_{1-x}$Se$_x$, comp. disorder-induced broadening for free excitons 79—15479
CdS$_{1-x}$Se$_x$ film, resonance between Se atom dipole vibr. and interference modes, IR spectra obs. *(Russian)* 80—2888
CdS$_{1-x}$Se$_x$, graded comp. semicond., tunable narrow-band filter, 5130 to 3700 Å 77—31128
CdS$_{1-x}$Se$_x$ gradient cryst., pseudointersection of dispersion curves n_o (λ) and n_e (λ) 79—15487
CdS$_{1-x}$Se$_x$, mixed cryst., electron-hole drops and plasma, luminesc. obs. *(Russian)* 78—92119
CdS$_{1-x}$Se$_x$ mixed crystals, free excitons, disorder effects 80—34365
CdS$_{1-x}$Se$_x$, mixed crystals, deformation effects on free excitons 80—76073
CdS$_{1-x}$Se$_x$ monocrystal petal lasers, single-photon excitation *(Russian)* 80—99736
CdS$_{1-x}$Se$_x$ single crysts., photocond. and excitonic luminesc. under high laser excitation 78—23127
CdS$_{1-x}$Se$_x$, spatial distribution and lasing modes under one photon optical excitation *(Russian)* 78—59012
CdS$_{1-x}$Se$_x$, zone edge phonon, IR absorpt. and Raman scatt. meas. 77—76508
CdS$_{1-x}$Se$_x$, zone edge phonons 78—76475
CdS$_{1-x}$Se$_x$-Cu, electrophotographic props. 77—45910
CdS$_x$Se$_{1-x}$, electron traps, DLTS meas. 80—24949
CdS$_x$Se$_{1-x}$, laser beam spontaneous action *(Russian)* 77—88820
CdS$_x$Se$_{1-x}$, laser damage, self-focusing influence 78—50844
CdS$_x$Se$_{1-x}$ laser electron-beam tube, possibility of acceleration voltage lowering 79—89929
CdS$_x$Se$_{1-x}$ mixed crystals, exciton spectra 78—92131
CdS$_x$Se$_{1-x}$ photoresistors, cutoff freq. extension by addition of Cr$_2$O$_3$, recrystn. *(Russian)* 78—84248
CdS$_x$Se$_{1-x}$, photosemiconductor, optically controlled deflector based on thin-film waveguide 80—33206

cadmium compounds continued
- CdS$_x$Se$_{1-x}$, photosensitive layer, in metal-photosemiconductor-insulator multilayered struct., charge pattern form. 80−47129
- CdS$_x$Se$_{1-x}$ photosensitive films, prep., props., and use for photodetectors 80−55298
- CdS$_x$Se$_{1-x}$, scanning semiconductor laser with transverse electron-beam pumping 80−9904
- CdS$_x$Se$_{1-x}$ solid soln. film by spray pyrolysis 77−81214
- CdS$_x$Se$_{1-x}$, strongly excited by electron beam, determ. of nonequilibrium carrier lifetime 80−39603
- CdS$_x$Se$_{1-x}$, thermoelec. and photothermoelec. power meas., inhomogeneity effects 80−54728
- CdS$_x$Se$_{1-x}$ thin-film position-sensitive photoresistor prod. and props. *(Russian)* 78−43503
- CdS$_x$Se$_{1-x}$ triode cathode sputtered films, electrophysical props. *(Russian)* 79−42642
- CdS$_x$Se$_{1-x}$, triode sputtered films, photoelec. props. *(Russian)* 79−15179
- CdS$_x$Se$_{1-x}$:In film, flash evaporated, prep. and elec. props. 80−20792
- Cd$_{1+y}$(S$_x$Se$_{1-x}$) single crysts., vapour phase transport and stoichiometry control 79−28940
- CdS(Se)(Te), determ. of wurtzite, zincblende and rocksalt phases 80−100219
- CdS(Se)(Te), epitaxial, condensation from gas phase of controlled comp., and props. 80−54562
- CdS(Se)(Te), evap. onto electron bombarded NaCl substrates, epitaxial growth and characts. 79−28948
- CdS(Se)(Te), excitons detect., precision method 79−19906
- CdS(Se)(Te):Co^{2+}, IR luminesc. quenching, Co^{2+} level position, ionisation energy 80−16079
- CdS$_x$Te$_{1-x}$, emission spectra at high excitation levels *(Russian)* 79−74004
- CdS$_x$Te$_{1-x}$, low temp. photoluminesc. *(Russian)* 78−43931
- CdS$_x$Te$_{1-x}$, recryst. from CdS$_x$Te$_{1-x}$-Cr$_2$O$_3$ mixtures, photocond. props. 80−96936
- CdS$_x$Te$_{1-x}$, surface layer conductivity type inversion by ruby laser radiation *(Russian)* 77−15948
- CdS; effect of halide (NaCl, CdCl$_2$, CdBr$_2$, CdI$_2$) and polysulphide (Na$_2$S$_x$, K$_2$S$_x$) on recrystn. 78−11171
- p-CdSb, elastic moduli depend. on hydrostatic press. up to 17 kbar 79−37755
- CdSb, elastic moduli temp. depend. 77−51430
- p-CdSb, elec. props. at low temp. 77−62866
- CdSb, energy spectrum, influence of chem. bonds, LCAO calc. 80−34356
- CdSb, free energy and heat of formation 79−77768
- CdSb, Hall coeff. and resist. 79−56216
- CdSb heterojunction, formation by laser irradiation, photoelec. meas. *(Russian)* 77−76915
- CdSb, layer growth in Cd-Sb diffusion couple at high press. 80−2217
- CdSb, layer growth in Cd-Sb diffusion couple at high press., elec. meas. 80−2218
- CdSb, monocrystalline film, prep., elec. props. 79−43159
- CdSb, phase diagram, region of homogeneity, elec. cond. 79−43219
- p-CdSb, photoconductivity and absorpt. in submm region, electroluminesc. 77−32046
- p-CdSb, photomagnetic and transverse Dember effects, 90 to 300K 77−4400
- CdSb resistance thermometer, characts. of cryogenic temps. 79−21760
- CdSb, self-diffusion of Cd, radioactive tracer investig. 77−24428
- CdSb single crystals, surface layer melting and recrystallisation due to laser irradiation *(Ukrainian)* 79−46699
- CdSb, thermodynamic props. 79−77767
- CdSb:Al, p-n junction formation by laser emission, photoelectric effects *(Russian)* 80−70815
- CdSb:Al(In)(Ga)(Te), p-n junction formation by laser radiation 80−96983
- CdSb:Au, solubility, thermal anal., microhardness, microstruct., elec. characts. 77−16557
- CdSb:Fe, self absorpt. edge, impurity effect *(Russian)* 80−97316
- CdSb:Ge, anisotropy of elec., mag. props. 78−34829
- CdSb:Te, photoconductivity characts. 77−43653
- CdSb-Ag, thermoelectric, thermal defect relax., elec. cond. and thermo-EMF effects *(Russian)* 78−14749
- CdSb-ZnSb, crystallisation characts., phase diagram 80−55383
- Cd$_2$Sb$_2$, phys. props. 78−26527
- Cd$_3$Sc$_2$Ge$_3$O$_{12}$, garnet, refined cryst. struct. 78−87654
- CdSe 78−80474
- n-CdSe, ^{133}Cd and ^{77}Se Knight shifts, impurity carrier wavefunction 78−35049
- CdSe 16 μm parametric amplification with HF laser pumping 80−78910
- CdSe (11$\bar{2}$0), surface electronic struct. and chem. struct. 78−14788
- CdSe, ambipolar diffusion meas. using nonlinear transient gratings 78−80000
- CdSe, biexcitonic state existence, 1.2 MeV binding energy *(Russian)* 77−39788
- n-CdSe, bipolar photocond. and acoustoelectric current 79−19636
- CdSe, charge transport 78−84233
- CdSe, charged dislocations, flow of charge with plastic deform. 80−85010
- CdSe, chemically sprayed thin films as photoanode in photoelectrochem. cells, power charact. meas. 80−85293
- CdSe, collisions between hot excitons and hot electrons 80−7415
- CdSe, comp. and evap. kinetics on vacuum heating, effects on deposited film characts. 77−85940
- CdSe, cryst. struct. and Bijvoet ratios, X-ray diffr. meas. 77−55268
- CdSe crystal, stimulated emission from electron-hole plasma, temp. depend. 78−88331
- CdSe crystals, photocurrent and electrorefl. spectra, stoichiometry defects revealed by annealing *(Russian)* 77−52134
- CdSe, dark current relaxation 80−44613
- CdSe, deep dislocation levels, TSC and luminesc. obs. 77−8050
- CdSe, defect struct. in Se vapour 78−64043
- CdSe, desorption of O$_2$, photostimulated desorption temp. depend. 80−24737
- CdSe, diffusion of Cu, effect of laser radiation on diffusion 79−10983
- CdSe down-conversion of LiNbO$_3$ broadly tunable picosecond IR source 80−74435
- CdSe, dynamic holographic gratings based on excitons 77−3556
- CdSe, effect of halide (NaCl, CdCl$_2$, CdBr$_2$, CdI$_2$) and polysulphide (Na$_2$S$_x$, K$_2$S$_x$) on recrystn. 78−11171

cadmium compounds continued
- CdSe, effect of heat treatment in Se vapour, photocond. acoustoelec. effect and surface morphology 78−39152
- CdSe, electrical cond. near metal-insulator transition 79−73550
- CdSe electrochem. photovoltaic cells, effect of thin film electrode prep. and conc. on efficiency 80−55847
- CdSe, electroless film deposition with variable comp. and polymorphic structs. 79−95952
- CdSe, electron irrad., edge emission 80−25461
- CdSe, electron-exciton elastic scatt. cross sections, central field and exchange approxs. 77−62919
- CdSe, electron-exciton inelastic collision cross sections 79−90967
- CdSe, electrorefl. and photocurrent of ground state excitons 79−99905
- CdSe, epitaxial film, gas-phase comp. effects on elec. props. 77−85354
- CdSe, epitaxial films, carrier scattering temp. depend. *(Russian)* 78−10583
- CdSe, epitaxial growth by transport reactions in closed system 77−52232
- CdSe, epitaxial growth on ZnTe (111), vacuum evaporated 78−14631
- CdSe epitaxial layers, on GaP-CdS substrates, absorption and electroabsorption 80−40178
- CdSe evaporated films, struct. and epitaxy, TEM, RHEED, and X-ray diffr. obs. 79−77939
- CdSe evaporated films, photoconductivity and effect of deposition conditions 79−95442
- CdSe evaporated films, elec. props. 80−2498
- CdSe, exciton-phonon luminesc. 77−16319
- CdSe, excitonic mol. transitions, optical gain and induced absorpt. spectra 80−11438
- CdSe film, as-deposited and recrystallised, struct. and fund. optical absorpt. 77−1753
- CdSe film, conductivity instability when exposed to the atmosphere 77−15980
- CdSe film, current noise due to thermal field ionisation 79−91110
- CdSe film, effect of growth conditions on electrophysical properties 78−44024
- CdSe film, Hall voltage meas. 77−69434
- CdSe film, laser annealing effects on surface struct. and elec. characts. 79−73605
- CdSe film, polycrystalline analogue elec. model 77−36000
- CdSe film, polycrystalline, analogue elec. model 77−39974
- CdSe film, resistivity rel. to vapour deposition parameters 77−12033
- CdSe film, soln. growth 80−66437
- CdSe, film, specific resist., deposition conditions, depend. 77−85363
- CdSe film, stimulated recrystallisation 77−4272
- CdSe film, stimulated recrystn. influence on photocond. 77−43754
- CdSe film, struct. props., influence of O$_2$ partial press. and substrate temp. during vapour deposition 77−39751
- CdSe film, thermally stimulated and isothermal discharges of capacitor across film 78−2582
- CdSe film, vac. condensed, growth and struct., HEED obs. 80−29292
- CdSe film, vac. deposited, stabilisation by heat treatment in vac. *(French)* 79−95532
- CdSe film, vac. deposited, elec. resist. and surface changes by laser annealing 80−2491
- CdSe, film, vacuum condensation thermodynamics, starting powder comp. effects 77−81220
- CdSe film, vacuum deposited, struct., resist. and Hall mobility 77−76974
- CdSe film deposition, and reaction sequence of H$_2$SeO$_3$ reduction 80−71603
- CdSe film photoanodes for electrochem. photovoltaic cells, fabrication and evaluation 80−76641
- CdSe film polycryst., thermal diffusion of Cr, 240-400°C 80−80001
- CdSe films, effect of annealing on resistivity and charge carrier mobility 77−8209
- CdSe films, electron irrad. effect on electrophys. props., prep. conditions depend. 79−28421
- CdSe films, growth kinetics and cryst. struct. during vacuum condensation 80−2305
- CdSe films, oriented, epitaxial growth by epitaxial nucleation in submicroscopic holes method 80−59834
- CdSe films, solar energy conversion using electrodeposited films for photoelectrochemical cell 80−94093
- CdSe, free-exciton multiphonon luminesc. 78−6741
- CdSe, fundamental absorpt. edge, influence of laser radiation intensity *(Russian)* 80−71445
- CdSe, fundamental vibrs., Raman scatt. and IR refl. obs. 78−60451
- CdSe, grown from melt, SEM exam. of dislocation boundaries 80−24456
- CdSe, growth rate, sublimation rate and etching behaviour along polar axis 80−24387
- p-CdSe, Hall density and mobility, in Se vapour atm., 600-1100K 78−52014
- CdSe, heat treatment effect on carrier mobility, role of defect centres 77−72861
- CdSe, heavily doped compensated piezoelectric semiconductor, sound absorpt. coeff. calc. *(Russian)* 79−15194
- CdSe, hexagonal, anharmonicity, X-ray intensity meas. 77−43286
- CdSe, hexagonal, Coulomb interaction at E$_1$ interband transition 78−19507
- CdSe, high intensity excited, exciton reflection spectra, reflection struct. 80−20692
- CdSe, high intensity photoexcitation, hot electrons and phonons 78−26905
- CdSe, highly photo-excited, time-resolved luminesc. spectra, 1.8K 78−35197
- CdSe, hot carrier distribution, optically excited, picosec. time resolved reflectivity obs. 78−76495
- CdSe, IR quenching and photocond., photon trapping energy depend. 79−56267
- CdSe image convertor, liquid-crystal, hybrid optical processors appl. 80−33166
- CdSe, kinetics of recomb. radiation 78−31243
- CdSe, LPE growth on ZnTe, characterisation of heterojunction 77−4745
- n-CdSe, laser excited stimulated emission, optical gain spectrum 80−76050
- CdSe layer, spectrophotometer-type filters of highest possible performance, 2.5-40 μm 80−14438
- p-CdSe layers, ion implantation prep., elec. props. 79−51699
- CdSe linear photopotentiometers, output characts. 77−1453

cadmium compounds continued
CdSe, low resist., mech. for nonradiative recombination of carriers, photoluminesc. and photocurrent characts. 78—19092
CdSe, luminesc. of high density electron-hole plasma at elevated temps. 80—20696
CdSe, MIS thin film capacitance, theory 79—87156
CdSe MIS thin film solar cell 80—45688
CdSe, magnetic susceptibility, grinding-induced states 79—61040
CdSe, magnetooptic study of P line at high excitations, biexciton binding energy values 78—48220
CdSe, magnetopolaritons in wurtzite-type crystals 79—78019
CdSe, magnetoreflectance spectra of anisotropic II-VI semiconds., by mag. field modulation 77—66519
CdSe, magnetoreflectance and magnetoluminesc. of A exciton 78—39597
CdSe, meas. of partial press., by optical absorption method *(Japanese)* 78—51661
CdSe, mol. model for exciton-impurity complexes 77—80740
CdSe, monocryst. layers and bulk specimens, spectral comp. of impurity luminesc. 77—16364
CdSe, NMR, ^{113}Cd nucl. mag. shielding 78—68395
CdSe, NMR, chemical shift and linewidth determ. 79—19792
CdSe, nonlinear freq. mixing 16 μm tunable source 78—9414
CdSe, nonstoichiometry, Cd and Se press. meas., up to 1400K 78—87664
CdSe, O_2 desorption by laser irradiation *(Russian)* 77—55462
CdSe, optical detection near absorption band edge 77—749
CdSe, optical gain spectra, exciton collision processes and electron-hole plasma 79—28814
CdSe, optical parametric devices, freq. tuning possibility by uniaxial press. 78—59084
CdSe, optical self-diffraction at induced phase lattice 77—3638
CdSe, optical spectroscopy, absorpt. coeff., lattice vibr. modes, band gap, acoustic approach 77—69822
CdSe, optically pumped, dynamic polarisation of nucl. moments 78—68411
CdSe, optoelectronic devices appl. *(German)* 77—7745
CdSe, oriented single-crystal films, edge luminescence at high excitation levels 77—1720
CdSe, oxidation by atmos. O_2 and SeO_2 vapour 77—52520
CdSe, parametric oscillator, grating-coupled, tunable 15.5 to 16.5 μm 77—58376
CdSe, partial press. meas. by optical absorption 80—15234
n-CdSe, partially illuminated single crystal, current-voltage characteristic and potential distrib. 79—65519
CdSe, phase diagram of electron-hole liqs. in polar semiconds. 77—89706
CdSe, phase gratings in semiconductors with one- and two-photon excitation 77—8546
CdSe photoanode improved efficiency by photoelectrochem. etching 80—104512
CdSe photoanodes, effect of Se substitution, photoelectron spectroscopy obs. 80—2463
CdSe photoanodes, S substitution during operation and mech. of surface protection 80—107906
CdSe, photoanodes in sulphide-polysulphide electrolytes, instability 78—80755
CdSe, photocond. film, plasma reson., IR refl. obs. 80—11037
CdSe, photoconductivity, recomb. characts. 77—8118
CdSe, photodetector, limiting sensitivity 79—63309
CdSe photoelectrode, immersed in polysulphide soln., S/Se substitution, XPS obs. 79—19656
CdSe photoelectrode, polycrystalline, for solar energy conversion 78—19147
CdSe, photoionization cross-section temp. depend., deep local levels 79—65408
CdSe, photoreflection exciton spectra *(Russian)* 77—20874
CdSe photosensitive film production from chelated metallo-organic compounds *(Russian)* 80—49813
CdSe, photosensitivity of elastic properties 78—92049
CdSe, photovoltage transients, expt. and model 77—89802
CdSe, pico-second time depend. of luminesc. line due to exciton-exciton collision 78—39587
CdSe, picosecond time-resolved luminesc. spectra 79—93890
CdSe, piezoelec. semicond., sound absorption 80—60051
CdSe, plastically deformed, luminescence line 0.96 eV 78—10950
CdSe platelets, determ. of localised level energies by Fermi level statistics 77—31980
CdSe, polar semiconductor, electron-hole liquid, electron-phonon interactions 80—6739
CdSe, polarisation correl. of resonant Raman scatt. or hot luminesc. 80—25384
CdSe, polaron IR cyclotron reson. 80—25347
CdSe, polycryst. film, photocapacitance, inductive effect and US oscills. *(Russian)* 77—8142
CdSe, positron annihilation study 80—60713
CdSe, ps. spectra, high density exciton system 78—19553
CdSe ps. spectra, high density exciton system 78—19554
CdSe, psec time resolved spectroscopy, electron-hole plasma 79—47500
CdSe, pulsed Hall photoeffect, transient processes in scattering of carriers 80—15546
CdSe, radiative recomb. process, P-band, 2-psec time resolution 79—24346
CdSe, recombination mechanism at dislocations, photoluminescence 80—103993
CdSe, reson. absorpt. of coherent IR radn. by acceptors, photocurrent and emission spectra 79—73974
CdSe, resonant Brillouin scatt. via free and bound excitons 79—24330
CdSe, resonant Faraday effect, optical orientation of excitonic polaritons 77—69821
CdSe, resonant Raman and Brillouin spectroscopy, review, book contrib. 80—49624
CdSe, saturation of optical absorpt. and photocond. 79—18487
CdSe, Se-annealed and Cu-diffused, photocond. props. 79—99580
n-CdSe semicond. liq. junction solar cells, photocurrent spectra, carrier recombination 78—76142
CdSe, signal and idler beam mixing device for optical parametric oscillator 79—14029
CdSe, single cryst., band parameters from optical exciton spectra 79—47021
CdSe, single cryst. elec. props., annealing in Se atm., expt. *(Japanese)* 77—1423

cadmium compounds continued
CdSe, single crystal, low-frequency current noise, effect of temperature quenching of photoconductivity 78—34874
CdSe single crystals, effects of impurities on photocond. *(Japanese)* 77—28221
CdSe single crysts., exciton luminesc. and polarisation spectra under one- and two-photon excitation 79—65391
CdSe, single crysts., luminesc. of electron-hole plasma 80—60675
CdSe, solubility of Cu and Ga 78—22856
CdSe, temp. depend. phase-matched nonlinear optical devices 80—99794
CdSe thermo-optic coefficient, dispersion 80—71396
CdSe, thin film, total current spectrosc. investig. 80—7454
CdSe thin film transistor and MISM struct., effect of annealing on electron mobility and conc. 79—78198
CdSe thin film transistor on Cr substrate, cryst. struct., substrate defect effects 80—70563
CdSe, thin films, exciton piezotransmission 79—24380
CdSe thin-film solar cells 80—93970
CdSe two-photon absorption, laser calorimetric obs. 80—33076
CdSe, uncoated and liq. layer coated, vaporisation mechanism, surface morphology 77—35683
CdSe, undoped and Cr doped, far IR transmission and reflectance spectra 80—71429
CdSe, vacuum deposited film, orientation axis tilt rel. to vapour angle of incidence 80—88456
CdSe, wave propag. 79—28042
CdSe, wavelength dependence of pressure coefficients of birefringence 77—20820
CdSe whiskers, growth in H_2 80—15425
CdSe, with dislocations, optical props. 79—83001
n-CdSe, with single deep electron trap, negative photocond. 77—15905
CdSe, X-ray diffuse scattering 80—14964
CdSe, X-ray topography 77—89441
CdSe:Ag, In, cryst., photocurrent and electroreflection, 77 to 300K *(Russian)* 78—23136
CdSe:Ar(N)(P), implanted, electroreflection obs. 80—40089
CdSe:Au impurity light absorpt. for current control in negative resistance region 80—11052
CdSe:Cd, Cu, photo-induced changes in absorpt. spectra 78—80382
CdSe:Cl(In), photoluminesc. props. near fund. absorpt. edge, impurity conc. effects 79—52003
CdSe:Co, impurity luminescence no phonon line depend. on temp., Debye temp. 80—66273
CdSe:Cu, doping profile rel. to photoelec. props. in alloyed surface layers *(Russian)* 77—85268
CdSe:Cu, impurity photocurrent, kinetics and oscills. 80—65624
CdSe:Cu,Cl film, induced impurity photocond., 0.6 to 1.2 eV 79—24012
CdSe:Cu surface layer of CdSe, microstruct., photoelec. props. 78—43221
CdSe:Fe, exciton electroreflectance spectra, impurity effects 77—16335
CdSe:In, epitaxial layers, synthesis and elec. props. 77—47909
CdSe:In, epitaxial layer, effect of activator distribution on conductivity 78—43047
CdSe:Li, pure and doped, reson. Raman and Brillouin scatt., elastic exciton-defect scatt. 80—80788
CdSe:P, effect of P on edge luminesc. 78—64399
CdSe:P(Zn), single crystals, luminesc. 79—87493
CdSe:Ti, optical and elec. investig. of shallow donor levels, reson. states 77—63437
CdSe:V (d^3), absorption and luminesc. spectra 78—15203
CdSe:Zn(Ga), epitaxial film, impurity distrib., current transfer features *(Russian)* 77—47908
CdSe-Al, Schottky barrier diode, I-V and C-V characts. 78—10555
CdSe-Al function formation, coupled interface plasmons, low energy electron energy loss spectra 77—24621
CdSe-As_2S_3($AsSbS_3$) heterostructure, energy bands and interface props., photoelectron spectroscopy 78—2551
CdSe-Au contacts, electronic states, vacuum UV photoelectron spectra 80—70827
CdSe-based photoelectrochem. cells, characts. 77—25287
CdSe-electrolyte boundaries, photo e.m.f. meas., semicond. energy bands 77—1481
CdSe-Ge (111) heterojunctions, epitaxial, azimuthal rotation 78—84085
CdSe-glass layered system, characts. of phase-velocity dispersion and struct. of surface waves 80—59775
CdSe-$LiNbO_3$, semicond.-piezoelec. layer struct., acoustic-wave-induced increase in cond. 77—59307
CdSe-$LiNbO_3$ structure, acoustoelectronic interaction between SAW and transverse drift current 77—69424
CdSe-$LiNbO_3$ structure, electroacoustic effects and signal convolution 80—10098
CdSe-metal interface, chemical reactions and local charge redistrib. 79—19661
CdSe-metal Schottky barrier form., transition with chemical reactivity 78—30986
CdSe-Mo, Schottky barrier, characts. study 79—51673
CdSe-O_2, photoactivated O desorption 80—100391
CdSe-Sb_2Se_3 heterojunction, photoelec. props. 80—70816
CdSe-Si n-n heterojunction, photovoltage sign reversal, energy band profile *(Korean)* 80—29469
CdSe-Si n-p heterojunctions, vacuum deposition, photovoltaic effects *(Korean)* 77—28243
CdSe-SiO_2 layered system, characts. of phase-velocity dispersion and struct. of surface waves 80—59775
CdSe-SiO_2 thin film transistors, fabrication and electronic characts. 79—33351
CdSe-SiO_2 thin film transistors, slow states, trapping state densities and cross sections 80—15613
CdSe-ZnO thin film n-n heterojunctions, prep. elec. and optical props. *(Korean)* 77—28244
CdSe-ZnTe, and CdSe-CdTe n-p heterojunction, photovoltaic props. 77—55600
CdSe-ZnTe single cryst. film heterojunctions, prep. and props. 79—19652
Cd_2Se_3, elec. resist., thermoelectromotive force, temp. depend., 300 to 1400K *(Russian)* 78—84243
Cd_xSe_{1-x}, streamer laser 77—79831
CdSe(Te) and solid solns., optimal synthesis conditions for single cryst. growth 80—100776
CdSe(Te), laser calorimetric meas. of two-photon absorpt. coeffs. at 1.06 μm 79—44934
CdSe(Te)-electrolyte photovoltaic cells, solar cell appls. 77—35990

cadmium compounds continued
- $CdSe_{0.65}Te_{0.35}$, polysulphide photoelectrochem. solar cell 80—72073
- $CdSe_xTe_{1-x}$ crystal, acoustoelec. oscillations affected by surface treatment *(Russian)* 78—10517
- $CdSe_xTe_{1-x}$ film, polycrystalline, deposition and physical props. 77—4741
- $CdSe_xTe_{1-x}$, solid solns., epitaxial layer prod. 78—23619
- $CdSe_xTe_{1-x}$, triode sputtered films, photoelec. props, *(Russian)* 79—15179
- $CdSe_yTe_{1-y}$ triode cathode sputtered films, electrophysical props. *(Russian)* 79—42642
- $CdSeTl_x$-$As_2Se_3Tl_x$ thin layer system, capacitance and I-V characts., charge transport mechanism 77—76985
- $CdSiAs_2$ chalcopyrite photovoltaic material 79—74526
- $CdSiAs_2$ diode, photoelec. props., potential photodetector and solar cell appl. 77—43655
- $CdSiAs_2$, electron irrad., defects, elec. and optical props. 79—19282
- p-$CdSiAs_2$, electron irrad. elec. props. annealing, lattice defects 80—100465
- $CdSiAs_2$, polarisation of photoluminesc. 77—16389
- $CdSiP_2$, birefringence meas. 78—56455
- $CdSiP_2$, birefringence, effects on hydrostatic pressure and temp. 80—45033
- $CdSiP_2$, bond strengths and bond lengths, thermal expansion coeff. meas. 78—87651
- $CdSiP_2$, electronic struct., X-ray spectroscopic investigation 80—108300
- $CdSiP_2$, one- and two-phonon Raman scatt. 79—78681
- $CdSiP_2$, optical activity near isotropic point, absorpt. spectra 79—69804
- $CdSiP_2$, PAC examination of deuteron irrad. damage, annealing effects 78—47446
- $CdSiP_2$, polarised Raman spectra 77—24853
- $CdSiP_2$, pseudodirect bandgap semiconductor, natural birefringence 79—65834
- $CdSiP_2$, pseudodirect chalcopyrite semicond., electronic band struct. 80—20079
- $CdSiP_2$, reflectance spectra at 300K 80—25407
- $CdSiP_2$, thermoreflectance spectra 77—81122
- $CdSiP_2$:Fe, EPR and optical absorpt. of Fe^+, Fe^{2+}, Fe^{3+} and Fe^{4+} on tetragonal sites 77—8397
- $CdSiP_2$:Na(Bi), single crystal, photocond. under laser excitation 80—44661
- $Cd_{16}Si_4S_{24}$, SHG obs. 78—46719
- $CdSnAs_2$, amorphous, SRO 77—84653
- $CdSnAs_2$, electron induced defects, p- to n-type cond. inversion, Hall meas. 77—24557
- p-$CdSnAs_2$, Hall effect, thermo EMF, thermomagnetic effects 80—107822
- p-$CdSnAs_2$, heavily doped, elec. transport props. under elastic deformation 80—96915
- $CdSnAs_2$, hydrostatic press. effect on resist. and Hall coeff., band struct. 77—47808
- n-$CdSnAs_2$, optical absorption rel. to energy spectra *(Russian)* 78—75994
- $CdSnAs_2$, solubility in Sn melt, temp. depend., enthalpy of melting 80—59658
- $CdSnAs_2$-Au(Al), surface barrier junction, elec. props., temp. depend. 80—65686
- $CdSnAs_2$-InP, n-p heterojunction, elec. props., electroluminesc., band struct. 80—75632
- $CdSnAs_2$-$ZnSnAs_2$, and $CdSnAs_2$-$CdSnP_2$, material distrib., possibility of heterostructure *(Russian)* 78—30979
- $CdSnAs_2(P_2)$ single crysts., refl. spectra, band struct., dielec. consts. 77—44022
- $CdSnO_3$ and Cd_2SnO_4, crystal growth by flux or high press. method, elec. and struct. props. 77—81206
- $CdSnO_3$, electric field gradient temp. depend. 78—39454
- $CdSnO_3$, single crysts., elec. props. 80—6978
- $CdSn_xO_y$, DC reactively sputtered film, elec. and optical props. 79—87022
- $CdSn_xO_y$ films, transparent conducting, deposited by RF sputtering from CdO-SnO_2 target 80—76179
- Cd_2SnO_4 and Cd_2SnO_4:CdO, thin film electrodes in H_2SO_4 electrolytes, reduction, AES and SEM 80—65674
- Cd_2SnO_4 anode for H_2O photoelectrolysis 80—108716
- Cd_2SnO_4, $CdSnO_3$ electrodes, spray coatings, elec. sheet resist. and optical transparency 78—27401
- Cd_2SnO_4 film, optical transmission and reflection, evaluation for solar heat collectors 77—52191
- Cd_2SnO_4 film, RF sputtered from powder targets, props. 77—43759
- Cd_2SnO_4, film, spinel struct., X-ray diffr. study 78—75644
- Cd_2SnO_4 film, sputter deposition and characterisation 79—43146
- Cd_2SnO_4 heat mirror on plastic sheet for radiation insulation of visible windows 80—95985
- Cd_2SnO_4 selective coatings, optical absorpt. edge 78—83046
- Cd_2SnO_4, single crysts., elec. props. 80—6978
- Cd_2SnO_4, transparent conducting coatings, book contrib. 78—10587
- $CdSnP_2$ crystal growth, DTA obs. of Cd-Sn-$CdSnP_2$ phase diagram 80—24394
- n-$CdSnP_2$, Hall coeff. and elec. cond. meas., 24-900K 80—54721
- n- $CdSnP_2$, Hall mobility of electrons meas., 120-300K 77—4373
- $CdSnP_2$, Hall mobility of holes 78—52015
- $CdSnP_2$, luminescent props. *(Russian)* 78—35201
- $CdSnP_2$, optical props., band struct. calcs., real space atomic potential parameters 79—95325
- p-$CdSnP_2$, photocond. meas., polarisation depend. 78—39157
- $CdSnP_2$, single cryst. growth, by means of temp. gradient 79—56927
- $CdSnP_2$:Cu, deep centres, emission transitions, polarisation *(Russian)* 78—84650
- $CdSnP_2$-$CdSnAs_2$, and $CdSnP_2$-$CdGeP_2$, solid solution form. and elec. characterisation 78—43125
- $CdSnP_2$-InP, n-n heterojunctions, growth, elec. characts. 77—11992
- $Cd_{1-x}Sr_xS$, solid soln., phase equilib. diagrams 80—108412
- $CdTa_2O_6$, force fields rel. to cryst. struct. *(French)* 80—107104
- CdTe, 10.6 μm absorption meas. using thermal emission 77—1649
- CdTe, aB glide dislocations, dissociated into two Shockley partials, stacking fault energy 78—43024
- CdTe AC Faraday rotation devices for far IR laser intracavity polarisation modulation 80—58613
- CdTe, absorbing precipitates, catastrophic laser damage threshold estimate 78—25913
- CdTe acousto-optic and electro-optic waveguide modulators 77—42624

cadmium compounds continued
- CdTe, amorphous, photocond., effective density of localised states 77—28210
- CdTe, amphoteric behaviour and solubility of Sn 79—33008
- CdTe and $Cd_xHg_{1-x}Te$, crystal growth by zone passing techniques 77—40360
- CdTe and CdTe:Cl, grown by travelling heater method, EPR defect charact. 77—40125
- CdTe and CdTe:Cl, semi-insulating, electroabsorpt. by impurities and defects, dichroism 77—40270
- CdTe, anodic oxidation as thin-layer removal technique for impurity distrib. profile determ. 79—34169
- p-CdTe, appl. as anode in stable photoelectrochemical cells for splitting of water 77—44484
- CdTe, applications review 77—72894
- CdTe, average number of phonons emitted in optical transition 77—8614
- CdTe, backward degenerate four-wave mixing obs. 80—53361
- p-CdTe, barrier heights of metals on etched surface 80—80378
- p-CdTe, bipolar photocond. and acoustoelectric current 79—19636
- CdTe, bipolar photoconductivity exam. 78—6410
- CdTe, bulk and surface states anal. using synchrotron radiation 77—66574
- CdTe cathodic deposition from aqueous electrolytes 78—64484
- n-CdTe, cathodoluminescence microscopy obs. of dislocations, compared with etch pit pattern 79—69105
- CdTe, charge carrier transport prop. meas. by time of flight technique 77—39850
- CdTe, charged dislocations, flow of charge with plastic deform. 80—85010
- CdTe, chem. laser window material 77—46769
- CdTe, Cl compensated detectors, polarisation suppression methods 77—61661
- CdTe, clean and oxidised surfaces, O_2 sticking coeff., ionicity effects, XPS expts. 77—85887
- CdTe, clean and oxidised surfaces, surface states, low-energy EELS study 80—11522
- CdTe, compensated single cryst., impurity centre parameters, elec. cond. and galvanomag. props. *(Russian)* 77—47811
- CdTe, creep activation energy and velocity *(Russian)* 78—56716
- CdTe, cryogenic refractive indices and temp. coeffs. meas. 80—7319
- CdTe, cryst. growth from vapour 77—24936
- CdTe crystal, refr. index, 10.6 μm ellipsometric meas. 78—24847
- CdTe crystal growth for γ-ray detectors 78—41889
- CdTe crystal in square waveguide, single sideband generation at 10.6 μm 79—55179
- CdTe crystal Pockels modulator, PCM of CO_2 TEA laser pulse 80—102742
- CdTe, crystal size depend. of photoplastic effect 80—92592
- CdTe, crystal structure stability, P-T diagrams 78—51886
- CdTe crystals, dislocation free growth by zone sublimation in Spacelab 79—78872
- CdTe crystals, exciton luminescence spectra rel. to shallow impurity conc. 80—97335
- CdTe, crysts., mech. behaviour, yield stress function of temp., stress relaxation 79—60427
- n-CdTe, deep trapping levels in high resistivity films 77—72930
- CdTe, defect struct., review 77—39581
- CdTe detector for radionuclide tracer biotelemetry 77—86587
- CdTe, detector grade semi-insulating crystals, determ. of product of mobility and carrier lifetime 80—39601
- n-CdTe, detector material, single crysts., activation energy anal. of defect levels 78—6321
- CdTe detectors, depletion layer extension 78—41891
- CdTe detectors, gamma and electron irradiation effects 78—41893
- CdTe detectors, photoscanning, determ. of crystal quality and contact behaviour 77—61664
- CdTe detectors, use in spectrometers, physical and electronic factors *(Czech)* 80—23259
- CdTe, diamond-like semicond., Mossbauer isomer shift meas. 77—16233
- CdTe, dielec. const. and loss tangent, temp. depend., 15.95 GHz 77—69763
- CdTe, diffusion and solubility of Ge, 630-800°C, prep. conditions depend. 80—103519
- CdTe, diffusion of Cu at 250 to 500°C, interstitial process 77—11737
- CdTe, diffusion of Sn and intrinsic defects role 79—33116
- CdTe diode, generation-recomb. and ionisation processes, temp. depend. *(Russian)* 77—39942
- p-CdTe diodes, X-ray escape peak variations 77—71723
- CdTe, donor impurity compensation models, impurity-vacancy complexes 77—39601
- CdTe, dynamic holograms, diffr. characts. using laser beam 79—46048
- p-CdTe, ESR optical detect., Overhauser shift, g-factor 78—80252
- CdTe, elec. and photoelec. props. due to double injection, quenching spectra 80—70765
- CdTe, electro-optic IR phase modulator, phase and freq. characts. 77—54805
- CdTe electrode, redox reaction due to complex $M(CN)_6^{3-/4-}$ *(French)* 80—89482
- CdTe, electron induced defect creation rates 78—41892
- CdTe, electron mean free path, 350-1450 eV 80—103707
- CdTe, electron-beam-controlled transmission of 10 μm radiation 79—81466
- CdTe, electron-hole liquid formation in pure and doped crystals, luminesc. study *(Russian)* 80—55184
- CdTe, empty surface states and surface order effects on sorption 77—85281
- CdTe, energy bands and optical props. calc., tight-binding model with spin-orbit interaction 80—65448
- CdTe epitaxial films, on CdS substrate, closed-tube vapour growth 80—55302
- CdTe epitaxial films, surface morphology, layer and spiral growth 80—10823
- CdTe epitaxial layers on GaAs, cryst. struct. and phys. props. 79—33202
- CdTe, equation of state 79—82310
- CdTe, excitation spectra, resonant Raman scatt. versus hot electron effects 79—38645
- CdTe, exciton magnetoreflectance spectra, multicomponent polaritons, Zeeman splitting 80—88974
- CdTe, far IR absorpt., two-phonon density of states 78—15155
- CdTe, film, anomalous-photovoltage, current-voltage characts. 79—69549
- CdTe film, between Ag electrodes negative differential resist. 78—19161

cadmium compounds continued
CdTe film, cathode sputtered, chemical composition and struct. 78—84100
CdTe film, excitation by H of anomalously high voltage *(Russian)* 78—60235
CdTe film, exciton spectra, press. and temp. depend. 80—80886
CdTe film, growth by photostimulated VPE, electrophys. props. 77—40390
CdTe film, low-resist., prep. by multi-source evaporation method, and characterisation 80—25582
CdTe film, photogenerated carrier transport props. 80—88590
CdTe film, photopolarisation 80—25286
CdTe, film, theoretical models of impurity levels 79—82557
CdTe film formation on glass substrates, influence of sublayers of recrystn. stimulators 77—43455
CdTe, film grown by hot wall epitaxy, elec. props. 79—82696
CdTe, film grown in quasi-closed volume, struct. *(Russian)* 78—75952
CdTe film. vac. condensed, growth and struct., HEED obs. 80—29292
CdTe films, oriented, epitaxial growth by epitaxial nucleation in submicroscopic holes method 80—59834
CdTe films, structural imperfections depend. on crystn. temp. 79—90661
CdTe films, switching obs. in sandwich structures 77—43752
n-CdTe films, uniform trap distrib., transient photocond. effects 79—28423
CdTe, films grown by hot wall epitaxy, elec. props. 79—28420
CdTe foils preparation, transparent, for TEM, ion sputtering technique appl. *(Czech)* 80—16619
CdTe, gas, identification by high-temp. mass spectrometry 80—45593
CdTe, grown by chem. transport, morphology, struct. and microhardness *(Russian)* 78—22729
CdTe, growth by travelling heater method, high resistivity charact., γ-ray detector appl. 78—84707
CdTe, growth by vapour phase chem. transport in I_2 77—40342
CdTe, growth from Cd rich soln. by solvent evaporation 77—40355
CdTe, growth from In solvents, self-compensation 77—28144
CdTe, growth from soln. in fused $CdCl_2$ 77—44138
CdTe, growth from Te soln. by slow cooling or travelling heater method, Te inclusions 77—40352
CdTe, growth from Te-rich soln. by travelling heater method, cond. and luminesc. 77—40351
CdTe, growth from Te-rich soln. in vertical Bridgman furnace 77—40354
CdTe, growth of epitaxial layers, activation by UV and IR radiation 80—71598
CdTe, growth on Te substrate by solid-state reaction 79—95287
CdTe γ-ray detector, resolution for 122 keV ^{57}Co and 59 keV ^{241}Am 77—75027
CdTe, H^+ ion implanted, optical waveguiding and electrooptic modulation 77—75679
n-CdTe, Hall effect and resist., close and distant donor-acceptor pairing effects 77—39881
CdTe, hexagonal film, effective birefringence 80—16004
CdTe, high purity crystal, growth from soln., γ-ray detector appls. 77—14310
CdTe, high-resistivity, carrier transport and trapping processes, growth parameter effects 77—39871
CdTe, high-resistivity, irradiation effects on carrier transport and trapping process 78—2164
CdTe homojunctions from VPE growth, solar cell appl. *(French)* 77—43453
CdTe, IR quenching of photocurrent and switch in type of photoconductivity 77—47862
CdTe, IR transmitting semicond., dn/dT, wavelength depend. 77—77163
CdTe, IR transparent materials, forward and backward scatt. data 78—59099
CdTe, in metal-semicond.-metal struct., as spectrometric detector of nucl. radiation 77—54460
CdTe, influence of heat treatment on carrier lifetime, photoelectromagnetic effect meas. 77—55576
CdTe intracavity electrooptic modulator, for high pulse repetition freq. CO_2 oscillator 77—88801
CdTe, irrad.-induced damage on γ-detector performance 80—23264
CdTe KO-6 optical ceramic component antireflection coatings 79—27345
CdTe, LPE in CdTe-$CdCl_2$ system 78—35323
CdTe, laser annealing, surface layer temp. distrib. 79—74029
CdTe, laser annealing of ion bombardment damage 80—25502
CdTe, laser window material, absorbing Te inclusions, damage threshold 77—46749
CdTe, laser window material, vap. deposition, mech. props. 77—46776
CdTe, laser window material, vap. deposition 78—27391
CdTe, lattice dynamics and phonon parameters bond bending force model 80—59595
CdTe, lattice mode, dispersive refl. meas. using modular interferometer 78—89568
CdTe layer deposition by ionised cluster beam technique 77—48351
n-CdTe layers, growth and characterisation, heterojunctions and Schottky barriers fabrication *(German)* 80—89151
CdTe layers, on CdS substrate, cryst. perfection and defects, X-ray diffr. obs. 79—56081
CdTe, Li diffusion, 300°C 77—43383
CdTe linear electro-optic translation of IR laser wavelengths 80—78878
CdTe, low temp. luminesc. *(Russian)* 79—91497
CdTe, low temp. themal cond., growth parameter influence 80—92725
CdTe, luminescence and reflect. investig. of excitons, stress and Zeeman splitting 77—40281
CdTe, MIS contacted small portable detector head for X-ray spectrometry 77—61662
CdTe, MSM detectors, charge collection 77—61660
CdTe, mag. susceptibility at 20-1400°C 77—12085
CdTe matrix γ-camera, biomedical appl. 80—76827
CdTe, meas. of partial press., by optical absorption method *(Japanese)* 78—51661
CdTe, melt-growth review, including liquid encapsulation method, defect charact. 77—40350
CdTe metal-semicond.-metal detectors, degradation characts. due to e and γ irradiation 79—45543
CdTe metal-semiconductor-metal γ-ray detector characts. 80—57451
CdTe, microwave cond. and dielec. permittivity using reson. cavity method 79—51620
CdTe, minority carrier diffusion length from photocurrent meas. in semicond.-electrolyte boundary 80—65584
CdTe, n- and p-type, elec. and galvanomag. props. 79—7830

cadmium compounds continued
CdTe, NMR, ^{113}Cd nucl. mag. shielding 78—68395
CdTe, NMR, chemical shift and linewidth determ. 79—19792
CdTe, NMR, dipole-dipole coupling between ^{111}Cd, ^{113}Cd and ^{125}Te 79—91305
CdTe, near-edge absorpt., effect of light illumination and elec. field 79—38547
CdTe, nearest-neighbour hopping cond., effect of electron irrad. induced compensating centres 77—43599
CdTe, negative and positive photoplastic effect 79—51192
CdTe negative dielectric relax. of hot electrons 78—52001
p-CdTe, nondoped, heat treatment in vacuum, dissoc. obs. effects on struct. and props. *(Japanese)* 80—60662
CdTe, nonlinear magnetoelec. susceptibility, three-dimens. model 80—39845
CdTe, nonlinear optical effects in rotationally twinned crysts., phase matching 77—42570
CdTe, obliquely deposited layers with reduced resist., photovoltaic props. and Cd doping effects 77—43755
p-CdTe ohmic contact with Pd and Pt, I-V characts., temp. depend. of cond., activation energy 78—39211
CdTe, on mica, substrate defects effect on epitaxy 78—26794
CdTe, optical absorpt. coefficient, photovoltaic determ. 77—39890
CdTe optical applications, review 77—42580
CdTe, optical detection of ESR 79—65770
CdTe, optical waveguide, fabrication by LPE using boat-slide technique 77—63570
CdTe, oscillatory magnetoabsorpt. spectra 80—40096
CdTe p-n homojunction, elec. and photovoltaic props. rel. to solar energy conversion 79—51668
CdTe p-n junction, short-circuited, estimation of surface recomb. rates, electron-probe meas. 77—43713
CdTe, partial press. meas. by optical absorption 80—15234
CdTe, phase diagram of electron-hole liqs. in polar semiconds. 77—89706
CdTe, phonon conductivity, 2 to 300K, scatt. mechanisms 79—4436
p-CdTe, photocond., photoluminesc., spectral studies 80—88593
CdTe, photoconductivity, extrinsic, contrib. by hopping through excited states of donors 78—6411
CdTe, photoelectron spectra at Schottky barrier *(Korean)* 79—11220
n-CdTe, photolum., plastic deform. effects 79—15509
CdTe, photoplastic effect, influence of plastic deform., heat treatment and doping 79—82277
CdTe, photoreflection exciton spectra *(Russian)* 77—20874
CdTe, physical props., review 77—39833
CdTe, picosecond absorption spectroscopy 79—47482
CdTe, plastic deformation activation anal. below room temp. 78—84935
CdTe, polycryst., laser window material, IR thermooptic coeff. meas. 77—36208
CdTe, positron annihilation study 80—60713
CdTe, properties and appls., conf., Strasbourg, France (Jun-Jul 1976) 77—39832
CdTe, purification, efficiency for extraction of Cu and Ag impurities, impurity scatt. meas. 77—8749
CdTe reactive close-spaced vapour transport, simplified theory 80—15396
CdTe, recombination radiation due to high-density excitons 80—93392
CdTe, relations pressure-volume under high pressure 80—39219
CdTe, reson. Brillouin scatt., book contrib. 79—42983
CdTe, reson. Raman scatt. by excitonic polaritons 80—11396
CdTe, Schottky diode, AC small signal capacitance 79—7899
CdTe Schottky solar cell, barrier height, open circuit voltage 77—43721
n-CdTe semicond. liq. junction solar cells, photocurrent spectra, carrier recombination 78—76142
n-CdTe, semiconductor electrode, electrochem. behaviour in nonaqueous media *(French)* 80—66808
CdTe, semiinsulating, anomalous photocond. and dark cond. 77—62959
CdTe, shallow donors, excited state transitions 78—6710
CdTe, shallow impurity spectral linewidths, 4-10K 77—63443
CdTe single cryst., linear electro-optical props., temp. depend. 80—71376
CdTe, single cryst. IR laser window, low absorption at 10.6 μm 78—79081
CdTe, single cryst. sublimation growth, X-ray topographic characterisation 80—29866
n-CdTe, single crystal, photoreflectance, temp. depend. of exciton spectra *(Russian)* 78—23488
CdTe single crystal IR window for CO_2 laser 77—75566
CdTe, single crystals, plastic deformation and dislocation struct. 79—8321
p-CdTe single crysts., photoreversal of Hall effect 77—43631
CdTe single-crystal film, switching and memory effects 78—76174
CdTe, solubility in Hg 78—35359
CdTe, spatial dispersion rel. to exciton reflection spectra *(Russian)* 80—40126
CdTe spectrometers for hard X-ray astronomy 77—13206
CdTe, sputter-deposited, electrical and optical props. 79—47181
CdTe, sputtered film, electrode effects in AC characts. from equivalence impedance meas. of metal-CdTe-Al struct. 79—82686
CdTe sputtered films, deposition conditions effects on struct. and props. 77—43452
CdTe sputtered films, struct., photocond., and trap distrib. 80—29489
CdTe, suitability for solar photocells, photovoltaic conversion props., band gap 77—43652
CdTe surface, nonpolar, electronic struct., tight-binding calc. 77—20383
CdTe surface, sputter cleaning and dry oxidation, XPS and LEED study 80—108618
p-CdTe, surface barrier struct., internal photoelec. emission 77—15958
CdTe, surface layers formed by etchants, XPS meas. 78—44240
CdTe, surface photovoltage 78—2540
p-CdTe, surface photovoltage spectroscopy in IR and visible range 80—39632
CdTe surfaces, SIMS, Rutherford scatt. and ellipsometry 79—56046
CdTe, temp. depend. Sellmeier coeffs. SHG coherence length 77—69789
CdTe, temp.-depend. of root-mean-square dynamic displacements, characteristic temp., X-ray study 78—83895
CdTe, temperature variation in bulk moduli in solids 79—73237
CdTe, thermal cond. and X-ray topography investig. of cryst. defects 77—39706
CdTe, thermostimulated capacitor discharge, trapping levels obs. *(Russian)* 78—10842
CdTe thick films, prep. by sintering and elec. props. 80—29451

cadmium compounds continued
CdTe, thin film, stopping power for protons and alpha particles, proton energy straggle values 77—89489
CdTe thin film on ferroelectric TGS, influence of polarisation reversal on elec. cond. 80—65720
CdTe thin film polycrystalline solar cells prepared by electrodeposition 80—93948
CdTe thin films, oriented, VPE growth, infrared transmission, photovoltaic cells 80—59825
CdTe, time-resolved spectra, carrier relax. time, phonon lifetime 80—11433
CdTe, trace anal. by heavy ion induced X-ray emission and SIMS 80—55755
CdTe, transmission spectrum under uniaxial compression 80—29714
CdTe, tunable high efficiency microwave freq. shifting of IR laser 78—71126
CdTe, two-photon absorption coefficient, 3-band model 79—78679
CdTe two-photon absorption, laser calorimetric obs. 80—33076
CdTe, undoped, high-resist.- characterisation, impurity level investig. 77—39801
CdTe, undoped and donor-compensated, cathodoluminesc. of 1.4 eV bands 77—40291
CdTe, undoped and halogen-compensated, defect conc. calc. 77—39602
CdTe, use in X-ray detectors 78—86745
CdTe, vacuum deposited film, orientation axis tilt rel. to vapour angle of incidence 80—88456
CdTe, vapour-phase-grown, cathodoluminesc. study 80—76086
CdTe, window material with absorbing inclusions, damage thresholds 77—38971
CdTe, Yb^{3+} implantation, nonstoichiometry effect 77—15440
CdTe:Ag, with microscopic p-n junction, photopolarisation in anomalous photovoltage 79—11175
CdTe:Ag film, photoelectret effect *(Russian)* 79—28676
CdTe:As^{2+}, photovol. props. of p-n junction prod. by ion implantation 78—43038
CdTe:As(P), ion implanted, elec. props. 80—65021
CdTe:Be, impurity modes and IR absorption 78—76506
CdTe:Cl, anomalous props., molecular centre with charge-state dependent config. 77—89728
CdTe:Cl, capacitance meas. and trapping, mol. centre model *(French)* 77—39872
CdTe:Cl, cryst., high resist., SCL currents, DC meas. 77—66170
p-CdTe:Cl, deep level characterisation, gamma-ray detector parameters 77—39802
CdTe:Cl, description of anomalous centres by non-purely electronic model 78—30886
CdTe:Cl, donor levels, anomalous press. effects, Hall const. meas. 77—51693
CdTe:Cl, electron irrad., defects 80—25460
CdTe:Cl, gamma-ray detector growth, travelling heater method improvement 77—40353
CdTe:Cl, grown by travelling heater method, carrier homogeneity investig. 77—39848
CdTe:Cl, heavily doped, elec. and photoluminesc. investig. of defect interactions 77—39603
p-CdTe:Cl, influence of gamma-irradiation on elec. props. 77—62951
CdTe:Cl, influence of lattice defects on electrical behaviour 78—2497
CdTe:Cl, interaction of impurities and lattice defects, changes in elec. props. and photoluminesc. 77—4685
CdTe:Cl, LPE from CdCl$_2$ soln., elec. props., defects 80—39689
CdTe:Cl, localisation of electrons, temp. depend. of cond. and Hall effect 78—14732
p-CdTe:Cl, mech. of electron recomb. 79—11176
CdTe:Cl, semi-insulating, Hall effect and cond. meas., carrier mobility 77—39849
CdTe:Cl, semi-insulating, impurity photocond. spectra, local state distrib. in band gap 80—107865
CdTe:Cl, semiinsulating, Hall effect and elec. cond., impurity levels 77—55532
CdTe:Cl, single cryst., photo Hall effect obs. 78—76094
CdTe:Cl(In), photoelectronic investig. of trap depths, TSC and SCL cond. 77—39893
CdTe:Co, impurity luminescence no phonon line depend. on temp., Debye temp. 80—66273
CdTe:Cr, impurity photoionisation transitions, EPR meas. 80—39857
CdTe:Cr^{2+}, absorpt. and luminesc. of Cr^{2+}(d^4), cryst. field theory interpretation 79—83000
CdTe:Cu, doping effects on evaporation kinetics and electronic props. during high-temp. annealing in vacuum 78—22743
CdTe:Cu films, impurity behaviour, Hall mobility and hole density meas. 80—80420
CdTe:Fe, annealed, magnetically ordered, Hall effect and photocond. 78—19060
CdTe:Fe, Mn, Cr, introduction of elec. active defects 80—103647
CdTe:Fe^{2+}, reson. relax. time for impurity electrons and localised phonons interaction, appl. to thermal cond. 80—59590
CdTe:Fe-group metals, mag. susceptibility *(Russian)* 79—56496
CdTe:Fe(Ni), luminesc. and refl. spectra, high temp. annealing effects 80—24472
CdTe:Ge, dopant behaviour 78—22742
CdTe:Ge, mag. props. 78—56289
CdTe:Ge, negative thermally stimulated cond. 79—19621
CdTe:H$^+$, ion-implanted, optical waveguiding and electrooptic modulation 77—7197
CdTe:In, lightly- and heavily-doped, cathodoluminesc., temp., injection level and freq. depend. 78—52584
CdTe:In, photoconductivity exam. and IR quenching 79—11181
CdTe:In, pure and heavily doped, electron-hole liq. form., luminesc. spectra 80—10884
CdTe:In, shift optical absorpt. edge with temp. and doping level 79—8165
CdTe:In precipitation and out-diffusion of solute during cooling 80—100840
CdTe:Li, excitation spectrum of Li acceptor and valence band parameters 79—28795
CdTe:Li(Cl), acceptor states study by donar acceptor pair excitation luminesc. 80—100683
CdTe:Mn, photoionisation absorption spectrum 78—23502
CdTe:Mn, spin-lattice coeffs. of Mn^{2+} 80—84646
CdTe:Mn^{2+}, exciton refl. spectra and mag. susceptibility 80—66253

cadmium compounds continued
CdTe:Mn^{2+}, luminesc. and magnetooptic reson., mag. field effect 80—93390
CdTe:Mn^{2+}, magneto-optical and microwave-optical double reson. meas. of exciton band *(Russian)* 77—81087
CdTe:Mn(Fe)(Ni), exciton refl., photoluminesc., and mag. suscept. meas., influence of impurities 77—39787
CdTe:P, annealing induced lattice defects, TEM obs. 80—2010
CdTe:p, defect model, from Hall effect meas. 77—43620
CdTe:S, reson. interaction of local S vibr. with lattice phonons 77—11654
CdTe:Si(Cl), force variation due to charged defects 80—92634
CdTe:Ti^{2+}, Jahn-Teller effect on $^3T_1(^3F)$ state, resonance on $^3T_1(^3P)$ state 78—27271
CdTe:Tl, growth by travelling heater method, elec. and optical characterisation 77—40356
CdTe:V,Cr, optical props. meas. 79—73969
CdTe:V (d^3), absorption and luminesc. spectra 78—15203
CdTe:Xe, anomalous Xe$^+$ ion implantation defect introduction, cathodolum. obs. 77—62554
CdTe:Yb, exciton emission, cathodoluminescence 78—39033
CdTe:Zn, TSC, carrier traps, depth and quenching by IR radiation 78—56420
CdTe/Hg$_{1-x}$Cd$_x$Te multilayers, LPE growth 80—80104
CdTe/HgTe superlattice, new IR material 79—72634
CdTe/SnCl$_2$/Pt, solar cell photoelectric props. *(Spanish)* 80—85290
CdTe-Ag diode, Schottky type, elec. and photoelec. props. 77—43719
CdTe-AlSb, phase diag. 77—52299
CdTe-Au contacts, electronic states, vacuum UV photoelectron spectra 80—70827
CdTe-Au Schottky barriers, quantum photoelectric yield, theoretical anal. 77—39939
CdTe-Au system, phase diagram rel. to doping 80—16282
CdTe-Au(Al) Schottky barriers, defect effects 79—60921
CdTe-Au(In) contacts, photo-effect in the 77-300K range, barrier height estimation 80—107850
CdTe-based p-n junction, photoeffect quantum efficiency depend. on photon energy *(Russian)* 79—78168
CdTe-CdS heterojunctions, growth by closed-tube chem. transport, elec. props. 80—60070
CdTe-CdS heterojunction, photocapacitance and photocond. 80—96978
CdTe-CdS p-n heterojunction, coordinate sensitive photoelements, longitudinal photovoltage 79—95440
CdTe-CdS solid solution phase diagram *(Russian)* 79—100120
CdTe-CdS thin film p-n solar cells, spectral response temp. depend. 80—93871
CdTe-CdS-CdSe system solid soln. single crysts., forbidden band width determ., comp. depend. 80—55083
CdTe-CdSe, and CdTe-ZnSe p-n heterojunction, photovoltaic props. 77—55600
p-CdTe-Cl, compensated, hopping cond. 77—76818
CdTe-Co(Mn) systems, reaction of components, DTA, microstruct. and microhardness obs. 79—38804
CdTe-electrolyte boundaries, photo e.m.f. meas., semicond. energy bands 77—1481
n-CdTe-electrolyte solar cells, interface changes during operation, AES, electrolum. and electroreflectance meas. 79—100525
CdTe-Fe, cross section and solubility of Fe 77—90334
CdTe-Ge heterojunction, photoelec. props., sensitivity in near IR region *(Russian)* 77—69405
CdTe-HgTe, neutron irrad. rel. to elec. props. 79—15141
CdTe-HgTe, semicond. solid solns., effect of reactor irrad. on electrophys. props. 77—51744
CdTe-HgTe ideal superlattice, electronic props. calc. 80—49885
CdTe-HgTe superlattice on CdTE layers, evanescent states, tight binding calcs. 80—70611
CdTe-In system, equilib. phase diagram and liq. phase epitaxial growth of CdTe from In soln. *(Japanese)* 80—71634
CdTe-In$_2$Te$_3$, composition depend. of energy gap, optical absorpt. obs. 77—80728
CdTe-InAs quasi-binary system, temp.-comp. diagram, physicochem. and thermodynamic analysis 80—104127
CdTe-InSb solid solns., electroreflectance spectra, Brillouin zone transitions 80—7330
p-CdTe-Langmuir film interface, prep., characters. and MIS struct. 80—92998
CdTe-Langmuir film MIS structures, C/V and G/V curves 79—65551
CdTe-metal, diode contact, elec. characts., generation-recombination space charge region *(Russian)* 78—39214
CdTe-metal contact, surface barrier exam. 78—64111
CdTe-PbTe(InSb) superlattices, laser deposition of multilayer heteroepitaxial structs. 80—44450
CdTe-Si heterojunctions, epitaxy and electrical props. *(Japanese)* 77—32074
CdTe-SnCl$_2$ electrolyte heterojunction photoelec. props., feasibility as solar energy convertors 77—76918
CdTe-Te film, prep. by combined hot-wall-flash evaporation method, and characterisation 80—55296
CdTe-Tl, quasibinary cross section 78—3102
CdTe-ZnS system, phase diagram and solid solubility 80—20909
CdTe-ZnS ternary mutual system, phase diagram 80—20904
CdTe-ZnSe pseudobinary system, phase diagram and equil., Bridgman single cryst. growth method 79—43213
CdTe-ZnTe n-p heterojunction, photovoltaic props. 77—55600
CdTe+ZnSe$\rightleftarrows$CdSe+ZnTe ternary mutual system, phase equilib. 79—52179
(CdTe)$_{1-x}$-(ZnSe)$_x$ system, mutual solubility and band gap energy *(Japanese)* 77—51501
(CdTe)$_x$-(CdSe)$_{1-x}$, diamond-type semiconductor, Mossbauer spectra, quadrupole interaction of ^{125}Te 80—44992
CdTeMoO$_6$, prep. and cryst. struct., X-ray diffr. obs. 79—1414
CdTe$_{1-x}$S$_x$, long-wavelength optical phonons, composition depend., IR and Raman spectra 78—67788
CdTe$_{1-x}$Se$_x$, multiband model of impurity complexes 80—65497
CdTe$_{1-x}$Se$_x$, Raman scatt. spectra, two-mode behaviour 78—60450
CdTe$_{1-x}$Se$_x$ solid solution films, prep., struct., and photocond. 80—54541
CdTh(MoO$_4$)$_3$, struct., DTA and X-ray diffr. obs. *(French)* 78—95024
CdTh(MoO$_4$)$_3$, X-ray cryst. struct. determ. *(French)* 80—64959
CdThNb$_2$O$_8$, monoclinic-quadratic phase transform. *(French)* 77—27998
CdTh(WO$_4$)$_3$, struct., DTA and X-ray diffr. obs. *(French)* 78—95024
CdTiO$_3$, CdSnO$_3$ perovskites elasticity meas. to 6 kbar 77—51428

cadmium compounds continued
$CdTiO_3$, electric field gradient temp. depend. 78−39454
$CdTiO_3$, form. entropy and tolerance factor 80−34204
$CdTiO_3$, perovskite, elec. quadrupole interactions, TDPAC meas. 78−31129
$CdTiO_3$, refl. and absorpt. coeffs. 3-3.5 eV, and refr. index dispersion *(Russian)* 78−39561
$CdTiO_3$, single cryst. growth and props. 79−100046
$Cd_2Ti_2O_5F_2$, single cryst. growth and props. 79−100046
$CdTl_2Se_4$, single cryst., preparation, elec. cond. 77−24554
$CdTl_2Se_4$:Au, solubility meas. by microhardness method 80−96650
$CdTl_2Se_4$:Au(Ag)(Cu), doping effect on surface tension of melt and cryst. microhardness 80−49464
$CdTl_2Se_4(Te_4)$:Au, elec. cond., density, dielectric const., changes on fusion 80−88553
$CdTl_2Te_4$, Hall and thermo-EMF coeffs., in solid, liquid states 80−54704
$CdTl_2Te_4$, single and polycryst. samples, linear expansion, heat capacity and thermodynamic props. 80−103489
$CdTm_2Se_4$, mag. susceptibility meas. 4.2 to 300K cryst. field approx. 77−66246
$CdUO_4$, phase transforms., anomalous oxidation state change 80−54369
$Cd_2V_2O_7$, elec. props. and EPR meas. 79−11114
$Cd_2V_2O_7$, V-O-V bridge stretching freq. correl. with bond angle 78−74636
$Cd_5(VO_4)_3I$, $Cd_5(VO_4)_3Br$, halogen atom distrib. determ. 78−2078
$Cd_5(VO_4)_3I$, $Cd_5(VO_4)_3Br$, X-ray diffr. cryst. struct. exam. and refinement 78−10000
$CdWO_4$, luminesc. efficiency, temp. and high-press. 78−23507
$CdWO_4$ single cryst., melt growth, defects and growth mechanism 80−29933
$Cd(WO_4)_{1-4}(MoO_4)_x$, growth and props. 80−71588
CdX_2, (X=Br, Cl), spectroscopic parameters of mols. from vibr. isotopic effects 78−74798
CdX_2, CdXY, (X,Y=Cl,Br,I), matrix isolated vibr. spectra, isotopic effects, force consts. 77−3358
CdX_2, CdXY, (X,Y=Cl,Br,I), matrix isolated, far IR spectra, thermodynamic props. 78−86869
CdX_4^{2-} (IO_4^-), (X=Cl,Br,I), force consts., compliance and Coriolis consts. calc. 78−42242
CdXY, (X, Y=Cl, Br, I), spectroscopic parameters of mols. from vibr. isotopic effects 78−74798
CdY_2S_4:Fe (Mn), superhyperfine interaction of Mn and Fe, ESR spectra 77−63271
$Cd_{3-x}Zn_xAs_2$, cryst., two-band and impurity conduction, 1.8 to 370K 78−19057
$Cd_{3-x}Zn_xAs_2$, electron mobility and carrier density calc. 77−80780
$Cd_{3-x}Zn_xAs_2$ press. and temp. depend. of Hall coeff. 77−69349
$Cd_{3-x}Zn_xAs_2$ solid soln., US wave prop. vel., composition depend. 77−20013
$Cd_{1-x}Zn_xCr_2Se_4$, ferromag. semicond., surface magnetism, magneto-optical meas. 77−20831
$Cd_{1-x}Zn_xCr_2Se_4$, mag. semicond., neutronographic obs. *(Russian)* 79−11297
$Cd_{1-x}Zn_xCr_2Se_4$, synthesis Curie pt., photomag. effect 77−51937
CdZnS thin films, growth and evaluation for fabrication of high performance photovoltaic solar cells 80−93501
CdZnS-CdS bifilm solar photocells, feasibility, study 78−76113
(CdZn)S-Cu_2S solar cell, film form. and characts. 78−68080
$Cd_{1-x}Zn_xS$ 10 μm film optical and electrical characterisation *(French)* 78−64153
$Cd_{1-x}Zn_xS$, electro-optical multilayer film, for data storage and display 78−71176
$Cd_{1-x}Zn_xS$, electroless film deposition with variable comp. and polymorphic structs. 79−95952
$Cd_{1-x}Zn_xS$, epitaxial growth of single crystal layers on (111) GaAs substrate, close-space geometry 78−92198
$Cd_{1-x}Zn_xS$, film, technical data, for low cost solar cell 79−48127
$Cd_{1-x}Zn_xS$ films, thermal evaporation prep., phys. props. 80−84410
$Cd_{1-x}Zn_xS$ heteroepitaxial single-cryst. layers, photoluminesc. props. 80−100692
$Cd_{1-x}Zn_xS$, RF sputtered electro-optical film for data storage and display 78−83047
$Cd_{1-x}Zn_xS$ reactively sputtered phtoconductive films for high field applications *(German)* 78−39154
$Cd_{1-x}Zn_xS$ solar cell thin films, microprobe characterisation *(French)* 80−61349
$Cd_{1-x}Zn_xS$ spray deposited film, for low cost solar cells 79−7915
$Cd_{1-x}Zn_xS$, use of parallel and monochromatic beams for comp. determ. by X-ray fluorescence 79−48000
$Cd_{1-x}Zn_xS/Cu_2S$ thin film heterojunction solar cells, operational charact. 80−45687
$Cd_{1-x}Zn_xS$-p-GaAs heterojunctions, elec. and photovolt. props. rel. to growth technique 80−29466
$Cd_{1-x}Zn_xS$-PbS heterojunctions prepared by spray pyrolysis 79−60917
$Cd_xZn_{1-x}S$ film, vacuum evaporated, struct. 78−38985
$Cd_xZn_{1-x}S$ films, chem. sprayed, carrier density and mobility 80−60121
$Cd_xZn_{1-x}S$, vibr. spectra, microscopic theory 79−73949
$Cd_xZn_{1-x}S$-Cu_2S solar cell, interface chemistry modification of current-voltage charact. 79−100523
$Cd_zZn_{1-z}S$-Cu_2S, heterojunction interface double layer, dislocation field, charge compensation 79−7855
$Cd_{1-x}Zn_xSe$, epitaxial layer growth with Zn content from doping to solid soln. formation 77−85094
$Cd_{1-x}Zn_xTe$, solid soln., vibr. spectra restructuring anomalies 79−4803
$CdZrO_3$, electric field gradient temp. depend. 78−39454
$Cd_5[PO_4]_3Cl$, X-ray diffr. study of cryst. struct. 78−10022
Cds film on metal substrate, resistivity 79−95522
Cds, photoconductive, convolution voltage enhancement due to carrier transverse drift in SAW convolver 80−1381
Cds, reson. Brillouin scatt. by piezoelectrically inactive TA phonon domains 78−84593
CeSe:Fe, long-wavelength fundamental absorpt. edge formation, role of Fe 77−16351
CeTe, surface characterisation by high resolution Rutherford backscatt. 80−25511
(Co,Cd)Cr_2S_4 and (Co,Cd)S solid soln., equilib. composition *(German)* 77−36486
CoS-CdS, phase study by X-ray obs., lattice const. 79−1854
$CsCdBr_3$, diamag. linear chain lattices, cryst. struct. 80−70172
$CsCdBr_3$:Gd^{3+}, EPR of coupled pairs of Gd^{3+} ions 78−19322

cadmium compounds continued
$CsCdCl_3$, phase transition under pressure 78−51664
$CsCdCl_3$:Co^{2+}, Zeeman Raman scatt. and Zeeman IR absorpt. spectra 79−56782
$CsCdF_3$:Cr^{3+}(Fe^{3+}), ligand polarisation and transferred hyperfine interactions 79−51535
$CsCdF_3$:Fe^{3+}, ENDOR meas. on Fe^{3+}-F^--Cd^{2+} struct. 78−31122
$CsCd(NO_2)_3$, pure and metal ion doped, cryst. struct., reflectance spectra and thermal decomp. 79−51081
Cu-Cd-Cl stretched photochromic glass, polorisation effects 79−95729
Cu-Cd-Se system, Cu-CdSe cross section and props. of cpds. formed 78−27491
Cu-CdP_2-Cu diode structure, switching effect obs. 77−4452
Cu-CdS, Schottky barrier, Cu diffusion and photovolt. mechanism 80−6980
Cu-$CdSiP_2$ surface-barrier diode, photoelec. props. 77−4442
P-Cu_{2-x}-n-CdS, heterojunction, energy band diagram 79−24070
$CuGa_{0.5}In_{0.5}Se_2/Zn_{0.29}Cd_{0.71}S$ heterojunction solar cell, preparation and props. 80−101110
$(CuGaTe_2)_{1-x}$-$(2CdTe)_x$, phase diagram and microstruct. DTA and X-ray diffr. 77−59762
CuI:CdI_2, ionic cond. obs. 77−15626
CuI:CdI_2, ionic cond., vacancy and interstitial mobilities, phase transitions 77−20116
CuO-CdO-Fe_2O_3, sintered ferrite, preparation, mag. susceptibility, DC resistivity 80−34598
CuS/Cds solar cells, developments, appls., and economics of solar photovoltaic conversion *(German)* 80−26132
Cu_2S/CdS solar cells, performance, obs. 80−30480
Cu_2S-CdS, heterojunction photocell, thin film structure, props., manufacture 77−51806
Cu_2S-CdS, photovoltaic junction, prep. by chemical deposition 79−66019
Cu_2S-CdS, solar cell, photocurrent, spectral depend. 79−7853
Cu_2S-CdS film junction formation by dry-barrier process 78−64109
Cu_2S-CdS heterojunction characteristics and CdS polarity *(Japanese)* 78−23154
Cu_2S-CdS heterojunction diodes, barrier model estimated from photovoltage and cathodoluminesc. spectra 79−78165
Cu_2S-CdS heterojunction, photoelectric props. 80−29467
Cu_2S-CdS heterojunction solar cells, carrier transport, nonmonotonic band profiles 80−61361
Cu_2S-CdS heterojunction interface, depth distribution profiles, Auger spectra 80−88622
Cu_2S-CdS heterojunctions, role of deep levels in controlling photovoltaic props. 80−92941
Cu_2S-CdS integrated thin film solar cell generators, fabrication techniques 80−55857
Cu_2S-CdS photocell characteristics, for various solar radiation incidence angles 79−83593
Cu_2S-CdS solar cell, fabrication using solid state reaction 77−16498
Cu_2S-CdS solar cell, interface recombination and junction field studies, exptl. technique 80−45683
Cu_2S-CdS solar cell fabrication by magnetron reactive sputtering deposition 80−61363
Cu_2S-CdS solar cells, Cu_2S film growth methods 80−80980
Cu_2S-CdS solar cells, EBIC and capacitance measurements, stability problems 80−45684
Cu_2S-CdS solar cells, interface recombination phenomena and tunnel effect 80−66978
Cu_2S-CdS solar cells, optical absorption coefficient changes in Cu_2S 80−93980
Cu_2S-CdS solar cells, optimised grid patterns 80−108798
Cu_2S-CdS solar cells in backwall configuration, model of photovoltaic effect 80−55861
Cu_2S-CdS solar cells with interdigitated grid, current-voltage analysis 80−93981
Cu_2S-CdS solar photopiles, tunnel conduction mechanism *(French)* 79−29480
Cu_2S-CdS sprayed solar cells, chemical spray deposition 80−93979
Cu_2S-CdS thin film planar junction devices, quantitative photon loss anal. 80−61362
Cu_2S-CdS thin film solar cells, Cu_2S layer separation, struct. 79−95282
Cu_2S-CdS thin film solar cell fabrication by electrophoresis 80−55862
Cu_2S-$Zn_xCd_{1-x}S$ and Cu_2S-CdS thin film solar cells by solid state reaction, comparison 80−101109
$Cu_{2-x}S$-CdS, solns. cell, photo-emf, depend. on degree of doping of CdS 79−52934
$Cu_{2-x}S$-CdS heterojunction V-I characteristic and max. photovoltage, long-term changes *(Russian)* 78−43468
$Cu_{2-x}S$-CdS heterojunctions, nature of longwave photo EMF 78−84284
$Cu_{2-x}S$-CdS p-n heterojunction solar cells, props., Burstein-Moss effects 80−21404
$Cu_{2-x}S$-CdS p-n heterojunction, optical energy convertor, struct. and recomb. props. 80−72065
$Cu_{2-x}S$-CdS p-n heterojunction, copper sulphide growth features during formation *(Russian)* 80−107898
Cu_xS-CdS heterojunction solar cells, time evolution of spectral characts. 80−30478
Cu_xS-CdS heterojunction solar cells spectral distrib. and photocapacitance 80−55864
Cu_xS-CdS solar cells, Cu_xS transform. behaviour rel. to topotaxial growth, cell efficiency 77−11814
Cu_xS-CdS solar cells, cu_xS growth kinetics and composition analysis by absorbance transient and galvanic electrochemical measurements 80−92797
Cu_xS-CdS solar cells, SCL current 80−76634
Cu_xS-CdS thin film solar cell using chem. sprayed CdS film 78−43465
Cu_xS-CdS thin film solar cells, using all film vacuum deposited process 80−93977
Cu_2S(Se)-CdS(Se) p-n heterophotoelements of optronic converters, props. on X-irrad. of scintillator 80−34505
Cu_2SnS_3-CdSe, diamond-type semiconductor, Mossbauer spectrum of ^{119}Sn 80−44991
$(Cu_2SnS_3)_x$-$(3CdS)_{1-x}$, diamond-type semiconductor, Mossbauer spectrum of ^{119}Sn 80−44991
$(Cu_2SnS_3)_x(3CdS)_{1-x}$, second co-ordination sphere atoms effect on ^{119}Sm Mossbauer spectra *(Russian)* 77−63348
Cu_2SnSe_3-CdS, diamond-type semiconductor, Mossbauer spectrum of ^{119}Sn 80−44991
$Cu_{2-x}Te$-CdSe heterojunction, elec. and opt. props. *(Korean)* 77−51811

cadmium compounds continued
cu$_2$S-CdS sprayed layer solar photopiles, CdS sprayed layer props. *(French)* 79—24901
dimethylammonium cadmium chloride, proton-^{14}N double reson. exam. of struct. phase transitions 77—4583
Di(methylammonium) cadmium tetrachloride, LF Raman spectra and phase transitions 77—63414
GaSb-Zn(Cd)Te, quasibinary system, phase equilibrium, intermol. interaction 77—12601
GdTe:P and CdTe:P,In(Ga)(Al), IR absorpt. investig. of localised vibr. modes of impurity centres 77—52136
GeO_2-CdO system, phase diagram anal. by differential thermal, X-ray anal. 77—8805
p-(Hg,Cd)Te, carrier lifetime, dominant Auger transitions comparison 80—49768
(Hg,Cd)Te IR detector array, 72-element, 8-12 micron, performance, FLIR system appl. 79—2829
(Hg,Cd)Te photodiode for 2 μm IR detection 77—82603
Hg-HgTe-CdTe system, equilib. phases comp. by dew point method 79—78941
$Hg_{1-x}Cd_xGe$, quantum oscillations of magnetoresistivity *(Russian)* 80—11007
$Hg_{0.985}Cd_{0.015}Se$, interband $\Gamma_6 \rightarrow \Gamma_8$ magnetoabsorption and band parameters 79—82960
$Hg_{1-x}Cd_xSe$, (x=0 to 0.15), Shubnikov-de Haas oscillations, influence of level broadening 79—11155
$Hg_{1-x}Cd_xSe$, IR absorpt. spectra, band struct., refr. index 80—50337
$Hg_{1-x}Cd_xSe$, zinc blende structure, optical and electronic properties 80—6723
HgCdTe, crystal and photodiode, imperfections and surface conditions using electron induced current technique 79—67385
HgCdTe, electron irradiated, high temp. defects 79—78122
HgCdTe IR photovoltaic detectors for 8-14 μm range, review *(Italian)* 78—54451
HgCdTe, interband magnetoabsorption and band struct. 79—82959
HgCdTe, ion implantation, junction form. 80—100260
HgCdTe MIS structure, modelling and appl. to CCD IR imagery 78—80058
HgCdTe, Magneto transport anomalies at low carrier densities, Wigner crystallisation 80—20222
HgCdTe, narrow band gap semiconductor IR devices, advances 80—48464
n-HgCdTe, photocond., Hall mobility and resist. 80—34478
HgCdTe photodiode IR detector, selection 79—58791
HgCdTe photodiodes formed by double-layer LPE 80—104078
HgCdTe, radiation effects on low-temp. carrier recombination lifetimes, photocond. meas. 78—6400
HgCdTe, recomb. effects, mag. quantum oscills. in Auger transition rate 79—82610
HgCdTe reverse-biased photodiodes for wideband appls., excess noise 80—107876
HgCdTe Schottky barrier diode and n-p diffused junction IR detectors, comparison 80—9039
HgCdTe solid solution photodiode for CO_2 laser active medium study 80—95868
HgCdTe, zero gap, unusual high electron mobility and related phenomena 79—82601
HgCdTe-CdTe IR detector arrays, 3 to 11 μm, fabrication techniques 80—9041
HgCdTe-CdTe photodiode, 1.33 μm, grown by LPE, phys. props. 80—107892
$Hg_{0.60}Cd_{0.40}Te$, LPE growth from Te-rich soln. 80—7508
$Hg_{0.6}Cd_{0.4}Te$, annealing temp. effect on carrier conc. 78—72167
$Hg_{0.6}Cd_{0.4}Te$ LPE layer growth from Te-, Hg-, and HgTe-rich solns., comparison 80—76199
$(Hg_{0.6}Cd_{0.4})_{1-x}Te_x$, defect anal., intrinsic material parameters 80—75519
n-$Hg_{0.61}Cd_{0.39}Te$ single crystals, flicker noise due to grain boundaries, meas. 79—1611
$Hg_{0.68}Cd_{0.32}Te$ photodiode, minority carrier lifetime determ. 79—38084
$Hg_{0.7}Cd_{0.3}Te$, 17 to 77K, photo- and cathodoluminesc. 78—52569
$Hg_{0.72}Cd_{0.28}Te$ semiconductor, two-mode reson. polaron 79—15105
$Hg_{0.74}Cd_{0.25}Te$ thin film deposition on Si substrates by RF triode-sputtering, large-area photodetector arrays 80—80965
$Hg_{0.75}Cd_{0.25}Te$, single crystal, reflection spectra 80—40140
$Hg_{0.75}Cd_{0.25}Te$, thermorefl. spectra, effect of excitons on E_1 and $E_1+\Delta_1$ structs. 80—16057
$Hg_{0.77}Cd_{0.23}Te$, near reson. spin-flip Raman scatt. 79—82983
$Hg_{0.77}Cd_{0.23}Te$ nonlinear optical IR generation 80—58642
$Hg_{0.77}Cd_{0.23}Te$, resonant four-photon and higher order mixing 79—41415
$Hg_{0.77}Cd_{0.23}Te$, spin-flip Raman laser, high conversion efficiency 77—79832
$Hg_{0.79}Cd_{0.21}Te$, ion implanted, elec. props. 80—20184
n-$Hg_{0.8}Cd_{0.2}Te$, microwave bolometer heterodyne receiver based on magnetic field induced phase transition 80—13135
$Hg_{0.8}Cd_{0.2}Te$ surface, sputter cleaning and dry oxidation, XPS and LEED study 80—108618
$Hg_{0.8}Cd_{0.2}Te$-ZnS MIS struct., nonparabolic bond semicond., surface state studies, capacitance measurements 79—78190
$Hg_{0.82}Cd_{0.18}Te$, electronic anomalous mass near reson. acceptor level, Shubnikov-de Haas meas. 80—80163
$Hg_{0.85}Cd_{0.15}Te$, acceptor states, galvanomagnetic effects study 79—82560
$Hg_{0.86}Cd_{0.14}Te$, spin-flip electron scatt., longit. magnetoresist. obs. 77—43622
$Hg_{1-x}Cd_xTe$ 0.1 eV, thermal conductivity meas. 77—24578
$Hg_{1-x}Cd_xTe$, acceptor bound exciton Auger and radiative transition rates, radiative recomb. 80—6733
$Hg_{1-x}Cd_xTe$, acceptor impurity band form. 80—20119
$Hg_{1-x}Cd_xTe$, acceptor levels due to local impurity potential 79—11084
$Hg_{1-x}Cd_xTe$, anodic oxide films, formation and props. 80—3212
$Hg_{1-x}Cd_xTe$, avalanche formation, high intensity IR transmission limit 79—78684
$Hg_{1-x}Cd_xTe$ breakdown-limited MIS device, increased charge capacity using ramped gate voltage 80—103751
$Hg_{1-x}Cd_xTe$, CESR *(Russian)* 78—23344
$Hg_{1-x}Cd_xTe$, CESR meas., four-photon mixing via spin-flip Raman scatt. 79—82873
$Hg_{1-x}Cd_xTe$, carrier conc., Hall effect, photocond., IR spectra meas. 80—49771
$Hg_{1-x}Cd_xTe$, cyclotron reson., 337 μm transmission expts., 77 to 150K 78—34750

cadmium compounds continued
$Hg_{1-x}Cd_xTe$, degenerate four-wave mixing of 10.6 μm radiation 80—95943
$Hg_{1-x}Cd_xTe$, doping props. of selected impurities, diffusion behaviour 77—72632
$Hg_{1-x}Cd_xTe$, Einstein relation for inversion layers 80—103706
$Hg_{1-x}Cd_xTe$, epitaxial layer, vapour phase growth 79—1829
$Hg_{1-x}Cd_xTe$, epitaxial layers, elec. properties in the range 4.2 to 300K *(French)* 80—65721
$Hg_{1-x}Cd_xTe$ epitaxial layers, elec. props. 80—96910
$Hg_{1-x}Cd_xTe$, far IR cyclotron resonance in inversion layer 77—69396
$Hg_{1-x}Cd_xTe$, far IR cyclotron reson., band edge effective mass and relax. time 79—19781
n-$Hg_{1-x}Cd_xTe$, far IR recomb. radiation in elec. field, acceptor states 77—16399
n-$Hg_{1-x}Cd_xTe$, far IR recomb. radiation with applied elec. field 78—27324
$Hg_{1-x}Cd_xTe$, Faraday effect at CO_2 laser freq. 78—64348
$Hg_{1-x}Cd_xTe$ films, Tamm surface states, Kane model 79—28395
$Hg_{1-x}Cd_xTe$, for appl. in IR detector arrays, comp. control 80—31872
$Hg_{1-x}Cd_xTe$, grown from melt, Kirkendall and Frenkel effects 80—100365
$Hg_{1-x}Cd_xTe$, high intensity IR transmission limit 78—79074
$Hg_{1-x}Cd_xTe$, high-pressure reflex growth technique, IR detector appl. 77—40347
$Hg_{1-x}Cd_xTe$, homogeneous single cryst., growth by modified Bridgman technique 78—39682
$Hg_{1-x}Cd_xTe$, Hooge's flicker noise MIS expt. 78—56233
$Hg_{1-x}Cd_xTe$ hot-electron photoconductive detection of near mm wave radiation 80—57377
$Hg_{1-x}Cd_xTe$, IR optical absorpt. and refr. index, 80 to 300K 79—91418
$Hg_{1-x}Cd_xTe$ IR photodetectors for night vision appl. 80—22429
$Hg_{1-x}Cd_xTe$ implanted detector 8 to 14 μm, performance, p-n junction characts. 77—15941
$Hg_{1-x}Cd_xTe$, implanted with Hg, Al, damage and lattice location study 80—103381
$Hg_{1-x}Cd_xTe$, interband magnetoreflectance 78—19448
$Hg_{1-x}Cd_xTe$ interface with native oxide, elec. props. 80—20318
$Hg_{1-x}Cd_xTe$, LPE current controlled 80—40272
$Hg_{1-x}Cd_xTe$, LPE growth and characterisation 80—50565
$Hg_{1-x}Cd_xTe$, LPE-grown and optically pumped crystal, continuous lasing at 2.79 μm 79—68397
$Hg_{1-x}Cd_xTe$, long-term Hall-type conversion by vacancy diffusion at room temp. 79—65498
$Hg_{1-x}Cd_xTe$, magnetooptical and impurity effects 80—6721
$Hg_{1-x}Cd_xTe$, magnetoreflection studies 79—82963
$Hg_{1-x}Cd_xTe$, material capabilities for 1 to 1.3 μm room temp. photodiodes 78—24859
$Hg_{1-x}Cd_xTe$, mixed crysts., band struct. and optical transitions, distorted atomic orbitals 77—69224
$Hg_{1-x}Cd_xTe$, mixed crystals, crystn. by chemical transport 80—20775
$Hg_{1-x}Cd_xTe$, n-surface inversion layers study 80—25017
$Hg_{1-x}Cd_xTe$, narrow-gap semiconductor, high intensity IR transmission limit 80—7361
$Hg_{1-x}Cd_xTe$, near band-gap photoluminesc., bound exciton luminesc. obs. 80—103973
$Hg_{1-x}Cd_xTe$, nonlinear absorption and saturation, 10.6 μm 77—746
$Hg_{1-x}Cd_xTe$, nonlinear optical effects 80—14389
$Hg_{1-x}Cd_xTe$, optical absorpt., quasilocal acceptor level effects, theory 80—92853
n-$Hg_{1-x}Cd_xTe$, optical phase conjugation 80—83644
$Hg_{1-x}Cd_xTe$, p-T diagrams, $p \rightleftharpoons n$ intrinsic-extrinsic lines 77—36481
n-$Hg_{1-x}Cd_xTe$, photoconductor, contact noise at 77K 78—88028
$Hg_{1-x}Cd_xTe$ photoconductors, gamma ray effects on surface props. and detector props. 79—17489
$Hg_{1-x}Cd_xTe$ photoconductive IR detector, optimum bias attainment with batteries 79—58789
$Hg_{1-x}Cd_xTe$ photodiodes, implanted n^+-p, improved performance using insulated field plates 80—52309
$Hg_{1-x}Cd_xTe$ photodiodes, long cutoff wavelength, effect of trap tunnelling on IR detector performance 80—73451
$Hg_{1-x}Cd_xTe$, photolum. and optical pumping 80—50424
$Hg_{1-x}Cd_xTe$, props. and appl. book 77—36250
$Hg_{1-x}Cd_xTe$, props. and appls., book contrib. 77—39834
$Hg_{1-x}Cd_xTe$, recombination processes using impact ionization capture cross sections 80—75577
$Hg_{1-x}Cd_xTe$, resonant acceptor level, single and multiple scatt. effect 77—47767
$Hg_{1-x}Cd_xTe$, segregation, compositional characterisation 80—107434
$Hg_{1-x}Cd_xTe$, semimetallic state, magneto-optical investig. of Landau levels and band parameters 77—63410
$Hg_{1-x}Cd_xTe$, semimetallic and semicond., Hall coeff., anomalous temp. depend., 4.2 to 70K 80—65604
$Hg_{1-x}Cd_xTe$, shallow acceptor contribution to near-resonance spin-flip Raman scatt. 79—95754
n$Hg_{1-x}Cd_xTe$, single-phonon and plasmon recomb. lifetime effect, with magnetically tuned bandgap 79—38098
$Hg_{1-x}Cd_xTe$, surface topographic stoichiometry variations, electrolyte electrorefl. obs. 78—27249
$Hg_{1-x}Cd_xTe$, Tamm surface states 77—55595
$Hg_{1-x}Cd_xTe$, theory of optical absorpt., contribution by quasilocal acceptor levels *(Russian)* 80—71451
$Hg_{1-x}Cd_xTe$, transverse magnetoresist. in extreme quantum limit 77—39885
$Hg_{1-x}Cd_xTe$, two-photon absorption coefficient, 3-band model 79—78679
$Hg_{1-x}Cd_xTe$, vaporisation under Knudsen effusion conditions 80—2154
$Hg_{1-x}Cd_xTe$, zero-bandgap state induced by press., galvanomag. props. 77—47725
$Hg_{1-x}Cd_xTe$, zero-gap semicond. with nonparabolic band struct., hot electron mobility and conc. 78—76080
$Hg_{1-x}Cd_xTe$, zero-gap semicond., reson. states 79—82558
$Hg_{1-x}Cd_xTe$-CdTe photodiodes, backside-illum., LPE growth and thermal noise characts. 79—40610
$Hg_{1-x}Cd_xTe$-In contact, diffusion of In 80—103520
$Hg_{1-x}Cd_xTe$-oxide interfaces, MIS capacitance characts. 80—49926
$Hg_{1-x}Cd_xTe$-type semimetals, kinetic props., local acceptor level effects 80—65557
$Hg_{a-x}Cd_xTe$, $(x<0.16)$, semimetallic phase, acceptor states and galvanomagnetic effects 80—6882
$Hg_{a-x}Cd_xTe$, single-LO-phonon and -plasmon recombination channels narrow-bandgaps 78—91728

cadmium compounds continued
- $Hg_xCd_{1-x}Te$, Hall effect and elec. cond., carrier density and mobility temp. depend. 77—4341
- n-$Hg_xCd_{1-x}Te$, narrow band gap, Auger effect under high mag. fields 79—82609
- $Hg_xCd_{1-x}Te$, photodiode, anomalous noise behaviour in heterodyne and background limited operation 79—69568
- $Hg_xCd_{1-x}Te$, zero-gap props. correlated to Γ_8 symmetry, review 80—6717
- $HgCr_2Se_4$-$CdIn_2S_4$ heterojunctions, prep. and photovoltaic prop. 78—34892
- HgI_2:CdI_2, cryst. growth from soln., doping rel. to elec. cond., phase transitions 77—55880
- HgI_2:CdS, photodielectric effect 77—11955
- HgI_2:CdS binder layer photoreceptor, surface charge characts. thickness depend. 80—57409
- HgI_2-CdS mixed system, photocond. depend. on composition and binder content 79—51625
- HgI_2-CdS photoconducting binder layers, surface charge decay characts. 77—43642
- HgSe/CdSe lattice-matched heterostructs. as Schottky barriers, CVD epitaxial growth and elec. props. 80—49877
- HgSe-CdSe pseudobinary alloy, phase diagram and cryst. growth 78—68620
- HgTe-CdTe, distrib. ratios of components during crystn. of melt 77—16485
- HgTe-CdTe, epitaxy by evap. and interdiffusion under isothermal conditions book contrib. 77—12549
- HgTe-CdTe, high intensity US effects on synthesis and growth 77—819
- HgTe-CdTe, mixed semiconductor with comp. fluctuation, kinetics of intraband absorpt. and magnetoabsorption coeff. 79—19865
- HgTe-CdTe, mixing energy and short-range order, diffuse X-ray scatt. 77—28006
- HgTe-CdTe solid solns. form., equil. vacancy conc. changes 77—43208
- $(HgTe)_x$-$(CdTe)_{1-x}$, diamond-type semiconductor, Mossbauer spectra, quadrupole interaction of ^{125}Te 80—44992
- In-CdS-In, tunnel junction light-induced DC Josephson current 79—47204
- In-CdS-In Josephson junction, exhibiting nonuniform max. current distrib. self-resonant modes 78—56263
- In-CdS-In structure, volt-ampere characts., carrier tunnelling emission *(Russian)* 80—49914
- In-CdS-In(Te) contacts, ohmic nature, monitoring method 77—39935
- In-Sb-Cd system, phase diagrams 79—87617
- InAs-CdTe, preparation, microhardness rel. to component interactions 77—24350
- $(InAs)_{1-x}(CdSe)_x$ solid solution, elec. props. 79—15146
- $(InAs)_x(CdTe)_{1-x}$, band gap and effective mass, IR spectra obs. 78—56491
- In_2O_3-SnO_2-CdTe:P, p-n homojunction solar cell, elec., photovoltaic props., photoluminescence 80—81463
- InP-CdS heterojunction, injection electrolum. 78—23153
- $In_{2-x}Sn_xO_{3-y}$-CdTe photovoltaic heterojunctions, surface and interface studies, efficiency 80—45691
- $In_{2-x}Sn_xO_{3-y}[SnO_2]$-CdSe-CdS:Cd,Cl sandwich photoconductor injection obs. *(Russian)* 80—54773
- $KCdCl_3$:Co^{2+}, Zeeman Raman scatt. and Zeeman IR absorpt. spectra 79—56782
- $K_2Cd_2(SO_4)_3$, ferroelastic phase transition, X-ray diffr. and dielec. temp. depend. meas. 79—55882
- $K_2Cd_2(SO_4)_3$, melt growth and ferroelastic transition, and K_2SO_4-$CdSO_4$ phase diagram 78—31335
- $K_2Cd_2(SO_4)_3$, piezoelec. langbeinite-type, cryst. struct. and ferroelastic transform. 78—6036
- $K_2Cd_2(SO_4)_3$, piezoelectric, cryst. struct., near ferroelastic transition 78—42984
- $KCd_4(VO_4)_3$, cryst. struct., Patterson and Fourier calcs. 77—19916
- KCl:$CdCl_2$, elec. cond., role of electrode material, surface precipitation effects 80—59985
- $K_2Mn_xCd_{1-x}F_4$, 2-dimens. antiferromag. sidebands on EPR lines 78—56370
- KNO_3-$Cd(NO_3)_2$ molten mixtures, elec. cond. 79—90813
- LiCd ferrite, dielec. const. and loss meas., 50-10^6 Hz 77—77135
- $LiCdBO_3$, cryst. struct., X-ray determ. 79—19226
- $LiCdBO_3$ triclinic cryst. struct., X-ray and Patterson function anal. 80—39055
- $LiHCd_4(Ge_5O_{15})$, cryst. struct., comparison with natural rhodonite 78—30600
- $LiNbO_3$-CdO, CdO addition effect on sintering 79—83157
- $LiNbO_3$-CdS, layered structure, transverse acousto-electric current 80—44669
- $LiNbO_3$-CdSe layer structure, SAW absorpt., elec. field effects 80—65355
- $LiNbO_3$-liquid-CdS-liquid-$LiNbO_3$ structure, acoustic wave propag. and amplification 77—42654
- $Mg_xCd_{1-x}Te$, electroreflection spectra, comp. depend. 80—66230
- $Mg_xCd_{1-x}Te$:P, vibr. modes of defects, IR absorpt. expts. 77—62601
- MgO-CdO, interface, coincidence-site-lattice relations 80—103588
- $(Mn,Cd)Cr_2S_4$ and (Mn,Cd)S solid soln., equilib. composition *(German)* 77—36486
- $Mn_xCd_{1-x}(NH_3)_2.Ni(CN)_4.2C_6H_6$, Hofmann type mixed cryst., mag. props. 79—4659
- $Mn_xCd_{1-x}Se$ single crysts., photoluminesc., composition depend. 80—80854
- $Mn_xCd_{1-x}Te$, far IR refl. spectra, phonon spectra 78—52497
- $Mn_xCd_{1-x}Te$, lattice vibrs., Raman and IR spectra meas. 80—93311
- $Mn_xCd_{1-x}Te$, phonons, Raman scatt. and IR absorpt. meas. *(French)* 80—97275
- MnO-CdO, solid solns. prep., struct. 78—95157
- $(NH_3$-$(CH_2)_2$-$NH_3)Cd_{1-x}Mn_xCl_4$, Mn^{2+} single ions, clusters and layers, ESR study 79—78507
- NH_4CdCl_3, X-ray cryst. struct. refinement by blocked least-squares method 79—1404
- $(NH_4)_2Cd_5Fe_3Al(SO_4)_{12}.18H_2O$, EPR above ferrimag. transition 78—10762
- $(NH_4)_2Cd_2(SO_4)_3$, dielec. and spontaneous polarisation, −195 to −180°C, particle size depend. 80—97200
- $(NH_4)_2Cd_2(SO_4)_3$:Mn^{2+}, $UO_2{}^{2+}$, luminesc., vibr. modes 79—38629
- $(NH_4)Cd[PO_3OH](OH)$, cryst. struct. of second modification 77—1115
- $(NH_4)Cd_6[P_2O_7]_2[P_3O_{10}]$, with mixed anion radical, cryst. struct. by X-ray anal. 79—86771

cadmium compounds continued
- $(NH_4)Cd[PO_4].H_2O$, B phase, cryst. struct. refinement, X-ray diffr. meas. 78—2095
- NaBr, XPS, satellite of Br 4s line 78—56556
- $Na_2CO.2CaCO_3$, shortite, cryst. struct. and space group, pyroelec. effect 79—23573
- $(Na_{1-x}Cd_x)Cd_2(PO_4)(PO_{3+x}(OH)_{1-x})$, cryst. struct. determ. 79—23589
- $(Na_{1-x}Cd_x)Cd_2[PO_4]\{PO_{3+x}(OH)_{1-x}]$, cryst. struct. determ. 77—15387
- $Na_2Cd_3Si_3O_{10}$, cryst. struct. 78—83801
- $Na_4Cd_2[Si_3O_{10}]$, cryst. struct. determ. 79—14778
- NaCl:$CdCl_2$, sintering in air, densification kinetics and mechanism 77—4750
- NaCl-CdO heterojunction form. in cathode-plasma dyeing, temp. depend. *(Russian)* 78—67710
- $NaHCd_4(Ge_5O_{15})$, cryst. struct., comparison with natural rhodonite 78—30600
- $NaHCd_2(Si_3O_9)$, synthetic cryst., refined struct. 79—86763
- $Ni_{1-x}Cd_xFe_2O_4$, mag. props. rel. to ionic struct. 80—75756
- $Ni_{1-x}Fe_2O_4$ ferrites, mag. thermal expansion anomaly 77—69595
- NiO-CdO-Fe_2O_3 system, phase equilibria 79—11582
- P_2O_5-CdO photochromic glasses, Weigert effect *(Russian)* 77—1690
- P_2O_5-K_2O-CdO-Na_2O glass:Nd^{3+}, highly doped, spectroscopic props. and CW laser action *(French)* 79—41385
- Pb-Cd-Te, microhardness meas. as function of applied load, elec. props. exam. 78—48493
- Pb-CdS-In Josephson junction, light-sensitive, structural fluctuations *(Russian)* 78—56265
- $Pb_{1-x}Cd_xS$, epitaxial, resist. and Hall coeff., substrate temp., thickness and comp. depend. 78—72290
- $Pb_{1-x}Cd_xS$ epitaxial layer, metastable, optical props. and electronic struct. 79—15543
- $Pb_{1-x}Cd_xS$ metastable epitaxial films, growth and physical props. 78—27417
- $Pb_{0.95}Cd_{0.05}Te$, solid solns., thermoelec. power and Hall effect under hydrostatic press. 79—23990
- $Pb_{1-x}Cd_xTe$, IR absorpt. study of Cd impurity levels, energy gaps 80—45081
- $Pb_3MgNb_2O_9$-CdS, electro-optical space-time light modulation 78—18056
- PbO-B_2O_3-SiO_2-Li_2O-ZrO_2-CdO, coloured, glass enamel, chemical durability and microstruct., CdO addition effect 79—29256
- PbS photocells, multicolour detectors in combination with Si photodiodes *(Czech)* 79—26126
- PbS-CdSe, phase boundary processes 78—71857
- PbSe-CdSe heterojunction, elec. props. 77—1478
- $xPbTiO_3+(1-x)PbCd_{1/3}Nb_{2/3}O_3$, phase transition spread, polarisation relaxation, dielectric susceptibility *(Russian)* 80—75922
- $PbZrO_3$-$PbCd_{0.5}W_{0.5}O_3$, phase transitions 78—43817
- Pd-CdS-In, tunnel junction, light induced DC Josephson current 79—47204
- $PdPb(OH)_6$, cryst. struct. determ. *(French)* 77—47419
- RbBr-$CdBr_2$-H_2O, Gibbs free energy, H_2O activity, 25°C *(Russian)* 78—31678
- $RbCdBr_3$, cryst. struct., X-ray diffr. 77—19917
- $RbCdBr_3$, polarised Raman spectra 78—76443
- $RbCdCl_3$, crystal struct., polarised Raman spectra and X-ray diffraction obs. 78—76443
- $RbCdF_3$:Cr^{3+}, EPR meas. of phase transition 79—61206
- $RbCdF_3$:Gd^{3+}, $O_h{}^1$-$D_{4h}{}^1$ struct. transition, ESR obs. 80—50178
- $Rb_2Cd_2(SO_4)_3$, pyroelectric and dielectric props., ferroelectric transitions 79—38458
- $Rb_2Cd_2(SO_4)_3$ single cryst., growth and phase transitions 79—33918
- RbCl-$CdCl_2$-H_2O, Gibbs free energy, H_2O activity, 25°C *(Russian)* 78—31678
- RbI-CdI_2-H_2O, Gibbs free energy, H_2O activity, 25°C *(Russian)* 78—31678
- Si-CdS heterojunction, radiation detector for integrated optics *(Czech)* 80—33227
- Si-CdS heterojunction memory diodes, switching process 78—80046
- $Sr_{1-x}Cd_xF_2$, lattice dynamics 78—75763
- p-Te, photocond. and lifetime, surface trapping, spectral distrib. 78—34840
- Te-CdS-Te contacts, ohmic nature, monitoring method 77—39935
- Te-Se-CdO struct., fabrication and characts. 78—76106
- $(Tl,NH_4)_2Cd_2(SO_4)_3$, langbeinite type mixed cryst., ferroelec. transitions, dielec. and elastic meas. 78—2810
- $Tl_2Cd_2(SO_4)_3$ single cryst., growth and phase transitions 79—33918
- V-CdS-In Josephson structures, light-sensitive 79—99660
- V-CdS-In preparation and behaviour obs. Josephson junctions 80—100559
- $(YCdYbBi)_3(FeAl)_5O_{12}$, cylindrical domain wall vel. anisotropy *(Russian)* 77—59440
- (Zn, Cd, Hg)S:Cu,In, electroluminesc. temp. depend. 77—1732
- (Zn,Cd,Hg)S:Cu,In, electroluminesc., brightness waves 77—59616
- $(Zn,Cd)Cr_2S_4$ and (Zn,Cd)S solid soln. equilib. composition *(German)* 77—36486
- (Zn,Cd)S:Cu,Al, luminesc. efficiency deterioration due to surface oxidation by $(NH_4)_2Cr_2O_7$ thermal decomp. 80—29810
- ZnCdS:(Cu+Ag) binder layer for electrophotography 80—4797
- ZnCdS:Ag, phosphor screen, electron beam excited, light ang. distrib., modulation transfer function 80—45150
- (ZnCd)S:Ag phosphor, absolute efficiency under fluoroscopy conditions 78—73203
- ZnCdS:Ag screen, electron beam excited, light emission spectra 80—25466
- ZnCdS:Cu, binders effect on electrophotographic characts. 79—80712
- ZnCdS:Cu, high field photoconduction in binder layer 79—47121
- ZnCdS-Ag binder layers, electrophotographic characts. eval. for use in charge transfer electrophotography 77—41714
- n-ZnCdS-PTA, photosensitive powder mixed with electrochromic material, photoinduced coloration and electrochem. bleaching 77—81082
- $Zn_{0.1}Cd_{0.9}S$, two-photon and two-step absorption of light 80—7389
- $Zn_{0.1}Cd_{0.9}S$:Cu, doping effect on two-photon absorpt. spectra, deep levels 77—69870
- $Zn_{0.1}Cd_{0.9}S$-CdTe p-n junction, prep. by spray pyrolysis, photovoltaic props. 78—60196
- $Zn_{0.35}Cd_{0.65}S$ binder layers, doped and undoped, xerographic characts. 79—56288
- $Zn_{1-x}Cd_xS$ films, polycryst., reactively sputtered, MSM struct. obs. of dielec. props. and cond. mechanism *(French)* 78—14841

cadmium compounds continued
$Zn_{1-x}Cd_xS$, graded comp. semicond., tunable narrow-band filter, 4272 to 4584 Å 77–31128
$Zn_{1-x}Cd_xS$ mixed crystals, Raman spectra between frequencies LO(Γ) to TO(Γ) 78–2854
$Zn_{1-x}Cd_xS$, reactively sputtered polycryst. film, cond. mechanism and grain boundary barriers *(French)* 77–76972
$Zn_{30}Cd_{70}S$ ceramic, electroluminesc., stationary thermostimulated cond. 79–87120
$Zn_xCd_{1-x}S$, bound-exciton lines, compositional fluctuation-induced broadening 80–2846
$Zn_xCd_{1-x}S$ epitaxial layers, elec. resist. and luminescence obs. 78–19540
$Zn_xCd_{1-x}S$ film, optimal synthesis conditions for single cryst. growth 80–100776
$Zn_xCd_{1-x}S$ film, prep. by soln. spray method, and struct., optical and elec. props. 78–52666
$Zn_xCd_{1-x}S$ film, prep. and use as heterojunction optical energy converters 79–95488
$Zn_xCd_{1-x}S$, film for heterojunction solar cell 77–8208
$Zn_xCd_{1-x}S$ films, spray pyrolysis, elec. props. 80–75657
$Zn_xCd_{1-x}S$, forbidden band width, exciton refl. and luminesc. meas. 78–10947
$Zn_xCd_{1-x}S$, graded single crysts., laser or electron beam excited, luminesc. 77–85792
$Zn_xCd_{1-x}S$, granulated films, optical reson. 79–4863
$Zn_xCd_{1-x}S$ laser beam spontaneous action *(Russian)* 77–88820
$Zn_xCd_{1-x}S$, laser damage, self-focusing influence 78–50844
$Zn_xCd_{1-x}S$, lasing modes and spatial distrib. under one-photon excitation, cavity model 78–74913
$Zn_xCd_{1-x}S$ layers on ZnS substrate, VPE growth 77–77420
$Zn_xCd_{1-x}S$ monocrystal, optical and nonlinear optical characts. *(Russian)* 79–98442
$Zn_xCd_{1-x}S$ monocrystal petal lasers, single-photon excitation *(Russian)* 80–99736
$Zn_xCd_{1-x}S$, platelet single cryst. one-photon optical excitation, spatial distrib. and mode struct. of laser emission 79–31912
$Zn_xCd_{1-x}S$, reflectivity spectrum, excitons and energy band struct. 77–55804
$Zn_xCd_{1-x}S$, resonance Raman scatt. involving exciton complexes 80–16039
$Zn_xCd_{1-x}S$ solid soln. film by spray pyrolysis 77–81214
$Zn_xCd_{1-x}S$ solid soln. films, reactive cosputtering, struct., comp. and opt. absorpt. edge *(French)* 78–6237
$Zn_xCd_{1-x}S$ substrate, rough, lattice mismatch with Cu_2S and InP films 78–43263
$Zn_xCd_{1-x}S$, thin solid soln. films, vapour deposited, elec. and optical characts. 80–60110
$Zn_xCd_{1-x}S$:Cu, photoluminesc., Birman effect *(Russian)* 79–28837
$Zn_xCd_{1-x}S$:Cu, photoluminescence 80–29783
$Zn_xCd_{1-x}S$:Cu, thermoemission of positive ions in simple gas atmos. *(Russian)* 77–28676
$Zn_xCd_{1-x}S$:Cu crystallophosphors, spectra of IR electrophotographic sensitivity *(Russian)* 80–50423
$Zn_xCd_{1-x}S$:In, low resist. film for solar cell window 78–71200
$Zn_xCd_{1-x}S/Cu_2S$ heterojunction solar cells, fabrication and performance 79–79397
$Zn_xCd_{1-x}S/Cu_2S$ heterojunction solar cells, junction anal. 79–92080
$Zn_xCd_{1-x}S$/GaAs heterojunction solar cells, meas. of minority carrier diffusion length 80–26158
$Zn_xCd_{1-x}S$-Cu_2S heterojunction solar cells, props., comp. meas. of interfacial region 80–81472
$Zn_xCd_{1-x}S_ySe_{1-y}$, energy bandgap and lattice constant contours 80–103622
$Zn_xCd_{1-x}S(Te)$, solid soln., broadening of exciton states, depend. on conc. 79–73449
$Zn_xCd_{1-x}S_yTe_{1-y}$, energy bandgap and lattice constant contours 80–103622
p-$Zn_{0.1}Cd_{0.9}Sb$, thermoelec. anisotropic semicond., carrier kinetics at low temps. 80–92893
$Zn_{0.1}Cd_{0.9}Sb$, thermoelectrically isotropic semicond., carrier kinetics in intrinsic cond. range 80–92894
$Zn_{1-x}Cd_xSe$, mixed crystals, antireson. in phonon spectrum, Raman spectroscopy 80–88992
$Zn_xCd_{1-x}Se$, exciton reflection spectra anomalies *(Russian)* 80–97304
$Zn_xCd_{1-x}Se$, vacuum condensates, forbidden band width determ. from transmission spectra 77–8670
$Zn_xCd_{1-x}Se_yTe_{1-y}$, energy bandgap and lattice constant contours 80–103622
$Zn_{1-x}Cd_xTe$ p-n junctions, LPE growth process, elec. props. 77–7981
$Zn_xCd_{1-x}Te$, absorpt. edge luminesc. on high-intensity excitation 78–6745
$Zn_xCd_{1-x}Te$ films, absorpt. spectra in 3.0 to 5.8 eV range 79–52034
p-$Zn_xCd_{1-x}Te$, negative photocond. excited by fundamental absorpt. region light 77–15905
$Zn_xCd_{1-x}Te$, reflection spectra, energy band struct. comp. depend. *(Russian)* 78–56500
$Zn_xCd_{1-x}Te$, relaxation processes, emission spectra *(Russian)* 78–72598
$Zn_xCd_{1-x}Te$, reson. Brillouin scatt. meas. using injected acoustic domains 78–27243
$Zn_xCd_{1-x}Te$, reson. Brillouin scatt., acoustic domain injection 79–38557
$Zn_xCd_{1-x}Te$, reson. Raman scatt. of light by longitudinal optical phonons 77–28577
$Zn_xCd_{1-x}Te$, resonant Brillouin scattering *(Japanese)* 79–15474
$Zn_xCd_{1-x}Te$-P, vibr. modes of defects, IR absorpt. expts. 77–62601
$ZnCl_2$-$CdCl_2$, molten, viscosity coeff. meas. *(Japanese)* 79–77662
$ZnCl_2$-$CdCl_2$ melt, Raman spectra, struct. anal. 79–38549
ZnO/CdTe heterojunctions and ZnO films preparation using spray pyrolysis 80–96985
ZnS-CdS, equimolar solid soln. formation kinetics 80–39289
ZnS-CdS, fluorescent screens for thermophotography 77–171
ZnS-CdS films, prep. by atomisation 80–16176
ZnS-CdS solid soln., phase transform. during crystn., 850 or 1150°C 77–48362
ZnS-CdS system, IR luminesc. and absorpt. centres, donor-acceptor pair model 77–44043
ZnS-CdS system, solid soln. form. mechanism 79–43177
ZnS-CdS:Ag, cathodoluminesc. yield, calorimetric method determ. *(Russian)* 77–20938
ZnS-CdS:Ag, Ni, Co, thermoluminesc. glow curves 78–95611
ZnS-CdS:Ag, Ni, Co phosphor, thermoluminesc. 77–66547

cadmium compounds continued
ZnS-CdS:Ag, Ni luminophor, temp. sensitive, biological effects of microwaves determ. appl. 80–36186
ZnS-CdS:Ag, phospors, nature of fluorescent centres and traps 79–91484
ZnS-CdS:Ag(Cu), cathodoluminesc. investig., appl. to cathode ray tube screening 80–108282
ZnS-CdS:Ag(Cu), cryst. struct., electron traps and glow curves 79–61437
ZnS-CdS:Ag(Ni)(Co), electron-irradiated phosphors, void formation mechanism 79–55780
ZnS-CdS:Tm,Ni, recomb. centre interaction, luminesc. quenching 78–10946
$(ZnS)_{0.2}(CdS)_{0.8}$, elec. props. effect of wurtzite-sphalerite boundary 77–55531
ZnSe-CdTe heterojunction, radiative recomb., electrolum. obs. 77–32445
ZnSe-CdTe heterojunction, cathodolum. and electrolum. 78–6782
ZnSe-CdTl, epitaxial film, cond. transition, laser switched memory *(Russian)* 77–8182
$(ZnSe)_x(CdTe)_{1-x}$, low temp. photoluminesc. *(Russian)* 78–43931
ZnTe-CdS(Se)(S_xSe_{1-x}) heterojunctions, prep. and electrolum. characts. 77–24610
ZnTe-CdSe, solid soln. formation and effects 78–27489
ZnTe-CdSe heterojunction, radiative recomb., electrolum. obs. 77–32445
ZnTe-CdSe solid solutions, phase equilib. *(Russian)* 79–43224

caesium
see also nuclei with ......
$6^2S_{1/2}$-$6_2P_{3/2}$ transition (λ=8521 Å) with hyperfine splitting, curves of growth 78–66513
absorbed layer on Pt(100) surface, LEED intensity spectra, τ-matrix interpretation method 77–15673
absorption on stainless steel oxides, meas. of contamination using washing test 78–62597
accommodation coefficients, of Na, Rb and Cs on Ni, 658-1095K 77–47666
adatom-Au surface interaction, polarisation energy from opt. data 77–72792
adsorbed Cs and Cs-O on Ag, surface plasma waves, ATR study 80–39451
adsorbed layer on Cu (111) surface, oxidation effect on UPS 79–78826
adsorbed layer on Pt (100), surface struct., LEED anal. 77–89654
adsorbed on Cu (100), work function influence of coadsorbed O_2 79–15014
adsorbed on Cu (111), XPS exam. of Cu surface state and Cs valence electrons 79–19647
adsorbed on graphite, dissolution, lamellar cpd. form. *(French)* 80–100399
adsorbed on metal, effects on photon and secondary ion emission during sputtering 80–35038
adsorbed on Ni (100) surface, electron binding energies of core levels 78–18896
adsorbed on Si and Ge (100), negative electron affinity surfaces, thermal stability of work fn. 78–92167
adsorbed on W (001), core-level photoemission anisotropy 78–11076
adsorbed on W (001) face, thermal desorption kinetics 79–28210
adsorption, jointly with O, on Mo (110) and (111) faces, and emission props. 78–2364
adsorption, on Cu (111), photoelectron spectra, angle averaging 79–83100
adsorption, on GaP (001), photoemission meas. 78–87874
adsorption, on Mo (100), negative ion form. by sputtering, work function depend. 78–39645
adsorption, on transition metal carbides, adsorpt. energy, thermionic emission 77–7978
adsorption, on W, work function, field emission meas. surface film effects 78–19645
adsorption, on W single cryst. faces, evap. isotherm 79–24829
adsorption and absorption on oxidised stainless steel 78–84061
adsorption and desorption on GaP and GaSb, LEED, AES, and photoemission meas. 80–70532
adsorption behaviour of Cs, trace quantities in NaCl soln., seawater *(Russian)* 77–73766
adsorption by Al_2O_3, radioactive waste storage 80–99240
adsorption of Cs, Cs+O on GaAs (111) epitaxial film, ellipsometric study 80–29282
adsorption of ions on surface coating constituent mats. 78–23843
adsorption of one atom on GaAs (110) face, mol. orbital study *(French)* 78–38958
adsorption on Cu(111), struct. and electronic props. 78–23147
adsorption on Cu (111), electronic surface band energy 80–2443
adsorption on Cu (111), surface band energy shift, angle-resolved UPS study 80–40228
adsorption on GaAs (110) 77–72794
adsorption on GaAs (InSb), LEED, AES, EELS study 78–68068
adsorption on GaAs epitaxially grown (001), (111) and $(\bar{1}\bar{1}\bar{1})$ surfaces 78–38924
adsorption on GaP (100), negative electron affinity surface prod. 80–10768
adsorption on Ge (111), effect on surface elec. props. 79–90880
adsorption on MgO, AES, LEED, work function, and secondary electron emission meas. 80–44407
adsorption on Mo covered with O_2, struct., emission props., thermal stability 80–66878
adsorption on MoS_2, LEED, Auger and work function meas. 78–71994
adsorption on n-GaAs (110) and p-Ge (111) surfaces, work function meas., adsorption site model 79–23839
adsorption on $NbSe_2$, 200-300K 78–26767
adsorption on oxygenated and oxidised W (110) 80–44424
adsorption on Pt, field-emission microscopy 78–51822
adsorption on Si (100)2×1 surface, LEED 77–62747
adsorption on Si (111), LEED, work function and thermal desorpt. 78–14590
adsorption on Ta, direct meas. of adsorpt. isobars 78–43235
adsorption on W (110)(112) and Mo (110), work function and thermal stability 80–44427
adsorption on ZnO $(000\bar{1})$ of alkali metals, anomalous behaviour of Na 78–79883
adsorption with O_2 on GaAs (110) 80–10793
arc, excitation and ionis. in nonequilib. plasma 78–18461
arc, low-voltage hot-cathode, plasma production and props. 77–27766

caesium continued
  arc, quenching at low Cs press. 78—5976
  atom, 16^2P states, reson., 3-photon ionisation, DC Stark effect 78—42026
  atom, 1st reson. level, effective electron-ionis. cross sections, plasma discharge method 78—13603
  atom, $4d^{10}$ shell, photoionisation cross sections, electron shell alterations determ. *(Russian)* 80—58144
  atom, $4d^{10}$ subshell photoionisation cross section, electron shell rearrangement 77—14400
  atom, 5^2D-n^2F series fine and hyperfine struct. 80—43201
  atom, $5p^56s^2\ ^2P_{3/2}$ autoionising level, ejected electron excitation function, reson. 77—58167
  atom, $5p^56s^2$ level, Hartree-Fock calcs. 79—59349
  atom, $6S_{1/2}$-$7P_{1/2}$ transition , photon echo polarisation rotation in mag. field 78—22180
  atom, $6s^2S_{1/2}$ to $5d^2D_{5/2}$ transition, stimulated electronic Raman scatt. 79—41411
  atom, 6s, photoelectron ang. distrib., anisotropic effects 78—50514
  atom, 6S-7S, parity violation search in highly forbidden mag. transition 78—82709
  atom, 6s-9p doublet, Xe perturbations, simultaneous additive effect on multiple satellite lines 79—76389
  atom, 6s-electron photoionisation, ab initio calcs. 80—91523
  atom, $7^2P_{3/2}$ sublevels, hyperfine struct., multiphoton elec. dipole transitions anal. 80—32692
  atom, 7^2P excited states, photoionisation cross section meas. 77—18858
  atom, $7P_{3/2}$-$6S_{1/2}$ transition, photon-echo quantum beats obs. 80—23373
  atom, 8S hyperfine splitting, two-photon transition and fluoresc. meas. 78—37585
  atom, 8S level lifetime meas., cooperative effects in EM cascade 77—30818
  atom, $^2P_{1/2}$ and $^2P_{3/2}$ levels lifetimes, Xe collisional effect 77—3307
  atom, ablated in hypersonic wake, excitation temp. meas. by atomic spectral line relative intensities 80—43732
  atom, analytic SCF HF ground state wave function, ionis. pot., mag. props. 77—18785
  atom, assoc. ionisation, in low press. discharge, 6P and 5D states effects 77—75284
  atom, assoc. ionisation, in low press. discharge, upper and intermediate states effects 77—75283
  atom, cascade-free radiative lifetime, modulated or deflected CW dye laser method determ. 78—25754
  atom, coherence of HFS excitations in optically orientated ats. mag. field modulation *(Russian)* 77—54530
  atom, coherent two-photon reson. and Doppler free population inversion 77—643
  atom, collisions between excited atoms, highly excited states excitation 78—17771
  atom, core charge polarisation effects, dipolar contributions 79—45631
  atom, cross-section meas. for four-photon ionisation 77—42297
  atom, direct meas. of 7P doublet state lifetimes by pulsed dye laser 79—786
  atom, discrete level raising into far continuum, oscillator strength to shape reson. transfer 78—78624
  atom, ejected electrons from autoionis. levels excited by electron impact 77—88573
  atom, elastic electron scatt., 0.8-20 eV, reson. structs. 78—5353
  atom, elec. dipole approx. and elec. quadrupole resons. allowed in multiphoton absorpt. *(French)* 78—5190
  atom, electron elastic scatt., polarisation and ang. distrib. meas. 79—89781
  atom, electron excitation cross sections for six autoion. config., Born approx. calc. 78—25713
  atom, electron impact excitation velocity consts. for reson. levels, meas. *(Russian)* 78—1086
  atom, electron-atom momentum transfer cross sections, from plasma electron thermal conductivity 78—42224
  atom, emission meas. in wing of self-broadened reson. line 77—50400
  atom, excited np states, fine struct., core electrons effect 77—18807
  atom, excited state, two-photon ionisation by ruby laser light 78—74621
  atom, excited states photoionis. cross-section, quantum defect method 78—25494
  atom, F Rydberg state emission oscill. strength minima 80—32662
  atom, F-levels lifetime meas. using partially superradiant population 80—9575
  atom, fine struct. meas. of highly excited F states 78—21871
  atom, fine-struct. of excited nd and nf states, at. core effect 78—58606
  atom, fluoresc., far wings profile of self-broadened reson. lines 79—76388
  atom, fluorescence spectra, time-resolved, collisional perturbation of Rydberg states 77—83529
  atom, forbidden M1 transitions, parity nonconserving effects 78—21844
  atom, four photon ionis., strongly interacting resons. theory 80—52955
  atom, four-photon ionis., near 6F reson., rate theory 80—9568
  atom, four-photon ionisation, new resonances 78—5187
  atom, four-photon ionisation, reson. effects 79—45689
  atom, four-photon resonant ionisation calculations 78—37613
  atom, g-factor anomalies and strongly forbidden M1 transitions 78—78825
  atom, ground state, photoionisation cross-section meas. 77—57949
  atom, He IIα $5p^{-1}$ photoelectron spectrum, config. interaction effects 80—5510
  atom, HFS of first doublet, He, Ne and Ar press. effects 77—38638
  atom, HFS pressure effect determ. from absorption coeff. profiles 80—106299
  atom, hook spectra, evaluation limitations 80—90905
  atom, hyperfine struct. density and temp. shift coeffs., at high buffer gas densities 79—18138
  atom, inner core neutral binding energies, relaxed orbital relativistic Hartree-Fock-Slater calc. 78—13433
  atom, L-shell internal excitation accompanying L-capture 80—95726
  atom, multiphoton ionis. cross sections, absolute meas. evaluation 80—14122
  atom, multiphoton ionisation, rel. to light statistics 79—72287
  atom, multiphoton ionisation, reson. peak amplitude, temporal effects 78—78760
  atom, multiphoton ionisation, reson. shift obs. 77—445
  atom, multiphoton ionisation, resonant, with intense monochromatic laser 80—32689
  atom, n=15-17 f-g interval meas. 80—91477
  atom, natural and effective lifetimes meas. for 10 P states 79—26934

caesium continued
  atom, optical pumping with second resonance light 80—23376
  atom, optical reson. line electron impact excitation cross sections, polaris. 78—55244
  atom, optical transitions, struct. of weak neutral currents *(Russian)* 77—88420
  atom, optically oriented, RF coherency on HFS transition excitation by AM UHF mag. field *(Russian)* 77—42278
  atom, orientation in CsI photodissociation by UV light *(Russian)* 80—69201
  atom, oscill. strengths of principal series doublets 79—13671
  atom, oscillator strength meas. by tunable laser interferometry 80—105697
  atom, oscillator strengths in principal series, Rozhdestvenskii hook obs. 80—37760
  atom, outer-shell photoelectron ang. distrib. 80—37797
  atom, P,D,F, and G Rydberg states, quantum defects and fine struct. 80—5496
  atom, parity non-conserving E1 matrix elements, many body calcs. 80—47924
  atom, parity nonconservation in light absorption 79—10086
  atom, parity violation in atomic electrons and electron-electron interaction effects 79—54788
  atom, photoabsorption oscillator strengths, $17<n<\infty$ transitions, interpolation formula 80—9559
  atom, polarisability constant, Stark interaction for excited states, laser spectroscopy 77—50404
  atom, polarised photoelectrons produced by circ. polarised synchrotron radiation 80—18830
  atom, proportional counter pulse height fluctuations, resonant ionisation studies 78—90025
  atom, pulsed 4-photon 6f-reson. ionis. 80—18831
  atom, quadrupole lines, oscillator strengths, broadening 77—18846
  atom, radioisotopes, hyperfine spectroscopy, nucl. charge radius, ground and isomeric states 80—57677
  atom, reson. lines, slow electron excitation cross section, low-lying D level coupling 77—23563
  atom, reson. multiphoton ionis. 79—41146
  atom, reson. multiphoton ionisation by pulsed excitation, Beers-Armstrong model 78—17645
  atom, reson. multiphoton ionisation by ultrashort laser pulses, 1.06 μm 78—58630
  atom, reson. multiphoton ionisation near 6f reson., effective nonlinearity order 80—32688
  atom, resonant multiphoton ionis. 79—36589
  atom, resonant multiphoton ionisation, spatio-temporal effects 80—37794
  atom, resonant multiphoton ionisation *(Russian)* 79—3421
  atom, resonantly excited in cylindrical discharge plasma, effective lifetimes 78—79413
  atom, Rydberg S and P states, hyperfine struct., RF spectroscopic meas. 77—57911
  atom, Rydberg states, diamag. and collisional perturbations 80—58181
  atom, scattering at high-energies, intermol. potential determ. 77—46609
  atom, self-broadened first reson. lines, near-wing asymmetries 80—9535
  atom, self-broadening of Doppler-free two-photon lines 79—41135
  atom, single pulse superfluoresc. 77—79573
  atom, strongly forbidden M_1 transitions, g-factor anomalies *(Russian)* 78—78648
  atom, superfluorescence, comparison with theory, quantum beat spectroscopy appls. 78—86837
  atom, superfluorescence, quantum beats 77—42275
  atom, superfluorescence *(Dutch)* 78—70780
  atom, superradiance triggering spectroscopy 80—52324
  atom, term dependence of position of 4f electron in $4d^94f$ configuration 77—26973
  atom, three-photon 16p reson. ionis. and DC Stark effect 80—14124
  atom, three-photon ionisation, reson. and AC Stark effects 77—68020
  atom, transition probability of valence shells, relativistic pseudopot. calc. 78—86803
  atom, transverse relax. in strong reson. RF field 78—5323
  atom, two photon ionisation, destructive interference effect 80—74153
  atom, two-photon, photoionisation theory 77—6741
  atom, two-photon ionis., profiles of $6^2S_{1/2}$-$7^2P_{1/2,3/2}$ lines 80—958
  atom, two-photon ionis. rates for linear and circular polaris. 77—50416
  atom, two-photon ionis. via $6^2P_{3/2}$ state, photoelectron spin polarisation 77—3328
  atom, two-photon ionis. via $7^2P_{1/2,3/2}$ intermediate states 77—57946
  atom, two-photon ionisation, 6s-6d quadrupole resons., ion asymmetry and spin polarisation 79—72286
  atom, two-photon ionisation, effective order nonlinearity var. 80—106304
  atom, two-photon ionisation rate, time depend. 79—31622
  atom, two-photon spectra, energy levels for highly excited ^{2}F states 78—70805
  atom, two-photon two-channel ionisation, laser bandwidth effect 79—59516
  atom, Xe broadened principal series lines, absorption meas. Cs-Xe pots. 77—79584
  atom, Xe collisions-induced 6s-ns transitions in absorpt. spectrum 78—9101
  atom, Xe perturbed emission lines, satellites in square well pot. approx. 78—46303
  atom, XPS, free atom core binding energy 78—74699
  atom+inert gas, D_2 line collisional broadening and shift, and HFS 79—22664
  atomic, photoionisation cross sections determ. in vacuum UV using Xe excimer laser 80—102494
  atomic beam, fast, collinear laser spectroscopy 78—37078
  atomic beam, optical pumping and detection of 0-0 transition 79—18158
  atomic beam frequency standard performance and environmental effects 77—37858
  atomic beam hyperfine optical pumping, appls. 77—75108
  atomic beam tube operation at HFS level transition in absence of Zeeman splitting 77—82482
  atomic beam tube velocity distributions 77—37856
  atomic beams, pulsed high-density source 78—17825
  atomic clock, laser synchronisation between observatories of Paris and San Fernando *(French)* 78—89461
  atomic clock, long beam, primary standard, accuracy, reliability 78—89454
  atomic clock, standard at Radio Research Lab., Japan 79—21714
  atomic clock using laser optical pumping of Cs beam 80—101785

caesium continued
atomic energy level ordering, in excited states 79—81162
atomic excited state, laser photoionisation theory, hyperfine coupling effect 80—102493
atomic excited states population in arc 78—26368
atomic freq. standards, Millman effect on freq. shift 78—32797
atomic frequency standard, Millman effect origin and expt. determination 77—5810
atomic frequency standard, optically pumped, buffer gas mixture optimisation 77—37859
atomic HFS of optically inaccesible excited states 78—37582
atomic photoionisation, ion alignment, many electron correl. effect 78—74622
atomic Rydberg states, principal series doublets, intensity ratio anomalies 79—18148
atomic Rydberg states collisional ionis. 79—64097
atomic time standard data combination 77—5814
atomic vapour, f-value determ. method using stimulated electronic Raman scatt., appl. to Cs 78—82693
atoms, 2-photon and 4-photon ionisation cross-sections, absolute determ. 80—83326
atoms, HFS, isotope shift related to nucl. charge rad. 78—78826
atoms, laser beam excitation, multipass, optical pumping and weak neutral current parity violation 80—58207
atoms, optically pumped, spin relax. in presence of N$_2$ 79—59420
beam clock development for satellites 78—57910
beam deflection system for time and freq. primary standard 78—89453
beam frequency standard design for satellites 78—57911
beam frequency standard drift and noise performance rel. to velocity distributions 78—57912
beam frequency standard errors due to excitation asymmetries 77—5816
beam frequency standards, quadrupole and hexapole magnet combination 77—5813
beam tube frequency standard design and construction 79—54103
cathode, hollow, Cs-film coated, intermediate press. arc operation 80—6305
CESR linewidth and g-shift in presence of spin-orbit perturbation, spin-phonon scatt. 77—63285
chemisorption on GaAs, isobars, LEED and loss spectroscopy meas. 77—4262
coadsorbed with O$_2$ on W (100), high photoemission efficiency 77—55862
coadsorption, with O$_2$, on W(110) surface 77—89656
coadsorption with Ba on W (110), work function of surface under equilibrium conditions 79—15025
coated GaAs film, secondary emission characts. 78—2957
coated GaAs photoemitter, negative electron affinity, fabrication and characts. 78—2979
coated graphite emitter, for thermionic cell 79—11494
coated oxidised W, thermionic emission, 450-800K 78—2972
coated Si photoemitter, achievement of negative electron affinity 78—2980
coated W and Ni surfaces, survival probabilities of H$^-$ ions 80—45187
coating on MgO secondary emitter, increasing of emission efficiency 78—2960
codeposition with O on W (110), Cs$_2$O form. 80—44425
condensation on fused quartz meas. by torsion microbalance *(German)* 77—35839
conduction-electron spin flip by phonons, expt. data anal. 79—61219
cooperative cascade emission transitions 80—14120
corrosion effect on stainless steel, Te effects 78—23866
corrosion of strontium alumoborosilicate glass by Cs vapour or liq. 77—16706
critical exponent β, for liq.-vapour coexistence curve 77—76538
crustacean neuromuscular junctions, synaptic facilitation obs. 79—39412
crystal struct., van der Waals and repulsive interaction 80—84137
crystal structure, effect of Van der Waals forces 79—99111
dense plasma, elec. and radiative heat cond. evaluation 78—71452
dense plasma, ionisation equilib. and cond., ion clusters effects 80—75032
dense vapour, anomalously large elec. cond., positive complex ions form. 80—19547
desorption dynamics on W, surface ionisation voltage modulation method 80—44426
desorption from graphite, release in nucl. reactor coolant 80—18431
detection, picogram sensitivity, in aq. soln., nonflame atomic fluoresc. spectroscopy with dye laser excitation 77—44528
diffusion in Ar, time-resolved meas. 77—90588
diffusion in Bi, mechanism 79—77819
diffusion in bitumen block coating, radioactive waste treatment *(Russian)* 80—52771
diffusion in graphite 77—7901
diffusion in high temp. alloys, AES, SIMS depth profile study *(German)* 78—84008
diffusion in Kr(Xe), determ. of diffusion coeffs. using π-pulse optical pumping method 79—68895
diffusion in Mo, W, divacancy mechanism *(Russian)* 80—70472
diffusion in Silumin, CsSi phase form. 79—38798
diffusion in stainless steel, study using ion beams 77—20125
diffusion pyrocarbon and SiC by post irradation annealing of coated 78—13247
diode with W emitter, current oscills. at low emitter temp. *(Russian)* 78—5952
discharge, high-press. pulsed, in capillary, energy balance diagnostics 77—65920
discharge, hollow cathode, volt-ampere characts. 78—71563
discharge, hot cathode diode, low-press., initial stage transient processes 78—51382
discharge plasma, optogalvanic effect characts. 78—63583
dual atomic beam tube performance 77—37857
EBR II, Cs control by C getter 80—13648
elastic scattering amplitudes, for high energy electron scattering, by ionised atoms, numerical calcs. 80—49057
electrical resistivity, data tables, 1-2000K 79—78072
electrical resistivity and thermal resist. calcs. 79—91016
electronic transition from self consistent APW Xα calcs. 78—51884
entropy change on melting of simple substances, thermal expansion, configurational entropy 80—59630
equation of state meas. 80—19905
equations of state determ. 80—24564
excimer states, molecular satellites of 6^{2}S-7^{2}P doublet 78—17632

caesium continued
exploding wire, striations produced at supercrit. press. 79—64952
exploding wire discharge, thermal instability of elec. cond. in metal vap. 78—1868
F states, radiative lifetime and g-factor determ. 79—41138
Fermi surface, de Haas-van Alphen meas. 78—2411
Fermi surface and quasiparticle props., density functional approx. 80—96771
Fermi-surface press. dependence 80—96772
field desorption and field ionisation on metal surface 80—104047
film, elec. props. *(Russian)* 77—47906
film, inert gas impurities, optical excitation spectra obs. 77—24876
film, on Mo substrate, ang. depend. XPS, depth profile determ. 78—88404
film, work function theory, size effect 78—43460
fission product, release and diffusion in fuel elements *(German)* 78—25298
fission product in coated-particle fuel, conc. determ. using YAG:Nd^{3+} laser 80—18416
flooded on noble metal surface, effect on sputtered negative ion yields 78—11056
fluid, metal-nonmetal transition and mag. interactions 80—49602
fluid, metallic and nonmetallic, mag. props. 80—44799
frequency standard, error due to second order Doppler shift 77—87745
frequency standard, frequency stability *(Japanese)* 77—108
frequency standard, NRLM-I, improvement of freq. stability 78—62184
frequency standard, Ramsey cavity and beam optics design, expt. 78—89456
frequency standard, time scale unit duration estimation 77—74368
frequency standard research at PTB, beam optics, Majorana transitions 79—21709
frequency standards, angular distribution of atomic flux diffusing from rectangular channels 77—87744
frequency standards, freq. offset due to spectral impurities 78—89455
frequency standards, freq. offset due to spectral impurities 79—21710
frozen solution in HMPA, Wannier-Mott impurity ground state, EPR 77—8054
fuel reprocessing waste ^{137}Cs, ^{90}Sr and rare earth radioisotope separation by cation exchange 78—78486
fully-ionised plasma hollow-cathode arc discharge theory 78—67533
gas, optically pumped, spatial distrib. of polaris. 79—76392
gas diffusion of Cs atoms in Ar-methane, by reson. ionis. spectrosc. 79—18984
gas discharge, two-photon ionis. by laser light 78—87534
gas fission product release, effect on LWR fuel performance calcs. 79—31054
GCFR fuel column, effect of Cs migration on fission gas permeability 79—67824
getter development for radiocaesium, obs. of Cs-SiO$_2$-Al$_2$O$_3$ system interactions 80—83208
graphite, Cs-intercalated, melting and staging, X-ray scatt. obs. 79—19180
graphite Cs-intercalated, theory of order-disorder phase transitions 80—19908
Hanle effect magnetometer characteristics and evaluation results 77—79586
heat of desorption from polycryst. W surfaces 80—75430
heat pipe, H atom anal. appl. for plasma 80—70043
hexamethylphosphoramide-K(Cs)(Rb), low temp. glass, EPR of solvated ats. 78—91927
high pressure effect on supercond. and high temp. resist. 77—47917
hollow-cathode plasma jet source 77—84463
impurity in N$_2$-Cu thermal plasma, effect on spectral line intensity *(German)* 78—30417
interaction with graphite, study of surface diffusion, computer simulation 78—30837
intercalation compounds with graphite, low temp. sp. ht. 78—71868
ion migration in basalt, velocities determ, from partition coeffs. 80—37525
ion source, CW monoenergetic, by photoionisation 80—63910
ion source, Penning discharge type, with hollow cathode, HF instabilities 80—43997
ion source, thermionic emission in SF$_6$ mol. gas 80—71557
ions, positive and negative, in thermionic converter, mass spectrometric study 79—19083
isostructural transition and lattice vibrs., relativistic LMTO calc. 80—20074
isotope, neutron deficient, supermultiplet mass predictions 79—85359
L-shell X-ray prod. by H(He) ion bombardment 79—47548
large aperture contact ionized Cs^{+1} ion source for an induction linac for fusion 79—76229
lattice dynamics, modified Bhatia model 77—51455
lattice sp. ht. and thermal vibrs. 78—30768
layer on p-Si(111) surface inversion layer, negative magnetoresist. in 2D impurity band 78—64135
leaching rates from calcined natural zeolites *(Japanese)* 77—67828
leaching rates from calcined zeolites, radioactive waste processing *(Japanese)* 77—61515
liquid, equation of state, vol. and compressibility meas. up to 22 kbar 77—47541
liquid, meas. of density at high temp. and pressures 78—55903
liquid, neutron diffr. struct. anal., density and viscosity temp. depend. 80—6352
liquid, radial distribution functions calc. at 100°C 78—22638
liquid, reduced density, screening, struct. and elec. resist. 78—19016
liquid, resist. and thermo-electric power using corrected parameters of Shaw model 79—19566
liquid, short range order parameters, from information theory 78—83730
liquid, specific heat meas., at temp. up to 1700K under pressure 78—51696
liquid, struct. factors, X-ray transmission diffr. expt. 77—47337
liquid, T$_c$, P$_c$, V$_c$, from eqn. of state 78—2228
liquid, transport coeffs., temp. and press. depend., Enskog theory 78—6170
liquid, vapour press., thermodynamic functions determ., Knudsen-effusion radiotracer method 78—26678
low-level transuranic storage, radwaste Sr, Cs, Co sorption meas. on soil sediment 80—95482
low-temperature erosionless cathode for high current densities 79—64953
LWR, LOCA, fission product source terms 80—13654
LWR fuel rods, power ramp induced I and Cs redistrib. 80—32343

caesium continued
LWR fuel-cladding gap, Cs-U-Zr-H-I-O system, chemical thermodynamics 78—82440
marine pollution, accumulation in muscle tissue of marine fishes 80—35797
maser, freq. standard, stability determ. method 77—83842
maser, optically pumped, cavity, buffer gas, press., temp., freq., characts. 77—10880
melting curve extrema from repulsive step potential, molecular dynamics calc. 77—59102
melting curve maxima simple model 77—43313
melting curve maximum at high press. 80—75337
metal impurity effect on residual elec. resistance *(Russian)* 80—84457
metallic compressibilities, general pseudopotential approach 80—54631
metrological Cs frequency standard MTs-1, description 77—79063
MHD generation appl. owing to low ionisation potentials *(Hungarian)* 80—3526
molecule, 6^2S-7^2P doublet, mol. satellites 79—85956
molecule, ion-pair form. in two-photon absorpt. 77—88507
monolayer on Cu(111), dilution of electron gas by O adsorption, plasmon energy losses 79—47036
multiphoton ionisation through $9D_{3/2}$ level 77—34602
muscle fibres, skeletal, resting, Cs^+ rel. to volt. depend. block of inward K currents 77—52756
muscle single fibres, Rb^+, Cs^+ and Na^+ localisation, autoradiographic demonstration at 77K 79—96726
nerve fibres, myelinated, diffusion of ions 79—24965
neutron activation analysis, in environmental materials, reliability aspects 78—40106
nonideal plasma thermodynamic props., shock wave obs. 78—71434
nonresonance spin echo, transverse relaxation time *(Russian)* 80—50224
NTS-2 satellite Cs frequency standard stability estimates 79—54110
nuclear mag:spin-lattice relaxation times 78—86889
nuclear reactor mixed-oxide fuel, Cs concentration effects 78—82452
one-atom detection by reson. photoionisation spectroscopy, demonstration 77—38742
one-atom detection by reson. photoionisation spectroscopy 77—79706
optical filter, ultrahigh-Q isotropically sensitive, using at. reson. transitions 79—55216
optical functions, effect of surface roughness 78—56447
optically pumped frequency standard stability limitations 79—54104
overlayer on GaAs (110), O_2 adsorption 80—50740
oxidation, adsorbate-induced structs., UPS obs. 79—47828
parametric frequency conversion, of CO_2 laser, by radiation mixing *(Russian)* 78—22175
phase transitions, shouldered hard-sphere pots. calcs. 77—2600
phonon frequencies and Gruneisen parameter, model pseudopotential calc. 77—35643
phonon spectral density, pseudopotential calcs. 80—39234
photoelectron energy distrib. curves, depend. on light polarization 79—15591
photoionisation, 3d subshell absorption spectra 77—10648
photoplasma, effect of H_2 impurities *(Russian)* 77—35320
photoplasma, optical excitation in radiation diffusion conditions 78—55227
plasma, arc hollow cathode, diagnostics 80—44043
plasma, are discharge, negative grid pulse effects, kinetics 80—38843
plasma, CW laser produced, dynamic response to loser modulations 80—14920
plasma, decay in presence of N_2, population inversion 79—55455
plasma, dense, in arc, elec. and heat conds., two-probe diagnostics 80—38560
plasma, dense, nondegenerate, electron transport, thermal cond. *(Russian)* 79—98865
plasma, elec. and radiative thermal conds., expt. data anal. method 78—42717
plasma, elec. cond. and eqn. of state, behind reflected shock wave 78—42716
plasma, elec. cond. meas. 79—64831
plasma, electron-ion pairs, correlated pairs, effect on conductivity 78—26249
plasma, eqn. of state, 30-140 atm, 3000-4000K, by adiabatic compression 78—14132
plasma, eqn. of state 78—42711
plasma, excited atomic state inversion obs. 78—71460
plasma, fully ionized dense, hollow cathode arc, V-I characts. and other props. 79—14627
plasma, generation by adiabatic compression, elec. cond. and thermodynamic parameters meas. 80—59180
plasma, highly ionised, conductivity and eqn. of state 78—26323
plasma, in thermionic convertor, ignited mode, electron energy distrib. meas. *(Japanese)* 80—3528
plasma, in thermionic convertor, spectroscopic meas. of Cs I *(Japanese)* 77—58902
plasma, in through-flow hollow cathode arc mode 79—27837
plasma, Knudsen discharge, longitudinal mag. field, emission polaris. 77—76211
plasma, low-voltage arc in 3-electrode system, grid influence 80—38844
plasma, nonideal plasma press. ionisation, short range forces, thermodynamic props. 80—33733
plasma, ohmic heating, electrical conduction temp. depend. 78—71442
plasma, prod. by resonant light irrad., density profile 77—7563
plasma, thermodynamics of nonideal low-temperature multicomponent plasma: chemical model 79—41796
plasma accelerator with pre-ionised Cs, closed electron drift, and extended accel. zone, I-V characts. 80—14944
plasma conductivity, effect of elastic electron scatt. by at. excited states 78—42715
plasma diagnostics by wire explosion 78—71516
plasma discharge, positive column constriction, ion conversion effect 80—44020
plasma elec. conductivity meas. 78—71450
plasma in vacuum diode, pre-discharge, electron impact excitation line emission polarisation 78—47170
plasma probe meas. in mag. field 78—63597
plasma source for ARAKS expt. 79—21142
plasma thermoelectronic laser energy convertor 78—90421
positronium, formation in positron+alkali metal atom collisions, first Born approx. 80—83525
positronium formation in positron+alkali metal atom collisions, pseudopot. calcs. 80—83524

caesium continued
prebreakdown elec. cond. of nearly saturated Cs vapour 80—48841
primary standard operation limitations 77—5812
pseudopotential, energy-depend., for Fermi surface distortion and phonon dispersion calc. 77—15737
pulsed high-density source of Cs atoms, comments 80—37123
pulsed sputter negative ion source 78—33347
pulsed vapour source for ion sources in heavy ion accelerators 80—63423
quantum current-frequency convertor using optical orientation of ^{133}Cs *(Russian)* 79—10275
quantum magnetometer with superconducting shield 77—18055
radioactive Cs in seawater, rapid determ. using Cs selective resin 78—85609
radioactive ions, sorption and fixation props. of shale, radioactive waste repository implications 80—32354
radioactive waste, low-level, radionuclide migration in soil 79—54610
radioactive waste storage, migration of ^{137}Cs in Magenta dolomite by aquifer 80—13718
radioactive wastes, leach behaviour of hydrofracture grout 77—10478
radiocaesium dynamics in herons inhabiting contaminated reservoir system 78—28092
radioisotopes, liquid effluents, aquatic radiological impact anal., radiocaesium transport in sediment 80—95486
radionuclide accumulation by oysters in reactor effluent, math. model 77—81589
relativistic model pseudopot., appl. to elec. resist. in liq. phase 78—51866
Rydberg atom system, microwave superradiance and transient maser action 79—86153
Rydberg atom-blackbody radiation interactions 80—37761
seeding of Ar induction HF discharge plasma in crossed fields, Hall parameter 79—55465
SIMS, semicond. doping profile anal. appls. 79—39265
skin transport, role of diffusion 78—20158
soft X-ray outer-shell absorption and emission, one-electron calc. 79—69904
solubility, diffusion and permeation in ZrC 78—51684
sorption in Ba-impregnated nuclear graphite, thermodynamic modelling of multicomponent sorption behaviour 80—102243
sorption in nuclear graphite, sorption kinetics modelling 80—102244
spin relaxation, effect of optical pumping in high mag. field 77—88430
strontium alumoborosilicate glass, effect of vaporous and liq. Cs 77—44509
structural energies, pseudopotential formalism 80—39519
structure factor determination, by X-ray and neutron diffr. 79—51046
submonolayer film, on W (011) or Mo (011), disordering, LEED obs. *(Russian)* 77—89655
submonolayers effect on electron stimulated desorption of O^- from O-Mo (100) chemisorption system 79—86991
superconducting film, A1-type quench-condensed, prep. and crit. temp. 77—69443
superconductivity, elec. resist. and phase transforms. under high press. *(German)* 80—107763
superfluorescence of vapour, effective initial tipping angle 79—22923
surface, caesiated negative ion emission *(French)* 80—108314
surface, H(He) positive ions impact, backscattering, fraction reflected 80—60741
surface (100), electronic states calc. by mixed-representation method 77—20399
surface energy, barrier height and work function, jellium model calc. rel. to fracture model 77—72907
surface energy, self-consistent calc. including ion pot. perturbation effect 77—8166
surface loss mechanism, in surface-plasma H^- beam source *(Russian)* 77—79196
thermionic converter, ion species mass anal. 77—89344
thermionic convertor, pulsed, plasma parameters, operating characts. 80—6293
thermionic discharge, auxiliary discharge to reduce voltage drop 79—10724
thermo-EMF, saturation effect, up to 1950°C and 140 atm. 77—51727
thin layer on Al thin film, surface plasma wave excitation photoemission obs. 80—50518
time/freq. standard, future prospects 77—74371
time/freq. standard of PTB, characts. 77—74369
trace identification in neutral-beam research 80—95401
transport in soil, evaluation of combined sorption model 79—8554
USSR State Standard of time and frequency 77—79062
UV absorpt. spectra 80—2780
UV absorption spectra, threshold singularities of p-shell absorpt. in XUV region 77—36261
vacuum preparation of pure Cs, by electrolysis of glass 77—8773
vapour, coherent anti-Stokes Raman scatt. 78—71146
vapour, corrosive effect on surface elec. resist. of Al_2O_3 ceramic 77—51802
vapour, elec. cond., tight binding approx. in Kubo formalism 79—60778
vapour, electrical cond. near saturation point 80—69967
vapour, electron drift vel. and momentum transfer cross section 79—82032
vapour, general higher-order effects of freq. shifts in optical-RF double reson. 78—21884
vapour, inelastic light scatt., mol. form. and fluoresc. *(Russian)* 77—61787
vapour, IR image up-conversion, two-photon reson. pumping by Nd:$La_2Be_2O_5$ laser 77—10968
vapour, IR picosecond pulse generation by stimulated Raman scatt.' 80—53371
vapour, Joule-Thomson effect, 768-1234K 78—71420
vapour, optical frequency down conversion and stimulated electronic Raman scatt. 79—50350
vapour, optically dense excited by resonance lines, spectral study of excited atomic distrib. *(Russian)* 77—23458
vapour, optically pumped, transverse relax. times and diffusion coeff., spin echo meas. 79—10062
vapour, oscill. in low voltage arc discharge growth 78—51386
vapour, parametric conversion of 3.39 μm He-Ne laser radiation to visible 78—83036
vapour, photon echoes on 6S-7P transitions 77—19369
vapour, plasma production by weak CW laser beam at 6010 Å 77—62388
vapour, pressure meas. using electric-discharge gauge for 0.1 to 10 torr range 79—17432

caesium continued
- vapour, self-phase modulation complete compensation at 1.06 μm 77—58395
- vapour, stimulated electronic Raman scatt., 2.7-3.5 μm 78—1300
- vapour, stimulated Raman scatt., appl. to tunable IR laser radiation generation by down conversion 77—10973
- vapour, thermal cond. coeff. meas., 600 to 2500K 77—35303
- vapour, thermal cond. in range 800 to 1100K 78—1782
- vapour, thermodynamic props. calc. from Joule-Thomson data 78—94886
- vapour, threshold for stimulated electronic Raman scatt. determ. using picosecond laser pulses 80—102768
- vapour, tunable IR generation using 6s-5d Raman transition 80—53365
- vapour, tunable IR source using stimulated electronic Raman scatt., appl. to HCN (001) relax. obs. 80—9696
- vapour, two-photon induced stimulated Raman scatt., optical Stark shifts 77—46756
- vapour, two-photon resonant parametric generation, 2 to 20 μm 77—42563
- vapour, two-photon resonant third harmonic generation 77—738
- vapour, viscosity up to 1620K 77—1254
- vapour, with dispersive delay line, optical pulse squaring effects 77—88808
- vapour dispersive delay line, pulse squaring effects 77—72035
- vapour heat pipe discharge tube pumping for 823 cm^{-1} tunable IR laser 78—63069
- vapour high-press. diode, ignition with low temp. emitting cathode 77—7623
- vapour in Ar, fog condensation in MHD generator, heat and mass transfer 80—1410
- vapour pressure measurement, 860 to 1060K, 340 to 2010 mm Hg 77—26313
- vapour source, thermionic energy convertor with Cs-He gas controlled heat pipe 80—64791
- volatilisation from zeolite in radioactive waste soln. processing at high temp. *(Japanese)* 79—13441
- VPE on W emitter, FEM obs. 80—70552
- wire, low temp. elec. resist., size and temp. depend. 77—76958
- wire, size effect and temp. depend. of resist. 79—51691
- wires, size effect and temp. depend. of resist. 79—51692
- Zircaloy-2, I_2 stress corrosion cracking, Cs_2O and Cs influence, in- and out-of-pile 80—3252
- ^{137}Cs, conc. variations in Baltic Sea 1973 to 1975 79—92100
- Ag-O-Cs surface, oxidation, role of Cs suboxides in low work function surface layers, XPS 80—76131
- Ar-Cs plasma, HF induction discharge, Hall effect *(Russian)* 77—43101
- Ar-Cs plasma stream, electrodynamic braking with strong MHD interaction 78—9763
- CO_2-He-Cs glow discharge, quenching cross section of resonant Cs(6P) state by CO_2 mols. 80—43860
- Cd-Cs, vapour, sensitised fluoresc. anisotropy transfer 77—57924
- Cd+Cs, excitation energy transfer in sensitized fluoresc. 79—98210
- $Co^+ + e^- + He \rightarrow Cs + He$, rate coeff., pulsed discharge at 625K 78—17789
- Cs and Cs-O, on GaP (100) surface, thermal desorption props. *(Japanese)* 80—15368
- Cs, Doppler-free two-photon spectrum, recorded using thermionic detector 78—46465
- Cs I, 560 to 1050 Å 79—31455
- Cs I, atomic wavefunctions collapse 78—70733
- Cs I, $n^2S_{1/2}$ and $n^2D_{3/2,5/2}$ states, energies 80—87066
- Cs I, plasma diagnostics, excited level populations, relative spectral line intensities *(Spanish)* 78—51344
- Cs I, radiative lifetime of 8S, 9S and 7D levels 77—34588
- Cs I, time-resolved fluoresc., lifetimes 77—58068
- Cs I isoelectronic series, transition probabilities, oscill. strengths, lifetimes, branching ratios 78—33470
- Cs II, HFS determ. by collinear laser-ion beam 80—52914
- Cs II, hyperfine struct., beam laser technique meas. 79—93951
- Cs II, radiation lifetimes of excited states 80—9558
- Cs IX, UV spectra (60-600 Å), resonance line identification and spectral line identification 78—33455
- Cs inert gas, pot. energy curves, collision induced oscillator strengths 79—22659
- Cs, Knudsen arc, electron beam heating and ionisation 80—75114
- Cs, photoelectron spectra obs., comparison with mol. spectra of CsCl 80—83419
- Cs principal series lines, self-broadening 77—46541
- Cs vapour, 3rd and 5th harmonic generation of Nd laser radiation quasireson. conditions *(Russian)* 78—25926
- Cs^-, in tetrahydrofuran soln., transient photoelectron nutation 79—3418
- Cs^-, multichannel photodetachment 78—42027
- Cs^+, $3d^94f$ config., collapse of 4f electron, X-ray spectra obs. *(Russian)* 80—58204
- Cs^+, analytic SCF HF ground state wave function, ionis. pot., mag. props. 77—18785
- Cs^+ blocking of inward rectification of starfish egg cell membranes, model 80—61523
- Cs^+ diffusion in molten (Li-K)NO_3, wave-front-shearing interferometry study 79—60535
- Cs^+ dipole and quadrupole polarisability fine struct. intervals and g-factor interval 80—91477
- Cs^+ excited levels, hyperfine struct. and lifetimes 80—63590
- Cs^+, free-ion polarisabilities, empirical values 77—20792
- Cs^+ impact, 5.5 keV, Cu and phosphor bronze surfaces, negative secondary ion emission obs. *(French)* 77—66562
- Cs^+ in He and Ne gas, ion mobility and longit. diffusion coeff. 78—67308
- Cs^+, in mol. gases, generalised Einstein relation, exptl. test 77—89224
- Cs^+, in mol. gases, ion mobility, drift tube mass spectrometer meas. 77—89228
- Cs^+ internal dialysis in Myxicola giant axons, Na inactivation 78—96036
- Cs^+, ion mobility in Ar, Kr, Xe, diffusion, generalised Einstein relation 78—67298
- Cs^+ ion sorpt. by ion exchanger $(NH_4)_{0.8}Ni_{1.1}PO_4.xH_2O$ 77—9121
- Cs^+, ion source for secondary ion mass spectrometry 78—32913
- Cs^+ mass spectrometer quadrupole mass filter transmission 79—21851
- Cs^+ primary ion source for ion microprobe mass spectrometer 78—4732
- Cs^+ voltage-dependent blockage of K^+ channel in fragmented sarcoplasmic reticulum 79—96524

caesium continued
- ^{137}Cs gamma-radiation source, measurement of activity for comparison of COMECON standards 80—42899
- Cs^{2+}, electron impact excitation studies by intersecting beam method 80—69239
- Cs^{2+} formation during electron-ion collisions, ultrasoft X-ray spectroscopic study *(Russian)* 80—43193
- Cs:Xe, optical absorption by rare gas, cluster Bethe lattic calc. 77—8612
- Cs:Xe film, metal-insulator transition, cond. and optical absorption meas. 77—24598
- Cs/W, work function measurement in SEM 80—80918
- $^{133}Cs^+$/Cs g-factor ratio, NMR and zeeman transition freqs. 78—17817
- Cs-Ar, low-pressure discharge, energy balance and Coulomb relax. 77—43098
- Cs-Ba, high current Knudsen arc discharge, spontaneous extinction, optical diagnostics 80—44044
- Cs-Ba discharge, high-current, low-press., spontaneous current cutoff 80—19626
- Cs-Ba Knudsen thermionic converter performance optimisation 79—27840
- Cs-Ba triode arc switch, high-current, low-voltage, pulsed control 78—71551
- Cs-Bi vapour saturated semiconducting film on collector, thermo-emission characts. *(Russian)* 78—23577
- Cs-CsCl, liq. mixture, enthalpy of fusion, Gibbs energy of mixing and excess entropy 80—19947
- Cs-D_2, vap., oscill. production of particulates, by CW laser beam 77—77794
- Cs-H_2 vapour, resonant character of laser induced formation of particles 80—89481
- Cs-He, new absorption/emission bands perturbed Cs transitions assignment, pot. energy curves 78—66486
- Cs-He afterglow, spectral emission from excited Cs ions, 380-750 nm 79—82116
- Cs-He plasma, steady-state discharge, role of inelastic collisions, spectroscopic diagnostics 78—42709
- Cs-N_2 discharge, Cs_2^+ form. rate, mass spectra obs., N_2 press. depend. 79—27853
- Cs-N_2 plasma, collision recomb. of charged particles *(Russian)* 77—80373
- Cs-NH_3, Cs-ND_3, solns., US absorption, metal-nonmetal transition 79—69194
- Cs-NH_3 solution, metal-nonmetal transition, cond. density and Hall coeff. meas. 77—51789
- Cs-Na_2KSb, semitransparent photocathodes, UV response 77—167
- Cs-O adsorbed films on Si (100), oxide formation, ionisation loss spectra, AES 79—69365
- Cs-O coated $Ga_{1-x}In_xAs$ photocathode, negative electron affinity, photoelectron scatt. in coating 79—28899
- Cs-O_2, desorption from W, activation energy 80—103562
- Cs-Se thermionic converter, output power, vap. source depend. 80—44000
- Cs-Sr(He) mixtures, photocond. at atm. press. 80—87844
- Cs-Xe, oscill. strength, for induced dipole transitions, pot. energy curves 77—75100
- Cs-Xe molecular bands, time-resolved fluoresc., lifetimes 77—58068
- Cs-Xe solar-pumped MHD excimer laser, modelling 80—95873
- Cs-Xe vapour mixture, possibility of solar direct energy conversion into laser radiation 79—59688
- Cs^+-Ar, gaseous ion transport, three-temp. theory appl., interaction pot. 80—6202
- Cs^+-Ar(Kr)(Xe), ion mobility and interaction pot., drift tube meas. at 300K 78—59537
- $Cs+(AuF_5)_n$, prod. of AuF_5^-, ionisation cross section energy depend. 80—81300
- $Cs+(SbF_5)_n \rightarrow Cs^+ + SbF_6^- + SbF_4 + (SbF_5)_{n-2}$, ionisation cross section energy depend. 80—81300
- Cs+Ar, laser two-photon ionisation, collisional line broadening, atomic forces 77—83543
- Cs+Ar, two-photon ionisation spectra, satellites, absorption line shape 78—82668
- $Cs+Ar^+(Kr^+)(H_n^+)(He^+)(N^+)(N_2^+)(Ne^+)(Xe^+)$, total charge-transfer cross-sections meas. 77—50527
- Cs+Ar(Kr)(Xe), spectral line breadth and shift, Van der Waals pot. calc. 78—90126
- Cs+Ar(Xe)(He), shift, halfwidth, satellite and absorpt line in square-well pot. 80—42993
- $Cs+CO_2$, in CO_2-Cs-He discharge, reaction rate meas. by IR absorption, press. depend. 78—44367
- $Cs+Cl_2(Br_2)(I_2)(ICl)(IBr)$, negative ion prod. cross sections 77—531
- Cs+Cs, nP, dD excited states, assoc. ionisation, state and thermal energy depend. *(Russian)* 79—5153
- Cs+Cs, Rydberg states collisional disalignment determ. by fluoresc. quantum beat damping 79—13789
- Cs+Cs, spin destruction, obs. 80—63781
- $Cs+Cs_2$, nuclear spin polarisation exchange collisions, optical pumping method obs. 77—16797
- $Cs+Cs^+$, charge exchange cross-section, temp. depend. 78—9244
- Cs+Cs(Rb), continuum- and bound-state pair absorption, 2300-3100 Å, 410-540°C 80—42970
- $Cs+D_2O$, ion-pair form., energy, angle and mass anal. of products 78—70970
- $Cs+D_2O \rightarrow Cs^+ + OD^- + D$, 100-200 eV, $D_2O^-(^2A_1)$ state 78—17770
- $Cs+F_2$, electronic excited states, chemiluminesc. in flame, spectra 77—52643
- Cs+F(Cl), quasiclassical charge transfer cross section, rel. vel. depend. 77—19073
- $Cs+H_2$, crystallisation of HCs, laser snow effect in ionized Ar laser 80—40712
- $Cs+H_2$, rot. excitation, infinite order sudden approx. 78—74740
- $Cs+H_2O(D_2O)$, ionising collisions in crossed-beam systems 78—48641
- $Cs+H^+$, 4 MeV beam-foil X-ray production cross-section 79—7003
- $Cs+H^+$, charge exchange collision producing H(2s), semiclassical differential cross-section 79—59551
- $Cs+H^+$, charge transfer processes with plasma gun, Lyman-α radiation exam. 78—46573
- $Cs+H^+$, elastic and charge exchange collisions, projected valence bond method 78—78804
- $Cs+H^+$, elastic scatt., differential cross-section calc., 13.4-24.2 eV 79—59530
- $Cs+H^+(H)$, single-electron capture total cross sections 80—91656

caesium continued
$Cs+H^+ \rightarrow H(2s)+Cs^+$, near reson. charge transfer, low energy 79−54964
$Cs+H(H^-)$ fast atom collisions, charge exchange, equilib. fractions calcs. 78−33601
$Cs+H(1s)$, differential electron attachment and elastic scatt., 30-528 eV 80−63745
$Cs+He$, interaction pot. and oscill. strength 80−91645
$Cs+He^+$, 5-100 keV, electron capture form. of fast metastable He 78−74760
$Cs+He^+$, spin dependent charge transfer in low-energy collisions 77−75293
$Cs+He^m(2^3S) \rightarrow Cs^+ + He+e$, reaction rate const., meas. in afterglow plasma 79−82116
$Cs+He(Ne)(Ar)$, optical pumping, spectral line shape *(Spanish)* 79−22662
$Cs+He(2^3S_1)$, Penning ionis. in stationary afterglow 78−42184
$Cs+I_2$, ion-pair form., differential cross sections, I_2 internal energy effects 77−61840
$Cs+I_2$, ion-pair form. cross section, 15-120 eV, mol. props. depend. 77−28996
$Cs+I_2$, ion-pair formation, energy transfer and differential scatt. 77−75272
$Cs+I_2$, ionising collision, trajectory surface hopping calc. 77−50509
Cs+inert gas, hyperfine struct., broadening and shift calcs. 77−58153
Cs+inert gas, three body interaction, fluoresc. spectra principal series lines and secondary satellites 80−83313
Cs+insert gas, $5d^2D_{5/2}$ level excitation by laser photon absorpt. 77−3438
Cs+methyl cyanide, collisional ionisation obs. 80−95716
$Cs+Mg^+$, charge exchange and excitation processes 78−17772
$Cs+O_2$, collisional ionisation, energy spectra of forward and backward directed positive and negative ions 80−87200
$Cs+O_2$, mol. target internal motion 80−78697
$Cs+O_2$, reaction kinetics, time-resolved meas. 77−90588
Cs+TCNQ, TCNQ-form., electron affinity, compound states 77−65530
Cs+Tl, Tl $6^2P_{3/2}$-state relax., NMR obs. 80−95653
$Cs+UF_6$, ion pair form. and atom abstraction reactions 79−1946
$Cs+UF_6$, ionisation reactions, absolute cross sections 80−99565
$Cs+UF_6(WF_6)$, collisional ionisation, crossed beam obs. 79−68299
$Cs+UF_6(WF_6)(MoF_6)(TeF_6)(SeF_6)$, crossed beams, reaction cross section 77−77740
$Cs+X$, ($X=N_2$, H_2, He, Ar, Xe), collisional relax. and population quenching of Cs 78−25467
Cs+Xe, Cs spectral line profile and absorpt. transitions 80−47944
Cs+Xe (neopentane), Cs line shape broadening, satellite data inversion, interaction pot. 78−74608
$Cs+Xe^{10+}$ depend. of charge transfer on ionisation pot. of atoms 79−64096
$Cs^+ + 2Cs \rightarrow Cs_2^+ + Cs$, gas phase reaction rate const. calc. 78−92457
$Cs^+ + Ar(Kr)(Xe)$, elastic beam scatt., repulsive pots. 79−98184
Cs^++benzyl chloride, beam reactions for 5.8 eV collision energy, mechanism 80−66777
$Cs^+ + Cs$, mol. ion form. rate, from mobility meas. 79−34299
$Cs^+ + Cs$, reson. charge exchange cross section at thermal energies 79−854
$Cs^+ + Cs^+$, charge transfer, ionis., 40-280 keV, rel. to fusion scheme 80−5615
$Cs^+ + Dy$ charge exchange, isotope separation of laser excited Dy atoms 80−83512
Cs^++t-butyl chloride, reactive scatt., stripping model, ang. and energy distrib. 80−35510
$Cs^+ + X$, $X=H$, H_2, He, C, N, O, cross-section, closure-Born approx. 78−66630
Cs_2, 4800 Å absorpt. band, classical method anal. 80−106330
Cs_2, absorpt. spectra, ground state pot. curves 77−75171
Cs_2, absorpt. spectrum in visible and near visible 78−46356
Cs_2, concealed weak absorpt. band, detect. by saturation spectroscopy 77−10675
Cs_2, detailed spectroscopic study, sub-Doppler spectroscopic techniques 80−52339
Cs_2, dimer and higher polymer IR absorpt. bands, triplet state 80−63629
Cs_2, fluoresc. at 6270 Å, rot. consts. 79−45744
Cs_2, fluoresc. spectra, kinetics, laser candidate 79−64027
Cs_2, fluoresc. spectra induced by laser, energy transfer and dissoc. 79−98141
Cs_2, ground state consts., pot. curve, laser spectroscopy 79−98247
Cs_2, laser-excited cross IR fluoresc. emission 79−76459
Cs_2, laser-excited fluoresc. in Cs-Xe mixture, pumping, level scheme 78−86909
Cs_2, laser-induced fluoresc. spectrum, diffuse band anal. 80−106346
Cs_2, laser-induced photodisintegration *(Russian)* 79−89719
Cs_2 molecules, magnetic shielding studies by NMR 77−42341
Cs_2, oscill. strengths 77−18846
Cs_2, rot. consts., Doppler-free polarisation spectrosc. 80−5555
Cs_2, saturation spectrum, 6250 Å band recorded using thermionic detector 78−46465
Cs_2, sub-Doppler laser spectrosc., high resolution 80−52320
Cs_2, thermal dissoc., optical pumping method obs. 77−16797
Cs_2, two-photon dissoc., spectrosc. obs. 80−32787
Cs_2^+, $^2\Sigma$ and $^2\Pi$ state pot. energy curves, two-centre model 79−26906
Cs_2^+, adiabatic pot. curves, ground and excited state, Hellmann-type model pots. 78−78647
Cs_2^+, core-core interaction potential calc. 78−25645
Cs_2^+, form. by $Cs+Cs$ assoc. ionisation, dissoc. energy 78−58804
Cs_2^+, form. by electron impact in elec. discharge, low-press. vap. 79−10738
Cs_2^+, pot. energy curve, pseudopot. calc. 77−6703
Cs_2^{2+}, interaction potential determ., comparison between all-electron frozen core and psuedo-potential results 80−69054
Cs_2^{2+}, low-lying states, MC SCF+CI 80−69053
Cs_2+halogens$(SnCl_4)(MoF_4)(UF_6)$, ionisation reactions, absolute cross sections 80−99565
$Cs_2+He(Ne)(Ar)$, exchange collisions, optical pumping method obs. 77−16797
$Cs_2+He(Ne)(Ar)(Kr)(N_2)(CH_4)$, collision-induced dissoc., atom-mol.-exchange optical pumping 78−22008
$CsAl(SO_4)_2.12H_2O$, third order elastic consts. from stress shifted reson. freqs. 78−55905

caesium continued
Cs(Ar-Cs) plasmas, electron momentum transfer cross section, cyclotron reson., temp., cond., and vel. meas. 80−106930
CsBr, linear dichroism spectra, stress-induced, reorientation of O_2^- and NO_2^- impurity ions *(Russian)* 80−45127
CsI, four-photon ionisation near 6f resonance 78−70801
CsI, isoelectronic series, oscill. strengths, relativistic HF calcs. 79−98035
CsI, linear dichroism spectra, stress-induced, reorientation of O_2^- and NO_2^- impurity ions *(Russian)* 80−45127
$Cs_2NaYbBr_6$, mag. behaviour, 3.5-251.3K *(German)* 80−50041
$Cs_2S_2O_6$, piezoelectric, crystal struct. studied by X-ray diffr. 80−100208
^ACs, A=133, 135, 137, isotope shifts and hyperfine struct. of 5s-7p transitions 79−13677
^ACs, A=138 to 142, nucl. moments and charge radii changes from hyperfine struct. and isotope shifts 79−17804
^{127}Cs, yield in I irrad. by α-particles 79−67760
^{129}Cs, yield in I irrad. by α-particles 79−67760
^{130}Cs, low energy ions systematic range meas. in Ar and N_2 gases 79−1472
^{132}Cs, contents in fish flesh 79−79718
^{133}Cs, filter cells for hyperfine optical pumping, optical detect. of 0-0 transition *(French)* 77−443
^{133}Cs, first excited D-level, hyperfine struct. meas. by cascade, fluoresc. spectrosc. 80−69101
^{133}Cs, freq. standard, optimum conditions for population inversion for 0-0 transition 80−78824
^{133}Cs, high-field quantum beats for $7^2P_{3/2}$ state 79−13682
^{133}Cs, Mossbauer isomer shifts, book contrib. 79−87363
^{133}Cs, Rydberg S and D states, hyperfine struct., lifetimes, depopulation cross sections 77−42270
^{133}Cs vapour external selective mirror for semiconductor laser 79−45961
^{134}Cs, activity meas. 79−59292
^{134}Cs and ^{137}Cs at Atlantic nuclear waste disposal site, radionuclide redistrib. 80−85309
^{134}Cs and ^{137}Cs in Clyde Sea Area 80−3541
^{134}Cs behaviour in sediments in laboratory-scale aquatic ecosystem 78−3831
^{134}Cs, errors in activity ratio determ. in reactor RA used fuel element 79−41061
$^{134}Cs/^{137}Cs$ activity ratio for LWR fuel burn-up determ. *(Russian)* 80−68804
^{137}Cs absorption through damaged and undamaged skins of guinea pigs 80−26383
^{137}Cs accumulation and elimination by naturally contaminated wood ducks 77−66865
^{137}Cs accumulation by marine organisms, sediment and sea water influences 78−80981
^{137}Cs accumulation in fruitbodies of Basidiomycetes 78−80977
^{137}Cs accumulation in rat liver, effects of altered thyroid states 78−24136
^{137}Cs adsorption by sediments near water-cooled nuclear reactors 77−78281
^{137}Cs and K contents in low-teens in areas of different fallout level in Japan 77−90922
^{137}Cs body burden in Japanese from 1967 to 1975 77−9283
^{137}Cs body burden in Japanese, biological half-life meas. 79−57795
^{137}Cs, contents in coastal sediments 79−57974
^{137}Cs, coyote scats, Hanford Reservation, radioactive waste distrib. 79−25120
^{137}Cs deposition on plate glass surface, contamination *(Japanese)* 78−29654
^{137}Cs, distrib. and behaviour in Urazoko Bay sediment 80−97825
^{137}Cs distrib. in upper layer of equatorial Indian ocean *(Russian)* 77−60426
^{137}Cs, errors in activity ratio determ. in reactor RA used fuel element 79−41061
^{137}Cs excretion in urine vs. total excreta following continuous intake of ^{137}Cs in fall-out 78−20294
^{137}Cs, fallout effects of Nagasaki atomic bomb 78−85393
^{137}Cs, fast neutron influence on fission product transport in UO_2 pyrocarbon-coated HTR fuel particles 80−42777
^{137}Cs, fixation on natural sorbents from phenol-polluted water 79−57506
^{137}Cs gynecologic insertions, expt. derived algorithm for computer calc. dose rates 80−101264
^{137}Cs γ-ray beams for perimeter security system 77−18713
^{137}Cs immobilisation in cement-waste composites 78−82466
^{137}Cs in alpine tundra habitats, effects of phys. habitat factors and plant morphology 77−37058
^{137}Cs, in atmosphere, bioindication using needles of common pine tree 79−100550
^{137}Cs, in molten alkali nitrates, diffusion coeffs. meas. 80−70437
^{137}Cs in sample soil and water, distrib. coeff., environmental effects 77−13092
^{137}Cs in Straits of Malacca marine environment 79−12135
^{137}Cs, intake by Bikini Island residents, model using bioassay data 80−109043
^{137}Cs, K, model for turnover in pike 79−8553
^{137}Cs leaching from ion-exchange resin incorporated in polyethylene or cement composite 77−65275
^{137}Cs levels in soils and vegetation of W.Malaysia 78−73263
^{137}Cs, long-term retention in Indian workers, dose commitment 78−35960
^{137}Cs movement and loss in small lake 78−24317
^{137}Cs needle implants, miniaturized, for radiation therapy 79−11995
^{137}Cs radiation effect on Chinese hamster cells, marker phenotype rescue 80−17005
^{137}Cs radioactive fallout and lacustrine sedimentation rates 80−4048
^{137}Cs, radionuclide leaching from hardened cement grout, container dimension depend. 79−13439
^{137}Cs removal from ocean waters, adsorpt. on hydrated MnO 78−3822
^{137}Cs, seasonal cycling in reservoir 79−100881
^{137}Cs, separation from nucl. waste using sodium zirconate 80−27760
^{137}Cs source for computerised tomography 77−60239
^{137}Cs sources, parametric definition 80−91346
^{137}Cs standardisation by 4π(PC)-γ efficiency tracing method 79−13577
^{137}Cs, study of absorpt. by Lemna minor 80−30677
^{137}Cs, time variation of low concentrations in rain water 79−43994
^{137}Cs transfer coefficient into cows milk rel. to level of milk prod. 78−80978
^{137}Cs, transmutation in high flux fission reactor, feasibility 79−85708

caesium continued
^{137}Cs, uptake by cotton rats inhabiting banks of radioactive liquid waste pond 79−25121
^{137}Cs whole-body content in a normal New Mexico population 1956-1977 80−26382
^{137}Cs/^{134}Cs radioisotopes in seawater, Cs-selective resin determ. 80−94137
^{137}Cs-irradiation, fractionated high dose-rate and continuous low dose-rate effect on pig skin 80−41127
^{137}Cs-irradiation, response of pig skin, various schedules of irrad. 80−72237
$\mathrm{Cs}^{*}+\mathrm{N}_2$, excited states quenching 78−5330
Cs_2^{*}, optically excited, cascade predissoc. *(Russian)* 79−10159
$\mathrm{Cs}^{*}(6\mathrm{D}_{3/2})+\mathrm{Cs}(6\mathrm{S}_{1/2})$, preferential excitation transfer from laser populated state 78−37732
$\mathrm{Cs}(5\mathrm{D}_{5/2,m=1/2})$+inert gas, dipole-induced transitions, pot. curves, oscillator strength 80−32816
$\mathrm{Cs}(6^2\mathrm{P}_{3/2})+\mathrm{He(Ne)(Ar)(Xe)}$, collisional depolaris., nucl. spin depend., by Zeeman scanning 77−19012
$\mathrm{Cs}(6s)+\mathrm{H}^+$, elastic scatt., pot. determ. from differential cross-sections meas. 78−78778
$\mathrm{Cs}(8^2\mathrm{P})+\mathrm{He(Ar)(Xe)}$, fine-struct. transition cross sections, semiclassical calcs. 77−30972
$\mathrm{Cs}(n^2\mathrm{D}_J)+\mathrm{Cs}(6^2\mathrm{S}_{1/2})$ collisions, inelastic cross sections 78−74753
$\mathrm{Cs}(n\mathrm{P})+\mathrm{Cs}(6\mathrm{S})$, assoc. ionisation, threshold energy, Cs_2^+ dissoc. energy 78−58804
Cu (111)/Cs, adsorption-induced changes of photoemission spectra and surface electronic struct. 80−55260
D+Cs, ang. scatt., neutral beam form. via negative ions 77−46636
D_3^++Cs, electron capture to D_3^- and D_3^0 repulsive states 79−59563
$\mathrm{D}^0(\mathrm{D}^+)$+Cs, D^- formation, ang. distrib., total cross sections 77−529
GaAs:Cs, oxidation process, UPS obs. 80−50511
GaInAs:Cs-O, occurrence of Schottky effect 79−8227
GaP:Cs-O simultaneous adsorption, oxidation interface chemical struct. 80−103584
$\mathrm{H}+\mathrm{Cs}\rightarrow\mathrm{H}^-+\mathrm{Cs}^+$, low energy cross sections 79−7009
H^0+Cs collisions, H^- production cross sections 80−78698
H^++Cs, electron capture, H metastable fraction of n=2 population 77−30988
H^++Cs(Rb)(K)(Na), charge exchange, H(2s) form. 79−64101
$\mathrm{H}^+ +\mathrm{Cs}\rightarrow\mathrm{H}^- +\mathrm{Cs}^{2+}$, proton conversion, 0.2 to 6.0 keV *(Russian)* 77−1920
H_2-Cs, H^- source for hollow beams 80−23228
He-CO_2-Cs mixture in rapidly circulating laser, interaction rate of Cs and CO_2, gasdynamic parameters 79−86173
He-Cs, turbulent plasma, characts., electron energy balance *(Russian)* 79−27779
He-Cs discharge plasma, high freq. oscills. in crossed elec. and mag. fields *(Russian)* 77−15189
He-Cs mixture, Cs ion conc. determ. by radn. absorpt. 79−34395
He-Cs mixture discharge, B-invariant transformation theory 78−67503
He-Cs plasma, HF instability in crossed fields, obs. 78−75305
He+Cs(Rb), interatomic pots., hyperfine shifts, diffusion coeffs., perturbation exchange theory 79−41220
Hg-Cs, vac. UV laser, charge exchange pumping 77−31095
I_2:Cs, doping effect on elec. cond., semicond. props. 80−49732
K_2+halogen mol., thermal energy mol. beam chemi-ionisation 77−9065
KCl:Cs^+, low-temp. heat capacity enhancement due to impurities 80−107442
Kbr:Cs, microcrystalline powders, isothermal decay of colour centres 80−2804
$\mathrm{Na}_2\mathrm{KSb(Cs)}$, photocathode, optical props. 79−78827
O_2+Na(K)(Cs), negative ion pair form., total cross sections 79−3550
Rb, absolute zero isotherms and polymorphic transition 79−73310
Rb-Cs plasma, electron collision induced charge exchange *(Russian)* 77−68740
Si:Cs, amorphous, ion implanted, control of cond. 79−60835
Si:Cs, high dose implantation profiles, determ. using low angle Rutherford He ion backscatt. 79−4327
n-Si:Cs, ion implanted, minority carrier lifetime and defect struct., annealing effect 78−6395
SiO_2:Cs film, implanted electronic cond. mechanism in MOS struct. 77−15983
Sr-Cs mixture, laser induced collisional two-photon ionisation, fluoresc. monitoring 80−91515
Tl-Cs vapour mixture, CO_2 CW laser radiation freq. conversion 80−74438
TlI:Cs, dielectric const. temp. and freq. depend. 77−32315
$\mathrm{(U,Pu)O}_2$ fuel pins 80−102250
UO_2 in UO_2-PuO_2, fast reactor fuel pins, Cs interaction 79−6743
^{133}Xe/^{133}Cs, implanted in various hosts, isomer shift values, Mossbauer spectra 80−7240
ZnO-Cs, fabrication, UPS meas. 78−15279
ZnTe:Cs, fluorescence spectra meas. 78−10949
ZrN_x:Cs, thermionic emission, metallic sublattice vacancy effects 78−68597

caesium alloys
charge transfer insulators, mechanism, resistivity 78−80070
surface plasmons at inhomogeneous liq. metal/dielec. interface, second dispersion branch 77−32059
Au-Cs, charge transfer, Mossbauer effect ^{197}Au isomer shifts, XPS valence-band spectra 80−2676
Au-Cs, liq. alloy, mag. susceptibility rel. to ionic charact. 77−1536
Cs-Ag, dil., electronic struct., density functional approach 80−44492
Cs-Au, disordered, min. metallic cond. 79−95372
Cs-Au, electron diffusion thermoelectric power calc. 77−28161
Cs-Au, ionic melts, elec. props. 79−99338
Cs-Au, liq., electronic struct., effects of short-range order 77−15755
Cs-Au, liq., exptl. evidence for ionic elec. transport 77−51534
Cs-Au, liq., molar vol. meas. 80−59546
Cs-Au, liq. alloys, ionic conductance 77−1251
Cs-Au, liquid, metal-insulator transition, mag. susceptibility, Knight shift, theory 80−44672
Cs-Au alloy, cryst., UV photoemission investig. of band struct. 77−24923
Cs-Au liq. alloy, formation of localised electronic states, NMR obs. 80−93201
Cs-Au(Sb), liq. alloys., mag. susceptibility and electronic struct. 77−1537
Cs-Hg, liq., elec. resist. meas. 77−51717

caesium alloys continued
Cs-K, thermal conductivity determ. 80−107760
Cs-K(Na), liq., thermodynamic props. at high temps. 80−15262
Cs-Na(K) liquid alloys as coolants, sp. ht. 79−86902
Cs-Rb(K)(Na), solute atom-grain boundary interaction energy, electron-statistical calcs. *(Russian)* 79−73175
Cs-Sb(Au), liq., metal-nonmetal transition and change in electronic and mag. props. 77−51790
Cs-Sn, disordered, min. metallic cond. 79−95372
Cs-Sn alloy, peritectic reactions, phase diagram *(Russian)* 80−40784
Cs-Tl, liq., elec. resist. meas. 77−51717
CsAu, band struct. and charge distrib., semicond. and metallic behaviour 77−20238
CsAu, electronic struct., XPS meas. 79−69403
CsAu, molten, equimolar, structural evidence of ionic nature 80−64882
CsAu, NMR line shape, Knight shift, X-ray diffr. study, struct. props. 78−68402
CsAu, optical absorpt. in liq. and solid 79−61397
CsAu, photoelectron spectroscopy and energy bands calc. 78−76581
$\mathrm{Cs}_{1-x}\mathrm{Au}_x$, liq., metal-nonmetal transition, electronic theory 78−79930
K-Cs, extreme UV absorpt. spectra 80−97294
K-Cs alloys, elec. resist., minima for $\mathrm{K}_2\mathrm{Cs}$, $\mathrm{K}_7\mathrm{Cs}_6$ concs. *(German)* 78−14708
K-Cs solution, activity and saturated vapour press. of Cs, reson. line absorpt. obs. 77−51509
$\mathrm{K}_2\mathrm{Cs}$ and $\mathrm{K}_7\mathrm{Cs}_6$, OPW calc. of struct., bonding and stability 77−43169
$\mathrm{K}_2\mathrm{Cs}$, Laves phase, chemical bonding, electronic charge density distrib. pseudopotential calcs. 79−77549
$\mathrm{K}_7\mathrm{Cs}_6$, μ-phase variant, chemical bonding, electronic charge density distrib. pseudopotential calcs. 79−77549
Na-Cs, internal energy, heat of mixing, entropy, dielectric function 80−88340
Na-Cs, liq., conc. fluctuations, X-ray transmission meas. 77−47329
Na-Cs, liq., form factors and transport coeffs., pseudopot. perturb. theory 80−44561
Na-Cs, liq., struct. factors, X-ray transmission diffr. expt. 77−47337
Na-Cs, liq., struct. factor, free energy of mixing, and electrochem. pot., thermodynamic calc. 80−96436
Na-Cs, liq., thermopower 78−23074
Na-Cs, liq. alloy, thermoelec. power and elec. resist. 77−47788
Na-Cs melt, density and molar volume *(Russian)* 78−15357
Na-Cs solution, saturated vapour pressure of Cs over solution 78−26688
Na-K-Cs alloys, liquid contact material, phase diagram calcs. 78−6145
$\mathrm{Na}_2\mathrm{Cs}$, OPW calc. of struct., bonding and stability 77−43169
Rb-Cs, liq., elec. resistivity, temp. depend. 78−39084
Rb-Cs, liquid, electron theory of chemical potential and activity *(Japanese)* 77−72702

caesium clocks *see atomic clocks*

caesium compounds
see also caesium alloys
acetate, molten mixtures, elec. cond., density 77−15613
n-alkanoates, phase transitions, differential scanning calorimetry 77−43315
aluminosilicate, containing Mo, Cu, Re or W, thermoelectronic emission characts. *(Russian)* 77−48301
caesium hydrogen tartrate, anomalous dispersion of Cs, refined struct. from modified least squares program 78−51522
caesium hydrogen tartrate, Cs $\mathrm{L}_{\mathrm{III}}$-edge anomalous X-ray scatt., meas. by synchrotron radiation 79−24389
caesium iodide screen for X-ray image intensifier 78−21311
caesium propanoate, solid state transitions and melting process, diffr. and conductometric meas. 80−10670
caesium uranyl propionate, low temp. absorpt., luminesc. spectra, intermol. interactions 80−2830
cryst., vibr. spectrosc. *(French)* 78−6667
GaP/$\mathrm{In}_x\mathrm{Ga}_{1-x}\mathrm{P}$/GaAs:(Cs-O) high sensitivity transmission photocathodes, photosensitivity, electron diffusion length 79−78832
graphite, structural ordering in intercalation compounds 78−26539
graphite intercalation compound, $\mathrm{C}_8\mathrm{Cs}$, Breit-Wigner line shape anal., Raman spectra 80−50336
graphite intercalation compound, CsC_8, polarised refl. spectra 78−31213
graphite-Cs compounds, intercalates, IR active lattice mode obs. 80−45072
graphite-Cs lamellar cpd., reversible intercalation of tetrahydrofuran 80−16211
halide, optical response function from Jahn-Teller systems, F-band absorpt. band shape 79−43005
halide, porous layers, electron bombardment induced cond. 78−56550
halide molecules, ionis. energy, relativistic Dirac-Slater and nonrelativistic HF-Slater calcs. 77−26983
halides, dielectric behaviour and optic mode Gruneisen parameters 79−10907
halides, dielectric const. meas. at 1 MHz 77−16238
halides, elec. field gradient at F_{Z1} electron site 78−22713
halides, electronic struct. of self-trapped excitons magneto-optic props. 79−33805
halides, F_x-centres, variational calc. of energy levels 79−82204
halides, F-centre energy levels, ion-size effects, calc. 80−96519
halides, F-centres, first excited degenerate states, props. of electron-phonon interaction 78−63824
halides, Gruneisen and Anderson-Gruneisen parameter determ. 80−59611
halides, He II photoelectron spectra, ionisation energy 77−18977
halides, luminesc. of interstitial atomic H 80−103986
halides, molten, structural props., computer simulation 77−84616
halides, photoelectric yield spectra, 10 to 40 eV photon energy 79−28887
halides, press. depend. of effective ionic charge 80−96462
intercalated donor cpds. of graphite, Raman scatt. 78−10890
intercalation compound with graphite, resistivity anomalies and phase transform. 78−26839
intercalation compounds with graphite, phase transitions, resistive anomalies, electronic props. 79−95405
perfluoro-octanoate/D_20, NMR of ^{2}D nuclei, response to three-pulse sequences in inhomogeneous B_0 field 79−42861
perfluoro-octanoate/$\mathrm{D}_2\mathrm{O}$, NMR of ^{2}D nuclei, response to three-pulse sequence in homogeneous B_0 field 79−42860
perfluoro-octanoate/$\mathrm{D}_2\mathrm{O}$ system, ^{2}H NMR quantum orders, RF pulses 80−103892
propylate, solns., conductivity meas., data anal. *(German)* 77−32806

caesium compounds continued
 salts, Raman and IR spectra of the dicyanoiodate (I) ion 80−60572
 suboxides film, work function theory, size effect 78−43460
 tartrate, optical rot. dispersion, dichroism and spectra, in soln. and cryst. *(Russian)* 77−90124
 TCNQ solt, $CS_2(TCNQ)_3$, cond. and thermopower meas., deep level acceptor model 79−42529
 ternary chlorides, $ABCl_3$ type, optical props. 78−35111
 tetracyanoplatinate conductors, IR and Raman spectra, cyanide stretching vibrs. 79−11415
 trichloroacetate, temp. depend. of ^{31}Cl NQR spectra 80−20495
 trisoxalatoferrate complexes, Mossbauer studies of electronic relax. phenomena 80−44973
 Zircaloy-2, I_2 stress corrosion cracking, Cs_2O and Cs influence, in- and out-of-pile 80−3252
 Ag-O-Cs photocathode, Ag colloidal particles and long wavelength response *(Chinese)* 80−45195
 Ag-O-Cs photocathode, role of Ag colloidal particles in photoemission *(Chinese)* 80−40215
 (Ag-Cs)Br molten mixture, transport nos. and external mobilities *(French)* 79−77787
 B_2O_3-K_2O-Na_2O-Rb_2O-Cs_2O glass, small angle X-ray scatt. exam. of struct. 80−38922
 $C_{24}Cs$ and $C_{36}Cs$, graphite intercalated, ordering of intercalant layers, X-ray diffuse scatt. 80−44182
 C_xCs intercalation compound with graphite, intercalation compounds with K and Cs 78−26693
 C_3PbCl_3, single crysts., X-ray and photoluminesc., and reflection spectra 77−69896
 CS, heat of formation from electron impact dissoc. of CS_2 and OCS 78−73074
 CS, valence electron photoionisation, ionisation pot. and spectral intensities 78−70883
 CSI:Na cryst., V_K-Na^0 centre pairs, tunnelling recomb. 78−91952
 CaBr(Cl)(I), Gruneisen γ and other thermodynamic props. at zero and elevated press. 78−43142
 $CaCeAl_3O_7$, melilite struct., prep. and props. 80−93524
 $CdCsP_3O_4$, cryst. struct. exam. *(French)* 78−2076
 CeS, atomic interaction effects in X-ray emission spectra *(Russian)* 79−69905
 $Ce_2(SO_4)_3$ dosimeter, mixed field of fast neutrons and γ-rays, absorbed dose meas. 78−74514
 Cs I, spectroscopic meas. of Cs plasma in thermionic convertor *(Japanese)* 77−58902
 Cs^+, adsorpt. potential determ., at soln.-solid interface 79−56068
 Cs^+, glycerol solns. quadrupole interactions, nucl. mag. relax., correl. time determ. 77−14449
 Cs-Cr-O, fission product compounds in irradiated nucl. fuels chemical thermodynamic data *(Japanese)* 79−22387
 Cs-Cr-O system, phase equilibrium 80−3012
 Cs-CsCl, liq. mixture, enthalpy of fusion, Gibbs energy of mixing and excess entropy 80−19947
 Cs-Graphite, interaction ordered and disordered cpd., Raman spectra 80−11393
 Cs-graphite intercalated compounds, anisotropy of Debye-Waller factor, Mossbauer meas. 77−55738
 Cs-inert gas molecule, excimer transitions, absorpt. spectra 77−475
 Cs-Mo-O, fission product compounds in irradiated nucl. fuels, chemical thermodynamic data *(Japanese)* 79−22387
 Cs-mordenite , dehydrated, positions of cations and molecules 79−1418
 Cs-O, low work function surface, prod. by Cs_2CO_3 decomp. and emission characts. 77−85882
 Cs-O, on GaP (100) surface, thermal desorption props. *(Japanese)* 80−15368
 Cs-O adlayer on GaAs photocathode, negative electron affinity, core level photoemission 79−19965
 Cs-O coated Ag cathode, photoemission mechanism *(Chinese)* 79−19966
 Cs-O coated $Ga_{1-x}In_xAs$ photocathode, negative electron affinity, photoelectron scatt. in coating 79−28899
 Cs-O coated GaAs, negative electron affinity, refl. of slow electrons, 0.4-3 eV 78−11038
 Cs-O coated GaAs and GaP, negative electron affinity, secondary emission characts. 78−11031
 Cs-O film, metallic, on Ag substrate, photoemission, surface plasmon excitation 77−16461
 Cs-O system, phase diagram and O_2 potential 80−3011
 Cs-SiO_2-Al_2O_3 system interactions, getter development for radiocaesium 80−83208
 Cs-U-O fission product compounds in irradiated nucl. fuels, chemical thermodynamic data *(Japanese)* 79−22387
 $Cs+Cl_2$, transient species, matrix isolation spectra 78−48635
 Cs_2 $CdBr_4$, room temp. struct. 80−29000
 (Cs-O)-Ag photocathode, operation mechanism involving Cs_2O_2 80−66384
 $CsAg_3Se_2$, crystal struct., X-ray study *(German)* 78−83795
 $CsAl_2Br_7$, ^{81}Br NQR and ^{27}Al NMR 78−6597
 $CsAlCl_4$, crystal struct. refinement 79−73145
 $CsAlCl_4$, solid state Raman spectra, 298-80K, vibr., struct. 79−28745
 $CsAlF_4$, dissoc. enthalpies, mass spectrometric determ., heat of form. 80−97720
 $CsAlF_4$, hydrothermal growth method in presence of hydrofluorhydric acid *(French)* 80−25543
 $CsAlF_4$, single cryst., prep. and struct. *(French)* 80−79762
 $CsAl_xFe_{(1-x)}(SO_4)_2$, solid soln., Raman and IR spectrum study *(French)* 79−47453
 $CsAl(SO_4)_2.12H_2O:Cr^{3+}$, ESR spectra 78−91944
 $CsAlSiO_4$, and $CsAlSi_5O_{12}$, cryst. evap., mass spectral investig. 80−49353
 $CsAlSiO_4$, prep. and X-ray characterisation 78−39728
 $CsAlSi_2O_6$, elec. cond. meas. 78−47787
 CsAr, 6dσ states, multiphoton laser spectrosc. obs. 79−85974
 $CsAsF_6$, γ-irrad., EPR spectra, hyperfine interactions and g-value determ. 77−81416
 $CsAsF_6$:BiF_6^-, gamma irrad., BiF_6^{2-} prod., EPR meas. 78−19329
 $CsAsO_4$, new compound, prep. and crystallographic characterisation *(French)* 79−66280
 $CsAsO_4$, polycrystalline, effect of mag. field on quadrupole spin echo 77−12245
 $Cs_2As_2O_7$, solid-state synthesis, X-ray powder data *(French)* 80−15079

caesium compounds continued
 Cs_3AsO_4, new compound, prep. and crystallographic characterisation *(French)* 79−66280
 $Cs_2Au^IAu^{III}Cl_6$, influence of high hydrostatic pressure on cryst. struct. in pressure range up to 52×10^8 Pa 79−51249
 $Cs_2Au_2Cl_6$, ^{197}Au Mossbauer high press. study of mixed valence compound 78−52387
 $Cs_2Au_2Cl_6$, electronic state of Au at high press., Mossbauer spectra 80−60467
 $CsBF_4$, ionic radii and chem. shifts, correl. with electronegativity 80−66054
 CsB_3H_8, IR, Raman and inelastic neutron scatt. spectra 79−42966
 $Cs_2B_{12}H_{12}$, cryst. growth from soln. and morphology 77−44145
 $Cs_2B_{12}H_{12}$.CsBr, cryst. growth from soln. and morphology 77−44145
 $Cs_2B_{12}H_{12}$.CsCl, cryst. growth from soln. and morphology 77−44145
 $CsBO_2$, mean geometrical config., vapour phase electron diffr. 77−50554
 $CsBO_2$, mol. struct. determ. by gas phase electron diffr. 79−10227
 $CsBO_2$, vapour over heated solid, XPS, obs. 80−87171
 $Cs(B_xW_{3-x})O_9$ (B=Na, Ca, Co, Ni, Cd, Ga, Bi, Nb, Ta) cryst. struct., temp. dielec. anomalies 80−1998
 $Cs_3Bi_2Br_9$, cryst. struct. determ. 77−80475
 $Cs_3Bi_2I_9$, hexagonal $Cs_3Cr_2Cl_9$ struct. type 78−34478
 $CsBi(MoO_4)_2$, low temp. phase transition, permittivity meas. 79−28698
 $Cs_5Bi(MoO_4)_4$, synthesis, X-ray and thermal investigations 77−36390
 $Cs_3BiSbBr_9(Cl_9)$, ^{121}Sb Mossbauer chem. shifts, optical reflectance spectra, solid state band populations 77−40162
 CsBr, (110) surface, electronic struct. of valence bands calc. *(Russian)* 80−75621
 CsBr, adsorption of methanol, IR spectrometric obs. *(French)* 78−46343
 CsBr, Br^- form., electron photodetachment cross section-determ. 77−3330
 CsBr, cryogenic temp. IR refractive index obs. 80−7320
 CsBr, crystal, short range interaction polarization, dielectric const. loss, and elec. cond. 10^2 to 10^7 Hz 79−99814
 CsBr, electron-phonon interactions of F-centres, first-order Raman scatt. 78−64370
 CsBr, electronic struct. anal. by reflectance and thermoreflectance studies 79−69855
 CsBr, emission spectra of O_2^- centres, at high hydrostatic press. 78−10943
 CsBr, evaluation of van der Waals dipole-dipole pot. 78−22692
 CsBr, exciton mechanisms of electron sputtering 77−55857
 CsBr, F-centre absorpt., uniaxial stress effects 80−60634
 CsBr, F-centre ESR in relaxed excited state, isotropic superhyperfine interaction consts. 79−65733
 CsBr, F-centres, EPR in relaxed excited state, detection via saturated optical pumping 78−6606
 CsBr, F-centres, relaxed excited state, ESR, detected via optical pumping 78−43693
 CsBr, far IR spectra, matrix isolated, monomers, dimers, trimers 78−66545
 CsBr, first-order Raman off- and on-reson. scatt. induced by F-centres 78−92073
 CsBr, gamma and additively coloured, dissolving in pure water, lyoluminesc. mechanism 80−100693
 CsBr, gamma irrad., EPR of Br_2 ions 79−51838
 CsBr, hyper-Raman spectra by single channel method 78−84591
 CsBr, IR active and silent modes, hyper-Raman scatt. obs. 79−61376
 CsBr, impurity absorpt. spectra after γ-irrad., aggregated colour centres 79−4829
 CsBr, irradiated with ultrasoft X-rays, thermolum. meas., surface energy losses 77−16408
 CsBr, isothermal eqn. of state *(Chinese)* 77−7836
 CsBr, lattice statics and dynamics, deformation shell model 77−20034
 CsBr, luminesc., mag. circ. polaris., self-trapped excitons, EPR 79−33805
 CsBr, luminesc. polarisation for free and bound excitons 78−10942
 CsBr, molten, structural props., computer simulation 77−84616
 CsBr, permittivity and polarisation behind shock wave front 77−52013
 CsBr, second relaxed excited state of F-centre, optically detected EPR 79−87335
 CsBr, self trapped exciton, optical detection of spin relax. processes 78−60358
 CsBr, self trapped hole, hopping motion equilib. lattice config., electronic excitation energy, activation energy calc. 78−10046
 CsBr, self-trapped exciton and F-centre form. by picosecond laser pulses 80−10546
 CsBr, self-trapped excitons, magneto-optical props., 1.3-50K 80−49606
 CsBr, single crysts., polarisation of luminesc. and reorientation of NO_2^- centres 79−95823
 CsBr solution, EPR of O_2^- luminesc. centres, 4.2K *(Russian)* 79−15339
 CsBr, spin-lattice relax. of F-centres, magneto-optical meas. 77−43884
 CsBr, storage layers stability under electron bombardment 78−27355
 CsBr, temp. depend. of Cs colloids absorption bands 80−40145
 CsBr, thermodynamic props., lattice dynamical calc. 77−20090
 CsBr, X-irradiated, release of stored energy 78−38753
 CsBr:$Ca^{2+}(Pb^{2+})(Ba^{2+})$ (MnO_4^{2-}), reorientation of dipolar complexes, ionic thermo currents meas. 77−80642
 CsBr:Cl(F), luminescence investig. of F_H-centre lifetime 77−20917
 CsBr:CrO_4^{2-}, coupling and fine struct., IR electronic and vibr. spectra obs. 80−45118
 CsBr:Cu, polarisation study of tetragonal Cu^{2+} aggregate centres 78−39590
 CsBr:Cu , excitation and absorpt. spectra 80−108255
 CsBr:Cu^+, γ-irradiated, thermolum. emission 80−104001
 CsBr:Cu^+, X-ray irrad., thermoluminesc. 80−16107
 CsBr:Cu^+ off-centre, optical absorpt. meas. 79−33740
 CsBr:$K^+(Na^+)(Rb^+)(Tl^+)$, impurity induced IR absorpt. spectrum, breathing-shell model 77−77256
 CsBr:K(Li)(Na)(Rb), optical absorpt. investig. of F_A-centres 77−44029
 CsBr:MNO_4^{2-}, optical and vibronic spectra 79−65909
 CsBr:Mn phosphor, luminesc. spectrum 77−59610
 CsBr:NO_2^-, luminesc. centre polarisation and reorientation *(Russian)* 78−76529
 CsBr:NO_2^-, vibronic and reson. Raman spectra of BCC cryst. 79−87468
 CsBr:O_2 , Stokes' losses on cryst. vibrs. in luminesc. spectra of mol. centres *(Russian)* 77−55827
 CsBr:O_2^- centres, luminesc., polarisation temp. depend. 78−87943

caesium compounds continued
CsBr:Pr, absorpt. and fluoresc. spectra, crystal field 78–2885
CsBr:Th, absorpt., excitation, fluorescence spectra 79–43032
CsBr:Tl, $[X_2^-]$ centre dynamic props. 79–65730
CsBr:Tl, emission bands, press. effect 79–33789
CsBr:Tl$^+$, ESR of $[X_2^-]$ centres 79–33533
CsBr:Tl$^+$, impurity induced Raman spectra, breathing shell model 78–39541
CsBr:Tl$^+$, perturbed lattice dynamics, breathing shell model calculation 78–75744
CsBr-dioxane-H_2O solns., elec. cond. calcs., computer program, data anal. *(German)* 77–32806
CsBr-$MgBr_2$ system, thermochem. and struct. investigation *(German)* 79–1423
CsBr-TlBr, phase diagram and pt. defect parameters 79–96017
CsBrICN, Raman and IR vibr. spectra, struct. 80–102513
$CsBrO_3$, ^{17}O NQR, spin echo double reson. method, electronegativity 80–54970
CsC_8 intercalation compound, cryst. atomic struct. study *(French)* 79–42021
CsC_x, lamellar cpds. with graphite, ^{13}C NMR studies 80–44936
CsCN, inelastic neutron scatt. by coupled rotational and translational modes 80–70333
Cs_2CO_3, ionic equil., mass spectra obs., heats of reaction and form. of ions 79–87867
Cs_2CO_3 thermal decomp., low work function surface prod. 77–85882
$Cs_2C_2O_4(SbF_3)_2$, growth from soln. and X-ray diffr. study *(French)* 77–80481
$CsCaCl_3$, birefringence, twinning and structural phase transitions 79–38480
$CsCaCl_3$ crystal, sp. ht. and thermal expansion coeffs. 80–10681
$CsCaCl_3$, optical characts. over wide spectral range 80–34875
$CsCaCl_3$:Co(Mn), EPR, 4.2 to 450K, ferroelec. transition 80–60414
$CsCaCl_3$:Pb, and undoped crystals, photolum. and thermolum. meas. *(Russian)* 77–85767
$CsCa_{0.95-x}Mg_xEu_{0.05}F_3$, blue luminesc. obs. 77–32428
$CsCdBr_3$, diamag. linear chain lattices, cryst. struct. 80–70172
$CsCdBr_3$:Cr^{3+}(Cr^+), EPR of impurities, charge compensation, X-ray effects 80–60407
$CsCdBr_3$:Gd^{3+}, EPR of coupled pairs of Gd^{3+} ions 78–19322
$CsCdBr_3$:Gd^{3+}, EPR spectra of mag. coupled Gd^{3+} ions 78–35032
Cs_2CdBr_4, struct. phase transitions, NQR study 80–71343
$CsCdCl_3$, NQR investig. of press. induced phase transition 77–12224
$CsCdCl_3$, phase transition under pressure 78–51664
$CsCdCl_3$, physical properties, application as lens or laser window materials 79–98450
$CsCdCl_3$:Co^{2+}, ground-state g-value, EPR meas. 77–16159
$CsCdCl_3$:Co^{2+}, Zeeman Raman scatt. and Zeeman IR absorpt. spectra 79–56782
$CsCdF_3$, nonlinear elastic behaviour, US velocity, 1 bar-3 kbar 78–59851
$CsCdF_3$:Cr^{3+}, ENDOR exam. of electron spin transfer 77–48089
$CsCdF_3$:Cr^{3+}(Fe^{3+}), ligand polarisation and transferred hyperfine interactions 79–51535
$CsCdF_3$:Fe^{3+}, ENDOR meas. on Fe^{3+}-F^--Cd^{2+} struct. 78–31122
$CsCd(NO_2)_3$, pure and metal ion doped, cryst. struct., reflectance spectra and thermal decomp. 79–51081
CsCl, (110) free surfaces, shell model surface acoustic mode dispersion 77–15675
CsCl, (110) surface, electronic struct. of valence bands calc. *(Russian)* 80–75621
CsCl, activation coefficients and solvation numbers in mixed methanol solvents 80–81334
CsCl, adsorbed on GaAs (110), adsorpt.-desorpt. processes and phase transitions 78–2361
CsCl, adsorption of methanol, IR spectrometric obs. *(French)* 78–46343
CsCl, aq. soln., density, isothermal compressibility, 293.15K, up to 200 MPa 80–44243
CsCl, aqueous soln., high precision viscosity meas. 80–10695
CsCl aqueous solutions, IR absorpt. ν_1 (CN) band parameter temp., conc. study *(Russian)* 80–80801
CsCl, Cl^- form., electron photodetachment cross-section determ. 77–3330
CsCl crystal, BCC and BCC ordered, core struct. of ⟨100⟩ dislocations, atomistic calc. 78–30637
CsCl, CsCl+KCl mixtures, osmotic coeffs. at 298.15K 78–92509
CsCl, electron beam excited luminesc., phase transition effects 77–85810
CsCl, electron-phonon interactions of F-centres, first-order Raman scatt. 78–64370
CsCl, electronic struct. anal. by reflectance and thermoreflectance studies 79–69855
CsCl, electrostatic energy calc. by planewise summation method 79–23564
CsCl emitter, secondary electron emission study 78–27356
CsCl, enthalpies of solution and formation 79–61892
CsCl, evaluation of van der Waals dipole-dipole pot. 78–22692
CsCl, F- and F_H-centres, luminesc. meas. 78–10397
CsCl, F-centre ESR in relaxed excited state, isotropic superhyperfine interaction consts. 79–65733
CsCl, F-centres, EPR in relaxed excited state, detection via saturated optical pumping 78–6606
CsCl, F-centres, relaxed excited state, ESR, detected via optical pumping 78–43693
CsCl, far IR spectra, matrix isolated, monomers, dimers, trimers 78–66545
CsCl films, kinetic electron emission when penetrated by H^+ ions with 0.3 to 30 keV energy 79–91554
CsCl, first-order Raman off- and on-reson. scatt. induced by F-centres 78–92073
CsCl, gamma and additively coloured, dissolving in pure water, lyoluminesc. mechanism 80–100693
CsCl, gas-surface collisions with Ni, ang. distribs. of mols. restituted to gas phase 80–6626
CsCl, hyperfine spectrum, mol. beam elec. reson. meas. 77–71797
CsCl, impurity and defect sites, elec. field gradient calc. 79–78034
CsCl, isothermal eqn. of state *(Chinese)* 77–7836
CsCl, lattice statics and dynamics, model calcs. 77–11647
CsCl, luminesc. in vac. UV range above and below phase transition temp. 80–93399
CsCl, Madelung pot. determ. by Ewald method 80–92475

caesium compounds continued
CsCl, molten, structural props., computer simulation 77–84616
CsCl, molten diffusion of Li^+, Na^+, Rb^+ and Cs^+ ions *(Japanese)* 78–14489
CsCl, phonon dispersion, temp. induced phase transition, deformable shell model calcs. 79–77698
CsCl, photoelectron spectra obs., comparison with atomic spectra of Cs 80–83419
CsCl, photofragment spectra, bond energies and excited state symmetries 80–87190
CsCl, positron-trapping colour centre dynamics, positron annihilation study 80–108294
CsCl, rot. excitation by electron impact, calc. cross sections 78–66670
CsCl, self trapped hole, hopping motion equilib. lattice config., electronic excitation energy, activation energy calc. 78–10046
CsCl soln., radioactive, tilt-pour melt caster for encapsulation 79–26580
CsCl solution, EPR of O_2^- luminesc. centres, 4.2K *(Russian)* 79 15339
CsCl, spin-lattice relax. of F-centres, magneto-optical meas. 77–43884
CsCl structure, evaluation of finite strain eqns. of state using lattice models 80–96620
CsCl structure, quantifying concept of coordination number 78–95008
CsCl structure solids, many-body effects on elastic consts. 77–1163
CsCl, thermal expansivity determ. at high press. 78–79787
CsCl, transition mechanism between CsCl-type struct. and NaCl-type struct. 77–31768
CsCl, twin form. by compressive stress during phase transform. 80–49358
CsCl type crystals, piezo-optic birefr. 78–39523
CsCl type crysts., elastic consts. Cauchy discrepancy, three-body force shell model 77–20004
CsCl:Ag film, EPR and optical exam. of Ag impurity centres 77–85562
CsCl:Ag phosphor, spectral characts., optical range 77–1724
CsCl:Cr^{3+}, ESR of Cr^{3+} centres, room temp. 78–91943
CsCl:Cu^+, γ-irradiated, thermolum. emission 80–104001
CsCl:Cu^+, X-ray irrad., thermoluminesc. 80–16107
CsCl:Fe, defect struct., Mossbauer spectra and X-ray diffr. obs. 80–7237
CsCl:K(Li)(Na)(Rb), optical absorpt. investig. of F_A-centres 77–44029
CsCl:Tl, $[X_2^-]$ centre dynamic props. 79–65730
CsCl:Tl$^+$, ESR of $[X_2^-]$ centres 79–33533
CsCl-AgCl, spectral luminesc. characts., optical range 77–1724
CsCl-$BaCl_2$:U^{3+}, melt, diffusion coeffs. and mechanisms 79–73330
CsCl-$BaCl_2$($LaCl_3$) molten binary mixtures, thermal cond. 79–86931
CsCl-H_2O-1-glyceryl 1-octanoate, Cs^+H_2O interaction in lamellar phase, NMR quadrupole splitting and chemical shift 80–50209
CsCl-NO_2^-, vibronic and reson. Raman spectra of BCC cryst. 79–87468
CsCl-NaCl melt, X-ray diffr. struct. determ. 79–41925
CsCl-structure compounds, lattice energy and elastic consts. for 3-body Van der Waals interaction 77–72580
CsCl-TlCl solid soln., point defect parameters 80–54224
CsCl-TlCl solid soln., determ. and computation of phase diagram 80–55379
CsCl-type crystal, cation vacancies migration energies 80–2192
CsCl-type lattice, (111) superlattice screw dislocation motion, computer simulation 80–79793
CsCl-UCl_3 melts, density, surface tension and viscosity 78–67764
CsCl-$ZnCl_2$, molten, US velocity, thermodynamic quantities and struct. *(Japanese)* 80–88270
CsCl-$ZnCl_2$, molten, US absorption coeffs. and bulk viscosity coeffs. *(Japanese)* 80–88271
CsCl+KCl mixtures, osmotic coeffs. at 298.15K 78–92509
CsCl+NaI→CsI+NaCl, solid-state displacement reaction 77–52635
CsCl+SF_6, collision induced dissoc., threshold behaviour 78–88627
$Cs_2Cl_2+SF_6$, collision induced dissoc., threshold behaviour 78–88627
CsCl(Br)(I), dielectric const. meas. at 1 MHz by immersion method *(Japanese)* 77–90087
CsCl(Br)(I), doped F_{Z1}-centre exam. 78–14341
CsCl(Br)(I), photoemission, electron-phonon interaction effects, Monte-Carlo calc. and expt. 78–11071
CsCl(Cs_2Cl_2)+Ar(Kr)(Xe), collision-induced ion-pair form., absolute cross sections 78–73029
CsClICN, Raman and IR vibr. spectra, struct. 80–102513
$CsClO_4$, AC elec. cond. temp. and freq. depend., obs. and unified defect struct. model 80–88554
$CsClO_4$, electrical conductivity, frequency dependence 80–65288
$CsClO_4$-$LiClO_4$, binary melt, Raman spectra, polarised line width, temp. depend. 78–84578
CsCl.2CuCl, and 3CsCl.2CuCl, phase transform. heats, DTA obs. *(Russian)* 80–55698
$CsCoBr_3$, ID Ising antiferromagnet, spin dependent Raman scattering from phonons and electronic excitations 80–103948
$CsCoBr_3$, quasi ID Ising antiferromag., polarised Raman scatt. from mag. excitations 80–66182
$CsCoBr_3$, quasi one dimensional antiferromag., magnon Raman scatt. 80–11395
Cs_3CoBr_5, optical anisotropies of mechanism of vibronic transitions in spectra 77–12372
Cs_3CoBr_5, single cryst. polarised vibr. spectra 78–39535
$CsCoCl_3$,$2H_2O$, pseudo one-dimens. Ising-like system, mag. heat capacity and metamag. transitions 77–66351
$CsCoCl_3$, 1-D Ising antiferromag., mag. phase transitions 79–51779
$CsCoCl_3$, 10 Ising antiferromag., mag. excitations, electronic Raman and IR absorption spectra 78–2668
$CsCoCl_3$, anisotropic antiferromag., inelastic neutron scatt. study 78–60274
$CsCoCl_3$, antiferromag., spin wave spectrum 79–28514
$CsCoCl_3$, antiferromag., ^{59}Co NMR spectrum obs. by spin echo method 79–51881
$CsCoCl_3$, covalency parameters estimation from nucl. quadrupole coupling 80–25246
$CsCoCl_3$, Ising antiferromagnet, electronic Raman scatt. on Co^{2+} 78–10878
$CsCoCl_3$, Ising like antiferromag., mag. phase transition, ^{133}Cs NMR 80–7184
$CsCoCl_3$, Ising-like antiferromag., spin dynamics 79–42747
$CsCoCl_3$, Ising-like antiferromag., instantaneous spin correlations 79–42746
$CsCoCl_3$, mag. excitation spectrum, spin-wave response, neutron scatt. study 80–50080

caesium compounds continued
$CsCoCl_3$, mag. struct., neutron diffr. meas. 78—43563
$CsCoCl_3$, one-dimensional antiferromag., neutron scatt. investig. of spin waves 77—47982
$CsCoCl_3$ spin dynamics, neutron scatt. study 80—80493
Cs_2CoCl_4, heat capacity below 1K, rel. to S=1/2 linear chain XY model 77—59415
Cs_2CoCl_4, mag. susceptibility and magnetisation curve meas. 80—11176
Cs_2CoCl_4, paramag. mag. exchange rel. to low temp. mag. characts. 77—55669
Cs_3CoCl_5, neutron diffr. struct. at 4.2K 80—54176
Cs_3CoCl_5, optical anisotropies of mechanism of vibronic transitions in spectra 77—12372
Cs_3CoCl_5, single cryst. polarised vibr. spectra 78—39535
$CsCoCl_3.2D_2O$, crit. behaviour along metamag. phase transition 77—59409
$CsCoCl_3.2D_2O$, metamag., thermodynamic props. near multicrit. pt. 77—66305
$CsCoCl_3.2H_2O$ interchain exchange low temp. susceptibility 78—19240
Cs_3CoI_5, cryst. struct. and thermal props. *(German)* 79—23578
$Cs_2Co_{1-x}Zn_xCl_4$, mag. sp. ht., effect of dilution, comparison with linear XY antiferromag. 77—66354
$Cs_3Cr_2Br_9$, Cr (III) trigonal pair, exchange interactions, absorpt., MCD and Zeeman spectra 78—19009
$CsCrCl_3$, α-β phase transition, dynamical aspects and thermodynamic theory 80—70404
$CsCrCl_3$, co-operative Jahn-Teller distorted struct. determ. 78—63713
$CsCrCl_3$, Jahn-Teller induced phase transitions 80—70391
$CsCrCl_3$, mag. structure and excitations, neutron diffr. and susceptibility meas. 80—44806
$Cs_2Cr_2Cl_9$, Cr (III) trigonal pair, exchange interactions, theory 78—19008
$Cs_3Cr_2Cl_9$, optical absorpt., MCD, exchange interactions 78—10917
$Cs_3Cr_3Cl_9$, thermo-optical spectroscopy, detection by mirage effect 80—47116
$CsCr_xFe_{(1-x)}(SO_4)_2$, solid soln., Raman and IR spectrum study *(French)* 79—47453
$CsCrI_3$, Mossbauer spectra, struct., electronic and mag. props. 79—91320
$CsCrI_3$, Mossbauer spectra, struct., electronic and mag. props. 80—15908
$CsCrI_3$, neutron diffr. expts. at 300, 77 and 1.2K 80—107163
$CsCrI_3$, X-ray cryst. struct. determ. *(French)* 79—73140
$CsCrO_4$, solid-to-solid transition temperature under hydrostatic pressures to 0.6 GPa 80—24586
Cs_2CrO_4, domain struct., ferroelastic 78—18702
Cs_2CrO_4, mol. beam obs. of evap., saturated vapour press., 656.8 to 1151K 80—107411
$CsCuBr_3$, quasi-1-dimens., NQR obs. 80—54987
$CsCuCl_3$, birefr. and opt. rot. near structural phase transition points 78—75823
$CsCuCl_3$, cooperative Jahn-Teller transition with trebling of period *(Russian)* 77—76557
$CsCuCl_3$, cryst., gyrotropy, anomalous dispersion curves 80—2719
$CsCuCl_3$, helical mag. struct., neutron diffraction study 80—107983
$CsCuCl_3$, Jahn-Teller induced phase transition, helical at. displacements 77—43301
$CsCuCl_3$, Jahn-Teller effect induced phase transitions 79—47439
$CsCuCl_3$, Jahn-Teller induced phase transitions 80—70391
$CsCuCl_3$, one-dimensional antiferromag., ^{63}Cu NMR mas. 78—2756
$CsCuCl_3$, optical props. rel. to IR electro-optical modulator appl. 78—42393
$CsCuCl_3$, phase transition, refr. index, electrooptic coeff., pyroelec. signal, and NQR meas. 80—70386
$CsCuCl_3$, phase transition obs., commensurate and incommensurate structural phase transitions in Jahn-Teller system 80—70403
$CsCuCl_3$, phys. props. 77—62511
$CsCuCl_3$, piezoelectricity, Jahn-Teller type phase transform. 80—40065
$CsCuCl_3$, quasi-1-dimens., NQR obs. 80—54987
$CsCuCl_3$ submillimetre spectra phasons, low freq. modes, phase fluctuations *(Russian)* 80—50333
$Cs_2CuCl_4.2D_2O$, quadrupolar interaction, 4-300K, reorientation 79—73848
$CsCuCl_4.2H_2O$, hyperfine and super-exchange interactions 80—103654
$Cs_2CuCl_4.2H_2O$, Bloch-wall NMR, anisotropic hyperfine interaction 79—51864
$Cs_2CuCl_4.2H_2O$, ferromag., hyperfine and exchange interactions, NMR study 80—50208
$Cs_2CuCl_4.2H_2O$, Heisenberg ferromag., exchange anisotropy by NMR 77—55714
$Cs_2Cu(SO_4)_2.6H_2O$, long exchange paths between mag. ion pairs, singlet-triplet separation determ. 77—69283
CsD_2AsO_4 crystals, SHG, temperature phase-matching curve hysteresis 80—91852
CsD_2AsO_4, ferroelec., elastic consts., HF meas. 77—8524
CsD_2AsO_4, ferroelect. phase transition, NMR study *(Chinese)* 79—33644
CsD_2AsO_4, ferroelectrics, Raman spectra, coupled tunnel-phonon modes and isotope effect 79—69205
CsD_2AsO_4 Fourier transform plane superposition multiplier, for optical processing 79—7084
CsD_2AsO_4, high efficiency SHG of Nd:YAG laser radiation 78—59088
CsD_2AsO_4, high efficiency freq. doubling of Nd:YAG laser light 78—79071
CsD_2AsO_4, SHG, electro-optic and piezo-optic tuning 78—46718
CsD_2AsO_4, shorted and free single crysts., piezoelec. coupled soft mode, Brillouin scatt. meas. 77—52109
CsD_2AsO_4, spectral phase-matching props. for SHG 77—83922
CsD_2AsO_4, temporal power variation of SHG of Q-switched YAG laser radiation 78—25922
$Cs(D_{1-x}H_x)_2AsO_4$, high temp. nondestructive phase transform. at 170°C 77—12337
$Cs(D_xH_{1-x})_2AsO_4$, cryst. struct. in ferroelec. and paraelec. phases neutron diffr. meas. 77—7694
$Cs(D_xH_{1-x})_2AsO_4$, isotope exchange during crystallisation from aqueous solns. 78—18569
$Cs(D_xH_{1-x})_2AsO_4$, phase transition exam. 77—12340
$Cs(D_xH_{1-x})_2AsO_4$, soln. cryst. growth, optical absorpt. and SHG phase match data 78—11095
$Cs(D_xH_{1-x})_2PO_4$, D distrib. during crystallisation from aq. soln. 77—11496
$Cs(D_xH_{1-x})_2PO_4$, isotope exchange during crystallisation from aqueous solns. 78—18569

caesium compounds continued
CsD_2PO_4, dielec. props., press. and temp. depend. 80—25317
CsD_2PO_4, ferroelec. transition, press. depend. 78—35101
CsD_2PO_4, neutron scatt. study of ferroelectric phase transitions 77—59538
CsD_2PO_4, one dimens. ordering, ferroelec. transitions, neutron scatt. study 80—25316
CsD_2PO_4, permittivity temp. depend., pseudo one-dimens. ferroelectric ordering and critical props., NMR 79—78635
CsD_2PO_4, pseudo one-dimens. ferroelec. ordering dynamics, ^{31}P NMR study 80—75971
CsD_2PO_4, pseudo-one-dimensional ferroelectric transition, ^{31}P chemical shift and relaxation study 80—66123
CsD_2PO_4, pseudo-one-dimens. ferroelec. transition, DMR and relax. study 80—71223
CsD_2PO_4, pseudo-one-dimensional ferrolec. and antiferroelec. transitions, phase diagram obs., soft modes 80—93245
$CsDy_2F_7$ and Cs_3DyF_6, cryst. symm. and cell parameters *(French)* 80—81040
$CsDy(MoO_4)_2$, effect of 38K phase transition on phonon spectrum, IR reflection spectra *(Russian)* 79—10902
$CsDy(MoO_4)_2$, trivalent ion impurity effects on structural phase transition temp., new transition 20-30K *(Russian)* 79—19367
$CsDy(MoO_4)_2:Eu^{3+}$, anomalous effect of impurity on struct. phase transition temp. *(Russian)* 77—69083
Cs_3EuF_6, $CsEu_2F_7$, cryst. struct. by X-ray diffr., equilib. in CsF-EuF_3 *(French)* 78—44107
CsF, adsorbed on Ag photocathode, work function decrease 79—78824
CsF, cryst., Debye characteristic temp. calcs. 79—37796
CsF, cubic NaCl-type cryst., Debye temp. 80—54333
CsF, dil. aq. soln., elec. cond., 25°C 77—69105
CsF, doped with F-centres, first order Raman scatt. 78—52492
CsF, EPR of self trapped exciton and MCd meas. 77—48091
CsF, electron impact, elastic scatt., model, static and static exchange calcs. 78—94321
CsF, electron-phonon interactions of F-centres, first-order Raman scatt. 78—64370
CsF, F-centre ground state distortion fields and optical absorption 80—55140
CsF, F-centre optical absorption bandshape calc. for transition to state with Jahn-Teller and spin orbit couplings 80—55135
CsF, far IR spectra, matrix isolated, monomers, dimers, trimers 78—66545
CsF, muon Coulomb capture ratio 78—62959
CsF, quadrupole coupling, vibr. and rot. effects, Morse oscill. calcs. 77—6805
CsF, rot. excitation by electron impact, calc. cross sections 78—66670
CsF, rot. inelastic collisions, mol. beam meas. 80—1049
CsF scintillator, pot. advantages for a time-of-flight positron camera 80—81706
CsF, second-order Raman spectra and phonon spectrum 77—90148
CsF, seeded in supersonic beam, vibr. relax. 78—37716
CsF, Stark effect, deviations from rigid rotator model 79—18234
CsF:Li(Na), F-centres, saddle-point configuration, molecular model parameter 80—107234
CsF-AlF_3, ion-molecule equilibria studied by mass spectrometric method, heats of dissoc. and form. calc. 80—104479
CsF-BeF_2 glass, anion conductivity, transport number radiometric meas. 79—86923
CsF-EuF_3 system, thermal anal. and X-ray diffr., phase equilibria *(French)* 78—44107
CsF+Ar, 87.7 meV, reorientation effects by approx. quantum methods 77—79680
CsF+Ar, elastic and rot. inelastic scatt., quantum mech. calcs. 77—14525
CsF+K collision complex, reactive decay branching ratio, rot. energy effect 77—66752
CsF+Ne, (Ar)(Kr)(Xe), sudden, body-fixed and semiclassical approx. calcs. 78—42164
$CsFeCl_3$, linear chain ferromag., optical absorpt. and dichroism in mag. field 77—77237
$CsFeCl_3$, linear chain cryst., quadrupole and mag. reson., rel. to $RbFeCl_3$ 79—38403
$CsFeCl_3$, pseudo-one-dimens. singlet ground state ferromag., mag. excitations, neutron scatt. study 80—97064
$CsFeCl_3$, single cryst. mag. susceptibility meas. 77—20560
$Cs_2FeCl_5(Br_5).H_2O$, antiferromag. props. and struct. 78—31056
$Cs_2FeCl_5.H_2O$, cryst. struct., superconducting susceptometer mag. meas. 79—73717
$Cs_2FeCl_5.H_2O$, mag. phase boundaries, susceptibility, 3D Heisenberg antiferromag. behaviour 78—84420
$CsFeCl_3.2D_2O$, cryst. and mag. struct., neutron scatt. and NMR expts. 79—7969
$CsFeCl_3.2H_2O$, rectangular Ising cpd., Mossbauer meas. 80—71252
$CsFeCrF_6$, $CsFeVF_6$, crystal struct., Mossbauer hyperfine spectra 78—52381
$CsFeF_4$, struct. phase transition at 250K 80—10663
$CsFeF_4$, two dimensional structural phase transitions, sp. ht., optical, dielec., X-ray diffr. meas. 79—69240
Cs_2FeF_5, mag. struct. and one-dimens. antiferromagnetism 80—60209
$CsFeS_2$, crystal ligand field theory, band assignment, absorpt. spectra study 80—20657
$CsFeSi_2O_6$, elec. cond. meas. 78—47787
$CsGa_{1-x}Fe_xS_2$, tetrahedrally coordinated Fe atoms in low spin state, mag. props. and neutron diffr. study *(German)* 80—88714
Cs_2GeF_6, A=Si, Ge, Sn, IR absorpt. spectra, integrated intensity 79—73944
Cs_2GeF_6, IR absorpt. spectra, integrated intensity, 100-300K 79—73945
$Cs_2GeF_6:Mn^{4+}$, magnetically circularly polarised emission and MCD of vibronic lines 77—16377
$Cs_2GeF_6.4HF$, cryst., H bond geometry, NMR obs. 79—42844
$Cs_2GeF_6.4HF$, molecular diffusion, spatial symmetry, HF molecule arrangement 79—42313
CsH, crystallisation in $Cs+H_2$ gas mixture, laser snow effect 80—40712
CsH, dissoc. energy calc. 78—90314
CsH, structural transition from NaCl to CsCl type under high press. 80—96458
CsH, $X^1\Sigma^+$ and $A^1\Sigma^+$ states, pot. energy curves, Rydberg-Klein-Rees methods 78—50486
CsH^+, Σ state pot. energy, Hellman pseudopot. calcs. 78—70764

caesium compounds continued
CsH_2AsO_4 and $Cs(H_xD_{1-x})_2AsO_4$, acoustooptical and photoelastic props. 78—27181
CsH_2AsO_4, and deuterated derivative, attenuation of LF elastic oscills. 77—7791
CsH_2AsO_4, and deuterated isomorph, E-mode splitting in ferroelec. phase, Raman scatt. meas. 77—16296
CsH_2AsO_4, and deuterated isomorph., ferroelectric mode and molecular vibr. press. depend. 78—19424
CsH_2AsO_4 crystals, dielectric radiation effects, γ-radiation 80—93234
CsH_2AsO_4, CsD_2AsO_4, SHG, laser heating effect 77—79891
CsH_2AsO_4, dielec. polarisation and dielec. const. 77—59527
CsH_2AsO_4, elastic props., photoelasticity near ferroelectric phase transition 80—29107
CsH_2AsO_4, ferroelec., temp. depend. of shear angle, neutron scatt. meas. 77—8524
CsH_2AsO_4, ferroelec., RF dielec. relax., loss mech. 79—38448
CsH_2AsO_4, ferroelectrics, Raman spectra, coupled tunnel-phonon modes and isotope effect 79—69205
CsH_2AsO_4, ferroelec., dielec. props., four-cluster approx. 80—97202
CsH_2AsO_4, high temp. phase transition 78—71856
CsH_2AsO_4, influence of γ-radiation on dielec. props. 79—46703
CsH_2AsO_4, laser accessory for freq. doubling 78—46725
CsH_2AsO_4, Mandelstam-Brillouin spectra and US vel. meas. near ferroelec. Curie point 79—38553
CsH_2AsO_4, pres. depend., LF dielec. response, ferroelec. props. 78—15120
CsH_2AsO_4, pyroelectric investig. in ferroelec. phase 77—12321
CsH_2AsO_4, RF dielec. response close to transition temp. 77—90099
CsH_2AsO_4, shorted and free single crysts., piezoelec. coupled soft mode, Brillouin scatt. meas. 77—52109
$CsHCl_2$, H bond bending vibrs., inelastic neutron scatt. obs. 79—89800
CsHClBr, H bond bending vibrs., inelastic neutron scatt. obs. 79—89800
CsH^-CsH^+(CsH), ab initio ground-state pot. energy curves, electron affinities 78—41946
$Cs(H_{1-x}D_x)_2PO_4$, dielec. props., temp. meas. 80—71335
$CsHF_2$, heat capacities, transitions and melting 79—10967
$CsHF_2$, struct. and phase transformation, NMR study 77—90047
$CsH(NO_3)_2$, inelastic neutron scatt. spectra, H bonds bending vibrs. 79—14893
CsH_2PO_4 and CsD_2PO_4, dielectric props. and ferroelec. transition temp. 77—12335
CsH_2PO_4, and deuterated phase, press. induced antiferroelec., switching behaviour 79—78634
CsH_2PO_4, dielec. props., press. and temp. depend. 80—25317
CsH_2PO_4, domain obs. in paraelectric phase 79—24277
CsH_2PO_4, ferroelec. transition, deuteration and press. effects 78—35101
CsH_2PO_4, ferroelec., press. induced antiferroelectricity 79—4774
CsH_2PO_4, ferroelec., X-ray and dielec. studies on phase transition 79—38477
CsH_2PO_4, ferroelec., critical behaviour of dielec. constant 80—34845
CsH_2PO_4, ferroelec. transition, electrooptic 80—76005
CsH_2PO_4, ferroelec., X-ray struct. study at room temp. 80—88113
CsH_2PO_4, ferroelec. transition, neutron diffr. study 80—93247
CsH_2PO_4, high press. phase diagram 78—52457
CsH_2PO_4, lattice consts., temp. depend. of dielec. const. and birefringence, high temp. phase transitions 79—56746
CsH_2PO_4, microhardness, expt. determ. 79—24603
CsH_2PO_4, NMR of ^{133}Cs, elec. field gradient 78—15034
CsH_2PO_4, neutron diffr. study of cryst. struct. 78—79592
CsH_2PO_4, one dimens. ordering, ferroelec. transitions, neutron scatt. study 80—25316
CsH_2PO_4, paraelectric phase, struct. exam. by neutron diffr. 79—37679
CsH_2PO_4, permittivity temp. depend., pseudo one-dimens. ferroelectric ordering and critical props., NMR 79—78635
CsH_2PO_4, press.-induced antiferroelectricity *(Japanese)* 80—15992
CsH_2PO_4, pseudo one-dimens. ferroelec. ordering dynamics, ^{31}P NMR study 80—75971
CsH_2PO_4, Raman scatt. and high temp. props. 80—16024
CsH_2PO_4, single cryst. growth, struct. and elec. props. 78—71693
CsH_2PO_4-d, antiferroelec. under hydrostatic press. 79—91384
$CsHSeO_3$, and deuterated analog, vibr. spectra 79—24311
$CsH_3(SeO_3)_2$, paraelec. phase, struct. determ. by neutron diffr. 78—34472
CsHe absorption bands associated with forbidden Cs transitions 79—27005
CsHe(Ne)(Ar)(Kr)(Xe), excited state IR emission bands 80—14140
$Cs_4Hf(C_2O_4)_4.nH_2O$, electric field gradient at metal site, γ-ray perturbed ang. correlation meas. 78—52380
$Cs_2HfCl_6:Mn^{2+}$, ESR of mol. jumps, zero-field splitting tensor 77—51944
$Cs_2Hf(MoO_4)_3$, X-ray cryst. struct. determ. 80—107182
Cs_2HgBr_4, phase transitions and singularities of cryst. struct., NQR study 80—19936
Cs_3HgBr_5, X-ray cryst. struct. determ. and refinement 79—46637
$CsHg(CN)_3$, CN and HgC stretching vibrations and HgCN bending vibration assignments 80—69140
Cs_2HgI_4, Cs_3HgI_5 and $Cs_2Hg_3I_2$, NQR spectra of ^{127}I and cryst. struct. 77 -12230
CsI, (110) surface, electronic struct. of valence bands calc. *(Russian)* 80—75621
CsI, {100} faces, form. of etch pits of different size and morphology, segregation influence 78—2130
CsI, acoustic NMR, role of incoherent phonons *(Russian)* 78—80230
CsI, adsorption of Ar-O_2 mixture, test of eqns. for gas mixture adsorption on heterogeneous surface 78—60030
CsI, adsorption of methanol, IR spectrometric obs. *(French)* 78—46343
CsI, and Na doped sample, elastically loaded, effect of annealing on optical absorption 77—44034
CsI, annealing effects on mech. and microstruct. props. 77—66686
CsI based powdered phosphors and screens possible appl. in X-ray radiography and fluorography 79—6245
CsI, correl. between UV emission band at 300 nm and self-trapped excitons, 4.2K 78—75998
CsI, cryogenic temp. IR refractive index obs. 80—7320
CsI cryst., dissolution, selective etching rel. to $CuCl_2.2H_2O$ additive in ethanol 77—72618
CsI crystal, growth time of scintillation pulse activator concentration and ionisation density 80—23251
CsI crystal, incoherent phonons, nuclear acoustic resonance 80—7180

caesium compounds continued
CsI crystals, in scintillation counters, nonstatistical counting rates due to phosphoresc. 78—95597
CsI crystals, relation of struct. and bond type to slip geometry 80—88165
CsI, crysts., microplasticity mechanism 78—30696
CsI, depth of emission of secondary photoelectrons 79—8228
CsI, electronic struct. anal. by reflectance and thermoreflectance studies 79—69855
CsI, evaluation of van der Waals dipole-dipole pot. 78—22692
CsI evaporated coating, photodetector sensitivity enhancement in VUV 79—85180
CsI, exam. of kinking process, using cholesteric liquid crystals 80—7629
CsI, exciton mechanisms of electron sputtering 77—55857
CsI, exposed to ultrasoft X-rays, thermal luminesc. and electron emission 79—8192
CsI, F- and F_H-centres, luminesc. meas. 78—10397
CsI, F-centre ESR in relaxed excited state, isotropic superhyperfine interaction consts. 79—65733
CsI, far IR spectra, matrix isolated, monomers, dimers, trimers 78—66545
CsI, far-IR optical props., shell-model calcs. 77—28557
CsI film, secondary emission yield, primary electron ang. of incidence effects 78—2961
CsI, free exciton reson. luminesc. lines 77—77272
CsI, high mass secondary ion clusters detected by SIMS 78—88400
CsI, hyper-Raman spectrum, optical phonons, nonlinear processes 77—4640
CsI, hyper-Raman spectra by single channel method 78—84591
CsI, IR active and silent modes, hyper-Raman scatt. obs. 79—61376
CsI in acetone, press. effects on Walden products, ion-solvent interactions 80—3398
CsI, isothermal eqn. of state *(Chinese)* 77—7836
CsI, isotope diffusion 78—75875
CsI, lattice statics and dynamics, model calcs. 77—11647
CsI, luminesc., mag. circ. polaris., self-trapped excitons 79—33805
CsI, mechanical props., effect of impurities 77—69034
CsI, molten, structural props., computer simulation 77—84616
CsI, nuclear spin echo for ^{127}I, magnetoacoustic excitation *(Russian)* 77—4578
CsI, optical props. in vacuum UV 77—24861
CsI photocathodes, efficiency evaluation for soft X-ray diagnostics 80—57442
CsI, photodissoc., UV, Cs atom orientation *(Russian)* 80—69201
CsI, photoionisation processes, expt. techniques, theory, review 77—14402
CsI, potential and limitations as dynode material for electron multiplier 78—23566
CsI, prep., 5-30 μ thick single cryst., for channellography appl. 78—80658
CsI, pure, influence of strain on photolum. 79—15527
CsI, pure and Na(Tl)-doped, luminesc. from bound excitons, UV absorpt. and EPR 77—77282
CsI, saturated photodissoc. by laser pulse, laser reson. ionis. obs. 77 -79661
CsI, secondary electron spectra, primary electron energies up to 30 eV 77—12473
CsI, secondary electron emission statistics, photomultiplier appl. 79—47564
CsI, selective etching, growth and dissolution in alcohols 78—71739
CsI, selective etching 78—19911
CsI, self trapped hole, hopping motion equilib. lattice config., electronic excitation energy, activation energy calc. 78—10046
CsI, self-trapped exciton and F-centre form. by picosecond laser pulses 80—10546
CsI, self-trapped exciton electronic struct., semi-empirical mol. orbital method 80—49605
CsI, self-trapped excitons, magneto-optical props., 1.3-50K 80—49606
CsI, single cryst., plastic deform. at 4.2K, temp. rise 77—15481
CsI, single crysts., polarisation of luminesc. and reorientation of NO_2 centres 79—95823
CsI, storage layers stability under electron bombardment 78—27355
CsI, temp. depend. of Cs colloids absorption bands 80—40145
CsI, thermal fields generated during plastic deform. 78—35457
CsI, thermodynamic props., lattice dynamical calc. 77—20090
CsI, ultralow loss optical fibre material, loss mechanism 80—78920
CsI, Wulf habits, ideal forms of soln. of crysts. 79—14718
CsI, yield point, obstacles to dislocation motion 77—43270
$CsI:CrO_4^{2-}$, coupling and fine struct., IR electronic and vibr. spectra obs. 80—45118
CsI:H , U-centres, force consts. using Green's functions 79—46775
CsI:K(Li)(Na)(Rb), optical absorpt. investig. of F_A-centres 77—44029
CsI:Mn phosphor, luminesc. spectrum 77—59610
$CsI:MnO_4^{2-}$, multiple-order Raman scatt., and absorpt. spectra 77—40229
$CsI:NO_2^-$, luminesc. centre polarisation and reorientation *(Russian)* 78—76529
$CsI:NO_2^-$, vibronic and reson. Raman spectra of BCC cryst. 79—87468
CsI:Na, crystal, kinetics of decay of surface solid soln. 79—23810
CsI:Na, electronic struct. and luminesc. 80—16080
CsI:Na, localised excitons, absorption and emission 77—32425
CsI:Na, photoluminescence spectra and lineshapes anal., exciton energies 77 77281
CsI:Na, self-trapped exciton emission polarisation 80—49607
CsI:Na, tunnelling recomb. of electron-hole pair, optical detection of ESR and circ. dichroism 79—47360
CsI:Na, UV irrad., thermoluminesc. 79—28846
CsI:Na, X-ray irradiated, optical and ESR studies in IR absorption band 80—80828
CsI:Na phosphor screen, absolute efficiency under fluoroscopy conditions 78—82084
$CsI:Na^+(K^+)$, luminesc. processes 80—103989
$CsI:Na^+(K^+),(Cu^{2+}),(Tl^{+}),(Eu^{3+})$, crysts., influence of impurities on yield stress 79--15748
CsI:Tl, [X_2] centre dynamic props. 79—65730
CsI:Tl, crystallophosphor, luminesc. characts., temp. and conc. depend. 80—55175
CsI:Tl, emission bands, press. effect 79—33789
CsI:Tl, gamma-scintillation growth front, external elec. field effect 80—34984
CsI:Tl, geometrical parameters of impurity centres by scattered-light method 80—2043

caesium compounds continued
- CsI:Tl, luminescence yield depend. on orientation of fast electron beam *(Russian)* 77—8665
- CsI:Tl, precipitation of Tl solid solns. 80—70419
- CsI:Tl, X-ray phosphor, influence of different factors on emission intensity 79—8171
- CsI:Tl, X-ray screens consisting of scintillating crystal fibers 79—6244
- CsI:Tl powdered phosphor screen for X-ray image intensifier 79—6246
- CsI:Tl single crystal gamma-optical converting screens, factors influencing relative afterglow intensity 79—8173
- CsI:Tl X-ray phosphor, spectral characts. 79—8172
- CsI:Tl^+, far IR props. of lattice resonant modes, hydrostatic press. effects 77—28574
- CsI:Tl^+, Jahn-Teller split luminesc., high press. study 78—52565
- CsI:Tl(Na), light yield under charged-particle bombardment 80—93409
- CsI-Hg-Ar discharge, high-press., temp. and plasma comp. determ. 79—10709
- CsI-KI, binary molten mixture, surface tension meas. 79—65294
- CsI-KI melt, X-ray diffr. struct. determ. 79—41925
- CsI+Ar(He), elastic and inelastic scatt. 77—58119
- CsI_3, solvent effects on electronic transitions of I_3^- 77—27080
- CsI_3, XPS, binding energies and bond orders 77—18976
- CsI(:Na), ionic cond. temp. depend. meas., effect of Na doping 78—18829
- CsI_2CN, Raman and IR vibr. spectra, struct. 80—102513
- CsI(Na) scintillating crystals in cosmic X-ray detectors, growth of deactivated layers 77—10554
- $CsIO_3$, hexagonal modification, temp. depend. of NQR freq., interpretation of long-wave spectra 80—25243
- CsI(Tl) crystal light output when exposed to protons at 3-15 MeV 78—78570
- CsI(Tl) thin film detectors, light output and resolution 78—9030
- $CsInCl_3$, mixed-valence cpd., structural phase transition *(German)* 80—70406
- Cs_2IrCl_6, hyperfine spectra of mag. ordered state at very low temp., Mossbauer meas. 77—69744
- $Cs_2KFe(CN)_6$, single cryst. neutron diffr. struct. determ. 80—28972
- $Cs_2KMO_3F_3$, (M=Mo, W), low temp. phase transitions *(French)* 78—92036
- Cs_2KPrF_6, Raman spectrum and cryst. field *(German)* 79—51940
- Cs_2KTiF_6, bonding, struct., ligand field splitting, electron gas calcs. 78—17557
- $Cs_2KTmBr_6(Cl_6)(F_6)$, mag. behaviour 2.9 to 251.3K, cryst. field levels, ang. overlap model *(German)* 80—29520
- Cs_2KYbF_6, mag. behaviour, 3.5-251.3K *(German)* 80—50041
- CsKr, 6dσ states, multiphoton laser spectrosc. obs. 79—85974
- $CsLaF_4$ and $CsCeF_4$, phase equilibria *(French)* 78—44107
- $CsLa(SO_4)_2$, X-ray cryst. struct. determ. 80—33939
- $CsLi_{0.5}(Al,Fe)_{1.5}F_6$ pyrochlore, Mossbauer contrib. to exam. of cationic order *(French)* 80—93224
- $Cs_2LiCo(CN)_6$, mol. vibr. in cryst., normal mode anal., Raman and IR obs. 77—76494
- $Cs_2LiCr(CN)_6$, cryst. struct., room temp., powder neutron diffr. obs. 77—19914
- $Cs_2LiCr(CN)_6$, room temp. struct., phase transitions 78—51491
- $Cs_2LiFe(CN)_6$, struct., phase transformations, temp. depend. Raman spectra 79—11416
- $CsLi_{0.5}Fe_{1.5}F_6$ pyrochlore, Mossbauer contrib. to exam. of cationic order *(French)* 80—93224
- $CsLiSO_4$, crystal structures of I and III phases, twins 80—70181
- $CsLiWO_4$, X-ray cryst. struct. determ., stuffed H-cristobalite struct. 80—54181
- $CsMF_3$:Mn^{2+}, (M=Ca,Cd), zero-field splitting of Mn^{2+}, superposition model *(French)* 79—15267
- $Cs_2MFe(CN)_6$, M=Ba, Mg, Ca, Sr, lattice instabilities 77—72668
- $CsMHoF_6$, (M=Na, K, Rb), mag. behaviour *(German)* 80—65774
- $Cs_{12}M_{33}O_{90}(.12H_2O)$, cation exchanger with intersecting tunnel struct. *(French)* 78—20014
- $Cs^+M^{III}(SO_4)_2$, $M=Al^{3+}$, Cr^{3+}, Fe^{3+}, Raman and IR spectrum study *(French)* 79—47453
- Cs_2MX_6(M=Se, Te, X=Cl, Br), $\Gamma_4^-(^3T_{1u})$ state, Jahn-Teller effect, luminesc. obs. 80—60650
- $CsMgBr_3$:$Cr^{3+}(Cr^+)$, EPR of impurities, charge compensation, X-ray effects 80—60407
- $CsMgBr_3(I_3)$, diamag. linear chain lattices, cryst. struct. 80—70172
- CsMgCl:Cr^{3+},Mo^{3+}, Cr^{3+}-Mo^{3+} exchange coupled pair, EPR study 79—42830
- $CsMgCl_3$, Raman spectrosc. investigation of struct. 80—49202
- $CsMgCl_3$:Co^{2+}, Zeeman Raman scatt. and Zeeman IR absorpt. spectra 79—56782
- $CsMgCl_3$:$Cr^{3+}(Cr^+)$, EPR of impurities, charge compensation, X-ray effects 80—60407
- $CsMgCl_3$:Mn^{2+}, EPR spectrum temp. depend. 78—19314
- Cs_3MgCl_5, Raman spectrosc. investigation of struct. 80—49202
- $CsMgCl_3(Br_3)$, quadrupole interaction meas. by NMR spin-echo modulation 77—85615
- $CsMgCl_3(Br_3)$:Gd^{3+}, EPR spectra of mag. coupled Gd^{3+} ions 78—35032
- $CsMnBr_3$, EPR linewidth anisotropies 80—103878
- $CsMnBr_3$, quasi-one-dimens. antiferromagnet, inelastic neutron scatt. 78—14929
- $CsMnBr_3$, triang. antiferromagnet, spin wave theory 79—7978
- $CsMnBr_3$:Nd^{3+}, nearly 1-dimens. cryst., emission spectrum, extensive energy transfer 79—15516
- $CsMnBr_3.2D_2O$, extended scaling in spin flop system 79—73737
- $CsMnBr_3.2D_2O$, mag. phase diagram near bicrit. point 79—15302
- $CsMnBr_3.2D_2O$, spin-flop systems, neutron scatt. expts. 79—61109
- $CsMnBr_3.2D_20$, spin-flop system, extended scaling near bicrit. pt. 79—51752
- $CsMnBr_3.2H_2O$, pseudo-one-dimensional mag. system, low-temp. sp. ht. 77—85471
- $CsMnCl_3$, antiferromagnetic resonance, parametric spin wave excitation *(Russian)* 80—93183
- $CsMnCl_3$, electron resonance linewidth anisotropy 79—28588
- $CsMnCl_3$, mag. anisotropy measurement 79—11310
- Cs_3MnCl_5, multilevel system, spin-lattice relax. from AC susceptibility 77—55702
- $CsMnCl_3(Br_3)$, rare earth doped, energy transfer, emission spectra obs. 80—20684
- $CsMnCl_3.2H_2O$, antiferromag. resonance and two-magnon absorpt. *(Russian)* 77—81014

caesium compounds continued
- $CsMnCl_3.2H_2O$, antiferromag. reson. and two-magnon absorpt. 79—61234
- $CsMnCl_3.2H_2O$, antiferromag. reson. temp. depend. *(Russian)* 79—87321
- $CsMnCl_3.2H_2O$, antiferromag. insulator, self-trapping of excitons 80—70619
- $CsMnCl_3.2H_2O$, diagonal elastic const., thermal expansion coeffs., ultrasonic velocity meas. 80—79853
- $CsMnCl_3.2H_2O$, Heisenberg antiferromag., linear mag. birefringence meas. 77—16277
- $CsMnCl_3.2H_2O$, linear antiferromagnet, specific heat, exchange interactions and anisotropy effects 77—1556
- $CsMnCl_3.2H_2O$, luminesc., electronic excitations localisation *(Russian)* 79—87492
- $CsMnCl_3.2H_2O$, mag. phase diagram near bicritical point 80—71021
- $CsMnCl_3.2H_2O$, nonequilibrium magnon population obtained by optical pumping *(Russian)* 80—11457
- $CsMnCl_3.2H_2O$, paramagnetic relax. rates, anisotropic diffusion model 77—69668
- $CsMnCl_3.2H_2O$, pseudo-one-dimensional mag. system, low-temp. sp. ht. 77—85471
- $CsMnCl_3.2H_2O$, quasi-onedimens., microwave absorpt. and antiferromag. reson. *(Russian)* 77—51962
- $CsMnCl_3.2H_2O$, quasi-one-dimensional antiferromag., luminesc. enhancement in mag. field *(Russian)* 79—91487
- $CsMnCl_3.2H_2O$, quasi-one-dimensional antiferromag., phase diagram *(French)* 80—20405
- $CsMnCl_3.2H_2O$, quasi one-dimensional mag. systems, impurity effects 80—71015
- $CsMnCl_3.2H_2O$, spin wave anal. 77—8292
- $CsMnCl_3.2H_2O$, subthreshold two-magnon absorpt., depend. on freq., temp. and mag. field, exchange coupling const. *(Russian)* 80—71184
- $CsMnCl_3.2H_2O$, thermal cond. in mag. field 80—70481
- $CsMnCl_3.2H_2O$:Cu, parallel susceptibility, impurity effect on spin-flop field *(French)* 78—43569
- $CsMnCl_3.2H_2O$:Cu(Co), quasi one-dimens. antiferromag., mag. impurity effect on Neel temp. and spin-flop field 79—61099
- $CsMn_{1-x}Co_xCl_32H_2O$, random mag. mixture, oblique-antiferromag. phase obs. 80—93142
- $CsMn_{1-x}Co_xCl_3.2H_2O$, impure Heisenberg linear chain, EPR meas. 78—43634
- $CsMn_{1x}Co_xCl_3.2H_2O$, random mag. mixture, mag. torque and sp. ht. expts. 80—60323
- $CsMn_{1-x}Co_xF_3$, ferrimag., mag. props. and cryst. struct. 77—77056
- $CsMn_{1-x}Cu_xCl_3.2H_2O$, impurities in quasi-one-dimens. Heisenberg systems, anisotropy effect 80—80502
- $CsMnF_3$, antiferromag., suscept. oscillations beyond threshold for parametric excitation of electronic magnons *(Russian)* 77—59398
- $CsMnF_3$, antiferromag., variation of spin wave spectrum in interaction between magnons 80—65841
- $CsMnF_3$, antiferromagnet, struct. with compensated magnetisation in noncollinear phase *(Russian)* 78—88095
- $CsMnF_3$, exciton migration, excitation and luminesc. study *(Russian)* 80—66264
- $CsMnF_3$, exciton-magnon interactions in optical transition, absorpt. and emission spectra meas. 80—70981
- $CsMnF_3$, hexagonal antiferromagnet, light interaction *(Russian)* 77—36257
- $CsMnF_3$, isotropic antiferromag., crossover behaviour of mag. phase boundaries 79—78370
- $CsMnF_3$, light absorpt. spectrum in mag. fields up to 300 kOe *(Russian)* 77—52115
- $CsMnF_3$, mag. field- and temp.-depend. of light absorption spectra 78—52528
- $CsMnF_3$, mag. phase boundaries, XY to Ising crossover, virtual bicritical point 80—50095
- $CsMnF_3$, mag. props. above T_n, NMR obs. of induced ferrimagnetism 79—99780
- $CsMnF_3$, mag. struct., phase transition, and magnon spectrum, random anisotropy effects 80—88722
- $CsMnF_3$, magnon absorption and luminesc. 80—7400
- $CsMnF_3$, NMR saturation, nuclear spin wave excitation, large freq. shifts *(Russian)* 80—50207
- $CsMnF_3$, new types of nuclear spin echo, single pulse and parametric echo 77—69726
- $CsMnF_3$, optical investig. of spontaneous tilt of mag. sublattices *(Russian)* 77—40215
- $CsMnF_3$, ordering temp., virtual bicritical pt. 79—61128
- $CsMnF_3$, parametric excitation of magnons, effect of RF modulation of mag. field 80—65842
- $CsMnF_3$, parametric magnon excitation, relaxation *(Russian)* 78—23352
- $CsMnF_3$, parametric nuclear magnon excitation, mag. field modulation *(Russian)* 80—107999
- $CsMnF_3$, RF modulation effect on parallel microwave pumping threshold *(Russian)* 80—29628
- $CsMnF_3$, solid and molten paramag. high-temp. e.p.r. linewidth meas. 77—4548
- $CsMnF_3$, specific heat, crossover from Heisenberg to XY like behaviour 77—85461
- $CsMnF_3$, spin echo form., parametric mechanism, spin dynamics *(Russian)* 78—23367
- $CsMnF_3$, spin wave propag. 77—63159
- $CsMnF_3$, spin wave spectrum obs., review 80—50081
- $CsMnF_3$, spin waves excitation 79—82772
- $CsMnF_3$, spin-wave dispersion relations, neutron inelastic scatt. obs. 77—51895
- $CsMnF_4$, planar ferromag., cryst. and mag. struct., Jahn-Teller effect 80—75715
- $Cs_2MnF_2.H_2O$, X-ray cryst. struct. anal. 79—4289
- $CsMnFeF_6$, mag. short-range ordered, neutron scatt. meas. 77—16048
- $CsMnFeF_6$, neutron scatt. and magnetisation meas. 77—66258
- $CsMnI_3$, Mossbauer spectra, struct., electronic and mag. props. 79—91320
- $CsMnI_3$, Mossbauer spectra, struct., electronic and mag. props. 80—15908
- $CsMn_{1-x}Ni_xF_3$, ferrimag., mag. props. and cryst. struct. 77—77056
- Cs_2MnNiF_6, cation distrib. and mag. struct. *(French)* 78—14935
- $CsMnX_3.2H_2O$ (X=Cl,Br), pseudo one-dimens. Heisenberg antiferromag., phase diagrams 79—61148
- $Cs_3MoO_3F_3$, ferroelec. and order-disorder phase transitions 78—92037

caesium compounds continued
$Cs_3MoO_3F_3$, ferroelec., transition obs. 80—75989
CsN_3, heat capacity from 5 to 350K 79—55901
CsN_3, polycryst., IR active lattice vibr., optical consts. 77—77185
CsN_3, Raman spectra, weaker features obs. 77—68045
CsNCS, long-wave lattice modes 78—59881
CsNCS, vibr. spectra, multiphonon modes 77—40230
$CsN_{1-x}Mn_xF_3$, hexagonal perovskites, struct. evolution and mag. props., effects of high pressure 79—41987
$CsNO_2$, NQR spectrum of ^{14}N at low temp., poss. ferroelec. transition 77—12223
$CsNO_2$-$CsNO_3$ solid solns., cryst. struct. and phase changes 79—51082
$CsNO_3$, anhydrous, kinetics of crystallisation 77—43164
$CsNO_3$, high pressure phases III and IV, X-ray struct. determ. 80—28953
$CsNO_3$, low-temp. cryst. modification, gyrotropy *(Russian)* 77—85684
$CsNO_3$, melt, NO_3^- ion struct., pulsed neutron diffr. obs. 78—22631
$CsNO_3$, molten, Brillouin spectra, 420-520°C, hypersonic vel. and sound absorption freq. depend. 77—28589
$CsNO_3$, molten, X-ray diffr. structural anal. 78—42887
$CsNO_3$, phase transition, IR spectra 80—7350
$CsNO_3$, Raman spectra temp. depend., NO_3^- ion external librational modes, I→II transition, Raman spectra temp. depend., NO_3^- ion external librational modes 79—78662
$CsNO_3$, single cryst., γ-irradiated, X-ray diffr. effects 79—46704
$CsNO_3$ solns. coagulation of amphoteric latex sols reversibility and specific ion effects 80—45567
$CsNO_3$-$LiClO_4$, binary melt, Raman spectra, polarised line width, temp. depend. 78—84578
$CsNO_3$-$Pb(NO_3)_2$, ht. of crystn. *(Russian)* 77—48418
Cs_2NaAlF_6, cryst. struct. determ. 78—95036
$Cs_2NaAl_3F_{12}$, cryst. struct. *(French)* 77—15348
$Cs_2NaBiCl_6$, optical props. 78—68549
$Cs_2NaBiCl_6$, optical, photoelastic, acoustooptic props. 80—55064
$Cs_2NaCe(III)Cl_6$ high symmetry complex, low temp. Raman spectrum CF splitting, paramag. susceptibility temp. depend. *(German)* 77—12380
$Cs_2NaErCl_6$, mag. susceptibility and IR and Raman spectra meas., crystal field splitting determ. 80—100652
$Cs_2NaEuCl_6$, luminescence Raman spectra, means for localisation of binding energy levels *(German)* 78—88304
$Cs_2NaEuCl_6$, mag. dipole transitions $^5D_3 \rightarrow {}^7F_4$, interpretation 79—42505
$Cs_2NaFe(CN)_6$, structural phase transformations 79—19178
$Cs_2NaLn(III)Br_6$, prep., cryst. genesis, and charact. by X-ray powder diffr. *(French)* 79—43135
Cs_2NaMCl_6, M=Eu, Tb, Er, Tm, Raman spectra 77—77205
$Cs_2NaM^{3+}Cl_6$ (M^{3+}=Bi,Nd,Pr), ferroelastic phase transitions, thermal expansion, elasticity, and X-ray anal. 80—70393
$Cs_2NaM^{3+}Cl_6$, (M=Bi,Nd,Pr), struct. transitions, polarisation optical expts. 79—99318
$Cs_2NaMO_xF_{6-x}$, M=Ti, V, Nb, Mo, W, high press. transforms. *(German)* 77—89400
Cs_2NaRCl_6 (R=Ce, Nd), tetragonal distortion from cubic symm., magnetisation and NMR meas. 80—34403
Cs_2NaRCl_6 (R=rare earth), low-temp. Raman spectra meas., cryst. field parameters calc. *(German)* 77—36228
Cs_2NaRCl_6, R=Pr^{3+}, Eu^{3+}, Tb^{3+}, Tb^{3+}, crystal field, ligand polarisability contributions 80—39536
Cs_2NaRCl_6:Er^{3+}(Gd^{3+}), R=lanthanide, EPR parameters and interpret. 77—59456
$Cs_2NaTbCl_6$, emission spectra, mag. dipole transitions assignments 78—23505
$Cs_2NaTbCl_6$, mag. circ. polarised emission, MCD, $^7F_J \rightleftarrows {}^5D_4$ transitions 77—77242
$Cs_2NaTbCl_6$, Tb^{3+} $^5D_4 \rightarrow {}^7F_J$ transitions, mag. and elec. dipole intensities 78—76033
$Cs_2NaTmCl_6$, UV absorpt. spectra, mag. circular dichroism spectra, vibr. obs. 80—29758
Cs_2NaTmF_6, mag. behaviour 2.9 to 251.3K, cryst. field levels, ang. overlap model *(German)* 80—29520
Cs_2NaYCl_6, Raman spectrum 77—59567
Cs_2NaYCl_6:^{249}Cf, mag. susceptibility of Cf^{3+} in octahedral site 77—12089
Cs_2NaYCl_6:Bi^{3+}, luminesc., cryst. growth, Stockberger method 79—8174
Cs_2NaYCl_6:Bi^{3+}, luminescence props., emission and excitation spectra 80—108262
Cs_2NaYCl_6:Ce, ENDOR evidence of noncubic distortion 79—11357
Cs_2NaYCl_6:Re,Tm, fluorescence, two-step blue up-convertors 78—95603
Cs_2NaYCl_6:Tb^{3+}, emission spectra, mag. dipole transitions assignments 78—23505
Cs_2NaYCl_6:Yb^{3+} electron spin-lattice relax. 77—63274
$Cs_2NaY_{0.99}Eu_{0.01}Cl_6$, cryst. field parameters of Eu^{3+} ion 77—31983
$Cs_2NaYbCl_6$, electronic struct., paramag. susceptibility and electronic Raman spectrum, cryst. field parameters *(German)* 77—63072
$Cs_2NaYbCl_6$, freq. depend. of spin-spin relax. rate from Mossbauer spectroscopy 78—48095
$Cs_2NaYbCl_6$, Mossbauer spectral lineshape in presence of paramag. relax. effects 77—69755
$Cs_2NaYbCl_6$, Mossbauer relax. spectra, breakdown of white noise approx. 78—27141
Cs_2NaYbF_6, mag. behaviour, 3.5-251.3K *(German)* 80—50041
$Cs_8Nb_{22}O_{59}$, melt growth and struct., dielec. and optical characterisation 78—35294
$Cs_{0.5}NbS_2$, supercond. props., alkali cation and topotactic solvation influences 79—87180
$Cs_2Nb_6TiO_{18}$, cryst. struct. *(French)* 78—6040
α-$CsNd(PO_3)_4$, single cryst. struct. and spectral-luminescent props. 80—96490
$CsNdP_4O_{12}$, X-ray cryst. struct. anal. 79—7590
$CsNiBr_3$, double ordering in mag. linear chain system, sp. ht. and NMR data 79—28545
$CsNiBr_3$, nearly one-dimensional antiferromag., thermal and mag. props. meas. 77—77041
$CsNiCl_3$, antiferromag. coupling in linear chains, molecular orbital approach 78—52239
$CsNiCl_3$, double ordering in mag. linear chain system, sp. ht. and NMR data 79—28545
$CsNiCl_3$, linear chain antiferromag., mag. props., 1.1 to 7K 79—61076
$CsNiCl_3$, linear-chain antiferromag., low temp. thermal expansion 80—39326
$CsNiCl_3$, mag. props. 79—73736

caesium compounds continued
$CsNiCl_3$, nearly one-dimens. antiferromag., mag. sp. ht. determ. 77—24702
$CsNiCl_3$, nearly one-dimensional antiferromag., spin-flop transition 78—6527
$CsNiCl_3$, noncollinear magnetic order and spin wave spectrum in presence of competing exchange interactions 80—65834
$CsNiCl_3$, nuclear spin-lattice relax., temp. depend., anisotropic effects 78—64293
$CsNiCl_3$, one-dimens. antiferromag., US attenuation, crit. behaviour 77—66308
$CsNiCl_3$, one-dimens. antiferromag., US attenuation 78—88156
$CsNiCl_3(Br_3)$, quadrupole interaction meas. by NMR spin-echo modulation 77—85615
$CsNiCl_3(F_3)$, one-dimensional anisotropic paramag., nucl. relax. rate and spin dynamics 77—69723
$CsNiF_3$, ^{19}F NMR, spin fluctuation suppression 78—91970
$CsNiF_3$, 1-dimens. ferromag., evidence for solitons, inelastic neutron scatt. study 79—78430
$CsNiF_3$, 1D ferromag., optical absorption and spin dynamics 80—71417
$CsNiF_3$, anisotropic Heisenberg chain, nonlinear excitations 80—70927
$CsNiF_3$, crit. exponent crossover, quasielastic neutron scatt. around Neel point 77—24693
$CsNiF_3$, demagnetising effects on antiferromag. reson. 80—15803
$CsNiF_3$, double-excitonic optical transition intensity, exchange and dimensionality effects 77—69591
$CsNiF_3$, easy-plane ferromagnet, one-dimens., dynamic props., review 80—15737
$CsNiF_3$, ferromag., Heisenberg chains with easy plane, validity of classical statistical mechanics 80—44786
$CsNiF_3$, field depend. mag. behaviour, mag. linear dichroism 79—73903
$CsNiF_3$, in mag. field, spin wave dispersion, inelastic neutron scatt. 77—77046
$CsNiF_3$, linear S=1 ferromag., easy plane anisotropy, low-temp. mag. props. 78—23250
$CsNiF_3$, longit. paramag. susceptibility, reaction field approx. 80—97059
$CsNiF_3$, low frequency dynamics in external mag. field 80—108020
$CsNiF_3$, NMR and relax. exam. 78—52371
$CsNiF_3$, nonlinear excitations, 1D-ferromag., neutron scatt. 80—70949
$CsNiF_3$, one dimens. ferromag., spin wave dynamics, inelastic neutron scatt. study 79—47270
$CsNiF_3$, one dimensional ferromag., magnetisation, FMR, 2.61-20K 77—20719
$CsNiF_3$, one dimensional planar model with symm. breaking fields, thermodynamics, static props. 80—97111
$CsNiF_3$, one-dimens. anisotropic paramagnet, EPR meas. 79—73799
$CsNiF_3$, one-dimens. ferromag. far IR investig. of ferromag. reson., temp. and mag. field depend. 77—66427
$CsNiF_3$, one-dimens. ferromag., solitons in external mag. field 79—19724
$CsNiF_3$, one-dimens. ferromag. phonon dispersion surfaces 79—42180
$CsNiF_3$, one-dimens. ferromag., solitons as gas of quasiparticles, inelastic neutron scatt. obs. 79—73679
$CsNiF_3$, one-dimens. ferromag., collective excitations in mag. field 80—44822
$CsNiF_3$, one-dimens. magnet, local magnon modes 80—65829
$CsNiF_3$, one-dimensional mag., Young's modulus softening along linear-chain direction 77—62578
$CsNiF_3$, one-dimensional magnet, dynamics, mol. field theory approach 80—34614
$CsNiF_3$, planar ferromagnet, US attenuation, spin-phonon coupling, magnons and magnetostriction contrib., calc. 80—34611
$CsNiF_3$, quasi one dimensional planar ferromag., low temp. NMR study im mag. field 80—97157
$CsNiF_3$, quasi-1D planar Heisenberg ferromag., thermal renormalisation of sine-Gordon soliton mass 79—54036
$CsNiF_3$, quasi-one-dimens. Heisenberg system, reaction field approx. and dipolar interaction 77—36088
$CsNiF_3$, quasi-one-dimensional ferromagnet, subthreshold parallel pumping of magnons 80—75745
$CsNiF_3$, quasielastic neutron scatt. around Neel-point 80—75768
$CsNiF_3$, single cryst. mag. susceptibility meas. 77—20560
$CsNiF_3$, solitons in one-dimens. ferromag., inelastic neutron scatt. 78—95450
$CsNiF_3$, solitons near crit. point, neutron scattering observation 80—34650
$CsNiF_3$, stochastic motion of Sine-Gordon-solitons, spin-correlation function 80—93105
$CsNiF_3$, subthreshold parallel pumping of magnons and antiferromag. reson. 80—71185
$CsNiF_3$:Mg, ferromag. chain system, temp. depend. of correlation length, quasi-elastic neutron scatt. meas. 77—16046
$CsNiFeF_6$ pyrochlore, Mossbauer contrib. to exam. of cationic order *(French)* 80—93224
$Cs_2Ni_3(P_2O_7)_2.nH_2O$, thermal dehydration 80—35513
Cs_2NpBr_6, prep., cryst. struct. and enthalpy of formation 78—10014
Cs_2NpCl_6, Mossbauer spectra and mag. susceptibility meas. 80—108140
$CsNpF_6$, cryst. field splittings for Np^{5+}, ab initio MO calcs. 77—20520
$CsNpF_6$, optical spectrum anal. 79—26963
CsO_2, low temp. phases, mag. order, EPR and antiferromag. reson. 79—95630
CsO_2, X-ray low temp. phase study, crystallographic domains and unit cell dimens. 78—63728
$Cs_{1-x}O_x$, metallic glass, prep., elec. props. and struct. 78—67652
$Cs_{11}O_3$, ionic clusters in alkali metal suboxide cryst., struct., vibr. freqs., Raman spectra 79—37772
Cs_2O film, Ag granules and colloidal particles in Ag-O-Cs photocathode *(Chinese)* 80—2279
Cs_2O profiled silicate glass, residual stresses 80—2107
Cs_2O-Ag photocathode, light absorption and photoemission 80—50510
Cs_2O-Al_2O_3-SiO_2, thermionic emission of ions and electrons 78—2969
Cs_2O-B_2O_3:Tl^+(Pb^{2+})(Bi^{3+}) glass, optical basicity, variation with probe ion and comp. 80—2800
Cs_2O-GeO_2 glass, He permeability, diffusivity and solubility 79—51308
Cs_2O-MgO-SiO_2 system, glasses, crystn. prods., composition, props. 79—41961
Cs_2O-P_2O_5 glass ESR of VO^{2+} ions 80—100610
Cs_2O-SiO_2 glass, low temp. heat capacity 80—49373
Cs_2O-SiO_2(-GeO_2) system glasses, X-ray diffr. anal., electron radial distrib. curves 78—87622
Cs_2O-TeO_2 glass, struct. and props. *(Japanese)* 79—32917
Cs_2O_3-CsO_2 corrosion of type 304 austenitic stainless steels 79—57141

caesium compounds continued
$CsOH$, liquid and vaporised, attack on stainless steel 78—68840
$CsOH$, quadrupole hyperfine struct., Δ-level splitting, microwave spectra 77—88446
$Cs_2O.Al_2O_3.4SiO_2$ (pollucite) for long term-storage of $^{137}CsCl$ 80—37467
$Cs_2O.4SiO_2$, glass, behaviour of VO^{2+} as spectroscopic probe 79—78510
$CsPFO/H_2O(D_2O)$ system, nuclear mag. relax. of water at identically oriented planar interface 77—36148
$CsPO_3$, form. from dihydroorthophosphate dehydration, reaction thermodynamics 79—52643
$CsPO_3$, He(I) photoelectron spectra, UTARC calc., assignments 79—72357
$CsPO_3$, vitreous, microhardness 80—25864
$CsPO_3$-$Ba(PO_3)_2$ system, equilibrium diagram *(French)* 77—28789
$CsPO_3$-$Sr(PO_3)_2$ system, physicochem. investigation 77—35666
$Cs_3P_3O_9.H_2O$, cryst. struct. determ. *(French)* 77—24298
$CsPbBr_3$, critical thermodynamic props. around successive phase transitions 79—33627
$CsPbBr_3$, $CsPbCl_3$, ionic semiconductors, electronic and optical props. 79—38594
$CsPbBr_3$, cubic-to-tetragonal phase transition, critical anomalies, phenomenological eqns. 80—39275
$CsPbBr_3$, electronic and optical props. 80—25414
$CsPbBr_3$, optical and photoelectronic spectra 79—24410
$CsPbBr_3$, optical props. and electronic struct. 78—48198
$CsPbBr_3$, struct., Debye-Waller factor, neutron diffr. study 79—90609
$CsPbBr_3$, US vel. around successive phase transition points 77—80581
$CsPbCl_3$, birefringence, twinning and structural phase transitions 79—38480
$CsPbCl_3$, critical thermodynamic props. around successive phase transitions 79—33627
$CsPbCl_3$, cubic-to-tetragonal phase transition, critical anomalies, phenomenological eqns. 80—39275
$CsPbCl_3$, elastic constants and thermal expansion, near struct. transitions 78—59849
$CsPbCl_3$, electronic and optical props. 80—25414
$CsPbCl_3$, electronic struct. and optical props. in fundamental absorpt. region 80—93367
$CsPbCl_3$, exciton states, magneto-optical investigation 80—29328
$CsPbCl_3$, high-resolution elastic neutron diffr. study 80—28984
$CsPbCl_3$, lattice thermal expansion, X-ray powder technique 80—19965
$CsPbCl_3$, NQR investig. of press. induced phase transition 77—12224
$CsPbCl_3$, n.q.r. spin-lattice relax. near cubic-tetragonal transition, soft modes 77—1616
$CsPbCl_3$, nucl. smearing functions, multipole analysis 80—88097
$CsPbCl_3$, $O_h{}^1$-$D^5{}_{4h}$ transition, US and thermodynamic props. 78—67826
$CsPbCl_3$, optical and photoelectronic spectra 79—24410
$CsPbCl_3$, optical props. and electronic struct. 78—48198
$CsPbCl_3$, phase transition under pressure 78—51664
$CsPbCl_3$, refr. index and birefr., struct. transition effects 77—90126
$CsPbCl_3$, struct. phase transitions, NMR obs. 78—83943
$CsPbCl_6(Br_6):ReCl_6{}^{2-}(ReBr_6{}^{2-})$, vibronic side bands 80—10609
$CsPbCl_xBr_{3-x}$, optical meas., LCAO band scheme 80—25437
$Cs_2PbCu(NO_2)_6$, α-modification, Jahn-Teller induced α to β transition, neutron diffr. obs. 79—1498
$Cs_2PbCu(NO_2)_6$, incommensurate Jahn Teller phase transitions 79—95156
$Cs_2PbCu(NO_2)_6$, incommensurate Jahn-Teller transition, Huang scatt. 80—70401
$Cs_2PbCu(NO_2)_6$, low-temp. γ-modification, struct., powder neutron diffr. study, 160K 80—84151
$Cs_2PbCu(NO_2)_6$, one-dimensional stacking order 80—28941
$Cs_2PbCu(NO_2)_6$, successive Jahn-Teller phase transitions, neutron and X-ray diffr. 78—95154
$Cs_2Pb(MoO_4)_2$, domain struct. and phase transition *(Russian)* 78—6159
$CsPbX_3$, (X=Cl,Br), anharmonic thermal vibrs., neutron diffr. study 80—29125
Cs_2PdCl_4, single cryst. growth from gel and soln., morphology 77—77360
$CsPr(MoO_4)_2$, energy levels and mag. props. of Pr^{3+} ion *(Russian)* 79—7810
$CsPr(PO_3)_4$, cryst. struct. 79—42022
$Cs_2(Pt(CN)_4)Cl_{0.3}$, elec. cond., 300-40K, 3-dimens. ordering temp. 79—78087
$Cs_2Pt(CN)_4.H_2O$, cryst. struct., neutron diffr. meas. 77—47393
$Cs_{1.75}(Pt(CN)_4).1.5H_2O$, 1-D cond., IR spectra 77—85703
Cs_2PtCl_6, physical properties, application as lens or laser window materials 79—98450
$Cs_2PtCl_4.H_2O$ single cryst. growth from gel and soln., morphology 77—77360
$CsR(MoO_4)$ R=Dy, Ho, Er, permittivity temp. depend., polymorphic transition 80—92670
$Cs_3R_2X_9$ (=Sc,Y,Ho-Lu, X=Cl and R=Sc,Sm-Lu, X=Br), prep. and Guinier-Simon X-ray study 80—49204
$Cs_{1-x}Rb_xMF_3$ (M=Mg, Co, Ni, Zn), hexagonal fluoride perovskite structural evolution by cationic substitution *(French)* 80—24430
$Cs_2RbMO_3F_3$, (M=Mo, W), low temp. phase transitions *(French)* 78—92036
$Cs_2RbMoO_3F_3$, ferroelec., transition obs. 80—75989
Cs_2RbTmF_6, mag. behaviour 2.9 to 251.3K, cryst. field levels, ang. overlap model *(German)* 80—29520
$Cs_2RbWO_3F_3$, ferroelec., transition obs. 80—75989
Cs_2RbYbF_6, mag. behaviour, 3.5-251.3K *(German)* 80—50041
Cs_2ReF_6, absorpt. spectra, splitting of $\Gamma_8({}^4A_{2g})$ ground state 78—74658
$Cs_2ReF_6(-Cs_2GeF_6)$ cryst., $ReF^{-2}{}_6$ ion electronic absorpt. spectra, Raman, visible, IR and UV, liq. H and room temps. 77—77193
$CsReO_4$, IR matrix-isolation spectra 80—87108
Cs_2S_2, synthesis and cryst. struct. *(German)* 79—46618
Cs_2SO_4, cryst., coord. and Raman intensity anal. 78—2831
Cs_2SO_4, IR absorpt. spectra, polymorphism, site group approx. and SO_4 stretching mode 78—52510
Cs_2SO_4, ionic equil., mass spectra obs., heats of reaction and form. of ions 79—87867
Cs_2SO_4 molecules isolated in inert gas matrices, low freq. IR spectra 78—50547
Cs_2SO_4, solid-to-solid transition temperature under hydrostatic pressures to 0.6 GPa 80—24586
Cs_2SO_4-$(NH_4)_2SO_4$ mixed cryst., ferroelec. transition, structural and dielec. props., proton spin-lattice relax. 78—39512
$Cs_2S_2O_6$, hexagonal, piezoelec., electro-optic, dielec., elastic, thermoelastic props., space groups 78—76388

caesium compounds continued
$Cs_2SO_4.Al_2(SO_4)_3.24H_2O$, $^{53}Cr^{3+}$ ENDOR Lines, RF ENDOR power and modulation freq. effects 80—75884
$Cs_2SO_4.3MoO_3$-In_2O_3, phase diags., chem. reactions 77—86008
Cs_3Sb photocathode, wavelength-modulated photoemission spectra 80—29857
Cs_3Sb vacuum deposited photoemitter, XPS study 80—89122
Cs_2SbCl_6, mixed valence compound, ^{121}Sb Mossbauer spectroscopy 79—51890
$CsSbF_6$, γ-irrad., EPR spectra, hyperfine interactions and g-value determ. 77—81416
$CsSbF_6$, high press. phase relations, vibr. spectra, and cryst. chemistry 80—108200
$CsSbF_4(OH)_2$, solid, IR and Raman spectra 80—40114
$CsSbF_5OH$, solid, IR and Raman spectra 80—40114
$Cs_3Sb_2I_9$, hexagonal $Cs_3Cr_2Cl_9$ struct. type 78—34478
$Cs_2Sb_{0.5}M_{0.5}{}^{IV}Cl_6$, ($M^{IV}$=Se, Te, Sn), ^{121}Sb Mossbauer effect 78—84506
$CsSbO_3$, solid state synthesis *(French)* 80—104438
$CsSbO_3.1/6CsF$, dielec. spectroscopy study, 100 Hz to 10 MHz, 238 to 417K *(German)* 80—108144
Cs_2SeO_4, single cryst., orthorhombic, Raman spectra 77—73140
Cs_2SeO_4, solid-to-solid transition temperature under hydrostatic pressures to 0.6 GPa 80—24586
$CsSiF_6:Mn^{4+}$, splitting of vibronic levels 78—60496
Cs_2SiF_6, A=Si, Ge, Sn, IR absorpt. spectra, integrated intensity 79—73944
Cs_2SiF_6, lattice dynamics from neutron scatt., Raman and IR absorpt. meas. 79—60449
$Cs_2SiF_6:Mn^{4+}$, IR absorpt. band, electron-vibr. effect 80—108238
$Cs_2SiF_6:Mn^{4+}$, Jahn-Teller effect in $^4T_{2g}$ state, Zeeman meas. 80—29367
$CsSnBI_3$, electronic struct., XPES and band theory calc. semimetallic behaviour 79—78837
$Cs_2SnBr_6:ReBr_6{}^{2-}$, luminesc. spectra and relax. processes 78—68552
$CsSnCl_3$, electronic struct., XPES and band theory calc. semimetallic behaviour 79—78837
$CsSnCl_6:ReBr_6{}^{2-}$, vibronic transition $\Gamma_7({}^2T_{2g})\rightarrow\Gamma_8({}^4A_{2g})$, intensity distrib. 80—45142
$Cs_2SnCl_6:ReCl_6{}^{2-}$, luminesc. and absorpt. spectra, relax. processes 77—85779
$Cs_2SnCl_6:UO_2Cl_4{}^{2-}$, luminesc., vibronic anal. 79—33767
$CsSnCl_6(Br_6):ReCl_6{}^{2-}(ReBr_6{}^{2-})$, vibronic side bands 80—10609
$Cs_2Sn_2Cl_3Br_3$, physical properties, application as lens or laser window materials 79—98450
Cs_2SnF_6, A=Si, Ge, Sn, IR absorpt. spectra, integrated intensity 79—73944
Cs_2SnF_6, thermal study and thermolysis *(French)* 78—10011
$Cs_2SnF_6.4HF$, cryst., H bond geometry, NMR obs. 79—42844
$Cs_2SnF_6.4HF$, molecular diffusion, spatial symmetry, HF molecule arrangement 79—42313
$CsSn_2I_5$, surface props., Auger study, elec. cond. meas., photochem. study 80—66339
$Cs_2SnPbCl_6$, physical properties, application as lens or laser window materials 79—98450
$CsSnX_{3(5)(6)}$ (X=Cl, Br, I), single cryst. gel growth, X-ray diffr. study 80—29870
$CsSrCl_3$, birefringence, twinning and structural phase transitions 79—38480
$CsSrCl_3$, phase transitions, dilatometric and press. studies 77—15578
$CsSrCl_3$, refr. index and birefr., struct. transition effects 77—90126
$CsSrCl_3:Mn^{2+}(Gd^{3+})$, structural transitions, EPR meas. 78—34619
$CsSrCl_3:Pb$, luminesc. spectral distrib., transitions identification *(Russian)* 77—40276
$CsSrCl_3:Tl$, absorpt. and luminesc. spectra 78—72586
Cs^+TCNQ^-, optical absorpt. spectra of small particles 78—19505
$Cs_2(TCNQ)_3$, elec. cond. and elastic const., mol. bending *(Korean)* 78—23090
$Cs_{0.33}TaS_2$, supercond. props., alkali cation and topotactic solvation influences 79—87180
$Cs_2Ta_6TiO_{18}$, cryst. struct. *(French)* 78—6040
Cs_2Te, photocathode for proximity focused image convertor, field enhancement of photoemission 78—72677
Cs_2Te_3, synthesis and cryst. struct. 80—88115
$Cs_2(TeBr_6)$, far IR and Raman spectra and phase transitions 80—11376
$Cs_2(TeCl_6)$, IR and Raman spectra, lattice and internal modes, phase transition 78—6659
$Cs_2TeCl_6:Re^{4+}$, vibronic transitions progressions, intensity distrib. 79—78735
$CsTeCl_6(Br_6):ReCl_6{}^{2-}(ReBr_6{}^{2-})$, vibronic side bands 80—10609
Cs_2TeI_6, ^{129}I Mossbauer spectra, coupling consts. 78—62833
Cs_2TiF_6, Raman spectra, internal and lattice vibrs. 77—8569
$Cs_2TiF_6:Mn^{4+}$, spin-orbit and field splitting, Jahn-Teller effect, Zeeman meas. 80—80234
$Cs_2TiF_6:MnF_6{}^{2-}$, $^4A_g\rightleftarrows{}^2E_g$ transition of Mn^{4+}, absorpt., emission, linear and MCD, MCE 78—10929
$CsTiMO_5$ (M=Ta, Tb), ion exchange props., synthesis and crystallographic props. *(French)* 80—28997
$CsTi_2NbO_7$, layer struct., X-ray and electron diffr. study 80—79753
$Cs_{1-x}(Ti_{1-x}Nb_{1+x})O_5$, layer compound, cryst. struct., nonstoichiometry 80—64972
$Cs_2Ti_4O_9$, preparation, cryst. struct. determ. 78—75646
$CsTl(SeO_4)_2$, $Cs_3Tl(SeO_4)_3$, and $Cs_5Tl(SeO_4)_4$, cryst. struct. *(French)* 80—84148
$CsTmO_2$, mag. props. of normal-temp. form, 2.9-251.3K *(German)* 79—91205
$CsUF_6$, D_{3d} distortion on octahedral $UF_6{}^-$ complex 77—47779
$CsUF_6$, D_3d distortion on octahedral $UF_6{}^-$ complex *(French)* 78—84173
$Cs_2U_2O_7$, cryst. structures of α-, β- and γ-phases, X-ray and neutron diffr. obs. 77—7696
$Cs_2UO_2Br_4$, force consts., IR spectra 78—5216
$Cs_2UO_2Cl_4$, electronic struct. of cryst., theory of uranyl ion 79—73476
$Cs_2UO_2Cl_4$, fluoresc. decay rate of pure and impure cryst. 79—47487
$Cs_2UO_2Cl_4$, low-lying excited electronic levels, fluoresc. decay meas. 79—47491
$Cs_2UO_2Cl_4$, luminesc. spectra of cryst., polarised, vibr. anal. 79—73983
$Cs_2UO_2Cl_4$ melts and mixtures, thermogravimetric determ. of uranyl cation state 80—101050
$CsUOF_5$, struct. obs. using neutron diffr. and NMR 79—32962
$Cs_4(UO_2)_2F_8$-$2H_2O$, IR absorpt. and Raman spectra, normal coordinate anal. *(French)* 78—52509
$CsUO_2(NO_3)_3$, ^{15}N isotope shifts in electronic spectrum, internal mode identification 80—55098

caesium compounds continued
$CsUO_2(NO_3)_3$, absorpt. spectra, MCD and natural dichroism, UV and visible 79−69853
$CsUO_2(NO_3)_3$, electronic struct. of cryst., theory of uranyl ion 79−73476
$CsUO_2(NO_3)_3$, fluoresc. decay rates, temp. depend. 80−25429
$Cs_4(UO_2)_4O_2Cl_8(H_2O)_4$, cryst. data 77−76367
$CsUO_2(PO_3)_3$, synthesis and struct. 79−86767
CsV primary clock performance of NRC 77−74370
$CsVCl_3$, antiferromag. coupling in linear chains, molecular orbital approach 78−52239
$CsVCl_3$, mag. behaviour of V^{2+} in one- and two-dimens. Heisenberg systems 77−66235
$Cs_3VCl_6.4H_2O$, magnetisation of ground state, field-induced level crossing 79−47068
$CsVF_4$, flux growth of crystal 79−78861
$CsVF_4$, structural phase transitions above room temp. 80−29167
Cs_xVF_3 (x=0.25,0.19), cryst. struct. examination by electron diffr. using TEM 79−23583
α-Cs_xVF_3, mag. props. *(French)* 77−80933
$CsVI_3$, Mossbauer spectra, struct., electronic and mag. props. 79−91320
$CsVI_3$, Mossbauer spectra, struct., electronic and mag. props. 80−15908
$CsVO_3$, cryst. struct. 78−6043
$CsVO_3$, polycryst., quadrupole coupling const., asymmetry parameter, chem. shift, NMR computer calcs. 78−6584
CsV_2O_5, cryst. struct. 77−35518
$Cs_{0.3}V_2O_5$, cryst. struct., semicond. behaviour 77−35516
$Cs_{0.35}V_3O_7$, cryst. struct., semicond. and antiferromag. behaviour 77−35515
$Cs_2V_5O_{13}$, cryst. struct. 77−35517
$Cs_2(VOF_4(H_2O))$, neutron and X-ray diffr. struct. determ. 79−90613
$CsVX_3$, X=Br, Cl, I, mag. props. *(French)* 77−16059
$Cs_{0.06}WO_3$, cryst. struct. determ. 79−23569
$Cs_{0.33}WO_3$, supercond. and special phonons, neutron scatt. obs. 80−15643
$Cs_6W_{11}O_{36}$, cryst. struct. determ. 78−26512
Cs_xWO_3, normal phase and supercond. props 80−25035
Cs_xWO_3, x=0.20 and 0.32, hexagonal W bronzes, X-ray cryst. struct. refinement 79−77577
$Cs_3WO_3F_3$, ferroelec. and order-disorder phase transitions 78−92037
$Cs_3WO_3F_3$, ferroelec., transition obs. 80−75989
CsX (X=Cl,Br,I), photodissoc. cross sections 77−6876
CsX, (X=F, Cl, Br), absorpt. fine struct. at Cs^+ 4d threshold 77−18940
CsXe excimer, laser-excited fluoresc. in Cs-Xe mixture, pumping, level scheme 78−86909
CsXe excimer laser, form. and dissociation rates, fluoresc. meas. 78−1216
CsXe+Xe, time resolved fluoresc. decay and collisional transition rates 77−27111
$Cs_9(XeO_3Cl_2)_4Cl$, neutron and X-ray diffr. struct. determ., Xe-Cl bonding 78−30591
$CsYbO_2$, normal-temp. form, mag. props. *(German)* 80−54864
$CsZnCl_4:Cu^{2+}$, electron spin echo, 35 GHz 80−13113
$Cs_2ZnCl_4:Cu^{2+}$, single cryst. and powdered single cryst., EPR, linear elec. field effect 80−11250
$Cs_2ZnCl_4:Cu^{2+}$ electron spin echo envelope, Fourier transform ^{133}Cs modulation 80−58291
$Cs_2Zn(N_3)_4$, IR and Raman spectra 77−43999
Cs_2ZrBr_6, $PtBr_4^{2-}$-$PtBr_6^{2}$ doped, mixed valence, absorpt. spectra, vibronic struct. 80−97308
$Cs_2ZrBr_6:Os^{4+}$, intraconfig. absorpt. and MCD spectra 80−80776
$Cs_2ZrCl_6:Mn^{2+}$, ESR of mol. jumps, zero-field splitting tensor 77−51944
$Cs_2ZrCl_6:Np^{4+}$, EPR obs. 79−33526
$Cs_2ZrCl_6:Np^{4+}$, EPR data interpretation for octahedral Γ_8 state in cubic cryst. field 80−2634
$Cs_2ZrCl_6:Np^{4+}{}_6$, EPR of np^{4+} ground state 80−44903
$Cs_2ZrCl_6:Os^{4+}$, intraconfig. absorpt. and MCD spectra 80−80776
$Cs_2ZrCl_6:Os^{4+}$, multiple state luminesc. 78−72584
$Cs_2ZrCl_6:Re^{4+}$, cryst., mag. circularly polarised emission 77−28613
$Cs_2ZrCl_6:UO_2Cl_4^{2-}$, luminesc., vibronic anal. 79−33767
^{133}Cs, Mossbauer isomer shifts, book contrib. 79−87363
^{133}Cs salts, powders, nucl. mag. shielding and quadrupole coupling 77−90056
$^{137}CsCl$, use of $Cs_2O.Al_2O_3.4SiO_2$ (pollucite) for long term-storage 80−37467
$Cs_2[Cu(H_2O)_6](SO_4)_2$, Tutton's salts, stereochem., neutron struct. determ. 78−18609
$Cs_2[FeCl_5(H_2O)]$, X-ray cryst. struct. determ. 80−107129
$Cs_2[M(CN_4)].H_2O$, M=Pt,Pd,Ni, cryst. data 79−51070
$Cs_2[M^{II}(H_2O)_6][(UO_2)_2F_8]$, M^{II}=Mn, Co, Ni, Cu, Zn or Cd, structural type, IR spectra 77−35525
$Cs_2[Pt(CN)_4](FHF)_{0.39}$, cryst. struct., X-ray diffr. meas. 78−59789
$Cs_2[Pt(CN)_4](FHF)_{0.39}$, one-dimensional elec. cond. 79−69504
$Cs_2[Pt(CN)_4].H_2O$, polarised emission, correlation to cryst. struct. 79−19917
$Cs_{1.75}[Pt(CN)_4].xH_2O$, one-dimensional, X-ray diffuse scatt. meas. 77−19937
$Cs[SbF_5OH]$, X-ray cryst. struct. determ. 79−55707
$Cs[SnI_3]$, X-ray cryst. struct. anal. 80−54192
$Cs_{12}[U(GeW_{11}O_{39})_2].13\text{-}14H_2O$, X-ray cryst. struct. determ. *(French)* 80−107136
$Cs[VOF_3].1/2H_2O$, cryst. struct. 79−60333
$Cs_2[ZnCl_4]$, Raman-active phonons, $[ZnCl_4]^{2-}$ distortion, press. effects 77−52073
$(Cu,Zn)Cs_2(SO_4)_2.6(H,D)_2O$ Tutton salt, proton spin-lattice relax. time, proton conc. depend. and spin diffusion role 80−71221
Cu-Cs diluted deuterated Tutton salts, electron non-Zeeman system, nuclear relaxation study 80−44951
DyF_3-CsF, phase diagrams and ternary fluorides *(French)* 80−81040
DyI_3/CsI/Hg arc, oscillations induced by external mag. field, arc constriction 79−60205
$FeCs_2(SO_4)_2.6H_2O:VO^{2+}$, EPR, spin Hamiltonian parameters 79−19771
Ge-CsI, narrow band interference filters for 8-15 μm 77−34951
$HfCl_4$-CsCl melt, equilib. phase diagram and vapour press., equilib. reaction 77−66764
K-Cs, liquid, resistivity calc. using general method pseudopot. 77−55506
K-Cs silicate glass, thermal expansion 77−4186
K+CsF(RbF), complex form., decay. branching fraction and cross-sections, translational energy depend. 77−21374
KCl-CsCl fused binary mixturs, electrocapillary phenomena on liq. Bi 77−40553
KCl-CsCl solid soln., SIMS, clustering distance critical to metal dimer form. 79−72379
$KClO_3$-$CsClO_3$, NQR, mag. susceptibility meas. 78−35059
K_2CsSb, evaluation as photocathode material 78−11072
K_2CsSb photocathodes, prep. and props. 78−84693
K_2CsSb, semitransparent photocathodes, UV response 77−167
K_2SO_4-Cs_2SO_4-MoO_3 system, fusibility diagram 79−87619
$(La,Cs)B_6$, single crystal growth for thermionic emission 78−92183
$(Li\text{-}Cs)NO_3$, molten, internal cation mobility meas. 79−60534
$LiCsSO_4$, thermal and dielec. props. 80−34860
$LiCsSO_3.2H_2O$, cryst. struct. *(French)* 80−24412
$MgCs_2(SeO_4)_2.6H_2O$, EPR, crystal field and hexahydrate distortion 78−91938
$(NH_4,Cs)Cl$, negative isotope effect on II-III phase transition *(German)* 78−95155
$(NH_4)_{1-x}Cs_xCl(Br)$, and $(ND_4)_{1-x}Cs_xCl(Br)$, phase diagrams, DTA and birefr. obs. *(German)* 79−83185
$((NH_4)_{1-x}Cs_x)_2SO_4$ mixed cryst., EPR of NH_3^+ and SeO_3^- radicals 80−50190
(Na,Cs)(F,Cl,I,) quaternary reciprocal system, calc. of phase diagrams 80−25666
Na-Cs, liquid, resistivity calc. using general model pseudopot. 77−55506
Na-Cs silicate glass, thermal expansion 77−4186
NaCl-CsCl-$CrCl_3$ system, melting diagram determ. by DTA, phase comp. *(Russian)* 77−63645
NaCl-CsCl-$CrCl_3$ system, phase struct. anal. by X-ray method *(Russian)* 78−3112
NaCl-CsCl-$MnCl_2$, molten salt system, molar volume and elec. cond. meas. 80−34217
NaCl-CsCl-$MnCl_2$, molten salt system, molar volume and elec. cond. meas. 80−34218
$NaClO_3$-$CsClO_3$, NQR, mag. susceptibility meas. 78−35059
NaI(Tl), well-detector, low-background γ-spectrometry, comparison with CsI(Tl) 78−86724
$NaNO_3$-$CsNO_3$-$Pb(NO_3)_2$, fusion diag. *(Russian)* 77−48418
Na_2O-Cs_2O-SiO_2 glasses, thermal diffusivity, heat capacity and thermal cond., laser flash method study 80−65310
Na_2WO_4-$CsWO_4$-WO_3, system form., melting point 79−43222
Rb_2CsSb, evaluation as photocathode material 78−11072
RbF-CsF, solid solution, fundamental absorption 79−11433
$ScCl_3$-NaCl-CsCl ternary system, cpd. form., thermographic investig. *(Russian)* 80−66490
ScOH, electron collisions, integrated and momentum transfer cross sections, cond. integrals 79−41238
$SnCl_2$-$AlkAlCl_4$ melts (Alk=Li, Na or Cs) 79−99874
Tb complex, in $Cs_2NaTbCl_6$, f-f transitions, mag. dipole intensities, vibronic coupling model 80−25404
TeO_2-V_2O_5-Cs_2O, glass, IR spectra of crystalline phases 79−38536
V_2O_5-CsV_2O_5 system, phase comp. and phase diagram for conditions of inert atmosphere 77−25030
V_2O_5-P_2O_5-Cs_2O glasses, enhanced secondary electron emission yield 80−93441
$ZnCl_2$-CsCl, molten, density meas. *(Japanese)* 79−19383
$ZnCl_2$-CsCl, molten, viscosity, 260 to 560°C *(Japanese)* 77−51537
$ZnCl_2$-CsCl melt, viscosity meas. by oscillating cylinder method *(Japanese)* 80−10696
$ZnCs_2(SO_4)_2.6H_2O:VO^{2+}$, optical absorpt. spectra obs. 80−40146
$ZrCl_4$-CsCl melt, equilib. phase diagram and vapour press., equilib. reaction 77−66764

caesium generators *see plasma diodes*

caesium plasma diodes *see plasma diodes*

calcium
see also nuclei with ......
657.3 nm line saturated absorption spectroscopy, photon-recoil component resolution 80−86457
absorption spectrum of Ca I in vac. UV, excitation of 3p-subshell 77−75085
adsorption on ZnO $(000\bar{1})$ of alkali metals, anomalous behaviour of Na 78−79883
aequorin luminescence during activation of single isolated smooth muscle cells 79−88064
alkali halide:Ca, impurity-vacancy complexes, association and orientation energies 78−51578
atmosphere aerosols over tropica N.Atlantic Ocean, water-soluble K, Ca and Mg contents 80−72598
atom, 2 keV electron excitation and ionis., ejected electron spectra 77−3466
atom, $3p^6$ subshell excitation by electron impact 80−1070
atom, $4p^2\ {}^1S_0-4s4p\ {}^1P_1-4s^2\ {}^1S_0$ cascade rate, two photon coincidence meas. technique 80−95576
atom, 4s4p $^1p_1$ level Hanle effect density depend., lifetime 80−91494
atom, 6573Å line photon recoil struct. 79−85925
atom, bound odd-parity J=1 spectra, multiphoton excitation 79−54795
atom, bound-even parity spectra, multichannel quantum defect theory anal. 77−34600
atom, direct meas. of excited state lifetimes 77−65435
atom, efficient ionis. by reson. laser pumping 80−32685
atom, electron impact, $3p^6$ subshell excitation, VUV spectra *(Russian)* 78−90117
atom, electron impact excitation, identification of low energy autoionising levels 79−31703
atom, electron impact ionis., ejected electron spectrum from autoionis. levels 78−33613
atom, in Ar matrix, multiphonon relax. processes emission spectra 78−37583
atom, in shock heated Ar, absorpt. line broadening obs. *(Japanese)* 80−83464
atom, intensities of reson. lines *(French)* 77−57912
atom, intercombination line, at. beam saturation and reson. fluoresc. spectroscopy 79−36580
atom, isotope shift in Ca I resonance line, nucl. charge distrib. 79−9461
atom, isotope shift meas. using enriched isotopes in atomic beam 78−17610
atom, laser excited, ionisation studies 80−83330
atom, metastable, prod. in N_2O-CO flame, u.v. spectra 77−9081
atom, multichannel quantum defect theory anal. to predict Ra states 80−52918

calcium continued
atom, multiphoton ionis. spectroscopy of even- and odd-parity states 78—86973
atom, multiphoton ionisation by Nd laser radiation *(Russian)* 78—21889
atom, multiphoton ionisation spectra of msnp$^3P^0$ states 77—83554
atom, oscillator strengths and excitation energy, valence shell states 78—17611
atom, photon recoil splitting, line widths, Doppler effects, saturated absorpt. optical interference spectroscopy 80—52922
atom, quantum defect theory of oscill. strength density 79—81183
atom, stable and radioisotopes, hfs, isotope shifts, dye laser saturation spectroscopy, beam expt. 80—58169
atom, Stark mixing of high-lying calcium levels by laser-produced charges 78—25469
atom, transition probability of valence shells, relativistic pseudopot. calc. 78—86803
atom, two-electron one-photon transition rate 77—71772
atom, weak intercombination line, Lamb-dips obs. by resonance fluorescence monitoring 79—3392
atom, X-ray production by protons by 0.5 to 2.0 MeV energy 78—66646
atom and ion, spectral lines collision broadening and shifts 78—58624
atom X-ray spectra, mass absorpt. coeffs. in ultrasoft region, spectral depend. 77—10622
atomic beam, time-of-flight spectrum using pulsed tunable laser fluoresc. detect. 77—49804
atomic polarisability, ground state electric dipole, electric beam deflection technique 77—10780
atomic resonance fluoresc. detection with intracavity at. beam laser spectrometer 77—19107
atoms, excitation series, potential barrier effects, single configuration HFC 80—78558
atoms, fluoresc. excitation profile, laser saturation broadening in flames obs. 80—95568
atoms, forbidden transitions, radiative lifetimes, MCSCF and CI calcs., time of flight spectra for metastable state 80—91498
atoms, quantum defect param., ab initio calcs. 80—78525
atoms, spectroscopy, masers and superradiance study 80—53248
atoms and ions, radiative lifetimes of excited states *(Russian)* 78—13472
axon, aequorin injected, Ca entry, crayfish 79—79513
axon, ATP as energy source for Ca pump in squid giant axons 78—77043
axon, squid, Ca buffering, review, book contrib. 79—5267
axoplasmic transport in mammalian nerve, role of Ca^{2+} 78—24052
binding energies, stable phase and elastic constants calc., appl. of reson. model pot. 77—69263
blood cells, red, Ca stimulated increase in K permeability, dog 79—62218
body content measurement, fate of ^{37}Ar prod. by fast neutron exposure 77—5075
body content measurement by neutron activation and ^{37}Ar meas. 78—3589
bone, human hand, CC Ca anal. by local neutron activation 79—83902
bone activation anal., prod. of uniform ^{38}K yield using range modulator 77—40735
bone C partial-body determ. by proton activation anal. 77—86605
bone Ca level meas. using computerised tomography, correl. with ACTA numbers 77—40756
brine, routine anal. by X-ray fluoresc. spectrometry applying matrix corrections 78—88690
Ca, A=40,42,43,44,46,48, laser spectroscopy, isotope shifts obs. 77—14392
Ca II K line emission widths in solar and stellar spectra 77—41373
cardiac intracellular pools, Ca dynamical modelling rel. to muscle contractive force 79—79568
catalytic effect on chemisorption of O_2 on Au, AES 79—15021
charcoal, catalytic graphitisation by gaseous species from Ca 80—11872
charge distribution in isotopes 40, 42, 44, 48, Hartree-Fock anal. *(Russian)* 78—70747
chemi-ionisation reactions of Ca, Sr, Ba, and Yb with halogens and interhalogens 77—32791
cochlear endolymph Ca content 78—61203
combustion, laser-initiated, time-resolved spectroscopy 77—77765
coral aragonite Sr/Ca ratio, ocean temp. determ. 80—12568
cosmic ray source abundance 78—28467
crustacean neuromuscular junctions, synaptic facilitation obs. 79—39412
cystic fibrosis, mitochondrial Ca uptake and O_2 consumption 79—43839
determ. by atomic absorption, using low temp. flames 80—30307
determination, by Zeeman effect at. absorpt. spectroscopy 77—32866
determination, image vol. samples 78—53308
determination, in lake sediments, by atomic absorption spectroscopy 78—95970
determination, in phosphates, chem. methods 78—23976
determination by intracavity at. emission spectroscopy 79—52830
determination in Greenland snow and ice, natural and anthropogenic origins 79—70815
determination in small bone biopsies by neutron activation 79—88154
diffusion in KCl simultaneously with Sr 78—79813
diffusion in Na_2O-Al_2O_3-SiO_2 glass, SIMS study 79—82387
electrical resistivity; 1-1000K, data tables 79—78073
electrical resistivity and thermopower, meas. at melting temp. 79—99524
endoplasmic reticulum in squid giant axon, Ca sequestering 79—83733
epithelium intercellular contacts, small intestine, permeab. and mech. props. regulation by Ca ions 77—81482
eye rod photoreceptors, vertebrate, opposing effects of Ca^{2+} and Ba^{2+} 79—24990
F-type supergiants in Magellanic Clouds, Ca abundances 80—98655
faecal samples, Ca determ. method using instrumental fast neutron activation anal. 80—104733
fast separation by ion exchange resin *(Rumanian)* 78—23922
film, imaginary part of permittivity determ., 2-5.6 eV *(French)* 77—4694
film, optical absorption and plasma reson. 77—40296
film, optical consts. meas., 2 to 5.6 eV *(French)* 78—52586
film, structure effects on work function, electron micrographs and photoemission meas. 79—83107
film, vacuum deposited, photoionisation coeff. from photoemission meas. 79—91569
films, thin and ultrathin, vac. deposited, struct. and photoemission meas. 80—11538

calcium continued
flame, luminesc., laser irrad. effects 77—77766
forced-flow chromatography, detection by photometric method 80—71965
glass surface, Ca^{2+} ion deposition as inhibitor to alkaline attack 80—50737
human body Ca meas. by neutron activation anal. 79—92350
in vivo measurement by ^{37}Ar method, inert gas elimination in humans 78—61247
interstellar Na I and/or Ca II lines, obs. towards 47 stars 79—25676
intestinal absorption of Ca and P in rat, simultaneous in vivo determ. using ^{47}Ca and ^{32}P 78—48882
intestinal epithelium, effect of Ca ions and pH on osmotic pot. 78—20156
intestinal epithelium, extracellular route for Ca transport *(Russian)* 78—40128
ion, 78—37760
ion implantation in Al, defect structures obs. 80—59494
ion levels in squid axons, influence of pCO_2 78—56960
ion recombination laser 78—17923
ion-selective electrode design 79—70404
ionophoretic model for Na-Ca counter transport 79—2017
ions, adsorbed on porous SiO_2 glass in distilled water medium, determ. 79—24814
ions, dielectronic recombination excitation in solar X-ray lines 80—51725
ions, two vacancies in K shell, 2 electron 1 photon, and hypersatellite transition probabilities 78—46294
isotope anomalies in Ca-Al-rich inclusions in Allende meteorite 78—32410
isotope fractionation on Earth and other solar system materials 79—20835
isotopic anal. using double vaporizer 80—106398
isotopic anomalies and lack of ^{26}Al in Allende meteorite unusual inclusion 79—40142
isotopic comps. of magnetic spherules in marine sediments 79—44423
K activation associated with intraneuronal free Ca 79—8494
laser, pumped via collision-induced absorpt. in Ca-inert gas mixture 79—7117
laser spectroscopic anal. of Rydberg series, multichannel quantum defect theory 80—18815
lattice dynamics, phenomenological model 80—44265
lipid bilayers, Ca^{2+} transport system of rat liver mitochondria 78—64966
liquid, density meas. at intermediate temps., method employs Archimedes' Principle 78—22784
liver, Ca balance and cooperative electrogenesis, rate 79—57608
lymphocyte stimulation rel. to early Ca flux 77—52758
magnetic hyperfine field in Fe, TDPAD meas. 78—52389
marine pollution determ. in Jordan Gulf of Aqaba 79—12142
membrane Ca in rabbit neutrophils, chemotactic factor-induced release 79—88095
membranes model using millipore-DOPH membrane, increase in elec. resist. with Ca^{2+} ions and its oscill. 80—40745
mitochondrial Ca^{2+} transport, effect of cations on temp. sensitivity, compared with liposome spermine uptake 78—11621
mitochondrial Ca^{2+} transport, rat liver, effect of Mg^{2+} and spermine 77—64015
molar surface enamel, rat, Ca content determ. using AAS 1 spectrophotometer 80—56303
molecule, optical spectra, inert matrices 78—58712
molecule, vibr.-rot. states, high accuracy wave functions and energies 80—74159
motor nerve endings, hyperosmotic neurosecretion rel. to internal Ca conc. 77—56368
muonic atom transition energy meas., tests of high-order vac. polarisation corrections 77—71895
muonic isotope shifts in Ca 78—33640
muscle, excitation and contraction processes, book contrib. 79—5262
muscle, skeletal fibres, intramembrane charge movement and Ca transients 79—66453
muscle, smooth, depolarised, tone change due to hyperpolarising current 77—86471
muscle, smooth, depolarised in hyper K medium, spontaneous relax. 77—86470
muscle, translocation of intracellularly stored Ca during contraction-relax. cycle 77—86474
muscle fibre post-synaptic membrane, ionophore-mediated Ca influx effects 78—11637
muscle mitochondria, fish, physiological correls. of Ca accumulating props 79—20527
myotonia, Ca induced, computer simulation 79—57633
myotonia and Ca permeab., math. model 78—11620
nerve cells, enhancement of Ca spikes 79—70545
nerve presynaptic terminals, ATP-depend. Ca storage 77—29126
nerve terminal Ca channel selectivity regulation by weak acid site 79—62231
nervous tissues, Ca dependent K activation, book contrib. 79—5266
neuro-secretion, role of Ca in control mechanism 77—64028
neuroblastoma cultured cells, membrane currents under volt. clamp 77—60193
neuromuscular junction miniature endplate current decay, effects of extracellular Ca^{2+} and Mg^{2+} 78—24064
neuron, intracellular Ca movement during pentylenetetrazole induced bursting activity 79—8495
neuron adaptation model allowing for Ca influence on membrane K permeability 79—79508
neuron late outward current, Ca-dependent depression, snail 78—7335
neuron membrane Ca channels, displacement currents assoc. with activation of gating mechanism 77—81486
neuron membrane inward Ca current, blocking effect of Cd^{2+} ions 77—81485
neutron activation anal., geochem. of genesis of ore deposits, atomic ratios in Ca-minerals *(German)* 80—30301
nuclear target, evaporation preparation 80—23224
ocean chemistry of N Pacific 80—90100
optical properties, 2-11 eV 78—15191
oxidation, low-temp., by water vapour 78—3256
pancreatic acinar cell stimulus-secretion coupling, fluoresc. probe detect. of cell Ca redistrib. 77—77872
pancreatic islet glucose-sensitive Ca pools, rel. to secretion 77—32883
parvalbumins, Ca-binding, lanthamide-substituted, of muscle, ^{13}C NMR obs. 79—96516
photoelectric cross sections at 52.4, 60, 72.2 and 84.4 keV 80—69187

calcium continued
- photoelectrode for recording intracerebral cellular Ca^{2+} transients 80—67307
- photoreceptor light adaptation, Ca^{2+} ion as putative intracellular messenger 78—15833
- pionic atom, 2p level shifts and widths 78—46469
- pituitary cell, Na and Ca action potential 77—48770
- PIXE anal. method 77—63973
- plant motor organ K, Ca distrib., ion microscope obs. 79—66466
- plasma, Gaunt factor temp. depends., from Ar II and Ca II Stark widths 78—87491
- plasma, laser produced, vac. UV emission 77—80372
- plasma temp. diagnostics from linewidth, inductively coupled plasma 77—43083
- plasmon excitation by oblique incidence of primary electron beam of medium energy 78—18987
- Purkinje fibres, calf, role of intracellular Ca in transient outward current 77—90748
- radiative decay of autoionisation states *(Ukrainian)* 78—82682
- recrystallisation of wires and filings by thermal processing encapsulated in metal tubulation 77—59810
- red cell Ca pump, ATP regulation 79—29511
- rod external segment fragment suspension, Ca^{2+} activity rel. to illum. 77—36918
- rod outer segments, vertebrate, role of Ca and H ions as transmitters 77—90776
- salivary gland cell junction, Ca^{2+} produces graded changes in membrane channel permeab. 77—64016
- saturated absorption optical Ramsey fringes 79—54204
- self-diffusion in molten Na_2O-CaO-SiO_2 glasses 78—10202
- serum automated electroanal. using ion-selective disc electrodes with neutral cation-carriers *(German)* 78—73269
- skeletal Ca, facility for regional in vivo neutron activation anal. 79—25088
- skeletal content estimation by exhaled ^{37}Ar meas., fast neutron dose requirement 77—16962
- skeletal muscle, excitation-contraction coupling, blockade by high extracellular concs. of Ca buffers 79—20528
- soil pollution indication, Ca and NO_3-N loss from microcosms 78—16019
- solar abundance, rel. to upper photosphere models and empirical damping parameters 77—33445
- solar quiescent prominance spectra, meas. of Ca^+ 8542 and 8498 Å 80—90373
- solubility in wustite and diagram Fe-Na-Ca-O at 1000°C *(French)* 78—31392
- spallogenic isotopes in Fe meteorites, radial distrib. 80—67488
- spectrochemical analysis of biological solns. using wall stabilised arc source 80—41343
- spine and forearm changes, meas. apparatus using ^{252}Cf neutron activation anal. 79—39490
- stars of solar neighbourhood, chromospheric Ca II H and K emission survey 80—109423
- steam enhanced segregation in dense Al_2O_3, AES and SEM obs. 79—83352
- steel, construction type, spectrochem. determ. of Ca 78—7275
- surface plasmons, excitation 79—28310
- surface segregation in dense Al_2O_3 exposed to steam and steam-CO 78—85013
- sweat secretion, role of Ca, in vitro meas. 78—40129
- tonoplast ionic channels in charophyte algae cell, role of Ca ions in excitation 77—81481
- tracheal ephithelium, effect of Ca on ion transport and elec. props. 79—34527
- transport properties, elec. resist., thermoelec. power, thermal cond. deviations from Matthiessen's rule 78—39086
- unilamellar lipid vesicles, Ca^{2+} initiation of fusion or lysis 79—2008
- US attenuation due to phonon-phonon interaction and thermoelastic phenomenon 79—77686
- vapour, optical SHG, quadrupole moment pot. by mag. field 77—46760
- vertebrate retinas, outer segment layer, light-induced Ca fluxes 80—94207
- water, natural, trace metals, energy dispersive X-ray fluoresc., at absorpt. anals., comparison 77—60175
- AgCl:Ca^{2+}, plasticity, impurity hardening effect 78—47466
- Al_2O_3, dense, exposed to steam, influence of Ca migration on strength reduction 80—11797
- α-Al_2O_3:Ca semicond. props. 80—54684
- Ba, oxidation, SXAPS 77—73189
- $Bi_{12}GeO_{20}$:Ga,Ca, photocond. suppression by simultaneous Ga and Ca doping, and appl. to electro-optic light valve 79—78134
- Br-Ca-Fe H_2O-decomposition cycles for thermochem. H prod. 80—35784
- Ca, electrical resistivity and thermoelectric power 78—26846
- Ca excess in snow and rain samples, Japan, from calcite source 79—39766
- Ca I, Ca II lines in solar spectra, non-mag. polarisation, centre-to-limb var. 80—67678
- Ca I, emission spectrum, level struct. 77—79562
- Ca I, inner shell absorpt. spectrum, 3d wavefunction collapse 77—23455
- Ca I 6102, 6122, 6162 Å multiplet, collisional broadening 80—37777
- Ca I 6573 Å and Ca II 7324 Å forbidden line, centre-to-limb behaviour 79—25572
- Ca I absorption spectrum, 1430-1340 Å 80—47930
- Ca I to XX, energy levels and ionisation energies, data compilation 80—14101
- Ca II, emission lines in solar quiescent prominences, theory 77—53523
- Ca II, Hanle effect, $^2P_{3/2}$ lifetime meas. 77—18852
- Ca II, in fast sporadic meteor spectrum, low-energy electron excitation 78—93170
- Ca II, in interstellar clouds, non-linear relationships between N(Ca II), N(K I) and N(H) 79—92832
- Ca II, interstellar, obs. in 30 Doradus nebula in LMC 80—46643
- Ca II, laser stimulation optimisation for intraresonator spectroscopy 80—77881
- Ca II, lifetime extraction from beam-foil decay curves 80—14107
- Ca II, reson. line broadening in shock tube plasma 77—35393
- Ca II, solar H and K line profiles vars. at solar minimum and cycle 21 onset 79—16907
- Ca II, unique interstellar K-line profile in 30 Doradus direction 80—51850

calcium continued
- Ca II 3737 Å emission line studies of prominences and flares *(Russian)* 80—51717
- Ca II 3934 Å K-line, temporal var. in solar spectrum 78—93186
- Ca II emission from stellar chromospheres 79—30061
- Ca II H and K line profiles of active solar limb filament 79—44446
- Ca II H and K lines in F0 to M2-type stars, high resolution absolute flux profiles 80—26842
- Ca II H and K lines in late type stars; photoelectric calibration 80—36617
- Ca II H and K lines in solar prominences, emission line intensities rel. to model calcs. 79—44447
- Ca II H and K-line, and abundance in globular star cluster giant stars 80—72940
- Ca II H and K-lines in binary star giants, emission intensity 80—82420
- Ca II H- and K-line complex structure in HD 190073 (A0ep-type) 77—60775
- Ca II H-K solar lines, non-mag. polarisation 80—63569
- Ca II H-line emission from Sun observed as star *(Russian)* 77—64727
- Ca II IR triplet lines in sunspot umbrae 80—85918
- Ca II interstellar absorption in NGC 4321 galaxy 80—51847
- Ca II K_3-line and solar chromospheric feature lifetime rel. to rotation 79—44442
- Ca II K-line asymmetry in A-type star Sirius unconfirmed 79—30062
- Ca II K-line asymmetry in A-type star Sirius, comments 79—30063
- Ca II K-line in α Cygni, core asymmetry 80—85981
- Ca II K-line in quiescent solar prominence, influence of spatial resolution on line width and shift 80—77364
- Ca II line width in late type stars, Wilson-Bappu effect 79—12464
- Ca II lines in solar chromosphere, vel. and temp. disturbances, weighting functions 80—67679
- Ca II network, giant cell circulations on Sun 79—8895
- Ca II solar chromosphere lines, mech. flux determ. 80—67680
- Ca II solar K-line, centre-to-limb obs. of K_2 component *(French)* 80—82331
- Ca II solar K-line network, giant cell circulation pattern 77—53546
- Ca III, atomic structure determ. by model pot. method 78—86777
- Ca III, autoionising transitions $ns^2np^6-nsnp^6mp$ 77—88419
- Ca III, photoionisation, multichannel CI calcs. 79—93931
- Ca ions activity change due to magnetisation as possible mechanism of biological effect *(Russian)* 79—39423
- Ca, whole-body, determ. method for rats using neutron activation anal. 80—51302
- Ca X, electron impact excitation, transition probabilities, oscill. and collision strengths 78—25718
- Ca X, wavelengths and energy levels, spectral obs. 77—428
- Ca XI, lasing action in far UV, 500 to 700 Å *(Russian)* 77—75491
- Ca XI, population inversion of transitions 77—75482
- Ca XI, vacuum UV lasing action 78—1213
- Ca XV, Ca XVI in solar flares, atomic data rel. to XUV electron density diagnostics 79—88633
- Ca XV, transition probabilities, energy spectra calcs. 78—70791
- Ca XVII, $2s2p(^3P_1{}^0)\rightarrow 2s^2(^1S_0{}^e)$ transition probabilities, CI calcs. 79—36544
- Ca XVII, energy levels and transition 79—59383
- Ca XVII, wavefunctions and oscill. strengths, CI calcs. 80—23317
- Ca XVIII wavelength, for line identification in solar corona radiation 77—79569
- Ca^+ cyclic laser, double-pulse excitation expts. 79—55118
- Ca^+, electron and ion Stark effects in plasma, widths and shifts 77—46526
- Ca^+, reson. line regularities in plasma Stark widths and shifts 80—43881
- Ca^+, resonance lines electron impact excitation, polarisability 78—42225
- Ca^+, transition probability of valence shells, relativistic pseudopot. calc. 78—86803
- Ca^{2+}, ATP driven pump in squid axon, physiological role 79—43865
- Ca^{2+} channel mediating asynchronous acetylcholine release by motor nerve impulse 78—11638
- Ca^{2+} concentration in extracellular fluids in body, digital simulation of short term regulation 79—83725
- Ca^{2+} conductance of acetylcholine-induced endplate channels 79—70546
- Ca^{2+} current in Paramecium, inactivation of Ca channel 79—79488
- Ca^{2+} effect on chromaffin granule electrophoretic mobility meas. by light scatt. 78—53357
- Ca^{2+}, effect on extracellularly-recorded photoreceptor pots. of cephalopod retina 79—62245
- Ca^{2+} effect on rat cell electrophoretic mobility after X-irrad. 79—92293
- Ca^{2+}, effect on thermotropic behaviour of E. coli cytoplasmic membranes 79—79482
- Ca^{2+} effects on bursting pacemaker neurons, modelling 78—44484
- Ca^{2+}, effects on intensity-response curve of toad rods 79—53091
- Ca^{2+}, effects on prolonged depolarising afterpot. in barnacle photoreceptor 80—8051
- Ca^{2+}, efflux from chick brain tissue, induction by RF radiation 80—56127
- Ca^{2+}, excitation-contraction coupling in frog myocardium model 79—70541
- Ca^{2+}, extracellular, effects of removal on excitation and adaptation in Lumulus ventral photoreceptors 77—9190
- Ca^{2+}, heart muscle excitation contraction coupling, mathematical model 79—96542
- Ca^{2+} in bursting pacemaker neurons, internal conc. changes meas. with arsenazo III 77—64021
- Ca^{2+} in pancreatic islet cells, effect on K^+ permeability 79—74615
- Ca^{2+} in seawater 80—31064
- Ca^{2+} incoming current obs. in trabeculae of frog atrium 79—79497
- Ca^{2+} influx, role in muscle excitation-contraction coupling 79—74616
- Ca^{2+}, interaction with bovine rhodopsin 79—100563
- Ca^{2+}, interaction with bovine thodopsin 79—100564
- Ca^{2+} intracellular changes in human erythrocyte ghosts, arsenazo III meas., rel. to K permeability 78—96032
- Ca^{2+} intracerebral transients, photoelectrode for recording 80—30961
- Ca^{2+} ion, efflux from cerebral tissue rel. to weak oscill. elec. fields 77—1984
- Ca^{2+} ion currents, presynaptic, rel. to synaptic transmission in squid, voltage clamp investig. 77—16926
- Ca^{2+}, K^+, blood concs. in rat, technique for continuous vivo meas. *(German)* 79—39533
- Ca^{2+}, marine sediment content, western continental shelf, India 80—8289

calcium continued

- Ca^{2+} mitochondrial transport, inhibition by antibodies directed to Ca^{2+}-binding glycoprotein 77−4990
- Ca^{2+}, passive and active fluxes across membranes, review 80−97886
- Ca^{2+} promotion of fusion of human erythrocyte ghosts, with PO_4 ions 77−4987
- Ca^{2+} regulation of chemotactic behaviour in bacteria 78−15851
- Ca^{2+}, role in Limulus photoresponse suppression during anoxia 79−62252
- Ca^{2+}, role in multiplication regulation of normal and transformed cells 79−2012
- Ca^{2+} transport across red blood cell plasma membrane, stimulation by calmodulin 80−12066
- Ca^{2+} uptake during mitosis in myxomycate Physarum polycephalum 77−90747
- Ca^{2+} voltage-depend. facilitated entry into voltage-clamped aequorin injected molluscan neurons 77−90763
- Ca^{2+}, X-ray microanal. of cultured skeletal muscle cells, calibration 79−100798
- Ca/H ratio in RR Lyrae variable stars in globular clusters 79−16962
- Ca^{2+}/Na^{+} extracellular ratio effect on photosensory membrane of Limulus ventral nerve photoreceptor 78−69067
- Ca-Ca symmetric collisions, molecular-K-X-ray anisotropy spectra, discrete struct. 77−14560
- Ca-H_2, single freq. laser, 5.54 μm emission, mag. field tuning 78−46634
- Ca-N_2O-CO flame, Ca catalyzed, gain meas., emission band assignment 78−66815
- Ca-N_2O-CO flame, candidate chem. laser reactions, intracavity dye laser absorpt. meas. 78−63108
- Ca-selective membrane electrodes, asymmetric, potentiometric meas. 77−77785
- Ca-Xe charge exchange system, optical gain meas. 79−10285
- Ca^{2+}-ATPase activity in brush border and basolateral membranes, rat duodenum 79−74613
- Ca^{2+}-dependent responses in Paramecium, effect of artificial deciliation 77−2017
- Ca^{2+}-induced aggregation of phospholipid vesicles 79−62202
- Ca^{2+}-induced luminesc. of aequorin, inhibition by anaesthetics 78−76985
- Ca^{2+}-induced release of Ca^{2+} in sarcoplasmic reticulum of skinned cardiac cells 80−3612
- $Ca+{}^{41}Ca$, transverse decoupling of hyperfine interactions in free atoms 77−18468
- $Ca+Ar$, quenching cross section of Ar atom for Ca reson. line 77−19021
- $Ca+Ar \rightarrow CaAr^{+}$, chemiluminescent 77−32781
- $Ca+CCl_4 \rightarrow CaCl+CCl_3$ reaction, laser-induced fluoresc. obs. 80−11916
- $Ca+Ca^{+}$(Rydberg Ca**), collision cross sections, $Ca_2{}^{+}$ pot. energy calcs. 79−27055
- $Ca+Ca(Mg)$(inert gas), metastable ^3P-state, quenching reactions, fluoresc. meas. 80−102477
- $Ca+Cl_2 \rightarrow CaCl+Cl$, chemiluminescent reaction, state-to-state cross-section, beam-gas expt. 80−45510
- $Ca+F_2$, crossed beam chemilum., kinetics and mechanisms 80−21264
- $Ca+H^{+}$, K X-ray production, 0.2-0.5 MeV, ionis. cross-section 79−31459
- $Ca+HF(DF)$, beam reaction, vibr. excitation 78−68877
- $Ca+Hd \rightarrow CaCl+H$, chemiluminescent reaction, state-to-state cross-section, beam-gas expt. 80−45510
- $Ca+He$, Ca, $^1P_1$ level lifetime, Hanle measurement 80−23365
- $Ca+He$, nonstatistical excitation of mag. substates of $^1P_1$ level 78−42194
- $Ca+He^{+}$, 2-1000 eV, spontaneous ionis. mechanisms 79−64090
- $Ca+He(Ne)$, press. broadening, line shifts 78−5290
- $Ca+He(2^3S_1)$, coherent $^2P_{3/2}$ levels excitation by Penning ionis., Hanle effect 80−5520
- $Ca+$inert gas, $^1P_1$-$^3P_1$ excitation transfer 80−102559
- $Ca+$inert gas, collision-induced dipole transitions, absorpt. study 80−37865
- $Ca+$inert gas, collision-induced dipole transitions assoc. with high-lying states 80−37866
- $Ca+N_2O+CO$ reaction, intracavity dye laser spectroscopy 77−86293
- $Ca+N^{+}$, X-ray production cross section, $K\beta/K\alpha$ ratio, 0.5-2.5 MeV/amu 77−54526
- $Ca+NH_4{}^{+}(CH_3NH_3{}^{+})(PH_4{}^{+})$, proton transfer reaction cross sections, 1-6 eV 78−20003
- $Ca+NaCl$, crossed beam reaction, collision complex lifetime internal state depend. fluoresc. 77−56217
- $Ca+O_2$ reaction, chemiluminesc. absolute cross sections, photon yields and CaO dissoc. energy 80−97697
- $Ca+O_2(CO_2)$, CaO form., product states obs. 78−92450
- $Ca+O_2(CO_2)(N_2O)$, reaction, electronic branching, statistical and dynamical influences 78−92451
- $Ca+S_2Cl_2 \rightarrow S_2{}^{*}+CaCl_2$, rearrangement reaction, crossed-beam chemiluminesc. 77−29009
- $Ca+Sr$, laser induced collisional and radiative energy transfer 80−53108
- $Ca+Sr$, laser-induced collisions, large cross sections meas. 79−64075
- $Ca+Sr$, laser-induced dipole-quadrupole collision 79−98207
- $Ca+Sr$, laser-induced inelastic collision, fluoresc. obs. 77−54603
- $Ca+Xe$, collision-induced dipole transition due to long range interaction, absorpt. obs. 80−63779
- $Ca^{+}+Ca$, 25, 30, 40 MeV, K-shell double ionis., $K\alpha\alpha$ and $K\alpha\beta$ obs. 77−57918
- $Ca^{+}+$inert gas atom collision, polarisation of emitted radiation, quasimol. interf. effect *(Russian)* 77−46633
- $Ca^{14+}+H^{+}$, collisional excitation of fine struct. transitions in ground state 77−19017
- $Ca^{20+}+H$, charge transfer, total and partial cross-sections calcs. 80−23542
- Ca_2, $A^1\Sigma_u{}^{+}$-$X\Sigma_g{}^{+}$ system, laser induced fluoresc., pot. energy curve and mol. consts. 80−58307
- Ca_2, ground state, multiple scatt. $X\alpha$ calcs. 80−58149
- Ca_2, in Kr matrix, 1- and 2-photon fluoresc. excitation 78−50567
- Ca_2, in solid Kr, discrete reson. Raman scatt. and vibr. relax. 79−18188
- Ca_2, laser-excited fluorescence in inert gas matrices 78−94273
- Ca_2, low-lying states binding energy, local spin density functional formalism calcs. 79−97994
- Ca_2, matrix isolated, vis. and near IR spectra 78−5214
- Ca_2, mol., vibr. quantum numbers of rotating vibrator 79−85949
- Ca_2, new ground state, photolum. obs. vibr. consts., dissoc. energy 80−5576

calcium continued

- Ca_2, rot. perturbed Morse oscillator eigenfunctions and Franck-Condon factors 77−42309
- Ca_2, transient species, matrix isolation spectra 78−48635
- Ca_2, van der Waals mol., in Kr matrix, absorpt. and emission spectra 77−83611
- Ca_2, vibr. relax. in rare gas matrices 78−58711
- $(Ca^{2+})_i$-linked K^{+} conductance in bullfrog, oscill. obs. 80−35867
- $CaCl_2$-Ca phase diagram, DTA study *(French)* 80−25672
- $Ca(^3P)+SF_6$, F_5S-F bond energy bounds from chemiluminesc. obs. 79−86081
- ^ACa, A=40, 42-44, 48, pionic X-rays, strong interaction and isotope shifts, π-nuclear optical pot. 80−53169
- $^{40}Ca(n,\alpha)^{37}Ar$, system for meas. total body Ca in man 79−25083
- ^{41}Ca, possible use for radioactive dating 79−21063
- ^{43}Ca, atomic beam and resonance spectroscopy 80−58180
- ^{43}Ca, isotope shift and hyperfine struct. by laser spectroscopy 79−41139
- ^{43}Ca, nucl. quadrupole moment, HFS in at. beam mag. reson. 79−63940
- $^{43}Ca^{2+}$, aq. ions, nucl. quadrupole relax. 78−64287
- $^{44}Ca+O_2(O_3)$, reaction products identification by IR spectra in N_2 matrix 78−9151
- ^{45}Ca and ^{32}P determination in biological samples by Cherenkov and liq. scintillation counting 80−98183
- ^{45}Ca, effect on spleen and thymus of Indian desert gerbil 80−8106
- ^{45}Ca, effects on bone marrow of Indian desert gerbil 80−45971
- ^{45}Ca, giant liver cell formation after administration to desert gerbil 79−92299
- ^{45}Ca, liquid scintillation counting in plant and soil material 77−44536
- ^{45}Ca tracer diffusion in silicate melt 79−90809
- ^{47}Ca, bone imaging radiopharmaceutical local accumulation model 78−24127
- ^{47}Ca, comparison with ^{32}P in profile scanning of skeletal disease 80−51218
- ^{48}Ca, and rare isotopes, beam prod. using Cs sputter source 78−29686
- ^{48}Ca beam prod. from isotopically enriched sputter targets 80−23221
- $Ca^{*}+Cl_2$, collision and reaction cross section meas. 79−59537
- $Ca^{*}+Cl_2(HCl)$, luminesc. reactive collisions 77−16816
- $Ca^{*}+HCl$, reaction performed under high resolution, luminescence obs. 80−95662
- $Ca^{*}+He(Ne)$, model pot. curves, including CI 78−42154
- $Ca(4p\ {}^3P_J)+Ba$, collisional deactivation and optical lifetime 80−48070
- $Ca^{+}(4s\ {}^2S_{1/2})+Sr(5s^2\ {}^1S_0)$, laser induced charge transfer to excited electronic state 79−81274
- $Ca(4s4p\,{}^3P)+N_2O$, absolute chemiluminesc. cross-section and photon yield 78−53208
- $Cl^{5+}+Ca(Sc)(Ti)$ thick targets, 30 MeV, near symmetry collisions, double-K-vacancy sharing 79−3391
- Cu II K-line in solar plage, peak separation due to microturbulence 80−109407
- $(Eu,Lu)_3Fe_5O_{12}$:Ga(Al)(Ca,Ge), bubble material, dynamic characterisation, comparison between transport and FMR methods 80−39833
- EuIG:Sb(Ca)(Ti), growth from PbO-B_2O_3 based flux, prop. depend. on Pb content 80−39824
- $Fe(OH)_3$, coprecipitation with Cu, Ag, Au; Ge, Sn, Pb; Mn and Ca 79−70415
- Ge:Ba, Ca, recomb. props. 78−56156
- Ge:Ca, elec. props. and effect of impurities on γ-radiation defect formation 78−10088
- Ge:Ca, positron annihilation angular distrib. 80−45165
- KBr:Ca, $F \rightarrow Z_1$ colour centre conversion, hologram recording appls. 78−17877
- KCl:Ba(Ca)(Sr), microstruct. and hardness, impurity distrib. effects 79−24529
- KCl:Ca, additively coloured, spectral and temp. depend. of initial yield of Z_3-centre form. 79−78716
- KCl:Ca, $F \rightarrow Z_1$ colour centre conversion, hologram recording appls. 78−17877
- KCl:Ca, microcrystalline powders, role of Z-centres in stabilizing coloration 80−54227
- KCl:Ca, optical studies of Z_4 centres 79−24336
- KCl:Ca, structural state of impurities, hydrostatic press. effect, thermostimulated depolarisation exam. 77−39614
- KCl:Ca, thermolum. and optical absorpt. spectra of Z_1 centres 79−52029
- KCl:Ca, thermoluminescence and colour centre thermal stability in irradiated sample 78−43941
- KCl:Ca, vol. holographic grating, modulation characts. 79−94197
- KCl:Ca, Z_2 and $Z_2{}^{+}$ centres, excited state, magnetooptical spectra 80−108233
- KCl:Ca, Z_2-centres, optical absorpt. and ESR spectra 79−91480
- KCl:Ca, Z_4 centres, thermal and optical bleaching 80−19802
- KCl:Ca effect of doping on dislocation distrib., in melt grown cryst. 80−6410
- $KCl:Ca^{2+}$, Ca^{2+} precip., flotation density obs. 78−51690
- $KCl:Ca^{2+}$, $Cl^{-}(Br^{-})$, diffusion traps for divalent ions, dielectric loss and ionic thermocurrent techniques 80−6566
- $KCl:Ca^{2+}$, conductivity, self-diffusion, lattice defect props. 77−4216
- $KCl:Ca^{2+}$, cryst., hydrolysed, IR absorpt. bands 77−32404
- $KCl:Ca^{2+}$, Z_1-centre thermolum. 80−80879
- $KCl:Tl^{+},Ca^{2+}$, electrolytic colouring, colour centre form., optical absorpt. spectra 79−15497
- $KCl(Br):Ca^{2+}$, $BeF_4{}^{2-}$ IR absorpt. spectra, impurity cation rel. to degenerate vibr. splitting *(Russian)* 80−2807
- $KCl_{0.5}Br_{0.5}$:Ca, X-ray irrad., Z_1-centres, thermoluminesc. and optical absorpt. meas. 80−16108
- $LaCoO_3$:Ca, anomalous $^{57}Fe^{m}$ charge states, Mossbauer study 80−40017
- LiF:Mg,Ca detectors, variation of parameters of thermally stimulated luminesc. 79−6793
- $LiH:Ca^{2+}$, two peaks in ionic thermocurrent curves 77−31807
- $MnCO_3$ crystals, gel. grown, Ca^{2+}, Ni^{2+} impurity influence, SEM study 80−20778
- NaCl:Ca, aggregation and precip. hardening in impurity vacancy, dipole decay 80−16322
- NaCl:Ca, cryst., radiation colouring, amplitude-phase hologram appls., diffraction efficiency 77−68191
- NaCl:Ca, hologram recording on R-centres 80−1157
- NaCl:Ca, holographic appls., diffr. efficiency 77−54679
- NaCl:Ca, irrad. at room temp., stored energy rel. to thermolum. 80−10574
- NaCl:Ca, light scattering coeff., effect of growing condition 78−55418

calcium continued

- NaCl:Ca, microhardness and thermoluminescence, hardness-quenching temp. variation 80−29813
- NaCl:Ca, precipitate form., transform. after annealing, critical flow stress 78−38848
- NaCl:Ca, reflection holograms recording 79−98320
- NaCl:Ca, single cryst., vaporisation kinetics meas. 78−18763
- NaCl:Ca, surface segregation and diffusion 77−43416
- NaCl:Ca, X- and gamma-irrad., thermostimulated electrons and luminesc. 79−91505
- NaCl:Ca, X-irradiated, Z_1-centre form. kinetics, thermolum. investig. 77−4693
- NaCl:Ca, Z_1 centre thermoluminescence study 80−16109
- NaCl:Ca crystals, optimum temp. for holographic recording *(Russian)* 80−1163
- NaCl:Ca crystals, surface recrystn., moisture effect 80−84950
- NaCl:Ca^{2+}, cryst., hydrolysed, IR absorpt. bands 77−32404
- NaCl:Ca^{2+}, dipole concs. determ. considering aggregation, expt. and theoretical comparison 80−59512
- NaCl:Ca^{2+}, highly doped, aggregation of point defects, NMR and dielec. loss meas. 79−10847
- NaCl:Ca^{2+}, spin-lattice relax. meas., 160 to 360°C, vacancy contrib. 77−28477
- NaCl:Ca^{2+}, X-irrad. effects on divalent metal aggregates, ionic cond. meas. 79−82263
- NaCl:Ca^{2+}, X-ray induced luminescence 78−23516
- NaCl:Ca^{2+},Mn^{2+}, EPR of Mn^{2+}, effect of Ca^{2+} on Mn^{2+} vacancy dipole decay 78−56371
- NaCl:Ca^{2+} crystals, influence of dipoles and dipole complexes on yield point 80−39208
- NaCl-Ca, single crysts., load-microhardness curves, heat treatment, impurity effects obs. 78−30694
- NaF:Ca, migration enthalpy and entropy, TSC obs. 80−54716
- NaF:Ca^{2+}, substitutional impurities, defect props. of (001) and (011) surfaces 77−47443
- NaI:Ca^{2+}, ionic thermocurrents meas. 80−80677
- NaI:Ca^{2+}, lattice defects, entropy and enthalpy of formation and migration 80−96687
- $NaNO_3$:Ca^{2+}, γ-irrad., damage species annealing 79−66324
- O_2+Be(Mg)(Ca)(Sr)(Ba), reaction kinetics in diffusion flame 77−90579
- Pb-Ca-Sn, effect of Sn additions on precipitation behaviour, of Pb-Ca alloys *(German)* 78−52821
- RbCl:Ca^{2+}, thermolum. and optical absorption studies 80−104002
- Sb-I-Ca process for thermochem. H_2 prod. by H_2O dissoc. 80−16824
- $Sr(5p^1P^0)+Ca(4s^2\ ^1S)$, laser-induced inelastic collisions, theory 77−14552
- YIG: Ca^{2+} epitaxial films, Fe^{4+} centres, MCD, optical absorpt., and thermoelectric power meas. 78−95595
- YIG:Ca, epilayer, reversible oxidation, ferromag. reson. 78−76781
- YIG:Ca, O diffusion depend. on defect conc. 78−67857
- YIG:Ca, oxidising effects of high temp. annealing in reducing atmosphere 80−66696
- YIG:Ca eddy current damping 80−39876
- YIG:Ca film, microwave losses induced by Fe^{4+} ions, ferromag. reson. study 79−1715
- YIG:Ca film, strong mag. reson. of Fe^{4+} 78−48047
- YIG:Ca films, rapid O diffusion at 25 to 250°C 77−85120

calcium alloys

see also calcium compounds

- Al-Al_4Ca, eutectic alloy, unidirectionally solidified, exam. of growth and crystallography 78−72771
- Al-Al_4Cin eutectic alloy, extruded and unidirectionally solidified, corrosion a neutral NaCl soln. 80−21154
- Al-Ca-Zn (5,5 wt.%) superplastic sheet alloy, mechanical properties, superplastic forming behaviour 80−60920
- Ba_2Cd and Ba_2Hg, cryst. struct. 77−11505
- Ca containing alloy systems, prep., glass form., thermal props. 79−24461
- Ca-Ag(In), liquid alloy, thermodynamic exam 78−75848
- Ca-Li-Mg, isothermal section calc. 79−29034
- Ca-Mg, liq. alloys, thermodynamic activities determ. using modified Ruff method *(German)* 80−11631
- Ca-Si, deoxidation of steel, thermodynamics *(Russian)* 80−16268
- $CaAl_2$, Laves phase, soft X-ray spectrum, band struct. calc. 77−77325
- Ca_3Cd_2, cryst. struct. 77−11505
- $CaCu_5$, γ-phase in Ca-Cu system, calorimetric determ. of enthalpy of form. *(French)* 80−84915
- $Ca_{0.65}M_{0.35}$, glass transition temp., comp. depend. 80−79702
- $CaNi_5$, Haucke compounds, low temp. heat capacity, Debye temp. 80−96663
- $Ca_{0.67}Pt_3B_2$, cryst. struct. and supercond. props. 79−38231
- $CaSn_3$, powdered, de Haas-van Alphen effect 80−59857
- $Ca_{31}Sn_{20}$, crystal struct. tetragonal phase 78−14310
- Ca_2X, X=Si, Ge, Sn, Pb, occurrence, struct. 78−38663
- $CaZn_3$, struct. with mixed $BaLi_4$- and $CeCu_2$-like ordering 80−107106
- Co-Ca, liq. alloy form. kinetics *(French)* 80−96652
- Cu-Ca-Mg, exam. of phase diagrams and thermodynamics props. 79−8275
- Eu_xCa_{1-x}, mag. ordering temp. conc. depend., Eu mag. hyperfine field temp. depend. 78−14971
- Fe-Ca, dil., mag. hyperfine field, TDPAC meas. 78−43699
- $Gd_{1-x}Ca_xAl_2$, mag. props. and phase relations 80−107991
- $La_{1-x}\ Ca_xNi_5$, H_2 sorption props. 78−91533
- Mg_2Ca, reversible alloys, hydrogenation for H_2 storage *(French)* 79−74549
- Mo-Ca, ion implanted, range distrib. of Ca^+ ions, work function and AES obs. 78−27365
- Ni-based superalloys, hot workability, effect of S, Ca, Mg, Y and Zr minor elements 80−66552
- Pb-Ca-Sn, chill cast and wrought, cyclic voltammetry and electrochemical meas. of anodic activity, PbO_2 form. 78−31582
- Pb-Ca-Sn, for battery grids, proposed phase diagram, grain struct. development, corrosion phenomena 77−16546
- Pb-Sn-Ca sheet, continuously cast, for battery grids, ageing behaviour 77−16603
- $Pr_{1-x}Ca_xAl_2$, mag. props. and phase relations 80−107991
- Zn-Ca, liquid alloy, exam. of thermodynamic props., using EMF method *(Russian)* 79−34003

calcium compounds

see also calcium alloys

- γ-irrad., EPR and luminesc. studies of U^{5+} and U^{6+} centres 79−51854

calcium compounds continued

- actinolite, optical spectra obs. 77−40284
- additives to MgO, effects on sintering *(Japanese)* 80−55340
- amosite in calcium silicate matrix, detection limit in X-ray diffr. analysis 77−84578
- anhydrite, shock compressed, vel. of sound meas. 78−10123
- apatite crystal growth in skeletal tissues 80−94181
- apatites with Ca deficiency, H atom stabilisation 78−23340
- aragonite, polymorphic transition kinetics, differential thermal anal. meas. 79−14722
- armstrongite, X-ray cryst. atomic struct. and refinement 79−60345
- Auger spectra, shake-up satellites 78−27369
- behenate monomolecular layers between Al electrodes, nonlinear dielec. props. 80−80405
- bie-solicylato-diaquo calcium (II), cryst. struct. 80−100222
- bytownite, quenched from 1723K, X-ray single cryst. struct. anal. and refinement 79−19193
- α-$Ca_3(PO_4)_2$, wet-process formation of nonstoichiometric $Ca_x(PO_4)_y(OH)_z$ *(Japanese)* 78−84752
- $Ca_3(PO_4)_2$ film form. on silicate glass surface bonding to bone 80−85212
- $Ca_3(VO_4)_2$-$Zn_3(VO_4)_2$, exam. of phase composition and phase diagrams 79−1851
- cabal glass:$SiO_2(TiO_2)$, microheterogeneity, and elec. cond. 78−83997
- $CaCO_3$, calcite, linear growth rate by pH-stat method *(German)* 79−74073
- $CaCO_3+Na_2CO_3$ solid state reactions, Hedvall effect 79−96300
- CaF_2:Na, Stark effect on Na disturbed F_2-centres 77−69279
- calcite, luminescence spectral anal. of polycyclic aromatic hydrocarbon impurities 80−71483
- calcite, sound emission on dislocation annihilation *(Russian)* 80−54246
- calcite rocks, experimentally deformed, texture development 79−83230
- calcite rocks, plastically deformed, texture transitions 79−83227
- calcium cadmium acetate hexahydrate, Mn^{2+} doped, EPR 79−65715
- calcium copper acetate hexahydrate, and deuterated cpd., tunnelling reson. effects in nonreson. spin-lattice relax. 79−86726
- calcium copper acetate hexahydrate, $CaCu(CH_3COO)_4.6H_2O$ and $CaCu(CD_3COO)_4.6H_2O$, antiferromag. transition obs. 78−2680
- calcium copper acetate hexahydrate, mag. susceptibility behaviour at low temp. 77−24679
- calcium copper acetate hexahydrate, mag. susceptibility field depend. 79−87241
- calcium copper acetate hexahydrate, PMR at low temp., atomic position determ. 77−20728
- calcium di-DL-glycerate dihydrate, Ca binding, X-ray cryst. struct. determ. 79−46642
- α-calcium formate, neutron diffr., cryst. struct., 100 and 296K 77−59004
- calcium oxalate trihydrate and monohydrate, dissolution kinetics charact. by SEM 79−42250
- calcium strontium propionate, compressed powder, dielectric props., particle size effects 77−59503
- calibo glass:Eu^{3+}, Ho^{3+}, energy transfer 78−76510
- CaO-SiO_2, wollastonaite, exam. of synthesis by hydrothermal sintering *(German)* 79−4934
- CaO-SiO_2-CO_2, subsolidus and liquidus phase relationships to 30 kbar 80−85643
- carboborite, cryst. struct. *(Chinese)* 78−18615
- carboborite, X-ray crystallographic investigation *(Chinese)* 78−18614
- chabazite, adsorption of Ar-N_2 mixture, test of eqns. for gas mixture adsorption on heterogeneous surface 78−60030
- chalk, grain size determ., sample preparation methods 79−24694
- chalk filled unsaturated polyester resin, props. *(German)* 80−104228
- composite glasses, high strength, prod. by overlayering 80−89193
- dicalcium barium propionate, ferroelec. in press. induced phase VI 79−91393
- dicalcium barium propionate, press. induced ferroelectricity, dielectric meas. 79−51920
- dicalcium lead propionate, effect of particle size on dielec. behaviour 79−38429
- dicalcium lead propionate, ferroelec., annealed, crit. exponents, dielec. const. temp. depend. 80−55050
- dicalcium lead propionate, Raman scatt., order-disorder type transform. 77−12373
- dicalcium lead strontium propionate, mixed cryst., phase diagram, dielec. and dilatometric anomalies 77−11689
- dicalcium strontium propionate, anomalous US attenuation near ferroelec. phase transition 79−91383
- dicalcium strontium propionate, cryst. symmetry in low temp. phase 79−37693
- dicalcium strontium propionate, effect of particle size on dielec. behaviour 79−38429
- dicalcium strontium propionate, elastic stiffness consts., determ. in US freq. region 79−37752
- dicalcium strontium propionate, ferroelasticity and optical activity rel. to transition 77−76547
- dicalcium strontium propionate, Landau theory breakdown in ferroelec. transition 77−12344
- dicalcium strontium propionate, Raman scatt., order-disorder type transform 77−12373
- dicalcium strontium propionate, temp. depend. of elastic const. c_{16} 79−28029
- diethylenetriaminepentaacetate, chelation therapy for transuranic elements, rats 77−44758
- dolomite, powders sintering, decarbonisation cycle effect 80−104102
- dolomite, shock compressed, vel. of sound meas. 78−10123
- ettringite, expansion by H_2O adsorption, exam. 78−64806
- ferrites, in sinters of Fe ores, texture anal. 80−18009
- fluorapatites, carbonated, B-type, EPR of F^+-centre after X-irrad. *(French)* 80−108065
- fluorite crystal gas-liquid inclusion meas. with microscope heating stage 80−76967
- fluoroapatite, IR spectra, H motion in nonstoichiometric cryst. 78−35125
- fluorochloroapatite, synthetic, defect struct. and colour centres obs. *(Russian)* 78−30612
- formate, intermolecular shielding contributions, proton mag. shielding 80−34783
- formate, selective high resolution ^{1}H NMR 79−61245
- garnet, Ca, Ge-substituted, LPE growth atm. effects on bubble props 77−20655

calcium compounds continued
gypsum, crystallisation 80−100766
gypsum, strength changes on setting *(Japanese)* 77−36619
gypsum, thermal conductivity thermal decomposition 78−2310
gypsum casts, improvement in impregnation method, exam. of mech. props. 78−48503
gypsum-high density polyethylene mixtures, flow props. *(Japanese)* 77−7357
gypsum-high density polyethylene mixtures, flow props. *(Japanese)* 77−7358
halophosphate, thermostimulated luminesc., mech. milling effects *(Russian)* 78−76537
halophosphate luminophors, grinding influence on thermolum. 79−95854
hydrogen dihomophthalate pentahydrate, cryst. struct. 77−15395
hydroxyapatites, dipolar reorientations, TSC study 80−60491
hydroxylapatite, dense, fatique and fracture strength from diametral tests, after various treatments 80−60953
hydroxylapatite, sintered bioceramic, prep. and props. 79−43174
hydroxylapatites, IR spectra, H motion in nonstoichiometric cryst. 78−35125
Iceland spar double refracting prism, rotated e-ray 77−769
ilvaite, electron delocalisation obs. in Mossbauer spectrum 79−33581
ilvaites, Mossbauer spectra and mag. features 80−7248
IR and Raman spectra 79−78671
lead formate, intermolecular shielding contributions, proton mag. shielding 80−34783
LPE growth, saturation magnetisation, collapse field, bubble diameter 78−95703
magnesite-dolomite refractories, tar bound, fracture and wear 80−104287
malonate dihydrate, cryst. struct. 77−59003
marble, ball mill grinding, wet, dry, rate constant determination *(Japanese)* 78−95827
marble, Italian Ondagata, diametral compressive strength, comparison with uniaxial tensile strength *(Japanese)* 78−72947
marble, powder, ultra fine, surface roughness effect on formation by rotating friction mill *(Japanese)* 78−95709
monticellite, solubilities of sesquioxides 79−69253
nifontovite, cryst. struct., H bonds 79−19232
omphacite, Mossbauer spectra study 79−65771
omphacite, P2/n to C2/c transform. study 79−65183
oxalate, biological mineralisation mechanism 78−31764
oxalate hydrates, crystn. kinetics, comparison for mono-, di-, and trihydrates 80−81528
particle size measurement by monoparticulate film method *(Japanese)* 78−95874
perovskite compound combination, Mossbauer spectroscopy study *(Russian)* 80−80666
phosphates, biological mineralisation mechanism 78−31764
phosphates, seeded growth, effect of solid/soln. ratio, calcification 78−15303
phthalate monohydrate, single cryst., X-ray cryst. struct. refinement 79−14790
plagioclase feldspar, deformed, elastic twinning, TEM obs. 77−62551
plaster of Paris based rechargeable cell 79−96433
polyester resin, unsaturated, $CaCO_3$ system, $CaCO_3$ addition effect on degradation in boiling water *(Japanese)* 78−11281
polyester resin, unsaturated $CaCO_3$ system, $CaCO_3$ addition effect on water absorption in boiling water *(Japanese)* 78−11282
polymer concretes, hydrothermally stable, hydraulic cement-type fillers 80−85144
polymer impregnated gypsum cast, mech. props. 79−100107
propionate monohydrate, cryst. struct. 77−76385
pyroxenes, high Ca, of diopside-hedenbergite series, change in struct. geometry with Fe^{2+} content 79−14783
rustumite, crystal structure, X-ray anal. 80−79766
rustumite, crystal structure determ. by X-ray diffr. method 80−70182
Si-CaF_2 film, dielectric const. and selective solar absorption 78−2937
silicates, entropy estimates at 298K from molar vols. 77−1243
soda lime glass, Ag^+ ion exchanged, planar optical waveguide, manufacturing tolerances 78−71212
soda lime glass, microparticle impact, high speed photography obs. 78−44223
soda-lime glass, depth profiles of Na and Ca by SIMS and AES 78−51805
soda-lime-silicate glass, dynamics of fracture mirror boundary formation 77−86132
sodalites, aluminogermanate- and aluminate-, IR spectra rel. to T-O bond length and T-O-T ang. 79−91445
stalactites, chem. decomp., ESR obs. 80−15788
stearate, Van der Waals forces, direct meas. 78−43461
stearate-stearic acid monomolecular films, multilayer deposition 80−54550
steel, sintered, Cr-Mo, CaF addition effects on struct. heterogeneity 78−60611
strontium calcium tartrate mixed crystal, growth in silica gel 77−48325
strontium calcium tartrate tetrahydrate, crystals grown by ion diffusion through silica gels, exam. of preps. 79−52102
strontium calcium tartrate tetrahydrate, gel grown mixed single crystals, defect characterisation 80−2027
tartrate tetrahydrate:Cu^{2+}, optical absorption spectra 80−45120
tartrate tetrahydrate:VO^{2+}, optical absorption spectrum 78−6713
tartrate tetrahydrate, X-irrad., EPR of free radicals 77−63936
tienshanite, cryst. struct. determ. 78−83800
torbermorite study by X-ray line profile anal. *(Japanese)* 80−33984
tremolite, optical spectra obs. 77−40284
tricalcium silicate paste, composition of solution in contact 77−81423
tris sarcosine calcium chloride:VO^{2+}, EPR and absorpt. spectra 78−60330
tris-sarcosine calcium bromide and chloride solid solns., Mn^{2+} doped, EPR linewidths and ferroelec. behaviour 79−24213
tris-sarcosine calcium chloride:Mn^{2+} ferroelec. dynamics, EPR and ENDOR study 80−75972
tris-sarcosine calcium chloride, ferroelec., ferroelasticity and hypothetical hexagonal to orthorhombic phase transition 77−63377
tris-sarcosine calcium chloride, ferroelec., US attenuation and vel., elastic consts., and permitt. near Curie temp. 79−37761
tris-sarcosine calcium chloride, phase transition, hydrostatic press. effect, dielec. const. meas. 80−71327
trisarcosine calcium chloride crystals, ferroelec., electrooptic and ferroelastic props. 80−34865

calcium compounds continued
trissarcosine calcium chloride, ferroelec. transition, press. effect 80−84681
vaterite, polymorphic transition kinetics, differential thermal anal. meas. 79−14722
$(YSmEuCa)_3(FeGe)_5O_{12}$, garnet film, ion implanted, bubble domain props. 78−88152
zeolites, type Y, containg catalysts, cryst. struct., IR spectra 79−42958
$16Na_2O.12CaO.72SiO_2$, self-diffusion of Ca^{2+} ions *(Japanese)* 78−6173
β-$2CaO$-SiO_2, hydration mechanism and rate, SEM and chem. anal. 79−79218
$3CaO.Al_2O_3$, hydration retardation by $CaSO_4$ 79−61856
$3CaO.SiO_2$, hydration in presence of lignosulphonates, glucose, Na gluconate 79−100330
$3CaO.SiO_2$ pastes, structural props., curing temp. effect 79−100332
$40CaO.20Al_2O_3.40SiO_2$ slag glass, self-diffusion of Ca^{2+} ions *(Japanese)* 78−6173
(Ag, Tl, Ca)NO_3, aqueous solutions, vapour press. meas. 80−6504
Al_2O_3:$CaTiO_3$, sintering temperature effect of titanate additions 80−60808
Al_2O_3-Ca (0.6 to 1.6 at.%), fracture behaviour, Ca segregation effect 80−40504
Al_2O_3-Ca_3SiO_5, solid solution, exam. of lattice defects 79−95167
Al_2O_3-CaF_2, phase relns. 78−23700
Al_2O_3-$CaTiO_3$, sintering *(Polish)* 79−100096
β- Al_2O_3-Na_2-CaO, microstruct. and ionic resistivity 80−44357
Al_2O_3-P_2O_5-Mg(Ca)(Sr)O glasses, Na^+, Sr^{2+} diffusion coeffs. rel. to temp. 78−30787
Al_2O_3-SiO_2-CaO-B_2O_3(1,1,1 wt.%) chemical analysis by photocolorimetry and titration 79−20483
Al_2O_3-SiO_2-Fe_2O_3-CaO-MgO-TiO_2, refractory, corrosion and mech. behaviour correlations 80−40563
Al_2O_3-SiO_2-MgO-CaO, blast furnace slag, viscosity, MP *(Russian)* 77−25039
$Al_2O_3.3H_2O$-H_3PO_4-CaO, phase equilib., $AlPO_4$ solid soln. 79−11586
B_2O_3-CaO-Fe_2O_3 glasses, semicond., cond. models, electronic props., 77-800K 80−54688
(Ba, Ca)(Ti, Zr)O_3, segregation of $CaTiO_3$ and effect on dielec. props. 78−38849
$BaCO_3$-$SrCO_3$-$CaCO_3$, phase inhomogeneity effects on oxide cathode props. 78−52614
$BaCaLu_2F_{10}$, site occupancy from excitation and emission spectra *(French)* 77−81145
Ba_2CaReO_6, new seignettomagnets and ferroelectrics 78−19425
$Ba_{0.92}Ca_{0.08}TiO_3$ ceramic, uniaxial stress effects, US dilatometric and dielec. meas. 78−52454
Ba_2CaUO_6, luminescence and energy migration 79−4837
$BaFe_{12}O_{19}$-CaO, Ca^{2+} additives effect on hexaferrite lattice and mag. props. 80−60243
$BaGeO_3$-CaF_2MgF_2-$Ca_2Al_2GeO_7(CaTiGeO_5)$ systems, glass forming and props. 80−19717
BaO-Al_2O_3-GeO_2-MF_2 ($M=0.45\ CaF_2+0.55MgF_2$), MgF_2 and CaF_2 effect on physicochem. props. 80−34876
BaO-PbO-GeO_2-MF_2 ($M=0.45CaF_2+0.55MgF_2$), MgF_2 and CaF_2 effect on physicochem. props. 80−34876
$Ba(PO_3)_2$-AlF_3-CaF_2, glass, elec. cond. and IR spectra 80−89005
$Ba(PO_3)_2$-CaF_2, IR absorption spectra exam. of hydrolytic stability 80−39291
$BaSr_xCa_{1-x}Fe_4O_8$, substituted hexagonal ferrites, mag. split Mossbauer spectra obs. and X-ray struct. data 80−71250
(BaSrCa)O, cathodes, thermionic emission characts., X-ray struct. obs. 78−48270
BeF_2-KF-CaF_2-AlF_3:Nd^{3+} (Er^{3+}) glass, multiphonon relax., fluoresc. obs. 78−15219
BeF_2-KF-CaF_2-AlF_3-EuF_3 fluoroberyllate glass, Eu^{3+} fluoresc. linewidth 80−66285
BeO_2-Al_2O_3-SiO_2-CaF_2 system glass, role of fluoride cations during crystn. 79−65176
$Bi_{3\ 2x}Ca_{2x}Fe_{3-x}V_xO_{12}$, crystallization in $Bi_{0.7}Ca_{2.3}Fe_{3.85}V_{1.15}O_{12}$-$Bi_2O_3$-PbO 77−48330
$BiCaVFe_5O_{12}$, magneto-optical near UV reflection-spectra, meridional and polar intensity effects *(Russian)* 78−39572
C-S-H gel, formed in hydration of C_3S pastes, chem. comp. 79−79346
CS_2, spectral splitting of stimulated Raman scatt. 78−50860
C_2S mineral, chem. and polymorphism 79−69051
(Ca,Fe)SiO_3, intracryst. Fe^{2+}-Ca^{2+} exchange, Mossbauer spectra 80−20548
$(Ca,Sr)_5(PO_4)_3Cl$, partially substituted chlorapatite, cryst. struct. from X-ray data 80−96478
Ca $0.4B_2O_3.2H_2O$, X-ray cryst. struct. determ. and refinement 79−94976
Ca $(PO_3)_2$ glass, crystallisation below glass transition temp. *(Japanese)* 77−62480
Ca complex, Ca-DTPA, comparison with Zn-DTPA for ^{241}Am removal from beagles 77−73599
Ca complex, Ca-DTPA, effect of inhaled aerosol on long-term $Pu(NO_3)_4$ effects 77−66861
Ca complex, Ca-DTPA treatment schedules for ^{239}Pu decorporation from simulated wounds 77−64137
Ca complex, Ca-DTPA vs. Zn-DTPA as chelate in removal of ^{242}Cm from rat 77−64141
Ca dichlorophosphate complexes, cryst. struct. ^{35}Cl NQR obs. 80−108108
Ca ferrite, composition and mag. props., anisotropy field, magnetisation 80−71109
Ca metaborates, endogeneous, H bonds in cryst. structs. 80−33975
Ca metasilicate glass, crystallisation kinetics 77−11486
Ca Mg $(CO_3)_2$ (dolomite), modulated struct. 79−100832
Ca-Mg-Ni hydrides, water form. on O_2 exposure 80−97727
Ca-Mg-Ni-B, hydriding behaviour 80−71942
Ca-Mg-Zr combustion sensor, pipe-form ceramics appl. *(Japanese)* 80−55761
Ca-Mn-O system, isobaric phase diagram and subsolidus phase relations 79−24508
Ca-Mn-S-Se system, multicomponent solubilities 80−108416
Ca-S-O system, sulphide-sulphate equil., solid state EMF obs. 79−83492
Ca-Sb, phase diag. 77−52284
$Ca_2\ Mn(PO_4)_2$, hydrothermal synthesis and cryst. growth 80−60762
$Ca_2(Al,Fe,Cr)O_5$ solid soln., planar interfaces, TEM obs. 80−65008
$Ca_4Al_2Fe_2O_{10}$, Portland cement clinker, formation kinetics 79−43191

calcium compounds continued
$Ca_2Al_2GeO_7$, gehlenite struct., synthesis and physicochem. props. 79—43181
$Ca_3Al_2Ge_3O_{12}$:Fe^{3+}, spin Hamiltonian parameters, g-factors, temp. depend. EPR obs. 77—48038
$CaAl_2O$:Eu^{2+}, activated phosphors, luminesc. efficiency, temp. and high-press. 78—23508
$CaAl_2O_4$ cement bond phases, corrosion in steam-CO at 199°C 79—29234
$CaAl_2O_4$, fine powder, prep. by evaporative decomposition of solns. 78—39725
$CaAl_2O_4$, high pressure modifications 80—104149
$CaAl_2O_4$ hydration, US wave propag. study 79—39114
$CaAl_2O_4$, phase transform. accompanying hydration, US and X-ray obs. 79—39115
$CaAl_2O_4$-$SrAl_2O_4$-BaA_2O_4, binary and ternary systems, solid solubility *(Japanese)* 80—35174
$CaAl_2O_5$, form by interdiffusion of CaO and Al_2O_3 79—28998
$CaAl_2O_5$, form. by solid state reaction of CaO and Al_2O_3, electric field effects 79—28997
$CaAl_4O_7$:Gd^{3+}, ESR, symm. effects 77—36130
$Ca_{12}Al_{14}O_{33}$, piezoelectric material, cryst. growth and characterisation 79—99825
$Ca_{12}Al_{14}O_{33}$, polar materials, appl. to SAW and other devices 80—66114
$Ca_3Al_2O_6$, cubic, X-ray powder diffr. data 79—94975
$Ca_3Al_2O_6$, retardation of hydration by sulphates 77—56249
$CaAl_2Si_2O_3$, cryst. struct. 78—63700
$CaAl_2Si_2O_8$-$CaSiO_3$-$CaMgSi_2O_6$, exam. of glass forming regions and properties of glasses 79—4958
$CaAl_2Si_2O_8$-$NaAlSi_3O_8$ (anorthite-albite) system, crystal growth rates and processes 80—4010
$Ca_2Al_2SiO_7$, gehlenite, new high-press. phase, rel. to Earth interior 79—29753
$Ca_2Al_2SiO_7$, single cryst. growth by floating zone method, opt. microscopy charact. 79—47623
$Ca_3Al_2Si_3O_{12}$, garnet, thermophysical props., 5 to 600K 79—60517
$Ca_3Al_2Si_3O_{12}$, grossular, cryst. struct. and compressibility to 60 kbar 78—63718
$Ca_3Al_2Si_3O_{12}$-$Mg_3Al_2Si_3O_{12}$, synthetic garnet, soln. grown, surface features 78—2346
$CaAl_2Si_3O_{10}.3H_2O$, scolecite, from Poona, India, X-ray cryst. struct. determ. 79—90605
CaB_6, ^{11}B nucl. quadrupole interaction, NMR meas. 80—2660
CaB_6, electrodeposition from molten salt baths, cathodic behaviour 79—11529
CaB_6, electronic struct. APW and muffin-tin calcs. 80—29320
CaB_6 electronic structures calc. and obs., by APW method and X-ray photoelectron spectroscopy *(Japanese)* 79—15074
CaB_6-SmB_6, mag. props., comp. depend. 80—50034
CaB_6-SmB_6 system complex borides, prep. and props. 78—52703
CaB_2C_2, cryst. struct. *(French)* 79—32969
$CaB_{12}H_{12}.10H_2O$, struct. dehydration, intermediate phases and thermooxidative degradation 80—33951
$CaB_{12}H_{12}.8H_2O$, cryst. growth from soln. and morphology 77—44145
$CaB_{12}H_{12}.8H_2O$, cryst. struct. 77—51351
CaB_4O_7, cryst. struct. determ. 78—10029
$Ca_2B_6O_{11}$, cryst. struct. determ. 77—11526
$Ca_2(B_5O_9)Cl.H_2O$, triclinic chilgardite, cryst. struct. determ. 78—63737
$Ca_2(B_4O_4(OH)_8)$, uralborite, accurate cryst. struct. 78—34492
$CaB_3O_4(OH)_3.H_2O$, order-disorder ferroelec., crit. dynamics, NMR data compared with dielec. data 78—76415
$CaB_3O_4(OH)_3.2H_2O$, NMR of ^{11}B in crit. region 77—16199
$CaB_2O_4.6H_2O$, crystal struct. determ. 77—15391
$CaBPO_5$:Eu^{2+}, activated phosphors, luminesc. efficiency, temp. and high-press. 78—23508
$CaBSi_2O_6$, B=Mg, Fe^{3+}, Al, pyroxenes, order-disorder interpretation 80—38987
$CaBaFe_4O_8$, Mossbauer study 79—38414
$CaBaFe_4O_8$, overlap contribution to $^{57}Fe^{3+}$ isomer shifts, nuclear size change 80—39903
$Ca_2BaFe_2TiO_8$, crystal struct., O vacancy ordering *(French)* 77—11520
$CaBa(PO_3)_4$, struct. from IR spectra 77—47421
$Ca_{0.2}Ba_{0.8}TiO_3$:Nb, conductive single cryst. growth by Verneuil method 77—85928
$CaBe_{13}$, thermal cond. coeff. determ. 79—1531
$Ca_{2x}Bi_{3-2x}Fe_{5-x-y}V_xIn_yO_{12}$, ferromagnetic relax. meas., 4.2-300K 80—44923
$Ca_{2x}Bi_{3-2x}V_xFe_{5-x}O_{12}$ ferrogarnet, magnetis. distrib., correl. with morphological habit 79—42802
CaBr, gas equilib. mass spectra, dissoc. energy meas. 77—65543
CaBr, thermally excited mol. emission spectrum 77—3377
$CaBr_2$, adsorption of NH_3, IR and far IR spectra 77—24478
$CaBr_2$, adsorption of NH_3 and ND_3, complex formation, IR and for IR spectra obs. 80—80063
$CaBr_2$-H_2O, ^{79}Br NQR, cryst. struct. 78—27110
$CaBr_2.4CH_3OH$, cryst. struct. determ. *(French)* 78—59788
$CaBr_2.4C_2H_5OH$, cryst. struct. determ. *(French)* 78—59788
$CaBr_2.6CH_3OH$ solvates, cryst. struct. *(French)* 78—34500
$CaBr_2.6H_2O$, cryst. struct. determ. 77—80474
CaC_2, solid-state ^{13}C NMR spectra 79—24220
CaC_2, solubility in CaF_2 and $CaCl_2$-CaF_2-CaO system *(French)* 79—70050
$CaCO_3$ (aragonite), transform. to calcite in marine gasteropod 79—62485
$CaCO_3$, acceleration of growth of particles, Lorentz forces, electric and mag. field effects 78—51455
$CaCO_3$ accumulation, Ontong-Java Plateau box cores, radiometric investig. 80—61793
$CaCO_3$ aerosols, coagulation rate meas. 79—96374
$CaCO_3$, aragonite, conical intensity distrib. 79—1747
$CaCO_3$, aragonite, split ν_4 mode of CO_3^{2-} ions 80—45077
$CaCO_3$, aragonite-calcite transformation, effect of impurities, DTA and IR studies 78—51662
$CaCO_3$, ball mill grinding, rate constant determination *(Japanese)* 78—95828
$CaCO_3$, birefr. and electronic polarisabilities of constituent ions 80—7322
$CaCO_3$, calcite, A_{1g} Raman mode obs., new technique appl. 79—61354
$CaCO_3$, calcite, coherent excitation of vibr., dephasing time meas. 78—35120
$CaCO_3$, calcite, complex dielec. const. at audio freqs., 5.5 to 380K 80—25272

calcium compounds continued
$CaCO_3$, calcite, cryst. preferred orientation in marble, mag. susceptibility anisotropy development 78—56286
$CaCO_3$, calcite, elec. cond., 300 to 1200°C at CO_2 pressure of 40 bars 80—20195
$CaCO_3$, calcite, form of end of free elastic twin *(Russian)* 80—6416
$CaCO_3$, calcite, form. temp. of fluid inclusions 77—56618
$CaCO_3$, calcite, gel grown crysts., spirals on rhombohedral faces 80—7486
$CaCO_3$, calcite, laser Raman line polarisation meas. 77—4641
$CaCO_3$, calcite, Nd laser second harmonic stimulated Raman scatt., comparison with nitrates 80—95949
$CaCO_3$ calcite, neutron irrad. effects 77—39617
$CaCO_3$, calcite, picosecond pulse stacking 79—61330
$CaCO_3$, calcite, polaris. relax. meas. using synchronously mode-locked dye lasers 79—44952
$CaCO_3$, calcite, quadrupole nonlinear coeff. dispersion meas. 78—37943
$CaCO_3$, calcite, random struct. of stimulated Raman scatt. lines 78—18019
$CaCO_3$, calcite, single-crystal, wave front reconstruction of light in stimulated Raman scatt. 80—93323
$CaCO_3$, calcite, spectral splitting of stimulated Raman scatt. 78—50860
$CaCO_3$, calcite, sputtering behaviour, optical and electron microscopy 78—43968
$CaCO_3$, calcite, tunnelling afterglows and retrapping 77—69902
$CaCO_3$, calcite, X-ray irrad., luminesc. and dielec. loss decays 77—12431
$CaCO_3$, calcite (aragonite), lattice energies, four-centre CO_3^{2-} charge distrib. 78—47272
$CaCO_3$, calcite crystal, higher-order CARS spectra 79—14035
$CaCO_3$ calcite linear polarizer, role in laser technology 80—64165
$CaCO_3$, calcite Raman laser, methods for increasing efficiency, optical damage avoidance 77—79853
$CaCO_3$ crystallisation from aqueous solutions, kinetic study 80—59419
$CaCO_3$, crystallization inhibition by phosphate and glycerophosphate ions 78—23593
$CaCO_3$ decarbonation for solar energy thermochemical conversion 80—94097
$CaCO_3$ decomp., rel. to CO_2 transport in CaO 79—23780
$CaCO_3$, decomposition, formation of Ca_3SiO_5 79—52651
$CaCO_3$, decomposition in deep oceans 79—25270
$CaCO_3$, dissolution rates in deep ocean, in situ expt. in N.Atlantic 79—34853
$CaCO_3$, growth dislocations obs. using Lang X-ray topography 78—2133
$CaCO_3$, γ-irrad. defects, absorpt. spectra obs. 77—63447
$CaCO_3$, hyper Raman scatt. of light by optical phonons 79—69844
$CaCO_3$, IR reflectivity, oblique phonons 78—60440
$CaCO_3$, Iceland spar, crack interactions with twin interlayers 77—7790
$CaCO_3$, Iceland spar, polarizing prism, struct. defects effect 78—18065
$CaCO_3$, Iceland spar natural crystals, optical characts. 77—10988
$CaCO_3$, influence of precipitation by organic phosphate molecules 79—43119
$CaCO_3$, luminesc. under N_2 laser excitation, and appl. to archaeological dating 80—60685
$CaCO_3$, marine sediment content, western continental shelf, India 80—8289
$CaCO_3$, nucleation mechanism accompanying Ostwald ripening 80—50641
$CaCO_3$, plastic deformation in compression parallel to (111) 78—38709
$CaCO_3$, point-dipole theory and optical birefringence 79—73896
$CaCO_3$ polydisperse particles, in $Ca(HCO_3)_2$ soln., growth, soln. in mag. field 78—53260
$CaCO_3$, precipitation from Mg^{2+} containing soln. *(French)* 77—85915
$CaCO_3$, precipitation induction errors, a method for determ. 79—5175
$CaCO_3$ production of mare incognitum, upper windward reef slope, Enewetak Atoll 78—7662
$CaCO_3$ single crystals, effect of defect struct. charact. on X-ray diffr. 79—65089
$CaCO_3$ single crysts., positron annihilation, two photon angular correlation 80—108295
$CaCO_3$, thermal decomp. in vacuo, ultrastruct. and crystallography 78—71864
$CaCO_3$, thermoluminesc. spatial distrib. using image intensifier technique 80—47115
$CaCO_3$, third order nonlinear optical difference frequency generation 78—22176
$CaCO_3$, with and without inversion centres, nonlinear susceptibilities *(Russian)* 78—13750
$CaCO_3$, with perfect struct., temp. depend. of rate of twinning 80—10561
$CaCO_3$, X-ray Ca K-edge meas. 79—6950
$CaCO_3$:Fe^{2+}, electronic spin relax., effect of second-order spin-orbit coupling 80—10935
$CaCO_3$:Fe^{2+}, Mossbauer spectra 80—108138
$CaCO_3$:Li, CO_3^{3-}-Li^+ centre, irradiated synthetic single crystal, bond angle and wave function 77—81006
$CaCO_3$:Li, synthetic calcite, $(CO_3Li)^{2-}$-Li^+ defect after X-irrad., EPR study 80—75852
$CaCO_3$:Mn, calcite, EPR and ENDOR absorpt. spectra of divalent Mn in single cryst. 79—47328
$CaCO_3$:Mn^{2+}, calcite, on axis half-field forbidden lines, numerical prediction 77—16161
$CaCO_3$-carboxymethylcellulose suspension, filtration eqn. 78—55690
$CaCO_3$-$NaAlSiO_4$, micromechanism for phase formation during sintering *(Russian)* 80—16253
$CaCO_3$-Pd, catalyst for H gettering of dimerised phenyl propargyl ether 77—18001
$CaCO_3+SiO_2$, in presence of NaF, thermal decomposition of Ca_2SiO_4 formation 78—68889
$Ca(CO_3H)_2$, effect on evaporation of aq. droplets in turbulent flow 79—90771
$CaCO_3.H_2O$, formation of aragonite 78—27427
$CaC_2O_4.2xH_2O$ (0<x<5 zeolite water fraction), weddellite, growth morphology, PBC analysis 80—24388
$Ca(Ca_xNb_{1-x})O_3$, perovskite, cryst. struct. determ. *(French)* 78—10021
$Ca_3(CaTa_2)O_9$, monoclinic symm., layer like cation ordering 77—1105
$(Ca_xCd_{1-x})CO_3$, cryst. struct. and cation isomorphous miscibility 80—33972
$CaCeAl_3O_7$, melilite struct., prep. and props. 80—93524
CaCl, aq., mean activity and osmotic coeffs., free energy, 298.15K, review 77—81411

calcium compounds continued
CaCl, $B^2\Sigma^+$-$X^2\Sigma^+$ system, laser excitation spectroscopy, rot. anal. 77-65500
CaCl, $B^2\Sigma-X^2\Sigma$ transitions, rot. anal. by laser spectroscopy 80-91536
CaCl, $D^2\Sigma$ and $X^2\Sigma$, two-photon vis. absorption, vibr. and rot. consts. 78-78764
CaCl, $E^2\Sigma$-$B^2\Sigma$ system, rot. anal., optical-optical double reson. obs., using two dye lasers 78-70855
CaCl, $E^2\Sigma$-$X^2\Sigma$ transition, rot. anal. 78-37652
CaCl, form., spectral bands, dissoc. energy calcs. 77-16816
CaCl, free radical, $A^2\Pi$-$X^2\Sigma^+$ system obs. by saturation spectroscopy 78-46353
CaCl, laser excitation and ODR spectra 78-82757
CaCl, laser excitation and fluorescence spectra, rotational anal. of $A^2\Pi=X^2\Sigma$ transition 80-43098
CaCl, spectral bands obs. in cool stars 77-53593
CaCl, $X^2\Sigma$ pot. energy curves, polarisability and dissoc. 80-91629
$Ca^{35}Cl$, radical, rot. spectrum, $X^2\Sigma^+$ state, laser MODR 78-5257
$CaCl_2$, adsorption of NH_3, IR and far IR spectra 77-24478
$CaCl_2$, adsorption of NH_3 and ND_3, complex formation, IR and for IR spectra obs. 80-80063
$CaCl_2$ aq. soln., vel. correls., time integral calcs. 80-59360
$CaCl_2$ aq. solns., viscosity meas. 79-77792
$CaCl_2$, aqueous soln., ion hydration 80-35518
$CaCl_2$ brine, subsurface, model for Sr behaviour, Dead Sea rift valley 80-17295
$CaCl_2$, $CaCl_2$-CaF_2-CaO eutectic melts, specific cond. meas. 77-59131
$CaCl_2$, cluster ions and mol. ions in salt field desorption 80-40238
$CaCl_2$ conc. solns., vel. correls. calcs., diffusion, cond. and transference props. 78-85166
$CaCl_2$, correlation between experimental and theoretical diffusion coeffs. 77-24421
$CaCl_2$, enthalpy calc. for solid and liq. phases 77-43349
$CaCl_2$, fused, exam. of hydrolysis at high temp. 79-11791
$CaCl_2$ in dipalmitoyl phosphatidylcholine, monodomain sample phase behaviour, birefr. obs. 79-83712
$CaCl_2$, isopiestic studies of aqueous solns., 382 to 474K 79-24815
$CaCl_2$, photoelectron spectra, geometry 78-29816
$CaCl_2$, solns. in methanol, conductance data anal., assoc. consts. 78-71875
$CaCl_2:Eu^{2+}$, fluorescence lifetime and quantum efficiency for 5d→4f transitions 80-100681
$CaCl_2:NO_2^-$, aqueous solns., luminesc., absorpt. and Raman spectra *(Russian)* 77-36291
$CaCl_2$-$BaCl_2$-H_2O ternary system, 45°C isotherm *(French)* 79-96004
$CaCl_2$-Ca phase diagram, DTA study *(French)* 80-25672
$CaCl_2$-CaF_2-CaO, phase diagram and CaC_2 solubility *(French)* 79-70050
$CaCl_2$-KCl, binary melt, viscosity *(Japanese)* 78-10209
$CaCl_2$-methanol thermochem. cycle for solar thermal energy storage 80-30587
$CaCl_2$-NH_3, isothermal dissociation and regeneration, appl. to solar refrigeration *(French)* 80-61300
$CaCl_2$-NH_3 dry absorption for solar refrigeration 80-61310
$CaCl_2$-NaCl-H_2O, conc. solns., vap. press. meas. 79-23713
$CaCl_2$-tryptophan, γ- and UV-irrad. solvent matrices at 77K, H^- fluoresc. 78-70779
$CaCl_2+8NH_3$ coolant for solar refrigeration *(French)* 79-24911
$CaCl_2(Br_2)$, aq. solns., IR spectral reflectance meas., Kramers-Kronig anal. 77-4633
$CaCl_2(Br_2)(I_2)$, glassy aqueous soln., LF region Raman spectra 80-84729
$CaClNO_3.2H_2O$, cryst. struct. *(French)* 78-42975
$Ca(ClO_3)_2$, mol. torsional oscills., cooperative study by NQR 80-25244
$CaCl_2\times5.99,5.33H_2O$, molar cond., compressibility, expansivity 78-51712
$CaCl_2.2CH_3OH$, solar heat pump and thermal storage system for space heating 80-85307
$CaCl_2.2H_2O$, cryst. struct., X-ray diffr. meas. *(French)* 77-47417
$CaCl_2.4H_2O$, β form, cryst. struct. *(French)* 78-42974
α-$CaCl_2.4H_2O$, redeterm. of cryst. struct., H bonding and Ca coordination *(French)* 79-37676
$CaCl_2.4NH_3$-$CaCl_2.2NH_3$, solar energy storage system heating and cooling 80-81484
$CaCl_2.6H_2O$, cryst. struct. determ. 77-80474
$CaCl_2.6H_2O$ heat of fusion system for solar energy storage 80-16846
$CaCl_2.6H_2O$, heat transfer props. for heat of fusion energy storage 80-76654
$CaCl_2.6H_2O$, liq., structural order 80-33871
$CaCl_2.8NH_3$-$CaCl_2.4NH_3$, solar energy storage system heating and cooling 80-81484
$CaCo_2$, aragonite, EPR of Mn^{2+} impurities, orthorhombic spin-Hamiltonian parameters 80-2631
$CaCo_3$, ball mill grinding, wet, dry, rate constant determination *(Japanese)* 78-95827
$CaCo_2(PO_4)_2$, dielectric permittivity and elec. resist., temp. depend. 77 59502
$CaCo_2(PO_4)_2$, growth by Bridgman method, crystn. speed depend. 77-59684
$CaCo_2(PO_4)_2$, reflection spectrum and mag. susceptibility meas. 77-59586
$CaCrF_5$, one-dimens. magnetism *(French)* 79-73670
$Ca_3Cr_2Ge_3O_{12}$, and $Ca_3Cr_2Si_3O_{12}$, absorpt. and luminesc. spectra, cryst. field and exchange interactions 77-73154
$CaCrO_4$-K_2CrO_4, phase diagram determ., struct. of double salt 77-15543
$CaCr_2O_4$, β to α transform. temp., effect of partial O_2 press. 80-84292
$CaCrO_4.H_2O$, cryst. struct. *(French)* 78-18593
$CaCu_3Ge_4O_{12}$, single crystals, high pressure synthesis, bond length determ. 78-14318
$Ca(Cu_{0.78}Mn_{0.22})_3Mn_4O_{12}$, mag. structure, neutron diffr. powder data, 350K ferromag. T_c 77-69502
$CaCu_3Mn_4O_{12}$, synthesis, struct. and mag. props. of perovskite-like oxides 77-68960
$CaCu_3Ti_4O_{12}$, mag. struct. and props. *(French)* 77-69495
$CaCu_3Ti_4O_{12}$, mag. struct., neutron diffr. powder data, 27K T_N 77-69502
$Ca_2Cu(UO_2)(CO_3)_4.6H_2O$, voglite, cryst. and powder diffr. data 80-24421
CaD, absorption spectra, extension of F-X system 79-18205
CaD_2, neutron diffr., NMR 77-15378

calcium compounds continued
$CaEuAl_3O_7$, mechanism of solid-phase reactions of formation and physicochem. props. 77-52622
$CaEuGa_3O_7$, synthesis, mechanism and kinetics, cryst. props. 77-52268
$Ca_{1-x}Eu_xSi_2$, solid solns., α-$ThSi_2$ struct. type, comp. and press depend. 78-91322
$Ca_5(F, Cl)(PO_4)_3$, apatite, Indian, fission track dating and annealing, U content determ. 79-57891
CaF, $^2\Sigma$ ground state, laser-RF double reson. spectrosc. 80-69171
CaF, $^2\Sigma_{1/2}^+$ ground state, spin-rot. and hyperfine splittings rot. depend., mol. beam laser-RF double reson. 80-43079
CaF, $A^2\Pi_r$-$X^2\Sigma$ band system, MODR 78-74685
CaF, $A^2\Pi$-$X^2\Sigma^+$ transition, HFS and fine struct., intermodulated fluoresc. spectra obs. 80-63695
CaF, $B^2\Sigma^+$-$X^2\Sigma^+$ system, rot. and vibr. anal. 80-74156
CaF, etched in H_2SO_4, dissolution kinetics of $CaSO_4$ on {111} faces 80-2028
CaF molecule, vis. spectrum, $B^2\Sigma$-$X^2\Sigma$ system 80-18863
CaF windows, process for vacuum tight joints prod. 77-26312
CaF:Eu(Gd)(Dy)(Tb), dimer reorientation activation volume 80-107285
CaF_2, ^{19}F NMR chemical shift, press. depend. 0-4 kbar 77-20733
CaF_2, 0.36 μ absorptance/fluence dependence obs. 79-15506
CaF_2 (100), elec.-mech. coupling of dislocations 78-75676
CaF_2 (fluorite), Gruneisen parameter at high press. 80-8299
CaF_2, (n,γ) induced lattice defects, struct., polarised ^{20}F NMR 77-20724
CaF_2, (n,γ) induced lattice defect annealing, polarised ^{20}F NMR 77-20725
CaF_2, (n,γ) induced point defects, struct. and annealing 78-59842
CaF_2 ⟨111⟩ oriented windows, optical distortion coeffs. at chem. laser wavelengths 79-94269
CaF_2, achievement of negative temp. *(French)* 78-74009
CaF_2 additive for celsian ceramics, props. obs. *(Bulgarian)* 80-50579
CaF_2, additively coloured, Ca colloid form. and size evolution during annealing 77-20895
CaF_2, additively coloured, new type of F_3-centre, absorption bands obs. 78-35172
CaF_2, additively coloured, photothermal bleaching of Ca colloids 79-15500
CaF_2, adsorbed water film internal reflection spectroscopy 79-15549
CaF_2, adsorption mechanism in selective etching 77-7727
CaF_2, anion motion at high temps., quasielastic nuetron scatt. obs. 80-59715
CaF_2, anion-void superlattices *(Danish)* 79-14796
CaF_2 antireflection coated, 3.8 μm CW laser damage threshold obs. 80-33053
CaF_2, appl. of theory of sputter-induced isotopic fractionation at solid surfaces 80-55244
CaF_2, association parameters of [Me^{3+}-Fi^-] dipoles (Me=Metal), ionic cond. meas. 78-30788
CaF_2, band struct. determ. by adjoint plane wave method 77-76750
CaF_2, barrier instability in strong elec. fields 79-69522
CaF_2, bleaching characteristics of crystals coloured by low energy electrons 78-76497
CaF_2, Brillouin scatt. and high temp. disorder 78-80365
CaF_2 bulk loss coefficient obs. 79-15488
CaF_2, cathodoluminescence, SEM 80-100700
CaF_2, cation jump freq., isotope effect, lattice dynamical calc. 80-88357
CaF_2 chip, discrimination of twin orientation in Au island epitaxial films on (111) surface 79-46983
CaF_2, colour centre thermal stability 78-83811
CaF_2, cond. meas. under controlled F_2 chem. pot. *(Japanese)* 78-59972
CaF_2, crack propag., cryst. props. effects 78-75720
CaF_2, cryst., (111) faces, selective etch rate and etch pit morphology, acid conc. and temp. effect 80-96524
CaF_2, cryst., dielec. props. in ULF range 80-7288
CaF_2, cryst. elec. field gradient determ., γ-ray anisotropy meas. after polarised neutron capture 77-12291
CaF_2 crystal active element for colour-centre laser, thermal strain anal. 80-91804
CaF_2 crystal structure, stability compared with TiO_2 *(Russian)* 80-64945
CaF_2 crystal under controlled F_2 chemical potential, cond. meas. 80-15301
CaF_2 crystal windows, transmission in vac. UV region, heat treatment effect 77-31137
CaF_2 crystals, elec. cond., O^2 effect 80-2431
CaF_2 crystals, mirror chips, in contact with liq. phase, ellipsometric investigation 80-11516
CaF_2, crysts., adsorption processes in selective etching 80-39098
CaF_2, damage by UV laser radiation, avalanche ionization mechanism 80-76110
CaF_2, dielec. const., 5.5 to 400K 80-50249
CaF_2, dielectric const. and polarisability strain derivatives 77-73125
CaF_2, dispersion calcs. of cubic nonlinear susceptibility near Raman resonance 79-94292
CaF_2, doped, colour centre form. by UV irrad., afterglow, thermolum. and EPR obs. 78-10047
CaF_2, doped and gamma irrad., high temp.-peak in thermoluminescence 80-50434
CaF_2, doped with trivalent rare earths, migration entropy for bound fluorine motion 80-71303
CaF_2, doubly doped, dielec. relax. 80-50263
CaF_2, EXAFS, intrinsic UV luminesc. excitation spectra 78-52567
CaF_2, elec. cond. at high temp. 78-72159
CaF_2, elec. cond. of shock-compressed monocrystals 77-9404
CaF_2 electrolyte for thermodynamic study of alkaline earth oxide compounds 78-53241
CaF_2, electron irrad. defect aggregates, ordering, U and Th impurity effects 80-75216
CaF_2, electronic band struct. determ., combined OPW and tight binding calc. 77-85145
CaF_2, electronic energy bands calc. 78-34762
CaF_2, electronic polarizability and dielectric const., strain derivatives 78-19406
CaF_2, etching behaviour in HCl vapour 78-59812
CaF_2, etching in H_2SO_4, etch pit morphology and $CaSO_4$ growth 80-6408
CaF_2, Eu^{2+} isomer shift, Mossbauer studies 79-56649
CaF_2, F diffusion 79-14964

calcium compounds continued
CaF_2, F^- interstitial and neighbours, mean-square displacements 80—29011
CaF_2, F-centre growth by neutron irrad. 79—55788
CaF_2, F-centres, muffin-tin approx. inadequacy 78—63761
CaF_2, fast ion transport, computer simulation 80—107485
CaF_2, fast Li^+ ion stopping, chem. bonding effects 77—27929
CaF_2 film, contamination by 1 MeV proton bombardment, backscatt. obs. 77—11811
CaF_2 film, IR absorpt. coeffs. meas. by laser calorimetry 78—25905
CaF_2 film, ionic migration study by Rutherford scatt., defects, secondary emission *(French)* 78—55982
CaF_2 film, refr. index and struct., deposition temp. depend. 79—4857
CaF_2, fine-grained, forging and bulk optical props. 80—33103
CaF_2, fluorine K absorpt. spectra using APS technique 79—99986
CaF_2, fluorite, electron irrad., {100} faceted anion voids 79—51153
CaF_2, fluorite, phase relations, to 60 kbar and 1800°C 78—84785
CaF_2, fluorite, solubility equilibria in geothermal waters 77—60368
CaF_2, fluorite, transmission spectrum 1200-800 cm^{-1} band, spectrophotometer scale calibration 79—12837
CaF_2, fluorite, use as standard specimen 80—96704
CaF_2, fluorite, use of proton irrad. to reveal growth and deform. features 80—84216
CaF_2, fluorite crystals, surface struct., growth mechanism 79—99096
CaF_2, fluorite crysts., lattice O^{2-} effect on thermal, elec., and thermoelec. props. 77—76599
CaF_2, fluorite-struct. compound, high-temp. elasticity, US pulse meas. 77—81878
CaF_2, force consts., mean amplitudes of vibr. 78—17647
CaF_2, Frenkel defect, entropy of form., Green function calc. 80—19898
CaF_2, glass-coating apparatus for Na resistance 80—90874
CaF_2, He isotopes prod. cross sections induced by 12-45 MeV protons 77—17310
CaF_2, heteronuclear mag. spin system relaxation in many pulse NMR expts. 80—93203
CaF_2, high resolution double NMR at low gyromag. ratio 78—25577
CaF_2, high-frequency phonon lifetimes 80—70338
CaF_2, hot forged, laser window material, fabrication, props. 77—46773
CaF_2, hot forged, refr. index, temp. coeff. 77—46772
CaF_2, hot pressed, dielectric, optical props. 79—56720
CaF_2, IR materials for measuring radiant flux *(Russian)* 80—48366
CaF_2, IR transparent materials, forward and backward scatt. data 78—59099
CaF_2 IR window refractive index var. with temp., −180° to +200°C obs. 79—14052
CaF_2, illuminated over large area, optical strength 77—75593
CaF_2, impurity effects on strengthening 77—63682
CaF_2, impurity modes due to interstitials, Green function formalism 80—24554
CaF_2 influence on melting of high ZrO_2 glass, surface crystallisation 80—84278
CaF_2, ionic clusters, struct., thermodynamic functions, energy surfaces and SIMS 80—63881
CaF_2, ionic cond., activation vols., freq. depend. cond., press. effects 80—100354
CaF_2, kinetics of thermoluminesc. buildup 79—65936
CaF_2, large optical crystals, quality 80—33097
CaF_2, laser window material, refr. index, temp. and stress effects 77—46771
CaF_2, laser window material, absorpt. at CO wavelengths, calorimetric meas. 78—25911
CaF_2, laser window material, surface and bulk absorpt., photoacoustic meas. 78—25912
CaF_2 laser window surface O_2 detection by X-ray photoelectron spectroscopy 79—14056
CaF_2, laser windows, intermediate temp. forging 77—46775
CaF_2, lattice dynamics in ang. force model, Debye-Waller factors, sp. ht., dispersion relations 77—59081
CaF_2, linear thermal expansion coeffs. meas., room temp. to 250°C 78—55416
CaF_2, localised vibrs. due to substitutional impurities 78—22803
CaF_2, long wavelength behaviour, elastic consts. 79—87441
CaF_2, low symmetry U^{5+} centres 78—76307
CaF_2 low-loss laser window material, surface absorpt. meas. at 2.8 and 3.8 μm 79—94267
CaF_2, melt, influence of B_2O_3, La_2O_3 and Y_2O_3 on elec. cond., ionic mech. 78—43157
CaF_2, melting curve, press. up to 40 kbar, rel. to high press. melting systematics 77—51475
CaF_2, melts, elec. cond., surface tension, viscosity, density *(Russian)* 80—92758
CaF_2, mid IR laser window material, absorption props. 77—46770
CaF_2, mixed cluster, doubly-doped with rare earths, elec. dipole relax. 79—82924
CaF_2, mol. dynamics studies of superionic conductors 80—107547
CaF_2, molten, struct., electrolyte 'general primitive model' prediction test 80—28902
CaF_2, muon Coulomb capture ratio 78—62959
CaF_2, NMR direct observation in rotating frame *(Russian)* 78—39422
CaF_2, natural fluorite colouring, effect of impurities on absorpt. spectra 79—56822
CaF_2, nucl. dipolar mag. ordering, dipole-dipole interactions, review 77—85475
CaF_2, nuclear ferromagnetism and antiferromagnetism 77—63124
CaF_2, O^{2-}-F_v^- dipoles association from ionic conductivity 77—43242
CaF_2, optical detection of acoustic phonons at THz freqs. 80—75320
CaF_2, optical material, thermal expansion, 60-300K 78—33791
CaF_2, optical props. of cation colloidal particles 78—23503
CaF_2, overlaid with Au and CaF_2 films, channelling meas. 78—67762
CaF_2, phonon resonances associated with vacancy 80—19893
CaF_2 photoelastic modulator, for vibrational circular dichroism spectrometer 78—54476
CaF_2, phototransfer of thermoluminesc. peaks 79—83040
CaF_2, picosecond laser-induced breakdown at 5321 and 3547 Å, freq. depend. 77—63495
CaF_2 piezo-optical coeffs. meas. at 0.6328, 1.15 and 3.39 μm 80—34888
CaF_2, planar channelling, minimum yields determ. 80—70280
CaF_2, plastic deform, work hardening regions, TEM obs. 80—3140
CaF_2, polarised Raman scatt. in fluorite crysts., anharmonicity, high-temp. disorder 78—35132
CaF_2, polished crysts., rocking curve meas. *(German)* 78—2347

calcium compounds continued
CaF_2, polycryst., laser window material, IR thermooptic coeff. meas. 77—36208
CaF_2, positron annihilation polarisation effects, electron momentum distribution 80—55225
CaF_2, powder, elec. cond. transition under high press. *(Russian)* 77—20370
CaF_2, press forged, mech. and optical props. 80—38079
CaF_2, press-forged laser window, polishing, cleaning and grinding 79—59849
CaF_2, pulsed RF radiation produced by scratching *(Russian)* 78—19607
CaF_2, pulsed-laser-induced damage, role of avalanche multiplication and multiphoton absorpt. 80—48316
CaF_2, radiation induced defects, nuclear Hanle effect 78—43734
CaF_2, Raman spectra, 15 to 1300K, anharmonic vibr. effects 77—43990
CaF_2, rare earth doped, force const. changes near impurity site, calc. 77—47529
CaF_2, rare-earth and transition ion doped, far IR absorption and Zeeman effect 77—40246
CaF_2, rare-earth-doped, cluster-associated relax., 5.5-400K 78—31153
CaF_2, refr. index, 20-85°C, temp. depend. 77—8536
CaF_2, relaxation rate calculation 78—15060
CaF_2, rigid lattice system, appl. of zero time resolution NMR 78—76325
CaF_2 scintillation counter activated with Eu, ^{85}Kr conc. determ. at high pressures using β-ray count 78—13385
CaF_2, single cryst., dislocation etch pit shapes, dislocation line inclination effects 77—7722
CaF_2, single cryst., linear thermal resistance temp. depend. 77—66048
CaF_2, slab, surface modes of vibr. 78—71935
CaF_2, slab with (110) free surfaces, lattice dynamics and thermodynamic functions 80—70519
CaF_2, soft diaphragms produced by induced absorption method at 1.06 micron 78—5477
CaF_2, solid, ^{43}Ca-^{19}F double NMR method, determination of ^{43}Ca 80—2668
CaF_2 solid electrolyte, meas. of O chem. pot. 80—3359
CaF_2 solid electrolyte use in galvanic cells for thermodynamic obs. on refractory double oxides *(French)* 80—85190
CaF_2, spin correlation function for free induction decay 77—8421
CaF_2, spin diffusion under magic angle conditions, calc. 78—19363
CaF_2, spin-diffusion const. 77—66432
CaF_2, strain induced splitting and oscillator strength anisotropy of IR transverse optic phonon 80—92625
CaF_2, strength-controlling fracture energy depend. on flaw-size to grain-size ratio 80—81152
CaF_2, stress fields of dislocation arrays *(German)* 79—23615
CaF_2 substrate, Au film 79—90922
CaF_2, substrate, for Au film, interphase coincidence boundaries 79—1560
CaF_2, superionic, computer simulation 78—43173
CaF_2, superionic conductor, theoretical investigation of Raman scatt. 78—80351
CaF_2 surface, adsorption of water, IR internal reflection spectra 79—77920
CaF_2, surface struct., Au decoration and C replica techniques 77—1286
CaF_2, thermal props. *(German)* 80—81355
CaF_2, thermo-optic coeff., 95-175K 77—63403
CaF_2, thermolum., F-centre annealing after neutron irrad. at 20K 79—55787
CaF_2, thermolum. dosimeter, neutron damage, displacement and ionis. fractions of fast neutron kerma 78—30669
CaF_2, thermoluminesc. and F-centre annealing, after neutron irrad. 80—7422
CaF_2 thin films, initial ionic thermocurrent meas. 80—97018
CaF_2, thin insulating film, lattice parameter meas. by electron microscope 77—65940
CaF_2, third-order elastic consts. from Lundqvist pot., many-body effects 80—39201
CaF_2, trace impurities, carrier distillation-spectrographic determ. 78—3412
CaF_2 trapezoid, ThF_4 and ZnSe coated, IR characterisation by internal-refl. spectra 78—71161
CaF_2, U-centre, electronic struct. and optical transition energies, SCF MS $X\alpha$ calc. 79—4532
CaF_2, undoped, H-centre prod. by reactor neutron irrad., optical absorpt. meas. 77—59010
CaF_2, vibr. anal., kinetic consts. method 80—18838
CaF_2, vol. depend. of refr. index 78—88275
CaF_2, whiskers and crysts., flux growth and charact. by morphology and fracture strength 79—19987
CaF_2, width of upper valence band, tight-binding calc. 78—26814
CaF_2, window for optical high press. cell at high temp., characts. *(German)* 80—47999
CaF_2 windows, in IR cell, appl. in wavelength calibration of UV-visible spectrophotometer 77—33808
CaF_2, X-ray mass attenuation coeffs. and anomalous dispersion corrections for wavelengths $IK\alpha_1$-$CuK\alpha_1$ 77—31559
CaF_2, XPS core electron peaks, satellite and loss structs. 77—66571
$Ca^{2+}F_2^-$, particle motions, ionic conduction, self-diffusion 77—15620
CaF_2: Ni crystals, X-irradiated, EPR study of Ni^+ and Ni^{3+} 80—75849
CaF_2: $Tm^{2+}(Yb^{3+})$, axial g-values of $4f^{13}$ ions with trigonal symmetry *(Korean)* 79—24135
CaF_2:^{241}Am, alpha-decay induced ^{237}Np charge state, Mossbauer obs. 79—47367
CaF_2:^{57}Co, γ-irradiated, Mossbauer spectra 77—81036
CaF_2:alkali metal cation, thermal depolarisation study 80—108147
CaF_2:CaO, optical scatt., absorpt. at 205 nm 80—20669
CaF_2:Cd^{2+}, X-irrad., ESR of Cd^+ centres 77—59459
CaF_2:Ce, Stark struct., phototransitions, g-factors 78—67995
CaF_2:Ce,Mn, heavily-doped phosphor, cathode-ray irrad., energy transfer 79—87509
CaF_2:Ce^{3+}, absorpt. peaks in the lowest $4f \rightarrow 5d$ band, effect of conc. 80—2798
CaF_2:Ce^{3+}, ENDOR meas. on Ce^{3+} photochromic centre 78—19372
CaF_2:Ce^{3+}, Kapitza limited spin-bath relax., paramag. Faraday effect meas. at liq. He temp. 79—95642
CaF_2:Ce^{3+}, Na^+, ^{23}Na ENDOR meas. 77—69730
CaF_2:Ce^{3+}, thermally modulated UV absorpt. spectra, 90K 77—28602
CaF_2:Ce(Nd)(Dy)(Ho)(Yb), props. of ionic thermocurrents 77—7897
CaF_2:Cm, fluorite-struct., self-luminesc. 78—27309
CaF_2:Co, X-irrad., F-centre form., optical absorpt. spectra and dichroism obs. 79—42998

calcium compounds continued
CaF_2:Co, X-irrad., luminesc. spectra 79−28801
CaF_2:Co, X-irradiated, optical absorption spectrum 78−35173
CaF_2:Co^{2+}, designation of optical transitions near 5.40 nm, temp. evolution of absorption spectra meas. 77−55806
CaF_2:Co^{2+}, elec. field effect on spectra induced by odd vibrs. 79−73973
CaF_2:Co^{2+}, Jahn-Teller split $^4A_{2g}\rightarrow{}^4T_{1g}(P)$ absorption band, elec. field effect 78−15202
CaF_2:Co^{2+}, MCD spectra 77−28603
CaF_2:Co^{2+}, parity-forbidden transitions, elec. field effect on electronic-vibr. spectrum 79−65905
CaF_2:$Co^{2+}(Mn^{2+})(Ni^{2+})$, far IR absorpt. spectra peaks 78−27265
CaF_2:D^{2+} submm. magnetospectroscopy, tunable far IR laser potential 78−52481
CaF_2:Dy, colour centres, antiresonance-type phenomenon in external fields 78−68529
CaF_2:Dy, TLD phosphor, γ-induced sensitisation and residual thermolum. 79−28844
CaF_2:Dy, TLD-200, thermolum. phosphor, photolum. and absorpt. spectra, thermolum. mechanisms 80−97321
CaF_2:Dy, thermolum. induced by 254 nm UV photons 80−55204
CaF_2:Dy (TLD-200), practical UV dosimeter 77−60258
CaF_2:Dy crystal with M centre, antiresonance line, mag. field effect 80−55138
CaF_2:Dy dosimeter crystals, γ-irrad. dose effect on thermoluminesc. response 77−64135
CaF_2:Dy sensitivity to UV and ionising radiations, temp. treatment effect 79−26763
CaF_2:Dy^{3+}, cubic cryst. field effects 80−2368
CaF_2:Dy^{3+}, cubic sites, Γ_7 state energy, e.p.r. 77−1590
CaF_2:Dy^{3+}, EPR of colour centres, spin-spin interaction of pair of Dy^{3+} ions *(Russian)* 79−69751
CaF_2:Dy^{3+}, fluoresc. spectra, A-centres and B-centres, Stark levels 80−25428
CaF_2:Dy^{3+}, Γ_8 quartets, orbit-lattice interaction, e.p.r. under stress 77−1591
CaF_2:Dy^{3+}, high temp. fluorescence using Ar^+ and N_2 lasers 78−56514
CaF_2:Dy^{3+}, Mossbauer obs. 78−64303
CaF_2:Dy^{3+}, spin-lattice interaction in Γ_8 quartets, models tested for EPR data 78−23336
CaF_2:Dy^{3+}, thermolum., associated luminesc. centres and traps 77−28638
CaF_2:Dy(Ho)(Pr)(Tb), V_k-centre recomb. kinetics, phosphoresc. 77−55817
CaF_2:Dy(Mn), thermolum. induced by monoenergetic parallel beam 81 MeV diffr. neutrons 77−52883
CaF_2:Dy(Tm), cryst. fields, overlap and covalency contribs. 77−1397
CaF_2:Er, defect structure, quenching effect, dielec. relax. and optical absorption 80−65031
CaF_2:Er, γ-irrad., photostimulated luminesc. meas. 77−66538
CaF_2:Er, hydrogenated and deuterated, optical and EPR specra 79−61209
CaF_2:Er, near-Debye dielectric responses 80−71291
CaF_2:Er^{3+}, fluoresc. spectra of charge compensated cryst., multiphonon and energy transfer relax. 79−87496
CaF_2:Er^{3+}, fluorite, defect equilibria cluster control 79−99231
CaF_2:Er^{3+}, laser active media, nonradiative losses due to $^4I_{11/2}$-$^4I_{13/2}$ transition 79−31911
CaF_2:Er^{3+} crystal laser, hologram form. at 2.76 μm, laser emission linewidth meas. 79−10270
CaF_2:Er^{3+} laser fluoresc. of Er^{3+} sites, defect equilibria 78−6748
CaF_2:ErF_3, clustering, defect struct., NMR study 78−80229
CaF_2:Eu, CaF_2:Eu,Mn(Gd), single crystal predisintegration phenomena, SEM cathodolum. obs. 80−59502
CaF_2:Eu, Mn, cathodoluminescence SEM appl., stroboscopic 80−70088
CaF_2:Eu, oxidation and reduction of Eu, EPR and optical studies 80−25199
CaF_2:Eu, scintillation detector, in STEM 80−101897
CaF_2:Eu, thermolum. in presence of lanthanide impurities 80−2870
CaF_2:Eu, X-ray luminesc. 79−99933
CaF_2:Eu^{2+}, circular polarisation in luminesc. and optical orientation 78−6740
CaF_2:Eu^{2+}, energy transfer to luminesc. centres, pulsed excitation obs. 77−85781
CaF_2:Eu^{2+}, fluorescence lifetime and quantum efficiency for 5d→4f transitions 80−100681
CaF_2:Eu^{2+}, nuclear spin diffusion barrier, ^{19}F NMR Obs. 78−64282
CaF_2:Eu^{2+}, photoluminesc. mag. circ. polaris. 80−89056
CaF_2:Eu^{2+}, second order perturbation in vibronic system 78−30893
CaF_2:Eu^{2+}, short high-energy pulse induced X-ray luminesc., anomalous kinetics 77−59608
CaF_2:Eu^{2+}, Sm^{2+}, relaxed resonance acoustic phonons in vibronic anti-Stokes luminescence *(Russian)* 80−93404
CaF_2:Eu^{2+}, tunable optical detection and generation of THz phonons 79−65149
CaF_2:Eu^{2+}, two-photon absorpt. spectra exam. of excited state of Eu^{2+} 77−77261
CaF_2:Eu^{2+}, X-ray excited luminesc., $^5D_0$-$^7F_1$ transition 80−2842
CaF_2:Eu^{2+}, X-ray induced luminesc. kinetics, energy transfer processes 79−8181
CaF_2:Eu^{2+} single cryst., temp. depend. of second-order spin-lattice coeffs. 77−90029
CaF_2:Eu^{3+}, dielec. spectrum 77−36171
CaF_2:$Eu^{3+}(Sm^{3+})$, VUV absorpt. spectra, dopant clustering 80−108230
CaF_2:Fe^{2+}, electronic props., Mossbauer and far IR spectroscopy 79−99803
CaF_2:Fe^{2+}, relax. meas., Mossbauer spectroscopy, 10-30K 80−44977
CaF_2:Gd, triply ionised, lowest energy 4f-5d transition 79−24345
CaF_2:Gd^{3+}, cubic, strain effects on EPR by UMER method 77−1592
CaF_2:Gd^{3+}, effect of strain on cryst. field, EPR longitudinal and shear strain parameters 77−90027
CaF_2:Gd^{3+}, Eu^{2+}, natural, EPR study of impurity centres 78−19318
CaF_2:Gd^{3+}, ITC spectra of impurity aggregate 78−71883
CaF_2:Gd^{3+}, $Li^+(K^+)$, elec. field gradient at nuclei on orthorhombic sites, vs. elec. zero-field splitting 79−87070
CaF_2:Gd^{3+}, ligand ENDOR, spin Hamiltonian and hyperfine parameters 77−43903
CaF_2:Gd^{3+}, ligand ENDOR cubic centres, elec. field effect *(Russian)* 78−60357
CaF_2:Gd^{3+}, Mn^{2+}, photo- and radioluminesc. investig. of intracentric energy transfer 77−16378

calcium compounds continued
CaF_2:Gd^{3+}, S-state splitting, investigation by ESR and ENDOR at high pressure 78−52345
CaF_2:Gd^{3+} evaporated film, struct. of impurity centres, substrate temp. effects 79−99943
CaF_2:Gd^{3+} film, Gd^{3+} luminesc. spectrum and kinetics 78−6763
CaF_2:Gd^{3+}-M^+, (M=Li, Na, K, Rb, Cs, Ag), electric field effect expts., EPR line breadths, lattice distortions 78−80210
CaF_2:Gd^{3+}-m^+, complex, cryst. field parameters, EPR 78−10768
CaF_2:H^-, mechanism of resonant absorption by impurities 78−6715
CaF_2:Ho^{3+}, fluoresc., relative intensities, lifetimes 78−27296
CaF_2:Ho^{3+}, site-selective spectroscopy 80−29791
CaF_2:La, pulse hologram recording 79−55091
CaF_2:La hologram recording medium, characteristic transfer curve description, using heuristic exponential model 80−78796
CaF_2:La^{3+}, thermal depolarisation of La^{3+}-F_i^- defect dipoles 80−75926
CaF_2:Li(Na)(K)(Rb), dielec. relax., activation energy, rel. to vacancy pair reorientation 80−88917
CaF_2:M, M=Mn, Fe, Co, Ni, X-irrad., impurity effects on defect prod. 80−92525
CaF_2:M^{3+}, M=activator ion, redox processes during growth 77−85924
CaF_2:Mn, EPR and optical absorpt. spectra 80−93171
CaF_2:Mn, low temp. X-irrad., Mn centres, optical absorpt. and emission props. 80−60635
CaF_2:Mn, TLD phosphor, γ-induced sensitisation and residual thermolum. 79−28844
CaF_2:Mn^{2+},Yb^{3+}, efficient luminesc. energy transfer from Mn^{2+} to Yb^{3+} 78−19536
CaF_2:Mn^{2+},Yb^{3+}, luminescent energy transfer efficiency obs. 78−6777
CaF_2:Mn(Co)(Ni), X-irrad., thermolum. 80−60686
CaF_2:Na, γ-irrad. cryst., spontaneous and induced colour centre emission 79−7131
CaF_2:Na, pulsed DNMR exam. 78−35066
CaF_2:Na, single cryst., X-irrad., optical absorpt. and thermoluminesc. 80−34952
CaF_2:Na, tunable room temp. laser action of M-centres, luminesc. and absorpt. spectra 79−31907
CaF_2:Na, vacancy motion activation vol., complex dielec. const. meas. 80−39356
CaF_2:Na^+, cryst., thermal depolarisation 79−82912
CaF_2:NaF (YF_3) thermal conductivity of single crysts., 80-300K 77−11747
CaF_2:Nd^{3+}, crystal field splitting 79−65418
CaF_2:Nd^{3+}, crystal field study, absorption spectra 80−20668
CaF_2:Nd^{3+}, Slater, Racah and Lande parameters, crystal bonding 80−16062
CaF_2:$Nd^{3+}(Eu^{3+})(Dy^{3+})(Ho^{3+})(Tm^{3+})$, ^{19}F NMR studies 80−60429
CaF_2:$Nd^{3+}(Yb^{3+})$, cryst. field at O_h sites 77−35899
CaF_2:Ni, X-irrad., optical absorpt. spectra and dichroism meas. 80−108239
CaF_2:Ni, X-irradiated, optical and EPR meas. 80−108235
CaF_2:$Np^{3+}(U^{3+})$, cryst. field splittings, ab initio MO calcs. 77−20520
CaF_2:O, absorpt., ionic cond., and thermal depolarisation 79−14960
CaF_2:O, absorption, ionic cond. and thermal depolarisation 78−14502
CaF_2:O_2^-, OH^-, ion incorporation by reaction with surrounding atm. 80−55143
CaF_2:O_2^-, struct. and dynamics, EPR and ENDOR obs. 79−33562
CaF_2:O^-, Jahn-Teller distortion, electronic struct., MS Xα calc. 78−23057
CaF_2:O^{2-}, CaF_2:Na^+, O^{2-} and CaF_2:Y^{3+},O^{2-}, thermal depolarisation obs. of defect clusters 80−71299
CaF_2:Pb,O, UV absorption, impurity centres 78−68534
CaF_2:Pb^{2+}, band struct., Jahn-Teller effect, UV luminesc. and optical absorpt. spectra 80−66243
CaF_2:Pr^{2+}, EPR data interpretation for octahedral Γ_8 state in cubic cryst. field 80−2634
CaF_2:Pr^{3+}, laser selective excitation and energy transfer 79−38612
CaF_2:Pr^{3+}, multisite system, laser selective excitation and energy transfer 78−84634
CaF_2:Pr^{3+}, wavelength and temp.-modulated UV absorpt. 80−2799
CaF_2:PrF_3, EPR of cubic Pr^{3+} 79−28607
CaF_2:R, R=rare earth, dopant effect on superionic state transition 79−60547
CaF_2:R^{3+}, dichroism, elec. field effects *(Russian)* 77−24823
CaF_2:R^{3+}, far IR Stark and Zeeman splitting 77−48190
CaF_2:R^{3+}, R=rare earth, dipole reorientation of charge compensation centres, ionic thermocurrents meas. 79−73880
CaF_2:RF_3, colour centre prod. by γ-irrad., absorpt. spectra obs. 78−72565
CaF_2:rare earth, defect model for nonlocally compensated trivalent impurities 77−72629
CaF_2:rare earth, electronic props., compared to CdF_2 *(French)* 80−49662
CaF_2:rare earth ion, elec. dipole-dipole interaction, ionic thermocurrent and EPR study 80−108060
CaF_2:rare earth ion, hydrogenated, local lattice modes, spectroscopy 80−50375
CaF_2:rare earth metal, thermal cond., 80 to 300K, defect centre struct. 77−15638
CaF_2:Sm, charge transitions, positron annihilation exam. 78−92143
CaF_2:Sm, positron annihilation polarisation effects, electron momentum distribution 80−55225
CaF_2:Sm^{2+}, coherent population oscills. and hole burning observed using polarization spectroscopy 80−71457
CaF_2:Sm^{2+}, luminesc. spectra, vibronic wing, 2K 79−8182
CaF_2:Sm^{2+}, optical absorption and magneto-optic. props. 77−59595
CaF_2:Sm^{2+}, phonon spectrum of thermal pulses by fluorescence 79−95860
CaF_2:Sm^{2+}, pseudo-Jahn-Teller effect 79−69476
CaF_2:$Sm^{2+}(Eu^{2+})$, cubic crysts., vibronic spectra, induced dichroism method 77−81131
CaF_2:Sm(Eu), capture of thermalised positrons by activator impurities 77−40299
CaF_2:Tb, EPR in new photoexcited centre 78−19319
CaF_2:Tb, spectra of radn.-induced defect form. 80−2801
CaF_2:Tb^{3+}, cubic Tb^{3+} centres, energy level and cryst. field parameters 77−52181
CaF_2:$Tb^{3+}(Eu^{3+})$, one- and two-photon luminesc. excitation spectra 79−83023
CaF_2:Ti^{2+}, electronic struct. and EPR of Ti^{2+} 78−76034

calcium compounds continued
- CaF_2:Tm temperature dependence of V_k-centre generation efficiency *(Russian)* 78–48203
- CaF_2:Tm thermoluminescent dosimeters, response to 14 MeV neutrons 79–49867
- $CaF_2:Tm^{2+}$, EPR, optical recording in weak mag. field 78–68376
- $CaF_2:Tm^{2+}$, EPR meas. of Tm^{2+} ion pair interactions 79–95641
- $CaF_2:Tm^{2+}$, single cryst., ^{19}F nucl. spin cooling of Tm^{2+} electronic spin *(French)* 77–66440
- $CaF_2:Tm^{2+}$, spin density parameters at ^{19}F nuclei 78–68001
- $CaF_2:Tm^{2+}$, ultra-low nuclear spin temp., low field behaviour, EPR study 80–100614
- $CaF_2:Tm^{2+}$, vibronic spectra and dynamics of impurity-contaiing lattice 79–1787
- $CaF_2:Tm^{2+}(Yb^{3+})$, evidence for covalency 77–85180
- $CaF_2:Tm^{2+}(Yb^{3+})$, trigonal centres, point-charge approx. 78–39072
- $CaF_2:Tm^{3+}$, 8.2 keV excited state, mag. props., Schottky ht. capacity, nucl. quadrupole splitting 78–76037
- CaF_2:U, charge conversion of U^{3+}, ESR spectra 80–7150
- CaF_2:U, U^{5+} centres, nonoctahedral symmetry 80–11266
- CaF_2:U single crystal, Czochralski-Kyropoulos grown, U ion localization 79–91580
- $CaF_2:U^{3+}$, anomalous magnetooptic props., optical detection of ESR and cross-relax. resonances 80–93287
- $CaF_2:U^{3+}$, cubic site substituent, EPR spectra obs. 78–72392
- $CaF_2:U^{3+}$, Na^+, EPR, orthorhombic U^{3+} centre 77–77100
- $CaF_2:U^{4+}$, EPR hyperfine struct. 80–15781
- $CaF_2:U^{5+}$, charge compensation, struct. 79–15124
- $CaF_2:U^{5+}$, rhombic centre EPR spectrum, heat treatment effects 78–72407
- $CaF_2:U^{5+}$, single cryst., EPR 78–19325
- $CaF_2:U^{5+}$, trigonal centres, hyperfine parameters, EPR 78–43643
- $CaF_2:U^{5+}$, trigonal EPR spectrum 78–15021
- CaF_2:U(Th), and pure, electron microscopy study of lattice deformation due to electron irrad. 79–65077
- CaF_2:Y, absorpt. spectra, radiation defect formation energy, F to M centre conversion kinetics 79–65079
- $CaF_2:Y^{3+}$, DC cond., high Y concs. influence 78–22887
- $CaF_2:Y^{3+}$, diffusion of bound and free $F_{(i)}^-$ interstitials, NMR meas. 79–78542
- $CaF_2:Y^{3+}$, ionic cond. and thermal depolarisation obs. of defect clustering 80–71298
- $CaF_2:YB^{3+}(Ce^{3+})$, point-charge approx. of tetragonal centres 77–47778
- CaF_2:Y(La), dielec. relax. spectrum, ion size trends 78–72460
- $CaF_2:Yb^{2+}$, cryst., stress polarisation of luminesc. and emitting states struct. 77–69897
- $CaF_2:Yb^{2+}$, divalent ion radiative state, magneto-optical obs. 77–69893
- $CaF_2:Yb^{2+}$, luminesc. polarisation, elastic uniaxial compression effect, radiative state model 78–6739
- $CaF_2:Yb^{2+}$, spectra, kinetics and polarisation of luminesc. 77–69892
- $CaF_2:Yb^{3+}$ vacuum UV absorpt. spectrum, rel. to other rare-earth ions 79–43001
- $CaF_2:YbF_3$, clustering, defect struct., NMR study 78–80229
- CaF_2-(Y,R)F_3 (R=any lanthanide except Pm, Eu), phase diagrams 78–84783
- CaF_2-(Y,R)F_3 systems (R=rare earth), phase diagrams, limiting solubilities and non-stoichiometry 79–47665
- CaF_2-AlF_3, phase equilibria, DTA and X-ray diffr. study 78–27493
- CaF_2-AlF_3-Na_3AlF_6(-Al_2O_3), phase equilibria, X-ray diffr. and DTA meas. 80–108409
- CaF_2-CaC_2, phase diagram and CaC_2 solubility *(French)* 79–70050
- CaF_2-CaO, elec. cond. meas., CaO solubility, O^{2-} diffusion const. 78–30760
- CaF_2-CaO-Al_2O_3, phase diagram contribution *(German)* 80–100830
- CaF_2-Ge(Si), cosputtered composite semiconductors, selective solar energy absorbers 79–56876
- CaF_2-LaF_3, solid soln. with fluorite struct., phase diagram 79–100119
- CaF_2-MgO-SiO_2, melts, elec. cond., surface tension, viscosity, density *(Russian)* 80–92758
- CaF_2-MgO(SiO_2), melts, elec. cond., surface tension, viscosity, density *(Russian)* 80–92758
- CaF_2-NaF crysts., F_A centres, 385 and 435 nm absorpt. bands of electron irrad. crysts. 78–2889
- CaF_2-Nichrome-(K_2O-BaO-CaO-SiO_2) glass multicomponent self-lubricating coating, prep. by plasma spraying, and props. 80–40604
- CaF_2-rare earth trifluoride, characts. of ordering of solid solns., superstructure form. 79–14725
- CaF_2-ScF_3, phase relationships at 100 kbar and 1200°C 77–43335
- CaF_2-SrF_2-$BaF_2:Gd^{3+}$, luminescence spectrum of Gd^{3+} ion and solid solution region obs. 78–84638
- CaF_2-UF_4-CeF_3 solid soln., surface degradation, complex admittance analysis 78–55980
- CaF_2-xCaO.ySiO_2, freezing point depression meas., effect of SiO_2 compound additions 77–28798
- CaF_2-YF_3, fluorite- and tysonite-related ordered phases *(German)* 79–23725
- CaF_2-$YF_3:Er^{3+}$, stimulated emission 77–52135
- CaF_2-$YF_3:Nd^{3+}$, selective excitation of activator centres, time resolved luminesc. 78–15223
- CaF_2-$YF_3:Nd^{3+}$, spectral migration of electronic excitation, selective laser excitation *(Russian)* 78–80417
- CaF_2-YbF_3 system, phase relationships *(German)* 79–24501
- $CaF_2+Dy_2O_3+KCl$, intermediate neutron detection by thermoluminescence 80–5444
- $CaF_2+SiO_2+Mg(OH)_2$ matrix, quantitative anal. of multocomponent powders, full-profile refinement of Guinier-Hagg X-ray film data 79–39249
- CaF_2+Yb^{3+}, Stark level Zeeman energies, mag. susceptibiltiy, Schottky specific heat, crystal field splitting 78–26831
- $CaF_3:Ho^{3+}$, laser excited fluoresc. rise and decay meas., expt. 80–22448
- CaFCl, cryst. struct. determ. 77–80465
- $CaF_{2-x}H_x$, IR spectra 80–34920
- $CaF_{2-x}H_x$, ionic cond. determ. from admittance and dielec. loss meas. *(French)* 80–107479
- $CaF_{2-x}H_x$, ionic conductivity study by NMR experiments *(French)* 80–29210
- $CaF_{2-x}H_x$, solid soln. prep. and struct. determ. *(French)* 78–51505
- $CaFPO_3$, colour centre form., X-ray and electron bombardment *(Russian)* 77–19948
- $Ca_5F(PO_4)_3$, colour centre accumulation deformation effects 77–84743

calcium compounds continued
- $CaF_2.SiO_2$, dehydration product of fluorapophyllite, X-ray powder and cryst. data 79–37686
- $CaF_2.3Ca(PO_4)_2$, apatite, fission damage detection, absorpt. spectra 78–84617
- $Ca_3Fe_xCr_{2-x}Ge_3O_{12}$, antiferromagnetic order below 12K, Mossbauer study 80–39945
- $CaFeF_5$, one-dimens. magnetism *(French)* 79–73670
- $CaFe_2{}^{2+}Fe^{3+}(OH)O(Si_2O_7)$, ilvaite, IR spectrum and Mossbauer effect obs. *(French)* 78–80321
- $CaFe_2{}^{2+}Fe^{3+}Si_2O_8(OH)$, Mossbauer spectra, temp. depend. electron delocalisation 80–20567
- $CaFe^{3+}Fe_2{}^{2+}(Si_2O_7)O(OH)$, ilvaite, electronic struct., press. and temp. depend. of ^{57}Fe Mossbauer spectrum 80–108129
- $Ca_3Fe_2Ge_3O_{12}$, antiferromagnetic reson., anisotropy and magnetoelastic interaction effects *(Russian)* 77–69712
- $Ca_3Fe_2Ge_3O_{12}$, antiferromag. single crystal garnet, magnetostriction *(Russian)* 79–8027
- $Ca_3Fe_2Ge_3O_{12}$ garnet, light absorpt. spectral study 80–93322
- $Ca_3Fe_2(Mn_2)Ge_3O_{12}$, single magnetic sublattice antiferromagnetic garnets 78–52652
- $CaFeO_3$, charge disproportionation, Mossbauer obs. 78–2778
- $CaFeO_3$, preparation, cryst. struct., mag. and elec. props. 78–44066
- $CaFe_2O_4$, overlap contribution to $^{57}Fe^{3+}$ isomer shifts, nuclear size change 80–39903
- $CaFe_3O_5$, cryst. struct., isotypism with $Ca_3Y_2Fe_{19}O_{30}$ *(French)* 77–43203
- $CaFe_5O_7$, cryst. struct. determ., unit cell parameters *(French)* 77–84709
- $Ca_2Fe_2O_5$, brownmillerite type, NO catalytic decomp. 79–43631
- $Ca_xFe_{3-x}O_4$, Ca^{2+}, Mossbauer study 78–10814
- $CaFeSbAs_2O_7$, stenhuggarite, cryst. struct. 77–58983
- $Ca_3Fe_2Si_3O_{12}$, andradite, hyperfine parameters, Huckel theory calc. 80–39542
- $Ca_3Fe_2TiO_8$, crystal struct., O vacancy ordering *(French)* 77–11520
- $Ca_3Fe_{3\,5}V_{1.5}O_{12}$, ferrogarnet, crystallisation field in CaO-V_2O_5-Fe_2O_3-PbO 77–16548
- CaFz crystals, grown from synthetic raw materials, quality, effect of impurities, composition 78–79083
- $Ca_3Ga_2Ge_3O_{12}$, appl. as substrate for mag. bubbles 77–28418
- $Ca_3Ga_2Ge_3O_{12}$, substrate, electron examination of microstruct. and microsegregation 78–67919
- $Ca_3Ga_2Ge_3O_{12}:Nd^{3+}$, stimulated emission at 300K 80–38019
- $Ca_3Ga_3Ge_3O_{12}:Fe^{3+}$, spin Hamiltonian parameters, g-factors, temp. depend. EPR obs. 77–48038
- $CaGa_2O_4$ and $CaGa_4O_7$, cryst., thermodynamic parameters of reactions of form., thermodynamic stability 80–108726
- $CaGa_2O_4$, Czochralski grown, and CaO-Ga_2O_3 phase diagram 80–29934
- $CaGa_2O_4$, high pressure modifications 80–104149
- $Ca_2GdFe_3O_8$, crystal struct., O vacancy ordering *(French)* 77–11520
- $Ca_{0\,5}Gd_{0\,5}H_n$, H_2 dissociation press., phase behaviour and struct. 78–2260
- $Ca_xGd_{2\,x}Sn_{2\,x}Sb_xO_7$, pyrochlorate struct. form. 80–92504
- $Ca_2Ge_2(GeO_4)(Ge_4O_{12})$, cryst. struct., X-ray anal. 80–19783
- $CaGeO_3$, reduction processes by C, kinetic analysis, reaction products *(Russian)* 80–55644
- $CaGe_2O_5$ crystal struct., X-ray and Patterson function anal. 80–39054
- Ca_2GeO_4, with K_2NiF_4-type struct., high press. decomp. 79–1507
- Ca_2GeO_4-$Ca_4(PO_4)_2$ system, phase equil. 77–36469
- $Ca_2Ge_7O_{16}$, cryst. struct. interpretation by symmetrisation method 80–107180
- $3CaGeO_3.H_2O$, synthesis, IR spectra 77–43986
- $Ca_4(Ge_3O_{10}).H_2O$, cryst. struct. determ. 79–90627
- CaH absorpt. spectra 2480 to 2550 Å, new electronic states and rot. anal. 79–36662
- CaH, absorption spectra, extension of F-X system 79–18205
- CaH, $D^2\Sigma^+$-$X^2\Sigma^+$ band system 80–18847
- CaH, Franck-Condon factors, rot. quantum number effect 79–31613
- CaH, in RF-excited heat pipe oven, efficient arc source 78–63162
- CaH, low lying electronic states, ab initio SCF-CI calcs. 80–52893
- CaH method of metal powders manufacture, $Ca(OH)_2$ separation 80–84878
- CaH, spin doubling, SCF calcs. 80–95649
- CaH_2, proton chemical shift tensor, heavy ion effects 79–19791
- CaH_2, simultaneous reduction of Nb_2O_5 and Al_2O_3, Nb_3Al prep. 80–100809
- CaH_2, XPS spectra, crystalline potentials 77–77344
- $Ca_x{}^+(H_2O)_y[NbS_2]^{x-}$, hydrate layered chalcogenide, anisotropic mobility of water, NMR 79–65744
- $CaHPO_4$, monetite, cryst. struct. refinement, H bonding, neutron diffr. meas. 77–47389
- $CaHPO_4$, monetite, low-temp. ordering of H atoms, X-ray and neutron diffr. study at 145K 80–39022
- $CaHPO_4$, powder and granules with starch mucilage binder, surface topography variation under compression 80–80998
- $CaHPO_4$, X-ray microanalysis, quantitative, microcrystal standards and excessive background 77–36842
- $Ca_2HPO_4SO_4.4H_2O$, synthetic, cryst. struct. and relation to brushite and gypsum 78–83785
- $CaHPO_4.2H_2O$, brushite, obs. of etch pits on as grown faces 79–73169
- $CaHPO_4.2H_2O$, gel grown crysts., quality study by X-ray topography 79–87572
- $CaHPO_4.2H_2O$ powder and crystals, vibrational spectra, factor group anal. 80–45076
- $CaHfO_3$:Ta, electric field gradient temp. depend., TDPAC 77–20768
- CaI, electronic band spectrum 6100 to 6600 Å 78–90176
- CaI, mol. dissoc. energy, high temp. mass spectra 78–58863
- CaI_2 aqueous solution, US study of apparent molar compressibility 78–10125
- CaI_2, mol. struct. parameters and geom. config., gaseous electron diffr. obs. 80–37883
- CaI_2, photoelectron spectra, geometry 78–29816
- CaI_2, polymorphic phase changes of adsorbed NO 77–31900
- CaI_2:Pb(Mn), recomb. processes, luminesc. characts. *(Russian)* 80–25450
- $Ca(IO_3)_2$, complex salts, phase transitions, cryst. struct. *(Chinese)* 80–70171
- $Ca(IO_3)_2$, synthetic lautarite, cryst. struct. determ. 78–26517
- $CaIr_xRe_{1-x}O_3$, (0<x<1), sintered, exam. of mag. and electrical props 78–80135
- $CaIr_xRe_{1\,x}O_3$, perovskite struct., X-ray and IR obs. 79–90621

calcium compounds continued
$CaIr_xTi_{1-x}O_3$, semiconductor, struct., mag. and elec. props. 79−91046
$CaK_2As_2O_7$, cryst. struct., bond lengths 77−31639
$Ca_2K_2NaTiO[Si_7O_{18}(OH)]$, tinaxite, X-ray cryst. struct. determ. *(German)* 80−39023
$CaLaBO_4$, crystallographic and Pb^{2+} luminesc. data 79−32971
$CaLaFeO_4$, two-dimens. mag. ordered, structural and mag. props. *(French)* 80−70173
$CaLaFeO_4$, two-dimens. mag. props. rel. to cryst. struct. 80−75776
$CaLaFeO_4$, X-crystallog. and Mossbauer spectrum *(French)* 77−66447
$Ca_2LaFe_3O_8$, crystal struct., O vacancy ordering *(French)* 77−11520
$Ca_2LaFe_3O_8$, Fe replacement by diamag. cation, Neel temp. *(French)* 79−73712
$Ca_2LaFe_3O_8$, physico-chemical characterisation, Mossbauer exam. and mag. props. *(French)* 77−28494
$Ca_2LaFe_3O_{8+x}$, influence of O_2 partial pressure on nature of point defects, characterisation by elec. cond. meas. *(French)* 79−42055
$CaLaGaO_4:Eu^{3+},Bi^{3+}$, luminesc. influenced by struct. transition 78−6773
$CaLaGaO_4:Eu^{3+}(Bi^{3+})$, luminesc. of α- and β-phases 77−90186
$CaLa_{1-x}Gd_xGaO_4$, $(0 \leq x \leq 1)$, Gd^{3+} luminescence and cationic distrib. *(French)* 79−78734
$Ca_8La_2(PO_4)_5(VO_4)O_2$, IR and Raman spectra 79−78671
$CaLa_4(SiO_4)_3O:Nd$, laser damage initiating inclusions 77−68246
$CaLa_4(SiO_4)_3O:Nd^{3+}$, spectra, stimulated emission 77−85755
$Ca_2La_8(SiO_4)_6O_2$, cation ordering, X-ray diffr. meas. 79−23577
$Ca_4La_6Si_4P_2O_{26}$, and derivatives, synthesis, physicochemical props. 77−21066
$Ca_8La_2(VO_4)_6O_2$, IR and Raman spectra 79−78671
$CaLn_4(SiO_4)_3O$ silicate oxyapatites, prep. and props. of single crystals 77−28704
$CaLu_2S_4$, cryst. struct., space group *(French)* 77−80479
$Ca_{18}M_2H_2(PO_4)_{14}$, (M^{2+}=Mn, Co, Ni, and Cu), hydrothermal synthesis and cryst. growth 80−60762
$CaMO_4:Mn^{2+}$, M=Mo,W, EPR spectrum, temp. depend. of zero field splitting 79−15346
$Ca_3(MTa_2)O_9$, M=Ca, Cd, Mn, Fe, Zn, Co, Mg, Ni, monoclinic perovskite-type struct. 77−84725
$Ca_2MTa_5O_{15}$(M=K, Rb, Tl, Cs), relative stability of struct. types, and piezoelec. props. *(French)* 80−49206
$Ca_2(Mg,Fe)_5(Si_4O_{11})_2$-$(OH)_2$, amphibole nephrite, planar defects termination, high resoln. electron microscopy 80−79772
CaMg, matrix-isolated, laser photoluminesc., van der Waals ground state 79−41192
$CaMg_2$, phonon spectra 77−20031
$CaMgB_2O_5$, crystal struct. determ. 77−15388
$Ca_3Mg(BO_3)_2(CO_3).0.36\ H_2O$, natural sacchite, cryst. struct. determ. 79−23590
$CaMg(CO_3)$, dolomite, kinetics and thermodynamics of decomposition to metastable solid product 78−80740
$CaMg(CO_3)_2$, dolomite, Raman spectra calc. 77−24848
$CaMg(CO_3)_2$, dolomite, partial dislocations and stacking faults obs. 78−3761
$CaMg(CO_3)_2$, dolomite, reaction with ZrO_2, mineralisation during roasting 79−43180
$CaMg_2Cl_6.12H_2O$, cryst. data, X-ray powder method 80−1978
$Ca_2Mg(Co)(Zn)(Mn)(Cd)(Ca)TeO_6$, optical SHG study of acentricity, ferroelec. of low temp. phases 80−71324
$CaMg_{0.95}Fe_{0.05}Si_2O_6$, pyroxene, Mossbauer line integrated intensity ang. depend. 77−90083
$CaMgGe_2O_6$-$CaFeGe_2O_6$, solid solns., phase equilibria, cryst. optical, X-ray struct. characts. 79−11577
$Ca_6Mg_5Mn(B_2O_5)_6$, kurchatovite, cryst. struct. 77−65967
β-$Ca_{3-x}Mg_x(PO_4)_2$, struct. and impurity distrib., stabilising role of Mg 78−10020
$(Ca_{1-x}Mg_x)RuO_3$, mag. props. 78−27027
$CaMg(Si, Ge)_2O_6$, solid solns., IR spectra 77−48156
$CaMgSiO_4$ (monticellite), high-press. phase transforms. and implications for upper mantle mineralogy 80−17255
$CaMgSi_2O_6$, diopside, elasticity, Brillouin scatt. meas. 80−6454
$CaMgSi_2O_6$, single cryst., IR reflection spectra, vibr. spectrum calc. 77−73142
$CaMgSi_2O_6$, thermal conductivity, 1.5-30K *(French)* 77−39704
$CaMgSi_2O_6$-$Ca_2MgSi_2O_7$-$KAlSi_2O_6$, phase diagram of ternary eutectic system 78−80529
$Ca_2MgSi_2O_7$, single cryst. growth by floating zone method, opt. microscopy charact. 79−47623
$(Ca_{0.15}Mn_{0.8}Fe_{0.05})SiO_3$, rhodonite lattice imaging of struct. defects 80−49240
$Ca_3Mn_2Ge_3O_{12}$, antiferromagnetic garnet, neutron diffr. study in mag. field 80−50060
$Ca_3Mn_2Ge_3O_{12}$, crystal struct. distortion due to cooperative Jahn-Teller effect *(Russian)* 77−1119
$Ca_3Mn_2Ge_3O_{12}$ garnet, metamagnetic transition, high anisotropy peculiarities *(Russian)* 80−60274
$Ca_3Mn_2Ge_3O_{12}$, highly anisotropic garnet, neutron diffr. obs. of mag. struct. 78−68168
$Ca_3Mn_2Ge_3O_{12}$, mag. struct. study 80−2554
$Ca_3Mn_2Ge_3O_{12}$, neutron diffr. in mag. field, metamagnetism, antiferromag. ordering 79−65651
$Ca_3Mn_2Ge_30_{12}$, mag. field induced transition 80−50094
$CaMnO_3$, microstruct., elec. cond., thermoEMF 78−23084
Ca_2MnO_4, with K_2NiF_4-type struct., high press. decomp. 79−1507
$Ca_2Mn_3O_8$, mag. props. 79−78339
$Ca_2Mn_3O_8$, mag. props. and EPR 79−91215
$Ca_2MnO_{4-x}F_x$, antiferromagnetic props. and elec. cond. *(French)* 80−29526
$CaMn_4(Si_5O_{15})$, rhodonite cryst. struct., compared with synthetic germanates 78−30600
$CaMn[B_2O_5]$, synthetic Mn-kurchatovite, cryst. struct. 79−14777
$Ca_2Mn_7[Si_{10}O_{28}](OH)_2.5H_2O$, inesite, cryst. struct., X-ray determ. 79−19227
$CaMoO_3$, perovskite-type cmpd., metallic conductivity, room temp. to 2.5K 79−65483
$CaMoO_4$, Davydov splitting of vibr. levels, short range interaction 80−71418
$CaMoO_4$, electrical cond. and ionic transport number meas., defect struct. model 80−2388
$CaMoO_4$, exam. of electrical conductivity, absorption spectrum 79−51301

calcium compounds continued
$CaMoO_4$, external lattice vibr. modes and elastic wave vels., dispersion relations 79−33050
$CaMoO_4$, form. by $CaO+MoO_3$ solid-state reaction 79−43579
$CaMoO_4$, luminesc. efficiency, temp. and high-press. 78−23507
$CaMoO_4$, precipitation from neutral equivalent solns., cryst. numbers, final morphology and sizes 78−23597
$CaMoO_4$, precipitation induction errors, a method for determ. 79−5175
$CaMoO_4$, refr. index, single crystals having scheelite struct. 78−79082
$CaMoO_4$, single crystal, growth and characterisation 77−36467
$CaMoO_4:Er^{3+}$, phase relax., EPR spin echo expts. 79−99767
$CaMoO_4:Er^{3+}$, phase relax. time rel. to g-factor anisotropy, electron spin echo obs. 80−29615
$CaMoO_4:Fe^{3+}$, single crystals, structure and kinetics, EPR meas. 79−99760
$CaMoO_4:Mn^{2+}$, of Mn^{2+}, EPR zero-field splitting 80−75531
$CaMoO_4:Mo^{5+}$, g-factor, ground state, line broadening, EPR obs. 80−39863
$CaMoO_4:Na(Y)$, pure and doped, luminesc. props., emission decay time 79−95835
$Ca(MoO_4)_{1-x}(WO_4)_x$, Raman scatt. meas. 77−28578
$CaNH_4HP_2O_7$, monoclinic, crystal struct. exam. 78−2070
$CaNH_4NaP_2O_7.3H_2O$, crystal data *(French)* 78−14316
Ca^+NO^-, $Ca^+NO_2^-$ in solid Ar, IR spectra at 15K 77−57996
$Ca(NO_3)_2$, aq. electrolyte, apparent molar heat capacity and volume, of 298.15K 79−65208
$Ca(NO_3)_2$, conc. aq. solns., ionic hydration and secondary dielec. relax. 79−24882
$Ca(NO_3)_2$ hydrous melts, proton spin relax. and mobility 77−77118
$Ca(NO_3)_2$, hydrous melts, correl. times, conc. depend., proton NMR relax. obs. 77−90059
$Ca(NO_3)_2$, Raman spectra temp. depend. anomalies in symmetric stretch region 79−61361
$Ca(NO_3)_2$-H_2O solns., ice I homogeneous nucleation temp., slow vitrification mechanism 78−26666
$Ca(NO_3)_2$-KNO_3 glasses, radiation products and recombination 79−57261
CaN_2O_3, vibr. spectra, assignments 77−38670
$Ca(NO_3)_2.2h_2O$, β- to α-phase orientational transform., struct. interpretation *(French)* 77−80448
α-$Ca(NO_3)_2.4H_2O$, cryst. struct., H bonds *(French)* 77−58986
$Ca(NO_3)_2.4H_2O$, high press. phase behaviour, dehydration and congruent melting 79−78947
$Ca(NO_3)_2.nH_2O$, aq. soln., conc., compressibility, elec. cond. 77−69024
$Ca_2NaHSi_3O_9$, pectolite, TEM obs., of microtwins and stacking faults 78−75677
$(Ca_{0.90}Na_{0.06}Mg_{0.71}Fe_{0.25}{}^{2+}Fe_{0.05}{}^{3+}Al_{0.03})(Si_{1.88}Al_{0.11}Ti_{0.01})_2O_6$, struct., space group, bond lengths, X-ray diffr. meas. 78−47298
α-$CaNa_2P_2O_7.4H_2O$, X-ray cryst. struct. determ. 80−64964
$CaNbF_7$, polymorphism, X-ray powder diffr. data *(French)* 80−19779
$Ca(NbO_3)_2$, thermally stimulated currents exam. 77−69766
$Ca(NbO_3)_2$-$LiNbO_3$, cryst. growth in baked mixture, Seignettoelec. phase *(Russian)* 79−47395
$CaNb_2O_6$, bonding characterisation 78−38680
$CaNb_2O_6$, columbite, polarised Raman and IR spectra, normal coord. anal. 77−76500
$CaNb_2O_6$, columbite struct., normal coord. anal. 78−964
$CaNb_2O_6$, columbite struct., IR and Raman spectra *(French)* 78−19485
$CaNb_2O_6$, force fields rel. to cryst. struct. *(French)* 80−107104
$CaNb_2O_{8-x}$, perovskite, cryst. struct. determ. *(French)* 78−10021
$Ca_2Nb_2O_7$, crystal struct. and phase transitions, rel. to isomorphous crystals *(Japanese)* 80−49208
$Ca_2Nb_2O_7$, crystal synthesis and SHG, solid laser freq. manipulation 79−41421
$Ca_2Nb_2O_7$, ferroelec., temp. depend. of SHG intensity 79−24267
$Ca_2Nb_2O_7$, ferroelectric phase transitions, dielec. constant and thermal expansion rel. to temp. 80−88934
$Ca_2Nb_2O_7$, monoclinic modification, cryst. struct., X-ray diffr. method 80−64955
$Ca_2Nb_2O_7$-$CaTiO_3$ system, mode of formation and stability of $A_nB_nO_{3n+2}$ phases *(French)* 78−3110
$Ca_2Nb_2O_7$-Sm_3NbO_7 system, phase equilib. 80−20907
Ca_xNbO_3, perovskite, cryst. struct. determ. *(French)* 78−10021
$Ca_{0.5}Nd_{0.5}H_n$, H_2 dissociation press., phase behaviour and struct. 78−2260
$CaNd_{3/2}Nb_{3/2}O_7$, pyrochlore struct., synthesis elec. props. 79−42543
$Ca_xNi_{1-x}Fe_2O_4$, initial permeability and Curie temp. 80−25130
$Ca_xNi_{1-x}Fe_2O_4$, X-ray struct. anal., determ. of lattice constant and interplanar distances *(French)* 80−96487
$Ca(No_3)_2$-H_2O system, induction period supercooling depend. meas. 80−19918
$Ca(No_3)_2.3.91H_2O$-$NiCl_2$ melts, glass forming, transport behaviour 78−59963
CaO, $^3T_{1u}$ of F-centre, EPR, unaxial stress effects 78−48040
CaO, $^3T_{1u}$ state of F-centre, ODMR spectra 78−43685
CaO, $^3T_{1u}$ state of F-centre, paramag. relax. optical detect. 78−43687
CaO (100), surface struct., LEED study 80−39396
CaO, (100) surface struct. using LEED meas. and rumpled ionic models 80−20019
CaO, absorpt. band identification of colour centres 77−40271
CaO, additive, effect on sintering struct., props. of corundum ceramic 79−15630
CaO, additive for sintered TiO_2 ceramics, effect on props. 78−35329
CaO and $CaO:Gd^{3+}$, crystal growth from molten solvent LiF-20 mole % CaF_2 77−77358
CaO, at. charge densities, X-ray struct. factors 78−79566
CaO, atomic interaction effects in X-ray emission spectra *(Russian)* 79−69905
CaO $B^1\Pi$-$X^1\Sigma$ and $C^1\Sigma$-$X^1\Sigma$ transition strengths, shock tube spectroscopic absorpt. meas. 80−53053
CaO, $B^1\Pi$-$X^1\Sigma$ and $C^1\Sigma$-$X^1\Sigma$ electronic transition strengths meas. 80−78602
CaO based refractory from industrial lime, with 5% added electrocorundum 80−89184
CaO, C-content determ. of single crystals grown by arc fusion 79−8456
CaO catalysed coal gasification 80−30339
CaO, catalyst, formation of cubic BN from hexagonal BN *(Japanese)* 80−54374
CaO, chemisorption of O_2, adsorboluminescence from surface F-centres 80−20723

calcium compounds continued
CaO, coherent/incoherent scatt. cross-sections of 136-278 keV γ-rays 78—70881
CaO, cohesive and thermophysical props., role of three-body interactions 80—92477
CaO, corrosion by K_2O melt, SEM obs. 77—44383
CaO, crystal growth by floating zone method, using thermal imaging system 77—77373
CaO, crystalline pots. from XPS data 77—77344
CaO, determ. in glass, at. absorpt. method *(Polish)* 79—24872
CaO, determination of contents in sintering charge, using X-ray spectral anal., assessment of error 79—52823
CaO, dielec. const., temp. and press. depend. 79—65789
CaO, dielectric behaviour 79—91343
CaO, displacement function calc. 80—34047
CaO dissoc. energy from $Ca+O_2$ chemiluminesc. 80—97697
CaO, dissociation energies, spectrometric determ. 78—74789
CaO, dissociation energy 77—550
CaO, doped, thermal stability of hole centres and hole recombination luminescence *(Russian)* 78—72614
CaO, EPR of colour centres, 295K *(Russian)* 80—84649
CaO, EPR spectra of Mn^{2+} along different mag. field orientations 79—47327
CaO, effect on carbothermic reduction of Cr_2O_3, to metallic Cr *(Japanese)* 78—48651
CaO, effect on corundum ceramic comp. and phase struct. 77—81244
CaO, effect on elastic modulus temp. depend. of silicate glass 79—61637
CaO, effect on high temp. creep of MgO 78—48450
CaO, effect on microstructure of glaze 77—21083
CaO, effect on PbO activity in molten PbO-SiO_2 system 78—60663
CaO, effect on props. of PbO containing cryst. glass 80—24637
CaO, elastic moduli, pressure and temp. derivs. 77—62577
CaO, electron irradiated, photocond. and luminesc. meas., F-centre electronic struct. determ. 78—6409
CaO, electron irradiated, symmetry assignment of new point defect 78—31261
CaO, electronic band struct., combined tight-binding and pseudopot. approach 77—47728
CaO, electronic struct., SCF calcs. 78—66462
CaO, electronic struct. calc. of F-centre, absorpt. and luminesc. bands 77—62859
CaO, electronic struct. of V^- and related centres 80—2355
CaO, electronic structure 80—2332
CaO epitaxial layer, on Mo, secondary electron emission, struct. effects, LEED and AES expts. 78—2959
CaO, epitaxial layer growth by chem. transport reaction 77—52254
CaO, epitaxial layers by CVD *(Russian)* 79—56934
CaO, eqn. of state at high press., appl. to Earth core and mantle 80—109122
CaO, F_A(Mo) centre, spin coherence zero-field double reson. 78—43689
CaO, F^+ centre, dynamic Jahn-Teller effect 79—28327
CaO, F^+ centre in octahedral Jahn-Teller system 79—42499
CaO F^+-centre, Lie group theory aspects of Jahn-Teller effect 77—20279
CaO, F-centre, selective excitation, detection of EPR 78—43688
CaO F-centre luminesc. and PMDR 79—95832
CaO, F-centres, ${}^3T_{1u}$ relaxed excited state, uniaxial stress effect and spin-lattice coupling 78—72405
CaO, F-centres, laser selective excitation and double reson. in Jahn-Teller systems 78—19379
CaO, form. from $Ca+O_2(CO_2)$, electronic states obs. 78—92450
CaO, formation of surface O_{2-} ion by O_2 adsorption, EPR 80—61155
CaO, gaseous chemiexcited mol., modulated transmission spectra 77—86316
CaO, heated on W, thermal anal. using mass spectrometric, technique, vaporisation behaviour 80—79932
CaO high pressure metallisation, tentative evidence 80—84427
CaO, interstellar, zero phonon lines rel. to origin of diffuse absorpt. bands 77—57073
CaO, interstellar grains, rel. to origin of diffuse interstellar absorpt. bands 77—9785
CaO, isotopically enriched target preparation using electron gun 80—23226
CaO, J=4-3 106 GHz undetected transition in stars and molecular clouds 79—71090
CaO, line broadening of EPR and zero phonon lines of F centres 78—43686
CaO, luminesc. single cryst., sharp IR absorpt. lines 77—1704
CaO, millimetre wave spectrum, spectrosc. consts. 77—61737
CaO, modified electron gas theory, high press. effect 77—19899
CaO, modified three-body shell model, lattice dynamics 77—4165
CaO, Mollwo-Ivey relation between peak-colour absorption energy and average O ion spacing 77—90179
CaO, muonium and positronium form. 79—56679
CaO, NaCl struct., elastic props., US meas. 78—18697
CaO, neutron irrad., MCD, optical absorpt. lines 77—77255
CaO, ODMR and spin coherences in phosphorescent state of exchange-coupled F^+-centre pairs 79—87336
CaO, obs. of dipolar induced spin dephasing, coherent optical-microwave spectroscopy 80—103900
CaO, phosphoresc. F-centre, phonon assisted conversion of Jahn-Teller states, ODMR under uniaxial stress 78—48084
CaO, photoionisation of F-centre, luminesc. and photocond. meas. 80—66270
CaO, produced from $CaCO_3$ powder decomp. in vac. and in CO_2 80—45255
CaO, random intrinsic strain effect on ODMR, PMDR, of F-centre in Jahn Teller states 78—84499
CaO, reduction by C, kinetics and mechanism *(Russian)* 80—93743
CaO, relax. in ${}^3T_{1u}$ state of F centres 80—24443
CaO, single cryst., tribolum. obs. 79—52031
CaO, single cryst. growth from molten $CaCl_2$ in wet atmosphere, habits 80—55287
CaO sintering, Cr_2O_3 addition effect *(Czech)* 80—45258
CaO, sintering of granular masses of ZrO_2, stabilisation 78—44064
CaO, smoke particles prep. by burning metal in Ar-O_2 gas, electron microscope obs. 77—52238
CaO, soln., chemisorpt. on quartz powders, effect on lattice parameters 79—37918
CaO solubility in $BaO.6Fe_2O_3$ 80—100333
CaO, solubility in Er_2O_3, elec. cond. and nonstoichiometry 79—11112

calcium compounds continued
CaO solubility products in molten NaCl-KCl, potentiometric determ 80—76488
CaO stabilised ZrO_2, preferred slip system 80—66585
CaO surface, AES peak height calibrations 79—43072
CaO, surface electron donor sites and acid-base props., adsorbed radical ESR 77—21417
CaO, thermal reduction with Al under reducing atmosphere 77—16864
CaO, transition, Earth mantle implications 80—79876
CaO, triplet state of F_A centres, ODMR obs. 79—28639
CaO, tunable optical gain at 3600 Å using F^+ centres 79—45947
CaO, undoped and Cl-, F- or Al-doped, X-ray and UV luminesc., electron-hole recombination processes *(Russian)* 78—76528
CaO with adsorbed metal, photoexcited ions and electron emission *(Russian)* 77—40324
CaO, XPS valence bandstruct. 80—89117
CaO:Ag(Au), electroluminesc. meas. 80—40162
CaO:Ag^{2+}, EPR spectrum, static, quasistatic and quasidynamic Jahn-Teller effect 77—85561
CaO:Bi surface, O_2 chemisorpt., positive ion emission determ. 80—92785
CaO:$Bi^{3+}(Pb^{2+})$, impurity centres vibronic spectra, lattice dynamics and electron-phonon interactions 80—7396
CaO:Ce,Gd phosphors, trap distrib., phosphoresc. decay characts. obs. 80—29773
CaO:Ce^{3+}, Gd^{3+}, sensitization of Ce^{3+} luminesc. by Gd^{3+} 80—97326
CaO:Cr^{2+}, APR spectra 79—87313
CaO:Cr^{2+} Jahn-Teller system, APR spectrum, zero strain site energy level diagram 79—99756
CaO:Cu(Ag)(Au), thermoluminesc., following UV excitation, 290-500K 77—40292
CaO:Dy, thermolum. induced by 254 nm UV photons 80—55204
CaO:Eu,Tb phosphor emission under X-ray excitation 79—52011
CaO:Eu^{3+}, influence of crystal field on luminesc. *(Russian)* 80—80834
CaO:Eu(Tb), phosphor, isothermal decay 80—55156
CaO:F(Cl)(Al), phosphon, luminesc., electron-hole recombination processes 79—65919
CaO:Fe^{2+}, octahedral symm., vibronic effects from Zeeman field induced Mossbauer spectra 77—8477
CaO:Gd^{3+}, quadrupole hyperfine interaction, ENDOR 78—23370
CaO:Ir, quadrupole interactions and static Jahn-Teller effect in EPR spectra 77—72842
CaO:Li, thermally quenched, generation of Li^0 centres 80—50382
CaO:$MMoO_4$; M=Cd,Pb, phase diag. cross sections and reactions 78—27487
CaO:Mg^+, EPR exam., hyperfine const. determ. 77—8388
CaO:Mg^+, g-shift anal. 80—29313
CaO:Mn phosphor, surface radical recomb. and cathodoluminesc. *(Russian)* 78—6787
CaO:Mn^{2+}, impurity pot. well shape calcs. 78—87950
CaO:Mo, spin coherence and Stark modulation effect of F_A-Mo centre excited state 77—69733
CaO:Ni^{2+}, vibronic splitting, effect of including higher vibronic states in calc. 79—55851
CaO:OH , room temp. IR spectra, heat treatment and electron irrad. effects 79—51992
CaO:$Pb^{2+}(Bi^{3+})$, luminesc. 77—73166
CaO:V^{3+} orbital triplet, intermediate Jahn-Teller effect, APR 80—34758
CaO:Y phosphor, chemical instability, thermoluminescence study 79—38682
$5CaO$-$3Al_2O_3$, cryst. struct. determ. 78—55840
CaO-(CaF_2)-Al_2O_3, IR absorption spectra and X-ray emission spectra obs. *(Japanese)* 77—52075
CaO-Al_2O_3, binary slag, reduction of Al_2O_3 by C saturated Fe *(Japanese)* 79—24733
CaO-Al_2O_3, molten binary slag, dissolved C study *(Japanese)* 78—60662
CaO-Al_2O_3 based glass development, water removal, use in IR to 5 μm 78—83052
CaO-Al_2O_3 melt, solubility of H_2O at 1600°C 78—51687
CaO-Al_2O_3 melts, density, atm. comp. effect 78—22624
CaO-Al_2O_3 melts in presence of graphite, solubility of C and N 78—38850
CaO-Al_2O_3 molten binary slag, C dissolution rate *(Japanese)* 79—23739
CaO-Al_2O_3-B_2O_3-SiO_2-FeO, glass, IR spectra at room and melt temp. 80—88986
CaO-Al_2O_3-CaF_2, electroslag remelting slag, solubility of N_2 and C, equilibria 78—44110
CaO-Al_2O_3-Fe_2O_3, and resonance spectroscopy study *(Russian)* 77—55733
CaO-Al_2O_3-Fe_2O_3-SiO_2, phase relations 77—12610
CaO-Al_2O_3-H_2O system, chemical degradation under high gaseous pressure and temp. 79—20464
CaO-Al_2O_3-P_2O_5, struct. energetics and charging under irrad. *(Russian)* 77—84791
CaO-Al_2O_3-P_2O_5, electron beam irrad., temporal change in electric field produced 79—4760
CaO-Al_2O_3-P_2O_5, exam. of electron beam irrad. effects on physical props. 79—4253
CaO-Al_2O_3-P_2O_5, sub-solidus relationships 79—66046
CaO-Al_2O_3-P_2O_5 irradiated electret glasses, relax. of external field intensity on heating 80—25282
CaO-Al_2O_3-SiO_2, effect of composition on mechanical props. 78—48435
CaO-Al_2O_3-SiO_2, glass ceramic prod. by TiO_2 nucleating agent 78—11189
CaO-Al_2O_3-SiO_2, rain erosion mechanisms 79—34154
CaO-Al_2O_3-SiO_2 additive to zircon ceramic, sintering and mech. props. 80—60814
CaO-Al_2O_3-SiO_2 based glasses, kinetic parameters of glass ceramic form. 77—24385
CaO-Al_2O_3-SiO_2 ceramic, chem. resist. and struct. 79—61756
CaO-Al_2O_3-SiO_2 diffusion triangular diagram, diffusion between lime and sintered kaolinite *(French)* 79—69296
CaO-Al_2O_3-SiO_2 glasses, density-of-states and structural forms, Raman spectra study 80—97255
CaO-Al_2O_3-SiO_2 melt, at 1723 to 1823K, determ. of inter diffusivities matrix 78—43161
CaO-Al_2O_3-SiO_2-TiO_2 system glass-crystal material, elec. cond. 79—60876
CaO-Al_2O_3-TiO_2-SiO_2, glass formation, structure of cations *(Russian)* 80—38933

calcium compounds continued
$CaO-Al_2O_3(B_2O_3)-SiO_2$ glass-forming additive, effect on Al_2O_3 ceramics sintering 80−89187
$CaO-B_2O_3-Al_2O_3-V_2O_5$ glass, cond. mechanism, current carriers, V_2O_5 conc. effects 77−62668
$CaO-B_2O_3-Fe_2O_3$ glasses, effect of heat treatment on electronic props. 78−2480
$CaO-B_2O_3-Fe_2O_3$ glass, dielec. relax., AC and DC cond., dielec. const. and loss 78−23393
$CaO-B_2O_3-GeO_2$ system glasses, physicochem. props., alkaline earth oxides effect 79−65827
CaO-CaF, hot pressed, effects of CaF_2 addition, sintering behaviours and microstructs. investig. *(Japanese)* 78−95721
$CaO-CaMnO_{3-x}-2CaO.Fe_2O_3$ pseudoternary system, equilibrium relationships between solid phases at 1300°C *(Italian)* 77−55951
$CaO-Ca(OH)_2$ reversible hydration-dehydration for solar energy storage 80−97810
CaO-Cu concentrate pellet, fluidised bed roasting 77−4934
$CaO-CuO-P_2O_5-V_2O_5$ glass EPR, Cu impurity effect on elec. props. 79−51849
$CaO-Fe_2O_3-Al_2O_3$ system, solid soln. of $Ca_2Fe_{2(1-x)}Al_{2x}O_5$ *(Russian)* 80−16284
$CaO-Fe_2O_3-B_2O_3$ glasses, phys. props. rel. to struct. and comp. 78−23331
$CaO-Fe_2O_3-SiO_2$ glass, struct. behaviour at melting, Mossbauer exam. 79−10802
$CaO-Ga_2O_3$, vitrification, spectroscopic and petrographic anal. 77−15556
$CaO-Ga_2O_3$ phase diagram and Czochralski melt growth of $CaGa_2O_4$ 80−29934
$CaO-Ga_2O_3-Bi_2O_3$, vitrification regions 77−15557
$CaO-Li_2O-Al_2O_3-SiO_2:Nd^{3+}$, CaO enriched, laser-type glasses, spectroscopic behaviour 78−60497
$CaO-Li_2O-B_2O_3$, calibo glass, $Dy^{3+} \rightarrow Ho^{3+}$ non-radiative energy transfer, diffusion limited relaxation 79−65925
$CaO-Li_2O-B_2O_3:Dy^{3+}$ glass, optical excitation energy transfer from $Dy^{3+} \rightarrow Nd^{3+}$ 79−15515
CaO-MgO, doloma, composition effect on creep, impurity effects 79−43318
CaO-MgO refractory, wettability by Fe melt *(Russian)* 78−10257
$CaO-MgO-Al_2O_3-Cr_2O_3-Fe-O_2-SiO_2$ system, exptl. determ. of periclase and spinel comps. 78−6906
$CaO-MgO-Al_2O_3-SiO_2-Fe_{(l)}$, heterogeneous equilib. calcs. *(Russian)* 77−59093
$CaO-MgO-Al_2O_3-SiO_2$, glass-ceramic prep. by hot pressing and crystallisation of powder 78−11192
$CaO-MgO-Al_2O_3-SiO_2$, glass ceramic, prep. by hot pressing and crystallisation, mech. props. 78−15351
$CaO-MgO-Al_2O_3-SiO_2$, shale glass, glass forming and dielec. props. 78−22660
$CaO-MgO-Al_2O_3-SiO_2$, shale glass, crystn. behaviour 78−22661
$CaO-MgO-Al_2O_3-SiO_2$ system, pyroxenes subsolidus phase relations rel. to geothermometry and geobarometry 79−16440
$CaO-MgO-Al_2O_3-SiO_2$, quartz sand-dolomite-magnesia-clay based glasses, crystn. 80−20915
$CaO-MgO-Al_2O_3-SiO_2$, glass formation, at molar ratio CaO: MgO=1 *(Russian)* 80−39269
$CaO-MgO-CeO_2$, fired, phase equilibrium diagram, 1700 to 1200°C 78−92248
$CaO-MgO-Cr_2O_3-Al_2O_3-ZrO_2-SiO_2$ system, subsolidus region characts. 80−97466
$CaO-MgO-NaPO_3$ system, subsolidus struct. 79−43215
$CaO-MgO-SiO_2$, diopside, exam. of synthesis by hydrothermal sintering *(German)* 79−4934
$CaO-MgO-SiO_2$, melts, mixing enthalpy, 1700-1873K 78−79785
$CaO-MgO-ZrO_2-SiO_2$, phase study, SiO_2 compatibility relationship 78−95734
$CaO-MgO-ZrO_2-SiO_2$, phase study, ZrO_2 compatibility relationship 78−95735
$CaO-MgO-ZrO_2-SiO_2$ refractories, phase diagram 80−11634
CaO-MnO system, solid soln. form. and analysis 80−28996
$CaO-MnO-SiO_2$ system glasses, vitrification and crystallisability 77−7853
$CaO-Na_2O-B_2O_3$, Raman scatt. studies of glass struct. 77−90147
$CaO-Na_2O-SiO_2$ glass, leaching studies by sputter-induced photon spectrometry 80−80004
$CaO-Na_2O-SiO_2$ glass, molten, metal ion diffusion and redox behaviour, electrochemical studies 80−81332
$CaO-Nd_2O_3-Fe_2O_3-Al_2O_3$ system, solid-state reactions 80−35173
$CaO-OsO_2$ system 79−24739
$CaO-P_2O_5$, glass, US velocity rel. to elastic props. 80−103425
$CaO-P_2O_5$ glass, diffusion of Cu^+, fluoresc. meas. 78−59980
$CaO-P_2O_5$ glass, ESR of VO^{2+} ions 80−100610
$CaO-P_2O_5$ glass, pulsed EPR study of Cu 78−84479
$CaO-P_2O_5:Cr^{3+}$ glass, absorpt. spectra, Fano antireson. and vibronic Lamb shift 80−71458
$CaO-P_2O_5-H_2O$ system, phase diagram at 200°C 80−45286
$CaO-P_2O_5-SiO_2$ glasses, photoelastic consts. and polarisability 79−65839
$CaO-SiO_2$, and $NaF-BeF_2$ systems, complex ionic liquids, corresponding-state principle *(Japanese)* 77−56245
$CaO-SiO_2$, arc electrode processes, thermodynamic approach *(Russian)* 77−27755
$CaO-SiO_2$, cements, effect of additives on compressive strength, carbonisation shrinkage, frost resistance 79−1897
$CaO-SiO_2$, melt, effect of cooling rate upon glass transition, X-ray analysis 79−27920
$CaO-SiO_2$, molten, corresponding state principle with $NaF-BeF_2$ and appl. 79−11589
$CaO-SiO_2$, molten binary, X-ray exam. of struct. 78−38610
$CaO-SiO_2$ DC arc plasma, meas. of conc. ratio of component atoms *(Russian)* 77−27754
$CaO-SiO_2$ glass, trimethylsilylation method for silicate ion anal. *(Japanese)* 80−71975
$CaO-SiO_2$ glass, two phase region, expt. and thermodynamic data 80 16288
$CaO-SiO_2$ glass prep. by gel method 80−100824
$CaO-SiO_2$ glasses, morphology effects on props. 80−49118
$CaO-SiO_2$ liquid, anal. expressions for heat capacities 79−77765
$CaO-SiO_2$ melt, ^{31}Si tracer diffusivity at 1600°C 80−54418
$CaO-SiO_2$ melt, tracer diffusivity of Ca^{45} and elec. cond. 79−60532
$CaO-SiO_2$ melt, viscosity and polymerisation *(Russian)* 78−26712

calcium compounds continued
$CaO-SiO_2$ slags, containing CaF_2 and B_2O_3, SO_2 capacity determ. by encapsulation method 80−11944
$CaO-SiO_2$ system glasses, IR absorpt. struct. obs. of phases and struct. 80−34918
$CaO-SiO_2/GeO_2-H_2O$ system, phase relations, influence of Si/Ge isomorphous substitution 79−52180
$CaO-SiO_2-Al_2-O_3$, 1500°C, ion transport coeffs., interdiffusivities 77−11718
$CaO-SiO_2-Al_2O_3$, metallurgical slag, dissolution of N_2 77−21109
$CaO-SiO_2-Al_2O_3$, slag phase, activity of components at 1873K *(Polish)* 78−52775
$CaO-SiO_2-Al_2O_3$, wollastonite, low dielec. loss factors, fabrication *(Japanese)* 80−55032
$CaO-SiO_2-Al_2O_3-Fe_2O_3$ mix, liquid phase sintering 79−91610
$CaO-SiO_2-Al_2O_3-MgO$, phase equilibria 77−86011
$CaO-SiO_2-Al_2O_3-Na_2O-CaF_2$ melts, surface tension and limit wetting angle in contact with C and CrNi steels *(Czech)* 79−37908
$CaO-SiO_2-Fe_2O_3$ glass, Mossbauer spectra 80−15850
$CaO-SiO_2-Fe_2O_3(MgO)$, melt, CaO dissolution *(Japanese)* 78−6909
$CaO-SiO_2-Fe_xO$ system, liq., steel making slag, Ca and Fe tracer diffusivities, O_2 press. depend. 78−38863
$CaO-SiO_2-MgO$ melt, elec. cond. meas., MgO behaviour *(Japanese)* 78−75857
$CaO-SiO_2-MnO$ molten mixtures, struct. and phys. props. *(French)* 80−24635
$CaO-SiO_2-MnO$ system, melts, densities, molar vols., thermal expansivity *(French)* 79−51183
$CaO-SiO_2-MnO$ systems, melts, elec. cond., struct. *(French)* 79−51287
$CaO-SiO_2-NiO$ melt, viscosity and elec. cond., effect of NiO conc. *(Japanese)* 79−23760
$CaO-SiO_2-NiO-MgO$ glass melt, interaction of NiO and MgO, elec. cond. and IR spectra obs. *(Japanese)* 80−24632
$CaO-SrO-Fe_2O_3$ system, phase relations, Sr hexaferrite field occurrence 80−93545
$CaO-TeO_2$, cryst. chem. study, X-ray diffr. powder data *(French)* 80−15080
$CaO-TeO_2$ glass, struct. and props. *(Japanese)* 79−32917
$CaO-V_2O_5-Fe_2O_3-PbO$, crystallisation field of Ca-V ferrogarnet 77−16548
$CaO-V_2O_5-SiO_2$ system, compatibility triangles 80−81037
$CaO-ZrO_2$ solid soln., thermodynamic investig., by EMF method 77−36485
$CaO-ZrO_2:Mn^{2+}$, EPR spectra, impurity substitution behaviour in various phases 77−16160
$CaO+\alpha-Fe_2O_3$, additive in ZrO_2 sintering 78−76617
$CaO+MoO_3 \rightarrow CaMoO_4$, solid state reaction 79−43579
$CaO+WO_3 \rightarrow CaWO_4$, solid-state reaction mechanisms 77−36750
$\beta-(CaO_2)-SiO_2-H_2O$, SEM and X-ray diffr. exam. of structure, crystallisation props. 78−73012
$Ca(O_2)_2$, standard heat, entropy and free energy of form. 79−87869
CaO_3, visible and absorpt, and reson. Raman spectra in Ar and N_2 matrices 77−65487
$Ca_2O:Bi$, positive ion nonequilibrium emission in heterogeneous chemical reaction, mass spectra 80−55277
$2CaO(Al_2O_3)_x(Fe_2O_3)_{1\ x}$, Fe^{3+} distrib. in struct. 79−94980
$(CaO_{1-x}BaO_x.6Fe_2O_3)_{97}(La_2O_3)_3$ ferrite magnets, anisotropic, BaO substitution effect on mag. props. *(Japanese)* 79−99697
$CaO(Ca_2O)-TiO_2-P_2O_5$, electrical resistivity *(Japanese)* 77−12719
$Ca(OD)_2:Cu^{2+}$, ESR, secondary spectra 78−88174
CaOH, dissociation energies, spectrometric determ. 78−74789
CaOH, laser excited mol. fluorescence, in an air-acetylene flame 78−86908
$Ca(OH)_2$ and $Ca(OD)_2$, molecular and lattice dynamics by IR^2 and Raman spectra 77−73134
$Ca(OH)_2$, dehydration, unsteady heat conduction, thermal conductivity change 80−76511
$Ca(OH)_2$, dissociation energies, spectrometric determ. 78−74789
$Ca(OH)_2$, energy storage medium for solar power systems 79−43790
$Ca(OH)_2$, mag. ordering of proton spins 79−73746
$Ca(OH)_2$ separation in CaH method of metal powders manufacture 80−84878
$Ca(OH)_2$, single cryst. NMR 77−48058
$Ca(OH)_2$, V-centres, EPR obs. 77−48051
$Ca(OH)_2:Ni^{2+}$ single cryst., X-irrad., Ni^+ EPR, g-factors and point-charge model 80−2626
$Ca(OH)_2$+silicate, reaction rates 80−26006
$Ca_5OH(PO_4)_5$, powder, precise study of electron diffr. patterns, diffr. interpretation at high tension *(French)* 79−37594
$(CaO)_3SiO$ cement pastes, electron microsc. anal. 80−108761
$(CaO)_3SiO_2$, effects of polymorphism on hydration, X-ray and TEM obs. *(Japanese)* 79−20046
CaO(100) surface, rumpling calc. 78−14559
$3CaO.Al_2O_3$ cement, high level radioactive waste disposal 78−78485
$\beta-CaO.Al_2O_3$, onset temp. of decomp. 77−81244
$CaO.Al_2O_3$, thermal expansion 77−84953
$3CaO.Al_2O_3-CaSO_4.2H_2O-CaO-H_2O$, citric acid effect on reactions 78−27725
$3CaO.Al_2O_3+CaSO_4.2H_2O$, effects of prehydration on liq. hydration 79−100354
$\beta-2CaO.SiO_2$, carbonation reaction kinetics, with CO_2 and H_2O vap. 79−79219
$\beta-CaO.SiO_2$, parawollastonite, rel. between structs. proposed 80−15056
$CaO.SiO_2$ pastes, structural props., hydrating cmpd. effect 79−100331
$ZCaO.SiO_2-2CaO.Na_2O.P_2O_5$ system, polymorphism and solid soln. 78−19731
$\beta-2CaO.SiO_2+H_2O+CO_2$, reaction conditions 80−26007
$(CaO)_3.SiO_2$, adsorption of H_2O, NMR exam. 78−48354
$CaO.SnO_2.SiO_2$, tin sphene, lattice parameters 77−7697
$CaO.V_2O_5$, reduction by Al powder for V production 78−44049
$10CaO.15Na_2O.75SiO_2$ glass, thermal cond., temp. depend. at low temps. 80−65322
$CaO.3B_2O_3,6H_2O$, thermal dehydration 78−43132
$CaO.3B_2O_3$, form. by dehydration of hydrated calcium borates *(Japanese)* 79−74378
$CaO.6Al_2O_3$, thermodynamic stability, reaction with Ti, Cr and Zr oxides 80−92687
$12CaO.7Al_2O_3$, composition of gases released on heating, crystallisation *(Russian)* 80−93820
$12CaO.7Al_2O_3$, hydration in presence of $Ca(OH)_2$ *(Japanese)* 79−20364

calcium compounds continued
$12CaO.7Al_2O_3$, single cryst. growth from melt 79—47614
$(CaO.nFe_2O_3)_{100-x}(La_2O_3)_x$ ferrite, permanent mag. material, mag. props. and preparation 79—83148
$Ca(PO_3)_2$ glass, crystallisation below glass transition, stress effect 80—19709
$Ca(PO_3)_2$ glass, rate of crystallisation, SiO_2 additive effects *(Japanese)* 77—68927
$Ca(PO_3)_2$, vitreous, microhardness 80—25864
$Ca(PO_3)_2:Eu^{3+}$, amorphous, phonon-assisted site-to-site electronic energy transfer, fluoresc. line narrowing obs. 77—81140
$Ca(PO_3)_2:Eu^{3+}$, anomalous spectral props. 79—38614
β-$Ca_2(PO_4)_2$ whitlockite ceramic fabrication for prosthetic applications 79—78924
β- and γ-$Ca_2P_2O_7$, IR and Raman vibr. spectra 80—25355
α-$Ca_2P_2O_7$, Raman, IR spectra, factor group anal. and band assignment 78—35126
$Ca_2P_2O_7$, solid state reaction with Al_2SiO_5 *(Japanese)* 78—19702
$Ca_2P_2O_7:Eu^{2+}$, activated phosphors, luminesc. efficiency, temp. and high-press. 78—23508
$Ca_2P_2O_7$:Sb, (Sb,Mn), luminesc., activation, colour centres *(Russian)* 78—92123
$Ca_2P_2O_7$:Sb(,Mn), luminesc., colouration 80—2828
$Ca_3(PO_4)_2$, amorphous, reduced intensity functions, thermal vibr. coupling 78—42910
$Ca_3(PO_4)_2$ ceramic, material science, bone implant 80—93523
α-$Ca_3(PO_4)_2$, cryst. struct. 77—47395
$Ca_3(PO_4)_2$, crystallisation kinetics 79—43119
$Ca_3(PO_4)_2$, new cryst. phase prep. and struct. *(French)* 78—83789
β-$Ca_3(PO_4)_2$, synthesis and fabrication, prosthetic appl. 79—24479
$Ca_3(PO_4)_2:Cu^{2+}$, ESR, high press. struct. transition 80—97134
$Ca_3(PO_4)_2$:Sb,(Sb,Mn), luminesc., activation, colour centres *(Russian)* 78—92123
β-$Ca_3(PO_4)_2$:Sb(,Mn) 80—2828
$Ca_3(PO_4)_2$-$CaCl_2:F^-$, electron excess colour centres, EPR experiments 78—10772
$Ca_3(PO_4)_2$-Mg_2SiO_4, partial system, phase diag. 77—86005
$Ca_4P_2O_9$ ceramic, material science, bone implant 80—93523
$Ca_5(PO_4)_3$, fluorapatite, far IR reflectivity to polarised light 79—56778
$Ca_x(PO_4)_y$, soln., coagulation effects on light scatt. obs., TEM, SEM 80—45090
$Ca_{10}(PO_4)_6Cl_2$, nonstoichiometry effect on X-irrad. induced electron-excess centres 77—62525
$Ca_2PO_4Cl:MnO_4^{3-}$, polarised electronic spectrum 77—52137
$Ca_5(PO_4)_3Cl$, structural interaction of Cl 78—55837
$Ca_{10}(PO_4)_6(F,OH)_2$, apatite, cryst. growth and habit, F ion conc. effect 78—30560
$Ca_{10}(PO_4)_6F_2:NO_2^{2-}$ apatite, ESR, struct. of ions *(French)* 78—43640
$Ca_5(PO_4)_3F$, cryst. struct., pattern-fitting struct. refinement method for X-ray powder diffractometer patterns 77—76251
$Ca_5(PO_4)_3F$, dislocation struct. exam. *(Russian)* 78—63770
$Ca_5(PO_4)_3F$, structural interaction of F 78—55837
$Ca_5(PO_4)_3F$: Cr^{5+}, spin-lattice relax. time and Debye temp., EPR obs. 79—28601
$Ca_5(PO_4)_3F:Cr^{5+}$, ESR, polymorphic transform., spin Hamiltonians 77—36117
$Ca_5(PO_4)_3F:Nd^{3+}$, luminesc. and absorpt. spectra, line shift and broadening 77—4678
$Ca_5(PO_4)_3F:Nd^{3+}$, optical fluorescence intensity and cryst. field parameters 78—52570
$Ca_5(PO_4)_3F:Nd^{3+}$, selective site laser spectroscopy and ESR studies 79—19909
$Ca_5(PO_4)_3F:Nd^{3+}$ site symmetries, EPR and spectral obs. 78—6571
$Ca_5(PO_4)_3F:Yb^{3+}(Nd^{3+})$, spin-lattice relax. times meas., Raman processes 77—51953
$Ca_5(PO_4)_3(F_{1-x}(OH)_x)$ apatites, lattice struct. NMR obs. 79—42845
$Ca_{10}(PO_4)_6(OH)_2$, dissolution in water at constant pH, exam. of kinetics 78—59949
$Ca_{10}(PO_4)_6(OH)_2$ dissolution kinetics, nucleation-controlled 80—59659
$Ca_{10}(PO_4)_6(OH)_2$ halogenated derivatives, IR absorpt. spectra *(Spanish)* 78—52489
$Ca_{10}(PO_4)_6(OH)_2$, hydroxyapatite, prep. by hydrotherm. recrystn. 79—33913
$Ca_{10}(PO_4)_6(OH)_2$, hydroxyapatite, aq. solution system, interfacial props. and equilibria 79—77751
$Ca_{10}(PO_4)_6(OH_2)$, IR spectra, stretching and librational bands of OH groups, and hindered rotation 78—2841
$Ca_{10}(PO_4)_6(OH)_2$ microcrystals, dissolution in non-stoichiometric solns. at constant pH 80—24597
$Ca_{10}(PO_4)_6(OH_2)$, polarised Raman and LF IR spectra, lattice vibr. 77—77192
$Ca_{10}(PO_4)_6(OH)_2$, solubility in aq. media 79—82341
$Ca_{10}(PO_4)_6(OH)_2$, synthesis and characterisation in dense polycryst. form 77—4749
$Ca_{10}(PO_4)_6(OH)_2$, UV induced thermolumin. glow peak obs. 80—29814
$Ca_{10}(PO_4)_6(OH)_2$:Mn, thermoluminesc. 77-500K, X-irrad. at 77K *(French)* 78—15234
$Ca_3(PO_4)_3(OH)$, automated scan of X-ray powder diffraction pattern 80—22492
$Ca_5(PO_4)_3OH$ ceramic, material science, bone implant 80—93523
$Ca_5(PO_4)_3OH$, prep. from sulphate, X-ray diffr. and IR spectrosc. 80—29893
$Ca_5(PO_4)_3OH$ prod. by hydrothermal synthesis, thermolum. props. 80—2877
$Ca_5(PO_4)_3OH$, structural interaction of OH 78—55837
$Ca_5(PO_4)_3OH$:Mn, synthesized by hydrothermal method in CaO-P_2O_5-H_2O, thermoluminescence study rel. to starting mixture 78—95612
$Ca_x(PO_4)_y(OH)_z$, nonstoichiometric, wet-process formation from α-$Ca_3(PO_4)_2$ *(Japanese)* 78—84752
$Ca_{10}(PO_4)_6(OH)_{2-2x}O_x\square_x$ polycryst. sintered bodies, prep. and thermal props. 80—25624
$Ca_{10}(PO_4)_6X_2$ (where X is F, Cl, OH or Co), influence of mech. treatment on struct. and reactivity *(German)* 79—43272
$Ca_{10}(PO_4)_6X_2$, halophosphate luminophor, forming during annealing of briquetted mixture 78—11173
$Ca_{10}(PO_4)_6X_2$:Sb, halophosphate luminophor, causes of Sb loss during synthesis 78—11172
$Ca_9(PO_4)_6.H_2O$, hydrolysis, activation energy *(French)* 77—73447
$CaPb(OH)_6$, cryst. struct. determ. *(French)* 77—47419
$Ca_{0.5}Pr_{0.5}H_n$, H_2 dissociation press., phase behaviour and struct. 78—2260

calcium compounds continued
$Ca(Pt(CN)_4)5H_2O$, transition energy tuning from 3.3 to 1.4 eV 79—61436
CaR_2S_4, R = rare earth, ternary sulphide with Th_3P_4 struct., vib. spectra 78—2844
$Ca_4R_6(SiO_4)_6F_2$, (R = Nd, Y or Yb), synthesis and characterisation 77—24992
Ca_3ReO_6, ordered or perovskite type struct., magnetic and elec. props. 79—65053
$Ca_{1+x}Re_2O_6(OH)_{2x}$ (x = 0,3), high pressure synthesis and structure *(French)* 78—51511
CaS, $A^1\Sigma^+$-$X^1\Sigma^+$, Franck-Condon factors and r-centroids 79—36700
CaS, absorpt. band identification of colour centres 77—40271
CaS, atomic and mol. centres of O, ESR and luminesc. methods *(Russian)* 80—84764
CaS, colour centres and photoluminesc., flash stimulation bands *(Russian)* 77—20923
CaS, dielectric props., effective ionic change 79—65783
CaS discs, sintering method prep., ionic cond. meas., 650 to 900°C *(Japanese)* 78—75869
CaS, EPR of colour centres, 295K *(Russian)* 80—84649
CaS, negative muon capture, rel. probability meas. 77—50550
CaS, oxidation kinetics 79—52407
CaS, phosphor, optical flash stimulation, optical absorption, MCD, thermally stimulated luminescence expts. 78—10951
CaS, phosphor, tunnel luminescence *(Russian)* 78—72577
CaS, phosphors, hole recombination luminescence *(Russian)* 78—72576
CaS, polycryst., cathodoluminesc. of point defects 79—78759
CaS, polycryst., point defects, EPR obs. 79—61214
CaS, single crystal, reflectance and absorption spectra, at edge of fundamental absorption *(Russian)* 78—56499
CaS, solid, tracer diffusion coefficient of S by ion microanalyser *(Japanese)* 80—34233
CaS:Bi, Tm, phosphor sensitisation mechanism, energy transfer 78—60507
CaS:Bi,Dy phosphors, thermoluminesc. 77—69921
CaS:Bi as UV dosimeter 80—34991
CaS:Bi phosphors, UV dosimetry by thermolum. 80—55199
$CaS:Bi^{3+}$, Pd^{2+}, phosphor, electroluminesc., brightness and mechanism 77—48248
$CaS:Bl^{3+},Na^+(Li^+)$ phosphors, luminescence of associated centres *(French)* 80—40155
CaS:Ce, Na, photon sidebands in emission and excitation spectra, pseudolocalised vibrs. 79—28800
CaS:Ce, Na phosphor, photoluminescence and excitation spectra 80—89049
$CaS:Cr^{3+}(Cr^+)$, EPR *(Russian)* 78—91946
CaS:Cu, colour centres, optical and thermal depths determ. 80—66275
CaS:Cu, colour centres and photoluminesc., flash stimulation bands *(Russian)* 77—20923
CaS:Eu, Eu^{2+} to Eu^{3+} charge transfer *(Russian)* 78—72403
$CaS:Eu^{2+}$, emission and excitation spectra obs. 80—55162
CaS:Mn,Ce, phosphor, fluoresc. spectrum, fine struct., ${}^4T_{1g}({}^4G)\rightarrow{}^6A_1({}^6S)$ transition 80—45130
CaS:Nd, Cu, phosphor, electroluminesc., spectral characts. 79—19936
CaS:Nd phosphors, X-ray powder diffr. anal. 80—100204
$CaS:Pb^{2+}(Bi^{3+})$, liminesc. 77—73166
CaS:Pd phosphor, thermally stimulated elec. cond., kinetics, 300-413K 78—76088
CaS:Pd phosphors, trap and luminescent centre location, photo-, thermo- and electroluminescence studies 80—71482
CaS:Tb,Eu phosphors, fluoresc. spectra under X-ray excitation 80—16083
CaS:Zn phosphor, photoluminesc. meas. 77—20913
CaS:Zr, Gd phosphors, thermoluminesc., trap distrib., activator effects 78 2929
CaS:Zr phosphors, photoluminesc. 79—28806
CaS:Zr phospors, photoluminesc. 79—28805
CaS-BaS:Cu phosphors, X-ray diffr. and fluoresc. spectra 80—40148
CaS-Bi, Mn, phosphors, thermoluminesc., phosphoresc. 78—2928
CaS-Pb,Mn, phosphors, thermoluminesc. and fluoresc. spectra 78—64396
CaS-Y_2S_3 (1 wt.%), solid electrolyte, elec. cond. under low partial pressures of S *(Japanese)* 80—49409
$Ca(SCN_2)$-water-n-butanol system with hypercrit. point, US absorpt. 80—49306
$CaSO_3$, thermal decomp., enthalpy of form. 77—73460
$CaSO_4$, (anhydrite), crysts., vibr. spectra, approx. calc. method *(Russian)* 78—35148
$CaSO_4$, anhydrite, resonance splitting of complex anion internal vibrs. 80—55081
$CaSO_4$, anhydrite and gypsum, phonon spectroscopy, lattice dynamical calc. 80—19889
$CaSO_4$, body centered matrix basis 80—79765
$CaSO_4$, cryst. growth kinetics at heated metal surfaces, thermal cond. morphology and crystn. 80—29867
$CaSO_4$ crystallisation, from liq. solns. as heat-transfer surface 80—100772
$CaSO_4$, dissolution kinetics on {111} faces of H_2SO_4 etched CaF 80—2028
$CaSO_4$, gypsum, growth curves, growth affinity presentation, for growth from soln. 79—27936
$CaSO_4$, γ-irradiated, ESR and bleaching studies of radical ion centres 80—2637
$CaSO_4$, hexagonal-orthorhombic transition kinetics 79—23724
$CaSO_4$, in KBr(KI) crysts., SO_4^{2-} vibr. spectra, press.-scanned Fermi reson. spectroscopy appl. 79—73937
$CaSO_4$ phosphors:Ce(Eu)(Dy)(Tm), gamma-irradiated valency conversions in rare-earth ions 80—55198
$CaSO_4$ TLD disc response to ${}^{131}I$ and ${}^{125}I$, influence of thyroid geometry 78—73250
$CaSO_4$, TLD material, kerma for monoenergetic neutrons, theory, expt. comparison 77—5086
$CaSO_4$, thermal decomposition, torsion-effusion cell obs. 77—77741
$CaSO_4$, thermal expsn., 22-1000°C 80—6530
$CaSO_4$, thermoluminesc. spectra, X-irrad. effect 78—35210
$CaSO_4$ with rare-earth and Y dopants, ESR, thermolum. correlation studies following gamma irradiation 77—59628
$CaSO_4$:Bi, cryst. growth, luminesc. props. 77—58993
$CaSO_4$:Ce(Eu) phosphors, fluorescence spectra, thermolum. glow curve 80—2879
$CaSO_4$:Dy, α and γ thermoluminescence response comparison 79—85814

calcium compounds continued
$CaSO_4$:Dy, Cd-covered TLD, thermal neutron dosimetry 77—90912
$CaSO_4$:Dy, competing deep trap model for thermoluminescence 79—83039
$CaSO_4$:Dy, cryst. growth from soln., thermoelec. and thermoluminesc. props. 79—56923
$CaSO_4$:Dy, γ-ray induced sensitization, competing trap model 80—2881
$CaSO_4$:Dy, high exposure UV response and sensitisation 79—91506
$CaSO_4$:Dy, phosphor, X-irrad., thermoluminesc., role of Na_2SO_4 as charge compensator 79—78764
$CaSO_4$:Dy, photo-stimulated thermolum., for high-exposure dosimetry 77—9262
$CaSO_4$:Dy, phototransferred TL studies 80—80875
$CaSO_4$:Dy, TLD during irrad. by γ-rays, X-rays, electrons, ambient atm. effect 78—19578
$CaSO_4$:Dy, TLD phosphor, gamma-ray induced sensitisation 78—74542
$CaSO_4$:Dy, TLD phosphor response, heating rate effect 80—26359
$CaSO_4$:Dy, TLD-900, thermolum. stability at low radiation doses 80—101272
$CaSO_4$:Dy, thermolum. dosimetry, high dose behaviour, comparison with trap depth model prediction 78—78588
$CaSO_4$:Dy, thermolum., studies for dosimetry 79—29634
$CaSO_4$:Dy, thermoluminescent glow peaks, post γ-irrad. annealing study 80—89077
$CaSO_4$:Dy embedded Teflon TLD phosphor photon energy dependence obs. 79—26761
$CaSO_4$:Dy fast-neutron TLD, efficiency increase by mixing with S 78—73251
$CaSO_4$:Dy phosphor, effect of Dy conc. on TL characteristics 79—93881
$CaSO_4$:Dy phosphor powder, effect of grinding on thermoluminescent sensitivity 79—33852
$CaSO_4$:Dy phosphors, photomag. susceptibility 78—2724
$CaSO_4$:Dy phosphors, dosimetric appls. 79—76154
$CaSO_4$:Dy photostimulated luminesc. for radiation dosimetry 77—90910
$CaSO_4$:Dy ribbon, dosimetric props. study 80—63395
$CaSO_4$:Dy sintered pellets, thermolum. response 80—93411
$CaSO_4$:Dy TLD, fading in high γ-dose region 78—90027
$CaSO_4$:Dy TLD, temp. effect during UV and gamma irradiation 79—38684
$CaSO_4$:Dy TLD phosphor, γ radiation changes in glow curve 80—60688
$CaSO_4$:Dy Teflon TL dosimeters, thin, development for β-dosimetry in personnel monitoring 80—63399
$CaSO_4$:Dy Teflon TLD discs, graphite-mixed, for beta dosimetry 77—86639
$CaSO_4$:Dy Teflon TLD discs, thermal history and reusability 79—89507
$CaSO_4$:Dy thermoluminescent dosimeters, low exposure rate depend. 78—20285
$CaSO_4$:Dy thermoluminescence sensitivity and glow curves, 700° to 1300°C 79—85815
$CaSO_4$:Dy thermoluminescent phosphor, effect of sensitisation on energy depend. 80—26358
$CaSO_4$:Dy-KBr thermolum. phosphor, thermal neutron detect. by activation 80—32581
$CaSO_4$:Dy$+Dy_2O_3+$KCl, intermediate neutron detection by thermoluminescence 80—5444
$CaSO_4$:Dy(Tm), thermolum. induced by 254 nm UV photons 80—55204
$CaSO_4$:Dy(Tm), thermolum. thermolum. phosphor, photolum. and absorpt. spectra, thermolum. mechanisms 80—97321
$CaSO_4$:Dy(Tm) thermoluminescent props. of non-commercial phosphors 78—58550
$CaSO_4$:Eu, origin of thermoluminescence 77—85813
$CaSO_4$:Mn, phosphor, thermoluminesc., low energy ion excitation 77—55838
$CaSO_4$:Sm phosphors, mag. susceptibility temp. depend. 300-453K 78—52196
$CaSO_4$:Sm phosphors, X-ray induced fluorescence and phosphorescence 80—55179
$CaSO_4$:Sm phosphors, X-irrad., thermoluminesc., charge compensation effects 80—97351
$CaSO_4$:Tm, Li, mixed field TLD 77—9263
$CaSO_4$:Tm, sensitised TLD phosphor, photon energy dependence 80—78498
$CaSO_4$:Tm, TLD phosphor, γ-induced sensitisation and residual thermolum. 79—28844
$CaSO_4$:Tm and nonluminous ^{6}LiF powders mixture, thermoluminesc. response to thermal neutrons 77—73588
$CaSO_4$:Tm composite TLD for γ-rays, X-rays, β-rays, and thermal neutrons 78—28076
$CaSO_4$:Tm intrinsic thermoluminescence stability for UV dosimetry 80—12262
$CaSO_4$:Tm/polythene mixture, thermoluminesc. response to fast neutrons 80—5340
$CaSO_4.H_2O$ (gypsum), hydration water isotopic comp. 79—20829
$CaSO_4.{}^1/_2H_2O$, (α and β-phase), surface chem. and porosity 78—85200
$CaSO_3.1/2H_2O$-$CaSO_4$ solid solution, prepared by coprecipitation from solns., exam. 79—20034
$CaSO_4.1/2H_2O$, transition to gypsum, mechanism 77—48390
$CaSO_2.2H_2O$, few thermodynamic invariants, proof from PMR 78—43657
$CaSO_4.2H_2O$, ball mill grinding, rate constant determination *(Japanese)* 78—95828
$CaSO_4.2H_2O$ crystals, linear growth rates in presence of additives 80—10515
$CaSO_4.2H_2O$, crystallisation 80—100766
$CaSO_4.2H_2O$, gypsum whisker, produced by desulphurisation *(Japanese)* 77—76712
$CaSO_4.2H_2O$, gypsum, cryst. growth at 298 and 313K, with and without mag. field influence *(Russian)* 78—9973
$CaSO_4.2H_2O$, gypsum, cryst. growth rates and nucleation *(French)* 80—80959
$CaSO_4.2H_2O$, H_2O intramol. force fields calcs. 79—51229
$CaSO_4.2H_2O$, mol. reorientations and mol. diffusion, PMR 78—43671
$CaSO_4.2H_2O$, occlusion formation during dendritic crystal growth, expt. 78—38993
$CaSO_4(.2H_2O)$, single cryst., SO_4^{2} vibr. levels, cryst. field effects, laser Raman spectroscopy 78—43847
$CaSO_4.2H_2O$, solid echo effect 77—51988
$CaSO_4.2H_2O$, solubility and activity coeffs. in synthetic seawater 79—91986
$CaSO_4.2H_2O$, supersaturated soln., nucleation induction time 79—69042

calcium compounds continued
$CaSO_4.2H_2O$, thermodynamic expression for crystal growth and dissolution affinity 80—24385
$CaSO_4.2H_2O$, Young's modulus in (010) plane, dynamical meas., natural cryst. 78—38768
$CaSO_4.2H_2O$-$CaHPO_4.2H_2O$ system, solid solns., IR study *(French)* 80—66165
$CaS_2O_6.4H_2O$, isomorphic substitution effect on optical activity 77—32347
$CaS_2O_3.6H_2O$, cryst. data and mag. susceptibility 77—76368
CaS(Se), crystalline pots. from XPS data 77—77344
$CaSb_{10}O_{10}S_6$, sarabauite, X-ray cryst. struct. determ. and refinement 79—14754
$Ca_3SbSnFe_3O_{12}$, mag. ordering and bond geometry rel. to tetrahedral Fe^{3+} 77—32163
$Ca_3SbSnFe_3O_{12}$, neutron diffr. patterns, group theory approach for determ. of mag. struct. *(Russian)* 79—51749
$Ca_3Sc_2Ge_3O_{12}$, garnet, refined cryst. struct. 78—87654
$Ca_3Sc_2Si_3O_{12}$, garnet, refined cryst. struct. 78—87654
CaSe: Sn^{2+}, dimer centre, emission and excitation spectra, temperature quenching *(French)* 79—99937
CaSe:Eu^{2+}, emission and excitation spectra obs. 80—55162
CaSe:Pb, luminesc. and EPR props. of Pb centres 80—55168
CaSe:Pb^{2+} phosphors, luminesc., refl., emission, and excitation spectra 79—11456
CaSe:Sn^{3+}, EPR study of octahedral Sn^{3+} centres, 4 to 290K *(Russian)* 80—84637
$Ca_x(Si,Al)_{12}(O,N)_{16}$, α'-Sialon ceramics, prep. and characterisation 78—84750
$Ca_{11}(Si,Al)_4O_{18}Cl$, alinite, cryst. struct. determ. 79—19215
$CaSi_2$, high press. transform. of three-connected Si nets 79—77744
$CaSi_2$, high-pressure phase transform., cryst. struct. 77—35693
$CaSi_2$, X-ray spectra, valence band struct. *(Russian)* 79—1798
$CaSiO_3$ (wollastonite), individual silicate chains obs. by high resolution electron microscopy 79—100829
β-$CaSiO_3$ fibre, continuous unidirectional crystallisation from melt 78—95739
$CaSiO_3$, fibrous, controlled crystallisation and anisotropy 80—59425
$CaSiO_3$ fibrous crystal reinforced matrix, unidirectional crystallization, anisotropic properties 79—56969
$CaSiO_3$, hydrated in Ca_3SiO_3 pore struct. 77—56213
$CaSiO_3$, production from xonolite slurry, using SiO_2 fibre 78—39730
$CaSiO_3$, structural transform. during hydration, IR spectra and X-ray diffr. meas. 77—76548
$CaSiO_3$, wollastonite, exptly. deformed, polytype transforms. 79—65021
β-Ca_2SiO_2, reaction kinetics with CO_2 and water vapour 80—76484
Ca_2SiO_4, bredigite-larnite rock from Scawt Hill, electron microprobe anal. 78—68952
β-Ca_2SiO_4, formation in presence of NaF, under different thermal treatments 78—68889
Ca_2SiO_4, gamma-irrad., ESR spectra 79—51853
β-Ca_2SiO_4, hydrating, composition of soln. in contact 78—11138
Ca_2SiO_4, K_2NiF_4-type structure, high pressure synthesis, crystal chemical and geophysical implications 79—69089
γ-Ca_2SiO_4, polymorphic transformation scheme 80—71642
β-Ca_2SiO_4, stabilisation, IR and Raman spectra 79—42265
β-Ca_2SiO_4, struct. redeterm., hydraulic activity 77—58981
Ca_2SiO_4, structural transform. during hydration, IR spectra and X-ray diffr. meas. 77—76548
Ca_2SiO_4, structurally related phases, high-temp. X-ray powder diffr. 80—81050
β-Ca_2SiO_4, very reactive powder, prep. 77—55924
Ca_2SiO_4-BaO, conditions and mechanism in cryst.-chemical stabilisation of unstable phases 80—39302
Ca_2SiO_4-$CaMgSiO_4$, T phase, review 80—50612
β-Ca_2SiO_4-CaO-SiO_2 paste, hydration, compression strength and composition 80—50584
Ca_2SiO_4-$CaSO_3$-CaO, region of homogeneity of Ca_2SiO_4 77—90332
Ca_2SiO_4-FeO, conditions and mechanism in cryst.-chemical stabilisation of unstable phases 80—39302
Ca_2SiO_4-MgO, conditions and mechanism in cryst.-chemical stabilisation of unstable phases 80—39302
Ca_2SiO_5, hydraulic reaction observed by microwave dielectric meas. 78—80745
Ca_3SiO_2, reaction kinetics with CO_2 and water vapour 80—76484
Ca_3SiO_3, hydrated, composition and morphology 78—26755
Ca_3SiO_5 form. by solid state reaction, mixture and firing condition effects 78—56602
Ca_3SiO_5, formation from $CaCO_3$ decomposition 79—52651
Ca_3SiO_5, fracture surfaces, quantitative anal. using energy dispersive X-ray spectrometry *(French)* 80—89571
Ca_3SiO_5, P containing, hydrated, microstruct. and IR struct. 79—29074
Ca_3SiO_5, polymorphism, X-ray diffr. data *(French)* 79—94973
Ca_3SiO_5, structural transform. during hydration, IR spectra and X-ray diffr. meas. 77—76548
Ca_3SiO_5, thermochem. effects on formation 80—16666
Ca_3SiO_5, thermomechanical effects on form. 79—15635
Ca_3SiO_5-$Cr_2O_3(Al_2O_3)(Fe_2O_3)$ solid solns., elec. cond., 800-1000°C, hydration 80—54683
$Ca_{11}Si_4O_{18}Cl$ alinite, cryst. struct. interpretation by rhombus method 80—39052
$Ca_2SiO_3Cl_2$, cryst. struct. 78—67694
$Ca_4Si_2O_7(OH)_2$, rustumite, crystal struct. 77—84727
$Ca_6Si_6O_{17}(OH)_2$, xonotlite, polytype identification from electron diffr. patterns 80—72519
$Ca_{10}(SiO_4)_3(SO_4)_3(OH,Cl,F)_2$, hydroxyellestadite, X-ray cryst. struct. determ. 80—96485
$Ca_6Si_6O_{18}.4H_2O$, tobermorite synthetic crysts., hydrothermal growth, TEM and X-ray diffr. characterisation 79—43122
$Ca_{1-x}Sm_xF_{2+x}$, luminesc. expt. suggesting Sm^{3+} ion pairing 80—76065
$Ca_{1-x}Sm_xS$, electron config. of Sm ions, X-ray L-absorpt. spectroscopy 80—60715
$CaSnCl_6$, Cl NQR anomalous temp. depend., crystal struct. and phase transitions 80—54977
$CaSnO_3$, ^{119}Sn conversion electron Mossbauer spectroscopy 79—33575
$CaSnO_3$, form. entropy and tolerance factor 80—34204
$CaSnO_3$, high-density ceramics prep. and elec. props. 80—60812
$CaSnO_3$, powder, electron scatt. from ^{119}Sn, effective range, Mossbauer obs. 77—63345
$CaSo_4$, exoelectron emission and radiation dosimetry *(Japanese)* 79—83110

calcium compounds continued

- $CaSo_4$, growth on CaF cryst. face etched in H_2SO_4, etch pit morphology 80–6408
- $CaSo_4$:Mn trap depth, thermolum. meas. 77–36301
- $Ca_{1-y}Sr_{y/2}Ba_{y/2}Zr_{1-x}Ti_xO_3$, ceramic system, dielectric props., microwave resonator application 80–80674
- $(Ca_{1-x}Sr_x)(Ca_{1/3}Nb_{2/3})O_3$ perovskites, cryst. struct. *(French)* 79–65044
- $Ca_{1-x}Sr_xF_2:Er^{3+}$ mixed crystal, luminesc. transition, inhomogeneous line broadening calc. 80–97332
- $Ca_{1-x}Sr_xFeO_3$, Mossbauer spectra, charge disproportionation 80–15891
- $Ca_{1-x}Sr_xFeO_3$, Mossbauer spectra, charge disproportionation 80–20542
- $Ca_2SrFe_2TiO_8$, crystal struct., O vacancy ordering *(French)* 77–11520
- $Ca_{10-x}Sr_x(PO_4)_6(OH)_2$, continuous cation migration, IR spectra study 80–93297
- Ca_2SrReO_6, ordered or perovskite type struct., magnetic and elec. props. 79–65053
- $(Ca_{1-x}Sr_x)RuO_3$, mag. props. 78–27027
- $Ca_{1-x}Sr_xSi_2$, solid solns., α-$ThSi_2$ struct. type, comp. and press depend. 78–91322
- $Ca_{1-x}Sr_xSi_2$, solid solution with type $SrSi_2$ struct., lattice parameters at high press. 80–54203
- $Ca(TCNQ)_2$, electronic absorpt. spectra, vibronic struct., charge transfer bands 79–24331
- Ca_2TaLaO_6, perovskite structure, cationic distrib. *(French)* 77–1109
- $CaTaRO_6$, (R=La, Nd, Gd, Sm, Er, Lu), synthesis and physicochem. props. 79–52139
- $CaTeO_4$, powder diffr. cryst. struct. determ. 79–42020
- $CaTe_3O_8$ (carlfriesite), cryst. struct., chemical formula revision, and synthesis 79–55709
- $CaThNb_2O_8$, monoclinic-quadratic phase transform. *(French)* 77–27998
- $Ca_6Th_4(SiO_4)_6O_2$, cryst. struct. by X-ray diffr., cation distrib. *(German)* 78–43001
- $Ca_n(Ti,Nb)_nO_{3n+2}$, (n=4.5,5 or 6), cryst. struct. determ. *(French)* 79–65039
- $CaTi_{0.7}Al_{0.3}O_{2.85}\square_{0.15}$, ionic conductivity 77–20119
- $Ca_2Ti_{2-2x}Fe_{2x}O_{6-x}$, antiferromag. phases, Neel temp. variation, vacancy long-range order *(French)* 78–34979
- $CaTiO_2$, $CaSnO_3$, $CaGeO_3$ perovskites, elasticity meas. to 6 kbar 77–51428
- $CaTiO_3$, crystallisation from melt, nucl. and final cryst. sizes 77–24951
- $CaTiO_3$, electrostatic lattice energy, optimisation of convergence of Ewald series 79–7569
- $CaTiO_3$, form. entropy and tolerance factor 80–34204
- $CaTiO_3$, O K_α X-ray emission band spectra *(Russian)* 79–15563
- $CaTiO_3$, perovskite, raw material activity and firing conditions as factors in sintering and grain growth 79–83161
- $CaTiO_3$, prep. from film forming soln. 80–60811
- $CaTiO_3$, protection against reduction during roasting in H_2 77–36426
- $CaTiO_3$, synthesis kinetics 79–15632
- $CaTiO_3$-$Ca_2Fe_2O_5$, Mossbauer resonance exam. of structure, phase equilibrium 78–76640
- $CaTiO_3$-$Ca_2Nb_2O_7$ system, mode of formation and stability of $A_nB_nO_{3n+2}$ phases *(French)* 78–3110
- $CaTiO_3$-$CaTiSiO_5$, sintering and dielectric props. 80–40307
- $CaTiO_3$-$LaAlO_3$ solid soln., phase redistrib. during roasting in H_2 78–52735
- $CaTiO_3$-$M_2Ti_2O_7$ system, mode of formation and stability of $A_nB_nO_{3n+2}$ phases, M=La, Nd *(French)* 78–3110
- $CaTiO_3$-TiO_2, ceramic, phys. props. 78–43784
- $CaTiO_4$, perovskite, sintering during synthesis 77–36422
- Ca_2TiO_3-La_3AlO_3, synthesis of solid solution by coprecipitation 79–1836
- $CaTiSiO_5$, sphere, effects of thermal annealing on track etching rate 78–65435
- $Ca_3Ti_{2x}V_{1.5-x}Fe_{3.5-x}O_{12}$. garnet, mag. and neutron diffraction investigation 77–16044
- $Ca_2TlTa_5O_{15}$, cryst. struct. *(French)* 79–86749
- $Ca_{1-x-y}U_xCe_yF_{2+2x+y}$, solid soln., ionic cond. 79–99356
- $CaUNb_2O_8$, monoclinic-quadratic phase transform. *(French)* 77–27998
- $Ca(UO_2PO_4)_2.6H_2O$, calc. and meas. of vibr. spectrum 77–76499
- CaV ferrite garnet, large grained, mag. props. 78–64222
- CaVG, polycryst. IR transmission spectra rel. to Faraday rotator and modulator appl. 78–10900
- $CaV_{12}O_{30}$, phase transitions, elec. cond., susceptibility and sp. ht. meas. 78–14776
- CaV_2O_6, elec. field gradient at ^{51}V, NMR meas. and ionic model calcs. 78–19370
- CaV_2O_6:Cr, EPR spectra temp. depend., paramagnetic ion point symm. 80–71166
- $CaV_2O_6:W^{6+},Mo^{5+}$, g-factors and hyperfine coupling parameters of V^{4+}, ESR 77–12196
- $Ca_{0.15}VO_2$, electrical cond., thermo-EMF, and lattice consts. 80–54685
- $Ca_2V_2O_7$, $Ca(VO_3)_2$, and $Ca_3(VO_4)_2$, thermal expansion, lattice constants temp. depend. 80–34211
- $Ca_2V_2O_7$, elec. props. and EPR meas. 79–11114
- $Ca_3(VO_4)_2$, linear and nonlinear optical props. 79–23010
- $Ca_3(VO_4)_2$, new high temp. ferroelectric, Curie temp. 78–43811
- $Ca_3(VO_4)_2$-$Mg_3(VO_4)_2$, exam. of phase composition and phase diagrams 79–1851
- Ca_xVO_2, oxygen vanadium bronze, phase comp., heating in air 77–40417
- $Ca_{10}(VO_4)_6(OH)_2$, solubility in aq. media 79–82341
- $CaWO:Mn^{2+}$, zero-field splitting of Mn^{2+}, EPR 80–75531
- $CaWO_4$, (scheelite), crysts., vibr. spectra, approx. calc. method *(Russian)* 78–35148
- $CaWO_4$ and rare-earth X-ray intensifying screen sensitivity to scattered radiation 78–7450
- $CaWO_4$, body centered matrix basis 80–79765
- $CaWO_4$, centrosymmetric cryst., linear electrogyration study 80–60540
- $CaWO_4$ collinear diffr. by oppositely directed acoustic beams 80–16007
- $CaWO_4$, cryst. growth from solns. in melts, kinetics parameters and thermodynamic props. 80–59424
- $CaWO_4$, crystal growth from soln. in Na_2WO_4 melts, by continuous cooling, growth kinetics exam. 78–48303
- $CaWO_4$, crystn. from solns. in $NaWO_4$ melts, kinetics obs. by DTA 80–40246
- $CaWO_4$, Czochralski grown, distrib. coeffs., cavity form., cellular struct. 77–11492
- $CaWO_4$, Davydov splitting of vibr. levels, short range interaction 80–71418
- $CaWO_4$, external lattice vibr. modes and elastic wave vels., dispersion relations 79–33050

calcium compounds continued

- $CaWO_4$, form., solid-state reaction mechanisms 77–36750
- $CaWO_4$, luminesc. efficiency, temp. and high-press. 78–23507
- $CaWO_4$ phosphor, interaction between intrinsic and impurity emission 79–8198
- $CaWO_4$, phosphors, energy storage, afterglow decay and thermolum. meas. 77–12422
- $CaWO_4$, radiographic intensifying screens, sensitivity to scattered radiation 77–77970
- $CaWO_4$, refr. index, single crystals having scheelite struct. 78–79082
- $CaWO_4$, scheelite, stella quadrangula as struct. building unit 80–15055
- $CaWO_4$, scheelite struct., intrinsic hole centres, EPR study 78–64274
- $CaWO_4$, single cryst. growth by Czochralski method and U incorporation, effective distrib. ratios, luminesc. characts. 79–42094
- $CaWO_4$, slow neutron inelastic scatt. spectra, Debye temp. calcs. *(Russian)* 80–59347
- $CaWO_4$, solid-phase synthesis, disordering and vacancy defect form. 77–8774
- $CaWO_4$ type compounds, system of polymorphic transitions 78–47268
- $CaWO_4$ undyed X-ray intensifying screen, role of reflective layer 80–62816
- $CaWO_4$, Yb^{3+}, Nd^{3+} phase relaxation electron spin echo spectra 80–29613
- $CaWO_4$:Er, spectroscopic parameters calcs. 80–50379
- $CaWO_4:Er^{3+}$, magnetocaloric behaviour, cryst. field theory 77–4520
- $CaWO_4:Er^{3+}$, phase relaxation, spin echo meas. 78–68375
- $CaWO_4:Eu^{3+}(Sm^{3+})$, energy transfer after red edge excitation 78–52552
- $CaWO_4:Fe^{3+}$, EPR, spin Hamiltonian parameters from anal. of Kramers' doublets 79–28595
- $CaWO_4$:Gd, site occupation 79–28608
- $CaWO_4$:Gd, thermally stimulated depolarisation current, 100 to 300K 80–7280
- $CaWO_4:Mn^{2+}$, polycryst., EPR spectra calc. using Bir's method, compared with expt. 79–1707
- $CaWO_4:Mn^{5+}$, new EPR center *(Russian)* 79–1709
- $CaWO_4$:Mo, P, thermoluminesc. traps, EPR meas. 77–90032
- $CaWO_4$:Na(Y), pure and doped, luminesc. props. 79–95835
- $CaWO_4:Nd^{3+}$, Slater, Racah and Lande parameters, crystal bonding 80–16062
- $CaWO_4:Nd^{3+}$, thermal behaviour of shape and width of 9145 Å laser line 78–6755
- $CaWO_4:Nd^{3+}$ $4f^3$ configuration, ground level energy state variation rel. to press. *(Russian)* 77–16358
- $CaWO_4:Nd^{3+}$ absorpt. spectra, hypersensitivity of $^4I_{9/2}$ to $^4G_{5/2}$ $^2G_{7/2}$ transition 80–97309
- $CaWO_4:Pr^{3+}$, anomalous hypersensitive $^3H_4 \rightarrow {}^3P_2$ transition 80–106296
- $CaWO_4:R^{3+}$, X=rare earth, cryst. field parameters, ang. overlap model 79–60772
- $CaWO_4:Tb^{3+}(Tb^{4+})$, new EPR centres *(Russian)* 79–1709
- $CaWO_4:Yb^{3+}(Nd^{3+})$, phase relax. time rel. to g-factor anisotropy, electron spin echo obs. 80–29615
- $Ca(WO_4)_x(MoO_4)_{1-x}$, Raman scatt. line shape 78–10898
- CaX-MnX, X=S, Se, Te, solubility limits 80–44320
- Ca_5X_3, α, intermediate phases, cryst. struct. (X=IIb, IIIb, IVb, Vb element) 78–83793
- Ca_2XRuO_6 (X=Y,La,Eu), ^{99}Ru Mossbauer spectra and other techniques 80–29659
- $CaYAlO_4:Nd^{3+}(Er^{3+})$, absorpt. and luminesc. spectra 77–69901
- $CaYAl_3O_7$, type of melting, crystallisation from melt 77–12515
- $Ca_{1-x}Y_xF_{2+x}$, fast ionic conduction of F^- ions 79–99360
- $Ca_{1-x}Y_xF_{2+x}$, solid anionic conducting electrolytes, struct., elec. props. 77–84977
- $Ca_2YFe_3O_8$, crystal struct., O vacancy ordering *(French)* 77–11520
- $Ca_4YFe_5O_{13}$, cryst. struct., electron microscopy and X-ray diffr. study 80–88116
- $CaY_2Ge_3O_{12}$:Nd, energy levels and laser action, fluoresc. meas. 79–81438
- $Ca_3Y_2Ge_3O_{12}:Eu^{3+}$, garnets, prep., struct., luminesc., absorpt. spectra, Eu^{3+} localisation 77–69884
- $Ca_{0.5}Y_{0.5}H_n$, H_2 dissociation press., phase behaviour and struct. 78–2260
- $CaY_2Mg_2Ge_3O_{12}$:Nd, CAMGAR, low threshold CW room temp. laser operation at 0.941 μm 78–1234
- $CaY_2Mg_2Ge_3O_{12}$:Nd, CW room temp. laser operation, 0.941 and 1.059μm 78–66842
- $CaY_2Mg_2Ge_3O_{12}:Nd^{3+}$, optical absorpt. and fluoresc. intensities 80–29793
- $CaY_4(SiO_4)_3O:Nd^{3+}$, absorpt. and luminesc. spectra 77–85755
- $CaZn(SiO_4).H_2O$, clinohedrite, cryst. struct., H bonds 78–79593
- $CaZrO_3$, form. entropy and tolerance factor 80–34204
- $CaZrO_3$, high-density ceramics prep. and elec. props. 80–60812
- $CaZrO_3$, perovskite type, X-ray K-absorpt. edge, chem. shift 79–91529
- $CaZrO_3:Pb^{2+}$, UV luminescence temp. depend., three-level model 77–4683
- $CaZrO_3:Pb^{2+}$ (Bi^{3+}) and related $Pb^{2+}(Bi^{3+})$-actuated hosts, cryst. struct. effects on luminesc. 77–16376
- $CaZrO_3$-$CaHfO_3$, solid soln. formation obs. 77–86003
- $Ca_3ZrSbFe_3O_{12}$, mag. ordering and bond geometry rel. to tetrahedral Fe^{3+} 77–32163
- ^{44}Ca substituted oxides, matrix isolated, IR spectra 78–9151
- $Ca2(NH_4)H_7(PO_4)_4.2H_2O$, X-ray cryst. struct., PO_4 ion with 3 symmetric H bonds 80–64956
- $Ca_8[Al_{12}O_{24}](WO_4)_2$, cryst. and powder diffr. data redeterm. 80–24423
- $Ca[B(OH)_4]_2$, frolorite, refinement of cryst. struct. 77–58996
- $Ca[B_2O_2(OH)_4]$, cryst. struct. determ. 77–15393
- $Ca_2[B_8O_{13}(OH)_2]$, refinement of cryst. struct., H-bonding 77–89421
- $Ca_2[B_3O_4(OH)_4]Cl$, solongoite, cryst. struct. refinement 78–26549
- $Ca[B_3O_4(OH)_3].H_2O$, differential thermal X-ray anal. of phase transitions in non isothermal conditions 79–52205
- $Ca[B_2O(OH)_6].2H_2O$, refined cryst. struct. 78–2092
- $Ca[B_3O_3(OH)_5].4H_2O$, differential thermal X-ray anal. of phase transitions in non isothermal conditions 79–52205
- $Ca_2[B_5O_9]Cl.H_2O$, hilgardite, PMR of water mol. 80–84655
- $Ca[Fe(CN)_5(NO)].4H_2O$, X-ray cryst. struct. determ., heavy-atom method 80–92494
- $Ca_5[GeO_4]_2(OH)_2$ monoclinic cell struct., crystallographic consts. 79–82191
- $Ca[Pt(CN)_4].5H_20$, energy band calcs. 77–39780
- $Ca_5[SiO_4]_2(OH)_2$, cryst. struct. refinement 80–107181
- $Ca_2[(UO_2)_3(PO_4)_2(OH)_2](OH)_2.4H_2O$, phurcalite, cryst. struct. determ 78–55849

calcium compounds continued
$Ca[ZnSiO_4].H_2O$, clinohedrite, cryst. struct., comparison with $(Mn,Mg)Mg(OH)_2[ZnSiO_4]$, herstmannite 79—19228
$3Ca.SiO_2$, carbonation reaction kinetics, with CO_2 and H_2O vap. 79—79219
Caf_2 current oscills. in elec. fields of $\sim 10^6\ Vm^{-1}$ *(Russian)* 77—20334
Caf_2, UV visible absorpt. by laser calorimetry, wavelength modulation spectroscopy 78—66876
$CdCa_2Cl_6.12H_2O$, X-ray cryst. struct. anal. *(French)* 79—4291
$Cd_xCa_{1-x}MoO_4$, intrinsic hole centres EPR study, thermoluminescence and thermal decay 79—99957
$Cd_{1-x}Ca_xS$, solid soln., phase equilib. diagrams 80—108412
$CdCo_3:Fe^{2+}$, electronic spin relax., effect of second-order spin-orbit coupling 80—10935
$CdF_2-CaF_2:Yb^{3+}$, Er^{3+}, IR to visible upconverting system 77—44035
CdS, diffusion length determ., resolution limit of EBIC technique 79—21865
CdS-CaS, solid soln., rock salt struct., high press. phase equilibrium study 78—52777
$Ce_{0.9}Ca_{0.1}O_{1.90}$, ionic cond. meas. 79—60543
CeF_2, ^{19}F NMR, free induction decay, initial behaviour 78—80227
$CeO-SiO_2$, molten and glassy state, X-ray diffr. determ. of struct. *(Japanese)* 78—9936
$CeO_2:CaO$, O ion cond. and defect struct. 80—107553
$Co_2Ti_{2-2x}Fe_{2x}O_{6-x}$ solid solution, extended defect model, X-ray diffr. and electron microscopy *(French)* 77—47446
$CsCaCl_3$ crystal, sp. ht. and thermal expansion coeffs. 80—10681
$CsCa_{0.95-x}Mg_xEu_{0.05}F_3$, blue luminesc. obs. 77—32428
$Cs_x^{+}(H_2O)_y[TaS_2]^{x-}$, hydrate layered chalcogenide, anisotropic mobility of water, NMR 79—65744
Cu-CaO concentrate pellet, oxidation kinetics 77—4894
$CuO-CaO-P_2O_5$ glass devices, memory switching 78—56192
$CuO-CaO-P_2O_5$ system glasses, DC cond., hopping transport, 300 to 620K 78—23096
$CuO.Al_2O_3.2SiO_2$, hydrothermal synthesis, phase transitions 77—48378
$(Eu,La,Ca)_3(Fe,Ga,Al)_5O_{12}$ film, LPE growth and induced orthorhombic anisotropy 77—20652
$Eu_{3-x}Ca_xSi_xFe_{5-x}O_{12}$, bubble film, LPE growth induced anisotropy 77—20659
$(EuLuCa)_3(FeGe)_5O_{12}$, mag. props. and growth of 2 μm bubbles 78—91910
EuTm-CaGe, magnetic FE garnet film, LPE growth and composition 78—23634
Fe-CaF (6 and 9 wt.%), sintered, elevated temp. mech. props. 77—28878
Fe-Mo-CaF (15, 9 and 6 wt.%), sintered, elevated temp. mech. props. 77—28878
$Fe-Mo-CaF_2$ sintered composite, struct. and mech. props., heat treatment effect 80—66526
$Fe_4Ca_3S_3O_6$, struct. and phase analysis *(Russian)* 77—58995
FeS_2-CaCO_3-C, reaction on heating, dissociation, reduction to Fe *(Russian)* 78—44041
GdCa garnets, solid soln., mag. and cryst. chem. props. 77—16057
HfO_2-CaO, elec. field gradient at ^{181}Ta, TDPAC meas. 79—33577
$Hg_{1-x}Cd_xTe$, semiconducting phase, acceptor states and galvanomagnetic effects 80—11017
$KCaCl_3$ impurity in NaCl cryst., precipitation and dissolution 79—42259
$KCaCl_3$, phase transitions, optical and dilatometric meas. 79—61394
$K_{2(1-x)}Ca_xSO_4:Tl^+$ phosphor, thermolum. characts. 77—90203
$K_2Ca(SO_4)_2.H_2O$, syngenite, space group refinement by vibr. spectroscopy methods 78—79507
$K_2Ca(SO_4)_2.H_2O$, single cryst., X-ray cryst. struct. refinement 79—14781
$K_2Ca(SO_4)_2.H_2O$, syngenite, thermal dehydration under nonisothermal conditions 80—3324
$K_2Ca(SO_4)_2.H_2O$, thermal dehydration, isothermal kinetics 79—15982
$KCl:CaCl_2$, KOH, complex form., U-centre influence, optical absorpt. bands 77—80502
$KCl-CaCl_2-NaCl$, ternary phase diagrams, interactive computer program 80—71629
$KLi_3Ca_7Ti_2(Si_6O_{18})_2F_2$, baratovite, cryst. struct. determ. by X-ray diffr. 77—76382
$3KNO_3-2Ca(NO_3)_2$, glass form. from liq., struct. transform., Raman spectrum obs. 80—64916
$K_2O-BaO-CaO-SiO_2$ glass-Nichrome-CaF_2 multicomponent self-lubricating coating, prep. by plasma spraying, and props. 80—40604
$K_2O-CaO-Al_2O_3-SiO_2$ glass, exam. of liquid phase separation phenomena 79—4417
$K_2O-CaO-B_2O_3:CuII$, immiscibility, ESR detect. 78—80200
$K_2O-CaO-BaO-B_2O_3$, glass, refraction, refractive index from 0.365 to 2.50 μm 80—88953
$K_2O-CaO-BaO-SiO_2$ (B_2O_3) (GeO_2), calc. of network refraction and exam. of glass structure 79—4783
$K_2O-CaO-SiO_2$ glass, composition-density relationship 77—90326
$(La,Ca)_nTi_nO_{3n+2}$, (n=4.5,5 or 6), cryst. struct. determ. *(French)* 79—65039
$La_{1-x}Ca_xCoO_3$, electronic and mag. props., itinerant ferromagnetism obs. 78—10660
$La_{0.9}Ca_{0.7}CrO_3$ polar semiconductor, elec. props., slight reduction effect 80—20183
$(La_{0.8}Ca_{0.2})MnO_{3+y}$, mag. sp. ht. and Debye temp. 79—61124
$(La_{0.8}Ca_{0.2})MnO_{3+y}$, mag. props., Faraday method meas. 80—103832
$(La_{0.8}Ca_{0.2})MnO_{3+y}$, non-stoichiometry and lattice consts. 80—100212
$(La_{0.8}Ca_{0.2})MnO_{3+y}$, sample preparation using O_2 partial pressure controller *(Japanese)* 78—73977
$La_xCa_{1-x}RuO_3$, metallic, mag., electronic and structural props., ^{99}Ru Mossbauer spectroscopy 77—48107
$La_{1-x}Ca_xVO_3$, struct., elec. and mag. props., temp. and conc. depend. *(French)* 77—4293
$(LaTmCa)_3(FeGe)_5O_{12}$, mag. loss and domain wall mobility 80—65980
$(LaTmCa)_3(Fe_{5-x}Ge_x)O_{12}$ film, high g, for mag. bubble applics. 77—85529
LiCa, $^2\Sigma^+$ and $^2\Pi$ states, mol. binding energy curves 80—58189
$LiF-CaF_2$, densities of binary molten salts *(Japanese)* 79—7644
$LiF-CaF_2$ binary molten salt, elec. cond. *(Japanese)* 77—76588
$LiF-NaPO_3-CaF_x$ glasses, IR spectroscopy study 80—16042
$LiO_2-CaO-SiO_2$ phase equilibria 78—64528
$LiO_2-Na_2O-CaO-SiO_2$ glass-ceramic coating, high temp. effects on steel substrate 79—61776
Li_2O-CaF_2 melts, component activities *(Russian)* 77—60104
$LiTaO_3-CaZrO_3$, struct. and dielec. props. 78—80298

calcium compounds continued
$(Lu, La, Y, Ca)_3(Ge, Fe)_5O_{12}$, temperature compensated high mobility bubble garnet, LPE and props. 77—20656
$Lu_{3-x}Ca_xFe_{5-x}Si_xO_{12}$ film on $Ca_3Ga_2Ge_3O_{12}$, mag. bubble props. 77—28418
$MgCa(CO_3)_2$, dolomite, partial thermal decomp. into MgO and $CaCO_3$, product cryst. growth 80—108706
$MgCaH_{3.72}$, synthesis and struct. *(Japanese)* 78—84751
$Mg_{1-x}Ca_xO$, epitaxial layers by CVD *(Russian)* 79—56934
$MgCl_2CaCl_2$, aq. soln., hydration, X-ray diffr. 77—43126
$MgGeO_3-Ca_{0.5}Fe_{0.5}GeO_3$, solid solns., physicochem. props. 77—44223
$Mg_{0.7}Na_{0.9}K_{2.0}Ca_{2.4}Al_{9.1}Si_{26.9}O_{72}.xH_2O$, erionite, cryst. struct. exam., stacking faults 78—2083
MgO (:CaO) powder compacts, sintering studies, SEM obs. 79—78918
$MgO:CaO(SiO_2)(B_2O_3)(Cr_2O_3)$, effective of impurities on high temp. creep 80—40455
$MgO-Ca_3Mg(SiO_4)_2(CaMgSiO_4)-NaPO_3$, phase conversions 77—66641
$MgO-CaMgSiO_4$, exam. of high temp. creep behaviour 78—80601
$MgO-CaMgSiO_4-(Al_{0.5}Cr_{0.5})_2O_3(Al_2O_3)(Cr_2O_3)$, spinel phase, phase equilibrium relations and spinel bonding 80—55376
MgO-CaO, thermal expansion coefficients of refractory ceramics 79—99336
MgO-CaO (58 wt.%), and MgO, comparison of high temp. creep and fracture 77—16658
$MgO-CaO-Al_2O_3-SiO_2(-TiO_3)$ systems, glass-ceramics, crystn. kinetics *(Russian)* 79—37626
$MgO-CaO-Fe_2O_3-Al_2O_3-SiO_2$, clinker production from dolomite and magnesite 80—55339
$MgO-CaO-FeO-Fe_2O_3-SiO_2-Cr_2O_3-Al_2O_3$ spinel refractories, physicochem. prod. conditions 80—89185
$MgO-CaO-SiO_2-Al_2O_3-Na_2O.P_2O_5$, effect of $NaPO_3$ on phase composition rel. to basic refractories 78—80528
$MgO-CaO-SiO_2-C$, equilibrium partial press. of Mg, SiO, Ca and CO 77—36482
$Mg_2SiO_4-Fe_2SiO_4-CaAl_2Si_2O_8-SiO_2$ system phase relations rel. to lunar basalts origin 78—65512
Mn-Si, liq. alloys, equilibria between $MnO-SiO_2-CaO-MgO$ slags 80—10639
$(Na,Ca)_2Zr[Si_6O_{15}].3H_2O$, Mongolian elpidite, cryst. struct. 78—95038
$Na_2-CaO-SiO_2$, rain erosion mechanisms 79—34154
$Na_{0.5}Ca_{0.5}Al_{1.5}Si_{2.5}O_8$, labradorite feldspars, lattice parameter determ. of exosolution structs. 77—84704
$Na_{7.5}Ca_{0.5}(AlSiO_4)CO_3.2H_2O$, cancrinite, proton-containing groups, PMR meas. 78—2094
$NaCa_2Mn_2V_3O_{12}$, antiferromag., spin wave contrib. to sp. ht., λ-anomaly at 25.05K T_N 77—77068
$NaCa(NH_2)_3$, cryst. struct. and cryst. chemistry *(German)* 79—51080
$NaCaPO_4-Ca_2SiO_4$ partial system, phase diagram 78—35364
$NaCaPO_4-Ca_3MgSi_2O_8(CaO)$ systems, phase diagrams of partial system 78—35369
$NaCaPO_4-Ca_3SiO_5$ partial system, phase diagram 78—35365
$NaCaPO_4-CaMgSiO_4$ system, phase diagram 78—35370
$NaCaPO_4-MgO$, $NaCaPO_4-NaMgPO_4$, $NaCaPO_4-Mg_2SiO_4$, $Na_2CaMg(PO_4)_2-MgO$, partial systems, phase diag. 77—86005
$NaCa_2Sb_2Fe_3O_{12}$, neutron diffr. patterns, group theory approach for determ. of mag. struct. *(Russian)* 79—51749
$NaCa_2Si_4O_{10}F$, agrellite, new type of silicate double chain 78—51514
$Na_8Ca_3SiO_{1.5}[Si_2O_7][PO_4]_3$, synthesis conditions, cryst. struct. and IR spectra characts. 80—108335
NaCaX zeolite, ion migration and $Ni(CO)_n^+$ form., EPR obs. 79—33522
$NaCl:CaCl_2$, quenched, aggregation process of Ca^{2+} ion-vacancy dipole, elec. cond. and dielec. loss meas. 77—80535
$NaCl-CaCl_2$, dislocation struct., etch pit obs. 78—43020
$NaCl-CaCl_2$, electrolyte mixture, evaporation from multi-component droplets, in stream of air 77—56255
$NaCl-KCl-CaCl_2$, solid soln., X-ray examination of final decomp. stage *(Russian)* 77—63681
$NaCl-NaBr-CaCl_2$, dislocation struct., etch pit obs. 78—43020
$Na_2MoO_4-CaMoO_4$, phase diagrams 77—36467
$NaNO_3-KNO_3-Ca(NO_3)_2.4.09H_2O$ melt, mixed alkali effect 80—34219
$NaNO_3-TlNO_3-Ca(NO_3)_2.4.09H_2O$ melt, mixed alkali effect 80—34219
NaO-CaO glass, melting speed, effect of struct. and grain shape *(Polish)* 79—29002
$NaO-CaO-SiO_2$ glasses, fluorinating agents effect on comp. and surface struct. 80—35364
$Na_2O-2CaO-3SiO_2$ glass, cryst. nucleation and growth, viscosity, thermodynamic props. 80—84079
$Na_2O-Ca_2O-SiO_2$ glass, crack nucleation about pointed indentations 79—91779
Na_2O-CaO glass, (K_I,V) diagram determ. *(French)* 80—108558
Na_2O-CaO glass, atomic absorption spectroscopy 79—43656
Na_2O-CaO glass, crack nucleation during indentation, micromechanics 80—30069
Na_2O-CaO glass, impacted with sharp SiC particles, strength degradation of annealed surfaces 79—61760
Na_2O-CaO glass, wettability, effect of cleaning procedures 80—65336
Na_2O-CaO glass phlogopite mica powders, composite fabrication, cellular struct. 80—84902
$Na_2O-CaO-Al_2O_3-SiO_2$ glass, exam. of liquid phase separation phenomena 79—4417
$Na_2O-CaO-Al_2O_3-SiO_2-F-B_2O_3-ZrO_2$ glaze, crystallisation, MgO, ZnO, BaO and SrO effects 79—60279
$Na_2O-CaO-Al_2O_3-SiO_2$ glass, crystn. for the purpose of obtaining vitroceramics *(French)* 80—75163
$Na_2O-CaO-B_2O_3-Fe_2O_3$ glass, Mossbauer expts., 85-500K 78—80260
$Na_2O-CaO-MgO-Al_2O_3-SiO_2$ glasses, ternary and quaternary, struct., Raman spectra obs. 77—36229
$Na_2O-CaO-MgO-Al_2O_3-SiO_2$, corrosion and microhardness, effect of detergents 80—16518
$Na_2O-CaO-P_2O_5:Co$ glass, bonding, symmetry meas. 79—46572
$Na_2O-CaO-SiO_2$, Al-coated glass, electron bombarded, SIMS analysis 79—66376
$Na_2O-CaO-SiO_2$, corroded glasses, electron microprobe analysis 77—4956
$Na_2O-CaO-SiO_2$, corroded, quantitative anal. by IR frequency shifts 78—19909
$Na_2O-CaO-SiO_2$, double torsion specimens, compliance and fracture load as crack length function 78—48508
$Na_2O-CaO-SiO_2$, dynamic hardness testing, pendulum attenuation, yield stress obs. 79—24699

calcium compounds continued
Na_2O-CaO-SiO_2, expt. errors in estimating time to failure 77−16666
Na_2O-CaO-SiO_2, foil, exam. of surface plasticity, and cracks, by electron microscopy 78−68733
Na_2O-CaO-SiO_2, for optical fibres, high purity glass production methods 78−87176
Na_2O-CaO-SiO_2, glass, elastic moduli meas., laser-target technique, for wide temp. range 77−27497
Na_2O-CaO-SiO_2, glass, composition-density relationship 77−90326
Na_2O-CaO-SiO_2, glass, transition from slow to fast crack propag., effect of different liquids 78−23828
Na_2O-CaO-SiO_2, glass, surface indentation effect on mech. strength, and thermal stress resistance 78−48463
Na_2O-CaO-SiO_2, glass, light scatt. rel. to heat treatment *(German)* 78−84598
Na_2O-CaO-SiO_2, glass, surface charge in aqueous electrolyte soln. 79−29245
Na_2O-CaO-SiO_2, glass, formation of colour centres, linear absorption of UV radiation 80−103328
Na_2O-CaO-SiO_2, multicomponent liq. state diffusion 78−55962
Na_2O-CaO-SiO_2, proof testing 80−108654
Na_2O-CaO-SiO_2, refining in glassmelting process 78−27467
Na_2O-CaO-SiO_2, soda-lime glass, hydration 79−87877
Na_2O-CaO-SiO_2 glass, optical props. characteris. in 0.006 to 22 eV region 77−16328
Na_2O-CaO-SiO_2 glass, Na surface conc. determ., by $^{23}Na(p,\alpha)^{20}Ne$ reaction 77−20171
Na_2O-CaO-SiO_2 glass, K_{IC} eval. by double torsion technique 77−90444
Na_2O-CaO-SiO_2 glass, Hertzian fracture characts., comp. influence 78−31522
Na_2O-CaO-SiO_2 glass, crack nucleation around plastic indents 78−92327
Na_2O-CaO-SiO_2 glass, water content effect on crystal nucleation and growth 79−55670
Na_2O-CaO-SiO_2 glass, SIMS anal. of aq. corrosion profile 79−66182
Na_2O-CaO-SiO_2 glass, surface viscous flattening kinetics, sinusoidal profile decay method 79−79139
Na_2O-CaO-SiO_2 glass, mm wavelength absorpt. 79−82978
Na_2O-CaO-SiO_2 glass, annealed and tempered, fracture strength studies under dynamic conditions 79−96132
Na_2O-CaO-SiO_2 glass, corrosion in alkaline soln. *(Japanese)* 79−96174
Na_2O-CaO-SiO_2 glass, sharp contact cracking, residual stress effects 79−100245
Na_2O-CaO-SiO_2 glass, electronic struct. and optical props. 80−2790
Na_2O-CaO-SiO_2 glass, microprobe anal. of corroded surface 80−7704
Na_2O-CaO-SiO_2 glass, effect of phase on liquids and gas diffusion *(German)* 80−38931
Na_2O-CaO-SiO_2 glass, thermal capacity meas. at low temps. 80−44334
Na_2O-CaO-SiO_2 glass, grain-cleaning procedures effect on crushed glass chem. durability tests 80−66678
Na_2O-CaO-SiO_2 glass, vol. relaxation and thermal history during forming process 80−70130
Na_2O-CaO-SiO_2 glass, redox phenomena evaluation in melting-fining process, SO_2 evolution 80−84900
Na_2O-CaO-SiO_2 glass, high-vel. liq. impact, oblique impact anomaly 80−89329
Na_2O-CaO-SiO_2 glass, hot erosion plastic flow and fracture 80−89354
Na_2O-CaO-SiO_2 glass microbubbles, permeation eccentricities of He, Ne and D-T 78−47598
Na_2O-CaO-SiO_2 glass foils, HVEM in-situ straining expts. 80−104216
Na_2O-CaO-SiO_2 glass:Fe, Mossbauer spectra of Fe^{2+}, Fe^{3+} impurities *(French)* 79−51893
Na_2O-CaO-SiO_2 glasses, ion-exchanged, mixed alkali effect rel. to elec. cond. 78−34653
Na_2O-CaO-SiO_2 glasses, elec. cond., room temp. to 450°C 80−107473
Na_2O-CaO-SiO_2 molten glass, electrolysis reactions 80−89496
Na_2O-CaO-SiO_2 sheet glass, pristine and scratched, fracture behaviour during bending 78−23829
Na_2O-CaO-SiO_2:Cr^{3+} glass, absorpt. spectra, Fano antireson. and vibronic Lamb shift 80−71458
Na_2O-CaO-SiO_2-Cr_2O_3 glass, redox equilibria of Cr ions, impurity effects 80−89477
Na_2O-CaO-SiO_2-Fe_2O_3 molten glass, optical props., temp. depend. *(French)* 80−100667
Na_2O-CaO-SiO_2-H_2O system gels, metastable nature 80−71952
$2Na_2O$-CaO-$XSiO_2$ glass, He mobility, interconnectivity, miscibility limits, effect of morphology 78−67864
$2Na_2O$-CaO-$3SiO_2$ glass, cryst. nucleation rate, viscosity, heat treatment 80−84081
Na_2O-K_2O-CaO-SiO_2 glasses, chemical durability, mixed alkali effect 79−8377
Na_2O-NaF-CaO_xZnO_{1-x}-Al_2O_3-SiO_2, opal glasses, strength, surface composition 80−30066
Na_2SiO_2-CaO glass, thermostimulated and tunnel luminesc. 80−45157
$(Nd,Ca)_nTi_nO_{3n+2}$, (n=4.5,5 or 6), cryst. struct. determ. *(French)* 79−65039
$Nd_{1-x}Ca_xVO_3$, solid solutions, elec. props. 80−96866
$NdVO_3$-$CaVO_3$ solid solns., mag. props. rel. to cryst. struct. 78−43571
Ni-Ca-B, Ni-B side of ternary diagram 77−59766
NiO-CaF_2 two-phase material, press. sintering, activation energy and compaction mechanism 79−47651
$NiO^{-}CaF_2$, hot-pressed, mech. props., thermal expansion rel. to CaF_2 additive 79−43321
P_2O_5-GO_3-CaO system, vitrification regions and physiochem. props. of glasses 77−11673
P_2O_5-MoO_3-CaO glasses, EPR study 79−82866
$PbCO_3$-$CaCO_3$ system, solid soln. form., regions of existence 79−11581
PbO-B_2O_3-SiO_2-LiO_2-CaO, glass enamel, chemical durability and microstruct., CaO addition effect 79−29255
PbO-CaO-SiO_2 system, melt, viscosity meas. in temp. range 950 to 1250°C *(Japanese)* 79−77663
$PbTiO_3$-$CaFe_{2/3}W_{1/3}O_3$, solid solutions 78−43816
Pd-$CaCO_3$ catalyst, hydrogenation rates of solid alkynes, H gettering 77−44510
$Pr_{0.9}Ca_{0.1}MnO_3$, mag. struct. neutron diffr. and magnetisation study 79−61061
$Pr_{1-x}Ca_xMnO_3$, struct. and magnetisation study 80−65804
$RbCaCl_3$, phase transitions, optical and dilatometric meas. 79−61394
$RbCaF_3$, ^{87}Rb NMR at cubic to tetragonal phase transition 79−82885
$RbCaF_3$, crit. scatt. at phase transition, Mossbauer diffraction 79−1733

calcium compounds continued
$RbCaF_3$, cubic to tetragonal phase transition, neutron diffr. obs. 79−23730
$RbCaF_3$, cubic to tetragonal phase transform., X-ray, neutron, Mossbauer diffr. study 80−49360
$RbCaF_3$, influence of domains on struct. phase transition 79−28097
$RbCaF_3$, NQR obs. of struct. transition at 198K 79−65191
$RbCaF_3$, nonlinear elastic behaviour, US velocity, 1 bar-3 kbar 78−59851
$RbCaF_3$, sp. ht. anomaly at struct. transform. 78−14426
$RbCaF_3$:Gd^{3+}, $O_h{}^1$-$D_{4h}{}^{18}$ struct. transition, ESR obs. 80−50178
$RbCa_{0.95-x}Mg_xEu_{0.05}F_3$, green luminesc. obs. 77−32428
$3RbNO_3-2Ca(NO_3)_2$, glass form. from liq., struct. transform., Raman spectrum obs. 80−64916
SO_2-lime plaster interaction *(German)* 77−86378
SiO_2-Al_2O_3-B_2O_3-MgO-CaO-Na_2O, strengthened by ion exchange, exam. of internal stresses using polarising microscope 78−88549
SiO_2-Al_2O_3-B_2O_3-CaO-Na_2O-K_2O system glasses, relax. of struct. stresses rel. to forming process 79−34088
SiO_2-Al_2O_3-CaO-BaO-SrO-ZnO-Na_2O-K_2O-B_2O_3, glaze effect of P_2O_5 additions 80−60824
SiO_2-Al_2O_3-CaO-K_2O system glass, phase separation and crystn., F catalytic effect 79−60280
SiO_2-Al_2O_3-CaO-MgO-TiO_2 system glasses, phase separation and crystn. 77−24384
SiO_2-Al_2O_3-CaO-MgO, liq. silicic and slag, struct, density, surface tension *(Polish)* 78−83711
SiO_2-Al_2O_3-CaO-MgO-Na_2O (1.58, 7.16, 3.59, 14.9 mole.%), polished sheet, strength in commercial state and after strengthening by ion exchange 79−1904
SiO_2-Al_2O_3-CaO-MgO-NaO-K_2O-B_2O_3-ZrO_2, glaze, exam. of zircon crystallisation 79−19155
SiO_2-Al_2O_3-CaO-MgO-Na_2O, ion exchange and electrodiffusion of Li ions in surface layer 79−20227
SiO_2-Al_2O_3-CaO-MgO, crystallized, prod. from inorganic waste *(Japanese)* 79−69017
SiO_2-Al_2O_3-CaO-MgO-Na_2O-K_2O effect of partial substitution of Na_2O by K_2O, on crystallisation 80−10499
SiO_2-Al_2O_3-CaO-MgO-FeO-Fe_2O_3 glasses, struct. transforms during heating 80−15014
SiO_2-Al_2O_3-CaO-Na_2O:Fe^{3+}, optical absorpt. due to Fe^{3+} ligand field and charge transfer 80−89020
SiO_2-Al_2O_3-Fe_2O_3-CaO-MgO-Na_2O-SO_3 glass, thermophysical props. 78−18849
SiO_2-Al_2O_3-Fe_2O_3-CaO-MgO-Na_2O-B_2O_3-SO_3, exam. of white flaky inclusions, causes and formation time 79−29237
SiO_2-Al_2O_3-Fe_2O_3-CaO, basalt glass ceramics, crystallite form. due to heat treatment 80−38917
SiO_2-Al_2O_3-Fe_2O_3-Na_2O-K_2O-CaO-MgO glasses, Mossbauer spectra study 80−39967
SiO_2-Al_2O_3-FeO-CaO-MgO pyroxene glasses, phase changes 80−15013
SiO_2-Al_2O_3-MgO-CaO-Fe_2O_3, glass ceramic, crystn., microstructures rel. to conditions 80−11638
SiO_2-CaO-Na_2O, glass, layers near surface, anal. using SIMS 80−88041
SiO_2-CaO-Na_2O-M_mO_n systems, M=Zr, Sn, Ti, Al, La, Ta, P, Mn, Fe, Pb, Cr, water, alkali, acid resist., chem. durability 79−34162
SiO_2-CaO-ZnO-B_2O_3-Na_2O-S, SrO effect on crystallisation 80−54135
SiO_2-Na_2O-$CaCO_3$ sheet glass, rupture upon local contact loading 80−50725
SiO_2-Na_2O-CaO (13, 11 wt.%) glass, phase separation, SiO_2 purity effect 80−44144
SiO_2-Na_2O-CaO glass, phase separation characts., melting atmosphere effect 80−44141
SiO_2-Na_2O-CaO:Fe(As)(Cr) glasses, optical absorpt. changes on heat treatment 78−31224
SiO_2-Na_2O-CaO-MgO-Al_2O_3, toughening by electrochemical treatment in Sn melt 80−11800
SiO_2-Na_2O-CaO-MgO-Fe_2O_3-Al_2O_3-SO_3-Sn thermally polished, exam. of strength of surfaces 80−25887
SiO_2-Na_2O-CaO-MgO float glass, surface SnO_2 distrib., ellipsometry and XPS study 80−84346
SiO_2-Na_2O-CaO-P_2O_5, BIOGLASS, surface, $Ca_3(PO_4)_2$ film form., bonding to bone 80−85212
SiO_2-Na_2O-CaO-TiO_2, thermal diffusivity in range 0-600°C, influence of TiO_2 80−29233
SiO_2-Na_2O-K_2O-CaO-MgO-Al_2O_3 glass melt, anodic dissolution of Ti 80−19949
SiO_2-NaO-K_2O-CaO-MgO-Al_2O_3 melt, anodic dissolution of Co and Ni in melt 78−88582
SiO_2-PbO-B_2O_3-Al_2O_3-CaO-Na_2O-K_2-O glaze, interaction with aluminosilicate glass-ceramics 80−84398
SiO_2-ZrO_2-Al_2O_3-CaO-Na_2O-K_2O-Li_2O, chemical resistant glass for glass fibres 80−21128
SiO_3-Na_2O-CaO-MgO-Al_2O_3 charge, silicate formation during heating 80−55342
$((SiO_2)_{45}(CaO)_{55})_{65}$ $(Fe_2O_3)_{35}$ glass, effect of melt atmosphere on mag. props. 78−68299
SmCaGe garnet LPE bubble film, coercivity, thickness depend. 78−68324
$Sm_{1-x}Ca_xS$, valence transition under high press. 79−73551
$Sm_{1-x}Ca_xS$, XPS, electronic struct. excitonic effects, insulator to metal transition 78−43988
$Sm_{0.3}Lu_{0.2}Tm_{0.2}Y_{1.45}Ca_{0.85}Fe_{4.15}Ge_{0.85}O_{12}$, LPE growth, saturation magnetisation, collapse field, bubble diameter 78−95703
$(SmLuYCa)_3(FeGe)_5O_{12}$ film, ion implant profile 79−78477
$(SmYCa)_3(FeGe)_5O_{12}$ epitaxial layer, growth kinetics and struct. as functions of cryst. lattice parameter mismatch 80−6677
SnCaV garnet polycrystal, ferrimag. resonance loss rel. to grain size 77−85581
$Sr_{1-x}Ca_xMnO_3$, Neel points, rel. to Curie point of $LaNi_{1/2}Mn_{1/2}O_3$, superexchange interactions 77−77055
$Sr_{1-x}Ca_xO$, epitaxial layers by CVD *(Russian)* 79−56934
$(SrCaR)_2(Cr_xGa_{1-x})O_4$, R=La or Sm, mag. 2-D oxide, phys. props. 78−47974
Sr_2CaReO_6, new seignettomagnets and ferroelectrics 78−19425
$SrFe_{12}O_{19}$-CaO, Ca^{2+} substitution effect on hexaferrite lattice and mag. props. 80−60243
SrO, mm wave spectrum, spectroscopic consts. 78−37629
$SrTiO_3$-$Bi_2Ti_2O_7$-$CaTiO_3$ system, solid solns., elec., optical props. 79−11375

calcium compounds continued
tartrate tetrahydrate:Cr^{3+}, optical absorpt. spectrum, cryst. field parameters 80–16067
ThO_2 ceramics, CaO and Y_2O_3 stabilised density, elec. cond., permittivity 78–47838
ThO_2-CaO, solid solns., defective oxides, ionic cond. 80–107548
ThO_2-CaO electrolyte, mixed and ionic cond. regions 77–8156
TiB_2-CaO, thermal stability of composite materials 78–60638
V_2O_5-As_2O_3-CaO, semicond. glass, electronic props. 80–88557
V_2O_5-P_2O_5-CaO system glasses, phase separation, crystn. and EPR spectra 77–76321
$(Y,Ca)_3(Fe,Ge)_5O_{12}$ LPE layer, exchange stiffness coeffs., 30-300K 79–78464
$(Y,Ca)_3(Fe)_2(FeGe)_3O_{12}$ film, exchange const., ferromag. reson. meas. 79–8023
$(Y,Eu,Lu,Ca)_3(Fe,Ge)_5O_{12}$, bubble memory chip, dynamic conversion comparison with $(Y,Sm,Lu,Ca)_3(Fe,Ge)_5O_{12}$ 78–68319
$(Y,Eu,Tm,Ca)_3(Fe,Ge)_5O_{12}$, Ca, Ge substituted garnet LPE films, elec. props., charge imbalance, Seebeck effect 78–68101
$(Y,Eu,Tm,Ca)_3(Fe,Ge)_5O_{12}$ garnet film coercivity, new annealing method 78–84459
$(Y, Eu, Yb, Ca)_3(Ge, Fe)_5O_{12}$, bubble film, LPE on $Gd_3Ga_5O_{12}$, mismatch and faceting 77–20657
$(Y,Sm,Ca)_3(Fe,Ge,Si)_5O_{12}$ single-crystal films, props. 78–64247
$(Y,Sm,Ca)_3(Fe,Ge)_4O_{12}$, garnet thin film, mag. anisotropy, Faraday effect meas. 79–42812
$(Y,Sm,Ca)_3(Fe,Ge)_5O_{12}$, domain wall, radial motion, method of dynamic collapse of mag. bubbles 79–8026
$(Y,Sm,Ca)_3(Fe,Ge)_5O_{12}$ epitaxial films, mag. props., growth condition effects 80–97124
$(Y,Sm,Ca)_3(Ge,Fe)_5O_{12}$ film, bubble wall state stability obs. 77–20651
$(Y, Sm, Lu, Ca)_3(Fe, Ge)_5O_{12}$:$Ne^+$, film, S=1 bubbles dynamic props., temp. depend. 77–20658
$(Y,Sm,Lu,Ca)_3(Fe,Ge)_5O_{12}$, bubble memory chip, dynamic conversion comparison with $(Y,Eu,Lu,Ca)_3(Fe,Ge)_5O_{12}$ 78–68319
$(Y,Sm,Lu,Ca)_3(Fe,Ge)_5O_{12}$ garnet film coercivity, new annealing method 78–84459
$(Y,Sm,Lu,Ca)_3(Fe,Ge)_5O_{12}$ bubble magnetic garnet film, LPE grown, props., $CaCO_3/GeO_2$ molar ratio influence 80–50152
$(Y, Sm, Lu, Ca)_3(FeGe)_5O_{12}$ LPE films, factors affecting coercivity 79–91267
$(Y,Sm,Lu,Ca)_3(Ga,Ge,Fe)_5O_{12}$, film growth and mag. props. for bubble-memory appl. 79–87297
$(Y,Sm,Lu,Cu)_3(Fe,Ge)_5O_{12}$, ion implanted, hard bubble suppression 80–11238
$(Y,Sm,Lu,Tm,Ca)_3(Fe,Ge)_5O_{12}$, epitaxial garnet film, temp. depend. mag. props. 80–39825
$(Y,Sm)_3(Fe,Ge)_5O_{12}$, Ca, Ge substituted garnet LPE films, elec. props., charge imbalance, Seebeck effect 78–68101
YAG:V_2O_5, CaO, V^{4+} ion impurity spectral anal. 79–78719
$Y_{1.6}Bi_{1.0}Ca_{0.4}Fe_{4.4}In_{0.4}V_{0.2}O_{12}$, cation distrib. 79–19211
$(YBiSmCa)_3(FeGe)_5O_{12}$ epitaxial layer, growth kinetics and struct. as functions of cryst. lattice parameter mismatch 80–6677
YCa garnets, solid soln., mag. and cryst. chem. props. 77–16057
$(YCaEuYb)_3(FeGe)_5O_{12}$, LPE, stripe end motion, effect of in-plane field 78–68330
$Y_{3-x}Ca_{2x}Fe_{2-y}In_yFe_{3-x}V_xO_{12}$, first magnetocryst. anisotropy const., ferrimag. reson obs. 78–68218
$(Y_{3-x}Ca_x)(Fe_{2-x}Sn_x)(Fe_3)O_{12}$, long and short range magnetic order 79–38419
$Y_{3-y}Ca_yFe_{2-y}Zr_yFe_3O_{12}$, first magnetocryst. anisotropy const., ferrimag. reson obs. 78–68218
$(Y_{3-x}Ca_x)[Fe_{2-x}Sn_x](Fe_3)O_{12}$, Mossbauer spectra of Fe^{27} and Sn^{119} nuclei 79–95578
$(YErCa)_3(Fe\ Ge)_5O_{12}$, mag. loss and domain wall mobility 80–65980
$(YErCa)_3(Fe_{5-x}Ge_x)O_{12}$ film, high g, for mag. bubble applics. 77–85529
$(YEuCa)_3(FeGeSi)_5O_{12}$, mag. loss and domain wall mobility 80–65980
$(YEuLuCa)_3(FeGe)_5O_{12}$ film, stable state of bubbles containing Bloch lines 78–76281
YEuTmCa garnet bubble films, domain wall transition 79–56584
$(YEuTmCa)_3(FeGe)_5$ bubble garnet films, ion-implanted, mag. susceptibility meas. 79–47311
$(YEuTmCa)_3(GeFe)_5O_{12}$ film, Bloch loop punch-through in mag. bubbles 77–59437
$Y_{1.52}Eu_{0.3}Tm_{0.3}Ca_{0.88}Ge_{0.88}Fe_{4.12}O_{12}$, bubble translation vel., ion-implantation effects 78–68327
$(YEuYbCa)_3(FeGe)_5O_{12}$, ion-implanted, in-plane mag. field effects on bubble props. 77–85521
$(YEuYbCa)_3(FeGe)_5O_{12}$ film, mag. σ-bubbles, automation props. 78–88150
$(YEuYbCa)_3(FeGe)_5O_{12}$ film, isolated straight stripe domain dynamic props. 79–33514
$(YEuYbCa)_3(FeGe)_5O_{12}$ bubble films, Ne^+-implanted, cryst. and mag. props., X-ray diffr. obs. 79–38362
$(YEuYbCa)_3(FeGe)_5O_{12}$, garnet film, isolated straight stripe domain, dynamic behaviour 80–39809
$(YEuYbCa)_3(GeFe)_5O_{12}$ bubble film with ion-implanted layer, FMR study 80–2643
$(YLuSmCa)_3(FeGe)_5O_{12}$ garnet film, bubble domain expansion, fuzzy wall struct. 80–71128
$(YLuSmCa)_3(GeFe)_5O_{12}$ bubble garnet film, coercivity 79–78459
$(YLuSmCa)_3(GeFe)_5O_{12}$ garnet films, bubble expansion saturation vel., sampling optical photography 80–75820
Y_2O_3-Lu_2O_3-Eu_2O_3-CaO-GeO_2-Fe_2O_3-PbO-B_2O_3 system, garnet crystn. fields 78–43995
$Y_{2.5}Pr_{0.5-x}Ca_xFe_5O_{12}$, magnetic aftereffect exam. 78–23304
$(YSmCa)_3\ (FeGe)_5O_{12}$ mag. bubble garnets, ion implantation induced stress influence on props. 79–91274
$(YSmCa)_3(FeGe)_5O_{12}$ LPE films, optimum growth conditions for low coercivity 78–95499
$(YSmCa)_3(FeGe)_5O_{12}$ LPE film, growth and coercivity 79–4707
$(YSmCa)_3(FeGe)_5O_{12}$ films, cc $(YSmLuCa)_3(FeGe)_5O_{12}$ films, mag. bubble props. mag. bubble props. and LPE conditions 79–74107
$(YSmCaLu)_3(FeGe)_5O_{12}$, bubble film inhomogeneity, spin wave reson. meas. 80–44439
$(YSmLuCa)_3(FeGaGe)_5O_{12}$, reproductibility in bubble garnet LPE growth 78–92204
$(YSmLuCa)_3(FeGe)_5O_{12}$, mag. props. and growth of 2 μm bubbles 78–91910

calcium compounds continued
$(YSmLuCa)_3(FeGe)_5O_{12}$, LPE growth, growth reproducibility of bubble props. 78–92208
$(YSmLuCa)_3(FeGe)_5O_{12}$ films, mag. bubble props. and LPE conditions 79–74107
$(YSmLuCa)_3(FeGe)_5O_{12}$ film, bubble propagation direction effects on high frequency bias margin 79–78480
$(YSmLuCa)_3(FeGe)_5O_{12}$, double layer struct., LPE growth from molybdate and Pb borate fluxes 80–39827
$(YSmLuCa)_3(FeGe)_5O_{12}$, bubble material, dynamic characterisation, comparison between transport and FMR methods 80–39833
$(YSmLuCa)_3(FeGe)_5O_{12}$, mag. loss and domain wall mobility 80–65980
$(YSmLuCa)_3(GeFe)_5O_{12}$, garnet film, refractive index dispersion 78–88273
$(YSmLuCa)_3(GeFe)_5O_{12}$, LPE low defect density films, prep. for mag. bubble device fabrication 79–87590
$YSm_{0.5}Lu_{0.7}Ca_{0.8}Ge_{0.8}Fe_{4.2}O_{12}$ film, magnetic bubble propagation with 8 μm period ion implanted propagation patterns 79–78475
YSmLuCaGeIG, mag. props. and defects, depend. on B_2O_3 conc. on growth in PbO-B_2O_3 solvents 78–68321
YSmLuCaGeIG films, epitaxial growth with 3 μm magnetic bubbles 79–61518
$(YSmTmCa)_3(GeFe)_5O_{12}$ film, YY pattern racetrack discrimination and state stability of S=1 and 0 bubbles 78–91908
Y_6WO_{12}:CaO, polycryst., elec. cond., 800-7400°C 80–15517
ZnCaSO, struct. and phase analysis *(Russian)* 77–58995
ZnF_4-BaF_2-CaF_2, vitreous phases, network formers, modifiers and stabilisers *(French)* 80–64909
ZrO_2:CaO, polycrystalline, grain boundary enhanced interdiffusion, flux density eqn. 80–29220
ZrO_2-CaO, microstruct., ordering, elec. props. 77–15374
ZrO_2-CaO, partially stabilised, growth morphology of tetragonal phase 79–4968
ZrO_2-CaO, phase equilibria and ordering 78–27498
ZrO_2-CaO, solid solns., defective oxides, ionic cond. 80–107548
ZrO_2-CaO, stabilised microspheres, structure, mechanical props. *(Russian)* 80–100379
ZrO_2-CaO (12-19 mole%), AC elec. behaviour, 300-900°C, grain size, electrode material, and sintering effects 78–34649
ZrO_2-CaO ceramic with grainy structure, props., effect of heating to 2000°C 80–104194
ZrO_2-CaO RF sputtered film, solid electrolyte, comp., struct. and AC cond. 77–39741
ZrO_2-CaO solid electrolyte, for O_2 flow regulator 80–57301
ZrO_2-CaO system, fluorite related ordered compd. prep., struct. 77–68958
ZrO_2-CaO thin film O_2 sensor, ionic transference number, cell design 77–70360
ZrO_2-CaO-SiO_2, relationship between texture parameters, and sintering, elec. cond. and mech. strength props. *(German)* 79–24474
ZrO_2-CaO-Y_2O_3, formation, stability and elec. props. of fluorite-like solid solutions 77–16550
ZrO_2-HfO_2-CaO, cubic solid solutions, thermal expansion 77–15598

calculating *see calculation*

calculating apparatus
desk, calculator-based instruments, meas. accel. due to gravity 80–73336
parametric sonar performance calculator 80–33392
programmable pocket calculator, short circuit current calc. *(German)* 80–68186
slide rule, to calc. transverse rupture strength for hard alloy bars 80–40530
slide rule for rot. and half integral spin states 78–45447
slide rule for rot. calcs., optical polarisation appl. 78–49594
sliderule for voltage loss calc. *(Russian)* 77–53869

calculating machines *see calculating apparatus*

calculation
see also graphs; nomograms
No entries

calculators *see calculating apparatus*

calculators (electronic) *see electronic calculators*

calculus
see also differentiation; integration; variational techniques
analysis, manifolds, calculus and other fundamental maths. book 78–28918
computing and appls., book 77–34
education, vector calculus and algebra geometrical meaning of curl operation 77–45639
ellipsometry, Mueller-Stokes calculus, conventions and formulas 80–102618
functional differentiation, heterogeneous, continuous, appl. to Feynman path integral 78–4504
global first integral for dynamical systems, importance of div. 77–82374
intertwiner algebraic struct. of superselection sectors 77–18185
macromolecular multicomponent system, phase separation, thermodynamic perturbation theory, calculus 78–18778
numerical-valued Fourier transform in two-sided operational calculus 77–67219
optical calculi, for phase modulation spectroscopy 77–88639
point of refraction boundary conditions and theorem *(Japanese)* 77–79743
sesquiholomorphic functions, symbolic calculus and second quantisation *(French)* 77–53804
square roots of measures 77–17765
teaching, discrete approach, using computer 79–80398
tensor calculus of stress anal. in glass reinforced plastic laminates *(Polish)* 77–12678
viscoelastic models formulation via fractional calculus 79–98627

calibration
see also measurement standards; standardisation
12 m discus and NOMAD buoy hull transfer function computations 80–46303
14UD Pelletron accelerator at ANU, energy calib. using $^{12}C(p,\alpha)$ 78–17449
20 and 30 GHz radiometers using ATS-6 satellite beacons 77–74500
600 MHz to 1 GHz coaxial thermal noise standard 80–98875
Abbe refractometer, self-calibration of polystyrene reference prism 77–55764
absolute, standardisation of radioactive sources and solns., 4π β-γ coincidence, program 77–18760

calibration continued
- absolute calibration of grating spectrograph for laser wavelength meas. 78—90528
- absolute ohm of ETL, determ. using calculable capacitance standard *(Japanese)* 79—6137
- absorbed dose calibration, ionisation chamber 77—40777
- AC portable digital voltmeter and calibrator 78—74019
- AC voltage measuring equipment, thermoelectric voltage convertor technique 77—53942
- AC voltage standard GK-10A 77—10055
- AC voltmeter, standard apparatus using thermoelectric convertors, 20 HZ to 1500 MHz 77—18036
- acceleration pick-ups, miniature vibrator for mechanical calibration *(German)* 80—95095
- accelerator calibration using ^{27}Al(p,n) threshold energy 79—36241
- accelerometer with centrifuge, linear, methods of eliminating systematic errors in calibration 79—71399
- accelerometers, gravimetric calibration 79—71444
- acoustic emission, structural calibration technique for quantitative appl. 78—9509
- acoustic emission transducer calibration temperature sensitivity checking technique 78—18144
- acoustic emission transducers and systems, spectral calibration by He gas jet 77—835
- adiabatic calorimeter for continuous specific heat meas. 800 to 1800K, design and calibration 80—57299
- AE transducer *(Czech)* 80—106697
- aerosol centrifuge, at unmatched relative humidities between stream and aerosol air 79—41775
- aerosol counters, photoelectric, sedimentation method 80—99031
- aerosol detector, in cryogenic systems 78—81986
- aerosol particle counter, optical, calibration oy Doppler shift spectrometry 80—68173
- AF hydrophone calibration intallation 77—75732
- air pollution measurement, particulates and gaseous pollutants anal. and calibration techniques 78—69531
- air pollution measuring instrument curves *(Dutch)* 77—66983
- air survey cameras, calibration techniques 80—18035
- airborne γ-ray spectrometer calibration, altitude effects 80—18754
- airborne expendable bathythermograph, for upper ocean temp. meas. 77—2262
- airborne IR scanners, temp. calibration 80—41572
- aircraft jet noise reduction test facility 77—11096
- airglow observatories intercalibration with AE-C satellite 77—41210
- albedo dosimeter, calibration using Sb-Be neutron source 78—33394
- albedo-type neutron dosimeter 77—65389
- Allen-Bradley resistor thermometers, one-point calibration, 2-20K 77—53922
- ammeter, demonstration apparatus, forces between parallel wires, calibration 77—33757
- analyser crystal, with automatically variable curvature, for three-axis spectrometer, construct., calibration 77—57797
- analytical methods, nonspecificity coeffs., estimation and verification 78—7306
- analytical methods, nonspecificity coeffs. 78—7305
- analyzer, automatic, calibration system, zero and span standardization 79—16107
- anemometer, const.-temp. hot-wire, for respiratory gas flow meas. 79—83967
- anemometer, hot film, calibration and use in fluids at varying background temp. 78—1767
- anemometer, hot-film, appl. to blood flow velocity meas. *(Japanese)* 79—29678
- anemometer, hot-wire, transonic flow 78—14103
- anemometer, low-speed, with const. temp. thermistor, experimental calibration *(French)* 77—21922
- anemometer probes, calibrating device operational principle *(Polish)* 77—72391
- anemometers, for indoor climate research, modification and calibration 77—3897
- anemometers, hot wire, comparison of dynamic and static calibration for vel. perturbation meas. 77—19644
- angle interferometer with 90° range, system set-up *(German)* 78—165
- angular scales, angle etalon constr. *(German)* 78—77852
- antenna calibration, radioastronomical methods, standard sources *(Russian)* 78—4103
- apparatus volumetric calibration by cryogenic Xe gas transfer 78—93653
- Ariel 5 Bragg spectrometer, calibration data 77—5441
- asbestos, airborne, X-ray diffr. anal., calibration standards 78—69517
- astronomical distance indicators, calibration rel. to Hyades distance scale 78—8121
- astronomical mm. obs., effect of Earth's atmosphere, two-layer model 78—53691
- astronomical photographic photometry, direct sensitometer *(French)* 77—13246
- astronomical photometer calibration for extended sources 77—9669
- astronomical photometry, Cousins VRI system, temp. and absolute flux calibration, appls. 80—26750
- astronomical spectrogram calibration by multiple exposure 77—22107
- astronomical spectrogram calibration using Lyot filter element 78—36466
- astronomical submillimetric multicolour photometry and calibration 79—35143
- astronomical telescope calibration, visible nd IR source, VISIR 80—36506
- astronomical UV spectrophotometry absolute calibration, 1750-3350 Å region 79—70963
- atmosphere N_2O measurements, laboratory intercalibration 78—81277
- atmosphere $NO/NO_2/O_3$ monitors, intercalibration 78—69529
- atmosphere O_3 concentrations meas., UV photometric standards interagency comparison 79—35000
- atmospheric CO_2 baseline monitoring station network, intercalibration 77—64491
- atmospheric O I 5577 and 6300 Å line widths meas., calibration using laboratory discharge lamp source 80—4148
- atmospheric pollutants meas., gaseous, sampling and calibration methods *(Dutch)* 79—83687
- atmospheric precipitation chemistry determ., calibration of collection procedures 77—37447
- atmospheric trace analysis, selection of calibration gas standards 77—91255

calibration continued
- atmospheric transmissometer/radiometer for electro-optical sensor evaluation 77—70884
- atomic, absorption analysis, calibration curves, theory *(Russian)* 77—21460
- atomic absorption calibration curves, initial slope, expt. conditions effect *(German)* 77—16891
- atomic absorption spectrometers, calibration algorithm for improved accuracy 79—39233
- atomic absorption spectroscopy, internal standards for sample introduction reproducibility 77—90666
- atomic absorption spectroscopy, Zeeman effect method, calibration curves 77—32866
- atomic emission spectroscopy, multi-element, with C furnace and optical MCA 77—40607
- attenuators, swept-frequency technique 77—18021
- audiometric circumaural earphones, using damped flat-plate 79—86316
- auditory ipsilateral acoustic reflex stimuli calibration 80—17170
- auroral data from DMSP 80—8443
- auto-collimating telescopes, angular measurement appl. *(German)* 78—77848
- autocalibration, capacitive displacement transducer *(Russian)* 80—36981
- autocollimator, photo-electric, with laser interferometer system and microcomputer 80—1304
- automatic digital magnetic recording system in Tihany Observatory 79—39989
- automatic image analysis, variables and errors, definition and quantitative description, nuclear carbons appl. *(German)* 78—25296
- automatic multirange calibrator of strain-gauge bridges 79—67285
- automatic network analyser, EM reflection coeff. meas. appl. 78—89463
- basic metrological operations and methods 78—41263
- beta-ray protection-level dosimeters, calibration quantities 77—52888
- biological precision rate calibrator 79—20731
- biomedical calibrator for ECG/respiration monitor 80—98159
- biomedical thermometry, use of salt-hydrate transition temps. as fixed points 80—104801
- biomolecular EPR and saturation transfer EPR spectra at high microwave field intensities 79—34488
- Bitter magnet development, stabilisation and calibration 79—30501
- blackbody for energy calibration of infrared equipment 80—86377
- blood gas analysers, review 78—69238
- blood pressure instruments, direct systolic/diastolic meas., review 78—69234
- bolometer, fast superconducting molecular beam detector 78—86383
- bolometer, for high-temp. integral normal radiating power meas., appl. to Nb 77—65667
- bone conduction vibrators, calibration force levels 78—65046
- Bonner spheres, calibration using Sb-Be neutron source 78—33394
- Borda inlet a-r flowmeters, performance characts. 78—22437
- brachytherapy source calibration using $Fe(NH_4)_2(SO_4)_2$-benzoic acid-xylenol orange dosimeter 77—5081
- British Calibration Service 80—22319
- broadband mm-wave calorimeter, design and calibration 79—26084
- buoy wave data analyses noise correction functions and error sources 80—46302
- burn-scarred human skin rheological props. in vivo meas. 78—31935
- calibration pressure generation, fundamental methods *(French)* 79—58670
- calibrator using band-gap voltage reference, oscilloscope appl. 78—65941
- calorimeter, circulated-liquid volume absorber, for intense laser pulses detect. 77—41617
- calorimeter, dynamic differential types comparison, in linear macromol. heat capacity meas. 78—89482
- calorimeter, energy calibration of liq. Ar detector for EM showers 78—37497
- calorimetric probes for gas stream enthalpy meas. 78—70126
- CAMAC-controlled calibration system for nucl. reactor systems 78—37532
- camera, resolving power type, sinusoidal targets design and construction 77—53999
- cameras, multi-, planar control in photogrammetric calibration for 3-D gait studies 80—67194
- cameras, wide-angle, astrometric reduction of photographs, calibration appl. *(Russian)* 78—28532
- capacitance transducer, calibrated, for detection of acoustic emission 78—71256
- capacitive grain moisture meter Standard Specimens 77—82481
- capillary viscometry, systematic error source identification 79—18982
- cardiac output analysers, equipment, maintenance and ccts., review 78—69239
- cardiotachometer, precision pulse generator, cct. 77—86682
- cellulose nitrate α-particle detector for Rn short lived daughters, results and calibration *(Czech)* 78—62663
- CERN muon storage ring, calib. of NMR magnetometers and mag. field meas. system 77—57780
- chamber calibration using ruby R_1 luminescence line shift, 80 to 550K 78—86284
- charged particle activation analysis, calibration 78—11587
- chemical anal. by counting meas. calibration determs., statistical uncertainties of anals. 78—92533
- chemical analysis, nonlinear calibration, theory 78—32784
- chemical analysis, systematic analytical errors of multicomponent materials, exposing and calc. methods 78—7274
- chemical analysis of water, dosing of vapour in vac. system to calibrate analysers 77—32850
- Cherenkov Pb glass large counter array, LED monitoring system 79—45565
- chromatographic method of calibrating leaks 80—77800
- chromatographs, for microconcentrations meas., improved calibration curve 80—26084
- chromatography, aqueous gel permeation 77—36824
- chromatography, nonlinear detector response quantification with lab. automation system 80—40775
- chromel-alumel thermocouples error statistical investigation 78—24794
- circular scale calibration by reflection grating polygon *(German)* 80—86250
- circumaural headset for hearing testing, calibration 77—9211
- colorimeter, three-colour, with spectral masks 77—30196
- colorimetric educational laboratory, calibration of set of surface colour standards 78—49625
- compression testing method of struct. fibreglass 78—23895

calibration continued
computed tomographic rotating fan-beam scanner, exptl. bench design 80−51230
computer peripheral pressure transducer calibration and metrological servicing 77−57314
computerised analysis, collaboration collection report 80−73106
computerised tomography X-ray beams, determ. of effective energies 79−20666
condensation nuclei counters, calibration and intercomparison 79−83684
condensation nuclei counters at South Pole, calibration 80−98470
condenser microphone, arrangement for precision reciprocity calibration 80−19203
conductance cell calibration, current practices 77−25274
conductance cell calibration technique, appl. molten bromides and iodides cond. meas. 77−80638
conduction flowmeter with calculable and controlled calibration characteristics *(Russian)* 79−7428
conductivity meter for in situ ocean meas., development, testing and calibration 79−5671
cone absorption calorimeter for pulsed laser meas. 80−98980
conference on analysis instrumentation, Charleston, West Virginia, USA (May 1977) 79−16100
constant volume gas thermometer for temps. 4-300K *(French)* 77−133
contact B-scanners, calibration method 79−23161
contactless speed meas., laser Doppler difference system *(German)* 77−17957
contactless temperature meas. methods *(Dutch)* 77−67433
contactless thermal flowmeter, calibration characts. 80−103085
convective heat loss assessment from humans in cold water 78−81093
coronagraph, white-light, on Skylab, radiance calibration 77−60606
cosmic ray particle telescope of Sydney Univ., calibration and results 78−25388
coupler for reciprocity calibration of microphones 77−75754
crack growth monitoring using finite element analysis, calibration of electric potential technique 79−32380
critical flow venturi nozzles, primary calibration in high pressure gas 80−53832
crop and soil bidirectional reflectance factor calibration, remote sensing field research 80−86382
crude-oil hydrometers calibration 78−73969
cryogenic construction material magnetisation meas. *(Slovak)* 78−93693
cryogenic resistance and diode thermometer 77−26311
cryogenically cooled IR sensors, calibration in space, AFGL expts. 79−5753
cutaneous blood flow meas. instrument, laser beam Doppler shift method 78−28030
cyclotron dee voltage calibration using an intrinsic Ge X-ray detector 80−99359
Danish temp. transducer calibration at Riso, in −150 to 1100C range *(Danish)* 79−54129
DC and AC analogue voltmeter and ammeter, digital voltmeter appl. *(Polish)* 78−45655
DC checking calibrators, output voltage filtering methods 77−53940
DC resistance decades, precision, integral verification 78−242
DC source (10^{-16} to 10^{-6} A) for electrometer testing 77−79112
decibel, definition, meter calibration and hi-fi equipment *(Spanish)* 79−54092
deep level transient spectrometer, automatic calibration cct 80−37067
deep sea temp. and pressure sensor and calibration techniques 77−37424
defibrillator energy meters, traceable calibration methods 80−30928
defibrillators, review of instruments and maintenance 78−69251
densitometer with resonating twin tube for ethane/propane flow meas. 77−38052
DePangher precision long counter and neutron dose-rate meters, calibration 80−47822
deuterated polarised target, calibration of deuteron polarisation 77−3200
development trends, length, press., mass, electrical and photometric standards 80−191
devices, made more accurate by improved basic standards 77−33980
dew-point hygrometer, fast-response, calibration *(Russian)* 77−13761
diagnostic probe for intense electron beams, calibration 78−12787
diamond anvil cell, calibration, 0-15 kbar, for X-ray diffr. expts. on polymers 77−41635
diamond turning precision machine tool system 80−69568
dichrograph calibration apparatus, 185 to 600 nm 77−5886
didymium glass filters for spectrophotometer wavelength scale calibration 80−43417
diffuse reflect. spect., standards and calibration rel. to chromatography 77−56278
diffuse reflectance spectroscopy, applics., standards and calibration 78−32848
diffuse reflectance spectroscopy, calibration of reflectance standards, review 78−32860
diffuse spectral reflectance, calibration of standards 77−53983
diffusion battery, screen type, theory 80−95208
digital calibration device for mag. field, appl. to EPR spectroscopy *(French)* 77−152
digital instrumentation, requirements 77−37907
digital laser-Doppler-velocimeters signal processor accuracy testing *(German)* 78−86242
digital phase shift for meter calibration 79−44898
digital temp. meas. instrument with automatic error compensation of thermoelectric thermometer 79−75526
digital voltmeter, self-calibrating high-resolution 77−57346
digital voltmeter *(German)* 78−93723
digital voltmeter calibration approaches and limitations 79−93126
digital voltmeters, simplified method 79−49248
digitization of mechanical meas. values by automatic calibration *(German)* 79−67247
dilatometers, tube type, calibration, standards 78−12669
diode laser, appl. to IR spectra of NH_3 mols. 78−58689
diode laser IR spectra, intermode calibration using tandem etalons 80−32982
distributed temperature sensor of optical path fluctuations, calibration 77−2688
Doppler signal simulator for optical heterodyne receiver parameter meas. 79−80684
dose meter calibration for radiation protection in European Community 80−58000
calibration continued
dose rate meter, use as X- and γ-ray secondary protection-level standard 77−81579
dosimeter, clear Perspex effect of storage temp. on calibration 77−60256
dosimeter, polymer sheets, calibration via differential calorimeter for electron radiation 79−6795
dosimeter, source storage and irradiation device 80−5339
dosimeter, thermoluminesc., calibration, γ-ray irradiator *(Japanese)* 78−66452
dosimeter calibration in terms of absorbed dose in water for ^{60}Co γ-radiation 80−18696
dosimeters, environmental and personal, calibration using ^{133}Xe 80−86992
dosimeters, radiochromic dye film dosimeter appl. 78−40330
dosimetric primary and secondary standardization within the European Communities 80−9415
dosimetry, calibration and meas. standards at Austrian Dosimetry Laboratory 80−5362
dosimetry, environmental radiation meas., instrument calibration 80−9426
dosimetry, Regional Calibration Laboratory, Cleveland, USA 80−5364
dosimetry, Regional Calibration Laboratory at the M.D. Anderson Hospital, Texas, USA 80−8189
dosimetry, secondary standard laboratory organisation in India 80−5366
dosimetry, secondary standards laboratory, role in a nuclear power utility 80−5365
dosimetry calibration, estimation of confidence levels 79−3247
dosimetry calibration problems in connection with radiation protection around nuclear facilities 80−9422
double Compton gamma-ray telescope, calibration in neutron beam 78−53827
double constant current source for cryogenic current comparators, standard resistor calibration appl. 78−93731
drag disc turbine transducer calibration for mass flow rate meas. in PWR coolant two-phase flow 80−37552
dual-grating direct-reading spectrograph mirror system design and performance 80−81397
Dynalyzer II, application to X-ray quality control 78−77896
dynamic, synthetic diamond grain thermoelectrodes, grinding temp. measurement appl. 77−55985
dynamic radiography, automatic control system design 77−60244
Dynamitron 4 MV accelerator, energy calibration of analysing magnet 79−54736
Dynamitron tandem, energy calibration of heavy ion beam analysing magnet 79−59287
dynamometer, for exact meas. up to 10 N *(German)* 77−53897
dynamometer standardisation machine method *(French)* 77−53894
dynamometers, multicomponent, practical experimental designs for calibration 79−35729
earphones, ear simulator const. meas. 78−27960
earphones, Telex 1470-A audiometric, calibration data 80−74685
Earth optical horizon, brightness-height calibration via photography of Moon 77−53186
earthquake magnitude calibration function for core phases, PKP1-PKP2 caustic 78−40509
ECG/VCG minicomputer digitising and preprocessing system 77−40863
eddy current inspection system with simulated signal, calibration 78−3285
electric rainfall intensity sensor 79−39888
electric soil moisture gauges, testing procedure 77−78481
electrical conductivity probe for NaCl stratified solns., conc. calibration 77−52718
electrical measuring instruments, portable, repair and test rooms *(German)* 77−2665
electrical standardising laboratory for developing countries 80−101774
electro-medical servicing, quality maintenance 78−77126
electro-optical pyrometer single-pulse calibration flash tube 78−12702
electroacoustic and aerodynamic calibrated sound sources compared 78−55543
electrochemical concentration cell ozonesonde, performance characts. 79−21039
electrochemical O_2 meter calibration in 10^{-7} bar range 78−80812
electron accelerators, energy calibration method based on Cherenkov effect in gases 80−18721
electron calibration of Mariner 10 instrumentation rel. to Mercury encounter meas. 80−12628
electron microscope, calibration using grating replica 79−2893
electron microscope calibration by photogrammetric technique 78−336
electron probe analysis, of lyophilised solns., calibration curve linearity limits 79−44075
electron spectrometer with laterally inhomogeneous sample, ang. and spatial depend. intensity 79−74468
electron spectrometers, energy calibration 78−24888
electronic thermometer circuit 79−54131
electrophysiological instrument calibrator 77−48970
electrostatic electron spectrometer, relativistic effects in calibration, toroidal analyser 78−29211
electrostatic electron spectrometer, relativistic effects in calibration, parallel plate and cylindrical mirror analysers 78−29212
electrostatic field parameter measuring instruments, calibration of transducers 79−75551
ellipsometer, in-process calibration, azimuth angle corrections 77−18070
EM blood flowmeter, comparison of dynamic calibration methods 78−40362
EM coating thickness gauge calibration using air gap 77−57300
EM flow meas. devices, theoretical aspects *(Dutch)* 78−22442
EM flowmeter dynamic calibration device 80−43817
EM flowmeters, dry calibration methods 80−43811
EM flowmeters, with non-uniform mag. field, liquidless calibration 77−72385
EM meas. and instrumentation, conf., Ottawa, Canada, 1978 79−21731
ends standards of length for calibration, alignment using autocollimator 79−54094
energy disperion X-ray analysers, evaluation, for water pollutant anal. 78−48712
energy dispersive X-ray analysis in STEM, semiquantitative analysis method using ref. spectra and empirical scale factors 78−24005
enthalpimetric analysis and calibration, new instruments and methods 79−43615
epoxy, three-component modified, development for dynamic photoelastic obs. of fracture 78−35474

calibration continued
equidensity fringe pattern lines on special film 77—18118
equipment calibration using standard frequency broadcasts 79—67258
ERG photostimulus calibration by standard photometer and photodiode 80—8222
errors in profiling instruments, analysis 80—8445
ESO-(B)-survey, characteristics curves from stellar image diameters *(German)* 79—70966
ethylene, supercritical, mass-flow meter inaccuracy 79—68842
ethylene gas-density meter, calibration method 77—84356
EUV spectroheliometer on Skylab Apollo Telescope Mount, photometric calibration 77—60595
exposure rate and absorbed dose meas. for 6-7 MeV 79—26766
extragalactic distance scale, tertiary distance indicators calibration 79—25708
extragalactic distance scale calibration, appl. to distance of giant spiral galaxy (M 101) 80—67852
F-type stars, absolute luminosity calibration 78—65612
Faint Object Camera calibration 79—25479
falling-weight equipment pressure pulse parameter calc. 77—67425
far IR and near MM wave power energy meter calibration 80—57373
far IR calibration source for balloon-borne telescopes 80—62027
fast neutron detector (long counter) absolute calibration by associated activity technique 79—6801
fast-response pyrometer 80—90852
FFTF startup, instrument calibration program 80—9337
fibre optics appl. in instrumentation 80—83665
field ion emitter, field calib., using energy distrib. of free space field ionisation 77—69971
film dosimeters, calorimeter for calibration in high intensity electron fields 78—73257
film thickness monitor, quartz crystal, based on SAW oscillator 78—3036
fine γ spectrometry and release meas. *(French)* 79—3258
fission track dating parameters 77—41207
flame, atm. press., ion mass spectroscopic sampling system characts. and calibr. 77—56270
flame temperature meas. using laser induced fluoresc. spectrosc. of OH 80—90839
flow calorimeters standardisation, calibration, thermal config. depend. *(French)* 77—67437
flow meas., two-dimensional nonsteady, X-hot wire probe method *(Japanese)* 80—59134
flow measurement, hot-wire calib., for vel. and temp. meas., low-freq. effects 79—50825
flow measurement, using orifice plates, interlaboratory comparison 79—68866
flow measurement, weighing method, accuracy 79—68891
flow measurement 80—92239
flow metrology, appls. of heat waves 79—68879
flowmeter, by comparison with standard instruments 77—76007
flowmeter, by electronic weighing 78—55700
flowmeter, calorimetric and heat-label, with IR or UHF sources 77—80243
flowmeter, critical venturi type, discharge coeff. meas. 79—68871
flowmeter, design advancements, microcomputer-controlled flow rigs 80—10320
flowmeter, electromagnetic, calibration using a flow simulator 79—68854
flowmeter, linear pad resistor type, calibration 79—68868
flowmeter, liquid, dynamic method 77—76006
flowmeter, open channel acoustic flowmeter, error sources and calibration 78—30389
flowmeter, throttle-type, standardisation in Soviet Union 77—76003
flowmeter calibrating devices, accuracy 79—68846
flowmeter calibration, Na-cooled reactor, signal anal. method 78—38425
flowmeter calibration method using sonic nozzles *(Japanese)* 77—65821
flowmeter methods with liquids, comparative survey 77—68720
flowmeter repeatability testing 77—84357
flowmeters, calibration at low flow rates 79—68847
flowmeters, differential, for large flow rate meas., tracer calibration 79—68885
flowmeters, irrigation water mains 80—96325
flowmeters, transfer-standard, calibration in water test rigs for comparison of laboratories 79—23389
flowmeters, V-notch weir, approach channel and sedimentation effects 78—30386
flowmeters for petroleum-gas industry measurements, Soviet standardisation 77—76004
fluxmeter measurement range extension 78—57993
FM pressure transducer using resonant diaphragm, multiple linear regression methods appl. 78—41295
force and meas. measurement, conf., Braunschweig, W.Germany (Sept. 1978) 79—35725
force measuring inductive transducer calibration characts., calc. and expt. *(Russian)* 77—10005
force standard machines, mass standards *(German)* 79—35735
force standards machines and measurement, 0.5 to 30 MN 79—35727
force transducers, calibration by absolute impulsive method 80—105627
force transducers, calibration using theoretical calcs. 79—35719
fusion thermal tracers, thermophys. characts. investig. 77—5837
galactic radio background emission, linear polarisation absolute calibration 77—2500
gamma beam densitometer calibration for mass flow rate meas. in two phase flow of PWR coolant 80—37552
gamma camera, phantom for simulating fast dynamic studies 77—16980
gamma radiation attenuation method using variable-thickness filter 77—83110
gamma radiation nationwide calibration system standardisation 77—38583
gamma ray sources for exposure rate meas. instrument calibration 80—32562
gamma ray spark chamber telescope for range 10-100 MeV 78—36459
gamma spectra obtained with Ge(Li) detectors *(Rumanian)* 80—5431
gamma-ray detector calibration for extended sources 79—724
gamma-ray measuring instruments, irrad. timer for shutter of ^{60}Co teletherapy head 77—66836
gamma-ray source, ^{60}Co, spectral meas. and data evaluation 77—6608
gamma-ray spectrometric logging and surface exploration equipment 78—85706
gamma-ray spectrometric meas., intrinsic calibration, isotope ratio determ. appl. 77—81440

calibration continued
gamma-ray standard sources using complex decay schemes 80—9081
gas analyser, based on thermocouple vacuum gauge 80—61183
gas concentration meas. using Raman intensity depend. on giant pulse laser polarization 80—98986
gas density transducer, by National Measurement Laboratory 78—36971
gas flow calibrator fibre-optic timing system 77—31408
gas flow generator transient process anal., controlled plunger movement method 77—72381
gas flow meas. standard methods review 78—94864
gas flowmeter, comparison of calibration methods *(Japanese)* 79—72970
gas flowmeter, using Laval nozzle theory *(Japanese)* 77—65779
gas mixture, reacting, atom conc. reson. absorb. meas., microwave discharge lamp calibration 79—92032
gas mixtures preparation (1 to 10^{-3})% molar range 80—99030
gas permeability measurement in high polymers, techniques and detectors 80—14854
gas volume counter and flowmeter, gravimetric standard method *(German)* 77—55112
GATE aircraft radiation instrumentation, anal., IR irradiance meas. 78—32134
gauge blocks, contact deformation and corrections 79—26028
gel permeation chromatography, calibration, appl. to polycarbonate 80—58424
gel permeation chromatography polymers, data treatment 79—92037
geomagnetic pulsations, Borok B-index recalibration for interplanetary mag. fields meas. 77—29589
glass micropipettes, comparative calibration by optical microscopy and SEM *(German)* 80—98201
glass-ceramic capacitance thermometers, low temp., accuracy and stability 77—61074
GLEEP reactor neutron thermal and epithermal flux calibration 79—93856
global calibration of terrestrial reference cells and errors involved in using different irradiance monitoring techniques 80—93951
graticules, highly accurate calibration technique 78—24762
gravimeter, based on inclination method 77—91313
gravimeter, HF, calibration and sensitivity 78—7812
grazing incidence spectrometer, 1.0 m, photometric calibration for plasma fusion diagnostics 80—92386
Grenvillian palaeopoles, calibration by ^{40}Ar/^{39}Ar dating 79—20778
hailpad calibration for Italian hail damage documentation 77—29488
hailpads calibration 78—93001
Hall magnetometer, system for calibration and checking in 0.3 to 6.0 T range 80—17964
halofluorocarbons, in ambient air, in situ quantification technique calibration 78—69530
Harwell linac II total scatt. spectrometer, Ni powder diffr. data 78—86725
Harwell type 95/0075 survey meter, calibration using Sb-Be neutron source 78—33394
headphones, low freq. calibration, effect of leakage 77—62119
HEAO-B X-ray telescope, mirror design, fabrication and expected performance 78—49330
heart volume determination by angiography, X-ray magnification estimation 78—73197
heat flux transducer calibration *(Russian)* 77—82505
heat gauge, transient heat flux meas. 77—49723
heavy ion and He dosimetry and instrumentation 79—20675
Hertzsprung-Russell diagram, age and mass calibration for H burning stars 80—51744
hierarchical systems, calibration errors influence on end item performance 80—98788
high press. apparatus with shaped Bridgman anvils, calibration 78—49856
high pressure chamber calibration, phase transitions in standard materials *(Russian)* 77—76544
high pressures, calibration via ruby fluoresc. R-lines at ambient and low temps. 77—18106
high resistance meas. circuit using matched pair of diodes 77—74455
high-pressure calibration scale based on Au, Ag and Cu melting curves, revision 80—39260
high-pressure devices with profiled anvils 77—82540
high-pressure gas equation-of-state meas. interferometry 80—77810
high-temperature meas. and calibration, above 1000°C, based on Au melting point *(Rumanian)* 80—47061
high-voltage spark source, characterisation, computational method 78—45717
high-voltage spark sources, calibration meas. methods 78—49908
hodoscopes for high intensity muon beam, high-rate photomultiplier-base and precise timing calibration 79—22544
holographic photoelasticity, technique for calibration of isochromatic and isopachic fringe pattern *(Rumanian)* 79—86388
hospital test instruments, scientific and medical instrumentation capability 78—69242
hot wire anemometer probes, X-configuration dynamic testing device 78—87421
hot wire anemometry, calibration at low vel., wire support correction 79—60077
hot wire tachometric probes, calibration instrument features *(Italian)* 79—72966
hot-film anemometer, calibration of low-vel., flow direction 78—91043
hot-film probe, calibration in liquids 79—27723
hot-film probe, in reversing flow, forced convection, finite difference soln. 80—12177
hot-film probe, vel. meas. in liquid metal MHD duct flow 80—75009
hot-film velocity sensors, cylindrical, low Reynolds number calibration 79—64815
hot-film wall-shear probes in liquids 79—50823
hot-wire anemometer, for air flow measurements, calibration at low vels. 79—27724
hot-wire probes, very low velocity calibration 80—75008
HS plexiglass flumes for open channel flows meas., calibration 77—62321
human motion 3-dimens. monitoring by optoelectronic means, calibration and meas. 78—31913
human motion three-dimensional monitoring by optoelectronic means 77—86658
humidity and dew point, standards and calibration 79—49240
HV instrument transformer calibration system based on LV inductive voltage divider 77—82567

calibration continued
- hydrocarbons, substituted, chemisorbed monolayers on Pt (100) surface, AES quantitative anal., calibration 78—31724
- hydrogenous scintillator, fast neutron sensitivity, calibration with ^{252}Cf fission neutrons 77—23376
- hydrophone, by modified piezoelectric balancing method 77—11097
- hydrophone, miniaturised, for biomedical uses, calibration apparatus *(Japanese)* 77—64144
- hydrophone LF calibration, field nonuniformity effect avoidance 78—42486
- hydrophones, calibration system using pseudo-Gaussian noise signals 77—84045
- hydrostatic pressure cells producing anisotropic strain 79—17410
- impact accelerometers, Impul's-3 calibration apparatus 80—8964
- impedance probe calibration, for vacuum meas. in single component two-phase mixture *(Italian)* 80—62677
- implantation type accelerator, 400 kV, energy resolution, stability and calib. using (p,γ) react. 79—30604
- incandescent lamp calibration for spectral irradiance by absolute radiometers 80—102788
- inductive voltage divider, calibration by step-up method up to 1 MHz 77—18031
- inductometer calibrator, U-738, description 78—74034
- industrial noise level meter calibration procedures 77—62125
- initial flowmeter for critical gas flow rate meas., principle 77—72382
- instrument quality not maintained by frequent calibration, statistical evidence 79—93090
- instrumentation for industrial noise meas. *(German)* 77—80039
- instruments, measuring NO$_x$ in flue gases 79—53015
- intensity meter calibration for 20 kHz to 300 MHz range 79—2786
- interference microscopes, calibration standards *(Slovak)* 79—71522
- interferometer, data handling in high vibration environment 80—95132
- interferometer calibration for atomic and molecular transition wavelength meas. 79—80696
- interferometric angle meas., 30°-60° range, accuracy *(German)* 77—79051
- international calibration cycles of field intensity and power density, measurements 80—82752
- international collaboration among calibration services 80—101773
- ion beam surface anal., appl. of bulk H standards to calibration 80—7884
- ion cyclotron resonance spectroscopy, sensitivity calibration of marginal oscillators 78—21177
- ion microprobe analysis, calibration using matrix ion species ratios, appls. 78—61070
- ion potentiometric continuous analysis, calibration method for minimizing errors 78—35748
- ion-selective electrodes, interpret. of non-ideal calibrations 77—90661
- ionisation chamber, tissue-equiv., response to 15 MeV neutrons 77—48874
- ionisation chamber calibration and testing using N$_2$ laser beam 80—27890
- ionisation chambers, calibration constants calc. for gaseous β-emitting nuclides *(Japanese)* 79—68142
- ionisation chambers, calibration methods for primary and secondary standards, in Hungary 80—5357
- ionisation chambers, calibration of dose to water for ^{60}Co γ-radiation 80—74032
- ionisation chambers, NB2 P-2 secondary standard, calibration with photon calorimeter 79—36469
- ionisation chambers, radiation exposure intercomparison 80—5363
- ionisation chambers calibration in absorbed dose units 78—20274
- ionisation current sources for electrometer calibration 77—79111
- ionisation detector of LW bremsstrahlung, evaluation of calibration constants 79—68147
- ionising radiation, metrology and calibration, French system *(French)* 80—5351
- ionising radiation calibration, meas. standards, CNEN, Italy 80—12273
- ionization-chamber-dependent factors for calibration of megavoltage X-ray and electron beam therapy machines 80—18704
- IR and millimetric waves and applications, conf., Miami Beach, USA (Dec. 1979) 80—57009
- IR and MM wave calibration standards requirements survey 80—57248
- IR calibrator, continuous-temp., for temp. measurement using IR scanner 79—75530
- IR detector, low-temp. modulated calibration method, space appls. 77—79152
- IR detectors, conf., Los Angeles, CA, USA (1978) 79—2822
- IR fluctuation hygrometer, design, calibration, field trial results 78—77368
- IR radiometer calibration, for atm. temp. remote sounding 77—41174
- IR sensor, long wavelength, uncertainties in calibration 77—170
- IR sensor test facilities 77—65647
- IR sensors, long-wave, for astronomical obs., ground calibration 79—5749
- IR spectra calibration using spline functions 77—27050
- IR spectrometer performance testing using CO line parameters 77—91275
- IR system for radiating source meas., calibration and spectral props. 77—49300
- IR thermometer and pyrometer calibration methods and standards 79—88958
- isothermal displacement calorimeter, for positive excess enthalpies 78—89483
- jacketed optical fibre residual stress diagnosis, pulse delay technique 80—53469
- laboratory condenser microphones, note concerning the implementation of IEC 327:1971 for pressure calibration 80—74686
- laser calorimeters, calibration system *(Chinese)* 80—228
- laser Doppler velocimeter calibration burst generator 79—77321
- laser energy meters, pulsed 79—27301
- laser energy meters for calibrations at most principal laser wavelengths 80—99741
- laser frequency, multipath optical cavities in saturated absorpt. expts. 77—65610
- laser frequency and spectral parameter check system 77—79880
- laser light energy distribution analysis, film calibration method 77—79875
- laser low level pulse simulation and calibration, tracking system evaluation 78—59074

calibration continued
- laser photoacoustic detector spectroscopy, calibration using HD 5-0 transition 80—77877
- laser power and energy meters, calorimeter system for calibration 80—38024
- laser power meas., scale comparison for calorimeter and radiometer systems 79—76729
- laser power meter, calibration, Si solar cell 80—46780
- laser power meter calibration for the range 5-1000 W using electrically calibrated calorimeters and beam splitters 78—1241
- laser wavelength and bandwidth calibration using optogalvanic effect 78—5514
- laser wavelength calibration using optogalvanic effect, atlas 80—62727
- laser-Doppler technique, local size and vel. probability distrib., two-phase suspension flow 78—59517
- lateral induction logging, calibration of apparatus *(Russian)* 79—39941
- layer thickness measuring device fixture *(German)* 77—74353
- layer thickness uniformity meas. instrums. *(German)* 77—74351
- leak detection, ultrasensitive, in vacuum devices 80—47065
- Leicester solar coronal Bragg spectrometer, wavelength calibration and resolution 77—5442
- level gauge, linearisation of scale eqn. for resonance level gauges *(Russian)* 80—68176
- level gauge reference installation for calibration 77—71294
- lidar systems, two- and three-freq., for aerosol meas. 78—36334
- lidar target calibration, backscatter refl. for circularly polarised radiation 80—102750
- light-scattering apparatus, low-angle for polymer films investigation, calibration 79—58803
- line hydrophone array, low-freq. technique for underwater calibration of individual elements 77—79997
- linear accelerator calibration monitor with a memory 80—3821
- linear accelerator calibration using Si diode detector, high-energy photon dosimetry 78—24143
- linear gauges, high precision, automatic interference comparator appl. *(German)* 78—77847
- liquid density transmitters, calibration 80—27265
- liquid flowmeter calibration automated secondary standard 77—37841
- LMFBR cooling circuit, calibration of EM flowmeters by average frequency method 80—570
- LMFBR fuel pin power calibration prediction, transient correction factor analysis 79—9719
- load cells, automatically controlled, method for digitizing measured values *(German)* 79—35721
- load transducer parallel operation tests *(German)* 77—79079
- loading machines, comparison with German PTB force scale *(German)* 79—35734
- long slip gauges, Fabry-Perot etalon appl. *(German)* 78—77849
- low density supersonic gas flow, temp. meas. probe 80—74913
- low energy proton accelerator, voltage or energy calibration using (p,γ) reaction 77—50316
- low flow generator and calibrator development 77—30125
- low level radiation monitors, calibration accuracy and precision 80—9428
- low pressure manometer calibration method using vacuum technique 78—74015
- low-impedance microphone calibrator for pressure transducers 78—59212
- low-temperature blackbody source 80—73355
- lubricant vapour pressure and evap. rate in vacuum, determ. using ambient press. meas. 78—29123
- luminosity and effective temp. calibration for B-type stars 80—17582
- luxmeter, development in Yugoslavia *(Croatian)* 80—105616
- luxmeters with large measuring ranges 80—13123
- α Lyrae, absolute energy distrib. from 3295 Å to 9040 Å 78—20828
- machinery acoustic noise meas. standards and reference sources *(French)* 78—83185
- magnetic circular dichroism recorder calibration at 10.6 μm 80—90876
- magnetic field strength meter calibration system *(Polish)* 80—51311
- magnetic induction calibration units, description 78—74035
- magnetic induction meters, electromagnet reference measure free from hysteresis effects 80—77817
- magnetic props. meas., using deviation ballistic method *(Polish)* 79—71498
- magnetic quadrupole spectrometer, calibration with thin-window He gas cell 79—93859
- magnetic resonance spectrometer calibration by EPR spectra recording 78—89513
- magnetic sensor, high permeability metal core solenoid absolute sensitivity calibration 80—31133
- magnetic spectrograph, calibration by electron capture reactions 80—63445
- magnetic susceptibility meas. calibration standard, low-field, using γ-Fe$_2$0$_3$ and glass powder mixtures 79—88989
- magnetic suspension densimeter, simplified calibration for absolute density meas. 77—30132
- magnetised Fe-scintillator sandwich total absorption calorimeter, performance at 15-140 GeV 78—55103
- magnetometers, vibrating sample, operation and appls. *(German)* 79—93172
- magnetostriction appls. in microdeformation transducer calibration *(French)* 78—12004
- manganin resistance gauge for high pressure meas. 77—10036
- Manganin stress gauges, technique for calibrating effect of resistive hysteresis on dynamic piezoresistive coeff. 79—54118
- manometer, capacitance diaphragm, electrostatic calibration between 10^{-4} and 10^{-1} Torr 77—2663
- manometers, in high- and ultrahigh-vacuum 78—16807
- mass spectrometer, space-borne, in-flight calibration device 78—93115
- mass spectrometer calibration by nonstationary flow method 78—4730
- mass spectrometer calibration using Li ion source 77—41727
- mass spectrometer leak detector, increasing sensitivity by selective gas accumulation 79—6215
- mass spectrometers for van der Waals dimers 78—89585
- mass standards, calibration by sets of weights intercomparison 78—54342
- mass standards (1000 kg) for electromech. balance testing *(German)* 77—79060
- Mauna Kea Observatory 33 μ photometry 77—67044
- measurement instruments, optimal intervals determ., generalised method *(Rumanian)* 78—49787
- medical intravenous infusion drop-rate calibrator 79—96705
- metallic bellows dilatometer 77—82487
- Meteosat, in-orbit, appl. to lunar thermal props. obs. 80—17511

calibration continued
metrological problems of the calibration of instruments used in radiology and radiotherapy *(Spanish)* 79—92377
metrology use in material inspection 78—95899
microgravimetric network for secular gravity studies in Scotland 78—36298
microphone, method for measurement of peak amplitude response and step-function decay 79—41548
microphone calibration at depth in dry hyperbaric chambers 80—38205
microphones, absolute calibration using laser-pistonphone 77—58519
microwave diathermy equipment and power indicator 77—40901
microwave radiation hazard monitors, measurement standards 80—26374
microwave radiometer blackbody calibration standard for MM wavelengths 80—269
microwave radiometer calibration standard with Brewster angle impedance matching 77—5918
microwave reflection coeff. meas., calibration error evaluation 79—21768
microwave survey instrument evaluation and calibration 77—37946
microwave wavemeter molecular rotational resonance investigation by spectrometer *(Polish)* 78—29866
mineral fission fragment track annealing characteristics for geochronology 79—100827
minicomputerised pressure transducer data logging system *(Russian)* 79—6102
mirror optical scatter meas. specification proposal 80—48390
modular electron calorimeter, relative and absolute calibration 78—78578
modulation meter development, special features *(French)* 77—53948
moisture measurement in porous ceramic components, equipment *(German)* 78—54378
moisture meters, representation as two series transducers, total error estimation 80—77792
monochromatic pyrometer, industrial type, methods *(French)* 77—5846
monochromatic pyrometer with silicon photocell as a detector *(Japanese)* 79—93145
monochromator, grazing incidence, intensity calibration *(Japanese)* 79—32062
monochromator, Littrow prism, wavelength calibration 78—25950
monochromator, normal incidence, intensity calibration by double monochromator method 79—94341
monochromators, grazing incidence and normal incidence, intensity calibration in VUV for plasma diagnostics 80—48995
mosaic sensor test and calibration facility for focal plane arrays 80—86425
Mossbauer 14.4 keV gamma-ray source, design, calibration and polarimeter 80—86535
Mossbauer data calibration using laser interferometer 77—88326
Mossbauer diffraction expts., calibration consts. 78—24906
Mossbauer spectrometer drive systems, improved interferometric calibration 77—18151
MPP-1 stationary precision proton magnetometer, errors and calibration 79—53535
multiples of the unit of mass, systematic search for orthogonal systems 80—82747
multiwire proportional chamber, frameless, cylindrically shaped, using charge division readout 77—38556
Nancay radioheliograph, Mark II, calibration and preliminary results 78—28517
National Bureau of Standards, calibration and related measurement services 79—168
Navy liquid flow correl. program 78—30380
NDT 79—11738
NE213 neutron counter, efficiency calibration 80—27877
nephelometer, meas. of Rayleigh scatt. props. of aerosols and gases 79—29865
neutral density filters, for UV-vis. spectrophotometry, calibration 78—45734
neutrino source at LAMPF, calibration from stopped π^+ decays in Cu beam dump 79—45503
neutron, dePangher long counter, calibration from 2 keV to 19 keV 77—88344
neutron activation in vivo total body anal. using 14 MeV neutrons, calibration and evaluation of system 78—53490
neutron beams at NBS reactor, prod. for calibration standards using reson. scatt. and filters 77—38539
neutron calibration technique for detectors with low neutron/high photon sensitivity 79—31344
neutron capture absolute yield calibration, saturated resonance technique 79—80935
neutron counter (60 element) calibration in energy range 8.5 to 450 MeV 79—6798
neutron detector, associated particle technique 77—26939
neutron detector, calibration of zero-angle direction 80—91185
neutron detector calibration, simple recipes for ground scatt. 80—106231
neutron detectors, 10-30 MeV range, absolute calibration by associated particle method 77—26937
neutron displacement cross section, radiation effects intercalibration, damage coeff. 79—23653
neutron dosimeter and monitoring instrumentation calibration using ^{252}Cf and ^{238}PuBe sources 80—13946
neutron filtered beams, 2 keV, 24 keV, 144 keV, calibration and use 79—9937
neutron flux absolute meas. at fast pulse reactors, calibration against ^{252}Cf source 77—23389
neutron monitor calibration, standard fields at Physikalisch-Technische Bundesanstalt 80—57999
neutron monitor calibration for radiation protection at 24.5 keV and 2 keV 78—89983
neutron personnel monitoring film, Kodak NTA, energy depend. 79—100753
neutron polarimeter, 3-D calibration procedure 80—18770
neutron precision long counters, calibration for use with filtered neutron beams *(German)* 78—58529
neutron rem counter, corrected calibration of Andersson and Braun type rem counter for divergently incident Am-Be neutrons 80—74031
neutron scintillation counter threshold 80—23258
neutron sensitive instruments, calibration using novel source emitting neutrons around 0.5 keV 77—6615
neutron source calibration at NBS for calibration checks of neutron radiation instruments 77—38540
neutron sources, anisotropic neutron emission 78—90009

calibration continued
neutron spectrometer, with pulse-height discrimination against γ-ray background 78—13378
neutron spectrometry, calibration and testing using moderator spheres *(Czech)* 80—47804
NMR, simple and inexpensive method for calibration of large magnetic field sweeps 78—261
NMR magnetometer for solenoid calibration 78—21187
NMR spectroscopy, frequency sweep nonlinearity, meas. and correction 78—24836
NMR spectroscopy, low-temp. thermometer for ^{1}H, ^{19}F, and ^{11}C samples 78—65949
noise source, high-level, for calibration of Johnson noise power thermometers 78—82005
nondestructive assay equipment, calibration using reference materials for fissile material assay 80—71880
NQR thermometer, calibration in 203-398K range 80—42222
nuclear materials accountability, tank volume calibration algorithm 80—83159
nuclear materials accountability tanks, automated calibrator 80—83158
ocean wave spectral density meas. with analogue filtering 77—41230
oceanographic instrumentation, international calibration standards 78—45043
oceanographic radio techniques, calibration and appls. 78—77337
open channel acoustic flowmeters, design, calibration and errors 78—55701
optical detector, calibration method for distorted optical short pulse 77—71373
optical devices for counting/detection of ice particles in mixed-phase clouds 77—41221
optical emission and X-ray spectrometry, synthetic calibration standards 79—24850
optical emission spectroscopy, emulsion calibration curve 79—43650
optical fibre absolute power meas. thermistor sensor 78—65971
optical fibre drawing, diameter control improvements 78—1445
optical fibre refracted near-field scanning, calibration technique 80—99823
optical fibre refractive index profile meas., near-field technique 80—91931
optical fibre variable attenuator, calibrated, expt. 77—39047
optical particle counter, aerodynamic particle size calibration 77—5879
optical scintillometer, large-aperture, fine calibration, optical estimate of turbulence inner scale 79—21026
optical single-particle-size spectrometer calibration and testing, monofilament fibres as substitute particles 80—58819
optical system for plasma temperature field determ., asymmetrical *(Czech)* 80—38704
optical transmittance, inverse-fourth photometric device 78—82021
optoelectronic scanning device accuracy, raster distortion and instability effects 79—72697
orthotropic composite model materials, photoelastic calibration 80—87715
oscilloscopes, deflection coeff. and sensitivity testing *(Rumanian)* 80—47048
oscilloscopes, new unit to calibrate for transient response bandwidth and gain 80—27288
OSO-8, LPSP expt, calibration and pre-launch performance 77—64649
outdoor noise monitoring microphone installation and calibration *(Japanese)* 78—42504
oximeter calibration, humans exposed to centrifugation 78—92734
parameters, InSb and Ge magnetooptical rotation standards 80—60551
particle velocity hydrophones, LF calibration in liquid layer 79—94443
particle-sizing device, Doppler shift spectrometer appl. 80—4827
particulate emission monitor calibration in gas-solid suspension 77—37454
peak detector circuits, use with single-particle detectors and multichannel analysers 80—37707
penetrameter cassette calibration to 400 kV and extra-focal radiation effects in X-ray tube filtration meas. 78—20242
personal integral dosimeters, calibration method *(Czech)* 80—27825
personnel dosimeter calibration, US NBS standard reference neutron fields 80—9417
personnel dosimeter design and use, physical requirements for dose meas. 80—9424
personnel dosimeters calibration techniques for electrons and photons 80—9419
personnel dosimetry photon calibrations, use of phantom 80—9425
personnel neutron dosimeters, calibration for use in different neutron fields 80—58001
pH meters, online, problems and solutions 78—53282
photodetector spectral response determ. using calibrated lamp and interference filters 79—71528
photodiode array, realtime hardwired data preprocessor, satellite earth resources survey sensor appl. 80—56693
photodiode detector calibration using synchrotron radiation 80—90810
photodiodes, down to 5 nm wavelength, synchrotron UV radiation appl. 78—77959
photoelastic frozen stress slices, fractional fringe order lines obtained by controlled density techniques, self-calibration 77—51001
photoelastic optical retardation determ. by colour photography 79—72865
photoelectric spectrophotometer, accurate absolute calibration in wide spectral region 79—96919
photoelectron spectrometer, calibration using binding energy scale 80—90930
photoelectron spectroscopy, biological appls., review 77—56558
photogrammetry, distortion calibration, lateral chromatic aberration effects, operational data reduction 79—35881
photogrammetry, orientation and calibration method for nontopographic appls. 79—35875
photographic emulsion, for spectrographic anal., calibration curve computer calcs. 78—4706
photographic film calibration for Q-switched ruby laser energy meas. 78—5517
photographic film detectors, γ-exposure efficiency, focal distance depend. *(Czech)* 79—89518
photographic plate calibration, new computerised method, galaxy photometry appl. 79—92677
photographic pyrometry technique and external calibration 79—93144
photometric gas analyser, method 78—49877
photometric light attenuation systems, comparative analysis 79—12839
photometry of white dwarf stars, calibration 78—85938

calibration continued
  - photon calibration of radiation protection instruments in an authorized metrology service 80—9423
  - photon counting system, pulsed reference light source 77—3640
  - photon irradiator calibration, compensation for geometry induced errors 80—18702
  - photopic response sensor, calibration rel. to photopic handbook data 80—62732
  - photosensor spectral responsivity calibration microprocessor system 80—86409
  - photothermophone, device for absolute calibration of photoacoustic spectrometers 78—16854
  - piezoelectric sound receivers, sensitivity determ. by impedance method 77—11104
  - piezoelectric transducers, absolute calibration 80—79099
  - piezoelectric transducers, reciprocity techniques for estimating the diffuse-field sensitivity 80—48538
  - piezoelectric triaxial cell for measuring occlusal force by human teeth *(German)* 78—20303
  - Pirani gauges, performance reproducibility 80—77806
  - PIXE analysis, MX-ray correction factors calcs., internal standard methods 80—45614
  - plane-wave microwave power density of hazard probe, power equation techniques 77—71341
  - planets, far IR brightness temps. recalibration 77—9683
  - plasma neutral atom, multichannel energy spectrometer, 0.3-10 keV, for fast pulsed expts. 79—73037
  - plastic detectors, calib., heavy cosmic ray charge distrib. 78—17500
  - plastic scintillation detector system for low level environmental radiation meas. 77—38567
  - plastic scintillators, radioluminesc. absolute output following ^{60}Co γ-ray irrad. *(Russian)* 78—92124
  - pneumatic force transducer, calibration 78—21128
  - pneumatic measuring/calibration system for strain meas. at up to 300°C 78—45610
  - pneumatic type anemometer *(Russian)* 77—37420
  - pohtometric calibrator, inverse fourth power, NBS optical density standards development and appl. 80—73412
  - polarimeter, illuminator with adjustable polarisation 77—57380
  - polychromator, Astro 7, UV, for zodiacal light obs., absolute radiometric calibration 78—49336
  - portable radiation meters, accuracy checking facility at Berkeley Laboratories, UK 78—74507
  - portable voltage source, ultrastable 79—67351
  - positron beam energy of NBS positron annihilation in flight facility 79—31306
  - potentiometric strip chart recorder calibrator/performance evaluator 77—87752
  - precision transducers with pneumatic output signals, reference air/water multitube manometer appl. 78—93717
  - precision voltage and current source [for thermoelectric transducer calibration] for thermoelectric primary transducer calibration 79—80605
  - pressure, above 10 GPa, fixed points 77—13765
  - pressure calibration by resistance-jump transitions up to 500 kilobars 78—54388
  - pressure instrument, automatic procedures 77—53880
  - pressure meas. in diamond anvil cell, improvement using ruby R_1 fluorescence 80—98928
  - pressure probe, omnidirectional, for wind meas. *(French)* 79—25349
  - pressure pulse sensors, by indirect piezoelectric effect *(Czech)* 77—5857
  - pressure transducer performance, effect of zero offset changes 80—56255
  - pressure transducers, interferometric techniques 78—21159
  - pressure-gradient hydrophone for particle vel. meas. in fluids, calibration *(German)* 77—72118
  - Preston tube calibration in transpired turbulent boundary layer 78—79397
  - primary dosimetric standards at the Memorial Sloan-Kettering Cancer Center, NY, USA 80—8190
  - prism IR spectrometer, calibration curve, non-min. deviation effect 77—13809
  - probe, five-hole, for complex flow field meas. 80—69951
  - probe, magnetometric, calib. by supercond. solenoid using NMR *(Czech)* 78—29130
  - probe, spherical Pitot, for flow meas. *(Italian)* 80—69957
  - process gas chromatographs, microprocessor based, calibration and data reduction 80—81402
  - proton beam calib., limits on differential hysteresis in Enge split-pole spectrograph 78—55082
  - proton induced X-ray emission anal. of autopsy tissues, calibration, correction methods 77—56466
  - proton polarisation standard using ^{12}C+p polarised scatt. 77—10573
  - pulse generator, spectrum amplitude measurement 77—18017
  - pulsed low current source for amplifier calib. in ion-molecule collision expts. 78—93724
  - pulsed plasma source temperature calibration spectropyrometer 77—7590
  - punched artificial defects for calibration of NDT equipment 79—34228
  - pyranometers for mesoscale solar irradiance network, test and calibration experience report 79—74499
  - pyrgeometer performance improvement 77—70860
  - pyroelectric radiometry, optical calibration system 77—61106
  - pyrometer, spectral ratio, scale correction by electric method *(Russian)* 80—37040
  - quadrupole mass filter specification and calibration *(Japanese)* 78—12784
  - quartz crystal oscillator checking against standard frequencies in LF/VLF ranges 77—74372
  - quick calibration checks, devices to calibrate commonly used meas. instruments 80—47010
  - radars calibration with raindrop disdrometers, field expt. 77—91311
  - radiant flux sensors, calib. with ball radiometer 78—282
  - radiation calibration, mobile laboratory design 77—38582
  - radiation calorimetry of single electron pulses from a LINAC 80—42872
  - radiation detector calibration in VUV, using wall-stabilised Ar cascade arc 79—80679
  - radiation detectors, appl. of monoenergetic standard X-ray sources 77—38078
  - radiation dosimetry standardisation, conf., Atlanta, GA, USA, Dec. (1977) 80—4469
  - radiation instrument, for radiant flux meas. of arbitrary source 77—34022

calibration continued
  - radiation irradiance scales intercomparison, 90 to 250 nm wavelength range 80—98963
  - radiation measurement, calibration program using NPL secondary standard ionisation chamber dosimetry system 77—38584
  - radiation monitor evaluation, techniques for producing standard EM fields 79—97341
  - radiation protection instrumentation test and calibration 80—9420
  - radiation pyrometer, near-infrared, using standard temp.-calibrated lamp with filter 77—53915
  - radiation pyrometry, high speed, review of problems and technology 77—26299
  - radiation standards for source spectral emission and detector spectral sensitivity 77—39007
  - radiation therapy, calibration and meas. standards in USA 80—8188
  - radiation therapy, chamber factor reliability review, United States institutions 79—20685
  - radiation therapy machines, calibration discrepancies, US institutions, data anal. 79—20686
  - radiation-force balance, portable, for diagnostic US transducer output power meas. 78—69163
  - radiation-pyrometer systems calibration device 79—80623
  - radio-isotopic density meter, temp. compensation method *(Russian)* 77—49713
  - radioactive release monitoring equipment test gas standard production *(French)* 79—3252
  - radioactive source calibration with $4\pi\beta$(CP)-γ coinc. counter 77—38545
  - radioastronomy, flux density meas. of calibration sources at 2295 MHz 77—37663
  - radiocarbon chronology and calibration of Late Minoan IB 79—26200
  - radiocarbon dates calibration, bristlecone pine and ancient Egypt 78—70234
  - radiochemical and chemical trace analysis, in environmental materials, reliability aspects 78—40106
  - radiography, exposure meas., energy depend. of correction factors for Victoreen 570 Condenser R-meters 78—3597
  - radiography, Hounsfield number definition and computerised tomography number conversion 78—35952
  - radiography instrument calibration, energy depend. of correction factors for Victoreen 666 Survey System 78—3596
  - radioisotope scanning, splenic sequestration meas. 77—2043
  - radiological instrumentation calibration by British Calibration Service 80—8186
  - radiometer, Crookes, calibration, student exercise 79—62978
  - radiometer, energy calibration, geometrical relationships 77—74482
  - radiometers, using high-temp. thermal radiation sources 80—17946
  - radiometric calibration, theory and methods 77—45878
  - radiometric exploration meas. standardisation advantages and methods 78—28325
  - radiometric field instruments, experiences with concrete calibration sources 79—5633
  - radiometric transfer standards calibration in UV and VUV by electron synchrotron radiation 79—12847
  - radiometrically calibrated imagery for thermography 77—40893
  - radiometry and photometry development and standards 79—6161
  - radionuclide calibrator, use in meas. mixed energy gamma radionuclides 77—14319
  - radiopharmaceutical dose calibrator performance and quality control 77—56470
  - radiotherapy, precision of dose meas. devices, therapy machines and patient dose delivery 77—40789
  - radiotherapy machines, instrumentation used by AAPM, Keithley-Farmer system 77—2055
  - Raman spectrometer, spectral sensitivity calibration 77—5930
  - Raman spectrometer calibration using AR ion laser lines 79—97446
  - Raman spectrometer calibration using Kr$^+$ laser plasma lines 80—57394
  - Raman spin-flip laser, multiply pumped, coherence effects 80—87398
  - rapid-scan polarising Michelson interferometer and InSb detector calibration 80—59305
  - rare-earth X-ray intensifying screens, in 15-70 keV range, for pulsed X-ray sources 77—26446
  - reactive components of resistors, measurement using precision dielectric cell 79—49255
  - recorders, direct-writing analogue type, biomedical appls., techniques and maintenance, review 78—69241
  - reference fission foils preparation by fluoride deposition, characterisation 80—23218
  - reference permeability meters, short cct. coaxial lines as inductance standards 80—77816
  - reference radiations for radiation protection dose meter calibration *(French)* 80—57998
  - reference sound sources, characts. 78—9515
  - reflectometers, thru reflect line, improved technique for calibrating dual six-port automatic network analyser 80—47073
  - refractive index measurement, calibration substrate for Abeles equipment 78—77965
  - remote radioactivity working level monitor, microprocessor assisted calibration 77—61616
  - remote sensors by time averaging *(Russian)* 77—78452
  - resistance strain gauges bonded to bone surface in vivo, post-mortem calibration 78—28135
  - resistance thermometer, cold-wire, in still air 77—5834
  - resistance thermometer, Cu and Pt sensors, method *(Polish)* 79—26055
  - resistance thermometer automatic calibration oven 80—98914
  - resistance thermometers, device for measurement of static characteristics 80—77784
  - resistance thermometers, thermodiodes and thermocouples, 4.2-300K range 78—45624
  - resistive voltage-ratio standard for 10 kV DC meas. 77—5873
  - respiratory measuring equipment, flow and vol. calibrator 79—96687
  - respiratory monitors, instrumentation and maintenance, review 78—69236
  - reverberant room, reverberation decay method appl. 77—19502
  - RF accurate voltage meas., review 77—18043
  - RF ammeter calibration method at 1 MHz 79—88905
  - RF signal level reference 77—115
  - RF standard magnetic field generator, with loop antenna, freq. charact. improvement 77—26348
  - RF voltage standard system for voltages from microvolt to 1 V *(Japanese)* 78—89491
  - rheograph, multichannel, with automatic calibration 80—3831
  - rheometer, high freq., operation, calibration, appls. 78—83345

calibration continued
- river bedload transport measurement, calibration of acoustic device 80—56620
- RMS digital voltmeter calibrator for VLF 78—86293
- rocks, igneous, crack porosity calibration from thermal cycling cracks 79—29759
- rod bundle void fraction in two phase flow, fast neutron scatt. technique calibration 79—82017
- roentgenocardiograph with photoelectronic sensors, calibration device 78—57061
- rolling ball viscometer, calibration for meas. on organic liquids 77—69107
- RONSARD atmospheric radar, calibration techniques 80—46278
- rotannular weight meters, for gas flow meter calibration 79—68843
- rotary-vane attenuator, automatic calibration on modulated subcarrier system 77—18022
- Rowland concave grating spectrometer, component alignment using optical bench *(French)* 79—98514
- Royco aerosol particle counter 225, data processing system and modified system props. 80—37005
- ruby R_1 fluoresc. press. gauge, calibration, 0.06-1 Mbar, specific vol. meas. for Cu, Mo, Pd, Ag 78—70150
- sailplane variometer, calibration and use to meas. vertical atm. vel. fluctuations 79—88480
- satellite IR radiometer, calibration 80—101440
- satellite solar cell calibration using high-altitude balloon *(Japanese)* 78—61700
- Savonius rotor current meter 77—33205
- scintillation counters, large area liquid, for EAS expts. 77—397
- scintillation techniques for calibration light sources 77—71720
- search-coil, magnetometer, mag. field simulation system, noise meas. *(German)* 77—49754
- Seasat, scanning multichannel microwave radiometer, calibration algorithm development 80—94682
- SEASAT-A satellite ocean surface truth expts. 77—5419
- seawater standard, preparation and chlorinity calibration 79—74898
- SEC Vidicon photometer, stellar photometry calibration and appl. to main sequence of ω Centauri 80—90491
- secondary radiation dosimeters, prep., sensitivity anal. and calibration 80—74034
- Secondary Standards Dosimetry Laboratory, review of role 80—5361
- seismic stations calibration, appl. of crustal spectrum characts. *(Russian)* 78—49158
- seismic systems, calibration using random binary signals 79—92604
- seismic systems, parametric models 79—92603
- seismograph, long-period, transfer function determ., temp. effects 77—9518
- seismometer calibration, in situ, modified step method 77—87101
- seismometers, automated high-precision amplitude and phase calibration 77—9519
- seismometers, EM and hybrid instruments, developments 79—39906
- SEM, metrical features of micrographs, calibration procedure 78—32922
- SEM linewidth meas. artifact fabrication and calibration 78—41375
- semiconductor dopant surface concentration determ. by IR reflectance 80—34036
- semiconductor packages, hermetically sealed, calibration and anal. of moisture by gas mass spectrometry 80—90928
- sensitometric sources, photometric and radiometric calibration, tutorial 77—34044
- ships compass adjustment in fog using atmosphere polarised sunlight cct. 78—24831
- short-time measurement instruments, pulse generator cct. *(German)* 78—12728
- SI system, need for periodic recalibration of laboratory equipment 80—31705
- signal generator reference voltage, testing with B3-24 compensation valve voltmeter *(German)* 79—54155
- simulated underwater partial launch system, photogrammetric data reduction system 77—79075
- sky background brightness meas., 4500-10600 Å *(Chinese)* 80—12540
- small liquid biological sample microwave complex permittivity meas. 80—17222
- soil, neutron moisture meter calibration, neutron absorpt. cross section meas. 77—9545
- soil-water system, γ-ray transmission studies, calibration 80—26629
- solar cell spectral response characterisation, 400 to 1000 nm 80—35675
- solar EUV output, meas. techniques and instruments recalibration 78—57535
- solar granulation, power spectrum calibration by Michelson stellar interferometry 77—17464
- solar heating systems, instrumentation principles for performance meas. 80—35743
- solar luxmeter 77—9661
- solar magnetograph calibration programme *(Russian)* 78—65499
- Solar Maximum Mission UV polarimeter design, operation and calibration 79—80225
- solar radiation meas. field instrument standard 78—88946
- solar radioflux, 1970 absolute calibration at 2800 MHz 80—17570
- solar simulator calibration photometer 79—26103
- solid state track detector, mass identification scale depend. on different track form. models 78—17515
- solid surface fluorescence analysis, calibration curves 78—31719
- sound measuring instruments, acoustical and electrical calibration 80—19197
- sound pressure in insert earphone couplers and real ears 78—65152
- southern standard stars, monochromatic flux relative and absolute calibration 80—51742
- Spar Buoy Oceanographic Telemetry System software engineering 80—46308
- spark-source mass spectrometry of metals, relative sensitivity coeff. 79—92045
- spark-source mass spectroscopic anal. of Al, Al alloys, sensitivity calibration 78—68962
- SPEAR transport line toroids, intensity monitors calib. system 77—88295
- speckle interferometric meas. of binary stars, calibration 77—78820
- spectra calibration, using Edser-Butler bands, for teachers 79—21504
- spectral radiance calibration of light sources in vac. UV using synchrotron radiation 78—65954
- spectral radiance calibrations, 165-300 nm, interlab. comparison 77 74478
- spectral radiation detectors, calibration and error anal. 78—46177

calibration continued
- spectrochemical analysis, photographic emulsion calibration technique 79—79321
- spectrochemical analysis, using induction-coupled plasma system 77—90708
- spectrometer, energy calibration, 110-280 nm 77—71386
- spectrometer, millimetre-wave astronomical, intensity calibration error evaluation 78—53821
- spectrometer calibration chamber for SURF II storage ring 80—91339
- spectrometer calibration samples, homogeneity investigations with LMA 10 laser microspectral analyzer 78—23983
- spectrometer for underwater gamma surveying, calibration 79—21066
- spectronephelometer, automatic scanning integrating, visible and IR spectra 77—79165
- spectrophotometer, four-channel, for stellar Ca II H and K flux meas., calibration obs. 78—73646
- spectrophotometer, photometric scale calibration using fluorite 1200-800 cm^{-1} transmission 79—12837
- spectrophotometer, UV absorbance standards, $K_2Cr_2O_7$ in perchloric acid soln. 78—32851
- spectrophotometer calibrator, nonlinearity of transmission coeff. scale 79—30571
- spectrophotometers, photometric accuracy verification, in visible range *(Czech)* 80—13159
- spectrophotometric standards, glass filter SRM 930 by NBS, clinical laboratory appl. 78—54331
- spectrophotometry, errors and calibration procedures 77—53988
- spectrophotometry, errors and calibration procedures 78—32849
- spectrophotometry, UV absorpt. and fluoresc., practical standards 77—49783
- spectrophotometry standardisation to ensure original calibration 77—38020
- spectropolarimetry, using d-10-camphorsulphonic acid ammonium salts 77—24816
- spectroradiometer, lone wavelength Exotech model 20C, Earth resource remote sensing appl. 79—88474
- spectroscopic instruments, 180-500 nm calibration via microwave lamps, photoelectric spectra 77—45899
- specular gloss of paint, calibration of reference standards 80—95061
- specular reflectometer-spectrophotometer, NBS reference, mirror refl. meas. 80—68236
- Speer C resistance thermometer, calibration and magnetoresist. effect 78—4624
- spinning magnetometer, absolute calibration method 78—54413
- spinning rotor gas friction gauge, calibration against fund. vac. press. standard 80—82787
- SQUID magnetometer, used for dilute magnetic alloy studies 79—67358
- standard capacitor, simple calibration method 77—82571
- standard cell, using supercond. junction device 77—18029
- standard cell calibration against Josephson voltage reference 77—5874
- standard resistors, cryogenic current comparators, double constant current source, appl. 79—21775
- standard stars, IUE photometric calibration, UV spectra 80—77383
- stars, luminosity calibrations from trigonometric parallaxes, practical improvement method 79—40083
- static and dynamic calibration using optical interferometric techniques 79—23178
- steel, tool and high-speed, high freq. induction melting and centrifugal casting in instrumental anal. 80—84886
- stellar absolute luminosity calibrations, consistency 80—62111
- stellar intermediate-band photometry, calibration of indices for late-type stars 78—49424
- stellar IR airborne spectrophotometry, 1.2-5.5 μm, spectra and absolute calibration 80—62117
- stellar luminosity systems calibration, trigonometric parallaxes appl. 80—4343
- stellar photographic photometry, calibration errors rel. to red dwarfs space density 77—5524
- stellar photometry, Hβ indices, calibration and instrumental considerations 79—96923
- stellar radiation, new absolute calibration of Vega 79—40193
- stellar spectra, photographic equivalent widths calibration against solar photoelectric equivalent widths, feasibility 78—73658
- stellar spectra, recalibration of quantitative three-dimensional classification for F8-K1 stars 77—78768
- stellar spectral energy distribution in 3500 to 7500 Å region, absolute calibration 80—67710
- stellar spectrophotometric standards calibration against α Lyrae 79—62760
- stellar uvbyβ photometric system, absolute luminosity calibrations check by means of small trigonometric parallaxes 78—57463
- stellar uvbyβ photometric system, calibration in terms of temp. and gravity 78—4198
- stellar uvby Hβ photometric system, empirical calibration for B-type stars 78—32454
- STEM, transmitted and backscattered electrons use 78—37118
- strain gauge, resistance device for calibration of low temps. 79—17413
- strain gauge calibration machine construction and parameters *(German)* 80—36970
- strain gauge for hip joint prosthesis, built in *(French)* 78—44705
- strain gauges, resist., in alternating sign deform., calibration 79—15901
- stylus tip instrums. for surface roughness meas. *(German)* 80—101782
- stylus-type surface texture meas. instrument against interferometrically measured step 78—77862
- subdwarf star 37-45 colour excess, calibration using Fe/H abundances 80—82363
- subsoil neutron moisture probe, lab. calibration, minimum soil sample size calcs. 77—57333
- sunlight polarisation, ships compass adjustment appl. in fog 78—24831
- superconducting susceptometer, automatic, sensitivity calibration, biological appl. 78—57154
- superconductive temperature fixed point device, prep. and calibration 80—82770
- superheterodyne mm wave spectrometers, intensity calibration 77—33353
- supersonic molecular beam source 80—82845
- SURF storage ring calibrations for NASA stratosphere and climate programs 80—94721
- surface barrier spectrometers for fast neutron calibration in MeV range 79—9961
- surface contamination monitors for hospital use 80—36153
- surface flatness meas., moire angular readout device 79—93209

calibration continued
  surface profile monitors for thin film thickness meas., calibration standards 80—17918
  surface tension meas. using filter paper Wilhelmy plates with insoluble monolayers 78—357
  surface wave meas. instruments, use of resistance wave gauge 80—24110
  synchrotron X-ray spectrometer, Si crystal wavelength calibrator 79—89051
  tandem Pelletron accelerator, calibration of 90° analysing magnet 77—57777
  Tarapur Atomic Power Station radioactive waste discharge monitoring 78—89989
  TDC, high precision calib. method 77—57831
  telescopes, auto-collimating, absolute calibration methods *(German)* 78—86239
  teletherapy alignment, simplified method of quality control 77—70528
  TEM, universal magnification curve 79—49340
  temperature calibration device, appl. of miniature sealed cells, and precision cyrostat 77—22559
  temperature calibration standard, melting point of pure Ga 77—41611
  temperature calibration standards using graphite-halogens for TEM 80—86510
  temperature distributions of powder particles in plasma stream, method and apparatus 78—14210
  temperature measurement by line shift method, internal temp. of Y_2O_2S:Eu phosphor 77—13750
  temperature sensors, Pt-100, stability, 20-273K range *(German)* 77—79094
  tensile/compressive strength test machine calibration *(German)* 77—77654
  test gas atmospheres, calibration standards, generated by gas phase titration 78—69507
  test leaks 78—53121
  thermal conductivity meas., 60 to 300K, USSR special standard 77—31205
  thermal diffusion column calib. technique, for dilute gas mixtures 78—22450
  thermal field analysers, digital, calibration curve 80—27293
  thermal IR scanner meas. technique for cooling water temp. 80—40947
  thermistor ebullioscopes, calibration and sensitivity uncertainty 78—12695
  thermocouple, PR, simplified calibration *(Japanese)* 79—93139
  thermocouple, thermometers, voltage generation, calibration 80—57295
  thermocouple calibrations, comparison, fixed point and melting wire methods 80—86252
  thermocouple instrumentation, field calibration 80—90840
  thermocouples, IR thermometers and optical pyrometers, standards 79—85141
  thermographic camera, calibration, transmittance and emittance meas. 78—45628
  thermogravimetric automatic temperature indicator 78—86257
  thermoluminescence dating, reassessment of fine grain dose-rate 77—34071
  thermoluminescent dosimetry, TLD 700, parameters affecting overall calibration accuracy 79—63821
  thermometer, in liq. He range, dipstick cryostat 80—37044
  thermometers, for low temp. meas., from 13.8K 77—26296
  thermometers, sealed metal freezing point cell 78—12696
  thermometers, surface contact, dynamic behaviour *(German)* 80—90843
  thermometers, time response calibration, concepts and model calcs. 78—54370
  thermometers, using Ga melting-point apparatus, enzymologic appl. 78—85460
  thermometers and thermistors using diphenyl ether triple-point cell 79—21750
  thermometry considerations in localised hyperthermia, review 78—53561
  thermopile radiometers for UV spectrum appl. *(Japanese)* 78—54422
  thermosphere, tidal struct. at equinox, model calibration 78—81476
  thermovision system, AGA 680, calibration procedure to extend versatility 78—4680
  thickness meter, eddy-current for thermal insulation meas. 80—73316
  thickness mode piezoelec. US probe design factors 79—68540
  thin film meas. tool calibration by cubic spline fitting 77—18063
  thin liquid films on inaccessible surfaces, thickness meas. 79—30412
  Thomson scattering, rot. Raman calibration 80—1844
  three dimensional computerised monitoring of human motion by optoelectronic means 77—48886
  time meas. system adjustment and calibration signal generator 78—57903
  time to amplitude converters, precision 1 GHz time calibration 80—27903
  TIROS N microwave sounder unit, blackbody calibration 78—93016
  tissue-equivalent ionisation chamber, photon calibration for neutron dosimetry 80—56221
  tissue-reflectance oximetry, simple homogeneous tissue model for calibration 77—40858
  TLD, calibration procedures in the Studsvik standardized personnel dosimetry system, Sweden 80—9418
  TLD, safety and reliability of decentralised reading in Sweden 77—40780
  TLD chip, individual calibration using a Texas instruments programmable calculator 80—36136
  TLD element, precise calibrator *(Japanese)* 80—23159
  TLD powders calibration for low expsoure rates 77—6632
  Tokamak diagnostic Fourier transform spectrometer calibration by liquid N_2 cooled microwave absorber 80—59304
  topology of calibration fields, theory *(Russian)* 80—8770
  torquemeters, calibration using rack with mobile primary transducer 79—80610
  track chamber slide processing, calibration programming problems *(Russian)* 80—73305
  track etch detectors, neutron energy depend. and threshold energy 80—61703
  transducer, with steady and pulsating flows, using computerised flowmeter system 80—79416
  transducers, alternating-voltage, analogue, Soviet methods development 80—98872
  transducers, calibration via radiation coupling of disc to plane back or to disc 77—46828
  transducers, reciprocity calibration in unconventional acoustic geometries 78—83200

calibration continued
  transfer standard radiometric sources and detectors, calibration using synchrotron radiation 78—65967
  transmission electron microscope, determ. defocus values, using Fourier images 80—47148
  transuranic element meas. in vivo at CRNL 77—77993
  triggered calibrated sweep for AC oscilloscope 80—67987
  turbine flowmeters, for solar collector testing facility 77—39387
  turbine meter uncertainty, uncertainty pattern statistical anal. 78—30381
  two-bulb cells, calibration via precise binary gas diffusion coeffs. 77—76019
  two-coordinate measuring device, interference band-object scanning, precision gauge block length standards *(German)* 78—89433
  two-photon absorption calibration via stimulated Raman gain 78—87098
  two-probe synchronized sampling technique for measuring flows behind rotors, calibrations 80—14865
  UHF-plasma torch emission spectrometry by metal hydride generation *(Japanese)* 78—92582
  UK 1.2 m Schmidt telescope plates, electronographic calibration 79—88703
  ultrafine capillaries with diameters between 0.5 and 60 μm, fabrication and calibration 77—30135
  ultrahigh pressure devices, appl. of acoustic vels. ratio in NaCl 77—27945
  ultrasonic testing probe *(German)* 79—81677
  underwater acoustic transducers, reciprocity calibration by FM signal correl. methods 77—68298
  underwater acoustic transducers using complex exponential signal representation 78—79183
  underwater sound transducers, parabolic reflector as nearfield calibration device 80—48528
  underwater transducers, steered planar nearfield calibration array 78—59214
  universal β-backscatter thickness gauge calibration method 77—32747
  US C-scan grey scale recorder, calibration method 78—95878
  US field calibration from acousto-optic data using Fourier techniques 77—84054
  US flowmeters, recalc. of characts. and calibration 80—103086
  US immersion testing, effects of curved entry surfaces on calibration, steel sample expts. 80—71849
  US measurements including medical device output meas. 77—39183
  US pulsed-echo thickness meters calibration using liquid-thickness model 79—37102
  US real time scanner, performance meas. 77—29191
  US reference block calibration procedures 77—62126
  US standard probe transducers, calibration 77—840
  US stress meas. method, experimental results *(German)* 80—53725
  US system for curved surface inspection 78—39977
  US thickness gauges calibration, thickness standards 79—35669
  US transducer absolute calibration by impulse techniques 79—23179
  US transducer calibration method using laser interferometry 79—23177
  US transducer evaluation and calibration conf., London 1977, May 79—23167
  US transducers, arbitrarily terminated, characterization using self-reciprocity calibration technique 80—53574
  US transducers, calibration by measuring total nearfield force, theoretical results 80—33400
  US transmitter, acoustic pressure meas. 77—65657
  US volume flowmeter, in vivo validation 79—83872
  UV and X-ray spectroscopy, synchrotron radiation as intensity reference 79—75619
  UV detection systems, calibration, using mol. emission cross sections 79—85996
  UV double-beam photometer, for atm. O_3 calibration 78—69505
  UV high-intensity narrow-band light source, 3130 Å, for photolysis expts. 78—22185
  UV photometer for atmospheric ozone monitors calibration 78—77960
  UV radiometric standards at NBS 77—38011
  UV spectral radiance calibration using H_2 plasma *(French)* 78—12774
  UV-visible range spectrophotometers, wavelength calibration by interference filters 77—33808
  UV-visible spectrophotometer, rapid scanning, computerised, automatic absorbance calibration method 77—67509
  VA meters, calibration at low flow rates 79—68847
  vacuum gauge, by static method 80—52258
  vacuum gauge, compact bakeable ultrahigh vacuum system design 78—21157
  vacuum gauge, mass spectrometer leak detector range extension 80—73375
  vacuum gauge, rate of rise method extension 77—57342
  vacuum gauge calibration, 10^{-4} to 10 Pa, by orifice flow method 78—82000
  vacuum gauge calibration, attenuation meas. on buffer gas scatt. of mol. beam *(French)* 79—58669
  vacuum gauge calibration, review 77—22563
  vacuum gauge calibration apparatus, flowmeter designs for gas throughput meas., review 77—26319
  vacuum gauge calibration techniques *(German)* 77—87778
  vacuum gauge testing and calibration for low absolute pressure 77—57341
  vacuum gauges, absolute pressure, automation 80—22378
  vacuum gauges, by expansion-reduction method 80—77807
  vacuum gauges, simple volume ratio method 80—31780
  vacuum monochromator, grazing-incidence, absolute calibration using Tokamak discharges 78—87492
  vacuum press. meas. considerations *(French)* 78—49846
  vacuum ultraviolet wavelength comparison of two copper sources using an imaging system 79—35686
  variable area flowmeter calibration, gas flow modelling 78—14115
  variable area flowmeter calibration, gas flow modelling 79—90353
  vascular pressure measurement systems 79—96691
  vector acoustic receivers, calibration method *(Russian)* 77—46876
  vector magnetometer sensor orientation, accurate calibration 78—53741
  velocity meter for cond. flow, characts., freq. depend. calibration *(Russian)* 77—65819
  velocity sensor, calibration equipment and technique, oceanographic appls. 80—8447
  VHF/UHF complex relative permittivity meas., lumped capacitance technique 77—74460
  vibrating wire stress gauge in soft rock 77—84199

calibration continued
vibration meas. devices, ring comparison meas. of equipment *(German)* 80—52189
Viking lander cameras, calibration and performance 78—20639
109 Virginis, absolute energy distrib. from 3295 Å to 9040 Å 78—20828
viscosity mesurements at high-temperature by gas percolation through porous medium 78—1781
volt-ampere meters, pointer type, automatic procedures 77—53937
voltage divider, inductive, between 10 kHz and 100 kHz, international comparison of calibration methods 80—13100
voltage standards and RMS voltmeters in 0.1 to 10 Hz range using AC voltmeter/calibrator 80—22385
voltage standards for testing AC voltage calibrators 79—35786
voltage transfer standard based on AC Josephson effect, standard cell calibration appl. 77—82553
voltameters and milliammeters, installation for determining freq. error over wide range 80—4734
voltmeter, digital, microprocessor appl. 79—40550
voltmeter, digital, using potentiometer, errors analysis 77—10059
volume calibration of nuclear materials accountability tanks 80—68829
vortex flowmeter, calibration and appl. 77—84374
vortex flowmeter calibration data and appl. 78—34231
vorticity indicators, vane-type, construction, calibration, streamwise vorticity meas. in swirling flows 79—60074
VUV calibration facility for radiation detector spectral sensitivity meas. *(German)* 78—82037
VUV detectors absolute efficiency meas. using VEPP-2M storage ring synchrotron radiation 80—82824
VUV light source, transfer standard, low-current AR arc with MgF_2 window 79—35856
VUV spectral irradiance calibrations, method and appl. 80—87452
water media, remote determ. of impurity conc. by laser spectroscopy, calibration by Raman scatt. 79—16090
water triple point cell prep. for calibrating thermometers 78—204
wattmeter, (3+3)-phase voltage and current source of high stability 77—18038
wattmeter, at zero power factor using digital sinewave generator 77—18039
wavelength calibration device for large dispersion spectrographs 80—41728
wavelength calibration of low dispersion objective prism plates, quasar redshift determ. 79—2485
wavelength measuring systems, calibration using freq. stabilised He-Ne lasers *(French)* 79—31935
wavenumber calibration of Pb salt tunable diode lasers, using etalons 78—45738
weather radar calibration, correl. with rain gauge data *(Japanese)* 78—85670
wedge opening load specimen, side grooved, stress intensity factor soln. and calibration 78—51130
Weissenberg rheogoniometer, computerised calib. and meas. of Newtonian fluids 78—87323
whole-body counter in vivo calibrations for quantitative retention estimation 78—3579
wind meas., airborne system, automatic calibration *(French)* 78—24386
wind tunnel calibration by shock standoff distance computation up to Mach 1.2, schlieren method 77—27557
wind-speed measuring instrums. using low-vel. airflow facility 80—1718
wind-tunnel balance, 6-component, using load cell techniques *(German)* 79—37268
wire temperature sensors, frequency response meas. by internal and acoustic heating 80—31123
worldwide flow meas. calibration facilities list 77—62322
X-ray astronomy, calibration of Bragg analyser cryst. polarimeters 77—64664
X-ray detector, photoelec. diode with Al photocathode, calibration 77—54033
X-ray detector calibration in 183 to 932 eV range 77—71717
X-ray detector calibration using low-energy X-ray sources 77—75016
X-ray detectors, energy-sensitive, simplified calibration procedure 77—38548
X-ray diffr. stress meas. calibration elastic const. meas. technique 78—7164
X-ray diffraction at high press., calibration via NaCl lattice parameters 77—11442
X-ray diffractometer furnace, temp. calibration using eutectic transitions of alloys *(Japanese)* 79—6128
X-ray diffractometers, monitor arrangements *(German)* 80—52374
X-ray fluoresc. anal., correction procedures, accurate coeff. method 77—56311
X-ray fluoresc. spectrometer, low energy, for air suspended particulate matter anal. 77—56321
X-ray fluoresc. spectrometers, energy dispersive, calibration standards development 77—60177
X-ray fluoresc. spectrometers, for air particulate anal., reference standard development 77—60176
X-ray fluorescence anal. of trace elements, calibration consts. *(French)* 78—61095
X-ray fluorescence analysis, energy dispersive, matrix correction method 77—70352
X-ray fluorescence analyzers, error estimates for calibration curve parameters 79—87931
X-ray fluorescence thin film calibration standards 80—22496
X-ray high intensity sub.-kV calib. facility using Cockroft-Walton proton accelerator 77—71714
X-ray low energy calibration sources for proportional counters using radionuclides 79—705
X-ray microanal. of cultured skeletal muscle cells 79—100798
X-ray powder diffractometer, APD3600, file searching techniques 80—24319
X-ray radiometric analyser, appl. of expt. planning 80—61186
X-ray source, industrial, use for electronic component radiation effects work 80—63402
X-ray spectral analysis, minerals 79—87904
X-ray spectrographic telescope, on Skylab, anal. of photographic X-ray images 78—49341
X-ray spectrographs, flat and convex curved cryst., wavelength calibration 79—40649
X-ray spectrometer, for at. electron impact ionis. studies 77—68116
X-ray spectrometry 77—48742
X-ray streak camera, calibration using Au 77—4713

calibration continued
X-ray survey instruments, automated calibration and recordkeeping system 77—37876
X-ray techniques, calibration facility at Lawrence Livermore Laboratory 79—49354
X-ray tubes and generators, calibration system 79—17583
Ag-activated Geiger counter calibration for neutron yield determ. in Frascati plasma focus expt. 80—99409
AlSi alloys, X-ray spectrometric anal. method *(Dutch)* 79—96394
$^{27}Al(p,\gamma)^{28}Si$, 2046 keV, gamma-ray intensity calibration standard 77—30698
^{11}B, radiative widths meas., 2.125 to 8.92 MeV levels, intensity calibration of photon spectrum 79—13242
Ba^{2+}, on calcite surface, ESCA, calibration 77—81432
C resistors as low temp. sensors in low temp. reactors, gamma, neutron irrad. investig. 77—45848
CO, gasdynamic laser, weak signal gain, calibration loss method meas. 78—17919
CO_2 infra red gas analyser, calibration method 78—20115
CO_2 isotope laser transitions, absolute freq. calibration, heterodyne technique 77—19230
CO_2 laser stability and heterodyne frequency calibration 78—59031
^{14}C absolute dating using low altitude European tree-ring calibration 78—16195
^{141}Ce standard, measured by dose calibrators, simulated $^{99}Tc^m$ standard 78—61261
^{252}Cf spontaneous fission spectrum irrad. facility for neutron reaction rate meas. 77—14294
^{60}Co, exposure-rate calibration of small radioactive sources 78—41881
^{60}Co gamma-rays, calibration in water vs. calibration in air for teletherapy units 77—21630
^{60}Co teletherapy unit dose calibration, comparison of methods 80—30900
Cs freq. standard, time scale unit duration estimation 77—74368
^{137}Cs, exposure-rate calibration of small radioactive sources 78—41881
^{137}Cs standardisation by $4\pi(PC)$-γ efficiency tracing method 79—13577
Cu-Mn alloy, manganin, hysteresis-corrected calibration under shock loading 80—74818
D lamp, operating time variation of spectral radiance 77—10992
D_2 lamp, spectral irradiance standard for UV, calibration 78—42397
DT miniature target assembly, neutron yield calib. with associated particle monitoring 79—45505
Fe, photoionis. cross section meas. 79—22674
Fe/plastic calorimeters, hadronic cascades induced by high-energy muons, calibration calcs. 77—54477
Fe-Ni film thermocouple, fabrication and calibration 77—37885
Ga, liq. particles-He(N_2)(CO_2)(air), nonequilib. Laval nozzle flow calib., numerical soln. 77—75967
GaAs LPE in situ etchback calibration 79—83114
GaAs resistance thermometers, thermometric characts. approx. in 4.2-100K range 80—31746
Ge detectors, calibration using precise relative γ-ray intensities 78—17469
Ge detectors, calibration using ^{152}Eu source uncertainties in peak area determ. 80—5436
Ge γ-ray spectrom, efficiency calibration in range 122-412 keV 80—37682
Ge, resistance thermometer, low temp., approx. of calibration curve 78—45620
Ge resistance thermometry, interpolation method 80—22357
Ge resistive sensing devices, temp. calibration and reproducibility, high mag. field effect *(Czech)* 80—37029
Ge spectrometer, energy and efficiency calibration in 100 keV to 3000 keV γ-ray energy range 78—17464
Ge spectrum, precise γ-ray energies for calibration up to 3.5 MeV 79—31311
Ge-Li spectrom., re-evaluation of precise γ-ray energies for calibration 78—90015
Ge(Li) and Ge spectrom., calibration using ^{228}Ra and ^{228}Th decay 79—85857
Ge(Li) detector, using linearly varying amplitude pulse generator 77—10526
Ge(Li) detectors, efficiency calibration using continuous external bremsstrahlung 78—46228
Ge(Li) detectors, gamma-ray intensity standards for calibration 80—74083
Ge(Li) detectors, relative γ-ray intensities for calibration 79—49896
Ge(Li) detectors, use of annihilation radiation for precision energy calibration 77—10528
Ge(Li) detectors for environmental assay, calibration using NBS mixed-radionuclide gamma sources 77—38541
Ge(Li) energy calibration using $^{13}C(\alpha,n)$ radioactive sources 79—13572
Ge(Li) gamma-ray spectrometer calibration for radioactive inert gas meas. 77—83442
Ge(Li) planar detector efficiency curve obtained using K_β/K_α X-ray intensity ratio 80—880
Ge(Li), spectrometer efficiency, dead time and pulse pile-up correction 78—50442
Ge(Li) spectrum, ^{236}Ra as calibration standard 77—38543
Ge(Li) system for low level radioactive gas monitoring 78—9038
Ge(Li) uncollimated detector, parametric representation of efficiency curves for X-rays 77—18740
H meters, on-line, calibration system 78—86236
H, optically thin plasma, UV spectral emission coeff., quantum statistics of recomb. continuum *(Russian)* 79—77348
H_2 flashlamp light pulse shape calibration, using synchrotron radiation excitation standard 79—72642
^3H calibration of photomultipliers on liquid scintillator *(Czech)* 79—31324
He, electron elastic scatt., 5 to 200 eV, cross-sections meas., calibration 80—63822
He gas jet noise source, absolute calibr. 78—59228
He-Ne laser wavelength stability, calibration and traceability 80—19050
$He+H^+$, differential scatt., 1-12 eV, high resolution beam meas. 80—58348
^3He ionisation chamber, calibration for use with filtered neutron beams *(German)* 78—58529
HgI_2 miniature probes for in-vivo medical appls., fabrication, spectroscopic evaluation 78—40308
^{123}I source sumpeak calibration absolute activity 77—57785
^{42}K technique, whole-body counters for estimation of whole-body K content 79—25086

calibration continued
LiF-polytetrafluorethane thermolumin. dosimeters, absorbed dose assessment 80—95470
^{6}Li tensor polarised beam prod. and calibration 78—46199
Mn, determination, in gasoline, by AAS using N_2O-H_2 flame, calibration methods 78—15729
N_2^-, 2 eV resonance as energy standard in low energy electron scatt. 77—71872
NO concentration meas. in gas mixtures, chemiluminescence method *(Russian)* 79—16094
^{14}N NMR chemical shift, external neat nitromethane scale 78—24834
^{14}N(n,γ), γ-ray energies, calibration standards 80—52613
NaI detector calibration using large diam. sources 78—33396
NaI scintillation counter, sex-dependent calibration factor, ^{42}K whole-body content meas. 79—29593
NaI(Tl) double crystal gamma ray spectrom., efficiency calibration 79—717
NaI(Tl) γ-spectrometer, calibration using 500 keV Van de Graaff proton accelerator 79—45524
NaI(Tl) large modularised detector, 50 MeV γ-ray meas. 79—76257
NaI(Tl) well type detector calib. for absolute counting of ^{85}Kr and ^{133}Xe 78—9036
NaI(Tl) well-type detector calibration 79—85858
Ni-Cr foldfoil strain gauge, for cryogenic anal. of supercond. structs. in high mag. fields, fusion reactors 78—54947
^{237}Np fission-foil dosimeter, calibration using Sb-Be neutron source 78—33394
O_2 consumption and CO_2 prod. continuous meas. for men in hyperbaric chambers 78—81008
O_3 calibration methods, accuracy 78—69506
O_3 calibration reference instrument calibration 78—73524
O_3 monitors calibration, modification of KI method for improved stoichiometry 79—88037
Pb glass counter, automated calibration system 80—106233
Pb^{2+}, on calcite surface, ESCA, calibration 77—81432
^{212}Pb inhaled body burden calibration, general phantom procedure 77—64138
Pt film resistance thermometer, fabrication, appls. 77—37890
Pt long stem resistance thermometers, Ar triple point realisation cryostat 77—26307
Pt resist. thermometers, 0-850°C range, principles and practice *(German)* 77—82512
Pt resistance standard capsule thermometer, for 13.81 to 273.15K, two-point calibration 79—206
Pt resistance standard low-temp. thermometer checking methods 78—37006
Pt resistance thermometer, Callendar coeffs. determ. 77—26287
Pt resistance thermometer calibration characts. linearisation methods *(Russian)* 78—70123
Pt resistance thermometers, simple Cu holder for calibration 80—98911
$Pt_{90}Rh_{10}$/Pt thermocouple, Inconel sheathed, MgO-insulated, decalibrations during 1200°C use, ion microprobe obs. 78—57957
Pu dosimetry, calibration of whole-body counters 80—21547
^{239}Pu, lung burden X-ray counting efficiency, from inhaled ^{103}Pd studies 78—85391
^{226}Ra, exposure-rate calibration of small radioactive sources 78—41881
^{88}Rb decay, γ-ray energy meas. 79—22530
resistor, improved thermal contacts 78—37015
^{103}Rh(n,n′)^{103M}Rh reaction rate, absolute calibration 79—85875
Rn continuous monitor response to transient Rn concs. 80—32519
SO_2 and nitrogen oxide automatic monitors, laboratory and field calibration *(French)* 77—37455
SO_2 small automatic monitoring network calibration and maintenance aspects 78—81462
Si photodiode absolute spectral response self-calibration 80—73448
Si, photovoltaic cell, absolute spectral sensitivity calibration, radiometry, photometry *(Chinese)* 80—86367
Si ring photodiode reflectometer for cavity reflectance 80—86376
Si, spreading resistance calibration, effect of specimen preparations 78—10450
Si surface barrier detector, pulse height-defect calibration 79—13602
Si whisker strain gauges, sensitivity to elastic pulses in −50 to 110°C range 79—17409
Si-thermometers, temperature-resistance relations, cryostat *(German)* 77—37897
Si(Li) uncollimated detector, parametric representation of efficiency curves for X-rays 77—18740
Si(Li) X-ray detector, efficiency calib. in range 1-5 keV 77—79504
Si(Li) X-ray detector, efficiency calibration in 1.5 to 60 keV energy range 80—47823
U II, oscillator strengths for calibration 77—42280
W ribbon-filament temperature lamps, radiation error estimation 80—64128
W-halogen quartz envelope lamp, polarization characteristics 80—95970
W-Re alloy thermocouples, calibration, 77 to 290K 77—57324
^{88}Y solution, standardisation using efficiency extrapolation method, β-γ coincidence meas. 78—21832
^{67}Zn spectrometer, double freq. interferometer for absolute velocity calibration of piezoelectric transducer 80—37146
Zr ribbon filament lamp, calibrated source for IR radiometer 80—83653
Zr, standard cylindrical calibration sample for long wavelength neutron scatt. meas., proposal 78—29722

californium
see also nuclei with ......
crystal structure at high press., X-ray diffr. 78—83766
determination in biological samples by solvent extraction and liquid scintillation counting 79—53260
neutron irradiation, ^{253}Es synthesis, separation and α-spectra identification 78—17435
separation with phosphororganic extractants 77—26854
surface valence state from surface tension props. 79—95462
target prpe. for synthesis of transactinide elements 80—23206
vapour pressure, thermodynamic functions 80—6509
^{252}Cb, polyethylene pellets in design, construction of storage safe, transport vessel, portable shield 79—5380
^{247}Cf, K-shell fluorescence yields from Auger electrons and X-rays, precision meas. 79—31462
^{249}Cf, IR spectrum, 3700-12000 cm^{-1} 77—68000
^{249}Cf metal, expanded FCC phase, mag. susceptibility meas. 77—28368
^{252}Cf, heavy metal shielding for neutron sources 79—9892

californium continued
^{252}Cf, human lymphocyte chromosome aberrations induced by neutron radiation 79—16169
^{252}Cf, measured neutron and γ spectra in a tissue equivalent medium 80—3805
^{252}Cf, medical appl., fast neutron therapy *(Japanese)* 80—98112
^{252}Cf source fabrication 77—26916
^{252}Cf source in tissue-equivalent phantom, neutron absorbed dose obs. 80—12278
^{252}Cf, status, application and prospects 77—26914
^{252}Cf, sub Cd thermal neutron fluxes in H_2O near the source 79—698
^{252}Cf wire neutron source distrib., meas. by autoradiography 77—61643
Cs_2NaYCl_6:^{249}Cf, mag. susceptibility of Cf^{3+} in octahedral site 77—12089

californium compounds
aqueous solution, electrochem. props., thermodynamic props., radiopolarography 77—29040
$^{249}CfCl_2$, prep. by reduction of $CfCl_3$, spectrochem. anal. 78—27756
$^{252}CfCl_3$ metabolism in rat and effect of in vivo DTPA chelation therapy 78—85387
CfI_2, cryst. struct. determ., X-ray diffr., optical spectra 78—75645
CfI_3, cryst. struct. determ., X-ray diffr., optical spectra, thermal expansion coeffs., 20 to 700°C 78—75645
CfO_x-O_2 system, for $1.50<O/Cf<1.72$, temp., press. and stoichiometry depends. 77—28009
Cf_xO_y, XPS meas. 77—48314
$^{249}CfBr_x$, spectral and X-ray diffr. data, 25 to 700°C 77—28584

calling equipment (telephone) *see telephone station equipment*

calorimeters
see also calorimetry
100 GHz bolometer mount efficiency meas. calorimeter *(Japanese)* 78—54460
absolute calorimeters for high-power high-energy CO_2 laser 78—93686
AC, automatic data acquisition system *(Japanese)* 80—52215
AC, high resolution, for organic liquids 78—70127
AC, high-resolution, for organic- and biological-material melting study 79—6127
AC calorimeter, computer-controlled, for sp. ht. meas. 79—85142
AC calorimeter, construction and design *(Japanese)* 78—89481
adiabatic, analogue differential wattmeter appl. *(Czech)* 78—23979
adiabatic, for use at superambient temps. 79—21754
adiabatic calorimeter for continuous specific heat meas. 800 to 1800K, design and calibration 80—57299
adiabatic for meas. of low-temp. specific heats 77—41614
adiabatic heat capacity small sample low temp. calorimeter, with automatic data acquisition system 78—12697
adiabatic laser calorimeter design for window and mirror evaluation 79—13971
adiabatic liquid-phase dynamic controlled reaction calorimeter, design and use 77—82519
adiabatic low temperature calorimeter, high resolution heat capacity meas. *(Japanese)* 80—52218
adiabatic scanning microcalorimeter specific heat capacity meas. of small samples 78—86274
adsorption calorimeter, dynamic characts. 78—24796
air chamber isothermal calorimeters for calorimetric nondestructive assay for in-field meas. of Pu-bearing materials 80—71874
automated, high precision, 200 to 400K, design and performance 79—17422
automated, without use of cmputer, 80 to 320K 79—88957
automated high precision calorimeter, for 200K to 400K, temp. controller design 80—86310
automatic heat flow calorimeter for heats of reaction meas. 78—54373
automatic power-spectrum density meter for pulsed laser beam 78—45698
BB2 meter, for high-power CW laser energy meas. 78—54372
bench scale, appl. to cyanomethylation process 79—97391
bench scale, appl. to exothermic elimination reaction, $XRCN+NaOH \rightarrow R'CN+NaX+H_2O$ 80—52214
biopolymer model compounds, calorimetric instrumentation used for studies 80—61746
bolometer mount, effective efficiency meas. using computerised system 78—86272
broad spectral EM calorimeter 77—2656
broad-band dry calorimeter for mm and sub mm wave power meas. 80—105646
broadband mm-wave calorimeter, design and calibration 79—26084
Bunsen ice calorimeter, meas. of ave. total decay power of Pu heat sources 77—6547
calibration of liq. Ar detector for EM showers 78—37497
calorimetry, applications of thermoelectric devices in various types of calorimeters 80—105648
Calvet microcalorimeter, adaptation for heat of soln. meas. *(French)* 77—44504
Calvet-type twin calorimeter, use of microcomputer-controlled integrator 80—77786
cell for US flow meas. 77—42674
circulated-liquid volume absorber calorimeter for intense laser pulses detect. 77—41617
classification, systematic criteria, exam. *(Rumanian)* 78—81975
compensation electrothermograph with pulse-width control 77—41612
computer controlled AC calorimetry technique *(Japanese)* 80—27306
conductive microcalorimeters, heat transfer 77—10025
conductive microcalorimeters, limiting potentialities, anal. 80—17942
cone absorption calorimeter for pulsed laser meas. 80—98980
constant-flow device, for US power meas., 1.5 to 3 MHz 77—50843
cosmic ray apparatus, transition radiation detector system for high energy hadron interactions research 77—61651
cosmic ray muon interactions meas. 80—37686
diathermal differential microcalorimeter, construction and appl. *(Russian)* 78—29118
differential, for materials with low thermal diffusivity, energy release determ. 80—47060
differential calorimeter, for meas. of absorbed energy in laser-produced plasmas 78—5942
differential calorimeter dosimeter for nonionising radiation 79—70649
differential calorimeter for electron radiation 79—6795
differential emissivity calorimeter, use in thermal stress energy studies of small mammals 78—40118

calorimeters continued
differential heat capacity flow microcalorimeter for thermal coefficients meas. of liquids and solids 80—52164
differential microcalorimeter for absorbed gamma-radiation dosage, 0.01-10 W *(Russian)* 78—85385
differential scanning calorimeter, thermochem. appls. 79—40578
differential scanning calorimeter for differential thermal analysis, in temp. range 100-800°C, exam. of design 79—52514
differential-flow mixing calorimeter, for gases at low densities, appl. to excess enthalpy meas. 78—12700
digital automatic thermodynamic enthalpy and specific heat determ. equipment 78—57951
direct heating pulse calorimeter for semicond. materials at high temps. 79—67302
dose measurements in fast neutron and ^{60}Co gamma-ray fields 77—40787
dosimetry, total absorption type calorimeter for 25 MeV electron beams *(Japanese)* 78—78501
double compensated calorimeter for absolute beam intensity meas., design, accuracy 77—6631
dry, mm wavelengths, power meas. 79—26085
DSM-2 differential scanning microcalorimeter (USSR), capabilities 80—62671
dynamic differential calorimeters comparison, in linear macromol. heat capacity meas. 78—89482
dynamic properties of nonisothermal-nonadiabatic calorimeters 79—40576
EBR-II active calorimeter design improvement 79—9967
emissivity measurement for solar-selective coatings of flat sheet using noval calorimeter 79—80621
enthalpies of mixing of condensable vapours, calorimeter for meas. 80—93791
enthalpy measurement, corrosive gases and liquids, particularly N_2O_4 77—79097
film dosimeters, calorimeter for calibration in high intensity electron fields 78—73257
flash chamber calorimeter, fine grain 78—37496
flow, meas. of isothermal Joule-Thomson coeff. 79—58688
flow calorimeter cell for measuring heats of solutions of solids 77—10027
flow calorimeter for condensable gases, low temp. and high press., design and eval. 80—37033
flow calorimeter for condensable gases, low temp. and high press., computer program prediction and exptl. data comparison 80—37034
flow calorimeters standardisation, calibration, thermal config. depend. *(French)* 77—67437
flow type, for closed-loop meas. in gas and liquid up to 100 MPa and 400°C descriptor 77—10024
fluorescent-wave-shifters and scintillators for calorimeters 79—59303
fusion reactor, Doublet III beamline calorimeter, three dimens. heat transfer anal. 80—99381
fusion reactor, TFTR, high energy heat sink, ion beam dump and calorimeter 80—99394
fusion reactor neutral beam injector, calorimeter and beam dump design 78—66382
graphite calorimeter, multisection, for energy distrib. in high current relativistic electron beam 77—46456
graphite calorimeter in water phantom for absorbed dose meas. 80—74032
hadron calorimeter modules, test of proportional wire shower counter 78—37499
hadron calorimeters, resolution determ. 77—30717
heat capacity meas. low temp., mag. fields to 4.5 T 78—16798
heat flow calorimeter for metal-H reaction studies 79—67301
heat transfer of rough cylinder in transverse water flow *(Russian)* 79—10449
high pressure liquid thermal capacity meas., design guidelines *(Russian)* 78—74001
high pressure mixture calorimeter *(German)* 78—16797
high temperature, automatic measurement of electrical energy 79—71451
high temperature, meas. of enthalpies of solids and liquids in 1200-300K range *(French)* 77—13754
high-pressure low-temp. differential scanning calorimeter 80—86311
high-rate amplifier-digitiser for liq. Ar calorimeter 78—46230
high-temperature, containerless, with sample heating by electron bombardment 80—73366
ice calorimeter reading unit with water indicator 80—31755
induction heating, HF generators, calorimeter for power output investigation *(German)* 79—40571
ion implanted impurities, absolute dosimetry using colorimeter-Faraday cup system 78—26590
ion implanter neutral beam component meas. 79—30605
ionisation calorimeter, energy resolution calc. using cascade characts. 77—61654
ionisation calorimeter, fluctuations in cascade showers generated by cosmic ray muons 79—84618
irradiation calorimeter for simultaneous, low-temperature measurements of energy release and of resistivity recovery in irradiated metals 80—31756
isothermal dilution calorimeter, for positive enthalpies of mixing 77—41615
isothermal displacement calorimeter, for positive excess enthalpies 78—89483
large aperture, for fusion laser meas., design 80—43382
laser absorption calorimeter, computer-controlled, for small absorpt. coeff. meas. 78—45680
laser absorption calorimeter automation 78—74084
laser calorimeter for absorpt. coeff. determ. of IR windows and mirrors 78—49838
laser calorimeter for optical coating absorpt. meas. at 1.06 μm 80—33066
laser calorimeter response, spatial var. 77—65603
laser calorimeter types and techniques 80—69441
laser calorimeters, calibration system *(Chinese)* 80—228
laser calorimetric energy meters, KDM and BKDM, for pulsed laser radiation 79—17494
laser calorimetric energy meters, KDS and BKD, for high-power laser pulses 79—17496
laser fusion experiments, calorimeters for meas. of ions, X-rays and scattered radiation 78—16800
laser low energy output meas. with absolute calorimeter 78—55396
laser plasma recording system for plasma blowoff and scattered light distributions 80—59287

calorimeters continued
laser power and energy meters, calorimeter system for calibration 80—38024
laser power meas., radiometric and calorimetric scales' equivalence 77—7115
laser power meas., scale comparison for calorimeter and radiometer systems 79—76729
laser pulse energy meas., 0.1 to 30 J *(Polish)* 78—29998
laser pulse energy meas. with absolute reference calorimeter 77—19268
linear heating method for calorimetric systems 77—49727
liquid, 2-compartment bomb calorimeter for combustion in F 80—57300
liquid, laser pulse energy measurement appl. *(Russian)* 78—22163
liquid Ar calorimeters, props. of EM and hadronic showers 79—45599
liquid crystal EM radiation monitor 77—79514
liquid crystal type, radiation characts. 77—71327
liquid evaporation rate meas. 77—87764
liquid metal enthalpy meas. up to 2100K 80—4715
liquids, complex thermophysical studies 78—57953
low temperature calorimetric investigations, simple off-line arrangement 80—90850
low-inertia differential, for appl. from 20-250°C 80—57298
low-temperature device for meas. heat capacity in 4 to 370K range 80—105647
macromolecules, study by scanning microcalorimeters 80—61747
mathematical simulation of calorimeters used for rapid nuclear fuel assay 80—95355
mechanical heat switch calorimeter to operate between 0.4 and 30K *(Portuguese)* 80—17943
micellar systems, aqueous, thermochemistry 80—61133
microcalorimeter, Calve type, use for kinetic characts. determ. of thermal effects in chem. reacting materials 77—57328
microcalorimeter, differential with thermoresistive elements for high temps. *(Russian)* 77—79098
microcalorimeter, meas. of excess enthalpy of volatile liquids 79—58689
microcalorimeter for nondestructive anal. of pacemakers and pacemaker batteries 79—57813
microwave irradiated mice, energy absorpt., equipment and obs. 80—55996
miniature, fast-acting, with changeable semicond. thermal detector 78—77916
modular calorimeter system for hadron detection in high energy physics 79—41070
modular electron calorimeter, relative and absolute calibration 78—78578
multichannel system, MIK-48, for laser pulse energy meas. 79—17497
multichannel system, MIS-20, for laser pulse energy recording 79—17495
nuclear reactor in-core nucl. heating rates meas. 78—25279
optical radiation measurement, practical considerations, rel. to enforcement of Federal standards 77—38012
opticophysical and physicochemical meas. instrum. 80—13121
pacemaker battery characteristic meas. microcalorimeter 80—30936
pacemaker battery internal loss characterisation calorimeter 80—30934
photocalorimeter, to determine moisture content of gases, exam. 78—56936
photometric calorimeter for proton flux measurements 80—4718
photon detection 79—36469
Picker flow calorimeter, accuracy anal., meas. apparent molar heat capacities and volumes 80—29179
plasma diagnostics and laser beam meas. 78—51361
polyamide-film calorimeter for measuring local electron-beam absorbed doses 80—83227
power meas. at higher microwave freq., conf., London, England, (Jan 1979) 79—26082
precision with isothermal jackets, mathematical model for temperature field 78—93687
probes for measuring high thermal flux 80—13080
pulse gas, for vacuum UV rad. meas. 80—251
pulse gas calorimeter, for vacuum UV radiation meas. *(Russian)* 78—93688
with quench-condensation facility, ht. capacity meas., 0.6-4.4K, for in situ produced metal films 78—41309
radiant flux density measurement, 1 to 40 W/cm^2, using calorimeter with 90° aperture angle 79—71452
reaction-solution rotating-bomb calorimeter, with air thermostat 80—4717
reading error anal. 78—12742
recycle-flow calorimeter, 2 to 20 MPa 90 to 400K 80—42228
relaxation calorimeter for temp. range 4-380K, automated 80—98915
remote measurement of heat release from irrad. nuclear field rods 77—46223
respiration calorimetry determination of O_2-calorie equivalence of thyroid patients and normal subjects *(German)* 78—85412
rod calorimeters using pyrolytic graphite, theoretical anal. 79—12804
scanning, with pyroelec. heat sensor, heat cond. eqn., model 77—10026
scanning ratio adiabatic calorimeter 80—62670
segmented calorimeter, high energy performance, Monte Carlo simulation 80—58029
snow melt calorimeter *(Japanese)* 78—88934
spark calorimeter, for locally generated cosmic ray penetrating particle beams obs. 79—84603
spark calorimeter for routine use 78—37010
specific heat of solids, 4.2 to 90K, USSR special standard 77—31207
spectrocolorimeter, SPEKOL, polymer characterisation by turbidimetric titrations 79—79301
spherical adiabatic calorimeter, minimization of thermal time const. 80—22363
standards for power meas. in mm. wave region 79—26083
temperature change meas., optimisation of Wheatstone bridge using thermistors *(German)* 78—86275
thermocouple microcalorimeters, Calvet-type, response time 78—45630
thermogenesis in flow calorimeters 79—88956
total radiation monitoring using liquid crystals and thermoluminescence 80—3819
transient heat flow anal., features *(Russian)* 78—86273
twin, for laser power meas. NBS and Calorimetrics Inc. developments 78—22161
two-cylinder, for combustion heat meas., of solid, liquid and gaseous fuels 77—79096
unit power standard for 53.57 to 78.33 GHz 80—90808
untuned cavity, for Hg arc lamp plasma props. study 77—82520
US, beam power meas. 77—39181

calorimeters continued
US beam power meas. calorimeter bridge for 1 to 15 MHz 77—27446
US transducer power meas. at MHz freq., calorimetric method 79—23180
variable aperture, for unstable laser resonator 77—7136
water calorimeter for absorbed dose meas. 80—76836
X-ray pulse dose determ. using calorimeter with medical thermometer 77—21628
Al plate calorimeter, meas. of local convective heat transfer coefft. by polarisation interferometry 80—82809
Ar, liquid, calorimeter, electron and proton response 80—47832
Ar liquid calorimeter with very thin sampling 77—34518
Fe scintillator calorimeter, segmented, structure of hadronic and EM showers 80—74078
Fe/plastic, hadronic cascades induced by high-energy muons, calibration calcs. 77—54477
^{3}He cryostat for calorimetric meas. of solids *(German)* 78—16805
O_2 bomb calorimeter modification for liquid metal reaction enthalpy meas. 79—201
Pb-plexipop calorimeter module viewed by wavelength shifter bars 79—81127
U plastic calorimeter, response to low GeV protons 79—93882
W alloy radionuclide calorimeter for liquid He range 4.2 to 8K 79—18093

calorimetry
see also calorimeters; specific heat; thermal analysis
absorption coefficient measurements using pulsed CO_2 lasers 80—9918
absorption coefficients meas. by transmission emittance and calorimetry 78—24839
absorption measurements by laser calorimetry 79—55308
absorption of laser window materials, calorimetric meas. of CO wavelengths 78—25911
AC, small sample specific heat recording appl. *(German)* 77—82518
AC calorimetry for press. up to 3 kbar 77—41616
accuracy of heat capacity evaluation, sample geometry effects 77—49726
accurate measurements of phys. const near phase transition pts. *(Japanese)* 80—52216
acetic acid+formic acid, liqs., mixing enthalpy 79—60515
adiabatic, for measurement of enthalpy of fusion of In 80—37037
adiabatic calorimetry, thermodynamic props. of biopolymers in helical and coiled state, 4 to 400K 78—20140
adsorption calorimetry for studying surface phenomena 79—40574
aerothermodynamic test techniques at AEDC von Karman gas dynamics facility 80—14863
air, afterglow plasma, interaction with glass, Cu, steel walls, calorimetric method obs. 78—14177
alkanes, mixtures, order, enthalpy of mixing, calorimetric obs. *(German)* 78—18773
anode potential drop, calorimetric meas. 77—35433
anthracene anion radicals, enthalpy of disproportionation, calorimetric determ. technique 79—96296
automatic data acquisition system with SI 1.2 standard interface for calorimetric meas. *(German)* 77—37898
bacteria, luminescent, calorimetric study of growth 77—25378
batch microcalorimetry, ballistic meas. 77—5843
battery self-discharge process assessment by microcalorimetry 80—30935
benzene, vapour-flow calorimetry 78—91058
biological macromolecules, conformation studied by calorimetry, review 80—97870
bremsstrahlung energy flux unit, 0.8 to 8 pJ, USSR special standard 77—30730
calibration standards requirements survey 80—57248
Calvet-type microcalorimeter, enthalpy of NaCl soln., at high temp. and press. 79—57286
cation-exchange sorption microcalorimetry, automatic micro-injection system 78—24777
CdSe two-photon absorption, laser calorimetric obs. 80—33076
cell, stainless steel, for differential scanning calorimetry of volatile systems 77—61067
chemical analysis methods, review 79—43660
chemical reactions, kinetics and mechanisms, theory 78—27733
chlorodifluoromethane, heat absorbed when laser irrad., laser calorimetry 79—16012
collagen-water system, phasic transition invesitgation by calorimetry and NMR 79—62167
combustion, use of DC comparator apparatus for voltage measurement 79—75529
comparative microcalorimetric method for heat capacity and conductivity meas. *(Russian)* 78—29116
compound glass rod absorption coeff. calorimetry 80—106631
computer controlled AC calorimetry technique *(Japanese)* 80—27306
continuous calorimetry for automatic reactor power meas. 78—17336
convective heat loss assessment from humans in cold water 78—81093
convective heat loss from horizontal cylinder, meas. under hyperbaric conditions 77—48760
α-corundum, enthalpy, 800-2300K, empirical eqn. 78—14478
cresyl violet, luminesc. quantum yield standard for red, calorimetric obs. 80—190
crown glass, corrosion by organic acid solns., exam. of corrosion depth by interferometry *(Japanese)* 79—20237
cryogenic calorimetry, review 79—40573
crystalline material optical absorption meas. 80—105718
DC arc thermal characts. determ., soln. 80—37036
n-decylammonium cadmium chloride, perovskite-type layer cmpd. n-decylammonium chain dynamics 79—99313
defibrillator energy meters, traceable calibration methods 80—30928
deformation calorimetry, for meas. change in stored energy with deformation 79—50682
deformation calorimetry, meas. of energy stored in plastic deform. of Al and Al alloys 78—84894
dialkylammonium zinc dichlorobromides, long chain cpds., phase transitions, calorimetric study 80—70390
dielectric loss factors meas. at 1 kHz and 4.2K 80—98921
differential microcalorimetry for direct meas. of difference between two thermal effects *(French)* 78—57950
differential scanning, computer-interfaced, heat capacity meas. 78—65935
differential scanning calorimetry, meas. of accurate heat capacities 80—8987
differential thermometer, high sensitivity, calorimetric appls. 78—4614

calorimetry continued
diffuse reflectance spectroscopy, applics., standards and calibration 78—32848
direct difference technique, for meas. of small changes in sp. ht., appl. to strong-coupling superconds. 77—33988
DNA film, dehydration and conform. state, differential scanning microcalorimetry 80—35830
DNA in water-ethanol solns., enthalpy of B-A transition 77—70412
dose measurement, 15 to 50 MeV electron beams in graphite, compared with ionometric meas. 77—2052
DTA and scanning calorimetry cell flow control system 79—67303
Eccobond solder 56 C, sp. ht., 1.3-300K 78—16804
electron beam energy flux density meas. using portable graphite calorimeters 80—307
electron dose distrib. for flat specimen using calorimetric method 79—49872
emissivity of solids and coatings at low temp., meas. technique 80—17941
emissivity of solids determ. 78—62201
enthalpy of soln., KCl, tris(hydroxymethyl)aminomethane standards appl. 77—73462
epoxies, low temperature specific heats, 4 to 40K 78—43138
ethane, solid, thermodynamic props. between double solid-to-solid transition and triple point temp. 78—75828
ethyl acetate, heat absorbed when laser irrad., laser calorimetry 79—16012
ethylene + N_2, gaseous, excess enthalpy, determ. by flow calorimetry 78—91057
excited electronic states, calorimetric detection 77—41692
excited states detection using calorimetric techniques 78—32847
explosives, secondary, thermal decomp., solid-state kinetics, differential scanning calorimetry 78—92449
fission reactor materials, gamma heating-effects, meas. using calorimetric and dosimetric techniques 80—658
flow microcalorimetry, bioassay and enumeration, drug biopotency meas. 80—95100
fluorescent screens, cathodoluminescent, yield, calorimetric method determ. *(Russian)* 77—20938
freeze-drying techniques; mass transfer, appl. of calorimetric instrumentation 77—25628
fusion reactor 120 keV neutral beam, calorimetric and optical beam diagnostics 78—54933
glass thermal diffusivity meas., calorimetric method 79—27349
glycerol, liq. and glass, thermal diffusivity meas. 79—82394
graphite-ICl intercalation compounds, anomalous sp. ht. due to order-disorder transform. 79—42235
heat and thermal diffusivity of liquid and free-flowing materials meas. 77—87765
heat capacity of materials, measurement using digital instrument 79—71453
heat of adsorption determ., expt. methods 79—42370
heat transfer equations, model of clothed man 79—24958
heat transfer to air-water stream, expt. meas. unit 77—42941
high-energy, IR laser component optical characterisation techniques 80—14347
high-temperature chemical processes, review, book contrib. 77—40545
high-temperature solution calorimetry, appl. to enthalpy of formation of B_4C at 1320K 79—11814
human body, heat loss meas. apparatus, evaporative and radiative, normal working mode 79—25178
ice, melting, in porous solid, NMR and differential scanning calorimetry obs. 77—62621
inorganic solids, high energy irradiation, energy storage meas. 78—51581
instrumentation development for nuclear transportable instruments 80—77787
inverse filtration, frequency limits, transference function analysis 80—47058
IR absorption measurement, interference calorimetric method, effect of crystal thermo-optic props. 80—47096
IR transparent materials, bulk and surface absorpt., calorimetric meas. method 79—27347
lamp, calorimetric meas. of radiant energy, student expt. 78—8191
laser beam heat flux and power profiling, using swept null point calorimetry 80—69439
laser calorimetric data, automated anal. 80—4714
laser calorimetric data analysis for surface and bulk absorpt. determ. 78—25904
laser calorimetric meas. of two-photon absorpt., appl. to CdSe(Te) 79—44934
laser energy standards inequivalence simplification 77—79876
laser flash, calibration and test on Al_2O_3 sp. ht. 80—4716
laser materials, absorpt. meas. by static profile calorimetry 78—25908
laser power meas. NBS and Calorimetrics Inc. developments 78—22161
laser power measurement by thermoelec. meter 78—63124
laser rate calorimetry analysis with coating absorption 80—33050
laser-flash calorimetry for small sample thermal capacity meas. *(Japanese)* 77—49725
light absorption, visible and near-IR for black surfaces 78—93685
liquid and solid state polymer at high pressure *(Russian)* 77—57327
liquid crystal phase transformations, size and surface effects 77—15555
liquid isobaric heat capacity, experimental apparatus using stationary flow-through calorimetry *(Russian)* 79—30480
lithium n-alkanoates, long-chain, thermal and phase props. 77—62619
low temp. specific heat measurement, electronic system *(French)* 80—27305
low temperature specific heat measurement, dynamic differential calorimetry 77—74405
lymphocyte cultures, human, heat prod. meas. with flow microcalorimeter 77—81473
lysozyme, cryst., dynamic sp. ht. capacity meas. 80—21447
macromolecule, linear, heat capacity meas., dynamic differential calorimeters comparison 78—89482
macromolecules, linear, heat capacities, scanning calorimetry meas. 80—61134
metal at low temperature, content investigation *(German)* 77—13753
methacrylates, cross-linked, structure-transformations, relations properties *(German)* 79—55677
microcalorimetry of isolated cells of mammalian brown adipose tissue 77—56343
microprocessor-controlled system for precise meas. of temp. changes 80—22361

calorimetry continued

- microwave irradiated mice, energy absorpt., equipment and obs. 80−55996
- microwaves, meas. of energy absorbed by biological systems by anal. of heating and cooling data 78−40343
- microwaves, meas. of energy absorbed by biological systems by Dewar-flask calorimetry 78−40344
- modulation method with SOTS-2 standard specimen 80−8988
- monoalkylcyclohexanes, heats of vaporisation by gas chromatography-calorimetry method 79−34344
- multi-jet dynamics in lepton induced reactions, granular struct. calorimeter anal. 79−9350
- nonadiabatic problem, transfer processes in suspensions of solids 79−23353
- nontransition element/alkali metal systems, direct calorimetric exam. 78−84775
- nylon 6, drawn yarn, origin of double melting peaks 78−3118
- optical, for laser energy meas., hollow graphite cone appl., absorption characts. determ. *(Slovak)* 79−40572
- optical fibre ribbons, loss meas. 78−87127
- optical fibres, light absorption and scatt., calorimetric meas. 78−46790
- optical glass and fibres, absorption coefficient measuremnt by calorimetric techniques *(Dutch)* 79−76774
- optical material absorpt. meas., real time holographic interferometry 80−83569
- organic compounds, enthalpies and related thermodynamic functions 79−42276
- organometallic compounds, standard for quantity-of-heat unit 79−17421
- oxidation of solids, improved calorimeter eqn. 79−66278
- pacemaker, batteries, characterisation of internal power losses by calorimetry 78−92747
- pacemaker battery microcalorimetric testing 80−30933
- pacemakers and batteries, microcalorimetric study 78−57130
- phase transitions, low thermal diffusivity materials, advantages of spherical samples 79−54134
- poly(β-benzyl L-aspartate), conformational transitions 77−88613
- poly-γ-benzyl-L-glutamate solutions, calorimetric study of fusion of liquid cryst. struct. 79−53022
- polyarylate-polyethylene oxide block-copolymers and mixtures, phase separation, DSC obs. *(Russian)* 79−55895
- polyethylene, high molecular weight, effect of density on properties 77−90403
- polyethylene, linear, quenching of thin films to amorphous state 80−28929
- polyhexamethylene adipamide, calorimetric, X-ray and IR study 80−10512
- polymer glasses, enthalpy relax., scanning calorimetry technique 80−90851
- polymer materials, chem. reacting, kinetic characts. of thermal effects determ. using Calve type microcalorimeter 77−57328
- polymer soln., dil. flow microcalorimetry, heat of mixing 77−56247
- polymers, glassy, optical absorpt., visible region, determ. by laser calorimetry 80−66218
- polypropylene-chloroform (chloromethane), χ-parameters, heat of mixing, vap. press. and microcalorimetric meas. 78−34626
- polystyrene glasses, transition temp. and thermodynamic state 78−75819
- porous solid, pore struct. determ. by capillary condensation calorimetry method *(French)* 77−25245
- powder catalyst, catalytic and sorption processes, calorimetric and adsorpt. kinetic methods 79−43629
- probe for determ. of heat flow *(Russian)* 78−12698
- probes for gas stream enthalpy meas., calibration 78−70126
- proteins, globular, crystalline, intermol. interactions, denaturation, DSC and X-ray diffr. obs. 80−16897
- proteins, phys. state in cryst., heating curves 77−70409
- proteins, phys. state in cryst., process of fusion of trypsin and pepsin cryst. 77−70413
- proteins, thermal denaturation, use of high heating rates to separate denaturation and aggregation 77−81470
- proton flux measurements using photometric calorimeter 80−4718
- pyridine, ethyl pyridine, heat of adsorpt. on sponge Fe, Fe_2O_3, CuO, adhesive wear, flow calorimetry 78−85193
- radiant heat flux detector, method of interpreting readings 78−211
- radiation dosimetry, automation of calorimetric measurements evaluation 79−67965
- radiation effects on material determ., thermal defect meas. using total-absorption calorimeters 80−99427
- real-time prediction of calorimeter equilibrium 79−75532
- refractories, integral radiant capacity, calorimetric meas. method 80−65259
- relaxation method using cryostat, 1.5 to 10K 80−68204
- rhodamine 6G solution, absolute fluoresc. quantum yield determ. by calorimetric method 80−78851
- sample container for solution calorimetry 80−52217
- second sound calorimetry, acoustic thermometry appl. to low temp. optical spectroscopy of solids *(French)* 77−87840
- self-balancing nanovolt potentiometric system for thermometry and calorimetry 77−53903
- sensitivity of calorimeter method 79−17423
- sheath temp. distrib. for material selection criterion 78−77917
- small sample AC-heating calorimetry at low temp. 77−5842
- small samples of low thermal diffusivity, heat capacity meas. technique 77−37894
- sodium n-alkanoates, long-chain, thermal and phase props. 77−62619
- solar selective surface absorption and IR emissivity calorimetry 79−62098
- specific heat, 2 to 30K, meas. equipment *(German)* 77−87763
- specific heat, meas. system for temp. range 3-300K with on-line computer 78−4620
- specific heat capacity of small samples using thermal relaxation method 79−49231
- specific heat determination, powders, meas. apparatus for 4.3-300K 80−227
- specific heat meas. method at arbitrary temp., simple and accurate 78−62202
- specific heat standards choice and certification, for liquids and vapours in 90 to 273.15K range 80−23877
- spinels, entropy of cation transitions 79−11812
- stearic acid, heat of adsorpt. on Fe_2O_3 powder, surface area meas. by flow calorimetry 78−81974

calorimetry continued

- steel, maraging, Ni-Co-Mo, ageing and evolution peak at 470°C, calorimetric anal. *(Japanese)* 79−100156
- steel, reflectivity at 10.6 μm, calorimeter meas. 78−55393
- stored energy, and increment in heat capacity due to plastic deform. 80−54302
- superconductor evaluation by sp. ht. meas. 77−32116
- surface area determination, calorimetric method, modified Harkins and Jura procedure 79−35667
- surface emittance, calorimetric emissometer 80−86309
- TCNQ salt, TMPD-TCNQ, enthalpy of combustion, calorimetric meas. 77−52663
- tensile testing, methods of measuring stored energy by calorimetry 79−29325
- tensile testing, methods of measuring stored energy by calorimetry 79−29326
- p-terphenyl, phase transition, heat capacity meas. 79−46801
- tetracene anion radicals, enthalpy of disproportionation, calorimetric determ. technique 79−96296
- thermoelectric devices application in various types of calorimeters 80−105648
- thermogenesis, harmonic analysis and inverse filter 80−27304
- thermogravimetric methods, review 78−3408
- thermokinetics, linear system output deconvolution for detn. of input 78−12699
- thermophysical meas. above 2500K, apparatus 77−45845
- thermophysical properties of liquids, quick method for determ. in region 30-95°C 78−21138
- titration calorimetry, research developments 79−40575
- transference function, analytic determ. 79−98590
- transparent solids, absorpt. coeffs. by laser calorimetry, wavelength modulation spectroscopy 78−66876
- triple point temp. of Ar and O_2 realisation 79−12806
- TTF-TCNQ, cryst. binding energy, enthalpy of form., calorimetric 77−52663
- tunable CO_2 laser calorimetry for bulk and surface absorption in NaCl and KCl in 9.2-10.8 μm region 79−95808
- Van der Waals film adsorbed on graphite, two-dimensional phase transitions 80−107653
- vinyl alcohol-vinyl acetate copolymers, mol. architecture and physiocochem. props. 80−44103
- vinyl monomers, specific heat, calorimetric method based on ^{60}Co source *(Italian)* 77−72694
- water, absorption coefficient at 488 and 541.5 nm, adiabatic laser calorimetry 77−73123
- water bath temp. control and temp. meas. devices 77−37893
- water heat transfer in calorimetric vessel and jacket study *(Polish)* 77−54996
- water solution calorimeter, determination of energy equivalent, with standard substance 78−23961
- water-methanol, heat of mixing, high-press. calorimetric obs. *(German)* 78−16797
- weakly absorbing material calorimetric meas., theory 79−76773
- yeast metabolism, microcalorimetry, diauxy during anaerobic growth of saccharides 78−3451
- Ag film, energy losses of electrons, microcalorimetric meas. 80−59543
- Ag halide crystals, relative dissolution rates meas. by flow calorimetry 80−85220
- Ag, tensile plastic deformation, energy storage efficiency 77−4807
- Al, tensile plastic deformation, energy storage efficiency 77−4807
- Al-Mg-Si, heterogeneous precipitation studies using differential scanning calorimetry 80−3062
- Al-Zn (10 wt.%), ageing behaviour, calorimetric study 80−45328
- Al-Zn-Mg, decomposition calorimetric study *(German)* 79−74165
- Al-Zn-Mg (4.8, 1.1 wt.%), second phase dissolution, calorimetry study 79−100193
- α-Al_2O_3, synthetic sapphire, enthalpy determ., 900-1900K, use as calorimetry reference standard 79−42275
- As_2Se_3 film on CaF_2, interface and bulk absorption meas. 80−35001
- Au film, energy losses of electrons, microcalorimetric meas. 80−59543
- Au film, laser absorpt. vs. temp., calorimetric meas. 79−98423
- Au, heat content between 300.05 and T (T from 400 to 1000K) drop calorimetry *(French)* 80−10682
- Au-Ag, plastic deformation, energy storage efficiency 77−4807
- Au-Cu alloy, internal oxidation, calorimetric meas. 79−43258
- Au-Mg alloy, internal oxidation, calorimetric meas. 79−43258
- Au-Te, thermodynamic props., calorimetric meas. 78−20051
- $Bi_{1-x}Te_xO_{3/2+x/2}$, solid solutions, phase transformations, dielectric and differential microcalorimetry *(French)* 79−55886
- C fibres, PAN-based, surface characts., investig. by flow microcalorimetry 78−48694
- $Cd_{0.010}Fe_{2.990}O_4$, heat capacity investigation of dopant effects on mag. disordering temp. 80−25143
- CdSe(Te), laser calorimetric meas. of two-photon absorpt. coeffs. at 1.06 μm 79−44934
- CdTe two-photon absorption, laser calorimetric obs. 80−33076
- $CeFeO_3$, enthalpy of formation determ. from heat of oxidation, calorimetric investig. 77−25300
- CoO-SiO_2 system calorimetric study of high press. phases stability 79−90779
- Cs, liq., specific heat meas., at temp. up to 1700K under pressure 78−51696
- Cu based dilute alloys, enthalpy of formation and excess entropy 80−55347
- Cu foil, total emissivity meas. by calorimetric technique 80−17941
- Cu, heat content between 300.05 and T (T from 400 to 1000K) drop calorimetry *(French)* 80−10682
- Cu single crystal, stored energy meas. by new deform. calorimetry method 78−39834
- Cu, tensile plastic deformation, energy storage efficiency 77−4807
- Cu-Au, plastic deformation, energy storage efficiency 77−4807
- Cu-In alloy, thermodynamics, calorimetric exam. *(French)* 77−21105
- Cu-Ni-Sn, liq. alloy, mixing enthalpies determ. using a SETARAM high temp. calorimeter *(German)* 80−44324
- Cu-Si, melt, enthalpy of formation at 1370K 80−26042
- β- Cu-Zn(47.4 wt.%), heat content between 300.05 and T (T from 400 to 1000K) drop calorimetry *(French)* 80−10682
- D_2, sticking and accommodation on low-temp. substrate, mol. beam expts. 80−84368
- Fe-Co-Cr, heats of form. adiabatic calorimeter determ. 78−35713

calorimetry continued
- $Fe_{40}Ni_{40}P_{14}B_6$, metallic glass, glass transition, viscous flow and differential scanning calorimetry meas. 80—96635
- $FeO-SiO_2$ system, calorimetric study of high press. phases stability 79—90779
- $FeSiF_6.6H_2O$, phase transform. exam. by X-ray and DSC methods 78—83948
- Ga/rare earth systems, direct calorimetric exam. 78—84775
- GaAs, absorption coefficients, method of meas. 78—83048
- H_2, sticking and accommodation on low-temp. substrate, mol. beam expts. 80—84368
- HCl-Xe, liq., enthalpy of mixing, calorimetric meas. 80—59661
- HF-cyclic ethers H-bonded complexes, calorimetry, IR spectra and MO calcs. 79—52738
- H_2O-acetic acid, liq. mixture, thermodynamic excess functions, calorimetric meas. 77—52666
- He, afterglow plasma, interaction with glass, Cu, steel walls, calorimetric method obs. 78—14177
- He cryostat for low temp. calorimetry 79—40577
- In, heat capacity and enthalpy of fusion, 300-1000K 79—14939
- InSb, heats of transformation for high pressure, orthorhombic modification, exam. 78—56627
- KCl, 10.6 microns absorption, calorimeter round robin meas. 79—35748
- KCl, absorpt. coeff. meas., using pulsed CO_2 laser, calorimetric method 78—18028
- KCl, bulk and surface absorpt. of CO_2 laser radiation, calorimetric data analysis 78—25904
- KCl, bulk and surface absorption comparison, 9.2 to 10.85 μm 80—33051
- KNO_2, polymorphism, calorimetric investigation 78—75827
- $Li-I_2$, primary battery, self-discharge rates using microcalorimeter 79—61963
- Li-Tl(In)(Bi), liquid alloys, calorimetry study *(German)* 80—25664
- $LiNbO_3$ waveguide absorption losses, laser calorimetric meas. 79—64311
- $MnSiF_6.6H_2O$, specific heat, thermal cond., simultaneous meas., method, 90-300K, near phase transition 77—37892
- MoF_6(l), enthalpy of form. by soln. calorimetry 79—47962
- N_2, afterglow plasma, interaction with glass, Cu, steel walls, calorimetric method obs. 78—14177
- NH_4Cl, specific heat, thermal cond. simultaneous meas. method, 90-300K, near phase transition 77—37892
- NaCl, bulk and surface absorption comparison, 9.2 to 10.85 μm 80—33051
- NaCl surface with adsorbed water layer, absorpt. and thickness meas. 80—16001
- NaF film on CaF_2, interface and bulk absorption meas. 80—35001
- $Na_2O-B_2O_3$, vitreous and cryst., enthalpy of form., calorimetric study 80—66861
- $NaPO_3$, heat content between 300.05 and T (T from 400 to 1000K) drop calorimetry *(French)* 80—10682
- Nb, liq. and solid, enthalpy meas. by levitation calorimetry 80—103499
- PLZT type ceramics, calorimetric meas. of energy of electrical polarisation 79—2770
- ^{32}P, half-life and mean beta distintegration energy determ by low-temp calorimetry 80—5094
- Pd-H system, thermodynamic props., 245-352°C, up to 34 atm. 79—23749
- Pu nondestructive analysis, calibration by calorimetric assay 80—71878
- PuO_2 heat sources, ave. total decay power meas. using Bunsen ice calorimeter 77—6547
- PuO_2, reactor grade, calorimetric assay 79—16116
- ^{239}Pu, calorimetric determ. of half-life 79—26405
- ^{239}Pu, specific power and half-life, calorimetric determ. 79—26406
- ^{242}Pu halflife from precise low-temp. heat capacity meas. on PuF_3, PuF_4, PuO_2 77—2952
- Se-Bi bilayers chemical reactions, differential scanning calorimetry technique and obs. results 78—2398
- Si microcalorimeter dosimetry system for transient radiation effects, radiation induced temp. rise meas. 77—26885
- Sn low-temp. specific heat meas. under pressure 78—77915
- Te-In alloys, direct reaction calorimetric study, 737 to 1340K *(French)* 80—49382
- U_3O_8, λ-type heat capacity anomalies 77—20080
- V-D, exam. of phase diagram, using DTA and calorimetry, isotope effect 78—80527
- W, sintered metal reference standard, sp. ht. at high temp. 78—89427
- Zn-HgO, primary battery, self-discharge rates using microcalorimeter 79—61963
- $ZnFe_2O_4$, heat capacity investigation of dopant effects on mag. disordering temp. 80—25143
- $Zn_xFe_yO_4$, heat capacity investigation of dopant effects on mag. disordering temp. 80—25143

caloristers *see calorimeters*

CAMAC
- acquisition system for high rate data 79—63197
- automated counting system, design philosophy 79—88923
- autonomous crate controller for sequential operations 77—34533
- autonomous system for control of scintillation and Cerenkov counters 78—21833
- BASIC overlay for CAMAC data and command handling 80—18772
- bit-slice microprocessor appl. 79—89566
- branch highway driver, high speed 79—89541
- Brilliant ADC, semi-autonomous controller for data acquisition 78—46245
- bubble chamber pictures, SNOOP module CAMAC interface to 168/E microprocessor 80—58103
- calibration system for nucl. reactor systems 78—37532
- calorimetric system for recording plasma blowoff and scattered light distributions from laser plasmas 80—59287
- CERN, Intel 8080 microprocessor development system 77—83314
- CERN ISR, control system, addition of local intelligence to CAMAC 79 72212
- CERN PS booster, microprocessors in control and beam obs. 77—88302
- CODAS, Joint European Torus, control and acquisition system 78—36982
- coincidence matrix, fast, programmable 79—97961
- computer interface for a linear accelerator 80—51226
- crate controller CC80 77—54491
- CRETA 74, improvement of PAL 11 A assembler for IML syntax implementation 78—33406

CAMAC continued
- cyclotron at MSU, computer control 79—54704
- data acquisition, high rate system 80—23281
- data acquisition, two-dimensional position sensitive detector system, CAMAC I/O module 80—47835
- data acquisition system testing 79—89568
- data acquisition systems, microcomputer-based 80—27277
- data collection station, based on autonomous CAMAC crate 80—61689
- data transfer in on-line systems 79—89571
- decade counter, 160 MHz, with digital readout 78—9041
- diagnostic module for on-line monitoring of CAMAC integrity 80—5459
- digital drift chamber digitizer system 79—45602
- direct time to digital convertor with multi-stop facility, appl. to neutron TOF meas. 77—14317
- dosimetry, automated data acquisition and anal. system at LAMPF pion therapy facility 78—53506
- drift chamber and pulse height readout systems using analog multiplexing 77—54490
- drift chambers, CAMAC/NIM for data acquisition and monitoring 77—88338
- event handler, a fast, programmable, CAMAC-coupled data acquisition interface 79—45608
- F-30 digital avometer, MUF-30 control module in CAMAC standard 79—88942
- far IR Fourier spectrometer automation *(Russian)* 79—6192
- fast 32-channel hodoscopic gating module, with memory and data output into CAMAC data way 78—7885
- FASTBUS—details of addressing and bus mastership 79—89554
- FFTF element measuring system 79—9729
- flexible CAMAC based data system for Space Shuttle scientific instruments 79—45603
- fusion experiments, 10 bit transient data recorded 80—13917
- fusion experiments, fibre optic signalling in control 80—13919
- fusion reactor ignition, eight-beam CO_2 laser system, minicomputer-CAMAC control system 78—58493
- gamma spectroscopy system control., appl. of CAMAC system 78—37531
- GEC Elliott CAMAC interface on PDP-11 computer running RSX-11M executive, software driver module 77—38590
- high energy physics CAMAC hardware, review 79—13617
- hodoscope read-out, fast sparse-data-scan system using CAMAC compatible elements 79—45609
- hodoscopic detector registration systems, data coding/reading block 78—78602
- hodoscopic recording system, coding and reading data unit 78—13397
- holographic store automated test using BASIC M-400 interpreter *(Russian)* 79—94180
- I/O struct., CAMAC/E extension 77—54487
- IBM 3630 modular data acquisition and communication system for industrial production *(German)* 79—30438
- instrument control via CAMAC to SPIB interface 78—36985
- instrumentation in European labs. 77—54482
- interface, for microprocessor controlled dual parameter ADC system 79—3337
- interface module for PACE ADC system 77—34534
- ion mobility measurement, in drift tubes, using CAMAC crate interfaced to microcomputer 78—93661
- IPNS time of flight neutron scattering instruments system 79—89558
- JET, control and data acquisition system, CODAS 78—62619
- Karlsruhe cyclotron, computerised diagnostics, control and extended beam optimization 79—54709
- KEK beam line magnets control by CAMAC serial highway 79—68007
- Knudsen torsion-effusion pendulum data acquisition system, computer-automated, for meas. of vapour pressures at high temps. 79—49214
- laboratory automation, standard modular interface 78—24768
- linkage module for CAMAC-CAMAC 77—10557
- Los Alamos P-9 accelerator facility, CAMAC data acquisition system 79—45607
- LSI-11 based auxiliary crate controller for beam line and experiment control 79—89565
- magnetic tape station interface to CAMAC for on-line data acquisition and reduction system 77—34532
- MBNIM, modular approach to fast trigger logic for high energy physics expts. 79—49920
- microprocessor based timed reading and time plot CAMAC modules 77—54484
- microprocessor-controlled target polarization monitor 79—88990
- mobile automated high speed transient data recording and transmission system 77—54488
- modular 125 ps resolution time interval digitizer for 10 MHz stop burst rates and 33 ms range 79—45591
- module for linking external equipment to computer 77—3245
- Mossbauer data acquisition system 79—30439
- multi-channel analyzer using a dedicated CAMAC memory 79—45592
- multi-faceted data gathering and analysing system 78—37530
- multi-microprocessor auxiliary crate controller, data processing in CAMAC 78—46246
- multi-parameter CAMAC compatible ADC scanner 79—31350
- multiparameter data acquisition and display program 79—89547
- multiple data streams, dynamically configured software system 79—89548
- multiwire proportional chamber readout system, CAMAC test 78—17510
- MWPC, CAMAC readout system 78—46248
- MWPC readout system 78—17505
- neutron diffractometer, computer-controlled CAMAC system *(German, English)* 77—19843
- neutron spectrometer, triple-axis, computer-control system with CAMAC interface, program functions 77—19840
- Niels Bohr Institute on line data acquisition system 79—89557
- nuclear chemistry laboratory, CAMAC automated 78—17542
- nuclear physics data acquisition with UNIX time-sharing system 79—41085
- nuclear physics expts., versatile data handling system based on PDP 11/03 microcomputers 79—76319
- oceanographic data acquisition, CMOS CPU, low power consumption *(Italian)* 77—82068
- parallel branch driver for Harris 6024/5 computer 77—42222
- particle beam phase space meas. at 2 MHz particle rate 77—54383
- particle track chamber, semi-automatic meas. instrum. register for camera photograph reduction 78—78575
- PDP-11 CAMAC system linking to PDP-10 on-line computer 79—21725

CAMAC continued
  peripheral node module allowing independent systems to share peripherals 77—57305
  photomultiplier HV readout system 77—54492
  physical instrum., CAMAC system and microprocessors 79—26041
  pion$^-$ biomedical beam line, CAMAC control 77—90886
  proton accelerator, target and collimator precision position control and monitoring via CAMAC 77—67927
  proton synchrotron slow extraction beam parameter monitoring and control system in CAMAC standard online with ES 1010 computer 78—29674
  pulse height anal. system, CAMAC based 77—87749
  pulse height analysers, CAMAC data acquisition interface 79—3336
  pulse sequence fast A/D conversion 78—55119
  pulse-train counter and recorder, automatic, with preset program 79—3319
  pulse-width modulation circuit for MWPC remote readout 79—26847
  Q signal as device-ready indicator 79—6809
  quadrupole CAMAC universal timer 78—9040
  rapid CAMAC data handling in FORTRAN real time programs 79—45616
  repetitive waveform generator for Fermilab booster 79—76214
  Rutherford Laboratory N5 expt. data acquisition system, program struct. and CAMAC hardware 78—90051
  SAR: a fast computer for CAMAC data acquisition 79—89569
  scintillation counter 77—3219
  serum samples, trace element anal., automatic data acquisition, on-line method 78—48726
  Shuttle/Spacelab missions, low power CAMAC and NIM modular system for spaceflight use 77—70973
  single crate CAMAC control system for negative ion source test facility 79—72216
  single crate controller, DMA-option for PDP-11 computers 77—10559
  SLAC beam, feedback system for steering and energy correction in beam switchyard 79—93852
  space science instrument testing, modular, CAMAC based computer controlled ground support equipment 79—25434
  space scientific instruments, standardised modular instrumentation system 77—71005
  spectroscopic data anal., electronics 80—5460
  spectroscopic data anal., programming techniques 80—5461
  storage ring, CESR control system, interface hardware 79—72069
  test system based on S-100 bus 78—36984
  Texas Experimental Torus, data acquisition and processing system 77—24217
  time coder with variable channel width for time-of-flight expts. 78—33403
  time digitiser for laser ranging, ps. resolution, built in CAMAC minicrate 78—36301
  time digitiser in CAMAC format 77—10558
  time to digital convertor in real time, low cost 78—55111
  Tokamak device, JT-60, microprocessor based distributed intelligence CAMAC system 80—59309
  TRIUMF data interface 77—88304
  two-channel data gathering and registration system for fast-action experiments 78—77877
  type U CAMAC controller for the Spacelab multi-crate, multi-processor system 79—45604
  universal branch driver, independent programmed control module 80—69046
  Van de Graaff target room control system, CAMAC and microprocessor appl. 78—37468
  vidicon systems, time digitiser in CAMAC format 80—14062
  weight data, computerised acquisition and processing methods *(German)* 79—30437
  wire spark chamber ferrite matrices data read-out device 77—46473
  wire spark chamber ferrite ring matrix, CAMAC-VECTOR standard readout system 77—46474
  ^{235}U(n,f), time correlated associated particle method, CAMAC experiment 80—52702

camera lenses *see photographic lenses*

camera tubes, television *see television camera tubes*

cameras
  see also coronagraphs; television cameras
  35 mm camera control cct. for automated time-lapse photography 78—58076
  35 mm camera systems for deep sea appls. 78—4003
  35 mm compact, with fully automatic exposure control 80—90916
  35 mm motion picture cameras necessity for production of number of apparatuses *(Russian)* 80—37111
  70 mm photographic camera, for scintillation camera, with roll film *(Japanese)* 77—70546
  aerial, stabilised camera mount anal. 80—9059
  aerial multispectral-photographic lenses, Pinatar 4/125, manufacture *(German)* 78—4717
  aerial photographic equipment developments, aerial survey camera and navigation telescope 77—66997
  Agat, streak image camera with picosecond time resolution used in plasma investig. 80—38717
  air survey cameras, calibration techniques 80—18035
  aircraft vibration isolation for high-performance cameras 77—74543
  Alban Press/Technical 79—21825
  amateur camera information capacity and image quality 79—49316
  amateur camera light scatt. coefficient factors 79—71559
  amateur camera objective lens production quality, MTF test freq. selection 79—81581
  anamorphic cameras for stellar spectrographs 80—41727
  Anger, dual head system for imaging of positron-emitting radionuclides 79—29598
  Anger camera dead-time, effect of window fraction 77—86598
  Anger camera field-uniformity correct., effect of spatial distortion 79—100721
  Anger camera/computer system using seven pinhole collimator for myocardial perfusion tomography 80—61663
  Anger scintillation camera, development since 1958 80—12234
  Anger scintillation cameras, state-of-the-art in suitable photomultiplier tubes 78—40304
  Anger tomographic scanner, comparison with 15 in. scintillation camera for Ga imaging 79—34658

cameras continued
  Arriflex 35BP-II motion picture camera mounted with 350PF-1A zoom lens for wide-screen filming *(Russian)* 80—95176
  Asahi Pentax 110, review 79—71544
  Asahi Pentax 110, review 79—71546
  astronomical cold camera, description 80—72779
  astronomical Schmidt camera, direct, quasi-telecentric and telecentric combinations of interference filters 78—57441
  astronomical speckle camera, Kitt Peak National Obs., design, double star meas. 79—62745
  astronomical spectrographic camera shorter than Schmidt 77—73951
  astronomical wide field UV cameras, Marseille Obs. *(Italian)* 78—32346
  Auger camera, Lixiscope, X-ray and gamma-ray telescope system 80—62020
  Auger camera collimator selection for ^{67}Ga imaging 79—57764
  Auger camera performance, effects of a reduction in crystal thickness 80—41187
  autofocus, mechanisms *(Japanese)* 79—75640
  automated for flash lamp photography, diaphragm adjustment 80—9058
  automatic control of exposure time, design and operation *(German)* 78—21249
  automatic control systems for high speed cine cameras *(Russian)* 80—285
  automatic exposure of photographic camera films 78—65992
  automatic focusing by US echo ranging in SX-70 cameras 79—93239
  automatic focusing mechanism principles and designs 79—30595
  automatic focusing of cameras using self-contained IC 78—82069
  automatic lens focusing using optolinear chip 78—54480
  automation developments 80—18027
  batteries, expendable, survey 79—71545
  battery, alkaline effect of discharge resistance obs. *(Polish)* 79—57420
  beta-ray, gas replacement monitor 80—95502
  Beurger precession camera, diffuse X-ray scatt. meas. *(Japanese)* 80—49049
  biomedical gamma camera systems, methods for MTF meas. 80—94324
  biomedical X-ray spot-camera of Medicor Works 80—85477
  Bonse-Hart X-ray diffractometer, asymmetrically cut, comparison with Kratky camera 80—77917
  brain imaging, positron camera appl. and charact. *(Swedish)* 78—28032
  C-CD camera, appl. to Einstein X-ray Observatory fields RI photometry 80—62315
  C-CD camera description performance and calibration 80—73499
  C-CD camera for streamer chamber appl. 78—37513
  cassette film camera for automatic and rapid prod. of colour pictures *(Russian)* 78—93780
  Chirana cylindrical cameras modification for Seemann-Bohlin focusing method *(Czech)* 79—26192
  Cine, guide elements, use of powdered polymer coatings 78—78021
  cine, time-lapse mechanism design, clouds and lightning photography appl. 78—85747
  cinematography, colour film processes and cameras, review, 1894 to date *(German)* 78—93773
  claws, principles for indexing and maintenance characts. for cine-cameras *(Russian)* 79—49325
  coded aperture imaging, review 80—101914
  cold camera, for astronomical cooled emulsion photography 80—56714
  colour strip film camera for microfilm retrieval systems *(Japanese)* 79—97455
  colour telecine camera KT 116 M *(Russian)* 78—29200
  compact solar camera, student project 80—67975
  computer assisted ring detector positron camera system for brain reconstruction tomography 78—40306
  computerised rotating laminar radionuclide camera 80—3796
  computerised tomography, picture documentation and filing 79—66554
  control IC, single chip, bipolar 78—21234
  coude camera for image tube work 77—22080
  CRO photographic recording status 79—93247
  CROs, photographic techniques for trace recording 77—38047
  data recording apparatus, based on LEDs and internal or external timing circuits 79—9251
  Debye-Scherrer camera conversion to back reflection camera 80—99024
  decorative trim quality 78—29197
  design of instrument optics from basic elements 77—58418
  Dicke camera, Lixiscope, X-ray and gamma-ray telescope system 80—62020
  digital control of Canon A-1 camera 78—70206
  drum camera, in eight-channel oscillograph for recording one-shot processes 77—37872
  for Earth exploration from satellite Soyuz 22, Raduga expt. *(German)* 77—56765
  earth terrain, Skylab photographs quality evaluation 77—2283
  EKTRAMAX camera lens design and performance 80—77894
  electro-optical deflector streak camera system, for picosecond laser pulse diagnostics 78—33909
  electrographic instrumentation for ultraviolet imaging and spectrography 80—46399
  electron diffraction, electronometric method of meas. intensities, efficiency 79—27881
  electron diffraction camera type EMR-100, industrial 79—2842
  electron exposure control, using electromechanical transducer *(German)* 79—80708
  electron microscope camera, electromech. arresting mechanism 77—74560
  electron-optical Feniks streak camera, quick change dyanamic processes application 79—50391
  electronic exposure sensor, Agfa Optima 535 and 1035, features *(German)* 77—82633
  electronic streak, vacuum arc promotion and development obs. *(French)* 77—7609
  electronographic camera, development and use 77—56829
  electronographic camera, polarisation maps of nebulae 77—57081
  electrooptic beam deflectors as streak cameras, theory 79—58809
  endoscopic miniature camera with fibre-optic faceplate 80—77896
  exposure error compensation in automatic cameras 80—52346
  exposure meter accuracy calc., CdS photoresistor errors 77—49773
  exposure meter for KSR-1M film camera *(Russian)* 78—93779
  external occulting disc as radially-graded neutral density filter, for solar coronal obs. during eclipses 79—80233
  Faint Object Camera calibration 79—25479
  Faint Object Camera on Space Telescope 79—25478

cameras continued
fast coincidence, gas-filled channel convertor 77—60276
fast solid-state camera for high-speed event diagnostics 80—78985
fast streak or frame camera appl. to plasma dynamics in plasma focus device 79—68950
FAUST, far UV camera on Spacelab 79—25476
field and aperture quantitative determ. *(Spanish)* 78—49921
field averaging spectrograph camera for remote sensing 77—45161
field-widened pinhole camera 79—97451
film camera construction impact of electronics *(German)* 77—79170
film transport rollers, fabrication accuracy improvement 78—18077
flare rel. to internal finish, student examination project 79—25782
fluorescence angiography, colour and black and white, use of interference filters 78—48856
fluoroscopic examinations, multi-image camera for spot radiography 80—109020
fly's eye intensifier-TV neutron counting camera, appl. to phase transform. studies 79—46519
focal plane camera shutters with independent curtain movements 78—29195
frame to hold 35 mm SLR to CRO, integral data display 80—68284
gamma, Anger-type, time resolution *(German)* 77—13000
gamma, performances under high counting rates 79—16277
gamma camera, 3-D particle track chamber using Compton interactions 77—86622
gamma camera, appls. for three-dimensional emission tomography using scattered photon information 80—98134
gamma camera, computer controlled, nuclear cardiology appl. 80—61682
gamma camera, electronically collimated, for single gamma emission computed tomography 78—44603
gamma camera, line spread function meas., practical considerations 79—17585
gamma camera, multidetector Ge, biomedical appls. 79—49353
gamma camera, multiple multiwire proportional chamber, improving the spatial resolution 79—49361
gamma camera, transverse-section emission tomography 77—86619
gamma camera data, evaluation in moving organ exam., use of OTF 80—30845
gamma camera imaging, recent advances 80—17127
gamma camera oscillosocpe display, performance meas., computer simulation 78—7425
gamma camera performance comparison 78—44595
gamma camera transfer function, statistical study 77—70541
gamma camera using CdTe detectors, medical appls. 79—49351
gamma camera with brightness amplifier *(French)* 77—37036
gamma camera-computer system for pulmonary function anal. using ^{133}Xe *(German)* 77—21600
gamma cameras, appl. of orthogonal light propag. 77—16979
gamma cameras, state of art 80—3802
gamma cameras, use of coded apertures with digital decoding 77—86620
gamma computerised camera for medical diagnosis *(Swedish)* 79—70607
gamma imaging, optical device 77—5056
gamma ray cameras, stereoscopic images 79—5365
gamma ray image intensifier camera, using Si posn. sensitive strip detector 77—81565
gamma scintillation camera, GSG-2 twin-transducer, colour shading, grey-scale photographic recording 79—34631
gamma scintillation cameras for radioisotope imaging *(Spanish)* 78—7428
gamma-camera for gated caroliovascular imaging 79—5367
gamma-ray cameras of Anger type, optimisation for medical diagnosis *(French)* 80—26328
gamma-ray type using Compton effect 78—10087
Gandolfi attachment, for Debye-Scherrer camera 79—37590
Gandolfi camera, modified for easy cryst. centring 79—14646
gonioscopy, foot-operated camera trip for Nikon photo slit lamp 78—80986
grainless focusing screen for light scatter reduction 80—101836
Guinier, appl. to X-ray powder diffraction anal., microcomputer automation 80—3454
Guinier X-ray powder diffraction camera, automatic scanning system 80—22492
Guinier-type focusing cameras, powder diffr. line profiles 79—58856
hard X-ray camera for study of gamma ray burst sources 79—25502
heat-camera system for panorama spectroscopy of extended laser medium 80—1257
high speed, with image commutation, calc. of reflex involute centre for image shift and defocussing *(Russian)* 80—90919
high speed magneto-optic camera system, for obs. of mag. bubble domain devices 77—79186
high speed movie recorders, human factor problems in artistic design 77—30212
high speed optical techniques, conf., San Diego, USA (Aug. 1976) 77—79182
high speed raster cameras, image dissection and mech. scanning for photographic recording *(Russian)* 80—95182
high speed shutter, appl. of PLZT ceramic 77—79187
high-speed, increase in image quality using plate polyhedral compensator *(Russian)* 79—35879
high-speed cine camera control desk type PIK-73M 79—2758
high-speed cineradiography, of projectiles 78—41395
high-speed intermittent cameras for research 77—49795
high-speed mirror photochronograph 78—37098
high-speed movie camera, angle measuring reticle insertion into field of view 77—30213
high-speed photographic camera for UV spectrum range *(Russian)* 77—34051
high-speed photography and photonic recording 78—86367
holocamera, clinically useful, for 3-D microscopy of unanaesthetised eye 78—48863
holocamera, investigation of hypersonic target material subject to impact with water droplet 78—42306
holocamera, lens assisted, motion pictures of microscopic plankton 78—48946
holocamera for 3-D micrography of the alert human eye 80—98057
holocamera for particulate studies 79—22919
holographic camera, automated thermoplastic for two-wavelength contouring 80—74318
holographic grating, calc., for very wide field camera *(French)* 78—81547

cameras continued
holographic interference camera 35 mm reflex 79—89867
holographic movie camera and projection system 80—78808
IAS triangulation camera for artificial clouds altitude determ. *(French)* 77—33192
image convertor, for laser and laser-plasma diagnostics 78—38550
image convertor camera, with microchannel intensifier, modular design 78—42427
image convertor camera for use with universal astrograting spectrograph 77—67037
image convertor streak camera 78—54484
image convertor tube, high-speed photographic recording, of exploding wires 78—41365
image convertor tubes for nanosecond, subnanosecond photography, dynamic range 78—38034
image convertor tubes for streak cameras, operating characts. comparison 78—38031
image intensifier cameras, channel-plate, for low light security and projectile photography 79—40639
image intensifier scintillation cameras for nuclear medicine 77—40732
image-convertor camera, high-speed, computer treatment of images 78—42295
image-shearing camera for surface strain direct meas. 79—58773
immunogram recording apparatus, self-contained, modified version using Polaroid film 80—17209
industrial electron diffraction camera EMR-100, description 79—50963
instrumentation camera, microprocessor technology, appl. to digital data recording 77—79189
intensified minification camera for low dose radiography 78—20262
International Ultraviolet Explorer (IUE), cameras in-flight photometric performance 78—96383
intervalometer using two cameras, sampling option 78—77367
IR single-line scanning 78—58029
IR sky survey telescope, wide field photography 80—105167
IR streak camera, high speed, appls. 77—79093
iris diaphragm with straight leaf edge, mechanism accuracy 80—28337
KA-102A EO LOROP camera for real-time tactical reconnaissance system 79—30599
Kodak instant-print colour film cameras *(German)* 78—21233
Kossel X-ray technique, for obtaining crystallographic data in the SEM 78—34391
Kron electrographic camera, spurious image mistaken as nebula 78—8101
Lang camera X-ray diffraction theory *(Japanese)* 79—86648
large field scintillation gamma cameras, performance characts. 78—7441
large format camera for Space Shuttle, cartography appl. 80—4232
Large Format Camera for Space Shuttle 79—101043
laser driven subnanosecond blast shutter 77—79842
laser fusion, image convertor camera optical measurement 78—38549
laser unequal path interferometer with electro-optical camera and minicomputer, fabrication/test appl. 80—77847
lattice period determ. by axial X-ray camera 79—68974
Laue camera, real-time back-reflection 79—37589
Leitz Vario-Orthomat, a new camera system for automatic photomicrography 80—82841
lens shutters, friction coefficient nonreproducibility evaluation 80—62765
lens-array focusing system tests, commercial reflex cameras 80—86479
lenses, automatic focusing systems 80—18028
lensless real-image camera 78—8456
lenslet array with periodic sampling structure, for image form. 78—37964
light detector using GaAs$_{1-x}$P$_x$ photodiode 79—89019
liver scintigraphy, optimisation of analogue-circuit motion correct. 79—39472
Lyman α camera, for high resolution solar Lyman α filtergrams 80—82323
magnetostriction spark cameras data readout cct. 78—78576
manual movie camera, Kinor 35P *(Russian)* 80—90917
market, status and growth prospects, USSR 80—27367
mass-produced camera objectives, effects of cosmetic defects 80—47135
MATEC (matched tandem etalon camera), appl. to auroral obs. 80—101442
McMullan 4 cm electronographic camera, appl. to high-dispersion stellar spectroscopy 78—73644
medicine, nuclear, digital filtering and edge detection 80—58065
medicine, nuclear, microprocessor systems for data acquisition, image processing, RIA anal., patient data retrieval 80—61670
MGH positron camera, medical transverse section imaging 79—66516
microfilm, appl. to patent information systems 79—75632
miniature flash camera, FlipFlash, with novel features *(German)* 77—82632
miniaturisation of design, 35 mm and 126 cartridge cameras 79—26153
mobile gamma camera with remote image processing computer system, for nuclear medicine 78—92700
Moire topography camera, simulator mounted, for constructing compensating filters 80—46024
motion picture camera device for shooting in movement *(Russian)* 78—93777
motion picture camera gyroscopic stabilisation system, anal. of dynamics and accuracy *(Russian)* 80—95173
movie camera, amateur, experience in developing company style 80—27369
movie cameras, design of lenses with long overall length and large diameter 79—30597
moving-fibre panoramic camera, image motion velocity calc. 79—26168
Muehllehner's tomographic camera, quantitative evaluation of depth effect 77—86609
multiple image shearing interferometric camera, displacement derivative meas. 80—33549
multipulse lightning discharge oscillogram scanning camera 78—61588
multispectral aerial imagery capabilities for military geographic information acquisition 77—82054
multispectral camera, use on Soyuz 22 spacecraft 78—40794
multispectral photography appl. using MKF-6 camera and MSP-4 projector 80—56633
multiwire proportional gamma camera for imaging ^{99}Tc^{m} radionuclide distribs. 78—53493
night identification appl., trade-offs consideration 78—54489
nuclear imaging, γ-ray detect., quantitative assessment field procedure 79—29611

cameras continued
nuclear medicine, camera aperture for data collection optimisation 80—67221
nuclear medicine, clinical and parametric evaluation of three large-field-of-view cameras 80—76823
nuclear-medicine image display system, dynamic physiological function visualisation 79—5396
objective matching with film channel in serial prod., tolerances 78—16885
Ohio-Nuclear Model 120, medical imaging using ^{125}I 79—49359
optical component fine diamond grinding on modernised equipment 79—46092
optical/X-ray framing camera tube 78—37121
oscillographs, photographic recording using Polaroid camera *(Italian)* 78—78007
particle camera, aircraft-borne, for in situ photography of cloud particles 78—85750
particle track chamber, semi-automatic meas. instrum. register for camera photograph reduction 78—78575
phased roller movement 77—79188
phosphor convertor camera for near IR laser beam profile recording 79—81468
photodiode arrays, characts. and appl. 79—89002
photoelastic dynamic studies of fracture 80—38358
photoelectronic streak camera tube, magnetically focused 78—33907
photofluorographic camera with electro-optical image intensifier 80—36128
photogrammetry, distortion calibration, lateral chromatic aberration effects, operational data reduction 79—35881
photogrammetry, orientation and calibration method for nontopographic appls. 79—35875
photographic materials, MTF automatic evaluation 80—95170
photographic techniques documenting CRT displays 79—21827
photorecorders, five-metre magnetic spark spectrometer, JINR (USSR) 80—87014
picosecond exposure scanning camera, and associated recording system *(French)* 78—42429
picosecond framing camera using a passive microchannel plate 79—49307
picosecond image convertor streak cameras, dynamic range 78—38032
picosecond streak camera, dynamic range and spatial resolution 78—42428
picosecond X-ray chronoscopy 78—38546
picture taking parameters display in amateur cameras, review 78—89578
pin bowing in AGR fuel elements, meas. by camera device 80—106146
pinhole camera, hole size required for no distortion 80—46028
pinhole camera, X-ray tube focal spot size meas., systematic error 79—75666
pinhole camera graphic design 79—35863
planar streak camera, picosec. recording appls. 79—44943
planetary lander camera, quasi-microscope for improved resolution 77—91426
polaroid camera, use in high school lab. to photograph oscilloscope trace 77—41443
Polaroid Sonar One-Step camera, US automatic focusing 78—78011
polymer composition coatings for rubbing mechanisms 78—29198
positron, circular ring transverse axial camera, 3-dimens. radioisotope imaging 77—77982
positron camera, 3-dimens., for nucl. medicine 78—73225
positron camera, 3-dimens. imaging using Fourier techniques 77—32951
positron camera, $Bi_4Ge_3O_{12}$ as potential scintillation detector 78—3586
positron camera, computed tomography, 3-D image reconstruction, Fourier deconvolution method 80—61669
positron camera, cylindrical, multilayer hybrid computed tomographic system, $Bi_4Ge_3O_{12}$ scintillation crysts. 78—48876
positron camera for brain imaging, appl. and charact. *(Swedish)* 78—28032
positron camera system, ring detector, brain research, computed transaxial tomography 80—61739
positron camera using ring detector system, for emission tomography of brain 80—30880
positron camera-computer system for various section images 79—66528
positron circular ring camera, in 3-dimens. radionuclide tomography 77—73566
positron circular ring camera tomographic system, resolution improvement anal. *(Korean)* 80—72312
positron circular ring cameras for computerised tomography, trends and prospects 79—66524
positron imaging device resolution limit 77—60243
positron ring cameras for emission computed tomography 77—44742
precession camera, resolution, transformation equation between reciprocal space and X-ray film 79—49313
precession camera furnace with indirect heating 77—10028
prism-scanning panoramic camera for reconnaissance aircraft 77—79181
programmed camera exposure setting accuracy 79—75639
pryroelectric vidicon, thermography appl. 77—54798
pulsed laser stereophotography, of electrically exploded bridges 77—79190
Radcliffe Cassegrain telescope, d-camera vel. system 78—73645
radioisotope hybrid scanner, design of detector and collimators 78—7423
reflecting all-sky cameras, design 79—40074
remote sensing, film and solid-state-array types comparison w.r.t. imagery 78—4723
resolving power type, sinusoidal targets design and construction 77—53999
retinal camera with infrared TV obs. *(German)* 79—2145
retrofocus lens system designs for film cameras *(German)* 77—54768
rotation camera data, empirical method correction for absorpt. and decay effects 80—14962
scintigraphic camera systems and their assessment by computer 78—57063
scintillation, deadtime meas., scatter conditions simulating nuclear cardiography 79—16276
scintillation, effect of photon energy on field uniformity tests 79—16278
scintillation, investigation of contribution functions 79—29603
scintillation γ, wide field, performance evaluations 79—29609
scintillation camera, ^{123}I imaging, detect. performance and quality factor 77—40743
scintillation camera, multidetector design with 254 channels 77—40739
scintillation camera, with 2 mm intrinsic resolution, biomedical appl. 77—70525

cameras continued
scintillation camera 3-dimens. gamma-ray imaging 78—11734
scintillation camera based on image intensifier tubes, for nucl. medicine appls. 77—5069
scintillation camera collimator image form. 80—89844
scintillation camera control, Pilotix module *(French)* 77—37040
scintillation camera data, recording method for low and moderate count rates 79—8539
scintillation camera dead time with and without computer 80—3777
scintillation camera deadtime in meas. of left ventricle ejection fraction 79—62355
scintillation camera electronics capable of high processing rates, clinical significance 77—40740
scintillation camera field uniformity, global and local, statistical features 80—61677
scintillation camera interface to scintigraphic data and computer 77—21613
scintillation camera nonuniformity, effects on cold lesion detectability 79—5352
scintillation camera performance monitoring, equally-spaced parallel-bar phantom 77—2041
scintillation camera systems, importance of correct photopeak setting 79—34660
scintillation camera transaxial tomograph, Humongotron 77—52867
scintillation camera upgrading, comparative study 80—12236
scintillation camera whole-body single-photon emission computerised tomography system 80—17086
scintillation camera/high energy collimator system, misleading results with a bar phantom image 80—12237
scintillation cameras, automatic field uniformity corrections 80—17128
scintillation cameras, large-field-of-view 78—44596
scintillation cameras using liq. and solid Xe detectors *(French)* 77—37034
scintillation gamma camera, anal. of basic characts. 78—57059
scintillation-camera simulator for remote-data acquisition testing 80—46020
Seeman-Bohlin X-ray camera, sample holder construction 77—67418
semiconductor gamma-cameras in nuclear medicine 80—81693
semiconductors and ICs used in modern equipment, review *(German)* 79—58813
septum visualisation and random collimator movement in γ-camera work 79—34648
SFR-2M (USSR), synchronisation with LG-36A gas laser 80—73489
short-focus cameras, semi-kinematic equatorial table 79—70958
shutters, efficiency rel. to picture quality 77—74531
sidereally driven satellite cameras, numerical corrections 78—40678
Sigma cameras, development since 1960 79—63328
simulated underwater partial launch system, photogrammetric data reduction system 77—79075
single lens reflex camera development *(Japanese)* 79—2846
single lens reflex through-the-lens, error in stopped-down metering *(Japanese)* 77—26416
single line CCD camera to improve microscope position 78—41347
solar ultraviolet Doppler camera 79—25485
solid state digital for glassware dimensional and sidewall inspection 78—16890
space telescope, design features 78—45229
spark chamber X-ray camera, AR filled, device description and performance evaluation 79—13598
speckle camera and analyser for surface displacement and tilt meas. 78—32790
spin scan camera system, on geostationary satellite, for global weather monitoring 78—61600
stereophotography, using camera slit lamp, ophthalmic applications 78—48904
streak, dynamic range measurements, picosecond time resolution 80—73490
streak, for immediate picosecond laser pulse meas. 78—33902
streak, picosecond spectroscopy, appl. to chem. and biological reactions 79—80697
streak, remote profilemeter 77—79058
streak camera, approx. 100 ps resolution, use of $LiNbO_3$ deflector 79—18533
streak camera, wide dynamic range, proximity focusing, visible and X-ray recording 77—89304
streak camera for subpicosecond chronoscopy 78—38030
streak camera intensified CCD readout system, sensor props. 79—27825
streak camera synchronisation using picosecond laser pulse activated Si switch, jitter reduction 80—53440
streak subpicosecond, for laser fusion experiments 77—5938
streamer chamber track recording with C-CDs 78—37515
subnanosecond X-ray framing camera, fibre array technique 78—41394
subpicosecond electro-optical cameras, progress report 77—5951
subpicosecond proximity-focused streak camera, for X-ray and visible light 77—79183
subpicosecond X-ray streak camera, for laser-fusion diagnostics 78—42822
super-8 silent movie camera *(German)* 78—86365
superconducting gamma camera, for clinical utilisation 79—63330
sweeping slit camera, characterisation of 1060 nm picosecond laser impulse *(French)* 78—42366
SX-70 system of instant photography, history of design 79—97457
synchroballistic camera, synchrospeed 78—41366
Synchroscan streak camera, picosecond chronoscopy of repetitive weak light sources 78—38033
synchrotron radiation camera and data acquisition system for time resolved X-ray scattering studies 80—99023
temperature scanning X-ray diffraction camera for liquid crystals 77—31558
thoracic electrical impedance camera for chest fluid meas. 77—40889
three dimensional imager, using mode-locked laser, beam splitter and streak camera 77—42597
time lapse shooting device, impulse generator scheme *(Russian)* 78—313
tomofluorographic camera with lens objective and angular tube 79—57750
tomography, single-photon emission, imaging capabilities of Ge camera 80—61668
topographic camera, high-sensitivity double-crystal, lattice parameter meas. 80—77915
transaxial tomography camera, photographic image reconstruction, analogue recording system 78—82085

cameras continued
triple frame camera, with beam-splitting prism 78—37097
underwater camera data correl. and interpretation, systems approach 79—5688
underwater lens system, metrical fundamentals 77—78457
underwater radiance scanner, design and implementation 78—61609
US camera for patient diagnosis *(French)* 77—37028
vacuum-cold camera, appl. to astronomical near IR photography 80—90341
videodensitometric camera and video disc system 77—40761
Viking Lander camera, optical system and design 78—53794
Viking Lander camera, stray light control 78—61713
Viking Lander camera design 77—41285
Viking Lander camera performance and data reduction 77—41286
Viking lander cameras, calibration and performance 78—20639
volume hologram superimposed information display 80—78807
wafer exposure camera, optical, step-and-repeat, with dark field automatic alignment 80—68283
wide-field filter, for astronomical appl. 78—49335
window for aerial photography large interferometer for testing 78—13821
X-ray, 10 cm diam. back-reflexion focusing, design and fabrication 78—18489
X-ray, 5-frame, for charged particle, inertial confinement fusion studies 80—57453
X-ray, attachment for aimed investigation of fractures 80—85102
X-ray, diamond and high-press. uniaxial stress component 78—38584
X-ray, low-angle, monochromatisation of primary beam on Borrmann principle 78—5985
X-ray, simple back-reflexion 78—32962
X-ray, small angle scattering camera for synchrotron radiation 78—66020
X-ray, topographic 80—84029
X-ray and optical cameras, laser fusion appls. 78—59686
X-ray and visible streak camera for subpicosecond laser fusion diagnostics 77—18122
X-ray camera, double focusing, use with synchrotron radiation 80—313
X-ray camera, photocathodes, characts., for X-ray diagnostics of laser-induced plasmas 77—54031
X-ray camera, wide field for astronomy, design, sensitivity and performance 80—85863
X-ray camera for orientation of large monocrystals 78—22600
X-ray convergent beam camera for struct. anal. of microcrystals 78—22602
X-ray diffraction, reciprocal lattice photographing with axis of film cylinder intersecting cryst. rotation axis at 45° 77—51274
X-ray diffraction camera, method for cryst. mounting on ends of fibres 78—93663
X-ray diffraction microcamera for analysis of cryst. defects in glasses 77—60002
X-ray pinhole camera, resolution improvement by image processing 77—30222
X-ray powder camera, for low temp. photography 79—58099
X-ray powder camera, high temp. focusing, new features 79—50942
X-ray powder diffraction camera, absorpt. attachment, appl. to gallstone study 77—41744
X-ray scatt. camera for low angle diffraction expts. with synchrotron radiation 77—87888
X-ray scattering camera, ORNL 10 metre small-angle 78—32961
X-ray small-angle camera using synchrotron radiation for structural studies 77—43108
X-ray streak camera, calibration using Au 77—4713
X-ray streak camera, for obs. of tightly pinched relativistic electron beams 77—49818
X-ray streak camera, high time resolution, with X-ray microscope *(French)* 78—42823
X-ray stream camera, ultrafast X-ray diagnostics for laser fusion experiments 77—79185
X-ray structural anal., high temp. system, for examining liquid metals 80—25950
X-ray topography, high speed, semiconductor lattice defects exam. appl. 77—11443
X-rays, S056 telescope camera on Skylab Apollo Telescope Mount 77—60596
CdTe matrix γ-camera, biomedical appl. 80—76827
CsF scintillator, pot. advantages for a time-of-flight positron camera 80—81706
Ge gamma camera resolution loss at depth, elimination technique 79—49352
Ge, high purity for nucl. medicine imaging 80—17113
$LiNbO_3$ electro-optic deflector based streak camera, 20 ps resolution 79—85189
NaI(Tl) scintillation cameras, image artifacts and counting losses 80—94345
Xe high pressure proportional, scintillation camera for X-and γ-ray imaging 80—99412

candoluminescence *see luminescence*

canted spin arrangements
see also weak ferromagnetism
amorphous ferromagnet with random uniaxial anisotropy, hysteresis, magnetisation 77—80963
antiferromagnet, magnetic phases, spin configurations in external field 80—70955
antiferromagnet, two-sublattice Neel-type, stable spin configurations, external mag. field and single-ion orthorhombic anisotropy effects 80—60249
antiferromagnet, uniaxial, spin configuration in ferromag. phase, field and temp. depend. 79—38321
chains of classical spins, weak ferromagnetism 79—15268
dialkylammonium iron tetrachloride, antiferromag., mag. susceptibility meas. 80—60220
dimethylamine iron tetrachloride, antiferromag., mag. susceptibility meas. 80—60220
dipropylammonium manganese tetrachloride, and tetrabromide, two-dimens. antiferromagnet, spin canting and exchange 80—34620
exciton spectra, optical props. 80—70622
Green function theory, dipolar crit. temps. 77—89962
heavily doped semiconductor, stability of canted antiferromag. order 77—12095
low-field magnetoresistance and domain drag 78—68014
magnetoacoustic resonance, elastic vibrations 80—29599

canted spin arrangements continued
manganese acetate tetrahydrate, Heisenberg ferrimag. magnetisation 79—47304
Neel ferrimagnets, phase transitions, field-induced spin-orientational 80—75767
1,3-propanediammonium tetrachloromanganate(II) mag. props. 4.2-220K 77—20567
singlet ground state system in mag. field, anisotropic exchange interaction effect on props. 79—91224
spin wave damping, magnetic materials with canted mag. struct., thermodynamic and high freq. props. 80—11184
two-sublattice ferromagnet, biquadratic exchange effects 77—4502
$BaMnF_4$, dielec. anomaly, mechanism, spin canting 78—10744
$Ca_2MnO_{4-x}F_x$, antiferromagnetic props. and elec. cond. *(French)* 80—29526
$CoNb_2O_6$, ordered state, field induced mag. transitions 77—16074
$Co(urea)_2Cl_2.2H_2O$, two-dimens. mag. props., cryst. struct., specific heat 80—75777
Cr_5Te_6, high press. effects on magnetisation and mag. transitions, 77 to 360K 77—77057
$DyCo_5$, rotational type spin reorientation, collinear to canted spin struct. change 77—63214
EuTe, high field Faraday rot., 1.7-3 eV 77—52131
EuTe, optical absorpt. in high mag. field 79—28726
Fe complex, $Fe(1,2,4\text{-triazole})_2(NCS)_2$, quasi-2-dimens. $S={}^1/_2$ antiferromag., mag. props., hidden canting 80—107986
Fe garnet, Bi-substituted, film, domain boundary transform. into canted phase at compensation point 77—24724
$FeBO_3$, Brillouin scatt. from parametrically excited phonons 79—73956
$FeBO_3$-MBO_3 solid soln., (M=Mn, Cr, Al, Ga, In), synthesis, crystal chem. and mag. props. 78—31058
FeGe, hexagonal, low-temp. mag. struct., neutron diffr. meas. 78—95418
$FeGe_2$ canted antiferromagnet, mag. susceptibility anisotropy and temp. dependence 80—25112
$FeGe_2$, collinear and canted antiferromag. structures 77—51887
$Fe_{1.2}Mg_{1.4}Ti_{0.4}O_4$, mag. ordering, Mossbauer effect in external mag. fields 80—71257
Fe_2MoO_4, magnetic struct. of low and room temp. by neutron diffr. 77—63100
$GdAlO_3$, canted antiferromagnetic, Mossbauer meas. 80—97171
GdIG, spin struct. obs. by Faraday rotation expts. in fields up to 200 T 77—69809
GdMg, canted mag. struct. in S-ion compound, neutron diffr. obs. 78—34962
GdMg, sp. ht., magnetisation and stability of canted struct. 79—78412
Ho_5Ge_4, mag. struct., neutron diffr. study 80—25093
HoIG, spin reorientation from Faraday effect meas. 79—51780
$Ho_2O_2SO_4$, antiferromag., mag. props. and Zeeman effect meas. 79—33464
$Ho_2O_2SO_4$, magnetic phase diagram, magnetisation and mag. susceptibility meas. 80—15720
$KNiF_3$, antiferromag. domain wall motion obs. by X-ray synchrotron topography 78—88139
$Li_{0.5}Fe_{1.25}Ga_{1.25}O_4$, ferrimag. with local canted struct. thermal expansion anomalies 79—73762
$Li_{0.17}Fe_{2.17}Zn_{0.66}O_4$, ferrimag. with local canted struct. thermal expansion anomalies 79—73762
$Li_{0.5-z/2}Zn_xFe_{2.5-z/2}O_4$, field magnetisation and susceptibility 79—82762
$Li_{0.5(1-x)}Zn_xFe_{2.5-0.5x}O_4$, canted spin struct., neutron diffr. study 78—68175
Mn complex, $Mn(SCN)_2(C_2H_5OH)_2$, two-dimens. Heisenberg magnet, cryst. struct. and mag. props. 79—60337
$Mn_3Al_2Ge_3O_{12}$, garnet, mag. ordering, neutron diffr. patterns 78—19220
MnZn ferrous ferrites, mag. permeability stress depend. 80—88822
$Mn_{1-x}Zn_xFe_2O_4$, prepared by wet method, neutron diffr. and high field Mossbauer expts. 80—75719
Ni-Mn alloy, disordered, mag. struct., high field twist deform. 78—68166
$NiCl_2.6H_2O$, antiferromag., phase diagram, low temp. canted paramag. boundary, bicritical point 79—47282
NiS_2, model for weak ferromag. 79—65632
$Ni_{0.25}Zn_{0.75}Fe_2O_4$, Mossbauer study, noncollinear spin struct. 80—60472
Pr_3Tl, hyperfine interactions, sp. ht. and magnetisation meas. 79—28531
$RbCoCl_3.2D_2O$, metamagnetic phase transition, crystallographic and mag. struct., neutron diffr. meas. 80—44174
$RbCoCl.2H_2O$, Dzyaloshinsky-Moriya linear chain magnet, spin counting 79—38304
$RbFeCl_3.2H_2O$, pseudo-one-dimens. canted Ising antiferromag., spin-cluster reson. 79—61233
$RbFeCl_3.2H_2O$, pseudo-one-dimens. canted Ising antiferromag., spin cluster reson. 79—61235
$RbFeCl_3.2H_2O$, pseudo-one-dimensional canted Ising antiferromag., spin-cluster excitations 80—70989
$RbFeCl_3.2H_2O$, spin cluster excitation expts. 80—66039
$RbFeF_3$, Mossbauer spectra, mag. phases 80—15878
TbF_3, mag. phase diagram, crit. and tricrit. behaviour 78—14959
Tb_5Ge_4, mag. struct. and mag. transitions, neutron diffr. expts. 78—43564
TbIG, Faraday rotation and transition of spin config. at high mag. fields 80—39776
$TbPO_4$, linear optical birefr. meas. near bicritical point 80—15719
$TbPO_4$, phase transitions at low temp. 80—15237
$TmAl_2$, ferromagnetic structs., elastic neutron scatt. obs. 80—50055
Tm_2Ni_{17}, magnetic structure by neutron diffr. 77—73000
$YCrO_3$, antiferromag., mag. domain walls, ^{53}Cr NMR study 79—11327
$YFeO_3$, mag. domain walls, photomagnetic effects, ^{57}Fe NMR obs. 78—95464
$Y_3Fe_{5-x}Sc_xO_{12}$, local spin struct., Mossbauer obs. 77—32305
$Y_3Ga_xFe_{5-x}O_{12}$, spin struct. obs. by Faraday rotation expts. in fields up to 200 T 77—69809
$YbFeO_3$:Co, mag. struct. factors, neutron diffr. study 79—47248
$Zn_xFe_{3-x}O_4$ ferrite, mag. struct., Mossbauer spectra and magnetisation study, 4.2K 80—103818
$Zn_xNi_{1-x}Fe_2O_4$, magnetic props. rel. to localised canting model 77—32161

capacitance
see also photocapacitance
bilateral capacity estimation, Ritz and Trefftz method *(Polish)* 77—14636
calcium behenate monomolecular layers between Al electrodes, nonlinear dielec. props. 80—80405

- **capacitance** continued
  - capacity estimation by means of Ritz and Trefftz's methods 78–5387
  - ceramics, granular, electrophysical props. depend. on porosity, temp., solid-phase props. 77–69764
  - chalcogenide glasses, localised states calc. rel. to contact capacitance and field effect 79–11090
  - charged disc or sphere in concentric hole of grounded sheet 77–14635
  - chlorophyll a film, charge injection and storage 78–53317
  - cholesterol, dielectric props. under UV excitation 80–6912
  - cholic acid, dielectric props. under UV excitation 80–6912
  - conducting bodies, capacity and energy calcs., for rotational symmetry *(Polish)* 79–875
  - conducting ellipsoid, capacitance bounds and equivalent radius 77–19126
  - conducting ribbon, ring shaped, capacitance, exact upper and lower bounds 79–36811
  - conformal transformations combined with numerical techniques, with applications to coupled-bar problems 80–83538
  - cracks, capacitance, mech. loads effects 80–84242
  - 4-4′-cyano-octyl-biphenyl, smectic A liq. cryst., elec. field effects, capacitance meas. 78–91237
  - 4-4′-cyano-octyloxy-biphenyl, smectic A liq. cryst., elec. field effects, capacitance meas. 78–91237
  - cylindrical conductor, between conducting surfaces, electrostatic field 78–9293
  - cylindrical conductor encircled by plane, capacitance calc. 79–36812
  - degenerate semiconductor-metal Schottky barriers, low temp. capacitance 80–60075
  - diamond:B, B conc. and impurity-to-band activation energy 79–56165
  - discontinuous metal film, AC equivalent circuit anal. 79–51690
  - double layers, image forces influencing capacitance and interaction 79–29367
  - electro-optic waveguide deflector performance characteristics 80–33213
  - electro-optic waveguide modulators, capacitance of electrode system rel. to modulation efficiency *(Russian)* 80–1359
  - electrocapacitance parameter change by physical distortion *(French)* 77–70564
  - electrochemical system, diffusion layer theory, exptl. test 78–35701
  - electrode, impedance meas., accuracy 80–61108
  - electrode metal-solvent interaction rel. to elec. double layer struct., adsorpt. 78–61023
  - electrode polarisation capacitance in bacterial growth detect. by impedance meas. 77–60325
  - electrode-electrolyte interfaces, theory, differential capacitances 77–48649
  - electrodes, smooth, solid, double-layer capacitance freq. dispersion 79–20379
  - fatty acid monolayers, electron tunnelling 77–69428
  - ferroelectrics, negative capacitances, comparison with negative viscosities 80–66118
  - fluid, local density variations, capacitive system of meas. *(French)* 77–41574
  - free space capacitance calc. for a square cylinder of finite length *(Chinese)* 78–66705
  - n-GaAs:O, press. depend. of deep level associated with O, transient capacitance meas. 78–64000
  - haemoglobin, dielectric props. under UV excitation 80–6912
  - hot carrier p-n junction as a contact with negative differential capacitance and conductance 79–69590
  - impedance of a p-n junction by direct currents *(Russian)* 78–84285
  - interface state energy determ. during capture of electrons and holes using DLTS 79–87107
  - IV-VI compounds, dielec. props., elec. meas. 78–15119
  - Josephson contact microwave detector sensitivity and cutoff frequency rel. to capacitance 78–49902
  - layer of symmetrical spherical dipoles, Poisson-Boltzmann treatment of capacitance 78–64844
  - lead phthalocyanine:O_2(I), Schottky barrier effect on AC current response 80–75623
  - least capacitance region, free boundary optimisation problem 79–13864
  - least capacitance regions, free boundary optimisation problem 79–13865
  - magnetite, electrode, polycrystn., differential capacitance 80–66136
  - metal-semiconductor junctions, capacitance, temp.-depend., by space-charge methods 78–91758
  - microstrip anisotropic electrostatic field problems, Green's function technique 78–70998
  - MIS, HF capacitance, minimum value and position 77–85338
  - MIS capacitance measurements, method of separating hysteresis effects, interface state density estimation 77–85324
  - MIS capacitor, freq. and temp. tests for lateral nonuniformities, C-V characts. 78–10563
  - MIS interface states and deep level impurities, DLTS, charge storage and charge release modes 80–49923
  - MIS Schottky barrier and conducting diodes with interface traps, capacitance and conductance 78–10564
  - MIS structure, accidental deep centre investigation using capacitance method 80–39677
  - MIS structure, accumulation regime, C-V data anal., insulator capacitance determ., interface states effects 77–12016
  - MIS structure, fast surface states density, photoelectric methods of determ. 80–70835
  - MIS structure, high- and low-freq. steady state capacitance 80–54796
  - MIS structure, semicond. surface states, capacitance, admittance, freq. depend. 80–49940
  - MIS structure, using low-temp. plasma oxidised GaAs 78–31546
  - MIS structures, unbalanced behaviour, external factors affecting *(German)* 78–43477
  - MIS structures with semiconductor layers of critical thickness, potential distrib. and capacitance calc. 78–95381
  - MOS C-V data in strong inversion, surface minority carrier redistrib. 78–72266
  - MOS capacitor, generation lifetime determ. from non-equilib. linear sweep current and capacitance meas. 78–47881
  - MOS capacitor, pulsed capacitance meas. anal. 79–38185
  - MOS capacitor, surface state distrib. determ. from transient capacitance plots 79–42658
  - MOS capacitors, pulsed relax. time meas., reln. to oxidation induced stacking faults 77–39943
  - MOS field-effect devices, mag. quantisation effect on surface capacitance 80–70834
  - MOS high frequency capacitance, simplified formula 77–72918

- **capacitance** continued
  - MOS structure, electron irrad. effects, pulsed CV charact. obs. 77–76935
  - MOS structure, flat-band capacitance, impurity concentration, approx. formulae 79–95497
  - MOS structure, generation lifetimes from C-t transients 78–88036
  - MOS structure, hole emission from interface states, transient capacitance meas. 78–14830
  - MOS structure, quenched-in bulk defects and interface states, transient capacitance spectroscopy 79–24081
  - MOS structure, semiconductor conductance and capacitance, extended AC conductance–bias method 80–96995
  - MOS structures, instantaneous characts. meas. *(French)* 77–55616
  - MOS structures, interface state density evaluated from charge-voltage data 79–11234
  - MOS structures, quasistatic and nonequilibrium phenomena with constant gate-current bias 80–80385
  - MOS structures of small-gap semicond., capacitance, effect of quantising mag. field 80–84513
  - MOS structures with semicond. layer under gate, C-V characteristic obs. 79–56322
  - MOS system containing interface traps, equilibrium and nonequilibrium response to linear voltage ramp 79–38173
  - n-n^+ step homojunction, theory 79–24056
  - negative, existence in stable steady state 77–43937
  - nematic cells, pretilted, Freedericksz transition in mag. field normal to director 79–99071
  - nematic layers, optical phase difference and capacitance, elec. and mag. field depend. 80–28911
  - nematic liquid crystal, capacitance response to elec. and mag. fields, appl. to elastic const. determ. 79–90545
  - open oscillating circuit, resonance characts., effect of spatial inhomogeneity of medium 79–41283
  - organic semiconductor Schottky barriers, capacitance meas. 79–82659
  - oxide-electrolyte interface, transition layer model 78–68895
  - p^+-n junction diffusion capacitance calc., discrepancy problems 80–60068
  - p-i-n diode, design technique for specific reverse bias characts. 78–34890
  - p-n diode, dynamic base capacitance and time const. 78–68076
  - p-n junction, abrupt, depletion layer capacitance, theory 78–52067
  - p-n junction, abrupt, space-charge layer capacitance, approximation eqns. 77–35989
  - p-n junction, conc. profile of singly charged deep impurity, capacitance meas. 78–26945
  - p-n junction, diffused, conc. profile of deep-level impurity by capacitance method 77–55299
  - p-n junction, diffused, transition capacitance calc. methods, comparison *(Rumanian)* 80–88625
  - p-n junction, GaAs and $GaAs_{0.6}P_{0.4}$ deep level profile anal. 77–80830
  - p-n junction in region of strong ferroelec. instability, barrier capacitance 79–11218
  - p-n junctions, capacitance, temp.-depend., by space-charge methods 78–91758
  - p-n junctions, determ. of arbitrary doping profile, depletion layer capacitance meas. 78–88021
  - p-n planar junction, capacitance calc. 78–30978
  - parallel plate condenser, mixed boundary value problem of electrostatic field 77–58222
  - pentylcyanobiphenyl, nematic, elastic and dielec. props. from capacitance-voltage curve 79–32894
  - planar electrodes, distributed capacitance, optic and SAW device appls. 77–27387
  - plasma probe, RF, ion sheath effects on impedance characts. 78–42818
  - plasmotron, capacitative, optimisation 79–55568
  - plastic clad metal, corrosion charact. by electrical resist. and capacitance meas. *(German)* 80–30171
  - polyethylene, electrical capacitance under high DC elec. field 80–54705
  - polyethylene, relation between electrostatic capacity and electronic space charges induced by high field 79–15154
  - polyethylene, structural changes induced by high elec. field *(Japanese)* 79–23532
  - polymer, in MIS struct, charge movement study using capacitance-voltage characts. *(French)* 80–39575
  - polymers, elec. capacity calc. strip electrodes system for dielec. props. study 80–25327
  - polymethylsiloxane, in MIS struct., C-V characts. and charge movements 77–85340
  - polystyrene film, in MIM struct., elec. conduction and free radicals 80–20340
  - polyvinyl chloride, dielec. props. at ULF, superimposed direct voltage *(French)* 78–15138
  - PTFE films, plasma-polymerized, cond. mechanism, AC cond. and capacitance meas. 79–24093
  - PVC, magnetoelectret form., RF thermomagnetic treatment, dielectric aftereffects 78–6625
  - RF sputtering, impedance matching networks, experimental and design information 80–50555
  - Schottky barrier, GaAs and $GaAs_{0.6}P_{0.4}$ deep level profile anal. 77–80830
  - Schottky barrier height approaching semicond. band gap, minority carrier injection effect 77–20434
  - Schottky diodes with deep acceptor impurities, inverse square capacitance curve, theory 80–2468
  - SCLC diode with traps, capacitance, depend. on freq. 79–11221
  - semiconductor, bulk deep centres, continuous energy spectrum, isothermal capacitance relaxation method 80–107741
  - semiconductor, deep level profile anal. by double deep level transient spectroscopy 77–20378
  - semiconductor, deep-level centre discrimination from capacitance versus time transients 78–10395
  - semiconductor, Gaussian diffusion determ., alternative method to angle lap and strain anal., depletion layer capacitance 79–86925
  - semiconductor defect characterisation by capacitance methods 77–51692
  - semiconductor device, surface recombination effect 79–82664
  - semiconductor junction, defect and impurity centre detection 78–10550
  - semiconductor on insulator substrate, capacitance meas. for Schottky barrier 80–39678
  - semiconductor or insulator, influence of states in gap on AC response 77–4362

capacitance continued
semiconductor-metal (electrolyte) contact, flat band potential from Mott-Schottky plot 78−34896
solid electrolyte-metal interface adsorption layer capacitance calc. *(Russian)* 80−59697
stearic acid film, in MIM struct., AC cond. and dielec. props., freq. depend. 80−55030
stearic acid films, evaporated, vac. effects 80−97435
tapered piezoelectric bar transducer with transversely polarised piezoceramic, capacitance and admittance 78−1537
testosteron, dielectric props. under UV excitation 80−6912
thermally stimulated capacitance method fitting anal. 79−47107
transient spectroscopy, book contrib. 78−10548
twisted nematic liq. cryst. layer, voltage depend. of capacitance 79−94894
unit realisation progress *(German)* 78−160
voltage transients, defect centres emission rates and density profile 78−10467
wax-graphite composite, specific capacitance, temp. and grain size depend. 80−50286
Ag, electric double layer of polycrysts. in NaF soln., diffuse capacitance minimum 79−91969
Ag filaments, cryst., electrolytic growth in Teflon capillaries, differential-capacity meas. 77−40552
Ag/(α-AgI) interface, impedance meas., equivalent circuit parameters. calc., electrolyte defect struct. 78−59975
Al-Al_2O_3-Au(Al), capacitance, water sorption effects 77−43738
Al-Al_2O_3-InSb MIS structures, recomb. processes and carrier lifetimes 79−38177
Al-Al_2O_3-metal capacitor, capacitance and power factor rel. to voltage and temp. changes 80−54802
Al-anodised Ta_2O_3/native oxide-n-GaAs MOS structure evaluation 80−84514
Al-CdTe-Al thin film VLF dielectric props. *(Slovak)* 79−7907
Al-GaAs-Al_xGa_{1-x}As Schottky barrier diodes, prep., characts. 80−6948
Al-SiO_2-Si capacitors, transient capacitance temp. depend., −40 to 70°C 79−47167
Al-SiO_x-GaAs, C-V characteristics 79−65553
Al-stearic acid-Al, low-loss thin film capacitor 80−71317
Al-tetracene-Au cell, depletion layer, LF capacitance meas. 79−56328
AlF_3 film, dielec. characts. 77−85650
n-$Al_{0.3}Ga_{0.7}$As, layer of (AlGa)As DH laser, deep levels 78−46605
Al_2O_3, anodic, passified, inhibition of reaction with water 80−89390
B″-Al_2O_3-Na_2O, bulk and grain boundary ionic cond. from conductance and capacitance meas. 80−2204
β-Al_2O_3-Na_2O, single cryst., non-Debye capacitance 80−107497
Au-AlF_3-Au structure, dielec. props. of RF sputtered AlF_3 film 77−36173
BaO-TiO_2-Nd_2O_3, exam. of compositional and dielectric props. 79−33601
$BaTiO_3$-$BaNb_2O_6$, semiconducting ferroelectric ceramic, nonlinearity of dielectric layer capacitance 79−8098
$BaZrO_3$-$LaAlO_3$ systems, sintering conditions, elec. props. 79−43184
Bi-NbO_2-Bi system, Schottky barrier effects in transport and dielec. props. 80−29486
Bi_2O_3 layer thermally grown on Bi film, thickness meas. by capacitance method 79−1554
Bi_2O_3 vacuum deposited films, dielec. props., 90 to 298K, freq. range 0.1 to 10 kHz, ageing effect 80−55036
Bi_2WO_6, ionic cond. and relaxation polarisation, capacitance, losses 80−24657
CdF_2-Au metal-semiconductor contact, capacitance and photocurrent, barrier height 77−85321
CdF_2-metal Schottky diode, photoemission, capacitance and I-V meas. barrier heights 78−26950
CdS, electron traps, DLTS meas. 80−24949
CdS, film for solar cells, struct. and elec. props., thickness depend. 78−72289
CdS_xSe_{1-x}, electron traps, DLTS meas. 80−24949
CdSe, MIS thin film capacitance, theory 79−87156
CdTe, Schottky diode, AC small signal capacitance 79−7899
CdTe thick films, prep. by sintering and elec. props. 80−29451
CeF_3 film, in MIM struct., dielec. props. *(Czech)* 80−25309
Cr, discontinuous thin film, AC equivalent circuit anal. 79−51690
Cr-phthalocyanine-Cr sandwich, I-V and C-V characts. 80−60106
Cr-Si, cleaved junction, interface states, capacitance meas. 79−91118
Cu-GeO_2/BaO-Cu thin film, amorphous, effect of electroforming on conductance and capacitance 80−34537
Cu-SiO/B_2O_3-Cu thin film, amorphous, conductance and capacitance, effect of electroforming 80−34537
Cu_2S-CdS heterojunction characteristics and CdS polarity *(Japanese)* 78−23154
Cu_2S-CdS heterojunction solar cell, interface recomb. vel. determ. by capacitance/collection efficiency variation 80−50959
Cu_2S-CdS solar cells, EBIC and capacitance measurements, stability problems 80−45684
D-T, liq., dielectric constant and elec. cond. 80−84680
Eu_xO_y film, dielec. props. rel. to annealing 79−99636
Fe passive film AC electroreflectance and impedance obs. 78−7093
Fe_xO_y thermal oxide film on Fe, capacitance, temp. and freq. depend., in aq. electrolyte soln. 80−54776
n-GaAlAs:Sn LED DH donor-level analysis, DLTS obs. 79−47040
$Ga_{1-x}Al_x$As electrodes, interface capacitance meas., flatband pot., conduction and valence band boundaries *(French)* 79−33339
$Ga_{1-x}Al_x$As:Si, linear-gradient p-n junction, barrier capacitance 77−43705
$Ga_{1-x}Al_x$As-$Ga_{1-y}Al_y$As p-n heterojunction, minority carrier lifetime, elec. characts. and electrolum. meas. 78−2554
GaAs anodic MIS system, dynamic props. of interface state bands 80−49933
GaAs anodic MOS structs., interface-state band model 80−11093
GaAs anodic oxide, electrical props. 79−38170
GaAs based MOS capacitors, scanning photovoltage investigation 80−80396
n-GaAs, deform. produced deep levels, DLTS meas. 80−54634
GaAs grown by VPE using organometallic method, deep trap levels 80 10923
GaAs MESFET, deep trapping effects at GaAs-GaAs:Cr interface 78−72245
GaAs MIS capacitor, transient capacitance and C-V characts. 78−95374

capacitance continued
GaAs MOS capacitor fabrication and transient response for minority carrier lifetime meas. 79−47103
In-GaAs, MOS capacitor struct., elec. props., annealing effects 80−34519
GaAs oxide film form., ion implantation effects 80−100266
GaAs Schottky barrier function capacitance meas., determ. of deep electron traps 77−39797
GaAs, temp. depend. of intervalley gap from Schottky diodes meas., thermionic emission theory generalization 79−73586
n-GaAs, undoped, proton radiation defect detect. by transient capacitance spectroscopy 79−11089
GaAs:Cr, deep acceptor level, DLTS and optical DLTS study 80−92852
n-GaAs:H(D), ion implanted, carrier removal, capacitance-voltage profiling 80−84195
GaAs-metal contacts, excess capacitance, depend. on nonlinear dielectric susceptibility 78−43475
$GaAs_{1-x}P_x$ electrodes, interface capacitance meas., flatband pot., conduction and valence band boundaries *(French)* 79−33339
$Ga_{1-x}In_X$As, VPE layers, main electron trap, transient capacitance spectroscopy obs. 78−34800
GaP anodic MOS structs., interface-state band model 80−11093
GaP, VPE, background deep level defects, transient capacitance obs. 77−62854
GaP:Zn, O LED, neutron irrad. effects on capacitance, I-V and electrolum. characts. 77−66543
Ge, pure, degree of compensation, capacitance meas., 4.2-150K 79−7624
Ge:Au, capacitance oscillations, trap recharging waves 77−43614
GeSe amorphous films in Al-GeSe-Al structs., AC cond. and capacity, thickness depend. 79−65566
^{3}He-A superfluid slab, magnetoelectric textures, capacitive meas. 78−22924
Hg/electrolyte contacts, adsorption model for double layer capacitance 80−44706
Hg/$Na_2B_4O_7.10H_2O$ contacts, double-layer capacitance, temp. depend. 80−44707
$Hg_{0.8}Cd_{0.2}$Te-ZnS MIS struct., nonparabolic bond semicond., surface state studies, capacitance measurements 79−78190
$Hg_{1-x}Cd_x$Te-oxide interfaces, MIS capacitance characts. 80−49926
HgI_2:CdS, photodielectric effect 77−11955
In-$SrTiO_{3-x}$ contacts, differential capacitance, elec. field depend. permittivity effect 80−54779
p-InAs-Au contacts, influence of free surface on elec. behaviour 78−95362
n-InP, hole traps by deep level transient spectroscopy and transient capacitance methods 79−51514
InP, inversion layers, C-V and surface transport meas. 80−49928
InP MIS capacitor, transient capacitance and C-V characts. 78−95374
InP-Langmuir film MIS structures, surface state distrib. obs. 77−89859
n-InP-SiO_2 system, interface and dielec. props. 80−49930
InSb, in MISIM struct., photovaractor effect and CV characs. obs. 77−8205
InSb, MIS thin film capacitance, theory 79−87156
InSb MOS capacitor, AC behaviour, semicond.-oxide interlayer effect 78−19151
InSb MOS struct., capacitance of n-channel inversion layers, elec. field effects 80−80393
InSb, n-type, anodic oxide film dielectric, MOS structure *(Russian)* 77−89874
LaF_3 films, electron beam evaporated, dielec. props. 79−91375
Na_2CO_3, phys. props. related to phase transitions 80−96643
Nb-Nb_2O_5-Nb structure, Schottky barrier effects on capacitance and loss tangent 77−8203
Nb-oxide-Pb Josephson tunnel junction, capacitance and ellipsometrically determined oxide thickness 77−4469
NiO and lithiated NiO, thermally grown, electrochemical capacitance variations 80−29475
PLZT ceramics, modified by $Ca^{2+}(Sr^{2+})(Nd^{3+})(Y^{3+})$, dielec. behaviour 80−60519
Pb, small Josephson junction, temp. and mag. field variations in resist., cos ϕ conductance and effective capacitance 78−84357
Pb-PbO_x-Pb small supercond. tunnel junctions, effect of capacitance in I-V characts., high-freq. obs. 80−80448
$Pb_5Ge_3O_{11}$, ferroelec., surface capacitance effect on dielec. props., DC cond. and dielec. const. meas. 79−91333
$Pb_{1-x}Ge_x$Te, ferroelec. phase transition, IR refl. and resist. meas. 80−11353
PbI_2 single crysts., photo-induced AC impedance meas., photodielec. effect 78−52034
PbS-Si heterojunction, space charge capacitance, PbSn film thickness depend. 80−88630
$PbSnF_4$, anionic conductor, thin films and ceramics 80−107556
PbTe substrate for MIS capacitor, C-V and G-V characts. 78−26962
Pb(Zr,Ti,Nb)O_3 ceramics, rel. dielec. const. and piezoelec. props. rel. to porosity 79−11388
Pb(Zr,Ti)O_3, piezoelectric ceramics, low fluence neutron irrad. effects 80−92564
Sb_2S_3, thin film, dielectric props. 79−15392
SbSI ferroelectric, dielectric behaviour, particle-size dependence 78−2811
Si, amorphous, Schottky barrier and p-n junction props. 79−28407
Si, amorphous film, electron beam evaporated, freq.-depend. dielec. behaviour 79−99549
Si based MOS capacitors, scanning photovoltage investigation 80−80396
Si, clean-cleaved, Schottky barrier height meas. accuracy 78−52081
Si, deep level transient spectroscopy *(French)* 79−11079
Si, defect form. during high press. low temp. steam oxidation 79−29238
Si, deformed, defect states associated with dislocations, capacitance transient spectroscopy 79−42483
Si, dislocation defect states, capacitance transient spectroscopy 79−82549
Si, dislocation electronic states, Schottky diode meas. 79−82548
Si, dopant distrib. in mono- and polycryst. samples, C-V technique 80−6425
n-Si, electron irrad., defect energy levels, energy depend., capacitance meas. 79−33262
Si, electron irrad. damage, capacitance meas. 80−24935
Si junction diode, diffused, with deep level traps, negative capacitance 80−96976
Si MIS capacitors, C-V curves, outer oxide surface conditions effects 80−97000

capacitance continued
  Si, p^+-n diode, neutron irrad., defect levels, G-T and C-T curves obs. 77—62986
  Si p^+-n junction diodes, flow fluence S implanted unequal defect densities, dynathermal obs. 80—20293
  Si, p-n junc. solar cell, forward bias capacitance and current meas. for lifetime and band narrowing detn. 79—7892
  Si p-n junction, dielectric props., freq. depend. of capacitance and conductance 78—43469
  Si p-n junction, negative annealing of γ-radiation defects 77—43246
  Si p-n step junctions, temp. depend. of capacitance 79—15210
  Si:Al, P-diffused, recomb. centres, thermally stimulated capacitance meas. 77—72834
  Si:Au, thermally stimulated capacitance method fitting anal. 79—47107
  Si:B, N-implanted junction capacitance meas., appl. of dynamic lateral photovoltaic effect 77—85304
  Si:F,H, amorphous, elec. and optical props. 80—60031
  Si:H, amorphous Schottky barrier solar cells, depletion region, capacitance study 80—50963
  a-Si:H Schottky barrier diodes, capacitance studies 80—49908
  n-Si:P, edge dislocation energy level, differential capacitance meas. 79—23927
  Si:P dislocation p-n junctions, capacitive props. 80—20300
  Si:Pd, deep levels, conc., activation energies, thermal emission rate, thermally stimulated capacitance meas. 79—51524
  Si:Pt, deep level, exam. by thermally stimulated current and capacitance techniques 79—1579
  Si:Re, diode, barrier capacitance and photocapacitance, uniaxial press. effect 77—20416
  Si:Rh(Pd), Schottky diode, capacitance characts., donor and acceptor levels 77—43697
  Si:S, existence of isotope shift for S deep level, isothermal transient capacitance meas. 78—63999
  a-Si/Au barrier, capacitance and cond. 80—2469
  a-Si/metal barrier, capacitance and cond. meas. interpretation 80—49909
  Si-electrolyte contact, implantation profile meas. from capacitance-voltage characts. *(German)* 77—1145
  Si-SiO_2, intentionally contaminated interface, transient capacitance meas. 79—33349
  Si-SiO_2, interface states from capacitance-voltage term spectra anal. 77—4446
  Si-SiO_2, MOS interface states density, meas. techniques and model development 80—92988
  Si-SiO_2 interfacial region on TCE/O_2 and CCl_4/O_2 oxidised Si, struct. and comp. 80—50741
  Si-SiO_2 layer formation by O_2^+ ion implantation, interface struct. and C-V characts. 77—1142
  Si-SiO_2 MOS interface states density, transient capacitance meas. eval. 80—92989
  Si-SiO_2-KCl_{aq}, interface, capacitance meas. 78—80051
  Si_3N_4, highly insulating film, current cond., CV curves, and IR absorpt. 79—38208
  Si_3N_4 thin film, reactively sputtered, struct. and elec. props. 80—88656
  SiO film, electrode effects in TSC and capacitance meas. 79—78203
  SiO_2 film, IR spectra and elec. props., influence of prep. conditions 79—87176
  SiO_2, pyrolytic, C-V characts., non-equilib. lowering in inversion mode 77—55630
  SiO_2 sputtered layers for semicond. devices, effect of impurities on elec. props. *(German)* 77—16495
  SnO_2-InP heterojunctions, elec. and photovoltaic characts. 80—75628
  $SrTiO_3$ semicond. electrode, electrochem., photoelectrochem. props. 80—3352
  Ta-Ti-O, reactive sputtered film, elec. props. 78—84336
  Ta_2O_5, anodic, on sputtered Ta_2N, dielec. props., 20-10^5 Hz, 150-500K 79—87386
  TeO_2 thin films, dielec. props. rel. to fabrication conditions 80—97199
  TeO_2-WO_2 glass, dipole correlations, capacitances and TSC meas. 79—28670
  TiO_2-Si, MIS capacitor, C-V characts. meas. 78—60208
  $Ti0_2$ electrodes, room temp. diffusions, capacitance, spectral response and volt-ampere characts. 80—15294
  Yb_2O_3 film, amorphous, electron beam deposited, dielec. props. 79—91339
  ZnO ceramic, nonohmic, drift phenomena of capacitance and current 80—39587
  ZnO film, high-resist., band and hopping cond., AC cond. and capacitance meas. 77—72928
  ZnO non-ohmic ceramic, degradation props. under AC and DC bias 80—80262
  ZnO pellets, and ZnO:Li single crysts., photo-induced AC impedance meas., photodielec. effect 78—52034
  ZnO-based nonohmic ceramic, dielec. dispersion and equiv. circuit 77—73110
  ZnTe, photoinduced dielec. loss and capacitance changes, rel. to space charge polarisation 80—2417
  ZnTe:Au, impurity identification and characterisation, capacitance, luminescence and IR absorption 80—60639
  ZnTe:Cu, elec. and optical identification of persistent acceptor 79—60764
  ZnTe-electrolyte interface, electrochem. behaviour of single crysts. 79—91138

capacitance measurement
  25 kV bias isolation unit for 1 MHz measurements using commercial C/G meter 78—54401
  72BD capacitance meter, Boonton *(German)* 80—22344
  accuracy improvement by variable coeff. elimination *(Russian)* 78—49789
  AF impedance bridge, 4-terminal-pair, 40 Hz to 2 kHz 79—88978
  antimonic caesium vacuum photocell, test instrument for contactless circuits *(Russian)* 79—58676
  astable multivibrator measures capacitor tolerance 78—4628
  automatic capacity/dissipation meas. device for LV/HV capacitors *(German)* 77—74459
  automatic test set, using capacitance to voltage convertor 78—24818
  ballistic method, 1 pF to 1 F range *(German)* 78—4655
  ballistic methods, using ICs and a comparator 77—74431
  bridge meas. system for assessment of deep levels in semiconductors 80 105674
  calculable 1 MHz capacitive Q standards 78—21176

capacitance measurement continued
  capacitance standard unit transmission techniques 77—53854
  capacitance standards, group storage errors, statistical analysis 77—53853
  capacitance/resistance meter, cct. *(Spanish)* 79—88946
  capacitoplethysmography for heart and lung meas. *(Japanese)* 78—53465
  capacitor, by three-voltmeter minicomputer multibridge system *(Russian)* 78—70159
  capacitor, stored energy meas. 80—77585
  capacitor loss measurement, using Q-bridges or resonant coaxial lines 77—34002
  capacitor loss-angle and capacitance checking cct. 77—61085
  capacitor transducer, noise-stable meas. cct. *(Russian)* 78—89493
  casting process, mould/metal, gap var. with time meas. method 77—52608
  charge-conversion meas. of nonlinear capacitance 77—79115
  CMOS capacitance evaluator, 50 pF-5 μF range 78—24827
  CMOS ICM 7555 capacitance meter cct., using radio receiver indicator 80—62692
  comparator for checking capacitance standard *(Polish)* 78—41331
  comparator used for testing 78—16811
  components of (30-100) Hz and (1-10) kV, Schering bridge amplifier system appl. *(Bulgarian)* 77—61083
  deep-level transient spectroscopy, using HP desk-top computer semiconductor processes and devices testing appl. 80—37091
  defibrillator, damped sine wave, intact, evaluation of operating parameters 78—57120
  dielectrography methods and apparatus, recording capacitance changes due to blood vol. fluctuations 78—57046
  digital, dynamic method *(Czech)* 79—63272
  digital capacitance meter, design and construction 80—57275
  digital capacitance meter, utilising CR discharge 79—12819
  digital capacitance meter *(Spanish)* 80—13062
  digital IC capacitance meter *(German)* 79—67339
  digital meter, using 555 oscillator 77—53926
  digital meter for inductance coil parameters meas. 78—12718
  direct, using phase sensitive detection and time encoded ballistic methods 78—4629
  direct reading capacitance meter 79—75513
  direct reading capacitance meters, using auto-ranging 78—32835
  direct reading linear capacitance meter, cct. *(French)* 78—237
  direct reading meter constr. 77—53927
  dispersion field transducers for granular material exam. 78—85078
  double layer theory, Pt, dropping Hg electrode results 77—53933
  DVM converted to capacitance meter, using diode pump cct. 80—62656
  electric double layer capacitance meas., potentiostatic method 78—85169
  electrochemical meas. system, using phase-sensitive detector, control circuit *(Spanish)* 80—55671
  electrolytic capacitors, 0 to 10000 μF in six ranges 80—27319
  electrolytic capacitors, series connection behaviour principle 77—53949
  electrometric voltmeter input capacitance absorption meas. 77—79107
  electron microscopes high-voltage supplies, capacitive meas. of slow fluctuations 77—13826
  electronic system, sampling of transient to estimate time-constant *(Spanish)* 80—47071
  enzyme reaction rate determ. by capacitance meas. 78—31997
  etching power determ. 77—44377
  faradmeters, errors checking with aid of tables 80—52271
  four-terminal high capacitance standard 77—5869
  high capacitance standard, four terminal device with auto transformers for scaling 77—18025
  high loss materials at high freqs. 80—62686
  IC for measuring amplitude of surface standing water waves 79—50833
  indicating instrument, operational amplifiers employing, for 10pF to 10μF range *(German)* 77—146
  insulation loss-angle and capacitance test trolley *(Russian)* 77—10041
  intracellular potential amplifier input capacitance determ. errors 77—60320
  junction capacitance, appl. of dynamic lateral photovoltaic effect 77—85304
  Kelvin double bridge, precison, for capacitance meas. up to 1 F, ratio arm adjustment 79—21776
  Lampard type electrostatic systems, analysis of the effect of the metrological properties *(Polish)* 78—77928
  Lampard-type electrostatic system, appl. of sensitivity criterion 80—98942
  large capacitances, meas. via modified commercial admittance bridge 78—4660
  linear meter, based on integrator 79—6146
  linear scale meter, improved cct. includes resistance measurement, transistor amplifier *(German)* 77—26327
  liquids, guarded cylindrical capacitance cell 80—86268
  lumped-capacitance method for complex dielec. permitt. in polar liqs. 78—77936
  meter, directly indicating, with linear scale *(Czech)* 79—97404
  meter, using ICs, 10 pF to 1 μF, design 79—6140
  meter construction, accurate, low cost, range 0 to 1 μF range 78—8423
  meter operation with 10 kV Bias Isolation Unit 77—57364
  meter with automatic range selector *(German)* 78—45648
  meters, new checking method for instruments having both uniform and non-uniform scales 80—62654
  method using laboratory oscilloscope and function generator 77—67463
  microstrip technique for theoretical capacitance determ. of concave capacitance sensor 80—198
  MIS structure capacitance-voltage charact. gauge 77—37923
  MIS structure surface characterisation by C(V) curves 78—72276
  monolithic timers form capacitive transducer-to-recorder interfaces 77—87781
  MOS capacitor, direct cap./surface-potential recording meas. method 79—91143
  MoS processing-related interface state meas., transient capacitance method 78—10574
  MOS structure dynamic volt-capacitance characteristic meas. 78—60207
  MOS structures, static technique for differential capacitance meas. 77—65044
  near zero signal source impedance measuring system, errors reduction 77—30186
  p-n junctions capacitance, using bridge circuit with analogue multiplication *(Bulgarian)* 78—57977

capacitance measurement continued
pacemaker lead fluid penetration detection by capacitance meas. 77−81749
precision thermostat and capacitor enclose, maintaining the unit of capacitance 80−95063
primary standard capacitor design 77−53944
quadrature or phase sensitive detection and time encoded ballistic methods 77−74454
RLC bridge, with oscillator and having ten ranges 79−2785
semiconductor, capacitive profilometry, accuracy 80−9005
semiconductor device, automatic display of CV and GV characts. at HF 77−26329
semiconductor device C-V and G-V measurements using automatic technique, 50 Hz to 300 KHz 80−31800
semiconductor junctions, transient capacitance instrumentation for deep level impurities spectrometry 77−51816
semiconductor-liquid junctions, differential capacitance measurement by desk calculator controlled system 79−78170
small capacitances by comparison, digital cct. 80−57327
small capacitances measurement by comparison, cct. 80−57327
standard capacitor, simple calibration method 77−82571
standard capacitors calc., with spherical caps *(Slovak)* 77−87783
standards, secondary *(German)* 79−71402
standards comparison, capacitance-inductance, transformer ratio bridge *(Polish)* 79−80645
standards unit reproduction, theoretical study 77−53943
stray, experimental methods with nanosec pulses 77−82548
student experiment, capacitance meas. of parallel-plate capacitor, fringing field effect 77−87604
student experiment, dielectric consts. and capacitor dissipation meas., RLC ccts. 77−82339
sulphide minerals-solvent boundaries *(Russian)* 78−10551
thermal expansion of solids, linear coeffs., capacitance meas. method 78−16772
thermometer for low-temp. measurements, bridge detector circuit 79−54132
transportable 1000 pF capacitance standard 77−5870
two plate capacitor with aerostatic electrode regulation for precise determination of capacitor loss factor *(German)* 78−74021
universal bridge, digital meter used to measure L, R, and C 78−12715
wide-range, on single scale of instrument, use of sinusoidal power generator 80−98935
n-Fe_2O_3, sintered and flame-oxidised, flatband pots. from capacity meas. 79−70355
p-GaP electrode, for solar cell, differential capacitance meas. for flatband potential determ. 78−72256
NaCl, capacitance determination of area thermal expansion and dielectric constant 79−80573

capacitance meters *see capacitance measurement*

capacitor storage
5 MeV electron accelerator modulator charging system 79−13563
Antares laser fusion project, 300 kJ, 200 kA Marx energy storage module 80−68954
arc gap with displacement by mag. field 78−87513
banks, optimum design rules, fusion reactor technology 78−74487
discharge mobile X-ray apparatus *(Japanese)* 79−88165
foil-and-paper 10 kV capacitors, low-cost energy storage for fusion reactors 78−74485
fusion reactor laser, Shiva pulse power, isolation and control system 78−54935
fusion reactor magnet coil, 125 kG, 1 m, design, fabrication 78−55008
HV capacitor banks and ccts. initiating by air driven fibre optic coupled pulser system 78−54943
inductive storage bank for rhodamine 6G dye-laser pumping 80−5742
neutral beam power supply, 40 kV, 25 ms, for fusion reactor 78−62610
NMR absorption peak voltmeter cct. error analysis *(Russian)* 79−26079
nuclear fuel rod scaling appl. 78−8910
plasma MHD flow in channel rel. to capacitative energy store element distrib. 79−86569
propylene film-paper-phthalate ester capacitors 78−74486
pulsed electron accelerator current density distrib. multichannel recorder 78−58520
rail accelerator, ambient medium heating expt. 78−75439
Shiva laser, 25 MJ energy storage and delivery system 78−55015
Shiva laser, 25 MJ energy storage and delivery system 78−59038
solid-state imaging charge injection devices 77−39083
solid-state laser miniature power pack 78−59015
THOR Tokamak toroidal field system design and manufacture 79−32807
N_2 laser, with discrete ceramic capacitors in Blumlein-type circuit 77−19330

capacitor stores *see capacitor storage*

capacitors
see also electrolytic capacitors; thin film capacitors; varactors
aerosol particles sizing, appl. of elec. capacitor 78−81471
antiferroelectric, appl. in TV sets, manufacture *(Chinese)* 79−33617
Brownian motion between capacitor plates, path integrals for inertial classical particles 78−57858
capacitance/loss-tangent meas. by three-voltmeter multi-bridge method *(Russian)* 78−70159
ceramic, nondestructive testing by scanning laser acoustic microscopes, comparison with SEM and optical microscopy results 80−58875
ceramic capacitor for N_2 laser, failure elimination 78−33740
ceramic multilayer capacitors, fracture mechanics approach to structural reliability assessment 80−89328
charge difference phenomena *(German)* 79−36810
charging polymer surfaces, injection times obs., with aid of computer 80−70796
conformal transformation, allowing for spatial dispersion *(Russian)* 80−53183
cylindrical, electron beam modulation mechanism 77−49808
cylindrical condenser, electrostatic prism appls. 77−6992
cylindrical condenser, finite length, elec. field distrib. calcs. 77−5957
cylindrical particle analyser, fringing field 78−94165
damping capacitors in pulsed N_2 laser, dynamics *(German)* 77−10957
deformation and strain in charging, Maxwell stress tensor, for teachers 77−33792
dense plasma focus, capacitor bank system design and safety 78−54889
dielectric, decay voltage and recovery voltage curves 79−61295

capacitors continued
dielectric constant meas. on fluids, parallel capacitor design 80−4737
displacement transducers, effect of tilt and surface damage 78−54356
distribution of concentration of electrically-conducting particles during autovibrational movement in plane capacitor *(Russian)* 80−48117
double layer capacitors, RF conduction in polar liqs., ion diffusion effect 80−107883
dumping capacitor modification for N_2 laser 77−14735
dumping capacitor system for Schenck-Metcalf N_2 laser 79−18439
education, capacitor complete discharge time, thermal noise 80−17727
electrometer measuring unit and component requirements 77−74445
electrometric fixed-capacitor and resistive methods compared 80−90866
electrostatic analyser with oblique cut plates, focusing props. 77−54667
electrostatic defectoscopy, of cylindrical specimens using cylindrical capacitors 78−40000
electrostatic problem of two staggered parallel strips in a bounded space 79−7052
Fermilab capacitor tree 77−83242
Fermilab neutrino focusing horn, pulse stretching in high current power supplies 77−83367
ferroelectric films, resonant autothermostabilisation *(Russian)* 78−52451
foil-and-paper 10 kV capacitors, low-cost energy storage for fusion reactors 78−74485
four terminal, high capacitance standard, four terminal device with autotransformers for scaling 77−18025
highly electrostrictive ceramic capacitor 79−47390
HV, Maxwell-Wagner dielectric polarisation 80−29676
HV deflection condenser operated under high vac. conditions 80−27861
interfacial polarisation effect on dielectric props., sandwich capacitor model 80−15614
Kelvin vibrating capacitor with pot. difference amplifier for current meas. *(French)* 77−22572
level detector for liq. He, using series of capacitors 77−30158
liquid level-to-frequency converter 79−6080
magnetic field between discharging plates, Ampere's law, for teachers 79−21490
magnetoplasma, coaxial and planar, impedance characts. 78−42837
MIS capacitor, capacitance-voltage characts., automatic computation method *(Polish)* 79−1624
MNOS capacitor, HCl annealing of memory oxide, effect on memory window size and location 79−70079
mosaic liquid crystal controlled transparency for holographic store data input *(Russian)* 79−94182
ohm, absolute determ. based on standard capacitors 77−82565
paper capacitor, dielec. loss, effect of simultaneous application of AC and DC voltages, freq. and temp. depend. 78−15091
parallel plate, variable space, capacitance determ. 77−87604
parallel plate condenser, mixed boundary value problem of electrostatic field 77−58222
parallel-flat plate condensers, thermodynamic treatment 79−6070
parallel-plate, props. in plasmon model 79−51511
PF correction, dielectric fluid test and anal., quality assurance 78−80272
plate-plate electrical configuration with injected unipolar space charge *(Portuguese)* 80−28132
poly Si gate MOS capacitor post-irradiation flat-band shift expts. 77−76939
polymeric, injection charging 77−76902
polypropylene, effect of corona treatment on dielectric props. for capacitor appl. 79−33607
potential fields calc., plane-parallel, in mixed boundary conditions *(Rumanian)* 78−82877
powder classification in electric field of plane capacitor 77−12775
power supply type selection for capacitor charging in pulsed laser 77−79838
propylene film-paper-phthalate ester capacitors, for energy storage 78−74486
push-me-pull-you capacitor, student discussion topic 79−97160
relativistic electron wave diffraction by cylindrical capacitor 80−5671
secondary ion emission from solid surface, meas. apparatus, spherical condenser *(German)* 77−44103
semiconductor capacitor, parameters of local states using thermally stimulated discharge, allowance for strong field effects 79−51528
sensors properties and uses *(German)* 78−36991
simulated spherical, for use in electron spectrometers 79−89043
standard, simple calibration method 77−82571
standard, with spherical caps, capacitance calc. *(Slovak)* 77−87783
stored energy meas. 80−77585
teaching two-capacitor problem, using circuit self-inductance 79−62960
temperature jump spectrophotometry using nanosecond resolution capacitor discharge 77−79159
toroidal, approx. capacities 80−28137
torquemeter transducer, with digital display *(German)* 77−34006
two plate with aerostatic electrode regulation for precise determination of capacitor loss factor, features *(German)* 78−74021
vibrating capacitor displacement transducer, eqn. of state 80−57281
vibrating capacitor probe for surface and adsorption studies 78−10274
vibrating-capacitor electrometer, current noise meas. 78−54398
$BaTiO_3$ ceramic dielectric capacitor, processing prop. relations, hysteresis, permittivity 80−80730
$BaTiO_3$, dielectric ceramic, interaction with metallic film during sintering 79−33958
$BaTiO_3$:La_2O_3 and $BaTiO_3$:La_2O_3.$3TiO_2$, permittivity ageing obs. *(Korean)* 80−25325
$Ba_{100}Ti_{101-x}Sn_x+0.3$ at.%Sb, intergranular capacitor, effect of microstructure on electrical props. 79−34160
GaAs crystals appl., with nipi superstructures *(German)* 78−95064
H_2O drops, acting as capacitors in corona discharge *(Russian)* 77−62420
PLZT modified high voltage dielectric, permittivity, Curie temp., loss meas. 80−80720
Si-SiO_2-Si capacitor, polycryst., capacitance voltage characterisation 80−70794
Ta capacitor, stress wave emission anal. in resistance welding 79−11739

capacity, channel *see channel capacity*

capillarity
see also bubbles; contact angle; drops; foams; liquid films; surface tension
adsorption and capillary condensation, adsorptive pot. boundary layer approx. 78−2366

capillarity continued
- air flow through capillary under action of ultrasound 80—6149
- air-water interface, adequacy of theories of capillary wave damping 77—72750
- band broadening, in microcapillary tubes, liq. chromatographic appls. 78—61085
- BBOA, pretransitional shear viscosity divergence near smectic A-smectic B transition 79—33077
- benzene adsorbent mesopores, capillary evaporation and struct. 80—107614
- bituminous pitch oils, flow curves, mag. field effect 80—33553
- blood, Fahraeus effect and cell screening rel. to dextran-induced aggregation 79—62273
- blood, Fahraeus effect and cell screening rel. to volume flow rate 79—62272
- brain capillary, microkinematic obs. of blood velocity *(Russian)* 79—5366
- bubble form in potential flow 79—86490
- bubble formation during gas injection into liq. through orifice, interfacial area, press. *(German)* 79—18937
- bubble formation during injection, system pressure and thermophysical effects *(German)* 79—41745
- capillary device construction for liquid introduction into analytic mass spectrometer 80—4805
- capillary mass transfer of porous solids based on pore distrib. curves 77—7443
- capillary rheometer, viscous heating from power law fluid, perturbation expansion anal. 78—63519
- capillary rise in random sphere packing, contact angle and film jumps 77—66076
- capillary surfaces, calc. by finite element methods 80—20009
- capillary surfaces approx. in gravitational field 77—55415
- capillary-porous bodies, heat and moisture transfer, analytical formulae 78—67013
- capillary-porous body, nonlinear heat/mass transfer problem, soln. using invariant groups 78—55688
- capillary-porous body, slit model 78—47031
- CBOOA, nematic and smectic, anisotropic shear viscosity meas. 77—15310
- cholesteric liquid crystal, oriented, Newtonian capillary shear flow, effective viscosity 79—18957
- classical theory generalisation 78—2335
- clinical capillary blood viscometer development 77—40844
- closed capillary method for radioactive tracer diffusion meas. in liq. 78—14491
- colloidal capillary-porous body, mass transfer parameters, adsorpt., osmotic moisture 78—11563
- compressible flow in permeable capillaries under deform., press. loss model 78—26141
- condensation and absorption processes 79—28175
- condensation and adsorption, Gibbs free energy, unitary approach 77—76643
- condensation theory, adsorbates liq. or gaseous props. 80—80028
- conducting liq. layer, surface tension effects, MHD convection stability and thermocapillarity *(Russian)* 78—47054
- constant pressure manometer with frequency read out, electrocapillary element appl. 80—73380
- convection driven by non-uniform surface tension 80—10116
- convective thermocapillary and thermomolecular fluid flow in low-g environment 79—73117
- counter-current system with capillary-size vessels, fluid movements due to hydrodynamic forces 77—5024
- countercurrent capillary saturation of porous media by active impurity solution 80—38489
- creeping flow over surface, angle of contact, viscous liq. 78—51149
- cryogen confinement for refrigeration and liquid control in zero gravity 78—43198
- cryogenic fluid boiling in capillary tubes, heat transfer 79—59915
- crystal growth, capillary phenomena during solidification 78—30564
- crystalline particles at sphere-plane contact, nondiffusional deform. under capillary forces 78—15329
- crystallisation stability during capillary shaping, general theory of capillary and thermal stability 80—107076
- crystallisation stability during capillary shaping for arbitrary small perturbations 80—107077
- cumene, films, thin, wetting, rheological characts. determ., capillary method 78—51788
- cyclohexane flow in capillaries, Washburn eqn. 79—64767
- cyclohexane menisci, exptl. verification of Kelvin eqn. for capillary condensation 79—33159
- decane, film flow calc., effect of temp. and press. gradients in conical capillaries 79—55416
- n-decane, films, thin, wetting, rheological characts. determ., capillary method 78—51788
- density measurement, using flexible capillary 80—98886
- diffusion near crit. point in solns. with large conc. gradients in capillary *(Russian)* 77—84958
- drop on fibre systems, contact angle, phase contact areas, drop vol. and Laplace excess press. meas. 77—7950
- drops, rotating, captive between co-rotating parallel faces, shapes and stability, capillarity eqns. 80—64592
- drops in immiscible liquid, intermittent elec. field heat transfer augmentation 78—94872
- dynamic liquid surface tension determ. from drop oscillation frequency and capillary jet instability 78—56026
- dynamic surface tension, meas. by excited capillary jet axisymmetric disturbance growth rate 78—95205
- elasticoviscous capillary jet stability 79—90303
- electrocapillary acceleration meters, electrolyte composition selection 80—73331
- electrocapillary acceleration meters with electrolyte in gel form 80—73330
- electrocapillary curves, automatic meas. eqpt. 78—40061
- electrocapillary theory, Lippmann relation, surface thermodynamics 78—61048
- electrode, porous, capillary equil. and percolation theory 79—91971
- electrokinetic flow in a narrow cylindrical capillary 80—92233
- electrokinetic parameters 77—48650
- electrolyte solutions, aq., wetting angle rel. to rate of meniscus movement capillary rise 79—65292
- electrostatic ink jet drop formation characteristics *(Japanese)* 78—25766

capillarity continued
- entrance effect in capillary flow of dilute and semi-dilute polymer solutions 79—60033
- epoxy resin adhesives, capillary flow and bond strength 80—71883
- epoxy resin bond layer, prep. methods, ultimate thickness 80—71884
- ethane, flow continuity in arterial capillary systems in cryogenic heat pipes 80—64536
- ethanol evaporating meniscus, capillary flow heat transfer model anal. 79—82416
- ethyl alcohol, free convection on turbulent horizontal layer, effect of thermocapillary forces 79—98722
- ethyl n-dodecoate, photocapillary effect, temp. depend. *(Russian)* 78—34682
- extensional flow capillary rheometer for extensional viscosity meas. 78—55704
- extruded polymer soln. through capillary, flow instability and electrostatic effects 79—60035
- ferromagnetic suspension, magnetorheological characts. meas., errors 80—33550
- flat plate streaming potential investigations: hydroynamics and electrokinetic equivalency 80—106777
- flotation, thin film capillary hydrodynamic theory 79—56038
- flow analysis, initial stage, relax. model 80—74977
- flow in rectangular channel, free surface shape *(Russian)* 77—51117
- flow measurement, NMR spin echo difference method appl. to plant stem 78—14110
- flow of generalized Newtonian and Bingham liquids in an annular capillary 79—41758
- flow of liquid-borne ultrafine particles in capillary, hydrodynamic chromatographic sizing 79—64759
- fluid bridges between solids in gravitational field, props. 80—88401
- fluid interfaces, flotation and mech. manipulation of solid spheres 78—63906
- fluid/fluid interfaces, capillary phenomena, review 80—70506
- foam with high press. gradients, syneresis in Plateau-Gibbs channels, capillary press. 80—74948
- fountain effect, flow boundary conditions 79—68784
- free boundary capillary MHD flows 80—43794
- free molecular gas flow in capillary, effect of absorption time differences 77—89164
- free surface equilibrium forms determination method *(Ukrainian)* 80—39386
- freesurface breakdown in rot. liq., wavelets 78—59402
- Galilean invariance of balance eqn. for singular surface in continuum 77—75792
- gas flow, through ultrafine capillaries 80—6151
- glass capillary columns, for gas chromatography 77—36814
- gravity-assist heat pipes with capillary flow, dry-out phenomena 80—79398
- gravity-capillarity waves, third-order reson. interactions 78—34148
- gravity-capillary surface waves, nonlinear interactions 78—18310
- heat and mass transfer in capillary-porous body, kinetic eqns. 78—5796
- heat pipe, with header and single or two-phase artery systems 78—90981
- heat pipe wick, liq. evaporation, drop carry-over phenomena in capillary struct., obs. 79—18948
- heat pipe with capillary struct., amount of coolant effect on operation 78—75037
- heavy hydrocarbons, surface transient deformation by laser-induced thermocapillarity 79—33157
- hexane, film flow calc., effect of temp. and press. gradients in conical capillaries 79—55416
- HPAM dilute polymer solutions, elongational flow 80—103047
- hydromagnetic capillary instability of a liquid jet with an axial flow 80—74990
- imbibition in 2-phase flow through porous medium with capillary pressure 79—20884
- immiscible liquid replacement, in capillary tube, moving contact line 77—55414
- jets, capillary instability, determ. of dynamic surface tension of inks 78—84031
- jets, Newtonian, axisymmetric, die-swell, Galerkin finite element method 80—83830
- Keller's solitary wave, capillary force effect 77—72313
- Knudsen flow, through periodically constricted pores *(Japanese)* 79—72911
- Knudsen to Poiseuille flow transition, capillary model 78—55689
- laminar flow, electrokinetic effects, analysis *(Russian)* 78—1748
- liquid, Laplace molecular pressure and internal pressure, rel. to capillary theory formulas 77—25303
- liquid crystal, reentrant nematic, oriented, capillary shear flow 80—49344
- liquid distribution across porous bodies 79—69326
- liquid film, disruption, variation in minimum thickness rel. to capillary forces 79—65297
- liquid film, free, squeezing mode relax., laser scatt. rel. to colloid interaction 78—87354
- liquid film draining deformation between rigid sphere and gas-liquid interface 77—66078
- liquid in capillary, evaporation above boiling point 77—66019
- liquid jet, capillary breakup, random initial perturbation, drop size distrib. 78—38380
- liquid jet, capillary instability, effect of harmonics 78—71378
- liquid meniscus in capillary, dynamics, wetting 77—85023
- liquid meniscus steady movement in capillary tube 77—69146
- liquid rise in capillary tube, rate meas. demonstration 80—73147
- liquid spreading on solid surfaces, static and dynamic contact lines, book contrib., review 80—20015
- liquid surface shape near stripwise heterogeneous wall, analytical soln. of Laplace eqn. 78—67890
- liquid-gas system between two plates, capillary curve 80—33660
- liquid-vapour interface, struct. at 110K, Monte Carlo method, for Ar-like fluid 80—54477
- low-temperature heat pipe wick evaporation *(Ukrainian)* 78—90639
- macromolecular fluid, stress-induced diffusion 78—10205
- magnetic fluid layer, thermocapillary instability with thermally insulated boundary 80—33595
- magnetic liquid surface equilibrium forms *(Russian)* 77—27605
- maltrose syrup, separation of elastic and shear thinning effects in capillary rheometer 78—42691
- manometers, liq., sensitivity, wetting hysteresis effect 80—98926
- mass transfer to power law fluids in fluidised beds 80—100032

capillarity continued
McLeod gauge, capillary depression phenomena, Hg vapour drag effect 80—98923
measurement of 1st normal stress difference, water rel. to polymer solns. 79—98829
melt adjoining solid phase, inhomogeneous temp. field influence on capillary phenomena *(Russian)* 80—20029
membrane, porous, hydrophobic, anomalous gas mixture flow into liqs. 80—40744
membrane and gradient models of capillary phenomena 79—99393
membrane oxygenator semiautomatic fabrication 79—20711
meniscus of air-liquid interface, evaporation 79—14224
meniscus thin film transition region, heat transfer 80—6058
metal drops in electrolytes, electrocapillary motion, elec. field strength effects 78—3346
moist materials, drying kinetics calc. method, heat (moisture) transfer 78—55555
multicapillary system capillary-tissue diffusion anal. 79—2095
multicomponent isothermal diffusion and forced flow of gases in capillaries 79—18914
nematic liquid crystal, circumferential surface orientation, in capillary, optical studies 77—47349
non-Newtonian fluid exit flow through capillaries, effect of vibrations 80—79358
nonlinear surface waves with gravity or surface tension restoring forces 78—22357
nonlocal theory of capillarity, static meniscus and shallow wave motion 80—10312
ocean bottom, capillary-gravity waves, development and stability *(Russian)* 78—16033
oil-water interface, electroadsorption and electrocapillarity 80—44393
oxygenator, membrane envelope type, capacity improvement *(German)* 79—2157
parallel-plate channel, theory of capillary rise of liq. 80—28567
particulates, glass, removal mech. from solid surface 79—50676
pendent drops, equilibrium and stability 79—23805
penetration of liquids into capillary tubes *(Japanese)* 79—99396
penetration problem, refined mathematical anal. 80—24713
periodic capillary tube, two phase fluid flow and hysteresis 80—107615
periodic capillary tube, two phase fluid flow and hysteresis 80—107616
physical chemistry of surfaces, book 77—25310
polybutadiene, high cis-1,4, orientation effects induced by shear rate in capillary rheometer 77—51014
polyethylene capillaries, for polarography in corrosive media, prep. 78—61090
polyethylene melt, oscillatory flow through capillary 80—103046
polyethylene oxide, dilute aq. soln., laminar viscous tube flow, scale-depend. effect 79—7367
polyisobutylene in toluene solution, effect of capillary materials on drag reduction *(German)* 80—87785
polymer additive effects on wall slip and viscosity in flow through capillaries *(German)* 80—59086
polymer melt, exit press. meas. from capillary or slit rheometer 77—72260
polymer melts, laminar and melt fracture flow through successive capillaries 80—59085
polymer solns., unstable flow, reservoir to capillary, jet instability onset and flow patterns, obs. 78—87364
polymer solution, laminar capillary tube, critical shear rate 78—34170
polymer solution, viscometric flow in capillary *(French)* 79—64711
polymer solution laminar capillary flow, excess press. drop 79—60038
polymer solutions, aq., capillary flow, thermal noise, low freq. oscills. 80—48754
polymerisable mass, unsteady viscosity meas. method *(Russian)* 79—23293
pores, cylindrical, appl. to pore size anal. 80—15340
porous bodies, capillary equilib. at surface 79—60059
porous body, drying, X-ray absorption obs., radiometry, temp. control 78—67023
porous body, sublimation, heat, mass transfer from parallel capillaries 79—37395
porous electrode type cells, electrochem. and capillary characts. 79—91967
porous media, capillary equilib., theory 80—24091
porous media, capillary rise, role of contact angle 77—24467
porous media, capillary rise, secondary phenomena 77—24466
porous media, capillary rise problem 77—24465
porous media, hydrophilic, uniform branched, capillary equilib., with correl., anal. 78—18877
porous media, random networks, gaseous Knudsen flow, capillary model 77—80212
porous media, thermomigration, capillary diffusion coeffs. *(French)* 77—89006
porous media, two-phase flow with end effect allowance, numerical simulation 80—33659
porous media wetting, capillary rise, contact angle effect *(German)* 78—84033
porous solid, blind porosity and capillary press. meas. 77—90545
porous solid, pore struct. determ. by capillary condensation calorimetry method *(French)* 77—25245
porous solid with below-freezing pt. adsorbate, isothermal adsorption and dimensional changes obs. 78—75925
profile curve of a cylindrical capillary surface *(German)* 79—81983
PVC cpds., rigid, plasticised, capillary flow 79—4046
Pyrex glass capillary tubes, effect of adsorbed water vapour on liq. water flow 80—92759
quartz, dynamic wetting angle of dry lyophilic surface 80—88405
random networks, interdiffusion of gases, struct. factor calc., Knudsen to gaseous diffusion transition 78—14080
Rankine-type capillary viscometer, for gases *(Japanese)* 80—14859
restricted withdrawal of vertical cylinders from quiescent liquids, numerical treatment 77—72756
rise rates in porous media with nonuniform pores, model 77—72747
rivulets, static, moving contact lines and rivulet instabilities 80—79264
rotationally symmetric fluid bodies in gravit. field, thermodynamic treatment of capillary phenomena 78—10262
rotationally symmetric fluid bodies with one asymptote, holms, capillary props. 77—66077
sands, poorly graded, moisture distrib. in capillary crack *(German)* 80—31066
semiconductor-liquid metal structure, electrocapillarity effect 79—73588

capillarity continued
sharp-lip capillary nozzle production and meas. precision 77—80246
silicon oil, separation of elastic and shear thining effects in capillary rheometer 78—42691
sintered composite-liq. metal interaction, mass transfer eqn. approx. soln. 78—67262
soil, heat and mass transfer with phase change 79—1093
soil moisture, capillary hysteresis model 79—53386
soil moisture, estimation of effective capillary press. in Green and Ampt infiltration eqn. 78—3844
solid bodies, capillary interaction 78—51792
solution of diffusion eqn. for capillary method with no external stirring 78—54518
steam condensation in capillaries 79—1066
steep water waves, surface tension effects 79—55398
styrene-butadiene copolymers, struct. study by pyrolytic capillary gas chromatography *(German)* 78—18557
surface condition, effect on crystallisation of aq. solns. in capillaries 79—56037
surface forces, interfacial press. and zero contact angle systems 77—55425
surface problems with prescribed contact angle, max. and min. principles 79—37907
surface tension measurement method, max. force exerted by meniscus formed by cone on free liq. surface 80—39390
surface tension temp. dependence from triple point to critical point *(German)* 80—100376
surfaces, rough adsorpt., capillary condensation 79—1544
swirling annular capillary jet flow *(Russian)* 78—75180
thermal transpiration, in circular capillary with small temp. difference 79—32191
thermally induced surface fluctuations on simple fluids 80—88403
thermocapillary convection, unevenly heated liq. stream near gas bubble 78—59460
thermocapillary gas bubble movement, liquid screening 80—19474
thermoplastic recording media, electrocapillary effect, tangential extension influence on ‘frost’ deform. *(Russian)* 77—68249
thin falling liquid films in tubes, ‘dry patch’ stability 80—53747
torsional-vibration fluid damper design 77—71309
tracer diffusion coefficients, open-eded continuous capillary method determ. 78—75861
transient thermocapillary flow in thin liquid layers 80—92226
transverse pressure existence in liquid filled capillary *(German)* 79—82418
transverse pressure existence in liquid filled capillary *(German)* 79—86964
two immiscible fluids, dynamic contact angles in capillaries 80—24715
ultrafine capillaries, diam. 0.5 to 60 μm, fabrication and calibration for leakage research 77—30135
unsaturated water flow within porous materials, obs. by NMR imaging 79—98840
van der Waals’ thermodynamic theory under hypothesis of continuous variation of density 79—56043
vapor-liquid energy transport in a porous medium 79—64762
variable pressure manometer, electrocapillary element appls. and properties 80—73379
vertical cylindrical tube, theory of capillary rise of liq. 80—28567
viscocapillary flows, interface shape and evolution eqns. 80—19507
viscoelastic capillary jets, stability 79—46352
viscometer, closed, effect of unsteady flow 78—9736
viscometer system, semiautomatic meas. *(German)* 79—94561
viscosity of liquids, capillarity method determ. 80—82619
viscous capillary jet, oscills., investigation of axisymmetric perturbation 79—37370
viscous or perfect incompressible fluids, gravity waves with surface tension and capillarity strain *(French)* 77—65749
water, films, thin, wetting, rheological characts. determ., capillary method 78—51788
water, spontaneous movement rate in capillary tube 79—65295
water flow in capillaries, Washburn eqn. 79—64767
water impurity concentration in steam-generating channels with capillary-porous structure 80—103071
water in capillary, freezing and melting behaviour, dilatometry, elec. cond. meas. 78—75908
water in single capillary, electrokinetic and rheological parameters 80—10220
water viscosity changes close to quartz surface, fine capillary calcs. 80—54422
water viscosity changes effect on electrokinetic phenomena in capillaries 80—53867
wave theory and mean field theory of interfaces 78—18309
wear effects, capillary, in interfacial tension meas. 78—26751
wetproofed electrode, pore filling degree with electrolyte and liq. reactant 80—40702
wetting film and capillary layer, transition layer 79—23807
wetting fluids, evaporating menisci 80—29248
wetting tension depend. on meniscus curvature, adjacent liquid film disjoining press. isotherm 80—2247
Bi, liq., in fused alkali chloride binary mixtures, electrocapillary phenomena 77—40553
Bi, liq., in fused KCl-KBr mixtures, electrocapillary phenomena 77—40554
CO_2, adsorption and capillary condensation on clays rel. to Mars volatile storage and atmospheric history 80—72833
Cu, sputtering, surface topography, appl. of thermodynamics of capillarity 80—20749
D_2O, temperature of maximum density in capillaries 78—51801
Fe and Fe-C(1.54 wt.%) alloy, electrocapillary curves in liq. sodium tetraborate 79—91968
^{3}He-^{3}He normal solution, size effect influence on capillary mass transport *(Russian)* 80—70497
^{4}He, adsorpt. and sp.ht. in 0.2 μm Nuclepore filters 77—35773
^{4}He, superfluid, capillary flow props., instabilities and vortex motion 77—55408
^{4}He, superfluid, capillary isothermal flow, persistent current obs. 79—55955
^{4}He, superfluid, flow, thermally-driven, in two coupled capillaries 79—86950
^{4}He, superfluid, fourth sound propag. and flow props. in very long capillaries 80—44384

capillarity continued
^{4}He, superfluid, in capillary geometry, effect of boundary conditions 79—69307
^{4}He superfluid, laminar flow through capillary tubes 79—55949
^{4}He, superfluid, stationary flow, 1.5K 79—73358
KCl, aqueous film on Hg, secondary electrocapillary effects, interfacial tension and entropy 77—55420
N$_2$ adsorbent mesopores, capillary evaporation and struct. 80—107614
N$_2$, capillary condensation and evap., apparatus and calc. method 80—2150
N$_2$, capillary condensation and evap., scanning curves within B-type hysteresis loops 80—2151
Na evaporation from slot type capillary structs., crit. heat fluxes 80—74854
Na, liquid, evaporation from capillary-porous struct., capillary restriction in initial stages 80—107609
Na, vaporisation from capillary-porous structs. (heat tubes, vap. chambers) crit. heat flux 78—90631
Pt, surface stress curves, electrocapillarity type curves 79—61866
Si, preshaped single crystal prep. by pendant drop method *(French)* 78—64466
Si ribbon grown by capillary action shaping technique, electron channelling analysis 77—76418
W, molten drop break up in gas flow, surface drag, capillary excitation *(Russian)* 80—100024
W, surface, self-diffusion coeff. at very high temp. using theory on tip evolution by capillarity forces and evaporation 79—11011

capillary phenomena *see capillarity*

capillary waves
active four-photon spectroscopy of capillary waves 79—41699
capillary wave slope meas., using laser optical instrument 78—36173
capillary-gravity waves, 2-dimens. wave packet 77—35154
capillary-gravity waves, exact eqn. numerical soln., closed bubbles 80—14715
capillary-gravity waves, linear problems 78—51178
capillary-gravity waves in viscous fluid 78—51177
capillary-gravity waves produced by moving press. distrib. 80—69859
development in two-layer fluid *(Russian)* 80—12421
dispersion relation, for isotropic liq., two-mode struct. 79—98741
Doppler scattering of EM waves by ripples due to acoustic and capillary waves 78—3807
fatty acid monolayers, capillary waves, photon correlation spectroscopy, viscoelastic props. 79—75608
finite-amplitude periodic progressive capillary waves, enclosed bubbles 80—79339
flow of gases and liquids through ultrafine capillaries 78—94822
flow velocity meas. in capillary using pulsed NMR 78—83506
formation on gravity water waves, model eqn., surface tension, viscosity 78—83421
gas-streamlined liquid film, quasiharmonic motion development in vertical flow 77—55014
generated by steep gravity waves, meas. 78—59409
gravitational-capillary, asymmetric, plane forced, wave shape on liquid surface of const. depth *(Russian)* 79—86448
gravity-capillarity waves, third-order reson. interactions 78—34148
gravity-capillary surface waves, nonlinear interactions 78—18310
gravity-capillary waves, reson. three-wave interaction, perturbation method 77—68608
gravity-capillary waves in two-layer fluid *(Russian)* 79—39733
infinite depth fluid, steady free surface gravity-capillary waves, integro-differential formulation 80—6072
jets, capillary oscillations, meas. 80—96291
jets, nonlinear capillary instability, satellite drop formation and control 80—33646
jets, nonlinear capillary instability, theory 80—33644
jets, nonlinear capilllary instability, behaviour effects before droplet formation 80—33645
large amplitude, on fluids sheets 77—7406
liquid, three-dimensional gravitationally-elastic, gravitationally-capillary surface waves *(Russian)* 79—32537
liquid-air interface, capillary waves, photon correlation spectroscopy 79—75607
liquid-vapour interface nature, non uniform classical fluids statistical mechanics 79—77468
liquid-vapour interface struct., Ar like fluid in equilib., thermodynamic states 78—10259
liquid-vapour interface structure near hard wall 80—14983
magnetisable liquid, thin layer instability 79—41762
MHD gravity-capillary waves in liq. film falling by permeable bed 78—67277
natural oscills. of two capillary fluids rot. in cylindrical vessel *(Russian)* 77—27542
non-stationary capillary-gravity waves in a shear flow *(Russian)* 79—34849
nonlinear propagation of wave-packets on fluid interfaces 77—47032
nonlinear surface waves with gravity or surface tension restoring forces 78—22357
nonlocal theory of capillarity, static meniscus and shallow wave motion 80—10312
ocean bottom, capillary-gravity waves, development and stability *(Russian)* 78—16033
ocean wave detection by microwave radar, gravity-capillary wave modulation 78—77333
ocean wind-generated surface waves, HF spectrum meas. 78—44857
oil-water interface, US emulsification drop form. by capillary wave instability 79—32643
progressive, arbitrary amplitude, nonlocal solution using Bernoulli eqn. nonlocal form 80—48727
progressive capillary-gravity waves, energy and momentum integrals 79—94637
propagation, experimental test of theories 80—69847
pulsating air bubbles in water, stability using optoelectrical method *(German)* 77—27578
ripples, generation by parametric subharmonic reson. with sound waves 77—46849
running stream, capillary-gravity wave problem 79—23333
short gravity-capillary waves modulation by longer-scale periodic flows 80—57106
solar photosphere, props. of surface (capillary) waves *(Russian)* 80—12726

capillary waves continued
stability in circular containers with convex spheroidal bottom 79—32462
steep water waves, surface tension effects 80—38424
surface tension restoring forces on gravity waves in narrow channels 80—28568
travelling, gravity-capillary, on liq. film surface falling past permeable bed 78—87351
two-layer stratified flow, entrainment at interface *(Japanese)* 79—14454
US atomization, cavitation-induced capillary waves 80—33328
water, capillary-gravity waves, nonlinear modulation 77—11206
water drainage, by capillary flow *(Japanese)* 78—95208
water waves in narrow channels: faster capillary waves 79—18905
wave theory and mean field theory of interfaces 78—18309
wave-slope spectra in capillary-gravity range, increasing wind, laser beam meas. 77—3836
wind driven capillary waves meas. in wave tank, rel. to ocean 79—64673
wind generated capillary waves, spectral characts. 80—59059
He, liq., surface, macroscopic electron lattice formation 79—77861
^{3}He-^{4}He, solution, capillary waves and second sound, mag. excitation 79—60594
UC, transient capillary wave generation on laser irradiated surface 78—21653

capture cross-sections, nuclear *see nuclear reactions and scattering*

Caratheodory's principle *see thermodynamics*

carbon
see also nuclei with ......
see also carbon fibres; charcoal; diamond; graphite
^{14}C evidence in tree rings 78—7962
abrasion against graphite, dusting wear regime 80—97595
abundance and distrib. in glassy rims of submarine pillow basalts 79—12111
abundance anomalies in QSO Q0353—383, UV and visible spectral obs. 80—82532
abundance in B-type stars in associations and general field 80—67702
abundance in globular cluster NGC 6752 first giant branch 80—67719
abundance in Orion Nebula and IC 418 from visible and IUE obs. 80—82451
abundance in red giant stars in 47 Tucanae cluster 79—97000
abundance in the ureilite meteorite Kenna 77—41365
acidic surface oxides, struct. investigation using diazomethane 79—52404
activated, adsorption in countercurrent flow 80—70524
activated, adsorption of 0.98 mol.% Ar, vol. adsorption capacity 78—75933
activated, adsorption rate constants prediction for various vapours 80—40735
activated, catalyst for H$_2$S oxidation, electrochem. model *(German)* 78—35717
activated, equil. adsorption coeffs. of Kr and Xe at low partial press. 77—52673
activated, interaction with H$_2$, alteration of paramag. props. 77—63957
activated, photoassisted decomposition at room temp. of H$_2$O over Pt/TiO$_2$ catalyst 80—55703
activated, vol. adsorption capacity, 25°C, org. trace gases 79—16036
activated, vol. adsorption capacity for selected trace contaminants 78—56031
activated and impregnated, adsorption and desorption isotherms of phosgene and chloroform 77—70333
activated and impregnated, adsorption of HCN and H$_2$O vapour mixtures 80—39412
activated and impregnated, temp. depend. adsorption of HCN 80—89522
activated C, adsorpt. of I$_2$, pure struct. 77—31870
activated C, surface oxidised, organic vapour adsorpt. rel. to paramag. props. 77—32238
activated C cloth for haemoperfusion 77—37105
activation analysis by photonuclear reaction *(Japanese)* 78—76945
active C, pore struct. anal. 77—32763
active C dust current, electrostatic field meas. using radioactive convertor 78—16812
active carbons, micropore filling and adsorption of simple gases, Dubinin theory 77—47661
adlayer, dissolution into (110) face of Ni, 600-913K 80—49504
adlayer effect on CO and H$_2$ adsorption and desorption on Fe(100) 80—71573
adsorbed layer on W FEM tips, conc. determ. by nucl. microanal. *(French)* 80—29860
adsorbed on Mo (110), oxidation, electron diffr., contact pot. difference, and AES obs. *(Russian)* 79—52430
adsorbed on Ni (100), LEED struct. anal., substrate distortion 80—6637
adsorbed on Ni surface, location of adsorbed atoms, surface channelling meas. 80—84373
adsorbed on Pt, determ. of monolayer coverage by AES 79—46916
adsorbed on Pt, stability and struct. of high Miller index forces in vacuum and with adsorbed C and O 77—76651
adsorbent, granules and artifacts, strength, mech. characts. 78—23771
adsorption, of Ar (methane), surface excess isotherms, gravimetric determ. 78—51816
adsorption, of CO$_2$, surface area meas., temp. and chemisorption effects 78—95225
adsorption, of Kr, Henry's constant, pre-exponential factor *(German)* 78—22961
adsorption, on CdS, AES study *(Japanese)* 78—88008
adsorption from methanol-benzene solutions 78—14568
adsorption of Ag and U, scanning-transmission electron microscope obs. 77—51597
adsorption of Br from CCl$_4$ soln. 78—10273
adsorption of gas, rate depend. on granule size and gas flow velocity 78—56033
adsorption of gases on graphitised surface 79—42366
adsorption on and diffusion into polycryst. Re *(French)* 77—28075
adsorption on Fe(100), adsorbate coverage determ. by LEED, AES and XPS 80—103566
adsorption on Fe (110), UPS and LEED/Auger meas. 77—72773
adsorption on Ni, coadsorbed Pb or Sn, AES study 80—54521
adsorption on Ni(Al)(Mg), internal and external sources of electrons 77—44097
adsorption on Ni (100), substrate reconstruction, LEED constant momentum transfer averaging study 80—39445
adsorption on W, Auger signal comparison using differential and integral Auger spectra 78—76561

carbon continued
adsorption on W, Auger signal intensity in differential and energy distrib. mode spectra 79—78799
aerosol of C spheres, black smoke opacity, particle size and refr. index depend. 79—72488
aerosol particles, size-fractionated, C, N and O determ. by particle elastic scatt. anal. 78—81466
aerosol particles, sonic agglomeration 77—29411
aerosol visibility vs. particle size distrib. 78—88911
AES, backscattering factor, Monte Carlo method calc. 80—7449
afterglow laser, recombination-pumped 77—50657
agglomerates, fractal dimension characterisation, dilation logic appl. 79—58673
amorphous, anomalous low temp. mag. and thermal props. 78—10647
amorphous, catalytic oxidation by Pd particles, TEM obs. 80—76555
amorphous, diamond-like 3-fold coord. 80—50323
amorphous, diffraction intensities, chem. bonding effects 77—72557
amorphous, elec. cond. and Hall effect, temp. depend. 78—60141
amorphous, heat treated, AC cond., 100 to 400K, electron hopping and Mott-Davis models 80—34443
amorphous, inelastic electron scatt., valence electron contrib. 80—55240
amorphous, Lifshitz constant for calc. of van der Waals force between two solids *(French)* 80—107658
amorphous, prepared by glow discharge method, elec. and optical props. 77—21036
amorphous, ranges of implanted 10-30 keV D^+ 78—83858
amorphous, X-ray and electron diffr. intensities, model struct. 78—26441
amorphous, X-ray diffr. investig. of coherence, strain, thermal vibr., preferred orientation 77—31595
amorphous char, mag. interactions between localised spins 80—34587
amorphous film, adsorpt., atomic imaging using the dark-field annular detector in the STEM 80—6331
amorphous film, catalytic crystallization by Ni particles 79—14683
amorphous film, elec. transport props. 78—6457
amorphous film, hopping cond., thickness depend. 77—89887
amorphous film, spin resonance, IR spectra, microhardness 80—71157
amorphous film, struct. props., Raman scatt. study 80—11417
amorphous film, vac. evaporated, density meas., microcrystalline model of struct. 80—2313
amorphous film struct., TEM obs. using bright field hollow cone illum. 78—22609
amorphous foil, electronic energy, straggling of light ions, at. number depend. 77—11612
amorphous foil, influence of detector geometry on STEM image props. 77—56554
amorphous grains, extinction coeffs., 0.21-340 μm, lab. meas., rel. to interstellar grains 80—73020
amorphous thin films, crack networks of voids 78—2399
amorphous thin films prepared by vac. evaporation, density meas. 77—80714
analysis, ultrasensitive, tandem facilities 78—33350
arc, low current, for props. of graphite near sublimation temp. 79—50901
arc anodes, fibre layers, props. and cooling behaviour 79—52245
arc in air, electron density meas. by CO_2 laser interferometry *(Japanese)* 80—28822
artificial carbons, graphitisation shrinkage kinetics 77—48385
asymmetric atom, case history for independent discovery, inductivist model 79—25821
atmosphere, global C cycle, modelling perturbations 80—31114
atmosphere aerosol, C particles causing Denver Brown Cloud 80—81961
atmospheric dust, imaginary refr. index rel. to particle size 78—7763
atom, $1s^22s^22p^2$ config., effective electron-electron interaction, many-body perturbation theory 80—47843
atom, $^3P \rightarrow {}^1D$ electron impact excitation, distorted wave approx., exchange and polaris. effects 77—34764
atom, ^3P state, valence shell correl. energy, IEPA-PNO method 77—10597
atom, ^5S-$^3P_2$ and $^5S_2$-$^3P_1$ transitions, ^{13}C isotope shift 80—58201
atom, and 1st row ats., Compton profiles, momentum distribs., correlation effects 77—88429
atom, beam-foil populations, charge state distribs., independent electron model 77—19035
atom, CNDO/S nucl. screening const. calcs. 78—86787
atom, correlated and HF electron density difference 78—46275
atom, effective valence shell Hamiltonian, ab initio calcs. 78—82611
atom, electron affinity, modified variational approx. 78—66679
atom, electron and proton interaction cross sections 77—50538
atom, electron attachment, low energy electron elastic scatt., review of theory 77—68111
atom, electron excitation cross section calc., Born approx. with Slater wave functions 80—69243
atom, electron impact, C K-ionisation, Auger and X-ray meas. 77—19096
atom, electron impact ionis., 7-1000 eV, cross-section 78—86956
atom, electron impact ionis. cross-section, accuracy of fast at. beam method 79—81283
atom, electron scatt., at. field bremsstrahlung, photon linear polaris. 78—62927
atom, electron scatt. and photoionis., correlation effects 78—58842
atom, electron scatt. Bethe-Goldstone and pseudostate approx. 77—68112
atom, excited states, quadrupole moments, Sternheimer shielding factors 78—82630
atom, excited states generalised Brillouin theorem multiconfig. method 77—67993
atom, fine struct. excitation by H impact 77—42384
atom, first-principles pseudopotential in the local-density-functional formalism 79—59328
atom, Gaussian basis sets, quality studies 79—59345
atom, ground and excited states, atomic polarisability calc. 77—83756
atom, ground state energy, HF calc., second-order correction 78—86784
atom, ground state fine struct., laser mag. reson. obs. 80—87062
atom, ground state static polarisability and hyperpolarisability, numerical SCF method 79—36567
atom, ground state wavefunction, SCF HF calc. 78—90070
atom, innershell ionisation, proton and electron impact equivalence at high vel. 77—14556
atom, intermediate coupling props., relativistic average of config. wavefunctions applicability 78—17574
atom, ionis. cross-section, accuracy of crossed at. beam method 79—81284
carbon continued
atom, lowest $^2P^0$ and $^4P^0$ states, variational Hylleraas-type wavefunction 79—10023
atom, min. basis of Slater-transform-Preuss functions 79—59343
atom, model pots., STO calcs. 77—408
atom, one-centre integrals of semiempirical theories of valence, ab initio calcs. 80—102441
atom, optical oscillator strengths, independent particle model, excited state wave functions, LS coupling and Born approx. 80—32674
atom, optimised one-electron wave functions 77—38598
atom, photoionisation cross section, CI calcs. 79—98050
atom, photoionisation of 2s shell, photoelectron ang. distrib. 78—86833
atom, polarisation functions for Gaussian basis sets 78—5126
atom, radiative lifetimes of visible and near IR transitions, solar abundance 78—50506
atom, reson. transitions, Stark widths and shifts of UV and VUV lines 77—88425
atom, SCF electron-gas local-spin-density model including correlation 80—9488
atom, structure, multiconfiguration optimised central pot. method calcs. 80—9515
atom, theoretical ionis. energies and oscill. strengths, excited s-, p- and d-levels 78—86823
atom, vac. UV spectral line broadening parameters meas. 80—23352
atom+H^+(He^+), K-shell ionisation, impact parameter depend. 78—62891
atom in molecule, K-shell fluoresc. yield, statistical scaling 80—78644
atom photoionisation, electron impact calcs. using R-matrix and linear algebraic methods 79—59579
atom X-ray spectra, mass absorpt. coeffs. in ultrasoft region, spectral depend. 77—10622
atom-atom pot. parameter in azabenzene, dispersion energy calcs. 80—23489
atomic correlation energies, perturbations and near degeneracy 79—3371
atomic laser, direct nucl. pumped in mixtures of He-CO(CO_2) 78—5460
atoms, metastable, prod. in cometary coma, detect. in comet West (1976 VI) 79—16885
atoms and ions, excited in single gas collisions, high-resolution Auger spectra 80—9717
automatic image analysis, variables and errors, definition and quantitative description *(German)* 78—25296
baked C mixes, anthracite, petroleum, metallurgical and pitch cokes as fillers, chracteristics study 79—57052
baked mix, optimum binder content estimation 77—73253
baked mixes, use of coal tar and petroleum pitches as binders 78—80483
bare nucleus+He, electron capture to excited states, X-ray cross-sections 77—71814
beam-foil spectra, excitation mechanism, investig. using C II-C VI projectiles 79—86060
bend strength testing, bench assembly with strain recording 79—57176
black, aerosol, coagulation, kinetics, particle size distrib. 79—39209
black, effect on cationic polymerisation of styrene by $SnCl_4$ 78—68891
black, effect on Fe whisker growth 78—30852
black, filled polybutadiene, ESR 77—90036
black, graphitized, adsorpt. of benzene and cyclohexane, exptl. determ. of models 78—6216
black, heat treatment, EPR rel. to temp., A-centers 78—43639
black, loaded paper, low temp. resist. characts., for resist. thermometry 77—74404
black, positron annihilation and positronium form. 79—28856
black, props. after extraction with organic solvents *(Polish)* 79—70010
black, pyrocarbon coating *(French)* 78—68921
black, reinforcement of elastomers, role of particulate fillers, review 80—29921
black, surface acidity effects on work function 78—2548
black, surface coating constituent mat., adsorpt. of Cs^+ 78—23843
black, surface S-containing group complexing 78—68920
black, thermal insulating props., furnace appls. *(French)* 78—44345
Black Pearls A, in butanol, electrophoretic mobility, charge origin 78—85211
black suspensions, simultaneous meas. of dichroism and birefringence in elec. field., photocurrent signal obs. 80—82801
blacks, powders, resistivity rel. to compression *(French)* 80—35349
blacks, surface, differently graphitised, two-dimensional freezing of N_2 or Ar 79—77896
blacks, surface polarity, surface activity, slurry pH, oxidation effects 78—68915
bonding to Tokamak walls, XPS studies 80—80942
brick, nondestructive acceptance testing by ultrasound *(German)* 77—4878
C_2, vibr. and rot. anal. of vis., UV spectra, RF discharges in N_2, H_2, CH_4 mixtures 78—5241
C III, excited states, transaction oscill. states and wavefunctions 79—59367
C IV, optical oscillator strength 80—47941
carbographite mats., elec. cond. temp. depend. 77—43592
carbon, metal-non-metal transition 79—60712
carbonisation, ESR study of kinetics, mesophase formation 79—96045
carbonisation of aromatic hydrocarbons, heterocyclic cpds. catalysed by $AlCl_3$ 77—63572
carbonisation of aromatic hydrocarbons, microscopic features of carbons obtained using catalysts 77—66597
carbonisation of steel, cementation process testing, foil samples method 79—70238
carbonisation under pressure, mesophase formation 77—44182
carbonmetalplastic, heating rate effect on thermal deform. in various atmos. 79—65226
carbothermal reduction, of Nb_2O_5, intermediate phases 79—11773
carbyne as possible constituent of interstellar dust 80—90514
carbyne forms, of C, in natural graphitic formations in Ceylon and California 79—77450
catalytic graphitisation, of carbons, by gaseous species formed from various metals 80—11871
catalytic graphitisation, three-phase, of phenolic resin C by Ni particles 78—68922
cathode, intercalation props. in Al reduction cell 79—43559
cathode damage and vapour/thermionic arc transition obs. 78—71603
channel and thermal blacks, graphitisation at high press. and temp. for diamond synthesis, Ni influence 80—60795
chaoite, a new allotropic form of carbon, produced by shock compression 80—80997

carbon continued
chars, heat treatment, EPR rel. to temp., A-centers 78—43639
chars, heat treatment, EPR rel. to temp., spin centres 78—48036
chars, thermally activated paramagnetism, mag. susceptibility, meas. 80—75709
chemisorbed on Ag film, reflectance and elec. resist. changes 80—11495
chemisorbed oxygen surface complexes, thermal desorpt. analysis 78—56032
chemisorption in steel, saturation kinetics for high-temp. carbonitriding *(Russian)* 79—52450
chemisorption of Cr, Mo and W, SXAPS obs. 79—52048
chemisorption on Ni (100), molecular cluster theory 77—1309
chemisorption on Rh (111) and (100) surfaces, LEED, AES and thermal desorption meas. 78—38951
chemisorption on Rh (755), (331), desorpt. temp. and decomp. characts. 79—65318
clay, Al_2O_3 and SiC recovery by C reduction 80—108704
coadsorption with N_2, on W {100}, AES obs. 77—35821
coating fusion applications 80—23146
coating on Ni-Fe (40%) (111) film, surface magnetism 77—73056
coating on Pt, temp. depend. of H_2^+ sputtering 78—95634
coke, anisotropic spheres obtained during needle coke form., struct. obs. 77—63573
coke, breakage behaviour rel. to struct. 80—85026
coke, graphitisation at high press. and temp. for diamond synthesis, Ni influence 80—60795
coke, imbedded in epoxy, X-ray diffr. 79—90495
coke, metallurgical, industrial strength meas. methods, critique 80—85117
coke, metallurgical, strength and struct. relationship 80—84997
coke, preparation for ESR exam. 77—90517
coke, pressure effects on structure, polymorphic transitions X-ray diffr. anal. 79—1859
cokes, acicular and spherulitic, high pressure effects on graphitisation 77—36414
cokes, graphitised, Raman spectra, effective Debye parameter, magnetoresist. 78—44231
cokes, metallurgical, struct. and strength 80—93610
cokes, raw, heat treatment, EPR rel. to temp., spin centres 78—48036
colloidal, refractive index determ. 79—66363
combustion products, appl. in CO_2 gasdynamic laser 79—27240
Comet Kohoutek (1973 XII), C and O spectra and prod. rates 77—49331
Comet West (1976 VI), model of C prod. in cometary coma 79—16885
composite, of PTFE and C black, electrochem. method for monitoring form. 77—36446
conference, Baden-Baden, Germany (June 1976) 78—43990
contaminant, effect on dissolution of quartz in liq. Si, rel. to melt growth of Si 80—70414
contaminant, in EFG Si ribbon, conc. determ. by nuclear techniques and SIMS 80—59506
contamination, of Al targets, in high vacuum electron excitation X-ray tube 79—44996
contamination of Al and Si surfaces, effect on characteristic energy losses 79—99997
contamination of ion irrad. Th surface, AES obs. 78—71775
contamination of metal surface, plasma etching and cleaning 80—97645
convoy electrons from solids, ion vel. and Z and target material depend. 78—84692
crystalline, intermediate form, CI lattice energy *(Russian)* 78—22693
crystalline diamond-like form, cryst. struct. *(Russian)* 79—99114
CVD coating, surface damage and erosion under energetic D^+ and $^4He^+$ irrad. 80—39174
cycle, rel. to land biota changes and atm. CO_2 77—70785
dense hard-type solids prep. from petroleum coke powder by grinding 79—20002
depletion in interstellar medium, from Cygnus Loop UV spectrum obs. 79—21398
deposition elimination in quartz:Ti tube for I photodissoc. laser 77—10945
deposition of columnar and laminar forms on Ni 78—63943
deposition of Ni, surface structural effects 77—28721
deposition on diamond powder from methane 77—11805
deposition on targets during beam bombardment 80—18741
depth profiling of ^3He ion implantation 78—59830
depth resolution for MeV $^4He^+$ backscattering in C, Al, Cu 79—14840
determination, combustion-gas chromatographic method, data processing 80—40762
determination, DC arc optical emission spectrosc. method 79—83527
determination, in alkaline earth oxide crystals, by nuclear reaction method 79—8456
determination, in Fe_3C melt, measurement using automatic device 79—39252
determination, in minerals, anal. of C and O_2, ZAF correction procedure *(French)* 80—11983
determination, in nonferrous metals by nucl. reaction method, surface treatment effects 78—11596
determination, in steel, by nuclear methods *(French)* 77—60160
determination, in steels, by spectrographic method using combined discharge 79—57327
determination, in UC_n-PuC_n refabricated fuel for breeder reactor 79—11877
determination by activation anal. (α,n), (α,p) reacts. investig. 80—61206
determination by alpha-induced X-ray spectrometry 78—53275
determination in B-C system 79—87907
determination in thin steel sheets by internal friction meas. *(German)* 78—27715
determination of C, O_2 purification and flux selection *(Japanese)* 78—92571
determination of Zr, chem. analysis by photon and proton activation *(French)* 79—43666
diamond:C^+, high temp. ion implantation 79—23623
diamond:Co-C, satellite phase, C content determ. *(German)* 77—72690
diamond polycrystal, sintering *(Chinese)* 77—59706
diamondlike layers, RF plasma deposited, frictional props. 80—71762
diamonds from Lesotho kimberlite pipes, isotopically light C obs. 79—48487
diffused C, influence on structure and oxidation of hot-pressed Zircaloy-2 80—61016
diffusion, in α-Ti, AES meas. 78—51735
diffusion, in MoO_3 77—11734

carbon continued
diffusion, in polycryst. hard mag. Fe-Co-Ni-Al-Cu alloy YuNDK24 79—77827
diffusion between C and austenitic steels, 773-1373K 79—19392
diffusion coeff. in Fe-Ni austenite, 950-1100°C 78—51747
diffusion dependence on Cu surface barrier on type 1Kh18N9T steel *(Russian)* 80—54434
diffusion dependence on W-Ni alloy surface barrier on type 1Kh18N9T stainless steel *(Russian)* 80—54434
diffusion from graphite to W coating prevention, in metal-graphite layer structure of X-ray tube *(German)* 80—105759
diffusion in α-Ni, β-Co, γ-Fe, high temp. vacuum metallography investigation *(Russian)* 77—72718
diffusion in α-Zr, 620 to 830°C *(Russian)* 79—46842
diffusion in austenitic steel, dislocation struct. 77—4223
diffusion in BCC Fe 77—4222
diffusion in Fe, and Cr diffusion, US effects *(Russian)* 77—59144
diffusion in Fe, coeff. meas. by mag. aftereffect 78—29129
diffusion in Fe, under US vibrs., initial struct. effect *(Russian)* 78—38876
diffusion in Fe-Cr 77—7907
diffusion in Mn steel, electron probe microanalysis *(Czech)* 77—59149
diffusion in steel, after high-temp. thermomechanical treatment *(Russian)* 78—39813
diffusion in transition metals, electronic states effect *(Russian)* 77—1264
diffusion in Zn and Y, radiographic meas. *(Russian)* 77—31809
diffusion into Ir, theory 80—6562
diffusion into liq. Fe *(Russian)* 78—79791
diffusion on Pt(111) surface, AES 78—71954
diffusivity in austenite, computer simulation 79—77803
diffusivity in Mo 77—43384
disordered, variable-range hopping cond. and negative magnetoresist. 80—34436
disordered anthracene char, density fluctuations effect on physical properties 78—51420
dispersions of C black, in polymer particles, photomicrography of submicrometer birefringent contaminants 80—62757
dissolution into Ni through (110) surface, 615-660K, AES, LEED 78—63932
dissolution mechanism in liquid Fe *(Russian)* 79—51264
dissolution rate in CaO-Al_2O_3 molten binary slag *(Japanese)* 79—23739
dissolution rate in molten Si, Fick's law calc. 79—99319
dissolved in molten CaO-Al_2O_3 binary slag *(Japanese)* 78—60662
dissolved organic C meas. in water, new approach 79—74582
distribution function in interplanetary corotating energetic particle streams 79—70938
distribution in cast Mo and low alloy Mo *(German, English)* 79—20059
Earth upper mantle, C abundance rel. to plate tectonics 80—81845
EBR II, Cs control by C getter 80—13648
Einstein force constants, harmonic and cubic, calc. 77—47515
elastomer reinforcement, carbon black-polymer interaction 79—83171
electric resistance, temp. depend., qualitative anal. by audible demonstration 80—46775
electrical contact generation by tattooing C into skin tissue 78—77122
electrode breakdown voltage dependence on adsorbed gases 78—75465
electrodes, used in emission spectrography, isotopic labelling study, plasma appl. *(Hungarian)* 80—106976
electromigration in α-Fe, current density and temp. effects 77—59145
electron degraded 1 keV energy spectra in water vapour and C foil 80—9474
electron dose distribs. from plane infinite oblique sources, Monte Carlo calcs. 77—65339
electron emission spectra produced by exploding wire photon sources, yield and energy meas. 78—31299
electron energy loss spectra, microanal. appl. 77—44099
electron microprobe local anal. of light elements, ultrasoft X-ray spectroscopy 80—99027
electron stopping power, continuous slowing down approx., range difference for 0.2 to 10 MeV electrons 80—39187
electron-energy-loss-spectra, extended fine struct. in K-ionis. edge 79—47566
electronic energy loss of protons (deuterons), 80-800 keV 79—23666
electronic stopping power of H_2^+ 79—10888
electronic stopping power of heavy ions, empirical relation 80—92571
electrotransport behaviour in Sc 77—11738
electrotransport in La 80—24674
emitter characts. for field desorption mass spectrometry of salts 77—63980
energy levels, position orbital calcs., electron repulsion integrals, teaching appl. 78—93494
energy loss of 120 keV heavy ions, range and range straggling determ. 79—45595
energy loss straggling of protons and He ions 78—18692
enhancement in nova envelope on surface accretion at white dwarf 80—85936
evaporated, paramag. and diamag. susceptibility meas., 77 to 1400K 77—28362
evaporated layers, thickness determ. by objective colorimetry 78—77844
evaporated thin films, yield tensile strength meas. 80—23214
excited electronic states contrib. to transport props., planetary probe heat shield ablation appl. 80—23326
in F- and G-type stars, abundances 77—91530
fabric reinforced plastic laminates, tensile and compressive strength determ., 20-1500°C 80—100880
felt, thermal insulating props., furnace appls. *(French)* 78—44345
fibre, Al-coated, stress rupture 78—80628
filamentous catalytic, rel. crystallographic orientations of C and metal 80—89240
film, amorphous, elec. struct., and optical props. 77—20474
film, amorphous, growth under ion impact in butane plasma, and IR transparency 78—52688
film, amorphous, struct. and semicond. props. and heterojunction form. with single cryst. Si 80—25002
film, amorphous, surface plasmon dispersion, electron energy loss spectra meas. *(French)* 77—63504
film, amorphous, two-dimensional variable range hopping cond. 80—10977
film, arc evap., optical props., 0.6-3.8 eV 77—81166
film, backscattered electron intensities, ang. depend. 77—40317

carbon continued
  film, colloidal, sputtering, chem. etching in DC glow discharge 78—27667
  film, deposited on (AlGa)As DH laser facet to prevent deterioration 78—87049
  film, deposited on Pt, H sputtering 77—69951
  film, deposition on RF target in butane plasma 77—16507
  film, depth distrib. on mild steel glow discharge emission spectrometry anal. *(French)* 79—87923
  film, diamond-like, ion deposited, hardness and mech. stability 80—2314
  film, diamond-like, ion-plated, electron energy loss spectra characterisation 80—2308
  film, diamond-like, plasma condensed, mech. props. 79—90924
  film, diamond-like, produced by RF glow discharge of hydrocarbon gases, props. and coating rates 80—21146
  film, diamond-like, produced in butane plasma, XPS anal. and elec. props. 79—82484
  film, high resolution dark-field images 78—26398
  film, image contrast, rel. to inelastic scattering 80—100154
  film, inelastic-elastic scatt. ratio of 80 keV electrons use for radiation damage monitoring 77—4127
  film, kinetic electron emission when penetrated by H^+ ions with 0.3 to 30 keV energy 79—91554
  film, large unsupported UV filter, production 78—38092
  film, orientating action of solid substrates, on liq. cryst. layer exam. 80—44111
  film, secondary electron emission rel. to energy loss 77—16438
  film, sputtered glassy, prep., mech. and struct. props. 77—66588
  film, surface struct., graphitisation, secondary electron spectra and AES 79—43077
  film, vacuum condensed, SRO from radial-distrib. curve analysis 77—89662
  film, vacuum-vapour-deposited, for prosthetic coatings, wear behaviour 79—43440
  film, work function, heat treatment 78—64563
  film automatic thickness control in freeze etching and related techniques, resist. monitor 78—49810
  film bolometer detection system with <0.1 μs response time 79—63226
  film deposition by ion beam methods 78—72728
  film resistor, high sensitivity temp. sensor, 1-10K 77—13757
  film with random structure, growth from ion impact damage in butane plasma 79—83139
  films, diamond-like, on Si, colour chart 80—97366
  films, hard and transparent, prep. by condensation of ionised organic species 79—83132
  films, ultrathin, H_2^+ recomb. yield upon emerging 79—50108
  films with high conductivity, prep. and props. 80—80983
  fine particle formation by C vapour condensation 79—52781
  fine structure characteristics of C materials, by integral method 77—43153
  fiom, vacuum condensed, graphitisation, electron microscopy 80—40265
  fluorophosphate glasses, C determ. by deuteron activation analysis 78—68961
  foam, thermal insulating props., furnace appls. *(French)* 78—44345
  foil, 2.2 MeV H_3^+ ions survival during traversal 79—64103
  foil, 40-100 keV He ions, electronic energy straggling 77—15471
  foil, $^4He^+$ and $^3He^{2+}$ impact, nonexistence of wake bound states 78—13571
  foil, Ag microcrystal condensate, size distrib. from electron micrograph obs., UV absorpt. spectra obs. 80—55121
  foil, breakage times under Ar^+ bombardment 78—25753
  foil, charge state distrib. of heavy ions 78—5334
  foil, electron impact knock-on damage at 4K, electron microscope obs. 79—55786
  foil, electron spectra from α-particle and fission product passage 77—24918
  foil, energy loss of Ne ions (40-120 keV), and Ar ions (40-240 keV), as function of emergence ang. 79—4357
  foil, energy loss spectra of transmitted electrons, straggling and plasmon excitation 79—95058
  foil, energy loss straggling meas. for low energy protons 78—47459
  foil, energy-angle distrib. of Ne and Ar ions below 250 keV, test of Meyer-Klein-Wedell theory 79—49916
  foil, extreme UV induced forward photoemission 80—76137
  foil, H_2^+ transmission field 80—100732
  foil, H and H^+ neutralisation at solid surface 79—74043
  foil, heavy ion impact energy loss 78—55902
  foil, HeH^+ impact, dissoc., emitted light polarisation meas. 80—58361
  foil, image restoration of TEM micrograph *(Japanese)* 79—71571
  foil, ion irrad., crystallographic transform. 79—55794
  foil, ion irrad., graphitisation rel. to lifetime, relevance to beam-foil spectroscopy 80—15166
  foil, Kr^+ incident, equilib. charge state distribs. and multiple scatt. angles 80—59532
  foil, OH^+ beam Coulomb explosion, charge state depend. 79—31649
  foil, passage of ^{14}N and ^{20}Ne ions, energy-angle distribs. 79—10889
  foil, secondary electron yield from heavy ion beam-tilted-foil expts. 78—62889
  foil, thin, for charging effects elimination in proton induced X-ray emission spectrometry 79—92024
  foil, transmission of fast H_3^+ mols. 79—76484
  foil, transmitted H^+ energy loss, ang. distrib. and charge fractions 80—2102
  foil$+H_2^+(H^+)$, 0.5-2.5 MeV, forward electron vel. distrib., peak shape 78—78794
  foil resistance, cause of stray electric field in H beam-foil spect. study 80—42978
  foils, forward photoemission and transmittance meas. 80—25516
  foils, He^+ and HeH^+ impact, quantum beat pattern depend. on foil thickness 80—58343
  foils, impurity anal. by PIXE 80—18740
  foils, stripping of heavy ions with energy 0.4-0.9 MeV/A, straggling, foil behaviour 78—33351
  foils for heavy ion stripping in tandem Van de Graaff 79—22516
  friction of graphitised and ungraphitised C materials in P_2O_5 vapour, 300-600°C 79—79116
  fusion reactor material, 0.6 to 3.5 MeV He^+ irrad., surface erosion, porosity effects 77—35602
  fusion reactor material, chem. interaction with H plasma discharge impurity ions 77—35357

carbon continued
  fusion reactor material, low energy ion erosion expts., Kaufman source appl. 80—68942
  gamma-ray attenuation coeff. meas., 1115, 1173, 1332 keV 77—55303
  gamma-ray buildup factors 80—27822
  gamma-ray scattering, incoherent, total at. cross section 79—13679
  gas phase abundances in planetary nebulae 78—28744
  gas-diffusion O_2 electrode in acid, electrochem. performance 78—31652
  glass, prep. and DC cond. at low temp. 79—95404
  glass-like C matrix, identification and props. of dispersed Fe particles 80—11229
  glassy, Compton profiles, momentum densities, comparison with graphite 80—2895
  glassy, crack form. during prod., propag. by thermal stress 79—11700
  glassy, electrodes, polymer film coated, prep., characterisation, electrochem. stability 78—76866
  glassy, electrolytic durability 80—66809
  glassy, graphitisation, density change 78—44142
  glassy, graphitisation kinetics 79—52246
  glassy, LMSC process prepared, exam. of props. by TEM and X-ray anal. 78—63675
  glassy, migration into steel during shock compression 80—24679
  glassy, negative magnetoresist. 78—23118
  glassy, reticulated struct., low temp. thermal cond. meas. 79—86938
  glassy, size effect on bending strength 79—52309
  glassy, struct. evolution due to thermal treatment at 1000 to 2700°C, layers evolution 77—68923
  glassy, struct. evolution due to thermal treatment at 1000 to 2700°C, tridimens. config. 77—68924
  glassy, struct. parameter var. with heat treatment temp. 77—11488
  glassy, surface erosion by ion bombardment crystal anisotropy effect 78—23845
  glassy, thickness imposed thermal diffusivity gradient 78—14521
  glassy C, prep. from liq. phenolformaldehyde resin, TEM obs. 79—83145
  glassy C electrodes for medical and physiological appl., meas. in saline 77—81764
  glassy C electrodes for photogalvanovoltaic and photovoltaic cells 80—89630
  glassy carbon foam, properties 77—24976
  glassy tip, field emission current stability 80—11544
  glassy-C, irradiation induced dimensional changes 80—65052
  global C budget and CO_2 from fossil fuel burning 80—77080
  global cycle, kinetic models stability anal. *(German)* 79—53414
  grain boundary segregation, in α-Fe 78—72778
  graphite, interstellar porous grains, free-space equilib. temps. calc., rel. to optical props. 80—62223
  graphite content, quantitative X-ray phase analysis 79—52820
  graphite-liquid-vapour triple point pressure and liq. C density 77—62618
  graphitic carbons, particle emission rel. to morphological changes during sublimation 77—47566
  graphitic overlayer on Ag electrode, pyridine adsorption, Raman spectra obs. 80—103954
  graphitisable, catalytic graphitisation by Cr, Mn and Mo oxides 80—89166
  graphitisation, catalytic, by various metals 80—3401
  graphitisation, cooperative accelerating effect of $CaCo_3$ and N_2 80—55429
  graphitisation stages of carbon materials 77—81235
  graphitised C black, adsorbent for gas chromotography 79—96358
  graphitised C black, adsorption of inert gases, gas-solid virial coeffs. 78—75928
  graphitised C black, adsorption of inert gases, Henry constant, rel. to intermol. interaction pot., review 78—22948
  graphitised C black, adsorption of methane, rot. tunnelling, neutron scatt. obs. 79—15000
  graphitised membrane, adsorption meas. in situ using steady state flows and time lags 79—33183
  graphitised thermal C black, coating for gas chromatography columns 77—77823
  graphitized C black, continuous phase transitions of adsorbed Kr monolayers 78—34698
  graphitized C black, virial coeff. theory of Kr adsorption 78—34697
  graphon, adsorption of Ar, high press. and temp., gas density profile theory 78—67903
  Graphon, colloidal, in butanol, electrophoretic mobility, charge origin 78—85211
  Graphon, colloidal dispersion in butanol, stability ratio 79—29413
  hard, heat-treated under pressure, characterisation of carbon phases by electron microscope 80—60855
  hard, surface wear characts. 80—108596
  hardness of C base materials, sclerometric determ. 77—77670
  heat capacities of synthetic mats., 50-3000K 77—84942
  heat-treatment and neutron irrad. effects on US atten. and Young's modulus 79—11644
  high energy arc, radiation loss measurement 77—7613
  high temperature behaviour, over 2600K, polymorphic carbyne forms 79—7575
  high-frequency heating, position regulator 79—80612
  HTGR fuel particles, inert gas intrusion as charact. procedure for pyrocarbon coatings 79—54512
  HTGR fuel particles, influence of pyrocarbon props. on as-produced gas permeability of coatings 79—54511
  HTGR spent fuel elements, ^{14}C determination, chemical anal. 80—42745
  HTR, pyrocarbon coated fuel, C density determ. by X-ray absorpt. 80—5301
  hydrology, C mass transfer and isotope evolution in natural water systems 79—20882
  IC 418, planetary nebula, C abundance from UV spectra 80—67832
  impregnated, reaction steps in gas sorption 78—68916
  impregnated oxide refractory melt, C oxidation 79—91828
  impurity in Cr_2O_3, effect on sintering behaviour 80—66461
  impurity in d-transition metals, integration with large-angle grain boundaries 80—39148
  impurity in GaAs epitaxial layers, from mixed Ga solns., C solubility 80—15392
  impurity in Si, equilib. of dissolved C and O with CO in ambient atm. 80—1949
  impurity in vitreous SiO_2 and quartz, determ. by isotopic spectral method 80—26093
  impurity in W and Mo, struct., mech. props. and purification 79—52277
  induced amorphous surface layers in Ti-implanted Fe 80—107287

carbon continued
internal strain rel. to strain tensor, group theory anal. 79–86835
interstellar C_2, Copernicus UV obs. of ζ Ophiuchi cloud 78–41022
interstellar C_2 molecules towards ζ Persei 80–12799
interstellar C, 492 GHz line detection 80–90508
interstellar medium, C depletion rel. to 2175 Å feature strength and origin 80–17638
interstellar southern molecular clouds, $^{12}C/^{13}C$ abundance ratio derived from H_2CO obs. 79–84838
interstitial in electron irrad. Si, photo EPR 77–16175
interstitial in V, neutron diffr. determ. of site 77–19944
interstitials, in transition metals, electronic structure 79–1583
ion, energy straggling in metal foils 80–27905
ion beam, heavy element ionisation cross-section ratio determ., X-ray method 77–6920
ion bombarded, chemical effects on secondary photon and ion emission 78–95637
ion energy selection by parallel-plate electrostatic analyser 78–83610
ion implantation in Fe(Ni)(Permalloy), MCP phase formation, electron diffr. study *(Russian)* 79–82469
ion implantation into $NbC_{0.89}$, supercond. transition temp. 77–69442
ion implantation of Si, SiC synthesis and struct. characterisation 77–76434
ion impurity in linear Z-pinch He plasma, outer 2s-shell electron excitation emission 78–22113
ion stopping power systematics, Z_1-oscills. 79–65130
ion-plated, on metal, deposition method, graphitic struct., and tribological props. 78–11440
ionisation states of energetic C and O emitted by the Sun 77–49249
ions, beam-foil excitation, relative initial populations, lifetime curves 80–14210
ions, collective accel. to 170 MeV by electron beam 80–9433
ions, energy loss in tissue-equivalent gas for elastic nuclear collisions 78–86759
ions, ionisation equilib. and radiative energy loss rates in low-density plasmas 78–87430
isotope enrichment in CVD system 77–23301
isotope geochemistry of small groundwater system, NE. Ontario 79–84324
isotope ratio, mass spectrometric anal. double inlet system with viscous gas flow 77–18131
isotope ratios in C stars, spectral analysis 79–30057
isotope record in coral growth rate (1944-74) 79–62524
isotope separation, by multiphoton dissociation of CF_3I 79–3592
isotopes, origin and $^{12}Cl^{13}C$ ratio evolution 78–93201
isotopic comp. of groundwater, correction for CO_2 outgassing effects during pH meas. 79–66718
isotopic composition determ. using RMO-4S omegatron mass spectrometer 78–5368
isotopic composition of brines and sediments in Orca Basin 79–88369
isotropic pyrolytic, for biomedical devices, mech. props. 78–65150
ISSEC selection for fusion reactor 80–57950
K-shell X-ray yield, following H^+ bombardment of foil 77–10624
K-shell X-ray yields, proton-induced, chem. effects 80–37820
kaolinite:C, high temp. reduction reactions, thermodynamic anal. 80–104426
kaonic ^{12}C, coupled channel formalism, role of Λ(1405), binding effect, Pauli blocking 78–55261
KERMA values, consistent set for H, C, N, and O for neutrons from 10 to 80 MeV 80–68967
laser, atomic, pulsed microwave discharges of CO_2, CO and CF_4 source gases 80–48233
laser, nuclear pumped. employing Ne(He)-CO(CO_2) mixtures, energy storage 80–63996
laser-heated electron emission from C-coated metal surface, appl. to emissive probe meas. 80–6270
late-type supergiants, C, N and O abundances for G AND K Ib stars 78–24509
lateral spread distribution widths MeV He ions in C, Al, Cu from energy spectra 79–14860
lattice dynamics of diamond type crysts., Keating's valence force field 78–79687
limiter for JFT-2 Tokamak 79–85768
low energy electron backscattering, 0.5-10 keV 77–52206
low temperature C, elec. cond. as function of freq. 79–23965
lunar regolith, C chemistry 77–60670
marine environment, stable C isotope comp. of dissolved and particulate organic C 79–20862
marine plankton, C isotope ratio rel. to surface water masses 79–29783
materials, thermodynamic props. rel. to struct. 77–80597
mechanical props., high temp., review 79–38897
mesocarbon microbead, heat treatment under high pressure 77–28736
metals, C content determ., isotope-spectral method *(Russian)* 80–55766
metastable phases, nature 77–89404
meteorites, thermal metamorphism, noble gases, C and S in Allende 79–92732
microneedles, grown on W wires under intense elec. fields, X-ray diffr. and AES 80–54580
micropore analysis 78–14570
micropore volumes from isotherm eqn. 78–14569
microporosity, determ. from isotherm eqns. 79–51419
microporous, gas adsorption 78–22956
microstructure, example of high resolution TEM application *(Hungarian)* 77–76267
migration on surface of solid solutions *(Russian)* 80–40360
mixes, extruded, preoxidation treatment effect on transverse breaking strength 77–63767
mixes, rheological props. at very low shear rates using capillary rheometer 77–65691
mixes, rheological props. using capillary rheometer, binder content depend. 77–65692
modulus of elasticity, interrelationship with crystalline struct., heat and irradiation effects 77–21210
molecular sieve prep. by pore blocking 78–15324
molecular vapour source for flowing systems 77–14616
molecules, long chain, explanation of diffuse interstellar lines in stellar spectra 79–53897
monatomic, transport properties, rel. to spacecraft entry into planetary atms. 78–87424
monofilaments, use as in-line electron beam energy monitors 77–61159

carbon continued
monolayer phase condensation on Ni (111), LEED and AES obs. 79–46960
morphology and growth mechanism of carbons formed by Ni-catalysed decomp. of hydrocarbons 78–35679
muonic X-ray transitions, nuclear charge radii 80–99589
natural rubber accelerator, effect on viscosity *(German)* 78–30688
neutron kerma factors for H, C, N, O and tissue, 20-70 MeV 77–73584
neutron yield calcs., electron beam incidence 78–95622
Ni, adsorption residual C removal by electron beam irrad. and heat treatment *(Chinese)* 80–88421
non-graphitic, two-dimensional X-ray reflections, anal. 80–24308
noncrystalline conversion to diamond, diffusion conversion enhanced rate due to shock compression 80–39221
nongraphitizable, catalytic graphitization by Cr_2O_3, MnO_2 80–97440
Nova Serpentis 1978, C grains condensation in circumstellar dust shell 80–90430
nuclear microprobe high sensitivity meas. of C in metals 80–50908
nuclear target backing foil 79–85201
on determination, in or on steel, XFA method 80–3466
optical microscopy, reflection, interference colours, terminology 78–42871
optically transparent electrodes, form. from reticulated vitreous carbon 78–3341
organic, decomposition in deep oceans 79–25270
organic, dissolved, determ. in methanol 80–16741
organic, non-methane, C in global troposphere 78–73462
organic, water quality indicator for Lake Superior 79–25287
organic C in marine atmosphere particulate matter conc. and particle size distrib. 78–32139
origin and abundances in terrestrial planets and meteorites 78–28559
Orion nebula, C and Mg abundances from UV spectrum 80–41882
α Orionis (Betelgeuse), C and O underabundances from UV flux 77–22231
overabundances in C star atmospheres 79–21284
oxidation in flow conditions at 1000 to 6000K 78–11445
oxidation kinetics, in Fe-C melts by CO_2 *(Russian)* 80–40680
oxidation kinetics on Ni (110), AES meas. 79–79291
paint type coating layer with spherical pigment, radiative transfer theory 80–61405
partially graphitised, K intercalation-desorpt. cycle rel. to stacking faults 78–47396
particle combustion, diffusion and reaction in stagnant boundary layer 77–68705
particle formation, C_2+C_3 as possible first step 78–68876
particle growth during hydrocarbon pyrolysis, model 79–91919
particles in flame, laser heating and sublimation 78–61012
particulate, identification in air pollution by Raman spectroscopy 79–5625
paste, viscoelastic props., depend. on coke grain size 80–1501
γ Pavonis, C and N abundances 77–91531
phase behaviour at high temps., meas. using laser heating system 77–77699
phenolic resin-derived, oxidation, ht. treatment effects 78–56790
phenolic surface, laser-induced impulse 79–43071
photoassimilated in soybean plants, γ-induced changes in distrib. and export 80–56139
photodesorption, role of C 77–36787
photoelectric cross sections, from total absorption cross sections, 5 to 130 keV 79–26947
photoemission spectra and total primary yields for exploding wire radiator source 80–32773
photoneutron yields released by incident electrons, improved calc. 80–27630
pionic, Auger electron emission *(Russian)* 80–69271
pitch, mesophase form. under reduced press. 77–63571
plasma, charge exchange in collisions of multi-charged ions *(Russian)* 79–98859
plasma, continuous absorpt. coeffs. 80–10362
plasma, graphite hollow cathode glow discharge C conc. determ. 80–44032
plasma, hot spot distribution, significance interpretation of laser produced plasma expts. 79–98945
plasma, laser produced, anomalous mag. field reversal, two-dimens. numerical results 78–87471
plasma, laser refl. and scatt. 77–19715
plasma, spectral and absorpt. coeffs. 80–69985
plasma extended source for short wavelength amplifiers 78–79447
plasma formation by CO_2 laser irrad. in strong mag. field mass loss and plasma blow-off 78–30455
plasma impurity, flux on wall of DITE Tokamak 80–28688
plasma impurity, high-temp. ionis. equilib. and radiative cooling 78–42712
plasma impurity, screening effect of divertor in T-12 Tokamak 80–28844
plasma production, laser irrad. of foil, mol. ions studied by mass spectrosc. 79–90429
plasmas produced by lasers, photoexcitation in the ionisation dynamics 78–91130
plate, interaction of laser with laser produced plasma 77–19734
plate, polarimeter for recoil proton polarisation meas. in $\gamma p \rightarrow \pi^\circ p$ reaction 79–93898
poisoning of LaB_6 cathodes in vac. systems, thermionic emission decay 78–27364
polarimeter, proton analysing power, 300-560 MeV 80–23279
polyester polymer-C black composition, elec. cond. under press. 77–28224
polygranular, flexural strength after heat treatment porosity correl. 80–84996
polymer chars, associated O_2 and H_2 78–11551
polymeric aspects of carbonization 80–2972
polymorphic modifications form. under low and high press. 79–15597
polystyrene melt, carbon-black filled, rheological study 80–48665
porous particle, internal combustion, model 78–92481
positron annihilation, differentiation between graphite and diamond structs. 79–28860
potential in equilibrium with impure high temp. inert gases 80–104135
powder, binary mixtures, bulk density, charact. curves interpret. 77–63574
powder behaviour in vibrating field from cond. obs. *(Japanese)* 78–95711

carbon continued
powder magnetisation thermometry for very low temps. 79—63219
precipitates with preferred orientation [100], from dissoc. of n-xylene *(Russian)* 80—45484
pregraphitic, diamag. suscept. rel. to temp., energy level calcs. *(French)* 78—34951
pregraphitic, negative magnetoresist. 80—34466
pregraphitic C crystallites, appl. of theory of diamag. susceptibility of condensed ring systems 77—16039
prostheses, cardiovascular devices, dental implants, review 77—44835
proteins, solid, NMR, detection of individual C resonances, appls. 80—51042
proton beam dosimetry, miniature Si dosimeter 80—47733
proton energy stagggling in ion backscatt. expt. 79—37750
proton impact X-ray emission, ang. distrib. and polarisation fraction 78—56546
proton induced X-rays as source for mass absorption coeff. meas. 78—2942
proton straggling determ., using 0.47 and 1.73 MeV elastic scatt. resonances of protons 79—4356
pyrocarbon:B, g-factor anisotropy *(Russian)* 79—47001
pyrocarbon, Ag diffusion 77—24441
pyrocarbon, coating for oxidation resistance 77—32704
pyrocarbon, deposition from fluidised bed, quantitative aspects 77—50239
pyrocarbon, deposition from gaseous hydrocarbons, kinetic model *(German)* 78—23851
pyrocarbon, desorption of D, activation energies 79—65330
pyrocarbon, diamagnetic susceptibility increase, mag. field intensity depend. *(Russian)* 79—82752
pyrocarbon, fuel particle coating, strength and Young's modulus meas., brittle ring test 77—8868
pyrocarbon, Hall effect and conductivity of specimens deposited at 2000 and 2200°C 78—23112
pyrocarbon, high-temp. deform. under mech. loads 77—16644
pyrocarbon, HTGR fuel particle coatings, struct. charact. 77—83034
pyrocarbon, irradiation-induced dimensional changes 80—65052
pyrocarbon, lamellar material, thermal expansion meas. appl. of interlayer spacing X-ray diffr. technique *(French)* 77—20096
pyrocarbon, low temp., isotropic, permeability study *(French)* 79—7549
pyrocarbon, methane formation during p and d irrads. and thermal release of H 77—36788
pyrocarbon, microstructure of coatings on fuel particles, TEM study 78—25293
pyrocarbon, oxidation behaviour at high temps. 80—55551
pyrocarbon cladding, gas permeability *(French)* 77—14234
pyrocarbon coated fuel, neutron effects in range 1273-1773k 77—79434
pyrocarbon coated particles, influence of fast neutrons on transport behaviour of solid fission products *(German)* 79—13427
pyrocarbon coating, isotropic, gas permeability, neutron irradiation effect *(French)* 80—63260
pyrocarbon coating, isotropic, gas permeability meas. *(French)* 80—63259
pyrocarbon coating deposition by gaseous hydrocarbon pyrolysis, theoretical anal. 77—40459
pyrocarbon coating of Biso fuel, neutron effects on stresses and strains 77—79436
pyrocarbon coating permeability effect on U redistrib. in HTGR fuel 77—40460
pyrocarbon coatings, deposition in fluidized bed, TEM, changes by irradiation 80—34084
pyrocarbon coatings, gas permeable isotropic, fluidised bed prep. 77—46381
pyrocarbon coatings, neutron induced fission gas permeation 77—79435
pyrocarbon coatings, quantitative chemical method to determ. disordered C component 77—79462
pyrocarbon coatings, refl. anisotropy and struct. determ. by perpendicular incidence microellipsometer 80—101824
pyrocarbon coatings, TEM anal. 77—79463
pyrocarbon coatings for Biso fuel, the permeability meas. 77—79433
pyrocarbon coatings on HTGR fuel particles, Bacon anisotropy factors meas. technique 79—13418
pyrocarbon deposition in fluidised bed, qualitative model, investigation with Stromungsrohr 78—56595
pyrocarbon deposition on C black *(French)* 78—68921
pyrocarbon nuclear fuel coating, props. and neutron irrad. behaviour *(German)* 77—67816
pyrocarbons, EPR, effect of motional averaging, anisotropy, skin effect rel. to heat treatment and neutron irradiation *(French)* 80—34752
pyroceramic, sputtering and blistering from H^+ and He^+ bombardment 78—79649
pyrolised non-graphitising, modified struct. model, interference function 78—67681
pyrolytic, electron induced irradiation creep, dislocation process obs. 77—47483
pyrolytic, energy depend. of methane prod. during deuteron bombardment 78—95939
pyrolytic, fast neutron flux effect on irradiation damage 78—22768
pyrolytic, graphitisation by Ni, activation energy and graphitisation rates 79—57010
pyrolytic, high temp. compatibility with Ni-Cu alloys 79—65261
pyrolytic, oxidation resist. in liq. corrosive medium 77—90471
pyrolytic, production in methane, AC arc discharge, plasma parameters 79—87843
pyrolytic, spiral growth rel. to temp., press., flow conditions, dislocations, props. *(German)* 78—42931
pyrolytic, tritium diffusion coeffs. and deuterium solubilities 80—37443
pyrolytic C, paracrystn. nature, bimodal statistics anal. 79—77451
pyrolytic film electrode, fabrication, electrochem. characterisation 78—92487
radiation creep, testing method 77—12769
Raman spectra in 2600-3300 cm^{-1} region, heat treatment temp. effect 79—42955
Raman spectra of carbons and graphite, new lines, exam. 78—48169
reaction with TiO_2, Cl_2 79—83450
reactive pulse plasma crystallisation, diamond like C 79—95938
reactive RF sputtering in N_2, paracyanogenlike film deposition 79—78886
reactivity with Y_2O_3, exam. by thermal anal. 78—85154
recombination line obs. of dark clouds 79—75260
red giant stars, meridional circulation and CNO anomalies 79—48786
red giant stars in globular clusters M92 and NGC 6397, C abundances 79—48785
reducing agent for $Al_2Ge_2O_7$, gaseous and metallic Ge yields *(Russian)* 80—40737
reduction in nonequilibrium plasma, effect of non-Boltzmann population of vibrationally excited states 79—20362
reduction of Cr_2O_3, mechanism 7573-2073K *(Russian)* 80—45483
reduction of Cr_2O_3 78—6877
reduction of GeO_2-SiO_2 and $3Al_2O_3$-GeO_2-SiO_2 in mixed diffusional kinetic regime *(Russian)* 80—66771
reduction of hematite 77—48687
reduction of MnO, surface reaction, CO regeneration *(Russian)* 80—66772
reduction of molten FeO, mechanism 77—48636
reduction of rare earth metal oxides *(Russian)* 80—93743
reduction of SnO_2 79—61901
reflection of H, D and He ions 78—95640
refractories, alkali attack as catalyst for oxidation 80—40562
reinforced metal sintered composite materials, form of C present *(German)* 79—95978
reinforced organic composite, graphite, or C-C, ablation, mathematical modelling 79—41564
removal from Fe, by dry H_2 method *(Japanese)* 78—11234
replica, stripped from pure and doped NaCl single crysts., elec. memory, Au and Ag deposition expts. 77—76691
replicas, single-stage, detaching using glue films 80—61038
residual carbonaceous material, in urban airborne particulates, Raman microprobe obs. 78—69441
resistors as low temp. sensors in low temp. reactors, gamma, neutron irrad. investig. 77—45848
ribbon, high modulus, strength, prep. 77—21062
roughness factor measurement, energetic D^+, He^+, Ar^+ irradiation of pyrolytic C 80—39172
rubber, C-black loaded SBR, elec. cond., effect of milling and thermal-oxidative ageing 77—55529
rubber mixtures, synthetic, natural ageing effects on dielec. props. 77—24778
rubber-channel black mixtures, natural ageing effects on dielec. props. 77—24777
saccharose char, catalytic graphitisation *(French)* 77—28739
secondary electron spectroscopy 77—85854
sedimentary distrib. rel. to O_2 in Precambrian atmosphere 77—5272
segregation in Fe, equilib. and struct. *(German)* 79—47690
segregation to Ni (100) surface, isosteres 77—1282
segregation to single cryst. surfaces from dil. solid solns. in Pd, Pt, Co 80—39301
shock compression for diamond production 80—11613
smokes, vapour-condensed, 800 to 130 nm extinction and interstellar extinction curve 80—82180
soft, low temp. sp. ht. anomalies, spin-spin interactions 79—15307
soft, sp.ht., 0.4-4.5K, rel. to localised spin transition 77—28389
solar C I multiplets at 1560 and 1657 Å, overlapping emission peaks obs. and theory 78—93178
solar flares, C-poor events, IMP 8 ULET sensor meas. 79—92739
solar flares, O I 1355.6 Å and C I 1355.8 Å lines obs. 80—90381
solar system, primordial C retention by terrestrial planets 79—40102
solid, electronic stopping function for He^+ and Li^+, 50-300 keV 79—69169
solid-liquid vapour triple point 78—48377
solid-liquid-vapour triple point pressure 79—14914
from solid-state reduction of carbonate ions, X-ray diffr. 78—56594
solubility and thermodynamic props. in solid Mo 80—15266
solubility in BCC transition metals 78—71861
solubility in CaO-Al_2O_3 melt in presence of graphite 78—38850
solubility in electroslag remelting type slag CaO-Al_2O_3-CaF_2 78—44110
solubility in Fe-Ga-C melts, thermodynamics *(Russian)* 80—39292
solubility in liquid Fe and alloys, donor-acceptor mechanism 80—49365
solubility in Mo-W solid soln. 77—25025
solubility in Ni *(Czech)* 79—77757
soot, airborne, photacoustic and absorption spectrum using tunable dye laser 80—4102
soot, granulated, thermal and elec. cond. 80—24687
soot and benzo(a)pyrene combined aerosol form., rel. to air pollution and health hazards 78—80796
soot in urban atm., determ. by optical absorption technique 80—108824
soot-CO_2-water vap. mixture, in luminous flames and smoke, IR mean absorption coeffs. calc. procedure 78—91061
soot-gas mixture, in luminous flames and smoke, IR mean absorption coeffs. calc. procedure 78—91061
spark gaps with C parallel plane electrodes, erosion characts. 80—70076
specific heat anomalies and spin-spin interactions in soft and hard C 79—69261
specimen preparation for TEM by ion beam thinning *(German, English)* 80—11861
spectra from CO_2 laser prod. plasmas 80—38711
spectra lines, charge exchange reaction effect 79—58243
sphere radiation in plasma, NRL fusion programme 78—59042
Spheron 6, surface group obs. using gaseous reagents, surface acidity evolution during heat treatments *(French)* 77—66767
sputtering, low energy, H, D and He ions 80—100734
sputtering by fast electrons 77—90226
sputtering of ice, MeV ions, erosion rate 78—48268
stainless steel:C, surface, obs. at very low accel. voltage (200 V-1 kV) by SEM 80—10764
steel, austenitic stainless, type 316, irradiated with 46.5 MeV Ni^{6+} ions, soluble C effect on void swelling and low dose dislocation structs. 80—49280
steel, carburisation, calc. of mass transfer in diffusional saturation 80—24676
steel welding, in Ar, resistance to cold cracking obs., C and H_2 content influence 77—21283
steels, ferritic and martensitic, C and N migration at low temps., monograph 80—22149
steels thermodynamics, C-C interaction energy 80—93793
STEM, bright field single atom images with half plane detectors 78—66010
stopping power determ. for heavy ions, 200 to 2000 keV 79—45596
stopping powers, low energy, determ. by TOF techniques 79—45594
stopping ratios of 50-300 keV H^+, He^+, $^7Li^+$, and $^8Be^+$ 80—42903

carbon continued
strength and struct., conf., Bath, London, England (Apr. 1979) 80—82566
stressed materials, mech. characts. analysis using acoustic emission *(German)* 79—15881
stripper foil, lifetime meas. 80—23216
stripper foil preparation, under heavy ion bombardment 80—18717
stripper foil prepared by cracking hydrocarbon vapour in glow discharge 79—31286
stripper foils, energy straggling of heavy ion beams at tandem energies, C foil appl. 78—33353
stripper foils, lifetime enhancement, heavy ion bombardment 78—94156
stripper foils, lifetime enhancement by slackening technique 80—23186
stripper foils under 4.8 MeV Ar^{++} ion bombardment, shrinkage, rupture, lifetime 78—33352
stripping foil, semiempirical formulas for heavy ion stripping data 78—33354
structure change, during thermal ordering, radiation disordering 80—54283
substrate, U atom motion at low temp., biomolecule marking appl. 79—25176
substrate amorphous, cluster migration in early stages of Au film growth 79—77964
substrate for B filament CVD technology, book contrib. 78—48352
substrate for Cr_3C_2 formation in Ar, CO and vac. atm. *(Russian)* 80—35570
substrate surfce, Pt crystallite behaviour on sintering 78—7235
sugar char, EPR in transition range 80—34751
support films for high-resolution STEM, prep. and observation 80—93496
surface, (001)-(2×1), reconstruction-induced mean-square displacements 80—15343
surface, interaction with D^+ ions, 5-30 keV temp. depend. of methane formation 78—79645
surface, SiC coatings, deposition by RF sputtering 80—25563
surface evaporation by Nd laser beam, spectral-line absorption 79—19951
surface groups, acidimetry, formation of derivatives 78—68918
surface groups, spectroscopy 78—68919
surface layer on Co (100), LEED and Auger expts. 78—38921
surface reconstruction-induced subsurface strain, theory 78—91516
surface-electron beam interaction, 0.4-5 mA ion beam extraction 77—84456
Swann band profiles in spectra of two comets 78—85909
swelling, blistering, 140 keV p, d and the ion irrads., porosity effects 77—35603
target, O^+ low energy ions, interaction obs. 79—34352
target impurity effect on laser produced expansion, ion spectrography 80—43945
terrestrial C reservoir changes rel. to atm. CO_2 78—57278
texture change on ht. treatment under press. 78—60687
thermal radiation detector sorbent test 79—29403
thermodynamic activity, in liquid Na, continuous method of determ. 77—56306
thermodynamic activity in austenite, computer simulation 79—37852
thermonuclear burning in degenerate stellar core, convection effects 80—41810
thermonuclear combustion neutrino mechanism, form. of neutrino stars and supernova outbursts *(Russian)* 77—87379
thin foil, irradiation with 1.2 MeV Ar^+, electron diffraction study 80—103397
thin foil thickness meas. using ^{148}Gd and ^{241}Am alpha-particles 79—30417
tissue composition measurement by fast neutron activation 77—64131
Tokamak limiter, plasma interaction, current profile evolution effect 80—10420
total organic carbon measurements for industrial water and wastewater 80—26071
transfer in clad materials *(German)* 77—50230
transmission electron energy-loss spectroscopy, energy-differential cross-section functional form 79—100000
trapping at 6 to 15 keV D in C, temp. depend. and depth profile 77—30664
turbostratic, formed in phenolic resin C by catalytic graphitisation of dispersed Ni, TEM study 79—77466
vacancy, tight-binding calc. 80—24844
vacuum deposited coatings for prosthetic devices 77—40374
valence electron radial and momentum distribs., X-ray form factors and Compton profiles 79—65956
vaporisation into nonequilib. stagnation point boundary layer, Jupiter probe heat shield 79—1264
vapour, Swan bands, oscillator strength 80—63712
vapour deposition, feasibility of fusion reactor first wall regeneration in situ 77—18701
vapour-deposited film, transparent and hard insulating layer, struct. and props. 80—10830
Viking C assimilation expts. on Mars 78—20708
vitreous, directional O ion beam etching, compared with reactive ion etching 80—71781
vitreous, disintegration by fluorophosphate optical glass melt 78—30101
vitreous, erosion in molten Si rel. to cryst. growth technology 78—3244
vitreous, low temp. sp. ht., thermal cond. and US vel. meas. 78—47533
vitreous, tensile strength, oxidation effects up to 2500K 80—3209
vitreous, wetting by Cu-Sn-Ti alloys 78—71904
vitrified, surface, wettability, surface tension, contact angles of liqs. 79—37901
whisker formation by Ar ion bombardment 78—30851
X-ray diffr. study of low cycle fatigue damage 77—66700
X-ray laser, pumping by C VII+Ar III charge exchange 78—5462
X-ray microanalysis determination, in austenitic stainless steel, X-ray microanal. method *(French)* 80—11981
XPS anal. of Ar and ^{57}Fe ion-bombarded 77—11769
zincblende structure group IVA covalent crystals, Murnaghan parameter estimates from Morse pot. 78—95014
$K_L{}^0C \rightarrow K_S{}^0C$ coherent regeneration in range 10-30 GeV/c 77—13955
Ag, oriented crystallisation on active amorphous C centres 79—7762
Al-C-Al sandwich, microwave irradiated, superconductivity at room temp. *(Russian)* 80—11138
Al-C-silaceous sand mixture in N_2 atmos., weight loss during heating, compaction *(Japanese)* 80—35151

carbon continued
Al-GeSe-C, effect of contact material on DC and AC behaviour of sputtered amorphous GeSe film 79—95513
$Ar+C^{4+}(C^{6+})$, K-shell X-ray prod. at high energy, charge state independ. 77—6905
Au-C, light ion large angle scatt. in weakly screened Rutherford region 80—84823
B C powders, effect of C on sintering 80—40312
B, tetragonal, X-ray diffr. and C doping obs. *(French)* 79—14731
β-B:C, rhombohedral, EPR meas. partly resolved absorpt. spectra 80—20449
B:C,H amorphous film, IR absorpt. spectra 77—77312
B-C system, electron probe microanalysis and destructive chem. methods of study *(French)* 80—11982
BN:C, hardening by doping, p-T diagram, cryst. struct. *(Russian)* 77—77491
$BaTiO_3$:C, solubility of C at low O_2 potentials, 800°C 80—100334
Be, of differing purities, C diffusion *(Russian)* 80—19984
C 1s contaminant buildup on conductors (insulators) in X-ray ESCA 78—95981
C and adsorbed acetylene on Fe, hydrogenation, C-1s XPS spectra obs. 80—84366
C and C^+, one-electron capture cross sections in alkali metal vapours 79—59553
C, C^+, interstellar, clouds cooling theory *(Russian)* 80—12801
C characterisation, using dark-field electron microscopy 79—77464
C depth profiling in solids using ^{12}C(d,p) 79—5212
C film, oxidation, IR spectroscopic study 79—96162
i-C, hard coating preparation by ion beam methods 80—25579
C I, abundances, UV grain albedos and pressures in interstellar medium 79—92818
C I, as continuous opacity source in late B-type main-sequence stars 77—87393
C I, C II, C III, C IV in solar flare, line profiles rel. to upper chromosphere model 79—40148
C I, C II, interstellar, fine struct. levels population ratios 79—35351
C I, in interstellar clouds, rel. to chemical evolution and formaldehyde abundance 77—13421
C I, interstellar, UV lines obs. in ζ Puppis and ζ Ophiuchi 79—35332
C I, m-representation approach 79—45645
C I, UV fluoresc. from photodissoc. of CO_2 79—13776
C I, weighted oscillator strengths for elec. dipole and forbidden transitions, data tables 80—37779
C I 1101 Å absorpt. edge in A-type stars, effect of $C+H^+ \rightleftharpoons C^+ + H$ charge transfer 80—90423
C I 5380 Å line sensitivity to temp. changes in static and oscill. systems 77—60743
C I IR forbidden emission lines obs. in Orion Nebula 78—85987
C I lines, Stark broadening in ARC plasma 77—10634
C I transition probabilities and oscillator strengths, rel. to H I regions 77—49448
C II, electron impact induced fine struct. transitions, collision strength 77—50540
C II, III, IV, radiative mean life meas. by beam-foil technique 78—90121
C II, interstellar, line emission rel. to Cl chemistry and H ionisation 79—40245
C II, low lying levels, excitation equilib. 79—12401
C II, UV line spectrum of active chromosphere star ε Eridani, models 80—77394
C II, UV lines Stark widths 79—6910
C II, Zeeman splitting of high-n recomb. lines 80—58210
C II and III, mean lifetimes of astrophysically important excited levels 77—46528
C II homologous ions series, Stark broadening trends 80—105157
C II line excitation by C I photoionisation 80—58223
C II lines in A-type star α Lyrae (Vega), Copernicus UV obs. 80—8627
C II to C VI, beam-foil excitation functions for optical transitions 80—14209
C III, atoms, static polarisability, lower bounds, oscill. strength calcs. 77—75074
C III, C IV, electron impact ionisation 78—70941
C III, electron collisional excitation, R-matrix calc. 77—58169
C III, electron impact excitation cross sections, Coulomb-Born approx. 77—75302
C III, electron-impact excitation calcs. 79—81286
C III, IV, V Auger lines obs., beam-foil excitation, ab initio calcs. 77—54601
C III, photoionization cross sections calc. 78—17625
C III, solar emission line ratios interpretation 78—28598
C III, transition probabilities 78—41987
C III 1909 Å emission line obs. of solar atmosphere 80—31277
C III 5696 Å in OB-type stars, transition from absorpt. to emission 79—67006
C III and IV, electron impact width of plasma lines, approximative semi-classical formula 80—43972
C III line intensity ratios, solar obs. by Skylab 79—53786
C III spectral lines, IUE obs. of optically thin emission regions 79—71089
C II(III)(IV), profile calc. method for stellar spectra *(Russian)* 79—92684
C IV, electron ionisation cross sections of excited atoms and ions 80—43186
C IV, in plasma, ion electron collisional radiative recomb. coeffs., bottleneck calc. 80—53942
C IV, lithiumlike ions, excitation by electron impact 78—13606
C IV, UV line identifications and lifetime meas. 80—106288
C IV, V, laser produced plasma, satellite spectra 78—5165
C IV 1548 Å line profiles of impulsive EUV bursts, OSO-8 obs. 80—90401
C IV 1548 Å profile in quiet solar region, interpretation 79—96980
C IV doublets in QSO spectra rel. to absorption redshift 79—35417
C IV in stars hotter than B 1, Copernicus obs. 79—44463
C IV interstellar column density towards early-type stars 80—73018
C IV interstellar lines in Wolf-Rayet star spectra, IUE obs. 80—67748
C IV resonance lines in B- and early A-type supergiant stars 80—46550
C IV/Si IV ratio for Be-stars, Skylab UV obs. 77—56987
C ion+Au, L-shell X-ray production and subshell ionisation cross sections meas. 80—91637
C ions+B(C), 10-40 MeV, soft X-ray spectra 77—75089

carbon continued
- C paste electrode with electrolytic pasting liq. and insoluble electroactive cpds., quantitative aspects *(French)* 79—79260
- C polymeric chains, reduced from poly(tetrafluoroethylene), reactivity 80—89488
- C, pyrolysis mechanism, electron microscopy, DTA, IR, ESR obs. 78—56593
- C stripper foils, ethylene cracking in glow discharge, irradiation lifetimes 80—23207
- C V, electron impact collision rates, reinterpretation of solar emission line ratios 80—98624
- C V, electron impact excitation cross sections calc. using nonrelativistic Coulomb-Born approx. 77—42414
- C V, ground-state electron impact excitation strengths, close-coupling calcs. 80—23561
- C V, ionisation rate coeff. in θ-pinch plasma, spectral meas. 77—6911
- C V, UV line identifications and lifetime meas. 80—106288
- C VI, and isoelectronic series, in laser-produced plasma, Balmer fine struct. (broadening) 80—48860
- C VI, cylindrical plasma, XUV gain calc. 79—72995
- C VI, laser plsma, electron density profile, Stark broadening meas. of vac. UV lines 78—59684
- C VI, n=3 and n=2 levels population inversion, possible extreme UV laser 77—7073
- C VI, XUV gain in expanding cylindrical plasma 77—15170
- C^-, effective valence shell Hamiltonian, ab initio calcs. 78—82611
- C , electron impact detachment, cross-section, 10-1000 eV 79—31702
- C_, electron impact detachment cross sections 79—89787
- C^-, free-free transitions, continuous absorpt. estimation 78—9098
- C^- ion source for radiocarbon dating using tandem accelerators 80—94620
- C^-, near-threshold photodetachment, IR meas. 77—42290
- C^+, adsorbed on metal, removal by 20-30 keV Ar^+, in plasma 77—76103
- C^+, association reactions, isotopic exchange, SIFT study, review 80—58435
- C^+, beam-foil excitation, absolute Auger yield meas. 80—14203
- C^+, beam-foil excitation; absolute Auger yield meas. 79—45685
- C^+, beam-tilted C foil interactions, charge-state distrib., photon emission, 100-400 keV 79—22814
- C^+, C^{++} ion beams, intense, production and postaccel. in magnetically insulated gaps 80—74041
- C^+, C^{2+}, electron impact ionisation cross section in hollow beam trap 78—25717
- C^+ charge transfer in diffuse nebulae 80—77463
- C^+, electron impact ionisation cross sections, autoionisation contrib. at low temp. 80—32838
- C^+, expt. results on $\bar{W}$-values for heavy particles 79—7000
- C^+, from exploding fast mol. ions, Auger spectra 80—32781
- C^+, gaseous diffusion in He gas, ion mobility and longit. diffusion of Ar^+ and CH_x^+ *(French)* 79—94766
- C^+ ions, beam-foil excitation, L-Auger decays, autoionisation 77—14569
- C^+, mobility in He, flow-drift tube meas. 80—43831
- C^+, reson. line regularities in plasma Stark widths and shifts 80—43881
- C^+, vacuum arc source 79—21853
- $^{12}C^+$, stopping power in Au at 50-500 eV 77—76478
- C^{2-}, parameters for analytical radial orbitals, total and binding energies 77—6668
- C^{2+}, Be-like, numerical many-body perturbation calcs. using multiconfig. model space 80—47907
- C^{2+}, dynamic multipole polarisability, coupled Hartree-Fock 78—82858
- C^{2+}, electron impact ionis. cross-section meas. 79—3577
- C^{2+}, Hund's first rule, new interpretation 78—78620
- C^{2+} ion energy loss spectra in Ti, Ni, Ge targets 80—65114
- C^{3+}, ^2S, $^2P^0$ and ^2D autoionising states, positions and widths 79—26944
- C^{3+}, 1s3s3p $^4p^0$ state, Hartree-Fock function, third-order energy 78—37569
- C^{3+}, electron impact, inner shell excitation cross-sections 79—59580
- C^{3+}, electron impact 2s-2p excitation, absolute cross sections 78—13605
- C^{3+}, electron impact excitation, relativistic Coulomb-Born approx. 79—68318
- C^{3+}, electron impact ionis. cross sections 79—22845
- C^{3+}, excitation by electron impact, resonance tabulation, cross sections 78—33616
- C^{3+}, fine struct. and lifetimes, doubly excited quartet system 78—78827
- C^{3+}, ionisation cross-section, excitation autoionisation effects 79—45850
- C^{3+}, partial photoionis. cross-sections and radiative recomb. rate coeffs. 80—52951
- C^{4+}, C^{5+}, production and acceleration in cyclotron *(Japanese)* 78—5084
- C^{4+}, electron impact excitation, cross-sections, modified Oppenheimer approx. 78—82843
- C^{4+}, few-parameter two-electron wavefunction of ground state 77—75051
- C^{4+} plasma, soft X-ray emission, electron-beam sliding spark device 78—79444
- C^{5+}, electron impact, continuum orbital approx., weak coupling theory 78—33417
- C^{5+}, plasma expansion, Balmer spectrum intensity inversion, charge transfer pumping 78—34371
- C^{5+}, resonant coherent excitation of channeled ions 79—51178
- C^{6+}, microdosimetric measurements of pretherapeutic heavy ion beams 80—72337
- C^{6+}, prod. in electron-beam superconducting ion source 77—23333
- C^{n+}, (n=1,2,3) effective valence shell Hamiltonian, ab initio calcs. 78—82611
- C^{n+}, collective accel. in vac. diode with C tip cathode, by 180 kV, pulses 78—37104
- C^{n+}, electron impact inner shell excitation/ionis. cross sections 77—23564
- C:H amorphous films, elec. cond. and optical absorpt. 80—49723
- C:H films, amorphous, elec. props., chem. modifications 80—84523
- C:Ni, X-ray photoemission studies 80—76138
- C/Au/C layer configuration, electron energy deposition meas. 77—24338
- C/C composite with S-modified pitch binder precursor, carbonisation and mech. props. *(German)* 77—44183
- C/Fe ratio in metal-poor stars from CH features 79—16945
- C/H, C/N in Jupiter, ratios determ. using new spectroscopic method 79—84734
- C/O ratio in massive stars, core convection effects 80—17579
- C/Pt-W (8 wt.%), desorption of K from C film surfaces 80—59784
- C/Re-W multilayer films for X-ray mirrors 79—44992
- C-Ar pot. parameters, from CO in Ar matrix, empirical evaluation 80—48057
- C-bearing gases, K X-ray yields induced by proton bombardment 79—45736
- C-C composite, structure model, Rosen model with fractional matrix 80—11719
- C-C composites, existence diagram and properties *(French)* 78—64517
- C-glass resistance thermometers, stability characts. 80—31751
- C-graphite materials, fluidised bed, carburising of metals, diffusion saturation 79—20276
- C-graphite materials for HTR and fusion reactors 80—73928
- C-H plasma, laser prod., spectral line emission 80—43969
- C-N bond in methylamine, nucl. mag. isoscreening line diagrams 80—78555
- C-PVC composite, fluctuation induced tunnelling conduction 78—52044
- C-PVC composite, transport props. 79—38073
- C-Tc(Mo)(V) film layer struct., obs. of supercond. transition temp. and crit. mag. field oscills. 77—69438
- C+Al(Sn), inner-shell multiple ionisation systematics, X-ray obs. 80—63790
- $C+B^{5+}(Li^{3+})(H^+)$, K-shell charge transfer cross sections, Bates-Born formalisms 79—45834
- C+C, K-shell excitation, Auger electron spectrosc. obs. 80—9714
- $C+CO_2$ Boudouard reaction, catalysed by Li_2O and Li_2CO_3, reaction rates 839-1050°C 79—16035
- $C+CO_2$ reaction, kinetics at low press. and hydrogen inhibition 77—63950
- $C+CO_2$ reaction, Langmuir-Hinshelwood kinetics at intermed. press. 77—66766
- C+C(N)(O) ions, 10-40 MeV, soft X-ray spectra 77—75089
- C+C(N)(O) ions, 4 to 40 MeV, beam-foil K-shell X-ray prod. cross sections 78—33461
- $C+H_2 \rightarrow CH+H$, pot. surface, HF calc. 80—16669
- $C+H^+$, absolute C K X-ray production cross sections, 18-26 MeV 77—83719
- $C+H^+$, electron capture cross sections 78—62912
- $C+H^+$, electron capture in foils 78—42203
- $C+H^+$, K-shell ionis., impact parameter depend., 90-200 keV 78—17775
- $C+H^+(H_2{}^+)$, vel. distrib. of convoy electrons, anal. 78—33600
- $C+H^+(H_2)^+(He^+)(He^{2+})$, ionisation processes viewed in forward direction 77—71866
- $C+H^+(He^{2+})$, K-shell Auger electrons ang. distrib. 79—89756
- C+He (methane), C atom K-shell binding energy by Auger spectra 78—50525
- C+He (methane), collisional excitation, prompt decay line energy, projectile Auger spectrosc. 79—85941
- $C+Li^+(Co^+)(Au^+)$, cross-section, closure-Born approx. 78—66630
- $C+N_2$ reaction, CNN radical prod., matrix isolation study 78—86880
- $C+N_2O \rightarrow CN+NO$, chemiluminesc., CN ($A^2\Pi_i$) vibr. distrib. 79—39152
- C+N(O), K-shell excitation, Auger electron spectrosc. obs. 80—9715
- $C+O^+$ ion-molecule reaction, 15 eV energy O^+ production system 80—84817
- $C+PbO \rightarrow CO+Pb$, chemiluminesc. from gas phase reaction 79—8426
- C+proton, charge transfer, target K-shell electron capture, impact parameter depend. 80—102552
- C+Ti self-propagating, high-temp. synthesis wave, radiating power 79—100377
- $C^-+CO(Mg)(N_2)$, electron detachment cross-sections, 20-150 keV 78—25690
- $C^-+H_2(He)(CO_2)(Ar)(Li)(Na)(Mg)$, negative ion stripping, at. beam form. 77—6926
- C^++alkali metal, charge exchange, negative ion form. 79—50128
- C^++ethylene (proplylene oxide), branching ratios 78—44354
- C^++H, fine struct. excitation cross section 77—38724
- C^++H, fine structure transition of C^+, collision cross section calc., validity of current approx. 78—25652
- C^++H_2, C^+ fine-struct. excitation, interstellar cloud cooling 78—25675
- C^++H_2, fine struct. transition excitation 77—42389
- $C^++H_2(D_2)$, $CH^+(D^+)$ $A^1\Pi$ rot.-vibr. population distribs. 80—23396
- $C^++H_2(N_2)$, reactant ion electronic states, effect on charge transfer cross sections 80—63809
- $C^++H_2 \rightarrow CH^++H$, classical trajectory anal. 78—53192
- $C^++H_2 \rightarrow H+CH^+$, energy spectrum and prod. vibr. excitation 77—77745
- $C^++H(H_2)$, 0.1-13 keV electron capture cross-sections meas. 79—36761
- C^++He(Ne), slow collision, ionis. obs. 79—10194
- C^++N_2, luminescent charge transfer, metastable and ground state ions 78—42202
- $C^++N_2(H_2)$, total charge transfer cross section, 5-100 keV 79—3561
- C^++NH_3, rate coeffs., ionised product distribs. 77—40522
- C^++Ne, energy loss collision spectrosc. 79—86037
- C^{2+}+Ar, intense low energy autoionisation lines 79—31674
- $C^{2+}+H_2(N_2)(O_2)$ (inert gas), charge transfer reaction rate consts. 80—7779
- $C^{2+}+H(H_2)$, electron capture cross-sections, 0.5-14 keV 78—42205
- $C^{3,4,5+}+H_2$, single and double electron capture cross sections, (0.3-1.2)10^8 cm s^{-1} 77—34756
- C^{3+}+Al(Si)(S)(Cl), chem. environment effect on $K\alpha$ satellites intensity 77—54527
- C^{3+}+H, charge exchange collisions, quantal calcs. 79—94079
- C^{4+}+H, charge transfer cross sections, ab initio potential energy curves 78—37741
- C^{4+}+He, charge-exchange total cross-sections 77—79691
- C^{4+}+Ti, ratio of single K-shell ionisation cross section to double K-shell ionisation cross section 80—53119
- $C^{5+,6+}$+C reson. charge transfer, population inversion, in laser generated plasma 77—50526
- C^{5+}+H, excitation distrib. following electron capture 79—36763
- C^{6+}+Ar, bound- and continuum-state electron capture in gas, strong correlations 80—9730
- C^{6+}+Ar, electron capture to continuum states, forward ejected electron spectra 79—45831
- C^{6+}+H, collisional electron removal, cross-sections, mechanisms 78—25683
- C^{6+}+H, electron capture by slow ions, pseudo-crossing 80—43176
- C^{6+}+H, low velocity charge transfer, two-state approximation calcs. 78—42207

carbon continued
- $C^{6+}+H(1s)$, low vel. cross-section, adiabatic mol. orbital basis 77−88553
- $C^{6+}+He$, electron capture and impact-ionis. cross sections, Monte Carlo calcs. 79−27083
- $C^{n+}+C$, 4 to 40 MeV, beam-foil K-shell X-ray prod. cross sections 78−33461
- $C^{n+}+H$, charge transfer cross sections, oscillatory behaviour in low-energy collisions 80−63806
- $C^{n+}+H$, electron capture cross-sections, Li and He-like ions 79−59559
- $C^{n+}+H_2$, electron capture cross-sections, Li and He-like ions 79−59559
- $C^{n+}+H(H_2)$, one electron capture and loss 80−18921
- $C^{n+}+Ne$, charge exchange contribution to K-vacancy production 80−102553
- $C^{q+}+Ar$, continuum electron capture and loss, 1.6-2.8 MeV/A 78−46443
- $C^{q+}+Ar$, continuum electron capture, projectile vel. and Z depend. 78−55222
- $C^{q+}+H(H_2)$, $q=1$-4, single electron capture cross sections 78−55233
- $C^{x+}+He$, electron capture, K X-ray emission ang. distrib. 77−57919
- C_{18} used in high performance liquid chromatograph, for multicomponent serum analysis 79−79334
- C_2, $(A^3\Pi_g$-$X'\,^3\Pi_u)$ band system, vibr. and rot. intensity distrib. 77−42332
- C_2, $(a^3\Pi_u)$, prod. from IR multiphoton dissoc. of acrylonitrile 80−63723
- C_2, A^3 pi_g-X'^3 pi_u bands, rot. struct., intensity alternation 79−41158
- C_2 $a^3\Pi_u$ state quenching, laser-induced fluoresc. obs. 79−31574
- C_2 absorption bands in stellar spectra, 876 nm obs. 80−12805
- C_2, band system transition moment ab initio SCF and CI calcs. 79−13770
- C_2, bond order values, ab initio calcs. and basis set depend. 80−32605
- C_2, bonding, spin density functional theory 78−17558
- C_2, calc. of bands strengths of Swann bands 77−61810
- C_2, canonical exchange energy modulation parameters, MTXα calc. 79−97997
- C_2, conc. meas. in oxyacetylene flame rel. to saturation spectroscopy 77−60148
- C_2, concentration in oxy-acetylene flame, $^3\pi_u$ state, saturation spectroscopy 77−77832
- C_2, electron affinity, vibr. struct. in radiative electron attachment spectra 77−88592
- C_2, Franck-Condon factors, rot. quantum number effect 79−31613
- C_2, ground state potential energy, non-muffin tin MS Xα calcs. 77−14355
- C_2, IR flame emission spectra, Ballik-Ramsay system 79−63999
- C_2 in comets, Swan/Phillips band ratio, statistical equilib. 79−96969
- C_2, in comets, synthetic spectra calcs. 78−28579
- C_2, in southern mag. white dwarf LP 790-29, spectrophotometric obs. 79−92765
- C_2, interstellar, detect. in spectrum of Cygnus 0B2 No.12 (VI Cygni No.12) 78−12332
- C_2, interstellar, detect. towards ζ Ophiuchi 78−49505
- C_2, interstellar, rot. fine-struct. lines obs. towards ζ Persei 80−67811
- C_2, interstellar, search in IR spectrum of ζ Ophiuchi 77−45423
- C_2, laser fluoresc. detection with high time resolution 80−9632
- C_2, laser stimulation optimisation for intraresonator spectroscopy 80−77881
- C_2, low lying $a^3\Pi_u$ state produced in intense IR field, fluoresc. and quenching obs. 80−11931
- C_2, magnetic susceptibility and anisotropy calc. *(French)* 78−37559
- C_2 molecule in solar spectrum, wavelength shift determ. method 78−49340
- C_2 molecule produced by laser irrad. of polyethylene 78−42777
- C_2, multiple photon dissoc. of C_2H_3CN, photofragment spectroscopy by laser-induced fluoresc. 80−11937
- C_2, multipole expansion of diatomic overlap, MEDO calcs. 78−46264
- C_2, Phillips system, 2.3-0.9 μm, rot. consts. 78−21925
- C_2, Phillips system, rot. depend. of Franck-Condon factors 77−27058
- C_2, pot. curves, binding and ionisation energies and config. variational cellular method 80−32597
- C_2, primary radicals, from ethylene photolysis, dye laser obs. 77−16851
- C_2, prod. by multiphoton dissoc. of organic compounds 80−5586
- C_2, reson. fluoresc. statistical equilib. calc., appl. to comets 78−1016
- C_2 resonance fluoresc. technique for transient flame investigs. 77−30894
- C_2 rotational temp. and solar photospheric models 80−62099
- C_2, solar rotational temperatures, centre to limb behaviour 79−84758
- C_2, Swan, Phillips, Deslandres-d'Azambuja, and Fox-Herzberg systems, rotational dependence 78−74701
- C_2, Swan band system, vibr.-rot. interaction on pot. energy curves 80−27965
- C_2, Swan bands, variation of electronic transition moment with internuclear separation 79−826
- C_2, Swan bands identification in mag. degenerate star LP 790−29 79−5815
- C_2, Swan transitions, relax. dynamics and two-photon excitation, in inert gas matrix 77−505
- C_2, total Xα energy, LCAO calc., rel. to local density models 80−32607
- C_2, transition moments of Swan band system, SCF-CI calc. 78−58746
- C_2, triplet ground state dissoc. continuum obs. $_{\rm is}$ UV spectrum of C_2 white dwarf (LP 145-141) 80−67715
- C_2, $X^1\Sigma^+{}_g$, $6^3\Sigma^-{}_g$ states, perturbations, ab initio CI calcs. 77−83490
- C_2^-, $A^2\Pi_u$-$X^2\Sigma_g^+$ lines, obs. in carbon stars 80−98661
- C_2^-, bound electronic states and electron affinity, IC calc. 79−76349
- C_2^-, matrix isolated, vibr. relax., absorpt. spectra 77−75172
- C_2^-, matrix isolated, vibr. energy transfer, fluoresc. 78−46382
- C_2^+, dissociative recomb. cross section determ., merged beam obs. 80−78715
- C_2^{6+}, total SCF energy estimation from orbital energies 79−63908
- C_2+acetylene, C_2 Swan band transition probabilities, collisional energy transfer effects 80−87214
- C_2+NO, laser-induced chemilum. reaction 80−61101
- $C_2+NO \rightarrow CN+CO$, chemiluminesc. reaction, crossed beam study 79−66299
- C_2+O_2, $C_2(X^1\Sigma_g^+)$ and $C_2(a^3\Pi_u)$ intersystem crossing and free radical kinetics 80−95668
- $C_2+O_2(NO)$, IR laser photolysis of polyat. mols. photochem. appls. 80−66835
- C_3, $\bar{A}^1\Pi_u$ state, orbital angular momentum 80−78514
- C_3, electron spectrum, ab initio MRD CI calcs. 78−90089
- C_3, ground and excited states, vibr., pot. curves, CI calcs. 77−83509
- C_3, ground state pot. surfaces, analytical functions 80−83304

carbon continued
- C_3, matrix isolated, vibr. relax. 78−66637
- C_3 production by IR multiphoton allene photolysis, vibr. relax., chem. kinetics 80−66820
- C_3, Renner effect, vibronic levels and wavefunctions, ab initio variational method 80−14127
- C_3, Swings band system, absorpt. cross section, oscill. strength meas 79−98116
- $C_3+O_2 \rightarrow C_2{}^*+CO+O$, chemiluminesc., rate consts. 77−44466
- C_n aggregates in equilib. C vapour, MINDO/2 calc., isomerism 78−29873
- $(C)_n$, cryst. struct. determ. from X-ray photoelectron and X-ray spectra 78−88384
- $C_2(A^3\Pi_g$-$X^3\Pi_u)$, obs. in optically-pumped CO-Ar(-N_2) 80−16701
- $C^{2+}B(F)$, K Auger electron spectra 79−89758
- $C_2(C_2^-)$ pot. energy curves calc. using SCF, MCSCF and CI methods, dissoc. energies, bond lengths, electron affinity 80−95523
- $C_2(\Delta v=+1)$ band in Comet Kohoutek (1973 XII) 78−20738
- CNO anomalies in spectra of OB stars 77−29835
- CO air pollution, statistical models with reference to Los Angeles Catalyst Study (LACS) data 80−30620
- CO-He(-O_2), glow discharge ion cluster in positive column, ion mass spectra diagnostics 80−38752
- CO_2, electron impact ionisation, dissoc. ionisation 78−13610
- $CO_2+C^+(N_2H^+)$, rate coeffs. meas. at 300 and 100K in flowing afterglow 79−20346
- $C(^3P)$ isoelectronic series, Sternheimer valence shielding and antishielding factors 80−18807
- $C^+(^2P)+CH_4$ reaction, 0.1-10 eV, complex formation 77−9073
- $C^+(^4P)+H_2$, reaction, energy and ang. distrib., energy spectra 77−1918
- $C(^3P)+O_2(^3\Sigma_g^-) \rightarrow CO(^3\Sigma^+)+O(^1D)$, pot. energy surface, vibr. population inversion, classical dynamics 77−52630
- $C^-(^4S^0)$, attachment energies, ab initio calc. 77−30768
- ^{11}C, absorbed dose comparison rel. to γ-ray emitters 79−70647
- ^{11}C, displacement visualisation in baboon brain 79−83730
- ^{11}C isotopes, production and transport system 78−46200
- ^{11}C labelled molecules, examples of use in medical research *(French)* 77−66833
- ^{11}C positron emission computerised tomography, pancreatic scanning obs. 80−30861
- ^{11}C production for nuclear medicine use 80−30889
- ^{11}C, production for studies on photosynthesis, transport and metabolism in plants 79−39502
- ^{11}C, racemic [1-^{11}C]-alanine and partially resolved [3-^{11}C]-alanine synthesis 79−88186
- ^{11}C radioisotope preparation at variable energy cyclotron of Frederic Joliot Hospital Service *(French)* 77−65361
- ^{11}C, scintigraphy, labelled thymidine, thymidylate, in vivo distrib. in rabbits 79−5344
- ^{11}C-acetylene, production by methane pyrolysis and irrad. 80−36129
- ^{11}C-iodomethane remotely controlled synthesis 79−88192
- ^{11}C-l-lactic acid, enzymatic synthesis 80−61695
- ^{11}C-pyruvic acid, enzymatic synthesis 80−61695
- ^{12}C 400 MeV/amu beam microdosimetry with wall-less proportional counters 80−26370
- ^{12}C ion, meas. of $\bar{W}$ in tissue equiv. gas, dosimetry appl. 80−19550
- ^{12}C kaonic atom, level shifts and widths, $\Lambda(1405)$ dynamics in nucleus 77−3495
- $^{12}C/^{13}C$, evidence for telluric ratio in atmospheres of Jupiter and Saturn 78−20723
- $^{12}C/^{13}C$, ratio in atmospheric of cool C star V460 Cygni 78−93223
- $^{12}C/^{13}C$ abundance ratio in C stars 77−33494
- $^{12}C/^{13}C$ in Jupiter, ratio determ. using new spectroscopic method 79−84734
- $^{12}C/^{13}C$ interstellar ratio, rel. to ^{13}C enriched matter ejection from red giants 77−9788
- $^{12}C/^{13}C$ ratio and stellar turbulent diffusion 80−21993
- $^{12}C/^{13}C$ ratio determination in atmospheres of C stars, peculiar red giants 80−17580
- $^{12}C/^{13}C$ ratio in atms. of luminous cool stars 77−13336
- $^{12}C/^{13}C$ ratio in atms. of giant and supergiant stars 77−13337
- $^{12}C/^{13}C$ ratio in C stars 79−35257
- $^{12}C/^{13}C$ ratio in G-K giant stars, explanation constraints 79−5817
- $^{12}C/^{13}C$ ratios in G-K giants and C stars, origin of freq. distrib. 77−78780
- $^{12}C/^{13}C$ ratios in Population I K-type giant stars, rel. to CN strengths 78−93229
- $^{12}C/^{13}C$ ratios in Sagittarius B2 and Orion A 79−21374
- $^{12}C/;\,^{13}C$, ratio in red giants after main-sequence mixing 77−33475
- $^{12}C^{5+}$ beam, 60 MeV, high-press. plasma production, electron props. diagnostics *(French)* 80−10407
- $^{12}C^{n+}$, partially stripped, energy straggling in thin Al foil, 3-36 MeV 79−41237
- $^{12}C+X$, $X=$Ti-Pb, atomic K-vacancy production 77−23543
- ^{12}C+alkane (alkene), thermal energy reaction, mass spectra 77−9067
- ^{13}C and D labelled paeonol and urinary metabolites, synthesis and physicochem. props. 80−67250
- ^{13}C, enrichment in multiphoton dissoc. products of trifluoromethyl halides 79−18302
- ^{13}C fractionation in calcite-depositing spring, chemical vars. and calcite precipitation 79−44202
- ^{13}C, from formaldehyde, ion laser induced photopredissociation 77−61871
- ^{13}C III, $1s^22s3p\ ^3P^0$ state,, HFS, beamfoil expt., CI and Hartree-Fock calcs. 77−75276
- ^{13}C, mechanism of spin transfer to next neighbours in complexes 78−86892
- ^{13}C NMR, chem. shift, effective excitation energy calcs. 77−14457
- ^{13}C NMR applications to cells 80−46110
- ^{13}C, NMR spectra assignment, proton-C splitting scaling 78−46372
- ^{13}C natural abundance dipolar interaction in hexamethylethane, NMR longit. cross relax. 80−93196
- ^{13}C, nuclei in molecules, isotope shifts calcs. 78−86917
- ^{13}C, palaeoclimatic features, based on stable isotope compositions, Lake Biwa, central Japan 79−12230
- ^{13}C V, high energy hyperfine struct. meas. 77−57915
- $^{13}C/^{12}C$, ratios in N.American ancient wood cellulose (9500-22000 BP) 77−60462
- $^{13}C/^{12}C$ dating of New Zealand kauri cellulose for last millennium 80−21819
- $^{13}C/^{12}C$ for rocks in Tertiary igneous complex of Skye 77−33012

carbon continued
  - $^{13}C/^{12}C$ from tree ring ^{13}C records, interpretation problems 79-62573
  - $^{13}C/^{12}C$ isotope fractionation of organic matter assoc. with U ores induced by alpha irradiation 79-57932
  - $^{13}C/^{12}C$ ratio analysis in carbonates by mass spectrometry *(Portuguese)* 80-7875
  - $^{13}C/^{12}C$ ratio in magmatic gases of Afar ridge volcanism 80-21732
  - $^{13}C/^{12}C$ ratio variations in Pinus longaeva (bristlecone pine) cellulose during the last millennium 79-44217
  - $^{13}C^{+}+^{12}CO$, isotopic exchange, interstellar implications 80-61087
  - ^{14}C absolute dating using low altitude European tree-ring calibration 78-16195
  - ^{14}C, abundance rel. to cosmic rays and solar activity cyclic vars. 79-16776
  - ^{14}C activity and distrib. in gaseous effluents from PWRs 79-85829
  - ^{14}C age errors for recent deposits with fluvially transported charcoal 78-36172
  - ^{14}C analysis of soil, dating 78-36299
  - ^{14}C anomaly in groundwater from regional carbonate aquifer, Great Basin, Nevada 77-45042
  - ^{14}C, autoradiography of thin laminars *(French)* 80-35438
  - ^{14}C beam prod. from isotopically enriched sputter targets 80-23221
  - ^{14}C β-rays, biological hazards, cell killing effects, E. coli expts. 80-89805
  - ^{14}C chronology of late Quaternary lakes in Arabian Desert 77-5161
  - ^{14}C concentration in Earth's atmosphere, corrections with astrophysical and geophysical phenomena 78-61477
  - ^{14}C, concs. in Florida annual coral rings 79-16513
  - ^{14}C content in tree rings correl. with solar cycle, 1744-1892 period *(Russian)* 78-16390
  - ^{14}C, continuous monitoring, sensitive method *(German)* 77-372
  - ^{14}C, cosmogenic conc. in Earth atm., diffusion distrib. 80-101510
  - ^{14}C dating, high energy mass spectrometer appls. 80-101917
  - ^{14}C dating of CO_2 sample with accelerator, blind meas. 79-25362
  - ^{14}C dating of mg geological samples with electrostatic accelerators 79-25361
  - ^{14}C dating of small samples via proportional counting 80-82102
  - ^{14}C dating rel. to magnetic and other dating methods 78-57359
  - ^{14}C dating technique using cyclotrons, or Van de Graaff as mass spectrometer 80-5414
  - ^{14}C dating using cyclotron as mass spectrometer 77-64489
  - ^{14}C dating using electrostatic accelerators and negative ions 78-32917
  - ^{14}C, detect. via small van de Graaff accelerator 79-11844
  - ^{14}C direct detection at natural concs. by mass spectrometry, for dating 78-32916
  - ^{14}C, dissolved in groundwater initial activity determ., new model and review 80-8458
  - ^{14}C, distrib. in submersible-taken deep sea cores from Project FAMOUS 77-37179
  - ^{14}C distrib. in W. Atlantic abyssal waters 77-5228
  - ^{14}C distribution, Ross Ice Shelf Project ice hole 79-88371
  - ^{14}C, dosimetry and metabolism of low energy β-emitters 79-8551
  - ^{14}C, dosimetry of labelled diethylenetriamine pentaacetic acid in the rat 79-62366
  - ^{14}C, enrichment method for radiocarbon dating 79-10220
  - ^{14}C fallout from nucl. weapons testing, human radiation burden 77-64091
  - ^{14}C fallout from nucl. weapons testing, use as biological tracer 77-64162
  - ^{14}C, formation, distrib. in nuclear fuel cycle *(Russian)* 80-5316
  - ^{14}C geochemistry in Galapagos Rise hot spring field, rel. to clam growth rate determ. 79-84300
  - ^{14}C in atmosphere, variability due to variable Sun 80-85730
  - ^{14}C in atmosphere content variation, past geomagnetic and cosmic ray intensity variations 78-61691
  - ^{14}C in groundwater, possible subsurface prod. rel. to dating 80-85690
  - ^{14}C, in red giant stars, nucleosynthesis and possible detectability 77-26005
  - ^{14}C, in solar wind, abundance 77-5407
  - ^{14}C in wines, abundance vars. with 11-year solar cycle, (1909 to 1952) 80-109249
  - ^{14}C labelled amino acids, optimisation factors in liquid scintillation counting 80-30951
  - ^{14}C labelled plant material, growth in simply constructed cabinet 79-84044
  - ^{14}C, liquid scintillation counting efficiency, volume and quenching effects 79-76270
  - ^{14}C low level liq. scintillation counting using small vol. teflon-Cu vial 80-16887
  - ^{14}C measurement in known age specimens, cosmic ray intensity determ. 80-101516
  - ^{14}C natural var. in atmosphere, Suess effect determ. accuracy 79-96801
  - ^{14}C, nuclear reactor radioactive gaseous effluents, abatement techniques 79-3221
  - ^{14}C on polyacrylamine gel, automated scanning 80-17221
  - ^{14}C pollution of Atlantic from nucl. weapons tests 80-89683
  - ^{14}C, prod. of intense negative beam from graphite 80-102361
  - ^{14}C produced in advanced FBR fuels, potential radiation doses 77-40799
  - ^{14}C production and discharge in BWRs 79-52979
  - ^{14}C production by nuclear power industry 77-54367
  - ^{14}C production in terrestrial atmosphere from Tunguska cometary impact 77-78720
  - ^{14}C, radioactivity meas. using Cherenkov liquid scintillator counter 79-26817
  - ^{14}C reactor radwaste, gas processing with low temp. rectification for quasi-null release 79-67877
  - ^{14}C released to atmosphere, dynamic model for estimating radiation dose to world population 80-89852
  - ^{14}C temporal atmospheric fluctuations 79-5591
  - ^{14}C trace elements in seawater estimation *(Dutch)* 77-29459
  - ^{14}C, use in dating, review of technique 79-49922
  - $^{14}C/^{13}C/^{12}C$ vars., Bermuda coral 200 yr. record 79-16570
  - ^{14}C-labelled bumetanide, whole body autoradiography in dogs by round saw method 80-72399
  - $C^{+*}+Ar(H_2)(N_2)(CO)(CO_2)(O_2)$, charge transfer cross-sections, 0.7-2.4 keV, $C^{+}(^{2}P)$ and $C^{+}(^{4}P)$ 78-58806
  - $C(2^{1}S_0)+H_2(O_2)$(ethylene) 80-74241
  - $^{13,14}C$, thermal diffusion separation column, effective vol. calc. *(German)* 78-42235

carbon continued
  - $C^{-}(4S)$+molecule, spin angular momentum conservation in proton transfer 77-16805
  - C=C bond, ^{13}C shielding tensor, NMR meas. 78-1005
  - CaO-Al_2O_3, binary slag, reduction of Al_2O_3 by C saturated Fe *(Japanese)* 79-24733
  - $C_2(a^3\Pi_u)+NO$(vinyl cyanide)(ethylene), laser-generated radical kinetics 79-100352
  - $C_2^{-}(a^4\Sigma)$, in Ar(Kr)(Ar-Kr) matrices, multiphonon vibr. relax., time-resolved emission obs. 80-18861
  - $C_2(a^3\pi_u)$, collisionless production in IR laser field 78-55206
  - $C_2(d^3\Pi_g)$ shock wave excitation, emission, excited state populations, in CO-N_2-Ar mixtures *(Russian)* 78-74638
  - Cl+He(C)(O)(Ne), K-shell ionising collisions, average L-shell ionisation probability, K_α spectra 79-72408
  - Cu:Au:C, surface, obs. at very low accel. voltage (200 V-1 kV) by SEM 80-10764
  - $Cu+C^{n+}$, radiative electron capture, target electron momentum distrib. 78-1075
  - D implanted, trapping of D, calibration for particle energy meas. in plasma boundary of Tokamaks 79-98983
  - F ions+Ne(Ar)(Kr) and C foil and slab, K shell X-ray spectra 78-17599
  - Fe, BCC, mag. relax. due to C and N meas., 210 to 410K 77-36102
  - Fe, cast, air-atomized powder, effect of particle size on C and O contents 78-15340
  - Fe film, vacuum-evaporated contamination, conversion electron Mossbauer spectroscopic obs. 78-23985
  - α-Fe, S and C diffusion, AES obs. 77-51543
  - Fe, structural stabilisation, influence of C interstitials, HF calc. 79-11611
  - Fe surface hardening, ion-carbo-nitriding in CO-N_2-H_2 gas mixtures, expt. *(Japanese)* 80-71670
  - Fe:$^{12}C(2_1^{+})$, PAC meas. of transient mag. fields 79-99800
  - Fe:^{13}C, transient mag. field for ^{13}C 79-47362
  - Fe:C, decarburisation by H_2, conversion electron Mossbauer obs. 78-85198
  - α-Fe:C, electron irrad., vacancy-C interaction, positron lifetime meas. 80-75264
  - α-Fe:C, electronic struct., Hartree-Fock calc. 78-14692
  - Fe:C, neutron irradiated at low temp., mag. disaccommodation 80-44881
  - α-Fe:C, valency effect of interstitials 80-65502
  - Fe:C(N), small concs. determ., mag. and mech. relax. methods 80-7879
  - Fe-Al-C, mag. permeability disaccommodation 78-88141
  - Fe-B-C amorphous alloys, effect of Si addition on mag. props. 80-34694
  - Fe-C, pearlite, eutectoid alloy, efficiency of directional transformation on orientated growth 78-76642
  - Fe-CR (26 wt.%), role of C and N in brittle fracture 80-16456
  - Fe-C(0.001 to 0.44 wt.%), C effect on low temp. brittleness *(Japanese)* 80-50711
  - Fe-C(1.54 wt.%), electrocapillary curves in liq. sodium tetraborate 79-91968
  - GaAs, C, O, Si impurities 78-59832
  - GaAs, epitaxial layer, C distrib., anal. by quasichem. reactions 77-11803
  - GaAs:C, diamagnetism quenching 80-6782
  - p-GaAs:C, ion implantation efficiency, elec. profile and compensation level meas. 77-27880
  - GaAs:C, ion implanted, laser annealing, ellipsometric and Hall meas. 79-73193
  - GaAs:C, MBE layers, photoluminesc. 80-29803
  - GaAs:C, Zeeman effect of effective mass acceptor, polarised luminesc. 79-4541
  - GaAs:C,O, impurity conc. determ. in LEC grown cryst. 77-39612
  - GaAs:C^{+},Ga^{+}, dual implantation of C^{+} and Ga^{+}, sheet resist. and Hall effect meas. 78-67728
  - GaAs-C, ion implanted, obs. of localised vibrational mode absorption, effects of annealing temp. 80-16068
  - GaP:C, excited acceptor state investig. by photoluminesc. 77-8632
  - GaP:C, IR photocond. response spectra 79-56257
  - GaP:C,S(Te), donor-acceptor pair luminesc., excitation spectroscopy 80-25440
  - GaP:C,Si, LPE, cathodo- and electrolum., residual impurity and struct. defect effects 78-19570
  - GaP:N,C, interimpurity recomb., acceptor binding energies 78-34796
  - n-GaP:N,O,S,C end, dielec. const. from S-C donor acceptor pair spectra 79-65788
  - H isotope backscattering, trapping, and depth profiles, model 79-99233
  - H-C, thermal desorption, one-phonon at. scatt., 3-dimens., continuum model 78-87860
  - $H+B^{q+}(C^{q+})(N^{q+})(O^{q+})$, $(2\leq q\leq 4, 5)$, cross sections at keV energies 80-78705
  - H+C, surface chemical reaction of thermal at. H 78-20071
  - $H+C^{+}(C^{3+})$, ionization model for NGC 7027 planetary nebula 78-36671
  - $H+C^{2+}(C^{3+})(N^{2+})$, radiative charge transfer, rate coeffs., pot. energy curves 77-88554
  - $H+C^{6+}(He^{2+})$, ionis. cross sections 79-22805
  - $H+H^{+}(Arq^{+})(Kr^{q+})(B^{q+})(C^{q+})(N^{q+})(O^{q+})$ charge transfer and impact ionis. cross sections calcs. 77-88555
  - $H+Li^{3+}(Be^{4+})(B^{5+})(C^{6+})$, charge transfer cross sections, distorted wave Born approx. 79-72415
  - H_2^{+}, energy loss in C foil, moving ion pot. determ. 78-33572
  - $He+B^{3+}(C^{4+})(N^{5+})(O^{6+})$, electron transfer 78-13598
  - HeH^{+}, energy loss in C foil, moving ion pot. determ. 78-33572
  - Hg-C optically transparent electrodes, prep., props. 78-7210
  - IV profiles at 1548 Å, OSO 8 time series rel. to solar chromospheric oscills. 79-53785
  - InP: C, O, impurity conc. determ. in LEC grown cryst. 77-39612
  - $Kr+C^{+}(H^{+})(N^{+})(O^{+})(S^{+})$, charge exchange cross-sections *(German)* 77-10753
  - LaB_6:C, AES, LEED and energy-loss spectra study of C layer on (100) surface 77-62715
  - Li ions stopping power and straggling 80-42908
  - Li_2O:C, conc. profile of C determ. by proton backscattering 78-10079
  - MgO:C, single cryst. grown by arc fusion, C content 77-68991
  - Mo, C and Ir impurities in single cryst. growth, effect on fine struct. *(German)* 77-28714

carbon continued
Mo, cast state, interaction nature between C, O_2 and N_2 *(Russian)* 79−70114
Mo:C (110) surface, segregation, precip. and desorpt. of C, AES and LEED study *(French)* 80−103480
N^{2+}, electron impact ionisation cross sections, autoionisation contrib. at low temp. 80−32838
N_2+C^+ collisions, luminesc. 80−1055
^{15}N-^{13}C spin-spin coupling constants calc. using SCF and INDO method 80−32609
Nb film, C impurity effects on supercond. transition temp. and transition width *(Russian)* 77−66222
NbC, C implanted, channelling crit. angle and min. yields 78−47458
Ni 200, C interstitial effect of yield point develop. during static strain ageing, model 78−88498
Ni, neutron irrad., void formation, C interstitial effects 77−76471
Ni:C, bulk-to-surface precip. and surface diffusion, AES meas. 77−11784
Ni:C, bulk-to-surface precip. and surface diffusion of C, AES data interpretation 78−34713
Ni:C, H(D), isotope effects of C-H and C-D complexes 77−20129
Ni-C system, satellite structs. of intermed. phases in diamond synthesis using Ni catalyst *(German)* 77−32538
Ni-Fe-C, 20 at.% Fe, vacancy-C interaction, induced mag. anisotropy *(French)* 79−55775
Ni_3Fe:C, mag. anisotropy depend. on C content, magnetometric study *(Russian)* 80−54887
NiO:C, surface charge, O(1s), C(1s) and Ni(2p) XPS 80−45196
$O_2+N^+(O^+)(C^+)$, rate coeffs. meas. at 300 and 100K in flowing afterglow 79−20346
$OH^-+C(N_2)$, electron stripping and breakup, proton spectra 77−83685
P-C, one-bond couplings, orbital and spin dipolar contribs., INDO approx. 79−31552
Pd membrane, C coated, H penetrability *(Russian)* 77−77808
Pd-Ag, Fermi energy influence on soln. behaviour of H, B and C *(German)* 80−44323
Pt:C, C layer formation on (111) surface, temp. depend., LEED, AES study 78−71911
Pt-C replicas, for rapid aimed replica prep. 80−61037
Re:C, work function, graphitic layer formation 80−96966
^{32}S ions+Be(C)(Ni), radiative electron capture, X-ray ang. distrib. 77−38729
Si, dislocation free, C and O impurity clouds, heat treatment influence on light scatt. 80−6427
in Si, effect on Au diffusion 78−10076
in Si, reaction of rare earth impurities with carbon during cryst. growth 79−38733
Si wafer C impurity IR absorption spectrometry, thickness fringe elimination 80−55132
Si:C, disorder profiles by proton backscattering, proton bombardment annealing 78−47449
Si:C, H^+ and He^+ beam impact phemomena, damage annealing rates 78−47450
Si:C, implant redistribution, annealing effects, SIMS meas. 80−96561
Si:C, impurity determ. by IR absorpt. spectroscopy, room temp. and low temp. meas. comparison 80−108237
Si:C, striated impurity distrib. calc. in melt-grown crystals 80−24488
Si:C, vibrational properties of the ⟨001⟩ split interstitial 78−91405
Si:C wafers, impurity meas. by Fourier transform IR spectra 80−89030
Si:C wafers, impurity meas. by Fourier transform IR spectra at low temp. 80−89031
Si:C(O), photoluminescence spectra, radiation damage investig. 77−28620
Si:In, C, 0.111-eV acceptor level, X-level defect conc. from IR absorpt. and Hall meas. 79−51512
Si:O, C, impurity conc. profiles and process-induced defects 78−6094
Si-C, one-bond couplings, orbital and spin dipolar contribs., INDO approx. 79−31552
Si-C interface on polycryst. Si ribbon, effect on solar cell efficiency *(French)* 80−54531
Si-C-O-Ar, high temp. plasma, prod. quenching mol. dynamics simulation 78−39711
Si-SiC struct. formation on ^{12}C ion implantation in Si, optical and photoelectric props. 79−91136
SiC-C, sputtering and blistering from H^+ and He^+ bombardment 78−79649
Si_3N_4:C film struct., oxidation, defects 79−51455
Si_3N_4-Y_2O_3 ceramic, thermal degradation, C impurity effect 80−50708
α,β-Si_3N_4+C, powders, high temp. reactions *(Japanese)* 77−48685
SiO_2 reduction, with C and SiC, forming SiO vap. 79−79240
T 79−5766
tetrafluoromethane+C react. in ionising radiation of nuclear reactor 77−63934
Ti-C system, reaction diffusion analysis 77−28049
TiI_4:C, deep doping during ion-beam welding, microhardness meas. 79−19294
TiO_2 reaction with C/Cl_2, high temp. chlorination, volatile species 79−83451
(U, Me)C, Me=Hf, Ti, Zr, Nb or Ta, effects of alloying and interaction with C 79−45350
V-C sandwiches, energy gap fluctuations *(Russian)* 78−34930
W, cast state, interaction nature between C, O_2 and N_2 *(Russian)* 79−70114
W-C point contact, compared with TGS pyroelec. detector, appl. to temporal coherence meas. of HCN laser 80−31871
W-Re/C multilayer, periodic and near-periodic, small-angle interferences of reflected X-rays 79−94846
Zr-C disordered systems, Hall effect depend. on composition conc. 79−95459
ZrC-C, disordered, Hall const. anomalies 79−56277
ZrC-C composite system, negative magnetoresist. 80−60008

carbon compounds
see also organic compounds
acetaldehyde+CO_2, vibr. relax., search for unquenchable species, room temp., 5-2200 torr 78−9229
air pollution removal mechanisms and processes *(Dutch)* 77−70824
alkali halide:CN^-, Kerr effect and birefringence from paraelectric CN^- defects 78−43838
carbide coating formation by chromising C steels 78−88571

carbon compounds continued
carbides, brittle materials, swelling, blistering, p, d, and He ion irrads. porosity effects 77−35603
carbonate chemistry of chalk water from Givendale, E.Yorkshire 79−66719
carbonate formation in Marslike environments 78−61778
carbonates, $^{18}O/^{16}O$ ratio analysis by mass spectrometry *(Portuguese)* 80−7875
carbonates, Isua sediments, W.Greenland, isotope averages and Archaean C and O cycles 79−84262
carbonates dissolved in groundwater, in Edwards artesian aquifer, Texas 78−73416
carbonates in deep sea rel. to deglaciation preservation spike in pteropods and foraminifera 77−86853
carbonyls, electric polarisability, in excited singlet and triplet states *(Bulgarian)* 80−52897
carboranes, bonding topology, graph-theoretical interpretation 78−33408
chemisorption on Co (10$\bar{1}$2), heating effects 79−4474
chlorotrifluoroethane, IR photoreaction *(Japanese)* 80−11885
$CO_2+^{18}OH$, evidence for at. exchange 79−47910
CO_2 laser construction as student project, design and building methods 79−97166
CO isotope mapping of L 134 N 79−30108
coadsorption with O_2 on Ru (001), uptake and flash desorption meas. 80−39450
CS_2, Raman laser as efficient excitation source for stimulated Raman scatt. 79−18480
cyanide, on Ag, at electrolyte interface, enhanced Raman effect 79−28767
cyanide deposits in CO_2 TEA lasers using amine additives 77−71991
cyanogen, thermal desorption on Pt (100) 77−31884
cyanogen adsorbed in Pt (100), UPS 77−36351
cytochrome P-450-CO complex, absorpt. spectrum, electronic transitions, PPP calcs. 77−71811
DF-CO_2 CW chemical transfer laser, comprehensive kinetics model 79−81422
diatomic molecules, linear, substituted fragment series, electronic struct. transferability, mutual at. influence 78−9066
ESCA shifts and effective charges 80−78648
ethylene-CO copolymer, dielec. absorpt. meas., permittivity *(French)* 80−103916
excited state props., by electrochromism in polymer matrix 79−22737
gas mixture, thermal diffusion const. 78−67300
graphite fluorides, $(CF)_n$ and $(C_2F)_n$, prep., struct., discharge characts., electrode props. 80−89502
graphite monofluoride, self-consistent semi-empirical LCAO calcs. of electronic band struct. 77−85142
graphite monofluoride, surface alteration by interaction with Ar^+ and Xe^+ beams 78−91347
graphite nitrate, $(C_{3.24})^+(NO_3)^-3HNO_3$, DTA, NMR and refl. meas., dynamical and electronic props. 77−59478
haemoglobin-CO complex, absorpt. spectrum, electronic transitions, PPP calcs. 77−71811
hexafluorethane, plasma etching characts., effect of dark space in RF glow discharge 79−15830
intercalation of graphite by $TiCl_4$ 80−40675
interconversion pot. energy surfaces, geometries, electronic structs. 78−35660
interstellar cloud gas phase chemistry 80−105319
lunar soil samples, C chemistry from Luna 16 and 20 77−22122
mass identified ions in O, N, CO and CO_2, transport properties, obs. and calc. 79−50837
metal carbonyls, excited metal atom prod. by UV multiphoton dissoc. 79--6974
mixtures, marginal comp., thermal diffusion column performance evaluation *(German)* 80−59157
molecular beams, nozzle-formed, energy parameter determ., time-of-flight method 79−64122
molecular cluster formation, in rarefied nozzle flowfield 80−5639
molecule, ground state MNDO calcs. 78−911
molecule, pot. curves, ab initio MRD-CI method 80−83293
molecules involving B and C atoms, self-consistent charge calcs. of core-electron binding energy shifts 80−69084
monocarbide, cubic, calc. of surface energy, rupture energy, and theoretical strength 77−11775
monocarbides of subgroups IVa and Va, kinetic props., review 78−47613
oscillatory oxidation over Pt 79−61905
oxides, glow discharge, excitation and ionisation mech., elec. and optical obs. *(Russian)* 78−59695
polyethylene, neutron penetration, Monte Carlo calculations for 30, 45 MeV *(Japanese)* 80−18677
pyrocarbon, agglomerate model 77−79458
pyrocarbon, coating process and model 77−79459
pyrocarbon, quality control techniques 77−79461
pyrocarbon, X-ray anal. of porosity, effect on radiation stability 77−79464
rapid anal. by mass spectrometry/mass spectrometry 80−61173
refractory materials, group IVa and Va, slip, microhardness, comments 78−84967
single and multiple free jet conc. meas., CW laser Raman spectroscopy 79−97447
Stark tunable molecular gases, absorption of laser radiation *(Rumanian)* 79−86157
thiocarbonates, mol. struct., S-substitution effect *(French)* 80−23335
triatomic molecules, linear, substituted fragment series, electronic struct. transferability, mutual at. influence 78−9066
trifluoroiodomethane, high press., selective isotope dissociation with pulsed CO_2 laser 79−72370
$^{12}CO(^{13}CO)+H_2$, vibr. relax. rate, stimulated Raman scatt. obs. 77−75269
Ag/CN, coverage meas. using surface enhanced Raman scatt. and radioisotope meas., electrochemical treatments 80−29260
$Al+CO_2 \rightarrow AlO+CO$, HTFFR kinetics obs., 300 to 1900C 77−90596
$Ar+CO_2$, rot. transitions, classical trajectory calcs. 77−50501
$Ar^++H_2(O_2)(CO_2)$, reactions in flow-drift tube, rate consts. 78−15664
$Ar^{2+}+O_2(CO_2)(C_2H_2)$, reactions in flow-drift tube, rate consts. 78−15664
B-C system, phase diagram review, book contrib. 78−48388
BCl_3-$COCl_2$, impurity removal by laser irrad., IR spectra meas. 78−15686
BF_3-CO_2 mixtures, ang. neutron flux distribs. meas. 77−54276

carbon compounds continued
- Ba+CO(CO_2), flame spectra, 500-1150 nm mechanism 77−48646
- Br_2-CO_2 chem. pumped photodissociation laser, output energy increase by WF_6 addition 79−45939
- Br_2-CO_2 IR laser with $Br^* \rightarrow CO_2$ electronic-vibr. energy transfer as pump mechanism 80−53260
- BrCN, ICN, and isotopic forms, force field calc., freqs., rot. consts. 79−22693
- BrCN, vacuum UV photodissociation spectroscopy, quantum yield, fluoresc. polarisation 80−32736
- ^{13}C, isotropic hyperfine coupling consts. in small radicals 80−52894
- $^{13}C/^{12}C$ ratio analysis in carbonates by mass spectrometry *(Portuguese)* 80−7875
- C-bearing gases, K-shell X-ray yields, proton-induced, chem. effects 80−37820
- C-C, C-H, vibr. amplitudes-internucl. distance relation validity, Badger's rule 77−68028
- C-H-O(-N) gas mixtures, high temp. emissivity, 4.8 μ region, shock waves 77−76027
- C-O-H-N-Si-Ar, computer calculations of heterogeneous equilib. 79−66044
- C-Si, amorphous, localised gap states, variable range hopping 77−72866
- ^{13}C-^{13}C spin-spin coupling consts., data compilation, meas. and appls. review 80−17725
- ^{13}C-^{13}C spin-spin coupling const. and stretching force consts., single and double bonds 80−63867
- C+CO_2 reaction, kinetics at low press. and hydrogen inhibition 77−63950
- C+CO_2 reaction, Langmuir-Hinshelwood kinetics at intermed. press. 77−66766
- C_2, $^3\Pi_g$ states, large CI wavefunctions, non-adiabatic coupling matrix elements 80−37744
- C_2, luminesc. assignments in excimer laser photolysis of CBr_4 and CF_2Br_2 79−39184
- C_2, valence states, CI calcs. 79−45642
- C_2+He, $C_2(A^3\Pi_g)$ vibr. relax. 80−53106
- C_3, linear, high temp., rot.-vibr., anharmonicity, thermodynamic function calcs. 80−43830
- $C_8{}^+AsF_6{}^-$, synthesis of first stage graphite salt, relationship to first stage graphite/AsF_5 intercalate 79−24738
- 2,4-$C_2B_5H_7$, polyhedral, spin coupled ^{11}B-^1H systems, 2-dimens. correl. NMR 80−69166
- $C_2B_{n-2}H_n$, n=5-12, localised orbitals, bonding, PRDDO calcs. 78−13431
- CBr_4, bubble departure radii at solidification interfaces 80−44295
- CBr_4, low gravity solidification, bubble behaviour 80−15219
- CCl, reaction rate const. determ. using laser-induced fluoresc. technique 80−97682
- CCl_2, reaction rate const. determ. using laser-induced fluoresc. technique 80−97682
- $C_{12}Cl$ and $C_{16}Cl$ intercalation compounds, form. and struct. *(French)* 80−40674
- CClF, reaction rate const. determ. using laser-induced fluoresc. technique 80−97682
- CCl_2FO_2+NO(NO_2), reaction, photolysis obs. 79−74931
- $CCl_2FO_2NO_2$, thermal dissoc., rel. to photodissoc. and stratospheric Cl budget 79−74931
- CCl_3O_2+NO+NO_3, photolysis, $CCl_3O_2NO_2$ thermal decomposition in stratosphere 79−57256
- $CCl_3O_2NO_2$, thermal decomposition, form. and lifetime in stratosphere 79−57256
- CCl_3PCl_4, cryst., libration freqs., temp. depend., combination light scatt. and NQR obs. *(Russian)* 77−66436
- $CCl(\bar{X}^2\Pi)$+methylhalosilanes, reaction rate const. determ. by kinetic absorpt. spectroscopy 80−97683
- CD^+, $A^1\Pi$-$X^1\Sigma$ band system, spectroscopic consts. and isotope shifts 79−59485
- CD^++HD(H_2), isotopic exchange, interstellar implications 80−61087
- CD_2 filled optical fibres, CW backward-wave generation by degenerate four-wave mixing 79−27327
- CD_2 target plasma, CO_2 laser produced, press. depend. of self-generated mag. field 78−26310
- CD_4, adsorbed film on PbI_2 cleavage faces, layer-like charact., neutron diffr. obs. 79−86994
- CF, electronic Rydberg states, dissoc. energy, multiconfig. HF calcs. 79−59360
- CF, low-lying electronic valence states, dissoc. energy, multiconfig. HF calcs. 79−59359
- CF_2, energy deposition and primary current profiles 80−39184
- CF_2, excitation by Hg 253.7 nm line, reson. fluoresc-spectra 80−63694
- CF_2, fluoresc. and radiative lifetime obs. in dibromodifluoromethane UV laser photolysis 80−16703
- CF_2, luminesc. assignments in excimer laser photolysis of CBr_4 and CF_2Br_2 79−39184
- CF_2 radical, UV emission in microwave discharge, assignments 77−50461
- CF_2+H, IR matrix isolation spectra 80−97706
- CF_2+He(Ne)(N_2)(SF_6), vibr. deactivation of CF_2 first excited single state 79−94061
- CF_3 radical, dipole moment from beam mass spectrometric anal. 79−59596
- CF_4, electron emission from thin W wire into gas under strong elec. fields 79−83108
- CF_4 laser, for 16 μm range, review *(Rumanian)* 80−87408
- CF_4, molecular laser operating in 16 μm region 77−50656
- CF_4 Nd laser excited stimulated Mendelstam-Brillouin scatt. phase fluctuations *(Russian)* 80−89014
- CF_4-UF_4 mixture, gas core fission reactor, fission based plasma engine 80−63366
- CF_x, exam. of graphite fluorination kinetics, meas. of activation energy, reaction rate 79−96284
- $(CF_x)_n$ rubbed films applied to different finished surfaces, obs. 79−83332
- CF_2Cl_2, electron emission from thin W wire into gas under strong elec. fields 79−83108
- CF_3Cl, ^{18}F-recoil labelling 80−23203
- C_8FeCl_3, behaviour with H_2 and CO, effect of activation 79−43623
- CH bond dipole calcs. 80−69067
- CH, formed by laser photolysis of methylamine fluoresc. obs. 80−97710
- CH, interstellar, detect. in NGC 4945, NGC 5128 and LMC 80−46673

carbon compounds continued
- CH^+, ‘π^-‘Σ band systems, vibr.-rot. interaction on pot. energy curves 80−27965
- CH^+, formation in diffuse interstellar clouds, problems 79−75266
- CH^+, gaseous diffusion in He gas, ion mobility and longit. diffusion of Ar^+ and $CH_x{}^+$ *(French)* 79−94766
- CH^+, ground state photodissoc. cross sections into $A^1\Pi$ state 78−82793
- CH^+ indirect nucl. spin-spin coupling const., Hartree-Fock and polarisation propag. calcs. 78−9170
- CH^+, photodissociation to C^+ and H, wavelength depend. and photofragment kinetic energies, visible obs. 80−58275
- CH^+, rot. excitation by electron impact 79−27094
- CH^+, rot. excitation by low-energy electrons *(Russian)* 79−94093
- CH^+, rot. excitation by slow electrons, calc. 78−5360
- CH+H_2, doublet and quartet states, abstraction reactions, pot. energy surfaces calcs. 78−31627
- CH^++HD(D_2), isotopic exchange, interstellar implications 80−61087
- CH_4, triple point, International Practical Temp. Scale, comparisons 79−40566
- $(CH_3)_3CH$, electron emission from thin W wire into gas under strong elec. fields 79−83108
- CH_3Cl, electron emission from thin W wire into gas under strong elec. fields 79−83108
- $(CH_3)_4NUO_2(NO_3)_4$, fluoresc. decay rates, temp. depend. 80−25429
- CH_2SiH_2, ab initio GO calc. 78−94187
- C_8K graphite intercalation compound, band structure calc., charge transfer effect 80−6692
- C_8K, intercalation compound, superconductivity 78−91827
- C_8K, K-graphite intercalation compound, electronic struct. using semi-empirical tight-binding scheme 78−6255
- CLi_3, desorption from graphite expt., ionis. pot. 79−34392
- CN $^4\Sigma^+$, identification and characterisation by anticrossing 77−6864
- CN, ($A^2Pi_i \rightarrow X^2\Sigma^+$) and ($B^2\Sigma^+ \rightarrow X^2\Sigma^+$) yields from HCN photodissoc. 80−87141
- CN ($A^2\Pi$-$X^2\Sigma^+$) transition, Franck-Condon factors, r-centroids, by Langer's approx. method 78−37685
- CN ($A^2\Pi$), chem. prod., CN number densities for gain, emission and absorpt. meas. 78−63112
- CN, ($B^2\Sigma^+$), polarised fluoresc. following synchrotron radiation photodissoc. of ICN 79−98130
- CN, ($X^2\Sigma^+$), prod. from IR multiphoton dissoc. of acrylonitrile 80−63723
- CN (X), free radicals, state distribs. rel. to prod. by photolysis of dicyanoacetylene 77−9107
- CN (0,0) band in Comet Kohoutek (1973 XII) 78−20738
- CN (0,0) vibr. band in Comet Mrkos (1957 V) 78−20734
- CN, A- and B-state lifetimes, collisional transfers and perturbations 78−78756
- CN, $A^2\Pi_i$ state vibr. distrib., chemiluminesc. 79−39152
- CN, abundance in comets from radiance of violet CN spectra bands 78−16348
- CN, $B^2\Sigma^+ \leftarrow A^2\Pi$ 0-0 and 1-0 bands, laser excitation spectra 80−91588
- CN, CN^-, HF electron affinity, SCF calcs. 77−67979
- CN, fluoresc. spectra, time resolved, radiative decay and radiationless deactivation in Ar 79−98142
- CN formed by laser photolysis of methylamine, fluoresc. obs. 80−97710
- CN, Fourier spectrometry of $A^2\Pi \rightarrow X^2\Sigma$ transition 77−57995
- CN free radical, $A^2\Pi$-$X^2\Sigma^+$ Red system, perturbation analysis 80−87247
- CN, free radical, anticrossing spectra for fine struct. consts. 79−68270
- CN, free radical, electron affinity 77−47375
- CN, from ICN photodissoc., internal state distrib., laser-induced fluoresc. 77−36773
- CN, high mag. field spectroscopy 79−72445
- CN, in arc, normalised temperature, localised emission, aureoles *(German)* 77−62413
- CN in F- and G-type stars, bands oscillator strengths rel. to C and N abundances 77−91530
- CN in neutral cometary atmospheres, prod. 80−82303
- CN in Population I K-type giant stars, band strengths rel. to $^{12}C/^{13}C$ ratios 78−93229
- CN, internal energy distrib. following vinyl cyanide photodissoc., temp. depend. 80−78638
- CN, interstellar, relationship with N_2H^+, HCO^+ and HCN 77−33587
- CN, interstellar, towards Cepheus OB2 association, spectral lines obs. 80−22052
- CN lines identification in cool Ap stars 77−91551
- CN, matrix isolated, interstate cascading radiationless transitions 77−46594
- CN molecular bands in N_2 and air-O_2 arcs, CN origin, band identification 80−38803
- CN, monolayer on Ag, picosecond Raman gain spectroscopy 80−25351
- CN, monolayer on Ag surface, vibr. spectra, picosec. Raman gain technique 80−91859
- CN photodissociation laser, IR stimulated emission due to BrCN photolysis 79−31888
- CN, prod. by RCN photodissoc., fluoresc. obs. 79−52725
- CN, r-centroids for $B^2\Sigma^+$-$X^2\Sigma^+$ transition 78−70811
- CN, RKR Franck-Condon factors and r-centroids for $B^2\Sigma$-$A^2\pi$ transition 79−81195
- CN, radical, ($A^2\pi$-$X^2\Sigma$) fluoresc. predissoc. in HCN photodissoc. 77−38691
- CN, radical, $A^2\pi$ state, collisional deactivation, fluoresc. quenching obs. 77−83642
- CN, radical, adiabatic electron affinity, CI calcs. 79−68197
- CN radical, effect on alkali-halide ion-induced luminesc. 77−16402
- CN, radical, electronic, vibr. and rot. energy partitioning obs. following ICN photolysis 77−16853
- CN, radical, nonradiative transition rates, matrix isolated molecule 78−78740
- CN radical, photofragment spectroscopy of A-X transition 79−52726
- CN, radical, $X^2\Sigma^+$ ground state, microwave absorpt. spectrum 78−17657
- CN, radical fluoresc. excitation spectrum and laser emission from ICN photolysis 78−76892
- CN radicals, electronic transition laser, using C_3F_7CN and $(CN)_2C_4F_8$ photodissociation 78−50769
- CN radicals, time behaviour in laser-initiated thermal isomerisation of CH_3NC 80−11887
- CN, red and violet band systems, rotational dependence of Franck-Condon factors 78−74701

carbon compounds continued
CN, red spectral system anal., mol. consts. 79−13728
CN, solar lines in 7100-7600 Å range, table 78−77495
CN, spectral absorpt. coeffs. for fundamental and first overtone vibr.-rot. bands 77−14405
CN strength differences in disk and halo giant stars 80−51750
CN towards interstellar clouds, EHF emission obs. 79−17037
CN variations among main-sequence 47 Tucanae stars 80−94794
CN, vibr. and rot. anal. of vis., UV spectra, RF discharges in N_2, H_2, CH_4 mixtures 78−5241
CN violet ($B^2\Sigma$-$X^2\Sigma$) band system, photoelec. intensity meas., transition probabilities 78−37649
CN violet (0,0) spectrum of Comet Kohoutek (1973 XII) 80−82308
CN violet system, rotational and vibrational analysis 80−52961
CN^-, adsorbed on Ag, giant Raman scatt. 79−95768
CN^-, adsorbed on Ag electrode, enhanced Raman effect 80−50348
CN^-, adsorbed on Ag surface, Raman active librational modes 80−65359
CN^-, bakeable hollow cathode duoplasmatron source 77−6602
CN^-, chemisorbed on AG (110), Raman scatt. 80−45075
CN^-, electron density distrib., theoretical and expt. determ. 77−61683
CN^-, electron density distrib., SCF mol. orbitals calcs. 78−9058
CN^-, enthalpy of formation and electron affinity 77−35506
CN^-, finite field method calc., moments, polarisability, field-induced shifts in mol. props. 78−74561
CN^-, first hyperpolarisability, Hartree-Fock-Slater calc. *(French)* 78−78625
CN^-, ground state pot. curve, CI and coupled pair method calcs. 79−68197
CN^- ion, gaseous, heat of form., solvation, proton affinity calc. 77−1092
CN^-, ionisation pot., CI and perturbation methods 79−31734
CN^-, ionisation pot. calcs. 77−75076
CN^-, leaches from gasworks site, Kingskettle, Scotland 79−88020
$(CN)^-$, monolayer on Ag, Raman spectra 78−72520
CN^- on Ag surface, bonding exam. by electrorefl. 77−80700
CN^-, proton affinity, enthalpies of form. and soln. 77−47375
CN^-, proton affinity, integral Hellmann-Feynman theorem 78−70767
CN^-, spectrosc. consts. for ground and excited states, ab initio, CI calcs. 80−78551
CN^- transformations by inner source based on $^{10}B(n,\alpha)^7Li$ 79−34341
CN^+, ab initio full CI calcs. 78−50480
CN^+, ground state, identity, ab initio CI calcs. 80−5468
CN^+, ground state, SCF pot. energy curves calcs. 79−13782
CN^+ ion, $^1\Sigma^+$ and $^3\Pi$ states, multi-reference CI study 80−83288
CN^+, lower states, pot. energy curves, equilib. distances SCF CI calcs. 80−27957
CN^+, lowest $^1\Sigma^+$ and $^3\Pi$ states, ab initio CI pot. curves calcs. 79−85905
CN^+, pot. curves, ab initio MRD-CI method 80−83293
CN· in solid Ne, internal conversions and relax. dynamics 77−34678
CN+H, bimolecular exchange reactions, dynamical-statistical method calcs. 80−104435
$CN+H^+$, perturbed rotational state approach 78−92469
$CN+H^+$, rot. excitation, decoupled l-dominant calcs. 77−6900
$CN+H^+$, scaling of energy and quantum no. for nonreactive collisions 80−9695
CN+NO, reaction rate constants 79−1935
$CN+O \rightarrow CO+N$, flash photolysis, absorption spectrosc. obs. 79−66289
$(CN)_2$, ^{14}N quadrupole coupling consts., ab initio calcs. 80−58283
$(CN)_n$ films, prep., RF sputtering by C in N_2 79−78886
C_2N_2, $2\nu_4$ band overtones, Raman intensities, bond polarisability theory 80−63639
C_2N_2, adsorbed on Pt (111) surface, Auger spectra 79−52077
C_2N_2, adsorption on Pt (100), backscatt. enhancement 77−90227
C_2N_2, adsorption on stepped Pt (111) surface 78−71992
C_2N_2, and $C_2N_2^+$, electronic struct. UV and PE spectra 80−23304
C_2N_2, $C^1\Pi_u$-state predissoc., vibronic effects 80−28078
C_2N_2, distrib. in 47 Tucanae red giant stars 79−71025
C_2N_2, electrostatic terms in lattice energy calcs. 79−51040
C_2N_2, gas, high resolution Raman spectra 78−17673
C_2N_2 gas, laser stimulation optimisation for intraresonator spectroscopy 80−77881
C_2N_2, gas phase 79−18191
C_2N_2, multiphoton dissociation in UV light 79−54928
C_2N_2, multiphoton UV photodissoc. 78−50602
C_2N_2, photolysis at 160 nm, $CN(X^2\Sigma^+)$ electronic-vibr.-rot.-translational partitioning 77−48667
C_2N_2, satellite struct. of electron spectra, CI and vibronic coupling, dynamical calc. 80−53044
C_2N_2, triplet state electronic energy delocalisation 77−3478
C_2N_2, valence and core photoionisation, spectral lines, many body effects 80−47853
C_2N_2, valence excitation and UV spectra by HAM/3, expt. photoelectron spectra 78−25454
$CN(B^2\Sigma)$, from electron impact dissoc., of HCN, near-threshold emission 79−54975
$CN(B^2\Sigma)$ shock wave excitation, emission, excited state populations, in CO-N_2-Ar mixtures *(Russian)* 78−74638
$CN(B^2\Sigma^+$-$X^2\Sigma^+)$, obs. in optically-pumped CO-Ar(-N_2) 80−16701
CNN, matrix isolation spectrum, 2600-1900 Å 78−86880
CNN, matrix-isolated, $^3\Pi$-$^3\Sigma^-$ system, laser-induced temporal and wavelength resolved spectra 77−83637
CNN radical, matrix isolation spectra, 23.5-25.6×10^3 cm^{-1}, vibr. relax. and Renner splitting 77−83612
$CN(X^2\Sigma^+)$, IR laser photofragmentation of cyanomethane, energy partitioning, rovibronic distrib. 77−61813
CN*, $B^2\Sigma^+$ state, fluoresc. decay dynamics, collisional quenching and radiative lifetimes 80−58306
$(CN^-;e^+)$ complex, ab initio LCAO SCF calc., positron affinity and excitation energy 79−49945
$CN^-.H_2O$, redox processes, MINDO/3 calcs. 79−47895
$CN^-.e^+$, positron energy levels, rel. to Rydberg levels of Na, NO 79−86089
$CN(\nu)+O(^3P)(O_2)$ reacts., prod. energy distribs. meas., CO vibr. level population *(German)* 78−76833
CO, ^{13}C chem. shielding, temp. and internuclear distance depend. 77−75068
CO, ^{13}C isotope enrichment by 123.58 nm Kr reson. radiation photolysis 78−33624
CO, ^{13}C NMR, density depend. mag. shielding in gas phase 77−75187

carbon compounds continued
β-CO, ^{13}C NMR, self-diffusion activation parameter, press. depend. 77−69719
CO, $^{13}C/^{12}C$ and $^{18}O/^{16}O$ liq.-vapour isotopic fractionation factors 79−90770
CO, $^1\Sigma$ state vibr. matrix elements, Dunham pot. *(French)* 79−54832
CO $^1\Sigma^+$, diatomic molecular form factors, vibr. average, study of convolution approx. 79−50926
CO, $^1\Sigma^+$ state, ionisation pots., dissoc. energy, atoms-in-mol. calcs. 77−88410
CO 115 GHz obs. of giant molecular cloud 79−71084
CO, 2.3 μ band strength in weak-G-band stars 78−12228
CO 2.7 mm line obs. of V645 Cygni 80−72956
CO 2.7 mm obs. towards L 43, filamentary cloud 79−62886
CO 4.7 μm rotation-vibration band obs. of quiet Sun variability 80−12729
CO, 600-W convective flow laser, characts. 78−17969
CO ($^1\Sigma^+$), X-ray and electron diffr. scatt. intensities, electron correlation effects 78−17577
CO, (CO^+), Franck-Condon factors, isotope effects calcs. 78−1031
CO, (4+) system, electronic transition probability 80−106332
CO ($d^3\Delta_i$-$X^1\Sigma^+$) fluoresc. from CO_2 photodissoc. 77−6836
CO ($\nu=1$)+Br_2, vibr. relax. rate consts. 77−6898
CO ($\nu=1$)+He, vibr. relax., collinear and 3D rate consts., temp. depend. 77−38717
CO ($\nu=1$)+He, vibr. relax., collinear and 3D rate consts., temp. depend. 77−38718
CO, A-X and B-X bands intensities in comets 79−35191
CO A-X system, rotational dependence of Franck-Condon factors 78−74701
CO $A^1\Pi$, Doppler free two-photon excitation 78−17641
CO, $A^1\Pi(\nu'=1)$, vibr. relax. by reversible intersystem crossing, fluoresc. obs. 80−14170
CO, $A^1\Pi \leftarrow X^1\Sigma^+$, (2-0) band, three photon excitation, fluoresc. obs. 78−13481
CO, $A^1\pi$-$X^1\Sigma$ system, Franck-Condon factors, r-centroids calc. program 77−27121
CO, $a^3\Pi$ and $A^1\Pi$ states, dipole moment, CI calcs. 77−79548
CO, $a^3\pi$ state, IR radiative decay of vib. levels 77−30870
CO, ab initio calcs. of the derivative of the static polarisability 79−3597
CO, absolute intensity meas., 4-0 vibr.-rot band 77−6854
CO, absorbed layer on Ni (111) surface, angle-resolved photoemission meas. 77−16463
CO, absorbed on Pt(111), photoemission, 40-150 eV 77−16465
CO, absorpt. spectra around 2100 cm^{-1}, Fourier transform spectroscopy appl. 78−58068
CO absorption and effective temp. of giants in globular cluster ω Centauri 80−51749
CO absorption meas. using long-path laser, system improvements 80−3563
CO, absorption on Ni/SiO_2, scavenging effect of H_2, in situ Fourier transform IR spectra obs. 80−39410
CO, abundance in air, IR spectrochem. anal. 78−15738
CO, acetone decomposition, near IR laser action 78−63055
CO, addition to CO_2 TEA laser for pulse stretching 77−14754
CO adlayer on Pd(100), band formation, calcs. and photoemission expts. 79−95463
CO adlayers, on Cu(100) and Cu(111), struct., LEED pattern reinterpretation 79−28209
CO adsoprt. on Al_2O_3-Ni catalyst in H_2-He, effect of H_2S on IR spectrum 78−71945
CO, adsorbed, lateral interactions on vibr. spectrum 79−46954
CO, adsorbed c(2×2) layer on Ni, Cu(001), struct. 80−88428
CO, adsorbed gas, on glassy AsSe, surface cond., photocond. 78−80038
CO, adsorbed layer, electron impact, electron impulsive ionisation spectroscopy obs. 80−60720
CO adsorbed layer on Ni surface, laser induced desorption 79−1548
CO, adsorbed layer on Ru (001) surface, electron induced dissociation 77−59215
CO adsorbed layer on Si (111) surface, ion scatt. obs. 80−59810
CO adsorbed layers, on W (210), surface struct., LEED obs. 79−82449
CO adsorbed layers on Ni (001), angle-resolved polarisation-dependent photoemission, adsorbate orientation 77−4716
CO, adsorbed layers on Pd (100), lateral interactions, effect on work function, UPS, and IR spectra 79−77904
CO adsorbed on Ag, Au films, enhanced Raman scatt. mechanism in ultrahigh vacuum 80−107645
CO, adsorbed on Ag films, Raman scatt. study 79−78672
CO adsorbed on $BaTiO_{3-x}$, Auger spectroscopy of surface layers 79−42343
CO adsorbed on clean metal solid surfaces, sputtering effects, combined analytical techniques 80−35047
CO, adsorbed on Co (0001), XPS and UPS study 79−74050
CO, adsorbed on Cu (100), Xα-scatt. wave cluster approach 80−49851
CO, adsorbed on Cu (100), vibr. excitation cross-sections 80−75441
CO, adsorbed on Cu film, optical constants 79−78645
CO, adsorbed on Cu film, work function 79−91570
CO adsorbed on graphite, fluid-registered solid transition 80−59796
CO, adsorbed on jellium, surface plasmon relax. energies 80−70537
CO, adsorbed on metal surface, collective vibr. modes, dipole interactions 78−50533
CO adsorbed on metal-sapphire interface, effect on shear strength 80−49485
CO, adsorbed on metals, valence photoemission book contrib. 78−95672
CO, adsorbed on metals, ion impact desorption, adsorption energy depend. 80−39442
CO adsorbed on Ni, adsorbed mol. bond config. and orientation, ang. resolved photoemission 77−44506
CO, adsorbed on Ni, core level spectrum, satellite struct., ab initio HF-LCAO calc. 80−40233
CO adsorbed on Ni, energy depend. of vibr. excitation, electron energy loss spectra 79−28201
CO, adsorbed on Ni, high press., low temp. Raman spectra 78−6219
CO, adsorbed on Ni, low energy electron scatt. 79−56896
CO adsorbed on Ni, valence band photoemission, SCF MO CNDO calc. 80−100754
CO, adsorbed on Ni, vibr. modes, anal. of electron-energy loss data 79−82461
CO adsorbed on Ni (100), UPS study 79−76473
CO, adsorbed on Ni (100), freq. and amplitude of localised vibrs., cluster calc. 80−6616

carbon compounds continued
CO, adsorbed on Ni (100), EELS and concomitant surface anal. 80—7453
CO, adsorbed on Ni (110), molecular desorption anal. 77—31874
CO, adsorbed on Ni (110), dissociation 77—31875
CO, adsorbed on Ni (111) face, CO stretching vibr., high resolution electron loss spectroscopy 78—14605
CO, adsorbed on Ni (111) surface, Raman spectra 79—28769
CO, adsorbed on Ni (111), isothermal desorption, UPS study, time-resolved approach 80—39440
CO, adsorbed on Ni (111) and (110), laser induced charge transfer, photoemission expts. 80—59798
CO, adsorbed on Ni and Cu, bond geometry, determ. using photoemission 78—71951
CO, adsorbed on Ni and Cu(100) surfaces, LEED study of c(2×2) struct. 79—86983
CO, adsorbed on Ni(Pt), intermediate UPS/XPS synchrotron radiation study 78—52633
CO adsorbed on Ni(001), orbital energy spectrum 78—2369
CO, adsorbed on Ni(001) surface, XPS for adsorbate geometry 79—65314
CO adsorbed on Ni(100), surface struct., LEED meas. 80—6647
CO, adsorbed on Ni(100)p(2×2)O surface and Ni(100)c(2×2)O surface, struct. and vibrs. 78—2375
CO, adsorbed on Pd, photoelectron spectra, 40-180 eV, adsorbate sensitivity enhancement 78—80453
CO, adsorbed on Pd, UPS of CO on Pd clusters, binding energy, d-electron emission particle size depend. 79—4888
CO, adsorbed on Pd (100), geometrical struct., LEED and high-resolution EELS study 80—20037
CO adsorbed on Pd (111) surface, metastable He impact, electron emission, energy and ang. distrib. 80—60744
CO, adsorbed on Pd (210), inclined bonding config., electron stimulated desorption and LEED obs. 80—39430
CO adsorbed on Pd surface, Penning ionisation by metastable He beam, theory 80—60735
CO, adsorbed on Pd/Al$_2$O$_3$, IR study 80—108193
CO, adsorbed on Pt, adsorbate induced electron losses 79—46959
CO, adsorbed on Pt, electron wave interference 79—33332
CO, adsorbed on Pt, internal optic modes, mol. dipole model 80—100395
CO, adsorbed on Pt, low temp. vibr. mode, site occupation, electron energy loss spectra 80—29263
CO adsorbed on Pt (100), electron energy loss 77—15688
CO, adsorbed on Pt (111), oxidation process, reflection-absorpt. IR study 78—76468
CO, adsorbed on Pt (111) surface, Auger spectra 79—52077
CO, adsorbed on Rh/Al$_2$O$_3$ catalyst, interaction with NO, IR study 79—70369
CO, adsorbed on Ru, adsorbed particle interactions, lattice gas quasi-chem. approx. 80—49529
CO, adsorbed on Ru (001), electron stimulated desorption, correl. with other meas 78—47658
CO, adsorbed on Ru (001), characteristic slow electron energy loss meas. 79—47562
CO, adsorbed on Ru (001), temp. depend. ordering processes 80—80773
CO, adsorbed on stepped Ni, adsorpt.-desorpt. behaviour, LEED, AES, thermal flash desorpt. study 78—71984
CO adsorbed on stepped Ni surface, vibrs. from electron energy loss spectra 79—73406
CO adsorbed on supported Pt catalysts, temp. programmed desorption 79—46915
CO, adsorbed on transition metal carbonyls, effect on photoelectron spectra 79—4897
CO adsorbed on transition metal zeolite, ^{13}C NMR study 79—52751
CO, adsorbed on transition metal surface, electronic struct., localised orbital pseudopot. method 80—39653
CO, adsorbed on W, electron beam induced C deposition, AES obs. 77—89651
CO, adsorbed on W, electron stimulated desorption of O$^-$ and O$^+$ ions 80—2270
CO adsorbed on W, electron-stimulated ion desorption 80—59797
CO adsorbed on W, electron-stimulated desorption, photoemission, relax. energy 80—100401
CO, adsorbed on W, FEM expt., pseudoclean pattern *(Japanese)* 78—34701
CO, adsorbed on W, He metastable atom bombard., secondary electron emission 79—47581
CO, adsorbed on W(210), surface struct., rel. to adsorbed N_2 79—15009
CO, adsorpt. on Cu (100), UV and X-ray photoelectron spectra, LEED 78—56037
CO adsorpt. on MgO, IR spectra 80—2751
CO, adsorpt. on Mo(100), LEED, AES, study 78—87873
CO, adsorpt. on Mo(110) face, adsorption/desorpt. expt. obs. *(French)* 77—85075
CO, adsorpt. on Mo(110) face, model *(French)* 77—85076
CO, adsorpt. on Mo(110) face, Auger yield attenuation interpret. *(French)* 77—85077
CO, adsorpt. on Pd(001), LEED, electron energy loss spectra study, surface struct. effect on weak chemisorpt. bonding 78—71987
CO, adsorpt. on Re 78—14594
CO, adsorpt. on W and Re filaments, temp. controller for filament heating appl. *(Japanese)* 77—51603
CO, adsorption, O_2-induced and reaction with other adsorbates on Ag(110) 80—55714
CO, adsorption, on Ni (100), bonding struct., vibr. excitations 77—15687
CO, adsorption, oxidation, and hydrogenation on Re, XPS, UPS, and thermal desorption study 80—71571
CO, adsorption and catalytic reactions with H_2 and O_2 on Pt 80—81362
CO, adsorption and desorption kinetics from clean and S covered Ru 80—6643
CO, adsorption and desorption on Fe(100), C, O, S and K adlayer effects 80—71573
CO, adsorption and dissoc. on Mo (100), comparison with carburised surface 77—15689
CO, adsorption and oxidation on Pt-Pb films, AES and ESCA obs. 79—52469
CO, adsorption and reaction with O_2 on Ir (110), transient study 80—30284
CO, adsorption by MgO, vibr. excitation on fracture 77—15488
CO, adsorption in evaporated Ir films, IR refl.-absorpt. spectroscopy 80—34925

carbon compounds continued
CO, adsorption of Ni (100)-p(2×2)C surface 79—91995
CO, adsorption of Ni(111) surface, carburisation, electron-beam induced effects, AES meas. 77—48588
CO, adsorption of Pt (111) using XPS, UPS, TDS and dynamic meas. of work function 79—65322
CO, adsorption on (110) plane of W, electron impact desorption, thermal desorption and work functions meas. 77—85064
CO, adsorption on Ag film, ellipsometric response 80—103571
CO, adsorption on Al, interatomic Auger transition spectroscopy 80—11521
CO, adsorption on alkaline earth oxides, reflectance spectra obs. 79—28781
CO, adsorption on Au, (100), LEED, AES, EELS, surface pot. 77—15691
CO, adsorption on CO films *(German)* 77—24485
CO, adsorption on clean and oxidised Pt (111), binding states and sticking coeffs. 77—72787
CO, adsorption on Cu, angle-resolved UPS and adsorbate induced struct. 78—71983
CO, adsorption on Cu (100) surface, EELS study 80—2260
CO, adsorption on Cu (110), electron energy loss vibr. spectra and LEED obs. 79—77902
CO, adsorption on Cu (311), electron energy loss spectra 77—63507
CO, adsorption on Cu-Ni (110), UPS, thermal desorption, AES,and LEED study 80—80087
CO, adsorption on Cu(110), LEED, surface pot., IR spectra 77—66092
CO adsorption on evap. Au films, effect on opt. consts. *(German)* 80—89081
CO, adsorption on evaporated Ni film, oscill. of galvanomag. props. 77—1496
CO adsorption on Fe, resistance changes, work function change and thermal desorption meas. 79—19450
CO, adsorption on Fe (110), UPS and LEED/Auger meas. 77—72773
CO, adsorption on Fe surface, core-level photoemission and LEED methods appl. 79—15003
CO, adsorption on Fe(001), random occupation of adsorption sites, LEED exam. 78—63930
CO adsorption on Fe(110) surface covered with C, O, N, S, photoemission study 80—54527
CO, adsorption on GaAs(Pt), surface electronic struct. (surface chem.) using synchrotron radiation 78—53254
CO, adsorption on Ge surface, adsorption potentials and trapped electrons role 79—90872
CO, adsorption on IR, field emission energy distrib. spectra 80—25535
CO, adsorption on In, AES study 79—82451
CO, adsorption on Ir (110) surface 78—38961
CO, adsorption on K promoted Fe (110), UPS, XPS, AES, and flash desorption obs. 79—82463
CO, adsorption on MgO powder, 77 to 150K, mol. motion anal. 78—84051
CO, adsorption on Mo, metastable He de-excitation spectroscopy and UPS study 80—34314
CO, adsorption on NaCl, electrostatic interaction energies 79—23831
CO, adsorption on Ni, binding and energy level shifts, NiCO and Ni$_2$CO electronic struct. 78—34882
CO, adsorption on Ni, electron field emission, energy distrib. 79—8231
CO, adsorption on Ni (100), SIMS and XPS meas. 79—42378
CO, adsorption on Ni (100), combined XPS/LEED/SIMS exam. 79—83075
CO, adsorption on Ni (110), electron bombard. effects, AES and electron stimulated ion desorption obs. 79—51430
CO adsorption on Ni (111), LEED and low-energy ion scatt. investigation 79—65324
CO, adsorption on Ni and Cu films, effect on resist. 77—85083
CO, adsorption on Ni and Cu metal clusters, mol. orbital calc. 78—18895
CO, adsorption on Ni and Mo, effect on ion and photon yields from ion bombard. surfaces 80—89098
CO, adsorption on Ni film, ferromag. reson. 78—15028
CO, adsorption on Ni films, effect on galvanomag. and mag. props. 79—33363
CO, adsorption on Ni films, effect on galvanomag. and mag. props. 79—33364
CO, adsorption on Ni ultrathin film, influence on field effect meas. 80—11108
CO, adsorption on Pd (111), catalytic oxidation, mol. beam investig. 78—88656
CO, adsorption on Pd(111), mutual interactions, transient product formation with O_2 78—87871
CO, adsorption on planar and O_2 etched Si (111), AES, SEM, ESD, flash desorption mass spectra 78—63934
CO, adsorption on polycryst. Re, work function *(French)* 77—28075
CO, adsorption on polycryst. Co, XPS and UPS *(French)* 77—36362
CO, adsorption on polycryst. metal, SIMS 78—14585
CO, adsorption on Pt, absolute coverage meas. using nucl. microanal. 80—54511
CO, adsorption on Pt, binding states, desorption and adsorption kinetics 77—85065
CO, adsorption on Pt, IR reflection absorpt. spectra, 1875 cm^{-1} band 79—65852
CO, adsorption on Pt, surface composition, AES and temp. programmed desorption meas. 80—34313
CO, adsorption on Pt, thermal desorpt. spectra 78—14607
CO, adsorption on Pt, UV photoemission spectra 78—14608
CO, adsorption on Pt (100), backscatt. enhancement 77—90227
CO, adsorption on Pt (110) clean and oxidised surfaces 77—28078
CO, adsorption on Pt (111), adsorption site investigation by IR reflection spectra 78—14565
CO, adsorption on Pt (111), cooxidation, AES *(German)* 78—14619
CO, adsorption on Pt (111) and Pt 6(111)×(111), EELS and thermal desorption spectroscopy 78—91547
CO, adsorption on Pt (111), XPS, UPS, thermal desorption, and work function meas. 79—77905
CO, adsorption on Pt and Pd, nature of chemisorption bond 77—51598
CO, adsorption on Pt and W, surface vibrs., electron energy loss spectroscopy study 77—69160
CO, adsorption on Re(0001), XPS, UPS and temp. programmed desorption 80—71574
CO, adsorption on Rh, inelastic electron tunnelling spectra obs. 79—46962

carbon compounds continued
CO, adsorption on Rh dispersed on Al_2O_3, ^{13}C NMR obs. of adsorbed states 80−96733
CO, adsorption on Ru (001), IR spectra, LEED, and thermal desorption meas. 80−70533
CO, adsorption on Ru $(11\bar{2}0)$, ellipsometry-LEED study 80−103570
CO, adsorption on Ru(001), IR spectra and LEED 79−37914
CO, adsorption on SiO_2-supported Pt or Pt-Pd, IR spectrosc. obs. 80−92780
CO, adsorption on SnO_2 gas sensor, effect on cond. 78−76067
CO, adsorption on stepped Pt (111) surface 78−71992
CO, adsorption on supported Rh catalyst particles, inelastic electron tunnelling spectra 79−3509
CO, adsorption on Ta, FEM and flash filament method exam. 78−43245
CO adsorption on Ti, SIMS expts. using 500 eV primary Ar^+ ions 77−72785
CO adsorption on Ti, W evaporated films, mutual replacement of CH_4, CO and NO *(Japanese)* 78−22949
CO, adsorption on transition metal, AES obs. 77−35818
CO, adsorption on V, effect on extended fine struct. above L-shell appearance pot. thresholds 78−92148
CO, adsorption on W, adsorbate characterisation by UPS, XPS and X-ray AES 77−15683
CO, adsorption on W, adsorption state at 300 to 80K *(Japanese)* 77−85057
CO, adsorption on W, field emission current instability, freq. spectrum 77−32509
CO, adsorption on W, surface reflectance spectroscopy on low index planes 78−71965
CO, adsorption on W (001) surface, electron energy loss spectra 78−71999
CO, adsorption on W (001) surface with adsorbed S layer 79−86981
CO, adsorption on W (100), displacement of H, photoemission and thermal desorpt. investig. 77−28079
CO, adsorption on W (100) and (110) surfaces, chemical effects in N_7 VV Auger spectra 77−32474
CO, adsorption on W (100), surface vibrs., EELS 77−62745
CO, adsorption on W (100) planes, LEED-AES obs. 77−69186
CO, adsorption on W (100) with ordered C overlayer, UPS meas. 79−77907
CO, adsorption on W (100), thermal desorption and work function meas. 80−29273
CO adsorption on W (111), angle resolved electron stimulated desorption, LEED and AES 80−6645
CO, adsorption on W and Ni, mol. orientation, ion scatt. 78−71949
CO, adsorption on W(100) surfaces, adsorbate density determ. 77−1320
CO, adsorption on ZnO surface, electron energy loss spectra meas. 78−14601
CO, adsorption on Zr, dissoc. and diffusion 80−80085
CO, adsorption sites on Pt (111), surface vibr. modes, electron energy loss meas. 77−43422
CO, adsorption sites on Ni (111) using IR reflection-absorption spectroscopy 79−69355
CO, adsorption sites on Ni (111), LEED, AES, thermal desorption, work function, and IR system meas. 79−77903
CO, adsorption sites on Mo (100), electron stimulated desorption and LEED meas. 80−49516
CO adsorption state on W, FEM obs. *(Japanese)* 77−62738
CO, adsorption/desorption on Pd clusters, AES and thermal desorption meas. 80−75436
CO, adsorption-desorption kinetics on Si and Ge surfaces 77−47684
CO, air pollution in Sheffield, conc. var. 80−16863
CO, air pollution rel. to HO tropospheric concs. in N and S hemispheres 78−32140
CO, air quality criteria using a COHb model 80−16864
CO, anal. of adsorption isotherm, determ. of porous texture of solids 79−77897
CO, analytic RKR pot. including higher-order WKB approx. effects 77−57901
CO and $(CO)_6$, electronic struct. and bonding, SCF-Xα-MSW calcs. 78−25431
CO, and CO_2, chemisorption on Rh (755), (331), desorpt. temp. and decomp. characts. 79−65318
CO and COS in atmosphere, biomass burning as source 80−26586
CO, and isotopic forms, fundamental bands, absolute wavenumbers, mol. consts. 79−59458
CO, and isotopic forms, laser freqs., Dunham coeffs. 79−64207
CO and N_2 binary diffusion in chamber and formed coke *(German)* 80−100356
CO and NO, coadsorbed on Ru(001), adsite symmetry by electron energy loss 79−99412
CO, anthropogenic emissions, implications for atm. CO-OH-CH_4 cycle 77−49160
CO, asymmetry parameter, angle resolved photoelectron spectra, multiple scatt. method 80−63708
CO, atm. absorption line parameters, AFGL, compilation update 79−21013
CO, atm. conc. meas. on aircraft flight 79−58010
CO, atm. press. laser, emission spectrum characts. 77−670
CO, atmosphere, global production by plants 77−86993
CO, atmospheric, production from oxidation of vegetation hydrocarbon emissions 78−88881
CO, atmospheric abundance, geographical, seasonal and secular vars. *(Russian)* 78−53700
CO, atmospheric abundance determ. by analysing solar spectra 78−85643
CO, atmospheric content meas. in N and S hemispheres *(Russian)* 77−13103
CO, Auger spectrum, ab initio MO LCAO SCF CI calc. many electron contribs. 80−87169
CO, Autler-Townes power splitting of rovibr. lines, direct obs. using intense IR laser 79−54854
CO, $b^3\Sigma^+$ state excitation, low-energy electron impact, $\nu'=3$ level lifetime 80−1072
CO, band emission detect. in Becklin-Neugebauer object 79−101184
CO binding, relation with conformational change of haemoglobin 79−8473
CO, boiling/condensation heat transfer props., cryogenic appls. 78−79192
CO, bonding, spin density functional theory 78−17558

carbon compounds continued
CO, boundary layer birefringence of rarefied heat conducting gas 77−80265
CO bremsstrahlung by CO^- free-free transitions continuous absorption calc. 79−63978
CO, broad emission lines obs. in Kleinmann-Low IR nebula 77−5556
CO bubbles in liq. Fe, homogeneous nucleation 77−60106
CO, C_{1s} ionis., CI calcs. of satellite peaks 78−916
CO, CO_2 in cometary nuclei, abundance ratio 78−12154
CO, CO^+, CO_2^+, airglow emissions from cometary inner comas 78−45282
CO, CO^+, emission spectra, 2100-5600 Å, electronic band systems and assignments 80−5560
CO, CO^+, MO correlation diagrams 77−61689
CO, CO-air, mol. rot. temp. determ., absorpt. spectra calcs. 77−30851
CO CW 80-kW supersonic elec. laser, elec. and laser diagnostics 79−98399
CO CW electric discharge laser, saturation parameter expt. determ. 78−50762
CO, CW electric laser, anal. model 78−25862
CO CW gas lasers, effect of Xe addition on room temp. operation 79−18407
CO CW gasdynamic laser, gain and population inversion 77−27278
CO, CW laser, spectral output 77−27292
CO CW laser emitting dominant spatial mode, output power stability rel. to CO_2 laser 80−32965
CO, CW preexcited supersonic laser, performance 77−14741
CO, c(2×2), adsorbed on Ni (100), photoemission orientation determ. 79−19974
CO, c(2×2), adsorbed on Ni(001), struct. by LEED, self-consistent scatt. pot. 80−70536
CO, c(2×2) adsorbed on Ni (001), surface geometry determ. by deep-core-level XPS 80−40224
CO, carbonyl group stretching freq. force const., CNDO/2 and localised orbitals calc. 77−30784
CO, catalytic interaction with H_2 on Ni (100), temp. programmed desorption study 80−66876
CO, catalytic oxidation on Pt, CO_2 product vel. and ang. distribs. 78−20065
CO, catalytic oxidation reaction over Pd(111) surface, reaction mechanism 78−40079
CO catalytic oxidation on spinel type ferrites, role of mag. exchange interactions 78−56916
CO, catalytic oxidation over NiO, activated complex struct., rate consts. 78−80786
CO, catalytic oxidation on polycrystalline Rh 79−79294
CO, catalytic oxidation on $Ni_xZn_{1-x}Fe_2O_4$ rel. to mag. props. and kinetic parameters 80−16723
CO, catalytic oxidation on ferrites, IR spectrosc. investig. 80−89524
CO, centrifugal distortion calcs. by perturbed Morse oscillator model including Dunham parameters 80−63862
CO, chem. form. from CS_2-O_2, laser dynamics and rot. relax. 77−10898
CO, chem. laser, book contrib. 77−10911
CO, chemical CW laser with CS_2-air mixture, output power press. depend. 79−72594
CO chemical laser, CS_2-O_2 mixtures in discharge 78−50766
CO chemical laser, flash photolysis of time-resolved spectra and gain 79−86172
CO chemical laser, high efficiency, CS/O_2 as fuel/oxidizer, chain reaction operation 80−23678
CO, chemical laser, supersonic combustor driven 78−87047
CO chemical laser, thermochem. generation of CS and S 77−68207
CO chemical laser using combustor-generated reactants 80−48288
CO, chemical shielding temp. depend. 78−5250
CO chemisoprotion as Fe and Ni films surface demagnetisation, ferromagnetic reson. study 80−80616
CO, chemisorbed, CNDO calcs. of mol. struct. *(German)* 79−96368
CO, chemisorbed and condensed on Rh(111) surface, energy level shifts 78−87865
CO chemisorbed and condensed on Rh(111) surface, UPS, meas. using synchrotron radiation 79−33902
CO, chemisorbed layer on Au(Pt), mag. phase transition obs. *(Russian)* 77−77083
CO, chemisorbed monolayer on Pt or Au, mag. phase transition, thermomagnetic study *(Russian)* 80−34319
CO, chemisorbed on Al_2O_3-supported Rh-Cu catalysts, IR spectra *(French)* 80−60559
CO, chemisorbed on alumina-supported transition metals, inelastic electron tunnelling spectra 77−31871
CO, chemisorbed on $\alpha+$Fe(111) surface, photoelectron spectra 77−62739
CO, chemisorbed on Cu (100) face, XPS of core levels 79−15589
CO, chemisorbed on Cu (100) surface, vibr. spectrum 79−69347
CO, chemisorbed on Cu (100), vibr. excitations and struct., EELS and LEED study 80−39437
CO, chemisorbed on Cu(111), coverage depend. photoelectron spectra, adsorption sites 78−95647
CO chemisorbed on Fe, low energy vibr. modes studied by tunnelling spectroscopy 80−78590
CO, chemisorbed on graphite, CNDO calc. using cluster model 80−54522
CO, chemisorbed on IR, electron states, electron field emission 78−84704
CO, chemisorbed on Ir(111) surface, electron beam induced desorption and dissociation 78−56043
CO, chemisorbed on metals, electronic struct., vibr. spectra, and chem. 79−42390
CO, chemisorbed on Mo (100), surface kinetics, photoemission study method 80−80941
CO, chemisorbed on Mo polycryst., substrate mediated C-O interaction, photoelectron spectra 79−34353
CO, chemisorbed on Ni, ab initio LCAO MO SCF calc. for NiCO 78−62712
CO, chemisorbed on Ni, ion bombard., particle ejection, SIMS obs. 79−78810
CO, chemisorbed on Ni, molecular cluster ejection on ion bombardment, model 79−87543
CO, chemisorbed on Ni, Raman spectra 80−2755
CO, chemisorbed on Ni (001), site determ. by angle-resolved UPS 78−71970

carbon compounds continued
CO, chemisorbed on Ni (100), photoemission angle-of-incidence depend. 77−32502
CO, chemisorbed on Ni (100) struct., dynamical LEED expts. 78−34710
CO, chemisorbed on Ni (100), contraction of mol. band, possibility 79−28202
CO, chemisorbed on Ni (111), bond energies 80−100398
CO, chemisorbed on Ni and Pd, catalytic activity, SCF-Xα-SW calcs. 78−15711
CO, chemisorbed on Ni(111), vibr. spectra from electron energy loss spectra *(French)* 78−22951
CO, chemisorbed on Ni(111), surface optical excitations, reflectance spectra, electron energy loss meas. 78−84064
CO, chemisorbed on Ni(111), adsorption sites and long range order, vibr. spectra 79−46946
CO, chemisorbed on Ni{001}, LEED study of mol. orientation in c(2×2) struct. 79−86982
CO, chemisorbed on Pd, Penning ionisation electron spectroscopy, metastable He impact, electron energy distrib. 79−52060
CO, chemisorbed on polycryst. Ti, secondary electron yield spectrum obs. 78−38933
CO chemisorbed on Pt, IR refl.-absorpt. spectra, absorbate island struct. 80−84385
CO, chemisorbed on Pt, photoemission meas. 77−63531
CO, chemisorbed on Pt (111) and Ni (111), orientation of CO from angle resolved photoemission 77−8721
CO, chemisorbed on Pt {111}, IR spectra, evidence for strong absorbate coupling interactions 78−14604
CO, chemisorbed on Rh, IR spectra, species identification 79−39198
CO, chemisorbed on Rh (111), dissociation probability, isotopic exchange and AES meas. 80−40743
CO chemisorbed on Rh/γ-Al_2O_3 disperse δ-phase, IR spectra, site distrib., mol. mobility 78−72496
CO chemisorbed on Ru(001), reaction with chemisorbed O_2, electron energy loss spectra 79−46924
CO, chemisorbed on W, IR vibration spectroscopy using refl. inelastic electron scatt. 78−14603
CO, chemisorbed on W {100}, electron beam effects, AES obs. 77−31897
CO, chemisorpt., surface struct. chemistry and electron impact props. on Rh(110) 78−6225
CO, chemisorpt. on Co (0001) 78−6222
CO, chemisorpt. on Cu(Ni)(Cu-Ni), SIMS, AES, desorpt. meas. 78−87875
CO chemisorpt. on evaporated Ni films, ellipsometric investig. *(German)* 80−61156
CO, chemisorpt. on Pd particles supported on mica, ultra high vacuum technique 78−71960
CO, chemisorpt. on Pt {111}, refl.-absorpt. IR spectroscopy 77−1306
CO, chemisorpt. on W(110), absolute coverage and work function meas. 100 and 300K 78−71986
CO, chemisorption, on Ir, XPS and UPS 77−16450
CO, chemisorption, on Rh dispersed on Al_2O_3, ^{13}C NMR obs. 80−1000
CO, chemisorption in Ni(100), mol. levels, angle depend. calcs. 78−90069
CO, chemisorption on AgNa mordenite 80−2752
CO, chemisorption on Al, interatomic Auger transition spectroscopy 79−7747
CO, chemisorption on α-Fe, surface deactivation effects 77−76669
CO, chemisorption on clean Fe (100) and (111) surfaces, LEED and thermal desorption 78−71996
CO, chemisorption on cleaved Si (111), Ge (111), electron energy loss spectra 78−79885
CO, chemisorption on clean and oxidised Ir (110) surfaces, kinetics obs. 79−11015
CO, chemisorption on Cu (111), IR spectra, LEED, and surface pot. meas. 80−39438
CO, chemisorption on Cu-Ni alloy surface, LEED, AES, thermal desorption, and work function meas. 79−90879
CO, chemisorption on Cu(100), angle resolved UV photoemission spectroscopy exam. 78−10284
CO, chemisorption on Cu(100), XPS shake-up satellites, Xα-SW cluster model calcs. 79−95899
CO, chemisorption on differently prepared Cu (111) surfaces 78−6223
CO, chemisorption on epitaxial Ni-Cu diffusion couple surface, AES 77−31891
CO, chemisorption on Fe (100) and Ir (100) surfaces, chemisorptive bonding and dissociation 77−59212
CO, chemisorption on Fe (110), UV photoelectron obs. 78−19629
CO, chemisorption on Fe fine particles, Mossbauer study 80−39415
CO, chemisorption on Ge (111) surface 80−10785
CO, chemisorption on Ir, photoemission, multiplets 77−15694
CO, chemisorption on Ir (111), XPS and UPS obs., comparison with Pt foil 78−38942
CO, chemisorption on Ir (110), preexponential factor and desorption energy 78−71963
CO, chemisorption on Ir(111), coverage dependent interaction, UPS 77−85897
CO, chemisorption on Mo, low energy SIMS and electron impact desorption expts. 78−38941
CO, chemisorption on Ni, CNDO calcs. *(German)* 78−29751
CO, chemisorption on Ni, surface struct. from ang. resolved UPS 78−31303
CO, chemisorption on Ni, carbonylation rate mag. field depend. 79−24828
CO chemisorption on Ni, Pd, Pt, Ir, mol. cluster calc. 80−100407
CO, chemisorption on Ni (100) and (111), tight-binding theory 77−20395
CO, chemisorption on Ni (001), final state relax. 77−62752
CO, chemisorption on Ni and Pt (001), localised orbital approach 77−69166
CO, chemisorption on Ni (100) surface, mol. cluster theory 77−69174
CO, chemisorption on Ni and Cu, electronic struct. of $(M)_5CO$ clusters 78−95948
CO, chemisorption on Ni (100), Hartree-Fock-Slater mol. cluster calcs. 79−51650
CO, chemisorption on Ni (100) and polycrystalline Ni, low energy SIMS and AES 80−34309
CO, chemisorption on Ni (001), back donation in chemisorption bond, UPS study 80−107642
carbon compounds continued
CO, chemisorption on Ni-Cu alloys, inhibition by Cu *(French)* 77−1295
CO chemisorption on Pd, Ag, PdAg, SIMS, XPS study 80−84382
CO, chemisorption on Pd surface, IR spectroscopic evidence for localised site adsorption 78−47669
CO, chemisorption on Pd (100), adsorbate band formation, UPS expts. compared with calcs. 79−77916
CO, chemisorption on Pd(111) surface, mol. beam scatt. expts. 78−79878
CO, chemisorption on polycryst. Ti surface, secondary electron yield obs. 78−71971
CO, chemisorption on Pt, LEED, AES obs. of surface struct. and states 77−1300
CO, chemisorption on Pt (111) surface 77−72781
CO, chemisorption on Pt (111) and Ni (100), (111), C-O bond lengths, electronic struct. 78−6210
CO, chemisorption on Pt (100) unreconstructed surface 78−38962
CO, chemisorption on Pt-Au, effect of surface segregation 77−51601
CO, chemisorption on Re (0001) surface, nonuniform attenuation of d-bond photoemission 79−74060
CO, chemisorption on Re (0001), role of d-orbitals, angular resolved UPS and thermal desorption meas. 80−40232
CO, chemisorption on Rh (111) and (100) surfaces LEED, AES and themal desorption meas. 78−38951
CO, chemisorption on Rh (110), LEED, AES, XPS, UPS, and desorption obs. 79−77899
CO, chemisorption on Rh (111), thermal desorption mass spectrometry and LEED meas. 79−77917
CO, chemisorption on Rh (111), high resolution EELS, thermal desorption, and LEED study 80−44419
CO, chemisorption on Ru (001), electron stimulated desorption ion ang. distribs. bonding geometry and bending vibrs. 79−33189
CO, chemisorption on Ru (001), overlayer struct., LEED obs. 79−51429
CO, chemisorption on Ru(101), surface structural chemistry and electron impact props. 77−1312
CO, chemisorption on Ru(10$\bar{1}$0) surface 77−72783
CO, chemisorption on Si(Ge), surface photoemission, adsorption gate geometry 78−73079
CO, chemisorption on supported Rh, activated surface processes, IR spectra 80−16724
CO, chemisorption on Tl film, quartz cryst. microbalance obs. of CO/Ti ratio 79−4475
CO, chemisorption on Th (111), LEED and AES obs. 77−89625
CO, chemisorption on Ti, flash desorption mass spectrometry obs. 77−89646
CO, chemisorption on Ti film, changes in work function 77−59221
CO, chemisorption on Ti (0001), LEED struct. anal. 78−71964
CO, chemisorption on Ti (10$\bar{1}$1), XPS, UPS, flash desorption mass spectra, and active ion bombard. obs. 79−11822
CO, chemisorption on Ti (0001), valence band struct., XPS and UPS 80−35062
CO, chemisorption on transition metals 78−2378
CO, chemisorption on W (110), LEED, XPS and Auger meas. 77−89647
CO, chemisorption on W (100) surface, mol. orbital study 78−71995
CO, chemisorption on W(100) surface, α and β states, AES and electron energy loss spectra 77−1313
CO, chemisorption with O_2 on Pt, SCF-Xα cluster calcs. 80−65365
CO, chemisorptive bonding on Ir (100), photoemission investig. using synchrotron radiation 77−12498
CO, chemisorptive bonding on metal surface, PES 80−10791
CO, circumstellar absorpt. obs. in α Orionis 4.6 micron spectrum 80−26858
CO, circumstellar lines discovery around B2-type supergiant 9 Cephei 79−84793
CO, co-adsorption with H_2 on Rh (111), segregation of co-adsorbed species 80−65361
CO, coadsorbed with hydrocarbons on Ni (111) and Pt (111), C$\equiv$O bond weakening 79−90863
CO coadsorption with H on Fe, effect of preadsorption of one on adsorption of other 79−19451
CO, coadsorption with H_2 on polycrystalline Pt 77−59220
CO, coadsorption with H_2 on W (100), CO/H surface complex obs. 79−4478
CO, coadsorption with H_2 on Rh, thermal desorption mass spectroscopy meas. 79−46948
CO, coadsorption with H_2 on Ni(111), surface carbide influence, vibr. electron energy loss obs. 79−52772
CO, coadsorption with H_2S on Ni (110), (100) and (111), surface coverage meas. by SIMS 79−90876
CO, coadsorption with H_2 on Rh (111) surface, 2-dimens. phase separation 80−107634
CO, collision-induced reorientation, direct meas. by IR double reson. 80−32800
CO, collisional excitation of interstellar molecule 78−81664
CO, combustion flow, passive optical diagnostics 77−44527
CO, combustion gas sampling system and valves for sampling during engine expansion process 78−24380
CO, computation of multiphoton IR rovibration spectrum 79−89660
CO concentration meas. in coal pulverising plant, IR gas analysers 80−89572
CO, condensed, vibr. excitation in photoemission spectra 77−28689
CO, condensed film, UPS linewidths 78−31294
CO, contamination of Co (0001) surface, LEED meas. 77−59188
CO cooled electron-beam-controlled laser, two-quantum transitions 79−45935
CO, core ionis., electric field depend. 78−13424
CO, core ionisation and single orbital relax. calcs. 78−5133
CO, core ionisation single orbital relax. energy, LCAO-SCF basis set depend. 79−89604
CO, core pseudopot. valence electron calc., orbital energy and bond length 79−72233
CO covered Ni films, adsorpt. of H, isotherms, resist., work function changes 78−75926
CO, cryst. at 5K, absorpt. and emission spectra, exciton interpretation 79−87481
CO, $d^3\Delta$ state, low energy electron impact excitation and radiative decay 80−91691
CO, $d^3\Delta_i$ state elec. dipole moment, vibr. depend. obs. 79−31548

carbon compounds continued
- CO, d$^3\Delta_i$ v=4 state dipole moment, laser-induced transition in mol. beam 78—25513
- CO, decomposition in corona discharge, qualitative chemical anal. of reaction products 78—60992
- CO, desorbed from W, thermal desorption and conversion kinetics, AES study 78—71959
- CO, desorpt. from graphite, kinetics 78—60025
- CO, desorption, from Cu surface, production and meas. of atomically clean surface environment 80—52250
- CO, desorption from clean and S covered Pt surfaces, binding energy meas. 79—46950
- CO, desorption from Ir (110), coverage dependence of kinetic parameters 79—19462
- CO, desorption from Ru(001) 79—15001
- CO, desorption from W(100), electron and photon-stimulated desorption 79—99414
- CO, detectability levels for CARS species sensitivity 80—43404
- CO, detection by Co_3O_4 MOS device 78—76908
- CO, detection of vibrationally excited state at 114 GHz from IRC+10216 C star 78—40941
- CO, determ. by portable IR tester 80—89569
- CO, determ. in air by reversible poisoning of electrocatalysts 77—37363
- CO, diffusion coeff. in laminar flames 78—51272
- CO diffusion in dog lungs, effect of static or slowing flowing blood 80—30970
- CO diffusion through cigarette papers 80—43824
- CO, dipole moment derivatives, MINDO/3 semiempirical calcs. 77—75055
- CO, dipole moment expsn. determ. from vibr. intensities *(French)* 78—42240
- CO, dipole moment functions for $d^3\Delta$ and $a'^3\Sigma^+$ states, MCSCF calc. 78—78636
- CO discharge, $C_2(A^3\Pi_g$-$X'\,^3\Pi_u)$ band system obs. 77—42332
- CO discharge, low-pressure laser striation obs. 78—66814
- CO discharge plasma, electron energy distrib. and kinetic coeffs., ground-state mols. 80—43867
- CO discharge plasma, electron energy distrib. and kinetic coeffs., vibr. excited mols. 80—43868
- CO, disordered overlayer on W (001), effect on electron spin polarisation in LEED 79—60632
- CO dispersal in city streets, wind tunnel modelling 78—3927
- CO, dissoc. attachment, differential cross-section meas. 77—50549
- CO, dissoc. chemisorption on Fe(Nli) *(German)* 78—53257
- CO, dissoc. sorption on Pt, XPS obs. 77—16863
- CO, dissociative chemisorption of Ru, isotope exchange 79—34354
- CO, dissociative electron attachment 77—42431
- CO, dissociative excitation by electron impact, metastable fragment energy 78—66672
- CO, dissociative ionisation 77—54616
- CO distribution in galactic equatorial plane, 115 GHz obs. 78—36689
- CO, distribution in galactic central regions 79—21416
- CO, Doppler-free two-photon vac. UV absorption spectra 78—86882
- CO dose meter for working places exposed to extreme peaks of CO contamination 78—81096
- CO, Dunham vibration-rotation coefficients, isotope dependence 80—83518
- CO, effect on electron loss spectra, Pt(111) surface *(German)* 78—52605
- CO, effect on field emission current stability of glassy C tip 80—11544
- CO, effect on SO_2 oxidation rate and aerosol form., smog chamber expt. 79—74925
- CO, effect on SnO_2:ThO_2, elec. oscill. phenomenon 78—68032
- CO, effects on surface pot. *(Russian)* 77—47686
- CO, efficient self-sustained pulsed laser 78—55377
- CO, ejected electron spectroscopy of autoionising states using electron-electron coincidence technique 79—3587
- CO, elec. and mag. props., mol. beam elec. reson. spectroscopy 77—61791
- CO, elec. excited overtone bands lasing at 2.7 to 3.1 μm 78—13684
- CO electric discharge laser using single vibr.-rot. transition, laser line selection 79—59687
- CO electric discharge laser, system efficiency *(Japanese)* 79—64206
- CO electric discharge lasers, vibr. kinetics, modelling and expts. 80—69374
- CO electric discharge supersonic laser, pulser-sustainer, construction and performance 78—25888
- CO electric discharge unstable resonator laser, computer model 78—58988
- CO, electrically excited gasdynamic laser, closed cycle operation *(German)* 80—43362
- CO, electrochemical oxidation in fused alkali metal carbonates 80—72040
- CO, electroionisation laser, generation efficiency *(Russian)* 77—58313
- CO electron beam controlled laser, stimulated emission characts. 78—1221
- CO electron beam controlled laser, energy and spectral characts., NO admixtures effect 80—9867
- CO, electron correl., quadrupole excitation in correl. energy theories 79—36538
- CO electron drift velocity and longit. diffusion coeff. time-of-flight meas. 77—80264
- CO, electron elastic scatt., differential cross-section meas. 77—3458
- CO, electron elastic scatt., low energy, static exchange approx. calcs. 80—69236
- CO, electron energy loss spectroscopy and IR reflection spectroscopy 77—85729
- CO, electron energy loss spectra, C K-shell excitation, vibr. struct. 79—22851
- CO, electron impact, absolute emission cross-sections meas., calibration appls. 79—85996
- CO, electron impact, energy loss spectra, electronic transitions obs. 78—17805
- CO, electron impact, reson. vibr. excitation calcs. 77—14595
- CO, electron impact, vibr. levels stepwise excitation 78—1095
- CO, electron impact desorption from W (110), isotope effects 77—76658
- CO, electron impact excitation, resonances in metastable and UV emitting levels 78—25727
- CO, electron impact excitation function, $b^3\Sigma^+ \rightarrow {}^3\Pi$ 79—31705
- CO, electron impact ionisation, metastable state mol. ion form. 77—14594

carbon compounds continued
- CO, electron impact K-shell ionis., ionic fragmentation, Auger decay post-collision interaction 77—75316
- CO, electron impact spectra, C atom inner shell excitation 77—10776
- CO, electron impact vibrational excitation, 1-4 eV 80—9747
- CO, electron reson. scatt., ang. distrib., vibr. and rot. excitation, theory 78—22044
- CO, electron scatt., absolute total cross-section meas. 78—74774
- CO, electron scatt., adiabatic polaris. pots. 79—10203
- CO, electron scatt., effective pot. calcs. 80—53131
- CO, electron scatt., elastic differential cross-section, 3-100 eV 79—27086
- CO, electron scatt., low energy, multichannel variational calcs., static exchange approx. 80—83483
- CO, electron scatt. at low energy, mechanisms *(Russian)* 78—90306
- CO, electron scatt. cross sections for momentum transfer and inelastic excitation 79—36782
- CO electron scattering, intermediate energy electrons 79—72418
- CO, electron scattering, iterative static exchange method 80—53155
- CO, electron stimulated desorption from W (100) and (110), threshold behaviour 77—47678
- CO, electron swarm motion simulation for high E/N 77—19667
- CO, electron-neutral energy exchange in AC field 77—42519
- CO, electronic states, oscill. strengths calcs. 78—9095
- CO, electronic struct., binding energy and interatomic distance, SCF variational cellular calc. 80—9498
- CO, electronic structure calcs., self-consistent, accelerating convergence of iterative process 80—87037
- CO, electrostatic interaction energies for point charge and NaCl (100) surface 78—74592
- CO, ellipsoidal Gaussian basis functions, integral formulas and test calcs. 77—23420
- CO emission from late-type galaxies 78—89250
- CO emission from mol. clouds assoc. with refl. nebulae, EHF obs. 80—82447
- CO emission in external galaxies, upper limits 78—36693
- CO emission in NQ Vulpeculae (Nova 1976), obs. during η Carinae stage 79—25609
- CO emission in W3 H II region, LF obs. 80—82446
- CO, emission intensity, CS_2-O_2 flame, rate of population of CO vibr. levels 78—7186
- CO, emission lines in UV spectra of solar flare and sunspots 79—53795
- CO, emission lines obs. from evolved stars expanding molecular envelopes 77—22219
- CO emission meas., Baden-Wurtemberg network *(German)* 79—52977
- CO, emissivity, computer calcs. 77—84386
- CO, emissivity calc. 78—90675
- CO, energy levels for perturbed Morse oscillators 80—78676
- CO, equilib. geometry, orbital energies, ab initio rel. to pseudopot. calcs. 78—82613
- CO, fast flow continuous-wave laser, with longit. elec. discharge 78—9373
- CO, field ionis. to excited states 77—19002
- CO, finite field method calc., moments, polarisability, field-induced shifts in mol. props. 78—74561
- CO, first hyperpolarisability, Hartree-Fock-Slater calc. *(French)* 78—78625
- CO, fixed-molecule, spectral variation of photoelectron ang. distribs. 77—14489
- CO flame, background-free CARS technique 79—94288
- CO flame rise vel. meas. by particle track method 80—89489
- CO, flowing laser plasma, spontaneous emission, A coeffs. 77—7070
- CO, fluoresc. of interstate intramol. perturbations 79—41194
- CO, fluorescence, lifetime meas. for rot. levels of (0,0) band, $A^1\pi$ to $X^1\Sigma^+$ transition 78—29808
- CO fluorescence in EUV solar spectrum, obs. 78—93184
- CO, form. in contracting interstellar clouds, thermal instabilities 78—81675
- CO formation at initial stages of H corrosion of nuclear graphite 78—11355
- CO, fourth positive system in 1115-4759 Å range 77—49291
- CO, Franck-Condon factors appl., rot. depend. 79—10154
- CO, Franck-Condon factors, rot. quantum number effect 79—31613
- CO from arctic surfaces during spring thaw 80—41511
- CO, gas, influence on field emission of glassy C tips 80—11543
- CO, gas, phase matched, IR third harmonic generation 77—38985
- CO, gas, rarefied flow, visco-magnetic heat flux 79—98844
- CO gas, third harmonic generation enhancement in metal-dielec. waveguides 79—50342
- CO gas discharge laser, optimisation of active media comps. and working parameters 79—64216
- CO gasdynamic laser, electrically excited, operation and performance *(German)* 78—33754
- CO gasdynamic laser, elec. excited, with closed-cycle gas flow, operation 80—102732
- CO, gasdynamic laser, energy characts. calc. 78—9367
- CO gasdynamic laser, increase of specific energy 77—31090
- CO, gasdynamic laser, optimum energy characts. 80—23665
- CO, gasdynamic laser, weak signal gain, calibration loss method meas. 78—17919
- CO, gasdynamic laser working media, energy characteristic 80—14319
- CO, geometry optimisation, using bond function augmented basis sets 78—905
- CO, glow discharge, O atom conc. determ. by mass spectrometry *(Russian)* 78—87512
- CO, ground level abundance, simultaneous determ. of CO_2, N_2O and H_2O 78—11969
- CO, ground state, radial matrix elements and dipole moment function 77—57973
- CO, ground state, third-order many-body perturbation theory 79—10015
- CO, ground state potential energy, non-muffin tin MS Xα calcs. 77—14355
- CO, ground states, anal. pot. function calcs. 78—78775
- CO, ground-state, absorpt. oscillator strengths for vibr. rot. transitions 78—62846
- CO group, NMR chem. shift, solvent's dielectric const. effect, mag. anisotropy 79—42847
- CO, HF calcs., compared with optimised LCAO results 78—5139
- CO, Hartree-Fock-Slater calcs., using pseudopot. method 77—57859
- CO, heat capacity, calc. by modified Redlich-Kwong eqn. of state 80—69963

carbon compounds continued
CO, high order vib. matrix elements, for dipole moment function and transition moments 77—6757
CO, high power discharge lasers, operational principles and design constraints 77—38931
CO, high press. pulsed elec. laser 77—79847
CO, high resolution lifetime meas., perturbation and collisional transfer correl. 78—78699
CO, high-press. electroionisation laser, lasing action *(Russian)* 77—7127
CO, highly excited vibr. states, double quantum V-V transitions *(French)* 77—61837
CO, hole burning in single quantum power spectrum due to Autler-Townes splitting 80—9671
CO, horizontal electric arc, in inhomogeneous mag. field, mass spectrometric anal. 80—79620
CO, hydrogenation kinetics, methane formation using polycryst. Ni ribbon catalyst 78—40078
CO, hydrogenation on Fe foil, AES and XPS study 80—7858
CO, hydrogenation to methane and higher mol. wt. compounds on Rh(Fe) surface 78—73034
α-CO, IR and Raman spectra, vibron band, vibron-phonon combination bands 78—68495
CO, IR band absorpt. derivation from vibr.-rot. band spectroscopic variables 77—14434
CO, IR band nonrigid rot. absorption 78—91060
CO, IR radiation spectral absorptance and transmittance, accurate modelling technique 78—91062
CO, IR vibr.-rot. overtone bands in Mira variable R Leonis 78—36574
CO, impurity in CO_2-gas dynamic laser, combustion-type, effect of residual CO on performance 79—68378
CO in Ar matrix, Ar-Ar, C-Ar and O-Ar pot. parameters, empirical evaluation 80—48057
CO in Ar matrix, fluoresc. and thermoluminesc. after photolysis 79—89700
CO, in Ar matrix, vibr. line shape, vibr.-phonon interaction 79—3493
CO in Ar matrix, vibr. freq. shift and interaction pot., force-field calcs. 80—47958
CO in atmosphere, abundance meas. method *(Russian)* 79—25343
CO, in atmosphere, comments on appl. of one-dimensional mixing models 77—45086
CO, in atmosphere, global prod. rate from methane surface flux meas. *(Russian)* 78—36223
CO, in circumstellar shells, millimetre line emission obs. 78—49423
CO, in circumstellar shell of 9 Cephei (B2 Ib), obs. 80—94795
CO, in combustion gases, high resolution spectroscopy 77—81434
CO in contracting interstellar clouds, influence on fragmentation 80—67838
CO, in cool giant stars, 5 μm obs. and anal. 78—36569
CO in evolved stars expanding envelopes, thermal and maser emission lines profiles 80—82334
CO, in galactic reflection nebulae, emission lines obs. 77—53658
CO in giant stars in globular clusters, IR obs. 78—93339
CO in globular cluster giant stars, line blanketing differences 80—4345
CO, in glow flow discharge, electronic states, excitation mechanism 80—53040
CO, in He bath, NMR spin-lattice relax., coupled states ang. momentum decoupling 77—77117
CO in IR C star CIT 6 (IRC+30219), line profile rel. to mass outflow 80—12761
CO in IR spectra of III-106, CH star in M22 globular cluster 80—62131
CO, in interstellar clouds, form. rel. to formaldehyde abundance 77—13421
CO, in interstellar clouds, isotopic abundance 77—29912
CO in interstellar dark clouds, evidence for isotopic fractionation 80—46638
CO, in intertstellar mol. clouds, line form. rel. to microturbulence and systematic motions 77—33586
CO, in Jupiter atmosphere, airborne spectroscopic obs. at 5 μm 78—36491
CO in Jupiter atmosphere, abundance 78—49374
CO in Jupiter upper atmosphere, extraplanetary source 78—93144
CO in Jupiter's upper atmosphere, Galilean satellites as source 79—40128
CO in Kleinmann-Low nebula, line profile rel. to radially moving cloud model 78—20865
CO, in M31, partial radial distrib. meas. 78—8117
CO in metal-deficient stars 2.2 and 2.4 μm obs. 79—58336
CO in molecular cloud complexes, structure of W75-DR 21 region 78—89232
CO in nearby galaxies, survey 80—62276
CO in quasar PHL 957 spectrum, absorpt. lines obs. *(Russian)* 79—101216
CO, in Sc galaxy NGC 5236 (M83), radio emission obs. 78—65689
CO in solar faculae, rot. temp. of mols. 77—78740
CO, in solar spectrum, centre to limb behaviour of first overtone vibr.-rot. transitions 79—8889
CO, in solid N_2, phonon-assisted v-v transfer rates 79—10901
CO, in Southern Coalsack, 115 GHz emission obs. 77—29902
CO in stars, equivalent widths of lines of (A-X) band 77—87368
CO, in symbiotic stars RR Telescopii and Henize 2-38, obs. 78—40970
CO in troposphere, interhemispheric transport study 80—31106
CO, in upper atmosphere, electron impact cross-section 78—28398
CO, in upper atmosphere, electron impact yield spectra 78—28401
CO, in Venus atmos., O_2, Ar, CO abundances, error of Pioneer Venus chromatography obs. 80—105189
CO in Venus upper atmosphere, dayglow spectrum obs., 1250 to 1430 Å 80—77311
CO in Venus' atmosphere nighttime luminescence spectra 77—78702
CO, indirect nucl. spin-spin coupling const., Hartree-Fock and polarisation propag. calcs. 78—9170
CO, influence on N absorpt. in plasma melting of steel *(Russian)* 79—39193
CO, initial reaction probability with Ba getter film, AES obs. 80—61153
CO, inner-shell ionisation, relax. effects calcs. 77—42351
CO, inner-shell ionisation, vibr. struct., sudden approx. calcs. 79—50002
CO, inner-valence ionisation, correl effects calcs. 78—9198
CO, integrated CARS power, press. depend. 78—59081
CO, interaction with adsorbed HD and D_2 on Re surface 79—86987
CO, interaction with Cu small particles, IR spectra obs. 77—20195
CO, interaction with Cu (100), molecular orbital calc. 77—31898

carbon compounds continued
CO, interaction with Cu clusters, Cu_nCO form., chemisorpt. bond 78—31631
CO, interaction with O_2 on Ru (101) 77—73471
CO, interaction with polycryst. CO surface, XPS, UPS *(French)* 77—73219
CO, interaction with ZnO nonpolar surface 79—65321
CO, interstellar, detailed struct. in NGC 6334 mol. cloud complex 78—4324
CO, interstellar, detect. in direction of supernova remnant (S147) 80—67836
CO, interstellar, distrib. around (l=30°, b=0°) 80—41868
CO, interstellar, effect on cosmic background radiation spectrum *(Russian)* 80—8719
CO, interstellar, in $^1\Sigma$ state, collisional excitation by H_2 80—109508
CO, interstellar, in S255 80—46637
CO, interstellar, in W3/W4/W5 direction, correl. with heavy optical obscuration 80—62301
CO, interstellar, isotope fractionation in Lynds 134 dust cloud 80—26924
CO, interstellar, J=2 to 1 line obs. in NGC 2024 (Orion B) nebula 80—8673
CO, interstellar, obs. in Perseus OB2 dark cloud and W44 mol. cloud 77—64836
CO, interstellar, obs. in H II region (NGC 281) 78—28740
CO, interstellar, obs. in young cluster (IC 5146) 79—48881
CO, interstellar, obs. in galactic star-forming region (W58) 80—67810
CO, interstellar, obs. in expanding mol. shell surrounding Pelican Nebula (IC 5070=W80) 80—105296
CO, interstellar, radio emission rel. to cold mol. clouds in inner Milky Way 80—4425
CO, interstellar, time-dependent form. and chem. fractionation 78—57602
CO, interstellar clouds, blister model for assoc. H II regions 79—25681
CO interstellar emission intensity rel. to H I absorption column density 79—35319
CO, ion transport in electrical discharge 78—87435
CO, ionis. pot., Koopman's theorem breakdown, rel. to N_2 photoelectron spectra 79—72354
CO, ionisation by electron bombard., empirical and semi-empirical calcs. 79—36784
CO, ionisation energies, self-consistent-charge Hartree-Fock-Slater calcs. 77—6687
CO, ionisation growth, spatial current growth meas. 77—19665
CO, isoelectronic sequence, Rydberg transitions, term value-ionisation pot. correl. 80—58276
CO, isotope effect in electron impact desorption 77—55460
CO isotopes in Ar matrix, vibr. energy accumulation 78—13485
CO, isotopic mols., Dunham pot. energy coeffs. 78—41979
CO isotopic rotational transitions in ultracold molecular gas 80—51826
CO, istopically enriched, Ar matrix isolation, laser-included vibr. fluoresc. 80—9707
CO J=1-0 and 2-1 obs. of Lynds 1551 dark interstellar cloud 80—105318
CO J=2→1 230 GHz obs. of IRC+10216 and related objects 79—62931
CO j=2→1 IR line obs. of Monoceros R2 assoc. 79—25654
CO, K-shell, excitation and ionisation, vibr. struct., electron energy loss spectra obs. 80—18943
CO, K-shell photoabsorption coeffs., 500-600 eV 80—9617
CO, LCAO method, improvement by directed variation of exponential parameters 79—41101
CO, LCAO-Xα method calcs., comparison with Hartree Fock and MS Xα methods 80—95539
CO, lack of C isotope exchange, methane and C oxides, high temp. 79—84263
CO laser, analytical theory, multilevel cascade emission *(Chinese)* 80—102702
CO laser, CS_2-N_2O-O_2 continuous combustion, performance characts. *(Russian)* 78—55348
CO laser, CW, with RF excitation in supersonic flow 80—74375
CO laser, chem. composition of plasma, room temp. 77—83866
CO laser, continuous flow longit. discharge high specific output energy 78—46585
CO laser, cooled electron-beam controlled, characteristics 80—19023
CO laser, cooled electroionisation type, in nucl. reactor active zone 80—64066
CO laser, discharge plasma, C combustion effect on vibr. excitation 77—50666
CO laser, electron-beam-controlled, short high-power pulse generation 78—25863
CO laser, externally sustained discharge, energy characts. 80—28207
CO laser, high power combustor driven system 78—87065
CO laser, liq. N_2 cooled, extended spectral distrib. of lasing transitions 79—89894
CO laser, longit. discharge, aerodynamically stabilized cathode 77—10955
CO laser, mass spectra of positive ions in discharge plasma 77—89315
CO laser, multiphoton amplification, HF removal of forbiddenness *(Russian)* 80—53262
CO laser, overtone generation, by pumping in elec. discharge *(Russian)* 78—22116
CO laser, radiation power, generation line selection influence *(Russian)* 77—83865
CO laser, sealed-off, output power and efficiency meas. 80—99743
CO laser, simple model for power and spectra 79—7119
CO laser, stable CW, step-tunable, pumping of external-resonator controlled Raman laser 80—9624
CO laser, steady state, parametric relation investigation 79—76677
CO laser, steady state operation, vibr. distrib., numerical calc. 79—36884
CO laser, theoretical and experimental developments *(Japanese)* 78—25857
CO, laser, vibr. distribs., O_2 addition effect 78—50757
CO laser, vibr. relax. in CO-Ar supersonic stream 77—14697
CO laser, water-sealed, efficiency increase by reducing resonator losses 80—64081
CO laser driven spectrophone, humidity trace detection in H_2 and air 79—20477
CO, laser gain measurements in acetylene+O_2 detonation products 78 33729
CO, laser lines, spectral coincidences with NO absorpt. lines 77—54559
CO laser lines, spectral coincidences with NO absorpt. lines 79—86162

carbon compounds continued
- CO laser output power, active species and buffer He isotope effects *(Russian)* 80—63986
- CO laser pumping with high-energy particles 79—64211
- CO laser with selective resonator, gain saturation law, lasing transition efficiency 80—48227
- CO lasers, scaling laws 80—95878
- CO, Lennard-Jones 12:6 parameters calc. from viscosity data 77—46612
- CO ligands, interactions with transition metal atoms, MO calcs., bonding props. of adsorption systems 79—85896
- CO light-dependent net prod. by intact plant shoots, rel. to photorespiration 79—2010
- CO, line broadening, short range force effects, semiclassical calcs. 79—98085
- CO, line parameters appl. to IR spectrometer performance testing 77—91275
- CO line profiles for dark molecular clouds 79—5877
- CO line radiation transfer in collapsing dark cloud, Monte Carlo method appl. 79—44357
- CO, liq., ^{13}C NMR for mol. diffusion and spin-rot. interaction, 0-1.73 kbar 79—99777
- CO, liq., IR four-wave mixing 78—18006
- CO, liq., pure vibr. Raman spectra 80—97262
- CO, liq., refr. index meas. by interferommetric technique 79—65816
- CO, liq., thermodynamic perturbation theory, equilib. props. 79—64976
- CO, liq., viscosity, density depend., theory 77—20105
- CO liq. and CO-O_2 (N_2)(Ar) mixtures, polarised vibr. Raman scatt. lineshapes 78—27199
- CO, liquid, Brillouin scatt. obs., US vel. and absorpt. 80—45085
- CO, long and short range electronic effects in bonding on Cu-Ni alloy 77—7974
- CO loss in glow discharges in CO, CO-He and CO-N_2-He mixtures 77—19788
- CO, low energy electron scatt., ab initio study, frame-transform. theory 77—83732
- CO, low transitions in discharge lasers, theory and expt. 77—3568
- CO low-press. laser discharge, effects of O_2 78—17914
- CO, mass spectrum. determ. in HTR individual coated fuel particles 77—56293
- CO, mass spectrum. determ. in HTR individual coated fuel particles 77—56294
- CO, matrix HF calcs. using universal basis sets 79—59354
- CO, matrix isolated, vibrational energy migration, vibr. fluoresc. obs. 79—91486
- CO, matrix-isolated, librational relax., IR line broadening 80—978
- CO, methanation over Ni catalyst 77—56250
- CO microconcentrations in air, metrological provisions for gas-analysing instruments 79—67248
- CO, microwave absorpt. coeff. 77—64378
- CO, microwave spectral line profiles, rotation effects in CRL 437 peculiar IR source 78—45426
- CO mixing ratio in mesosphere from ground-based microwave meas. 79—58036
- CO, mm wave emission and visual extinction in interstellar dark cloud L134 77—13425
- CO, mobility on (110) plane of W 79—46955
- CO, mol., nucl. spin-spin coupling, diamag. contrib. 79—36665
- CO, mol. potential energy functions, extended accuracy 79—64066
- CO, mol. transition freqs. in resonant optical field, Stark shift 77—14487
- CO molecular adsorbed on Mo (110) surface, electronic states, photoemission spectra 80—65363
- CO molecular layer optical depth and rotational temp. on Sun 79—96988
- CO molecules, IR spectra obs. 77—46655
- CO monolayers, on Pd (100), electronic states, tight-binding method appl. 80—49564
- CO, multiphoton UV photolysis, isotope effects obs. 80—55679
- CO, multipole expansion of diatomic overlap, MEDO calcs. 78—46264
- CO near highways, line source dispersion models, comparison 79—12247
- CO, near resonant V-V transfer rates for high-lying vibr. states 79—3536
- CO, negative-ion resons. associated with inner-shell-excited states, electron impact 77—88580
- CO, nondispersive IR analyzer with compensation for optical bias 79—16103
- CO, nonempirical PRDDO scheme and calcs. 80—37739
- CO, nonequilib. dissoc. induced by electron-vibr. and IR laser pumping 79—86016
- CO, nonlinear optical polarisability meas. 79—54991
- CO, nucl. elec. shielding tensor calcs. 80—83296
- CO nuclear pumped lasers, electron impact cross section meas. 80—63985
- CO nuclear pumped laser, fission fragment excited with gas cooling, performance obs. 80—63997
- CO, numerical coupled Hartree-Fock parallel polarisability, partial wave SCF calc. 78—9079
- CO, obs. in Maffei 2 galaxy 78—16530
- CO obs. of molecular cloud assoc. with NGC 7023 at 2.7 mm wavelength 78—41008
- CO on Co surface, adsorption-desorption kinetics, surface carbide form. effects 80—103574
- CO, on CoO, catalytic oxidation 80—71945
- CO, on Cu surface, cluster calc. using SCF-Xα-scatt. wave method 77—62742
- CO on Jupiter, implications for atm. convection 78—36500
- CO on Ni, Pd, and Pt, absolute coverage, desorption expts. 80—49493
- CO, on Ni (100), adsorbate vibr. EELS, large-ang. defl. 80—44405
- CO, on Ni (111), desorption preexponential factor 80—49515
- CO on Pd, catalytic oxidation and chemisorption 77—70339
- CO on Pt, oxidation, surface struct. effects on rate, data assessment 78—43251
- CO, on Pt surface, IR spectrum obs. in presence of free CO 78—74654
- CO, on Re, effects of surface steps on CO β state adsorption *(French)* 78—43250
- CO, on W surface, interaction of He metastable atoms with surface 79—91558
- CO, one electron props., SCF-Xalpha scattered wave method 80—83279
- CO, one-election props., SCF and CI calcs. 80—27951
- CO, one-electron props., corrections, Moller-Plesset perturbation theory calc. 80—95519
- CO, optical excitation function by electron impact near threshold 77—6942

carbon compounds continued
- CO, optical parametric oscillator, resonantly enhanced four-wave pump intensity 78—9412
- CO, orbital contribs. to relax. energies accompanying core ionis., ΔSCF HF calcs. 78—82642
- CO, ordered overlayer on Ni(100) surface, angle resolved UV photoemission 78—56570
- CO, ordered overlayer on W (001), effect on electron spin polarisation in LEED 79—60633
- CO, ordered surface structures on W (110), LEED meas. 77—59213
- CO, orientated mol., (e,2e) spectra, electron momentum density 79—98236
- CO, oriented molecule, photoelectron ang. distrib., energy depend. 80—76152
- CO, oriented molecules, vibrationally inelastic electron scatt. 78—67907
- CO, oriented mols., inelastic low energy electron scatt. 78—72653
- CO, oscill. oxidation on Pt surface, kinetic model 77—4926
- CO, oscill. strengths for shape resonances near K edges 77—75224
- CO oscillatory oxidation over Pt, theory 80—85215
- CO oscillatory oxidation over Pt, theory 80—85216
- CO, output spectra from CS_2-O_2-CO_2(N_2O) flame lasers 80—83601
- CO oxidation by NO on Ir surface XPS and UPS 78—15702
- CO, oxidation on Co (0001) 79—60631
- CO, oxidation on Ir films, IR absorpt. spectroscopy 80—71398
- CO oxidation on Pt, AC pulsing technique 79—100439
- CO, oxidation on Pt and Pd, kinetics 79—61903
- CO, oxidation over Ir, tracer studies on reaction path and kinetics of CO oxidation 80—7857
- CO oxidation over Pt, kinetics determ. using ^{13}C tracer 79—29400
- CO, oxidation reaction over Ir (111) surface, appl. of XPS 77—31886
- CO, P(6) line absorpt. coeff. and halfwidth, temp. depend. 80—78618
- CO, partial photoionisation cross-section determ. using synchrotron radiation 77—75243
- CO, photoabsorpt. cross section, 10 to 50 nm 77—61797
- CO, photoabsorpt. cross-section, photoionis. continuum 77—68029
- CO, photoabsorpt. cross-section, 50-340 Å, as sum of empirical at. cross-sections 78—58718
- CO, photoabsorption, photoionisation cross section, separated channel static exchange Stieltjes-Tchebycheff calc. 79—3502
- CO, photoabsorption and photionisation, UV region meas. 78—42087
- CO photodesorption from metal, forming CO_2 79—52777
- CO, photodissoc. ionis., 16-41 eV 77—18995
- CO, photoelectric cross section and angular distribution calcs. 80—58323
- CO, photoelectron ang. distrib., energy depend. 79—22760
- CO, photoelectron ang. distrib., multiple scatt. calc. 79—81238
- CO, photoelectron ang. distrib., photon energy depend. , 16-25 eV 80—53046
- CO, photoelectron ang. distributions, wavelength and vibr. state depend., reson. effects, asymmetry parameters 80—91602
- CO, Photoelectron angular distrib. of C and O K-shell ionisation 78—52628
- CO, photoelectron spectra, 21.2-151.4 eV and soft X-ray, ionis. cross-section 78—37683
- CO, photoelectron spectra ang. distrib., vibr. transitions, autoionis. state 79—31609
- CO, photoelectron spectra, fourth band system assignment 79—72361
- CO, photoionis., vibr. intensity distrib., shape reson. effects 79—98167
- CO, photoionis. cross section calc., for YMζ line, HF vs OPW method 77—42353
- CO, photoionisation, expt. techniques, processes, theory, review 77—14402
- CO, photoionisation cross sections, at. extrapolation, ground state inversion method appl. 80—18787
- CO, photoionisation cross sections and asymmetry parameters, SCF Xα scatt. wave calcs. 80—63542
- CO, physisorption and chemisorption on Cu and Au, UPS 78—39666
- CO, poisoning effect on D_2+H_2O exchange reaction on Pt surface 79—11824
- CO, polarisability derivatives, bond length depend., SCF and CI calcs. 80—58162
- CO, pollution from road traffic, street level conc. 80—81500
- CO, pollution from vehicle emission in urban area cold engine startups 80—104527
- CO, population inversion mechanism for rot. levels, interstellar medium appl. 79—21406
- CO, pot. curve, variational cellular method, electronic struct. calcs. 80—54591
- CO, pot. curves, binding and ionisation energies and config. variational cellular method 80—32597
- CO, pot. energy functions, virial theorem calcs. 77—88519
- CO presence effect on $FeCl_3$ pyrolysis 79—43623
- CO, press. depend. of melting and α-β phase transition temp. 77—69075
- CO, pressure-induced spectral linewidth and line shifts, vibr. depend., IOS scatt. approx. 79—68267
- CO, prod. in Venus atmosphere by thunderstorms 80—98587
- CO production by lightning 79—70836
- CO production in electric discharge 79—96786
- CO, production in O(^{3}P)+1-butyne (2-butyne) reaction, dynamics and mechamisms 78—11510
- CO production using fusion reactor heat and gas dynamic compression heating 80—35793
- CO production using fusion reactor heat, from $2CO_2 \rightarrow 2CO+O_2$, CO+-steam$\rightarrow CO_2+H_2$ 80—67014
- CO, proton affinity, integral Hellmann-Feynman theorem 78—70767
- CO, pulsed laser, characts. 80—43325
- CO pulsed laser, stimulated emission dynamics, transition lines for isotope enrichment 80—48225
- CO pulsed laser emission with line selection, analytical theory 80—53277
- CO pulsed TE laser and pulsed CS_2/O_2 chemical laser, comparative study 79—31876
- CO, π face bonding of cyclobutadiene 79—98180
- CO, quadratic vibr. force const., from X-ray scatt. factors 79—45864
- CO, quadrupole moment from K^+(Ar)(Kr)(Xe) scatt. total cross sections 77—50495
- CO, quasi-energy states and stability in light wave field, width of unsteady zones *(Russian)* 79—94039
- CO, radiative lifetimes and electron impact absolute emission cross-sections 77—88503
- CO, rate of entry into myoglobin 79—8471
- CO, ratio of lateral diffusion coeff. to mobility for electrons 79—50840

carbon compounds continued
CO, reaction with adsorbed O_2 on Pd, kinetic behaviour, AES obs. 77–90640
CO, reaction with adsorbed O_2, N_2O on Cu (100) surface 80–103583
CO reaction with H_2, C_8FeCl_3 behaviour, effect of activation 79–43623
CO, reaction with H_2 on Ni(001), extended muffin-tin orbital theory 80–76557
CO, reaction with NO on polycrystalline Pt surface at low press., reaction kinetics study *(German)* 79–15989
CO, reaction with NO on polycrystalline Pt at low press., reaction kinetics study *(German)* 79–15988
CO, reaction with O_2 adsorbed on Cu (111), AES, LEED and ellipsometric meas. 79–65317
CO reaction with O_2 adsorbed layer on Cu, ellipsometry, AES, LEED study 80–6635
CO, reaction with O_2 chemisorbed on Pt, AES expts. 77–90639
CO, reactions, catalysis by ferroelectric $KNbO_3$ 80–30282
CO, reactions with dissolved O, and C in liquid Fe, equilibria 78–44397
CO, reactions with NO over Rh flash desorption spectra, titration, reaction kinetic calcs. 78–61045
CO, reactivity with metal surfaces, electron spectra 77–62748
CO reduction in solar nebula, kinetic inhibition 80–85875
CO, reduction of SO_2 in presence of H_2O and O_2, catalyst effects 79–24819
CO, relative Raman scatt. cross section 80–100061
CO, remote sensing using freq. doubled CO_2 laser radiation 80–67025
CO, reson. transitions, radiative lifetimes, astrophys. appls. 78–62767
CO room temperature nuclear pumped laser, parameter optimisation and spectral props. obs. 80–63995
CO, rot. distrib. in supersonic beam, IR bolometry using tunable diode laser 80–63869
CO, rot. line strengths in multiphoton transitions 80–48051
CO, rot. population transfer, IR laser double reson. expt. 78–50566
CO, rot. spectra, 714-1667 μm, Fourier interferometric spectrometer 77–83765
CO, rot. transitions obs. in interstellar molecular clouds 77–33612
CO, rot.-vibr. matrix elements, fourth-order contribs. 77–46553
CO, rotational Raman intensities and polarisability anisotropy change meas. with internuclear distance 80–63641
CO, rotational-level populations of interstellar molecule 79–97054
CO, rovibr. multiphoton spectra comput., hole burning effect 80–9672
CO sealed laser, approximate analytic theory 78–58994
CO, sealed TE laser, UV preionisation 78–17966
CO, second virial coeffs. 80–83440
CO, selective detection by SnO_2:ThO_2, hydrophobic and hydrophilic silica effect 79–97372
CO, sensitive optoacoustic detection by reson. absorpt. 78–44981
CO, simple high energy TEA laser 79–3714
CO, simple high-power TEA laser operating in IR 79–94251
CO, single and double ionisation by electron impact, energy depend. and ionisation pot. 79–13827
CO, single breath diffusing capacity in man, meas. by rapid CO anal. 80–46115
CO, single breath diffusing capacity, theoretical anal. 80–67328
β-CO, single cryst., adiabatic elastic consts., at triple pt., Brillouin scatt. obs. 79–47466
CO, solar, equivalent widths of (A-X) band lines 77–17501
CO, solar IR spectrum rel. to atm. struct. and C abundance 78–28608
CO, solid, anisotropy of chem. shift tensor, ^{13}C NMR obs. 77–90054
CO, solid, CO laser excited, strong vibr. population inversion 80–58547
CO, solid and liq., vibr. relax. and vibr. diffusion rates, 66-79K 78–17757
CO, solid and matrix isolated, IR and Raman spectra 78–48156
CO solid film, contaminant on cryocooled Ge optical window, IR transmission 79–32007
CO solubility in water and seawater at 10^{-5} atm partial press., 0-30°C 79–100870
CO, solubility parameters, calc. from eqn. of state 77–11660
CO, sticking coeff. on W (110) and (100) planes 79–82464
CO, stimulated emission behind overdriven detonation wave front in CS_2-O_2 *(Russian)* 77–23668
CO, stratosphere and troposphere content, circumpolar airliner flight obs. 80–51475
CO submillimetric high-resolution Fourier transform spectra 79–31509
CO, supersonic laser mixture, double discharge stabilisation 78–5461
CO supersonic lasers, CW double elec. discharge performance 80–69416
CO supersonically driven chem. laser, kinetics of physical processes 79–45937
CO, surface, (110), chemisorpt. effects on dielec. function, refl. spectra chemisorption on W(110) surface, effects on dielec. function, refl. spectra 80–75616
CO surface contamination of Ti thin film, effect on deuteriding 77–35814
CO, surface coverage of Ni crystal faces, backscattering coeff. from ^{14}C radiation 78–30824
CO survey of mol. clouds, use as galaxy spiral struct. survey 80–105346
CO, temp. meas. technique using IR tunable diode laser 78–86268
CO, thermal desorption from Mo, effect of temp. gradient along sample 77–62735
CO thermal desorption from Re single cryst. surface *(French)* 78–22959
CO, three-body electron attachment in discharge 80–24245
CO, titration of pre-adsorbed O on Ir (111), XPS investigation 79–91994
CO, total Xα energy, LCAO calc., rel. to local density models 80–32607
CO, triplet state, form. from spin transfer reaction with Ar *(French)* 79–34289
CO, triplet state electronic energy delocalisation 77–3478
CO, troposphere vertical profile, eastern USA in winter 80–77035
CO, tropospheric latitude distrib., model involving production and transport 80–41483
CO, two-photon excited vac. UV fluoresc. 78–5264
CO, two-photon spectroscopy with tunable ArF laser 80–37843
CO, UV photodissoc., O I 1304 angstrom emission 80–32652
CO uptake in respiration, computer aided measuring system *(German)* 80–3875
CO, $v=0\rightarrow1$ vibr. excitation, electron impact cross sections 80–83507
CO, vac. UV absorpt. spectrum, Doppler-free two-photon excitation 79–41185
CO, vacuum UV molecular photoabsorpt. cross-section meas. 80–37096

carbon compounds continued
CO, valence excitation energy and UV spectra, HAM/3 calc. 78–25453
CO, valence X-ray photoelectron spectrum, satellite struct. 77–61800
CO, vaporisation temp. and press., state eqn. *(French)* 77–43323
CO, variable 2.6 mm emission in o Ceti (Mira) and χ Cygni 78–12241
CO, vehicle generated, in atmosphere, correl. study 79–21012
CO vel. features in OMC rel. to shock fronts and expansion of Orion H II region 80–41880
CO, vibr. excitation calc., in gas mixture discharge 79–77442
CO, vibr. excitation using steady state chemical reaction between CO and N_2O 80–50851
CO, vibr. excitation via high-energy shape resonances 80–91693
CO, vibr. excited, form. in charge transfer reactions 77–3455
CO, vibr. excited, in Ar matrix, information theoretic anal. 78–91386
CO, vibr. intensity meas. in photoelectron spectra for ionic ground states 77–18972
CO, vibr. population distrib. in supersonic expansion 78–71364
CO, vibr. relax. at glass surface, glow discharge meas. 79–18409
CO, vibr. relax. in unsteady expansion wave, vibr. temp. distrib. 77–68096
CO, vibr. struct., core and valence ESCA spectra, Frank-Condon and HF anal. 80–32602
CO, vibr. struct. of K_α emission spectra 78–86886
CO, vibr. transition moments, elec. and mech. anharmonicity influences 80–23459
CO, vibr.-rot. absorpt. line., shock tube spectroscopy 77–71890
CO, vibr.-rot. interaction, high excitation transitions in solar IR spectrum 77–68040
CO, vibrational structure in X-ray spectra, calcs. 77–30884
CO, vibrational transitions dipole matrix elements, numerical calc. 80–95594
CO vibrationally excited transition at 114 GHz in IRC+10216, identification refuted 80–51829
CO, viscomagnetic heat flux, in a Burnett regime 78–71400
CO waveguide CW laser, 280-290K *(Russian)* 77–71975
CO, waveguide laser operating near room temp., design and construction 78–22144
CO, $X^1\Sigma^+$ state, diagrammatic many-body perturbation theory, pot. curves 79–10014
CO, $X^1\Sigma^+$ state elec. dipole moment function, transitions, vibr.-rot. band calcs. 77–14410
CO, $X^2\Sigma^+$, vibr. levels, UPS electron attachment obs. 80–95683
CO, X-ray and electron scatt. first Born approx. calcs. 77–61867
CO, X-ray and high-energy elastic electron scatt., vibr. averages 79–81279
CO, X-ray K-absorpt. spectra, vibr. fine struct., ab initio restricted HF calc. 78–86883
CO, X-ray K-absorpt. spectra, reson. obs., near fine struct. 80–37817
CO, Xe matrix-isolated and solid, UPES obs. 79–45762
CO , electron impact dissoc., to positive ion states, negative-ion reson. effects 79–54977
CO^+ ^{14}C and ^{18}O isotope shifts, vibr. anal. of first negative, comet-tail and Baldet Johnson systems 80–28029
CO^+, A-X and B-X bands intensities in comets 79–35191
CO^+, $A^2\Pi$-$X^2\Sigma^+$ system, (2,0) band, rot. anal., $^2\Pi$ state Λ-doubling *(French)* 77–10681
CO^+, ab initio pot. energy curves, full valence CI with minimal STO 79–72361
CO^+, appearance potential by anal. of field-dispersed ions 78–85234
CO^+, $B^2\Sigma^+$ state, radiative lifetimes of 0, 1, 2, 3 vibr. levels, intensity decay meas. 79–98157
CO^+, CN^+, interstellar, radio search 78–24534
CO^+ collective accel. in vac. diode with C tip cathode, by 180 kV pulses 78–37104
CO^+ detection at outburst in Periodic Comet Schwassmann-Wachmann I (1974 II) 80–72881
CO^+, dissoc. energy determ. from pot. energy curve 79–13837
CO^+, electron impact rot. excitation, Glauber approx. with Coulomb effect 80–63840
CO^+, electronic absorpt. spectrum, rot. lines, laser/ion beam reson. 77–54564
CO^+, electronic struct., CO(e, 2e) reaction meas., CI calcs. 77–34769
CO^+, electronic transition moments for ($B^2\Sigma^+$-$X^2\Sigma^+$) and ($b^3\Sigma^+$-$a^3\Pi$) systems and matrix elements for ($X^1\Sigma^+$) and ($B^2\Sigma^+$) 77–38696
CO^+, exploding fast mol. ions, Auger spectra 80–32781
CO^+, fluoresc. and production cross-sections by photoionis. of CO 78–9204
CO^+, fluoresc. spectra of ion beam, laser and electron excitation 79–45743
CO^+ in Comet West (1976 VI), brightness profiles of $A^2\Pi$-$X^2\Sigma$ system (2-0) band 80–85896
CO^+ in cometary coma, dissoc. recomb. rel. to C prod. 79–16885
CO^+ in cometary tails, surface brightness rel. to H_2O^+ 80–72880
CO^+ in Periodic Comet Schwassmann-Wachmann 1 near minimum brightness 80–82305
CO^+, radical, $+NH_3(PH_3)$, thermal energy charge transfer reaction 77–16796
CO^+, UPS by threshold photoelectron spectrosc. by electron attachment method 79–89708
CO^+, vibr. ($A^2\Pi_i$) states, radiative lifetimes 77–3397
CO^+, vibr. intensity distribs. for electronic states prod. by photoionis. 78–25614
CO^+, vibr. relax., laser-induced fluoresc. 77–83632
CO^+, vibr.-excited $A^2\Pi$ state, radiative and radiationless vibronic deactivation rates with He 79–10134
CO^+, violet-degraded B-A bands, rotational analysis 79–18199
^{11}CO inhalation for imaging small pulmonary ischaemic lesions 77–2035
$^{12}CO^+$ and $^{13}CO^+$, sub-Doppler laser spectroscopy using fast ion beams 80–9655
$^{12}C^{16}O$, ^{13}C ^{16}O, Heizberg system, rot. anal. 79–59423
$^{12}C^{16}O$ and $^{12}C^{18}O$ $J=2\rightarrow1$ transitions obs. towards galactic H II regions 80–73022
$^{12}C^{16}O$ in Ar matrix, vibr. level energy cascades 77–79598
$^{12}C^{16}O$, in Ar matrix, vibr. population time evolution temp. depend., master eqn. 78–9180
$^{12}C^{16}O$, near UV emission bands of fourth positive system, vibr. and rot. anal. 77–58054
$^{12}C^{18}O$ 78–82768
$^{12}C^{18}O$, $A^1\pi$-$X^1\sigma^+$(13,0) band, monochromatic excitation 78–82767
$^{12}C^{18}O$, Herzberg system of $C^1\Sigma^+$ state 78–90185
$^{12}C^{18}O$, IR emission, vibr.-rot. lines 77–3355

carbon compounds continued
^{13}CO in external galaxies, ^{12}CO/^{13}CO intensity ratios 80−4416
^{13}CO, in interstellar molecular clouds, column density rel. to submillimetre optical depth 77−45508
^{13}CO self-absorption in the ρ Ophiuchi dark cloud 80−90500
^{13}C^{16}O, fluoresc. and electronic quenching cross sections 78−82768
^{13}C^{16}O, IR emission, vibr.-rot. lines 77−3355
^{13}C^{16}O^{+} (2,0) band, comet-tail system, rot. anal. 80−74157
^{14}CO, atmospheric, measurement, method for tropospheric OH radical conc. determ. *(German)* 80−8419
^{14}CO, pure rot. far IR spectra, rot. consts. 80−47996
^{14}C^{16}O, fourth positive band system, near UV meas. 78−66559
C^{16}O and C^{18}O, adsorption on Rh, inelastic electron tunnelling spectra obs. 79−65331
^{12}C^{16}O:CO isotopes, IR and Raman spectra, vibron band, vibron-phonon combination bands 78−68495
CO/H_2 ratio in interstellar dark clouds, meas. 78−96513
CO/H_2 surface complex, on W (100), flash desorption and AES obs. 78−73083
^{13}C^{16}O/^{12}C^{18}O double ratio, isotopic fractionation evidence in interstellar dark clouds 80−73017
CO-^{3}He nuclear pumped laser, optimisation with 2 MeV protons 80−64000
CO-air streams, selective oxidation of H_2 before CO electrochem. anal. 77−63978
CO-alkane, liq. soln., vibration-rot. IR spectra, rot. diffusion 77−83584
CO-Ar, cryst. at 5K, absorpt. and emission spectra, exciton interpretation 79−87481
CO-Ar, glow discharge, ion cluster in positive column, ion mass spectra diagnostics 80−38752
CO-Ar, non-self-sustained discharge instability, negative differentiated cond. *(Russian)* 80−38740
CO-Ar gasdynamic laser, output power, specific output energy and efficiency 78−46583
CO-Ar glow discharges, positive ion spectra, ion clusters obs. 80−64807
CO-Ar mixture non-self-sustained discharge instability obs. 78−71612
CO-Ar(-N_2), C_2 and CN form. by optical pumping, room temp. 80−16701
CO-Ar(-N_2), high press., arc assisted elec. discharges 77−3606
CO-CS_2, laser system, interaction between vibr. states, theory 77−23670
CO-cycloalkane solns., CO IR vibr.-rot. spectra, solvent mol. struct. 77−83585
CO-H_2O-NH_3-methanol, solid mixture vibr. modes, IR spectra 80−90504
CO-HBr, weakly bound, rot. spectra 80−91544
CO-HCN complex, charge transfer theory, Mulliken population, ab initio calc., multiconfiguration scheme 80−106392
CO-HCl, weakly bound, rot. spectra 80−91544
CO-HF, weakly bound, rot. spectra 80−91544
CO-haemoglobin reaction kinetics, relax. meas. on photolytic illum. 77−70405
CO-He, heat of mixing, low press., theories comparison 78−26230
CO-He, plasma-injection-stabilised discharges at low temp. 78−17959
CO-He glow discharge, positive column, ionisation processes 80−79618
CO-He glow discharges, positive ion spectra, ion clusters obs. 80−64807
CO-He low press. mixture, CO vibr. distrib. to high level 78−58985
CO-He nuclear pumped laser, high energy beam deposition 80−63999
CO-He-O_2, species concentrations in glow discharge and afterglow, mass spectra, laser conditions 78−14241
CO-He-O_2 gas discharge laser plasma, positive ion generation mechanism *(Russian)* 79−99005
CO-He-O_2-H_2O laser discharge, stability, influence of recombination and ion chem. 78−17915
CO-He-Xe, laser, Xe effect on gas temp. 77−19238
CO-hydrocarbon mixtures, phase equilib. calcs., modified Soave eqn. of state 79−19353
CO-myoglobin, mol. tunnelling, isotope effect, time resolved IR Fourier transform obs. 80−72126
CO-N_2, (Ar), (He), pulsed non self sustained discharges, peculiarities 80−38811
CO-N_2, liq., N_2 Raman scatt. parameters, high resolution coherent active spectroscopy 80−66207
CO-N_2 and CO lasers, energy and spectral characteristics 80−14327
CO-N_2 discharge, energy balance influence of N_2 rot. level reson. excitation 78−17903
CO-N_2 discharge, plasma characts. and vibr. kinetics anal. 80−59331
CO-N_2 plasma mixture decay, effective recombination coeffs. *(Russian)* 77−47144
CO-N_2-^{3}He, laser mixture, excitation in externally maintained discharge in reactor core 80−28193
CO-N_2-Ar mixture, supersonic expansion, CO vibr. level populations, gasdynamic laser appl. *(French)* 77−23659
CO-N_2-He laser, cooled electron-beam-controlled, characteristics 80−19024
CO-N_2^{3}He, nucl. reactor active zone, plasma and sustained discharge props. 80−5729
CO-N_2O gasdynamic laser, CO_2 vibr. level superequilibrium chem. pumping, mixture composition, He effects 79−76666
CO-N_2O reacting gas mixture, gain due to CO_2 $00^{0}1$-$10^{0}0$ transition 80−74337
CO-NO mixtures, Ar matrix isolation, laser-included vibr. fluoresc. 80−9707
CO-Ne, cryst. at 5K, absorpt. and emission spectra, exciton interpretation 79−87481
CO-O_2 liq. mixture, enhancement of nonlinear optical processes with double-pass tight-focusing geometry 79−18472
CO-O_2 liq. mixture, IR four wave sum and difference freq. generation 78−33771
CO-O_2 liquid, IR third harmonic generation 77−88849
CO-O_2-SF_6, efficient CO_2 laser radiation 3rd harmonic generation, for fusion ignition 78−59087
CO-O_2-SF_6, liquid, phase matched IR third harmonic generation 78−42384
CO-O_2(Ar)(N_2) dil. liq. solns., resonant IR third harmonic generation 77−31116
CO-OCS-N_2, liq. mixture, vibr. energy relax. and exchange, laser induced fluoresc. obs. 78−70905
CO-protohaeme binding dynamics, flash photolysis, activation energy, entropy 77−21472
CO-SF_6, single-photon absorption reaction chemistry in solid state 77−73454

carbon compounds continued
CO-Xe-N_2-He gas laser power rel. to mixture composition *(Russian)* 79−7114
CO+ perfluoroalkyl halides, collisional relax. 79−13799
CO+^{12}C^{+}(HCO^{+}), isotopic exchange, interstellar implications 80−61087
CO+^{14}N_2, vibr.-vibr. energy transfer, long and short range pot. effect 80−99556
CO+^{14}N_2 (^{14}N^{15}N),(^{15}N_2), vibr. energy transfer, laser fluoresc. obs. 80−28050
CO+^{14}N^{15}N, vibr.-vibr. energy transfer, long and short range pot. effect 80−99556
CO+^{15}N_2, vibr.-vibr. energy transfer, long and short range pot. effect 80−99556
CO+^{18}OH, evidence for at. exchange 79−47910
CO+^{3}He(^{4}He), vibr. relax., deactivation rates, pulsed fluoresc. meas. 79−89698
CO+Ar, charge transfer cross sections 77−34751
CO+Ar, intermolecular pots. from Thomas-Fermi-Dirac functional 77 19009
CO+Ar, molecular fluid mixtures, equilibrium props. 80−64867
CO+Ar, shock heated steady state dissoc. rate consts. calc. 78−40039
CO+Ar^{+}(He^{+})(Ne^{+}), charge transfer, thermal energy, product distrib. obs. 78−25656
CO+Ar^{+}(Kr^{+})(Xe^{+}), near-resonant charge transfer, 4-45 keV 77−27176
CO+Ar(CO), rot. band, line shape, collisional broadening, impact approx. 78−42134
CO+Ar(He)(Ne)(Kr)(Xe), intermol. pot. energy surfaces from electron gas model, ang., distance, and vibr. depend. 79−3520
CO+aromatic molecule, vibr. energy transfer, quenching efficiency 79−3539
CO+Ba, radiation quenching of metastable Ba (5d ^{1}D) in gas 79−85932
CO+Br^{-}, total electron detachment cross sections for energies around threshold 80−99550
CO+C^{-}(O), electron detachment cross-sections, 20-150 keV 78−25690
CO+C^{+}*, charge transfer cross-sections, 0.7-2.4 keV, C^{+}(^{2}P) and C^{+}(^{4}P) 78−58806
CO+CO, d$^{3}\Delta$ state vibr. relax. in glow discharges 79−18271
CO+CO, V-V master equation, numerical inversion 79−18265
CO+CO, vibr. energy transfer, collinear and 3-dimens. rate consts. 80−48065
CO+CO, vibr -vibr. energy exchange among highly excited states 79−76490
CO+CO, vibr.-vibr. energy transfer, rot. effects and long-range collisions 80−14194
CO+CO_2, CO_2 1st vibr. levels collisional deactivation, photoacoustic study 79−98187
CO+CO_2, exchange rates behind reflected shock waves for C^{18}O and ^{13}CO 79 29363
CO+CO_2, vibr. level depend. quenching of CO(ν=1-16) 80−32808
CO+CO_2, vibr. relax., optoacoustic obs. *(French)* 78−42178
CO+Cd($^{3}P_{0,1}$), absolute quenching cross section, phase-shift method 80−58340
CO+chemisorbed O_2, on Pt surface, transient kinetics obs. 78−7229
CO+Cl^{-}, total electron detachment cross sections for energies around threshold 80−99550
CO+Cl^{+}→O+CCl^{+}, reaction cross section, heat of form., mass spectrometric obs. 79−61843
CO+CsF, rot. inelastic collisions, mol. beam meas. 80−1049
CO+DCl, V-V energy transfer 80−78695
CO+e, momentum transfer cross sections, effect of non-spherical short range interactions 80−9745
CO+e, static pot. calcs. by INDO/1s and INDOX/1s 77−27192
CO+F in Ar matrix, vibr. and electronic spectra, valence force potential determ., mol. photodissoc. obs. 80−85170
CO+H, total differential collision cross section meas., interstellar gas clouds appl. 79−45786
CO+H_2, (oriented), total collision cross-sections, anisotropic pot. parameters calcs. 78−13568
CO+H_2, adsorpt. on Rh, reflection-absorption IR and thermal desorpt. obs. 78−6226
CO+H_2, interaction on Ni (100), reaction rate, AES and UPS obs. 79−79290
CO+H_2, pot. energy surface anisotropy in nonreactive region, ab initio calcs. 78−29832
CO+H_2, Raney Ni catalyst, absorption co-absorption and reaction, neutron inelastic spectroscopy method 79−99408
CO+H_2, rot. excitation, rel. between tensorial cross sections 80−83454
CO+H_2, thermal energy collision, ab initio pot. energy surface 79−45788
CO+H_2, vibr. deactivation, 250 to 2000K, Morse pot. calcs. 78−46428
CO+H_2 combustion in air, gasdynamic laser operating on combustion products, construction, amplification coeff. *(Russian)* 77−7075
CO+H_2^{+}, excited product dissoc., proton transfer dynamics, correl. diagram anal., crossed beam obs. 80−48079
CO+H_2^{+}(He^{+}), dissoc. charge transfer, energy transfer processes 78−74759
CO+H_2^{+}→H+HCO^{+}, 1.89 eV crossed beam study 80−21287
CO+H_2O^{+}, rate constants determ. as function of relative kinetic energy 80−81292
CO+H^{+}, computed cross section vibr. threshold effects 80−63759
CO+H^{+}, electron capture into n=3 states, 2.2-8.2 keV 79−50129
CO+H^{+}, ground state pot. energy surface, ab initio SCF calc., protonated equilib. geometry 80−83301
CO+H^{+}, vibr. excitation, 5-90 eV, forward scatt. differential cross section 78−9228
CO+H^{+}, vibr. excitation, differential scatt., low energy meas. 79−89749
CO+H^{+}, vibr. excitation calc., close coupling and sudden approx. 80−78561
CO+H^{+}(He^{+})(O^{+}), dissociative ionis. 79−10188
CO+HBr, rate consts. for vibr. energy transfer meas. using laser. induced fluorescence technique 80−87206
CO+HCN (001), relax. rate consts., using Cs vap. IR source 80−9696
CO+HCl, HCl linewidth, impact parameter calcs. 79−89714
CO+HF, HF(v=3) relax. and rate consts. 80−61069
CO+H(He), vibr. state distrib., charge exchange 150-2400 eV 78−42195

carbon compounds continued
  CO+haemoglobin reaction kinetics, using various regimes of photolytic illum. 78−48753
  CO+He, anisotropic intermol. pots., crossed beam expts. 79−31639
  CO+He, energy sudden approx., beam scatt. meas. mol. anisotropy effects 78−78802
  CO+He, nuclear mag. shielding consts., interaction geometry depend., chemical shift, gauge invariant method 78−62866
  CO+He, polarised mol., differential scatt. cross-sections calcs. 79−89733
  CO+He, press. broadening cross-section, ang. momentum approx. calcs. 77−34696
  CO+He, press. broadening, rot. energy transfer, infinite order sudden approx. 78−22011
  CO+He, rot. excitation, infinite order sudden approx. 78−74740
  CO+He, rot.-translational energy transfer, nonlinear vs. linear rotors, surprisal anal. 79−76492
  CO+He, vibr. relax., unitary distorted-wave approach 79−36738
  CO+He, vibr.-rot. energy transfer, stochastic theory 79−54944
  CO+He differential scatt. 0 to 5×10^{-2} rad. detector angle, 800 eV He *(Russian)* 77−79674
  CO+He_2, collisionally excited neutral and ionic emission, flowing afterglow 77−51248
  CO+He(H), scattering cross-sections, factorisation and fitting, IOS approx. 78−33575
  CO+He(Ne)(Ar) Penning ionisation, electron spectra, vibr. transfer 77−14555
  CO+$Hg(^3P_1)$, quenching rate constants determ. with nanosecond light pulser with Hg vapour 80−100111
  CO+$Hg(6^3P_1)(6^3P_0)$, electronic-vibr. energy transfer collision, IR obs. 79−45716
  CO+$I_2(ICl)(NO_2)$, E-V energy transfer reactions, electronically excited target mol. 78−64814
  CO+I^-, endoergic ion-molecule reaction 77−25262
  CO+inert gas, collision-induced intersystem crossing, reversibility 77−50465
  CO+inert gas, collision-induced intersystem crossing mechanism 78−74689
  CO+inert gas, state-to-state rates from press.-broadened linewidths, data reduction method 78−46430
  CO+K, anisotropy of the repulsive intermolecular potential from rotationally inelastic scattering 79−41226
  CO+K, atom electronic excitation, vibr. to electronic energy transfer, seeded mol. beam studies 80−47919
  CO+K, bulge effect, in rot. inelastic scatt., isotope shift 79−86047
  CO+K, rot. inelastic scatt., quantum effects, simple model surfaces 80−48064
  CO+Kr^{2+}, charge transfer reactions, rate coeffs. and product-ion distributions meas. 80−104431
  CO+$Kr(^3P_1)(^1P_1)$ $A^1\Pi$-$X^1\Sigma^+$ and $b^3\Sigma^+$-$a^3\Pi$ sensitised fluorescence, isotope effects 78−82761
  CO+Li^+, 4-7 eV, final rot. state distrib., small ang. depend. 79−68300
  CO+Li^+, comparison with classical small-ang. pot. scatt. theory 80−1043
  CO+Li^+, differential cross-sections, classical trajectory calcs. 78−29841
  CO+Li^+, differential cross-sections, ab initio CI vibrotor pot. energy surface calcs. 78−46421
  CO+Li^+, pot. energy surface, equilib. distance, SCF calcs., correl. effects 77−3430
  CO+Li^+, rot. excitation, ab initio CI pot. energy surface, classical mech. and coupled states calcs. 78−25665
  CO+Li^+, rot.-vibr. energy transfer, 1-10 eV, calc. 79−45799
  CO+methane (tetrafluoromethane), vibr. deactivation 80−37862
  CO+methyl cation, ternary assoc. reaction, rate coeffs., 100-300K 79−61845
  CO+N_2, adsorption on ZrC-W eutectic alloy 79−69951
  CO+N_2, collinear collisions, anharmonicity effects, vibr. excitation 79−31656
  CO+N_2, electronically inelastic collision, distorted wave calc. and pot. energy curve 80−9709
  CO+N_2, in matrix, vibr. energy transfer and relax. 78−46426
  CO+N_2O, adsorption on NiO, catalysed reaction in Neel transition region 78−53258
  CO+N_2O, CO_2 vibr. temps. under gasdynamic laser conditions 80−21276
  CO+N_2O, use of steady state chemical reaction for vibr. excitation of CO_2 and N_2 80−50851
  CO+N_2O catalytic reaction on Sc_2O_3 and MgO, kinetic obs. 79−29389
  CO+N_2O+Ca(Sr) reaction, intracavity dye laser spectroscopy 77−86293
  CO+N_2*, vibr. excitation and quenching, long contact time effect 79−86040
  CO+$N_2(CO_2)$, line broadening, short range force effects, semiclassical calcs. 79−98085
  CO+$N_2(CO)$, ionis. at low energy 78−58791
  CO+N^+, charge exchange, 1-3 keV, $N^+(^3P)$ and (^1D) states 79−36760
  CO+N^+, integral reactive cross-section calcs. 78−27750
  CO+NO, electronic energy transfer, spectroscopic obs. 78−82716
  CO+NO, NO $\gamma(0,0)$ band, oscillator strength and line broadening 80−106356
  CO+NO+H_2 interaction over Pt, Rh, Ru and Os, NH_4OCN formation 78−73082
  CO+$NO(O_2)(D_2)$, (ν=1) relax., temp. depend. 78−17760
  CO+Na, 13d-13f transition, collisional dephasing, Ramsey method investig. 79−54791
  CO+Na velocity-changing collisions, stimulated photon echo obs. 79−81258
  CO+$Na^*(3^2P)$, electronic to vibr.-rot. energy transfer, differential cross sections 77−38715
  CO+$Na(3p^2P_{3/2})$, electronic energy quenching dynamics, crossed beam expt. 80−9683
  CO+Ne^+, thermal energy, reaction rate coeffs. and product distrib. 79−29333
  CO+Ne^{2+}, charge transfer reactions, rate coeffs. and product-ion distributions meas. 80−104431
  CO+Ne*, quenching rate const. for metastable $Ne(^3P_2)$, flowing afterglow 78−46295
  CO+Ni, complex form. in NiCa-Y zeolite, EPR, UV obs. 77−63949
  CO+$Ni_{1-x}Cu_x$, $Ni(CO)_4$ form. activation energy, mag. phase depend. 80−3409
  CO+NiF_2 react., Ar matrix isolated, ab initio MO calcs. 78−92458

carbon compounds continued
  CO+O, adsorbed on Ir (111), Langmuir-Hinshelwood reaction mechanism 79−29408
  CO+O, vibr. deactivation 78−94305
  CO+O_2, vibr. deactivation of CO, 80-300K, laser fluoresc. study 78−25661
  CO+O_2 interaction on Ag (110), ellipsometry-LEED expts. 78−91542
  CO+O_2 on Ag (111) ordered and damaged surfaces 78−14583
  CO+O_3, double-quantum vib. energy transfer 77−6897
  CO+$O^+(^4S)(^2D)$, charge transfer reactions, cross-sections meas. 78−92462
  CO+$O^{n+}(Xe^{n+})(Pb^{n+})$, 50 keV, multiple scatt., target at.+energetic ion spatial correlation influence 79−27062
  CO+OH, reaction rate consts. and quenching kinetics, reson. fluoresc. obs. 79−72349
  CO+OH radical, reaction rate consts. meas. 78−35663
  CO+OH˙, rate consts. 77−16781
  CO+OH˙, reaction rate 77−52610
  CO+OH(+isobutane), reaction rate consts., press. depend. 78−35654
  $CO+O+M \rightarrow CO_2+M$, time-resolved and flame-band emissions in shock tube expts. 77−36729
  CO+$O(^1D)$, deactivation rate consts. temp. depend., 113-333K 78−88629
  CO+PH, collisional deactivation of $PH(b^1\Sigma^+)$, time resolved quenching 79−54948
  CO+Si*, collisional quenching, reson. line absorpt. expt. 78−46297
  CO+$U^+(UO^+)$, reaction cross-sections, ion beam apparatus study 80−97691
  CO+X^{n+}, X=Ar,Kr,Xe,U, Auger emission line shape after dissoc. 78−86838
  CO+Xe, ^{129}Xe chem. shielding, second virial coeff. 78−66563
  $CO^+ + 2CO_2 \rightarrow 2CO_3^+$, reactions of electronically excited CO^+ 77−1915
  CO^++CO, metastable and $X^2\Sigma^+$ states dissoc. 78−33587
  CO^++CO (methane), charge transfer cross-section, low energy 78−58791
  CO^++D, reaction, ion cyclotron reson. mass spectrometric obs. 79−64098
  CO^++D_2, state selected reaction cross-sections, coincidence technique obs. 80−66797
  CO^++H_2, ion-molecule reaction detection of laser-induced ion spectrum, rot. components 78−74671
  CO^++He, $CO^+(A^2\Pi_i)$ vibr. relax. 80−53106
  $CO^+ + NO \rightarrow CO_2^+ + N$, crossed beam study 80−104436
  $CO^{+\cdot}$+fluoromethanes, thermal energy charge transfer reactions mechanism 77−63889
  $^{12}C^{16}O + {}^{13}C^{16}C$, vibr. energy transfer, laser-induced fluoresc. obs. 80−78690
  $^{13}CO^+$+CO, charge-exchange detection of $^{13}CO^+$ electronic absorption spectrum, hyperfine consts. calc. 78−70822
  CO_1, temp. and press. relax. behind shock wave, M=10-30 78−38490
  CO_2, $^{12,13}C$, $^{16,17,18}O$ isotope analysis by PbS diode laser absorpt. spectroscopy 77−44529
  CO_2, ^{13}C NMR, chem. shift., determ. of virial coeffs., rovibr. motion 78−58720
  CO_2, ^{13}C NMR, density depend. mag. shielding in gas phase 77−75187
  CO_2, $^1\Delta_u$ valence state, vertical energy level MC-CI wavefunction 79−45644
  CO_2 00^01-10^00 transition in CO-N_2O reacting gas mixture, gain 80−74337
  CO_2, 1 mJ line tunable optically pumped laser 78−66840
  CO_2 1KJ laser system for laser-plasma interaction expts. 78−5502
  CO_2, 10 μm absorption line profile, high resolution meas. 77−42359
  CO_2, 10^000-$00^00_{I,II}$ absorpt. band profile temp. depend., integral and spectral binary absorpt. coeffs. 80−43049
  CO_2, 100 kJ laser, optical design and components 78−82990
  CO_2, 1060-1175 Å photodissoc. quantum yield and $O(^1S)$ decayplots 78−27798
  CO_2, 10.6, 9.4 μm laser bands high-press. absorpt-spectra 78−66543
  CO_2, 10.6 μm absorption, 300-650K 78−5207
  CO_2 10.6 μm laser, freq. modulation and demodulation 80−43378
  CO_2, 10.6 μm reson. absorpt. behind shock front 78−42707
  CO_2 15 μ band radiant energy inflow in disturbed LTE *(Russian)* 78−40657
  CO_2, 15 μm band rel. to non-LTE radiative transfer in Earth atmosphere *(Russian)* 78−36341
  CO_2, 16 μm, kinetic mechanisms, model simulation 79−98338
  CO_2 16 μm laser, pumped optically in 4.3 μm, 9.6 μm bands, energy characts. 79−18398
  CO_2, 16.5 micron band generation, HF laser pumped, threshold characts. *(Russian)* 77−83846
  CO_2, $1\pi_g{}^3\,2\pi_\mu{}^1$ config., ab initio eqn. of motion excitation energies 77−50376
  CO_2, 200 J TEA laser, injection mode locking 78−79049
  CO_2, $201_{II} \leftarrow 000$ band, press. broadened coeffs. and absolute intensities, temp. depend., IR obs. 80−53054
  CO_2, 30 ps laser pulse generation by free induction decay 77−14738
  CO_2, $30^01_{II} \leftarrow 00^00$ band, meas. at different temps. of absolute intensities, line half-widths and broadening by Ar and N_2 78−86865
  CO_2, $30^01_I \leftarrow 00^00$ and $30^01_{IV} \leftarrow 00^00$ bands, absolute intensity meas. at different temps. 78−86864
  CO_2, 4854 cm^{-1} $201_{III} \leftarrow 000$ band, intensities and half-widths, 197, 233, 294K 79−89713
  CO_2, 4.3 micron absorption band, collision-broadened lineshape theory appl. 79−89711
  CO_2, 4.3 micron band, band model parameters 80−43026
  CO_2, 4.3 μ absorption spectrum appl. to atm. temp. sounding 78−16166
  CO_2 4.3 μ band radiance meas. of internal combustion engine gas temp. *(Japanese)* 78−29119
  CO_2, 4.3 μm airglow, excitation mechanism involving OH and N_2 79−16731
  CO_2 4.3 μm aurora and related phenomena 77−70904
  CO_2, 4.3 μm band, spectral absorpt. coeff. 78−5211
  CO_2 4.3 μm band absorpt. in atmosphere, solar occultation sounding for temp. and press. profiles meas. 80−98452
  CO_2 7883 Å band in Venus spectrum, high-dispersion obs. 78−53851
  CO_2 9 μm band laser amplifier, using saturable gas absorber 79−76709
  CO_2, 9.6 μm region emission spectrum, rot. consts. 77−3353
  CO_2 (00^01)+Br_2, vibr. relax. rate consts. 77−6898
  CO_2 (00°1) vibr. relax. in H_2 and D_2 below room temp., fluoresc. decay obs. 77−42381

carbon compounds continued
CO_2, (001)→(000) fluorescence following dye laser photolysis of s-tetrazine 78–88652
CO_2, [100] symmetric stretch mode excitation 79–76523
CO_2, ab initio SCF calcs., force consts., vibrs., pot. energy surface 78–5209
CO_2, absorpt. spectrum recorded by intracavity Nd:glass laser spectrometer 77–74530
CO_2, absorption, spectrum calibration, 14-15 μm, using diode laser source 77–18917
CO_2 absorption at 2.7 μ in atmosphere at large optical thicknesses, mechanisms *(Russian)* 78–40659
CO_2 absorption in H_2O, aq. solns. with interfacial turbulence due to microstirrers 80–64527
CO_2 absorption in leaves, sun vs. shade 78–80850
CO_2, absorption spectrum line parameters *(Rumanian)* 77–42326
CO_2, accumulation in atmosphere, effect on climate and harvests 80–40940
CO_2, acetone decomposition, near IR laser action 78–63055
CO_2, activation of C, paramag. props. rel. to interaction with H_2 77–63957
CO_2, addition to photoionis. plasma 80–10359
CO_2, additive effect on HCl helical TE laser output power enhancement 79–98397
CO_2, adsorbed film, on KBr, density fluctuations 79–42391
CO_2, adsorbed gas, on glassy AsSe, surface cond., photocond. 78–80038
CO_2, adsorbed on Al_2O_3, Raman spectroscopy study 80–65358
CO_2, adsorbed on alkali halide cryst., field induced vibr. splitting, IR spectra 78–46334
CO_2, adsorbed on α-cyclodextrin, positron annihilation, effects of adsorbed gases 79–65952
CO_2, adsorbed on quartz, effect on surface cond. 77–85297
CO_2, adsorbed on W, electron beam induced C deposition, AES obs. 77–89651
CO_2, adsorpt. on $Fe(OH)_3$ rel. to prep. method 79–39192
CO_2, adsorpt. on ice surface, gas capture by crystallising aq. aerosols investig. 79–39191
CO_2, adsorption, O_2-induced and reaction with other adsorbates on Ag(110) 80–55714
CO_2, adsorption (with H_2), on Ta surface, field-emission and mass spectra obs. 77–76673
CO_2, adsorption and capillary condensation on clays rel. to Mars volatile storage and atmospheric history 80–72833
CO_2, adsorption of Ni(111) surface, carburisation, electron-beam induced effects, AES meas. 77–48588
CO_2, adsorption on C, surface area meas., temp. and chemisorption effects 78–95225
CO_2, adsorption on η-Al_2O_3, IR and microgravimetric meas. 78–14578
CO_2, adsorption on $Fe(OH)_3$ 79–66344
CO_2, adsorption on In, AES study 79–82451
CO_2, adsorption on microporous C 78–22956
CO_2, adsorption on Mo (200), adsorbed O effect, LEED and AES obs. 80–39443
CO_2, adsorption on NaCl, atomic interaction pot. on (100) face *(German)* 80–15380
CO_2, adsorption on Ni (110), electron bombard. effects, AES and electron stimulated ion desorption obs. 79–51430
CO_2, adsorption on Ni (100)-p(2×2)C 79–91995
CO_2, adsorption on polycryst. Co, XPS and UPS *(French)* 77–36362
CO_2, adsorption on Ta, FEM and flash filament method exam. 78–43245
CO_2, adsorption on Ti, SIMS expts. using 500 eV primary Ar^+ ions 77–72785
CO_2, adsorption on water, 0-50°C, press. effects on surface tension 78–56024
CO_2, adsorption potential on NaCl cryst. surface 80–24738
CO_2, adsorption-desorption kinetics on Si and Ge surfaces 77–47684
CO_2 aerosol/hypersonic air stream interaction, gasdynamic CO_2 laser energy characts. 80–48211
CO_2, afterglow, press. effects on spectral features excitation 78–38563
CO_2, air composition at Barrow, Alaska, wind direction depend. 80–85704
CO_2, alveolar, technique for meas. in infants 79–66564
CO_2 amplifier, method for radiation pulse shape control 80–43367
CO_2 amplifier, pulsed, large-vol., small-signal gain meas. 80–91772
CO_2 amplifier, spatial and temporal fluctuations of nanosecond radiation pulses 79–14009
CO_2, anal. of adsorption isotherm, determ. of porous texture of solids 79–77897
CO_2 analysis, amplifier and lineariser for Beckman LB-1 analyser 77–29215
CO_2, and CO binary diffusion in chamber and formed coke *(German)* 80–100356
CO_2 and chlorofluoromethanes in stratosphere, simultaneous effects on O_3 column density 79–74940
CO_2 and climate, model of geographically nonuniform effects 80–90143
CO_2, and isotopic forms, bending fund. region, IR spectra, rot. consts. 80–47988
CO_2 and isotopic species, high-resolution Fourier spectra near 4.3 micron 80–47982
CO_2 and O_2 exchange and cardiopulmonary control interaction model, duck 80–3600
CO_2 and stratospheric O_3, two-dimens. model calc. 79–62564
CO_2, anharmonic pot., determ. of zeroth approx. 77–75255
CO_2, anomalous energy minima surfaces 78–86791
CO_2, anomalous Zeeman effect, nonlinear optical techniques, book contrib. 78–9279
CO_2, antisymmetric vibr., energy relax. rate, rel. to IR luminesc. kinetics *(Russian)* 78–82826
CO_2 antisymmetric vibr. mode relax. rate, luminesc. meas 79–94067
CO_2, aqueous solution, photoelectrochemical reduction on p-type GaP in liq. junction solar cells 78–88649
CO_2 as intracavity absorber in TEA CO_2 laser, multiline operation 79–94206
CO_2, as volatile component in magmas, influence on physical props. and comp. 80–41418
CO_2, asymmetry parameter, angle resolved photoelectron spectra, multiple scatt. method 80–63708
CO_2, atm., fast response sensor design, for eddy correl. flux meas. 79–5622
CO_2, atm., land biota changes rel. to C cycle 77–70785

carbon compounds continued
CO_2, atm. absorpt. and emission over mean long optical paths 77–49163
CO_2, atm. absorption line parameters, AFGL, compilation update 79–21013
CO_2, atm. conc., logistic source function calcs. 78–24368
CO_2, atm. conc. meas., comparability 78–20495
CO_2, atm. increase rel. to future climate, coupled atm.-ocean model 79–58082
CO_2, atm. press. laser pulse duration reduction by stimulated emission quenching 79–18400
CO_2, atmos. greenhouse effect, surface temp. calc. 80–26587
CO_2, atmos. var. at Mauna Loa Obs., Hawaii during 1964-71 period 77–37365
CO_2, atmos. var. at S.Pole in 1957-71 period 77–37366
CO_2, atmospheric, biosphere as source and/or sink 79–88030
CO_2, atmospheric, climatic effects of increasing content 79–88029
CO_2 atmospheric, climatological significance of doubling of conc. 80–101426
CO_2, atmospheric, conc. vars., cycles and trends 79–84381
CO_2, atmospheric, conc. meas. at Baring Head, New Zealand 79–100931
CO_2, atmospheric, concs. rel. to ^{13}C vars. in N.hemisphere trees during last 150 years 80–17363
CO_2, atmospheric, correl. with Pacific sea surface temp. 77–29307
CO_2, atmospheric, decrease during 1963-69 period 79–84380
CO_2, atmospheric, effect on climate *(French)* 79–84360
CO_2, atmospheric, emissions reduction approach *(German)* 78–49121
CO_2 atmospheric, fossil fuel generated, models for ocean uptake 79–88031
CO_2, atmospheric, gas chromatographic meas. using electron capture detect. 79–57549
CO_2, atmospheric, global problem of increasing levels 79–88032
CO_2, atmospheric, IR transmissivity 78–11998
CO_2, atmospheric, impact on snow and water surfaces cooling 79–92569
CO_2, atmospheric, recent trends of $^{13}C/^{12}C$ ratio, rel. to tree ring studies 79–25311
CO_2, atmospheric, short-term disturbances in record at Mauna Loa Observatory 78–88879
CO_2, atmospheric, thermal radiation detect. 79–16669
CO_2, atmospheric, uncertainties associated with effect on global climate 79–88028
CO_2, atmospheric, wood vs. fossil fuel as source 77–53162
CO_2, atmospheric conc., effects of different future energy strategies, rel. to global climate 79–83640
CO_2 atmospheric conc. increase, radiative-convective model 77–66977
CO_2, atmospheric content rel. to temp. changes since 1665, statistical study 79–8680
CO_2, atmospheric content variation meas. *(Dutch)* 79–70838
CO_2, atmospheric content, climatological consequences *(Dutch)* 80–98411
CO_2, atmospheric environmental control technology 80–104529
CO_2, atmospheric gases condensation on cold metal surfaces, nucleation barrier 78–22838
CO_2, atmospheric input from burning wood 78–81368
CO_2, atmospheric levels rel. to agricultural expansion in late 19th century 78–53717
CO_2 atmospheric line freqs. in 4.3 μ region 78–88910
CO_2, atmospheric meas. at Hauna Loa Obs. 1974-76 period 78–7685
CO_2 atmospheric pollution, report summary *(German)* 78–44993
CO_2, atmospheric problem, increase from fossil fuel combustion 79–16623
CO_2, atmospheric sealed CW laser, gain characts. 79–36871
CO_2, band model parameters prediction, 4.3 micron, 200-3000K 80–43047
CO_2 beam alignment by Seebeck effect position sensor 80–5772
CO_2, beam molecules capture probability on surface 79–32578
CO_2, bending vibr. quanta intramol. exchange, interpretation of obs. 77–58144
CO_2, bipropellant, advanced fuel-rich and screen mixing gasdynamic laser concepts, performance 79–36878
CO_2, blood conc. meas. using P electrodes 79–20725
CO_2 blood level in artery and vein, quantitative continuous meas. 78–40363
CO_2 bond distribution functions, anharmonicity effects on electron diffr. pattern 80–69234
CO_2, breathing pattern and ventilatory response in divers 80–45934
CO_2 bubbles, coalescence time in water 77–42899
CO_2, C $1s^{-1}$, π^*-state decay, fragment ion relative abundance by electron-ion coincidence technique 80–9743
CO_2, CO_2-CCl_2F_2 under pressure, breakdown voltage data *(Rumanian)* 77–19782
CO_2, CO_2-H_2, adsorption on ZnTe, manometric and mass-spectroscopic obs. 77–35808
$CO_2 \to CO + O$, dissoc. pathways, pot. energy surface and vibr. anal. of IR and Raman spectra 78–64826
CO_2 CW capillary waveguide laser for optically pumping D_2O 80–48278
CO_2 CW closed-cycle technological laser with 6 kW output power 79–27291
CO_2 CW coaxial discharge laser, props. and advantages 79–81442
CO_2 CW continuous flow laser, unstable resonator props. using dihedral corner reflector 78–29983
CO_2, CW electric discharge lasers, mode medium interaction 79–36876
CO_2 CW electric discharge laser, output beam props. 79–36877
CO_2 CW gasdynamic laser, determ. of saturation parameter 78–37871
CO_2 CW gasdynamic mixing lasers, pumped by N_2 or air, low stagnation temp. characts. 78–63053
CO_2 CW high power lasers, appls. for metal working 78–79026
CO_2, CW high power recycled electric discharge laser *(Chinese)* 79–98410
CO_2, CW high power TE electron initiated laser, small signal gain profile calcs. 79–72550
CO_2 CW laser, axial gain distribution 80–58502
CO_2 CW laser, electron-beam-controlled, closed-cycle 80–14315
CO_2 CW laser, sealed-off design, NaCl Brewster angle mirrors 78–55370
CO_2, CW laser, tunable simultaneous double wavelength operation 79–72583
CO_2 CW laser, vibr. temp., dissoc. and gain limitation determ., new technique 80–87369

carbon compounds continued
CO_2 CW laser burning CO in air for pump energy, saturation parameters 78—71077
CO_2 CW laser emitting dominant spatial mode, output power stability rel. to CO laser 80—32965
CO_2 CW laser model, electron beam ionisation 80—32954
CO_2 CW laser radiation, freq. conversion in Tl-Cs vapour mixture 80—74438
CO_2, CW sequence band laser, optical pumping of $^{15}NH_3$ far IR laser 78—46578
CO_2 CW sequence laser lines generated using incavity NH_3 cell 79—18438
CO_2 CW waveguide laser, freq. stabilised, operation and performance characts. 78—42349
CO_2, CW waveguide laser, anodised Al waveguide construction 78—55376
CO_2, CW waveguide laser, nearly atm. press., using plasma injection technique 78—74925
CO_2, capacitative discharge, high-freq. gas overheating suppression 80—38856
CO_2, change of state, student demonstration expt. 79—40325
CO_2, chem. laser, $CO+0.5\ O_2$ oxidation reaction in supersonic stream 77—677
CO_2 chemisorbed molecules, surface flow through $MgCr_2O_4$ 77—47083
CO_2, chemisorbed on $MgCr_2O_4$, mobility of CO_2 mols. 77—51595
CO_2, chemisorbed on W (100) surface, UPS studies 79—23841
CO_2, chemisorption on clean Fe (100) AND (111) surfaces, LEED and thermal desorption 78—71996
CO_2, chemisorption on goethite, IR spectra 80—7855
CO_2, chemisorption on Ni, Cu, Pd and Ag, semiempirical calcs. 78—14611
CO_2, chemisorption on Rh (111) and (100) surfaces, LEED, AES and thermal desorption meas. 78—38951
CO_2, chemisorption on Rh (111), high resolution EELS, thermal desorption, and LEED study 80—44419
CO_2, chemisorption on Ti film, changes in work function 77—59221
CO_2 chemisorption on ZnO, differential heat 79—52759
CO_2, circulation in human organism, model *(Russian)* 79—2093
CO_2 climate and society, IIASA conf. (Laxenburg, Austria, 1978 February 21-24) 79—8679
CO_2, closed cycle CW electrodeless pulse ionisation discharge *(Russian)* 77—75474
CO_2, coadsorption with O_2 on MgO surface, ESR 78—6572
CO_2, coadsorption with O_2 on Mo, AES and SIMS obs. 79—46928
CO_2, collision induced Raman scatt. at ν_2 and ν_3 inactive vibrs. 78—90175
CO_2, collision relax. 180-400K, spectrophone method 77—61832
CO_2, collision-induced absorpt. at 4.6 cm^{-1} 78—78679
CO_2, collision-induced Raman spectrum, theoretical studies 80—63646
CO_2, collisional laser-induced vib. excitation 77—27155
CO_2, combination and difference bands, IR intensities 77—466
CO_2, combustion gasdynamic laser, working cpds. simulation *(Russian)* 79—27239
CO_2, combustion-driven gasdynamic laser, effect of N_2 preheat 77—38854
CO_2, compact cylindrical TEA laser 77—703
CO_2, compact electro-ionising laser, 1 kJ radiation energy *(Russian)* 77—19316
CO_2 compact high PRF TE laser 78—46643
CO_2, compact high-repetition-rate double-discharge TEA laser 77—23693
CO_2 compact pulse-periodic laboratory laser 80—9903
CO_2, compact pulsed double transverse discharge laser 80—53324
CO_2 compact repetitively pulsed superatm. press. laser with high output power density 80—102731
CO_2 compact sealed TEA laser, single mode operation 79—968
CO_2 compact sealed waveguide laser, design, construction and performance data 77—10947
CO_2 compact TEA laser with ladder-type preionization discharge *(Japanese)* 77—23694
CO_2, comparison of dielectric and refractive virial coefficients and collision induced absorption bands 79—86547
CO_2, compression to 34 kbar, apparatus and technique, diamond anvil cell 78—74017
CO_2 conc. and temp. in flames, Raman spectroscopy 80—32720
CO_2 conc. increase effects on stratospheric O_3 78—57250
CO_2, concs. in lower thermosphere 78—96336
CO_2 concs. over native grassland in Saskatchewan 77—45120
CO_2, condensation and sublimation in Mars polar regions 78—49363
CO_2 condensed layers, cryosorption pumping characts. for He, thermal spike effects 79—80635
CO_2 content of atmosphere, role of C storage by forests and oceans 78—53718
CO_2, content of atmosphere, continuous automatic monitoring by coulometric method 79—53537
CO_2 content of atmosphere, response to deep-sea injections of fossil-fuel CO_2 80—31090
CO_2 content of ocean water, gradual increase 79—29786
CO_2 content of polar ice, 20000 yr BP 80—61891
CO_2, continuous slowing down approx., range difference for 0.2 to 10 MeV electrons 80—39187
PCO_2, continuous transcutaneous meas., electrochem. sensor 77—13020
CO_2, continuously tunable high press. monochromatic laser for spectroscopy 80—5762
CO_2 continuously tunable laser, optical pumping of NH_3 laser 80—83596
CO_2 continuum absorpt. contrib. to atm. transmission, 4.0 to 5.3 μm 79—92589
CO_2, continuum rel. to atm. absorpt. spectra near 2400 cm^{-1} 78—11968
CO_2 convection laser discharge, negative ion effects 78—55335
CO_2, core electron ionis., vibronic coupling, symmetry breaking, O1s line vibr. struct. 78—5279
CO_2, corrosion of graphite, CO production, radiolytically induced gas pressure effects 80—106115
CO_2 cross-flow CW laser output and gain rel. to discharge instability 78—46563
CO_2 cycle, effects of soil organic C 79—58063
CO_2 cycling in environment, non-proportionality between flux and reservoir content 80—46261
CO_2, decaying discharge plasma, contraction in const. elec. field *(Russian)* 79—37447

carbon compounds continued
CO_2 decomposition, plasma radiolysis by high current relativistic electron beam 79—91947
CO_2, desorpt. from graphite kinetics 78—60025
CO_2, desorption from ZnO powder during electron irrad. and interaction with atomic H 77—89638
CO_2, determ. in rocks and minerals by inorganic gas chromatography 80—85767
CO_2, development of miniature high-power high-press. UV and IR lasers 78—46642
CO_2, diagrammatic perturbation theory, using universal even-tempered basis set 80—58131
CO_2, dibutyl sebacate diffusivity, from aerosol drop evap. obs. 79—43639
CO_2, diffusion in nonuniform chemically reactive atmosphere, three-dimensional time depend. modelling 79—66846
CO_2 diffusion processes in stationary membrane blood oxygenator 77—78046
CO_2, diffusion rate in Au thin layers 80—100359
CO_2, diffusion through polymer membranes, determ. using McInnes glass electrode 78—20067
CO_2 diffusivities in aq. mixed electrolyte solns. 79—95190
CO_2, dimer, geom. struct., by mol. beam deflection 79—27102
CO_2 dimer, photoionisation efficiency curve, supersonic mol. beam expt. 78—46406
CO_2, dimer struct. CNDO/2 and ab initio calcs. 77—71753
CO_2 dimers in rare gas matrices, struct. determ. from IR spectra 79—10101
CO_2, dipole moment derivatives, MINDO/3 semiempirical calcs. 77—75055
CO_2, dipole moment functions 80—87094
CO_2, discharge, DC, plasma microwave propag. const. determ. by slab technique 80—53992
CO_2, dissoc., high temp. effect 78—35675
CO_2, dissoc. in high-press. nonequilib. plasma 79—15991
CO_2, dissoc. in nonequilib. plasma of stationary plasma-beam discharge *(Russian)* 79—99006
CO_2, dissoc. in shock tube, interferometric meas. 77—9071
CO_2 dissociation in a nonequilibrium plasma 80—87851
CO_2, dissociation into CO and O_2, H_2 production from CO+steam, fusion reactor heat 80—67014
CO_2 dissociation obs. in flow system with cylindrical hollow cathode 78—66674
CO_2 dissociation obs. in hollow-cathode glow discharge 78—70946
CO_2, dissociative chemisorption on Rh (111), EELS and thermal desorption spectra meas. 80—6656
CO_2, dissolved gas mass transfer through tubular membranes 77—35225
CO_2 diurnal and seasonal vars. in air over Tehran 77—37396
CO_2 doped TEA laser, Penning ionisation 79—3678
CO_2 Doppler-tuned CW IR radiation for highly excited atomic beam source 77—27204
CO_2, double ionis. by photon impact 77—88506
CO_2 dual beam laser system for fusion ignition *(Japanese)* 79—81456
CO_2, Dunham coeffs., high-order contribs. 78—46285
CO_2 effects on geothermal fluid buoyancy 79—44203
CO_2 effects on long-term global sea surface temp. vars. 78—73398
CO_2, elastic and inelastic electron scatt. differential cross section, obs. and calc., struct., binding energy 80—28110
CO_2, elastic electron scattering and rot. excitation calcs. 79—22834
CO_2, elec. discharge, negative ions and volt.-current characts. 78—71574
CO_2, electric breakdown, Paschen curves *(French, English)* 77—76221
CO_2, electric breakdown voltage, 300-2100K *(Russian)* 78—51370
CO_2 electric discharge excited 16 μm laser for isotope separation meas. 77—88746
CO_2, electric discharge gasdynamic 16 μm laser, high average power, high repetition rate 78—55381
CO_2, electric discharge convection laser, saturation characts. *(Chinese)* 78—90408
CO_2 electric discharge laser, free oscill. stimulated emission, nanosecond pulse duration 79—31860
CO_2 electric discharge CW laser beam properties 79—76736
CO_2 electric-discharge mixing laser, 30 kW output, 9% efficiency 80—87410
CO_2, electro-optical parameters determ. from IR absorpt. 79—98128
CO_2, electrochem. reduction for use in energy storage 78—92490
CO_2 electrochemical reduction for H storage 80—7934
CO_2 electrode, dynamic response 79—92025
CO_2, electrodeless discharge closed cycle laser theory *(Russian)* 77—75475
CO_2 electroionisation laser plasma mirror, soft X-ray emission for biological radiography 79—43983
CO_2, electroionisation pulsed laser 79—89922
CO_2, electron and negative ion swarms 80—28595
CO_2, electron beam controlled laser, with grid-controlled electron gun 78—46635
CO_2, electron beam controlled laser with plasma mirror, stimulated emission dynamics 78—50799
CO_2 electron beam controlled laser, emission pulse synchronisation with plasma mirror 79—89930
CO_2, electron correl., quadrupole excitation in correl. energy theories 79—36538
CO_2, electron diffraction cross-section, finite scatt. geom. in mol. beam expt. 78—74803
CO_2 electron drift velocity and longit. diffusion coeff. time-of-flight meas. 77—80264
CO_2, electron drift vels., time-of-flight meas. 80—28855
CO_2, electron elastic scatt., 0 to 100 eV 80—23547
CO_2, electron elastic scatt. and vibr. excitation by 4, 10, 20 and 50 eV electrons 80—83484
CO_2, electron emission from thin W wire into gas under strong elec. fields 79—83108
CO_2, electron energy deposition, rel. to Venus and Mars atms. 79—45857
CO_2, electron energy loss spectra, low-lying and triplet states 78—46454
CO_2, electron energy loss spectra, C K-shell excitation, vibr. struct. 79—22851
CO_2, electron excitation-relax., time resolved Fourier spectra 78—58070
CO_2, electron impact, 3.8 eV resonance 77—42430
CO_2, electron impact, 50-400 eV, secondary electrons double differential cross section 80—37897
CO_2, electron impact, cross sections for rot. excitation 78—17809

carbon compounds continued
CO_2, electron impact, energy loss spectra, electronic transitions obs. 78−17805
CO_2, electron impact, reson. vibr. excitation calcs. 77−14596
CO_2, electron impact, transitions, generalised oscill. strengths 78−94327
CO_2, electron impact dissoc. excitation, O^{**} fragment translational spectra 79−54979
CO_2, electron impact excitation, electron cooling in Mars and Venus atms. 78−57481
CO_2, electron impact shape-reson.-enhanced vibr. excitation, 10-40 eV 80−5629
CO_2, electron impact single and double ionisation cross-sections 79−3584
CO_2, electron impact spectra, 35 keV electrons, Bethe surface and Compton profile 79−27091
CO_2, electron scatt., 0.07 to 10.0 eV, cross-sections by coupled-channel approach 77−75300
CO_2, electron scatt., absolute total cross-section meas. 78−74774
CO_2, electron scatt., effective pot. calcs. 80−53131
CO_2, electron scatt., Glauber eikonal approx. calcs. 80−53130
CO_2, electron scatt., vibr. struct. in resonances 78−17813
CO_2, electron swarm parameters for high E/N, Monte Carlo simulation 80−19548
CO_2, electron transmission function and mean energy per ion pair, obs. 80−23566
CO_2 electron transport coeff. calc. in counting gas mixtures 79−32727
CO_2, electron-beam-controlled closed-cycle laser, pulse periodic conditions 78−46632
CO_2, electron-beam-controlled laser, operation characts., 1 to 10 atm range 78−71118
CO_2, electron-beam-controlled laser, pulse forming network power source 78−74928
CO_2 electron-beam-controlled gas-flow laser, CW and pulse periodic lasing 79−7111
CO_2, electron-beam-induced desorption from ZnO, phase sensitive detection 80−54502
CO_2, electron-neutral energy exchange in AC field 77−42519
CO_2, electrooptic constants, IR absorption spectrum in $2\nu_3$ vibration band 79−3442
CO_2, electrooptical consts., $2\nu_3$ band induced component 80−78626
CO_2, electrostatic terms in lattice energy calcs. 79−51040
CO_2, emissibility, correl. for high temp. and large optical thicknesses 77−15156
CO_2 emission meas., Baden-Wurtemberg network *(German)* 79−52977
CO_2, energetics of sorption in poly(ethylene terephthalate) 80−29270
CO_2 enhancement in Mars atmosphere and palaeoclimate 80−46450
CO_2 enriched in $^{17,\,18}O$, diode laser spectroscopy of Q branches 80−78621
CO_2, equations of state, molecules interacting via Kihara pot. with spherical core *(Spanish)* 77−31749
CO_2 equilibrium partial pressure, temp. coeff. in seawater 79−74903
CO_2, exchange in Mars atmosphere-regolith system, rel. to atm. press. 78−73668
CO_2, excited by CO_2 laser, sub-Doppler optoacoustic spectrum 80−5545
CO_2 expiratory concentration analysis by computer 78−57106
CO_2 facilitated transport in monoethanolamine solns. 79−91992
CO_2 fast flow laser, active medium parameter input fluctuations, intensity response 80−53257
CO_2 fast flow laser, combined pulse and DC discharge as pump 78−71117
CO_2, fast flow laser, meas. of N_2 vibr. temps. 80−32955
CO_2, fast transverse flow discharge laser, stimulated emission stability 77−75478
CO_2, fast-flow CW laser using atm. air-CO_2 mixtures 77−75559
CO_2 fast-flow CW laser characts., DC self-sustained excitation 80−53259
CO_2 fast-flow closed-cycle laser, output power, medium comp. effect 80−48213
CO_2 fast-flow electric-discharge laser, dynamic characts. 80−32956
CO_2, fast-flow laser, elec. discharge chamber characts. 77−79854
CO_2, fast-flow laser, pumping efficiency by AC discharge 78−50801
CO_2 fast-flow laser with nonself-sustained discharge, active medium characts. 80−28194
CO_2, Febetron radiolysis in the presence of O_2 and CO 80−35557
CO_2, Fermi reson, effect on vibr. bands relative intensities 80−965
CO_2, filtering gases, mixing zone in different porous media *(Russian)* 77−51112
CO_2 flow in heated tubes, with near critical parameters, turbulent flow, heat transfer 80−59022
CO_2, flux meas. in atm. boundary layer, eddy correl. method 79−25303
CO_2, forced air convection cooled waveguide laser 77−38921
CO_2, form. from fossil fuel combustion in atm., effect on climate 79−2359
CO_2, formation, during Fe oxide reduction, kinetics 79−83449
CO_2, formative time lags, expt. 77−1025
CO_2, Franck-Condon transition amplitudes for mol. dissoc., semiclassical evaluations 78−62860
CO_2, free expsn. of jet, nonequilib. effect 79−27676
CO_2 free jet, rarefied flow, homogeneous condensation scaling law 80−6121
CO_2, free molecule flow and interdiffusion, through porous glass 79−32658
CO_2, freq. stabilised laser with OsO_4 absorber, output freq. reproducibility 78−50800
CO_2, from fossil fuel burning, climatic effects, proposed CO_2 disposal in deep ocean 78−57301
CO_2 from fossil fuel burning and global C budget 80−77080
CO_2, frost streaks in south polar cap of Mars 80−31226
CO_2, fugacity at high temps. and press. from exptl. decarbonation reactions 79−16439
CO_2 fundamental condensation cycles in steam and nucl. power plants, performance characts. 80−63368
CO_2, fundamental vibr. bands in liq. phase 79−54856
CO_2, future atm. level prediction using atm. and ocean models 78−61549
CO_2 gain-switched laser oscillators, analytic modelling 77−7052
CO_2 gas, electron impact ionisation, electronic fluoresc. spectra 80−95664
CO_2 gas, electron mobility to lateral diffusion coeff. ratio 80−43836
CO_2, gas, electron-ion recombination, at 292K, three-body interaction 79−46418

carbon compounds continued
CO_2, gas, flow through aperture into vacuum 78−9621
CO_2, gas, second virial coeffs., intermol. pot. at low temp. 79−46416
CO_2, gas, sparking pots., ionisation and electron attachment coeffs. 78−42705
CO_2, gas, total ionization created by completely stopped H^+ ions 79−46419
CO_2, gas, virial coeffs., from theory of system of nonpolar mols. of arbitrary symmetry 78−9743
CO_2, gas discharge laser, 14 and 16 μm emission *(Russian)* 77−10885
CO_2 gas flow impinging on heating surface, heat transfer radiation 80−43710
CO_2 gas flow laser, vibr. and translational temp. fields, panoramic spectrosc. obs. *(Russian)* 79−12868
CO_2 gas laser, glow discharge electron irrad. rel. to output characts. 79−64198
CO_2 gas refractive index meas., 150 GHz to 6 THz 77−5892
CO_2 gas sensing probe, potentiometric, micro-size 78−61071
CO_2, gas standard enthalpies of solution and formation, standard Gibbs energies of formation and standard entropy 79−57285
CO_2 gas transport laser, discharge and power extraction characts. *(Rumanian)* 80−95869
CO_2, gas-liquid crit. pt. region, depolarised light scatt. 78−34612
CO_2 gasdynamic 16 μm laser, performance determ. using multipass cavity 79−81443
CO_2 gasdynamic laser, 16 μm radiation, modified Anderson's time-depend. anal. 80−106505
CO_2, gasdynamic laser, combustion driven, thermally pumped 77−34871
CO_2 gasdynamic laser, contaminants effect on gain and power 78−25847
CO_2 gasdynamic laser, CW operation, specific output energy and efficiency 80−48212
CO_2 gasdynamic laser, depopulation of lower active level by CO_2+NO collisions 80−74336
CO_2 gasdynamic laser, energy characts. calcs. 80−95866
CO_2, gasdynamic laser, flow inhomogeneity effect on gain distrib. 78−1205
CO_2 gasdynamic laser, gain prediction, comparison of vibr. models 78−29928
CO_2 gasdynamic laser, gain supersonic flow heating effect, condition optimisation 78−82947
CO_2 gasdynamic laser, gas heating by electrically induced explosion, parameter optimization 79−64250
CO_2 gasdynamic laser, HCl, HF, DCl and DF effects on physical kinetics 78−5451
CO_2 gasdynamic laser, IR spectroscopic determ. of vibr. level populations 80−32952
CO_2, gasdynamic laser, optimisation of gain coeff. in nozzle stream *(Russian)* 77−27272
CO_2 gasdynamic laser, operating on combustion products, gain coeffs. of complex working media 80−58506
CO_2 gasdynamic laser, peak small-signal gain, closed-form correl. 77−42518
CO_2 gasdynamic laser, population inversion, press. effect 80−102692
CO_2 gasdynamic laser, resonator action, output power 78−13681
CO_2 gasdynamic laser, resonator design, lasing medium model 78−29984
CO_2, gasdynamic laser, specific power optimisation 77−712
CO_2 gasdynamic laser, supersonic-after-mixing-type, gain charact. *(Japanese)* 77−23647
CO_2, gasdynamic laser, simplified model for cavity flow, population inversion calc. 78−46567
CO_2 gasdynamic laser, two-stage expansion of N_2, supersonic nozzle 78−71076
CO_2, gasdynamic laser, unstable resonator selection 77−23701
CO_2, gasdynamic laser, using methane-O_2-N_2-Cl_2 mixture combustion products 77−50649
CO_2 gasdynamic laser, vibr. temp. meas. method 80−9854
CO_2 gasdynamic laser power, free-piston shock tube expts. *(Japanese)* 79−76661
CO_2, gasdynamic laser possibility, transitions between levels of paired modes 79−89885
CO_2 gasdynamic laser with gas mixing, excitation efficiency 79−22934
CO_2 gasdynamic laser with partial inversion at 16 μm, gain calcs. 80−78833
CO_2 gasdynamic lasers, amplifying characteristics, combustion product utilisation 79−27240
CO_2 gasdynamic lasers, combustion driven, effect of residual CO on small signal gain 80−63973
CO_2 gasdynamic lasers, multicomponent working media, energy characts. calcs. 80−95867
CO_2, gaseous impurity, role in H_2 embrittlement of steel 77−59904
CO_2 glow discharge, acoustic wave influence on F^- forward ionisation wave 78−67521
CO_2, glow discharge, O atom conc. determ. by mass spectrometry *(Russian)* 78−87512
CO_2 glow discharge chemical processes and rate coefficients 78−63626
CO_2, ground level abundance, simultaneous determ. of CO, N_2O and H_2O 78−11969
CO_2, ground state props., coupled cluster and MBPT methods appl. 80−47881
CO_2, γ-radiolysis in glass packed vessels, CO yields rel. to packing, baking 77−12811
CO_2 H^+, geom. struct., ab initio mol. orbital study 78−62939
CO_2, HF laser irrad. visible luminesc. 77−46593
CO_2, harmonic force consts., vibr. freqs., integrated intensities, MINDO/3 method 80−58411
CO_2, heat transfer at critical point, heat transmission coeff. determ. *(German)* 77−35133
CO_2, helical TEA laser, spectral output, charging voltage depend. 77−61936
CO_2, helical TEA laser, output power as function of discharge inductivity 79−10278
CO_2, high density behaviour, extrapolated $P\rho T$ surfaces and critical density 80−87834
CO_2, high power amplifier, energy and time characts. 77−79797
CO_2 high power elec. discharge laser, multielement cathode design and operational characts. 78−82983
CO_2, high power electrical laser technology 77−88777
CO_2, high power electron beam controlled laser for fusion research 77−709

carbon compounds continued
CO_2, high power pulse, single-stage, electroionisation laser, tens of gigawatts 79—3704
CO_2, high power pulse laser with unstable resonator 77—75564
CO_2, high press. sealed-off laser amplifier characts. 79—18397
CO_2, high repetition rate hybrid TEA laser freq. and amplitude characts. 78—37897
CO_2, high repetition rate TEA laser, sealed operation 78—46623
CO_2, high resolution UV photoelectron spectra 80—91603
CO_2 high stability CW waveguide laser, for high resolution saturation spectroscopy 78—71112
CO_2, high temp. absorpt. meas. in 10.4 μm laser band 79—36870
CO_2, high-power discharge lasers 77—34872
CO_2 high-power elec. discharge laser, holographic interferometry during power extraction 80—28172
CO_2, high-power laser for fusion reactor appl. 77—7062
CO_2, high-power lasers, review 80—32950
CO_2, high-power multibeam CW laser, parallel packed tubes in common resonator 79—13984
CO_2 high-power pulsed laser continuously tunable over wide freq. range 79—45925
CO_2 high-power pulsed laser, wave-optical resonator modelling, gain saturation law 80—99693
CO_2 high-power pump laser, direct narrow-line tuning 80—58579
CO_2, high-power rapid flow CW laser with combined-discharge pumping, I-V characts. 80—14318
CO_2, high-power tunable laser for 9 to 12.5 μm range 77—83884
CO_2, high-press. laser, gain contribs. from 00°2 and 00°3 sequence bands, theory 78—46565
CO_2 high-press. laser with cascade discharge 79—68407
CO_2, high-press. tunable IR lasers 78—59030
CO_2 high-pressure discharge, sequence-band lasing 78—46570
CO_2, high-pressure ionization chamber for spatial growth meas. 77—46657
CO_2 high-pressure Q-switched electron-beam-controlled laser characts. 79—59669
CO_2 high-pressure reinjection oscillator design and performance 80—78867
CO_2 highly multimode pulsed electron beam laser, beam divergence 79—3731
CO_2, horizontal electric arc, in inhomogeneous mag. field, mass spectrometric anal. 80—79620
CO_2 hybrid laser, operating regimes 79—22932
CO_2 hybrid laser, transverse mode struct., effect on laser induced acoustic waves in liq. 79—77683
CO_2 hybrid laser operation 79—64246
CO_2, hypersonic flow, in shock tunnel, mass spectrometric analysis 77—31328
CO_2, IR absorpt. in regions of weak absorpt., lab. meas. rel. to atm. windows 79—64005
CO_2, IR absorpt. spectrum, press. and conc. depend. 77—3362
CO_2, IR absorpt. spectrum, line parameters, spectral transmittance function *(Russian)* 77—57998
CO_2, IR absorption bands integrated intensities, liquid and gas 77—493
CO_2, IR absorption spectrum using Nd:glass intracavity spectrometer *(Russian)* 78—33512
CO_2, IR band intensity 80—83425
CO_2, IR band nonrigid rot. absorption 78—91060
CO_2, IR bands transmission functions 80—106324
CO_2, IR energy levels and line intensities 78—85691
CO_2 IR laser, line tunable and optically pumped 77—88747
CO_2 IR laser, transients obs. by modulation of intracavity absorber 78—74933
CO_2, IR laser induced fluoresc. as spectroscopic probe 79—89704
CO_2, IR radiation spectral absorptance and transmittance, accurate modelling technique 78—91062
CO_2, IR spectra, $401 \leftarrow 000$ and $411 \leftarrow 010$ absolute intensities 78—21976
CO_2, IR spectra, lineshape and Q-branch head absorpt. profile 79—59452
CO_2 IR Zeeman spectra utilizing copropag. wave reson., diamag. shift obs. 80—53055
CO_2 ice clouds on Mars, brightness temp. and radiative props. 80—105192
CO_2 ice on Mars surface, evidence from reflectance spectroscopy 80—72834
CO_2 ice spheres, IR scatt. and absorpt. props. 80—97269
CO_2, impact on climate 80—31118
CO_2 in Ar matrix, fluoresc. and thermoluminesc. after photolysis 79—89700
CO_2 in atmosphere, $^{13}C/^{12}C$ vars. in last 22 yrs. 80—104530
CO_2 in atmosphere, climate sensitivity study with global climate mathematical model 80—31117
CO_2 in atmosphere, climate-C budget model 80—98381
CO_2 in atmosphere, increasing concs. effect on heating rates 80—17376
CO_2, in atmosphere, possible influence on temp. 80—51486
CO_2 in atmosphere, rel. to C reservoir changes 78—57278
CO_2 in atmosphere, significance of deforestation 79—74572
CO_2, in burnt gases of combustion engines, laser action 79—45924
CO_2 in climate feedback systems, involving sea-ice, ocean temp. and CO_2 80—98443
CO_2 in comet comae, effect of solar photodissociative ionisation 80—90370
CO_2 in comet nuclei, vaporisation rel. to lifetimes and orbits 80—56772
CO_2 in dark interstellar clouds, abundance 79—35322
CO_2, in H_2O, D_2O, soln., Raman spectra 77—65467
CO_2 in Mars atmosphere, press. seasonal var. as affected by S polar cap 79—84716
CO_2, in Martian atmosphere, photochemistry 77—91458
CO_2, in N_2, 20-140 bar, dipolar correlation function meas., IR band shape anal. 77—61743
CO_2 in stratospheric ion chemistry, reactions with $O_2^+.O_2$ 79—2343
CO_2, in surface-troposphere system, radiation energy balance and temp. 80—12498
CO_2, in tropical atm., IR cooling rate rel. to H_2O vapour 78—81405
CO_2, in troposphere under stable anticyclonal conditions, CO_2 laser radiation absorpt. 78—20515
CO_2, in upper atmosphere, electron impact cross-section 78—28398
CO_2, in upper atmosphere, electron impact yield spectra 78—28401
CO_2 in urban atmosphere, dependencies and trends 80—16870
CO_2, in various solvents, IR absorpt. spectrum, Fermi-reson. doublet and intermolecular interactions 80—18856

carbon compounds continued
CO_2 increase in ocean water masses, direct obs. 79—34854
CO_2 increase rel. to Mesozoic greenhouse and climatic warming 79—20963
CO_2 induced absorpt., 3-4μm, temp. depend. 80—983
CO_2, induced absorpt. spectral moment, mol. calcs. 80—63737
CO_2 induced atmospheric temp. rise, Arctic sea ice decay 80—61802
CO_2, industrial pollution affecting ^{13}C tree ring dating method 80—51586
CO_2 influence on level of ionised Ca in squid axons 78—56960
CO_2 infra red gas analyser, calibration method 78—20115
^{15}O-CO_2 inhalation, for left heart imaging 77—9240
CO_2, initial rate of decomposition in volume discharges 79—50905
CO_2, initial reaction probability with Ba getter film, AES obs. 80—61153
CO_2 injection into supersonic stream containing CO, gain 79—31861
CO_2 injection mode-locked TEA laser, extra-cavity feedback into unstable resonators 79—72601
CO_2, intense sub ns CO_2 laser pulse attenuation and reshaping 77—88870
CO_2, interaction with Cu (100), molecular orbital calc. 77—31898
CO_2, interaction with polycryst. CO surface, XPS, UPS *(French)* 77—73219
CO_2, interaction with ZnO nonpolar surface 79—65321
CO_2, intrapulmonary haematocrit maldistrib., effect on O_2, CO_2, inert gas exchange 80—8033
CO_2, inversion transitions in aerodynamic cooling region *(Russian)* 77—34869
CO_2, inverted, on-resonant phase-conjugate refl. and amplification at 10.6 μm 79—64275
CO_2, inverted, wavefront reversal, high efficiency 80—74436
CO_2, inverted rot.-vibr. population, in blunt body shock layer, amplification factor change 78—5828
CO_2, ion drift velocities and mobilities 80—43834
CO_2, ion transport in electrical discharge 78—87435
CO_2, ionisation, energy dependence of $\bar{W}$ for alpha particles 79—6999
CO_2, ionisation and attachment coefficients 78—42706
CO_2, ionisation current growth, Townsend swarm coeffs. 78—59541
CO_2, ionisation energy, LCAO $X\alpha$ calcs. 77—50353
CO_2, ionisation meas. and $\bar{W}_n$ derivation for neutron irradiation 79—36430
CO_2, ionised states, core and valence, ab initio HF calcs. 77—79597
CO_2, isentropic decompression from crustal and mantle press., thermodynamics 79—79769
CO_2, isotope effect on spectroscopic parameters *(Russian)* 77—54577
CO_2 isotope laser transitions, absolute freq. calibration, heterodyne technique 77—19230
CO_2, isotope ratios, optical anal. method 78—85228
CO_2, isotopic relations, harmonic freq. calc. 77—23486
CO_2, isotopically mixed crysts., IR spectra ν_2 vibr. exciton band 77—73136
CO_2, isotropic Raman scatt., Fermi reson. vibr.-rot. spectra 77—38741
CO_2 jets, axisymmetric, turbulent mixing of gases with different densities 77—58749
CO_2 jets, homogeneous condensation, similarity law 79—42229
CO_2, Joule-Thomson coeff. at 20-583°C 77—42956
CO_2, K-shell photoabsorption coeffs., 500-600 eV 80—9617
CO_2, kinetic cooling by laser radiation 79—31621
CO_2, lack of C isotope exchange, methane and C oxides, high temp. 79—84263
CO_2 laer, excitation by NO+N reaction, tranverse flow, output power, intensity distribs. 77—79796
CO_2, laminar free convection at supercrit. press. under cooling conditions, heat transfer analysis 79—86428
CO_2, large angle elastic and inelastic electron scatt. differential cross section, exchange corrections 80—28111
CO_2 large aperture TEA laser, injection mode locking 77—14737
CO_2, large-volume pulsed laser amplifier 79—64253
CO_2 laser, 10 ns pulse generation, rotating mirror technique 80—33042
CO_2 laser, 10.17 μm R(32) transition, appl. to He-Ne laser freq. meas. 77—31113
CO_2 laser, 14-μm and 16-μm, CW and improved pulsed operation 78—17900
CO_2, laser, 16 GHz tunable sideband generation 78—90428
CO_2 laser, accurate frequency meas. *(Japanese)* 80—9850
CO_2 laser, active medium obs. using heat camera system 80—1257
CO_2 laser, Antares system, 100 kJ, for fusion expts. 78—46665
CO_2 laser, atmospheric pulsed photoionisation, active medium optical homogeneity 80—58508
CO_2, laser, beam up-conversion, pulse temporal struct. determ. 77—3603
CO_2 laser, CW, construction and power calibration *(Korean)* 78—17961
CO_2 laser, CW, electrically excited *(Japanese)* 79—3676
CO_2, laser, CW, transverse mode suppression by cavity length control 77—14762
CO_2 laser, compact flowing gas system 78—87067
CO_2 laser, computer modelling, book 79—41364
CO_2 laser, construction, industrial appls. *(German)* 77—88731
CO_2 laser, construction and excitation circuit 79—22968
CO_2 laser, continuous, fast flowing, thermal discharge contraction *(Russian)* 79—99009
CO_2 laser, controlled multiline oscillator 78—1259
CO_2 laser, convective-cooled, fast-flow, pulse discharge stability 78—94389
CO_2 laser, coupling modulation near intermode spacing freqs., freq. response 77—38956
CO_2 laser, cutoff filter 77—88938
CO_2 laser, detuning effects of FM mode-locking 80—69434
CO_2 laser, double transverse pulsed discharge characteristics 78—71617
CO_2 laser, E-beam sustained large amplitude discharge, for fusion appls. 78—55382
CO_2 laser, effect of H_2 addition on gain coeff. in expanding CO_2-N_2 stream *(Russian)* 77—27271
CO_2 laser, effects of added gases *(Rumanian)* 77—27273
CO_2 laser, efficiency at 14 and 16 μm 79—59670
CO_2, laser, electron beam controlled, plasma mirror 78—17976
CO_2 laser, Faraday effect optical isolation at 10.6 μm using chalcogenide spinels 78—50816
CO_2 laser, fast modulator using CdS two-photon magnetoabsorpt. 77—88805
CO_2 laser, for 16 μm range, review *(Rumanian)* 80—87408

carbon compounds continued
CO_2 laser, forced oscill. by injection of weak external optical signal 77–19347
CO_2 laser, freq. stabilisation expts. *(Japanese)* 77–68225
CO_2, laser, freq. tripling in DCl gas 79–76751
CO_2 laser, frequency control by spectrally depleted destructive two-beam interf. 78–74941
CO_2 laser, frequency stabilisation method, phase-locking 80–74401
CO_2 laser, gain spiking and mode-beating control by signal injection 77–71999
CO_2 laser, gaseous saturable absorber cell to suppress parasitic oscillations 78–87066
CO_2 laser, Gaussian beams energy profile 79–64247
CO_2 laser, glow discharges at high press., voltage-current characts. 78–87036
CO_2 laser, high power, CW, electron beam sustained, performance, theory and expt. 78–71074
CO_2, laser, high press., continuous tuning, electron beam controlled 77–713
CO_2 laser, high press. stabilised discharge 78–17904
CO_2 laser, high press. with nonself-sustaining discharge 79–98339
CO_2 laser, high pressure, passive mode-locking characteristics *(Japanese)* 80–14357
CO_2 laser, high repetition rate-pulsed, weak shock wave effect 78–90409
CO_2 laser, high voltage microsec. pulse-forming network 78–5494
CO_2 laser, high-field preionised discharge for transversely excited waveguide laser 77–83844
CO_2 laser, high-power, multi-atmosphere, photoionization stabilized system 77–38919
CO_2 laser, high-power high-energy, using an absolute calorimeter 78–93686
CO_2 laser, high-power photopreionisation stabilised, operation at press. up to 13 atm. 78–63131
CO_2 laser, high-press., homogeneous self-sustained discharge 80–9852
CO_2 laser, high-press. cathode preionis. pulse type, design 77–65596
CO_2 laser, high-press. ns pulse generation *(Russian)* 77–75581
CO_2 laser, high-press. CW, output power fluctuations 80–74333
CO_2 laser, IR freq. absolute meas. *(Russian)* 80–9851
CO_2 laser, IR luminesc. of active layer *(Russian)* 79–31862
CO_2 laser, in-cavity hot cell 78–5495
CO_2 laser, influence of tripropylamine admixtures 80–23669
CO_2 laser, intense high-press. sequence-band 78–33749
CO_2 laser, intermode beats, use in automatic frequency control system 80–48209
CO_2, laser, internal modulation 80–23728
CO_2 laser, Lamberton and Pearson type, shock wave detect. 79–36946
CO_2 laser, line selection using metal film reflection filter 78–55368
CO_2 laser, long and short pulse formation, optimum conditions 78–87037
CO_2 laser, longit. pulsed, appl. in TEA lasers single-mode operation 77–68229
CO_2 laser, mode locking obs. by intracavity plasma injection 80–83624
CO_2 laser, modulation and freq. stabilisation by Stark effect in difluoroethane 79–59667
CO_2 laser, multiphoton amplification, HF removal of forbiddenness *(Russian)* 80–53262
CO_2 laser, NASA high power system for laser appls. 78–5493
CO_2 laser, non-self sustaining discharge for CW laser excitation, review 78–42849
CO_2 laser, nsec pulse amplification at efficiencies greater than 20% 78–50818
CO_2 laser, optical coupling modulation in travelling-wave cavities 77–42553
CO_2 laser, output characts. at high pump levels 80–58509
CO_2 laser, p-Ge broadband passive isolator, pulse shaping 78–46662
CO_2, laser, passive Q-switching by CH_3F 78–9402
CO_2 laser, passive Q-switching using heated CO_2 saturable absorber 78–25900
CO_2 laser, passive Q-switching by FIR laser gas CH_3I 80–1246
CO_2 laser, periodically pulsed, heating of oxidising metal 80–7445
CO_2 laser, periodically pulsed, power supply inductive pulse shaping 80–53311
CO_2 laser, photoinitiated impulse-enhanced elec. excited struct., operational characts. 79–27283
CO_2 laser, photoionis. TEA type, output pulse characts. calc. 80–32953
CO_2 laser, photoionisation, atm. press., high sp. energy output 78–29975
CO_2 laser, possible freq. stabilisation using 1-1 difluoroethane in external Stark cell 79–94266
CO_2 laser, power stabilisation *(Russian)* 78–22145
CO_2 laser, preamplifier capabilities for low level 10.6 μm direct detectors 77–53976
CO_2 laser, preionisation effect on discharge characts. 77–61938
CO_2 laser, preionization by pulse electron accelerator 77–88780
CO_2, laser, pulse evolution 77–10884
CO_2 laser, pulse flow stretching *(Chinese)* 78–90435
CO_2 laser, pulsed, broadening of lasing spectrum 79–94205
CO_2 laser, pulsed, elec. field distrib. in vol. discharge controlled by electron beam 80–58505
CO_2 laser, pulsed, high repetition rate, average power limitations at 10.6 and 16 μm 80–58503
CO_2 laser, pulsed, high-press., high-power, electron-beam-controlled, continuously tunable 80–64065
CO_2 laser, pulsed, with transverse discharge operating at atmos. press., energy characts. of emission 77–42520
CO_2 laser, pulsed low-pressure far IR, for use in plasma diagnostics 80–53332
CO_2 laser, pulsed transverse electrodeless discharge excitation 79–45958
CO_2 laser, pulser-sustained, gain and optical extraction meas. 79–27284
CO_2 laser, Q-switched, single rot. line-selection *(German)* 78–46562
CO_2 laser, radiation absorpt. by propane and propane-N_2 gas mixture 77–58366
CO_2 laser, radiation detection by PbSnTe detector and preamplifier modules 78–32875
CO_2 laser, radiation duration control, expts. and devices 78–22156
CO_2 laser, saturable absorber using doped KCl 79–10363
CO_2 laser, sealed-off, parameter meas. 77–3614
CO_2 laser, selected two-colour operation for length meas. scheme 80–99747
CO_2 laser, self sustaining discharge, medium effect on output energy 77–14690

carbon compounds continued
CO_2 laser, self-focusing parallel-plate waveguide, transverse excitation 77–7139
CO_2, laser, semi-self-sustained discharge, optical homogeneity, mol. gas heating 80–37990
CO_2 laser, Sharplan 791, for clinical surgery 78–35904
CO_2 laser, short pulse generation from intracavity laser breakdown plasmas 78–37924
CO_2, laser, short-pulse high-energy operation 77–88758
CO_2, laser, signature curve anal. 77–654
CO_2 laser, single frequency, using unstable resonator 77–38939
CO_2 laser, single mode locked pulse selection, semicond. refl. switching 77–3609
CO_2, laser, small-gap multiatm. press. system 78–74921
CO_2, laser, smooth high power pulse form. 78–17990
CO_2 laser, spark photoionisation, tripropylamine additive 78–13679
CO_2 laser, Stark cell noise reduction 78–59059
CO_2 laser, Stark effect modulation by iodomethane 78–17992
CO_2 laser, successively excited sections, duration of emission pulses 79–94257
CO_2 laser, supersonic jet utilizing $D+O_3+CO_2$ mixture, gain meas. 79–89902
CO_2 laser, TE, injection mode locking, press. up to 8 atm. 77–10883
CO_2 laser, TEA, double helical, computer simulation study of dynamics *(Chinese)* 80–74390
CO_2 laser, TEA, equilib. gas temp. and its distrib. 77–54691
CO_2, laser, TEA, freq. chirp reduction, improved stability 77–10959
CO_2, laser, TEA, multifreq. injection locking, resonator config. 77–7141
CO_2, laser, TEA, pulse stretching by CO addition 77–14754
CO_2 laser, TEA, single longit. mode, various prod. techniques 80–106547
CO_2 laser, TEA, tunable simultaneous double wavelength operation 77–61970
CO_2 laser, TEA, with seed gas, Penning ionisation 78–5449
CO_2, laser, TEA discharge, arc suppression 77–7056
CO_2, laser, TEA oscillator, injection locking, mode selection 77–653
CO_2 laser, thermally pumped, output power enhancement by Ar gas addition 78–55336
CO_2 laser, thermodynamic approach *(Rumanian)* 79–7109
CO_2 laser, transitions, linewidth, temp. depend. 80–69360
CO_2 laser, transverse double-discharge, spectral characts. *(Russian)* 77–656
CO_2 laser, transverse flow CW, glow discharge stabilization 78–37900
CO_2 laser, transverse mode-medium instability anal. 79–76662
CO_2 laser, tri-n-propylamine in working gas 79–22935
CO_2 laser, tripropylamine additive on amplification characts., CO_2+N_2+He gas *(Russian)* 78–25848
CO_2, laser, tunable linearly polarized TEM_{00} operation, concave diffr. grating 77–19344
CO_2 laser, tunable stabilised single-mode TEA 78–5485
CO_2 laser, unstable resonator, gain, spatial inhomogeneity effect 77–34870
CO_2, laser, using CdS fast optically controlled modulator 78–13736
CO_2 laser, vac. UV preionisation source spectral characts. 79–31938
CO_2 laser, variable pulse width generation, 100 ps to 1 ns range 78–46691
CO_2 laser, versatile high-power industrial system 78–55380
CO_2 laser, vibr. energy transfer by current modulation 78–1204
CO_2 laser, volume discharge excited by electron beam, mag. field influence 79–27241
CO_2 laser, with anisotropic resonator, radiation polarisation *(Russian)* 79–27309
CO_2 laser, with anisotropic resonator, output polarisation 80–28253
CO_2 laser, with foreign gas additives, time delay in pulsed operation 77–7058
CO_2 laser, with transverse excitation and preliminary photoionisation 78–1254
CO_2 laser active medium study using heterodyne photoreceiver 80–95868
CO_2 laser amplifier, double-discharge at 1800 torr 78–50815
CO_2 laser amplifier, high power large aperture electron beam controlled, development *(Japanese)* 78–66846
CO_2 laser amplifier, short pulse amplification calcs. 78–58979
CO_2 laser amplifier, short pulse propagation calcs. 79–76730
CO_2 laser amplifier, with UV preamplification 80–48284
CO_2 laser amplifier chain, laser plasma isolator for retropulse 79–22959
CO_2 laser amplifier design, IR laser optical pumping appl. 78–63133
CO_2 laser amplifier multipulse energy extraction 80–78832
CO_2 laser Antares fusion system power amplifier optics 80–74394
CO_2 laser Antares fusion system beam alignment 80–74422
CO_2 laser Antares fusion system optical diffraction computation 80–74424
CO_2 laser Antares system, power amplifier module 78–46666
CO_2 laser Antares system, optical design and anal. 78–46667
CO_2 laser Antares system, energy extraction, pulse shaping 78–46668
CO_2 laser beam, intensity fluctuations, spatial distrib. 79–18458
CO_2 laser beam meas. using pyroelectric vidicons 78–49907
CO_2 laser beats, technical line width, acoustic interference and current fluctuations influences obs. 80–48210
CO_2 laser cavity and Ge phase-conjugate 10 μm reflection expts. 80–78894
CO_2 laser compact wideband ring modulator 77–88803
CO_2 laser discharge, positive ion processes, mass spectrometric obs. 77–89337
CO_2 laser discharge, special case of effect of initial conditions on homogeneous discharge development 78–63613
CO_2 laser discharge, TEA, glow form. and glow-to-arc transitions, high speed camera obs. 78–25846
CO_2 laser discharge tube, phase distortions due to heating differential 80–95865
CO_2, laser discharges, determ. of recombination coeff. 78–90407
CO_2 laser discharges, electrode surface field and preionisation effects on spatial distrib. of arcs 78–63054
CO_2, laser eight-beam-system, power amplifier stabilisation by saturable absorbers 78–46619
CO_2, laser electron beam pulsed, sealed electron guns 78–71119
CO_2, laser excitation by RF discharge with rot. elec. field, linear and circular polarisation 80–37991
CO_2 laser excitation using double pulse discharge excitation scheme 77–19319

carbon compounds continued
CO_2, laser excited, dealignment relaxation meas. by fluorescence 78−25587
CO_2 laser excited by capacitative AC discharge, expt. model 80−9853
CO_2 laser freq. stabilization for far IR laser pumping 77−68223
CO_2, laser frequency measurements: a review, limitations, extension to 197 THz (1.5 μm) 78−81952
CO_2 laser fusion effort at Los Alamos Scientific Lab. 78−33290
CO_2 laser fusion system optical design and analysis 80−74391
CO_2 laser fusion system alignment by IR Smartt interferometer 80−74425
CO_2 laser fusion system wavefront correction, deformable mirror design 80−74427
CO_2 laser fusion system, optical design considerations 80−78868
CO_2 laser fusion target alignment 78−46706
CO_2 laser gain switch, pulse characts., approx. evaluation 80−58504
CO_2 laser gas mixture, vol. photo-preionisation by VUV radiation 80−87966
CO_2 laser gas mixture seeded with tripropylamine, photoionisation meas. 80−78829
CO_2 laser Gemini fusion system optical performance 80−74392
CO_2 laser Gemini fusion system, wavefront error correction by deformable mirror 80−74426
CO_2, laser generation by pulsed microwave excitation 78−74879
CO_2 laser Helios fusion system, multicomponent gaseous saturable absorber optimisation 80−74393
CO_2 laser Helios fusion system, beam simultaneity system 80−74419
CO_2 laser Helios fusion system alignment 80−74420
CO_2 laser Helios fusion target positioning with orthogonal telescopes 80−74421
CO_2 laser Helios fusion system beam diagnostics 80−78882
CO_2 laser heterodyne meas. of 01^11-11^10 hot band transition frequencies 77−7063
CO_2, laser hot-band transitions, heterodyne freq. meas. 77−88695
CO_2, laser intensity distrib., hot spot detect. using Ag halide film 78−82945
CO_2 laser intracavity freq. modulation, transient behaviour 80−14374
CO_2 laser irrad. of air, breakdown plasma prod., elec. field meas. by probes *(Russian)* 80−59334
CO_2 laser light pulse amplification calc. Fortran program PULSAMP 77−58312
CO_2 laser line, electro-optic frequency shift *(Chinese)* 80−43379
CO_2 laser method in stabilisation of ionisation-thermal instability 77−19302
CO_2 laser microsurgery and laryngology applics. 78−35905
CO_2 laser mixtures, high press. glow discharge, collision freq. 77−55184
CO_2 laser modulation, plasma injection into cavity 80−83626
CO_2 laser nanosecond pulse coherent interactions with amplifying media *(Russian)* 80−14314
CO_2 laser noise, fluctuations and output power stabilisation, 1 Hz to 150 kHz *(Polish)* 78−5447
CO_2 laser operating under free-oscillation conditions, nanosecond pulse emission 79−22933
CO_2 laser plasma, electron beam spreading, field variations 78−5446
CO_2, laser plasma electron energy distrib., exp. 80−37989
CO_2 laser power variation detection via plasma tube impedance changes 80−69437
CO_2 laser processing of materials, interfacing with modern prod. engng. technology 78−33767
CO_2 laser prod. microballoon plasma, fast ion emission 80−103172
CO_2 laser produced plasma, nonlinear scattering of laser radiation by fast ion waves in plasma 80−106916
CO_2 laser pulse, nonlinear propagation, computer simulation *(Japanese)* 80−95963
CO_2 laser pulse, nonlinear propag. characts., computer simulation 80−106575
CO_2 laser pulse duration discrimination, transient versus steady-state mol. absorption 77−79865
CO_2, laser pulse generation, cavity dumping by NH_2D Stark active mol. 77−88800
CO_2 laser pumped by energy transfer from Br, line tunable 78−5448
CO_2 laser R(18) line, wideband modulation with NH_3 Stark cell 77−23704
CO_2 laser radiation, saturated absorpt. by SiF_4 mol. 80−37811
CO_2 laser radiation, single pulse, thermal blooming 80−19080
CO_2 laser radiation amplification in reaction products of $CO+N_2O$, nonequilib. chem. pumping effects 77−83848
CO_2 laser radiation two photon pumped InSb laser 79−86182
CO_2 laser resonator, gasdynamic, optimal parameters determ. from vibr. energy exchange kinetics 80−14317
CO_2 laser self-modulation by means of nonlinear absorbing filters, anal. 78−37925
CO_2 laser self-sutained discharge, effect of low-ionisation-potential additives 78−71616
CO_2, laser sequence band transitions, heterodyne freq. meas. 77−71970
CO_2, laser sequence lines, pumping of methanol far IR laser lines 78−9369
CO_2 laser short pulse propagation and energy extraction 80−74335
CO_2, laser sideband spectroscopy *(German)* 79−26975
CO_2 laser small-signal gain coefficient calc. 80−78831
CO_2 laser stabilisation using 4.3 μm fluorescence technique 77−75557
CO_2 laser stability and heterodyne frequency calibration 78−59031
CO_2 laser stabilization for use in far IR laser pumping 79−72551
CO_2 laser stationary discharge positive column, electron density distribution *(Russian)* 80−54031
CO_2 laser system, broadband gas isolator mixes 78−46663
CO_2 laser system, eight beam, optical anal. 78−50814
CO_2 laser system, multipass power amplifier stabilisation using saturable absorbers 78−46664
CO_2 laser system, zero small signal gain 80−48271
CO_2 laser systems, multiline oscillator 79−72584
CO_2 laser systems for laser fusion appls. 78−50817
CO_2 laser transition absolute freqs. by multiplication of difference freqs. 80−37992
CO_2 laser velocimeter, optical design for long-range anemometry 78−36333
CO_2 laser waveguide, photoionisation stabilisation using Blumlein-type pulser 77−54734
CO_2 laser with partial population inversion, 16 μm steady state action 79−36873
CO_2 laser-plasma amplifier, 11-16 μm range 78−22173

carbon compounds continued
CO_2 laser-produced plasma-initiated neutral gas recomb. lasers 80−48286
CO_2 lasers, CW, high-power appl. of photoinitiated impulse-enhanced electrically excited discharge 78−50785
CO_2 lasers, double discharge and photopreionisation types, comparison *(French)* 79−31855
CO_2 lasers, effect of supersonic nozzle 78−46564
CO_2 lasers, freq. stabilisation through saturated absorption in SF_6 77−75556
CO_2 lasers, freq. stabilisation using OsO_4 narrow resonance, expt. *(Russian)* 78−33747
CO_2 lasers, high flow rate, gain and discharge characteristics 77−38855
CO_2 lasers, high-power, book contrib. 77−50651
CO_2 lasers, IR saturable absorpt. in benzene, chlorobenzene and bromobenzene 80−69465
CO_2 lasers, optically pumped, use of crystalline reflector in cavity 80−64080
CO_2 lasers, transition strength of 00°2 9.4 μm sequence band, appl. to IR isotope anal. 79−18395
CO_2 lasers for selective interactions with matter 77−27296
CO_2, lattice energies, non-additive three body contributions, triple-dipole term 80−54168
CO_2, Lennard-Jones 12:6 parameters calc. from viscosity data 77−46612
CO_2 levels rel. to global C cycle, modelling perturbations 80−31114
CO_2, lifetimes from collision induced absorption spectra, IR line broadening 78−33554
CO_2, light scattering, multiple scattering contribs. to depolarisation 80−87842
CO_2, light transmission functions for 15 μm band, calc. and expt. *(Russian)* 77−64428
CO_2, line broadening, short range force effects, semiclassical calcs. 79−98085
CO_2, line width effect on atmospheric 15 μm emission 77−21903
CO_2, linear, high temp., rot.-vibr., anharmonicity, thermodynamic function calcs. 80−43830
CO_2, liq., 100 to 3000 atm., depolarised Rayleigh spectra, orientation dynamics, wings 78−92084
CO_2, liq., mol. dynamics of '2-Lennard-Jones centres' pair pot. liq. 79−73082
CO_2, liq., thermodynamic and struct. props., pair pots. calcs. 77−58939
CO_2, liq., thermodynamic perturbation theory, equilib. props. 79−64976
CO_2, liq., transient stimulated vibr. Raman scatt. 78−71144
CO_2, liq., viscosity, density depend., theory 77−20105
CO_2, liq. and gas, state of aggregation effect on 1-4 μm absorpt. bands intensities 79−27042
CO_2, liq. phase vibr. spectra, anharmonicity effects 79−50022
CO_2, localised mol. orbitals, ab initio PRDDO SCF calc., isoelectronic struct. 78−25441
CO_2 long-pulse 2 GW single longit. mode source for laser-matter expts. 80−78860
CO_2, low energy electron (positron) collisions, ab initio adiabatic polarisation pots. 80−14240
CO_2, low energy electron scatt. cross sections, vibr. excitation, Boltzmann eqn. 80−18942
CO_2 lowest triplet state, Ar matrix isolation spectra 80−91569
CO_2, mantle related thermodynamic props. and reactions at high press. and temp. 80−81874
CO_2, matrix isolated Raman and IR spectra, fundamental freqs., isotope effects 77−88457
CO_2 measurement in air, using glass sample tubes and gas chromatography 77−4959
CO_2 mixed isotope multiatmosphere laser, lasing action 80−19016
CO_2 mixing gasdynamic laser 78−71073
CO_2 mixtures with methane and n-butane, oxidation under RF discharge conditions 78−15670
CO_2, mobility of Li^+, NO^+, and $O_2{}^+$, obs. using injected-ion drift tube mass spectrometer 78−1784
CO_2 mode-locked hybrid TEA laser, variable width stable pulse prod. 79−76726
CO_2, mol. beam apparatus, appl. as target for storage ring 77−6586
CO_2, mol. beam; interaction with cooled surface, AC excitation effects *(Russian)* 77−62744
CO_2, mol. quadrupole moments, mag. shielding and spin-rot. tensors 79−22609
CO_2, molecular charge density contours for cryst. struct. 78−38645
CO_2, molecular correlation energies, estimation from semi-transferable orbital correlation energies 78−82650
CO_2, molecular discharge, externally sustained, thermal instability 77−58915
CO_2, molecular fluid, Rayleigh and Raman light scatt. props., orientational and collision induced effect 80−63644
CO_2, mud volcanoes, Copper River Basin, Alaska, composition of emitted gases 79−84308
CO_2, multi-atm. TE laser, 10.6 μm ultrashort pulse generation by injection mode-locking 77−88799
CO_2 multi-rotational line TEA laser, theoretical model 80−69361
CO_2 multiatmosphere laser, mode-locked pulses 80−1248
CO_2 multiatmosphere laser tuning for methyl fluoride laser pumping 80−69421
CO_2 multiatmosphere UV preionized laser, elec. and gain characts. 80−14313
CO_2 multiatmospheric UV-preionised lasers 78−50805
CO_2 multistage laser, amplifier module, discharge and optical characts. 80−28248
CO_2, narrow band TEA laser for far IR laser pumping 77−54729
CO_2, narrow reson., elastic scatt., spectroscopic studies 80−53094
CO_2, near critical point Rayleigh and Raman scatt., Fermi diad 80−80765
CO_2, near IR absorpt. band props. 77−30872
CO_2 needle laser improvements, preionization influence 79−31926
CO_2, negative ion form., photodissoc., mass spectrometric obs. 78−13558
CO_2, negative point-plane corona, electrical characts. 78−71567
CO_2, negative Van der Waals polymer mols., formed by nozzle expansion 78−90307
CO_2, neutron flux preionised laser, operation in nuclear reactor active zone 78−17975
CO_2, new impurity analysis method 80−66908
CO_2 nighttime luminescence, Venera 9 and 10 spectroscopic obs. in Venus atmosphere 77−78701

carbon compounds continued
CO_2, non-symmetric parametric eqn. of state for extended crit. region 77−35296
CO_2, nonbending, vibr. motion calc. using SCF-SI theory 80−23399
CO_2, nonempirical PRDDO scheme and calcs. 80−37739
CO_2, nonequilib. expansion, retardation temps. $\leq$1200K, vibr. relax. and condensation influences 78−5777
CO_2, nonlinear optical polarisability meas. 79−54991
CO_2, nucleate boiling, heat transfer rate 77−39199
CO_2, $\nu_2+\nu_2$ biexciton transition in Raman spectra 77−48158
CO_2, O_2 and heat transport in the placenta, construct. and usefulness of models 80−3604
CO_2 optical gain in TE channel waveguides, discharge-related limitations 78−17951
CO_2, optical pumping in stimulated Raman scatt., tunable laser emitting at 14,16 μm, theory 78−46568
CO_2, optical reson. widths, nonlinear press. depend. 77−42358
CO_2, optically pumped laser, simultaneous lasing in bands of sequence 80−5725
CO_2, optoacoustic laser spectroscopy of excited vibr. molecular states 77−19106
CO_2 optogalvanic stabilised laser 79−89923
CO_2 oscillating laser transition, band width meas. 79−3677
CO_2 oscillator, high power nsec. pulse selection 79−98382
CO_2 oscillator, multiatm. injection mode-locking, high-power subnanosec. pulses 78−29988
CO_2 outgassing during pH meas., effects on groundwater chemistry and C isotopic comp. 79−66718
CO_2 oxidation of C in Fe-C melts, kinetics *(Russian)* 80−40680
CO_2 oxidation of structural steels in gas-cooled reactors 80−45447
CO_2, P ρ T surfaces, butterfly catastrophe 79−86546
CO_2, P-branch transitions, accurate wavelength meas. 77−38667
CO_2, P(26)-P(32) laser transitions, high temp. absorpt. meas. 80−14137
CO_2, partial photoionisation cross-sections, branching ratios, synchrotron radiation meas. 78−42141
CO_2, partial photoionisation cross-sections meas. 20 to 60 eV 79−31624
CO_2 partial pressure in blood, meas. by rapid response electrode system *(German)* 78−85409
CO_2, periodically operated laser, pulse repetition freq. limits 78−50750
CO_2 periodically pulsed laser, appl. isotope separation 79−27287
CO_2 permafrost on Mars, effect on topography 78−65535
CO_2 permeability in hard elastic polypropylene films, extension effects 80−40412
CO_2 permeability in polyethylene terephthalate above and below glass transition 79−73340
CO_2, photo-electrochemical production of C-C bonds from carbon dioxide using solar light 80−21407
CO_2, photoabsorpt. cross section, 10 to 50 nm 77−61797
CO_2, photoacoustic Raman spectroscopy under pulsed laser excitation 80−82825
CO_2 photochem. reduction to organic fuels using photoelectrochem. solar cells 80−55880
CO_2, photodesorption by ZnO powder, surface cond. 77−11980
CO_2, photodesorption from ZnO, rel. to surface cond. 77−47671
CO_2, photodesorption from ZnO, pulsed-laser-dynamic-mass-spectrometer study 80−35568
CO_2, photodissoc., C I UV fluorescence spectrum obs. 79−13776
CO_2, photodissoc., CO fluoresc. 77−6836
CO_2, photodissoc., isotope effects 77−75238
CO_2, photodissoc. CO($A^1\Pi \rightarrow X^1\Sigma^+$) transitions, vibr. population 77−58100
CO_2, photodissoc. ionis., 16-41 eV 77−18995
CO_2, photoelectrocatalytic reduction in aq. suspensions of semicond. powders 79−39141
CO_2, photoelectron ang. distrib. asymmetry parameter for 30.4 nm photons 79−98151
CO_2, photoelectron spectra, 21.2-151.4 eV and soft X-ray, ionis. cross-section 78−37683
CO_2 photofixation to formic acid in water, photosynthesis mimicking 78−88650
CO_2 photoionisation, expt. techniques, processes, theory, review 77−14402
CO_2, photoionisation, nuclear motion effects 80−58324
CO_2, photoionisation, partial oscill. strengths 79−6973
CO_2 photoionisation and photoelectron energy distrib. in thermosphere of Mars and Venus 79−2506
CO_2, photoionisation efficiency curve, supersonic mol. beam expt. 78−46406
CO_2 photoionisation laser, elec. and stimulated emission characts. 77−71971
CO_2 photoionisation laser with 300 J output energy 79−31939
CO_2 photoionisation laser, breakdown effect on output 79−68379
CO_2 photoionisation TEA laser, characteristics calculation using computer model *(Russian)* 80−83589
CO_2, photolysis, 1470 and 1302-1306 Å, absolute O atom yield 78−48681
CO_2, photolysis, O(^{1}S) absolute quantum yield spectral depend. meas. using XeO luminesc. 80−35561
CO_2, physisorbing on Ni, stay time meas. 78−56044
CO_2 pin-bar TEA laser, internal arcing, ultra high speed photography 78−9357
CO_2, planar hollow-core doubling grating DFB laser, characts. 78−46673
CO_2 plasma, 10000-13000K, VUV continuum radiation 78−91152
CO_2 plasma, atm. press. opt. props., 400-1200 nm spectral range and 10^4-2×10^4K temp. 80−33753
CO_2 plasma, microwave discharge, electron energy distrib. function *(Russian)* 77−11415
CO_2 plasma, surface treatment of polyester fabric, effect on surface struct., props. 78−95831
CO_2, plasma-chemical dissoc. in nonequilib. UHF and high freq. discharges 79−15990
CO_2, plasma-sheet pulsed laser 77−23696
CO_2, polarisabilities, quadrupole and dipole moments, nucl. geom. effects 79−63899
CO_2, polymer degradation products, chem. anal. by UV photoelectron spectroscopy 78−53300
CO_2, positive and negative ion reactions 77−40540
CO_2, press. broadening coeffs. at 4.2 μm, rot. quantum number 78−74704
CO_2 pressure, end-tidal and arterial diff. obs. 80−72193

carbon compounds continued
CO_2 pressures in dogs during acute hypercapnia, arterial-expired differences 80−72198
CO_2, primary ionis. coeff., electron attachment coeff. rate coeff. 77−4900
CO_2, proton affinity, cluster ion stability, mass spectrometer obs., appl. Martian ionosphere 77−77760
CO_2, Pt-catalysed recombination of CO and O_2 in sealed TEA lasers 78−46566
CO_2, pulmonary gas exchange model, effect of ventilation-perfusion, diffusion-perfusion ratios *(French)* 79−8516
CO_2, pulse laser, UV photoionisation, impurities effect 78−1206
CO_2, pulse periodic laser with non-self-sustaining discharge 78−1263
CO_2, pulse periodic open cycle laser, 500 W average output power 77−61974
CO_2 pulse-periodic elec. pumped gasdynamic laser, possibility of spontaneous circulation 79−45926
CO_2 pulse-periodic laser, preionisation by electrodeless capacitative pulses 79−31937
CO_2 pulse-periodic laser utilising air-CO_2 mixture, emission characts. 79−89886
CO_2 pulse-periodic laser, gas stream gasdynamic perturbations, heated gas convective removal 79−94207
CO_2 pulse-periodic laser, gas stream gasdynamic perturbations, acoustic waves 79−94208
CO_2 pulse-periodic laser, multiphoton molecular dissociation 80−9931
CO_2 pulse-periodic TEA laser freq. stabilisation by low press. CW laser signal injection 80−74408
CO_2, pulsed elec. discharge laser, UV ionisation at atm. press. 78−46630
CO_2 pulsed electric discharge laser with stable parameters 80−48283
CO_2, pulsed electrical breakdown at high temps. *(Russian)* 78−34379
CO_2 pulsed electroionisation laser with controllable emission parameters 80−78865
CO_2, pulsed electron-beam-controlled laser, parameters optimisation 78−71116
CO_2 pulsed gas discharge laser, emission on molecular transitions at 14, 16 μm 80−53261
CO_2, pulsed gas-discharge laser, skimming discharges for preionisation 80−99740
CO_2, pulsed laser, 23 J, Lamberton-Pearson config., parameters 77−19317
CO_2, pulsed laser, high power, oscill. spectrum expansion *(Russian)* 78−74882
CO_2, pulsed laser, laser induced medium perturbation 78−58977
CO_2 pulsed laser beam, thermal coupling 78−63145
CO_2, pulsed laser characts., UV preionisation 77−7059
CO_2 pulsed laser system, acoustic suppression 80−74378
CO_2 pulsed laser with combined current discharge 77−14689
CO_2 pulsed laser with transverse electric discharge 77−38913
CO_2, pulsed photoacoustic Raman spectrosc., gaseous trace anal. 80−40769
CO_2, pulsed TE laser, tunable single-mode operation by means of selective absorbers 79−36940
CO_2, pulsed TEA laser, tuning by 9.55 μm CO_2 laser radiation injection 77−38908
CO_2 pulsed transversely excited waveguide laser design 79−27280
CO_2, pump laser for far IR gas laser in common resonator 77−38950
CO_2, pure and CO_2-He mixture, optically pumped continuously tunable lasers 78−13678
CO_2, pure gas, enthalpy, Carlson-Thodos van der Waals eqn. calcs. 80−83878
CO_2, pure rotational stimulated Raman photoacoustic spectroscopy 80−32724
CO_2, Π_u symmetry transition probabilities, dipole moment and electro-optical consts. calc. 80−43115
CO_2, quadrupole moment from K^+(Ar)(Kr)(Xe) scatt. total cross sections 77−50495
CO_2 quantum amplifier, high power radiation pulse generation, efficiency 78−13680
CO_2, quenching of laser-excited O_2 80−99515
CO_2, R-branch head of ν_3 band, up to 985K laser spectrometer 80−47983
CO_2 R-branch line intensities and press.-broadened line widths at 15 μm 80−102508
$(CO)_2$, RF lab. meas. and interstellar search 80−43035
CO_2, radiative transfer, Curtis-Godson approx. 78−67019
CO_2, radiative transfer in 4.2 μm band with non-LTE in terrestrial atm. *(Russian)* 78−88914
CO_2 rapid discharge TEA laser, construction and performance characts. 79−3710
CO_2, rapid wavelength switching probe laser, J-line scan gasdynamic laser diagnostic 78−59044
CO_2, rarefied jet beam, Raman scatt., for rot. temp. and density 80−6185
CO_2, ratio of lateral diffusion coeff. to mobility for electrons 79−50840
CO_2, ratio of lateral diffusion to mobility for electrons at moderate E/N 80−59160
CO_2, Rayleigh linewidth, vap. near crit. pt., gravitationally induced effects 79−82035
CO_2, Rayleigh scatt. props., nephelometer meas. 79−29865
CO_2, reaction with W at high temps. and low press. 77−86379
CO_2, reactions with dissolved O, and C in liquid Fe, equilibria 78−44397
CO_2 rebreathing, contrib. of rib cage and abdomen-diaphragm to tidal vol. 79−100650
CO_2 rebreathing studies, microcomputer-based data acquisition and anal. system 80−36161
CO_2, refr. index and Lorentz-Lorenz functions, 944 cm^{-1} and 15803 to 22002 cm^{-1} 78−59543
CO_2 refractive index meas., intermolecular interaction effects 80−33728
CO_2, relative Raman scatt. cross section 80−100061
CO_2 relativistic electron beam transport at low pressures 78−75373
CO_2, relativistic electron beam propag. 79−76569
CO_2 removal from simulated HTGR fuel reprocessing off gases 79−26577
CO_2 repetitively pulsed electron beam laser operation 79−31943
CO_2, reson. absorpt. of CO_2 laser radiation 78−20514
CO_2, reson. electron impact vibr. excitation, 3-5 eV 78−25726
CO_2, resonant vibr. excitation cross section in electron scatt. 77−19098
CO_2 respiratory output, continuous meas. in man 77−29216

carbon compounds continued
CO_2 responses of conscious rabbits at ambient temps. of 5, 20 and 35°C 80−56085
CO_2, rot. Raman and IR lines, self-broadened linewidths 77−42357
CO_2, rot. Raman spectra, $01^{1}0$ state effects on intensity distrib. *(German)* 77−10679
CO_2, rot.-vibr. bands, absorpt. coeff. calc. method, Fermi reson. effect on spectral lines 80−32696
CO_2 rotating-mirror Q-switched TEA laser, mode sweeping effects 80−99769
CO_2, SCF vertical spectrum for valence, mixed character and Rydberg states 77−50375
CO_2 saturable absorber, heated, for passive Q-switching of CO_2 laser 78−25900
CO_2, saturable absorpt. and rot. relax., (00°0) vibr. level 77−19367
CO_2, scatt. electron angular distrib. 78−74766
CO_2, sea-air flux meas., eddy correl. method 78−32191
CO_2, seabed gas seep, Norton Sound, Alaska 80−67361
CO_2 sealed high-pressure pulsed laser, gas equilibrium chemical comp. 80−63972
CO_2 sealed photoionisation TEA laser, limiting processes 78−82946
CO_2 sealed TEA lasers, with external control of gas chemistry 77−88738
CO_2 sealed type laser using metal construction *(Chinese)* 79−81459
CO_2, sealed UV-preionization TEA laser 78−46627
CO_2 sealed-off TEA lasers, size reduction and improved efficiency 79−31942
CO_2, seeded laser mixture, photoabsorption and ionisation cross sections 77−23645
CO_2, selected fragment vibr. energy distrib. in dissoc. processes 78−1036
CO_2 self-pumping on pulsed periodic energy input *(Russian)* 80−106506
CO_2 self-sustained laser system, electron avalanche and electron-ion recomb. coeffs. meas. 80−102694
CO_2, sequence bands, laser power and gain meas. 77−79795
CO_2 shape resonances in [100] symmetric stretch excitation *(French)* 79−86074
CO_2, short pulse laser, efficiency rel. to discharge parameters 77−708
CO_2 short-pulse laser high-pressure amplifiers, design engineering 79−36936
CO_2, short-pulse oscillator, variable pulse repetition freq., pulsewidth and wavelength control 77−88801
CO_2, simple high-power TEA laser operating in IR 79−94251
CO_2, simple preionised waveguide TE laser with continuous discharge electrodes 77−54721
CO_2, single and multiple free jets, CW laser Raman spectroscopy 80−32727
CO_2, single axial mode laser, digital feedback stabilization 79−89928
CO_2, single freq. atmospheric press. laser 78−13728
CO_2, single mode laser, internal freq. modulation up to 350 MHz 77−19308
CO_2 single-discharge self-sustained laser, 5 cm gap distance, high power output 80−102735
CO_2 single-pulse laser, emission spectrum photographic recording by parametric conversion 79−10357
CO_2, small high press. UV preionised laser, continuous tuning characts. 79−59722
CO_2, solid, adsorption of Ar, density functional theory, computer simulation 80−24735
CO_2, solid, as adsorbing walls separated by Lennard Jones liq., Monte Carlo calc. of force 80−15363
CO_2, solid, energy loss of 0.5 to 2 MeV ^{4}He ions, from backscattering meas. 79−4346
CO_2, solid, Fermi reson. press. tuning, Raman spectra 80−93293
CO_2, solid, high press. mol. libration calc. with Kihara core pots., Gruneisen parameter and lattice 80−65173
CO_2, solid, IR spectra and refr. index, Martian implications 80−72821
CO_2, solid, melting curves, Lennard-Jones Devonshire theory 80−65201
CO_2 solid film, contaminant on cryocooled Ge optical window, IR transmission 79−32007
CO_2, solid pellets, for on-top seeding of convective clouds 78−73531
CO_2, solubility in cellulose acetate, 0.-70°C, up to 45 atmos. 78−83957
CO_2, solubility in liq. solutions of $ZnCl_2$ in NaCl and KCl 79−90785
CO_2, solubility in molten Na_2CO_3 79−69251
CO_2, solubility in plasticized PVC *(Polish)* 79−69252
CO_2, solubility under magma genesis conditions, petrological implications 78−11886
CO_2 solution in ocean surface waters, role of homogeneous buffer factor 80−21783
CO_2, sorption on hydrated Ce_2O_3 rel. to dehydration conditions 79−66345
CO_2, sorption on ThO_2 sol-gel for nucl. applics. 77−4940
CO_2, specific heat, meas., near crit. point 77−51490
CO_2, spectra, Fermi reson. and classical motion 80−28000
CO_2, spectral line breadth in 15 μm band, N_2 broadened, 200-300K 79−22765
CO_2, spin polarised photoelectrons, synchrotron excited 80−43101
CO_2, spontaneous emission probabilities and collisional broadening of $00^{0}1$-$10^{0}0$ lines 77−23649
CO_2, stability of parallel pin electrode laser discharges, theoretical investigation 80−83588
CO_2, static polarisabilities, ab initio SCF HF calcs., internucl. separation depend. 78−9073
CO_2, stretch-stretch interaction force const., electron correlation influence, ab initio CI study 80−58161
CO_2, submillimetre wave laser operating in passive Q-switched intracavity pump mode 77−83885
CO_2, supercooled, IR absorpt. spectrum 77−23574
CO_2, supercritical, natural convection to cooled horizontal cylinder 79−98724
CO_2 supercritical, vertical plate, laminar natural convection heat transfer 80−64544
CO_2 supercritical boilers, forced flow, frictional pressure drop 80−14689
CO_2, supercritical fluid coolant for CANDU reactors, feasibility study 79−76064
CO_2, supersonic chem. laser, mixing of $D+O_3+CO_2$ streams 77−676
CO_2, supersonic jet, $(CO_2)_n^-$ cluster formation and electron attachment 78−5385
CO_2, supersonic radiation waves, excitation by CO_2 laser 79−90433
CO_2, Σ-diads, Raman spectra, O isotope effects 77−83610

carbon compounds continued
CO_2 TE laser, longit. mode control using intracavity gas-phase absorbers 79−72579
CO_2 TE laser, passive mode locking using p-Ge saturable absorber 78−71127
CO_2 TE laser, performance improvement with tripropylamine additives 78−78991
CO_2 TE laser, waveguide, role of elec. field to press. ratio 78−17901
CO_2 TE laser amplifier, characts., with different UV preionisation at superatmospheric press., tripropylamine doped 77−14686
CO_2, TE multiatmos. laser, 10 μm pulse generation and amplification 79−45981
CO_2 TE pulsed 4.3 μm laser 79−89926
CO_2 TE unstable resonator laser, operation using additives 79−98403
CO_2 TEA amplifier, gain meas. on sequence bands 78−78990
CO_2 TEA helical laser, axial mode behaviour 79−55108
CO_2 TEA high-power tuned laser using three-mirror confocal unstable resonator 80−23719
CO_2, TEA injection laser, single-mode pulse prod. 77−54722
CO_2 TEA laser, 4.3-μm radiation pulse generation 80−5724
CO_2 TEA laser, actively modelocked multiline, controlled by NaCl etalon 80−23713
CO_2, TEA laser, attachment loss of photoionisation electrons 78−5450
CO_2, TEA laser, catalytic control of gas chemistry 79−76663
CO_2 TEA laser, compact sealed single mode operation 78−50810
CO_2 TEA laser, compact sealed photopreionised, without heterogeneous catalysis or gas recycling 79−59709
CO_2 TEA laser, construction and optimisation with pin electrodes *(German)* 77−23697
CO_2, TEA laser, energy extraction improvement in multiline double band mode 78−63129
CO_2, TEA laser, field uniformity requirements 79−3675
CO_2 TEA laser, fine freq. tuning 79−98405
CO_2 TEA laser, high power, construction and performance 77−3566
CO_2 TEA laser, homogeneous discharge development, preionisation conditions influence 79−18399
CO_2 TEA laser, injection mode locking on P and R transitions in 9, 10 μm bands 79−89883
CO_2 TEA laser, injection tuning and mode locking on low gain rot. lines 80−95928
CO_2, TEA laser, intense pulsed lasing at lines of P and R branches of $00^{0}2$-$(10^{0}1,02^{0}1)_{I,II}$ 79−89887
CO_2 TEA laser, isolation between amplifiers using absorbing gases 80−95911
CO_2 TEA laser, laser output depend. on initial photoelectron density 80−43320
CO_2, TEA laser, mode characts. using unstable resonators 79−3719
CO_2 TEA laser, mode-locked, cavity-dumping 80−87415
CO_2 TEA laser, multiline oscill. temp. control., intercavity etalon method 79−98337
CO_2, TEA laser, optical pump source for high-energy NH_3, CF_4 lasers 79−89927
CO_2 TEA laser, optimum operational conditions with double discharge at atm. pressure *(Bulgarian)* 78−33720
CO_2 TEA laser, picosecond pulse generation using Ge optical switch 79−7159
CO_2, TEA laser, pulse shape and duration, excitation method *(German)* 78−83010
CO_2 TEA laser, pulse shaping by independent excitation of coaxial discharge systems 79−7150
CO_2 TEA laser, pulse shape and gain 80−1181
CO_2, TEA laser, pulse-forming and line-broadening in AM mode locking 77−54743
CO_2, TEA laser, self sustained discharge excitation, efficiency 77−655
CO_2, TEA laser, self-sustained discharge excitation 77−7061
CO_2 TEA laser, sequence band effect on 10.4 μm band multiline oscillation 80−74334
CO_2 TEA laser, shortening of pulses *(Rumanian)* 79−86199
CO_2 TEA laser, tri-n-propylamine doped, parametric meas. 80−78830
CO_2 TEA laser, UV preionisation, parametric studies 80−64040
CO_2 TEA laser, UV preionised, characts. 80−69414
CO_2, TEA laser amplifier, high power short-pulse, efficiency enhancement 79−36872
CO_2 TEA laser design and construction *(Italian)* 78−55360
CO_2 TEA laser discharges 77−14687
CO_2, TEA laser discharge form., electrode and preioniser geometry effects 77−27269
CO_2 TEA laser discharge, influence of additives and contaminants evaluated by electrical meas. 78−94388
CO_2 TEA laser electrical excitation rates, theory and expt. 78−71078
CO_2, TEA laser emission on sequence bands 78−71075
CO_2 TEA laser injection locked, tunable single longitudinal mode operation, O_3 absorpt. spectra 80−33018
CO_2 TEA laser mode locked by positive Ge, pulse shape meas. 78−46694
CO_2 TEA laser operation, effect of low-ionisation gas additive along with UV photopreionisation 77−50683
CO_2 TEA laser oscillator, longit. mode rejection, cavity length tuning effect 79−86189
CO_2 TEA laser oscillator, transverse mode locking by short pulse injection 80−38045
CO_2 TEA Laser pulse, PCM with CdTe crystal Pockels modulator 80−102742
CO_2, TEA laser pumping efficiency increased by longitudinal mode control 77−38924
CO_2 TEA laser stability 77−38935
CO_2 TEA laser system, 20-J nanosecond pulse, based on injection-mode-locked oscillator 80−99752
CO_2, TEA laser transverse discharge electrode system, relax. and plasma homogeneity 77−23648
CO_2, TEA laser tube, helical electrodes, convergent lensing effect *(French)* 77−75472
CO_2 TEA laser with long optical resonator, mode-locked operation 78−79041
CO_2 TEA lasers, one-step photoionisation, preionisation discharge effect on electron density 80−53256
CO_2 TEA oscillator, injection mode-locking using N_2 laser-controlled semicond. switching of 10-μm radiation 80−1247
CO_2 TEA oscillator, simultaneous freq. stabilisation and injection 78−55362

carbon compounds continued
CO_2 TEA pulse-periodic laser, utilisation efficiency of gas flow 79−64201
CO_2 TEA pulsed, UV preionized, high power laser, development and performance 80−106539
CO_2, TEA sealed laser, seed gas compatible system with unheated oxide catalyst 78−63130
CO_2 TEA single longit. mode laser with tilted intracavity etalon 78−5484
CO_2 TEA UV preionized laser, non-dispersive tuning 79−31856
CO_2 TEA waveguide laser, high power 80−91814
CO_2 technological closed-cycle laser optimisation to 10 kW power 79−94254
CO_2, tectonic processes causing emission from crust, seismicity prediction possibility 80−94470
CO_2 tension dynamics in brain, math. model 77−36965
CO_2, thermal accommodation coeff. on W, gas saturated system 77−70335
CO_2, thermal accommodation coeffs., on Al(Fe), translational (internal) gas-solid energy exchange 78−92506
CO_2, thermal activity coeff. meas., periodic-heating method 80−42218
CO_2 thermal cond., simple relation, 1000-3000K 77−24048
CO_2, thermal cond. at 350 to 1300K 77−35304
CO_2, thermal cond. meas. at room temp., and pressures up to 35 MPa 79−86551
CO_2, thermal conductivity, 400 to 1500K, vibr. internal energy calc. 79−18986
CO_2, thermal conductivity meas. at elevated temps. by hot wire method 80−6199
CO_2, thermal conductivity meas. at elevated temps. by hot wire method 80−6200
CO_2, thermal conductivity, corresponding states model 80−69964
CO_2, thermal diffusivity and cond. in crit. region meas. by holographic interferometry *(German)* 78−59942
CO_2, thermal gasdynamic laser energy parameters 77−75479
CO_2, thermal transpiration, theory and expt. comparison, molecular and transition flow 79−32579
CO_2, thermally pumped gas-dynamic laser based on deformation and symmetric modes 79−36874
CO_2 thermally pumped laser, He and Ar gas addition effect on small signal gain 79−22931
CO_2, thermochem. reduction using solar energy to provide C-based fuels 80−76610
CO_2, three-body electron attachment in discharge 80−24245
CO_2, threshold photoelectron and photoionisation spectra 77−14491
CO_2, time-depend. of radiation in pulse discharge regime *(Russian)* 77−84548
CO_2, time-resolved IR single-shot absorpt. spectra 79−58808
CO_2, total scatt. cross sections for intermediate-energy positrons 80−91692
CO_2 transfer in membrane blood transfer 79−25154
CO_2 transition, $10°0 \rightarrow 01'0$ 13.9 μm, in pulsed elec. discharges, laser emission 77−88692
CO_2, transition calibration, rotational constants, absorption spectrum, 4.82-μm region 78−58868
CO_2, transition moment and probabilities of IR spectra 79−3498
CO_2, transition moment of IR band near 7740 cm^{-1} 78−90224
CO_2, transition moment of IR band near 7740 cm^{-1} 78−90225
CO_2, transport kinetics through porous CaO formed by carbonate decomposition 79−23780
CO_2, transverse discharge laser, spatial gain distrib. meas. 77−696
CO_2 transverse discharge flow type laser, theoretical model *(Chinese)* 80−53255
CO_2 transverse flow CW laser, modelling and props. meas. 80−43321
CO_2, transversely excited laser, advances in control 77−88748
CO_2, transversely excited waveguide laser, high field preionisation, design considerations 77−88751
CO_2, Trichel corona, negative ions 78−30503
CO_2 triple point, overheating and undercooling phenomena 80−2142
CO_2 tunable waveguide laser 79−64249
CO_2, turbulent cooling tube flow, at supercrit. press. 78−14005
CO_2, turbulent flow field, mol. vibr.-rot. bands, spectral absorpt. coeff., temp. depend. 80−52987
CO_2, two-scale factor universality near crit. point 78−55936
CO_2, UV photodissoc., O I 1304 angstrom emission 80−32652
CO_2 UV preionised laser discharge, large scale, aero-acoustic effects 79−36875
CO_2 UV preionised TEA laser, parametric study 80−102738
CO_2 upper hybrid and whistler mode laser radiation anomalous penetration in overdense magnetoplasma 79−77386
CO_2, upper laser level population, active medium gain in waveguide discharge channel 79−86158
CO_2, VV processes, estimation of almost resonant molecular energy transfer due to multipolar pot. 80−91642
CO_2, valence excitation energy and UV spectra, HAM/3 calc. 78−25454
CO_2, valence shell ionic photofragmentation, oscill. strengths, EELS and electron-ion coincidence meas. 80−37879
CO_2, valence shell ionis. spectra, theory and dipole (e-2e) spectra expts. 79−76522
CO_2, valence states study by (e,2e) momentum spectroscopy 78−22039
CO_2, vapour-liquid and vapour-solid equilib. data, mass spectroscopic tracer pulse chromatography 80−37115
CO_2, ventilatory response in sprint swimmers *(Japanese)* 80−8077
CO_2, Venus IR absorpt. bands, 3900-10000 cm^{-1}, assignment 78−7896
CO_2, vertical valence ionis. pot., many-body Green's functions 78−22051
CO_2, vibr. distrib., effect of laser radiation 77−34868
CO_2, vibr. excitation and de-excitation by electronic collisions, calc. of cross section 78−66669
CO_2, vibr. excitation calc., in gas mixture discharge 79−77442
CO_2, vibr. excitation threshold struct., low-energy electron scatt. 80−5625
CO_2 vibr. luminesc., excited by DC discharge, rot. and vibr. mol. consts. 78−58867
CO_2 vibr.-rot. band shape calcs. 80−969
CO_2, vibr.-rot. spectrum, absolute line intensity, vibr. transition moment 77−83655
CO_2, vibr.-rot. transitions power broadening by laser irrad. 77−3420
CO_2, vibr.-rot. transition overtones, active Raman spectra obs. 78−50550
CO_2, vibration and electronic excitation results obtained with magnetically collimated electron impact spectrometer 79−49334

carbon compounds continued
CO_2 vibrational problem, Rayleigh-Schrodinger and contact transform techniques *(French)* 77−3340
CO_2 vibrational temperature determ. in gasdynamic laser with $CO_2+N_2+H_2$ mixture 80−9849
CO_2 vibrational temps. at 40 to 140 km altitude 77−70762
CO_2 vibrational temps. in reaction products of $CO+N_2O$ under gasdynamic laser conditions 80−21276
CO_2, viscosity, density expansion near critical temp. 80−53909
CO_2, viscosity meas. at 298 to 473K *(German)* 77−42954
CO_2, viscosity meas. at low temps. 80−6193
CO_2, viscosity near liquid-vapour transition point 80−2189
CO_2, viscosity rel. to ionis., skin friction of wetted oscill. disc 78−34252
CO_2, viscous hypersonic flow over blunted cone, numerical anal. 79−77171
CO_2, W-value for pion$^-$ 77−56473
CO_2 wave numbers, intercomparison at 800 to 600 cm^{-1} with diode laser spectrometer 79−98082
CO_2 waveguide amplifiers, temp. depend. of small signal gain and saturation power 78−46569
CO_2 waveguide high press. laser, line selection and tunability 78−59026
CO_2 waveguide laser, CW, optical pumping of far-IR molecular lasers 80−83615
CO_2, waveguide laser, coherent optical pulse generation 77−38907
CO_2 waveguide laser, design and performance characts. 80−9909
CO_2 waveguide laser, dynamic gain, discharge tube depend. 80−23668
CO_2 waveguide laser, electrooptically Q-switched 79−98416
CO_2, waveguide laser, gain calcs. 78−25849
CO_2 waveguide laser, gain and saturation *(Rumanian)* 80−23667
CO_2, waveguide laser, low prime power, gain and discharge power meas. 77−88749
CO_2 waveguide laser, multibeam, excited by AC discharge 80−99754
CO_2 waveguide laser, parameters meas. 79−31859
CO_2 waveguide laser, performance characts. *(Japanese)* 77−19318
CO_2, waveguide laser, population and gain, kinetic eqn. soln. 79−64200
CO_2 waveguide laser, pulsed operation 78−42353
CO_2 waveguide laser, saturation intensity, effect of wall deexcitation 79−924
CO_2 waveguide laser, saturation parameter 79−94209
CO_2 waveguide laser, saturation parameter meas. method 80−87372
CO_2 waveguide laser, small signal gain, saturation intensity and volumetric output power 78−74880
CO_2 waveguide laser, transversely excited multiatmosphere, construction and characts. 77−79845
CO_2 waveguide laser, transversely RF excited 78−63127
CO_2 waveguide laser, tunability calc. *(Rumanian)* 80−87371
CO_2 waveguide laser 79−98380
CO_2 waveguide laser amplifier, using short BeO ceramic discharge tube, gain meas. 80−33027
CO_2 waveguide laser amplifier with strong discharge tube 80−74398
CO_2 waveguide laser and appls. 77−75568
CO_2 waveguide laser discharge, cooling, gas temp. meas. 78−17958
CO_2, waveguide laser structures, design, construction and performance 77−88750
CO_2, waveguide laser with BN channel 77−14743
CO_2 waveguide laser with plane parallel mirror resonator 79−3715
CO_2 waveguide laser with pulsed high-freq. discharge 80−99755
CO_2 waveguide lasers, engineering aspects 79−31941
CO_2 waveguide lasers, high stability 77−3615
CO_2 waveguide lasers, high-power, high-press., photoionisation-stabilised 78−46641
CO_2, waveguide TE laser, modes of operation 79−81451
CO_2, weak laser lines around 10.6 μm, wavenumber meas. 78−17998
CO_2, weak laser transitions, freq. and gain meas. using diode laser 77−88693
CO_2, weak nonlinear waves, struct. and propag., effect of vibr. relaxation 79−64683
CO_2 whispering-gallery CW laser, design and operation 79−81447
CO_2 wire-triggered high press. pulsed laser 79−89935
CO_2 Xe-He plasma discharge, electron conc. and temp., optical diagnostics method 79−41871
CO_2^-, adsorbed on MgO, g-tensors, spin densities, CNDO calc. 78−46270
CO_2^-, dissoc., $^2\Sigma_g^+$ state, Wall Porter pot. surface, autodetachment and vibr. level population inversion 80−21275
CO_2^-, hydrated anion stable gas phase heteronuclear clusters, mass spectra, autodetachment rates 80−14266
CO_2^+, $^1\Pi_g$, mixed charact. state, vertical energy level MC-CI wavefunction 79−45644
CO_2^+, $A^2\Pi_u$-$X^2\Pi_g$ band emission spectrum, rovibronic anal. 80−9613
CO_2^+, appearance potential by anal. of field-dispersed ions 78−85234
CO_2^+, electron impact ionisation, cross section obs. 80−58397
CO_2^+, fluoresc. quantum yields and lifetimes, meas. method, ion form. 77−6815
CO_2^+, fluoresc. quantum yields, isotope effects, photon-photoion coincidence meas. 78−90200
CO_2^+, ion mobility in N_2, flow drift tube obs. 77−19663
CO_2^+, laser excitation spectra, $A^2\Pi_u \rightarrow X^2\Pi_g$ fluoresc., rot. struct. 78−1019
CO_2^+, mobility in Ne gas 78−14125
CO_2^+, photoelectron and ion emission quantum yields, interelectronic state effects 79−6967
CO_2^+, photoionisation reson. spectra and threshold electron-ion coincidence meas. of fragmentation 77−38700
CO_2^+, radiative lifetimes, threshold electron-phonon coincidence meas. 78−13550
CO_2^+, radical, $+NH_3(PH_3)$, thermal energy charge transfer reaction 77−16796
CO_2^+, thin foil impact, dissoc. struct. effects in ionic fragment energy spectra 78−50631
$^{12}CO_2$, absorpt. spectrum at 4.3 microns 78−58692
$^{12}C^{16}O_2$, double-discharge Pyrex waveguide CW laser 78−9393
$^{12}C^{16}O_2$, Herman-Wallis coeff. for band affected by reson. *(French)* 77−61805
$^{12}C^{16}O_2$, ν_3 band, IR single line strength 80−83370
$^{12}C^{16}O_2$, vibr.-rot. Raman spectrum, in Fermi reson. region 78−42073
$^{13}C^{16}O_2$, emission spectrum near 4.5 μm, nu$_3$ region spectroscopic consts. 77−38664
$^{13}C^{16}O_2$, IR line strength 80−83371
$^{13}C^{16}O_2$ laser, isotopically enriched, appl. in optically pumping far IR laser 80−58507

carbon compounds continued
$^{13}C^{16}O_2$, ν_3 band, absorpt. spectrum 78—58693
$^{13}C^{16}O_2$, ν_3 fundamental at 4.4 μm 78—86862
$^{13}C^{16}O_2$, Q-branch spectrum of $(01^{1d}0\text{-}00^00)$ transition 78—42061
$^{14}CO_2$, activity meas. in air 79—66388
$^{14}CO_2$ breath analysis tests, plastic scintillation filament detector system 78—65122
$^{14}CO_2$, in liq. scintillator, determ. of low radiocarbon activity by absorption 78—74550
$^{14}CO_2$ released to atmosphere, population dosimetry 78—35958
$^{14}CO_2$, respiratory, determ. by $Ba^{14}CO_3$ decomposition in sample oxidiser 79—88153
$^{14}CO_2$, tunable diode laser spectroscopy, absorption coeffs., appls. 77—83583
$^{14}C^{16}O_2$, band centre at 4.5 μm, tunable diode laser spectroscopy 78—33503
$C^{15}O_2$ inhalation for left heart imaging 77—64126
$C^{18}O_2$, isotope exchange with $CeMoO_4$, $LaMoO_4$, $PrMO_4$, $NdMoO_4$, 300-500°C 77—63884
$C^{18}O_2$, Raman spectra in Fermi reson. region 78—74664
CO_2:Cr I, hypersonic flow, excitation temp. meas., hook method 77—58200
CO_2:He:N, glow discharge instability in afterglow 80—6313
CO_2:N_2:He plasma, lasing action, gain limiting attainment possibility 79—89884
$CO_2/^{192}OsO_4$ laser, absolute light oscill. freq., universal const. variation meas. possibilities *(Russian)* 80—5723
CO_2-^{14}C animal exhalation meas. by liquid scintillation counting *(French)* 79—48384
CO_2-^{222}Rn, thermal diffusion, expt. method for study 80—5922
CO_2-2,2-dimethylpropane, liquid, -vapour equili., 220 to 300K and 6.7 MPa 80—62821
CO_2-air, heat transfer from cylindrical anemometer probe 77—84256
CO_2-air, open cycle laser, generated power depend. on pulse repetition freq. *(Russian)* 77—19231
CO_2-air binary mixtures, flowing, probe for conc. meas. 79—4098
CO_2-Ar, thermal diffusion factors meas. 80—10344
CO_2-Ar atmosphere melting plasmatron arc characts. *(Russian)* 80—38573
CO_2-Ar mixture, Ar* prod. by electron excitation, transfer reaction kinetic study 80—63824
CO_2-Ar solution, diffusion near crit. point in solns. with large conc. gradients in capillary *(Russian)* 77—84958
CO_2-Ar(He), natural diffusion coeffs., press. effects 78—26229
CO_2-Ar(He), stepwise pulsed photoionisation 77—50479
CO_2-Br laser, pulsed, electron-vibr. energy exchange from Br* 78—29930
CO_2-Br_2-He mixture, possible gas lasers with solar excitation 80—99695
CO_2-CO, He free TE laser, variable pulse length. operational characts. 78—22151
CO_2-CO laser, optical transfer, saturation behaviour and tunability *(German)* 77—23650
CO_2-CO-N_2-He in CO_2 lasers, ionisation wave, slow changes, dispersion curves 80—38822
CO_2-Cs-He discharge, CO_2+Cs reaction rate meas. by IR absorption, press. depend. 78—44367
CO_2-DF-He CW optically reson. pumped transfer laser 77—75471
CO_2-ethane(propane)(n-butane) mixtures, viscosity, diffusion coeffs. 80—1722
CO_2-ethylene gaseous mixture, thermoosmotic conc. difference across membranes 79—83508
CO_2-F_2-Ar mixture, vibr. relax. in shock wave, 4.3 μm radn. 78—1062
CO_2-gas dynamic laser, combustion-type, effect of residual CO on performance 79—68378
CO_2-H halide, pulsed chem. transfer lasers, book contrib. 77—10906
CO_2-H_2 turbulent flow heat transfer, expt. and numerical anal. 78—94690
CO_2-H_2-He 10.6 μm scan laser with programmable VO_2 mirror 80—38026
CO_2-H_2O, IR radiation transfer 79—80028
CO_2-H_2O-O_2, gas mixture, photodetachment and photodissoc., mass spectra meas. 77—500
CO_2-H_2O-peridotite system, phase relationships, rel. to planetary mantles 78—77506
CO_2-$H_2O(D_2O)$-mineral oils, radiolysis products form. in nucl. reactor 78—689
CO_2-He, binary diffusion coeffs., press. depend., 300 and 323K, Thorne's eqn. 80—1724
CO_2-He, species concentrations in glow discharge and afterglow, mass spectra, laser conditions 78—14241
CO_2-He UV photopreionisation TEA laser, role of He excited atoms 78—17902
CO_2-he volume discharge, electron recombination and attachment 77—19799
CO_2-He-Cs glow discharge, quenching cross section of resonant Cs(6P) state by CO_2 mols. 80—43860
CO_2-He-N_2, absorpt. coeff. for 10.6 μm CO_2 laser radiation, 295 to 650 K 80—92252
CO_2-He-N_2, gas dynamic laser, gain coeff. numerical estimates, book contrib. 80—1183
CO_2-hydrocarbon mixture, phase equilibria and critical phenomena at high press. 78—51648
CO_2-hydrocarbon mixtures, phase equilib. calcs., modified Soave eqn. of state 79—19353
CO_2-methane, shock wave refr. at slow-fast gas interface 79—32573
CO_2-methane reforming-methanation cycle for Solchem thermochemical solar energy transport 80—94096
CO_2-N_2, CW gasdynamic laser, qualitative comparison with N_2O-N_2 laser 78—25856
CO_2-N_2, CW mixing gasdynamic laser, saturation parameter and small signal gain 79—45923
CO_2-N_2, gasdynamic laser mixture, vibr.-nonequilib. nozzle flows, numerical and approx. solns. 78—74881
CO_2-N_2, gasdynamic laser, gain-optimisation, theory 79—76664
CO_2-N_2, gasdynamic laser, theoretical gain-optimisation, parametric study 79—76665
CO_2-N_2, gasdynamic mixing laser, performance for various injection techniques 77—38917
CO_2-N_2, glow discharge instability, non self sustained ionisation source, mechanism 80—38819
CO_2-N_2, high temperature gas diagnostics by spectral remote sensing, 700-1350K 78—74002

carbon compounds continued
CO_2-N_2, highly efficient gas for nanosecond pulse CO_2 laser system *(Japanese)* 80—48214
CO_2-N_2, hot gas mixture, spectral and integral emission capacities calcs. *(Russian)* 77—68054
CO_2-N_2, ionisation current growth, Townsend swarm coeffs. 78—59541
CO_2-N_2, kinetic cooling effect by CO_2 laser radiation, temp. dependence 80—10347
CO_2-N_2, non self sustained repetitively pulsed discharge instability obs. 80—38820
CO_2-N_2 electroionisation laser mixture, ionisation instability of semi self maintaining discharge 80—63971
CO_2-N_2 fast-flow laser with unstable resonator, self-oscillation instability 80—95870
CO_2-N_2 gas mixture, kinetic cooling by CO_2 laser radiation *(Russian)* 77—89229
CO_2-N_2 gasdynamic laser, amplification coeff. rel. to water vapour content *(Russian)* 77—7057
CO_2-N_2 gasdynamic laser, thermal nonequilibrium heating of active medium by elec. arc 80—53258
CO_2-N_2 laser, high-pressure, numerical optimisation 77—10882
CO_2-N_2 laser mixture, electron drift vels., time-of-flight meas. 80—28855
CO_2-N_2 mixture, strongly excited, vibr. relax. 80—102555
CO_2-N_2 mixture, temperature measurement by spectrum line reversal 80—73358
CO_2-N_2 mixture gasdynamic laser, energy characts. 80—69362
CO_2-N_2-^3He, laser, plasma diagnostics of media capable of lasing in nucl. reactor environment 79—10279
CO_2-N_2-^3He laser, nonautonomous continuous discharge due to thermal neutrons from reactor 78—29929
CO_2-N_2-^3He laser mixture, excitation in externally maintained discharge in reactor core 80—28193
CO_2-N_2-H, laser discharge circuit parameters, effect on energy imput mode 77—75476
CO_2-N_2-H_2, non-self-maintained glow discharges at atm. pressure, elec. characteristics and energy exchange 78—71606
CO_2-N_2-H_2 electron beam controlled laser, efficiency and output energy depend. on H_2 78—58978
CO_2-N_2-H_2O fast flow discharge laser, output power time depend. 80—99697
CO_2-N_2-H_2O gas mixture, oscillatory nonequilib. in planar supersonic nozzle flow 78—1758
CO_2-N_2-H_2O gasdynamic laser, water vapour condensation and mol. relax. processes 79—13946
CO_2-N_2-H_2O gasdynamic laser, nonequilib. flow calc. by relaxation formula *(Chinese)* 79—31853
CO_2-N_2-H_2O gasdynamic laser, small signal gain and vibr. wall accomm. 79—98340
CO_2-N_2-H_2O mixture, unstable-oscillatory expansion *(Russian)* 78—1637
CO_2-N_2-He, coefficient of optical amplification behind an axisymmetric shock wave *(Russian)* 77—89153
CO_2-N_2-He, discharge ionisation growth, diffusion coeffs. 78—83636
CO_2-N_2-He, gasdynamic laser utilizing selective thermal excitation and supersonic mixing, numerical analysis 79—64202
CO_2-N_2-He, non-self-sustained plasma discharge instability, electron collisions *(Russian)* 77—76050
CO_2-N_2-He, pulse-periodic operation of electron-beam-controlled discharges, energy characts. changes 80—102695
CO_2-N_2-He, pulsed discharge with temp. and density gradient in cathode sheath 79—41899
CO_2-N_2-He, transverse combined discharge laser, 10-20 kW *(Russian)* 77—54703
CO_2-N_2-He, vol. discharge, negative ions effect 80—14956
CO_2-N_2-He, vol. discharge with UV preionisation by capillary discharge, ionis. pots. depend. 80—44065
CO_2-N_2-He (H_2O) gas mixture, method for obtaining vibrational population inversion 79—94210
CO_2-N_2-He CW gasdynamic laser, closed-cycle, construction and operating parameters 80—23717
CO_2-N_2-He discharge, voltage drop, impedance 77—47291
CO_2-N_2-He discharge, energy balance, influence of N_2 rot. level reson. excitation 78—17903
CO_2-N_2-He discharge, electron distrib. relax., numerical study 80—54070
CO_2-N_2-He electroionisation laser, freq. mode, lasing conditions 80—63970
CO_2-N_2-He flowing gas mixture, glow discharge produced population inversion 78—78992
CO_2-N_2-He gas mixtures, fluorescent IR radiation from glow discharge 78—94386
CO_2-N_2-He gas mixtures, time-of-flight meas. of electron transport parameters 78—94387
CO_2-N_2-He gasdynamic laser, effect of weak flow perturbations on gain 80—14316
CO_2-N_2-He laser, civr. temp. approx. for N_2, applicability limit 78—5452
CO_2-N_2-He laser, pulsed microwave discharge pump, skin effect and gain 79—13945
CO_2-N_2-He laser, vibr. population distrib. of N_2, vibr. temp. determ. 77—14688
CO_2-N_2-He laser media excitation by electron beams admitted through gasdynamic windows 80—99694
CO_2-N_2-He laser mixtures, self-sustained glow discharges, low ionisation pot. organic additives effects *(French)* 77—88694
CO_2-N_2-He laser mixtures, electron swarm parameters, Boltzmann eqn. anal. 79—18396
CO_2-N_2-He laser mixture in nonself-sustained discharge, direct heating mechanism 80—28195
CO_2-N_2-He mixture, ionisation and attachment coefficients 78—42706
CO_2-N_2-He mixture in gas-dynamic system with independent thermal excitation, population inversion in two-step mixing 79—89888
CO_2-N_2-He mixture supersonic adiabatic expansion, population inversion and gain 80—19017
CO_2-N_2-He mixture volumetric glow discharge formation at atm. pressure 78—71615
CO_2-N_2-He nozzle flows with boundary layer, gain coefficients 80—14312
CO_2-N_2-He pulsed transverse discharge, investigation of gain 80—9855
CO_2-N_2-He self-sustained TEA discharge laser, config. for high beam qualtiy 77—14753

carbon compounds continued

CO_2-N_2-He system, CO_2 TEA laser discharge development, high-speed-camera investigation 79—55109

CO_2-N_2-He volume discharge, self-sustained, with UV preionis. 79—60211

CO_2-N_2-He-CO, electron diffusion perpendicular to elec. field, second order theory 80—43322

CO_2-N_2-He-CO gas laser mixture, electron motion anal. 79—64199

CO_2-N_2-He-O_2 discharge mixture, three body electron attachment to O_2 80—64779

CO_2-N_2-He(H_2) laser mixtures, composition effect on excitation efficiency in dicharge 78—5453

CO_2-N_2-Ne-H_2O mixture IR laser *(Russian)* 79—10323

CO_2-N_2-O_2 mixtures, thermalisation under reson. excitation by laser radiation *(Russian)* 78—26231

CO_2-N_2O, laser optical pumping in 4.3 μ band 77—7060

CO_2-N_2O, mixed cryst., librational motion, Raman obs. 78—6661

CO_2-n-butane, freejet flow, vibr. relax. time 79—98760

CO_2-O_2, negative ion form., photodissoc., mass spectrometric obs. 78—13558

CO_2-O_2, O_2 electron attachment coeff. meas., O_2 partial press. depend. *(German)* 79—13821

CO_2-O_2-H_2O, mixture, mol. negative ions, photodissoc. and photodetachment cross section 77—27129

CO_2-O_2-H_2O, photodissoc. and photodetachment of negative ions 80—14182

CO_2-O_2^- radical, on MgO surface, ESR spectrum, mobility effects 80—43076

CO_2-O_3 coupling in Cl free stratosphere, photochemical-radiative column model 80—85723

CO_2-O_3 stratosphere coupling, photochemical radiative column model with Cl chemistry 80—85724

CO_2-polar component binary mixtures, up to 1000 bar, phase separation, critical phenomena 77—35695

CO_2-propane, freejet flow, vibr. relax. time 79—98760

CO_2-propane system, radiolysis by fission fragments, CO form., G-values 77—48657

CO_2-SF_6, AC particle initiated breakdown, compressed gas mixture 78—87556

CO_2-SF_6(O_2)(CF_4) mixtures, viscosity and diffusion coeffs. 77—89225

CO_2-soot-water vap. mixture, in luminous flames and smoke, IR mean absorption coeffs. calc. procedure 78—91061

CO_2-T_2-F_2 chemical laser using energy transfer from TF to CO_2 77—58322

CO_2-TF, chem. laser, rate const. of energy transfer from TF($\nu=1$) to $CO_2(00^\circ0)$ 77—675

CO_2-type cryst., transl.-vibr. absorpt., hexadecapole moment effects 77—90134

CO_2-water, saturated two phase flow system, non-equilib. state transient process 80—59096

CO_2-water vapour mixtures, 2.7 micron band absorption, 1000 to 2200K, 0.25 to 3 atm. 77—58006

CO_2-water vapour slug flow, radiative and convective transfer interaction 77—58529

CO_2-Xe laser, sealed-off, high efficiency, low impedance 77—3614

CO_2^+-D_2, DCO_2^+ and DCO^+ formation 77—60056

CO_2+ perfluoroalkyl halides, collisional relax. 79—13799

CO_2+Ar, drift properties of tubular drift chambers in high magnetic fields 80—53917

CO_2+Ar, press. broadening, rot. energy transfer, infinite order sudden approx. 78—22011

CO_2+Ar, rot. inelastic wide angle scatt., differential cross sections 77—14536

CO_2+Ar, rot. line width of vibr. bands 78—33552

CO_2+Ar, short-range intermol. pots., combined interatomic pots. calcs. 80—87198

CO_2+Ar, total differential scatt., IOS approx. calcs. 79—98194

CO_2+Ar^+, reaction kinetics, mass spectrometer with selective introduction drift tube *(French)* 79—11839

CO_2+Ar^+(He^+)(Ne^+), charge transfer, thermal energy, product distrib. obs. 78—25656

CO_2+Ar^{12+}, C K-shell Auger effect 77—6908

CO_2+Ar(N_2), 301_{III}-000 band, intensities, press.- and self-broadening coeffs. meas. 78—78695

CO_2+B, gas phase rate consts., 300K, at. absorption obs. 79—83445

CO_2+Ba, crossed beam kinetics, BaO recoil velocity spectra 80—76500

CO_2+BaO, in Ar flame, rot. and translational relax. by sub-Doppler optical-optical double reson. 80—95583

CO_2+Br, quenching of $4^2P_{1/2}$ state, vib. excitation, temp. depend. 78—58792

CO_2+Br_2 mixture, Raman laser optical excitation, electron phototransition theory *(Russian)* 80—99711

CO_2+Br , total electron detachment cross sections for energies around threshold 80—99550

CO_2+Br($4^2P_{1/2}$), electronic to vibrational energy transfer rates 78—29839

CO_2+C Boudouard reaction, catalysed by Li_2O and Li_2CO_3, reaction rates 839-1050°C 79—16035

CO_2+C_2H_4O, quad. moment eval. from rot. line broadening 80—28065

CO_2+C^-(O^-)(F^-)(Cl^-), negative ion stripping, at. beam form. 77—6926

CO_2+C^{+*}, charge transfer cross-sections, 0.7-2.4 keV, $C^+(^2P)$ and $C^+(^4P)$ 78—58806

CO_2+C^+(N_2H^+), rate coeffs. meas. at 300 and 100K in flowing afterglow 79—20346

CO_2+CO, bending mode excitation 77—10738

CO_2+CO, line broadening, short range force effects, semiclassical calcs. 79—98085

CO_2+CO, vibr. level depend. quenching of CO(ν=1-16) 80—32808

CO_2+CO_2(N_2), IR spectral absorpt. induced by press. in atmos. *(Russian)* 80—56600

CO_2+CO_2(N_2)(LiH)(H_2)(H_2), intermol. forces, multipole results validity, charge overlap effects 79—89730

CO_2+COS mixture, Raman laser optical excitation, electron phototransition theory *(Russian)* 80—99711

CO_2+CO(Ar), bending vibr. mode deactivation rate meas., 150 to 1500K 77—10738

CO_2+CO(N_2), vibr. relax., optoacoustic obs. *(French)* 78—42178

CO_2+Ca, CaO form., product states obs. 78—92450

CO_2+Ca, reaction, electronic branching, statistical and dynamical influences 78—92451

carbon compounds continued

CO_2+Cd($^3P_{0,1}$), absolute quenching cross section, phase-shift method 80—58340

CO_2+Cl^-, total electron detachment cross sections for energies around threshold 80—99550

CO_2+CsF, rot. inelastic collisions, mol. beam meas. 80—1049

CO_2+D_2, near reson. V-V exchange 77—27165

CO_2+DF, vibr. relax., laser-induced fluoresc. obs. 79—64028

CO_2+deuteromethane, time resolved fluoresc. for vibr. relax 79—31659

CO_2+e, momentum transfer cross sections, effect of non-spherical short range interactions 80—9745

CO_2+ethane system, isothermal vapour-liq. equilibrium data, 10 to 25°C and high press., critical points 78—79754

CO_2+formaldehyde, cross sections meas. *(French)* 79—76487

CO_2+H_2, (oriented), total collision cross-sections, anisotropic pot. parameters calcs. 78—13568

CO_2+H_2, exponential gap relation, rot. inelasticity 80—78693

CO_2+H_2, rot. transfer, ab initio intermol. pot. energy surface 80—58354

CO_2+H_2, V-V transfer, pulsed fluoresc. obs. 77—14540

CO_2+H_2, vibr. de-excitation of $CO_2^*(\nu_3)$, 200K 79—45802

CO_2+H_2, vibr. relax. rate, stimulated Raman scatt. obs. 77—75269

CO_2+H_2O, collision broadened H_2O absorpt. line, laser radiation intensity effects 77—83661

CO_2+H_2O, photoassisted reaction on $SrTiO_3$ (111) face, methane form. 78—76878

CO_2+H_2O, pressure-temp. curves under conditions of New Zealand geothermal field 77—51488

CO_2+H_2(CO_2)(Ne)(NH_3)(CH_3F), rot. transfer collisions, momentum transfer distributions 77—523

CO_2+H_2(D_2), ab initio LCAO-MO-SCF intermolecular pot. energy surface, V→T transfer 77—50489

CO_2+H^+, electron capture into n=3 states, 2.2-8.2 keV 79—50129

CO_2+H^+, vibr. excitation in differential scatt. 77—50503

CO_2+H^+(D^+), vibr. excitation, 10-30 meV 80—58358

CO_2+H^+(D^+), vibr. excitation, isotope and time effects 80—63773

CO_2+HBr, rate consts. for vibr. energy transfer meas. using laser. induced fluorescence technique 80—87206

CO_2+HBr, V-V energy transfer, 300-900K 79—59539

CO_2+HCN (001), relax. rate consts., using Cs vap. IR source 80—9696

CO_2+HCl, vibr. relax., 300-900K, by laser fluoresc. 79—31658

CO_2+HCl, vibr. relax. rate, chemiluminesc. depletion method meas. 79—72400

CO_2+HCl collisions, semi-empirical non-Lorentzian line shape determ. 77—34699

CO_2+HF, HF(v=3) relax. and rate consts. 80—61069

CO_2+HF, vibr. relax. , laser fluoresc. obs. 77—14484

CO_2+HF, vibr. relax. dye laser pumping effects 80—9703

CO_2+HF, vibr. relax. laser induced fluoresc. obs. 79—64037

CO_2+HF, vibr. relax. of HF (ν=3,4) 79—50117

CO_2+HF(DF), vibr. relax. rate, chemiluminescence depletion method meas. 79—72399

CO_2+H+Xe plasma, elec. parameters, Xe effects *(Russian)* 77—84507

CO_2+He, anisotropic intermol. pot. for differential scatt. cross-section 79—13788

CO_2+He, collinear atom-triatom transition probabilities for anharmonic triatom pots., quantum mech. calcs. 80—83455

CO_2+He, collisionally excited neutral and ionic emission, flowing afterglow 77—51248

CO_2+He, Penning ionisation of target mol., for He(2^3S) 79—41228

CO_2+He, rot. and vibr. inelastic scatt., rot. IOS approx. calcs. 78—46433

CO_2+He, rot. inelastic, moments of final state distrib., direct method 78—33562

CO_2+He, rot. inelastic collision, ab initio SCF, electron gas and pot. energy surfaces 80—83468

CO_2+He, rot. transition classical integral cross section, surprisal predictions 77—54594

CO_2+He, translational-vibrational energy transfer, quantum dynamical study 80—63746

CO_2+He^+, 0.7-2 MeV, charge-changing collisions, electron capture 80—58372

CO_2+He^+, dissociative charge exchange kinematics 80—3318

CO_2+He^+(Ar^+)(Ne^+)(Kr^+), electronically excited CO_2^+, $A^2\pi_u$ state bending vibrs. 77—3454

CO_2+He^+(H_2^+), charge transfer, energy transfer, product ion excitation and fluoresc. 77—75288

CO_2+He(Ar), dipole and Raman line press. broadening temp. depend. 79—68265

CO_2+He(Ar), repulsive pot. energy surface, approx. calc. and differential scatt. expt., comparison 79—22788

CO_2+He(Ar), rot. relax. rates and cross sections 79—848

CO_2+He(Ne)(Ar) Penning ionisation, electron spectra, vibr. transfer 77—14555

CO_2+hydrocarbon in mixtures, vibr. energy transfer, laser induced fluoresc. obs. 78—58731

CO_2+hydrocarbon mixtures, vapour-liq. equilibrium, crit. locus curve, Soave eqn. 78—83913

CO_2+I_2(B^3Pi_{0u}+), collisional energy transfer, quenching effects 80—14193

CO_2+inert gas, intramol. energy transfer, 153-393K, photoacoustic obs. 79—54943

CO_2+inert gas, reactant decomp., rot.-vibr. energy transfer, relax. analytic soln. 80—55650

CO_2+inert gas, vibr. and rot. energy transfer, quasiclassical trajectory study 78—33578

CO_2+Kr, collision dynamics, generalised Langevin eqn. approach 78—70900

CO_2+Kr, collisional energy transfer, anharmonicity effects 80—28097

CO_2+Kr, vibr. energy transfer rate, anharmonicity, quasi-classical calc. 78—46431

CO_2+Kr 80—83455

CO_2+Kr(Xe), ^{13}C-mag. shielding density depend. 78—9173

CO_2+Li^+, collisional excitation, quasiclassical trajectory calcs. 80—83467

CO_2+Li^+, rot. vibr. energy transfer, 1 to 10 eV, many body theory 80—28093

CO_2+methyl cation, ternary assoc. reaction, rate coeffs., 100-300K 79—61845

CO_2+monobromomethane mixture, Raman laser optical excitation, electron phototransition theory *(Russian)* 80—99711

CO_2+N_2, energy transfer, semiclassical calc. 79—86042

carbon compounds continued
CO_2+N_2, ionis. at low energy 78–58791
CO_2+N_2, near IR absorpt., collisional broadening 77–30872
CO_2+N_2, semiclassical energy transfer method, Coriolis coupling 78–90266
CO_2+N_2, vibr. energy transfer, time-resolved laser induced fluorescence 78–29842
CO_2+N_2O, vibr. energy transfer, relax. times 79–72401
CO_2+N_2+He, glow discharge positive ion species identification *(Russian)* 80–84014
CO_2+N_2+benzene, electronically excited, mol. fluoresc., vibr. relax. cross sections and equilibration rates determ. 80–87205
$CO_2+N_2(CO)$, CO_2 1st vibr. levels collisional deactivation, photoacoustic study 79–98187
$CO_2+N_4^+$, reaction rate determ. 78–60985
CO_2+N^+, charge exchange, 1-3 keV, $N^+(^3P)$ and (^1D) states 79–36760
CO_2+N^+, product distribs., rate consts., ion cyclotron reson. obs. 77–52618
CO_2+NH_3 collisional broadening of NH_3 inversion spectrum lines 80–99521
CO_2+NO, NO $\gamma(0,0)$ band, oscillator strength and line broadening 80–106356
CO_2+NO_2, continuum quenching in upper atmosphere 79–88520
CO_2+NO^+, reaction rate consts. meas. 80–7782
$CO_2+Na^*(3^2P)$, electronic to vibr.-rot. energy transfer, differential cross sections 77–38715
CO_2+Ne, energy transfer, anharmonic coupling terms, semiclassical calcs. 80–37861
CO_2+Ne, energy transfer rate consts., semiclassical method 80–91640
CO_2+Ne, fluoresc. spectra, mol. bands, 0.1 to 6 atm., 3000-8200 Å 79–3394
CO_2+Ne, intermol. pot. in repulsive short-range region, ab initio 80–69204
CO_2+Ne^+, thermal energy, reaction rate coeffs. and product distrib. 79–29333
CO_2+Ne^+, three dimens. quadrupole ion storage, ion mobility, effect of charge exchange reactions, Monte Carlo calcs. 80–55738
CO_2+Ne^{2+}, charge transfer reactions, rate coeffs. and product-ion distributions meas. 80–104431
$CO_2+O_2(N_2)$(air), bending mode vibr. deactivation rate, 1500-350K, shock tube meas. 77–38714
$CO_2+O_2(NO)$, Senftleben-Beenakker effect, saturation field, Kohler-Raum theory and obs. 80–28596
$CO_2+O_3 \rightarrow CO_2+O^- +O_2$, long-lived excited (or isomeric) state of O_3 78–5318
CO_2+O^+, in Mars thermosphere, effects of energetically produced O_2^+ on ion temps. 79–96945
$CO_2+O^+(^4S)(^2D)$, charge transfer reactions, cross-sections meas. 78–92462
$CO_2+O^{n+}(Xe^{n+})(Pb^{n+})$, 50 keV, multiple scatt., target at.+energetic ion spatial correlation influence 79–27062
CO_2+OCS, collisional line broadening of microwave spectra, semiclassical theory, calcs. 78–25516
CO_2+OCS, collisional line broadening of microwave spectra, semiclassical theory 78–29776
CO_2+OCS, gas, EPR of rot. transitions, T_1 press. depend. 80–9621
CO_2+OCS, rot. relax. parameters, microwave spectra linewidth parameters 80–28009
$CO_2+OH^- \rightarrow HCO_3^-$ react., MO-LCAO-SCF calcs., energy barrier 78–76846
$CO_2+OH^+(H_2O^+)$, reaction, ICR obs. 79–8429
$CO_2+O(^1S)$, product channels 78–46422
$CO_2+O(2^1D_2)$, collisional deactivation meas., 295K, rel. to atmospheric processes 80–16663
CO_2+p-dichlorobenzene, monochlorobenzene quantum yield in collision induced photodecomposition 79–79270
CO_2+polyatomic molecule, (00^01) mode deactivation, laser induced fluoresc. obs. 80–83453
CO_2+propyl alcohols, collisional deactivation, of CO_2 (00^01), 303-514K 78–17759
CO_2+SO_2, collisional quenching of $^3B_1$ state, 8-1300 torr 78–86906
CO_2+steam, H prod., plasmochem. cycle 80–45772
CO_2+triplet methylene, reaction rate constant determ. 77–36727
$CO_2+U^+(UO^+)$, reaction cross-sections, ion beam apparatus study 80–97691
CO_2+X^{n+}, (X=Ar,Kr,Xe,U), Auger emission line shape after dissoc. 78–86838
CO_2+Xe^{2+}, charge transfer from ground and metastable states 79–31677
$CO_2^- +O_2$, nanosec. pulse radiolysis, react. rate const. meas. 77–16843
$CO_2^+ +2CO_2 \rightleftharpoons (CO_2.CO_2)^+ +CO_2$, reaction rates 77–36745
$CO_2^+ +$ethylene, rate coeffs. and product distribution determ. 80–97693
$CO_2^+ +H_2$ (D_2), HCO^+ and DCO_2^+ form., threshold form. energy 80–50844
$CO_2^+ +H_2O$, reaction rate consts., product distrib., ICR obs. 79–8428
$CO_2^+ +H(D)$, reaction, ion cyclotron reson. mass spectrometric obs. 79–64098
$CO_2^+ +O$, in Mars thermosphere, effects of energetically produced O_2^+ on ion temps. 79–96945
$CO_2^+ +SO_3$, in mass spectroscopy of SO_3 mixtures 78–3415
$CO_2^+ +Th$, charge transfer cross-section, 1-500 eV 78–82835
$CO_2^+ +U$, charge transfer cross-section, 1-500 eV 78–82835
CO_2^+ +fluoromethanes, thermal energy charge transfer reactions mechanism 77–63889
$^{12}CO_2+Br(4^2P_{1/2})$, electronic-vibr. energy transfer, temp. depend. meas. 79–10136
$(CO_2)_2$, struct., stability, electron affinity of neutral dimer, Hartree Fock calc. 79–63912
$(CO_2)_2^+$, ion-mol. reaction product distribs. and rate coeffs. 80–50852
$(CO_2)_2^+$, photodissoc., mass spectrometric obs. 77–6867
CO_3, and isotopic forms, struct., normal coord. anal. 78–965
CO_3^-, form. by photodissociation and ion-mol. reactions in CO_2 and CO_2-O_2 mixtures 78–13558
CO_3^-, formation and dissociation in CO_2 77–60058
CO_3 , laser photodissociation, tandem quadrupole study 80–81343
CO_3 , photodissoc. cross-section, excited state vibr. mode determ. 77–6870
CO_3 , thermally relaxed, photodetachment cross-section and solar detachment rate determ. 77–58094

carbon compounds continued
CO_3^{2-} chemistry of groundwater from tropical tower karst, S.Thailand 79–79906
CO_3^{2-}, electronic struct., X-ray spectra obs. 78–55185
CO_3^{2-}, localised mol. orbitals, ab initio PRDDO SCF calc., isoelectronic struct. 78–25441
CO_3^{2-}, molecular orbital anal., anisotropic X-ray emission obs. of components 80–18786
CO_3^{2-}, X-ray fluorescence, electronic struct. determ. 78–86887
CO_4^-, form. by photodissociation and ion-mol. reactions in CO_2 and CO_2-O_2 mixtures 78–13558
$C_2O+NO(O_2)$(isobutene), absolute reaction rate consts. meas. by laser induced fluoresc. 80–93738
C_2O_3, liq., mol. conform. and orientation correlation 79–32877
C_3O_2, $3\nu_7^{1f}+\nu_2 \leftarrow 2\nu_7^0$ $4\nu_7^0+\nu_2 \leftarrow 3\nu_7^{1f}$ Q-branches, diode laser analysis 78–74660
C_3O_2, bending pot. function, vibr. depend. 80–48058
C_3O_2, CCC bending mode, two-dimens. anharmonic oscill. calcs. 77–14415
C_3O_2, far IR absorpt. spectra, 20 to 100 cm^{-1}, temp. depend. 79–59450
C_3O_2, far IR and Raman spectra, vibr. mode and quasilinear config. 78–62940
C_3O_2, IR Fourier transform spectroscopy, interaction between vibr. levels 77–75152
C_3O_2, IR spectra, P-branch of ν_6 fundamental 79–98092
C_3O_2, large amplitude bending mode, rot.-vibr. calc., assignments 77–18905
C_3O_2, liq., neutron diffraction studies at high momentum transfer 79–46525
C_3O_2, mol., pot. functions of bending modes 80–9753
C_3O_2, ν_2, $\nu_2+2\nu_7^0$ and $2\nu_7^0$ Raman band-accumulations 79–3449
C_3O_2, $\nu_2+\nu_7$ bands, Q-branch spectra, 12 μm region, l-doubling const. 77–65459
C_3O_2, $\nu_4+2\nu_7^0$ and $\nu_4+3\nu_7^1-\nu_7^1$ bands, high resolution IR spectrum 79–72311
C_3O_2, ν_7 vibrational states, rigid-bender model 80–47964
C_3O_2 polymer, as source of UV absorpt. in Venus clouds 78–20665
C_3O_2 polymers in primitive atmosphere rel. to living systems genetic code 79–83690
C_3O_2, Raman bands, vibr. assignments 79–59463
C_3O_2, semirigid bender, rot.-vibr. energy level separations obs., struct. and pot. functions determ. 80–83446
C_3O_2, vibr. IR spectra anal. 80–47984
C_3O_2, vibr.-rot. band, microwave, spectrum obs. 80–5536
CO_2(-He) discharge, UV-initiated, electron ion recomb. and CO_2 dissoc. 80–44068
CO_2(-ethane)-N_2O, gas phase thermal electron N_2O attachment mechanism, 5-120 torr 79–27085
$CO_2CO_2^+$, photodissoc. cross sections meas., 3500-8600 Å 79–24763
$CO_2^+(CO_2^{2+})$+atom(mol.), dissoc. and charge transfer 77–65532
$CO_2(CS_2)(COS)$, Penning ionisation and photoelectron spectra 77–83653
$CO_2^+(C^2\Sigma_g^+)$, formation and predissoc., photoelectron spectra 78–5300
$COCl_2$ (phosgene) in ambient air of California 77–13119
$COCl_2$, phosgene, Cl_2 nuclear quadrupole coupling tensor, microwave spectra 80–52982
$COCl_2$, photodissociation, C isotope effects, photocatalysed isotope exchange with CO 77–36764
$COCl_2$, Raman line intensities, modified CNDO/2/INDO calc. 78–25621
$COCl_2+Xe(6s,^3P_2)$, vibr. energy disposal from XCl* spectrum 79–100345
COF_2, centrifugal distortion analysis including P^6-terms 77–14413
COF_2, dipole moment from compact formulation of polar tensors on bond moment hypothesis 80–58108
COF_2, force field analysis using parametric represent. method 80–27990
COF_2, laser excited IR fluoresc. C=O and C-F stretching modes 78–21960
COF_2, soln. in liquid Ar, transition freq., halfwidths and relative intensity, IR absorpt. spectra 80–55101
COF_2+COF_2, collisionally induced relax. processes and vibr. energy transfer 80–53107
CO_2H^+, SCF CI equilib. struct. calc., CO_2 proton affinity 77–10599
COO^-, bond lengths and angles relations 80–53158
$COOCH_3$, bond lengths and angles relations 80–53158
COOH, bond lengths and angles relations 80–53158
COS, air pollution conc. meas. 77–73830
COS, asymmetry parameter, angle resolved photoelectron spectra, multiple scatt. method 80–63708
COS, density and refractive index, volumetric meas. by Burnett method 80–29707
COS, detect. in stratosphere 79–58014
COS, dissoc. photoionisation, mass spectrometric obs. 79–72366
COS, electron energy loss spectra, low-lying and triplet states 78–46454
COS, electron energy loss spectra, C K-shell excitation, vibr. struct. 79–22851
COS, high resolution UV photoelectron spectra 80–91603
COS, in stratosphere, effects on sulphate aerosol layer 80–109212
COS, mole. potential surface, evaluation from spectroscopic observations 80–43207
COS oxidation rel. to stratospheric S budget 79–84423
COS, photoionis., vibr.-excited ions form. in Franck-Condon gaps, threshold photoelectron spectra obs. 79–68262
COS, vapour pressure and critical properties 79–95149
COS^+, fluoresc. quantum yields and lifetimes, meas. method, ion form. 77–6815
COS^+, photoionis. reson. study of $(^2\Pi)$ and $(^2\Sigma^+)$ states, vibr. freqs., ionis. pot. 78–29821
$COS+Br(4^2P_{1/2})$, electronic to vibrational energy transfer rates 78–29839
$COS+CH_n^+$, (n=Q-4), reactions at 300K 78–44357
$COS+Cl^+$, reactions at room temp. 80–93749
COS+He(Ne)(Ar) Penning ionisation, electron spectra, vibr. transfer 77–14555
$COS+Ne^+$, thermal energy, reaction rate coeffs. and product distrib. 79–29333
COS+OH, reaction rate consts., 299-430K 78–35653
$COS+U^+(UO^+)$, reaction cross-sections, ion beam apparatus study 80–97691
C_3OS, vibrational assignment, calc. of normal modes and valence force consts., IR spectra 79–50014

carbon compounds continued

$CO(^1\Sigma^+)$, total X-ray scatt., two-electron density functions 78–70889
$CO(^1\Sigma^+)+O(^1D_2)$, collisional quenching, energy transfer processes 80–23501
$COX^1S^++Na(3^2P)$, electronic-vibr. energy transfer reaction 79–64084
$CO(X^1\Sigma^+)+O(^3P)$, vibr. deactivation and atom exchange, rate consts., Monte Carlo anal. 77–48627
$CO_2(X^1\Sigma_g^{\ +})+Ar^*(^3P)$, differential elastic and quenching cross-sections 78–58773
$CO_2(X^1\Sigma_g^{\ +})+Ar^*(^3P)$, T-R and T-V energy transfer, collisional energy depend. 79–18262
$CO_2(00^01)+H_2(D_2)$, intramol. vibr.-vibr. transfer cross sections calc. 100-3000K 78–1053
$CO_2(01^10)+N_2(CO)(O_2)$, collisional deactivation rate const., 160-375K, photoacoustic obs. 79–10179
CO^* prod. from Ar^*+CO_2, use in laser systems 80–63824
CO^*, $X^1\Sigma^+$ state, dipole moment functions calc. 77–65429
$CO_2^*+SO_2$, near-reson. energy transfer, fluoresc. obs. 80–106348
$CO_2^*(\nu_3)$ fluoresc. obs. of $N_2^*+H_2O(H_2S)$(methane) deactivation 80–63776
$CO_2^*(\nu_3)+H_2O(H_2S)$(methane), deactivation 80–63776
$CO(1)+CO(\nu)\rightarrow CO(0)+CO(\nu+1)$, vibr. energy accumulation, reaction rate anal. 80–78692
$CO^+.CO$, lateral diffusion in CO, mass spectra meas. 78–91055
$(CO_2.CO_2)^++CO\rightarrow(CO_2.CO)^++CO_2$, reaction rates 77–36745
$CO_2.CO_2^{\ +}$+ethylene, rate coeffs. and product distribution determ., dissoc. energy and heat of form. 80–97693
$CO_2.CO_2^{\ +}+SO_2$, reaction rate coeff. and product distrib. 80–3305
CP^+, pot. curves, ab initio MRD-CI method 80–83293
CS, $A\ ^1\pi$ state, collisional transfer and radiative decay, time resolved obs. 79–89809
CS, $A^1\Pi(\nu=0)$, radiative lifetimes and quenching rates, laser-induced fluoresc. obs. 79–59496
CS, as origin of 3.9 micron absorpt. band in C stars 78–93231
CS, CS^+, emission band systems after $He(2^3S)+CS_2$ reaction 77–14473
CS, collisional excitation of interstellar molecule 78–81664
CS, core pseudopot. valence electron calc., orbital energy and bond length 79–72233
CS, dissoc. energy by photodissociative ionisation study of CS_2 79–94044
CS emission in W3 H II region, LF obs. 80–82446
CS, heat of form calc. 80–102581
CS, interstellar, numerical solns. to radiative transfer and statistical equilib. eqns. 78–12319
CS, isotopic variants, IR absorpt. spectra, vibr.-rot. transitions 79–45720
CS, isotopic variants, IR absorpt. spectra, $\nu=2\leftarrow1$ hot band 79–45721
CS J=1-0 transition at 49 GHz in southern molecular clouds 78–65674
CS molecule, calc. of HeI photoelectron spectrum, ionisation pot., vibr. struct. 77–3415
CS, near UV spectra, rot. anal. of $a^3\pi_r=X^1\Sigma^+$ transition 78–5242
CS, nonexponential decay of $a^3\Pi$-$X^1\Sigma^+$ luminesc., Π sublevel radiative lifetimes, matrix isolated spin-orbit 79–89699
CS, perturbation parameters between valence states 77–26975
CS, population inversion mechanism for rot. levels, interstellar medium appl. 79–21406
CS, presence or absence in solar atm., theory 78–69765
CS, prompt emission and internal energy distrib. of $X^1\Sigma^+$ state 80–106364
CS, rotation analysis of $d^3\Delta_i$-$a^3\Pi_r$ transition, IR spectra 80–78591
CS, rotational-level populations of interstellar molecule 79–97054
CS, S isotopic composition, spectroscopic meas. *(Russian)* 80–91696
CS, spin-orbit and spin-spin parameter calcs. 77–27044
CS, thermochem. generation for CO lasers 77–23666
CS, thermochemical generation for CO chem. laser 77–68207
CS, turbulent cores in giant molecular clouds 80–51822
CS, ultraviolet vibronic spectra, for ^{34}S isotopic anal. *(Russian)* 79–50041
CS, vibr. states in RF discharge plasma, microwave spectrosc. obs. 80–14133
CS, vibr. struct. calcs. from photoelectron spectra 77–18973
CS, $X^1\Sigma^+$ ground state, diagrammatic perturbation theory calcs. 78–29737
CS^+, red emission spectrum, rot. anal. and perturbation effects 78–55193
$^{12}C^{32}S$, $(^{12}C^{34}S)$, IR spectra, 2-0 vibr.-rot. bands, spectroscopic consts. 77–75153
CS/O_2 as fuel/oxidizer, chain reaction operation of high efficiency CO chem. laser 80–23678
$CS+H_2$, rot. excitation, classical and quantum calcs. 78–1059
$CS+H_2$, rot.-translational energy transfer, nonlinear vs. linear rotors, surprisal anal. 79–76492
$CS+H_2$, scattering cross-sections, factorisation and fitting, IOS approx. 78–33575
$CS+He$, $CS(A^1\Pi)$ vibr. relax. 80–53106
$CS+He$, Penning ionisation, $CS^+(B^2\Sigma^+\rightarrow A^2\Pi_i)$ fluoresc., flowing afterglow 80–14197
$CS+O\rightarrow CO+S$, rate const. temp. depend., ESR-mass spectrometer obs. 78–20013
$CS+O\rightarrow CO+S$, shock tube reaction, chemiluminescence and lasing 77–16824
CS_2, $^3A_2$ state, triplet bands, MCD spectrum, near UV absorpt. spectrum 80–48010
CS_2, $^3A_2$-state, MCD and UV spectrum, theoretical anal. 80–48011
CS_2, 193 nm laser dissoc., prompt emission and internal energy distrib. of CS 80–106364
CS_2, $\bar{a}^3A_2$-state detect. by reson. enhanced multiphoton ionis. spectrosc. 80–95551
CS_2, absorpt. spectra, Rydberg series converging to $A^2\Pi_u$ states of $CS_2^{\ +}$ 78–90182
CS_2, adsorpt. on Ti(Ta)(Nb) evaporated films, 195 to 473K 79–33197
CS_2, aerosol form. by laser, kinetics study and photoreaction products chem. nature study 80–21324
CS_2, air pollution conc. meas. 77–73830
CS_2, amplified phase-conjugate refl. and optical parametric oscill., 4-wave mixing obs. 78–74946
CS_2, ang. distrib. of stimulated Raman scatt. 78–83039
CS_2, anti-Stokes stimulated Raman scatt., anomalous behaviour 77–50723
CS_2, as candidate for 3150 Å Venus band 79–40108

carbon compounds continued

CS_2, asymmetry parameter, angle resolved photoelectron spectra, multiple scatt. method 80–63708
CS_2 binary liquid mixtures with acetonitrile, nitromethane and acetic anhydride, crit. behaviour of elec. resist. 78–6422
CS_2 bond distribution functions, anharmonicity effects on electron diffr pattern 80–69234
CS_2, CARS with counterpropagating beams, three-laser phase matching geometry 79–72626
CS_2, COS, atmospheric, oxidation as SO_2 sources 80–4085
CS_2, coherent Brillouin spectrum, Raman induced Kerr effect, acoustic phonon excitation study 79–59754
CS_2, coherent Raman scattering with three lasers 79–23016
CS_2, condensation vibr. shift, intermol. interaction, vap. press. isotope effect 77–61742
CS_2, crystalline, far IR spectra 77–24834
CS_2, dissoc. photoionisation, mass spectrometric obs. 79–72366
CS_2, electron elastic scatt., 0 to 100 eV 80–23547
CS_2, electron energy loss spectra, low-lying and triplet states 78–46454
CS_2, electron impact excitation of low-lying electronic states 79–10215
CS_2, electron impact excitation and ionisation 80–63837
CS_2, electronic autoionisation branching 80–91614
CS_2, electronic transitions, solid phase UV spectra 77–3380
CS_2, emulsion theory, appl. to the permittivity of nonpolar dielectrics *(French)* 78–39497
CS_2 filled waveguide, time-reversed wave generation by nonlinear refraction 78–90447
CS_2, fluoresc. from third excited singlet state 79–22749
CS_2, fluorescence due to laser excitation, Hanle effect 78–25628
CS_2, fundamental vibr. bands in liq. phase 79–54856
CS_2 gas binary diffusion coeff. obs. in H_2, He, N_2, air and Ar *(Japanese)* 79–10627
CS_2 gasdynamic laser, increased efficiency 77–27283
CS_2, high resolution UV photoelectron spectra 80–91603
CS_2, high resolution X-ray emission, valence electron struct. and chemical bonding 79–31545
CS_2, high-power tunable laser for 9 to 12.5 μm range 77–83884
CS_2, IR spectra, $\nu_1+2\nu_2^{\ 0}+\nu_3$ band *(French)* 79–41162
CS_2, in alkane soln., ^{33}S NMR linewidth for mol. correl. times 79–95661
CS_2, in Ar, medium perturbations of extravalence excitations, VUV absorpt. 78–1002
CS_2 in benzene, third-order nonlinear susceptibility ratio by CARS 78–46713
CS_2, in CCl_4, orientational fluctuations, depolarised Rayleigh relax. time obs., temp. and conc. depends. 79–4809
CS_2, in carbon tetrachloride soln., Raman scatt. 79–65850
CS_2 in cooled supersonic expansion, electronic absorpt. spectra obs. 80–78629
CS_2, in external transverse resonator, Rayleigh wing stimulated scatt. line, anomalous shift 78–13763
CS_2, in liquid binary mixtures of optically anisotropic molecules, depolarized Rayleigh scatt. 80–40122
CS_2, intensity dependent total refl., ps pulses 77–14781
CS_2, ionisation and fragmentation by monoenergetic electron impact, mass spectrometric study 80–102581
CS_2, isotopic variants, $2\nu_1+\nu_3$ band IR spectra, rot. and rovibr. consts. 79–41166
CS_2 Kerr liquid filled nonlinear Fabry-Perot 79–27316
CS_2 laser, for 16 μm range, review *(Rumanian)* 80–87408
CS_2, laser excited fluoresc., time and freq. resolution, assignments 77–14476
CS_2, laser fluoresc., discrete and continuum, time and freq. resolved obs. 79–41195
CS_2, laser transition, rel. dipole strengths calcs. 77–61937
CS_2, lattice dynamics of 0K cryst., phonons and lattice energy 79–73269
CS_2, liq., ^{33}S NQR, quadrupole coupling const. from linewidth data 78–91985
CS_2, liq., diamagnetism, mass mag. suscept. meas., temp. depend. 80–97054
CS_2, liq., electronic optical Kerr effect, subpicosec. optical gating 79–46548
CS_2, liq., Kerr effect in UV region, mol. optical anisotropy dispersion 78–72488
CS_2, liq., light scatt. intensities, struct. models 78–60476
CS_2, liq., props. from allowed light scatt. spectra 80–25364
CS_2, liq., ratio of Brillouin to total light scatt. intensity 78–52515
CS_2, liq., S partial struct. factor, 20°C, from X-ray and neutron diffr. data 77–80407
CS_2, liq., struct. and equilib. optical props. 80–45026
CS_2, liq., time-reversed replica generation of image-bearing optical beam 80–69459
CS_2, liq., two-photon absorpt. meas., using nonlinear light-mixing spectroscopy 77–79620
CS_2, liq., vap. press., isotope effects, mass spectrometric determ. 77 24412
CS_2, liq., wavefront restoration during stimulated Brillouin scatt. 78–18013
CS_2, liq. phase vibr. spectra, anharmonicity effects 79–50022
CS_2, liq. struct., mol. dynamics simulation 79–77488
CS_2, liq. struct. factor determ. rel. to short-range correlations 77–1060
CS_2, liquefied gas solns. bound exciton model for Rydberg bands 78–31214
CS_2, liquid, light field reconstruction accuracy after stimulated scatt. 80–78911
CS_2, liquid, Raman spectra, effects of intermolecular forces 79–41177
CS_2 liquid, Rayleigh and Raman bands, intensities of interaction induced components 80–63645
CS_2 liquid for efficient IR AC Kerr switches 80–19078
CS_2, mag. quenching of fluoresc. 79–31582
CS_2, magnetic quenching, enhancement of radiationless decay, direct and indirect mechanisms 77–42345
CS_2, matrix isolated Raman and IR spectra, fundamental freqs., isotope effects 77–88457
CS_2, measurement of Kerr electro-optical effect, 170 to 300K 80–52199
CS_2, mol. quadrupole moments, mag. shielding and spin-rot. tensors 79–22609
CS_2 molecular fluid, hard-core triatomic, Monte Carlo simulations 80–38880
CS_2, non-polar liq., microwave induced Kerr effect meas. 78–76435

carbon compounds continued
- CS_2, ν_2 bending fundamental, high resolution IR spectrum 80—91559
- CS_2, ν_3 band, dipole moment correl. function, isotope splitting and band contour 78—74650
- CS_2, optical Kerr const., electronic and orientational contribs., obs. by coherent Raman techniques 77—88874
- CS_2 optical shutter, time resolution, group velocity dispersion and beam geom. effects 77—58452
- CS_2, orientational correlation parameter for liquid 79—73090
- CS_2 oxidation rel. to stratospheric S budget 79—84423
- CS_2, phase conjugate mirror for optical resonator 80—14392
- CS_2, phase conjugated wavefronts by stimulated Brillouin and Raman scatt. 80—5791
- CS_2, photodissoc., fragment energy distrib. 80—69200
- CS_2, photodissoc. below 1600 Å, $CS(a^3\Pi)$ production, quantum yield, rate const. 77—48658
- CS_2, photoelectron ang. distrib. asymmetry parameter for 30.4 nm photons 79—98151
- CS_2, photoelectron spectra (He II), Green's function anal. 79—27031
- CS_2, photoelectron spectrum, spin-orbit splitting, excited state form. 80—43102
- CS_2, photoionis., vibr.-excited ions form. in Franck-Condon gaps, threshold photoelectron spectra obs. 79—68262
- CS_2, photoionisation and dissociative ionisation due to 60-129 nm light, mass spectra study 79—94044
- CS_2, precursor for atm. COS 79—53490
- CS_2, proton affinity, cluster ion stability, mass spectrometer obs., appl. Martian ionosphere 77—77760
- CS_2, pulse-sequenced CARS spectroscopy 80—53375
- CS_2, $\pi\pi^*$ and Rydberg bands, cryogenic solvent effects 78—55182
- CS_2, radiation self synchronisation on Rayleigh edge time stimulated scatt. in external resonator *(Russian)* 80—69461
- CS_2, S atom $L_{II,III}$-absorption spectra 78—86807
- CS_2, second order Raman spectrum in condensed phase 80—93299
- CS_2, shock heated, visible emission 80—58274
- CS_2, single-photon isotope separation using ArF laser 78—55211
- CS_2, solid, lattice vibrs., group theoretical anal. by computer 77—80590
- CS_2, solid, tailoring of potentials, in lattice dynamics 78—79679
- CS_2, solns. with liq. Ar, Kr, Xe, CH_4 and CF_4, Rydberg band positions, temp. depends. 78—17686
- CS_2, spectral determ. in atmosph. of Venus *(French)* 79—62776
- CS_2, symmetric stretch mode, moments and polarisability derivatives, SCF calcs. 80—901
- CS_2, thermodynamic ionis. energy, rel. to benzene and photoionis. energy 77—16858
- CS_2 travelling wave Kerr cell, ultrafast pulse shaping and picosecond rise time elec. pulses 80—33152
- CS_2, UV spectra, Stark modulation of a^3A_2-$X^1\Sigma_g^+$ system 79—86003
- CS_2, VUV photolysis in Ar matrix, thermoluminesc. 77—52659
- CS_2, vapour pressure, ^{13}C and $^{33,34}S$ isotope effects 78—18756
- CS_2, vibr.-rot. bands at .46 μm, isotope effects 78—94245
- CS_2, vibrational dephasing meas. with CW mode-locked dye lasers 79—65846
- CS_2, wavefront inversion for stimulated Raman scatt. *(Russian)* 77—34912
- CS_2, wavefront reprod. obs. by stimulated Brillouin, Raman scatt. 80—53369
- CS_2, X-ray scatt., reference-site-interaction model, intermol. pot. function 77—11459
- CS_2^-, adsorbed on MgO, g-tensors, spin densities, CNDO calc. 78—46270
- CS_2^+, and $(CS_2)_2^+$, photoionis. in supersonic mol. beam 79—98165
- CS_2^+, CS_2^{2+}, CS^+, S^+, S_2^+, 10 eV impact on Pb surface, chem. modification, ESCA obs. 77—24916
- CS_2^+, dissociation mechanism 79—59601
- CS_2^+, electronic transitions, solid phase UV spectra 77—3380
- CS_2^+ fluoresc. quantum yields and lifetimes, meas. method, ion form. 77—6815
- CS_2^+, matrix isolated, laser induced fluorescence spectrum 79—50068
- CS_2^+, photodissociation cross section, UV and visible spectral obs. 80—28077
- CS_2^+, photoionis. reson. study of $(^2\Pi)$ and $(^2\Sigma^+)$ states, vibr. freqs., ionis. pot. 78—29821
- $^{12}CS_2$, $^{13}CS_2$, vibration-rotation bands 2700-2900 cm^{-1} *(French)* 78—25521
- $^{12}C^{32}S_2$, ν_1-ν_2 difference band assignments 79—45719
- $^{12}C^{34}S_2$, $^{13}C^{34}S_2$, high resolution IR spectra *(French)* 80—58249
- $^{13}CS_2$, laser emission at 6.9 μm, HF laser optical pump 78—58995
- $^{13}CS_2$, optically pumped by pulsed HF laser, emission obs. at 6.9 μm 79—50283
- CS_2/O_2 additive flame laser, design and performance 80—78870
- CS_2-acetone, liq. mixture, excess Gruneisen parameter, intermol. interaction 78—67635
- CS_2-ethanol mixture, in external transverse resonator, Rayleigh wing stimulated scatt. line, anomalous shift 78—13763
- CS_2-ethanol mixture, Rayleigh and depolarised Raman scatt. lines near crit. temp. 77—20863
- CS_2-ethanol mixture, thermal diffusion ratio determ. by forced Rayleigh scatt. 78—75858
- CS_2-glass boundary, optical bistability at nonlinear interface 80—33094
- CS_2-niromethane, crit. resist. of binary liq., 10 Hz-100 kHz 78—76123
- CS_2-nitromethane, elec. resistance, crit. phenomena, freq. depends. 79—60884
- CS_2-O_2 flame, rate of population of CO vibr. levels, CO emission intensity 78—7186
- CS_2-O_2 mixture, stimulated emission of CO behind overdriven detonation wave front *(Russian)* 77—23668
- CS_2-O_2 pulsed chemical laser and pulsed CO TE laser, comparative study 79—31876
- CS_2+acetic anhydride, elec. resist. near crit. soln. temp. 78—71874
- CS_2+acetonitrile liquid mixture, elec. cond. crit. phenomena 77—4212
- CS_2+Ar^*, Penning ionisation and dissoc. fluoresc, collisional energy depend. 78—33584
- $CS_2+Br(4^2P_{1/2})$, electronic to vibrational energy transfer rates 78—29839
- CS_2+fluoromethane, fluoromethane laser, buffer gases collisional narrowing 80—99710
- CS_2+He^+, dissoc. charge-transfer, $CS^+(B^2\Sigma^+$-$A^2\Pi_i)$ emission prod., Morse pot. Franck-Condon factors calc., vibr. anal. 80—99539
- $CS_2+He(Ar)(N_2)$, perturbed rot. diffusion of CS_2, IR spectra 78—75245
- $CS_2+He(Ne)(Ar)$, Penning ionis., electron spectra, vibr. transfer 77—14555
- CS_2+I^-, endoergic reaction, time-of-flight mass spectral obs. 77—12786
- CS_2+inert gas, translational excitation, energy transfer, cross spectra 77—50559
- CS_2+nitromethane liquid mixture, elec. cond. crit. phenomena 77—4212
- CS_2+O, reactive scatt., O atoms seeded in Ne supersonic nozzle beam 78—48637
- CS_2+O, reactive scatt. in supersonic at. beam 79—36753
- CS_2+O_2, vibr. relax., effect of atomic O 79—66300
- CS_2+OCS (methyl bromide), spectral line broadening, quadrupole moment meas. 77—6848
- CS_2+OH, flash photolysis reson. fluoresc. rate consts. determ., global S cycle 78—95914
- CS_2+OH, lower atmosphere chem. 80—61870
- CS_2+OH, reaction rate consts., 299-430K 78—35653
- $CS_2+O(^3P) \rightarrow CS+SO$, reaction rate enhancement, triat. mol. symmetric vs. asymmetric stretch excitation 79—91927
- $CS_2+O \rightarrow CS+SO$, vibrational distribution of CS, laser-induced fluorescence meas. 80—71895
- CS_2+S, electronically excited atom, reson. fluoresc. 80—99476
- $CS_2+U^+(UO^+)$, reaction cross-sections, ion beam apparatus study 80—97691
- $CS_2^+ + Kr$, collision-induced dissociation, mass spectra *(Russian)* 77—88549
- $CS_3+N_2O+O_2$ combustion, CO laser performance characts. *(Russian)* 78—55348
- C_2S, influence of polymorphic transform. on sinter stability *(Russian)* 80—66503
- C_3S_2, electronic struct., optical and photoelectron spectra 78—70745
- CSFCl, sextic centrifugal distortion consts., microwave spectra *(German)* 77—75140
- $CS_2^* + CS_2 \rightarrow CS_3^+ + CS + e^-$, chemiionisation, mol. beam photoionisation 80—76495
- $C_{12n}(SbCl_5)$, magnetothermal oscill. and electronic struct. 78—84129
- CSe, atomisation energies, enthalpy of form. 78—33631
- CSe_2, atomisation energies, enthalpy of form. 78—33631
- CSe_2, liq., partial struct. factor, neutron diffraction meas. 80—79672
- CSe_2, photoionis. mass spectrum, Rydberg states props., heat of form., CSe dissoc. energy and ionis. pot. 77—46604
- $^{13}C^{16}0$, $A^1\pi$-$X^1\sigma^+$(13,0) band, monochromatic excitation 78—82767
- $^{12}C^{16}O$ emission, unsuccessful search at 2.6 mm wavelength of globular clusters 78—41000
- $^{12}C^{16}O+{}^{13}C^{16}O$, vibr. distrib., electron impact excitation, isotopic composition, interaction depend. 79—29332
- ^{13}CO, interstellar, emission in galactic plane, rel. to giant mol. clouds distrib. in Galaxy 79—101183
- $^{14}CO_2$, radiometric estimation of the replication time of bacteria in culture 79—16170
- $^{14}CO_2$ meas. in Karlsruhe Reprocessing Plant exhaust air 79—3231
- $^{14}CO_2$ trapped in solns. of NaOH, reliable scintillation counting method 79—62410
- Ca-N_2O-CO flame, Ca catalyzed, gain meas., emission band assignment 78—66815
- Ca-N_2O-CO flame, candidate chem. laser reactions, intracavity dye laser absorpt. meas. 78—63108
- $CaCO_3$ filled polymer melts, viscous props. 80—19311
- $CaCO_3$ in seawater and scale formation on OTEC heat exchangers 80—41461
- $CaCO_3$ inorganic precipitation in calcite-depositing spring 79—44202
- Cl_2-CO_2 system, vapour-liquid equilib. *(Japanese)* 79—42258
- ClCF, radical in Ar matrix, vibr. relax., multiphonon processes, fluoresc. 77—65430
- ClCN, and isotopic species, force field calc., freqs., rot. consts. 79—22692
- ClCN, vacuum UV photodissociation spectroscopy, quantum yield, fluoresc. polarisation 80—32736
- ClCO radical, struct. and props. calcs. 80—74112
- Cl_2CS, fluoresc. decay from second excited singlet state 78—25600
- $ClO^- + NO(NO_2)(SO_2)(CO_2)$, rate consts. at 300K 78—76829
- Cn free radical, $B^2\Sigma^+$ state lifetime, photon-photon cascade meas. 78—5273
- Co emission in Markarian and Seyfert galaxies, unsuccessful search 80—26975
- Cs-graphite intercalated compounds, anisotropy of Debye-Waller factor, Mossbauer meas. 77—55738
- Cu, liq., deoxidation rates by CO_2-CO gas mixture *(Japanese)* 80—89394
- D_2-CO_2, laser system, interaction between vibr. states, theory 77—23670
- DCl-cycloalkane solns., CO IR vibr.-rot. spectra, solvent mol. struct. 77—83585
- DF-CO_2, CW and pulsed chem. transfer lasers, book contrib. 77—10907
- DF-CO_2, chem. amplifier of short light pulses, photolytic or fast electron initiation 78—13696
- DF-CO_2, chem. laser, vibr. energy transfer from DF to CO_2 mols. 77—23669
- DF-CO_2, chem. laser, high performance characts. 77—34881
- DF-CO_2, chem. laser utilising ClF_5, ClF_3, ClF and F_2, energy transfer characts. 79—94225
- DF-CO_2, chem. transfer laser, efficient performance 77—34886
- DF-CO_2, laser system, interaction between vibr. states, theory 77—23670
- DF-CO_2 CW chemical transfer laser, high pressure operating charact. 79—81449
- DF-CO_2 chemical laser, possibility of increasing generation quantum yield and specific energy output 80—19025
- DF-CO_2 chemical laser, photon branching in chain reactions, IR radiation initiation 80—91785
- DF-CO_2 chemical laser, amplification of long and short pulses 80—95883
- DF-CO_2 pulsed chemical transfer laser, analysis of calc. model 79—94226
- DF-CO_2 pulsed photoinitiated chem. laser, characts. rel. to HF laser 79 64219
- FCN, and isotopic forms, force field calc., freqs., rot. consts. 79—22691
- FCN, IR laser Stark spectra, C-F stretching mode, dipole moments, rot. consts. 78—1022
- FCN, photoelectron spectrum 77—30920
- FCO, radical, struct. and props. calcs. 80—74112
- FCP, microwave spectrum, struct., dipole moment and vibr.-rot. props. obs. 80—91549

carbon compounds continued
F_2CS, pot. surfaces, X^1A_1, a^3A_2 and $a^3A_2(b_1)$ states, ab initio SCF calcs. 78−86795
FeO_2 nucleation, kinetics of formation of H_2O and C_2O 79−83449
H_2+CO, coadsorption on Cu-Ni (110) single cryst. surface, TDS and UPS obs. 80−80052
H_2+CO_2, rot. excitation, semiclassical calc. using exponential approx. 77−42379
H_2+CO(CS)(OCS), rot. excitation, classical and quantum calcs. 78−1059
H_2+O_2+CO, 500°C, rate consts. involving OH and HO_2 radicals 78−35646
HCO, pot. energy functions for ground state surfaces 79−89620
HCO, radical formation in acetaldehyde photodissoc., wavelength depend. 79−83490
HCP, force fields and force consts. of electronically excited states 80−69116
$HCl+O^-(O_2^-)(NO_2^-)(CO_3^-)(CO_4^-)$, rate consts. at 300K 78−76829
$HF-CO_2$, laser system, interaction between vibr. states, theory 77−23670
$HO+CO \rightarrow H+CO_2$, 700 and 100 torr, 25°C, FT-IR anal. 77−25247
$HONO+NO+NO_2+CO$+air, UV irradiated, computer simulation, peroxynitric acid form., smog 77−63885
$He-CO_2$, nuclear pumped laser, use of fast burst Caliban reactor *(French)* 79−89889
$He-CO_2$ atomic C nuclear pumped laser collision processes, output delay 80−38002
$He-CO_2$ pulsed atomic C laser, time and energy characts. in mag. field *(Russian)* 78−22108
$He-CO_2-Cs$ mixture in rapidly circulating laser, interaction rate of Cs and CO_2, gasdynamic parameters 79−86173
$He-CO_2-Xe$, supersonic elec. discharge TEA laser, mag. field effects 79−7110
$He-CO_2-Xe$ electrical discharge laser pumped by crossed electric and mag. fields 78−42320
$He-Co_2$ mixtures, thermal diffusion 80−1726
$He-N_2-CO_2$ mixture, IR laser output from elec. discharge after X-ray preionisation 79−64205
$He-N_2-CO_2$ mixture in supersonic nozzle, shock activation with overexpansion, jet form. 78−18330
He+CO, rot. inelastic scatt., coupled eqns. for single initial state, variation-iteration method 79−68301
He+CO, unitary approx. for inelastic collisions 78−13569
$He+CO_2$, IOS opacities and integral cross sections, partial wave parameter identification effects 77−38719
He+CO(HCl), effective pot. and coupled states approx., differential and gas kinetic cross sections 77−61827
He+CO(HCl), rot. excitation, classical and quantum calcs. 78−1059
He+OCS, emission spectra in He afterglow 80−87139
$He_2^+ + Ne(Ar)(N_2)(CO)(CO_2)(Ch_4)$, bimol. and termol. charge transfer reactions, rate coeffs. 77−1910
$He^+(He_2^+)+N_2(CO)(CO_2)(H_2S)$, charge transfer Penning ionis. 78−17784
$He_2(^3\Sigma_u)+Ne(Ar)(N_2)(CO)(C_2)(CH_4)$, excitation transfer reaction rates 78−5332
$He(2^3S)+CS_2$, CS^+ and CS fluoresc. spectra assignments, vibr. populations, transition moments 77−14473
$Hg(^1P_1)$+CO, $Hg(^3P_1)$ production mechanisms 78−29847
$I^- + COS(CS_2)(H_2S)$, endoergic reaction, time of flight mass spectral obs. 77−12786
$IBr:CO_2$ photolysis, electron-vibr. pumping, 2.7 μm Br and 4.3, 10.6 μm CO_2 laser transitions 80−28196
$IBr-CO_2$ IR laser with $Br^* \rightarrow CO_2$ electronic-vibr. energy transfer as pump mechanism 80−53260
ICN, vacuum UV photodissociation spectroscopy quantum yield, fluoresc. polarisation vacuum UV photodissociation spectroscopy, quantum yield, fluoresc. polarisation 80−32736
K+CO, rotational inelastic scatt., uniform semiclassical sudden approx. 80−99544
$KBr:CN^-$, neutron scatt. studies of $(CN)^-$ defects 80−92620
$KBr^*+Ne(Ar)(CO)(N_2)(CO_2)$, information theoretic anal. 77−521
KC_8 intercalation compound, H_2 chemisorption *(French)* 79−43624
$KCl:CN^-$, phonon-internal mode hybridisation, neutron scatt. 78−2217
$KCl:CO_3^{2-}$, $Sr^{2+}(Ba^{2+})$, shift and broadening of local vibr. bands, temp. depend. 78−87755
$Li^+ + CO_2(N_2O)$, vibr. excitation, time of flight meas. 77−79682
$Mg-N_2O-CO$ flame, efficient chem. generation of $Mg(^3P)$ 78−63109
$Mg-N_2O-CO$ flame, Mg catalyzed, gain meas., emission band assignment 78−66815
Mn-Al-C, metallic magnets investigations, present state *(Polish)* 80−107987
$N^+ + CO(CO_2)$ (methane)(NO), product distribs., rate consts., ion cyclotron reson. obs. 77−52618
N_2:CO, IR and Raman spectra, vibron band, vibron-phonon combination bands 78−68495
$N_2:CO_2(N_2O)$(methane-d_4), liq., vibr. relax., Raman scatt. obs. 78−92061
N_2-CO, angularly resolved CARS 80−22453
N_2-CO, electrical discharge excitation, vibr. level population distrib., electron beam fluoresc. obs. 80−48031
N_2-CO, liquid, high resolution CW CARS spectra 80−63635
N_2-CO mixed cryst., librational motion, Raman obs. 78−6661
N_2-CO_2, N_2 non-self-maintained discharge, high press., ionisation instability, pulse discharge train *(Russian)* 77−47282
N_2-CO_2 jet, molecular rot. level population during condensation 79−86481
N_2-CO_2 mixture non-self-sustained discharge ionisation instabilities, obs. 78−71610
N_2-CO_2 nonequilibrium aerosol flux mixing, inverse population of vibrational levels *(Russian)* 77−10743
$N_2-CO_2-H_2O$ gasdynamic laser mixture, electron beam diagnostics 77−83845
N_2-CO_2(-He) volume discharge, N_2 vibr. levels, stepwise excitation, effect on electron energy balance 80−54071
NH+CO, vibrational energy transfer in solids, rot. mode participation 78−63815
NH_3-CO_2 complex, matrix isolation IR spectrum, struct., ab initio SCF calcs. 78−5209
N_2O-CO, flame, alkaline earth atom catalysed combustion 77−9081
N_2O-CO flame, alkaline earth catalyzed chain reaction chemiluminesc. 77−40548
N_2O-CO flame, Mg catalyzed chain reaction chemiluminesc. 77−36758

carbon compounds continued
N_2O-CO_2, optically pumped transfer lasers, continuously tunable 78−13678
N_2O-CO_2 mixtures, predicted values of viscosity and thermal cond coeffs. 77−84383
N_2O-CO-He mixture, radiation amplification factor in supersonic expanding stream of gas 77−10896
N_2O+CO, Na catalysed, Na chemiluminesc., excitation mechanism, appl. chem. laser 77−63916
N_2O+CO, nonequilibrium reaction in shock waves *(Russian)* 78−76845
$NO_2^*+CO \rightarrow CO_2+NO$, laser-stimulated reaction 77−9075
$NO_2^*+CO \rightarrow NO+CO_2$, laser stimulated reaction, rate const. 78−40044
$Na-CO_2$ mixing-type gasdynamic laser, experimental and theoretical studies *(Japanese)* 80−23666
$Na+CO(CO_2)$, total cross sections 79−27064
$NaCl:Mn^{2+}$, CN^-, EPR spectrum rel. to Mn^{2+}-vacancy-CN^- complex 80−54942
$Na(n^2D)+N_2(CO)$, collisional l-mixing, highly excited states, fluoresc. obs. 77−83686
$Ne+CS_2$, metastable atoms, energy transfer processes 80−83466
Ni (001)/CO(O) system, adsorbate geometries determ. from final state scattering in X-ray photoemission 80−54488
NiCO, hypothetical mol., adsorbate bond geometry, determ. using photoemission 78−71951
$O+CS_2 \rightarrow OCS+S$, branching ratio meas. 79−52656
$O+Cl_2(CS_2)$, reactive scatt. of beams, vel. distribs. 77−73443
$O+I_2(CS_2)$(OCS), crossed-beam investigation of translational energy 79−5145
O+OCS (ethylene), reaction dynamics, IR laser excitation, vibr. effects 77−12788
$O^- + CO \rightarrow CO_2^+ + e^-$, vibr. chemiluminesc. 78−3340
O_2-CO coadsorbed complexes evolving from Ag surface, mass analysed thermal desorption spectra 77−60121
O_2-CO_2 mixture, temp. difference of molecular vibr. relaxation freq. from 300 to 675K 80−74238
O_3-CO, photorecombination laser, shock wave triggered, waveguide mode optical gain 80−5730
O_3+H_2S(OCS), SO chemiluminesc. in Ar matrix 79−5146
$O_3^- + CO_2 \rightleftharpoons CO_3^- + O_2$, rate const., 200-600K in flowing afterglow 78 7193
(O_2-O_2), thermal electron attachment meas., microwave cond., pulse radiolysis 80−28592
$OCBr_2$, IR spectra in Ar matrix, force consts. *(German)* 79−36641
OCS, 5.3 μm vibr.-rot. bands, rot. consts., spin-flip Raman laser obs. 77−34631
OCS, atmospheric concs. in S.W. and E.United States 78−20466
OCS, collisional excitation of interstellar molecule 78−81664
OCS, collisional rot.-line widths and shifts, microwave region 78−25619
OCS, detect. of new interstellar transitions 77−60808
OCS, dipole moment, laser microwave double reson.-Stark effect meas. 78−55191
OCS, electron elastic scatt., 0 to 100 eV 80−23547
OCS, electron impact dissoc., CS heat of form. determ. 78−73074
OCS, electron impact excitation and ionisation 80−63837
OCS, electron scatt., absolute total cross-section meas. 78−74774
OCS, fundamental vibr. bands in liq. phase 79−54856
OCS, gas, EPR of rot. transitions, T_1 press. depend. 80−9621
OCS, high-intensity laser photolysis at 157 nm, $S(^1S)$ prod., photoionisation, and loss, laser appl. 80−21306
OCS, IR spectra, diode laser calibration 80−83363
OCS, IR spectra using spin-flip Raman laser, combination band near 1890 cm^{-1} 78−37640
OCS, IR spectral moments and mean squared torques, rare gas effects 78−62944
OCS, IR spectroscopy 79−98088
OCS in Ar matrix, photolysis, S_2 and S_3 absorpt. spectra 79−5149
OCS, in atmosphere, contrib. to stratospheric aerosols and climate 80−41524
OCS in n-alkane, rot. relax., solvent hydrodynamic props., Raman and IR spectra 80−45055
OCS laser, two-quantum excitation, photolysis, energy transfer, for fusion expts. 78−59003
OCS, laser Stark spectra, 9.5 micron, band origins, dipole moments 77 18969
OCS, M-resolved rot. Stark levels, four-level microwave-microwave double reson., collision induced 77−10696
OCS, MM wave spectrum, centrifugal distortion const. 77−34618
OCS, MODOR in $\nu_2=1$ state, nondipolar collision-induced transitions 77−6812
OCS, microwave absorpt. coeff. 77−64378
OCS, microwave rot. absorpt. lines, press. broadened width and shift 77−61807
OCS, microwave rot. lines, self-broadening 78−58668
OCS, microwave rot. transitions, phase shift effect, collisional effects 79−98073
OCS, microwave spectrum, width and shift parameters 77−18985
OCS, microwave spectra, rot. Q-band *(Polish)* 78−29866
OCS, microwave spectral lineshape of J $1 \rightarrow 2$ line 79−68225
OCS, microwave spectra, Ku-band Fourier transform spectrometer appl. 80−68265
OCS, microwave-microwave double resonance 80−53029
OCS, millimeter wave rot. spectra, isotope shifts, freqs. and mol. consts. 80−78611
OCS mixtures, rot. energy collisional transfer, M-depend., microwave double reson. 78−46435
OCS, mol. consts. of ν_2 levels 77−14429
OCS, mol. quadrupole moments, mag. shielding and spin-rot. tensors 79−22609
OCS, motion, regular and irregular spectra, theory 80−9590
OCS, multiphoton dissociation by IR laser 79−36710
OCS, multiphoton i.r absorption, optoacoustic detection 77−507
OCS, ν_3 band absolute wavenumbers *(French)* 79−98099
OCS, optically pumped roto-vibr. mol. laser, rate eqn. model 78−37874
OCS, optically pumped CW subMM emission lines 80−95876
OCS photodissociation, $S(^1S)$ prod. and props. in liq. Ar and N_2 80−43064
OCS photolytic laser, for fusion reasearch 78−59002
OCS, pure and seeded beams, rot. cooling, electric reson. meas 79−13795
OCS, r_m struct. determ. from rot. consts. 78−42236

carbon compounds continued
OCS, rot. relax. cross section, beam maser meas. 79–31654
OCS, rot.-vibr. levels and semiclassical energy levels 80–37804
OCS, roto-vibr. mol. laser, low-temp. performance 80–9871
OCS, seeded beam, rot. cooling 79–18266
OCS, self-broadening linewidth parameters 79–18268
OCS, semiclassical energy levels calc., vibr. freqs. 78–46315
OCS, spectroscopic reference freqs. in 9.5 μm band, heterodyne freq. meas. 80–18850
OCS, stratosphere content, solar spectra meas. by 12 km attitude aircraft 80–41486
OCS, submillimetre rot. lines, press. shifts 80–23463
OCS, T_2 relax. meas. using budge-type superhet. microwave spectrometer 80–91551
OCS, UV photolysis producing $S(3^1D_2)$ 79–79274
OCS, vibr. energy transfer map 80–99560
OCS^+, photodissociation cross section, UV and visible spectral obs. 80–28077
$^{16}O^{12}C^{34}S$ and $^{16}O^{13}C^{34}S$, IR spectra, v_3 band anal. 80–95620
OCS-N_2-SF_6 mixture laser, OCS photodissociation, electron dipole forbidden transition, absorpt. spectra 79–68389
OCS+benzene, microwave line width and quadrupole moments, perturbation theory 80–69190
OCS+benzene (S_1), V-V reson. energy, transfer, microscopic reversibility, level degeneracies role 79–86045
OCS+bromomethane, microwave spectral line width, dipole-dipole interaction calc. 78–74648
$OCS+CO_2(H_2)(N_2)(OCS)$, collisional line broadening of microwave spectra, semiclassical theory, calcs. 78–25516
$OCS+H_2$, rot. excitation, infinite order sudden approx. 78–74740
$OCS+H_2$, scattering cross-sections, factorisation and fitting, IOS approx. 78 33575
OCS+He, translational-vibrational energy transfer, quantum dynamical study 80–63746
$OCS+He^+$, dissoc. charge-transfer, $CS^+(B^2\Sigma^+$-$A^2\Pi_i)$ emission prod., Morse pot. Franck-Condon factors calc., vibr. anal. 80–99539
OCS+He(Ar), rot. lines, collisional broadening 79–18267
$OCS+He(Ne)(Ar)(Kr)(H_s)(0_2)(C0_2)$, gas, EPR of rot. transitions, T_1 press. depend. 80–9621
OCS+methanol (H_2)(He), collisional rot. energy transfer, microwave-microwave double reson. obs. 77–19016
$OCS+N_2^*$ 80–48063
OCS+nonpolar perturber, J1-2 line broadening 77–6848
OCS+nonpolar perturbation, $J=1\rightarrow2$ microwave line press. broadening 80–9644
OCS+O, reaction dynamics, IR laser excitation effects 79–66288
$OCS+O_3$, double-quantum vib. energy transfer 77–6897
OCS+OCS, rot. transition, interpolation scheme 79–22776
OCS+OCS(He)(Ar), rot. spectral line shift and widths, collision induced phase shifts 77–75222
OCS+S, electronically excited atom, reson. fluoresc. 80–99476
$OCS+S\rightarrow S_2+CO$, reaction kinetics of $S(3^1D_2)$ reactions 79–79274
OCS+Si(Ge), SiS and GeS multiple collision chemiluminesc., intercombination systems 80–45505
OCSe, isotopic species, microwave and IR spectra 77–38658
OCSe, photolysis, $Se(^1S)$ prod., quenching of high concs. 79–6904
OCSe, quantum yields for Se, $^1S_0$, $^1D_2$, and $^3P_{0,1,2}$ atoms determ. in photolysis, lifetime and quenching rate meas. 80–97741
$O(^1D)+O_2(N_2)(CO_2)(O_3)(H_2O)$, 100-350K, reaction rate consts. 77–21355
OH+CO, HOCO and HOCO* form., thermochem. props. 78–27805
OH+CO, reaction mechanism, HOCO radical stability 77–73436
OH+CO, reaction rate consts. at 296K, press. effect 77–73435
$^{13}O^{16}O$ and $^{12}C^{18}O$, emission bands of $E^1\Pi$-$A^1\Pi$ transition 78–90177
$O(^3P)+C_3O_2\rightarrow 3CO$, reaction dynamics and monoxide vibr. distrib., laser reson. absorpt. method 78–68882
$4PbO.PbSO_4$, paste mixing and curing for Pb acid batteries, effect of CO_2 79–61968
QCS, static polarisability, ab initio SCF wave functions 80–74106
S-O-C, equilibrium 550 to 1100°C 79–38807
SCN^-, associated with metallic cations in aq. soln., press. effect, Raman spectra *(French)* 78–80333
SCN^-, positronium formation, Doppler broadened annihilation line shapes 80–45164
$(SCN)_2$, and $(SCN)_2^-$, vibr. anal., bond strengths 80–9582
$(SCN)_2$, prep., UV photoelectron spectrum and structure 80–28059
SCO, S atom $L_{II,III}$-absorption spectra 78–86807
$SO_2+CO(C_2H_2)$, photochem. reactions, rate consts. 78–23956
SeO_2+CO_2, radiative lifetime and quenching rates 80–95685
α-SiC, sintered, influence of B, C additives on microstructure, SEM exam. 79–8262
SiO-CO gas phase, Si and C transfer to Fe-C liquid alloys 80–55655
SiO_2-C mixture, nitridation to form. Si_3N_4 additives effects, exam. 78–44068
Sr-N_2O-CO flame, candidate chem. laser reactions, intracavity dye laser absorpt. meas. 78–63108
Sr-N_2O-CO flame, Sr catalyzed, gain meas., emission band assignment 78–66815
Th-Zr(Nb)(Ru)(Rh)-C, phase diagrams *(German)* 77–48413
Ti-B-C system, complex carbide phase synthesis by crystallisation from gas phase 77–16526
Ti-Si-C system, complex carbide phase synthesis by crystallisation from gas phase 77–16526
Ti-V-C-N, solid solns., quasibinary cross sections 78–23676
$Tl+CO_2$, relax. of $6^2P_{3/2}$ and $7^2S_{1/2}$ states 79–64094
WC-Co cemented carbides, transverse-rupture strength obs., w.r.t. domain size of binder phase *(Japanese)* 80–11741

carbon fibre reinforced composites
aligned, prep. and theoretical strength agreement 80–84906
bonded Al-CFRP single lap joint strength 79–29328
bonding with epoxide-isoprene copolymer 77–52280
coating of fibres with Si, SiC whiskers, shear strength improvement 78–3093
damping capacities, cantilever beam tests *(Japanese)* 79–91869
diaphragm for loudspeaker, with high specific modulus, flexural rigidity and loss factor *(Japanese)* 80–53596
elastic moduli 77–86069
electropolymerisation, on electrodes, book contribs. 80–50854
epoxide resin matrix, torsion creep 78–44172

carbon fibre reinforced composites continued
epoxy cross ply laminates, transverse cracking and long. splitting, strain effects 79–61723
epoxy laminates with Kevlar 49/C fibre reinforcement, impact props. 78–44164
epoxy matrix, cryogenic tensile, compressive and shear props. 78–6983
epoxy matrix, deterioration in water, hydraulic press. effect *(Japanese)* 80–55470
epoxy matrix, deterioration in water, immersion time effect *(Japanese)* 80–55471
epoxy matrix, effect of material variability on predicted environmental behaviour, numerical anal. 78–90733
epoxy matrix, strength in twisting, stretching and transverse bending 80–11622
epoxy matrix, thermal expansion, thermal and elec. conductivity, 2 to 290K 79–60528
epoxy matrix, use in construction of cryogenic telescopes 80–22414
epoxy matrix laminate, containing interlaminar paper inclusions, AE monitoring 79–34229
epoxy matrix with activated C fibres, storage life effect on shear strength *(Russian)* 78–35483
epoxy phenol matrix, oxidation, effect on props. 80–40574
epoxy resin, Cu electroplating, coating props. *(Japanese)* 77–36412
epoxy resin, diamag. susceptibility as fibre alignment characterisation method 78–84381
epoxy resin, dynamic Young's modulus and internal friction 80–25754
epoxy resin, thermal expansion, influence of fibre type and orient. 77–35722
epoxy resin $DX210/BF_3400$, reinforced with Morganite C-fibres, thermal cond. 79–65264
epoxy resin matrix, crack form. *(German)* 78–19887
epoxy resin matrix, transverse creep compliance, time and temp. depend. *(Japanese)* 80–45358
fibre, wettability, relative, evaluation 78–43209
fibre reinforced epoxy, thermal cond., diffusivity and sp. ht., determ. 80–24613
filament wound C-fibre reinforced composites, thermal residual stresses 80–49290
fracture, C fibre surface effects 80–11777
fusion reactor first wall, limiter, beam dump appl. 80–32458
glass C matrix, graphitisation 79–15643
glass fibre reinforced epoxy resin composites, thermal expansion, thermal and elec. conductivity, 2 to 290K 79–60528
glass matrix, SiC fibre coating, hot pressing production method *(German)* 78–95724
glass-carbon fibre-reinforced composite disc, rot. strength 79–74198
glass/C reinforced epoxy resin, hybrid effects, conditions for positive or negative effects vs. rule of mixtures, mech. props. 78–68769
graphite, fibre reinforced epoxy, fibre orientation effect on friction and wear 79–79125
graphite, reinforced epoxy angle-ply laminate wave propag. during transverse impaction 79–83295
graphite, Type-A, surface comp. and energetics 77–70024
graphite fabric reinforced organic-matrix, interlaminar fracture studies 80–55495
graphite fiber reinforced epoxy, transversely isotropic moduli 79–83246
graphite fibre epoxy composites, exposed to high temp., degradation of tensile and shear props. 80–81113
graphite fibre reinforced Al, temp. and press. effect on interface chemistry, mech. prop. meas. 78–64595
graphite fibre reinforced Al, US effect on molten Al wetting of graphite during prep. 79–15629
graphite fibre reinforced epoxy, correlation of tensile strength with US stress wave factor 79–87798
graphite fibre reinforced epoxy, fracture mechanics 80–35294
graphite fibre reinforced epoxy, impact damaged, acoustic emission 79–91875
graphite fibre reinforced epoxy, laminate, splitting process charact. 80–25843
graphite fibre reinforced epoxy, laminated plate under tension, stacking sequence and lay up angle effect on free edge stresses round hole 78–88524
graphite fibre reinforced epoxy, mositure absorption in liquids and humid air 79–61897
graphite fibre reinforced epoxy, notched, fatigue initiation 77–52471
graphite fibre reinforced epoxy, stress transfer to brittle coating, failure 79–96106
graphite fibre reinforced epoxy, US attenuation as an indicator of fatigue life 80–85118
graphite fibre reinforced epoxy laminate, fracture, comparison of anal. and expt. 79–61713
graphite fibre reinforced epoxy laminate tension-compression fatigue loading, fatigue residual strength degradation model, comparison with expt. results for 78–35491
graphite fibre reinforced epoxy laminates, expt. investigation of tensile moduli and strength 78–52870
graphite fibre reinforced epoxy matrix laminates, microscopical anal. 78–3288
graphite fibre reinforced epoxy resin, hygrothermal microstresses, in material exhibiting inelastic behaviour 77–84141
graphite fibre reinforced epoxy resin, radiographic technique for resin content meas. 78–3286
graphite fibre reinforced metals, tribological behaviour, fibre origin effects 79–96158
graphite fibre reinforced panels, low energy impact testing 78–72845
graphite fibre reinforced polyimide, correl. of US attenuation and shear strength 78–19968
graphite fibre reinforced polyimide acoustic emission spectral anal. 79–47850
graphite fibre reinforced polyimide composites 79–52381
graphite fibre reinforced Sn-Pb (38 wt.%) alloy, effect of interface on fracture characts. 78–76723
graphite reinforced epoxy, 0° graphite/epoxy and ±45°/0° graphite/glass/epoxy, fatigue damage, early detection by NDT 77–28951
graphite reinforced epoxy, accelerated characterisation procedure 79–34263
graphite reinforced epoxy, B fibre addition as radiographic inspection aid 78–95880
graphite reinforced epoxy, combined torsional-bending fatigue tests 77–28951

carbon fibre reinforced composites continued
graphite reinforced epoxy, NDT 79—96254
graphite reinforced epoxy, scale effect in fatigue 79—91780
graphite reinforced epoxy angle ply laminates, statistical fatigue in shear 79—11690
graphite reinforced epoxy composites, moisture detection by nuclear reaction anal. 80—30306
graphite reinforced epoxy laminate, cantilever shells and late, natural modes 79—91737
graphite reinforced epoxy laminate, edge effects 78—19803
graphite reinforced epoxy laminate, fracture behaviour 79—83294
graphite reinforced epoxy laminate, fracture by three point bend 79—83297
graphite reinforced epoxy laminate, mech. strength meas., comparison with theory, tensor polynomial failure criterion 78—39886
graphite reinforced epoxy laminate plates with cracks, strain and failure anal. 79—29170
graphite reinforced epoxy laminate with arbitrarily symmetrical struct., stability 79—61649
graphite reinforced epoxy laminates, cracked, deformation and failure in biaxial stress fields 79—47763
graphite reinforced epoxy laminates, imminent fracture detection using acoustic emission 79—20302
graphite reinforced epoxy resin, average stress failure criterion appl. 78—88519
graphite reinforced epoxy steel scarf joint, adhesively bonded, exam. of failure 78—92350
graphite reinforced epoxy/Al laminate, cantilever shells and late, natural modes 79—91737
PAN graphite-Al composites, fracture characteristics and props. 80—11779
graphite-epoxy composites, Thornel 300/Fiberite 1034, effects of thermal spiking on moisture absorpt. characts., tensile strength and buckling modulus 79—43330
graphite-epoxy laminates, AS/3501-5, compressive fracture strength 79—43396
graphite/epoxy composite, high elec. cond., engineering appl. 80—70780
graphite/epoxy composite, single ply, elec. cond. meas. 80—92953
graphite/epoxy laminates, statistical fatigue, high load effect 80—93642
graphite/epoxy laminates, stress meas. by X-ray diffr. from fillers 79—43331
graphite/epoxy laminates, stress wave damage 80—93611
graphite/epoxy laminates, T300/5208, effect of curing stresses on first ply failure 79—43329
high work of fracture composites, prep. and mech. tests 80—81029
HTGR fuel rods, carbon-carbon composites designed for high weight and low strength 77—71684
hybrid C and glass fibre, fracture energy 78—95801
hybrid C fibre and glass fibre reinforced plastics, review of physical properties 80—55496
hybrid glass fibre/C fibre reinforced epoxy-phenolic, elastic characts. prediction 80—108491
hydrothermal ageing 77—52367
implanted prostheses applics. of C fibre reinforced C 77—64150
integral composite joints, finite element and expt. eval. 79—11670
interlaminar shear strength, effects of fibre surface treatment, resin type and fabrication process 78—35346
Kinel, mech. props., 20 to 300°C *(French)* 77—56018
kinking as structural degradation mode 78—52893
laminate, elastically orthotropic or isotropic, stress around pin loaded holes 77—84143
laminate, elasticity modulus *(Russian)* 80—39199
laminate, non Hookean behaviour in fibre direction, effect of fibre waviness on tensile props. 78—19804
laminates, C/epoxy, moisture distribution determination, low cost method 79—65252
mechanical properties, environmental cycling effects 77—86207
mechanical properties and residual stresses in wound components of glass-C fibre composition 77—52436
mechanical properties rel. to aircraft appl. 77—81289
mechanical property determ. of C fibres 77—81287
metal matrix, wear, effect of fibre orientation 79—87744
multicomponent composites, mech. props. 79—52329
multilayer plastic sheets, strength props., deformation *(Russian)* 80—30019
notched, biaxial fatigue loading 78—19879
Nylon 6, unidirectionally reinforced, mech. props. and fracture 77—21252
nylon matrix, design parameters, fibre orientation effect 80—81141
orthopaedic implants appl., exam. of mech. props. 79—20706
orthotic bone plate, variable-stiffness, absorbable 79—79691
oxidation and mech. strength at intermediate temps. 77—81330
phenol resin matrix, karbovoloknits, improving transverse tensile, interlaminar shear and compressive strengths 79—87691
plastic, epoxy resin DLS 351/BF$_3$400, thermal expansion, 90-500K, fibre vol. fraction effects 78—26703
plastic, fractography of fracture surface under three-point bending *(Japanese)* 80—55506
plastic, fracture energy improvement by delamination promoters 77—8909
plastic, nonlinear stress strain relations, under continuous static loading 77—59872
plastic, shear props., effects of flaws and voids 77—44334
plastic laminates, US evaluation of hygrothermal effects 80—7730
plastic matrix, ±45° orientation, creep, fatigue, repeated loading and crack growth 78—68729
plastic matrix, aircraft structural appl., non destructive testing, review, AE appl. 78—35599
plastic matrix, angle ply specimen, calc. of strength and elastic response 79—20108
plastic matrix, bonded joint fatigue life, stress distrib. analysis 80—55497
plastic matrix, cross ply, defect location by natural frequency meas. method 80—30191
plastic matrix, deform. and failure using AE method *(Russian)* 80—40630
plastic matrix, degraded, study of strain, 20 to 1000°C 80—71680
plastic matrix, failure under compression, tension and bending 79—96142
plastic matrix, fatigue behaviour visualised by moire fringe method 80—21110
plastic matrix, fatigue failure mechanism identification, AE detection using piezoelectric strain gauge 79—96239

carbon fibre reinforced composites continued
plastic matrix, fatigue props. and flexural rigidity *(Japanese)* 80—55510
plastic matrix, laminate, free-free plates, predicted and expt. natural modes 79—10520
plastic matrix, moisture content effect on elec. resist. 79—38992
plastic matrix, props., implications for structural design 80—81174
plastic matrix, SEM obs. of fatigue 80—11737
plastic matrix, shear strength of glued joint, combined effect of temp. environment moisture, fibre orientation 79—96100
plastic matrix, strain response to acoustic excitation, statistical props., comparison with Al alloy 79—43502
plastic matrix, strength, specimen size effect, statistical anal. 78—68724
plastic matrix, stress analysis of butt strap joint 79—43300
plastic matrix, tensile testing using ring specimens *(Japanese)* 79—29148
plastic matrix, under complex stress-state conditions, mech. props., method for studying 80—50799
plastics, for polymeric joint replacements 79—83999
plastics, strength props., effect of SiC coating on fibre 80—104224
plastics matrix, prep. with large breaking strain C fibre 78—44077
plastics matrix with mixed fibres, exam. of fracture toughness and shear strength 79—20151
polyacetal matrix, friction and wear against glass and steel 78—56783
polyamide thermoplastic, stiffness and strength 78—27600
polycarbonate matrix, design parameters, fibre orientation effect 80—81141
polyester matrix, interlaminar shear fatigue 78—56742
polyester resin matrix, crack form. *(German)* 78—19887
polyethylene matrix, ultra high molecular weight, wear limit, γ-irradiated and unirradiated *(Japanese)* 78—27649
polyethylene matrix, ultra-high mol. wt., for medical appls., tensile and flexural props. 78—31969
polyethylene total joint replacement, props. improvement by C fibre reinforcement, SEM obs. 78—24183
polylactic acid polymer-filamentous carbon tissue scaffold, for ligament and tendon replacement 79—92434
polymer, review 78—11196
polymer, strength props., fibre surface treatment effects 78—27636
polymer coated graphite fibre-epoxy resin composites, prep., adhesion 79—15644
polymer matrix, hybrid, impact props., strategic reinforcement 78—15502
polyphenylsiloxane matrix, long-time strength, and influence of protective coatings 80—3133
preparation, properties and structure for spacecraft use 80—71625
PTFE matrix, friction and wear against glass and steel 78—56783
resin, multilayer IR mirror design and fabrication *(French)* 77—54770
resin matrices and their contribution to composite properties 80—81028
resin matrix, optimisation of thermally stable structures using holographic interferometry *(German)* 79—90804
review 77—21082
space appls. rel. to mech. and thermal props. 78—7016
Spacelab pallet, C fibre reinforced plastic appl. 78—45186
strength, surface treatment effect analysis and obs. *(Japanese)* 77—77596
stress/strain behaviour, split Hopkinson press. bar test, opt. and strain gauge methods comparison 80—85132
testing, using burn test apparatus with metal grid and indicator lamp 80—76441
thermal expansion, in low temp. range 78—83978
thermal expansion, influence of resin type 78—95164
thermal expansion, matrix curing effects 79—55909
thermal expansion, ply multidirectional effects 78—95165
thermal expansion 79—1513
Thornel 300/Fiberite 1034 graphite epoxy composite, elastic moduli, environmental effects 77—86068
Thornel 300/Fiberite 1034 graphite epoxy laminates, tensile strength, 200 to 422K, moisture effects 77—48486
transient hygrothermal stresses, coupled diffusion of heat and moisture 80—33451
unidirectional model for longit. tensile strength prediction 78—95778
US determ. of lay-up order 77—60007
Young's modulus, depend. on cross-sectional area of fibre 77—4804
Al alloy, new production method with continuous fibres 77—66610
Al alloy matrix corrosion resistance, electrochemical characts. 80—11806
Al composite, CVD fibre coating, diffusion barrier and wetting agent 77—40458
Al composite, formed by ion plating and vacuum hot pressing, mech. strength 78—11165
Al, factors affecting struct. formation and some props. 78—15346
Al matrix, C-Al contact interaction kinetics 79—20007
Al matrix, matrix-fibre interaction depend. on metallic dopants *(Russian)* 80—76479
Al matrix, mech. props. 80—11708
Al matrix, wear volume/sliding time relationship 79—61743
Al, matrix interaction between components and compatibility, mech. props. effect 80—11761
Al-vitreous C composite, microchem. inhomogeneity of transition zone 77—24985
C based, appl. as refractories, toughness props. 79—38782
C binder and filler, oxidation behaviour, rate-controlling steps 80—55550
C fibre reinforced epoxy resin, eddy current methods of exam. 77—12760
C glass fibre hybrid plastics, review of mech. props 79—20107
C matrix, fibre-matrix interactions 78—84725
C matrix, processing, room temp. mech. props., and low temp. expansion 80—25820
C matrix, wear, oxidation contribution 79—52383
C-fibre reinforced epoxy resin, laminated structs. mech. props. 80—50672
C-fibre reinforced plastic insert molding strength *(Japanese)* 80—66588
Cu matrix, electrodeposited, tensile strength *(Japanese)* 79—43333
Cu matrix, fatigue strength under constant strain *(Russian)* 78—95796
Cu matrix, mech. props. *(Japanese)* 77—63723
Cu matrix, specific elec. resistivity, 77 to 550K *(Russian)* 77—72895
Cu matrix, thermal cond., temp. depend., 80 to 350K 77—24452
Cu matrix, thermal expansion and thermal fatigue *(Russian)* 79—38936
Cu-Sn matrix, exam. of high speed tribological props. in friction expts. against steel 79—15809
CuO-H$_3$PO$_4$ microconcrete, effect of C fibre on props. 79—43192
Mg 78—11164
Na-S cells, S electrode potential distrib. model 79—96435
Ni matrix, hot pressed and electrodeposited, strength 79—38898

carbon fibre reinforced composites continued
  Ni matrix, struct. and strength change at high annealing temp. *(Russian)* 79—66076
  Si-Al C fibre composite technological coatings, liquid phase method preparation *(Russian)* 80—108375
  SiC (TiC) coated C-fibre reinforced SiO_2-glass, prep. for high temp. appl. 80—45267
  TaC-C fibre composite, neutral beam target appls. 78—66399
  TiC-coated C fibres in Ni, diffusion barrier effectiveness 78—60624
  ZrN-coated C fibres in Ni, diffusion barrier effectiveness 78—60624

carbon fibres
  see also carbon fibre reinforced composites
  activated C, storage life effect on shear strength of expoxy composites *(Russian)* 78—35483
  arc anodes, layers on, props. and cooling behaviour 79—52245
  Beslon based, coeff. of linear thermal expansion, sag method for determ. 79—77774
  biomedical electrode, elec. props. and EEG appls. 80—72355
  cathode prebreakdown field emission transition to vacuum breakdown 78—75462
  cementation technique for coating with metal 79—39000
  coated with Si or ZrC, mech. props. 77—70197
  coating with SiC, effect on strength props. of C fibre reinforced plastics 80—104224
  conference, Baden-Baden, Germany (June 1976) 78—43990
  density of states, magnetoresistance theory appl. 80—44620
  diagmagnetic susceptibility meas. for fibres from pitch mesophase, pitch and PAN 79—69649
  diamagnetic studies of as-processed fibres 77—25165
  durability, elastic props. and struct., heat treatment temp. effect, US meas. methods 80—40446
  elastic moduli 77—86069
  electrical resistivity, temp. dependence 77—20311
  electrolytic oxidation treatment for fibre struct. studies 78—22649
  electron field emission, energy distrib. of post-accelerated electrons 77—16468
  engineering applications, production requirements and mech. props. 80—89168
  fibril dimension estimation, using lubricostatic structural models 80—54171
  flexural fatigue and surface abrasion 78—15504
  friction, expt. and adhesion theory 77—1877
  friction and wear, individual fibres rubbing on rotating cylinder 77—52498
  glass tip, surface and crystallographic struct. using field-ion and electron microscopy 80—10767
  graphite, electrical hazards 79—91111
  graphite, surface anal. by XPS and polar/dispersive free energy anal. 80—65340
  graphite, transversely isotropic moduli 79—83246
  graphite, Type-A, surface comp. and energetics 77—70024
  graphite fibres, elec. resist., mech. props. after nitration 77—32698
  graphite fibres, HM, surface comp. and energetics 80—54480
  graphitisable, prepared by benzene decomp., stepwise heat treatment, TEM expts. 77—85950
  graphitised, Br_2 and ICl intercalation and its removal 79—43561
  graphitised viscose fibre, fluorination, change in struct. 80—88039
  high modulus, and mesophase from pitch 79—94867
  high strength, from mesophase pitch, tensile strengths, Weibull parameters, SEM study 79—79031
  irradiation-induced dimensional changes 80—65052
  lattice images, of C fibres treated with intercalating agents, TEM study 79—64993
  layered compounds with alkali metals, prep. 80—20809
  mechanical properties, thermal stability up to 2000°C 80—60929
  mechanical property determ. from C-fibre reinforced plastics 77—81287
  mesophase pitch based, resist., magnetoresist., EPR and mech. props. rel. to struct. 79—78116
  mesophase-pitch-derived, Young's modulus and tensile strength, struct. flow elimination 80—80995
  metal-coated with Cu, Co or Ni, coating struct., SEM study 80—97605
  metallic coated, increased temp. effect on strength *(Russian)* 78—35429
  microelectrodes, neurophysiology appl. 80—67314
  microvoids in pitch and lignite based fibres, X-ray scatt. exam., heat treatment and stretching effects 79—20091
  morphological charact. rel. to fracture, SEM obs. 77—63791
  neutron irradiation effects 78—78496
  optical anisotropy caused by strain birefringence 79—56760
  oxidation, coated with pyrolytic SiC 78—60857
  oxidation, effect on props. 80—40574
  oxidation, surface props. *(French)* 78—44238
  oxidation by NO_2, struct., props. modification 78—44237
  PAN based, layered compounds with metal chlorides, struct. and elec. cond. 79—91600
  PAN fibres, neutron irradiated, struct. and props. *(Russian)* 80—25763
  PAN-based, surface characts., active surface area, microporosity 78—35536
  PAN-based, surface characts., investig. by flow microcalorimetry 78—48694
  PAN-based, type I, II and III, TEM study of structural heterogeneity 79—77465
  physicomechanical props. stability, tensile strength versus fibre cross section 77—52387
  plasticizing and wettability-enhancing coatings 79—29252
  preparation, mech. props., struct., incorporation into C fibre reinforced plastics 78—44077
  production from coal tar pitch, heat treatment *(German)* 78—44033
  production processes, properties, and applications 77—63623
  reinforced plastic pressure vessel, immersion technique for acoustic emission detection 77—1902
  struct. and physical props. effects of B additions and heat treatment temp. 78—68715
  structural and mech. characts. 77—28737
  structural changes with stepwise heat treatment up to 3000°C, for fibres prep. from benzene 77—12649
  structural parameters obtained by electron microscopy and X-ray diffr., comparison 77—47353
  structure, recent advances 80—81069
  structure obs., Raman microprobe-microscope appl. 80—62737

carbon fibres continued
  substrate for crystallisation of Ni, Ni-B films, struct. evolution *(Russian)* 80—75455
  supersonic wave propag. and damping as function of thermal treatment temp. 77—89499
  surface treatment with tetra-(octadecyl) titanate, X-ray and electron microscope study *(Japanese)* 79—74280
  surfaces, effect on fracture of C fibre-polymer composites 80—11777
  technology advancements, Indian developments 80—93562
  tensile strength, heat treatment and flaw effects 80—81173
  tensile strength, Young's modulus, high temp. obs. 79—20139
  tensile testing, high-temp. equipment 77—40497
  thermal expansion coeff. meas. using TEM fitted with furnace 80—102966
  thermal treatment temp. effect on struct. and props. 78—23743
  thermoelectric power meas., fibre prep. by benzene decomp. 78—2507
  tip, field emission characts. 80—11543
  US attenuation factors 77—39631
  vapour-grown, growth mechanism and props., review *(Japanese)* 77—66598
  wettability, relative, evaluation 78—43209
  yarn, prep. of B_4C continuous yarn 78—48365
  Al coated, effect of annealing on ultimate tensile strength and fracture 78—56744
  C characterisation, using dark-field electron microscopy 79—77464
  Cu-plated C fabric, plasma sputtering influence on strength and elec. cond. *(Russian)* 80—21008
  Ni coated, high-temp. compatibility 78—19829
  SiC coating, CVD, relation between surface morphology and coating conditions *(Japanese)* 78—39704
  SiC coatings, oxidation protection *(Polish)* 79—52408
  SiC-coated C fibre, compatibility with Al *(Japanese)* 80—71700
  TiC coating on C fibre, by CVD TiC coated C fibre compatibility with Al *(Japanese)* 79—78898

carbon microphones *see microphones*

carbon steel
  80Kh5G5, austenite hot deform. effect on martensitic transform. *(Russian)* 77—48434
  120N12, austenite hot deform. effect on martensitic transform. *(Russian)* 77—48434
  abnormal decomposition kinetics and mechanism of austenite *(Russian)* 80—55344
  abrasive wear resistance, effect of C content, annealing, quenching 77—56115
  accelerated deform. by to H_2 absorption *(Japanese)* 79—70121
  accumulation of longitudinal strain under cyclic torsion 78—64615
  acoustic emission characts., effect of pressurisation during tensile testing 78—92304
  acoustic-emission signals, rel. to struct. of type 45 79—52297
  adhesive bonds with polymers, shear resist., polymer crystn. effect 80—89462
  adsorption of Hg, effect on mech. strength, creep, fatigue embrittlement *(Russian)* 79—29267
  alloying addition effect on austenite-cementite boundary *(Czech)* 77—85991
  AISI 1010, corrosion susceptibilities in synthetic geothermal brines 77—86223
  aluminised, hot dipped, phase composition anal. of alloy layer by X-ray, electron probe and hardness meas. 79—34192
  annealed, roller, macroscopic and microscopic changes in surface layer due to rolling contact 77—77518
  annealed, rolling wear under dry contact conditions 79—52391
  annealed low C, X-ray stress anal. using position-sensitive proportional counter 80—1498
  annealed roller, rolling contact fatigue life, effect of changing rolling direction 77—77519
  annealed S45C, multiple repeated low cycle torsion fatigue under controlled strain *(Japanese)* 78—27610
  anticorrosion films, quality rating using colour indication method 80—21209
  antifriction material, sintered, determination of elastic moduli 79—96070
  austempered, exam. of running in and wear 80—16485
  austenite, supercooled, decomposition, exam. of carbide formation *(Russian)* 78—35388
  austenite grain size, determ. 79—74332
  austenitic, recrystallisation and grain growth obs. with photoelectron microscope 79—47730
  austenitic grain size determination, exam. of methods used 78—85071
  with austenitic stainless steel cladding creep-rupture strength in corrosive environment *(Russian)* 77—52533
  austenitic transformation, temp.-conc. range of product formation 79—100135
  autectic, sintered, isothermal transformation behaviour, porosity effects 80—3031
  bainitic, microstruct. and cleavage resistance 77—52481
  bainitic, morphological characteristics 78—68682
  ball bearings, surface comp., AES and ion sputter profiling 77—40465
  beams with bracket plates welded to tension flange 78—7008
  bending, effect of strain rate on dynamic stress factors 77—56046
  bending fatigue, difference between strain energy changes *(Japanese)* 78—39894
  bending fatigue resistance, size effect and prediction 79—43411
  boride coatings, spectroscopic thickness determ. 80—85099
  boride coatings, under elec. heating conditions, hydroabrasion wear resist. 80—55543
  brazed butt joint, static torsional deform. 77—16657
  brazed joints used in thermal power plants, corrosion resistance 79—43492
  brittle fracture, grain size and precipitate thickness effect 78—60786
  brittle fracture resistance, C effect 80—3163
  built-up edge form., direct SEM obs. 80—104303
  carbide coating by CVD, interlayer form. 80—11574
  carbide coating formation by chromising C steels 78—88571
  carbide deposition on surface, exam. *(Russian)* 79—34200
  carbide formation during chromising, exam. in terms of ternary phase diagrams 78—56818
  carbide residues after deform. and tempering, X-ray diffr. investig., type U10A *(Russian)* 77—81275
  carbide transitions during post-strain ageing and tempering *(Russian)* 78—95741

- **carbon steel** continued
  - carburising kinetics, in endothermal atm. 80—76410
  - cast, C and C-Mn steels, fracture toughness 77—4836
  - cast, fatigue from notches 77—16678
  - cast 18OSKhNM, fractographic investigation 77—21266
  - cast cylinders, fragmentation tests 78—35519
  - castability, in metal mould, mechanical props. *(Japanese)* 80—25681
  - casting by C diffusion solidification 78—52792
  - casting properties, correlation anal. *(Bulgarian)* 79—83192
  - cavitation erosion, exam. of mechanism and rates 79—5063
  - cementation process testing, foil samples method 79—70238
  - cementite decomposition during plastic deform., alloying element effects 78—84768
  - cementite formation and properties 80—45313
  - cementite precipitation cryst. geometry singularities during decomposition of U12, U15, U17 high-C martensite *(Russian)* 80—7577
  - channelling contrast, to investigate fatigue crack propag. 80—66609
  - chemical polishing for opt. microscopy 77—9021
  - chemicothermal treatment, diffusional basis 80—104343
  - chromisation, influence on surface roughness *(German)* 79—11729
  - clad plate of middle and low C, inhomogeneity and residual stresses, heat treatment effects *(Japanese)* 78—6955
  - coarsening of dispersed particles, in solid matrices 78—56651
  - coated with Fe powder layers, sinter-bonded, hot-pressed 79—95976
  - coated with TiC, prep. and props. 80—76414
  - coating with NbC, deposition technique, struct. and props. 79—52462
  - cold deformation hardening, effect of C content and cementite shape 78—92277
  - cold formability *(French)* 78—60681
  - cold rolled sheet, spot welded joints, static fracture appearance 80—55538
  - cold rolled St3Kp, annealed, mag. nondestructive inspection of strip and ribbon 78—60913
  - cold rolling rolls, high C-Cr type 9Kh2, hardness determ. 79—87713
  - cold strained effect of rapid treating on strain ageing *(Russian)* 79—11642
  - cold worked, original struct. effect on softening during heating 80—60882
  - cold worked and recrystallised, attenuation behaviour *(German)* 78—48445
  - cold-rolled, recovery of lattice defects in cementite 77—90370
  - cold-worked, Mossbauer obs. of cementite decomp. and restitution 78—64558
  - composite layered specimen influence of contact strengthening by intermediate layer, on fracture toughness *(Russian)* 79—15768
  - compression, high strain rate, 1023 steel 79—34099
  - contact fatigue strength, effect of austenite grain size 79—100254
  - corroding surface in nuclear reactor, mixed cation spinel form. 78—35565
  - corrosion, alternating current effect 80—30141
  - corrosion, cold working effect on corrosion behavior 79—74299
  - corrosion and self protection in hot saline soln. 79—1925
  - corrosion behaviour in reducing environment of coal fired MHD generator 80—104322
  - corrosion behaviour in simulated HTGR He environment 79—54495
  - corrosion by aq. H_2S solns. 80—100946
  - corrosion by freshwater *(Russian)* 79—1921
  - corrosion by hot concentrated saline solutions, aerated and nonaerated environments 80—25926
  - corrosion by wet elemental S, exam. as function of pH and particle size 78—92388
  - corrosion cracking by sulphide, effect on props. 80—55587
  - corrosion during cyclical exposure, to wet elemental S, and He atmosphere 78—92391
  - corrosion fatigue, cathodic coatings effects *(Russian)* 77—52532
  - corrosion fatigue, effect of corrosion inhibitors *(Russian)* 77—59977
  - corrosion fatigue, with anodic coating *(Russian)* 77—70206
  - corrosion fatigue resistance in cavitations, bainitic and martensitic structs. *(Russian)* 78—56815
  - corrosion fatigue strength determ. *(Japanese)* 80—25910
  - corrosion in concentrated H_2SO_4 78—64767
  - corrosion in H_2S soln., Fe dissolution 79—79145
  - corrosion inhibition by 2-ethylamino-ethanol in aerated 3% NaCl soln., pH effect 80—21160
  - corrosion products, chem. state anal. by conversion electron Mossbauer spectroscopy 80—40595
  - corrosive reactions obs. by polarimetric Mossbauer spectroscopy 80—40594
  - corrosivity in conc. chloride soln. 79—96193
  - crack, with straight front perp. to wire under tension, strain energy release rate, C 0.75% *(French)* 79—1136
  - crack growth, Weibull analysis 78—92319
  - crack growth in high-temp. water 80—108636
  - crack initiation and propagation life under repeated impact tensile loads *(Japanese)* 80—104264
  - crack initiation lives at stresses near endurance limit, probability distribs. 77—86127
  - crack opening displacement, rel. to flow stress 78—68810
  - crack profile meas. and correlation with mech. props. *(German)* 80—21108
  - crack propag. and sealing, effect of thermal working *(Russian)* 79—34078
  - crack propag. under combined creep and fatigue, J-integral approach in type S15C *(Japanese)* 79—83303
  - crack propagation energy rel. to temp., time factors 79—29179
  - crack resistance, preliminary loading condition effects on crack appl. 78—56739
  - cracking in NH_3 at 600°C 79—70207
  - creep, expt. investigation above 900°C 80—81134
  - creep crack propagation, J-integral application 80—35331
  - creep deformation, under reversed cyclic stresses in type S15C *(Japanese)* 80—81114
  - creep rupture tests, at 500°C loading times up to 300000 hours *(German)* 80—25828
  - cumulative damage rule, based on reduction in fatigue limit, experimental confirmation 78—92358
  - CVD hardfacing using W, for coal gasification unit components 77—40472
  - CVD protective coating using Cr, struct. and carbide form. 77—40387
  - cyclic loading and fracture toughness 80—35298

- **carbon steel** continued
  - cyclic strain induced creep, relation between modes of stress and strain superposition 78—60733
  - cylindrical parts, centreless smoothing 77—90507
  - cylindrical specimens with crack. fracture characts. in inelastic strain, test methodology 80—25839
  - deep-drawing, texture problem after processing through continuous annealing 79—87659
  - deformation, tension, torsion compression test exam. *(Russian)* 78—31455
  - deformation ageing, of medium and high C steel, entropy, free energy, dislocations *(Russian)* 80—66581
  - deformation peculiarities at high temp. under superplasticity with cyclic thermal load *(Russian)* 78—95776
  - deformation strength and strain rate depend. under plain strain state *(Japanese)* 80—30028
  - density and thermal expansion in liq. and solid states 80—96668
  - deposition of composite, wear resistant Ni-B-Cr coating on type 45 78—11420
  - diffusion coating by Cr and Pb melt bath, kinetics *(Korean)* 78—60873
  - diffusion coatings, Ti-Al, struct. and props. 79—57156
  - diffusion couple with austenitic steel, diffusion of C, 773-1373K 79—19392
  - diffusion melting in Fe-C melts, heat transfer correl. 80—54348
  - diffusion of H_2, effect of quenching and tempering 77—7908
  - diffusion of H_2, SCC via martensite form. cooling rate changes on Mn and Ni addition *(Russian)* 78—56813
  - dissolution of Cr_7C_3 in austenite *(Russian)* 80—103479
  - dry lubrication by Cd film, tribological behaviour 80—89364
  - dual phase structures (martensite and ferrite), effect of martensite composition on content, mech. props. 78—76717
  - ductile fracture, role of hydrogen 79—57103
  - ductile fracture criterion for cracked plate in fully plastic state *(Japanese)* 78—38253
  - ductile fracture under cold forming conditions, press. effect 78—52938
  - ductile fracture under cold metal forming conditions, metallurgical struct. influence 79—34125
  - ductility, effect of temp., deform. rate and stress state *(Russian)* 78—35428
  - elastic const. meas., X-ray diffr. technique 78—5714
  - elastic props., effect of additional tempering temp. 77—21192
  - elastic-plastic plane waves with combined stresses 78—90764
  - elastic-plastic stress anal. by photoelasto-plastic method and X-ray method *(Japanese)* 78—13978
  - electric resistance welded pipe, grooving corrosion in seawater 78—35556
  - electroheated, thermal cycling and corrosion behaviour 80—61006
  - electron bombardment, microstruct. and hardness 79—38956
  - electrophoretic Cr_3C_2 alloy coatings on C steel, sintered, struct. form., Ni-P undercoat effect 80—61027
  - EM excitation of US at high temps. 80—33412
  - erosion-corrosion in aqu. H_2S soln. up to 120°C, 1.6 MPa press. 80—21155
  - eutectic, YU8, effect of segregating structurally free ferrite *(Russian)* 79—15677
  - eutectoid, anisothermal strain with phase transform., effect on tensile strength *(Russian)* 80—40431
  - eutectoid, deformed, back stress decrease on annealing and H embrittlement 80—20981
  - eutectoid, high strength, unnotched specimens, fatigue crack init. and propag. 77—56098
  - eutectoid, mech. behaviour, thermomech. treatment effects 80—84970
  - eutectoid, microhardness determ., acoustic emission 79—15889
  - eutectoid, notch toughness, tempering at moderate temps., effect of quenching temp. 77—21193
  - eutectoid, schematic isothermal transform. diagram 78—48393
  - eutectoid, Si partitioning during pearlite transform., analytical electron microscopy applic. 80—108458
  - eutectoid, U8, cold hydraulic press. forging effect on transform. and heat treatment *(Russian)* 79—52235
  - eutectoid, wear due to impulsive friction, device for exam. 80—25957
  - eutectoid and hypoeutectoid, stress relaxation during rapid heating transform. *(Japanese)* 78—11258
  - eutectoid schematic transform. diagrams 79—56958
  - eutectoid thermomechanically treated, textural studies 80—29978
  - explosively fractured, struct. of white etching band 79—61722
  - explosively strengthened, cause of anomalous increase in H_2 of low cycle endurance *(Russian)* 77—16729
  - extra mild, use of limiting forming curves, deform. distribution, assessing deep drawability *(French)* 77—21232
  - fastener holes, cold-worked, residual stress meas. 78—7163
  - fatigue, crack form. mechanism in type 45 79—38957
  - fatigue, low cycle, cyclic stress-strain curve eval. 77—44347
  - fatigue, mean stress effects *(German)* 78—56721
  - fatigue, residual stress and crack growth expts., notch and surface treatment effects 79—8356
  - fatigue, residual stresses, surface cracks *(Japanese)* 77—25121
  - fatigue behaviour of NiAl precipitation hardening 78—84983
  - fatigue crack exam. using slip initiation phenomena *(Japanese)* 77—8930
  - fatigue crack features, in S 35 C and SK 5, anal. by precision matching method *(Japanese)* 78—52955
  - fatigue crack growth in air and seawater, under constant amplitude and random loading 78—64679
  - fatigue crack growth rate in high temp., high purity oxygenated water 80—40622
  - fatigue crack plasticity, effect of water vapour 78—64678
  - fatigue crack propag., crack closure, dislocation struct., electron microscopy obs. *(Japanese)* 80—25845
  - fatigue crack propag., transient effects 77—56053
  - fatigue crack propag., transient effects *(Czech)* 77—63775
  - fatigue crack propag. and crack closure, of part through cracks *(Japanese)* 78—72842
  - fatigue crack propag. and crack closure behaviour, under various loading conditions 78—68795
  - fatigue crack propag. and crystallographic orientation *(Japanese)* 78—7027
  - fatigue crack propag. and fractography under periodic overstressing, exam. *(Japanese)* 78—52958
  - fatigue crack propag. under periodic overstressing, design criterion *(Japanese)* 79—20166

carbon steel continued
fatigue crack propagation, effect of mean stress on crack closure 77—73315
fatigue crack propagation, in biaxial stress fields 80—40494
fatigue crack propagation in sheet, influence of struct. of ferrite-pearlite bands *(French)* 80—76338
fatigue crack resistance, temp. effect 79—52375
fatigue crack tip, observation of crack closure phenomena, by electron microscopy 78—68794
fatigue cracks, in NaCl, oil and water vapour *(Japanese)* 78—11414
fatigue cracks, transition from initiation to propagation 78—68802
fatigue damage, under sawtooth wave strain cycling at elevated temp. *(Japanese)* 78—84977
fatigue damage accompanying nonstationary modes of cyclical loading, coeff. of heredity *(Russian)* 79—52349
fatigue damage accumulation and nonuniform microscopic strains, development features 79—91770
fatigue damage detection, using optical correlation technique 78—35511
fatigue damage indicators, non-destructive 80—25932
fatigue deformation, phenomenological exam. 78—64691
fatigue failure, inelastic response, energy criterion, of low and medium C steels 77—73333
fatigue failure in type 45, strength charact. 79—52373
fatigue fracture after Fe and Ce diffusion coating, microstruct. investigation *(Russian)* 79—52446
fatigue life, fluctuating overstresses, effects 77—90524
fatigue life, reliability analysis, reliability-based design safe lives *(Japanese)* 77—8939
fatigue life and cumulative fatigue damage under const. stress cycling, plastic strain range effect *(Japanese)* 77—8940
fatigue life estimation, under combined torsion and bending *(Japanese)* 80—93647
fatigue life prediction under programmed loading *(Japanese)* 79—20167
fatigue limit, in plane specimen microfatigue cracks and understressing effects *(Japanese)* 77—52480
fatigue limit during bending, inelastic strain effects 77—44355
fatigue of AISI 1010, effect of Se, Te additions 78—92359
fatigue strength, atmospheric press. effect *(Japanese)* 77—77573
fatigue strength, low cycle, reduction factor for type SFVV1 *(Japanese)* 80—104259
fatigue strength, of notched specimens with regard for cyclic plastic strains of type 45 79—43414
fatigue strength, push-pull, effect of high tensile load during stress cycling *(Japanese)* 78—92332
fatigue strength, small defect effect 80—104255
fatigue strength and damping capacity, short term cyclic overload effect 79—66157
fatigue strength criterion, of a bar, subjected to combined static and repeated bending and torsion 80—40496
fatigue strength improvement, by subcritical quenching 78—44153
fatigue subsurface crack initiation, result of residual stresses 80—25833
fatigue tests, low cycle, material variance distrib. law, type 45 79—91799
fatigue under reversed tension-compression stresses, photoelasticity investig. *(German)* 78—31493
fatigue-freq. relationship for S20, 45, 0.1%C types 79—11707
ferrite, transform. kinetics, grain size, alloying element effect, carbide precip. 80—93560
ferrite-martensite microstructure, microstructural parameters effect on fatigue strength *(Japanese)* 80—71735
ferrite-pearlite, cyclic behaviour, fatigue, chem. comp. and microstruct. effects 78—60833
ferrite-pearlite transformation, tensile strength, cooling rate effect 80—7549
ferritic, fatigue crack growth micromechanisms at low stress intensities 80—108570
ferritic, low-C, deform. microstruct., electron microscopy *(German)* 78—64589
ferritic-pearlitic transform., kinetics, struct. aspects *(French)* 78—68685
ferromagnetic, U8, magnetic method of martensite transform. study *(Russian)* 79—87631
ferromagnetic parts, mech. property meas., method and instrument 80—35469
ferromagnetic rods, direct and inverse electromagnetic conversion 79—52569
fibre reinforced Cu matrix, deformation parameters controlling dislocation motion, flow stress, activation volume 79—57055
filament reinforced hypoeutectoid C steel, strength characts. after deform. and quenching 80—35271
filaments, Cu platings porosity determ. 79—70239
forgings, austenite grain refining, in type 25KhN3MFA 79—38864
fracture, dynamic, testing apparatus 77—44450
fracture, effect of cementite *(Russian)* 78—7037
fracture characteristics, notch sharpness effect in impact tests 79—52536
fracture criterion determination, using 3-point bending 79—29216
fracture dynamics at high frequency loading *(Czech)* 80—45391
fracture resistance after low temp. tempering, P content and grain size effects for steel 35KhGSA *(Russian)* 78—48490
fracture surface obs. during fatigue failure 77—86185
fracture toughness, low temp., non-metallic inclusions influence *(Russian)* 79—52346
fracture toughness testing, obs. of crack initiation and stable growth processes *(Japanese)* 78—52954
fretting fatigue, microstructural and environment effects 78—64734
fretting fatigue damage, SEM exam. 78—88541
fretting fatigue tests, effects of environmental H_2O, O_2 78—92407
Fretting-induced damage between contacting steel-polymer surfaces 78—15539
friction faces, S, O content, secondary ion-ion emission obs. 80—55545
friction in liq. Sn, Rebinder effect *(Russian)* 79—29269
friction pair with Armco Fe, bronze or Cu, seizure centre on contacting surface *(Russian)* 77—70185
galvanized, Fe-Zn phases, Mossbauer study 80—50233
gas turbine disc, thermal fatigue 77—52452
glass-enamel coating on C steel tubes, prod. by induction fusion method, heating rate of steel effect 80—11825
grain size and substruct. control by alloying and thermomech. treatment, review 80—3082
hard, developments, properties and fabrication processes *(Dutch)* 77—70021
hard patch of rubbed surface, tempering effect *(Japanese)* 78—7054

carbon steel continued
hard-alloy/U8 C alloy steel weld, local internal stress region boundaries 77—59846
hardened, martensite struct. characts., Cu and Al additions effect *(Russian)* 78—19709
hardened and tempered parts, nondestructive magnetic inspection 79—1929
hardened and temperred parts, nondestructive magnetic inspection 78—95889
hardened by HF current, mech. testing method 80—61053
hardened layer structure and props. with intensive spray cooling and hardening, in type 45 79—38859
hardness, correl. with macrostress intensity under plastic strain 79—87708
heat exchanger, gas-flame spray deposited Fe-Si protective coating 80—61025
heat treated, exam. of microfractographic aspects of fatigue cracks *(Japanese)* 78—52959
heat treated, stresses and cracks form. *(Czech)* 80—20977
herringbone specimen weld stresses rel. to heat-affected zone rigidity 79—29130
heterogeneous structure, fracture characts. 79—38961
high C, 0.7% C, welded zone, fatigue strength and microstruct. *(Japanese)* 80—89339
high C, boriding, boride case struct. 79—24665
high C, Burgers vector of dislocations in cementite crystal 77—27891
high C, ductile fracture, role of second phase particles 79—52359
high C, graphite nucleation on surface *(Russian)* 80—40360
high C, high Cr, rapidly quenched, in situ carbide reactions during tempering *(Japanese)* 78—84862
high C, investigation of transformations during tempering by nuclear gamma resonance method *(Russian)* 80—76256
high C, pearlitic, non-metallic inclusion effect on threshold behaviour of fatigue 79—91786
high C, piano wire, mean stress effect on low cycle torsional fatigue life *(Japanese)* 79—96114
high C, plate, rolling residual stress meas. by X-ray diffr. *(Japanese)* 79—66081
high C, quenched and tempered, hydrostatic press. effect on brittle fracture stress 79—61727
high C, resist. to crack propag. and abrasive wear, role of retained austenite 79—83330
high C, thermomech. treated, strengthening factors 77—8862
high C, type 7KhFNSh, plastic deform. influence of X-ray interference line breadth *(Russian)* 80—93599
high C, wear tests in fuel oil, O_2 conc. effect in oil *(Russian)* 77—16694
high C, weld heat affected zone, impact and fatigue props. *(Japanese)* 80—11668
high C and mild, roughness and wear characteristic of spark-eroded surfaces 79—52390
high C wire, fatigue and fracture 80—55531
high speed, made by liquid infiltration 77—55906
high strength 0.77%C, plastic deform., surface dissolution effect 77—8883
high-C, ShKh15, interaction with controlled atmospheres during annealing 77—44269
high-C steel, strength characts. with controlled hardenability after bulk-surface hardening 77—56156
hollow pipe body with internal crack pattern, ingot segregation, hot shortness 77—32693
hot plastic deform., vac. colour etching investigation 80—61036
hot rolled, ultrasonic echo inspection method 79—87772
hot-rolled high quality sheet use of stat. maths. for NDT determ. of mech. props. 79—11749
hydrogen *(Russian)* 79—29175
hydrogen attack, effect of H_2S on type 1020 79—96192
hydrogen attack, steelmaking effects 79—100076
hydrogen attack morphology, effect of hydrogen press. 80—85052
hydrogen embrittlement, elastic interaction of H_2 with precipitates 78—92340
hypereutectoid, austenite dissociation depend. on strain at intercritical temps., pearlite transform. *(Russian)* 80—40362
hypereutectoid, form. of surface graphitisation centres *(Russian)* 79—11720
hypereutectoid, thermomech. treatment, Fe_3C distrib. and yield point *(German)* 79—52243
hypereutectoid, type ES-01, brittle fracture, fragmentation due to blast loading 80—50699
hypo-eutectoid unalloyed, basis of naturally fibrous composites, strength analysis 78—3190
hypoeutectic, texture development from frictional stress *(German)* 78—53003
hypoeutectoid, alloying effect of graphitisation *(Japanese)* 79—52270
hypoeutectoid, C22, recrystn., influence of carbides distrib. *(German)* 79—38850
hypoeutectoid, fracture toughness, effect of Widmanstatten ferrite 80—35315
hypoeutectoid, morphology and stability of Widmanstatten struct. *(Slovak)* 79—70094
hypoeutectoid, recrystn. initiation, carbide particle size effect 77—12641
hypoeutectoid Widmanstatten struct. form., contrib. to the laws *(Slovenian)* 78—84817
hysteresis loop behaviour under fatigue load, dislocations model 79—74197
impact deposited white-layer on X65 78—48566
impact fatigue, failure mechanisms 80—40493
impact fatigue strength under −100°C low temp. atm. 77—52451
impact fatigue tests under −50°C low temp. atm. 77—52450
impact testing, pseudo-brittleness 79—79111
impact torsional test by means of dropped bar, appl. to low C steel 79—100304
impact-fatigue strength, notch strength, rel. to comp. and ductility of core 77—56093
implanted with N, surface hardness and abrasive wear resist. 80—50746
inclusions, influence on toughness and fatigue props. 80—40533
induction hardened, surface durability, optimum case depth 80—30137
inelasticity in steel 45, under cyclic strain in active media 78—80613
interface with Al-Zn alloy coating, struct. 79—52466
intergranular segregation of C and P in as-quenched state, AES *(Japanese)* 78—19764

carbon steel continued
- ion nitrided and ion-softnitrided, comparison of compound layers in S15C and S48C *(Japanese)* 79−8386
- ion nitriding, wear resistance *(Japanese)* 77−63828
- ion-softnitriding effects on metallurgical props. of nitrided layer in S15C and S48C *(Japanese)* 79−5079
- ion-softnitriding of type S15C with N_2-H_2-CH_4 mixture, mech. props. of surface *(Japanese)* 79−61780
- isoforming and warm rolling, effect of mech. props. 80−11673
- isotropic-kinematic strengthening during plastic deform. *(Russian)* 77−20007
- joints, with interference, increasing supporting capacity, by electrophysical methods, exam. 78−85055
- kinetic friction re-examination using modified pin and disc machine 80−55547
- lamellar pearlite, containing proeutectoid cementite, brittle fracture study *(Japanese)* 80−93648
- laser surface melted, topographical characts., for type 1018 79−70200
- law-C, hot deform., austenite strengthening and weakening 80−76282
- loading surface parameter, temp. effect in type 45 79−66084
- loading wave shape effect on deform., failure, impact tensile strength of smooth specimen *(Japanese)* 79−29146
- low, type 30KhGSN2A *(Russian)* 79−74148
- low and high C, rephosphorised, mag. props. and texture 77−20634
- low and medium C, fatigue crack growth rate, kinetic eqn. of temp. depend. *(Russian)* 77−25136
- low and medium C, tempering 79−61629
- low C, *(Japanese)* 79−8343
- low C, 79−24551
- low C, 10Kh2G3M, development of plastic deform., slip and dislocation struct. *(Russian)* 79−15722
- low C, $\gamma \to \alpha$ transform., martensitic mechanism *(Russian)* 79−47682
- low C, absolute dimensions effect on logarithmic decrement of torsional vibrs. 80−3150
- low C, AISI 1010, low-cycle fatigue at temps. up to 1200°F 78−35516
- low C, Al-killed, effect of V on mag. props. 79−83339
- low C, annealed, fatigue crack propag. law under elastic-plastic and general yield conditions *(Japanese)* 77−48538
- low C, austenite transform., TTT diagrams 77−70031
- low C, bainitic, optimal struct., heat treatment effects 77−16624
- low C, brittle fracture of notched specimens, ferrite grain size and notch geometry effects 78−19860
- low C, brittle fracture susceptibility, low temp. deform. effects 77−56103
- low C, C content effects in corrosion fatigue in nitrate solns. *(Russian)* 78−56811
- low C, capped, cold rolled sheet, deep drawability, effect of carbide size, cold reduction, annealing 78−64559
- low C, carburizing hot plastic deform. effects 77−90377
- low C, close coiled helical spring, corrosion under axial deflection and const. load 79−52428
- low C, cold rolled, graphite precip. and S segregation, AES investigation *(Japanese)* 80−89222
- low C, cold rolled and recrystallised, containing Nb(CN) dispersion, struct. and textural aspect of deform. 79−47712
- low C, cold rolled sheet, Cu effect on recrystallization texture *(Chinese)* 79−74173
- low C, cold rolled sheet, strain rate effect on yield *(Japanese)* 79−96084
- low C, containing P, Mg effect on annealing texture, mech. props. and plastic anisotropy 78−27536
- low C, corrosion, heat treatment and plastic deform. effects 77−63825
- low C, corrosion fatigue strength, soln. pH effects *(Japanese)* 77−52545
- low C, corrosion in HCl inhibited by 2-hydroxy-3-(2-undecyl, pentadecyl or heptadecyl amidoethylamine) propane-1-triethyl ammonium hydroxides, acid-corrosion inhibitors 80−50761
- low C, corrosion inhibition by Na_2MoO_4 77−86221
- low C, crack initiation at root of circumferential notch of round bar specimens *(Japanese)* 80−60947
- low C, creep, prestrain effects *(Korean)* 77−21227
- low C, creep rupture strength, precracked round bars under torsion *(Japanese)* 77−59908
- low C, current density and voltage effect on cpd. layer growth by ion-softnitriding *(Japanese)* 80−35402
- low C, cyclic loading, change in mech. props. rel. to heat treatment 80−104282
- low C, cyclic plasticity and low cycle fatigue life in variable amplitude loading 80−16433
- low C, cyclic strain ageing effect on crit. stress for crack propag. 79−34124
- low C, cyclic stress-strain response under spectrum loading *(Slovak)* 78−19886
- low C, deep drawing sheets, influence of strain- and stress-ratios on preferred orientation change 79−91690
- low C, deep-drawing, mechanism of recrystn. texture formation 79−87658
- low C, deform. form effect on texture *(Russian)* 78−3141
- low C, deformed, comp. of precipitated carbonitrides, X-ray diffr. anal. *(Russian)* 79−20051
- low C, delamination study by impact testing 78−3218
- low C, dual phase, impact props., microstruct. element influence 80−40525
- low C, dual-phase, law of mixtures, applicability 80−89346
- low C, ductile fracture, in situ obs. of microprocess of failure *(Chinese)* 80−55492
- low C, dynamic and static strength, strain rate and temp. depend. of flow stress 80−85139
- low C, dynamics of cyclic plastic deform. and fatigue life at low temps. 77−16670
- low C, dynamics of cyclic plastic deform. at low temps. *(Czechoslovakian)* 77−32679
- low C, effect of heat treatment on resistance to fatigue crack propag. 80−11675
- low C, effective stress determ. during the loading cycle 79−38879
- low C, electroboronising by superimposed cyclic current, Na_2CO_3, B_4C, NaCl, NaOH activator studies 80−85081
- low C, endurance limit, effect of coatings *(Russian)* 77−25145
- low C, etchant for revealing austenite grain boundaries 80−85098
- low C, fatigue, stability of energy dissipative charact. 77−21209

carbon steel continued
- low C, fatigue crack development, at temps of +20 and −160 degrees C, 08Kp sheet steel 78−35505
- low C, fatigue crack propag. and cumulative damage under periodic overstressing *(Japanese)* 77−12692
- low C, fatigue crack propag. prestrain effect *(Japanese)* 79−96116
- low C, fatigue crack propagation in smooth specimen, strain ageing effect *(Japanese)* 79−20163
- low C, fatigue endurance limit, metallurgical technology, and mech. treatment effect 80−55536
- low C, fatigue fractographs *(Japanese)* 78−92335
- low C, fatigue life, variable strain ranges *(Czech)* 80−60956
- low C, fatigue life under programmed loading including stress lower than the fatigue limit *(Japanese)* 77−8934
- low C, fatigue limit, statistical interpretation on basis of extreme theory 80−30056
- low C, fatigue limit, strain ageing effect *(Japanese)* 77−8933
- low C, fatigue strength, influence of mech. stress level in preliminary corrosion 80−55579
- low C, fatigue strength, low-cycle, effect of shock wave press. 79−29205
- low C, fatigue strength and fatigue failure at complicated states of stress 77−56057
- low C, fatigue strength of notched specimen, low-temp. quenching and quench ageing effects 79−100173
- low C, fatigue strength under rotating bending and torsion, understressing effects *(Japanese)* 78−44201
- low C, ferrite grain nuclei form. during polymorphic transform. *(Russian)* 80−50626
- low C, ferrite grain size effect on cyclic stress-strain response 79−100203
- low C, ferritic, static yield prop. changes during fatigue cycling 77−52427
- low C, flow stress variation after unloading, tensile load/strain diagrams *(Russian)* 78−76703
- low C, forming limit diagram, eval. of applicability of theoretical anal. 78−60682
- low C, fractographic study of stage 1 cracking, endurance limit *(Japanese)* 77−8936
- Low C, frictional behaviour, effect of mechanical properties 80−55548
- low C, gas nitrocarburized, cyclic stressing 79−57098
- low C, grain size effect on fatigue strength, high temps. 78−68759
- low C, grain size influence on size of brittle transgranular shear facets 80−35327
- low C, HF oscillations during electron beam welding *(Russian)* 80−76273
- low C, high frequency fatigue limit, external factor effects *(Czech)* 77−59988
- low C, high strength, thermomech. treatment, microstruct. 79−57015
- low C, high strength, thermomech. treatment, strengthening mech. 79−57014
- low C, high temp. plastic flow under thermal cycling in superplasticity interval 77−70130
- low C, high-temp. heating effect on oxide inclusions 79−96051
- low C, highcycle fatigue, crack initiation model *(Japanese)* 80−104258
- low C, hot rolled and cold deep drawn, nonmetallic inclusion distrib. in microcavities *(Russian)* 79−52265
- low C, hot rolling effects on struct. *(Russian)* 78−19793
- low C, hot-rolled sheet, drawability improvement by Al addition *(Ukrainian)* 79−78996
- low C, hysteresis loop initiation mechanism under repeated load *(Japanese)* 78−39851
- low C, impact and tensile props., effect of Si 77−36526
- low C, impact specimen fractures, stress concentrator sharpness effect on size of tough component 78−7015
- low C, impact strength and crit. brittleness temp., sample thickness and notch radius influence 80−85018
- low C, improvement of props. by ion implantation 80−16601
- low C, influence of cold rolling reduction on elastic stored energy 79−91731
- low C, initial stages of plastic deform. *(Japanese)* 80−93618
- low C, instability obs. by large strain compression 80−35253
- low C, kinematic hardening models, use in multi-axial cyclic plasticity 80−25717
- low C, kinetic aspects of diffusion zone and compound layer formed during ion-softnitriding *(Japanese)* 79−15866
- low C, long life corrosion fatigue strength under continuous and alternate immersion in 1% NaCl *(Japanese)* 77−12736
- low C, low cycle fatigue, cumulative damage, absorbed plastic energy anal. 79−38932
- low C, low cycle fatigue props. with variable strain ranges *(Czech)* 80−45390
- low C, low endurance fatigue at low temps. 77−21274
- low C, low temp. effect on rate and fractographic features of fatigue cracks 78−39909
- low C, low-cycle failure investigation, elec. resist. meas. appl. 80−85109
- low C, lower yield stress, grain size effects, Petch slope, temp. depend. *(Japanese)* 78−39852
- low C, martensitic, fracture toughness variations during tempering 78−60812
- low C, mech. characts., specimen size and shape effects 80−66715
- low C, mechanical props., NDT methods 79−29176
- low C, microhardness of nonmetallic inclusions and metallic matrix 79−96127
- low C, microplasticity at high and low loading freq. *(Slovak)* 79−38910
- low C, Mn, laws of banding structure form. *(Slovenian)* 78−83776
- low C, natural, discrete microlamellar composite based on steel M16C *(Russian)* 78−39810
- low C, Nb effect on cold resist. 79−38954
- low C, NbN and VN dispersion hardening effect on mech. props. 78−3137
- low C, nil ductility transition temp. 80−100896
- low C, non-ductile transition temp., tensile speed, effect of prestrain *(Japanese)* 78−72839
- low C, non-oriented, texture and mag. props., effect of Mn and S content 77−86047
- low C, normalised, plastic deform., using microhardness and grain strain meas. 77−4810
- low C, notched, fatigue strength, crack propagation, plastic torsional prework depend. *(Japanese)* 79−15744
- low C, notched sheet under tensile loading notch tip opening/contraction, J-integral relationship *(Japanese)* 77−4840

carbon steel continued
low C, notched specimens, brittle fracture stress, effect of ferrite grain size, notch acuity and notch length 79—20187
low C, nucleation and increase of discontinuities in environment of nonmetallic inclusions *(Polish)* 79—79022
low C, orientation distribution function anal. in maximum shear planes 79—82172
low C, oxide scale removal from fractured surfaces, improved techniques 78—95886
low C, P, plastic anisotropy and mech. props., dynamic strain ageing effect 78—64608
low C, plastic props., fracture, effect of strain rate in static tensile tests *(Czech)* 77—59866
low C, plasticity role during low temp. fracture 78—39905
low C, positron annihilation, influence of fatigue 78—76551
low C, precipitation of Nb and V, critical temperature identification by meas. electric resistance *(Slovak)* 77—4781
low C, pressurised, strain rate sensitivity prior to serrated yielding onset 78—48482
low C, quench-hardened, plastic deform. effect on mech. props. and struct. *(Russian)* 77—70102
low C, quenched, hardening during explosive forming 79—87650
low C, quenched, interphase precipitates obs. *(Russian)* 80—29957
low C, quenched, struct. and props. after plastic deform. and tempering 78—23734
low C, rapidly solidified laser surface alloyed, electron microprobe obs. 79—70201
low C, relation between low yield behaviour and tensile speed, preloading and temp. effect *(Japanese)* 78—6982
low C, rephosphorised, static strain ageing 77—70079
low C, rimmed, structural damage in sheet metal forming 78—64614
low C, rimmed and killed, exam. of impact fatigue behaviour *(Japanese)* 78—88528
low C, rolled, analytical vectorial method for crystallographic texture *(French)* 80—20956
low C, rolled, nondestructive impact strength testing by coercive force meas. 79—52601
low C, rolling deform., effect on NbC particle size distrib. 79—47717
low C, serrated flow and thermomechanical treatment *(Korean)* 80—30026
low C, Si effect on gas nitriding, surface hardness *(Japanese)* 77—48582
low C, slip band expt. studies during fatigue process 80—45374
low C, slip line development 78—15480
low C, specimens with notch and fatigue crack, fracture surface features 79—43417
low C, spheroidised, H_2 embrittlement, fracture characts., electron probe anal. of inclusions 79—57109
low C, spheroidization of pearlite, global microstruct. evolution 80—108482
low C, strain ageing, effect of prestrain *(Korean)* 77—8865
low C, stress ageing embrittlement under short term thermally stressed cycle *(Russian)* 80—60885
low C, stress dip technique for effective stress determination in cyclic straining 80—2113
low C, stress-controlled and strain-controlled tests, S/N curves comparison *(German)* 80—40476
low C, struct. changes during decarburisation in intercritical temp. interval *(Russian)* 77—25075
low C, structural, AE rel. to crack tip plasticity *(Japanese)* 79—66150
low C, structurally free cementite formation 78—23697
low C, surface damage produced by pulsating impact contact load *(Japanese)* 80—104263
low C, surface layer struct. under sliding friction 79—52393
low C, surface shot blasting, prep. for plasma deposition 80—16586
low C, temp. effect on hysteresis loop under cyclic load *(Japanese)* 79—20096
low C, texture hardening in maximum shear planes during expansion 79—91704
low C, thermomechanically processed, martensitic fibre development, fatigue fracture 78—64572
low C, thin walled tube, fatigue behaviour, low endurance, under bending and torsion 77—86129
low C, Ti-stabilized, recrystn. texture development 79—83231
low C, transition behaviour, bending speed effect *(Japanese)* 78—11222
low C, type 08Yu, influence of nonmetallic inclusions on microfailures, during strain *(Russian)* 79—34128
low C, type 17G2SF, crack critical opening evaluation using plasticity diagram 80—45382
low C, type 38NCD4, fatigue life improvement by N ion implantation, dose depend. 80—76328
low C, type AISI 1018 79—61718
low C, type En3, high strain deform., struct. and props. 80—89301
low C, type KAS, fracture toughness meas. using elect. potential method *(Japanese)* 80—93722
low C, type SAE 1008, finite fatigue life distribs., various load-time histories 80—97589
low C, under rotating bending and torsion, overstressing effects *(Japanese)* 77—8935
low C, unnotched specimens, brittle fracture beyond general yielding, tensile-torsional stresses 77—56096
low C, V(C,N) precipitation and twinning in $\gamma \rightarrow \alpha$ transform. *(Polish)* 78—52807
low C, wear charact. on MgO single crystal 78—15541
low C, weldment, AE monitoring 79—87800
low C, with various strain ageing potentials, tension compression fatigue *(Japanese)* 79—20162
low C, yield point, effect of ageing stress 79—96091
low C, Young's modulus and internal friction meas., apparatus for elevated temp. *(Polish)* 79—96279
low C (0.01-0.05 wt.%), structural and mech. props., report *(French)* 80—25691
low C (0.04 wt.%), strain distribution near notch tip under mixed plane stress-plane strain condition *(Japanese)* 77—8891
low C conc. determ. using laser excitation in vac. UV *(Russian)* 77—12867
low C ductile-brittle transition behaviour, grain size effects 78—52942
low C fatigued, appl. of microbeam X-ray technique to plastic zone size evaluation 80—3199
low C S10C, fatigue strength under repeated stresses of superposed wave pattern *(Japanese)* 79—61705

carbon steel continued
low C sheets, effect of N_2 content on recrystn. texture 79—83233
low C steel, explosive-thermal treatment, sulphide cracking decrease, hydrogen embrittlement *(Russian)* 80—108477
low C structural, fracture toughness and X-ray diffr. obs. of surface *(Japanese)* 80—66634
low C type 08KP, plastic deform. depend. on grain size *(Russian)* 80—66580
low stability, vibratory magnetometer for high temp. anal. 77—28946
low temperature strength, preliminary plastic deform. effect 80—81128
low-C, 510 C and 520 C, tensile fracture at low temps. *(Japanese)* 80—81163
low-C, aged after quenching, rel. between micro-cracks and coaxing effect *(Japanese)* 80—81159
low-C, Al-stabilised, texturing during annealing *(Russian)* 78—19777
low-C, bond form. between powder layer and dense basis during hot pressing 79—24669
low-C, cast, SC49, rel. between rotating and flexural bending strengths *(Japanese)* 80—81117
low-C, coherent precip. of VC 78—35392
low-C, Cr, ferritic, optimal heat treatment development 79—38869
low-C, crack growth rate and crack tip shapes, fatigue, cyclic bending *(Russian)* 80—71740
low-C, creep rate and fracture, effects of prior stress history 77—4829
low-C, fatigue strength and crack propag. behaviour under impact program loading conditions *(Japanese)* 80—66635
low-C, fracture toughness, electroscopy remelting effect 77—63788
low-C, fully pearlitic, struct. and mech. characts. rel. to cooling conditions *(French)* 80—40425
low-C, gas nitrocarburised, aged, fatigue behaviour 80—40514
low-C, high-strength low alloy, Nb(CN) precipitation and coarsening during hot compression 80—97514
low-C, HSLA, austenite recrystn. 80—97512
low-C, kinetics of void development in fracturing A533B tensile bars 80—76357
low-C, Nb microalloyed, interaction between deform., recrystn. and precip. 80—97515
low-C, phosphorus effect on annealing texture, plastic anisotropy and mech. props. 77—25069
low-C, pitting resist. in low salinity geothermal brines 80—93681
low-C, preliminary thermomech. treatment, cold deform. effect on struct. and props. 79—38847
low-C, transformed by cooling in ferritic-pearlitic range, relations between cooling rate, struct. and mech. props. *(French)* 77—32570
low-C, type dynamic stress intensity factor meas., possibilities and limits Ni-Cr-Mo 37, dynamic stress intensity factor meas., possibilities and limits *(German)* 80—93719
low-C, types 535C, SB 42-B, fatigue crack propag. and crack closure behaviour under plain strain conditions *(Japanese)* 80—81160
low-C, types SS41, SB42, SM50A, STK55, liq. Zn embrittlement *(Japanese)* 80—81164
low-C, with Nb-B addition, transform. characts. and mech. props. *(French)* 79—43253
low-C containing Ti, sheets, recrystn. texture effects on plastic strain ratio and deep-drawing *(Chinese)* 80—66527
low-C electric sheet, struct. and coercive force after second cold rolling 77—44270
low-C sheet, texture anisotropy determ. using inverse pole figures *(German)* 77—44431
low-C-Si, LS1.2, LS1.5, phase transformation 80—45302
low-cycle fatigue effect of plastic strain and stress factor 77—63766
low-cycle torsional fatigue under multiple repeated loads of S45C steel *(Japanese)* 77—8925
low-temperature thermomechanical treatment of U8A, struct. 79—79008
machined, microdefects on surface 80—16607
machining, adhesion mechanism of built-up edge and layer on rake face of cutting tool 79—47784
machining theory, for chip geometry, cutting forces etc. 80—93629
magnetomechanical acoustic emission for residual stress NDT 80—71149
martensite, electron irrad., reversible C at. redistrib. 77—65991
martensite, quenched, and heated to 293K, struct., Mossbauer obs. *(Russian)* 77—59784
martensite, struct. transforms. during low temp. tempering *(Russian)* 77—59737
α-martensite decomposition in medium-C steels, low temp. singularities *(Russian)* 77—8814
martensite-ferrite combined microstructure, two-phase, tensile fracture strength 78—60783
martensites, fractography, facets classification *(Slovak)* 79—20173
martensitic, tempering induced decomposition and segregation, atom probe study 80—3112
martensitic by quenching 80—3038
martensitic needle size, effect on mech. props. after induction hardening in type 45 80—11672
martensitic points, effect of cooling rate *(Russian)* 79—43247
massive martensitic transformation kinetics 80—81060
mechanical properties after warm extrusion 77—12668
mechanical props., DIN ST 35, FBR safety anal. 78—60966
mechanical props. rel. to heat treatment, ferrite-pearlite transform. *(French)* 79—20043
medium, C, fatigue crack propagation under repeated two-step loadings above and below threshold condition *(Japanese)* 79—38945
medium, C, type 35 laser treatment effect on struct. and mech. props. 79—39041
medium, C, US attenuation, mag. field effect 80—89428
medium, Nb addition, effect on transformation and strength 80—7607
medium C, 45, fatigue strength increase by plasma steel coatings, fretting corrosive cond. 79—15875
medium C, 45, Ti+Al coated, failure during high temp. creep in NH_3 79—11731
medium C, behaviour under combined fatigue and wear 78—3236
medium C, Cr-Mn-Mo, austenising temp. effect on microstruct. and fracture toughness *(Chinese)* 80—66542
medium C, deform. hardening, plasticising action of Sn-Zn melts 80—55415
medium C, deformed, H_2 enhanced load relaxation 79—61635
medium C, drilling in liq. Sn-Zn eutectic, cutting conditions rel. to tool parameters *(Russian)* 79—34187
medium C, ductile fracture, in situ obs. of microprocess of failure *(Chinese)* 80—55492
medium C, ductility, fracture, effect of H_2 *(Russian)* 77—25131

carbon steel continued
- medium C, dynamic and static strength, strain rate and temp. depend. of flow stress 80—85139
- medium C, electrolytic Fe coated, distrib. of bounded fatigue limits 80—81198
- medium C, etchant for revealing austenite grain boundaries 80—85098
- medium C, fatigue crack accel. and closure in rotating bending tests, in annealed or quenched/tempered state 79—43383
- medium C, ground, residual stresses, X-ray evaluation 80—79863
- medium C, hardened, Mossbauer spectroscopy study of austenite and carbide 79—56646
- medium C, high-temp. heating effect on oxide inclusions 79—96051
- medium C, interface temp. meas. in fretting 78—64741
- medium C, internal cracks in continuous casting billet and rolling products *(Chinese)* 79—43375
- medium C, S45C, hardening temp. determ. using pulsed laser 78—72942
- medium C, S45C notched specimens, Charpy impact tests, notch angle effects *(Japanese)* 80—85124
- medium C, S 45 C, influence of mean strain on low-cycle torsional fatigue life *(Japanese)* 79—8348
- medium C, shell-shaped fracture due to B embrittlement *(Chinese)* 80—55493
- medium C, static and dynamic stress effect on hardenability and grain growth *(Korean)* 78—35404
- medium C, stress corrosion cracking, effect of H_2S, aggressive components of gas condensates and moisture *(Russian)* 77—16726
- medium C, tempered, normalised or quenched, statistical property of fatigue limit, press-fitted axles *(Japanese)* 77—12693
- medium C, thermomechanical working influence on mech. props. *(Russian)* 80—93578
- medium C, type 45, Cr galvanic coating thickness determ. by profilography 80—85095
- medium C, type 45, electroerosion, white-layer structures detection method 79—52485
- medium C, type 45, fatigue strength improvement after glow discharge treatment 80—108573
- medium C, type 45, sheet, working life, effect of dynamic loading type 77—21278
- medium C, wear charact. in unidirectional and reciprocating friction *(Japanese)* 79—100266
- medium C quenched, tempered, relation between wear and worn surface layers *(Japanese)* 77—52499
- medium C type JIS S45C, multiple notched specimens, fatigue props. 79—61729
- medium Cr, B effects on struct. and toughness 77—21265
- microcracks, non-propagating, opening and closing behaviour in rotating bending and torsional fatigue *(Japanese)* 80—25846
- microduplex, ferritic-martensitic, struct. effect on tensile fracture *(Japanese)* 79—96113
- microflow and strain hardening under cyclic loading 80—104182
- microstructural inhomogeneity, influence on formability and fracture 80—11682
- mild, 1019 AISI, acoustic emission generated during deform. 80—60921
- mild, AC effect on fatigue and static props. 80—45372
- mild, AC-induced corrosion 79—15864
- mild, activation energy for strain ageing 78—56677
- mild, adiabatic viscoplastic deform. at high strain rate, negative strain hardening *(French)* 77—21212
- mild, adsorbed H distrib. rel. to electrochemical treatment in pure alkali 80—16589
- mild, aerosol container, electrochemical cell for corrosion study 80—30180
- mild, AISI 1009 and 1018, corrosion incipient processes in hypersaline geothermal brine at 90°C 80—50753
- mild, alloying constituents, XES determ. 78—73126
- mild, and cold-rolled, diffusion, permeation, and accumulation of H_2 *(Japanese)* 77—39692
- mild, annealed, fatigue crack init., microstructure and strain ageing effect 77—86162
- mild, annealed, plastic flow under proportional and non-proportional straining 80—40465
- mild, anodic polarisation behaviour in hot alkaline sulphide solns. 80—100949
- mild, biaxial fatigue, data compilation and anal. 77—4856
- mild, cantilever beams, structural response under random loading conditions, memory model 77—3784
- mild, cathodic protection against corrosion fatigue cracks 79—74281
- mild, cavitation erosion rate, effect of stress level 78—15545
- mild, cold rolled, deformation texture *(French)* 79—70082
- mild, cold rolled, texture and plastic anisotropy rel. to alloying and precipitation *(French)* 80—108475
- mild, cold rolled sheets, microstruct. and strain path in deep-drawing 78—19775
- mild, cold-deformed, struct. changes during annealing, electron microscope obs. *(Russian)* 78—23722
- mild, cold-rolled, rate-sensitive, fracture initiation, loading rate and temp. effects 80—40532
- mild, conical rider on Cu surface, plastic deform. and wear at friction junction, SEM exam. 78—88542
- mild, constitutive eqn. covering wide range of strain rates *(Japanese)* 80—79862
- mild, contact resist. against metals, for high compressive stress and high current density 77—59324
- mild, corrosion, by applied alternating currents 79—70205
- mild, corrosion behaviour of borided and nitrided steels in aqueous media 78—95837
- mild, corrosion by Fe^{3+}, inhibition by potassium oxalate 79—39019
- mild, corrosion in complex aq. environment, linear polarisation investig. 78—76782
- mild, corrosion in lime water, stress effect 80—11815
- mild, corrosion inhibitor, zinc potassium chromate 78—95839
- mild, corrosion kinetics in presence of cyanoguanidine formaldehyde resin 78—19926
- mild, corrosion rate meas. in H_2SO_4 using microprocessor controlled potentiostat 80—71798
- mild, creep in low endurance fatigue 78—19865
- mild, critical soil moisture content in underground corrosion 79—96186
- mild, cyclic plastic deform. effect on electrode reactions in aq. chloride soln. of varying pH 77—52548
- mild, cyclic strain enhanced dissolution in NH_4NO_3, corrosion fatigue props. 80—85083

carbon steel continued
- mild, cylindrical shells, limit loading under loop bending moment 78—80581
- mild, descaling by HCl *(French)* 80—108642
- mild, ductile fracture of cracked plates, nonlinear boundary-value problem 77—81318
- mild, dynamic flat fracture resistance, shear lip effects 77—44451
- mild, effect of elastic stress on mag. props. *(Russian)* 77—8329
- mild, effects of CO_2-O_2 mixture compositions on hot cracking resistance 77—21239
- mild, elastic stress meas. using X-ray diffraction, wavelength effect 77—84202
- mild, elastic-plastic analysis of yield process 77—36571
- mild, electrodes, in H_2SO_4, H evolution reaction kinetics 80—97630
- mild, etching method for revealing plastic deformation 78—72825
- mild, etching of plastic zones 77—60013
- mild, eval. of cold rolling oils and boundary lubrication characts. by SEM 80—85068
- mild, exam. of fatigue damage, using thermography 78—92356
- mild, experimental analysis of junction growth with a junction model 79—47783
- mild, explosively welded, 0.1% C tube to 0.2% C plate, microstructure 77—70221
- mild, fatigue crack arrest and retardation, load stepdown effect 80—108527
- mild, fatigue crack growth and threshold measured at very high frequencies 80—71742
- mild, fatigue crack growth from a surface flaw 78—68803
- mild, fatigue crack growth in compression, notch effect 80—30065
- mild, fatigue crack initiation 77—86163
- mild, fatigue crack propag., stress ratio effect *(Japanese)* 79—38946
- mild, fatigue crack propag. study using servohydraulic test system 80—76431
- mild, fatigue crack propagation, acoustic monitoring 79—86313
- mild, fatigue crack propagation, stress ratio effect 80—71733
- mild, fatigue life, effect of H_2S and SO_2 gas 79—15871
- mild, fatigue limit, effect of grain size, cold work, temp., loading frequency 77—32685
- mild, fatigue softening and hardening detected from Barkhausen noise 80—76428
- mild, fatigue strength, effect of grinding surface *(Japanese)* 77—48533
- mild, fractography study of shear mode fatigue crack growth by etch pits *(Japanese)* 80—108545
- mild, fracture toughness meas. with reinforced-double-cantilever-beam specimen 77—4842
- mild, fretting fatigue, shot-peening effect 79—87733
- mild, fretting wear, role of adhesion and delamination 78—35533
- mild, friction welded joint, strain distrib. and fatigue damage under rotary bending *(Japanese)* 80—30076
- mild, grain size depend. of cleavage fracture toughness 79—8359
- mild, ground/sandblasted interfaces, tangential displacement, contact press. and lubricating film distrib. effect 80—16484
- mild, H_2 embrittlement, effect on design requisites for H energy systems 80—30109
- mild, hardness and protective props. of Cr film 78—11436
- mild, high temp., generation and reception of US surface waves test head device 78—95901
- mild, high temp. fatigue, effect of temp. variation 78—64685
- mild, hot shortness mechanism, surface enrichment of residual elements and oxidation *(Chinese)* 79—74230
- mild, impact velocity effect on fracture surface *(Japanese)* 79—96118
- mild, in Na_2SO_4 soln., anodic polarisation study of corrosion by AC 80—40582
- mild, inelastic beam flexural behaviour and lateral buckling anal. under cyclic loads *(Japanese)* 78—87283
- mild, interface between corrosion fatigue and stress corrosion cracking 77—86172
- mild, ion implantation of Ni and Cr, conc. profile 77—81339
- mild, junction growth mechanism during friction *(Japanese)* 79—32391
- mild, laser microspectral anal., Si and Cr trace element identification 80—108769
- mild, Luders band front 78—3168
- mild, Luders bound front, elastoplastic anal. by finite element method 78—3169
- mild, mech. behaviour, deform. rapidity influence *(French)* 79—57056
- mild, microbehaviour of notch tip during increasing load in brittle fracture beyond general yield 78—35487
- mild, microstructure effect on cleavage fracture stress 79—8358
- mild, mild, transgranular stress corrosion cracking in H_2SO_4-KCl soln., XPS obs. 80—16556
- mild, mode II fatigue crack growth threshold 78—92362
- mild, N_2 on oxidation resistance 79—61786
- mild, nitrided, oxidation resistance 78—95846
- mild, nonmetallic inclusion effect on pitting 80—35381
- mild, notch effect on impact fatigue strength *(Japanese)* 79—43400
- mild, orientation distribution function, representation of texture and slip directions 80—11665
- mild, origin of spherical particles on fatigue fracture surfaces and ferrograms 79—79112
- mild, oxidation of contaminated crevices exposed to CO_2 79—20243
- mild, panels, electrodeposition painting, effect of surface pinholing 79—43493
- mild, photoetched profiles 80—25907
- mild, pitting corrosion in O_2 bearing water, nonpassivating metal/environment system 80—30147
- mild, plastic deform. and pitting corrosion in neutral media 79—52415
- mild, plastic deform. around fatigue cracks, X-ray microbeam and recrystn. studies 80—35258
- mild, plastic deform. during fatigue, detection by Barkhausen noise meas. 79—43524
- mild, plastic deform. energy const. 77—32658
- mild, plastic flow, photoelastic investigation of temp. and strain rate effects 77—86238
- mild, plastic flow localisation under dynamic torsional loading, crit. variables 80—85015
- mild, plastic flow under proportional and non-proportional straining at controlled rates 79—57084
- mild, plastically deformed, X-ray meas. of stress and TEM 77—48496
- mild, plastically pretorsioned, dynamic props. 79—83267
- mild, plate, effect of striking velocity on perforation energy 78—68818
- mild, plate, explosive hardening of one end 77—36531

carbon steel continued
mild, precracked Charpy bars, plasticity spread 80—16415
mild, programmed fatigue crack propag., crack tip residual stresses 77—36644
mild, protection by Zn-rich paint in flowing aerated 0.5 M NaCl solution, Zn particle size effect 78—95840
mild, protection by Zn-rich paint in flowing aerated 0.5 M NaCl solution, exposed area ratio effect 78—95841
mild, protection by Zn-rich paint in flowing aerated 0.5 M NaCl solution, zinc content effect 78—95842
mild, protection by Zn-rich paint in flowing aerated 0.5 M NaCl solution, zinc oxide addition effect 78—95843
mild, reinforcing bars, stress strain charact. under cyclic loading 79—87688
mild, residual stress meas., acoustoelastic, in a patch-welded disc 79—27604
mild, resistance to slow stable crack growth, use of J integral 78—68809
mild, rolled, critical angle US reflectometry of stressed bar, book contrib. 79—100324
mild, rolled, texture analysis, vector method 79—83218
mild, S45C and SS41 types, dynamic yield condition under dynamic torsion and static tension 79—34214
mild, shear mode of ductile fracture 79—91785
mild, sheet, with low Al content, annealing, AlN recrystn., precipitation kinetics *(French)* 79—20083
mild, sliding contact in magnetic field, model for cross diffusion 79—79121
mild, SM41, brittle fracture initiation characts., under biaxial loading, exam. 78—60803
mild, solderability, annealing effect *(Japanese)* 80—89244
mild, stress corrosion cracking in NH_3 vapour above liquid NH_3 77—28926
mild, stress history effect on fatigue crack retardation 78—64627
mild, stress/strain relation formulation for plastic deform. for strain trajectory 78—52913
mild, subject to three point bending and tensile load, acoustic emission 80—3154
mild, surface hardness improvement by dynamic recoil implantation 80—61008
mild, surface oxide effect on acid corrosion inhibition 78—11384
mild, surface segregation induced by heat treatment *(French)* 77—59831
mild, susceptibility of underclad cracking, rel. to chem. comp. 77—21280
mild, tempered and quenched, dynamic fracture toughness 77—36665
mild, tensile and cyclic loading effect on Barkhausen noise 80—40560
mild, thin sheet, biaxial tensile deform., effect on crystallographic texture *(French)* 77—59814
mild, transgranular stress corrosion cracking in H_2So_4-KI soln. 80—71797
mild, tubes, crushed between rigid plates, large deformation compression 80—66579
mild, tubes between rigid plates, lateral compression, strain hardening effect 78—48422
mild, two sandblasted interfaces, tangential displacement, contact press. and lubricating film distrib. effect 80—16484
mild, under transverse loading 77—36567
mild, US detect. of H embrittlement 80—71822
mild, UV cured coating, protective and elec. props. 79—43489
mild, wave propagation in thin-walled tube, energy dissipation 77—7326
mild, wear exam. 79—87738
mild, wear mechanism against oriented fibre reinforced plastics 78—56782
mild, welded struct., dynamic initiation of brittle fracture, testing 77—36716
mild, with different grain sizes, surface strengthening by high frequency loading *(Czechoslovakian)* 77—28934
mild, with different sensitivities to strain ageing, cyclic plastic strain amplitude *(Japanese)* 77—8932
mild, work hardening and strain ageing during fatigue *(Japanese)* 77—8931
mild, X-ray meas. of conc. stress at crack tip *(Japanese)* 77—77570
mild, yield strength and fracture toughness, microstruct. effect, heat treatment 78—27615
mild, Zn gluconate inhibitor against corrosion in sea water 77—56136
mild steel, circular plate perforation and deformation by square section punch 79—34100
mild steel, fatigue of V-bent specimens 77—16681
mild steel, surface analysis rel. to annealing *(French)* 77—32857
mild steel pipe corrosion, mass transfer coeffs. under isothermal flow conditions 80—97628
mild wettability, effect of relative humidity 78—18872
Mossbauer effect exam. of effect of alloying elements 78—2781
natural reinforced composite 80—30039
naval, corrosion in harbour anaerobic sediments, rolling direction and tensile stress effects 80—30135
naval, corrosion in natural seawater, rolling direction and tensile stress effects 80—30134
nitrided layer, NH_3 gas addition to N_2-H_2(-C_3H_8) gas mixture and its effect on props. of layer *(Japanese)* 80—35403
nitriding, effect on struct. and internal stresses 80—30162
nonmetallic inclusion segregation during cooling *(Russian)* 80—100330
nonmetallic inclusions, improved metallographic technique for examining 78—72956
nonstrain-ageing state 77—52349
normalising device, for decarburisation determ. 79—87663
notched beam, fatigue crack emanates from notch root, fracture strength 78—72866
nuclear process liquid waste containers, stress corrosion cracking 77—46311
optical constant dispersion and emissivity, up to 900K 78—52464
pearlite, coercivity temp. depend., −196 to 770°C 77—20637
pearlite, deform. and fracture mechanisms, HV SEM obs. 80—104243
pearlite grade ShKh15, struct. transformations, hot plastic strain influence *(Russian)* 80—20927
pearlite growth, effect of Co additions 77—90359
pearlite in C steels (0.08 to 1.6 wt.%), exam. of temp. depend. of mag. coercivity 78—52304
pearlite interlamellar spacing, alloying additions effect *(German)* 80—40327
pearlite spheroidization, quantitative meas. 77—44275
pearlites, microplastic deform. of drawn and undrawn samples *(French)* 79—1894

carbon steel continued
pearlitic, deform. microstruct. and cementite fracture, −196 to 700°C 78—27576
pearlitic, struct. variations under plastic strain and subsequent heating, cementite decomp. *(Russian)* 80—84954
pearlitic eutectoid, cleavage fracture, grain size effect 78—60784
phosphide analysis using nonaqueous electrolyte potentiostatic etching method *(Japanese)* 80—89221
pipes, welded branch, stresses calc. 80—108493
pitting corrosion and scaling in geothermal brine 79—91843
plain C, cyclic induced creep at room temp. 80—25765
plain C, Nb microalloyed, interaction between deform., recrystn. and precip. 80—97515
plasma melting, N_2 absorpt., CO form. influence *(Russian)* 79—39193
plastic deform., −150 to 200°C, effect on loading surface 79—66130
plastic deform., study of loading surface 77—44322
plastic deformation by pencil glide, r-values and yield loci 80—7654
plastic relaxation, time dependent at crack tip 77—63765
plastic strain, high-temp., influence on austenite transformation kinetics of type Kh2G2P *(Russian)* 80—21004
plate, rolling direction determ. with notched bend test specimen *(German)* 77—60003
plates, comparison of dynamic tear and Charpy V notch impact props. 78—92357
plates, residual elements effect on through-thickness props. 80—66660
plating with Ni, Zn and Cu, barrel plating efficiency 80—100964
Poisson ratio, plastic prestrain effect in type 20 79—70103
pore formation in surface layers, during As diffusion redistrib. 80—49421
potentiodynamic behaviour, in conc. NaOH, cyclic voltammetric obs. 79—16006
powder forged, fatigue, surface treatment effect 80—85048
precipitation of VC in ferrite, pearlite, during direct transformation, TEM exam. 78—52812
predeformed, anisotropy temp. effect on yield point 78—39878
pressure vessel and piping, factors affecting notch toughness 79—61730
prestrain effect on non ductile transition temp. and bending speed relationship *(Japanese)* 78—84919
prior austenite grain size, effect on near threshold fatigue crack growth 78—92341
prior austenite grain size, effect on near threshold fatigue cracks growth 78—92342
push-pull fatigue strength, effect of tensile preload on plastic strain range *(Japanese)* 78—64625
quality, effect of methodic factors on quality of S replicas 79—24691
quench ageing avoidance, critical cooling rate *(German)* 79—52244
quenched, restoration of austenite grains during rapid heating *(Russian)* 80—76272
quenched and tempered, ductility, effect of hydrostatic press. 78—44190
quenched and tempered, struct.-prop. relationships 80—7599
radioactive contamination under applied potential in high temp. water 79—24646
recrystallisation textures, and deformation formed by dry sliding against steel 79—91698
recrystallization annealing, grain growth, effect of type of deform. 80—100847
relax. resist. rel. to struct. 78—23788
relaxation of residual stress with fatigue loading 77—56051
residual elements, effect on props. 80—66643
residual stress induced by uniaxial deform., mag. meas. 77—73390
residual stresses rel. to heating temp. in hardened, cold-drawn or shot peened samples *(French)* 77—77494
resistivity, thermal and elec., spin disorder scatt. anal. 78—76063
restricted durability, subject to pure bending with rotation 77—90431
reverse flow behaviour in spheroidized 1090, exam. 78—80610
reversible temper brittleness kinetics *(French)* 78—35498
ribbed surface, continuous hard layer *(Japanese)* 77—52501
rimming, effect of addition of Al to Zn on phase composition and morphology *(Polish)* 78—53014
rolled products, H flaking 80—50719
rolling contact fatigue, tufftriding effect on 0.2% C cylindrical specimen 80—100954
rolling wear study of misaligned cylindrical contacts 80—108590
rotating bending fatigue strength, high tensile load effect during stress cycling *(Japanese)* 77—52477
rotating bending fatigue strength, periodic high tensile load effects *(Japanese)* 78—11313
rotating bending fatigue strength of S15C, S35C, S55C, annealing in vacuum effects *(Japanese)* 78—11314
rotating disc electrode in 3 wt.% NaCl solution, corrosion rate meas. *(French)* 79—43470
rotational hysteresis 78—91889
rust prevention control by changing sulphide type 79—47813
SAE 1045, thick walled cylinder, finite strain pressure-tension loading 77—32632
sheet, thin, residual stresses determ. after bending 78—60708
sheet deformation, criteria for determ. of deformation limit G *(German)* 80—21000
siliciding in US field 79—39043
sintered, diffusional boronizing, exam. of process 79—96219
solidification singularities in C and low-C steels *(Russian)* 78—80532
spheroidised, fracture toughness, cementite particle effects, optic and electron obs. 78—60785
spheroidised, fracture toughness, cementite particles effect., obs. 77—70165
spheroidization at 680 to 690°C, struct. changes *(Russian)* 78—15431
spheroidized, medium C, strain hardening 78—52845
spheroidized, shear mode of ductile fracture 79—61714
spinning machine ring, increasing wear resist. by boriding 80—21115
spring, 60C2A, tempered under stress, influence of tempering conditions on mech. props. *(Russian)* 79—47724
spring, compressed, patented wire, reverse elastic aftereffect and fatigue strength 79—38881
stainless steel, alloyed with C, magnetron-sputtered, microstruct., and cryst.-amorphous transition 80—19719
statistical fatigue props. eval., heat-to-heat variations, low C S25C, medium C S45C 78—7048
statistical fatigue props. of heat treated JIS steel S 45 C and SK 5 78—44222
steel, 35, fracture characteristics, notch sharpness effect in impact tests 79—52536

carbon steel continued
steel, boride coatings from induction heating microstruct. and props. 80—30165
steel, C, bainitic hardenability, overheating effect 79—38866
steel, C, pearlite grade ShKh15, struct. transformations, hot plastic strain influence *(Russian)* 80—20927
steel, C, rod, breakdown charact. by longitudinal stress waves 78—38773
steel, low C, cyclic plasticity and low cycle fatigue life 80—21058
steel, medium C, 40MnB, dissoln. and precipitation of $M_{23}(C,B)_6$ *(Chinese)* 80—66511
steel, medium C, Ni-Cr-Mo, overheated, fractographic study *(Chinese)* 80—66616
steel, mild, bolt thread strain meas. 78—60972
steel, mild, ground/sandblasted interfaces, tangential displacement, contact press. and lubricating film distrib. effect 80—16484
steel, mild, two sandblasted surfaces, tangential displacement, contact press. and lubricating film distrib. effect 80—16484
steel, plain C, quench ageing avoidance, critical cooling rate *(German)* 79—52244
steel C, fatigued, strengthening by surface plastic deformation 78—88505
steel St3, kinetics of form. and struct. of thermodiffusional protective coatings 77—56158
strain ageing, essential work of plane stress ductile fracture 79—29187
strain ageing, of types AISI 1008, 1020, 1035, renitrogenized 1010 and 1522, changes in tensile notch impact and fatigue props. 79—43288
strain ageing and fatigue limit 80—40378
strain ageing contribution to fatigue hardening 78—23817
strain hardening parameters, determination from stress-strain curves 78—80562
strength, fracture, effect of H_2, varying C content *(Russian)* 77—25129
strength, static, dynamic, interrelation 79—15725
stress and temp. short time effects, room and elevated temp. tensile tests, creep fracture tests 78—35462
stress corrosion cracking in radioactive waste storage tanks 79—70226
stress corrosion cracking susceptibility in liquid NH_3 *(Japanese)* 78—11411
stress depend. of US velocity *(Japanese)* 78—26629
strip, low-temp. strength and brittle fracture susceptibility of type 1792AF 79—38966
structural, ductile and brittle fracture resist. in stable crack growth stage 79—52369
structural, fatigue softening, temp. and load freq. influence *(German)* 79—61614
structural, grain boundaries, AES 79—24524
structural charges after deformation and annealing, Mossbauer spectroscopic exam. *(Russian)* 78—35446
structural strength, increase by high temp. mech. treatment with austenite isothermal decomp. 79—24555
structural transform. and surface hardening by laser treatment 77—70233
substrate, ion plating of hard TiN decorative coatings 78—11441
substrate, load-bearing capacities of TiC layers 80—40606
sulphide cracking resistance 80—108640
sulphides, obs. and anal. using non-aqueous electrolyte-potentiostatic etching method *(Japanese)* 80—89433
superplastic characteristics, carbon content influence *(Russian)* 77—21218
superplasticity due to successive deformations *(Russian)* 80—55464
surface, heated, water droplet evaporation, heat transfer characts. 78—59269
surface alloyed with nitride forming elements, nitriding *(Russian)* 78—31569
surface burnishing effect on low cycle corrosion fatigue *(Russian)* 77—16730
surface crack exam. by eddy current technique 77—9007
surface damage during friction, struct. effect 80—35339
surface damage produced by pulsating impact contact load *(Japanese)* 80—104263
surface deposit of ZrC, exam. of composition *(Russian)* 79—34201
surface tension and limit wetting angle in contact with $CaO-SiO_2-Al_2O_3-Na_2O-CaF_2$ melts *(Czech)* 79—37908
surface wearing ability, surface finishing method and running-in effects 80—11794
surfacing, self-shielding flux-cored wire development 79—8402
temperature monitoring system used during mech. deform., stress anal. appl. 79—12796
tempered, with different Ni contents, scaling behaviour obs. 80—71817
tempering, associated microstresses 80—3111
tempering, second stage 79—61627
tempering effect on struct. and mech. props. of types 70, U8, and U12 *(Russian)* 80—50655
tensile fracture surface in high press. H_2 at room temp. *(Japanese)* 80—108540
tensile props. in high press. H_2 at room temp. *(Japanese)* 80—108501
tensile strength, effect of specimen length *(Japanese)* 78—84920
tensile strength, working and heat treatment effects *(Japanese)* 80—104209
tensile strentgh, thermomechanically treated eutectoid steel as in situ composite material 80—7649
tensile testing, acoustic emission signals interpretation 77—9030
texture effect on mech. props./magnetic props. relationship, NDT appl. 79—96274
textured, rolled, REK and lattice strain distrib. *(German)* 79—29095
thermal diffusivity meas., const.-rate heating method *(Japanese)* 78—79976
thermal fatigue, effect of temp. difference in fatigue tests on fatigue life *(Japanese)* 78—84978
thermal stresses, spontaneous relaxation 79—1892
thermal stresses in submerged arc welded joint, consideration of phase transformations 79—61683
tool, 45, self lubricating composite, frictional props., Ag-Cu-Zn-Cd lubricant 78—11340
tool steel transformation hardening by CO_2 laser 80—16483
torsional fatigue process, obs. by electron microscope *(Japanese)* 77—12690
torsional fracture strain, effect of pre-straining *(Japanese)* 80—3183
torsional prework effect on fatigue strength, crack propagation *(Japanese)* 80—55514
transformation kinetics, heat cond. and elastic-plastic stresses during quenching *(Japanese)* 80—25688
trapping mechanism, detection, positron meas. 80—84798

carbon steel continued
tube blanks, mech. props., statistical determ. 79—29316
tufftrided, fatigue strength and microstructure change by reversed stressing *(Japanese)* 78—15511
tufftrided steel, type S15CK, fatigue strength, estimation of size effect *(Japanese)* 80—81166
type S15CK, tufftrided, fatigue strength at elevated temp., under reversed axial strength *(Japanese)* 78—84980
ultrahigh C, heat treated, mechanical properties and microstructure 79—57012
ultrahigh C, superplastic, mech. behaviour at elevated temps. 80—21028
ultrahigh C, superplastic struct. development by heat treatment 80—11703
US wave velocity meas., rel. to cold working in type $38NiCrMo_4$ 80—99908
vanadisation by CVD 80—44454
wear, struct. changes in centres of galling 79—38985
wear charact. of worn surface layer under lubrication *(Japanese)* 78—35526
wear during impact, effect of C content 79—38986
wear of Cr, Zn protective coatings, exam. using nuclear radiation excited X-ray fluorescence 80—21206
wear property, of S25C gas nitrosulpherising steel 80—50729
wear resistance, change through hardened layer 79—96153
wear resistance during friction, effect of retained austenite 77—21288
wear resistance in liquid Sn and Bi *(Russian)* 77—59941
wear resistant, review of abrasive adhesive and rolling wear *(Korean)* 79—24624
weldable, ferrite-pearlite, Widmanstatten structs., resist. to fracture 79—29203
weldable, precipitation hardening rel. to low cycle fatigue *(Czech)* 79—15686
welded joint in corrosive environment, S-N data determ. 79—66227
welds, residual stresses, evaluation by Barkhausen noise meas. 80—76436
white layers effects on stress-corrosion resistance rel. to C content *(Russian)* 78—11393
wire, drawing effect on spheroidization *(Korean)* 77—66656
wires, pre-strained electroheated, corrosion behaviour, direct resist. heating technique study *(German)* 80—40580
X-ray diffraction correlation between cyclic loading and residual stress *(German)* 78—48583
X-ray fluorescence anal. of carbon content in surface layers and in bulk 80—3466
X-ray line fitting by Gram-Charlier distrib., appl. to tension test *(French)* 79—15689
X-ray stress meas., appl. of position sensitive proportion counter *(Japanese)* 78—64791
yield and breaking strength, US exam. 79—15755
yield point determ. rel. to grain size, deform., ageing and temp., dislocation theory *(Serbian)* 79—34120
yield strength, anisotropy in relation to temp. of deformation 78—80612
B-Al coated, creep and long term strength in NH_3, type 45 79—91854
BN thick film, crystn. and semicrystn. CVD on C steel substrate 79—87586
C-Mn, stress corrosion cracking failure, predictive approaches 80—97611
cold swaged, exam. of H_2 attack mechanisms 78—76791
Cr diffusion coating ductility, on types 45, 50, U8, U10 79—43357
Cr effect on carbon steel weld metal hot cracking resistance 79—79061
Cr-Ni steel, carburised, effect of atm. during heating to quenching temp. on austenite decomp. 77—56157
Cu-mild steel explosively welded interface, SEM examination *(German, English)* 80—96746
Fe-C, pre-eutectic melt, struct. anomalies *(Russian)* 77—28794
Fe-C (0.11, 0.23, 0.42 wt.%), grain boundary ferrite allotriomorphs, growth kinetics 77—44244
Fe-C (1.0 wt.%), mixed powder compact, sintering, C diffusion meas. 77—90293
Fe-Cu-C, fatigue behaviour for tempering at 500°C, precip. hardening 77—40442
Fe-P-C alloys, amorphous, mag. anisotropy, Mossbauer obs., prior cooling effects *(Russian)* 77—32300
H attack kinetics and service behaviour 78—39951
H permeation, and trapping meas. in plain C type 1045, rel. to cryst. microstruct. 80—84328
low-C, Nb, microalloyed, hot rolled, Nb(CN) precip. and austenite recrystn. 80—97513
Mg cast iron, microstruct. of spheroidal graphite, rel. to polishing and annealing treatments 77—56160
Mo coated, fretting wear and fatigue strength assessment 78—88583
Ni-Cr, surface hardened, rolling contact fatigue failure 80—16608
S determination, flame chemiluminesc. method 78—48711
SiO_x inclusion formation on introduction of solid SiO into molten steel *(Russian)* 78—80530
steel, C, eutectic, YU8, effect of segregating structurally free ferrite *(Russian)* 79—15677
Ti-coated C steel, effect of heat treatment on struct. and props. 77—56159

carbon tetrachloride, CCl_4 *see organic compounds*

carcinotrons
relativistic millimetre, electron beam in high current accelerator 79—68359
wideband carcinotron tunable submillimetric source 77—41304

cardiology
see also blood; electrocardiography; haemodynamics
9.712 GHz irradiation effect on vagal heat membrane bound acetylcholinesterase 80—3593
acoustic model for computer-aided surface acceleration mapping 78—35791
action potential, cond. and propag., equiv. cct. 78—31791
adaptation and hypertrophy, ventricle model *(Japanese)* 78—31828
afferent innervation of heart and great vessels, vagal rel. to sympathetic components 79—83726
ambulatory noninvasive monitoring of physiological data, recording systolic time intervals 79—66574
aneurysms, possibility of blow out 79—88100
angiocardiogram computer analysis, pot. energy distrib. rel. to left ventricular efficiency 77—40757
angiocardiogram objective quantitative processing, Cardiac Image Analysis System 79—70629
angiocardiographic image computer quantitation 80—36118

cardiology continued
  angiocardiography, digital multiprocessor system 80—94362
  angiocardiography, improved digital real-time processing and storage 79 70624
  angiocardiography, quantitative radionuclide, in dogs with atrial septal defects 78—85362
  angiographic computerised evaluation of left ventricular wall motion 79—70634
  angiographic definition and quantification of regional left ventricular contraction 79—70637
  angiographic images of left ventricle, system for off-line anal. using minicomputer 78—80964
  antithrombotic prosthetic surfaces development, bioelectrochemical approach 78—40414
  aorta, root of, functional anatomy and deform. props. 80—67136
  aorta valves, crescent-shaped, deform. props. by holographic interferometry 80—61616
  aortic and mitral valve prostheses, in vitro flow visualisation 77—86703
  aortic ejection click and first heart sound description 80—30827
  aortic heart valves, blood pressure drop across, steady and pulsatile flow 79—74707
  aortic regurgitation rel. to thoracic impedance cardiogram, dog expt. 77—40890
  aortic stiffness noninvasive determ. methodology, echocardiographic recording 79—83875
  aortic valve, closing behaviour, model 79—53170
  aortic valve, expansible nature of base, rel. to prosthetic design 78—40232
  aortic valve, human, finite element stress analysis 77—44699
  aortic valve, vortex motion and induced pressures 79—62288
  aortic valve leaflet stress anal., pig 79—53168
  aortic valve leaflets, stress anal. with smoothed geometrical data 77—52815
  aortic valve mechanics, anal. in diastole 80—35928
  aortic valve mechanics, material props. of natural porcine valves 79—39440
  aortic valve opening, haemodynamics 78—20208
  aortic valve prostheses, hydrodynamic losses eval. 80—72378
  aortic valve prosthesis, Hancock porcine xenograft, comparison of models 242 and 250 77—56532
  aortic valve prosthesis, Reul-Ghista optimal tri-leaflet, in vitro performance tests 79—92432
  aortic valve prosthesis water hammer pulse effect *(Japanese)* 78—3676
  aortic valve replacement, computerised simultaneous press./vol. anal. before and after 80—85531
  aortic valve replacement with subcoronary ball valve, early expts. 77—56524
  aortic valve study, by holographic interferometry and shadow Moire methods 80—104613
  aorto-coronary saphenous bypass surgery, ^{201}Tl myocardial perfusion scintigrams 79—25068
  apexcardiogram, math. model of endogenous thoracic forces 78—31849
  arrhythmia monitoring, 15-channel analogue selector 77—40898
  arrhythmia monitoring, ARGUS/RT microcomputer system 78—81014
  arrhythmia simulation device 78—44636
  arrhythmia treatment by temporary cardiac pacing 77—81648
  arrhythmia treatment with permanent cardiac pacing 77—81674
  arterial stenoses, fluid mechanics 80—35948
  arterial system and cardiac activity, optimum tuning model *(German)* 79—16225
  arterial system impulse response determ. 79—79594
  arterial vasa vasorum deformation/hydraulic resist. study *(Japanese)* 78—3544
  artifical heart, stroke vol. and cardiac output meas. by echographic technique 80—41319
  artificial, mitral valves, insufficiency, press. and work losses *(German)* 78—88764
  artificial blood pump fabrication for durability 79—84026
  artificial heart, bench test technique 79—48366
  artificial heart, microcomputer based automatic controls 80—67289
  artificial heart, rigid-vane system development 79—84025
  artificial heart, simulation of fluid dynamics *(Japanese)* 79—43954
  artificial heart, transfer function governing ventricular ejection in assisted circulation 80—104817
  artificial heart 79—84016
  artificial heart and assisted circulation apparatus, hydrodynamic test bench rigs 79—48372
  artificial heart designs compared 79—48367
  artificial heart performance, role of cardiac valves 80—21575
  artificial heart valve closing element, kinematics photoelectric recorder 79—48370
  artificial heart valve closing element surface pressure distrib. 79—57811
  artificial heart valves, dynamics 80—72379
  artificial valve with convex closing body *(German)* 78—81066
  atrial and/or arterial blood pressure servo control in expt. animals 78—31986
  atrial contraction, model anal. of contrib. to ventricular filling 80—85424
  atrial electrode placement, transmediastinal retrocardiac and transvenous endocardial methods 77—81685
  atrial muscle, cyclic GMP rel. to negative isotropic effect of acetylcholine 77—48781
  atrial pacing stress test quantification, normal, abnormal values, coronary artery disease in man 78—85449
  atrial septal defect assessment by echocardiography 79—70600
  atrial septal defect repair, sinus node dysfunction and atrioventricular conduction disturbances 77—81647
  atrial trabecula membrane, frog, accommodation, repeat responses and anode-breaking excitation 78—64956
  atrial-triggered cardiac pacing method and long-term results 77—81690
  atrioventricular block, ventricular overdrive test evaluation 77—81632
  atrioventricular block natural history and diagnosis 77—81626
  atrioventricular conduction disturbances with permanent pacemakers 77—81672
  atrioventricular region of rabbit heart, passive elec. props. rel. to intercellular link 78—48767
  atrium, bullfrog, mechanisms for positive inotropism of low-K Ringer soln. 77—77884
  atrium of bullfrog, tension components and temp. effects 77—52760
  atrium trabecula membrane, changes in elec. props. due to elec. stimulus 77—36891
  avian heart rate meas. using autocorrel. techniques 78—31989

cardiology continued
  ballistocardiogram compared with HF ECG 78—77123
  ballistocardiograms, statistical pattern recognition 80—26408
  beat-to-beat stroke volume estimation from pulmonary arterial pressure contour 79—53178
  biofocal diverging collimator for equilibrium radionuclide ventriculography 80—72310
  biological material, laser stereometry light-scatt. technique, cardiac images 80—56310
  biomagnetic instrumentation and meas. 80—36181
  biomechanics of intact heart, relationship between velocity, muscle length, force and contractile state 78—44543
  biomedical engineering seminary, Brno, Czechoslovakia (Sept. 1976) *(Czech)* 77—17001
  biopotential distribution laws rel. to functional state 78—65142
  biotelemetry, conf., Garmisch-Partenkirchen, W.Germany (May, June 1978) 79—43980
  birth monitoring by cardiotocography, interference effect by infusion pumps *(German)* 78—85416
  Bjork-Shiley aortic prosthesis, in vitro vel. meas. using laser-Doppler anemometer 80—17196
  Bjork-Shiley tilting disc heart valve 77—56525
  blood flow, numerical anal. 78—15854
  blood flow detection in human heart, US pulsed Doppler flowmeter system, microcomputer based 80—104690
  blood flow distribution within the myocardium *(Japanese)* 79—96590
  blood flow meas., computerised system 80—36051
  blood flow through heart valves, vortex method calcs. 80—72189
  blood flow visualisation, clinical usefulness of US pulsed Doppler technique *(Japanese)* 79—96638
  blood gas and acid-base calculations, electronic data computing 79—25139
  blood pool, dynamic radio-isotopic images, time-motion display 79—5347
  blood pool imaging over complete cardiac cycle using multiformat imager 77—40737
  blood pool visualisation, ^{99m}Tc labeled red blood cells and serum albumin 79—29601
  blood pressure control, racial differences 80—30757
  blood pressure control model 77—21557
  blood pressure control system dynamic behaviour identification 79—2097
  blood pressure waves, physiological interpretation of spectra, heart rate, respiration waves 79—29540
  blood pump regulation with pressure controlled servo-drive *(German)* 79—84003
  blood velocity measurements in vicinity of aortic prostheses 79—74706
  blood-pool imaging in ^{99m}Tc myocardial scintigraphy 80—12228
  bradycardia, during face cooling, selective brain cooling as possible cause 80—30670
  capacitoplethysmography for heart and lung meas. *(Japanese)* 78—53465
  cardiac electrodes, safe voltage limits 79—16344
  cardiac function, reliability of noninvasive methods for meas. during exercise 79—16231
  cardiac function modification by synchronised oscill. accel. 80—56089
  cardiac mechanical activity, noninvasive mag. detect., instrumentation 80—89820
  cardiac noise, automatic segment anal. *(German)* 78—88759
  cardiac output, meas. from respiratory tracer gas nonlinear computer anal. 79—62395
  cardiac output analysers, equipment, maintenance and ccts., review 78—69239
  cardiac output and shunt calc. from dye dilution curves using automated catheterisation system 78—81023
  cardiac output automatic determ. by indicator dilution in computerised monitoring system 78—81022
  cardiac output control mechanism modelling *(Japanese)* 78—69133
  cardiac output estimated by impedance cardiography 79—57741
  cardiac output on-line determ. by thermodilution in coronary care unit 78—81021
  cardiac pacing, symposium, Tokyo, Japan (Mar., 1976) 77—81666
  cardiac stimulator for evaluation of mech. and elec. responses 79—44058
  cardiac synchronised augmented pulsation pressure concept, prototype 77—78058
  cardiac-assist in-series devices, controller 78—81075
  cardio-pulmonary system, thermal indicator heat and mass transfer, pulsatile flow 79—25018
  cardio-pulmonary system, thermal indicator heat and mass transfer, pulsatile flow 79—25017
  cardio-vascular structures, new examination method, short range sonar 78—87221
  cardiograms, image processing, cardiac function meas. *(Japanese)* 80—94354
  cardiomagnetism, high resolution 80—104698
  cardiomyopathy scintigraphic diagnosis by ^{99m}Tc-labelled pyrophosphate, method sensitivity 80—17061
  cardiopulmonary analysis, computerised data reduction 77—44814
  cardiopulmonary bypass, portable, appl. to emergency instrumentation 78—44679
  cardiopulmonary control and lung O_2 and CO_2 exchange interaction model, duck 80—3600
  cardiopulmonary monitoring of high-risk infants using microprocessor-controlled memory 78—31962
  cardiopulmonary readjustments in passive tilt 80—56084
  cardiopulmonary resuscitator, programmable, for evaluation of standards 80—72374
  cardiopulmonary stress test data acquisition and control systems 79—79673
  cardiopulmonary stress testing in children 80—30911
  cardiostimulator, implanted, contactless rhythm indicator 79—39602
  cardiosynchronisation method for assisted circulation apparatus, problems 78—7534
  cardiotachometer calibration, precision pulse generator, cct. 77—86682
  cardiotocograph for foetal heart-rate monitoring *(German)* 77—86566
  cardiotocography, Partecust equipment, effect of technical recording conditions 77—44783
  cardiovascular activity, piezoceramic acceleration transducer recording 79—39536
  cardiovascular and other physiological signals, 7-channel data averager/printer 78—40366
  cardiovascular and respiratory system dynamics *(French)* 79—34585
  cardiovascular changes associated with age, US obs. in dogs 77—25504

cardiology continued
cardiovascular computerised modelling, pressure regulation in hypertension 79—88098
cardiovascular computerised monitoring in medical intensive care unit 78—20304
cardiovascular control dynamic test method evaluation, model considerations *(German)* 77—52813
cardiovascular disease diagnosis, US appls. *(Russian)* 79—39456
cardiovascular dynamics instrumentation evolution (1940-80) 79—83983
cardiovascular effects of positive-pressure ventilation in normal subjects 80—41081
cardiovascular emergency clinical assessment, use of ECG telemetry 78—44677
cardiovascular function, effects of noise exposure, rhesus monkey study 79—5322
cardiovascular function, effects of normal and loaded spontaneous inspiration 80—56088
cardiovascular measurements, conf., Bellingham, USA (Sept. '78) 80—31419
cardiovascular medical diagnosis, bicycle ergometer AM 368 *(Italian)* 80—30918
cardiovascular modelling of pressure regulation effects, hypertension 77—73539
cardiovascular nuclear medicine, an overview 80—85480
cardiovascular nuclear medicine, instrumentation and data processing, ventricular function evaluation 80—85481
cardiovascular radiopaque marker tracking algorithm 78—40329
cardiovascular research database system 78—53549
cardiovascular response to acute aquatic and treadmill exercise in the untrained rat 80—8085
cardiovascular response to dynamic/static exercise monitoring, four-channel radiotelemetry 78—3633
cardiovascular shunts, detection and quantitation with commonly available radioisotopes 80—94356
cardiovascular simulator for the undergraduate physics laboratory 79—84889
cardiovascular surgery, endothelial lesions associated with vascular clamping 79—53278
cardiovascular system, analogue circuit and compartmental model, normal and defective states 79—57700
cardiovascular system, early adaption to simulated zero gravity 80—3827
cardiovascular system, haemodynamic obs. in awake rabbits during hyperbaric He-O_2 exposure 80—101200
cardiovascular system, identification and parameter estimation 80—35947
cardiovascular system, mathematical models and identification problems 80—89780
cardiovascular system contractility characterisation by programmed premature contractions 79—88113
cardiovascular system simulation by elec. compartmental model 79—5388
catheter flow probe for left ventricular source parameters meas. 79—92324
catheterisation, automated processing and storage system 79—70694
catheterisation computer system 79—70695
catheterisation data analysis programs 78—36017
catheterisation data analysis via remotely located hybrid computer system 77—40869
catheterisation data on-line analysis by remote access computer system 77—40870
cellular electrophysiologic-clinical correlations using a relational data base 80—89890
cerebral echo-pulsation curve and plethysmograms anal. of cardiac arrhythmia 78—7413
Chagas' cardiomyopathy treatment with implantable pacemakers 77—81681
Chagas' disease, sinus node dysfunction obs. 77—81776
chemical power, appl. of power, work and efficiency eqns. to left ventricular energetics in man 80—16912
chemical power, derivation of chem. power eqn. and determ. of eqn. consts. 80—16911
chest motion due to heart action, imaging by holographic interferometry 79—20699
chest X-rays automated screening, image segmentation and cardiac silhouette anal. 79—88178
chronic arrhythmias produced by focused ^{60}Co γ-irrad. of canine atria 80—41136
cineangiocardiograms, automatic anal. using TV system on line with minicomputer 78—92699
cineangiocardiography, accuracy of ventricular models and localisation of contraction anomalies 80—89845
cineangiograms, computerised anal. system 80—72284
cineangiography, automatic detect. of apex of heart 80—89847
cineangiography, left ventricular contour segmentation from anatomical landmark trajectories and its application to wall motion analysis 80—94363
cineanigiocardiogram of left ventricle, automatic processing and cardiac function display techniques *(Japanese)* 80—72311
circulation-assist, steady state anal. of press. and flow 80—17193
circulatory system polynomial model *(Japanese)* 77—70488
circulatory variables, power spectra of spontaneous variations 79—29538
circumferential fibre shortening vel., computer anal. for eval. of cardiac performance mechanics 77—37095
circumferential fibre shortening vel. determ. from meas. left ventricular dimensions 77—48867
clinical applications of US techniques 79—79619
clinical vascular laboratory instrum. management using computer 78—7460
colour scintiphotographic radionuclide angiography, aide to isotope ventriculography 80—12239
computed tomography 80—98088
computer applications, conf., Rotterdam, Netherlands, (Sep.-Oct. 1977) 78—81013
computer applications, conf., Stanford, USA, (Sept. 1978) 79—62387
computer cardiotomography, methods and results of morphological anal. 79—34647
computer graphic techniques for heart damage quantification 79—29654
computer system SYSCORMORAM for haemodynamic and cineangiographic data treatment 78—81030
computer-aided monitoring after open-heart surgery, appl. to adrenaline effects meas. 78—81059
computer-controlled stimulator for ventricular myocardial function analysis 77—60267

cardiology continued
computerised data processing system 80—56236
computerised fluoroscopy for non-invasive cardiovascular imaging 80—17121
computerised positron emission tomography for assessment of myocardial integrity 80—36120
computerised radionuclide cardiography, hardware and software techniques 79—57806
computerised tomography, dynamic 3D imaging system for cardiac structures and functions 78—44600
computerised tomography, ECG-gated, motion phantom 80—98115
computerised tomography, multislice reconstruction from twin-cone beam scanning 79—66546
computerised tomography, resource sharing computer hierarchy for 3D image reconstruct. 80—26345
computerised tomography, scanner for early detect. and evaluation of heart disease 79—66521
computerised tomography of heart and circulation, dynamic spatial reconstruction system 79—66520
computerised tomography system, high speed heart imaging 79—66544
computing conf., Geneva, Switzerland, (Sept. 1979) 80—82582
conference on cardiac defibrillation and cardiopulmonary resuscitation, Lafayette, USA (Sept. 1979) 80—67929
congenital defect detection using roentgen densitometer, patient dose 77—9239
congenital defect evaluation from dynamic tracer meas. 78—40378
contractile filament and series elastic work and power, clinical correls. 80—16982
contractile filament and series elastic work and power, mathematical model 80—16981
contractility, muscle tissue quality and sliding filament micromechanism *(Dutch)* 78—73171
contractility, optimal, minimal O_2 consumption, theoretical approach 79—74694
contraction, left ventricular wall and fluid dynamics 78—44523
contraction kinetics recording using thorax elec. fields *(Czech)* 78—77138
contraction mechanism modelling 80—72204
control of heart rate in man, system anal. 77—25478
Cooley-Cutter heart valve prosthesis 77—56526
coronary angiogram computer quantitation 80—41233
coronary arteriography, current techniques and equipment 78—35940
coronary artery blood flow thermographic visualisation during by-pass surgery 79—53265
coronary artery bypass graft patient recovery trajectory classification algorithm 80—94411
coronary artery disease, abnormal left ventricular contraction pattern cineangiography 79—83930
coronary artery disease, sensitivity and specificity of ^{201}Tl perfusion scintigrams 79—25069
coronary artery disease, significance of abnormal rest ^{201}Tl myocardial image 80—17060
coronary artery disease extent prediction by ^{201}Tl myocardial images 80—26336
coronary artery quantitation using digital image processing techniques 80—85517
coronary blood flow, calc. from myocardial clearance of systemically administered ^{133}Xe 77—16967
coronary blood flow meas., precordial counting collimator 77—77967
coronary bypass surgery, left ventricular function and myocardial metabolism evaluation by atrial pacing 77—81646
coronary care unit emergency cardiac pacing experience 77—81651
coronary care unit equipment failure finding and prediction 78—44648
coronary heart disease, demand pacing hazards 77—81668
coronary heart disease screening, direct-writing ECG recorder ST segment distortion assessment *(German)* 77—90945
coronary lesions of left anterior descending artery, exercise ECG diagnosis 79—70692
coronary perfusion pressure programmable control circuit 79—92278
coronary regional intravascular resist. determ. 78—31853
coronary sinus blood flow on-line computerised assessment by thermodilution 78—81024
counterpulsation assist pumping, optimum performance determ. under computer control 78—24181
counterpulsation dynamics simulation, rel. to heart assist. blood pump 80—16996
cross-sectional shape change during beats, simulation 77—44714
current noise parameters in embryonic heart cell aggregates 80—21459
cytosol, aspartate transaminase, electron density map interpretation 80—55990
data collection station, based on autonomous CAMAC crate 80—61689
data processing in real time by hybrid computer, optical link 77—86677
defibrillation, multiple-shock, effect of shock separation time 78—57053
defibrillation, myocardial damage rel. to high-energy elec. current 78—57051
defibrillation, performance characteristics of three commercial instruments in transthoracic ventricular defibrillation of animals 78—57048
defibrillation, transchest, strength-duration curves for trapezoidal waveforms of various tilts, dogs and ponies 78—57054
defibrillation, transchest damped sine wave shocks producing cardiac damage 78—57052
defibrillation, transchest ventricular, comparative efficacy of damped sine wave and square wave in dogs and ponies 78—57055
defibrillation, transthoracic, square-wave, experience in dog and calf 78—57050
defibrillation, transthoracic ventricular, in adults, success rate rel. to energy used 78—57049
defibrillation conference, Lafayette, USA, (Sept. 1977) 78—57047
defibrillator, automatic, implantable, cardiac pumping detect., optimal electrode spacing 80—72373
defibrillator electrodes, recovery curves for different materials 80—67283
diagnosis, analysis of signals from pulsating arteries 77—48831
diagnosis, US real time system for simultaneous image displays 80—41148
diastolic semilunar valve vibrations, heart sounds, one-dimensional model 79—79580
digital cardiac defibrillator tester 80—41286
digital pulse counter for cardiovascular monitoring 78—35978
dipole apparent orientation, vol. conductor effects 78—28108
dipole moment variation with body size, double-layer model 77—56358
disc mitral valve in left ventricle, computer model of motion 80—8

cardiology continued
  disease prognosis, appl. to haemorrhagic shock, nonlinear dynamical model 79—83838
  Dopper echocardiography sample vol. tracking unit 79—57730
  Doppler US equipment design and biological applications *(Spanish)* 78—7409
  dynamic cardiac imagery, gross and segmental motion analysis 79—25093
  dynamic imagery, gross and segmental motion anal. 79—70632
  dynamic phantom for radionuclide cardiology 80—12232
  ECG and VCG data analysis by computer, advantages *(Swedish)* 78—24163
  ECG continuous monitoring on commercial pilots using portable cassette recorder 77—86659
  ECG gated acquisition cardiac imaging, quantification of left ventricular function 79—70638
  ECG gated radionuclide cardiac imaging system 79—70639
  ECG S-T segment elevation meas. instrument, programmable 78—31956
  ECG U-wave correlation with repolarisation of Purkinje system 78—28122
  ECG-gated radiography, interlaced system for improved chest X-rays 80—26344
  ECG-gated scintigraphy 78—7440
  ECG-triggered scintigraphy of intracardiac space 78—28033
  echocardigram, automatic anal. and VTR recording 80—8112
  echocardiogram, M-mode, automatic computer anal. *(Japanese)* 80—72274
  echocardiogram, M-mode, computer-assisted anal. 78—80942
  echocardiogram analysis in a pattern recognition framework 79—83864
  echocardiogram computer-assisted interactive interpretation 78—80938
  echocardiogram Fourier analysis 78—28028
  echocardiogram on-line computer anal. 78—80941
  echocardiogram processing, microprocessor-based system 77—40726
  echocardiograms, 1D and 2D, computer processing *(German)* 80—81665
  echocardiograms, computer assisted left ventricular anal. *(German)* 80—81667
  echocardiograms, M-mode, microcomputer editing for semiautomatic anal. 80—94299
  echocardiograms displayed on CRT using multilayer 3D adapter 79—18498
  echocardiograph signals, M-mode, analogue storage using video tape 80—94298
  echocardiographic, graphic representation of 2-dimens. structs. in motion 79—70597
  echocardiographic and systolic time interval processor 79—83869
  echocardiographic images, video recorded, interactive segmentation 80—89817
  echocardiographic images enhancement by lateral filtering 79—70592
  echocardiographic left-ventricular diameter time curve automated analysis 77—21578
  echocardiographic tracking, digital range-gating 79—16260
  echocardiographic tracking system, microprocessor-controlled 80—67169
  echocardiography, 2D, transducer beam profile effects on tissue aperture detection 78—73185
  echocardiography, automatic range gate tracker 79—83868
  echocardiography, bidirectional, for detect. of cardiac cycle 78—15877
  echocardiography, binocular stereoscopic display system 79—48297
  echocardiography, clinical appls. of new techniques 80—36050
  echocardiography, clinical significance *(German)* 80—81664
  echocardiography, contrast cross-sectional *(Japanese)* 80—101237
  echocardiography, pulsed Doppler, variable sample vol. dimension 80—76816
  echocardiography, safe method for acquiring morphological and functional data *(German)* 79—16261
  echocardiography, two-dimens., wall motion and thickening quantification by computer-aided contouring 78—80937
  echocardiography, US, picture processing of 2-dimens. data 77—77958
  echocardiography and pulsed Doppler, off-line data processing of left ventricle performance 79—62323
  echocardiography appl. of pattern recognition 78—35898
  echocardiology, book 77—64103
  echocardiophone, CW swept freq. US echo location system 77—70514
  echographic information related to left ventricle and mitral valve in diastole, anal. by small computer 78—80939
  effects of increased lung vol. and decreased pleural press., man 80—41073
  ejection cct., age and compliance effects on cardiac function curves and systolic pressures of rat heart *(French)* 79—34588
  ejection fraction determ. from left ventricular time-activity curves, noise effects 77—40741
  ejection fraction rel. to ventricular vol., computer anal. 80—104599
  electric shocks, 50/60-Hz AC, ventricular fibrillation tests on animals *(German)* 80—101154
  electrical activity, mag. detect. *(Japanese)* 77—81515
  electrical and mechanical monitoring on extensometer 80—45944
  electrical axis, electronic tracing on CRT from ECG waveform generator 77—13022
  electrical generator integral characts. in normal humans 78—69244
  electrical generator integral characts. in period of repolarization 77—70442
  electrical heart stimulator, versatile, wide-range, for animal expts. 80—89912
  electrocardiographs, portable, Phillips Cardiopan 531, clinical/electronic evaluation 78—11757
  electromechanical field model and computation, inverse problems 79—39400
  electromedical devices of the angiohaemodynamical catheterisation laboratory 80—85515
  electromedical instruments, charact. and appl. 78—3642
  electrophysiological mechanisms of cardiac arrhythmias *(German)* 77—44631
  ellipsoidal model, appl. to left ventricular contractions study 80—104608
  emission computerised tomography, ECG-gated, cardiac blood pool 80—98117
  emission computerised tomography of normal and infarcted patients 80—30859
  endocardial unipolar pacing, long term, importance of stimulation threshold 77—81710
  endocardium motion during contraction, anal. method 80—109072
  energy density function encompassing elastic and contractile props. 79—62279

cardiology continued
  epicardial excitation pattern spherical double layer model, using human multipole data 78—27928
  epicardial mapping, DC, during exptl. coronary occlusion, digital data acquisition system 80—85527
  epicardial mapping with clock electrode array 78—28109
  epicardial potential derivation from torso skin potential obs. 77—64148
  equilibrium left ventricular ejection fraction determ., background noise estimation 80—94365
  equipment and techniques, development progress 78—3646
  ergometric test, computer interpretation of heart-rate var., anal. of cardiac control in exercise 78—85430
  esophageal accelerometers, use in monitoring cardiovascular system 80—26403
  excitable medium, auto-oscillatory, 1-dimens., stability complex regimes 78—15752
  excitable medium self-sustained activity, role of inhomogeneity 78—64968
  excitation spread in smooth muscle and myocardial tissues, fibre interaction 80—51068
  exercise cardiopulmonary response analysis, breath-by-breath computer system 78—35995
  exercise-radionuclide ventriculograms, methods for eliminating motion 80—41193
  FFT applied to heart rate, beatquency domain 77—81595
  fibre optic, catheter transducer, side hole type, for intracardiac press. meas. *(Japanese)* 78—73272
  fibre optic catheter, for intravascular press. and sound meas. 78—44638
  fibre optic catheter oximeter system, solid-state, using three single optical fibres 78—44637
  fibre optic catheter-tip micromanometer as intracardiac press. transducer *(Japanese)* 78—73270
  fibrillation, reduced risk using conductive catheter 78—35972
  fibrillation threshold for intracardiac catheter, vs. current flow duration and electrode area 77—37101
  fibrillation threshold for intracardiac catheter as function of 60 Hz current duration and electrode area 77—86675
  fibrillation thresholds for 60 Hz currents and voltages directly applied to heart 80—101301
  first-heart-sound spectra, temporal and heart-size effects 80—41276
  flowmeters, digital 2D full range Doppler velocity meter for cardiovascular diagnosis 78—88731
  fluoroscopic cardiac imaging, real-time computerised system 80—36123
  flying fitness assessment, cardiology and pulmonary function findings, conf., London, England (Oct. 1977) 79—39531
  foetal ECG and heart rate radiotelemetry monitoring 78—3651
  foetal heart and uterus diagnostic monitoring and functional mechanics 78—36009
  foetal heart rate on-line data management during labour, prediction of one-minute Apgar scores 78—44655
  foetal heart rate recording, interference due to infusion pump *(German)* 78—85414
  foetal heart rate variability anal. using spectral anal. 78—28111
  foetal heart rate variability monitoring by digital filtering 79—48353
  foetal heartbeat semiautomatic monitor for nontechnical operators 77—56501
  foetal valve movement, automated detect. using Doppler US 77—40727
  foetal ventricular ejection time, registration and clinical significance 78—85417
  fourth sound studied by FFT 80—94397
  gamma camera, computer controlled 80—61682
  gamma-camera adaptive gating device for heart synchronisation 78—31898
  gamma-camera for gated caroliovascular imaging 79—5367
  gammagraphy, 3-dimens. image processing appl. to coded aperture imaging *(French)* 78—57067
  ganglion, frog, impulse blockage, partial denervation in changing synaptic organisation 79—53081
  gated blood pool scan, radioisotope evaluation of ventricular performance 80—85483
  gated cardiac scintigram anal., digital boundary detect. techniques 80—98106
  gated cardiac scintigram analysis, digital boundary detection techniques 80—98081
  gated cardiac studies, data processing system 79—25091
  geomagnetic activity correl. with heart attacks 77—13049
  graphic analysis using microprocessor-based system 79—70665
  haemodynamic data processing in intensive care unit *(French)* 77—40903
  haemodynamic parameter estimation using elec. analogue 77—37092
  haemodynamic problems associated with cardiac prostheses *(French)* 79—34590
  haemodynamic research, human, physiological signal acquisition and processing 77—44768
  haemofoil mitral valve, results of flow visualisation expts. 80—104632
  heart adaptation to large loads structural changes simulation 79—5258
  heart attack as biological effect of geomag. fluctuation 79—83812
  heart attack early diagnosis appl. of statistical pattern recognition, results 78—40388
  heart attacks, no correl. with geomag. activity 80—21482
  heart attacks correl. with geomag. activity 79—39424
  heart beat frequency monitoring circuit *(Bulgarian)* 77—78006
  heart conduction system modelling 79—83741
  heart disease, haemodynamical parameters optimal control 79—53182
  heart imaging from computerized tomography 78—88741
  heart model time-position mode scanning in obstetrics, heart model practice aid 78—24111
  heart monitor, using IR transducer, design and construction 79—83891
  heart muscle preparations, isolated, viscoelastic props., math. model *(German)* 79—53167
  heart rate analyser for long-term continuous ECG recordings *(German)* 78—3649
  heart rate and blood pressure biofeedback, literature review 80—21484
  heart rate and blood pressure biofeedback theoretical models review 80—16974
  heart rate and cardiac function regulation in normal and pathological states *(Japanese)* 77—40688
  heart rate changes due to sustained voluntary isometric contracts. 80—3628
  heart rate changes due to sustained voluntary isometric contracts. 80—3629

cardiology continued
  heart rate control device, appl. for cardiac rehabilitation 79—83995
  heart rate meas. (foetal), adaptive correlation ratemeter, US signals 78—88732
  heart rate measurement system using phaselock loop device 77—52906
  heart rate on-line statistical anal., using special-purpose computer 78—35984
  heart valve prosthesis, theoretical limit to flow design 77—60302
  heart valves, fluid-mechanical study 79—53171
  heart-beat monitoring circuit with missed beat alarm 77—56500
  heart-rate digital meter, instantaneous, precision 77—86681
  heart-rate variability measurement, clinical and neural cardiovascular research appl. 77—81610
  high-pressure convolutions in rodents, associated heart rate changes 80—67124
  Hippuran plasma clearance meas. using gamma camera and cardiac background subtraction 77—52870
  His-Purkinje conduction system, human, mag. study 80—89818
  human heart consistent rectangular/spherical coordinate system for EEG and magnetocardiography 77—86679
  hybrid computer for dye-dilution curves 78—40365
  hydromechanical simulation facility 79—20708
  hydrophone, miniaturised for internal use, calibration apparatus *(Japanese)* 77—64144
  image description and analysis, interactive knowledge-based systems approach 78—81031
  image processing, tracer kinetics, nuclear medicine, cardiology appls. 78—48873
  imaging, comparison of red blood cells labelled with $^{99}Tc^m$ in vitro and in vivo 78—65109
  imaging, left side, following inhalation of $C^{15}O_2$ 77—9240
  imaging with ^{11}C-palmitate and PETT IV system 80—89849
  impedance cardio-telemeter *(Japanese)* 77—44790
  impedance cardiography, problems 80—41285
  impedance during elec. stimulation, depend. on electrode, pulse duration and acid-base balance 78—27929
  implantable accelerometer for cardiac performance telemetering 77—86670
  implantable cardiac pacemakers, non-polarizable stimulating electrode development 79—92428
  implanted cardiac pacemaker experience and trends 77—81701
  impulse circulation in excitable medium, critical size of closed circuit 79—92200
  in-series assistance using balloon pump, effects on left ventricular afterload/aortic power dissipation 78—3669
  in-series cardiac assist devices, expt. and theoretic observations 78—36063
  indicator dilution method, Stewart-Hamilton eqns. 79—16334
  injury potentials, inadequacy of solid angle formulation 77—44633
  intensive care instrumentation, book 77—17006
  interactive computer program for measurement of data obtained using the extra-stimulus technique during electrode-catheter studies 78—24156
  intercellular communication and membrane elec. noise in embryonic cell culture 77—44612
  intra-aortic balloon pumping efficacy evaluated by nonlinear cardiovascular system model 78—44732
  intra-aortic balloon pumping in-series cardiac assistance, haemodynamic responses, computer model 79—96711
  intracardiac blood flow measurement, noninvasive ultrasonic technique 77—86569
  intracardiac pressure measurement, using fibre optic catheter tip press. transducer 79—2150
  intracardiac shunt noninvasive quantitation using cardiovascular sound complexes 78—48918
  intracellular transmembrane action pots., automated anal. 79—70729
  intracoronary radiolabelled particulate imaging 80—94360
  intractable tachyarrhythmia treatment with pacemaker and β-receptor blocking agents 77—81675
  intramural resistivity of cardiac tissue, canine obs. 79—92319
  intraoperative angiography in surgery 77—90880
  intraoperative coronary arteriography for graft patency prediction 79—92343
  intrapulmonary shunt, influence of cardiac output 80—8086
  intravenous angiography, digital video subtraction system 80—41234
  intravenous antiarrhythmic drug infusion, automated delivery 78—81058
  intravenous fluid overload, cardiopulmonary effects, radiologic manifestations 79—92259
  ischaemia, exptl. study on dogs using body surface pot. mapping 78—44750
  ischaemia index using peak diastolic dV/dt of heart chambers from ECG-gated radiocardiogram 78—44602
  ischaemic heart disease determ. by heart beat interval anal. and medical questionnaire evaluation 78—65145
  ischaemic heart disease diagnosis using respiratory sinus arrhythmia 78—65147
  ischaemic heart disease studied by cardiac pacing 77—81628
  isobaric contraction system for left ventricular performance analysis *(Japanese)* 79—29677
  isolated heart preparation computer control for biomedical research 78—53603
  kinematics of the beating heart 80—76777
  kinetocardiography, non-contact technique using air-coupled US transducer 77—86568
  left heart and systemic circulation, 2-stage identification scheme 80—41071
  left heart bypass, partial and subtotal systems compared 77—81660
  left heart failure, effects on lung regional differences 79—25076
  left heart imaging following $C^{15}O_2$ inhalation 77—64126
  left venticular ejection fraction meas. in equilib. radionuclide angiography 80—46009
  left ventricle, 3D image expression, nuclear medicine 80—104731
  left ventricle, contractile filament stress rel. to wall stress 80—56096
  left ventricle, effects of external pressures on pressure-volume relation 79—11954
  left ventricle, human, geometric modelling using biplane cineangiograms 80—35955
  left ventricle, infarcted, source impedance and internal reactive power 77—37007
  left ventricle, math. model of mechs. 80—101195
  left ventricle, model study of isovolumic and non-isovolumic contracts 80—85428

cardiology continued
  left ventricle active model deform., nonlinear finite element anal. 78—35877
  left ventricle and systemic vascular bed model parameter estimation 77—21548
  left ventricle blood flow field off-line computation from Doppler US velocimetry 79—62324
  left ventricle dynamic geometry in intact unanaesthetised man, midwall motion 80—85491
  left ventricle ejecting beats, estimation of hydromotive source press. 80—76776
  left ventricle ejection fraction meas., scintillation camera deadtime 79—62355
  left ventricle function, nucl. medicine equilib. meas. 79—62357
  left ventricle model, diastolic pressure-vol. relations and wall pressure distrib., fibre extension 80—8079
  left ventricle pressure distribution 77—37006
  left ventricle prosthesis, pneumatically regulated, in-vitro/in-vivo performance 78—3681
  left ventricle regional wall motion, spatial resolution and correl. between segments 79—62359
  left ventricle stress analysis, computerised finite element procedure 77—86518
  left ventricle stress and power, computer simulation 77—56406
  left ventricle time-varying capacitance model, driving energy and cardiac O_2 consumption *(Japanese)* 80—21486
  left ventricular angio processing using Contouromat hard-wired system 79—16325
  left ventricular angio processing using Contouromat hard-wired system 79—16326
  left ventricular apex outlet-abdominal aorta valved composite conduit for outflow obstructions 77—56542
  left ventricular assist device, transapical 79—84021
  left ventricular assist device design and performance 79—96708
  left ventricular assist device development and utilisation 77—25600
  left ventricular assist system microprocessor controlled electromechanical convertor 78—15928
  left ventricular boundary determ., automated analogue method 77—60281
  left ventricular boundary extraction from radioisotope angiocardiogram *(Japanese)* 77—81562
  left ventricular bypass performance, influence of power waveform 78—40433
  left ventricular cineangiograms, computing techniques wall movement 77—90891
  left ventricular diameter-time curve shape from M-mode echocardiogram, automated anal. 78—80940
  left ventricular diastole mechanics 80—94261
  left ventricular diastolic press.-area curves, shifting with positive end-expiratory press. 80—104604
  left ventricular dimensions and dynamics during coronary occlusion determ. by B-scan US in dog model 78—48849
  left ventricular ejection and valvular regurgitant fraction determ., noninvasive radiocardiographic data parameter estimation 78—48886
  left ventricular ejection fraction determ., comparison of three radionuclide techniques with contrast angiography 78—31889
  left ventricular ejection fraction determ. by equilib. radionuclide angiography 80—12227
  left ventricular ejection fraction determ. using multicryst. scintillation camera 78—73213
  left ventricular ejection fraction determ. using radionuclides 78—80962
  left ventricular ejection fraction meas., scintigraphic count-volume and geometric methods compared 79—83896
  left ventricular equilib. radionuclide angiography, arrhythmia effects correction method 80—17089
  left ventricular flow pattern index of pumping efficiency 79—96601
  left ventricular function, correlation with myocardium deformation 79—16244
  left ventricular function, effects of intracoronary nitroglycerin, computer anal. 79—70575
  left ventricular function, normal and abnormal, vel.-strain relationship 78—69119
  left ventricular function, radioisotope evaluation with nonimaging probes 80—85484
  left ventricular function assessment using radionuclide techniques, technical considerations, review, book contrib. 80—101261
  left ventricular function evaluation by myocardial scintigraphy and radionuclide angiocardiography *(Japanese)* 80—81724
  left ventricular function evaluation using ECG synchronised scintillation camera 78—65110
  left ventricular function obs. 79—74749
  left ventricular function quantitative evaluation by 2D ultrasonography system 80—85457
  left ventricular haemodynamics during respiration, dog expts. 80—81635
  left ventricular hypertrophy, model based on myocardial infarction simulation 77—37005
  left ventricular images digital processing *(Japanese)* 80—12224
  left ventricular localised wall motion abnormality assessment, usefulness of quantitative parameters 80—89848
  left ventricular mech. behaviour, orthotropic elastic moduli 79—57695
  left ventricular mural force changes rel. to myocardial pump performance 80—8092
  left ventricular parameter meas., noninvasive radioisotope images with digital prefiltering and boundary detection 78—48887
  left ventricular performance, respiration effects model 80—3670
  left ventricular performance characteristics in trained and sedentary dogs 80—97969
  left ventricular performance parameters rel. to max. dZ/dt 80—101159
  left ventricular pressure volume anal. in eval. of heart diseases 79—70628
  left ventricular pressure/volume relation, large-deformation model *(Japanese)* 79—2091
  left ventricular regional function anal. from cineangiogram, computer system appl. 78—80963
  left ventricular turbulence 77—48834
  left ventricular volume meas. by ECG-gated scintillation probe system 78—31891
  left ventricular wall finite element stress analysis, humans 77—64079
  left ventricular wall force, comparison of models used in calc. 80—56093
  left ventricular wall motion anal., externally referenced polar coord. system 80—89846

cardiology continued
left ventricular wall motion assessment from computer-processed fluoroscopy 79−62358
left ventricular wall motion determined by echocardiography in elderly subjects 80−98039
left-heart haemodynamics, mathematical model 78−65074
left-to-right cardiac shunts, deconvolution anal. in radionuclide quantitation 80−12229
left-ventricular aneurysm, reliability of gated scintigrams in detect. 80−30856
left-ventricular ejection fraction and segmental wall motion by peripheral first-pass radionuclide angiography 78−61246
left-ventricular ejection fractions meas. by equilib. radionuclide angiography 80−12226
lidocaine infusion regimes, computer assisted planning, clinical studies 77−40919
long-term adaptation modelling, oscillatory phenomena *(Russian)* 78−40212
magnetic heart vector components, simultaneous meas. with unipositional lead system 80−104697
magnetic heart vector meas., in humans 78−35873
magnetic measurement of cardiac bloodflow 78−44517
magnetocardiogram, effect of torso geometry 77−60222
magnetocardiogram, PR segment theory rel. to current sources within heart 80−101191
magnetocardiogram and cardiac output meas. with integrated system 80−104709
magnetocardiogram and ECG, medical appls. of SQUID *(Japanese)* 80−12290
magnetocardiogram enhancement by applied mag. field 80−104701
magnetocardiogram meas. first order gradiometer and DC-thin film SQUID 80−89877
magnetocardiogram study using computer model 78−3528
magnetocardiograms from normal hearts, interpretation *(Japanese)* 78−53433
magnetocardiograms of normal and abnormal subjects, anal. using 2D displaying method *(Japanese)* 80−67177
magnetocardiography, clinical appls., instrumentation and methods 80−35927
magnetocardiography, magnetometers for very weak fields 79−30510
magnetocardiography and ECG, R and T waves 80−104699
magnetocardiography in weak DC ambient magnetic fields 79−79567
magnetocardiography overview 79−92246
magnetometer, induction type, for biomag. fields *(German)* 79−88207
magnetometry of human heart in small ferromag. enclosure, using SQUID 78−92726
measurement of central venous-, pulmonary artery end-diastolic- and pulmonary capillary wedge-pressure 77−90955
mechanical activity, noninvasive mag. detect., theory 80−89819
mechanical function assess., left ventricular wall stress and strain anal. *(Japanese)* 79−96589
mechanical function assessment methods *(Japanese)* 79−2148
mechanical heart computer simulation 79−70709
mechanical properties and biochem. composition of human cardiac arteries, effect of age 80−8091
mechanics, elastic props., forces, stresses and press. *(Dutch)* 78−73170
mechanomyocardiography, left ventricular, technique for detect. of diseased myocardial elements and states 80−72363
mechanopressography, left-ventricular, noninvasive intrinsic assessment of pumping efficiency 80−72203
medical evaluation of function and anatomy, echocardiography and radionuclide imaging, book contrib. 80−101241
microcomputer based biomedical signal processor 80−26390
microprocessor-controlled output meter 80−36162
microwave apexcardiography 79−74737
microwave effects, insensitivity of frog heart rate to p.m. energy 77−2020
microwave irradiation effect on embryonic quail heart rate, 2450 MHz irrad. 80−89794
microwave irradiation of isolated rat heart after treatment with ANS blocking agents 78−40251
microwave-induced chronotropic effects in isolated rat heart 78−69137
microwaves as potentiating factor in cardiovascular disease in North Karelia, Finland 77−12959
minicomputerized automatic radiocardiogram analysis *(Japanese)* 79−29614
mitochondria of bovine heart, EPR investigation of two forms of Fe-S centre N-2 78−69014
mitral valve, conditions of closure 80−85439
mitral valve, natural, human, turbulent flow 77−36975
mitral valve leaflets, mathematical anal. 79−39435
mitral valve replacement, prediction of postoperative systolic left ventricular wall stress 78−40427
mitral valve velocity meas. by digital echocardiographic tracking system 77−21579
mitral valve vibration anal. to detect first heart sound freq. 78−40233
monitoring instrument, digital socially acceptable, for heart beat counting 78−40367
monitoring output by computerised transthoracic admittance plethysmography *(Japanese)* 77−86693
monitoring system for stroke patients 80−26394
motion kinetic anal., force-displacement relation 78−40222
motor reactivity, isolated heart of grass snake, pH and temp. effects 80−26219
motor reactivity of isolated heart of the grass-snake 80−67100
multipole moments rel. to activated parts of epicardium and endocardium 79−100588
multitrack video tape recorder, exercise ECG examination and cardiological telemetry appl. 77−70561
muocardial infarction ECG diagnosis in patients with transvenous ventricular pacemakers 77−81624
muscle, behaviour of myosin projections during staircase phenomenon 78−53362
muscle, contraction variable preload and afterload independence, thermodynamic and clinical consequences 79−79576
muscle, excitation contraction coupling, mathematical model 79−96542
muscle, excitation-contraction coupling 79−96547
muscle, mathematical contractile model *(Japanese)* 79−57632
muscle, passive, viscoelastic theory and obs. 80−94273
muscle, resting, activation monitored by intensity fluctuation spectroscopy 80−108953

cardiology continued
muscle and heart, apparent source resistance 79−25005
muscle biomechanics *(Japanese)* 80−72201
muscle cells, bivalve mollusc, fine structure 79−92188
muscle cells, leaky, heavy water effects 79−62220
muscle cells, Na current, electrophysiological studies, rat 79−43838
muscle cells, paraffin-embedded, cryofracture, SEM and TEM obs. 78−57148
muscle contractile force in unskinned rat heart fibre 80−30955
muscle contractility calc. using analogue computer *(German)* 78−7378
muscle contractility modelling of atria and ventricles 79−53079
muscle contraction force, rhythm influence modelling, intracellular pool Ca 79−79568
muscle contraction simulation 77−12954
muscle fibre, stresses in left ventricular wall, biaxial stress-strain relations 79−29558
muscle force-velocity relation, anal. in time domain 80−35943
muscle isolated preparation, determ. of segment length by mag. induction 77−48982
muscle mechanics, relation with zero-load aortic flow 79−29548
muscle model activation parameter behaviour, numerical study 78−11686
muscle preparations, viscoelastic props. anal., meas. and model *(German)* 79−83817
muscle series elasticity, effects of mech. history and time in twitch 77−37004
muscle stress/strain relationship determ. by computerised tomography 79−92262
muscle V_{max} determination from intraventricular press., on-line digital computation 77−40866
myocardial ^{201}Tl perfusion images, computer anal. method 80−30860
myocardial ^{201}Tl perfusion scintigrams in the evaluation of aortocoronary sapheneous bypass surgery 80−12235
myocardial ^{201}Tl scintigram anal., nonredundant coded aperture tomographic method 80−94364
myocardial ^{201}Tl scintigram anal. by coded aperture imaging 79−79647
myocardial activity determ. at surgery using shrinking stress meas. 78−31966
myocardial blood flow, ^{133}Xe studies, theoretical, technical and practical aspects 80−94355
myocardial blood flow, meas. by fractional uptake of ^{84}Rb and microspheres 79−34656
myocardial blood flow and haemodynamic responses to exercise training, dog expts. 80−3678
myocardial cell transmembrane potential QRS-T wave simulation *(Japanese)* 77−90740
myocardial contrast accumulation, densitometric evaluation 78−69216
myocardial damage, induction by open-chest low energy countershock, rabbit expts. 80−72150
myocardial damage from defibrillator discharges at various dosages 80−72368
myocardial dimension measurement system using pulsed Doppler US 80−26313
myocardial dimensioning system, pulsed ultrasound method 79−48298
myocardial dosimetry of ^{99m}Tc-pyrophosphate used in infarct imaging 77−40771
myocardial energy status, ^{31}P NMR of perfused working rat hearts 77−29236
myocardial excitability evaluation, strength-interval curves generation under computer control 80−41336
myocardial fibre accommodation, role of incoming currents 77−36898
myocardial fibre excitation and contraction uncoupling on slow Na-Ca channel block 78−15810
myocardial fibre shortening velocity dependence on inotropic and haemodynamic conditions 78−31833
myocardial fibres, ionic nature of repeated responses 77−70441
myocardial function studies, exptl. approaches using C^{15}O$_2$ and ^{81m}Kr 77−40755
myocardial imaging, rationale and radiopharmaceuticals 77−40747
myocardial imaging agents, comparison of ^{201}Tl, ^{129}Cs, ^{43}K, ^{81}Rb 77−2037
myocardial imaging studies, prod. and characts. of ^{81}Rb 79−29628
myocardial imaging using ^{201}Tl, collimator evaluation 79−34657
myocardial imaging with ^{123}I-hexadecenoic acid, distrib. in animals 77−16970
myocardial imaging with ^{13}NH$_4^{+}$, prod., distrib. and imaging 77−40752
myocardial imaging with ^{201}Tl, clinical usefulness analysis based on Bayes theorem 79−88170
myocardial imaging with ^{201}Tl, exptl. model for anal. of myocardial and background components 78−11727
myocardial imaging with ^{201}Tl, human distrib. and phys. imaging props. 77−37042
myocardial imaging with ^{201}Tl, interinstitutional study of observer variability 78−85361
myocardial imaging with ^{201}Tl, subtraction imaging using ^{201}TlCl and ^{99m}TcO$_4^{-}$ 80−72318
myocardial imaging with ^{201}Tl 77−40751
myocardial imaging with time-modulated coded aperture, results with ^{201}Tl 79−92372
myocardial infarct imaging with ^{43}K and analogues 77−40750
myocardial infarct imaging with ^{99m}Tc complexes 77−40749
myocardial infarct imaging with ^{99m}Tc-phosphates 77−40748
myocardial infarct scintigraphy, inexpensive rib phantom 77−56461
myocardial infarct size computerised quantification from ^{201}Tl scintigrams 78−44601
myocardial infarct sizing, comparison of noninvasive methods, dog expt. 77−66869
myocardial infarct sizing using computer programming and 3-dimens. model 77−90888
myocardial infarction, ^{99m}Tc pyrophosphate scintigrams for diagnosis, localisation 79−5350
myocardial infarction, acute, ^{99m}Tc imaging in dogs, emission-computed tomography appl. 79−79638
myocardial infarction, acute, comparison of ^{99M}Tc pyrophosphate with ^{99M}Tc hydroxymethylene diphosphonate 80−94342
myocardial infarction, nontraumatic radionuclide assessment of ventricular wall motion and stroke vol. 77−52865
myocardial infarction, perioperative, comparison of ECG, scintigraphy and enzyme diagnosis 80−30855
myocardial infarction, topographic relation between myocardial ^{201}Tl uptake and left ventricular kinetics 78−61243

cardiology continued
myocardial infarction diagnosis in endocardially paced patients 77−81625
myocardial infarction diagnostic data anal. database 79−70693
myocardial infarction dimension model and FORTRAN program *(Russian)* 79−2038
myocardial infarcts, acute modified ^{99M}Tc heparin for imaging, dog expts. 80−81733
myocardial infarcts rel. to blood rheology thermal factors 79−79573
myocardial inhomogeneity effect on left ventricular circumferential stress distrib. 79−92267
myocardial injury, correlation of US and enzymatic indices 77−21581
myocardial interaction between ventricles 77−12946
myocardial ischaemia, zero-load aortic flow 77−37003
myocardial left lateral images using ^{201}Tl, effect of patient positioning 79−100714
myocardial O_2 sufficiency, noninvasive IR monitoring 78−44583
myocardial performance index from left ventricular area ratios 77−56465
myocardial perfusion evaluation by coded aperture tomographic technique 80−21537
myocardial perfusion images using ^{201}Tl, quantitative evaluation methods 79−39479
myocardial perfusion imaging, quantitative aspects, review 80−94358
myocardial perfusion imaging using ^{201}Tl, algorithm for background activity calc. 80−56195
myocardial perfusion imaging using ^{201}Tl, computer processing 79−62356
myocardial perfusion imaging with ^{201}Tl, single photon emission computerised tomography *(Japanese)* 80−98114
myocardial perfusion index calculator for prediction of subendocardial ischaemia in cardiac surgery 77−40915
myocardial perfusion scan interpretation, computer technique 78−80960
myocardial regional blood flow from dynamic anal. of ^{201}Tl 79−70627
myocardial regional function and coronary blood flow study during ischaemia in baboons, telemetry system 78−44752
myocardial regional perfusion, tomographic scintigraphy 78−3584
myocardial scans and wall motion studies using ^{99m}Tc pyrophosphate 79−96654
myocardial scintigrams, specificity of ^{99M}TC pyrophosphate in prior infarction cases 79−39476
myocardial scintigraphy, computerised extraction of organ contours *(German)* 78−88735
myocardial scintigraphy, sequential, following myocardial infarction, using ^{99M}Tc stannous pyrophosphate 79−39474
myocardial scintigraphy in stressed state using ^{201}Tl, segmental anal. 77−66840
myocardial scintigraphy using ^{99M}Tc pyrophosphate, correls. with coronary-artery bypass surgery 79−39475
myocardial threshold, pharmacological influence determ. 77−81643
myocardial tissue, relationship between collagen and US attenuation 79−43973
myocardial tissue, US attenuation depend. on time after excision and temp. 78−11711
myocardial transmural heat gradient instantaneous meas. 78−44661
myocardial uptake of ^{201}Tl, correl. with local perfusion, dog expts. *(French)* 80−104740
myocardial uptake of ^{99m}Tc stannous pyrophosphate in expt. viral myopericarditis, mouse obs. 80−46019
myocardial-stress perfusion scintigraphy, predictive value in patients without previous infarction 78−73205
myocardium, acoustic microscopic anal. 80−45995
myocardium, contractility determ., anal. of differential quotients 79−34584
myocardium, detect. of viable muscle in dysfunctional regions of left ventricle 77−37093
myocardium, frog, model of excitation-contraction coupling 79−70541
myocardium, normal and ischaemic, US attenuation 80−45954
myocardium, quiescent, anal. of some theological and mech. props., rat 79−74709
myocardium adjacent portions, mutual elec. influence genesis of arrhythmias 79−92202
myocardium contraction amplitude depend. on freq. of elec. stimulation, frog 78−77027
myocardium mitochondria lipid composition and phase transitions rel. to depth of hypothermia, rats and dogs 78−53350
myocardium of frog, temp. effects on membrane currents 77−52759
myocardium of human left ventricle, stiffness distrib. rel. to shape change in diastole 80−41095
myocardium prosthetic, haemodynamic results 79−84019
myosin, struct. and functional changes in chronic cardiac insufficiency 77−36887
myosin heads movement during a heart beat 79−48207
natural pacemaker of heart, modelling as pulse-freq. modulator 78−40135
neonate cardiorespiratory monitoring, automatic system with microprocessor 80−94399
NMR zeugmatographic imaging of heart and lungs 80−17053
Noble model, spread of excitation through node of branching 77−16899
noradrenaline release during nerve stimulation, regulated by α-adrenoceptor mediated negative feedback 77−29139
nuclear, beat-by-beat validation of ECG gating [nuclear medicine] 80−98071
nuclear, computer system 79−25094
nuclear angiocardiogram anal. program for radiology trainees 80−8143
nuclear angiocardiography, computerised, ECG-gated, automatically generated LV regions of interest 79−70626
nuclear angiocardiography, first pass technique, automation during anal. 79−70625
nuclear cardiography, deadtime meas. in scintillation cameras 79−16276
nuclear cardiology, automated chest parsing algorithm 80−61678
nuclear cardiology, status and prospects 79−70605
nuclear images, digital technique for accurate change detect. 79−48326
nuclear medical instrumentation, mobile, review 80−101262
nuclear medicine, appls. to cardiovascular studies 77−40746
nuclear medicine, coded-aperture imaging of the heart, improved aperture 80−98072
nuclear medicine, conf., London, England (June 1979) 80−36759
nuclear medicine, digital data collection system, portable, cost-effective 80−41195
nuclear medicine, left ventricular edges detect. methods 80−98132

cardiology continued
nuclear medicine conference, Karlovy Vary, Czechoslovakia (May, 1979) 80−12840
nuclear medicine for clinicians, book 80−98765
nuclear medicine in acute myocardial infarction, ^{99M}Tc pyrophosphate rel. to ^{99M}Tc methylene diphosphonate 80−17070
nuclear medicine instrumentation, review, book contrib. 80−101260
nuclear medicine technology conference, Louisville, USA (Feb. 1980) 80−51949
nuclear performance characts. of a commercial ECG gate 80−98073
nuclear ventriculograms, processing and display 77−86627
nuclear-medicine image display system, dynamic physiological function visualisation 79−5396
oesophageal accelerometer, cardiovascular function indication 80−104798
oesophageal accelerometer evaluation for cardiac function noninvasive meas. 79−92458
oesophageal phonocardiogram, correl. of freq. components with non-meas. physiological parameters 77−52836
one-sided cardiac failure differentiation by planimetric electrokymography 79−43990
output and right ventricular residual fraction determ. with rapidly responding pH sensor 77−40860
output and shunts, automatic computation from indicator dilution curves 79−48359
output determ. by computer, using Stewart-Hamilton method, algorithm 77−86691
output determination by N_2O technique, corrections for press. and temp. 77−16948
output estimation by N_2O rebreathing method in adults and children 77−12953
output estimation during exercise by rebreathing technique, automated system 77−37090
output estimation from aortic pressure curves, simulation model 79−53177
output estimation from isotope dilution and residue detect., time-varying flow and vol. effects 80−101194
output flow wave calculator *(Japanese)* 77−70489
output meas. by US transoesophageal probe 79−92315
output meas. method evaluation by impedance cardiography *(Japanese)* 77−90948
output measurement, continuous electronic thermodilution meas. 77−40859
output measurement, in vitro comparison of six commercially available thermodilution systems 78−77135
output measurement, tracer transport model accounting for recirculation 77−36978
output measurement error due to nonuniform dye distrib. 77−36979
P-R segment non-invasive information, clinical pot. of elec. and mag. methods 80−36182
pacemaker activity, phase resetting and annihilation 80−81565
pacemaker base rate follow-up reliability for long-term pacing 77−81694
pacemaker current obs. in chick embryo heart cells 80−51066
pacemaker epicardial electrode implantation 77−81703
pacemaker implantation surgery, intracardiac ECG derivation during electrocoagulation 78−40397
pacemaker patient and medical education journal 77−81700
pacemaker patient routine monitoring using telephone-telemetry system 77−90957
pacemaker patient surveillance by automatic pacemaker function analyser 78−3679
pacemaker patients, late survival prognostic determinants 77−81693
pacemaker treatment principles and experience 80−8213
pacemakers, diathermy interference, simulation models 79−84007
pacemakers, fixed-rate type, safety of competition with intrinsic ventricular beats 77−81706
pacemakers, implantable, for increasing heart rate 78−7533
pacemakers, survey of 2243 pacemaker implantations in 1228 patients 77−81689
pacemakers, survival of heart block patients 77−81686
pacemaking, role of catecholamines 77−70437
pacing, aortic shear stress reduction 78−40239
pacing, meas. of ohmic electrode-tissue contact resistance and voltage applied to myocardium 80−67284
pacing, survey of clinical results over 10 years 77−81687
pacing as diagnostic tool 77−81629
pacing electrodes, implanted, signal source impedance 80−56275
paediatric patient, radiation exposure from cardiac catheterisation and angiography 80−41241
papillary muscle fibres, rabbit, effect of preliminary stimulation on repeat responses 78−48768
papillary muscle in rat, dynamic behaviour stochastic model 78−35821
papillary muscle selection and testing, some mech. considerations 80−89919
parameter estimation, cadiovascular, nonlinear filter statistical parameters optimal choice 79−5308
paroxysmal supraventricular tachycardia management by scanning pacemaker system 77−81676
paroxysmal supraventricular tachycardia termination by overdrive pacing 77−81649
particulate myocardial perfusion scintigraphy in eval. of coronary artery disease 77−40753
patient heart condition monitoring during bath therapy using immersed electrodes 78−3665
pediatric cardiac catheterisation, absorbed dose in presence of contrast agents 80−30897
performance criteria for optimisation of cardiac assistance 79−74782
perfusion and intraaortic balloon pumping system, Biopul's-3 78−7536
pericardial effusion, malignant, myocardial accumulation of labelled phosphate 80−17068
pericardial potential simulation and mapping in dog 79−39399
pericardium, role in cardiac mechanics 80−35938
permanent pacing, analysis of 536 patients 77−81688
personnel exposure during cardiac catheterisation, calc. technique using time-lapse photography 79−39504
pervenous atrial sensing and pacing 77−81684
phase invariant signature algorithm (PISA) processing of ECG and phonocardiogram for cardiac anomaly detect. 78−40395
phonocardiogram and phonothyreogram frequency spectrum analysis by minicomputer, ECG reference time signal 79−83966
phonocardiogram automatic classification, linear predictive anal. processing *(Japanese)* 80−36036

cardiology continued

- phonocardiogram classification, linear prediction analysis appl. *(Japanese)* 78−36010
- phonocardiogram detection algorithm using spectral tracking 80−41151
- phonocardiogram pattern classification using linear prediction analysis 77−90950
- phonocardiogram quantitative anal. for murmur detect. 80−56270
- phonocardiographic microphones, air cavity characteristics, effect of vibrations, room noise 77−81611
- phonocardiography, Fonokard type instruments 80−56229
- photocardiogram contact microphone 77−21634
- photoplethysmography, audio-visual heart monitor based on light transmission through skin 79−53206
- physiological compartment tracer flow modelling and digital imaging 80−101257
- pivoting disc heart valve prosthesis, clinical results and new all-C model 77−52923
- plethysmogram detection and its clinical usefulness *(Korean)* 79−62380
- postoperative cardiac surgical patient care, automation of meas. and interventions 78−20310
- potential function represented by chains of maps, analysis 77−37062
- pressure meas., computer aided anal. *(Swedish)* 77−44779
- pressure measurement, by US resonant scatt. from bubbles 77−37029
- pressure noninvasive US measurement, scatt. from encapsulated bubbles 80−36048
- pressure pulse LF wave synthesizers, mammalian cardiac system 77−9301
- prostheses, cardiovascular, corrosion and thrombogenesis 77−9300
- prostheses pumping, effect on mech. props. of vascular walls 78−40429
- prosthetic, heart valves, load cell for meas. of dynamic forces 80−104815
- prosthetic aortic heart valve dysfunction computer-assisted detection 77−40922
- prosthetic aortic heart valves, wall shear stress meas. in near vicinity 79−83829
- prosthetic aortic valve mechanics, apparatus for in vitro study 79−44054
- prosthetic cardiac valve, concave-convex pivoting disc two-dimensional model 79−84028
- prosthetic disk valves, max. opening rel. to aortic blood flow characts. 80−108941
- prosthetic heart valve, disk-type, numerical soln. for steady axisymmetric flow 80−35952
- prosthetic heart valve, trileaflet, design, fabrication and evaluation 80−94415
- prosthetic heart valve models, effect of channel diffusion, cut-off element on hydrodynamic resistance *(Russian)* 79−44053
- prosthetic heart valves, laser Doppler anemometer for velocity meas. 79−57814
- prosthetic heart valves, rigid leaflet and caged-ball types, diastolic ventricular mechs. 78−81079
- prosthetic material mech. props., effects of physiological environment, cardiovascular appls. 80−8212
- prosthetic mitral valve, pressure drop and flow pattern obs. 79−92430
- prosthetic myocardium, functional left ventricular wall replacement 77−52931
- prosthetic valve testing 77−56530
- prosthetic valves, insufficiency, pressure loss and energy loss obs. *(German)* 79−83818
- prosthetic valves, past and future 77−52924
- protein kinases, cAMP-depend., membrane-localised, and regulation, of slow inward current, frog heart 80−81567
- proton spin-lattice relaxation times prolongation, regionally ischemic dog heart tissue 80−101216
- pulmonary blood pressure, flow and vol. in man, effects of sitting up 79−88103
- pulse rate, blood press. and rate-press. product automatic meas. during rest and exercise *(German)* 78−35974
- pulse rate meas. by pulsilogium of Sanctorius 79−71215
- pulse rate meter for heart monitoring 78−31915
- pulse rate monitor, digital, IR absorpt. detect. 80−26322
- pulse-wave velocity measurement in humans *(German)* 80−81751
- pulse/phono pick-up appls. in ambulant cardiological practice 78−40377
- pulsed Doppler flowmeter, development and cardiac appls. *(Japanese)* 80−36037
- pulsed Doppler velocimetry, clinical appls. 80−46003
- pump stimulation, association with positive inotropy in cat 79−16196
- pumping ability of left heart rel. to end-diastolic vol. and inotropic state 78−31851
- Purkinje fibers, delay, block, oneway conduction model 80−21462
- Purkinje fibre, Na current 79−43861
- Purkinje fibres, calf, role of intracellular Ca in transient outward current 77−90748
- Purkinje fibres, canine, activity-dependent extracellular K^+ fluctuations 80−89733
- Purkinje fibres, intracellular Na^+ activity rel. to tension, sheep obs. 80−51060
- Purkinje fibres, rabbit, Na channels 79−43828
- Purkinje fibres, sheep, intercellular clefts effect on elec. props. 79−34522
- Purkinje terminal electrical connection with muscle fibres in canine ventricle 77−86460
- Purkinje-myocardial junction conduction rel. to ventricular overload 77−81775
- pyrophosphate myocardial imaging, review 80−94359
- QRS-onset and offset in children, detection using parametrised templates 78−85438
- quantitation of infarct size using radionuclides 80−85492
- radiation induced ultrastructure changes, fission neutrons vs. ^{60}Co gammas, mouse 77−5047
- radiation ultrastructural effects, aged mouse, fission spectrum neutrons rel. to γ-rays 80−41138
- radiocardiogram parameter identification *(Slovene)* 78−44586
- radiocardiograph equipment TESLA NRG 724, description 78−28062
- radiocardiography, noninvasive meas. in clinical cardiology 77−40754
- radiographic display of heart internal image *(Dutch)* 79−70623
- radiographic image sequence analysis and recording 78−57069
- radiographic images of heart, automatic extraction of location of surgically implanted markers 79−88175
- radiography, cardiac catheterization laboratory sensitometric system application and clinical evaluation 78−20263
- radioimmunoassay of acute myocardial infarction markers 80−3809

cardiology continued

- radioisotope angiocardiograms, image enhancement and left ventricular contour extraction techniques appl. 80−72283
- radioisotope angiocardiographic image, left ventricular contour extraction and vol. computation *(Japanese)* 80−3798
- radioisotope angiography, heart shunt diagnostics, anal. by PASD computer program 78−20250
- radioisotope cardiac scan computer-aided anal., using ECG gate 78−40328
- radioisotope functional imaging, clinical experience 78−80958
- radioisotope image, anal. of high speed multicrystal gamma camera recording 79−25077
- radioisotope sequential meas. of ventricular vols. and cardiac output 80−94319
- radionuclide, left ventricular systolic ejection rate assessment of cardiac function 79−79633
- radionuclide angiocardiography, exercise techniques 79−57762
- radionuclide angiography, gated, use of computer-generated functional images to define ventricular boundaries 80−85487
- radionuclide angiography of the left ventricle using the first-pass technique *(German)* 80−109019
- radionuclide angiography technique for assessment of regional wall motion abnormalities 80−85488
- radionuclide cardiac motion study, computer-processed, ECG gating device 78−73210
- radionuclide cardiac output determination, automated computer program 80−56196
- radionuclide cardiology, using dedicated minicomputer, ischemic heart disease appl. 79−96661
- radionuclide cineangiography, clinical utility of real-time computer-based system 78−80957
- radionuclide computer-assisted cardiology, off-line viewing using videotape 78−65119
- radionuclide evaluation of cadiac trauma 80−94361
- radionuclide images, digital image superposition algorithm, accuracy and reproducibility 78−73209
- radionuclide imaging techniques, book contrib. 80−36113
- radionuclide left ventriculography with slant hole collimator 78−3588
- radionuclide ventriculography, computerised, assessment of LV wall motion and regional kinetics 80−89850
- radiopaque marker clinical usefulness in left ventricular function 80−36119
- rat cardiac muscle, mech. props., effect of 1 MHz ultrasound 78−96062
- rate measurement using digital cardiotachometer 77−56503
- rate meter, based on analogue low-frequency meter *(Czech)* 77−37084
- ratemeter based on analogue divider, heart rate determ. from ECG and arterial press. curve 78−40368
- real time digital echocardiography using burst analogue sampling 77−9234
- recirculation maths. and cardiac output meas. 77−56404
- regional left ventricular wall motion in coronary heart disease 80−85490
- regional left-ventricular dyskinesis, paradox nuclear image as noninvasive index 80−56190
- regional myocardial function quantitative parameters 79−25095
- regional myocardial perfusion determ. from H_2 washout curve 79−92459
- relaxation parameters, digital anal. of isovolumic press. fall, dogs 80−94276
- renal/iliac bloodflow telemetering from exercising dogs 77−90822
- resistance and facilitation gradient demonstration in cardiac pacing 77−81669
- respiratory gating mechanism for cardiac slowing 77−12902
- RF EM noninvasive transcutaneous measurement technique *(Italian)* 78−85352
- RF SQUID, use in magnetocardiography *(Dutch)* 79−79670
- rheocardiography, 4-electrode, in computer-aided cardiac output determ. 80−61718
- rheoplethysmograph type RPG-202 79−92405
- rhythm disturbances, Markov process model *(German)* 79−2019
- rhythmic heart-cell clusters, fluctuations in interbeat interval, membrane voltage noise role 80−30705
- right atrial diameter meas. dynamic/static, using US sonomicrometer technique *(Japanese)* 78−3568
- right bundle branch block patterns during permanent right ventricular pacing 77−81704
- right ventricular angiogram computer quantification 79−62360
- right ventricular wall thickness meas. by echocardiography, comparison with necropsy 78−40277
- rotation coronary angiography 80−104744
- safe voltage differences, practical equipot. limits 78−44649
- saline conductivity method for measuring cardiac output simplified 79−92318
- sarcolemmal permeability changes during early myocardial anoxia 80−85371
- sarcoplasmic reticulum of skinned cardiac cells, Ca^{2+}-induced release of Ca^{2+} 80−3612
- saturation dive, 17-day 18.6 ATA exposure effects 79−92256
- scintigraphic cineangiography with ECG gating 77−9255
- scintigraphic image handling using microprocessor system 80−85489
- scintigraphy and angiography, equipment for quant. evaluation and off-line operation *(German)* 78−88736
- scintigraphy of cardiac function using Bonn System III 78−73198
- scintigraphy-radiocardiography, left ventricular ejection fraction and regurgitation meas. *(French)* 77−29194
- scintillation probe detector in assessment of cardiovascular disease 80−3800
- sector scanning sonar, use in fish heart rate telemetry 80−8225
- segmental myocardial wall motion velocity during cardiac cycle 77−37094
- semilunar leaflet contrib. to turbulent blood flow 80−3666
- semilunar valvular motion vibr. model during early diastole, rel. to second heart sound 78−44533
- semilunar valvular vibration in early diastole, rel. to second heart sound 78−44544
- senile dementia patients, unrecognised intermittent bradycardias, rel. to cardiac pacing 77−81644
- shape descriptors, Fourier-Walsh, radiographic image processing appls. 80−8153
- shunt detection with the short-lived radioactive gases 80−94357
- sick sinus syndrome, cardiac pacing problems 77−81680
- sick sinus syndrome applications of cardiac pacing 77−81679
- sick sinus syndrome pathology 77−81774

cardiology continued
simulator for cardiac activity signals 80−56230
sinatorial node of rabbit heart, vagal stimulation, K$^+$ permeability and extracellular transients 78−92608
single myocardial fibre model, source-field relationships 79−39385
sinoatrial bradycardia treatment by transvenous atrial synchronised pacing 77−81683
sinus node and AV junction, automaticity model based on weakly coupled relax. oscillators 78−24017
sinus node function electrophysiology rel. to long-term cardiac pacing 77−81673
sinus node of rabbit heart, intercellular coupling 78−20159
sinus node response to premature atrial stimulation, microelectrode analysis 77−81630
sleep depth determ. by cluster anal. of heart rate data 78−44659
Smeloff-Cutter heart valve prosthesis 77−56527
SOLO monitor, microcomputer bedside monitor 80−94404
sound and vibration recording, electro-optical sensor 77−21648
sound frequency shifting stethoscope 79−29647
SQUID gradiometer, second-derivative, magnetocardiogram meas. 80−104696
statistical pattern recognition for early diagnosis of heart attacks 77−25584
stenosed valve, energy losses in flow calcs. 80−41082
stenoses model disorder distal, steady and pulsatile flow 79−57688
stenosis densitometric analysis from remote terminal 79−83900
stenotic flow, vascular anal. model 79−79593
stimulation threshold, time var. 77−25609
stimulation threshold noninvasive meas., long-term follow-up 77−81711
stimulator, isotropic power supplies appl. *(Spanish)* 78−15922
stimulator, microprocessor-controlled dual-channel 80−56279
stimulator power supply battery selection 77−48931
strength interval curve rapid generation, computer system 78−40456
stress ^{201}Tl scintigram anal. methods comparison 80−89851
stress exercise facility automation using microcomputer system 79−70682
stroke index determination from impedance cardiography 77−25569
stroke volume and systolic time interval adjustments during bicycle exercise 80−3679
stroke volume calc. from transthoracic impedance plethysmogram 78−7381
stroke volume calc. using noninvasive pressure pulse contour method *(German)* 78−3631
stroke volume meas. from impedance, rel. to aortic flow waveform 77−86522
submitochondrial particle succinic dehydrogenase, interaction of ubisemiquinone with Fe-S centre, EPR 78−69016
surgery, data acquisition and processing during operation by multiplexer *(German)* 78−92743
surgery, interference suppression for EEG recording 79−100784
surgical aspiration automatic control device for cardiac surgery *(French)* 78−61282
surgical patient postoperative computerised meas., analysis, and treatment 78−36044
surgical patient postoperative management, computerised intensive care 77−40918
sympathetic preganglionic neurons, raphe inhibition 79−92211
synapse formation between parasympathetic neurones deprived of preganglionic innervation, frog heart 77−77888
synchronised diagnostic and treament techniques 80−61727
systemic lupus erythematosus treatment with permanent pacemakers 77−81682
systolic time interval, off-line processing of exercise data 77−40868
systolic time interval meas. microprocessor system for heart malfunction detect 79−79681
systolic time interval processing system, STIPS 78−81029
systolic time intervals during $+G_z$ accel., appl. to cardiovascular function estimation 77−5087
systolic time intervals during exercise 79−70668
systolic time intervals from surgical patients, continuous real-time computation and display 77−37098
T-wave rise time rel. to heart rate, exercise vector cardiograms study 78−85434
tachometer, digital, for heart rate measurement 80−17162
tachycardia suppression by programmed premature stimulation 77−81650
tachycardia termination system, microcomputer-based 80−56280
tachycardia treatment by implanted pacemaker 77−81677
telemetered cardiovascular changes with free-ranging and treadmill exercise in dogs 77−90821
telemetry, low power PAM/FM system for ventricular press. and cardiac dimension meas. 78−44747
telemetry system, implantable, multichannel, inductively powered, for animal cardiovascular data recording 77−86662
telemetry system for wild animal heart rate activity monitoring 77−86713
temporary artificial elec. stimulation 80−56272
thalassaemic tissue, Mossbauer spectra of Fe deposits 78−73202
therapy/measuring combined unit for pacemaker implantation *(German)* 78−7519
thermal entrainment device for cardiovascular investigation 80−104793
thermodilution cardiac output meas. in small animals, thermistor probe contruction 77−64161
thermodilution method, bidirectional shunt quantification 80−3837
thoracic electrical impedance sensitivity to blood volume changes 79−34543
thoracotomy, calves, physiological variables obs. 79−53280
three-dimensional image reconstruction for cone-beam X-ray sources 78−77111
tissue parameter identification by digital processing of real-time US clinical cardiac data 80−51191
tissue resistivity, intramural meas. 79−39388
tissue response to retraction during open-heart surgery 80−26254
tomography, cylindrical scanning, high temporal resolution, appls. to physiology and medicine 80−30885
tomography, myocardial perfusion, Anger camera/computer system using seven pinhole collimator 80−61663
total artificial heart and left ventricular assist device 79−84017
total artificial heart haemodynamic study 79−84018
total artificial hearts, pneumatic powered, telemetric monitoring system, in calves 77−90956

cardiology continued
total cardiac monitoring integrated microcomputer/minicomputer system 78−35997
trabecula membrane of frog auricle, electrophysiological characts. from ionic currents on pot. clamping 78−24049
trabeculae of frog atrium, Ca^{2+} incoming current obs. 79−79497
transmission computed tomography, cardiovascular imaging 80−36121
transverse-sectional imaging with Na^{18}F in myocardial infarction 80−46015
trophic influences on frog heart during cold acclimation 79−83754
two-dimensional echocardiographic images enhancement by lateral filtering 80−81677
ultrasonotomography with electronic sector scanning, features, appl. 77−66829
US and nuclear medicine, complementary roles 80−98051
US appl. in echography and bioecholocation, progress and prospects 80−21509
US cardiotomography, cardiovascular system diagnosis appl. *(German)* 77−77944
US data, moving heart surfaces extraction 80−8114
US Doppler returns from foetal heart, processing, valvular timing information extraction 80−101238
US Doppler signal processing, swept-frequency transient signal filtering 78−48848
US echoaortocardiography, Kymo-two-dimensional, aortic root diagnosis appl. 78−24110
US echocardiographic system, two-and three-dimensional, computerised, atrial septal defect detection appl. 78−20237
US electronic sector-scanning cross-sectional echocardiograph, model SSH-10A 79−57732
US image feature enhancement via digital processing 78−73183
US image sequences, logical neighbour operations appl. 80−8113
US imaging systems, high-resolution, real-time 78−69160
US imaging techniques and appls. 78−49620
US intraoesophageal dynamic imaging 80−94303
US monitor for fetus cardiac pre-ejection period continuous meas. 79−74732
US pulse echo digital processing 77−32948
US pulsed Doppler techniques for cardiovascular meas. 77−77947
US range-gated echo Doppler techniques for cardiac output and aortic flow meas. 78−40276
US real-time echographic imaging system, acoustic field study *(Italian)* 79−96636
US real-time image computerised anal. 79−70598
US scanner, real-time rotating transducer, for heat and abdomen exams. 79−20603
US scattering, quantitative meas. 80−45959
US tomography in cardiology 80−30824
US transducers arc array with automatic sector scan echo signals presentation system *(Italian)* 79−96637
US two-dimensional images, extraction of cardiac parameters 77−25533
valve bioprosthesis, porcine 77−56529
valve dynamics, fluid physics appls. *(French)* 79−34589
valve motion obs. CW FM sonar 78−61230
valve prostheses development 77−56523
valve prosthesis design, role of simulation studies 79−12033
valve prosthesis mean press. gradient meas. under in vitro pulsatile flow 77−56531
valve tissue, glutaraldehyde preserved, stress/strain and fatigue behaviour 78−40217
valve vibrations, aortic and mitral, anal. and role in heart sound production 80−101214
valves, appraisal of power loads on elements 80−104811
valves, blood flow, vortex-grid method 80−41105
valves, diseased and prosthetic, assessment of haemodynamic function 77−48830
valves, natural and prosthetic, simple stress estimation method 80−8210
valvular bioprosthesis, devel. from xenograft (1965-77) 77−56528
valvular regurgitant fraction meas. by radionuclide angiocardiography, iterative estimation 79−34668
varifocal imaging 79−70631
vector cardiograph for pacemaker pulse display 80−41325
vector magnetocardiogram meas. using supercond. magnetometer 77−29213
vector magnetocardiography, practical lead system 77−44698
vectorcardiogram automatic anal., computer system 78−20302
vectorcardiographic P loop correlation with left atrial volume echocardiogram 79−44025
velocity-strain loop in normal and abnormal left ventricular function 78−31850
ventilator-patient coupling, effects of positive press. ventilation on cardiac output and pulmonary arterial flow 78−31852
ventrical, left, haemodynamical parameters meas., frame rate requirements 79−100715
ventricle, left, boundary detection from cineangiocardiograms 80−8168
ventricle, left, cineangiographic images automatic processing 79−83927
ventricle, left, contour extraction from radioisotope angiocardiograms, and wall motion classification 79−88180
ventricle, left, human, 3-D time-varying reconstruct error sources and magnitude estimation 80−85454
ventricle, spherical, dynamic press. distrib. 79−70562
ventricle dynamic model, using optimisation concept of systolic elastance 77−16951
ventricle excitation spread, computer simulation *(Japanese)* 80−3847
ventricle regional wall motion parameters, angiography vs. echocardiography 79−62392
ventricle volume characts., nuclear medical determ., appl. of computer system *(German)* 78−88737
ventricular, pressure, noninvasive meas. based on Doppler effect 79−5384
ventricular action potential, mammalian, analysis 79−62227
ventricular aneurysms, mechanical behaviour, mathematical model 79−11953
ventricular arrhythmias and depolariation effect of simultaneous biventricular pacing 77−81642
ventricular circumferential segmental shortening, from US sector scanning images in ischaemic dogs 79−70599
ventricular defibrillation, transthoracic 100 kg calf, truncated and untruncated exponential stimuli 80−41306
ventricular defibrillation thresholds with capacitor discharge, dogs 80−17182

cardiology continued

- ventricular defibrillation with myocardial electrodes in the dog, calf pony, and pig 80—72369
- ventricular dimensions noninvasive meas. in awake dog by echocardiography 77—44863
- ventricular ejection fraction determ. by radionuclide angiocardiography, correction of noisy data 77—48868
- ventricular excitation, digital simulation, computer model evaluation 78—85302
- ventricular failure, synchronous mech. cardiac massage, dog expt. 77—78036
- ventricular fibrillation alerting device 77—78024
- ventricular fibrillation and defibrillation 80—81769
- ventricular fibrillation for AC shocks at 50-60 Hz, threshold considerations 80—51065
- ventricular fibrillation/defibrillation threshold energy-time anal. 77—48924
- ventricular function, left, dual-probe system for rapid bedside assessment using radionuclide 77—2039
- ventricular function computer simulation, development of model and parameter estimation 78—53439
- ventricular function evaluation, comparison of systolic and diastolic parameters 79—70636
- ventricular function monitor, ambulatory, CdTe detector, cardiac ejection fraction meas. 80—61680
- ventricular function quantitative meas. by torque ballistocardiography 78—44660
- ventricular functionanalyser, microprocessor-based 80—26402
- ventricular mean transit time, right, using radiocardiography 77—2040
- ventricular muscle, mammalian, slow inward current depression by acetylcholine 79—92210
- ventricular muscle excitation threshold current rel. to electrode area, volume effect 77—81670
- ventricular myocardium plastic cast global Young's mod., calc. from angiograms 77—48827
- ventricular performance, 1st pass radioisotope assess. 80—85482
- ventricular pressure and ECG continuous monitoring during angina attacks, computer anal. 78—85436
- ventricular programmed pulse generator, testing by waveform generator and cardiac simulator 79—16351
- ventricular Purkinje fibre, electrophysiological and histological props. 79—39396
- ventricular septal defect, prediction by non-invasive examination using interactive terminals 78—31954
- ventricular septal defect plastic repairing instrument 78—7522
- ventricular tachycardia termination by rapid ventricular pacing bursts 77—81678
- ventricular volume determ. from indicator dilution curves, dog expts. 79—57696
- ventricular wall dynamics and obs. on blood flow 78—80896
- ventricular wall motion assessment, terminology 80—85528
- ventricular wall regional motion extent and sequence, clinical study 79—70635
- ventriculography, algorithm for automatic selection of end diastolic and end systolic cine frames 78—88757
- vibration effects sensitivity of response to time relationship between vibr. and cardiac cycles 77—56407
- vibration quantitative characterisation by multipolar acoustic heart model, minicomputer method 78—85429
- vibration responses of dogs to nonsynchronous and heart synchronous whole-body vibration 80—3675
- video processor for computer calc. of press.-vol. indices from left ventriculograms 78—53495
- video-angiocardiographic image series storage improvement by digital signal processing *(German)* 78—92723
- video-sync mixer for cassette videotape recording of computer images 79—29604
- videodensitometric camera and video disc system 77—40761
- videodensitometry via an S-100 bus microcomputer angiocardiograms appl. 80—26434
- volume determination by angiography, X-ray magnification estimation 78—73197
- wall motion abnormality detect. using regional changes in ventricular shape and vol. 79—70633
- wall motion and regional ejection fraction, comparison at rest and during isometric exercise 80—30857
- wall motion cine display using ^{99}Tc^{m}-labelled red blood cells 80—17129
- wall motion quantification using computerised US technique 78—40279
- weightlessness, bedrest analogue studies of exercise response 80—61713
- work, anal. using general energy equation of thermodynamics 78—20207
- X-irradiation effects, dog expts. 80—104679
- X-radiology, criteria of cardiac insufficiency *(German)* 79—53237
- X-ray apparatus, practical aspects in cardiac work 79—96659
- X-ray computed tomography, 3-dimens., of heart, lungs, and circulation 79—53224
- x-ray diffraction studies of the heart, review, book contrib. 80—109079
- Ca transients in aequorin-injected frog cardiac muscle 78—61149
- Ca^{2+} transients during excitation-contraction coupling 80—97896
- K arrested left ventricle finite deformation anal. in canine hearts *(Japanese)* 78—3543
- O_2 mass transport and regulation, microelectrode and math. modelling study 78—44534
- ^{31}P NMR investigations of metabolism, pH and contractile performance 78—69018
- ^{31}P NMR of the perfused heart 80—77534
- ^{99m}Tc labelled human serum albumin kits, evaluation for cardiac blood pool imaging 80—17130
- ^{201}Tl distribution in stressed rats, imaging, organ uptake and myocardial kinetics 78—65114
- ^{201}Tl myocardial imaging, eval. of right-ventricular overloading 79—53230
- ^{201}Tl myocardial imaging, redistrib. rel. to rest images 80—12225
- ^{201}Tl scintigraphy of the myocardium, effect of gate width 80—41172

carrier avalanches *see impact ionisation*

carrier communication

see also carrier telephony

- brain unit and slow-wave field activity, telemetry with FM pulse subcarrier 77—25625

carrier density

see also current density; electron density; electron density (metals)

- A15 compounds, quasi-one-dimens., theoretical group anal. of electron spectrum 79—82511
- amorphous materials, non-Markov carrier diffusion 80—6841
- benzophenone, cryst., charge carrier generation by exciton-exciton collisions 80—88568
- C-CD, signal charge and surface pot., steady-state distrib. calc. 80—100525
- chalcogenide lone-pair semicond. charged impurities, effect on carrier concs., Street-Mott model 78—67984
- charge carrier conc., temp. depend., computer data anal., effect of band parameter errors *(Russian)* 78—52006
- compound semiconductor, nonstoichiometry and carrier conc. control in MBE 79—95941
- conducting crystals, kinematical and dynamical inelastic light scatt. 78—80368
- copper phthalocyanine, imperfect cryst., elec. transport phenomena, charge carrier conc. 77—1421
- current fluctuations in strong elec. field, interelectron collisions, drifted Maxwellian distribs. *(Russian)* 80—2436
- defect cluster scatt. and removal of carriers, model 78—76069
- defect semiconductor, or insulator, carrier densities, elec. cond. and Fermi level 77—43532
- degenerate materials with position depend. band struct. carrier densities and emitter efficiency calc. 78—43378
- degenerate semiconductors, heterogeneous state, first-order phase transition, Ginzberg-Landau method analogue 80—70372
- DH, nonequilib. carrier distrib., local excitation of active region, influence of diffusion of luminesc. 79—73574
- DH laser diodes, impedance characts. 80—23690
- diagnostics of radiation plasma, electrode method *(Russian)* 78—14200
- diamond, natural semicond., isothermal annealing of electron radiation damage 77—7764
- dielectric, free charge carrier density calc., error in quasistationary approx. *(Russian)* 80—65544
- dielectric breakdown with picosecond laser pulses, large carrier conc. prod., SHG increase 80—102769
- dielectrics containing impurities, carrier distribs. and currents, numerical simulation *(French)* 80—70718
- disordered semicond., random field effect on carrier conc. *(Russian)* 77—51762
- distribution function, high energy asymptote in strong elec. field *(Russian)* 78—72163
- drift solutions, discontinuities, hot carriers injection and accumulation 78—51999
- electrical noise in equilibrium conditions 79—56274
- electron-hole paired systems, ferromagnetic ordering phase diagram 80—97097
- electron-hole plasma, strongly degenerate, helical density waves 80—15550
- electron-hole plasma stratification on heating by light or elec. field *(Russian)* 77—11951
- epilayer structures, transition regions 79—78167
- EPR line shape, magnetoresist. effect 80—84638
- extrinsic semiconductors, carrier concs. and Fermi levels 77—66112
- ferroelectric and antiferroelectric crystals, perovskite type structure, semiconductor props. *(Polish)* 78—56437
- ferroelectric semiconductor, phase boundary structure 79—11398
- ferroelectric semiconductor, phase transition temp., rel. to free carrier conc. 78—10860
- ferromagnetic degenerate semiconductor, magnon spectrum near instability of homogeneous state 79—28516
- ferromagnetic nondegenerate semiconductor, magnetoresistance 80—11019
- ferromagnetic semiconductor, electronic spectrum, influence of finite carrier conc. 78—76220
- film, electrophysical properties measurement apparatus 78—4654
- film, polycrystalline, carrier conc. depend. on crystallite size 77—85361
- films, elec. and galvanomag. props., microstruct. 80—70859
- free carrier profile measurement on thin-layers, fast current pulse MOS deep-depletion technique 78—80075
- gain-guiding double-heterostructure laser transverse carrier diffusion effects 79—55139
- gain-guiding stripe-geometry DH semiconductor laser oscillation characteristics 79—45945
- galvanomagnetic-recombination field effect, theoretical model 78—43420
- graphite, galvanomagnetic and thermomagnetic effects at low temp. 80—44618
- graphite, galvanomagnetic effects, low field data and free carrier densities 78—87986
- graphite, galvanomagnetic effects, trigonal warping of constant energy surfaces 78—87987
- graphite, neutron irradiated, effect on quantum limit Shubnikov-de Haas oscills. 78—95304
- graphite, thermoelec. and thermomag. props., cylindrical band model 80—39616
- graphite intercalation compounds, electronic props. in dil. limit 77—47714
- graphite-SbF_5 intercalation cpd., carrier density from ^{19}F NMR line shapes 80—25224
- Gunn diode, anode domain disappearance dynamics, computer simulation calcs. 80—6859
- heat treatment effects on elec. props. 78—43411
- heavily doped semiconductors and devices, review 79—47039
- HMTSF-TNAP, organic low temp. cond. 78—43368
- hopping in two-dimensional impurity bands, activation energy depend. 80—88561
- Hubbard model, half-filled, charge ordered solution local mag. moments, repulsion energy renormalisation 79—61034
- III-V compounds, n-type, new meas. method for compensation and spatial fluctuations of impurities 78—6404
- inhomogeneous system, with spherical inclusions, Hall coeff. and average carrier density 79—69533
- injection laser, reson.-like peak reduction in direct modulation due to carrier diffusion 78—74905
- injection stripe lasers, current carrier conc. distrib. *(Russian)* 78—13712
- insulator-semicond. interface, impurity-band hopping conduction in surface layers 80—75649
- ionic crystal, sublattice disorder, phenomenological models 77—35663
- junction device, injected carrier detect. by IR emission 79—38151

carrier density continued
Kapton, pyrolysed, cond. polymer, transport and mag. props. 80—96887
magnetodiode and magnetoconcentration effects, influence of field effect 80—107903
magnetoresistance four-probe method for free carrier density and mobility meas. 77—43626
many-valley semiconductor, impurity band for screened impurities 79—47053
many-valley semiconductor, metal-insulator transition at finite temp., calc. 80—49603
metal, non-cubic, electric field gradient, press. and temp. depend. 77—8057
MIS, HF capacitance, minimum value and position 77—85338
MIS structure, radiation induced charge storage 80—6997
MIS structure, time depend. of carrier density semicond. bands and surface states 79—69603
MISIM struct. inversion layer, symmetrical, carrier conc. calc. 80—75651
MNOS memory device, trapped charge behaviour, UV light effects 77—12014
MOS structures, total dose effects on carrier conc. and mobility 77—20443
MOSFET, ionic scatt. effect on Shubnikov-de Haas amplitudes in Si inversion layers 79—42653
n-n homojunction, calc. of free carrier density profile in a semicond. near ohmic contact 80—70810
narrow-band semiconductors, current-carrier conc. distrib. nonuniformity, contactless meas. 77—76853
negative differential cond. of hot electrons in mag. field due to carrier density nonlinearity 77—55540
nematic liquid crystal, elect. conduct. based on injection-contact phenomena theory *(Russian)* 80—107807
nonhomogeneous semiconductor, galvanomagnetic effects 79—91077
nonuniform band structure materials, Shockley like equations for current density and carrier density 80—60001
nonuniformity monitoring by relative thermoEMF meas., limits of applicability 77—36702
p-n heterojunctions, nonequilib. carrier behaviour at high current density 80—6968
p-n junction, abrupt, forward-biased, transition region behaviour anal. 77—76909
p-n junction injection characteristics in strong elec. fields 77—76913
p-n junctions, linearly graded, characterisation 80—6962
paramagnetic semiconductor, heavily doped, linear response functions and magnetoresist. 77—51770
photoconductivity, short-pulse, transit time effects 80—70754
photovoltage for doping factor, mobility ratio and excess conc. determ. extreme band bendings 78—91726
piezoelectric semiconductors, dependence of US attenuation 78—72206
poly(γ-methyl L-glutamate), electric conduction mechanism *(Japanese)* 80—54696
polyacetylene conductivity mechanism, Peierls phase one dimensional cond. *(Russian)* 80—88546
polycrystalline layer, carrier conc. and effective Hall mobility 77—4375
polycrystalline semiconductor thin film, effective mobility and concentration 77—28264
polyethylene, linear, films, elec. cond. rel. to drawing, annealing *(Japanese)* 79—15817
polymer film electret, charge distrib., generalized model 80—6873
polystyrene atactic carrier transport and photogeneration 80—80318
quantised inversion layer, hot carrier transport 78—30993
rare earth chalcobismuthites, $RBiTe_3$, prep., elec. props., and crystallographic date 80—59981
Schottky barrier, charge carrier conc. determ. from low-field electrorefl. spectra 77—85320
self-oscillatory semiconductor medium, coupled temp. and carrier density self-oscills., photoelectron heating, microwave field 79—11166
semiconductor, Auger recombination, carrier density depend. 79—38089
semiconductor, carrier concentration distribution by scanning IR absorption 79—61356
semiconductor, carrier distribution function 78—26856
semiconductor, carrier intrinsic conc. and effective mass determ. by IR refl. 79—51580
semiconductor, charged impurity diffusion 80—6563
semiconductor, current-voltage characts. of hot electrons under phonon heating and recomb. conditions 79—51591
semiconductor, dark conductivity anomalous temp. depend. 77—20319
semiconductor, distrib. function in presence of external elec. field, anal. 77—1415
semiconductor, doped with mag. impurity, ordering mechanism 80—2572
semiconductor, double injection characteristics under high voltages 79—51590
semiconductor, effect of effective lifetime modulation 78—47808
semiconductor, Einstein relation for degenerate carrier concentrations 78—72143
semiconductor, electron distribution function, temp. gradient effect 78—72145
semiconductor, electron-hole plasma and elec. field, stratification at low temp. 80—60020
semiconductor, ferromag., anomalous carrier density mag. field depend., EuSe appl. 80—49774
semiconductor, free carrier density profile near ohmic contact calc. 80—70810
semiconductor, galvanomagnetic-effects in strong elec. field 78—56163
semiconductor, graded-gap, internal photo-effects, excess carrier distribs. 80—107847
semiconductor, impurity band props. 79—23888
semiconductor, inhomogeneous, carrier statistics and thermal relax. *(Russian)* 77—4333
semiconductor, large-band-gap, self-compensation, role of impurities 80—92850
semiconductor, near intrinsic magnetoresist. effect determ. of carrier density and mobility 78—2501
semiconductor, nonlinear conductivity, vortex waves, carrier mobility and lifetime 80—96893
semiconductor, optical generation of carriers under Franz-Keldysh effect conditions, instability 79—24017
semiconductor, optical heating, coupled diffusion eqns. for heat and excess carrier density 80—60718
semiconductor, self-oscillatory medium, modelling 77—20811

carrier density continued
semiconductor, superlattice doping, electronic states, elec. props. 79—95480
semiconductor, theory of carrier multiplication and noise due to avalanche processes 80—6865
semiconductor, transport equations, initial approxs. for numerical soln. 78—14741
semiconductor, trap-free lifetime and relaxation, bulk boundary conditions for injection and extraction 78—72169
semiconductor, two-photon absorpt., free carrier storage by deep centres *(Russian)* 78—23131
semiconductor containing traps, minority, carrier lifetime 78—60137
semiconductor crystal surface, nonequilib. electron effects due to chem. excitation 78—72238
semiconductor device, surface recombination, effect on steady-state relationships 78—39191
semiconductor electron-beam-pumped laser, carrier distrib. and collection efficiency 79—31902
semiconductor epitaxial layer, free-carrier density determ. by Hall meas., surface and interface depletion corrections 79—91170
semiconductor epitaxial layer, p-n junc. and Schottky barrier differential capacitance obs. 77—12036
semiconductor epitaxial layers, fast characterisation by MESFET 79—87170
semiconductor Fabry-Perot interferometer retuning by optical excitation *(Russian)* 80—98970
semiconductor film, carrier temperature and density self-oscills. near instability threshold 80—11118
semiconductor film, photoconductor, thermal-density hysteresis 79—51631
semiconductor heating, thermal domain investigation, current voltage characts. 80—70711
semiconductor in highly excited state, thermodynamic theory, photocond. 77—47742
semiconductor in mag. and US wave fields, electronic density of states *(Russian)* 78—72056
semiconductor isotype heterojunction barriers, cond. band discontinuity, C-V profiling meas. method 80—70801
semiconductor junctions, quantum statistical theory in thermal equilibrium 78—39197
semiconductor laser, dynamic behaviour, lateral mode and carrier density profile effects 78—82968
semiconductor layers, measurement technique using a long gate MOSFET structure 79—47178
semiconductor non-equilibrium periodic stratification by diffusion 77—55544
semiconductor or insulator, theory for flow of Hall current in sample of arbitrary shape 79—73532
semiconductors, determ. using calibrated polarimeters and the Faraday magnetooptical effect 80—60551
semiconductors, dopant distrib. from carrier drift distrib. in high elec. field 79—51140
semiconductors, doped, IR absorpt. in Drude tail, effect of finite electron densities 79—47449
semiconductors, free carrier density in strong electric and quantised mag. fields 80—6860
semiconductors, generalised transport equations 79—95398
semiconductors, heterogeneous, anisotropic, Hall coeffs., Hall mobility, carrier density *(Russian)* 80—70734
semiconductors, narrow gap, hot electron phenomena, I-V curve calc. 80—34457
semiconductors, photocarrier distrib. and photomagnetoelectric effect near stimulated emission threshold 80—80320
semiconductors, photomagnetoelectric effect, expt. parameters rel. to material props. 79—99584
semiconductors, quasi elastic hot electron impurity scatt. in quantising mag. field 80—24938
semiconductors, van Hove critical point region, electron-phonon interactions, dispersion law 80—70344
semiconductors free-carrier concentration, contactless meas., IR polarimeters, Faraday effect 77—73135
semimetal, two-stage drag of electrons by phonons 77—15843
semimetals, two-dimensional, electron-hole rearrangements in high mag. fields 79—87028
Si, on sapphire, Schottky magnetodiode, integrated mag. sensor 80—68223
small Hall effect transducer potential, elec. field and majority carrier density distrib. 79—67290
solid surfaces props. characterisation, structural, chemical and electronic, use of LEED methods *(Italian)* 80—49467
solid-state diode, carrier mobility, carrier density depend., scaling law 77—8179
solid-state electronics, introductory theory, book 80—22160
space charge limited current with diffusion theory, for exponential trap distribution 80—10992
spreading resistance meas., multilayer correction factor calc. 77—76823
sputtered films, optical props. and appls. 78—72623
superconductors, critical temp. correlation with electronic and phonon props. 79—69620
superlattice semiconductor impurity photoconductivity electron spectrum reconstruction 80—24966
surface magnetoplasmon type polaritons, LF, existence criterion in Faraday config. 80—96961
teracene, photoionisation of triplet excitons 77—62837
tetracene surface states, electric field effects, exciton-charge carrier interactions *(Russian)* 80—24989
thin surface layer, interactions between nondegenerate electrons, effect on cyclotron resonance, mag. cond. *(Russian)* 80—15802
TTF-TCNQ, semicond., driven oscills. of carrier conc. 80—15551
wide-gap semiconductor, recomb.-trap barriers 77—8119
$Ag_{1-x}Sn_{1+x}Se_{2-y}$, supercond. and normal state props. 77—36008
Ag_8SnSe_6, cryst., Hall effect investigation of polymorphic transform. 80—39605
Ag_2Te, low temp. thermal cond., thermoEMF 78—43423
Al-Al_2O_3-$SnTe$, junction, tunnelling, Fermi level depend. on carrier conc., influence of surface states 80—25016
Al-Al_2O_3-$SnTe$ structure, tunnelling characts., model anal. 80—29480
AlAs-GaAs, heterostructure electroluminesc. characts., active region electron density depend. 77—12446
AlAs-GaAs:Ge double heterojunctions, efficiency of radiative recombination 77—77286

carrier density continued
AlGaAs buried heterostructure lasers, gain and absorpt. spectra meas. 80—91792
AlGaAs DH laser, self-pulsations due to proton bombarded region self-annealing during ageing 80—99728
AlGaAs DH stripe geometry lasers, spontaneous radiation, carrier conc., and threshold current, luminesc. meas. 79—36898
AlGaAs p-n diodes, I-V characts., tunnelling 80—100510
p- (AlGa)As:Zn, MBE grown, elec. props., shallow junction solar cell use 79—91175
n-$Al_xGa_{1-x}As$, electrical props. 78—6381
$Al_xGa_{1-x}As$ MBE layers, ionized beam doping, elec. and optical characts. 79—37721
$Al_xGa_{1-x}As$, organometallic VPE growth, and characterisation 79—78899
$Al_xGa_{1-x}As$, VPE growth and characterisation 78—35315
$Al_xGa_{1-x}As$:Mg doping characteristics, elec. props., effective hole masses 79—78117
$Al_xGa_{1-x}As$:Te, epitaxial film, elec. cond. and Hall coeff. rel. to donor levels 77—24630
$Al_xGa_{1-x}As$:Zn epitaxial layers, composition and Zn carrier conc. 80—25585
AlGaAsSb, photodiode, lattice-matched to GaSb 79—71527
$Al_xGa_{1-x}Sb$:Zn, impurity diffusion, p-n junction depth 80—24678
$Al_xGa_{1-x}Sb$:Zn(Si)(Ge)(Sn)(Pb), doping of solid solns. during LPE *(Russian)* 77—85087
α-Al_2O_3, energy levels of donor and acceptor dopants and electron and hole mobilities 80—59911
As chalcogenides, deep levels, photoluminesc. and photocond. 80—70641
As, rhombohedral, nucl. quadrupole spin-lattice relax. 79—15373
a-As_2Se_3 chalcogenide glass, influence of thermally induced defects on transport props. 80—49766
As_2Se_3 glassy films, current-voltage characts., temp. depend., SCL current 80—92902
Au, thin film, discontinuous, high resist., Hall effect meas. 80—65716
(Ba,La)TiO_3, defect chemistry and elec. cond., conc. of conduction electrons, thermogravimetric meas. 77—39580
Ba-ferrite, temp. range 303 to 353K 79—42564
$Ba_{1-x}Sm_xB_6$, prep., elec. cond. and thermoelec. props. 80—49697
$BaTiO_3$, acceptor-doped defect equilibria, elec. cond. 77—39579
$BaTiO_3$, H_2-reduced, elec. cond. mechanism, EPR, resist. and Seebeck coeff. meas. 80—10976
$BaTiO_3$, SCL currents, carrier mobility and trapping 77—15863
Bi, diffusion thermoelectric power in mag. field, calcs. 78—56167
Bi epitaxial films, size effect in elec. props. 80—54813
Bi film, carrier conc., mobility and 1/f noise 80—44748
Bi film, carrier conc. and mobility, resist., galvanomag. and thermoelec. meas. 78—52111
Bi film, kinetic props. of electrons 77—63011
Bi, Shubnikov-de Haas effect in high mag. fields 80—2404
Bi, transverse magnetoresistance, field depend., static skin effect 79—11149
$Bi_{12}GeO_{20}$ crystals, principal carriers obs., in dark and under laser illumination *(Russian)* 80—80312
$Bi_{12}GeO_{20}$, hopping cond., carrier mobility and density 78—19040
n-BiSb, cyclotron mass meas., high hydrostatic press. 79—77991
$Bi_{0.88}Sb_{0.12}$, semiconducting transport props., 2 to 100K 80—59989
$Bi_{0.9}Sb_{0.1}$, epitaxial film, defect struct. and galvanomagnetic props. 77—89889
$Bi_{1-x}Sb_x$, growth by horizontal zone refining, low charge carrier conc. 77—21020
$Bi_{1-x}Sb_x$, semicond.-semimetal transition, temp. and press. depend. of transport props. 78—76120
$Bi_{1-x}Sb_x$ thin films, elec. props., 4.2-300K, charge carrier conc. *(Russian)* 79—24087
$Bi_{88}Sb_{12}$-Sn, current carrier energy spectrum *(Russian)* 78—60139
$Bi_{2-x}Sb_xTe_{3-y}Se_y$ solid solution, density-of-states effective mass, carrier mobility temp. depend. 80—24931
Bi_2Te_3, Shubnikov-de Haas effect, high press. effect on band struct. 77—51767
Bi_2Te_3-Bi_2Se_3 solid solns., bladed cryst. growth, electrophysical props. 78—43387
Bi_2Te_3-Bi_2Se_3-Sb_2Te_3, solid solution, single crystal, elec. cond., thermoelectric props. 80—88550
$Bi_2(Te_{1-x}S_x)_3$, quasi 2-D cryst., I-V and magnetocond. meas. 77—85360
$Bi_2Te_{3-x}Se_x$ films, surface band struct. and scatt. mechanism 80—34535
$Bi_2Te_{3-x}Se_x$ solid solution, Hall effect anisotropy parameter, thermoelectric power, depend. on carrier density 79—69536
C pregraphitic, negative magnetoresist. 80—34466
$CaCO_3$, calcite, elec. cond., 300 to 1200°C at CO_2 pressure of 40 bars 80—20195
Cd_3As_2, depend. of g-factor on electron conc. at low temps. 77—69218
Cd_3As_2, elec. resist. and HF dielec. const. calcs. *(French)* 77—59284
p-$CdCr_2Se_4$:Ag, electrical props., 100-300K 80—54692
$CdCr_2Se_4$:Cu, elec. props., temp. depend. *(Russian)* 78—72181
n-$CdCr_2Se_4$:In, electrical props., 93-168K 80—49713
$Cd_{0.96}Cu_{0.04}Cr_2Se_4$, single cryst., temp. depend. 79—7848
CdF_2:Ge^{3+}, Ce^{3+}, in semicond. state, elec. cond. and Hall meas. 78—10443
$CdGeAs_2$, elec. and optical props., acceptor levels and energy gap determ. 77—85218
n-$CdGeAs_2$:In(Te), resist. and Hall coeff. meas., influence of press. 77—47810
n-Cd_2GeO_4, electronic and cond. props. rel. to prep. conditions and defect struct. 80—107787
$CdGeP_2$:Cu, impurity behaviour 77—15857
Cd_xHg_{1-x} Te, elec. characts., impurity effects 80—92890
n-$Cd_xHg_{1-x}Te$ crystals, carrier recomb. in extrinsic conduction range 80—70722
$Cd_xHg_{1-x}Te$, current-voltage characts., pinch effect, mag. field effects 80—6858
$Cd_xHg_{1-x}Te$, electron mobility and conc. near gapless state, influence of hydrostatic press. 79—65486
$Cd_xHg_{1-x}Te$ epitaxial graded gap layers, plasma reflection and magnetoreflection 80—71391
$Cd_xHg_{1-x}Te$ films, epitaxial growth, optical, elec., and photoelec. props. 79—11512
$Cd_xHg_{1-x}Te$, fine-graded gap struct., electrophysical props. *(Russian)* 78—60144
$Cd_xHg_{1-x}Te$, intrinsic carrier conc., Fermi level calc. 77—55481

carrier density continued
$Cd_xHg_{1-x}Te$, low temp. piezoresistance, Hall effect, elec. cond., plastic flow 80—6844
$Cd_xHg_{1-x}Te$, photomagnetic and galvanomagnetic effects in quantising mag. fields 80—20223
$Cd_xHg_{1-x}Te$, resistivity, Hall effect and magnetoresist. in strong elec. field 77—28199
$Cd_xHg_{1-x}Te$, strong elec. field effect on galvanomagnetic effects 79—11159
CdP, electron mobility, carrier density depend. calc. 79—56229
Cd_3P_2, thermomagnetic transport effects obs. 77—15883
CdS, carrier density nonlinearity of interacting acoustic fluxes 77—51781
CdS, chem. sprayed film, struct. and morphology 78—72020
CdS, epitaxial film, conductivity control by S vacancy form., light modulation appls. 77—4455
CdS, epitaxial film, structural and electron transport props. 79—82481
CdS film, chemically sprayed, carrier conc. and mobility, thermoelec. and photothermoelectric meas. 80—2503
CdS film, Hall effect meas. 79—65570
CdS film, prep. by hot wall technique, morphology and semicond. props. 79—95292
CdS film, spray pyrolysis prep., elec. transport props. 78—2590
CdS, film for solar cells, struct. and elec. props., thickness depend. 78—72289
CdS, single crystal, growth by modified Piper-Polich method, props. *(Japanese)* 79—100036
CdS single crystals, depend. of radiative props. on equilib. carrier density 79—19932
CdS sprayed films, elect. and optical props. 78—39241
CdS, surface photovoltage, characterisation 80—60033
CdS, thermal decomp. kinetics, in vacuo, free electron density depend. 77—59111
CdS:Cu, photocurrent, elec. field effect on recombination processes *(Russian)* 80—100484
n-CdS:In, containing excess Cd, effects of In on elec. props. 79—56217
CdS:In film, flash evaporated, prep. and elec. props. 80—20792
CdS:Li chemically deposited filter, elec. props. 80—11113
n-CdS:Te, grown from Te soln., elec. props. 79—65475
CdS-type semiconds., Dember effect, theory 78—72189
CdS_xSe_{1-x}:In film, flash evaporated, prep. and elec. props. 80—20792
CdSb, monocrystalline film, prep., elec. props. 79—43159
CdSe, defect struct. in Se vapour 78—64043
CdSe, epitaxial film, gas-phase comp. effects on elec. props. 77—85354
CdSe film, Hall voltage meas. 77—69434
CdSe film, vacuum deposited, struct., resist. and Hall mobility 77—76974
p-CdSe, Hall density and mobility, in Se vapour atm., 600-1100K 78—52014
p-CdSe layers, ion implantation prep., elec. props. 79—51699
CdSe thin film transistor and MISM struct., effect of annealing on electron mobility and conc. 79—78198
CdSe:Cl(In), photoluminesc. props. near fund. absorpt. edge, impurity conc. effects 79—52003
CdSe:In, epitaxial layers, synthesis and elec. props. 77—47909
CdSe-Mo Schottky barrier, tunnelling and majority carrier density 79—51673
$CdSnP_2$-$CdSnAs_2$, and $CdSnP_2$-$CdGeP_2$, solid solution form. and elec. characterisation 78—43125
CdTe, film grown by hot wall epitaxy, elec. props. 79—82696
CdTe, laser window material, vap. deposition 78—27391
p-CdTe, nondoped, heat treatment in vacuum, dissoc. obs. effects on struct. and props. *(Japanese)* 80—60662
CdTe:Cl, grown by travelling heater method, carrier homogeneity investig. 77—39848
CdTe:Cl, heavily doped, elec. and photoluminesc. investig. of defect interactions 77—39603
p-CdTe:Cl, influence of gamma-irradiation on elec. props. 77—62951
CdTe:Cl, interaction of impurities and lattice defects, changes in elec. props. and photoluminesc. 77—4685
CdTe:Cl, LPE from $CdCl_2$ soln., elec. props., defects 80—39689
CdTe:Cu, doping effects on evaporation kinetics and electronic props. during high-temp. annealing in vacuum 78—22743
CdTe-HgTe, semicond. solid solns., effect of reactor irrad. on electrophys. props. 77—51744
$Cd_{3-x}Zn_xAs_2$, electron mobility and carrier density calc. 77—80780
$Cd_xZn_{1-x}S$ films, chem. sprayed, carrier density and mobility 80—60121
CeO_2:S, acceptor properties of S, free electron concentrations 80—34395
CeO_2:S, in $O_2+CO_2+SO_2$ atmosphere, elec. cond. study 80—39583
$Ce_{3-x}S_4$, $Ce_{3-x}Sm_xS_4$, elec. cond. mechanism, thermoelec. power, Hall and absorpt. coeffs. 77—24559
Co_3O_4:S, defect struct. and elec. props., electron, hole conc. 80—44601
Co_2RhS_4, mag. semicond., mag. and elec. props. 80—93121
$CrSi_2$ based solid solns., prep., elec. cond. and thermoelec. props. 80—49697
Cu_3Au, electrical resistivity and LRO, energy gap formation in Fermi surface 80—88533
$Cu_{0.67}Cr_{1.78}Se_{2.67}Br_{1.34}$, polycrystalline mag. semicond., mag. and elec. props. 79—7846
$Cu_yCr_2Se_{4-z}Br_x$, degenerate ferromag. semicond., resist. minimum 79—73517
$CuCr_2Se_4(S_4)(Te_4)$, binary and ternary solid solns., mag. and elec. props. 80—2407
$CuGaSe_2$ thin films, on GaAs substrates, structural and elec. props., photoluminesc. meas. 79—65564
$CuGaTe_2$, elec. and optical props. 80—6829
$CuGaTe_2$ epitaxial layers, elec. props. as function of growth temp. 79—65565
p-$CuInSe_2$ film, prep. from vac. evaporation of $CuInSe_2$, optical and elec. props. 79—82697
$CuInTe_2$ epitaxial layers, on GaAs, growth and props. 80—108359
$CuInTe_2$, grown from near stoichiometric comp., elec. and optical props. 78—68504
$CuInTe_2$, vac. deposited film, growth, struct. and elec. characts. 77—69995
$Cu_2Mo_6S_8$, normal state and superconducting property measurements 78—91660
$Cu_xMo_6S_8$, Hall effect and magnetoresistivity 78—95400
Cu_2O, positive and negative photomemory, IR luminesc. spectra, illum. effect 79—69557
Cu_2O:Mn, photomemory mobility components, charged centre conc. 80—103725

carrier density continued
- Cu_2S film, reactively sputtered, Hall effect meas., 90-300K 80—15541
- $Cu_{2-x}S$ single crysts., comp. depend. 77—24302
- $Cu_{2-x}Te$, x=0 to 0.3, elec. cond., Hall const., carrier mobility, conc., thermoelec., density, lattice parameter 77—11915
- $Cu_{2-x}Te$-CdSe heterojunction, elec. and opt. props. *(Korean)* 77—51811
- EuB_6, correlation between mag. struct. and elec. props. 77—63192
- EuO, Eu doped, temp. depend. of carrier conc. and mag. susceptibility 77—69483
- EuO nonstoichiometric film, ESR spectra and exchange interaction 80—93176
- EuO:Eu, doped ferromag. semicond., carrier density and mag. susceptibility rel. to M-S transition 77—72820
- EuO:Gd, elec. cond. under hydrostatic press., Curie temp. 80—96881
- EuO(Se), complex elec. cond. anomalies 80—107812
- $Eu_{0.98}Sm_{0.02}O$, ferromag. semicond., elec. cond. meas. 80 to 370K, press. effect to 20 kbar 77—51751
- Fe-Al (45%), ordered and disordered states, optical and elec. props. 77—85826
- Fe-Al-Ni-Co-Cu alloys, Ti alloying and deoxidising addition *(Russian)* 78—80181
- Fe_3Al, electrical resistivity and LRO, energy gap formation in Fermi surface 80—88533
- α-Fe_2O_3 electrode, carrier density determ. by optical absorpt. and photoelectrolysis spectra 80—71462
- α-Fe_2O_3, polycryst., pure and TiO_2 doped, flatband potentials, donor densities, photocurrent meas. 78—76089
- $FeRh_2S_4$, mag. semicond., mag. and elec. props. 80—93121
- GaAS, proton isolation layer, lateral spread, elec. meas. 77—80520
- GaAS:Cr, mag. field depend. of single carrier parameters, mixed cond. anal. 79—91043
- GaAlAs DH laser, narrow stripe geometry, spontaneous carrier lifetime 80—87392
- GaAlAs:Zn recombination radiation drift, charge carrier photon induced drift in varigap semicond. 80—50418
- $Ga_{1-x}AlAs$:Zn, acceptor energy level and elec. props. 80—65482
- $Ga_{1-x}Al_xAs$, LPE growth and characterisation 80—50566
- $Ga_{1-x}Al_xAs$, non-shallow levels and cond. band struct. from Hall carrier conc. meas. 80—39607
- $Ga_{1-x}Al_xAs$, p^+-n-n^+ heterostructure, distrib. of injected carriers, forward V-I characts. *(Russian)* 80—6973
- $Ga_{1-x}Al_xAs$:Si, LPE, phase diagram, Hall effect meas., carrier conc., donor ionisation energies 77—72803
- $Ga_xAl_{1-x}As$, LPE, charge carrier conc. distrib. *(Russian)* 78—52694
- $Ga_xAl_{1-x}As$ stripe-geometry laser, current carrier conc. distrib. and threshold props. 77—68212
- n-GaAs, and Te doped, homogeneity, IR introscopy investig., carrier density and mobility calc. 79—15446
- GaAs, anodic oxide film, annealing effect on carrier density profile 78—88040
- GaAs, CVD, S doping behaviour during growth, electron conc. 78—26784
- n-GaAs carrier compensation by O ion implantation, C-V meas. 77—7747
- GaAs, carrier conc. and compensation microprofiles 80—80820
- GaAs, carrier conc. variations using electrolyte electroreflectance, topographical features 79—99562
- GaAs, carrier concentration determ. using electroreflectance 78—23483
- GaAs, carrier removal after $H_1{}^+$, $H_2{}^+$, and $H_3{}^+$ implantation 77—8115
- n-GaAs, crystal growth by Czochralski method kinetics, total emittance determ. 80—75193
- GaAs, defect clusters induced by γ-rays and neutrons, effect on elec. props. 80—29408
- GaAs, domain elec. instability in two-valley semiconds. 77—76842
- GaAs, elec. effects of dislocations 79—82586
- GaAs, electrical conductivity and thermoelectric power charge due to melting 80—100490
- p-GaAs, electronic props. 78—68040
- GaAs epilayers and p-n junctions, anisotropic phonon generation 79—37784
- n-GaAs, epitaxial, thermoelec. power, temp. depend. in mm wavelength range 79—23996
- GaAs epitaxial film on GaAs substrate, IR characterisation 78—23544
- GaAs epitaxial layers, non-doped, from Ga-$AsCl_3$-H_2 system, TEM and RHEED study of micromorphology and defects 79—65340
- GaAs epitaxial layers fast characterisation, electroless plating of Au 79—33347
- n-GaAs epitaxial wafers, IR reflectance and elec. characts. 79—56293
- GaAs, epitaxy using TMG and AsH_3, chloride etching effect 78—76606
- n-GaAs, far IR propag. of surface EM waves 79—42615
- p-GaAs, Fe-compensated, photocond. under strong excitation 77—15904
- GaAs, heavily doped, electron effective mass, Kane equation calcs. 79—77989
- p-GaAs IR plasma reflectivity spectra calc., rel. to carrier conc. 78—52511
- n-GaAs, implanted, IR refl. meas. of free carrier parameters 77—36244
- p-GaAs, impurity band Hall mobility 80—70730
- GaAs, in MIS system, nature of surface carrier depletion layers 77—1469
- p-GaAs, influence of light holes on transport props. 77—4367
- GaAs, injection lasers with filament, junction current and carrier-conc. profiles *(Chinese)* 79—50292
- GaAs, ion implantation, review 78—6080
- GaAs, ion implanted, effect of channelling on elec. props. 77—8114
- GaAs, LPE, charge carrier conc. distrib. *(Russian)* 78—52694
- n-GaAs, LPE, deep trapping centre characterisation by Hall and photo-Hall meas. 80—88578
- n-GaAs, LPE, impurity compensation photolum. and free carrier conc. meas. 77—62558
- GaAs LPE from Ga soln., carrier conc., growth condition depend. 80—71584
- GaAs, LPE layers, ambient O_2 effect on defects and elec. props. 77—76683
- GaAs layers and p-n junctions grown by current-controlled LPE, elec. characts. 78—6436
- GaAs, MBE, growth temp. depend. and characts. 79—28946
- GaAs, MBE, SnTe source of donor impurities 79—95035
- n-GaAs, mechanical polishing damage effect on IR refl. and ATR spectra 77—20848
- n-GaAs, mechanism of cyclotron reson. induced cond. 78—43396

carrier density continued
- p-GaAs, minority carrier mobility calcs., including screening, scattering mechanisms 79—99545
- GaAs multilayer with abrupt carrier conc. profile, vapour growth technique 78—11123
- GaAs, n^+-n-n^+ and n^+-p^--n^+ structs., ballistic electron motion at room temp. 80—80360
- GaAs n^+2n^+ epitaxial multilayers, carrier conc. from Fourier transform anal. of magnetoresist. signal 79—38205
- n-GaAs, non-equilibrium acoustic phonon generation by hot electrons 80—6477
- GaAs, p- and n-type, and Zn-diffused, spreading resist. meas. 79—28343
- GaAs, p^+-n^0-n^+ struct., control of modulation of base resist. 79—91133
- GaAs, photon transfer of excitation of nonequilib. carriers, conc. profile and relax. time 77—69907
- GaAs, produced by VPE using trimethylgallium and arsine, controlled doping 78—6855
- n-GaAs, proton irrad., E_p=30 MeV, defect form., orientation depend. 78—55898
- GaAs pure and Se-doped, photoluminescence at dislocations, band gap electronic levels 79—99926
- GaAs, semi-insulating, elec. characts., correl. with mass spectra anal. 78—39104
- GaAs, semi-insulating, surface layer thermal conversion mechanism, Hall effect meas. 80—49772
- GaAs, Si ion implantation and annealing, damage recovery, surface carrier profile 77—4119
- n-GaAs, surface recomb. vel. meas., diffr. from transient optical grating 79—1604
- GaAs, surface wetting with Hg, doping degree influence 80—92762
- GaAs, thermalisation of electron-hole plasma 79—95439
- GaAs, transmutation doping by thermal neutrons 80—10581
- GaAs, unintentionally doped layer grown by MBE, elec. props. 79—91167
- n-GaAs, VPE, hi-lo, carrier conc. profiling by electrochem. methods 80—49958
- GaAs, VPE film growth in Ga-$AlCl_3$-H_2 system, O_2 injection effect 79—100057
- GaAs, VPE layer growth with abrupt doping profile 80—24746
- GaAs, VPE on Ge substrate, and characterisation 78—72736
- GaAs, wide-gap semiconds., HV diodes, current-voltage characts. 79—24068
- GaAs:Ag, diffusion of Ag at 1000°C, profiles, Schottky barrier and Hall effect meas. 80—54435
- GaAs:Be, ion implanted, elec. profiling and optical activation expts. 77—89457
- p-GaAs:Be, ion implanted, annealing characts., defect cond. profiling, electron diffr. obs. 79—4318
- GaAs:Be, ion-implanted, IR refl. and transmission meas. 80—34908
- GaAs:Cr, Be, ion-implanted, semi-insulating, carrier mobility and conc. temp. depend. 77—76808
- GaAs:Cr, Mg, ion implanted, elec. meas. and optical activation studies 79—86806
- GaAs:Cr, parameters determ. using cond., Hall effect and magnetoresist. meas. *(Slovak)* 78—47802
- GaAs:Cr, Se implantation, carrier conc. and mobility profiles depend. on dose and annealing temp. 77—47479
- GaAs:Cr, Se layers, ion implanted, ohmic contact form., contact resist. meas. 79—91158
- GaAs:Cr, semi-insulating, thermal conversion suppression by arsine-controlled capless-anneal, ion implantation 80—49245
- p-GaAs:Cr, semi-insulating, mobilities and carrier concentrations, temp. depend. 80—70702
- GaAs:Cr, Te implantation, electron conc. and mobility profiles depend. on dose and annealing temp. 77—39607
- GaAs:Cr, VPE growth, carrier conc. profiles 79—74099
- GaAs:Cr, Zn(Se) shallow impurity implantation, elec. props. after annealing 80—24465
- GaAs:Cr diffusion profile meas. 80—6554
- GaAs:Cu, diffused layers, photocond. spectra, hole conc. and mobility *(Russian)* 78—14758
- GaAs:Cu, LPE, photoelec. meas. of electron density for different Cu introduction methods 78—43437
- GaAs:Ge, VPE, doping, electrophysical characts. meas. 78—43493
- GaAs:Ge, vap. grown, diatomic complex donor and acceptor model 78—80003
- n-GaAs:Ge epitaxial layer, ion-implantation doped, anomalous behaviour of impurities 78—18669
- GaAs:Ge film, MBE grown, heavily doped, elec. props. rel. to growth parameters 80—100537
- GaAs:n, ion implantation, hole conc. and mobility profile meas. 78—23082
- n-GaAs:O film, influence of O on elec. props. 79—11252
- GaAs:S^+ film, ion implanted carrier characterisation by cyclotron reson. 77—20472
- GaAs:Se, Ga, dual species ion implantation, elec. characts. 80—103377
- GaAs:Se ohmic contacts, pulsed electron beam annealing donor density, mobility 80—65678
- GaAs:Se(Sn), annealing kinetics of implanted donor ions 78—6079
- GaAs:Se(Te), laser annealed, donor implanted, elec. props. 79—4556
- GaAs:Se(Zn) polycrystalline film, Hall effect, resistivity meas. 80—96911
- GaAs:Si, electrical activity of Si 79—15145
- GaAs:Si, LED, effect of struct., defects on quantum efficiency 79—11211
- GaAs:Si, Li, IR absorpt., microstruct., charge compensation 80—107565
- GaAs:Si, pulsed laser annealing of implanted layers, defect structure and Hall effect meas. 79—69118
- GaAs:Si, thick LPE layer growth and characterization 77—12511
- n-GaAs:Si LEC crystal, carrier conc., B acceptor centres, Hall meas. and IR spectra 78—6717
- GaAs:Si(Sn), ion implanted, laser annealed, high doping levels 80—88181
- GaAs:Sn, influence of growth process in doping profile and mobility profile during LPE 79—70000
- GaAs:Sn, LPE layers, electronic props., depend. on Sn incorporation 78—87883
- GaAs:Sn, Te, luminescence props. 79—52017
- GaAs:Sn epitaxial layer, electronic props. and epilayer-substrate interface props. 77—89886

carrier density continued
- n-GaAs:Sn(Te), pure and doped, diffusion of Sn, radiotracer profiles 79—23782
- GaAs:Zn, diffusion of Zn by two-temp. method, LED fabrication 80—49416
- GaAs:Zn, implanted, hole conc. and mobility profiles meas. 78—23081
- GaAs:Zn, pulsed laser annealing, expt. 78—34828
- GaAs:Zn, sign inversion of the linear photogalvanic effect *(Russian)* 80—80321
- GaAs:Zn epitaxial layers, composition and Zn carrier conc. 80—25585
- GaAs:Zn ion implanted ionic alloy, electrophysical props., annealing 80—39133
- GaAs:Zn MBE layers, ionized beam doping, elec. and optical characts. 79—37721
- GaAs-Al_xGa_{1-x}As heterojunction interface, two-dimensional hole gas obs., Shubnikov-de Haas meas. 80—80357
- GaAs-electrolyte interface, surface barrier electroreflection anisotropy *(Russian)* 80—34895
- GaAs-$Ge_{1-x}(GaAs)_X$ n-p heterojunctions, hydrostatic press. effect on elect. and photoelectric props. 80—20304
- GaAs-S VPE layers, thickness and carrier conc. variations 79—100060
- $GaAs_{1-x}P_x$ based structs., carrier conc., mobility calcs. from Hall effect meas. 78—60138
- $GaAs_{1-x}P_x$ epitaxial layers, charge carrier conc. determ. from low-field electrorefl. spectra 77—85320
- $Ga_xIn_{1-x}As_{1-y}P_y$:Ge(Sn)(Te), epitaxial film, elec. and optical props. 79—11251
- $Ga_xIn_{4-x}PyAs_{1-y}$, In rich bulk single crysts. growth from melt via gradient freeze method, and characterisation 78—68618
- $Ga_{1-x}In_xSb$, LPE on GaSb by stepwise grading, and characterisation 78—72745
- n-GaN elec. props., electron mobility calc. 78—30923
- GaN film, thermoelec. power and Hall coeff. meas. 77—55627
- GaN, high-press. VPE and elec. characts. 78—14627
- GaN:Mg, and undoped, epitaxial growth from vapour, orientation, elec. props. 77—4740
- GaP, LPE layers high purity, invest. *(German)* 78—31353
- GaP layers, LPE growth, elec. props., residual impurities 79—38202
- GaP, luminesc. from electron-hole drops, 2 to 77K 79—11454
- GaP, rare earth doped, photolum. and elec. props. *(Russian)* 78—52545
- GaP, soln. growth of bulk crysts., luminesc. and elec. props. 78—92181
- GaP:Fe n-i-n epitaxial struct., photoconductivity, recombination scheme *(Russian)* 80—15569
- GaP:Fe^{3+}, deep impurity states investig. 77—15794
- GaP:Mg, ion implanted, elec. profiles 79—77628
- GaP:Te, Hall effect and elec. cond., 80-400K 78—91705
- GaP:Zn, Hall effect and elec. cond., 80-400K 78—91705
- GaP:Zn, implanted, elec. profiling using anodic oxidation in N-methylacetamide 80—54690
- GaP:Zn, Sn doped epitaxial layers, Hall const., hole mobility and conc. 80—15143
- $GaS_xSe_{(1-x)}$ solid solns., electrical props. meas. 78—84216
- GaSb and $GaSb_xAs_{1-x}$ films, MBE growth and elec. props. 79—23863
- GaSb, bulk and epitaxial, IR reflect. meas., carrier conc. and mobility determ. 80—80769
- p-GaSb, elec. cond., Hall effect, mobility and carrier concentration *(Russian)* 79—19603
- GaSb:Gd(Yb), elec. props., dopant effects 79—87115
- GaSb:Li, dopant behaviour 77—51696
- p-GaSb:Te, effective radiative recombination centre nature, photoluminescence spectra 79—90998
- n-GaSb:Te, Hall coeff., carrier conc. and mobility, elec. cond., 290 to 550K *(Russian)* 79—19604
- GaSb-InSb solid solns., heavily doped, electronic props. 77—80727
- GaTe, Hall mobility, resistivity anisotropy 79—11150
- Gd_2GeSe_5, elec. props., 300 to 1100K 79—51585
- GdN, and $GdN_{1-x}O_x$, mag. interactions 80—60218
- GdN, mag. interaction and carrier conc. 80—71005
- $GdN_{1-x}O_x$, magnetic interaction and carrier conc. 80—71005
- GdP-GdS systems, mag. exchange interactions, free carrier conc. 78—60278
- $(Ge,Pb)_{1-x}Mn_xTe$, mag. and elec. props. meas. 80—29534
- Ge bicrystal cleavage plane, Shubnikov-de Haas oscills. *(Russian)* 78—64094
- p-Ge, bleaching, optical heating and cooling of electrons involving intraband transitions 79—10365
- Ge, carrier conc. variations using electrolyte electroreflectance, topographical features 79—99562
- Ge, carrier density in electron-hole drops, plasma reson. determ. 77—24522
- n-Ge, carrier generation, depend. on laser intensity 79—69548
- p-Ge, carrier heating by weak electric field 77—11927
- n-Ge, current carrier-dislocation interactions, resistance in UHF range *(Russian)* 80—54732
- n-Ge, deform. induced point defects, Hall coeff. meas. 80—19800
- n-Ge, deformed, 1/f noise, resist., mobility, and carrier density 77—8161
- n-Ge, doped, dopant distrib. from carrier drift distrib. in high elec. field 79—51140
- p-Ge, double injection characteristics under high voltages 79—51590
- Ge, elec. cond., optically injected carrier density and temp. depend. 78—68046
- Ge, electron-hole correlation density depend., in electron-hole liq., under uniaxial stress 79—15090
- Ge, electron-hole drop drag by ultrasound *(Russian)* 80—100437
- Ge, electron-hole drop magnetoplasmas, radius-independent elec. and mag. reson. 79—73446
- Ge, energy-gap narrowing and state filling under laser irrad. 79—42441
- Ge epitaxial film, ion implantation and electron beam anneal effects on carrier conc. 80—75255
- Ge, epitaxial film, ion sputtering, growth mechanism, struct., props. 77—31917
- Ge, exciton condensation, electron-hole drop investigation in UHF field, nucleation *(Russian)* 80—80193
- Ge, Fermi level, minority carrier conc., effective intrinsic conc., Einstein relation 77—85209
- Ge film, elec. props., prep. by DC sputtering *(Japanese)* 79—78237
- Ge film, polycrystalline, structural and elec. props. 78—76173
- Ge, galvanomagnetic-recombination field effect, theoretical model 78—43420
- n-Ge, group V doped, point defect form. due to γ-ray irrad., carrier density, mobility meas. 78—71759

carrier density continued
- n-Ge, γ-irrad., nonlinear steady-state recomb., nonequilib. carrier lifetime and density 80—20215
- n-Ge, Hall mobility in fast electron irradiated samples 77—55551
- p-Ge, IR light free hole absorpt., nonvertical optical transitions *(Russian)* 80—80802
- n-Ge, impact ionisation at 4-9.5K 80—10994
- Ge, inhomogeneous mag. field effects on conductivity 77—4374
- Ge, irradiation by 3.5 MeV electrons at high temp., carrier density and lifetime changes 77—4128
- Ge, laser induced elec. damage, carrier removal, mobility degradation 77—80791
- n-Ge, laser irrad., accumulation of defects, effect on elec. props. 80—107317
- Ge, low temp. recombination into shallow donors, transient case 79—38092
- Ge, microwave absorption by nonequilibrium carriers, carrier density determ. method 77—8148
- Ge, microwave absorption by nonequilib. current carriers, book contrib. 80—11042
- Ge, nonequilibrium carrier excitation by CO_2 laser radiation 77—89803
- Ge, nonuniformly deformed, electron-hole drop density depend. on size *(Russian)* 80—20092
- p-Ge, optical cooling and carrier heating, intraband photocond. meas. 79—11174
- Ge, oscillatory exciton breakdown, microwave cond. 80—103716
- Ge p-n junction injection characts. in strong elec. fields 77—76913
- Ge, phonon cond. correction term and electron-photon scatt. relax. rate, appl. to doped and undoped samples 80—39369
- Ge, photoconductivity, carrier lifetimes in excited states of impurities *(Russian)* 77—76864
- n-Ge, plastically deform., dislocation state spectrum, photocond., elec. cond., and Hall const. meas. *(Russian)* 80—2362
- Ge, quenching temp. effect on annealing rate of quenched-in acceptors 79—82590
- Ge, size effects in small electron-hole drops 79—82530
- Ge surface Hall effect and cond., electron, hole conc. and mobility *(Russian)* 80—44619
- p-Ge, uniaxial compression influence on carrier heating by weak electric field 80—10978
- Ge, uniformly deformed, free carrier cyclotron resonance, electron-hole drops *(Russian)* 80—71182
- Ge, voltage-current curves, specimens of variable cross-section 77—8113
- Ge:Al, limiting solubility, rel. to charge carrier conc. 80—24596
- Ge:Au, gamma-irradiated and electron irradiated, elec. props. meas. 77—62950
- Ge:Au,Sb, electron irradiated, Hall effect, photocond., and photomagnetic effect meas. 77—4369
- p-Ge:Au,Sb,Hg(Zn), radiation-defect form., Au influence 80—92911
- n-Ge:Au piezoresistance in presence of deep levels, stress anisotropy 80—10979
- Ge:Cu, electron irrad. effects on carrier density, defect form. 80—19843
- Ge:Cu, quenched, energy levels of thermal acceptors, annealing effect 78—34798
- Ge:Cu(Sb), electron irradiation effects on elec. props. 78—6103
- p-Ge:Ga, carrier heating by weak elec. field, hole-hole collision influence 78—72161
- Ge:Ga, cryst. defects due to neutron irrad., elec. cond. and annealing 79—55789
- Ge:Hg, Sb, influence of electron irradiation on elec. props. 77—20318
- Ge:metal, polycrystalline film, electron transport props. 79—99642
- Ge:Mn, Sb, recombination waves, convective instability development 80—70721
- n-Ge:Ni p^+-n-n^+ structs., double-injection current-voltage characts. 80—60074
- p-Ge:Nz, Sb, influence of electron irradiation in elec. props. 77—20318
- Ge:O, elec. props., O interaction with point defects 79—11081
- Ge:Sb, cryst. defects due to neutron irrad., elec. cond. and annealing 79—55789
- n-Ge:Sb, electron irrad., impurity photoconductivity 77—15900
- n-Ge:Sb, fast electron irrad. at 77K, radiation defect changes by annealing at 220K 79—37737
- Ge:Sb, limiting solubility, rel. to charge carrier conc. 80—24596
- Ge:Sb,Cu, photoelec. props., fast electron irrad. effects 80—60036
- Ge:Sb(Au) cleaved surface, influence of impurities on local surface states 79—78150
- Ge-GeO_2 boundary, electrophysical parameters *(Russian)* 77—85327
- Ge-In-Te system, region of solid soln. of In in GeTe 77—51499
- Ge-InAs based MIS struct., avalanche carrier multiplication 80—88566
- p^+-Ge-n-GaAs abrupt heterojunction, reverse currents *(Russian)* 78—10542
- Ge-Si, UHV-produced epitaxial structs., electrophys. props. 78—3060
- Ge-Si alloy, epitaxial growth by getter sputtering, characts. 79—28915
- Ge-Si alloys, n-type, phosphorous doped, precipitation effects due to heat treatment 80—107833
- GeTe, concentration of carriers, rel. to stoichiometry 80—6847
- GeTe, effect of phase transition on mech. and elec. props. 77—51746
- GeTe film, elec. props. 77—51831
- GeTe, high pressure effects on hole conc. and thermoelec. props. 78—26894
- GeTe-Ga_2Te_3, electrophys. props. 77—48403
- HgCdTe, 0.1 eV photodetector performance background dependence 77—32038
- $Hg_{0.6}Cd_{0.4}Te$, annealing temp. effect on carrier conc. 78—72167
- $(Hg_{0.6}Cd_{0.4})_{1-x}Te_x$, defect anal., intrinsic material parameters 80—75519
- $Hg_{0.79}Cd_{0.21}Te$, ion implanted, elec. props. 80—20184
- $Hg_{1-x}Cd_xTe$, carrier conc., Hall effect, photocond., IR spectra meas. 80—49771
- $Hg_{1-x}Cd_xTe$, epitaxial layer, vapour phase growth 79—1829
- $Hg_{1-x}Cd_xTe$ epitaxial layers, elec. props. 80—96910
- $Hg_{1-x}Cd_xTe$, high-pressure reflex growth technique, IR detector appl. 77—40347
- $Hg_{1-x}Cd_xTe$, ionized intrinsic pt. defects, effect on carrier density 77—47835
- $Hg_{1-x}Cd_xTe$, LPE growth and characterisation 80—50565
- $Hg_{1-x}Cd_xTe$, zero-gap semicond. with nonparabolic band struct., hot electron mobility and conc. 78—76080
- $Hg_xCd_{1-x}Te$, Hall effect and elec. cond., carrier density and mobility temp. depend. 77—4341
- $HgCr_2Se_4$, electronic props. rel. to departure from stoichiometry 80—100472

carrier density continued
- $Hg_{1-x}Mn_xSe$, band struct. from anomalous Shubnikov-de Haas effect 80—20080
- HgSe, Bridgman growth at hydrostatic press. to 3 kbar, free electron conc. and mobility 77—52245
- HgSe, CVD crysts., electrophys. characts. 77—85910
- HgSe, point defect model rel. to elec. props. and phase diagram 77—4339
- HgSe, Shubnikov-de Haas oscills., electron conc., g-factor and Dingle temp. 77—69354
- HgSe, Shubnikov-de Haas determ. of electron g factors 80—6704
- HgTe, contrib. of resonant states to conductivity 79—51577
- HgTe, electron conc. temp. depend., 1.6 to 32K, Hall effect and cond. meas. 80—24952
- HgTe, vacancy doping, effect on elec. characts. 79—82595
- HgTe, vacancy doping by off-stoichiometry, influence on transport props. 78—55862
- HgTe:Cu, effect of prep. conditions on impurity distrib., hole conc. 77—8743
- $HgTe_xSe_{1-x}$, solid soln., intrinsic carrier density and energy band struct. 78—39134
- n-InAs, edge luminescence band, shape depend. on degree of doping, band gap 80—7405
- InAs, elec. props. after heating for 300 to 900°C for 1 to 100 hours 78—47793
- InAs, electrical conductivity and thermoelectric power charge due to melting 80—100490
- n-InAs, electron irrad., carrier introduction rate, annealing 80—24948
- n-InAs, electron mobility dependence on conc. Hall effect at 300K 78—47794
- InAs, epilayer, MBE growth parameters, relationship with elec. props. 80—2296
- InAs, epitaxial, laser action mechanisms with electron beam excitation 80—28240
- InAs epitaxial layers, on GaAs substrate, electron diffr. and SEM exam., electronic props. 79—1552
- InAs heteroepitaxial layers, VPE grown, effect of $AsCl_3$ mole fraction on elec. props. 79—11255
- InAs, heteroepitaxial layers, $AsCl_3$ mole, fraction and substrate orientation effects on elec. parameters 80—39690
- InAs, intrinsic point defects, nature and influence on electrophys. props. 78—79609
- InAs, MBE growth, SEM, RHEED, optical microscopy and elec. meas. 78—18925
- n-InAs, Shubnikov-de Haas oscills., conduction electron density, phonon scatt. 77—15768
- p-InAs, surface conductance of Ar-ion-bombard. samples 79—60910
- InAs, surface space charge investig., reson. enhanced Raman scatt. 77—20849
- n-InAs, undoped, electron irrad., Hall coeff., elec. resistivity, optical absorption 77—89479
- n-InAs, VPE layers, on GaAs substrate, electronic profile 79—95525
- InAs:Cd, Te, donor-acceptor interaction, elec. cond. and Hall coeff. meas. 80—59988
- InAs:Cd,Te interaction between impurities, effect on elec. props., Hall effect. 80—19832
- InAs:Cr, high-resist., energy positions of deep levels, elec. and optical props. 79—7807
- InAs:Sn, single crysts., defect formation 80—88606
- InAs:Zn, optical absorpt. and refl. spectra 79—91479
- p-InAs-Au contacts, influence of free surface on elec. behaviour 78—95362
- InAs-FeAs, eutectic, growth from melt, electrical props. 77—11911
- InAs-GaSb superlattice, semiconductor-semimetal transition obs. 80—44710
- InAs-GaSb superlattices, semicond.-semimental transition obs. 80—49882
- p-$In_{0.53}Ga_{0.47}As$:Zn on InP, elec. and optical props. 80—75662
- $In_{1-x}Ga_xAs$, LPE layer on InP substrate, phys., elec. and optical props. 78—39235
- n-$In_xGa_{1-x}As$ film, epitaxial, on GaAs, evaluation 77—1812
- $In_xGa_{1-x}As$, MBE layers on InP substrates, elec. props., photoluminesc., X-ray and Auger obs. 79—51450
- $In_xGa_{1-x}As$, VPE on (100), (111)A, and (111)B InP substrates 80—15382
- $In_{1-x}Ga_xAs_yP_{1-y}$, Hall mobility, comp. depend. 80—75587
- $In_{1-x}Ga_xAs_yP_{1-y}$ LPE layers, background carrier conc. and electron mobility. 79—95523
- $In_{1-x}Ga_xAs_yP_{1-y}$:Be, ion implantation, hole conc. and mobility, junction depth 79—46685
- $In_{1-x}Ga_xP_{1-y}As_y$ LPE films, hot electron and magnetotransport props. 78—26977
- $In_xGa_{1-x}P_yAs_{1-y}$, electron effective mass and Dingle temp., Shubnikov-de Haas oscills. 80—59859
- InO_3:Sn film, prep. by spray hydrolysis, struct., elec. and optical props. *(Japanese)* 79—42678
- In_2O_3 films, reactively evaporated, elec. props. 80—84521
- In_2O_3, polycrystalline, electron conc. and mobility, 25 to 700°C, O_2 partial press. depend. 77—76811
- In_2O_3, Seebeck coeff., density of states effective mass 78—56171
- In_2O_3, transparent electrode deposition on PLZT ceramic, elec. and opt. props. 78—74848
- In_2O_3, transparent heat mirror formation by ion plating on ambient temp. substrates and props. 80—25578
- In_2O_3:Sn, film, HF sputtered, cond., Hall mobility, oxidation, charge carrier density 78—72287
- In_2O_3:Sn films, pure and doped, prod. by ion plating, elec. and optical props. 80—2488
- In_2O_3:Sn films; vac. deposited, elec. props. 80—100542
- In_2O_3-SnO_2 thin film, Hall mobility, temp. depend., grain boundary effects 80—75658
- In_2O_3-SnO_2/SiO_x/Si diode solar cells, loss mechanisms, characts., band struct. 80—26135
- InP, automatic electrochemical carrier conc. profiling 79—99614
- InP carrier profiling using liq. barrier contact 78—76087
- n-InP, epitaxial, Hall effect, electron mobility and density, temp. depend. 78—72288
- n-InP film, polycrystalline, elec. props. 77—76965
- InP, free carriers, freq. depend. relax. time 80—2385
- InP growth from soln. and LEC, photolum. and elec. meas. 79—87575
- n-InP, heat treatment effect on surface carrier conc. 77—11936

carrier density continued
- InP, ion implanted, anodic oxidation and elec. carrier conc. profiles 79—70185
- InP, n- and p-type, surface recomb. vel. meas., diffr. from transient optical grating 79—1604
- InP, planar reactive deposition on CdS, heterostruct. formation and elec. evaluation 78—72738
- n-InP, room temp. electron irrad., Hall coeff. meas. 77—89478
- p-InP, single crysts. and epilayers rel. to prep method 77—81211
- InP, synthesis solute diffusion grown, elec. props., photoluminesc., etch pit profiles 79—4914
- InP, vapour phase epitaxial growth in presence of O_2, elec. props. 79—46971
- InP, Zn diffused single-crystal, substitutional dopant and hole conc. meas. 80—75260
- InP:Be, ion implantation, hole conc. and mobility, junction depth 79—46685
- InP:Be, LPE, Be distrib. coeff., carrier conc. 79—90694
- InP:Sn, LPE growth from Sn soln., elec. props., 80 to 300K 79—11250
- p-InP:Zn, electrical meas., doping levels hole conc. 78—14745
- InS, prep., and elec. and optical props. 77—77361
- n-InSb based MIS struct., carrier generation under nonequilibrium conditions 80—88640
- InSb, carrier conc. variations using electrolyte electroreflectance, topographical features 79—99562
- n-InSb, elec. props. changes during ht. treatment 77—85213
- InSb, electron irrad. effects on elec. props. and recomb. 79—51584
- InSb, electron irradiated, kinetics of changes in carrier density 79—56228
- n-InSb film, degenerate, electron conc. and resist. temp. depend., band struct. 77—76971
- InSb film, degenerate, concs. and ionisation energies of defect levels, Hall effect meas. 79—91087
- n-InSb film, galvanomagnetic meas. of surface layer carrier conc. and mobility 77—55628
- InSb film, heteroepitaxial, MBE growth and elec. props. 80—2301
- n-InSb film, low energy electron irrad. effect on elec. props. 80—7009
- InSb, high-resistivity p-type or crystals of n-type, recombination processes, photocond. and photomag. effect meas. *(Russian)* 80—88567
- InSb, horizontal zone melting in vacuum 79—47624
- n- InSb, hot electron energy relax. in quantizing mag. fields 78—31259
- InSb, ion bombard. and defect annealing, n- and p-type cond. layer prod. 78—26606
- InSb lattice, static dielec. const. and carrier conc. meas. via gyrotropic sphere reson. 80—97143
- InSb, low-temp. annealing effect 77—8091
- InSb, MISS struct., surface electron and hole mobility and conc. *(Russian)* 80—44701
- InSb, magneto-surface transport props. 77—43693
- p-InSb, magnetophonon reson. of holes 79—95424
- n-InSb, microwave helicon resonances, carrier density, mobility, dielectric const. 80—96930
- p-InSb, mobility, diffusion and thermoelectric power of hot holes 80—39595
- InSb n-type, heavily doped, effects of hydrostatic pressure on electron mobility and conc. 77—4390
- n-InSb, negative longit. magnetoresist., carrier conc. and mobility depend., 77K 80—60007
- n-InSb, photoconductivity, recombination processes 80—11030
- p-InSb plate in crossed E and H fields, even magnetoconcentration effect *(Russian)* 77—85244
- n-InSb, proton irrad. defects energy level scheme, transport props. meas. 80—96576
- n-InSb, stationary energy transport velocity of light scattered from bunched solid-state plasma 79—95720
- InSb, surface carrier accumulation in crossed elec. and mag. fields 80—20205
- n-InSb, undoped, press. induced slow relax. of free electron conc., Hall coeff. meas. 77—47833
- InSb:Cd (Zn) (Ge), ion-irradiated, p-n conversion during heat treatment 80—96558
- p-InSb:Cu(Zn) film, heavily doped, ionized impurity scatt., Hall effect and DC cond. meas. 79—99643
- p-InSb:Ge, proton irrad. defects energy level scheme, transport props. meas. 80—96576
- InSb:S, ion implanted, Hall effect meas. 77—20342
- InSb:Te, anomalous anisotropy of magnetoresist. and g-factor 77—47831
- n-InSb:Zn, Zn diffusion out of implanted layers, free hole distrib. 79—10984
- n-InSe, layered semiconductor, current-voltage characts. investig., 130 to 400K 77—4342
- InSe, photoelec. props. 79—73543
- In_2Se_3-Cu_2S system, electrophys. props., influence of 1-4% Cu_2S 80—20219
- P-In_6Se_7, electrophysical props. 110 to 400K, hole conc. at 300K *(Russian)* 77—35867
- $(In_{1-x}Sn_x)_2O_{3-y}$, pyrolytic selective coating, Sn additions effect 78—43499
- In_2SnO_3 film, effect of ambient atmosphere during annealing, elec. props. 80—97510
- In_2Te_3-type semiconductor, mechanism of electrically inactive impurities 80—24834
- La_2GeSe_5, elec. props., 300 to 1100K 79—51585
- $La_{1-x}Sr_xCoO_{3-y}$, Seebeck coeff. meas., small polaron hole conduction model 80—20233
- $La_{1-x}Sr_xCrO_3$ ($0 \leq x \leq 0.4$), localised level hopping transport 80—10974
- Li-Pb liquid alloys, elec. resistivity, negative temp. coeff. 80—88527
- Mg-In dil. alloys, effect of alloying on Fermi surface, pseudopot. model 77—76733
- Mg-Li dil. alloys, effect of alloying on Fermi surface, pseudopot. model 77—76733
- $MnAs_{1-x}P_x$ mixed crystals, metallic magnetically ordered, Hall effect 80—65536
- Mn_3O_4:S, defect struct. and elec. props., electron, hole conc. 80—44601
- NH_4ClO_4, elec. field effect on decomp., novel charge-carrying species detect. method 79—15987
- NbO_2, sustaining and decaying of the high conductance on state 79—95454
- Nd-Gd-Te alloys of R_2Te_3-T_3Te_4 region, physicochem. props. 78—52017
- Nd_2GeSe_5, elec. props., 300 to 1100K 79—51585

carrier density continued
$Ni_{0.5}Zn_{0.5}Fe_2O_4$, Hall mobility, elec. cond. and carrier conc., 30 to 180°C 77—51765
$Pb_{1-x}Ge_xTe$, degenerate semiconducting ferroelectric, structural phase transition temp., mag. field effects 80—45017
$Pb_{1-x}Ge_xTe$:Ga, Fermi level stabilization, transport props. meas., 77-400K 78—56065
$Pb_{1-x}Ge_xTe$:Ga, influence of hydrostatic compression on elec. props. 79—73516
PbI_2, electron hole elec. polarisation expt. 79—24023
$PbMo_6S_8$, Hall effect and magnetoresistivity 78—95400
$PbMo_6S_8$, normal state and superconducting property measurements 78—91660
PbO_2 pressed powder, Hall voltage and change of cond. in transverse mag. fields 79—4567
p-PbS, dispersion law investigation, valence band density of state effective mass 79—95314
PbS, low carrier conc., prep. and props. 77—39846
PbS:Tl, self-compensation of acceptors by vacancies, Hall coeff. meas. 80—92913
$PbS_{1-x}Se_x$, diffused homojunction diode laser, carrier conc. profile photon confinement 79—18415
PbSe, carrier density depend. of cyclotron mass, Shubnikov-de Haas effect 79—73533
PbSe, electron gas magnetisation, energy band parameters determ., use of Faraday effect 80—45047
PbSe:Tl, self-compensation of acceptors by vacancies, Hall coeff. meas. 80—92913
$Pb_{1-x}Sn_xGe$:In, press.-induced transition to gapless state, galvanomag. effects 78—19108
$Pb_{0.59}Sn_{0.41}Se$, struct. phase transition, temp and hydrostatic press. influence, Hall effect, resistivity *(Russian)* 78—51675
$Pb_{0.93}Sn_{0.07}Se$ crysts., sublimation growth, controlled carrier concs. for IR lasers and detectors 77—52237
n-$Pb_{0.94}Sn_{0.06}Se$ solid solns., Burstein-Moss effect and energy band struct. 80—40118
$Pb_{1-x}Sn_xSe$, band struct. parameters, thermoelectric power meas. in strong mag. fields 79—51474
$Pb_{1-x}Sn_xSe$, carrier density depend. of cyclotron mass, Shubnikov-de Haas effect 79—73533
$Pb_{1-x}Sn_xSe$, valence zone struct. effect on mobility/inherent conc. ratio *(Russian)* 79—73437
$Pb_{0.76}Sn_{0.24}Tc$, background radiation, influence on elec. props. 80—20226
PbSnTe IR detectors, spectral response depend. on surface carrier concentration *(Japanese)* 79—44929
PbSnTe, optical dielectric const. variation with carrier conc. 80—84709
p-$Pb_{0.65}Sn_{0.35}Te$, transport coeffs. and dispersion law 80—44629
$Pb_{0.72}Sn_{0.28}Te$, Hall effect and elec. cond., 77 to 480K, energy band struct. 77—76817
$Pb_{0.8}Sn_{0.2}Te$, hole conc. at 77K from room temp. thermoelec. meas. 78—56155
$Pb_{0.8}Sn_{0.2}Te$, single cryst. and epitaxial film, far IR refl. spectra, carrier density, Hall const., and plasma freq. 80—20629
$Pb_{0.8}Sn_{0.2}Te$, susceptibility effective mass, carrier conc. depend. 80—20069
$Pb_{0.8}Sn_{0.2}Te$:Cd, influence of Cd doping on high field magnetoresist. and Hall effect 80—75590
$Pb_{0.8}Sn_{0.2}Te$:La, evaporated thin films, low carrier conc. 80—65414
$Pb_{0.82}Sn_{0.18}Te$, Hall mobility, scatt. mechanisms, temp. and carrier conc. depend. 77—55548
p-$Pb_{0.82}Sn_{1.8}Te$, Hall coeff. sign-inversion temp. 78—52010
$Pb_{0.84}Sn_{0.16}Te$ single cryst., anelastic relax., helicon wave dispersion *(Russian)* 77—51437
$Pb_{0.85}Sn_{0.15}Te$ homostructure diode laser, LPE growth, with controlled carrier conc. 80—95903
$Pb_{1-x}Sn_xTe$ ($x=0.15$ to 0.20), SEM study, dislocation density, and carrier density and mobility 79—69107
$Pb_{1-x}Sn_xTe$, ($x<0.35$), permittivity and soft modes, carrier density and comp. effects 80—7256
$Pb_{1-x}Sn_xTe$, Cd-In diffusion, changes in elec. props. 78—91348
$Pb_{1-x}Sn_xTe$, cryst. growth rel. to IR detector fabrication 77—85911
$Pb_{1-x}Sn_xTe$, DH laser, gain-freq.-current relation, k.p band model 77—61951
$Pb_{1-x}Sn_xTe$, diffusion of Cd, Hall effect, cond. and solubility meas. 79—69292
$Pb_{1-x}Sn_xTe$, effective mass of holes, thermoelec. power, Hall coeff., carrier conc. 79—65371
$Pb_{1-x}Sn_xTe$ epitaxial films, adsorption-induced accumulation layer form. on surface 80—60117
$Pb_{1-x}Sn_xTe$ film, deposition, elec. and piezoresist. props. 78—6465
$Pb_{1-x}Sn_xTe$ film, sputtered, for IR detector appl. elec. and optical props. 80—35084
$Pb_{1-x}Sn_xTe$ heterojunction lasers, instantaneous vacuum evaporation grown, threshold current density 80—5759
p-$Pb_{1-x}Sn_xTe$, LPE layer, carrier conc. and mobility 79—99639
$Pb_{1-x}Sn_xTe$, large non-seeded single cryst. growth by sublimation method, and characterisation 79—78860
$Pb_{1-x}Sn_xTe$, lattice instability and phonon-width, carrier conc. and composition depend. 79—14906
$Pb_{1-x}Sn_xTe$ narrow gap solid alloys, hole Fermi surface, galvanomag. and oscill. effect obs. *(Russian)* 77—69345
$Pb_{1-x}Sn_xTe$, narrow gap solid solns., mag. susceptibility and energy band spectrum 79—28276
$Pb_{1-x}Sn_xTe$, soft mode, carrier conc. depend. of ferroelec. transition temp. 77—8530
$Pb_{1-x}Sn_xTe$, solid-liq. phase equilib. above 750°C 79—82316
p-$Pb_{1-x}Sn_xTe$, thermoelec. power, carrier conc. and temp. depend., interband scatt. 80—24957
$Pb_{1-x}Sn_xTe$:Cd, Cd diffusion obs. using Hall mobility and Cd solubility expts. 78—26584
$Pb_{1-x}Sn_xTe$:In film, anomalous elec. props. 78—10477
$Pb_{1-x}Sn_xTe$-PbTe heterostructures, MBE produced on mica and $LiNbO_3$, elec. props. study 80—88629
$(Pb_{1-x}Sn_x)_{1+y}Te_{1-y}$ system, VPE parameters influence on epitaxial film props. 79—28229
PbTe (111) epitaxial films, localised electron irrad. effects on elec. props. and O_2 sorption 80—49472
PbTe, carrier conc. inhomogeneity 78—52019
PbTe, diffusion of Cd, Hall effect, cond. and solubility meas. 79—69292
n-PbTe, epitaxial, time dependent negative weak field magnetoresist. 78—64151

carrier density continued
n-PbTe, epitaxial layers, elec. characts. rel. to explosive evap. in closed vol. 77—89885
p-PbTe, Fermi surface parameters depend. on carrier density, Shubnikov-de Haas oscills. 79—42435
PbTe film, ion-implantation-induced lattice defects 77—68985
PbTe, ion implantation induced damage and reson. levels 80—49255
n-PbTe, LPE layer, carrier conc. and mobility 79—99639
PbTe layers, quality control of carrier conc. using Hall effect graphical representation 77—1500
p-PbTe MIS capacitors 5 μm IR detector appl. 78—52101
p-PbTe, MIS struct. inversion layer sub-bands, IR magnetoreflectance obs. 80—44731
n-PbTe, noncubic (111) oriented epitaxial films, weak field magnetoresistance 80—75584
PbTe, solidus line anal., carrier conc. 78—75806
PbTe, uncontaminated films on mica sustrates, elec. props. obs. 77—76967
PbTe, uncontaminated films prepared by mol. beam deposition, elec. props. meas. 78—15316
PbTe:As, hole conc. control, in LPE layers, plasma reflectivity and thermoelec. probe meas. 79—99640
PbTe:Bi(Sb)(Cr)(Ag), thermoelec. props., thermal and elec. cond. 79—82616
PbTe:Cd, Cd diffusion obs. using Hall mobility and Cd solubility expts. 78—26584
PbTe:Ti, effect of impurities on transport props. 79—11158
PbTe:Tl, thermoelectric power, elec. cond., Hall coeff. and optical absorpt. coeff. 80—39584
p-PbTe-M, M=In, Pb, Zn, Cu, barrier props. 79—7898
PbTe-SnTe, solid soln. single crysts., TSM growth and elec. characts. 78—68625
Pr_2GeSe_5, elec. props., 300 to 1100K 79—51585
$(SN)_x$, quasi-one-dimens., theoretical group anal. of electron spectrum 79—82511
Sb, carrier density at press. up to 80 kbar, magnetoresist. and Hall effect obs. 79—73534
Sb, carrier transport, magnetoresistivity, field-dependent tensor study 80—39609
Sb, current carrier concentration charge, under pressure *(Russian)* 79—7824
Sb-Ge (1.2 to 2.2 at.%), carrier transport, magnetoresistivity, field-dependent tensor study 80—39609
Sb-Sn (0.5 to 1.0 at.%), carrier transport, magnetoresistivity, field-dependent tensor study 80—39609
$Sb_{1-x}Bi_x$ alloys, Shubnikov-de Haas *(Russian)* 78—23007
$Sb_{1.5}Bi_{0.5}Te_3$ solid solution, temp. influence obs. *(Slovak)* 78—30946
Sb_2O_3 anodic layers on Sb, semicond. props. 79—56303
Sb_5O_7I, polytypes 2MC and 2MA, photoferroelastic phenomena 79—95447
SbSe, amorphous thin film high field charge transport and quasi-Fermi level location 80—70863
Sb_2Te_3, $Sb_{1.5}Bi_{0.5}Te_3$, Te- and Se-doped cryst. growth and elec. props. 77—48334
Sb_2Te_3-Bi_2Te_3 solid solns., bladed cryst. growth, electrophysical props. 78—43387
ScN_x, region of homogeneity, physicochem. props. 78—52018
Si, amorphous and crystalline, heating by Q-switched laser radiation 80—84963
Si, Auger recomb. coeff. meas. using laser excitation 79—38654
Si, Auger recombination, localized and free carrier comparison 79—38090
Si, carrier conc. determ., electrochem. method 78—60200
Si, carrier conc. variations using electrolyte electroreflectance, topographical features 79—99562
Si, carrier concentration distribution by scanning IR absorption 79—61356
n-Si channel ⟨100⟩ inversion layer MOSFET, valley splitting, conductivity 80—70840
Si, complex doping effects on limiting electron conc. 78—22740
n-Si, current carrier-dislocation interactions, resistance in UHF range *(Russian)* 80—54732
p-Si, deformed, 1/f noise, resist., mobility, and carrier density 77—8161
n-Si, deformed, thermal treatment effect on elec. cond. and dislocation mobility 80—107265
Si, dense plasma dynamics during pulsed laser annealing, carrier density, recombination 80—84479
Si devices, obs. of carrier densities via IR emission 77—72707
Si, diffusion coeff. of Se, by sheet Hall coeff. meas. 79—46843
Si, diffusion coefficient determ. from carrier conc. depth profile 80—107566
Si diode, Auger recombination coefficient at very high injection rates 78—47863
Si, elec. props., plastic deform. and annealing temp. depend., dislocation effects *(Russian)* 77—89765
Si, electrical props. affected by heat treatment *(Russian)* 78—11352
Si, electrochemical carrier conc. profiling 80—2461
p-Si, electron irrad., influence of acceptor impurity conc. and irrad. temp. on defect formation 79—19281
Si, electron irrad. induced defect form., carrier density, mobility and lifetime changes 77—43250
n-Si, electron radiation defect annealing, negative stage, Hall coefficient, defect levels 79—90701
Si, electron-hole drops, thermodynamical parameter determ. from luminescence data 80—2845
Si, Fermi level, minority carrier conc., effective intrinsic conc., Einstein relation 77—85209
Si films, polycrystalline, elec. props., grain size and dopant conc. influence 80—29492
n-Si films on sapphire, crystalline defects effect on elec. props. 77—20470
n-Si, gamma ray irrad., impurity composition influence on recombination centre formation 80—6872
n-Si, heavily doped, carrier conc., comparison of expt. and theory, screening effects 77—85216
Si, heavily doped, excess intrinisic carrier density, deionisation of impurities as explanation 80—96864
Si, high level photogeneration, absorpt. and free carrier distrib. 79—33309
Si, high O conc., electrical and mechanical props., influence of heat treatment 77—35934

carrier density continued
- p-Si, high ohmic material, deep level investigation, vacuum growth *(Russian)* 80—54654
- Si, impurity conc. from MOS DC transfer characts. 78—2155
- Si ingots, polycrystn., growth and characterisation from metallurgical grade source material 79—87576
- Si, intrinsic, electronic properties, temp. depend. *(German)* 77—76822
- n-Si, inverted MOSFET surfaces, quantum oscills., valley splitting, line-shape in state density effects 79—56318
- Si, ion implanted, structural and elec. profiles for double damage layers 78—2169
- n-Si, ionisation of low donor levels and recomb. of hot electrons at low temp. 79—51596
- Si, laser induced dense plasma, dynamics 80—65612
- Si, laser induced elec. damage, carrier removal, mobility degradation 77—80791
- p-Si, laser irrad., accumulation of defects, effect on elec. props. 80—107317
- Si, laser measurement, of semiconductor materials and devices *(Rumanian)* 78—52035
- Si, local electron irrad., Frankel pair separation, influence on photo EMF 80—44203
- Si, local pseudopotential, Gaussian band charge model 80—88477
- Si, neutron doped, γ-irrad. influence on elec. props. 80—6845
- n-Si, neutron or γ-irrad., elec. props., in strong elec. fields 79—95416
- Si, nonequilib. carrier excitation by CO_2 laser radiation 77—89803
- Si, nonequilibrium carrier density relax., lifetime determ. using light absorption 78—15170
- Si on sapphire, gettering effect by O implantation, Hall and Rutherford backscattering meas. 79—65103
- n-Si plate, effect of nonequilibrium carriers on IR transmission 79—38548
- p-Si polycrystalline films on graphite substrates *(French)* 78—64154
- Si, radiation-doped and annealed, carrier density and mobility meas. 78—56145
- n-Si, relaxation of electron energy, carrier-density dependence 80—107809
- Si ribbons, roller quenching method of prep., grain sizes and carrier conc. 80—40275
- p-Si, surface elec. behaviour after chem. treatment 80—20185
- n- Si, surface electron states, props. determ. at 77K 77—55598
- Si, surface inversion layers, intersubband optical absorpt., Auger-type transition 80—29741
- Si surface space charge layers, cyclotron reson. of holes 77—76932
- Si, temp. depend. of Auger recomb. coeff. 80—24942
- Si, thermal donor energy levels, Hall effect meas. 78—6335
- Si, thermal donor generation in temp. range 600-800°C 79—11121
- Si, voltage-current curves, specimens of variable cross-section 77—8113
- Si wafer, automatic meas. system for resist. profiles 80—39574
- Si wafer doping, by thermal neutron irradiation, charge carriers behaviour obs. *(Japanese)* 79—42484
- p-Si, X-irrad., subthreshold defect prod., Hall meas. of carrier conc. and photocond. spectra 77—89470
- p-Si, X-ray bombard. effects on elec. resist., and carrier density, annealing effect 77—4125
- Si:0, electrical activity due to heat treatment, Hall effect meas. 80—15543
- Si:As, effects of recoil-implanted O on elec. activation of As 79—99227
- Si:As, heavily As-diffused, Hall mobility and resist. rel. to carrier conc. 80—107815
- Si:As, implanted through SiO_2 films, elec. props., defect struct. 80—54264
- Si:As, ion implanted, annealing characts., elec. props. 77—19974
- Si:As, ion implanted, beam techniques 80—24474
- Si:As, ion-implanted, laser recrystallisation by freq.-doubled Nd:YAG laser 79—77613
- Si:As, shallow junctions by high-dose implants 80—96694
- Si:B, implanted, free carrier conc. and impurity location, Raman scatt. obs. 77—55295
- Si:B, polycryst., effect of laser annealing on struct. and elec. props. 79—11243
- p-Si:B epitaxial layer, proton-implanted, annealing characts., carrier conc. profiles 77—32097
- Si:B film, sputter-deposited, elec. props., struct., SEM and TEM obs. 79—95298
- Si:B(P), ion implanted, polycryst. annealing characts. 77—24324
- Si:B(P), ion implanted layers, carrier distrib. meas. precision 77—43603
- Si:B(P) impurity conc. profile determ. by anodic oxidation 79—28010
- Si:Bf_2^+ layers, ion-implanted, anomalous carrier tail generation mechanism 80—19819
- Si:Cd n^+-n-n^+ structs., photoresist. props. under exclusion conditions 80—39666
- Si:Ga^+, influence of annealing on carrier conc. 79—69152
- Si:Ga(Sb), epitaxial film, doping efficiency *(Japanese)* 79—73201
- p-Si:Gd, irradiated, elec. props. 79—51613
- Si:In, neutron irrad. to compensate for residual B, photocond., IR focal plane array 78—67727
- Si:Li, electron-phonon scatt., in intermediate conc. region 80—65180
- Si:Na ion implanted, Hall effect temp. depend., electron surface density and mobility 80—11018
- Si:O, electrial and infrared spectroscopic investigations 80—34389
- p-Si:P, annealing behaviour, recovery, surface carrier density and Hall mobility meas. 77—32012
- Si:P, BF_2^+ ion implantation, anomalous carrier profiles 80—2048
- Si:P, carrier mobility and distrib. rel. to annealing, 400-910°C 78—79995
- Si:P, effect of annealing on charge carrier conc. on floating zoned crystals 78—47805
- n-Si:P, heavily doped, carrier conc., Hall coeff. and elec. cond. meas. 77—8094
- Si:P, heavily doped, electron mobility carrier conc. relationship 79—65470
- Si:P, implantation damage of channelled P ions, elec. activity recovery stages 77—59034
- Si:P, implanted, SiO_2-film-covered, laser annealing behaviour 79—86808
- Si:P, implanted low temp. annealed, elec. activation, damage depend. 80—88182
- Si:P, impurity band states 77—8047
- Si:P, incoherent light flash annealing, elec. props., backscattering spectra 80—97504
- Si:P, ion implantation defect annealing investig. by CESR 77—8404

carrier density continued
- Si:P, ion implanted, selective annealing of amorphous layers by Nd^{3+}:YAG laser irrad. 79—14823
- Si:P, ion-implanted, carrier conc. reduction caused by wet O_2 oxidation 80—10565
- Si:P, ion-implanted, damage-dependent elec. activation 79—55793
- Si:P, low energy and high dose ion implantation, through SiO_2 film 77—15435
- n-Si:P, low-compensated, Hall factor, electron-phonon interactions 79—4570
- Si:P, neutron transmutation doping, elec. props. rel. to neutron fluence 80—96555
- n-Si:P, piezoresist. under strong uniaxial elastic deform. 77—15858
- Si:P, polycryst., neutron transmutation doped, elec. props. 78—34836
- Si:P film, CVD polycrystalline, low press. and atmos. press., oxidation 80—3214
- Si:P film, polycryst., heavily doped, mobility and carrier conc., optical determ. 80—66314
- Si:P implanted, multiscanning electron beam annealing 80—75242
- Si:S, γ-irrad. influence on elec. props. 80—6845
- Si:Sb, epitaxial film, growth by mol. beam technique 80—2292
- Si:Se, energy levels, resistivity and Hall coeff. 79—69528
- n-Si:Sm,P, electron irrad. effects *(Russian)* 77—66168
- Si-Au-P system, partition coeff. of P, temp. depend. 79—43158
- Si-Ge, solid solns., doping characts. 78—22745
- Si-Ge alloy, thermoelec. material, lattice thermal conductivity rel. to grain size and carrier conc. 78—91495
- Si-Ge:Al(B)(P), hot-pressed alloy, thermoelec. props. 78—91711
- Si-In(Rh)(Au) Schottky diodes, X-ray irradiated, radiation-accelerated diffusion of impurities in Si 78—26952
- SiC, 6H polytype, elec. and thermal cond., carrier concentrations 80—2223
- SiC, self-focusing of ruby laser radiation, free carrier conc. depend. *(Russian)* 77—42579
- Si_3N_4-GaAs, layer struct., carrier density in EH liquid, temp. depend. 79—69434
- SiO_2 film grown by Si oxidation in O_2-H_2-HCl mixture, elec. props. 80—40569
- SiO_2-Si:A, effects of recoil-implanted O on elec. activation of As 79—99227
- Si(100) inversion and accumulation layers, effective mass and collision time of electrons, oscillatory magnetoconductance 78—34909
- SmB_6, mixed valent, large low-temp. Hall effect and resist. 80—39611
- Sm_2GeSe_5, elec. props., 300 to 1100K 79—51585
- SmS, press. depend., change near semicond.-metal transition 77—62968
- $Sn_{1-x}Mn_xTe$, degenerate mag. semicond., thermoelec. power meas. 80—29392
- SnO_2 film, doped, electron effective mass and elec. props., carrier density depend. 77—43750
- SnO_2, transparent electrode deposition on PLZT ceramic, elec. and opt. props. 78—74848
- SnO_2:P, CVD films, elec. props., cryst. to amorphous transition effects 80—107933
- SnO_2-InP heterojunctions, elec. and photovoltaic characts. 80—75628
- $Sn_{1-x}Pb_2Te$, elec. and struct. props. of epitaxial layers *(Russian)* 78—64147
- SnSe, single crysts., growth by Bridgeman technique, electron diffr. anal., lattice consts., carrier conc. 79—47616
- SnSe, sublimation growth, deviation from stoichiometry, elec. props. 78—76594
- SnTe, annealed, iodide method of prep., props. meas. 80—71591
- SnTe, carrier density depend. of soft TO-phonon, Raman scatt. meas. 78—6684
- SnTe, carrier density rel. to temp.-depend. ^{119}Sn isomer shift 77—8457
- SnTe, solidus line anal., carrier conc. 78—75806
- SnTe-InTe, SnTe-In_2Te_3, solid soln. region, lattice constant variation 77—35697
- SnTe-PbSe mixed system layers, struct. and props. *(Russian)* 77—28082
- $(TSeT)_2Cl$ complex, metal-semimetal transition, magnetoresist. and cond. *(Russian)* 79—38138
- Ta film, RF sputtered, thermoelec. power, Hall coeff. and struct. props. 77—43743
- Ta_2O_5 films, Poole-Frenkel effect and cond., effect of heat treatment in oxygen and in vacuum 80—39693
- Te, carrier density nonlinearity of interacting acoustic fluxes 77—51781
- Te, dislocations influence on galvanomag. props. 80—54722
- Te, elec. props. anisotropy, influence of deform. and annealing 77—15859
- Te film, evaporated, crystallinity and electronic props., annealing effect 77—85107
- Te film, on TGS substrate, ferroelec. field effect 79—42675
- Te film, thermally evaporated, elec. cond., Hall voltage and thermoelec. power 77—47913
- Te films, elec. props., 77 to 450K, thermal width of band gap 79—51698
- Te, lightly doped, galvanomagnetic props. in fields up to 140 kOe 78—91707
- Te, thin evaporated films, 130 Å, temp. depend. of elec. props. 79—95529
- Te thin film, thermoelec. EMF, Seebeck coeff., elec. cond. structural depend. 79—78230
- Te, undoped, elec. cond., magnetoresist. and Hall meas., hydrostatic press. effect 77—47830
- Te, warm hole conductivity 78—72160
- Te:Sb, 96 to 500K, cond. Hall const., hole mobility, conc., dislocation effects *(Russian)* 78—64039
- $Te_{81}Ge_{15}As_4$, Hall effect in electrically switched memory state 80 —2403
- TiO_2 electrode, carrier density determ. by optical absorpt. and photoelectrolysis spectra 80—71462
- TiO_2, rutile, optoelectronic props., band struct., theory 80—80175
- TiO_2:S, acceptor properties of S, free electron concentrations 80—34395
- TiO_2:S, in $O_2+CO_2+SO_2$ atmosphere, elec. cond. study 80—39583
- TiS_2, evidence for semicond. props., Hall coeff., refl., cond., thermoelec. power 80—20220
- TiS_2, transport props. and semicond. nature 80—44598
- $TiSe_2$, semimetal, electronic props., superlattice form. 77—15532
- Tl-S melts, Hall effect 77—85239
- $TlInSe_2$-$TlPrSe_2$ system, struct., elec. cond., and thermoelec. props. 79—87119
- Tl_2O_3 single crystal, elec. cond., cryst. grown from vapour in air 77—85219

carrier density continued
Tl_2O_3, single crystal, elec. cond., annealing at 923K in O_2 effects 77—85220
Tl_xTe_{1-x}, liq., rigid band behaviour, elec. cond. and thermopower 77—35845
VO_2, film, semicond.-metal transition, carrier density, mobility and Hall meas. 77—43751
V_2O_5, ferroelec. semicond., dielec. and elec. meas. 80—60516
V_2O_5-P_2O_5 glass, dielec. relax. mechanism, SDRC investigation, Schottky barrier formation in metal-glass-metal systems 78—60388
V_2O_5-P_2O_5 glass, electrical 1/f noise and DC cond. 79—91109
$Zn_xCd_{1-x}S$ films, spray pyrolysis, elec. props. 80—75657
$ZnGeP_2$, synthesis, characts., applic. to laser windows *(French)* 78—80467
$Zn_xHg_{1-x}Se$, band struct. from Shubnikov de Haas effect and hydrostatic press. meas. 80—49599
$Zn_xHg_{1-x}Se$, galvanomagnetic effects, Shubnikov-de Haas oscill. determ. of band struct. 80—6884
ZnO ceramic varistors, trapping by localized states, effect on dielec. and elec. props. *(Russian)* 79—28671
ZnO epitaxial film on Al_2O_3 substrate, recombination radiation in intense single photon excitation 80—7410
ZnO epitaxial layers, rel. between elec. and photoluminesc. props. and their deposition conditions 79—95530
ZnO, field-effect mobility in accumulation layers on polar surfaces 79—73509
ZnO films, RF sputtered single-cryst., on sapphire, struct. and SAW props. 80—80105
ZnO single crystals, quantised accumulation layers, electron Hall mobility, surface electron density var. 79—60909
ZnO sputtered films, undoped and Ga doped, props. rel. to deposition conditions 80—107935
ZnO surface, quantised accumulation layer magnetoresistance, spin scattering model 79—69529
ZnO surface extreme accumulation layers due to He^+ ions 77—72909
ZnP_2, pure and doped, carrier mobility and conc., donor and acceptor energy levels, 190 to 380K 78—84217
Zn_3P_2, elec. cond., Hall effect, P interstitial effects 80—84465
p-Zn_3P_2, temp. dependence of resistivity and Hall constant 77—35937
ZnSe, laser induced modulation of opt. absorpt. 78—88324
ZnSe MIS LED, donor density calc. from C-U meas. 78—47878
ZnSe, self-compensation, role of impurities 80—92850
ZnSe:Al(Mn), elec. and luminesc. props. 77—39844
ZnTe, elec. active intrinsic defects, Hall meas. of carrier conc. 77—51700
ZnTe films, residual conductivity, Kikuchi lines of electron diffr. pattern 79—91173
ZnTe, single cryst., electron-hole drop conc. *(Russian)* 79—11460
ZrO_2:Y_2O_3, solid electrolytes, charge carrier conc. and diffusion 77—11930
ZrO_2-CeO_2, semiconducting ceramics, electronic conductivity and oxido-reduction *(French)* 78—26919

carrier diffusion length *see carrier lifetime*

carrier lifetime
alkali halides, F-centre trapping of conduction electrons, photocond. study 78—56179
alkali metal halides, hole self-localization and capture, temp. depend. 80—92526
amorphous materials, exponential trap distrib., majority carrier lifetime determ. 78—14760
anthracene, trapping effects on emission-limited current flow 80—29413
auramine single crystal, lifetime and mobility of photogenerated charge carriers 78—2516
bulk trapping processes and trap occupancy 77—39876
cascade capture of charge carriers in quantised mag. field, appl. to many-valley semicond. *(Russian)* 79—4572
creep discharge surface injected carrier half-life meas. 80—15972
degenerate semiconductor, band to band radiative recombination *(Russian)* 78—35200
DH devices, interface recomb. effects on transient response anal. 78—22127
DH laser diodes, impedance characts. 80—23690
p-diamond, synthetic, semicond., free hole lifetime reduction due to their capture by excited states 79—69550
diffusion length and lifetime meas. and assessment by SEM 80—96902
diffusion length and surface recomb. vel. determ., light excitation 78—91725
disordered systems, elec. cond. and Hall mobility, theory 80—54697
EBIC technique, resolution limits in determ. of diffusion lengths in semiconductors 79—21865
electron-beam-induced current, minority carrier generation vol. influence 80—84475
electron-hole plasma current layering, electron cooling length, momentum scatt. 80—6890
equilibrium carrier trapping by centres localised in disordered regions 77—43618
generation lifetime, surface generation velocity determ., linear sweep MOS-CV method *(Chinese)* 80—107916
Gunn diodes, population inversion condition 77—77251
heat treatment effects on elec. props. 78—43411
heavily doped emitter structures, electron beam technique for lifetime profile meas. 80—15538
heterogeneous semiconductor systems, elec. cond. and EMF relax., pulsed radiation effects 77—89842
homojunction solar cells, superposition principle 80—81449
hydrocarbon, long chain single cryst., carrier transport meas. 80—6874
II-VI semiconductor, self-interaction dynamics of Nd laser radiation 79—27342
III-V epitaxial layers, minority carrier lifetime, correl. with defect props. 77—89835
III-V semiconductor epitaxial structures as wide-gap substrates, minority carrier diffusion length determ. by photoluminesc. 80—103992
injection laser, reson.-like peak reduction in direct modulation due to carrier diffusion 78—74905
n-InSb, photoconductivity relax. temp. depend., carrier recomb. processes 77—4363
insulator, charge carrier injection, Onsager model 78—80001
LED, DH, output power and response time, thickness depend. 79—95479
LED, diffusion lengths and near-junction luminescence-efficiency profiles from SEM scans 77—77301

carrier lifetime continued
lifetime of carriers and excitons before self trapping 77—85236
measurements from transient elect. photoresponses in solar cells 80—61346
minority carrier diffusion length, Schottky barriers, electron bombard. investigation 78—68037
minority carrier diffusion length determ., using angle-lapped p-n junctions 79—42631
minority carrier diffusion length determ. near p-n junction, SEM appl. *(French)* 78—43466
minority carrier diffusion length meas. using electron microprobe 77—39867
minority carrier exclusion 79—42561
minority carrier generation rate meas. using transient response of MOS capacitor with guard ring 78—2576
minority carrier lifetime mapping by SEM 80—96903
minority carrier lifetime-meas. technique using SEM-electron beam induced current 80—59999
minority carrier recombination at surfaces, dislocations and microdefects, luminesc. evaluation 78—6769
minority carriers, spectrometric determ. *(Russian)* 78—84230
MIS, minority carrier, lifetime and generation determ., graphical technique 78—95378
MIS structure, hysteresis pulsed C-V method for minority-carrier lifetime and surface generation velocity determ. 80—70839
modulation of effective lifetime, surface recomb. and mag. field effects 77—28193
molecular crystals, electronic transport theory, local linear electron phonon coupling 80—65545
MOS capacitor, comparison of lifetime meas. techniques 78—56232
MOS capacitor, generation lifetime determ. from non-equilib. linear sweep current and capacitance meas. 78—47881
MOS capacitor, minority carrier generation time and surface generation rel. determ. from Q-t meas. 78—72265
MOS capacitor, minority carrier lifetime, effects of swirls and stacking faults 77—32088
MOS capacitor, pulsed, transient response calc. 77—85341
MOS capacitor switched from inversion to accumulation, minority carrier lifetime meas. 77—39957
MOS diodes, minority carrier lifetime determ. from photocurrent spectra 80—49920
MOS pulsed capacitor, minority carrier lifetime meas. influence of Si-wafer surface state density 80—60098
MOS structure, bulk lifetime determ. by voltage step response method 78—47882
MOS structure, quench-in defects and interface states exam. by transient capacitance techniques 78—39225
MOS structure under strong inversion conditions, freq. response of bulk traps. 77—39958
MOS tunnel diodes characterisation, solar cell appls. 77—32089
narrow gap semiconductors, recombination mechanisms, review 80—96905
negative differential cond. of hot electrons in mag. field due to carrier density nonlinearity 77—55540
optical beam size effects on diffusion length meas. by surface photovoltage method 80—60002
p^+-n^--n^+ pulsed diodes, forward pulsed case, voltage transient response 80—60071
p-i-n diode, influence of high temp. processes on props. of high resistivity region 77—35988
p-i-n diodes, step recovery, analytical expressions 80—25000
p-n diode minority carrier storage effect reduction by F ion implantation damage 78—72243
p-n junction, diffusion length meas. of minority carriers, accel. voltage of primary electrons effect *(Czech)* 78—34844
p-n junction, impedance determ. from direct currents *(Russian)* 78—84285
p-n junction diodes, emitter and base lifetimes determ. 77—43701
p-n junction minority carrier diffusion length meas. by short-circuit current ratio 80—31849
p-n junction solar cells, determ. of lifetime and recombination currents 80—89637
p-n junctions, minority carrier surface recombination velocity, lifetime, AM electron beam determ. 79—87145
p-n junctions, photoeffect, quantity effective diffusion length *(Russian)* 78—56212
pentacene layers, photogeneration, charge carrier transport *(Russian)* 78—56181
photoconductor, electron trapping kinetics at broadened levels, transient behaviour 77—47826
photoconductor, measurement technique, using linearly increasing intensity light source 77—35960
photoconductor carrier lifetime, nonequilibrium, phase method for determ. 80—65629
photoelectric cell, continuous exposure mode, discharge model, surface generation of pairs *(Russian)* 77—72890
photovoltaic cell, grain boundary effects on performance 79—83603
poly-N-vinyl carbazole, trap-free lifetime, neutral traps, hopping systems 80—65566
polydiacetylene-bis(toluenesulphonate), transient photocond. meas. 78—30951
polyethylene, elec. props. and oxidation after electron beam irradiation and heat treatment 79—87092
polymer film, carrier transport meas. 80—6874
sapphire, Czochralski-grown, excess charge carriers, generation, transport and trapping 79—82646
Schottky barrier, real and ideal, photosensitivity losses 80—2452
Schottky barrier solar cell, doping density effect on efficiency 80—101100
SEM electron beam induced conductivity obs. of semicond. using Schottky barriers 78—34898
SEM meas. of diffusion const., lifetime and surface recomb. vel. 78—91701
SEM measurement of minority carrier diffusion lengths in semicond. interpretation 78—80002
semicondctor diffusion length and surface recombination velocity determ. by intensity modulated SEM 78—10472
semiconducting photocathodes, carrier transport simulation, Monte Carlo method 80—71575
semiconductor, absorption of strong EM waves, weak electric field effects 79—95400

carrier lifetime continued
semiconductor, ambipolar diffusion meas. using nonlinear transient gratings 78—80000
semiconductor, carrier capture by attractive centres in strong elec. fields 79—11144
semiconductor, carrier capture cross section by attractive Coulomb centres, piezoelec. scatt. 78—72170
semiconductor, carrier generation lifetime profiles meas. in diffused layers 78—47803
semiconductor, carrier lifetime profiles meas. in diffused layers 78—47811
semiconductor, cathodoluminescence meas. of minority carrier lifetime, appl. to GaP 78—19572
semiconductor, compensated, electron capture probability by Coulomb centre in case of optical phonon emission 80—20214
semiconductor, effect of effective lifetime modulation 78—47807
semiconductor, effect of effective lifetime modulation 78—47808
semiconductor, elec. parameters determ. by electron probe method 79—9259
semiconductor, homogeneous, nondegenerate, single-level Schockley-Read-Hall recomb. centres, flicker noise 80—70779
semiconductor, influence of long-range dislocation pots. on de Haas-van Alphen effect 77—8009
semiconductor, lifetime meas. by photoconductivity null apparatus 78—56184
semiconductor, lifetime of carriers recombining in disordered regions, injection depend. 78—14742
semiconductor, minority carrier injection 78—60136
semiconductor, minority carrier lifetime determ. by relative amplitude method 77—72869
semiconductor, n-type, inhomogeneous, nonequilib. carrier diffusion and lifetime 80—60005
semiconductor, narrow gap, mag. quantum oscills. of Auger transition rate 77—69340
semiconductor, nonequilibrium processes exam. by method of transient holograms 78—23105
semiconductor, nonlinear conductivity, vortex waves, carrier mobility and lifetime 80—96893
semiconductor, nonuniform diffusion length and elec. field determ. 78—72166
semiconductor, optical absorpt. coeff. and minority-carrier diffusion length, differential photocurrent method of meas. 80—96896
semiconductor, photoexcitation, electron lifetime and capture by trapping centres *(Russian)* 77—32047
semiconductor, photomagnetoelectric effect, injection-level dependent lifetime 80—80319
semiconductor, polycryst., electronic processes at grain boundaries under optical illum. 77—55561
semiconductor, self-oscillatory medium, modelling 77—20811
semiconductor, SEM electron beam induced current images of dislocations and stacking faults, computer simulation 80—70198
semiconductor, spatial resolution of SEM electron beam induced conductivity images 80—6327
semiconductor, spin-dependent recomb. and scatt. in presence of optical orientation of electrons 80—96908
semiconductor, superlattice doping, electronic states, elec. props. 79—95480
semiconductor, three-electron recombination processes 78—43413
semiconductor, two-photon absorpt., free carrier storage by deep centres *(Russian)* 78—23131
semiconductor bicrystal, charge carrier interface recomb., photocond. meas. method 79—99431
semiconductor containing traps, minority, carrier lifetime 78—60137
semiconductor crystals, with high quantum efficiency, minority carrier lifetime meas. *(Japanese)* 80—54711
semiconductor depth profiling by electron beam induced junction current meas. 80—96977
semiconductor detector with alternating bias, energy resolution 77—10553
semiconductor device characterisation using electron beam induced current technique, review 78—21302
semiconductor devices, resistivity and lifetime inhomogeneities, laser scanning method detect. 79—30489
semiconductor diode transient process calcs., minority nonequilibrium carriers, postinjection EMF 80—6971
semiconductor heterostructure, multipass, effective lifetime of nonequilibrium carriers 78—6435
semiconductor heterostructure laser, carrier diffusion length using differential electron beam induced current 79—55137
semiconductor laser, photopumped, III-V semiconductor, book contrib. 80—99732
semiconductor laser, stimulated emission threshold, surface recombination influence 79—10311
semiconductor laser damage, role of carrier diffusion 79—19954
semiconductor lasers, generalised expressions for turn on delay 79—94233
semiconductor layers, double injection in transverse mag. field, theory 80—80421
semiconductor layers, thin, theory of lifetime meas. with SEM, transient anal. 80—88573
semiconductor phonon-assisted nonradiative recomb. phenomena, review *(Polish)* 77—69339
semiconductor surface eval. using SAW convolver 80—97677
semiconductor wafer characterisation by photonic injection + microwave meas., appl. to Si *(French)* 78—23106
semiconductors, disordered, carrier mobility and transient pulse dispersion for hopping mechanisms 80—44586
semiconductors, free carrier density in strong electric and quantised mag. fields 80—6860
semiconductors, generalised transport equations 79—95398
semiconductors, hot electron recombination at impurity centres 80—10995
semiconductors, minority carrier diffusion lengths meas. 79—60848
semiconductors, photoconductivity measurement at UHF and at high excitation levels 80—65627
semiconductors, photomagnetoelectric effect, expt. parameters rel. to material props. 79—99584
semiconductors, polycryst., opto-electronic processes at grain boundaries 77—43667
semiconductors, scatt. influence on Auger transition, depend. of impact ionisation on electron energy 80—44608

carrier lifetime continued
semiconductors, two-photon conductivity calc., nano-pico sec. pulse excitation 78—72188
semiconductors and insulators, non-radiative processes multiphonon recomb. 78—6752
semiconductors with deep impurities, double injection currents 77—55543
shallow junction devices, minority carrier diffusion lengths 78—72168
n-Si, recombination centres and carrier lifetimes after γ-irrad. 80—60004
small signal electrical response theory, generation-recomb. and trapping kinetics 77—89772
solar cell, diffusion equation, surface boundary condition 80—66975
solar cell, interaction of electron beam, minority carrier diffusion length 80—7943
solar cell, p-n junction, photoinjected carrier lifetime meas. by reverse voltage pulse response 80—45664
solar cells, minority carrier lifetime meas., open-cct. to short-cct. switching method 79—79392
solar cells, minority carrier lifetime meas. from photo-induced open-cct. voltage decay 79—87990
solar cells, output monitoring, design and utilization of a microprocessor-controlled absolute spectral response system 80—81476
solar cells, polycryst., recomb. at grain boundaries, effect on photoresponse 80—108796
solar cells, surface recombination velocity and diffusion length meas. 80—93965
solid-state electronics, introductory theory, book 80—22160
SOS films, carrier recomb. props., magnetosensitive method 79—38186
SOS films, surface recomb. profile and transport parameters 79—33357
superlattice semiconductor impurity photoconductivity electron spectrum reconstruction 80—24966
Teflon, non-destructive charge release 80—24946
Teflon FEP, N implanted, TSC spectra 80—88912
tetracene, layers, photogeneration, charge carrier transport *(Russian)* 78—56181
tetracene, trapping effects on emission-limited current flow 80—29413
transmutation doped, stabilisation 78—10449
TSC and isothermal decay currents, influence of blocking contacts 77—28182
tunnel MIS solar cells, grain boundary effect on performance 79—79394
UV transparent material, multiphoton-induced cond. and free carrier lifetime 79—19629
Si:P, sheet resistance of Gaussian n-type ion-implanted layers 79—87103
AgBr, photoexcited electrons and holes in latest image form., review 80—73496
β-AgI:Cu, pure and doped, photoconductivity, band struct., trap nature 79—95449
Al-Al_2O_3-InSb MIS structures, recomb. processes and carrier lifetimes 79—38177
Al-SiO_2-Si capacitor C-V characteristic determ. of surface minority carrier lifetime *(Polish)* 77—89855
AlAs-GaAs double heterostructure, effective lifetime of nonequilibrium carriers 78—6435
AlGaAs lasers, relaxation oscillation rel. to carrier diffusion length, spontaneous emission 80—32986
AlGaAs-GaAs heterostructure, minority carrier lifetime, photon recycling effect *(Japanese)* 79—42556
AlGaAs-GaAs proton irradiated solar cells, deep level defects and recombination parameters 80—94032
n-$Al_xGa_{1-x}As$, variable-gap solid solns., diffusion length, photolum. meas. 79—38659
$Al_xGa_{1-x}As$:Cu, variable-gap semicond., impurity props., carrier recomb. 80—96907
$Al_xGa_{1-x}As$-GaAs heterostructure, effect of photon recycling on diffusion length and internal quantum efficiency 77—39929
$Al_xGa_{1-x}As$-GaAs long life laser, initial degradation, minority carrier lifetime reduction 77—71984
AlSb as high-energy photon detector 77—75026
$(As_2S_3)_{0.55}(Sb_2S_3)_{0.45}$ vitreous film, dispersive charge transport, time-of-flight meas. 79—19594
As_2Se_3, glassy, drift mobility of holes, 20 to 120°C 79—51583
BN glass transfer process 80—107459
Bi_2O_3 anodic films, struct. and electronic props., photoeffects 80—44749
Cd, positron trapping at low temp. lifetime spectra 80—84799
Cd_xHg_{1-x} Te, photodetectors, recomb. processes, photoconductive decay obs. 79—38129
$Cd_xHg_{1-x}Te$, Auger effect, temp. depend. of Auger lifetime 79—38097
$Cd_xHg_{1-x}Te$, carrier lifetime, effect of comp. fluctuations and second-phase inclusions 80—80294
n-$Cd_xHg_{1-x}Te$ crystals, carrier recomb. in extrinsic conduction range 80—70722
$Cd_xHg_{1-x}Te$, electron irradiated, elec. and recomb. characts. 78—39113
$Cd_xHg_{1-x}Te$ films, epitaxial growth, optical, elec., and photoelec. props. 79—11512
$Cd_xHg_{1-x}Te$, photoelectric props. at high temp. 77—4403
n-$Cd_xHg_{1-x}Te$, recombination due to surface excitation, photoconductivity, impurity states *(Russian)* 80—60042
$Cd_xHg_{1-x}Te$ single crystal, photoconductivity spectral distrib. rel. to surface condition 79—78136
$Cd_xMg_{1-x}Te$, inhomogeneous composition effects, photosensitivity *(Russian)* 79—73526
CdP_2:Cu, photoluminescence and photocond. characts., interimpurity recomb. of carriers 77—8637
CdS crystals, electron-hole plasma, carrier optical orientation 80—100689
CdS, defects formed by laser radiation of subthreshold intensity, bulk photo-EMF investigation 79—91098
CdS, electron-hole liq., effect of excited electron states lifetime on gain spectra 77—85748
CdS, photosensitivity degradation mechanism due to photocurrent, phtot-carrier lifetime 80—6903
n-CdS:Cu, Si, photocond., carrier lifetime, X-ray effects 77—59300
CdS:Cu(Cl) thin films, surface and bulk photoconc. 80—88653
CdS:Na thin film, photoconducting props. 80—39623
CdS-Cu_xS solar cells, electron diffusion length determ. using spectral response meas. 80—81475
CdS-$CuInSe_2$ solar cells, grain boundary and interface recomb. effects 79—39311
CdS_xSe_{1-x}, strongly excited by electron beam, determ. of nonequilibrium carrier lifetime 80—39603
CdSe, charge transport 78—84233

carrier lifetime continued
- CdSe film, effect of growth conditions on electrophysical properties 78—44024
- CdSe, photoconductivity, recomb. characts. 77—8118
- n-CdSe, with single deep electron trap, negative photocond. 77—15905
- CdTe, detector grade semi-insulating crystals, determ. of product of mobility and carrier lifetime 80—39601
- CdTe, film, theoretical models of impurity levels 79—82557
- CdTe, influence of heat treatment on carrier lifetime, photoelectromagnetic effect meas. 77—55576
- CdTe, minority carrier diffusion length from photocurrent meas. in semicond.-electrolyte boundary 80—65584
- CdTe p-n homojunction, elec. and photovoltaic props. rel. to solar energy conversion 79—51668
- p-CdTe:Cl, mech. of electron recomb. 79—11176
- CdTe-CdS thin film p-n solar cells, spectral response temp. depend. 80—93871
- Cr-SiO_x-Si MIS solar cells, photovoltaic performance and interface states, nucl. radiation effects 80—94004
- $CuInS_2$, minority carriers lifetime, photoelectromag. effect meas. 79—47125
- p-$CuInSe_2$, minority carrier lifetime and surface recomb. velocity, photoelectromag. meas. 78—19085
- $CuInSe_2$ thin films for solar cells, radiofrequency sputtering technique, elec. props. 80—93487
- Cu_2O, pure and Fe doped, carrier cyclotron resonance impurity scattering effects, polar mass extrinsic origin 79—56614
- Cu_2O-Cu diode junction, Schottky barrier, electronic structure and minority carrier diffusion length *(French)* 80—65682
- Cu_2S, diffusion length meas. using scanned laser beam tech. 80—93886
- Cu_2S epitaxial films, reactive sputtering prep. and electronic props. 79—78885
- Cu_2S/CdS heterojunction solar cells, diffusion length determ. using minority carrier SEM 80—61359
- Cu_2S-CdS heterojunctions, electron trap characterisation by capacitance transient meas. 79—78163
- Cu_2S-CdS solar cells, EBIC and capacitance measurements, stability problems 80—45684
- $Cu_{2-x}S$-CdS p-n heterojunction, optical energy convertor, struct. and recomb. props. 80—72065
- Cu_xS, photon and electron excitation phenomena 79—7865
- Cu_xS-CdS solar cell, minority carrier diffusion length, SEM determ. 77—72911
- α-Fe_2O_3 electrode, carrier density determ. by optical absorpt. and photoelectrolysis spectra 80—71462
- FeSi and $FeSi_2$, inner level ESCA spectra, many particle effects, hole lifetime *(Russian)* 79—91560
- GaAlAs DH laser, narrow stripe geometry, spontaneous carrier lifetime 80—87392
- GaAlAs DH laser, optimum p-n junction depth, photoluminesc. method 79—4598
- GaAlAs DH laser diode, deep level associated with slow degradation 78—87050
- GaAlAs DH lasers, electron-hole recomb. effects 79—45944
- GaAlAs-GaAs heteroface solar cells, 1 MeV electron irrad., analytical and expt. study 79—70450
- $Ga_{0.5}Al_{0.5}As$-GaAs(:Ge) DH structure, minority carrier lifetime and internal quantum efficiency of surface-free GaAs 79—43013
- $Ga_{1-x}Al_xAs$-$Ga_{1-y}Al_yAs$ p-n heterojunction, minority carrier lifetime, elec. characts. and electrolum. meas. 78—2554
- $Ga_{1-x}Al_xAs$-GaAs p-n and p-p-n heterojunction solar cells, high efficiency, prep., eval. and characters *(Japanese)* 80—61342
- $Ga_{1-x}Al_xSb$ p-n homojunction LPE and photovoltaic effect obs. *(French)* 78—64108
- Ga(As,P)/(In,Ga)P DH laser, red-emitting, optical and elec. characts. 78—66826
- GaAs, diffusion and power spectral density and correl. function of vel. fluctuation for electrons 80—65576
- GaAs diode, quantum efficiency and nonequilibrium carrier lifetime 77—12442
- GaAs, electron and neutron irrad., defect clusters, carrier lifetime changes, doping level depend. 80—2077
- GaAs, electron beam induced defect annealing 77—80790
- n-GaAs, electron irrad. defects, carrier removal rate, annealing effects 80—75269
- n-GaAs epitaxial films, residual cond. meas., struct. perfection rel. to photomemory 80—7010
- p-GaAs, Fe-compensated, photocond. under strong excitation 77—15904
- GaAs film, vapour-grown, effect of gas-phase stoichiometry on deep levels 78—10393
- GaAs Gunn diodes, population inversion condition 77—77251
- GaAs, hot photoluminescence depolarisation in mag. field, 0.4 eV energy state electron lifetime *(Russian)* 80—16086
- GaAs, illuminated, carrier lifetime profile, depth depend. 78—68036
- GaAs injection lasers, longitudinal mode spectrum, effect of carrier diffusion 78—71099
- GaAs, intervalley electron transfer, drift velocity and diffusion coefficient 80—39594
- GaAs LED, minority carrier lifetime determ. 79—42560
- GaAs LED, optimum p-n junction depth, photoluminesc. method 79—4598
- GaAs, LPE layers, outdiffusion of recomb. centres from substrate during growth 80—39466
- n-GaAs, Landau level lifetimes for electrons 79—87112
- GaAs, laser heating of lightly damaged material, carrier diffusion effect 80—84809
- GaAs layers, electroepitaxy and thermal LPE growth, defect struct. and electronic characts. 80—2290
- GaAs layers and p-n junctions grown by current-controlled LPE, elec. characts. 78—6436
- GaAs, lightly doped, p-n structure, parameters of nonequilib. carriers, transient photoeffect method 79—11143
- GaAs MOS capacitor fabrication and transient response for minority carrier lifetime meas. 79—47103
- GaAs, minority carrier diffusion length, reabsorbed radiation effect 77—28191
- GaAs, minority carrier diffusion lengths, contact metal effects 78—72260
- GaAs, minority carrier diffusion length, photon absorption reemission 79—87109
- GaAs, minority carrier lifetime at high temp., solar cell performance appl. 80—24947

carrier lifetime continued
- GaAs p^+-n^0 junction, photocurrent, hole diffusion length in lightly doped n-type region 77—28246
- GaAs, photoconductive carrier lifetime meas. by optoelectronic gating technique 77—47857
- GaAs, polycrystalline films, meas. of effective diffusion length by SEM 80—80424
- GaAs, proton irradiated, low energy, deep level defects and hole diffusion length meas. 80—60000
- GaAs, radiation induced changes 77—8664
- n-GaAs, Raman scatt. by wavevector depend. coupled plasmon-LO phonons 77—40232
- GaAs, relaxation of photoexcited carriers 78—19080
- n-GaAs Schottky barrier junction, SEM meas. of hole diffusion length, surface effects 79—87110
- GaAs, Schottky barrier solar cells, diffusion length meas. 79—61973
- GaAs, semi-insulating, magnetophotoconductivity as function of etching time 79—56265
- GaAs solar cell polycrystalline conducting substrate, minority carrier diffusion length spatially-resolved meas. 80—94084
- GaAs, surface recomb. velocity, determ. from SEM expts. on p-n junctions 77—55601
- n-GaAs, surface recomb. vel. meas., diffr. from transient optical grating 79—1604
- n-GaAs, two-valleyed semicond., hot electron diffusion coeff., random walk calc. 78—68033
- GaAs, VPE, hole diffusion lengths, surface prep. and heat treatment effects, etchant evaluation 80—15627
- GaAs, VPE, hole diffusion lengths, effect of transition metal diffusional doping 80—15628
- GaAs VPE layers, role of diffused Ga vacancy in degradation 78—95050
- GaAs, valence-band dispersions, electron and hole lifetimes, angle-resolved photoemission 80—80947
- n-GaAs vapour phase epitaxial film electrophysical props. rel. to growth temp. *(Russian)* 80—49961
- GaAs:Cr excess electron lifetime determ. by US method *(Czech)* 77—20336
- GaAs:Ge, vap. grown, diatomic complex donor and acceptor model 78—80003
- GaAs:Se cathodoluminescence decay obs. with SEM and streak camera, 90 to 300K 80—97348
- GaAs:Si, heteroface solar cells, diffusion lengths 78—47849
- GaAs:Si(Mg), doped and undoped, sputtered epitaxial films, elec. props. 79—78234
- GaAs:Te, microcathodoluminesc. of effect of struct. defects on radiative recomb. 79—11475
- GaAs:Te Schottky barrier solar cells, diffusion length determ. using minority carrier SEM 80—61359
- GaAs-$Al_xGa_{1-x}As$ heterostruct., photon recycling, diffusion length and lifetime determ. 79—47499
- GaAs-$Al_xGa_{1-x}As$ multilayer, photoluminesc., electron spin orientation 80—25453
- n-GaAs-electrolyte interface, surface pretreatment rel. to photocurrent, spectral response 80—3204
- GaAs-$Ga_{1-x}Al_xAs$ DH lasers, electron beam induced current microscopy 80—95899
- GaAs-GaAlAs double heterostruct., self-absorpt. effects on radiative lifetime 77—39928
- $GaAs_{0.6}P_{0.4}$, VPE, hole diffusion lengths, surface prep. and heat treatment effects, etchant evaluation 80—15627
- $GaAs_{0.6}P_{0.4}$, VPE, hole diffusion lengths, effect of transition metal diffusional doping 80—15628
- GaInAsP/InP lasers, LPE grown, effect of p-doping on carrier lifetime and threshold current density 80—99726
- $Ga_{1-x}In_xAs_{1-y}P_y$-InP DH laser, carrier lifetime meas. 77—61955
- n-$Ga_xIn_{1-x}P$ photoelectrochemical cells, bandgap energy, electronic transition mode, and diffusion length 80—72070
- GaInSb, intervalley electron transfer, drift velocity and diffusion coefficient 80—39594
- $Ga_{1-x}In_xSb$, LPE on GaSb by stepwise grading, and characterisation 78—72745
- n-GaP, deep state controlled minority carrier lifetime 80—20211
- GaP, epitaxial layer, thickness and diffusion length, photocurrent meas. 77—32096
- GaP, epitaxial layers, dislocation recomb., SEM cathodoluminescence studies 79—42558
- GaP, frozen-in pt. defects annihilation 79—99949
- n-GaP, interface-recomb.-controlled minority carrier lifetime obs. 77—12027
- n-GaP, LPE, minority carrier bulk lifetime and diffusion coeff. meas. 77—11932
- GaP, minority carrier lifetimes at dislocations, SEM meas. using photon counting 78—23109
- GaP p-n junction, diffusion length, space-charge region width, barrier electron voltaic effect meas. 79—69587
- n-GaP, shallow trapping centres, electron lifetime from photocond. meas. 79—99563
- GaP:N VPE LED, deep level centres, DLTS studies 79—42493
- GaP:N VPE layers, thermal emission energies, trapping, and carrier lifetimes, deep level capacitance spectroscopy 79—42487
- GaP-In LPE layers, carrier diffusion lengths and escape probabilities optical absorpt. and photoemission meas. 79—87559
- p-GaSb:Zn film, epitaxial, lifetime of nonequilib. carriers, determ. from circular polarisation of luminesc. 77—24898
- p-GaSe, back wall Schottky barrier cells, diffusion length, RT spectral response meas. 80—107806
- GaSe, layered, photoelectromag. effect meas. of transport parameters 77—59301
- n-GaSe, photomagnetoelec. and photocond. current spectral distrib. 79—42585
- Gap-Ge, compensated, photosensitivity 79—19624
- Ge, charge carrier diffusion coeff. 78—84218
- Ge, compensated by thermal defects, recomb. and optical props. 80—64989
- Ge, cyclotron resonance and radiative recomb. with laser excitation, book contrib. 80—11472
- p-Ge, detector-grade single crysts., impurity background effect on minority-carrier lifetime 79—11088
- Ge diode, influence of mechanical stresses on effective carrier diffusion length in base region 77—35987
- Ge, dislocation energy band width, carrier lifetime anal. 77—11874

carrier lifetime continued
p-Ge, electron bombard. at high temp., carrier lifetime and defect levels 77—55306
n-Ge, electron irradiated, high temp. annealing, nonequilibrium carrier lifetime and Hall effect 77—4370
Ge, electron-hole correlation density depend., in electron-hole liq., under uniaxial stress 79—15090
Ge, electron-hole fluid drift in crossed electric and mag. fields, photocurrent dynamics *(Russian)* 79—99487
n-Ge, γ-irrad., nonlinear steady-state recomb., nonequilib. carrier lifetime and density 80—20215
n-Ge, γ-irrad. and subjected to arbitrary excitation and rate, recombination 79—38101
Ge, irradiation by 3.5 MeV electrons at high temp., carrier density and lifetime changes 77—4128
Ge, magnetic field influence on 1/f noise, surface origin evidence 79—99592
Ge, microwave absorption by nonequilibrium carriers, carrier density determ. method 77—8148
Ge, photoconductivity, carrier lifetimes in excited states of impurities *(Russian)* 77—76864
p-Ge, photoexcited charge carrier capture by shallow impurity centres *(Russian)* 80—15571
Ge, photomagnetic effect, space inhomogeneous nonequilibrium carrier lifetimes *(Russian)* 80—71152
n-Ge, proton and γ irrad., minority carrier recombination 80—65591
Ge recombination characteristics used in design of semicond. devices *(Russian)* 79—42557
Ge, surface electronic props. meas. by SEM, sand-blasting effect 77—62976
Ge:Au, recomb. at repulsive centres, photocond. lifetime meas. 77—43617
Ge:Ba, Ca, recomb. props. 78—56156
Ge:Cu, hot photoexcited holes at low temp. 78—30954
p-Ge:Ga, dislocation density effect on carrier lifetime and deep recomb. centres 79—51598
p-Ge:Ga(Sb), proton irradiated, kinetics of accumulation of radiation defects, minority carrier lifetime 79—10885
n-Ge:Ni, quasi-surface conduction effects on photocond. spectrum and IR quenching 77—1452
n-Ge:Ni p^+-n-n^+ structs., double-injection current-voltage characts. 80—60074
Ge:P(Sb)(Bi), γ-irrad., carrier trapping and recomb. at point radiation defects 80—107810
Ge:Sb, γ-irrad., electron capture mechanism by radiation defects 78—26885
n-Ge:Sb, γ-irradiated, trapping and recomb. coeffs. 77—43616
Ge:Zn photoresistor, current responsivity rel. to nonequilib. hole lifetime 80—60035
Ge:Zn^{II} carrier lifetime, nonequilibrium, phase method for determ. 80—65629
Ge-metal Schottky barrier photodetectors, near IR interband transitions and optical parameters 80—73449
Ge-Te-Se/Si amorphous film-cryst. heterojunction, electron-beam-induced current 79—24060
GeS film, photocond. kinetics 77—39897
p-(Hg,Cd)Te, carrier lifetime, dominant Auger transitions comparison 80—49768
HgCdTe, 0.1 eV photodetector performance, geometrical enhancement 77—32040
n-HgCdTe, photocond., Hall mobility and resist. 80—34478
HgCdTe, radiation effects on low-temp. carrier recombination lifetimes, photocond. meas. 78—6400
HgCdTe, recomb. effects, mag. quantum oscills. in Auger transition rate 79—82610
$Hg_{0.68}Cd_{0.32}Te$ photodiode, minority carrier lifetime determ. 79—38084
$Hg_{1-x}Cd_xTe$, Einstein relation for inversion layers 80—103706
$Hg_{1-x}Cd_xTe$, long-term Hall-type conversion by vacancy diffusion at room temp. 79—65498
$nHg_{1-x}Cd_xTe$, single-phonon and plasmon recomb. lifetime effect, with magnetically tuned bandgap 79—38098
$Hg_xCd_{1-x}Te$, photodiode, anomalous noise behaviour in heterodyne and background limited operation 79—69568
HgI_2, and photomagnetoelectric and photocond. meas., carrier lifetimes 77—55562
HgI_2 crystals, native defect compensation, doping, mobility-lifetime and TSC meas. 77—55492
HgI_2, layered, photoelectromag. effect meas. of transport parameters 77—59301
HgI_2, photo-EM effect and photocond., trapping effects 77—32042
InAs and solid solutions, recombination mechanisms of excess carriers, luminesc. obs. 80—97337
InAs, intrinsic point defects, nature and influence on electrophys. props. 78—79609
InAsP, intervalley electron transfer, drift velocity and diffusion coefficient 80—39594
InGaAsP, epitaxial layer, defect evaluation by cathodoluminescence 80—2866
p-InGaAsP, on InP surface, diffusion coeff. and surface recombination velocity 80—39598
InGaAsP-InP, double heterostructure laser, temp. sensitive threshold current 79—59700
InGaAsP-InP DH lasers, carrier lifetimes meas. 78—66828
InGaAsP-InP DH lasers, threshold characteristic 79—81430
InGaAsP-InP DH lasers, low temp. behaviour of threshold current and carrier lifetime 79—98374
InGaAsP-InP DH laser, threshold current, temp. depend. 80—106521
$In_xGa_{1-x}As_{1-y}P_y$ epitaxial layers, characterisation and relation to lattice matching 80—100540
$In_{0.5}Ga_{0.5}P$-GaAs heterojunction, interfacial recomb. vel. determ. 77—51809
$In_xGa_{1-x}P$-GaAs heterojunction, interface recomb. velocity determ. 77—89838
$In_xGa_{1-x}P$-GaAs lattice mismatched heterojunction, recomb. props. 78—13707
InP Gunn diodes, population inversion condition 77—77251
InP, impact ionisation by electrons and holes 80—100467
InP, intervalley electron transfer, drift velocity and diffusion coefficient 80—39594
InP, n- and p-type, surface recomb. vel. meas., diffr. from transient optical grating 79—1604

carrier lifetime continued
InP, photoemission and LEED meas., minority carrier diffusion length 77—69959
InP substrate, LEC-grown, defect evaluation by cathodoluminescence 80—2866
InSb, Auger-governed decay of laser-induced plasma, optical probing 80—76105
InSb, carrier heating by microwave field, inertia effects 80—65580
InSb, Einstein relation for inversion layers 80—103706
InSb, Ettingshausen effect, influence of surfaces, narrow-gap semicond. characterisation 77—24571
n-InSb, high-resist., recomb. of carriers at 77K 77—51761
InSb, high-resistivity p-type or crystals of n-type, recombination processes, photocond. and photomag. effect meas. *(Russian)* 80—88567
n- InSb, hot electron energy relax. in quantizing mag. fields 78—31259
InSb, intrinsic, photoinjected electron hole pairs, Auger lifetime, photoconductive decay obs. 80—39629
n-InSb, Landau-level-electron lifetimes, saturation meas. of magnetoabsorption 78—48150
InSb, low-temp. annealing effect 77—8091
p-InSb, magnetoconcentration effect in extrinsic cond. range 80—65593
p-InSb, mobility, diffusion and thermoelectric power of hot holes 80—39595
InSb, photoconductive and photoelectromag. effect spectral distrib., sample thickness depend. 77—4394
n-InSb, photoconductive lifetime, surface pot. effects 80—11029
n-InSb, photoconductivity, recombination processes 80—11030
n-InSb, proton irrad. defects energy level scheme, transport props. meas. 80—96576
n-InSb, recomb. of hot electrons, photoelectromag. and dynamic photocond. meas. 79—38081
InSb:Cr, electron and hole lifetimes, recomb. at trapping and acceptor levels 77—51760
InSb:Cr(Zn)(Mn)(Ge), recombination of nonequilibrium carriers 79—65496
p-InSb:Ge, proton irrad. defects energy level scheme, transport props. meas. 80—96576
$LiNbO_3$:Fe, hologram writing, beam coupling and transport length in bulk photovoltaic effect 79—94190
NaCl crystal with aggregate colour centres, photocond. kinetics 78—19100
NbO_2, threshold switching recovery curve, distribution trapped carrier lifetime 80—20258
(Pb,Sn)Te, (Pb,Sn)Se IR detector diodes, junction resist. comparison, minority carrier lifetimes 78—24858
PbI_2, layered, photoelectromag. effect meas. of transport parameters 77—59301
PbI_2, photoelectromagnetic investigation, expt. 79—24010
PbO single crystals, current-voltage characts., electrolum. *(Russian)* 80—2863
$Pb_{0.86}Sn_{0.14}Te$/PbTe, interface recomb. velocity in DH laser diodes 79—64222
$Pb_{1-x}Sn_xTe$ DH laser, minority carrier lifetimes and lasing thresholds 80—19031
$Pb_{1-x}Sn_xTe$, epitaxial layers, carrier lifetime meas. 79—42559
$Pb_{1-x}Sn_xTe$, narrow gap, many-body interaction effects, Bloch electron scatt. lifetimes, energy renormalisation 80—49637
$Pb_{1-x}Sn_xTe$, photoconduct., photoelectromag. effect, laser intensity depend., carrier lifetimes 77—15896
$Pb_{1-x}Sn_xTe$, photomagnetic effect at low temps. 77—62960
$Pb_{1-x}Sn_xTe$:Cd, photocond., photomag. effect, carrier lifetimes 80—44658
$Pb_{1-x}Sn_xTe$:In, with low carrier conc., transport phenomena 80—49783
$Pb_{1-x}Sn_xTe$-PbTe heterojunction, Sn diffusion and elec. effects of dislocations, elec. and metallurgical expts. 77—89839
$Pb_{1-x}Sn_xY$. Y=Te, Se, S, photocond. anisotropy rel. to lifetimes 78—52032
PbTe, Auger recomb., photocond. decay time expts. 77—72879
PbTe epitaxial films, carrier recomb. and deep levels, photocond., Hall effect, and luminesc. meas. 79—38024
PbTe, epitaxial layers, carrier lifetime meas. 79—42559
PbTe IR diode, epitaxially grown and ion implanted, minority carrier lifetimes, efficiency 77—20411
p-PbTe MIS capacitors 5 μm IR detector appl. 78—52101
PbTe p-n junction, minority carrier lifetime, step pulse recovery 77—11995
Se, amorphous, carrier lifetime and drift mobilities 78—87985
n-Si, A-centre ionisation energy change due to uniaxial deform. 78—71733
Si, adsorbed Pd impurity, effect on surface electronic props. *(Russian)* 79—91124
Si, Auger recombination, localized and free carrier comparison 79—38090
Si, CVD film, transport props. 79—24089
Si, carrier capture at amphoteric deep level defects 80—88569
Si, carrier generation in depletion layer, effect of stacking faults 79—23983
Si, carrier lifetime, comparison of meas. by photocond. decay and surface photovoltage 78—68038
Si, carrier lifetime degradation at room temp. 78—95301
Si, carrier lifetime depth distrib. due to Ar ion implantation 80—70232
Si, compensated by thermal defects, recomb. and optical props. 80—64989
P-Si, conductivity and carrier lifetime, high injection effects 80—70719
n-Si, defect charge states, complex form., gamma-ray effects 80—96564
Si, defect formation kinetics during charged particle irrad. 80—29096
Si, deformed, annealed and recrystallized, struct., implications for solar cells 80—60922
Si, diffused p-n junction, computer calcs. of photoresponse using Gummel-de-Mari algorithm 78—56221
Si, diffusion and power spectral density and correl. function of vel. fluctuation for electrons 80—65576
Si, diode. minority-charge-carrier lifetime rel. to abrasion of surface *(Russian)* 80—11805
Si diode, transient switching duration, linear carrier lifetime, emitter efficiency and Auger recomb. coeff. determ. 79—11207
Si, electrical properties of single crystal, dislocation effects *(Rumanian)* 79—73504
Si, electrical props. affected by heat treatment *(Russian)* 78—11352
Si, electron irrad. devices, dominant recomb. centres 77—72912

carrier lifetime continued
Si, electron irrad. induced defect form., carrier density, mobility and lifetime changes 77—43250
n-Si, electron radiation defect annealing, negative stage, Hall coefficient, defect levels 79—90701
Si, electrophysical props. of single crysts. with and without dislocations 77—47812
Si, epitaxial, minority carrier lifetime and impurity conc. meas. *(Japanese)* 80—25025
Si epitaxial film, correlation between electrooptical and electrical props., IR absorpt. spectra *(Russian)* 78—60453
Si epitaxial layer, minority carrier lifetime obs. *(Russian)* 80—49765
Si epitaxial layer substrate junctions *(Korean)* 78—47888
Si, epitaxial layers, minority carrier lifetime and diffusion length meas., photocurrent technique 78—95302
Si, film, polycryst., for photovoltaic appl., grain size effects 78—72034
Si, float zone, process-induced effects on carrier lifetime and defects 80—81216
n-Si, gamma ray irrad., impurity composition influence on recombination centre formation 80—6872
Si, gettering by ion damage, minority carrier lifetime and backscatt. study 80—100286
n-Si, γ-irrad, ($E_{max}=100$ MeV), carrier recomb. 78—56158
Si, heat treated, minority carrier lifetime, effect of swirl defects 77—39868
Si, heavily doped, approx. of Einstein relation, carrier diffusivity to mobility ratio 79—65494
Si, heavily doped, bandgap narrowing and diffusion length meas. 79—7781
Si, heavily doped, carrier recomb. through shallow donor and acceptor states 80—15535
n-Si, heavily doped, meas. of minority carrier transport parameters 80—15537
Si, heavily doped layer, electronic characts., electron beam induced current obs. 78—10473
Si, heteroepitaxial films, photomagnetoelectric effect 77—85264
Si, highly doped and highly exerted, Auger coeffs., radiative band to band recomb. lifetime meas. 77—85764
Si, hot holes, drift and diffusion 79—78110
n-Si, influence of deform. on capture of electrons by divacancies 77—1449
Si, ion beam damaged, minority carrier lifetime distribs., electron beam meas. 79—87108
n-Si, ionisation of low donor levels and recomb. of hot electrons at low temp. 79—51596
Si junction diodes, fabrication by LPE on Si:B substrates, and characts. 80—80363
Si, laser annealed, charge collection microscopy, carrier lifetime determ. 79—69136
Si, laser annealed, elec. props. 79—69609
Si, laser heating of lightly damaged material, carrier diffusion effect 80—84809
Si, laser measurement, of semiconductor materials and devices *(Rumanian)* 78—52035
Si, laser pulsed annealing, carrier diffusion role in lattice heating 80—45172
Si, lifetime control through impact sound stressing 77—85238
Si, lifetime in Ar^+ ion implant damage gettered, MOS voltage ramping 80—75247
Si MIS solar cells, spectral response and diffusion length 79—92077
Si, MOS diode, dependence of minority carrier bulk generation on HCl concentration 80—88639
Si MOS struct., space-charge generation props. of Au 80—2475
Si, metallurgical grade, purification and charact. 78—56573
Si, minority carrier lifetime and surface recomb. vel. meas. 77—28194
Si, minority carrier lifetime profiles meas. 77—39873
Si minority carrier lifetime degradation effect of $POCl_3$ emitter diffusion 77—76917
Si, minority carrier lifetime and diffusion length meas. contactless nondestructive technique 77—80789
Si, minority carrier lifetime and surface recomb. vel. determ. 77—89771
Si, minority carrier lifetime degradation by $POCl_3$ emitter diffusion 78—2496
Si, minority carrier lifetime and surface recombination velocity meas. by photocurrent 78—10515
Si, minority carrier lifetime meas. by contactless technique 78—23102
Si minority carrier lifetime meas. methods and results *(Hungarian)* 79—56241
Si, minority carrier lifetime, effect of SiO_2 coating deposited by sputtering 80—11003
Si, minority carrier lifetime in neutron doped samples 80—20218
p-Si, minority carrier lifetime, effect of low dose ion implantation *(Japanese)* 80—54715
Si, minority carrier lifetime improvement through laser damage gettering 80—65589
Si, minority-carrier diffusion length and drift mobility determ. using a modulated SEM beam 79—19607
Si multilayer structure dopant distrib. and minority carrier diffusion length, SEM obs. *(Russian)* 78—10543
Si n^+-p diffused diode, optical lifetime meas. in heavily doped diffused regions 77—80829
Si, n^+-p diode, γ-radiation defects, annealing and recomb. props. 80—65045
Si, neutron and electron bombard., radiation defect recomb., photoelec. props. meas. 80—60039
Si, neutron irradiated, resistivity and minority carrier lifetime, radial inhomogeneity *(Russian)* 78—26881
Si, neutron transmutation doping, annealing, deep defect levels 80—20123
Si, nonequilib. carriers generated by Nd laser, relax. rate temp. depend. 78—26911
Si, nonequilibrium carrier density relax., lifetime determ. using light absorption 78—15170
Si, nonideal, lifetime and diffusion length rel. to solar cell appl. 79—15192
Si oxides, grown in Cl-containing ambients, correl. between elec. and material props. 80—39479
Si, p^+-n junction, irrad. with α-particles, defect form 80—24509
Si p^+-n-n^+ back-surface-field solar cells, physics underlying performance 80—85283

carrier lifetime continued
Si p^+n diodes, minority carrier lifetimes, gettering of Cu and Au during Ga diffusion 78—91350
Si p-n diode, 1/f noise calc., free carrier mobility interpretation 80—54774
Si p-n junction, charge carrier recomb. at dislocations, combined SEM and TEM study 80—15105
Si, p-n junction, dopant conc. diffusion length and lifetime variations, SEM obs. 79—82604
Si p-n junction, forward bias capacitance and current meas. for lifetime and band narrowing detn. 79—7892
Si p-n junction diodes and solar cells, minority carrier diffusion length 80—107894
Si, photodiode, shallow junction n^+-p, spectral response limitation mechanisms 78—37058
Si planar structures, Haynes-Shockley expt. for students 78—28888
Si, polycryst., elec. and photovolt. props., grain size effects 80—49800
Si, polycrystalline, grain boundary effects on minority-carrier diffusion length and solar-cell efficiency 79—48124
Si, polycrystalline, large grain size, gross defects effect on effective carrier lifetime 77—80793
Si, polycrystalline films, meas. of effective diffusion length, by surface photovoltage meas. 80—80424
p-Si polycrystalline films on graphite substrates *(French)* 78—64154
Si, proton irradiation, energy depend. of rate of degradation of cond. 77—62944
p-Si radiation defects due to 30 MeV proton irrad., rel. to solar energy convertors 78—71776
Si, rapidly grown RTR sheet, props. and solar cell processing 79—100048
Si recombination characteristics used in design of semicond. devices *(Russian)* 79—42557
Si ribbon crystal evaluation for solar cells 77—76813
Si ribbon solar cell, EFG, diffusion length enhancement under illum. 78—14756
Si ribbon solar cells, var. of minority-carrier diffusion length with light intensity, heavy metal doping effects 80—93937
Si ribbons, capillary action shaping tech., lifetime charact. 78—34847
Si, ribbons produced through capillary action shaping, elec. and struct. characts. 78—47804
Si, shallow p-n junction, energy loss and escape depth of hot electrons 79—78159
Si slice, minority carrier diffusion lengths, surface photovoltage meas. 78—72168
Si solar cell, carrier lifetime meas. from transient photoresponses of pulsed laser *(French)* 79—24898
Si, solar cell, minority carrier lifetime *(Korean)* 78—23103
Si, solar cell, minority carrier excess charge and time const. 78—30938
Si solar cell parameters, grain size dependence 80—94049
Si solar cells, effect of Ti, Cu, and Fe 80—72064
Si solar cells, inhomogeneities and their influence on cell performance 80—93967
Si solar cells, ion-implanted, expt. study of efficiency controlling factor 80—93997
Si solar cells, light-enhanced diffusion length obs. by DC photocurrent meas. 79—39301
Si solar cells, low-cost sheet fabrication structural defects, effect on electronic props. and cell performance 80—50977
Si solar cells, minority carrier lifetimes determ. from spectral and transient meas. 79—100533
Si solar cells, radiation damaged, origin of reverse annealing 80—76630
Si, trichloroethylene and HCl grown oxides compared 77—76988
Si wafer, nondestructive method for meas. of spatial distrib. of minority carrier lifetime 80—13098
Si wafers, Czochralski-grown, lifetime improvement by two-step annealing 80—49916
Si:Ar, ion implant gettering of MOS capacitors using linear voltage ramp and N^+ backscattering 79—95502
Si:Ar^+(Si^+). implantation effect on carrier lifetime, damage obs. by TEM 79—65493
Si:Au Ar ion implant gettering obs. by MOS and Rutherford backscatt. techniques 80—39119
Si:Au p^+-i-n^+ diode, double injection switching, effect of trapped space charge 77—1473
Si:Au p^+-i-n^+ diode, I-V characts., recomb. centre influence 78—19134
Si:B, diffusion length, SEM-EBIC/Schottky diode 79—82605
Si:B, hot-carrier scatt. and recomb. characts. 79—91069
Si:B photodiode front region collection efficiency models 80—96899
Si:B radiation damage and minority carrier lifetime, SEM-EBIC obs. 80—96573
p-Si:B(Al), radiation defect form. and annealing study using Hall effect, cond. and carrier diffusion length 80—84214
Si:B(P), minority carrier diffusion coeffs. 79—99559
Si:Cd n^+-n-n^+ structs., photoresist. props. under exclusion conditions 80—39666
Si:Cd(Zn), n^+-n-n^+ structure, photocond. lifetimes, deep level occupancy in exclusion region 78—72253
Si:Co, diode minority carrier lifetime, Lax method meas., effect of Co diffusion 79—69525
Si:Co, minority carrier lifetime investigation 80—80292
n-Si:Cs, ion implanted, minority carrier lifetime and defect struct., annealing effect 78—6395
Si:Fe(Al), compensated substrates for solar cells, effects of Fe and Al 80—94009
p-Si:Gd, irradiated, elec. props. 79—51613
Si:Gd, radiation defect form., effect of Gd impurities, elec. and optical meas. 78—71764
Si:Gd, radiation defects effect on elec. props. 77—28184
Si:H, amorphous, in p^+-i-n^+ struct., hole diffusion length meas. 80—44712
n-Si:H, amorphous, photoelectromagnetic effect 80—107845
Si:H, amorphous, solar-cells, charge collection and spectral response 80—85275
Si:H, amorphous, surface activated, photoemission spectra, minority carrier diffusion length 80—40235
Si:H amorphous semiconductors, prep. from SiH_4 and characts. 78—48326
p-Si:Li, dislocation free, minority carrier lifetime, effects of heat treatment *(Japanese)* 79—65492
Si:O, annealed, minority carrier lifetime 79—23985
Si:O, carrier recomb. processes, role of vacancy-O complexes 80—65592

carrier lifetime continued
Si:O, heat treated, excess carrier recomb. rate, defect levels 80—75579
Si:P, impurity doped, electron lifetime and transport in upper Hubbard band 79—95452
Si:P solar cell, minority carrier lifetime degradation during ion implanted processing, surface photovoltage 79—39305
Si:P(B) solar cells, minority carrier lifetime mobility rel. to impurity conc. 80—55848
Si:Zn, minority carrier lifetime investigation 80—80292
Si:Zn p-n junction diode, computer-aided study of carrier lifetimes 80—24999
Si-Ge, amorphous, solar cells, tandem multiple gap 80—94029
Si-metal contact, transport theory of Schottky barriers 80—80372
Si-SiO_2 MOS interface, surface-state density and minority carrier generation rate, meas. by DLTS, hot hole effect 80—100527
SiH_x discharge produced amorphous film, gap state role in carrier transport 79—73608
SiO_2, amorphous, defect-controlled carrier transport 79—91049
SiO_2, amorphous charge transport and storage 80—6864
p-Si_2Te_3, photoelectric props., luminesc., hole lifetime and trapping 77—39892
$^{30}Si(n,\beta)^{31}P$ transmutation doping and electrical characterisation 78—10071
SnO_2 chemically sprayed antireflecting films on Si solar cells 79—72639
SnO_2-Si n-n photodiode, 5.4 MeV electron irrad. effects 77—80806
p-Te, photocond. and lifetime, surface trapping, spectral distrib. 78—34840
TiO_2 electrode, carrier density determ. by optical absorpt. and photoelectrolysis spectra 80—71462
TiO_2 electrode, sensitised, for photoelectrolysis of water in sunlight, minority carrier diffusion length 78—19143
$Zn_xCd_{1-x}S$/GaAs heterojunction solar cells, meas. of minority carrier diffusion length 80—26158
ZnO, single crysts., photocond. lifetimes, Zn^+ hole traps 80—75581
p-ZnP_2:S(Se)(Te), photocond., carrier generation and recomb. at high excitation levels *(Russian)* 78—64059
Zn_3P_2, characteristics for photovoltaic appl. 79—7839
Zn_3P_2 thin polycrystalline films for solar photovoltaic cells 80—97797
Zn_3P_2-Al(Mg)(Be), diode, spectra response meas. of minority carrier diffusion length 79—78131
ZnS, photocond. excited with laser radiation near fundamental absorpt. edge 77—76867
ZnSe, minority carriers diffusion length by surface photovoltage method 80—60003

carrier mean free path
see also electron mean free path (metals)
Bloembergen-Rowland approximation, indirect exchange interaction, mean free path effects 80—60238
cadmium arachidate, monolayer, electron mean free path length, XPS obs. 79—74051
dielectric solid, current limitation in injected beam of fast electrons, stationary MFP *(Russian)* 77—4349
electron gas, two dimensional, elec. cond., mean free path *(Russian)* 80—44702
exchange interactions in semiconductors and insulators, mean free path and energy gap effects 80—88522
heterojunction multilayered structs., effective impact ionisation rates 80—88621
indirect exchange in Bloembergen-Rowland approx., ellipsoidal Fermi surface and relax. process effects 80—107754
insulating films, hot electron energy distribs., Monte Carlo study 77—51832
magnetic semiconductor, indirect exchange interaction, mean free path effects 80—97088
MNOS structures, transport processes of electrons 80—34523
poly(p-xylylene), electron MFP as function of kinetic energy, XPS 78—52114
poly-(bisphenol) carbonate, photocond., of double layer polymer systems doped with charge transfer complexes 79—87124
polydiacetylenes, band struct., ab initio cryst. orbital method, and transport props. calc. 78—26811
polyglycine chain, electronic struct. and transport props., ab initio Hartree-Fock crystal orbital calc. 79—42448
polyglycine chain with hydrated side group, electronic struct., transport props. 79—16146
polyvinylcarbazole, photocond., of double layer polymer systems doped with charge transfer complexes 79—87124
semiconductor, carrier distribution function in inhomogeneous regions 79—11146
semiconductor, doped, in model for RKKY interaction between localised mag. momenta 77—66296
semiconductor thin films, degenerate one-valley and many-valley, photogalvanic effect calcs. 80—34487
semiconductor-plasma with two-hole species, parametric instability 80—2410
semiconductors, charge carrier transport operator, soln. for device in cct. 77—39836
semiconductors, hot electron recombination at impurity centres 80—10995
TCNQ complex salts, with pyridinium cations, cond. and structural studies 79—87087
TCNQ salts, (N-methyl pyridine) $(TCNQ)_Z$, struct. and cond., 280 to 340K 79—23955
Teflon, negatively corona charged, new model of isothermal charge transport 80—34536
Ar film, electron MFP, vacuum UV photoemission data 77—28690
Bi, film, evaporated, elect. and elastoresistance props. 79—33367
Bi, film, Hall effect, magnetoresist., resist. and TCR expts. 78—2589
Bi thin film, structure and electronic props. 80—70562
Cd, carrier mean free path, temp. depend. 79—7822
CdTe, electron mean free path, 350-1450 eV 80—103707
CdTe:As^{2+}, photovol. props. of p-n junction prod. by ion implantation 78—43038
GaAs, surface (111), $(\bar{1}\bar{1}\bar{1})$, (110), XPS, photo-Auger ionisation cross section, electron mean free paths 78—56558
$InAs_{1-x}Sb_x$ p-n junctions, avalanche multiplication 80—6965
InP, impact ionisation by electrons and holes 80—100467
Kr film, electron MFP, vacuum UV photoemission data 77—28690
Mo, skin effect, Gantmakher-Kaner effect peculiarities *(Russian)* 80—49796

carrier mean free path continued
NaCl:Ag, diffusion parameters of hot holes created by ionising radiation 78—47800
PbTe films, thermal cond. and elec. props., 4.2 to 300K 79—28162
Si, shallow p-n junction, energy loss and escape depth of hot electrons 79—78159
Si:F,H, amorphous efficient carrier generation for solar photovoltaic energy conversion 80—92906
Si-SiO_2 interface, avalanche injection of charge carriers, oxide current decay 77—43728
TiO_2, rutile, electron mean free path, four-step transition and Auger spectra investig. 80—97389
Xe film, electron MFP, vacuum UV photoemission data 77—28690
$Zn_xCd_{1-x}S/Cu_2S$ heterojunction solar cells, fabrication and performance 79—79397

carrier mobility
see also carrier mean free path; carrier relaxation time; current density; electron-hole recombination; electron mobility (metals)
2,4-hexadiyne-1, 6-diol, bis(p-toluene sulphonate), dark-current meas. 80—15520
alkali halide, dynamics of nonrelaxed and self-trapped holes *(Russian)* 80—80607
alkali halide, hole capture kinetics, influence of autolocalised and zone holes *(Russian)* 80—54714
alkali halides, F-centre trapping of conduction electrons, photocond. study 78—56179
alkali metal-NH_3 solution, Hall effect and cond. at metal-nonmetal transition 78—2530
alkali metal-V_2O_5 bronzes, single cryst., elec. cond., 300 to 900K 77—20369
alkanes, electron mobilities through liq. and critical regions 78—2536
amorphous, high field transport, impact ionisation, carrier mobility 80—80286
amorphous layers, injected charge drift and localisation *(German)* 78—91794
amorphous material, trap-controlled transient current injection 79—23984
amorphous materials, non-Markov carrier diffusion 80—6841
amorphous semicnductors, DC and AC cond., high field effects, magnetoresist., EPR, carrier transport, review *(Japanese)* 77—35943
amorphous semiconductor, charge transport behaviour, model 79—91048
amorphous semiconductor, electronic properties and localised states, review 77—62871
amorphous semiconductor, mobility gap temp. derivative calc., polar contrib. 78—26861
amorphous semiconductor, size and field variation of activation energy for drift mobility 80—49769
amorphous semiconductor, substantially doped, electronic props., review 79—87175
amorphous semiconductors, dispersive charge transport 80—39585
amorphous semiconductors, thermopower, conductivity, statistical shift, doping effects 79—69537
anisotropy determ. by photoelectromag. effect and photocond., method and appl. to HgI_2 79—38126
anthracene:perylene crystal, trapping factors anisotropy 77—59291
anthracene, and deuterate, electron drift mobility temp. depend., transient photocond. obs. 77—66164
anthracene, drift mobility expts., arrival-time detection 79—33308
anthracene, electron and hole generation under electron bombardment 79—73524
anthracene, electron bombardment, field and temp. depend. of carrier yield 77—8117
anthracene, excess electron and excess hole cryst., band struct., drift and Hall mobilities, depend. on press. 79—60709
anthracene, field depend. of photocond. 79—99578
anthracene, hole mobility mechanism interpretation of cyclotron reson. results 78—10438
anthracene, laser-induced photocond., excited charge carriers 77—28211
anthracene, liq. chromatography, sublimation, zone refining, exciton fluoresc., mobility meas., melt grown crystal 79—38736
anthracene, off-diagonal electron mobility and lateral space charge drift 78—72192
anthracene, phonon-assisted mobility due to intermol. vibrs. 78—6383
anthracene, photogeneration of charge carriers through two photon excitation 80—11033
anthracene, temp.-independent mobilities, phonon-induced electron hopping 79—28347
anthracene crystals, carrier trapping in deformed surface region 78—47806
anthracene-PDMA, weak donor-acceptor complexes, electron mobility model 80—15511
anthroquinone, temp. depend. and anisotropy of electron drift mobilities 78—19089
aromatic molecular crystal, electron-intramol. vibr. coupling, rel. to carrier mobility 77—15854
auramine crystal, photocond. and intermol. electron interaction, tight binding approx. 77—15765
auramine single crystal, lifetime and mobility of photogenerated charge carriers 78—2516
azulene, drift mobility expts., arrival-time detection 79—33308
benzophenone, charge carrier generation and mobility 78—84231
biological system, advantage to low electronic mobility 79—39346
biphenyl, electron mobility and photogeneration temp. depend., polaron hopping 78—19033
bipolar conductivity investigs. using ohmic and acoustoelec. currents in Hall effect 77—32027
bipolymer, charge carriers origin and mobility, adsorbed water effects 79—92461
Boltzmann eqns. field depend. collision terms 77—51714
β-carotene, hole mobility meas. by transient photocond., Poole-Frenkel effect 77—11957
cellulose acetate, I_2 doping effect on elec. props. 80—49757
chalcogenide glass, elec. cond. parameters rel. to charge carriers 77 35970
chalcogenide glass film, switching field calc. 78—14775
chalcogenide glasses, field effect, localised states and electronic transport 77—66187
charge carrier with anisotropic energy spectrum, cond. oscills. in quantised mag. field *(Russian)* 80—6886
charge-transfer solid, quasitone dimens., Hall effect and transverse mobility 77—4326

carrier mobility continued
charged particle mobility, elec. field depend., parity and differentiability restrictions in liquids and gases 79—38141
cholesteryl benzoate, elec. drift mobility, 140 to 185°C *(Korean)* 79—65481
coeff. and surface conc. 80—39122
compensated semiconductors, low temp. mobility, unscreened charged impurities effects calcs. 80—75562
Coulomb relaxation of electrons with oriented spins 80—6801
crystal, ionic, X-ray K absorpt. fine struct., relative hole mobility influence *(Russian)* 79—47542
crystalline grain interfaces, distrib. functions, boundary conditions 77—55503
cubic semiconductors, bulk hot-electron props., review 79—99553
$CuPbBiS_3$ aikenite, ferroelec. semicond. electrophysical props. 77—47822
cyclohexane, cation-electron pair distrib. irrad. and elec. field effects 77—81419
cyclohexane, liq. and solid, mobility of excess charge carriers 78—2489
trans-decalin, liq., irrad., positive charge mobility meas. by microwave absorpt. 77—20100
trans-decaline-cyclohexane liq. mixtures, hole mobility, percolation model 80—65551
defect cluster scatt. and removal of carriers, model 78—76069
degenerate semiconductor, amplification of sound by temp. gradient 77—20366
degenerate semiconductor, diffusivity-mobility ratio under mag. quantisation, band non-parabolicity effects 77—20339
degenerate semiconductors, empirical approxs. appl. to generalized Einstein relation 79—23970
degenerate semiconductors, hot electron transport in parabolic energy bands, kinetic theory, transport coeffs. 80—29412
diamond, ion-doped with Li electron transport 80—92917
diamond, natural, electron effective mass and lattice scatt., Monte Carlo anal. 80—44484
diamond, natural, lattice scattering and effective mass of holes 79—60842
diamond, semicond., electron irrad., charge carrier mobility 77—11921
diamond, semicond., energy band struct., elec. and optical props., review 77—35862
diamond detectors, elec. props. and performance for α- and β-particles 79—36481
9,10-dichloroanthracence, monoclinic, photocond. carrier mobility 80—39630
α-9,10-dichloroanthracene, crystal, hole mobility temp. depend. 78—26858
β-9,10 dichloroanthracene, hole mobility anisotropy and cryst. struct., transient photocond. 78—95310
dielectric, carrier-dominated, low-frequency dispersion 79—47380
dielectric charge carrier drift simulation using stochastic graphs 80—15539
dielectric liquid, drift mobility and conduction band energy of excess electrons 77—4348
dielectric liquid, polarity effect on breakdown voltage in inhomogeneous field 77—52018
dielectric liquids, cond. band minima, rel. to electron mobility maxima 78—80029
dielectric liquids, high-field electron transport *(Japanese)* 78—2495
dielectric space charge distrib., carrier mobility and interface injection mechanism identification 80—15974
1,1′-diethyl-2,2′-quinocyanine-[TCNQ]$_2$ anion radical salt single crystals, photovoltaic effect *(Japanese)* 78—2522
disordered semiconductor, hopping mechanism of dispersive transport 80—10971
disordered semiconductor, mobility edge exam. by new perturbation theory 78—47790
disordered system, conductivity and mobility edge, square and diamond lattice calc. 78—43347
disordered system, electron mobility in Gaussian random pot. 77—24543
disordered system, props. of mobility edge 77—4330
disordered systems, elec. cond. and Hall mobility, theory 80—54697
double injection of holes and electrons, semicond. with carrier mobility gradients *(Russian)* 77—35948
drift solutions, discontinuities, hot carriers injection and accumulation 78—51999
durene, photoconductivity, charge carrier mobility 77—47852
durene, transient photocond. and charge carrier mobility anisotropy, temp. depend. 77—80805
edge, mobility, particle in random potential 80—34409
electrode and volume controlled photocurrents 80—6908
electron conductivity in random pot., diffusive mode existence 79—65421
electron in random field in 4-ε dimensional space 78—47756
electron-hole plasma, strongly degenerate, helical density waves 80—15550
EPR line shape, magnetoresist. effect 80—84638
ethyl cellulose films, secondary ion injection 79—24094
ferrite-semiconductor hybrid struct., magnetoelastic wave interaction with drifting carriers 80—54934
ferroelectric and antiferroelectric crystals, perovskite type structure, semiconductor props. *(Polish)* 78—56437
ferromagnetic nondegenerate semiconductor, magnetoresistance 80—11019
ferromagnetic semiconductors, carrier mobility, electron-two magnon scatt. Hall effect 78—51992
film, vacuum-deposited, struct. and props., basic relationship 78—6236
films, elec. and galvanomag. props., microstruct. 80—70859
fluid, conf., Banff, Alberta, Canada, (5-11 Sept. 1976) 77—89680
fluid, effect of disorder on electron mobility and localisation 77—89682
fluorene, hole mobility temp. depend., transit time meas. *(German)* 77—66169
fluorenone derivatives as electron transport materials, electron affinity and electrochemistry, rel. to photocond. 79—38127
free and trap modulated mobility transition 79—82598
n-Ge, noise and hot carrier diffusion in mag. fields 79—11193
glass, electron migration and spectral relax., random-walk model 80—80280
graphite, artificial, electrophys. props. 77—51745
graphite, carrier mobility, temp. depend. determ. from magnetoresist. expts. 80—11009
graphite, electron-phonon interactions, rel. to elec. transport 80—34156
graphite, galvanomag. props., temp. depend. between 4.2 and 298K 77—32024

carrier mobility continued
graphite, pyrolytic, galvanomag. effects, effect of fast neutron irradiation 80—34465
graphite, resistivity and magnetoresistance, 4.2 to 293K 80—100459
graphite, thermoelec. and thermomag. props., cylindrical band model 80—39616
graphite intercalation cpds. with K, Rb, or Cs, phase transitions, resistive anomalies, electronic props. 79—95405
Hall effect, 1/f noise, mobility fluctuations 80—92950
Hall effect noise, explained as carrier mobility fluctuations 77—62949
Hall mobility, microwave meas. method 79—54154
Hall mobility measurement in specimens in strong pulsed elec. fields 79—35779
heavily doped semiconductor, with Gaussian band tails, modification of Einstein relation 80—80270
heterogeneous material, scatt. theory, effective medium approx. 78—56116
hexafluorobenzene liq., electron mobility, percolation model 80—65551
hexafluorobenzene-benzene liq. mixture, electron mobility, percolation model 80—65551
n-hexane-ethanol liq. mixtures, electron mobility, percolation model 80—65551
hexatriacontane, single crystal, elec. props. *(Japanese)* 79—51592
hexatriacontane single cryst., elec. cond. and dielec. breakdown 80—6849
high-resistivity semiconductors, theory and expt. *(Japanese)* 80—6850
higher polymer films, steady Gunn type oscillations, origins *(French)* 79—28351
homojunction solar cells, superposition principle 80—81449
hopping transport kinetic theory, localised state separation, Pauli master eqn. 80—80276
hot electron semiconductor, capture of charge carriers rel. to I-V curves, phonon heating 79—51589
hydrocarbon, long chain single cryst., carrier transport meas. 80—6874
hydrocarbon liq., effect of mol. struct., temp. and elec. field on electron mobility 78—2535
hydrocarbon liquid, model for thermalisation of quasifree electrons rel. to electron mobility 77—40316
ice film, low-temp. diffusion of electrons, evidence for polaron bands 77—1380
IGFET, velocity-field curves for surface-free carrier in Si 80—60095
II-IV p-n amorphous heterojunction, phenomenological model 80—54769
III-V compounds, n-type, new meas. method for compensation and spatial fluctuations of impurities 78—6404
III-V mixed semiconductor, electron mobility theory 78—84210
III-V semiconductor, anisotropic carrier mobility due to dislocations 78—60124
III-V semiconductor, disorder scatt. 78—47780
III-V semiconductor, low temperature, high mobility transistor materials 78—87970
III-V semiconductors, transport phenomena, review 79—19587
inert gas, liquid, Ramsauer-Townsend minimum in electron scatt. cross section 77—89821
inert gases, liq., model for thermalisation of quasifree electrons rel. to electron mobility 77—40316
inflowing structure, Anderson localisation, elec. cond. temp. depend. *(Russian)* 80—103639
inhomogeneous semiconductor, nonequilibrium carrier mobility 77—15879
inhomogeneous strain field scatt. deform. potential, theory 77—35905
p-InSb:Ge, single cryst. field dependence of Hall effect, cond. and carrier mobility *(Bulgarian)* 78—34848
n-InSb, Hall mobility of free electrons, determ. using radioelectric effect 77—69327
insulator-metal transition, electron-phonon interaction, electronic transport props. 77—89702
inversion layer in quantising mag. field, Einstein relation 78—19156
ion pair, in irrad. medium, transport, transient elec. field effects 77—81419
ionised impurity scatt. limited mobility in semiconductors with spatially variable dielec. function 78—51986
isotropic semiconductor, differential relax. times and diffusivities of hot carriers 77—62936
Kapton, pyrolysed, cond. polymer, transport and mag. props. 80—96887
lattice scattering mechanism in quantised inversion layers 79—78187
layer semiconductor system, theory of Hall effect 79—69589
linearised transport equations, explicit solns. 78—43375
liquid crystal, smectic, anisotropy of carrier mobility and electro-optical effects *(Japanese)* 77—43605
liquid dielec., ionic-cond. and -dissociation under low elec. field 77—8089
liquid dielectrics, electrical conductivity and breakdown, liquid impurity effects 80—11340
localization aspect of electron phonon-coulomb system 79—7793
magnetic semiconductors, electron propag., s-d model, red shift theory 77—51736
magnetoresistance four-probe method for free carrier density and mobility meas. 77—43626
many valley semiconductor, intervalley transfer of population by ambipolar diffusion 79—11128
MBBA, nematic, transient elec. current obs. 77—20324
MBBA, nematic liq. cryst., charge carrier drift mobility 78—87801
measurement, contactless measurement of sheet conductivity and mobility of semiconductor wafer by using eddy current 80—62693
measurement of Hall mobility, automatic *(Polish)* 77—41638
metal-semiconductor junction layer charge migration with localised state participation *(Russian)* 80—49913
methane, liquid, compressed, excess electron mobility, density depend. 77—11924
methane, liquid, Ramsauer-Townsend minimum in electron scatt. cross section 77—89821
minority carrier conc. determ., integral eqn. approach to abrupt depletion approx. 77—32022
minority carrier exclusion 79—42561
MIS inversion channel hole mobility rel. to field treatment in active media 78—91774
MIS structure, charge-transfer, surface mobility and Hall mobility determ. 78—23175
MIS transistor's inversion channel *(German)* 80—6996
MNOS structure, model for degradation mechanisms 80—29477
molecular crystal, charge carrier mobility temp. depend. 78—10376
molecular crystal, mixing between Frenkel excitons, and charge transfer states, effect on charge carrier transfer 77—89707

carrier mobility continued
  molecular crystals, electronic transport theory, local linear electron phonon coupling 80—65545
  molecular crystals, exciton-phonon coupling and exciton transport 80—84430
  Monte Carlo simulation 79—33274
  MOS, many-body effects in n-Si inversion layers, excitation to higher subbands 77—62997
  MOS inverted-channel carrier scatt., effect of oxidation in Cl media 78—76156
  MOS structures, hot electron transport, expt. review 78—30994
  MOS structures, total dose effects on carrier conc. and mobility 77—20443
  MOS structures with superthin gate dielectric, hole mobility in inversion layers 80—29482
  MOST struct., gamma irrad., interface states and carrier mobility 79—73593
  MOST structure, determ. of hole mobility in Si 77—66204
  n-type semiconductor with grain-boundary barriers, elec. cond. 77—55523
  naphthalene, charge carrier drift mobility, semi empirical anal. 80—65553
  naphthalene, electron and hole off-diagonal mobility component determ. 80—65552
  naphthalene, electron band hopping transition 78—39155
  naphthalene, hole mobility, anomalous current transients 78—76091
  naphthalene, pure and deuterated, band-hopping mobility transition 80—6833
  naphthalene, temp.-independent mobilities, phonon-induced electron hopping 79—28347
  narrow band-gap semiconductor, energy depend. relax. time, EM response of electrons 78—60142
  narrow gap semiconductor, modification of Einstein relation for inversion layers in strong elec. field 80—96959
  negative electron diffusivity in high fields 78—30935
  nematic liquid crystal, elect. conduct. based on injection-contact phenomena theory *(Russian)* 80—107807
  neopentane:n-butane, electron mobility and electron-ion recombination rate const. 79—73557
  NLC, effective ion mass and mobility calcs. *(Russian)* 80—79694
  nonhomogeneous semiconductor, galvanomagnetic effects 79—91077
  nylon (N12), uniaxially oriented, anisotropy of elec. cond. 79—87095
  one-dimensional disordered system, analytical expression for mobility edges 79—51487
  one-dimensional phenomenological transport equation set 78—39102
  one-dimensional semiconducting polymer, demonstration of high mobility 80—20212
  Onsager model, time-depend. quantum efficiency 79—11194
  organic liquid mixtures, percolation model of electron and hole mobility 80—29452
  organic molecular crystal, electron mobility, temp. independent, theory 79—69509
  organic molecular crystal, temp.-independ. mobilities, elec. field and defect scatt. effects 80—10963
  organic molecular crystals, anomalous elec. field depend. of temp. independ. electron mobilities 79—42548
  organic semiconductor films, Schrieffer effect 80—60118
  organic semiconductor layers, injected charge drift and localisation *(German)* 78—91794
  oxide glass, elec. cond. parameters rel. to charge carriers 77—35970
  p$^+$-i-n$^+$ double-injection struct., regional approx. 78—14805
  p$^+$-n-n$^+$ heterostructure, variable gap base, carrier injection, quasielectric field, transient process anal. 80—44716
  p-n heterojunctions, nonequilib. carrier behaviour at high current density 80—6968
  p-n junction, impedance determ. from direct currents *(Russian)* 78—84285
  p-n junction, majority carrier flow model, diffusion effects in equilib. field distrib. 77—51808
  p-n junction injection characteristics in strong elec. fields 77—76913
  paraffin, liq., electron mobility, mol. struct. depend. 77—4350
  pentacene layers, photogeneration, charge carrier transport *(Russian)* 78—56181
  phenazine, charge carrier transport rel. to cryst. and band struct. 79—95403
  phenothiazine derivatives, semicond. elec. props., optical spectra, and EPR 80—103693
  photoconductor, drift mobility meas., arrival time detection using interdigital electrode 77—11954
  photoconductors, noise theory and measurements for modelling electronic processes and transport phenomena 79—56264
  photovoltage for doping factor, mobility ratio and excess conc. determ. extreme band bendings 78—91726
  phthalocyanine thin layers, metal-free, mobility and thermally stimulated polarisation meas. 79—73527
  piezoelectric and deform. pot. scatt. of free carriers, due to screw dislocations 77—1416
  piezoelectric semiconductor SAW convolver, effect of transverse drift of carriers on operation, theory and expt. 80—14529
  piezosemiconductors, second harmonics of acoustoelectric current 80—80329
  planar diode, heavily doped, collection efficiency and surface recomb. vel. modulation 80—20291
  Poisson's equation, linear and nonlinear numerical solution including spatially variable dielectric const. 80—6825
  polar semiconductor, HF mobility in longitudinal quantising mag. field 79—51619
  polar semiconductor, surface inversion layers, energy loss of warm and hot carriers 77—11981
  polar semiconductors, peak electron velocity, simple method for estimation 77—8129
  poly(γ-methyl L-glutamate), electric conduction mechanism *(Japanese)* 80—54696
  poly(N-vinylcarbazone), charge transport and struct., bromination effect 78—11516
  poly(p-phenylene), AsF$_5$ doped, highly cond. charge transfer complexes, elec. and optical props. 80—70778
  poly-γ-methly-L-glutamate, uniaxially oriented, anisotropy of elec. cond. 79—87095
  poly-n-epoxypropilcarbazole electrophotographic layers, photogeneration and drift mobility 79—19631

carrier mobility continued
  poly-N-epoxypropylcarbazole layers, optical and photoelec. props 77—39896
  poly-N-vinyl carbazole, and Br-substituted derivative, transient hole hopping transport, 150-500K 78—39108
  poly-N-vinyl carbazole, hole hopping mobility, transit pulse dispersion 80—65565
  poly-N-vinylcarbazole, electrophotographic film, dark discharge 78—34864
  poly-N-vinylcarbazole films, drift mobility of photocarriers, polymerisation method influence 77—76986
  poly-N-vinylcarbazole thin amorphous film, hole drift mobility, mol. mass. depend. 80—75663
  poly-N-vinylcarbazole-polycarbonate mixture, hole drift mobility and photosensitivity 77—85260
  polyacene quinone radical polymers, two-dimens. variable range hopping 79—51608
  polyacetylene:AsF$_5$, Hall effect meas. 80—24955
  polyacetylene, doped, elec. cond. and thermopower 80—96951
  polycrystalline layer, carrier conc. and effective Hall mobility 77—4375
  polycrystalline semiconductor thin film, effective mobility and concentration 77—28264
  polydiacetylene bis-(toluenesulphonate), single cryst., charge carrier mobility and recomb. 77—8132
  polydiacetylene-bis(toluenesulphonate), transient photocond. meas. 78—30951
  polydiacetylenes, band struct., ab initio cryst. orbital method, and transport props. calc. 78—26811
  polydiacetylenes, photocond. action spectrum of single crysts., charge transport obs. 80—15557
  polydimethylsiloxane liquid film, non-pure, dielec. behaviour 80—29672
  polyethylene:Br$_2$(I$_2$), films, electron-beam induced carrier mobility and elec. breakdown 80—80429
  polyethylene, γ-irradiated, effect of elec. field on TSC 79—65790
  polyethylene, carrier mobility determ. by current oscillation method 79—28344
  polyethylene, corona charged, direct drift mobility meas. 78—10837
  polyethylene, elec. cond. of high and low density samples, oxidation effects 80—107784
  polyethylene, halogen-doped, carrier transport and breakdown characteristics *(Japanese)* 80—96889
  polyethylene, high density, carrier transport 79—33288
  polyethylene, oxidised, charge carrier, transport phenomena 80—15515
  polyethylene, space-charge storage under high DC voltage condition, TSC meas. *(German)* 80—75576
  polyethylene film, high density, anomalous transient currents around 50-70°C 79—33368
  polyethylene film, surface pot. decay, drift mobility determ. 77—11979
  polyethylene films, electron beam irrad., carrier mobilities 79—1600
  polyethylene terephthalate films, current peaks obs. with linearly increasing voltage 80—88654
  polyethylene terephthalate thin films, electronic mobility 80—15634
  polyglycine chain, electronic struct. and transport props., ab initio Hartree-Fock crystal orbital calc. 79—42448
  polyglycine chain with hydrated side group, electronic struct., transport props. 79—16146
  polymer, molecularly doped, carrier drift, percolation approach 80—2390
  polymer film, carrier transport meas. 80—6874
  polymer film electret, charge distrib., generalized model 80—6873
  polymeric capacitors, injection charging 77—76902
  polypropylene, electron bombarded electret, trapped charges ESR study 80—7170
  polystyrene:Br$_2$(I$_2$), films, electron-beam induced carrier mobility and elec. breakdown 80—80429
  polystyrene, atactic, bulk and surface elec. props., contact charging obs., dielec. const. 80—15615
  polystyrene, electron-beam-induced conduction 80—2397
  polystyrene, halogen-doped, carrier transport and breakdown characteristics *(Japanese)* 80—96889
  polystyrene atactic carrier transport and photogeneration 80—80318
  polystyrene thin films, TSC and surface charge meas. 80—103769
  polyvinylcarbazole, amorphous, hopping transport, reinterpretation of mobility meas. 79—42563
  polyvinylcarbazole, Coloumb trap controlled hopping mobility model tests, mobility and permittivity meas. 79—56226
  polyvinylcarbazole, fast hole transport 79—51628
  polyvinylcarbazole, photocond., of double layer polymer systems doped with charge transfer complexes 79—87124
  polyvinylcarbazole xerographic film, discharge kinetics 77—13810
  polyvinylidene fluoride, dielectric relax. mechanism 80—55023
  polyvinylidene fluoride drift mobility meas., I$_2$ charge transfer from surface charge decay technique 80—49744
  powder combinations, compressed, mixing ruler concerning Hall effect and Hall mobility *(German)* 78—84234
  prep. by electron beam evaporation, and optical and elec. props. 80—20793
  protein-methylglyoxal complex, electronic props., energy band cond. 79—24936
  proton semiconductors, with H-bonds, quantum theory of proton cond. 80—65641
  pyrazoline-based carrier transport layers use in layered photocond. systems for electrophotography 77—69375
  pyrene-TCNE, vapour-grown cryst., transit-time meas. of photocarriers 78—39149
  pyrocarbon, Hall effect and conductivity of specimens deposited at 2000 and 2200°C 78—23112
  quantum resonance impedance oscillations *(Russian)* 78—91781
  quasi-two dimensional conductor, galvanomagnetic props., optical analogy *(Russian)* 80—60108
  quasilocal acceptor states, effects on band gap and electron mobility *(Russian)* 78—60082
  p-quaterphenyl oriented layers, charge carrier transport, hopping model 80—2506
  p-quaterphenyl oriented layers, field depend. mobility 79—91169
  quinolinium (TCNQ)$_2$, charge transport, proton spin-lattice relaxation 80—88545
  rare earth chalcobismuthites, RBiTe$_3$, prep., elec. props., and crystallographic date 80—59981
  recombination kinetics controlled simultaneously by diffusion and tunnel effect, transient case 77—8120

carrier mobility continued
  relaxation process in quantising mag. field, elastic scatt. mechanisms, relax. matrix 79—15166
  relaxation semiconductor, theory of carrier transport in p^+-ν junction 79—60914
  rubrene, orthorhombic cryst. photogenerated carriers, transit time meas. 80—49811
  sapphire, Czochralski-grown, excess charge carriers, generation, transport and trapping 79—82646
  Schottky barrier solar cell, doping density effect on efficiency 80—101100
  SCL current charge distribution discharge, with shorted and open electrodes 80—6863
  self-oscillatory semiconductor medium, coupled temp. and carrier density self-oscills., photoelectron heating, microwave field 79—11166
  semiconductor, 1/f noise origin 80—11060
  semiconductor, ambipolar diffusion, electron-hole scatt. effect 80—59976
  semiconductor, amorphous or disordered, cond. mechanisms, model of medium-range comp. disorder 78—79994
  semiconductor, anisotropic conductivity and ambipolar drift noise 77—20375
  semiconductor, carrier scatt. and mobility transient processes, pulsed Hall photoeffect 80—15546
  semiconductor, carrier scattering by impurity potentials with spatially variable dielec. functions 79—69507
  semiconductor, carrier transport, in presence of temp. gradient, flux method 78—72144
  semiconductor, containing screw dislocations, impurity centres 78—72111
  semiconductor, damage by 10.6 μm CW CO_2 laser beam 77—63497
  semiconductor, defect interactions, radiation physics *(Russian)* 79—46702
  semiconductor, diffusivity of charge carriers, in strong elec. fields 77—35950
  semiconductor, displaced Maxwellian distribution function and warm electrons problem 78—26864
  semiconductor, dopant, transverse inhomogeneity, effect on ambipolar drift and field effect 80—6834
  semiconductor, drift mobility determ. from photoresistor noise meas. 77—4414
  semiconductor, drift mobility temp. depend. in presence of trap-recombination centres *(Russian)* 78—26880
  semiconductor, effect of overlap function on electron mobility in quantising mag. field 78—43374
  semiconductor, Einstein relation for degenerate carrier concentrations 78—72143
  semiconductor, elec. cond., hopping model, semi-classical, effective mass and carrier mobility calc. 80—96872
  semiconductor, electro-optic effects anisotropy and hot electron cond., free carrier-impurity scatt. 77—4626
  semiconductor, electron distribution function, temp. gradient effect 78—72145
  semiconductor, electron drift vel. and phonon multiplication 80—6848
  semiconductor, electron quantum states, nonequilibrium current fluctuations in quantised mag. fields *(Russian)* 80—107704
  semiconductor, electron transport phenomena, high-field transport and quantum transport in strong mag. fields *(Japanese)* 77—55526
  semiconductor, electron-hole plasma drift due to carrier mobility gradients 78—26896
  semiconductor, electron-hole plasma in crossed fields, renormalised diffusion coeffs. 79—87123
  semiconductor, exact calc. of mobility due to point defect scatt. 78—19029
  semiconductor, gapless, current-voltage charact. in longit. quantizing mag. fields 77—55524
  semiconductor, Hall current method generalisation to arbitrary magnitude mag. fields *(Russian)* 80—29421
  semiconductor, highly doped, flicker noise in terms of number fluctuation model, surface effects 79—60882
  semiconductor, hot electron fluctuations with displaced Maxwellian distrib. 80—29418
  semiconductor, hot electron mobility in mag. field 77—4368
  semiconductor, inhomogeneous, anomalous elec. props. in mag. field 80—44621
  semiconductor, inhomogeneous, theory of residual cond. 78—14739
  semiconductor, inhomogeneous elec. fields in oscillatory photocond. 80—2421
  semiconductor, intrinsic and injected electron-hole plasmas, one-dimensional drift and diffusion of carriers 79—11163
  semiconductor, inversion layer, Einstein relation, modification 77—12015
  semiconductor, ionised impurity scattering, theory 80—20181
  semiconductor, irradiated, Hall mobility, dark and photo-conductivity calc. 78—47835
  semiconductor, kinetics of photoinjection currents 78—47834
  semiconductor, microwave magnetoconductivity in large quantising mag. field, effect of band non-parabolicity 79—47112
  semiconductor, models for transport and accumulation 78—87975
  semiconductor, near intrinsic magnetoresist. effect determ. of carrier density and mobility 78—2501
  semiconductor, nonequilibrium carriers, diffusion in alternating elec. field 79—11133
  semiconductor, nonlinear conductivity, vortex waves, carrier mobility and lifetime 80—96893
  semiconductor, one-dimensional with deep levels 77—4356
  semiconductor, optical generation of carriers under Franz-Keldysh effect conditions, instability 79—24017
  semiconductor, partly disordered, with mobility threshold, transport props. and thermoelec. parameters 80—34449
  semiconductor, polar, mobility in mag. field, extreme quantum limit, iterative technique 78—2498
  semiconductor, transient and alternating currents, influence of deep traps 79—73525
  semiconductor, two-band system, acoustic scatt., appl. to hole transport props. 79—60823
  semiconductor, two-valley, carrier vel.-field characts. under high elec. field 80—70713
  semiconductor, unipolar, n-type, field-effect mobility, energy spectrum of surface states 80—39657
  semiconductor, variable-gap, with high band-gap gradient, characts. of radiative recomb., carrier drift lengths determ. 79—56858
  semiconductor alloy, disorder scatt., Green's function calc. 77—11906

carrier mobility continued
  semiconductor carrier scattering by ionized impurity potentials incorporating spatially variable dielectric functions 79—42535
  semiconductor device characterisation using electron beam induced current technique, review 78—21302
  semiconductor devices, theoretical foundations 77—39835
  semiconductor diodes, minority and majority mobilities, transit time effect determ. 78—14753
  semiconductor diodes in radiophysical devices, minority carrier charge-accumulation effect *(Russian)* 79—73569
  semiconductor electron-hole-plasma, instability in heating elec. field 80—15552
  semiconductor epitaxial layers, fast characterisation by MESFET 79—87170
  semiconductor epitaxial layers, varizonal, parameter determ. by photoluminescence method *(Russian)* 80—108291
  semiconductor film, carrier mobilities and doping conc., Hall meas. in MISIM struct. 77—76975
  semiconductor film, electric-field-induced anisotropy, differential carrier mobility tensor derivation 77—39973
  semiconductor film, polycryst., Hall and drift mobilities 79—95531
  semiconductor film, spin relaxation due to electric fields 77—62928
  semiconductor film, trap-limited model for dispersive transport 78—6378
  semiconductor heating, thermal domain investigation, current voltage characts. 80—70711
  semiconductor junction lasers, transport phenomena, junction effects and devices, book 80—98766
  semiconductor junctions, sublinear current-voltage characts., field-opposed diffusion of free carriers 78—47862
  semiconductor layers, measurement technique using a long gate MOSFET structure 79—47178
  semiconductor non-equilibrium periodic stratification by diffusion 77—55544
  semiconductor nonhomogeneous, dimens. localisation of electrons *(Russian)* 78—19000
  semiconductor or insulator, theory for flow of Hall current in sample of arbitrary shape 79—73532
  semiconductor resistivity and Hall effect meas., nondestructive four-electrode characterization 80—49743
  semiconductor solid solutions, influence of lattice disorder on elec. props. 77—8100
  semiconductor thin film, carrier redistribution in strong crossed elec. and mag. fields *(Russian)* 77—72927
  semiconductor thin films, degenerate one-valley and many-valley, photogalvanic effect calcs. 80—34487
  semiconductor thin films, fabrication for device appls. 80—100418
  semiconductor wafer, influence of discontinuous resist. distrib. on results of four-point probe method meas. 77—39841
  semiconductor with disordered regions, carrier mobility, theory and expt. 78—56166
  semiconductor with position depend. band struct., electron and hole currents 78—43377
  semiconductor with position depend. composition, carrier generation, recomb., trapping and transport 77—43613
  semiconductor with two types of hot carriers, under overheating instability conditions, current-voltage characts. 77—62943
  semiconductor-ferrite composite struct., bulk magnetostatic wave instability, theory 77—12186
  semiconductors, anisotropic, voltage fluctuations associated with carrier drift 79—51644
  semiconductors, carrier mobility-meas. technique on inverted surfaces near cond. threshold, appl. to Si 79—69602
  semiconductors, charge carrier transport operator, soln. for device in cct. 77—39836
  semiconductors, charged-impurity scatt. formulae, third-body interference 77—55520
  semiconductors, disordered, carrier mobility and transient pulse dispersion for hopping mechanisms 80—44586
  semiconductors, drift mobility and Hall factor, nonpolar optical scatt. mechanism 79—51579
  semiconductors, drift velocity relation to low-field mobility and high-field saturation velocity 80—75563
  semiconductors, elec. props., mag. field effect determ., method 80—44623
  semiconductors, electron scattering by deep level impurities 80—10968
  semiconductors, electron-phonon interactions, combined phonon resonance *(Russian)* 80—75321
  semiconductors, exciton-impurity state with low binding energy 80—103646
  semiconductors, free-carrier mobility associated with dislocation strain fields 77—51738
  semiconductors, heterogeneous, anisotropic, Hall coeffs., Hall mobility, carrier density *(Russian)* 80—70734
  semiconductors, hot electron maximum mobility in longitudinal quantising mag. fields 79—69519
  semiconductors, impurity electron scatt., resonance scatt., Hall and drift mobility 80—65487
  semiconductors, intravalley carrier transfer, transverse photo-EMF for various absorpt. coeffs. 79—69551
  semiconductors, light induced electron drift, two-photon transitions *(Russian)* 80—107853
  semiconductors, mobility-fluctuation description of 1/f noise 80—84496
  semiconductors, n-type, metal-insulator transition and negative resist. effects 79—24026
  semiconductors, nondegenerate, flicker noise, mobility fluctuation possibility 79—91108
  semiconductors, photomagnetoelectric effect, expt. parameters rel. to material props. 79—99584
  semiconductors, polycrystalline, electrical conductivity theories *(Czech)* 79—42537
  semiconductors, polycrystalline, phenomenological theory of Hall effect 79—11160
  semiconductors, pure, carrier mobility and electron state damping at low temps. *(Russian)* 80—15530
  semiconductors, quasi elastic hot electron impurity scatt. in quantising mag. field 80—24938
  semiconductors, relaxation regime, generalised transport eqns. 78—56139
  semiconductors, spatially variable dielectric functions, ionized impurity limited mobility 79—42534
  semiconductors, temp. depend. electronic cond. 80—59975
  semiconductors, variable gap, carrier transport and fluctuation effects due to changes in gap width 80—107793

carrier mobility continued
- semiconductors with impurities, electron cond. temp. and freq. depend., two band model *(Russian)* 80—75564
- semimetal, degenerate, anisotropic scattering at low temp. *(Russian)* 78—95298
- ρ-Si, deionisation effect on hole mobility evaluation 77—35945
- n-SiC, 6H and 15R polytypes, (0001) plane, influence of uniaxial mechanical stress on resist. anomaly 78—10445
- silicone oil, ionic behaviour, carrier mobility and viscosity 80—107453
- SIS system, mutual drag of carriers 78—6430
- size-quantising film pulsed inversion of adsorbed molecules 79—90889
- solar cell, diffusion equation, surface boundary condition 80—66975
- solar cell, low resistivity, rel. to open cct. voltage improvement 80—93910
- solar cells, $Cu_{2-x}S$-CdS, collection coefficient theoretical anal. at conjunction 80—101094
- solar cells, metal-semiconductors contacts, collection vel. of excess minority carriers 77—15954
- solid-state diode, carrier mobility, carrier density depend., scaling law 77—8179
- solid-state electronics, introductory theory, book 80—22160
- SOS, cryst. perfection rel. to MOS transistor mobility 78—75956
- SOS film, electron mobility 78—91792
- SOS films, surface recomb. profile and transport parameters 79—33357
- SOS MOS devices, elec. characts., cryst. defects and residual stress effects 78—34906
- SOS MOS devices, hole mobility under residual stress, Hall meas., valence band struct. 78—88039
- spatially inhomogeneous magnetic field effect on semiconductor carriers 80—92916
- sputtered films, optical props. and appls. 78—72623
- stilbene, single cryst., free charges and excitons generated by electron pulses 78—63988
- stilbene, single cryst. under pulsed electron excitation, spectral and elec. characts. 79—7838
- strongly degenerate plasma, double injection, vol. controlled current regime 79—51658
- surface CCDs, electron mobility surface diffuse scatt. model 78—47879
- TCNB complexes, hole mobility, photocurrent meas., 260-300K 78—60161
- TCNE, hole drift mobility, temp. depend. and anisotropy, photocond. meas. 80—80314
- TCNQ, electron mobilities from 210 to 350K using transverse photocond. meas. 79—19618
- TCNQ complex salts, with pyridinium cations, cond. and structural studies 79—87087
- TCNQ complexes with N-methyl derivatives of pyridine, cond. and thermoelec. power meas., band model anal. 80—10952
- TCNQ salt, (N-methylphenazinium)$_x$(phenazine)$_{1-x}$, 1 band filling, carrier mogility and disorder effects 80—24904
- TCNQ salt, (NMP)$_x$(Phen)$_{1-x}$(TCNQ), band filling and disorder 78—87968
- TCNQ salt, HMTSeF-TCNQ, Hall effect, temp. and press. depend. 77—35929
- TCNQ salts, (N-methyl pyridine) (TCNQ)$_Z$, struct. and cond., 280 to 340K 79—23955
- TCNQ salts, Qn(TCNQ)$_2$ impurity effects on electronic coherence length 79—73500
- Teflon, TSC, trap modulated electron and hole mobilities 78—10441
- Teflon FEP, N implanted, TSC spectra 80—88912
- Teflon film, TSC studies of carrier trapping and mobility 80—7016
- Teflon films, hole transit, trap modulated mobility and dispersive hopping discussion 79—69616
- ternary alloy semiconductors, disorder effects on electronic props. *(Japanese)* 80—49709
- p-terphenyl, carrier generation and transport, temp. depend. around phase transition at 180K 78—47783
- p-terphenyl, hopping cond. among localised states 80—70861
- p-terphenyl film, polycryst., charge carrier transport and DC cond. 80—70858
- tetracene, cryst., hole drift mobility, photoexcitation 77—1444
- tetracene, hopping cond. among localised states 80—70861
- tetracene, layers, photogeneration, charge carrier transport *(Russian)* 78—56181
- tetracene, polycrystalline, charge carrier drift mobility 78—34835
- tetracene, polycrystalline layer, carrier mobility and AC cond. 79—65569
- tetramethylsilane, liq., electron drift vel. saturation, skeletal vibr. 80—34451
- tetramethylsilane, liq., electron mobility up to crit. point 77—76809
- thermal conductivity, electronic contribution, mobility threshold effects 80—65570
- thermopiezosemiconductor critical drift velocity for US amplification 78—60169
- transient current injection, trap-controlled 77—24565
- transition metal oxides, 3d-, microwave cond. at high temp. *(Japanese)* 78—91715
- trinitrofluorenone, amorphous, hopping transport, reinterpretation of mobility meas. 79—42563
- triphenylamine-bisphenol-A-polycarbonate solid soln., pot. discharge technique for hole transport meas. 78—43438
- TSC technique, trap modulated electron and hole mobility meas. in insulators 78—10441
- TTF-TNCQ, mobility due to mol. optical phonon scatt. 77—85202
- TTT film, Schrieffer effect 80—60118
- two-dimensional electron-impurity system, theory 78—43457
- very pure semiconductor, mobility calcs. including low impurity conc. limit 77—28173
- violanthrene-A film, amorphous and crystalline, carrier mobility differences 78—60125
- wave hierarchy interpretation of multiple trapping model 80—6894
- Si:P, sheet resistance of Gaussian n-type ion-implanted layers 79—87103
- AgBr, photoexcited electrons and holes in latest image form., review 80—73496
- AgBr(I) microcrystals, photohole motion 78—26903
- AgCNS, mixed conductor, elec. cond. props. 80—65639
- β-AgI, drift mobility of holes 77—47814
- AgI, growth, elec. and optical props. 79—77805
- β-AgI:Cu, pure and doped, photoconductivity, band struct., trap nature 79—95449
- $AgInS_2$, and $AgIn_5S_8$, spray pyrolysis, film struct., elec. and optical props. 80—71592

carrier mobility continued
- $AgIn_5S_8$, cryst. growth and props. 78—39677
- AgN_3, high-resist. explosive cpd., elec. and galvanomag. props., temp. depend. 80—103728
- Ag_2S(Se)(Te), changes in elec. cond. and thermoelec. power at melting point 79—15147
- Ag_2Se, electronic and electrogalvanic props. in α-phase region *(French)* 80—107820
- Ag_8SnSe_6, cryst., Hall effect investigation of polymorphic transform. 80—39605
- p-Ag_2Te, electrophysical props. 77—39842
- Ag_2Te, low temp. thermal cond., thermoEMF 78—43423
- p- (AlGa)As:Zn, MBE grown, elec. props., shallow junction solar cell use 79—91175
- AlGaAs-GaAs DH laser, carrier leakage, physical mechanisms 78—66824
- $Al_xGa_{1-x}As$, compensated, electron mobility temp. depend. 80—96868
- n-$Al_xGa_{1-x}As$, electrical props. 78—6381
- $Al_xGa_{1-x}As$, electron mobility illumination, compensation, space charge regions, carrier scatt. 80—70691
- p-$Al_xGa_{1-x}As$ film, variable-gap photo-EMF 80—65626
- $Al_xGa_{1-x}As$, VPE and LPE growth, electron mobility 79—91165
- $Al_xGa_{1-x}As$, VPE growth and characterisation 78—35315
- n-$Al_xGa_{1-x}As$, variable-gap solid solns., diffusion length, photolum. meas. 79—38659
- p-$Al_xGa_{1-x}As$:Ge layer on GaAs substrate, Hall and elec. cond. meas., Hall mobility 80—2402
- $Al_xGa_{1-x}As$:Mg doping characteristics, elec. props., effective hole masses 79—78117
- $Al_xGa_{1-x}As$:Te, epitaxial film, elec. cond. and Hall coeff. rel. to donor levels 77—24630
- $Al_xGa_{1-x}N$ epitaxial layers, growth and props. 79—11522
- α-Al_2O_3, energy levels of donor and acceptor dopants and electron and hole mobilities 80—59911
- Al_2O_3 polycrystalline, effects of space charge, grain-boundary segregation and mobility differences on conductivity 80—79979
- AlSb as high-energy photon detector 77—75026
- Ar, condensed, electron drift, Davydov electron energy distribution function, diffusion *(Russian)* 80—80339
- As, thermopower and thermal cond. from 8K down to 0.3K 79—19610
- As-Se-Te, amorphous, electron and hole drift mobilities 80—34442
- As-Se(Te)-Ge, fabrication of amorphous semicond. thin films with graded band struct. *(Japanese)* 77—55623
- As-Te-Cu system glasses, elec. cond. and thermo-EMF 79—42540
- As_2S_3, drift mobility, along molecular direction, 207-465K 77—43643
- As_2S_3, electron drift mobility temp. depend., transient photocond. obs. 77—66164
- As_2S_3, temp.-independent mobilities, phonon-induced electron hopping 79—28347
- As_2S_3 thin glassy films, hole drift mobility, interaction with deep localised levels 80—11117
- As_2S_3, vapour-deposited, pure and doped, hole mobility 80—49728
- As_2S_3 vitreous film, hole transport obs. 80—49727
- As_2S_3:Te glasses, doping influence on AC conductivity, electron transport by hopping 79—78106
- As_2S_3-Sb_2S_3, vitreous, dispersive charge transport analysis 79—95418
- $(As_2S_3)_{0.55}(Sb_2S_3)_{0.45}$ vitreous film, dispersive charge transport, time-of-flight meas. 79—19594
- As_2Se_3, amorphous, electron and hole transport, charge defect model 79—15162
- As_2Se_3, amorphous, hole mobility expt., transient photocurrent shape 79—99582
- As_2Se_3, amorphous, photocond. and photoinduced optical absorpt. 79—82645
- As_2Se_3, amorphous, transient hole transport props., trap controlled hopping model 77—47820
- As_2Se_3, crystalline, electron drift mobility and DC cond., trapping model 77—47815
- As_2Se_3, glassy, drift mobility of holes, 20 to 120°C 79—51583
- As_2Se_3, vitreous, hole drift mobility, temp. and field depend. 77—76830
- As_2Se_3:I, hole drift velocity enhancement by I doping 77—39883
- a-As_2Se_3:Mn(Fe)(Ni)(Cu)(Zn)(Ga)(Tn)(Il)(Na), hole drift mobility depend. on impurity conc. 79—60846
- $As_{0.3}Te_{0.48}Ge_{0.1}Si_{0.12}$, amorphous film, transient switching processes 78—84232
- Au-p-n-Si Schottky barrier solar cell, photovoltaic characts., barrier heights, carrier mobility 79—83601
- B, β-rhombohedral, field effect on hopping cond. 79—82589
- α-B, rhombohedral, elec. cond., thermoelec. power, and Hall coeff. 80—6843
- Ba-ferrite, temp. range 303 to 353K 79—42564
- $Ba_{1-x}Sm_xB_6$, prep., elec. cond. and thermoelec. props. 80—49697
- n-$BaTiO_3$, elec. transport props., theoretical discussion and expt. 78—84215
- $BaTiO_3$, H_2-reduced, elec. cond. mechanism, EPR, resist. and Seebeck coeff. meas. 80—10976
- $BaTiO_3$, melt grown, drift mobility meas. 79—19596
- $BaTiO_3$, SCL currents, carrier mobility and trapping 77—15863
- $BaTiO_3$, transport and optical props., small polaron hopping theory 79—47096
- Bi alloy, mag. field depend. electron scatt. rates, de Haas-van Alphen meas. 78—10436
- Bi epitaxial films, size effect in elec. props. 80—54813
- Bi film, carrier conc., mobility and 1/f noise 80—44748
- Bi film, carrier conc. and mobility, resist., galvanomag. and thermoelec. meas. 78—52111
- Bi film, high-mobility, quantum size effects, struct. and kinetic characts. improvement 79—91174
- Bi film, kinetic props. of electrons 77—63011
- Bi, intervalley scatt. influence on mobilities, thermopower calc. 78—26866
- Bi, resistivity at ultralow temp., high precision meas., scatt. mechanisms 77—80776
- Bi, single crystal, drift velocity of charge carriers *(Russian)* 78—84208
- Bi, thermoelec. power, influence of mag. field reversal, drift vel. method 77—69363
- Bi(:Si)(:Sb), mag. field dependent electron and hole scatt., quantum limit 77—15878
- $Bi_{12}GeO_{20}$ crystals, principal carriers obs., in dark and under laser illumination *(Russian)* 80—80312
- $Bi_{12}GeO_{20}$, hopping cond., carrier mobility and density 78—19040

carrier mobility continued
Bi_2O_3 anodic films, struct. and electronic props., photoeffects 80—44749
BiSb (>20 wt.%), electronic band struct. 80—107698
$Bi_{0.88}Sb_{0.12}$, semiconducting transport props., 2 to 100K 80—59989
$Bi_{0.89}Sb_{0.11}$, effect of band structure on the dispersion of magnetoplasma waves 77—47845
$Bi_{0.9}Sb_{0.1}$, epitaxial film, defect struct. and galvanomagnetic props. 77—89889
$Bi_{0.91}Sb_{0.09}$, magnetoresistance anisotropy in strong magnetic field 79—82613
$Bi_{1-x}Sb_x$, solid soln., temp. depend. of weak-field galvanomag. coeffs. *(Russian)* 80—70724
$Bi_{1-x}Sb_x$ thin films, elec. props., 4.2-300K, charge carrier mobility meas. *(Russian)* 79—24087
$Bi_{2-x}Sb_xTe_{3-y}Se_y$ solid solution, density-of-states effective mass, carrier mobility temp. depend. 80—24931
BiTeI-SbTeI solid solns., form., crystn., elec., thermal props. 78—44003
$Bi_{2/3}Te_{1-x}S_x$, single cryst. film, field effect mobility, peaked struct. 77—66207
$Bi_2Te_{3-x}Se_x$ solid solution, Hall effect anisotropy parameter, thermoelectric power, depend. on carrier density 79—69536
Cd_3As_2, effect of annealing on elec. transport props. 80—49739
Cd_3As_2 film, size effects, electrical properties 78—2600
Cd_3As_2, ionised-impurity mobility and static dielec. const. at 4.2K 77—32017
p-$CdCr_2Se_4$:Ag, electrical props., 100-300K 80—54692
$CdCr_2Se_4$:Ag, magneto-electrical props. temp. behaviour depend. on dopant conc. *(Russian)* 80—11006
n-$CdCr_2Se_4$:In, electrical props., 93-168K 80—49713
$CdCr_2Se_4$:In, ferromag. semicond., carrier mobility, electron-two magnon scatt. Hall effect 78—51992
$Cd_{0.96}Cu_{0.04}Cr_2Se_4$, single cryst., Hall mobility 79—7848
$CdGeAs_2$, elec. and optical props., acceptor levels and energy gap determ. 77—85218
n-Cd_2GeO_4, electronic and cond. props. rel. to prep. conditions and defect struct. 80—107787
$Cd_xHg_{1-x}Se$, 77-400K *(Russian)* 78—2485
$Cd_xHg_{1-x}Se$, carrier mobility, 4.2 to 300K, scatt. mechanisms 79—4561
$Cd_xHg_{1-x}Se$, Hall coeff. and electron mobility, band parameters 79—73506
$Cd_xHg_{1-x}Se$ mixed cryst., electron mobility and electron scatt. 78—95296
$Cd_xHg_{1-x}Te$, disorder scatt. 78—39137
$Cd_xHg_{1-x}Te$, electron mobility and conc. near gapless state, influence of hydrostatic press. 79—65486
$Cd_xHg_{1-x}Te$ films, epitaxial growth, optical, elec., and photoelec. props. 79—11512
$Cd_xHg_{1-x}Te$, graded-gap layers, galvanomag. props. at low temp. and in weak mag. field 80—75664
n-$Cd_xHg_{1-x}Te$, single crystal, scattering mechanism on intensity of 1/f noise 80—39642
$Cd_xHg_{1-x}Te$, strong elec. field effect on galvanomagnetic effects 79—11159
$Cd_xHg_{1-x}Te$, vac. evap. film struct. rel. to carrier scatt. 77—85116
$Cd_xHg_{1-x}Te$, vacancy electron states, acceptor behaviour, electron mobility 80—70193
$Cd_xHg_{1-x}Te$, vacancy mech. of resorption of Hg droplets 80—39070
$Cd_2Nb_2O_7$, photolum. and carrier drift mobility at ferroelec. transition 80—71469
CdP, electron mobility, carrier density depend. calc. 79—56229
Cd_3P_2, energy band struct. and electron mobility at low temp. 79—37984
CdS, acoustoelectric mobility measurement for X-ray excited carriers 77—15916
CdS, drift mobility in presence of trapping-recomb. centres 78—19054
CdS, electron drift vel. and phonon multiplication 80—6848
CdS, epitaxial film, conductivity control by S vacancy form., light modulation appls. 77—4455
CdS film, chemically sprayed, carrier conc. and mobility, thermoelec. and photothermoelectric meas. 80—2503
CdS film, Hall effect meas. 79—65570
CdS film, prep. by hot wall technique, morphology and semicond. props. 79—95292
CdS, irrad. with high doses of fast reactor neutrons, investigation of electron mobility 79—73221
CdS, photocond. on supplementary X-irrad. *(Russian)* 77—28212
CdS SAW convolver, effect of transverse drift of carriers on operation 80—14529
CdS, semicond. piezoelec. crysts., US determ. of electron mobility 77—1456
CdS single cryst., melt growth, improvement of elec. characts. 79—38734
CdS single cryst. Hall effect, temp. depend., 800-1200K *(Russian)* 77—80797
n-CdS single crystals, effect of high-temp. annealing on electrical transport props. 79—78098
CdS sprayed films, elect. and optical props. 78—39241
CdS:$CuCl_2$, sintered film, dopant conc. effects on carrier mobility 78—2484
n-CdS:In, containing excess Cd, effects of In on elec. props. 79—56217
CdS:In film, flash evaporated, prep. and elec. props. 80—20792
CdS:In films, vacuum deposited, growth, elec. and optical props. 79—51460
CdS:Li chemically deposited filter, elec. props. 80—11113
n-CdS:Te, grown from Te soln., elec. props. 79—65475
CdS-$LiNbO_3$, layered structure, acoustoelectric surface current kinetics 78—43232
n-CdS(Se), bipolar photocond. and acoustoelectric current 79—19636
CdS_xSe_{1-x}:In film, flash evaporated, prep. and elec. props. 80—20792
p-CdSb, elec. props. at low temp. 77—62866
CdSb, monocrystalline film, prep., elec. props. 79—43159
CdSb, phase diagram, region of homogeneity, elec. cond. 79—43219
CdSe, charge transport 78—84233
CdSe, dark current relaxation 80—44613
CdSe, defect struct. in Se vapour 78—64043
CdSe, epitaxial film, gas-phase comp. effects on elec. props. 77—85354
CdSe, epitaxial films, carrier scattering temp. depend. *(Russian)* 78—10583
CdSe film, effect of growth conditions on electrophysical properties 78—44024
CdSe films, effect of annealing on resistivity and charge carrier mobility 77—8209

carrier mobility continued
p-CdSe, Hall density and mobility, in Se vapour atm., 600-1100K 78—52014
CdSe, heat treatment effect on carrier mobility, role of defect centres 77—72861
CdSe, pulsed Hall photoeffect, transient processes in scattering of carriers 80—15546
CdSe thin film transistor and MISM struct., effect of annealing on electron mobility and conc. 79—78198
CdSe:In, epitaxial layers, synthesis and elec. props. 77—47909
p-$CdSnAs_2$, heavily doped, elec. transport props. under elastic deformation 80—96915
n-$CdSnP_2$, Hall coeff. and elec. cond. meas., 24-900K 80—54721
n- $CdSnP_2$, Hall mobility of electrons meas., 120-300K 77—4373
$CdSnP_2$, Hall mobility of holes 78—52015
$CdSnP_2$-$CdSnAs_2$, and $CdSnP_2$-$CdGeP_2$, solid solution form. and elec. characterisation 78—43125
p-CdTe, bipolar photocond. and acoustoelectric current 79—19636
CdTe, bipolar photoconductivity exam. 78—6410
CdTe, charge carrier transport prop. meas. by time of flight technique 77—39850
CdTe, detector grade semi-insulating crystals, determ. of product of mobility and carrier lifetime 80—39601
CdTe detectors, gamma and electron irradiation effects 78—41893
CdTe, film grown by hot wall epitaxy, elec. props. 79—82696
CdTe, films grown by hot wall epitaxy, elec. props. 79—28420
n-CdTe, Hall effect and resist., close and distant donor-acceptor pairing effects 77—39881
CdTe, high-resistivity, carrier transport and trapping processes, growth parameter effects 77—39871
CdTe, high-resistivity, irradiation effects on carrier transport and trapping process 78—2164
CdTe metal-semiconductor-metal γ-ray detector characts. 80—57451
CdTe negative dielectric relax. of hot electrons 78—52001
p-CdTe, photocond., photoluminesc., spectral studies 80—88593
CdTe, undoped, high-resist.- characterisation, impurity level investig. 77—39801
CdTe:As^{2+}, photovol. props. of p-n junction prod. by ion implantation 78—43038
p-CdTe:Cl, deep level characterisation, gamma-ray detector parameters 77—39802
p-CdTe:Cl, mech. of electron recomb. 79—11176
CdTe:Cl, semi-insulating, Hall effect and cond. meas., carrier mobility 77—39849
CdTe:Cl, semiinsulating, Hall effect and elec. cond., impurity levels 77—55532
CdTe:Cl, single cryst., photo Hall effect obs. 78—76094
CdTe:Cu films, impurity behaviour, Hall mobility and hole density meas. 80—80420
CdTe-HgTe, semicond. solid solns., effect of reactor irrad. on electrophys. props. 77—51744
$Cd_{3-x}Zn_xAs_2$, cryst., two-band and impurity conduction, 1.8 to 370K 78—19057
$Cd_{3-x}Zn_xAs_2$, electron mobility and carrier density calc. 77—80780
$Cd_xZn_{1-x}S$ films, chem. sprayed, carrier density and mobility 80—60121
$Cd_{1-x}Zn_xSe$, epitaxial layer growth with Zn content from doping to solid soln. formation 77—85094
CeO_{2-x}, conductivity and Seebeck coeff., small polaron and hopping mechanisms 77—76812
CeO_{2-x}, small polaron mobility, elec. cond. and nonstoichiometry meas. 78—47785
Co-Ga liquid and solid alloys, elec. resistivity at high temps., partial struct. factors 80—6806
$CoSnTe_2$, thin films, metallic elec. props. 79—78212
$Cr_{1-x}Mn_xSi_z$, semicond. props. 78—79992
Cr_2O_3 carrier mobility temp. dependence 77—35958
$Cr_2S_{3-x}Se_x$, elec. resist., thermal cond. and Seebeck coeff. meas. 80—24958
$CrSi_2$ based solid solns., prep., elec. cond. and thermoelec. props. 80—49697
$CrSi_2$, semicond. props. 78—79992
$CuCr_2Se_4(S_4)(Te_4)$, binary and ternary solid solns., mag. and elec. props. 80—2407
$CuGaSe_2$ thin films, on GaAs substrates, structural and elec. props., photoluminesc. meas. 79—65564
$CuGaTe_2$ epitaxial layers, elec. props. as function of growth temp. 79—65565
$CuGdTe_2$, synthesis and elec. props. 78—26529
$CuInSe_2$, acceptor levels, elec. props. study 80—39578
n-$CuInSe_2$, single cryst., elec. props. 78—43397
$CuInTe_2$, vac. deposited film, growth, struct. and elec. characts. 77—69995
$Cu_xMo_6S_8$, Hall effect and magnetoresistivity 78—95400
Cu_2O, hole mobility, scatt. mechanisms, elec. field effect 77—80786
Cu_2O, odd photomag. effect. meas. 77—89805
Cu_2O, positive and negative photomemory, IR luminesc. spectra, illum. effect 79—69557
Cu_2O:Mn, photomemory mobility components, charged centre conc. 80—103725
$Cu_{1.8}S$ film, vacuum evaporated, props. rel. to elec. cond. 77—36001
Cu_2S film, reactively sputtered, Hall effect meas., 90-300K 80—15541
Cu_2S, rel. to band models of Cu_2S-CdS heterojunctions *(Japanese)* 78—23154
Cu_2S-CdS heterojunction solar cells, carrier transport, nonmonotonic band profiles 80—61361
$Cu_{2-x}S$, carrier mobility rel. to x 78—43389
$Cu_{2-x}S$ single crysts., comp. depend. 77—24302
$Cu_{2-x}Se$, carrier mobility rel. to x 78—43389
$Cu_{2-x}Se$, elec. props. and band struct. 79—73513
$Cu_{2-x}Te$, carrier mobility rel. to x 78—43389
$Cu_{2-x}Te$, x=0 to 0.3, elec. cond., Hall const., carrier mobility, conc., thermoelec., density, lattice parameter 77—11915
$Cu_{2-x}Te$-CdSe heterojunction, elec. and opt. props. *(Korean)* 77—51811
Er_2O_3:CaO, elec. cond. and nonstoichiometry 79—11112
EuO:Gd, electron mobility below Curie temp. 78—91696
EuO(Se), complex elec. cond. anomalies 80—107812
EuO(s), mag. semicond., s-f model, intermediate coupling theory 79—95326
α-Fe_2O_3 electrode, carrier density determ. by optical absorpt. and photoelectrolysis spectra 80—71462

carrier mobility continued
- $Fe_{3-x}Ti_xO_4$, elec. transport near Verwey transition, thermoelec. power and cond. meas. 79—95455
- GaAS, semi-insulating and n-type, doping by neutron transmutation 80—96553
- GaAS:Cr, mag. field depend. of single carrier parameters, mixed cond. anal. 79—91043
- GaAlAs:Zn recombination radiation drift, charge carrier photon induced drift in varigap semicond. 80—50418
- $Ga_{1-x}AlAs$, LPE layers, electron mobility, scatt. processes 80—84519
- $Ga_{1-x}Al_xSb$, melt growth and elec. props. 79—65999
- p-GaAs, 100 μm minority carrier diffusion lengths from photoluminescence 80—29807
- α-GaAs, amorphous, mobility gap temp. derivative calc., polar contrib. 78—26861
- n-GaAs, and Te doped, homogeneity, IR introscopy investig., carrier density and mobility calc. 79—15446
- GaAs, automatic electrochemical Hall mobility profiling 79—99615
- GaAs, ballistic and near ballistic transport 80—96867
- GaAs, CVD in $Ga-AsCl_3-H_2$ system with different input supersaturations *(Russian)* 78—68098
- GaAs, carrier diffusion in transient response regime 80—103688
- GaAs, carrier mobility profiles meas. at room temp. by Corbino effect 78—60128
- GaAs, circuit effects in time-of-flight diffusivity meas., Monte Carlo method 80—88563
- GaAs, compensated, electron mobility temp. depend. 80—96868
- GaAs compensated VPE thin film, electron Hall mobilities 80—107932
- GaAs, defect clusters induced by γ-rays and neutrons, effect on elec. props. 80—29408
- GaAs, diffusion coeff. of hot electrons 79—15156
- GaAs, domain elec. instability in two-valley semiconds. 77—76842
- GaAs, dynamical response of electron distrib. to high elec. field fluctuations 77—51758
- GaAs, elec. effects of dislocations 79—82586
- n-GaAs, electron drift vel. meas. at high elec. fields 77—39861
- GaAs, electron heating under hydrostatic pressure, Monte Carlo calcs. 77—69334
- n-GaAs, electron mobility, free-carrier absorpt., and compensation ratio 79—56218
- GaAs, electron mobility temp. depend. 79—91084
- GaAs, electron mobility illuminaticn, compensation, space charge regions, carrier scatt. 80—70691
- GaAs, electron transient vel. characts., Γ-L-X cond. band ordering 78—79997
- p-GaAs, electronic props. 78—68040
- n-GaAs, epitaxial, electron mobility calc. 77—69435
- n-GaAs, epitaxial, high temp. carrier transport 80—65725
- n-GaAs, epitaxial film, defect clusters, charge-carrier mobility temp. depend. anal. 80—54701
- GaAs epitaxial film on GaAs substrate, IR characterisation 78—23544
- GaAs epitaxial films on strongly doped substrate, basic parameter meas. utilising magnetoresist. and SEM techniques under cathodoluminesc. conditions 80—65728
- GaAs epitaxial layers, characterisation Hall effect and Schottky diode profile meas. 78—91791
- GaAs, epitaxial layers, MBE grown, Hall mobilities, substrate temps. 80—20335
- GaAs epitaxial layers fast characterisation, electroless plating of Au 79—33347
- GaAs, epitaxy on semiinsulating GaAs, elec. props. of transitional layers rel. to growth conditions 77—15977
- GaAs, epitaxy using TMG and AsH_3, chloride etching effect 78—76606
- GaAs for MOSFETs, native oxides, annealing effects and inversion layer mobilities 78—6452
- GaAs, Gunn oscillator, magnetoresist. meas. of mobility and noise 77—62948
- GaAs, heavily doped electron mobility due to scatt. by pot. fluctuations 80—2387
- n-GaAs, heavily-doped, with Gaussian band tails, modification of Einstein relation 80—80270
- GaAs, high press. electron transport props., three band model 80—15516
- n-GaAs, high temp. mobility anal. in three-valley ($\Gamma_6{}^c$-$L_6{}^c$-$X_6{}^c$) model 79—99544
- GaAs hot electrons drift rate/field strength characteristic in microwave fields *(German)* 78—43430
- n-GaAs, implanted, IR refl. meas. of free carrier parameters 77—36244
- p-GaAs, impurity band Hall mobility 80—70730
- p-GaAs, influence of light holes on transport props. 77—4367
- GaAs, ion implantation, review 78—6080
- GaAs ion implantation parameter determ. by microwave contactless mobility meas. 78—10527
- n-GaAs, LPE, deep trapping centre characterisation by Hall and photo-Hall meas. 80—88578
- GaAs LPE layers, effect of baking on mobility and doping conc. 79—99641
- GaAs layers, electroepitaxy and thermal LPE growth, defect struct. and electronic characts. 80—2290
- GaAs layers and p-n junctions grown by current-controlled LPE, elec. characts. 78—6436
- GaAs, MBE layers, H_2 effect on residual impurities, photolum. obs. and elec. characts. 79—47636
- n-GaAs, mechanical polishing damage effect on IR refl. and ATR spectra 77—20848
- GaAs, melt grown, improve elec. and luminesc. props. after short time heat treatment 77—63452
- p-GaAs, minority carrier mobility calcs., including screening, scattering mechanisms 79—99545
- GaAs, N_2 laser pumped under appl. elec. field, gain anisotropy 77—61958
- GaAs, negative differential mobility and geometrical magnetoresist. calc. 77—43624
- GaAs, optical cond. of free carriers 78—19436
- GaAs, organometallic VPE, with varying As/Ga ratios, deep states 80—65480
- GaAs orientation dependence of ballistic electron transport and impact ionisation 80—49758
- n-GaAs, photo-Hall effect meas. of ionised impurity scatt. 78—56182
- n-GaAs, piezoelectric semiconductor, influence of acoustic phonon disturbances on conductivity 78—91697

carrier mobility continued
- n-GaAs, proton irrad., $E_p=30$ MeV, defect form., orientation depend. 78—55898
- GaAs, self-scattering in Monte Carlo calcs. of transient dynamic response 80—103687
- GaAs, semi-insulating, cond. mechanism, model explaining temp. depend. of elec. props. 79—51571
- GaAs, semi-insulating, conduction model 80—10986
- GaAs, semi-insulating, elec. characts., correl. with mass spectra anal. 78—39104
- GaAs, semi-insulating, undoped and Cr-doped, compensation mechanisms, Hall effect and optical absorpt. meas. 80—84477
- GaAs, Si ion implantation and annealing, damage recovery, surface carrier profile 77—4119
- n-GaAs, three valley band struct., high temp. Hall mobility 80—29318
- n-GaAs, transferred electron effects under hydrostatic pressure 77—32018
- GaAs, VPE, electron Hall mobility meas., attempted correlation with growth parameters 78—43417
- GaAs, VPE film growth in $Ga-AlCl_3-H_2$ system, O_2 injection effect 79—100057
- n-GaAs VPE layers, Hall mobility, effect of Cu contamination, photolum. expts. 80—54810
- GaAs VPE layers, role of diffused Ga vacancy in degradation 78—95050
- GaAs VPE layers for FET devices, impurity characterisation 80—29491
- GaAs:Be, implantation and annealing, elec. props. 79—99540
- GaAs:Cr, Be, ion-implanted, semi-insulating, carrier mobility and conc. temp. depend. 77—76808
- GaAs:Cr, carrier transport in p^+-ν junction based on relaxation semiconductors 79—65543
- GaAs:Cr, epitaxial layers, MBE grown, Hall mobilities, substrate temps. 80—20335
- GaAs:Cr, FET, influence of Cr on mobility of electrons 80—92910
- GaAs:Cr, parameters determ. using cond., Hall-effect and magnetoresist. meas. *(Slovak)* 78—47802
- GaAs:Cr, Se implantation, carrier conc. and mobility profiles depend. on dose and annealing temp. 77—47479
- p-GaAs:Cr, semi-insulating, illumination effect on mobilities 77—32043
- p-GaAs:Cr, semi-insulating, mobilities and carrier concentrations, temp. depend. 80—70702
- GaAs:Cr, Te implantation, electron conc. and mobility profiles depend. on dose and annealing temp. 77—39607
- GaAs:Cu, diffused layers, photocond. spectra, hole conc. and mobility *(Russian)* 78—14758
- GaAs:Ge, ion implanted, elec. props., comparison with Sn, Se and Te ion implanted samples 77—39879
- GaAs:Ge, VPE, doping, electrophysical characts. meas. 78—43493
- GaAs:Ge, vap. grown, diatomic complex donor and acceptor model 78—80003
- GaAs:Mn epitaxial layers, fabrication and electrical props. 77—80859
- GaAs:n, ion implantation, hole conc. and mobility profile meas. 78—23082
- n-GaAs:Ni, negative photocond. at low temps., impurity levels 80—6900
- n-GaAs:O film, influence of O on elec. props. 79—11252
- GaAs:S^+ film, ion implanted carrier characterisation by cyclotron reson. 77—20472
- GaAs:S(Se), ion implanted, evaluation by contactless mobility meas. 79—1448
- GaAs:Se ohmic contacts, pulsed electron beam annealing donor density, mobility 80—65678
- GaAs:Se(Zn) polycrystalline film, Hall effect, resistivity meas. 80—96911
- GaAs:Si, electrical activity of Si 79—15145
- GaAs:Si, pulsed laser annealing of implanted layers, defect structure and Hall effect meas. 79—69118
- GaAs:Si,Cr, under layer of SiO_2, effect of annealing, on electron concentration and mobility, and impurity distrib. 79—4323
- GaAs:Si epitaxial films, elec. and photoelec. props., impurity distrib. 80—7006
- GaAs:Si(Mg), doped and undoped, sputtered epitaxial films, elec. props. 79—78234
- GaAs:Sn, LPE layers, electronic props., depend. on Sn incorporation 78—87883
- GaAs:Sn epitaxial layer, electronic props. and epilayer-substrate interface props. 77—89886
- GaAs:Sn films, MBE grown, doping profiles, carrier mobilities, RHEED and AES obs. 79—1447
- GaAs:Sn(Be) MBE films, elec. characterization 79—91168
- GaAs:Te, superdilation and defects, lattice parameter meas. and carrier mobility 80—10569
- GaAs:Zn, implanted, hole conc. and mobility profiles meas. 78—23081
- p-GaAs:Zn, luminescent, ion doped MBE growth 80—44436
- p-GaAs:Zn, optical absorpt. spectra and photocond. after 2 MeV electron irrad. *(Russian)* 77—69859
- GaAs:Zn, pulsed laser annealing, expt. 78—34828
- GaAs:Zn ion implanted ionic alloy, electrophysical props., annealing 80—39133
- $GaAs-Al_xGa_{1-x}As$ modulation-doped heterojunction superlattices, electron mobilities 79—7877
- $GaAs-Al_xGa_{1-x}As$ superlattice, electronic props. 80—11080
- GaAs-AlGaAs heterojunction superlattices, electron mobilities 80—29473
- GaAs-AlGaAs:Si heterojunction interface, two-dimens. electron gas, Hall effect and cyclotron reson. meas. 79—65530
- $n-GaAs-Ga_{1-x}Al_xAs$, heavily doped superlattice, electronic props., perpendicular low temp. mobility 80—65660
- GaAs-metal contacts, intervalley scatt. effect on current-voltage characts. 77—89845
- $n-GaAs-n^+-Al_xGa_{1-x}As$ heterostructure production, by MBE *(German)* 80—44711
- GaAs-oxide, IGFET, electron mobility meas. 79—66188
- GaAs-Si ion implanted, impurity profiles elec. props. 80—96550
- $GaAs_{1-x}P_x$ based structs., carrier conc., mobility calcs. from Hall effect meas. 78—60138
- $GaAs_xP_{1-x}$, energy band struct., CPA based on LCBO *(Japanese)* 80—44495
- $GaAs_{1-x}Sb_x$ electron intervalley transfer and drift velocity calc. 77—80778
- $GaAs_{1-x}Sb_x$ ternary phase diagram, LPE, band gap and elec. props. 77—55896
- GaInAs-InP, growth by low-pressure metalorganic CVD 80—71595
- $Ga_{0.47}In_{0.53}As$, HF carrier mobility, temp. depend., theory 80—75593

carrier mobility continued
$Ga_{0.47}In_{0.53}As$, LPE growth and characterisation 80—10845
$Ga_{1-x}In_xAs$, IR reflectivity, cluster effect on optical phonons 80—97259
$Ga_{1-x}In_xAs$ solid solns., electron scatt. by isoelectronic impurities in covalent crysts. 79—11129
$Ga_xIn_{1-x}As$, on ⟨111⟩B InP, LPE growth, characterisation of high purity lattice 80—104082
$Ga_xIn_{1-x}As_{1-y}P_y$:Ge(Sn)(Te), epitaxial film, elec. and optical props. 79—11251
$Ga_{1-x}In_xP_{1-y}As_y$, carrier compensation and alloy scatt. 80—29490
$Ga_{1-x}In_xP_{1-y}As_y$, drift vel. elec. field characts., Monte Carlo simulation 77—39839
$Ga_{1-x}In_xP_{1-y}As_y$, electron transient drift vel., influence of effective mass and alloy scatt. 80—2384
$Ga_xIn_{4-x}PyAs_{1-y}$, In rich bulk single crysts. growth from melt via gradient freeze method, and characterisation 78—68618
$Ga_{0.3}In_{0.7}Sb$, negative differential mobility and geometrical magnetoresist. calc. 77—43624
$Ga_xIn_{1-x}Sb$, electron transport props. calc. by Monte Carlo method 77—76834
n-GaN elec. props., electron mobility calc. 78—30923
GaN, high-press. VPE and elec. characts. 78—14627
GaN:Mg, and undoped, epitaxial growth from vapour, orientation, elec. props. 77—4740
GaP complex band semicond. photogalvanic effect mechanism 80—11036
n-GaP, cryst. growth, synthesis solute diffusion method, elec. characts. *(Korean)* 78—52653
n-GaP, electron mobility, 77 to 300K, intervalley scatt. of electrons *(Russian)* 79—95407
GaP, epitaxial layer prep. and elec. props. 77—85096
GaP layers, LPE growth, elec. props., residual impurities 79—38202
GaP, rare earth doped, photolum. and elec. props. *(Russian)* 78—52545
GaP, scatt. mech., mobility tensor 80—6826
GaP, soln. growth of bulk crysts., luminesc. and elec. props. 78—92181
n-GaP, uniaxially deformed, piezoresist. exam. of donor levels 77—4346
GaP:Mg, ion implanted, elec. profiles 79—77628
n-GaP:S, Hall effect and resistivity meas. *(Japanese)* 77—39840
GaP:Te, Hall effect and elec. cond., 80-400K 78—91705
GaP:Zn, Hall effect and elec. cond., 80-400K 78—91705
p-GaP:Zn, Hall effect determ. of hole mobility temp. depend., scatt. mechanisms 77—4364
GaP:Zn, implanted, elec. profiling using anodic oxidation in N-methylacetamide 80—54690
GaP:Zn, Sn doped epitaxial layers, Hall const., hole mobility and conc. 80—15143
$GaS_xSe_{(1-x)}$ solid solns., electrical props. meas. 78—84216
GaSb and $GaSb_xAs_{1-x}$ films, MBE growth and elec. props. 79—23863
GaSb, bulk and epitaxial, IR reflect. meas., carrier conc. and mobility determ. 80—80769
p-GaSb, elec. cond., Hall effect, mobility and carrier concentration *(Russian)* 79—19603
n-GaSb, galvanomagnetic effects 78—72172
p-GaSb, heavy and light holes scattering 78—91692
GaSb LEC single crystal growth, novel encapsulant material 80—93475
GaSb, sputtered films, on GaAs, growth, Hall effect, impurity levels 80—20334
n-GaSb:Te, Hall coeff., carrier conc. and mobility, elec. cond., 290 to 550K *(Russian)* 79—19604
p-GaSb:Zn, hole transport props. from 77 to 300K 79—73530
GaSe, Hall mobility anisotropy 78—68041
GaSe, lamellar crystal, exciton translational mass from magneto-Stark effect *(Russian)* 78—48153
p-GaSe:Sn, majority carrier drift mobility meas. 80—92895
GaSe:Sn, single crystal, transient photoconductivity *(Russian)* 79—11171
GaTe, transport anisotropy 79—23975
Gd_2GeSe_5, elec. props., 300 to 1100K 79—51585
n-Ge accumulation layers, effect of low-energy Ar^+ ion bombardment on electron scatt. 77—66205
p-Ge, carrier drag by photons, comparison with p-GaAs 79—11185
p-Ge, carrier scatt. by ionised impurities, rel. to carrier mobility calc., 10-70K *(Russian)* 78—39103
n-Ge, cathodically treated, surface mobility of electrons 77—51801
Ge, charge carrier scatt. and compensation effect on Hall mobility of majority carriers *(Russian)* 77—32026
n-Ge, deformed, 1/f noise, resist., mobility, and carrier density 77—8161
p-Ge, diffusion coeff. for hot holes in mag. field 80—39614
Ge, diffusion coeff. of hot holes meas. 78—6387
Ge, drift mobility and Hall coeff. factor of holes 78—43379
Ge, drift velocity of plasma cloud, at high elec. field 80—6887
Ge, effective masses of heavy and light holes, from ohmic mobility data 80—80160
Ge, electron mobility in Δ_{1c} minima, temp. depend. 79—65473
Ge, electron mobility is semiconductors based on dielectric function modification of Dingle pot. 79—60836
Ge, electron-hole fluid drift in crossed electric and mag. fields, photocurrent dynamics *(Russian)* 79—99487
Ge, electronic inversion channel anomalous Hall factors *(Russian)* 79—95467
Ge, epitaxial film, ion sputtering, growth mechanism, struct., props. 77—31917
Ge epitaxial film, vac. deposited on GaAs, doping effect of annealed GaAs surface 80—65718
Ge, exciton condensation, electron-hole drop investigation in UHF field, nucleation *(Russian)* 80—80193
Ge, Fermi level, minority carrier conc., effective intrinsic conc., Einstein relation 77—85209
Ge film, elec. props., prep. by DC sputtering *(Japanese)* 79—78237
Ge film, polycrystalline, structural and elec. props. 78—76173
Ge film, prep. by low press. reactive deposition process and characterisation 79—24449
n-Ge, group V doped, point defect form. due to γ-ray irrad., carrier density, mobility meas. 78—71759
n-Ge, Hall coeff. and cond. mech. in intermediate conc. at He temps. 79—95422
Ge, high purity, surface inversion layer electron and hole mobilities 77—76937
p-Ge, highly deformed, hole scattering 77—20309
p-Ge, hole drift vel. in high field 79—95415
Ge, hole drift velocity, effect of impurity scatt. 78—60127
Ge, hole drift velocity, time-of-flight meas. 78—10444

carrier mobility continued
p-Ge, hole-hole collisions, effect on carrier mobility above 80K 80—6838
Ge, impurity-ion potential, electron-conductivity mobility, spatially variable dielectric function calcs. 79—78105
Ge, injection current in presence of electron and hole mobility, gradients 77—69326
Ge, ionised impurity scatt. limited mobility in semiconductors with spatially variable dielec. function 78—51986
Ge, laser induced elec. damage, carrier removal, mobility degradation 77—80791
n-Ge, minority-carrier injection and extraction 80—49767
Ge, multivalley struct., helical instability *(Russian)* 79—47101
Ge, nonequilibrium charge carrier-mag. field interaction electron-hole drops, recombination *(Russian)* 80—75511
Ge, oscillistor effect in strong mag. fields, ambipolar drift and breakdown 78—2511
Ge p-n junction injection characts. in strong elec. fields 77—76913
Ge, p-type, hole conductivity anisotropy 77—4360
Ge, semiconductors, intravalley carrier transfer, transverse photo-EMF for various absorpt. coeffs. 79—69551
Ge, sputtered hydrogenated amorphous, steady-state and transient photocond. meas. 78—10506
Ge, surface, Hall effect study, channel cond. *(Russian)* 80—92909
n-Ge, surface electron mobility, Hall effect and cond. meas. 79—56281
Ge surface Hall effect and cond., electron, hole conc. and mobility *(Russian)* 80—44619
Ge, transport props. of high density electron-hole plasma at low temp. 77—47864
Ge:As, NMR, conduction electrons in impurity band, metal-nonmetal transition 79—78544
p-Ge:Cd,Sb, electron irrad. at 300K, elec. props. 80—6435
Ge:Cu, hot photoexcited holes at low temp. 78—30954
Ge:Hg, Sb, influence of electron irradiation on elec. props. 77—20318
Ge:Mn, Sb, recombination waves, convective instability development 80—70721
n-Ge:Ni, recombination of hot electrons on Ni impurity centres 80—44612
p-Ge:Nz, Sb, influence of electron irradiation in elec. props. 77—20318
Ge:O, elec. props., O interaction with point defects 79—11081
n-Ge:Sb, electron irrad., impurity photoconductivity 77—15900
Ge:Sb(Au) cleaved surface, influence of impurities on local surface states 79—78150
Ge-As-Te glass, thermoelec. power and DC cond., temp. depend. 77—62955
Ge-GeO_2, MIS struct., electrophysical characts. 79—82680
Ge-GeO_2 boundary, electrophysical parameters *(Russian)* 77—85327
Ge-Si, UHV-produced epitaxial structs., electrophys. props. 78—3060
Ge-Si alloy, epitaxial growth by getter sputtering, characts. 79—28915
Ge-SiO_2, MIS struct., electrophysical characts. 79—82680
Ge-SiO_2-Si_3N_4, MIS struct., electrophysical characts. 79—82680
n-$Ge_{1-x}Al_xAs$:Te, long-lifetime photocond. effect obs., Hall effect meas. 77—89795
GeS film, photocond. kinetics 77—39897
$GeSe_2$, drift mobilities of electrons and holes, photocurrent decay meas. 80—2424
Ge_xSe_{1-x} chalcogenide glasses, trap-controlled carrier mobility, time of flight meas. 79—4557
Ge_xSe_{1-x} chalcogenide glasses, drift mobility of optically injected carriers 79—19627
p-$Ge_{1-x}Si_x$, $0.004 \leq x \leq 0.08$, hole mobility and hopping cond. rel. to composition fluctuations 77—76819
$Ge_{0.5}Sn_{0.5}Te$ film, elec. and optical props. 77—12028
GeTe, single cryst., hole mobility 78—6379
He, crystalline, charge carrier mobility temp. depend., diode volt-ampere characts. meas. *(Russian)* 77—31838
He, liquid, surface electron high freq. cond., electron system heating, I-V characts. *(Russian)* 80—29244
He, solid, charge carrier mobility in strong electric fields *(Russian)* 77—62706
He, solid, charge motion, singularities in temp. and time depend. *(Russian)* 78—56019
He, solid, peculiarities of charge motion *(Russian)* 78—95202
^{4}He, electron localisation, mobility in dense low temp. gas 80—92247
^{4}He, liq., HF cond. of electrons trapped at surface 78—10238
^{4}He, liquid, surface warm electrons, non-Ohmic transport, scatt. mechanisms 77—20142
^{4}He, solid, charge mobility, plastic deform. effect *(Russian)* 79—60599
$Hg_{1-x}Cd_xSe$, zinc blende structure, optical and electronic properties 80—6723
n-HgCdTe, photocond., Hall mobility and resist. 80—34478
HgCdTe, zero gap, unusual high electron mobility and related phenomena 79—82601
n-$Hg_{0.785}Cd_{0.215}Te$, slightly compensated, transport props. of photo-excited carriers 78—47832
$Hg_{0.79}Cd_{0.21}Te$, ion implanted, elec. props. 80—20184
$Hg_{1-x}Cd_xTe$, Einstein relation for inversion layers 80—103706
$Hg_{1-x}Cd_xTe$, epitaxial layers, elec. properties in the range 4.2 to 300K *(French)* 80—65721
$Hg_{1-x}Cd_xTe$ epitaxial layers, elec. props. 80—96910
$Hg_{1-x}Cd_xTe$, high-pressure reflex growth technique, IR detector appl. 77—40347
$Hg_{1-x}Cd_xTe$ photoconductors, gamma ray effects on surface props. and detector props. 79—17489
$Hg_{1-x}Cd_xTe$, props. and appls., book contrib. 77—39834
$Hg_{1-x}Cd_xTe$, quasi-local acceptor levels and electron mobility 78—67974
$Hg_{1-x}Cd_xTe$, zero-gap semicond. with nonparabolic band struct., hot electron mobility and conc. 78—76080
$Hg_xCd_{1-x}Te$, Hall effect and elec. cond., carrier density and mobility temp. depend. 77—4341
$HgCr_2Se_4$, electronic props. rel. to departure from stoichiometry 80—100472
HgI_2 crystals, native defect compensation, doping, mobility-lifetime and TSC meas. 77—55492
HgI_2 detectors, recent improvements 78—37507
HgI_2, electrons and holes cyclotron reson. 78—72061
HgI_2, mobility anisotropy determ. by photoelectromag. effect and photocond. 79—38126
HgI_2, photoexcited, Hall effect, magnetocond., and cyclotron reson., carrier mobility and effective mass 77—59294
HgI_2, photomagnetoelectric effect anisotropy, photocond. 77—15897

carrier mobility continued
HgSe, Bridgman growth at hydrostatic press. to 3 kbar, free electron conc. and mobility 77—52245
HgSe, CVD crysts., electrophys. characts. 77—85910
HgSe-Se, photo-field model, rel. to anomalous photocond. in Se:Hg 77—43658
HgTe film, vac. deposited, elec. props., 78-420K 80—11119
HgTe, mobility of electrons and holes, 4 to 100K 80—107821
HgTe, vacancy doping, effect on elec. characts. 79—82595
HgTe, vacancy doping by off-stoichiometry, influence on transport props. 78—55862
HgTe, vacancy electron states, acceptor behaviour, electron mobility 80—70193
HgTe, vacancy mech. of resorption of Hg droplets 80—39070
HgTe:Mn, impurity scatt. contrib. to electron mobility and thermoelec. power 77—15852
InAs, elec. props. after heating for 300 to 900°C for 1 to 100 hours 78—47793
n-InAs, electron mobility dependence on conc. Hall effect at 300K 78—47794
InAs, epilayer, MBE growth parameters, relationship with elec. props. 80—2296
InAs epitaxial layers, on GaAs substrate, electron diffr. and SEM exam., electronic props. 79—1552
InAs films, MBE grown on GaAs, electron mobilities, lattice mismatch effect 80—80419
InAs, heteroepitaxial film, orientation and struct. investigation 79—82480
InAs heteroepitaxial layers, VPE grown, effect of $AsCl_3$ mole fraction on elec. props. 79—11255
InAs, intrinsic point defects, nature and influence on electrophys. props. 78—79609
InAs, laser excitation, photocond., optical absorpt., electron-hole scatt. 77—43661
InAs, MBE growth, SEM, RHEED, optical microscopy and elec. meas. 78—18925
p-InAs, surface conductance of Ar-ion-bombard. samples 79—60910
InAs, thin film prep. and elec. props. 79—1633
n-InAs, transport props., influence of higher energy bands, calcs. 79—19598
n-InAs, VPE layers, on GaAs substrate, electronic profile 79—95525
InAs:Cd, Te, donor-acceptor interaction, elec. cond. and Hall coeff. meas. 80—59988
InAs:Cd,Te interaction between impurities, effect on elec. props., Hall effect. 80—19832
InAs:Sn, single crysts., defect formation 80—88606
$In_{0.53}Ga_{0.47}As$, Hall mobility and Hall factor, temp. and donor conc. depend. 80—49773
$In_{0.53}Ga_{0.47}As$, LPE layer on InP, electron mobility and energy gap 77—24627
p-$In_{0.53}Ga_{0.47}As$:Zn on InP, elec. and optical props. 80—75662
$In_{1-x}Ga_xAs$, LPE, electron mobility and max. drift vel., microwave device appls. 77—77431
$In_{1-x}Ga_xAs$, LPE layer on InP substrate, phys., elec. and optical props. 78—39235
$(In_{1-x}Ga_x)As$, scattering of electrons by potential clusters 77—15842
$In_xGa_{1-x}As$, electron drift vel. in high elec. fields 78—30928
n-$In_xGa_{1-x}As$ film, epitaxial, on GaAs, evaluation 77—1812
$In_xGa_{1-x}As$, heteroepitaxial, MBE grown, props. 78—84328
$In_xGa_{1-x}As$, MBE layers on InP substrates, elec. props., photoluminesc., X-ray and Auger obs. 79—51450
$In_xGa_{1-x}As$, VPE on (100), (111)A, and (111)B InP substrates 80—15382
$In_{1-x}Ga_xAs_yP_{1-y}$, evidence for alloy scatt. from press. induced changes of electron mobility 80—88548
$In_{1-x}Ga_xAs_yP_{1-y}$, Hall mobility, comp. depend. 80—75587
$In_{1-x}Ga_xAs_yP_{1-y}$, hole mobility over temp. range 77 to 300K 80—60111
$In_{1-x}Ga_xAs_yP_{1-y}$ LPE layers, background carrier conc. and electron mobility. 79—95523
$In_{1-x}Ga_xAs_yP_{1-y}$:Be, ion implantation, hole conc. and mobility, junction depth 79—46685
n-$In_{1-x}Ga_xP$ solid solns., electron scatt. mechanisms *(Russian)* 79—4568
$In_xGa_{1-x}P_yAs_{1-y}$, electron effective mass and Dingle temp., Shubnikov-de Haas oscills. 80—59859
$In_{1-x}Ga_xSb$, drift velocity of electrons 77—20327
$(In_{1-x}Ga_x)Sb$, scattering of electrons by potential clusters 77—15842
InO_3:Sn film, prep. by spray hydrolysis, struct., elec. and optical props. *(Japanese)* 79—42678
n-In_2O_3 film, RF sputter grown, substrate bias effect on elec. and optical props. 78—64150
In_2O_3 films, reactively evaporated, elec. props. 80—84521
In_2O_3, polycrystalline, electron conc. and mobility, 25 to 700°C, O_2 partial press. depend. 77—76811
In_2O_3, thermally evaporated film, struct. and elec. props. 80—104066
In_2O_3, transparent electrode deposition on PLZT ceramic, elec. and opt. props. 78—74848
In_2O_3, transparent heat mirror formation by ion plating on ambient temp. substrates and props. 80—25578
In_2O_3:Sn films, pure and doped, prod. by ion plating, elec. and optical props. 80—2488
In_2O_3:Sn films; vac. deposited, elec. props. 80—100542
In_2O_3-SnO_2 thin film, Hall mobility, temp. depend., grain boundary effects 80—75658
n-InP, compensated, elec. props., space-charge effects 80—65569
n-InP, compensated impurity conduction and negative magnetoresist. 79—28360
InP, compensation ratio, electron mobility and free-carrier absorpt. 80—80261
InP, diffusion and power spectral density of velocity fluctuations for electrons, Monte Carlo calc. 79—51572
n-InP, epitaxial, Hall effect, electron mobility and density, temp. depend. 78—72288
n-InP, epitaxial, subthreshold velocity-field charact., 77K 78—64038
InP epitaxial films, grown on heavily doped substrates, carrier mobility study, magnetoresist. meas. 80—60116
n-InP film, polycryst., deposited on Mo sheets, elec. props. obs., w.r.t. varying deposition conditions 79—4608
n-InP film, polycrystalline, elec. props. 77—76965
InP film, prep. by low press. reactive deposition process and characterisation 79—24449
InP films, organometallic VPE grown, props. 80—96753
InP, free carriers, freq. depend. relax. time 80—2385

carrier mobility continued
InP growth from soln. and LEC, photolum. and elec. meas. 79—87575
InP, Gunn oscillator magnetoresist. meas. of mobility and noise, contact effects 77—62948
InP, ion-implanted n- and p-type layers, characts. 78—6075
InP, negative differential mobility and geometrical magnetoresist. calc. 77—43624
InP, planar reactive deposition on CdS, heterostruct. formation and elec. evaluation 78—72738
p-InP, single crysts. and epilayers rel. to prep method 77—81211
InP VPE, growth kinetics and controlled doping 79—87569
InP, vapour phase epitaxial growth in presence of O_2, elec. props. 79—46971
InP, weak field Hall mobility and Hall mobility and Hall ratio 78—23116
InP:Be, ion implantation, hole conc. and mobility, junction depth 79—46685
InP:Si, implantation at high temp., elec. mobilities 79—99541
InP:Si, pulse electron annealing, carrier activation and mobility 80—15124
InP:Sn, LPE growth from Sn soln., elec. props., 80 to 300K 79—11250
n-InP/SiO_2 capacitors, minority carrier generation 79—95496
InSb, carrier heating by microwave field, inertia effects 80—65580
InSb, charact. and phys. props., review *(Japanese)* 80—39576
n-InSb, compensated, impact ionisation temp. depend. 77—20331
InSb, current-voltage characteristics at room temperature and high hydrostatic pressure 80—88560
InSb, Einstein relation for inversion layers 80—103706
n-InSb, elec. cond., press. dependence 80—6830
n-InSb, elec. props. changes during ht. treatment 77—85213
InSb, electron drift velocity in fields up to 800 V/cm in presence of impact ionisation 78—39120
n-InSb electron heating and energy relaxation time in quantising mag. field 80—10996
n-InSb, electron heating dynamics in longitudinal electric and quantising magnetic fields 79—69520
InSb, electron irrad. effects on elec. props. and recomb. 79—51584
InSb, electron mobility, low-field, Monte Carlo calc. 80—10973
n-InSb, electron mobility at 77K in avalanche regime 79—33295
InSb, electron-hole plasma instabilities, impact ionisation conditions, microwave emission 80—107840
p-InSb, excess In, polycryst. thin film, elec. transport props., non-stoichiometric effect 79—95528
InSb, extrinsic and intrinsic, interaction of transverse magnetoresist. effects 80—65596
p-InSb film, elec. transport props. 78—72291
InSb film, for monolithic elastic surface wave amplifiers of continuous operation 77—80023
n-InSb film, galvanomagnetic meas. of surface layer carrier conc. and mobility 77—55628
InSb film, heteroepitaxial, MBE growth and elec. props. 80—2301
n-InSb film, low energy electron irrad. effect on elec. props. 80—7009
InSb, galvanomagnetic props. of annealed single crystals 80—96909
InSb, gamma irradiated, changes in energy spectrum of impurity spectrum 78—51937
InSb, heteroepitaxial film, orientation and struct. investigation 79—82480
n-InSb, hole mobility temp. depend. after electron bombardment 79—33290
InSb, horizontal zone melting in vacuum 79—47624
p-InSb, influence of plastic deform. on elec. props. 80—103711
InSb, ion bombard. and defect annealing, n- and p-type cond. layer prod. 78—26606
p-InSb, ion bombardment using 30-80 keV ions, isochronous annealing, elec. props. obs. 79—19295
InSb, ion irrad., isothermal annealing effects 80—6424
n-InSb, ionized impurity scatt. limited mobility, expt. 80—80274
InSb, low temp. electron mobility, theory and expt. 77—89759
InSb, MISS struct., surface electron and hole mobility and conc. *(Russian)* 80—44701
InSb, magnetic freeze out *(Japanese)* 78—39130
InSb, magneto-surface transport props. 77—43693
p-InSb, magnetoconcentration effect, negative differential conductance 80—70729
n-InSb, microwave helicon resonances, carrier density, mobility, dielectric const. 80—96930
p-InSb, mobility, diffusion and thermoelectric power of hot holes 80—39595
InSb, mobility from soln. of Boltzmann eqn. for electron-LO phonon scatt. 79—19586
n-InSb, mobility in mag. field, extreme quantum limit, iterative technique 78—2498
InSb n-type, heavily doped, effects of hydrostatic pressure on electron mobility and conc. 77—4390
n-InSb, negative longit. magnetoresist., carrier conc. and mobility depend., 77K 80—60007
InSb, neutron irrad., defect cluster form., effect on elec. props. 80—65062
n-InSb, photoconductivity, 1.8K, hot-carrier and free-carrier absorption. effects 78—84254
InSb, polycryst. film, Hall and drift mobilities 79—95531
n-InSb, proton irrad. defects energy level scheme, transport props. meas. 80—96576
InSb recrystallised thin films on mica substrate, elec. props. 80—70867
n-InSb, spin polarisation, anisotropic size effect, effect on CESR signal 80—70743
InSb, thin film, Hall mobility of carriers at room temp. 79—65568
InSb, thin film prep. with remelting, elec. props. 77—52255
InSb thin films prepared by ion beam epitaxy system *(Japanese)* 78—22976
n-InSb, transverse magnetophonon reson., oscillatory amplitude and damping 78—47813
InSb:Cr, press. effects on transport props. 78—56146
p-InSb:Cu(Zn) film, heavily doped, ionized impurity scatt., Hall effect and DC cond. meas. 79—99643
p-InSb:Ge, proton irrad. defects energy level scheme, transport props. meas. 80—96576
p-InSb:In, two-phase polycryst. films, negative magnetoresist. 80—11011
InSb:S, ion implanted, Hall effect meas. 77—20342
InSb:S(Se)(Te), reson. states and reson. scatt., elec. props. 80—49738
n-InSb:Zn, Zn diffusion out of implanted layers, free hole mobility 79—10984

carrier mobility continued
- InSb-NiSb two-phase system, electron scatt. mechanism *(Russian)* 78—6373
- InSb-type semiconductor, inelastic scatt. of electrons by optical phonons 78—76073
- $InSb_{1-x}Bi_x$, multitarget RF sputtering, metastable phase, conductivity transition 80—76178
- n-InSe, layered semiconductor, current-voltage characts. investig., 130 to 400K 77—4342
- In_2Se_3-Cu_2S system, electrophys. props., influence of 1-4% Cu_2S 80—20219
- In_6Se_7, single cryst. prep. and electrophys. props. 79—43129
- In_2SnO_3 film, effect of ambient atmosphere during annealing, elec. props. 80—97510
- KCl, coloured, trap-controlled photoelectron mobility, transit-time expts. 77—72880
- KCl:Tl, hole capture kinetics, influence of autolocalised and zone holes *(Russian)* 80—54714
- $KNbO_3$ reduced, phase hologram recording sensitivity, energy transfer, photovoltaic effects 80—78799
- LaB_6 film, prep. by electron beam evaporation, and optical and elec. props. 80—20793
- La_2GeSe_5, elec. props., 300 to 1100K 79—51585
- La_2O_2S:Tb, cathodoluminesc., nonlinear depend. on activator concs. 79—8190
- $La_{1-x}Sr_xCrO_3$ ($0 \leq x \leq 0.4$), localised level hopping transport 80—10974
- $La_{1-x}Sr_xVO_3$, high-temp. transport meas. 77—11917
- α-$LiIO_3$, neutron diffr. intensity enhancement under DC field, investig. 80—10462
- $LiNbO_3$, reduced, electron Hall mobility, photo-Hall meas. 77—8121
- $LiNbO_3$:Cu(Fe), light induced charge transport, photovoltaic effects, impurity states 80—80317
- $LiNbO_3$:Fe, electro-optic cryst., light induced charge transport, holographic obs. 80—70747
- $LiNbO_3$:Fe, optical damage induced by laser light, X-ray irrad., carrier mobility effects 79—33657
- $LiTaO_3$:Cu(Fe), light induced charge transport, photovoltaic effects, impurity states 80—80317
- $LiTaO_3$:Fe, electro-optic cryst., light induced charge transport, holographic obs. 80—70747
- $LuRhO_3$, elec., mag. and photoelectrochemical props. 80—96925
- MBBA(:TEAI), elec. drift mobility, carrier identification *(Korean)* 78—51998
- $Mn_{1-x}Fe_xSi_{1.7}$, solid soln. system, temp. depend of conductivity and thermo-EMF, conc. depend of Hall const. 77—11913
- MnO, electronic cond., rel. to basic processes of Mn corrosion 77—25198
- β-MnO_2 powders, Hall carrier mobility mixing rule *(German)* 78—52008
- MnTe film, elec. props. 78—43498
- $(MnTe)_{1-x}(Bi_2Te_3)_x$ ($x \leq 0.05$) solid solution, electrophys. props. 80—24925
- MoS_2, elec. cond. and Hall coefficient temp. depend. 77—28180
- $MoSe_2$, elec. cond. and Hall coefficient temp. depend. 77—28180
- $MoTe_2$, elec. cond. and Hall coefficient temp. depend. 77—28180
- NaCl:Ag, diffusion parameters of hot holes created by ionising radiation 78—47800
- Nb-Al_2O_3 cermet-type film, thermoelec. power and annealing effects 77—47911
- Nb_2O_5, electron energy spectrum by optical and thermal methods 79—69418
- $NbSe_2$(2H), low field magnetoresist. and anomalous transport props. 80—65602
- Nd_2GeSe_5, elec. props., 300 to 1100K 79—51585
- Ni film, evaporated, elec. resist. and galvanomagnetic props. 80—80411
- Ni-n-GaP:Si(Ge) contacts, doping effect in elec. props. 80—6983
- Pb-Sn-Te, solid solution, scattering mechanism of carriers 80—49710
- p-Pb_{1-x} Sn_xTe, carrier mobility, acoustical phonon and impurity scatt., deform. impurity const., conc. depend. 80—39570
- $PbBr_2$, determ. of sign and drift mobility of majority carriers *(Russian)* 79—69512
- $Pb_{1-x}Cd_xS$, metastable epitaxial films, elec. props. 78—26979
- $PbCl_2$, determ. of sign and drift mobility of majority carriers *(Russian)* 79—69512
- PbI_2 (2H), electronic transport and cyclotron reson. 79—28369
- PbI_2, determ. of sign and drift mobility of majority carriers *(Russian)* 79—69512
- PbI_2, electron hole mobility, elec. polarisation expt. 79—24023
- $PbMg_{1/3}Nb_{2/3}O_3$, carrier mobility and photoluminesc. near ferroelec. transition *(Russian)* 78—2813
- $PbMg_{1/3}Nb_{2/3}O_3$, ferroelec., crit. electron-phonon phenomena and diffuse phase transition in elec. field 79—38497
- $PbMg_{1/3}Nb_{2/3}O_3$, photolum. near ferroelec.-paraelec. phase transition 80—16100
- $PbMg_{1/3}Nb_{2/3}O_3$, photolum. and carrier drift mobility at ferroelec. transition 80—71469
- $PbMo_6S_8$, Hall effect and magnetoresistivity 78—95400
- PbO_2 and pyrolusite compressed powder mixtures, mixing rules concerning Hall effect and Hall mobility *(German)* 78—84234
- PbO_2 compressed powder magnetoresistance and apparent carrier mobility 80—35669
- PbO_2 pressed powder, Hall voltage and change of cond. in transverse mag. fields 79—4567
- PbS, microwave incremental conductivity, high-field, 77K 80—11026
- PbS:Tl, Hall and Seebeck coeffs., Hall mobility, impurity states 80—15545
- PbS_xS_{1-x} epitaxial film, Hall mobility meas., surface charge transport 77—20473
- PbSe, polycryst. film, low temp. illumination, residual cond. 77—43756
- $PbSe_xTe_{1-x}$ epitaxial layers, growth, struct., elastic strain and Hall mobility 77—15717
- n-$Pb_{0.83}Sn_{0.17}Se$, carrier mobility, 77-300K, scattering mechanism *(Russian)* 78—2486
- $Pb_{1-x}Sn_xSe$ epitaxial film, Hall mobility meas., surface charge transport 77—20473
- $Pb_{1-x}Sn_xSe$, film struct. and elec. props. 77—80708
- $Pb_{1-x}Sn_xSe$, valence zone struct. effect on mobility/inherent conc. ratio *(Russian)* 79—73437
- $Pb_{0.76}Sn_{0.24}Te$, background radiation, influence on elec. props. 80—20226
- $Pb_{0.41}Sn_{0.59}Te$, Hall coeff., elec. cond. meas. 80—44615
- $Pb_{0.72}Sn_{0.28}Te$, Hall effect and elec. cond., 77 to 480K, energy band struct. 77—76817

carrier mobility continued
- $Pb_{0.72}Sn_{0.28}Te$, Hall mobility, temp. and carrier conc. depends. *(Russian)* 77—39877
- $Pb_{0.78}Sn_{0.22}Te$:In, low current carrier conc., Hall effect, lattice constant 79—82603
- $Pb_{0.78}Sn_{0.22}Te$:In, transport phenomena, below 20K *(Russian)* 79—38074
- $Pb_{0.8}Sn_{0.2}Te$:Cd, influence of Cd doping on high field magnetoresist. and Hall effect 80—75590
- $Pb_{0.82}Sn_{0.18}Te$ films, VPE, hot wall technique, struct., elec. props. 79—37926
- $Pb_{0.82}Sn_{0.18}Te$, Hall mobility, scatt. mechanisms, temp. and carrier conc. depend. 77—55548
- $Pb_{0.83}Sn_{0.17}Te$, carrier tunnelling through potential barrier in p-n junctions *(Russian)* 78—52074
- $Pb_{1-x}Sn_xTe$ (x=0.15 to 0.20), SEM study, dislocation density, and carrier density and mobility 79—69107
- $Pb_{1-x}Sn_xTe$, Cd-In diffusion, changes in elec. props. 78—91348
- $Pb_{1-x}Sn_xTe$, cryst. growth rel. to IR detector fabrication 77—85911
- $Pb_{1-x}Sn_xTe$ film, pure and Bi doped, polycryst., struct., elec., optical props. 79—42542
- p-$Pb_{1-x}Sn_xTe$, LPE layer, carrier conc. and mobility 79—99639
- p-$Pb_{1-x}Sn_xTe$, mobility meas., impurity and phonon scatt. mechanisms 78—23091
- $Pb_{1-x}Sn_xTe$ solid solution, electron scatt. by charged Te vacancies 77—69328
- $Pb_{1-x}Sn_xTe$:In, energy spectra modifications due to comp. changes and press. appl. 80—10915
- $Pb_{1-x}Sn_xTe$:In epitaxial layers, growth, elec. props., and luminesc. 80—54542
- $Pb_{1-x}Sn_xTe$-PbTe heterostructures, MBE produced on mica and $LiNbO_3$, elec. props. study 80—88629
- PbTe, effect of pressing and sintering, study of induced defects by SEM 80—59983
- p-PbTe, energy band struct. and scattering of holes 80—10874
- n-PbTe, epitaxial, time dependent negative weak field magnetoresist. 78—64151
- n-PbTe, epitaxial layers, elec. characts. rel. to explosive evap. in closed vol. 77—89885
- PbTe film, elec. transport props. 79—42679
- n-PbTe, free carrier absorpt. and electron mobility 78—43392
- PbTe, high mobility polycrystalline layer, mol. beam deposition 79—83138
- n-PbTe, LPE layer, carrier conc. and mobility 79—99639
- n-PbTe, low temp. elec. cond. 80—20227
- n-PbTe, low temperature electrical transport, Hall effect 80—84478
- n-PbTe, noncubic (111) oriented epitaxial films, weak field magnetoresistance 80—75584
- p-PbTe, quantum oscillations in inversion layer 77—85245
- p-PbTe, relax.-time anisotropy 77—35954
- PbTe, uncontaminated films on mica sustrates, elec. props. obs. 77—76967
- PbTe, uncontaminated films prepared by mol. beam deposition, elec. props. meas. 78—15316
- PbTe, VPE film growth under near equilib. conditions 77—32526
- PbTe:As, hole conc. control, in LPE layers, plasma reflectivity and thermoelec. probe meas. 79—99640
- PbTe:In, electron mobility, temp.-independent part, Hall effect and elec. cond. meas. 80—92914
- n-PbTe:In(Cu) epitaxial films, elec. transport props. 80—75659
- PbTe-InTe, solid solns., anomalies in electron mobility 77—80772
- PbTe-SnTe, solid soln. single crysts., TSM growth and elec. characts. 78—68625
- $PbTiO_3$, photolum. and carrier drift mobility at ferroelec. transition 80—71469
- Pd_2Si film on Si, metallic, resist. and Hall mobility meas. 78—47886
- γ-PtPc, Pc=phthalocyanine, single crystals, energy band structures and carrier mobilities 77—72817
- S, flash-excited charge-transits, electrode-edge effects, meas. 80—2396
- $(SN)_x$ crystal, galvanomagnetic effects meas. 77—85246
- $(SN)_x$, elec. cond., galvanomag. effects 79—91091
- $(SN)_x$ single crystals, galvanomag. effects 79—19582
- Sb, carrier transport, magnetoresistivity, field-dependent tensor study 80—39609
- Sb-Ge (1.2 to 2.2 at.%), carrier transport, magnetoresistivity, field-dependent tensor study 80—39609
- Sb-Sn (0.5 to 1.0 at.%), carrier transport, magnetoresistivity, field-dependent tensor study 80—39609
- $Sb_{1.5}Bi_{0.5}Te_3$ solid solution, temp. influence obs. *(Slovak)* 78—30946
- Se, amorphous, carrier lifetime and drift mobilities 78—87985
- Se, amorphous, electronic props., xerographic use 80—20242
- Se, amorphous, hole diffusion obs. 77—76828
- Se, amorphous, TSC, dielec. relax. modes 77—90090
- Se liquid, pure and I doped, DC cond. and thermoelectric power *(French)* 79—56223
- Se, trigonal, acoustoelectric current saturation 80—60053
- Se:As, amorphous, pure and doped, photoelectronic preps. in glass transition region 79—4583
- Se:Tl, hole drift mobility meas. by light pulse technique 78—19086
- Se-Te film, evaporated, drift mobility of holes, elec. field and comp. depend. 77—39977
- Se_xTe_{1-x}, acoustoelectric current saturation 80—60053
- Se_xTe_{1-x}, liq., thermoelec. transport at mobility edge 80—49787
- $Se_{12}Te_{49}As_{29}Ge_{10}$ semiconductor amorphous films, field effect, trapping 80—84472
- p-Si, $^{49}BF_2$ ionised mols. obtained by implantation of 78—31003
- Si, (100) inversion layer, electromigration in two dimensional electron gas, driving force 80—84441
- n-Si (100) inversion layer mobility depend. on intersubband scatt. at low temps. 79—95506
- Si, amorphous, control of dihydride bond density using RF sputtering, dark anal. and photocond. 80—34327
- Si, amorphous, doped, density of states determ. from transport meas. 80—49720
- Si, amorphous, doped, drift and Hall mobility, photocond. 79—65477
- Si, amorphous, electron and hole drift mobility meas. 78—19027
- Si, amorphous, hydrogenated, electron drift mobility meas. 80—75565
- Si, amorphous, substantially doped, electronic props., review 79—87175
- Si, amorphous, transport results interpretation 80—44590
- Si, amorphous, transport results, interpretation 80—80260
- Si, amorphous CVD film photodetector for picosecond pulses 80—47101
- Si, amorphous film, drift mobility and photocond. 79—15143

carrier mobility continued
Si, amorphous film, hole drift mobility, temp. depend. 79—23973
Si, amorphous film, RF plasma deposition from $SiCl_4$-H_2, characterisation 80—66435
n-Si, carrier scatt. anisotropy, Hall mobility calcs. 77—24552
Si, charge transport properties, review 77—39851
Si, conductivity of holes at low temp., electric field depend. 77—28179
p-Si, deformed, 1/f noise, resist., mobility, and carrier density 77—8161
n-Si, deformed, thermal treatment effect on elec. cond. and dislocation mobility 80—107265
Si, doped amorphous, transport props., conductivity, thermopower, temp. depend. 79—73512
Si, drift mobility and Hall coeff. factor of holes 78—43379
Si, effective masses of heavy and light holes, from ohmic mobility data 80—80160
Si, electron drift in high elec. fields, long-time tail of autocorrelation function 80—103702
n-Si, electron heating by static elec. field 80—96894
p-Si, electron irrad., influence of acceptor impurity conc. and irrad. temp. on defect formation 79—19281
Si, electron irrad., limiting position of Fermi level, elec. cond. and optical absorpt. meas. 79—65484
Si, electron irrad. induced defect form., carrier density, mobility and lifetime changes 77—43250
Si, electron irrad. induced defects, bulk photo-EMF meas. 80—39160
Si, electron mobility is semiconductors based on dielectric function modification of Dingle pot. 79—60836
n-Si, electron-two phonon scatt. 77—47527
Si epitaxial film, correlation between electrooptical and electrical props., IR absorpt. spectra *(Russian)* 78—60453
Si, epitaxial layer deposition by ion beam methods 80—100417
Si epitaxial thin film growth on sapphire and spinel by MBE 80—76186
Si, Fermi level, minority carrier conc., effective intrinsic conc., Einstein relation 77—85209
Si film, high electron mobility, grown on sapphire at high growth rate 77—81225
n-Si films on sapphire, crystalline defects effect on elec. props. 77—20470
p-Si, heat-treated, majority-carrier mobility, anomalous temp. depend. 79—69531
Si, heavily doped, approx. of Einstein relation, carrier diffusivity to mobility ratio 79—65494
Si, heavily doped, carrier diffusion coeff. 79—47099
Si, heavily doped, carrier mobility calc., 300K 79—56215
Si, heteroepitaxial growth using SiH_4 in H_2-He atm. 80—20049
Si, high O conc., electrical and mechanical props., influence of heat treatment 77—35934
Si, high-resistivity, characterisation by Hall meas. 78—10480
p-Si, highly deformed, hole scattering 77—20309
Si, hole diffusivity, time-of-flight and noise meas. 79—56233
p-Si, hole drift vel. in high field 79—95415
Si, hole mobility temp. depend., valence bandstruct. 77—80771
Si, hot electron diffusivity, theory 77—62940
Si, hot holes, drift and diffusion 79—78110
Si implanted layers, utilisation coefficient of impurities after laser annealing 77—76437
Si, impurity-ion potential, electron-conductivity mobility, spatially variable dielectric function calcs. 79—78105
Si, influence of surface recombination rate and carrier diffusion on photocond. 80—44660
Si ingots, polycrystn., growth and characterisation from metallurgical grade source material 79—87576
Si, intrinsic, electronic properties, temp. depend. *(German)* 77—76822
Si, inversion layer, Hall effect meas. 78—56199
Si inversion layer, high field drift vel., Monte Carlo calc. 77—32087
Si, inversion layer, impurity scatt., self-consistent calc. 79—28415
Si inversion layer, press. depend. of struct. of field effect mobility 78—60216
Si inversion layers, mobility temp. depend., Coulomb and surface roughness scatt. 80—80390
n-Si inversion layers, resist. temp. depend. at liq. He temps. 80—80391
Si, ion implanted, structural and elec. profiles for double damage layers 78—2169
Si, ionised impurity scatt. limited mobility in semiconductors with spatially variable dielec. function 78—51986
Si, laser induced elec. damage, carrier removal, mobility degradation 77—80791
Si, low dislocation density, plastically deformed, electron mobility anisotropy anomaly *(Russian)* 77—80777
Si MBE layer resistivity and carrier mobility obs. *(Russian)* 80—49962
Si MNOS structures with tunnelling-thickness SiO_2 films, surface channel hole mobility obs. 78—95380
Si MOS inversion layer, subband struct., many body effects 78—64131
n-Si MOS inversion layers, Hall cond. meas. 80—39676
Si, magnetodiode, effect of mag. field on current-voltage characts. at low temp. 79—91134
Si, metallurgical grade, purification and charact. 78—56573
n-Si, microwave and far IR hot carrier mobility, Monte Carlo calc. appl. to mm. transit time oscill. efficiency 78—72184
Si, minority-carrier diffusion length and drift mobility determ. using a modulated SEM beam 79—19607
n-Si, mobility and resist. as functions of dopant density and temperature 78—2487
Si, multivalley struct., helical instability *(Russian)* 79—47101
Si, negative differential mobility and geometrical magnetoresist. calc. 77—43624
n-Si, neutron irradiated, characts. of changes in mobility 78—39135
Si, neutron transmutation doping, annealing, lattice damage 80—15163
Si neutron-prod. defects, investigation by transcond. meas. of JFETs 77—15455
Si on sapphire, residual strain effect on elec. props. *(Japanese)* 80—84522
n-Si on sapphire magnetoresistance anisotropies and electronic struct. obs. 77—20471
Si on sapphire thin film, Hall effect, magnetoresistance *(French)* 80—65601
Si p-channel MOS structure, stress effects on elec. props., press. transducer props. 80—100526
Si p-n diode, 1/f noise calc., free carrier mobility interpretation 80—54774

carrier mobility continued
Si p-n junction in surface region obtained by evaporation in UHV 78—39198
Si p-n junction radiation detectors in DC mode, temp. response nonlinearity 77—38565
n^+nn^+Si planar device, hot electron flicker noise at 78K 80—103732
Si planar structures, Haynes-Shockley expt. for students 78—28888
Si, polycryst. films, transport props. and grain boundary charact. by TEM 80—50980
Si, polycrystalline, Hall mobility 80—60006
Si, polycrystalline, phenomenological model for mobility 80—65564
p-Si polycrystalline films on graphite substrates *(French)* 78—64154
n-Si, quadratic piezoresistance, ang. depend. *(Russian)* 78—47782
Si, radiation defects, influence of dislocations on accumulation, elec. props. 80—92558
Si, radiation-doped and annealed, carrier density and mobility meas. 78—56145
Si resistivity and carrier mobility effects of dissolved interstitital O_2 77—76824
Si ribbons for solar cells, ultra high speed growth, elec. props. 80—89162
n-Si, shear deformed, Smith-Herring and mobility change piezoresistance 80—6842
n- Si, surface electron states, props. determ. at 77K 77—55598
Si, thermally oxidised surfaces, electron mobility in inversion and accumulation layers, MOS devices 80—103753
Si, transport phenomena in strong elec. fields, intervalley electron scatt. 79—56240
n-Si, uniaxially deformed, intervalley scatt., 78-300K 77—20330
Si:As, amorphous, field effect and thermoelectric power 79—33289
Si:As, effects of recoil-implanted O on elec. activation of As 79—99227
Si:As, implanted As redistrib. during annealing in oxidising ambient, carrier distrib. meas. 79—19275
Si:As, implanted through SiO_2 films, elec. props., defect struct. 80—54264
Si:As, polycrystalline, As segregation at grain boundaries, elec. props. meas. 80—75259
Si:B, dopant density and temp. depend. of hole mobility and resistivity 79—38075
Si:B, hole mobility calc. for dopant density and temp. var., resistivity meas., effective mass calcs. 80—54703
p-Si:B-SiO_2 interface in MOS structures, carrier mobility and impurity distrib. 78—34902
Si:B(Al), (P)(As)(In), ion implanted film, elec. prop. impurity depend. 80—24467
Si:B(P), ion implanted, polycryst. annealing characts. 77—24324
Si:B(P), ion implanted layers, carrier distrib. meas. precision 77—43603
Si:B(P), minority carrier diffusion coeffs. 79—99559
Si:Cr, specific resistance, activation energy of deep levels, and carrier mobility *(Russian)* 78—72146
Si:Ga (Al)(In) extrinsic detector material props. 77—89797
Si:Ga(Al), MBE, growth, struct. and elec. props. 77—89458
Si:Gd, radiation defects effect on elec. props. 77—28184
Si:H, amorphous, geminate recombination model for photoluminescence decay 80—71481
n-Si:H, amorphous, photoelectromagnetic effect 80—107845
Si:H, amorphous, Schottky diode, spectral response and hole drift mobility 80—39673
Si:H, amorphous, solar cell struct., photocurrent meas., absorpt. coeff. 80—50960
Si:H, amorphous, solar-cells, charge collection and spectral response 80—85275
Si:K, ion implanted, influence of doping and annealing on carriers 78—38742
Si:Li, amorphous, elec. cond. and thermopower 79—73537
Si:Li, amorphous electronic transport, depend. on activate carrier mobility 79—69142
Si:Na ion implanted, Hall effect temp. depend., electron surface density and mobility 80—11018
Si:O, effect of interstitial O on elec. props. 77—76846
Si:P, carrier mobility and distrib. rel. to annealing, 400-910°C 78—79995
n-Si:P, electron mobility and resist., dopant density and temp. depend. 77—76816
Si:P, heavily doped, electron mobility carrier conc. relationship 79—65470
Si:P, heavily doped, influence of impurities and crystalline defects on electron mobility 79—78095
Si:P, incoherent light flash annealing, elec. props., backscattering spectra 80—97504
Si:P, neutron transmutation doping, elec. props. rel. to neutron fluence 80—96555
Si:P, polycryst., neutron transmutation doped, elec. props. 78—34836
Si:P film, polycryst., heavily doped, mobility and carrier conc., optical determ. 80—66314
Si:P(B) solar cells, minority carrier lifetime mobility rel. to impurity conc. 80—55848
Si:Sb, epitaxial film, growth by mol. beam technique 80—2292
n-Si:Sm,P, electron irrad. effects *(Russian)* 77—66168
Si:Sn, thermal conductivity, Hall mobility depend. on Sn conc., phonon-defect scatt. 80—29232
p-Si-As_2S_3 isotype crystalline-amorphous heterojunctions, electrophysical props. 79—24063
Si-As-Te glass, thermoelec. power and DC cond., temp. depend. 77—62955
Si-H amorphous film, reactively sputtered, prep. and props. 79—78889
Si-SiO_2, interface free carrier mobility in inversion layer, influence of polar phonon scatt. 79—73597
Si-SiO_2 boundary, surface charge transport in valence band of Si 80—70789
Si-SiO_2 in MOSFETs, inversion layer carrier mobility, theory 80—60094
Si-SiO_2 interface, effect of thin transition layer on electron mobility and energy levels 77—20458
Si-SiO_2 interface, effect of N_2 annealing on electron scatt. 79—42660
Si-SiO_2 interface, remote polar phonon scatt. in Si inversion layers 80—80095
n-Si-V_2O_5 system, carrier transport mechanisms 77—62999
$Si_{1-x}B_x$:H, amorphous films, thermopower and cond. for mixed band and broad tail state cond. 80—49786
n-SiC, 6H, epitaxial layer, saturated electron drift velocity meas. 78—19168

carrier mobility continued
n-SiC, 6H polytype, expitaxially grown, electronic props. meas. 77−39975
SiC, cubic, magnetoresistance and Hall mobility, field and orient. depend. *(Russian)* 77−69346
SiC, growth from soln. in fused Si, temp. gradient method in Tb vap. 78−35301
SiC polytypes deformed, resist. anisotropy in (0001) plane 80−20198
n-SiC, saturation of electron drift velocity in strong electric field 77−76840
SiO_2, amorphous, defect-controlled carrier transport 79−91049
SiO_2, amorphous, high-field transport of excess electrons and holes 77−89767
SiO_2, amorphous, time-resolved hole transport, small polaron model 77−43598
SiO_2, amorphous charge transport and storage 80−6864
SiO_2, amorphous electron transport and breakdown at high elec. fields 79−78108
SiO_2 layers, thermally grown, undoped and ion implanted, elec. props. 78−23187
SiO_2, mobility and trapping of ions, Si-SiO_2 interface states 80−92985
SiO_2-Si MOS capacitor, two-stage process for building up of radiation induced interface states 80−20313
SiO_2-Si MOS system, ion irrad. effects on struct. and electrophysical props. 80−6995
SiO_2-Si:A, effects of recoil-implanted O on elec. activation of As 79−99227
Si_2Te_3, passivated single cryst., elec. conductivity 78−95299
p-Si_2Te_3, photoelectric props., luminesc., hole lifetime and trapping 77−39892
Si_3Te_3, photoconductivity of cryst. with clean surface 77−4395
$Si_{12}Te_{48}As_{30}Ge_{10}$ amorphous film, high-field transient conduction 78−43500
$Si_{12}Te_{48}As_{30}Ge_{10}$, amorphous film, elec. cond. mechanisms, temp. depend. *(Japanese)* 78−80078
$^{30}Si(n,\beta)^{31}P$ transmutation doping and electrical characterisation 78−10071
Si(100) inversion layers, magnetoelec. and piezoresist. evidence for mobility domains 77−4447
Si(100)-SiO_2 interface, mobility in Si inversion layers, screening and neutral impurity effects 79−28412
SmB_6 film, prep. by electron beam evaporation, and optical and elec. props. 80−20793
Sm_2GeSe_5, elec. props., 300 to 1100K 79−51585
SmS, Hall effect near semicond.-metal transition 77−62968
SmS, metallic, determ. from transmission, refl. and absorpt. spectra 78−19587
SnO_2 doped films for spectral-selective surfaces, refl. and elec. props. meas. 79−74013
SnO_2 film, doped, electron effective mass and elec. props., carrier density depend. 77−43750
SnO_2 film, mobility limitation by intercrystalline potential barrier, tunnelling effect 77−66210
SnO_2, transparent electrode deposition on PLZT ceramic, elec. and opt. props. 78−74848
SnO_2:P, CVD films, elec. props., cryst. to amorphous transition effects 80−107933
$Sn_{1-x}Pb_2Te$, elec. and struct. props. of epitaxial layers *(Russian)* 78−64147
$Sn_{1-x}Pb_xTe$, film, production under quasi-equilibrium conditions 80−45241
SnSSe, electron mobility, elec. cond. and Hall effect meas. 78−80004
$SnS_{2-x}Se_x$, electron mobility elec. resist. and Hall constants 79−28346
SnSe, sublimation growth, deviation from stoichiometry, elec. props. 78−76594
SnTe, film, heat treatment in air, effect on struct., props. 79−11037
SnTe-MnTe, degenerate semicond., anomalous Hall effect 80−29420
SnTe-PbSe mixed system layers, struct. and props. *(Russian)* 77−28082
$SrTiO_3$, photolum. and carrier drift mobility at ferroelec. transition 80−71469
$SrTiO_3$, pure and Nb doped, heat treated, Hall effect, electrical cond., optical absorpt., defect states 78−47812
$SrTiO_3$:B layers, ion implanted, conductive props. Hall mobility, defect energy levels 79−82693
Te, a-edge dislocated crystals, mobility anisotropy 80−107781
Te, cryst., hole mobility anisotropy, effect on Hall coeff. 79−7847
Te, dislocations influence on galvanomag. props. 80−54722
Te, elec. props. anisotropy, influence of deform. and annealing 77−15859
Te, electron irrad., mobility increase due to defect prod. 80−24501
Te, electron irradiated, dose-depend. and recovery behaviour of transport props. 78−71761
Te, electron mobility, elec. field depend., 77K 77−85233
Te film, Hall consts., thickness depend. of mobility 79−87171
Te film, on TGS substrate, ferroelec. field effect 79−42675
Te film, polycryst., hole mobility, influence of tunnelling through barriers on grain boundaries 77−43748
Te film, thermally evaporated, elec. cond., Hall voltage and thermoelec. power 77−47913
Te films, elec. props., 77 to 450K, thermal width of band gap 79−51698
Te, films, elect. and galvanomag. characts. 79−33365
Te, hole mobility anisotropy in edge dislocated cryst. 80−24936
Te, induced acceptor levels and free-carrier mobility due to $\vec{c}$-screw dislocations 77−89730
Te, mag. inversion of Hall effect *(Russian)* 77−4376
Te, photoconductivity spectrum in 1.6-4.2K band, nonequilibrium electron mobility *(Russian)* 77−11960
Te, photoconductivity under pulse excitation conditions, scatt. mechanism and carrier mobility meas. 80−2425
Te, piezoelectrical free-carrier scatt. by screw dislocations, Hall effect and cond. meas. 80−24926
Te thin film, thermoelec. EMF, Seebeck coeff., elec. cond. structural depend. 79−78230
Te, two types of carriers 80−60013
Te, undoped, elec. cond., magnetoresist. and Hall meas., hydrostatic press. effect 77−47830
Te, warm hole conductivity 78−72160
Te:Cu films, elec. transport props. 80−60120
Te:Sb, 96 to 500K, cond. Hall const., hole mobility, conc., dislocation effects *(Russian)* 78−64039
$Te_{81}Ge_{15}As_4$, Hall effect in electrically switched memory state 80−2403

carrier mobility continued
TiO_2 electrode, carrier density determ. by optical absorpt. and photoelectrolysis spectra 80−71462
Ti_4O_7 and $(Ti_{1-x}V_x)_4O_7$, metal-insulator transitions, EPR, elec. and mag. props. 80−2336
TiS_2, evidence for semicond. props., Hall coeff., refl., cond., thermoelec. power 80−20220
$TlInSe_2$-$TlPrSe_2$ system, struct., elec. cond., and thermoelec. props. 79−87119
VH_x, reluctance, Hall effect 79−38102
VO_2, film, semicond.-metal transition, carrier density, mobility and Hall meas. 77−43751
V_2O_5 containing melts, activation energy of electron mobility and electronegativity 77−35971
V_2O_5, ferroelec. semicond., dielec. and elec. meas. 80−60516
V_2O_5, hydrated amorphous, EPR, struct. and electron mobility *(French)* 77−15319
V_2O_5-P_2O_5 glass, in metal-semicond.-metal struct., TSC of dielec. relax. *(Russian)* 77−35998
WSe_2, elec. cond. and Hall coefficient temp. depend. 77−28180
YIG-InSb system, surface magnetostatic wave interaction with drift electrons *(Russian)* 77−12185
Zn_3As_2:Cu(Te), single crysts., gas phase growth, elec. props. 79−15598
$Zn_{1-x}Cd_xS$, reactively sputtered polycryst. film, cond. mechanism and grain boundary barriers *(French)* 77−76972
$Zn_xCd_{1-x}S$ films, spray pyrolysis, elec. props. 80−75657
$ZnGeP_2$, synthesis, characts., applic. to laser windows *(French)* 78−80467
$Zn_xHg_{1-x}Se$, band struct. from Shubnikov de Haas effect and hydrostatic press. meas. 80−49599
$Zn_xHg_{1-x}Se$, current carrier scattering mechanism 80−65546
$Zn_xHg_{1-x}Se$, galvanomagnetic effects, Shubnikov-de Haas oscill. determ. of band struct. 80−6884
$Zn_xHg_{1-x}Te$, vacancy electron states, acceptor behaviour, electron mobility 80−70193
$Zn_xHg_{1-x}Te$, vacancy mech. of resorption of Hg droplets 80−39070
$Zn_{1-x}Mg_xTe$ alloys, high purity, metallurgical and analytical methods of prep. 80−40247
ZnO epitaxial layers, rel. between elec. and photoluminesc. props. and their deposition conditions 79−95530
ZnO, field-effect mobility in accumulation layers on polar surfaces 79−73509
ZnO films, RF sputtered single-cryst., on sapphire, struct. and SAW props. 80−80105
ZnO, polar faces, space charge layers, anomalous electron mobility 77−62981
ZnO single crystals, quantised accumulation layers temp. depend. of electron Hall mobility 79−60909
ZnO sputtered films, undoped and Ga doped, props. rel. to deposition conditions 80−107935
ZnO surface extreme accumulation layers due to He^+ ions 77−72909
ZnP_2, pure and doped, carrier mobility and conc., donor and acceptor energy levels, 190 to 380K 78−84217
ZnP_2, trapping levels, TSC and thermolum. meas. 79−15115
ZnSe, carrier mobility and deform. pot. const. determ. 79−91051
n-ZnSe crystals, electron scatt. mechanisms, high mobility 80−34433
a-ZnSe, elec. and optical meas., Mott-type model for amorphous semicond. 78−2414
ZnSe film, MBE and resistivity 79−100059
n-ZnSe, impurity band, Hall effect, elec. cond., mobility and magnetoresist. expts. 77−35888
ZnSe:Al(As), high temp. electron mobility, lattice scatt. and ionized impurity scatt. 79−91042
ZnSe(:Ga)(Al), effect of thermal treatment and doping on elec. props. 77−85223
ZnTe films, residual conductivity, Kikuchi lines of electron diffr. pattern 79−91173
ZrO_2, cubic single crystal, colour centres 77−15410
ZrO_2:Y_2O_3, solid electrolytes, charge carrier conc. and diffusion 77−11930
ZrO_2-Y_2O_3 (10 mole%), electron transport, elec. induced p-n junction 77−43597
ZrS_3, quasi one-dimens. semicond., elec. transport props. 80−107790

carrier relaxation time
see also electron relaxation time (metals)
amorphous semiconductors Hall mobility be modified relaxation time approx. 80−24950
anthracene, excess electron and excess hole cryst., drift mobility, depend. on press. using constant-relaxation-time approx. 79−60709
bipolar semiconductor, strong EM wave propagation, effect of generation-recombination processes *(Russian)* 79−78115
compensated semiconductor, theory of transient processes 80−24930
electron-electron relaxation in ultraquantum mag. fields, electron-phonon interactions 77−4371
electron-hole plasma current layering, electron cooling length, momentum scatt. 80−6890
energy relaxation of photoexcited hot electrons at very low temperatures 78−91724
ethyl cellulose films, secondary ion injection 79−24094
ferromagnetic semiconductor, hot electron relax. *(Russian)* 79−51593
ferromagnetic semiconductors, hot electron relax. time 80−59996
free charge carriers in solids, high order harmonic generation 77−76804
p-GaAs, spin relaxation of photoelectrons 77−85207
graphite intercalation compounds, electronic props. in dil. limit 77−47714
heavily doped semiconductor, correction to static elec. cond. due to many-centre scatt. 80−2374
heavily doped semiconductors, static conductivity in terms of transport relax. time 79−56213
III-V mixed semiconductor, electron mobility theory 78−84210
inhomogeneous semiconductor, negative photocond. and IR quenching of residual cond. 77−24587
injection lasers, intraband electronic relaxation effect on relaxation oscillation 79−81433
n-InSb, photoconductivity relax. temp. depend., carrier recomb. processes 77−4363
isotropic semiconductor, differential relax. times and diffusivities of hot carriers 77−62936
isovalent impurity long range potential, role in electron scatt. 80−10966

carrier relaxation time continued
metal, neutral and charged impurity scattering, Matthiessen's rule 79—47081
metallic films, grain boundary scatt., Hall coeff., theory 80—88649
MOS structure, nonequilibrium depletion layer relaxation 79—56325
narrow band gap semiconductor multilayers with p-n junctions, relaxation and photocurrent analysis 79—7883
narrow band-gap semiconductor, energy depend. relax. time, EM response of electrons 78—60142
p-n junction, US wave effect on effective current relaxation time in base 77—4434
p-type semiconductor, effective mechanism of hot electron energy relax. 78—26878
phenazine, charge carrier transport rel. to cryst. and band struct. 79—95403
piezoelectric semiconductor, scatt. anisotropy in longit. quantizing mag. fields 78—26890
piezoelectric semiconductor film, mobility of hot electrons 78—56247
polar semiconductor, nonlinear transport, field-dependent relaxation time 80—6866
polymer electret, absorpt. and relax. of charge 80—6942
prep. by electron beam evaporation, and optical and elec. props. 80—20793
quasi-two-dimensional semiconductor, warm carrier relax. via acoustic phonons 77—43694
relaxation process in quantising mag. field, elastic scatt. mechanisms, relax. matrix 79—15166
semiconductor, barrier cond. mechanism, effects due to emptying of local levels by electric field 79—65468
semiconductor, carrier relax. time and effective masses determ. by microwave photocond. meas. *(Russian)* 78—19071
semiconductor, carrier relaxation time anisotropy effect on free carrier dispersion studies 80—84474
semiconductor, electron relaxation, electron-hole interaction effect 78—10437
semiconductor, gapless, bottleneck effect at low temp., hole heating 78—10470
semiconductor, hot electrons, photoexcited in quantizing mag. field, energy distrib. calcs. 79—42586
semiconductor, influence of strong inelastic scatt. on electron energy relax. 79—23959
semiconductor, inhomogeneous, carrier statistics and thermal relax. *(Russian)* 77—4333
semiconductor, IR absorpt. and optical relax. time of free carriers 80—66206
semiconductor, monopolar, anisotropic, US amplification at intermediate freq. *(Russian)* 77—35965
semiconductor, n-type, carrier waves instabilities electron relax. time 77—4382
semiconductor, optical orientation of electrons, surface quality effects 79—11466
semiconductor, phonon conduction and relaxation times 80—107585
semiconductor, photoexcitation phenomena, low density 78—27319
semiconductor film, spin relaxation due to electric fields 77—62928
semiconductor surfaces, relaxation time spectrum of slow traps *(Russian)* 77—15937
semiconductors, pure, carrier mobility and electron state damping at low temps. *(Russian)* 80—15530
semiconductors, quasi elastic hot electron impurity scatt. in quantising mag. field 80—24938
semiconductors, relaxation regime, generalised transport eqns. 78—56139
semiconductors, spatially variable dielectric functions, ionized impurity limited mobility 79—42534
semiconductors, thermoelectrically anisotropic, carrier kinetics at low temp. 80—92893
semiconductors, thermoelectrically anisotropic 80—92894
semiinsulator, minority carrier injection effect on TSC 78—10466
solid with parabolic electron band, relaxation time oscillations in strong mag. field 79—60855
Stark-Ladder current theory 78—68035
superlattice semiconductor impurity photoconductivity electron spectrum reconstruction 80—24966
surface electrical resistivity of thin semiconductors, semimetallic films 78—91751
time resolved reflectivity of ps pulses 78—31217
very pure semiconductor, mobility calcs. including low impurity conc. limit 77—28173
zero-gap semiconductor, reson. scatt. of electrons 80—10938
zincblende narrow-gap mixed crystals, disorder scatt. 78—51985
n-Si, deep levels in p-n junctions or Schottky barriers determ., hybrid method 79—24067
AlGaAs injection lasers, undoped, estimation of intra-band relax. time 80—43335
As_2S_3-HgSe structure, anomalous photocond., relax. curves 77—55567
a-As_2Se_3 chalcogenide glass, influence of thermally induced defects on transport props. 80—49766
Au/oxide/n-GaAs struct., photocurrent relax. 80—92978
B, residual photoconductivity in single crysts. 80—20241
BaO-B_2O_3-SiO_2 system glass, electronic cond. of Ti ions 78—23095
Bi alloy, mag. field depend. electron scatt. rates, de Haas-van Alphen meas. 78—10436
Bi, diffusion thermoelectric power in mag. field, calcs. 78—56167
Bi, hole relaxation time, temp. depend., cyclotron reson. 79—47108
Bi:Sb, semimetallic alloy, microwave spectroscopy 78—87908
$Bi_{0.88}Sb_{0.12}$, semiconducting transport props., 2 to 100K 80—59989
n-$Cd_{0.3}Hg_{0.7}Te$, photoelec. props. at 78K, relax. time, minority carrier extraction 80—107864
CdSe, dark current relaxation 80—44613
CdTe, time-resolved spectra, carrier relax. time, phonon lifetime 80—11433
GaAs, compensated, Shubnikov-de Haas oscills. 77—11941
n-GaAs, conductivity relax. times in warm electron range, intervalley transitions 77—55537
GaAs, distribution function relax. times 77—55541
GaAs, epitaxial, nonequilibrium carrier relax., recombination radn. 80—7416
GaAs epitaxial film recombination props. *(Russian)* 80—49812
GaAs, film, radiative relax. time, nonequilibrium carriers 78—84657
n-GaAs, high temp. mobility anal. in three-valley ($\Gamma_6{}^c$-$L_6{}^c$-$X_6{}^c$) model 79—99544

carrier relaxation time continued
GaAs, impurity centres ionis. by Auger electrons, carrier relax. *(Russian)* 79—51594
GaAs, optical absorption spectrum dynamics using sub-ps. optical pulses 80—11431
GaAs, optical cond. of free carriers 78—19436
GaAs, photoexcited, carrier relaxation determ. from time resolved transmission spectrum changes 79—99583
GaAs, photon transfer of excitation of nonequilib. carriers, conc. profile and relax. time 77—69907
p-GaAs, piezoresistance, relax. time for heavy and light holes determ. 79—19599
n-GaAs, submillimetre cond. and carrier heating, two-electron-temp. model 77—20349
GaAs, temp. depend. of intervalley gap from Schottky diodes meas., thermionic emission theory generalization 79—73586
GaAs, time-resolved spectra, carrier relax. time, phonon lifetime 80—11433
GaAs, transient and steady-state electron transport props. 77—39812
n-GaAs, uncompensated, mech. of energy relax. at low temps. 77—62921
n-GaAs:Sn epitaxial layer, free carrier relax. time, transverse magnetoplasma refl. 77—90212
GaAs-$Al_xGa_{1-x}As$ multilayer, photoluminesc., electron spin orientation 80—25453
$GaAs_{1-x}P_x$ solid solution, disorder scatt. Hall mobility meas. 77—69350
GaInAsP-InP DH laser, relaxation and delay in oscillations 78—13709
GaSe:Sn, single crystal, transient photoconductivity *(Russian)* 79—11171
$Ga_{0.25}Te_{0.75}$, amorphous film, off-state recovery after nonosecond switching 80—44681
Ge bicrystal cleavage plane, Shubnikov-de Haas oscills. *(Russian)* 78—64094
n-Ge, carrier relax. time, mag. field effects, rel. to Hall effect 80—39608
Ge, carrier relaxation rate temp. depend. and pair density in large electron-hole drop 80—75509
Ge, compensated, impurity photocond. relax times 80—88592
Ge, electron scatt. by charged impurities under cyclotron reson. conditions 77—63286
p-Ge, hot hole relax., IR saturated absorption, LO phonon emission 77—28569
Ge, hot phonon influence on energy relax. of high-density carriers 79—82608
p-Ge, hot-hole relax. rates by saturation spectroscopy 77—65611
Ge, irradiated and annealed, cyclotron reson. linewidth investig. of electron scatt. 77—55707
p-Ge, noise, energy relax. time and diffusion of hot holes 77—76839
N-Ge, phenomenological cond. relax. time, uniaxial stress and electron-electron scatt. effects 77—15862
p-Ge, photoexcited charge carrier capture by shallow impurity centres *(Russian)* 80—15571
Ge, plasma excitation, ultrafast optical props. 78—31248
p-Ge, relaxation dynamics and photoconductivity 79—51636
Ge surface, X-irradiated, slow relaxation of surface states 77—62980
Ge:Au under laser illumination, non-equilibrium conduction 80—6896
Ge-GeO_2, MIS struct., electrophysical characts. 79—82680
^4He, liq., HF cond. of electrons trapped at surface 78—10238
$Hg_{1-x}Cd_xTe$, quasi-local acceptor levels and electron mobility 78—67974
HgTe-type crystals, inverted band structure, influence of interband scattering on cond. *(Russian)* 79—51563
n-InAs, photoelectric props., inhomogeneous impurity distrib. 80—107867
InP, free carriers, freq. depend. relax. time 80—2385
n-InP, submillimetre cond. and carrier heating, two-electron-temp. model 77—20349
InP, transient and steady-state electron transport props. 77—39812
n-InSb electron heating and energy relaxation time in quantising mag. field 80—10996
InSb, electron spin levels resonant excitation, photolum. 80—25454
n-InSb, helicon wave propag., quantum mechanical features 79—42571
InSb, hot electron energy relax. time 77—80783
n-InSb, hot electrons relax. in quantising mag. field *(Russian)* 80—6876
p-InSb, magnetophonon reson. of holes 79—95424
n-InSb, undoped, press. induced slow relax. of free electron conc., Hall coeff. meas. 77—47833
InSb:Cr(Zn)(Mn)(Ge), recombination of nonequilibrium carriers 79—65496
$In_{0.25}Te_{0.75}$, amorphous film, off-state recovery after nonosecond switching 80—44681
LaB_6 film, prep. by electron beam evaporation, and optical and elec. props. 80—20793
MnP_2, nonequilibrium luminesc. and relaxation processes, 25 to 300K *(Russian)* 78—80415
MoO_3, film and cryst., long range potential centres 78—30920
NaCl:Ag, diffusion parameters of hot holes created by ionising radiation 78—47800
PbS, conduction band nonparabolicity and carrier scattering mechanism 79—11065
PbSe, film with pot. barrier, magnetoresistance anisotropy 79—91172
n-PbSe, polar semicond., mag. field influence on high-freq. relaxation time 79—95438
$Pb_{1-x}Sn_xSe$, plasma reflection spectra, carrier effective masses and relax. times determ. 78—2858
$Pb_{0.82}Sn_{0.18}Te$, narrow band gap, relax. time for Shubnikov-de Haas effect 78—80006
$Pb_{1-x}Sn_xTe$, energy spectrum under hydrostatic pressure 79—65381
n-$Pb_{1-x}Sn_xTe$, galvanomag. effects, alloy scatt., 4.2K 77—39880
p-$Pb_{1-x}Sn_xTe$, increase in relax. time on transition to zero-gap state under press. 79—69413
$Pb_{1-x}Sn_xTe$ narrow gap solid alloys, hole Fermi surface, galvanomag. and oscill. effect obs. *(Russian)* 77—69345
p-PbTe, relax.-time anisotropy 77—35954
Si, (100) surface, effective mass and collision time 78—64081
Si, amorphous evaporated, picosecond optoelectronic detect., sampling and correlation meas. 80—100478
n-Si, carrier relax. time, mag. field effects, rel. to Hall effect 80—39608
Si, electrical conductivity, inertia of electron heating, expt. and theory 80—65613
p-Si, millimetric and far IR cond., evidence for interband transitions 78—52022
p-Si, millimetric and far-IR cond., freq.-depend. carrier relax time 80—34460

carrier relaxation time continued
Si on sapphire thin film, Hall effect, magnetoresistance *(French)* 80—65601
n-Si, phenomenological energy relaxation time, temp. depend. 78—43409
n-Si, relaxation of electron energy, carrier-density dependence 80—107809
Si surface, metal doped, recomb. of nonequilib. carriers at high excitation rates 79—7835
Si, transport phenomena in strong elec. fields, intervalley electron scatt. 79—56240
n- Si:O, charge carrier scattering on neutral centres 80—49762
Si(100)-SiO_2 interface, mobility in Si inversion layers, screening and neutral impurity effects 79—28412
SmB_6 film, prep. by electron beam evaporation, and optical and elec. props. 80—20793
Te, interband photocond. at up to 10 kbar, 1.6-200K 77—47850
p-Te, photocond. and lifetime, surface trapping, spectral distrib. 78—34840
n-ZnSe, long persistent cond. relax. and frozen cond. 80—54735
p-ZnTe, cyclotron resonance from photoexcited electrons 79—69723
carrier scattering at surfaces *see surface scattering*
carrier scattering by dislocations *see dislocation scattering*
carrier scattering by impurities *see impurity scattering*
carrier scattering by point defects *see point defect scattering*
carrier telephony
2.1 km optical cable link installation, TV and telephonic transmission expt. *(German)* 78—33890
fibre optics in telephone carrier systems 79—81528
PCM system, optical fibre cable development 78—9458
carrier traps *see electron traps; hole traps*
carry circuits *see adders*
CARS *see coherent antiStokes Raman scattering*
cartography
aerial photographic analysis and stereographic mapping with electro-optical pattern recognition 77—19186
aerial photographic equipment developments, aerial survey camera and navigation telescope 77—66997
aerial photography rapid screening by optical power spectrum analysis 78—63033
aerial survey image interactive hybrid optical/video processing system 77—53254
aerotriangulation by Skylab Earth terrain camera photography 77—33209
Africa CITHARE project, soil thermal inertia and humidity cartography by geostationary satellite 80—76980
air pollution effects indicators, provisional map 78—81387
air survey cameras, calibration techniques 80—18035
airborne bathymetric charting using pulsed blue-green lasers 77—29447
albedo maps from global surface model, land use basis 80—12394
Arctic Ocean, bathymetry, seismicity and gravity maps in geophysical review *(French, English)* 79—48452
Arctic Ocean, bathymetry and sea-floor features morphology 79—48453
E.Asia, atmospheric noise source contour maps 77—91245
tropical Atlantic, element charts, construction method *(Russian)* 77—60485
Atlantic, MODE-I region bathymetry 77—56615
N.Atlantic, precipitation maps 80—51523
atmospheric pollution, cartography *(French)* 80—7989
automated pattern recognition with hybrid optical/digital systems 78—63037
automatic, using electron beam film recording equipment 77—10120
automatic contouring of faulted subsurfaces 77—45170
automatic drafting system, appl. to problems of geodesy *(German)* 78—15952
base metal exploration with rapid pyroclastic mapping 77—53052
bathymetry, deterministic and random error model of multibeam hydrographic sonar system 79—3873
Bavaria, development of present 1:500000 outline map *(German)* 77—2081
S.Brazil, structural mapping, mineral deposits rel. to tectonics 77—81855
Brazil Patanal, drainage network mapping from Landsat-2 imagery 80—81944
Bucharest, seismic microzonation map 79—88280
cadastral maps and new technical developments *(German)* 77—70589
camera, remote sensing, film and solid-state-array types comparison w.r.t. imagery 78—4723
Canada, vertical crustal movements, map 80—109130
Caucasus, max. possible earthquake and shakeability maps 77—70607
Chaudes-Aigues region, surface anomaly, aerial thermographs and isopleth map 77—21714
coastal photogrammetric mapping 80—104960
color map automatic digitisation, spectral classification scanner technique 80—17424
colour IR film for mapping and multispectral photointerpretation 79—25356
colour maps from black and white photographs in remote sensing 80—109270
colour plotter system, application to computer graphics 80—4130
computer-aided spatial derivatives mapping 77—40965
computerised file system, for geologic index maps updating 77—2252
contour maps, evaluation method for determ. relative accuracies 77—90989
contour maps, structural description, weather map appls. 80—101419
contour maps classification problems 79—79999
contouring from digital terrain models, accuracy 79—84085
coordinate system for aerial frame photography 79—2179
coordinatograph, precision, 120×120, accuracy of applicability 80—52158
cultivated and natural vegetation mapping 77—56781
curvimeter for meas. of rivers, contours and basins on maps 80—26650
Dakota landforms and drainage patterns, IR thermal imagery remote sensing 80—81892
data bank model, appl. to geological data 77—53199
Death Valley, geological interpretation from composited radar and Landsat imagery 80—56647
deep sea floor mapping instrumentation 77—5358
densification of ground control networks, computer program package *(German)* 80—94452
desert environment mapping and monitoring, worldwide 77—78489
cartography continued
digital map revision 80—17422
digital stereo mapping, flexible algorithm 79—84543
Digital Terrain Model, use of electronically controlled drawing machines *(German)* 78—20348
digital terrain modelling, symposium (St. Louis, Missouri, 1978, May 9-11) 79—84083
distributed data bases for structured data 77—53200
Earth conductivities, mapping via multifreq. airborne EM system 79—5446
Earth resources satellite data information processing *(French)* 79—53526
Earth surface, three-dimensional mapping onto telluroid 78—65171
earthquake acceleration hazard map, sensitivity to input seismic parameters 79—44111
earthquake risk maps for Western Central Europe *(German)* 79—8600
EEG field plotting method for isopotential maps 79—39542
energy balance maps from remotely sensed imagery 77—37433
estuary mapping, classification algorithms for Landsat data 78—40567
Europe, preliminary heat flow map and tectonic and geophysical implications 79—70765
European USSR, heat flow map 79—70766
feature space mapping, linear transformation for improved colour image interpretability 77—78499
Friuli earthquake, 1976 May 6, isoseismal map 78—24245
Friuli earthquake (1976, May 6), isoseismals map 79—44137
geodetic solutions based on NAVSTAR Global Positioning System satellites Doppler meas., accuracy 79—100803
geological, automatic pattern recognition applic. 77—21953
geological map automatic compilation system design *(Russian)* 77—41025
geological surveys, Quaternary, automation 77—53209
geomagneic field map of USSR, use of aeromagnetic control network 77—21676
geomagnetic contour maps, optical filtering 77—25797
geophysical mapping and remote sensing by optical filtering 80—101458
Georgia Strait, British Columbia, seismic risk maps 79—88274
GEOSAT, geological industry reommendations on remote sensing from space 78—69495
geoscientific maps for planning 79—84080
Ghana, gravity mapping and interpretation 77—78080
graphical approximation methods applied to mapping of free water surfaces *(French)* 79—96771
gravity contour maps, optical filtering 77—25797
gravity from 60°N to North Pole, free-air anomaly maps 79—48391
Great Britain, global solar radiation distrib. on horizontal surface, monthly maps 79—79959
Great Britain triangulation, geocentric positioning via satellite Doppler techniques 79—29695
gridded data convolution and padding algorithm 78—69475
groundwater contour mapping in Venice, stochastic interpolator method, theory 80—8353
groundwater contour mapping in Venice, stochastic interpolators method, results 80—8354
Guatemala City, 1976 February 4, map of landslides during earthquake 79—88276
Gulf Stream, large-scale frontal study using Geos 3 radar altimeter data 79—5488
heterodyne optical correlation, photogrammetric appls. 77—42497
holographic terrain displays in 3D 78—78979
hydraulic fractures mapping technique 78—69543
hydrographic charting by multispectral and ocean colour scanners 77—5368
hydrographic charts preparation, appl. of LANDSAT MSS imagery 79—29894
hydrothermal alteration mapping, airborne spectroradiometric data anal. and LANDSAT data appl. 79—34973
image evaluation methods, project SENTINEL SIGMA for Air Force, resolution meas. 79—31826
image scanner technology for digital mapping systems 80—85773
inland wetland photointerpretation evaluation, cell analytical method 79—29898
interactive computer graphical systems appl. *(German)* 79—21023
International Orthophoto Expt. 1972-76 results 77—44903
ionosphere F_2-layer, analytic description of geometric parameters maps by spherical functions 79—53616
Irish gravity map, trend surface anal. 77—2080
ISO FORTRAN IV program for generating isopleth maps on small computers 78—57157
isoseismal map, Warrnambool earthquake, (1903 July 14) 79—92506
S.Italy, seismic risk map preliminary results 79—44113
Japanese Islands region, geophysical data compilation and maps *(Japanese)* 80—67332
lake level fluctuations since 30000 yr BP, global maps 80—51447
Lake Lugano, bathymetric map 78—96252
Lambert, Johann Heinrich, 1728-1777, biography *(German)* 79—17174
land use mapping by radar imagery, techniques 80—8449
land use mapping using radar imagery 77—73886
land use maps, remote sensing and computer appls. 77—5349
land-use map, remote sensing derived, accuracy test method 78—7805
land-use map accuracy testing, sampling designs 80—17226
land-use mapping, evaluation of LANDSAT image data 80—101443
land-use mapping by machine processing of LANDSAT-1 data 77—78467
land-use maps extraction, from satellite data 80—76899
land-use/land-cover mapping from aerial photographs 80—41569
LANDSAT digital thematic maps, radiometric interpretive legend 77—78468
Landsat imagery geometrical correction *(French)* 80—81889
Landsat MSS points location on maps, methods and accuracy 79—2389
LANDSAT scene- and map-corrected images using mini computer 78—7806
LANDSAT snow mapping data 77—82061
large format camera for Space Shuttle, cartography appl. 80—4232
laser bathymetry for near-shore charting appl., preliminary field test results 79—5679
laser point transfer machine, TRANSMARK, performance testing 78—81438
Light-Behind Camera photography for sea floor mapping 77—5359
line scanning sensor, spatial filtering design 79—53527

cartography continued
lunar colorimetric map, absorpt. strip intensity distrib. at 0.95 μm *(Russian)* 79—44381
macroseismic intensity map of Friuli, 1976 May 6 earthquake 78—65203
magnetic anomaly map of Republic of Djibouti, reduction techniques 80—61753
magnetic maps for Italy, regional survey 78—65175
map intensification from small format camera photography 79—25354
Mapsat (Automated Mapping Satellite System), proposed parameters 80—17468
marine boundary delineation, geodetic aspects *(German)* 77—91155
Mars, synthetic topographic contour mapping 78—45253
microfilm mine maps, correlation with topographic maps 78—32259
mountain territories, formal morphostructural zoning 77—73876
nautical, near-shore charting, laser appls. 80—8463
ocean floor, real-time optical mapping system [ocean floor] 80—8464
ocean tides mapping with satellites, computer simulation 79—39880
oceanic rainfall maps, global climatic features 78—65379
offshore shoal positioning using LANDSAT imagery 77—73883
orthomapping review 78—88777
orthophoto mapping, accuracy prediction 77—40970
orthophotography, history, advantages and uses 77—66995
orthophotography, system errors of differential rectifiers with optical projection 77—40971
N.Pacific, precipitation maps 80—51523
Pakistan, northeast, near Skardu, structural geology mapping 77—86872
palaeocontinental maps for Early Phanerozoic and Proterozoic 79—44150
Palaeozoic base maps, palaeogeography and plate tectonics 80—41441
photogrammetric mapping, unique surface interpolation via linear prediction *(German)* 77—9321
photogrammetric meas. for field mapping *(German)* 78—92776
photogrammetry, point transfer error determ. 80—17227
photomapping, Gestalt computer-controlled system features 78—40714
photomapping using earth terrain camera, Skylab photographs quality evaluation 77—2283
planetary mapping by airbrush technique 78—53833
polynomial and Fourier trend surfaces computation 78—32245
population exposure to air pollution, satellite-aided evaluation 79—92116
position location and navigation, conf., San Diego, CA, USA, Nov. (1978) 79—25374
position meas., satellite surveyor MX 1502, microprocessor controlled ground based system 79—25377
production mapping with orthophoto digital terrain models 79—84545
quantitative cartographic analysis, SYMAP auxiliary programs, geoenvironmental appls. 79—70469
Queen Maud Land, Antarctica, ice elevation map from balloon altimetry 79—53374
radar image interpretation, line detection technique 78—61630
remote sensing system for nationwide data bank 77—78512
remote sensing using artificial satellites, Space Shuttle and European Spacelab 78—69494
resistivity mapping using combined telluric profiling technique *(French)* 78—69285
river drainage patterns, link magnitude var. with map scale 77—25723
Salt Lake City, ground response maps 79—88287
satellite imagery, anal., distortion free map projection 79—34986
satellite imagery, computer-generated gridding 77—21930
satellite mapping, by synthetic aperture radar 80—12572
sea floor mapping on Mid-Atlantic Ridge, integrated approach 77—5360
sea floor relief mapping considerations 80—46169
sea-floor mapping in real time, sonar-microprocessor equipment 80—26646
seismic microzoning, mapping method based on subsoil conditions 79—44108
seismic microzoning map of Tokyo 79—88282
seismic risk map, new proposal for Japan 79—88281
seismic velocity anomaly mapping by graphical method 80—77146
seismic zoning map, new elements 79—44105
seismic zoning problems, effect of earthquake freq.-magnitude statistical parameters 79—44112
selenodetic control network 77—37515
side-looking airborne radar appl. 78—20561
Skylab spectral channel evaluation for classification and thematic mapping 77—78500
soil moisture and geology mapping, thermal inertia method 80—8344
solute loading and chem. denudation rate mapping in Devon, England 78—69375
sound immission, city noise mapping for noise abatement 80—48533
Space Oblique Mercator projection 79—2178
stereo photogrammetry, prism correlator appl. 78—86368
stereo side-looking radar mapping, accuracy anal. 80—56646
stereo-orthophotography, method and accuracy 77—44904
stereo-orthophotography in cadastral and general mapping 77—40972
stereomapping processes 78—61631
STEREOMETROGRAPH model G with fast motor drive 77—66996
stereophotogrammetry, digital profile to contour convertor, display 77—9501
stereoplotter, orthoprinting system, TOPOMAT, appls., accuracy 78—81437
stereoplotter, TOPOCART B, accuracy and performance study 78—81436
stratigraphic units correlation from geological maps 79—62508
structural map construction for Precambrian strike complexes *(Russian)* 78—12014
structural mapping using two methods, optimal combination *(Russian)* 79—62617
Sun, orthographic projection rel. to use of solar graticules 78—16299
Taiwan, seismic zonation risk map 79—88277
Taiwan velocity risk mapping for seismic resistant building design 80—31002
W.Tennessee, wetland mapping and classification, high altitude photography 80—8340
terrain, reflexive prediction and digital modelling 79—2175
terrain evaluation methods, Mackenzie Transportation Corridor, Canada 78—20344
terrain height data and orthophoto accuracy 79—2176
thematic map accuracy, statistical testing of remote sensing 78—77372
thematic mapper, time-delay and integration CCD imager appl. 79—35098
three-dimensional geodesic mapping eqns., rel. to Earth best-known figure determ. *(German)* 78—73304

cartography continued
Tokyo, liquefaction susceptibility map 79—88309
TOPOCART-ORTHOPHOT C system for prod. of stereo orthophotos 77—66994
topographic mapping, digital terrain model appls. 79—84544
TOPOMAT all-automatic photogrammetric system for aerial photography 77—66993
Ukrainian Shield, rock mag. props. map rel. to composition and metamorphism 80—17229
United States, national seismic hazard and zoning maps status and prospects 79—44109
United States seismic hazard maps, prospects for geological data appl. 79—44110
vegetation and crop development mapping, table look-up procedure 77—78531
Venus, radar mapping by Pioneer Venus orbiter 79—48723
Venus radar mapping, Pioneer Venus Orbiter mapper design and operation 80—67495
video stereophotogrammetry, interactive computerised, for Mars Viking 1975 Lander data 78—81557
Viking Orbiter rectified photography, planimetric Martian triangulation 77—87276
volcanic eruption risk mapping 78—11856
wetland mapping in New Jersey and New York 78—77265
Windward Passage sill, bathymetric chart 77—56616
world soil map 79—57937
Zoom Transfer Scope, data transfer system for maps 80—8450

cascade control
U enriching gas centrifuge cascade, reflux effect, enrichment enhancement control 77—54346

cascade networks
see also ladder networks
linear sonar array processor finite impulse response digital filter design 80—43549
monolithic cascade CCD ultrasonic lens applications 78—22231
π-section cascade networks, appl. to wideband elec. matching of transducers 78—5626

cascade showers *see cosmic ray showers and bursts*

Cassegrain antennas *see reflector antennas*

casting
ABA poly(styrene-b-butadiene) copolymer, physical props., casting solvent effects 77—55935
aliphatic-aromatic block copolyamides, synthesis, struct. and dynamic viscoelasticity, DTA and X-ray anal. *(Japanese)* 78—31377
alloy, crystallising, impurity distrib. under suppressed natural convection temp. *(Russian)* 77—28795
austenitic crystals, inverted casting process for very rapid growth of large crystals 78—84791
brass, free cutting, machinability and mech. props., cooling rate effects *(Korean)* 77—63695
bronze 905, partially solid, die thermal behaviour in machine casting 78—6917
ceramic mould accelerated shell heat treatment models 79—76896
ceramics, slip moulding method development 78—68661
chemically hardening material cast in elastic cylindrical mold, transient thermal stresses 80—7589
continuous ingots, two phase zone critical parameters during casting *(Russian)* 80—93549
cylinder lining alloys, centrifugally cast, compatibility with hardfacing alloys 77—32726
elasto-viscoplastic thermal stress model, appl. to continuous casting of metals 79—18740
Epon 828, simple procedure for casting plates for 2D photoelastic models 79—39061
epoxy tensile coupons, method for producing silicone rubber moulds 78—72957
Fe, ingot, cast, exam. of nonmetallic inclusions, size freq. distrib. 78—39989
fluorophosphate optical glass development 80—106588
glass deformation degree rel. to optimum moulding prod. rate 79—50456
gypsum casts, improvement in impregnation method, exam. of mech. props. 78—48503
heat flow in 3-phase ESR slab production 80—10241
heat transfer anal. by finite element anal. 78—30167
heat transfer model, of direct-chill continuous casting process 80—43592
inward solidification with black body radiation at boundary, asymptotic and perturbation solns. 77—55346
liquid metal continuous casting, solidification process, convective heat transfer, anal. 78—84789
mathematical model for closed mould horizontal continuous casting 77—28801
melt extraction technology, advances 80—76207
metal, continuous coating of slab, solidification interface shape 79—15656
metal, freezing at mean heat exchange intensity in irregular mode stage *(Russian)* 79—52193
metal ingots, cast, nonmetallic inclusions, size frequency distrib. determ. 78—39989
metal ribbon, amorphous, fluid-flow-temp. model for casting by melt extraction 79—56942
metal ribbons, amorphous Newtonian-quenched, formed by melt spinning and melt extraction, dimens. variations 79—56943
MHD conduction pump for filling casting mold 80—43798
micaceous-crystalling material, cast prep. and props. 77—12591
molten metal binary mixtures with wide immiscibility range, gravitational layering of components *(Russian)* 80—104092
mould/metal gap var. with time meas. method 77—52608
Nimonic, IN100, γ' precipitates, casting conditions effect on morphology 80—7548
noise abatement methods in foundry operations 77—72115
Nylon-12 film, casting conditions effect on polymorphism 80—84903
permanent magnet alloys manufacture, Co-mishmetal alloys *(Polish)* 80—35132
piezoelectric ceramics, bimorph element for loudspeakers manufacture *(Japanese)* 80—53597
polymer processing, US effects casting appl. *(German)* 77—48388
pyrometer, radiation, for molten cast Fe, design and field test *(Japanese)* 80—98917
rheocasting, review 77—4757
skin technology, industrial appl. of space processing 79—28991

casting continued
solidification, impurity distrib. effect of thermal-gravitational convection, numerical study *(Russian)* 78−19734
solidification science 79−78952
solidification simulation, use of general purpose software 77−52312
space environment, dendrite remelting and macrosegregation in low-gravity 79−47669
steel, austenitic stainless, cast struct., determination of origin using etching techniques 78−39985
steel, C, casting by C diffusion solidification 78−52792
steel, C and alloyed props., correlation anal. *(Bulgarian)* 79−83192
steel, cast, nonmetallic inclusion size frequency distrib. determ. 78−39989
steel, cast struct. form. in continuous casting *(German)* 78−92256
steel, continuous casting machine design, based on heat flow analysis, review 77−21048
steel, continuously cast slab, liquid-solid interface obs. by Pb additions to mould 77−21128
steel, Cr-Mo, cast and forged, difference in mech. props. 77−48465
steel, crack form. during continuous casting 78−7038
steel, cylindrical ingot, continuous casting, elastic-plastic temp. stresses and deformation *(Russian)* 79−61576
steel, Hadfield, cast and crystallised, deform. resist. of grain boundaries *(Russian)* 77−21216
steel, high alloy, instrumental anal., use of HF induction melting and centrifugal casting *(Japanese)* 77−56280
steel, high alloy, preparation for instrumented anal., HF induction melting, casting 78−48607
steel, high speed R8F8K7M6, cast, forged, sintered, struct. and props. 77−77516
steel, medium C, cast cylinders fragmentation tests 78−35519
steel, medium C, internal cracks in continuous casting billet and rolling products *(Chinese)* 79−43375
steel, Mn-Nb-Al-C, crack progag. and hot ductility during straightening concast strand 80−66646
steel, molten, heat loss during solidification hydrodynamic eqns., hardening front kinetics *(Russian)* 80−55385
steel, rimming, continuous casting and solidification *(French)* 80−25685
steel, solidification of castings in mould *(Russian)* 78−27502
steel, solification during continuous casting, cooling regime comparison *(Russian)* 80−93548
steel, tool and high speed samples, high frequency induction melting and centrifugal casting method for prep. in instrumental anal. *(Japanese)* 79−43232
steel, tool and high-speed, high freq. induction melting and centrifugal casting in instrumental anal. 80−84886
steel, type 27KhGSNL, castings, exam. of cracks due to treatment 78−44205
steel, US study 79−66252
steel casting, calc. method of thermal and thermo-visco-elasto-plastic processes *(German)* 80−79859
steel continuous casting, thermal, thermo-visco-elasto-plastic processes *(German)* 80−81044
steel ingot, state of viscoelasticoplastic stress deformation, in process of solidification *(Russian)* 80−45295
steel production, heat treatment, computer based interpretation of heat and cooling *(German)* 79−78995
styrene-butadiene triblock copolymer films, mech. props., effect of casting solvent 79−11651
Superinvar alloy casting for optical instruments 79−81580
surface alloy layer on casting by flame spraying technique *(Japanese)* 77−48586
ternary polymer systems, diffusion controlled formation of porous structures 80−7539
thermal contact resistance, determ. for solidifying metal and mould 78−39759
thermal stress simulation in continuous casting, finite element method 78−30170
TNT, role of HNS in grain modification 79−100129
u.s. testing in casting quality control *(German)* 77−4876
vacuum melting furnaces and casting techniques 78−84727
Ag_3Sn, dental alloy, prod. by melt extraction technique, exam. of mech. props. 78−48349
Al alloy, cast, forging and heat treatment effects on diamond planishing treatment 79−43237
Al alloy, cast struct. form. in continuous casting *(German)* 78−92256
Al alloy die casting, heat transfer coeff. 79−81685
Al alloy-mica particle composite, cast prep. and mech. props., bearing appl. 80−71613
Al alloys, columnar struct. of alloys solidified in flowing melt in centrifugal casting 80−71640
Al alloys, die casting, steel mould thermal fatigue 79−24619
Al, cast and directionally solidified, porosity 79−74145
Al, crystallisation thermokinetics calc. of pure cylindrical specimen *(Czech)* 77−63654
Al, heat transfer during cooling with water *(German)* 80−23873
Al-Cu, cast and directionally solidified, porosity 79−74145
Al-Cu alloy, chilled zone composition and thickness obs. *(Japanese)* 80−7541
Al-$CuAl_2$ eutectics, microstruct. after solidification, heat pipe influence 80−76243
Al-Mg alloy, chilled zone composition and thickness obs. *(Japanese)* 80−7541
Al-Mg alloy, crystallisation front form. props., casting in EM field *(Russian)* 80−55384
Al-Mg alloys, relationship between props. and nonequilib. phase diagram 79−96000
Al-Si alloys, eutectics and hypoeutectics, mech. props. and thermal cond., P impurity effect 79−83271
Al-Si alloys, penetrability coeffs. for two-phase zone of solidifying castings *(Russian)* 77−55956
Al-Si-Cu-Ni alloy casting, thermal props. 78−95814
Al-SiO_2 (2wt.%), dispersion hardened particulate composite, prep. 80−7588
Al-Zn-Mg-Li alloys, effect of Li on thermal props. 79−24515
Al_2O_3, aqueous acid slip, casting in gypsum mould 79−83165
α-Al_2O_3 fibre FP reinforced Al and Mg composites, fabrication and props. 80−81004
β-Al_2O_3, new slip casting technique for fabrication of ceramics 78−84745
Al_2O_3 substrates, tape-casted, fracture strength analysis 80−60948

casting continued
Be, produced in zero gravity environment, BeO particles uniform distrib. 78−72753
Cd-Zn eutectics, microstruct. after solidification, heat pipe influence 80−76243
$Cd_xHg_{1-x}Te$, cast-recrystallise-anneal growth 79−91578
Co-base superalloy, machine thixocast, mech. prop. deficiencies 79−74244
Cu alloys, optimal secondary cooling condition estimation in continuous casting *(German)* 77−73295
Cu, continuous casting, heat transfer and surface temp. meas. apparatus *(Russian)* 77−66631
Cu, heat transfer during cooling with water *(German)* 80−23873
Cu ingot, cast, nonmetallic inclusion size frequency distrib. determ. 78−39989
Cu ingots, solidification, quality and optimal modes of solidification, prediction from temp. fields 79−83187
Cu-Nb, exam. of monotectic reaction, using chill casting technique 78−68679
Cu-Nb alloy, chill casting, consumable arc melting, ingot prep. techniques 80−84879
Cu-Nb alloys for superconducting wire, casting of dendritic structure 80−2976
Fe and steel, centrifugal casting method and high frequency induction melting, sample prep., emission spectral anal. 77−48367
Fe and steel, macrosegregation of S and form. of equiaxed crystals, autoradiographic study, cast struct. effect 77−63658
Fe, cast, spheroidal graphite form., role of interphase boundary adsorption 77−63657
Fe, thermoelec. method of Si, Mn, C content monitoring, thermo EMF meas. 77−73490
Fe-B amorphous ribbons formation, high-speed photography investigation 80−76216
Fe-base samples, for working curves, HF induction melting and centrifugal casting 80−22340
Fe-Cr-Mo alloy castings, thick-section, factors affecting 80−108374
Fe-Ni-B glassy ribbons melt spinning, gas boundary layer effects 80−76217
$Fe_{40}Ni_{20}B_{20}$, metallic glassy ribbon, casting conditions *(Japanese)* 80−55386
$Fe_{40}Ni_{40}B_{20}$, amorphous, casting conditions effect on mag. props. *(Japanese)* 80−34698
$Fe_{40}Ni_{40}B_{20}$, amorphous ribbon, anal. of casting conditions 79−95965
$Fe_{40}Ni_{40}B_{20}$, molten, jet streaming, planar and cylindrical, instabilities rel. to glassy alloy casting 80−35129
Nb_3Sn-Cu multifilamentary wires, in situ prep., supercond. and mech. props. 79−38768
NbZr(Hf)-C(N) alloys, phase comp. after casting and annealing, precip. 79−56983
Ni alloys EhP539L, heat-resist., heat treatment effect on props. and hardening phase morphology 80−29995
Ni base superalloy, instrumental anal., use of HF induction melting and centrifugal casting *(Japanese)* 77−56280
Ni base superalloy, preparation for instrumented anal., HF induction melting, casting 78−48607
Ni, heat transfer during cooling with water *(German)* 80−23873
Ni-Co-Cr-Al-Ti-Mo superalloy IN738, casking porosity removal using hydrostatic press. sintering 80−55322
Ni-Cu semiconducting cast ingots, effect of EM stirring on struct. *(Russian)* 78−6915
NiTaC eutectic superalloy, casting, furnace atm. effects 80−84880
NiTaC-13, directionally solidified eutectic alloy, chem. compatibility with ceramic materials 79−87623
Pb-Sb battery grids, ageing behaviour obs. 79−100517
Si multicrystalline solar cell material prep., fast-pulled float zone, CZ and cast ingot and foil methods 80−93483
Si, polycryst. with columnar struct., crystn. using casting technique and microstruct., book contrib. 79−43137
Si sheet casting for solar cells 80−89139
Si, single cryst. growth in clear SiO_2 crucibles, heat exchanger method 79 33919
Si single crystal growth by heat-exchanger casting 78−11104
SiO_2-base cores, for superalloys, shrinkage and expansion during casting 80−10640
steel, C, castability, in metal mould, mechanical props. *(Japanese)* 80−25681
U-Pu-Zr metal fuel remote alloying and casting 79−89477
V_3Ga, cast, effect of hydrostatic extrusion on supercond. props. *(Russian)* 77−21215
$ZrSiO_4$-Al_2O_3 (SiO_2) suspensions for slip casting, prep. and props. 80−104103

castings
cast iron with lamellar graphite, tensile strength, reactor appl. 77−57718
continuous casting cylindrical ingot, development of elastic-plastic temp. stresses and deformations *(Russian)* 79−29151
cylindrical ingot, continuous casting, elastic-plastic temp. stresses and deformation *(Russian)* 79−61576
defects, NDT 78−27690
dimensional instability of CF8 stainless-steel castings at elevated temperatures 78−82448
economic testing, by mag. powder method *(German)* 80−3277
epoxy resins, AC breakdown-voltage characts. *(Japanese)* 80−88927
flexible scanning industrial X-ray/fluoroscopic inspection 80−89459
fracture toughness characteristics, using double torsion method 78−68863
ingot, temp. field calc. approx. by equiv. cylinder *(German)* 78−84788
nonferrous metals, integral degrees of blackness 77−35725
permanent magnets, semifinished, columnar structure castings 79−54157
pressure diecast automatic components, processing condition effect on performance 78−88623
quality control by NDT 79−29321
rare earth cobaltide, RCo_2, 'as cast', fibre texture 78−3117
refractories, casting-pit, quality control, specific non-standardized test development *(French)* 77−90297
Rheocast high performance alloys, solid-liquid phase charact. 77−28803
solidification and cooling in mold, temp. field *(Russian)* 79−29038
solidifying ingot, temp., strain and stress distrib. *(Russian)* 77−25041
steel, 12Kh18N9T-TiB_2, eutectic alloy, high temp. props. 78−84931
steel, casting, C-scan method of US inspection, developments 79−29294

castings continued
steel, continuously cast, optimum conditions for annealing castings during dynamic working *(Russian)* 78—44134
steel, continuously cast slabs, formation of longitudinal midface cracks 79—83315
steel, effect of non-uniform struct. on props. 78—84850
steel, Mn, solutioning of castings in salt baths 78—23871
steel, radiography with the 25000 R/min Linac 80—97656
steel, Rheocast, struct. and props. 77—28804
steel, rimming, continuously cast, nonmetallic inclusion distrib. *(Russian)* 78—80534
steel casting surface alloying feasibility trials 79—83395
steel shot, impact fracture *(Japanese)* 78—92338
white cast Fe, abrasive wear 80—108587
Al castings, grain refinement by gas-generating mold coatings containing hexachloroethane 79—83355
Al-Mg-Si alloys, precip.-rich zones on grain boundaries, soln. heat treatment conditions effect on mech. props. 80—104176
Al-Mn alloys, study of solidification by rapid cooling *(Japanese)* 78—88459
Al-Si, hypereutectic silumins, P and Na modification 78—84792
Al-Si eutectic, pressure effect on metal-die heat transfer coeffs. during solidification 80—7544
B-Al cast braid, crystallisation and structuring of Al matrix *(Russian)* 78—52725
Be ingot, high-purity, TEM obs. of BeO dispersion 80—104165
Cr, and Cr alloys, cast, B additions effect on struct. and props. *(Russian)* 78—19891
Cu-Al-Ni-Fe, (10, 5, 5 wt.%), cast microstruct. 78—80535
Cu-Ni cast alloy, effect of alloying and residual elements 78—85033
Fe casting in metal mould, strength before, after heat treatment *(Japanese)* 77—48461
Fe, electron probe determ. of traces of modifying agents in spheroidal graphite 79—52814
Fe, Mg-modified, scale for shapes eval. of graphite inclusions 78—35609
Fe nodular castings, comparison of sonic-resonance and US velocity techniques for quality control 80—97654
Fe-Cr-Mo alloy castings, thick-section, factors affecting 80—108374
Fe-Mn, as cast, pseudo-composite struct. resulting from interdendritic segregation, cryogenic materials appl. *(French)* 80—93556
Pb-Ca-Sn alloys for battery grids, proposed phase diagram, grain struct. development, corrosion phenomena 77—16546
Pb-Sn-Ca alloy sheet, continuously cast, for battery grids, ageing behaviour 77—16603
Ti-A-V (6, 4 wt.%), castings, fatigue crack initiation 79—29186
Ti-Al-V (6, 4 wt.%), hot isostatically pressed casting, fatigue crack initiation 79—79078

cataloguing
see also library mechanisation
USSR-East German joint optical glass catalogue 79—76775

catalysis
see also catalysts; reaction kinetics
acetic acid, chemisorbed on MgO, decomposition mechanism 78—92502
acetic acid, photocatalytic oxidation, photoacoustic spectroscopic obs. 79—16010
acetylene, adsorbed on Ni(111), benzene form., vibr. spectra 78—95952
acetylene, on Pt surface, electron energy loss spectra, surface vibrs. 78—15701
acetylene, reaction with Ni (100) and (110), room temp., UPS expts. 80—61151
acetylenic material, solid, on $Pd\text{-}CaCO_3$ catalyst, H getter, hydrogenation rates 77—44510
adsorbed species, catalytic reaction, high temp. IR obs. 78—88655
air pollution control, evaluation of catalysts for vapour phase oxidation of odorous organic compounds 79—70482
alloy surface chemistry, sample morphology effects 78—7233
amino acid photodegradation in presence of TiO_2 78—11531
α-aminoacids, stereoselective catalysed hydrolysis of esters *(French)* 79—66438
anthracene, oxidation to anthraquinone, in fixed bed catalytic reactor with KS-14 catalyst *(Russian)* 79—66268
aromatic compounds, oxidative bromination, chem. oscills. 80—3335
aromatic hydrocarbons, carbonisation of heterocyclic cpds. catalysed by $AlCl_3$ 77—63572
atom recombination, heterogeneous, Smith-Linnett theory, H_2 appl. 77—48634
autocatalysis, multiplicative stochastic processes in statistical physics appl. 80—22289
autocatalysis in stoichiometric model of energy metabolism 77—36860
autocatalytic deposition of Sn 80—100965
autocatalytic kinetic system, asymmetric multiple steady states 79—86527
autocatalytic reaction system, sustained oscills., deterministic and stochastic theories 78—95922
autocatalytic reactions, symmetry breaking, spatial struct. striation theory 77—12778
autocatalytic system, concentration waves, multiplicity and stability 79—16037
Belousov-Zhabotruskii reaction, existence of solitary travelling wave solns. 80—35525
benzene, bromination on zeolite adsorption complex, Raman spectroscopic anal. 80—16670
benzene, deep oxidation on Al-Pt catalyst, kineti model depend. of reaction rate 77—90583
bidisperse pore catalysts effectiveness factors 80—16719
Bray reaction, kinetics obs. *(French)* 80—7788
butan-2-ol, catalytic dehydrogenation and dehydration, MgO catalyst selectivity obs. 79—24820
carbonaceous chondrite meteorites, surface catalysis rel. to organic matter origin in early solar system 78—20767
carbonic anhydrase, active site substrate binding, environmental effects, CNDO and SCF LCAO calcs. 80—8002
catalytic beds, effect of granulometry and nature of catalyser on heat transfer *(French)* 77—68689
catalytic reactive flow, normal velocity in laminar boundary layer *(French)* 77—75988
catalytic reactors, runaway inhibition 79—47983
catalytic surface boundary layer struct., kinetic, diffusion reaction phases 80—33706

catalysis continued
catastrophe theory of n^{th} order reactions, uniqueness and multiplicity criteria 79—70296
cell energy metabolism, ATP effect on initiator stage enzyme activity and conc. 78—64950
charcoal, catalytic graphitisation by gaseous species from Ca 80—11872
chemical rectifiers, one-way catalysis 80—71901
chemically reactive flow in porous catalyst, conc. and temp. profiles, computation method 79—86523
chemisorption kinetics, determ. from substrate current fluctuations 80—84383
chemisorption on metal films, use of external mag. field, review 78—72003
chemisorption on metals, appl. in heterogeneous catalysis 77—35815
cholesterol, T-labelled, prod. by catalysed exchange with T_2 *(German)* 77—90599
chromatographic reaction and separation in pulse-fed catalytic reactor 78—64880
Clusius separation column, appl. to catalytic prod. of highly conc. H_2 79—24832
cluster systems, program for calc. electronic struct. with double self-consistency-Bersuker's method 80—69289
coal, new catalysts for $CO\text{-}H_2O$ induced liquefaction 80—30335
coal gasification, preliminary research 79—52871
coal gasification, using K catalyst, predevelopment research 79—52870
coal liquefaction, up-grading of solvent refined coal by catalytic hydrogenation 80—30331
colour image amplification by redox couple reaction 79—24802
controlled atmosphere electron microscopy obs. 77—29042
cooperative instability phenomena, catalytic site arrays, nonlinear mechanisms 77—66770
cybernetic significance by coordination complexes *(French)* 77—12797
β-cyclodextrinylbisimidazole, ribonuclease model, catalysis of cyclic phosphate substrate 78—85287
cyclohexane dehydrogenation, limitations of kinetic studies of catalysis on single-cryst. surface in UHV system 77—9126
cyclohexanol, dehydrogenation on Cu-Mg catalyst, kinetic model depend. of reaction rate 77—90583
cylinder array, convective mass transfer with surface reaction 78—79369
deactivation, model soln. by nonlinear partial differential eqns. 79—39123
defect processes, theory, rate eqns., chemical rules 80—33990
diamond polycrystal growth, phenomenon of catalyst movement *(Chinese)* 77—77806
diamond synthesis by graphitisation of carbon materials at high press. and temp., Ni influence 80—60795
diamond synthesis using Ni catalyst, intermed. phases of Ni-C system, satellite structures *(German)* 77—32538
diffusion-controlled reactions on a two-dimensional lattice 80—71940
3,5- dimethylphenol formaldehyde resin carbon, catalytic graphitisation from various metals 80—11871
dissociating air, non-equilibrium laminar boundary-layer flow 77—952
dissociatively chemisorbed molecules, desorption kinetics 79—86977
dual function catalysts, macroscopic distribution of components, selectivity effect 79—47967
electrocatalysis, radiotracer method investig. appls. 80—70525
electrocatalysis, surfaces modified by metal adatoms, review 80—61110
electrocatalytic O_2 evolution on reactively sputtered electrochromic IrO films 80—26125
electronegativity, spin-orbital, and catalytic activity 78—73078
enzymatic activity, quantum cooperative mechanism 77—40632
enzymatic catalysis, dynamic theory, conform. rearrangements 77—36858
enzymatic catalysis, orbital perturbation anal. 78—31623
enzymatic charge transfer across oil-water interface, effect of dielec. const. 77—70419
enzymatic reactions in water pools, interface processes 80—26050
enzyme, elasticity of polymer globule 77—70404
enzyme, intramol. reacts., review 80—40953
enzyme, oligomeric, catalysis of reversible flow reaction 77—36859
enzyme catalysis, electron pairing as source of cyclic instabilities 78—95953
enzyme catalysis, electron pairing in thermodynamically consistent pathways 79—5179
enzyme dynamics, statistical phys. 80—21439
enzyme particle, encapsulated, reactor systems, effects of mass transfer resistances 79—96522
enzyme-catalysed reactions, network thermodynamic modelling 80—89463
enzymes, chem. active sites 79—52757
enzymic kinetics, rate constants estimation 79—70505
epoxy cure, autocatalytic reaction, kinetic parameter estimation 79—70327
ethanol, chemisorbed on MgO, decomposition mechanism 78—92502
ethylene, adsorption on Ni, Pd and Pt films, reactivity with adsorbed H, surface pot. meas. 79—86995
ethylene, adsorption on W (100) and decomposition to acetylene, AES obs. 79—66353
ethylene, on Pt surface, electron energy loss spectra, surface vibrs. 78—15701
ethylene, polymerisation kinetics, heterogeneous Ziegler-Natta catalysts, polyethylene struct. and morphology 79—96307
ethylene to acetylene conversion on Ni (111), UPS 78—88657
ethylene-Co copolymers and $\text{-}SO_2$ copolymers prep. by catalysis and ^{60}Co γ-radiation, mech. props. 80—66841
first order reaction in catalyst particle, conc. depend. diffusion coeff., effectiveness factors 78—48693
first order reactions, uniqueness criteria 79—79281
Fischer-Tropsch synthesis, N isotope fractionations, appl. to carbonaceous chondrites 80—46496
fixed bed reactor catalyst decay, dynamic phenomena study *(German)* 78—7201
formaldehyde, adsorbed on W(100) single cryst., XPS obs. of decomp. 77—4927
formaldehyde, chemisorbed on Rh, catalytic decomposition, transmission IR spectra 79—39199
formaldehyde, decomp. and absorpt. on hot W filament 77—90641
formamide oxidation at Pt alloy catalytic electrodes 79—57245
formic acid, adsorpt. and decomp. over Ni surface, obs. using combined SIMS-FDS-AES system 78—40076
formic acid, decomp. on W (100), flash desorption obs. 79—29402

catalysis continued
- formic acid, decomposition, using Ni (110) catalyst, reaction kinetics and mechanism, mol. beam relax. spectroscopy 77—70340
- fuel cell electrocatalytic O_2 reduction mechanism with metal chelate coating 78—23951
- gas mixture, multicomponent, transport equations near catalytic surfaces 80—43821
- gas phase catalytic reactions, periodic press. cycling, viscous flow effects 80—19521
- gas-solid catalysed reactions effect of nonuniform activity distrib. 79—96362
- gas-solid reactions solid catalysed, effectiveness factors 79—47966
- gaseous heterogeneous reactions, interpretation of power kinetic eqns. 77—60117
- gaseous mixtures, conc. fluctuations meas. using catalytic wire 77—26291
- glycerides, high mol. wt. species prod. after contact with lunar grains 78—3333
- graphite, Fe-catalysed gasification, electron, microscopy 80—104358
- graphite catalytic gasification using Pt, Ir, Pt-Ir, small bimetallic particle identification by controlled atm. electron microscopy 79—83502
- graphitisation, catalytic effect of S, 1400-2000°C 77—28735
- graphitisation, three-phase, of phenolic resin C by Ni particles 78—68922
- heat of adsorption determ., expt. methods 79—42370
- heterogeneous, basic eqns. and examples *(Dutch)* 78—80788
- heterogeneous, bimolecular surface reactions, defect renormalised propagator stochastic theory 78—95955
- heterogeneous, kinetic transport, deactivation rate interactions on steady state and transient response 78—68914
- heterogeneous, mechanism, symposium, contrib., Florida, USA (March 1979) 80—51946
- heterogeneous, research using IR spectroscopy, literature review *(German)* 78—53256
- heterogeneous, role of surface science expts. 78—15710
- heterogeneous, vibr. excitation, classical trajectory calcs. 80—26045
- heterogeneous atom recombination on surface sites, kinetics of Langmuir-Rideal mechanism 79—87876
- heterogeneous catalysis, conference, Varna, Bulgaria (Oct. 1979) 80—82578
- heterogeneous catalysis reaction mechs., electron pair behaviour and surface orbitals 80—55705
- heterogeneous catalysts, gas phase diffusion and reaction calcs., viscous flow importance 79—47970
- heterogeneous reactions, bimolecular, following Langmuir-Hinshelwood mechanism, rates 79—84907
- heterogeneous surface with mass transfer, boundary layer transport 79—70371
- heterogeneously catalysed reactions, kinetic instabilities, oscill. instabilities 79—24717
- heterogeneously catalysed reactions, kinetic instabilities rate multiplicity 79—20341
- heterogeneously catalyzed oscillatory reactions 80—108732
- historical review, rel. to stochastic models of chem. kinetics 80—105483
- hydrocarbons, Ni-catalysed decomp., morphologies and growth mechanisms of carbons 78—35679
- hydrodesulphurisation, intermediate radical formation ESR expts. on used catalysts 77—70342
- impurity analysis, laser emission spectroscopy, material evaporation, auxiliary spark gap effects 79—87924
- inelastic electron tunnelling spectroscopy, surface chem. and heterogeneous catalysis appls. 78—92512
- inhibitory additives, for anatase-rutile transition *(Japanese)* 78—95744
- interstellar H_2, form. by catalysis process 78—54005
- interstellar oxide grains, catalytic props. rel. to mol. prod. 79—25690
- ion implantation studies, review 77—43236
- isobutane hydrogenolysis, limitations of kinetic studies of catalysis on single-cryst. surface in UHV system 77—9126
- isomerisation, apparent failure of Box-Hill procedure for model discrimination 77—63951
- isomerisation, catalytic activity of solid acids *(Chinese)* 78—31635
- isopropanol, decomp. on α- and β-V_2O_5 bronzes, 186-300°C, kinetics and mechanism 78—11553
- isopropyl alcohol decomposition using MoO_3:Li catalyst 78—60122
- isotopically selective heterogeneous reactions, stimulation with laser light 77—25309
- kinetic model depend. of reaction rate 77—90583
- kinetic studies on single cryst. surface in UHV system limitations 77—9126
- laser driven, LASL developments 79—31719
- macrocyclic receptor mols., chem. reactivity, mol. catalysis, transport processes 80—21280
- metal cluster growth and props., appl. to catalysis, conf., Villeurbanne, France (Sep. '79) 80—105431
- metal surface, chem. active sites 79—52757
- metal surface $H_2 \rightleftarrows H+H$ reaction rel. to catalysis, friction coeff. calc. 77—77807
- metal-insulator interface, catalytic reactions studied by work function meas. 80—55711
- metallic surface, catalysed thermal desorption and dissoc. processes, microscopic theory 80—75439
- metallic surfaces, thin film appls. 78—75943
- metals, electron waves, tight-binding description, appl. to heterogeneous catalysis 79—60700
- methane, dissoc. by adsorption-desorption process on W 78—92511
- methane formation, CO hydrogenation kinetics, using polycryst. Ni ribbon catalyst 78—40078
- methanisation plant ADAM I, nuclear long-dist. energy circuit *(German)* 78—25335
- methanol, adsorption and decomp. on Al, UPS, XPS and thermal desorption obs. 79—82441
- methanol, adsorption and decomposition on W 77—31887
- methanol, catalytic decomp. on NiO, mol. beam relax. spectrometry using surface temp. modulation 79—29401
- methanol oxidation mechanisms at Pt electrodes in acid electrolytes in methanol-air fuel cells 80—45661
- methyl propionate$-H_2O(Ba^{2+})$ mixtures, in DMSO, acetonitrile solns. IR, assoc., solvent, catalytic effects *(French)* 79—87827
- methylradioiodide, catalytic trapping by beds of impregnated charcoal 78—21681
- micelles, organic reaction kinetics 79—29416
- micelles, reversed, solubilisation and catalysis, review 80—45545

catalysis continued
- microreactor assembly to study heterogeneous catalyst system, IR emission spectra anal. 80—98988
- modeling of elementary step of chemical transform. of crysts., appl. to decomp. 79—15985
- molecular metal clusters rel. to chemisorpt. and catalysis 77—76668
- Mossbauer effect appl., conference, Kyoto, Japan (Aug.-Sept. 78) 80—7199
- multiroute systems, optimum characts. 79—39124
- myosin catalysed O_2 exchange, evidence for cooperative interaction between globular heads 77—32870
- NH_3 synthesised on Fe, promoter action of K 79—29390
- nonlinear diffusion-reaction problem, dissipative structs., stability anal. 79—1938
- nonlinear diffusion-reaction with autocatalysis and saturation law, single perturbation approach 80—35502
- nucleation and growth at surfaces, kinetic studies, review 78—72046
- orbital perturbation approaches 78—80783
- orbital phase condition for stabilising three systems 77—1923
- organic compounds, photocatalytic oxidation on Mars 78—85883
- organometallic compounds, chem. active sites 79—52757
- pellet, isothermal n-order decomposition reaction, steady state stability anal., topological degree and Lypunov method 80—30280
- phenol formaldehyde resin carbon, catalytic graphitisation from various metals 80—11871
- phenol-urethane composition based, properties and production methods, reactivity as function of catalyst *(German)* 79—56951
- phenolic resin carbon catalytic graphitisation by Al powder 77—28734
- phospholipid vesicle walls, photosensitised electron transport 78—80787
- photoelectron spectroscopy, review *(French)* 77—29045
- photographic development process, electrocatalysis 79—20400
- Photoinduced heterogeneous catalysis, review 78—40080
- physical chemistry of surfaces, book 77—25310
- polybutadiene, hydrogenation 80—26008
- polyelectrolyte 'catalysis' of chem. reactions 79—57217
- polyethylene, supermolecular structure, polymerisation at low pressure *(Russian)* 79—64126
- polypropylene on oxidised Cu, degradation, ion scatt. anal. 77—40463
- porous catalyst pellets, singular perturbation anal. of boundary value problems modelling reactions 78—76906
- porous solid boundary layer flow catalytic reaction, model 78—31684
- powder catalyst, catalytic and sorption processes, calorimetric and adsorpt. kinetic methods 79—43629
- propanol, chemisorbed on MgO, decomposition mechanism 78—92502
- propene soft oxidation, gas-solid catalytic reaction, kinetics, automatic meas. *(French)* 77—1912
- propylene, oxidation on MgO:Mo catalyst, surface structs., IR absorpt spectra obs. 80—66868
- protein dynamic states, role of geometry and elastic strains 78—48745
- PVC thermal degradation, reinitiation mechanism of HCl catalysis 80—71944
- quinoline, photooxidation on rutile, ESR and effects of surface states 79—66352
- rare earth manganites, catalytic activity 80—71941
- rare-earth compounds, catalytic props. 80—66875
- rare-earth-Cu double oxides, catalytic props., mag. props., elec. conductivity 79—66350
- reaction model, instability and spread of excitation waves, non-trivial modes 78—20161
- reaction rate, influential factors, new definition 79—1943
- reaction scheme, stochastic model, with autocatalysis and saturation law 79—52623
- recycle reactors for catalyst evaluation 80—3402
- retinals, catalysed cis-trans isomerisation by crude tissue extracts 78—64925
- saccharose char, catalytic graphitisation *(French)* 77—28739
- semiconductor catalytic kinetics, complex mech. of excitation, constant state problems 80—85213
- semiconductors, catalytic kinetics, excitation-complex mech. *(Chinese)* 77—70337
- slurry catalyst with particle size distrib., internal effectiveness factor 79—34355
- sodium 10-undecanoate, γ-ray induced polymerisation in aq. micelle solns. 80—61093
- solid surface, mol. dynamic processes interaction with laser radiation 80—71943
- solid surfaces, surface processes, and solid/gas interactions 80—73125
- solid surfaces *(Japanese)* 80—16731
- steel, superheated-steam oxidation, exam. of catalyst influence 78—85030
- styrene, cationic polymerisation by $SnCl_4$ in presence of C black 78—68891
- supported metal catalyst active centre, appl. of metal cluster theory 77—20219
- surface, problem areas, review 77—4928
- surface activity investigation using combined IR cell and differential single-pass reactor 79—80683
- surface mag. field effect on mol. dissoc. rate 80—16721
- surface phenomena, Raman spectroscopy using rot. vacuum cell 78—16852
- surface processes investigated by alpha-particle effect on electron work function 78—2547
- surface reactions at high press. 79—47972
- surface science rel. to catalysis, review 80—40740
- TEM, advances, catalytic chem. appls. 80—85214
- thermal desorption and dissociation catalyzed by a solid surface 80—108734
- thymocyte, calf, tritiation by catalytic hydrogenation 79—88152
- toluence, hydrogenation catalysed by Pt implanted cryst. supports 79—20462
- transition metal surface electronic struct., influence of size and roughness 78—14785
- transition mtals, hydrocarbon catalysis 78—11550
- transition state characterisation by struct.-reactivity coeffs. 78—40026
- trimethylgallium, product catalysed reaction with PH_3 or AsH_3, CVD mechanism for GaP or GaAs 77—48345
- unimolecular laser photodissoc., reson. photocatalytic effect 80—3377
- urease shear inactivation, metal ion effect, rel. to shear deform. effects in enzyme catalysis 78—76982
- N-vinylcarbazole, polymerisation in presence of C black 79—20366
- water-cetyltrimethylammonium bromide-haxanol system, ^{13}C NMR, catalysis in micellar and liq. cryst. phases 79—61909

catalysis continued
- weakly coordinated molecular systems, mutual vibronic effects in chem. reactions and catalysis 78–64821
- zeolites, type Y, Sc-, Zr-, catalytic activity, NMR, mechanism 79–29405
- Zhabotinski system, ferroin catalysed, period of homogeneous oscills. 80–30225
- Ziegler-Natta type catalysis, reaction pathway, ab initio SCF-LCAO-MO calcs. 78–56891
- Ag_2S film reduction, effect of Ag interdiffusion on the catalytic activity of Pt and Pd films 78–14519
- Al oxidised surface, EXAFS in soft-X-ray region 79–37921
- γ-Al_2O_3, hydrate covering, surface struct., IR spectra meas. 77–89622
- Al_2O_3, pure and SiO_2 coated, surface props., catalytic activity 79–79287
- BCl_3-H_2, photochem. with Ti, Pb catalysts, isotopic excitation by laser 78–64882
- BN, cubic, water catalysed form. 78–53199
- BN, cubic struct. form. from hexagonal struct. at high press., catalytic effects *(Japanese)* 77–90308
- $Bi_2Mo_2O_9$, thermal decomp. rel. to catalytic oxidation 80–35520
- Bn, cubic, formation from hexagonal BN using Cao and Li_3N catalysts *(Japanese)* 80–54374
- Br_2, adsorbed layer on zeolites, Raman spectra, aromatic bromination catalysis 80–3408
- C, amorphous, catalytic oxidation by Pd particles, TEM obs. 80–76555
- C gas-diffusion O_2 electrode in acid, electrochem. performance 78–31652
- C, graphitisable, catalytic graphitisation by Cr, Mn and Mo oxides 80–89166
- C graphitisation, catalytic, by various metals 80–3401
- $C+CO_2$ Boudouard reaction, catalysed by Li_2O and Li_2CO_3, reaction rates 839-1050°C 79–16035
- C_8FeCl_3, behaviour with H_2 and CO, effect of activation 79–43623
- CO, adsorbed on Pd (111) surface, catalytic oxidation, mol. beam investig. 78–88656
- CO, catalytic oxidation on Pt, CO_2 product vel. and ang. distribs. 78–20065
- CO, catalytic oxidation reaction over Pd(111) surface, mechanism 78–40079
- CO catalytic oxidation on spinel type ferrites, role of mag. exchange interactions 78–56916
- CO, catalytic oxidation over NiO, activated complex struct., rate consts. 78–80786
- CO, catalytic oxidation on ferrites, IR spectrosc. investig. 80–89524
- CO on Pd, catalytic oxidation and chemisorption 77–70339
- CO oxidation by NO on Ir surface XPS and UPS 78–15702
- CO oxidation over Pt, kinetics determ. using ^{13}C tracer 79–29400
- CO, reaction with adsorbed O_2 on Pd, kinetic behaviour, AES obs. 77–90640
- CO, reaction with O_2 chemisorbed on Pt, AES expts. 77–90639
- $CO+H_2$, interaction on Ni (100), reaction rate, AES and UPS obs. 79–79290
- $CO+N_2O$, adsorption on NiO, catalysed reaction in Neel transition region 78–53258
- $CO+N_2O$ catalytic reaction on Sc_2O_3 and MgO, kinetic obs. 79–29389
- CO_2, photoelectrocatalytic reduction in aq. suspensions of semicond. powders 79–39141
- CO_2 production, kinetics of CO oxidation reaction over Ir (111) surface, appl. of XPS 77–31886
- CO_2, TEA laser, catalytic control of gas chemistry 79–76663
- $COCl_2$, photodissociation, C isotope effects, photocatalysed isotope exchange with CO 77–36764
- Ca catalytic effect on chemisorption of O_2 on Au, AES 79–15021
- Ca-Mg-Ni hydrides, water form. on O_2 exposure 80–97727
- $CaCO_3$-Pd, catalyst for H gettering of dimerised phenyl propargyl ether 77–18001
- $Ca_2Fe_2O_5$, brownmillerite type, NO catalytic decomp. 79–43631
- β-$Ca_2(PO_4)_2$ whitlockite ceramic fabrication for prosthetic applications 79–78924
- $ClNO_2$, catalysed by ClNO, thermal decomposition spectral photometric investig. *(German)* 78–95925
- Co/Na zeolite, -A and -Y type, local coordination of Co(II) ions studied by X-ray absorpt. fine struct. spectroscopy 80–93434
- $Co(NH_3)_5\ Br^{2+}$, aquation, polyelectrolyte catalysis, high pressure effect 80–55656
- $Co(NH_3)_5Br^{2+}\ +OH^-$, polyelectrolyte catalysis, high pressure effect 80–55657
- Cr carbides, catalytic oxidation of H_2 80–104462
- Cu-Ni alloys, surface comp. and catalysis, AES and thermal desorption meas. 79–46898
- D_2+H_2O, isotope exchange on Pt, CO poisoning effects 79–11824
- D_2+H_2O, isotope exchange on Pt over hydrophobic support 79–11823
- D_2O moderator, of reactor KS-150, purification from organic impurities by catalysis *(Slovak)* 77–67811
- ^{18}F-F_3COF-^{18}F radiopharmaceutical synthesis procedure 79–29619
- Fe (110), K promoted, adsorption of CO, rel. to heterogeneous catalysis 79–82463
- Fe, membranes, effect of electrodeposited metals on H permeation, proposed catalytic mechanism 78–53252
- Fe_3C, catalytic oxidation of H_2 80–104462
- n-Fe_2O_3 electrodes, enhanced photoeffects by electrocatalysis and peroxide effects 80–16815
- GaN film, heteroepitaxial deposition, growth kinetics and catalytic effects 79–4487
- Ge, adsorption-desorption kinetics of H_2, O_2 and other gases, catalysis 77–47684
- H, dissociated, heat transfer to catalytic surfaces, shock tube investigation 80–64551
- H, para-ortho conversion, action of TiP catalyst 80–55316
- H-D exchange, catalysis by α-$Cr_xAl_{2-x}O_3$ solid solutions 77–52631
- H_2, interstellar, form., catalytic prod. on transition metal grains 78–57616
- H_2, nonempirical calc. for molecules in electric field 78–25459
- H_2, ortho-para conversion, magneto-catalytic reaction, quantum formulation 80–108750
- H_2, ortho-para conversion on paramagnetic crystal impurity, mag. field effects, theory 78–61050
- H_2 oxidation on Pt, OH radical form., laser diagnostics 80–5572
- H_2 photocatalytic production by carbohydrate conversion using $RuO_2/TiO_2/Pt$ photocatalyst powder 80–94120
- H_2, selective oxidation in air streams before CO anal. 77–63978

catalysis continued
- H_2-D_2, exchange on stepped Pt surface 77–1945
- $H_2+D_2 \rightleftharpoons 2HD$ catalysis, MgO surface, SCF UHF calc. 77–9120
- H_2+N_2O, HO radical form. on Pt surface, laser-induced fluoresc. obs. 80–108738
- $H_2(D_2)(T_2)$, ortho-para transition, catalytic-, radiation-, and self-induced conversion, review 77–90633
- H_2O, electrochem. splitting, solar energy assisted, on MoS_2 layer cryst. surface 77–90612
- H_2O, gaseous, photodecomposition over TiO_2 and TiO_2-RuO_2 surfaces 80–85194
- H_2O photocatalysis on TiO_2 using solid C, appl. to H prod. 80–26150
- H_2O, photoelectrolysis with TiO_2 catalyst 80–60755
- H_2O photolysis, for H fuel prod. using organic and metallic catalysts. *(French)* 80–55776
- H_2O photolysis using biological and artificial catalysts for H prod. 80–61444
- H_2O_2 decomposition, IO_3^- catalysed, oscillatory Bray-Liebhafsky reaction 79–91931
- H_2S oxidation by active C, electrochem. model *(German)* 78–35717
- H_2SO_4 formation in urban atmosphere, flame photometric obs. *(French)* 77–41136
- $Hg+Cl_2 \rightarrow (HgCl_2)_n$, surface catalysed reaction 79–100430
- Ir evaporated film, ethane hydrogenolysis kinetics 79–100436
- K, Na, superthermal neutral beams impact on W surface, stimulated chemical reaction 77–9123
- $KNbO_3$ catalysts, ferroelectric, for reactions involving CO and NO , and adsorption of NO 80–30282
- $K_2S_2O_8$, thermal transitions, catalytic effects of CuO and ZnO 79–15983
- $LaMn_{1-x}Cu_xO_{3-y}$, prep., struct., selected catalytic props. 77–36433
- LiH, form. on polycryst. Mo membrane, from diffusing gases, mass spectrometric obs. 77–66771
- Mg-Mg_2Ni eutectic alloy and Mg_2Ni, catalytic effect in hydrogenation, surface analysis 80–30283
- Mg_2Cu polycrystals, surface study by AES, XPES and X-ray induced AES 80–65346
- MgO, O_2 adsorption, $(O_2^-)_s$ form., thermal activation, reducing gas effects, EPR 77–9119
- Mo, adsorpt. of NH_3, and catalytic decomposition, field emission study 78–14596
- N, assoc. on metal catalyst surface, chemical energy accommodation, flow reactor obs. 79–24816
- N, at. recombination, Smith side tube method obs. 78–68881
- N atom recomb. on Fe, vibr. energy of desorbing N_2, electron beam induced fluoresc. 80–61149
- N heterogeneous atom recomb. on glass, Langmuir-Rideal mechanism 80–7853
- N_2 fixation, semiempirical INDO study 80–16898
- N_2, nonempirical calc. for molecules in electric field 78–25459
- N_2+methane, N_2 fixation, catalytic processes in non-equilibrium plasma chemical reactors *(French)* 80–89483
- N_2+O_2, N_2 fixation, catalytic processes in non-equilibrium plasma chemical reactors *(French)* 80–89484
- NH_3, adsorpt. and decomp. on stepped Pt surface, LEED, AES and desorpt. expts. 78–38943
- NH_3, chemisorption and decomp. on clean and N-covered Fe (111) and Fe (100) 78–40077
- NH_3, chemisorption on Ni (111) and reaction, LEED, desorption and photoemission expts. 80–59799
- NH_3, decomposition, on supported FE catalyst, kinetics, IR obs. 79–11792
- NH_3, flow in steel tubes, wall heat transfer with catalytic dissoc. 78–14099
- NH_3 on Pt surface, heterogeneous reaction of decomp., stimulation by CO_2 laser 78–61052
- NH_4OCN formation, in interaction of CO, NO and H_2 over Pt, Rh, Ru and Os 78–73082
- NO, adsorpt. and decomp. on stepped Pt surface, LEED, AES and desorpt. expts. 78–38943
- NO, adsorpt. on W (100), 300K and 100K, XPS, UPS and XAES, rel. to catalytic decomp. 79–28204
- NO, catalytic decomp. over brownmillerite like compounds 79–43631
- NO, catalytic reduction with CO by rare earth oxides 77–81422
- NO, dissociative adsorpt. on Ru $(10\bar{1}0)$, LEED and AES expts. 77–90642
- NO, electrocatalytic decomp. on electrochem. reduced zirconia surface 80–61113
- NO, reduction with NH_3 and laterite catalyst 79–91993
- NO_x reduction on Fe-based catalysts containing V 79–12285
- NO_x to NO_2 conversion in metallic materials, expts. *(German)* 80–55716
- N_2O, decomposition on titanate catalyst, energy reson. hypothesis 78–95947
- N_2O-CO, flame, alkaline earth atom catalysed combustion 77–9081
- N_2O-CO flame, alkaline earth catalyzed chain reaction chemiluminesc. 77–40548
- N_2O-CO flame, Mg catalyzed chain reaction chemiluminesc. 77–36758
- N_2O+CO, Na catalysed, Na chemiluminesc., excitation mechanism, appl. chem. laser 77–63916
- $Na_2S_2O_8$, thermal transitions, catalytic effects of CuO and ZnO 79–15983
- Ni (100), interaction of adsorbed H_2, CO, and methanol, temp. programmed desorption study 80–66876
- Ni (110), effect of surface O on catalytic and chemisorptive behaviour, ligand effects and oxide states 77–85066
- Ni (111), chemisorption and reaction of NH_3, LEED, desorption and photoemission expts. 80–59799
- Ni catalyst, H_2+CO, adsorption, co-adsorption, reaction, neutron inelastic spectroscopy method 79–99408
- Ni catalysts for fuel cells, thermoanalytic investigation *(German)* 79–74420
- Ni, of CO, catalytic activity, SCF-Xα-SW calcs. 78–15711
- Ni-Co-Cr/Al_2O_3 catalyst, IR spectra of adsorption and interaction with pyridine 80–71946
- Ni-Cu alloy, surface comp. and catalysis 80–54489
- Ni-P, electroless deposition on Al, X-ray and SEM obs. 79–90907
- $Ni(CO)_4$, form. reaction rate, substrate mag. phase depend. 80–108737
- NiO, adsorption of $CO+N_2O$, catalysed reaction in Neel transition region 78–53258

catalysis continued
Np(V)/Np(IV) catalytic redox reactions, kinetics and mechanisms 77—29006
O , form. from O_2 adsorbed on reduced Mo_2O_3-Al_2O_3 catalysts 78—85197
O_2, nonempirical calc. for molecules in electric field 78—25459
O_2+CO interaction on Ag (110), ellipsometry-LEED expts. 78—91542
O_2+CO isotope exchange reactions on Re 77—70338
O_3 destruction by catalysis in stratosphere 79—34879
O_3 heterogeneous decomposition in stratosphere, lab. study 79—70850
O_3, stratospheric, reduction by natural NO_x and man-made pollution, model 77—60461
Pd, adsorption of NH_3, NH_x and N, decomposition of NH_3 and hydrogenation of N 77—1315
Pd, chemisorption of O_2 and CO, catalytic activity, SCF-Xα-SW calcs. 78—15711
Pd film, work function changes due to adsorbed H_2, surface and interface dipoles 80—96972
Pd-Ag alloy, surface comp. and catalysis 80—54489
Pd-Ni alloys, surface comp. and catalysis, AES and thermal desorption meas. 79—46898
Pt, adsorption and catalytic reactions of H_2, CO, and O_2 80—81362
Pt, catalysts, supported, characterisation, hydrogenation and H_2-D_1 equilib. 78—76910
Pt, chemisorption of O_2, catalytic activity, SCF-Xα-SW calcs. 78—15711
Pt complex, coordinatively unsaturated, electronic struct. and catalytic activity 78—72228
Pt, hydrocarbon reactions catalysed by surfaces with variable kink concs., surface O_2 effects 80—35576
Pt on C, crystallite behaviour on sintering 78—7235
Pt/Al_2O_3, electron accepting sites by pyridine absorpt. 80—71947
Pt-Pd(Au) alloys, surface comp. and catalysis, AES and thermal desorption meas. 79—46898
Pu(IV) catalytic redox reactions, kinetics and mechanisms 77—29006
Re, catalytic activity during adsorption of HD 79—69358
Re-O_2, surface interactions and catalysis, 77 to 773K 79—79286
Rh (111), catalytic reaction between adsorbed O_2 and H_2, LEED obs. 79—52773
Rh, (111) surface, chemisorbed O_2, catalytic reaction between adsorbed O_2 and gaseous H_2 79—83503
Rh, catalytic oxidation of CO on polycrystalline sample 79—79294
Ru (110), methanol reaction, thermal desorpt. meas. 78—31685
RuO_4, catalytic reduction in radioactive liquid waste processing 79—76092
S, glass, catalytic crystallization in organic media at room temp. 77—84657
SO_2, aerosol-catalysed oxidation, expt. under atm. conditions 79—1941
SO_2 oxidation in stored rainwater samples, rel. to Mn content 79—84352
SO_2, reduction by CO in presence of H_2O and O_2, catalyst effects 79—24819
Se film, crystallisation using org. catalysts, struct. and elec. props. 77—51613
Se, glass, catalytic crystallization in organic media at room temp. 77—84657
Si, adsorption-desorption kinetics of H_2, O_2 and other gases, catalysis 77—47684
Si, controlled etching in catalysed ethylenediamine-pyrocatechol-water solns. 80—3223
Si, oxidation, solubility and transport behaviour of water, dissolution 80—93801
p-Si:P(P^+) photolytic props. in HF 80—89504
SiO_2 on Si, chem. stability of films produced by catalytic oxidation 77—86353
SiO_2:Cu(Ag)(Au), isolation matrix, XPS, atomic electronic struct. 79—89655
SiO_2-Al_2O_2-CaO-K_2O system, phase separation and crystn., F catalytic effect 79—60280
$Sm_{0\,5}M_{0\,5}CoO_3$, (M=Ca, Sr, Ba), catalytic props. 80—66875
$Sr_2Fe_2O_5$, brownmillerite type, NO catalytic decomp. 79—43631
$SrTiO_3$ photocatalyst for H_2O decomp. 80—85202
T removal from air streams of reactors by catalytic oxidation and water adsorption 77—50292
ThO_2:Pr^{3+}, luminesc., calcination temp. and excitation process depend. 79—33749
TiC whiskers, growth by CVD, catalytic effects of various metals and refractory oxides 79—33211
$TiCl_4$-$MgCl_2$, high activity catalyst for polyethylene, struct. and mechanism investig. 80—11951
TiO_2, nonstoichiometric anodic films, O incorporation kinetics 80—97733
TiO_2-Ni, electronic props., struct., comp., chemical bonding 80—84499
$Ti(OC_4H_9)_4$, pyrolysis, autocatalysis, TiO_2 film form. 80—55311
V_2O_{5-x}, O_2 equilib. press. as measure of O_2 binding energy in oxide system 79—16030
WC electrode, for hydrogen oxidation in acid, effect of starting material, obs. 79—100500
WO_n, (n=2-3), adsorption of O_2 (propene), struct., rel. to catalysis 78—51826
ZnO powder, effect of dry grinding in EPR and catalytic activity *(Japanese)* 80—84640
$Zr(BH_4)_4$ catalytic reactions on Al_2O_3, inelastic electron tunnelling spectra 80—75425
ZrC, whiskers, CVD on Ni, catalytic effect 78—51865

catalysts
see also catalysis
activity, determ. using interference oxide film 79—83501
AGR coolants, CO oxidation 77—54282
alkaline earth metal oxides, new catalysts for CO-H_2O induced liquefaction of coal 80—30335
aluminium and boron hydrides of titanium(III) bis-cyclopentadienyl, exam. of catalytic props. 80—30278
aromatic hydrocarbons, carbonisation, microscopic features of carbons obtained using catalysts 77—66597
atomically rough surfaces, mag. excitations 77—69664
auto-catalytic systems, kinetics rel. to symbiosis and origin of life 77—90979
automotive exhaust gas catalysts, dissolution of Pt and Pd 79—100433
automotive exhaust gas catalysts, radiometric determ. of Pt and Pd attrition 78—31740
bidisperse structured catalysts, diffusion in pores, gas chromatography obs. 79—70372

catalysts continued
catalyst for water photolysis, I-V model 80—108721
ceramic coating, self-cleaning for ovens and grills *(Japanese)* 80—55557
chlorophyll a dihydrate, photocatalysis of H_2O photolysis for H_2 prod. 80—61458
crystallites of supported catalysts, size distrib. from wide-angle X-ray meas. *(German)* 77—84566
dispersed metal catalyst clusters, EXAFS obs. 79—91530
dual function catalysts, macroscopic distribution of components, selectivity effect 79—47967
dynamic response of single catalyst pellet 79—79282
electrical conductivity measurement of non-metallic catalyst during adsorption and catalysis using bifilar conductivity probe 80—13096
electrocatalysts, reversible poisoning by CO, air pollution detection appl. 77—37363
ESCA, quantitative surface anal., limitations, depth profiling, catalyst surface anal. 78—53298
fluidisable cracking catalysts, microstruct. 77—28738
gas-solid reactions solid catalysed, effectiveness factors 79—47966
granular bed, static, flow transfer processes 80—45554
graphite intercalation compounds, as catalysts for polymerisation *(French)* 78—27822
heterogeneous, development for up-grading of solvent refined coal by catalytic hydrogenation 80—30331
heterogeneous, energy resonance hypothesis 78—95947
heterogeneous catalysis, basic eqns. and examples *(Dutch)* 78—80788
heterogeneous catalysis, conference, Varna, Bulgaria (Oct. 1979) 80—82578
heterogeneous oxidation catalysts, effects of Pb compounds 79—24817
hydrodesulphurisation catalysts, Co, Mo and Ni determ. by at absorpt. spectroscopy 77—9145
K-22 solid catalyst, H_2O_2 decomp. rel. to Mossbauer spectra 80—34826
KS-14, oxidation of anthracene to anthraquinone, in fixed bed catalytic reactor *(Russian)* 79—66268
laser Raman spectroscopy in controlled atm. rot. cell 80—86437
laterite, for reduction of NO by NH_3 79—91993
macroscopic metal catalysts, morphology and etching processes, review 80—7856
mag. excitations, atomically rough surfaces, isolated cluster of overlayer spin 78—31102
magnetic characterisation, review 78—64881
metal catalysts, structural exam. of monometallic and bimetallic systems 79—95264
metal oxide, convergent beam electron microscopy obs. 80—108689
metal oxides, thermodesorption of O_2, expt. technique *(French)* 78—64884
metal particles, small, characterisation and props., book contrib. 80—84417
metal surfaces, N atom assoc., chemical energy accommodation, flow reactor obs. 79—24816
metallic fine particles, theory of melting in the Percus-Yevick limit, appl. to particles on SiO_2 and C substrates 80—20060
metallic oxides, electrochemical behaviour 80—45516
methanation catalysts, nonreduced, IR spectra 78—88288
methylhydropolysiloxanes, equilibration by catalysts *(German)* 78—35722
nitrogenase, structure and function, role of Mo 77—86367
oxidation, Auger spectra 78—14600
pellet, transient diffusion-react. eqns., approximation using Galerkin technique 79—96357
perovskite type compounds, electrode catalysts for cathodic reduction of O_2 79—29371
phosphoric acid, for afterpolymerisation of ε-caprolactam under reduced press. *(Japanese)* 78—95929
photoactive catalyst used in light induced photocuring of coating systems 80—7820
PIXE appl. to design and evaluation of catalysts 80—61201
polybrene, catalysis of $Co(NH_3)_5Br^{2+}$ alkaline hydrolysis, high pressure, effect 80—55657
polymer, Mossbauer spectroscopy 77—12798
propane, radiative thermal cracking on porous glass *(Russian)* 79—39205
rare earth nickelates, form. conditions and props. 80—21270
rare earth perovskites, prep. and props. book contrib. 80—44193
rare-earth-Cu double oxides, catalytic props., mag. props., elec. conductivity 79—66350
redox enzyme, Fe-, Cu-, or Mo-containing, electron transfer peculiarities 80—16896
sandwich compounds, prep. from free atoms of metals *(French)* 80—21281
SIMS, solid surface investig. applications *(Rumanian)* 80—49510
sodium polyethylene sulphonate, catalysis of $Co(NH_3)_5Br^{2+}$ alkaline hydrolysis, high pressure, effect 80—55657
sodium polyethylene sulphonate, catalysis of Co(NH%d3)$_5$Fr^{2+} aquation reactions, high pressure effect 80—55656
sodium polystyrene sulphonate, catalysis of Co(NH%d3)$_5$Fr^{2+} aquation reactions, high pressure effect 80—55656
sodium-napththalene, catalyst for polymerisation of methacrylamide by H transfer *(Japanese)* 78—95726
STEM, atomic number contrast, supported catalyst particles 80—79651
superacids, props. and appls. *(French)* 79—74482
supported metal catalysts, particle growth, models 77—8830
supported metal catalysts, particle growth, obs. of Pt on alumina 77—8831
surface, laminar film boiling with chem. react., model 80—45553
surface characterisation by cyclic voltammetry, review 78—40092
surface investig. methods 78—14546
surface structure, molecular beam expts. 79—47971
thermal desorption theory for catalyst surfaces 80—26052
titanites, decomposition of N_2O, energy reson. in catalysis 78—95947
transition metal complex, surfaces, and supported catalysts, analogies among active sites 78—56917
transition metal hydrides, synthesis and physicochemical props., conf., Moscow, USSR (Jan. 1978) 80—27032
transition metal hydrides (binary ternary systems with metallic cond.) review of research on catalytic props. 80—30273
transition metal oxide catalysts, reduction, cryst. defects influence, in-situ electron microscopy 80—81322
ultramarine, catalyst struct., binding energies, ESCA 77—21420
zeolite, Faujasite type, varied Si/Al ratio, absorption of H_2S 78—60029
zeolite, synthetic, ZSM-11, synthesis and struct. 78—87657

catalysts continued
  zeolites, type Y, containg catalysts, cryst. struct., IR spectra 79−42958
  Ag, adsorption of O_2^-, catalytic oxidation mechanism 78−61046
  Ag catalysts, multiply-twinned particles 80−15114
  Ag clusters on Si substrates, opt. spectra investig. of struct. *(German)* 80−25492
  Ag, for oxidation of rubber, prep. of diene oligomers with hydroxyl groups *(German)* 80−85175
  AgX, X=halide, form. and migration of catalytic nuclei *(Russian)* 79−70378
  Al-Pt catalyst, deep oxidation of benzene, kinetic model depend. of reaction rate 77−90583
  Al_2O_3 based catalysts, porous pellets, thermal cond. 79−86936
  γ-Al_2O_3, heat treatment rel. to texture 78−72789
  δ-Al_2O_3, isomerisation of adsorbed 1-butene, IR study 80−76554
  Al_2O_3, pure and SiO_2 coated, surface props., catalytic activity 79−79287
  Γ-Al_2O_3, with Pt on, STEM, atomic number contrast, supported catalyst particles 80−79651
  Al_2O_3-supported, X-ray fluoresc. anal. using matrix correctional procedure 78−80817
  Au, for amorphous Si whisker growth characts. by SiH_4 thermal decomposition 80−34342
  $Ba_2Bi(Y)RuO_6$, perovskites, prep., struct., emission control catalysts 77−68957
  Bi, molybdates on SiO_2, EPR rel. to catalytic reactions *(French)* 78−64271
  Bi_2O_3-WO_3, X-ray diffraction studies 78−38677
  C, graphitisable, catalytic graphitisation by Cr, Mn and Mo oxides 80−89166
  CaO catalysed coal gasification 80−30339
  CaO, form. of cubic BN from hexagonal BN *(Japanese)* 80−54374
  CdO_2, catalyst on isopropanol, surface active sites during dehydrogenation 79−43621
  $CdTeMoO_6$, prep. and cryst. struct., X-ray diffr. obs. 79−1414
  CeO_2, for reduction of NO by CO 77−81422
  $CeRh_{3-x}Pd_x$, electronic and cryst. struct. comparison, catalytic behaviour 78−84398
  $ClSO_2OH$, superacid, props. and appls. *(French)* 79−74482
  (Co,Mo)/Al_2O_3, hydrodesulphurisation catalyst, prep., props. and appls. 77−86360
  (Co,Mo)/Al_2O_3 hydrodesulphurisation catalysts, physical props. and activities 77−86358
  (Co,Mo)/$Al_2O_3(SiO_2)$, and unsupported, catalyst for hydrodesulphurisation 77−86355
  $(Co,Mo)S_2$ hydrodesulphurisation catalyst, defect struct. and activity 77−86357
  Co, catalytic effect on W carburization 80−3255
  Co, magnetooptical investigation of mag. props. 79−69858
  Co/γ-Al_2O_3 catalyst, ESCA and EPR meas. after hydrodesulphurization reaction *(French)* 79−52755
  Co-Mo catalyst, Mossbauer spectra 80−7222
  Co-Mo oxidic precursory state, supported on SiO_2 and γ-Al_2O_3 hydrotreating catalysts 79−61898
  Co-Ni, selective catalytic surface behaviour, tight-binding approx. calcs. 78−76924
  $Co_xMg_{1-x}Al_2O_4$, struct., catalytic activity, Co^{2+} ion distrib. 78−30595
  CoMo/γ-Al_2O_3 catalyst, ESCA and EPR meas. after hydrodesulphurization reaction *(French)* 79−52755
  $Co(NH_3)_5Br^+$ volume of activation for spontaneous aquation anionic polyelectrolyte catalyst 79−39206
  CoO, and CoO_4, surface reequilibration kinetics 77−55449
  CoO, for catalytic oxidation of CO 80−71945
  CoO-MoO_3, catalyst pellets, Raman spectra 77−40216
  Co_3O_4, evaluation for organic compounds oxidation in air 77−37353
  $Cr_2O_3.Mo_2O_3$, effect of Al_2O_3 additives on catalytic activity, in oxidation of methanol to formaldehyde *(Russian)* 79−66346
  Cu catalyst, Al_2O_3 supported, effect on reduction of SO_2 by Cu 79−24819
  Cu, clusters, size, geometric effects, catalysis implications 78−73131
  Cu-Mg catalyst, cyclohexanol dehydrogenation, kinetic model depend. of reaction rate 77−90583
  $CuAl_2O_4$, pure and NiO promoted catalysts, surface oxidation state and comp., XPS study 80−76134
  CuO-Cr_2O_3 based oxide, catalyst, adsorption of fluorobenzene, binding energy of F 1s electrons *(French)* 79−69346
  D exchange reaction between H_2 and water a hydrophobic catalyst supporting Pt 80−30208
  Fe, corrosion in O_2 free water, catalytic effect of certain metals 79−47804
  Fe film, polycryst., heat of adsorpt. of H_2 and D_2 78−91530
  Fe, gasification of graphite, electron microscopy 80−104358
  Fe industrial catalysts for NH_3, XPS studies 79−70370
  Fe on Al_2O_3 substrate, controlled vapour growth of small particles 78−75958
  Fe particles, motion on graphite surface 79−90850
  Fe wires, catalytic, electrically heated, steady state temp. multiplicity, resist. meas. 77−32828
  Fe-M-SiO_2 (M=Ru,Pt), supported catalysts, Mossbauer spectra 80−11296
  Fe-MgO system, decomp. reactions, ferromag. reson. obs. 77−9058
  Fe-Mo catalyst, Mossbauer spectra 80−7222
  Fe-Mo/SiO_2 oxide catalyst for methanol oxidation 79−100440
  Fe-SiO_2 supported catalysts, Mossbauer spectra 80−11296
  $Fe_2(MoO_4)_3$, pure and Bi-doped, chem., struct. and catalytic modifications 77−86362
  Fe_2O_3 based catalysts for NH_3 synthesis, sintering of powders 79−61551
  Fe_2O_3-MoO_3, on SiO_2 and Al_2O_3, Mossbauer effect 79−47365
  $Fe(OH)_3$-Cr_2O_3 catalysts, for water-gas shift react., porous struct. 79−29407
  γ-FeOOH-Cr_2O_3 catalysts, for water-gas shift react., porous struct. 79−29407
  H_2O dissociation on polynaphthoquinone catalyst for H_2 prod. 80−16825
  Hf-Ni-H, catalytic activity, exam. by conversion of toluene, and bicyclic aromatic hydrocarbons 80−30276
  Hf-Ni-H, catalytic props. 80−30274
  In, for Mg/H_2 reaction, kinetics 78−76851
  Ir, catalysts, supported, Cl determ. by X-ray photoelectron spectroscopy 77−9146
  Ir(111), chemisorption of O_2, LEED-Auger expts. 77−20191
  K_2O-Al_2O_3-SiO_2 system, crystallisation of glasses in primary phase field of leucite 78−67658

catalysts continued
  La-Co-H, catalytic props. in hydrogenation of propylene, dehydrogenation of propane 80−30277
  La-Ni-H, catalytic props. in hydrogenation of propylene, dehydrogenation of propane 80−30277
  $LaMn_{1-x}Cu_xO_{3-y}$, prep., struct., selected catalytic props. 77−36433
  $LaMn_{1-x}Cu_xO_{3+y}$, O_2 stoichiometry by thermogravimetry 77−36434
  $LaNiO_3$, form. conditions and props. 80−21270
  $LaPO_4$ catalyst crysts., high resolution electron microscopy, morphological characts. rel. to catalytic activity 80−107193
  $La_{1-x}Pb_xMnO_3$, spin polarised XPS and UPS, elec. struct. 77−8717
  Li_3N, form. of cubic BN from hexogonal BN *(Japanese)* 80−54374
  $Li_xV_2O_5$, α- and β-phases, decomp. of isopropanol, 186-300°C 78−11553
  $Mg_{0.8}Mn_{0.2}Fe_{1.8}Al_{0.2}O_4$, grade 6SChl ferrite, milling conditions effect on fine cryst. struct. and activity 79−24483
  MgO, catalytic behaviour, rel. to XPS obs. 79−24820
  MgO, for $CO+N_2O$ reaction, kinetic obs. 79−29389
  MgO powder, decomp. of chemisorbed ethanol, propanol and acetic acid 78−92502
  MgO:Mo catalyst, adsorpt. of propylene, oxidation reactions, surface structs., IR absorpt. spectra obs. 80−66868
  $MgTeMoO_6$, prep., cryst. struct., and catalytic props. 80−108709
  MnO_2 dispersion mode on Al_2O_3 and SiO_2 powder supports, N adsorption obs. 80−81363
  Mo, chemical binding to dinitrogen and dinitrogen hydrides 77−86368
  Mo complex, dithiocarbamate, model for molybdoenzymes, thermochem. meas. 77−86365
  Mo complex, $MoOCl_3L_2$ ($L=Ph_3PO$ or $(Me_2N)_3PO$), O transfer reactions and molybdoenzymes 77−86306
  Mo complex, Mo(V) cysteine, reduction of cytochrome c 77−86371
  Mo complex, nitrate reductase, reduction mechanism and kinetics in dimethylformamide 77−86366
  Mo complexes, bis-carboxylate Mo(V), struct. and catalytic reactivity 77−77804
  Mo complexes, monomeric Mo(V) and Mo(IV) species 77−77803
  Mo complexes, mononuclear, EPR ligand superhyperfine interactions, implications for enzymes 77−86372
  Mo complexes, oxo- and sulphido-bridged, binuclear, in aprotic media, electrochem. and redox mechanisms 77−86324
  Mo complexes and catalytic activity, synthesis 77−77805
  Mo compounds, low-valent, stoichiometric and catalytic reactions with azobenzene 77−86370
  Mo compounds, reductive cleavage of azo link, implications in N_2 fixation 77−86370
  Mo cpds, chemistry and uses, conf., Oxford, Eng., Sep (1976) 77−77749
  Mo, membrane, polycryst. LiH form. on surface from diffusing $Li+H_2$ 77−66771
  Mo oxycyano complex, reaction with reducible substrates, biological N_2 fixation 77−86369
  Mo, substitution and redox reactions in oxidation states III to VI, role in enzymes 77−86364
  Mo/$MgO(SiO_2)(\gamma$-$Al_2O_3)$ catalyst, diffuse refl. spectra 77−86363
  Mo/SiO_2, supported catalyst, EPR and UV-visible spectra of $Mo_6O_{19}^{3-}$ 79−99764
  Mo-Al_2O_3 based hydrosulphurisation catalyst, used, ESR of SO_2^- and Mo^{5+} 77−70342
  Mo-containing (2Fe, 2S) protein, isolation from Desulphovibrio gigas, sulphate reducer 77−86375
  Mo-containing catalyst, unsupported, for isomerisation of n-hexane 77−86361
  Mo-containing enzymes, investigation using EPR 77−86373
  Mo-deficient plant, nitrate reductase form. by apoprotein recomb. with Mo complex 77−86374
  MoO_3 supported on aluminas, Raman obs. of struct. 79−28734
  MoO_3:Li, elec., catalytic props. 78−60122
  MoO_3-Al_2O_3 catalyst, state during thiophene hydrogenolysis 77−86359
  MoO_3+Ni^{2+} interaction on Al_2O_3, Raman spectrum 80−108742
  Mo_2O_3-Al_2O_3, reduced catalyst, adsorption of O_2, O^- form. 78−85197
  MoS_2, catalytic activity of basal and edge planes 77−86356
  MoS_2 hydrotreating catalysts, Co, Fe and Ni effects on microstruct., TEM, SEM and EPMA obs. 79−52762
  MoS_2, layer cryst. surface, for solar energy assisted electrochem. splitting of H_2O 77−90612
  MoS_2, MoS_3, catalysts struct. ESCA, binding energies 77−21420
  MoS_2, unsupported hydrosulphurization catalyst promoted by group VIII metals, catalytic, structural and textural props. 79−79289
  Na_2CO_3, new catalyst for CO-H_2O induced coal liquefaction 80−30335
  $Na_xV_2O_5$, α- and β-phases, decomp. of isopropanol, 186-300°C 78−11553
  Na_xWO_3 bronzes, reaction with Fe powder, reaction mechanism and reactivity 80−108712
  (Ni,Mo)/Al_2O_3, hydrodesulphurisation catalyst, prep., props. and appls. 77−86360
  Ni (100), kinetics of C deposition from adsorbed CO 80−76553
  Ni (100) face, O-Ni system vibrs. rel. to struct. during oxidation 77−66089
  Ni (110), kinetics of surface C oxidation, AES meas. 79−79291
  Ni, Al_2O_3 supported, CO adsorpt. in H_2-He, effect of H_2S on IR spectrum 78−71945
  Ni catalyst, chemisorption of benzene, Raman and vibr. spectra 80−108747
  Ni chemisorption and methanation of CO 77−56250
  Ni, diamond synthesis by graphitisation of carbon materials at high press. and temp. 80−60795
  Ni, dispersed catalyst on Al_2O_3 and SiO_2, epitaxial and textural effects, ferromag. reson. 78−23963
  Ni dispersions, semi-amorphous, on Al_2O_3-graphite, mag. characterisation 80−44876
  Ni films, CO-covered, adsorpt. of H, isotherms, resist., work function changes 78−75926
  Ni, in diamond synthesis, growth mech. *(Japanese)* 77−60122
  Ni, magnetooptical investigation of mag. props. 79−69858
  Ni polycrystalline foils, methanation reaction, kinetic information 78−73081
  Ni/Al_2O_3, sintered, mag. and catalytic props. for methanation reaction 79−79296
  Ni/Al_2O_3 catalysts, coprecipitated methanation type, metal-support interaction, XPS obs. 80−80936
  Ni/$Al_2O_3(SiO_2)$ methanation catalysts, nonreduced, IR spectra 78−88288

catalysts continued
- Ni-Al, Raney nickel catalyst, surface texture studied by N_2 adsorption and ESCA *(French)* 79−69348
- Ni-Cr/$MgSiO_3$, methanation catalysts, S resistant, XPS characterization 79−83506
- Ni-Fe, (100) surface, O interaction, Fe segregation, LEED and XPS studies 79−82437
- Ni-SiO_2 supported catalysts, particle size, H_2 chemisorption, Mossbauer study 80−7219
- Ni-Th (1 at.%), surface comp., temp. and O_2 exposure effects, AES study 80−80914
- NiO catalyst, superparamagnetic, elec. props. 79−65506
- NiO, undoped and Li_2O doped, surface reequilibration kinetics 77−55449
- NiO:$Li^+(Na^+)$, finely divided catalyst, low-temp. doping 79−51128
- NiO/SiO_2, catalyst, XPS for surface struct. and composition 79−43093
- NiO-Al_2O_3 powders, coprecipitated particle-size distrib. meas. 78−39726
- NiO-Al_2O_3/SiO_2 catalyst, XPS for surface struct. and composition 79−43093
- NiO-Cr_2O_3-$MgAl_2O_4$, methanation catalyst, struct. changes, IR obs. 79−73912
- NiO-Cr_2O_3-$MgSiO_3$ methanation catalyst, S-resistant, IR and Raman spectra 80−93290
- $Ni_xZn_{1-x}Fe_2O_4$, catalytic oxidation of CO, mag. props., kinetic parameters and composition depend. 80−16723
- Os, interaction of CO, NO and H_2, NH_4OCN formation 78−73082
- Pb, BCl_3-H_2 photochem. with Ti, Pb catalysts, isotopic excitation by laser 78−64882
- Pb_xMnO_2, synthesis, chem. stability, use *(French)* 78−80525
- Pd black, adsorpt. props. rel. to PdO irrad. 77−11796
- Pd, catalyst hollow cone dark field microscopy on γ-alumina substrates 78−61049
- Pd catalytic clusters, electronic structure, XPS obs. 77−77345
- Pd, chemisorbed O_2, reaction with CO, AES obs. 77−90640
- Pd, clusters, size, geometric effects, catalysis implications 78−73131
- Pd, for oxidant impurities elimination, in viologens electrochromic solutions 80−78922
- Pd on Al_2O_3, controlled vapour growth of small particles 78−75958
- Pd on Al_2O_3, surface atomic composition by AES 77−86377
- Pd, on glass, used in electroless deposition, proton backscattering anal. 80−16749
- Pd particle array, on amorphous SIO_2 substrate, model catalyst, electron microscopy and UPS expts. 79−4899
- Pd surface chemical reactions using MOS structure 77−73470
- Pd, Z-contrast, in STEM 79−46530
- Pd/Al_2O_3 catalyst, contact poison 2-methylthiophene damage reduction by neutron irrad. *(Russian)* 79−20467
- Pd/Ni/Cr layered catalyst for H_2-O_2 recombination in BWR coolant 80−18504
- Pt, adsorption of cyclopropane, NMR and PMR obs., chem. shift 77−51591
- Pt and Pt/Ru electrocatalysts for methanol oxidisation in acid electrolyte with improved steady state activity for fuel cell appls. 80−76629
- Pt black, adsorpt. props. rel. to PtO irrad. 77−11796
- Pt black anode of implantable fuel cells, effect of O_2 77−60309
- Pt, CO oxidation by NO, XPS and UPS 78−15702
- Pt, catalyst, dispersed onto silica support, EXAFS meas. 78−48258
- Pt catalyst surface morphology, faceting induced by NH_3 and propane oxidation 77−52669
- Pt catalysts, supported, adsorbed CO, temp. programmed desorption 79−46915
- Pt catalytic clusters, electronic structure, XPS obs. 77−77345
- Pt, chemisorbed O_2, reaction with CO, AES expts. 77−90639
- Pt electrode, powdered, aggregation in disperse system 79−11830
- Pt, H_2+D_2 mol. beam exchange reaction on stepped Pt surface, incidence angle depend. 78−31686
- Pt, interaction of CO, NO and H_2, NH_4OCN formation 78−73082
- Pt, limitations of kinetic studies on single cryst. surface in UHV system 77−9126
- Pt, on C electrode, surface area loss in H_3PO_4 80−101091
- Pt, oxidation kinetics of CO, determ. using ^{13}C tracer 79−29400
- Pt polycrystalline foils, methanation reaction, kinetic information 78−73081
- Pt, small particles, contraction and relax. of interatomic distances using EXAFS 79−47546
- Pt small particles, on graphite substrate, crystallographic struct., electron microscopy study 79−99465
- Pt, stepped surface, adsorption of H_2 and D_2, reaction probability, reactant ang. of incidence effects 77−47670
- Pt surface, adsorption of H_2, rel. to electrocatalysis 78−38935
- Pt surface, oscill. oxidation of CO 77−4926
- Pt, surface reactions analysis by spectroscopy of surface vibrs. 78−15701
- Pt, Z-contrast, in STEM 79−46530
- Pt/MgO, H_2 adsorption, 300-873K *(French)* 78−38967
- Pt/TiO_2 catalyst for photoassisted decomposition at room temp. of H_2O and ethylene 80−55703
- Pt/TiO_2 catalysts, photodecomp. of water 80−81337
- Pt-Fe alloys, supported, mag. prop. meas. in H_2 and O_2, 77 to 700K 79−91257
- Pt-graphite catalyst, H adsorption, ESR obs. 79−24818
- Pt-Sn/Al_2O_3 catalyst, Mossbauer effect, reactivity 80−11298
- Re, supported, chem. anal. method 77−25332
- Re/Al_2O_3, surface interactions and catalysis, 77 to 773K 79−79286
- Rh, interaction of CO, NO and H_2, NH_4OCN formation 78−73082
- Rh supported catalyst particles, adsorption of CO, inelastic electron tunnelling spectra 79−3509
- Rh/Al_2O_3 catalysts, surface interaction between NO and CO, IR study 79−70369
- Rh/γ-Al_2O_3 disperse δ-phase, chemisorpt. of CO, IR spectra, site distrib., mol. mobility 78−72496
- Rh-Cu catalyst, Al_2O_3 supported, chemisorbed CO, IR spectra *(French)* 80−60559
- Rh-TiO_2 catalyst, adsorpt. of H_2, surface states, NMR spectrosc. investig. 80−103891
- Ru $(10\bar{1}0)$, adsorption of NO and CO 77−72783
- Ru $(10\bar{1}0)$, dissociative adsorpt. of NO, LEED and AES expts. 77−90642
- Ru (110), kinetics of C deposition from adsorbed CO 80−76553
- Ru catalysts, chemisorption of O_2, EXAFS obs. 78−15708
- Ru complex, tris-(2.2′-bipyridyl)-Ru(II) complex, photoelectrochemical systems, solar energy utilisation *(German)* 80−45713

catalysts continued
- Ru, interaction of CO, NO and H_2, NH_4OCN formation 78−73082
- Ru-Cu catalyst, electron spectroscopy exam. 78−44405
- Ru-Cu clusters, EXAFS study 80−84804
- RuO_2, catalyst on isopropanol, surface active sites during dehydrogenation 79−43621
- RuO_x, catalyst at anode of solid polymer electrolyte cell, corrosion 79−20376
- Sc_2O_3, for $CO+N_2O$ reaction, kinetic obs. 79−29389
- SiO_2 gel, $SiO_2Al_2O_3$, SiO_2MgO, pore structure influence on X-ray intensity in EPMA *(Japanese)* 80−26046
- SiO_2, new catalyst for CO-H_2O induced coal liquefaction 80−30335
- SiO_2-Al_2O_3 porous catalysts, EPMA quantitative anal., new correction calc. method, modified ZAF method *(Japanese)* 80−93822
- SiO_2-MgO porous catalysts, EPMA quantitative anal., new correction calc. method, modified ZAF method *(Japanese)* 80−93822
- SnO_2, catalyst particles, converger beam electron diffr. 78−83685
- $Sr_2Bi(Y)RuO_6$, perovskites, prep., struct., emission control catalysts 77−68957
- $ThNi_5$, methanation catalyst, AES and characteristic energy loss spectra 78−56915
- Ti, appl. in laser photochem. isotope separation of B 77−61612
- Ti, BCl_3-H_2 photochem. with Ti, Pb catalysts, isotopic excitation by laser 78−64882
- Ti-H, deposited on carriers, synthesis, structure and catalytic props. 80−29890
- Ti-H (Ni-H)(Cu-H), catalytic props. 80−30274
- $TiCl_4$-$MgCl_2$, high activity catalyst for polyethylene, struct. and mechanism investig. 80−11951
- TiO_2:V, localisation and migration of V^+ ions *(French)* 79−33529
- TiO_2-V_2O_5 interface, role of struct. props. in interfacial reactions 78−31688
- TiP, iodide synthesis, and catalytic props. 80−55316
- U-SbO_3 catalyst, dynamic measurements of electrical conductivity during adsorption and catalysis 80−13096
- V-Mn-O system, phase comp. during oxide prep. 78−27447
- V_2O_5, (001) surface modification, during catalytic oxidation of propene *(French)* 80−45557
- V_2O_5 and lower oxides, defect structures and related props., review 80−59454
- V_2O_5, α- and β-phases, decomp. of isopropanol, 186-300°C 78−11553
- α-$VOP0_r$, VPO_4, $V_4(P_2O_7)_3$ and $(VO)_2P_2O_7$, IR absorpt. spectra, bond freqs. 80−108192
- $VSbO_4$, catalyst particles, converger beam electron diffr. 78−83685
- W (100), CO/H_2 surface complex, flash desorption and AES obs. 78−73083
- W (100), formic acid decomp., flash desorption obs. 79−29402
- W, catalytic activity during adsorption of HD 79−69358
- W, hot filament, adsorpt. and decomp. of formaldehyde 77−90641
- WC electrode, for hydrogen oxidation in acid, effect of starting material, obs. 79−100500
- WC, microcrystalline, mol. dynamics, motion of H_2O and H_2 mols. adsorbed on surface, catalytic activity 78−71941
- WC, small clusters, electronic struct., rel. to catalytic activity 77−59253
- WCs, preparation method effects on catalytic activity for H_2 evolution 80−101024
- WS_2 unsupported hydrosulphurization catalyst promoted by group VIII metals, catalytic, structural and textural props. 79−79289
- $ZnCrFeO_4$, ferrite spinel, unsupported and SiO_2 supported, structural and catalytic studies 80−44191
- $ZnFeO_4$, ferrite spinel, structural and catalytic studies 80−44191
- Zr-H, deposited on carriers, synthesis, structure and catalytic props. 80−29890
- Zr-Mo(Co)(Fe)(Cu)(Ni-Cu)-H, catalytic props. 80−30274
- Zr-Ni-Cu-H, catalytic activity, exam. by conversion of toluene, and bicyclic aromatic hydrocarbons 80−30276
- Zr-Ni-H, catalytic activity, exam. by conversion of toluene, and bicyclic aromatic hydrocarbons 80−30276
- Zr-Ni-H, surface segregation of Ni, influence on catalytic activity 80−30275
- ZrNi, surface segregation of Ni, influence on catalytic activity 80−30275
- $ZrNi_5$, methanation catalyst, AES and characteristic energy loss spectra 78−56915
- ZrO_2 solid electrolyte, electrochem. reduced, electrocatalytic decomp. of NO 80−61113

cataphoresis *see electrophoresis*

catastrophe theory
- atmospheric circulation flow patterns 78−40721
- beam, buckled, forced oscillations, global bifurcations and chaos 79−27580
- bibliographic overview 78−32665
- bifurcation from rotationally invariant states 78−77671
- biological applications, elementary approach 79−11881
- biological statistical mechanics, ensemble methods 79−66437
- biological systems coherent oscillations 78−44490
- bistable system, catastrophe prediction using externally applied force 78−77823
- black holes, Hawking particles production 79−2553
- butterfly catastrophe in high density behaviour of real fluids 80−87834
- chemical kinetics, chaos and strange attractors 80−7760
- chemical reactions, oscill., kinetic model based on catastrophe theory 79−43557
- chemical reactions analysis 78−7170
- chemical reactions of n^{th} order, uniqueness and multiplicity criteria 79−70296
- climate model, zero-dimens., with ice-albedo and greenhouse feedback, catastrophes and resilience 79−80007
- compound branching, imperfection sensitivity 78−13934
- crack propagation anal. technique using catastrophe theory 79−55342
- critic's view of appls. 79−25828
- description for scientists 78−41136
- discontinuous transitions into chaos after single bifurcation, hysteresis existence 80−73264
- elastic structure buckling models for higher order catastrophes 79−1122
- electrochemistry, steady-state conversion rate rel. to surface reaction process, catastrophe theory 80−108717
- electron density orthogoral trajectories 79−9995
- elementary catastrophe theory modelling of Duffing's equation for seismic excitation of nuclear power facilities 79−31240

catastrophe theory continued
elliptic umbilic diffraction catastrophe 79—50213
end-loading ring in rigid cavity, elementary catastrophe theory modelling 79—68585
ferromagnetism, mol. field theory, appl. of catastrophe theory, for teaching 79—35467
Feynman path integrals on/near caustics, semiclassical approx. using catastrophes 79—53992
fission electric cells, synergetics using catastrophe theory 80—45761
fission fragments, mass-yield curves, topological classification *(French)* 79—76043
flow fields and other vector field struct. and evolution 78—77733
fold field, evolving, structural stability 80—8802
fundamental catastrophe states and applications, review *(Chinese)* 79—35534
gas-liquid phase transition, press., temp. and density 79—55864
gases, chem. pot. near crit. density, Thom's catastrophe theory 78—91063
global behaviour of experimentally determined μ, ρ, to surfaces of real gases and cusp and butterfly catastrophes 78—26226
infinite dimensional spaces, biefurcations in variational problems 80—8789
infinite dimensions and the fold catastrophe, particle modelling 80—8788
instability of charging systems 78—44442
interacting electron system, orthogonality catastrophe 80—6757
introduction and appl. 78—69967
L-equivalence classes of submanifolds in complex projective spaces 79—75323
Legendre transforms and thermodynamics, catastrophe theory 79—26012
materials testing appls. *(German)* 78—64797
mechanical aspects *(Polish)* 78—20966
molecular homeomorphism, structural, between nuclear pot. and electronic charge density 80—42968
natural philosophy, role played by castastrophe theory 80—8772
natural sciences applications 78—32665
nonconservative hyperbolic systems, gradient catastrophe in soln. 78—69992
nongradient systems, nonlinear instability behaviour 79—75331
optical caustics and diffraction catastrophes 80—9801
optical caustics from liquid drops under gravity, obs. of parabolic and symbolic umbilics 79—72485
orthogonality catastrophe due to local electron interaction 79—1566
phase diagram classification 80—22313
phase diagram classification by catastrophe theory 80—17905
phase diagrams, critical points 80—8946
phase transitions, critical phenomena 80—8948
phase transitions, Landau theory, as example of catastrophe theory 79—12750
phase transitions with several order parameters 78—32782
phase-space projection identities for diffraction catastrophes 80—27162
phonon Focusing catastrophes 80—59591
pituitary thyrotropic responsiveness to protirelin, CUSP catastrophe model 78—81095
plasma, Vlasov, mathematical model 79—55503
plastics, crack growth stability anal. using catastrophe theory 80—74810
pseudo-groups applied to symmetry and defects ordered media 80—10541
quantum topology of mol. charge distribs., mol. struct. and its change 79—68175
quasi-geostrophic flow, bifurcation and catastrophe 79—88430
random waves, intensity fluctuations 80—8811
reaction-diffusion systems, bifurcation theory, classification 80—108713
real gas, P ρ T surfaces, butterfly catastrophe 79—86546
Riemann-Hugoniot catastrophe and P, ρ, T surfaces of real gases 79—6066
self-immunisation mechanisms of applied mathematics 78—65745
semiclassical path integrals in terms of catastrophes 80—8860
singularities, discontinuous changes, bridge between mathematics and physics 80—8786
singularities, folds, cusps, bifurcation sets, examples, Thom 80—8785
stability predictions through a succession of folds 79—76991
statistical biophysics applications 79—39334
stellar dynamical stability 79—8906
stochastic processes nonequilibrium transitions 79—12720
structural stability in physics (conference, Tubingen, Germany, May and Dec. 1978) 80—8739
swallow tail catastrophe and ferromagnetic hysteresis 78—56349
symmetry and higher order cuspoid catastrophes 79—9085
synergetics, universal approach, bifurcation theory 80—8787
tachyon quasi-catastrophe theory, tachyon existence, imaginaries, and causality, book contrib. 79—44815
teaching, soap film simulation of phase changes, catastrophes 79—62974
time scales and conventions 80—42173
triple points, 180° Rule, Butterfly model 80—8945
two mode buckling problems 78—34042
umbilic catastrophes, bifurcations, local diffeomorphisms 80—4511
visual behaviour modelling 79—83784
wavefront dislocations, anal. 80—8812

cathode followers
see also emitter followers
resonance bar damping meas. system, cathode follower cct. 77—2649

cathode-ray oscilloscopes
see also oscillographs
1 GHz laboratory instrument, design techniques 77—22540
25 MHz, laboratory, LBO 515, performance and serviceability *(German)* 78—41294
1000 series (Telequipment), design approach 79—35701
AC crest voltage superimposed on DC levels, measurement using static HV valve voltmeter *(German)* 79—58757
AC vector diagram, demonstration using CRO 77—37685
accurate time measurement *(German)* 79—30423
alternated double time base oscilloscope design and applications *(French)* 77—87784
analogue system for fast light curve registration, lunar occultations appl. 79—53725
automation developments 78—24821
axisymmetric electrostatic post-deflection lenses third-order distortion 80—32898
beam splitter using operational amplifier as square wave generator 78—77884

cathode-ray oscilloscopes continued
biomedical oscilloscope with digital storage for elec. signal obs. and storage 80—104786
calibration, deflection coeff. and sensitivity testing *(Rumanian)* 80—47048
calibration unit, transient response bandwidth and gain checks 80—27288
calibrator, Y amplifier, cct., constr., amateur radio appl. 77—30183
camera frame, integral data display 80—68284
circuitry techniques incl. triggering, hold-off, auto-fix and logic control system *(Italian)* 78—77882
colour display technique for NMR imaging 77—57373
combined instruments provide several test functions DMM, oscilloscopes, frequency counters, signal generators 77—34000
combined multimeter/oscilloscope, type D4000, features *(German)* 78—16783
compact, easy to use 78—49814
design using modular systems 78—93671
diffraction grating, electronic analog 80—46753
digital, operation and transients *(Danish)* 78—8392
with digital storage, OS4000, features *(Spanish)* 79—6116
digital storage memory oscilloscope *(Chinese)* 80—8976
digital storage oscilloscope principles and applications *(Danish)* 80—62647
digital storage oscilloscopes, Gould Advance OS4000 using A/D and D/A convertors 78—93673
double insulated 25 MHz oscilloscope, PM 3212 77—71338
double time multiplier *(Rumanian)* 78—86252
double-beam, for home constructor 77—37910
dual delayed-sweep capability added to oscilloscopes, low cost 77—18004
dynamic magnetization curves display, apparatus 79—17451
echoencephaloscope, two-probe three-mode design 78—44567
eight channel store for digital signals, single-beam oscilloscope accessory, cct. *(German)* 78—45607
fast, new general purpose oscilloscope capable of capturing subnanosecond events clearly 80—27287
fast signal averager based on sampling oscilloscope interfaced to minicomputer 77—57308
ferrometer with CRO display 77—71353
FET probes used for reducing rise-time meas. error 78—93667
fibre optic, recording modes and appl. 79—27389
frequency and current characteristics meas., conversion to proportional voltage signal *(German)* 77—13766
frequency differences indicated using a flip flop 79—88919
gamma camera oscilloscope display, performance meas., computer simulation 78—7425
GHz bandpass general purpose types 79—88936
Grundig, inexpensive and compact, technical data *(German)* 77—87785
Grundig model GO 15, detailed description, performance information *(Italian)* 79—54120
hard copy systems, digital storage 79—88937
harmonic waveforms, Fourier analysis using SR56 calculator 78—36986
HF CRO design, using cold switching for front panel operation 78—93672
high-speed oscillographic investigation, subnanosecond Nd glass pulse oscillator 80—74411
high-speed storage oscilloscope, Tektronix 7104 *(Danish)* 80—62646
HV probe, with subnanosec. rise time 77—10061
instrument selection tables, recent developments 80—13055
intelligent oscilloscopes used for production testing, dynamic analysis 77—37929
interface for X-Y recorder, cct. *(French)* 77—53951
Japanese, technical trends, review 77—37925
Japanese 1978 status and development trends 79—40554
lightning stroke current measurement, automatic observation system *(Japanese)* 77—29506
low repetition trigger cct., for high speed pulse observation *(Spanish)* 80—62657
maintenance- and service-types, operation, selection guideline 78—86259
measuring techniques, trends *(German)* 78—74020
multipulse lightning discharge oscillogram scanning camera 78—61588
NMR weak signal recording by second-harmonic oscillogram 77—10080
operation and appl. *(French)* 77—60884
optical fibre transmission characteristic meas. by digital processing oscilloscope 79—12787
peak-detecting window discriminator for neuronal spikes 77—60323
Philips PM2361, 120 MHz, recorded digital time base *(Italian)* 77—26325
Philips PM3244, 50 MHz, portable, 4 channel input *(Italian)* 77—26325
Philips PM 3244, four channel, 50 MHz, battery driven capability *(French)* 77—13780
photographic recording status 79—93247
photographic techniques for recording CRO traces 77—38047
photographing trace in high school lab. using polaroid camera 77—41443
plug-in type used for spectrum and logic analysis, timers, computer interfaces 77—41648
polar coordinate display CRO 78—86253
price/performance ratio improvement *(German)* 78—12723
PW Purbeck oscilloscope, construction of Y amplifier 79—6114
recording fibre-optic, characts. 77—37911
sampling, minicomputer controlled, NBS automatic pulse measurement system, capabilities 77—18018
sampling instrum. for recording/meas. instantaneous values of periodic events *(German)* 77—53876
sampling oscilloscope's capabilities extended by adding vertical channels 78—65914
sampling stroboscopic transformation of pulsed photocurrent from electron beam multiplier ELUFT-01 (USSR) 80—73471
self-test facilities in μP-equipped oscilloscopes 79—88935
seven segment display, using ROM and TTL IC 77—37933
signal time-interval measurement using digital meter 79—35702
simple harmonic motion demonstration on CRO 78—12518
specifications and user requirements 77—30138
state-of-art and trends *(German)* 77—65028
stereo vector CRO 80—90833
stochastic instantaneous signal recording, add-on cct. *(German)* 78—74031
storage, for measuring parameters of high-speed physical processes by means of time-scale conversion 80—8968
string instruments tuning to overtones appl. 77—50839
switch, four-channel, IC *(German)* 77—65030

cathode-ray oscilloscopes continued
  technological improvements and applications *(French)* 77—61091
  technology trends *(German)* 79—71437
  Tektronix 7104 specification includes 1-GHz bandwidth and rise time of 350 ps 80—13051
  Tektronix 7104 specification includes 1-GHz bandwidth and rise time of 350 ps 80—13052
  Telequipment D 61, dual channel, low cost *(German)* 77—18049
  test instrument survey *(German)* 78—8394
  time interval measurement using CROs 79—6098
  time interval measurements, very short intervals 78—36975
  time response, optoelectronic sampling in picosecond range 77—58451
  time-mark circuit with controlled delay 79—35703
  transients, shutter mechanism for photography *(Danish)* 78—234
  transistorised, S61 'Telequipment', construction and performance *(French)* 78—21123
  triggered calibrated sweep for AC oscilloscope 80—67987
  types and props., reviews *(Swedish)* 78—62189
  US grey scale display 78—3569
  very short time interval measurement appl. 78—81948
  visualizer for infrared laser emission field 80—23732
  voltage calibrator using band-gap technique 78—65941
  wide-band, photographic attachment for increased recording speed 79—21732
  wideband, 20 MHz, construction details *(German)* 78—24825
  CO$_2$ laser pulse meas., single sweep 5 GHz oscilloscope detector system 77—88817

cathode-ray tube displays
  see also cathode-ray oscilloscopes
  adapter mounted on CRT face for multilayer 3D display 79—18498
  artificial heart experiments with animals, data acquisition and monitoring system *(German)* 79—8582
  biocular magnifier design for display system viewing 79—27361
  coherent light valve optical modulator 79—72712
  colour CRT-observer interaction 77—77901
  colour TV imaging computer peripheral 79—20667
  CRT man-machine communication system in nuclear power stations 79—45364
  ECG atrioventricaulr transmission intervals, automatic recording and processing 77—25568
  ECG long period signals, reading by pages 77—25580
  electro-optic signal representation by implicit sampling 79—76620
  electron microscope video monitor with colour-coded CRT display 79—80729
  EMG activity in extraocular muscles, visual display 77—40834
  fast recording of information on external carrier 78—12682
  film exposure device, gamma correction method 77—10125
  gamma-camera for gated caroliovascular imaging 79—5367
  grating patterns, moving digital technique for generation on oscilloscope 77—40957
  half-tone image displays using MIR-2 computer 80—62641
  high performance liquid chromatography, with CRT display, microprocessor-controlled 79—20478
  image facsimile synthesized with Gaussian spot, fine structure 79—76604
  implanted pacemaker patient long-term surveillance unit 77—81722
  intelligent oscilloscopes used for production testing, dynamic analysis 77—37929
  ion beams, display device for beam profile 77—5960
  liquid chromatography, high performance, with CRT display 79—57321
  medical, equipment and maintenance, review 78—69240
  modules of 'Summa' system for information output to oscilloscope, digital display and digital printing 77—3244
  nuclear medicine images, minimum detectable grey-scale differences 78—61249
  nuclear physics experiments, displays for data output 78—9046
  nuclear reactor neutron flux level CRT state indicator 77—79444
  phosphor types, contrast sensitivity of human eye 79—11933
  photographic techniques documenting CRT displays 79—21827
  plasma, non-equilibrium, props. display using short-time pulsed probe analyser 77—15240
  plasma wave group velocity measurement by FM technique, delay versus freq. display 79—73047
  pseudorelief image of microstructures and photographic images, production on CRT screen *(Russian)* 78—93674
  real time interferogram simulation by analogue device, aberration generation, CRT display 79—54181
  retino-tectal mapping using microprocessor controller 78—31995
  screen image distortion corrections in R7912 transient digitiser. FORTRAN programs 79—30440
  series RLC circuit, phase relationships demonstration 79—58466
  single-fibre EMG oscilloscope trace selective gain control 77—44864
  small-area ultrasonotomogram magnification and smoothing 77—86572
  speech trainers, with visual display system, systematic use for hard of hearing children *(Japanese)* 79—39596
  speech trainers using visual display system, for hard of hearing children *(Japanese)* 79—39595
  static campimeter with CRT display 77—90941
  swept-frequency heterodyne receiver with CRT display for spectral analysis *(Spanish)* 77—37875
  text TV display for visually handicapped *(German)* 79—2162
  thermal image recording, scale and luminance distortion elimination 79—50398
  three-dimensional optical display unit 80—1297
  underwater US video system *(German)* 78—94471
  US imaging sonar, design and construction 79—3831
  US materials testing, gray tone display processor, cct. 78—44284
  US pulse echo material testing method *(German)* 78—7153
  USA National Weather Service graphic display network 79—12320
  viewability improvement, using optical absorptive filters 78—24820
  visual stimulator, computer-controlled, for electrophysiology expts. 78—69230
  visual trend display, an electronic equivalent to the chart recorder 77—37930
  weak luminescence visual investigation unit 78—12763
  n-GaAs semiconductor optical inhomogeneities visualisation *(Russian)* 77—90123
  PLZT electro-optic shutter stereoscopic display applications 80—90826
  Pu laboratory stack monitoring, computerised system 79—3256
  ZnO-GeO$_2$-MnO-B$_2$O$_3$ wideband cathodoluminescent phosphor 80—55196

cathode-ray tube screens *see cathode-ray tubes; fluorescent screens*

cathode-ray tubes
  see also image convertors; image intensifiers; image storage tubes; television camera tubes; television picture tubes
  alternative scanned light sources 80—69477
  charge degree, CsI and CsBr, storage layers stability under electron bombardment 78—27355
  development trends, CRT/observer interface improvements 78—24076
  dome-shaped grid utilisation, thick film losses, and vert. output *(Italian)* 78—77882
  double deflection scheme CRT for automatic film scanner KAMA 77—38552
  fast, new design incorporating microchannel plate as electron multiplier 80—27287
  fast recording of information on external carrier 78—12682
  fibre optic face-plate for high-efficiency photographic recording *(German)* 77—54801
  holographic TV, appl. of CRT with electro-optic crystal *(Russian)* 80—37974
  laser screens using single cryst. CdS, CdS$_x$Se$_{1-x}$ and ZnSe ingots 77—75561
  mass spectrometer three-dimens. quadrupole electron gun, compact tube assembly poisoning resistant 78—54493
  microspot CRT, non-deflected spot position stability testing device 77—82500
  phosphors, cathodoluminesc. investig., appl. to cathode ray tube screening 80—108282
  photography, self developing film utilisation, applications 79—58811
  screens, luminescent-cathodochromic sodalite powders, prep. and props. 77—20925
  SEM positive print photography of CRT image 78—82082
  semiconductor laser screens, scanning optical microscopy appl. 80—86398
  speckle patterns appl. to surface inspection 77—26385
  tester based on ohmmeter and adaptor 79—35711
  video photography in computed tomography and US imaging, film selection 80—41224
  vidicon, Si-intensified-target, low intensities meas., astronomy appl. *(German)* 80—98545
  La$_2$O$_2$S penetration phosphor, penetration and cathodoluminescent props. 80—20718

cathode rays
  focusing optimisation with specified image parameters 78—86385
  radiological physics, early history 79—80410

cathodes
  see also electron emission; oxide coated cathodes; photocathodes; thermionic cathodes
  aerodynamically stabilised cathode, for CO longit. discharge lasers 77—10955
  air, discharge, high-current, nanosecond, explosive cathode processes and contraction 80—10449
  arc, axial flow stability, cathode emission mechanism change effect 78—83638
  arc, cathode spot current density determ. 77—62425
  arc spot crater form. model 77—62414
  arc spot temp., Joule heat liberation effect 78—26361
  atomic absorption spectroscpy, cathode preparation by electroplating 79—43655
  bakeable hollow cathode, ion-molecule reaction study in discharge gas mixtures 80—37117
  Berkeley type ion source, long life cathode 78—66375
  biomedical implant electrode, function in induced bone growth 80—41312
  butyl alcohol cathode, hot electron emission from NaCl single-crystal film, inhomogeneous current flow due to cathode roughness 79—15244
  cathode surface heating by high pressure glow discharge, catastrophic bridging 78—87574
  cold cathode arc starting, probe and high speed photography obs. 80—38832
  cold cathode low press. arc retrograde motion in strong mag. field, theory 79—27858
  combined field cathode lenses, for electron optical system, optimisation, influence functions 79—76575
  condensed arc, in hydrocarbon, cathode processes 77—35415
  conference, Washington, DC, USA (Jan.-Feb. 1978) 79—43068
  cupric oxalate cathodes for seawater cells 79—92067
  current transport at the surface of a hollow cathode, current distrib. technique 80—54048
  damage from 300 ns, 4.5 A arc, material comparisons 78—87579
  DC vacuum arc emitted particle flux 78—75470
  dense gas nanosecond discharge, cathode region field amplification 80—38855
  disc LaB$_6$ cathode for plasma production in magnetic field 80—106951
  electric field averaging at cathode in space charge sheath 77—19806
  electrochemical treatment cathode with honeycomb arrangement of drain apertures *(Russian)* 79—96164
  electron beam production, high current relativistic plasma diodes [-] beam with $>10^{-5}$ sec duration *(Russian)* 77—10135
  electron gun, glow-discharge type, with plane-frustrum cold cathode, characts. 79—7495
  erosion and energy condits. in explosive electron emission 79—19111
  erosion components, vac. arc, fusion temp. and charge transfer depend. 77—4010
  explosive cathode process, high current diffuse discharge 80—38785
  explosive electron emission, cathode plasma emission surface processes 78—71569
  explosive electron emission, drop fraction of Cu cathode erosion 80—44063
  explosive emission multiple-tip cathodes, improved stability 79—64887
  field at the surface of a field-emission cathode 80—100757
  field emission, film with Mo cones, phys. props. 77—24931
  field emission, oxygen processing method 78—64448
  field emission current density, max., rel. to cathode geometry and kinetic props. 78—72704
  field-emission peak current, size effect 80—29863
  film cathodes, arc spot theory 77—39495
  flare, fast ion emission 77—62426
  flash X-ray tubes with new type of cathode 78—58101
  fuel cell, voltage losses 80—104503
  gas discharge, low press., emitted photon probe for electron swarm parameters 80—43839

cathodes continued
glow discharge, HV, electrode surface effects 79—64955
glow discharge, investigation with cylindrical hollow cathode in Ne and He *(Russian)* 80—28856
glow discharge, ion flow mass-energy relations, near hollow cathode 77—84563
glow discharge cathode region microscopic model 78—67524
graphite, intercalation compounds as cathodes 78—27780
heat sources of the arc cathode spot ion impact and neutralisation heating 80—38733
heavy ion source cathodes, lifetime improvements 79—72167
high current discharge from cold LaB$_6$ cathode 80—107011
high-current, graphite cathode vaporisation, composition and temp. spectral determ. 78—14228
HIP-1 hot ion plasma, effect of anode-cathode geometry on performance characts. 77—24112
hollow, electric discharge, electrical characts. 77—68890
hollow, glow discharge effect based on cathode fall theory 77—35413
hollow arc with reduced gas flow, operation mode 80—38783
hollow cathode, glow discharge, current balance and secondary electron emission 80—75108
hollow cathode, with plane-parallel geometry, current and radiation mechanisms 78—18474
hollow cathode arc, alkali plasma, low-press. current limiting 80—6304
hollow cathode discharge, Al spectral line, pulse feeding 80—64797
hollow cathode discharge, radiating ions 79—73054
hollow cathode discharge, slow electron energy distrib., density and temp. 77—55197
hollow cathode lasers, high voltage, spectroscopy appls. 79—27274
hollow cathode of special design for determ. traces of Br and Cl in semiconducting Si *(Russian)* 77—29083
hollow-cathode glow discharge with static stepped V-I characteristic *(Russian)* 78—75443
hot cathode Penning discharge plasma, HF oscills. and electron beam relax. 80—38614
hot cathode temperature, thermionic emission meas. method *(Czech)* 78—70121
ion sources, arc-discharge-type, cathode lifetime and stability problems 80—32558
ionisation manometric transducer, PMI-2, cathode protection 77—74416
iron phthalocyanine, performance in fuel cells with H$_2$SO$_4$ electrolyte 80—21293
laser tube design, cathode fall theory studies 80—58560
lenses, with combined elec. and mag. fields, third order aberration theory 79—41317
liquid cathode arc, cathode sheath model, liquid K in Ar *(French)* 77—1032
liquid K, erosion rate estimation in Ar arc *(French)* 80—44056
liquid metal, 78—87578
metal, electrically stressed surface elec. phenomena, electrolum. and breakdown with medium gap spacings 80—20710
metal cathodes, oxidised and clean, basic erosion processes in electric arcs 80—103211
metal cathodes subjected to pulsed electric fields, electron field emission charact. 80—71580
metal-Al$_2$O$_3$-Au type uniformly emitting MIM thin film cathode with evaporated insulator *(German)* 79—19675
metallic cathodes, electroluminescent impurities causing vacuum breakdown, obs. 78—84660
metallic heated cathodes, physics of electron emission *(French)* 80—104033
MHD generator, cathode spot erosion, thermal conduction-diffusion 78—5955
microscopic metal points, explosive emission characts. 77—7624
microscopic metal points, explosive emission characts. 77—7625
MIM, LF noise sources and reduction 80—108328
MIM, radial temp. distrib. *(Russian)* 78—6833
MIM cathode, local electron emission and electroluminescence patterns obs. 80—108327
MIM cold cathode emission density improvement, pinhole and compound insulator methods *(German)* 78—39670
motion of the cathode spot of a vacuum arc 80—54069
moving arc, parametric study of current density distrib. at electrodes 77—24239
MPD arc, thermal analysis of conical cathode 80—24270
multicavity, pressure effects 77—39482
multielement cathode, for high power elec. discharge laser, design and operational characts. 78—82983
multiplier assisted discharge, new type of cold cathode 79—55591
multirod design for high current plasma source 78—26308
MWPC, lateral distrib. of cathode charge 79—36470
nanosecond discharge in vac., cathode polishing effect 80—79599
needle field emitter, ion bombardment effects, field emission microscope obs. 77—55869
Nier-Bernas type ion source, factors affecting cathode performance 77—18723
oxide cathode conductivity model 79—15159
Penning discharge, cathode sheath, RF impedance study 80—106935
photoelectrochemical cells, cathodes and anodes for splitting of water 77—44484
plasma valve design with liq. metal cathodes, high-power conversion/switching appls. 78—9865
plasmatron, W cathode unit operation 78—75433
polyiodide materials in I$_2$-Ag current source, compatibility with solid electrolyte RbAg$_4$I$_5$ 77—40555
porous cathodes for implantable hybrid cells, recent improvements 77—40933
porous metal cathodes, emission props., work function 80—100502
positive ion source, hollow cathode design 80—99399
pulsed desorption slot, operating stability 80—87002
pulsed hollow cathode lamp, transient emission characts. in microsecond region for atomic absorption spectrophotometry *(Japanese)* 77—70365
quenching of residual conductivity in metal-semicond. system 79—7902
rectangular cold cathode, for high current electron accelerator 78—25358
scanning electron excited AES, appl. to cathode studies 79—40643
secondary electron emission by metastable N$_2$ interaction 80—38830
SEM field emission sources, review 78—21299
semiconducting point cathodes, explosive electron emission 77—59678
sheaths in K$_2$CO$_3$ seeded petroleum MHD combustion plasma 80—87870
single crystal whisker field effect, activation efficiency improvement in triodes 78—27377

cathodes continued
single-point electron field emission cathode, limiting current 77—8729
spectroscopic light source cathodes, of Al(graphite), glow discharge and hollow cathode types 78—82047
spot, halo and core prod. meas. 80—38829
spot pinning with pulsed discharge current 79—55601
spot shape and kinetics, cathode photoeffect from discharge UV irradiation 80—38836
spots of the first kind, erosion rate resistivity and thermal cond. depend., explosive model 79—14630
temporal space-charge field change meas. at high voltage electrodes in negative corona 80—38770
thin film, Al-Si$_3$N$_4$-Al struct., pulsed emission obs. 77—8728
thin film evaporator with cooled rotatable RF cathode 79—78876
tissue O$_2$ electrode design criteria and perform. characts., recessed cathode 79—39543
Townsend discharge spark voltages, cathode surface state effects *(Korean)* 80—19643
transient electron emission, for high-current cathodes 78—3001
twin hollow cathode interferometer-spectrometer, strongly cooled, imaging system *(German)* 77—61143
twin-hollow-cathode interferometer-spectrometer, discharge characts. for He and Ar *(German)* 78—67461
twin-hollow-cathode of interferometer-spectrometer, radial electron temp. *(German)* 78—67462
ultra high vacuum, erosion phenomena on contaminated cathodes due to electrical discharges 79—41889
ultrahigh vacuum discharge cathode erosion minimum conditions 78—75461
vacuum arc, cathode spot, review 80—24290
vacuum arc, cathode spots and erosion craters 80—10442
vacuum arc cathode, cathode spot phenomena, classification 77—24223
vacuum arc cathode plasma interaction with transverse mag. fields 78—75468
vacuum arc cathode spot dynamic models 78—75481
vacuum diode, laser produced cathode plasma, streaming, electron emission temp. determ. 78—91162
Ag cathode, underpotential deposition of Pb 78—52692
Ag, cathode spots on vac. arc discharge electrodes, model 78—91179
Ag electrode, evaporation rate from cathode spot in vac. arcs. 80—49024
Ag, hollow cathode discharges, IR laser transitions, discharge conditions, excitation mechanisms 79—68383
Ag-InP contact in InP Gunn device, relationship between microwave efficiency and metallurgical state of cathode contact 80—6981
Al, production of D ion beam impurities 79—86592
for Al smelting, comp. and props. 77—28740
Al smelting cell, effect of anthracite calcination and formulation variables 78—39719
Al, X-ray phototube, X-ray laser detector appl. *(German)* 77—10107
Al-Al$_2$O$_3$-Au thin-film cathode anomalous electron emission 79—8232
Al-Si$_3$N$_4$-Al, fluctuation noise 78—2998
Al-Si$_3$N$_4$-Al thin-film cold cathode, electrical forming, expt. 78—76160
Al-Si$_x$N$_y$O$_z$-Al thin film cathode, physical model from expt. study 80—100535
Al-SiO$_x$-Au cathode, emitted electron energy distrib. 78—52645
Al-Ti alloy spark alloying, cathode weight change and hardened layer obs. *(Russian)* 80—61005
Al$_2$O$_3$, production of D ion beam impurities 79—86592
Ar arc, new cathode shape for UV spectral radiance transfer standard *(French)* 80—38082
Ar, electron transmission factor numerical determination 80—10350
Au electrode, evaporation rate from cathode spot in vac. arcs. 80—49024
Au-SiO$_2$-Si structures, electron and ion emission from MOS field cathodes *(German)* 77—12499
BN, production of D ion beam impurities 79—86592
BaO epitaxial films, cathode poisoning due to O$_2$, CO$_2$, and S, surface anal. 79—42600
C cathode damage and vapour/thermionic arc transition obs. 78—71603
C fibre cathode prebreakdown field emission transition to vacuum breakdown 78—75462
Cd cathodes arced in vacuum, erosion structs. 80—1872
Cd electrode, evaporation rate from cathode spot in vacuum arcs 79—37566
Cs hollow-cathode plasma jet source 77—84463
Cs low-temperature erosionless cathode for high current densities 79—64953
Cs-film coated hollow cathode arc, intermediate press. operation 80—6305
Cu, broad area type, electrolum. regions, current-voltage characts. 80—84019
Cu cathode, electroluminesc. from semicond. impurities on surface 77—90200
Cu, cathode, ns voltage pulse breakdown of emitting sites, field emission microscopy obs. *(German)* 77—63547
Cu cathode, vacuum arc, current parameters, theory 80—54068
Cu cathode spot, MHD generator channel conditions, temp. calc. 78—26359
Cu, cathode spots on vac. arc discharge electrodes, model 78—91179
Cu cathodes arced in vacuum, erosion structs. 80—1872
Cu, electrically stressed, broad area, surface elec. phenomena, electrolum. K-spot radiation identification with electron emission 80—20711
Cu, erosion, vacuum to atmospheric press. arcs 78—79482
Cu, hollow cathode discharges, IR laser transitions, discharge conditions, excitation mechanisms 79—68383
Cu, moving arc, microcrater current and spectral fluctuations, simultaneous meas. 80—38828
Cu, point cathodes, explosive electron emission 77—55873
Cu upper electrode effect on MIM cathode emission 77—85344
CuII lasers with cylindrical hollow cathodes, performance 80—5751
Fe electrode, evaporation rate from cathode spot in vacuum arcs 79—37566
Fe plating cathode current distrib. influences *(Russian)* 79—96197
Fe, X-ray phototube, X-ray lasers detector appl. *(German)* 77—10107
GaP negative electron affinity cold cathodes, vidicon appls. 78—19133
GaP, surface cleaning by oxidation and heating, characterisation for electron emitter appl. 78—35548
GaP-GaAlP, heterojunction cold cathode 79—69965
Ge, electrode, cathodic characts. rel. to halide ions 79—57238
H$_2$-N$_2$ hollow cathode effect discharge 79—86639
He, electron transmission factor numerical determination 80—10350

cathodes continued
He, hollow cathode, 1-4 torr, population of excited levels, excitation and decay mechanisms 77—80267
He spark, cathode spot conversion kinetics 80—44067
He-Cd, hollow cathode discharge tube, voltage, ion spectral line intensities and metastable states 79—46505
He-Cd hollow-cathode laser tube, description and performance *(Bulgarian)* 79—27279
Hg DC vacuum arc anchored cathode spot current density obs. 78—75467
Ir electrode, evaporation rate from cathode spot in vac. arcs. 80—49024
LaB_6 cathodes for Kohler illum. and brightness meas. 80—68296
LaB_6 hollow cathode for dense plasma production 78—55729
LaB_6, hollow cathode mag. multipole ion source 80—102369
LaB_6, porous, field emitter cathode sputtering and surface damage 79—11492
LaB_6, single cryst., highly stable, for conventional electron microprobe instruments 78—78043
LaB_6, synthesis and props. *(Japanese)* 80—40255
Li pacemaker battery similarities and differences 77—81737
Li-$(CF)_n$ high energy density battery, cathode materials evaluation 80—97780
Li_xMO_2 (M=transition metal), thermodynamic investigations 80—89210
$LiNO_3$ solution cathodic gas evolution rate rel. to electrode material *(Russian)* 80—26020
Mg, in Ar, spark discharge, evidence for ionic post discharge environment 77—84551
MgO surface, secondary electron emission effects on voltage breakdown curves in Penning mixture for insulated electrode discharges 78—19616
Mo cathode, H_2 glow discharge, FCC surface layer form., electron diffr. obs. 77—55311
Mo cathode, ns voltage pulse breakdown of emitting sites, field emission microscopy obs. *(German)* 77—63547
Mo cathode surface contamination effect on erosion by nanosecond vacuum discharge 78—75463
Mo cathodes arced in vacuum, erosion structs. 80—1872
Mo fine tip cathode, field emission stability, rel. to passivation 80—100760
Mo, H penetration of Mo cathode in glow discharge, point defect depend. 79—41903
Mo, production of D ion beam impurities 79—86592
Mo-Cu cathode, spot motion and nature in UHV 80—79597
MoS_3, prep., use as Li battery cathode 80—29892
N_2 discharge, flowing, electron-beam maintained, cathode shape effects 79—27850
NH_4NO_3 solution cathodic gas evolution rate rel. to electrode material *(Russian)* 80—26020
$NaNO_3$ solution cathodic gas evolution rate rel. to electrode material *(Russian)* 80—26020
Nb-Zr-Ti, needle field emitter, ion bombardment effects, field emission microscope obs. 77—55869
Ne hot cathode discharge plasma, second order harmonic surface wave generation 80—38849
Ni, cathode spots on vac. arc discharge electrodes, model 78—91179
Ni electrodeposition cathode polarisation, influence of unsaturated sulphates *(Russian)* 79—91963
Ni electrodeposition from alkaline citrate electrolytes, cathodic process rate *(Russian)* 79—8440
Ni sputtered coating microstructure on mechanically activated cathode *(Russian)* 79—91586
Ni-Fe alloy, Ni base cathodes, powder metallurgy technique 80—29903
$PbCrO_4$, cathode material for Li cells evaluation 78—11525
PbF_2, cathode materials for Li cells, evaluation 78—11525
PbO_2, cathode material for Li cells, evaluation 78—11525
Pd electrode, evaporation rate from cathode spot in vac. arcs. 80—49024
Pt electrode, evaporation rate from cathode spot in vac. arcs. 80—49024
Rh electrode, evaporation rate from cathode spot in vac. arcs. 80—49024
Ta auto-cathodes, effect of O_2 on emission and surface diffusion *(Russian)* 79—77892
Ta autocathode, influence of electric field and heating on work 80—7478
TiB_2, production of D ion beam impurities 79—86592
TiS_x, cathodes in secondary Li batteries, operating characts. 77—86320
W, cathode spots on vac. arc discharge electrodes, model 78—91179
W cathodes arced in vacuum, erosion structs. 80—1872
W, cylindrical hollow-cathode, heavy-current temp. investig. 80—38763
W, field cathode with (001) orientation preparation technique 80—15241
W fine tip cathode, field emission stability, rel. to passivation 80—100760
W, high-current hollow cathode, energy balance *(Russian)* 77—58910
W, impregnated with Ba and BaO, AES and work function meas. 77—24921
W microneedles, field electron emission, suitability for electron source investigation 78—52644
W multicavity cathode, Ar discharge, V-I and power characts. 78—26360
W, needle field emitter, ion bombardment effects, field emission microscope obs. 77—55869
W points, micro-size, change in shape and electron field emission 79—74067
W:La, B coadsorption and work function, FEM and FIM obs. 79—52087
W:ThO_2, uncarburized filament activation by sputtering 78—52608
Zn electrode, evaporation rate from cathode spot in vacuum arcs 79—37566

cathodes, electrochemical *see electrochemical electrodes*

cathodochromism
carnegieite, metastable cathodochromic, prep. by zeolite decomposition *(French)* 79—95719
holosodalites, synthesis, cathodochromism, reflectivity spectra 77—40399
luminescent sodalite powders, prep. and props. 77—20925
$NaAlSiO_4$, carnegieite, cathodochromic props., storage CRT appl. 77—8604
$Na_3Al_6Si_6O_{24}X_2$, optically erasable colouring and luminesc. *(Russian)* 77—85801
$Na_8Al_6Si_6O_{24}$.Cl(Br)(I), cathodochromic sodalites, coloured crysts., tunnel and recomb. luminesc., temp. depend. *(Russian)* 80—66261
$Na_6Al_6Si_6O_{24}.NaX_{(2-n)}$, (X=Cl, Br, I), X-ray irrad., thermal-erase cathodochromism and dihalide mol. centres *(Russian)* 80—66236

cathodoluminescence
ageing of cathodoluminophors 78—10994
alkali halides, luminescence quenching by defects *(French)* 77—26378

cathodoluminescence continued
anthracene:tetracene crysts., mag. field modulation of scintillation under α-irrad. 77—48256
bibliography, including papers on appl. to semiconductor technology, SEM, TEM etc. 79—21482
bibliography 78—23536
biological material microscopy, improved resolution 77—56549
biomedical appls. of SEM cathodoluminescence method 80—72400
cathode fall in electron beam controlled stationary non-self-sustained discharges 78—71613
cathodoluminophors, characteristic calcs. 78—10993
chalcopyrites, for electrolum. device appl., props. and technology, book contrib. 77—73175
clinoenstatites in Indarch enstatite chondrite 80—36596
corundum, vac. UV luminesc. spectra *(Russian)* 77—24903
crystal, optical parameters meas. apparatus *(French)* 77—26378
diamond, cathodoluminescence of defects *(French)* 80—34988
diamond, dynamic Jahn-Teller distortions at trigonal optical centres 79—87069
diamond, frictional anisotropy, cathodoluminesc. study 80—35340
diamond, industrial, anal. cathodoluminesc. studies in SEM 80—81410
diamond, natural, defect struct., recent obs. by new methods 78—30628
diamond, natural, free exciton luminesc. line shape 80—40165
diamond, natural, subthreshold defect formation due to electron irrad., cathodoluminescence study *(Russian)* 80—45152
diamond, natural type-IIb, single dislocations, cathodoluminescence obs. by STEM 80—80871
diamond, planar defects, in {100} planes, electron microscopy 77—11569
diamond, polarised cathodoluminescence in near IR, from platelet defects 77—48253
diamond, semicond., energy band struct., elec. and optical props., review 77—35862
diamond, semiconducting, GR1 cathodoluminescence, fine struct. 78—68566
diamond, synchrotron electron beam damage, study by optical, cathodolumінesc. and X-ray topography 80—39155
diamond, synthetic, external crystal morphology, SEM obs. 79—73078
diamond, synthetic semiconductor, IR spectroscopy and cathodoluminesc. *(Ukrainian)* 79—78758
diamond cathodoluminesc. at dislocations 79—47524
diamond subsurface damage exam. using cathodoluminescent mode of SEM 77—80398
diamonds, synthetic, polarised infra-red cathodoluminescence 80—89073
diamonds, topographically identifiable sources of cathodoluminescence 77—55836
direct gap semiconductors, exciton energy determ., electron beam excited luminesc. 79—38680
electron beam instruments for cathodolum. meas., EPMA and SEM, review 78—4740
emission, applic. of microscopy and spectroscopy for finding distrib. of impurities in minerals *(French)* 79—5630
energy transfer, random walk model, comment 78—72610
energy transfer, random walk model, reply to comment 78—72611
ferroelectrics, O-octahedric, cathodlum. spectral and temp. depend. 78—84665
fluorescent screens, cathodoluminescent, yield, calorimetric method determ. *(Russian)* 77—20938
$GaSe_xTe_{1-x}$, temp. range 7 to 150K 78—10992
Giemsa stain, detection of cathodoluminescence and its appls. 80—67323
growth-layering effect on optical symmetry in cubic crystals, rel. to cathodolum. data 80—88072
heterojunction properties analysis and control, cathodolum. appls. *(French)* 79—69892
III-V multilayer structure, as-grown, assessment of defects by differentiated cathodolum. topography 80—59819
inerg gas excited molecules formation, rate const. determ. 80—9859
inert gas, solid, electron impact excited, exciton recomb. spectrum, temp. variation 78—48239
information display technology, symposium, San Francisco (1978) 79—9209
ionic compounds, electron irrad., broad band radioluminesc. 77—32446
ionic crystal, electron beam excited, luminesc. and cond. of nonideal degenerate electron-hole plasma 78—10488
ionic crystal containing self-localising excitons, cathodolum. 78—6785
IR imaging methods, crystal lattice defects appl. 78—22201
LED, diffusion lengths and near-junction luminescence-efficiency profiles from SEM scans 77—77301
measurement techniques 78—41354
metal, surface plasmon light emission due to low energy electron irrad. 80—34997
metal film, luminescence, electron beam excited *(Russian)* 79—47526
metals, luminescence of electron irrad. surfaces 79—65934
microprobe analyser, scanning cathodolum. 80—81409
mineralogy, appl. of cathodolum. microscopy and spectrometry 77—69919
minerals, ionisation enhanced diffusion effect obs. 80—71497
minority carrier lifetime mapping by SEM 80—96903
naphthalene, fluorescence decay induced by electron pulse, exciton interactions 77—16403
noise, in particle flux, due to reduction and multiplication processes 79—21672
optical microprobe for high-resolution anal. 77—13806
phosphor efficiencies, rel. to other material props. 77—81158
phosphors, cathodoluminesc. investig., appl. to cathode ray tube screening 80—108282
phosphors, containing O, kinetics of buildup 78—10952
phosphors, quantum efficiency meas. 77—41699
photon counter design for low light detection systems, spectroscopy, cathodolum. materials appl. 80—105711
photon statistics for cathodoluminesc. of characteristic phosphor 77—59620
quantum and radiant efficiency meas. methods, standard materials 78—32899
quartz in granites, cathodoluminescence rel. to granites microcracking and healing 80—51391
quartz overgrowths, on quartz, cathodoluminescence and microstruct., SEM exam. 79—25239
rare earth activated phosphor, use of internal reference 77—44071
rare earth double orthophosphates with alkali metals, conc. depend. of luminesc. props. 80—100673

cathodoluminescence continued
rare earth double orthophosphates with alkali metals, spectroscopic obs., struct. and chem. nature 80—100674
rare earth vanadates, electron energy loss spectra, primary excitation processes in cathodolum. 79—11490
rough surface, polarisation and spectral comp. of radiation from interaction with nonrelativistic electrons *(Russian)* 80—29812
screens, cathodoluminescent, luminous emittance, photometric characts. *(Russian)* 77—1739
SEM, cathodoluminescence mode, efficient spectroscopic detection system 77—5964
SEM, detector system 80—101898
SEM, polarisation contrast of cathodolum. 79—7529
SEM, spatial resolution enhancement for cathodolum. and electron beam induced current modes 78—21293
SEM, stroboscopic cathodolum., appls. 80—70088
SEM, theory of cathodoluminesc., spatial resolution anal. *(Russian)* 77—32448
SEM cathodoluminescence analysis of impurities, localisation and sensitivity 78—95985
SEM cathodoluminescence detection system for transmission optical fluorescence analysis 78—23999
SEM cathodoluminescence microscopy, mirror detector system 78—24000
SEM cathodoluminescence probing of biomol. species at 100 Å resolution or below 78—24197
SEM specimen, meas. of local temp. 79—9258
SEM use for cathodoluminescence analysis 78—32949
semiconductor, cathodoluminescence meas. of minority carrier lifetime, appl. to GaP 78—19572
semiconductor, effect of surface space charge region 78—43939
semiconductor, ferroelectric props., paraelec. phase transition, cathodoluminescence *(Russian)* 78—23535
semiconductor, micron scaled cathodoluminescence with SEM, review 78—23537
semiconductor, recomb.-enhanced defect reactions 77—51377
semiconductor, spatial distrib. of traps obs. with SEM *(Russian)* 77—32449
semiconductor, STEM spectroscopic techniques for simultaneous electronic and defect obs. 80—100145
semiconductor, TEM/SEM observations comparing diffr., elec. and luminesc. contrast from dislocations 78—38714
semiconductor, two stage model for deep level capture 78—10396
semiconductor defects, spectroscopic techniques to study of electronic props. 80—84446
semiconductor electron-hole pair creation and migration 77—77304
semiconductor induced current obs., using stroboscopic SEM 77—19855
semiconductor minority carrier diffusion length meas. using electron microprobe 77—39867
semiconductor optical characterization 80—50352
semiconductor viewing in a stroboscopic SEM, spatial resolution of luminescence and spectra 77—20936
semiconductors, II-VI cpds., dislocation motion obs. by SEM in cathodolum. *(Japanese)* 79—46666
semiconductors, quasi-equilib. approx. 80—84779
small particles, characterisation and microanal. by STEM combined with other techniques 80—50901
spectroscopic techniques, anal. with STEM for electronic anal. and obs. of defects in semiconductors 79—14812
spectroscopy using Weierstrass sphere geometry 77—49777
STEM, use for cathodoluminescence analysis 78—32950
surface plasmon light emission induced by fast electrons on modulated surface 78—80424
ureilite meteorites, fluorescent accessory phases in carbonaceous matrix 79—40143
wet objects, cathodolum. mode obs. in raster electron microscope 78—11782
Ag, film and polycryst. samples, low energy electron irrad., visible and UV emission 78—2921
Ag polycrystal, luminesc. spectra due to slow electron bombard. 78—10995
Ag, surface and volume plasmon light emission due to low energy electron scatt. 80—40177
Ag, surface plasmon light emission induced by fast electrons on modulated surface 78—80424
$AgGaSe_2$, reabsorpt. of excitonic luminesc. in direct band gap semiconds. 77—63469
AlGaAs, LPE layers, growth initiation and cathodoluminesc. irregularities 79—87010
$Al_xGa_{1-x}As$ DH laser material, Ar laser induced catastrophic damage 79—86178
$Al_xGa_{1-x}As$ epitaxial diode, neutron and γ-irrad. effects on cathodolum. in SEM 79—11473
$Al_xGa_{1-x}As$, LPE, cathodoluminesc. obs. 78—68565
$Al_xGa_{1-x}As$, solid soln., synthesis by ion implantation Al^+ ions 78—38741
$Al_xGa_{1-x}As$:Ge(Te)(Zn), photo- and cathodolum., comp. depend. *(Russian)* 77—48215
p-$Al_xGa_{1-x}Sb$ epitaxial layers, cathodoluminescence. investig. for varying x *(Russian)* 77—20931
AlN, epitaxial film growth by MBE, physical and optical props. 80—2293
AlN film on Si and Ge, growth, struct. and props. 77—55468
AlN, impurity-doped film, cathodoluminescence spectra 79—83038
AlN:O, UV spectra of deep impurity centres, radiative recombination 79—87490
α-Al_2O_3, defects in unirradiated cryst., optical absorpt. spectra 79—61409
Ar, condensed electron beam excited, exciton radiative lifetimes 80—6727
Ar jet, supersonic, electron beam-excited, continuous VUV emission spectrum origins 79—6964
Ar, liquid, triplet state of self-trapped exciton states, evidence of existence, luminescence meas. 78—72608
Ar, liquid and solid, absorpt. and luminesc. spectra of self-trapped excitons 79—65893
Au, film and polycryst. samples, low energy electron irrad., visible and UV emission 78—2921
Au polycrystal, luminesc. spectra due to slow electron bombard. 78—10995
BN external crystal morphology, SEM obs. 79—73078

cathodoluminescence continued
$BaTiO_3$ ceramics, grain boundary pot. barriers, cathodoluminesc., electron probe anal. 80—2864
Ba_2ZnS_3:Mn, luminescent props. 77—77292
BeO with/without admixtures, TV picture tubes appl. *(Polish)* 80—2869
CaF_2, SEM 80—100700
CaF_2:Ce,Mn, heavily-doped phosphor, cathode-ray irrad., energy transfer 79—87509
CaF_2:Eu, CaF_2:Eu,Mn(Gd), single crystal predisintegration phenomena, SEM cathodolum. obs. 80—59502
CaF_2:Mn, CaF_2:Eu,Mn, single crystal predisintegration phenomena, SEM cathodolum. obs. 80—59502
CaO, electron irradiated, symmetry assignment of new point defect 78—31261
CaO:Mn phosphor, surface radical recomb. and cathodoluminesc. *(Russian)* 78—6787
CaS, polycryst., cathodoluminesc. of point defects 79—78759
CdF_2:Eu(Gd)(Nd), semicond., symmetry of optical centres, optical and elec. props. 77—59592
CdF_2:R^{3+}, cooperative luminescence influenced by symmetry of centres 78—6791
CdI_2 (Br_2), cathodoluminescence, 300 and 80K *(Russian)* 79—78760
CdS, cathodolum. in red and exciton regions, surface treatment influence 77—77303
CdS, doped laser mechanism and output study 80—43340
CdS, exciton cathodoluminesc. of semicond. with surface pot. barriers 78—88366
CdS, exciton-LO phonon interactions under high excitation and temp. conditions 77—69899
CdS, influence of surface annihilation of excitons on cathodolum. meas. 77—20937
CdS, ion irrad. damage, obs. using SEM in cathodolumin. mode 79—7633
CdS, local cathodolum. of single crysts. under colour contrast conditions in SEM 79—8191
CdS, stimulated and spontaneous emission from degenerate electron-hole plasma at 300K 80—29762
CdS, temp. depend. of edge emission band shape 77—20934
CdS:Cu, Fermi level position, luminesc., and photosensitivity, electron irrad. effects *(Russian)* 78—14652
CdS:Ga crystal cathodoluminescence, SEM analysis 80—97349
CdS:In(Ga)(Al), cathodolum. on diffusion front 77—32447
CdS-based phosphor, microstruct. and luminesc. efficiency 78—10959
CdS(Se), with dislocations, optical props. 79—83001
$CdS_{1-x}Se_x$, chem. comp. and luminescence obs. 80—80869
CdS_xSe_{1-x} mixed crystals, exciton spectra 78—92131
n-CdTe, cathodoluminescence microscopy obs. of dislocations, compared with etch pit pattern 79—69105
CdTe, undoped and donor-compensated, cathodoluminesc. of 1.4 eV bands 77—40291
CdTe, vapour-phase-grown, cathodoluminesc. study 80—76086
CdTe, Yb^{3+} implantation, nonstoichiometry effect 77—15440
CdTe:In, lightly- and heavily-doped, cathodoluminesc., temp., injection level and freq. depend. 78—52584
CdTe:Xe, anomalous Xe^+ ion implantation defect introduction, cathodolum. obs. 77—62554
CdTe:Yb, exciton emission, cathodoluminescence 78—39033
CsCl, electron beam excited luminesc., phase transition effects 77—85810
CsI:Tl, luminescence yield depend. on orientation of fast electron beam *(Russian)* 77—8665
Cu, film and polycryst. samples, low energy electron irrad., visible and UV emission 78—2921
Cu, hot cathodoluminescence study, electron-hole recombination 80—93410
$Cu_{1-y}Ag_yInS_{2(1-x)}Se_{2x}$, lattice consts. and band gap variations 79—78000
$Cu_{1-y}Ag_yInS_{2(1-x)}Se_{2x}$ pentenary alloy system, appl. to photovoltaic solar energy conversion, cathodolum. determ. of band gap 80—35680
CuCl, exciton luminesc., reabsorpt. and polariton effects 80—50430
$CuGaS_2$, reabsorpt. of excitonic luminesc. in direct band gap semiconds. 77—63469
CuI, single crysts., growth and optical props. 80—93470
$CuInS_2$, cathodolum. spectra, heat treatment and electron irrad. effects 78—10996
Cu_2S-CdS heterojunction diodes, barrier model estimated from photovoltage and cathodoluminesc. spectra 79—78165
Cu_xS film for Cu-Cd-S solar cell, cathodolum. spectrum rel. to prod. method 79—56866
Cu_xS, photon and electron excitation phenomena 79—7865
Cu_xS-CdS solar cell, p-n junction shape and struct. 77—55599
Cu_3SbSe_4, cathodoluminesc., 90-298K 77—40290
(Ga,Al)As:Si(Ge), epitaxial layers, radiative recomb., compensation, cathodolum. study 80—66307
GaAlAs 79—64964
$Ga_{1-x}Al_xAs$ structures, STEM and scanning deep level transient spectroscopy in defect centre anal, cathodoluminesc. techniques 80—103642
$Ga_{1-x}Al_xN$ heteroepitaxial films, photoluminesc., cathodoluminesc. 80—66292
$Ga_xAl_{1-x}N$, epitaxial film, cathodoluminesc. 80—25469
$Ga_xAl_{1-x}N$ film, growth and props. 78—39702
$Ga_{1-x}Al_xP$:N epitaxial films, ion implanted, cathodoluminescence study 80—60684
GaAs, doped with Group IV elements, etching, electron spectra, cathodoluminesc. study of inhomogeneities 77—11556
GaAs epitaxial films on strongly doped substrate, basic parameter meas. utilising magnetoresist. and SEM techniques under cathodoluminesc. conditions 80—65728
GaAs film, electron scatt., cathodoluminesc. meas., energy depend. of electron deposition depth determ. 80—104023
GaAs LPE layers, dopant tracing of terrace growth 78—75948
GaAs, SEM defect study, transmission cathodoluminescence 79—64964
GaAs, stimulated and spontaneous emission from degenerate electron-hole plasma at 300K 80—29762
GaAs VPE layers for FET devices, impurity characterisation 80—29491
GaAs:Cr, fine structure in cathodoluminescence spectrum 78—56524
GaAs:Cr, luminescence and absorption spectra, temp. depend. of fine structure 80—6779
GaAs:Cr, semi-insulating, i.r. induced modulation of cathodoluminescence, and specimen current 77—1737

cathodoluminescence continued
GaAs:Cr(W), deep trapping centre exam. by thermally stimulated capacitor discharge method and luminesc. 77–55495
GaAs:Cu melt grown, 1.36 eV band luminescence studies, edge emission 79–87510
GaAs:P films, epitaxial growth from melt with components introduced by ion bombardment 77–21044
GaAs:Se cathodoluminescence decay obs. with SEM and streak camera, 90 to 300K 80–97348
GaAs:Si defect density before and after Zn diffusion, SEM and TEM obs. 80–96529
GaAs:Si(Ge) LPE layers, luminesc. props. rel. to substrate quality 78–52583
GaAs:Sn, selective LPE, orientation dependent growth, luminesc. 77–12551
GaAs:Sn, Te, luminescence props. 79–52017
GaAs:Te, impurity cond., microcathode-luminesc. investig. 77–8666
GaAs:Te, microcathodoluminesc. of effect of struct. defects on radiative recomb. 79–11475
GaAs:Te influence of fluctuations of impurity pot. on Burstein-Moss effect 78–48240
$GaAs/Al_xGa_{1-x}As$ heterostruct., anomalous elec. and optical characts. 80–2865
GaAs-Cu:Tl, cathode luminescence spectra, Hall effect, cryst. defects 80–76087
$GaAs\text{-}Ga_xAl_{1-x}As$ DH laser material crystal cathodoluminescence, SEM analysis 80–97349
GaAs-GaAlAs wafers, defects and degradation, transmission cathodolum. evaluation 80–65395
$GaAs_{1-x}P_x$, solid soln., synthesis by ion implantation P^+ ions 78–38741
$GaAs_xSb_{1-x}$, spontaneous and stimulated emission, electron beam excitation 77–58333
$GaAs_xSb_{1-x}$-GaAs epitaxial films and multilayer heterostruct., SEM obs. under cathodolum. conditions 79–11023
$(GaAs)_{1-x}(ZnSe)_x$, LPE growth, resist., Hall effect and cathodoluminesc. meas. 77–28270
$(GaAs)_x(ZnSe)_{1-x}$ single crystal, visible cathodoluminesc. spectra 80–20716
$Ga_xIn_{1-x}As$, spontaneous and stimulated emission, electron beam excitation 77–58333
$Ga_xIn_{1-x}As_{1-y}P_y$, spontaneous and stimulated emission, electron beam excitation 77–58333
$Ga_xIn_{1-x}As_yP_{1-y}$, LPE layers, growth and characterisation 78–38983
$Ga_xIn_{1-x}As_ySb_{1-y}$, epitaxial film and DH, luminesc. props. 77–686
$Ga_xIn_{1-x}P$, real struct. exam. by electron microscopy and channelling 78–2143
$Ga_xIn_{1-x}P$, with indirect band struct., radiative recomb. of free excitons, cathodolum. meas. 77–90202
$Ga_xIn_{1-x}P$:N layers, LPE growth, luminesc. and direct exptl. obs. of band struct. effects 77–52157
GaN and GaN:Zn epitaxial layers, doping effect on cathodoluminesc. 77–20935
GaN, epitaxial, 78-300K 78–19575
GaN epitaxial films, cathodoluminesc. spectra 80–71496
GaN, epitaxial layer, characts. from cathodoluminesc. 78–35208
GaN epitaxial layers, exciton cathodolum. *(Russian)* 78–76543
GaN epitaxial layers, exciton cathode luminesc. 79–65933
GaN film, preparation by pyrolysis of $Ga(CH_3)_3$ in NH_3, cathodoluminesc. 77–4691
GaN, pure and Zn-doped epitaxial layers 78–10955
GaN, VPE growth rate influence on elec. and luminesc. props. 80–100702
GaN, VPE on sapphire, and characterisation 78–2387
GaN:Al, VPE grown, luminesc. and elec. props. depend. on doping conc., bound excitons 80–20688
GaN:As(P), implanted single cryst. film, cathodolum. 78–60523
GaN:Zn, cathodolum. obs., recomb. model 79–11474
GaN:Zn, cathodoluminesc., photocapacitance 79–38679
GaN:Zn, epitaxial layer, effective electroluminesc., blue regime *(Russian)* 77–77302
GaN:Zn epilayers, growth parameters effect on props., device struct. 78–26975
GaP, dopant dislocations, scanning electron micrographs, cathodoluminesc. 78–91340
GaP, electron-hole liq., cathodolum. spectra meas., 4.2-20K 77–63470
GaP, electron-hole liquid, emission band from time-resolved spectra 78–43938
GaP, epitaxial layer, carrier recomb. at dislocations 77–20932
GaP epitaxial layer, crystal defects influence on luminesc. obs. 79–87511
GaP, epitaxial layers, dislocation recomb., SEM cathodoluminescence studies 79–42558
GaP, epitaxial struct., cathodolum. in SEM 78–10991
GaP, first order Mott transition of exciton gas 78–76535
GaP, frozen-in pt. defects annihilation 79–99949
GaP, green cathodolum. from cryst. defects, SEM, TEM study 80–80870
GaP, green luminesc. efficiency, review 77–28636
GaP, growth and props. of LPE layers on Si substrates 78–6864
GaP, LEC crystal, cathodolum. and photolum. around dislocations 78–84663
GaP LED, SEM study of charge collection and cathodoluminesc. 80–65661
GaP, LPE, cathodo- and electrolum., residual impurity and struct. defect effects 78–19570
GaP, light emitting diode structure, effect of neutron irradiation on cathodoluminesc. 79–28843
GaP, minority carrier lifetimes at dislocations, SEM meas. using photon counting 78–23109
GaP, Mott transition of exciton gas, cathodoluminesc. 79–33845
GaP polycrystals, subgrain boundaries, cathodolum. in SEM 79–1440
GaP, radiative and non-radiative recombination around dislocations 78–19576
GaP, SEM, cathodoluminesc., impurity and defect detect. 78–83695
GaP:N, epitaxial layer, determination of nitrogen concentration from cathodoluminescence spectra 78–38744
GaP:N, N doping profiles in GaP grown by LPE, cathodoluminesc. data 79–23631
GaP:N LED structures, local dopant conc. determ. using SEM cathodolum. spectra 80–101057

cathodoluminescence continued
GaP:N(N,O) epitaxial struct., luminesc. study of degradation during heat treatment 80–45139
p-GaP:Zn,O-n-GaP:Te,N diode struct., radiative recomb. 80–7419
GaSe, cathodolum., 115 and 285K 79–87512
GaSe, electron beam excited free exciton luminesc. 79–19940
GaSe, exciton-phonon quasibound states, photocond. and luminesc. study 80–96800
GaSe, radiative transitions, cathodoluminescence 78–10997
$Hg_{0.7}Cd_{0.3}Te$, 17 to 77K, photo- and cathodoluminesc. 78–52569
α-HgS, band gap shrinkage, cathodolum. under very strong excitation 77–85146
HgS, cathodoluminescence, evidence of donor-acceptor type transition 77–24902
α-HgS, cinnabar, donor-acceptor transitions, cathodolum. meas. *(French)* 77–48250
HgS, cinnabar powder, 1.65 eV pair recomb., thermal quenching and total light decay 78–27330
α-HgS, green cathodoluminesc., impurity effects 78–2924
α-HgS, natural, yellow emission 78–68567
n-In Ar:Te(Sn), heavily doped, cathodoluminescence, doping effect on luminesc. band position and spectral profile 80–45153
In-ZnSe:Al-In, MSM structure, mechanism of current flow *(Russian)* 79–78208
$In_{1-x}Al_xP$:Bi(N)(Zn,O) radiative recombination at isoelectronic centres 79–52027
InAs and solid solutions, recombination mechanisms of excess carriers, luminesc. obs. 80–97337
n-InAs, cathodoluminescence, radiative recomb. of hot carriers 77–8667
InAs, electron beam excitation, luminesc. and stimulated emission 77–16339
InAs, epitaxial, laser action mechanisms with electron beam excitation 80–28240
InAs, heavily doped, Burstein-Moss effect and near-band-edge luminesc. 79–47525
InBr, metastable exciton emission, electron excitation mechanism 77–66546
InGaAsP, epitaxial layer, defect evaluation by cathodoluminescence 80–2866
$In_xGa_{1-x}As_ySb_{1-y}$ laser, nonequilibrium carrier recombination, luminesc. study 80–50431
n-$In_{1-x}Ga_xP$, direct-gap semiconductor, cathodoluminesc., electron irrad. effects 80–108283
$In_{1-x}Ga_xP$, epitaxial film, cathodolum. obs., recomb. mechanisms 78–72613
$In_{1-x}Ga_xP$, LPE, on $GaAs_{1-y}P_y$, photo- and cathodolum. 78–19559
$In_{1-x}Ga_xP$, luminesc. props. from cathodoluminesc. and electroluminesc. meas. 80–2281
$In_{1-x}Ga_xP$:Bi(N)(Zn,O) radiative recombination at isoelectronic centres 79–52027
$In_{1-x}Ga_xP_{1-z}As_z$ luminesc. props. from cathodoluminesc. and electroluminesc. meas. 80–2281
$In_{1-x}Ga_xP_{1-z}As_z$ solid solution, radiative transitions 79–11476
$In_{1-x}Ga_xP_{1-z}As_z$, stimulated yellow-green emission under electron excitation, 80K 79–33846
InP substrate, LEC-grown, defect evaluation by cathodoluminescence 80–2866
InP:Te(S), heavily doped, dislocation imaging using transmission cathodoluminesc. 80–29023
InP:Zn heavily doped X-ray topography, cathodolum., and TEM obs. 79–99197
K film, splitting of surface plasmon emission spectra 79–99954
KBr, optical conversion, luminesc. and colour centre formation 79–24354
KCl, electron irradiation, tunnelling recombination luminescence, between neutral Ag atoms and V_k centres 79–61442
KCl:Na^+, self trapped excitons, optical absorption and emission 77–43503
KCl:Tl, temp. depend. of cathodolum. *(Russian)* 80–80868
KI, electron irrad., polariton effects in reson. emission 79–33843
KI, exciton diffusion, luminesc. quenching, meas. 4 to 77K 77–32433
KI, free exciton-F^- centres interaction, electron excited emission 79–83036
KI, luminesc. polarisation for free and bound excitons 78–10942
KI, polariton effects in resonant emission 78–76533
KI, self trapped exciton form. time at ${}^1\Sigma_u{}^+$ state under pulsed electron beam in ps range 80–97347
Kr, liquid, triplet state of self-trapped exciton states, evidence of existence, luminescence meas. 78–72608
Kr, liquid and solid, absorpt. and luminesc. spectra of self-trapped excitons 79–65893
Kr supersonic jet, electron beam excited, vac. UV spectrum 77–88414
$LaAlO_3:Tb^{3+}$, cathodo- and photoluminesc. 77–12448
$LaF_3:Nd^{3+}(Er^{3+})(Tm^{3+})$, VUV fluorescence and tunable coherent sources from 1650 to 2600 Å 77–688
$LaGaS_3:Ce^{3+}$, phosphor, luminesc. props. 80–103979
La_2O_2S penetration phosphor, penetration and cathodoluminescent props. 80–20718
La_2O_2S:Tb, cathodoluminesc., nonlinear depend. on activator concs. 79–8190
La_2O_2S:Tb, cathodoluminesc. efficiency changes due to processing, XPS meas. of surface changes 79–99951
La_2O_2S:Tb based barrier layer phosphors, prep. and cathodum. props. in penetration phosphors 77–1738
LiD, luminesc. of free and localised excitons, UV, X-ray and electron irrad. luminesc. 79–87483
LiF crystal, contact damage obs. by cathodoluminesc. 80–71728
$LiGaO_2$:Fe, phosphor, luminesc. 78–92108
LiH (D), single crystals, electronic excitations, review *(Russian)* 78–72574
LiH, excitons, reflection, cathodolum. and photocond.-excitation spectra 78–10989
LiH, luminesc. of free and localised excitons, UV, X-ray and electron irrad. luminesc. 79–87483
LiH, single crysts., refl. photolum., cathodolum., and photocond. meas. 77–52186
LiH:LiF, luminesc. of free and localised excitons, UV, X-ray and electron irrad. luminesc. 79–87483
$LiYF_4:Nd^{3+}(Er^{3+})(Tm^{3+})$, VUV fluorescence and tunable coherent sources from 1650 to 2600 Å 77–688

cathodoluminescence continued
- LuF$_3$:Nd^{3+}(Er^{3+})(Tm^{3+}), VUV fluorescence and tunable coherent sources from 1650 to 2600 Å 77—688
- MgAl$_2$O$_4$, spinel, vac. UV luminesc. spectra *(Russian)* 77—24903
- MgF$_2$, transient absorption and luminesc. following electron beam excitation 77—69920
- MgO, cathodoluminesc. at dislocations 79—47524
- MgO crystal, contact damage obs. by cathodoluminesc. 80—71728
- MgO crystal cathodoluminescence, SEM analysis 80—97349
- MgO, deformed, cathodlum. obs. by STEM 80—76088
- MgO, electron irradiated, luminescence, radiative recombination kinetics 80—7421
- MgO, electronic excitations and luminescence, review *(Russian)* 78—72575
- MgO, exciton luminesc. spectrum, fine struct. 80—20715
- MgO film, vacuum deposited on NaCl-type alkali halides, struct. characterisation 79—82490
- MgO, local loss of stoichiometry caused by plastic deform., cathodoluminesc. spectra 78—35209
- MgO, pure and doped, luminesc. of free and relaxed excitons 79—74008
- MgO single crystal, grain boundaries, cathodolum. in SEM 79—1440
- MgO, single crystals, compressed, SEM exam. of cathodoluminescence 78—56525
- MgO:Be epitaxial layers, vacuum UV luminescence 80—11480
- MgO:Fe, cathodolum. after plastic deform. 79—95849
- MgO:Li(Al)(F), impurity-induced UV luminesc. 79—83037
- MgO:S, cathodoluminesc. spectrum *(Russian)* 80—55197
- Mg$_x$Zn$_{1-x}$Te, high purity, luminesc. and band gap 78—68553
- N$_2$ crystals, luminesc. and biexcitons 79—69893
- N$_2$ film, on metal or sapphire substrates, luminescence and nonradiative energy transfer to surfaces 80—97350
- N$_2$, solid, electron impact excited, luminesc. spectra 77—48252
- N$_2$, solid 77—28634
- N$_2$, solid 79—19939
- Na film, slow electron bombarded, light radiation 80—40168
- Na$_4$Al$_3$Si$_3$O$_{12}$Cl:Br,Ge, sodalite, reflectance and luminescence obs. 79—4839
- NaCl, electron and ion beam excited luminesc. spectra 79—52026
- NaCl electron excited luminescence yield orientational depend. 80—40169
- NaCl, electron irradiation, tunnelling recombination luminescence between neutral Ag atoms and V$_k$ centres 79—61442
- NaCl, exciton luminesc. obs. 77—12449
- NaCl, optical conversion, luminesc. and colour centre formation 79—24354
- NaI, luminesc. polarisation for free and bound excitons 78—10942
- Ne, liquid and solid, absorpt. and luminesc. spectra of self-trapped excitons 79—65893
- Pb halides, above-edge cathodolum. from metastable excitons 78—6786
- PbBr$_2$, metastable exciton emission, electron excitation mechanism 77—66546
- PbCl$_2$, metastable exciton emission, electron excitation mechanism 77—66546
- PbI$_2$, metastable exciton emission, electron excitation mechanism 77—66546
- PbS-(PbSO$_4$)$_x$(PbO.PbSO$_4$)$_y$ heterosystem, cathodoluminescence spectra 79—24370
- Pb$_{1-y}$Sn$_y$Se, ($0 \leq x \lesssim 0.08$), spontaneous emission investigated 78—10990
- Pb$_{1-x}$Sn$_x$Te, ($0 \leq x \lesssim 0.2$), spontaneous emission investigated 78—10990
- RbBr, self trapped exciton form. time at $^1\Sigma_u{}^+$ state under pulsed electron beam in ps range 80—97347
- RbI, electron irrad., polariton effects in reson. emission 79—33843
- RbI, luminesc. spectra induced by pulsed Ne$^+$ and electron beams and X-rays 80—80851
- Se, trigonal, cathodolum. at 10K *(German)* 78—2923
- Si, electron beam irrad. at 31 GeV, polarised photon emission *(Russian)* 80—29811
- Si, intrinsic, two-phonon assisted free exciton recomb. radiation 78—2922
- Si: Li, absorpt. and luminesc. transitions involving exciton excited hole states 79—78038
- Si:As(Sb)(Bi)(P), luminescence associated with transitions from bound exciton excited states 78—23534
- Si:B(Al)(Ga)(In)(Tl), high resolution recomb. radiation, investigation, electron excited 78—15233
- Si:P, excitation density depend. of cathodoluminesc. from bound multiexciton complexes 78—72609
- SiC, cathodoluminescence, comparison with other materials 78—92130
- SiC:Al,N, blue cathodolum. spectra obs. 78—19574
- n-SiC:N, O, cathodolum. spectra meas. 78—19573
- SiO$_2$, amorphous and crystalline, with O vacancy, cathodolum. meas. 77—24901
- SiO$_2$ coatings on SiO$_2$ substrate, cathodoluminescence spectra, electron irrad. 80—76085
- SiO$_2$ layers in LSI cct. device, cathodoluminesc. obs. 80—80867
- SiO$_2$, undoped film, 2 to 5 eV *(Russian)* 80—40164
- SiO$_2$:Nd^{3+} films, cathodoluminesc. 80—20717
- SiO$_2$-Si, cathodoluminesc. and AES rel. to struct. 78—43937
- SnO$_2$, rare earth ion doped, luminesc. and charge compensation 78—76532
- SnO$_2$:Eu film, RF cosputtering, cryst. site of Eu, cathodolum. obs. 77—7987
- SnO$_2$:Eu powder phosphor, prep., low energy electron excitation 78—39608
- SnO$_2$:Eu^{3+}, luminesc. and charge compensation 77—28618
- p-SnTe, cathodoluminescence and Fermi level hole effective mass 80—25467
- SrO, luminesc. band edge, 4-6.5 eV, optical absorpt., photoluminesc., cathodoluminescence, photocond. obs. 80—50411
- Th, O$_2$ adsorpt., and oxidation, electron-induced luminesc. expts. 78—38946
- W, surface adsorption processes following electron excitation, cathodeluminescence studies 80—100390
- Xe, condensed electron beam excited, exciton radiative lifetimes 80 6727
- Xe film, decay times meas. of 1750 Å intrinsic luminesc. band 77—59619
- Xe, liq., α-particle and electron excited luminesc., time depend., specific ionisation density effect 80—71495
- Xe, liquid, triplet state of self-trapped exciton states, evidence of existence, luminescence meas. 78—72608

cathodoluminescence continued
- YAG, undoped and Ce^{3+}-doped, cathodolum. intensity and decay time, 10-480K 79—99952
- YAG:Ce, cathodoluminescence meas., temp. depend. 79—61443
- YAG:Ce phosphors, luminesc. efficiency, prep. and dopant effects 80—45151
- YAG:Ce^{3+}(Eu^{3+})(Gd^{3+})(Tb^{3+}), cathodoluminesc. efficiency rel. to activator conc. 80—11479
- YAG:R^{3+}, CRT and X-ray phosphor lattice-activator energy transfer model 78—6792
- YAG-Ce^{3+}(Eu^{3+})(Tb^{3+})(Gd^{3+}), cathodolum. intensity, temp. depend., comparative study 79—99953
- YF$_3$:Nd^{3+}(Er^{3+})(Tm^{3+}), VUV fluorescence and tunable coherent sources from 1650 to 2600 Å 77—688
- Y$_3$Ga$_5$O$_{12}$:Tb^{3+}, luminesc. 77—48251
- Y$_2$O$_3$, rare earth activated, use of internal reference 77—44071
- Y$_2$O$_3$:Eu, fluoresc., cathodoluminesc. and thermal quenching 79—47488
- Y$_2$O$_3$:Eu^{3+}, absorpt. spectra, fluoresc., electron beam excitation 78—92093
- Y$_2$O$_2$S:Eu phosphor, luminescence saturation effects due to N$_2$ laser and cathode-ray excitation 80—40151
- Y$_2$O$_2$S:Tb, cathodoluminesc. efficiency at low electron energy 78—6790
- Y$_2$O$_2$S:Tb, cathodoluminesc. efficiency changes due to processing, XPS meas. of surface changes 79—99951
- Y$_2$O$_2$S:Tb^{3+},Eu^{3+}, energy transfer mechanism 78—6793
- Y$_2$O$_2$S:Tb^{3+}(Pr^{3+}), enhancement of cathodolum. efficiency 79—69891
- Y$_{1-x}$Tb$_x$Al$_3$B$_4$O$_{12}$ phosphors, conc. quenching, impurities effect 77—73177
- YVO$_4$:Eu, fluoresc., cathodoluminesc. and thermal quenching 79—47488
- YVO$_4$:Eu^{3+}, absorpt. spectra, fluoresc., electron beam excitation 78—92093
- YVO$_4$:Eu^{3+} phosphor, cathodoluminesc. and photon statistics 77—59621
- (Zn,Cd)S:Cu,Al, luminesc. efficiency deterioration due to surface oxidation by (NH$_4$)$_2$Cr$_2$O$_7$ thermal decomp. 80—29810
- (Zn,Mg)$_3$(PO$_4$)$_2$:Mn^{2+}, cathodoluminescence obs. 80—71492
- ZnCdS:Ag, phosphor screen, electron beam excited, light ang. distrib., modulation transfer function 80—45150
- ZnCdS:Ag screen, electron beam excited, light emission spectra 80—25466
- Zn$_x$Cd$_{1-x}$S, graded single crysts., laser or electron beam excited, luminesc. 77—85792
- Zn$_{1-x}$Mg$_x$Te alloy, efficiency *(French)* 77—21019
- Zn$_{1-x}$Mg$_x$Te alloys, high purity, metallurgical and analytical methods of prep. 80—40247
- ZnO epitaxial film, ionized-cluster beam and reactive ionized-cluster beam deposition, cathodolum. characterisation 80—16202
- ZnO film, prep. by reactive ionized cluster beam deposition, and characterisation 80—10829
- ZnO, hexagonal spot pattern production with light source and electron beam 77—69148
- ZnO, low energy cathodolum., surface effects 78—60522
- ZnO:Li, effect of LiOH mineraliser on struct. and optical props. 77—8737
- ZnO:Li(Na), band-edge emission obs. 77—20933
- ZnO-GeO$_2$-MnO-B$_2$O$_3$ wideband cathodoluminescent phosphor 80—55196
- ZnP$_2$, cathodoluminesc. 4.2 to 200K 79—52028
- α-ZnP$_2$, local centre parameters, photoelectron transition scheme, recomb. process anal. 80—44654
- ZnP$_2$, monoclinic, cathodoluminesc. spectra exam. 79—15534
- ZnS, cathodolum. emission spectra, exciton lines 80—76084
- ZnS, low voltage cathodoluminescence 78—52585
- ZnS platelets, cathodolum. analysis using STEM 78—32950
- ZnS, single electron excitation study, cathodoluminescence image contrast using STEM 80—89072
- ZnS striated platelets, SEM studies of local variations in cathodolum. 78—15232
- ZnS, temp. depend. of edge emission band shape 77—20934
- ZnS:Ag, Al and ZnS:Cu, Al, LV cathodoluminesc. 79—33844
- ZnS:Ag, luminesc. efficiency deterioration due to surface oxidation by (NH$_4$)$_2$Cr$_2$O$_7$ thermal decomp. 80—29810
- ZnS:Ag, photon counting statistics of cathodoluminesc. light emission 79—24371
- ZnS:Cl, shape of self-activated cathodoluminesc. band 80—34987
- ZnS:Er^{3+}, ion-implanted, annealing, cathodolum. obs. 80—2868
- ZnS:Mn film, luminesc. of highly efficient DC diodes 77—8630
- ZnS:Mn film, spectral and electro-optical props. 77—1736
- ZnS:RF$_3$ in Ta-Ta$_2$O$_5$-ZnS:RF$_3$-Au struct., electrolum. and cathodolum. meas. *(French)* 77—16398
- ZnS-based phosphor, microstruct. and luminesc. efficiency 78—10959
- ZnS-O, single cryst., fast neutron irrad., optical props. 78—27331
- ZnS$_x$Se$_{1-x}$, VPE, characterisation of defect centres by photoelectronic meas. 80—10914
- ZnS$_x$Se$_{1-x}$, VPE on CaF$_2$ substrate, in flowing H$_2$, growth and characterisation *(French)* 80—107678
- ZnSe, reabsorpt. of excitonic luminesc. in direct band gap semiconds. 77 - 63469
- ZnSe:Al(Mn), elec. and luminesc. props. 77—39844
- ZnSe:B(F), ion implantation, photocond. and cathodoluminesc. meas. 78—26586
- ZnSe:Cu, Al, single cryst., low-voltage red cathodolum. 78—80423
- ZnSe:Cu,Al, LV cathodoluminesc. 79—33844
- ZnSe-CdTe(ZnTe) heterojunction, cathodolum. and electrolum. 78—6782
- Zn$_2$SiO$_4$:Mn film, electron beam depth-dose functions, cathodoluminesc. 80—2867
- Zn$_2$SiO$_4$:Mn phosphor, efficiency enhancement by AlPO$_4$ substitution 80—11452
- ZnTe, edge luminesc. excited by electron bombard. 80—66308
- ZnTe, elec., SEM and TEM studies of impurity segregation during long annealing 80—30001
- ZnTe, electro- and cathodoluminesc., impurity segregation 79—43042
- ZnTe, extrinsic luminesc., bands, temp. injection level, and freq. depend. 80—20714
- ZnTe, ion implantation defect introduction, cathodolum. studies 80—75250
- ZnTe, low voltage green LED, struct. double diffusion procedure 80—100697
- ZnTe, SEM and luminesc. study of Li segregation 79—38657
- ZnTe:Cu, doping behaviour, SEM in cathodoluminesc. and photoluminesc. exam. 79—65927
- ZnTe:Li, diffusion investigation by SEM and TEM 80—10706

cathodoluminescence continued
ZnTe:Li, impurity segregation during short annealing and quenching, SEM, TEM and elec. meas. 80—10676
ZnTe:O,Zn, dual ion implantation, luminesc. spectra obs. 78—87697
ZnTe:P(As), ion implanted, cathodoluminescence emission spectrum 80—108281
ZnTe-ZnSe(CdSe), LPE growth, elec., photoelec. and luminesc. meas. 77—4745
cathodophosphorescence *see cathodoluminescence*
cathodothermoluminescence *see cathodoluminescence*
catholytes *see electrolytes*
CATV *see cable television; community antenna television*
causality *see physics fundamentals*
causticity *see pH*
cavitation
see also bubbles; vortices
acoustic, threshold conditions for onset 78—59433
acoustic field generated cavitation, review 80—74934
acoustic wave reflection from fluid-solid boundary, bubble collapse, US cleaning and cavitation erosion 80—65158
activity in acoustically excited spherical flask, obs. 78—42488
adhesion determination appl., metal film on polymer base, US test device 79—91865
air bubble growth meas. by rectified diffusion at 22.1 kHz 80—96155
alkali metal salt solution, Ar saturated, sonoluminesc. as acoustic cavitation probe 79—60437
alloys, creep cavitation control, intergranular precipitates role 80—66664
amplitude-spectrometric study of acoustic cavitation erosion 77—52505
AMTE/OUEL underwater jet noise rig, working report for 1977/78 80—79286
approximate analysis with allowance for surface tension and gravity 80—92191
approximate soln. of cavity allowing for surface tension and force of gravity *(Russian)* 79—86475
auger-centrifugal pump entry sections, cavitational cavities and cavitational resistance, return flow effects 79—18921
axisymmetfic cavity shape, asymptotic solution for infinite steady flow *(Russian)* 77—31344
axisymmetric cavitational flow of vertical liquid stream around a body *(Russian)* 79—90297
baffles, critical cavitation parameters at high flow vel. 80—38462
bicrystals, diffusion growth of pores under creep conditions 77—15404
bituminous coal emulsification by ultrasonics 79—47997
blade pump, oscill. study, linear math. model 77—35187
blood, volume expansion effects, gas cavities 80—67134
blood platelet morphology and function modification by US exposure 77—77929
bluff bodies, cavitating, constrained flow, drag and vortex shedding 78—47006
boiling water in annular channel, acoustic emission *(Russian)* 77—54302
boundary motion of cavity in weighable liquid *(Russian)* 77—55054
brain injury and instabilities 80—45943
α-brass, Al bearing, high temp. relief cavitation, SEM, STEM, TEM, SIMS and EDX anal. 79—5039
α/β brass, cavitation during superplastic deform. 79—5011
brass, comparison of liquid impact erosion and cavitation erosion 80—104302
α/β brass, grain boundary sliding and intergranular cavitation during superplastic deformation 79—5009
bubble, ellipsoidally deformed, near wall, cumulative jet form. 77—934
bubble, in magnetisable fluid, mag. field and press. effects on shape *(Russian)* 77—27608
bubble cavitation in inviscid compressible liq. 80—28553
bubble cavitation problem, numerical soln. 78—79347
bubble collapse, num. simulation 77—58747
bubble collapse, shadowgraph study 80—48827
bubble collapse in liq. during laser-induced breakdown 77—89171
bubble collapse in water shock tube 78—67231
bubble collapsing near free surface, cavitation 78—47026
bubble formation by action of focused laser radiation *(German)* 77—42882
bubble generation at aperture in submerged surface and associated pressure pulses in liquid *(Russian)* 77—68650
bubble in liquids with polymer additives, small pulsations 77—68647
bubble rupture between two solid walls, effect of drag-reducing polymers on cavitation 80—106822
bubble-produced elec. pulses in water 79—47407
bubbles, amplitude distrib. of pulses produced by shock waves 80—64252
bubbles, gas and vapour, dynamics, review 79—98788
bubbles, linear stability of growth or collapse, slightly viscous liquid 78—90947
cascade hydrofoil SC$_2$ in oil, pitch-chord ratio=0.667, cavitation characts. 78—18323
cavitating fluid model *(Russian)* 78—55668
cavitation inception in liquids 80—38465
cavitation mechanical strength, US assessment of materials in various media 77—16772
cavitation tunnel, for high-temp. operation 78—63521
caviton in incompressible liquid, boundary stability 77—80190
ceramic, cylindrical cavity effect on fracture 79—66144
ceramic, spherical cavity effect on fracture 79—66145
chemical reaction rate increase in US cavitation, diffusion model 79—96312
cloud development *(French)* 78—22388
collapse and expansion of underwater gas bubbles, surface tension effects 77—42880
collapse of cavity artifically cheated downstream of disc 77—58746
collapse of cavity induced by underwater spark 78—42636
columnar vortices in cavity flow 80—24037
compressibility effects in cavity flows, in channel for wedge shaped obstacle 79—77256
cone revolving in tube, finite cavity flow, drag force coeffs., cavitation 80—33641
conf., New Orleans, LA, USA, March 1980 80—105430
conference, cavitation and polyphase flow, Niagara Falls, New York, USA (Jun. 1979) 80—4475
constant pitch inducer pumps, solidity effect limits 80—6108
control valve noise level estimation 77—84076
controlled by surface diffusion, numerical study 79—90668
cavitation continued
creep crack propag. by cavitation near crack tips 80—107364
creep damage and rupture criteria, cavity config., use of density meas. 78—60818
creep failure by cavitation under non-steady conditions, exam. 78—56774
creep fracture model, plastic growth of cavities at tip of grain boundary wedge cracks 77—52446
creep mechanisms, independent and sequential 80—55480
cylinder placed transversely to flow, dil. aqueous polymer solns. effect on cavitation onset 77—68645
cylinders, elliptic 2-D, cavitation shock-noise measurement for different eccentricities 80—79368
damage prediction 79—74265
diffusional growth of intergranular cavities in uniform stress field and ahead of crack-like stress concentrator 80—107366
diffusive cavitation of grain interfaces, non-equilib. models 79—46668
disc motion in presence of collapsing cavity *(Russian)* 77—31342
disc wake, cavitating flows with perturbations 80—92190
dissolved gas liberation kinetics in turbulent liquid stream 77—11226
driven, Navier-Stokes eqn. soln. numerical stability 80—92147
drop impact on solid surface 79—64747
dynamic instability phenomenon, governing eqn. 78—59434
entrainment and thermodynamic effect, viscous effects, review 79—10598
erosion, book contrib. 78—11350
erosion, non-spherical bubble collapse near a solid wall, analytical soln. using matched asymptotic expansions 80—106824
erosion, observation of eroded surface by SEM 78—15536
erosion damage due to cavitation, expt. studies in plasticine 80—1490
erosion intensity in hydrodynamic wakes *(Russian)* 80—53790
erosion of alloys in venturi 80—108602
erosion of ductile Al ogives, cavitation damage scaling 78—5773
erosion with plain jets and jets with cavitation inducers 79—15805
explosions in liquids, slow detonation, vapour explosions and bubble reson. explosions *(German)* 78—34150
failure, incorporating cavity nucleation with strain 80—16451
fatigue high temp., hold time effects, cavitation nucleation, creep interaction 78—60734
film cleaning by ultrasonic liquid cavitation and acceptable solvents 80—62769
flow around circular cylinder, pressure distrib. *(French)* 78—67234
flow boundary rel. to cavity shape near solid walls *(Russian)* 77—68646
flow motion and heat transfer in cavities, fixed and floating boundaries *(Russian)* 77—35144
flow turbulence influence on the inception and growth of cavitation 78—90948
flow visualization of cavitation in water jets and nuclei distribution measurement by holography 80—106862
flow-induced, suppression by dilute polymer solutions 78—67233
fluid, multiphase system, vapour bubble collapse, charact. functions 78—18156
fluid, radio band pulse radiation due to spark initiated cavity dynamics, sonoluminescence *(Russian)* 80—66313
fluid-solid boundary, cavitation by incident P-wave, bubbles 80—6107
free convective heat transfer, from inclined plate in water, effect of US vibr. 77—51055
free gas content and cavitation *(Italian)* 78—22389
free gas content in water, variations during press. fluctuations *(French)* 78—22390
gas bubble in acoustic field, effect of diffusion on evolution, stability 77—15105
gas bubble in compressible liquid, influence of inhomogeneous sound field on motion 80—6131
gas nuclei, radii determ. by filtering gelatin 79—81612
gas nuclei, stabilization using skins of varying permeability 79—81611
gas-liquid systems, vibs. stabilisation of dynamic equilib. and mixing *(Ukrainian)* 80—10291
gaseous cavitation, effect on fluid transients 79—77194
gaseous microbubble growth in laminar separation bubbles 80—106821
gel, gas cavitation nuclei, physical props. of surrounding nonionic surfactants 79—100444
growth in restricted flow 79—18922
growth mechanisms, stress depend., rel. to creep fracture 79—99266
history Berthelot's first publication, 1850, subjection of liqs. to tension 78—32639
holocinematography, high-speed, of cavitation bubbles 78—37841
holography for cavitation and flow research 78—38436
hydraulic liquids, cavitation-erosion props. assessment using ultrasonic dispergator 80—71832
hydrodynamic, at a circular cylinder, characts. 78—1701
hydrodynamic cavitation in nonuniform mag. fields 80—19518
hydrodynamic cavitation in viscous liquid, investigation using HF US probing method 80—87676
hydrodynamic siren, acoustic excitation of cavitation 78—94776
hydrofoil, partially cavitating 79—32596
hydrofoil cavitation noise and inception, boundary layer development 77—55057
hydrofoil characteristics, in supercavitating flow, press. gradient effect *(Japanese)* 77—68649
hydrofoil profile for accelerating cascade, surface press. distribs. 78—18321
hydrofoils, supercavitating, in subsonic liq. flow, linearised theory 77—89173
hydrofoils, tail-loaded, fully cavitating, avoidance of turbulent separation 78—94659
hypersonic cavitation of high and low gas mixtures at low density *(German)* 80—1651
implosion of cavitation bubble, near solid boundary or free surface *(French)* 77—55056
inception characteristics, viscous effects on a two dimens. cylinder 79—4050
incompressible perfect fluid, collapse or expansion of prolate and oblate spheroidal bubbles *(French)* 80—74933
inertial confinement targets, hollow H$_2$ droplet prod. by acoustic excitation of superheated liq. H$_2$ jet 79—85766
insulating oils elec. breakdown at solid-liquid interface with EHD motion, expt. 77—76226
ionizing radiation and cavitation threshold 78—94774
jet development in pulsating bubbles 80—33640
jet pump cavitation with ambient and high temperature water 79—76071
jet-flapped hydrofoil, cavitating flow, second-order theory on wall effect 77—42879

cavitation continued
large-scale spatial oscillations of a cavity in a sound field 78−94775
laser cavitation meter, design and testing 77−68715
laser induced, bubbles obs. by holocinematography 77−46704
laser induced breakdown, high speed holography 78−18360
laser produced water bubbles, behavioural study by holo-cinematography *(German)* 78−87371
laser-produced bubbles, appl. of HF holography with ruby laser *(German)* 77−75437
Laval nozzle, hot water flow 78−75181
liquid, effects of simultaneous action of US vibrations of different freqs. 79−94396
liquid, laser breakdown, photoacoustic and photohydrodynamic parameters 78−52597
liquid cavitation and droplet impact erosion, predictability of prototype machine from lab. tests 78−64723
liquid cavitation technique for cleaning cinefilm 80−31918
liquid cavity collapse, accompanied by RF emission 80−87790
liquid containing gas bubbles, struct. of supersonic waves and cavitation development 80−33643
liquid filtration US enhancement 78−59526
liquids, generalised model 79−68770
liquids, response to dynamic tension, conf., Ispra, Italy (Sept. 1977) 79−69175
lubrication, boundary conds. and cavity-fluid interface, review 77−55058
lubrication, cavity-fluid interface, wavy interface anal. 77−55059
marine propellor, noise emission from cavitation zone 77−14853
mechanism of cavitation emulsification employing high-speed photography *(Chinese)* 78−14049
metal, cavitation erosion resist., increase by case hardening, possible mechanism 80−11845
metal, FCC, cavitation erosion 77−86191
metals, cavitation erosion 78−48538
metals and alloys, relative cavitation strength 77−12672
microbubbles due to ultrarelativistic particles, acoustic emission for particle detection 77−61653
molten metal cavitational bubble collapse and erosion intensity in constant mag. field *(Russian)* 80−60987
natural flow and US cavitation erosion comparison 78−59435
nematic liquid crystal, laser breakdown, plasma-acoustic cavitation phenomena *(Russian)* 77−65947
Nimonic 80A, creep in tension and torsion 77−25113
Nimonic 80A, intergranular creep fracture under const. cavity density 78−60825
noise, subharmonic component 77−14851
nonlinear acoustics 8th symposium, conf., Paris, France, July 1978 80−33277
nonlinear interaction of deformable body with liquid pressure wave *(Ukrainian)* 78−65777
nonNewtonian lubricant, bubble behaviour 78−56786
nonpolar liquids, cavitation threshold under ionising acoustic radiation 79−37074
nozzle-type venturi, cavitation pressure meas. to determ. mechanism of cavitation erosion 79−90298
nucleate boiling, active sites role 77−15569
nucleation at second phase particles in grain boundaries 78−59819
nucleation by plastic deform. 79−29127
nucleation of boiling and cavitation 77−89008
n-octane fluid, spontaneous cavitation 80−69886
oil-water emulsification, by US, large primary oil drop breakup 79−32644
oil-water interface, US emulsification drop form. by capillary wave instability 79−32643
optic, laser-produced bubbles 80−38463
optical breakdown in liquids caused by ruby laser pulses *(German)* 77−75949
orifice, cavitating, under reattached flow conditions, noise and vibration characteristics 80−83829
p-α-τ equation of state in Lagrangian codes 79−68771
partially cavitating hydrofoil, linearised theory, singularity method *(Japanese)* 78−14050
PET film, crystallised by nonreactive liquids and vapours, exam. of diffusion of liquids and vapours 79−42314
pipe flow, spatial cavitation-nuclei-measurements by means of laser velocimeter 80−64593
plastically deforming solid, creep cavitation by vacancy diffusion 78−48471
plates, partially cavitating, boundary layer and drag *(Russian)* 77−27504
polyacrylamide, additive to water supply, effect on cavitation and erosion in pipes 78−83441
polyacrylamide solutions, dil., static and dynamic breaking tensions 79−23346
polymer solns., vap. bubble growth from gas nuclei, viscoelasticity effect 77−89172
polymer solution, bubble behaviour, Denn model 78−79343
polymer solution, bubble behaviour, second-order fluid model 78−79344
polythene, finite element anal. of crazing and cavitation by dil. aq. detergent 78−53006
prebreakdown events in liquid dielectrics, optical studies 77−20797
precipitate hardened material, intergranular cavity growth inhibition 80−50677
pressure pulse acting on cavity in viscous liquid 79−68769
pressure transient analysis in piping systems including the effects of plastic deformation and cavitation 80−74775
propeller cavitation tunnel hydroacoustic transfer function, meas. and anal. *(Croatian)* 80−92002
protecting coating for erosion damage prevention 77−21306
protein synthesis in human fibroblasts in vitro, US stimulation, role of cavitation 80−8100
pulsation amplitude threshold for surface waves on oscillating bubbles 79−18900
pulsation of cylindrical cavity in incompressible fluid, rel. to detonation *(Russian)* 77−24001
pulsed radiolysis, nonlinear radiation-acoustic phenomena 80−79029
pumps, cavitating, dynamic characts., bubbly flow model 79−32646
PVC, cold drawn, plastic fracture around cavities 79−56994
PWR coolant water pump, detection, methods, brief review *(German)* 77−74906
reactor coolant cavitation in dynamic containment loading 80−32326
reactor fluid piping systems, transient cavitation effects 78−29554

cavitation continued
reactor pool swell dynamics during depressurisation, exact anal. soln. by method of characteristics 78−29555
recompaction waves, propagation calcs. 79−68752
rectified gas diffusion effect on cavitation bubble *(Japanese)* 77−42881
review, book contrib. 77−47050
screw pump nonsteady-state press. component, cavitation flow 80−19455
self focusing of acoustic waves 79−3821
separate-bubble cavitation tests, nucleation meas. by Venturi tube *(French)* 79−55402
shape of non-sysmmetric cavity rel. to inclination of cavity *(Russian)* 77−55055
sharp-edged disc, semiempirical anal. of cavitation in wake 77−35188
ship propeller induced underwater acoustic disturbance obs. 79−68463
shock pressures in venturi, 10 kHz-1 MHz 77−24002
shock wave theory, appl. to acoustic and hydrodynamic cavitation 77−27567
shock waves, investigation by coherent optical methods 78−38431
singularity at free streamline separation pt., capillary modification 80−1655
size distribution of cavitation nuclei in liquid flows, meas. technique 77−68716
slender permeable profile, cavitation flow 80−38466
sonochemical reactions, cavitation induced, rate dependence on US intensity 77−36732
spherical cavity in compressible liquid in sound field, eqns. for dynamics 80−87612
spillway surfaces, flow around three dimens. projections 78−67232
spray mixing, effect of sharp-edged orifice type and cavitation 77−51107
steel, austenitic and martensitic, cavitation failure in liq. 77−44405
steel, austenitic Cr-Ni, intergranular damage parameters in creep *(Czech)* 80−89342
steel, austenitic stainless, cavitation erosion resistance, martensitic transform. effect *(Russian)* 78−35524
steel, austenitic stainless, deformation induced cavitation, exam. 79−43363
steel, austenitic stainless, flow cavitation erosion, initial part of incubation period 78−44224
steel, C, cavitation erosion, exam. of mechanism and rates 79−5063
steel, C, corrosion fatigue resistance in cavitations, bainitic and martensitic structs. *(Russian)* 78−56815
steel, cavitation during superplastic flow, affecting factors 78−60728
steel, Cr-C (18, 0.9 wt.%), cavitation, abrasion resistance, effect of unstable austenitic struct. *(Russian)* 77−16695
steel, Cr-Mo (1, 0.5 wt.%), heat treated creep failure, role of stress state 79−5047
steel, Cr-Mo (2.25, 1 wt.%), interrelationship between creep deform. and creep rupture 79−61664
steel, Cr-Mo-V, rupture ductility rel. to cavitation, density and SEM obs. 79−34142
steel, Cr-Mo-V low-alloy with high residual element content, cavitation control 80−66663
steel, Cr-V (1.5, 0.5 wt.%), ferritic, effect of temp. and microstruct. on creep damage 79−5023
steel, low C, type 08Yu, influence of nonmetallic inclusions on microfailures, during strain *(Russian)* 79−34128
steel, mild, cavitation erosion rate, effect of stress level 78−15545
steel, stainless, aged 304, twin boundary cavitation during creep 77−86099
steel, stainless, cavitation erosion in chemically aggressive liquids, acetic acid effects *(German)* 79−39050
steel, stainless, cavitation-erosion in fresh water, electron microscope and electrochem. study 80−55580
steel, stainless, Cr-Ni (18,10 wt.%) Ti stabilised, cavitation failure, relationship of corrosive and erosive factors *(Russian)* 77−16722
steel Cr-V (1.5, 0.5 wt.%), cavitation effect of temp. and C content 78−64638
stress produced in solid, rel. to erosion and deform. 77−24354
supercavitating blocked flow, finite cavity, anal. for wake displacement thickness 78−18322
supercavitating flat plate hydrofoil, leading edge correction 79−32595
supercavitating hydrofoils with pseudo Kirchhoff noses, drag, nose press. 77−27566
supercavitation flow, cylinder between parallel walls, Efros' model 78−42637
supercavitation flow past thin lifting surfaces *(Russian)* 78−34171
supercavitation mechanisms, isoperimetric problems *(Russian)* 78−75177
supercavity hydrofoil, wall effects, nose rounding 80−64594
superheated liquid, growth of spherical bubbles, anal., numerical calcs. 77−24399
superplasticity, cavity growth anal. 80−60923
surface tension and gravity, combined influence, nonlinear theory of perturbed motion *(Russian)* 78−75178
surface tension and gravity effects on cavity form. 79−64719
tap water, tension pulse propag. in column 79−69176
tensile stability, effect of crack and cavitation generation 77−16659
tension pulse propagation in a liquid column 79−69176
tension waves, propagation calcs. 79−68752
thermodynamic nondimensional parameters *(Italian)* 79−76959
threshold meas. for polyalkylene glycol and castor oil, underwater sound transducer appl. 80−107374
transient, on marine propellers, high-speed photography 78−38432
tunnels with continuous and perforated walls, cavity size 80−92193
turbulent jets, influence of drag reducing polymers on cavitation inception 80−106823
two dimensional cavitation problem, cylindrical bubble, numerical soln. *(German)* 80−14764
two-dimensional laminar flow between porous walls 79−14477
underwater spark discharge, vapour-gas cavities generation and space-time evolution characts. 80−19650
underwater steam cavity during spark discharge *(Russian)* 77−31345
unstable axisymmetric cavity, independent expansion eqns. *(Russian)* 77−31343
US, in water, effect of transducer radiating surface coatings *(German)* 77−42653
US, production of pressure and light impulses *(French)* 80−33297
US activation effect on gas-filled intercellular channels of Elodea leave at 1 MHz 78−24093
US and laser cavitation in liquid crysts. 80−87633
US atomization, cavitation-induced capillary waves 80−33328

cavitation continued
  US cavitation emission from insonated plant tissues 78—59185
  US cavitation intensity in liquids, organic comparisons 80—106820
  US cavitation intensity measurement, chlorine solvents appl. *(Polish)* 80—38464
  US field, kinetics of number of cavitation bubbles 77—15085
  US radiation force variation with differing propagating media gas content 79—32128
  US shock waves emitted by cavitation at rotating perforated plate, wear, thickness effects 77—27565
  US wave in cavitating liquids, optical visualisation, nonlinear effects 80—106651
  vapour bubble growth in US field 80—87608
  vapour/gas joint flow in pumps, oscill., kinetic model 77—35186
  variational methods, book contrib. 79—32456
  velocity exponent for erosion and noise due to cavitation 79—77193
  venturi, characts. of cavity flow past cylindrical inducers 77—31347
  vertical axisymmetric cavitating flow around a body, independ. cavity expansion method 80—92192
  vertical axisymmetric cavitation flow about bodies of revolution 80—33642
  viscoelastic liquid, polymer additives effects on bubble motion and cavitation noise intensity 77—68648
  void swelling, nucleation theory 80—65038
  water, acoustic cavitation threshold and tensile strength, theory 79—42131
  water, cavitation, gas supersaturation thresholds under high press. 77—16861
  water, cavitation due to ultrasound, radn. force balance method 80—24063
  water, cavitation expts. in steel Berthelot tube 80—87788
  water, cavitation expts. using shock tube 80—87789
  water, cavitation mechanism 120°-250°C, bubble growth 80—14762
  water, content of cavitation nuclei 77—31346
  water, matching optimisation for magnetostrictive transducers 78—94503
  water, statistical anal. of cavitation strength 77—11227
  water flow through orifice, polymer additives effect on cavitation and noise 79—98768
  water flow with air contents, partially- and super-cavitating hydrofoils in cascade, analysis method *(Japanese)* 80—14763
  water jet, influence on wall-attachment element, Coanda effect *(Japanese)* 77—39321
  wedge oscillations in confined vesicle *(Russian)* 80—43651
  wing-tip vortex cavitation, vapour core characteristics eval. by asymptotic expansion 80—106825
  wood chip refiners, cavitation effects in two-phase flow 80—35348
  Zircaloy-4, creep damage at LWR temp. 79—52312
  Zircaloy-4, oxide coating effect on ductility 79—47819
  AL, thermal sprayed coating on steel substrate, cavitation and corrosion resist. in sea water 80—35427
  Ag, implanted grain boundary cavities effect on cavity growth kinetics and creep fracture 78—52935
  Ag, large grain boundary cavity coalescence during tension creep 78—52894
  Ag-MgO (0.1 wt.%), intergranular cavity growth at elev. temps. 79—66068
  Al and Al-Cu(Mg), comparison of liquid impact erosion and cavitation erosion 80—104302
  Al, cavitation erosion considering bubble collapse and pulse height spectra 80—16503
  Al, cavitation erosion in water flow, initial stage 78—27648
  Al, soft, type 1100-0, erosion tests in cavitating venturi 80—35347
  Al, wear particles, spheroid form. by cavitation erosion 79—52382
  Al-Cu(Mg), age-hardenable, US cavitation erosion mechanisms, effects of comp. and heat treatment 78—53002
  Al-Mg, fracture during superplastic flow 78—60729
  Al-Zn-Mg, cavitation during superplastic deform. *(Japanese)* 78—15464
  Al-Zn-Mg superplastic alloy, cavity growth under creep conditions 80—60940
  Al_2O_3, cylindrical cavity effect on fracture 79—66144
  Co, single crystal, cavitation erosion, role of twinning 80—107272
  Cr_3C_2-(WC)-Ni, sintered, cavitation erosion resistance *(Japanese)* 77—52500
  Cu alloy, fatigue cavitation, high temp. 77—36658
  Cu alloys, cavitation during superplastic flow, affecting factors 78—60728
  Cu and alloys, intergranular damage parameters in creep *(Czech)* 80—89342
  Cu electrodeposit, US agitation effect on hardness, porosity and grain size, work-hardening 77—60075
  Cu, gas content and temperature effects in vibratory cavitation tests 79—61744
  Cu, grain boundary morphology effect on void form. 78—48533
  Cu, high purity, creep cavitation topology, high temperature region *(Czech)* 80—65138
  Cu-Ni-Zn, microduplex, superplastic deform., cavitation and fracture 78—64640
  Cu-SiO_2 systems, cavity nucleation, by plastic deform. 79—29127
  Cu_3Au, ordered and disordered, cavitation induced erosion 77—16743
  Fe, cast, cavitation erosion rate, effect of stress level 78—15545
  α-Fe, cavitation and sliding distrib. changes during creep at 500°C 78—6991
  Fe, cavitation erosion, exam. of mechanism and rates 79—5063
  Fe, comparison of liquid impact erosion and cavitation erosion 80—104302
  Fe-Fe_2C, cavity nucleation, by plastic deform. 79—29127
  H_2O, cavitation nuclei conc., holographic and hydrodynamic obs. 78—83440
  H_2O, neutron irradiation and mag. field effects on cavitation and nuclei spectra 77—62568
  He, liq., bubble formation mechanism, on surface of deformed crystal *(Russian)* 78—85066
  ^{4}He, superfluid, tensile strength and visible US cavitation 77—7920
  Mg-Zr alloy, cavitation during diffusion creep 77—44296
  Mo wire, laser shock induced microstructural changes, rel. to explosive shock induced phenomena 78—67768
  Mo-Zr-Ti-C(0.1, 0.15, 0.004 wt.%), alloy TsM2A, cavitation failure mechanism 77—70169
  NaCl, rock salt, progressively mined soln. cavities, struct. behaviour 78—61409
  Ni, He$^+$ irradiated, cavity depth distrib. determ. technique 79—51161

cavitation continued
  Ni, oxidation, high temp., effect of C on cavity form., SEM study 80—97638
  Ni-Cr, wrought, fatigue at high temp., microstruct. assessment 79—29208
  Ni-Cr-Mo steel, corrosion and cavitation-erosion resist. *(Russian)* 78—11395
  Pb-Sn eutectic, cavitation during superplastic flow, affecting factors 78—60728
  Pb-Sn microduplex eutectic, cavitation during superplastic flow due to hard particles 77—36575
  Si_3N_4-Mg_2SiO_4-Si_2N_2O, compressive creep, composition effect 80—50674
  Sn-Pb-(Bi)(Ag)(Sb) (Cu), microduplex eutectic, cavitation during superplastic flow 78—48457
  Ti-Al-V (6, 4 wt.%), cavitation induced erosion, under mill annealed, soln. treated and aged, and beta annealed conditions 79—8371
  W wire, laser shock induced microstructural changes, rel. to explosive shock induced phenomena 78—67768
  W wires, KSiAl doped cavity formation *(German)* 78—31524
  Zn monocrystal, cavitation induced multiple slip, twinning and fracture 78—39872
  Zn, thermal sprayed coating on steel substrate, cavitation and corrosion resist. in sea water 80—35427
  Zn-Al (15 wt.%), thermal sprayed coating on steel substrate, cavitation and corrosion resist. in sea water 80—35427
  Zn-Al (22 wt.%), superplastic eutectoid cavitation evidence 77—63741
  Zn-Al (22 wt.%), superplastic, of very high purity, cavitation 79—24586
  Zn-Al (22 wt.%) superplastic alloy, cavitation and neck form. 80—30022

cavity resonators
  see also acoustic resonators; laser cavity resonators
  2.148 GHz SAW oscillator using AlN/Al_2O_3 delay line 80—74680
  absorptive optical bistability, two-level atom system, photon antibunching 80—58486
  air, microwave breakdown field calc., resonator and rectangular waveguide expt. 79—41789
  anisotropy meas. at microwave freq., experimental results 80—52279
  beam induced e.m. fields, coupling impedance struct. above tube cutoff frequency 77—375
  bistable nonlinear Fabry-Perot resonator switching speed and energy calc. 80—64095
  calorimeter with untuned cavity for Hg arc lamp plasma props. study 77—82520
  cavity, scalar Green's function, numerical calcs. using integral eqn. *(French)* 79—32110
  cavity-coupled Josephson device, parametric dependences, I-V characts. 80—20356
  CESR cavities, HF modulation technique 77—37956
  charge bunch radiation losses in pill-box resonator, time domain numerical computations of EM fields 79—31781
  circulating resonance masers, parallel magnetic and electric fields, theory of operation *(Russian)* 77—75464
  coaxial, with lumped capacitance, appl. to complex permittivity determ. for wide range of materials *(Polish)* 80—73382
  coaxial lumped capacitance resonators design for dielec. material investigs. 77—67460
  coaxial microwave cavity for improved EPR sensitivity with loss solvents 80—62705
  coaxial resonator technique for microwave cond. meas. 77—4384
  conference on cyclotrons and their appl., Bloomington, USA (Sept. 1978) 79—54626
  confocal cavity imaging characts., mode decomposition method 79—31816
  cryocurrent comparators, ring cavity elements, field attenuation 77—144
  cyclohexane loss meas. at 35, 72 and 144 GHz 77—82560
  cylindrical, H_{01n} mode, accurate complex permittivity, meas. for wide range of materials *(Polish)* 80—73383
  cylindrical cavities in E_{010} mode relations for dielec. parameter eval. 79—35783
  cylindrical cavity resonator in H_{01n} mode, for complex permittivity meas., approx. method *(Polish)* 80—73384
  cylindrical hole in wall of infinite thickness, elec. and mag. polarisabilities determ. 78—71004
  cylindrical TE_{01n} cavity, measurement of complex permittivity using approx. anal. method 79—49254
  cylindrical unstable resonators, ray-optical anal. 79—72652
  DC permeameter for ring specimens 80—98954
  dielectric loss angle/permittivity meas. as function of temp. at 9-10 GHz 77 82559
  dielectric loss tangent meas., microwave resonator bridge method 77—37914
  dielectric thin film permittivity calc. in partly-filled resonator cavity 78—45652
  disc and washer structure, RF props. 79—72170
  discrete modes of a system subject to an inhomogeneous, high-frequency force 80—43237
  dual-mode microwave cavity for harmonic power meas. 78—41333
  Earth-ionosphere cavity, Schumann resonances, book 80—86050
  eccentric spheres, interior and exterior boundary-value wave problems 77—75384
  eigenvalue translation method for mode calculations 79—71515
  electro-optical nonlinear Fabry-Perot resonator, for optical signal processing 78—42460
  electron accelerators, elimination of electron multipacting in supercond. structs. 78—9004
  electron cyclotron maser, fundamental mode, linear theory 80—58496
  electron cyclotron maser device theory 80—58494
  electron cyclotron maser in overmoded cavity, nonlinear multimode formulation 80—58495
  EM conservative fields, canonical formulation 78—33310
  EM eccentric spherical cavity, resonant frequencies 79—72457
  EM field meas., imaging using thermoluminophorous sensor 79—93168
  EM fields in resonance systems used in charged-particle accelerators 80—37641
  EM open resonator, complex source point theory 79—50196
  EM spherical cavity resonator, amplitude of standing gravitational waves *(Russian)* 78—73906
  empty off-axis unstable resonators with rectangular mirrors, modes 79—76787
  ENDOR cavity for electron spin echo experiments 78—82013
  EPR high-temp. cavity for easily oxidised fluorides 80—77831

cavity resonators continued
EPR spectrometer, 2 mm band, with re-entrant resonator 78—86311
Fabry Perot resonator containing electrooptical element, light processing appls. 78—38001
Fabry-Perot cavity, absorptive bistability, mean-field approx., truncated Bloch hierarchy 80—83631
Fabry-Perot cavity, instabilities for coherently driven absorber 80—53387
Fabry-Perot cavity, optical bistability, spatial effects 80—83632
Fabry-Perot cavity, optical bistability, standing wave effects 80—91837
Fabry-Perot hemispherical resonator, effect of mirror aperture *(Russian)* 77—31085
Fabry-Perot non-linear optic media devices, instability and regenerative pulsation phenomena 78—46685
Fabry-Perot nonlinear electro-optic device, using refl. light feedback 78—55457
Fabry-Perot resonator, bistable, use as optical switch, limiter or memory element 77—39024
Fabry-Perot resonator cavity, dielectric film effect on characts. 79—94134
Fabry-Perot resonator for CESR studies at 34 GHz 80—37065
Fabry-Perot resonators, second-order perturbation theory 79—18451
Fabry-Perot type microwave wideband open resonator 77—57351
feedthrough waveguide resonator Q-factor meas. 77—10053
Fermilab 500 GeV main accelerator RF cavity 128 MHz mode damper 77—83299
frequency shift, surface roughness effect 77—19131
fusion reactor, ELMO Bumpy Torus, microwave coupling 80—99328
gyromonotron, operating characteristics at 35 GHz 80—58497
gyromonotron design, 240 GHz, using supercond. magnet system 80—58498
Hall mobility, microwave meas. method 79—54154
harmonic generation at microwave frequency in bounded magnetoplasma 80—48897
helical electron beam in resonator of gyro device with uniform EM field, nonlinear eqns. soln. 79—81348
helix resonators, supercond., elec. freq. control 79—72169
HF field distrib. meas. 80—98930
integrated optical device used as switch, amplifier, limiter and memory logic element 79—32090
intracavity absorption, CW dye laser, Ba at. beam line shape obs. 80—47120
ISR RF cavities, beam load compensation, feedback system 77—83294
Josephson junction, semiconductor-barrier, cavity resonances 78—84352
KVI cyclotron, dee voltage and beam RF phase stabilisation 79—54688
linac, Argonne superconducting heavy ion accelerator 77—38459
linear accelerator, closely-coupled cavity chain, unit cell reson. freq. meas. method 77—83179
linear accelerator, heavy-ion spiral loaded cavities 77—38455
linear accelerator, RF cylindrical cavity, evaluation by computer code SUPERFISH 77—38463
linear accelerator, superconducting slow-wave structures 77—38458
linear accelerator cavity code, based on finite element method 78—33307
linear accelerator EM field in cavity, by MESSYMESH computer program 77—38462
linear accelerators, ion acceleration at 4.4K by superconducting resonators 77—34483
linear accelerators, postacceleration and bunching of 150 MeV ^{58}Ni ions 77—34484
linear accelerators, resonator sensor for the parameter of charged-particle beams 80—68991
liquid dielec. complex permittivity meas. method 77—82558
loaded with periodically inhomogeneous active medium, spatial struct. of field 79—81462
marginally-stable, analytical solns. of Fresnel-Kirchhoff integral equation 79—94262
measurement of dielectric parameters at microwave freq. by cavity perturbation technique 80—9002
microtron accelerating resonator, coupling coeff. with waveguide rel. to high-freq. path 77—65367
microwave, automatic monitor of resonant freq. and bandwidth 77—22567
microwave, containing dielec. sample, num. soln. of charact. eqn. *(French)* 78—13649
microwave, partially filled with temp.-anisotropic uniform hot plasma, eigenmodes 78—75362
microwave, spherical absorpt. cavity for freq. meas. in upper microwave bands 77—5868
microwave, visualisation of hypersonic sphere in air, obs. with open microwave resonator 79—77301
microwave cavity, transient response 79—72027
microwave cavity for EPR at high hydrostatic pressures 78—89518
microwave cavity gravitational radiation detectors 79—21647
microwave deflector for cryogenic phase selector of electrons 80—27845
microwave discharge source with extended cavity design for H beam production 79—67427
microwave IC substrate permittivity meas. in cylindrical cavity 78—77942
microwave resonant cavities, thermal expansion correction methods *(French)* 77—61087
microwave spectrometer 77—53929
Milan superconducting cyclotron, RF cavity model study 79—54682
muffin tin cavity, computer calc. of EM fields 79—9923
muffin-tin structure, deflecting modes *(French)* 79—45469
multicavity IR electro-optical tunable filter 80—102831
Multipass optical cavities for laser spectroscopy 78—17982
natural frequencies of coaxial and concentric cavities, universal tables and diagrams *(French)* 79—31760
nonlinear Fabry Perot devices, integrated optic format 78—38087
nonlinear Fabry-Perot filled with Kerr liquids CS_2 and nitrobenzene 79—27316
nonlinear optical resonator filled with Raman or Brillouin active medium, theory 77—50722
normal modes and normal freqs., Green's function numerical study *(French)* 79—32111
ocean wave energy conversion techniques and subsystems 80—45627
open resonator with cylindrical confocal mirrors, plane EM wave excitation *(Ukrainian)* 78—55280
open sector injector cyclotron, for SIN 600 MeV ring accelerator, design of RF system 79—54685
optical bare resonator eigenvalue analysis, matrix methods 80—78927

cavity resonators continued
optical bistability, absorptive and dispersive, in Fabry-Perot and ring-cavity geometries 80—95942
optical bistability, dressed mode dynamics 80—19013
optical bistability, exact semiclassical treatment of ring cavity 80—58627
optical bistability equations for standing wave cavity, analytic solns 80—48328
optical bistability in bad cavity limit, Fokker Planck eqn. approach 80—64116
optical bistability of a homogeneously broadened medium with dispersion 80—83630
optical cavity filled with Kerr dielectric, nonlinear effect of powerful laser radiation field 80—99787
optical dispersive resonators with system of reflective gratings *(Russian)* 80—96029
optical microscope, scanning resonant cavity, nonlinear interaction enhancement 78—93758
optical rotation sensor, passive ring cavity, drift performance 80—1343
orthogonality properties of optical resonator eigenmodes 80—38042
parallel coupled RF cavity struct. for e^+e^- storage ring 77—83295
particle accelerator, nonidentical resonators with narrow coupling slits, dispersion and field distrib. characts. 79—41047
permittivity meas. using resonator terminated by infinite sample 79—21777
perturbation technique for microwave measurement of dielec. const. 80—31802
phase free rectangular storage device for relativistic electrons 77—10504
picosecond bunching system at the Munich MP-tandem accelerator 79—85835
precision electrical meas. using superconductivity *(German)* 77—79124
Prony method for symmetric matrix in scalar resonator calc. 80—5807
proton linear cavity, calc. methods for field distrib. 77—38505
Q-factor meas. by analytic method using reflection coeff. vs. freq. 80—98937
quasi-optical open resonators, phase struct. of field, meas. method *(Russian)* 78—29925
Raman oscillator, shared resonator config. 77—88853
ray-optical analysis of unstable resonators with spherical mirrors 80—14415
RCNP AVF cyclotron, outline of RF system and latest developments 79—54686
re-entrant, RF breakdown, rel. to lower hybrid reson. in Tokamak plasma 78—26364
reflection from moving boundary between two dielectrics in waveguide 77—584
relative dielectric constant for insulators in range 1-10 GHz, State Special Standard 80—13037
relativistic electron storage device, phase free cavity resonator + mag. mirrors 77—83172
resonator, transient process, excited by beam 79—81347
RF cavities for e^+e^- storage rings, damping antennas for spurious RF modes 78—70659
RF cavities with cylindrical symm., evaluation by computer program SUPERFISH 77—18714
RF superconducting resonators for booster linac 79—54623
ring cavity, chaotic behaviour of transmitted light, optical turbulence 80—102760
Schumann resonance in ionosphere-Earth waveguide, line splitting detection, chirp-z transform 78—3861
self-acceleration of electron bunches, emission spectra 78—33331
semiconductor microwave conductivity meas. by eddy current loss method 78—8417
semiconductor thin film conductivity monitoring by microwave resonator absorption *(Russian)* 78—23182
SHG, optimum, in thin-film external resonator 79—18485
single-cavity double-frequency buncher 79—68076
single-ended cavity resonator loaded Q-factor meas. using reflection bridge 78—54405
slab line cavity for excitation of electrodeless discharge tubes 77—7166
small frequency shifts meas. using two open resonators at mm wavelengths 78—81949
solid dielectric props. meas. with superconducting resonators 78—21180
spherical open resonator, approx. theory *(French)* 80—48301
spiral resonators for heavy-ion accel., meas. at high field levels 77—10503
Stanford superconducting heavy ion linac, reentrant cavities 77—83124
Stark microwave, for continuous NH_3 monitoring 80—61500
stimulated Rayleigh wing scatt. line, anomalous shift in external transverse resonator containing CS_2, CS_2-ethanol, o-xylene 78—13763
superconducting, Q-factor depend. on mag. flux line motion 77—32110
superconducting accelerating cavities for high-energy e^+e^- storage rings 79—97924
superconducting cavities for heavy ion LINAC, beam tests and phase locking 77—26896
superconducting cavity in microwave noncontacting accelerometer for gravitational wave antenna 77—30076
superconducting FM resonators, analysis and appls. 77—26893
superconducting heavy-ion resonator, microprocessor based feedback system 77—88292
superconducting microwave resonators used for high sensitivity dielectric loss meas. 77—10043
superconducting Nb_3Sn cavities with high microwave qualities 77—26890
superconducting Nb_3Sn coatings, for RF cavities, props. 77—26891
superconducting Nb split-ring resonator as heavy-ion accelerating struct. 77—26895
superconducting Pb resonators, polishing procedure for high surface electric fields 77—83197
superconducting resonators, high stability oscillators, appl. to fundamental physics, metrology 79—26034
superconducting split-loop resonator as heavy ion accelerating element 77—26894
superconducting X-band Pb cavity expt., closed-cycle mech./adsorption refrigeration appl. 78—93708
toroidal resonator, successive approxs. for reson freqs. 78—17841
transducer for subatomic mech. vibr. 77—82436
travelling wave periodic struct. props., computer calcs. 79—72165
tubular dielectric, complex permittivity and loss angle meas. in X-band using H_{011} cavity resonator method *(German)* 80—62690
two-resonator CRM oscillator with external feedback 80—87362
unstable, selective props., mirror-edge shape 77—23754

cavity resonators continued
- VICKSI cyclotron, methods and results of RF system stability meas. 79−54687
- Wonderstone ENDOR cavity 78−70174
- X-band, high Q, design procedure, frequency standard appl. *(Polish)* 77−26342
- X-ray resonator based on successive refls. of surface wave 80−99021
- Cs maser, optically pumped, cavity, buffer gas, press., temp., freq., characts. 77−10880
- Cu, resonant cavities, RF loss reduction at 35 GHz by cryogenic cooling 78−93761
- H atomic passive frequency standard 77−37860
- H maser cavity, tuning using variable capacitance diode 79−72545
- H maser microwave resonator, miniature design 79−55097
- H masers, with automatic tuning 80−95859
- H passive maser frequency standard 79−55100
- H spacecraft maser, operating development model 79−54105
- NH_3 molecular beam maser with semi-confocal cavity, output power spectral distrib. 80−43311
- Nb, microwave cavity of muffin-tin type, for accelerator use 77−26905
- Nb, RF superconductivity, appl. to particle acceleration, overview 79−31244
- Nb superconducting C-band cavities for linear accelerator appl. 79−36432
- Nb TM_{010} superconducting RF cavities for high energy storage rings, 700 MHz meas. 79−68059
- Nb_3Sn disc loaded waveguide, for linear accelerator appl., fabrication and props. 77−26892
- $Nb_{30}Ta_{70}$, microwave props. of 8.6 GHz supercond. cavity 77−28297
- $OHX^2\Pi$ radical, ground and vibr.-excited ($\nu\leq6$) levels, microwave spectrum 79−63985
- Pb-Te-Pb Josephson junction, cavity resonances 78−84352

c.c.d. circuits *see charge-coupled device circuits*

CCTV *see closed circuit television*

celestial mechanics
- *see also N-body problems; stellar motion*
- 1976 AA, Apollo asteroid, orbital elements and relation to Earth *(Danish)* 77−60706
- 1977 UB (Chiron), past and future orbit calc. 79−35171
- 1977 VB, Phocaea-type Mars-crosser, ephemeris (1977 November 13 to December 13) 78−7913
- 1978 RA (=1975 TB), Apollo object, orbital elements and ephemeris 78−93141
- 1978 SB, orbital elements and ephemeris, (1978 September 9 to October 29) 78−93143
- 1979 BA, fast-moving object, discovery and orbital elements 79−35177
- 1979 BA, orbital elements and ephemeris, (1979, March 18 to June 16) 79−40121
- 1979 QB, Amor-type object, orbital elements and ephemeris (1979 August 25 to October 4) 79−92693
- 1980 LB, improved orbital elements rel to 2:1 Jupiter librator hypothesis 80−94744
- accuracy of Ptolemaic and Copernican theories using curve fitting techniques 78−32325
- 2101 Adonis, orbital problem soln. 80−72842
- algebraic aspects of perturbation theories 80−31539
- aligned triple collision, new study *(French)* 78−85832
- analemma, photographic representation inc. year-long solar images 80−12649
- analytical satellite theory in extended phase space 80−67524
- Apollo asteroids, orbits secular evolution rel. to Farmington meteorite last parent body non-discovery *(Russian)* 79−101124
- applied modern mathematical techniques *(German)* 78−45211
- area-preserving polynomial mapping, instability 78−77463
- Ariel 1 satellite orbit at 29:2 reson., geopot. 29th order harmonics determ. 77−56572
- Ariel 4 (1971-109A), defenitive orbit 78−73604
- articial satellite motion, orbitally stable multistep methods 78−85834
- artifical Earth satellites, gravit. harmonics from shallow reson. orbits 78−40805
- artifical satellite geodesy techniques *(German)* 77−64190
- artifical satellites, role of orbit determ. in altimeter data anal. 78−77177
- artificial counter-orbiting satellites orbit perturbation, general relativity test 78−45554
- artificial Earth satellite, near-circ. orbit dispersion 79−44349
- artificial Earth satellite, resonance due to solar radiation pressure 79−25456
- artificial Earth satellites, second order perturbation soln. *(Chinese)* 80−77270
- artificial Earth satellites, theory of motion in coordinates in arbitrary intermediate orbit case 79−62720
- artificial Earth satellites radial and cross track errors analysis 77−45297
- artificial satellite, determ. of elliptical orbit from parameters of apparent motion 77−53403
- artificial satellite, determ. of orbit sections where instruments are under critical illumination 78−49288
- artificial satellite, disturbing function for orbital perturbations by direct solar radiation press. 77−78605
- artificial satellite, Global Positioning System, computationally efficiency modelling for long-term prediction of orbits 79−80198
- artificial satellite, SEASAT-A, orbit analysis 79−80199
- artificial satellite, spin-stabilised, nutation damping *(Russian)* 77−64626
- artificial satellite, spinning, symmetric, in planar periodic orbit, attitude stability 80−4220
- artificial satellite, unstabilized weakly perturbed, orientation determ. 79−8809
- artificial satellite, Vinti problem, extended phase space representation, luni-solar perturbations 79−35101
- artificial satellite atmospheric drag perturbations 77−17342
- artificial satellite coordinates determ. from nonsynchronous data 78−7870
- artificial satellite eccentric orbit motion analysis, von Zeipel perturbation method 77−45295
- artificial satellite geodesy, twin probes method 79−25443
- artificial satellite gravit. accel., recurrent calc. 77−56818
- artificial satellite in highly eccentric orbit, decay and re-entry date prediction 77−25931
- artificial satellite inclination, gravity effect, first order theory error determ. 80−17475

celestial mechanics continued
- artificial satellite motion, error evaluation, averaging method for canonical eqns. *(French)* 77−67028
- artificial satellite motion, error evaluation, averaging method for canonical eqns. *(French)* 77−67029
- artificial satellite motion, numerical integration of near-parabolic orbits 77−25925
- artificial satellite motion, third-order soln. 78−16285
- artificial satellite motion eqns., time element for general time transform. 77−25928
- artificial satellite near-circular orbits, lunisolar perturbations 77−49278
- artificial satellite nodal period, direct solar radiation pressure effects 77−70987
- artificial satellite orbit data, M_2 ocean tide parameters and Moon's meas. longit. decel. determ. 80−31048
- artificial satellite orbit determ. using Hills method *(Russian)* 79−40067
- artificial satellite orbit perturbations due to Earth, ocean and atmospheric tides 77−87243
- artificial satellite orbit perturbations due to tides 77−64187
- artificial satellite orbital inclination changes due to resonance 77−17334
- artificial satellite orbital vars. *(French)* 79−58240
- artificial satellite orbits and general relativity, motion in Schwarzschild metric 77−64622
- artificial satellite S3-1, atm. winds and aerodynamic lift effects on orbit inclination 77−53262
- artificial satellite stability criterion, derivation for GYROLITE 79−92649
- artificial satellite theory, appls. of Pfaff's equations of motion 79−12386
- artificial satellite theory, Hansen's coeffs. 77−49276
- artificial satellite with ecliptic plane orbit, solar radiation orbit perturbation 78−4088
- artificial satellites, analytical orbiter theory based on Lie transform 77−17340
- artificial satellites, analytical theory 80−46373
- artificial satellites, anomalistic period, solar radiation press. effects 80−77255
- artificial satellites, critical inclination problem with small eccentricity 80−67525
- artificial satellites, eqns. of motion in nonsingular variables 77−60581
- artificial satellites, influence of tidal forces rel. to Love number determ. 77−91410
- artificial satellites, non-stationary gravitational problem *(Russian)* 78−32328
- artificial satellites, orbital element improvement using photographic or laser obs. *(Russian)* 80−46364
- artificial satellites, orbits, short periodic drag perturbations 80−67522
- artificial satellites, transition of Keplerian elements to apparent motion *(Russian)* 78−32330
- artificial satellites elliptical orbits, eccentricity probability characts. 77−64599
- artificial satellites orbit analysis for upper atm. zonal wind determ. 77−56785
- artificial satellites orbit changes, 14th order geopot. harmonics calc. 79−29694
- artificial satellites second order perturbation computation *(Chinese)* 79−80207
- Aryabhata artificial satellite orbit computations 79−84655
- Aryabhata satellite, spin decay calc. 80−21900
- asteriods, regular proximities concept and approximate perturbation methods 80−72843
- asteriods, resonant, theory based on quasi-periodic solns. of restricted three-body problem *(Russian)* 79−48727
- asteroid, equation of motion for elliptic Jupiter orbit 79−25455
- asteroid, mean motion resonant with Jupiter, short-periodic perturbations 78−53803
- asteroid 108 Hecuba, motion in restricted three-body problem, nonlinear oscills. *(German)* 78−57488
- asteroid 1977 UB, orbit of mini planet between Saturn and Uranus 78−20721
- asteroid belt, Kirkwood gaps, kinematic theory 77−60712
- asteroid belt, Kirkwood gaps, spectral anal. 77−60711
- asteroid belt depletion by gravit. forces, numerical calc. of orbits 79−35173
- asteroid belt truncation, theory of tidal torques on infrequently colliding particle discs in binary systems of tidal torques on infrequently colliding particle discs in binary systems 80−98596
- asteroid families, concs. in proper elements space statistics and mapping 78−96420
- asteroid family detection by new criterion, orbital data 80−82256
- asteroidal belt, restricted three-body problem rel. to orbital characts. 79−8874
- asteroids, dynamical families correl. with spectral classes 77−91464
- asteroids, invariant relation in elliptic restricted three body problem 79−88616
- asteroids, Kirkwood gaps origin 79−16867
- asteroids, Munich meridian obs. (1941-61), orbital elements determ. *(German)* 80−77306
- asteroids, orbital dynamics rel. to cosmogony 77−13275
- asteroids, orbital evolution near 1:3 Kirkwood gap 80−36541
- asteroids, secular orbital vars., seminumerical calc. method 80−51686
- astrodynamics, perturbed boundary-value problems, variational formulae 79−21161
- astrometry and celestial mechanics, book 79−12384
- Astronomical Netherlands Satellite, orbit prediction 79−21139
- asymmetric Maxwell theory, additional universal inverse square forces 80−27149
- asymmetric periodic orbits in three dimensions 78−77476
- asymmetric periodic solutions, numerical determ. 77−49270
- asymptotic solution to problem involving two simultaneous small divisors 77−49272
- autonomous Hamiltonian system near equilib. point, formal integrals 78−89047
- autonomous Hamiltonian systems, orbital stability of periodic Lyapunov motions *(Russian)* 78−69664
- averaging method and two-timescale method, common derivation 78−85835
- axisymmetric rigid body, periodic motions in gravit. field of sphere 78−36446
- axisymmetric satellite, periodic motion rel. to centre of mass in evolutionary circular orbit 80−21899

celestial mechanics continued
- axisymmetric satellite, periodic motions rel. to centre of mass in circular orbit *(Russian)* 79—11284
- axisymmetrical body, translational-rotational motion in gravitational field of sphere, averaging methods applic. *(Russian)* 78—21049
- Babylonian lunar theory 80—94729
- bifurcation of periodic orbits of the planar circular restricted N-body problem to the three-dimensional general N-body problem 79—16803
- bifurcations of straight line oscills., rel. to Stormer and spring pendulum problems 78—71278
- binary collisions regularization in N-body problem *(French)* 77—22045
- binary star, eccentricity of apparent orbit 80—51807
- binary stars formation by three-body encounters, probability and effects on cluster evolution 77—13396
- canonical systems of differential eqns. in resonant case, periodic solns. 79—44345
- capture problem 78—77477
- Cassini's laws 79—8812
- Castor satellite, accels. below 10^{-9} g meas. by Cactus accelerometer, flight results synthesis 80—77251
- central configurations, families *(Russian)* 80—90327
- central dynamical configurations addendum to note 79—66911
- Charon (1978 P 1), satellite of Pluto, positions and dynamical parameters 80—62069
- China 2 rocket (1971-18B), orbit determ. and geophysical interpretations 80—4231
- 2060 Chiron, orbital history and evolution 80—36543
- circular and rectilinear motions of axisymm. body under gravit. effect of two spheres 77—13222
- circular orbits, existence and stability in a Schwarzschild field with non-vanishing cosmological constant 79—92660
- circular orbits in the problem of n fixed centres *(Russian)* 79—12392
- circular restricted three body problem, soln. method *(Russian)* 77—60588
- circular restricted three body problem , three-dim. stability of plane periodic orbits 77—17333
- circular restricted three-body problem, periodic solns. and arcs for zero mass parameter 79—8803
- circular restricted three-body problem, props. of solns. for zero mass parameter 79—8804
- circular restricted three-body problem *(French)* 78—93084
- Clairaut eqn., connection to satellite geodesy and Jupiter 78—11795
- classical Kepler problem in momentum space, education 78—36764
- close binary systems, effects of libration on light curves 78—57579
- close encounter computation, new method 79—35099
- close near-circular orbits, optimal multimomentum transfers 77—41290
- close-Earth satellite perturbations due to lunar inequalities 78—53786
- close-Earth satellite perturbations due to radiation pressure of reflected sunlight from Earth 77—91411
- coasting artificial satellites, first-order effects of Earth's oblateness 77—60582
- colliding bodies in gravitational field, numerical simulation of standard model 77—29634
- colliding bodies systems in gravit. field, effect of transversal viscosity 77—67026
- colliding particles in gravitational field, numerical simulations 79—16802
- collinear N-body problem, homothetic solns. structural stability 79—75086
- collision avoidance method, 2 counter orbiting polar satellites, relativity mission appl. 77—45296
- collisional systems, statistical mechanics of Keplerian orbits 78—20625
- collisions in Keplerian systems, numerical analysis 80—109342
- comet belt beyond Neptune, orbital diffusion rel. to short-period comets origin 80—94759
- Comet Bowell (1980b), precise posn. and orbital evolution 80—56770
- Comet Bradfield, parabolic elements and ephemeris, 1978 July 31 to (1979 January 7) 78—65551
- Comet Bradfield (1978c), positions, orbital elements and ephemeris 78—40875
- Comet Bradfield (1978o), parabolic orbital elements and ephemeris, (1978 October 29 to 1979 January 27) 79—2524
- comet dynamics, exact solns. of diffusion eqn. 80—82304
- Comet Fujikawa (1978n), orbital elements and ephemeris (1978, October 9 to December 8) 78—93168
- Comet Giclas (1978k), precise positions, orbital elements and ephemeris 78—89122
- Comet Kohler (1977m), improved parabolic elements and ephemeris 78—7937
- Comet Kowal (1979a), parabolic and elliptical orbital elements 79—35195
- Comet Macholz (1978l), orbital elements and ephemeris (1978, September 19 to October 9) 78—89126
- Comet Meier (1978f), precise positions, orbital elements and ephemeris 78—53884
- Comet Meier (1979i), improved parabolic orbital elements 80—4306
- comet motion, data processing for comparison of obs. and theory 77—41307
- comet orbital elements distrib., effect of galactic forces *(Russian)* 80—77353
- comet orbits, evolution under perturbing influence of giant planets and nearby stars 80—98613
- comet orbits, three-dimenx. model construction 78—61808
- comet orbits influenced by solar companion 80—31260
- Comet Schuster (1975 II), precise positions, 1977, February 12 to 25, and orbital elements 77—37579
- Comet Seargent (1978m), parabolic orbital elements and ephemeris, (1978, September 29 to October 29) 78—93164
- Comet Seargent (1978m), precise positions and parabolic orbital elements 78—96432
- Comet Torres (1979e), parabolic orbital elements and ephemeris, (1979 July 26 to November 23) 79—84749
- cometary equations of motion, recurrent power series integration 80—72882
- cometary orbits, dynamic charact. based on orbital elements phase distance 80—56774
- cometary orbits, perihelion distrib. asymmetry 78—96429
- cometary orbits, reciprocal semimajor axes accuracy 80—62074
- comets, ancient and medieval, orbits 80—62077
- comets, long-period, distribs. of inclination of perihelion dynamical implications 80—101563
- comets, long-period, nongravit. perturbations 79—70998

celestial mechanics continued
- comets, long-period, perihelion points distrib. statistical tests 80—4304
- comets, long-period, statistical study of orbits evolution 79—53775
- comets, lost one appearance objects, orbit recalc. and motion *(Russian)* 80—46487
- comets, nearly parabolic orbits, distrib. of nodes and perihelia 80—67661
- comets, nineteenth century, new orbits 80—56771
- comets, orbital evolution of short-period objects, Monte Carlo simulations 80—62073
- comets, orbits for one-appearance objects in 1840-94 period 79—96975
- comets, original, orbital inclinations distrib. anomalies rel. to origin of comets 80—98615
- comets, osculating orbits and anal. of original orbits 78—32395
- comets, perihelion distance differences between new and old comets 78—36513
- comets, short-period, distrib. of Jovian perturbs. on orbital elements 78—40871
- comets and asteroids close approaches to Earth, list of events 78—73621
- comets capture by Laplace scheme, orbital elements statistical consequences 78—53888
- comets capture by planets, Laplace hypothesis 78—28592
- comets motion, correction for nongravitational effects, comparison of methods 78—61811
- comets origin, celestial mechanical aspects of planetary ejection hypothesis 80—62080
- comets perihelia longitudes concentration, reality from discovery probability anal. 80—67660
- commensurabilities in solar system 80—109418
- complete class of potentials forming vel. field of given multiplicity, determ. method *(Russian)* 78—69665
- conference, Washington, DC, USA (Nov.-Dec. 1978) 80—90605
- conical precession stability of symmetrical rigid body *(Russian)* 78—4091
- Copenhagen problem, classification of vertical and periodic orbits 79—75081
- σ Coronae Borealis (=ADS 9979), binary, mass and orbital elements *(French)* 80—77449
- counter-orbiting drag-free satellites in Earth polar orbit, general relativity test and geodetic meas. 77—22047
- Cowell's difference formula, modification for two-body problem *(Russian)* 78—32329
- Dalembertian functions, props. *(Russian)* 78—24454
- P/Daniel, predicted orbital elements 78—53883
- degenerate Hamiltonians, von Zeipel method appl. 79—48655
- degenerate Lagrangian systems *(French)* 80—41710
- Dhajala meteorite, orbit and props. 78—32425
- direction field gradient along normal to trajectory 77—78618
- diurnal motion of Sun seen from Mercury, computer aided soln., teaching aspects 78—61969
- drag perturbations of near-circular satellite orbits in oblate diurnal atm. 77—25915
- drag-free satellite, anal. modelling of orbital motion *(French)* 77—73936
- dual-spin satellites, nutational motion damping *(Russian)* 77—60570
- Dynamical Astron. Division of Am. Astron. Soc. meeting/Stanford, CA, 28 Feb.-2 Mar. 1979 80—36762
- dynamical astronomy, AAS meeting (Chapel Hill, N.Carolina, USA, 2-4 December, 1976) 77—91409
- dynamical astronomy, integrable and stochastic behaviour 80—12650
- dynamical astronomy numerical simulation, new Runge-Kutta algorithms 79—12387
- dynamical systems, asymptotic orbits and instability zones 79—101055
- dynamical systems, averaging method 78—77469
- dynamical systems, effects of integrals on totality of solns. 77—25924
- dynamical systems, relation in families of periodic solns. 77—64627
- dynamical systems evolution with time-varying gravity, theory 78—24459
- dynamical systems linearization using integrals of motion 77—49274
- early solar system, mass removal by outer planets 78—53841
- Earth, classical perturbation theories rel. to computation of barycentric radial vel. 77—45291
- Earth, cyclical orbital variations detect in S.Australian beach ridges chronology rel. to Milankovitch ice age theory 80—98307
- Earth, motion, numerical theory using radar, optical and Venera satellite obs. data 78—16325
- Earth, nutation and tides in time-service obs. 79—96733
- Earth, orbit, determ. from radar obs. of Venus in 1962-1977 period 79—88570
- Earth, orbit determination on basis of radar and visible observations 80—90323
- Earth, orbital vars. influence on abrupt palaeoclimatic events 80—51531
- Earth, support for astronomical theory of climatic change 77—87058
- Earth artificial satellites motion, relativistic effects 79—2465
- Earth astronomical parameters corrections determ. ill-conditioned systems least squares soln. 80—26747
- Earth climate, astronomical theory, teaching approach 79—84891
- Earth elliptical orbital elements long term vars. 77—64625
- Earth grazing fireball, eqns. of motion, vel., orbit and mass determ. 80—67663
- Earth motion from self consistent FORTRAN subroutines 80—85845
- Earth orbit variations as cause of climatic fluctuations, geological support 80—72509
- Earth orbital elements, periodic vars. influence on insolation *(Russian)* 78—53605
- Earth orbital elements rel. to caloric insolation long-term vars. 78—73502
- Earth orbital variations, rel. to gravitation and inertia corpuscular model *(Russian)* 79—40439
- Earth orbital variations, rel. to Pleistocene ice fluctuations 77—37346
- Earth orbital variations, role in causing glaciations 79—20961
- Earth resources rocket, enriched air propulsion system 77—2259
- Earth satellite, low-eccentricity, at critical inclination, orbital motion 79—12388
- Earth satellite, periodic and quasi-periodic orbits 77—13214
- Earth satellite orbits with resonance lunisolar perturbations, dependent on inclination 80—90326
- Earth satellites, loci of nongravitational foci, apsides of set of paths analysis 78—7867
- Earth survey satellites, orbit determination 79—25442
- Earth-Mars min. time orbit transfer, conjugate gradient method 77—87244
- Earth-Mars-Venus orbital transfer minimal flight time calc. 78—4090
- Earth-Moon system, lunar laser ranging results 80—21933

celestial mechanics continued
Earth-Moon system, new kind of three-body problem 78—45210
Earth-Moon system, palaeodynamics from nautiloid growth 80—41713
Earth-Moon system history, palaeontological data 80—17224
Earth-Moon-Sun force function 79—80208
education, alternative derivation of Kepler's laws from conservation principles 78—49583
education, astronomy, orbital elements, nonlinear least squares minimisation 77—33761
education, Kepler's third law, synodic period statement 77—87601
education, Kepler ellipse, some props. 79—97151
elastic object in central force field, programmed motion control 80—17481
elliptic motion, mean anomaly as random variable 80—67523
elliptic motion of solid body in primordial solar nebula, gas drag effect 77—33362
elliptic orbit determ. by applying least squares method to observation residues *(French)* 78—40799
elliptic restricted three-body problem, invariant relation 78—69662
elliptic restricted three-body problem, invariant relation for Trojan asteroids 78—69726
elliptical orbits and inverse square law of gravity 80—46755
equatorial satellite in J_2-field, periodic solns. *(French)* 78—45205
Euler motion kinematic eqn. reduced to Kepler's eqn. 79—8813
Euler-Lambert problem, approximate soln. for circular orbits 77—53410
extended ideal resonance problem, comment 77—22055
families of three-dimens. periodic orbits bifurcating from plane periodic orbits around both primaries 78—57432
FK5, equinox and equator of new fundamental reference coord. system 80—109341
flight trajectories to Jupiter using Mars gravit. field 79—62712
flight trajectory between satellite orbits of Earth and Moon, variational problem 80—72754
fluid bodies, dynamic eqns. *(Russian)* 78—36444
fluid bodies, dynamics, Navier-Stokes eqn. *(Russian)* 78—12093
force function between two solid celestial bodies 80—41701
force function of nonspherical body in arbitrary coord. system *(Russian)* 80—46366
force function of two general celestial bodies 78—73620
form factors α and β product asymptotic limit for celestial bodies 79—84653
formulae for programmable calculators, book 79—88571
foundations of mechanics, book 79—25837
four body Newtonian problem reduction to 14th order *(French)* 80—21894
four fixed centres problem, new interpretations and appls. 78—28493
four fixed centres problem, real motions qualitative anal. and classification 79—96901
four-body problem, gyrostat near three spherical bodies subject to gravitational forces, motion, orient. *(French)* 77—5422
four-body problem, relative equilib. solns. 79—8805
four-body problem, restricted planetary case 80—41742
four-body problem asymptotic solns., periodic orbits 77—64621
four-body systems, statistical theory for disruption 80—101531
four-impulse planetary landing and return under time constraints 79—62711
fragmented celestial bodies, particles asymptotic distrib. 78—32326
fundamental astrometry rel. to celestial mechanics and radioastronomy *(German)* 78—45200
galaxy collinear configs. of point masses, three body problem 77—71139
galaxy models, numerical orbit computation algorithms comparison 79—12497
Galilean satellites, de Sitter ephemerides rel. to Jupiter oblateness 77—29715
Galilean satellites, photometric eclipses anal. rel. to theory of motion 78—53864
Galilean satellites, pole positions 79—66954
Galilean satellites motion, new theory and improved ephemerides 80—62066
Galilean satellites motion theory 77—45352
Galilean satellites of Jupiter, orbits long period behaviour 78—40864
Galilean satellites orbital reson. locks rel. to Io tidal heating 79—75145
Galileo's theory of motion, conceptual changes in period 1604-1610 77—82356
Geminid meteor stream, orbital period 78—53889
general N-body problem, three-dimensional, periodic orbits families existence 79—16805
general planetary theory in elliptic variables 77—13212
general three body problem, distances upper estimate *(Russian)* 77—53412
general three body problem, stability of solns. 77—53408
general three body problem, Sundman's inequality and Jacobi's integral derivation *(Russian)* 77—45299
general three-body problem, M_8 manifold topology *(Chinese)* 79—16808
generalised Kepler motion, Lie groups of motor integrals 78—85831
generalised two-dimens. problem of three fixed centres, classification of motions *(Russian)* 78—77465
generalized circular restricted three-body problem, periodic orbits of second genus in 2-D coord. system 79—29980
generalized elliptic restricted three-body problem, libration points 78—53799
generalized three-body problem with force centre term 77—37499
geocentric and selenocentric gravit. constants refinement from lunar probe tracking data *(Russian)* 77—73940
geometric quantisation for multidimensional harmonic oscillators and Kepler problem, Maslov theory 80—17833
Geos 3, orbit determ. expt. 80—4226
Geos 3, orbital positions rel. to gravity model improvement (GEM 9 and 10) 80—3909
Geos 3 orbit determination expt., results of Geos 3/ATS 6 satellite-to-satellite tracking 80—4225
geostationary satellite, orbit determ. by single ground station tracking 80—109329
geostationary satellite orbit, relationship between arc and min. angle of elevation from Earth's surface area 77—13223
geostationary satellites, libration points rel. to position of Earth's mass centre 79—21156
geostationary satellites, methods for numerical integration of eqns. of motion 78—69659
geostationary satellites, orbit determ. using VLBI 80—4238
geosynchronous satellites, libration centre shift 79—84649

celestial mechanics continued
giant planets, representation of perturbations due to Pluto *(French)* 80—26724
giant planets, second order perturbs. *(French)* 79—12385
giant planets second-order perturbations, semi-major axis secular vars. *(French)* 79—2474
gradient of field of directions normal to trajectory, and forms of potential 78—65662
gravitational attraction between two quickly moving bodies, energy depend. 77—2597
gravitational movements of two invariable solid bodies *(French)* 79—29982
gravitational potential of a body of revolution, representation by finite system of mass points *(Russian)* 80—72757
gravitational potentials, Stachel harmonic pot. in elliptic and parabolic cylindrical coordinates 79—96898
gravitational problems, programmable pocket calculator appl. 78—4438
gravitational spring-pendulum problem, numerical treatment of non-integrable dynamical systems 79—58234
gravity potential derivatives evaluation using Bernstein multidimens. inequality *(German)* 78—93081
gyroscope, Earth orbiting, rot. motion according to general relativity 79—84651
gyrostatic satellite in circular orbit, regular precessions 78—93082
gyrostatic satellite in Kepler orbit, rot. motions 80—86080
halo orbits in Earth-Moon restricted three body problem 80—36483
Hamilton-Jacobi equation, complete integral of motion *(Russian)* 78—16283
Hamilton-Jacobi equation integrable cases, rel. to nonsteady problems 79—35103
Hamilton-Jacobi generalised theory, phase space approach 80—36891
Hamiltonian systems instability, examples 79—62732
Hamiltonians linear in momenta, note 78—77468
handbook for pocket calculators 80—8745
Hecuba family resonance asteroids intermediate orbit, three fixed centres generalized problem internal variant 79—84726
Hecuba-type asteroids, evolution of orbits *(Russian)* 77—49328
Henon-Heiles Hamiltonian 80—36485
high altitude Earth satellite, elimination of short and intermediate period terms 77—17339
high altitude Earth satellite orbit, doubly averaged effect of Moon and Sun 77—17335
higher order resonances in dynamical systems 79—5738
Hilda group asteroids, resonant orbital motion of Palomar-Leiden Survey objects 77—9690
Hill's curves, geometric prop. 78—77474
Hill's curves perturb. due to oblateness of one primary in restricted 3-body problem 79—53705
Hill's equation, new exact method *(Chinese)* 80—105152
Hill's lunar problem, literal soln. 79—66909
Hill's problem in Lunar theory 78—77473
Hill's relativistic problem, periodic solns. 78—40804
historical background for teachers, gravitation as Newton saw it 78—4436
homoclinic points and resonance in dynamical systems 80—4240
hyper-periods and Kirkwood Gaps 80—105153
hyperbolic orbits, differential eqns. *(Russian)* 77—78622
hyperbolic orbits, differential eqns. for non-angular elements *(Russian)* 78—16284
Iapetus, theory of motion, perturbations 78—28577
inclination functions, recurrent relations *(Chinese)* 80—8525
infinitesimal librations with variable primary masses, orbit evolution 77—22046
initial orbit determ. using angles and angular rates of movement of artificial satellites 78—53795
inner planetary systems, stability 79—70975
inner planets, second order perturbation theory *(French)* 80—72801
inner planets orbits, discrepancies in motions of perihelia 80—67531
integrable Hamiltonian systems 80—41712
integrals of motion, disappearance in multi-resonance conditions 78—77471
integrals of motion for hamiltonian of coupled harmonic oscillators, calculation program 79—58239
intermediate anomaly, integration for Keplerian motion 78—45209
interplanetary dust particles, effects of solar radiation on orbits 77—5493
interplanetary trajectories computing, ESTEC program 79—21129
interplanetary trajectories determ. procedure *(Italian)* 79—44341
invariant sets and polhodes in the rigid body problem 80—41706
inverse-square orbits; A geometric approach 79—44662
85 Io, definitive orbit from obs., (1865-1977) 80—4284
Jacobi's virial eqn. soln. for celestial bodies 79—8832
Jacobi's virial equation soln. for nonconservative systems, anal. of depend. on parameters 80—4243
Jacobi integral constant for Moon, annual and monthly vars. 78—49301
Jupiter, close encounters with minor bodies 79—35184
Jupiter, orbital and solar resonance of inner three Galilean satellites 80—56753
Jupiter close encounter with planet crossing objects, orbit changes 80—77329
Jupiter close encounters with minor bodies, importance of nearly tangent orbits 80—82248
Jupiter first order theory, perturbed by Saturn, critical term elimination 79—35183
Jupiter orbiter motion and risk of collision with Galilean satellites 77—2322
Jupiter outer satellites, origin rel. to libration-point capture theory 77—29636
Jupiter ring, orbit changes depend. on dust charge 80—82273
Jupiter-Saturn-Sun systems, long-term numerical solns. 78—24450
Kalman filtering, use of Givens transformation techniques 78—4473
Kepler's celestial mechanics, dynamical theory 79—88787
Kepler's eqn., starting value for iterative soln. 79—48657
Kepler's equation, generalisation using Banach's contraction principle 80—105151
Kepler's equation for elliptic orbits, soln. using general algorithm 80—21898
Kepler's laws, inverse square law of gravit., Cartesian coords., for teaching 77—33802
Kepler's laws of planetary motion, conservation principles 77—13538
Kepler's problem, stabilisation 78—24445
Kepler's third law, mean radius calcs., teaching 78—24612

celestial mechanics continued
- Kepler discretization in regular celestial mechanics 80−46374
- Kepler initial value problem, geometry, two-circle calcs. 79−71182
- Kepler orbit, from initial conditions via Lenz vector 78−16602
- Kepler problem, time transformation stabilisation *(German)* 78−89333
- Kepler problem and geodesic flows, in spaces of const. curvature 78−40807
- Kepler problem regularisation 77−64630
- Kepler symmetry problems, Hamiltonian dynamical systems 79−12586
- Keplerian motion, canonical transform. of the eccentric anomaly *(German)* 79−70945
- Keplerian motion, isochronous derivatives and uniform formulae of Langrange multipliers *(Russian)* 80−72756
- keplerian motion and gyration 78−77472
- non-Keplerian orbit, Keplerian representation 80−90324
- Keplerian orbital motion, Lagrange parenthesis and perturbation eqns. *(Spanish)* 77−49280
- Keplerian orbital motion, systematic formulation of perturbation formulae *(Spanish)* 77−49279
- Keplerian orbits, revised flux vector for collisional evolution 78−93080
- Keplerian systems, collisonal evolution, improved general theory 79−21152
- Keplerian systems, computer simulations 80−26720
- Keplerian transition matrices for elliptical orbits 78−36442
- Keplerian tritangential orbit analysis 77−5421
- Kirkwood gap 1:3, width *(Russian)* 80−36559
- Kirkwood Gaps and stability of conservative periodic systems 78−65544
- Kolmogorov entropy, of dynamical system with increasing number of degrees of freedom 79−80562
- KS-transformation and inverse Newton problem 77−17344
- Kustaanheimo-Stiefel regularisation, appl. of nonclassical canonical transforms. 77−60586
- Kustaanheimo-Stiefel regularizing transformation derivation 78−93086
- Kustaanheimo-Stiefel two-point boundary-value problems 77−25927
- LAGEOS orbit, long-term evolution 80−94676
- Lagrange's inversion formula, soln. 80−31484
- Lagrangian equations generalization, KS transform. extension *(French)* 77−25922
- Lagrangian points L_4 and L_5, positions rel. to radiation and gravity forces ratio 80−85843
- Lagrangian solutions stability at critical relation of masses *(Russian)* 78−69666
- Lambert and planetary and cometary orbit determ. 80−42024
- Lambert boundary value problem, uniform soln. 77−49275
- Laplace, P.S., chronology and citations of early work, 1770-1773 period 78−93505
- launching directions, influence on pencil of orbits 80−26723
- Legendre series summation, recursive procedure, gravit. potential evaluation 80−31486
- Lense-Thirring effect and satellite relativistic nodal precession meas., covariance anal. 78−126
- libration points location and stability in restricted problem, effect of perturbs. in Coriolis and centrifugal forces 79−5737
- Lie series use in studying nonlinear Hamiltonian systems 79−8811
- linear difference equation, optimal estimates for soln. on circle 77−25920
- lunar capture 80−56728
- lunar capture hypothesis, effect of planetary bodies deform. energy 78−81570
- lunar centre of mass displacement from geometric centre, comment 78−69937
- lunar ephemeris, Earth oblateness effects, corrections 77−22043
- lunar motion, literal soln., formal convergence *(French)* 80−36482
- lunar orbit, evolution 77−29671
- lunar orbit, evolution 80−8565
- lunar orbit evolution, relation of contracting Earth 77−41331
- lunar theories, main problem, comparison between ELP and SALE *(French)* 80−85844
- lunar theory, new soln. to main problem 79−75083
- lunar theory, non-Newtonian corrections *(German)* 77−25960
- lunar theory of Hill and Brown 80−46370
- luni-solar nutation tables, Earth liquid core effects 80−98210
- magnetic-binary problem, stationary solns. and stability when primaries are oblate spheroids 80−41697
- major planets, estimate of stellar perturbs. in motion 77−78621
- major planets motion, numerical study 79−92657
- many-body problem solutions, symmetry conservation in moving coordinate system 80−17480
- Mars, orbit determination on basis of radar and visible observations 80−90323
- Mars, oval orbit construction and rejection by Kepler, physical hypotheses 78−62027
- Mars descent spacecraft, ballistics 77−33319
- Mars moons, dynamical evolution and origin 78−89104
- Mars orbit emplacement using atmospheric braking, control algorithm 78−69639
- Mars satellites, orbits and perturbations 78−89100
- mass distrib. of disrupting three-body systems 77−49277
- mass point motion in gravitational field of rotating solid *(Russian)* 80−46375
- masses for which triple collision is regularizable 80−41704
- masses in anisotropic parametrised post-Newtonian gravitational metric field 77−5720
- massive protoplanets orbital stability in terrestrial planet region 79−66931
- material test point, statistics of distant perturbs. 78−28494
- mathematical methods, conf., Oberwolfach, Germany (Aug. 75) 77−25916
- mathematical methods, conf. (Oberwolfach, Germany, 1978 Aug. 14-19) 80−36763
- Mercury, escape of natural satellite 78−16323
- Mercury, perihelion precession, nonrelativistic contrib. 79−71184
- Mercury orbited motion, Lorentz-covariant model of the system of two gravitating particles 80−8865
- Mercury perihelion precession, appl. of relativistic force equation *(Afrikaans)* 79−97270
- Mercury rotational motion theory *(Russian)* 78−93134
- Mercury-Jupiter synodic period, coincidence with Red Spot 90 day oscill. 77−82158
- meteor stream dissintegration, solar radiation and planetary perturbation effects *(Russian)* 80−46495

celestial mechanics continued
- meteor trajectories and orbits, visible obs. 80−72887
- meteorioids, trajectories and orbits of fireballs photographed incentral Europe 78−36534
- meteoroid flight trajectory azimuth from Sikhote-Alin field craters 80−72893
- meteoroids and dust, orbits from radio and photographic meteor obs. 80−101555
- meteors, trajectories and orbits from NASA-NMSU Meteor Observatory 77−74014
- Mimas and Tethys, orbital theory including perturbs. 80−36568
- minimally classifying relative equilibria 77−67027
- minimum-time trajectory, interstellar drag effects 78−49286
- minor planet orbit determ. using Chebyshev's approx. *(French)* 80−94720
- minor planet satellites, occultations of stars 80−94741
- minor planets, orbital elements probability distribs. 80−46461
- modified conservation laws in the classical Kepler problem 80−72755
- modified Hill method for perturb. calc. in rectangular coords. 77−78617
- Monte Carlo orbit evolution simulations for comets becoming asteroids 80−82261
- Moon, 18.6 year nodal cycle effect on shallow seas surface temp. due to tidal mixing vars. 78−73387
- Moon, correction for solar terms in lunar ephemeris 80−12684
- Moon, fast evaluation of Fourier series for Brown-Eckert Improved Lunar Ephemeris 80−56711
- Moon, libration, literal theory for laser ranging interp. 77−64677
- Moon, libration in longit. due to Giordano Bruno AD 1178 impact, consistency with laser ranging 78−69717
- Moon, moments of inertia calc. 77−25961
- Moon, orbit and physical libration rel. to universal time meas. from lunar laser ranging 78−85854
- Moon, orbital history rel. to palaeogravimetry and palaeofigure 77−71023
- Moon, orbital theory rel. to lunar laser ranging 77−64676
- Moon, peculiarities of translatory-rotatory motion caused by force function third and higher harmonics *(Russian)* 80−90349
- Moon, secular motion of mean longit. and perigee due to gravit. fields perturbations 77−78679
- Moon, tidal accel. calc. 79−16849
- Moon main problem, ELP soln. *(French)* 80−62044
- Moon orbital dynamics results from anal. of VLBI and laser data 77−29672
- Moon orbital motion, Earth tidal potential multiple expansion 79−12062
- Moon planetary perturbations, formulation and Brown separation *(French)* 77−29664
- Moon pre-capture orbits 77−37525
- Moon secular acceleration, calc. from oceanic tide semidiurnal waves *(French)* 79−8634
- Moser twist mapping theorem, new proof 77−25919
- motion around a source whose luminosity changes 79−12394
- motion in spherically symmetric force fields, vector consts. 78−85833
- motion up to second post-Newtonian approx. in general relativity 79−75079
- mutual gravitational potential of N solid bodies, harmonic coeffs. expansion 79−12390
- n fixed centres problem, particular soln. *(Russian)* 77−17346
- N-body calculations, statistical results validity 78−12084
- N-body central configurations 80−41702
- N-body planetary problem, dynamical coupling of periodic systems, resonance *(French)* 77−73938
- N-body problem, continuations existence 79−84652
- N-body problem, double encounter regularization *(Russian)* 80−46367
- N-body problem, existence of families of periodic orbits 78−24449
- N-body problem, numerical solution accuracy 80−21896
- N-body problem, translational-rotational motion of six bodies *(Russian)* 80−67528
- N-body problem, variation eqns. and eleventh integral *(French)* 77−25921
- n-body problem and integral invariants *(French)* 77−91413
- N-body problem in Euclidean E^4 space, central configurations and relative equilib. 80−41703
- N-body problems, asymptotic behaviour of solns. as time approaches infinity 77−25918
- N-body problems, symmetrical solns. 79−96895
- near circular Earth satellite orbits, element perturbation 79−21165
- near-Earth satellite, perturbations due to sunlight diffusely reflected from Earth 78−24444
- Neptunee encounter with massive body rel. to chaotic satellite system and Pluto origin 79−84743
- New South Wales fireball, 7 April 1978, trajectory and ground track 80−82313
- Newton's laws of motion, planets and rocket dynamics, for schools 78−12509
- Newtonian cosmology, extension to whole of space *(Italian)* 79−21475
- Newtonian dynamics of systems of extended bodies 79−21160
- Newtonian gravitational systems of specified ang. momentum, improbability of collisions 79−53706
- Newtonian mechanics and expansion of the universe *(Italian)* 79−21472
- non-gravitational foci and apexes, of paths with common launching point and common apsidal distances 79−16804
- nonrestricted double-averaged three body problem, Hill's approx. 77−22051
- numerical method stability, appl. to circular motion *(Chinese)* 80−8526
- numerical simulation of 3-dimens. gravitating systems of colliding masses 77−9654
- 1206 Numerowia, improved elements of lost object 78−7906
- obliquity of ecliptic, historical obs. anal. 79−44076
- obliquity of ecliptic 2000 years BP, calc., error correction 79−29688
- obliquity of ecliptic in geological time *(Chinese)* 78−69270
- one-dimensional self-gravitating isothermal systems, stability 80−73008
- optimal m-fold Runge-Kutta algorithm 77−25930
- optimal trajectory-meas. program and meas. error effects 77−53409
- optimum low-thrust multiple rendezvous between inclined orbits 78−4086
- orbit and attitude manoeuvres for spin stabilised satellites, semianal. soln. 77−17338
- orbit computation, appl. of Urabe's method to Moon and artificial satellite cases 80−17477
- orbit computation, semi-analytical method *(Chinese)* 79−8798
- orbit design for geomagnetic tail mission 79−92647

celestial mechanics continued
- orbit determ. contrib. of C.F. Gauss 78–19
- orbit determ. method from observational results 79–84654
- orbit determ. using probe satellite relative motion 77–33316
- orbit determination for comets and minor planets, method for study of error propag. 77–25914
- orbit determination for cosmic object, Green's functions appl. 80–61992
- orbit determination method by filter technique for asteroids and satellites *(French)* 79–101050
- orbit generation for stable close encounter periodic solns. of restricted three-body problem 78–28489
- orbit improvement, vis-viva and Lambert equations, partial differentiations 78–7864
- orbit transfer of rocket between elliptic orbits, globally optimal solns. 78–8236
- orbit-orbit resonances, appl. of spin-orbit theory to Titan-Hyperion case 78–24451
- orbit-orbit resonances in the solar system, varieties and similarities 78–4093
- orbital dynamics and rigid body dynamics, analogy 80–98537
- orbital equations in the relativistic two-body problem 79–44805
- orbital evolution of short-period comets treated as a Markov process 80–46484
- orbital motion, book 78–40809
- orbital motion, potential and travel directions 79–5735
- orbital motion on an interactive-graphics terminal, teaching appl. 80–73152
- orbital motion perturbations determ., analytical method 78–24455
- orbital motion stability for two free ideal conducting current rings *(Ukrainian)* 79–35102
- orbital resonance in dissipative medium rel. to asteroids and Saturn's rings 78–28491
- orbital resonances in solar system, review 77–25998
- orbital transfer, optimal, low-thrust, limited power, elliptical orbits 78–4087
- orbiter around large satellite of giant planet, perturbations due to primary planet oblateness 77–17343
- orbits in Earth's gravitational field 78–40460
- orbits in vicinity of 1:3 commensurability with Jupiter, evolution, model calcs. results *(Russian)* 80–36486
- osculating elements reduction to proper elements for entire solar system 80–21897
- pairs of focal curves in orthogonal planes and movable bar frames *(German)* 77–60927
- particle motion from L_2 Lagrangian point, elliptic orbits 77–91579
- particle motion round variable luminosity source, stochastic scatt. accretion and ejection 79–44338
- particle streams, self-focusing, computer simulations 79–53704
- peculiar direct motions, loops made by objects in strange orbits 80–109346
- pendulum like systems, diagrammatic transition theory 79–44342
- periapsis passage for bitangential turn of path by given angle, anal. 79–44340
- periastron advance in the second post-Newtonian approximation in general relativity 79–75078
- perihelion advance in post-Newtonian gravitation with correction 77–70986
- perihelion displacement, gravitational wave effects 80–61998
- Periodic Comet Ashbrook-Jackson, orbital evolution in 1660-2060 period *(Russian)* 78–49377
- Periodic Comet Boethin (1975 I), libration around 1/1 resonance with Jupiter 80–72883
- Periodic Comet Chernykh (1977l), definitive orbit at first apparition (1977 to 1978) 80–62079
- Periodic Comet Denning-Fujikawa (1978n), orbital elements and ephemeris 79–5780
- Periodic Comet Encke, spin axis precession, nongravitational motion and sublimation 80–46483
- Periodic Comet Giclas (1978k), improved elliptical orbital elements 78–85916
- Periodic Comet Halley, 1986 apparition, student lab. expt. 77–45652
- Periodic Comet Halley, orbital evolution, 1000 BC to present 80–12710
- Periodic Comet Halley, orbital evolution tendency and ancient history *(Chinese)* 79–16886
- Periodic Comet Halley orbital motion, 837-2061 AD 77–74011
- Periodic Comet Haneda-Campos, orbital elements and ephemeris 78–89121
- Periodic Comet Haneda-Campos (1978j), orbital elements 78–89127
- Periodic Comet Kowal 2 (1979a), elliptical elements and ephemeris, (1979, March 28 to June 16) 79–40140
- Periodic Comet Kowal 2 (1979a), improved orbital elements and ephemeris (1979, May 7 to July 6) 79–48739
- Periodic Comet Taylor (1916 I), nuclei separation vels. during disintegration 78–61812
- Periodic Comet Wolf (1884 III), motion in interval 1925-1967, and precalc. of 1975-1976 apparition 78–24493
- periodic comets, missing objects, uncertain orbits and Jupiter effects 77–67072
- periodic Hamiltonian flows, generalised Bertrand's problem, Kepler system 78–86131
- periodic motions close to Lagrangian solns. of three-body problems, orbital stability 78–53804
- periodic orbits, three-dimens. circular restricted to general three-body problem 79–44343
- periodic orbits around oblate spheroid *(French)* 80–31200
- periodic orbits around rotating ellipsoid 78–77464
- periodic orbits of second generation and regions of stability, in restricted three-body problem 78–24453
- periodic oscillations of artificial satellite in plane of elliptical orbit 79–8810
- periodic oscills. around Lagrangian points 79–58236
- periodic solution of $d^2x/dt^2=-V'(x)$, approx. value determ. for period 79–8802
- periodic systems dynamical coupling, particular case of homographic soln. 80–36480
- periodic three body orbits in the case of small third mass 78–77467
- Perko timing condition for second species orbits in restricted three body problem 77–13211
- perturbation eqns., elementary derivation 77–6
- perturbation theory in rectangular coordinates 79–21158

celestial mechanics continued
- perturbed Hamiltonian systems, soln. via accelerated elimination technique 77–60585
- perturbed Hamiltonian systems, transformation-elimination technique 79–44346
- perturbed motion rel. to KS transformation osculating variables 80–109344
- perturbed two body motion Poincare-similar elements development 77–17341
- perturbing celestial bodies, non-spherically symm. gravit. fields, tidal potential study 80–12654
- perturbing planet coordinates, expression through perturbed planet eccentric anomaly 80–67530
- Phobos, orbital inclination evolution 80–67628
- Phobos and Deimos orbital evolution 80–26770
- Phoebe (Saturn IX), orbital motion 1904 to 1969 and Saturn mass determ. 79–88621
- photogravitational restricted circular three-body problem, triangular libration point stability 79–21164
- physical librations, resonances in analytical soln. for libration in longit. 79–84648
- Pioneer 11 post-Jupiter trajectory midcourse manoeuvre sequence for Saturn targeting options 78–7857
- Pioneers 10 and 11, tracking data rel. to gravity field of Jupiter and satellites 77–37554
- planar magnetic binaries problem, areas of motion 78–96386
- planar magnetic-binary problem, equilib. points 80–82178
- planar magnetic-binary problem, stationary soln. stability 79–75080
- planar N-body problem, circular-elliptic type periodic solns. 78–93083
- planar restricted (N+1)-body problem, periodic elliptic motions 78–40806
- planar restricted three-body problems, effect of oblateness on triangular solns. at critical mass 79–44339
- planar three body problem, bifurcation points 78–24446
- planar three body problem, eqn. system adoption for triple collision *(French)* 80–21895
- planar three body system, asymptotic solns. 77–49273
- planar three- and four-body problem, families of periodic solns. 77–25917
- plane circular three-body restricted problem, Hamilton-Jacobi eqn. integrability, separation of variables method *(Russian)* 78–36445
- plane motion with two-fold vel. field, eqns. for potentials *(Russian)* 80–67527
- plane orbit estimation using discrete timing of range measurements, Hermite polynominals appl. 80–21890
- plane periodic motions of solid body in gravit. field of sphere 77–78619
- plane planetary three body problem, quasi-isosceles movement characterisation *(French)* 80–21893
- plane problem of n fixed centres, soln. *(Russian)* 78–24448
- plane restricted three body problem, asymptotic solns. *(Russian)* 77–22049
- planet gravitational field, appl. of satellite model to pot. at physical surface 79–62774
- planet stability, three-body problem using hydrodynamical model 77–87245
- planet-satellite systems of solar system, tidal friction secular effects 79–8860
- planetary, solar and lunar positions, low-precision formulae 80–61990
- planetary capture, satellite aided, of external body, patched conic anal. 79–75087
- planetary disturbing function expansion, convergence of Newton's iteration 77–64629
- planetary dynamics obs. by satellite geodesy 77–81785
- planetary formation by coalescence, averaging of orbital eccentricities 77–17388
- planetary motion calc. method 77–53411
- planetary orbits, analytical method for asteroid belt effects 79–75082
- planetary orbits computation using Chebychev polynomials, appl. to minor planets *(French)* 80–61997
- planetary satellite ejecta, effect of proximity to Roche limit on dynamics 80–98592
- planetary satellite orbit calc. for almost circular-near equatorial plane situation *(Russian)* 77–82115
- planetary satellite orbits, third and fourth-order perturbations rel. to flattening of planet 80–67529
- planetary satellites, true circular orbit 80–46368
- planetary satellites synchronous rotation theory *(Russian)* 78–93134
- planetary system stability, Hill's concept generalisation 79–92656
- planetary systems, stability with bifurcation theory 77–53406
- planetary terms in lunar ephemeris 79–84645
- planetary theory developments in 1973-6 period 78–77505
- planets, Munich meridian obs. (1941-61), orbital elements determ. *(German)* 80–77306
- planets, orbit stability in binary systems, Hill's method appl. 80–94834
- planets, Taylor-Steffensen series appl. to integration of eqns. of motion *(Russian)* 78–49352
- planets capture into resonance rotation, tidal friction 77–78620
- planets gravitational spectra, determ. from planetary orbiters tracking 80–41744
- Pluto, 1978 P 1, possible satellite, orbit and eclipses ephemeris 78–93152
- Pluto, long-term motion, semi-analytical theory 78–69741
- Pluto, orbital motion, long term librational character 80–94753
- Pluto, orbital motion solutions comparison 78–93151
- Poincare periodic solns. and rotational stability according to Cassini laws *(Russian)* 79–40066
- Poincare periodic unstable orbits classification *(French)* 79–29981
- Poincare problem, unconditional stability criterion for Hamiltonian system 78–28492
- Poincare unstable periodic orbit classification *(French)* 79–21157
- point mass motion in one conservative force field, appl. to celestial mechanics 78–24456
- Poisson's theorem in heliocentric variables, applicability to planetary orbits major axes invariability *(French)* 78–85829
- potentials satisfying resonance assumptions 78–20626
- power series expansions by computer 79–84679
- precession constant, new adopted value and effect on stellar proper motions 79–25459
- precession theory, vector-matrix notation 80–51642
- precessional constant and general catalogue for southern stars, proper motions in α *(Russian)* 79–92685

celestial mechanics continued

- precessional corrections to AGK3 system in polar region, rel. to stellar proper motion system anal. *(Russian)* 80—12647
- predictive relativistic mechanics for gravitational interaction, perihelion shift of planet 77—2541
- preliminary orbit determination, method having no co-planar singularity 77—60578
- Proton 4 satellite, orbit determ., geophys., implications 77—64632
- Ptolemaic system, success as kinematic predictor 77—78941
- Quadrantid meteor shower, orbit 78—61815
- Quadrantid meteor stream, effect of orbital evolution on meteoroids influx 80—56776
- Quadrantid meteor stream, long-term orbital evolution 80—17551
- Quadrantid meteor stream, orbital evolution between (AD 1830 and 2030) 80—21948
- quasi-elliptical coplanar transfer in an arbitrary central gravitational field *(Russian)* 79—12391
- quasi-integrals from Von Zeipel transformations in Hamiltonian mechanics 80—46372
- quasiperiodic motions stability in Hamiltonian systems 78—93085
- rectilinear isosceles restricted problem, numerical study 80—4242
- regularised numerical method based on Taylor-Steffensen power series *(Russian)* 78—49300
- relative equilibria and the virial theorem 79—48658
- relative motion of noninteracting particles in force field 77—29635
- relativistic, astron. meas. and coord. systems 80—36481
- relativistic Kepler problem, field asymptotic behaviour in infinite past 79—88575
- relativistic Kepler problem, orbits with gravitational radiation damping, behaviour in distant past 79—88574
- relativistic restricted three body problem, appl. of Gauss method to periodic solns. 77—13215
- relativistic two-body problem, nonlinear effects 79—8799
- resonance in restricted problem of two rigid spheroids 77—45294
- resonance problems, Delaunay-Zeipel transformation analytical props. 80—46378
- resonance problems, regularising function 80—94693
- resonance rotation stability 79—96897
- resonances of higher order in conservative Hamiltonian systems 78—53800
- resonant inclination variations of ten satellites, 30th order gravity harmonics determ. 79—84071
- resonant motion, extremal props. 77—87246
- resonant orbits comparison, theoretical results 80—56889
- resonant stellar systems, formal third integral of motion *(Russian)* 77—82284
- restricted averaged elliptical three-body problem, periodic orbits 79—8807
- restricted circular three-body problem, stabilisation of collinear libration points 77—64624
- restricted elliptic three-body problem, motion near triangular points 79—40064
- restricted elliptical three body problem, difference between solns. of exact and averaged problem *(Russian)* 77—45298
- restricted Jupiter orbiter problem, introduction 77—13216
- restricted problem, effect of perturbed potentials on libration points stability 80—4241
- restricted three body problem; transform. to generalized rot. and pulsating coord. system 78—49298
- restricted three body problem, asymptotic solns. near collinear libration points 77—91414
- restricted three body problem, bifurcations and trifurcations 78—4084
- restricted three body problem, critical generating orbits for second species, periodic solns. 78—4089
- restricted three body problem, near intermediate orbits of point of small mass 79—62731
- restricted three body problem, new connection between families of periodic orbits 78—45204
- restricted three body problem, second species periodic solns. with near-Moon passages 77—49271
- restricted three body problem, stability of second species periodic orbits 78—61717
- restricted three body problem, three dimensional asymmetric periodic orbits 77—64631
- restricted three body problem, three-dim. periodic orbit flattening 77—82116
- restricted three body problem in three dimensions, axisymmetric periodic orbits 77—64620
- restricted three-body problem, asymm. quasiperiodic orbits 79—8801
- restricted three-body problem, asymmetric, periodic and asymptotic orbits 79—16807
- restricted three-body problem, asymptotic solns., plane form and symmetry 79—8814
- restricted three-body problem, commensurability induced by oblateness 79—8806
- restricted three-body problem, effect of larger primary oblateness on collinear libration points 78—40803
- restricted three-body problem, effect of mass ratio on existence of retrograde satellites 77—13210
- restricted three-body problem, form. of periodic solns. by appl. of mean schemes 79—25457
- restricted three-body problem, iterative soln. *(Russian)* 77—91416
- restricted three-body problem, L_4 and L_5 points, stability at pot. maxima 79—7
- restricted three-body problem, numerical extrapolation of periodic solutions 78—69663
- restricted three-body problem, periodic solns., Sun-Jupiter case 79—25454
- restricted three-body problem, perturbations of Lagrangian points 78—32327
- restricted three-body problem, second species periodic solns. with one near-Moon passage 78—45207
- restricted three-body problem, Sun-Jupiter-satellite system, three dimens. orbit determ. 80—67526
- restricted three-body problem, surface fitting of three-dimens. closed solns. 79—8800
- restricted three-body problem, symm. of first integrals *(Russian)* 79—21166
- restricted three-body problem, theory and appl. 79—58241
- restricted three-body problem, three-dimens. branchings of plane periodic solns. 77—64623

celestial mechanics continued

- rigid bodies, translational-rotational motion eqns. in osculating elements 78—28495
- rigid bodies under mutual gravitational attraction, motion 80—61996
- rigid body, motion in Newtonian force field, phase coords. determ. *(Russian)* 78—89049
- rigid body, perturbed motion about centre of mass, element formulation 78—41150
- rigid body, regular motions in gravit. field of sphere 80—62000
- rigid body, regular motions stability in Newtonian gravit. field 77—26165
- rigid body near Earth's surface, stability of flight *(Russian)* 78—89048
- rigid body resonance translational-rotational motion in sphere gravit. field, intermediate theory 79—96899
- rigid body translational-rotational motion in gravit. field of sphere, Poincare periodic solns. of third kind 80—46377
- rigid Earth rotation, theory 77—60332
- Roche problem, for polytropes in central orbits 80—82179
- rotating finite bodies, motion eqns. in extended parametrised post-Newtonian formalism 77—64628
- rotation of rigid body in central Newtonian field, stability *(Russian)* 77—33328
- satelite motion around spheroidal planet *(Russian)* 77—73939
- satellite, differential eqns. of motion, numerical integration 77—33327
- satellite, gravity oriented, with thermally flexed appendages, librational dynamics 78—7868
- satellite, orbits near Jupiter and Saturn, post-Newtonian effects 79—101054
- satellite 1966-51C orbit anal., upper atm. zonal wind speeds determ. 77—56786
- satellite dynamics, appl. of higher-order stroboscopic method 79—66913
- satellite escape or capture duration, simple lower bound 79—2475
- satellite gyroscopic motion, differential eqns. stabilisation procedure including perturbing torques 80—4244
- satellite in resonance with second-degree sectorial harmonic, motion 78—24452
- satellite mission analysis, orbit selection and mission constraints 78—40790
- satellite motion, recurrence relations for inclination functions 77—22054
- satellite motion in vicinity of triangular libration points 78—12488
- satellite motion prediction by extrapolation methods *(Russian)* 78—49299
- satellite orbit, time regularisation of Adams-Moulton-Cowell algorithm 78—45208
- satellite orbit contraction due to atmospheric drag, analytic theory 80—17474
- satellite orbit determ. by astromeas. optimisation 78—16279
- satellite orbit determ. from two posns. and radial vel. 80—8521
- satellite orbit determ. using range meas. *(Italian)* 78—24439
- satellite orbit perturbations, semi-analytical method 80—8522
- satellite orbital lifetimes, prediction methods 78—73605
- satellite orbital motion, flexible appendage effects 78—77456
- satellite orbital motion in resonance with second-degree sectorial harmonic, comments 79—66910
- satellite orbits, initial determ., multiple obs. using angles and angular rates 80—56694
- satellite oscillating orbit utilisation, determ. by apparent motion *(Russian)* 80—26717
- satellite rendezvous trajectories determ., autonomous system 77—53392
- satellite systems stability, Hill's concept generalisation 79—92656
- satellite-derived ocean tide parameters, lunar tidal accel. determ. 78—73662
- satellite-gyrostat in nearly circular orbit, eccentricity var. 78—16280
- satellite-satellite resonances, origin 79—16867
- satellites, cable-connected in Earth orbit, mag. force effect 79—44347
- satellites, orbital speed, in Kepler ellipse, theory 77—70984
- satellites, spin-stabilised, effect of orbital eccentricity and nodal regression on gyroscopic motion 78—45206
- satellites direct and retrograde orbits, limiting radii and appl. to solar system and stellar systems 79—88572
- Saturn, orbital elements of satellites rel. to Saturn's position and mass 77—74007
- Saturn's rings, thickness caused by satellite and solar perturbs. and planetary precession 80—36569
- Saturn rings, coherent solar and satellite perturbations rel. to vertical struct. and thickness 80—4296
- scale invariance, metrical connection and the motions of astronomical bodies 79—44648
- Schwarzschild field geodesic, Newtonian limit 78—86056
- secular planetary theory of first order up to fourth power in eccentricities and inclinations 79—96894
- semirestricted three body problem 77—25932
- separable potential in spheroconical coords. satisfying Laplace eqn. 79—25458
- solar sail trajectories, long-term evaluation 79—48641
- solar system, distrib. of mean motions of planets and satellites rel. to development 77—91451
- solar system, higher-order stability in restricted problem 77—13208
- solar system, numerical values of consts. of IAU Commission 4 Working Groups Joint Report 78—40845
- solar system, relativistic effects verification, comparison of obs. results with theoretical data *(Russian)* 79—80209
- solar system, Titius-Bode law for planet distances from Sun 80—82236
- solar system bodies, orbital perturbations by solar companion star 78—12198
- solar system dynamics and long-term stability 79—40095
- solid bodies, general expansion of force function 78—7877
- solid bodies in solar system, gravitational potential 78—77550
- solid body rotation in Newtonian force field *(Russian)* 79—35546
- space craft motion in gravitational and mag. dipole fields *(Russian)* 80—36487
- space vehicle, motion in vicinity of collinear libration point, semianalytical method 78—4066
- space vehicle motion in vicinity of collinear libration point, statistical estimates in control problem 78—4067
- space vehicle orbit determ. optimization with incomplete inform. on error covariance matrix and expectation 79—8808
- space vehicle orbiting oblate planet, optimal low-thrust takeoff 77—60580
- space vehicles, relative motion computation using time transformations 77—22050

celestial mechanics continued
space vehicles, thrust-aided sub-orbits 78—45181
space vehicles relative motion computation with increased precision 77—22048
space vehicles station-keeping manoeuvre, operational requirements and geometry 78—45180
spacecraft, flexible, eigenvalues and eigenvectors for hybrid coordinate eqns. of motion 79—75085
spacecraft orbital plane, autonomous determ. via landmarks on central planet surface 77—64595
spacecraft trajectory optimisation using closed soln. of constant thrust-accel. motion 77—25926
spacecraft with solar sail, eqns. of motion from geocentric orbit 77—53394
spacecraft-artificial satellite closest approach times calc. 79—62713
spherical motion of satellite with varying mass geometry in Newtonian gravitational field *(Russian)* 78—16282
spherical stellar systems submitted to aspherical perturbations, second variation of energy *(French)* 77—53646
spheroidal balloon satellite, orbital perturbations due to direct solar radiation press. 80—4219
spin precession in the relativistic two-body problem 79—49118
spin-orbit resonance, mathematical aspects 79—12389
stability of plane periodic motion of satellite in circular orbit *(Russian)* 78—16281
Starlette satellite, precision orbit computation 78—65478
stationary satellite, arbitrary integration constants in approx. analytical theory *(Russian)* 78—32331
stationary satellites, equations of motion, numerical integration methods *(Japanese)* 78—85837
stationary satellites of Earth, Moon and Mars, coordinates of gravit. fields stationary points 78—53805
statistical mechanics of Keplerian orbits, perturbations 77—49269
stellar aberration, classical rel. to relativistic theory 80—67517
stellar reson. orbits comparison, 2/1 reson. 80—67796
Stormer problem, family of asymm. periodic oscills. 77—78586
Stormer problem, periodic motions in mag. dipole meridian plane 78—85841
Stormer problem, periodic motions in mag. dipole meridian plane 78—89053
Sun-Earth-Moon system, stability limits for restricted three body problems 79—75084
Sun-Earth-Moon system stability, Hill's problem 77—70985
Sun-Jupiter case, plane symmetric periodic orbits in restricted three-body problem 79—58235
Sun-Jupiter-asteroid circular and elliptic problem comparison at commensurabilities 77—56819
Sun-Jupiter-Saturn mass ratio, families of periodic orbits and their stability 77—13209
synchronization mode of rotating solid celestial body 78—7869
Szebehely equation, modification 78—24447
Szebehely equation for potential of prescribed family of orbits, solns. 78—40808
teaching, demonstrational appliances *(Hungarian)* 78—36772
teaching, Newtonian motion anal. using micro-computer simulations *(Japanese)* 80—31462
terrestrial longit. determ., without time, from obs. of lunar altitude 78—85836
thee-body problem, restricted case secular post-Newtonian effects, Treder dynamics 80—72753
third integral of motion, construction in reson. cases 77—53647
three body averaged plane restricted problem, first integrals, computer calc. *(Russian)* 77—56820
three body problem, generalized circular restricted, triangular libration points *(Russian)* 79—48659
three body problem, Lagrange equilateral triangle, Euler collinear solns., generalisation to nongravit. forces 78—54178
three body problem, planar circular restricted case, stochastic behaviour, reson. overlap criterion 80—105150
three body problem near triple collision 77—17336
three body restricted problem, stability of generating soln. 77—72146
three fixed centres problem, soln. 77—60584
three fixed centres problem 77—25933
three rigid bodies problem, particular solns. for translational motion *(Russian)* 80—61999
three-body, circular plane restricted problem, stable orbits 79—44348
three-body, elliptic three-dimens. restricted problem, recurrence relations in integration 79—48656
three-body, planar general problem, isosceles triangle config. 79—48654
three-body gravitational scattering 79—44344
three-body problem, classical restricted, Coriolis asymm. and Jacobian integral 80—61994
three-body problem, colinear positions of relative equilibrium *(French)* 78—36443
three-body problem, conditionally periodic solns., KAMo method 80—109343
three-body problem, doubly averaged elliptical restricted, first integrals 80—17479
three-body problem; doubly-averaged elliptical restricted, trajectories 80—46376
three-body problem, elliptic, Jacobian integral development *(German)* 79—92655
three-body problem, elliptical restricted case, Lagrangian soln. stability *(Russian)* 80—94695
three-body problem, families of 3-dimens. periodic orbits 80—41698
three-body problem, forms of motion qualitative anal. in new model problem 79—62733
three-body problem, general, families of three-dimens. periodic orbits 80—26721
three-body problem, general, regions of motion *(Chinese)* 79—80206
three-body problem, general, three-dimens., biparametric family of symm. periodic orbits 80—61995
three-body problem, general case, families of 3-dimens. periodic orbits 80—41700
three-body problem, general case, topology of M_8 manifold 80—8528
three-body problem, general planar case, families of vertical periodic orbits 80—41699
three-body problem, general planar case, periodic solns. of Poincare's second sort 80—41707
three-body problem, generalised, Lagrangian and Eulerian solns. in absolute axes *(French)* 79—66912

celestial mechanics continued
three-body problem, generalized restricted, zero relative vel. curves 79—84650
three-body problem, limited circular, Delaunay-Hill method averaging error estimation *(Russian)* 80—8530
three-body problem, model for close encounters in planetary system 78—61718
three-body problem, periodic orbits continuation 79—16806
three-body problem, photogravitational restricted circular case, triangular libration points stability *(Russian)* 80—77272
three-body problem, photogravitational restricted core, Lagrangian points 80—26725
three-body problem, planar case, reduction of eqns., of motion 80—41711
three-body problem, planar case, variational eqn. 80—46371
three-body problem, planar hyperbolic-elliptic motion, central configurations 80—41705
three-body problem, planar to three-dimens. general core, periodic orbits 79—66908
three-body problem, plane averaged restricted case, qualitative analysis 80—109345
three-body problem, rectilinear case 80—41708
three-body problem, redundant variables for global regularization 77—25923
three-body problem, restricted, bifurcation orbits, Sun-Jupiter case 79—84647
three-body problem, restricted, families of three-dimens, double-symm. periodic orbits, Sun-Jupiter case 80—26722
three-body problem, restricted, in resisting medium, particular solution *(Italian)* 80—90325
three-body problem, restricted case, Poincare's second species solutions 80—41709
three-body problem, restricted case, Sun-Jupiter case, doubly symm. periodic orbit determ. 80—77269
three-body problem, restricted case, u-type families of periodic orbits 80—101530
three-body problem, restricted planar elliptic case, stationary solns. 80—46369
three-body problem, restricted plane case, formal integrals 79—96900
three-body problem, spatial periodic orbit families 80—77271
three-body problem, stability of interplay motions 77—60583
three-body problem, sufficient conditions for absence of collisions 78—24457
three-body problem, Sun-Jupiter case, axisymmetric periodic orbits 79 58237
three-body problem, three-dimens. general case, periodic orbits determ. 80—56696
three-body problem, three-dimens. periodic orbit families, Hill's problem 80—56695
three-body problem, triple collision and tri-parabolic escape 80—67521
three-body problem, unrestricted, Lagrangian solns. stability problem *(Russian)* 80—4245
three-body problem, unrestricted, Laplace solns. stability *(Russian)* 80—8529
three-body system disruption, statistical theory for three-dimens. motion 78—77475
three-body systems disruption, statistical theory for high ang. momentum 77—13220
three-dimens. circular restricted three-body problem, simplified variant 79—8815
three-dimensional periodic orbits around Moon and planets 78—20627
three-impulse min.-time orbital transfer generation, numerical method 78—73607
115 Thyra, astrometry and orbit improvement *(German)* 80—85881
tidal force acting on Moon due to Earth and Sun *(Russian)* 77—78616
time elements for time transformations, numerical aspects 77—25929
time standard differences and celestial mechanics *(Italian)* 78—93087
time transformations and Cowell's method 78—77466
Titan-Hyperion resonances and close approaches, restricted three-body problem anal. 80—77347
Titius Bode Rule for solar planets and planetary satellites, c.f. Bohr atomic orbitals 79—101057
Titius-Bode law, existence of space for more than ten planets 78—40851
Titius-Bode relation, modified 79—84684
topology of phase levels for a point motion in a non-central field *(Russian)* 79—12393
1685 Toro, orbital resonances with Earth and Venus 79—2513
trajectory analysis of Vikin 1 Orbiter encounter with Phobos 80—12641
trajectory optimisation for ion-propelled space tug 78—53798
trajectory prediction errors for geocentric motion of apparatus with solar sail *(Russian)* 79—88576
translational-rotational motion of two mutually gravitating rigid bodies 79—96896
translatory-rotary motion of gravitating spheroids *(Russian)* 78—73841
translatory-rotary motion of three rigid bodies, Euler solns. *(Russian)* 78—53802
trapping of particles in time-depend. Hamiltonian 77—13217
triple collision in rectilinear three body problem, neighbouring solutions *(French)* 77—13213
triple collision manifold in planar three-body problem *(French)* 79—58238
triple collisions 80—56697
triple rectilinear collision, Siegel matrix, eigenvectors *(French)* 77—70988
Trojan asteroids, asymptotic soln. of plane elliptic restricted three body problem 77—60587
Trojan asteroids, long-period effects in motion and problems of 1/1 resonance 80—41755
Trojan asteroids, long-periodic solution in restricted three body problems 77—17337
Trojan asteroids, orbital theory 79—12419
Trojan asteroids, perihelion motion 79—84725
Trojan asteroids, restricted three body problem 77—74003
Trojan asteroids, three-dimens. motion 79—5773
Trojan asteroids and fictitious objects at 1/1 resonance, long-period effects 78—85830
Trojan asteroids with large orbital inclination, dynamics 80—77323
tropical year, its astronomical meaning, for teachers 79—97136
two bodies of variable mass problem, relative orbit 79—62730
two body problem, time transformations and local truncation errors 77—22053

celestial mechanics continued
- two body problem, time transformations effect on local truncation errors 77—22052
- two body problem in invariant mechanics *(French)* 80—94696
- two finite bodies problem, development of force function *(French)* 77—13218
- two point-masses bound system, influence of weak gravit. wave 80—21903
- two rigid body motion under mutual gravitational attraction 78—28490
- two-body motion under inverse square central force and equiv. geodesic flows 77—91412
- two-body orbital mechanics, solution to Kepler's problem for orbital position 78—73622
- two-body problem, expansions of functions of velocity 77—91415
- two-body problem, first and second isochronous derivatives 80—8527
- two-body problem, general case, translating-rotating motion, force function determ. 80—17478
- two-body problem, general time elements 78—77470
- two-body problem, orbits from Lenz vector, education 78—36763
- two-body problem, with decreasing gravit. const. 77—13219
- two-body restricted problem, almost circular orbits in general relativity *(Ukrainian)* 79—101056
- two-body variable-mass problem, osculating orbital elements estimation 77—13221
- two-position orbit-determination problems 79—88573
- two-terminal trajectories, global anal., geometric and kinematic family struct. 78—4085
- unpowered spaceprobe ejected from circularly orbiting space station, trajectories calc. 80—36484
- unrestricted 3-body problem, Laplace soln. instability *(Russian)* 78—4092
- Uranus, ε-ring, variable width and ellipticity, orbital considerations 78—40870
- Uranus, rings origin, orbital reson. effects 78—53874
- Uranus ε ring, precession 80—26804
- Uranus ring system, influence of tiny Miranda 78—4148
- Uranus ring system, quantitative anal. of Dermott-Gold theory 78—4147
- Uranus rings, reson. orbit theory and prediction of undiscovered satellite 78—81585
- Uranus rings, three-body resons. rel. to ring radii 78—89117
- Uranus-Neptune general planetary theory, short-periodic term elimination 79—75153
- US Navy navigation satellites, mean elements for 1974-6 period 79—48642
- variational eqns. of a class of dynamical systems 77—17345
- Venera-9 and -10, dynamical flattening of Venus from meas. of trajectories 79—35168
- Venus, escape of natural satellite 78—16323
- Venus, motion, numerical theory using radar, optical and Venera satellite obs. data 78—16325
- Venus, orbit and radius determ. from radar obs. in 1962-1977 period 79—88570
- Venus orbit determ. using radar obs., appl. to spacecraft navigation 80—109386
- Vinti problem, extended phase space formulation 78—53801
- zodiacal dust cloud, charged dust particles motion in interplanetary space 80—4299
- zodiacal light dust, orbits from Doppler shift meas. 78—85904

cell model (liquids) *see liquid theory*

cell motility
- axonal transport, components, mechanisms and specificity, book contrib. 79—96551
- bacteria, diffusing and motile, light scatt. props. calc., RGD approx. accuracy 79—92193
- bacteria, motile, rot.-translational models for interpretation of quasi-elastic light scatt. spectra 79—11906
- bacteria, motion, quasi-elastic light scatt. 77—23617
- bacteria, proton pump as molecular engine 78—40130
- bacteria magnetotaxis, Mossbauer study 80—41056
- bacterial chemotaxis, cyanine fluorescent dye membrane probe effects on cell props. 78—35815
- bacterial dispersal tracking by three dimens. microscope 80—30965
- bacterial flagella, protonmotive driving force 78—48774
- bacterial flagella rotating in bundles, helical geometry study 77—52825
- bacterial flagella rotation rel. to ion transport down electrochem. gradient 77—73515
- bacterial migrating chemotactic bands, quasi-elastic light scatt., E. coli 78—77018
- bacterial motility, E. coli, struct. effects in quasi-elastic light scatt. 78—77024
- bacterial movement tracking using one-dimens. fringe system 78—73299
- bacterial sensory electrophysiology, motility depend. on membrane pot. and chemotaxis 78—53373
- Biophysical Society, 23rd annual meeting, conf., Atlanta, USA (Feb. 1979) 79—34468
- blood, red cells as fluid droplets, erythrocyte membrane dynamics in shear flow 79—74711
- chemotactic bacteria travelling bands, model 78—44516
- ciliary activity obs. by laser light-scatt. spectroscopy 78—36076
- ciliated cell activity during exposure to ionising radiation, temp. effect 77—70493
- ciliated cell response during irrad. at different dose rates 78—61216
- cytoplasmic streaming, in green plants, review, book contrib. 79—5265
- cytoplasmic streaming in amoeboid movement, review, book contrib. 79—5264
- cytoplasmic streaming vel. change during action pot., meas of birefringence change 79—100585
- enkaryotic cells, roll of dynein, book contrib. 79—16178
- erythrocyte tank-treading motion in a shear flow, model 80—104568
- Euglena gracilis, effects of EM fields on motion 79—16174
- Euglena gracilis, motion parameters meas. by laser light scatt. 79—16173
- fibroblast spreading kinematics, individual locomotor activity 78—69006
- flagella, laser damage, high speed cinematography 80—81785
- flagella bend propagation, derivation of eqns. of motion and simulation 78—77074
- flagella bend propagation, dynein cross-bridge kinetics 79—43942
- flagellar fragments of long insect sperm, motion characts. 80—51056
- fluid mechanics of propulsion by cilia and flagella, book contrib 77—48833

cell motility continued
- granulocytes, human, spatial trajectories in isotropic medium 79—34523
- interactive film anal. system 80—3876
- leukocyte motility and chemotaxis parameters meas., quantitative anal. of under agarose migration assay 79—96525
- lymphocyte sensitisation meas., electrophoretic mobility test improvements 79—25138
- Markov chain model of motility and adhesion 77—66804
- molecular basis of movement rel. to proteins 79—100586
- movement, droplet on surface model 78—22934
- pancreatic cell moving granules anal. by digital moving image processing 79—84063
- Paramecium, artificial deciliation causes loss of Ca-depend. responses 77—2017
- Paramecium, central tubules rotation during ciliary beat 79—70536
- Paramecium membrane potential changes during chemokinesis 80—26209
- photon correlation spectroscopy meas. of bacterial translation 78—44738
- protoplasm streaming in Nitella flexilis, vel. distribs., laser Doppler spectrum 77—40684
- red cell extensional recovery, determ. of membrane viscosity 79—57683
- red cell membrane thermoelasticity obs. 79—57684
- saltatory motility of uninserted trichocysts and mitochondria in Paramecium tetraurelia 78—24044
- self-propelled uniflagellated micro-organism, hydromechanical model 79—92199
- silicone rubber substrata, appl. to study of cell locomotion 80—104835
- sperm, human, flagellar propulsion in cervical mucus, interaction hydrodynamics model 80—97878
- sperm flagella equation of motion 78—80895
- spermatozoa, bull, motility evaluation by photon correl. spectroscopy 77—48964
- spermatozoa, bull, swimming speed distribs. determined by quasi-elastic light scatt. 78—44478
- spermatozoa, human, motility evaluation, photon correlation meas. 80—61745
- spermatozoa, swimming, quasi-elastic light-scatt. spectra 80—30760
- spermatozoa after deep freezing, kallikrein effect on motility 79—66463
- spermatozoa flagellation, observation by depolarised laser light scatt. 80—40978
- spermatozoa mobility, photon correlation study 80—12063
- spermatozoa mobility meas. by laser light scatt. *(French)* 78—36083
- spermatozoa motility, depolarised laser light scatt. obs. 77—90749
- spermatozoa motility evaluation by laser scatt. 78—48864
- spermatozoa motility evaluation by photon correl. spectroscopy 79—92440
- spermatozoa motility meas. by laser light scatt. *(German)* 79—12056
- spermatozoa motility meas. by light scatt., appl. to reproduction immunology *(French)* 79—34628
- spermatozoa swimming in cervix, effects of dynamical interaction and peripheral layer viscosity 78—69126
- subcellular motions in Nitella flexilis, photon correl. spectroscopy 79—66465
- tracking microscope, design and operation 80—36214
- trap action model 79—16176
- Ca^{2+} effect on rat cell electrophoretic mobility after X-irrad. 79—92293
- Ca-dependent sensory-motor response of marine dinoflagellate to CO_2 78—57026

cells (electric)
- *see also fuel cells; photoelectric cells; photoelectrochemical cells; primary cells; secondary cells*
- air-bath enclosure for standard cell group monitoring by AC Josephson effect 77—82556
- alkaline cell, creepage rate of electrolytes 79—61967
- anodic oxidation of Mn in solns. of Mn salts, appl. to cells. *(French)* 78—11520
- batteries 1978 progress and development trends *(Japanese)* 79—83579
- battery monitor, operates on only a few microamperes 77—18005
- calibration of conductance cells, current practices 77—25274
- capillary Hg-electrolyte cells, elec. characts. rel. to mag. field 77—1937
- catecholamines, HPLC and continuous flow anal. using flow cell based on rotating disk electrode 80—66894
- CdTe thin polycrystalline film for photoelectrochemical cell 78—23162
- concentration-cell electrochemical convertors for seismic registering device, data readout 77—2287
- conference, Electrochem. Society fall meeting, Las Vegas, USA (Oct. 1976) 77—16831
- conference, electrochem. society fall meeting, Las Vegas, USA (Oct. 1976) 77—77787
- convective diffusion eqn. for electrochem. cell, computer soln., numerical methods 77—16830
- coulometric data unit, oxygen, long lifetime 79—39243
- cylindrical, for making standard samples of metal coatings 80—85106
- diaphragm-type electrolysis cells, current yields of alkali 79—100402
- electrical double layer, props., nonlinear AC methods obs. 78—3345
- electrochemical cell, AC component effect on convective diff. processes, characts. 77—63929
- electrochemical cells, photovoltaic phenomena and mechanisms 78—8198
- electrochemical cells with capillary membrane, electrochem. and capillary characts. 79—61874
- electrochemical commercial, characts 79—70334
- electrochemical corrosion of metals and alloys, corrosion conditions simulation *(Russian)* 79—52445
- electrochemical current source, exergetic efficiency 77—44488
- electrochemical gas concentration cells for the conversion of ocean wave energy 80—40821
- electrochemical oscillations, of voltage and current, spontaneous, maths. anal. of mechanisms, in book, for teaching 78—8201
- electrochemical storage, of H in $LaNi_5$ alloys, nature of H bond 79—24917
- electrolyser, rotating, flow field 79—52682
- electrolytic cell resistance meas., differential recorder 78—86297
- fast ionic conductors, review, device appls. 78—51724
- fission electric cells, synergetics using catastrophe theory 80—45761
- galvanic cell, electrochemical transient investigations 77—11930
- Galvanic cells for in-situ AES study of metal oxide surfaces 78—19615
- impedance theory and experimental data review 80—55667
- internal resistance of energy source meas., student expt. 79—30176
- magnetoelectrolytic cell, hydrodynamics, mass transport 77—36759
- materials needs, in energy conservation and storage 80—66958

cells continued
- matrix-type electrochemical cell, preparation of porous Ti-MnO_2 anodes 77—81414
- metal-cellulose-metal sandwich system, spontaneous elec. current induced by heating 80—40700
- metal/β-alumina/metal, complex admittance diagrams, grain boundary effect *(French)* 80—45653
- metal/metal ion system, instantaneous corrosion rate deform. by Faradaic rectification 78—80667
- metal/metal ion systems, instantaneous corrosion rate determ. by Faradaic rectification 78—80666
- metallic oxides used as battery cathodes, electrochemical behaviour 80—45516
- multicomponent impedance diagrams, resolution technique 80—66959
- NASA space power technology program 79—96883
- nuclear energy, nonconventional conversion systems *(Rumanian)* 78—86705
- pacemaker energy sources, clinical use 77—81731
- pacemakers and batteries, microcalorimetric study 78—57130
- photoelectrochemical, water photoelectrolysis by irradiation of platinized n-type semicond. $SrTiO_3$ and $KTaO_2$, appl. 77—86332
- photoelectrolysis, $SrTiO_3$ electrodes defect surface states obs. 78—14815
- photoelectrolysis cell for solar energy conversion 77—20423
- polypropylene-covered galvanic cell, O_2 consumption anal. 78—31923
- porous electrode type cells, electrochem. and capillary characts. 79—91967
- porous electrodes, flow-through, math. modelling 77—16832
- potentiostat, microprocessor controlled, for electrochem. meas. 79—85133
- prosthetics, energy sources for long-term implantable devices 80—98175
- purpose-built battery development 79—79388
- resistive electrode current density distribution 80—21302
- reverse electrodialysis of brine solns., elec. cell design and cost 80—85271
- reversible galvanic cell, thermodynamics, EMF rel. to temp. 77—1935
- semiconductor electrodes, light energy conversion and storage 78—14813
- sodium polyaluminate, impedance parameters in electrochemical cell, Mn ions effect 80—21296
- sodium tetraphenylborate soln., electrolyte, steady state electrochemiluminesc. 79—57250
- solid electrolyte, unipolar cond. model 79—28144
- solid electrolyte cells, inductive effects and AC meas. 78—6623
- solid electrolyte containing systems, electronic self-discharge currents 79—100502
- solid electrolyte electrochem. cells, V(I) characts. 78—35704
- solid electrolyte galvanic cell for gas sensing, response speed 77—60149
- solid electrolytes appl. *(Czech)* 77—77779
- solid film, electrolyte systems, materials characts. and appls., review 77—77781
- solid state chemistry of batteries, electrodes, and electrolytes, conference, Miami Beach, Florida, USA (Sept. 1978) 79—100393
- solid-electrolyte, for conc. EMF meas. of sulphide melt 77—40571
- standard cell intercomparison system for reference groups, microcomputer-controlled 80—22384
- standard cell voltage monitor using AC Josephson effect 77—82552
- standard cells with low temp. coeff., characts. 80—101090
- testing aqueous caustic electrolyzers at high temperatures 80—45655
- theoretical efficiency limit of water electrolysis and practical means to approach it 80—45656
- thermal battery, react. prods., electron probe anal. 79—43601
- thermal energy, electrochem. conversion using cells with reversal of pot. with temp. 80—26124
- thermocell, solid electrolyte, twin, for entropy of O_2 in mixture determ. 78—27812
- three dimensional gauze electrode in new cell design, mass transfer enhancement by counter-electrode gases 79—43590
- voltage cell using Josephson junction, computer simulation 79—93089
- voltage transfer standard based on AC Josephson effect, standard cell calibration appl. 77—82553
- Zn(Hg)/KOH, ZnO(sat.), rates, instantaneous, Faradaic rectification, experimental verification part II 78—80667
- Ag sintered electrode production for concentrating cell *(Portuguese)* 78—88637
- $Ag/Na_2SO_4(WO_4)$, and $Ag/Ag_2SO_4(WO_4)$ solid cell systems interface form., intergrain contact growth 77—16827
- AgI-Ag oxosalt systems, solid electrolytes with glass-like struct., thermodynamic and electrochem. props. 79—10978
- AgI-$Ag_2O.B_2O_3$ system, ionic cond., struct., electrochem. prop. in galvanic cell 78—95181
- $AgNbO_3.4AgI$ room temp. solid electrolyte and galvanic cell performance 78—79803
- $Ag(T_1)/AgI/Ag(T_2)$ cell, thermo-EMF of highly conducting solid electrolytes 80—24659
- β-$AgVO_3.4AgI$ room temp. solid electrolyte and galvanic cell performance 78—79803
- $Ag(s)/Ag_2SO_4+Na_2SO_4(l)$ high temp. ref. electrode, study 80—76622
- Al-air, mechanically rechargeable, for automotive propulsion 79—48103
- β-Al_2O_3 polycryst. electrolyte containing cells, impedance and cond. relax. 79—100401
- Al_2O_3-Na_2O, β' and β'' phases, engineering props. data compilation, rel. to energy storage 80—49415
- CaF_2 solid electrolyte use in galvanic cells for thermodynamic obs. on refractory double oxides *(French)* 80—85190
- CeO_2 doped electrolyte cell, polarisation phenomena associated with CeO_2 reduction 80—55827
- Cl cells, diaphragms action 80—21294
- $Cu/CuBr/Cu_{2-x}Te/C$, galvanic cell, use in $Cu_{2-x}Te$ phase diagram construction 80—6917
- $Cu(Hg)/CuSO_4(m)/Hg_2SO_4$, Hg, EMF, standard electrode pot. 78—76874
- $Cu_xMo_6S_{8-y}$, mixed conductor, equilib. partial thermodynamic props. 80—85270
- Fe-thiamine solution, modified, photogalvanic effect 78—91722
- α-Fe_2O_3:TiO_2 electrode, water photooxidation appl. 78—15684
- H-O electrochemical matrix-type cells, transport effects study 80—26027
- H_2S oxidation by active C, electrochem. model *(German)* 78—35717
- Hg-Cd cell, EMF rel. to temp., thermodynamics 77—12805
- Hg-electrolyte capillary cell, capacitative control of interelectrode gap 77—90610
- Li cells, electrochemical charact. of VSe_2 79—1959
- Li-H_2O_2, 600 kWh reserve power system 79—48104
- Li-Si, electrode pot., Li utilisation determ. 80—81427

cells continued
- $Li_xUO_2F_2$, $0 \leq x \leq 2$, use in electrochemical batteries 80—50858
- MnO_2 powder electrical characts. obs. battery grade, highly hydrated 79—100501
- $Mo|Cr$, $CrF_2|CaF_2$, $CO|Mo$ galvanic cell, EMF meas., thermodynamic props. of CaF_2 determ. 77—7874
- $Pb/PbF_2/BiF_3/Bi$ thin solid film reversible galvanic cell 79—52928
- $Pb(Sb)/H_2SO_4$, $PbSO_4$(sat.), rates, instantaneous, Faradaic rectification, experimental verification part II 78—80667
- ^{147}Pm small-size nuclear battery, characts. of luminophores and photoelements *(Bulgarian)* 80—72084
- Pt 79—48340
- Pt/Y_2O_3-ZrO_2/Pt cell, Faradaic reaction kinetics, impedance dispersion anal., electrode/electrolyte interface process 79—11798
- WCs, preparation method effects on catalytic activity for H_2 evolution 80—101024
- ZrO_2, electrochemical cells for O_2 sensing, EMF oscills. 79—47999

cellular arrays
- computer-controlled liquid-crystal transparency array *(Russian)* 77—58430
- computer-generated pure binary hologram analysis and expt. 79—55092
- image processing nonlinear nonmonotonic function synthesis 77—50633

cellular automata *see finite automata*

cellular biophysics
- *see also biomembrane transport; biomembranes; cellular effects of radiation; cellular transport and dynamics; lipid bilayers*
- Acetabularia cell electrical parameters and equiv. cct. 77—56350
- Acetabularia cell wall, deform. rel. to genetic and geometric factors 77—56348
- Acetabularia cell wall deform. and morphogenesis, local control of viscoelastic deform. 77—56349
- acetylcholinesterase, membrane bound, activity rel. to struct. changes induced by cAMP 80—30674
- action potentials from cultured neurons, recording by extracellular microcircuit electrodes 80—72382
- actomyosin-ATP system kinetics, energy transform. anal. 77—81476
- adenocarcinoma cells, population anal. of DNA content, flow microfluorometry obs. 80—16913
- adenylate kinase, photokinetic microassay using the firefly luciferase reaction 80—56306
- adhesion, review 78—15803
- adhesion and motility, Markov chain model 77—66804
- adhesion models, reaction kinetics and forces 78—80844
- aerobic Escherichia coli cells, metabolism, high resolution ^{31}P NMR studies 77—90741
- afterpotentials influence on shape and magnitude of extracellular pots. 80—3625
- ageing, evolutionary view 78—11789
- ageing process, role of cell membranes, review 78—15809
- algae, Chlorella pyrenoidosa, delayed emission, temp. effects 77—29118
- algae, living electrode for biophotolysis of water, long-lived photoconvertor 80—104510
- algal suspension, light scatt. expts. and theory, ang. depend. 79—16166
- algal suspensions, light scatt. and absorpt. props., 380-720 nm 78—92604
- alveolar brush cells of rats, SEM obs. 79—34517
- 1,8-anilinonaphthalene sulphonate in bacterial suspension, fluoresc. spectra 79—88052
- animal behaviour, neural control, book contrib. 79—2041
- anterior pituitary cell action pots., stimulation by thyrotropin-releasing hormone 78—48771
- antigen-antibody complexes, dissociation, net repulsive van der Waals forces between different particles, macromolecular, or biological cells in liqs., appls. 80—34274
- antigenic nature of mammalian cell surfaces, review 78—15805
- antitumor drug dosage schedule, cell cycle kinetics approach 77—86700
- apatite crystal growth in skeletal tissues 80—94181
- arterial smooth muscle, pig, estimates of cellular mechanics 79—16229
- Aspergillus niger dying spores, electron refl. and transmission SEM expts. after irrad. 80—56111
- ATP, chemiosmotic theory of manufacture in cells 78—61151
- ATP content meas. in single red blood cell, using firefly bioluminescent reaction with optical instrument 79—79695
- ATP measurement in single red blood cells using firefly biolum. reaction 78—48951
- ATP synthesis, participation of free radicals 79—92183
- ATPase kinetics in E. coli cells, ^{31}P NMR meas. 78—77022
- atrial trabecula membrane, frog, accommodation, repeat responses and anode-breaking excitation 78—64956
- atrioventricular region of rabbit heart, passive elec. props. rel. to intercellular link 78—48767
- atrium trabecula membrane, changes in elec. props. due to elec. stimulus 77—36891
- auditory neurone phasic sensitivity as function of sound signal freq. 79—57666
- auto-immunity, math. model of cell dynamics 77—16900
- automatec cell sorting with flow systems, book contrib. 79—5435
- autoradiography, double radionuclide methods for tissue sections or cell smears, using light microscopy 77—5113
- axon, squid, Ca buffering, review, book contrib. 79—5267
- axon diameter changes concurrent with action pot., crayfish, laser interferometer meas. 77—64029
- axon membrane admittance change during action pots., squid 79—57621
- axonal branching in brain ascending raphe and nigral projections, fluorescent retrograde double labelling obs. 79—79504
- bacteria, freshwater magnetotactic, identification of magnetite, Mossbauer obs. 80—3657
- bacteria, luminescent, calorimetric study of growth 77—25378
- bacteria, photosynthetic, EPR line shape of partially aligned cells 79—87305
- bacteria, polydisperse suspensions, angular light scatt. calcs. 79—94151
- bacteria, radiometric estimation of replication time in culture using $^{14}CO_2$ 79—16170
- bacteria, Rayleigh-Gans-Debye scatt. theory for nonspherical particles 78—46510
- bacteria, yeast and leukaemic cells, dynamic struct. obs. by Overhauser enhanced ^{15}N NMR 77—90742
- bacteria as biogenic sources of freezing nuclei 79—20948
- bacteria in H_2O, detection by resonance Raman spectra 80—94418
- bacteria light scattering patterns, appl. of Mie theory and cubic splines 79—36838

cellular biophysics continued
bacteria species identification and conc. estimation by light scatt. 77—56564
bacteria-like layered prolate spheroids, angular scatt. calcs. 79—64179
bacterial biomass production, efficiency bypasses that of photosynthesis 80—21408
bacterial cell wall, surface charge and morphogenesis of regular arrays of macromols. 80—85366
bacterial cell wall structure study by STEM, S/N enhancement by interactive computation 79—5427
bacterial cells, active, reson. between 10^{11} and 10^{12} Hz obs. by laser Raman spectroscopy 77—36893
bacterial culture, Degn-Harrison reaction scheme, multiple steady state 78—88700
bacterial luminescence, yellow light, Photobacterium fischeri 77—66802
bacterial photosynthesis, low-temp. electron transfer 78—44470
bacterial picosecond fluorimetry obs. 79—92178
bacterial sensory electrophysiology, motility depend. on membrane pot. and chemotaxis 78—53373
bacterial single cells, bioluminesc. obs. 80—108860
bacterial suspension, physico-chem. changes on cooling, cell elec. cond. anal. 77—86458
bacteriochlorophyll absorption polarisation, in liq. cryst. cell 79—24950
barnacle photoreceptors, lateral vs. median, elec. props. and early receptor pots. 77—44651
baroreceptor Na sensitivity mediating reflex changes of blood press. and urine flow 77—48818
benzodiazepine receptors in brains of humans and animals, autoradiographic localisation 79—83752
binding, role of surface carbohydrates 78—15804
bioabsorbable polymers, standards for in vitro and in vivo comparison and qualification 78—3677
biochemical model, phase transition induced by external noise 79—17377
biochemical reactions, fast, in solns. membranes and cells, conf., Airlie, USA (Apr. 1978) 79—8485
bioelectrochemistry and bioenergetics (book) 80—8749
bioenergetics, entropy changes 80—3609
bioenergetics and proton-electron systems of membranes, review 78—96030
biomass determ. in immobilised cell biocatalyst by luminol assay for haem 79—66590
biopolymer negative resistance, rel. to living cell props. 78—64923
bipolar cell, catfish, receptive field and input signals 77—12921
Birbeck granule-containing cells of mice, occurrence of cored tubule 79—34515
birefringence analysis in biological materials 78—56954
bladder smooth muscle impulse propag., math. anal. *(Japanese)* 78—53359
blood, magnetic relax. time of H_2O protons 79—11898
blood, red cell flexibility, effect on blood flow through tubes of 30-500 μm 80—67111
blood, sickle cell, effect of deoxygenation on US absorpt. coeff. 78—44477
blood, sickle cell rheology, press.-flow curves 77—25503
blood, US propag., effects of red cell shape and orientation 78—24104
blood, viable cells, automated differential cell counting 79—74777
blood cell, red, Fe content anal. by electron microprobe and scanning electron microscopy 79—53065
blood cell aggregation, conductometric meas. 77—25614
blood cell damage in extracorporeal circulation, haemorheological effects of mech. factors 79—62280
blood cell K^+ ion X-ray absorpt. edge fine struct., frog 79—66459
blood cell leukocytes, automatic recognition and classification systems *(Italian)* 80—81780
blood cell membrane phospholipid asymm. rel. to coagulation 77—73511
blood cell preservation at low temps. 78—24043
blood cell profile direct meas. using SEM beam reference lines 78—81094
blood cell suspensions, deep-freezing improvements by thermal history automatic detect *(German)* 79—88215
blood cells, computerised spectral meas. 79—25058
blood coagulation and fibrinolysis under influence of direct elec. current 78—48766
blood exam. by scanning electron microscopy 79—74812
blood oxygenation simulation in stirred membrane cell 78—40421
blood red cell effect on blood flow velocity profiles in small tubes 79—25014
blood red cell shape, laser differential scatt. system for continuous monitoring 77—90873
blood red cells separation in vivo, transfusion therapy appl. 79—92190
blood rheology, erythrocyte rigidity effects on viscoelastic dilatancy 80—61610
blood white cells classification, automation using computer, expt. 78—3663
blue-green algae, absorpt. spectrum, struct. resolution 80—76715
bone, hydroxyapatite nucleation energetics 78—40127
bone, marrow and leucocyte preservative freezing apparatus 79—39617
bone tissue preservation, effect of treatment on chemilum., rel. to bone fragment transplantation 77—86709
Brumberg, Y.E., biographical note 79—75309
burst-generating neuron model, field effect transistor analogue 77—25411
bursting pacemaker neuron, internal Ca^{2+} changes meas. with arsenazo III 77—64021
cancer cell cycle kinetics, flow microfluorometric DNA distribution representation 77—21669
cancer chemotherapy, cell kinetics system model 79—48229
cancer problem cell kinetic study based on automatic control theory 77—40639
cancerous cell culture, phonons, long-range coherence, microwave effects 78—35816
cardiac cell membrane electrogenesis, selective adaption 79—57617
cardiac chemical power, appl. of power, work and efficiency eqns. to left ventricular energetics in man 80—16912
cardiac chemical power, derivation of chem. power eqn. and determ. of eqn. consts. 80—16911
cardiac injury potentials, inadequacy of solid angle formulation 77—44633
cardiac intracellular transmembrane action pots., automated anal. 79—70729
cardiac muscle model activation parameter behaviour, numerical study 78—11686

cellular biophysics continued
cardiac pacemaking, role of catecholamines 77—70437
cardiac tissue, pacemaker activity, phase resetting and annihilation 80—81565
carotid body, model for chemoreceptive process *(German)* 77—29162
cataract formation in vitro, rel. to protein synthesis control and intracellular Na^+/K^+ ratio 78—11646
cell analysis, high speed light scattering system 79—12042
cell division, model relating cell deformation to elastic props. of cell membrane 80—3606
cell division simulation, deform. of viscous droplet due to surfactant deposition 78—18876
cell size meas., laser flowthrough microphotometer, double-beam technique, internal calibrated 79—17391
cell size meas. by static light scatt. Fourier transform 80—81793
cell water polarized multilayer theory expt. confirmation 79—62213
cellular system growing, graph generation by parallel rewriting 79—66458
central axons, remyelination restores secure conduction 79—83753
cerebellar cortical current appl. rel. to underlying cellular activity 77—60195
cerebellum, neuronal organisation, informational capacity of Purkinje cell and climbing nuclear unit 77—25409
cerebral tissue, Ca^{2+} binding rel. to weak oscill. elec. fields 77—1984
cervical smear screening with coherent optical processing 77—21653
charged disk interactions in various dielectric media, biological cell modelling 78—66706
chemical reactions and ion transport in brown adipose tissue, network thermodynamics 78—92606
chemiluminescence of aldehyde-preserved plant tissues on exposure to salts of heavy metals 78—77160
chemoreception physics 78—15850
Chinese hamster cells, combined effects of hyperthermia and X-rays 80—45977
chlorella, delayed fluoresc., ns laser pulse excited, fast phase kinetic anal. 79—24951
chlorophyll, a and b, lowest singlet-singlet transition, solvent effects 79—24952
chlorophyll, energy migration between native forms at −196°C using sensitised fluoresc. 77—70429
chlorophyll a, fluoresc. and absorpt. spectra, resolution into components 79—57584
chlorophyll a delayed fluoresc. in absence of electron transport on acceptor side of photosystem 2 77—70428
chlorophyll a in photosynthetic material, luminesc. 79—34498
chlorophyll c absorpt., fluoresc. and fluoresc. excitation spectra in alga cell at −196°C 78—53329
chlorophyll in aqueous solns., electrochem. behaviour, cathodic reduction 79—29373
chlorophyll in leaves and algae cells, phosphorescence obs. 79—92142
chlorophyll monolayer electrodes, light energy conversion, photosynthesis electrochem. simulation 79—43833
chlorophyll-a arrays, exciton transition calculations 78—35802
chloroplast, bean, effect of salts on form of EPR II signal 78—64952
chloroplast, EPR signal II and Mn-water splitting, factors influencing stability 78—24038
chloroplast conformational variations study 79—92177
chloroplast conformational vars., auto-correl. anal. 80—30680
chloroplast fragments, paramagnetic centres and photochemical reactions 79—53061
chloroplast in intact cell of green alga Haematoccus pluvialis, fluoresc. 78—24037
chloroplast membrane proton gradient and osmotic vol. determ. 78—28143
chloroplast millisecond afterglow, activation and suppression 78—96025
chloroplast photosystems, exciton annihilation at 100K 77—25371
chloroplast-ribosomal RNA, in situ hybridisation with isolated nuclei in Euglena gracilis 79—66457
chloroplasts, bean, chromatic transitions of fluoresc. 77—25389
chloroplasts, EPR investigation of state of Mn^{2+} 78—69008
chloroplasts, in suspension, near IR radiation dispersion *(Russian)* 78—24045
chloroplasts, spin glass type structs., mag. anisotropy obs. 79—79490
chloroplasts and subchloroplast fractions, linear dichroism 77—90744
chloroplasts conformational fluctuations 79—53060
CHO cells exposed to hyperthermia, radiosensitivity and recovery from radiation damage 80—72250
CHO fibroblast, press., inhibited thermal killing obs. 80—81564
chromaffin granule electrophoretic mobility meas. by light scatt., effect of Ca^{2+} and Mg^{2+} 78—53357
chromatin, factors affecting the heat-induced increase in protein content 80—97882
chromatin packings, scanning microscope photometric image analysis *(German)* 79—5409
chromatin protein, increase kinetics for heated cells, possible role in cell killing 80—40980
chromatin structure of cell nuclei using scanning microphotometry and TV image anal. 79—34720
chromosome band online linear scanning, human, BANDSCAN computer program 78—92758
chromosome banding pattern technique, human, automatic classifying system 79—84062
chromosome classification system, banding technique 80—67320
chromosome classifying system based on banding technique 79—84060
chromosome density profiles, description and classification 79—43830
chromosome examination under light transmission microscope *(German)* 78—92685
chromosome identification, mammals, banding technique developments 77—56561
chromosome metaphase spread, automatic finding, prep. and eval. of object spectra 80—98168
chromosome size meas., fast karyotype approach 78—61153
chromosome spread automated detect. and classification 77—60328
chromosome-classification system based on banding technique 80—36199
chromosomes, banded human, contrast enhancing filter 78—92755
chromosomes, human, satellite associations 79—34518
cilia of mollusc, gill, effective stroke bending process 80—30756
clonal survival curves with cellular recovery, parameter fitting 77—56352
clone growth computer model 77—40643
cochlea hair cell tuning props. 77—64054
collagen fibril, ultrastruct. 79—48226

cellular biophysics continued
- collagen fibrils cholesteric analogue packing in Holothuria forskali 80—8035
- communicating cells, gap junction observed with electron microscope 80—45873
- compound eye of worker honey bee, cell junctions, electron microscopy 80—85383
- conditioned random walk, absorpt. time moments, appl. to tumour growth and multigene evolution 79—62165
- cones, superposition images formed by refl. in eyes of some oceanic decapod. crustacea 77—4997
- control system stability properties 77—40640
- cooperative behaviour, Bose condensation, Frohlich model 78—35797
- cortex ensemble distribution patterns in different functional states 77—48774
- Coulter electrical sizing principle, appl. to new multiparameter system 80—89911
- cryobiology, H_2O-NaCl-sucrose phase diagram 78—15777
- cultured cell obs., SEM STEM comparison 79—74801
- cultured cell time lapse cinemicrographs, computer-aided analysis 78—92756
- cylindrical cell with time-variant membrane resist., passive parameter meas. 77—29113
- cylindrical surface crystals in biological structures, dislocation interactions 78—95055
- cytochemical leucocyte differentiation and radioimmune assay *(German)* 79—5412
- Cytocomputer biomedical image analysis 79—92419
- cytogenetics, applications of photomicrography 80—21577
- cytological preparation evaluation, optical preliminary data reduction *(German)* 79—5392
- cytology, digital picture anal., in book 77—17962
- cytology, digital picture analysis 77—21650
- cytometry, fast flow-through, pattern recognition by light scatter meas. 79—88228
- cytomorphological contour classification for mass cancer screening 79—79682
- cytophotometric histogram, computer aided analysis of cell-cycle phase 78—92759
- cytophotometry, multiparametric pulse technique for cell and radiation research *(German)* 77—78060
- cytoplasm spherical drop with effective surface tension influenced by oscillating enzymatic reactions 80—108862
- cytoplasmic membranes in somatic cell interaction and hybridisation, review 78—15792
- cytoskeletal proteins of human erythrocyte, in vitro complex formation 79—96514
- cytosol-ribosomal RNA, in situ hybridisation with isolated nuclei in Euglena gracilis 79—66457
- cytotic processes of unicellular organisms, microcinematographic analysis 79—100800
- Deiter's cells of organ of Corti, well developed gap junctions 77—29155
- deoxygenated sickle cell blood, acoustical props. 78—3453
- diatom recognition and counting, matched-filter and statistical method 80—101304
- dielectrophoretic levitation, dynamic, of living individual cells 80—51062
- diffractometric method for meas. of cellular deformability 80—98187
- diploid cell culture mutation models 77—73514
- diploid fibroblasts, human, nuclear morphometry 79—43831
- discrimination of cells, paraxial anal. of light scatt. in flow system 79—11907
- disturbed cell renewal control system modelling and simulation 79—29510
- disturbed cell renewal systems, simulation by microprocessor system 80—35859
- division control by tension or diffusion 78—64962
- DNA distributions automatic processing and interpretation 78—92757
- DNA histograms from flow cytometry, program for anal. 80—41337
- DNA kinetoplast, ultrastruct., interpretation of dark field electron microscopy images of isolated purified networks 80—85369
- DNA natural storage of information, comparison with digital mag. recording 79—2009
- DNA strand breaking and rejoining in UV irrad. normal human and xeroderma pigmentation cells 77—4986
- double-barrel ion-sensitive microelectrodes, extra thin tip diameters, intracellular meas. appl. 80—101298
- dynamic receptor pattern generation model 79—62207
- E. coli, membrane struct. rearrangements in presence Ca^{2+} induced by heating 79—79482
- E. coli B, active, evidence for non-thermal excitation of energy levels 78—15800
- E. coli cells, anaerobic metabolism, ^{1}H correlation NMR spectra 79—43978
- E. coli cells, iron-storage protein, Mossbauer spectra obs. 80—8022
- E.coli strains in aq. suspension, polarisability anisotropy and aminoglycoside antibiotic effects 80—85441
- E.coli suspensions, dielec. anal., interfacial polarisation theory appl. 80—97876
- egg cell membrane elec. props 80—21455
- elastin ultrastruct., freeze-fracture electron microscopy 80—8036
- electric circuit model, alternating signal interaction 78—77011
- electric circuit model, alternating signal interaction 78—77012
- electric circuit representation of the cell, voltage gain 80—40977
- electric fields, extracellular, Fourier transform anal. 79—62223
- electrical control of development, review 77—86467
- electrical excitation of liver cells, DC 77—56565
- electrolyte localisation by electron probe microanal., freeze-substitution of plant and animal tissue 77—37115
- electromyographic electrodes, small-size, meas. of uptake area 79—74799
- electron microscopy, characterisation of cell membranes 80—104841
- electron microscopy symposium, Toledo, Ohio, USA (Aug. 1979) 80—82571
- electron transfer reaction energetic coupling to endergonic reactions, mol. mechanism 78—96026
- electrophoresis, medical appl., Zeiss rectangular chamber cytopherometer 77—13034
- electrophoretic analysis of cell suspension, Doppler spectra line shape smoothing 79—84053
- electrophysiological responses of Didinium nasutum to Paramecium capture and mechanical stimulation 80—56001

cellular biophysics continued
- electrotonic coupling, effective sign reversal by inhibitory neurons 77—29141
- ellipsometric monitoring of mol. and cellular biological processes in vitro 77—48852
- ellipsosomes in fish cones, ultrastruct. and staining props. 79—11924
- embryo, mouse, innocuous freezing during warming 80—94175
- embryonic skeletal muscle differentiation, electrophysiological and biochem. membrane props. 78—53363
- energy metabolism, ATP effect on initiator stage enzyme activity and conc. 78—64950
- energy metabolism, stoichiometric model, energy metabolism 77—36860
- energy transformation, intracellular, phys. aspects 77—86462
- epipelic biocenoses, self-cleaning capacity, water pollution abatement, fluorescence microscopy 79—79702
- epithelial cells of Hydra, mechanically dissociated, spontaneous and evoked pots. 77—21499
- epithelial tissue pattern recognition 79—25145
- epithelioid fibre system decoration by sera, immunofluorescence microscopy visualisation 78—15801
- epithelium, tight, impedance anal. using distributed resistance model 79—62201
- epithelium of small intestine, mech. props. of intercellular contacts 78—53351
- EPR of ^{125}IUdR-labelled and X-irrad. cells at 4.2K and above 80—72211
- EPR spectra of animal tissues in vitro, 13 to 43K, Fe-S proteins in mitochondria 77—16919
- erythrocyte, human, dynamic osmotic haemolysis and ghost repair, resistive pulse spectra 79—62208
- erythrocyte, human, steady rate of glycolysis rel. to ATP conc., quantitative model 78—53354
- erythrocyte, rheological models *(French)* 78—24083
- erythrocyte, sectioned, generalised theory of geometrical shape 78—65071
- erythrocyte, surface area and vol. calcs. from scanning electron micrographs 79—5259
- erythrocyte deformability, viscometric flow and laser diffractometric technique 78—35879
- erythrocyte deformation in centrifugal field 78—27976
- erythrocyte distribution profiles during sedimentation as determ. by HeNe laser light 80—81563
- erythrocyte flexibility, pharmacological effects, aging model *(German)* 79—79583
- erythrocyte ghost membrane, human, electron density, small-angle X-ray diffr. 77—73510
- erythrocyte ghost membrane struct. effects of fusogenic agent, fusion mechanism 78—31782
- erythrocyte ghosts, human, fusion promoted by Ca^{2+} and PO_4 ions 77—4987
- erythrocyte haemolysis, human, thermodynamic and kinetic model 79—92191
- erythrocyte high gradient magnetic separation 78—53585
- erythrocyte mechanical properties, determ. by US scatt. 77—81542
- erythrocyte membrane, carbocyanine dye orientation, microscopic fluorescence polarisation obs. 79—83694
- erythrocyte membrane, cooperative pH-sensitive state transition, Raman spectroscopy 77—36881
- erythrocyte membrane, phys. state of lipids, X-ray diffr. 78—80835
- erythrocyte membrane, viscoelastic props., theoretical and expt. studies 79—16157
- erythrocyte membrane alterations, rheological technique evaluation 80—61611
- erythrocyte membrane protein alterations in Huntington's disease, EPR 77—56347
- erythrocyte membrane struct. changes due to cAMP, spin-probe study 78—31779
- erythrocyte membrane viscoelastic props., area and vol. of cells entering micropipette 77—29114
- erythrocyte membranes, ESR study of abnormalities in Duchenne muscular dystrophy 78—96111
- erythrocyte membranes, interaction of lucensomycin with cholesterol, spectral parameters 77—9177
- erythrocyte nucleosomes, chicken, temp. dependence of ^{31}P-NMR spectra 80—94280
- erythrocyte osmotic fragility curve, statistical synthesis 78—65070
- erythrocyte survival after slow freezing in glycerol, temp. depend., human cells 78—77019
- erythrocyte thermal fragility, expt. obs. 79—62198
- erythrocytes, determ. of relative refractive index, dimensions and conc. from turbidity spectrum 79—79698
- erythrocytes, haemolysing action of u.s. 77—2019
- erythrocytes, human, cholesterol-loaded, rheological and kinetic dysfunctions 80—45867
- erythrocytes, human, haemoglobin's suspending medium, dielec. props. obs. 80—76716
- erythrocytes, membrane protein vertical displacement, rel. to microviscosity changes 77—44608
- erythrocytes, slowly frozen human cells, phys.-chem. basis of protection by glycerol 78—77020
- erythrocytes, surface area calc. method in elastic deform. 79—70571
- erythrocytes, technique for observing 3D dim. struct. with a cryo-SEM 78—92765
- erythrocytes, X-ray small-angle scatt. *(German)* 78—35812
- erythrocytes labelled with stable Rb, survival determ. by fluoresc. excitation anal., rabbits 80—81788
- erythrocytes of human blood, diameter meas. by specific elec. cond. 78—53353
- Escherichia coli, aq. colloid suspension, electrophoretic mobility and elec. polarisability 78—35813
- eukaryotic cell cycle, long-range dielec. aspects 80—94182
- eukaryotic cells, circular form of RNA in cytoplasm, electron microscopy 79—83703
- excitable cell model, numerical method 78—53376
- excitable medium self-sustained activity, role of inhomogeneity 78—64968
- excitable membrane analysis, computer calcs. 80—56004
- extracellular potentials generated by curved fibres in a vol. conductor, modelling 80—97889
- eye, bovine receptor cell outer segment, Ca^{2+}-depend. ATPase activity 77—29147

cellular biophysics continued
eye, direction-selective cells formation modelling in developing retina 80—30721
eye, rod outer segments, shedding behaviour under constant light, darkness 79—2050
eye crystalline lens, frog, elec. props. of struct. components 79—24982
eye slow cell responses in insects, colour adaptation 78—64988
fever and pasteurisation at supra-optimal temps. 79—62211
fibroblast DNA, damaged by UV or N-acetoxy-2-acetylaminofluorene, rate-limiting steps in excision repair 77—90865
fibroblast spread kinematics, population anal. 78—53352
fibrosarcoma cells, buoyant density, effect of hypoxic growth conditions in vitro 80—104601
filtering method for biomedical specimens, C-calculus appl. 79—84061
flow cytometry, fluoresc. polarisation meas., appl. to fluorescein in mammalian cells 77—52942
fluid distribution rel. to bioimpedance in living tissues 77—32879
fluid disturbances, compartmental anal. *(Japanese)* 80—3607
fluorescein, excitation and emission polarisation spectra, cell cycle changes 78—96013
fluorescein excitation and emission polarisation spectra obs., involvement of mitochondria 80—30683
fluorescence polarisation measurements in flow systems, epi-illumination optical design 80—89908
fluorescence polarisation of chlorella cells and pea chloroplasts orientated in a mag. field 80—51055
fluorescent probe interaction with surface structs. of E. coli 78—69007
fluorescently labelled molecules as probes of living cells struct. and function, review 80—67321
fluorometry, nanosec. system, appl. to biological samples at cell and tissue levels 77—17010
freeze conservation control unit *(German)* 79—5410
freeze fractured chicken erythrocyte nuclei, 3D view of chromatin 80—8229
freeze-fracture technique, appl. to study of animal plasma membranes 80—104842
freeze-fracture techniques and appls. in struct. anal. of mammalian plasma membranes, book contrib. 80—30960
frozen cell structure and function, freezing patterns and post-thaw survival 78—64960
frozen cells, mechanism of dehydration on thawing 77—81478
ganglion cell recordings from pigeon retina 79—57655
ganglion cells, adjacent, serial reconstruct. in the retina 80—89749
gap junction structure and cell coupling, Ca^{2+} effects 78—31786
genes, mouse, heavy chain immunoglobulin, nuclear transcripts 80—26208
genetic and physiological process control by magnetic methods *(Russian)* 79—2088
globin genes, human fetal, charact. of deletions of DNA 79—70519
glucose-deprived hypoxic cell killing with moderate hyperthermia 79—92157
green bacteria, resolution of absorpt. and fluoresc. spectra into components 78—20152
green-rod pigment of frog, Rana temporaria, long-lived photoproducts 77—25433
growth in vitro, rel. to cell surface, review 78—15808
growth regulation modelling 79—2014
haemolysis kinetics, US differential absorption meas. 77—77877
haemopoietic stem cell population and proliferation model 77—44610
hair cell, vertebrate, response to controlled mechanical stimuli 78—15852
hair cell voltage noise during mech. stimulation 77—90817
hair cells, inner, role of in hearing 79—43932
Halobacterium, Mossbauer spectrum of whole cells and ferredoxin, EPR spectrum of ferredoxin 78—76998
Halobacterium halobium membrane microstruct. 77—25386
heart adaptation to large loads structural changes simulation 79—5258
heart contractility, muscle tissue quality and sliding filament micromechanism *(Dutch)* 78—73171
heart muscle, behaviour of myosin projections during staircase phenomenon 78—53362
heart muscle cells, bivalve mollusc, fine structure 79—92188
heart muscle contraction simulation 77—12954
heart physiology, ^{31}P NMR investigations of metabolism, pH and contractile performance 78—69018
heart tissue and mitochondria, bovine, heterogeneity of N-2 Fe-S centres 77—86461
heat survival curves of normal and thermotolerant CHO cells, Arrhenius anal. 80—35849
HeLa cell nuclei protein content, effect of hyperthermia 80—40972
HeLa cells, high electron microscope autoradiography 78—36077
HeLa cells, hypothermic potentiation of radiation lethality 80—45978
hepatocytes, adhesive strength of ultrastructural elements 79—57682
histological and cytological reflection contrast microscopy 80—72389
host cell membranes in animal virus reproduction, review 78—15791
human carcinoma cells, binding and internalization of epidermal growth factor 79—92189
human red cell membranes, surface adsorpt. of dextrans 78—15799
human retinal image processing, two-channel model 80—94215
human serum and erythrocyte microwave complex permittivity meas. 80—3889
hydra, simple nervous system and behaviour 79—83738
hydrated cells, heavy ion microradiography with SEM imaging 79—16360
hydrocarbon carcinogenesis, fluoresc. meas. in cells 79—39343
hydrophobic effect, organisation of living matter 79—11887
hyperthermia effect on nonhistone proteins isolated with DNA 78—80843
hyperthermia lethality in mammalian cells under oxic and hypoxic conditions 78—40124
hyperthermia-induced lethality, 41 to 44°C, pH effect 77—64014
hyperthermia-induced sensitisation of tumour cells to antibody-complement cytotoxicity 80—104570
hyperthermia/radiation interaction, survival surface 78—11616
hyperthermia/radiation interaction, temp. coeff. of interaction 78—11617
hyperthermic cell death, influence of membrane lipid composition and procaine 78—27907
hyperthermic effect on ascites tumour cells in vitro, depend. on environmental pH 77—86465
hyperthermic tumour-cell devitalisation in vivo 77—70424
image anal. in cytology/cytogenetics, using Golay transform processor 78—61152

cellular biophysics continued
image processing, boundary trace transform: an edge and region enhancement transform 79—70713
image processing algorithm for distortion anal. 79—88229
image processing for identification of human chromosomes 79—62418
image segmentation using multispectral information 79—88224
immobilised enzyme systems, industrial appls. 79—29399
immune cell membrane receptors, rel. to memory *(German)* 77—66811
immunonephelometric assays 79—84046
impedance transient response characterisation 79—53066
intercellular junctions in FANFT-induced carcinomas of rat urinary bladder in tissue culture 80—8230
interference effects on observation of cells 79—84055
interference reflection microscopy, image interpretation theory and appl. to cells 79—80677
intestinal crypt cells, mouse, effect of local hyperthermia 79—88054
intracellular potential amplifier input capacitance determ. errors 77—60320
intracellular pressure measurement system 80—109084
intracellular recording from pulsating cerebral cortex 77—48960
intracellular water, effect of paramag. impurities on proton spin-lattice relax. 80—51134
ion localisation, plant tissue prep. by freeze-substitution 77—9309
ionic balance during cultivation of cell populations in a spatially homogeneous medium 80—81557
iontophoresis circuit isolated current monitor for cell membrane studies 77—60311
isopycnic centrifugation method for rapid separation of murine thymocytes 80—104832
kinetic parameters estimation from flow microfluorometry 78—73143
kinetic proofreading in biosynthetic pathways, thermodynamic constraints 80—108861
kinetics stochastic model using DNA microfluorometric data 79—83723
Krebs II ascites cells, subcellular localisation and paramag. props. of observed signals 80—108952
laser diagnostic irradiation of fluid-suspended cell flow 77—21594
laser diffractometer for rapid anal. of microparticles and biological cells 79—66589
laser Doppler meas., scattering characts. of intersecting beams *(Russian)* 80—3874
laser microirradiation for struct. and function investigation 79—66599
laser Raman spectra of living cells, review 80—56113
lateral geniculate nucleus, monkey, cell size changes in undeprived laminae after monocular closure 80—16927
lateral geniculate nucleus in cat, struct. of identified X and Y cells 80—26231
lateral geniculate nucleus in dark-reared cats, Y cell loss without cell size changes 80—3644
lecithin-water systems, bilayer connecting passages 78—96028
leucocyte, human, fluorochromed with acridine orange, spectral characts. 78—96024
leucocyte, PMR relax. times in peripheral blood of cancer patients 77—86579
leucocytes, differential counts, comparison between light and electron microscopic results 79—5429
leucocytes, radioactive-labelled, appl. for proof of inflammations 80—67218
leukaemia cells locomotion analysis 80—40983
light absorption and scattering, effect of struct. of three-layer spherical particles 78—31785
light absorption in non-homogeneous objects, sieve effect 79—22896
light scattered from microscopic regions, photon correlation spectroscopy 79—44933
light scattering, low-angle, from cell model, eikonal approx. 78—44466
light scattering by biological particles, shell and nucleus effect on indicatrix and polarisation 79—74608
light scattering from biological cells, backscatter depend. on membrane thickness and refr. index 79—48225
light scattering measurement with photodiode array, for biological cell anal. 78—28146
light scattering model, anomalous diffr. approx. 77—25396
light scattering problem, integral formulation, appl. to biological particles 78—63010
light single particle scattering, asphericity effects 79—7069
lipid bilayer membrane interaction forces in zone of contact 78—53345
lipid bodies, saturated, in organ pipe cactus visualisation by cytochem. technique 80—76873
lipid cell membranes, thermal structural rearrangements 79—92163
liquid crystal, lyotropic, form. in biological systems 77—86454
liquid crystal technological appls., role in biological systems *(Croatian)* 79—10788
liquid crystals in living and dying systems, review 77—44602
liver, Ca balance and cooperative electrogenesis, rat 79—57608
liver, rat, ion movements during energy-linked mitochondrial structural changes 80—12065
liver cells, rat, isolated, ^{31}P NMR studies 78—61150
liver cytochrome concentrations at different stages of cold adaptation 79—62196
liver growth protein metabolism and turnover, radiotracer obs. 79—88062
liver tissue, mouse, appearance of free radical centres on low temp. oxidation 78—69013
liver tissue and transplantable hepatoma, EPR spectrum and paramag. centre conc. 77—86459
liver tissue and tumour proton mag. relaxation rel. to Fe content 79—39355
living cell metabolism, laser Raman spectrosc. obs. *(German)* 79—29577
living cell volumetric changes in freezing and thawing, thermodynamic model and expt. 79—92192
lung cancer detection by Kr laser fibre-optic bronchoscope *(German)* 79—12024
lymphoblast automated morphological anal., subclassification of acute leukaemia 77—81620
lymphocyte cultures, human, heat prod. meas. with flow microcalorimeter 77—81473
lymphocyte surface morphology, human, SEM obs., review 78—53599
lymphocytes, Quantimet 720 meas. of proportion of actively growing cells 79—74606
lymphocytes exposed to temps. of 37-45°C, two types of interface death 80—104566
lyophilisation, effect on free radical states of animal cells 77—25391

cellular biophysics continued
lysosomal hyperthermic response rel. to heat-induced thermal resistance 79—57595
magnetic field effects, 5000 Oe, morphological and physiological transform. of mammalian cells 77—21500
malignant cells, evidence for a condensed phonon state 79—62214
malignant transformations, optical detect. of cell-surface changes 79—79703
mammalian cell culture, thermal sensitivity rel. to cholesterol level 80—51058
mammalian cell line sensitivities to hyperthermia, γ-rays and UV 77—66800
mammalian cell membranes, plasma membrane responses, book 78—15787
mammalian cell membranes and cellular functions, book 78—15784
mammalian cells, interactions with liposomes, review, book contrib. 79—5261
mammalian cells, NMR relax. time meas. of bulk water 80—21454
mammalian surface membrane turnover, review 78—15788
mammary tumours, paramagnetic changes during development in rat 79—39425
mammographic US image correlation with histopathologic sections 80—101240
marrow cells, SEM and optical microscope correlation before and after culture 79—74605
mechanical calorimetry of red cell membranes 80—45854
mechano-sensory receptor of crayfish stretch receptor organ, effect of D_2O 77—44696
mechanoreception, Millipore-DOPH model membrane showing excitation with press. stimulus *(Japanese)* 78—3526
mediastinal lymphoscintigraphy, use in observing cell kinetics of developing malignant ascites 79—92176
medical image structural analysis, fast feature extraction *(German)* 79—5393
medically relevant class determ., scatt. light cluster anal., cervical smear tests *(German)* 78—92686
medullary interneurons of goldfish, elec. and chem. inhibition in vertebrate central nervous system 77—36911
megakaryocytes, guinea pig, membrane elec. responses 78—44472
membrane, elec. excitable, phys. model, excitation mechanism 77—36902
membrane asymmetry, review 77—48768
membrane electric properties measurement method using glass electrode impaled into single cell 80—89916
membrane energetics, conf., Bloomfields Hills, USA (Jul. 1979) 80—94923
membrane fluidity modification, mechanism of hyperthermic cell killing and therapy appl. 80—104569
membrane fluidity of fatty acid auxotroph, EPR study 79—70574
membrane interaction theory of molecular level mechanics 79—92174
membrane nuclear hydrodynamic shear, non-equil. Ising model, master eqn. 78—61146
membrane particle diameters meas. by computer from electron micrographs 80—101307
membrane particles diameter meas. via picture processing 79—84065
membrane phase transitions 78—35808
membrane potential generation by submitochondrial particles, direct meas. 80—35852
membrane potential levels in Acetabularia 77—70427
membrane properties, influence of solute environment, review 78—15789
membrane regulation of cell cycle, mathematical model 79—92180
membrane slide support for living cell microscopic obs. 79—74809
membrane structure and solute transport, review of current ideas 77—32878
membrane suspension physiology and induced pathophysiology, noninvasive analysis using EM method 79—2125
membrane thermal fluctuations and mechanoreception problem 79—53057
membrane ultrastructure rel. to function, review 78—15785
membrane-covered cubes in cubic array at high conc., analogue soln. of elec. capacity 77—40642
membranes, effects of hydrostatic pressure, review 78—15790
membranes and energy control, review 78—15807
memory of temporal sequences, model, simulation studies 77—9181
metabolism intensity relation with embryonic cell determ. process 80—85367
metabolism regulation, conformational phase transitions in macromolecule adsorption on charged surface 77—19118
Methanobacterium thermoautotrophicum, DNA organisation, evolutionary implications 80—30686
microalgae, correl. of light scatt. patterns from pure and mixed asynchronous cultures 78—44737
microbe thermistor for metabolite anal. 77—78063
microbial cell vibratory spectra, interpretation 77—70425
microbial prod. of tritiated and ^{14}C methane from radioactive waste 80—45868
microcalorimetry of isolated cells of mammalian brown adipose tissue 77—56343
microdosimetry, role in radiobiology 80—61705
microelectrodes, Na-selective liquid ion-exchanger, for intracellular meas. 80—3888
microorganisms, lack of intracellular bubble formation at very high gas supersaturations 80—81562
micropipettes of very low resistance for intracellular meas., production method 80—61738
microscope bidirectional illumination and viewing, living cells 80—51304
microscope-photometer for visible region absorpt. of single living cell *(German)* 79—66588
microscopic cell images classification by feature extraction 79—88225
microscopic image anal. system, cell cycle, cancerous blood and bone marrow cells appls. 79—88223
microscopic images, computer processing *(Japanese)* 79—39373
microtubule structure, temp. depend. 78—85288
microwave dielectric properties of tissue, rel. to rot. mobility of tissue water 77—29092
mitochondria, absorbance changes after ADP addition, rel. to ATP synthesis 78—27908
mitochondria, energetic state indication using pyronin dye fluoresc. 77—66790
mitochondria, giant, elec. props. study by double impalement technique 79—92446
mitochondria, interaction of cationic dyes, absorpt. spectra 77—52752

cellular biophysics continued
mitochondria and submitochondrial fragments by high resolution NMR 77—16918
mitochondria and submitochondrial particle membrane pot. generation in anaerobic conditions 78—69015
mitochondria in rat liver and monkey cardiac muscle, SEM obs. 79—34516
mitochondria membrane Ca^{2+} interaction, influence of oestrogens 78—53349
mitochondria of bovine heart, EPR investigation of two forms of Fe-S centre N-2 78—69014
mitochondria phosphorylation and respiration, EPR 78—31784
mitochondrial cytochrome b, evidence for two or more components 79—24944
mitochondrial DNA, nucleotide sequence in human, replication origin identification 79—29502
mitochondrial inner membrane, ribbon struct. 78—11618
mitochondrial membrane pot., respiratory chain study by method of penetrating ions 78—64951
mitochondrial membrane potential meas. with microelectrodes 77—48769
mitochondrial permeability, transport and energy-coupling processes, effect of fatty acids and acyl-CoA 77—21498
mitochondrial regulators, membrane-active 77—25397
mitosis, spherical reaction diffusion systems, steady state spatial patterns, secondary bifurcation theory 80—40672
mitotic aortic cells of swine, origin and fate of paired cisternae 79—74604
mitotic growth of cell systems, model 78—11619
molecular computer, coding during intracellular processes of information processing 77—70400
monoamine-containing neurone connectivity in leech central nervous system 77—44639
monochromatic coherent plane wave scatt. by living cell *(Russian)* 78—48765
morphogenesis model 79—83722
morphological parameters extraction from diffr. pattern of cells, Fourier optical approach 78—92749
morphology transformation by UV, effect of X-irrad. and chem. carcinogens 77—1981
morphometric cytology pictorial pattern recognition appl. 79—25179
motoneuron firing rates with strong random synaptic excitation 77—9184
motorneurons of different geometry and size principle 77—36908
multicell spheroid cycling, noncycling, and hypoxic cell response to hyperthermia 79—92156
multicellular development growth, L system strategy 78—27906
multiplication regulation in normal and transformed cells, role of Ca^{2+} and Mg^{2+} 79—2012
multispike train, anal. techniques 77—44868
muscle, active frog skeletal, isometric tension, slow stretch effect, X-ray diffr. study 78—80906
muscle, Ca transients in frog slow muscle fibres 77—77892
muscle, cell surface, heterogeneity of acetylcholine receptor molecules 80—16910
muscle, cross-striated, effect of uncouplers of oxidative phosphorylation on conc. of ATP 78—20149
muscle, cross-striated, mol. mechanisms of sarcomere struct. reorganisation in contraction 77—81462
muscle, excitation-contraction coupling in voltage-clamped cut skeletal fibres, rel. to transparency 77—29138
muscle, fast and slow myosin in developing fibres 78—64961
muscle, force-length relations of glycerinated rabbit psoas 77—48828
muscle, frog, spin-lattice relax. times for ^{13}C in isotope-enriched glycine 77—44605
muscle, frog, spin-spin relax. times rel. to temp. and water content 78—56952
muscle, frog, vacuolation and subcellular comp. in fatigue, electron probe anal. 79—24963
muscle, glycerinated fibres, filament overlap rel. to number of Ca binding sites 78—44465
muscle, glycerol-extracted fibrillar fibres, cross-bridge slippage induced by AMP-PNP and stretch 78—77075
muscle, insect, chemo-mech. coupling in oscillatory contraction-relax. cycles 77—48829
muscle, isometric contractile props. of single isolated smooth muscle cells 77—29137
muscle, mechanochem. contractile system as thermodynamic machine 78—20201
muscle, mouse, ^{13}C NMR and PMR 77—86463
muscle, multifibre preparation, intercellular clefts influence on pot. and current distrib. 80—72145
muscle, myosin regulated, changes in crossbridge attachment 78—53361
muscle, myosin subfragment-1 attachment to actin, effect on equatorial X-ray refls. 78—27880
muscle, of barnacle, transverse nucl. mag. reson. relax., bounds on bound water 77—4989
muscle, of guinea pig, force-vel. characts. for Ca-activated slow- and fast-twitch skeletal fibres 77—44643
muscle, skeletal, birefringence signals rel. to Ca transients 78—24041
muscle, skeletal, bond graph simulation of glucose metabolism 77—36894
muscle, skeletal, effect of stretch on EMF *(Japanese)* 77—36886
muscle, skeletal, intact, energy transduction depend. on time in tension 77—52754
muscle, skeletal, IR spectra of mitochondria and endoplasmic reticulum 77—70434
muscle, skeletal, K-contractures and membrane pot., rat 77—29117
muscle, skeletal, Na relaxation, spin echo study, evidence of Na ion binding inside a biological cell 78—88698
muscle, skeletal, quantitative model of actin-myosin interaction 77—52753
muscle, skeletal, tension development, F-actin subunits struct. non-equiv. model 78—64959
muscle, smooth, cell plasma membrane, inhomogenous distrib. of filipin-sterol complexes 79—83720
muscle, smooth, effect of hyperosmolar soln. on elec. connections between cells 78—69027
muscle, striated, mol. basis of force development 78—40126
muscle, striated, reversible loss of Ca control of tension assoc. with removal of regulatory light chains, scallop 78—53360
muscle, tryptophan fluorescence polarisation 80—97877
muscle, vertebrate striated, thick filament linked Ca^{2+} regulation 78—69020

cellular biophysics continued
  muscle cell cultures, skeletal, myosin synthesis increased by elec. stimulation 77—1988
  muscle cell cultures biology, book contrib. 79—2031
  muscle cell membrane fluidity rel. to fusion 77—77873
  muscle chemomechanical energy transduction, mol. basis 80—72143
  muscle contraction, elementary catastrophe theory model, reliability anal. 78—44471
  muscle contraction, protofibril reciprocal sliding and thick filament shortening 77—56331
  muscle contraction cross-bridge model 78—44475
  muscle contraction kinetics, 3-state model 78—48769
  muscle cross bridge rotation during contraction, fluctuations in polarised fluoresc. 80—97856
  muscle crossbridge stroke and activity revealed by optical diffr. 78—69021
  muscle dynamic stiffness rel. to crossbridge action 78—48819
  muscle exponential rate processes rel. to MgATP conc., head rot. and dissoc. 78—44468
  muscle fibre, skeletal, helicoids in T system and striations, HV electron microscopy 78—53356
  muscle fibre tension fluctuation meas. during contraction 78—20153
  muscle fibres, Ca^{2+}-activated, effect of MgATP on stiffness meas. at 5 and 100 Hz 78—48822
  muscle fibres, computed extracellular pots. 79—43843
  muscle fibres, computed extracellular pots. 79—74620
  muscle fibres, fibrillar, tension transients affected by stretch-dependent binding of AMP-PNP 79—20562
  muscle fibres, rabbit psoas, stiffness and tension after sudden length changes 79—25007
  muscle fibres, skinned, swelling 77—73513
  muscle fibres, slow and twitch type, of frog, contractile activation 77—32884
  muscle mechanics thermodynamic model 78—80908
  muscle membrane, skeletal, lanthanide ionic radius selecting 78—24042
  muscle model ultra-relaxation in medium with high Ca ion conc. on exposure to MgATP 77—25388
  muscle power flows, bond graph model 79—92260
  muscle single fibres, Rb^+, Cs^+ and Na^+ localisation, autoradiographic demonstration at 77K 79—96726
  muscle water proton and deuteron relax. over wide ranges of reson freqs. 77—52740
  muscle water transverse and longit. NMR relax. rates 78—35810
  muscle-tendon junction strength, ultrastruct. elements 77—25485
  muscles, smooth, of elastic arteries, biophys. props. 78—69011
  muscular strength, relationship with muscle energy sources, Wistar rat 79—11904
  mutation theory, physical model of genetic stability 79—8486
  myelin sheath, thickness irregularities distrib., paracryst. struct. 77—12892
  myocardial cell transmembrane potential QRS-T wave simulation *(Japanese)* 77—90740
  myocardial cells, cats, improved techniques for studying surface topography by SEM 79—34712
  myocardial energy status, ^{31}P NMR of perfused working rat hearts 77—29236
  myocardial fibre accommodation, role of incoming currents 77—36898
  myocardial multicellular preps., voltage clamping methods 79—84056
  myocardium mitochondria lipid composition and phase transitions rel. to depth of hypothermia, rats and dogs 78—53350
  myoepithelial cells, SEM examination 79—34713
  myosin, struct. and functional changes in chronic cardiac insufficiency 77—36887
  nerve cell cultures biology, book contrib. 79—2031
  nerve cell kinetics, appl. of Interactive Simulation Language 77—21507
  nerve cell membrane detection of HF EM fields, possibility discussion *(Russian)* 80—76785
  nerve cell unitary discharge automatic recognition *(French)* 77—37072
  nerve conduction in squid axon, Hodgkin-Huxley equations, large amplitude periodic solns. 78—20166
  nerve fibres, mammalian, demyelinated, continuous cond. 77—4995
  nerve membranes, cell excitation detect. using birefringence changes *(Japanese)* 77—66876
  nerve presynaptic terminals, ATP-depend. Ca storage 77—29126
  neural inhibitory network, probabilistic and stochastic anal. *(Japanese)* 79—39410
  neural nets, rhythmic movement generation, lobster, leach, book contrib. 79—5273
  neural structure histological exam., Epon block sectioning technique 79—74814
  neuroblastoma tumour, thermal conductivity and diffusivity meas. 79—5252
  neuromuscular transmission, prejunctional role of cyclic nucleotides 77—1987
  neuron firing rate meas. by freq.-to-voltage converter 79—70715
  neuron hydrodynamics, numerical methods for creeping flow investigation 77—5019
  neuron inhibitory synapse, influence of presynaptic irregularity on action pots., stretch receptor 77—9185
  neuron multi-input model diffusion approx. 77—29135
  neuron response to stationary and moving visual stimuli, cat superior colliculus 79—43893
  neuron soma model with high reliability and low power consumption 80—72392
  neuron with shunting inhibition, stochastic modelling 77—9183
  neuronal activity firing pattern evoked by monosynaptic inputs, stochastic model 77—29134
  neuronal average firing frequencies, digital display 77—5117
  neuronal models, spike trains, and the inverse problem 77—52764
  neuronal population density estimation, robust distance method 79—70721
  neuronal units in cortical projection area of vagus nerve, discharge during hypoxia 77—25407
  neurone compartmental chain model membrane voltage changes 77—29124
  neurones, visual cortex, pattern-selective adaptation, cats 79—53090
  neurons, cat, cytoplasmic laminar body identification by phase contrast microscopy 79—48385
  neurons, cat eye, stereotaxic method for recording from single cells 80—89913
  neurons, developing, optimal stimulus distrib. model 77—25419

cellular biophysics continued
  neurons, harmonic-sensitive, mustache bat auditory cortex 79—43933
  neurons, section embedding technique for sequential light and electron microscopic exam. 80—67317
  neurosecretory cell IR photomicrography 80—30959
  neurotransmitter synthesis and uptake by isolated sympathetic neurones in microcultures 78—7333
  neutrophils rabbit, chemotactic factor-induced release of membrane Ca 79—88095
  Nitella, fluctuation and instability in membrane pot. near threshold 80—89723
  NMR, pulsed, of ^{39}K in frog striated muscle 77—16920
  NMR, simultaneous multinucl., by alternate scan recording of ^{31}P and ^{13}C spectra 80—26426
  NMR applications, ^{31}P and ^{13}C studies 80—46110
  NMR intensity of ^{23}Na in rat liver homogenate, effects of alkali cations 77—12893
  NMR of ^{31}P for anal. of living tissue 77—37117
  NMR of H_2O, classical diffusion to explain 'H spin relax. 79—83721
  Noble model, spread of excitation through node of branching 77—16899
  normal and tumour-like cell growth model 77—12894
  nuclear fibre framework in interphase nucleus *(Chinese)* 79—92187
  nuclei and tissue denaturing process, cooperative charact. 79—57593
  nuclei structural change in the physiological pH interval 79—79492
  ocellus of phalangium opilio, electrical response 79—53095
  oedema resulting from reduced efficiency of cellular membranes at low body temp. 77—29225
  oocyte membrane, existence of acetylcholine receptor 78—24040
  oocyte paracrystalline structs., mouse, Mus cervicolor poppaeus 80—89731
  optic nerve fine structure in lamprey 77—60201
  optical analysis system for agar-cultured micro-organism colonies, microcomputer-based 80—56304
  optical device for time lapse studies in vitro *(German)* 79—74813
  optical microscopy, cell deposition system for deposition at predefined locations on microscopic slide 80—76876
  organelle lipid anti-radical activity change due to freezing at −78 and −196°C 77—70426
  organelles, SEM of thick sections etched by O plasma 80—21584
  oscillatory biochemical model, spatial differentiation 78—44476
  osmotic pressure effect on contacts and surface of liver cells 77—56354
  oxidative phosphorylation, role of respiratory chain 78—15795
  oxidative phosphorylation mechanism, depend. of functional indices on mitochondrial incubation medium 78—69009
  oxidative phosphorylation mechanism, nature of residual current 78—20151
  oxidative phosphorylation mechanism, role of closed condition of mitochondrial membranes 78—77013
  pacemaker transmembrane potential generation in fish heart sinoatrial cells 79—39395
  pancreatic acinar cell stimulus-secretion coupling, fluoresc. probe detect. of cell Ca redistrib. 77—77872
  pancreatic acinar cells, acetylcholine null pot., mouse 77—4988
  pancreatic acinar cells, acetylcholine-like effects of intracellular Ca^{2+} appl. 77—66801
  pancreatic islet cells, plateau pots. as voltage-dependent action pots. 80—94180
  pap smear inspection, segmentation approach 80—8124
  papillary muscle fibres, rabbit, effect of preliminary stimulation on repeat responses 78—48768
  paramagnetic centres in lyophilised animal tissues 80—30681
  Paramecium membrane potential changes during chemokinesis 80—26209
  parastriate cortex, cat, rabbit, selective response of single units 79—74624
  pattern formation in Gierer Meinhardt morphogenesis model 79—62210
  pea roots, circadian rhythms of ultra-weak chemiluminesc. 77—70432
  peripheral polymorphonuclear leucocyte system model, humans 78—56956
  Petri dish autoradiographed cell counter 79—70723
  phospholipid membrane thermotropic transitions rel. to fusion and endocytosis 77—48765
  phosphorescence microscopy 78—3454
  photoactive complexes of chlorophyll precursor, energy migration, and spectroscopic characts. of pigmnets 77—36889
  photodiode camera improvement of shading correction 80—56325
  photon emission from biological systems *(German)* 79—96527
  photoreceptor, Drosophila mutant with phototransduction defect 77—90777
  photoreceptor form dichroism in vertebrates 78—56969
  photoreceptor membrane, protein-lipid interactions on peroxide oxidation of lipids 77—21522
  photoreceptor membrane rhodopsin orientation model 77—90775
  photoreceptor mutant of Drosophila, protein role in intermediate steps of phototransduction 77—48799
  photoreceptor potentials rel. to charge displacements of rhodopsin in model membranes 77—52785
  photoreceptor sensitising pigment, fly 77—90796
  photoreceptor transduction mechanism, conf., Julich, Germany, Oct., (1976) 77—90774
  photoreceptors, arthropod, prolonged light-induced cond. change on recovery from anoxia 77—12915
  photoreceptors, Limulus ventral eye, effects of removing extracellular Ca^{2+} on excitation and adaptation 77—9190
  photosynthesis, biophysical processes, review 78—92605
  photosynthesis, electron path across membrane rel. to chlorophyll 77—44607
  photosynthesis, picosecond relax. meas., book contrib. 77—64166
  photosynthesis, role of phycobilin pigments 78—48752
  photosynthesis, use of picosecond lasers 77—81480
  photosynthesis measurements in wheat using IR analyser and Geiger counter *(German)* 77—70436
  photosynthesis of higher plants, energy migration and electron transport 78—20150
  photosynthetic electron transport in isolated chloroplasts, effects of purine nucleotides 77—64013
  photosynthetic membrane, optical and electrochromic props., chloroplast chlorophyll orientation 77—48763
  photosynthetic membranes, supramolecular organisation model based on freeze-fracture electron microscopy 77—29106
  photosynthetic reaction centres, dark reduction kinetics of photo-oxidised bacteriochlorophyll P870 77—36888

cellular biophysics continued
photosynthetic systems, magnetoorientated, fluorescence polarisation theory 79—16165
photosynthetic unit, bimol. quenching of excitons and fluoresc. 77—16908
photosystem I of higher plants, model of donor-acceptor energy transfer *(Ukrainian)* 77—70435
physicochemical properties of intra- and extra-cellular media at low temps., effect of non-electrolytes 78—53355
pigmented biomembranes, photoelec. and magneto-orientation effects, review 77—48766
plant cell wall and cytoplasm refr. index determ. by interference microscopy 78—57151
plant cell walls, viscoelastic props., hysteresis loop in the stress-strain curve 79—25009
plant cell walls, viscoelastic props., mathematical formulation for stress relax. 79—25008
plant cell walls, viscoelastic props., pre-extension rate effect on stress relax 79—29542
plant cell walls, viscoelastic props. 80—67106
plant roots extracellular chemiluminescence obs. 79—70534
plant tissues, herbicidal activity of N_1-aryl-N_2-alkyl thioureas, structure relationships 79—62176
platelet adhesion to solid surfaces, effects of plasma proteins and substrate wettability 78—35814
pneumocytes, isolated type II, effects of high O_2 exposure on bioenergetics 80—30685
pollutant exposure, effect of chem. variability of fly ash particles 79—16172
poly (N^{α},N^{ϵ}-terephthaloyl-L-lysine) membrane for artificial red blood cells, interaction with serum proteins *(Japanese)* 80—12061
population auto-activation, math. model 78—77017
population auto-oscillations, influence of delay 77—36892
populations exposed to supraphysiological temp., haemolysis time history 80—35850
Porphyridium cruentum, energy transfer efficiency from photosystem II to photosystem I 77—40641
presynaptic facilitation as mechanism for behavioural sensitisation in Aplysia 77—36912
prokaryote epigenetic control mechanisms, distributed model 77—77879
protein synthesis mechanisms, genetic codes 77—56353
proteins, UV fluorescence detect. of conformational rearrangements in plants 79—53031
Purkinje cells of cerebellar cortex, histogram analysis of interpulse intervals 78—96042
Purkinje terminal electrical connection with muscle fibres in canine ventricle 77—86460
purple membrane, of Halobacterium halobium chromophore excitonic interaction, protein location 77—21497
purple membrane of H.halobium, bacteriorhodopsin luminesc. 77—36890
quantitative microscopy, object delineation program 80—41338
R. spheroides, triplet state electron spin echoes, fluoresc. detection 78—70856
radiation dose of labeled neutrophils and platelets 79—100749
Raman scattering, enhanced anti-Stokes, of C. pyrenoidosa living cells 79—16171
random effects in tracer and cell cycle kinetics 78—44445
reactive polymers, for enzyme immobilised enzymes 79—29398
red blood cell, human, axial trajectory meas. in high-gradient magnetic separation 79—53165
red blood cell aggregation detect. during blood flow by US 79—84068
red blood cell diameter meas. from He-Ne laser beam diffr. pattern 77—86582
red blood cell elastic deforms. 77—56400
red blood cell ghosts, light scatt., ang. depend. struct. 77—81475
red blood cell membrane, surface tension and deform. rel. to 2-D phase transform. 77—1980
red blood cell orientation, effect on elec. impedance *(Japanese)* 80—21513
red blood cell plasma membrane, Ca^{2+} transport stimulation by calmodulin 80—12066
red blood cell sizing, evaluation of automated Electrozone Celloscope in haemolysis study 78—40455
red blood cell suspensions, haemoglobin NMR relax., T_1 and T_2 meas. 78—80832
red blood cells, ^{99m}Tc labelling 80—41236
red blood cells, equilib. shapes in osmotic swelling 80—85368
red blood cells, in vivo labelling with ^{99m}Tc with stannous pyridoxylideneaminates 80—46049
red blood cells, minimum energy anal. of membrane deform. 80—72141
red blood cells, type O, using optical system for light scatt. expts. 79—76786
red blood cells of thalassemia, sickle-cell anaemia, and haemoglobin Hammersmith, ferritin-like Fe, Mossbauer study 80—8018
red blood cells ultrafiltration technique for labelling with ^{99m}Tc 80—51243
red cell haemolysis rates in subsec. to sec. range, normal human cells 78—15796
red cell membrane, human, surface elasticity and viscosity 80—61608
red cell membrane, temp. dependence of viscoelastic recovery 80—40979
red cell membrane protein monolayers, viscoelastic props. 79—48224
red cell suspensions, backscatt. of light 80—41107
red cell-hydrocarbon surface long-range attraction 77—77874
resin-embedded unicellular organism preparation for ultrathin sectioning 79—70724
resting pot., eqns. according to surface adsorption theory 80—35861
retina, cephalopod, extracellularly-recorded photoreceptor pots. 79—62245
retina, cephalopod, intra and extracellular pots. obs., dark adaption dynamics 79—79541
retina, frog, morphometric anal. of internal horizontal cells 80—108892
retina, goldfish, X-like and not X-like cells obs. 79—43837
retina, inner, of teleosts and reptiles, proximal negative response 77—21521
retina, light-adapted, of carp, intercellular junctions between pigmentary epithelium and cones *(French)* 77—12911
retina, of river lamprey, electroretinogram recordings 77—60205
retina, pigeon, extensive lateral transmission in inner plexiform layer 77—48794
retina electrical activity and lipid peroxidation 79—43885

cellular biophysics continued
retina of developing frog eye, free radical reactions rel. to mitosis, daily vars. 77—56376
retina of turtle, horizontal cells influence on bipolar cells' membrane pot. 78—88708
retina outer plexiform layer lateral interactions after atropine block of horizontal cells, turtle 77—70457
retina physiology, single cell studies on lower vertebrates, book contrib. 79—96558
retina receptor layer current spatial distribution, frog, electrical model 77—40666
retinal cell sensitivity to movement of stimuli and flickers, histochem., frog 77—86490
retinal cone chromatic organisation, baboon, using light-stimulated NBT reduction 77—64031
retinal ganglion cell functional pathways, book contrib. 79—96559
retinal ganglion cell responses in dark-reared rats 79—53102
retinal ganglion cell responses to flashing and moving stimuli, mudpuppy 77—12917
retinal ganglion cells, abnormal response in Siamese cats 77—90785
retinal ganglion cells, bovine, size and distrib. 79—100596
retinal ganglion cells, frog, species differences in optimal stimulus sizes 77—21519
retinal ganglion cells, mudpuppy, hyperpolarising ON/OFF responses 77—25427
retinal ganglion cells, struct. basis for on- and off-centre responses 77—1997
retinal ganglion cells action pots., goldfish, function of lighting conditions 79—43888
retinal ganglion cells of 3 week old kittens, physiological props. 77—36922
retinal ganglion cells of pigeon, concentric receptive fields 77—44653
retinal horizontal cell reaction to non-uniform illum., model 77—56375
retinal horizontal cells, amplification of graded pots. 77—32889
retinal light responses, simultaneous recording by extra- and intracellular electrodes in crayfish 78—69055
retinal neuronal network of photoreceptors and horizontal cells 78—3482
retinal neurones, differential labelling by ^{3}H-2-deoxyglucose 79—92447
retinal photoreceptor and horizontal cell synaptic connections 77—90787
retinal pigment epithelium, defective phagocytosis of isolated rod outer segments RCS rat cells 78—11647
retinal rod discs, intradiscal surface, photoreceptor membrane carbohydrate 77—4998
retinal rod external segment mag. anisotropy decrease after total photolysis 77—52838
retinal rod outer segment membranes and liposomes of extracted phospholipids, proton spin-lattice relax. rates 77—90782
retinal rod outer segments, presence of Lubrol activated latent Na^+, K^+-ATPase 77—12920
retinal rod photoreceptor membrane orientation in intact eye, X-ray diffr. 77—48790
retinula cell response properties, fly 77—44658
retinular cells, arthropod, light-induced membrane cond. change rel. to membrane pot. 77—5001
rhodopseudomonas sphaeroides, reaction centre triplet state fluoresc. mag. field depend. 78—53358
rhythmic heart-cell clusters, fluctuations in interbeat interval, membrane voltage noise role 80—30705
ribosomal particles, electron microscopic investigation using tilting technique 79—34514
ribosome subparticle fine struct. investigation by optical filtration of electron microscope images 80—81779
ribosomes of Escherichia coli, partially deuterated subunit, protein and RNA distrib., neutron scatt. 78—77021
rigidity increase of material of bioconstructs. during morphogenesis 80—94249
tRNA, genetic code origin, kinetic proofreading 79—92126
RNA, spliced viral messenger 79—92175
rod, amphibian, dark adaptation processes 78—15835
rod external segment membrane, phospholipid auto-oxidation during conform. changes 77—21523
rod outer segment, Rana pipiens, birefringence meas. of struct. inhomogeneities 78—77048
rod outer segments, intact, GTP hydrolysis rel. to transmitter cycle in visual excitation 79—83773
rod photoreceptor model sensitivity, depend. on level of background light intensity 78—20179
sarcomere dynamics in single skeletal muscle fibre, light diffr. spectra 78—15797
sarcomere shortening in striated muscle, stepwise pattern 77—77893
sarcoplasmic reticulum hydrated oriented multilayers, lamellar X-ray diffr. 78—11614
SEM visualization method for concanavalin A receptors on lymphoid cells 79—74800
separation of living cells, local conc. gradient determ. by conductivity meas. *(German)* 79—5411
serial section models of human lung endothelial cell nuclei, estimation of mean caliper diameter 79—29679
serial section models of rat lung cell nuclei, estimation of mean caliper diameter 79—25165
sickle cell anaemia sickling kinetics, multiangle laser scatt. spectrophotometer 79—79494
single motor unit, recording during strong effort 79—11908
size analysis of single particles in flow, appl. of differential light scatt. photometer 80—77834
size and shape of cells, light scatt. photometry compared with microscopy for meas. 79—84030
skeletal muscle fibre with helicoidal T system, linear elec. props. 78—80852
skin response to heat alone or with X-rays, mouse ear 78—27902
small intestine, mouse, transient heat-induced thermal resistance, crypt survival assay 80—108850
smooth muscle, single isolated cell, Ca^{2+} indicator aequorin luminesc. during activation 79—88064
solid tumour growth model, apoptosis as volume loss mechanism 78—96027
space research, biology and medicine 80—41265
spermatozoa, bull, laser light-scatt. studies, orientational effects 80—89786
spherical three-layer particles as cell models, light scatt. and attenuation, shell effect 78—82913

cellular biophysics continued
- spin labels and biomembranes, review 78—69265
- spinal cord, transient synapses in the embryonic primate 79—74623
- spirostomum, mag. field effects on drug induced contractility and mortality 79—74607
- stereological method for estimating relative membrane surface area 77—64158
- stereology conference, Salzburg, Austria (Sep. 1979) 80—22134
- streaming potential measurements of biosurfaces 77—2074
- Streptococcus mutans 10449, size determ. by laser light scatt. 80—109062
- Streptococcus mutans aggregation, dextran-induced, laser light scatt. meas. 80—89729
- stress-strain meas. on living cells using cell poker 80—76880
- stretch receptor neuron excitation and inhibition summation, crayfish 77—2015
- striate cortex cat, orientation selectivity of single cells 79—2053
- striate visual cortex, spatial freq. rows 77—32888
- striated muscle contraction, intracellular control of force development 79—48228
- striato-nigral fibres, feedback loop vs. output pathway 77—29136
- structural change dynamics in biological particles, rapid light scatt. meas. 79—39615
- structure and surface, high-speed analysis, laser absorpt. and scatt. meas. *(German)* 78—92687
- submitochondrial particle semiquinone Q_{10}, EPR signal qith unusual relax. parameters 77—56338
- submitochondrial particle succinic dehydrogenase, interaction of ubisemiquinone with Fe-S centre, EPR 78—69016
- surface immunoglobulins, characts., mobility and role in immune phenomena, review 78—15806
- surface labelling techniques for eukaryotic cells 77—56560
- suspension analysis, dielec. theory, interfacial polarisation 80—45563
- suspensions of ellipsoidal particles covered with shell, dielec. behaviour, rel. to biological cells 80—51057
- synaptic facilitation and behavioural sensitisation in Aplysia, role of serotonin and cyclic AMP 77—36913
- synaptic transmitter release, modulation by repetitive postsynaptic action pots. 77—4996
- syncytia, spherical, electrical props. 79—24962
- syncytium, passive three-dimens. and anisotropic, modelled as continuous medium 77—16898
- systemic muscular arterial wall medial smooth muscle orientation obs. 79—70572
- taste cells, insect, special purpose amplifier for spike train recording 80—72394
- tectal cells, frog, intracellular recordings 79—79525
- temperature effects on proliferation and viability, normal and malignant human cells 80—21449
- testis, mouse, ^{239}Pu distrib. and significance of interstitial tissue ultrastruct. 79—57610
- thermal history of cells during freezing of biological materials 79—62419
- thermal injury kinetics, HeLa cells 78—56955
- thermal sensitivity of mammalian cells to pulsed CO_2 laser irrad. and hyperthermia 78—15802
- three-dimensional cellular tree structure meas. semiautomatic system 79—70720
- thylakoid membranes of wheat chloroplasts, proton spin-lattice relax. time, −8°C phase transition 80—108853
- thymocyte, calf, tritiation by catalytic hydrogenation 79—88152
- thyroid epithelial cell, methodology of thickness determ. 78—20330
- time-optimal control theory appl. to cell growth 77—40638
- tissue change detection in rabbit urinary bladder, holographic laser interferometry appl. *(German)* 79—34625
- tissue coagulation, effects of HF current parameters, rel. to electrosurgery 80—3746
- tissue damage and death rel. to mech. props., US interaction 80—51151
- tissue LET dose distrib. calcs. for 14 MeV neutrons 79—96664
- tissue molecular dynamics and freezing phase transition studied by proton spin relax. 78—68983
- topography of cell surface ionogenic groups 77—1982
- trace element conc. factors, mag. field effects 77—70438
- transition-probability theory of cell proliferation, cell cycle kinematics 78—24039
- tumour cells, human, from pancreatic carcinoma xenograft, in vitro and in vivo radiosensitivity 77—5041
- tumour growth simulation, in vitro, with aid of computer 77—86464
- urinary tract infections, radiorespirometric testing of antibiotic sensitivity 80—81705
- uterine cancer cells automatic classification via cellular differentiation 79—88226
- uterine cytology, automated, adenocarcinoma recognition 79—88227
- valonia cellulose, pole figures and orientation functions 77—86439
- van der Waals interactions between surfaces of biological interest 77—44609
- vascular smooth muscle cells adventitial aspect visualisation under SEM 79—20523
- vertebrate retina modelling and simulation, extended networks 80—108884
- vertebrate retinal horizontal cells, spatial integration, computer analysis 77—36920
- vertical plane serial sectioning of identified tissue culture cells 79—74807
- VERTIVAL microscope with interference contrast equipment after NOMARSKI for gonorrhoea types classification 80—56301
- virus-cell interactions, early molecular events, fluorescence and radioactivity obs. 79—100561
- virus-cell interactions, early molecular events, kinetic study 79—100562
- vision, neural light intensity analyser model 79—57648
- visual cell, proposed role of cyclic GMP 78—64997
- visual cells, daily rhythms and vision research 78—61176
- visual cells, hierarchical detection structures 79—79523
- visual cortex simple cells, spatial resolution and nonlinearities, cat 77—9187
- visual neuron receptive field mapping with visual stimulus generator 79—74817
- visual photopigments and pseudo-pigments, spectral sensitivity and neural interaction 77—25425
- visual spectral sensitivity analysis, math. techniques 77—52786
- visual Wulst, barn owl, neurons selective for orientation and binocular disparity 77—1996
- vitamin B_6 fluorescence 77—21496

cellular biophysics continued
- vitamin D, role of free radicals in conversions and mechanisms of physiological action 77—70430
- voltage clamp of multicellular preps. 77—40955
- voltage measurement using voltage sensitive dyes 79—57833
- volumetric changes during freezing and thawing, thermodynamic model 80—108863
- von Neumann cellular automata appls. 78—31754
- water, at biological interfaces, struct. and functional aspects 78—40121
- water NMR *(French)* 77—90739
- water PMR obs. in obligately halophilic blue-green alga 79—96526
- white blood cell images boundary finding 79—12021
- X-ray microanal. of cultured skeletal muscle cells, calibration 79—100798
- Xeroderma pigmentosum fibroblasts infected with γ-irrad. adenovirus, decreased viral repair obs. 80—61650
- yeast cell IR spectrum, effect of membrane components 77—70433
- yeast cell wall component contrib. to IR spectra 79—39371
- yeast cells, singular, dielec. props. 78—88699
- yeast cells in suspension, vacuole detect. by transmittance radiometry 80—26418
- yeast metabolism, microcalorimetry, diauxy during anaerobic growth of saccharides 78—3451
- ^{11}C, production for studies on photosynthesis, transport and metabolism in plants 79—39502
- Ca sequestering by endoplasmic reticulum in squid giant axon 79—83733
- HeLa cell chromatin, effects of hyperthermia on protein-to-DNA ratio 79—11905
- ^{31}P NMR analysis of intact tissue, review 80—26432
- T content in organs, and DNA of rat liver cells, after doses of tritiated food, protein or water 80—56226
- T distribution in cells exposed to HTO 80—72142
- ^{99m}Tc radiolabelling of mouse spleen leucocytes 79—100739

cellular effects of radiation
- *see also biological effects of .... (type of radiation)*
- *see also photosynthesis*
- 10 GHz pulse irradiation effect on bacterial growth 80—3721
- 27.12 MHz selective heating of cutaneous tumours 78—24179
- α-particles, multiple track, cell survival obs. 79—66488
- abdominal epidermis histogenesis and age depend. of X-ray sensitivity in flesh fly metamorphosis 78—65084
- AC signal interaction, approx. soln. of distributed parameter model *(Czech)* 78—31855
- acetylcholine receptor response to rapid photochem. prod. increases in agonist conc. 77—36909
- acid phosphatase activity following hyperthermia of mouse spleen, rel. to heat potentiation of X-ray damage 78—48842
- adenocarcinoma cells, mouse, MADCAP 37, hyperthermia and irradiation response 80—40971
- adoptive antibody responses in DBA/2 and BALB/c mice, differential effects of preirrad. 78—80926
- alga, filamentous blue-green, effects of high and low UV fluences 79—48294
- alkaline endonuclease activity in thymus and spleen of irrad. mice 78—28004
- alveolar macrophages, effect of X-irrad. in mice 80—98024
- amino acid absorption by rat intestinal prep., effect of supralethal X-irrad. 77—56444
- amino acid stimulatable transport system in rat liver after hole-body γ-irrad. 78—65098
- amino acid transport hormonal control in liver of rats exposed to whole-body γ-irrad. 78—65099
- amino acid transport in rat liver after whole-body gamma irrad. 77—9232
- amino acid utilisation in cultured insect cells, X-irrad. effects 77—5043
- amoeba, combined effects of thermal neutrons and agents which interact with DNA 78—20219
- amoeba irradiated by thermal neutrons, absorbed dose estimation 78—53449
- Anacystis nidulans, unstable protein mediated UV light resist. 77—86536
- aneuploidy in mouse fetuses after paternal exposure to X-rays 79—79607
- anoxic kidney cell sensitivity to 35 MeV electron single pulses 80—26292
- Artemia eggs, effects of 645 MeV and 9.2 GeV protons 80—45969
- arterial wall damage, fast neutrons vs. X-rays 77—29183
- Aspergillus nidulans, mutation induction by γ-irradiation in presence of O_2 or N_2 80—94297
- Aspergillus niger dying spores, electron refl. and transmission SEM expts. after irrad. 80—56111
- atomic bomb survivors' carcinogenesis and mortality (1950-74) 79—88136
- ATP content meas. in single red blood cell, using firefly bioluminescent reaction with optical instrument 79—79695
- autotrophic microorganism, repair of potentially lethal γ-ray damage 80—3735
- bacteria, E. coli B, microwave radiation effects on colony formation and mol. struct. 78—24097
- bacteria survival, E. coli effect of membrane fluidity 77—21568
- bacterial cell microwave absorption at spectral singularities 77—40712
- bacterial cells, heavy ion irrad., long range effects, comparison with γ-irrad 80—101236
- bacterial culture viability under negative ion irrad. in elec. field *(Russian)* 79—83855
- bacterial membrane, light-induced generation of elec. pot. difference 78—28001
- bacterial photosynthesis, and model systems, electron transfer, ps studies 79—48214
- bacterial photosynthesis, light collection and harvesting processes investig. on psec. time scale 77—90743
- bacterial photosynthesis, primary electron transfer processes, psec. dynamics 78—80841
- bacterial photosynthesis, ultrafast events, picosecond obs. 79—39375
- bacterial photosynthetic reaction centre, fast electron transfer processes 79—8479
- bacterial spores, breaking survival curves and O_2 removal times obs. 80—81658
- bacterial spores, loss of optical density due to partial cell electron irrad. 77—32943
- bacterial spores, thermorestoration of mutagenic radiation damage 79—20524

cellular effects of radiation continued
bacteriochlorophyll, photochem. oxidised, kinetics of dark reduction, R. rubrum chromatophores 77—25390
bacteriochlorophyll-800, implication in picosec. electron transfer to bacteriopheophytin in R.rubrum reaction centres 80—35844
bacteriophage λ superinfecting E. coli, induction and repair of DNA strand breaks 80—72228
bacteriophage ϕ29 in B. subtilis host, effects of temp. and UV irrad. 77—86539
bacteriophage T1 radiosensitivity on various host strain mutants of E. coli 78—20228
bacteriorhodopsin, enthalpy changes during photochemical cycle 79—34602
bacteriorhodopsin, photoelec. conversion in charged synthetic membranes 80—108954
bacteriorhodopsin generated photocurrents on planar bilayer membranes 80—51050
bacteriorhodopsin proton pump, elec. demonstration of rapid light-induced conform. changes 77—44597
bacteriorhodopsin-containing membrane fragments, quantum yield of flash-induced proton release 79—34601
bacteriorphage λ, inactivation by combined X-ray and UV light exposure 80—3732
barley coleoptile growth behaviour under low LET radiations 79—88122
benign tumours, spontaneous and radiation-induced, in parabiont rats 79—88133
beta-emitting radionuclides from reactor accident, ingestion, acute toxicity 78—65082
beta-rays from ^{14}C, biological hazards, cell killing effects, E. coli expts. 80—89805
beta-rays from ^{45}Ca, effects on bone marrow of Indian desert gerbil 80—45971
binucleate cell formation induced by X-irradiation 80—17015
biochemical indicators of radiation injury 79—34607
blood adenylate energy charge changes of lymphocytes, platelets, erythrocytes after γ-irradiation 79—57718
blood cell banding in US standing wave field 79—62291
blood cell permeability to K$^+$, Na$^+$ repair after X-ray, fast-neutron damage 79—57615
blood cells, electrokinetic props. on exposure to phys. factors 77—70431
blood lymphocytes, peripheral, chromosome aberrations due to ^{222}Rn rich water 79—70587
Bloom's syndrome fibroblasts, UV sensitivity and delayed DNA chain maturation 77—29185
blue-green alga, UV dose modifying effects of acriflavine 79—43963
blue-green bacterium Anacystis nidulans, resist. to UV in dark phase 77—16957
bone, granulocyte and macrophage precursor cells, mouse, microwave effects in vitro 80—76789
bone cancer induction by α radiation 78—15871
bone marrow, effect of a 600 MeV neutron beam, mouse 79—96630
bone marrow, mouse, late effects of X-irrad on ability to support haematopoiesis 77—70496
bone marrow ^{32}P effects during postnatal development of Swiss albino mice 78—53450
bone marrow cell inactivation with ^{60}Co γ-rays, depth-related differences 78—7406
bone marrow cell-culture, RBE of different-energy neutrons 79—34508
bone marrow colony-forming units in beagles, response to whole-body γ irrad. 79—25043
bone marrow electronic cell sizing and counting, biological dosimetry of irradiated rat 79—100744
bone marrow erythrocytes of mice, X-ray induced micronuclei 78—77088
bone marrow regeneration from cortex after segmental fractionated irrad. 77—70495
bone marrow stem cells of C$_3$H mice, long term radiation effects 80—30787
bone-tissue interface, fast neutron dosimetry 79—25113
brain tumour cells, rat, anal. of interaction of 2 nitrosourea compounds and X-radiation 80—72230
brain tumour cells, rat, BCNU-modification of in vitro X-ray response 77—70498
brain tumour cells, Z-ray-BCNU interactions in vitro, isobologram anal., rats 80—81662
breast carcinoma, appearance of non-specific suppressor cells in the blood after local irradiation 79—20597
bronchial cancer induction by α-emitting warm particles 78—96078
bronchial tumour reaction to combined neutron-telecobalt therapy 79—20642
cancer thermographic diagnosis enhancement by US irradiation 79—79614
cancer treatment by microwave hyperthermia *(French)* 80—3764
cancer X-ray sensitivity increased by 434 MHz EM irradiation 78—24180
cancerous cell culture, phonons, long-range coherence, microwave effects 78—35816
capillary endotherlial cells, repair of sublethal radiation damage, beagle cornea 79—100672
carcinogenesis, shape of dose-response curve, extrapolation to low doses 78—15866
carcinogenesis, stochastic model, obs. from chemical and radiation dose-response data 79—2110
carcinogenesis theory, cell survival-depend. dose-rate effects 79—11973
carcinogenetic action of fluoresc. light on mice cells 80—98014
carcinogenetic risk estimation, comparison of radiation therapy and chemotherapy 79—20592
carcinoma cell metabolism, Ehrlich ascites, effects of microwave radiation 79—2104
cartilage, baby rat tails, hyperthermia and X-irradiation, O$_2$ enhancement ratio 79—57712
caudal fin regeneration in mosquito fish, for in vivo study of UV damage 77—52844
cell killing and the sequencing of hyperthermia and radiation 79—100673
cell permeability polarity and control by phytochrome, red light irrad. of mass 78—77025
cellular repair mechanism, investigation by high dose rate electron beam 79—53195
charged particle track evaluation, distance distrib. and intratrack dose 80—26368
chemical carcinogenesis, redox model 80—26298

cellular effects of radiation continued
chemotherapy enhancement by US, time/intensity studies using cell suspension and mechlorethamine 77—29175
Chinese hamster cell, γ-dose survival, seasonal variations 79—43959
Chinese hamster cell, repair of potentially lethal damage after X- and α-irrad. 78—28014
Chinese hamster cell sublethal damage repair after fast neutron irrad. with or without X-irrad. 78—20218
Chinese hamster cell survival and sublethal repair, ultra-high dose rate electron irrad. compared with X-rays 78—40272
Chinese hamster cells, ^{60}Co-irrad., computer anal. of survival curve data 78—85344
Chinese hamster cells, additive action of ionising and non-ionising radiations throughout cell cycle 77—48845
Chinese hamster cells, combined effects of hyperthermia and X-rays 80—45977
Chinese hamster cells, DNA replication after X-irradiation 79—11986
Chinese hamster cells, enhanced killing by ^{238}Pu α-particles in the presence of cordycepin 80—72233
Chinese hamster cells, hyperthermic radiosensitisation to X-rays 80—21450
Chinese hamster cells, pot. lethal damage rel. to sublethal damage 80—36012
Chinese hamster cells, X- and UV-irradiation obs. 79—96627
Chinese hamster ovary cell colony size and giant cell form. after 1 MHz US irrad. 78—28000
Chinese hamster ovary cell recovery from damage due to fast neutron radiotherapy beams 78—20231
Chinese hamster ovary cell X-ray induced division delay, effect of hydroxyurea 78—31865
Chinese hamster ovary cells, changes in cellular heat and/or radiation sensitivity obs. 79—74727
Chinese hamster ovary cells, response to fast neutron radiotherapy beams 80—21497
Chinese hamster ovary cells, X-ray response during latter part of G$_2$ 80—30775
Chinese hamster V79 cells, mutation and inactivation by heavy ion beams 80—35982
Chinese hamster V79 cells, synchronised, inactivation with charged-particle track segments 80—108966
Chinese hamster V79 cells grown as spheroids or monolayers, radiation-induced DNA damage 80—41130
Chinese hamster V-79 cells, US lethality obs. 80—85443
Chlamydomonas reinhardi, dividing, X-ray and proton-induced ultrastruct. changes 78—65085
Chlorella, quantum productivity of synchronous culture in different spectral regions 77—25392
chlorella cells, effects of light and low temp. on chlorophyll content and metabolism 80—56118
Chlorella microalgae cells, laser damage mechanism 78—3550
Chlorella microwave photocond., rise/fall kinetics, depend. on physiological state 78—15793
Chlorella pyrenoidosa synchronised cultures, effect of extremely low doses of secondary radiation from ^{32}P 78—73176
chlorophyll, energy trapping dynamics in photosynthetic unit model 78—88697
chlorophyll, photosynthesis mechanism, upconversion, EPR and O$_2$ evolution data anal. 78—35811
chlorophyll in marine dinoflagellates, photosynthetic characts. and organisation 79—5260
chloroplast EPR signal props., effect of ferricyanide, dark adaption, ageing 79—57607
chloroplast photosystem II photoinduced EPR centres 79—39372
chloroplast suspension, photoinduced changes in oxidation-reduction pot. rel. to photosystem II activity 77—25399
chloroplast thermoluminescence, effect of medium redox. props. 79—57609
chloroplast thylakoid, light-induced absorbancy and scatt. changes about 520 nm rel. to struct. 78—69019
chloroplasts, chlorophyll a fluoresc. duration rel. to ferricyanide and vitamin K$_3$ conc. 77—25393
chloroplasts, EPR investigation of state of Mn^{2+} 78—69008
chloroplasts, EPR signal in response to illum. sequence of four flashes 78—7325
chloroplasts, isolated, broken, fluoresc. changes and involvement of elec. double layer 78—44464
chloroplasts, photoinduced dielectric const. shift *(French)* 78—61147
chloroplasts and subchloroplast particles, optical absorpt. at 700 nm and EPR spectra 77—25394
chloroplasts in pulsed illum. regime, photophosphorylation 78—64958
chloroplasts in pulsed illumination, light-dependent reactions of Mn^{2+} and P700$^+$ 79—53062
CHO cells, alterations in radiosensitivity by anisotonic treatments 80—72251
CHO cells, asynchronous, fractionation of combined heat and radiation, radiation sensitivity obs. 80—76806
CHO cells, asynchronous, fractionation of combined heat and radiation, cell-cycle redistrib. 80—76807
CHO cells, comparative effects of water-bath- and microwave-induced hyperthermia on survival 80—55997
CHO cells, cyclic AMP levels rel. to X-ray induced mitotic delay 80—51170
CHO cells, effects of X-irrad. and hyperthermia on SCE freq. 80—36021
CHO cells, O$_2$ sensitisation at ultrahigh dose rates 80—36000
CHO cells exposed to hyperthermia, radiosensitivity and recovery from radiation damage 80—72250
CHO synchronous cells, ionising radiation induced 6-thioguanine-resistant clones 80—98027
cholecalciferol, UV dependent synthesis in a green plant 80—35860
Chorella cell microwave photocond., long wave illum. and Emerson effect 78—15794
chromatid aberrations, UV induced, in cell lines of Chinese hamster with different repair activity 79—57711
chromatin from cultured mammalian cells, radiolysis, DNA-protein cross-links formation 80—81655
chromatophores of R. rubrum, induction of elec. pot. diff. by laser flash 80—81560
chromosomal aberrations as radiobiological quantitative end-point 80—12188

cellular effects of radiation continued
chromosomal aberrations for tritiated water dose, Swiss albino mice 79—2112
chromosomally aberrant cells, Japanese A-bomb survivors, dose-response relationship of neutrons and γ-rays 80—94295
chromosome aberration form. by gamma irrad. in lymphocytes, protection by free radical scavenging 78—20216
chromosome aberration of human lymphocytes, microdosimetric expts. 80—26289
chromosome aberration specificity, X-irrad. human T-cell line 78—80921
chromosome aberrations, alteration in freqs. of different classes throughout first cell cycle after irrad. 80—104672
chromosome aberrations, dose-effect relationship, population exposed to increased natural radioactivity 80—72254
chromosome aberrations as biological dose-response indicator in U miners 80—17019
chromosome aberrations as dosimetric technique for fission neutrons at 0.2 to 50 rad 78—69145
chromosome aberrations in swine leukocytes after in vitro and in vivo exposure to fission neutrons 78—28011
chromosome aberrations in Syrian hamster lung cells due to inhaled $^{238}PuO_2$-ZrO_2 particles 77—56440
chromosome aberrations in vivo effect of US alone and in combination with X-rays 78—20210
chromosome aberrations induced by low doses of X-rays in human lymphocytes in vitro 80—72235
chromosome aberrations of peripheral lymphocytes in rabbits exposed to whole body X-irradiation 79—43834
chromosome aberrations rel. to overexposure in accidents 78—53519
chromosome condensation and X-induced G_2 arrest 79—34510
chromosome inactivation in UV irrad. E. coli during growth 77—86551
chromosome observation, estimation of radiation effects *(Japanese)* 79—83845
chromosome recombination during oogenesis in silk worm 77—2030
chromosomes, interaction of X-ray induced primary breaks in form. of dicentrics 77—12963
chromosomes, irradiated, identification by pattern classification system 77—37114
chromosomes of human female lymphocytes, distrib. of X-irrad. induced lesions, dose-effect relation 80—51175
ciliated cell activity during exposure to ionising radiation, temp. effect 77—70493
ciliated cell response during irrad. at different dose rates 78—61216
clonal survival curves with cellular recovery, parameter fitting 77—56352
clonal survival model generalisation, eqns. for families of curves for fractionated irrad. 77—2029
clonal survival of Chlorella and chloroplastic survival of Euglena gracilis after irradiation 79—79606
clonogenic normal cells, new derivation of the complete survival curve 80—41137
cochlear, struct. and functional changes following US irrad. 80—89791
collagen synthesis stimulation, human fibroblasts, role of US-induced cavitation 80—85442
colon crypt survival after whole- or partial-body irrad. of mouse 77—56427
colon crypts, mouse, induction of radioresistance by X-rays 80—45970
colonic epithelium, compensatory proliferative response to multi-fraction irradiation 79—88128
cone ionic channel closure, turtle 78—15830
conference, Brussels, Belgium (Oct. 79) 80—105416
conference, Osaka, Japan (Nov. 1979) 80—98756
conference, Rotterdam, Netherlands (Aug. 1980) 80—105425
continuous diploid yeast cultures, radiosensitivity to continuous ^{60}Co gamma-ray exposure 77—52843
cosmic ray nuclei, $Z=30$-40, Earth orbit expts. 80—3828
Crepis seeds, heat rel. to storage in X-ray injury modification 79—88118
Critical Human Organ Radiation Dosimetry operators for cell survival models and insult assessment 78—20221
crypt system, mouse, alternating fractionation formula of cumulative radiation effect 80—104652
cultured mammalian V79-S171 cell response, rel. to SO_4 salt soln. conc. 78—48833
cutaneous telanagiectasia after electron beam radiation, dose-time relationships 78—3552
cyanine fluorescent dye membrane probe effects on cell props., rel. to bacterial chemotaxis 78—35815
cyclic nucleotide changes in X-irradiated synchronized Tetrahymena 79—25046
cytochromes ratio in radiation-induced leukemia cells, mouse 80—21500
cytogenetic findings 30 years after low level exosure to Nagasaki atom bomb 77—90862
cytotoxicity of X-rays rel. to ^{238}Pu 4.4 MeV α-particles 80—72265
damage model, radiation chemistry approach for direct and indirect effects 79—11974
delta-electrons prod. in water by high-energy electrons and X-rays 77—29178
delta-ray model of track effects, applicability to physical, chemical and biological systems 77—65407
deoxyribonucleoprotein, thin fibres revealed after γ-irrad., calf thymus 80—30794
dicentric chromosome induction in human lymphocytes by 30 kV X-rays, RBE 78—3563
dihydropyrimidine bases in aq. soln., spin-trapped OH radical reactions, EPR obs. 79—88053
dimethyl sulphoxide radioprotection of mammalian cells, exposed to X-rays, heavy charged-particle beams 79—79609
dipalmitoyl phosphatidyl choline vesicle damage by picosecond laser pulses 79—79599
diploid populations, human, acute and late effects of single exposure of X-rays 80—98029
diploid yeast, liquid-holding recovery, nature of damage after α- and γ-irradiation 79—16256
diploid yeast, O_2 effect in killing by photon irrads. of different energies 80—36018
diploid yeast, response to radiations at different LET 80—21501
diploid yeast, split dose and liq.-holding recovery after X-irrad., growth phase depend. 77—64088
diploid yeast, split-dose and liq.-holding recovery after X-irrad. 77—86547
diploid yeast cell inactivation by accelerated heavy ions 80—26295

cellular effects of radiation continued
diploid yeast cell ribosomal RNA gene inactivation curves and cross-sections 80—26297
division delay, effect of ^{125}I-UdR and ^{3}H-TdR 77—29179
DNA, damage from ionising radiation, repair mechanisms 79—11987
DNA, double strand breaks, recombination, formation of chromosomal rearrangements 78—85289
DNA, Escherichia coli, γ-irradiation induced damage, enzyme labile sites 80—35993
DNA, high mol. wt., sedimentation data, radiation-induced single-strand breakage, additives effect 80—30667
DNA, mammalian, organisation of repeated nucleotide sequences in replicons 77—73506
DNA, single-strand break repair after X-irradiation, cultured insect and mammalian cells 79—74725
DNA, subchromosomal synthesis in X-irradited V-79 cells 80—41141
DNA, thymine base damage release, γ-irrad. Tetrahymena pyriformis 80—72268
DNA, thymine damage production and excision, mammalian cells, high-LET irrad. obs. 80—72261
DNA, transforming, shape of UV inactivation curve 77—66797
DNA, transmutation effects of incorporated ^{32,33} P 80—26283
DNA, UV and gamma-ray damaged, defective repair in Fanconi's anaemia 77—44725
DNA, X-ray induced damage in rat cerebellar neurons and brain tumour cells 78—80922
DNA, X-ray induced single-strand breaks, yield and repair, E. coli cells 77—9173
DNA base damage detection method, UV induced pyrimidine dimers in human cells 79—44067
DNA break rejoining capacity rel. to mouse age 78—69148
DNA breaks in E. coli and superinfecting phage λ, repair rel. to buffer. 77—25376
DNA chain growth in vivo in intestinal crypt cells, effect of ^{60} gamma and hydroxyurea 77—66795
DNA damage and repair in γ-irrad. rat brain tumour, detect. by S_1 nuclease 78—48838
DNA damage of Chinese hamster ovary cells on X-irradiation after preheating 79—34493
DNA degradation in Escherichia coli after UV irrad. 78—48841
DNA double strand breaks rel. to radiation dose, yeast cell obs. 80—72232
DNA double-strand breaks, repair in isolated nuclei of Physarum polycephalum 80—72248
DNA double-strand breaks during γ-irrad. of Micrococcus radiodurans, O_2 effects 78—7393
DNA double-strand breaks in irradiated yeast cells, survival and yield, O_2 influence 80—35992
DNA end group characterisation after low dose γ-irrad. of thymocytes 78—11613
DNA inactivation by γ-rays in vitro, O_2 effect in presence of metalloporphyrins 79—92303
DNA methylation after UV irrad., of HeLa cells 77—12979
DNA non-rejoining break induction by high LET radiation, rel. to cell death 77—44596
DNA repair, human cancer, radiation hazards assessment 80—41143
DNA replication and repair in human melanoma cell-line resist. to UV irrad. 77—44721
DNA replication fork struct. in UV irradiated human cells 79—88117
DNA replication kinetics in X-irrad. Chinese hamster ovary cells 78—20226
DNA single strand break yield and survival curves for E.coli B/r 80—26282
DNA single-strand breaks, ultra-fast repair in γ-irrad. Chinese hamster cells 77—21569
DNA single-strand breaks in preheated cells irrad. under N_2 and N_2O saturation 78—28017
DNA single-strand breaks in rat thymocytes due to irrad. histidine and γ-rays 77—56438
DNA strand breaks, lymphoma cells, detected by hydroxyapatite chromatographic technique 79—43819
DNA strand breaks in ^{60}Co γ-irrad. thymocytes 78—7395
DNA strand breaks induced by ^{125}I in cultured human kidney cells, repair 80—12192
DNA synthesis, nucl., in yeast, UV and gamma-ray effects 77—56428
DNA synthesis by DNA-membrane complexes from electron irradiated E. coli 79—16167
DNA synthesis in chick embryonic Mullerian ducts, X-ray dose response obs. 79—88130
DNA synthesis in X-irrad. HeLa cells, depend. on dose and time after exposure 77—37025
DNA synthesis inhibition in vitamin-E-depleted lymphosarcoma cells by X-rays and cytostatics 77—56429
λDNA transcription, effect of UV irrad. 77—66827
DNA unscheduled synthesis in diploid yeast after X-irrad. in different phases of cell cycle 77—44722
DNA unscheduled synthesis in UV irrad. spleen lymphocytes after X-irrad., rat 78—69156
dose planning expts. for radiation therapy 78—15879
dose-LET spectra and radiobiological effects 80—26265
dose-modifying factors test 80—21544
dose-rate effects in plateau-phase cultures of S3 HeLa and V79 cells 80—76796
dose-rate model testing with Chlamydomonas reinhardi 80—21543
Drosophila germ cells, decrease of γ-induced mutations by visible light 80—67159
E. coli, damage induced by T decay, secondary lethality under nongrowth conditions 80—104654
E. coli, DNA repair in radiation resistant and radiation sensitive strains 79—34489
E. coli, effect of US at 1.5 MHz 80—72212
E. coli, photodestruction of zinc-porphyrins in presence of O_2 79—79601
E. coli, photoreactivable component in the mutagenic action of ionising radiations 80—72225
E coli, photoreactivation following ionising irrad. rel. to Cherenkov emission 80—108969
E. coli, photoreactivation of ionising radiation induced damage 80—3734
E. coli, relative rates of repair of single-strand breaks and postirradiation DNA degradation 79—16149
E. coli, repairability of chromosomal and cytoplasmic DNA after γ and UV irrad. 80—30796

cellular effects of radiation continued
E. coli, UV-irradiated, DNA double-strand breaks from single photochemical events 79—16151
E. coli, UV-irradiated, DNA single-strand breakds and alkali-labile bonds 79—16152
E. coli, value of photoreactivable component after exposure to ionising radiation 80—72224
E. coli ^{125}I and X-ray damage, effect of cell DNA content 78—28006
E. coli B$_{s-1}$, response to tritium-β particles rel. to 7 MeV electrons 79—57714
E. coli B, combined US and gamma irrad. 78—20211
E. coli B irrad. with 0.8 MeV electrons in oxygenated and anoxic states, mol. alterations 78—24031
E coli B/r, UV sensitivity rel. to DNA content obs. 80—108960
E. coli B/r radiosensitisation by paracetamol, mechanisms 77—86544
E. coli fatty acid auxotroph, factors influencing survival after γ-irradiation 80—17007
E. coli inactivation, 365 and 254 nm radiation synergism 79—25044
E. coli K-12 cells, inhibition of X-ray induced UV resistance by nitrofurantoin 78—85342
E. coli K-12 X-irrad. cells., influence of uvrD mutation on survival and repair 77—86540
E. coli photoreactivation after electron irrad., O_2 effect 78—20213
E. coli strains, two with lambda lysogens, induced radioresist. 78—69140
E. coli strains differing in DNA repair capability, survival after fission-spectrum neutrons irrad. 80—98031
E-coli, enzymatic activities in UV-induced DNA degradation 80—36011
E.Coli, lambda prophages induction by mm microwaves 79—100663
E.coli, lethality by 365 nm radiation under various conditions 80—61624
E.coli, radiation killing, role of membrane fluidity, hypothermia and local anaesthetics 80—104653
E.coli, radiation response of thymine-starved bacteria 79—11981
E.coli, respiration cessation obs. after far UV irrad. 80—76799
E.coli AB2463 recA response to fast neutron beams, 4 to 27 MeV, rel. to dosimetry intercomparison 78—65077
E.coli repair-deficient mutant, microwave irradiation obs. 79—100666
egg, sea urchin, radiation-induced mitotic delay rel. to S-phase 79—96625
Ehrlich ascites carcinoma cell fluoresc. after X-irrad. 78—69143
Ehrlich ascites carcinoma cells, effects of pions rel. to electrons and X-rays 80—26267
Ehrlich ascites tumour cell, thymidine transport kinetics and DNA synthesis, X-ray effects 78—20215
Ehrlich ascites tumour cell membranes damaged by X-rays, biochem. interaction of heparin 78—31864
Ehrlich ascites tumour cell mitotic activity, H_20_2 and gamma-ray effects 77—52854
Ehrlich ascites tumour cells, influence of O_2 tension of X-ray-induced fall in anodic mobility 79—34526
Ehrlich ascites vital cell UV primary fluoresc. rel. to ^{60}Co γ-ray dose 78—69142
electric circuit model, alternating signal interaction 78—77011
electric circuit model, alternating signal interaction 78—77012
electron beams, 10, 20 and 30 MeV, RBE vs. depth for mouse leukaemic cells 77—5037
electron microscope superconducting lens system for reduction of radiation damage 79—34718
electrons, O_2 diffusion into mammalian cells following ultrahigh dose rate irrad. 80—30694
ELF EM field effects, myxomycete obs. 80—41117
Elkind recovery rel. to sublethal damage 77—64085
Elodea, cell death thresholds for 0.45-10 MHz US 80—67149
Elodea, US induced pulsations of gas-filled channels 79—53185
EM control of cell functions 80—85535
EM fields, direct influence on nerve and muscle cells of man in 1 Hz-30 MHz range 80—51160
EM nonionising weak-field interaction with brain tissue, freq. and power windows 80—35974
EM pulse environment, tests of biological integrity in dogs 79—39448
EM wave on excitable nerve membrane, surface change density variation 78—85334
embryo C3H10T1/2 cells, mouse, high-energy neon particle irrad., viral transformation enhancement 80—104668
embryo of 2 cells, mouse, cell cycle-dependent radiosensitivity obs. 80—104669
embryonic bone and cartilage, effects of in vitro gamma irrad. 78—65089
embryonic cell viability and survival in mouse, preimplantation X-irradiation effects 79—88137
embryos of mouse, one-cell and two-cell effects of UV, X-rays and carcinogen 77—12967
EMT6 cell, RBE, OER and recovery of potentially lethal damage of 645 MeV He ion beam 78—20229
EMT6 cells, changes in repair of potentially lethal damage with culture age 79—74723
EMT6 tumour cell response to single fractions of X-rays and cyclotron neutrons 78—20230
EMT-6 cells in vitro, potentially lethal damage recovery following X-ray or neutron irrad. 79—62308
endothelial cells, human, replication in culture, X-ray induced inhibition 77—21571
endothelial cells and adjoining tissue, effects during laser surgery 79—66505
endotoxin of S. typhimurium, radiation-induced alterations 78—7391
energetic heavy ion beam model for radiobiology 80—26293
energy metabolism of blood morphotic elements, ionising radiation effects 80—61645
enzyme activities of kidney after gamma irrad. 77—12976
enzyme induction in X-irrad. E. coli B and B/r 78—28005
epidermal cells, mouse dorsal skin, regeneration and dose-response characts. 77—5031
epidermal mitotic activity during mouse skin wound healing, X-irrad. 77—56436
epidermal mitotic activity during wound healing in adrenalectomised mice, effect of head irrad. 78—20220
epidermia, enzymatic behaviour rel. to age and lesion location 77—64089
epidermic regeneration cytokinetics, β-irrad., guinea-pig 78—15870
epidermis, ultrastruct. stereology after X-irrad., rat tail expts. 80—36003
epithelial cell proliferation, mouse, ^{3}H-thymidine effects on circadian rhythms 77—21572

cellular effects of radiation continued
epithelial stem cell survival parameters, considerations in use of mouse foot system 80—36017
EPR of ^{125}IUdR-labelled and X-irrad. cells at 4.2K and above 80—72211
erythrocyte, toad, X-ray induced changes 78—11699
erythrocyte electrophoretic mobility, effect of UHF EM radiation 78—53442
erythrocyte ghost IR spectra in region of amide I and II bands on microwave irrad. 77—86531
erythrocyte membrane, spin-label study of γ-irrad. effect 80—51168
erythrocyte membrane struct., intrinsic fluorescence obs. 79—74724
erythrocyte membrane-haemoglobin interaction, γ-ray effects, EPR 78—7402
erythrocyte membranes, fluidity change after X-irrad., pyrene excimer fluoresc. obs. 80—72262
erythrocyte membranes of rabbit, dog, man, microwave irrad. effects obs. 80—56130
erythrocyte radiosensitivity for cells with increased level of superoxide dismutase 77—44726
erythrocyte surface charge decrease, target of X-irrad. and dislocation of sialic acid 77—52853
erythrocyte survival in mice, effects of polymeric ^{239}Pu 77—9227
erythrocyte survival in mice, effects of polymeric ^{239}Pu 80—45973
erythrocytes, avian, US effects on transport 79—96613
erythrocytes, gas reactions, shape changes microspectrophotometry obs. 79—8488
erythrocytes, investigation of thermal and athermal effects of microwave irradiation 79—70581
erythrocytes, rabbit, increased passive efflux of ^{22}Na and ^{86}Rb on microwave irrad. 80—108957
erythropoiesis and survival of tadpole after whole-body X-irrad. 77—52845
erythropoietic activity, UV effects in rabbits and rats 77—32940
erythropoietic differences in mice after whole-body irradiation 79—25045
erythropoietin action, identification of two components by irrad. in vitro 78—65094
Escherichia coli radiation-damage inducible system, rel. to UV light mutagenesis 78—53458
Euglena cells, light and dark grown, sensitivity to gamma-irradiation 80—35989
Euglena gracilis, differential response to γ-ray radiation in light and dark 79—57710
Euglena gracilis, effects of EM fields on motion 79—16174
eukaryotic cells, improved method to detect small amounts of DNA radiation damage 80—36205
excitable cellular membranes, nonthermal interaction of RF and microwave fields, squid giant axon model 80—67150
excitable nerve membrane exposed to optical radiation, surface-charge density variation, comment 79—8524
extra-retinal photoreceptor model for Aplysia californica 78—44506
extracorporeal irradiation of blood and lymph, in adrenalectomised calves 77—5055
eye, light damaged, albino rat photoreceptor survival, ERG 77—36927
eye, rod outer segments, shedding behaviour under constant light, darkness 79—2050
eye lens fibre damage after laser irradiation, rat 79—39374
face, solar dosimetry, natural UV exposure rel. to basal cell carcinoma localisation 79—92382
fast neutron and photon therapy, randomised clinical trials 79—20638
fast neutron effects on multicell spheroids 77—56423
fast neutron induced DNA strand breaks and repair obs., cultured mammalian cells 80—61651
fast neutron irradiation of cells cultured in monolayer, dosimetric aspects 78—69218
fast neutron RBE comparison for Edinburgh and Hammersmith hospital 78—11698
fast neutron sublethal damage and cell division delay expts. 79—20588
fast neutron teletherapy, preliminary clinical results 79—20639
fast neutron therapy with medical cyclotron, clinical results 79—20643
fast neutrons in normal tissue, early and late damage obs. 79—20590
fetal fibroblasts, UV induced chromosomal abnormalities, New Zealand Black mice 79—43836
fibroblast cells, human, comparative response to 50 MeV neutrons 79—34512
fibroblast L-929F, mouse, radiosensitivity and recovery during cell cycle, 200 kVp X-irrad. 78—28019
fibroblasts, human, UV-irrad., effects of radioactive labelled DNA on excision repair 80—94289
fibroblasts, mouse embryo, clonogenic survival after UV irradiation 79—74722
fibroblasts and smooth muscle cells in culture, acute and long term laser beam effects 78—40268
fibroblasts human, non-transformed, ionizing radiation effect on life span 80—41125
fibrosarcoma cells, murine, separated by centrifugal elutriation, radiation sensitivity obs. 80—76808
fibrosarcoma selected tumour cell populations, fast neutron irrad. in situ 78—44560
flagella, laser damage, high speed cinematography 80—81785
flagellate alga, photoinduced bioelec. reactions 79—70579
fluoresceindiacetate hydrolysis and transport in mammalian cells after UV and gamma irrad. 77—56333
fluorescence photobleaching recovery for meas. of mol. motion, cell surface heating 77—48956
fluorescent light induced DNA crosslinkage and chromatid breaks, mouse cells 79—96615
fluorescent light intermittent exposure, effect on lifespan of human diploid fibroblasts in culture 77—77936
fractionation, math. models 77—5049
free plant cell, suspension-cultivated, survival after X-ray and fission neutron irrad. 79—92296
gamma rays, lack of lethality threshold obs. 80—76810
gamma-rays, conference, Tokyo, Japan (Apr. 1979) 80—27034
gastrointestinal crypt stem cells, murine, single-dose—response curve 77 37022
generation times in two successive generations of X-irrad. FM3A cells 78—31872
genetic and cytogenetic effects in mice fed on gamma-irrad. wheat 77—86545

cellular effects of radiation continued

- germ cell and embryo development effects after X-irradiation, toad 80—8107
- germ cell determinant UV effect, rel. to germ cell form. in Xenopus embryo 77—70503
- giant cell formation, influence of conditions enhancing potentially lethal damage repair 77—25519
- glioma cells, cultured, influence of microwave irradiation 79—100661
- gliosarcoma 9L cells, response to hyperthermia and X-irrad. 80—36030
- graft-versus-host reactivity, single irrad., bone marrow reconstitution and continuous irrad. 77—9229
- gram (cicer arietinum L.), γ irradiation effects 79—34609
- granulocyte growth enhancement on peritoneal cell-coated membranes following irradiation 80—21504
- green alga, 2 species of Sirogonium with different chromosome types, γ-irrad. effects 80—81651
- greening bean leaf low-temp. fluorescence induction obs. 79—39354
- growth inhibition of Vicia faba roots by neutron (pion) beams, RBE and OER values 80—26276
- growth retardation in Chinese hamster V-79 cells by 1 MHz ultrasound 79—62293
- guard cells, anion, light-sensitive membrane pots. 78—11622
- H. halobium, light-induced surface pot. changes in purple membranes and bacteriorhodopsin liposomes 80—98015
- haematological findings significance for medical exam. of radiation employee *(Japanese)* 79—11971
- haematopoiesis progenitor and effector cells, expt. murine system, whole body irrad. obs. 80—98034
- haematopoietic microenvironment, progenitor cells radiosensitivity, mouse expts. 80—45983
- haematopoietic stem cells, effects of dose rate, mouse bone marrow 79—100674
- haematopoietic stem cells, susceptibility to ^{55}Fe radiation damage 79—11975
- haemopoiesis, kinetic basis for compensation during continuous irrad. with low doses 80—36010
- haemopoietic repopulation and stromal cell viability in X-irrad. mice 78—15872
- haemopoietic stem cells, mouse, effect of ^{239}Pu 80—51174
- haemopoietic stem cells, mouse, proliferative and differentiative ability, ^{226}Ra and X-irrad. effects 79—79611
- haemopoietic stem cells of shielded bone marrow, role of migration 77—9225
- haemopoietic system of mice, X-irrad., damage repair modification by microwaves 78—24096
- Halobacterium halobium R_1 cells, photogeneration of two-vector transmembrane gradient of protons 78—80845
- Halobacterium halofium, photo-products spectral conversions, purple membrane formation 79—57605
- halophilic bacteria, effect of illum. on thermogenesis of growing culture 77—86530
- heart, ultrastruct. changes, fission neutrons vs. ^{60}Co gammas, mouse 77—5047
- heavy ion and He effectiveness on tumour systems 79—20587
- heavy ion and He inactivation of mammalian cells, radiobiological characterisation 79—20585
- heavy ion peak-to-plateau relative biological effectiveness ratios, fractionation enhancement 79—62309
- heavy particle comparison for therapy, cell survival, OER and RBE 78—85337
- heavy particle comparison for therapy, cell survival vs. depth 78—85336
- HeLa cell, RNA synthesis sensitivity to UV irradiation 79—57591
- HeLa cell chromosome, UV induced repair pattern 79—57611
- HeLa cells, DNA repair after γ-irradiation, action of hyperthermia 79—100577
- HeLa cells, first postirrad. division obs. 80—72258
- HeLa cells, hypothermic potentiation of radiation lethality 80—45978
- Hela cells, recovery from sub-lethal damage when irradiated at ultra high dose rates 79—79608
- HeLa cells, S3, dose-rate effects on cell cycle and survival 80—76794
- HeLa S3 cells, cell damage resulting from labelling with ^{111}In oxine 80—56145
- heritable lesions, radiation induced, in proliferating mammalian cells, review 79—20602
- herpes simplex virus in carcinogen-pretreated cells, enhanced survival after UV irrad. 78—35894
- herpesviruses, survival and immunological characts. after gamma irrad. 78—77089
- heteroallelic reversion induction, in diploid yeast fission neutron O_2 enhancement ratio 79—88139
- high LET constraint on low LET survival 80—17012
- high LET constraints on low LET radiation survival 80—12199
- high LET constraints on low LET survival of cells, RBE theory 78—92679
- Hiroshima A-bomb survivors, whole-body doses estimation by chromosome aberrations 80—109035
- human, multinucleate and micronucleus formation obs. 80—72219
- human diploid fibroblasts, mutation and inactivation by heavy ion beams 80—35983
- hybrid X-ray resistant cell line, response to X-irrad., UV, actinomycin D and cordycepin 77—86541
- hydra, elimination of interstitial cells by γ-rays 80—21495
- hyperthermia, nonintrusive meas. by US temperature tomography 79—53282
- hyperthermia and X-ray combined effects on CHO cells, rel. to temp. and order of appl. 78—65088
- hyperthermia combined with radiotherapy, normal and cancer cell effects obs. 80—45972
- hyperthermia dosage definition form in vitro thermal cytotoxicity data 78—24178
- hyperthermia interactions with radiations of different LET, C ions and X-rays 77—48846
- hyperthermia modification of X-ray damage in Chinese hamster ovary cells, 40 and 45°C 77—86557
- hyperthermia/radiation interaction, survival surface 78—11616
- hyperthermia/radiation interaction, temp. coeff. of interaction 78—11617
- hyperthermia/X-ray survival response of plateau-phase V-79 cells, effect of delay 78—3555
- hyperthermic treatment of tissue, biological effectiveness estimation, minimum inactivated cell ratio 79—100574

cellular effects of radiation continued

- hypoxic cell fraction determ. in transplantable murine sarcoma 77—64164
- hypoxic cell radiosensitisation by respiratory inhibitors in in vitro tumour model 77—52852
- hypoxic cells, rel. to O prod. in anaerobic water by X-rays 77—25514
- hypoxic tumour cells, hyperthermia effect in vivo 77—70499
- ileum, guinea-pig, immediate X-ray induced contractions, localisation of effect by drugs 77—56443
- immune function changes in irradiated patients with carcinoma 79 16251
- immune response of mice to 2450 MHz microwaves, lymphoid splenic cells 78—40257
- immune system, RF induced alterations due to hyperthermia, mouse obs. 80—35975
- immunological effects of irrad., review 80—81660
- immunological processes after laser irrad. of exptl. tumours *(German)* 78—40242
- in vitro transformation, conf., Toronto, Canada (May 78) 80—67931
- inactivation by γ-rays, depth-related, serum-mediated differences 79—96629
- intenstinal crypt cells, extreme sensitivity to X- and γ-irrad. 77—90864
- intestinal cell sublethal damage after mixed treatment with X-rays and fast neutrons, mouse 77—64086
- intestinal epithelium of rat, fine-struct. effects of 1200R abdominal X-irrad. 78—3561
- intestinal proliferation after multiple fractions of gamma irrad. 78—20223
- intestinal stem cells and crypts of γ-irrad. mice, cell-survival characts. 80—72255
- intestine, mouse, response to 14 MeV neutrons 79—66490
- intestine, small, acute and late damage following fractionated neutron and X-irrad. mouse 78—11706
- ionising radiation, effects of small doses, fundamental biophys. characts. 78—15863
- jejunum, mouse, effect of hyperthermia on radiation response 79—25038
- jellyfish electrically-coupled photosensitive neurons controlling swimming 77—90756
- keratinocytes, dose-dependent vol. changes after X-irrad. 80—61652
- KHT sarcoma cells, effect of intercellular contact on radiation sensitivity 80—30801
- kidney cells, cultured human, fast neutron effects on reproductive capacity 79—62307
- kidney cells, hamster, photodynamic induction of oncogenic virus 79—25029
- kidney cells, inactivation by high-energy monoenergetic heavy-ion beams 80—72256
- kidney radiation injury, mouse, light microscopy 78—35891
- killing, by ionising radiation, mechanistic state vector model 78—11707
- killing by π on glass and plastic surfaces 79—92305
- L-cells, γ-irrad. effect on chromatin struct., mouse 80—30793
- laser effects on cell ultrastruct. *(Chinese)* 79—53187
- laser emission for functional activity regulation of human cells 79—43957
- laser exposure of mammalian cells using evanescent fields created in optical waveguides 78—73298
- laser flash absorption change kinetics spectroscopy at 820 nm, photosynthesis study appl. 78—92769
- laser radiation on immunocompetent human cells, abscess removal example *(German)* 77—77960
- leaf, Saintpaula, dose-effect curve shape rel. to radiation-stimulated repair 80—26291
- leaf $P700^+$ reaction centre reduction in higher plants 78—64954
- leaf radiation stochastic model 77—32880
- leaves of higher plants, electron transport chain, rapid induction of fluoresc. 77—81477
- lecithin bilayers, reaction kinetics of radicals, OH, e_{aq} 79—11886
- LET dependent radiosensitivity of E. coli K-12 rec and uvr mutants 78—15874
- lethality computation, dose-time relationship, fractionated radiation therapy 79—20598
- lethally X-irradiated hamster cells, viable hybrids with unirrad. mouse cells 77—5034
- leucocyte, human, fluorochromed with acridine orange, spectral characts. 78—96024
- leucocytes, human, US effects, sister chromatid exchange anal. 79—96612
- leucocytes, microsonation effect, cell destruction critical threshold determ. 78—20212
- leukaemia cell radiosensitisation by hyperthermia and nitroimidazoles, rel. to hypoxia 77—86555
- leukaemia cell reproductive survival and hypoxic protection rel. to ionisation density 77—86554
- leukaemia in children associated with nuclear weapon test fallout 80—12186
- leukaemic cell line, mouse, radioprotection by procaine 78—65080
- light induced quenching of atebrin fluoresc. and photosynthetic electron transport, pea chloroplast 77—56351
- light response and kinetics in Aplysia giant neuron 78—53381
- Light-regulated body ion balance in marine slug Elysia virdis (Montagu) 78—73146
- lipid free radical oxidation, UV effect on lipid-protein complexes and membranes 77—36874
- lipid membrane models, dose-rate and O_2 effects, linoleic acid 77—48841
- lipid metabolism disorder in mice due to microwave exposure *(French)* 79—34600
- lipid photoperoxidation in isolated chroroplasts, role of superoxide anion radicals and superoxide dismutase 78—77016
- liposomal membrane permeability, radioresist. 78—80919
- liposome, photoinduced electron transport across phospholipid wall using methylene blue 79—74614
- liposome proton permeability increase on peroxide photo-oxidation of lipids 78—69024
- liver, giant cell formation after ^{45}Ca administration, desert gerbil 79—92299
- liver, in vivo repair of injury leading to interphase death, rat 77—52850
- liver biomembranes of gamma-irrad. animals, postradiation recovery 80—35976
- liver cell proliferation, rat, failure of X-ray hepatoma production 79—25050

cellular effects of radiation continued
liver chromosome aberrations, mice, effect of continuous intake of HTO 77—25518
liver membrane alternations after X-irrad., normal and vitamin E deficient ducklings 80—41139
liver membranes, mouse, X-irrad., dose-rate effects 80—94293
liver microsomes, γ-induced lipid peroxidation and membrane-bound enzymes 80—104660
living system biophysical interaction mechanism with RF and microwave radiation 79—79602
low-dose radiation carcinogenesis 80—12198
lung, ^{218}Po, ^{214}Po, α-particle effects in Syrian golden hamster 79—16304
lung, pathological changes following single and multi-fraction irrad. 78—3553
lung, specific early fine struct. changes after X-irrad. 78—31859
lung cancer in histoculture, continuous isotopic X-irrad. 77—73550
lung carcinogenesis in rats, induced by inhaled high-fired ^{239}PuO$_2$, BeO 78—96077
lung cells, mouse, radiosensitivity, in vitro colony method obs. 80—101230
lung early radiation dose-response, ultrastruct., dog 78—35890
lung epithelial cells, type 2, proliferative response after X-rays and fission neutrons 80—108974
lung lipids, biochem. effects of inhaled ^{239}PuO$_2$ 77—25510
lungs, alveolar macrophage number and index of effect 78—31869
lymph node metastases, radiosensitivity rel. to initial subcutaneous tumours, nude mice 80—36029
lymphocyte, hog, energy metabolism effect of ionising radiation 79—92301
lymphocyte, human, dicentric yield, γ dose rate dependence calc. 79—92294
lymphocyte B and T cell membrane receptors, human effects of ^{60}Co gamma-rays 77—21575
lymphocyte cell DNA damage by US diagnosis 80—67148
lymphocyte chromosomal aberrations of people exposed to ^{226}Ra and ^{3}H paints 77—37011
lymphocyte chromosome aberrations, influence of blood storage after X-irrad. 77—66828
lymphocyte chromosome aberrations, irrad. in vitro and in vivo, monkeys 77—37012
lymphocyte chromosome aberrations, pion peak expansion to range of depths useful in radiotherapy 78—20243
lymphocyte chromosome aberrations and the Poisson distrib. 79—100675
lymphocyte chromosome aberrations in humans induced by photon and electron irrad., sublesion interaction model 80—26279
lymphocyte death and transform., effects of X-ray and neutrons 78—69144
lymphocyte dicentric yield on X-irradiation, human and feline blood 79—96624
lymphocyte function evaluation after 2450 MHz CW microwave exposure, mouse 79—100667
lymphocyte homing patterns, radiation induced alterations 80—17014
lymphocyte in vivo migration modulation by whole-body hyperthermic RF irradiation, mouse 79—100668
lymphocyte morphology and chromosomes, effect of 2450 MHz microwaves 78—40252
lymphocytes, acentric fragments formation, anal. of primary processes, X-irrad. 80—72272
lymphocytes, chromosome aberrations rel. to radiation dose, A-bomb survivors 79—43835
lymphocytes, comparative effects of γ-rays on T and B cells 79—11968
lymphocytes, human, chromosome aberration yields due to 15 MeV electrons 77—48843
lymphocytes, human, chromosome aberrations induced by ^{252}Cf neutron radiation 79—16169
Lymphocytes, human, effect of irrad. on hexose monophosphate shunt pathway 80—76798
lymphocytes, human, effects of heat and radiation 80—97864
lymphocytes, human, effects of low-dose radiation on repair processes 80—98023
lymphocytes, human, effects of US irradiation 79—96609
lymphocytes, human, homogeneous sensitivity to radiation-induced chromosome damage 79—53197
lymphocytes, human, lethally-irrad., ultrastruct. events in cytoplasmic death 77—48842
lymphocytes, human, prediction of dose-rate effects for dicentric production by X- and γ-rays 80—72226
lymphocytes, human, RBE for d(42 MeV)-Be neutrons based on chromosome-type aberrations 80—104663
lymphocytes, human, sister chromatid exchanges obs. after γ-irrad. 80—41140
lymphocytes, human, variation in neutron RBE values compared to X-rays 80—101229
lymphocytes, human peripheral, chromosome sensitivity to various X-ray doses and subsequent storage 80—17011
lymphocytes, human peripheral blood grown in γ-irrad. medium, sister chromatid exchanges 80—104658
lymphocytes, in vitro ^{60}Co gamma-ray response of leucoagglutinin stimulated human cells 78—57041
lymphocytes, mouse thymus, X-irradiation effects on UV fluorescence 79—66491
lymphocytes, of equine peripheral blood, stimulated with phytohaemagglutinin, X-irrad. 77—5032
lymphocytes, perinatal rats, effects of 2450-MHz CW microwave irrad. 80—56133
lymphocytes, peripheral, function in dog, impairment by chronic pulmonary ^{144}Ce irradiation 79—88135
lymphocytes, peripheral, population changes following radiation therapy to limited and extended fields 80—72236
lymphocytes, pig, chromosomal aberrations after neutron and gamma irrad. in vitro 77—64095
lymphocytes, rat, cell damage resulting from labelling with ^{111}In oxine 80—56145
lymphocytes, stimulated, cell cycle progression perturb. by tritiated thymidine radiation 79—57726
lymphocytes, survival of T- and B-cells after X-irrad. in vitro 77—12969
lymphocytes and thymocytes, human, radiosensitivyt 77—37026
lymphocytes irrad. in vitro, effect of radiotherapy on mitogenic response to phytohaemagglutinin 78—24100
lymphocytes of man, rabbit and swine, chromosome aberrations induced by ^{60}Co gamma rays 80—56146

cellular effects of radiation continued
lymphoid cells, peripheral, functional changes after breast carcinoma radiotherapy 79—88125
lymphoma, murine, effect of synchrony on survival of L5178Y cells after neutron irrad. 80—72227
lymphoma cell line, murine, inverse X-irradiation split-dose effect 80—17008
lymphoma cell survival after X-irrad., effect of vitamin E 78—92677
lymphoma cells, mouse, of differential sensitivity to X-rays, expt. obs. 80—72221
lymphoma cells, Murine L5178Y, production of radioresistant mutants 80—76809
lysosomal enzyme activation in gamma-irrad. mammary tumours 77—5050
lysosomal hydrolase redistrib. in rat spleen homogenates under γ irradiation 79—88132
lysosomal hydrolases of rat serum and spleen 77—52848
magnetic field effects on tetrahymena pyriformis 79—83814
magnetic fields, weak, effect on growth of tissue culture cells 79—62271
magnetic sensitivity test of 3 different biological systems 79—92247
malic dehydrogenase isoenzymes in wheat shoots and chloroplasts, effect of light 78—11696
malignancy analysis based on somatic mutation 78—69147
malignant melanoma, relationship between total dose, fraction number, fraction size 79—5341
malignant melanoma, thermal neutron capture therapy, in vitro radiobiological anal. 80—104657
mammalian, influence of radiation quality on effectiveness of small doses 80—30785
mammalian cell, survival of normal and hybrid X-ray resist. lines exposed to X-rays and protons 78—80929
mammalian cell growth and genetics under constant mag. field exposure 79—34520
mammalian cell hybridization ability rel. to X-ray dose 79—88138
mammalian cell line sensitivities to hyperthermia, γ-rays and UV 77—66800
mammalian cell mutation and activation by radiations of differing LET 77—56431
mammalian cell radiosensitivity, anal. using radio-sensitive and radio-resist. clones in vitro 77—9226
mammalian cell radiosensitivity, effect of hypertonic soln. 77—90853
mammalian cell radiosensitivity, effect of NaCl solns. containing radiosensitisers and radioprotectors 78—69146
mammalian cell survival in vitro, average vs. viable cell multiplicity 79—92304
mammalian cells, Chinese hamster, human kidney, radiation studies with modulated C ion beam 79—11978
mammalian cells, cultered, effectiveness of 0.3 keV C X-rays in inactivation and mutation 80—35979
mammalian cells, cultured, dose-rate effects obs. 80—76795
mammalian cells, cultured, interpretation of mutation and inactivation obs. 80—72229
mammalian cells, drastic G$_2$ arrest after heavy-ion beam irrad. 80—45979
mammalian cells, dual radiation action of diatomic deuteron beams, interaction distance effects 79—53196
mammalian cells, effect of low dose rate radiation on cell growth kinetics 80—8103
mammalian cells, effects of ultrahigh electron dose from field emission accelerator 79—53194
mammalian cells, enhancement of X-ray induced potentially lethal damage by low temp. storage 77—37010
mammalian cells, heavy ion effects, irrad. facilities and methods 80—35981
mammalian cells, in vitro US irrad. at hyperthermic temps. 80—94282
mammalian cells, lack of correlation between heat and radiation sensitivity 79—20599
mammalian cells, laser radiation effects obs. using optical waveguide evanescent fields 80—12183
mammalian cells, lethally damaged, proliferation obs. after irrad. by various particles 80—108971
mammalian cells, microdosimetric determ. of radiation quality factors 77—37027
mammalian cells, premature chromosome condensation following X-irrad. 80—45984
mammalian cells, replicon sizes estimated by X-ray plus bromodeoxyuridine photolysis method 79—16353
mammalian cells, thermal enhancement of γ-irradiation effectiveness of reproductive death induction 79—34509
mammalian cells, transformation by α-particles 80—45968
mammalian cells, UV-irradiated, DNA repair kinetics 79—20513
mammalian cells in culture, continuous and fractionated irrad., growth rate effect 79—66493
mammalian cells in vitro, 300 keV X-ray, 14 MeV neutron and pion^{-} effects 78—69155
mammalian cells irrad. with π^{-} and Co γ-rays, cell cycle progression 78—40269
mammalian cells irradiated at ultra-high dose rates, sublethal damage repair 80—36006
mammalian cellular DNA; breaks induced by accelerated heavy ions, impaired repair capacity 80—41129
mammalian chromosomal DNA, single-strand breakage, sensitive detect. by sedimentation anomaly appl. 80—104825
mammalian cultured cell survival after US exposure, synergism with X-ray effects 78—11693
mammalian liver structural changes, US thresholds 79—48287
mammalian tissue mitotic activity inhibition by strong mag. fields 79—34519
mammary adenocarcinoma cell lines, mouse, radiation response and characts. 78—65095
mammary adenocarcinomas, effects on tumor cell survival after irradiation, mice 79—25036
mammary carcinoma C3H response to fractionated irrad., rel. to fractionation number and intertreatment interval 78—53453
mammary cell survival following irrad. in vivo, single dose-survival curve 78—31870
mammary gland cells, rat, damage repair obs. 80—36005
mammary gland cells, rat, survival after X-irradiation under different endocrinological conditions 79—34513
mammary tumours, mouse, cytokinetic basis for efficacious radiotherapy protocols design 79—88124

cellular effects of radiation continued
- marker phenotype rescue, effects of BUdR sensitisation, hypoxia and high LET 80—17005
- marrow colony-forming units, dose-dependence of the split-dose response 80—61701
- melanoma and radiation, mouse tumour cells and clonal lines obs. 80—76800
- melanoma cell radiosensitivity in culture rel. to radiotherapy of malignant melanoma 77—73548
- melanoma cell strains, human, γ-radiosensitivity and growth parameters 79—29574
- membrane damage caused by light irradiation of fluorescent concanavalin A 80—56123
- membrane diffusion measurement by fluorescence photobleaching recovery method, bleaching light effect 80—94434
- membrane fatty acid composition effect on E. coli K-1060 radiosensitivity 79—92306
- membrane of Herpetomonas samuelpessoai, concanavalin A binding, UV effect 78—48835
- membrane permeability, of sheep erythrocytes, O_2 effects with X-ray and neutron irrad. 77—5039
- membrane potential changes on X-irradiation 79—39369
- membrane radiobiology, impact on radiation protection 79—70585
- membrane translational dynamics, fluorescence redistrib. after photobleaching obs. 80—21491
- membranes, ionising and UV radiation effects, review 78—15875
- micellar system, photoinduced redox processes kinetics, intramicellar electron transfer 78—92603
- micro-algae layers for various sun elevations and uniformly bright sky, capture cross sections determ. 79—23039
- micro-organisms, radiation injury, repair and sensitisation, review 78—11700
- micro-organisms irradiated with monoenergetic X-rays, biological consequences of Auger effect 79—11969
- microbial genetic response to 2.45 GHz CW and 8.5-9.6 GHz pulsed microwaves 80—56120
- microorganisms, effects of laser and ordinary UV irradiation 79—70586
- microorganisms, photobehaviour, review, book contrib. 79—5329
- microsurgery using UV laser beam *(German)* 77—60235
- microtubule polymerisation in vitro, effects of ^{60}Co gamma irrad. 78—20222
- microtubules and axonal transport in rabbit tissue after 3.1 GHz pulsed microwave irrad. 77—64097
- microvasculature in rabbit ear chamber, electron microscope obs. 77—64092
- microwave cellular, subcellular and molecular effects *(Russian)* 79—16249
- microwave effects of membrane level, athermal electrophysiological mechanisms and experimental test 79—2108
- microwave long-term effects on ultrastruct. of cerebral cortex and haematologic profiles of rats 78—40267
- microwave radiation on cells in vitro, study using waveguide exposure chamber 79—5327
- microwave-diathermy, pulsed, expt. obs. 79—83849
- microwaves thermal and non-thermal effects, review and German research *(German)* 80—51159
- mitochondria, rat liver, vitamin E deficient, effect of X-irradiation on proteins 79—34511
- mitochondria isolated from bean, respiration and cation accumulation effects of X-irrad. 80—56141
- mitochondrial protein synthesis in rat liver after whole-body X-irrad. 78—80925
- mitotic accumulation of HeLa cells during continuous irrad., cinemicrography obs. 77—64094
- mitotic crossover increase in Nicotiana tabacum after 150 kVp X-irrad. 78—61219
- molecular theory of survival, anal. of synergistic interaction with Pt complex 77—21565
- monocyte function rel. to irrad. in breast cancer patients 80—72238
- monocytosis observation during ^{60}Co radiotherapy 77—70501
- Moss cells, regeneration and photoreactivation after UV irradiation 79—88120
- mouse lung tumour growth delay by bleomycin with 2.45 GHz local hyperthermia 79—83894
- mouse ovaries, X-ray effect on population of granulosa cells *(Russian)* 78—73177
- multi-target survival curve linear transform 78—65078
- multicell spheroid low dose-rate irrad. 79—62304
- murine L5178Y cells, correl. of cell cycle parameters with radiation sensitivity 80—98016
- murine leukemic lymphoblasts, deficient repair and degradation of DNA after X-irrad. 80—72249
- murine leukemic lymphoblasts, deficient repair and degradation of DNA after X-irrad. 80—72253
- muscle cell osmotic state and membrane permselectivity repeated microwave irrad. effects quantitation 80—56131
- mutagenicity of X-rays rel. to ^{238}Pu 4.4 MeV α particles 80—72265
- natural radiation, high levels in Brazil, cytogenetical effects on scorpions 77—5048
- natural radioactivity in Southwest France and its possible genetic consequences for mammals 80—36007
- necrosis of normal tissue, mouse tail expt. 78—40270
- neoplastic and nontransformed human cell radiosensitivity 80—12194
- neoplastic transformation and dose fractionation, role of damage repair 80—72242
- neoplastic transformation in vitro induced by neutrons and X-rays, rel. to radiation quality and repair 80—51178
- neoplastic transformation of 10T1/2 cells by ^{60}Co γ-rays 80—104659
- neoplastic transformation of hamster embryo cells irrad. in utero and assayed in vitro 77—32941
- nephropathy, glomerular and juxta-glomerular lesions 77—9233
- nerve and muscle isolated preps., 2450 MHz radiation effects 78—53443
- nerve cells, microwave reception by brain 77—12958
- nerve membrane, excitable, charge density due to optical irrad. 79—8526
- nerve membrane, excitable, surface-charge density when exposed to optical radiation 77—29176
- neuroblast, mitotic effects of UV, rel. to cell cycle, nucl. membrane breakdown 77—12972
- neuroblast, mitotic effects of UV rel. to cell cycle, nucl. membrane breakdown 77—12973

cellular effects of radiation continued
- neuronal DNA damage accumulation rel. to death after whole-brain irrad., rats 80—76804
- neurons, pigmented, of pond snail, effect of light on electrogenic processes 77—81528
- neurons, single, rapid killing by irrad. of intracellularly injected dye 80—81795
- neutron collimated beam RBE for cell survival rel. to lineal energy spectral differences 80—12200
- neutron relative biological effectiveness in different exptl. tumours, 15 MeV neutrons 79—20591
- neutron therapy beams, radiobiological intercomparisons 80—3739
- neutron therapy clinical trial programme in USA 79—20640
- neutron therapy radiobiology, review 77—5076
- neutrons, 15 MeV, RBE for jejunal crypt cells, oesophagus and lung 77—44728
- neutrons, cyclotron-produced, repair of radiation damage 80—3740
- neutrons, high energy, from Fermilab 500 BeV synchrotron, OER 77—70500
- neutrons, high-energy, prod. by 80 MeV deuterons on Be, OER 77—81538
- neutrons generated by 70 MeV protons on Li, OER and RBE meas. 78—65079
- Nitellopsis obtusa, photo-induced H^+ transport 80—81645
- p-nitroacetophenone charge transfer reaction with triplet state of guanine for radiosensitisation 79—92146
- nonthermal effects of radio and microwave fields on biological membranes 77—86534
- normal tissue protection by irrad. of tumour-bearing mice in hypoxic hypoxia 77—5051
- nSD and cell survival in fractionated irradiation 79—74720
- nuclear lesions induced by X-irradiation of Chinese hamster cells, ultrastruct. anal. 80—21494
- nuclear peripheral DNA critical site for radiation-induced reproductive death 79—88131
- nuclear-dockyard workers, radiation-induced chromosome aberrations 79—34606
- nucleic acids in trigeminal neurons, γ-irrad. expts., rats 80—72270
- nucleoside effect, dependence on LET 80—35980
- nucleoside metabolism effects of γ-rays, Physarum polycephalum 80—30797
- nucleus, radiotoxicity of ^{125}I atoms not bound to DNA 80—104655
- OER for bacteria and cultured mammalian cells irrad. in frozen state, γ and neutron irrad. 77—90856
- oncogenic transformation of mouse 10T1/2 cell line in vitro, by UV light 77—12971
- oncogenic transformations in cultured mouse embryo cells rel. to X-ray dose fractionation 78—35893
- one-hit chromosome exchanges 78—3566
- oocyte nondisjunction in aged mice 77—16958
- oocytes, bovine, late effects of ^{60}Co gammas, oocyte survival, follicular devel. and reproduction 77—9231
- oocytes of Drosophila melanogaster, class B, repair of X-ray induced sublethal damage 80—35987
- oocytes of Drosophila melanogaster, Elkind-type recovery from X-ray induced damage 80—35988
- optic lobe neurosecretory cells of Poekilocerus pictus, effects of visual stimulation 79—5279
- oral epithelium, rat, ultrastruct. effects of X-irrad. 77—56434
- osteocytes from mouse proximal tibial metaphysis, early ultrastruct. changes after ^{224}Ra incorporation 77—37020
- osteosarcoma, human, in vitro, evidence for unusual cellular repair activity 77—48847
- ovarian cortex effect of daily prenatal gamma irrad. in beagle pups 80—85453
- ovary cells, Chinese hamster, heat killing and thermal radiosensitization at 42°C 80—45860
- oxidative phosphorylation in cauliflower mitochondria, radiation inactivation 78—48844
- pacemaker neurons, Aplysia, effects of irradiation with 20 MeV electrons 80—17013
- particle track structure analysis advantages over classical microdosimetry 80—26284
- pea roots, circadian rhythms of ultra-weak chemiluminesc. 77—70432
- pea roots, effects of localised US irradiation 79—48285
- peripheral reticulocyte count as biologic dosimetry of ionising radiation, mouse expts. 80—46051
- permeability changes after X-irradiation 79—39370
- phage ϕX 174 inactivation by accelerated ions, enhancement by δ-ray effect 80—36008
- phage T7, action spectra for UV and visible light inactivation 80—21498
- pheophytin reduction obs. in higher plant photosystem II 79—43817
- phosphorescence microscopy of X-irrad. cells 78—3454
- photo-dependent ^{14}C-alanine transport into H.halobium cells 77—70439
- photobiological conversion of solar energy *(German)* 79—2013
- photobleaching, meas. of cell membrane diffusion coeffs. 77—48962
- photodermatological uses of dye lasers, erythema production, psoriasis treatment, tumour destruction *(German)* 80—56164
- photoinduced H_2 evolution by Chlorella due to flashing lights primary processes 77—25398
- photoreactivation in E. coli bacteria after gamma-irrad. 77—29184
- photoreceptor electric potential in phototaxis of alga Haematococcus pluvialis 78—27909
- photoreceptor electric response, in invertebrates and vertebrates, quantitative model 77—44656
- photoreceptor function, rel. to prolonged depolarising afterpot. 78—15832
- photoreceptor light adaptation, Ca^{2+} ion as putative intracellular messenger 78—15833
- photoreceptor membrane fragment modified artificial lipid membranes, effect of light 77—77898
- photoreceptor membrane photostable pigments and possible role 78—15837
- photoreceptor membrane potential reconstruction from simultaneous intra- and extracellular recordings, S. atlantica 77—86494
- photoreceptor model, light-induced transmembrane channel form. in rhodopsin-containing bilayer membranes 77—52784
- photoreceptor voltage signal at visual threshold 77—16930
- photoreceptors, ventral, light-induced conductance changes in Limulus 79—8506
- photoreceptors, vertebrate, light-activated GTPase 78—3481

cellular effects of radiation continued
photoreceptors of Limulus ventral eye, sensitivity rel. to Ca^{2+} injection and light adaptation 78—44500
photorespiratory NH_3 cycling, reassimilation involving glutamine synthetase 79—2011
photosensory mechanism for Halobacterium, rel. to visual photoreception 77—90738
photosensory retinal pigments in Halobacterium halobium 80—97860
photosynthesis, Blinks effect rel. to two-photosystem hypothesis 79—57590
photosynthesis, delayed light 77—86466
photosynthesis, effect of bivalent cations on photo-induced redox conversions of P700 78—77014
photosynthesis, electron spin polarisation and mechanism of electron transfer in photosystem I 78—40122
photosynthesis, energy upconversion and minimum quantum requirement 77—29115
photosynthesis, fluoresc. and energy transfer, time resolved obs. 79—48216
photosynthesis, fluoresc. induction modelling by elec. diagram 79—57589
photosynthesis, in vitro models 78—77023
photosynthesis, interaction of paramag. probe I (12,3) with bean chloroplast membranes 78—77015
photosynthesis, nonadditiveness in action of light 78—40123
photosynthesis, O_2 formation rate on pulsed illumination 79—57606
photosynthesis, oceanic, in situ quantum efficiency determ. using photoelec. sensor chlorophyll simulator 79—39760
photosynthesis, picosec. spectroscopic investig. 78—68964
photosynthesis, picosecond fluorometry in primary events 79—8476
photosynthesis, primary, selectively excited by tunable ps parametric oscillator 79—48163
photosynthesis in green plants, principle of nonadditiveness, two photosystem concept 78—80842
photosynthesis of green plants, tripartite model for photochem. apparatus 78—44474
photosynthesis of higher plants, energy migration and electron transport, theoretical results 78—64957
photosynthesizers, contrived, biosystems and photoelectrochem. conversion 79 ·52953
photosynthetic efficiency of green spectral region for Chlorella 78—69010
photosynthetic electron transport in higher plants, adaptation rel. to light intensity 78—64953
photosynthetic energy conversion, quantum efficiency 78—44473
photosynthetic membrane, in vivo, light collection and exciton dynamics 79—48215
photosynthetic membrane model, electron transfer and charge separation in photoexcited chlorophyll aggregates 77—81468
photosynthetic membranes, exciton dynamics, picosecond pulse train study 79—8483
photosynthetic organisms, reson. energy transfer, fluoresc. decay times 77—81479
photosynthetic reaction centre, chlorophyll function 79—5251
photosynthetic reaction centres, primary electron transfer rate 79—8481
photosynthetic reactions of leaf discs and chloroplast preps. of crop species, 298 nm radiation effects 78—61220
photosynthetic systems, computer assisted scanning and kinetic spectrophotometry 78—68963
photosynthetic systems of higher plants, electron transport, P700 redox conversions, EPR 77—21494
photosynthetic systems of higher plants, electron transport, P700 redox conversions, EPR 77—21495
photosynthetic unit of H_2 evolution 77—77875
photosystem II, fluoresc. when electron transport on acceptor side is blocked 78—7324
phototropic response of Phycomyces, rel. to intracellular rot. 77—48837
phototropism of coprophilous Zygomycetes, review 77—90851
physical, molecular, cellular and macrocolony level obs. 80—12193
picosecond flash photolysis in biology and biophysics, book contrib. 79—5328
pigment reversible changes due to illumination of leaves 79—43818
pigmented biomembranes, photoelec. and magneto-orientation effects, review 77—48766
pine pollen, localisation of site of action of tube growth stimulation by micro UV-irrad. 77—56445
pine pollen grains, tube growth stimulation, site of action localisation 80—45982
pineal unitary response to light stimulation in frog central nervous system 77—52780
$pion^-$, cell survival over the depth profile after irradiation 80—26268
$pion^-$, chromatid breaks induced in Chinese hamster cells, rel. to X-irradiation 80—26270
$pion^-$, effects on monolayers and spheroids of Chinese hamster cells 80—26269
$pion^-$, genetic and cellular response, depend. on intrinsic props. of reaction systems, RBE 78—3562
$pion^-$, OER and RBE for beams of different peak widths, Chinese hamster cells 79—62301
$pion^-$, pre-clinical studies at TRIUMF 80—26264
$pion^-$, radiobiological data for clinical dosimetry in pion tumour therapy 80—26266
$pion^-$, radiobiological evaluation of suitability for tumour therapy 80—67166
pion biological effectiveness and O_2 enhancement ratio obs. 79—20595
pion cancer radiotherapy, RBE in and near large beam 80—12245
pion radiotherapy, biological effect prdiction, star distrib. for high LET dose determ. 80—12248
pith cell, growth in vitro after γ irradiation 79—92295
planarian, regeneration of epidermis and basement membrane after total-body X-irrad. 80—36022
plant growth and development regulation, role of light, review 78—11695
plant photosynthesis, solar energy conversion, book contrib. 79—43781
plant tissue acoustic microstreaming induced by Doppler foetal heart detector 79—62292
plants, light-induced intracellular and extracellular bioelec. reactions 77—56422
plasmid molecular weight determ. from UV sensitivities 78—44458
plateau phase cells, hyperthermia and radiation response, potentiation and repair 77—64099
platelet morphology and function modification by US exposure 77—77929

cellular effects of radiation continued
platelets, human blood, adenine nucleotide content and release reaction after ^{60}Co γ-irrad. 78—28021
pollen, Petunia, post-X-irradiation effects on germination 79—29569
Pollen, Pinus Silvestris, effect of X, UV irradiation on NAD(P), NAD(P)H, hydroxyproline levels 79—20582
pollen mother cells, tradescantia, meiotic chromosomes, stage sensitivity and dose response to X-ray 80—104648
polymorphonuclear granulocytes and FL-cells, effect of X-rays on membrane pot. and electrophoretic mobility *(German)* 77—56442
polyribosome distribution in regenerating livers of irrad. adrenalectomised rats 78—7398
population kinetic parameter derivation from clinical statistical data 79—43965
postreplication repair enhancement of Chinese hamster cells by UV light 78—92678
postreplication repair enhancements in UV-irrad. Chinese hamster cells by irrad. in G_2- or S-phase 78—77085
postreplication repair in mammalian cells after UV irrad., model 78—80918
pre-implantation embryos and implantation reaction in mouse, acute X-irrad. effects 78—69154
preimplantation mouse embryo sensitivity to UV irrad. in vitro, postreplication repair 78—20224
primordial germ cells in embryos of Oryzias latipes, γ-ray effects 78—48843
primordial germ cells of fish Oryzias latipes, nucl. size changes after γ-irrad. 78—53451
progression, in broad bean roots, monoenergetic neutron effects 78—65086
protein synthesis control studies, exptl. probe using psoralen and near UV light 77—66881
protein synthesis in human fibroblasts in vitro, US stimulation, role of cavitation 80—8100
protein-containing membranes, photoinduced electron transport 80—30768
proton RBE for normal tissue reactions and fractionated dose schedules 78—31858
proton relative biological effectiveness, microdosimetric interpretation of biological data 79—62306
proton relative biological effectiveness, microdosimetric parameters 79—62305
protoplast response to X-irradiation and a chemical mutagen 79—88121
pulmonary metastases, artificial, of EMT6 tumour in mice, cell response 77—12977
pulmonary metastases, artificial, of Lewis lung carcinoma, cell radiosensitivity 77—12978
pupillary sphincter, light-induced Ca release in photosensitive vertebrate smooth muscle 78—64994
purple membrane light energy transduction, bacteriorhodopsin photoreactions 77—90726
purple membrane light-driven proton pump mechanism in Halobacterium halobium 78—35820
purple membrane of Halobacterium halobium, energy transfer 78—44467
purple membrane of Halobacterium holobium, review 77—86457
purple membrane of H.halobium, effect of 560⇄570 transition and blue light on photochem. 80—30673
purple membrane protein chromophore, fluoresc. 78—44454
purple membrane protein chromophore photoisomerisation rel. to proton pump 78—35804
purple membrane structure, effects of bleaching and regeneration, H-halobium 77—86532
purple membrane suspensions, light-induced conductivity changes, pH and temp. effects 80—51157
purple membrane thin layers, hydration effects on bacteriorhodopsin photocycle 78—7320
pyri pyriformis,→pyriformis, 80—61648
pyrimidine dimers, excision repair of UV damage in monkey kidney cells 78—53332
quail embryo exposure to 2.45 GHz microwave radiation during development 78—20214
quality factor recommendations and dose limits 80—26369
R. sphaeroides, polarisation of photosynthetic membranes and reaction centres in elec. field 80—94277
radiation therapy, equivalence of quantitative models for tumour response 80—30770
radiography, foetal vs. parenteral radiosensitivity 80—51271
radionuclide therapy, pot. future appl. 80—36031
radionuclides incorporated into mammalian cell DNA, microdosimetry 80—12191
radionuclides incorporated into stem cell DNA, biological damage, radiation protection implications 80—12187
radiosensitivity of 6 human cell lines, comparative study with different statistical models 80—108967
radiosensitivity of CHO cells, negative pions rel. to X-rays at various cell stages 80—17021
radiosensitivity of mammalian cells, effect of salt solns., specific ion effects 77—86549
radiosensitivity of mammalian cells, effect of salt solns., treatment with hypotonic solns. 77—86550
radiotherapy, optimal fractionation for tumour cells with wide-shouldered survival curves 79—53192
radiotherapy treatment time and sub-lethal repair, CHO cell obs. 80—30773
radiovaccine of S. typhimurium cells 77—56426
rat embryo acute viral infection inhibition by whole-body microwave heating 80—3769
rat metastatic growth effect of local tumour hyperthermia 78—24115
renal damage following perinatal gamma irrad. in beagle 78—31866
repair and prolonged hypoxia 79—74721
repair competency changes after 5-bromodeoxyuridine pulse labelling and near UV light 79—83854
repair of potentially lethal and sublethal X-ray damage, effect of hypoxia and glucose, mammalian cells 78—7404
repair of potentially lethal X-ray damage, effect of hyperthermia 77—5054
repair of sub-lethal and potentially lethal damage in plateau-phase hamster cells 77—21567
repair rates determined by split-dose and dose-rate methods, comparison 80—104680

cellular effects of radiation continued
reproductive death and chromosomal aberrations in mammalian cells, RBE/LET 80−12189
reproductive death and chromosome aberrations obs. 80−30795
respiration in Halobacterium halobrium cells, photoinduced inhibition and stimulation 78−96066
reticuloendothelial system, granulopectic activity modification in mice exposed to 1 to 10 GHz fields *(French)* 77−21560
retina, effect of illum., colour photography obs. of Boll's phenomenon 78−24072
retina, light-damaged, rhodopsin content and electroretinographic sensitivity, rat 77−64033
retina, teleost, enhancement of hyperpolarising S-potentials of surround illumination 79−2051
retinal bipolar cell dark noise and stability of rod rhodopsin 78−11644
retinal damage by visible light, role of singlet O 78−15858
retinal damage from suprathreshold Q-switch laser exposure 79−5274
retinal ganglion cell activity induced by ELF mag. fields, method for study 80−56321
retinal ganglion cell response to sinusoidal flicker, mudpuppy 78−48798
retinal photocoagulation by laser beam, temp. and bleaching dynamic meas. *(German)* 79−2098
retinal pigment epithelium, variations in phagosome content rel. to cyclic lighting 77−90772
retinal rod external segment mag. anisotropy decrease after total photolysis 77−52838
retinal tissue damage, by single ultrashort laser light pulses 78−96065
retinular cell spectral sensitivities in bumblebees, optical method meas. 79−2057
RF radiation effects on inflammation, white cell counts 78−40253
RF wave applicator for investigating effects on mammalian cells 79−100802
RF-field interactions with biological systems, elec. props. and biophys. mechanisms 80−35957
rhabdomyosarcoma, rat, response to Ne and He ion irrad. 79−25042
rhodopsin membrane at oil-water interface, effect of illumination, rel. to cephalopod visual cells 77−44646
rhodopsin phosphorylation as possible mechanism of visual adaptation 78−15836
ribonucleotide reductase of E.coli, in vivo photoinactivation by near-UV 77−52841
RNA, heterogeneous nucl., effects of UV irrad. and postirrad. incubation on size in murine cells 78−69139
RNA of Novikoff Hepatoma ascites cells, effects of sparsely-ionising radiation after in vivo labelling 78−7389
RNA specific activity, Novikoff Hepatoma ascites cells 78−3560
RNA synthesis in regenerating liver of irrad. adrenalectomised rats 77−64087
RNA synthesis in slime-mould, effects of electrons and neutrons, caffeine modification 77−12962
rod external segment fragment suspension, Ca^{2+} activity rel. to illum. 77−36918
rod outer segment birefringence changes following intense light flashes, frog 77−90789
rod outer segment disc shedding in rat retina, rel. to cyclic lighting 77−32887
rod outer segment membrane, bovine rhodopsin conform. 77−44587
rod outer segment membrane current, light-induced fluctuations recorded in single toad rod 77−86493
rod outer segment shedding, intraocular initiation 78−85309
rod outer segment tip shedding in frog retina, rel. to light stimulation 77−29148
rod outer segments, accel. membrane renewal after light exposure 77−64035
rod photoreceptor disc membrane, cooperative conform. change induced by bleaching 77−81499
rod photoresponse, contrib. of Cs^{+}-sensitive cond. increase 78−44501
root meristem cells, 2 MHz US effects on DNA, RNA and protein synthesis 77−9218
root meristem cells, Vicia faba, micronuclei induction, X-ray rel. to US exposure 79−96633
root meristem cells, Vicia faba, subnuclear chromosome aberrations rel. to neutron energy deposition 80−26280
root meristem cells of Pisum sativum, increased G_2 duration after sonication obs. 80−56117
root meristems, Pisum, inhibition of cell-cycle progression by unincorporated ^{3}H-thymidine 77−56425
root meristems, Vicia faba, X- and neutron-induced cell progression delay 77−56437
Salmonella typhimurium LT2 mutants, effects of microwave radiation and heat 80−108958
sarcoma, dose fractionation studies on mice breathing air or O_2+CO_2 78−35889
sarcoma in vivo response, effect of pre-irrad. breathing times of O_2 and CO_2+O_2, mouse 78−35888
sea-urchin egg radiosensitivity during early cleavage stages, split-dose ^{137}Cs γ-irrad. 78−7392
seasonal oscillation of radiosensitivity of cells in culture 78−7397
sensitivity to radiation, physical aspects 80−67162
shouldered dose-response curve shape 77−64090
single-strand breaks at short times after irrad., radiation chem. and enzymatic processes 77−12965
sister chromatid exchanges, X-induced, cultured mammalian cells 79−43832
skin, cell migration following irrad., effect of shielding minute areas, mouse 78−24099
skin, cumulative radiation effect, cell survival description 80−30771
skin, mouse, effect of dose rate on prod. of early and late X-ray damage 77−70497
skin, rats, cellular survival kinetic parameters after fractionated irradiation 80−21496
skin, swine, response to single acute X-ray exposures, epidermal cell changes quantification 80−72245
skin γ and neutron responses, dose fractionation effects 79−20593
skin acute response, human, pion^{-} relative biological effectiveness 79−20596
skin fibroblasts from retinoblastoma patients, X-ray sensitivity 77−48848
skin growth regulation, mouse, after X-irradiation, possible role of chalones 79−16168
skin melanoma therapy by laser irradiation *(German)* 80−12208
slime mold, Physarum polycephalum, effects of ELF fields 80−56129

cellular effects of radiation continued
slime mould mitotic cycle lengthening by ELF waves 79−25032
slime moulds, γ-irrad. effects on species-specific cell sorting-out 77−44720
small intestinal cryptogenic cells in W/W^{v} mutant mice, survival curves after X-irradiation 79−11980
small peptide antibiotic and protein solns., US absorption 79−48286
soft fruit cell walls, histochem. effects of γ-irrad. 80−81652
soft X-rays, RBE, rel. to ^{125}I therapy 78−7405
somatic cell hybrid, intraspecific, radiation response obs. 80−72246
somatic cell hybrids, X-ray sensitivity 77−21574
spatially correlated ions studies, background and theory 80−36024
spatially correlated ions studies, cell survival obs. using diatomic deuterium 80−36026
spatially correlated ions studies, multiple scatt., expt. facility and dosimetry 80−36025
sperm cells of eri silkmoth, γ-ray induced chromosomal breaks 80−41123
sperm count reduction and abnormal sperm increase after X-irrad. or ^{22}Na injection, mouse 80−108961
spermatocytes, mouse, stage-sensitivity and dose-response after gamma-irrad. 77−29182
spermatogenesis cell population kinetics under longterm fractionated irrad., mice *(Russian)* 77−48849
spermatogenesis in sugarcane root borer, γ irradiation effects 79−34608
spermatogenesis of fish Oryzias latipes, fast neutron effects 77−86553
spermatogenic cell damage in fish exposed to tritiated water 78−28016
spermatogonia, role in recovery from temporary sterility in fish 77−5038
spermatogonia, stem and differentiating cells, ^{60}Co gamma-ray effect, postpuberal rat 77−25515
spermatogonia of fish, Oryzias latipes, X-irrad. effects 77−5045
spermatogonial stem cell survival in mouse, split dose neutron and X-irrad. 78−28012
spermatogonial stem cells, mouse, survival after split-dose irrad. with fission neutrons 80−72244
spheroids, V79, split-dose survival and cycle progression 77−56430
spheroids grown in different O_2 concs., survival obs. 80−76792
spheroids of V79 Chinese hamster cells, variable radiobiological responses 80−98028
spinach chloroplasts, laser photoinduced changes in high freq. dielectric constant 80−85449
spinal cord, rat, neuroglial cell population changes after local X-irradiation 79−100671
splenic cells, rat, enhanced cytotoxic reactivity after X-irrad. 78−85343
splenocyte locomotion, X-ray inhibition and bacterial protection 79−25047
spore radiobiology, conf., Tokyo, Japan (May 1979) 80−101660
spores exposed to pulsed electron irrad., decay of potentially lethal O_2-depend. damage 78−20217
spores of Bacillus megaterium, wet, anoxic damage enhancement by electron pulses 80−26296
spores of Bacillus pumilus E601, radiation resist. changes 77−52846
spores of Bacillus subtilis, inactivation by heavy ion irradiation 80−26294
spores of Bacillus subtilis, mutagenic effect of water-t 78−80928
spores of Bacillus subtilis inactivation rel. to heavy ion impact parameters 80−26288
squamous-cell carcinoma, spontaneous, in mice, comparison of neutron- and X-irrad. effects 80−98033
sterilisation modes, cell killing and early differentiation 78−65093
stomatal function, blue light-stimulated swelling of guard cell protoplasts 77−77885
Streptococcus, effect of ionising radiation on transmembrane pot. 80−36019
structural model, of radiation effects in living cells 77−37016
sub-lethal damage accumulation site, evidence for location in Chlamydomonas 78−7390
subcellular particle membrane pot. diff., proton channels in oxidative phosphorylation 78−64964
sublesion combination probability, molecular ion expt. 80−26285
sublesion production and interaction, primary ionisation cluster nanodosimetry 80−26278
sublethal damage repair in multi-cell spheroids, fast neutrons vs. X-rays 77−25512
supralinear photographic emulsions, radiobiological aspects 80−26290
surface photoelectron micrographs and quantum yields 78−61148
surfactant early release following lung irrad. of alveolar type II cells 80−94291
survival, fractionation and dose-rate effects at lowered temps. 78−28013
survival as function of depth, modulated negative pion beams 79−43966
survival curve, initial part-implications for low-dose, low-dose-rate radiation responses 78−15864
survival curves, biological variability model 80−108978
survival data, new approach to anal. 80−30800
survival dependence on radiation quality, models and exptl. data analysis 80−26287
survival derivation method using tissue damage obs. after fractionated irrad. 80−36016
survival formulation, nature and limitations of approx. 80−98017
survival kinetic parameters for cell populations derived by computer simulation of radiobiological data 77−56433
survival model appls., fixation time picture 78−65087
synchronised cultured human liver cell survival after UV-irrad. 77−56439
synchronous HeLa cells exposed to low LET radiation, OER 77−37019
synchronous HeLa cells in culture, dose-rate effects 78−28010
synergism of radiation and other DNA damaging agents 80−26299
testes, γ-irrad., glycogen a metabolising enzymes following radiation-induced atrophy 78−15869
testes, glucose 6-phosphate dehydrogenase studies following partial body γ-irrad. 78−80924
testes, inorganic pyrophosphatase and pyrophosphate following γ-irrad. of rat 78−15868
testes, isocitrate dehydrogenase studies after partial-body γ-irrad. 78−80923
testes, mice, comparative effects of various radiations on weight loss and spermatogenic stem-cell survival 80−108976
testes, monovalent electrolytes rel. to radiation injury of germinal epithelium 78−31862
testicle, influence of duration of Ra irrad. 78−3556
testicular stem cell, mouse, regeneration after γ irradiation 79−25048

cellular effects of radiation continued
testicular tissue, mouse, morphological changes from in vivo US irrad. 80—35959
testis, interstitial cell tumour induction by X-irrad. 77—90860
testis cells, mouse, radiation damage from $^{99m}TcO_4$ 78—24103
testis damage by ^{125}I in partially blocked thyroid of rats 78—3565
testis radiosensitivity, rel. to alternating rhythm of cellular mitoses 78—3557
Tetrahymena, γ-irrad., role of DNA damage and repair in eukaryotic gene function 80—104677
thermal neutron beam response of hamster and HeLa cells containing various concs. of ^{10}B 78—73178
thermal sensitivity of mammalian cells to pulsed CO_2 laser irrad. and hyperthermia 78—15802
thermocytes, rat, US-induced changes in rates of influx and efflux of K^+ in vitro 80—89793
thylakoid membrane of green plants, simulation of electron transport in primary photosynthesis reaction, in PL/1 *(German)* 77—86468
thymine damage in chromatin from heated cells after X-irrad., excision obs. 80—45980
thymine dimer excision from DNA of UV-irrad. plant seedlings 78—61221
thymine dimer excision kinetics in UV-irrad. human cells 78—53331
thymine dimer induction by UV as function of cell stage 79—57715
thymocyte membrane props. modification by hyperthermia and gamma-rays 78—69017
thymocytes, negative surface charge reduction and thymic phagocytosis after X-irrad. 80—81663
thymocytes, rat, reduction of interphase death by hyperthermia 80—108970
thymus dividing cells, recovery response, in whole-body gamma-irrad. mice 77—12968
thyroid, mouse, cellular and tissue changes after local X-ray irrad. 77—66826
thyroid cell survival after irrad., directly generated single dose survival curve 80—36014
thyroid cells in culture as radiobiological model, sheep, culturing method 80—41327
thyroid radiobiological response, sheep cells, single X- and γ-doses 80—41122
tight junction disruption and recovery after sublethal γ-irrad. 80—36027
tissue response to multiple small dose fractions 78—15865
total body irradiation, radiobiological bases 80—104667
track structure theory in radiobiology and radiation detection 78—50446
track theory of survival appl. to neutrons 77—12970
Trandescantia, somatic mutations induction by low-dose irrad. from ^{131}I 80—72266
transcriptase switch-on perturbed by ionising radiation 80—3733
transducer noise in locust photoreceptor, intracellular responses 79—34560
transplantable tumour response to fractionated fast neutrons plus Ro-07-0582 77—86558
triton bombardment of human blood cells, morphological detail of radiation damage 77—60230
tumour, effect of vascular occlusion on thermal sensitization and X-irradiation in mouse 79—16253
tumour, murine, cure, cell survival and tumour growth delay, X-ray effect 77—48840
tumour and normal cell microwave transmission 79—2107
tumour cell chromosomes, effect of electrostatic fields 79—62212
tumour cell in vitro radiosensitivity and recovery, effect of 1400 gauss mag. field 77—44723
tumour cell optimal radiotherapy for exponential-quadratic survival curves and exponential repopulation kinetics 77—81555
tumour cell survival with fractionated doses, pitfalls in use of in vitro survival curves 78—77084
tumour cells, acutely hypoxic, recovery from sublethal damage 79—88116
tumour cells, Ehrlich ascites, lethal effects of ^{64}Cu-bleomycin complex 79—57709
tumour cells, explanted, reproductive survival after exposure to nitrogen mustard or X-irrad. 77—37023
tumour cells, human, effect of irrad. feeder cells on X-ray survival curve shape 80—98032
tumour cells, human, from pancreatic carcinoma xenograft, in vitro and in vivo radiosensitivity 77—5041
tumour cells, human, X-ray sensitivity in vitro 80—104665
tumour cells, interaction of hyperthermia with fast neutrons or X-rays on local tumour response 77—9230
tumour cells, thermotolerant, hyperthermic radiosensitisation 79—74600
tumour curability, cellular radiosensitivity and clonogenic cell number 78—3551
tumour growth inhibition in mice, microwave irradiation, 3000 MHz 79—2101
tumour model, potentiation of radiation lethality by hyperthermia 79—25037
tumour model in vitro, repair and reoxygenation following irrad. 77—44727
tumour regrowth after irradiation in rat hepatoma 79—92292
tumour response to fractionated fast neutron irrad. rel. to X-rays 77—12974
tumour response to neutron radiation therapy, animal expts. 79—20594
tumour X-irrad. in vivo, enhanced lymphocyte-mediated killing of tumour cells 78—77086
tumour X-radiation response after prior exposure to reduced O_2 environment 79—88127
tumours, biological effect of 27.12 MHz SW diathermy 79—2102
tumours, effect of wide field irrad. on uniradd. tumours in same host 77—70502
tumours, fractionated irrad., math. derivation of optimal treatment schedules 80—98078
tumours, spontaneous, in dogs and cats, treatment by ultrasound-induced hyperthermia 79—62290
US, 1 MHz, lysis and viability of cultured mammalian cells 78—7384
US, 2 MHz, effects on growth and mitotic index of Pisum sativum roots 78—7385
US, biochem. effects on mouse and human cells and tissues 80—30764
US activation effect on gas-filled intercellular channels of Elodea leave at 1 MHz 78—24093
US cellular inactivation, thermal and non-thermal components 77—48835
US effects on mammalian cells and chromosomes in vitro 78—40240

cellular effects of radiation continued
US effects on pregnant mice and embryos in utero 78—35880
US irradiated cells, temp. distrib. calcs. 80—61623
US perturbation obs. at cellular level 78—61214
US therapeutic level effect on HeLa cells 78—24092
US treatment of Chinese hamster cells at high intensities and long exposures 77—5026
uterine cervical squamous cell carcinoma, biological props. and radiation repsonses, hamster 80—36023
UV, correls. in human diploid fibroblasts after potentially lethal damage 80—21493
UV, dNA repair and longevity assurance in Paramecium tetraurelia 80—3741
UV and X-ray damage, interaction in Chinese hamster cells 79—11977
UV induced unscheduled DNA synthesis, chromosomal localisation 77—25520
UV irradiated human strain cells, herpes virus production as repair marker 80—30783
UV sensitive mouse neuroblastoma cells, DNA replication and post-replication repair 77—5027
V79 cells, dose-rate effects on cell cycle and survival 80—76794
V79-spheroids, survival and kinetic response after heavy ion beam exposure 80—104651
vascular permeability in rat ears after X-irradiation 79—5330
vibrios UV inactivation kinetics 77—90854
visible fluorescent light, mutagenicity and toxicity to cultured mammalian cells 77—48838
visual adaptation 78—15834
visual cell membrane cond. control, arthropod 78—15831
visual cortex increase on exposure of dark-reared rats to light 78—24069
vitamin C radioprotective effects obs. in Chinese hamster ovary cells 77—73546
vitamin E distribution among tissues and subcellular fractions in sublethally irrad. mice 77—64098
VUV, broad-band synchrotron radiation, effects on wet yeast cells 80—108972
wallaby cells, absence of effect of photoreactivation on sub-lethal damage accumulation 79—11970
X-irradiation, survival after hypoxic irradiation 79—74719
X-irradiation, vitamin E deficiency and lipid peroxidation, mouse obs. 80—72263
X-irradiation of diploid cell culture, neoplastic transformation 80—51172
X-ray, cell survival at low O_2 tension and dose build-up in Ar 80—72220
X-rays and hyperthermia, effect of post-exposure incubation conditions 78—40273
yeast, diploid, liq.-holding recovery in γ- and α-irrad. cultures 77—2028
yeast, diploid, OER rel. to exposure temp., hyperthermia 77—5036
yeast, diploid, radiation sensitive mutants, γ-ray response and recovery obs. 80—101227
yeast, haploid, sulphydryl content var. rel. to radiosensitivity 78—7394
yeast, hyperthermic inactivation and interaction of hyperthermic and γ-irradiation damage 79—96518
yeast, inducible enyzme synthesis, UV effects on regulation and activity per cell 78—69157
yeast, sensitivity to ionising radiations and damage repair 80—81659
yeast, UV-inactivation kinetics and division delay during different growth phases 77—25517
yeast Candida guilliermondii, photoprotection and reversible inactivation by 313 nm light 77—25509
yeast cell, caffeine inhibition of liquid-holding recovery from UV induced budding delay 79—11985
yeast cell electrophoretic mobility, X-ray effect 78—31868
yeast cell mutagenesis by storage in tritiated water 80—17017
yeast cell suspensions, vac. UV irrad., 163 nm, lethal and genetic damage 77—21573
yeast cells, alpha-irrad., UV-induced reactivation 78—80920
yeast cells, budding, genetic control of X-ray resist. 77—37024
yeast cells, determ. of thermal equivalent to MM microwaves 80—67151
yeast cells, dried, inactivation by accelerated heavy ions of very high LET 80—108965
yeast cells, elevated temp. effect on radiation sensitivity 79—79610
yeast cells, irrad. by weak microwaves, reson. growth rate response 78—3549
yeast cells, reparable and irreparable damage induced by sparsely ionising radiation 80—51167
Yoshida sensitive and resistant cells, dimer form., excision and DNA strand growth after UV irrad. 77—90858
π^- irradiation of Chinese hamster cells, OER 79—88126
Al ultrasoft X-rays, mammalian cell inactivation and mutation, theory of dual radiation action 77—86548
Al ultrasoft X-rays, phys. props. and Chinese hamster cell expts. 77—86542
Al ultrasoft X-rays, vs. different LET radiations, response of Chinese hamster and human diploid cells 77—86543
Ar ions, high-energy, chromosome aberrations in aerated and hypoxic Vicia faba root meristems 78—7403
Ar ions, high-energy, RBE OER and cell cycle response 78—3558
CO light-dependent net prod. by intact plant shoots, rel. to photorespiration 79—2010
Ca^{2+} effect on rat cell electrophoretic mobility after X-irrad. 79—92293
Co teletherapy, T3-carcinoma in Bilharzial bladder, hyperfractionation and conventional fractionation comparison 80—41179
^3H induced lethal and genetic changes in yeast Saccharomyces cereinsiae 78—28015
^3H-thymidine, cell survival and cytogenic responses, mammalian cells 77—5046
He^{2+} 650 MeV beam relative biological effectiveness as function of depth 80—26281
He^{2+} 650 MeV ions study for possible radiation therapy applications *(French)* 77—66835
HeLa cells, changes in sensitivity after split doses of X-rays 79—74726
HeLa cells, synchronised, DNA damage from UV irradiation 79—25034
^{125}I thyrotoxicosis management, dosimetry, radiobiology, clinical aspects 77—2048
^{125}I toxicity in cultured mammalian cell, primary site for division delay 77—52851
^{125}I-iododeoxyuridine, cell survival and cytogenic responses, mammalian cells 77—5046
5-^{125}I-iododeoxyuridine as prototype for radionuclide therapy with Auger emitters 77—29186

cellular effects of radiation continued
  ^{131}I in tissue, specific energy calc. in accordance with crit. cell concept 77−2031
  ^{131}I-iododeoxyuridine, cell survival and cytogenic responses, mammalian cells 77−5046
  K^+ permeability of E. coli, membrane lipid role in radiation damage 78−48834
  ^{20}Ne, high-LET, effects on brain, eyes and other hand structs., mouse 79−66489
  O_2 effect, rel. to cellular glutathione 78−31861
  O_2 effect fast kinetics in electron irrad. mammalian cells 78−48836
  O_2 effect throughout cell-cycle of human cell line NHIK 3025 cultivated in vitro 77−44724
  O_2 enhancement effect, photo-reactivation of γ-radiation damage 78−77087
  O_2 enhancement ratio, hypothesis test and microdosimetric implications 80−26212
  O_2 radiobiological effect, molecular and cellular basis 80−26211
  O_2^- superoxide ion as cause of O_2 effect, X-ray induced cell lethality 77−25513
  Pt complex potentiation, of X-irrad. lethal effects, rodent cells 78−85345
  ^{239}Pu in tissue, specific energy calc. in accordance with crit. cell concept 77−2031
  $^{239}PuO_2$ alpha-particle freq. in lung cells 78−69151

cellular method
  disordered system, scaling near mobility edge 77−11835
  extended rigorous cellular method, theory and appl. to films 78−52055
  linear rigorous cellular method, modified 79−51468
  nonspherical potential calc., appl. to Cu and graphite 78−56063
  variational cellular model for mol. and cryst. elec. struct. 78−29726
  Na, variational cellular method, electronic struct. calcs. 80−54591
  UN, density of states calc. 80−6715
  US, density of states calc. 80−6715

cellular transport and dynamics
  see also cell motility
  acetylcholine receptor electrophoretic movement in embryonic muscle cell membrane 78−85298
  acetylcholine receptor response to rapid photochem. prod. increases in agonist conc. 77−36909
  action potential propagation, effects of cellular geometry on current flow 80−94196
  action potential sources and their volume conductor fields 77−44640
  active transport, rel. to second law of thermodynamics 77−9178
  active transport, review 78−15814
  active transport and energy transformation, quantum mechanism 78−53364
  ^{14}C-alanine transport, photo-depend., into H.halobium cells 77−70439
  alga intracellular potential, effect of ionic composition of external medium 78−20157
  algal host cells, kinetics, mechanism and thermodynamics of cyanophage A-1 absorpt. 79−57614
  amino acid, permeability of E. coli K-12 78−77029
  amino acid absorption by rat intestinal prep., effect of supralethal X-irrad. 77−56444
  amino acid stimulatable transport system in rat liver after hole-body γ-irrad. 78−65098
  amino acid transport hormonal control in liver of rats exposed to whole-body γ-irrad. 78−65099
  amino acid transport in lymphoid cell lines, differences in ionising irrad. effects 80−72264
  amino acid transport in rat liver after whole-body gamma irrad. 77−9232
  anterior pituitary cell action pots., stimulation by thyrotropin-releasing hormone 78−48771
  antibody binding and complement interactions at the cell surface, dynamics, book contrib. 80−30689
  aortic wall, albumin transport during acute angiotensin induced hypertension 77−44619
  apical membrane of toad gallbladder, K^+ selective channels 79−2018
  asymmetrically permeable membrane channels in cell junction 80−94187
  Na^+, K^+-ATPase, identification of membrane-embedded segment of large polypeptide chain 78−3447
  atrial muscle, cyclic GMP rel. to negative isotropic effect of acetylcholine 77−48781
  atrium, bullfrog, mechanisms for positive inotropism of low-K Ringer soln. 77−77884
  atrium of bullfrog, tension components and temp. effects 77−52760
  autorhythmicity and entrainment in excitable membranes 80−108866
  axon, giant, Myxicola, internal Cs^+ dialysis, Na inactivation 78−96036
  axon, giant squid, current fluctuations obs. 79−24973
  axon, squid, Ca buffering, review, book contrib. 79−5267
  axon, squid, Na channel inactivation, removed by high internal pH or tyrosine-specific reagents 79−20534
  axon, squid, physiological role of ATP driven CA^{2+} pump 79−43865
  axon, squid giant, exponentiated exponential model g Na^+ and K^+ cond. changes 78−44493
  axon, squid giant, temp. effects on gating currents 78−96037
  axon, squid giant, transient polarisation currents 77−86477
  axon asymmetry currents and admittance, squid 77−73518
  axon membrane, squid, freq. domain anal. of asymmetry current 80−51064
  axon membrane asymm. current, squid, freq. domain anal. 78−44494
  axon Na conductance and Ca transport, squid, mol. model 78−85305
  axonal K^+ transport, single-file model for squid giant axon 77−73517
  axonal membrane of mammals (myelinated fibres), K channel conduction 80−61538
  axonal transport, components, mechanisms and specificity, book contrib. 79−96551
  axonal transport, theoretical approach to anal. 80−67064
  axonal transport and microtubules in rabbit tissue after 3.1 GHz pulsed microwave irrad. 77−64097
  axonal transport of vasoactive intestinal peptide in sciatic nerve 80−21463
  axons, squid, effects of internal and external cations and ATP on Na-Ca and Ca-Ca exchange 77−90745
  axoplasmic transport, slow, asymm. in branches of bifurcating axons 78−80848
  axoplasmic transport in mammalian nerve, role of Ca^{2+} 78−24052
  axoplasmic transport of proteins, review 80−21464

cellular transport and dynamics continued
  bacteria, attachment to solid surface, influence of substratum critical surface tension 79−79493
  bacteria, motion, quasi-elastic light scatt. 77−23617
  bacteria chemotactic behaviour regulation by Ca^{2+} 78−15851
  bacteria motility, proton pump as molecular engine 78−40130
  bacterial cells, tethered, rot. rate and direction detect. apparatus 77−73620
  bacterial chemotaxis in Escherichia coli, membrane pot. changes 77−44695
  bacterial flagella, protonmotive driving force 78−48774
  bacterial flagella rotation rel. to ion transport down electrochem. gradient 77−73515
  bacterial movement in viscous environments 79−43840
  barbiturate-induced slow outward currents in Aplysia neurones 78−80866
  bimolecular lipid membranes, electrophoretic mobility 79−79479
  bioenergetics and proton-electron systems of membranes, review 78−96030
  biological n-compartment model, identification by filtering techniques 79−34507
  biomagnetic fields and cellular current flow 80−101192
  biomembrane transport catalysis, ADP,ATP carriers of mitochondria *(German)* 79−29512
  Biophysical Society, 23rd annual meeting, conf., Atlanta, USA (Feb. 1979) 79−34468
  black lipid membranes, permeability of cyclic nucleotides 79−39376
  blastocyst, rabbit, amiloride-sensitive rheogenic Na^+ transport 78−15812
  blood, effect of flow channel thickness on surface-induced damage 79−39439
  blood, Fahraeus effect and cell screening rel. to dextran-induced aggregation 79−62273
  blood, Fahraeus effect and cell screening rel. to volume flow rate 79−62272
  blood, flowing, electrical resistivity changes *(Japanese)* 79−2015
  blood, transport of catecholamines from adrenomedullary cells 79−66464
  blood cell banding in US standing wave field 79−62291
  blood cell motion dynamics tracking and quantification, automatic picture processing method 79−53074
  blood cell permeability to K^+, Na^+ repair after X-ray, fast-neutron damage 79−57615
  blood cell speed absolute meas. in retinal vessels, using laser Doppler velocimeter 79−83884
  blood cell suspensions, stability to small disturbances in circular Couette flow 80−56099
  blood cells, electrokinetic props. on exposure to phys. factors 77−70431
  blood cells, red, Ca stimulated increase in K permeability, dog 79−62218
  blood corpuscle settling rate automatic fast meas. *(German)* 79−5413
  blood flow through narrow capillaries, rheological mechs. 80−97961
  blood mech. transfer function, modifications by some biological factors and study method 80−16969
  blood vessel walls, active and passive transport of Na^+ and K^+ 77−44618
  blood viscosity and red cell aggregation changes after haemodilution 80−97952
  blood volume control after haemorrhage, model and implication for intravenous fluid therapy 77−40697
  bone, transport mechanism between blood supply and osteocytes in long bones 77−86472
  brain capillary endothelial cells, Na^+-dependent neutral amino acid transport 79−57616
  brain mitochondria, mechanism of oxidative phosphorylation 79−53068
  brush border of renal proximal tubule and intestinal mucosa, review 78−15815
  burn-induced leakage of macromolecules in living tissue 79−29514
  burnt skin heat and water losses, thermal modelling 78−31790
  cameral liquid transport rel. to buoyancy control in chambered nautilus 80−89732
  capillary permeability determ. from multiple indicator data, effects of finite red cell permeab. 78−44483
  capillary permeability evaluation from multiple indicator data, effects of red cell and tissue exchange 80−101193
  capillary tracer exchange, 4-phase model 80−101152
  carbohydrate active transport in membrane vesicles of Acholeplasma laidlawii cells 78−64965
  cardiac blood pool visualisation, ^{99m}Tc labeled red blood cells and serum albumin 79−29601
  cardiac conduction and propag., equiv. cct. 78−31791
  cardiac intracellular pools, Ca dynamical modelling rel. to muscle contractive force 79−79568
  cardiac Purkinje fibres, intracellular Na^+ activity rel. to tension, sheep obs. 80−51060
  cardiac Purkinje fibres, sheep, intercellular clefts effect on elec. props. 79−34522
  cell permeability polarity and control by phytochrome, red light irrad. of mass 78−77025
  centripetal particle transport, local inhibition where LETS protein pattern appear, 3T3 cells 77−32881
  cerebellar Purkinje cells, synaptic action depression by inferior olive destruct. 79−34544
  cerebral angiography, cortical pO_2 and K^+ dynamics rel. to contrast agent neurotoxicity 78−35954
  cerebral ventricle, intact, site for allografted mature superior cervical ganglion fragments in rats 79−8493
  charge transfer in thin membranes, discrete models, nonsteady state at high polarising voltages 78−69023
  chemically reacting system, temporal oscillations 77−25359
  chemoreception physics 78−15850
  chloroplasts, isolated, effect of temp. on photo-induced pH gradient 80−81566
  cholesterol transmembrane movement in human erythrocytes, radioactive tracer expt. 78−3459
  cholinergic channel without const. field, permeab., phase-boundary pot. and conductance 77−60191
  cholinergic synaptic vesicles, morphological and biochem. heterogeneity 77−64024
  chromaffin granules, osmometer model for changes in buoyant density 77−90737
  chromatophores of photosynthesising purple bacteria, sorption and desorpt. of water 78−69012

cellular transport and dynamics continued
chromatophores of Rhodospirillum rubrum, cyclic rel. to non-cyclic electron transport 79—53067
ciliary motor responses, intracellularly recorded receptor currents 79 11916
cochlea, mammalian, fluid flow permeability through hair cell cilia 79 53157
cochlear endolymph Ca content 78—61203
colon Na transport in vitro, rabbit, amiloride effect blocked and reversed by p-chloromercuribenzene sulphonate 78—44479
conductance fluctuations in cultured spinal neurones induced by γ-aminobutyric acid 78—80867
cone ionic channel closure, turtle 78—15830
cone outer segments, light-induced changes in membrane current, tiger salamander and turtle 80—108899
corneal hydration endothelial control theory 78—35841
cortical spreading depression, math. model 78—80857
crustacean neuromuscular junctions, synaptic facilitation obs. 79—39412
current noise parameters in embryonic heart cell aggregates 80—21459
cystic fibrosis, mitochondrial Ca uptake and O_2 consumption 79—43839
D-leucine, exchange diffusion in mouse Ehrlich ascites tumour cells, temp. reduction effect 80—67053
digitalis inotropy rel. to enhanced slow inward Ca current 78—61155
digitalis receptor binding, Na^+,K^+-ATPase as model 78—40111
directed locomotion arising from strongly biased turn angles 77—21502
disturbed cell renewal systems simulation via microprocessor system 79—48227
drug radioreceptor analysis applications 80—94315
dystrophic muscle, neuromuscular transmission in abnormal fibres 78—27932
E. coli migrating chemotactic band, spatio-temporal struct. 79—62215
eel electroplaque, temp. dependence of four ionic processes of spike electrogenesis 77—36899
egg cell membrane elec. props 80—21455
egg cell membranes, starfish, inward rectification blocking model 80—61523
Ehrlich ascites tumour cell, thymidine transport kinetics and DNA synthesis, X-ray effects 78—20215
Ehrlich ascites tumour cells, influence of O_2 tension of X-ray-induced fall in anodic mobility 79—34526
electrical connection of cells without highly permeable cell contacts 77—70440
electrically excitable membrane, phys. model, voltage-current characts. 77—25382
electro-orientation and dielectrophoresis meas. devices *(Russian)* 80—51300
electrodiffusion, steady-state, scaling, exact. soln. and phase plane 77—25403
electrogenic Na pump, role in slow synaptic inhibition 77—48780
electrolyte transport across a simple epithelium 79—88063
electron and proton transport in membranes 80—67052
electron flow, photosynthetic and respiratory, in dual functional bacterial membrane 80—16914
electrophoresis along cell membranes 77—25405
electrophoresis of concanavalin A receptors along embryonic muscle cell membrane 77—29121
electrophoresis of proteins in intercellular bridges 80—89734
electrophoretic mobility test, diagnosis of malignant tumours 79—79680
endocrine tumours, silent, feedback system cell number change effects, steady-state anal. 79—20526
endocytosis, review 78—15816
endplate acetylcholine-induced channels and transmitter release, humans 78—24063
endplate channel lifetime and cond. alteration by permeant cations 78—3467
enzymes, membrane bound, influence of membrane fluidity on activity, book contrib. 80—30688
enzymes, monosubstrate inhibited, conc. response, multiplicity and memory in membrane transport 80—30679
epithelia, pathways for hydraulically and osmotically-induced water flows 77—29112
epithelial cell, phospholipase A and mechanism of aldosterone action 78—24053
epithelial cells, of unpoisoned non-depolarised frog skin, intercellular junctions 77—12897
epithelial K active transport system of insect midgut, pump-mediated efflux 78—80846
epithelial membrane conductance rel. to extracellular shunting, rabbit salivary duct 77—77881
epithelium, fluid-transportin, tight junctions in an insect 80—3613
epithelium, fluid-transporting, ion distrib. determ. by electron-probe X-ray microanal. 77—4991
epithelium, leaky, effect of plant cytokinins on microfilaments and tight junction permeab. 77—12899
epithelium, living, size and shapes of lateral intercellular spaces 78—77032
epithelium, small intestine, asymm. behaviour under influence of osmotic press. 77—52747
epithelium intercellular contacts, small intestine, permeab. and mech. props. regulation by Ca ions 77—81482
epithelium membrane permeability, effect of intracellular Na conc. 77—32882
erythrocyte, flow resistance into pores 80—61609
erythrocyte, human, chloride distrib. and transport, cell membrane struct. 77—1983
erythrocyte Ca transport in myotonic muscular dystrophy patients 78—80849
erythrocyte filtration through polycarbonate filter determ. method *(German)* 79—79708
erythrocyte flow behaviour, particle motion in ghost cell conc. suspensions 80—3605
erythrocyte ghosts, human, Ca^{2+} intracellular changes, arsenazo III meas., rel. to K permeability 78—96032
erythrocyte $H^{32}PO_4^{-2}$ transport, inhibition by high press. 77—12900
erythrocyte integral membrane protein lateral mobility, human cells 77—66805
erythrocyte membrane, pulse NMR meas. of water exchange 79—43826
erythrocyte membrane fluidity, adult and neonatal human cells 77—36885
erythrocyte membrane hydraulic cond. determ. 79—34528

cellular transport and dynamics continued
erythrocyte membrane thermal transitions identified from ANS permeability 79—53055
erythrocyte membrane water permeability defect in human epilepsy, NMR 77—29122
erythrocyte sedimentation rate in inclined tubes 80—67048
erythrocyte surface charge decrease, target of X-irrad. and dislocation of sialic acid 77—52853
erythrocyte suspension, laser-induced fluoresc. of intact human membrane cell 77—90733
erythrocyte suspensions, human, HCO_3^-, Cl^- exchange 79—8487
erythrocytes, avian, US effects on transport 79—96613
erythrocytes, elec. characts. of flowing blood 80—36053
erythrocytes, frozen human cells, conc. polarisation effect 78—3460
erythrocytes, gas reactions, shape changes microspectrophotometry obs. 79—8488
erythrocytes, human, effect of hydration on water content 77—16921
erythrocytes, human Li efflux through Na/K pump 78—48775
erythrocytes, motion and deform. in the microcirculation 79—29513
erythrocytes, rabbit, increased passive efflux of ^{22}Na and ^{86}Rb on microwave irrad. 80—108957
erythrocytes, rat, ^{99m}Tc labelled, factors affecting splenic deposition of heat damaged cells 79—29596
erythropoietic activity clinical assess., distrib. model of Fe kinetics 79—100587
excitable fibre, steady speeds of spread of stable and unstable impulses, depend. on membrane ionic currents 78—53382
excitable membrane, rapid transient changes in Na ion conductivity 77—44613
excitable membrane conductivity, acetylcholine and Ca ion binding rel. to receptor protein 77—40649
excitable membrane K^+ conductance temp. dependence *(Japanese)* 78—24051
extra-retinal photoreceptor model for Aplysia californica 78—44506
extracellular Na transient meas., appl. of Na liq. ion exchanger microelectrode 77—52949
eye centrifugal fibres in nonavian vertebrate, source revealed by horseradish peroxidase transport 77—36921
fibroblast spread kinetics 78—64955
fibroblast spreading kinematics, individual locomotor activity 78—69006
FitzHugh-Nagumo equations, perturbation anal. of slow periodic wave soln. 78—24060
fixed charge membrane modules, pot. controlled transient gating mechanism, book contrib. 80—12067
flagellar hydrodynamics, resistive-force theory compared to slender-body theory 79—24961
flagellar propulsion, hydrodynamic anal. 79—53072
flagellar propulsion hydrodynamics, helical waves 79—92185
flow cytometric data, computerised display and anal., review, book contrib. 80—109082
fluorescein uptake, fibre optic micro-spectrophotofluorimeter for in vivo animals studies 77—60327
fluoresceindiacetate conversion to fluorescein, in living cells and in vitro, kinetics 77—56332
fluoresceindiacetate hydrolysis and transport in mammalian cells after UV and gamma irrad. 77—56333
fluorescence photobleaching recovery for meas. of mol. motion, cell surface heating 77—48956
fusion rosettes in Paramecium, possible function as Ca^{2+} gates 78—56958
GABA uptake or exchange by synaptosomal fractions 77—12907
gallbladder epithelial cells, compartmental anal. of osmotically induced permeability changes 78—3455
gallbladder epithelium Na^+ pump site distribs., frog 78—27914
gastro-intestinal electrical activity model, frequency entrainment of oscillators 77—81489
gating charge immobilisation by inactivation-simulating substance 78—61154
gating currents, role of nonlinear capacitive currents of electrostrictive origin 77—48771
gland cells, stimulus-response coupling, review, book contrib. 80—108864
glial smooth endoplasmic reticulum acid phosphatase transport into damaged axons, role of microtubules 80—85381
glial-neural interaction demonstrated by Na^+ and Li^+ injection into cortical glia 77—36905
glomerular permeability in foetal rabbit 80—85372
glucose transport in human red cell ghosts, effect of chlorpromazine and temp. 78—77026
glutamate Na-stimulated uptake in membrane vesicles of E. coli, role of ion gradients 78—48776
glycolipids, regional synthesis, axonal transport, in neuron of Aplysia californica 79—83755
glycoproteins, fast axonal transport in guinea pig auditory neurons 80—104573
growth control of cell motion, diffusion coeff. model 77—40645
growth regulation, effects of cell density and metabolite flux on dynamics 78—85296
growth regulation, effects of cell density and metabolite flux on dynamics 78—88701
guard cells, anion, light-sensitive membrane pots. 78—11622
haemoglobin, human and Lumbricus terrestris, conc. depend. of self-diffusion 78—68984
haemopoietic stem cells, functioning kinetics study 79—53063
haemorheology related to blood cells, conf., Hamburg, Germany (Aug. 1979) 80—62365
hair cell receptor pot., ionic basis in vertebrates, bullfrog obs. 80—26239
Halobacterium halobium R_1 cells, photogeneration of two-vector transmembrane gradient of protons 78—80845
Halobacterium species, passive elec. props., membrane ionic flow 79—24970
heart, muscle cells, Na current, electrophysiological studies, rat 79—43838
heart cells of chick embryo, pacemaker current obs. 80—51066
heart muscle cells, leaky, heavy water effects 79—62220
hippocampal burst-firing neurons, slow inward current, voltage clamp obs. 80—94194
5-hydroxytryptamine receptors on visceral primary afferent neurones in rabbit nodose ganglion 77—56364
ileum, guinea-pig, immediate X-ray induced contractions, localisation of effect by drugs 77—56443

cellular transport and dynamics continued
ileum epithelial cells and intercellular spaces, microprobe meas. of Na, K and Cl conc. profiles, rabbit 78—35819
insulin secretion neural control, math. model 78—31796
intercellular contact high permeab. 78—48773
internodal cell, Nitella, mebrane pot. instability 79—92204
intestinal epithelium, effect of Ca ions and pH on osmotic pot. 78—20156
intestinal membrane transport of oligopeptides, intracellular study of underlying ionic events 80—104572
intestinal smooth muscle cells, non-cholinergic excitatory transmission 77—77891
intestine, small, effect of pH on permeability and mech. props. of intercellular contacts 79—57613
intracellular conductivity meas., indirect method 77—40950
intracellular control and intercellular transfer of molecules, multichannel anal. 79—53073
intracellular water, two-fraction fast-exchange model of spin-lattice relax. 77—60192
ion channel formation in artificial lipid bilayer membranes by synthetic peptides 77—90750
ion channels in development, book contrib. 79—96549
ion exchange membrane, unstirred layer effects on pot. difference calcs. 77—48680
ion transport and chem. reactions in brown adipose tissue, network thermodynamics 78—92606
ion transport model, intracellular osmoregulation mechanism 77—25400
ionic channel formation in living cell membrane, microelectrode obs. 78—53372
ionic channels and gating currents in excitable membranes, review 77—90764
ionic channels in excitable membranes, current problems and biophysical approaches 78—53369
ionic mechanisms of excitation in Paramecium, review 80—21458
ionophoretic model for Na-Ca counter transport 79—2017
ions, active transport through membranes, elec. events, book contrib. 80—12068
iontophoretic isolated current monitor for cell membranes 77—25626
junction membrane form., quantum jumps of cond. 78—73145
junctional membrane channels, size limit of permeating mols. 77—36900
K activation associated with intraneuronal free Ca 79—8494
kidney, isolated, perfused in vitro, sugar reabsorpt. rel. to Na transport, rabbit 78—20155
kidney preservation, analogue model of perfusion dynamic changes 79—83724
kinetic schemes theory, integral method 79—53064
laser Doppler spectroscopy, flow meas. appl. 79—66598
lateral geniculate nucleus neutron classes, morphological effects of monocular deprivation 77—52781
leaf CO_2 absorption and diffusion, sun vs. shade leaves 78—80850
leucocyte β-glucoronidase release on exposure to shear stress 78—40125
leucocyte adhesion studied quantitatively by multiple internal reflectance-IR spectroscopy 77—56562
leukocyte migratory patterns, use of ^{99m}Tc as radioactive label for study 80—51222
leukocytes in motion, surface struct., SEM 77—29116
light induced quenching of atebrin fluoresc. and photosynthetic electron transport, pea chloroplast 77—56351
light scattering by cells in flow system, paraxial anal. 79—11907
Light-regulated body ion balance in marine slug Elysia virdis (Montagu) 78—73146
liposome, photoinduced electron transport across phospholipid wall using methylene blue 79—74614
liposome suspension, coupled transport of K^+, Cl^-, H^+ and OH^- ions 79—53069
liposome-cell interaction, transfer and intracellular release of trapped fluoresc. marker 77—36901
liver, distributed model for transcapillary exchange and solute removal 79—34524
liver, rat, ion movements during energy-linked mitochondrial structural changes 80—12065
liver cells, regenerating, specific resist. and electrophoretic mobility, effect of RNase and neuraminidase 77—25402
liver membrane potential in situ, effect of blood flow changes 78—48772
lymphocyte homing patterns, radiation induced alterations 80—17014
lymphocyte in vivo migration modulation by whole-body hyperthermic RF irradiation, mouse 79—100668
lymphocyte plasma membrane components, distrib. and mobility, book contrib. 80—30690
lymphocyte stimulation rel. to early Ca flux 77—52758
Lymphocytes, human, effect of irrad. on hexose monophosphate shunt pathway 80—76798
lymphocytes, living and dead, mag. props. and mag. sedimentation 80—35925
lymphosarcoma development, rat, EPR studied of serum transferrin bound Fe^{3+} 77—77878
macromolecular transport, conc. systems 79—57567
macromolecular transport in living cells, fluid mechanical hypothesis 79—62219
magnetic force between moving cells 77—70486
mammal cell junction, permeability of cell-to-cell membrane channel 80—51061
mast cells, rat, electrophoretic mobility distrib. alteration after immunological activation 80—67047
melanoma cells, human, uptake of ^{67}Ga and ^{59}Fe 79—62217
membrane, dynamic interfacial electrochem. phenomena, toad urinary bladder membrane system 78—27912
membrane, thin, ionic transport, jump vs. electrodiffusion description, for steady transfer 77—36895
membrane, thin, ionic transport, jump vs. electrodiffusion description, volt. clamp 77—36896
membrane, thin non-uniform, jump vs. electrodiffusion description, volt. clamp 77—36897
membrane admittance, integral representation 78—15811
membrane charge transfer, possible role of α-helical proteins 80—81524
membrane conductance fluctuations and ionic pores, review 77—90752
membrane current separation using Paramecium mutant 77—66806
membrane diffusion coeffs. meas. 77—48962
membrane diffusion measurement by fluorescence photobleaching recovery method, bleaching light effect 80—94434
membrane dynamic equation solving, practical algorithm 78—77038

cellular transport and dynamics continued
membrane electrical noise and intercellular communication in embryonic heart cells 77—44612
membrane excitability, review 78—15786
membrane H^+ channels and mol. electrostatic generators 77—21501
membrane integral proteins, mobility increase in spherocytic erythrocytes obs. 80—81569
membrane organisation dynamics, book contrib. 80—30687
membrane permeability, review 78—15813
membrane permeability changes after X-irradiation 79—39370
membrane permeability of sheep erythrocytes, O_2 effects with X-ray and neutron irrad. 77—5039
membrane translational dynamics, fluorescence redistrib. after photobleaching obs. 80—21491
membranes, axon and bilayer props., excitable and ion-selective artificial membranes 77—86451
membranes, non-bilayer lipidic, props., excitable and ion-selective artificial membranes 77—86452
membranes, volt.-depend. tetrodotoxin action 77—44620
mesenteric artery Na kinetics, digital simulation of 3 compartment model 77—44616
methotrexate effects, cellular response simulation 77—40647
microelectrophoresis, intracellular, contrib. of volumetric charge to mobility of nuclei 77—86710
microtubules in optic nerves of temperature acclimated goldfish, electron microscopy 80—85395
mitochondria and submitochondrial particle phosphate transport, influence of thiol oxidation 78—27913
mitochondria membrane Ca^{2+} interaction, influence of oestrogens 78—53349
mitochondrial Ca^{2+} transport, effect of cations on temp. sensitivity, compared with liposome spermine uptake 78—11621
mitochondrial Ca^{2+} transport, inhibition by antibodies directed to Ca^{2+}-binding glycoprotein 77—4990
mitochondrial Ca^{2+} transport, rat liver, effect of Mg^{2+} and spermine 77—64015
mitochondrial membrane monovalent Tl^+ ion transport 78—31787
mitochondrial outer membrane, permeability pathway obs. 79—74602
mitochondrial proton pump coupled to cytochrome c oxidase 77—25406
mitochondrion, elec. props. and struct. transitions 79—24943
monosynaptic potentials onset and propagation, discrete-dynamic equations 78—77040
motoneurone survival during normal cell death in chick embryo, effect of neuromuscular blockade 78—27933
motor nerve endings, hyperosmotic neurosecretion rel. to internal Ca conc. 77—56368
motor nerve impulse, conventional Ca^{2+} channel mediating asynchronous acetylcholine release 78—11638
motor nerve terminals, cyclic nucleotide-mediated Ca flux 77—73524
motor neuron firing pattern in Aplysia 79—48244
moving semipermeable boundary, diffusion transport in liquid solution 77—80639
muscle, Ca diffusion in transient and steady states 78—3457
muscle, frog skeletal fibres, mesh model of tubular system, elec. props. 77—25395
muscle, K^+ concentration effect on Na^+ efflux rate obs. 79—79495
muscle, locust, pot.-depend. transition temp. of ionic channels induced by glutamate 77—77882
muscle, single ionic channels obs. in tissue cultures 80—30699
muscle, single postsynaptic channel currents in tissue cultures 80—30700
muscle, skeletal, Na:K rel. to Na:Na exchange by Na pump 77—66807
muscle, smooth, depolarised, tone change due to hyperpolarising current 77—86471
muscle, smooth, depolarised in hyper K medium, spontaneous relax. 77—86470
muscle, smooth, effect of hyperosmolar soln. on elec. connections between cells 78—69027
muscle, smooth, intestinal cell, voltage clamp studies of hyperpolarising inactivation 78—80847
muscle, striated, possible gating signal for K channel 77—64018
muscle, translocation of intracellularly stored Ca during contraction-relax. cycle 77—86474
muscle cell osmotic state and membrane permselectivity repeated microwave irrad. effects quantitation 80—56131
muscle cells in tissue culture, acetylcholine-induced current fluctuations 77—29119
muscle contraction activation, membrane mechanisms, guinea-pig 79—53071
muscle endplate, desensitisation rel. to selective alteration of Na^+ channels 77—77890
muscle fibre end-plate current pot. depend., effect of phenylalkylamines, frog 78—31799
muscle fibre membrane pot., effect of eserine, frog 77—56345
muscle fibre post-synaptic membrane, ionophore-mediated Ca influx effects 78—11637
muscle fibre resting pot. in cricket, influence of ions 78—24046
muscle fibres, skeletal, resting, Cs^+ rel. to volt. depend. block of inward K currents 77—52756
muscle fibres of giant barnacle, cyclic GMP levels associated with contraction 77—56369
muscle innervation-like effect, substances moved by axonal transport, released by nerve stimulation 79—16197
muscle membrane, insect, permeation of Mn, Cd, Zn and Be through Ca channels 77—56357
muscle mitochondria, fish, physiological correls. of Ca accumulating props 79—20527
muscle Na channel use-depend. block by local anaesthetic, pH effect, frog 78—20160
myelin swelling and meas. of forces between membranes 79—62204
myelin vesiculation simulated by nerve exposure to Ca ionophore 77—29128
myelinated axon impulse cond. simulation, sensitivity to nodal and internodal parameters 78—35831
myoblast membrane lateral transport of lipid probe and labelled protein 77—40646
myocardial fibre excitation and contraction uncoupling on slow Na-Ca channel block 78—15810
myocardial fibres, ionic nature of repeated responses 77—70441
myocardium contraction amplitude depend. on freq. of elec. stimulation, frog 78—77027
myocardium of frog, temp. effects on membrane currents 77—52759

cellular transport and dynamics continued
myotonia and Ca permeab., math. model 78—11620
myotubes, human, cultured, acetylcholine-induced conductance fluctuations 78—61157
Myxicola axons, Na tail currents compared with membrane asymm. currents 77—66808
nerve action potential, molecular events and energy changes 78—44497
nerve axon, phys. model, ionic distrib., pot. profile and resting pot. 77—12901
nerve axon adsorption model, action pot. and excitation currents, volt. clamp test 80—56018
nerve cell membrane, flow of Na^+ and K^+ through ion channels 79—74644
nerve cells and circuits, insights into construct. by genes 79—39411
nerve excitability, interactions between intrinsic membrane protein and elec. field 78—53377
nerve fibre, substance flow transport *(German)* 80—45878
nerve fibre membrane analogue-code conversion, ionic mechanisms 80—81575
nerve fibre membrane Na permeab. reversible blockage by increase in temp. of medium above 45°C 80—81576
nerve impulse, physical mechs., ion transport through membranes, review 78—85306
nerve impulse equation, dynamic responses of impulse 78—64972
nerve impulse propagation, subthreshold solns. of Hodgkin-Huxley eqns. 78—77044
nerve ionic permeability of K, Na and Cl, regulation by fixed charges and pH, crayfish 77—66809
nerve membrane permeability changes, fluctuation anal. 78—11636
nerve membranes, protein channels for Na and K ions, mol. mechanisms 77—4994
neural repetitive firing, Hodgkin-Huxley axon modification suggested by crustacean axon results 77—48776
neural transmitter kinetics model anal. 78—3465
neuro-secretion, role of Ca in control mechanism 77—64028
neuroblastoma cells, quiescent, rapid ionic conductance changes, serum induced 79—74612
neuroblastoma cultured cells, membrane currents under volt. clamp 77—60193
neuromuscular blockade by amantadine by suppression of acetylcholine receptor ionic cond. 78—64975
neuromuscular development, synaptic channel gating props. changes 79—16195
neuromuscular ectopic synapse, gating props. of acetylcholine receptor 78—27934
neuromuscular frequency-depend. block and temp.-induced seizure in ts mutant of Drosophila 78—56963
neuromuscular junction, crustacean, ethanol effect on excitatory postsynaptic current duration 77—48777
neuromuscular junction, frog, acetylcholine diffusion barrier 78—7334
neuromuscular junction, frog, Ca-depend. presynaptic action 77—52773
neuromuscular junction, frog, volt.-depend. effect of curare 77—52775
neuromuscular junction, snake, synaptic channel gating differences at twitch and slow junctions 78—80868
neuromuscular junction channel, in frog, endplate current fluctuations 77—25416
neuromuscular junction transmitter release during repetitive stimulation, effect of Sr^{2+} and Ba^{2+} 78—3469
neuromuscular synapse, response to acetylcholine 77—40660
neuron, intracellular Ca movement during pentylenetetrazole induced bursting activity 79—8495
neuron adaptation model allowing for Ca influence on membrane K permeability 79—79508
neuron hydrodynamics, numerical methods for creeping flow investigation 77—5019
neuron input current, Helix pomatia, rel. to membrane pot. and extracellular Sr and Ca ion concs. 80—81577
neuron late outward current, Ca-dependent depression, snail 78—7335
neuron membrane, electrostatic plasma probe physical analogue 80—79573
neuron membrane Ca channels, displacement currents assoc. with activation of gating mechanism 77—81486
neuron membrane inward Ca current, blocking effect of Cd^{2+} ions 77—81485
neuron model as universal element of self-learning network 77—44621
neuron model of burst generation, FET analogue 77—44630
neuronal adaptation to osmotic stress and facultative blood-brain barrier in marine osmoconformer 77—29127
neuronal ensembles, spike transfer 79—57631
neurone Ca conduction units, Helix aspersa 78—77041
neurone electrical activity modulation by cholesterol, Aplysia 78—7329
neurone impulse activity, limiting behaviour of a model 79—57630
neurone membrane, asymm. displacement currents and effect of internal F anions 77—48773
neurone regeneration in leech, form. of elec. synapse on severed axon segment 77—52776
neurones of large horse-leech, electrophysiological characts. rel. to intracellular Na^+ conc. 78—53374
neurons, Aplysia, effects of NH_4^+ and HCO_3CO_2 on intracellular Cl^- level 78—44485
neurons, burst firing, prolonged inhibition obs. 79—66469
neurons, transport of substances 80—89745
neurosecretory structure particle motion, effect of increased K^+ concs. 78—77046
nicotinic transmission, role of voltage-sensitive receptors 78—44492
Nitellopsis obtusa, photo-induced H^+ transport 80—81645
nonmyelinated nerve fibre conduction vel. 77—90759
nonspiking neurones, pharmacological evidence for fast Na channels 78—73151
oocytes, salamander, free and bound intracellular solutes, reference phase anal. 79—24966
oocytes, salamander, free and bound intracellular solutes, reference phase anal. 79—24967
opercular epithelium of killifish, isolated, membrane rich in Cl^- cells, active Cl^- transport 77—36882
osmotic behaviour of unperfused tissues 80—104574
ouabain resistance, contact-mediated resist. in mammalian cells in culture 77—77883
oviductal egg transport, stochastic model 80—51059
pancreatic acinar cell basolateral membrane, α-amylase transport 78—44481
pancreatic islet cells, effect on K^+ permeability of Ca^{2+}, glucose 79—74615
pancreatic islet glucose-sensitive Ca pools, rel. to secretion 77—32883
papillary muscle in rat, dynamic behaviour stochastic model 78—35821
papillary muscle Na kinetics, diffusional and compartmental models 77—44617
Paramecium, artificial deciliation causes loss of Ca-depend. responses 77—2017
Paramecium excitation, model anal. 80—61524
particle absorption rates at high cell concs., Monte Carlo simulation 80—94141
periodic conversions in biological system solns., optical mixing method obs. 78—96029
phospholipid bilayer membranes, voltage depend. channel form. by colicin K 79—8490
phospholipids, exchange between membranes, book contrib. 80—30695
photoelectrode for recording intracerebral cellular Ca^{2+} transients 80—67307
photoreception, transmitter-mediated, diffusion and reaction modelling system 79—70547
photoreceptor model, light-induced transmembrane channel form. in rhodopsin-containing bilayer membranes 77—52784
photoreceptor rod cells, vertebrate, visual transduction, book contrib. 79—96561
photoreceptor visual response rel. to metarhodopsin transitions, barnacle 78—69050
photosensory membrane of Limulus ventral nerve photoreceptor, effect of extracellular Ca/Na ratio 78—69067
photosynthetic electron transport in higher plants, adaptation rel. to light intensity 78—64953
photosynthetic electron transport in isolated chloroplasts, effects of purine nucleotides 77—64013
phototropic response of Phycomyces, rel. to intracellular rot. 77—48837
Physarum polycephalum, true slime mold, surface membrane simulation using liquid ion-exchange membrane *(Japanese)* 78—31781
pituitary cell, Na and Ca action potential 77—48770
plant motor organ K, Ca distrib., ion microscope obs. 79—66466
plant protoplast membrane, osmotically induced changes in elec. props. 78—27910
plant root transport studies using ion localisation, freeze substitution method 80—85569
plant sieve tube sucrose loading, role of pH gradient and membrane ATPase 77—52757
plant tissue acoustic microstreaming induced by Doppler foetal heart detector 79—62292
plants, flow and transport, book contrib. 77—48832
plants, transfer cells and their roles in transport of solutes 78—73148
plasma membrane, electrophoresis and diffusion obs. 79—57599
plasma membrane H^+ and K^+ circulation, role in bacterial growth 77—90751
plasma membrane of mouse egg, effect of fertilisation on lateral diffusion of lipids and proteins 78—44480
plasmalemma of Nitella flexilis, selective centres of excitable channels of early ionic current 80—81568
platelet diffusivity estimation in flowing blood 79—25010
platelet interaction with vessel surface, blood rheological factor influences 80—61612
platelets, shear-induced activation 79—74704
polarised spherical cell, ionic conc. profiles and charge distrib. 78—73144
polymorphonuclear granulocytes and FL-cells, effect of X-rays on membrane pot. and electrophoretic mobility *(German)* 77—56442
Porphyra osmoregulation, struct. aspects 80—85370
portal currents rel. to intramembrane charge displacement, one-dimens. approx. 78—31789
presynaptic Ca^{2+} current rel. to synaptic transmission, in squid giant synapse 77—16926
protein biosynthesis, role of guanine nucleotides 78—68982
protein kinases, cAMP-depend., membrane-localised, and regulation, of slow inward current, frog heart 80—81567
protein secretion by pancreas, accounted for by diffusion-like process 80—21457
protein transfer across microsomal membranes reassembled from separated membrane components 78—69029
protein two-dimensional analytical electrophoresis 79—96528
protoplasm streaming in Nitella flexilis, vel. distribs., laser Doppler spectrum 77—40684
Purkinje fibres, calf, role of intracellular Ca in transient outward current 77—90748
Purkinje fibres, canine, activity-dependent extracellular K^+ fluctuations 80—89733
purple membrane light-driven proton pump mechanism in Halobacterium halobium 78—35820
purple membrane of Halobacterium holobium, review 77—86457
purple membrane protein chromophore photoisomerisation rel. to proton pump 78—35804
random walk model for cell mixture sorting 77—44606
Ranvier nodes exposed to DDT, asymm. currents and Na currents 77—48778
receptor-mediated endocytosis and coated pits, coated vesicles 79—74611
red blood cell, human, rheologic effects of shape transform. 79—62216
red blood cell shape, optimality, O_2 diffusion approach 80—30693
red blood cell suspensions, steady state O_2 diffusion 77—40644
red blood cells, hydrodynamic and diffusion considerations in rapid mix expts. 80—40982
red blood cells, rheological props. meas. by Couette viscometer 80—97992
red blood cells, viscoelastic study of aggregation 80—97960
red cell, human, increased passive permeability below 12°C 80—94185
red cell Ca pump, ATP regulation 79—29511
red cell ghosts, human, Ca-depend. K efflux, effect of carbocyanine dyes 77—12896
red cell ghosts active transport, cytoplasmic contamination, electron microscopic obs. 80—45874
red cell membrane, Li transport in manic depressives 80—61525
red cell membrane elastic area compressibility meas., osmotic correction 78—20147
red cells, intact, use of ionophore A23187 to meas. and control free and bound cytoplasmic Mg 77—52755
red cells in dilute suspensions, turbulent flow and effect on O_2 uptake kinetics 77—60223

cellular transport and dynamics continued
renal brushborder membrane vesicle, proline and glycine uptake 77−44614
Renshaw spinal interneuron repetitive firing, model 77−90760
retina physiology, single cell studies on lower vertebrates, book contrib. 79−96558
retinal ganglion cell functional pathways, book contrib. 79−96559
retinal on-centre bipolar cell, ionic mechanisms of rod and cone signals 78−61177
retinal pigment epithelium, identification of membrane protein binding retinol 77−21515
retinal rod, localisation of Na$^+$, K$^+$-ATPase and Ca^{2+}-activated Mg^{2+}-depend. ATPase 77−44652
retinol-binding proteins in retinal pigment epithelium 79−20525
rheological behaviour of stored blood cells *(French)* 80−67110
rod, Ca-depend. regenerative responses 78−3480
rod disc membrane ion transport props. 78−15829
rod external segment surface membrane, lateral diffusion of rhodopsin 78−15828
rod network in turtle retina, elec. spread 78−80874
rod outer segment adaptation anal. based on a simple equiv. cct. 78−73157
rod outer segment membrane current, light-induced fluctuations recorded in single toad rod 77−86493
rod outer segments, vertebrate, role of Ca and H ions as transmitters 77−90776
rod photoresponse, contrib. of Cs$^+$-sensitive cond. increase 78−44501
rods, toad, effects of Ca^{2+} on intensity-response curve 79−53091
salivary gland cell junction, Ca^{2+} produces graded changes in membrane channel permeab. 77−64016
salt gland, avian, significance of extensive leaky cell junctions 77−77880
saltatory motility of uninserted trichocysts and mitochondria in Paramecium tetraurelia 78−24044
sarcolemmal permeability changes during early myocardial anoxia 80−85371
sarcoplasmic Ca pump, efficient ion translocating system 77−90746
sarcoplasmic reticulum Ca^{2+},Mg^{2+}-ATPase transient kinetics obs. by fluoresc. 78−61156
sarcoplasmic reticulum membrane rearrangements on peroxide oxidation of lipids 78−69025
sarcoplasmic reticulum of skinned cardiac cells, Ca^{2+}-induced release of Ca^{2+} 80−3612
saturation density, evidence against diffusion-limited process 78−48770
Schwann cell layer of squid axon, diffusion models 80−40985
sedimentation process for biological isotope separation 79−44066
serotonergic excitation, unconventional response in Aplysia 77−86484
sessile organism flagellar motions, feeding current generation, optimum motion 79−92184
sickle cell disease, capillary diffusion and transport compensation 79−92198
sickle-cell blood, flow in capillaries 80−41066
sinatorial node of rabbit heart, vagal stimulation, K$^+$ permeability and extracellular transients 78−92608
single-file ionic transport theory, reduced flow diagrams 78−69022
sinus node of rabbit heart, intercellular coupling 78−20159
skeletal muscle, excitation-contraction coupling, blockade by high extracellular concs. of Ca buffers 79−20528
skeletal muscle of frog, displacement currents, K cond. channel contrib. 79−39409
skin, frog, Na$^+$ transients, network thermodynamic approach to compartmental anal. 79−24968
skin of frog, radioactive Na washout rate anal., numerical simulation 78−3456
soleus muscle, rat, electrogenic Na$^+$-K$^+$ transport obs. 80−21456
spectrin-actin monolayer, adsorbed at Hg-H$_2$O interface, ionic permeability 80−12064
spinal motoneurones refractoriness accumulation and secondary range firing model 77−1985
squid giant axon, response of delayed K$^+$ channels to time-dependent clamping functions 79−39382
stability and control of cell cycle kinetics, cancer chemotherapy appl. 79−34521
stomatal function, blue light-stimulated swelling of guard cell protoplasts 77−77885
subcellular particle membrane pot. diff., proton channels in oxidative phosphorylation 78−64964
subcellular particle membrane pot. difference, compensation meas. method 77−56547
subcellular particle pot. difference, chemiosmotic and chemielec. generation mechanism 77−52751
suction capillary for holding moving cells during intracellular elec. recording 79−100793
sugar transport system dependent regulation of adenylate cyclase, review 78−69031
supraoptic neurons, rat hypothalamus, osmosensitivity obs. 80−104578
surface anisotropic molecular motion 80−97883
surface component rotational diffusion, time-resolved phosphoresc. anisotropy 80−97885
surface organisation, dynamic aspects, book 80−27047
surface receptors, molecular movements 80−45866
sweat secretion, role of Ca, in vitro meas. 78−40129
synaptic action of pentylenetetrazole, selectivity for Cl cond. 78−7336
synaptic active zone functional unity, evidence from quantum and amplitude distribs. 78−3468
synaptic terminal, choline transport obs. 79−70544
synaptic transmission, long-lasting potentiation by postsynaptic mechanism 77−32885
synaptic transmission modulation and information processing model 77−29142
synaptic vescles and synaptosomal membranes, electrokinetic props. 80−67055
syncytia, cylindrical, and muscle fibres, elec. pots. induced by current point source 79−74610
syncytial tissues, elec. pot. induced by current point source 79−74609
testing potential, membrane pot. rel. to ionic diffusion *(French)* 80−94184
tetanus toxin retrograde axonal transport, α vs. γ fibres 77−29120
thalamus, cat, stimulus induced and seizure related changes in extracellular K conc. 80−35870
thermocytes, rat, US-induced changes in rates of influx and efflux of K$^+$ in vitro 80−89793

cellular transport and dynamics continued
thylakoid membrane of green plants, simulation of electron transport in primary photosynthesis reaction, in PL/1 *(German)* 77−86468
thymocyte membrane props. modification by hyperthermia and gamma-rays 78−69017
tonoplast ionic channels in charophyte algae cell, role of Ca ions in excitation 77−81481
trabecula membrane of frog auricle, electrophysiological characts. from ionic currents on pot. clamping 78−24049
tracheal ciliary beat, improved device for freq. recording 80−109070
transepithelial current-voltage relationships of toad urinary bladder and colon 79−92195
transepithelial electrical parameters in midgut of Lepidoptera larvae 78−20154
transepithelial ion transport endogenous regulation, implications of ouabain-like activity in toad skin 78−73147
transport in biomembrane, NME determ. methods *(Rumanian)* 80−94435
tumour electrolyte exchange kinetics, meas. using fast neutrons 77−64125
unmyelinated nerve Na channels optimum density, analytic treatment 78−24061
urophysis, transport across isolated skin of a marine teleost 79−74617
vesicular transport and endothelial membrane interaction, theoretical models 80−45869
viral infection, membrane leakiness, rel. to development of antiviral agents 78−53371
visual cell membrane cond. control, arthropod 78−15831
visual cell microvilli membrane fragment protonic and ionic processes, cephalopod 78−73159
water, self diffusion in frog muscle 80−8037
water diffusion meas. by pulsed gradient NMR, cell struct. size determ. 78−77159
water diffusion through narrow pores of biomembranes, ^{1}H NMR obs. 79−92194
water flux through aortic tissue, model 79−48230
water molecule exchange rel. to NMR relax. in living and ischaemically damaged tissue 77−12895
water permeability during freezing and thawing, cryomicroscope multiple nonlinear regression analysis 79−92197
yeast cell membrane, water transport study, pulse NMR obs. 80−40981
yeast cell suspension in salt soln., dynamic effects of freezing 79−70533
yeast cells, translational mobility of water, pulsed NMR obs. 79−57612
yeast metabolism, microcalorimetry, diauxy during anaerobic growth of saccharides 78−3451
Ca conductance, inactivation without facilitation in Cs-loaded Aplysia neurones 78−56965
Ca ion levels in squid axons, influence of pCO$_2$ 78−56960
Ca pump driven by ATP in squid giant axons 78−77043
Ca spike enhancement during neurite in tissue culture 79−70545
Ca transients in aequorin-injected frog cardiac muscle 78−61149
Ca^{2+} concentration in extracellular fluids in body, digital simulation of short term regulation 79−83725
Ca^{2+} conductance of acetylcholine-induced endplate channels 79−70546
Ca^{2+} current in Paramecium, inactivation of Ca channel 79−79488
Ca^{2+}, excitation-contraction coupling in frog myocardium model 79−70541
Ca^{2+} influx, role in muscle excitation-contraction coupling 79−74616
Ca^{2+} intracerebral transients, photoelectrode for recording 80−30961
Ca^{2+}, passive and active fluxes across membranes, review 80−97886
Ca^{2+}, role in Limulus photoresponse suppression during anoxia 79−62252
Ca^{2+} uptake during mitosis in myxomycate Physarum polycephalum 77−90747
Ca^{2+} voltage-depend. facilitated entry into voltage-clamped aequorin injected molluscan neurons 77−90763
Ca-Na channel of cell, reconstruction in lipid bilayer 77−25404
Cl$^-$ active transport inhibition by piretanide, in teleost intestine cell 78−64967
^{57}Fe transport and storage compounds 77−12875
H$^+$-K$^+$ exchange and cell enlargement in maize coleoptile segments treated with auxin and fusicoccin 77−86469
K channel blocking agent, 3,4-diaminopyridine 78−69028
K channel ionic interactions, squid giant axon 78−3458
K currents induced by acetylcholine in Aplysia neurones, slow relax. 78−80865
K$^+$ ion flux through membrane channels, nerve impulses, random walk anal. 78−77045
K$^+$ ion transport inducing compound identification in mitochondria and bilayer lipid membranes 78−31788
K$^+$ permeability of E. coli, membrane lipid role in radiation damage 78−48834
K$^+$ permeability of mitochondrial and artificial bilayer membranes 78−53365
Li$^+$ ion entry through Na channel in cultured mouse neuroblastoma cells, biochem. obs. 77−81487
Na$^+$,K$^+$-ATPase generation of pot. jump at octane-water interface 77−81484
Na channel, fully coupled excited state model, conductance in volt. clamped case 78−85297
Na channel, fully coupled transient excited state model, action potential generation, threshold, accommodation and repetitive firing 79−57634
Na channel density in myelinated nerve fibres and nature of axonal membrane 77−52777
Na channel fluctuations, phys. nature, microscopic model 80−35869
Na channels in nerve, evidence for two conductance states 78−11634
Na current in cardiac and nervous tissues, validity of dV_{max}/dt as meas. 78−77037
Na exchange in tissue, incorporating diffusion effects into multicompartment models using digital simulation 80−3611
Na permeability inactivation in squid giant nerve fibres, review of exptl. work 78−73154
Na pump, electrogenesis in model of boundary transfer 77−25401
Na pump activation by external cations in squid axon, effect of ATP levels 78−35818
Na pump in red blood cells, cholesterol interactions 77−12898
Na transport mediation by ionophore A23187 in absence of divalent cations 78−11623
Na$^+$ activity of epithelial cells, liquid-ion exchanger microelectrode estimates, resistive artifacts 80−89909

cellular transport and dynamics continued
- Na^+ intracellular activity rel. to Na^+ transport across a tight epithelium 80—67051
- Na^+ pump, unphosphorylated, occlusion of K ions 79—88065
- Na^+ pump rel. to increasing thermogenesis in cold acclimation in rats 78—7326
- Na^+ saturation kinetics in frog skin, compartmental aspects 80—67050
- Na-K pump reversal and apparent affinity for intracellular K 77—86473
- O_2 diffusion and reaction in biological tissue, Michaelis-Menten kinetic model 78—31793
- O_2 diffusion distance and necrosis development in multicell spheroids 80—81570
- O_2 diffusion into mammalian cells following ultrahigh dose rate irrad. 80—30694
- ^{133}Xe diffusion through frog skin, toad bladder and water boundary layer 77—66803

cement industry
- cement kiln dust emission control by electrostatic precipitator, meas. 79—52989
- dust content in exhaust gas meas. by laser *(French)* 77—64486
- dust generation, peak short term dustfall meas. and effect on residential development 78—81386
- dustfall from isolated cement works, implications for residential development 77—37403
- IR pyrometer performance parameters and applications *(German)* 80—86315
- noise meas., fundamental principles *(Hungarian)* 79—86290
- Portland cement mortar, micromorphology and interfacial zone around aggregates, SEM obs. 79—61598
- Ca_3SiO_5, thermochem. effects on formation 80—16666

cements (building materials)
- *used only for those materials which bind together particulate matter so as to form a coherent mass of considerable strength. For cements that cause two or more separate masses to adhere see adhesion*
- admixture, for making high strength concrete *(Japanese)* 80—89297
- alite paste, mature, microstructure study by SEM, TG and X-ray diffr., corrosion 78—92381
- asbestos cement, resistance to crack growth 79—29185
- asbestos fibre reinforced cement, strength and fracture props. 80—108533
- asbestos fibre reinforced cement mortar, strength and fracture properties 79—100241
- asbestos fibre reinforced Portland cement analytical fracture resistance curve expression 78—76756
- atomic absorption spectrometric determ. of Cu, Mn, Pb and Cr by direct atomisation *(Japanese)* 79—70413
- basalt fibres, alkali resist. in cement soln. 80—89377
- binding properties, PMR obs. 78—23355
- cement raw-material mix, main component determ. by atom absorption spectrophotometry 80—45615
- coated cement stone heat and mass transfer obs. *(Russian)* 79—14219
- corrosive effect on zirconosilicate glass fibres, rel. to composite strength 77—44335
- fatigue hardening 79—29086
- fibre reinforced, mech. and rheological props. *(German)* 79—20129
- flexural strength, loading rate effect on crack growth 77—77556
- glass fibre reinforced cement, glass fibre volume fraction determ., using photodiode 78—48578
- glass fibre reinforced cement, progress report 79—91905
- glass fibre reinforced cement, review of reinforcing theory, ageing, stress/strain relations 78—44165
- grog bodies, high Al_2O_3 cement, creep characts. obs. 80—66578
- gypsum content effect on compressive strength, in concrete cured by accelerated methods 77—63615
- hardened paste, internal stresses and microcrack form. caused by drying 78—92325
- hardened paste, transitional thermal creep 80—25785
- high alumina cement pastes, accelerated conversion, acoustic emission 77—36726
- high-temperature high-strength composite based on $Ca(OH)_2$ and polymethylphenylsiloxane 77—36439
- hot pressed, type III, role of admixtures on pastes and H_3O cured cement, exam. 78—44073
- hot-pressed paste, strength, X-ray diffr., DTA, IR spectra, microstruct. exam. 77—8864
- hydration, SEM, new technique 77—40503
- hydration kinetics, microwave obs. 79—34255
- ion beam etching 80—30117
- jute fibres, alkali resist. in cement soln. 80—89377
- Kevlav fibre reinforced cement composites, cement boards, exam. of mech. props. 78—48499
- mathematical models for stress relaxation and deformation 77—14923
- mortar, cured by 28-day standard and accelerated methods, strength correlation 77—16762
- mortar, deform. charact., expt. study *(Japanese)* 78—56704
- mortar, impact bending capacity *(Japanese)* 80—89341
- mortar bars, aggregate particle size influence as expansion caused by alkali-SiO_2 reaction 80—66762
- mortar containing Ca lignosulphonate, creep, effect of degree of hydration 77—63731
- mortar-epoxy resin mortar, durability of jointing of successive pours with epoxy resin adhesive *(Japanese)* 77—8793
- mortar-K cement mortar, durability of jointing of successive pours with epoxy resin adhesive *(Japanese)* 77—8793
- nuclear reactor containment vessels, cement selection criteria *(Polish)* 79—49876
- nuclear waste constituents, stabilisation in Portland cement 80—13630
- paste, direct tensile tests and tied crack model 78—11306
- paste, direct tensile tests and tied crack model 78—11307
- paste, elasticity modulus and strength, aggregate conc. effect 80—66591
- paste, heat-cured, recoverable and irrecoverable deform. 77—63732
- paste, mathematical model relating flow curve to water/cement ratio 78—34100
- pastes, flow behaviour, specific surface and conc. of solids influence 80—65132
- pastes, setting at positive, subzero temps., PMR exam. 80—55625
- polyethyl acrylate modified mortars, inner struct. and flexural props., suspension and emulsion studies *(Japanese)* 77—86092
- polymer-cement composite, review 79—70039

cements continued
- polypropylene fibrillated film reinforced cement, loading capacity, cracking 78—72759
- polypropylene fibrillated film reinforced cement matrix for low cost sheeting 80—80996
- porous solid with below-freezing pt. adsorbate, isothermal adsorption and dimensional changes obs. 78—75925
- Portland, containing Cr, superhigh-early-strength, early hydration 77—21072
- Portland, static and fatigue cracking morphology, SEM obs. 77—52493
- Portland cement, a model describing the hydration process 78—23654
- Portland cement, absorbed H_2O, pulsed NMR study 80—84665
- Portland cement, corrosion by H_2S 80—21129
- portland cement, doped with ZnO, struct. and props. 80—60914
- Portland cement, HVEM and gas reaction cell for microstructural investigation 80—40649
- Portland cement, hydration mechanism 78—35349
- Portland cement+silicate, reaction rates 80—26006
- Portland cement clinker, elec. props. 78—59976
- portland cement clinker with Ti_2O additions, property changes *(German)* 78—23714
- portland cement concrete, determination of hydrated cement content by differential thermal analysis 79—79335
- Portland cement paste, hardened, creep under cyclic temp. 79—8320
- portland cement paste, microstructure study by SEM, TG and X-ray diffr., corrosion 78—92381
- Portland cement-fly ash, physico-mech. props., SEM and X-ray diffr. anal. 79—74239
- regulated set, sulphate resistance and long term strength 78—35438
- resin mortar, flowability, viscosity meas. with rotational viscometer *(Japanese)* 78—11260
- review, physics and chemistry 78—73013
- sisal fibre reinforced cement, flexural strength 80—11692
- soil-cement mixture for earthfill dam embankment *(Japanese)* 78—39729
- steel fibre reinforced cementitious material, radiographic anal. of fibre distribs. 78—52747
- steel wire reinforced Portland cement mortar, wire pull out, inelastic behaviour 78—56681
- strength, fracture mode, statistical props. *(Japanese)* 78—31520
- suspension, settling and flow props., effect of cellulose ethers and lignosulphonates 77—11242
- wood fibre reinforced Portland cement composite, strength 80—100822
- $3CaO.SiO_2$, hydration in presence of lignosulphonates, glucose, Na gluconate 79—100330
- $3CaO.SiO_2$ pastes, structural props., curing temp. effect 79—100332
- Al_2O_3-P_2O_5-H_2O system, phase diagram 80—3014
- B_2O_3-PbO(ZnO) glass-ceramic-cement composites, review 79—38783
- $BaAl_2O_4$-Ba_2SiO_4-$BaZrO_3$, fusibility diagram 79—83184
- Ba_2SiO_4 cement, hardened, H_2SO_4 resistance *(Japanese)* 77—77602
- $Ca_4Al_2Fe_2O_{10}$, Portland cement clinker, formation kinetics 79—43191
- $CaAl_2O_4$ compounds and cements, quantitative thermogravimetry after hydrothermal treatment 80—16737
- $CaAl_2O_4$ hydration, US wave propag. study 79—39114
- $CaAl_2O_4$, phase transform. accompanying hydration, US and X-ray obs. 79—39115
- $Ca_3Al_2O_6$, retardation of hydration by sulphates 77—56249
- CaO-SiO_2, cements, effect of additives on compressive strength, carbonisation shrinkage, frost resistance 79—1897
- $(CaO)_3SiO$ cement pastes, electron microsc. anal. 80—108761
- $3CaO.Al_2O_3$, high level radioactive waste disposal 78—78485
- $3CaO.Al_2O_3$-$CaSO_4.2H_2O$-CaO-H_2O, citric acid effect on reactions 78—27725
- $3CaO.Al_2O_3+CaSO_4.2H_2O$, effects of prehydration on liq. hydration 79—100354
- β-$2CaO.SiO_2$, carbonation reaction kinetics, with CO_2 and H_2O vap. 79—79219
- $CaO.SiO_2$ pastes, structural props., hydrating cmpd. effect 79—100331
- β-Ca_2SiO_4, hydrating, composition of soln. in contact 78—11138
- β-Ca_2SiO_4, very reactive powder, prep. 77—55924
- Ca_2SiO_4-$CaSO_3$-CaO, region of homogeneity of Ca_2SiO_4 77—90332
- Ca_3SiO_5, thermomechanical effects on form. 79—15635
- $3Ca.SiO_2$, carbonation reaction kinetics, with CO_2 and H_2O vap. 79—79219
- ^{137}Cs immobilisation in cement-waste composites 78—82466
- H_2O adsorption, NMR relaxation exam. 78—48354
- MgO-$MgCl_2$-H_2O, cement paste, reaction products, X-ray diffr. study 78—23689
- $Mg_3(OH)_4(NO_3)_2$, nitrate based cement binder formed from MgO powder 79—15634
- $Mg(PO_4)_2.xH_2O$, x=8, 22, dehydration and water bonding 77—44456
- T leaching behaviour from hardened cement paste 80—18443
- ZnO-B_2O_3-SiO_2 glass-ceramic-cement composites, review 79—38783
- ZnO.$ZnCl_2$.H_2O cement, phase equilibrium diagram 77—86013

centrifuges
- accelerometer with centrifuge, linear, methods of eliminating systematic errors in calibration 79—71399
- aerosol centrifuge, calibration at unmatched relative humidities between stream and aerosol air 79—41775
- aerosol mass distribution, meas. using centrifuge with quartz oscills. *(German)* 79—92004
- aerosol size distribution, meas. by combined light scatt. and centrifugation 77—10083
- analytical ultracentrifugation technique for direct meas. of DNA sedimentation consts. *(French)* 80—8004
- bacteriological testing of medical grade papers using filtering centrifuge tube 79—84045
- binary isotopic gas mixture, convection-diffusion eqn. soln. for centrifuge axisymm. vel. field 78—17434
- collimating optics for analytical ultracentrifuge *(German)* 79—71443
- crossed-field plasma centrifuge, effect of ion wind on separation 79—31722
- discharge, cylindrical, rotation by elec. and mag. fields, isotope separation appl. 77—39486
- dust-air cyclone separator, operation anal. 78—57362
- earthquake modelling, appl. of centrifuge 78—81429
- enrichment by plasma centrifuge, rotational velocity meas. 78—74502
- FBR fuel reprocessing, using centrifugal extractor, mixing and separation obs. *(Japanese)* 80—52775

centrifuges continued
fission reactor fuel reprocessing, extractor for mass transfer examination by single drop method 77—67848
gas, compressible flow in rot. cylinder, linearised anal. 78—71345
gas, for separation of U isotopes 79—3227
gas, liquid, appls., review 79—53289
gas, pressure recovery of supersonic flow in diffuser 78—29104
gas centrifuge, fluid flow anal., computer calcs., appl. to UF_6 77—75924
gas centrifuge, isotope separation of ^{235}U, separative performance transients 79—67957
gas centrifuge, numerical anal. of weakly compressible rotating flows 80—47726
gas centrifuge rotating differentially, non-rotating side wall 77—67895
gas centrifuge with differential rot., U enrichment 77—54363
gas centrifuge with insulated end walls, Stewartson layer struct., temp. distrib. 78—46973
gas centrifuge with insulated side wall, Stewartson layer struct., linearised eqns. 78—46974
gas centrifuges, axisymmetric flow driving mechanisms 77—15039
gas centriguge, effect of compressible flow on max. separating power 78—70644
high-pressure liquid MP determ. centrifuge cell 80—31783
high-temperature centrifuge construction 78—57938
impulse plasma centrifuge with circulation, theory *(Russian)* 80—38553
inert gas rotating arc meas. in plasma centrifuge 78—75438
interference optics of analytical ultracentrifuges, background suppression of multiplexer-gated modulatable laser 80—73430
isotope centrifuge, effect of thermal convection on separative power, numerical anal. 78—58500
mechanical strength obs. of low-density fibrous struct. using centrifugal method 80—71823
nuclear fuel reprocessing by Purex process, adaptation of centrifuge technology to active conditions 79—26684
nuclear powdered target prod. by centrifugal precipitation method 78—841
particle separation, high-resolution, by sedimentation field-flow fractionation 77—73473
plasma, fluid flow analysis, third-order differential equation solution *(Japanese)* 80—53949
polymer systems, sedimentation field-flow fractionation in macromolecule characterization 80—66879
polystyrene monodisperse ^{51}Cr tagged aerosol prod. using aerosol centrifuge 78—92519
rotating annular jets, velocity distrib. and profile meas. 79—50829
rotating plasma, separation of metals 78—75436
rotating plasmas, balance and separation processes 78—1911
rotating structures finite element analysis, cylindrical shell with end plate subjected to centrifugal force *(Japanese)* 79—1104
steam turbine lubricating oil, filter separators and centrifuges eval. for effects on props. 78—3283
two-fluid spin-up 78—30301
two-phase flow distribs., nuclear power appl. *(German)* 77—6574
ultracentrifugation, rotor matching, laboratory use 79—40556
ultracentrifugation of polymers, absolute mol. wt. and mol. heterogeneity determ. from sedimentation vel. *(German)* 80—14261
ultracentrifugation pattern analysis, FORTRAN program DIANA 2 77—40549
ultracentrifuge, flow, isotope conc. field, numerical model 79—1199
ultracentrifuge, thermally-controlled, for isotopic separation, gasdynamic features 77—54362
ultracentrifuge enrichment of uranium, ^{235}U to ^{238}U, present status and development 77—18680
ultracentrifuge with magnetic suspension, contactless meas. of adhesivity and cond. appl. 77—16776
velocity sedimentation, separation of mammalian cells 80—101293
vibration monitoring, safety and economic aspects 79—49218
U enriching gas centrifuge cascade, reflux effect, enrichment enhancement control 77—54346
U enriching gas centrifuge cascade, computer program for performance anal. 79—85805
U enrichment, centrifuge process, LWR fuel *(German)* 80—68905
U enrichment, HAGA radial separating nozzle centrifuge process, cost 78—46155
U enrichment, layout of gas centrifuge cascades 79—26587
U enrichment by plasma centrifuge, partial pressure distrib. obs. 78—74501
U fuel enrichment, flow profile meas. of gas in rotating cylinder 77—46382
U isotope separation using gas centrifuge 79—49815
UF_6 centrifuge cascade, power supply loss accidents anal. 79—13502
Xe-He(Ne), gas mixture, element and isotope separation in impulse plasma centrifuge *(Russian)* 80—38725

ceramals *see cermets*

ceramic industry
automated sintering and hot pressing system 79—33961
manufacture of ceramic ware, mechanisation and automation 79—61548
porcelain techno-economic form. by linear programming 78—39721
waste heat recovery, from ceramic tunnel kilns, using tetra-chloroethylene Rankine cycle 79—52955
weighing, automatic, application in ceramics industry 80—95074

ceramics
see also ceramic industry; refractories
β-alumina, Na heat engine appl., principle and thermal efficiency 79—48179
β-eucrypite, glass-ceramics, internal stresses 79—15770
β-spodumene, glass-ceramics, internal stresses 79—15770
abrasive wear, role of plastic deform. and fracture 80—108594
acid-resistant, based on Artemov clay and obsidian 80—20852
acoustic wave attenuation mechanisms for ceramics containing volatiles 80—74560
adamantine, structural, thermophysical and electrophysical props. 80—6918
AE meas. under maintained load *(German)* 79—43315
α-Al_2O_3, production rel. to props. of dense corundum refractories 80—25627
β-Al_2O_3-MgO ceramic, formation and structure of atomic scale cracks 80—45395
β- and β''-Al_2O_3-Na_2O, fast ion conductors, TEM obs. 79—86920
alkali metal polyaluminates, synthesis, solar furnace appl. 78—84746

ceramics continued
alkali-alkaline earth ceramic solid solutions, with tetragonal tungsten bronze struct., low freq. optical modes 78—76477
allophane adsorber, removal of atmospheric gaseous hydrocarbons *(Japanese)* 77—78412
alumina, diametral compression test, parametric study 78—44282
β''-alumina, K^+ ion nonuniformity, in contact with $NaNO_3$ and Na_xS_x melts 78—10215
alumina, multiaxial fracture, general approach to statistical anal. 78—90785
alumina, polycryst., compressive strength, microplasticity 77—36620
alumina, polycrystalline, subcritical crack extension and crack resist. 77—8911
alumina, wear, effect of liquid environment, use of pendulum scratching sclerometer *(Russian)* 77—16693
alumina based ceramics containing Mn and Ti compounds, sintering and paramag. props. 77—21069
alumina ceramic artificial hip joint wear tests *(German)* 79—8567
alumina on stainless steels and Inconel, gasless ion plated films 77—40476
alumina powder, particle size analysis, using centrifugal sedimentation *(German)* 78—57890
aluminous porcelain, electrical conductivity of function of O_2 partial press. *(German)* 77—1419
anadalusite, thermal expansion and cell parameters 79—90801
anatase fibres synthesis from K_2TiO_3 fibres, hydrothermal leaching *(Japanese)* 79—56949
ancient pottery, characterisation by neutron activation anal., suitable element selection 78—8484
annular crack at spherical voids, stress intensity factor estimates 80—106757
anorthite, chem. resist. and struct. 79—61756
applications in fusion systems, neutron effects, review 80—32473
archaeologic samples age determining, using thermoluminescent dosimetry *(Czech)* 77—5972
archaeology, dating by alpha-recoil tracks in mica 78—70237
artificial hip joint, wear and friction tests *(German)* 79—8568
atomic pile fuel *(Polish)* 79—22394
automatic US defect detection for tile grading and packing processes 78—23885
bakor beams, residual thermal stresses, expt. determ., theoretical anal. 77—66667
ball mill grinding, wet and dry, rate const. *(Japanese)* 80—29895
barium aluminosilicate glass coating on NbZr, d and He ion irrad., blistering 77—35605
bending test results processing 80—97672
bioceramic, SnO_2 coated, for artificial heart valves, mech. props. *(German)* 79—12028
bioceramics in orthopaedic surgery, internal struct. of inorganic parts in bones *(Polish)* 79—20714
biomedical implants, interfacial tensile strength and bone form., effect of elec. stimulation 77—5108
bonding using synthetic adhesives made in Poland, resistance tests *(Polish)* 80—35365
bone bioceramic implants, surface structure *(German)* 79—44057
bone china body, MgO effect on vitrification mech. props. *(Japanese)* 79—78922
bone replacement *(Polish)* 78—20316
bone substitute materials, sintered hydroxylapatite as bioceramic 79—12036
borides, lightweight ceramic armour appls., ballistic tests, computer simulation, book contrib. 78—48556
borosilicate glass, transform. to glass ceramic, fixation of long-lived fission products 77—61558
brittle, heat-transfer variables effect as thermal stress resist., meas. by quenching expts. 80—79871
brittle, non metallic materials, wear chart, exam. *(German)* 78—35521
brittle, post thermal buckling resistance, role of physical props. 78—64585
brittle, specimen prep. for optical and SEM obs. *(German, English)* 80—35457
brittle ceramics, partially absorbing, thermal stress anal. subjected to symmetric radiation heating 80—59570
brittle ceramics, phys. props. role in resist. to failure by thermal buckling 79—77673
brittle fracture, mechanisms interpreted on basis of material mechanics *(German)* 78—35471
brittle model mats., porous and nonporous, strength and struct. 77—4849
building materials, breakdown kinetics by X-ray diffr. 80—108526
building materials, high-temp. microscopy interpretation *(Polish)* 80—66743
building product, nonmetallic, first crack determ. device, during load test *(Czech)* 80—45471
bulk defects and surface cracks determ. by US means 80—76473
$Ca_3(VO_4)_2$-$Zn_3(VO_4)_2$, exam. of phase composition and phase diagrams 79—1851
CaO-SiO_2, wollastonaite, exam. of synthesis by hydrothermal sintering *(German)* 79—4934
carbide fusion cast ceramics, crystn., microstructures rel. to conditions 80—11638
carborundum, oxidation protection via phosphate impregnation 77—44374
cast stoneware, quality control, use of US methods 78—11490
celsian, chem. resist. and struct. 79—61756
celsian, with CaF_2 and ZnO additives, props. obs. *(Bulgarian)* 80—50579
cement grog bodies, high Al_2O_3 content, creep characts. obs. 80—66578
ceramic-ceramic composites, high temp. high performance materials *(French)* 79—83166
ceramic-glass-glass composites, crack growth, elec.-mech. analogue 80—85022
ceramic-metal composite using metal-coated alumina powder 77—21081
ceramic-metal seal technology, history and trends 78—81992
ceramics, photovoltaic effect application to information storage 80—80316
ceramics, polycrystn., strength-grain size relations 79—79081
chamotte glazed masses, deformation occurring during heat treatment 78—84747
characterisation with analytical electron microscope 80—84068
chemical plating of glass ceramic with Ni and Cu 77—44379
chemical reactions, high temp., diffusion controlled 79—91935

ceramics continued
- chemical reactions in plasma generated near ferroelectric surface, obs. 78—68931
- chemical resistance for medical laboratory techniques 79—88926
- chinaware, semivitreous, eval. of crazing resistance by stress meas., after autoclaving *(Japanese)* 79—20235
- chinaware, vitreous, elimination of crazing by repeating glost firing *(Japanese)* 79—20236
- clay, sintering tendency, effect of basalt and chemical-mineralogical composition 78—11177
- clays, heat treatment, effect on rheological props. of enamel slips 80—60809
- coating, vapour deposition by plasma activated process 79—57125
- coating by physical vapour deposition processes *(Japanese)* 80—55306
- compact, morphological investigations significance 79—33988
- compaction during pressing, green strength, effect of adsorbed layers *(German)* 78—6880
- compatibility with liquid Na and Li 77—44387
- composite, mech. props. *(Polish)* 78—31481
- composite, toughening by oriented nucleation of microcracks 77—8921
- composite strip piezoceramic US receiving array 78—42511
- cordierite, dense ceramic prep. with sintered condition over 300°C interval 79—33983
- cordierite, synthesis rel. to WC addition 77—8787
- cordierite, thermal expansion 78—6165
- cordierite electroceramic, thermal expansion coeff. meas., 80-300K 79—60526
- cordierite glass, effect of crystn. on thermal diffusivity 79—33127
- cordierite glass ceramics, effect of TiO_2 and ZrO_2 content on phase sequence during heat treatment 78—48381
- corundum, behaviour in reducing conditions at temps. above 1700°C 77—16522
- corundum, composition and phase struct., effect of Na_2O and CaO 77—81244
- corundum, crack jump determ. from specific failure and elastic energy 79—87712
- α-corundum, enthalpy, 800-2300K, empirical eqn. 78—14478
- corundum, optical, polished, surface layer obs. by IR reflection spectra *(Russian)* 78—19458
- corundum, polycrystalline, creep under low partial pressure of O_2, 1200-1600°C 80—35255
- corundum, powdered mixture, compaction, optimum porosity and particle sizes 77—85971
- corundum, shaped crystal, grown from melt, struct. perfection 78—3021
- corundum ceramic, high-temp. treatment, powder medium effect on microstruct., comp., strength and dielec. props. 79—33984
- corundum ceramic, roughness depend. on initial grain size of alumina *(Polish)* 78—30816
- corundum refractory ceramic deformation curve analysis *(Russian)* 79—90716
- corundum synthetic raw materials, sintered and fused, use in refractories industry, slagging, creep, thermal shock resistance *(German)* 79—4937
- corundum transparent ceramic prod., synthesis of initial alumina 77—52270
- Cr_2O_3, pure, hydrothermal reactive sintering 77—36431
- crack and inclusion detection, NDT microwave evaluation 78—95866
- crack extension micromechanisms, review 80—108567
- crack initiation threshold, subject to elastic/plastic indentation 79—70157
- crack propagation, cracking velocity-stress intensity factor data *(German)* 78—35469
- crack propagation, microstructural aspects 79—15771
- crack tip, process zone, theory for stress field 78—67154
- cracking, spontaneous, grain-size depend. 80—44253
- cracking characterisation by double torsion test *(French)* 80—104369
- creep, porosity depend. 80—97530
- creep for polycryst. ceramics with ambipolar diffusion incl. grain size 77—73304
- creep measurement, samples with initially nonlinear axis creep, expt. errors *(Russian)* 77—25224
- creep stress exponents rel. to slip and ductility 77—90400
- cristobalite, irreversibility of initial beta to alpha transition, relevance to ceramic bodies 78—39761
- critical stress intensity factor and fracture energy concepts applic. *(French)* 77—32672
- crystalline materials, IR transmission, review 78—55417
- cylindrical cavity effect on fracture 79—66144
- deformation mechanism map 79—34109
- density measurement, true and apparent, specimen liquid saturation cell 80—62636
- deposition of Au with Cr interlayer 77—20202
- detects in materials, direct observation and characterisation 78—88617
- development from organosilicon polymers by heat treatment 80—81014
- developments for electrical industry appls. 79—78925
- diamond, elec. cond., temp., freq. depend. 80—54687
- diamond ceramic, elec. cond., thermal cond. rel. to temp. 79—15140
- dielectric, laser induced microwave damage, space simulation 77—81050
- diffusion constants, melting pt. diffusivity activation energy and volume correls. 80—96679
- diffusion creep activation energy 78—11274
- dimensional stability, internal and external gas pressure within pores 80—11606
- directionally solidified eutectic 78—27503
- disilicate, piezoelectric glass ceramic, recrystallisation, pyroelectric response, permittivity 80—80703
- drying mechanicsms, electrical transducer for automatic recording 77—52561
- DTA application in ceramic technology 80—20913
- dunite-dolomite mixtures, sintering and minerogenesis 77—66613
- dynamic fatigue tests, statistical reproducibility of crack propag. parameter 80—25842
- efficient transducer arrays for NDT 79—57194
- elastic behaviour, finite element anal. model, thermal props. 78—31449
- elastic moduli, effect of inhomogeneous porosity distrib. 79—87674
- electrical conductivity, porosity effects, 20 to 1000°C *(Polish)* 78—6385
- electroacoustic sensitivity, right circular cylinders 78—2805
- electroceramic development involving grain boundary structural analyses *(Japanese)* 77—85977
- electroceramics, thermoluminescent and dosimetric characts. 79—8196
- electroceramics and magnetoceramics, microstructure and physical props. 78—72756

ceramics continued
- electrodes, high dielectric constant materials for ultraminiature high power N_2 discharge lasers 80—58572
- electron and ion conductivity, instrument for meas. up to 2000°C 79—96247
- electron diffraction and imaging, at high resoln., characterisation of alloys and ceramics 80—104050
- electronic materials, analysis by fluorescent X-ray spectroscopy *(Japanese)* 77—86417
- electrooptic ceramics and ferroelec. glasses *(Japanese)* 79—65840
- electrotechnical porcelain, bend tests, fracture stress distrib. at various loading rates 78—15529
- enamel, melted vitreous, for protective coating appls., gas generation in highly viscous phase *(Russian)* 77—73360
- endoprostheses (total hips), mech. and tribological props. *(German)* 79—84005
- engineering materials, nature and props., book 78—72707
- enstatite-type glass-ceramic, crystn. kinetics and mechanism 77—55241
- erosion in high temp. steam and H atmosphere 80—35334
- eucryptite, chem. resist. and struct. 79—61756
- eucryptite-cordierite binary system, sintering of polycrystalline bodies *(Japanese)* 77—12588
- failure mechanisms, at high temps. 80—39210
- failure prediction under thermal loading, Weibull eqn. 78—88534
- fatigue, subcrit. crack extension charact. *(German)* 80—100888
- fatigue data analysis, lifetime predictions for ceramic materials 78—95870
- fatigue strength investigation, hip prostheses appl. *(German)* 77—56514
- fatigue testing, subcrit. crack extension meas. with double-torsion specimens *(German)* 80—104359
- FBR Sphere-Pac carbide fuels, SPECKLE-I, computer modelling of thermal aspects of fuel response 80—18427
- feldpsar in porcelain, melting behaviour *(German)* 79—90758
- feldspars, sintering props. 79—29006
- ferrite, microwave mag. props., grain size effect 78—10722
- ferrite (Li-containing)-BiO_2, phase diagrams and sintering conditions 79—52141
- ferrites, Li-containing, conditions for obtaining high-density one-phase mag. ceramic 79—52141
- ferrites, M type anisotropic, powder prep. and, sintered, effect of powder and pressing technology on alignment *(German)* 79—24472
- ferrites, manufacture, modified technology development *(German)* 77—21073
- ferrites, sintering, strength and mag. props., vacuum effects 79—70028
- ferrites, soft, production and props. 80—88801
- ferroelectric, axially loaded, nature of elec. field and resulting voltage 78—72468
- ferroelectric, dielec. losses due to domain wall oscill. 78—84541
- ferroelectric, elec. and thermoelec. props. of grains and grain boundaries 78—43382
- ferroelectric, mech. and elec. losses, correl., theory and expt. 80—66133
- ferroelectric, optical modulation by electrostriction during electron beam charging, spatial characts. 79—7224
- ferroelectric, polarised, acoustic vel. anisotropy 79—55835
- ferroelectric, tetragonal, 90° domain-rot. fraction after polarisation, X-ray determ. 80—75992
- ferroelectric, with external inductive-resistive load, linear electromechanical responses 79—51909
- ferroelectric ceramic, polycryst., elasticity props., neutron bombardment effects 80—79856
- ferroelectric ceramic, tetragonal TsTS-23 and TBK-3, 90° domain rot. in fixed elec. field 80—7315
- ferroelectric ceramic-photoconductor structure, as optically controlled transparency 80—28343
- ferroelectric ceramics, 1-D linear dynamic electromechanical responses 79—47397
- ferroelectric ceramics, elastic and piezoelec. eigenstate spaces 79—42901
- ferroelectric ceramics, materials and dielec. props., review 80—75957
- ferroelectric films, resonant autothermostabilisation *(Russian)* 78—52451
- ferroelectric hysteresis cycle computing from a statistical model *(French)* 79—11393
- ferroelectric solid solns., perovskite struct., physical props., review *(Russian)* 77—48134
- ferroelectricity, conference, Leningrad, USSR (1977) 79—15406
- fibre reinforced, design and prod. *(Polish)* 78—11188
- fine ceramic masses, organic plasticizer, plasticity model and plastic behaviour meas. by cyclic shear test *(German)* 79—96080
- fine powder, compaction during pressing and green strength, absorbed layer effect *(German)* 77—77450
- fine-grained, cyclic plastic deform. as cause for thermal expansion hysteresis 80—89290
- fireproof materials, for use in direct energy conversion *(Czech)* 79—70455
- firing in tunnel kiln, direct current and counter current in gases and waves 77—52264
- fission reactor fuel, effect of gas composition on thermal conductivity 79—93733
- fission reactor fuels, high temperature chemistry, nonstoichiometry, review 77—14238
- flashover behaviour, of spacers at low temps. 80—25882
- flat parts containing Ti, efficiency increase in fine diamond polishing 79—20228
- fluoride systems, fundamental condition for glass formation 80—44135
- fluorite ceramics, doped, short range order anal. by electron diffr. 78—83672
- fluorophlogopite mica, glass-ceramic, thermal diffusivity, crystallisation effects 78—6190
- fracture by single pulse 10.6 μm irrad. 79—99988
- fracture mech., probability, micromech. models of crack growth 80—108571
- fracture mech. appl. 79—43426
- fracture mechanics, and mech. props., fragile materials *(French)* 80—104274
- fracture mechanics, review 80—45373
- fracture mechanism maps for materials which cleave 79—91774
- fracture processes, adsorption-sensitive, control and appl. 77—52468
- fracture strength, dimensional anal. of grain size depend. 80—70299
- fracture stress, rel. to flaw and fracture mirror sizes 78—11309
- fracture stress rel. to flaw and fracture mirror sizes 79—11689

ceramics continued
- fracture toughness, exam. of methods of enhancing, merits and limitations 78—60771
- fracture toughness specimens, wedge indentation technique for precracking, appl. to Al_2O_3 and SiO_2 78—85087
- fracture-mirror boundary formation, criterion 80—70297
- fuel, irradiation device for creep and swelling study 77—42063
- fuels, vibro-compacted, initial stages of sintering and hot-pressing 80—16254
- fusion reactor applications, design methodology and anal. 80—32475
- fusion reactor design criteria for blanket and first wall regions 80—32474
- fusion reactor materials, effects of radiation on electrical insulators 78—95082
- gas turbine engine, substitution of ceramics for high temp. alloys 80—97678
- glass, heat treated, thin foil prep. for TEM obs. 78—7154
- glass, low temp. heat capacity, glassy and devitrified states 78—22862
- glass, surface prep. for Si thermosprayed coating 78—11367
- glass, thermal expansion variation with ratio of phases and comp. 77—35719
- glass and oxide glasses, microstructure 78—88442
- glass applications, review 78—3306
- glass ceramic, form. characts. in slag glasses 77—8794
- glass ceramic, machinable, elastic moduli press. and temp. derivatives, specific heat 78—52873
- glass ceramic, nucleation and growth studies by small angle neutron scatt. 79—32913
- glass ceramic mineralogy 80—60826
- glass ceramic prep. by hot pressing and crystallisation of glass powder, mech. props. 78—15351
- glass ceramic protective coatings for Ti, synthesis and props. 80—25900
- glass ceramic rods, strengthened, residual stress determ. 78—23830
- glass ceramics, machinable, vac. compatibility 79—93152
- glass ceramics, radioactive high level waste management 80—5271
- glass ceramics highly radioactive waste management 80—5271
- glass fibre ceramics, manufacture 80—40304
- glass phase of 22KhS, valence state of Ti and Mn ions, ESR determ. 77—43871
- glass technology and applications, review of advances 77—66618
- glass-ceramic, aligned, hot extrusion method for prep. 77—32552
- glass-ceramic, dispersion strengthened glass matrix 77—40425
- glass-ceramic, machinable, elastic const. temp. depend. 80—79852
- glass-ceramic, randomly oriented, physical props. 78—48501
- glass-ceramic, randomly oriented, physical props. 78—48502
- glass-ceramic, strength, effects of moisture-assisted slow crack growth 78—27593
- glass-ceramic composite, internal stress effects on mech. props. 77—21250
- glass-ceramic machinable, machining techniques 78—77881
- glass-ceramic/bone histological and mechanical bonding *(German)* 79—8569
- glass-ceramics, transient heterogeneous nucleation of glass-forming systems 80—88042
- glass-ceramics and photosensitive glass, microstructure rel. to properties *(German)* 80—38926
- glass-ceramics based on β-spodumene solid solns., dielec. const. calcs. 77—52008
- glassy, struct. and electron beam sensitivity 80—79841
- glassy phase, struct. study through electron-beam-induced ionisation effects, HVEM obs. 80—14978
- glaze, abrasion resistance 79—38984
- glaze-porcelain system, intermediate layer investig. by electron probe microanalysis 77—8965
- glazed ceramic insulators, surface quality monitoring 79—61813
- glazes, opaque, with ZnO, microstruct. 79—60281
- glazes, Pb, Zn and added chromogenic ions release, as function of colouring oxide mill additions, voltammetric exam. 78—39920
- glazing with gaseous P_2O_5 80—108609
- grain and phase boundaries between crystals, conf., Konigstein, Germany (Oct. 1977) 78—72762
- grain boundary segregation 78—15410
- granular, electrophysical props. depend. on porosity, temp., solid-phase props. 77—69764
- graphite, neutron damage at 1200°C, fusion reactor first-wall appl. 79—93829
- graphite, porosity effect on strength variation 78—31369
- grinding induced tempering, in ceramics containing ZrO_2 80—89260
- growth micromechanism in corrosive environment 80—108616
- $(H_3O)_{5-x}Ta_{11+x/t}O_{30}$, synthesis, non-stoichiometry, density and ionic cond. meas. *(French)* 78—52741
- high Al_2O_3 fired bars, modulus of rupture, relative humidity depend. 80—40473
- high performance, review and fabrication methods 77—8785
- high temp. props., conf., Baden-Baden (Feb. 1978) *(German)* 79—70135
- high-power US transducer performance rel. to ceramic location 79—50561
- high-temperature materials, technological requirements, R and D, report 80—45222
- high-temperature transmission/wavelength characteristics *(French)* 79—7188
- highly electrostrictive ceramic capacitor 79—47390
- hot pressing ferrite and ceramic, bulk interaction *(Russian)* 80—40277
- Humiceram-III, multifunctional sensor to detect humidity and gases *(Japanese)* 80—105659
- hydrogen embrittling effects from acoustic emission meas. 80—11742
- hydroxylapatite, sintered bioceramic, prep. and props. 79—43174
- impact toughness testing device 80—25941
- insulation joints for Frascati fusion reactor Torus 80—18653
- intergranular thin film detect. by high resolution electron microscopy 80—4824
- internal microstresses in glass-ceramics 78—30542
- ion accelerators for fusion ignition, neutron resistant ceramic insulator development 80—37639
- ion beam irradiation techniques for simulation of 14 MeV neutron irradiation 80—10584
- ion etched surface microstructures 79—83362
- ion-selective membrane electrodes development, Ag^+ and F^- based materials appl. *(Japanese)* 80—61203
- K-ramic^R, ultrahigh vac. compatibility, outgassing characts. 79—81080

ceramics continued
- kaolin bodies, effect of mineralizers on firing shrinkage, microstruct. and strength 80—97488
- kaolin grog particles, shape and density 80—97450
- kaolinite, decomposition 77—52627
- kaolinite to mullite reaction series, reexam. of solid state phase transformations 78—64535
- kaolinite-mullite reaction sequence, interpretation from IR absorption spectra, comment 78—48720
- kaolinite-mullite reaction sequence, spectroscopic anal. of Al coordination changes 78—48719
- kaolinite-mullite thermal sequence, intermediate cubic phase 80—25652
- kaolinite-mullite thermal sequence, structural analysis and transition phases 77—36484
- KER 110 hard porcelain corrosion in conditions of practical use *(German)* 79—100270
- laser induced explosion 77—40308
- laser-assisted hot spot machining, advantages and potential 79—70199
- layers on metallic substrates, mech. props. meas. *(French)* 80—104375
- leading in glazed caramics, colorimetric method *(Spanish)* 80—73414
- leucosapphire, spectral absorption coeff., 0.25-1.25 micron, up to 1800K, and 3.5-5.2, up to 1200K 78—27204
- lifetimes and slow crack growth prediction *(German)* 80—104250
- liquid, sp. ht. eqn. for high temp. 77—51510
- LMFBR carbide fuel cladding damage anal. at TREAT 80—13602
- local in depth anal. by neutral beam SIMS 80—89565
- LV switchgear contacts *(Slovak)* 78—56603
- lyophilisation parameters of ceramic compounds, freeze-drying synthesis 80—97453
- material analysis by electron beam bombardment *(Japanese)* 77—86416
- material processing facilities and expts. on Spacelab. 78—36431
- MC planar, design based on TMS 9980 *(Italian)* 79—21697
- mechanical behaviour, book 79—38983
- mechanical engineering props. and applics., conf., London, England (Dec. 1977) 79—38840
- mechanical failure, porosity effects *(Polish)* 77—59934
- mechanical properties measurement, apparatus for up to 1700°C *(French)* 80—104374
- mechanical properties measurement, using disc-shaped specimens *(French)* 80—104367
- mechanical strength and brittle fracture behaviour, microstruct. and microcrack effects *(German)* 78—31500
- mechanical test apparatus for up to 2200°C *(French)* 80—104372
- membrane, chalcogenide ceramic, Cu-selective electrode *(Chinese)* 80—81357
- metal layer/crystalline ceramic adhesion mechanism for metallization of electronic ceramics, elec. props. *(German)* 80—76381
- metal oxides, polymorphic (chemipolymorphic) transitions 79—11603
- metal to ceramic joint, problems of characterizing the adherence 79—43552
- metal-ceramic containing diamond, impact hardening 79—15828
- metallic oxide powders and mixtures, hydrostatic pressing, density and hardness variation 79—70029
- metalloceramic materials, NDT of microstructure and porosity using mag. props. 77—73416
- metallographic method for polishing specimens, of ceramics and metal-ceramic mixtures 78—56850
- $MgO\text{-}ZrO_2$ ceramic reinforced with filamentary crystals, mech. and thermal props. 80—45262
- MHD generator duct wall, semi-hot, thermal stress design study *(Japanese)* 78—13890
- MHD generator insulation wall deterioration *(Japanese)* 77—24200
- mica glass-ceramics, near perfect shape-memory solid 77—48492
- microcracked brittle, thermal stress resistance anal. 80—40472
- microcracking as mechanism to improve thermal shock resistance and insulating props. 77—28885
- microcracks, and thin intergranular films obs. by TEM 80—68295
- microstructural consequences of phase transformations 80—3034
- microstructure dependence of mechanical behaviour 78—88533
- microwave permittivity and dielectric loss method for ceramic low-loss foils *(Polish)* 78—37028
- mineral, exam. by X-ray diff. at high temp. *(French)* 79—96234
- mirror surface manufacture on pyroceramic blanks 77—62079
- moisture measurement in porous ceramic components, equipment *(German)* 78—54378
- monoxide, high resolution electron microscopy 79—90501
- mould accelerated shell heat treatment models 79—76896
- moulding material containing SiC, moisture content measurements in UHF range 79—34404
- mounting and polishing technique, for microstruct. exam. 78—48580
- mullite, crystallisation from $SiO_2\text{-}Al_2O_3$ melts 78—47243
- mullite, high temp. mech. props. in compression 77—56033
- mullite, polycrystalline, prep. by hot pressing aluminosilicate glasses 78—60639
- mullite, quantitative X-ray anal., standardisation, texture *(German)* 78—11176
- mullite, refractory ceramic creep, struct. effects 77—66679
- mullite, synthetic raw materials, sintered and fused, use in refractories industry, slagging, creep, thermal shock resistance *(German)* 79—4937
- mullite fibre reinforced mullite, in vitro degradation, bending strength, Young's modulus, density meas. 78—85011
- mullite rollers, heat treatment effects 79—61616
- mullite-corundum, thread-like crystals reinforced, props. 80—108525
- mullite-corundum ceramics, electron microscopy of damaged surface 80—88413
- mullite-corundum electroceramic, thermal expansion coeff. meas., 80-300K 79—60526
- multichannel ceramic blanks, produced from a refractory material 79—83163
- multilayer capacitors, fracture mechanics approach to structural reliability assessment 80—89328
- NASICON solid electrolyte, processing and phys. props. 80—60820
- nepheline concentrate, low Fe, phase composition 77—21110
- nepheline containing ceramic masses, phase transform. during firing 77—66611
- nickel calcine, reactivity, contact I-V meas. 77—85975
- niobate based ceramics, synthesis, struct., elec. cond., mag. props. *(Czech)* 80—45259
- non-oxide, hot pressing review 79—74113
- non-oxide, hot pressing review 80—25641

ceramics continued
- nondestructive testing, scanning laser acoustic microscopy, appl., comparison with SEM and optical microscopy results 80—58875
- nonsymmetric vibrations of piezoelectric ceramic rings polarized along the thickness 80—7299
- nuclear ceramics, grain boundary energy to surface energy ratio, as determ. from pore geometry 80—34291
- nuclear ceramics, quantitative image anal. using light and SEM obs. 79—12912
- nuclear fuel, irradiation induced creep 77—42056
- nuclear fuel, porosity characterization, optical and electron microscope exam. 78—44302
- nuclear fuels, mech. props. at compressive deformation 80—651
- nuclear high-temp. reactor, advanced system, materials for core-specific and primary circuit components 77—26842
- nuclear reactor materials developments for advanced HTR systems 77—46297
- nuclear reactor plant materials developments for HTGR systems 77—46298
- one dimensional cooling, effect of particle orientation on frost damage *(Japanese)* 77—12701
- optical, KO-1, IR scatt. and brightness indacatrices meas. 78—71164
- optical ceramic, gas-moulded, characteristics and application prospects 79—81495
- optical ceramic, KO1, homogeneity in terms of refr. index 80—64125
- optical ceramic KO-1 strain, yield limit, and stress relaxation obs. 79—46018
- optical ceramics, dispersion, double refraction and storage effects, material appls. *(German)* 80—69471
- optical glass ceramic, (sital) surface operation parameters, selection using bending strength tests 79—32101
- optical materials, nephelometer for light scatt. meas. 77—10084
- oxide, TEM study of deform., review 79—87686
- oxide, thermal conductivity and emissivity at high temp. 77—28051
- oxide ceramics, dependence of props. on raw materials, exam. using ceramic magnets as model *(German)* 79—4936
- oxide ferrolectric, perovskite structure type, cond. and polarisation 77—12325
- oxide fuels, in-pile densification by vacancy boil-off and vacancy knockout, model 79—8259
- oxide systems, quasibinary and quasiternary, data base development for phase diagram calc. 79—96006
- oxide thermal-sprayed coating on steel, acoustic emission 80—21247
- oxides, semi-sintered, as press. transmitting media 80—52259
- paste, direct tensile tests and tied crack model 78—11178
- periclase, fused, and periclase-chromite blocks, produced from beneficiated starting meterials, struct. and props. 79—87600
- perlite, low temp., processes occurring during firing 80—11607
- phase diagrams, exam. of compilation activities 79—8287
- phase diagrams for ceramists 78—15380
- phase equilibria, use in development of high temp. structural ceramics 79—11595
- phosphate bonded synthetic mica ceramics, form., physical props., texture 77—21063
- phosphate containing materials, technological prod. processes, review 80—97452
- phosphate glass-Al alloys seals, elec. and mech. props., glass transition 80—81018
- photoacoustic effect in piezoelectric ceramics 80—84252
- piezoceramic, compression tests, fracture stress distrib. at various loading rates 78—15529
- piezoceramic, polarisation method effect on mech. strength 78—39879
- piezoceramic, statically compressed layer, electrical energy of instantaneous discharges *(Russian)* 78—39503
- piezoceramic aperiodic transducer, mech. load study 80—87700
- piezoceramic articles, nonuniform polarisation investig. by microwave polaris. method 78—72969
- piezoceramic benders, circular, bond stresses 78—21124
- piezoceramic cylinders, finite axially polarised, vibr. anal. 77—11081
- piezoceramic disc resonators, dispersion of thickness vibrs. 78—22237
- piezoceramic elastic compliance and mechanical Q-factor at high drive levels 78—60395
- piezoceramic material, SAW, nonsynchronous interaction *(Russian)* 78—26002
- piezoceramic medium, electroelastic waves, magnetic accompanying effects *(Russian)* 79—28680
- piezoceramic microwelding transducer component oscillation amplitudes 79—26046
- piezoceramic planar Poisson ratio variation with poling conditions 79—11391
- piezoceramic plate, electroelastic equilibrium *(Russian)* 78—43795
- piezoceramic plates, bending strains, electromechanical transformation, energetic method of calc. *(Ukrainian)* 80—71320
- piezoceramic Poisson ratio rel. to electromech. coupling and energy trapping 78—43796
- piezoceramic SAW propagation loss reduction by hot pressing 78—2356
- piezoceramic sphere, radially polarised, equivalent cct. parameters calc. 80—14538
- piezoceramics, converters of shock wave mech. energy into elec. power 80—61429
- piezoelectric, artificial poling procedures and transducer appls. 77—12314
- piezoelectric, bend and compressive strength, stressing rate effect 77—52409
- piezoelectric, bimorph element for loudspeakers props. and preparation *(Japanese)* 80—53597
- piezoelectric, electromechanical energy conversion in nonuniformly deformed bodies *(Russian)* 78—19418
- piezoelectric, filters for HF appl., using $Pb(Zn_{1/3}Nb_{2/3})O_3$-$PbTiO_3$-$PbZrO_3$ and $Pb(Mg_{1/3}Nb_{2/3})O_3$-$PbTiO_3$-$PbZrO_3$ *(Japanese)* 80—60507
- piezoelectric, meas. using autocorrel. anal., stress characts. 77—1639
- piezoelectric, nonlinear charge release under uniaxial press. 80—80706
- piezoelectric, phase method of microwave flaw detection 78—72968
- piezoelectric, reflection and transmission of elastic waves at boundary with water 80—87588
- piezoelectric, TsTBS-3, mech. strength, effect of glass powder additions 78—31370
- piezoelectric, US instrument for determ. characts. 80—66752
- piezoelectric acoustic Lamb wave focusing devices 80—79093
- piezoelectric buzzers for high sound levels 80—92005

ceramics continued
- piezoelectric ceramic materials, reviews appl. and recent developments 79—78628
- piezoelectric ceramic platelets, geometry effect, effect on props. of flexural oscillator *(German)* 79—32168
- piezoelectric ceramic transformers, optimal transducer design *(Japanese)* 77—13770
- piezoelectric ceramic vibrator, resonant freq. temp. stability anal. *(Chinese)* 78—68454
- piezoelectric cylindrical shell, longitudinal wave propagation 78—92026
- piezoelectric effects due to polarisation, expt. *(Polish)* 77—77151
- piezoelectric material for electrostatic voltage sensor *(Japanese)* 80—105632
- piezoelectric materials, piezoelec. props. review *(Japanese)* 77—73115
- piezoelectric resonators, eigencoupling state space vector representation 80—2697
- piezoelectric transducer, anomalous radiation pattern due to parasitic Lamb wave generation 80—96170
- piezoelectric transducer parameters testing equipment 79—50555
- piezoelectric transducers, broadband, production 80—61044
- piezoelectric US transducer, shear-wave vel. meas., bone elastic moduli determ. 78—83201
- pigments, willemite struct., NiO, MnO, and FeO based, synthesis 80—20855
- pile fuel *(Polish)* 79—17985
- plasma sprayed ceramic coating for turbine engine components 80—40616
- plastic deformation, grain and grain boundary processes 77—4814
- plasticity determ. using drying process and shrinkage 79—20307
- PLZT, optically induced birefr. change 78—43832
- PLZT ceramic modulator for 1064nm laser Q-switching 77—38964
- PLZT ceramics, ferroelec., special props. 79—42916
- PLZT ceramics as electro-optic shutter material for IR appls. 79—72679
- PLZT coarse-grained solid solutions, electro-optical processes induced by longitudinal electric field *(Russian)* 80—80750
- PLZT electrooptic ceramic, electron beam surface charging, rel. to optical modulation 80—6952
- PLZT ferroelectric ceramic, anomalous bulk photovoltaic effect and cond. *(Russian)* 80—54733
- polished section prep. using pedepin *(German)* 78—19983
- polycrystalline, fracture mirror form. 77—48541
- polymer filled ceramic, ZrO_2 stabilised, fracture mechanism *(Russian)* 80—100895
- polymorphism and defect characts. *(Japanese)* 80—15075
- porcelain, conventional and rapid fired, comparison of texture and props. *(German)* 78—64510
- porcelain, correlation between wear, crack resistance and stress intensity factor *(German)* 77—36666
- porcelain, crack propag. data applicability to failure prediction 80—81154
- porcelain, elec., comparative assessment of methods of determ. strength 80—40429
- porcelain, elec., high-strength, development from ceramic raw materials, mech., elec. props. 79—24630
- porcelain, electrotechnical, compressive strength 80—100882
- porcelain, equipment for translucency testing *(Polish)* 78—19985
- porcelain, flashover behaviour at low temps. 80—25882
- porcelain, neutron-retardation behaviour for continual moisture determ. *(German)* 80—105660
- porcelain, relation of crazing to stress in porcelain glaze, method of stress determ. *(Japanese)* 78—31537
- porcelain, sintering, theoretical treatments and exp. procedure 78—44067
- porcelain, sintering charact. 79—83156
- porcelain, strength eval. after grinding 77—52518
- porcelain body dynamic equation, during sintering process *(German)* 78—27455
- porcelain enamel, electrocoating, appl. 79—33947
- porcelain enamel, resistance to aqueous attack, expt. results 78—56788
- porcelain enamel, resistance to aqueous attack, prediction eqn. 78—60853
- porcelain enamel layers on steel, H_2 induced fracture of layers 78—76752
- porcelain enamel panels, TiO_2-opacified, quantitative X-ray diffr. anal. of anatase, rutile 79—32857
- porcelain raw material, ion exchange chromatography method, for separate determ. of Na_2O and K_2O 78—7272
- porcelain wave, crazing resistance, glaze fitness *(Japanese)* 79—74278
- porcelains, sintering props. 79—29006
- porosity, exam. using image analyser and optical microscopy *(French)* 79—15880
- porous, capillary mass transfer 77—7443
- porous, eval. of frost resistance by holography *(Japanese)* 78—19987
- porous, frost resistance under 1-d cooling, pore size distrib. effect *(Japanese)* 78—44069
- porous, longitudinal US wave velocity 77—55323
- porous ceramics, frost action under one dimens. heat flow *(Japanese)* 79—79140
- porous ceramics, with non-spherical holes, US wave vel. and elastic moduli evaluation 77—60031
- portland cement, doped with ZnO, struct. and props. 80—60914
- potsherds, Melian, instrumental neutron activation anal. 78—8485
- potsherds, S.W. African, neutron activation anal. of trace elements, characterisation 78—8486
- potsherds, Turkish, neutron activation anal. 78—8487
- pottery, sigillated, trace element archaeochem. using neutron activation anal. 78—8488
- powder, thermal stresses during spheroidisation process *(Russian)* 80—40386
- powder pressing review 79—47652
- powder synthesis from laser-heated gas phase reactants 80—93525
- powders, electron microscope determination of particulate sizes *(German)* 78—57891
- powders, equipment for sublimation drying, exam. 80—25733
- preparation from metal-containing organic cpds., state-of-the-art 77—55922
- pressure-mode soft-metal vacuum seal, for glass and ceramics 80—17952
- procelain, unglazed, membrane, thermoosmotic conc. difference meas. for gaseous membranes 79—83508
- processing before firing, book 78—56608
- proof testing 80—104207
- proof testing 80—108654

ceramics continued
- pyroceramic, stress in working zone under biaxial compression, Moire-band method 77−81369
- pyroceramic end gauge, high-precision stability 79−76778
- pyroceramic lightweight mirror blank fabrication using standard metal-working equip. 80−102871
- pyroceramic plate scribing by pulsed CO_2 laser 79−52410
- pyroceramic plate surface quality obs. after mechanical polishing 79−72732
- pyroelectric, high power continuous laser emission meas. appls. *(Russian)* 78−16845
- pyroxene slag glass ceramics, exam. of synthesis conditions, influence of catalysts 79−4942
- PZT, ferroelec. ceramic, mechanical props. determ. by acoustic techniques 79−28685
- PZT, ferroelec. energy conversion under shock loading 80−108163
- PZT, polycrystn., thermal expansions, elasticity and internal friction 80−35238
- quartz, elastic property changes on sintering 77−90301
- quartz, physiomech. props., influence of surfactant incorporated during synthesis 80−20856
- quartz, quantitative X-ray anal., standardisation, milling effect on degree of disorder *(German)* 78−11176
- quartz ceramic, SiO_2-Cr_2O_3-TiO_2, creep and porosity, for ceramics with different structures 80−21011
- quartz ceramics, thermal and temp. cond. in range 500-1900K 80−39370
- quartz glass based, organosilicon binder, spalling-resistant, prod. 80−40313
- quartz glass-ceramics, atm. influence on sintering rate 79−38784
- quartz porcelain fast fired, development of microstruct. *(German)* 78−60625
- quasibinary and quasiternary ceramic oxide systems, calculation of phase diagrams 78−60660
- radioactive high level waste storage 77−6542
- radioactive waste, high-level, evaluation of products for solidification 77−61555
- radioactive waste disposal, synthetic mineral nuclear waste ceramics 80−42813
- radioactive waste encapsulation, using powder metallurgical process *(German)* 78−33281
- rare earth aluminates, effects of roasting in reducing and oxidizing media on elec. props. 78−52736
- rare earth elements, use in glass and ceramics *(Polish)* 80−97455
- rare earth niobates, pyrochlore structure, synthesis and props., 79−11533
- rare earth oxyphosphates, x Ln_2O_3.y P_2O_5, synthesis, characterisation and thermal stability 80−16256
- rare earth perovskites and garnets, prep. and props. book contrib. 80−44193
- rare earth pyrochlores, $R_2(V_{4/3}W_{3/3})O_7$, (R=Gd, Tb, Dy, Ho, Er, Tm, Xb, Lu), synthesis and elec. props. 80−29914
- rare earth zirconate, $R_2Zr_2O_7$, Raman spectra, anion disorder characterization 80−25358
- rational molecular engineering 78−11179
- raw kaolin, acoustical investigations of the effect of additives on elastic props. 80−66559
- recrystallisation and grain growth, survey 78−76660
- recycling, residual and additive elements control by specifications 80−66522
- red shaped, elastic moduli and Poisson ratio determ. method 80−55606
- refractory, high-temperature creep testing, at different loadings, laboratory equipment *(Russian)* 78−19970
- refractory ceramic, creep testing, equipment combination 78−11477
- refractory ceramic, deform. test apparatus and method *(Russian)* 78−35613
- refractory ceramic, heterogeneous, significance of non-elastic deform. in fracture 79−47765
- refractory ceramic creep meas. in tension and compression 78−31486
- refractory coatings, for high temp. use, current status *(Japanese)* 80−71619
- relaxor ferroelectrics, electrostrictive effects 80−66112
- rheological meas. device for 20° to 90°C and constant moisture content 78−85079
- ring assemblies, brazing techniques for TFTR injector and pumping ports 80−32476
- Rochelle-type, controllable transparency, birefringence effect *(Russian)* 77−630
- rollers for conveyor lines, bending strength as func. of wall thickness 80−11699
- ruby, spectral absorption coeff., 0.25-1.25 micron, up to 1800K, and 3.5-5.2, up to 1200K 78−27204
- ruthenates, $ACu_3Ru_4O_{12}$, A=Na,Ca,Sr,Cd,La,Pr,Nd, synthesis, cryst. struct., mag. and elec. props. *(French)* 80−107151
- rutile ceramic anomalous conductivity effect analysis 80−15512
- sapphire, shaped single crystals, porosity, microstruct. 78−2125
- sapphire, work hardening 77−16604
- sapphire filaments in Al_2O_3:MgO matrix, single cryst. boundary migration 80−44369
- SAW filter development and applications 79−23156
- sculpture from Oaxaca, Mexico, authentication by thermolum. and style 78−70238
- self vitrifying, consisting of quartz, feldspar and kaolin, compaction press. during firing effects 80−29909
- self-cleaning catalysts for ovens and grills *(Japanese)* 80−55557
- SEM and anal. techniques *(German)* 78−56832
- semiconducting, low resistance contacts 77−1483
- semiconducting, meas. cell and setup for elec. resist. meas. 300-1400°C 79−30488
- semiconducting ferroelectric glass-ceramics, dielectric dispersion *(Russian)* 79−8097
- sherds, macroporosity determ. by replica techniques 77−34065
- shirasu volcanic-ash ceramics, sintered and bloated, props. and appls. *(Japanese)* 77−73252
- shrinkage kinetics meas., high-temp. dilatometer system 79−17396
- Si_3N_4-Ce_2O_3-SiO_2 materials: phase relations and strength 80−97465
- Sialon, high resolution electron microscopy 79−90501
- β-Sialon, high strength, reaction sintering 80−7525
- sialon, oxidation 77−56126
- Sialon, reaction sintered, mech. props., effect of composition and X-phase 77−56013
- β'-sialon compositions, reaction sintering obs. 80−55337

ceramics continued
- SiAlON X-phase, X-ray diffr. data 80−49198
- sialons, ceramic material fracture mechanics, review 80−45373
- silicate+$Ca(OH)_2$, reaction rates 80−26006
- silicate+Portland cement, reaction rates 80−26006
- SiN, hot-pressed, creep 80−16380
- sintered, thermal diffusivity meas. by flash with negative pulse, plasma jet heating 79−37888
- sintered glass-ceramics prep. from calcined simulated high level radioactive waste 77−28770
- sintering, rate controlled 80−20871
- sintering kinetic laws, with involvement of a liq. phase 80−55335
- SiO_2-Al_2O_3-MgO(-K_2O-F) glass ceramic crystn., microstructures rel. to conditions 80−11638
- sital, technical, compressive and bending strength 77−70131
- Sitall-based composite mat., grinding 77−63822
- sitalls, thermal conductivity, at various stages of heat treatment 79−60562
- slip moulding method development 78−68661
- solar cavity receivers for thermal electric systems 80−30549
- space flight applications in materials science 79−47885
- Space Shuttle external insulation, acoustic emission inspection 78−16276
- specific surface area meas. by gas adsorption 78−11144
- specimen prep., time saving methods *(German, English)* 80−35459
- specimen preparation, thin sections, for optical microscopy 79−52562
- specimen preparation, with Pedemax-Planopol automatic grinder and polisher 79−74333
- spherical cavity effect on fracture 79−66145
- spinel oxide, dissociation of dislocations and plastic deform., temp. effects 79−7613
- spinel single crystals, mech. props., 1350-1650°C *(French)* 80−104374
- spinel transparent glass ceramics, colour centre form. due to alkali metal vapour and X-ray irradiation 79−87316
- spodumene, chem. resist. and struct. 79−61756
- β-spodumene-mica glass ceramic, thermal expansion thermal shock and moduli of rupture and elasticity 78−60736
- β-spodumene-mica glass ceramics, phase evolution and TiO_2, MgF_2 additive effects, exam. 78−44089
- SQUID coupled to piezoelectric transducer, detection of gravitational waves 78−21218
- Steatit ceramic strength determination by measuring US dynamic elastic modulus *(German)* 79−43301
- steatite, dielectric ceramic 77−32546
- steatite, exam. of thermal damage by strength meas. 78−84997
- steatite, glass-ceramics technology appl. 80−104097
- steatite, sintering and crystn., depend. on original powder state 79−61527
- steatite electroceramic, thermal expansion coeff. meas., 80-300K 79−60526
- steel, stainless, fibre reinforced wustite, strength and toughness 78−27602
- strain intensity criterion for crack branching in brittle mats. 78−55592
- strength and deformation testing, wide temp. range, universal apparatus 79−57177
- strength and failure predictions 77−21256
- strength recovery by diffusive crack healing 77−77555
- stress intensity factor estimates for a peripherally cracked spherical void and a hemispherical surface pit 79−29196
- stress-relaxation technique for deformation studies in four point bending 79−100200
- stress-strain diagrams, anal. and classification of low deforming materials by their behaviour under stress 79−15753
- structural, state-of-art review and survey of R&D techniques 77−63605
- structural characterisation, automatic structure analyser, EPIQUANT, quant. microscopic meas. 79−83409
- structural components, design criteria and structural testing 79−39083
- structural integrity in severe thermal environments 77−36544
- structural stresses measurement using X-ray diffr. meas. *(German)* 78−52744
- substrate, ion plating and microstruct. of metal coatings 78−11132
- surface, glow-discharge treated, adhesion of vacuum deposited oxide *(Russian)* 77−44372
- surface cracks, acoustic surface wave meas. 80−61055
- surface flaw detection by SAW scatt. 79−47866
- surface metrology using peak counting, quality control 80−95065
- surface spark discharge, channel spreading and substrate vaporisation 77 89336
- suspended particle, effect of electrolyte on charge, in cermet electrodeposition 78−68665
- suspension, automated meas. of viscosity 79−37258
- suspension, ceramic body growth, diffusion theory *(Czech)* 79−69269
- suspension, ferromagnetic filtration apparatus improvement 78−11561
- suspension, ferromagnetic treatment, optimum system construction with FOL instruments 78−4666
- suspension, rheological properties, effect of grainy filler ceramic suspensions 80−43685
- SYNROC-B ceramic for radwaste disposal, feasibility of subsolidus sintering 80−83198
- SYNROC-B sintered ceramics for high-level radwaste fixation, comp. and phase charact. 80−106126
- synthetic raw materials, exam. of chemical preparation methods *(German)* 79−4930
- synthetic raw materials, sintered and fused, use in refractories industry, slagging, creep, thermal shock resistance *(German)* 79−4937
- TBK-3, ferroelectric ceramic, 90° electric domain processes, mech. stress, X-ray diffr. 78−72478
- TEM, high-resolution, ceramic science applic. 78−35397
- TEM study of precipitation 79−87637
- TEM study of radiation damage, review 79−86816
- tensile and bending strengths, error sources in testing *(German)* 78−35421
- tensile and compressive creep behaviour, bend tests 78−48455
- tensile strengths, uniaxial and equibiaxial in bending statistical comparison 80−25775
- tensometric equipment, for determ. of properties, during vacuum pulse drying 80−20965
- Terra Sigillata from La Peniche, Switzerland, chem. comp., mineralogy and porosity 79−26198
- thermal conductivity, effect of decrease in thermal resistance of pores and microcracks 78−75892

- **ceramics** continued
  - thermal conductivity, temp. depend. with rarefaction of gas medium 77—7914
  - thermal expansion at high temps., meas. via laser interferometry of two fibres 77—26270
  - thermal expansion hysteresis, cyclic plastic deform. explanation 80—89290
  - thermal fatigue life prediction 78—19873
  - thermal fatigue life prediction 79—38939
  - thermal shock resistance determ., new heat flux method *(Japanese)* 79—39075
  - thermal shock resistance meas. by AE *(German)* 79—70233
  - thermal stability determ. by US monitoring 77—44441
  - thermal stress and thermal shock, review of test methods, thermal stress theory industrial problems 77—63805
  - thermal stress failure mode, effect of data scatter, brittle ceramics 80—60949
  - thermal stress resistance, enhancement, for materials with thermal cond. gradient 78—48506
  - thermal stress resistance, figures of merit, review 79—83290
  - thermal stresses in ceramic elements of MHD generator channel walls 77—70075
  - thermodynamic props., calc. for liq. and solid phases 77—43348
  - thermoluminesc. dating, comparison of results 80—84791
  - thermophysical properties at high temp., conference, Moscow, USSR (May 1976) 77—28012
  - thoria effusion membrane, production techniques based on that of incandescent gas mantles 78—39724
  - tile, resistance to fracture, Weibull statistics *(German)* 77—7338
  - toughened, stress corrosion characts., exam. 78—71295
  - toughened, stress corrosion characts. 78—19912
  - transducer, spatially-bounded US wave response 80—48542
  - transformation toughening, martensitic transforms. in crack-tip stress fields 80—104154
  - transition elements, 3d, ESR for valency assessment, appl. to ceramics and glass industries *(German)* 80—34757
  - translucent systems, absorption and scatt. coeffs. for visble light, Kubelka-Munk theory 80—60627
  - transparent ferroelectric, composition selection for appl. in light modulators *(Russian)* 80—91869
  - transparent glass-ceramics, microstruct. and props. 78—59960
  - trapped-energy ceramic resonator with improved response characts. *(Japanese)* 78—9522
  - treatment methods, drying, cooling, heat treatment, reln. to material props. *(French)* 77—90296
  - tricalcium silicate paste, composition of solution in contact 77—81423
  - TsTS polarized ceramic film, Lamb waves near. crit. freq. study *(Russian)* 78—52039
  - TsTS-19, dynamic peizoelec. modulus *(Russian)* 79—28681
  - TsTS-23, ferroelectric ceramic, 90° electric domain processes, mech. stress, X-ray diffr. 78—72478
  - turbine disc, subjected to centrifugal stresses, failure probability, photoelastic model 79—18816
  - ultrafine powder, prod. by cryochemical, freeze drying, spray drying or soln. techniques 80—55336
  - ultrahigh vacuum and cryogenic feedthrough, with 48 pins 79—97399
  - ultrasonic NDT techniques, low-frequency 78—80690
  - unfired, cavity form. by electron beam machining 78—80660
  - unfired, precision e-beam machining, kinetic focusing 78—80661
  - unplated piezoceramic plate frequency response meas. 78—248
  - US attenuation 78—67772
  - US attenuation and velocity, 5-500 MHz 77—39634
  - US attenuation meas., pulse-echo method 77—28969
  - US investigation, porosity, mech. and dielectric strength *(Polish)* 79—52565
  - US transducers array, transducer elements tuning 80—87684
  - US treatment, without abrasion suspensions 77—44375
  - utilisation in nuclear industry 80—9341
  - utilization in fission reactors 79—93718
  - utilization in nuclear industry, current status and future trends, review 79—45349
  - utilization in nuclear industry, review 80—32350
  - vacuum hot pressing, continuous, of transparent ceramics, press design criteria 78—23643
  - Verneuil method of crystal growth 78—3082
  - vitreous ceramics, slow neutron irradiation effect *(Spanish)* 80—57816
  - vitreous china, crazing tendency, rel. to thermal expansion and quartz and cristobalite content *(Japanese)* 78—44243
  - vitreous enamel, bubble struct. and flaw forecasting 78—53118
  - vitreous enamel coating, method of quantitatively assessing blistered structure 78—53108
  - vitroceramic-metal composite materials development, Spacelab appl., mech. props. *(French)* 78—92229
  - Weibull distribution, adding static and dynamic fatigue effects 80—70298
  - white Cl-containing slag glass-ceramic, synthesis with nonsulphide catalyst 78—52748
  - X-ray analysis of inhomogeneities, using STEM with field emission gun 80—59354
  - zeolites, synthetic, effect of sintering on elec. cond., porosity and microstruct. 79—29009
  - Zerodur, glass-ceramic, thermoelastic props. 78—27550
  - zircon, dissociated, form. in plasma furnace, comp. and microstruct. 77—36429
  - Zircon ceramic, exam. of development and fabrication 80—11608
  - zirconate-titanate ceramics, K_{IC} eval. by double torsion technique 77—90444
  - $2ZrSiO_43Al_2O_3$, identification of stages in reactive hot-pressing 79—11542
  - $3CaO.Al_2O_3$, hydration retardation by $CaSO_4$ 79—61856
  - $3Y_2O_3.5Al_2O_3$, garnet, synthesis by firing mixed oxides 79—61545
  - Al_2O_3, heat of formation 79—91982
  - Al-C-silaceous sand mixture in N_2 atmos., weight loss during heating, compaction *(Japanese)* 80—35151
  - Al-Si-N-O system, comps. corresponding to β'-sialon phase reaction hot-pressing 80—84891
  - Al_4C_3-Be_2C-SiC system, phase analysis and TEM struct. obs. 80—108420
  - AlN, activating sintering process 80—25639
  - AlN, creep during hot pressing 78—23650
- **ceramics** continued
  - AlN filamentary crystal reinforced mullite-corundum ceramics, filaments strength, eval. 80—104230
  - AlN, polycrystalline, stress-strain data up to 1.25 GPa 80—100899
  - AlN powder, plasma-chem. and self-propag. high-temp. thermoplastic slips, synthesis 80—25633
  - AlN-Al_2O_3 composites, phys. and mech. props. of hot-pressed 77—52275
  - AlN-Al_2O_3 powders, hot pressing, crystalline phase obs. 78—95720
  - AlN-Si_3N_4-Be_3N_2 system, phase equilibria 80—60844
  - $AlNbO_4$, polycrystalline, thermal diffusivity, effect of microcracking 78—26743
  - AlO_2, corrosion resistance of phosphate bonded castable, and dense fired types in steam CO at 199°C 79—20222
  - α-Al_2O polycrystalline grain orientation, permeable pressing effect *(Japanese)* 78—15349
  - Al_2O_2, sintering, rate contolled 80—20871
  - Al_2O_3 *(Russian)* 80—50552
  - Al_2O_3 (96 wt.%), fractographic criteria for subcritical crack growth boundaries 80—81155
  - Al_2O_3, abrasive, wear in simulated hot grinding 78—56784
  - β-Al_2O_3, additive modified charact. by NMR 78—10785
  - Al_2O_3, adhesion of thick films, destructive and nondestructive meas. 80—50809
  - Al_2O_3, alumina, deformed by prismatic slip, HV TEM obs. of dislocations 80—108517
  - Al_2O_3, ambipolar diffusion in deformation mechanism maps 78—48454
  - Al_2O_3, aqueous acid slip, casting in gypsum mould 79—83165
  - α-Al_2O_3, atomic disorder, dominant type 78—63757
  - Al_2O_3 based ceramic sintering conditions effects on props. *(German)* 78—56604
  - Al_2O_3 based ceramics, ladder structures, interference phenomena explanation 78—72898
  - Al_2O_3 based coating produced from separated flow vacuum arc plasma *(Russian)* 78—31548
  - Al_2O_3 based electroceramic, thermal expansion coeff. meas., 80-300K 79—60526
  - Al_2O_3, bending strength, surface roughness effect at high temp. *(Japanese)* 79—70131
  - Al_2O_3, biaxially stressed, exam. of localised impact damage 78—72846
  - Al_2O_3 bicrystals, grain boundary obs. 80—39106
  - Al_2O_3 bioceramic synthesis, for orthopedic purposes, props. *(Polish)* 80—66465
  - Al_2O_3 brittle ceramic fracture toughness meas. notch requirements *(German)* 77—59937
  - Al_2O_3, calcined, exam. of morphological changes during calcination by SEM, exam. of sintering behaviour *(German)* 79—4931
  - Al_2O_3, ceramic, delayed fracture 77—44342
  - α-Al_2O_3, ceramic, prod. from etching wastes of Al foils 80—108376
  - Al_2O_3 ceramic, thermal expansion coeffs., represented by Gaussian spline polynomials 80—44341
  - Al_2O_3, ceramic compact, morphology 79—33988
  - Al_2O_3, ceramic Sinoksal, strength variation dependence on type of loading and temperature 79—57080
  - Al_2O_3 ceramics, elastic props. meas. in 100 to 300°C range 80—55445
  - Al_2O_3 ceramics, with thermoplastic bond, prep. 80—45254
  - Al_2O_3 ceramics in surgery for artificial limb-joints *(German)* 77—25593
  - Al_2O_3, commercial, Na_2O impurity removal and modifier in corporation 79—43183
  - Al_2O_3, composite base ceramic coating, hot pressed, H_2 permeability 77—56164
  - Al_2O_3, compressive stress state strength determ. in brittle material 77—16757
  - β-Al_2O_3, conduction and dielec. loss mechanisms, paired interstitialcy model 80—107468
  - β''-Al_2O_3, conductive, Li_2O stabilised, sintering and annealing 77—59724
  - Al_2O_3, corundum ceramic, effects of Na_2O, CaO additions on sintering struct., props. 79—15630
  - Al_2O_3, creep and long term strength 78—23802
  - α-Al_2O_3, cryst. struct. determ. at 2170K 80—39015
  - Al_2O_3, crystallite size and lattice distortion, determination using X-ray line broadening analysis, appl. to ceramic powders 79—8261
  - Al_2O_3 cutting tool, performance relationships, porosity determ. 78—11169
  - Al_2O_3, cutting tools, effect of acid etching on cutting performance 79—96169
  - Al_2O_3, cylindrical cavity effect on fracture 79—66144
  - Al_2O_3, cylindrical voids, exam. of instability 78—79603
  - Al_2O_3, D plasma interaction, surface structure, chemistry and resistivity changes 78—53010
  - Al_2O_3, deformation mechanism map 79—34109
  - Al_2O_3, dense, effects of oxide sintering additions on strength *(German)* 77—1866
  - Al_2O_3, dense, exposed to steam, influence of Ca migration on strength reduction 80—11797
  - Al_2O_3, dense, surface segregation of Ca under exposure to steam and steam-CO 78—85013
  - Al_2O_3, derived from gels, sintering behaviour, microstruct. 80—20875
  - Al_2O_3, derived from metalalkoxides, sintering behaviour 79—29005
  - Al_2O_3 detonation deposited coatings, porosity and adhesion, processing parameters effects 79—70227
  - Al_2O_3, dielec. breakdown mechanism determ. acoustic signature anal. techniques 80—11337
  - Al_2O_3 discharge tube for cataphoresis lasers 77—75551
  - Al_2O_3 dispersion hardened by Ba mica, thermal diffusivity 80—25713
  - Al_2O_3 dispersion in polycryst. NaCl, diffusive creep 80—97531
  - Al_2O_3, dynamic deform., stress-wave response 80—21020
  - β-Al_2O_3, effect of furnace atmosphere on sintering, and densification 79—20010
  - Al_2O_3, effect of quenching hardening on mech. strength, for various quenching mediums *(German)* 78—35403
  - Al_2O_3, elastic behaviour, finite element anal. model, thermal props. 78—31449
  - high-Al_2O_3, electrode in compact high-voltage vacuum feedthrough 77—26315
  - α-Al_2O_3, energy levels of donor and acceptor dopants and electron and hole mobilities 80—59911
  - Al_2O_3, evaluation of crack resistance and crack velocity, using controlled fracture experiments 78—72881
  - Al_2O_3, explosively compacted powder, struct. and annealing 77—55926
  - Al_2O_3, extraction from coal wastes, sinter process investigation 77—28769

ceramics continued

Al_2O_3, fatigue, static and dynamic in moist air 79−39002
α-Al_2O_3 fibre FP, manufacture, strength and modulus 80−81013
Al_2O_3, fibrous, thermal diffusivity and conductivity 78−10232
α-Al_2O_3 filamentary crystal reinforced mullite-corundum ceramics, filaments strength, eval. 80−104230
Al_2O_3, fine grained, basal slip and nonaccommodated grain boundary sliding 80−60916
Al_2O_3, fine grained, interface-controlled diffusional creep 80−60915
Al_2O_3, fine powder, prep. by evaporative decomposition of solns. 78−39725
Al_2O_3 for technical ceramics, extraction and prep. *(German)* 78−53200
Al_2O_3 fracture resistance, exam. 78−76826
Al_2O_3, fracture toughness specimen, appl. of wedge indentation technique for precracking 78−85087
Al_2O_3, fracture toughness testing by AE *(German)* 79−70234
Al_2O_3, fracture toughness meas. using Knoop indentation method *(German)* 80−25830
Al_2O_3 fracture toughness determ. using four-point-bend specimens 80−108536
Al_2O_3 fusion cast ceramics, crystn., microstructures rel. to conditions 80−11638
Al_2O_3, gamma irradiated single crystal, defect centres 79−65117
Al_2O_3, glass resistant, plasma coating props. 79−34164
Al_2O_3, grinding and polishing, quantitative control and optimization *(German, English)* 80−35460
Al_2O_3, grinding material, grain shape optimization *(Polish)* 80−29916
Al_2O_3 hard anodic coatings, effects of cellular structures 78−11448
γ-Al_2O_3, heat treated, SO_2 adsorpt., IR spectra 79−56070
Al_2O_3, high purity, sintering, impurity effects, analysis *(German)* 78−6881
Al_2O_3, high-purity, modulus of rupture, expt. test of Weibull scaling theory 77−21258
β-Al_2O_3, hot isostatic press. 80−108377
Al_2O_3, hot pressed, crack-growth boundaries, subcritical, fractographic criterion 79−100243
Al_2O_3, hot pressed, fracture stress-reflecting spot relations 80−71731
Al_2O_3 hot pressed, high density, effect of grain size on grinding 78−39723
Al_2O_3 humidity sensor, ageing improvement *(Japanese)* 80−100863
Al_2O_3, initial sintering, method for obtaining surface diffusion coeffs., appl. to shrinkage data 78−95713
Al_2O_3, insulator, electrical puncture strength at high temps. *(German)* 79−70175
Al_2O_3 insulators, surface treatment with Mn-Ti, effect on voltage-holdoff in vacuum 79−24261
β-Al_2O_3, internal friction and Na transport 80−59578
Al_2O_3, laser drilling and cutting, anal. of results using computer model 79−70180
Al_2O_3, layer, obtained by reactive evap., surface struct. and morphology *(Polish)* 79−28242
β''-Al_2O_3, Li_2O-stabilised, deterioration under electrolytic conditions 80−40592
Al_2O_3, liq., viscosity determ., oscill. cup technique 79−23758
Al_2O_3, liquid, exam. of diffusion parameters, using Al^{26} 79−1518
β-Al_2O_3, long-period structs., electron microscope obs. 80−92501
Al_2O_3, mechanical props. charact. by dynamic elastic modulus meas. up to 1400°C *(German)* 79−70101
Al_2O_3, melting speed, effect of struct. and grain shape *(Polish)* 79−29002
Al_2O_3, microhardness as function of grain size 79−79084
Al_2O_3, molten, structural, conform. and solidification 77−36491
β-Al_2O_3, new fabrication methods 79−78916
β-Al_2O_3, new slip casting technique for fabrication of ceramics 78−84745
β-Al_2O_3 phases, synthesized, effect of starting Al_2O_3 composition and halogen ion additions, on structural state 78−76620
β-Al_2O_3, polycryst. with preferred grain orientation, hot pressing of gibbsite and Na_2CO_3 *(Japanese)* 79−56948
Al_2O_3, polycrystalline, conditions for formation of anion vacancies 79−10844
Al_2O_3, polycrystalline, diffusion creep activation energy 78−11274
Al_2O_3 polycrystalline, effects of space charge, grain-boundary segregation and mobility differences on conductivity 80−79979
Al_2O_3, polycrystalline, fracture probability under static bending and tensile loading at 800°C *(German)* 78−23806
Al_2O_3, polycrystalline, stress-strain data up to 1.25 GPa 80−100899
Al_2O_3, polycrystn., high-temp. fatigue and strength 80−60954
β''-Al_2O_3, polycrystn. electrolyte tubing, prepilot process for fabrication 79−87597
Al_2O_3, polymorphic transitions during heat treatment at 900-1500°C 79−11607
Al_2O_3 porcelain for high voltage insulators, increased mech. strength 78−11269
Al_2O_3, porous, sintered, delayed failure, static fatigue in distilled water 78−64750
Al_2O_3 powder, active, sintering 80−20870
Al_2O_3, powder, phase composition, sintering, effect of explosive treatment 77−21079
Al_2O_3, powder sinterability, prep. history effects *(Japanese)* 77−66616
Al_2O_3, powder sintering, isochronal temp. depend. data interpreation 77−77453
Al_2O_3, prefired substrate, acid treatment, improvement in as-fired surface finish 79−24636
η-Al_2O_3, prep. and struct. *(Japanese)* 77−55930
Al_2O_3 prep. from purification of technical gibbsite *(German)* 79−100091
Al_2O_3 pressing method, for the telecommunications industry *(Hungarian)* 78−52728
Al_2O_3 production, removal of S compounds in Na_2O-CaO sintering *(Chinese)* 80−55323
α-Al_2O_3, pure and doped, rapid sintering 79−74123
α-Al_2O_3, radiation damage in HVEM, at high temp. and high dose 79−46707
α-Al_2O_3, radiation damage in HVEM, temp. depend. of displacement threshold 79−46706
α-Al_2O_3, rapid firing, XPS study of cryst. struct. 78−68663
Al_2O_3, reactive hot pressing, exam. of pressing characteristics 78−80499
Al_2O_3, residual stress reduction by ultrasonics 79−24575
Al_2O_3 rich substrate, surface smoothness and metallization props. *(German)* 78−19906

ceramics continued

Al_2O_3 rod, damaged, mech. strength, surface defects effect, appl. as insulators *(German)* 80−76330
Al_2O_3, single cryst., O self diffusion, ion-probe meas. 80−59701
Al_2O_3, single crystal, fracture mirror formation, anisotropy of fracture surface energy and elastic constants 78−68824
α-Al_2O_3 sinterability, dependence on crystallinity of $NH_4AlO(OH)HCO_3$ parent salt *(Japanese)* 78−6883
Al_2O_3, sinterability, $NH_4AlO(OH)HCO_3$ synthesis conditions effect *(Japanese)* 78−52710
Al_2O_3, sinterability, $NH_4AlO(OH)HCO_3$ crystallinity effect *(Japanese)* 78−52711
Al_2O_3 sintered, and hard metal alloys, comparison of stress intensity factor depend. on notch base dia. *(German)* 78−35470
Al_2O_3, sintered, containing $MgAl_2O_4$ precipitates, Mg distribution at grain boundaries 78−80498
Al_2O_3, sintered, electron microprobe anal. of impurity and additive distribs. 80−40359
Al_2O_3, sintered, MgO-enhanced densification, test of second phase and impurity segregation models 78−64511
Al_2O_3, sintered, strength, effects of moisture-assisted slow crack growth 78−27593
Al_2O_3, sintered, TEM ons. of K containing β''' precipitates 78−27522
α-Al_2O_3, sintered or hot-pressed, porosity effect on positron mean lifetime 78−27463
Al_2O_3 sintered surfaces, premetallizing with Mo-Mn-SiO_2 79−47792
Al_2O_3 sintered tubes, H_2 permeability 80−24675
Al_2O_3, sintering, calcination cond. effect *(German)* 80−16251
Al_2O_3 sintering, effect of SrO, MgO and Y_2O_3 additives on α-Al_2O_3 mineralisation 80−89186
Al_2O_3 sintering, role of MgO 80−81010
Al_2O_3 sintering and props., glass forming additive effect 79−61544
Al_2O_3, sintering behaviour and props. of 24 aluminas *(German)* 79−4932
Al_2O_3 sintering in liq. phase presence, particle rearrangement 79−29004
Al_2O_3, sintering in presence of wetting phase 80−25640
Al_2O_3, sintering in reducing atmosphere, Na effect on density and strength 77−63613
Al_2O_3, sintering mechanism and kinetics, glass-forming additives effect 80−89187
Al_2O_3, sintering of single phase and multiphase components *(German)* 78−80494
Al_2O_3, sintering response with const. rate of heating, depend. on processing related pore distrib. 79−28992
Al_2O_3, sintering under press., survey *(Polish)* 78−31368
Al_2O_3, sintering with $SrTiO_3$ admixture *(Polish)* 78−19699
Al_2O_3, solid solubility in MgO 80−15247
Al_2O_3, spalling and cracking by compression 77−81313
Al_2O_3, spatial distrib. of β- and β''-phases 79−66045
Al_2O_3, spray dried agglomerates, compaction response, fracture, deform. 79−43172
Al_2O_3, stress value determination by bending tests, comparison with crack tip theory 78−67154
Al_2O_3 surface diffusion coefficient obtained by free sintering 77−72765
Al_2O_3, surface elec. resist. in Cs vapour 77−51802
Al_2O_3, surface energy measurement by const. temp. method data for liquid Cu-Sn and Au-Ag 78−6208
Al_2O_3, surface energy meas. by temp. variant method for liquid metals 78−6209
Al_2O_3, surface smoothness and densification, effects of SiO_2 additives 78−27462
Al_2O_3 suspensions, grinding method influence on rheology and suitability for high-density sintering 79−29001
Al_2O_3, tensile and compressive strengths of fine powder bed *(Japanese)* 80−25780
Al_2O_3, therm. characts. using constant power source method 79−95222
Al_2O_3, thermally shocked, strengthening kinetics 77−8920
Al_2O_3 thin film used in inelastic electron tunnelling spectroscopy, X-ray photoelectron spectrum 80−108319
Al_2O_3, translucent, fabrication by high press. sintering 78−11167
Al_2O_3, transparent, evaluation of freeze drying and spray drying for prep. 77−4761
Al_2O_3, transparent, polycrystalline, prep. by sol-gel method *(Japanese)* 78−19698
Al_2O_3, transparent ceramic manuf., characts. of powder and process 77−48383
Al_2O_3, transparent hot-pressed, transparent and translucent properties 80−60533
Al_2O_3, unflawed polycryst., tensile failure, SEM and acoustic emission expts. 78−27598
α-Al_2O_3, unintentionally doped, defect struct. 79−60755
Al_2O_3, vacuum compacted using $MgCl_2$ soln. moistener and MgO additive 79−61546
Al_2O_3, validity of high pressure Hg intrusion porosimetry 79−24697
Al_2O_3, vitreous-bonded, eval. of proof testing to assure against delayed failure 78−84954
Al_2O_3, vitreous-bonded, mech. behaviour under various stress-time schedules 79−38968
Al_2O_3, wear chart, exam. *(German)* 78−35521
α-Al_2O_3, wear resistant coatings on cemented carbide machine tools *(German)* 79−74297
Al_2O_3, wetting by Cu-Sn-Ti alloys 78−71904
α-Al_2O_3:Cr(Ti)(V), impurities effect on thermoluminesc. 80−40170
Al_2O_3:MgO, grain boundary segregation of Ca and Mg X-ray spectrosc. and STEM study 80−107269
β-Al_2O_3:MgO, strength and delayed fracture behaviour 80−35290
α-Al_2O_3:Ti, defect struct., electronic and ionic cond., optical absorption meas. 78−30603
Al_2O_3:Zr ceramic, elec. props., additives effect, and interaction with steel melt 80−104305
β-Al_2O_3/metal, field assisted bonding 80−45474
Al_2O_3/Nb, fracture mech. parameter determ. at high temps. *(German)* 79−70136
Al_2O_3/Nb/Al_2O_3 joint, solid state bonded, exam. of bond fracture strength 78−76826
Al_2O_3/stainless steel, adhesive energy, meas. techniques 80−50803
Al_2O_3-Al, disordered, energy diagram model 79−56110
Al_2O_3-AlN, creep 77−21235
Al_2O_3-AlN phase diagram and reaction sintering of transparent cubic ALON spinel 80−25669

ceramics continued
Al_2O_3-B_2O_3-SiO_2 system, liq. phase calc. for commercial quartzite powders 80—25671
Al_2O_3-based ceramics, high rate reactive ion etching 80—85070
Al_2O_3-Cr_2O_3 melt, exam. of surface tension and density 79—1541
Al_2O_3-Dy_2O_3, phase diagram at high temps. *(Japanese)* 79—38810
Al_2O_3-Gd_2O_3 system, phase diagram at high temp. *(Japanese)* 80—45290
β-Al_2O_3-$H^+(H_2O)_n$, p-type conductor, stability *(French)* 79—38063
β-Al_2O_3-Li_2O-Na_2O, spin-lattice relaxation and Li motion 80—70451
Al_2O_3-MgO, MgO addition role in sintering 79—91608
Al_2O_3-$MgTiO_3(CaTiO_3)(BaTiO_3)$, sintering *(Polish)* 79—100096
Al_2O_3-$MoSi_2$, for use as heating element, fabrication method and prop. *(Japanese)* 79—95989
β-Al_2O_3-NH_4^+, p-type conductor, stability *(French)* 79—38063
β-Al_2O_3-Na_2O, AC impedance, microstruct. and strength 80—100349
β-Al_2O_3-Na_2O, ceramic and powder specimens, various Na_2O content, NMR study 79—61240
β-Al_2O_3-Na_2O, development for Na/S battery 80—71615
β-Al_2O_3-Na_2O, fracture stress, effect of microstruct. defects 77—44338
β-Al_2O_3-Na_2O, hot pressing and phys. props. 79—4940
β''-Al_2O_3-Na_2O, Li_2O stabilized, texture conductivity relationship 79—47788
β''-Al_2O_3-Na_2O, Li_2O stabilised, electrolyte polarisation anal. by complex admittance method 80—2689
β-Al_2O_3-Na_2O, MgO stabilised sintering *(German)* 78—19696
β-Al_2O_3-Na_2O, preferable orientation for Na^+ cond. 80—35144
β-Al_2O_3-Na_2O, single crystal ionic conductor, migration losses 77—80643
β''-Al_2O_3-Na_2O, solid electrolyte, behaviour at high current density, sodium heat engine mode 80—61330
β-Al_2O_3-Na_2O, superionic anisotropic ceramic, prod. by microwave sintering *(French)* 78—52742
β-Al_2O_3-Na_2O, synthesis, ceramic form., sintering, cond. 79—11537
β-Al_2O_3-Na_2O, synthesis by chem. methods 77—24993
β-Al_2O_3-Na_2O, vacuum hot pressed, densification kinetics 78—72758
β-Al_2O_3-Na_2O electrolyte development for Na-S battery 79—29461
Al_2O_3-Na_2O solid electrolytes phase composition 77—36468
β''-Al_2O_3-Na_2O solid electrolyte, tube fabrication from cast ceramic tape 80—60819
β''-Al_2O_3-Na_2O solid electrolyte, processing and phys. props. 80—60820
β''-Al_2O_3-Na_2O solid electrolyte, strength degradation under electrolytic conditions 80—61329
β''-Al_2O_3-Na_2O solid electrolyte, heat treatment effects on ionic cond. and microstruct. 80—65293
β-Al_2O_3-Na_2O tube life determ. for Na-S battery 79—29462
β-Al_2O_3-Na_2O:Mg, ionic cond., effect of microstruct. and phase composition 78—67859
Al_2O_3-Na_2O-Li_2O, phase transformations during firing 80—3036
β''- Al_2O_3-Na_2O-Li_2O (8.85, 0.75 wt.%) pressing powders, prep. by spray drying 80—40294
Al_2O_3-Na_2O-LiO_2 (8.8, 0.75 wt.%) exam. of Na^+ resistivity as function of temp. grain size model 78—80654
β-Al_2O_3-Na_2O-SiO_2, solid electrolytes, exam. of microstruct. ionic resistivity 78—80566
β''-Al_2O_3-NaO-LiO_2, stabilised, effect of phase composition, grain size, on Na ion cond. 78—47582
Al_2O_3-Nd_2O_3, phase diagram at high temps. *(Japanese)* 77—63649
Al_2O_3-polymethylsiloxane composite, thermoreactive compaction 80—20879
Al_2O_3-SiO_2, derived from metalalkoxides, sintering behaviour 79—29005
Al_2O_3-SiO_2, mullite, powder, synthesis using silicic acid, clay and $AlCl_3$ *(German)* 79—4933
Al_2O_3-SiO_2 (3 wt.%), J-integral meas. at high temps. *(German)* 80—93624
Al_2O_3-SiO_2 glass ceramic, surface streaks and blisters, UV fluoresc. study 80—84347
Al_2O_3-SiO_2 melt, exam. of surface tension and density 79—1541
Al_2O_3-SiO_2 system, evidence for metastable miscibility gap 80—71632
Al_2O_3-SiO_2 system, solid state transform. of andalusite to mullite 80—16281
Al_2O_3-SiO_2-CaO-B_2O_3(1,1,1 wt.%) chemical analysis by photocolorimetry and titration 79—20483
Al_2O_3-SiO_2-MgO, cordierite, powder, synthesis using silicic acid, clay and $AlCl_3$ *(German)* 79—4933
Al_2O_3-SiO_2-TiO_2-B_2O_3-Fe_2O_3, exam. of porous structure, using a combinational method 79—29303
Al_2O_3-SiO_2-ZrO_2, liquidus surface, discussion 77—44231
Al_2O_3-Sm_2O_3, phase diagram at high temps. *(Japanese)* 78—19732
Al_2O_3-TiC, multiphase ceramics, mech. strengthening due to dispersion of non-metallic particles *(German)* 78—60674
Al_2O_3-TiC sinter products, grain size meas. by combination etching process 79—74331
Al_2O_3-TiO_2 powder, plasma-prepared, morphology and phase constitution 80—100833
Al_2O_3-Y_2O_3, corrosion protective W coating 80—35367
Al_2O_3-ZrO_2, dispersion hardened, fracture toughness improvement by induced microcracking *(German)* 78—31501
Al_2O_3-ZrO_2, microstructure effect on friability 78—64515
Al_2O_3-ZrO_2, multiphase ceramics, mech. strengthening due to dispersion of non-metallic particles *(German)* 78—60674
Al_2O_3-ZrO_2, tetragonal to monoclinic transform. of ZrO_2 particles *(German)* 79—43240
Al_2O_3-ZrO_2 composite, fracture toughness increase by microcracking in energy dissipative zone near crack tip 79—20156
Al_2O_3-ZrO_2 dispersed system, thermal diffusivity/conductivity, effect on microcracking resulting from phase transform. 78—10231
Al_2O_3-ZrO_2 dispersed system, fracture toughness, inclusion induced microcracking effect 78—11296
Al_2O_3-ZrO_2 mixture, stress induced transformation of tetragonal ZrO_2, exam. 78—48392
Al_2O_3-$ZrSiO_4$ mixture, reaction sintering, correlation between densification and reaction 80—29911
Al_2O_3+TiC system, elastic and fracture charact. at elev. temp. *(German)* 79—43299
$Al_2O_3+TiO_2$, reaction on sintering in reducing media 78—27457
$Al_xO_y^+$, spark source mass spectrometric study of species 79—29423
$Al(OH)_3$ based ceramics containing Mn and Ti compounds, sintering and paramag. props. 77—21069
$Al(OH)_3$, derived from metalalkoxides, sintering behaviour 79—29005
β-$Al_2O_3(Na_2O.11Al_2O_3)$, prep. by diffusional transform. during sintering of Al_2O_3 in presence of $NaAlO_2$ 80—25637

ceramics continued
β-$Al_2O_3.Na_2O$, ceramic tube fabrication, crystallite preferred orientation, ionic cond. 77—8781
$Al_2O_3.SiO_2.H_2O$, new materials from pianlinite minerals *(Chinese)* 79—95982
$3Al_2O_3.2SiO_2$, mullite, synthesis by freeze drying 80—16252
$3.5Al_2O_3.2SiO_2$, mullite, decomposition by SiO_2 volatisation 80—61082
$3Al_2O_3.2SiO_2$-ZrO_2 composites, sintered, in situ-reacted, fracture props. 80—81158
$Al_4Si_2C_5$, synthesis, X-ray diffraction pattern, lattice constants 80—50581
Al_2SiO_5, solid state reaction with $Ca_2P_2O_4$ *(Japanese)* 78—19702
Al_2TiO_5, eutectoid decomposition, kinetic study *(Japanese)* 77—55941
Al_2TiO_5 powders, decomposition kinetics using nucleation and growth-rate constants *(Japanese)* 80—35156
Al_2TiO_5, sinterability improvement by partial decomposition 79—28994
Al_2TiO_5, sintering and annealing effect on decomposition *(Japanese)* 79—87606
Al_20_3, corundum, abrasive, evaluation of brittleness, contact endurance by cyclic microhardness 79—15890
α-Al_20_3, thermoluminescent trap stability, 450 to 1400°C 79—24372
B content by emission spectrosc. with high freq. plasma excitation *(French)* 80—76477
BC, physical and chemical interaction with energetic T 79—97902
BN based, sintered, oxidation kinetics 79—96171
BN ceramic with organosilicon polymer additions, strength and oxidation resistance 80—20880
BN, channel for CO_2 waveguide laser 77—14743
BN composites, polymer impregnated 80—7526
BN films, humidity sensitive elec. props. and switching characts. 80—107938
BN films, optical and electrophysical props. *(Russian)* 77—20941
BN, O content depend. on heat treatment temp., neutron activation analysis 80—16356
BN, production kinetics of gasification of organosilicon binders 78—60635
BN, toughening by stress-induced phase transforms. 78—80635
BN, turbostatic, hot pressing, struct. rearrangement, temp., residence time effects 77—8789
BN-SiO_2, sintered, oxidation kinetics 79—96171
B_2O_3, microprobe state anal. by X-ray OK and BK emission band spectra *(Japanese)* 78—19606
B_2O_3, molten, growth and dissolution of air, N_2, O_2 gas bubbles 77—20070
B_2O_3-containing ceramic glaze, neutron probe anal. for control of prep. process *(Polish)* 80—97751
B_2O_3-Nb_2O_5 system, phase equil. and phase struct. obs. by high resolution TEM 80—108419
B_2O_3-PbO(ZnO) glass-ceramic-cement composites, review 79—38783
BPO_4-$AlPO_4$, non-equil. phase diagram, electron microscope obs. 79—43225
(Ba, Ca)(Ti, Zr)O_3, segregation of $CaTiO_3$ and effect on dielec. props. 78—38849
(Ba,La)TiO_3, defect chemistry and elec. cond., thermogravimetric meas. 77—39580
Ba ferrite powder, effect of lattice defects on coercivity *(German)* 79—24194
BaB_6 powder prep., thermionic emission charact. *(Japanese)* 80—11610
$BaCO_3$-$SrCO_3$-$TiO_2(ZrO_2)$, ternary systems, solid-phase synthesis 78—52733
$Ba_{0.8}Ca_{0.08}Pb_{0.12}TiO_3$, piezoelectric ceramic solid soln. *(Polish)* 77—55755
$Ba_{0.95}Ca_{0.005}TiO_3$, piezoelectric ceramic solid soln. *(Polish)* 77—55755
$(Ba_{0.95}Ca_{0.05})TiO_2+CaCO_3$ (0.75%), piezoelectric ceramic solid soln. *(Polish)* 77—55755
BaF_2, optical ceramic, hot pressing in vacuum, rel. to spectral transmission 78—52730
$BaFe_{12}O_{19}$, effect of impurity concentrations, and sintering conditions on grain size *(German)* 79—23630
$Ba_2Ga_2GeO_7$, gehlenite struct., synthesis and physicochem. props. 79—43181
$BaHfO_3$, $BaSnO_3$ and $BaZrO_3$, high-density ceramics prep. and elec. props. 80—60812
$Ba_2KNb_5O_{15}$, Raman scatt. experiments in tetragonal tungsten bronze compounds 80—40113
$BaMnO_{3-x}$, O_2 deficiency induced polymorphs 78—26531
$Ba_2NaNb_5O_{15}$, effect of substituting Gd, Cr on lattice parameters 78—47291
$Ba_2NaNb_5O_{15}$, Raman scatt. experiments in tetragonal tungsten bronze compounds 80—40113
$Ba_2NaNb_5O_{15}$, X-ray powder diffraction data determ. *(Chinese)* 80—70170
$BaNb_2O_6$, solid-phase formation reaction, thermographic, X-ray phase and chemical anal. 77—12783
BaO-Al_2O_3-SiO_2, chem. resist. and struct. 79—61756
BaO-Al_2O_3-SiO_2-H_2O system, phase transitions during hydrothermal treatment 79—43216
BaO-Al_2O_3-SiO_2-Ta_2O_5-Mo glass ceramic metal composites, cermet prep. 80—11618
BaO-Nd_2O_3-TiO_2-Bi_2O_3 system ceramics, high stability low loss dielectric preparation 80—81008
BaO-SiO_2 glass ceramic, nucleation, effect of electric fields 78—83742
BaO-SiO_2 glass ceramic, growth and nucleation kinetics 80—7528
BaO-SiO_2 glass-ceramic, crystallisation mechanism 79—90559
BaO-SiO_2-Fe_2O_3 permanent mag. ceramics, exam. of phase diagram, using X-ray analysis, optical microscopy, electron probe anal., and thermal analysis *(German)* 79—29012
BaO-SrO-Al_2O_3-TiO-SiO_2 glass ceramics, cryst. phases form., BaO/SrO ratio influence 80—19705
BaO-TiO_2-Nd_2O_3, exam. of compositional and dielectric props. 79—33601
$BaO.Al_2O_3.2SiO_2$, hydrothermal synthesis, phase transitions 77—48378
$BaO.2SiO_2$, glass, spherulitic growth and recrystallisation 77—4046
BaO.n Fe_2O_3, magnet, effect of SiO_2 on texture and densification behaviour *(German)* 79—24631
$BaPb_{1-x}Bi_xO_3$ film, RF sputtered, T_c as function of comp. and annealing conditions 79—24100
$Ba_3SiAl_{10}O_{20}$, Ce^{3+} activated, X-ray diffr. and luminesc. props. 80—49199
$Ba_{1.35}Sr_{0.65}NaNb_5O_{15}$ crystals, struct., dielec. and pyroelectric characts. 79—51913

ceramics continued
$Ba_xSr_{1-x}Nb_2O_6$ crystals, struct., dielec. and pyroelectric characts. 79—51913
$Ba_{1-x}Sr_xTiO_3$ ceramic pyroelec. responsivity, −140° to +160°C obs. 78—23405
$Ba_2TiGe_2O_8$-$Ba_2TiSi_2O_8$, pseudobinary system, pyroelectricity and related props. 78—95553
$BaTiO_3$, 3d element doped, phase stability, phase transition temp., mag. susceptibility meas. 78—38835
$BaTiO_3$, 90° electric domain processes, mech. stress, X-ray diffr. 78—72478
$BaTiO_3$, acceptor doped, exam. of electrical conductivity 130 to 300°C 79—33286
$BaTiO_3$, acceptor-doped defect equilibria, elec. cond. 77—39579
$BaTiO_3$, $BuTi_4O_9$, Ba_2TiO_4, synthesis from coprecipitation products 77—48382
$BaTiO_3$ ceramic, degradation under high AC elec. field 80—60499
$BaTiO_3$, ceramic, effect of grain size on nonlinear dielec. props. 77—8522
$BaTiO_3$ ceramic, electromechanical coupling caused by electrostriction, reson. props. meas. 77—20802
n-$BaTiO_3$, ceramic, expt. and theoretical investigation of grain-boundary resist. 79—56235
$BaTiO_3$ ceramic, semiconductive sintering 77—36430
n-$BaTiO_3$, ceramic, systematic expt. and theoretical investigation of grain-boundary resist. 79—56236
$BaTiO_3$ ceramic dielectric capacitor, processing prop. relations, hysteresis, permittivity 80—80730
$BaTiO_3$ ceramic films, dielec. strength, statistical anal. 80—75935
$BaTiO_3$ ceramic surface, neutralisation of bombarding ion beam 80—71528
$BaTiO_3$ ceramics, calcination effects, TiO_2 powder eval. *(Japanese)* 78—64516
$BaTiO_3$ ceramics, grain boundary pot. barriers, cathodoluminesc., electron probe anal. 80—2864
$BaTiO_3$, chemically precipitated, exam. of sintering behaviour by isothermal shrinkage *(German)* 79—4935
$BaTiO_3$, crystn. from melts, comparison of different prospective oxy-anion solvents 80—71583
$BaTiO_3$, defect chem., elec. cond. obs. 77—4097
$BaTiO_3$, defect chemistry and elec. cond. improved positive temp. coeff. model 77—39859
$BaTiO_3$, dielec. and elastic consts., temp. depend. *(Russian)* 78—64307
$BaTiO_3$, dielectric ceramic, interaction with metallic film during sintering 79—33958
$BaTiO_3$, donor doped, exam. of heterogeneous microstructure *(German)* 79—24632
$BaTiO_3$, doped, defect chemistry and elec. cond. kinetics of equilib. restoration 77—39700
$BaTiO_3$, doped-undoped ceramic composites, sintering behaviour 79—100094
$BaTiO_3$, effect of phase transformation on fracture behaviour 78—48507
$BaTiO_3$, exam. of anomalous pyroelectric effect above Curie point 79—33613
$BaTiO_3$, exam. of PTC effect as function of Ti excess *(German)* 79—23960
$BaTiO_3$, ferroelec. ceramic, mech. strength, for single crysts. and Ca and Co modified specimens 78—64332
$BaTiO_3$, ferroelec. ceramic, 90° domain rot. in fixed elec. field 80—7315
$BaTiO_3$, ferroelectric ceramic, dielec., piezoelec. and elastic props., orientational contrib. 78—68468
$BaTiO_3$, ferroelectric, internal stress and strength, failure mechanism 80—66128
$BaTiO_3$ fibres synthesised from $Ba(OH)_2+2K_2O.11TiO_2.3H_2O$ fibre hydrothermal reaction *(Japanese)* 80—93527
$BaTiO_3$ film, ferroelec., composition profiles by Auger electron spectra anal. 79—66391
$BaTiO_3$, Mossbauer spectroscopy, sample prep. and results 80—66078
$BaTiO_3$, PTC-type, grain boundary study using TEM 80—107267
$BaTiO_3$, PTC-type, voltage contrast imaging for low and high Ti excess 77—28183
$BaTiO_3$, piezoceramic, nonlinear piezoeffect 79—42900
$BaTiO_3$, piezoceramic, elastic normal wave propagation, phase transitions *(Russian)* 80—40067
$BaTiO_3$, piezoelectric ceramic solid soln. *(Polish)* 77—55755
$BaTiO_3$, piezoelectric, secondary electron emission yield 79—91546
$BaTiO_3$, polycryst., elec. resist. anomaly in phase transition region 78—43381
$BaTiO_3$, polycryst., form. from coprecip. products 77—24997
$BaTiO_3$, polycryst., prep. from coprecipitated $BaCO_3$-BaF_2-$TiO(OH)_2$ 77—24996
$BaTiO_3$, polycrystalline, exam. of effect of freq., temp. and DC electric field strength, on elastic consts. 79—1890
$BaTiO_3$, positive temp. coeff. resistivity as function of Ti-Ba ratio 78—72151
$BaTiO_3$ powder, dispersion effect on meas. in electrical sensing zone particle size counter 79—17383
$BaTiO_3$, powder compacts, sintered, physical and chem. inhomogeneities 79—87594
$BaTiO_3$, rare earth doped ceramics, thermolum. and microwave induced thermolum. fading 79—1792
$BaTiO_3$, semiconducting ceramic, AC thermopower measurement 80—44624
$BaTiO_3$ surface voids, Auger spectrochem. anal., organic contamination 79—24467
$BaTiO_3$, synthesis by solid-solid reactions 79—38776
$BaTiO_3$, synthesis by solid-solid reactions 79—38777
$BaTiO_3$, synthesis from barium titanyloxalate 77—48381
$BaTiO_3$, thin film, obtained by modified doctor blade method grain orientation *(Japanese)* 77—77455
$BaTiO_3$:Al, 0.05-0.3 wt.%, ceramic dielectric, dielec. and mech. props. 79—8091
$BaTiO_3$:$BaTi_3O_7$, dielec. props. and microstruct. 80—60481
$BaTiO_3$:Dy ceramic, sintering, grain size, characterisation and props. 77—55923
$BaTiO_3$:Fe ceramic, dopant distrib., STEM obs. 79—82255
$BaTiO_3$:La, Sb, second phase effect on elec. and mag. props. 80—60986
$BaTiO_3$:La and undoped, defect chemistry elec. cond. at high temp. meas. 77—39858
$BaTiO_3$:Mn, polycrystn., annealing effect on transition temps. 80—3100

ceramics continued
$BaTiO_3$:X(X=Cr, Mn, Fe, Co, Ni, Zn, Ga), annealed in H_2 and O_2, valence change in phase stability 80—20600
$BaTiO_3$-$BaNb_2O_6$, semiconducting ferroelectric ceramic, nonlinearity of dielectric layer capacitance 79—8098
$BaTiO_3$-$BaNbO_3$ system, solid solns., thermal ionic relaxation, vacancy form. 77—8499
$BaTiO_3$-based ceramics, impurity atoms chem. state, Mossbauer spectra 80—15902
$BaTiO_3$-based nonpiezoelectric ceramic, acoustic convolution in paraelectric phase 80—6467
$BaTiO_3$-CeO_2 liquid immiscibility region, X-ray diffr. anal. 80—50611
$BaTiO_3$-$CuO(TiO_2)(ZrO_2)$ mixture, exam. of liquid phase sintering, densification 79—33979
$BaTiO_3$-$Ni(Co, Mn)Fe_2O_4$, ceramic, exam. of prep. and physical props. 78—68655
$BaTiO_3$-PbO-B_2O_3, liquid phase sintering, effect on props. *(German)* 79—33980
$BaTi_4O_9$ effect of chemical treatment on loss quality, at microwave wavelengths 79—34159
$Ba_2Ti_9O_{20}$, effect of chemical treatment on loss quality, at microwave wavelengths 79—34159
$Ba_2Ti_9O_{20}$ single crysts., prep. and unit-cell parameters 80—103302
$Ba_{100}Ti_{101-x}Sn_x+0.3$ at.%Sb, intergranular capacitor, effect of microstructure on electrical props. 79—34160
$(Ba_{1-x}Y_x)TiO_3$ ceramic, resistivity rel. to donor dopant content 79—65474
$BaZrO_3$-$LaAlO_3$ systems, sintering conditions, elec. props. 79—43184
Be-Si-Al-O-N ceramic, phase assemblages, relationships with props. 80—60848
Be-Si-N system polytypes, struct. obs. using TEM 80—107192
Be-Si-O-N polytypes, X-ray study 78—27496
Be-Si-O-N system, polytype periodicities, direct obs. 78—18662
$BeAl_2O_4$, chrysoberyl, kinetics and mechanism of formation, in presence of V_2O_5 79—11535
BeO, appl. as material for US delay lines 77—51447
BeO, ceramic, sintered, thermoluminesc., EPR, emission spectra, energy level diagram 77—81163
BeO ceramic, unlapped and lapped with diamond powder, thermally stimulated exoelectron emission 78—11086
BeO ceramics, thermally stimulated exoelectron max., effect of H_2 adsorption 79—43109
BeO, ceramics, thermally stimulated exoelectron emission *(German)* 79—100028
BeO ceramics, thermostimulated exoemission and adsorption centres 78—27386
BeO, EPR-ENDOR study of [Li]° centre 77—85569
BeO, exoelectron emission from hydrated and dehydrated surfaces 80—11545
BeO, low-Z material, outgassing expts. 79—209
BeO, polycrystalline, stress-strain data up to 1.25 GPa 80—100899
BeO powder, sinterable and unsinterable, sintering processes, electron microscope exam. 79—33986
BeO TLD, operational characts. and problems 77—42216
BeO, TSEE, effect of surface SiO_2 80—76159
BeO, thermoelectret props. 80—7269
BeO, thermoelectret state, effect of gamma radiation 80—7270
BeO, thermolum. glow curves 79—47527
BeO:Li, ceramics, thermally stimulated exoelectron emission *(German)* 79—100028
BeSiN ceramics, glass free grain boundary 79—90671
$Be_9Si_3N_{10}$, TEM, direct obs. of cryst. struct. 79—60339
$Be_4Ti_2O_{12}$ grain oriented ferroelectric ceramic, prep. by molten salt synthesis-tape casting method 80—40296
$Bi_{12}GeO_{20}$, X-ray sensitive ceramic, sintering 80—25621
$Bi_{2-x}La_xWO_6$, synthesis and crystallography 80—66459
Bi_2MoO_6 ceramic, permittivity, ferroelec. T_c and hysteresis 79—82932
Bi_2MoO_6, superplasticity during phase transitions 80—108498
Bi_2O_3, powder diffr. patterns and struct. 79—27961
$Bi_4Ti_3O_{12}$ ceramics, ferroelectric, hot-forged, grain orientation and dielectric props. 80—40076
Bi_2WO_6 grain oriented ferroelectric ceramic, prep. by molten salt synthesis-tape casting method 80—40296
Bi_2WO_6, superplasticity during phase transitions 80—108498
$Bi_2W_2O_9$, struct., dielec. props., melting character and thermal stability 79—23572
bonde fusion cast ceramics, crystn., microstructures rel. to conditions 80—11638
C pyroceramic, sputtering and blistering from H^+ and He^+ bombardment 78—79649
Ca aluminophosphate foam glasses, for prosthetic appl., porosity and mech. props. 79—74128
Ca-Mg-Zr combustion sensor, pipe-form *(Japanese)* 80—55761
$Ca_2Al_2GeO_7$, gehlenite struct., synthesis and physicochem. props. 79—43181
$CaAl_2O_4$ cement bond phases, corrosion in steam-CO at 199°C 79—29234
$CaAl_2O_4$, fine powder, prep. by evaporative decomposition of solns. 78—39725
$CaAl_2O_4$-$SrAl_2O_4$-BaA_2O_4, binary and ternary systems, solid solubility *(Japanese)* 80—35174
$CaAl_2O_5$, form by interdiffusion of CaO and Al_2O_3 79—28998
$CaAl_2O_5$, form. by solid state reaction of CaO and Al_2O_3, electric field effects 79—28997
$CaCO_3$-$NaAlSiO_4$, micromechanism for phase formation during sintering *(Russian)* 80—16253
$CaCeAl_3O_7$, melilite struct., prep. and props. 80—93524
CaF_2, press-forged laser window, polishing, cleaning and grinding 79—59849
CaF_2, strength-controlling fracture energy depend. on flaw-size to grain-size ratio 80—81152
CaF_2-AlF_3, phase equilibria, DTA and X-ray diffr. study 78—27493
$CaFeO_3$, preparation, cryst. struct., mag. and elec. props. 78—44066
$Ca_{1+x}Ga_{1-x}N_y$, prep. *(French)* 77—44206
$CaMg(CO_3)_2$, dolomite, reaction with ZrO_2, mineralisation during roasting 79—43180
$Ca_2Mg(Co)(Zn)(Mn)(Cd)(Ca)TeO_6$, optical SHG study of acentricity, ferroelec. of low temp. phases 80—71324
$Ca_2Nb_2O_7$-Sm_3NbO_7 system, phase equilib. 80—20907
CaO, C-content determ. of single crystals grown by arc fusion 79—8456
CaO sintering, Cr_2O_3 addition effect *(Czech)* 80—45258

ceramics continued
$CaO-Al_2O_3-Fe_2O_3-SiO_2$, phase relations 77—12610
$CaO-Al_2O_3-SiO_2$, chem. resist. and struct. 79—61756
$CaO-Al_2O_3-SiO_2$, glass ceramic prod. by TiO_2 nucleating agent 78—11189
$CaO-Al_2O_3-SiO_2$ based glasses, kinetic parameters of glass ceramic form. 77—24385
CaO-CaF, hot pressed, effects of CaF_2 addition, sintering behaviours and microstructs. investig. *(Japanese)* 78—95721
CaO-MgO, doloma, composition effect on creep, impurity effects 79—43318
$CaO-MgO-Al_2O_3-SiO_2$, glass-ceramic prep. by hot pressing and crystallisation of powder 78—11192
$CaO-MgO-Al_2O_3-SiO_2$, glass ceramic, prep. by hot pressing and crystallisation, mech. props. 78—15351
$CaO-MgO-Al_2O_3-SiO_2$, shale glass, glass forming and dielec. props. 78—22660
$CaO-MgO-Al_2O_3-SiO_2$, shale glass, crystn. behaviour 78—22661
$CaO-MgO-Al_2O_3-SiO_2$, quartz sand-dolomite-magnesia-clay based glasses, crystn. 80—20915
$CaO-MgO-CeO_2$, fired, phase equilibrium diagram, 1700 to 1200°C 78—92248
$CaO-MgO-NaPO_3$ system, subsolidus struct. 79—43215
$CaO-MgO-SiO_2$, diopside, exam. of synthesis by hydrothermal sintering *(German)* 79—4934
$CaO-MgO-ZrO_2-SiO_2$, phase study, SiO_2 compatibility relationship 78—95734
$CaO-MgO-ZrO_2-SiO_2$, phase study, ZrO_2 compatibility relationship 78—95735
$CaO-Nd_2O_3-Fe_2O_3-Al_2O_3$ system, solid-state reactions 80—35173
$CaO-SiO_2-Al_2O_3$, wollastonite, low dielec. loss factors, fabrication *(Japanese)* 80—55032
$CaO-SiO_2-Al_2O_3-Fe_2O_3$ mix, liquid phase sintering 79—91610
$CaO.Al_2O_3$, thermal expansion 77—84953
$3CaO.SiO_2+H_2O+CO_2$, reaction conditions 80—26007
$\beta-Ca_2(PO_4)_2$ whitlockite ceramic fabrication for prosthetic applications 79—78924
$Ca_3(PO_4)_2$ ceramic, material science, bone implant 80—93523
$\beta-Ca_3(PO_4)_2$, synthesis and fabrication, prosthetic appl. 79—24479
$Ca_4P_2O_9$ ceramic, material science, bone implant 80—93523
$Ca_{10}(PO_4)_6(OH)_2$, synthesis and characterisation in dense polycryst. form 77—4749
$Ca_5(PO_4)_3OH$ ceramic, material science, bone implant 80—93523
$Ca_{10}(PO_4)_6(OH)_{2-2x}O_x\square_x$ polycryst. sintered bodies, prep. and thermal props. 80—25624
CaS discs, sintering method prep., ionic cond. meas., 650 to 900°C *(Japanese)* 78—75869
$Ca_x(Si,Al)_{12}(O,N)_{16}$, α'-Sialon ceramics, prep. and characterisation 78—84750
$CaSiO_3$, fibrous, controlled crystallisation and anisotropy 80—59425
$\beta-Ca_2SiO_4$, stabilisation, IR and Raman spectra 79—42265
$Ca_2SiO_4-CaMgSiO_4$, T phase, review 80—50612
$\beta-Ca_2SiO_4-CaO-SiO_2$ paste, hydration, compression strength and composition 80—50584
Ca_3SiO_5 form. by solid state reaction, mixture and firing condition effects 78—56602
$CaSnO_3$ and $CaZrO_3$, high-density ceramics prep. and elec. props. 80—60812
$Ca_{1-y}Sr_{y/2}Ba_{y/2}Zr_{1-x}Ti_xO_3$, ceramic system, dielectric props., microwave resonator application 80—80674
$CaTaRO_6$, (R=La, Nd, Gd, Sm, Er, Lu), synthesis and physicochem. props. 79—52139
$CaTiO_3$, prep. from film forming soln. 80—60811
$CaTiO_3$, protection against reduction during roasting in H_2 77—36426
$CaTiO_3$, synthesis kinetics 79—15632
$CaTiO_3-CaTiSiO_5$, sintering and dielectric props. 80—40307
$CaTiO_3-LaAlO_3$ solid soln., phase redistrib. during roasting in H_2 78—52735
$CaTiO_3-TiO_2$, ceramic, phys. props. 78—43784
$CaTiO_4$, perovskite, sintering during synthesis 77—36422
$Ca_2TiO_3-La_3AlO_3$, synthesis of solid solution by coprecipitation 79—1836
$Ca_3(VO_4)_2-Mg_3(VO_4)_2$, exam. of phase composition and phase diagrams 79—1851
$CaWO_4$, crystal growth from soln. in Na_2WO_4 melts, by continuous cooling, growth kinetics exam. 78—48303
$CaWO_4$, crystn. from solns. in $NaWO_4$ melts, kinetics obs. by DTA 80—40246
$CdAl_2O_4$, LWR burnable poison, irradiation and corrosion beahviour *(German)* 79—67846
$CdFe_{1/2}Nb_{1/2}O_3$, high temp. X-ray exam. 77—11527
$Cd_2Mg(Co)(Zn)(Mn)(Cd)(Ca)TeO_6$, optical SHG study of acentricity, ferroelec. of low temp. phases 80—71324
CdO, effect of compacting pressure on consolidation and elec. cond. 79—29007
CdO, influence of initial compacting press. on elec. resis. Hall coeff. 80—20872
CdS, dry process formation from CdO and S *(Spanish)* 78—56607
CdTe KO-6 optical ceramic component antireflection coatings 79—27345
Ce-Si-Al-O-N ceramic, phase assemblages, relationships with props. 80—60848
$CeNbO_{4+x}$, oxidation-reduction reactions 78—39930
CeO, high press. synthesis, struct. and lattice consts. *(French)* 80—29913
CeO_2:Y, slow transient phenomenon 80—107550
$CeO_2La_2O_3$, ceramic, thermal stability, sintering, deform., effect of La_2O_3 79—11532
$3Ce_2O_3.2Si_3N_4$, ceramic, prep. by cold compaction and firing, struct. anal. 77—21070
$3Ce_2O_3.2WO_3$, X-ray charact. and thermal props. 77—43194
$CeTaO_{4+x}$, oxidation-reduction reactions, phase equilibrium, thermogravimetry and magnetic susceptibility meas. 78—39930
$CoFe_2O_4$ synthesis, chem., thermal histories rel. to fine cryst. struct. 79—43186
$Co_{1-x}Fe_{2+x}O_4$, prep. by wet and ceramic methods, struct., mag. and surface props. 78—52307
$Co_{0.5}Mg_{0.5}O$, sintered pellets, oxidation mechanism and kinetics, optical and SEM study 79—79137
$Co_{1-x}Mg_xO$ ceramics as O_2 sensors, phase stability, elec. cond. and thermoelec. power meas. 78—3420
CoO, pressure sintering densification model, computer program 78—44040

ceramics continued
CoO single crystal, compressive creep morphology 77—56034
CoO, sintered pellets, oxidation mechanism and kinetics, optical and SEM study 79—79137
CoO, under controlled atmosphere, exam. of composition and temp. dependence, of lattice parameter *(French)* 79—19214
$CoO-MgO-Al_2O_3-Cr_2O_3-TiO_2$, form. and colour of spinel solid soln. *(Japanese)* 77—32550
$CoO-ZnO-Al_2O_3-Cr_2O_3-TiO_2$ system, form. and colour of spinel solid soln. *(Japanese)* 77—25001
Co_xO_y (x=1, 2 or 3, Y=1, 3, 4), conducting oxide prod. by amorphous citrate process 79—95985
$CoO.Al_2O_3$, prep. from film forming soln. 80—60811
$CoTiO_3$, prep. from film forming soln. 80—60811
CrB_2, electrodeposition mech., onto metal electrodeposit, cermet prop. 79—33992
$CrNbO_4$, elec. cond. meas. 80—100463
CrO_2, synthesis and morphology 79—24481
Cr_2O_3, active, block growth in crystallisation 77—85972
Cr_2O_3 corrosion, high-temp., in Cl_2 and Cl_2-O_2 mixtures 78—15601
Cr_2O_3, grain growth during sintering *(Japanese)* 80—16261
Cr_2O_3, influence of TiO_2 on sintering behaviour, densification as function of temp. 79—78919
Cr_2O_3 powder, activation and sintering 77—21078
Cr_2O_3, solid solubility in MgO 80—15247
$Cr_2O_3-Al_2O_3$ solid soln., Vickers micro-hardness 80—66629
$Cr_2O_3-WO_3$, phase relations 78—92249
$CrVO_4$, elec. cond. meas. 80—100463
$CsAlSiO_4$, prep. and X-ray characterisation 78—39728
Cu-coated TiO_2 particles, prep. for composites 80—89159
Cu-Mg-FeO system spinel solid solns., synthesis, struct., and mag. props. 79—52142
Cu-U-O system, equilib. relationships *(German)* 80—35163
$CuFe_5O_8$, sintered, eutectoid decomposition study by elec. resist. meas. *(Japanese)* 78—19711
Cu_2O, creep tests, exam. of a creep machine mech. ability *(French)* 79—20325
$CuO.Al_2O_3.2SiO_2$, hydrothermal synthesis, phase transitions 77—48378
Dy_2O_3-based ceramic, preparation, mech. props. 77—24998
Er_2O_3, densely sintered and granular ceramics prep. physicomechanical props. 77—32548
Er_2O_3, of Hf, vol. and grain boundary diffusion coeffs., tracer sectioning technique 79—7712
Er_2O_3, pure and HfO_2-doped polycryst., Er self-diffusion 80—29207
$Er_2O_3-ZrO_2$, subsolidus phase relations, X-ray diffr. and thermal expansion exam. 78—31382
$Eu_{0.5}Ba_{0.5}TiO_3$, ferromag., ferroelec., ceramic, Curie temps. determ. 78—68230
Eu_2O_3 ceramic powder, in situ deposition of metal coating, cermet form. 77—32713
Eu_2O_3, cubic to monoclinic transform. 77—8815
$Eu_2O_3-Ta_2O_5$, microcracking, elastic props., internal friction 78—92326
Fe-containing glass-ceramics, effect of Mn_2O_3 on strength 77—48380
$Fe-SiO_2-Al_2O_3$ Lisakovskii concentrate mixture, sintering process, temp. thermal treatment *(Russian)* 80—55317
$Fe^{2+}Cr_x{}^{3+}Al_{2-x}{}^{3+}O_4{}^{2-}$, finely divided, oxidation kinetics 80—50848
$(Fe^{2+}Fe_{2-x}{}^{3+}M_x{}^{3+})O_4{}^{2-}$ ($M^{3+}=Al^{3+}$, Cr^{3+}), oxidation to γ lacunar spinels, rate law vs. O_2 press. 80—50849
Fe_2O_3 based catalysts for NH_3 synthesis, sintering of powders 79—61551
Fe_2O_3, diffusion in gas phase during firing of $MgO-Cr_2O_3$ bricks *(French)* 78—80495
Fe_2O_3, powder, compression in moulds, meas. apparatus *(Dutch)* 77—44205
$\alpha-Fe_2O_3$, prep. by evaporative decomposition of $Fe(NO_3)_3.6H_2O$ soln. 79—20011
$\alpha-Fe_2O_3$, reduction to active magnetite and direct air oxidation to $\alpha-Fe_3O_4$ *(German)* 78—7060
$\alpha-Fe_2O_3$, semiconducting, gas sensor for city gas appl. *(Japanese)* 80—61498
Fe_2O_3-FeO, sinter, heating and reduction effect of phase transform. and fracture *(Russian)* 78—15375
Fe_2O_3-FeO, sintered and pellets, reduction in H_2 *(Russian)* 78—15705
$Fe_2O_3-WO_3$, phase relations 78—92249
Fe_2O_y, powder, sintering, surface area reduction, exam. 78—44039
Fe_3O_4, low temp. sintering 78—92221
Fe_3O_4, partial thermal dissociation in air, using solar concentrator *(French)* 79—20015
$Gd_3Al_5O_{12}$ phase obtained by crystallisation of amorphous $Gd_2O_3.5/3Al_2O_3$ by quenching 78—92224
Gd_2O_3 densely sintered and granular ceramics prep. physicomechanical props. 77—32548
Gd_2O_3, polycryst. monoclinic, Gd self-diffusion 80—24655
$Gd_xZr_{1-x}O_{2-x/2}$, elec. cond. of ceramic solid solutions 80—107554
$Gd_xZr_{1-x}O_{2-x/2}$, fluorite and pyrochlore solid solutions, electrical conductivity meas. 80—65287
HF adsorption, by smelter-grade aluminas, during Al smelting 80—80075
HFO_2, polycrystalline, monoclinic, elastic props. at room temp. 78—27548
HFO_2, powder, preparation technique for highly sinterable powder 78—39714
HfB_2, oxidation in O_2 atmosphere, exam. 80—11814
HfO_2, monoclinic, microcracking, elasticity, internal friction, thermal expansion meas. 79—29195
HfO_2, zero and low coeff. of thermal expansion 80—39325
$HfO_2:Er_2O_3(Y_2O_3)(Eu_2O_3)$, elastic props., sonic reson. meas. 80—7612
$HfO_2-Eu_2O_3$, phase equilibrium, 960 to 1900°C, X-ray anal. 78—23688
$HfO_2-Gd_2O_3$, phase relations 78—72769
HfO_2-MgO system, intermediate phases existence, X-ray diffr. and IR obs. 79—38805
$HfO_2-Sm_2O_3$, X-ray diffr. obs. of phase relations 79—61566
HfO_2-TiO_2, phase relations and thermal expansion 77—21121
HfO_2-TiO_2, thermal expansion coeff. and dynamic response to pulsed energy deposition 78—26705
HfO_2-TiO_2 system, zero and low coeff. of thermal expansion 80—39325
$(HfO_2)_y(In_2O_3)_{1-y}$, bulk resistivity 77—35936
$HgO_2-Y_2O_3$, solid soln., elastic and photoelastic props., Mendelstam-Brillouin scatt. 78—6693
$(K,Na)NbO_3$ ceramic, hot pressed, dielec. props. 79—87375
$KEuHP_3O_{10}$, synthesis of K_2CO_3, Eu_2O_3 and phosphoric acid, exam. of structure 79—1837

ceramics continued
$KEu(PO_3)_4$, synthesis of K_2CO_3, Eu_2O_3 and phosphoric acid, exam. of structure 79—1837
KNO_3-$K_2Cr_2O_7$ 77—44232
$KNbO_3$ powder synthesis, unit cell determ. 78—11168
K_2O-Al_2O_3 system, high temp. thermodynamics and phase equilibria 78—80521
$K(Ta,Nb)O_3$ ceramic, prep. and electro-optical props. 80—25620
$KTaO_3$, defect struct. and elec. props. 78—91695
$K_2Ti_3O_7$ fibres, synthesis by kneading, drying, calcination process *(Japanese)* 79—38779
$K_2Ti_6O_{13}$ fibre synthesis from melt reaction of TiO_2 and K_2CO_3 *(Japanese)* 78—44070
$K_2V_8O_{16}$, Hollandite type compound, synthesis, struct. and magnetic props. 79—11543
La-Si-O-N system, new compound form. with fluorapatite struct. 79—4941
LaB_6, chemical vapour growth of whiskers, and single crystals 78—72710
$La_{0.003}Ba_{0.66}Sr_{0.34}TiO_3$ ceramic, positive TCR near Curie temp. rel. to charge dispersion *(Russian)* 80—16511
$LaCoO_3$, conducting oxide powder prod. by freeze drying 79—95984
$LaCoO_3$, conducting oxide prod. by amorphous citrate process 79—95985
$LaCr(Co)O_3$, conducting oxide prod. by amorphous citrate process 79—95985
$LaCrO_3$, vaporization in oxidizing atmos. 80—24579
$LaCrO_3$-Cr ceramic, prep., phase comp. and elec. cond. *(Polish)* 80—71621
$LaCrO_3$-MgO, LC20M electrode material in open cycle MHD systems, thermionic emission characts. 80—97394
$LaMn_{1-x}Cu_xO_{3-y}$, prep., struct., selected catalytic props. 77—36433
$LaMn_{1-x}Cu_xO_{3+y}$, O_2 stoichiometry by thermogravimetry 77—36434
La_3NbO_7, synthesis and cryst. growth 80—71590
La_2O_3, thermal expansion, 100 to 300K, X-ray method 79—99335
La_2O_3-Al_2O_3 system, alumina rich phase, X-ray obs. 79—29030
La_2O_3-Mn_2O_3-Cr_2O_3, synthesis and properties of solid solutions 78—44038
La_2O_3-Y_2O_3 phase, diagram at high temps. *(Japanese)* 77—1218
$3La_2O_3.2WO_3$, X-ray charact. and thermal props. 77—43194
$La_4Si_2O_7N_2$ single cryst. growth by floating zone method with SiO_2-Si_3N_4 additions 80—93481
$La_{0.5}Sr_{0.5}CoO_3$, conducting oxide powder prod. by freeze drying 79—95984
$La_{0.5}Sr_{0.5}CoO_3$, conducting oxide prod. by amorphous citrate process 79—95985
$La_{1-x}Sr_xCoO_3$, $(0.5 \leq x \leq 0.9)$, ferromag., elec. props., itinerant electron model 80—107785
$La_{1-x}Sr_xCrO_3$, densification 77—8780
$La_4(TiO_4)_3$, electrical props., effect of initially used La_2O_3 *(Polish)* 77—59508
$(Li, Na)NbO_3$ ceramic, dielectric and electromechanical props. 77—40183
Li aluminosilicate, formation of glass-ceramic in $LiCl_3$ vapour 77—16536
Li solid electrolytes, synthesis and characts. 78—18831
$LiAlSiO_4$, crystalline, glass and glass-ceramic form, effect of composition changes, substitutions and press. on ionic cond. 78—43172
$LiAlSiO_4$ glass-ceramics, percolative ionic cond. 77—76605
$LiAlSiO_4$ glass-ceramic, fracture phenomena as function of initial flaw size and temp. 78—95797
LiB_4O_7, crystal growth from undercooled melt 77—52248
$Li_4B_7O_{12}Cl$, new solid electrolytes, conductivities and activation energies 79—28137
LiF, ceramic, characts. on pressing in vacuum and in air 78—52734
LiF compact, particle size rel. to pore characts. 78—60631
LiF tile and sheet for thermal neutron shielding *(Japanese)* 78—74510
LiF-AlF_3-Na_3AlF_6-Al_2O_3 system, phase equilibrium, X-ray diffr., DTA, quenching, optical microscopy study 80—50610
$LiFe_5O_8$, hysteresis and other mag. props. rel. to microstruct., TEM investig. 77—20636
$Li_{0.5}Fe_{2.5}O_4$ milled ferrite powder, substruct. and sinterability 80—84894
$Li_{0.5}Fe_{2.5}O_4$-$Bi_2O_3(V_2O_5)$ systems, phase diagrams, sintering conditions 78—35366
$LiGaO_2$, single crystal ionic conductor, migration losses 77—80643
Li_2GeO_3 piezoelectric glass ceramic, recrystallisation, pyroelectric response, permittivity 80—80703
Li_2MgSiO_4-Li_2ZnSiO_4, form. of solid soln. *(Japanese)* 77—25037
LiNa ferrite, effect of sintering temp. on oxidation kinetics, conductivity meas. 77—21298
$LiNbO_3$, electromigration in ion bombardment 78—26601
$LiNbO_3$, ion-bombardment erosion of single cryst., prep. for TEM exam. 79—38996
$LiNbO_3$, piezoceramic, elastic normal wave propagation, phase transitions *(Russian)* 80—40067
$LiNbO_3$-CdO, CdO addition effect on sintering 79—83157
$Li_xNi_{1-x}0$ $(x=0$ to $0.03)$, solid soln. effect of Li on densification during sintering 80—25638
LiO_2-Na_2O-CaO-SiO_2 glass-ceramic coating, high temp. effects on steel substrate 79—61776
Li_2O pellets, sintered, reaction with Mo and Ho alloys 79—47913
Li_2O-(Al_2O_3)-SiO_2 glass-ceramic, crystallisation mechanism 79—90559
Li_2O-Al_2O_3-Cr_2O_3 system, subsolidus equilibria 80—60843
Li_2O-Al_2O_3-SiO_2, chem. resist. and struct. 79—61756
Li_2O-Al_2O_3-SiO_2, glass ceramic form. obs. using positron annihilation 77—7762
Li_2O-Al_2O_3-SiO_2, glassy and polycryst., interdiffusion coeffs. for ion exchange 78—26738
Li_2O-Al_2O_3-SiO_2, glass ceramic, elastic props. at high press., US meas. 78—83863
Li_2O-Al_2O_3-SiO_2, kinetics of glass-ceramic formation, by modified broken total internal reflection method 77—36444
Li_2O-Al_2O_3-SiO_2 glass ceramic, fracture initiation, influence of temperature and composition 79—100246
Li_2O-Al_2O_3-SiO_2 glass-ceramic, near-zero thermal-expansion heat treatment effect in fracture behaviour 80—66537
Li_2O-Al_2O_3-SiO_2-TiO_2 system glasses, Raman spectra obs. of glass-ceramics form. 80—60825
Li_2O-Cr_2O_3-SiO_2 system, phase equilibria 79—78944
Li_2O-MgO-Al_2O_3 system, subsolidus phase equilibria 80—81036
Li_2O-Nd_2O_3-P_2O_5 phase diagram, $LiNdP_4O_{12}$ single crystal growth 80—25668
Li_2O-SiO_2, glass ceramics, phase transformation processes 80—3025

ceramics continued
Li_2O-SiO_2 glass ceramic, aligned, prep. by hot extrusion and microstruct. 77—32552
Li_2O-SiO_2-P_2O_5 glass ceramic fibres, heat treatment, crystn., tensile strength 80—84995
$(Li_2O$-Al_2O_3-$SiO_2)$:Fe_2O_3, glass, pyroceramic form., colour centres, magnetochem. investig. 77—16537
$Li_2O.2SiO_2$ ceramics unidirectionally solidified, porosity *(Japanese)* 79—38816
$Li_2O.2SiO_2$, directionally solidified, thermal and mech. props. *(Japanese)* 80—16295
$Li_2O.2SiO_2$ glass and glass-ceramic, fatigue props. in various environments 79—91820
$Li_2O.2SiO_2$ glass and glass ceramic, Auger electron signal decay, crystn. effects 80—25503
$Li_2O.2SiO_2$, polycrystalline, oriented, fabrication by unidirectional solidification from melt *(Japanese)* 78—31371
$Li_2O.2SiO_2$, prep. from film forming soln. 80—60811
$Li_2O.2SiO_2$, prep. of oriented microstructure by unidirectional solidification of melts 80—71614
$100(Li_2O.2SiO_2).3B_2O_3(3Na_2O)(3MgO)(3Al_2O_3)(3SiO_2)(3P_2O_5)$, directionally solidified, thermal and mech. props. *(Japanese)* 80—16295
$Li_2O.nAl_2O_3(7.3\text{-}n)SiO_2$, metastable solid soln., Al^{3+} vacancy incorporation 77—12593
$Li_x(Si,Al)_{12}(O,N)_{16}$, α'-Sialon ceramics, prep. and characterisation 78—84750
Li_2SiO_4, piezoelectric glass ceramic, recrystallisation, pyroelectric response, permittivity 80—80703
$Li_2Si_2O_5$, pyroelectric glass-ceramics 80—75950
$LiTaO_3$ glass-ceramics, transparent fabrication by crystn. of aluminosilicate glasses 77—59734
$Li_{1+y}Ta_{1-5y}Ti_{6y}O_3$ $(0 \leq y \leq 0.028)$, non-stoichiometric phase, crystallographic and dielec. props. 80—75212
$LiTi_2O_4$, prep., characterisation and supercond. props. 77—40010
Li_2TiO_3-MgO (20 to 40 at.%), order-disorder transitions, DTA and X-ray anal. 79—29050
LiTiZn ferrites, elec. resist., mag. props., effect of Bi addition 78—95474
$Li_{14}Zn(GeO_4)_4$, LISICON, AC meas. of ionic cond., 298 to 573K 80—107526
Mg ferrite, sintered, cation redistribution, microstructural effects 77—55356
Mg-Al spinel, hot pressed ceramic, annealing effect on transparency and microstruct. *(Japanese)* 79—74188
Mg-Al spinel ceramics, mech. strength, non-stoichiometry and microstruct. *(Japanese)* 80—21054
Mg-Cu-Mn-Ni-Fe-O, UHF ferrites, synthesis, physicochem. state, mag. and dielec. parameters 79—11536
Mg-Si-Al-O-N, grain boundary segregation, combined X-ray microanal. and lattice fringe imaging determ. 79—15681
Mg-Si-Al-O-N ceramic, phase assemblages, relationships with props. 80—60848
$MgAl_2O_4$, active spinel, prep. and crystallite growth mech. 78—27465
$MgAl_2O_4$, composition rel. to ceramic microstruct. form., light transmission 79—43188
$MgAl_2O_4$, form. from amorphous substance prep. by homogeneous precipitation *(Japanese)* 79—56950
$MgAl_2O_4$, powder effect of precursory sulphate solution anion on sintering 78—56605
$MgAl_2O_4$, pure and Fe-doped spinel, elec. cond. 80—59702
$MgAl_2O_4$ spinel, kinetics of form. from oxides in thin films *(Russian)* 79—52144
$MgAl_2O_4$, spinel materials press forged, mech. props., IR appl. 78—39722
$MgAl_2O_4$, strength-controlling fracture energy depend. on flaw-size to grain-size ratio 80—81152
$MgAl_2O_4$ transparent ceramic, transmittance, grain size and dopant effects *(Japanese)* 80—19083
$Mg_{1.86}Al_{1.67}Si_{2.47}O_{3.19}N_{3.81}$, 12H polytype, intergranular phases and compositional variations 80—79645
$MgCO_3$ powder, high speed method of porosity determ. 77—90543
$MgCr_2O_4$ spinel, exam. of expansion during synthesis 79—20012
$MgCr_2O_4$-TiO_2, porous ceramics, humidity-sensitive electrical conduction 80—107782
$MgCr_2O_4$-TiO_2 porous ceramic humidity sensors 80—86325
MgF, polycryst., quartz particle impacts no. effect on erosion in elastic-plastic response regime 80—81209
MgF_2, optical ceramic, synthesis 78—52729
MgF_2, polycrystalline, elastic moduli, press. and temp. depend. US meas. 77—21202
$Mg_{0.8}Mn_{0.2}Fe_{1.8}Al_{0.2}O_4$, grade 6SChl ferrite, milling conditions effect on fine cryst. struct. and activity 79—24483
MgO (:CaO) powder compacts, sintering studies, SEM obs. 79—78918
MgO bicrystals, formed by welding single crystals with H_3PO_4, exam. 78—56796
MgO, boundary segregation of Ca, Fe, La and Si 79—70069
MgO brick, particle-size distrib. depend. of texture and struct. *(Japanese)* 78—84753
MgO briquets, prep. by shock compaction and characteris. 79—43178
MgO, compressive stress-strain behaviour at high temps. 80—25774
MgO crystal, chemical etchant for old and fresh dislocations 79—65088
MgO crystal, diffusion of ^{51}Cr 77—35754
MgO crystals, etching and polishing, inorganic or organic acids effect 80—40573
MgO crystals, etching behaviour rel. to chem. reactions 80—3229
MgO crystals, kinetics and mechanism of dissoln., etch rates in H_2SO_4 solns. 79—79136
MgO, crysts., adsorption processes in selective etching 80—39098
MgO, dense layer form. in pitch bearing magnesite brick, kinetics and mechanism 79—11717
MgO, dislocation creep, creep deform. predictions 78—19815
MgO, dislocation motion 79—4309
MgO, EPR of Mn^{2+} diffusion 78—91477
MgO, effect of B_2O_3, CaO and SiO_2 minor additives on high temp. creep 78—48450
MgO, effect of Cl^- and F^- ions on calcination and sintering *(Japanese)* 78—95719
MgO, electron irradiation induced mobility of substitution H 77—55390
MgO, filamentary crysts., synthesis and props. 77—52267
MgO fusion cast ceramics, crystn., microstructures rel. to conditions 80—11638
MgO, hardness anisotropy obs. 79—79085

ceramics continued

MgO, hot pressed, microstruct. influence on microhardness 79—38971
MgO, lattice defects., calcination temp. effect 80—15091
MgO, lattice misorientation and displaced vol. for microhardness indentation 78—64617
MgO, molten K_2SO_4 treated, phys. and chem. props. *(Japanese)* 79—57133
MgO, plastically deformed, recovery of internal friction at room temp. *(French)* 78—80577
MgO, polycryst., creep diagrams inc. ambipolar diffusion and grain size for polycryst. ceramics with ambipolar diffusion, incl. grain size 77—73304
MgO, polycrystalline, diffusion creep activation energy 78—11274
MgO, polycrystalline, ductile, porous, model 79—47653
MgO, polycrystalline, grain growth and grain boundary migration, pore effects *(Japanese)* 78—19701
MgO, polycrystalline, stress depend. of creep 79—70120
MgO polycrystals, hot-pressed, effect of annealing on props. 79—34073
MgO polycrystals, mech. props., 900-1150°C *(French)* 80—104374
MgO polycrystals, ultrafine grained, compressive creep 77—32639
MgO polycrystals, ultrafine-grained, creep microstruct. 80—35246
MgO, pore distrib. and grain size in intermediated sintering stage *(Japanese)* 79—74124
MgO powder, active, sintering 80—20870
MgO, powder activation during grinding 77—90300
MgO powders, hot pressing, mechanisms 80—40300
MgO, precipitate morphology, strain energy effects 80—40358
MgO refractory, erosion resistance in reaction products flow *(Russian)* 77—25173
MgO, segregation of aliovalent solutes adjacent {100} surfaces 79—78979
MgO short time chemomechanical effects, dislocation generation and motion, drilling simulation 79—87749
MgO single cryst., impact wear characts. 80—76374
MgO single cryst., impact wear damage 80—76375
MgO, single cryst., order hardening by large precipitated vol. fraction of spinel particles 80—3085
MgO single crystal, absorbed fluid effect on rolling contact deform. 78—64719
MgO single crystal, corrosion by BOF slag 79—24635
MgO, single crystal, thermolum. meas. *(Japanese)* 78—19577
MgO, single crystal, wear damage, surface cracks 78—68825
MgO single crystals, chem. polishes for {100}, {110} and {111} surfaces, spectrochem. anal. for impurity content 79—29241
MgO, single crysts., work hardening and creep 79—43262
MgO sintered-ceramic separator plate development, Li-Al/LiCl-KCl/FeS battery applications 80—61321
MgO, solid solubility of Sc_2O_3, Al_2O_3, Cr_2O_3, SiO_2 and ZrO_2 80—15247
MgO, spherical particle impact damage, effect of crystallographic orientation 79—79135
MgO, stresses on hot pressing 77—36425
MgO, tensile and compressive strengths of fine powder bed *(Japanese)* 80—25780
MgO, tensile creep of single crystals, substruct. effect 79—66113
MgO, thermal characts. using constant power source method 79—95222
MgO, thermally shocked, strengthening kinetics 77—8920
MgO, thermoluminescence mechanism 79—15538
MgO, ultrafine grained Fe doped, high temp. creep 79—15727
MgO, vaporization in O_2-H_2O atmos. *(Japanese)* 79—74279
MgO, X-ray and electron diffr. crystallite size determ. *(Polish)* 79—100153
MgO:(Li), polycrystn., internal friction *(German)* 80—59577
MgO:CaO(SiO_2)(B_2O_3)(Cr_2O_3), effective of impurities on high temp. creep 80—40455
MgO:Fe, Fe^{2+} oxidation and Fe^{3+} reduction kinetics, EPR obs. 79—70399
MgO:Fe^{3+}, defect structure, and oxidation reduction behaviour of Fe 79—99181
MgO:Li, internal friction, mech. and dielec. relax. *(German)* 80—34135
MgO-Al_2O_3 transparent spinel ceramic, fabrication by reactive hot pressing *(Japanese)* 77—77454
MgO-Al_2O_3-Cr_2O_3, vacuum vaporisation, Langmuir method 78—95149
MgO-Al_2O_3-Fe_2O_3-SiO_2, cordierite, in ceramic, effect of heat treatment on cordierite content 79—20039
MgO-Al_2O_3-SiO_2, glass ceramics, phase transformation processes 80 - 3025
MgO-Al_2O_3-SiO_2, glass ceramic, structure and props. *(German)* 80—38927
MgO-Al_2O_3-SiO_2, sintered, cordierite, mineralogy and props. 80—60827
MgO-Al_2O_3-SiO_2 based cordierite glass-ceramic, strength and thermal shock, surface treatment effect 80—25884
MgO-Al_2O_3-SiO_2 glass ceramic, nucleation, effect of electric fields 78—83742
MgO-Al_2O_3-SiO_2 system glasses and glass ceramics, EPR obs. of transition elements, crystn. effects 78—23332
MgO-Al_2O_3(Cr_2O_3)(Fe_xO_y)-CuO, phase relations and microstruct. 79—74140
MgO-C dispersion, creep, effect of C on grain size and growth 79—100213
MgO-$Ca_3Mg(SiO_4)_2$($CaMgSiO_4$)-$NaPO_3$, phase conversions 77—66641
MgO-CaO refractory ceramics, thermal expansion coeffs. 79—99336
MgO-CaO-Al_2O_3-SiO2(-TiO_2) systems, glass-ceramics, crystn. kinetics *(Russian)* 79—37626
MgO-Cr_2O_3, reaction sintering *(German)* 78—11174
MgO-Cr_2O_3, vaporisation rate, O_2 partial press. effect *(Japanese)* 78—63848
MgO-NiO, STEM microanal., absorpt. effects 80—80902
MgO-NiO, solid soln. formation, initial stage obs. 77—81243
5 wt.% MgO-Si_3N_4, hot-pressed, dielec. props. 78—10822
MgO-Si_3N_4, hot-pressed, electrical props. 78—39136
MgO-SiO_2, molten, corresponding state principle with LiF-BeF_2 and appl. 79—11589
MgO-ZrO_2, dispersion hardened, fracture strength and texture, rel. to temp. *(German)* 79—43378
MgO-ZrO_2 ceramic sublimation at optical furnace focal spot *(Russian)* 79—95983
MgO_2 powder exam. of packing behaviour *(Japanese)* 79—20016
$Mg(OH)_2$, and calcination product, relations between particle size, shape and surface area 78—48355
MgO.Al_2O_3.2SiO_2, hydrothermal synthesis, phase transitions 77—48378
MgO.nAl_2O_3, nonstoichiometric spinel, DTA 77—28791

ceramics continued

$MgTiO_2$, Mg_2TiO_4, $MgTi_2O_5$, formation mechanism 77—48373
$MgTi_2O_5$, thermal diffusivity, grain size and microcracking effects 78—10233
MgV_2O_4-Mg_2VO_4 spinel solid soln., quenching and lattice const. 77—90307
(Mn,Zn)Fe_2O_4:Si, Ca, Ti, second phase effect on elec. and mag. props. 80—60986
$Mn_xCo_yNi_7O_4$, spinel ceramic, current noise in thermistor bolometer 77—51793
MnO, EPR spectra of ceramic and epitaxial monocrystalline thin film samples *(Russian)* 80—11252
MnO_2 porous powders, Al_2O_3 and SiO_2 coated, changes in surface free energy for N adsorption 80—84363
Mn_2SiO_3, effect of vibration during sintering, on electrical resistivity 80—16258
MnZn ferrite, laser drilling and cutting, anal. of results using computer model 79—70180
MnZn ferrite, props. rel. to raw materials *(German)* 77—21074
MnZn ferrite powder prep., wet method 80—89180
MnZn ferrites, doped; determ. of grain boundary composition, using Auger spectroscopy *(German)* 79—23618
Mo-Mn-Fe-Si/Al_2O_3 ceramic seal, interfacial phases 78—72011
$MoCr_2O_6$, hydrothermal cryst. growth, 40 kbar, 873K, cryst. struct. *(French)* 78—35342
$MoSi_2$, ceramic additives effect on sintering, recrystallisation 80—40306
$MoSi_2$, effect of Al on oxidation behaviour *(German)* 78—31587
$MoSi_2$-$TiSi_2$, high-temp. oxidation 79—83341
$(NH_4)_2Cd_2(SO_4)_3$, dielec. and spontaneous polarisation, −195 to −180°C, particle size depend. 80—97200
(Na,Li)NbO_3, ceramics, electrophys. and struct. props. near morphotropic transition 78—2816
(Na,Li)NbO_3 ceramic, optimum prep. conditions and characterisation 78—3079
Na-βAl_2O_3 ceramics, synthesis 80—40305
$Na_{0.5}Bi_{4.5}Ti_4O_{15}$, hot-forged ferroelec. ceramic with layer struct. 79—43175
NaF powder, porous, of skeleton struct., grain size effect on strength *(Russian)* 77—24991
$Na_{0.5}K_{0.5}NbO_3$, piezoelectric ceramic solid soln. *(Polish)* 77—55755
$(Na_{0.5}La_{0.5})_xBa_{1-x}TiO_3$, dielec. and IR spectra exam., ferroelec. transition 78—23418
$NaNbO_3$-$BaTiO_3$, unidirectionally solidified transparent ceramics 80—25677
$NaNbO_3$-$BaTiO_3$ solid soln. form. and props. *(Russian)* 78—48378
$NaNbO_3$-based ferroelec. solid solns., morphotropic transitions and elec. props., enhanced vacancy conc. 80—55048
$NaNbO_3$-$SrNb_2O_6$, phase diagram, props. meas. 79—11576
β-Na_2O-Al_2O_3, thermal dissoc. at high press. 77—36435
Na_2O-Al_2O_3-SiO_2, glass, nucleation, crystn., ceramic form. 80—84082
Na_2O-BaO-Al_2O_3-SiO_2, glass, nucleation, crystn., ceramic form. 80—84082
β-Na_2O-CaO-Al_2O_3, impurity conc. at grain boundaries, AES obs. 77—35570
Na_2O-Li_2O-Al_2O_3, local electrode current density and flow decoration 80—100935
Na_2O-MgO-Al_2O_3, β''''-alumina, high-resolution electron microscopy 80—75208
β''-Na_2O-MgO-Al_2O_3, thermal dissoc. at high press. 77—36435
Na_2O-PbO-SiO_2 glass-ceramic composite, directionally crystallised 80—107058
$Na_2O.Li_2O.Al_2O_3$, comp. and props. for use in Na-S battery 79—87745
$Na_2O.SiO_2$, prep. from film forming soln. 80—60811
$Na_2O.11Al_2O_3$, polycrystalline with preferably orientated grains, preparation *(Japanese)* 80—81012
$Na_2O.7Al_2O_3.0.2Mn_3O_4$ impedance parameters in electrochem. cells 80—21296
$Na_2O.y(Al_{1-x}Fe_x)_2O_{3-m}$, β''-Al_2O_3 phase stability, lattice constants 80—45283
$Na_{5-x}Ta_{11+x/5}O_{30}$, synthesis, non-stoichiometry, density and ionic cond. meas. *(French)* 78—52741
$Na_5YSi_4O_{12}$, high Na^+ ion conduct. 78—91479
NbC, NbC-ArC, right-through sat. prep., strength and plasticity, temp. depend. 77—40432
NbC, physicomechanical props. within the homogeneity range 77—1848
NbC_X powders, nonstoichiometric, sintering kinetics 79—100099
Nb_2O_5-V_2O_5-P_2O_5, glasses and glass ceramics, elec. cond., struct. 80—84466
$Nd_{1/3}NbO_3$, $NdNbO_4$, structural characteristics and residual polarisation 77—15361
$3Nd_2O_3.2WO_3$, X-ray charact. and thermal props. 77—43194
$NdTiO_3$, physicochem. props. 80—25625
$Nd_xZr_{1-x}O_{2-x/2}$, elec. cond. of ceramic solid solutions 80—107554
$Nd_xZr_{1-x}O_{2-x/2}$, fluorite and pyrochlore solid solutions, electrical conductivity meas. 80—65287
Ni-ceramic coating structure, influence of micropowder inclusion *(Russian)* 80—59820
Ni-Eu_2O_3, specific resistivity and emissivity, 1000 to 1500K 77—43675
$NiFe_2O_4$, hysteresis and other mag. props. rel. to microstruct., TEM investig. 77—20636
$NiFe_2O_4$ milled ferrite powder, substruct. and sinterability 80—84894
$NiGa_2O_4$ spinel form., effect of Ga^{3+} chemical diffusion in NiO *(German)* 78—22894
NiO, chemical diffusion 79—60544
NiO, under controlled atmosphere, exam. of composition and temp. dependence, of lattice parameter *(French)* 79—19214
NiO-Al_2O_3 powders, coprecipitated particle-size distrib. meas. 78—39726
NiTaC, eutectic alloys, chem. incompatibility of ceramic nitrides for directionally solidifying 80—81046
NiTaC-13, directionally solidified eutectic alloy, chem. compatibility with ceramic materials 79—87623
$NiTiO_3$, synthesis from products of soln. spray drying, kinetics 77—16519
NiZn ferrite, laser drilling and cutting, anal. of results using computer model 79—70180
NiZn ferrite, ZrO_2 additions influence on sintering and physicochem. props. 80—108369
$^{237}NpO_2$ powder, oxalate based, prep. and charact. 78—11166
PLZT ceramic, ageing, dielec. props. 80—88940
PLZT ceramic, bonded lens assembly manufacture 80—79018

ceramics continued
PLZT ceramic, dielectric anisotropy, role of 90° domain processes 77–63384
PLZT ceramic, modulator for optical communication 80–78964
PLZT ceramic, optical gate, dielec., optical props., electro-optical effect meas. 78–42418
PLZT ceramic, possible construction of matrix-addressable controlled transparency 78–71222
PLZT ceramic, proton implanted, photoferroelectric effect for image storage and display devices 80–80315
PLZT ceramic, thin waver electrode slotting process 80–79017
PLZT ceramic, thin wafer production polishing process 80–81214
PLZT ceramic, transverse electro-optical effect, matrix-addressable transparency 79–27431
PLZT ceramic birefringence props., transverse electro-optical meas. 78–72487
PLZT ceramic photoferroelectric image storage device, characts. 77–55756
PLZT ceramic with memory, domain reorientation, alternating elec. field effect 79–47405
PLZT ceramic;, visible light scatt. depend. on photoferroelectric space charge fields 80–80806
PLZT ceramics, electro-optical props. *(Korean)* 79–11406
PLZT ceramics, electro-optic; defect struct. and prop. 79–42910
PLZT ceramics, elastooptic effect, stress induced birefr. 80–60543
PLZT ceramics, modified by $Ca^{2+}(Sr^{2+})(Nd^{3+})(Y^{3+})$, dielec. behaviour 80–60519
PLZT ceramics, optical recording *(French)* 77–31078
PLZT ceramics, photoferroelectric effects, image storage device appl. 79–42924
PLZT ceramics, photoinduced charge transfer process 79–50362
PLZT ceramics, SHG, anomalous phase transition 79–45996
PLZT ceramics, short circuit photocurrent, depend. on polarization 79–38121
PLZT ceramics, stress-induced ferrelec. transition, pseudoelasticity and shape memory, bending meas. 79–24274
PLZT ceramics, transparent ferroelec., photorefraction and photocond. study 79–42581
PLZT ceramics photosensitivity enhancement by H- and He-ion implantation 80–96934
PLZT composition, effect on its switching characts. 79–42917
PLZT, diffuse phase transitions and thermodynamics 80–29694
PLZT, effect of ageing on temp. depend. of permittivity, for ferroelectric and antiferroelectric compositions 78–48121
PLZT, electro-optic characts., w.r.t. future instrument applics. *(German)* 78–33792
PLZT, electro-optical, physical, elec. and optical props. and fabrication *(Polish)* 78–56458
PLZT, electrooptic systems *(Japanese)* 79–65840
PLZT, exam. of grain growth in hot pressing, and liquid phase sintering 79–33981
PLZT, Fe doped, photochromic effect 77–16347
PLZT ferroelec. ceramics, piezoelec. props. 79–42897
PLZT, ferroelectric domain struct. obs. by SEM and optical microscopy *(Japanese)* 78–15136
PLZT, ferroelectric devices for optical systems 78–90473
PLZT ferroelectric ceramic, photovoltaic effect 79–99585
PLZT, ferroelectric and struct. transitions, crystallographic, thermal, and dielec. anal. 80–29693
PLZT, fine grained 90° electric domain wall movement, interpretation of dielectric losses *(German)* 79–33646
PLZT, light scattering, IR laser radiation recording 78–4695
PLZT, mech. and elec. losses, correl., theory and expt. 80–66133
PLZT optical ceramic, as high speed shutter 77–79187
PLZT, phase transitions induced by elec. fields 80–29695
PLZT, photoferroelectric image storage in antiferroelectric-phase PLZT ceramics 80–71353
PLZT porosity and transparency affected by vacuum hot pressing 77–12556
PLZT powder preparation, hyrolysis ball mixing 80–81006
PLZT powders, chemical prep. and hot pressing 78–44059
PLZT, prep. by liquid phase sintering of oxides 79–38778
PLZT, pure and doped solid soln. powders, synthetic process prep. 79–78920
PLZT, reduced, exam. of ageing phenomena, using dielectric hysteresis *(German)* 79–33647
PLZT, refr. index, 405-764 nm, surface layer 78–35110
PLZT slim-loop and linear ceramics, longit. electrooptic effects, display appl. 80–80751
PLZT slugs, powder hot pressing technique 80–81007
PLZT, Sn substituted, antiferroelectric ceramics research and their applications *(Chinese)* 79–33617
PLZT thermal, flash, ferroelectric protective goggles 80–81746
PLZT, transparent, optical exam. of small signal behaviour, of 90° electric domain walls *(German)* 79–33645
PLZT transparent ceramics, electro-optical anisotropy due to hot pressing 77–12720
PLZT transparent ceramic laser modulator *(German)* 78–5553
PLZT, transparent ferroelectric, ceramics obtained by hot pressing, optimum conditions *(German)* 79–43176
PLZT type, variation of light scatt. during field induced AF→F transition *(French)* 77–90158
PLZT type ceramics, calorimetric meas. of energy of electrical polarisation 79–2770
PLZT/TFPD thermal/flash protective lens assembly, polarised delamination investigation 80–78929
PLZT-based polarised ceramic, electro-opt. props. 77–52041
PLZT-ceramics, cathodlum. spectral and temp. depend. 78–84665
(PLZT)(PLZN) system, ferroelec. transparent, prep. and study 79–42911
PZT paraelectric ceramic one-dimensional spatial light modulator 79–55240
PZT, PbO content estimation using analytical procedure *(German)* 78–53279
$(Pb,La)(Zr,Ti)O_3$, ferroelec. ceramic, polarisation distrib. obs. using electro-optic effect 80–25278
$(Pb,Sr)(Zr,Ti)O_3$, piezoceramic, effect of glass additions on props. during hot pressing 79–24475
Pb ceramic glaze, Cu^{2+} doped, Pb^{2+} release 80–49101
Pb glazes, Cu^{2+} doped, alkaline substitution, crystal field modifications, EPR study 79–95634

ceramics continued
$(Pb_{1-y}Ba_y)_{1-x}La_xNb_{2-x/5}O_6$, transparent ferroelec. ceramic, optical transmittance, electrooptic props. and Curie temp. 77–32395
$(Pb_{1-y}Ba_y)_{1-x}La_xNb_{2-x/5}O_6$, ferroelec., phase transitions 79–38487
$Pb_{0.6}Ba_{0.4}Nb_2O_3$, piezoelectric ceramic solid soln. *(Polish)* 77–55755
$Pb_{0.94-x/2}Ba_{0.6}Nb_xZr_{1-x}O_3$, Nb dopant morphology effect on microstructure 80–81005
$(Pb_{0.715}Ba_{0.285})_{0.991}(Zr_{0.707}Ti_{0.293})_{0.981}Bi_{0.019}O_3$, slim loop ferroelec. ceramic, shock wave compressed, elec. response 78–80293
$(Pb_{0.8}Ba_{0.2})(Zr_{0.8}Ti_{0.2})O_3$, ferroelec. ceramic, pulse-like voltage generation using polarisation reversal 78–2809
$PbBi_2Nb_2O_9$, bend strength, grain orientation effects 80–40375
$PbBi_2Nb_2O_9$ ceramic, grain oriented, dielectric and piezoelectric props. 79–42896
$PbBi_2Nb_2O_9$, hot-forged ferroelec. ceramic with layer struct. 79–43175
$PbBi_4Ti_4O_{15}$, dielec. props., temp. depend. 78–95561
$PbBi_4Ti_4O_{15}$, hot-forged ferroelec. ceramic with layer struct. 79–43175
$Pb_2Bi_4Ti_5O_{13}$, hot-forged ferroelec. ceramic with layer struct. 79–43175
$PbCo_{0.33}Nb_{0.66}O_3$, ferroelectric, exam. of permittivity and dielectric props. 79–1742
Pb_2CrO_5, thermal X-ray and dielec. investigations 79–47403
$Pb(Cu_{1/4}Nb_{3/4})O_3$-$Pb(Li_{3/4}Nb_{3/4})O_3$-$PbTiO_3$-$PbZrO_3$, piezoelec. ceramic materials for SAW devices 79–11390
$Pb(Cu_{1/4}Nb_{3/4})O_3$-$Pb(Li_{1/4}Nb_{3/4})O_3$-$PbTiO_3$-$PbZrO_3$, optimisation of composition for SAW devices 79–33609
$Pb(Fe_{1/2}Nb_{1/2})O_3$-$La_2O_3(CeO_2)$ ferroelec. ceramics, electrophysical props. 78–35099
$2PbFe_{1/2}Nb_{1/2}O_3$-Pb_2FeReO_6, comp., struct., dielec. and mag. props. 80–2704
$2PbFe_{1/2}Ta_{1/2}O_3$-Ba_2FeReO_6, comp., struct., dielec. and mag. props. 80–2704
$2PbFe_{1/2}Ta_{1/2}O_3$-Pb_2FeReO_6, comp., struct., dielec. and mag. props. 80–2704
$PbFe_{2/3}W_{1/3}O_3$-$BaTiO_3$ system ferroelec., antiferromag., ESR and dielec. props. meas. 77–40172
$Pb_5Ge_3O_{11}$ bonded $Pb(Zr,Ti)O_3$ composites, piezoelec. props. 79–78629
$Pb_5Ge_3O_{11}$, ultrafine-grained crystallized from glass, ferroelectricity 78–39508
$PbHf_{1-x}Ti_xO_3$, phase diagram, influence of poling treatment, ferroelec. antiferroelec. transition *(French)* 77–63374
$Pb_{0.97}La_{0.02}(Zr_{0.92}Ti_{0.08})O_3$, ferroelec. ceramic, stress effects 80–2119
$Pb(Mg_{1/3}Nb_{2/3})O_3:PbTiO_3$, ceramic dielectric, electrostriction, relaxation, polarisation 80–80700
$PbMg_{1/3}Nb_{2/3}O_3$-$BiMg_{2/3}Nb_{1/3}O_3$, dielectric polarisation of solid solutions 78–43776
$Pb(Mg_{1/3}Nb_{2/3})O_3$-$PbTiO_3$-$PbZrO_3$, piezoelec. PCM ceramic, formation process *(Japanese)* 77–85978
$Pb(Mg_{1/3}Nb_{2/3})O_3$-$PbTiO_3$-$PbZrO_3$, piezoceramics for high frequency use 78–95555
$Pb(Mg_{1/3}Nb_{2/3})O_3$-$Pb(W_{1/2}Mg_{1/2})O_3$, struct. and dielec. props. 80–25312
$Pb_3MgNb_2O_9$-$PbTiO_3$, relaxor ferroelectrics, electrostrictive effects 80–66112
$PbMg_{0.33}Ta_{0.66}O_3$, ferroelectric, exam. of permittivity and dielectric props. 79–1742
$Pb(Mn_{1/2}Ta_{1/2})O_3$, ceramic, for thermal and dielectric isolation at low temp. 80–39365
Pb_2MoO_5, form. conditions 80–20853
Pb_2NbFeO_6, form. reacts., thermogravimetric investig. 78–35340
$PbNb_2O_3$, piezoelectric ceramic solid soln. *(Polish)* 77–55755
$PbNb_2O_6$, O defects and elec. props. anomalies 79–42898
$PbNb_{0.5}Sc_{0.5}O_3$, ceramic, dielec. props. 79–11392
$Pb_{0.98}Nb_{0.02}(Zr_{0.95}Ti_{0.05})_{0.98}O_3$, PZT 95/5, ferroelec. ceramic, resist. meas. under shock wave compression 78–19031
$Pb_{0.99}Nb_{0.02}(Zr_{0.95}Ti_{0.05})_{0.98}O_3$, ferroelec. ceramic, stress effects 80–2119
PbO, microprobe state anal. by X-ray OK and BK emission band spectra *(Japanese)* 78–19606
PbO-GeO system, pyroelec. and TSC props. 78–43798
PbO-ZnO-B_2O_3, glass ceramic cements, crystallisation kinetics and character 77–85982
PbO_2, corrosion in HBF_4, redox mediator effects 77–90480
$4PbO.GeO_2$, X-ray phase and thermal anal., new antiferroelectric 79–1744
3PbO.2GeO, TSC in thermoelectret state during ceramic synthesis, pyroelec. currents and energy struct. of capture centres 80–55014
$Pb_{1-\alpha x}R_xTiO_{3+x(1.5-\alpha)}$, R=La or Sm exam. of permittivity as function of temp. 79–33586
$Pb_{1-nx}R_xTiO_{3+x(1.5-n)}$, R=rare earth, ferroelec. Curie temp. comp. depend. 77–16258
$Pb(Sb_{1/3}Mn_{2/3})O_3$-$PbTiO_3$-$PbZrO_3$, remanent dielec. polarisation of poled ceramic, heat treatment 79–87390
$Pb(Sc_{0.6}Ta_{0.5})_3$ ceramics, ordering and diffuse phase transitions 80–29699
$PbSnF_4$, anionic conductor, thin films and ceramics 80–107556
$Pb_{0.94}Sr_{0.06}(Ti_{0.47}Zr_{0.53})O_3$-NiO, modified, dielec. and piezoelec. props. 80–11342
$Pb_{0.94}Sr_{0.06}Ti_{0.47}Zr_{0.53}O_3$, piezoelectric ceramic, stress relax., time depend. deformation 80–60899
$Pb_xSr_{1-x}(Zr,Ti,Nb)0_3$, hydrophone ceramic, effect of one-dimensional uniaxial stress 80–80705
$(Pb_{0.95}Sr_{0.05}(Zr_{0.53}Ti_{0.47})O_3)_{99\%}+Ta_2O_5(Nb_2O_5)$ piezoelectric ceramic solid soln. *(Polish)* 77–55755
$(Pb_{0.97}Sr_{0.03})Zr_{0.51}Ti_{0.49}O_3$, ferroelec. phase transition under high press. 77–36188
$Pb_{0.95}Sr_{0.05}(Zr_{0.53}.Ti_{0.47})O_3$, low temp. internal friction in ferroelectric ceramic 77–21200
Pb_2TaFeO_6, form. reacts., thermogravimetric investig. 78–35340
Pb_2TaMnO_6, reaction of form. from oxides, ferroder. props. 80–55326
$Pb(Ti,Zr)O_3$, kinetics of initial stage of sintering 77–85973
$Pb(Ti, Zr)O_3$, piezoelectric-ferroelectric ceramic, polarisation processes, X-ray obs. 80–34847
$Pb(Ti,Zr)O_3$ solid solutions, phase coexistence discrepancies 80–96662
$Pb(Ti,Zr)O_3:Fe(Mn)(Al)$, internal bias field and hysteresis relaxation 78–43823
$PbTiO_3$, ferroelec. ceramic, mech. strength 78–64332
$PbTiO_3$, ferroelectric ceramic, dielec., piezoelec. and elastic props., orientational contrib. 78–68468
$PbTiO_3$ glass-ceramics, transparent, fabrication method by crystn. 77–59733
$PbTiO_3$, piezoceramics for high frequency use 78–95555
$PbTiO_3$, temperature-compensated, for SAW appl. 80–15355

ceramics continued

- $PbTiO_3$-$CaFe_{2/3}W_{1/3}O_3$, solid solutions 78—43816
- $PbTiO_3$-$La_2O_3.3TiO_2$, struct. and dielec. props. 80—54200
- $PbTiO_3$-$PbZrO_3$-$In(Li_{3/5}W_{2/5})O_3$, piezoelec. ceramic characteris. for surface wave filters 78—95215
- $PbTiO_3$-$PbZrO_3$-$Pb(Ni_{1/3}Sb_{2/3})O_3$ solid solutions, dielec. and electromech. anomalies *(German)* 77—20800
- $PbTiO_3$-$PbZrO_3$-$PbNb_{2/2}Zn_{1/3}O_3$(-$PbNb_{2/3}Co(Mg)_{1/3}O_3$) solid solutions, dielec. and piezoelec. props. 79—87393
- $PbTiO_3$-$PbZrO_3$-based multicomponent ferroelec. solid solns., morphotropic transitions and comp.-temp. phase diagrams 80—55047
- $PbTiO_3$-$Pb(Fe_{1/2}Nb_{1/2})O_3$ based modified ceramics, struct. and elec. props. 79—87392
- $PbTiO_3$-$Pb(Fe_{1/2}Nb_{1/2})O_3$-$PbZrO_3$, with additions, exam. of electrical characteristics 80—2698
- $xPbTiO_3+(1-x)PbCd_{1/3}Nb_{2/3}O_3$, phase transition spread, polarisation relaxation, dielectric susceptibility *(Russian)* 80—75922
- $Pb_3WFe_2O_9$, form. reacts., thermogravimetric investig. 78—35340
- $Pb(Z,Ti,Mg,W)O_3$, low-Q ceramics, props. and transducer appl. 80—75944
- $Pb(Zn,Ti)O_3$ piezoelectric electrically deformable diffraction grating 80—78963
- $Pb(Zn_{1/3}Nb_{2/3})O_3$, perovskite type, high-press. high temp. synthesis *(Chinese)* 78—68654
- $Pb(Zr,Ri)O_3$:Ni-silicon rubber flexible composite pyroelectric, dielectric props. 80—80704
- $Pb(Zr,Ti,Ge)O_3$, antiferro-ferroelectric transition 78—95565
- $Pb(Zr,Ti,Nb)O_3$ ceramics, rel. dielec. const. and piezoelec. props. rel. to porosity 79—11388
- $Pb(Zr,Ti,Sn)O_3$ ceramics, ferroelec., doped with tri- and pentavalent oxides, piezoelectric props. 78—19413
- $Pb(Zr,Ti)O_2$ ceramic, surface barrier electroreflectance, hysteresis, ageing 80—80752
- $Pb(Zr,Ti)O_3$, axially loaded, nature of elec. field and resulting voltage 78—72468
- $Pb(Zr, Ti)O_3$ cast tape, densification by pressing for piezoelec. devices 79—87595
- $Pb(Zr,Ti)O_3$ ceramics, low field depoling charact. 77—8492
- $Pb(Zr,Ti)O_3$ ceramic, permittivity and resonant frequency ageing, space charge field effects 77—85657
- $Pb(Zr,Ti)O_3$ ceramic-polyvinylidene fluoride composite film, complex piezoelec. props. 78—64323
- $Pb(Zr,Ti)O_3$ ceramic, substrate for In_2O_3 film, ferroelec. field effect 79—47177
- $Pb(Zr,Ti)O_3$ ceramics, piezoelectric characts. *(French)* 79—56727
- $Pb(Zr, Ti)O_3$ ceramics for IR detectors, pyroelectric characts. 79—56736
- $Pb(Zr,Ti)O_3$ ceramic/polymer, composite systems, piezoelec. props. 79—99823
- $Pb(Zr,Ti)O_3$ ceramic, X-ray investigation before and after polarisation *(Chinese)* 80—2712
- $Pb(Zr,Ti)O_3$ ceramic, interconnected porous, props. 80—43579
- $Pb(Zr, Ti)O_3$ ceramics, low temp. sintering, elec. and mech. props. 80—71616
- $Pb(Zr,Ti)O_3$ ceramics with ladder type struct., prep. and props. 80—75945
- $Pb(Zr,Ti)O_3$ ceramics, DC field sintering preparation, piezoelectric props., ageing behaviour 80—81211
- $Pb(Zr,Ti)O_3$, dielectric response in solid-medium high-pressure device 78—43766
- $Pb(Zr,Ti)O_3$, effect of spherical pores on strength 77—70103
- $Pb(Zr,Ti)O_3$, electrooptic ceramic *(Japanese)* 79—65840
- $Pb(Zr,Ti)O_3$, excitation of mechanical vibr. by ionising radiation beams 77—24799
- $Pb(Zr, Ti)O_3$, ferroelectric ceramics in solid matrix, high pressure effect on dielectric props. 77—16259
- $Pb(Zr,Ti)O_3$, ferroelec. ceramic, mech. strength 78—64332
- $Pb(Zr, Ti)O_3$, ferroelectric ceramic discs, axial-current-mode shock depoling 79—78631
- $Pb(Zr,Ti)O_3$ fibre arrays in epoxy cement, ferroelectric ceramic-plastic composites 80—81015
- $Pb(Zr,Ti)O_3$ films, ion beam sputtering, dielec. and ferroelec. props. 79—78881
- $Pb(Zr, Ti)O_3$, formation 79—43185
- $Pb(Zr,Ti)O_3$, fracture and deform. 80—79870
- $Pb(Zr,Ti)O_3$, internally electroded with Pt, resonance behaviour 80—84701
- $Pb(Zr,Ti)O_3$, K_{IC} eval. by double torsion technique 77—90444
- $Pb(Zr,Ti)O_3$, modified, measurement of electrical field-polarisation using automated system 79—67268
- $Pb(Zr,Ti)O_3$, PCD ceramic, pyroelectric props. 80—100635
- $Pb(Zr, Ti)O_3$, piezoceramic, explosive synthesis 77—16525
- $Pb(Zr,Ti)O_3$ piezoceramic, phase transition under shock loading *(Russian)* 77—69041
- $Pb(Zr,Ti)O_3$, piezoceramic, nonlinear piezoeffect 79—42900
- $Pb(Zr,Ti)O_3$, piezoelec., coexistence of tetragonal and rhombohedral phases 77—7845
- $Pb(Zr,Ti)O_3$, piezoelectric material, effect of processing on props. *(Polish)* 77—85655
- $Pb(Zr,Ti)O_3$ piezoelectric ceramic, CeO_2 additive effect on struct. and props. 79—52140
- $Pb(Zr,Ti)O_3$, piezoelectric ceramics, low fluence neutron irrad. effects 80—92564
- $Pb(Zr,Ti)O_3$, polarisation effect on deform. and strength, Curie pt. region 79—42902
- $Pb(Zr,Ti)O_3$ polycrystalline ceramic, fracture and strength, surface treatment effects 80—11704
- $Pb(Zr,Ti)O_3$, porosity-permittivity relations, depolarising factors determ. and pore effects *(Japanese)* 80—97189
- $Pb(Zr,Ti)O_3$, prep. and reactivity from butoxide precursors 78—84749
- $Pb(Zr,Ti)O_3$ pyroelectric ceramics 79—47649
- $Pb(Zr,Ti)O_3$, research grade, hydrophone ceramic, effect of one-dimensional uniaxial stress 80—80705
- $Pb(Zr, Ti)O_3$, Sc modified, sintering 77—44204
- $Pb(Zr,Ti)O_3$, shock depoling, for pulse charging of nanofarad capacitors 79—42913
- $Pb(Zr,Ti)O_3$, shock depoled ferroelec. ceramic, anal. of ideal response 80—60511
- $Pb(Zr,Ti)O_3$ solid solutions, elec. and thermoelec. props. appl. *(Polish)* 77—28203
- $Pb(Zr,Ti)O_3$, space charge field meas. by ferroelec. domain switching current, piezoelec. reson. freq. ageing characts. 80—7296

ceramics continued

- $Pb(Zr,Ti)O_3$, synthesis from cryochem. mixtures, chem. reacts. in sublimation drying 79—11538
- $Pb(Zr,Ti)O_3$, tetragonal ferroelec. ceramic, 90° domain-rot. fraction after polarisation, X-ray determ. 80—75992
- $Pb(Zr,Ti)O_3$, thermodynamic properties and formation data 80—29939
- $Pb(Zr,Ti)O_3$ type 1 ceramic, appl. in Langevin type sonar transducer, performance characts. 80—79095
- $Pb(Zr,Ti)O_3$:Ba, paraelectric ceramic, giant electrostrictive effect 79—91378
- $Pb(Zr,Ti)O_3$:Ba, paraelectric ceramic, electrostrictive effect 80—80701
- $Pb(Zr,Ti)O_3$:Cr_2O_3 ceramic, electrical cond. and dielectric const. meas. 80—2389
- $Pb(Zr,Ti)O_3$:Cr_2O_3 ceramics, reson. freq. comp. and temp. depend. 80—70413
- $Pb(Zr,Ti)O_3$:Fe(Nb) ceramic, elec. and electromechanical props., depend. on dopants 80—81212
- $Pb(Zr,Ti)O_3$:La(Cd,W), electro-optical ferroelec. ceramic, secondary electron emission yield 79—91546
- $Pb(Zr,Ti)O_3$:Mn, crystal struct. and electrophysical props., piezotransformer props. 78—43806
- $Pb(Zr,Ti)O_3$:Mn ceramics, anomalous dielec. losses 79—42892
- $Pb(Zr,Ti)O_3$:Nb ceramic, stress effects on ferroelec. hysteresis, macroscopic strain, US vel. 79—4778
- $Pb(Zr,Ti)O_3$:$Nb_2O_5(Sc_2O_3)$, elec. cond. investigation with and without various dopants and stoichiometry 79—11120
- $Pb(Zr,Ti)O_3$-$Pb_3Ge_5O_{11}$ ceramic, sintering conditions rel. to piezoelec., dielec. props., microstruct. 77—16252
- $Pb(Zr_{0.53},Ti_{0.47})O_3$, piezoelec. ceramic, HF filter appl. *(Korean)* 79—27472
- $PbZrO_3$ based ferroelec. ceramic, pressure-temp. phase diagrams 79—24273
- $PbZrO_3$, phase transitions, X-ray, dielec., and thermal anal. 80—45020
- $PbZrO_3$-Pb_2FeNbO_6-$PbTiO_3$, pyroelectric props. of ferroelec. rhombohedral transition 77—12336
- $PbZrO_3$-$PbCd_{0.5}W_{0.5}O_3$, phase transitions 78—43817
- 1-$xPbZrO_3$-$xPbSc_{0.5}Nb_{0.5}O_3$, $0 \leq x \leq 1$, phase transitions, X-ray, dielec., and thermal anal. 80—45020
- $Pb(ZrTi)O_3$ type piezoelectric ceramics, compressive properties 79—33612
- $Pb(Zr_{0.42}Ti_{0.58})O_3$, hot-pressed piezoelec. ceramic, effect of nonferroelectric phase 77—43936
- $PbZr_{0.95}Ti_{0.05}O_3$ ceramics, of ABO_3 type, dopant distrib. between A and B sites 79—42093
- $PbZr_{0.95}Ti_{0.05}O_3$, impact loading, mech. and elec. response, elec. state effect 78—64317
- $PbZr_{0.95}Ti_{0.05}O_3$:oxide doped, A and B site dopant distrib., antiferroelec.-ferroelectric transition 78—34532
- $Pb(Zr_{1-x}Ti_x)O_3$ ceramics, double isovalent substitution effect on piezoelectric characts. *(French)* 79—51908
- $Pb(Zr_{1-x}Ti_x)O_3$ solid solution, piezoelectric ceramic, prop. improvement by multiple substitution 80—80702
- $PbZr_{1-x}Ti_xO_3$:Nb_2O_5 ceramic, ferroelec. transitions, polarisation meas. *(French)* 80—66124
- $Pb(Zr_xTi_{1-x})O_3$, anomalous photovoltaic effect 79—19625
- $PbZr_xTi_{1-x}O_3$ ceramics, morphotropic phase boundary 80—81035
- $Pb(Zr_xTi_{1-x})O_3$, high density, sol-gel technique prep., piezoelec. props. 80—20596
- $Pb(Zr_xTi_{1-x})O_3$, meas. of Hugoniot curve with commercial manganin stress gauges 80—70362
- $Pr_2 NiO_4$, elec. props., 300 to 1000°C 78—91694
- $PrFeO_3$, elec. props., 300 to 1000°C 78—91694
- $Pr(NbO_3)_3$ form. mechanism, struct., dielec. props. 77—16235
- PrO, high press. synthesis, struct. and lattice consts. *(French)* 80—29913
- $3Pr_2O_3.2WO_3$, X-ray charact. and thermal props. 77—43194
- $Pr_2Zr_2O_7$, synthesis from carbonates 77—85974
- Pt coatings on glass, quartz, ceramic or sitall, method 77—44376
- PuN, fabrication and high-temp. thermodynamic and transport props. 77—28774
- PuO_2-UO_2 mixed oxide fuel, plutonia particle behavior during sintering in Ar-H_2 (8%) atmosphere 79—8258
- $Rb_{5-x}Ga_{11+x/5}O_{30}$, synthesis, non-stoichiometry, density and ionic cond. meas. *(French)* 78—52741
- Sc_2O_3, heat treated, elec. cond. rel. to O_2 partial press. 77—15845
- Sc_2O_3, polycrystalline, elastic props., porosity and temp. depend. 77—52384
- Sc_2O_3, solid solubility in MgO 80—15247
- Sc_2O_3-R_2O_3 (R = rare earth or Y), phases and phase transitions at high temp. *(French)* 79—100126
- Sc_2O_4, polycryst., form. conditions of anion vacancies, phase comp. 80—54220
- Si based ceramics, stepped temperature stress rupture testing 79—61804
- Si on ceramics, coating with inverted meniscus (SCIM) technique, solar cell appl. 80—89163
- Si/SiC ceramic composite, elastic moduli and bend strength meas., anisotropy 77—59838
- Si/SiC ceramic composite, room temp. props., effect of SiC content and orientation 78—27599
- Si-Al-O-N, ceramics, thermal decomposition 79—91936
- Si-Al-O-N, compression creep, comparison with SiC and Si_3N_4 79—15728
- Si-Al-O-N, high-temp. fracture and diffusional deform. mechanisms 80—40509
- β'-Si-Al-O-N, Mg-containing phases, crystn. 80—39297
- Si-Al-O-N, mullite like cpd. comp., EPMA, X-ray and chem. anal. obs. *(Japanese)* 80—35175
- Si-Al-O-N, oxidation mechanisms 80—40570
- Si-Al-O-N ceramic, grain boundary desegregation and intergranular cohesion 80—100872
- Si-Al-O-N ceramic, single-phase, prep. by hot-pressing, microstruct. investig. 77—8792
- Si-Al-O-N ceramic, single phase form. using hot pressing *(Japanese)* 79—70031
- Si-Al-O-N ceramic systems, layer struct. 80—6382
- Si-Al-O-N ceramics, elec. and therm. cond. 79—86934
- Si-Al-O-N ceramics, grain boundary segregation, combined X-ray microanal. and lattice fringe imaging determ. 79—15681
- Si-Al-O-N composites, dense direct prep. from naturally occurring SiO_2 and Al powder 78—11187

ceramics continued
Si-Al-O-N compounds, decomposition in N_2 atm. at high temp. 79—57226
Si-Al-O-N polytypes, hot-pressed, microstruct. 80—3023
Si-Al-O-N sintered ceramic, microstruct., phase composition and transformation mech., mech. props. 80—40309
Si-Al-O-N system, exam. of compounds and properties 78—48387
Si-Al-O-N system, ionic cond. from 850 to 1400°C 80—2203
Si-Al-O-N system, phase analysis and TEM struct. obs. 80—108420
Si-Al-O-N system, TEM exam. of X phase structure 78—56606
Si-Al-O-N systems, behavioural diagrams 79—24507
Si-Al(Ti)C, sintered, exam. of props. 80—25644
Si-C-Al-O-N and related systems, new materials 78—95159
Si-Na-B-O-N glass, synthesis and characterisation 80—108381
Si-O_2-N_2 system, Si_2N_2O, corrosion in O_2, sintered in the presence of magnesia *(French)* 78—23837
Si-Ti-O-N system, formation of TiN and SiO_2 80—71617
Si_5-Al-O-N_7, hot pressed, exam. of fracture mechanisms 78—72879
$Si_{(6-z)}Al_zO_zN_{(8-z)}$, sialons, hot-pressed, dielec. props. 78—10822
SiAlON ceramic, pressureless sintering 78—27449
SiAlON, oxidation 77—56130
SiAlON powder, prod. by reaction clay+C+N_2 80—40295
SiAlON, prepared from siliceous sand and Al powder, hot pressing, steatite contamination effects *(Japanese)* 80—93528
SiAlON, pressureless sintered with low amounts of sintering aid 79—66029
SiAlON system, β′, 15 R phases, oxidation resist. *(French)* 78—72899
$Si_{6-x}Al_xO_xN_{8-x}$, x=1.5, 3, 4, Sialon ceramics, elec., thermal cond. 79—33124
$Si_{6-z}Al_7O_zN_{8-z}$, β-Sialon, form. from Si_3N_4-SiO_2-AlN system *(Japanese)* 80—45261
$Si_{6-z}Al_zO_zN_{8-z}$, hot pressed, DC elec. props., 18-500°C, fields up to 1.1×10^4 V cm^{-1} 78—26860
$Si_{(6-Z)}Al_ZO_ZN_{(8-Z)}$ 78—39136
SiC and Si_3N_4, hot pressed, comparison of high-temp. thermal fatigue resistance 77—36623
SiC, ceramic, mass loss in inert gas stream *(Russian)* 79—7686
SiC, ceramic material fracture mechanics, review 80—45373
SiC, compression creep, comparison with Si_3N_4 and sialon 79—15728
SiC, corrosion in gases and alkaline melts 77—8967
SiC, corrosion resist. in residual fuel oil fired environment 79—39010
SiC, cryst. surface layers treatment and study by HF ion-plasma etching *(Russian)* 80—16517
SiC, electrode and container material in Na/S cell 80—35355
SiC, electrodeposition mech., onto metal electrodeposit, cermet prop. 79—33992
SiC, engng. ceramic, lattice resolution studies 78—27510
SiC, exam. of N solubility, in epitaxial layers 80—6520
SiC, exam. of T_2 diffusion coeffs. and D_2 solubility 78—79816
SiC, failure prediction technique derived from fracture mech. 77—7343
SiC fibre, development from organosilicon polymers by heat treatment 80—81014
SiC fibres, microcrystalline state anomalous characts. 79—74122
SiC filament reinforced phosphate foam ceramics, bending strength 80—11716
β-SiC, fluidised bed deposited coatings for nucl. fuel granules, microstructural obs. by SEM 77—14233
SiC, fracture toughness specimen, appl. of wedge indentation technique for precracking 78—85087
SiC, fuel particle, coating meas. of strength and Young's modulus, brittle ring test 77—8868
SiC, hot pressed, brittle fracture and subcritical crack growth 78—72885
SiC, hot pressing, role of grain boundaries, addition of B, B_4C and Al_2O_3 77—24999
SiC, identation plasticity and microfracture 79—70158
SiC, impact resistance, instrumented drop weight test 78—11265
SiC, instrumented Charpy impact testing 77—36719
SiC, meas. of critical stress intensity factor and subcritical crack propag. rates 78—72880
SiC, mechanical props. charact. by dynamic elastic modulus meas. up to 1400°C *(German)* 79—70101
SiC, microrelief of fracture failures *(Ukrainian)* 77—32729
SiC, monocryst., and epitaxial layer growing, temp. distrib. study in high temp. furnaces 79—65989
α-SiC monocrystalline grains, mech. props. and grain separation *(Polish)* 80—40554
SiC, nondestructive evaluation, scanning photoacoustic microscopy 80—85115
SiC, oxidation protective coating on C fibres *(Polish)* 79—52408
SiC, pellet, rise in temp. involving reaction sintering 77—12555
β-SiC, polycrystn., C^{14} self diffusion 80—2200
SiC, polycrystn., crack length and indentation dimension versus indentation load 79—70157
SiC polytypes, quantitative calcs. from X-ray diffr. peak intensities 79—82174
SiC, reaction densified, controlled surface flaw initiated fracture 77—8919
SiC, reaction sintered, microstruct. *(Japanese)* 77—1825
SiC, reaction sintered, TEM exam. of recrystallisation, phase transformation 78—80567
SiC, self-bonded, microstruct., electrical props., sintering effects 77—1822
SiC single cryst., reaction-bonded and hot pressed, hardness and wear behaviour 79—38970
SiC single crystal, friction and fracture in contact with itself and Ti 80—11780
B SiC, sintered, effect of Al trace amounts on specimen props. 79—83289
SiC, sintered, high resolution electron microscopy 79—90501
α-SiC, sintered, influence of B, C additives on microstructure, SEM exam. 79—8262
SiC, spiral growth of polytype struct. from faulted matrix, 15R and 4H struct. 77—4778
SiC, strength-grain size relation, surface finish effects 77—81333
SiC surface, H^+, D^+ and Ar^+ bombardment, 5 to 15 keV, meas. of erosion yield 78—79647
SiC, surface defect annealing, following Ar ion and electron irrad. 80—7603
SiC, tensile strength distrib. 80—40471
SiC, uncommon mode of morphological development among coherent phases, optical and electron microscope exam. 78—80544

ceramics continued
α-SiC-Al_2O_3, sintering 80—11611
SiC-Ni based superalloy reaction, at elevated temps. 80—3287
SiL, neutron damage at 1200°C, fusion reactor first-wall appl. 79—93829
Si_3N_4, and Si_3N_4-MgO, hot pressed, DC elec. props., 18-500°C, fields up to 1.1×10^4 V cm^{-1} 78—26860
Si_3N_4, biaxially stressed, exam. of localised impact damage 78—72846
Si_3N_4, CVD, struct., optical and mech. props. 77—1816
Si_3N_4, CVD, structural props., effect of deposition parameters 77—55272
Si_3N_4, CVD, Vickers microhardness, effect of deposition parameters 77—56079
Si_3N_4 capped GaAs, Ga precipitation 79—79127
Si_3N_4 ceramic, surface and subsurface struct. by photoacoustic spectroscopy 78—68481
Si_3N_4, ceramic inclusions meas. and characterisation using US 80—76474
Si_3N_4, ceramic material fracture mechanics, review 80—45373
Si_3N_4, consolidation by hot isostatic pressing 80—11605
Si_3N_4, corrosion resist. in residual fuel oil fired environment 79—39010
Si_3N_4, cracking characterisation by double torsion test *(French)* 80—104369
Si_3N_4, deposition by SiC reactive RF sputtering in N_2 79—78886
Si_3N_4, effect of Al on oxidation behaviour *(German)* 78—31587
Si_3N_4, effect of oxide impurities on physicomechanical props. 80—16396
Si_3N_4, engng. ceramic, lattice resolution studies 78—27510
Si_3N_4, evidence for cavitation crack growth, SEM study 79—79086
Si_3N_4, exam. of fracture resistance 78—76826
Si_3N_4 fabrication by rate-controlled react. sintering, nitridation react. control 79—24468
Si_3N_4, growth of α and β phases 78—95717
Si_3N_4, HS-130, dynamic mode I fracture toughness and flexural strength 77—21248
Si_3N_4, high temp. thermal fatigue, role of activation energy of slow crack growth 77—44340
Si_3N_4, high-speed rolling bearings, fatigue strength 80—93655
Si_3N_4, hot press, high resolution electron microscopy 79—90501
Si_3N_4, hot pressed, flawed plate under combined stresses, failure prediction 78—72884
Si_3N_4, hot pressed, fracture phenomenology, fracture surface energy, crack propagation 79—57090
Si_3N_4, hot pressed, high temp. compressive cracking, optical and electron microscopy exam. 78—76733
Si_3N_4, hot pressed, slow crack growth from controlled surface flaws 78—80632
β-Si_3N_4, hot-pressed, containing small amounts of Be and O in solid soln. 80—2985
Si_3N_4, hot-pressed, dielec. props. 78—10822
Si_3N_4, hot-pressed, electrical props. 78—39136
Si_3N_4, hot-pressed, impact resistance, instrumented drop weight test 78—11265
Si_3N_4, hot-pressed, thermal cond. by laser flash method 79—69302
Si_3N_4, impure, oxidation, phase equilibria 79—70045
Si_3N_4, meas. of critical stress intensity factor and subcritical crack propag. rates 78—72880
Si_3N_4, mechanical props. charact. by dynamic elastic modulus meas. up to 1400°C *(German)* 79—70101
Si_3N_4, MgO-fluxed, hot pressed, grain boundary phases 78—27464
Si_3N_4, nondestructive evaluation, scanning photoacoustic microscopy 80—85115
Si_3N_4, optimization of props. as tool material, for high fracture toughness and hot pressing prod. 79—95987
Si_3N_4, oxidation, 1300 to 1500°C 77—8966
β- Si_3N_4, oxidation 77—56130
Si_3N_4, oxidised ceramic, O_2 depth profiling using ^4He backscatt. 77—89463
Si_3N_4, phase content determ., using X-ray diffr. anal. 78—44281
α-Si_3N_4 powder, hot pressing, kinetics 77—55925
Si_3N_4, prep. by CVD, effect of raw gas flow rate *(Japanese)* 77—48348
Si_3N_4, preparation, effect of Fe and $FeSi_2$ on nitriding of Si powder 79—33985
Si_3N_4, pyrolytic, crystn. and amorphous, thermal diffusivity, thermal cond., specific heat 79—69303
Si_3N_4, reaction bonded, exam. of strength as function of nitrided density, microstruct. design 78—68731
Si_3N_4 reaction bonded, microstructure, formation, properties, phase composition 79—56947
Si_3N_4, reaction bonded, Na assisted oxidation, exam. 78—56795
Si_3N_4, reaction bonded and hot pressed. exam. of thermal shock behaviour *(German)* 78—64561
Si_3N_4, reaction bonded and hot pressed, compression creep, comparison with sialon and SiC 79—15728
Si_3N_4, reaction-bonded, hexagonal (wurtzite) form of Si 77—1112
Si_3N_4, reaction-bonded, microstructural analyses 77—8782
Si_3N_4, reaction-bonded, Na ion assisted oxidation, 800 to 1300°C 79—39011
Si_3N_4, reaction-bonded, struct., form. mechanisms and kinetics 77—4760
Si_3N_4, reaction-bonded and hot pressed, hardness and wear behaviour 79—38970
Si_3N_4, reaction-sintered, non-axial dislocs. 77—19956
Si_3N_4, room temp. fracture strength data, statistical anal. 78—64619
α-Si_3N_4 single crysts., growth, morphology, hardness and slip system 79—83112
Si_3N_4, sintering under high press., modulus of rupture tests 77—44202
Si_3N_4, sintering with Al_2O_3 and Y_2O_3 *(Japanese)* 78—19703
Si_3N_4, slip casting from aqueous suspension, reactions with HCl and NaOH 80—16259
β-Si_3N_4 solid soln., form. from SiO_2-AlN sintering 78—23655
β-Si_3N_4 solid soln. prod. by reaction sintering SiO_2-AlN mixture 80—25645
Si_3N_4, static fatigue, fitting of data to iterative trivariant analysis 78—76732
Si_3N_4, stress corrosion 77—8917
Si_3N_4, synthesis in Cl_2 system 80—40308
Si_3N_4, tensile strength distrib. 80—40471
Si_3N_4, thin sheets, reaction sintered, exam. of oxidation in damp air 78—48552
β-Si_3N_4, X-ray cryst. struct. and refinement, struct. rel. to α-Si_3N_4 79—46605
Si_3N_4, Zr-based hot pressing aids effect on oxidation resist. 77—8971

ceramics continued

- Si_3N_4:MgO, hot-pressed, linear thermal expansion rel. to MgO content 80−70430
- Si_3N_4/Zr joint, solid state bonded, exam. of bond fracture strength 78−76826
- Si_3N_4/ZrO_2, hot-pressed, compressive surface stresses developed by oxidation induced phase change 80−60992
- Si_3N_4-Al_2O_3, Sialon, pressure sintering 77−55919
- Si_3N_4-Al_2O_3-AlN, isothermal sections, free energy of formation 80−55363
- Si_3N_4-Al_2O_3-AlN, Sialon, fabrication and reaction sintering 77−44201
- Si_3N_4-Al_2O_3-SiO_2 systems, glass forming regions 80−84070
- Si_3N_4-Al_2O_3-Y_2O_3, sintered, observation of a noncrystalline phase 78−64536
- Si_3N_4-Al_2O_3(25.5, 37.0, 47.8 and 57.8 mol.%) thermal diffusivity 77−7913
- Si_3N_4-AlN-Al_2O_3-SiO_2-Y_2O_3, phase equilibrium study by X-ray diffr. and optical microscopy 80−50614
- Si_3N_4-CeO_2, surface stress development during oxidation 80−50736
- Si_3N_4-Mg_2SiO_4-Si_2N_2O, compressive creep, composition effect 80−50674
- Si_3N_4-MgO, compressive creep, source of viscoelastic effect 80−50675
- Si_3N_4-MgO, compressive creep, oxidation induced compositional change 80−50676
- Si_3N_4-MgO, hot pressed, oxidation kinetics 79−29243
- Si_3N_4-MgO, hot pressing and α-β phase transform. 78−27461
- Si_3N_4-MgO (2-5 wt.%) hot pressed, tensile creep testing 80−40423
- Si_3N_4-SiC-Y_2O_3 (La_2O_3)(Ce_2O_3)(Eu_2O_3)(Gd_2O_3), reactively sintered, microstruct. and strength 80−25631
- Si_3N_4-SiO_2-AlN mixture, reaction sintering forming β-Si_3N_4 solid soln. 79−52145
- Si_3N_4-SiO_2-MgO, phase relations and interrelation with mech. strength, and oxidation 78−48386
- Si_3N_4-SiO_2-Y_2O_2, subsolidus phase relations 80−60845
- Si_3N_4-SiO_2-ZrN-ZrO_2, X-ray diffr. phase anal. and reactions $Si_3N_4+ZrO_2$, SiO_2+ZrN 80−50613
- Si_3N_4-Y_2O_3 (8.0 wt.%), hot pressed, mech. props. 79−70134
- Si_3N_4-Y_2O_3 ceramic, thermal degradation, C impurity effect 80−50708
- Si_3N_4-Y_2O_3(CeO_2), hot pressed, sintered, microstruct., flexural strength and fractographic anal. 80−40293
- Si_3N_4-Y_2O_4-Al_2O_3 (4-17, 4 wt.%), sintering 80−81009
- Si_3N_4-ZrO_2, tetragonal to monoclinic transform. of ZrO_2 particles *(German)* 79−43240
- α,β-Si_3N_4+C, powders, high temp. reactions *(Japanese)* 77−48685
- Si_3N_4+MgO, hot pressing and effects 77−63614
- Si_3N_4+MgO, reaction during hot pressing 78−68658
- Si_3N_4AlN-Al_2O_3 system, reaction sintering forming β-Si_3N_4 solid solns. 80−50585
- Si_2N_2O, emissivity determ. by IR thermography 77−59130
- Si_2N_2O, fast neutron irradiation, variation of lattice parameters 80−24504
- Si_2N_2O, sintered with MgO or BeO additives, effect on oxidation *(French)* 79−20233
- Si_2N_2O, thermal decomp. 80−81311
- Si_2N_2O-Al_2O_3, solid soln., prep., effect of Si_3N_4 powder reactivity 80−45256
- $Si_3N_4.Y_2O_3$ prepared by hot press, cryst. struct. 80−10534
- $Si_3N_4.15Y_2O_3$, sintering under high N_2 pressure 80−29907
- SiO_2, crack propag. and bifurcation 78−72888
- SiO_2 films, microporous, sintering effects, IR ATR, transmission investigs. 79−66031
- SiO_2, fused, fibres, lifetime predictions, applicability of crack velocity date 77−52467
- SiO_2, fused, refractive index dispersion, thermal history depend. 80−25331
- SiO_2, fused, surface crystn. by Li^+ ion implantation and annealing 80−89383
- SiO_2 gel, $SiO_2Al_2O_3$, SiO_2MgO, pore structure influence on X-ray intensity in EPMA *(Japanese)* 80−26046
- SiO_2, microprobe state anal. by X-ray OK and BK emission band spectra *(Japanese)* 78−19606
- SiO_2, molten, struct., X-ray radial distrib. anal. 78−67651
- SiO_2, molten, viscosity, 2300 to 2600K 79−37863
- SiO_2 nonporous film, plasma deposition method, appl. to semicond. device manufacture *(Russian)* 80−16197
- SiO_2 particles, movement and heating in air plasma jet *(Russian)* 80−7522
- SiO_2 phase equilibrium and microstructure interpretation 80−60847
- SiO_2 reduction, with C and SiC, forming SiO vap. 79−79240
- SiO_2, sitall coating, control of phase composition, microstruct. and props. 77−32545
- SiO_2, solid solubility in MgO 80−15247
- SiO_2, surface reactivity modification by Ar/O_2 plasma treatment 78−64890
- SiO_2, tensile and compressive strengths of fine powder bed *(Japanese)* 80−25780
- SiO_2, transfer in quartz capsule 79−4902
- SiO_2, vaporisation in steam atmosphere 80−44306
- SiO_2, vitreous, strengthening by coating application 77−32636
- $SiO_2:Al_2O_3$, ultrafine and ultrapure powder prep., SEM study 79−70025
- SiO_2-Al_2O_3, calculated thermodynamic data and metastable immiscibility 78−27495
- SiO_2-Al_2O_3, minerals, phase equilibrium *(German)* 77−73261
- SiO_2-Al_2O_3, mullite, sintering behaviour and microstruct. 80−20876
- SiO_2-Al_2O_3, sintering theoretical treatments and exp. procedure 78−44067
- SiO_2-Al_2O_3 (36.6 wt.%) plasma prep. powder, metastable immiscibility and microstruct. during sintering 80−35143
- SiO_2-Al_2O_3 (8 mol.%) glass, heat treated, devitrified phases 80−66469
- SiO_2-Al_2O_3 melts, densities 79−99259
- SiO_2-Al_2O_3 mixture, depend. of phase comp. on nuclei available 79−11584
- SiO_2-Al_2O_3-CaO-MgO-NaO-K_2O-B_2O_3-ZrO_2, glaze, exam. of zircon crystallisation 79−19155
- SiO_2-Al_2O_3-CaO-MgO-Fe_2O_3 glass ceramic crystn., microstructures rel. to conditions 80−11638
- SiO_2-Al_2O_3-CaO-MgO-B_2O_3, E-glass, acid resist. studies 80−60991
- SiO_2-Al_2O_3-Fe_2O_3-CaO, basalt glass ceramics, crystallite form. due to heat treatment 80−38917
- SiO_2-Al_2O_3-K_2O glass ceramic interaction with Pb borosilicate glaze 80−84398

ceramics continued

- SiO_2-Al_2O_3-Li_2O glass ceramic, crystn., microstructures rel. to conditions 80−11638
- SiO_2-Al_2O_3-Na_2O-BaO-TiO_2, glass ceramic interaction with Pb borosilicate glaze 80−84398
- SiO_2-Al_2O_3-R_2O_3-MgO-TiO_2, T=rare earth of Ce group, glass-ceramic permittivity comp. depend. 77−43928
- SiO_2-Al_2O_3-Si_3N_4, isothermal sections, free energy of formation 80−55363
- SiO_2-AlN mixture sintering, form. of β-Si_3N_4 solid solns. 78−23655
- SiO_2-$Al(OH)_3$, derived from metalalkoxides, sintering behaviour 79−29005
- SiO_2-Li_2O-K_2O-ZnO-P_2O_5, glass ceramic, phase changes and crystn. processes 80−7562
- SiO_2-Li_2O-K_2O-ZnO glass ceramic, prep., phase transformations and physical props. 80−45299
- SiO_2-MgO porous catalysts, EPMA quantitative anal., new correction calc. method, modified ZAF method *(Japanese)* 80−93822
- β-SiO_2-MgO reaction, diffusion controlled 78−6882
- SiO_2-MgO-BaO, steatite, glass-ceramics technology appl. 80−104097
- SiO_2-Na_2CO_3, sodium Erevanit-25, sintering, struct. 79−43284
- SiO_2-RO-Na_2O-Li_2O (RO=MgO, CaO, SrO) glass-ceramic coating, optimisation of props. by selective oxide action 80−55552
- SiO_2-TiO_2-Al_2O_3-SrO(BaO), glasses, ceramic form. rel. to Al_2O_3 content 77−25005
- SiO_2-ZnO-Na_2O-Li_2O, glass-ceramic coating, optimisation of props. by selective oxide action 80−55552
- Si_2ON_2 needle crystals, growth by nitridation of Si-SiO_2 powder compacts *(Japanese)* 79−56921
- Si_2ON_2, thermal diffusivity meas. by flash with negative pulse, plasma jet heating 79−37888
- Si_2ON_2-Y_2O_3-Al_2O_3 phase relations at 1400°C *(Japanese)* 79−38811
- Si_3ON_2 needle crystal growth by nitriding Si-SiO_2 system in powder compacts *(Japanese)* 78−68609
- $Sm_2Zr_2O_7$ pyrochlore phase, O ion conduction 80−24654
- SnO_2, activated sintering, mechanism and kinetics, additives role 79−38771
- SnO_2 based ceramics, sintering qualities 79−61547
- SnO_2 powders, specific area, granulation and sintering *(Polish)* 79−52146
- SnO_2-NiO(ZnO)(Nb_2O_5), activated sintering mechanism 80−60810
- SnO_2-VO_x-PdO, switching and oscill. phenomena 78−6417
- $Sr_2Al_2GeO_7$, gehlenite struct., synthesis and physicochem. props. 79−43181
- $SrBaNaNb_5O_{12}$, X-ray powder diffraction data determ. *(Chinese)* 80−70170
- $Sr_{0.5}Ba_{0.5}Nb_2O_6$:Fe(Mn)(Cr)(La), ceramic, additive effects on ferroelec. and pyroelec. props. 77−16256
- $Sr_{0.75}Ba_{0.25}Nb_2O_6$, ceramic ageing dielec. props. 80−88940
- $SrCoO_3$, conducting oxide prod. by amorphous citrate process 79−95985
- SrF_2, press-forged laser window, polishing, cleaning and grinding 79−59849
- $SrFe_{12}O_{19}$ ceramic compact, sublattice magnetisation and textures 78−68426
- $SrFe_{12}O_{19}$, exam. of factors affecting reaction kinetics, thermal analysis *(German)* 79−24471
- $SrFe_{12}O_{19}$, ferrite, powder effect of SiO_2 during sintering, exam. of grain growth and phase diagram *(German)* 79−24473
- $SrFe_{12}O_{19}$, prep. by fluidized bed technique, ceramic and magnetic props. 79−43445
- $SrFe_{12}O_{19}$:Si, Sr, second phase effect on elec. and mag. props. 80−60986
- $Sr_2KNb_5O_{15}$, Raman scatt. experiments in tetragonal tungsten bronze compounds 80−40113
- $Sr_2Mg(Co)(Zn)(Mn)(Cd)(Ca)(Sr)TeO_6$, optical SHG study of acentricity, ferroelec. of low temp. phases 80−71324
- $SrMnO_{3-x}$, O-deficiency induced polymorphs and elec. cond. 80−71643
- $Sr_x(Na_{0.5}Bi_{0.5})_{1-x}TiO_3$ ferroelec. ceramic, hot pressing, numerical simulation *(French)* 80−76220
- $Sr_2NaNb_5O_{15}$, Raman scatt. experiments in tetragonal tungsten bronze compounds 80−40113
- $Sr_{2.05}Na_{0.90}Nb_5O_{15}$, X-ray powder diffraction data determ. *(Chinese)* 80−70170
- SrO-SiO_2-Fe_2O_3, permanent mag. ceramics, exam. of phase diagram, using X-ray analysis, optical microscopy, electron probe anal., and thermal analysis *(German)* 79−29012
- SrO_2-Al_2O_3-SiO_2 fusion cast ceramics, crystn., microstructures rel. to conditions 80−11638
- $SrO.6Fe_2O_3$, ultrafine, microstruct. development during sintering, mag. props. 79−70022
- $SrO.nFe_2O_3$ isotropic ferrite magnets, manuf. process and mag. props. *(Japanese)* 80−29915
- $Sr_{1-x}Pb_xTeO_3$, ferroelec. soln., prep. at room temp. *(French)* 79−43190
- $Sr_7Sb_2O_{12}$, prep. and cryst. struct. *(French)* 79−32967
- $Sr_3SiAl_{10}O_{20}$, Ce^{3+} activated, X-ray diffr. and luminesc. props. 80−49199
- $SrSnO_3$ and $SrZrO_3$, high-density ceramics prep. and elec. props. 80−60812
- $Sr_6Ti_2Nb_4O_{20}$, new class of layer ferroelectrics. X-ray anal. and permittivity meas. 77−16266
- $SrTiO_3$ ceramic, electrocaloric effects for refrigeration at cryogenic temp. 80−77789
- $SrTiO_3$, for electrocaloric refrigeration, 4 to 15K 79−80624
- $SrTiO_3$ glass ceramics, polarisation and dielec. const., 4-77K 77−32319
- $SrTiO_3$, Mossbauer spectroscopy, sample prep. and results 80−66078
- $SrTiO_3$, prep. from film forming soln. 80−60811
- $SrTiO_3$, sintering kinetics rel. to added SrF_2, ZrO_2 78−44037
- $SrTiO_3$, Sr_2TiO_4, $Sr_3Ti_2O_7$, prep. from coprecipitates of Sr and Ti 77−48374
- $SrTiO_3$-$Bi_2Ti_2O_7$-$CaTiO_3$ system, solid solns., elec., optical props. 79−11375
- Sr_2TiO_4-Eu_2O_3, synthesis, luminesc. of materials 79−11534
- $SrZrO_3$ ceramic, high-temp. corrosion resist. *(Polish)* 79−52409
- Sr_2ZrO_3, resist. to corrosion by Al_2O_3, CaO, MgO, SiO_2, K_2CO_3 and coal ash 80−16516
- (Th,U)O_2, thermal conductivity model for temps. to melting 79−93732
- Th ceramic recycle fuels, metal-clad, fabrication technology 79−59244
- ThO_2 ceramics, CaO and Y_2O_3 stabilised density, elec. cond., permittivity 78−47838
- ThO_2 single crystals, crystal growth, using crucibleless skull melting technique 78−39681

ceramics continued
ThO_2, thermally stimulated depolarisation currents, grain size and growth determ. 79−65792
ThO_2/Ni, adhesive energy, meas. techniques 80−50803
$ThO_2/Ni-Cr$, adhesive energy, meas. techniques 80−50803
ThO_2-based ceramic impurity diffusion, electrotransport method 78−67869
$Ti-Si_3N_4$ system, reactions under heating and plasma conditions 79−95988
TiB_2, hardness of sintered material 78−60636
$TiB_2-Al_2O_3$, thermal stability of composite materials 78−60638
$TiB_2-Al_2O_3$ system-based composites 77−85979
TiB_2-CaO, thermal stability of composite materials 78−60638
TiB_2-MgO, thermal stability of composite materials 78−60638
$TiB_2-Y_2O_3$, thermal stability of composite materials 78−60638
TiC, high temp. thermal cond., ambipolar diffusion contrib. 78−26742
TiC, ion plating and applics. *(Japanese)* 77−63565
TiC, mag. suscept. rel. to temp. in homogeneity region 78−34953
TiC single crystal, vapour deposited on Mo and W wires, electron microscope study 77−1795
TiC, ultrafine powder prep. by plasma jet *(Japanese)* 77−52273
TiN, powder, plasma-chem. and self-propag. high-temp. thermoplastic slips, synthesis 80−25633
TiN, ultra-fine powder prep. by reaction in N_2 plasma jet *(Japanese)* 78−72757
TiN-AlN composites, struct. and props. 77−40413
TiN_2, ultrafine synthesis in RF plasma, X-ray diffr. chem. and electron microscopy anal. 79−70026
Ti_xN_y, synthesis by nitriding Ti and TiH_2 77−44200
TiN_zO_y, cubic, concentration dependence of the degree of filling of unit cell 78−44063
TiN_zO_y, cubic, thermal expansion coeffs., Ti-Ti bond screening 79−10970
$TiO-ZrO_2$, pseudo binary system, effect of Ti addition on struct. and props. of zirconia 79−11583
TiO_2 amorphous film, alkali resistance, refractive index, IR spectra *(Japanese)* 78−23546
TiO_2 based ceramic dielec. materials, medium permittivity, elect. charact. 78−35086
TiO_2 based ceramics, variation of dielectric constant and resistivity with temp. 80−2683
TiO_2 based construction ceramics, fibre-like cryst. reinforced, mech. props. 80−55341
TiO_2 brookite synthesis from Ti in NaF or Ti compounds, form. mechanism *(Japanese)* 80−93529
TiO_2 polymorphs, transform. enthalpy 79−100131
TiO_2, porosity-permittivity relations, depolarising factors determ. and pore effects *(Japanese)* 80−97189
TiO_2, rutile, ageing in strong electric field TiO_2 *(Polish)* 78−52869
TiO_2, rutile, ferroelectric ceramic, dielec., piezoelec. and elastic props., orientational contrib. 78−68468
TiO_2, rutile, mass transport mech. determ. by sinusoidal profile decay method 78−6178
TiO_2, rutile ceramics, space charge effects 80−24945
TiO_2, sintered ceramic, props. rel. to additives, impurities 78−35329
TiO_2, sintering, hardness, density, elec. cond. and colour *(Japanese)* 78−68659
TiO_2, sintering, struct., pressing, atm., and doping effects 80−20873
$TiO_2:Nb_2O_5$, preparation method, effect on semiconductive props. and sintering temp. 77−16527
TiO_2-based ceramics, impurity atoms chem. state, Mossbauer spectra 80−15902
TiO_2-containing slag-glasses, phase separation and glass-ceramic formation 78−51424
TiO_2-SiO_2 fibre, prep. from metal alcoholates, prep. of spinnable soln. *(Japanese)* 78−44071
TiO_2-SiO_2 powders, anatase-rutile transition, mechanism investigation *(Japanese)* 78−95746
TiO_2-ZrO_2, submicron powders, vapour phase production from $TiCl_4-ZrCl_4-O_2$ system 80−40301
Ti_2O_3, new synthesis method *(French)* 79−100095
$TiO_2(-Cr_2O_3)$, rutile, Cr_2O_3 effects on O_2 tracer diffusivity, depth profile meas. by SIMS 80−24651
$TlNbO_3$, ceramics, hysteresis loops and dielec. props. 79−42885
$TlTaO_3$, ceramics, hysteresis loops and dielec. props. 79−42885
$Tl_{5-x}Ta_{11+x/5}O_{30}$, synthesis, non-stoichiometry, density and ionic cond. meas. *(French)* 78−52741
$Tl_2Ti_4O_9$ ceramics, hysteresis loops and dielec. props. 79−42885
Tm_2O_3, polycrystalline, elastic props., porosity depend. 77−52384
(U, Pu)C, ceramic fuel, plastic deform. behaviour at stress changes 80−35261
(U,Pu)C, fracture and crack healing, SEM study 79−79080
$(U,Pu)O_2$, microsphere fabrication, hydrolysis process 77−23204
$(U,Pu)O_{2-x}$, mixed oxide fuel, final stage densification 79−49681
$(U,Th)O_2$, γ-active pellet fuels fabrication, conceptual design of remotely operated plant 80−32340
UAsSb, prep. and struct. 77−68951
UC FBR fuel fabrication by reaction sintering of UO_2 and UC_2 80−812
UC-(PuC), ceramic fission reactor fuels, fabrication and performance, review 78−58392
UCr_2O_6, hydrothermal cryst. growth, 40 kbar, 873K, cryst. struct. *(French)* 78−35342
UFe_2O_6, hydrothermal cryst. growth, 40 kbar, 873K, cryst. struct. *(French)* 78−35342
$UMnNiO_6$, hydrothermal cryst. growth, 40 kbar, 873K, cryst. struct. *(French)* 78−35342
UMn_2O_6, hydrothermal cryst. growth, 40 kbar, 873K, cryst. struct. *(French)* 78−35342
UN microspheres, prep., effect of process variables 78−8956
UN-(PuN), ceramic fission reactor fuels, fabrication and performance, review 78−58392
UO_2 ceramic fuel fabrication, simulation of thermal processes by emanation thermal anal. 80−811
UO_2 compact, density distrib. determ. using autoradioagraphy 77−25234
UO_2, crystn., specific heat anomaly 80−84299
UO_2, fine grained, low-stress creep study, metallographic obs. 79−43312
UO_2 fuel, density, thermal conductivity, specific heat, thermal diffusivity, flash method 77−55362
UO_2 fuel elements cores, electrically conducting inclusions detection, using eddy current flaw detector 77−90560
UO_2 fuel fabrication by the AUC powder process 80−13744

ceramics continued
UO_2 fuel pellet, bending strength, fabrication and microstruct. effect 80−2986
UO_2, grain boundary diffusion, sintering and creep correlation, reinterpretation of creep mechanism 79−66111
UO_2, in reactor densification 78−21648
UO_2, microwave heating in nuclear fuel preparation 80−37556
UO_2, modified Ashby's computer method for constructing sintering diagrams 79−43165
UO_2, non-stoichiometric, oxidation reactions and dopants 79−42087
UO_2 pellets, sinterability, particle size effect 80−104098
UO_2 pellets, thermal densification *(Korean)* 78−44065
UO_2 powder, precompaction effect on compressibility 78−41846
UO_2 powder, temp. depend. of atomic thermal displacements, Rietveld profile-refinement procedure 80−49190
UO_2 powder compaction, friction between particles and die walls 80−71620
UO_2 powders, sintering characterisation 79−43189
UO_2, sintered, production by gel calcination and drying, thermal anal. *(Czech)* 80−45260
UO_2, sintered pellets, relationship between intercept length and grain diameter 78−52743
UO_2 sintering, thermal anal., hexavalent uranium xerogel drying, thermal treatment modelling *(Czech)* 79−36378
UO_2, sintering, use of NH_3, grain size changes 77−55920
UO_2 spectral emissivity meas. up to 3800K 80−24625
UO_2, stoichiometric, sintering diagram *(Rumanian)* 79−87602
UO_2 waste material, dry recovery 79−63787
$UO_2:Nb_2O_5$, additions on elec. cond. 80−49712
$UO_2-(PuO_2)(BeO)$, ceramic fission reactor fuels, fabrication and performance, review 78−58392
UO_2-PuO_2, ceramic fuel, plastic deform. behaviour at stress changes 80−35261
UO_2-PuO_2 fuel pin, hyperstoichiometric, post irradiation examination 80−63258
UO_2-PuO_2 powder compacts, homogenization kinetics study by X-ray diffr. technique 79−37883
UO_2-UC_2-C microspheres, carbothermic prep., rate-controlling preps. 80−45257
$UO_2+Nd_2O_3$, sintering, initial stage kinetics, diffusion coeff. 80−2987
UO_{2+x}, ternary sintering diagram, grain boundary diffusion 79−59234
$UO_{2\pm x}$, model of response of fission gas bubbles to dynamic behaviour of point defects 79−37735
UO_3, microwave heating in nuclear fuel preparation 80−37556
U_3O_8, microwave heating in nuclear fuel preparation 80−37556
U_3O_8, supported fission foils for laser excitation, preparation method 77−68218
$UO_2(-Nb_2O_3)$, kinetics of initial state of sintering stoichiometric and nonstoichiometric oxide 79−91609
VC, damage sustained during neutron irradiation 77−1841
$V_2O_5-Cr_2O_3$, phase diagram 77−70040
$V_2O_5-In(Tl)_2O_3$, ceramic, elec. resist., dielec. props., porosity 77−8093
W, metal-ceramic, mech. props. and structural nonuniformity 79−15705
WO_2, struct. refinement by powder neutron diffr., profile anal. 79−99139
WO_3, ceramic, Raman spectra, 80-300K, inhibited ferroelectric phase transition 77−32378
$W(ZrO_2.La_2O_3)$, structural changes during reduction and sintering 80−25636
Y-Si-Al-O-N ceramic, phase assemblages, relationships with props. 80−60848
YAG, production of densely sintered ceramic, exam. of recrystallisation during sintering 80−11609
YAG single crystal growth by flux method *(Japanese)* 78−19655
$YAlO_3$, with perovskite structure comparative assessment of methods of prep. 79−95980
$YCrO_3-MgCr_2O_4$ sintered ceramics, elec. cond. 80−24927
YIG, transient flash effect on peremability 78−27024
Y_2O_3 binder, sintering 79−24469
Y_2O_3 ceramic, elec. resistance rel. to density 79−82594
Y_2O_3, ceramic structs., thin-walled fabrication, plasma spraying technique 79−33978
Y_2O_3, effect of roasting temp. of $Y_2(C_2O_4)_3$ on crushing, compressibility, sintering props. 77−8790
Y_2O_3, grain size depend. of fracture energy, SEM study 79−34130
Y_2O_3, high temp. sintering *(Japanese)* 77−55928
Y_2O_3, hot cast ceramic, prod., used as dielectric 78−11181
Y_2O_3 hydroxy salt binder phase form., X-ray, thermal anal. obs. 79−28999
Y_2O_3, polycrystalline, high temp. O ion bombard., TEM microstruct. investig. 77−27923
Y_2O_3 powder, active, sintering 80−20870
Y_2O_3, prep. of transparent ceramic, exam. of light transmission preps. 79−20013
Y_2O_3 sintered bodies, thermal cond. and diffusivity *(Japanese)* 79−55944
Y_2O_3 sintered body, blackness study thermoluminescence anal. *(Japanese)* 78−23541
Y_2O_3 sintered body, luminous pipe of high press. Na discharge lamp, corrosion resistivity *(Japanese)* 78−19915
Y_2O_3 sintered-ceramic separator plate development, LiAl/LiCl-KCl/FeS battery applications 80−61321
Y_2O_3, strength under mech. and thermal actions 80−97554
Y_2O_3, strength-controlling fracture energy depend. on flaw-size to grain-size ratio 80−81152
Y_2O_3, translucent ceramic, prep. effect on struct. and props. 79−87601
Y_2O_3 transparent ceramic, transmittance, grain size and dopant effects *(Japanese)* 80−19083
Y_2O_3, U, C interactions, thermal anal. 78−85154
$Y_2O_3:ThO_2$, IR absorpt., 2-4 μm 77−55805
Y_2O_3-AlN, creep 77−21235
$Y_2O_3-HfO_2(ZrO_2)$ systems, solid soln. form. mechanisms 79−11579
$Y_2O_3-Mn_2O_3$, solid-phase reactions 77−48405
$Y_2O_3-Nb_2O_5$, solid state reactions, 1275 to 1350°C, electron microscopy, EPMA, X-ray diffr., dilometry *(Japanese)* 78−63883
$Y_2O_3-Sc_2O_3$ fused powders, production of ceramics of good thermal strength 77−63607
$Y_2O_3-TiB_2$, ceramic, production by sintering in vacuo, or hot moulding at 1500°C 78−60629
$Y_x(Si,Al)_{12}(O,N)_{16}$, α'-Sialon ceramics, prep. and characterisation 78−84750

ceramics continued
$Y_3Si_2O_8Cl$; Ce phosphor, prep. and luminescence props. 78–52740
$Y_2(V_{4/3}W_{2/3})O_7$ pyrochlore, synthesis and elec. props. 80–29914
Yb_2O_3-based ceramic, preparation, mech. props. 77–24998
$Zn_{30}Cd_{70}S$ ceramic, electroluminesc., stationary thermostimulated cond. 79–87120
$(Zn_{0.2}Co_{0.8}(Ni_{0.8}))O.Al_2O_3$, ZnO evaporation in vac. 80–59640
$ZnFe_2O_4$, duplex struct. formation during sintering, grain growth study 79–11541
$ZnFe_2O_4$-Fe_3O_4 solid solns., form. of α-Fe_2O_3 during oxidation 80–25889
ZnMn ferrites, prepared by wet chemical and ceramic methods, comparison of struct. and mag. props. *(German)* 79–24470
ZnO, adsorpt. of H_2O vapour, annealing and grinding effects 78–68656
ZnO based varistors, evolution and role of chem. constituents rel. to prep. method, influence on elec. props. *(French)* 78–31367
ZnO ceramic, nonohmic, drift phenomena of capacitance and current 80–39587
ZnO, ceramic, nonohmic props. 77–85229
ZnO ceramic, with additives, nonohmic thermally stimulated current meas. 77–20325
ZnO ceramic containing rare earth metal oxides and Co_3O_4, non-ohmic props. 77–76833
ZnO, ceramic varistor, physical props. of elec. barriers by AES and electron microscopy 77–20326
ZnO ceramic varistors, I-V characts., single grain junction meas. 79–15225
ZnO ceramic varistors, trapping by localized states, effect on dielec. and elec. props. *(Russian)* 79–28671
ZnO ceramics, heat treatment effect on cryst. phases, microstruct. and elec. props. 79–100268
ZnO ceramics, non-Ohmic, cond. mech. 78–68034
ZnO ceramics, non-Ohmic transient cond. phenomena, current-voltage overshoots 79–91057
ZnO ceramics, nonohmic, cryst. phases 78–26530
ZnO, doped, dielec. losses 77–81049
ZnO, fully dense, grain growth 80–93526
ZnO, ground powder, X-ray Fourier anal. *(Japanese)* 78–39727
ZnO, microstructural evaluation 79–55750
ZnO non-ohmic ceramic, degradation props. under AC and DC bias 80–80262
ZnO, nonhomic ceramic, current oscillation phenomena 79–69515
ZnO, nonohmic ceramic, current creep 79–69514
ZnO nonohmic ceramic, formation mechanism 80–60813
ZnO, powder, sintering, surface area reduction, exam. 78–44039
ZnO powders, direct meas. of intrinsic cond., using emulsion 79–99595
ZnO, sintered, impurity ion effects on crystalline state *(Japanese)* 77–28768
ZnO sintered electrode, for dye-sensitive solar photocell 80–16816
ZnO varistor ceramics, current-voltage characts., inhomogeneities and single barriers 80–80273
ZnO, wurtzite structure, hydrothermally grown exam. of thermal expansion coefficient 78–75854
$ZnO:{}^{31}P^+$ implanted nonlinear resistor production and characteristics *(Russian)* 80–49252
ZnO:Bi, Sb, Co, second phase effect on elec. and mag. props. 80–60986
ZnO/Al_2O_3, microstratified mixing of suspensions, viscosity dependence 79–70023
ZnO-Al_2O_3-SiO_2, transparent glass-ceramics, EPR obs. of glass crystallisation 78–80507
ZnO-Al_2O_3-SiO2, transparent glass ceramics, heat treatment effect on microstruct. 78–56667
ZnO-$Al_2O_3SiO_2$, transparent glass-ceramic, microstruct., physical props., crystallisation ht. treatment depend. 78–80506
ZnO-B_2O_3-SiO_2 glass-ceramic-cement composites, review 79–38783
ZnO-based ceramic microstructure and nonlinear props., B diffusion effects *(Russian)* 80–49423
ZnO-based ceramic varistors, current-voltage characts., leakage and breakdown regions, 100 to 1300°C 79–56231
ZnO-based nonohmic ceramic, dielec. dispersion and equiv. circuit 77–73110
ZnO-Bi_2O_3, ceramic semiconductor, injection currents 79–11141
ZnO-Bi_2O_3 varistor, grain boundary segregation, STEM study 79–78980
ZnO-Bi_2O_3-CoO-MnO-Sb_2O_3 (97.5, 0.5, 0.5, 1.0 mole%), exam. of elec. props. at different annealing temps. 80–3099
ZnO-Bi_2O_3-Sb_2O_3-Co_2O_3-MnO_2-Cr_2O_3, nonohmic ceramic, microstruct. exam. 78–47292
ZnO-CoO_4 (Fe_2O_3), ceramics, impurity at. states, elec. cond. 79–11130
ZnO-$NiO:Li_2O$ n-p heterojunction, contact resist., effects of water vapour 80–34506
ZnO-PbO-B_2O_3, exam. of glass formation and its props. 79–8283
ZnO-SnO_2-M_xO_y, M_xO_y = glass-forming additive, I-V characts., heat treatment effects 77–43595
ZnO-TiO_2 system, heat treated, X-ray anal. of phase form. sequence 79–1850
ZnSSe:Cu, Br, SCL currents and electrolum. via rad. recomb. 77–44065
$ZnS_{1-x}Se_x$:Cu,Br ceramic, current oscills. and electrolum. under high elec. fields 79–38677
ZnSe, commercial feasibility for optical ceramic manufacture 79–87598
ZnSe:Cu, I, electroluminescent ceramic, electric field induced switching effect under illum. 77–1460
ZnSe:Cu, I ceramic, injection electroluminesc. of p-n microjunctions 80–40163
Zr-Al_2O_3 couple, diffusion welding, 1000 to 1300°C *(German)* 79–28155
ZrB_2, oxidation in O_2 atmosphere, exam. 80–11814
ZrC, brittle mat. discs, ultimate thermal stresses 77–4210
ZrC coating on refractory metal fibre, diffusion barrier, deposition 77–4759
ZrC, factors affecting CVD 77–8760
ZrC, fracture by laser beams, macrocrack propag. 79–15789
ZrC, NbC-ZrC, right-through sat. prep., strength and plasticity, temp. depend. 77–40432
ZrC, solubility, diffusion and permeation of Cs 78–51684
ZrF_4 based glass, elec. and dielec. props. in freq. and temp. ranges 5-500 kHz and 130-280°C *(French)* 79–23772
ZrN, physicomechanical props. with the homogeneity range 77–1848
ZrN-Al_2O_3, effect of N on sintering 79–33991
ZrN-AlN composites, struct. and props. 77–40413
ZrO corrosion layer, specimen preparation for TEM by ion beam thinning *(German, English)* 80–11861

ceramics continued
ZrO_2 amorphous film, alkali resistance, refractive index, IR spectra *(Japanese)* 78–23546
ZrO_2, CaO stabilized, O_2 permeability at low O_2 partial press. 79–47980
ZrO_2 ceramic, dense nonstabilized, fabrication by hydrothermal reaction sintering 80–97451
ZrO_2 ceramics, microstruct. and props., monoclinic to tetragonal transition 80–3035
ZrO_2, containing metastable tetragonal phase, stress induced phase transform. effect on props. 78–68683
ZrO_2, crystallisation from $Zr(OH)_4$, effect of water vapour, heat treatment and grain size *(Japanese)* 79–19170
ZrO_2, cubic, nitride stabilised 78–92223
ZrO_2, electrode fabrication for MHD generator by plasma deposition 77–39474
ZrO_2 electrolyte cells, sintering 79–24476
ZrO_2 electrolyte cells, elec. props. 79–24477
ZrO_2 foils, production for TEM 79–74087
ZrO_2, hydrous particles, crystal texture *(Japanese)* 77–25002
ZrO_2, isoelec. points, effect of pH on electrophoretic mobility 80–35548
ZrO_2, metastable, tetragonal, erosive damage depth, martensitic transform. effect 79–61738
ZrO_2, metastable, tetragonal, strengthening by surface grinding 80–71777
ZrO_2, MgO partially stabilized, microstruct. development during ageing 79–91710
ZrO_2 microsphere stabilised ceramic, fracture characts., thermal stability *(Russian)* 80–76335
ZrO_2, near-surface phase transforms., effect of grinding and polishing 78–15557
ZrO_2, obtained by coprecipitation with different oxides, props. 78–64514
ZrO_2, partially stabilised, toughening mechanism 77–56084
ZrO_2, partially stabilised, high temp. effect on strength *(German)* 79–43316
ZrO_2, partially stabilised ceramics, strengthening, post-sintering heat treatment 80–97518
ZrO_2, partially stabilized, precipitation hardening effect on fracture mode 77–90353
ZrO_2, partially stabilized, precipitation effects on fracture mode 77–90354
ZrO_2, partially stabilized, transform. toughened, fracture toughness 79–91775
ZrO_2, partially stabilized, processing defects 80–97558
ZrO_2 particles, influence of ionic treatment on formation of Al coatings *(Russian)* 80–50552
ZrO_2 particles in ceramics, grinding induced tempering 80–89260
ZrO_2, plasma sprayed coatings, elec. cond. and gas permeability 79–82478
ZrO_2, porous, sintered stabilised microspheres, strength and fracture studies 80–85019
ZrO_2, powder, preparation technique for highly sinterable powder 78–39714
ZrO_2 powders, vapour phase reaction production 78–68660
ZrO_2, produced by coprecipitation with stabiliser, sintering 77–66614
ZrO_2 products from granules, props., prep. method effect 80–25628
ZrO_2, Raman spectra, temp. depend. 78–6668
ZrO_2 shock wave treatment of powders *(Russian)* 77–44186
ZrO_2, sintering of granular masses, stabilized with CaO and Y_2O_3 78–44064
ZrO_2, sintering response with const. rate of heating, depend. on processing related pore distrib. 79–28992
ZrO_2, solid solubility in MgO 80–15247
ZrO_2, spray dried agglomerates, compaction response, fracture, deform. 79–43172
ZrO_2, stabilised, coating for turbine components, degradation due to internal stresses 79–24671
ZrO_2, stabilised, fabrication by hot petroleum drying method, X-ray diffr. and thermal anal. study 80–40297
ZrO_2, stabilised microspheres, sintered, temp. depend. of strength, 20 to 1700°C *(Russian)* 78–23766
ZrO_2, stabilised voltage-current-time charact. with point contact Pt electrode in Ar gas ambient 77–1461
ZrO_2 stabilised with Y_2O_3, ultrafine grained, fabrication and flexural strength 77–1829
ZrO_2, stabilised with Y_2O_3 synthesis and eval. for H_2 prod. 77–85976
ZrO_2, stabilized, thermal barrier coating system, spectral emission and absorpt., 300 to 1590K 79–24672
ZrO_2, stabilized by Y_2O_3, corrosion and thermal shock resist. in diesel engines 79–24675
ZrO_2, synthesis by solid state reaction 80–100821
ZrO_2, technical grade containing CaO, polymorphic transform. up to 1200°C 78–64539
ZrO_2, tetragonal polycryst., sintering and props. 79–29008
ZrO_2, tetragonal to monoclinic phase transf. by ball-milling 80–25687
ZrO_2, wear chart, exam. *(German)* 78–35521
ZrO_2, Y_2O_3 stabilised, hydrothermal growth 78–15302
$ZrO_2:Y_2O_3$, low-temp. specific heat, oxygen vacancy effects 80–49376
ZrO_2-based solid solutions, effect of added B_2O_3 and Nb_2O_5 on sintering and stability 77–40410
ZrO_2-CaO, phase equilibria and ordering 78–27498
ZrO_2-CaO (15 mol.%), precipitation and ordering 80–100837
ZrO_2-CaO-SiO_2, relationship between texture parameters, and sintering, elec. cond. and mech. strength props. *(German)* 79–24474
ZrO_2-CaO(MgO)$(YO_{1.5})$, partially stabilised, growth morphology of tetragonal phase 79–4968
ZrO_2-CaO(Y_2O_3) ceramics with grainy structure, props., effect of heating to 2000°C 80–104194
ZrO_2-CeO_2, semiconducting ceramics, electronic conductivity and oxido-reduction *(French)* 78–26919
ZrO_2-Gd_2O_3, solid solution with fluorite and pyrochlore structure; exam. of elec. conductivity *(German)* 79–23766
ZrO_2-HfO_2, monoclinic solid soln., ceramic prep. and use 80–55338
ZrO_2-HfO_2-CaO, cubic solid solutions, thermal expansion 77–15598
ZrO_2-MgO system, intermediate phases existence, X-ray diffr. and IR obs. 79–38805
ZrO_2-Nd_2O_3 system, solid solns., evaporation, mass spectroscopy investig., thermodynamics 79–10938
ZrO_2-$Nd_2O_3(Sm_2O_3)(Dy_2O_3)$ eutectic, unidirectional solidification, microstruct. and crystallographic characterization 80–35176
ZrO_2-Sc_2O_3, phase system, X-ray and thermal anal. 78–27494

ceramics continued
- ZrO_2-Sc_2O_3 system, high-temp. phase transitions, elec. cond., thermal props. 77—16573
- ZrO_2-Y_2O_3, solid soln., elastic and photoelastic props., Mendelstam-Brillouin scatt. 78—6693
- ZrO_2-Y_2O_3 (9 mol.%), precipitation and ordering 80—100837
- ZrO_2-Y_2O_3 ceramic powder, in situ deposition of metal coating, cermet form. 77—32713
- ZrO_2-Y_2O_3 microspheres, stabilised, from HF air plasma, struct. 79—78917
- ZrO_2-Y_2O_3 powder, prep. for plasma spheroidisation, sputter drying *(Russian)* 80—55324
- ZrO_2-Y_2O_3/Ni sputtered multilayered ceramic/metal coatings, props. 80—40620
- ZrO_2-Y_2O_3/(Cr-Ni) sputtered multilayered ceramic/metal coatings, props. 80—40620
- ZrO_2-ZrO_2, multiphase ceramics, mech. strengthening due to dispersion of non-metallic particles *(German)* 78—60674
- $(ZrO_2)_x(In_2O_3)_{1-x}$ ceramic, bulk resistivity 77—35936
- $ZrO_2Y_2O_3$/Ni-Cr-Al-Y, NASA two-layer thermal barrier coating, for gas turbine engines, test results 80—40617
- $((ZrO_2)_{0.92}(Y_2O_3)_{0.08})_{1-x}(Fe_2O_3)_x$, Fe solubility and elec. cond. 79—99354
- $6.14ZrO_2.Nb_2O_5$, elec. cond. meas. 80—100463
- $ZrO_2.SiO_2$-αAl_2O_3 mixed powders, solid state reactions 80—40337
- $6.14ZrO_2.Ta_2O_5$, elec. cond. meas. 80—100463
- $ZrSiO_4$, Fe_2O_3 and TiO_2 additions effect on stability 77—48377
- $ZrSiO_4$ zircon ceramic with glass-forming additives, sintering and mech. props. 80—60814
- $ZrSiO_4$, zircon yellow pigment, synthesis *(Polish)* 80—66466
- $ZrSiO_4$-Al_2O_3 mixture, reaction hot pressing 79—38775
- $ZrSiO_4$-Al_2O_3 system, particle rearrangement kinetics due to densification 80—25626
- $ZrSiO_4$-Fe_2O_3, pink colour form. kinetics 79—60360
- $ZrTiO_4$, form. mechanism from spray drying of solns., precip., of hydroxides and reactions of hydrates and solns. 79—43182

Cerenkov counters *see Cherenkov counters*

Cerenkov radiation *see Cherenkov radiation*

cerium
- *see also nuclei with ......*
- abundance in chert, indication of form. in marine environment 77—37200
- abundance in HD 18474 giant star *(Spanish)* 79—25605
- addition to Cr-Mo and Ni-Cr-Mo-V low-alloy steels, remedy for temper brittleness 80—66659
- addition to Ni-Cr austenitic stainless steel, effect on heat resist. and comp. of non-metallic inclusions 80—76315
- adsorption and absorption of $H_2(D_2)$ 77—4257
- allotropic phase above 121 kbar, X-ray diffr. obs. 77—35509
- aluminate:Ce^{3+}, hexagonal, luminesc. rel. to host lattice structure 78—6776
- aluminates:Ce^{3+}, luminesc. exam. 78—56513
- atom, optically oriented, hyperfine transition struct. parametric reson. *(Russian)* 77—54522
- atom, photoionis. of 6s electron, spin-orbit interaction, ab initio calc. 79—81191
- atomic excitation, $fds^2 \rightarrow d^2s^2$, theoretical calc. of energy 77—62639
- beta phase, elec. resist., mag. susceptibility, 2-300K 77—4320
- bremsstrahlung resonances and APS near 3d threshold 77—69937
- chemically collapsed, valence transition 79—28325
- cold working, deform. induced struct. effects 80—25719
- Compton profile study of γ-α phase transition 80—11503
- Compton scattering study of γ-α phase transition 80—59650
- critical isomorphic $\gamma \rightleftarrows \alpha$ transition, phase equilibrium curve *(Russian)* 80—55397
- crystal structure, α'' high pressure phase 79—23565
- crystal structure of α' phase, X-ray diffr. data, reappraisal 77—55260
- crystal structures at high pressures 77—19890
- density functional theory 80—15442
- depletion in Melrose-b howardite 80—101566
- diffusion and solubility in Be 77—35757
- elastic properties up to 84 kbar, US vel. meas. *(Russian)* 79—60434
- electrical resistance, temp. coeff., 20 kbar at 300K 78—83973
- electrical resistance behaviour at press. induced α'-tetragonal phase transform. 77—35916
- electronic energy band calcs. by KKR method for β-phase 79—95317
- electronic structure, 4f band *(German)* 77—55479
- electronic structure, Compton profile meas. 80—10867
- electronic structure vol. depend., rigorous cellular method, γ- and α-forms 77—20233
- FCC, ground-state props. 78—75989
- film, vapour-quenched, unsuccessful search for supercond. above 0.3K 77—12053
- getter beds, T removal from inert gases, CTR appl. 78—41861
- gettering of H, mass spectrometry and microgravimetry study, rel. to HTGR gas purification 80—73374
- glasses:Ce (III) and (IV), u.v. absorpt. 77—4658
- ground state properties of f band metals 78—91607
- heat capacity redeterm. 77—20617
- high pressure phase transition, anomalous Gruneisen parameter behaviour 80—79934
- implantation on Cr-Ni Nb stabilized austenitic stainless steel surface, effect on oxidation behaviour 80—71791
- impurities in superconductors, unified description of demagnetisation, sp. ht. jump 77—69450
- inelastic neutron scatt. cross-section, effect of cryst. field 79—65642
- intermediate valence, renormalisation of collective excitations, acoustic wave vel. near electronic transition 79—82539
- IR spectrum, isotope shift *(French)* 77—54523
- isostructural solid-solid phase transitions, core collapse, cell theory 80—59620
- Kondo-like anomaly in FCC phase 80—96857
- lattice and spin dynamics, inelastic neutron scatt. obs. 79—86859
- liquid, 4f electron susceptibility temp. depend. 80—20378
- liquid, resist. and thermoelec. power, t-matrix calc. 78—26840
- liquid, struct., neutron diffr. meas. 77—51305
- localised vibration of interstitial H impurities in FCC γ-Ce 80—75322
- magnetic properties and sp. ht. of α-phase 79—28512
- marine sediment Ce composition, determination method 80—104543

cerium continued
- melting curve extrema from repulsive step potential, molecular dynamics calc. 77—59102
- metaphosphate glasses, $n(M_2O.P_2O_5).(1-x)Y_2O_3.xTb_2O_3.3P_2O_5$, $M=Li$, Na, K, Ce-doped, excitation and emission spectra 80—40150
- neutron scattering, inelastic, under press. near first order γ-α phase transition 77—63102
- neutron scintillating glasses activated by Ce^{3+}, luminesc. 79—38668
- normal spectral emittance above 1000K 77—28028
- oxidation, ESCA and UPS meas., core levels 77—63542
- oxidation agent for Fe-Armco, grain size and strength depend. on nonmetallic inclusions *(Russian)* 80—100894
- oxidised surface, comparative sputtered neutral mass spectrometry and SIMS studies 79—90856
- phase boundary between α' and tetragonal polymorphs, resistance anomaly meas. 79—60500
- phase transition, high press., $\alpha \rightarrow \alpha'$, volumetric study 78—83940
- phase transitions, shouldered hard-sphere pots. calcs. 77—2600
- phosphate glass:Ce^{3+},Tm^{3+}(Tb^{3+}), temp. depend. of energy transfer $Ce^{3+} \rightarrow Tm^{3+}$, $Ce^{3+} \rightarrow Tb^{3+}$ 77—24882
- photochemical separation from rare earth mixtures in aq. soln. 79—39165
- photoelectron spectra, 4f level position 80—25519
- photometric determ. in cast Fe and steel *(German)* 78—68955
- polymorphic $\gamma \rightleftarrows \alpha$ transform. and volume anomalies under press. 80—34189
- Precambrian Fe formations, rare earth elements evidence for changing oxidation states 77—64284
- purification, laser induced photochem. separation methods, review 79—61883
- rare earth ethyl sulphates:Ce^{3+}, Kramers ions, virtual phonon exchange, field theoretic formalism 80—20137
- rare earth pentaphosphates:Ce^{3+},Tb^{3+}, energy transfer between dopants, excitation spectra, laser appls. 78—10961
- resonant photoemission, time-depend. density-functional technique 80—89114
- reversible mech. memory effect, α to γ transition *(Russian)* 78—15396
- solid-state phase transformation, γ-α, energetics, rel. to atomic excitation $fds2 \rightarrow d^2s^2$ in atomic Ce 77—62639
- specific heat, 0-16 kbar, press. depend. 77—51512
- specific heat, up to 20 kbar at 300K 78—83973
- specific heat at 300K, up to 20 kbar *(French)* 79—95177
- superconducting film, A1-type quench-condensed, prep. and crit. temp. 77—69443
- superconductivity, high press., phonon softening 78—14852
- surface and volume props., flow props., surface layer thickness *(Russian)* 80—59760
- surface implantation in stainless steel, effect on oxidation resistance at high temp. 77—8977
- SXAPS from 0 to 1400 eV 77—4703
- target prpe. for synthesis of transactinide elements 80—23206
- TCR, to 15 kbar *(French)* 79—95383
- thermal conductivity at low temps. *(Russian)* 79—11100
- thermo-EMF up to 75 kbars 80—24882
- thermochemical water-splitting cycles based on Ce and alkaline earth phosphates for H_2 prod. 80—55945
- thermoelectric power up to 6 GPa 79—51556
- thermopower behaviour under press. up to 7500 MPa γ-α and α-α' transitions 79—47083
- transport properties at high temp., scatt. mechanisms 77—15825
- vacancy formation enthalpy in γ phase, positron annihilation meas. 79—99182
- valence band exam. by XPS and UPS 79—37977
- valence band photoemission intensity, giant enhancement in α-phase 79—19972
- valence mixed state, Kondo lattice, Anderson localisation models *(Japanese)* 78—51945
- X-ray 4d-absorption spectra, similarity for atomic and metallic states 77—12463
- XPS valence band spectra meas. 77—48306
- α-induced X-ray anal. of Y, La, Ce, Nd content of apatite minerals 79—16084
- α-Al_2O_3:Ce, semicond. props. 80—54684
- B_2O_3-SiO_2:Ce glasses, radiation resistance mechanism, optical absorpt. and luminesc. obs. *(Polish)* 79—86825
- BaF_2:Ce^{3+}, EPR of low-symmetry sites 79—47332
- BaO-Al_2O_3-B_2O_3:Ce^{3+} glass, EPR spectra, before and after X-irrad. 78—19320
- $Ba_3SiAl_{10}O_{20}$, Ce^{3+} activated, X-ray diffr. and luminesc. props. 80—49199
- $Ba_xSr_{1-x}Nb_2O_6$:Ce, photoelec. props. and photorefraction 80—60538
- CaF_2:Ce, Stark struct., phototransitions, g-factors 78—67995
- CaF_2:Ce,Mn, heavily-doped phosphor, cathode-ray irrad., energy transfer 79—87509
- CaF_2:Ce^{3+}, absorpt. peaks in the lowest $4f \rightarrow 5d$ band, effect of conc. 80—2798
- CaF_2:Ce^{3+}, ENDOR meas. on Ce^{3+} photochromic centre 78—19372
- CaF_2:Ce^{3+}, Kapitza limited spin-bath relax., paramag. Faraday effect meas. at liq. He temp. 79—95642
- CaF_2:Ce^{3+}, point-charge approx. of tetragonal centres 77—47778
- CaF_2:Ce^{3+}, thermally modulated UV absorpt. spectra, 90K 77—28602
- CaO:Ce,Gd phosphors, trap distrib., phosphoresc. decay characts. obs. 80—29773
- CaO:Ce^{3+}, Gd^{3+}, sensitization of Ce^{3+} luminesc. by Gd^{3+} 80—97326
- $Ca_5(PO_4)_3OH$:Ce^{3+}, thermolum. props. 80—2877
- CaS:Ce, Na, photon sidebands in emission and excitation spectra, pseudolocalised vibrs. 79—28800
- CaS:Ce, Na phosphor, photoluminescence and excitation spectra 80—89049
- CaS:Mn,Ce, phosphor, fluoresc. spectrum, fine struct., ${}^4T_{1g}({}^4G) \rightarrow {}^6A_1({}^6S)$ transition 80—45130
- $CaSO_4$:Ce, gamma-irradiated valency conversions in rare-earth ions 80—55198
- $CaSO_4$:Ce phosphors, fluorescence spectra, thermolum. glow curve 80—2879
- CdF_2:Ge^{3+}, Ce^{3+}, in semicond. state, elec. cond. and Hall meas. 78—10443
- α-Ce, exchange-enhanced, elec. resist. T^2 depend., press. effect 80—96845
- γ-Ce, field induced mag. form factor 78—68151
- Ce II, isotope shift and screening, pseudo-relativistic HF calc. 78—90096

cerium continued
- Ce III, 3d and 4f energy level parametrisation, Slater parameters and correl. corrections 80−87041
- Ce XII, UV spectra, 60-600 Å reson. lines 78−33455
- Ce^+ formed by electron impact in CeI_3 vapour, appearance potential 77−23567
- Ce^{3+} impurities in cubic crystals, 5d→4f radiative transition probability calc. 80−71474
- Ce^{3+} in paramagnet, cryst. field effects on EPR and NMR *(Japanese)* 77−43880
- Ce^{3+}, in Van Vleck paramagnets, EPR meas. 77−12199
- Ce^{3+}, local symmetry in frozen aq. solns., EPR and linear electric field effect 77−16169
- Ce^{3+} oxidation kinetics in X zeolite on O_2 adsorpt. 78−3373
- Ce:^{143}Pr, mag. dipole moment of Pr 57 keV state, PAC meas. 77−46110
- Ce:LaF_3 286 nm laser, optically pumped 80−99738
- Ce:$LiYF_4$, tunable UV laser at 325, 309 nm, KrF laser excitation 80−38022
- Ce^{3+}:LaF_3, UV fluoresc. potential tunable laser 2760 to 3220 Å 78−15206
- Ce^{3+}:$LiYF_4$, UV laser at 325 nm, stimulated emission obs. 79−72574
- Ce^{3+}:LuF_3, UV fluoresc. potential tunable laser 2760 to 3220 Å 78−15206
- Ce^{4+}/Ce^{3+} dosimeter, adsorbed doses, potentiometric determ. 78−94146
- Ce-Cl cycle for thermochemical H production 80−35783
- Ce-S-O equilibrium in molten Fe *(Chinese)* 80−104423
- Ce(IV), biamperometric iodometric determ. using Pt-graphite electrode system 77−70359
- $Ce_{1-x}Th_x$ solid mixture, isostructural phase transitions 77−84884
- ^{139}Ce, use in biomedical meas. of stable I conc., absorpt.-edge transmission technique 80−56194
- ^{140}Ce magnetic hyperfine field in Ni, TDPAC meas. 79−11363
- ^{141}Ce, diffusion behaviour in SiC, 1650 to 1850°C 78−79814
- ^{141}Ce standard, measured by dose calibrators, simulated $^{99}Tc^m$ standard 78−61261
- ^{144}Ce absorption through damaged and undamaged skins of guinea pigs 80−26383
- ^{144}Ce, anodic deposition on Pt anode, electrochem. separation 79−91958
- ^{144}Ce, errors in activity ratio determ. in reactor RA used fuel element 79−41061
- ^{144}Ce gastrointestinal absorpt. and distrib. in suckling pig 78−15942
- ^{144}Ce, inhalation exposed mice, toxicity, dosimetry and ^{144}Ce retention 80−89874
- ^{144}Ce, intravenous injection, wound site absorption, comparison of metabolic behaviours in rats 79−8545
- ^{144}Ce, radiation dose-response curves, hazard function method of resolution 79−66556
- ^{144}Ce, removal rate in lower stratosphere, seasonal vars. 80−55957
- ^{144}Ce/^{144}Pr miniature radioisotope generator 79−49885
- Cr^{4+} concentration oscillations, in Belousov-Zhabotinskii system; detection of BrO_2 *(German)* 79−29351
- Cs_2NaYCl_6:Ce, ENDOR evidence of noncubic distortion 79−11357
- ^{144}e inhalation effect of influenza virus infection on pulmonary retention and mouse survival 78−85340
- GaP:Ce epitaxial films, photoluminesc. spectra 80−66294
- H, and He, stopping powers meas. 80−42904
- H isotope removal from flowing Ar, U and Ce as hydriding materials 78−17438
- $He(2^3S, 2^1S)+Ba(Y)(Ce)$, Penning process, double ionisation 77−3439
- HfO_2:Ce^{n+}, impurity valence transitions 77−51694
- $LaAl_2$:Gd(Ce), supercond., electronic thermal cond. 77−12063
- LaB_6:Ce, Kondo system, magnetoresist. down to 0.04K, anisotropy 77−11904
- LaF_3:Ce, cryst. field parameters, optical transitions and g-factor determ. 78−2456
- $LaGaS_3$:Ce^{3+}, phosphor, luminesc. props. 80−103979
- $La_2Mg_3(NO_2)_{12}.24H_2O$: Ce^{3+}, electron spin-lattice relax. under uniform compression 77−90028
- $La_2Mg_3(NO_3)_{12}.24H_2O$:$Ce^{3+}$, mag. circular dichroism of Ce^{3+} 77−69869
- $La_2Mg_3(NO_3)_{12}.24H_2O$:$Co^{2+}$, Ce^{3+}, relax. and ESR in magnetically cooled systems 78−88225
- $La_2Mg_3(NO_3)_{12}.24H_2O$:Ce, bottlenecked Orbach relax. process, phonon lifetime 79−65151
- LiH:Ce, thermolum., appl. as X-ray detectors 79−6794
- MgO-Al_2O_3-SiO_2:Ce^{3+} glass scintillator, energy transfer, luminesc. efficiency under UV and charged-particle excitation 79−95821
- MgS:Ce^{3+} phosphors, emission and excitation spectra *(French)* 80−93380
- Na_2O-SiO_2:Ce photochromic glass absorption centres 79−27352
- SiO_2-MgO-CaO-Al_2O_3:Ce,Fe, redox equilib., expt. 80−85171
- $(Sr,Ba)Nb_2O_6$:Ce, high sensitivity holographic storage 77−71953
- SrF_2:Ce, dipolar complex exam. 79−38435
- SrF_2:Ce^{3+}, cryst. field energies 80−59941
- SrF_2:Ce^{3+}, dipole reorientation, Ce^{3+} conc. effect 78−10841
- SrF_2:Ce^{3+}, EPR of low-symmetry sites 79−47332
- $Sr_3SiAl_{10}O_{20}$, Ce^{3+} activated, X-ray diffr. and luminesc. props. 80−49199
- ThO_2:$Ce^{3+}(Ce^{4+})$, mixed ionic and electronic transport 80−107875
- $ThOF_2$:Ce,Tb, photolum. obs. 77−77270
- YAG:Ce, γ-irradiated elec. cond. meas. 77−43601
- YAG:Ce phosphors, luminesc. efficiency, prep. and dopant effects 80−45151
- YAG:Ce^{3+}, cathodolum. intensity and decay time, 10-480K 79−99952
- YAG:Ce^{3+}, cathodolum. intensity, temp. depend., comparative study with other YAG:R^{3+} crysts. 79−99953
- YAG:Ce^{3+}, cathodolum. efficiency rel. to activator conc. 80−11479
- YAG:Ce^{3+}, excited-state absorpt. meas., tunable laser model system 79−42994
- YAG:Ce^{3+}, new fast scintillator for SEM 78−86394
- YAG:Ce^{3+}, photoluminescence excitation energy, crystal field and temp. effects 80−11460
- YAG:Ce^{3+}, recomb. processes, spectral, kinetic and relative quantum intensity meas. 79−61443
- YAG:Ge^{3+}, excited state absorpt. loss, 5d→4f rare earth lasers 78−90417
- YAG:Nd,Ce,Cr, effect of γ-rays, fast electrons on optical props., annealing and colour centre destruction 77−8608
- YAG:Nd^{3+}, Ce^{2+}, sensitisation, luminesc., absorpt. and emission spectra *(Russian)* 78−10982
- $YAlO_3$:Ce, fast decay UV phosphor 80−71471

cerium continued
- YF_3:Nd, Ce, energy transfer between 5d electronic states 80−2808
- YPO_4:Ce, luminesc. and optical spectra 79−65921
- Y_2SiO_5:Ce^{3+}, EPR and spin-lattice relax. 80−108063
- $Y_3Si_2O_8Cl$; Ce phosphor, prep. and luminescence props. 78−52740
- ZnO:Ce phosphor, electrolum. brightness, voltage and freq. depend. 80−60681
- ZnO+Ce phosphors, electrolum. 79−99946

cerium alloys
- abnormal ordered Kondo lattice 78−47947
- Alnico alloys, effect of Ce addition on mag. props. 78−2699
- Anderson model, exchange parameter, Kondo temp., mag. susceptibility 79−1656
- binary and pseudobinary intermetallics, struct. and mag. data 80−20129
- cubic intermetallics, interconfig. fluctuations 80−20130
- dilute, elec. resist. in presence of external mag. field 78−19022
- Kondo effect, mag. suscept. exam. 77−8270
- Kondo system, crystal field effects on thermopower and Kondo effect 77−66163
- misch metal, improvement of Al alloy 51S, for space appl. 80−55466
- Mischmetal-Ni alloy, H_2 adsorption and desorption *(Japanese)* 77−47668
- mischmetall-Co system, phase relations, microstruct., mag. props. 80−104118
- steel, austenitic, Cr-Ni-Ce(La,Nd,Pr), nonmetallic inclusions modification using rare earth metals *(Russian)* 80−40369
- steel, Ce, Nb, addition effects on hot plasticity *(Russian)* 77−66680
- steel, Cr-Ni-Mo-V-Nb (12,8,1,1.5,0.4 wt.%) Ce addition effects on strength and hardness *(Russian)* 78−15454
- steel, low alloy, Mn-P, temper brittleness, rare earth mischmetal effect *(Chinese)* 80−104249
- transition metal intermetallics ESR of Nd^{3+} and Gd^{3+} 79−87315
- transition metal-Ce alloys, valence state of Ce 79−77545
- valence transition, scaling studies 80−20135
- Al-Ce, very dil. alloy, low temp. sp. ht. 79−51745
- Al-Ce (0.06 at.%), rapidly quenched from melt, vacancy loops and precipitates, TEM 77−59769
- Al-Ce foil, alloying effect on strength characts. and weldability 80−55475
- Al_2Ce, Al_3Ce, nucl. orientation exam. of Ce ground state at very low temp. 78−67999
- Al_3Ce and $Al_{11}Ce_3$, Kondo cpds., mag. behaviour obs. by neutron diffr. 80−50049
- Al_3Ce, thermal expsn. below 1K 79−90803
- $Al_2La_xCe_{1-x}$, low temp. mag. props. 80−20564
- $(Ce,La)Al_2$, collective phenomena 80−65933
- $(Ce, La)Al_3$, near stabilisation of Ce moment upon dilution 79−91209
- $(Ce, La)In_3$, heat capacity and elec. resist. 80−71049
- $(Ce,Y)Al_2$, collective phenomena 80−65933
- Ce-Al, XPS valence band spectra meas. 77−48306
- Ce-Bi, heat of formation, calorimetric meas. 78−44392
- Ce-Co, liq., charge transfer effect 78−94967
- Ce-Co-Al (0-33.3 at.% Ce), isothermal section, X-ray study *(Ukrainian)* 80−39002
- Ce-Co-Cu-Fe-Ti, sintered magnet, prep. and mag. props. 77−73043
- Ce-Co-Si, thermoelectromotive force and electrocond. *(Ukrainian)* 80−54670
- Ce-Co-Si system, mag. props. in 77-300K range *(Russian)* 78−56290
- Ce-Cu, liq., charge transfer effect 78−94967
- Ce-Cu, liquid, normal spectral emissivity 80−103506
- Ce-Fe-Si, thermoelectromotive force and electrocond. *(Ukrainian)* 80−54670
- Ce-Fe-Si system, mag. props. in 77-300K range *(Russian)* 78−56290
- Ce-Ga, phase diagram *(Russian)* 78−27478
- Ce-Ga (Al)(In)(Sn)(Pb)(Bi)(Zn) liquid, solubility and thermodynamic props. *(Russian)* 78−19717
- Ce-Ga system, phase equilib. and cryst. struct. of phases 80−35159
- α-Ce-Gd(Dy)(Er), dil., ESR study of mag. prop 78−39398
- Ce-In, phase equilibrium and cryst. struct. 80−66483
- Ce-La, DHCP, low temp. mag. and elec. props. 77−62911
- Ce-La, mag. ordering, sp. ht., susceptibility and resist. 78−68238
- Ce-La H_2 charging effect on nodularizing efficiency of Ce-La additions to cast Fe 78−27544
- Ce-M intermetallic cpds., M=3d transition metal, sorption of H_2, structural charges 80−88429
- Ce-Mg-Fe master-alloy innoculated cast Fe, struct. and props. 80−100843
- Ce-Mn-Co, temp. conc. limits of homogeneous compounds *(Russian)* 78−23666
- Ce-Mn-Co(Fe)(Ni), cryst. struct. determ. 77−11508
- Ce-Mn-Cu systems, phase equilibria at 600 and 400°C *(Ukrainian)* 80−11625
- Ce-Mn-Ni system, phase diag. 77−52283
- Ce-Nd, reversible mech. memory effect, α to γ transition *(Russian)* 78−15396
- Ce-Nd-Si, phase diagram, X-ray anal. *(Ukrainian)* 79−38792
- Ce-Ni, hydriding characts., applicability for H_2 storage material 78−83955
- Ce-Ni liq., X-ray diffr. exam. of struct. 77−62465
- Ce-Ni-Si, thermoelectromotive force and electrocond. *(Ukrainian)* 80−54670
- Ce-Ni-Si system, mag. props. in 77-300K range *(Russian)* 78−56290
- Ce-Pr powder, DHCP⇄FCC transition, X-ray, DTA and resistivity studies 80−50629
- Ce-Pt, paramag. suscept. 79−61047
- Ce-Sm-Co-Fe-Cu, permanent magnet props. 79−8013
- Ce-Sn, liq., elec. resistivity negative temp. coeff., CPA calcs. 79−42515
- Ce-Th, mag. suscept. and sp. ht. 79−78411
- Ce-Tl, phase equilibrium and cryst. struct. 80−66483
- CeAg, mag. and structural phase transition at hydrostatic press., elec. resist. meas. 79−61102
- $CeAg_xIn_{1-x}$, cubic to tetragonal phase transform., conc. dependence by resist. meas. 78−2252
- CeAg(Mg)(Zn), magnetic struct. and cryst. field, neutron diffr. exam. 78−72328
- $CeAg_2Si_2$, ^{29}Si NMR and mag. susceptibility 79−61246
- CeAl, mag. props. and mag. struct. 78−6517
- $CeAl_2$, and $CeAl_3$, magnetisation and sp. ht. 80−20418
- $CeAl_2$, Anderson lattice system, thermal expansion meas. 1.5 to 10K 79−37860

cerium alloys continued
CeAl$_2$, Anderson lattice system, volume collapsed strongly mixed valent state 79−38033
CeAl$_2$, Anderson lattice system, ground state props. 80−20443
CeAl$_2$, anisotropic magnetostriction near antiferromagnetic transition 78−88157
CeAl$_2$, antiferromag. ordering between 4f shells, Kondo effect 80−20417
CeAl$_2$, antiferromag. ordering and Kondo behaviour, ^{27}Al NQR study 80−71231
CeAl$_2$, CeAl$_3$, Kondo lattice theory 80−20380
CeAl$_2$, collective phenomena 80−65933
CeAl$_2$, conf. Kondo system, sp. ht. meas. 78−52210
CeAl$_2$, dynamic Jahn-Teller effect, neutron energy loss obs. 79−78060
CeAl$_2$, electronic transition under pressure, resist. meas. 79−33311
CeAl$_2$, low temp. mag. behaviour, neutron diffr. 78−84395
CeAl$_2$, low temp. mag. props., Kondo effect 80−20381
CeAl$_2$, mag. anisotropy, transition, crystal field splitting 78−52243
CeAl$_2$, mag. behaviour 2.5 to 300K, neutron scatt. meas. 77−63110
CeAl$_2$, mag. ordering, neutron diffr. meas. 78−6518
CeAl$_2$, mag. ordering and anomalous ground state, neutron diffr. obs. 79−78331
CeAl$_2$, magnetic ordering, 24 component Ginzburg-Landau model 80−97095
CeAl$_2$, magnetisation curves under high mag. field and hydrostatic press. 77−63233
CeAl$_2$, magnetoelasticity, rot. invariance and magnetoacoustic birefringence 79−87304
CeAl$_2$, mode softening due to magnetoelastic interaction, elastic consts. meas. 1.5 to 280K 77−32233
CeAl$_2$, multiple q mag. struct. 79−78330
CeAl$_2$, multiple-q mag. struct. 80−25100
CeAl$_2$, multiple-*q* structure or coexistence of different mag. phases, neutron diffr. study 80−107985
CeAl$_2$, NMR, cryst. field effects and mag. order in low temp. phase 78−68391
CeAl$_2$, neutron diffr. at low temp., magnetism 80−20383
CeAl$_2$, press.-induced electronic transition 80−20147
CeAl$_2$, resistivity and volumetric meas., phase diagrams, comparison with CeS 80−107789
CeAl$_2$, skew scatt., evidence of cryst. field effect, Hall effect meas. 78−2466
CeAl$_2$ sound vel. in high mag. fields 79−78500
CeAl$_2$, sp. ht. in high mag. fields, Kondo effect 78−52284
CeAl$_3$, anomalous resistivity maxima in metallic magnetic system 78−79977
CeAl$_3$, cryst. field effects, inelastic neutron scatt. meas. 77−51710
CeAl$_3$, effect of disorder on cond. transition into ground state 77−89755
CeAl$_3$, inelastic neutron scatt. meas. 79−47066
CeAl$_3$, magnetic susceptibility, dense Kondo system 77−63087
CeAl$_3$, singlet ground state at T=0, mag. ordering 2.5-6K 78−84388
CeAl$_3$, sp. ht., Kondo effect and ferromag. order coexistence 80−65927
CeAl$_3$, sp. ht. anomalies due to presence of CeAl$_{11}$ 79−19745
CeAl$_3$, valence mixed state, Kondo lattice, Anderson localisation models *(Japanese)* 78−51945
Ce$_3$Al$_{11}$, competition between ferro- and antiferromag. interactions 80−60258
Ce$_3$Al$_{11}$, mag. ordering at low temps. under press., relation to CeAl$_3$ props. 79−19745
Ce$_3$Al$_{11}$, sp. ht., Kondo effect and ferromag. order coexistence 80−65927
Ce$_{30}$Au$_{20}$, amorphous, cryst. field effects and mag. interactions, magnetisation and transport props. meas. 78−68191
Ce$_{80}$Au$_{20}$, metallic glass, mag. ordering and cryst. field effects, speromagnetism 80−80531
CeAu$_2$Si$_2$, ^{29}Si NMR and mag. susceptibility 79−61246
CeBe$_{13}$, intermediate valence state, XPS, resist. and susceptibility study 80−71565
CeBe$_{13}$, lattice spacings and susceptibilities 80−65778
CeBi, lattice distortion modes and mag. structural transitions 79−78325
CeBi(Sb), anisotropic mag. ordering and mag. structural transitions 79−78324
CeCo$_2$, of Co, interdiffusion exam., growth kinetics of intermediate layers 78−2304
CeCo$_3$, and ternary hydride, mag. props. 80−108007
CeCo$_3$-H$_2$, phase equilibria, from dissociation isotherms 80−50591
CeCo$_5$, adsorption and desorption charact. of H$_2$ *(Japanese)* 77−47667
CeCo$_5$ hard magnets, characteristics and appl. *(German)* 77−80966
CeCo$_5$, magnetisation and coercive strength 77−55688
CeCo$_{5+x}$, Cu and Fe modified, coercive force *(Czech)* 79−42805
CeCo$_x$, sorption at press. up to 1500 atm. 80−97819
Ce$_2$Co$_7$, and ternary hydride, mag. props. 80−108007
Ce$_3$Co, absorpt. of D, heats of reaction and equilib. press., T-getters for CTR 78−51683
Ce$_{5.3}$Co, absorpt. of D, heats of reaction and equilib. press., T-getters for CTR 78−51683
CeCoAl$_4$, X-ray anal. of crystal struct. *(Russian)* 77−55263
Ce$_2$Co$_5$B$_2$, crystal struct. *(Ukrainian)* 79−51050
CeCo$_{3.5}$Cu$_{1.5}$, and alloys of similar comp., cryst. structs., X-ray diffr. exam. 79−99120
CeCo$_{5-x}$Cu$_x$, $0 \leq x \leq$ internal oxidation kinetics, oxide struct., X-ray study 80−104329
Ce(Co$_{1-x}$Ni$_x$)$_5$, mag. props. and mag. reversal phenomena *(Russian)* 77−51924
CeCoSi$_2$ film, Hall effect and magnetoresist. *(Russian)* 80−11109
Ce(Cu,Ni)$_2$, pseudobinary phases, struct. and mag. props. rel. to Ce valence 78−6032
CeCu$_4$ Knight shifts and mag. susceptibility 79−95656
CeCu$_5$, Knight shift and mag. susceptibilities 79−95656
CeCu$_2$Si$_2$, collective phenomena 80−65933
CeCu$_2$Si$_2$, local mag. moments, neutron scatt. study 79−61058
CeCu$_2$Si$_2$, resistivity, thermal conductivity and thermopower between 1.5 and 300K 78−87963
CeCu$_2$Si$_2$, strong Pauli paramagnetism, superconductivity obs. 80−29499
CeCu$_2$Si$_2$, transport anomalies 80−20148
CeCu$_2$Si$_2$, tunnelling anomalies due to intermediate valence phenomenon 77−62873
CeCu$_2$Si$_2$, valence fluctuations, ^{29}Si NMR and mag. susceptibility 79−61246
CeFe$_2$, ferromagnetic cpds., mean field exchange consts., Stoner itinerant model calcs. 80−50084
CeFe$_2$, H$_2$ absorption effect on mag. props. and struct. 77−40045
CeFe$_2$, magnetostriction in polycryst. samples 77−73065

cerium alloys continued
CeFe$_2$, magnetostriction and magnetisation 80−39844
Ce$_{8.5}$Fe, absorpt. of D, heats of reaction and equilib. press., T-getters for CTR 78−51683
CeFe$_4$Al$_8$, mag. props. 78−52250
CeGa$_2$, mag susceptibility, 1.5-300K and Neel temp. 78−68184
Ce$_{1-x}$Gd$_x$Ru$_2$, superconductivity and ferromagnetism coexistence, 60 mK-4.2K, spin echo NMR 78−84349
Ce$_{1-x}$Gd$_x$Ru$_2$Zr$_2$Co, spin-pairing state investig. via Josephson effect 77−47942
Ce$_{11}$Hg$_{55}$, cryst. struct. determ. 79−77555
Ce$_{0.73}$Ho$_{0.27}$Ru$_2$, spontaneous mag. order below superconducting transition temp., Mossbauer study 80−39701
Ce$_{0.73}$Ho$_{0.27}$Ru$_2$, superconductors, mag. correlations and crystal-field levels 80−34547
(Ce$_{1-c}$Ho$_c$)Ru$_2$, superconducting, mag. props., neutron scatt. study 80−44808
Ce(In, Sn)$_3$, heat capacity and elec. resist. 80−71049
Ce(In, Sn)$_3$, mag. susceptibility, temp. depend., intermediate valence 80−65779
CeIn$_3$, crystalline elec. field parameters, exchange and Coulomb contrib. 77−20278
CeIn$_3$, Kondo effect, mag. suscept. exam. 77−8270
CeIn$_3$, Kondo system, mag. susceptibility calc. in Anderson model 77−55661
CeIn$_3$, mag. struct., neutron diffr. study 80−80481
CeIn$_3$, magnetisation and sp. ht. 80−20418
CeIn$_3$, Neel temp., hydrostatic press. depend. 80−29549
CeIn$_{3-x}$Sn$_x$, conduction electrons role in valency fluctuations 78−47741
CeIn$_{3-x}$Sn$_x$ mixed valence system, low-temp. susceptibility, paramagnon study 80−97077
CeIn$_{3-x}$Sn$_x$, scaling behaviour near valence instability, mag. susceptibility and mag. transitions 80−25111
CeIn$_{3-y}$Sn$_y$, electrical resist. and thermal expansion meas., 1.5-300K 80−34400
CeIr$_2$(Rh$_2$), ESR of Nd^{3+} and Gd^{3+} 77−85564
Ce$_{1-x}$La$_x$ alloy, thermoelectric power 79−78080
Ce$_{1-x}$La$_x$, dil., $\gamma-\alpha$ transition temp. and press., elec. resist. meas. up to 10 kbar 80−59643
Ce$_{1-x}$La$_x$, electrical resist. T^2-depend. under high press. 80−29383
Ce$_{1-x}$La$_x$, thermoelectric power, mag. transition temps. 80−20154
Ce$_{1-x}$La$_x$Al$_2$, extraordinary Hall effects, 4.2-300K, cryst. field interaction 78−79980
(Ce$_x$La$_{1-x}$)Al$_2$, inelastic neutron scatt. cross-section, effect of cryst. field 79−65642
Ce$_x$La$_{1-x}$Al$_3$, Kondo system, mag. susceptibility, 1.5 to 20K 79−78310
(Ce$_x$La$_{1-x}$)Be$_{13}$, mag. intermediate valence behaviour 79−24131
Ce$_{1-x}$La$_x$Sn$_3$ (x=0 to 1), mag. susceptibility and magnetisation, lattice parameters, X-ray and neutron diffr. meas. 80−49675
Ce$_{0.9-x}$La$_x$Th$_{0.1}$, mixed valence state, static and dynamic mag. response 80−103816
Ce$_x$(La$_y$Y$_{1-y}$)$_{1-x}$Al$_2$, local mag. moments, neutron scatt. study 79−61058
Ce$_x$(La$_{0.76}$Y$_{0.24}$)$_{1-x}$Bi, mag. phase diagrams 79−56535
Ce$_x$(La$_{0.76}$Y$_{0.24}$)$_{1-x}$Sb, mag. phase diagrams, exchange interaction variation-thermodynamic model 79−65673
CeM$_2$:Nd^{3+}, M=Ru, Rh, Ir, ESR investigation 79−78514
CeMM$_{0.8}$Sm$_{0.2}$Co$_5$, (MM=mischmetal), thermal props. *(German)* 77−8359
CeMg$_{12}$, reversible alloys, hydrogenation for H$_2$ storage *(French)* 79−74549
Ce$_x$Mg$_y$, hydrogen storage materials *(French)* 79−66419
CeMg$_2$Si$_2$ type structure, role of elongated rhombic dodecahedron in alloy structures 79−32946
CeMg$_{11}$V(Cr)(Mn)(Fe)(Co), hydriding and appl. in H$_2$ storage 80−51009
CeMn$_2$Si$_2$, cryst. and mag. struct. determ. 78−52225
CeMn$_2$(Si$_x$Ge$_{1-x}$)$_2$, Ce(Mn$_{1-x}$B$_x$)$_2$Si$_2$, (B=Fe, Cu) mag. props. 80−25134
CeNi$_2$-CePt$_2$ system, structural and mag. studies on valence behaviour of Ce 80−103809
CeNi$_3$, and ternary hydride, mag. props. 80−108007
CeNi$_x$, sorption at press. up to 1500 atm. 80−97819
Ce$_{4.5}$Ni, absorpt. of D, heats of reaction and equilib. press., T-getters for CTR 78−51683
CeNi$_4$Al, mag. susceptibility, H adsorption-desorption cycle effects 80−107990
CeNi$_{8.5}$Si$_{4.5}$, X-ray cryst. struct. determ. 80−88089
CePb$_3$, crystalline elec. field parameters, exchange and Coulomb contrib. 77−20278
CePd$_3$, dil., local mag. moments, neutron scatt. study 79−61058
CePd$_3$ fluctuating-valence compound, anomalous far IR absorption 80−66210
CePd$_3$, intermediate valence system, mag. neutron scatt. cross-section meas. 77−20552
CePd$_3$, magnetic neutron scatt. cross-section and linewidth, temp. depend. 77−63080
CePd$_3$, mixed valence cpd., theory of inelastic mag. neutron scatt. 79−15284
CePd$_3$, mixed-valence, 3d and 4d core levels, XPS study 80−89111
CePd$_3$, neutron scatt., spontaneous relax. of 4f magnetisation, interconfig. fluctuations 77−77025
CePd$_3$, susceptibility, sp. ht. and magnetisation 79−28512
CePd$_3$, tunnelling anomalies due to intermediate valence phenomenon 77−62873
CePd$_3$, unstable valence system, model for thermodynamics props. 77−69487
CePd$_3$-Er, dil., low field mag. susceptibility, electro-nuclear effects 80−60189
CePd$_3$-Er(Gd)(Yb), dil., EPR spectra 80−25201
CePd$_3$-Gd, EPR of Gd^{3+} impurities in host with interconfig. fluctuations 78−56377
CePd$_3$-Gd, ultralow interaction temp. and cryst. field effects for Gd impurities 79−61100
CePd$_3$-MPd$_3$ mixed valent systems, nonlinear conc. depend. of resist. 80−65528
CePd$_{3-x}$Rh$_x$, resistance behaviour and intermediate valence effects 79−78068
Ce$_{1-x}$Pr$_x$Al$_2$, mag. struct., comp. depend., neutron diffr. and mag. susceptibility meas. 80−50054
Ce$_{1-x}$Pr$_x$Al$_2$, mixed mag. phase at low temp. 78−68228

cerium alloys continued
$CePt_2$, ESR of Er^{3+} 79—87315
$CePt_3$, ^{195}Pt NMR and susceptibility meas. 77—63299
$CePt_5$, mag. susceptibility, 4.2 to 295K *(German)* 79—47233
Ce_3Pt_2, structure determ., rhombohedral Er_3Ni_2 type 77—80443
Ce_3Rh_2, structure determ., rhombohedral Er_3Ni_2 type 77—80443
$CeRh_{3\ x}Pd_x$, electronic and cryst. struct. comparison, catalytic behaviour 78—84398
$CeRh_{3-x}Pd_x$, lattice spacing and mag. suscept., effect of prep. and hydrogenation 77—58976
$CeRh_{3-x}Pd_x$, powdered alloys, catalytic behaviour correlation with electronic struct., lattice struct. and surface comp. 79—82181
$CeRu_2$, change of valence of Ce ions, induced by H absorption, supercond. disappearance 79—47185
$CeRu_2$, H absorption induced Ce valence change, mag. and supercond. props. 80—50042
$CeRu_2$, spin-pairing state investig. via Josephson current between weakly-coupled superconductors 77—47942
$CeRu_2$, type II supercond., ESR of Nd^{3+} meas. 79—28444
CeSb, commensurate-commensurate transitions and devil's staircase 79—78317
CeSb, ferromag., mag. excitation spectrum, inelastic neutron scatt. obs. 79—78352
CeSb, mag. phase transitions, zero applied mag. field 78—31070
CeSb, mag. transition, effect of applied mag. field 78—43590
$Ce_{1-x}Sc_xAl_2$, fluctuating valence system, quadrupole interaction temp. depend. 80—54972
$Ce_2Sc_3Si_4$, X-ray cryst. struct. determ. 80—92480
$CeSn_3$, crystalline elec. field parameters, exchange and Coulomb contrib. 77—20278
$CeSn_3$, field induced form factor, temp. depend. 79—78308
$CeSn_3$, induced magnetic form factor, polarised neutron studies 80—25078
$CeSn_3$, intermediate valence cpd., search for phonon anomalies, inelastic neutron scatt. 80—100317
$CeSn_3$, low temp. mag. behaviour, press. induced valence change 77—63078
$CeSn_3$, mag. susceptibility and magnetisation, lattice parameters, X-ray and neutron diffr. obs. 80—49675
$CeSn_3$, mixed valence cpd., electronic struct. and mag. props. 80—70649
$CeSn_3$, mode softening and elastic consts., acoustic vel. meas. 80—88242
$CeSn_3$, phase diagrams, lattice props., electron hole symmetry 79—91002
$CeSn_3$, polarised neutron study of induced magnetisation 80—34594
$CeSn_3$, valence instabilities 79—78546
Ce_5Sn_3, low temp. modification with tetrogonal struct. 80—1963
$Ce_{0.736}Th_{0.264}$, induced mag. form factor 79—78307
$Ce_{0.74}Th_{0.26}$, induced magnetic form factor, polarised neutron studies 80—25078
$Ce_{0.74}Th_{0.26}$, mixed valence alloy, spin dynamics 78—10708
$Ce_{0.8}Th_{0.2}$, inelastic neutron scatt. meas. 79—47066
$Ce_{1-x}Th_x$, mixed valence systems, spin dynamics and mag. ordering 78—68162
$CeTl_3$, mag. susceptibility, magnetisation, neutron diffr., elec. resist., and sp. ht. meas. 80—75733
$(Ce_xY_{1-x})Fe_2$, mag. susceptibility and Mossbauer meas., lattice parameters 80—97068
CeZn, cryst. field and exchange effects, inelastic neutron scatt. study 80—24855
CeZn, mag. struct. and cryst. field effects 78—52223
$(Co, Cu, Fe)_5Ce$, sintered permanent magnets, magnetic charact. 78—60608
$(Co,Cu,Fe)_5Ce$, sintered, mag. props. 78—68302
Co-Ce Mischmetal powder, sintering 77—21055
Co-Cu-Fe-Ce, mag. characteristics of sintered permanent magnets 78—60312
Co-Cu-Fe-Ce alloys, sintered permanent magnets, mag. characts. 77—43855
$(Co_{0.83}Cu_{0.17})_6Ce$, cryst. struct. and mag. props., decomp. during ageing *(Russian)* 79—37661
Co_4CuCe, cryst. struct., mag. characts., ageing and decomposition *(Russian)* 79—4272
$Co_4CuCe_{0.9}$, correl. of cryst. struct. and coercive force *(Russian)* 77—80962
Cr-Ce-N, Ce and N effects in ductile-brittle transition, microstruct., hardness, *(Russian)* 78—35497
Cr-V-Ce-N, (2.4 to 2.6, 1.7 to 2.3, 0.005 to 0.23 wt.%) V effect on hardness, and ductile to brittle transition temp. *(Russian)* 79—34138
Cu-Ce, effect of alloying additions on electrical cond., and mech. strength 78—44233
Cu-Ge-La, Cu+Misch metal, eutectic alloy, internally oxidised, mech props. *(Japanese)* 77—52411
$Dy_xCe_{1-x}Ru$, supercond., mag. order 79—87189
$Dy_xCe_{1-x}Ru_2$, supercond., mag. props. 79—11267
$Er_cCe_{1-c}Pd_3$, cryst. field spectra, neutron scatt. study 80—50047
Fe, cast, Ce effect on graphite nodularisation *(Japanese)* 77—55999
Fe, cast, Ce hypoeutectic, new phase formation sequence during crystallisation, X-ray obs. *(Russian)* 78—95731
Fe, cast, ferritic, Ce addition effect on impurity distrib. Mossbauer study *(Russian)* 78—18673
Fe, cast, modular graphite form., Ce effect *(Japanese)* 77—56000
Fe, cast, P and Ce effect on struct. *(Russian)* 79—52224
Fe, cast, spheroidizing effect of Mg and Ce modifiers 80—35193
Fe, cast hypoeutectic, Ce distrib. in graphite grains 80—100279
Fe-Cr-Al-Ce, Ce effect on high temp. oxidation 79—100301
Fe-Cr-Al-Ce, high temp. oxidation *(Japanese)* 78—11413
Fe-Si-Mn-C, east, Ce additions, nonmetallic inclusions *(Russian)* 78—19710
ε-FeTi, Ce addition effect on H_2 absorption capacity 79—61899
ε-FeTi, effect of Ce on H_2 absorption 79—73315
Gd-Ce, magnetocrystalline anisotropy, magnetisation and torque curve meas. 80—65859
$Gd_xCe_yLa_{1-x-y}Be_{13}$, high electron lattice relax., Gd EPR meas. 78—2736
$Gd_xCe_{1-x}Ru_2$, magnetic ordering by ^{155}Gd Mossbauer spectroscopy 78—27139
$Gd_xCe_{1-x}Ru_2$, coexistence of supercond. and spin glass mag. freezing 77—28283
$Gd_xLa_{1-x}Be_{13}$, high electron lattice relax., Gd EPR meas. 78—2736
Ge-Ce liquid alloys, enthalpies of mixing, exothermal effects *(Russian)* 80—34192
In_3Ce, nucl. orientation meas. 78—39415

cerium alloys continued
Ir-Ce (0.4 wt.%), field emission characts., crystallography and heat treatment effects 78—2994
$(La,Ce)Al_2$, conf. Kondo system, sp. ht. meas. 78—52210
$(La,Ce)Al_2$, magnetic impurity effect on thermal cond., normal and supercond. states 77—63027
$(La,Ce)B_6$ dil. alloy, Kondo effect, impurity-impurity interaction, mag. susceptibility, mag. to non mag. transition 78—47948
$(La,Ce)Ru_2$, supercond. transition temp., its press. depend., and structural phase transform. 78—6473
$(La, Ce)Sn_3$, dil. alloys, supercond. and normal state props. 78—76184
(La,Th)-Ce, dilute alloys, mag.-nonmag. transition of impurity moments, environment effects 77—40034
(La,Y)Ce, dil., Kondo supercond., transition temp., susceptibility and resist. 80—65733
La-Ce, dil., cryst. fields and Kondo effect 77—43809
La-Ce, Kondo system, intermediate temp. supercond. under hydrostatic press. 79—24097
La-Ce alloy, press. induced spin glass to Kondo phase transition, resist. meas. 79—24174
$La-Ce-Al_2$, dilute alloy, cryst. fields and Kondo effect 77—43809
La-Ni-Ce, H absorption for storage appls. 80—45790
La-P-Ce, dilute, NMR investig. of anisotropic cond. electron exchange 77—63309
$LaAl_3$-Ce, dil., linewidth of cryst. field excitations 78—67988
$La_{1-n}Ce_n$, supercond. mag. alloy, effect of interconfigurational fluctuations 78—19175
$(LaCe)Al_2$, unstable valence system, model for thermodynamic props. 77—69487
$La_{1-c}Ce_cAl_2$, Kondo superconductor, self-consistent theory of pairbreaking 78—26989
$(La_{1-n}Ce_n)_3Al$, mag. impurity effects in normal and supercond. state, NMR 78—2622
$(La_{1-x}Ce_x)Al_2$, Kondo supercond., tunnelling density of states 78—14900
$(La_{1-x}Ce_x)Al_2$, Kondo supercond., tunnel junction fabrication with wax barriers, tunnelling meas. 78—19191
$La_{1-x}Ce_xAl_2$, Kondo system, mag. susceptibility calc. in Anderson model 77—55661
$La_{1-x}Ce_xAl_2$, Kondo system, low temp. thermal expansion behaviour 79—19382
$(La_{1-x}Ce_x)Al_2$, Kondo system, antiferromag., specific heat 79—24179
$La_{1-x}Ce_xAl_2$, supercond., nucl. relax. and impurity magnetism 77—20495
$La_{1-x}Ce_xPd_3$, resistance behaviour and intermediate valence effects 79—78068
$La_{1-x}Ce_xSn_3$, electrical resist. and thermal expansion meas., 1.5-300K 80—34400
$La(Ce)Sn_{3-x}Pb_x$ system, mag. impurities in supercond., supercond. transition temp. and sp. ht. 78—39244
LaCeY, three normal supercond. transitions 78—26989
$La_{0.80}Th_{0.20}Ce$, re-entrant supercond. matrix-impurity system additive pair breaking 77—69460
$(La_{1-x}Th_x)_{1-n}Ce_n$, supercond. mag. alloy, effect of interconfigurational fluctuations 78—19175
$(La_{0.80}Y_{0.20})Ce$, three superconducting crit. point behaviour 78—10625
$La_{1-y}Y_y(Ce)$ system, mag. impurities in supercond., supercond. transition temp. and sp. ht. 78—39244
$(La_{1-x}Y_x)_{1-y}Ce_yAl_2$, resistivity meas., Kondo temp. enhancement 77—62917
Mg-Ce, appl. to H_2 storage 80—72093
Mg-Ce, diffusion coeff. determ. during hydriding *(German)* 79—29288
Mg-Ce, workability, aging characts. and tensile strength 80—55416
Mg-Mn-Ce, MA8, dislocations at grain boundaries and grain-boundary glide 78—64605
Mg-Mn-Ce, structural changes and deformation during superplastic flow 78—15472
Mg-Mn-Ce (1.5, 0.3 wt%), superplasticity role of diffusional creep *(Russian)* 80—97528
Mg-Mn-Ce (1.5%, 0.3%), dislocation slip during superplastic deform. *(Russian)* 77—21214
Mg-Mn-Ce alloy, superplastic deform., role of grain boundaries 78—19843
Ni-C-Ce, overmodification *(Russian)* 80—40432
Ni-Cr-Ce, Ce effect on oxidation 79—43484
Ni-Fe-Ce superalloy, vacuum melted, Ce effects on microstruct. 77—36552
Pb_3Ce, nucl. orientation meas. 78—39415
Pd-Ce (5.75 at.%), H_2 permeability and solubility, comparison with other Pd solid soln. alloys 79—23738
Pd-Ce alloy, SRO determ. 77—7738
Pr-Ce, mag. order onset, elec. resistivity 80—20416
Sb-Ce system, heats of form. 80—89517
$Sm_{1-x}Ce_xCo_5$, mag. props., domain boundary pinning on statistical conc. heterogeneities *(Russian)* 79—99728
$Sm_{1-u}Ce_u(Co_{1-x-y-w}Fe_xCu_yCr_w)_z$, permanent mag., improved mech. props. 79—87593
Sn-Ce system, heats of form. 80—89517
Th-Ce-H, hydride form. and supercond. 77—36007
Th-Y-Ce, supercond., magnetisation of Ce impurities, sp. ht. meas. 78—47904
$Th_{65}Sc_{35}Ce$, supercond., magnetisation of Ce impurities, sp. ht. meas. 78—47904
U-Ce-C system, phase equilibrium exam. *(German)* 78—23670
Y-Ce, dilute alloy, cryst. fields and Kondo effect 77—43809
Y-Ce, Kondo system, spatial extent of Ce moment, neutron diffr. meas. 78—68159

cerium compounds
see also cerium alloys
alkaline earth fluoride solid solns., $MF_2-UF_4-CeF_3$, surface degradation, complex admittance anal. 78—55980
antiferromagnetic Ce-group V cpds., temp.-renormalised longit. mag. excitations 77—51862
chalcogenides, low temp. thermal props. 78—84445
ethylsulphate, elec. susceptibility evidence for electronically driven lattice dilation 77—76781
formate, IR spectra and phase transitions, under pressure 78—31179
halides and oxides, stability study, energy difference between trivalent and tetravalent Ce states 78—79553
hexa-antipyrene iodide of Ce or CIP, heat transfer with dil. ^3He below 50 mK 79—51413
Kondo coupling, hyperfine and exchange interactions 79—65647

cerium compounds continued
- mixed valence compounds, charge dominated fluctuation props. comparison, mag. moments and ordering 80—54659
- monochalcogenides, cryst. field effects, phase transitions 80—24853
- monochalcogenides, mag. ordering, expt. test for ε-expansions with n=4 80—60259
- monopnictides, anomalous mag. props., planar coupling theory 80—60245
- monopnictides, cryst. field effects, phase transitions 80—24853
- pnictides, low temp. thermal props. 78—84445
- Si_3N_4-Ce_2O_3-SiO_2 materials: phase relations and strength 80—97465
- triindenylcerium pyridinate, X-ray cryst. struct. determ. 79—32984
- Al_2O_3-MgO/ZrO_2-CeO_2/MgF_2 triple layer antirefl. coating for crown glass in visible region 78—13777
- $BaTiO_3$-CeO_2 liquid immiscibility region, X-ray diffr. anal. 80—50611
- CMN-^{3}He, superfluid thermal boundary resistance, preliminary meas. 77—66060
- CMN-^{3}He(^{3}He-^{4}He), heat capacity and heat transfer meas. instrum. *(French)* 79—1097
- CaO-MgO-CeO_2, fired, phase equilibrium diagram, 1700 to 1200°C 78—92248
- (Ce,Ta)Ta_6O_{19}, disordered struct., convergent-beam electron diffr. symmetry 80—54178
- Ce complex, Ce (III) 1,2-dioxy-3-sulphoanthraquinone, soln., absorpt. spectra *(Russian)* 78—76975
- Ce-H(D), inelastic neutron scattering exam. of lattice dynamics 80—29128
- Ce-S system, L-X-ray absorpt. spectroscopy, conc. of ions with various numbers of f electrons 77—28646
- Ce-Si-Al-O-N ceramic, phase assemblages, relationships with props. 80—60848
- Ce_2ASe_5, A=Ge, Sn, diffuse refl. spectra and band gaps 79—51963
- $CeAl_2$, Anderson lattice system, mag. moment reduction, press. effects 80—7093
- $CeAl_2$, specific heat between 0.02 and 1K 79—1680
- CeAs, compressibility, room temp., from neutron diffr. meas. of lattice parameter variation up to 41 kbar 77—27940
- CeAs, evidence for valence fluctuations, ^{75}As Knight shift data 78—91966
- CeAs, low temp. thermal, elec. and mag. props. 78—27051
- CeAs, XPS exam. 79—38717
- CeAs, XPS for electronic struct. determ. 79—33888
- CeAsS, and homologs, struct. determ. *(French)* 77—51361
- CeB_6, anomalous sp. ht. intrinsic mag. phase transitions obs. 80—108027
- CeB_6, crystal preparation, elec. resistance, phase transitions 80—97427
- CeB_6, field emission patterns and emission characts. *(Japanese)* 77—85900
- CeB_6, mag. and electronic props. 80—71048
- CeB_6, magnetostriction, US absorpt. and thermal expansion 80—66004
- CeB_6, Raman spectra of phonons 79—82972
- CeB_6, resist. anomaly and mag. ordering obs. 79—61110
- CeB_6, single cryst. work function, thermionic emission, evaporation 77—24922
- CeB_6, single crystal growth for thermionic emission 78—92183
- CeB_6, thermionic emission rel. to surface state 78—39654
- CeB_6, work functions from thermionic and field emission retarding pot. methods 79—65537
- $Ce(BH_4)_3$, synthesis from chloride salts and $NaBH_4$ in tetrahydrofuran 80—30222
- $CeBO_3$:Tb^{3+}, vacuum UV excitation spectra and quantum efficiencies 79—28811
- CeBi, magnetoelastic effects, anisotropic mag. behaviour 80—25176
- CeBi, phase diagram in mag. field, hydrostatic press. effect 80—25132
- CeBi, thermal expansion, 20-800°C 79—14942
- CeBi, unusual anisotropy mechanism due to virtual valence fluctuation 80—96828
- $Ce_{1.25}Bi_{3.78}S_8$, cryst. struct. determ. *(French)* 77—80467
- CeBi(Sb), enhanced lattice-displacement effects on cryst. field and anomalous mag. anisotropy 79—73477
- $CeBi_xSb_{1-x}$, mag. props. and press. effects 80—71026
- $CeBr_6$, work function, thermionic and field emission retarding pot. meas. 77—90233
- $Ce(BrO_3)_3$-malonic acid, multiple stationary states in oregonator 78—20061
- CeC_2, mag. props. 80—108008
- $Ce(CO_3)_5^{6-}$, in Na and guanidinium salts, struct./props. correlation *(French)* 78—95032
- $Ce_{0.9}Ca_{0.1}O_{1.90}$, ionic cond. meas. 79—60543
- $CeCl_3$, complex Raman tensors, irreducible tensor method, antisymmetric scatt. 78—37623
- $CeCl_3$, doubly degenerate phonon states, mag. field dependent splitting 77—16320
- $CeCl_3$, mag. field depend. of polaritons 79—33246
- $CeCl_3$, Raman spectra circ. polaris., Faraday effect phonon state splitting 78—43855
- $CeCl_3(Br_3)$, interaction parameters, high freq. meas. of adiabatic differential susceptibility 78—68211
- $CeCl_3.7H_2O$, X-ray cryst. struct. determ. 79—46606
- $CeCrOS_2$, single cryst. X-ray diffr. struct. determ. *(French)* 79—23581
- $CeCrOS_2$, X-ray cryst. struct. determ. *(French)* 80—92485
- $CeD_{2.12}$, lattice vibrs., coherent neutron scatt. meas. 77—62598
- $CeD_{2.12}$, neutron cryst.-field spectroscopy 80—14967
- $CeD_{2.12}$, phonon dispersion relations 78—30716
- $CeD_{2.72}$, phonon dispersion relations 80—88287
- CeD_x, $1.94 \leq x \leq 2.74$, Ce^{3+} ground state crystal field splitting from inelastic neutron scattering 79—99517
- CeD_x, (x=1.94 to 2.75), phonon dispersion, crystal field splitting, neutron scatt. study 79—60452
- $Ce_xDy_{1-x}C_2$, mag. props. 80—108008
- $CeDyS_3$, cryst. struct. determ. *(French)* 78—6034
- $Ce_xEu_{1-x}B_6$, mag. susceptibility, 80-1000K 79—73674
- CeF_3, ^{19}F spin-lattice relax. and mag. couplings 79—65753
- CeF_3, CeF_3+, MS Xα electronic struct. calc., inner shell photoelectron spectra 77—10594
- CeF_3, coating materials for IR laser components 80—33105
- CeF_3, doped with aliovalent cation dopants, ionic cond. 77—20115
- CeF_3, Faraday rot., paramag. temp. *(French)* 79—65841
- CeF_3 film, in MIM struct., dielec. props. *(Czech)* 80—25309
- CeF_3 film, refr. index and struct., deposition temp. depend. 79—4857
- CeF_3, force consts., Coriolis coupling consts., vibr. amplitudes 78—17650
- CeF_3, ionisation energies, satellite struct., photoelectron spectra, MS Xα calcs. 78—13425

cerium compounds continued
- CeF_3 MIM structs., dielec. props. temp. irreversibility *(Czech)* 80—15616
- CeF_3, mol. consts., kinetic consts. and L-approx. methods 80—18839
- CeF_3, mol. force, compliance and Coriolis consts. 79—31726
- CeF_3, new coating materials for IR laser optical components 79—65821
- CeF_3, protective overcoating material for inhomogeneous interface laser mirror coatings 80—1252
- CeF_3:Pr^{3+}, absorpt. spectrum, 400-700 nm, 78K, 22 kbar press. effects 77—81133
- $CeFe_4As_{12}$, synthesis and cryst. struct. 80—84154
- $CeFeO_3$, enthalpy of formation determ. from heat of oxidation, calorimetric investig. 77—25300
- $CeFe_4Sb_{12}$, prep. and cryst. struct. 80—100211
- $CeFe_2Si_2$, CeFeSi, absence of effective mag. field at Fe nuclei *(Russian)* 78—19397
- $CeFe_2Si_2$, charge state of 3d shell, state of Fe atoms, atomic bonds *(Russian)* 80—47884
- $CeH_{1.98}$, $CeH_{2.98}$, elastic props. at high press. 77—84825
- $CeH_{2,2.7,2.96}$, low-temp. sp. ht., mag., elec., and cryst. field splitting effects 80—49379
- $CeH_{2.70}$, low temp. phase transition, sp. ht. meas. 78—47535
- $CeH_{2.70}$, sp. ht., 2 to 260K, second-order phase transitions and cryst. field splitting 79—82355
- CeH_4, Dirac-Fock one-centre calcs. 79—6837
- CeH_x, phonon features in IR and Raman spectra 80—93310
- $Ce(HPO_4)_2 \times 1.33H_2O$, crystalline, thermoanal. meas. 79—91938
- CeI^+, CeI_2^+ and CeI_3^+ formation in CeI_3 vapour by electron impact, APS 77—23567
- CeI_3 vapour, negative ion formation by electron irradiation 77—27190
- $Ce_5Ir_{3(4)}$, cryst. struct. determ. 80—64960
- $CeKFe(CN)_6.4H_2O$, struct., X-ray diffr. obs. 79—51065
- $Ce_x(La,Y)_{1-x}Sb$, and $Ce_x(La,Y)_{1-x}Bi$, antiferromag. spin arrangement, neutron diffr. obs. 77—63106
- $Ce_xLa_{1-x}B_6$ solid solutions, Weiss const. antiferromagnetic ordering calcs., mag. props. *(Russian)* 79—91212
- $Ce_cLa_{1-c}F_3$, Raman spectra circ. polaris., Faraday effect phonon state splitting 78—43855
- $Ce_xLa_{1-x}F_3$, paramag. mixed crystal, scattering of optical phonons by rare earth ions 78—68518
- $Ce_xLa_{1-x}F_3$, phonon self-energy and electron-phonon interaction 79—65159
- $(Ce_xLa_{1-x})_2Mg_3(NO_3)_{12}.24H_2O$, mag. susceptibility meas., AC method meas., appl. as thermometer in mK region 77—17999
- $(Ce_xLa_{1-x})_2Mg_3(NO_3)_{12}.24H_2O$, adiabatic demagnetisation temp., mag. entropy *(Russian)* 80—65892
- $Ce_xLa_{2-x}Mg_3(NO_3)_{12}.24H_2O$, magnetically diluted thermometer 79—17420
- $Ce_xLn_{1-x}P_5O_{14}$, UV luminescence lifetimes obs. 78—6775
- $CeMgAl_{11}O_{19}$:Tb^{3+} phosphors, for low press. fluoresc. lamps, luminesc. characts. 78—10960
- $Ce_2Mg_3(NO_3)_{12}$, AC mag. susceptibility, mag. field depend., 1-4K 79—56516
- $Ce_2Mg_3(NO_3)_{12}$, heat capacity meas., 0.15 to 0.6K, origin of anomaly 77 -35707
- $Ce_2Mg_3(NO_3)_{12}$, spin-lattice relax., dynamic susceptibility meas., liq. He contact effects 80—66011
- $Ce_2Mg_3(NO_3)_{12}.24H_2O$, Mandel'shtam-Brillouin light scatt. by hot phonons 77—52110
- $Ce_2Mg_3(NO_3)_{12}.24H_2O$, La diluted, mag. thermometry to below 1 mK 79—30469
- $Ce_2Mg_3(NO_3)_{12}.24H_2O$, pure and dil., heat transfer with dil. ^{3}He below 50 mK 79—51413
- $Ce_2Mg_3(NO_3)_{12}.24H_2O$ demagnetization cryostats, appls. of nucl. cooling in nucl. orientation studies 79—63230
- $Ce_2Mg_3(NO_3)_{12}.24H_2O$, EPR detection at mK temps. using SQUID magnetometer 79—63290
- $Ce_2Mg_3(NO_3)_{12}.24H_2O$, EPR of Ce^{3+} appl. of SQUID detection system 79—75560
- $Ce_2Mg_3(NO_3)_{12}.24H_2O$, ground state with dipole-dipole and exchange interactions in external mag. field 80—84582
- $Ce_2Mg_3(NO_3)_{12}.24H_2O$/He Kapitza resist., appraisal of expt. results 79—51414
- $Ce_2Mg_3(NO_3)_{12}.24H_2O$-^{3}He interface, Kapitza resist. around the mK, effect of ^{4}He impurity 79—55999
- $Ce_2Mg_3(NO_3)_{12}.24H_2O$-solid ^{3}He boundary, thermal contact below 35 mK 79—60598
- $Ce_2(MoO_4)_3$, crystn. from Na_2MoO_4 based melt 80—20920
- $Ce_6Mo_{10}O_{39}$, 22 77—76373
- $Ce_6(MoO_4)_8(Mo_2O_7)$, X-ray examination crystal struct. 78—67687
- $Ce_xMo_6Se_8$, mag. props., 0.7 to 295K 77—32113
- CeN, electronic struct., XPS exam. 78—6269
- CeN, interconfiguration fluctuation, temp. and press. depend. 79—38031
- CeN, m.p. N_2 press. depend., Pirani-Alterthum meas. 78—43103
- CeN, miscibility with UC *(German)* 80—96654
- CeN, optical props. and valence mixture 78—56450
- CeN, XPS exam. 79—38717
- CeN, XPS for electronic struct. determ. 79—33888
- CeN-RN systems, (R=La,Nd,Gd), mutual solubilities *(German)* 79—19374
- $CeNH_4P_4O_{12}$ and $Ce(NH_4)_2(PO_3)_5$, synthesis by solid-phase reaction, characts. 80—60778
- $Ce(NO_3)_3$:^{143}Pr, aqueous soln., mag. dipole moment of Pr 57 keV state, PAC meas. 77—46110
- $CeNbO_4$, cryst. chemistry exam. 78—38678
- $CeNbO_{4+x}$, oxidation-reduction reactions 78—39930
- $CeNbO_x$, redox processes, elec. resist., phase anal., mag. suscept., thermogravimetric meas. 78—34482
- $CeNb_3O_9$, $CeNbO_4$, $CeNbO_{7.6}$, electron config. of Ce ions, mag. sucept., L_3 absorpt. edge, resist. 79—43063
- Ce_3NbO_x, redox processes, elec. resist., phase anal., mag. suscept., thermogravimetric meas. 78—34482
- $CeNb_3Ox$, redox processes, elec. resist., phase anal., mag. suscept., thermogravimetric meas. 78—34482
- $CeNiC_2$, struct. determ. using X-ray diffraction *(Ukrainian)* 80—33949
- $Ce_6Ni_6P_{17}$, synthesis and cryst. struct. 78—75634
- CeO, C_1-X_1 and D_3-X_3 systems, fluoresc., vibr. spectra, laser spectroscopy obs. 80—32761
- CeO, dissoc. energy, rel. band strengths of a_2-X_2 and b_2-X_2 systems 80—99495
- CeO, fabrication of Fresnel lens for thin-film waveguide 78—94452

- **cerium compounds** continued
  - CeO, gas, electronic spectrum 79—41178
  - CeO, high press. synthesis, struct. and lattice consts. *(French)* 80—29913
  - CeO, identification in S-type stars, new s-process mol. 77—33488
  - CeO, identification in S-type stars 79—21280
  - CeO_2 additive to $Pb(Zr,Ti)O_3$ piezoelectric ceramic, effect on struct. and props. 79—52140
  - CeO_2, catalyst for reduction of NO by CO 77—81422
  - CeO_2, chemisorption of H_2, kinetics and characts. at different pressures and temps. 78—51821
  - CeO_2 coating of laser optical components, electron microscope obs. 80—43342
  - CeO_2 coatings on Gd-Fe amorphous films, Kerr magneto-optical effect enhancement 79—19866
  - CeO_2, conductivity at high O press. 77—20367
  - CeO_2 doped electrolyte cell, polarisation phenomena associated with CeO_2 reduction 80—55827
  - CeO_2, elec. cond. and dielectric props. at low temp. 78—72447
  - CeO_2 film, Rayleigh scatt., 441.6 nm, scatt. losses correl. with deposition parameters 79—78782
  - CeO_2 film, refr. index and struct., deposition temp. depend. 79—4857
  - CeO_2 in O_2 atmos., adsorption and elec. cond. props. 79—23836
  - CeO_2, ionic conduction, doping effects and defect interactions 80—19978
  - CeO_2, nonstoichiometric, defect struct. and elec. props. 79—60827
  - CeO_2, plasma deposition of crysts. and their characterisation 80—20800
  - CeO_2, rare earth doped, ionic cond. meas. 79—60543
  - CeO_2, single cryst. whiskers, electron field emission 78—27378
  - CeO_2, X-ray absorpt. spectrum, 4d absorpt. edge region, chem. binding effects 77—12467
  - $CeO_2:CaO(Y_2O_3)$, oxygen ion cond. and defect struct. 80—107553
  - $CeO_2:Nb_2O_5$, sintered, elec. cond. and solid solubility, 800 to 1329°C 79—99546
  - $CeO_2:S$, acceptor properties of S, free electron concentrations 80—34395
  - $CeO_2:S$, in $O_2+CO_2+SO_2$ atmosphere, elec. cond. study 80—39583
  - $CeO_2:S$, influence of S on elec. props. *(Russian)* 79—51566
  - $CeO_2:Y$, slow transient phenomenon 80—107550
  - $CeO_2:Y_2O_3$, bias sputtering, film growth and characts. 77—40366
  - $CeO_2:Yb^{3+}$, axial g-values of $4f^{13}$ ions with trigonal symmetry *(Korean)* 79—24135
  - $CeO_2:Yb^{3+}$, ENDOR, evidence for covalency 78—80247
  - $CeO_2:Yb^{3+}$, trigonal centres, point-charge approx. 78—39072
  - $CeO_2:Yb^{3+}$, trigonal sites of Yb^{3+}, ENDOR meas. 79—95677
  - CeO_2-La_2O_3 system, surface microphases investigation by X-ray electron spectral anal. 79—51269
  - CeO_2-$LaCrO_3$, and CeO_2-La_2O_3, quadrupole interactions and moments, ^{137}La Mossbauer obs. 78—27121
  - CeO_2-Mo-CeO_2 thin-film selective coatings for solar energy collectors 78—94422
  - CeO_2-PrO_x system, mixed cryst. phase characterisation 79—14936
  - CeO_2-rare earth oxides, complexes of the ‘two impurity ions-vacancy’ type 79—95004
  - CeO_2-SiO_2, RF cosputtered optical film, prep. and props. 78—6849
  - CeO_2-$SiO_2(MgF_2)$, multilayer refractory oxide interf. coatings 79—7192
  - CeO_2-Y_2O_3 film, surface characterisation, XPS, ESCA, and AES expts. 78—72028
  - CeO_2-Y_2O_3 solid soln. phases, synthesis 80—104132
  - CeO_2+SiC, high temp. chem. reactions, products obs. by X-ray diffr. 78—17312
  - CeO_2+ZrC, high temp. reactions 80—3320
  - CeO_{2-x}, $1.5<O/Ce<2$, physicochemical equilibria, statistical thermodynamics model *(French)* 78—38688
  - CeO_{2-x} $(0<x<0.3)$, oxidation-reduction study, Cahn electrobalance appl. 77—79084
  - CeO_{2-x}, conductivity and Seebeck coeff., small polaron and hopping mechanisms 77—76812
  - CeO_{2-x}, small polaron mobility, elec. cond. and nonstoichiometry meas. 78—47785
  - CeO_n, redox reactions, quasiisothermal thermogravimetric obs. 79—15980
  - Ce_2O_2, CeO_2, atomisation energies and stand. ht. of formation 77—54622
  - Ce_2O_3, hydrated, sorption props. rel. to dehydration conditions 79—66345
  - Ce_2O_5-P_2O_5 glass, crystallisation 77—51326
  - $Ce(OH)_3$, mol., XPES, satellite phenomena 79—27035
  - $Ce(OH)_3$, X-ray cryst. struct. determ. 80—19758
  - $CeO_2La_2O_3$, ceramic, thermal stability, sintering, deform., effect of La_2O_3 79—11532
  - Ce_2O_2S, free energy of formation and nonstoichiometry of CeO_2 79—83498
  - Ce_2O_2S-Ga_2S_3, exam. of preparation and props. *(French)* 78—80504
  - $Ce_4O_4S_3$ and $Ce_6O_6S_4$, synthesis and cryst. struct. *(French)* 79—32965
  - $Ce_4O_4S_3$, X-ray cryst. struct. determ., using Patterson and Fourier synthesis *(French)* 79—14753
  - $Ce_6O_6S_4$, X-ray cryst. struct. determ., Fourier and Patterson synthesis *(French)* 79—73139
  - $CeOSO_4.H_2O$, struct. refinement 77—15359
  - $3Ce_2O_3.2Si_3N_4$, ceramic, prep. by cold compaction and firing, struct. anal. 77—21070
  - $Ce_2O_3.2Si_3N_4$, preferred unit cell for indexing powder diffr. pattern 80—49200
  - $3Ce_2O_3.2WO_3$, X-ray charact. and thermal props. 77—43194
  - $CeOs_4As_{12}$, synthesis and cryst. struct. 80—84154
  - $CeOs_4Sb_{12}$, prep. and cryst. struct. 80—100211
  - CeP, compressibility, room temp., from neutron diffr. meas. of lattice parameter variation up to 41 kbar 77—27940
  - CeP, low temp. thermal, elec. and mag. props. 78—27051
  - CeP, XPS exam. 79—38717
  - CeP, XPS for electronic struct. determ. 79—33888
  - CeP(As)(Sb), microwave resist. meas. 77—4383
  - CeP_3O_9, X-ray powder data 79—51079
  - CeP_5O_{14}, photoemission spectra, 4f, 5p and 5s giant reson. enhancement 78—95660
  - $CeP_5O_{14}:Gd^{3+}$, EPR and emission spectra *(French)* 77—69686
  - CeP_5O_{15}, IR absorpt. and luminesc. spectra 80—55079
  - $CePd_3$ single crystal Czochralski growth and characterisation 80—60767
  - $CeRe_4Si_2$, cryst. struct. determ. 78—2098
  - $CeRu_4As_{12}$, synthesis and cryst. struct. 80—84154
  - $CeRu_4Sb_{12}$, prep. and cryst. struct. 80—100211
  - CeS, mag. props., sp. ht. and thermal expansion 78—60292

- **cerium compounds** continued
  - CeS, resistivity and volumetric meas., phase diagrams, comparison with $CeAl_2$ 80—107789
  - CeS_2, orthorhombic, prepared at 1773K and 5.5 GPa X-ray single cryst. struct. determ. 79—19198
  - Ce_2S_3-1.8 Ga_2S_3 glass, vibr. spectra, electronic transitions, short range order 77—69820
  - Ce_2S_3-Ga_2S_3 system, phase diag. *(French)* 78—3108
  - $Ce_{3-x}S_4$, $Ce_{3-x}Sm_xS_4$, elec. cond. mechanism, thermoelec. power, Hall and absorpt. coeffs. 77—24559
  - $Ce_{3-x}S_4$, mag. ordering and elec. cond. 78—10681
  - $Ce_2(SO_4)_3$ soln., adiabatic and apparent molal compressibility determ. from US vel. meas. 78—63797
  - $Ce_2(SO_4)_3.8H_2O:Gd^{3+}$, single cryst., EPR study, spin Hamiltonians 80—80606
  - $Ce_2(SO_4)_3.9H_2O$, grown from solution, exam. of Raman spectra and physical props. 79—52104
  - $Ce_2(SO_4)_3.9H_2O(D_2O)$, polarised Raman spectra, vibr. props. and role of lattice H_2O 80—66201
  - CeSb, antiferromag., first-order transitions, mag. phase diagram 80—60252
  - CeSb, commensurate-commensurate transitions, devil’s stairs theory 79—19740
  - CeSb, compressibility, room temp., from neutron diffr. meas. of lattice parameter variation up to 41 kbar 77—27940
  - CeSb, crystal field effect in thermal expansion 78—19305
  - CeSb, forbidden band gap and electrotransfer parameters 80—39497
  - CeSb, mag. excitations dispersion 80—25121
  - CeSb, mag. phase diagram and mag. struct., neutron diffr. determ. 77—63182
  - CeSb, mag. phase diagram for mag. field applied along ⟨111⟩ direction 79—33458
  - CeSb, magnetoelastic effects, anisotropic mag. behaviour 80—25176
  - CeSb, phase diagram and mag. struct. 77—85422
  - CeSb phonon dispersion curves, lattice dynamics of rare-earth monopnictides 79—37780
  - CeSb, press. effect. on mag. props. 78—23315
  - CeSb, unusual anisotropy mechanism due to virtual valence fluctuation 80—96828
  - CeSb, XPS exam. 79—38717
  - CeSb, XPS for electronic struct. determ. 79—33888
  - $CeSb_XAs_{1-x}$, mag. props. and press. effects 80—71026
  - $Ce_{1-x}Sc_xPd_3$, intermediate valence of Ce, susceptibility, lattice const., ESR meas. 80—103648
  - CeScSi, Laue obs. of crystal structure *(Ukrainian)* 79—51064
  - CeSe, mag. ordering, expt. test for ε-expansions with $n=4$ 80—60259
  - CeSe, mag. ordering, ε expansion predictions, neutron diffr. obs. 79—61060
  - CeSe, mag. props., sp. ht. and thermal expansion 78—60292
  - Ce_2Se_3-$SnSe_2$, solid-solution region, physical properties 78—43391
  - $Ce(SeO_4)_2.4H_2O$, cryst. struct., X-ray powder diffr. meas. 78—34483
  - $CeSiO_2N$, cryst. struct. 78—10017
  - $CeSiO_2N$, cryst. struct. 78—10018
  - $CeSiO_2N$, cryst. struct. 78—10019
  - $Ce_4Si_2O_7N_2$, crystal struct., resemblance with lanthanite and yttrium analogues 80—39035
  - $Ce_4Si_2O_7N_2$, lattice consts., X-ray diffr. anal. 80—28986
  - $Ce_4Si_2O_7N_2$, preferred unit cell for indexing powder diffr. pattern 80—49200
  - $Ce_5(SiO_4)_3N$, X-ray powder diffr. data 80—39036
  - $Ce_{4.67}(SiO_4)_3O$, role in densification of Si_3N_4 79—61549
  - $Ce_ySn_xMo_6S_8$, supercond. props. 80—97023
  - CeT_2, ^3He detrapping and release after ^3H decay, strain model 77—60101
  - $CeTaO_4$, $CeTa_7O_{19}$, cryst. chemistry exam. 78—38678
  - $CeTaO_{4+x}$, oxidation-reduction reactions, phase equilibrium, thermogravimetry and magnetic susceptibility meas. 78—39930
  - $CeTa_7O_{19}$, crystal struct. 79—60323
  - CeTe, mag. ordering, expt. test for ε-expansions with $n=4$ 80—60259
  - CeTe, mag. ordering, ε expansion predictions, neutron diffr. obs. 79—61060
  - CeTe, mag. props., sp. ht. and thermal expansion 78—60292
  - $CeTiNbO_6$, electrophys. props. 78—23388
  - $CeTiO_3$, water-splitting reactions for thermochem. H_2 prod. 80—55929
  - $CeTi_2O_6$, cryst. chemistry exam. 78—38678
  - $Ce_2Ti_2O_7$, ferroelec., layer type struct., cryst. growth 80—108348
  - $Ce_2Ti_2O_7$, ferroelec., temp. depend. of SHG intensity 79—24267
  - $CeVO_4$, monazite struct., IR and NMR spectra 79—78534
  - $CeVo_3$, phase transitions and Jahn-Teller distortions 79—28548
  - $Ce_2(WO_4)_3$, mag. susceptibility, paramag. Curie temp., 300-900K 79—82753
  - CeX ($X=P$, As, Sb, Bi), neutron inelastic scatt. expts. 80—19674
  - $Ce_{0.08}Y_{0.92}Sb$, dilute f-electron system in cluster regime, crystal field and exchange splittings 80—97062
  - $CeYb_3S_6$ type mixed sulphides, struct. organisation *(French)* 77—11519
  - $^{144}CeO_2$, effects of repeated inhalation exposure, mouse obs. 80—104676
  - $^{144}CeO_2$, inhalation by mouse, effect on pulmonary clearable of S. aureus 80—36013
  - $^{144}CeO_2$, repeated inhalation exposure of mice, retention and dosimetry 80—109034
  - CrF_3, gamma-ray effects, absence of coloration 77—35586
  - Eu-Ce-Fe-O system, solid solns. of ferrogarnet and ferroperovskite type 78—27488
  - HfO_2-CeO_2, solid solutions 77—16549
  - $K_2CeSi_6O_{15}$, cryst. struct., X-ray diffr. meas. 78—18619
  - $K_2CeSi_6O_{15}$, synthesis and X-ray structural anal. 78—2096
  - K_2O-BaO-SiO_2-$Ti(Ce)O_2$ laser glasses, TiO_2 and CeO_2 antisolarisation additive effects 79—94309
  - $(La,Ce)B_6$, low temp. mag. props. 79—61043
  - $La_{1-x}Ce_xB_6$, Kondo system, low-field impurity susceptibility, 0.03 to 8K 77—63095
  - La_2O_3-CeO_2, microstruct. of La_2O_3 rich crystallites, electron microscopy and diffr. *(French)* 78—35374
  - $(La_2O_3)_{1-x}$-$(CeO_2)_x$:Mn, valence state of Mn, effect of annealing in H_2 atm., ESR obs. *(French)* 80—71164
  - $(La_2O_3)_{0.95}(CeO_2)_{0.05}:Mn^{2+}$, X-band EPR study 80—60409
  - $La_{1-x-y}Pr_xCe_yCl_3$, satellite lines in optical absorpt. spectra, Zeeman effect 79—65912
  - $(NH_4)_2Ce(NO_3)_6$, acid soln. photolysis, NO_3 radical study 79—52717
  - $(NH_4)_2Ce(NO_3)_6$, proton spin-lattice relax., temp. depend. 79—42859

cerium compounds continued
- $NaCeS_2$, mag. susceptibility, 3.7 to 297K, extended mol. field model 79-87227
- $Na_3La_{1-x-y}Ce_xTb_y(PO_4)_2$, optical props. *(French)* 80-103991
- Na_2O-SiO_2:Au+CeO_2, Au particle nucleation 80-81066
- Nd:glass:CeO_2, TiO_2, lasing action, stabilisation *(Russian)* 78-13715
- $Pb(Fe_{1/2}Nb_{1/2})O_3$-$La_2O_3(CeO_2)$ ferroelec. ceramics, electrophysical props. 78-35099
- Si_3N_4-CeO_2, hot pressed, sintered, microstruct., flexural strength and fractographic anal. 80-40293
- Si_3N_4-CeO_2, surface stress development during oxidation 80-50736
- Si_3N_4-CeO_2 additive, hot-pressing and oxidation behaviour 80-71618
- Si_3N_4-SiC-Ce_2O_3, reactively sintered, microstruct. and strength 80-25631
- SrF_2:CeF_3, absorpt. spectra of γ-irrad. cryst., 77K, 200-700 nm 78-84615
- (U,Ce), U self-diffusion 80-92711
- UO_2-20CeO_2 mixed powder, X-ray and microprobe exam. of homogenisation 80-25609
- Y-W(Mo)-B, phase equilibria, struct. of crysts. 77-21122
- ZnS-CeF_3, single-layer vac. antirefl. coatings for near IR spectral region 80-33099
- $ZrH_mCe_n(PO_4)_2.XH_2O$, cryst., self-diffusion of Ce^{3+} ions 78-34648
- ZrO_2-Ce_2O_3, stabilised, reaction with Cr_2O_3 77-36438
- ZrO_2-CeO_2, semiconducting ceramics, electronic conductivity and oxido-reduction *(French)* 78-26919

cermets
- adhesion mechanism for metallization of electronic ceramics, elec. props. *(German)* 80-76381
- armour, lightweight, appls., ballistic tests, computer simulation, book contrib. 78-48556
- cemented carbide, porosity 77-59722
- cemented carbide, simple evaluation method 77-32748
- cemented carbides, physical and chem. nature 80-76265
- dielectric constant, Maxwell-Garnet and effective medium theories 77-47760
- effective bulk dielec. const., analytical props. 78-56414
- effective medium theory: mathematical determination of the physical solution for the dielectric constant 80-93230
- electrodeposition, effect of electrolyte in charge carried by suspended ceramic particle 78-68665
- film, as solar selective absorbers, production, struct. and optical props. 79-29485
- film, dense, regular, optical props, rel. to appl. as selective solar absorber 79-79408
- film, elec. props., effect of distrib. of particle size 77-66209
- flame heated thermionic convertors, development of cermet electrodes 80-40891
- gas turbine engine, substitution of ceramics for high temp. alloys 80-97678
- GCFR cermet cylindrical core swelling *(Russian)* 79-13425
- granular media, dielectric function theory, permittivity, percolation transport props. 80-88498
- grinders with fillers, performance 77-72103
- high-temperature materials, technological requirements, R and D, report 80-45222
- high-temperature phenomena, conf., Helsinki, Finland, June 1975 77-52295
- laminated cermet coating on Cu, thermal shock performance 78-7081
- layers deposited by silk-screen printing, microscopic struct. obs., cond. matrix form. mechanism *(Czech)* 77-48386
- metal-insulator composite solar selective absorbers optical props. 79-52037
- porcelain-metal cermet, stress determ., meas. method *(German)* 80-76425
- porous cermet, heat transfer and stability for moving evaporating coolant 80-64563
- production by electrodeposition of ceramic onto metal electrodeposit 79-33992
- rare earth chromite based electrode material development for MHD generators 80-84893
- sintering, optimum conditions for electric heating elements 77-90287
- small particle composite, optical properties from periodic multiple scatt. theory 78-56444
- solar selective absorber design, optimal comp. profiles for max. solar absorptance 80-101129
- steel, high-speed, sintered, refractory carbide additions effect on hardness and cutting performance 77-66608
- tunnel conduction, temp. depend. 77-20467
- Ag-CdO, coprecipitated carbonates and hydroxides, physicomech. props. 80-25706
- Ag-MgF_2 layered system, optical excitation of surface plasma waves 78-6803
- Ag-SiO_2 cermet film, optical props., comparison of effective medium theories 79-24379
- Ag-SiO_2 film, elect. and struct. props., ion beam sputtering 78-80071
- Al-Fe_3O_4 binary thermite powder mixture, compaction 79-74125
- Al-SiC cermet elasticity, porosity meas. by US means 80-81101
- AlN-Mo cermets, ZrO_2 and mullite whisker reinforced, strength var. with temp. 80-104232
- $Al_{2+x}O_3$, sintered, elec. cond. temp. and comp. depend., thermoelec. power 80-2438
- Al_2O_3 based cermet, protective coating for blast furnace tuyeres *(German)* 79-66193
- Al_2O_3/Al clad powder prep. and physicomech. props. 79-29010
- Al_2O_3/Nb, fracture mech. parameter determ. at high temps. *(German)* 79-70136
- Al_2O_3-Au, cermet coatings, solar energy photothermal conversion, Bruggeman effective medium theory 79-83627
- Al_2O_3-Au cermet, optical constants, incl. proximity effects 78-56446
- Al_2O_3-Cr cermet, Ti effect on sinterability 79-61552
- Al_2O_3-Fe cermet, microstruct. and physical props. 79-42279
- Al_2O_3-Mo, dielectric cermet, thermophysical props. 77-51557
- Al_2O_3-Mo (20 wt.%) cermet, ZrO_2 crystal addition effect on thermal fatigue resistance 80-40528
- Al_2O_3-Mo cermets, effect of processing factors on props. 79-100103
- Al_2O_3-Mo cermets, ZrO_2 and mullite whisker reinforced, strength var. with temp. 80-104232
- Al_2O_3-Nb, cermet thin film, electrical transport and thermoelectric power 77-20462

cermets continued
- Al_2O_3-Nb, dielectric cermet, thermophysical props. 77-51557
- Al_2O_3-Ni cermets, prep. and props. *(French)* 80-20877
- Al_2O_3-Pt metal-ceramic reaction, micro/macro obs. 80-66467
- Al_2O_3-W, dielectric cermet, thermophysical props. 77-51557
- Al_2O_3-W cermet, phase bonding 78-52745
- Al_2O_3-W cermet, sintered pressed compact, compressive and transverse rupture strength 78-19850
- Al_2O_3+W interaction, 2200 to 3200°C *(Russian)* 79-39194
- $Al_2O_3(Al_2O_3$-MgO)-Ag(Au)(Cr)(Cu) cermet selective surfaces for evacuated solar collectors 79-43785
- Au-Al_2O_3 film, dense, regular, optical props., rel. to appl. as selective solar absorber 79-79408
- Au-dielectric cermets, optical constants, incl. proximity effects 78-56446
- Au-WO_3, electrochromic material, optical and electrical props. 79-33674
- Au-WO_3, electrochromism 77-90129
- Au-WO_3 electrochromic cermets, resist. and optical density meas. 79-8201
- B_4C-304 stainless steel cermet for nuclear shielding appls. 80-102352
- B_4C-Cu cermet fabrication for neutron shielding appls. 80-102354
- BaO-Al_2O_3-SiO_2-Ta_2O_5-Mo glass ceramic metal composites, cermet prep. 80-11618
- BamSrmPb hexaferrites, prep. by cernet procedure, mag. props. 77-32174
- Bi-SiO_2 cermet films, elec. and optical props. 79-78775
- $Bi_{0.52}Sb_{1.48}Te_3$-Te, phase-equilibrium boundary, Hall coeff. meas. 78-44094
- Cr, powder, plasma deposition for production of contact portions of cermet electric heating element 78-11364
- Cr-Al_2O_3 powder targets for plasma-ion spray deposition of resistance films 80-84897
- Cr-Cr_2O_3, black chrome electroplating for solar energy photothermal conversion, prep. and struct. 79-74544
- Cr-Cr_2O_3, black chrome electroplating for solar energy photothermal conversion, optical props. 79-74545
- Cr-Cr_2O_3, chrome black, electroplated selective surface, thermal emittance, solar absorpt., refl., and roughness 79-79406
- Cr-Cr_2O_3 composite mixture, preferential sputtering, XPS expts. 79-87544
- Cr-$NdAlO_3$, dielectric films, phase composition and structure 80-39464
- Cr-SiO cermet film, silicide form. during deposition 77-12535
- Cr-SiO cermet thin films, thickness effect on density, resist., adhesion and annealing coeff. 77-69432
- Cr-SiO film, elec. props., effect of P^+ and Ar^+ implantation 79-11239
- Cr-SiO film, RF sputtered, substrate bias effect obs., on electrical resistivity 78-60573
- Cr-SiO_2 film, deposition by RF sputtering of powder target, elec. resist. and TCR 79-78890
- Cr_2O_3/Cr cermet film, RF sputtered, for selective black absorbers 78-30046
- Cr_2O_3/Cr solar-absorber surfaces, chemical and struct. anal. 79-95283
- Cr_2O_3-Cr, RF sputtered cermet film, selective black absorber 77-58399
- Cr_2O_3-Cr black, selective coating, optical and topographical props. 80-26165
- Cr_2O_3-Cr cermet films, for selective black absorbers 79-29483
- Cu-Al_2O_3, composite coatings, prep. by precip., props. 78-23841
- Cu-Al_2O_3 cermet films, temp. depend. of AC and DC cond. 79-87166
- Cu-Al_2O_3 film, solar absorbing, production by dual cathode DC magnetron sputtering 80-16186
- Cu-Al_2O_3 thin film ceramets, TEM study of composition and struct. 79-99437
- Eu_2O_3/metal cermet prep., in situ deposition of metal coating and hot pressing 77-32713
- Fe-Al_2O_3 granular film, interface props., Mossbauer spectroscopy 80-34336
- Fe-Fe_2O_3 composite mixture, preferential sputtering, XPS expts. 79-87544
- Fe-SiO_2 film, solar absorbing, production by dual cathode DC magnetron sputtering 80-16186
- Fe-SiO_2 granular film, interface props., Mossbauer spectroscopy 80-34336
- Fe-$SiO_2(Al_2O_3)(ZrO_2)$ granular films, superparamag., Mossbauer effect 80-7131
- Fe-ZrO_2 granular film, interface props., Mossbauer spectroscopy 80-34336
- $(Fe$-$Ni)_{1-x}(SiO)_x$, cermet film, internal strsses *(Russian)* 78-75951
- GeTe, nonstoichiometric, homogenisation 78-44004
- $GeTe_x$ cermet specimens, density, 25 to 412°C, depend. on nonstoichiometry and annealing temp. 77-25004
- KCl-Al composite, optical and IR reflectance 78-56465
- KCl-Al(Pd) composite, far IR absorption 78-56466
- $LaCrO_3$-Cr effect of explosive compacting on props. 77-12557
- Mg-MgF_2, sputtered films, opt. props. 78-80430
- MgF_2-Au, cermet coatings, solar energy photothermal conversion, Bruggeman effective medium theory 79-83627
- MgO/Ni-Cr (80, 20 wt.%) cermets, sintered, elec. resist. temp. effect 80-3206
- MgO-Au, cermet coatings, solar energy photothermal conversion, Bruggeman effective medium theory 79-83627
- MgO-Au cermet film, high intensity electron bombard. effect on secondary electron yield 77-81184
- MgO-Au cermet film, selective black absorbers 77-1747
- MgO-Au cermet films, for selective black absorbers 79-29483
- MgO-Pd metal-ceramic reaction, micro/macro obs. 80-66467
- Mn-MgF, cermet film, evaporated, variation of elec. resist. with prep. conditions 77-43746
- Mn-MgF, cermet film, variation of resist. with deposition rate 77-43747
- Mn-MgF_2 cermet, heat treated, lattice distortion, resist. meas. 79-19492
- Mn-MgF_2 cermet film, resistivity-temperature variation 79-24085
- Mn-SiO, annealed cermet films, elec. resist., composition depend. 80-97007
- Mn-SiO cermet film, silicide form. during deposition 77-12535
- Mn-SiO cermet films, DC and AC resist. 80-54804
- Mn-SiO cermet films, elec. resist., annealing behaviour 80-54803
- Mn-SiO cermet thin film, DC resist., activation energy, thickness depend. 80-84518
- Nb-Al_2O_3 cermet-type film, thermoelec. power and annealing effects 77-47911
- Nb-Al_2O_3 composite, semicond. films, cond. on localised states 77-24628

cermets continued
  Ni cermet selective absorbers, photothermal conversion appls. 80—21413
  Ni-Al_2O_3, fabrication and mech. characts. 79—38781
  Ni-Cr-Al_2O_3 powder targets for plasma-ion spray deposition of resistance films 80—84897
  Ni-Cr-MgO system, elec. resist. variation with comp. and prep. method 78—60637
  Ni-NiO composite mixture, preferential sputtering, XPS expts. 79 87544
  Ni-NiO_x-NiS_y, black Ni, struct.-depend. thermal and optical props., rel. to solar thermal conversion 79—79404
  Ni-SiC composite coatings, phase composition calc., wear resistance *(Russian)* 79—11709
  Ni-SiO cermet film, elec. resist., percolation effects 77—76954
  $Pb_3Rh_7O_{15}$ thick film, temp. coeff. of resist., cond. mech. 78—84315
  Pt-SiO_2 cermet films, struct. and props. 80—96956
  Pt-WO_3, electrochromic material, optical and electrical props. 79—33674
  Re+rare earth oxide cermets, prep. and props. 78—27466
  SiC, wetting by Cu-Ti and Cu-Sn-Ti melts 78—68664
  SiO_2-Ag, CW CO_2 laser deposited dielect. thin film, optical and struct. props. 80—7506
  Ta(C,N)-Ni-HfC(HfN)(Mo_2C)(VC), sintering, prod. of hard metals 78—11155
  TaC-NiC, powder for plasma arc spray coating appl. 78—15591
  (Ti,Cr)B_2, sintering kinetics and props. 80—100811
  (Ti,V)C carbides, prep. and mech. props. 78—64518
  Ti-Cr_3C_2 composite, TiC and struct. form. during sintering 79—29011
  TiC film, Au-dispersed, struct., hardness and wear rate 77—77493
  TiC-Mo_2C-Ni cermets, influence of anomalous phases on strength 78—92228
  TiC-Ni, reaction kinetics under simulated liq.-phase sintering 78—52746
  TiC-Ni-Cr(Mo) hard alloy mixtures, pressing 77—63596
  TiC-steel alloys, structure formation during sintering 77—59732
  TiC-steel cermet with Cu additions, precip. hardening and ht. treatment temp. 77—40414
  TiC-VC(ZrC) carbide alloys, thermophys. props., temp. depend., specific elec. resist. 79—86908
  $TiCrB_2$-Ni(Ni-Mo) systems, interphase reactions, electron probe anal., metallography and hardness exam. 80—2990
  U_3O_8-Al cermet fuel for research reactors 79—9835
  (V,Ti)C+(Ni,Mo) cermets, carbide-binder interface ledges 80—29283
  (V,Ti)C+Ni cermet, binder grain size 80—44401
  VC-Ni, fracture mode determination, using Auger electron spectroscopy 80—7680
  W-Al_2O_3 cermet films, oxide evaporation deposited on Mo, Ti, Al_2O_3 substrates, struct., props. 80—25581
  W-SiO_2 film, deposition by RF sputtering of powder target, elec. resist. and TCR 79—78890
  WC, friction against FeO compacted powder, effect of wall groove orientation and wall lubricants 78—23831
  WC-Co, dynamic SEM wear obs. 77—36667
  WC-Co, fracture mode determination, using Auger electron spectroscopy 80—7680
  WC-Co, rupture of bending specimens, use of quantitative metallography and stereology *(French)* 77—28899
  WC-Co (10 wt.%), vacuum sintered, short-time bending creep rupture strength *(Japanese)* 78—15508
  WC-Co alloys, microstresses in two phases, mag. investig. 77—59879
  WC-Co cemented carbides, effect of Co form and distrib. in prep. starting mixture 78—44072
  WC-Co hard alloy, preheating influence on explosive shock hardening *(Russian)* 79—29083
  WC-Co hard metal, stress conc. factor and stress intensity factor, rel. to wear *(German)* 78—11335
  WC-Co hard-alloy cermets, strength, fatigue, static tests 79—29314
  WC-Co hardmetal, defect initiated fracture and bond strength 78—11319
  WC-Co sintered carbide tips, microscopic stress anal. 78—5663
  WC-Co-Cu, interdiffusion up to 1120°C 78—11492
  WC-TiC, powder for plasma arc spray coating appl. 78—15591
  WC-TiC-Co, powder for plasma arc sprayed coating 78—15591
  WC-TiC-Co alloys, microstresses in two- and three-phases, mag. investig. 77—63758
  WC-TiC-TaC, powder for plasma arc spray coating appl. 78—15591
  $YCrO_3$-Cr (40 wt.%) cermet, effect of Cr preoxidation on props. 79—87603
  ZrB_2-Nb, reactions between components 80—100812
  ZrB_2-SiC-C(-V)(-Nb), refractory cermet, hot pressing and oxidation resist. 80—3231
  ZrB_2-ZnS:Ag(Ag,Ni)-glass binder, thermally stable, comp. 77—63617
  ZrC based cermets, strength and gas-abrasive wear resistance 77—25163
  ZrN-Mo, cermet, sintering reaction thermodynamics 80—2989
  ZrO_2/Al clad powder prep. and physicomech. props. 79—29010
  ZrO_2-Ta and ZrO_2-Y_2O_3-Ta aligned eutectic composites, solidification and fracture behaviour 77—48387
  ZrO_2-W, eutectic microstruct. 78—27499
  ZrO_2-Y_2O_3/metal cermet prep., in situ deposition of metal coating and hot pressing 77—32713
  ZrO_2-Zr cermet composite, hot pressed, fracture toughness 78—27604

CESR
  alkali halide, CESR of dendritic metal phase precip. 77—24744
  casein-methylglyoxal complex, electronic props. 77—52736
  chars, heat treatment, EPR rel. to temp., spin centres 78—48036
  degenerate semiconductor, conduction electron acoustic spin resonance, oscillations of absorbed power 80—108075
  density matrix formalism for coupled dynamical systems 78—95522
  Fabry-Perot resonator for CESR studies at 34 GHz 80—37065
  ferromagnetic semiconductor, CESR in strong alternating electric field 78—35038
  ferromagnetic semiconductor, CESR line width, two-magnon exchange splitting 80—29621
  p-GaAs, spin relaxation of photoelectrons 77—85207
  graphite intercalation compounds with acceptor molecules, CESR 78—48042
  II-VI semiconductors, electron-electron spin-flip scatt. and spin relax. 80—44916
  III-V semiconductors, k.p perturbation theory 77—43484
  III-V semiconductors, optical detect. of CESR, giant Overhauser shifts 78—80251
  III-V semiconductors 80—44916

CESR continued
  line profile, indirect spin spin interaction 79—28616
  line-width and g-shift anisotropy, singularities, appl. to Ag 77—20705
  metal, CESR and inhomogeneous broadening due to local moments 79—99769
  metal, CESR for arbitrary probability of scattering at surface *(Russian)* 78—68378
  metal, CESR line shape, strong surface relax. case *(Russian)* 78—56378
  metal, paramagnetic, CESR spin-orbit perturbation, spin-phonon scatt. 77—63285
  metal, spin scattering and spin-orbit coupling 80—29369
  metal, surface scattering of conduction electrons and kinetic phenomena *(Russian)* 79—56210
  metal CESR, mm waves, surface effects 80—66036
  metal colloids in ionic cryst., preparation, optical, mag. resonance, elec. props. 80—59459
  metal film, CESR line width and shape, surface relax. contrib. *(Russian)* 77—32260
  metal particles, conduction electron spin echo modulation, theory 80—39872
  metal spherical particles, CESR line shape 77—43886
  metals, cond. electron and spin scatt. due to dislocations 80—75856
  metals, conduction-electron spin flip by phonons, expt. data anal. 79—61219
  metals, non-S-state impurities, coupled ESR 79—47326
  metals, paramagnetic, conduction electron spin transmission 77—69693
  metals, surface relax. time of conduction electron spins 78—91814
  modulation technique for CESR cavities 77—37956
  narrow band gap semiconductors effects, review 79—95437
  nonferromagnetic metal, two-component electron Fermi fluid, in mag. field *(Russian)* 77—20252
  optical detection of ESR, in excited states *(Japanese)* 77—81029
  particles, quantum size effect obs. by CESR and NMR 77—20700
  pure metal, derivation and validity of Elliott relation 79—19780
  rare earth alloys, cryst. field effect on EPR and NMR 78—56391
  relaxation times for cond. electrons due to indirect spin-spin interaction via phonon field *(Russian)* 77—90035
  semiconductor, conduction electron paramag. relax., Coulomb mechanism 78—88191
  semiconductor, mixed, EPR theory 78—39402
  semiconductor, paramagnetic phonon resonance, theory 80—50187
  semiconductor, spin-depend. recomb. effect 78—34841
  semiconductor without inversion centre, conduction electrons spin relaxation *(Russian)* 78—52355
  semimetal, degenerate, conduction electron acoustic spin resonance, oscillations of absorbed power 80—108075
  superconductor, slightly dirty, CESR due to exchange and spin-orbit scatt. 77—28300
  superconductors, zero-gap dirty, cond. electron spin resonance theory 80—103888
  surface relaxation in CESR, evidence of spin lattice character 79—28615
  tetramethylaminelithium(0), $Li(CH_3NH_2)_4$, existence, conduction- and localised-electron spin reson. 80—66035
  $(TMTSF)_2PF_6$, ESR g-factor, linewidth, spin susceptibility, metal-insulator transition 80—103887
  $(TMTSF)_2PF_6(AsF_6)$, linear-chain conductor, semicond.-metal transition in small elec. field 80—103730
  transmission, surface relax. effects 79—61218
  TTF conducting salts, ESR of itinerant spins 77—66424
  TTT film, hopping cond. AC and DC meas. and EPR 80—11111
  type II superconductor, EPR of paramagnetic impurities and conduction electrons *(Russian)* 79—1641
  Ag, CESR due to edge dislocations 78—19328
  Ag film, CESR linewidth exam., sample size effect 79—33536
  Ag foil, or film, conduction electron spin disorientation at surface 80—75855
  Ag, obs. of CESR using reflection technique 77—20702
  Ag, resonant and nonresonant conduction-electron-spin transmission 80—75857
  Ag-Dy(Er), dil., cryst. field and spin exchange parameters, susceptibility and ESR expts. 77—40129
  $AgCl:Cd^{2+},Pb^{2+},Br^-$, mechanism for photoinduced decomposition 78—80219
  Al, CESR due to edge dislocations 78—19328
  Al, CESR lineshape and A/B and g-values 77—63284
  Al, CESR linewidth, freq. effects 78—10775
  Al foil, CESR at 20.98 and 9.27 GHz 77—28445
  Al, spin wave excitations, CESR expts., 79 GHz 77—40128
  Al, with plastic surface coating, g-factor and spin relax. time of cond. electrons 77—32258
  Al, with plastic surface coating, CESR obs. at 60 GHz in refl. spectrometer 77—32259
  Al:Fe(Cu), CESR, effect of ion implantation 77—20701
  Al-Er(Tm)(Lu) alloy, dil., transmission ESR expts. 77—20704
  Au, CESR, influence of freq. and surface effects 79—51856
  Au, CESR obs., spin orbit relax. by phonons 77—24743
  Au, resonant and nonresonant conduction-electron-spin transmission 80—75857
  BN, EPR, book contrib. 78—48041
  CESR due to edge dislocations 78—19328
  Cu, CESR, influence of freq. and surface effects 79—51856
  Cu, CESR linewidth and *g*-value, freq. and temp. influence, 4.2-50K 79—87318
  Cu foil, conduction electron spin disorientation at surface 80—75855
  Cu, resonant and nonresonant conduction-electron-spin transmission 80—75857
  Cu, selective transmission method, 4.2K 78—39401
  Cu, surface spin-flip probability from TESR 78—91953
  Cu-Fe, interface, ferromagnetic and cond. spin reson. mode coupling 79—78521
  Cu-Ni, interface, ferromagnetic and cond. spin reson. mode coupling 79—78521
  Cu-Permalloy, interafce, ferromagnetic and cond. spin reson. mode coupling 79—78521
  $Ga_{1-x}Al_xAs$, optical detection of CESR 77—36155
  GaAs, electron-spin relaxation and recomb. kinetics, time-resolved luminesc. study 80—108074
  GaAs, optical detection of CESR 77—36155
  $Ga_{1-x}In_xAs$, optical detection of CESR 77—36155
  p-GaSb. CESR, optically detected, giant Overhauser shift 79—4722

CESR continued
p-Ge, free-carrier reson., photoconductivity spectra in submillimetre wavelength 79—15353
$Hg_{1-x}Cd_xTe$, CESR *(Russian)* 78—23344
$Hg_{1-x}Cd_xTe$, CESR meas., four-photon mixing via spin-flip Raman scatt. 79—82873
InSb, CESR at high mag. fields, scatt. mechanisms 80—93177
n-InSb, cond. electron spectra in quantised mag. field, impurity resonance scatt. *(Russian)* 80—93178
n-InSb, effective g-value of electrons determ. by spin flip Raman scatt. and electric-dipole-excited ESR 78—52494
InSb, elec. paramag. reson. and combined reson. of cond. electrons at 24 GHz 77—1596
InSb, electron-electron spin-flip scatt. and spin relax. 80—44916
n-InSb, nonlinear optical susceptibility spin reson. *(Russian)* 79—59749
n-InSb, spin polarisation, anisotropic size effect, effect on CESR signal 80—70743
K, microwave transmission modes at cryogenic temps. 79—42473
K, Pauli susceptibility and Knight shift meas., electron wave functions 80—44937
$La_{3-x}\square_xS_4:Gd^{3+}$, indirect mag. interaction *(Dutch)* 77—63277
$La_{3-x}\square_xS_4:Gd^{3+}$, localised moment-cond. electron interactions, EPR data interpretation 77—63280
Li, first Landau spin parameter, transmission ESR obs. 77—20703
Li, metallic, obs. of intrinsic spin-lattice relax. of conduction electrons 78—10774
Li, microwave Faraday effect, relation to CESR 79—99855
Li particle size distrib. meas. by SEM 80—101775
Li, Pauli susceptibility meas. by CESR method 79—42735
Li, Pauli susceptibility meas. by CESR transmission 79—61217
Li/Sb(Cu) interface, CESR meas. 78—80218
Mg, CESR meas., 4.2-300K 78—48043
Mg-Mn, dil., cryst. field and spin parameters, transmission ESR obs. 77—40130
Na, CESR, influence of freq. and surface effects 79—51856
Na, microwave transmission modes at cryogenic temps. 79—42473
Na, Pauli susceptibility meas. by CESR method 79—42735
Na, Pauli susceptibility meas. by CESR transmission 79—61217
Na small particle, model calc. of size depend. of CESR g-shift 79—61220
$NaCl:Mn^{2+}(Zn^{2+})(Sn^{2+})$, electrolytically coloured, CESR 77—16174
Nb_3Ge film, superconductivity, relevance of mag. interactions, EPR study 80—100545
Pd, CESR obs., g-factor and susceptibility enhancement factor 79—65734
Pd, expts. using transmission technique 78—91954
Pd, Lande g-tensor for d-holes 79—61221
Pt-graphite catalyst, H adsorption, ESR obs. 79—24818
Rb, Landau Fermi-liquid-theory parameters, conduction-electron spin wave meas. 79—42472
Rb, microwave transmission modes at cryogenic temps. 79—42473
Si amorphous film, EPR rel. to elec. cond. 77—69692
n-Si, heavily-doped, EPR near metal-nonmetal transition 77—28446
Si, optically stimulated ESR, dielec. effects 77—73080
Si p-i-n structure, ESR of conduction electrons 80—93179
Si, surface, spin-depend. carrier recomb., photocond. expt. 78—19096
Si:B amorphous film, CVD prep., EPR, elec. and optical props. 79—4558
Si:P, ESR-induced changes in DC resistance 78—35037
n-Si:P, heavily depend., spin-lattice relax. at high temp. 78—39403
Si:P, heavily doped, metallic region, resist. decrease due to ESR 77—16178
Si:P, ion implantation defect annealing investig. by CESR 77—8404
Si:P, ion implanted, resist. changes induced by ESR 78—68377
Si:P, ion-implanted layers, CESR meas., impurity distrib. inhomogeneity 78—2738
Si:P, optical excess charging $D^0 \rightarrow D^-$, photoelectron spin relaxation *(Russian)* 79—78572
Si:P, polycryst., CVD, elec. activation of impurities, EPR obs. 80—34774
Si:P,Sb(Te), impurity implantation effect on CESR, spin-orbit interactions 77—36133
Si:P amorphous films, doping and annealing effects on localized states, ESR meas. 79—38380
Si-Au, amorphous, ESR linewidth var. with temp. and comp. 77—48033
Si-Ge amorphous films, effects of annealing and crystn., ESR microstruct. and elec. meas. 78—26790
Si-Ge film, amorphous, ESR line intensity anal., rel. to cond. mechanism 78—43645
$Si-SiO_2$ interface, anisotropic photoinduced ESR 78—23345
W, resonant and nonresonant conduction-electron-spin transmission 80—75857
ZnO, accumulation layer, ESR and NMR studies of adsorbed H_2 *(Japanese)* 80—50186

chalcogenide glasses
AC conduction, theory 78—23077
AC conduction mechanism, electronic versus atomic 80—29409
AC conductivity, temp. dependence 78—72153
AC conductivity due to intimate pairs of charged defect centres 79—4563
amorphous semiconductors, localised gap states, chemical trends 78—39067
antireflection coating, two-layer low-absorpt., for KCl laser window 78—37927
antireflection coating for KCl, design, prep. and performance 79—14063
As_2S_3, luminescence with short decay time 78—2906
a-As_2Se_3, diffusion of Ag and Au 77—51549
chalcogenide glasses, localised states calc. rel. to contact capacitance and field effect 79—11090
chalcogenide lone-pair semicond. charged impurities, effect on carrier concs., Street-Mott model 78—67984
charge screening lengths 79—23974
charged dangling bond model reassessment 77—72813
charged defect states, model 80—24847
charged defects, influence of ionicity 79—87063
conductivity, doping effect 79—38062
contact projection of micro-objects by X-ray synchrotron radiation 79—26193
crystallisation and decomposition 79—41959
crystallisation process, 60-240°C, elec. field influence 77—76315
current filamentation on switching, analytical theory 77—15922
defect chemistry and states in gap, models 79—38030

chalcogenide glasses continued
defect model, neutral diamagnetic quasimolecules, excess orbital bonds *(Russian)* 80—70647
defect models, optical, versus transport processes. 80—84449
defect pairing and effect on AC cond. 80—49725
defect reactions, ionicity dependence, negative-U states 80—88510
defect states 78—39066
defects, band gap states 80—80215
defects, cooperative charge disproportionation, rel. to field effect behaviour 80—54649
diamagnetic glassy semiconductors, at. tunnelling states, dielec. and elastic losses 79—87385
diffusion phenomena, mechanisms and meas. 77—76608
dispersive transient transport in disordered solids, expt. and theory 79—28342
doping effect and nature of localised states 78—14696
electrical conduction mechanism, review of developments 78—26854
electrical conductivity, percolation-controlled 78—72150
electrical conductivity, press. effects 78—56142
electrical conductivity, super-linear freq. depend. 79—28348
electrical conductivity, weakly freq.-depend. 77—1425
electrical conductivity at room temp., contact effect 77—20354
electrical conductivity increase on addition of Cu, Mn impurities 77—11920
electrical conductivity parameters, rel. to charge carriers 77—35970
electron physics of vitreous materials *(French)* 79—33225
electron-hole recombination, mech. 78—72196
electronic gap states, origin, structural relax., electronic transport and trapping 80—54648
electronic properties of glasses 79—42495
electronic props., xerographic use 80—20242
electronic transport mechanisms and coeffs. 80—80282
ESR studies of doped Mn, review *(Japanese)* 77—90019
filament waveguides for signal transmission in far IR region *(Czech)* 80—96017
film, drift and thermal diffusion of Au electrodes, α-particle backscatt. meas. 79—4434
film, electrothermal switching and current filament form., cond. model 77—76886
film, kinoform optical elements and integrated optics elements prod. 77—75634
film, M-Sb-S-I (M=Ge, Sn, Pb, Cd, Cu), prep. by laser evaporation, and characterisation 77—12533
film, monostable switching obs. 77—8157
film, opt. inform. recording uses 77—75633
film, optical waveguide form. by laser and electron beam irrad. 77—79978
film, photoinduced optical anisotropy, spectral responses 79—65948
film, photostructural effect, phase tuning in optical directional coupler 77—83963
film, reversible photostructural change obs. in IR absorption spectra 78—10897
film, switching field calc. 78—14775
film, switching phenomena 77—39976
film, weak field behaviour 77—36004
films, high field, short pulse cond. expt. 80—49751
films, threshold switching 80—96950
gap states, electronic behaviour 78—2452
gap states electronic behaviour 79—87098
glass formation, in chalcogenide systems 80—35152
glass formation regions, calc. using empirical theory of glass form. 80—33894
Hall effect, review of expt. data 79—51606
heteropolar, coordinations of ground state and of negative U defects 80—54137
hologram recording on surface *(Russian)* 77—19199
hologram recording with IR readout, diffr. efficiency 78—46548
holographic recording, effectiveness of chalcogenide film *(Russian)* 77—71960
holographic recording materials and devices, book contrib. 78—25838
inhomogeneous thin amorphous chalcogenide films, reversible switching, thermal stability criteria 80—70856
ionicity dependence of defect reactions and negative-U states in glasses 80—88511
IR planar waveguide with chalcogenide glass-BaF_2 emitting grating, mech. fabrication 79—50443
IR transmitting materials, appl. in 1 to 6 μm range, mech. props., review 79—4250
IR transparent materials and components 77—19374
IV-VI material production and physical props. for microelectronics *(Russian)* 78—11108
kinoform lens production and optical testing *(Russian)* 79—98310
layered acoustic waveguide, group delay time, temp. coeff. var. 78—83152
local order as determined by electronic and vibrational spectroscopy 79—37627
localised gap states, Mott-street model 79—37968
localised states, two-electron excitations, low temp. props. 77—15786
localised states role in cond. in high elec. fields 77—76841
Luminescence, temp. depend. rel. to nonradiative transitions 80—71485
luminescence centres, evidence for neutrality 78—88356
melts, glass-forming, miscibility criteria and phase separation 77—76569
memory effect, local doping, switching 80—107873
metal-chalcogenide glass-metal structure, freq. response characts. 77—76951
metal-chalcogenide glass-metal structures, elec. field influence on opt. parameters, electrostimulated chem. transforms. 77—76950
multicomponent, Hall-thermopower sign anomaly 77—35957
neutron irradiated, paramag. centres 79—82872
non-radiative recombination of electron-hole pairs 78—6759
optical and electrical props., comparison with amorphous SiO_2, review 78—6721
optical constants, cooling rate influence, O_2-free glasses in crit. annealing region 80—88952
optical directional coupler phase tuning by chalcogenide glass film loading 78—1373
optical grating direct writing using SEM 78—83121
optical information media role of amorphous materials 77—54764
optical integrated circuits, SEM written gratings in chalcogenide films 79—32087
optical memory material, density of recorded information 77—75433

chalcogenide glasses continued
optical properties rel. to electron states, lecture 78—27263
optical transitions and electronic struct., review 77—76741
optically induced metastable paramag. state, optical absorpt. and ESR meas. 77—40113
optimal polynomials in calcs. of complex glass's properties 78—68026
optronic receiver with simultaneous direct and memory effect 77—75706
oxychalcogenide, phase separation 77—8803
p-n heterojunctions with GaAs, InP, fabrication, characterization, switching 80—49892
partial values and structure features 79—41969
photoconductivity, analysis 78—72197
photoelastic properties, optimum glasses for acoustic delay lines and deflectors 78—55420
photogeneration of charge carriers and recomb. 77—81147
photographic materials, chalcogenide glass-metal light sensitive systems with barrier layer 77—75635
photoinduced structure changes, interferometric meas. 77—49769
photoluminescence props., review 79—56862
photostructural changes, photodarkening, thin film and melt-quenched samples 80—49121
point defect exam. by positron annihilation 78—72637
Poole-Frenkel effect, charged dangling bonds model 80—59994
Poole-Frenkel effect, nonlinear current voltage characts. 80—7007
positive photorecording effect on layers *(Russian)* 79—59781
quartz-chalcogenide glass IKS-25 system, mech. of contact interaction, mech. and optical props. 78—88375
radiative emission during threshold ON-state 78—76119
radiative recombination obs. as efficient luminesc. 78—2914
rare earth sulphides-1.8 Ga_2S_3 glasses, vibr. spectra, electronic transitions, short range order 77—69820
rare earth-gallium sulphide glass, R_2S_3-1.8Ga_2S_3, vibr. and electronic spectra, short-range order 78—27228
real-time kinoform synthesis using chalcogenide glass films *(Russian)* 78—13669
refractions, atomic, determ. using optimum polynomial method 79—65828
refractive index, temp. coeff., O free glasses 77—58403
review of properties, current and potential applications 78—30539
review of structural and electronic props. 80—64901
selenide systems, binary, glass transition behaviour, model, comp. depend. 78—26673
SEM written diffraction gratings for integrated optics, characts. 79—68450
semiconductor device developments and future trends 77—69386
semiconductor film kinoform production *(Russian)* 77—14670
semiconductor-metal system, photochemical transformations rate rel. to light-stimulated diffusion coeff. 77—76626
short-range order, theory and probes 80—79698
small-polaronic glass, dynamics of optically induced props. 80—49630
stress-induced birefringence meas., 1-12 μm 77—24818
structure and growth kinetics, topological principles 80—49123
structure and low temp. props. 79—37631
structure modelling by Monte Carlo method *(Russian)* 79—55672
structure of simple inorganic amorphous solids, review 80—15004
switches, relaxation processes in memory and threshold switches 78—60172
switching components, amorphous thin film chalcogenide semicond. *(French)* 77—72710
switching devices, reliability 79—11238
technology and applications, review of advances 77—66618
ternary, correlation between specific volume and composition 77—9038
ternary layer sensors, imaging by photo- and thermal doping 78—1342
ternary semiconductor amorphous film comp. monitoring by EPR 77—51940
tetrahedrally coordinated, pnictide and chalcogenide, defect energies 80—54647
theory of glass formation 79—86713
thermal conductivity, 1.5 to 30K *(French)* 77—39704
thermal mechanism for bias-induced switching effects in inhomogeneous thin films 80—11057
thermopower in Anderson model 78—84241
thin film, thermal diffusion of Au electrode layer, α-particle backscatt. obs. 78—10228
threshold switch, high resist. state 77—15924
threshold switch, on-state model 79—56270
threshold switch, on-state model 79—99588
threshold switch response to pulse burst waveforms 78—10523
threshold switching mechanism in chalcogenide glass thin films, review 78—76122
trap controlled transient photocond. 80—44641
Urbach tail, rel. to Mott-Street model 77—47771
xerography, defect control 79—97454
Ag-As chalcogenide glass systems, reaction and diffusion 79—77826
Ag-As-S system, struct., props. and vibr. spectra 79—65901
Ag-As-Se system, glass-forming 79—65001
Ag-As-Se system glasses, soln. rate 79—43456
Ag-As-Te glasses, elec. props. *(Russian)* 77—85211
Ag-As-Te system, vitrification region, physiochem. props. 79—41960
Ag-Ge-S glasses, X-ray determ. of struct. *(Japanese)* 80—10501
Ag-Sb-S, prep. and props. of glasses in the system 77—20053
$AgAsS_2$, $AgSbS_2$ and $AgBiS_2$, cryst. and vitreous, refl. spectra, energy spectrum 77—8596
$AgAsS_2$, band struct. photoemission and refl. spectra obs. 77—66581
Ag_2S-As_2S_3-AgI, temp. and comp. depend. of ionic cond. *(French)* 80—34229
$Ag_{19}Sb_{29}Te_{52}$, single-phase, thermoelectric efficiency 80—107826
Al-chalcogenide glass thin layer struct., EMF in elec. field *(Russian)* 77—39936
$Al_{20}As_{40}Te_{40}$, amorphous alloy, radial distribution function anal., X-ray diffr. *(Spanish)* 80—28915
$3Al_2S_3.La_2S_3$:Ho^{3+}, radiative and multiphonon relax. 79—33794
$Al_{23}Te_{77}$ glasses, crystallization 79—51000
As chalcogenides, deep levels, photoluminesc. and photocond. 80—70641
As-Ge-S(Se), glass films, photostruct. changes 77—85822
As-Ge-Se and As-Ge-Se-Sb systems, acousto-optic props. 77—27327
As-Ge-Se based glasses, refr. index, 1-11 μm 78—39520
As-Ge-Se system, synthesis and phys. props. of amorphous layers 77—52252
As-Ge-Se system glasses, alkali-free, optical absorpt. 79—65883
As-Ge-Te, chalcogenide glass, elec. cond. and dielec. const. 80—75567

chalcogenide glasses continued
As-Ge-Te glass, dielectric meas. 79—87382
As-S, amorphous, glass transition and specific heat, intermolecular bond saturation 80—15011
As-S, glass, IR vibr. spectra, optical characts. calc. 80—40119
As-S, glassy film optical props., photostimulated effects and hologram recording 79—27215
As-S, spectral variation of SKβ emission with S content 79—8209
As-S amorphous chalcogenide thin film, transient photoinduced phenomena 80—80884
As-S amorphous film, photo-induced optical changes, annealing effect 78—27345
As-S chalcogenide glass holographic recording efficiency, photocond. and annealing effects *(Russian)* 80—15556
As-S chalcogenide glassy semiconductors, induced anisotropy 79—32013
As-S film, amorphous, photo-induced dynamical changes in refr. index 79—28705
As-S film, guided light reversible control by electron beam irrad. 78—1331
As-S glass media, temp. control of hologram props. 78—17883
As-S glasses, acousto-induced structural changes, optical props. 80—49122
As-S glasses, heat of solution in alkaline soln. 79—91989
As-S glasses, resonance Raman scatt. 80—50325
As-S glassy film, photobrightening effect 80—11498
As-S semiconducting glass film holographic recording media *(Russian)* 77—10864
As-S system, glass forming ability and phase diagram 78—59760
As-S system glasses, photostruct. transforms. under laser radiation, use in holographic recording 77—76316
As-S systems, temp. depend. of conductivity and photocond. at 632.8 nm *(Russian)* 80—44666
As-S-Br, IR spectra 79—95780
As-S-I system, glasses, Raman spectra, struct. 79—65857
As-S-I system glasses, IR transmission spectra, structure-chem. comp. 79—42974
As-S-Se, solubility, photostimulated changes 80—24602
As-S-Se-Ge with low softening temp., IR characts. *(Czech)* 80—25332
As-S-Te, vitreous semiconductor, photoconductivity *(Russian)* 79—11172
As-S-Te, vitrification, density and elec. cond. measurements 79—7645
As-S-Tl, viscosity and elastic props. 80—100180
As-S(Se), solubility, photostimulated changes 80—24602
As-Sb-S-I system, vitrification and volt-ampere characts. 77—31756
As-Se, amorphous, glass transition and specific heat, intermolecular bond saturation 80—15011
As-Se, amorphous film, kinetics of photo-induced processes *(Russian)* 79—69896
As-Se, glassy, surface phenomena, gas adsorption effects on elec. props. 79—42621
As-Se, optical parameter optimisation for holographic recording appl. *(Russian)* 80—43299
As-Se, relation between glass-transition temp. and optical memory-eraser temp. 80—10650
As-Se amorphous film, density of upper valence band states, annealing effects, UPS obs. 80—29845
As-Se amorphous film, optical props. change under high-power light pulse action 79—47534
As-Se amorphous films, photo-induced changes in IR vibr. spectra 79—91514
As-Se amorphous system, photocond. props. 80—88587
As-Se amorphous system, Raman scatt. 80—88984
As-Se and As_2S_3 films, electron-stimulated changes in optical props. and dissolution rate 80—29709
As-Se based glasses, refr. index, 1-11 μm 78—39520
As-Se chalcogenide glass, semicond. film, laser stimulated refr. index change, writing/erase cycle 77—50677
As-Se chalcogenide glass, optical const. photoinduced changes mechanism 80—7321
As-Se film, MgF_2 film coated, effectiveness for optical holographic recording *(Russian)* 77—71960
As-Se film, photoinduced absorpt. changes 79—87519
As-Se film, photostimulated changes in microhardness 77—15723
As-Se films, chalcogenide vitreous semiconductors, reversible photoinduced changes in optical, physicochem. and contact props. 79—24378
As-Se glass, magnetic susceptibility meas. at room temp. *(Japanese)* 79—82748
As-Se glass thin-film waveguide, for 10.6 μm range 77—50770
As-Se glasses, elec. transport studies 80—103695
As-Se glasses, low temp. photocond. 80—49808
As-Se glassy system, mag. susceptibility 77—55657
As-Se system, chalcogenide vitreous semiconductors, darkened films, thermal and optical bleaching, light transmission obs. 80—50447
As-Se system glasses, electronic props. and localised states, review 77—62871
As-Se system glasses, opt. absorpt. edge shift on densification 77—77250
As-Se system glasses, point defects, positron lifetime spectra meas. 78—88380
As-Se system glasses, structural and electronic transitions 77—76890
As-Se system glasses, thermal expansion coeff. and free vol. at transition temp. *(Japanese)* 79—55876
As-Se:^{197}Au, glassy, Au impurity influence, elec. cond., optical absorpt. and Mossbauer meas. 77—24558
As-Se-Bi, semicond. chalcogenide glasses, crystallisation and electrophys. props. 78—9955
As-Se-Cu system glass films, elec. and photoelec. props. variation with photostruct. transforms. 77—76980
As-Se-Ge film, master for hologram copying 78—29912
As-Se-Ge(-S), photostructural change in Urbach tail 80—76021
As-Se-S glasses, isothermal sintering, surface area reduction 77—8779
As-Se-S-Ge chalcogenide glass films, appls. to passive optical waveguide components 79—37048
As-Se-S-Ge chalcogenide amorphous film, computer-generated holograms using electron beam irrad. 80—95846
As-Se-Sb, crystallised glasses, struct. from Mossbauer spectra 80—64917
As-Se-Te, amorphous, electron and hole drift mobilities 80—34442
As-Se-Te, glass form., charact. temp., density, thermal expansion and dynamical viscosity, struct. model 78—26672
As-Se-Te glasses, electron transport props. 78—10439
As-Se-Te system glasses, AC cond. and permittivity, freq. and temp. depend. 77—76857

chalcogenide glasses continued
As-Se-Te thin films, laser induced crystn. kinetics 77–76317
As-Se-Tl system, NMR spin-lattice relax. time meas. 79–95671
As-Se(-Ge) system, mode-guiding layer in IR microwaveguides 80–28329
As-Se(Te) films, laser-beam recordings by thermal creation of holes 80–35010
As-Se(Te) systems, mag. susceptibility comp. depend. 77–80908
As-Te system glasses, DC and AC cond., thermo-EMF, 140 to 350K 79–42549
As-Te-Cu system glasses, DC and AC cond., thermo-EMF, freq. depend., 100 to 370K 77–76827
As-Te-Cu system glasses, elec. cond. and thermo-EMF 79–42540
As-Te-Cu(Ag) system glasses, absorpt. coeff. and optical band gap 79–65829
As-Te-Ga, glass, elec. cond., 190-300K *(Russian)* 80–54702
As-Te-Ga system, glass-forming region and props. 80–25674
As-Te-Ge films, thermally induced transformations, TEM obs. 79–94917
As-Te-Ge system thin films, effect of S, Se, Sb, Bi, Tl on volt-ampere characts. 77–15976
As-Te-Ge/n-Si, film on cryst., heterojunction, elec. and photovolt. props. 80–100514
As-Te-Ge-Si, film, high speed switching mechanisms 77–8153
As-Te-Ge-Si sandwich type amorphous films with metal electrodes, space-charge-limited switching, pre-breakdown characts. *(Japanese)* 77–69385
As-Te-In, glass-forming, density and microhardness 80–103257
As-Te-Si-Ge amorphous chalcogenide semiconductor, thin film interface, electrical charact. *(Korean)* 80–97014
As-Te-metal amorphous film, switching, memory effects 80–44677
As_2-Se_3-Bi_x amorphous system, elec. and photocond. props. 79–51574
AsGe amorphous semiconductor layers for recording information *(German)* 78–42395
As_2Ge_2SeTe, semiconducting glass, elastic props., US vel. meas. 78–26628
$As_2Ge_3T_{15}$, semiconducting glass, elastic props., US vel. meas. 78–26628
AsGeTe, semiconducting glass, elastic props., US vel. meas. 78–26628
$As_{10}Ge_{15}Te_{75}$, glass, cond. and switching characts. 77–32054
$As_{10}Ge_{15}Te_{75}$:Ag glasses, elec. props. 79–91045
$As_{25}Ge_{10}Te_{65}$, chalcogenide glasses, dielectric relaxation 80–55027
$As_xGe_{10}Te_{90-x}$, cond. and dielec. const. from 77 to 383K and from DC freq. to 5 MHz 79–23964
$As_{10}Ge_{15}Te_{75}Ag_x$, elec. and dielec. props., Ag additions effect 80–65558
As_2O_3, vitreous, Raman and IR spectra 79–73933
$As_2(S,Se,Te)_3$ glasses, Hall mobility composition depend. 78–68042
$As_x(S,Se)_{1-x}$, covalent non crystalline topology, short range order 80–15009
$As_{1-x}S_x$ glasses, building blocks and bonds 80–54141
$As_{2-x}S_{3+x}$, hydrogenated chalcogenide glasses, prep. by plasma decomposition 80–49735
As_2S_3 (Se_3), electron irradiated, effects on elec., photoelec. and optical props. 80–49806
As_2S_3, acousto-optical effects *(Japanese)* 79–82946
As_2S_3, Ag, Cu, Sn and Ge impurities effect on electrophys. props. 77–76826
As_2S_3, amorphous, AC cond. magnitude and variation *(French)* 79–47095
As_2S_3, amorphous, acousto-induced struct. change, Brillouin scatt. meas. 79–27928
As_2S_3, amorphous, band to band radiative recomb. 80–25435
As_2S_3, amorphous, band-to-band luminesc., electronic band states 79–61432
As_2S_3, amorphous, charged defect pair photolum. meas. 80–16078
As_2S_3, amorphous, electrodiffusion profile meas. of Ag migration 78–87822
As_2S_3, amorphous, low temp. US meas., two-level systems role 78–30703
As_2S_3, amorphous, luminesc. and optically detected ESR, photoinduced struct. change 80–50399
As_2S_3, amorphous, optical detection of ESR 79–38408
As_2S_3, amorphous, photodissolution of Ag film 78–26737
As_2S_3, amorphous, quantum efficiency and fatiguing behaviour of luminesc. processes 80–7402
As_2S_3, amorphous, temp. below 1K, props., tunnelling 80–49576
As_2S_3, amorphous, time resolved spectroscopy of valence alternation pair luminesc. 80–50400
As_2S_3, amorphous, time resolved luminesc. 80–66288
As_2S_3, amorphous, time-resolved photolum., spectrosc. 79–24360
As_2S_3, amorphous, US attenuation obs. 79–46756
As_2S_3, amorphous, ultrasonic velocity, 1.5 to 296K 79–37764
As_2S_3, amorphous film, photodissolution of Ag, struct. changes 77–11815
As_2S_3, amorphous film, photooxidation, substrate depend. 78–64866
As_2S_3 amorphous film waveguide and grating coupler 80–53448
As_2S_3 amorphous films, meas. of photoinduced transformations by optical waveguiding 79–43050
As_2S_3 amorphous films, photo-induced changes in IR spectrum 79–52033
As_2S_3, amorphous semicond., photo-induced optical and structural changes *(Japanese)* 78–47244
As_2S_3, amorphous thin films resonant Raman scattering 78–68505
As_2S_3 and As_2S_3-Sb_2S_3 system glasses, long-term photocond. relax. 77–76874
As_2S_3 and As_4S_4 vapour-deposited films, valence states, thermal and photo-induced changes UPS study 80–93459
As_2S_3, antireflection coating for KCl, design, prep. and performance 79–14063
As_2S_3, As_2Se_3, optical props., electronic struct., photocond., book contrib. 77–44024
As_2S_3, at. struct. changes due to irrad., comp. variations and annealing 77–76323
As_2S_3, build-in mechanism of impurities, electronegativity influence 77–76313
As_2S_3 chalcogenide film surface relief hologram selective etching *(Russian)* 79–94181
As_2S_3, chalcogenide glass, effect of press. on elastic props. 80–10590
As_2S_3 coating defects and impurities affecting damage threshold and absorptance 79–14065
As_2S_3, cryst., vitreous or amorphous, nonlinear light absorption, temp. depend. *(Russian)* 77–48199

chalcogenide glasses continued
As_2S_3, cryst. and glassy, two-photon spectrum at room temp. 79–24334
As_2S_3, cryst. and vitreous, nonlinear light absorpt. 77–75605
As_2S_3, crystalline and amorphous, inelastic neutron scatt. spectra 77–24276
As_2S_3, crystalline and vitreous, nonlinear absorption of ruby laser radiation *(Russian)* 78–22165
As_2S_3, deep struct. changes, NQR obs., high-press. and temp. effects 80–54139
As_2S_3, density of valence states, XPS and UPS obs. 77–48308
As_2S_3, determination of stoichiometric discontinuity, using US velocity 79–5242
As_2S_3, diffusion, elec. transport and first group impurities effect on elec. and opt. props. 77–76623
As_2S_3, drift mobility, along molecular direction, 207-465K 77–43643
As_2S_3, elec. cond. mech. obs., in bulk material and evaporated thin films *(Japanese)* 80–11028
a-As_2S_3, energy gap meas., by Faraday rotation 80–66161
As_2S_3, Faraday rotation, 0.7-2 μm 77–16307
As_2S_3 film, amorphous, deposited at different temps., IR spectra 80–40102
As_2S_3 film, amorphous, opt. const. changes under illumination 77–77316
As_2S_3 film, amorphous, photo-induced dynamical changes 80–66142
As_2S_3 film, diffr. efficiency of continuously etched gratings 78–38019
As_2S_3 film on KCl, strain-induced refractivity anisotropy, 10.6 μ ellipsometric obs. 79–14064
As_2S_3 film optical constants, wedged-film meas. 79–14066
As_2S_3 film waveguide, integrated optical functional elements based on holographic gratings 77–79972
As_2S_3 films, amorphous, structural implications from Raman spectra of As_4S_4 polymorphs 79–61385
As_2S_3 films, kinetics of light-enhanced vaporisation rel. to photocond. 77–84919
As_2S_3 films, photographic Ag photodoping to produce negative relief image 80–59490
As_2S_3 glass, band gap and trap levels, determ. from elec. props. 77–4337
As_2S_3 glass, localised paramag. states, As_4S_6, As_4S_4 units, mol. analogue models 78–60087
As_2S_3 glass, melt-quenched, reversible photostruct. change 77–68925
As_2S_3 glass, natural optical activity and related phenomena 79–73895
As_2S_3 glass, natural optical activity and related phenomena 79–95727
As_2S_3 glass, press. effect on optical props. 80–50363
As_2S_3, glass, US attenuation, enhanced after elec. field removal 79–65145
As_2S_3 glass fibre, elongation, force depend., deviations from linearity 80–45334
As_2S_3 glasses, DC elec. cond. and thermo-elec. power 80–96865
As_2S_3 glasses, quasi-eutectic structure, X-ray and IR investig. 77–15320
As_2S_3, glassy, interface with metal, photoelec. props. 79–73589
As_2S_3, glassy, photoinduced defects, EPR and absorpt. spectra 80–59398
As_2S_3, glassy, thermally stimulated depolarisation 77–24782
As_2S_3 high-resist. vitreous, photopolarisation and photoelectret effects 77–76876
As_2S_3, LF inelastic light scatt. meas. 78–15181
As_2S_3, luminescence 80–80862
As_2S_3, optical absorption spectra after 4.5 MeV electron bombardment *(Russian)* 77–32408
As_2S_3, optically induced changes, ps. spectroscopy 80–48326
As_2S_3, photoreactive diffusion of Ag 80–19991
As_2S_3 photosensitive etching in nonoxidising etchants 80–78813
As_2S_3 radiator bonded LED's, with optical guide struct., efficient coupling to optical fibres 77–39043
As_2S_3, rain erosion mechanisms 79–34154
As_2S_3, relation between glass-transition temp. and optical memory-eraser temp. 80–10650
As_2S_3, secondary electron emission, fluctuation state effect 80–40193
As_2S_3, semiconducting glass, elastic props., US vel. meas. 78–26628
As_2S_3, shear wave attenuation and high freq. elec. cond. 80–11027
As_2S_3, struct. determ. by electron spectroscopy 79–65979
As_2S_3 structure simulation of some tellurite and chalcogenide glasses quasi-crystalline structural diffusion method *(Russian)* 80–54147
As_2S_3, thermal capacity, 300 to 600K 80–103492
As_2S_3 thin films for integrated optics, photodetector elements, relief-type diffraction gratings 79–32094
As_2S_3 thin glassy films, hole drift mobility, interaction with deep localised levels 80–11117
a-As_2S_3, time-resolved photoluminescence study 80–89057
As_2S_3, two photon light absorpt. dispersion, induced linear light absorpt. *(Russian)* 80–66231
As_2S_3, two-phonon vibrational spectra, crystalline and amorphous forms, Raman and IR spectra 78–39537
As_2S_3, vaporisation, mass spectrometric analysis 78–22843
As_2S_3, vapour-deposited, pure and doped, hole mobility 80–49728
As_2S_3 vitreous film, hole transport obs. 80–49727
As_2S_3 vitreous film, photodecomp. and photostruct. changes 77–76318
As_2S_3, vitreous local struct., elec. field gradient tensor asymmetry obs. 79–73847
As_2S_3, X-ray induced paramag. colour centres 78–19327
As_2S_3:Ag, AC conductivity determ. 77–66167
As_2S_3:Ag, amorphous US props. 78–51616
As_2S_3:Ag, doping influence on photolum. at 77K 77–77293
As_2S_3:Ag film, Ag photodoping rate, localised struct. transform. effect, absorpt. meas. 77–31914
As_2S_3:Ag glassy films, optical transmission spectra, photodoping effect 80–66317
As_2S_3:B glass, impurity effect on photoluminesc. and optically induced EPR 79–65918
As_2S_3:Fe glass, photolum. and ESR, Fe impurities as non-radiative recomb. centres 80–29788
As_2S_3:Ga system chalcogenide glasses, thermophysical and struct. props. 80–15007
As_2S_3:Te, doping influence on AC conductivity, electron transport by hopping 79–78106
As_2S_3-Ag system, photosensitivity depend. on As_2S_3 thickness *(Russian)* 80–54784
As_2S_3-Ag system, photosensitivity depend. on metallic layer thickness *(Russian)* 80–54785
As_2S_3-Ag_2S, Ag diffusion, 50-120°C 78–18828
As_2S_3-$AsBr_3$, glass, exam. of combination scatter spectra in IR 78–88315

chalcogenide glasses continued
As_2S_3-$AsBr_3$ and As_2Se_3-$AsBr_3$ systems, phase diagrams 77−8804
As_2S_3-PbS, DC elec. cond. and photocond. 78−39107
As_2S_3-PbS glasses, structural props. 79−27925
As_2S_3-Sb_2S_3, vitreous, dispersive charge transport analysis 79−95418
As_2S_3-Se, glass-forming system, phase diagram 77−16551
As_2S_3-Si, isotype amorphous-crystalline heterojunctions, electrophys. props. 79−24063
As_2S_3-Tl_2S, As_2Se_3-Tl_2Se and As_2Te_3-Tl_2Te systems, vitrification and reaction characts. 77−15560
As_2S_3-Tl_2S and As_2Se_3-Tl_2Se system glasses, comp. depend. of IR absorpt. props. 77−16292
As_2S_3-Tl_2S glass, phase relns. and crystallisation 78−23675
As_2S_5, amorphous, struct., vibr. and electronic spectra 80−64908
As_2S_5, deep struct. changes, NQR obs., high-press. and temp. effects 80−54139
As_2S_5, thin film optical waveguide, for acoustooptic modulators 78−83051
As_2S_5-AsSI glasses, IR and Raman spectra, struct. rel. to comp. *(Russian)* 77−81107
As_2S_x, Raman and IR spectra, struct. model 78−80330
$As_{40}S_{60}$ glass, structure modelling by Monte Carlo method *(Russian)* 79−55672
As_xS_{1-x} glass, Raman spectra, chem. struct. *(Russian)* 78−76469
As_xS_{100-x} amorphous film, composition depend. of photo-induced refr. index changes 79−78644
As_xS_{100-x} amorphous film, photoinduced changes in optical props. 80−50445
As_xS_{100-x} amorphous films, optical props. and photoinduced changes 80−60700
As_xS_{100-x} glasses, band gap and neighbouring order *(Russian)* 79−60694
As_xS_{100-x} glasses, Raman spectrum and structure 80−60593
As_xS_{100-x}, TSC *(Russian)* 79−91074
As_xS_{100-x}, thin film, absorption in range of large optical densities *(Russian)* 80−11428
As_xS_y, bulk and vapour deposited films, comparison of struct., X-ray diffr. meas. 77−69195
$As_{15}S_{40}Ag_{45}$ glass, photosurface deposition of metallic Ag discs 77−76650
$(As_2S_3)_{1-x}(AsBr_3)_x$ glass, struct. interpretation of Raman spectra 79−65856
$(As_2S_3)_x(AsI_3)_{1-x}$, glass, Raman spectra, chem. struct. *(Russian)* 78−76469
$(As_2S_3)_{1-x}(As_2Se_3)_x$ and $(As_2Se_3)_{1-x}(As_2Te_3)_x$ pseudobinary glasses, comp. depend. of opt. props. 77−90157
$(As_{0.4}S_{0.6})_{100-x}Cu_x$, glassy, struct. and elec. cond. study 80−59399
$As_2S_3Ge_x$ glasses, vibr. props. and struct., IR refl. and Raman scatt. 79−78682
$(As_2S_3)_{1-x}(GeS_2)_x$ and $As_2S_3Ge_x$ glasses, struct. and vibr. spectra 79−91440
$(As_2S_3)_{1-x}(GeS_2)_x$, LF inelastic light scatt. meas. 78−15181
AsSI, struct. determ. by electron spectroscopy 79−65979
AsSI, X-ray diffr. study in vitreous and fused states 77−7675
$(AsSI)_x(GeS_2)_{1-x}$, Raman and long-wave IR spectra obs. of struct. 79−51964
$(As_2S_3)_{1-x}(PbS)_x$, high field effects 79−42553
$(As_2S_3)_{0.55}(Sb_2S_3)_{0.45}$ vitreous film, dispersive charge transport, time-of-flight meas. 79−19594
$As_{1-x}S_x(Se_x)$, bulk-quenched glasses, opt. freq. dielec. const., chem. ordering effects 78−23472
$As_2S_{2.66}Se_{0.34}$, X-ray photoelectron spectra, electron binding energy, effect of Ag alloying 79−11499
$As_2S_{3-x}Se_x$, amorphous, picosecond relax. of optically induced absorption 80−97302
$As_2S_{3-x}Se_x$, ps. relax., optically induced absorpt. 80−48325
$As_2S_3(Se_3)$, amorphous, network dynamics, vibr. band splittings 79−42199
$As_2S_3(Se_3)$, elastic moduli, hydrostatic press. effect, US wave vel. meas. 80−34115
$As_2S_3(Se_3)$ evaporated films, struct. and thermally induced effects 79−41963
$As_2S_3(Se_3)$ evaporated films, optical absorpt. and thermally induced effects 79−42989
$As_2S_3(Se_3)$, photoconductivity dependences applied elec. field 80−107857
$As_2S_3(Se_3)$, thermal expansion at low temperatures 78−83982
$As_2S_3(Se_3)$, X-ray induced paramag. states and luminesc. 78−95520
$As_2S_3(Se_3)$:Ag glassy films, doped by photodiffusion and thermodiffusion, photocond. 80−29441
$As_xS_{100-x}(Se_{100-x})$, localised states density near valence band edge *(Russian)* 80−103638
$As_{40}S_{25}Se_{25}Si_{10}$ film, transient photoinduced absorpt. 77−40295
$As_2S_3(Se_3)(Te_3)$, electronic struct., calc. by extended Huckel theory 78−23012
$AsS_{3.5}Te_{2.0}$ glass, gamma-irradiated, TSC meas. 77−66166
$As_2S_{3-x}Te_x$, opt. and mag. props., comp. influence 77−77225
$As_2S_{3-x}Te_x$, optical absorption, magnetic susceptibility and AC conductivity meas. 80−55125
$As_4Sb_2Se_9$ glassy semiconductors, electronic props. 80−103712
$As_2(Se,Te)_3$ glasses, X-ray absorption and photoelectron spectroscopy study 80−7463
AsSe and As_2Se_3, electrical cond. freq. depend., hopping cond. contrib. 77−76856
AsSe, efficiency of optical recording and erasing, temp. depend. *(Russian)* 77−79908
AsSe film, light-induced light absorption changes 77−73181
AsSe-$GeSe_2$-PbSe, glass form., struct. defects, elec. cond., assoc. *(Russian)* 80−54144
$AsSe_{10}$, stable thermoelectret, effects of anisotropic external perturbation *(Russian)* 77−63361
$AsSe_{1.2}$:Fe, Fe effect on physiochem. props. of glass 80−24370
$As_{1-x}Se_x$, ave. energy gap, optical freq. dielec. const. and refr. index 77−76739
$As_{1-x}Se_x$ glass, refr. index comp. depend. and photo-induced variation 79−91398
$As_{2-x}Se_{3+x}$, hydrogenated chalcogenide glasses, prep. by plasma decomposition 80−49735
As_2Se_3, AC cond. and photo-induced states 79−87128
As_2Se_3, amorphous, AC cond. magnitude and variation *(French)* 79−47095
As_2Se_3, amorphous, DC Hall effect, elec. cond. mechanism 78−23121

chalcogenide glasses continued
As_2Se_3, amorphous, dark discharge, relaxation current meas. *(German)* 80−49760
As_2Se_3, amorphous, defect states, exptl. study. 80−54645
As_2Se_3, amorphous, electrophotographic props., photodecomp. effect 78−49918
As_2Se_3, amorphous, electron and hole transport, charge defect model 79−15162
As_2Se_3, amorphous, hole emission defect states 80−49759
As_2Se_3, amorphous, hole mobility expt., transient photocurrent shape 79−99582
As_2Se_3, amorphous, modulated photocurrent 78−10500
As_2Se_3, amorphous, modulated photoconductivity anal. 80−44650
As_2Se_3, amorphous, nonradiative recombination of photocarriers 80−11046
As_2Se_3, amorphous, optically broadened lattice vibration spectra 79−77712
As_2Se_3, amorphous, photoconductivity exam. 78−30953
As_2Se_3, amorphous, photocond. and photoinduced optical absorpt. 79−82645
As_2Se_3, amorphous, theoretical calc. of defect states 80−49657
As_2Se_3, amorphous, time resolved meas. of photoinduced optical absorpt. and photocond. 80−49807
As_2Se_3, amorphous, ultrasonic velocity, 1.5 to 296K 79−37764
As_2Se_3, amorphous and single cryst., ODMR expts. 80−50230
As_2Se_3 amorphous film, comp. ratio variation by annealing and laser irrad., ESCA meas. 79−99447
As_2Se_3 amorphous film, pulse hologram recording 79−55091
As_2Se_3 amorphous layers with Al electrodes, photoelectrochem. process 77−76953
As_2Se_3, amorphous radiative interband recombination 80−66286
As_2Se_3 amorphous thin films, illumination-induced change in contact pot. 80−20251
As_2Se_3, and $As_{1-x}Se_x$, struct. models 79−37628
As_2Se_3, and $As_2(Se,Te)_3$ glasses, as ion-selective materials for solid-state electrochem. sensors 80−50897
As_2Se_3, AsSe and As_3Se_2 films, photostimulated changes in opt. and elec. props. 77−76979
As_2Se_3 bulk glass, physical parameters anisotropy, cooling effects 77−36545
As_2Se_3 chalcogenide film surface relief hologram selective etching *(Russian)* 79−94181
a-As_2Se_3 chalcogenide glass, influence of thermally induced defects on transport props. 80−49766
As_2Se_3 coating defects and impurities affecting damage threshold and absorptance 79−14065
As_2Se_3, contact influence on AC cond. 78−76076
As_2Se_3, cryst. and amorphous, optically induced absorption in band gap, picosec. dynamics 79−87439
As_2Se_3, crystalline and amorphous, inelastic neutron scatt. spectra 77−24276
As_2Se_3, Cu, Ag and O impurities influence on electronic energy spectrum and mol. vibr. spectrum 77−90181
As_2Se_3 disordered films in flash evap. systems, nonsteady-state behaviour of interface states 77−76952
a-As_2Se_3, doped film, photoluminescence intensity and lineshape study 80−50448
As_2Se_3, effect of Cu and I, investigated by Mn^{2+} EPR spectra 77−73075
As_2Se_3, effect of gamma-radiation on solution kinetics 77−19986
As_2Se_3, effect of impurities on paramagnetic gap states 80−24848
As_2Se_3, film, amorphous, fatigue and recovery of electrophotographic props. 78−21253
As_2Se_3, film, influence of electric field on crystallisation kinetics 78−42914
a-As_2Se_3 film, metallic impurity effect on transport props. 80−49963
As_2Se_3 film on KCl, strain-induced refractivity anisotropy, 10.6 μ ellipsometric obs. 79−14064
As_2Se_3, glass, density of optically induced localised paramagnetic states 78−52354
As_2Se_3 glass, heat capacity and struct. relaxation of enthalpy 77−55360
As_2Se_3 glass, microwave elec. cond. and struct. 80−49793
As_2Se_3 glass, mol. struct. model 80−100179
As_2Se_3, glassy, dielectric const. determ. 78−72449
As_2Se_3, glassy, drift mobility of holes, 20 to 120°C 79−51583
As_2Se_3, glassy, with adsorbed $H_2O(NH_3)(NO_2)(O_2)(CO_2)(CO)$, surface cond., photocond. 78−80038
As_2Se_3, glassy defect electron states, tight binding calc. 80−96818
As_2Se_3 glassy films, current-voltage characts., temp. depend., SCL current 80−92902
As_2Se_3, hole drift mobility, temp. and field depend. 77−76830
As_2Se_3, IR spectra and intrinsic band assignments 77−77223
As_2Se_3, impurity effect on photoluminesc. and optically induced EPR 79−65918
As_2Se_3, in evaporated layer systems, electric field forming and ageing processes 77−12021
As_2Se_3, influence of oxygen added in As_2O_3 and SeO_2 forms on phys. props. 77−76314
As_2Se_3, LF inelastic light scatt. meas. 78−15181
As_2Se_3, laser radiation induced struct. changes, electron microdiffr. obs. 79−10874
As_2Se_3 layers for electrophotographic use *(German)* 80−42283
As_2Se_3, localised gap states estimated by dielec. relax. 78−35087
As_2Se_3, lone-pair semiconductor, defect chemistry 80−25421
As_2Se_3, luminescence 80−80862
As_2Se_3, luminescence with short decay time 78−2906
As_2Se_3, mech. props. var. due to high press. phase change 77−76481
As_2Se_3, modulated photocurrent, analysed for trap-limited case *(Japanese)* 80−60030
As_2Se_3, neutrality of luminescence centres 78−88356
As_2Se_3, optical absorption spectra after 4.5 MeV electron bombardment *(Russian)* 77−32408
As_2Se_3, photodarkening and photostructural effects, Raman, IR and NQR studies 80−16036
As_2Se_3, photostimulated changes in contact props. 78−19162
As_2Se_3, richardson-Schottky type photoinjection current from photoconductor into insulating liquid 80−15608
As_2Se_3, semiconducting glass, elastic props., US vel. meas. 78−26628
As_2Se_3, solid and liq., elec. cond. meas. 77−28185
As_2Se_3, struct. changes, Mn^{2+} EPR expts. 78−79534
As_2Se_3, struct. determ. by electron spectroscopy 79−65979

chalcogenide glasses continued
As_2Se_3, thermal capacity, 300 to 600K 80—103492
As_2Se_3, thermally reversible photodarkening effects obs. 80—103970
As_2Se_3, threshold switches, turn-on state maintenance mechanism *(Russian)* 77—85271
As_2Se_3, transient electrical transport, general and unified treatment 80—59977
As_2Se_3, vitreous, elec. and opt. prop. changes on densification 77—11958
As_2Se_3, vitreous, hologram recording light sensitivity spectral distrib. *(Russian)* 78—1191
As_2Se_3 vitreous film, photodecomp. and photostruct. changes 77—76318
As_2Se_3 vitreous films, crystn. stimulated by org. subst. and electrophotographic parameters 77—76319
As_2Se_3, X-ray induced paramag. colour centres 78—19327
As_2Se_3:Ag, amorphous, US props. 78—51616
As_2Se_3:Ag amorphous, freq. depend. cond. 80—88565
As_2Se_3:Al, glassy, energy spectrum of deep localized states, thermal dielectric relaxation 78—15088
As_2Se_3:B:, devitrification kinetics, Bi impurity effects 77—35675
As_2Se_3:Bi, annealing kinetics, cond. activation energy and density 79—73503
As_2Se_3:Fe, glassy, mag. susceptibility investig. of doping effect 77—77024
As_2Se_3:I, hole drift velocity enhancement by I doping 77—39883
As_2Se_3:In, amorphous, photoluminesc. fatigue, metallic additive effect 79—61434
$As_2Se_3:Mn^{2+}$ film, reversible photostructural change, ESR obs. 77—32411
a-As_2Se_3:Mn(Fe)(Ni)(Cu)(Zn)(Ga)(Tn)(Il)(Na), hole drift mobility depend. on impurity conc. 79—60846
As_2Se_3:Pt, glass, effect of impurities on elec. props. 80—103699
As_2Se_3:Tl, hole transport, photoluminesc. and photoinduced ESR 79—8183
As_2Se_3:X (X=Cu, Ag, Tl, I, Ge), effect of doping, NMR meas. 80—11282
As_2Se_3-As_2Te_3, crystallisation 77—43156
As_2Se_3-As_2Te_3, localised states role in cond. in high elec. fields 77—76841
As_2Se_3-As_2Te_3, solid and liq., elec. cond. meas. 77—28185
As_2Se_3-As_2Te_3 glass thermoelec. power, and transport mechanism 80—2408
As_2Se_3-based glasses, crystallization, DTA investig. 78—22658
As_2Se_3-Bi_2Se_3, semiconducting crystallized glasses, elec. conductivity mechanism 77—39843
As_2Se_3-Cu (10-20%) film, darkening kinetics, and hologram diffr. efficiency 77—62027
As_2Se_3-Ge glassy thin films, flash photoresponse 80—107863
As_2Se_3-$GeSe_2$ glass, bulk and impurity IR absorpt. 80—71455
As_2Se_3-$GeSe_x$-$SnSe_x$ (x=1,2), exam. of Sn valency and physical props. 79—4753
As_2Se_3-InI_3, glass system, IR spectra 78—64365
As_2Se_3-metal system, time-resolved dark injection 79—91139
As_2Se_3-Sb_2S_3 glass, threshold and memory switching, expt. data 78—39170
As_2Se_3-Si amorphous-cryst. heterojunction, energy band diagram construction 77—55602
As_2Se_3-Ti_2Se (Tl_2Se_2) (Tl), glass, hot pressed, temp. dependence of optical absorption edge 78—88328
As_3Se, vitreous, optical transparency, photostimulated changes *(Russian)* 79—65941
As_3Se_2 amorphous film, photocond., TSC, light-induced changes 80—49810
As_3Se_2 chalcogenide film surface relief hologram selective etching *(Russian)* 79—94181
As_3Se_2 chalcogenide semicond. film, thermoptical transitions with photostructural transformations *(Russian)* 80—16016
As_3Se_2, electron irradiated, effects on elec., photoelec. and optical props. 80—49806
As_3Se_3:Cu, glassy, broadening of electrodiffusion profiles at high elec. fields 79—55939
$As_{50}Se_{50}$ and $As_{20}Se_{80}$ semicond. glasses, densified, photoluminesc., inelastic deform. effect 80—66293
$As_{60}Se_{40}$, amorphous films, spectral characts. of photodarkening 78—76494
As_xSe_{100-x} glasses, temp. depend. of mag. susceptibility and EPR 77—63073
As_xSe_{100-x}, thermally stimulated cond. *(Russian)* 79—91074
$As_xSe_{100-x}:Mn^{2+}$, $0 \leq x \leq 70$, EPR, composition depend. and struct. 77—24736
$As_2Se_3Ag_x$ glassy semicond. film, prep. by photodiffusion of Ag, negative photocond. 80—92934
$As_2Se_3Ag_x$, optical absorpt. coeff. and DC cond. 80—54699
$(As_2Se_3)_{1-x}(As_2Te_3)_x$ amorphous films, changes in optical props. under elec. fields and optical excitation 79—61455
$AsSe_{1.5}Bi_{0.05}$ glasses, soln. rate in alkali solns. 80—16531
$As_{10}Se_{67.5}Ge_{22.5}$, film as master for PVC copied holograms 77—23632
As_4Se_5Ge, glass, light irrad. induced changes in optical and elec. props. *(Japanese)* 78—68031
As_4Se_5Ge, struct. changes, Mn^{2+} EPR expts. 78—79534
$As_4Se_5Ge_1$, amorphous, optically broadened lattice vibration spectra 79—77712
$As_2Se_3Hg_x$, semicond. glassy system, struct. 77—35489
AsSeI, struct. determ. by electron spectroscopy 79—65979
AsSeI, X-ray diffr. study in vitreous and fused states 77—7675
$AsSeI_{0.1}$, photostimulated changes in contact props. 78—19162
$AsSeI_x$, cond. and photocond. 80—20253
$As_2Se_3(S_3)$, glassy film, photostructural effects, NQR study 80—49549
$As_{40}Se_{50-x}S_xGe_{10}$ film strip-loaded waveguide formed in graded-index $LiNbO_3$ planar waveguide 78—74965
$As_2Se(Se_3)$, photostimulated light absorpt. 77—77221
$AsSe_{1.5}Sn_x$ glasses, crystallisation, Mossbauer obs. 77—47557
$(AsSe)_{1-x}Te_x$, thermal props. and viscosity, temp. and conc. depend. 77—76324
$AsSe_{1.1}Te_{0.2}$:Fe, Fe effect on physiochem. props. of glass 80—24370
$AsSe_{1.5-x}Te_x$ glasses, physical props. 78—68028
As_2SeTe_2, between Al and Sb electrodes, rectifying effects 80—75654
As_2SeTe_2, field effect, localised states and electronic transport 77—66187
$As_2(Se_{1-x}Te_x)_3$ semiconducting glasses, solid and liquid, thermal cond. 80—6574
$As_2(Se_{1-x}Te_x)_3$, thermal cond., temp. and press. depend. 79—82396

chalcogenide glasses continued
$As_2Se_{1.5}Te_{1.5}$, thermally reversible photodarkening effects obs. 80—103970
As_2Se_2Te, electrical conductivity at strong elec. fields and high hydrostatic press. *(Czech)* 77—24560
As_2Se_2Te, field effect, localised states and electronic transport 77—66187
$As_2Se_xTe_{3-x}$ chalcogenide glasses, cond. meas., field strength and temp. depend. 78—84225
$As_{40}Se_xTe_{60-x}$ amorphous system, resistivity press. depend. 79—82592
$As_{60}Se_xTe_{40-x}$ glasses, crystallisation 77—35488
As_2Te_3, amorphous, defect states and impurity states 80—54650
As_2Te_3 and As_2Te_3Ge, amorphous, AC cond. at low temps. 80—80269
As_2Te_3, field depend. elec. cond. and localised states role 77—76829
As_2Te_3, field effect, localised states and electronic transport 77—66187
As_2Te_3 film, charge screening length 79—23974
As_2Te_3, localised gap states, hopping cond. and chem. bonding 78—23052
As_2Te_3, phase transitions and elec. cond. 78—10440
As_2Te_3, press.-induced semicond.-metal and supercond. transitions 77—43671
As_2Te_3, solid and liq., elec. cond. meas. 77—28185
As_2Te_3, struct. determ. by electron spectroscopy 79—65979
As_2Te_3, thermal capacity, 300 to 600K 80—103492
As_2Te_3-Tl_2Te system, phase diagram 77—16559
$As_2Te_3+Tl_x$, glassy system, composition depend. of activation energy, thermopower meas. 78—64052
$As_{25}Te_{75}$, and $As_{45}Te_{55}$, vitreous, local struct., elec. field gradient tensor asymmetry obs. 79—73847
$As_{50}Te_{50}$, amorphous films, metal and semicond. contacts, threshold switching, IR emission 80—49831
$As_{50}Te_{50}$ amorphous switches, light emission charact. 79—78139
As_xTe_{100-x}, glassy system, composition depend. of activation energy, thermopower meas. 78—64052
$As_xTe_{100-x}:Mn^{2+}$, $40 \leq x \leq 70$, EPR, composition depend. and struct. 77—24736
$AsTeCu_x$ ($0 \leq x \leq 0.4$) glass, effect of Cu on elec. cond. and thermoelectricity, 100 to 370K 78—87978
$AsTeE_x$, E=S, Se, Sb, Bi, annealing effects on elec. cond. of films 77—43594
$As_{10}Te_{75}Ge_{15}$, dielec. props. 77—63355
$(As_2Te_3)_{1-x}Ge_x$, amorphous, AC cond. magnitude and variation *(French)* 79—47095
$As_xTe_{90-x}Ge_{10}$, $As_{35}Te_{55}Ge_{10-x}Si_x$ glasses, elec. and optical props., comp. depend. 77—24555
$As_{35}Te_{28}Ge_{16}S_{21}$, chalcogenide semiconductor study of electric properties *(French)* 80—29414
$As_4Te_5Ge(Si)$, struct. changes, Mn^{2+} EPR expts. 78—79534
$As_4Te_5I_2$, struct. determ. by electron spectroscopy 79—65979
$As_{50}Te_{45}I_5$, glass, semicond., elec. switching, high press. effects 78—72212
$As_xTe_xS_xSe_{100-3x}$ glasses, IR absorpt. spectra 77—12378
$AsTeS_x(Se_x)(Sb_x)(Bi_x)$, thin film crystallisation 79—7758
$As_2Te_{3-x}Se_x$, ^{125}Te Mossbauer expts., comparison of amorphous and cryst. samples 78—88232
$As_xTe_xSe_{100-2x}$, x=2.5 and 5.0, IR absorpt. spectra 77—24842
$As_{30}Te_{48}Si_{12}Ge_{10}$, film, charge screening length 79—23974
$As2S_3$ amorphous chalcogenide film inorganic photoresists, holographic resolution evaluation 79—76629
Bi-Sb-S-I system glasses, vitrification and volt-ampere characts. 77—31756
Bi_2Se_3, thin film, charge transport at high fields *(Rumanian)* 79—60841
CC $Si_{12}Ge_{10}As_{30}Te_{48}$, thermally stimulated depolarization current meas. *(Japanese)* 78—34875
Cd-As-S, prod. and acoustooptic props. *(Russian)* 78—63158
$Cd_6Ge_3As_4$, semiconducting glass, elastic props., US vel. meas. 78—26628
$CdGe(P_xAs_{1-x})_2$ static current-voltage characteristics *(Russian)* 77—15925
$CdSeTl_x$—$As_2Se_3Tl_x$ thin layer system, charge transport 77—76985
Cu-As-Se glass, localised states exam. *(Russian)* 78—34806
Cu-As-Se glasses, recording and erasure by laser beam *(Russian)* 78—71170
Cu-P-Se system, glasses, semicond., density, microhardness, softening point rel. to conc. 77—7674
$Cu_x(As_{0.4}Se_{0.6})_{1-x}$, amorphous, ^{77}Se NMR, comp. depend. 78—76329
$Cu_{10}As_{31}Se_{38}O_{21}$, chalcogenide glass, exam. of electron mechanism of photo induced changes 78—87998
Eu, anomalous Hall effect, anal. 77—20344
Eu-As-S, glass forming region, Raman and IR obs. *(French)* 79—99080
EuS-Ga_2S_3-GeS_2, chalcogenide glasses, conditions of form. of glassy prod. *(French)* 80—100325
Fe doped in equil. conditions, impurity cond. and Mossbauer effect 80—49726
$GE_{40}S_{60}$-Ag glass, EPR exam. 78—23334
Ga-Ge-Se chalcogenide glasses, rare earth element doped, elec. props. 80—96885
n-GaAs/chalcogenide glass, elec. props. and band diagram 79—99609
Ga_2S_3-La_2S_3-$Nd_2S_3:Nd^{3+}$ chalcogenide glass, Nd^{3+} emission and absorption spectra, nonradiative relax. 77—40268
$3Ga_2S_3.La_2S_3:Ho^{3+}$, radiative and multiphonon relax. 79—33794
$Ga_{0.25}Te_{0.75}$ time evolution of nanosecond switching 80—6921
$Ga_{20}Te_{80}$, amorphous, splat cooled, thermoelectric props. 78—43426
Ge amorphous film, effects of alloying chalcogen atoms 80—49670
Ge-As-S-I system, acousto-optical parameters 77—36199
Ge-As-Se, amorphous film, condensation formation and struct. props. *(Russian)* 78—38629
Ge-As-Se, appl. in 8 to 12 μm thermal imaging system 78—25935
Ge-As-Se, elastic moduli, US vel. and reson. freq. meas. 78—23756
Ge-As-Se, Se-As, and Se-Ge, for IR appl., prod. using H_2 distillation 77—32551
Ge-As-Se films, light irrad., heat treatment rel. to optical props. *(Russian)* 79—4858
Ge-As-Se IR transmitting glass composition, prep. and props. 80—69474
Ge-As-Se system, thermal capacity, 300-600K 79—65210
Ge-As-Se-Te glasses for 8-12 μm IR optics 80—69475
Ge-As-Te, between metal electrodes, contact props. determ. 79—7908
Ge-As-Te, thin chalcogenide glass film, high-field switching effects 77—32052
Ge-As-Te glass, thermoelec. power and DC cond., temp. depend. 77—62955
Ge-As-Te system, glasses, magnetochemical exam. 78—88092

chalcogenide glasses continued
- Ge-Bi-S system, semicond., elec. cond., glass transition temp. and optical absorption meas. 77—16329
- Ge-Bi-S system glasses, opt. props. and glass transition temp. 77—77224
- N-Ge-Bi-Se glass, elec. and optical props. 80—65550
- Ge-P-S glass system, EPR of intrinsic and Mn^{2+} impurity centres 80—88870
- Ge-P-Se system, glasses, semicond., density, microhardness, softening point rel. to conc. 77—7674
- Ge-P-Se system glasses, penetration by indentor, activation parameters, microhardness 79—43419
- Ge-Pb-S, glassy, photoconductivity dependences applied elec. field 80—107857
- Ge-Pb-Se-Te, glass form., DC cond., and mole volume 79—90560
- Ge-S, amorphous, photocond., photo-induced ESR, optical edge shift 80—49809
- Ge-S, Ge-S-Ag, amorphous prop. and origin of paramagnetic defects 79—10801
- Ge-S, glass, ESR, model of paramag. defects 79—78517
- Ge-S, melt-quenched photoinduced ESR, annealing behaviour and glass comp. depend. 80—71156
- Ge-S amorphous film, defect states, ESR 80—49670
- Ge-S glasses, Cu doped, thermal, structural and dielectric props. 79—60283
- Ge-S glasses, EPR study 78—43644
- Ge-S system glasses, thermal expansion coeff. and free vol. at transition temp. *(Japanese)* 79—55876
- Ge-S-Ag glasses, bulk and film, EPR study 78—43644
- Ge-S-Cu, phase separation in melt centrifugal quenching 80—25701
- Ge-S-Ga amorphous thin film, memory switching effects 80—88605
- Ge-S-Ga(In) system glasses, photoinduced changes 80—24365
- Ge-S-In, determ. of glass phases, phys. props. meas. 79—23526
- Ge-S-Sb glasses, microgravity effect on recrystn., optical and elec. props. 80—49127
- Ge-S-Se, glass formation 80—103251
- Ge-S-Se system, glass-forming, struct. and props. 80—19713
- Ge-S-Te system, glass forming 80—19718
- Ge-S(As)-Se, solubility, photostimulated changes 80—24602
- Ge-Sb-Se glass, elec. props, comp. depend. 80—70697
- Ge-Sb-Se glass, physical props., purification method for Sb, Se from surface oxides 78—46735
- Ge-Sb-Se system, thermal capacity, 300-600K 79—65210
- Ge-Se, elastic props. under press., US interferometry 78—79658
- Ge-Se, glassy, photoinduced photolum. fatigue *(Russian)* 78—60520
- Ge-Se, vibr. props., Raman and IR spectra obs. *(Japanese)* 77—43989
- Ge-Se based glasses, refr. index, 1-11 μm 78—39520
- Ge-Se film, photoinduced absorpt. changes 79—87519
- Ge-Se glass system, effect of changes in local surrounding of atoms on optical props. *(Russian)* 78—80414
- Ge-Se glasses, radiative localised centres, photoluminesc. 79—83025
- Ge-Se system glasses, thermal expansion coeff. and free vol. at transition temp. *(Japanese)* 79—55876
- Ge-Se-Fe phase system, amorphous films, mag. and elec. props. 79—51695
- Ge-Se-Ga(In) system glasses, vitreous phase struct. 77—76320
- Ge-Se-Te amorphous alloys, prep. and calorimetric obs. 77—11675
- Ge-Se-Te glasses, form. region, elec. props. 79—94904
- Ge-Se-Tl, vitrification region 77—43154
- Ge-Se(Te) films, laser-beam recordings by thermal creation of holes 80—35010
- Ge-Si-S system, glass formation, transition temp., crystallisation and melting 80—100178
- Ge-Te alloy films, amorphous, semicond. props., refr. index, struct. study 78—26978
- Ge-Te and Ge-Te-As system glasses, local struct., ^{119}Sn Mossbauer obs. 79—41968
- Ge-Te binary glass, eutectic, DSC obs., thermodynamic and thermokinetic characts. 80—39309
- Ge-Te-As-In quaternary compounds, elec. resist. of thin sheets, Mott's theory *(Spanish)* 77—69320
- Ge-Te-As-In quaternary compounds, elec. props., Hall effect *(Spanish)* 77—69344
- Ge-Te-As-In quaternary compounds, thin sheets elec. props., thermoelec. power *(Spanish)* 77—69358
- Ge-Te-Se/Si amorphous film-cryst. heterojunction, electron-beam-induced current 79—24060
- $Ge_{100-x}As_x$ glass, elec. props. 77—76966
- GeAsS, X-ray photoelectron spectra, valence electrons density of states *(Russian)* 79—15583
- $Ge_xAs_xS_xSe_{100-3x}$ and $Ge_xTe_xS_xSe_{100-3x}$ glasses, IR absorpt. spectra 77—12378
- $Ge_{33}As_{27}S_{15}Te_{25}$, chalcogenide thin films, coupled carrier theory test, high field conditions 80—100466
- $Ge_{33}As_{27}S_{15}Te_{25}$ glass, switching, microstructural changes 79—65523
- $Ge_{0.3}As_{0.2}Se_{0.5}$, IR optic materials, characteristics *(German)* 80—38081
- $Ge_xAs_xSe_{100-2x}$, x=2.5 and 5.0, IR absorpt. spectra 77—24842
- $Ge_{15}As_4Te_8$, film, influence of electric field on crystallisation kinetics 78—42914
- $Ge_{10}As_{40}Te_{40}I_{10}$, film, switching delay time 78—26926
- $Ge_{10}As_{40}Te_{40}I_{10}$, threshold switch, high resist. state 77—15924
- $Ge_{30}As_{17}Te_{30}Se_{23}$, antireflection coating for KCl, design, prep. and performance 79—14063
- $Ge_{30}As_{17}Te_{30}Se_{23}$-$As_2S_3$, two-layer antirefl. coating, error considerations in design 80—74477
- $Ge_xAs_xTe_xSe_{100-3x}$, IR absorpt. spectra 78—23448
- n-$Ge_{20}Bi_{10}Se_{70}$ glass, preparation and elec. props. 79—74126
- $Ge_{20}Bi_xSe_{80-x}$, semicond. glass, resist., thermoelec. power, optical absorpt. 80—88555
- $Ge_{20}Bi_xSe_{70-x}Te_{10}$, n-type semiconducting glasses, resistivity and thermoelectric power meas. 80—54695
- $Ge_{20}Bi_xSe_{70-x}Te_{10}$, semicond. glass, resist., thermoelec. power, optical absorpt. 80—88555
- $Ge(S,Se)_2$ glasses, comparison A_1 Raman line, microscopic origin 80—29740
- $Ge_x(S,Se)_{1-x}$ covalent non crystalline topology, short range order 80—15009
- GeS, amorphous, UPS and XPS, valence band struct. 77—90247
- $GeS_{1.1}$ glass, neutron irrad., thermal and elec. props. 79—19286
- $GeS_{1.5}$ glass, TSD evidence for ionic cond. 77—76598
- $GeS_{1.35}$ glass, neutron irrad., AC elec. cond. 80—24924

chalcogenide glasses continued
- $GeS_{1.5}$, high-resistivity, uniform and space charge polarisation, thermally stimulated depolarisation anal. 78—15085
- $GeS_{1.5}$:Cu, interpretation of dielectric behaviour 79—33595
- GeS_2, amorphous film, reversible and irreversible photostructural changes 79—74061
- GeS_2, cryst. and glass, Raman spectra, struct. *(Russian)* 79—51966
- GeS_2 glass, melt quenched, reversible photostructural change, optical transmission spectra obs. 80—45109
- GeS_2 glass, molecular to band-like modes 77—66012
- GeS_2, glass, structure correlation range, Raman Brillouin light scatt. determ. 77—20857
- GeS_2 glass, temp. and press. depend. of elastic props. 77—15476
- GeS_2, glassy, high freq. vibr. bands, central force model 80—49330
- GeS_2, hollow cluster model of atomic structure 80—6366
- GeS_2, IR optic materials, characteristics *(German)* 80—38081
- GeS_2, LF inelastic light scatt. meas. 78—15181
- GeS_2, thermal expansion at low temperatures 78—83982
- GeS_2-GeS-Ag_2S, Ag diffusion, 50-120°C 78—18828
- GeS_8 glass, activation energies after neutron irradiation, elec. cond. and transmission coeff. 78—83850
- GeS_x glass, x=1.25 to 1.5, softening and crystallization kinetics 79—32906
- GeS_x, neutron irrad. effects on thermal parameters 77—11597
- GeS_x, optical props., chem. struct. effects 77—63460
- $Ge_{1-x}S_x$ glasses, building blocks and bonds 80—54141
- $Ge_{100-x}S_x$, film, effect of alloying chalcogen atom on elec. cond., optical transmission and ESR 79—78101
- Ge_2S_3, electron irradiated, effects on elec., photoelec. and optical props. 80—49806
- Ge_2S_3, glass form. and characterisation *(German)* 80—64913
- Ge_2S_3-Ag contact, photoinduced diffusion of Ag in amorphous semicond. film 80—49418
- Ge_2S_3-Ge_2Se_3, glass, photoluminesc. spectra, solid soln. form. *(Russian)* 78—23525
- $Ge_{25}S_{75}$:Mn, bond struct. and character in Ge-S system, EPR obs. 80—66014
- $Ge_{30}S_{70}$ glass film, Ag photodoping sensitivity 80—39121
- $Ge_{40}S_{60}$, $Ge_{25}S_{75}$ glasses, Mn^{2+} EPR spectra investigation 79—11340
- $Ge_{40}S_{60}$ glass, Cu doped, EPR study 79—65713
- $Ge_{40}S_{60}$:Mn (Ag)(Cu), bond struct. and character in Ge-S system, EPR obs. 80—66014
- $Ge_{42}S_{58}$, amorphous, bulk and film forms, elec. props. and ESR study 80—103691
- $Ge_{42}S_{58}$:Cu(Ag)(I), impurity effect on e.p.r., dangling bonds 77—4553
- Ge_xS_{1-x} glasses, sp. ht., 2 to 18K 79—65214
- GeS(S_2) amorphous films, photostructural changes, UPS study 80—49550
- $Ge_{1-x}S_x(Se_x)$, bulk-quenched glasses, opt. freq. dielec. const., chem. ordering effects 78—23472
- $Ge_{20}Sb_{25}S_{55}$ glasses, optical props., absorption edge temp. depend. 80—2789
- $Ge_{2.33}SbSe_5$:Fe, Fe effect on physiochem. props. of glass 80—24370
- GeSe, amorphous, film, thermally induced effects, UPS study 80—104042
- GeSe, amorphous, pair distrib. function, anomalous X-ray scatt. 80—49126
- GeSe, amorphous, UPS and XPS, valence band struct. 77—90247
- GeSe, amorphous film, optical properties 78—39620
- GeSe amorphous films, blocking metal contacts characteris. and photo/EMF obs. 77—76924
- GeSe amorphous films, photoconductivity measurements, recombination model 78—64061
- GeSe-Si amorphous-cryst. heterojunction, energy band diagram construction 77—55602
- $GeSe_2$, amorphous, film, thermally induced effects, UPS study 80—104042
- $GeSe_2$ amorphous film, laser induced light absorpt. oscillation, exciton model 80—50446
- $GeSe_2$, amorphous film, photocond., photo-induced ESR, optical edge shift 80—49809
- $GeSe_2$ amorphous layers, photoconductance meas. 80—65632
- $GeSe_2$, and $Ge_{1-x}Se_x$, struct. models 79—37628
- $GeSe_2$ chalcogenide film, struct. changes due to laser induced transmittance oscill., SEM obs. 78—6240
- $GeSe_2$, cryst. and glass, Raman spectra, struct. *(Russian)* 79—51966
- $GeSe_2$, DC conductivity, calorimetric, and X-ray diffr. meas. 79—78107
- $GeSe_2$, drift mobilities of electrons and holes, photocurrent decay meas. 80—2424
- $GeSe_2$ evaporated films, optical absorpt. and thermally induced effects 79—42989
- $GeSe_2$ evaporated films, struct. and thermally induced effects 79—41963
- $GeSe_2$ film, glassy, self-controlled laser-beam chopping effect 78—60528
- $GeSe_2$ film, light-induced light absorption changes 77—73181
- $GeSe_2$ glass, photoluminesc. spectrum, rel. to cryst. forms 77—55819
- $GeSe_2$, glassy, powdered and bulk, fatigue of photolum. 80—80855
- $GeSe_2$, glassy photoinduced photoluminescence fatigue 79—28827
- $GeSe_2$, hollow cluster model of atomic structure 80—6366
- $GeSe_2$, LF inelastic light scatt. meas. 78—15181
- $GeSe_2$, photoluminescence at 77K 77—63456
- $GeSe_2$-As_2Se_3-Sb_2Se_3 system glasses, vitrification and elec. cond. 79—50996
- $GeSe_2$-As_2Se_3-Sb_2Se_3, quenched glass system, elec. cond., low temp. heat treatment effect 80—39586
- $GeSe_2$-As_2Se_3-Sb_2Se_3, elec. cond. over wide range of temp. 80—88564
- $GeSe_2$-$SnSe_2$-As_2Se_3, GeSe-SnSe-As_2Se_3, Mossbauer investigation 77—20052
- $GeSe_4$ film, self-controlled laser beam chopping effect 78—31266
- $Ge_{1-x}Se_x$, ave. energy gap, optical freq. dielec. const. and refr. index 77—76739
- $Ge_{1-x}Se_x$ film, EPR, elec. and optical props. meas. 78—48038
- $Ge_{1-x}Se_x$ glass, refr. index comp. depend. and photo-induced variation 79—91398
- $Ge_{1-x}Se_x$, photolum. and optical props. meas. 77—20908
- $Ge_{100-x}Se_x$ film, effect of alloying chalcogen atom on elec. cond., optical transmission and ESR 79—78101
- Ge_2Se_3, glass form. and characterisation *(German)* 80—64913
- Ge_2Se_3, vitreous, evaporation kinetics and amorphous film deposition 80—97434
- Ge_8Se_{92}, electrical cond. freq. depend., hopping cond. contrib. 77—76856

chalcogenide glasses continued
Ge_xSe_{1-x}, $0<x<0.2$, crystallisation in amorphous bulk and thin films 78−55813
Ge_xSe_{1-x}, amorphous, AC cond. *(Korean)* 80−44591
Ge_xSe_{1-x}, amorphous, excitation spectra of photolum. fatigue and creation of paramag. centres 80−50402
Ge_xSe_{1-x}, amorphous, exponential absorpt. edge rel. to struct. 79−99902
Ge_xSe_{1-x}, amorphous, X-ray diffr. and local order modelling 80−49125
Ge_xSe_{1-x} amorphous film, photocrystallisation, elec. cond. meas. 79−32911
Ge_xSe_{1-x} amorphous film, photocrystn., elec. cond. and optical microscopy obs. 79−87024
Ge_xSe_{1-x}, amorphous semicond., elec. props. 78−84219
Ge_xSe_{1-x} chalcogenide glasses, drift mobility of optically injected carriers 79−19627
Ge_xSe_{1-x} glass, $1/3\leq x\leq 1/2$, Raman scatt., local order 78−23442
Ge_xSe_{1-x} glasses, DC cond. and static dielectric const. meas. *(French)* 77−62925
Ge_xSe_{1-x} glasses, defect states, photoluminesc. and ESR obs. 79−61418
Ge_xSe_{1-x} glasses, optical props. and local struct. *(French)* 77−77162
Ge_xSe_{1-x} glasses, trap-controlled carrier mobility, time of flight meas. 79−4557
Ge_xSe_{1-x} glasses, vibr. props. 78−2219
Ge_ySe_{1-y}, glass, bulk and film, IR transmission and reflectivity meas., struct. mode assignments 78−79537
α-Ge_ySe_{1-y}, photoluminescence and fatigue effects 78−84648
$(GeSe_2)_x(As_2Se_3)_{1-x}$, vibr. excitations of large atomic clusters, Raman and depolarisation spectra 77−20856
$(Ge_{1/3}Se_{2/3})_{100-x}Ni_x$, ESR, rel. to elec. cond. 80−7155
$GeSe(Se_2)$ amorphous films, photostructural changes, UPS study 80−49550
$Ge_{20}Se_{40}Te_{40}$ amorphous alloys, thermal crystn. study 78−26789
$Ge_3Se_2Te_4$ film, Hall effect freq. depend. 77−1436
Ge_4Se_5Te, amorphous layer, Poole-Frenkel controlled charge carrier transport, model of charged dangling bonds 80−49750
Ge_4Se_5Te, amorphous layers, charge carrier transport mechanism 80−54708
Ge_4Se_5Te amorphous layers, prep. and elec. props. 80−97436
$(Ge_{0.32}Se_{0.32}Te_{0.32}As_{0.4})_{100-x}Ni_x$, ESR, rel. to elec. cond. 80−7155
a-GeSi film with Mo contacts, AC performance *(German)* 77−63012
$Ge_{10}Si_{12}As_{30}Te_{48}$, monostable chalcogenide glass threshold switch, temp. meas. *(German)* 77−4412
$Ge_7Si_9As_{39}Te_{35}Ga_{10}$, chalcogenide thin films, coupled carrier theory test, high field conditions 80−100466
$Ge_{1-x}Sn_xTe$ film, amorphous, elec. cond. 80−93016
GeTe, amorphous, UPS and XPS, valence band struct. 77−90247
GeTe film, amorphous, evaporated and annealed, variable range hopping cond. 78−80077
GeTe film, amorphous, specific current noise power 77−66190
GeTe, film, local order, electron diffraction study 79−77485
GeTe, high temp. mass spectrometric obs. of vaporis. 77−76542
$GeTe$-As_2Te_3 system, phase diagram, eutectic comp., thermographic and X-ray anal. *(Russian)* 77−63646
GeTe-Si amorphous cryst. heterojunction, energy band diagram construction 77−55602
$Ge_{0.5}Te_{0.5}$, strucutral anal. by neutron diffr., radial distribution functions 80−15010
$Ge_{100-x}Te_x$ film, effect of alloying chalcogen atom on elec. cond., optical tranmission and ESR 79−78101
$Ge_{15}Te_{85}$, amorphous, splat cooled, thermoelectric props. 78−43426
Ge_xTe_{1-x}, amorphous, struct., quadrupole splitting of $^3/_2$ spin state of ^{125}Te calc. 77−65950
$Ge_{15}Te_{81}As_4$ film, amorphous, characts. of optical switching 78−18031
$Ge_{15}Te_{81}As_4$, influence of O_2 on phase separation of chalcogenide glasses 77−47354
$Ge_xTe_{10-x-y}E_y$, E=impurity, glass-crystn. transition, memory effect 77−47870
$Ge_{15}Te_{81}Sb_2S_2$ film, amorphous, characts. of optical switching 78−18031
$Ge_{15}Te_{81}Sb_2Se_2$, electrical cond. freq. depend., hopping cond. contrib. 77−76856
$Ge_xTe_xSe_{100-2x}$, x=2.5 and 5.0, IR absorpt. spectra 77−24842
$Ge_{20}Te_2Se_{80-x}Si$, amorphous-cryst. heterojunctions 79−65546
Hg-As-S, prod. and acoustooptic props. *(Russian)* 78−63158
Hg-As-S modulating glasses, optical parameters and struct. *(Russian)* 78−63159
Hg-As-S system glasses, photoelectron X-ray spectroscopy study 80−29858
In-As-Se-I system, glass form. obs. 77−77466
In_xSe_{1-x}-SnO_2 heterostructure, anomalous temp. depend. obs. on photovoltage 78−56209
$In_{0.25}Te_{0.75}$ time evolution of nanosecond switching 80−6921
$In_{20}Te_{80}$, amorphous, splat cooled, thermoelectric props. 78−43426
In_3Te_2 amorphous film, pulse hologram recording 79−55091
$La_2S.3GaS_3$:Ho^{3+}, fluoresc., visible and IR spectra assignments 77−52150
$La_2S_3.3Ga_2S_3$, fluoresc. and possibility of lasing 78−23514
La_2Se_3-Ga_2Se_3-$GeSe_2$ ternary system, phase diags., glass formation *(French)* 78−3109
Li_2S-GeS_2, glass forming region, struct. and ionic cond. 80−88358
Mo-chalcogenide glass-Mo-Al struct., strong elec. field effects 80−97004
Na_2S-P_2S_5, glass forming region, struct. and ionic cond. 80−88358
Na_2S-$SiS_2(GeS_2)(P_2S_5)$, synthesis, structure and ionic conduction *(French)* 80−65291
Na_2S-XS_2, X=Si, Ge, glass forming region, struct. and ionic cond. 80−88358
P-As-Se glasses, mag. susceptibility, dielec. const., opt. props. 78−64184
P-S, amorphous, glass transition and specific heat, intermolecular bond saturation 80−15011
P-Se, amorphous, glass transition and specific heat, intermolecular bond saturation 80−15011
P-Se, effect of Ag electrodiffusion on volt-ampere characteristics 79−7869
P-Se, phase diag. and crystallisation of glasses at high press. 77−52297
P-Se, solubility, photostimulated changes 80−24602
P-Se glass system, IR spectra 78−64365
P-Se system, glass form. props., effect of P concentration *(Russian)* 78−2019
P-Se system glasses, magnetochem. investig. 77−51325
P-Se-Te system glasses, mag. susceptibility and opt. props. 80−25079
P-Se-Te system glasses, vitrification region 78−51425
P-Se-Tl, NMR of ^{31}P and ^{205}Tl 80−15812

chalcogenide glasses continued
P-Se-Tl system glasses, polarisation, refr. index and dielec. const. meas 80−20608
P_2S_5-Ag_2S, Ag diffusion, 50-120°C 78−18828
$P_2Se_xS_y$, thermophysical props., 303-413K, struct. interpretation 78−47615
P_2Se_xSy glass, vitrification temp., elec. props. and hardness meas. *(Russian)* 77−28177
Pb-As-S semiconductor glasses, far IR transmission and Raman scattering 77−63419
Pb-Ge-S semiconducting glasses, far IR transmission and struct. 79−65855
Pb-Se-As-Ge, phase separation in melt centrifugal quenching 80−25701
PbS-As_2S_3 glass, elastic props. temp. depend. 78−71780
$(PbS)_x(As_2S_3)_{1-x}$, high field effects 79−42553
PbSe-GeSe-AsSe, glass form., elec. cond., struct. defects, assoc. *(Russian)* 80−54145
S-Se amorphous alloys, crystn. kinetics, elec. cond. meas. 78−34441
S-Se-Te semicond. glasses, mag. suscept. meas., refractive index 78−34952
SSe_{20}, crystalline phase growth in amorphous solid and liquid samples 78−43107
$SSe_{22.5}$, amorphous, photo-effect on crystn. kinetics, elec. cond. obs. 79−77522
SSe_{40}, amorphous alloy, crystn., elec. cond. meas. 78−34440
SSe_9, stable thermoelectret, effects of anisotropic external perturbation *(Russian)* 77−63361
Sb-Ge-Se system glasses, thermal capacity, 80 to 300K 79−42272
Sb-Ge-Se system glasses, activation energy of elec. cond. calc. 79−51568
Sb-S films, laser-beam recordings by thermal creation of holes 80−35010
Sb-S-I, activation energy of crystn. 80−64920
Sb-S-I system crystals and glasses, adhesion levels, TCE spectra 77−24529
$SbGe_xSe_y$, with const. Sb content, heat capacity, thermal expansion, US vel. and elastic moduli 77−76574
Sb_2S_3 (Se_3), photoconductivity dependences applied elec. field 80−107857
Sb_2S_3, amorphous and crystalline thin films, optical consts. 79−91518
Sb_2S_3, amorphous layer, scattering of visible light, rel. to substrate temp. during deposition 79−65950
Sb_2S_3, density of valence states, XPS and UPS obs. 77−48308
Sb_2S_3 film, amorphous and crystalline, optical props. 79−95867
Sb_2S_3, glassy, interface with metal, photoelec. props. 79−73589
Sb_2S_3, vitreous, prep. elec., opt. and struct. props. 77−76889
$Sb_2S_3(Se_3)$, IR spectra rel. to bonding, amorphous film and cryst. 77−16410
SbSe, amorphous thin film high field charge transport and quasi-Fermi level location 80−70863
Sb_2Se_3-Se-SbSeI, exam. of glass formation, IR transmission spectra 78−88452
Sb_2Te_3 field effect, localised states and electronic transport 77−66187
Se, bonding coordination defects 80−59927
Se, electronic props., xerographic use 80−20242
Se glass, flexural strength in transition range 77−56032
Se, liquid-glass transition, P-V-T relations 77−24387
Se, photoelectronic behaviour, in glass transition region 80−60045
Se, transient electrical transport, general and unified treatment 80−59977
Se:As, continuous crystn. kinetics 77−24382
Se-As, photoelectronic behaviour, in glass transition region 80−60045
Se-As film, evaporated, thickness, substrate temp. effects 79−15610
Se-As_2Se_3 system glasses, vibr. spectra and partial vols. of components 79−42973
Se-As-Ge, glass alloy system, annealed light irradiated, photoinduced absorption change, random network model 79−59773
Se-based, band gap variation 78−90461
Se-Bi-I, high sensitivity visible-near IR photoconductor, development and characterisation 78−39153
Se-Fe system, amorphous films, mag. and elec. props. 79−51695
Se-Ge, amorphous, Raman spectra and average band gap 80−50327
Se-Ge, amorphous thin film, photocontraction rel. to surface struct. 80−49551
Se-Ge, chalcogenide glass, Raman scatt. and bond struct. 79−95772
Se-Ge, lattice vibr. spectra, photostruct. change, far IR absorpt. 78−72494
Se-Ge amorphous films, obliquely deposited, photoinduced chem. changes 80−76385
Se-Ge amorphous system, AC elec. cond., near T_g, temp. depend. 80−49791
Se-Ge glasses, extreme far IR absorpt. meas. 80−50318
Se-Ge system, amorphous, press. depend. of AC cond. 77−76858
Se-Ge-As, self-diffusion, investigation using radioactive tracers 79−23770
Se-Ge-Sb alloy glass, crystn. kinetics 77−20057
Se-Ge-Te, chalcogenide glass, elec. cond. and dielec. const. 80−75567
Se-Ge-Te glass, dielectric meas. 79−87382
Se-S, glassy alloy, order-disorder transition kinetics 78−67650
Se-Si, vibr. IR spectra 80−20643
Se-Te crystallised glasses, struct. transforms. and IR spectra 80−19712
Se-Te film, evaporated, drift mobility of holes, elec. field and comp. depend. 77−39977
Se-Te-As-Ge glasses, absorpt. spectra, diffuse reflectivity loss correction 79−82995
Se-Te-As-Ge glasses, elec. transport 79−60833
Se-Te-Ge, amorphous, off-state thermal switching 79−65524
Se-Te-Ge and Se-Sb systems, amorphous, electrical transport, activation energy 79−95406
Se-Te-$Ge_{0.5}Sb_{0.5}$, DTA, critical cooling rates determ. *(French)* 77−72682
Se-Te-Sb glasses, electronic transport 80−88579
a-$Se_{97.5}As_{2.5}$, trapping, photo-stimulated and thermally-stimulated current obs. 77−28192
$Se_{0.84}Ge_{0.16}$ glass, sp. ht. excess rel. to far IR absorption 77−84874
$Se_{1-x}Ge$, amorphous, AC cond. magnitude and variation *(French)* 79−47095
$Se_{75}Ge_{25}$, obliquely deposited amorphous films, photo-induced optical effects 79−56871
$Se_{0.09}Te_{0.05}$, crystallisation, effect of an alternating electric field 80−88054

chalcogenide glasses continued
  $Se_{1-x}Te_x$ amorphous films, sublinear and superlinear I-V characts. 79—82695
  $Se_{1-x}Te_x$, film, photo-crystallisation 80—59839
  $Se_{1-x}Te_x$, film, struct. and props. 79—99079
  $Se_{1-x}Te_x$, optical and elec. props. 80—84506
  $Se_{1-x}Te_x$ systems, amorphous and liq. states, short range order, neutron scatt. study 80—49124
  Se_xTe_{1-x}, amorphous, structural relaxation and crystallisation kinetics study by DTA 80—59394
  $Se_{12}Te_{49}As_{29}Ge_{10}$ semiconductor amorphous films, field effect, trapping 80—84472
  $Se_{60}Te_{30}Ge_{10}$, amorphous, neg. magnetoresist. 79—51603
  Si-As-Te glass, thermoelec. power and DC cond., temp. depend. 77—62955
  Si-As-Te glasses, crystallisation kinetics under influence of water vapour 78—59762
  Si-Ge-Te system glasses, structural and electronic transitions 77—76890
  Si-Te system, structural changes rel. to memory effect *(Russian)* 78—71679
  Si-Te system glasses, local struct., ^{119}Sn Mossbauer obs. 79—41968
  $Si_{12}Ge_{10}As_{30}Te_{48}$ chalcogenide glass threshold switch conductivity in high ohmic state *(Russian)* 78—43502
  $Si_{12}Ge_{10}As_{30}Te_{48}$, conducting filaments and switching phenomena 79—87134
  $Si_{12}Ge_{10}As_{30}Te_{48}$, dark cond. and thermoelec. power, thermal activation energies interpret. 78—23123
  $Si_{12}Ge_{10}As_{30}Te_{48}$, energy-controlled switching obs. 77—35973
  $Si_{12}Ge_{10}As_{30}Te_{48}$, energy controlled switching obs. *(Japanese)* 78—34867
  $Si_{12}Ge_{10}As_{30}Te_{48}$, film, switching delay time 78—26926
  $Si_{12}Ge_{10}As_{30}Te_{48}$ glass, nonlinear I-V characts. 79—99557
  $Si_{12}Ge_{10}As_{30}Te_{48}$, localised states role in cond. in high elec. fields 77—76841
  $Si_{12}Ge_{10}As_{30}Te_{48}$ surface, heat treatment and electron bombard. effects. SEM obs., rel. to switching filament form. 77—47700
  $Si_{12}Ge_{10}As_{30}Te_{48}$, switching filament, direct obs. 77—24595
  $Si_{12}Ge_{10}As_{30}Te_{48}$, switching in thin layers with semicond. electrodes 79—4586
  $Si_{12}Ge_{10}As_{30}Te_{48}$, threshold switch, high resist. state 77—15924
  $Si_{12}Ge_{10}As_{30}Te_{48}$, threshold switches, turn-on state maintenance mechanism *(Russian)* 77—85271
  $Si_{12}Te_{48}As_{30}Ge_{10}$ amorphous film, high-field transient conduction 78—43500
  $Si_{12}Te_{48}As_{30}Ge_{10}$ amorphous film, current-voltage characts. 79—87104
  $Si_{12}Te_{48}As_{30}Ge_{10}$ film, temp.-depend. of non-ohmic current and switching characts. 77—8158
  $Si_{12}Te_{48}As_{30}Ge_{10}$ film, transient cond. characts. in preswitching regime 77—32055
  $Si_{12}Te_{48}As_{30}Ge_{10}$ film, amorphous, Poole-Frenkel cond. for centres with screened Coulomb pot. 78—19044
  $Si_{12}Te_{48}As_{30}Ge_{10}$-Au, Schottky barrier props. 79—7897
  $Si_{10}Te_{40}As_{30}P_{20}$, amorphous films, optically assisted mono-stable switching 77—11968
  $SnSe$-$GeSe_2$-As_2Se_3 glasses, vitrification region and elec. cond. 80—15008
  $SnSe_2$-$GeSe_2$-As_2Se_3 system glasses, vitrification and elec. cond. 79—50997
  SnTe film, amorphous, evaporated and annealed, variable range hopping cond. 78—80077
  Sr-Te-O system, amorphous thin film, vacuum deposited, elec. cond., current cut-off *(Japanese)* 77—24625
  Te rich ternary chalcogenides, glass transition temp. predictions 78—38823
  Te-As-Ge, RF sputtering, temp. and bias effects on comp. 77—40367
  Te-based, thermal cond., 100-500K, and sp. ht., 373-600K 77—20138
  Te-Ge-As-Si amoprhous film, voltage controlled negative resistance type characts. 79—69614
  Te-Ge-Sn(Pb), Te rich, structural phase transformation concurrent with glass crystallisation, thermal evidence 79—4965
  Te-Si glassy alloys, IR transmission and sp. ht. changes in glass interval, vibr. modes, struct. models 78—23474
  $Te_{40}As_{35}Ge_7S_{18}$ film, threshold switching in relax. oscill. mode 77—69389
  $Te_{40}As_{35}Ge_7Si_{18}$, amorphous, threshold switching, expt. 80—49830
  a-$Te_{40}As_{35}Ge_7Si_{18}$, trapping, photo-stimulated and thermally-stimulated current obs. 77—28192
  $Te_{40}As_{35}Ge_7Si_{18}$ with pyrolytic graphite electrodes, threshold switching characts. 77—24593
  $Te_{48}As_{18}Ge_6Si_{28}$ amorphous film, I-V curve, memory switching 79—69615
  a-TeAsSiGe film with Mo contacts, AC performance *(German)* 77—63012
  $Te_{39}As_{36}Si_{17}Ge_7P_1$ amorphous film, electroluminescence from on state 79—8188
  $Te_{80}Ge_{20-x}A_x$ glasses, rapid melt cooled, glass transition and stability range 80—75170
  $Te_{0.81}Ge_{0.15}As_{0.04}$, sp. ht., 1-20K 78—22864
  $Te_{81}Ge_{15}As_4$, Hall effect in electrically switched memory state 80—2403
  $Te_{80}Ge_{12.5}Pb_{7.5}$, phase-separated system, overlapping effects of glass transition and crystn., DSC results 78—83739
  $Te_{80}Ge_{15}Pb_5$, DSC sensitivity to controlled ageing in glass transition region 80—71673
  $Te_{80}Ge_{20-x}Sb_x(Bi_x)$, DSC studies of struct. phase transformation 80—66505
  $TeSe_{12.5}$, amorphous alloy, thermal and elec. cond. during devitrification 78—26922
  $TeSe_{19}$ glass, crystallisation kinetics 77—35484
  $TeSe_{19}$, glasses, crystallisation kinetics, elec. cond. meas. 77—43155
  $TeSe_{20}$, vitreous alloy, elec. and thermal cond. during crystallisation 79—7550
  $TeSe_{50}$, amorphous to cryst. transition, kinetics 79—73099
  Te_xSe_{1-x}, chemical bonding from ^{129}I and ^{125}Te Mossbauer spectra 79—73867
  Te_xSe_{1-x}, localised gap states estimated by dielec. relax. 78—35087
  $Te_{43}Se_{30}Sn_7$ in MSM struct., switching effects 78—19164
  $Te_{50-x}Se_{50}Sn_x$, thin films, elec. cond. and thermoelectric power meas. *(French)* 80—80335
  Te_xSi_y, ($x=78,87$, $y=22,13$), amorphous, struct., X-ray diffr. study 80—6362
  $Te_{80}Si_{20-x}Pb_x$ glasses, phase separation, double T_g presence 80—88306

chalcogenide glasses continued
  Tl-B-Se system, vitrification region, primary crystallisation fields 77 15321
  Tl-Ge-S system, glass forming 80—19716
  Tl-Ge-Te, glass formation 80—103255
  $TlAsS_2$, crystallisation, effect of an alternating electric field 80—88054
  $Tl_xAs_{2-x}S_{3-x}$ glasses, opt. and mag. props., comp. influence 77—77225
  $TlAsS_2(Se_2)(Te_2)$, vitreous, crystn. kinetics 80—64918
  TlS_2, struct. and origin of crystn. process 77—76322
  TlS_x, struct. from radial electron density distrib. curves 79—23527
  $TlSe_x$ amorphous phase struct., rapid electron density distrib. curves 80—33896
  $Tl_{1-x}Se_x$, IR spectra, structure 77—77194
  Tl_2Se-As_2Se_3-SnSe system alloys, covalent component of chem. bond effect in vitrification processes, Mossbauer obs. 77—36156
  Tl_2Se-As_2Te_3 and Tl_2Te-As_2Te_3, vitreous, photo-EMF kinetics 77—76877
  $Tl_2SeAs_2Te_3$, amorphous semicond., nuclear spin-lattice relaxation by localised electronic states, modification by spin diffusion 78—52372
  $Tl_2SeAs_2Te_3$, electrical cond. freq. depend., hopping cond. contrib. 77—76856
  $Tl_2SeAs_2Te_3$, secondary electron emission, fluctuation state effect 80—40193
  $TlSe.As_2Se_3$, $Tl_2Se.As_2Se_3$, γ-irrad. effects on mech. props. 77—80567
  $Tl_2Se.As_2Te_3$, vitreous, thermal switching process in high electric fields 80—2432
  Tl_3TaSe_4 SAW coupling and temperature coefficients 79—51410
  Tl_xTe_{1-x}, amorphous, bonding and electrical conduction 79—90951
  $Tl_2Te.As_2Te_3$, temp. depend. of cond. and thermopower, electron energy spectrum 77—76831
  Tl_3VS_4 SAW coupling and temperature coefficients 79—51410
  Zn-As-S, prod. and acoustooptic props. *(Russian)* 78—63158

change of state *see phase transformations*

channel capacity
  acoustic logging, channel requirements for elastic waves recording *(Russian)* 79—39955
  atmospheric scintillation effect on capacity of polarisation and amplitude modulated links 77—75428
  electrocutaneous stimulation, energy threshold meas. and channel capacity estimation *(Japanese)* 78—53573
  multilevel pulsed phase modulation in optical links 78—78934
  optical communication laser light and fibre optics techniques *(German)* 80—5827
  parallel optical fibre channels, pulse skew model 77—68279

channelling
  see also energy loss of particles
  accelerator irradiation, heavy ion irradiation damage 80—100291
  amorphous medium, radiation suppression *(Russian)* 78—30686
  angular sputter yield peak position, ion reflection theories 77—59662
  anthracene, (100) and (110), scintillation response of α-particles in planar channelling and blocking expts. *(German)* 79—14869
  apparatus, for channelling meas. at torr press., test results on LiF crystal at 4 torr H_2O 79—2779
  atom location, continuum approx. calc. of ion scatt. yield 77—7778
  atomic chain, discreteness, effect on electron dechannelling 80—6448
  atomic collisions in solids, book contrib. 78—75697
  atomic collisions of channelled ions in crystal lattices, resonant coherent excitation 80—15170
  axial, and interatomic pot. 77—11610
  axial, in monatomic and diatomic crystals, multistring model computer simulation, foreign atom location appl. 79—42128
  axial hyperchannelling theory, momentum approx., difference eqns. 77—20001
  backscattering channelling surface peak calc. 79—8219
  backscattering use for radiation damage studies, review *(Japanese)* 77—72640
  bending of high energy beams using axial and planar channeling 80—88225
  beryl, natural and synthetic, ion channelling transmission ratios 80—75277
  Bloch wave channelling as electron diffr. 78—83860
  charged particle beam focusing, collimation and deflection 80—48132
  charged particle channelling in deformed single crystal 79—14867
  charged particle energy loss in cryst., theory 80—79847
  charged particle motion in curved axial channel, effects of dislocation 77—55314
  charged particles in single crystal, physical principles, uses and future trends *(Russian)* 79—82269
  coaxial atomic and light beams, simultaneous self-focusing and self channelling *(Russian)* 80—28292
  coherent and magneto-blocking effects of relativistic particle radiation in crystal *(Russian)* 80—92577
  coherent radiation and bremsstrahlung 80—65079
  coherent Roentgen radiation prod. from channelled charged particles in a monocrystal *(Russian)* 78—92138
  computer simulation determ. of atomic posn. in solids 77—80563
  conference, atomic collisions in solids, Hamilton, Canada (Aug. 1979) 80—62375
  conference on ion beam anal., Washington, USA (June-July 1977) 79—5194
  continuum planar potential 79—51177
  continuum-model planar channeling and the tangent-squared potential 79—42125
  crystal, axial blocking shift of scatt. nuclear products 79—82268
  crystal, channelled particle γ-quanta generation in external ultrasonic field 80—70282
  crystal, charged particle energy loss *(Russian)* 80—75280
  crystal, ion beam channelling, at inner shell excitation, impact parameter dependence 77—19047
  crystal channelling measurements, experimental system, components, capabilities 77—22617
  crystal orientation determ. from selected area channelling patterns 80—70092
  crystals, EM rapid cascades *(Russian)* 80—107348
  crystals, relativistic electron channelling, overbarrier states *(Russian)* 80—92576
  curved crystal, charged particle channelling, EM radiation emission 78—75698
  dechannelling, by dislocations *(Japanese)* 80—34106
  dechannelling, defect enhanced, energy and temp. depend. 79—4365

channelling continued
- dechannelling (aligned-to-random beam transition), WKB approx. 80—34109
- dechannelling by dislocation loop, energy depend. 79—42127
- dechannelling mechanism due to dislocations, anal. 80—59538
- dechannelling theory, γ-factor and diffusion processes 77—7775
- dechannelling theory, axial and planar conditions, anal. methods for dechannelled fraction calc. 79—4359
- dechannelling theory, particle lifetime, evolution 80—19857
- defect analysis 79—95063
- deformed crystal, optical method for quantitative evaluation of electron channelling patterns *(German, English)* 77—7777
- deformed crystals, radiation from channelled electrons and positrons 80—49283
- diamond:Sb, implanted, radiation damage and annealing study 80—100263
- diamond:Sb, ion implanted under channelling conditions, depth profile, distribution tail 80—2057
- diamond, accelerator irradiation, heavy ion irradiation damage 80—100291
- diamond, channelled electrons, gamma emission 80—54293
- diamond, channelling of 4.7 GeV electrons, γ-quanta yield *(Russian)* 79—69170
- diamond, electron channelling, γ-ray spectra *(Russian)* 79—61280
- diamond, electron channelling gamma-ray spectra 80—40023
- diamond, electron channelling radiation comparison with coherent stopping radiation *(Russian)* 80—103403
- diamond, energy loss of protons, alpha particles and ^{7}Li 80—42905
- diamond, gamma radiation angular distribution of channelled 900 MeV electrons *(Russian)* 80—19858
- diamond, half wavelength and stopping power of planar channelled protons 80—65087
- diamond, ion channelling and dechannelling meas. 80—65090
- diamond, light ion damage, channelling investigation 80—65068
- diamond, natural type Ia, dechannelling and nature of defect structures 80—49282
- diamond, proton channelling, transverse energy evolution in planar channels, computer simulation 80—79849
- diamond, sound excitation orientational effect due to channelled electrons 80—84254
- diamond crystal, radiation of channelled 800 MeV electrons 79—61274
- diffraction of radiation from channelled charged particles 78—75699
- digital scattering angle pre-processors 80—23268
- dislocation imaging, electron channelling appl. with SEM 80—70214
- dislocation loops, dechannelling 79—19299
- disorder distribution extraction, semiempirical method of applying dechannelling correction 78—22781
- doping of channelled ion implantations, apparatus for spatial uniformity 78—51569
- elastic scattering and bremsstrahlung theory of fast charged particles in crystals *(Russian)* 79—28853
- electron, axial channelling, quantum mechanical treatment 80—65091
- electron, radiation spectrum in channelling regime, complex and anomalous Doppler effect 77—84819
- electron and positron relativistic channelled beams, X-ray and γ-ray emission 77—36304
- electron bunching, scattering and bremsstrahlung in cryst. lattice in strong EM field 80—65113
- electron channeling pattern, large angle, generation and appl. 80—100296
- electron channelling, induced radiation *(Russian)* 78—64425
- electron channelling band width, SEM study *(Chinese)* 78—91366
- electron channelling imaging in SEM 80—10471
- electron channelling pattern, indexing method *(Chinese)* 80—103402
- electron channelling patterns, contrast mechanisms, lattice-defect images, in SEM 79—27884
- electron collimation, coupled-state model and weak coupling approx. 80—10588
- electron diffraction symmetries 80—100138
- electron flux anisotropy behind extended heterogeneities in material 78—17541
- electron gas, nonuniform, energy loss of charged particles 79—37748
- electron patterns and crystallographic contrast in SEM 79—86657
- electron radiation characts., approx. real potential calcs. 80—39191
- electron relativistic channelling radiation, energy and temp. depend. of freq. characts. 79—73236
- electrons, characteristic radiation, sharp lines obs. 80—65111
- electrons, emission of γ-quanta on plane channelling *(Russian)* 79—8205
- electrons, in crystals with extremal mag. field 77—65996
- electrons, planar-channelled, emission spectrum 80—44240
- electrons, relativistic, 10-130 keV channelling spectra in Si 80—24516
- electrons, relativistic, quantum beats 80—88226
- electrons, relativistic, scattering of photons 80—39190
- electrons and positrons, quantum theory of spontaneous and stimulated emission *(Russian)* 78—49999
- electrons and positrons channelled between cryst. planes, full average radiation 80—2097
- electrons in crystals, quasi-synchrotron radiation characts. 80—92572
- EM, Schwinger scattering of fast neutrons in crystals *(Russian)* 80—70286
- EM radiation from channelled particles, influence of medium polarisation 79—69168
- EM radiation of relativistic channelled electrons and positrons, spectral and ang. distrib. 78—23549
- EM wave emission by channelled particles in cryst. *(Russian)* 78—14394
- energy loss of channelled ions, effect of screw dislocations 78—67761
- fast channeled ions, electronic states calcs. 80—24517
- fast channelled particles with low charge, energy loss calcs. 78—55899
- fast charged particle, dechannelling from planar channel, stochastic theory 80—96579
- fast electron, strongly interacting bound states 78—34563
- fast electron bound states on axial channelling in single cryst. *(Russian)* 77—80562
- fission nuclei lifetimes from ^{235}U(d,f) study using blocking technique 80—63216
- gamma quanta emission effect on motion of channelled particles *(Russian)* 80—15173
- gamma quanta spontaneous emission by channelled charged particles *(Russian)* 77—52198

channelling continued
- generalized transport equations in quantum theory of channelling 78—10110
- GeV region, density effect 80—65085
- graphite, electron channelling, γ-ray spectra *(Russian)* 79—61280
- heavy ions, channelled, stopping power Z_1 oscillation vel. depend. 80—65101
- heavy ions, electron pick-up from free electron gas in thin solid film 80—107349
- heavy ions, low vel., channelling stopping power oscills. 80—103404
- heavy-particle channelling, diffr., probe for correlated lattice dynamics 78—30687
- high frequency phonon stimulated emission by fast charged particle channelling 79—73267
- high resolution Rutherford backscatt. techniques, appl. to near surface anal. 79—5207
- highly energetic ion beam thermalisations on channelling in crystals 80—2100
- ice, intrinsic surface order near melting point 79—14986
- ice, monocrystalline, radiation damage, 100 keV proton channelling 80—34102
- ice surface, near 0°C, 100 keV proton channelling meas. 78—14549
- improved depth resolution of channelling meas. in Rutherford backscatt. by detector tilt 79—5209
- impurity lattice location, using channelling effect *(Japanese)* 80—24513
- interatomic potential in channelling calcs., simplicity considerations 79—82267
- ion, appl. to surface studies 79—95064
- ion, flux peaking, lattice location 79—95062
- ion, material characterisation, conf., Aleria, Corsica (Sept. 1976) 79—96403
- ion axial channelling analytical model, point defect scatt. 80—39192
- ion backscattering under planar channelling conditions, ion-atom pot. and stopping power 80—24519
- ion beam penetration in lattice, general description 79—95061
- ion beam surface crystallography, channelling and blocking effects, double alignment backscattering 80—65350
- ion channelling, coherent excitation 79—46727
- ion implantation, book 77—31691
- ion implantation by laser annealing, characterisation, solar cell applications 80—70247
- ion motion in crystal, effect of polarisation field 80—103406
- ion path identification in cryst. surface channels 79—15576
- ion reflection, surface semichannelling effects 79—46728
- ion scattering, 180°, on solid targets, evidence for yield enhancement, channelling case 80—70281
- ion scattering, medium and high energy, two-atom model for surface blocking calc. 79—4886
- ion-induced X-ray prod., solid-effects 77—77326
- ion-lattice interactions, modelling displacement correls. in computer simulations 78—2179
- ions, inner-shell vacancy production in collisions with lattice atoms 80—24514
- ions, multiply charged, electron loss *(Russian)* 79—69171
- ions at small depths, theory 77—55316
- ions in crystals, electron losses and excitation *(Russian)* 79—95059
- kinetic equation for fast particles moving in cryst. at small anlge to crystallographic axes *(Russian)* 78—26609
- Kronig-Penney potential, charged particle motion, band struct. and Bloch wavefunctions 80—65112
- laser beam acceleration of particles along cryst. channel axis 77—30677
- lattice isolation of impurities from hyperfine interaction and channelling results 78—43731
- lattice vibration correlations in computer simulations 80—65086
- leptons, coherent radiation emission 80—65080
- light atoms in crystal lattices, position determ. by α-particle channelling and backscatt. 79—65113
- metal, ion implanted H(D), interstitial positions and vibr. amplitudes, fast ion channelling study, review 80—79848
- metal, irrad., self-interstitial type defects, combined single-double alignment channelling backscatt. 78—34561
- metal, radiative electron capture by channelled ions, theory 78—30685
- metal, solute atom displacement in mixed dumbbell interstitials for FCC lattice 78—79631
- metal target preparation for stopping power meas. of channelled ions in low energy region 80—63431
- metals, FCC, H implantation, lattice location and trapping, ion beam anal. 79—55769
- metals, metastable phases, ion implantation, review 80—49254
- metals, mixed dumbbells, ion channelling studies 80—70277
- MgO, temp. depend. of int. angles for proton axial channelling 80—10586
- molecular-type states in fast-electron channelling 78—87731
- monocrystals, EM radiation of relativistic positrons and electrons during axial and planar channelling 80—79845
- naphthalene single crystal, 4.50 MeV α bombardment, scintillation response, planar channelling, blocking *(German)* 78—6780
- neutron beam channelling and focusing in ferromagnets *(Russian)* 80—107351
- neutron focus in radiation field of relativistic channelled particles 79—85852
- Ni foils, proton beam channelling micrographs, defect struct. 77—11445
- nuclear inelastic channel suppression, nuclear reson. and electronic scatt. of γ-quanta, hyperfine transitions 78—60361
- nuclear reaction modulation for high-energy negative particles 79—77655
- nuclear reactor shielding anal., spatial channel theory 77—6569
- Okorokov effect, reson. excitation of electrons bound in channelling ion 77—15468
- particle beam cooling, by channelling in monocrystals *(Russian)* 80—52806
- particle motion through a cryst., dynamic statistical approach 80—34111
- particle radiation spectra, emitted quanta angular distrib. 80—96578
- periodic lattice, theory of channelling 80—29099
- photon production by channelled electrons 80—79846
- planar, α-particles, 1 to 5 MeV, stopping power of solids, effect of extended defects 78—51602
- planar, envelopes of ion trajectories 80—10585
- planar, oscill. behaviour of backscatt. spectra from small depths 80—6447
- planar, statistical equilib. spatial density computation using the continuum model 79—4364

channelling continued
- planar channelling, yield oscills. of inelastic processes at angles greater than crit. angle 79–77657
- planar channelling at small depths, theory 79–73232
- planar dechannelling of ion, simple model for calc. 79–77661
- planar dislocation channelling in modified continuum model 80–65089
- planar-channelling spatial density under statistical equilib., derivation for continuum model 79–4368
- positron, radiation spectrum in channelling regime, complex and anomalous Doppler effect 77–84819
- positron (electron), coherent radiation 77–76476
- positrons, planar channelled, Compton scatt. anal. 79–7639
- positrons, planar channelled, radiation characts. 79–55797
- positrons, relativistic, radiation at channelling 80–70279
- proton channelling, planar, depth depend. analysis *(Japanese)* 77–55315
- proton fast channelled continuum states, Gaussian flux peaking calcs. of electron capture, appl. to Au 79–86827
- protons, relativistic, channelling in bent crysts., theory 80–96581
- protons, theory of energy loss 78–38765
- γ-quanta channelling effect in periodic struct. *(Russian)* 80–96584
- quantum channelling theory, channelled particle multiple scatt. by electrons, contrib. to dechannelling rate 80–107350
- quantum theory, particle dechannelling with phonon scatt. 78–18695
- radiation, multiple scatt., remanent effects 79–77659
- radiation damage cascades, validity of energy partitioning 78–43056
- radiation of relativistic channelled particles 78–22779
- radiation spectrum of relativistic channelled particles, theory 78–83859
- radiative damping effect for ultrarelativistic channelled particles 78–67758
- radiative electron capture by channelled heavy ions, theory 77–47498
- rapid-scan polarising Michelson interferometer and InSb detector calibration 80–59305
- reflection of charged particles, surface channelling, two-wave approx. 78–6822
- relativistic, quantum theory of spontaneous γ-radiation 77–19997
- relativistic channelled nuclei, effects of Coulomb excitation and electrodisintegration 80–59539
- relativistic channelled particle beam, induced radn., tunable laser prod. 79–18391
- relativistic channelling particle, spontaneous γ quanta emission 77–63481
- relativistic charged beams, radiation cooling by channelling 77–72641
- relativistic charged particle in electric field, spin rot., curved crystal p,e^+ channelling *(Russian)* 80–63907
- relativistic charged particle motion, axial and planar channelling 80–39189
- relativistic electron and positron bremsstrahlung in crystals, theory *(Russian)* 79–61459
- relativistic electrons, axially channelled, spontaneous EM radiation *(Russian)* 77–84813
- relativistic electrons, self-acceleration in single cryst. planar channelling 80–65084
- relativistic electrons, spontaneous EM emission in channel pot. 78–83848
- relativistic particle channelling in cryst., spontaneous emission of γ-quanta, new effect 78–15243
- relativistic particles, energy loss in solids 80–39188
- relativistic particles, Fokker-Planck eqn. 79–60413
- relativistic particles, possible resonance radiation *(Russian)* 79–23661
- relativistic particles emission spectrum, rel. to interplanar pot. 80–65115
- relativistic positron and electron bremsstrahlung under conditions, theory 79–19301
- relativistic positron beam collimation in single cryst. 79–23669
- relativistic positron channelling, radiation intensity and spectrum calcs. 80–2098
- relativistic positron EM energy emission spectra *(Russian)* 79–78785
- resonance acceleration of channelled particles in intense laser field 80–88236
- resonance dechannelling under axial-to-planar transition conditions 80–59540
- resonant coherent excitation in planar channeling 80–65081
- resonant coherent excitation of channeled ions 79–51178
- resonant coherent excitation of channeled ions 80–65082
- resonant excitation, H-like and He-like channelled ions in Au and Ag 78–43058
- review 78–2184
- Rutherford scattering, anomalous, quantum-mech. treatment for swift electrons 78–43059
- Rutherford scattering of fast electrons during channelling, temp. depend. *(Russian)* 78–83857
- Schrodinger equation separation in electron diffr. and channelling, case of systematic refls. 79–46522
- SEM, contrast mechanism of electron channelling patterns 78–1965
- SEM, contrast of electron channelling patterns, estimation from low index refl. 78–9921
- SEM, electron channelling patterns 78–83697
- SEM, HV, for electron channelling pattern anal. 79–4213
- SEM channelling contrast technique for material deform. obs. 78–23917
- SEM channelling patterns, review 77–55217
- SEM selected area channelling patterns, optimum instrumental procedures 78–34408
- SEM selected area channelling patterns determ. of dislocation density 78–34407
- semiconductor, ion-implanted, post annealing meas. using Rutherford backscatt. and channelling 79–69121
- semiconductor materials, channelling-blocking measurements, (n,α) method for B-depth profiling 80–70276
- semiconductor microstructure fabrication, ion channeling effects 80–70230
- semiconductors, ion-implanted, laser pulse annealing, TEM and channelling study 80–100264
- semistatistical model for interatomic pot. 79–33024
- SOS films, cryst. quality improvement by Si ion channelling, annealing 80–44222
- spatial density quantum oscills. of channelled particles 77–39620
- spontaneous radiation, coherent bremsstrahlung and synchrotron radiation 80–6446
- spontaneous radiation higher harmonics of ultrarelativistic channelled particles *(Russian)* 80–75281

channelling continued
- steel, low C, channelling contrast to investigate fatigue crack propag. 80–66609
- steel, stainless sheet, texture effect on sputtering erosion by Ar^+, SEM-electron channelling study 79–91856
- stratified crystal structs., strongly bound γ-rays 80–80895
- surface and defect studies by channelling 79–4358
- surface hyperchannelling, crit. angle calcs. 80–2099
- surface semi-channelling, ion scattering *(Japanese)* 80–50501
- surface semichannel effects on fast ion recoil energy distribs. 80–65092
- thick targets of single crysts., meas. of charge state distribs. of channelled ions 79–23665
- thin crystals, axial channelling, momentum density calcs. 79–42126
- trajectory focusing of channelled ions, surface scatt. and surface struct. anal. 78–68594
- transition metal carbides, influence of implanted ions on supercond. transition temp. 77–28276
- transition metals, influence of implanted ions on supercond. transition temp. 77–28276
- transverse energy damping in the channeling process 79–55799
- two-fluid dissipative plasma, energy principle in Lagrangian form, tearing modes 78–42794
- ultrahigh vacuum system, for channelling backscattering experiments *(Japanese)* 79–26061
- ultrarelativistic channelled particles, spontaneous radiation, theory 80–92573
- ultrarelativistic electron and positron radiation in planar channeling 80–65083
- ultrarelativistic electrons, spectral distribution of radiation *(Russian)* 80–49285
- ultrarelativistic particle channelling in crystal lattice *(Russian)* 79–30690
- ultrarelativistic particle spin rotation, in cryst. 80–6449
- uniaxial channelling-blocking and single-alignment channelling-backscatt. anal. 77–84816
- pN, 2-15 GeV/c, in Ge, Si, influence of channelling on scattering 80–73729
- π^- mesons, fast, effects obs. on channelling in cryst. *(Russian)* 77–84812
- π^--meson channelling in crystals 78–6115
- $\pi^{\pm}N$, 2-15 GeV/c, in Ge, Si, influence of channelling on scattering 80–73729
- Ag, electron channeling pattern, large angle, generation and appl. 80–100296
- Ag, radiative electron capture by channelled O ions 79–77658
- Al, Ar^+ ion bombard., photon and secondary ion emission, single cryst. struct. effect 77–59660
- Al, blocking of α-particles from $^{27}Al(p,\alpha)^{24}Mg$ reaction, nuclear lifetime meas. problems 77–47500
- Al, dechannelling of α-particle by dislocation loops *(French)* 79–95056
- Al, defect structures depend. on Ca and Ga implanted species 80–59494
- Al, diffusion of Zn along grain boundaries, effect of grain boundary struct. *(Japanese)* 77–15628
- Al, displacement of Mn impurities during He irradiation, computer simulation 77–80563
- Al film, electron transmission less than 3 keV *(French)* 78–10109
- Al, interstitial trapping configuration study by ion channelling 78–47455
- Al, ion-implanted, dechannelling by dislocations, backscatt. expts. 79–7642
- Al, quasichannelled and randomly scattered proton, orientation rel. to closed-packed ⟨110⟩ direction 79–14864
- Al, single crystal, $^{18}O^+$ ion implantation in channelling directions, expt. conditions and range profile obs. 80–65022
- Al single crystal, $^{18}O^+$ ions implantation in channelling directions, stopping power meas. from max. range 80–65078
- Al-Ag, dil., radiation damage by channelled and random He^+ ion beams 79–46719
- Al-Ag (0.10 at.%), channelling meas. of trapping efficiencies of solute atoms for self-interstitials 79–86829
- Al-Ge (0.1 wt.%), channelling meas. of Al interstitial atom trapping by Ge atoms 80–59537
- Al-Mn(Cu)(Ag), solute atom displacement in mixed dumbbell interstitials for FCC lattice 78–79631
- α-Al_2O_3, diatomic cryst., channelling of He ions 78–38764
- α-Al_2O_3, noncubic cryst., axial-to-planar channelling transition 79–4367
- α-Al_2O_3:Pb, implantation, lattice disorder 77–80525
- Au, 70 keV ion bombardment, analysis of obs. shadow pattern 77–32488
- Au (110) surface, proton reflection, influence of channelling 80–54295
- Au, ang. distrib. of relfected keV ions 79–65127
- Au, channelling of H^+, planar channelling and blocking profile, transfer matrix method 78–22780
- Au cryst., ion bombarded, Ar^+ ions, time-of-flight spectra of sputtered atoms 80–89103
- Au, curved cryst., planar and axial channelling of protons, numerical simulation 79–65132
- Au curved crystal planar channelling effects for relativistic protons and π^- mesons, deflection effects 79–77656
- Au, electron channeling pattern, large angle, generation and appl. 80–100296
- Au, higher order z, effects and effect of screening by bound K electron on electronic stopping of channelled ions 77–51424
- Au, irrad., self-interstitial type defects, combined single-double alignment channelling backscatt. 78–34561
- Au, proton impact, blocking profile calcs. 78–18694
- Au surface, high energy ion backscatt., computer simulation *(German)* 77–59664
- Au, surface proton and electron channelling on reflection 80–39193
- Au, thin single cryst., coherent electronic excitation of channelled He^+ 78–22778
- Au, transmission sputtering by $Ag^+(Ar^+)(He^+)$ ions 79–4885
- Au-Ag (35 at.%), dechannelling of energetic He ions at dislocations 80–70275
- BP:Zn(Se)(Cd), epitaxial layers, ion implantation, defects and lattic locations, channelling obs. 80–88179
- BaF_2, planar channelling, minimum yields determ. 80–70280
- $BaTiO_3$:Co, voltaic current appearance on proton irrad. 80–104032
- Be, ion-implanted, impurity lattice location, channelling meas., Monte Carlo calc. 80–107291
- Be, lattice location results for implanted impurities, Rutherford backscatt./channelling technique 79–4329

channelling continued
- Be, neutron forces in relativistic electron radiation field in crystal, channelling *(Russian)* 80−70287
- Be, oscillatory channelled $^{4}He^{+}$ ion scatt. yield 78−52610
- Be:Li, lattice location of implanted ^{6}Li, ion beam channelling study 79−37730
- Be:Zn, lattice location of implanted Zn, ion-beam channelling meas. 77−68992
- $Be_3Al_2Si_6O_{18}$, beryl, 350 keV proton irrad., superchannelling effects 79−4344
- $CaCO_3$, calcite, sputtering behaviour, optical and electron microscopy 78−43968
- CaF_2, overlaid with Au and CaF_2 films, channelling meas. 78−67762
- CaF_2, planar channelling, minimum yields determ. 80−70280
- CdS, defect struct. and config. produced by irrad., elastic scatt. expts. 80−84178
- CsI, prep. 5-30 μ thick, preparation for channellography 78−80658
- Cu, channelling of Xe ions, Xe(M) radn. yield 79−73234
- Cu, electron-irradiated crystals, electron diffr. channelling effect on atom displacement 80−39158
- Cu, energy depend. of surface channelling of Ar ions, 10-35 keV 77−27928
- Cu foil, polycrystalline struct. influence on transmitted 300 keV ion energy loss 79−95057
- Cu, implanted with Cu^{+}, effect on cryst. orientation, Kr penetration meas. 80−88174
- Cu, interstitial trapping configuration study by ion channelling 78−47455
- Cu, ion channelling, continuum approx. calc. of scatt. yield for atom location 77−7778
- Cu metastable alloy layers, Ag^{+} and Ta^{+} implanted, structure obs. by MeV He^{+} channelling 78−71709
- Cu, O^{+} implantation along channelling directions, stopping power 77−69021
- Cu, positron implantation profiles in mono- and polycryst. samples, channelling 77−48273
- Cu, range of Ni^{+} ions, increase due to ion bombardment induced crystalline reorientation 78−26611
- Cu, self ion irrad., axial channelling along ⟨110⟩, by Rutherford backscatt. of He ions 79−4342
- Cu single crystal, surface semichannelling effects on spatial distrib. of reflected ions, computer simulation 80−35030
- Cu single crystals Au ion implanted, pulsed electron beam irrad. 80−65019
- Cu spheres, Shewmon rotation mechanism, selected area channelling patterns obs. in SEM 79−38759
- Cu surface, conditions for total refl. of low-energy atoms 79−19958
- Cu, vacuum deposited layer, ion bombardment induced preferential orientation 80−100290
- Cu:O single crystal, $^{18}O^{+}$ ion implantation in channelling directions, expt. conditions and range profile obs. 80−65022
- Cu:O single crystal, $^{18}O^{+}$ ions implantation in channelling directions, stopping power meas. from max. range 80−65078
- Cu-Ag, ion implantation as an ultrafast quenching technique for alloy production, ion channelling and TEM 77−55902
- Cu-Ag(Ta) metastable alloy form. by ion implantation, combined TEM and ion channelling obs. 78−34530
- Cu-Be, solute atom displacement in mixed dumbbell interstitials for FCC lattice 78−79631
- Cu-Be (0.25 at.%), channelling meas. of trapping efficiencies of solute atoms for self-interstitials 79−86829
- Cu-Be (0.25 at.%), cryst., Cu self-interstitial atom, trapping, nucl. reactions and ion channelling obs. 78−14384
- Cu-Ni textured alloys, grain boundary effusion of Ni to surface 79−90680
- Fe, radiation induced defects, annealing exam. using channelling tech. 78−47316
- Fe:^{169}Yb, lattice location of implanted Yb, annealing temp. depend., channelling meas. 77−48100
- Fe:Bi, impurity site distrib., channelling and nucl. orientation obs. 77−15447
- Fe:F, F lattice location, channelling and proton-induced nuclear reaction obs. 77−59041
- Fe:Yb(Au), radiation-damage evolution, influence on lattice-location meas. 80−6426
- Fe-Si (3 wt.%), Al-bearing, grain orientation by selected area electron channelling 77−12714
- $FeGe_2$, single cryst. perfection, proton diffr. obs. 80−55284
- FeS_2, diatomic crysts. electron induced X-ray emission, channelling effects 79−56888
- GaAs, 40 keV N^{+} implantation, disorder profiles meas. by Rutherford backscatt. and channelling 80−54270
- GaAs, amorphous layers, ion-implanted, low-temp. epitaxial regrowth 80−92790
- GaAs, disorder distrib. extraction, semiempirical method of applying dechannelling correction 78−22781
- GaAs, ion beam induced annealing effects 80−59530
- GaAs, ion channelling meas. for lattice location of S and Mn implanted in single crystals 79−4332
- GaAs, ion implanted, effect of channelling on elec. props. 77−8114
- GaAs, surface chem. changes on annealing, α-particle Rutherford scattering and channelling study 79−73383
- GaAs, X-ray and Rutherford backscatt. yields from channelled $^{4}He^{+}$ ions 79−46730
- GaAs:^{11}B, physicochem. and resistivity meas. 80−24933
- GaAs:Cr, epitaxial, ion implanted, Cr conc., depth distrib. and diffusion coeff. 80−49243
- GaAs:Cr pulsed electron beam induced recrystallisation and damage, amorphous layer formation 80−34052
- GaAs:Si(Se), ion implanted, laser annealing, microwave device appl., channelling meas. 79−69139
- GaAs:Te, implanted and laser annealed, surface crystallinity, refl. and channelling meas. 79−95036
- GaAs:Te, ion implanted, surface crystallinity and stoichiometry of laser annealed samples 79−73198
- GaAs-$Ga_{0.7}Al_{0.3}As$ channelled substrate buried heterostructure injection lasers 77−38932
- GaAs-metal ohmic contacts, solid phase epitaxy formation, AES and channelling meas. 79−60658
- GaAs(P), ion irrad. damage, strain effect contrib., channelling meas. 78−67752

channelling continued
- $Ga_xIn_{1-x}P$, real struct. exam. by electron microscopy and channelling 78−2143
- GaN, epitaxial layer, cryst. quality meas. by channelling 78−38986
- GaP, disorder distrib. extraction, semiempirical method of applying dechannelling correction 78−22781
- Ge, 15 GeV/c pion and proton nucl. interactions under random and channelling conditions in single crystals 79−13348
- Ge, amorphous, laser reordering of implanted amorphous layer 79−19270
- Ge, bremsstrahlung spectra for 1 GeV electrons and positrons, planar and axial channelling *(Russian)* 77−32465
- Ge, channelling effects for 15 GeV/c π^{-} 78−21831
- Ge, channelling of 160 MeV protons, deuterons and α particles, stopping powers 79−86826
- Ge, channelling of H^{+} and He ions, backscatt. particles ang. distrib. 79−51174
- Ge crystals, 1 GeV protons, pions and deuterons energy loss 77−89488
- Ge, modulation of nucl. interactions due to protons and pions 80−37373
- Ge, mol. and atomic ion damage, Rutherford backscatt./channelling meas. 77−59056
- Ge, planar dechannelling of protons, (100) direction 77−20000
- Ge, proton bombardment damage, irrad. energy depend., channelling meas. 80−24511
- Ge, solid-phase epitaxial growth through PdGe layers, channelling and backscatt. obs. 77−85936
- Ge, stopping power for fast channelled α-particles 78−79654
- Ge:Pb, ion implanted, lattice reordering, channelling and sheet resist. meas. 77−35577
- Hg electric field gradients at different Be lattice sites, gamma-spectral study 80−80224
- Hg, quadrupole interactions in Zn, lattice location, gamma spectral study 80−80227
- $Hg_{1-x}Cd_xTe$, implanted with Hg, Al, damage and lattice location study 80−103381
- InAs-GaSb superlattices, crystallography, Rutherford backscatt. and channelling obs. 80−49533
- InP, anal. of anodically oxidised (111) layers by MeV $^{4}He^{+}$ channelling effect meas. and AES 79−4492
- InP, Zn diffused single-crystal, substitutional dopant and hole conc. meas. 80−75260
- InSb, of ^{4}He, 800 keV, measurement, dose rate and orientation dependence of radiation damage 77−89482
- KBr, 5-30 μ thick, preparation for channellography 78−80658
- KCl, channelling of MeV H^{+} and He^{+}, zero dose meas. 78−18689
- KCl, dechannelling of H^{+}, temperature and energy dependence calculation 77−89490
- KCl, influence of elec. field on proton channelling 78−26614
- KCl, radiation damaged, proton and $^{4}He^{+}$ channelling, F-centre production, optical absorpt. meas. 78−79656
- KCl(I), electron range-energy relation, thermally created lattice vacancies effect 80−92574
- LiF, channelling of MeV H^{+} and He^{+}, zero dose meas. 78−18689
- LiF, radiation damaged, proton and $^{4}He^{+}$ channelling, F-centre production, optical absorpt. meas. 78−79656
- Mg, defect solute atom interaction investigation using channelling techniques 78−47442
- Mg-Ag, dil., ion irradiated, interaction between Ag and defects, channelling meas. 78−38766
- Mg-Ag (0.18 at.%), channelling meas. of trapping efficiencies of solute atoms for self-interstitials 79−86829
- MgO, 1.7 MeV proton channelling, axial to planar transition 78−30684
- MgO, H^{+} axial dechannelling temp. depend. 79−28022
- MgO, planar channelling of He ions along (100), (110) and (111) directions 79−28023
- Mo, electron irrad. in HVEM, channelling effect on damage prod. 80−107322
- Mo, fission fragment bombardment, channelling effects *(Russian)* 78−38762
- Mo single crystals, ion implanted, energy dependent channelling and backscatt. anal., $^{4}He^{+}$ ions, 1 to 2.8 MeV 79−4360
- NaCNaCl, 5-30 μ thick, preparation for channellography 78−80658
- NaCl, channelling of MeV H^{+} and He^{+}, zero dose meas. 78−18689
- NaCl electron excited luminescence yield orientational depend. 80−40169
- NaCl, Ne^{+}, Ar^{+}, Kr^{+} bombard., sputtering and ionoluminescence 80−96583
- NaCl preirradiation effect on proton channelling, thermoluminescence study 80−19860
- NaCl, radiation damaged, proton and $^{4}He^{+}$ channelling, F-centre production, optical absorpt. meas. 78−79656
- NaCl:Tl, luminesc. yield, effect of fast electron channelling 78−84646
- NaF, channelling of MeV H^{+} and He^{+}, zero dose meas. 78−18689
- NaF, radiation damaged, proton and $^{4}He^{+}$ channelling, F-centre production, optical absorpt. meas. 78−79656
- NaI:Tl, and unactivated NaI, scintillation response to random and channelled ions 77−48255
- NaI:Tl, triple-peaked scintillation pulse height spectra for MeV channelled ions 77−48254
- Nb, bremsstrahlung spectra for 1 GeV electrons and positrons, planar and axial channelling *(Russian)* 77−32465
- Nb channelling study of $^{4}He^{+}$ irradiation damage, effect of dissolved O_2 79−82270
- Nb, channelling study of $^{4}He^{+}$ irradiation damage, effect of irradiation temp. 79−82271
- Nb, electron diffraction axial channelling Kossel patterns, Bloch wave model, obs. 78−42869
- Nb, lattice location measurements of O using $^{3}He/^{16}O$ and $^{1}H/^{18}O$ prompt nucl. reactions, ion irrad. effects 79−86813
- NbC, C implanted, channelling crit. angle and min. yields 78−47458
- NbO, ion channelling, 1 MeV deuterons 79−60416
- NbO, ion channelling, neutron and deuteron radiation damage 79−65131
- Ni (101), light emission by scattered 195 keV He^{+} ions after focusing and channelling interactions 78−35240
- Ni (101) surface, optical excitation of He projectiles during reflection under channelling conditions 79−47576
- Ni (110), surface relax., O_2 coverage effects, medium energy ion scatt. obs. 79−28181
- Ni, (110), surface relaxation and composition, medium energy ion scatt spectra 78−63916

channelling continued
- Ni absorbers, deuteron distrib., depend. on direction of implantation *(German)* 77—4123
- Ni, anodically oxidised, 100 keV proton channelling investig. of oxide layer struct. 77—84820
- Ni, ion-implanted and virgin, laser irrad. effect, Rutherford backscatt. and channelling obs. 80—108306
- Ni, magnetisation effect on channelling and blocking of proton beam 77—69022
- Ni, Si ion projectile bound s electron polaris. rel. to transient mag. fields 79—33023
- Ni single crystal, surface hyperchannelling, scatt. of low energy Ar ions, computer simulation 80—34110
- Ni surface, location of adsorbed atoms, surface channelling meas. 80—84373
- Ni, surface channelling of Ar ions at (110) face 79—73233
- Ni, with Te overlayer, surface sensitivity of MeV He ion scatt. 79—56904
- Ni:Bi, impurity site distrib., channelling and nucl. orientation obs. 77—15447
- Ni:F, F lattice location, channelling and proton-induced nuclear reaction obs. 77—59041
- Ni:He, implanted, profile meas. technique 77—80524
- Ni:O, single crystal, $^{18}O^+$ ion implantation in channelling directions, expt. conditions and range profile obs. 80—65022
- Ni:O single crystal, $^{18}O^+$ ions implantation in channelling directions, stopping power meas. from max. range 80—65078
- Ni-Si(111), interface, reactivity and struct., ion channelling meas. 80—92788
- $NiCr_2O_4$, cooperative Jahn-Teller phase transition, channelling obs. 78—38839
- $NiCr_2O_4$ single crystal, appl. of particle channelling to the study of a cooperative Jahn-Teller phase transition 79—4413
- $NiSi_2$, epitaxial film on Si, ^4He ion channelling meas. and RHEED anal. 80—10834
- $NiSi_2$ epitaxial film on (111) Si substrate, interfacial order, backscatter, channelling study 80—65390
- $NiSi_2$, layer, on Si, ion implantation damage, channelling obs. 78—30676
- $NiSi_2$ layer, on Si, struct. modelling, using axial and phase channelling techniques 79—4489
- O ion channelling techniques, radiative electron capture anal. 77—35350
- PbS-PbSe epitaxial bicrystals, direct scatt. of channelled He ions at dislocations 80—65110
- PbTe film, ion-implantation-induced lattice defects 77—68985
- $PbTiO_3$, channelling of 1 MeV He ions 80—39194
- $PbTiO_3$ single crystal, channelling of He^+ ions, polarisation effects 79—99258
- Pd-C solid solution, dechannelling of α-particles by C atoms *(French)* 79—7643
- $(Pd_{0.8}Au_{0.2})D_{0.04}$, lattice location of D, ion channelling obs. 78—67708
- $(Pd_{0.8}Au_{0.2})D_{0.04}$, thermal vibr. temp. depend., ion channelling exam. 78—47457
- α-$PdD_{0.007}$, lattice location and thermal props. determ. of D by ^3He channelling 78—38747
- Pd_2Si, epitaxial film on Si, ^4He ion channelling meas. and RHEED anal. 80—10834
- Pd_2Si layer, on Si, ion implantation damage, channelling obs. 78—30676
- Pd_2Si layer 79—4489
- Pt, (100) surface, phase transition and relax. by MeV ion backscatt. and channelling 79—86970
- Pt (111), relax. effects, and thermal vibrs., medium energy ion scatt. 79—28182
- Pt (111) and (100), surface struct. anal. by MeV ion backscatt. and channelling 78—71916
- Pt, (111) surface, backscattering, channelling spectra, H adsorption, surface relaxation 80—71552
- PtSi, epitaxial film, cryst. perfection and thermal stability, channelling and backscatt. meas. 79—99255
- PtSi, epitaxial film on Si, ^4He ion channelling meas. and RHEED anal. 80—10834
- Si, 1 MeV He well-channelled ions with greater-than-random energy loss 77—80564
- n-Si, 300 keV proton irrad., temp. depend. of defect prod. 78—6113
- Si, 40 keV N^+ implantation, disorder profiles meas. by Rutherford backscatt. and channelling 80—54270
- Si (100), H adsorption, MeV ion scatt. study 80—80071
- Si (100), P implanted, dechannelling by edge dislocations, obs. by backscatt. spectrometry and TEM 79—4308
- Si (100), self-ion implanted, laser annealing, channelling and TEM meas. 80—24466
- Si, (110) plane, quantum state observation during fast electron channelling *(Russian)* 80—59541
- Si, (111) surface, proton dechannelling under channelling, blocking and double alignment conditions 80—88235
- Si, amorphous, Si implanted, substrate-orientation depend. of epitaxial regrowth rate, channelling effect meas. 78—79900
- Si, amorphous, substrate orientation effect on regrowth by laser pulses, channeling, backscatter 80—84409
- Si amorphous layer, ion-beam induced epitaxial regrowth 79—69378
- Si, amorphous to polycrystalline transition induced by laser beam, depth analysis by channelling 77—84771
- Si, ang. distrib. of electrons, beyond single cryst., diffr. patterns 78—1962
- Si, axially channelled protons, transmission meas. using two-dimensional position-sensitive detector 79—1471
- Si, bent crystal, γ-radiation beam deflection due to 900 MeV channelled electrons 80—84223
- Si, bent single crystal, proton beam trajectory control *(Russian)* 80—19859
- Si, bremsstrahlung spectra for 1 GeV electrons and positrons, planar and axial channelling *(Russian)* 77—32465
- Si, channeled B and P implantation along ⟨111⟩ and ⟨110⟩ axes 78—22739
- Si, channelled and random proton stopping power, 30-1000 keV 78—67760
- Si, channelled protons, energy loss to valence electrons, dielec. calc. 77—55312
- Si, channelled-ion implantation of group III and group IV ions 78—75682
- Si, channelling of 160 MeV protons, deuterons and α particles, stopping powers 79—86826

channelling continued
- Si, channelling of fast electrons, flux redistrib. meas. 80—19856
- Si, channelling of H^+ and He ions, backscatt. particles ang. distrib. 79—51174
- Si, channelling of π^- and π^+ 79—60414
- Si, channelling of relativistic electron beam, anal. of low-energy bremsstrahlung meas. 77—36304
- Si, channelling surface peak rel. to thin film anal. 78—43966
- Si, dechannelling by twins, ^4He backscatt. spectra 78—18691
- Si, dechannelling of H^+, generalised Fokker-Planck eqn. calc. 77—19999
- Si, deep amorphous layer implantation, laser effects, channelling diffr. study 80—25494
- Si detector, ionisation energy for channelled 160 MeV α-particles 78—62680
- Si, diffracted X-ray channelling by special deform. fields 80—100295
- Si, dislocations, depth distrib. planar channelling anal. with 2 MeV He backscattering 79—7640
- Si, disorder depth distrib. prod. by N^+ irrad. 79—73227
- Si, disorder distrib. extraction, semiempirical method of applying dechannelling correction 78—22781
- Si, disorder produced by high-dose implantation, channelling meas. 77—11573
- Si, displacement of group III, IV, V, and VI impurities in Si by He^+ and H^+ analysing beam 79—4330
- Si, elec. activation of implanted As during low temp. anneal, channelling meas. 78—51571
- Si, electron channelling patterns, contrast mechanisms, lattice-defect images, in SEM 79—27884
- Si electron diffraction axial channelling Kossel patterns, Bloch wave model, obs. 78—42869
- Si, electron scattering energy distrib., channelling effect *(Russian)* 78—2183
- Si epitaxial layers, dechannelling by stacking faults, channelling effect technique using He^+ and D^+ ion backscatt. 79—4361
- Si, epitaxial layers, stacking defect distrib. anal. using ion channelling tech. 80—100294
- Si, fast electron bound states on axial channelling *(Russian)* 77—80562
- Si, gamma radiation angular distribution of channelled 900 MeV electrons *(Russian)* 80—19858
- Si, half wavelength and stopping power of planar channelled protons 80—65087
- Si, heavy ion induced disorder in surface and at shallow depths 80—59535
- Si, implanted, dechannelling of MeV He ions by twinned regions 78—75700
- Si, implanted ^{16}O, lattice location of ^{16}O by α-particle backscatt. method 78—10080
- Si, implanted and annealed, effect of twins on dechannelling charged particle beam 79—4315
- Si, implanted annealed layers, amorphised structure formation mechanism and crystallographic nature 80—29091
- Si, impurities displacement by H^+ or He^+ irrad. 79—86824
- Si, impurity solubility limit after laser induced melting, Rutherford backscatt. spectrum 80—107426
- Si, inelastic stopping of medium energy light ions, channelling meas. 77—59058
- Si, ion bombardment, anomalous surface damage from channelling-backscatt. meas. 80—84222
- Si, ion implantation, channelled, through metal silicide film 80—70231
- Si, ion implantation, channelling, alignment effects 80—88183
- Si, ion implantation, high dose, solid phase epitaxial regrowth 80—103380
- Si, ion implantation, off-axis channelling disorder anal. 77—24325
- Si, ion implantation and pulsed laser annealing of group III and group V dopants, supersat. alloy form. 80—54267
- Si, ion implanted, annealing of heavy ion cascade damage, channelling meas. 80—89255
- Si, ion implanted, damage profiles, Rutherford backscattering 80—100733
- Si, ion implanted, spin density effect on laser annealing 80—11517
- Si, ion implanted and laser annealed, characterisation 80—29043
- Si, ion irrad. damage, strain effect contrib., channelling meas. 78—67752
- Si, ion irradiated, room temp., depth distrib. of disorder 79—37745
- Si, ion-implanted layers, epitaxial regrowth by laser beam and flash annealing 80—100420
- Si, laser pulse induced amorphous to cryst. transition, thickness depend. 78—47678
- Si, monocrystal, channelling of 5 MeV protons *(Rumanian)* 79—14863
- Si, new materials properties achievable by ion implantation doping and laser processing 79—69127
- Si, of electrons and positrons, correspondence between classical and quantal descriptions 78—18682
- Si, P^+ implantation, induced disorders. 80—6422
- Si, Pb implantation, channelling and RHEED anals. 78—30657
- Si, planar dechannelling of protons, (100) direction 77—20000
- Si, polycrystalline layer, laser-induced single cryst. transition, RHEED and backscatt. obs 78—87704
- Si, positron channelling, 56 MeV, producing radiation 79—51176
- Si, positron channelling, possible tunable X-ray source 79—69167
- Si, postimplantation defect annealing in samples heavily damaged by 140 keV Si^{2+} ions 77—11602
- Si proton damage, depth profile anal. by channelling 78—43054
- Si, radiative electron capture by channelled O ions 79—77658
- Si, random and channelled energy loss for positive and negative, 2-15 GeV/c pions, kaons and protons 79—3332
- Si, resonance dechanneling of fast protons in axis to plane transitions 79—14861
- Si ribbon grown by capillary action shaping technique, electron channelling analysis 77—76418
- Si, self-implanted, ⟨100⟩ and ⟨111⟩, crystallised layers by laser annealing, struct. 78—47644
- Si single crystal, planar channelling of fast electrons, 0.8-2.0 MeV 77—59059
- Si single crystal, planar channelling of fast electrons 78—2178
- Si single crystal surface, He^+ bombardment, damage production, defect diffusion 80—39181
- Si, stopping power for channelled 160 MeV α particles, expt. 78—26613
- Si, surface radiation damage cross sections, influence of distortions 80—6442
- Si wafers, channelling dips for K and L X-ray prod., PIXE and Rutherford backscatt. anal. 79—4363

channelling continued
Si: As(Pb), high-dose ion implanted and annealed, implant redistribution 80—107309
Si:Ar, As, ion implanted, laser annealing, doping profiles, channelling 80—97506
Si:As, anomalous tail generation, As ion channelling 80—49246
Si:As, As implantation damage and atom location, channelling meas. 77—59032
Si:As, CW CO_2-laser annealing, comparison with thermal annealing 80—84193
Si:As, displacement effect beam energy depend., vacancy trapping 80—33996
Si:As, electron induced displacement, channelling study 80—29058
Si:As, ion implanted, recrystallisation by free running ruby laser 79—73185
Si:As, ion-implanted, CW IR laser annealing 80—34022
Si:As, ion-implanted, channelling anal. of CW Ar laser annealing 79—73186
Si:As, ion-implanted, laser annealing, channelling obs. of As cluster form. 79—69128
Si:As, laser annealing, channelling, optical obs., and resist. meas. 79—1444
Si:As, planar and axial channelling of 800 keV As 77—19995
Si:As, scanning electron beam annealing, spreading resistance, junction depth 80—75267
Si:As, solid solubility and thermal behaviour of metastable 80—75359
Si:As(Sb), implanted, pulsed ruby-laser annealing, Rutherford backscatt., TEM and ion channelling study 79—86805
Si:As(Sb), ion implant lattice location after pulsed ruby laser annealing 79—73204
Si:B, implemented laser annealed samples, unidirectional contraction 78—71747
Si:B, ion implantation, channelling and random distrib. of B ions meas. 77—47473
Si:B, ion-implanted, influence of US waves on charged particle channelling 79—23668
Si:B, low noise avalanche photodiode fabrication by channelling implantation 79—35827
Si:B, self-interstitials location by Rutherford backscatt. of channelled ions 80—2101
Si:B (0.2 wt.%) ion implanted, B atom displacement due to low temp. irrad. 80—88234
Si:B ion implantation, proton channelling effects, anal. using Promiss protonograph 80—19823
Si:BF_2^+, ion implantation appl. in semicond. device production 80—103383
Si:B(Be)(Li) ion implanted, channelling and random equivalent depth distrib. 80—100293
Si:Bi, ion implanted, channelling obs. of pulsed Q-switched ruby laser annealing 80—59542
Si:Co, ion implanted, Co lattice location, channelling meas. 80—88201
Si:Cr, ion implanted, Cr conc., depth distrib. and diffusion coeff. 80—49243
Si:D, ion implanted, struct. of impurity centre 79—7623
Si:Fe(Cu), impurity segregation by pulsed laser irrad., channelling and ion scatt. meas. 79—82254
Si:Fe(Cu)(Pt), implant redistrib. and enhanced solubility following laser irrad. 79—69129
Si:Ga, heavily damaged, channelling investigation of diffusion behaviour 79—37877
Si:Ga(As), laser-doped, impurity distrib., Rutherford backscatt. and channelling anal. 80—59507
Si:Ge, regrowth behaviour from backscatt. and channelling meas. 80—2300
Si:H, 50-250 keV H^+ irrad. damage distrib., $^4He^+$ channelling obs. 78—26587
Si:H(D), H-related defects, channelling and IR meas. 80—25422
Si:Ne ion implanted, channelling anal. of disorder struct., ^4He ions, 0.7 to 2.2 MeV 79—4321
Si:O, implanted O location, channelling effect meas. 78—26593
Si:P, implantation damage of channelled P ions, elec. activity recovery stages 77—59034
Si:P, ion implanted, subsurface damage, TEM and channelled Rutherford backscatt. study 80—107337
Si:P, polycryst., channelling of implanted P during MOS device processing 80—65017
Si:Pb, He^+ Rutherford backscatt. and TEM exam., implant species effect on recrystn. 78—47452
Si:Pb, ion-implanted and annealed, dose depend. of residual lattice disorder 77—43228
Si:Sb, ion implanted, annealed, dislocation generation, channelling and Rutherford backscatt. meas. 80—88158
Si:Sb, ion implanted, annealing, Sb behaviour above solid solubility, channelling meas. 80—88200
Si:Sb(Ga)(Bi)(In), dopant solubility limit, laser irrad. effects 80—84295
Si:Te(Sm), implanted impurity location, Mossbauer and channelling expts. 80—39128
Si:Th, meas. of stopping power of channelled B ions 79—28025
Si/Pd system, solid phase epitaxial growth control by C ion implantation 80—75466
Si-$CoSi_2$Si, double heteroepitaxy, solid phase and MBE 80—104063
Si-epitaxial film, ionised-cluster-beam deposited, cryst. and elec. characts. 80—70553
Si-H (up to 15 at.%), amorphous, ion implanted, laser annealing obs. 79—69133
Si-saphhire, Si ion implanted wafer, laser annealing 79—99989
Si-SiO_2, two layer system, P^+-ion penetration tails, expt. and computer anal. 80—75249
Si-SiO_2 interface, backscattering-channelling study 80—34320
Si-SiO_2 interface, MeV backscatt. channelling meas. of Si monolayers 79—11020
Si(Bi), elimination of He^+ beam effect on channelling dips 80—54292
SiC, on Si and metal silicides, formation characteristics and mechanism, by ion backscattering techniques 79—60653
SiO_2, amorphous anodic layer on Si, MeV light ion multiple through-scatt., backscatt. obs. 79—86828
Si⟨111⟩/Al/Si, growth kinetics study of Si⟨111⟩ through Al by He^+ backscattering and channeling 79—28236
Ta, transmission channelling of MeV ions to study edge dislocations, expt. setup 80—29098
$TaD_{0.10}$, lattice location of D, ion channelling obs. 78—67708

channelling continued
Ti ferrite, magnetisation effect on channelling and blocking of proton beam 77—69022
Ti:O, channelled ions, flux peaking study using protons, H_2^+ and H_3^+ ions 79—1450
Ti-Al-Sn-Zr (6.19, 1.92, 1.43 wt.%), fatigue fracture facet investigation by selected area electron channelling 80—89344
Ti-Al-Zr-Mo-Si (5.97, 4.73, 0.49, 0.34 wt.%), fatigue fracture facet investigation by selected area electron channelling 80—89344
TiO_{2-x}, slightly reduced rutile, Ti interstitials, proton channelling obs. 77—35551
TiO_{2-x}, slightly reduced semiconducting, channelling expts. with 6 MeV protons, defect structs. 78—2117
UO_2 epitaxial films, epitaxial, channelling studies 79—49683
V, lattice location study, of 0, 1 MeV deuteron channelling 79—10846
V single crystals, ion implanted, energy dependent channelling and backscatt. anal., $^4He^+$ ions, 1 to 2.8 MeV 79—4360
V, trapping of D by O interstitials, channelling study using ion induced nuclear reactions 79—4316
V-$D_{0.01}$, enrichment of D during the ion bombardment 80—54288
V_3Si, ^4He induced damage, channelling effect meas. 77—62570
V_3Si, channelling, at displacements and electron phonon/defect interactions 77—84815
V_3Si, He irrad., computer simulation of channelling 79—55800
V_3Si, ion irradiated, influence on struct., resist., and supercond. transition temp. 80—54823
V_3Si, single cryst., computer simulation of channelling meas. 79—51180
V_3Si single crystals, channelling effect studies using He ions and $^{28}Si(d,p_8)$ reaction 79—4362
W (001), surface reconstruction and reordering by H adsorption, MeV ion scatt. 79—23835
W, (001) surface, reconstruction and reordering by H adsorption, MeV ion scatt. studies 79—82443
W (001) surface structure by MeV ion backscattering, channelling 80—6605
W (110), D^+ depth distrib., effect of surface impurities, channelling model 79—1451
W, ang. distrib. of particles emitted on 1200 MeV electron irrad. *(Russian)* 79—33025
W, atomic density, effect on proton energy loss and dechannelling 80—65088
W, axial to planar channelling transition, proton induced X-ray yield meas. 77—31704
W, channelled proton energy losses 77—1161
W, channelling of H^+ and He ions, backscatt. particles ang. distrib. 79—51174
W, channelling of He atoms, calc. 80—34108
W crystal, backscatt. energy spectra, channelling particles energy loss determ. 78—2181
W, D electro-fission on relativistic channelling *(Russian)* 80—54294
W, electron channelling in (111) direction, 200 to 1000 keV 78—2182
W, electron channelling in (111) direction, 1000 to 2000 eV energy range 78—38763
W, electron channelling map *(Chinese)* 79—73229
W, electron-channelling patterns, crit. voltage effects 80—79647
W, enhanced penetration of low energy He along ⟨100⟩ channel 80—65093
W, single cryst., proton integral dechannelling functions *(Russian)* 78—10111
W single crysts., surface scatt. by MeV He ions 77—69952
$(Y,Sm,Lu,Cu)_3(Fe,Ge)_5O_{12}$, ion implanted, hard bubble suppression 80—11238
ZnS, diatomic crysts. electron induced X-ray emission, channelling effects 79—56888
ZnSe, diatomic crysts. electron induced X-ray emission, channelling effects 79—56888
ZnTe:Au, impurity identification and characterisation, capacitance, luminescence and IR absorption 80—60639
ZnTe:Bi, laser annealing, channelling, reflectivity spectra 80—66215
Zr, defect solute atom interaction investigation using channelling techniques 78—47442

character recognition
see also optical character recognition
component letter perceptibility rel. to gross vision of word, quantitative model 79—53145
digital picture analysis, book 77—17962
symbol discrimination, human visual performance predictor 78—40178

character recognition equipment
automatic recognition of printed characters, heuristic algorithm, optical reading machine parameters *(French)* 77—48933
voice synthesis machines, principle and appl. 79—98564

character sets
Braille display cassette tape recording for text reproduction *(Spanish)* 79—39612
Kanji character memory and display system 78—9351

characteristic temperature *see Debye temperature*

characteristics measurement
see also headings for specific characteristics, e.g. gain measurement; viscosity measurement
amateur radiotelescope testing, test equipment 79—16830
angle modulated optical signals, modulation parameter meas. *(Russian)* 78—37047
Canadian seismographs, operations and characts., (1977) 79—66837
diode, thermometric characts., 15 to 300K 78—8403
fast-response photocell time characteristics meas. 77—5913
high-energy, IR laser component optical characterisation techniques 80—14347
high-resistance specimen conductivity nonlinearity meas. instrument 79—67341
image converter, UMI-93ShS, investigation of time frequency-contrast characts. 79—18520
jet displacement tranducers, relation between dynamic and precision characts. 80—64660
metal-dielectric-semiconductor structs., capacitance-voltage characts. gauge 77—37923
micro-organism electrical characteristics meas., elec. cond. and dielec. props. *(Italian)* 78—3684
MOS structures, instantaneous capacitance-voltage characts. meas. *(French)* 77—55616

characteristics measurement continued
- optical fibres, multimode, loss and mode-conversion parameter meas. principle 78—22192
- p-n junction, volt-farad characts. meas. with semiautomatic installation 77—41643
- p-n junction impurity profile meas., two-freq. method 79—23633
- pacemaker battery characteristic meas. microcalorimeter 80—30936
- photodetector parameter meas. via optomechanical/electronic unit 78—284
- photomultiplier linearity, meas. in pulsed mode using GaAs injection laser 77—37961
- piezoelectric receivers, sensitivity determ. by impedance method 77—11104
- plasmatron with arc chamber of variable radius, characts. meas. 77—35407
- pressure transducers, amplitude-frequency and phase-frequency characts. 80—62650
- pulsed injection light sources, installation for meas. their characteristics 77—75640
- recording systems, determination of complete dynamic characts. 80—62651
- ring laser output characteristic coefficient determ. 77—7123
- SAW device impedance, amplitude and phase characts. meas. in freq. domain 77—75755
- semiconductor, elec. parameters determ. by electron probe method 79—9259
- semiconductor device, automatic display of CV and GV characts. at HF 77—26329
- SQUID, low-inductance, with two microwave junctions 77—82579
- thyristor p-n-p-n structure turnon parameter meas. by optical probe 77—57358
- turbine blade arrays, turbulence characts. of stream, obs. 78—71319
- US pulsed transducer effective directivity meas., semi-automatic method 77—84102
- US transducer constants, automatic meas. method *(Japanese)* 78—33972
- volt-ampere characts., visual obs. of low-resistance semiconductor structure 78—4646
- X-ray image intensifier freq.-contrast charact. curves determ. 78—7427
- Al-Al_2O_3 thin film system, electrical conductivity and I-V characts. meas. *(Polish)* 79—56310
- Al-SiO_2-Si capacitor C-V characteristic determ. of surface minority carrier lifetime *(Polish)* 77—89855
- GaAs injection laser, appl. to meas. of photomultiplier linearity in pulsed mode 77—37961
- He-Zn, coaxial type hollow cathode laser, oscillation charact. *(Japanese)* 78—13692
- Si solar cell, I-V charact. meas., effect of voltage ramp, theoretical anal. using linear model 80—61354

charcoal
- *see also carbon*
- activated charcoal with oxine, adsorption of ^{60}Co waste water 78—58365
- active, heat-treated, spiral growth structs. *(German)* 78—44141
- adsorbed fission gas release in spill accident 77—50262
- adsorbed H_2 monolayers, H_2 dynamics 79—66341
- adsorption of Se, in environmental water, preconc., neutron activation anal. appl. 77—44551
- adsorption of V, from sea and surface waters, neutron activation anal. appl. 77—44549
- artificial liver support, protein-bound metabolite adsorbent equilibrium props. 79—20709
- artificial liver support, protein-bound substance removal kinetics 79—20710
- catalytic graphitisation by gaseous species from Ca 80—11872
- cryosorption pumping of He by charcoal, cryopump design for fusion reactor 80—105654
- filter, adsorpt. of radioactive I, safety evaluation *(Japanese)* 78—33267
- filters, NDT of residual adsorption capacity 80—89523
- fluvially transported charcoal causing erroneous ^{14}C ages for recent deposits 78—36172
- microporosity, determ. from isotherm eqns. 79—51419
- palaeoatmosphere O_2 content, since Lower Carboniferous, fossil charcoal evidence 80—51542
- polymer charcoal, adsorpt. isotherms of organic vapours 80—96731
- thermal conductivity meas. at room temp. 78—63889
- wood, prep., chem. activation 79—28973
- $Ag(CN)_2$, adsorption on activated charcoal 79—82455
- $Ag(CN)_2$, adsorption on activated charcoal, kinetics and thermodynamics 79—82456
- $Au(CN)_2$, adsorption on activated charcoal, kinetics 79—82457
- ^{54}Mg, removal from waste water by oxine-impregnated activated charcoal 80—9344

charge (electric) *see electric charge*

charge compensation
- *see also crystallography*
- β-Al_2O_3-Na_2O, mechanism of diffusion 80—2202
- alkaline earth fluoride, doped with trivalent rare earths, migration entropy for bound fluorine motion 80—71303
- amethyst, Fe^{3+} diffusion, associated phenomena 77—36269
- cd CdTe, growth from In solvents, self-compensation 77—28144
- compensated semiconductors, low temp. mobility, unscreened charged impurities effects calcs. 80—75562
- fluorite type crystal; $Tm^{2+}(Yb^{3+})$, axial g-values of $4f^{13}$ ions with trigonal symmetry *(Korean)* 79—24135
- heavily doped closely compensated semiconductor, density of states tail 78—47689
- III-V compounds, n-type, new meas. method for compensation and spatial fluctuations of impurities 78—6404
- ionic crystals, evaluation of association parameters of quadrupoles 77—43365
- phthalocyanines, elec. cond., compensation effect 80—100455
- plasma, streaming, in laser vac. diode, electron emission temp. 78—91162
- polyacetylene, n- and p-type doping, and compensation, p-n junction formation 78—76070
- α-quartz, X-irrad., paramag. Ag_2^+/AlO_4 centre, EPR obs. 79—28612
- semiconductor, carrier scattering by impurity potentials with spatially variable dielec. functions 79—69507
- semiconductor, cluster scattering, DC resist., energy-loss method 80—96862

charge compensation continued
- semiconductor, compensated, solid-state inductance, theory and expt. 78—56138
- semiconductor, doped and strongly compensated, fluctuation pot. and density of states *(Russian)* 79—95366
- semiconductor, electron-hole plasma and elec. field, stratification at low temp. 80—60020
- semiconductor, impurity characterisation from thermal carrier meas. 80—65595
- semiconductor, large-band-gap, self-compensation, role of impurities 80—92850
- semiconductor, lightly doped, compensated, percolation level, Monte Carlo calc. 80—59923
- semiconductor impurity bands, one-dimens. AMO-MT model validity 79—33256
- semiconductors, heavily doped, compensated, long wavelength recomb. radiation 80—7403
- strontium formate dihydrate:Cr^{3+}, optical absorption spectrum 80—50380
- TCNQ salt, $Qn(TCNQ)_2$, organic transfer salt, impurity effects on cond. 77—76799
- TGS, vacuum-cleaved cryst., charge compensation, ferroelec. field effect obs. 78—95556
- n-$AgInSe_2$, press.-induced compensation, resist. expts. 78—30919
- $Al_xGa_{1-x}As$, compensated, electron mobility temp. depend. 80—96868
- p-$Al_xGa_{1-x}As$:Ge layer on GaAs substrate, Hall and elec. cond. meas., Hall mobility 80—2402
- β-Al_2O_3-K_2O-MgO, cryst. struct., nonstoichiometry, ion-ion correlations 80—88129
- $Ba_x(Ba_{1-x}Al_x)Fe_2S_6[S_{1-y}(S_2)_y]$, cryst. struct., Mossbauer and mag. behaviour 77—55273
- $BaF_2:Er^{3+}$, single-site multiphonon and energy transfer relax. 78—52547
- $BaF_2:Gd^{3+}$-m^+ complex, cryst. field parameters, EPR 78—10768
- $Ba_2NaNb_5O_{15}$, effect of substituting Gd, Cr on lattice parameters 78—47291
- CaF_2:Ce, Stark struct., phototransitions, g-factors 78—67995
- $CaF_2:Gd^{3+}$-M^+, (M=Li, Na, K, Rb, Cs, Ag), electric field effect expts., EPR line breadths, lattice distortions 78—80210
- $CaF_2:Gd^{3+}$-m^+, complex, cryst. field parameters, EPR 78—10768
- $CaF_2:O^{2-}$, $CaF_2:Na^+$, O^{2-} and $CaF_2:Y^{3+}$,O^{2-}, thermal depolarisation obs. of defect clusters 80—71299
- $CaF_2:R^{3+}$, R=rare earth, dipole reorientation of charge compensation centres, ionic thermocurrents meas. 79—73880
- $CaF_2:U^{3+}$, Na^+, EPR, orthorhombic U^{3+} centre 77—77100
- $CaF_2:Y^{3+}$, ionic cond. and thermal depolarisation obs. of defect clustering 80—71298
- $CaF_2:YB^{3+}(Ce^{3+})$, point-charge approx. of tetragonal centres 77—47778
- $CaSO_4$:Sm phosphors, X-irrad., thermoluminesc., charge compensation effects 80—97351
- Cd compound with XO_4 tetrahedral, complex, var. of cation coordination numbers 79—86768
- $CdF_2:R^{3+}$, cooperative luminescence influenced by symmetry of centres 78—6791
- $CdGeP_2$:Cu, impurity behaviour 77—15857
- $Cd_xHg_{1-x}Te$ crystals, donor compensation, low temp. cond. study 80—75571
- CdS, interaction of excitons with charged impurities 78—43906
- CdS:Cd(In), Cu- or defect-compensated, optical ageing rel. to storage cond. 78—84247
- CdTe:Cu, doping effects on evaporation kinetics and electronic props. during high-temp. annealing in vacuum 78—22743
- $Cd_zZn_{1-z}S$-Cu_2S, heterojunction interface double layer, dislocation field, charge compensation 79—7855
- $CeO_2:Nb_2O_5$, sintered, elec. cond. and solid solubility, 800 to 1329°C 79—99546
- $CsCdBr_3:Cr^{3+}(Cr^+)$, EPR of impurities, charge compensation, X-ray effects 80—60407
- $CsMgCl_3(Br_3):Cr^{3+}(Cr^+)$, EPR of impurities, charge compensation, X-ray effects 80—60407
- EuIG:Pb, valence of Pb in Fe-garnets 77—47480
- $Fe_{10.92}K_{1.55}O_{17}$, ferrite, cryst. struct., nonstoichiometry, ion-ion correlations 80—88130
- GaAs, carrier conc. and compensation microprofiles 80—80820
- GaAs, compensated, electron mobility temp. depend. 80—96868
- GaAs, compensated, photoabsorption, expt. 78—19521
- n-GaAs, density of states tail in heavily doped closely compensated semicond. 78—47689
- GaAs, dual implantation of C^+ and Ga^+, sheet resist. and Hall effect meas. 78—67728
- n-GaAs, electron mobility, free-carrier absorpt., and compensation ratio 79—56218
- GaAs, impurity-point defect complexes 78—6097
- GaAs, interaction of excitons with charged impurities 78—43906
- n-GaAs, LPE, impurity compensation photolum. and free carrier conc. meas. 77—62558
- n-GaAs, melt-grown, stoichiometry, photolum. obs. 78—72583
- GaAs, self-compensation due to shallow and deep levels 80—24837
- GaAs, semi-insulating, conduction model 80—10986
- GaAs, semi-insulating, undoped and Cr-doped, compensation mechanisms, Hall effect and optical absorpt. meas. 80—84477
- GaAs:Cr, semi-insulating elec. compensation, Hall and resist. meas. 77—62855
- n-GaAs:Cu, contaminated single cryst., deep level photoluminesc. model 78—68554
- GaAs:Cu, diffused layers, photocond. spectra, hole conc. and mobility *(Russian)* 78—14758
- GaAs:Mg(Be)(Cd)(Zn), implanted, low temp. photolum. spectra 78—39583
- GaAs:Si, Li, IR absorpt., microstruct., charge compensation 80—107565
- GaAs:Si epitaxial films, elec. and photoelec. props., impurity distrib. 80—7006
- GaN:As(P), implanted single cryst. film, cathodolum. 78—60523
- Gap-Ge, compensated, photosensitivity 79—19624
- $Gd_3Fe_3O_{12}$, electron irrad., primary-ion charge compensation using SIMS 79—57322
- Ge, compensated by thermal defects, recomb. and optical props. 80—64989
- Ge, impurity breakdown field increase due to strong compensation 80—20204
- p-Ge, Li-compensated, carrier capture 77—15792
- Ge, transmutation-doped, impurity cond., 1.5-4.2K 77—89758

charge compensation continued
- Ge:Cu photodetector, I-V characts. 78—19141
- Ge:Ga,Sb, compensated, low temp. props. rel. to appl. in bolometry 80—31867
- Ge:In(Hg), impurity characterisation from thermal carrier meas. 80—65595
- Ge:Ni compensated, hot electron recomb. anisotropy 78—39125
- Ge:P(As)Ga, lightly doped semicond., electron-phonon scatt., role of compensation 79—60456
- n-Ge:Sb, fast neutron irrad. effects on donor conc., and annealing 78—56107
- n-Ge:Sb, γ-irrad. effects on donor conc. and compensation by acceptors 78—56106
- Ge:Sb, neutron irrad., carrier mobility theory and expt. 78—56166
- Ge:Sb,Cu, exactly compensated, impurity absorpt. and photocond. spectra 78—56189
- n-Ge:Sb,Cu, exactly compensated, static photocurrent-voltage characts. 79—38131
- n-Ge:Sb,Cu, exactly compensated, unipolar injection influence on photoconductivity 79—42592
- Ge:Sb,Cu, photoelec. props., fast electron irrad. effects 80—60036
- Ge:Sb,In, lightly doped semicond., electron-phonon scatt., role of compensation 79—60456
- n-InAs, photoelectric props., inhomogeneous impurity distrib. 80—107867
- n-InP, compensated, elec. props., space-charge effects 80—65569
- n-InP, Hall effect, 10-300K ,thermal activation energy and influence of compensation 78—72171
- n-InSb, compensated cryst., influence of surface cond. on Hall coeff. and elec. resist. 79—69579
- n-InSb, high-resist., prep. using radiation compensation 80—34016
- p-InSb:Cu(Ag), ionisation energy of multiply charged impurities, compensation effects 78—18996
- KBr, electron irrad. at 4K, role of V_K centres in equilib. among centres 78—67712
- KF:U, X- and γ-irrad., EPR of U^{5+} centre charge compensation mechanism 77—90030
- LiF:U, X- and γ-irrad., EPR of U^{5+} centre, charge compensation mechanism 77—90030
- LiF:U, X-ray and γ-ray irrad., EPR of U^{5+} centres 79—91295
- $MgO:Cr^{3+}$, axial centres, EPR and fluoresc. meas. 78—2731
- MgO:Li, thermally generated $[Li]^0$ defects, valence compensation 79—77598
- $(NH_4)_2SO_4:Cu^{2+}$, ESR parameters, effect of pH of mother soln., trapping sites 80—15791
- NaF:U, X- and γ-irrad., EPR of U^{5+} centre, charge compensation mechanism 77—90030
- $Na_2HAsO_4.7H_2O:Cu^{2+}$, ESR, Cu lattice location 78—52342
- $NaH_3(SeO_3)_2:Cr^{3+}$, deuterated, phase transitions, EPR 77—48135
- $Na_2S:Mn^{2+}$ single crystal, EPR expts. and interpretation 79—1708
- n-PbS, $PbS_{1-x}Se_x$ layers prepared by hot-wall epitaxy 77—16481
- PbS:Tl, self-compensation of acceptors by vacancies, Hall coeff. meas. 80—92913
- PbSe:Tl, self-compensation of acceptors by vacancies, Hall coeff. meas. 80—92913
- $Pb_{1-x}Sn_xTe$, diffusion of Cd, Hall effect, cond. and solubility meas. 79—69292
- PbTe, diffusion of Cd, Hall effect, cond. and solubility meas. 79—69292
- Sc_2O_3:MgO, defect struct., X-ray diffr. and pyrometric density 78—34524
- Si, compensated by thermal defects, recomb. and optical props. 80—64989
- Si, Overhauser effect in optically pumped compensated samples 79—73857
- p-Si photoresistor, compensated with radiation centres, current responsivity and detectivity 79—17492
- Si:Cd n^+-n-n^+ structs., photoresist. props. under exclusion conditions 80—39666
- Si:In, neutron irrad. to compensate for residual B, photocond., IR focal plane array 78—67727
- Si:P, ion implanted with small doses, defect annealing by nanosecond laser pulses 80—107297
- Si:P, neutron transmutation doping, elec. props. rel. to neutron fluence 80—96555
- Si:P, neutron transmutation doping, resist. homogeneity rel. to compensation ratio 80—96556
- Si:Zn, P^+-n-n^+ struct., deep doubly ionized centres, impedance calc. 79—11202
- SiO_2, glass, irrad., EPR of Al E_1' centres 80—11268
- SiO_2:Na, film, depth profiling by SIMS 78—79624
- SnO_2, rare earth ion doped, luminesc. and charge compensation 78—76532
- $SnO_2:Eu^{3+}$, luminesc. and charge compensation 77—28618
- $SrCl_2:Gd^{3+}$-m^+ complex, cryst. field parameters 78—10768
- SrF_2:La, type-I dipole reorientation, activation vol. determ. from dielec. const. 80—88916
- SrF_2:rare earth ion, elec. dipole-dipole interaction, ionic thermocurrent and EPR study 80—108060
- TiO_2:Cr(Ta), slightly doped, elec. cond. and defect struct., charge compensation and point defect model 80—75568
- TiO_2:Nb, rutile, elec. cond., 1273-1623K, O_2 press. depend., charge compensation mechanism 77—85217
- $VO_2:M^{3+}$, M=Al,Ga,Fe, anisotropy of thermoelec. power, hole conductivity 77—11946
- V_2O_5-Fe_2O_3-Li_2O ternary system, charge compensation of Fe ions, Mossbauer obs. 78—52410
- YIG: Ca^{2+} epitaxial films, Fe^{4+} centres, MCD, optical absorpt., and thermoelectric power meas. 78—95595
- YIG:B,Pb, IR spectrum, localised modes, rel. to impurities and O vacancies 80—50377
- YIG:Pb, valence of Pb in Fe-garnets 77—47480
- ZnS, ion implantation effects on luminesc., thermo-EMF 80—88178
- ZnS:Cu, film effect of Cu valency on cond. 79—11246
- ZnSe, self-compensation, role of impurities 80—92850
- ZnSe:In, heavily compensated, galvanomag. props. and thermopower 79—51600
- ZnSe:In, heavily doped, Hall effect and DC cond. expts., compensating acceptors 78—52013
- ZnSe:In, heavily doped, impurity band cond., Hall coeff. and cond. expts. 78—72147
- ZnTe, growth from In solvents, self-compensation 77—28144
- $ZrSiO_4$, isomorphous replacement of Zr^{4+} by Tb^{3+}, charge compensation 77—47424

charge-coupled device arrays *see charge-coupled device circuits*

charge-coupled device circuits
- analogue CCD and SAW filters 77—39172
- analogue memory charge-coupled devices, nucl. data acquisition 78—46250
- area imaging CCD low light level performance 77—39089
- astronomical ultralow light level imaging by intensified CCD 77—41287
- automatic measuring machine for star images *(Japanese)* 80—82212
- bandpass transversal filtering technology 77—27440
- biomedical signal conditioning CCD transversal filter 77—52901
- body motion computer-aided tracking using CCD image sensor 78—61269
- bucket brigade delay line, delayed auditory feedback unit, stammer inhibition appl. 78—31825
- C-CD/SAW devices for signal and image processing, conf., Ottawa, Canada, 1977, Oct. 79—32159
- camera, description performance and calibration, astronomical appl. 80—73499
- channel vocoder based on CCD discrete Fourier transform processors 80—53568
- charge injection device as stellar tracking sensor 80—85861
- charge injection devices for astronomy 77—41317
- control system for Si cryst. growth 78—68623
- correlators using split-electrode CCDs for sampling considerations and FM compression system 79—18625
- CTEM image recording appls. 80—68329
- digicons, image detection with semicond. array for multichannel photon counting 77—83989
- digital image store for Earth resource surveying 79—34964
- digital images from 800×800 detector arrays on Space Telescope 80—109370
- dynamically focused array imaging systems, induced Doppler distortions 79—46117
- dynamically focused electronic sector scanner based on CCDs 80—98042
- ECG signal automatic evaluation using analogue circuits *(German)* 78—92717
- electrical charge injection methods 77—39082
- electron spectrometer using new multidetector based on charge-coupled imaging device 80—86502
- electronic delay, dynamically variable, for real-time US imaging 79—46142
- electronic detectors to enhance optical information from telescopes, image intensifiers and CCDs *(French)* 80—67569
- fast event recorder utilizing a CCD analog shift register 79—45578
- fibre-optic communication receiver designs 77—68281
- Galileo Jupiter Orbiter Mission CCD camera 80—85859
- hybrid IR/CCD focal planes, performance, appls. 79—3798
- hybrid signal processor using SAW/CCD technologies 79—32163
- image convertors, solid state, with integrated fixed-pattern noise suppression 80—14458
- image sensor, microscope TV for nucl. emulsion track detection 79—3290
- image sensor readout organisations 77—39080
- image sensors, dynamic sampling of object pattern 79—50414
- image sensors, evaluation techniques 77—83990
- image sensors, intensified, development 79—32086
- imager, edge enhancement using 3×3 pixel neighbourhood operator functions 80—102644
- imaging devices, sensitivity comparison with Kodak SO-143 film for streamer chamber appls. 78—21820
- imaging systems, conf., Washington, DC, USA, 1978 79—32085
- imaging systems, large area, for deep space photography 77—57426
- integrated CCD imaging array, coupled with channel waveguide 78—38077
- integrated optical channel waveguide-CCD transversal filter 80—58797
- integrated optical waveguide and CCD image array 77—34962
- intensified CCD photon counting array photometer 77—37964
- intensified CCD test results 77—41318
- IR charge injection and CCD focal plane arrays 77—39088
- IR charge transfer device imaging arrays 78—77990
- IR charge transfer devices with Si detectors 77—83991
- IR detection techniques, for low background satellite expts. 78—49343
- IR image sensors, operation *(German)* 78—63190
- IR imagery, modelling and appl. of HgCdTe MIS struct. 78—80058
- IR imaging appl., book contrib. 78—38026
- IR imaging appl., development trends *(Czech)* 79—97383
- large imaging CCD array development and test results 77—41316
- line sensors, telecine FDL 60 appl. 80—278
- linear array waveguide coupled detector device for signal processing and communication 79—59847
- linear sensor, diameter meas. of Fabry-Perot interf. rings 79—93210
- low light level performance of CCD in electron-bombarded mode 77—39092
- low-background astronomical integrated IR detector array development 80—85860
- monolithic cascade CCD ultrasonic lens applications 78—22231
- MOS capacitor, neutron damage mechanisms in CCDs 79—19672
- MOS photosensor charge integration and storage 77—39079
- MTF of C-CDs, charge transfer inefficiency compensation techniques 80—10026
- multichannel photon counting image detector arrays 78—65970
- multielement IR detector array technology 77—45893
- multiplexer, direct coupling with 5 μm (Hg,Cd)Te photovoltaic detector 77—83987
- optical channel waveguide array coupled to integrated C-CD, appl. 80—102860
- optical channel waveguide arrays coupled to integrated CCD 80—33244
- optical spark chamber data automatic digitisation using CCD 79—89517
- optoelectronic devices and optical imaging techniques, book 80—27059
- P^2CCD line sensors for slide scanner, photography appl. *(German)* 79—49308
- pattern recognition, transversal filter anal. 78—71052
- photoarray, as mol. absorpt. spectrophotometric detector 79—80689
- photodetector for optical information processing 80—91753
- photographic speed of solid-state image sensor arrays 79—17543
- photosensor array aliasing and MTF effects 77—39086

charge-coupled device circuits continued
- prototype CCD system for the time projection chamber 79−45575
- pushbroom CCD time-delay-and-integration mode image sensors 77−39087
- real-time multispectral feature classification by analogue CCD 78−24438
- remote sensing, sensors and detectors in NASA's future mission 79−5656
- satellite onboard feature classification by CCD analogue signal processing 77−70980
- satellite solid-state imaging for meteorology and astronomy 77−39074
- SAw/CCD accumulating correlator for analogue signal processing 79−72757
- SAW/CCD buffer memory device, operation 79−46137
- SAW/CCD high-speed analogue programmable tapped delay line 77−39167
- SAW/CCD programmable matched filter 80−5896
- Schottky IR C-CD staring sensors, operation and performance 80−10029
- signal processing in ultrasonics, conf., London, England, Jan. 1980 80−33351
- single line CCD camera microscope position control 78−41347
- single photon X-ray detection with a CDD image sensor 79−35836
- sleep EEG automatic K-complex detector 78−53557
- soft X-ray imaging experiments, astronomical appls. 79−35138
- solid-state imaging devices, conference, San Diego (1977) 78−66944
- sonar beam steering, time delay and integrate CCDs 79−18623
- sonar beamforming by CCD scan conversion for SAW chirp-Z transform 80−43552
- sonar signal processing, conf., London, England, 1978, Nov. 79−18618
- sonar system, chirp Z-transform implementation 79−18626
- sonar system appls. 80−53535
- sonar system design, beamforming and signal processing systems 80−33325
- sonar time delay design 80−43570
- space-borne Earth imager, high resolution, features 79−35097
- spark chamber digitisation using CCD 80−27902
- spatial light modulator with CCD address 80−48445
- star pattern sensors for real time spacecraft attitude determination 78−96380
- star tracker, microprocessor controlled CCD, STELLAR design 78−53792
- streak camera intensified CCD readout system, sensor props. 79−27825
- streamer chamber track recording with C-CDs 78−37515
- streamer chamber tracks recorded with charge-coupled devices 77−88336
- surface channel CCD image sensors 77−39081
- thermographic diagnosis, high resolution dynamic method, detector system 80−41167
- thinned back-illuminated CCD, for extreme UV direct detect. 80−77852
- time delay and integrate CCD device for pulse sector scanning in sonar 79−18624
- time-delay and integration mode imager, Earth resource thematic mapper appl. 79−35098
- transient data recorder, DC to 200 MHz 79−89540
- TV camera, colour, marine life forms obs. appl. 80−51301
- US imaging system, CCD devices appl. in electronic focusing 80−56148
- UV sensitized Si detector for space astronomical appl. 79−84668
- visible imaging CCD and charge injection device arrays 77−19446
- X-ray imaging, MOS solid-state detector arrays 78−47180
- X-ray sensitivity of CCD array 77−71413
- GaAs signal processing optical electronic devices 80−33242
- He speech unscrambler using charge-transfer devices 79−98559
- InSb charge injection device IR imaging arrays 77−79962
- $LiTaO_3$/CCD hybrid focal plane, IR imaging and detection, crosstalk 80−77856
- PtSi Schottky-barrier monolithic IRCCD focal plane 80−86427
- Si, phase transformation, lattice dynamics, microscopic theory 80−107387

charge-coupled devices
- *see also charge-coupled device circuits*
- abdominal CCD camera for continuous video recording of sheep ovary images during reproductive cycle 78−40442
- analogue signal processing C-CD and SAW devices appl. 77−27439
- astronomical CCD spectrometer for 500 to 900 nm range 80−82207
- astronomical instruments, cosmic ray background effects 80−51669
- buried channel, thermal carrier generation obs. 79−56313
- C-CD/SAW devices for signal and image processing, conf., Ottawa, Canada, 1977, Oct. 79−32159
- charge transfer inefficiency affecting modulation transfer function of CCD 79−94175
- double channel, surface and bulk charge transport 78−30990
- heterojunction isotypic, under transient depletion conditions, information-carrying charge 78−26944
- insulator-semiconductor interface, electrostatic field, Green's function calc. 77−76933
- MIS structure, charge-transfer, surface mobility and Hall mobility determ. 78−23175
- MIS structure, SAW charge transfer theory 79−56327
- MOS, charge motion, surface state effects 78−2573
- MOS inversion layers, freq. response of charge transfer 80−88638
- MOS structure, n-channel, evidence for impact ionised electron injection in substrate 78−88031
- MOS structures, inversion layer near electrode edge, pot. and charge density distribution 80−88642
- parallel signal injection using integrated optical channel waveguide array expt. 78−37996
- processing, elimination of stacking faults 78−10065
- radiometer, single-cell for artificial satellite measurement system 80−13147
- resistive gate image sensor 77−75681
- signal charge and surface pot., steady-state distrib. calc. 80−100525
- signal processing appls., comparison with digital devices 79−32145
- signal processing technology assessment seminar, Aviemore (1976) 77−39166
- solid-state array and camera tube imagers compared 77−39090
- solid-state imaging application 77−37707
- streamer chamber appl. of CCD camera 78−37513
- surface CCDs, electron mobility surface diffuse scatt. model 78−47879
- surface channel, interface trapping noise calc. 80−11058

charge-coupled devices continued
- surface channel CCDs, surface state parameters, transfer loss meas. 79−56279
- surface trapping phenomena rel. to surface states 77−39916
- surface wave interaction CCD prototype 77−23818
- survey of component technologies in subsystem signal processing 79−32160
- wide-band measuring system for studying charge-coupled device characteristics 79−45585
- X-ray image sensor, direct soft X-ray response 77−74565
- Al-anodised Ta_2O_3/native oxide-n-GaAs MOS structure evaluation 80−84514
- $Cd_xHg_{1-x}Te$ narrow gap semiconductor, charge transfer device for IR detection appl. *(French)* 79−30563
- GaAlAsSb-GaSb p-n heterojunction CCD, charge transfer, charge exchange 80−65658
- GaInSb, Be ion implantation, device appl. 80−24478
- InAsSb, Be ion implantation, device appl. 80−24478
- Si charge transfer by SAW in ZnO 77−27415
- Si, thermal oxidation technology, improved using 1,1,1-trichloroethane as optimised additive 79−29239
- Si/SiO_2, incomplete charge transfer, fringing fields and interface states effects 77−15964

charge density waves
- ϕ-particle model for charge density wave systems 79−82537
- actinide compounds, electronic configurations correlation 80−6385
- alkali metals, Matthiesen rule deviations rel. to CDW 80−29385
- alloy, stabilisation of long-period superlattices 79−95348
- BGD model, collective modes and response functions 79−60734
- bilinear organic addition compound, cryst. struct. and cond., rel. to lateral elastic interaction between chains 77−39827
- chain conductors, CDW ordering 78−79731
- chaotic states of anharmonic systems in periodic fields 80−22288
- coexistence with spin density waves, appl. of multicritical point anal. 79−77717
- collective modes of CDW near lock in transition 78−30879
- commensurability effects and collective excitations in systems with CDWs *(Russian)* 78−60074
- commensurate one-dimens. CDW system, lattice dynamics and elec. props. 79−38057
- commensurate-incommensurate CDW phase transition in one-dimensional electron-phonon system 78−67959
- commensurate-incommensurate transition in the quasi-one-dimensional Frohlich model with a nearly half-filled band 80−80199
- condensates, commensurability-pinned, solitary-wave solns. 79−58553
- condensates, soliton pair creation and low temp. elec. cond. 79−4550
- Coulomb gas in strong mag. field analogy with electron gas with backward scatt. 80−24817
- coupled incommensurate charge density waves, 3D ordering, mean field theory calcs. 80−107719
- cummulene type infinite chain cryst., energy bands, ab initio Hartree-Fock orbital calc. 78−60066
- distorted linear chain, electronic response and longit. phonons 79−11074
- domain-like incommensurate CDW states and collective modes 79−4521
- dynamics in presence of free-carriers 80−6760
- electric field depinning of charge density waves 79−73454
- electrical conduction, CDW, sliding condensed-matter system model 80−44258
- electron gas, dielectric function, dynamical exchange decoupling, plasmon dispersion, SDW and CDW 80−59900
- electron gas, dielectric transition temp. in strong mag. field 80−24813
- electron gas, one dimensional, dynamic interaction screening, spin and charge density wave instabilities 80−24819
- electron gas, one-dimens., interacting, ground-state energy in mean field approx. and instabilities 80−88493
- electron gas, optical props. in generalised HF approx. 80−24825
- electron gas, screening props., CDW and singlet supercond. response functions 77−47745
- electron gas, two-dimens., polarisability, many-body correction 78−60071
- electron gas, two-dimensional, Hartree-Fock soln. of CDW in mag. field 79−28302
- electron gas, two-dimensional, in strong mag. field, phase diagram properties 79−78024
- electron gas, two-dimensional, variational approach to ground state, CDW instability 80−39517
- electron gas instability in strong mag. field 78−79950
- electron-phonon scattering, effect on CDW phase transition 78−95265
- exciton ferromagnet, incommensurate mag. structs., inhomogeneous magnetisation *(Russian)* 80−29566
- exciton ferromagnet, spin-lattice relax., light and US absorption *(Russian)* 79−7960
- excitonic insulator, quasi-one-dimens. 79−90966
- ferromagnet, magnetic susceptibility, spin and charge density waves, Curie temp. *(Russian)* 80−100581
- ferromagnetism and ferroelectricity, coexistence in systems with electron-hole pairing 80−7310
- frictional force on drifting CDW 78−56123
- Ginzburg-Landau theory of weakly coupled metallic chains 78−60068
- graphite acceptor intercalation cpds., modulated electronic struct. 79−95310
- graphite intercalation compounds with K, Rb, Cs, resistivity anomalies and phase transform. 78−26839
- group V transition metal dichalcogenides, layered, CDW effect on thermoreflectance spectra 77−52120
- group-V layer compounds, 2H-polytypes, origin of CDW, elec. susceptibility, electron-phonon interactions 77−51679
- hexagonal layers, lattice distortions, chem. bond model 78−79560
- high frequency cond. of charge density wave condensates at low temps. 79−95392
- Hubbard model, generalised, charge ordering 80−39513
- Hubbard model, one-dimens., extended, $2k_F$ and $4k_F$ correl. functions, computer renormalisation group calcs., appl. to one-dimens. conductors 80−54625
- Hubbard model, one-dimensional $2k_F$ and $4k_F$ correl. functions, computer renormalisation-group calcs. 79−78029
- Hubbard model, phase transition due to CDW *(Russian)* 79−4526
- Hubbard model calc. *(Russian)* 79−65395
- Hubbard model calc. *(Russian)* 79−65396
- impurity pinning, phonon localization, in incommensurate modulated lattices 80−39238

charge density waves continued
  impurity pinning in single chain, CDW dynamics 78—47716
  incommensurate CDW structure, phase fluctuations, Coulomb effect and long-range order 77—43524
  incommensurate lattices, optical absorption and neutron scatt., lattice dynamics 79—33039
  incommensurate Peierls systems, amplitude solitons, implications for TTF-TCNQ 80—92841
  incommensurate structural phase transformations, recent neutron scatt. studies, review 79—42205
  incommensurate-commensurate transition, impurity pinning effect on commensurate CDW state 79—65394
  instabilities, incommensurate struct. phase transitions, neutron scatt. study, review 79—51231
  inversion layers, n-type, collective modes in charge density wave state 79—78200
  isotropic metals, CDW, Fermi-surface instability 78—79947
  Israel Physical Society 1980 annual meeting, Rehovot, Israel (April 1980) 80—94909
  itinerant-electron ferromagnetism, possible coexistence with itinerant-electron antiferromagnetism 78—39286
  jellium, attenuation of collective excitations 78—84157
  jellium, two- and three-dimens., CDW, appl. to liq. He surface and semiconductors 80—65476
  Landau model, anisotropic one dimens., correl. length complex order parameter amplitude fluctuation effect 80—46995
  lattice distortion and statical charge wave theory 77—72828
  lattice dynamics and charge density distortions, appl. to Nb 78—30714
  lattice instabilities, electronically driven, theory 78—10158
  layer compounds, structural phase transitions 77—59116
  layer structures, intercalation with N_2H_4, charge density waves or artefacts 80—100221
  layer systems, intercalates, order-disorder phase transforms., CDW and mass density waves 80—39281
  layered compound, supercond. and charge-density waves 80—34542
  layered compounds, effect of exchange on CDWs 78—60078
  layered compounds CDW instability rel. to supercond. T_c 78—14856
  layered crystal, three-dimens. ordering of CDWs *(Russian)* 78—2439
  layered materials, struct. changes rel. to CDW, TEM, electron diffr., dichalcogenides appl. 80—39042
  linear aggregates, small, polarisability determ., CNDO method and analytical models *(French)* 80—29298
  linear chain, CDW distorted, longitudinal phonon spectrum 80—24814
  linear conductor, CDWs and impurity effects 80—59967
  linear conductor, interchain coupling role 78—6294
  linear conductor role of interchain coupling 77—47751
  localisation of electrons in a magnetic field 79—60752
  lock-in and onset transitions of CDWs, triple point 78—67960
  lock-in transition, effect of thermal fluctuations on harmonics 79—19338
  magnetic order coexistence with charge density waves 80—97096
  magnetodynamics of incommensurate CDW 78—30915
  many-electron system, Wigner cryst., electron chain and CDW in strong mag. fields 78—60067
  many-valley semiconductor, inversion layers, electronic ground state 77—43731
  many-valley semiconductors, inversion layers, optical props. of CDW ground states 77—43732
  metal, K-like, noncommensurate charge density wave dynamics 78—30913
  metal, mag. susceptibility of cond. electrons 80—44523
  metal filament surrounded by polarisable mols., metal-insulator transition, electron density waves 77—24519
  metal simple, CDW detection by angle-resolved photoemission 78—95658
  metallic chain, weakly coupled, Ginzburg-Landau theory 78—91626
  metals, heat capacity, ultra-low temp., anomalies due to CDWs 79—42271
  modulated structures, phase amplitude decoupling, Landau Ginzburg approach 80—34375
  MOS, n-type inversion layers, two-valley model low temp. phase study, CDW coupling consts. 78—72275
  nonlinear amplitude-phase interaction 80—88490
  nonlinear conduction mechanisms in CDW condensates in two and three space dimensions 79—60807
  nonlinear de Haas-van Alphen effect 77—43523
  nonlinear one-dimens. Hamiltonian dynamics for lattice distortion 80—20171
  one dimensional condensate, nonlinear oscillating dipolar excitations 79—38007
  one dimensional Fermi gas model in relation to spin and field theoretical models 80—24816
  one-dimensional, commensurability pinning versus impurity pinning 79—11075
  one-dimensional complex order parameter model, mol. dynamics 78—34787
  one-dimensional conducting chain array, long-range Coulomb effects, CDW dynamics 78—47717
  one-dimensional conductor, CDW in random pot., interaction with impurities *(Russian)* 77—69264
  one-dimensional conductor, dynamic Peierls instability, mean-field model, CDW soln. 77—47748
  one-dimensional conductor, impurity pinning 80—6819
  one-dimensional conductors, disordered, elec. props., coherence length, impurity effects 80—24903
  one-dimensional conductors, incommensurate CDW 80—20174
  one-dimensional electron system, generalised susceptibilities in mag. field *(Russian)* 77—80750
  one-dimensional electron system, with short-range attraction, case of one electron per atom 77—4281
  one-dimensional electron-phonon system, CDW commensurate-incommensurate phase transition 78—14682
  one-dimensional Fermi gas with backscattering, coupling between charge and spin degrees of freedom 80—17861
  one-dimensional Hubbard model, Friedel oscills. around a nonmagnetic impurity 80—25073
  one-dimensional lattice, props. of commensurate CDW system 78—75796
  one-dimensional materials, nonlinear transport due to bound quantum solitons 79—51558
  one-dimensional materials, nonlinear transport due to bound quantum solitons 79—78089
  one-dimensional metal, phonon drag and sliding CDW 80—20173
  one-dimensional metals, incommensurate sliding CDW 80—20156

charge density waves continued
  one-dimensional metals, Peierls and CDW transition *(Chinese)* 79—51502
  one-dimensional metals and charge density wave effects in these materials, review 79—78085
  one-dimensional Peierls-Frolich state, impurity pinning of charge density wave 78—6298
  one-dimensional system, cond. and longitudinal sound attenuation above Peierls transition point 77—28168
  one-dimensional system, supercond. order and CDW coexistence, Peierls instability *(Russian)* 77—69445
  one-dimensional systems, impurity effects on ordered phases 80—24905
  ordered state in coupled chains of BGD model, props. 80—6756
  organic linear chain cpds., diffuse $4k_F$ refls., small intramolecular Coulomb interaction 80—34376
  parametric excitation of charge density fluctuations in classical and quantum electron-hole plasmas 79—50856
  Peierls condensate, phase solitons 77—43463
  Peierls transition, Frohlich model, one-dimens., CDW stability, electron-phonon coupling 80—65452
  Peierls-Frohlich dielectric, metallic screening, with pinning to impurities at finite temps. *(Russian)* 79—56208
  Peierls-Frohlich state, effect of Umklapp processes on dynamics *(Russian)* 77—47752
  Peierls-Frohlich state on many-phonon-coupling model, dynamical props. 78—47773
  Peierls-Frohlich system, nearly 1/3 filled band ground state, charge density waves 77—51681
  phase excitations of CDWs 78—43317
  phase transition between commensurate and incommensurate charge-density wave states, nearly half-filled Frohlich model 80—107723
  phase transition to incommensurate excitonic phase 80—75510
  polyacetylene, continuum model for solitons 80—65472
  polyacetylene type infinite chain cryst., energy bands, ab initio Hartree-Fock orbital calc. 78—60066
  polyene, energy bands, ab initio Hartree-Fock cryst. orbital calcs. 77—89717
  polyenes, long chain, electronic struct. in Peierls-PPP model 80—84423
  quasi one dimensional crystals, Frohlich collective mode and dielectric permittivity *(Russian)* 77—89722
  quasi one-dimensional conductor, CDW onset and pinning 80—70690
  quasi one-dimensional conductor, phonon drag conductivity in Frohlich Peierls phase, effect of impurities 78—60114
  quasi two dimensional, phason and sound wave coupling 80—92839
  quasi-one-dimensional CDW distorted solid, charge density fluctuations and dielec. matrix 80—107726
  quasi-one-dimensional CDW systems, commensurability pinning of fluctuation cond. 80—75555
  quasi-one-dimensional conductor, chiral charge density waves form. 78—6302
  quasi-one-dimensional conductor, high temp. struct. instability, tight-binding approx. and fluctuation model 78—6292
  quasi-one-dimensional conductor, impurity effects, interchain interaction 78—72138
  quasi-one-dimensional conductors, order in coupled metallic chains problem 78—6358
  quasi-one-dimensional conductors, review 78—60070
  quasi-one-dimensional cryst., three-dimens. ordering of CDWs *(Russian)* 78—2439
  quasi-one-dimensional electron gas with strong on site interactions 77—4306
  quasi-one-dimensional electron systems, effect of interchain electron transfer on phase transition 78—51911
  quasi-one-dimensional electron systems, instabilities, mean field approx. 78—23036
  quasi-one-dimensional electron-lattice system, three dimensional CDW ordering temp. 78—23037
  quasi-one-dimensional metallic system, effect of one-dimensional correlations on phase transition 77—24525
  quasi-one-dimensional metallic system, phase transitions problem, Gorkov-Dzyaloshinskii model 78—6296
  quasi-one-dimensional metallic systems, crit. behaviour, Ginzburg-Landau theory 79—56147
  quasi-one-dimensional metals, narrow-band, exchange-correlation effects on plasmons and on CDW instability 80—44525
  quasi-one-dimensional solid, CDW distorted, macroscopic dielec. function 80—39515
  quasi-one-dimensional system, Frohlich cond. in fluctuation region 78—84203
  quasi-one-dimensional system, phase ordering *(Japanese)* 80—2352
  quasi-one-dimensional systems, three-dimens. ordering in system of weakly coupled chains 78—6295
  quasione dimensional structures, collective excitation of CDW 78—18981
  random Gaussian pot., one dimens. charge density wave *(Russian)* 79—19534
  rare earth compounds, valence mixed state, Kondo lattice, Anderson localisation models *(Japanese)* 78—51945
  review, impurity effects, saddle-point model 77—51678
  rotating electron-plasma column space-charge wave propagation 77—55137
  scattering effects on CDW transition temperature 80—107720
  semiconductors, density waves in one, two and three dimensions 79—95353
  sine-Gordon ϕ-particles, quantum dynamics and statistical mechanics 79—42475
  sliding Frohlich waves, lack of superconducting behaviour 78—10378
  sliding waves in periodic and disordered lattices, pinning 78—14717
  $(Sn)_x$ chain, energy band struct., Hartree-Fock and CDW solns. 79—23885
  soliton lattice melting, functional integral method 80—17883
  soliton pair creation by elec. fields in CDW condensates 77—69309
  space modulated cryst. struct., theory of symmetry 79—38004
  spin-orbit coupling, charge and spin density wave effects 79—91009
  structural Peierls transition in quasi-one-dimensional systems with anisotropic electronic and elastic properties 79—7671
  surface, itinerant antiferromagnetism and density waves 79—82743
  1T-TaS_2, nearly commensurate phase, harmonics effect on phase transitions 78—14462
  TCNQ, optical IR antireson. absorption, characts. rel. to cryst. parameters 77—77183

charge density waves continued
TCNQ salt, acridizinium, one-dimens. cond., permittivity 25 to 60 GHz, 4.2K 78−88248
TCNQ salt, quinilinium, one-dimens. cond., permittivity 25 to 60 GHz, 4.2K 78−88248
TCNQ salt, TSeF-TCNQ, CDWs, X-ray study 79−28301
TCNQ salt, TSeF-TCNQ, nonlinear transport in pinched one-dimensional CDW system 77−89754
TCNQ salt, TSeF-TCNQ, Peierls transition and CDW ordering, X-ray study 80−20101
TCNQ salts, complex, with aromatic donors, interchain coupling and disorder 78−6314
TCNQ salts, complex, with symmetric and asymmetric donors, transport and mag. props. 78−6315
TCNQ-HMTTF, struct. evidence of CDW 78−51912
TEA$(TCNQ)_2$, linear chain semicond., phase phonons, intramol. electron-phonon coupling 77−32373
thallium hexanoate, soliton conduction, elec. cond. field and temp. depend. anomaly *(Russian)* 80−103703
$TiSe_2$, anomalous behaviour and excitonic insulator mechanism 77−39782
TMTTF-TCNQ, quasi one-dimens. conductor, diffusive hopping, theory 80−54677
transition metal, 2H layer compound, theory of superstructures 79−99291
transition metal, dichalcogenide layer cpds., bonding and phase transitions 80−34186
transition metal chalcogenides, $MS_3(Se_3)$, present status of research *(Japanese)* 80−20100
transition metal chalcogenides, quasi-one-dimens., elec. mag., and supercond. props., review *(Russian)* 80−93022
transition metal compounds, electron density periodic modulation 79−56148
transition metal compounds, localisation of electrons, review 80−49650
transition metal dichalcogenide, stacking layer study, appl. of convergent beam electron diffr. 80−39116
transition metal dichalcogenides, 2H polytype, rel. to Hall coeff. sign reversals 77−80795
transition metal dichalcogenides, electronic struct. and band theory 80−44497
transition metal dichalcogenides, periodic lattice distortions, charge density waves 79−82536
transition metal dichalcogenides, phys. props. *(Japanese)* 77−69225
transition metal dichalcogenides, phys. props. and CDWs, review *(Japanese)* 80−49635
transition metal dichalcogenides, physical props., review *(Japanese)* 80−33969
transition metal dichalcogenides, trigonal-prismatically coordinated layers, phenomenological theory of CDW state 80−80200
transition metal layer compounds, Fermi surface anisotropy effect on struct. transitions 77−51661
$TTF_{0.4}TSeF_{0.6}$-TCNQ, $2k_F$ and $4k_F$ CDWs, X-ray study 80−65474
$TTF_{0.97}Se_{0.03}$-TCNQ, Peierls-superlattices and soft phonon anomalies, X-ray scatt. meas. 78−75795
$TTF(SCN)_{0.588}$, Peierls instability, strain coupled charge density waves, X-ray scatt. obs. 78−79949
$(TTF)_7I_5$, superstruct. modulation, X-ray obs. 78−14333
$(TTF)Cl_x$, disorder transition, cond. decrease and commensurate charge density waves 80−70153
TTF-SCN, quasi one-dimens. conductor, CDW phase transform., X-ray scatt. study 80−24594
TTF-TCNQ, $4k_F$ anomaly, explanation 77−35875
TTF-TCNQ, anal. of harmonic microwave mixing 80−44635
TTF-TCNQ, and related 1D conductors, temp. depend. microwave dielec. const. 77−31967
TTF-TCNQ, and related cpds., partial charge transfer and CDW modulation 79−95349
TTF-TCNQ, CDW and phase transition exam. 78−6283
TTF-TCNQ, CDW instability, classical vs. crit. behaviour 78−39041
TTF-TCNQ, CDW transition with tripling of period along chains 80−96805
TTF-TCNQ, collective-mode conductivity in metallic phase 78−64031
TTF-TCNQ, controlled defects effect on microwave cond. and dielec. function 80−24885
TTF-TCNQ, crit. behaviour near 53K phase transition, Ginzburg-Landau theory 79−33249
TTF-TCNQ, deuterated, phase transition exam. by elastic neutron scatt. 77−4194
TTF-TCNQ, electron-molecular distortion coupling near Peierls transition, IR spectra obs. 80−25390
TTF-TCNQ, fluctuation cond. and commensurability pinning 80−34429
TTF-TCNQ, implications of amplitude solitons in incommensurate Peierls systems 80−92841
TTF-TCNQ, impurity effects on CDW fluctuations 80−44576
TTF-TCNQ, interchain tunnelling effect on nucl. spin-lattice relax. time, interchain coupling of CDW 80−20163
TTF-TCNQ, Landau free energy function, CDW-libron interaction, sp. ht. near phase transitions 80−19963
TTF-TCNQ, Landau theory of phase transitions 78−30914
TTF-TCNQ, Landau theory of phase transitions 80−92666
TTF-TCNQ, linear CDW, melting of phase locking *(Japanese)* 77−43522
TTF-TCNQ, low. temp. phase stochastic theory of nonlinear DC cond. 77−80768
TTF-TCNQ, microscopic model for three low temp. phases 79−73303
TTF-TCNQ, neutron and X-ray diffuse scatt., phase transitions, one-dimens. behaviour and interpret. 78−10381
TTF-TCNQ, non-linear elec. transport by pinned CDW 80−20172
TTF-TCNQ, nonlinear electronic transport, microwave harmonic mixing obs. 80−20168
TTF-TCNQ, nonlinear transport at low temp. 77−8079
TTF-TCNQ, ordering types below 54K, perp. phase depend. 78−6300
TTF-TCNQ, Peierls instability and consequences 78−6303
TTF-TCNQ, Peierls-superlattices and soft phonon anomalies, X-ray scatt. meas. 78−75795
TTF-TCNQ, periodic lattice distortions, charge density waves 79−82536
TTF-TCNQ, phase transition model, interchain coupling of CDW 77−76558
TTF-TCNQ, phase transitions and CDW state, controlled disorder effects 80−15507

charge density waves continued
TTF-TCNQ, phase transitions and CDW state, induced defect depend., transport and mag. studies 80−24980
TTF-TCNQ, phason and metal-insulator microdomain model, Young's modulus temp. depend. anal. 77−31964
TTF-TCNQ, phason instability at 49K phase transition 77−4303
TTF-TCNQ, physical properties, reviews *(Japanese)* 80−24883
TTF-TCNQ, pinned CDW in very far IR 80−25391
TTF-TCNQ, pinned charge density wave, far IR bolometric observations, damping 79−60735
TTF-TCNQ, pure and irrad. crystal, nonlinear transport at low temp. 79−4552
TTF-TCNQ, short-range and long-range order of phason clusters 77−35874
TTF-TCNQ, struct. phase transitions, coupled phasons model 78−83942
TTF-TCNQ, struct. rel. to quasi one-dimensional elec. props. 78−14716
TTF-TCNQ, symmetry changes and phase transitions 78−6299
TTF-TCNQ, two-chain inverted band model 78−6313
TTT_2I_3, charge transfer salt, Coulomb effects 79−28308
tunnelling of solitons and CDWs through impurities 78−51913
two dimensional electrons in mag. field 79−90978
two dimensional periodic lattice, electron ordering, CDW-disordered state transition, Hubbard model *(Russian)* 80−6754
two-dimensional CDWs, pinning and cond. in mag. fields 79−42610
two-dimensional electrons, in strong mag. fields, CDW 78−43316
two-dimensional layer, model, electron-correlated density-wave states 78−51919
Wigner crystal, long-wavelength excitations in strong mag. fields 79−82533
Wigner crystal, two-dimens., in strong mag. field, classical and quantum theory 78−79948
Wigner glass, effect of coexistence of random potential and electron-electron interaction 79−56169
Al-3d transition metal, dil., pre-asymptotic charge oscills. 80−20099
Br-graphite, intercalation cpd., magnetothermal oscill. and charge-density waves 80−11199
C_8K, K-graphite intercalation compound, electronic struct. using semi-empirical tight-binding scheme 78−6255
Cr alloys, localised magnetic moments in band antiferromagnets, impurity interactions *(Russian)* 80−54888
Cr and alloys, itinerant antiferromagnetism and density waves at surface 79−82743
Cr, spin density wave, CDW and strain wave, effect of spin polarisation of reservoir and imperfect nesting 78−56284
Cr, spin density wave, temp. depend. of second and third harmonics 77−12094
de Haas-van Alphen freq. and Fermi surface anisotropy press. depend. 80−59856
Fe_3O_4, electronic struct. and charge density oscills. near Verwey transition, Mossbauer expt. 78−27150
Fe_3O_4, Verwey transition, charge density-phonon condensation 80−65217
1T-$Fe_{0.1}Ta_{0.9}S_2$, mag. modulation of lattice electric field gradient 77−85628
Ga ultrathin metallic filaments, appearance of dielec. instability, coexistence with supercond. 80−103784
GaAs-Al_xGa_{1-x}As multilayers, two-dimens. transport at high mag. fields 80−65724
H, adsorbed on jellium surfaces, charge density oscills. and adatom-adatom interaction 79−42389
Hg ultrathin metallic filaments, appearance of dielec. instability, coexistence with supercond. 80−103784
$Hg_{3-\delta}AsF_6$, one dimens. fluctuations and chain ordering transform 80−24593
$Hg_{3-\delta}AsF_6$, one-dimens. fluctuations and chain ordering transform., neutron scatt. calc. 78−59923
In ultrathin metallic filaments, appearance of dielec. instability, coexistence with supercond. 80−103784
InSb, submillimeter radiation diffr. by electron-density waves 80−7328
n-InSb, Wigner cryst., long-wavelength excitations in strong mag. fields 79−82533
K, CDW, detection attempt by neutron diffr. 80−49634
K, CDW vector orientation, positive ion lattice distortion 80−6759
K, phasons, transverse, freq. dispersion relation in CDW state 80−96804
K, residual-resist. anisotropy due to cond. electrons in static charge-density-wave state 79−19571
K, resistivity, anomalous temp. depend. below 1.6K 79−78074
K, theory of residual resistivity anomaly 77−80765
KC_{24}, intercalated graphite cpd., anisotropic mag. susceptibility and phase transitions 79−19370
$K_2Pt(CN)_4$, quasi-one-dimens. Peierls system, phonon dispersion and neutron scatt., calc. 80−24550
$K_2Pt(CN)_4Br_{0.30}.3H_2O$, dynamic ^{195}Pt NMR meas. below metal-insulator transition 80−34810
$K_2Pt(CN)_4Br_{0.3}.3H_2O$, struct. rel. to quasi one-dimensional elec. props. 78−14716
$K_2Pt(CN)_4Br_{0.3}.3H_2O$, quasi-one-dimens. conductor, Br^- distrib. long-range Coulomb interaction, effect on structure and CDW 79−7591
$K_2Pt(CN)_4Br_{0.3}.3H_2O$, CDW system, nonlinear amplitude-phase interaction 80−88490
$K_2Pt(CN)_4Br_{0.3}.3.2H_2O$, deuterated, coupling of charge density wave and water mode 77−4646
metals, one- and two-dimens., periodic lattice distortion and CDWs 79−60678
Mo (001) surface, surface CDW phase transitions 78−43455
Na_xVS_2, Na_xVSe_2, charge density waves, electron localisation 79−47038
$Na_xVS_2(Se_2)$, mag. and elec. props. rel. to struct. transitions 78−91848
Nb, charge density distortions and lattice dynamics 78−30714
NbO_2, low temp. sp. ht. and Debye temp., role of phonon-like CDW excitations 77−80632
NbS_2, 2H layer cpd., electronic susceptibility and CDWs 78−39040
$NbS_3(Se_3)$, phase transitions and elec. props. 80−20178
$NbSe_2$, 2H layer cpd., electronic susceptibility and CDWs 78−39040
$NbSe_2$, 2H polytype, effect of incipient CDW on second-order Raman spectra 78−80357
$NbSe_2$, 2H polytype, Fermi surface and CDWs 77−51641
$NbSe_2$, 2H polytype, layered cpd., thermal props. at CDW transitions 77−47750
$NbSe_2$ (2H), CDW amplitudes determ. by ^{77}Se NMR 77−77116
$NbSe_2$ (2H), charge density wave transitions, neutron diffr. exam. 77−89515
$NbSe_2$ (2H), charge density waves state, NMR meas. 78−39421

charge density waves continued

- $NbSe_2$ (2H), effect of CDW fluctuations on Raman active optic phonon freq. 78—87750
- $NbSe_2$ (2H), electronic response function including electron-phonon matrix elements 79—28300
- $NbSe_2$ (2H), Raman scatt. from supercond. gap excitations 80—93340
- $NbSe_2$ (2H), Raman scatt. by supercond. gap excitations, coupling to CDWs 80—103956
- $NbSe_2$, charge density wave state, NMR meas. 77—8430
- $NbSe_2$, layered dichalcogenide, US vel. rel. to CDW 77—76490
- $NbSe_2$:Fe, local moment form., mag. susceptibility meas. 79—82756
- $NbSe_2$:Fe (2H), pure and doped, magnetoresist. and elec. resist. temp. depend. rel. to CDW form. 80—44574
- $NbSe_3$ and $Nb_{1-x}Ta_xSe_3$, thermoelec. power meas., 10-300K 80—20177
- $NbSe_3$ and related cpds. bands, bonds and charge density waves 79—95327
- $NbSe_3$, CDW, cryst. struct., X-ray and electron diffr. studies 79—14768
- $NbSe_3$, CDW condensate, soliton pair creation by elec. fields 77—69309
- $NbSe_3$, CDW form., direct electron diffr. 78—30877
- $NbSe_3$, CDW form., non-linear props., temp. and press. depend. 80—49753
- $NbSe_3$, CDW form., supercond. and Fermi surface determ., press. study 80—70891
- $NbSe_3$, CDW linear chain metal, two band model in ohmic region 79—38056
- $NbSe_3$, CDW noise, temp. and freq. depend. 80—103681
- $NbSe_3$, CDW transitions *(Japanese)* 78—30880
- $NbSe_3$, conductivity anisotropy and transverse magnetoresistance 79—38055
- $NbSe_3$, depinning props. of lower CDW, weak pinning model *(French)* 80—70630
- $NbSe_3$, elec. field depend. thermopower 79—56204
- $NbSe_3$, elec. resist. anomalies down to 7 mK associated with CDWs 79—60811
- $NbSe_3$, freq. depend. conductivity 80—107838
- $NbSe_3$, Frohlich sliding mode, nonlinear resist. and noise 79—60808
- $NbSe_3$, incommensurate CDW, X-ray scatt. and elec. field studies 79—42471
- $NbSe_3$ interference effects of CDW motions 80—88544
- $NbSe_3$, linear chain metal, anomalous transport props. 78—14718
- $NbSe_3$, linear-chain metal, Hall effect meas. 78—76058
- $NbSe_3$, mag. anomalies at CDW transitions 80—11158
- $NbSe_3$, mag. susceptibility, CDW effect 80—88716
- $NbSe_3$, metallic, non-ohmic cond., CDW pinning 80—39563
- $NbSe_3$, non-Ohmic conduction, depinning of charge density waves 79—65459
- $NbSe_3$, non-ohmic transport props. near phase tranistions 78—72213
- $NbSe_3$, phase transitions, phys. props. meas. 77—8005
- $NbSe_3$, quasi one-dimens. conductor, CDW phase transform., X-ray scatt. study 80—24594
- $NbSe_3$, satellite electron diffr. below 59K, Fermi surface features 78—84136
- $NbSe_3$, transport props. 80—20175
- $NbSe_3$, two charge density wave locking 79—95350
- $NbSe_3$:Ta, elec. cond., anomalous, and microwave absorpt. 79—42527
- $NbSe_3$:Zr, dopant effect on supercond. transition temp. rel. to CDW 80—39699
- $NbSe_2$(2H), CDW layered cpd., phase diagrams 79—69243
- $NbSe_2$(2H), CDW onset temp. and supercond. crit. temp., press. effects up to 20 kbar 77—39987
- $NbSe_2$(2H), effect of electron-phonon scattering on CDW phase transition 78—95265
- $NbSe_2$(2H), I-free, anomalous resist. 77—51732
- $NbSe_2$(2H), layered metallic magnetoresist. and Fermi surface above and below CDW onset temp. 79—19578
- $NbSe_2$(2H) microscopic theory of charge density wave instability 78—79732
- $NbSe_2$(2H), Raman spectra of soft modes at CDW transition 77—16301
- $NbTe_2$, CDW and accompanying periodic structural distortions 78—72094
- $Nb_{1-x}V_xSe_2$, elec. and mag. anomalies at CDW transition 80—107722
- $Nb_{0.87}V_{0.13}Se_2$(4Hb), stacking layer study, appl. of convergent beam electron diffr. 80—39116
- $Nb_{1-x}W_xSe_2$ $x=0$ to 0.15, elec. resist., mag. suscept., heat capacity, structural, supercond. transition *(Russian)* 78—31006
- $nbSe_2$ (2H) single crystal, elec. resistivity, effect of hydrogen intercalation *(Russian)* 78—84338
- PbTe, CDW in strong mag. fields, Peierls-type transition 80—34362
- Pt complex, KCP, periodic lattice distortions, charge density waves 79—82536
- Pt complex, $Mg_{0.82}Pt(C_2O_4)_2.xH_2O$, X-ray diffuse scatt., 1-D Peierls-Kohn anomaly and struct. transforms. 78—14680
- $(SN)_x$, quantum chem. calcs. of electronic struct. 78—6257
- Si (111) inversion layers, CDWs, effect of four valley interaction terms 79—33324
- n-Si (111) MOS charge layer, optical spectrum of inter-subband transition 78—64133
- Si, (111) surface, electron inversion layers, obs. of sixfold valley degeneracy 79—38176
- n-Si inversion layer, exchange instabilities 78—52052
- Si inversion layers, CDW mag. fields and stability 78—10533
- n-Si, inversion layers, many-valley electron-phonon interactions, piezoresistance, anisotropic cond., Shubnikov-de Haas oscillations 78—52096
- Si inversion layers, random pair attractive interaction model of carrier correl., compared with expt. 78—60212
- Si-SiO_2 interface, electronic props. of n-Si inversion layers, stress and temp. depend 78—19113
- Si-SiO_2 inversion layers, applied stresses, cyclotron masses and CDWs 77—55596
- Si(III) inversion layers, CDW induced cyclotron reson. harmonics 78—64085
- Sn ultrathin metallic filaments, appearance of dielec. instability, coexistence with supercond. 80—103784
- TCNQ salt, TSeF-TCNQ, anal. of harmonic microwave mixing 80—44635
- TTF-TCNQ, nonlinear transport in pinched one-dimensional CDW system 77—89754
- TTF-TCNQ single crystal, nonlinear electronic transport, microwave harmonic mixing 78—91684
- Ta-chalcogenides, domain-like incommensurate CDW states and first order incommensurate-commensurate transition 78—26824

charge density waves continued

- $Ta_{0.97}Hf_{0.03}S_2$ (1T), charge density waves, ESCA, XPS investigs. 77—12490
- TaS, (1T), effect of CDW on optical spectra 79—95738
- TaS_2, 1T, anomalous magnetoresist., CDW state 78—72173
- TaS_2, 1T, quasi-octahedral layer compound, band struct. and Fermi surfaces 77—76747
- TaS_2, 1T and 1H polytypes, fast neutron irrad., defect prod., effects on resist. and charge density waves 80—65060
- TaS_2, 1T polytype, charge density waves effects on phonon modes, Raman spectra meas. 77—36245
- TaS_2, 1T polytype, intercalated with Li(Na)(K)(Eu), CDW's and superlattice patterns 77—47746
- TaS_2 (1T), CDW and accompanying periodic structural distortions 78—72094
- TaS_2 (1T), CDW-transition temp., press. depend. 77—51730
- TaS_2 (1T), charge density waves, ESCA, XPS investigs. 77—12490
- TaS_2 (1T), commensurate and incommensurate CDW state, far IR reflection spectra 79—95755
- TaS_2 (1T), domain-like incommensurate CDW states and first order incommensurate-commensurate transition 78—26824
- TaS_2 (1T), generalised electronic suscept. and CDW 77—43471
- TaS_2 (1T), Hall effect 79—38103
- TaS_2 (1T), low temp. elec. props. 77—85205
- TaS_2 (1T), nonlinear cond. in two-dimens. CDW system 80—10997
- TaS_2 (1T) and (2H), bonding and charge density wave phase transitions 80—44282
- TaS_2 (1T) electron irradiated, lattice contraction 80—59520
- TaS_2 (2H), quantum oscillations and Fermi surface 79—37960
- TaS_2 (2H), Raman scatt. 77—1679
- TaS_2 (2H), sp. ht. and resist. near CDW phase transitions 78—34786
- TaS_2 ($4H_b$), press. effects on CDW transitions 77—51680
- TaS_2 (4Hb) layer cpd., oscillatory magnetotransport obs. 77—85241
- TaS_2, charge density waves, mol. beam diffr. obs. 79—73453
- 4Hb-TaS_2, Fermi surfaces and charge transfer 78—79926
- TaS_2, layered dichalcogenide, US vel. rel. to CDW 77—76490
- 1T-TaS_2, nearly commensurate phase stabilisation 77—15588
- TaS_2, non-linear conduction in two-dimensional CDW 78—91685
- TaS_2, polytypes, charge density waves and superlattice effects, intercalation with hydrazine 78—39043
- TaS_2 polytypes, in situ intercalation in TEM, using N_2H_4 gas 79—8254
- TaS_2, TDPAC meas., CDW, structural and charge transfer effects 78—39468
- TaS_2:Fe, local moment form., mag. susceptibility meas. 79—82756
- TaS_3, CDW state, Raman spectroscopy obs. 78—60439
- TaS_3, electron diffr. evidence for one-dimens. Peierls distortion 78—10024
- TaS_3, phase transitions and elec. props. 80—20178
- TaS_3, Raman spectra, CDW induced metal-semicond. transition 80—11404
- $TaS_{2-x}Se_x$ layer compound, Hall coeff., 4-200K 78—95305
- $TaS_2(Se_2)$, 1T phase, CDWs, electronically driven phonon anomalies and phase transforms. 78—63834
- $TaS_2(Se_2)$, 2H and 4Hb polytypes, layered cpd., thermal props. at CDW transitions 77—47750
- $TaS_2(Se_2)$, 2H polytype, effect of incipient CDW on second-order Raman spectra 78—80357
- 1T$TaS_2(Se_2)$, Hall effect meas., 1.4-360K 80—44616
- $TaS_2(Se_2)$, intercalated with ethylenediamine, Raman spectra 78—48182
- TaS_2(1T), anomalously large negative magnetoresist. at ultra low temps. 79—60852
- TaS_2(1T), surface CDW, obs. by atomic beam diffr. 80—39195
- TaS_3(1T), inequivalent lattice sites in charge density distorted phases 80—15835
- TaS_2(1T)(2H), nucl. quadrupole interactions, high press. effects 78—35072
- $TaS_2(4H_b)$, electrical cond. and CDW transitions under press., rel. to supercond. 77—43574
- $TaSe_2$, 1T, quasi-octahedral layer compound, band struct. and Fermi surface 77—76747
- $TaSe_2$, 2H, action on Fermi surface 77—76736
- $TaSe_2$ 2H, CDW effect on thermoreflectance spectra 77—52120
- $TaSe_2$, 2H phase, CDW band struct. and IR and visible thermoreflectance meas. 77—28556
- $TaSe_2$ (1T and 2H), charge density waves, ESCA, XPS investigs. 77—12490
- $TaSe_2$ (1T), CDW obs. by Mossbauer reson. of ^{57}Fe impurity 77—73104
- $TaSe_2$ (1T), commensurate and incommensurate CDW state, far IR reflection spectra 79—95755
- $TaSe_2$ (1T), generalised electronic suscept. and CDW 77—43471
- $TaSe_2$ (2H), anisotropy in mag. susceptibility 78—43558
- $TaSe_2$ (2H), broken hexagonal symm., incommensurate charge-density wave struct. 80—96646
- $TaSe_2$ (2H), CDW amplitudes determ. by ^{77}Se NMR 77—77116
- $TaSe_2$ (2H), CDW and accompanying periodic structural distortions 78—72094
- $TaSe_2$ (2H), CDW and discommensurations, ^{77}Se NMR study 80—88883
- $TaSe_2$ (2H), charge density wave transitions, neutron diffr. exam. 77—89515
- $TaSe_2$ (2H), domain-like incommensurate CDW and first order commensurate-incommensurate transitions 78—56084
- $TaSe_2$ (2H), effect of CDW fluctuations on Raman active optic phonon freq. 78—87750
- $TaSe_2$ (2H), effect of CDW on optical spectra 79—95738
- $TaSe_2$ (2H), Fermi surface, de Haas van Alphen meas. 77—20229
- $TaSe_2$ (2H), first-order phase transition, thermal expansion meas. 79—51256
- $TaSe_2$ (2H), magnetoresistance in commensurate CDW state, Fermi surface topology 77—43576
- $TaSe_2$ (2H), optical absorpt., band struct., plasmons, and CDW 80—45104
- $TaSe_2$ (2H), Raman scatt. from CDW 80—93340
- $TaSe_2$ (2H), softening of CDW excitation, at superstructure transition 78—79728
- $TaSe_2$ (2H), sp. ht. and resist. near CDW phase transitions 78—34786
- $TaSe_2$ (2H), thermal and elastic props., X-ray diffr. exam. 79—37754
- $TaSe_2$ (2H) and (1T), Raman spectroscopy of CDW state 78—35141
- $TaSe_2$, (2H) CDW, reentrant lock in transition at high press. 80—88320
- $TaSe_2$ (2H) microscopic model of CDWs 77—89719

charge density waves continued
$TaSe_2$ (4Hb), atomic displacements in CDW induced superstructure 80—10536
1T-$TaSe_2$, CDW obs. by ^{181}Ta Mossbauer effect 78—39469
2H-$TaSe_2$, commensurate superlattice vibr., Raman spectra 77—16299
$TaSe_2$:Fe, competition between charge and spin density waves, Landau-Ginzburg theory 79—95352
$TaSe_2$:Fe, local moment form., mag. susceptibility meas. 79—82756
$TaSe_2$/(2H) layer cpd., oscillatory magnetotransport obs. 77—85241
$TaSe_2$(2H), CDW layered cpd., phase diagrams 79—69243
$TaSe_2$(2H), effect of electron-phonon scattering on CDW phase transition 78—95265
$TaSe_2$(2H), layer cpd. commensurate-incommensurate transition 79—69244
$TaSe_2$(2H), plasmon behaviour at charge density wave onset 80—10900
$TaSe_2$(2H), Raman scatt., charge density wave mode softening at superstruct. transition 77—8584
$TaSe_2$(6R), stacking layer study, appl. of convergent beam electron diffr. 80—39116
$Ta_{1-x}Ti_xS_2$ (1T), magnetoresist. near metal-nonmetal transition at ultra low temps. 80—88600
$Ta_xTi_{1-x}Se_2$, cryst. struct. and elec. props. 79—47133
$Ta_{1-x}Zr_xSe_2$ (1T), CDW stacking order, interlayer interactions and impurity effects 77—7699
$Ti_{50}Ni_{47}Fe_3$, premartensitic phases, neutron scatt., sp. ht. and electron microscopy obs. 79—96025
$TiSe_2$ (IT), structurally induced semimetal-to-semicond. transition, ab initio LCAO calc. 78—51896
$TiSe_2$ (1T), effect of CDW on optical spectra 79—95738
$TiSe_2$ (1T), lattice dynamics and phase transitions 78—79727
$TiSe_2$ (1T), phonons and CDWs, inelastic neutron scatt. meas. 79—28059
$TiSe_2$, CDW and accompanying periodic structural distortions 78—72094
$TiSe_2$, CDW transition temp. and transport props. pressure depend. 79—99550
$TiSe_2$, lattice dynamics, charge density waves transverse phonon dispersion curves, model 80—49322
$TiSe_2$, mechanism for 200K transition, sp. ht. meas. 78—22853
$TiSe_2$, semimetallic behaviour band struct. from local-density functional approach 78—56070
$Ti_{1+x}Se_2$, superlattice form. and phase transition, IR reflectivity meas. 79—24322
α-U, CDW at 43K 80—80198
α-U, charge density wave, first order transition 80—10664
$V_{1-x}Nb_xSe_2$, CDW anomalies, Nb substitution effects, mag. susceptibility, 16-300K 79—38005
VO_2, metallic, electronic struct., lattice instability 78—14664
V_2O_3:Cr, anomalies in X-ray diffuse scatt. at high temp. metal-insulator transition 79—87042
V_nO_{2n-1} ($3\leq3\leq9$), Magneli phases, mag. susceptibilities at low temp. 80—20389
VSe_2, 1T, band struct. calc. 79—95324
VSe_2, 1T, quasi-octahedral layer compound, band struct. and Fermi surface 77—76747
VSe_2, 1T polytype, layer cpd., thermal props. at CDW transition 77—47750
VSe_2 (1T), deform. modulated superstruct., electron diffr. expts. 78—51515
VSe_2 (1T), incommensurate periodic lattice distortion, X-ray diffraction study 80—107414
VSe_2, angle-resolved UPS, Fermi surface determ. 80—55257
VSe_2, CDW and accompanying periodic structural distortions 78—72094
VSe_2, CDW states, correl. mag. and transport props. 79—73494
VSe_2, CDW states, intrinsic mag. props., mag. susceptibility and NMR obs. 78—68397
VSe_2, k-dependent photohole scatt. in photoemission 79—56912
VSe_2, metallic behaviour obs., anomalous elec. and mag. props., temp. effects 77—15819
VSe_2, press. depend. of CDW transitions, role of Coulomb correlations, elec. props. 78—87927
V_3Si, anharmonic mode softening effects 78—79734
$V_xTi_{1-x}Se_2$, cryst. struct. and elec. props. 79—47133
W (001) surface, surface CDW phase transitions 78—43455
W (100) surface, fluctuation, thermal impurity depinning and commensurate-incommensurate transition of CDWs 79—42611

charge exchange
for charge exchange in particle and nuclear physics see elementary particle interactions and nuclear reactions and scattering
see also charge transfer states; ionisation
2,4-hexadiyne-1,6 diol bis(p-toluene sulphonate) ester, demonstration of high mobility 80—20212
AB system, molecular calcs., electric dipole moments and electronic valence population, CNDO study 80—37742
accelerated atom+O_2, chemiionisation, crossed beam obs. 77—9085
acceptors, randomly distributed, direct energy transfer via exchange from excited donor 80—65483
acetone, thermal energy charge transfer reactions 79—87828
acetylenic compounds, 1- and 4-octyne, hydrogen bonding effects on Raman line $\nu(\equiv$C-H), solvents effects *(French)* 77—71805
N-acetylglucosamide, substrate-inhibitor of lysozyme, localisation of unpaired electrons 78—68992
AH system, molecular calcs., electric dipole moments and electronic valence population, CNDO study 80—37742
alcohol+H_x^+, methanol to butanol, x=1-3, charge exchange ionisation *(German)* 77—83700
alcohol+H_x^+, methanol to octanol, x=1-3, charge exchange and ionisation *(German)* 77—83699
alkali atom+H^+ charge exchange, eikonal approx. 80—32830
alkali atom+hexafluoride molecule, collisional ionisation 78—55226
alkali atom+methane derivative, collisional ionisation, nitromethane, perfluoromethyl bromide (iodide) electron affinities 78—66639
alkali ion+alkali atom, differential scatt. cross sections 77—28999
alkali metal+$H^+(C^+)(O^+)(S^+)$, negative ion form. 79—50128
alkali metal atoms, charge exchange, exciplex or excimer form. in plasma 80—75026
alkali metal ion+atom, cross sections 79—26871
alkali metal vapour-H plasma, charge exchange role in optical props. 80—59284
alkyl iodide-$I_{(atom)}$ complex, multiple charge-transfer bands in liquid-phase 77—32776

charge exchange continued
anthracene, single crystal, contact charging and photoemission 79—47586
anthracene-amine cation radicals, electron transfer with heterocyclic and carbonyl anion radicals, triplet state electrogeneration 80—63803
anthracene-dimethylpyromellite-imide, CT complex, reaction yield detect. double reson., delayed fluoresc. quenching *(Russian)* 78—88230
aqueous soln., ion luminesc. quenching by electron transfer 78—76511
aromatic compounds and oxygen, at 10K, contact charge transfer interactions 77—46637
aromatic compounds mixture, charge transfer equilib. consts., adiabatic ionis. energies, entropy changes 78—37738
aromatic hydrocarbons, oxygen quenching of triplet states, charge-transfer interactions 77—23516
aromatic substitution mechanisms 77—9056
ascorbic acid adduct model systems, SCF calc., rel. to protein internal charge transfer 80—69072
astrophysical plasmas, charge transfer rel. to Si lines appl. as spectral diagnostics 80—41717
atom+highly ionised ions, charge exchange cross-sections calcs. 78—9246
atom+ion, nonadiabatic electron transition in EM field *(Russian)* 79—86064
atom+ion, rainbows, interference, and diffr. effects *(Dutch)* 79—50110
atom+ion, two-electron exchange interaction 79—59565
atom+ion multielectron collisions, charge transfer at intermediate energy, atomic model 80—91652
atom+multicharged ions, charge exchange *(Russian)* 79—86063
atom+multiply charged ion, charge exchange 78—58813
atom-ion collision, eikonal approximation, reson. charge exchange ang. distrib. and atom refl. *(Russian)* 77—34759
atom-ion collisions, charge transfer between target inner shells, projectile K shells 79—89778
atomic and molecular collisions in intense light beams, quantum aspects *(Russian)* 79—6903
atomic beam in vapour, ang. scatt., neutral beam form 77—46636
atomic collisions, avoided-crossing, approx. partitioning procedure 78—33599
atomic collisions, charge exchange, one or two electrons, symmetry effects *(Russian)* 79—3562
atomic particle stripping analysers with solid and gaseous targets 79—1341
atomic resonance charge exchange in laser field, secondary emission 79—27081
atomic scattering, many-particle theory 77—10715
atoms, highly-ionised Coulomb-Born calc. of charge transfer cross sections 77—10752
bacterial photosynthesis, and model systems, electron transfer, ps studies 79—48214
bacterial photosynthesis, low-temp. electron transfer 78—44470
bacteriochlorophyll a, bacterial photosynthesis primary electron transfer processes, psec. dynamics 78—80841
bacteriochlorophyll-800, implication in picosec. electron transfer to bacteriopheophytin in R.rubrum reaction centres 80—35844
bacteriopheophytin, bacterial photosynthesis primary electron transfer processes, psec. dynamics 78—80841
benzene, and substituted forms, thermodynamic ionis. energy, rel. photoionis. energy 77—16858
benzene, cation radical, charge exchange reagent appls. 78—70929
benzene+molecular ion, fragmentation and electron transfer collisions 79—79229
benzophenone-N,N-dimethylaniline, intramolecular exciplex systems, laser photolysis obs. 80—35550
biacetyl, thermal energy charge transfer reactions 79—87828
biological photo-induced charge transfer, mechanism and range 77—60182
biomembrane charge transfer, possible role of α-helical proteins 80—81524
biomolecules+chloranil, charge transfer interaction, equilib. const., enthalpy and entropy determ., mol. polarisability 80—89708
blue proteins, activation of electron transfer reactions 78—44446
bromanil, electron affinity, bound and excited negative ion states, lifetimes, electron and alkali metal collisions 79—869
cis-2-butene, charge transfer mass spectra and photoelectron spectra 80—40778
CA(s)+$B^{++}\rightarrow A^{+}+B^{+}$(p), charge exchange, at term pseudointersection, level degeneracy effect 79—27084
carbocyanine dyes, triplet state quenching by nitroxyl radical, charge transfer complexing 78—25585
carbon tetrachloride, charge exchange mass spectra 80—43177
carbonyl anion radicals, electron transfer with anthracene-amine cation radicals, triplet state electrogeneration 80—63803
carrier-molecule complexes, probability description of electron transport processes 78—53314
casein-methylglyoxal complex, electronic props. 77—52736
chalcogenide, charge transfer, influence of cryst. field 79—99516
charge transfer electroradiography, physical processes 79—17594
chemical laser systems, ion-molecule reactions, thermal energy, book contrib. 77—50668
chemical reactions with inner sphere complex charge redistrib., polar solvent reorganisation energy 80—40730
chemical reacts. in condensed phase at low temps., at.-mol. transforms. 77—25253
chemiluminescence reactions, electron exchange initiated, kinetics correl. with free energy changes 80—50856
chemisorption, phys. significance and terminology 77—25307
chloranil, electron affinity, bound and excited negative ion states, lifetimes, electron and alkali metal collisions 79—869
chloroform, charge exchange mass spectra 80—43177
chloromethane, charge exchange mass spectra 80—43177
chlorophyll-duroquinone photochemical interaction, photopot. 77—16903
N-5′-chlorosalicylideneaniline, photochromism and thermochromism, NQR spectra, temp. and UV irrad. depend. 80—54968
clusters, small, formation, struct. and props. 80—58437
cofacial diporphyrins, electron transfer reactions following picosecond excitation, CT state lifetimes, optical difference spectra 80—25995
collision spectroscopy, book 79—27065
complexes, electronic absorpt. spectra calcs., rel. to H-bonded complexes *(Russian)* 78—37628
contact charge transfer complexes of organic molecules with O_2, CNDO/S calcs., absorpt. spectra obs. 80—69076

charge exchange continued
- Coulomb centres with different charges, asymptotic expansions 80—69211
- coumarin 102, excited state protonation kinetics, laser pH jump and picosecond spectroscopy 80—25992
- cycloalkane, mol. ion struct., photodissoc., charge transfer, ICR obs. 79—45774
- cytochrome c, electron tunnelling to cytochrome c peroxidase 79—20507
- cytochrome c, trifluoroacetylated, electron transfer reactions 79—20505
- cytochrome c-Fe$(CN)_6$ electron transfer, verification of vibronically coupled electron tunnelling 78—48750
- cytochrome c-Fe$(CN)_6$ electron transfer, vibronically coupled tunnelling description 77—52737
- between degenerate states 77—38727
- diatomic ion+molecule, reson. charge exchange *(Russian)* 79—98218
- diatomic molecular ion mobility in gas, drift vel., resonant charge transfer 77—65832
- diatomic molecules, diamag. susceptibility and second moments, intramol. charge transfer effects 80—78702
- dichloromethane, charge exchange mass spectra 80—43177
- dielectric liquid, charge exchange mechanism between impurities and electrodes 79—91356
- differential cross-sections, static Brinkman-Kramers approx. 77—83723
- dimethylaminophenyl-$(methylene)_n$-(1-pyrenyl), intramolecular charge transfer, heteroexcimer formation processes 78—27783
- dimethylether-HCl(I)(Br) mixture in N_2 matrix, IR induced proton transfer isotope effects, bond strengths 79—29335
- 2,6-diphenyl-1,4-benzoquinone+aromatic amine, triplet exciplex quenching, H-transfer mechanism 79—79228
- diphenylamine, in nitrobenzene soln., dry hole capture in pulse radiolysis expt. 79—79266
- 9,10-diphenylanthracene, electrogenerated chemiluminescence, T_2 state emission 78—60524
- dissociative charge transfer collisions, vibr. enhancement 78—33597
- double scattering mechanism involving target electron recoil, quantum mech. description 79—86062
- double well damped motion, proton tunnelling, transfer rate temp. depend. *(German)* 80—87058
- double-charge transfer processes in gaseous nebulae 79—30112
- electrochemical electron transfer at electrodes in soln., review, in book, for teaching 78—8203
- electrochemical kinetics at interface with space charge layer, appls. *(German)* 77—32807
- electrode processes possessing charge transfer mechanism, overvoltage theory, in book, for teachers 78—8204
- electrode systems, nonequilib. polaris. states props. overvoltage theory, in book, for teachers 78—8205
- electrode-redox system electron transfer reacts. time-depend. perturbation theory 78—61027
- electrogenerated chromophores, electrochemical conc. profiles, mass transfer, charge transfer, laser absorpt. spectroelectrochem. obs. 80—40765
- electron and exciton transfer rates, effect of nucl. degrees of freedom 78—60057
- electron attachment to mol. and mol. clusters, electron-mol. collision, Rydberg electron exchange 80—63843
- electron donor-acceptor complex formation, equilib. const. determ., reson. Raman spectroscopy 78—3329
- electron exchange reactions, stochastic solvent model 79—68312
- electron transfer between multicharged ions and neutral targets 77—72407
- electron transfer collisions time independ. quantum theory with nonorthogonal basis and R-matrix propag. 79—89769
- electron transfer limiting efficiency and rate constant meas., step excitation method expt. 79—91929
- electron transfer reactions, damping mechanisms effects calcs. 77—21381
- electron transfer reactions, free energy, anharmonic intramol. quantum mode depend. 77—12781
- electronic and at. collisions, conference, Kyoto, Japan (Aug.-Sept. 1979) 80—62394
- electrostatic pot. energy of atoms in mols., electronegativity, charge transfer and polarisation 79—63885
- ethanethiol, rare gas sensitised radiolysis and charge exchange mass spectra 77—48664
- ethyl carbazole, in nitrobenzene soln., dry hole capture in pulse radiolysis expt. 79—79266
- ethylene, twisted, intervalence charge transfer and reson., sudden polarisation effect 80—69230
- ethylene+$F^{\cdot}(CH_3^{\cdot})$, transition state, ab initio calc. 78—48640
- exciplexes and excited aromatic molecules, donor-acceptor props., comparison of fluorescence quenching 80—69174
- excited state process ps. kinetics, geometrical and solvent polarity effects 77—30986
- excited states, interpretation charge-transfer numbers 80—78530
- F ions recoiling in gases, hyperfine interactions 78—74735
- fast ion+atom, energetic electron emission as charge transfer process, Born approx. 80—53126
- fast ion+atom collisions, one electron charge transfer and capture 78—70931
- fast molecular ions, break-up on collision with solids 80—66353
- fast multiply charged ions, electron loss cross sections, semiempirical calcs. 79—86054
- Fermi one dimensional gas with long range potential, renormalisation group, exchange, Umklapp interactions 80—2351
- fixed-bed electrodes, three-dimensional, mass and charge transfer *(French)* 80—71920
- fluoranil, electron affinity, bound and excited negative ion states, lifetimes, electron and alkali metal collisions 79—869
- fluorinated ethylene-propylene copolymer, charge transfer by non wetting liquid contacts 77—4420
- fluoromethanes+$Ne^{+\cdot}(He^{+\cdot})(Ar^{+\cdot})(Kr^{+\cdot})(Xe^{+\cdot})(N_2^{+})(CO^{+\cdot})(CO_2^{+\cdot})(N_2O^{+\cdot})$, thermal energy charge transfer reactions mechanism 77—63889
- force decomposition anal. along reaction coord. 78—27741
- formamide-glyoxal, charge transfer theory, Mulliken population, ab initio calc., multiconfiguration scheme 80—106392
- formic acid, monomer, cyclic dimer, charge transfer through H bonds, Hartree-Fock calcs. 77—58157
- frozen media, electron transfer reactions and multiphonon transition theory 80—7812
- gas, partly ionised, viscosity calc., simplified expressions 79—18983
- glow discharge, secondary electron emission mechanism 77—19800
- glyoxal, electron affinity at centrosymm. trans geometry 80—87225

charge exchange continued
- graphite nitrate, charge transfer, ionic salt model 79—11780
- graphite-AsF_5 intercalation compounds, de Haas-van Alphen effect, charge transfer rate 80—54595
- graphite-Br_2 intercalation cpds., EXAFS study 80—71515
- graphite-K intercalation compounds, electronic props., de Haas-van Alphen effects and Fermi surfaces 80—75498
- graphite-K intercalation compounds, electronic props., resistivity, Hall effect and magnetoresistance 80—75585
- heavy ion collisions, inner and outer shell contribs. to charge state distribs. 80—14228
- heavy ion small impact parameter collisions, dynamic screening model 77—50525
- heavy ion stripping in dilute gases and C foils, data anal., semiempirical formulas 78—33354
- heavy negative ion beam prod. in range 15-90 keV by charge exchange with Mg vapour 78—25366
- heavy negative ion prod., 10-80 keV, charge exchange in Na vapour 78—33341
- heavy-ion collisions, charge transfer, target K-shell electron capture, impact parameter depend. 80—102552
- heavy-ion collisions, K-vacancy production, 1sσ excitation of transient mol. orbital 77—83718
- heterocyclic anion radicals, electron transfer with anthracene-amine cation radicals, triplet state electrogeneration 80—63803
- heterogeneous charge transfer kinetic effects, deconvolution by FFT faradaic admittance meas. 78—20091
- high-energy 77—27137
- high-Rydberg state high-impact-velocity forward charge transfer as classical process 79—22824
- highly charged ions in neutral atoms 78—62913
- hole-burning spectroscopy, electron phototransfer in reaction centres of Chlorella photosystem I 80—81561
- hydrazones, protonation energy and basic strength 80—37719
- hydrocarbon, (C_nH_{2n+2}, n=1-4)+H^+, electron capture and loss cross-sections 1-20 keV *(French)* 77—38728
- hydrocarbons, simple ions, reaction with simple mols. at thermal energies 77—40532
- 2-hydroxy, 3-allyl, 4,4′-dimethoxybenzophenone, methyl methacrylate copolymer, excitation singlet, internal H^+ transfer, visible spectra 80—32728
- 2-hydroxybenzophenone, excitation singlet, internal H^+ transfer, visible spectra 80—32728
- 3-hydroxyflavone, excited state proton transfer, luminesc. 80—35818
- ice crystals collision with simulated hailstones, lab. study of charge transfer 78—49112
- impurity ions in Tokamaks, charge transfer excitation 79—4103
- indole, fluorescence quenching by chloromethanes due to electron transfer 79—94027
- inert gas+O^{n+}, (n=4 to 7) small impact parameter collisions, dynamic screening model 77—50525
- inert gas+S^{n+}(n=5 to 9), small impact parameter collisions, charge exchanging processes, electron promotion 80—14227
- inert gas atom+H^+, outer S-shell ionisation cross-sections calcs. *(French)* 78—42212
- inert gas atom+ion, radiative charge transfer coeffs. 79—7010
- inert gas atom+$Ne^{2+}(Ar^{2+})(Kr^{2+})(Xe^{2+})$, low energy reactions, SIFT and drift tube obs. 80—97705
- inert gas dimer+atom, IOSA calc. for total integral cross sections for excitation, exchange and dissoc. 80—1044
- inert gas halides, exciplex mol. form., rel. to laser operation 80—81318
- inert gas hollow cathode arc, mol. beam sampling of metastable atoms as electron temp. probe 80—43967
- inert gas ion, in parent gas, transverse diffusion coeff., reson. charge exchange effects 78—63533
- inert gas ion+atom electron transfer collisions, cross section meas. 79—5143
- inert gas-halogen mixture, ion form., ion-mole. reactions, mass spectra 77—61841
- inert gases, doubly charged ions, thermal energy charge transfer 79—91946
- inner shell charge transfer, asymptotic, distorted-wave eikonal approx. calcs. 77—50528
- inorganic molecular crystals, metal complexes electronic spectra and intermolecular interactions 80—55137
- integrated spatial electron populations, evaluations for simple mols. 80—78524
- interstellar dense molecular clouds, chem. evolution 78—28749
- interstellar ion-dust grain collisions, electron transfer 78—77591
- intramolecular electron transfer amplitude, basis function overlap effect 78—9080
- iodide, charge transfer to solvent spectra, spectral shift data, Madelung const. determ. 80—85204
- ion+atom, impulse approx. by impact-parameter formulation 78—1076
- ion+atom, nonadiabatic transitions between decaying states *(Russian)* 77—10754
- ion+atom, projectile charge dependence *(Dutch)* 79—50121
- ion+atom collision, symmetric charge exchange, below 1 keV, cross sections calcs. 77—532
- ion+atom collisions, ionis., charge transfer, model 77—75278
- ion+atom collisions, K-shell hole, multiple hole production, charge transfer and antisymmetry 80—43168
- ion+ion, reson. charge exchange collisions 77—1921
- ion+ion collisions, charge exchange Coulomb scatt. 80—69232
- ion+ion mutual neutralisation rate coefficient parametrisation 80—81301
- ion+ion mutual neutralisation rates, approx. scaling formula 79—72411
- ion+molecule, charge transfer, energy disposal and reaction mechanisms 80—28103
- ion+molecule, slow reactions, proton transfer, rate consts. rel. to struct. 80—30232
- ion beam transport system, charge transfer cross sections 79—30609
- ion equilibrium negative charge state fractions 78—90288
- ion kinetics in high-pressure laser plasmas 80—64002
- ion mobility, resonant charge transfer effect 79—37440
- ion motion and charge exchange in quadrupole elec. field, Monte Carlo calcs. 77—9060
- ion pair forming collisions, dynamics 78—66661
- ion-atom collision, radiative charge exchange, high energy 78—55234
- ion-atom collisions, charge transfer, new integral eqn. calc. method 79—45832
- ion-ion collisions, crossed beam expts. 78—58843

charge exchange continued
- ion-metal atom processes, charge exchange cross sections, calcs. and computer program 78—55236
- ion-Rydberg atom collision cross sections, classical trajectory Monte Carlo calcs. 80—43174
- ion-surface scattering, low-energy inelastic case, review 80—40212
- ionic crystals, coupling of interfacial charge transfer and bulk transport 80—79986
- ionic motion, 3-D quadrupole electric field, simulation model 78—9315
- ionisation reactions, review 77—60053
- ions emerging from C foils, mean charge, inner-shell vacancy effects 80—87219
- isoqinoline, solns., dielec. polarisation, π-electron system effects 77—90096
- laser pumping, quasi-reson. energy and charge exchange processes, new transitions 80—58526
- linear accelerator, Na vapour charge exchange cell 77—38542
- linear sweep voltammetry, charge transfer, diffusion control 80—45583
- lysine, aq. solns., $H^+(D^+)$ exchange rates, ^{17}O NMR linewidths, pH depend. 80—91661
- lysozyme complex with substrate-inhibitors, photosensitised electron transfer, role of Cu^{2+} 80—30638
- Mattauch-Herzog mass spectrometer, charge exchange 80—86486
- merocyanine dye monolayer on p-chloranil cryst. in sandwich cell, electrochromic detection of internal charges 78—11549
- mesosphere, ion-neutral bunches charge exchange rel. to ion bunching 78—73424
- metal atoms, investig. in ion source for twin mass spectrometer 80—106215
- metal cluster ion energy spread from molten metal, charge exchange with neutral vapour 80—37922
- metal polymer contact, charge transfer and contact charge spectroscopy 80—65680
- metal polymer contact, charge transfer and contact charge spectroscopy 80—65681
- metal-ionic crystal-Cl system, charge transfer mechanism 78—11527
- methane+$H^- \rightarrow H$ +methane, force decomposition anal. along reaction coord. 78—27741
- methane+inert gas ion, thermal energy charge transfer 78—37739
- methane+$N_2^+(CO^+)$, charge transfer cross-section, low energy 78—58791
- methyl glyoxal, electron affinity at centrosymm. trans geometry 80—87225
- 9-methyladenine single crysts., protonic cond. 77—55388
- micellar system, photoinduced redox processes kinetics, intramicellar electron transfer 78—92603
- MIN, negative ion injector, Na charge exchange cell 80—99386
- model for nearly symmetric charge transfer 78—33598
- molecular crystal-metal interface, exciton decay, random-walk model 78—10356
- molecular interactions, weak, competitive preferential solvation theory 79—27051
- molecular solid, electron tunnelling, long-range electron transfer processes, orbital overlap model 80—7813
- molecule+ion charge transfer, vibr. excited mol. form. 77—3455
- multichannel charge-exchange energy analyser with high time resolution, plasma energy spectrum 79—41882
- multicharged ion thermal charge exchange reaction, rel. to astrophysics 80—63815
- multiple electron transfer to highly charged ions, scaling of cross sections 77—83711
- multiply charged heavy ions, charge exchange, and prod. method 78—58816
- muonic D+He, μ^- transfer rate 77—42447
- naphthalene radical anion+TCNQ, electron transfer reactions, theory 78—15661
- nebulae, charge exchange reactions rel. to N and O abundances 78—8093
- negative ion+atom (molecule), electron stripping, at. beam form. 77—6926
- negative ions, form. processes and props., review *(Japanese)* 80—53127
- NGC 7662, planetary nebula, photoionisation model with charge transfer reactions rel. to emission-line spectrum 80—62233
- p-nitroacetophenone charge transfer reaction with triplet state of guanine for radiosensitisation 79—92146
- p-nitroanilines, intramol. charge transfer satellites, XPS 80—78650
- nitroaromatic compound+anion radical, photo-CIDNP, acid-base equilib. effects 77—75185
- nitronaphthylamines, ESCA and UV photoelectron spectra, assignments 78—50588
- NMP-TCNQ, partial charge transfer effect, one dimensional disordered Hubbard model study 80—70687
- nucleic acids, H_2 exchange kinetics and internal motions 80—21440
- octane-water interface, water photo-oxidation in presence of adsorbed porphyrins 78—64933
- one-dimensional system, solitary electron, charge transfer without resist. 79—23691
- organic charge transfer salt process for high-density video storage 80—43269
- organic ion, excited electronic state correlation with mass-spectral fragmentation pattern 80—45482
- outer-sphere electron transfer in polar solvents, Debye theory 80—93762
- oxide electrodes, electron transfer reactions, tunnelling through a space charge barrier 78—80050
- oxide film on metal electrode, nonadiabatic theory of electron transfer 77—28237
- 2-oxyphenylbenzoxazol, proton intramolecular transfer, light absorpt. and emission, dichroism, polarised fluoresc. 80—87166
- paraaminophenol and paraphenylenediamine analogue molecular complex, free radicals of developers, EPR obs. *(Russian)* 80—7814
- parallel-plate sputtering system deposition rate model 79—87579
- particle beam, flux control, charge exchange method *(Russian)* 78—70662
- peptides, 1-electron reactions, pulse radiolysis obs. 80—45848
- peptides and derivatives, mol. electron acceptor groups 80—30637
- phenylpolyenes, donor-acceptor disubstituted, INDO calc. of hyperpolarisability 79—93924
- photo-copiers, organic photoconductors, charge acceptance calc. 78—80020
- photoactive pigment electrophotographic imaging system, dark charge exchange process 80—62758

charge exchange continued
- photochemical reactions, isomerisation, complexing, proton transfer, initiation of internal conversion processes 80—40713
- photoconductor image charge transfer to electrographic film 80—101864
- photon assisted, nonreson., optimal photon energy 77—75289
- photon-assisted, nonresonant, mol. model 77—16803
- photosynthetic reaction centres, primary electron transfer rate 79—8481
- phthalocyanine compounds, XPS and change transfer 80—95681
- phthalocyanine-alkane interface, charge transfer, rel. to photoelectrophoretic image form. 80—65616
- pigments, photochemical ionisation reactions in soln., automatic conductimetric instrument for kinetic studies 77—4971
- planetary corona, charge exchange effects on H distrib. and escape 77—29674
- planetary nebulae, charge transfer and He II Ly α photons absorpt. rel. to forbidden lines intensities 80—67833
- plasma, axially symmetric, Doppler broadened optical line emission interpretation model 78—75276
- plasma, charge exchange in collisions of multi-charged ions *(Russian)* 79—98859
- plasma, ion drift velocity in EM fields, charge transfer effect 78—83527
- plasma, resonant charge exchange, polarisation effect 80—43859
- plasmas, laser-produced, expansion, ion energy distrib., charge transfer effects 80—106953
- pnictides, charge transfer, influence of cryst. field 79—99516
- polar mol.+ion, statistical and thermodynamic theory 80—99562
- polar solvents, charge transfer, general oscillator model 77—21390
- polarized source based on nuclear polarization by charge-exchange 79—22514
- poly(p-phenylene), AsF_5 doped, highly cond. charge transfer complexes, elec. and optical props. 80—70778
- polyatomic ions, energy deposition on high-energy collision, angle-resolved mass spectrometry obs. 80—32825
- polyethylene terephthalate charge transfer from metallic electrodes 80—15605
- polymer, contact charge exchange spectrum, electronic struct., polarisation fluctuations effect 77—72833
- polymer film, proton intramolecular transfer, light absorpt. and emission, dichroism, polarised fluoresc. 80—87166
- polypeptides, in aq. poly(L-glutamic acid) soln., helix-coil transition, US relax. times 80—45849
- porphyrin-water interface, photoinduced charge separation 77—81408
- positive ion formation energetics by negative ion charge stripping 80—78700
- potential energy surfaces, qualitative, from linear comb. of fragment configs. 78—44349
- prelumirhodopsin, psec. kinetics, primary photochem. event in vision, proton translocation 78—44508
- protein internal charge transfer, ascorbic acid adduct model systems, SCF calc. 80—69072
- proteins, folded, models for H exchange 78—76981
- proteins, H_2 exchange kinetics and internal motions 80—21440
- proton relay model systems, reaction field theory of solvent effects 78—44346
- PVC+$Br_2(I_2)$, reaction in surface-modified film subject to thermal-radiative and photochem. action *(Russian)* 77—21385
- pyridine, solns., dielec. polarisation, π-electron system effects 77—90096
- quantum mechanical and impact parameter capture amplitude 80—87226
- quantum scattering theory, R-matrix propagation methods in inelastic and reactive collisions 79—59534
- quasiresonant atomic collisions, asymptotic calcs. 80—23512
- quercetin, excited state proton transfer, luminesc. 80—35818
- quinoline, solns., dielec. polarisation, π-electron system effects 77—90096
- rare earth oxysulphides:Eu^{3+}, effect on luminescent props. 78—15214
- rare-earth ions, charge transfer and crystal field theory 80—70654
- reactive and charge transfer collisions, between ions and molecules 78—62914
- resonant charge transfer, spin depend. *(Russian)* 78—29850
- resonant ion charge exchange collective modes 80—33736
- resonant transfer, eqns. of classical system interacting with quantum system 79—76498
- rhodamine dyes, triplet state, role in intermediate prod. 77—29018
- ring current ions, charge exchange lifetimes in magnetosphere 79—25409
- ring current ions+geocoronal H, charge exchange rel. to low-latit. E-region ionisation 78—77415
- rubrene film, excited complex with charge transfer, fluoresc. obs. of mag. reson. *(Russian)* 77—8454
- rubrene-in-benzene, excited state migration and charge transfer 77—55559
- Rydberg state reactions, time of flight mass spectrometric obs. 77—71867
- salicylidene-2-chloroaniline, photochromism and thermochromism, NQR spectra, temp. and UV irrad. depend. 80—54968
- shake-up and UV charge transfer transitions, comparison 80—102567
- slow ion+atom collisions, coherent excitation and decay of autoionising states 79—45789
- small molecules, diamag. susceptibility and second moments, intramol. charge transfer effects 80—78702
- solar wind, charge exchange with interstellar medium in unstressed deceleration model 79—53692
- spherical particle, max. charge imparted by pulse-charging 80—6945
- spherical particle with extremely high resistivity, corona charging 80—6944
- strongly interacting systems, energy decomp. scheme 79—31431
- subtilisin charge-relay system, electrostatic pot. map, STO transferable bond calc. 80—3571
- surface, charge exchange scatt. 78—43974
- symmetrised non-resonance, multicomponent kets theory 79—31676
- TCNE-benzene, charge transfer theory, Mulliken population, ab initio calc., multiconfiguration scheme 80—106392
- TCNE-substituted benzene complexes, isomers, stability, rel. to charge transfer band intensity 77—68051
- thermosphere, charge exchange of metastable ^2D O ions with N_2 78—20571
- thionine-monohaloaniline triplet exciplex, quenching position dependent heavy atom effect, intersystem crossing 78—53197
- three-centre systems, charge transfer effects and Huckel parameters, mapping concept *(German)* 79—22604
- Tokamak impurity problems, atomic and mol. struct. and collision data, review 80—43959
- tolyl cation+alkyl nitrate, reactions and ion struct. 77—52619

charge exchange continued

- total probability in collision processes, approximations 77−34753
- transition intermetallic cpds., CsCl struct., charge transfer and heat of form. 78−22689
- transition metal complexes, O containing, coordinate bonding, charge transfer electronic bands, complex struct. determ. 80−52977
- transition metal complexes, reaction mechanisms and solvent effects 80−26012
- triethylamine, gas (soln.), fluoresc. quenching by 'inert' perfluoromethylcyclohexane 78−46438
- trypsin inhibitor, soybean, folded, models for H exchange 78−76981
- two-atom system, with weakly bound electron, s-term passing through continuum parabolic boundary 79−72392
- two-centre charge distrib., Fourier transform, STO general expression derivation 80−58119
- two-level atomic collision system 78−62893
- ubiquinone-Fe complex, bacterial photosynthesis primary electron transfer processes, psec. dynamics 78−80841
- upper atmosphere H escape flux, charge exchange induced, diurnal and solar cycle vars. 78−93022
- valence and core photoionisation, spectral lines, many body effects 80−47853
- variationally consistent approximation scheme 79−22825
- very high energy, cross sections, second Born approx. 79−45827
- water, solvated electrons, photon-induced electron transfer transitions 79−8154
- X-ray laser pumping and charge transfer, book contrib. 79−31852
- Ag, hollow cathode discharges, IR laser transitions, discharge conditions, excitation mechanisms 79−68383
- Ag, population mechanism, highly-excited states, hollow cathode discharge *(Russian)* 78−63610
- Al-polymer contacts, charge transfer and contact charge spectroscopy 79−56305
- $Al+N^{n+}(O^{n+})(F^{n+})$, X-ray prod. and electron transfer cross-section 79−45790
- Ar^{+}, in Ar, transverse diffusion coeff., reson. charge exchange effects 78−63533
- Ar-Ti hollow cathode afterglow, energy transfer mechanisms and excited metallic ion prod. 80−43857
- $Ar+Ar^{+}$, charge exchange, Σ oscill. and spin change 80−74247
- $Ar+Ar^{+}$, differential cross section, pot. curve fitting, reson. electron exchanges 77−58118
- $Ar+Ar^{2+}$, charge transfer, energy defect and sealing laws 80−48083
- $Ar+H_2^{+}$ endothermic charge transfer reaction, low energy crossed beam study 80−95720
- $Ar+H_2^{+}\rightleftharpoons Ar^{+}+H_2$, electronic transitions, collinear reaction, curve crossing model, DIMZO surface 79−74373
- $Ar+H^{+}$, charge transfer and ionisation cross sections 79−89766
- $Ar+H^{+}$, importance of d-state couplings, inner shell charge transfer 79−89760
- $Ar+H^{+}$, subshell electron capture cross sections 79−89771
- $Ar+He^{+}$, (Ne^{+}), charge transfer reaction rate coefficient 79−91932
- $Ar+He^{+}(He^{2+})$, ionisation, differential cross-sections, 0.3 to 2 MeV 79−81271
- Ar+highly charged ion, inner-shell charge transfer calcs. 77−50528
- $Ar+K^{+}$, inelastic collisions, emission cross sections, quasimol. state interference 77−61848
- $Ar+Li^{+1,2,3}$, K-shell ionisation depend. on projectile charge state 77−34743
- Ar+negative ion, electron-loss cross sections 80−37877
- Ar+proton, charge transfer, target K-shell electron capture, impact parameter depend. 80−102552
- $Ar^{+}+(N_2)(H_2)(O_2)$, charge exchange reaction rates 77−86295
- $Ar^{+}+Ar$, charge transfer, fine-structure transitions 80−63808
- $Ar^{+}+Ar$, elastic scatt. and charge exchange, differential cross section, 2.7-20 eV 78−66660
- $Ar^{+}+Ar$, quasi-resonant charge transfer at thermal energies 80−48082
- $Ar^{+}+Ar$ collision, cross section meas. 78−25697
- $Ar^{+}+Ar(He)$, 100-550 keV, 3s vacancy production 79−13809
- $Ar^{+}+CO(CO_2)(N_2)(N_2O)(NO)(O_2)$, charge transfer, thermal energy, product distrib. obs. 78−25656
- $Ar^{+}+H_2$, charge transfer kinematics 78−9242
- $Ar^{+}+H_2(D_2)(N_2)$, small angle charge exchange, 0.5 to 1.0 keV, time of flight spectra 78−33604
- $Ar^{+}+H_2(N_2)(O_2)(CO)(NO)$, charge transfer cross sections 77−34751
- $Ar^{+}+Kr(Xe)$, thermal energy charge transfer reaction rates, mass spectrometric obs. 78−61000
- $Ar^{+}+N_2$, energy transfer, vibronic excitation, emission spectra 78−66578
- $Ar^{+}+O_2$, charge transfer mech., implication of inner-shell level mixing 77−61852
- $Ar^{+}+O_2\rightarrow Ar+O_2^{+}$, thermal energy charge transfer, energy disposal determ. 79−64099
- $Ar^{+}+Y\rightarrow Ar+Y^{+}$, (Y=He, Ne, Ar), keV energies, translational spectroscopy 78−5339
- $Ar^{2+}+Ar\rightarrow 2Ar^{+}$, thermal rate const. in negative glow 78−9241
- $Ar^{2+}+He(Ne)(Ar)(Kr)$, electron transfer cross-section, <100 eV 78−66654
- $Ar^{2+}+Kr(Xe)$, thermal energy charge transfer reaction rates, mass spectrometric obs. 78−61000
- $Ar^{2+}+Na$, Ar^{+} form, electron capture, Ar^{+} excited states relative population distrib. 80−23544
- $Ar^{3+}+He$, electron transfer cross-section, <100 eV 78−66654
- $Ar^{6+}+H_2$ collisions, ionisation and excitation resulting from electron capture 80−78683
- $Ar^{n+}+He$, $3\leq n\leq 8$, single and double electron transfer cross-sections 77−6924
- $Ar^{+}(Kr^{+})(Xe^{+})+H_2(N_2)(O_2)(CO)$, near-resonant charge transfer, 4-45 keV 77−27176
- $Ar^{*}+O_2$, ion pair form. explained by charge transfer model 80−99546
- $B^{+}+He(Ne)$, charge transfer and excitation, differential cross sections, 2-5 keV 79−36764
- $B^{3+}+H$, charge transfer cross sections, ab initio potential energy curves 78 37741
- $B^{3+}+He$, total cross-sections 77−79691
- $B^{5+}+He(C)(Ne)$, K-shell charge transfer cross sections, Bates-Born formalisms 79−45834
- $BeSO_4$ soln., high press. conductance meas., transfer mechanism 77−76586
- $BiCl_3$.nitrile complex, NQR spectra changes during complex form. 77−12242

charge exchange continued

- Br_2-pyridines, charge transfer complexes, ν_{Br-Br} vibr., Raman intensity obs. 79−36644
- C lines, charge exchange reaction effect 79−58243
- C VII+Ar III, laser produced plasma, C VI X-ray laser pumping 78−5462
- C^{+} charge transfer in diffuse nebulae 80−77463
- C^{5+}, plasma expansion, Balmer spectrum intensity inversion, charge transfer pumping 78−34371
- $C+H^{+}$ collision, electron capture cross section 80−63804
- $C+H^{+}(H_2^{+})$, vel. distrib. of convoy electrons, anal. 78−33600
- $C+H^{+}\rightleftharpoons C^{+}+H$, effect on C I 1101 Å absorpt. edge in A-type stars 80−90423
- C+proton, charge transfer, target K-shell electron capture, impact parameter depend. 80−102552
- C^{+}+ethylene (propylene oxide), branching ratios 78−44354
- $C^{+}+N_2(H_2)$, total charge transfer cross section, 5-100 keV 79−3561
- $C^{2+}+H_2(N_2)(O_2)$ (inert gas), charge transfer reaction rate consts. 80−7779
- $C^{4+}+H$, charge transfer cross sections, ab initio potential energy curves 78−37741
- $C^{4+}+He$, total cross-sections 77−79691
- $C^{5+,6+}+C$ reson. charge transfer, population inversion, in laser generated plasma 77−50526
- $C^{6+}+H$, low velocity charge transfer, two-state approximation calcs. 78−42207
- $C^{6+}+H(1s)$, low vel. cross-section, adiabatic mol. orbital basis 77−88553
- $C^{q+}+Ar$, continuum electron capture and loss, 1.6-2.8 MeV/A 78−46443
- $CH_4^{+}+CH_4(CH_2D_2)$, dissoc. charge transfer reactions, H and D atoms elimination 78−85141
- C_8K graphite intercalation compound, band structure calc., charge transfer effect 80−6692
- $CO+H_2^{+}(He^{+})$, dissoc, charge transfer, energy transfer processes 78−74759
- $CO^{+}+2CO_2\rightarrow 2CO_3^{+}$, reactions of electronically excited CO^{+} 77−1915
- $CO^{+}+CO$ (methane), charge transfer cross-section, low energy 78−58791
- $^{13}CO^{+}+CO$, charge-exchange detection of $^{13}CO^{+}$ electronic absorption spectrum, hyperfine consts. calc. 78−70822
- CO_2, positive and negative ion reactions 77−40540
- $CO_2+He^{+}(Ar^{+})(Ne^{+})(Kr^{+})$, electronically excited CO_2^{+}, $A^{2}\pi_{u}$ state bending vibrs. 77−3454
- $CO_2+He^{+}(H_2^{+})$, charge transfer, energy transfer, product ion excitation and fluoresc. 77−75288
- $CO_2^{+}(CO_2^{2+})$+atom(mol.), dissoc. and charge transfer 77−65532
- $^{12}C^{n+}$, partially stripped, energy straggling in thin Al foil, 3-36 MeV 79−41237
- $C^{+*}+Ar(H_2)(N_2)(CO)(CO_2)(O_2)$, charge transfer cross-sections, 0.7-2.4 keV, $C^{+}(^{2}P)$ and $C^{+}(^{4}P)$ 78−58806
- C (4S)+molecule, spin angular momentum conservation in proton transfer 77−16805
- Ca-Xe charge exchange system, optical gain meas 79−10285
- $Ca+Ca^{+}$(Rydberg Ca**), collision cross sections, Ca_2^{+} pot. energy calcs. 79−27055
- CaF_2:Eu, oxidation and reduction of Eu, EPR and optical studies 80−25199
- $Ca^{+}(4s\ ^{2}S_{1/2})+Sr(5s^{2}\ ^{1}S_{0})$, laser induced charge transfer to excited electronic state 79−81274
- $Cd+He^{+}$, thermal energy charge transfer reaction, ion states, relative yields 79−45840
- $Cd(^{1}P_{1})$ excited state quenching by mols., cross sections, chem., phys. exit channels 79−779
- CdTe electrode, redox reaction due to complex $M(CN)_6^{3-/4-}$ *(French)* 80−89482
- n-CdTe, semiconductor electrode, electrochem. behaviour in nonaqueous media *(French)* 80−66808
- Ce-Co, liq., charge transfer effect 78−94967
- Ce-Cu, liq., charge transfer effect 78−94967
- CeI_3 vapour, electron irradiated, negative ion formation 77−27190
- Cl^{-}, far UV spectra in solns. 78−94208
- Cl+highly charged ion, inner-shell charge transfer calcs. 77−50528
- $Cl_2+2Br^{-}\rightarrow Br_2+2Cl^{-}$, aqueous soln., specific rate determ., competition technique 78−44348
- $Cr(CO)_6$, MCD spectra, charge transfer transitions 80−95658
- $Cs+(AuF_5)_n$, prod. of AuF_5^{-}, ionisation cross section energy depend. 80−81300
- $Cs+(SbF_5)_n\rightarrow Cs^{+}+SbF_6^{-}+SbF_4+(SbF_5)_{n\ -2}$, ionisation cross section energy depend. 80−81300
- $Cs+Ar^{+}(Kr^{+})(H_n^{+})(He^{+})(N^{+})(N_2^{+})(Ne^{+})(Xe^{+})$, total charge-transfer cross-sections meas. 77−50527
- $Cs+Cl_2(Br_2)(I_2)(ICl)(IBr)$, negative ion prod. cross sections 77−531
- $Cs+Cs^{+}$, charge exchange cross-section, temp. depend. 78−9244
- Cs+F(Cl), quasiclassical charge transfer cross section, rel. vel. depend. 77−19073
- $Cs+H^{+}$, charge exchange collision producing H(2s), semiclassical differential cross-section 79−59551
- $Cs+H^{+}$, charge transfer processes with plasma gun, Lyman-α radiation exam. 78−46573
- $Cs+He^{+}$, spin dependent charge transfer in low-energy collisions 77−75293
- $Cs^{+}+Cs$, reson. charge exchange cross section at thermal energies 79−854
- $Cs^{+}+Cs^{+}$, charge transfer, ionis., 40-280 keV, rel. to fusion scheme 80−5615
- $Cs_{1-x}Au_{x}$, liq., metal-nonmetal transition, electronic theory 78−79930
- Cu, hollow cathode discharges, IR laser transitions, discharge conditions, excitation mechanisms 79−68383
- Cu, low energy noble gas ion refl., surface thermal vibrs. effect 77−69955
- Cu, low energy noble gas ion refl., surface thermal vibrs. effect 77−73203
- Cu, population mechanism, highly-excited states, hollow cathode discharge *(Russian)* 78−63610
- Cu+He ion, neutralisation and ionisation of low energy He ions scatt. from (100) face 78−23572
- $CuCr_{2\ x}Fe_{x}O_4$, charge transfer, Mossbauer spectroscopy 80−15836
- D^{-} ions, equil. charge state fractions of 3.3-39 keV D atoms and ions in Mg vapour 77−57788

charge exchange continued
- D+alkaline earth, D^- ion production, multiple charge-transfer collisions 79−89776
- D+Cs, ang. scatt., neutral beam form. via negative ions 77−46636
- $D+D_2^+(CO_2^+)(CO^+)(N_2^+)(HCN^+)$, reaction, ion cyclotron reson. mass spectrometric obs. 79−64098
- $D+H^+(D^+)(He^+)(Ne^+)(Ar^+)(Kr^+)$, reson. charge charge transfer from photoexcited donor state 79−22820
- $D+M \rightarrow D^- + M^+$ (M=alkali metal atom), ion-pair form. 78−58779
- $D^+ + Rb \rightarrow D^{-,0} + Rb$, equil. fraction of D^- ions, charge transfer cross section 77−65375
- $D^+ + Xe$ double charge exchange, D^- prod. *(French)* 79−94080
- D_3^+ +inert gas, ion decay, 1-40 eV *(Russian)* 78−90286
- D_2O, $H^+(D^+)$ exchange rates, ^{17}O NMR linewidths, pH depend. 80−91661
- Dy atom isotope separation, laser excitation, charge exchange with Cs^+ ions 80−83512
- ^{151}Eu (^{153}Eu) excitation transfer, effect on selective photoionisation 80−99538
- $Eu+H^+$, two-step laser isotope enrichment using charge transfer ionisation 79−867
- $F^+ + H_2$, empirical and ab initio correlation diagrams, pot. energy surfaces 78−40041
- F^{n+} +Ag foil, 10-40 MeV, Ag L-shell X-ray production 77−71856
- ^{19}F NMR solvent shifts, charge transfer contribs. 77−50454
- ^{19}F, nuclear dealignment of multiply ionised 3 and 6 MeV atoms recoiling in gases 80−78267
- Fe group elements, singly ionised, charge transfer, rel. to laser action 80−74246
- Fe microspheres, impact on mech. polished electrodes, contact pot. influence on charge transfer *(French)* 78−47198
- Fe XXII, XXIV, XXV, charge exchange recomb. in Princeton large torus during beam heating 80−100067
- Fe^{2+} and Fe^{3+} hydrate clusters, aq. electron exchange reaction, ab initio RHF MO calc. of inner shell reorganisations, vibr. freq. 80−102564
- Fe^{26+} +H, electron removal by collision 79−76508
- Fe^{n+} +H, electron transfer cross-section meas. 78−17787
- FeAl B2 struct., band struct. and density of states, KKR calc. 78−63969
- $Fe_{3-x}Cr_xO_4$, electron transfer and spin density distribs., Mossbauer spectra 79−24243
- Ga, liq., electron transfer of rare earth metal impurities *(Russian)* 77−59132
- H atoms on nuclei of multicharged ions, charge exchange with allowance for degeneracy of final states *(Russian)* 78−46444
- H bond system, charge transfer theory, relation between vibr. spectra and energy 77−3334
- H, change in spectral line intensity of multiply charged ions *(Russian)* 78−58814
- H, charge exchange involving excited states, Born cross sections 79−45836
- H excited atoms, charge transfer processes, perturbed stationary state method 79−89770
- H, H^+ and H^- beams, charge transfer cross sections in gases and vapours, 10 eV to 10 keV, graphs and tables 80−32824
- H, inverted, optical gain at Lyman-α spectral line 80−95880
- H ion sources, plasma reaction cross sections data 77−38538
- H polarised ion source, Lamb-shift type, charge exchange processes *(Rumanian)* 77−46445
- H, positron charge exchange, positronium form., two state approx. 77−79710
- H, positron impact ionisation, charge exchange problem 79−50139
- H, positron scattering, positronium formation 79−89772
- H species, on C foil, 800 keV amu^{-1}, electron loss and capture cross-sections 80−65066
- H^- form. by surface and vol. processes, neg. ion source appl., review 80−58375
- H-bonded model systems, intermolecular charge transfer, biological implications 80−3572
- H-like atom+bare ion, electron capture to continuum, cross-section cusp 78−90289
- H-like ion+H charge stripping processes 77−19072
- H-like ions, electron impact excitation to S states exchange effects 78−58835
- H-like ions$+H^+$, charge transfer cross sections 79−18286
- $H+{}^3He^{2+}({}^4He^+)$, electron loss, capture cross-sections 78−22026
- $H+{}^4He^{2+}$, electron capture and charge exchange cross sections 77−68108
- $H+A^{7+}$, charge transfer for ground and metastable states 77−42399
- $H+B^{n+}(C^{n+})$, one electron capture and loss 80−18921
- $H+Be^{2+} \rightarrow H^+ + Be^+$, charge transfer total cross-sections 79−3559
- $H+C^+(C^{3+})(N^{2+})(O^{2+})(Ne^{2+})(S^+)(S^{3+})(N^+)$, ionization model for NGC 7027 planetary nebula 78−36671
- $H+C^{2+}(C^{3+})(N^{2+})$, radiative charge transfer, rate coeffs., pot. energy curves 77−88554
- $H+C^{3+}(N^{3+})$, charge exchange collisions, quantal calcs. 79−94079
- $H+C^{6+}$, collisional electron removal, cross-sections, mechanisms 78−25683
- $H+Cs \rightarrow H^- + Cs^+$, low energy cross sections 79−7009
- H+H collisions in laser field, excitation, charge exchange and ionis. *(Russian)* 79−94078
- $H+H_2^+(HeH^+)(CO_2^+)$, reaction, ion cyclotron reson. mass spectrometric obs. 79−64098
- $H+H^+$, charge exchange and differential scatt., theoretical calcs. 77−10729
- $H+H^+$, charge exchange probability 79−98216
- $H+H^+$, charge transfer, Born approx. 79−59552
- $H+H^+$, classical 3 body collision, cross section, energy transfer, computer calcs. 78−17783
- $H+H^+$, coupled state calc., charge transfer and direct ionis. 79−22810
- $H+H^+$, cross section for production of metastable H(2S) state 78−13588
- $H+H^+$, electron capture, 25 to 200 keV 77−88551
- $H+H^+$, electron capture in 3s level, distortion approx. 80−37876
- $H+H^+$, excitation and charge transfer to 2s(2p) states, 49-125 keV 80−18910
- $H+H^+$, fast proton total electron capture cross section, fixed scattered approx. 79−22819
- $H+H^+$, in plasmasphere, rel. to atmospheric H escape rate 77−37469
- $H+H^+$, low energy, optimised translation factors 80−18813
- $H+H^+$, nuclear repulsion, contrib. to charge transfer 80−18922
- $H+H^+$, resonant charge transfer in presence of lower field 79−64072

charge exchange continued
- $H+H^+$, transition probabilities and total cross-sections, high energy behaviour 78−9245
- $H+H^+(Arq^+)(Kr^{q+})(B^{q+})(C^{q+})(N^{q+})(O^{q+})$ charge transfer and impact ionis. cross sections calcs. 77−88555
- $H+H^{2+}$, electron capture in 3s level, distortion approx. 80−37876
- $H+He^{2+}$, charge transfer cross sections, molecular bases calcs. 79−98217
- $H+He(N_2)$, stripping cross-section, 0.3 to 3 keV 78−78807
- H+highly stripped ions, S-matrix construction 79−3527
- H+ion, charge exchange and ionis. cross sections *(Russian)* 79−50130
- $H+Li_2$, collinear reactions, SCF correl. diagram for Li_2H form. 77−70292
- $H+Li^{3+}(Be^{4+})(B^{5+})(C^{6+})$, charge transfer cross sections, distorted wave Born approx. 79−72415
- $H+N^{3+}$, charge exchange, assoc. reaction, rel. to interstellar gas 80−7763
- $H+Ne^{10+}(Si^{14+})(Ca^{20+})$, charge transfer, total and partial cross-sections calcs. 80−23542
- $H+O^+$, in upper atm., rel. to H^+ loss during solar cycle 78−93021
- $H+O^{8+}$, electron removal, charge transfer and impact ionisation cross-section 79−76504
- $H+O^{8+} \rightarrow H^+ + O^{7+*}$, during neutral beam injection into Tokamak 77−58899
- $H+O^{n+}(N^{n+})(C^{n+})(B^{n+})$, charge transfer cross sections, oscillatory behaviour in low-energy collisions 80−63806
- H+positive ion collisions, producing H atoms in arbitrary p-state, charge transfer 79−64074
- H+positron, charge exchange, excited positronium states form. 78−58873
- $H+X^{n+}$, sub-barrier charge exchange cross section calc. *(Russian)* 79−7004
- $H^- + (He),(Ar),(Xe),(N_2)$, 1 to 5 keV, production cross sections for 3d,3s,4s,5s states of H 78−33603
- H^- +atom, electron loss high energy cross sections 78−13597
- H^- +Cs, fast atom collisions, charge exchange, equilib. fractions calcs. 78−33601
- H^- +H, electron detachment cross-sections, 100 keV-10 MeV 79−59561
- $H^- + H_2$, electron detachment cross-sections, 100 keV-10 MeV 79−59561
- $H^- + H_2(He)(Li)$, 50-150 keV, scatt. angle of neutral H 78−5340
- $H^- + H^+$, charge exchange, one or two electrons, symmetry effects *(Russian)* 79−3562
- $H^- + H^+$, double charge transfer, 30-200 eV 79−45837
- $H^- + H^+$ charge exchange, quantum transition probabilities calc. 80−9557
- $H^- + H^+ \rightarrow H(1S)+H$, level degeneracy effect on charge exchange at term pseudointersection 79−27084
- H^- +He, electron detachment cross-sections, 100 keV-10 MeV 79−59561
- H +He, electron detachment cross-section, target distortion calcs., 100 keV-100 MeV 79−59562
- H^++ hydrogenic ion, electron capture in highly excited s-state 79−45839
- H^+ +alkali metal, charge exchange, eikonal approx. calcs. 80−78703
- H^+ +alkali metal, valence and core electron capture collisions 79−94081
- H^+ +Ar, charge exchange excitation, alignment tensor components, coincidence method 80−63795
- H^+ +Ar, inner-shell charge transfer calcs. 77−50528
- H^+ +atom, ionisation, proton polaris. meas. 80−9482
- H^+ +Cs, elastic and charge exchange collisions, projected valence bond method 78−78804
- H^+ +Cs(Rb)(K)(Na), charge exchange, H(2s) form. 79−64101
- $H^+ + Cs \rightarrow H^- + Cs^{2+}$, proton conversion, 0.2 to 6.0 keV *(Russian)* 77−1920
- $H^+ + D \rightarrow H + D^+$ near threshold rel. to HD molecule formation in interstellar medium 78−89239
- H^+ +Ge collisions, charge exchange 77−6922
- H^+ +H, 1-7 keV, H(2s) form. and Lyman-α polarisation 80−14221
- H^+ +H, 15-200 keV, excitation and charge transfer cross sections, Sturmian expansion 77−19024
- H^+ +H, 1s charge exchange amplitudes, impact parameter calcs. 77−534
- H^+ +H, charge transfer collisions, angular distribution 78−13599
- H^+ +H, charge transfer cross section calc., up to 100 keV 78−55235
- H^+ +H, in radiation belts, as source of energetic interplanetary H 77−9645
- H^+ +H, inelastic collision, time depend. Schrodinger eqn. for electron motion 79−89774
- $H^+ + H_2$, charge transfer into continuum 79−89765
- $H^+ + H_2$, electron capture into ground and excited s states 79−76509
- H^+ +H , merged beams, double charge transfer cross section 79−22818
- H^+ +H(D), elastic scatt. and charge exchange, resonances 78−78777
- H^+ +H(O), in upper atm., rel. to H^+ loss during solar cycle 78−93021
- H^+ +H(1s), radiative charge exchange, 1-50 MeV 78−55234
- H^+ +H(1s), reson. charge transfer, spin depend. *(Russian)* 78−29850
- $H^+ + H(1s) \rightarrow H(nl) + H^+$, cross-sections, continuum distorted-wave approx. 77−68108
- $H^+ + H(1s) \rightarrow H(nlm) + H^+$, highly excited states rearrangement collisions 79−59564
- $H^+ + H \rightarrow H + H^+$, charge exchange, atomic scattering, many-particle theory 77−10715
- H^+ +He, electron capture total cross sections 78−5322
- H^+ +He, proton energy degradation, approx. yield spectrum 79−31643
- $H^+ + He^+$, charge transfer and ionis. cross sections, coincidence meas. 78−50634
- $H^+ + He^+$, fast collision, ionisation and charge transfer, cross section meas. 78−25698
- $H^+ + He^+$, He^{2+} form. by charge exchange and ionis., cross sections 77−83708
- $H^+ + He^+$, ionis. and charge transfer cross sections 78−42186
- $H^+ + He^+$, ionisation and charge transfer using intersecting beams 77−68104
- H^+ +He(Ar), charge exchange, differential cross sections 79−7006
- H^+ +He(Ar), emitted electron's energy and angular distrib. support for charge transfer to continuum theory 78−37740
- H^+ +He(Ar), H(n=4) s-d coherence, zero-field quantum beats obs. 80−32676
- H^+ +He(Ar) electron transfer cross sections 78−58809
- H^+ +He(Ar)(C), ionisation processes viewed in forward direction 77−71866

charge exchange continued
$H^+ + He(Ar)(O_2)$, charge transfer to $H(n=2)$, mixed parity elec.-dipole oscillations 79−31678
$H^+ + He(C)(Ne)$, K-shell charge transfer cross sections, Bates-Born formalisms 79−45834
$H^+ + He(Ne,Ar)$, charge transfer into continuum 79−89765
$H^+ + He(Ne)(Ar)$, ionisation, projectile energy depend., secondary electron energy distrib. 78−42211
$H^+ + He(Ne)(Ar)(Kr)$, charge exchange, 80 to 1500 eV, total cross sections 77−61854
$H^+ + He(1s^2) \rightarrow H^* + He^+(1s)$, continuum distorted wave approx., total cross section 77−68109
H^+ + inert gas, 4s-state electron capture cross-section meas. 78−82836
$H^+ + Kr$, mol. orbit approach, spin-orbit interaction, adiabatic pot. and projected valence band treatments 77−533
$H^+ + Kr(Ar)$ charge exchange, oscillating cross sections 77−58158
$H^+ + Li$, charge exchange, eikonal approx. calcs. 80−78703
$H^+ + Li^+$, charge transfer and ionisation, total cross sections for production of Li^{2+} determ. 80−91657
H^+ + metal ion, pot. curve, for exchange, Landau-Rosen and Rosen-Zinner model *(Russian)* 77−75287
$H^+ + Mg(Ba)$, metastable H form. by charge exchange 79−81275
$H^+ + O_2$, energy transfer, vibronic excitation, emission spectra 78−66578
$H^+ + Si$ collisions, charge exchange 77−6921
H_2 beam, D diffusion studies by pulsed injection in He Tokamak plasma 80−28611
H_2, vib. excited state production in charge transfer reactions 77−30968
H_2^+ differential cross section rel. to charge exchange cross sections of fragments 80−78704
$H_2 + {}^3He^{2+}({}^4He^+)$, electron loss, capture cross-sections 78−22026
$H_2 + Ar^{n+}(Kr^{n+})$, charge transfer, collision defects and dynamics, cross section meas. 80−53099
$H_2 + B^{n+}(C^{n+})$, one electron capture and loss 80−18921
$H_2 + C^+(N^+)(O^+)$, reactant ion electronic states, effect on charge transfer cross sections 80−63809
$H_2 + H_2$, van der Waals pot., electron tunnelling, charge transfer 77−54588
$(H_2 + H^+, H_2^+ + H)$ collinear system, electronically nonadiabatic effects 78−1063
$H_2 + He^+$, 0.5-3.0 keV, direct and charge-exchange scatt. 77−75263
$H_2 + He^+$, charge transfer, appl. of atom-photon coincidence meas. 79−45829
$H_2 + He^+$, DIM approx. pot. energy surfaces and nonadiabatic coupling 80−23330
H_2 + negative ion, electron-loss cross sections 80−37877
$H_2 + X^{Z+}$, $Z \geq 4$, 1-20 keV, electron capture 80−37875
$H_2^+ + Ar$, low energy proton transfer reactions, crossed beam studies 80−108697
$H_2^+ + Ar(He)(H_2)$, 10 keV dissoc. charge exchange collisions 78−94319
$H_2^+ + H_2$, pot. energy surface and nonadiabatic regions, charge exchange and reaction, VB calc. 78−40027
$H_2^+ + H^- \rightarrow H_2^* + H$ recombination react., calcs. *(Russian)* 80−55659
$H_2^+ + He(Ar)$, emitted electron's energy and angular distrib. support for charge transfer to continuum theory 78−37740
$H_2^+ + He(Ar)(C)$, ionisation processes viewed in forward direction 77−71866
$H_3^+ + Ar(H_2)$(air), dissoc., 400-800 keV, product charge state distrib. model 78−82838
$H_3^+ + C$ foil, 2.2 MeV, ion survival during traversal 79−64103
$H_3^+ + H_2$ charge transfer collisions, 10 keV, H_2-H fragmentation 79−853
H_n^+ multispecies beam, particle species evolution in neutral-beam injection lines 79−85846
HCN-CO complex, charge transfer theory, Mulliken population, ab initio calc., multiconfiguration scheme 80−106392
HCl, charge exchange mass spectra 80−43177
HD^+ scattering states, elastic and charge transfer cross sections 78−9221
$H(D) + Cs$, 40 keV, prod. of polarised H^- or D^- ions, low emittance 78−55078
$H_3^+(D_3^+) + H_2(D_2)$ collisions, slow ion production, charge transfer cross sections 80−106378
$H^+(H_2^+) + C$ foil, $v_i = v_e$ electron prod., charge transfer to continuum theories 78−13583
HNC^+, radical cation, charge exchange mass spectrometry, HNC^+ ion recombination and ionisation pot. 78−76838
H_2O, $H^+(D^+)$ exchange rates, ${}^{17}O$ NMR linewidths, pH depend. 80−91661
$H_2O + Ar^+$, thermal-energy charge transfer, H_2O^+ product internal and kinetic energy 80−16654
H_2O + inert gas ion, thermal energy charge transfer 78−37739
${}^3H(p,n){}^3He$ charge exchange reaction, multifold diffr. scatt. theory *(Russian)* 80−78303
$H(1^2S) + H_2$ (inert gas), electron capture, electron loss and deexcitation cross sections meas. 78−22025
$H(1s) + He^{2+}$, charge transfer, Coulomb-Born approx. calc. 80−43175
$H(1s) + O^{8+}(He^{2+})(H^+)$, charge transfer, 0.025-200 keV/amu 79−22823
$H(2^2S) + H_2$(inert gas), electron capture, electron loss and deexcitation cross sections meas. 78−22025
$H(2s)$ + energetic projectile ion, charge exchange, cross-sections calcs. 79−59554
$H = H^+$ collisions, H(2s), H(2p) production, 1-7 KeV, differential, total cross sections 80−32818
$He\ (2^3P) + Ca(Sr)$, collisional quenching of metastable states, excitation transfer cross sections 78−66653
He I 2^3P-3^1D intercombination line, collision-induced, obs. by laser absorpt. spectroscopy 80−58194
He ions backscatt. from solids, charge state distribs., target temp. depend. 79−95887
He, positron scattering, positronium formation 79−89772
He species, on C foil, 800 keV amu^{-1}, electron loss and capture cross-sections 80−65066
He^+, electron impact excitation to S states exchange effects 78−58835
He-Cd, afterglow, Cd^+ excited state prod. by Penning and charge exchange reactions 77−15252
He-Cd discharge, enhancement of rate of charge exchange collisions 77−83862
He-Cd mixture, Penning ionis. and nonreson. charge exchange in afterglow 79−72414
He-Hg afterglow plasma, time resolved double probe study 78−18444

charge exchange continued
He-Hg nuclear pumped laser, charge exchange pumping 80 63996
He-Ne gas mixture plasma, role of charge exchange in form. of optical props. 80−28600
$He + Ar^{+Z}$ (Z=3 to 7), electron capture into different electron states by multiply charged ions *(Russian)* 78−17788
$He + Ar^{2+}$, charge transfer, energy defect and sealing laws 80−48083
$He + B^{3+}(C^{4+})(N^{5+})(O^{6+})$, electron transfer 78−13598
$He + H^+$, charge transfer, approx. close-coupling calcs. 77−23560
$He + H^+$, electron ejection, energy and ang. distrib. calcs. 77−6914
$He + H^+$, ionising collision, first-order Faddeev approx. 79−22827
$He + He$, He^- decay cross section oscills. *(Russian)* 77−19038
$He + He^+$, double collision spectroscopy 80−58378
$He + He^+$, resonant charge transfer cross sections, 2 to 100 eV 78−66655
$He + Mg^+(Ne^+)$, charge exchange, Rydberg state excitations 77−58159
He + negative ion, electron-loss cross sections 80−37877
$He + OCS$, emission spectra in He afterglow 80−87139
$He + X^{n+}$, X^{n+} = completely stripped positive ion, charge-transfer eqns. 77−75294
$He^{+,2+} + Ar$, 2 MeV, ejected electron spectra, 20-450 eV, 0-10° 77−34746
He^+ + acetylene-d_0($-d_2$), $CH^+(CD^+)$, A-X luminesc., in near-thermal charge exchange 78−50632
He^+ + alkali metal, charge exchange, He metastable beam form., composition 79−89775
$He^+ + Ar$, charge exchange, quasimolecule model, four-state calcs. 77−14571
$He^+ + Ar$, charge transfer cross section, kinetic energy dependence in low energy region *(Japanese)* 78−90100
$He^+ + Ar$, direct excitation and charge exchange processes 77−75279
$He^+ + Ar$, low energy charge transfer collisions, kinetic energy depend. 78−86947
$He^+ + As^* \rightarrow He + (As^+)^*$, He-As CW laser, excitation mechanism 79−3685
$He^+ + CO_2$, dissociative charge exchange kinematics 80−3318
$He^+ + CO(CO_2)(N_2)(N_2O)(NO)(O_2)$, charge transfer, thermal energy, product distrib. obs. 78−25656
$He^+ + CS_2$, dissoc. charge-transfer, $CS^+(B^2\Sigma^+ - A^2\Pi_i)$ emission prod., Morse pot. Franck-Condon factors calc., vibr. anal. 80−99539
$He^+ + H_2$, charge transfer at 1.5 and 3 keV, $He({}^3P)$ excitation 78−66658
$He^+ + H_2$, dissoc. charge transfer, vibr. enhancement 78−33597
$He^+ + H_2(D_2)$, dissociative charge transfer, 78-330K 80−61079
$He^+ + H_2(D_2)(N_2)$, small angle charge exchange, 0.5 to 1.0 keV, time of flight spectra 78−33604
$He^+ + He$, 2^1P level, direct and charge-exchange excitation, 150-1000 keV 78−70913
$He^+ + He$, charge exchange cross section, drift-vel. meas., 0.3-8 eV 78−25694
$He^+ + He$, charge transfer, appl. of atom-photon coincidence meas. 79−45829
$He^+ + He$, charge transfer collision, approx. diabatic mol. representation 80−9728
$He^+ + He$, elastic scatt. and charge exchange, differential cross-section, 0.4-30 eV 78−66659
$He^+ + He$, $He(2^3S)$ formation, elastic and resonance charge exchange perturbations 77−42386
$He^+ + He$, reson. charge transfer, merging-beam technique 79−41235
$He^+ + He$, symmetric reson change transfer, 0.1-3 keV, 3-state close-coupled calcs. 77−50524
$He^+ + He$ collision, cross section meas. 78−25697
$He^+ + He^{2+} \rightarrow He^{2+} + He^+$, 10-1700 eV, absolute. cross-sections meas. 79−3560
$He^+ + Hg_0 \rightarrow He_0 + (Hg^+)^* + \Delta E$, cross sections, rate consts. 78−17785
$He^+ + N_2$, $\lesssim 0.1$ eV, UV and visible luminesc. spectra 77−83722
$He^+ + N_2$, charge exchange, time-resolved emission probe 78−86946
$He^+ + N_2$, collisional excitation processes, visible emission, cross-sections 80−99571
$He^+ + N_2O$, in afterglow, N_2^+ optical emission obs. 79−68251
$He^+ + Ne^* \rightarrow He^* + Ne^+$, cross sections 79−22821
$He^+ + Ne(Ar)$, attenuation and single electron charge exchange cross sections, 500-5000 eV 77−34752
$He^+ + O_2$, (N_2), charge transfer reactions, product ion distribs. 77−73445
$He^+ + O_2$, charge transfer product state distribs., time of flight obs. 80−87223
$He^+ + O_2$, thermal energy charge transfer, O^+ product ion obs. 79−64100
$He^+ + OCS$, dissoc. charge-transfer, $CS^+(B^2\Sigma^+ - A^2\Pi_i)$ emission prod., Morse pot. Franck-Condon factors calc., vibr. anal. 80−99539
$He^+ + Pb$, at. beam and surface interaction, scatt. ion yield oscills. 78−55221
$He^+ + SO_2$, dissoc. charge transfer reaction, SO^+ $(A^2\Pi - X^2\Pi_r)$ emission 80−95659
$He^+ + Xe$, internal energy distrib. at 100 eV 80 ·99564
$He^+ + Xe$ charge transfer, optical emission cross sections 77−61853
$He^{2+} + H$, mol. treatment, cross sections and charge exchange probabilities 77−58128
$He^{2+} + H_2 \rightarrow He^+ H^+ + H^+$, two-electron capture 78−58811
$He^{2+} + He$, 5 to 100 keV, elastic and double charge exchange, mol. treatment 78−82813
$He^{2+} + He$, radiative single charge transfer cross section 79−7011
$He^{2+} + He$, single charge exchange, reson. contrib., thermal 79−76511
$He^{2+} + He^+$, ionis. and charge transfer cross sections 78−42186
$He^{2+} + Li$ collisions, soft X-ray emission obs. 80−83591
$He^{2+} + N_2$, 200-600 eV, 0-20°, comparison with $He^{2+} + Ne(Ar)$ 78−74732
$He^{2+} + Ne(He)$, electron transfer cross-section, <100 eV 78−66654
He_2^+, rate coeffs. for bimol. and termol. ion-mol. reactions 78−53188
$He_2^+ + Ne(Ar)(N_2)(CO)(CO_2)(Ch_4)$, bimol. and termol. charge transfer reactions, rate coeffs. 77−1910
$He_2^+ + O_2$ charge exchange laser 78−50759
$(HeH)^+$, breakup in single dissociative collision, fragment charge states 80−74226
$He^+(He^{2+}) + H$, charge transfer and direct excitation processes 78−25696
$He^+(He^{2+}) + He(Ar)(C)$, ionisation processes viewed in forward direction 77−71866
$He^+(He_2^+) + N_2(CO)(CO_2)(H_2S)$, charge transfer Penning ionis 78−17784

charge exchange continued
^{3}He-Ar nuclear pumped laser, first order model, lasing action depend. on Ar conc. 79—76668
$^{3}He^{2+}+H^{*}\rightarrow{}^{3}He^{+}+H^{+}$, merged beams, cross section 77—75292
$^{4}He^{+}+{}^{3}He^{2+}$, charge exchange, cross section meas. 80—32827
He*, Rydberg state charge transfer reactions, time of flight mass spectrometric obs. 77—71867
He*+He, (*=excitation or charge), differential scatt. inversion procedure, symmetric exchange, classical, semiclassical theory 79—13802
$He^{+}(1s)+H^{2+}$ symmetric resonance charge transfer 80—32826
Hg+He, afterglow, $Hg^{+}(7^{2}P_{1/2}, 7^{2}P_{3/2})$ excitation processes, rate consts. *(Russian)* 78—29848
$Hg+He^{+}$, thermal energy charge transfer reaction, ion states, relative yields 79—45840
$Hg^{+}+Cs$, pumping of vac. UV laser 77—31095
I^{-}, aq., in supercooled water, and glass forming solns., charge transfer to solvent spectra 77—50447
$I^{-}+CO$, endoergic ion-molecule reaction 77—25262
$I^{-}+COS(CS_2)(H_2S)$, endoergic reaction, time of flight mass spectral obs. 77—12786
$I^{-}+SO_2$, endoergic reaction, time-of-flight mass spectral obs. 77—12785
I_2 solid charge-transfer complexes, determ. of thermodynamic form. values 80—45540
I_2, solns., visible absorpt. spectra, temp. effects 77—61760
$^{129}I_2$, frozen soln. in o- or p-xylene, Mossbauer effect obs. 80—78637
IBr-benzene in n-decane soln., IR line broadening by chemical exchange 80—87111
InS(Se)(Te), fused, charge transfer nature 77—89757
K atomic beam form. by charge transfer for ion-pair form. expts. 79—59555
$K+Br_2$ (Cl_2), electron transfer crossed beam reaction, energy and ang. differential cross section 79—20358
$K+Br_2(BrI)(I_2)$, stripping reactions at hyperthermal energies 77—16815
$K+Cl_2(Br_2)(I_2)(ICl)(IBr)$, negative ion prod. cross sections 77—531
$K+Cl_2\rightarrow K^{+}(Cl+Cl^{-})$, 5.5—14.0 eV, energy loss, spectrum maxima, mechanism 77—75286
K+F(Cl), quasiclassical charge transfer cross section, rel. vel. depend. 77—19073
$K+K^{+}$ collisions, charge exchange cross section 80—58374
$K+NO_2$, charge transfer reactions, energy and ang. differential cross-sections meas. 80—53125
$K+O_2\rightarrow K^{+}+O_2^{-}$, electron transfer kinematics 77—6903
$K^{+}+Na$, differential scatt. cross section, electronic excitation via. rot. coupling in NaK^{+} 78—13579
K_2+halogen mol., thermal energy mol. beam chemi-ionisation 77—9065
KCl, charge transfer and pair polarisability anisotropy 80—43173
KCl:Cu,Tl, plastic deform., charge exchange of hole centres *(Russian)* 77—11876
Kr, at. beam, partially metastable, composition, charge exchange 79—85914
$Kr+C^{+}(H^{+})(N^{+})(O^{+})(S^{+})$, charge exchange cross-sections *(German)* 77—10753
$Kr^{+}+Kr$, quasi-resonant charge transfer at thermal energies 80—48082
Kr^{+}+molecule, $^{2}P_{3/2}(^{2}P_{1/2})$ doublet ground state reactions at 300K 80—108702
$Kr^{+}+O_2$, charge transfer mech., implication of inner-shell level mixing 77—61852
$Kr^{2+}+H_2(N_2)(O_2)$ (inert gas), charge transfer reaction rate consts. 80—7779
$Kr^{2+}+H_2(N_2)(O_2)(CO)(CO_2)$(methane), charge transfer reactions, rate coeffs. and product-ion distributions meas. 80—104431
$Kr^{2+}+Kr$, symm. reson. double charge transfer, 0.04-20 eV 78—66657
KrHF, ^{83}Kr nucl. quadrupole coupling, charge transfer 80—53012
$Kr^{*}(Kr^{+})+NF_3$, rate consts., electron attachment coeffs., flowing afterglow 78—13578
Li^{+}-H_2O complex, charge transfer theory, Mulliken population, ab initio calc., multiconfiguration scheme 80—106392
$Li+Cl_2(Br_2)$, ion pair form., double differential cross sections, 8-30 eV 78—11507
$Li+F_2(Cl_2)(NO_2)$, $4^{2}S_{1/2}$ excited atom crossed beam collisional ionisation 79—64087
Li+LiH, collinear reactions, SCF correl. diagram for Li_2H 77—70292
$Li^{+}+K$, differential scatt. cross section, electronic excitation via. rot. coupling in LiK^{+} 78—13579
$Li^{+}+Li$, charge exchange, relative differential cross-sections 79—81273
$Li^{+}+Li(Na)(Cd)$, electron capture cross sections 10-60 keV 80—48084
$Li^{+}+Na$, charge exchange, generalised Rosen-Zener model 77—50497
$Li^{+}+Na$, charge transfer and elastic scatt., two state model 78—58805
$Li^{+}+Na$, direct and charge exchange scatt., differential scatt. cross-sections meas. 78—42158
$Li^{+}+Na\rightarrow Li+Na^{+}$, electron transfer collisions time independ. quantum theory with nonorthogonal basis and R-matrix propag. 79—89769
$Li^{3+}+He(C)(Ne)$, K-shell charge transfer cross sections, Bates-Born formalisms 79—45834
LiC_6, intercalated, charge-transfer and non-rigid-band effects 80—44496
LiCl, charge transfer and pair polarisability anisotropy 80—43173
$Li_{1-x}Pb_x$, liq., metal-nonmetal transition, electronic theory 78—79930
Mg-polymer contacts, charge transfer and contact charge spectroscopy 79—56305
Mg+Ar(Xe), plasma, near reson. charge exchange, spectra *(German)* 77—31425
$Mg+He^{+}(He_2^{+})$, inelastic collisions, 2-800 eV, excited state form. 78—94312
Mg^{+}+alkali metal, effective charge exchange cross section, 20 to 1000 eV 77—42398
$Mg^{+}+H^{+}$, Mg^{2+} form. by charge exchange and ionis., cross sections 77—83709
$Mg^{+}+Mg$ and $Mg^{2+}+Mg$, resonant charge transfer, phase interference effect 79—10199
$Mg^{+}+Na(K)(Rb)(Cs)$, charge exchange and excitation processes 78—17772
MgO, dissoc. under heat and electron bombardment 80—7834
$Mo(CO)_6$, MCD spectra, charge transfer transitions 80—95658
$Mo_3S_4(Se_4)$, channel-type, topotactic redox reactions 77—90598
N IV+H charge exchange cross section rel. to intercloud gas 77—45514
N^{-}, form., by double electron transfer, cross-section meas. 78—78806
N^{x+}, (x=1-7), electron loss and capture in He, N_2, Ne and Ar *(Russian)* 78—13600
$N^{+}+Ar(H_2)(N_2)(O_2)(CO)(NO)(CO_2)$, charge exchange, 1-3 keV, $N^{+}(^{3}P)$ and (^{1}D) states 79—36760

charge exchange continued
$N^{+}+H$, charge transfer reaction in astrophys. nebulae rel. to ionization struct. 80—46384
$N^{+}+H_2$, electron capture and ion-loss cross-section, 2.4-24.3 keV 80—58373
N^{+}+inert gas, electron capture (loss) by metastable (ground-state) ions, 2-30 keV 78—25695
N^{+}+methane, charge transfer reaction, dissoc., isotope effects, mass spectra 77—21382
$N^{+}+N_2$ collisions, 2.0 MeV ion energy, electron capture and loss cross section 77—34754
$N^{+}+N_2(H_2)$, total charge transfer cross section, 5-100 keV 79—3561
$N^{+}+O_2$, branching ratio kinetic energy depend. 80—97703
$N^{+}+O_2$, electron capture and ion-loss cross-section, 2.4-24.3 keV 80—58373
$N^{2+}+He$, electron transfer cross-section, <100 eV 78—66654
N_2-He laser, charge transfer pumping at atm. press., in elec. avalanche discharge 79—10286
$N_2+C^{+}(N^{+})(O^{+})$, luminescent charge transfer, metastable and ground state ions 78—42202
$N_2+H_2^{+}\rightarrow N_2^{+}+H_2$, rot. energy distrib., 10 and 25 keV 79—76507
N_2+H^{-}, 1 to 5 keV, production cross sections for 3d,3s,4s,5s states of H 78—33603
N_2+H^{+}, electron capture and loss cross-sections, 1-20 keV *(French)* 77—38728
$N_2+H^{+}(He^{+})$, K-shell ionisation, AES meas. 77—10749
N_2+negative ion, electron-loss cross sections 80—37877
$N_2^{+}+2N_2\rightarrow 2N_3^{+}$, reactions of electronically excited N_2^{+} 77—1915
$N_2^{+}+He$, ion loss cross-section, 2.4-24.3 keV 80—58373
$N_2^{+}+Li(Na)(K)$, 50-1000 eV, crossed beams, electron transfer and excitation 80—14226
N_2^{+}+methane, charge transfer cross-section, low energy 78—58791
$N_2^{+}+O_2$, electron capture and ion loss cross-section, 2.4-24.3 keV 80—58373
$NH_3+H_2^{+}(He^{+})$, dissociative charge transfer reactions, energy transfer depend. 77—25258
NH_3+radical ion, thermal energy charge transfer, reaction mechanism 77—16796
NH_n^{+}+molecule (n=0 to 4), reactions, selected ion flow tube obs. 80—45489
NH_4F, electron distribution and charge transfer in NH_4^{+} ion 78—91291
NO^{+} +molecule, reaction rate consts. meas. 80—7782
NO^{+}, symmetric charge transfer reaction cross section, selected kinetic energies, vibr. states 77—16813
NO+aromatic compounds mixture, charge transfer equilib. consts., adiabatic ionis. energies, entropy changes 78—37738
$NO+Kr^{+}$, charge-transfer reaction rel. to vibr. state of NO^{+} 77—1916
$NO+S^{+}\rightarrow NO^{+}+S+1.1$ eV, rate consts. kinetic energy depend., drift tube meas. 80—7778
$NO^{+}+NO_2^{-}$ neutralisation reaction, spectroscopic study 79—13819
$^{15}NO^{+}+{}^{14}NO$, charge transfer in state selective NO photoionis., mass spectra obs. 80—43119
$NO_2+O^{-}(O_2^{-})$, charge exchange excited NO_2^{-} formation 77—75236
N_2O+inert gas ion, mol. ionis., emission obs. 79—31707
N_2O+Ne^{+}, charge transfer excitation, down to 1 eV 79—45835
N_2O+X^{+}, charge transfer excitation channels, emission cross-sections meas. 77—61851
$N^{2+}(^{2}P^{0})+H$, charge transfer, ab initio CI pot. curves and coupling-matrix elements 80—37878
$N^{3+}(^{1}S)+H$, charge transfer, ab initio CI pot. curves and coupling-matrix elements 80—37878
$N(^{4}S)+N^{+}(^{3}P)=N^{+}(^{3}P)+N(^{4}S)$, gerade-ungerade splitting of N_2^{+} pots., cross sections 77—30987
$Na+Cl_2(Br_2)(I_2)(ICl)(IBr)$, negative ion prod. cross sections 77—531
Na+F(Cl), quasiclassical charge transfer cross section, rel. vel. depend. 77—19073
$Na+H^{+}$, charge transfer cross section and equilibrium fractions, 1-25 keV 80—5616
$Na+H^{+}$, charge transfer processes with plasma gun, Lyman-α radiation exam. 78—46573
$Na^{+}+K$, differential scatt. cross section, electronic excitation via. rot. coupling in NaK^{+} 78—13579
$Na^{+}+Li$, direct and charge exchange scatt., differential scatt. cross-sections meas. 78—42158
$Na^{+}+Ne$, excitation and charge transfer, 0.2-12 keV collision 79—68314
Ne^{x+}, (x=1-8), electron loss and capture in He, N_2, Ne and Ar *(Russian)* 78—13600
Ne-N_2, charge transfer kinetics, weak H^{+} beam effects 78—9243
$Ne+Ar^{2+}$, charge transfer, energy defect and sealing laws 80—48083
$Ne+C^{N+}(N^{n+})(O^{n+})$, charge exchange contribution to K-vacancy production 80—102553
$Ne+H^{+}(He^{+})$, K-shell ionisation, AES meas. 77—10749
$Ne+H^{+}(He^{+})(Ne^{+})$, multiple ionisation of Ne 2s and 2p electrons 80—18918
$Ne+Li^{+1,2,3}$, K-shell ionisation depend. on projectile charge state 77—34743
Ne+proton, charge transfer, target K-shell electron capture, impact parameter depend. 80—102552
$Ne^{+}+CO(CO_2)(N_2)(N_2O)(NO)(O_2)$, charge transfer, thermal energy, product distrib. obs. 78—25656
$Ne^{+}+Co_2$, three dimens. quadrupole ion storage, ion mobility, effect of charge exchange reactions, Monte Carlo calcs. 80—55738
$Ne^{+}+H_2(N_2)(CO)(CO_2)(N_2O)(O_2)(NO)(NH_3)(SO_2)(COS)(H_2O)$, thermal energy, reaction rate coeffs. and product distrib. 79—29333
$Ne^{+}+He$, multiple ionisation of Ne 2s and 2p electrons 80—18918
$Ne^{+}+Kr(Xe)$, thermal energy charge transfer reaction rates, mass spectrometric obs. 78—61000
Ne^{+}+methane(chloromethane)(ethylene), thermal energy, reaction rate coeffs. and product distrib. 79—29333
$Ne^{+}+N_2$, charge exchange, time-resolved emission probe 78—86946
$Ne^{+}+Ne$, quasi-resonant charge transfer at thermal energies 80—48082
$Ne^{+}+Ne$, reson. transitions, direct and charge-exchange excitation 77—19020
$Ne^{+}+O_2\rightarrow O^{+}+O+Ne$, thermal energy charge transfer, energy disposal determ. 79—64099
$Ne^{+}+Zn$, charge exchange and Penning ionisation in pulsed discharge afterglow 79—7007
$Ne^{2+}+H$, charge transfer process, astrophys. plasmas appl. 79—59550
$Ne^{2+}+H_2(N_2)(O_2)(CO)(CO_2)$(methane), charge transfer reactions, rate coeffs. and product-ion distributions meas. 80—104431

charge exchange continued
  Ne^{2+}+He, charge transfer rate coeff. and astrophysical appls. 80−56701
  Ne^{2+}+He(Ne)(Ar), electron transfer cross-section, <100 eV 78−66654
  Ne$_2$+Ar, total integral cross sections for excitation, exchange and dissoc. 80−1044
  Ne$_2$+Kr total integral cross sections for excitation, exchange and dissoc. 80−1044
  Ne$_2{}^+$+Kr(Xe), thermal energy charge transfer reaction rates, mass spectrometric obs. 78−61000
  Ni-polymer contacts, charge transfer and contact charge spectroscopy 79−56305
  O ion+inert gas, small impact parameter scatt., charge distrib. 77−30989
  O ions, non-equilibrium charge state distrib. charge exchange cross-sections in solid targets 80−65109
  O$^+$-O, in F-region, experimental estimate of reson. charge transfer cross-section 77−45231
  O$^-$+O$_2$→O$_2{}^-$+O, cross sections, 0-100 eV *(German)* 77−32785
  O$^-$+O$_2$→O$_2{}^-$+O, cross section kinetic energy depend., rate consts. meas. and Monte Carlo calcs. 80−78701
  O$^+$+H, cold dense H plasma, charge exchange, impurity losses, Monte Carlo simulation 78−34260
  O$^+$+N$_2$, charge exchange collision, rate coeff. and ionosphere implications 80−87224
  O$^+$+N$_2$(H$_2$) 79−3561
  O$^+$+N$_2$(O$_2$), excited ion reactions, charge transfer coeffs. at thermal energy 80−95721
  O$^+$+N$_2$(O$_2$), reaction rates, 300-900K 79−8434
  O$^+$+NO, charge transfer, reaction rates and cross-section determ. 77−60052
  O$^+$+O$_2$, charge exchange collision, rate coeff. and ionosphere implications 80−87224
  O^{2+}+H, charge transfer process, astrophys. plasmas appl. charge transfer process, astrophys. plasmas appl. 79−59550
  O^{2+}+H, charge transfer rate coeff. and astrophysical appls. 80−56701
  O^{2+}+He, electron transfer cross-section, <100 eV 78−66654
  O^{2+}+inert gas, electron transfer meas., 60-200 keV 80−83480
  O$^{4,5,6,7+}$+Ne(Ar)(Kr)(Xe), 10-30 MeV, charge exchange 77−34757
  O^{q+}+Ar, continuum electron capture and loss, 1.6-2.8 MeV/A 78−46443
  O$_2{}^+$, symmetric charge transfer reactions, selected states, photo-ion, electron coincidence 78−73028
  O$_2$+F$^-$(Cl$^-$)(Br$^-$)(I$^-$), 0.2-100 eV, reaction differential cross sections energy depend. meas., exoergicity 77−63902
  O$_2$+negative ion, electron-loss cross sections 80−37877
  O$_3{}^-$+molecule reactions, thermochemistry, electron affinity and rate consts. 78−40040
  O$^+$(^{2}D)+N$_2$, charge exchange rate coefficient, effect of N$_2{}^+$ recomb. on aeronomic determ. 78−88954
  O$^+$(^{2}D)+N$_2$ charge exchange, rate coeff. temp. depend. 80−77179
  OH, in inert gas matrix, H-bonding and charge transfer, fluoresc. 78−25602
  O$^+$(^{4}S)(^{2}D)+Ar(H$_2$)(N$_2$)(O$_2$)(CO)(NO)(CO$_2$), charge transfer reactions, cross-sections meas. 78−92462
  O$_2$−, electron transfer reactions, singlet O$_2$ form. and quenching 77−29002
  ^{16}O^{x+}+Al, energy-loss straggling, charge exchange effects 78−58799
  O^{+*}+O$_2$(N$_2$), metastable ion reactions, rate consts. and ion mobility at 300K 80−95722
  PH$_3$+radical ion, thermal energy charge transfer, reaction mechanism 77−16796
  ^{210}Po, nucl. alpha decay, electron inner shell vacancy creation, semi quantal approach 80−68607
  Pt-polymer contacts, charge transfer and contact charge spectroscopy 79−56305
  Rb, radiatively excited states, ionis. rate coeffs. in two atom collisions 80−43160
  Rb-Cs plasma, electron collision induced charge exchange *(Russian)* 77−68740
  Rb+He$^+$→Rb$^+$+He^0, cross section, 1-36 keV 77−1919
  Ru bipyridine ion, electron transfer limiting efficiency and rate constant meas., step excitation method expt. 79−91929
  Ru complex, (2,2′-bipyridyl)$_3$ruthenium^{2+}, excited-state redox processes, electron transfer theory 79−39126
  Ru complexes, Ru(NH$_3$)$_6{}^{2+}$ and Ru(en)$_3{}^{2+}$ in soln., UV spectra, solvent effects 79−94010
  S$^+$ charge transfer in diffuse nebulae 80−77463
  SF$_6$, equilib. electron-transfer reactions in gas phase involving long-lived neg. ion radicals 78−58807
  SF$_6$+H$^+$(He$^+$), F K-shell ionisation, AES meas. 77−10749
  SF$_6$+X$^-$→SF$_5{}^-$+F+X (X=O, S, F, Br, I), electron affinity of SF$_5$ radical 80−45495
  SO$_3$, electron impact mass spectrometry, proton affinity, ion-mol. reactions 78−3415
  o-semiquinone, radicals, intra- and intermolecular H$^+$ transfer, ESR 77−16840
  Si (111), with chemisorbed Cl and F, electronic energy struct. calcs. 79−78144
  Si+Li$^{+1,2,3}$, K-shell ionisation depend. on projectile charge state 77−34743
  Si^{2+}+H, charge transfer reactions in interstellar medium 77−9789
  SiO$_2$ charge transfer from metallic electrodes 80−15605
  ^{28}Si$^{\bar{n}+}$+Sc(Ti)(Cu)(Ge), K-shell ionisation, projectile charge state depend., theory 78−17786
  Sr+Ca$^+$, laser induced charge transfer 80−53108
  Sr+D(D$^+$), 2.7 to 31 keV, D$^-$ equilib. charge-state fractions 78−17750
  SrII, near IR laser transitions in hollow cathode discharge 80−1194
  T$_2{}^+$+T$_2$, charge transfer reactions rel. to vibr. states 77−9070
  Ta surface, nonstationary heating and oxidation in low temp. plasma flow, heat and charge transfer obs. *(Russian)* 80−104341
  Ta$_x$O$_y$ on Ta, anodic film, electrochem. reactions by tunnel current 77−81340
  Th+X$^+$, X=O, N, N$_2$, CO$_2$, charge transfer cross-section, 1-500 eV 78−82835
  Ti, heat- mass- and charge transfer in high temp. oxidation 79−83369
  Ti XX 80−100067
  Ti+Ar$^+$, charge exchange obs. through spectral line enhancement 79−7005
  TiC, TiN and VC, charge distrib. and bond ionicity 78−63961

charge exchange continued
  U ion beam prod. at 50 keV by charge exchange in gas and metal vapour targets 78−70675
  U+X$^+$, X=O, N, N$_2$, CO$_2$, charge transfer cross-section, 1-500 eV 78−82835
  U^{36+}+N(Ne)(Ar)(Kr), radiative charge exchange, 16, 64, 256 MeV/amu 78−55234
  UF$_6$ on C-coated Pt(Pt-W), mol. negative surface ionisation 78−56913
  UO$_6{}^{6-}$, octahedral uranate group, charge transfer transition and luminesc. 80−97324
  VC, TiC and TiN, charge distrib. and bond ionicity 78−63961
  VO$_4{}^{3-}$, charge transfer transition, bond length effects calcs. 77−83721
  W(CO)$_6$, MCD spectra, charge transfer transitions 80−95658
  WF$_6$, electron and fluoride affinities, ICR spectra 79−39130
  WF$_6$+Na(K) electron transfer, WF$_6{}^-$ form., dissoc. energies, electron affinity 77−19071
  Xe$^+$, symmetric charge transfer reaction cross section, selected kinetic energies 77−16813
  Xe+H$^+$ charge exchange, H spin polarisation 77−61688
  Xe+Xe$^+$, differential cross section, pot. curve fitting reson. electron exchange 77−58118
  Xe$^+$+molecules, ^{2}P$_{3/2}$(^{2}P$_{1/2}$) doublet ground state reactions at 300K 80−108702
  Xe$^+$+O$_2$→O$_2{}^+$+Xe, O$_2{}^+$+Xe→Xe$^+$+O$_2$, charge transfer, photoionisation mass spectra 77−16793
  Xe$^+$+Xe, quasi-resonant charge transfer at thermal energies 80−48082
  Xe$^+$+Xe$^+$, charge transfer and ionisation Xe^{2+} prod. 80−91659
  Xe^{10+}+He(Ne)(Ar)(Kr)(Xe)(Cd)(Na)(Cs), depend. of charge transfer on ionisation pot. 79−64096
  Xe^{2+}+Ar(Xe)(H$_2$)(N$_2$)(O$_2$)(CO$_2$), charge transfer from ground and metastable states 79−31677
  Xe^{2+}+H$_2$(N$_2$)(O$_2$) (inert gas), charge transfer reaction rate consts. 80−7779
  Xe^{2+}+Xe, symm. reson. double charge transfer, 0.04-20 eV 78−66657
  Xe^m+Ne$^+$→Xe$^+$(7s^{2}P$_{1/2,3/2}$)+Ne, in negative flow 80−38857
  Xe^{n+}+Xe, electron transfer cross-sections, 15 keV to 1.6 MeV 79−59557
  Xe$^+$(^{2}P)+Ca(Sr), collisional quenching of metastable states, excitation transfer cross sections 78−66653
  Zn+He$^+$, thermal energy charge transfer reaction, ion states, relative yields 79−45840
  ZnO-polystyrene photoreceptors sensitised by β-Cu phthalocyanine 79−17552
  n-ZnO-rubrene, radical cation reduction, triplet state formation, luminesc. 77−16825
  ZnTe electrode, redox reaction due to complex M(CN)$_6{}^{3-/4-}$ *(French)* 80−89482
  Zr, heat- mass- and charge transfer in high temp. oxidation 79−83369

charge measurement
  see also electrometers
  aerosol particle mass and charge determ. by one electron differentials 79−66368
  aerosols, meas. via variable freq. electrostatic mobility analyser 78−77945
  capacitive discharges, charge transfer meas. 80−52265
  contact-charging apparatus using flexing cantilever 79−80585
  dielectric film, spatial charge distrib. meas. technique 77−32327
  dielectric liquid, new method for charge density meas. 80 4743
  electrets, influence of meas. method *(French)* 77−41637
  electrets, meas. of charge distrib. 77−30184
  electrolyte timing cell and coulometer 80−68216
  electrometers, high-speed general-purpose, features 77−74448
  electron beam charge monitor, single pulse toroidal coil type 78−78036
  electrostatic charge measurement and effects *(French)* 79−64140
  electrostatic charge meter IEZ-P 79−75553
  electrostatic charges meas. and localisation, neutralised during lightning flashes 80−77097
  electrostatic potential distrib. in dielectrics, meas. method 77−26336
  electrostatic potential distrib. in dielectrics, new meas. method *(French)* 77−143
  electrostatic precipitation, charge measurement, positive and negative corona 80−96403
  flare discharge, dielectric coated anode, surface and excess vol. charge meas. 77−11426
  fractional charge, $^1/_3$e, expt. determ. on Nb sphere 79−21694
  fractional charge obs. on Nb ball, exptl. reliability 78−12666
  fractional charge on matter, obs. by mag. levitation of Nb spheres 77−49709
  fractionally charged ions, search in He gas 80−8954
  metal-H system, permeation technique for electrotransport studies 77−7903
  microcoulombmeter, for accelerated ion beams meas., with mean current meas. facility *(Czech)* 77−67476
  microscopic particles using small collector 80−13095
  MIS structure charge distrib., optoelectric determ. methods *(Polish)* 80−39675
  mobile charges in MIS structures, using triangular voltage sweep methods *(German)* 80−4740
  nucleonic dual charge sensitive preamplifier 78−55110
  plasma density IF phase meas. using three-mirror interferometer 78−75414
  polymer foil, charge distrib. determ., thermal pulse technique, meas. accuracy 78 -80287
  polymer powder layers, by electrostatic method *(Russian)* 77−10042
  polystyrene latex particles, suspension in CTAB (Na$_2$SO$_4$), gas bubble surface charge meas. 78 -21100
  rotating sector type instrument, edge effect *(Japanese)* 80−86269
  surface charge, on small gas bubbles, meas. method 78−21100
  surface charge distribution determ. and potential probe meas. anal. 77−10051
  surface charge meas. by vibrating electrode method, ultrahigh vac. apparatus 78−12708
  surface charge measurement by electrostatic induction 78−49807
  textile fibre, moving dielectric 79−75549
  time measurement experiment in phys. education, mass and charge meas. using electronic time counter *(Japanese)* 78−41127
  two-layer dielectric interface polarisation charge expt. 80−15946
  Al-SiO$_2$-Si, charge measurement in MIM and MIS struct., MOS system appl. 78−2572

charge measurement continued
- Hg-polymer interface, contact potential and charge exchange determ. 80–75642
- Pb-acid battery charge determ. from internal impedance 79–96436
- W ions, fractionally charged, search 78–29083
- W particles, search for fractional charge 77–74349

charge-ordered states
- charge and orbital ordering in crystals 78–34738
- collective electronic excitations, low-lying, NQR studies 79–78561
- collective excitations and charge-ordered state 77–28138
- conductivity of charge-ordered systems at const. elec. field 78–19013
- critical temperature of charge ordering in localised state 79–69456
- crystal with intraband electron attraction, electronic spectra and parametric instabilities 79–51504
- electron charge ordering, Peierls distortion, quasi one-dimensional spinless fermion model 79–87050
- electronic excitation spectra in band model, pair correl. effects 77–72829
- electronic spectra and EM props. 78–14683
- Hubbard model, charge-ordered soln. 77–39759
- Hubbard model, doubly degenerate, functional integral approach 79–99711
- Hubbard model, generalised, charge ordering 80–39513
- Hubbard model, half-filled, charge ordered solution local mag. moments, repulsion energy renormalisation 79–61034
- Hubbard model, half-filled, charge-ordered ground state 80–39487
- Hubbard model, two band, mag., orbital and charge ordered states 78–27012
- lattice distortion and statical charge wave theory 77–72828
- magnetic collective excitations and charge-ordered state 77–35876
- magnetic properties 78–18979
- Mott insulator, magnetism and charge ordering 79–60751
- narrow partially filled S-band, charge ordering *(Russian)* 78–76015
- non-conducting chain systems, 3-d Coulomb coupling and charge ordering 78–18980
- nonconducting linear chain systems, 3D Coulomb coupling and charge ordering 78–60075
- orbital-charge ordering in crystals 77–35884
- Orbital-charge ordering in crystals 78–18988
- polar crystal model, instabilities in electron energy spectrum, max. polarity state 79–82534
- supernonradiative phase transition, appl. to paramag. impurities in strong mag. field 79–14898
- TCNQ salts, complex, with aromatic donors, interchain coupling and disorder 78–6314
- TCNQ salts with asymmetric donors, transport props. 79–23953
- CoO, Mossbauer evidence for relax. valence averaging 77–1626
- CsAu, molten, equimolar, structural evidence of ionic nature 80–64882
- Fe_3O_4, magnetite, charge order-disorder and insulator-metal transition 77–20241
- Fe_3O_4, Verwey transition, charge density-phonon condensation 80–65217
- Fe_3O_4, Verwey transition, cond. processes 80–96787
- NiO, Mossbauer evidence for relax. valence averaging 77–1626
- $(Ti_{1-x}V_x)_4O_7$, mag. susceptibility calcs. 78–91850
- YFe_2O_4, Mossbauer spectra of ^{57}Fe in antiferromag. and paramag. states 80–15834

charge storage diodes
- dual dielectric charge storage cells, writing and erasing, differential studies 78–80059
- laser diode 1ns pseudo-random pulse modulation cct. 78–50836
- SAW p-n diode storage correlator, charging process 78–9500
- variable-gap semiconductor, feasibility of use 80–11076
- Si MIS switch diode, charge storage effects, threshold depend. on driving voltage pulse freq. 80–49939
- Si photodetector storage-mode operation 77–39075

charge transfer *see charge exchange*

charge transfer states
- A15 compound trends, self consistent band calcs. 78–79925
- acceptor-donor-acceptor complex, Frenkel excitons and ionic excited states 80–92824
- acceptors, randomly distributed, direct energy transfer via exchange from excited donor 80–65483
- acetic acid-aliphatic amide intermol. H-bonded systems, charge transfer bands 77–58041
- acridizinium ion, fluoresc. quenching by external heavy atom, via charge-transfer complex 78–42112
- alkali halide: $Tl^+(In^+)(Sn^{2+})(Pb^{2+})(Cu^-)$, charge transfer absorpt. band 79–73977
- alkali metal:halogen, charge transfer excitations 79–95815
- alkali metal alloy, charge transfer and percolation 79–95372
- alkyl iodide-$I_{(atom)}$ complex, multiple charge-transfer bands in liquid-phase 77–32776
- alkylammonium iodides, solns., MCD spectra of iodide ions 78–94268
- alkylbenzenes, electronic struct., photoelectron spectra rel. to semiempirical CNDO/S CI calcs. 79–54770
- alloy, binary, charge transfer and alloy binding, Thomas-Fermi-Dirac approx. 77–76775
- alloy, nearly-free-electron, random, charge transfer rel. to stability 78–6316
- γ-aminobutyric acid, cryst., film, matrix IR spectra, low temp., neutral and zwitterion forms. 77–18920
- 14-aminopyridine-I_2, charge-transfer complexes, hyperpolarisability 77–34568
- amorphous semiconductor, charge transport behaviour, model 79–91048
- anthracene:chloranil, charge transfer spectra line shape 79–78700
- anthracene:cyclohexadienyl type radicals, charge transfer reactions 78–52535
- anthracene:tetracyanobenzene charge transfer complex, cryst. struct., temp. effects 80–96508
- anthracene like crysts., charge-transfer electron-exciton bound states, theory 78–10365
- anthracene-d_{10}-s-tetracyanobenzene, rotational mode coupling in phase transition 78–71827
- anthracene-dimethylpyromellitimide, CCT crystals, mag. field effect on fluorescence 78–19543
- anthracene-dimethylpyromellitimide charge-transfer complex, photoconductivity mechanism 77–47860
- anthracene-PDMA, weak donor-acceptor complexes, electron mobility model 80–15511
- anthracene-phenanthreen-TCNB, exciton transport obs. 80–65461

charge transfer states continued
- anthracene-phenanthrene-tetracyanobenzene, CT-cryst., mini-excitons and lattice dynamics, ESR, optical and Raman spectra 80–60406
- anthracene-PMDA, charge transfer cryst., 2K, zero-phonon lines, singlet spectra 78–23484
- anthracene-PMDA crysts., phosphorescence blue shift of charge transfer config. 77–36278
- anthracene-pyromellitic dianhydride, cryst., charge transfer exciton transitions, refl. spectra obs. 78–72540
- anthracene-pyromellitic dianhydride, mol. charge transfer cryst., Raman scatt. meas. 80–29743
- anthracene-pyromellitic dianhydride complex, optical and photoelectric props. *(Russian)* 80–15570
- anthracene-pyrometallitic dianhydride cryst., refl. and absorpt. spectra of singlet charge transfer excitons 80–71442
- anthracene-TCNB, 1:1 charge transfer complex, phase transition at 206K, NMR meas. 79–7690
- anthracene-TCNB charge transfer cryst., phosphoresc. and delayed fluoresc. detected mag. reson. 79–33565
- anthracene-tetracyanbenzene, magnetic resonant modulation of photoconductivity 78–64062
- anthracene-tetracyanobenzene, charge transfer complex, phase transitions, deuteration effect, mag. reson., spectral and thermal meas. 79–4412
- anthracene-tetracyanobenzene 1:1 charge transfer complex, low temp. phase, cryst. struct. 80–6397
- anthracene-tetracyanobenzene charge-transfer complex, EPR of triplet excitons, phase transitions 77–28425
- anthracene-tetracyanobenzene charge-transfer complex, RYDMR of triplet excitons annihilation 78–39448
- anthracene-tetracyanobenzene cryst., triplet exciton annihilation, time correlated delay fluoresc., ODMR 80–39895
- anthracene-trinitrobenzene complex, neat and mixed cryst. and glass opt. spectra 77–40274
- anthracene/TCNB, charge-transfer cryst., fluoresc., 1.2-300K, mobile triplet excitons 78–43913
- anthracenes, anthronyl substituted, solvent-assisted form. of luminesc. intramol. exciplexes 78–25589
- p-(9-anthryl)-N,N-dimethylaniline derivatives, excited emitting states in polar solvents, fluoresc. 78–5263
- benzene:I_2, charge transfer spectra line shape 79–78700
- benzene, reson. Raman effect in gas, liq., and solid phases 79–31531
- benzene-acetone donor-acceptor pair, energy transfer cross sections rel. to generalised oscill. strengths 78–46452
- benzene-Br_2 charge transfer complex, Raman spectra, bending modes, electronic excited states 78–56485
- benzene-I_2, binary soln., charge transfer spectrum 78–90183
- benzenes, para-disubstituted, liq., 2nd order hyperpolarisabilities, regularities, intramol. charge transfer 79–10353
- benzyl radical-halide ion, form. by dissoc. electron attachment in matrix, charge transfer bands 77–16854
- benzyl radicals, monomtheyl- and dimethyl-substituted, electronic spectra and electron affinity 80–63618
- bimolecular mixed-valence metal complex, intramol. intervalence charge transfer 79–76405
- binary alloys, charge transfer and transport props. in tight-binding model 79–82577
- binary compounds, energy gap trends, correl. with electron transfer parameters from optical spectroscopy 80–80174
- carbazole, spin-unrestricted study, donor and acceptor states 78–9077
- CdS:Cu, V, photoluminescence spectra 79–83027
- chlorides, I^- or Br^- doped, optical investigation of atomic hydrogen centres 78–88351
- chloroaluminium phthalocyanine, sublimed layer, IR absorption, vibr. assignments 78–55174
- chlorophyll, photosynthesis mechanism, upconversion, EPR and O_2 evolution data anal. 78–35811
- chymotrypsin, charge relay system, H-bond models, IR spectra 78–64935
- cofacial diporphyrins, electron transfer reactions following picosecond excitation, CT state lifetimes, optical difference spectra 80–25995
- complexes, geometries, CNDO/2 and EHT calcs. 79–36530
- complexes, solid, positron annihilation and ang. correl. meas. 79–87521
- copper phthalocyanine, polycryst. film, charge transfer state and optical spectra *(Russian)* 78–84607
- copper porphine, Xα multiple scatt. calcs., EPR and electronic spectra 78–13426
- coronene-TCNQ, solid complexes, spectra, stoichiometry 78–23435
- CT complex, equilib. distances and stabilisation energy, PCILO calc. 78–41963
- cyanine dye monolayer/p-chloranil crystal, charge carrier injection rate const. determ., energy transfer vs. charge transfer method 79–83031
- p-cyano-dialkylanilines, twisted intramol. charge transfer states, dual fluoresc. 79–36683
- 6-cyanobenzquinuclidine, intramol. electron-transfer excited state 80–58295
- cyclic polyphenylacetylene, thermally excited paramag. props. 77–88614
- cyclophanes, double and triple-layered, triplet state zero field splitting parameters, HMO calc. 77–50366
- dialkylaniline derivatives, twisted intramol. charge transfer states, dual fluoresc. obs. and form., dipole moments 80–18881
- dialkylanilines, p-substituted, twisted internal charge transfer excited state form. 79–22683
- diamagnetic susceptibility, interatomic charge transfer in diatoms, mol. second moments, additivity formulas 78–70961
- dicarbaclosododecaboranes, icosahedral, electron transfer phenomena in isolated borane units 80–18871
- 9,10-dichloroanthracene, quasi 1D α-cryst., exciton transitions, optical refl. spectra obs. 77–81116
- p-dichlorobenzene, charge transfer complexes, NQR shifts 78–55186
- 9,10-dicyanoanthracene, exciplexes, electronic struct. by electro-optical expts. 78–25581
- 1,1′-diethyl-2,2′-cyanine iodide, sensitising dye 77–72602
- trans-4-dimethylamino-4′-nitrostilbene, mol. hyperpolarisability in soln., UV dispersion of charge transfer contrib. 79–31986
- N,N-dimethylaniline, exciplexes, electronic struct. by electro-optical expts. 78–25581
- 1,8(6′,7′-dioxododecamethylene) phenanthrene, intramol. electronic energy transfer, emission obs. 79–31571
- DNA, Hg (II) and Ag (I) complexes in soln., theoret. interpret. of elec. dichroism obs. 80–85347
- donor-acceptor electron transfer kinetics *(Russian)* 79–38029

charge transfer states continued
double charge transfer and two to one charge transfer adducts, energetics 79—82561
dyes in polymer matrices, intramol. charge transfer, electrochromism 79—73901
electron and exciton transfer rates, effect of nucl. degrees of freedom 78—60057
electron donor-acceptor complexes, excited state dipole moments, electro-optical expts. 77—46586
electronic excitation of mols., charge transfer and localisation 79—41119
EPR conversion-rate meas., charge transfer band identification 78—76297
ethane, barrier and one electron charge transfer states in strong orthogonal group function theory 78—13421
ethylene-LiF complex, transfer from ethylene to LiF molecule of 0.056 e 78—29745
exchange coupled ions, electron transfer, optical intervalence transition 80—44556
excited charge transfer systems, in polar solvents, dynamic behaviour obs. 78—58772
exciton transport, low-dimensional in mixed charge transfer crystals, statistical model and expts. 80—65461
extended correlated electronic systems, charge transfer transitions 80—29362
fluorescence, depolarisation, orientation factors, excitation energy transfer between isolated donor-acceptor fluorophore pairs 79—22740
Frenkel exciton-charge transfer state mixing near charged defect model of photocond. 77—51663
graphite intercalation compounds, C_nK, electronic struct. and elec. props. 80—44471
graphite lamellar cpds., ^{13}C NMR studies 80—44936
graphite-DNO_3, intercalation cpd., mol. dynamics 79—28631
group IV, V and VI elements, XPS, bond ionicity, struct. stability and charge transfer 77—44127
haematoporphyrine, complexed with chloranil and tryptophane, energy spectra, transition moments and intermolecular distances 80—72127
Heisenberg antiferromagnetic chain, random, low temp. thermodynamic props. in zero mag. field 80—34657
hexacyanobenzene-naphthalene, charge transfer triplet states, electron distrib., ESR 77—3388
hexamethylbenzene charge-transfer complexes, heavy atom effect on radiative and radiationless transitions 78—25607
hydronaphthyl radicals embedded in naphthalene cryst., optical transition energies and ionisation energies 80—78595
impurity centre-external elec. field interaction, charge transfer processes influence 78—87944
indole, aq. alkaline soln., charge transfer, luminesc. obs., 77 and 300K 79—69876
inert gas-halogen atom contact charge transfer interaction, UV transient absorption following flash photolysis 79—61879
insulators, charge transfer, density functional approach 80—44492
insulators, charge transfer processes influence on cryst. field 80—92865
insulators, tightly bound, collective excitations 79—51492
inter-electron repulsion integrals for three open shell configurations in cubic symmetry 78—90061
intermolecular interactions, PCILO method for fixed wavefunctions 78—17571
intervalence charge transfer transitions, solvent effect, appl. to Ru complexes 77—75127
intramolecular, electron propagator method 77—34560
intramolecular electron transfer rate, purely electronic effects, simple model Hamiltonian 77—10592
ion equilibrium negative charge state fractions 78—90288
IV-VI compounds, XPS, bond ionicity, struct. stability and charge transfer 77—44127
lanthanide, trivalent, hypersensitive transitions, intensity parameters, charge transfer mixing 77—55498
lanthanide-porphyrin complexes, upper $\pi\pi^*$ electronic states, fluoresc. 80—83410
linear crystal, donor-acceptor complex, Frenkel excitons and ionic excited state mixing 79—99485
linear molecular crystal, effect of mixing between Frenkel excitons and charge transfer states on charge carrier transfer 79—33242
linear molecular crystal, mixing of Frenkel excitons and ionic excited states 77—15771
linear molecular crystal, mixing of Frenkel excitons and ionic excited states 77—15772
liquid, electron-hole interactions and double proton transfer, picosec. laser obs. 79—45773
liquid, low-viscosity, Forster kinetics breakdown, time-depend. rate const. 79—86033
liquid alloys, electron charge transfer 77—1388
liquid mixtures, associating, mol. hyperpolarisability, SHG 77—552
liquid semiconductor, metal-insulator transition model 77—1368
localisation and local phenomena in excited and ionisation stationary states 77—34563
luminescent system, orientation factor in conc. effects due to nonradiative energy transfer 80—25425
mesitylene:tetracyanoethylene, charge transfer spectra line shape 79—78700
metallic alloy, binary, ordered and disordered, transfer of charge 77—15785
methacrylate polymer, carbazolyl substituted, excimer and charge transfer complex trapping of excitons 80—34367
methanol, effect of hydrogen bonding on Raman spectrum 79—18197
methiodides of nitrogen heteroaromatics, frequencies of multiple charge transfer bands 79—94009
methylated benzene + tetracyanobenzene, fluorescent exciplex form., electronic relax. 80—5573
1-methylpyrene, fluoresc. quenching by Cu^{2+} in micellar system, general kinetic model 80—32753
mixed donor-acceptor stacks, mag. gap and partial charge transfer, VB calc. 78—76008
mixed valence system, far IR intervalence tunnelling transition, vibronic coupling model 78—58646
molecular charge transfer complex, Raman scatt. intensity enhancement model 79—13720
molecular charge transfer complexes, mol. and cryst. struct. 78—62942
molecular crystal, charge transfer biexciton spectra, theory 77—51664
molecular crystal, charge-transfer electron-exciton bound states, theory 78—10365

charge transfer states continued
molecular crystal, electronic transport mechanisms, asymmetry role 78—6370
molecular crystal, Frenkel excitons, effect on charge carrier transfer 78—79936
molecular crystal, mixing between Frenkel excitons, and charge transfer states, effect on charge carrier transfer 77—89707
molecular crystal, multicomponent, energy migration master eqn. 80—16075
molecular crystals, charge transfer exciton-phonon interactions 77—84857
molecular crystals, charge-transfer electron-exciton bound states 77—43543
molecular electron-donor-acceptor complexes, solvent effect on charge transfer absorpt., thermodynamic props. 77—83615
molecular pair, fluoresc. depolarisation, using stochastic Liouville eqn. with radiative terms 80—16074
molecule, π-bonded, polarisability, atom monopole-dipole interaction model with charge transfer 79—22860
molecules adsorbed on metal surface, giant Raman scatt. mechanisms 79—51960
monolayer assemblies, molecular cooperation in photo-induced electron transfer 79—73985
Mott-Hubbard insulator, one-dimens., charge transfer absorpt. 79—37958
multiply-ionized species, thermal energies, in astrophysical plasmas 78—33596
myoglobin , oxyhaeme complex, single cryst., visible spectrum, electronic struct., coord. geometry 78—44456
naphthalene:1-hydrodynaphthyl, cryst., charge transfer optical transitions 77—44027
naphthalene, inclined dimers, transition energies and moments, excitation energy, four-electron MO-CI treatment 77—42237
naphthalene charge transfer complexes, cryst., vibr., factor group splittings 79—7658
naphthalene charge transfer complexes, orientational disorder, spt. ht. meas. 79—46813
naphthalene TCNE π-π three mol. complexes, absorpt. spectra, assoc. consts., extinction coeffs. *(German)* 77—35465
naphthalene-TCNB, charge-transfer cryst., donor mol. orient. and dynamics 79—32926
naphthalene-TCNE π-π three mol. complexes, UV-visible spectra assoc. const., extinction coeff. determ. *(German)* 77—35464
naphthalene-TCPA charge transfer triplet states, electron-phonon coupling 79—38601
naphthalene-tetrachlorophthalic anhydride charge-transfer cryst., electronic states 77—32415
naphthalene-tetracyanobenzene, charge transfer complex, phase transitions, deuteration effect, mag. reson., spectral and thermal meas. 79—4412
naphthoquinone series charge transfer complexes, cryst. and electronic structs. 79—73474
nitrile complexes, RCN...Cl-Cl′ and RCN...$HCCl_3$, charge transfer and distrib., NQR 77—12244
p-nitroaniline, exciton level directional dispersion, absorpt. band profiles 78—48192
p-nitroaniline, mol. hyperpolarisability in soln., UV dispersion of charge transfer contrib. 79—31986
nitroanilines, hyperpolarisability, intromolecular charge transfer effects 77—54624
nucleic acid-TCNQ complex, charge transfer interaction 80—3576
one-dimensional system, energy and charge transport theory *(German)* 80—15506
organic charge transfer complexes, refl. spectra, excitons 79—47477
organic charge transfer salts, valence bond theory 79—73473
organic charge-transfer salts, comparison of ESR spectra 80—50164
organic donor-acceptor compounds, incomplete charge transfer stability 78—30883
organic linear chain cpds., diffuse $4k_F$ refls., small intramolecular Coulomb interaction 80—34376
organic molecules, conjugated, nonlinear props. of new class of cpds. 79—41413
organic salts, neutral-ionic interface, energy states and mag. props., VB anal. 79—4537
organic salts, strongly correlated, interband absorpt., long-range Coulomb interaction 79—4525
pentamethylbenzene-TCNB, charge transfer triplet states, electron distrib., ESR 77—3388
phanes, glassy and cryst., ODMR meas. 79—19812
phenanthrene-PMDA, cryst., triplet charge transfer state symmetry 77—72836
phenanthrene-PMDA, spin polarization of charge-transfer excitons, EPR meas. 79—19766
phenanthrene-pyromellitic acid dianhydride, single cryst., EPR, delocalised and localised charge transfer excitons 77—85545
phenanthrene-pyromellitic dianhydride, single cryst., charge-transfer triplet excitons, spin polaris. 79—11069
phenothiazine derivatives, semicond. elec. props., optical spectra, and EPR 80—103693
photoluminescence of solutions, decay and self-depolarisation 79—24351
phthalimide derivative-tetramethyldiaminodiphenylmethane exciplexes, luminesc. props. 77—68070
phthalocyanine, optical density spectra, charge transfer states 79—95800
pigment associations, conc. effects, luminesc., absorpt. spectra and dichroism obs. 80—1007
pigments of visual and purple membranes, charge stabilisation mechanism 79—34500
poly(halo-N-vinylcarbazoles):2,4,7-trinitro-9-fluorenone charge transfer complexes, dark DC cond. 80—39626
poly(n-vinylcarbazole)-trinitrofluorenone films, charge carrier trapping 78—14846
poly-2,4-hexadiyn-1,6-diol bis(p-toluene sulphonate), exciton theory of excited states 77—80733
poly-p-phenylene, charge transfer complexes, elec. cond. 79—91031
polyacetylene:I charge transfer complex, struct. 79—74052
trans-polyacetylene, halogen doped, elec. cond. 79—19589
polyacetylene, soliton form. 79—76540
polyaromatics, elec. cond. correl. with chem. struct. and synthesis, charge transfer complexes *(German)* 80—15514
polycrystalline charge-transfer complexes, NMR spin-lattice relax. *(French)* 77—32279
polymer films, electret state and adsorption during injection 79—69770
polystyrene-metal contact-charge-exchange expt., charge induced relaxation 77—4309

charge transfer states continued
polyvinylidene fluoride drift mobility meas., I_2 charge transfer from surface charge decay technique 80−49744
potassium chloranil, IR spectra, mag. and optical props., phase transition and solvation 77−43983
potassium oxalate monohydrate:VO^{2+}, cryst., IR absorpt. 80−55134
n-propylhalides, gauche conformer stability, exchange interactions effects 79−13817
proteins, electron transfer mechanism 79−96510
PTZ:PMDA, purification, growth, struct., optical and elec. props. 80−54216
PVC thin films, pure and I doped, photoconductivity study 80−44646
pyrazine, intensity of intercombination transitions, influence of n-σ-type complex form. *(Russian)* 77−26980
pyrene picrate, charge transfer complex, thermally stimulated discharge current 79−78610
pyrene-tetracyanobenzene, charge transfer complex, phase transitions, deuteration effect, mag. reson., spectral and thermal meas. 79−4412
pyridine iodine complexes, charge transfer complexes, vibr. spectra, laser Raman obs. 80−52990
pyridine-bromine charge transfer complexes, Raman spectra 77−6788
pyridine-$I_2(Br_2)$ charge transfer complexes, vibr. spectra, vibronic contrib., intensity enhancement 80−53048
pyridine-I_2(ICl), charge-transfer complexes, hyperpolarisability 77−34568
pyridine-I_2 charge transfer complex, hyperpolaris., SHG obs. 77−553
quartz, rose, charge transfer mechanism for origin of colour, EPR and optical expts. 78−52537
rare earth ions, trivalent, in O-dominated host, high energy states, reflectance spectra 77−69849
rare earths, trivalent, 5d states charge transfer and intershell spectra, separation and overlap 78−10966
rare gas adsorbates on simple metals, optical excitation, configurational switching, charge transfer 80−107643
retinal, highly polar excited electronic states, electron transfer 78−48757
rhodamine 6G+BBOT donor-acceptor system, intermol. electronic energy transfer 78−17702
rhodopsin, bathochromic shift origin 78−31767
semiconductor electrode, surface state charge transfer in photoelectrolysis of water 79−28405
spectral sensitisation, electron and energy transfer mechanisms, review *(German)* 79−39172
spectral sensitization theory, review *(German)* 79−39174
stilbene derivatives, hyperpolarisabilities, four-wave mixing and SHG meas. 77−83925
styrene derivatives, hyperpolarisabilities, four-wave mixing and SHG meas. 77−83925
surfactant adsorption on metal surface, effect on electrochem. reaction kinetics 80−40703
TCNE aromatic donor/acceptor complexes, reson. Raman excitation and absorpt. profiles, model theory 77−18982
TCNE electron donor/acceptor complexes, photoionic dissoc., photocurrents 77−14502
TCNE-benzene, charge-transfer complex, change of C≡N and C=C band intensities 77−88448
TCNE-paraxylene, charge-transfer complex, change of C≡N and C=C band intensities 77−88448
TCNE-stilbene complexes, and analogs, charge transfer energy calc. isomer prediction 78−21854
TCNQ, charge transfer complexes, changes in valence electronic structure 80−7477
TCNQ, semiempirical CNDO calcs. of electronic struct. and absorpt. spectra 78−995
$(TCNQ)_2$, dimeric interactions, MO calcs., applicability to crystal struct. 80−75215
TCNQ alkali salts, charge transfer enhanced IR absorpt. spectra 77−28558
TCNQ alkaline salts, in dimethylsulphoxide, and aq. solns., Raman and IR spectra 78−46344
TCNQ anion radical charge transfer salts, semiconducting behaviour 79−11118
TCNQ charge transfer complexes, elec. cond. 79−38058
TCNQ complex, Adn $TCNQ_2$, nuclear-spin-lattice relaxation 80−39886
TCNQ complex with 5-phenyl-[1-thiol]-3-selenol-2-thione, charge-transfer salt, cryst. and mol. struct. 80−33986
TCNQ derivatives, intramol. charge transfer, electronic absorpt. spectra obs., electron density calcs. 77−65490
TCNQ donor-acceptor complexes, refl. and absorpt. spectra 79−73965
TCNQ salt, HMTTF-TCNQ, Madelung energy, intermol. charge transfer, 1-dimens. disorder 79−7572
TCNQ salt, K-TCNQ, single crystal, charge transfer band interpretation, refl. spectrum obs. 80−25353
TCNQ salt, NMP-TCNQ, X-ray diffuse scatt. rel. to charge transfer 77−80496
TCNQ salt, Rb-TCNQ, ^{14}N NQR, Zeeman perturbation study, charge transfer 78−39438
TCNQ salts, charge transfer, mode shift study, Raman scatt. *(German)* 79−28731
TCNQ salts, charge transfer and cond. 80−20164
TCNQ salts, charge transfer and ionic bonding 77−39558
TCNQ salts, complex, with aromatic donors, interchain coupling and disorder 78−6314
TCNQ salts, conducting, Raman spectra, estimation of degree of charge transfer from vibrational frequencies 80−50344
TCNQ salts, K(TCNQ), $Ba(TCNQ)_2$ and $Ca(TCNQ)_2$, electronic absorpt. spectra, vibronic struct., charge transfer bands 79−24331
TCNQ salts of 1:1 stoichiometry, kinetic models of form. 79−46596
TCNQ salts of ionene polymers containing triethylenediammonium or 4,4′-bipyridilium ring, chem. struct. correl. with cond. 79−91032
TCNQ salts with alkali metals, intensities of IR absorpt., electronic transfer magnitude 78−6691
TCNQ-NMP, incomplete charge transfer, NMR relax. and line-shift meas. 80−20485
TCNQ-NMP, nucl. relax. and spin dynamics 78−52370
TCNQ-perylene, electronic absorpt. spectra, vibronic struct., charge transfer bands 79−24331
$TCNQF_4$, charge transfer complexes and salts, C(1s) and N(1s) XPS anal. of shake-up satellites 77−14492
terylene film, electret state prod. using electrochem. injection, adsorbed states, frozen field 79−91344
tetracene, double quantum external photoelec. effect 79−87564

charge transfer states continued
tetracene, optical obs. of charge transfer 78−35199
1,2,4,5-tetracyanobenzene complexes, electron donor-acceptor interaction, ionic photodissoc. yield 79−6975
tetracyanoethylene(d), charge-transfer complex, fluoresc. quantum field and decay time 78−42107
tetracyanoethylene charge transfer complex, nonradiative decay of excited states, D isotope effect 79−31580
tetracyanoethylene-benzene(-toluene), and isotopic forms, excited charge-transfer state nonrad. decay, vibrs. role 78−82765
tetracyanoethylene-hexamethylbenzene, electron-donor/acceptor complex, reson. Raman scatt. 77−24831
di-(tetraethylammonium)tetrahalomanganate, mag. circular and linear dichroism obs. 80−29725
N,N,N′,N′-tetramethyl-p-phenylenediamine-p-chloranil, soln., optical spectra, temp. and environment effects 79−54861
tetrathiotetracene, charge transfer state parameters, evaluation by mag. field effect *(Russian)* 80−10924
TGS:Fe^{3+} and aq. solns., optical absorpt. spectra 79−82997
three open shell configs., inter electron repulsion integrals 77−55499
TMBP.HCNB and TMBTP.HCNB complexes, elec. and mag. props. 78−6512
TNF-carbazolyl compound charge transfer complexes, equilib. consts. 78−64877
transition metal alloys, vol. corrected isomer shifts 78−39470
transition metal carbides, charge transfer from XPS core level chem. shift anal. 77−72837
transition metal complex anions, ligand-bridged, binucl., reson. Raman spectra 78−42067
transition metal ion pairs, simply reducible symmetry group crystal fields, kinetic exchange theory 80−39541
transition metal-Al, X-ray spectra, electronic structure 79−78793
p-tricyanovinylphenyldicyanomethide ion, donor props., cyclic voltammetry and π-complex form. 80−88520
Triton X100-water-coumarine 1-rhodamine 6G, micellar dye soln., energy transfer 80−45581
tryptophan, aq. alkaline soln., charge transfer, luminesc. obs., 77 and 300K 79−69876
tryptophan, aq. soln. charge transfer, luminesc. obs., 77 and 300K 79−69875
TTF_x $TseF_{1-x}$TCNQ solid soln., DC conductivity, struct. 78−10423
(TTF^+) radical cation, optical props. in mixed-valence and monovalent halide salts and solns. 79−61399
TTF, TTF-TCNQ, $(TTF)_7I_5$ and TCNQ, Raman scatt. and charge transfer 77−69817
$(TTF)_{12}(SCN)_7$ and $(TTF)_{12}(SeCN)_7$, charge-transfer salts, elec., mag. and optical props. 77−43575
$(TTF)_2$, dimeric interactions, MO calcs., applicability to crystal struct. 80−75215
TTF halides, charge transfer effect on internal modes, Raman scatt. 80−25392
TTF salts, charge transfer, mode shift study, Raman scatt. *(German)* 79 28731
TTF-(2,5-diethyl)TCNQ, cryst. and mol. struct. temp. depend. 77−35531
TTF-$Br_{0.79}$, charge transfer and ionic bonding 77−39558
TTF-TCNO, optical evidence for Coulomb interactions, review 78−6704
TTF-TCNQ, and related cpds., partial charge transfer and CDW modulation 79−95349
TTF-TCNQ, charge transfer, mode shift study, Raman scatt. *(German)* 79−28731
TTF-TCNQ, charge transfer change with press. 80−39564
TTF-TCNQ, charge transfer determ. from spectral line shift using Raman scatt. 80−25392
TTF-TCNQ, covalon conduction 78−10427
TTF-TCNQ, dimeric interactions, MO calcs., applicability to crystal struct. 80−75215
TTF-TCNQ, Madelung energy, electronic struct. *(Russian)* 78−6253
TTF-TCNQ, mixed valency in organic crystals *(Japanese)* 79−78051
TTF-TCNQ complex, trans-diethyl-dimethyl TTF-TCNQ, one-dimens. cond. 80−96853
TTF-TCNQ complexes, charge transfer, X-ray photoelectron spectra determ. 77−73210
TTF-TCNQ crystal, charge transfer, dipolar polaris. binding energy 77−80754
TTF-TCNQ series, cryst. struct., elec. cond., and EPR meas., steric factor effects 80−19789
TTT, dark cond. and photocond. effect of strong mag. field, at charge carrier injection *(Russian)* 79−69607
TTT, dark injection current, sign inversion of low mag. field *(Russian)* 79−73602
TTT, neutral, cation and conducting complex reson. Raman spectra, vibr. lines, charge transfer 79−4794
TTT salts, charge transfer salts, optical props. 79−61403
TTT salts, charge transfer salts, optical props. 79−73970
TTT salts, IR spectra, mixed-valence salts 80−40121
TTT-$I_{1.6}$, dimensionality and disorder 77−66160
twisted intramol. charge transfer states, dual fluoresc. 79−36683
two-centred bonds, CNDO calcs. of electrostatic energy components, complexing effects 77−18791
uranocene, reson. Raman spectra, anomalously polarised electronic band, energy level assignment 79−59451
uranyl complexes, MCD spectra, electronic struct. of lowest excited states *(Japanese)* 79−27014
vanadyl phthalocyanine, sublimed layer, IR absorption, vibr. assignments 78−55174
vinyl acetate, model for exciton theory of excited states in poly-2,4-hexadiyn-1,6-diol bis(p-toluene sulphonate) 77−80733
vinyl polymers quenched with electron donor (acceptor) in soln., ionic photodissoc. 79−11800
X-ray photoelectron spectra of solids, satellite lines *(French)* 77−36363
ytterbium etiophorphyrin, electronic energy transfer with porphines and metalloporphyrins, luminesc. 77−474
Ag halide photochromic glass, darkening mechanisms under pulsed laser excitation 78−25938
AgCd, charge transfer, core-electron binding-energy shift 80−2676
$Ag_xMo_3S_4$, chevrel phase, charge transfer and valence electron conc. 78−6029
Ag_2SO_4:CrO_4^{2-}, polarised electron spectrum assignments, red colour explained 77−85753
Al-Mg alloy, charge transfer, X-ray emission spectra exam. 77−47774

charge transfer states continued

- $AlBr_3.SrBr_3$, $AlBr_3.BiBr_3$ complexes, NQR 77—20747
- α-Al_2O_3:V^{3+}(V^{4+})(Co^{3+})(Co^{2+}), optically and thermally stimulated reactions, absorpt. spectra 80—80825
- Au-Cs(Mg)(Rb)(Zn), charge transfer, Mossbauer effect ^{197}Au isomer shifts, XPS valence-band spectra 80—2676
- Au-M (M=Cd, In, Sn, Sb, Te), charge-transfer and valence-band behaviour using ^{197}Au Mossbauer and X-ray photoemission spectra 79—60695
- Au-Te, elec. field gradients and charge transfer, Mossbauer spectra 80—25268
- $AuAl_2(Ga_2)(In_2)(Sn_2)(Sb_2)(Te_2)$, core-level binding energy shifts and charge transfer 80—25268
- BaO-Al_2O_3-B_2O_3-V_2O_5 glass, spectra, oxidation-reduction behaviour, DC cond. 77—76814
- BaO-B_2O_3-SiO_2:Ti^{3+}, optical absorpt. spectra 78—72564
- $Ba_{1-x}Sm_xS$, electron config. of Sm ions, X-ray L-absorpt. spectroscopy 80—60715
- Bi, oxidation, charge transfer obs. from final state changes 77—51703
- Br_2, organic solvent effects on Raman parameters 79—26998
- $C_{6.6}FeCl_3$ intercalation compound, charge transfer, acceptor sites, XPS study 80—49218
- $CaFe_2^{2+}Fe^{3+}Si_2O_8(OH)$, Mossbauer spectra, temp. depend. electron delocalisation 80—20567
- $CaFeO_3$, charge disproportionation, Mossbauer obs. 78—2778
- Ca_2PO_4Cl:MnO_4^{3-}, polarised electronic spectrum 77—52137
- $Ca_{1-x}Sm_xS$, electron config. of Sm ions, X-ray L-absorpt. spectroscopy 80—60715
- Cd etiochlorin complex, visible spectrum, intracomplex electron phototransfer, vibr. effects 79—72330
- Cd_2 as 470 nm absorber, multiconfig. SCF calcs. 80—32731
- $CdBr_2$:Fe^{2+}(Co^{2+})(Ni^{2+}), charge transfer near UV spectra, 4.2K, mag. circular dichroism 78—80378
- $CdCl_2$:Fe^{2+}(Co^{2+})(Ni^{2+}), charge transfer near UV spectra, 4.2K 78—80378
- CdF_2:Eu^{3+}, luminesc., charge transfer states 79—33799
- CdS, Wannier exciton-ionised donor complex, binding energy 80—44509
- Cd^*_2, 470 nm absorber, multiconfiguration SCF calcs. 80—27963
- $Co_{49.6}Al_{50.4}$, Compton scatt., 59.54 keV γ-rays, charge transfer study 78—68578
- $Co_{1-y}Fe_{2+y}O_4$, role of vacant and chemisorbed O and charge transfer effect 78—79868
- $^{57}CoMn_2O_4$, after effects of orbital electron capture 79—73870
- $^{57}CoY_2O_4$, after effects of orbital electron capture 79—73870
- Cs alloys, charge transfer insulators, mechanism, resistivity 78—80070
- CsAu, band struct. and charge distrib., semicond. and metallic behaviour 77—20238
- Cu complex, bis(triphenylphosphine) phenanthroline copper (I), luminesc. spectra, decay times 80—60648
- Cu complex phthalocyanine, optical density spectra, charge transfer states 79—95800
- Cu-Zn, charge transfer, core-electron binding-energy shift 80—2676
- $CuM_2X_4.2D_2O$, MX=alkali or ammonium halide, quadrupolar interaction, 4-300K, reorientation 79—73848
- $Cu_xMo_3S_4$, chevrel phase, charge transfer and valence electron conc. 78—6029
- ^{64}Cu decay in Cu-Ag, electron density change 79—99519
- $EuCl_3.6H_2O$-$NdCl_3.6H_2O(HoCl_3.6H_2O)$, in DMSO soln., $Eu^{3+}\rightarrow Nd^{3+}(Ho^{3+})$ radiationless energy transfer 80—5499
- $Eu(NCS)_3$ solns., luminesc. quenching of Eu^{3+}, charge transfer states 77—90190
- $Eu_{1-x}Sm_xS$, electron config. of Sm ions, X-ray L-absorpt. spectroscopy 80—60715
- (Fe, Ti) silicate glasses, optical absorption and Mossbauer spectra 80—55136
- Fe complexes, Fe (III) bis(dithiocarbamato) iodides, transferred hyperfine interactions and mag. ordering 77—20759
- Fe-Y(Th)(Zr), amorphous, charge transfer and mag. props., ^{57}Fe Mossbauer spectra 79—19719
- $Fe_{49.7}Al_{50.3}$, Compton scatt., 59.54 keV γ-rays, charge transfer study 78—68578
- $FeBr_4^-$, in various solvents, $^4A_1$ ^4E d-d band reson. Raman spectra, solvent depend. 80—55085
- $Fe_{3-x}Co_xO_4$, charge transfer, ion distribs., Mossbauer effect 77—20767
- Ga complex, photoluminesc. spectra, $\pi\rightarrow\pi^*$ and charge transfer L→M transitions, Stokes shift 78—64407
- GaAs:Fe, impurity atom charge exchange, Mossbauer spectroscopy 79—47050
- $GaAs$-Ta_2O_5, charge transfer, influence of field-aided thermionic emission 79—61769
- GaP:Fe, impurity atom charge exchange, Mossbauer spectroscopy 79—47050
- GaX_3, (X=Cl,Br,I), charge transfer spectra 79—76441
- GdFe(Co), amorphous film, XPS meas. 79—87295
- $Gd_xZr_{1-x}O_{2-x/2}$:Tb^{3+}(Eu^{3+}), energy transfer, luminesc. 79—51999
- Ge-$Na_2S_2O_3$ interface anodic oxidation electron transfer 79—56304
- H^+ in $(H_5O_2)^+$ and $(H_3O_2)^-$, CNDO/2 simulation 79—94054
- H_4, excited potential energy hypersurfaces, trapezoidal geometry, rel. to photochem. 2s+2s processes 77—30797
- H_n^+ (n=3,5,7,9,11), stability, struct., ab initio MO calcs. 78—74810
- H_2O-$(HF)(F_2)$ complexes, CNDO/2 calcs. for electronic struct. and props. 78—25442
- I complexes, charge transfer states, Mossbauer spectra 80—15907
- I complexes, ICl.L (L=organic radical), charge transfer and quadrupole-interaction consts. calc. 77—10590
- In complex, photoluminesc. spectra, $\pi\rightarrow\pi^*$ and charge transfer L→M transitions, Stokes shift 78—64407
- $In_xMo_3S_4$, chevrel phase, charge transfer and valence electron conc. 78—6029
- IrF_6, in mixed crysts., Jahn-Teller effect, $\Gamma_{8g}(t_{2g})^3$ state, 6800 Å 78—76032
- IrF_6, ligand field theory analysis of spectra 79—72248
- KCN, ionic mol. cryst., exciton struct. 78—79935
- KCl:I , H, fluorescence of interstitial H-centres 79—73987
- KMF_3, M=Mg, Ni, Co, Mn, reflectivity, 8-60 eV, excitonic struct. 77—20871
- $LaCoO_3$, structural phase transition involving changes in spin and valency 78—79765
- La_2O_2S:Eu, high press. effect on luminesc. efficiency and lifetime, charge transfer absorpt. 80—66266
- La_2O_2S:Yb^{3+}, charge transfer type luminesc. 79—33797
- $LaPO_4$:Yb^{3+}, charge transfer type luminesc. 79—33797

charge transfer states continued

- Li Al, electronic struct., mol. cluster calc. 78—14649
- Li_5B_4, molecular and electronic struct. 80—20107
- $LiBr$:Cu^{2+}(Ni^{2+})(Co^{2+})(Fe^{2+})(Mn^{2+}), optical absorpt., charge transfer spectra 80—2797
- LiC_6, intercalated graphite, band struct. determ. by angle-resolved photoemission 80—45203
- $LiCl$:Cu^{2+}(Ni^{2+})(Co^{2+})(Fe^{2+})(Mn^{2+}), optical absorpt., charge transfer spectra 80—2797
- Lu_2O_2S:Yb^{3+}, charge transfer type luminesc. 79—33797
- $LuPO_4$:Yb^{3+}, charge transfer type luminesc. 78—64392
- $LuPO_4$:Yb^{3+}, charge transfer type luminesc. 79—33797
- Mg_2, Mg_2^+, electronic struct., pot. energy curves, multiconfig. SCF calcs. 78—5124
- MgO:Ni, optical absorpt. spectrum in mag. field, and 2p-3d charge transfer 77—52141
- MnO, SCF CI calcs., ground and first excited states, bonding mechanism 77—14347
- N_2 fixation, semiempirical INDO study 80—16898
- NH_3-$(HF)(F_2)$ complexes, CNDO/2 calcs. for electronic struct. and props. 78—25442
- NH_3-lithium halide complex, ab initio calcs., Li bond rel. to H bond 77—14343
- NH_4Cl:$[MoOCl_5]^{2-}$, single cryst., struct. investigations 77—66524
- NO^++metal atom reaction, obs. using magnetically confined afterglow 77—34750
- Na_3, EPR spectrum, Ar matrix, bonding models 77—14462
- $Na_2MoO_4(S_4)(Se_4)$ crystals, charge transfer spectra of MoX_4^{2-} complexes 80—54658
- $Na_2O.3B_2O_3$, effect of Fe_2O_3 conc. and temp. on UV absorption 77—16340
- $Nb_3Al(Ge)$, bonding, electronic charge distribs. and struct. transform. from self-consistent pseudopotentials 79—69054
- Ni, (001) surface, local density of states, asphericity of pot. and charge transfer, ab initio self-consistent calcs. 79—15064
- Ni (111) and (110), laser-induced charge transfer to adsorbed CO, photoemission expts. 80—59798
- NiF_2, ESCA, charge transfer satellite struct., hole state localisation intensity depend., MS-MO calc. 77—66139
- PbI_2 intercalated with organic mols., energy band splitting *(Russian)* 78—76027
- Pd-Zr alloy, activity coeff. rel. to electronic props. *(German)* 77—20084
- $PdBr_n(H_2O)_{4-n}^{2-n}$, electronic absorpt. spectra, band assignments 78—50553
- $PdCl_n(H_2O)_{4-n}^{2-n}$, electronic absorpt. spectra, band assignments 78—50553
- Pt-Zr alloy, activity coeffs. rel. to electronic props. *(German)* 77—20084
- $PtCl_n(H_2O)_{4-n}^{2-n}$, electronic absorpt. spectra, band assignments 78—50553
- $Rb+Rb^+$, total resonant charge transfer cross section determ. using model pot. simulation 79—64073
- RbC_8, intercalated graphite, band struct. determ. by angle-resolved photoemission 80—45203
- RbCl:I, H, fluorescence of interstitial H-centres 79—73987
- $RbMnF_3$, reflectivity, 8-60 eV, excitonic struct. 77—20871
- Ru complex, (2,2′-bipyridyl)$_3$ruthenium^{2+}, excited-state redox processes, electron transfer theory 79—39126
- Ru complex, Ru(II)-polypyridine, excited charge transfer states, multiple emissions 79—3468
- Ru complexes, $[Ru(bipy)_n(pq)_{3-n}]^{2+}$ mixed-ligand, electronic absorpt. and emission spectra meas. 80—71441
- Ru dimers, mixed-valence, electron transfer rate consts. calc. from intervalence transfer absorpt. bands 79—81164
- $(SN)_x$, electronic struct., X-ray and UV photoemission obs., OPW and pseudopot. calcs. 78—6832
- $(SN)_x$, electronic struct. and opt. props. 78—6256
- $(SN)_x$, quantum chem. calcs. of electronic struct. 78—6257
- S_2N_2, gas phase and solid state core level XPS 80—66401
- S_4N_4, solid state core level XPS 80—66401
- $(SNBr_{0.04})_x$ and $(SNBr_{0.25})_x$, solid state core level XPS 80—66401
- $(SNI_y)_x$ crystals, reson. Raman scatt. meas. 80—66203
- Sb complexes, $SbCl_5.L$ (L=organic radical), charge transfer and quadrupole-interaction consts. calc. 77—10590
- Sb complexes, $SbCl_5.L$ (L=organic radical), charge transfer and charge distrib. calc. using NQR data 77—12243
- ScH_2, self-consistent bond struct., charge transfer 80—49590
- SiO_2-Al_2O_3-CaO-Na_2O:Fe^{3+}, optical absorpt. due to Fe^{3+} ligand field and charge transfer 80—89020
- Sn complexes, $SnCl_4.L$ (L=organic radical), charge transfer and quadrupole-interaction consts. calc. 77—10590
- $Sn_xMo_3S_4$, chevrel phase, charge transfer and valence electron conc. 78—6029
- $Sr_{1-x}Sm_xS$, electron config. of Sm ions, X-ray L-absorpt. spectroscopy 80—60715
- TTF-TCNQ, transport props. of dynamically disordered chains 78—72137
- Ta-Nb-V, solid solutions, superconductivity and charge transfer 79—7926
- 4Hb-TaS_2, Fermi surfaces and charge density waves 78—79926
- TaS_2 intercalated with NH_3, charge transfer, PAC meas. 78—76366
- TaS_2, mixed coordination polytypes, optical props. 0.5-6.0 eV range, interlayer charge transfer 79—15476
- TaS_2, TDPAC meas., CDW, structural and charge transfer effects 78—39468
- $TbCl_3.6H_2O$-$PrCl_3.6H_2O(ErCl_3.6H_2O)$, in DMSO soln., $Tb^{3+}\rightarrow Pr^{3+}(Er^{3+})$ energy transfer mechanism 80—5498
- tetraselenatetracene, neutral, cation and conducting complex reson. Raman spectra, vibr. lines, charge transfer 79—4794
- TiNi, soft X-ray spectra, electronic struct. 77—44091
- TiO_2, ESCA, charge transfer satellite struct., hole state localisation intensity depend., MS-MO calc. 77—66139
- TiO_2-Ni, electronic props., struct., comp., chemical bonding 80—84499
- UF_6, matrix isolated, laser fluoresc. spectrosc. at 12K 79—68253
- UF_6, neat and mixed cryst. emission spectra, lowest charge transfer state, Jahn-Teller effect 78—67992
- UF_6, UV spectra, electronic and vibronic states in gas and solid phases 77—14445
- UGe_3, induced magnetisation density and f-d bonding, polarised neutron diffr. study 80—50063
- UO_2, uranyl cpds., X-ray photoemission spectra obs. of electronic struct. 77—28695

charge transfer states continued
UO_6^{6-} in oxides, excitation and emission transitions involved in green luminesc. obs. 77−16372
$^{57}CoV_2O_4$, after effects of orbital electron capture 79−73870
WO_3, amorphous coloured film, charge transfer, XPS 77−12491
WO_6^{6-}, in lattice electronic struct., luminesc. ab initio calcs. 78−6337
Xe-MF_6, M=W, Mo, U, Re, Ir, charge transfer interactions, VUV and IR obs. 78−50664
XeCl, energy curves and transition moments 80−28210
XeF, energy curves and transition moments 80−28210
XeO, Ar-matrix-isolated, UV absorpt. spectra 77−3375
YIG, epitaxial layer, n and p-type, UPS, elec. struct. 77−4710
Y_2O_2S:Eu phosphor, luminescence saturation effects due to N_2 laser and cathode-ray excitation 80−40151
$Y_2O_2S:Yb^{3+}$, charge transfer type luminesc. 79−33797
$YPO_4:Yb^{3+}$, charge transfer type luminesc. 78−64392
$YPO_4:Yb^{3+}$, charge transfer type luminesc. 79−33797
$Yb_{1-x}Sm_xS$, electron config. of Sm ions, X-ray L-absorpt. spectroscopy 80−60715
ZnO, surface charge transfer in presence of photosensitising dyes 78−68049
ZnO, surfaces, charge transfer in presence of photosensitising dyes, photovoltage spectra 78−72193
ZnS:Cu, O, Co, photocurrent spectral distrib., killer impurity effects 77−8135

charge transfer transitions *see charge transfer states*

charged dislocations *see dislocation dipoles*

charm particles
see also D mesons; psi mesons
0^--mesons in broken SU(4), improved mass formula 77−30352
$1/2^+$, baryons, vector mesonic decay, charm changing mode, SU(4) and SU(8) 80−47283
1/N dual unitarisation convergence due to SU(4) breaking, charm and strangeness implications 79−6321
$3/2^+$ charmed baryons, mass splitting by weight diagrams, parallelogram law sum rules 77−49915
$\Delta S=\Delta Q$ isolation, charmed particle at SU_3 27-plet effect 77−26501
accelerator proton collisions, 200 to 400 GeV, review of charm particle prod. in nuclear emulsions 79−63534
associated photoprod. of charmed hadrons by 9.3 GeV photons 77−18301
associated prod. search in proton-emulsion nuclei 300 GeV/c interactions 77−18348
associated strange and charm prod. in dual unitary approach 77−41824
asymptotic energy scale factors for pseudoscalar meson scatt. and charmed meson couplings 78−8620
asymptotic freedom and charmonium 78−54534
asymptotic symm. for charmed mesons, new duality 78−21348
axial vector meson prod. in e^+e^- at $\sqrt{S}\simeq 4.1$ GeV 77−13969
baryon, charm changing weak decays $1/2^+\rightarrow 3/2^+ + 0^-/\gamma$ in SU(4) and $SU(8)_w$ 79−3021
baryon, EM mass differences in charmed-quark model 77−71515
baryon, spectrum in SU(4) breaking 15-plet dominance scheme 77−74663
baryon decay obs. 79−67548
baryon decays, EM and weak, U- and V-spin generalisations 80−47284
baryon decays, nonleptonic, parity-violating, single-quark and two-quark transitions 80−68453
baryon decays, weak hadronic, SU(3) dynamical scheme 80−68454
baryon diffractive prod. at ISR energies 77−41818
baryon EM mass differences 77−65155
baryon EM mass differences in charmed quark model 77−82741
baryon hadronic decay, $3/2^+$ decuplet isobars in SU(3) symmetry, dynamical assumption 79−26333
baryon hadronic decays, parity violation in SU(8) 79−89077
baryon mag. moment sum rules in SU_4 charm symmetry scheme 77−30380
baryon mass and F/D ratio, colour magnetic interaction 80−62957
baryon mass formulae via SU(4) Regge trajectory anal. 77−79257
baryon non-leptonic parity violating decay in SU(8) 77−26523
baryon non-leptonic weak decays 77−2829
baryon non-leptonic weak decays in SU(8) 77−49963
baryon nonleptonic weak decay, SU(4)-20″-dominance 78−45917
baryon prod. in e^+e^- annihilation 78−17034
baryon prod. of neutrinos, quark-model calc. 78−45909
baryon production in electron positron annihilations 79−49530
baryon reson. prod. cross-sections in νN reactions 77−26513
baryon semi-leptonic decay and quark effective masses, SU_4 symmetry 78−58185
baryon spectrum due to chromomagnetic and electromagnetic hyperfine interaction 79−13123
baryons, $\Delta C=\Delta S=1$ nonleptonic decays, amplitude relations 79−54339
baryons, binding to single nucleon, finite nuclei, exam. 78−21511
baryons, charm changing radiative weak decays in AFS model 80−47285
baryons, charmed, mag. dipole moments and mag. quarks 79−97573
baryons, charmed, weak nonleptonic multibody decay, interpretation of $\bar{\Lambda}$-multi π peaks in photoprod. data 77−34153
baryons, classification in SU(4) charm symm. model, mag moments. 77−61257
baryons, dipole mag. moments, new U_3 scheme using u, d, c quarks 78−58165
baryons, elec. and mag. quarks rel. to Dirac mag. monopoles 80−402
baryons, EM mass splitting, quantitative meas. in chiral SU(4)×SU(4) model 79−93311
baryons, ground state, production by neutrino interactions 79−93400
baryons, inclusive yields of $\bar{p}$ and λ as function of energy 78−78199
baryons, mag. moments in higher symmetry schemes 77−57538
baryons, magnetic moments, broken SU_3 subsymmetries of SU_4 79−63382
baryons, magnetic moments by SU_3 and SU_4 symmetry 78−82209
baryons, mass spectrum from $SU_{1,3}$ dynamical group theory 80−62956
baryons, mass splitting and weight diagrams 79−26314
baryons, mass splitting sum rules 79−89083
baryons, nonleptonic decays 78−66118
baryons, one-parameter mass formula 77−10232
baryons, ordinary and charmed, magnetic moments in broken SU(4) 80−18136
baryons, parity violating and conserving decays, $(1/2^+\rightarrow 3/2^+ + 0^-/1^-)$ in Abe, Fujii and Sato model 79−97623

charm particles continued
baryons, quark-diquark model of nonleptonic decays 79−13120
baryons, Regge spectroscopy 77−38148
baryons, static and transition magnetic moments in quark model 77−46050
baryons, SU(1,4) dynamical group, anal. of discrete representations, mass formulae 77−45982
baryons, tensorial mass operators, SU(8) model mass formulae 77−54091
baryons, weak decays, quark model framework 80−62976
baryons in quark model with hyperfine interactions 79−97601
beam dump experiments, prompt neutrinos and charm particle lifetime 79−63535
beauty and charm photoprod. in QCD, $q\bar{q}\rightarrow b\bar{b}$ or $c\bar{c}$ mechanism 80−32079
bound states near charm threshold, charm molecules 78−45857
bound states of charmed baryons and antibaryons 78−8608
Brayshaw and Peierls mechanisms for generating hadron peaks, N*(1470), 0(1020) and charm 79−404
bubble chamber detection technique 79−22543
channel coupling effects and resonance phenomena in pp interactions, N/D eqn. study 79−71765
charm as possible source of prompt leptons 77−225
charm meson decay, inclusive electron spectrum 77−13970
charm particles, inclusive production cross sections, correlating quark rearrangement model 79−54320
charm photoprod. with linearly pol. photons, QCD calcs., gluons 80−68464
charm quark prod., scaling violation as threshold effect 78−66088
charmed baryon nonleptonic decays, sum rules for $\Delta C=\Delta S=1$ S-wave decays 79−58957
charmed meson spectra from effective quark-quark interaction, D^0 mass 79−36018
charmed quark fragmentation functions in a Monte Carlo quark recombination model 79−97570
charmonium, $^1P_1$ state, mass, branching ratios, decay rates 78−62370
charmonium, ψ and χ states, hyperfine struct. 78−12878
charmonium, C-even, decay sum rules in QCD 77−54081
charmonium, generation of spin depend. forces through scalar-vector admixture 78−33038
charmonium, hyperfine interaction, nonperturbative treatment 80−62944
charmonium, non-singular confining pot., order of levels anal. 77−65189
charmonium, radially excited states, small Q-value channel dominance in decay 79−54335
charmonium, rel. to gluons, quantum chromodynamics theory 78−62362
charmonium, review of exptl. results and theoretical advances *(German)* 78−66184
charmonium, Schwinger partial symmetry, quark flavour EM interaction 79−93335
charmonium, spin structure of the quark-confining potential 79−22042
charmonium, strazonium and baryonium dual S-matrix approach 80−52526
charmonium and asymptotic freedom in QCD 79−6327
charmonium and QCD, review 78−82157
charmonium and similar two fermion systems, effective Hamiltonian 78−21381
charmonium atomic physics, ψ, ψ', η_c, η_c' masses and $\psi\rightarrow\eta_c\gamma$ decay 79−40740
charmonium decay, effective strong coupling constant for timelike Q^2 80−99091
charmonium electromagnetic decay, relativistic eval. 80−68459
charmonium from QCD $q\bar{q}$ β-function 79−343
charmonium hyperfine quadrupole moment, orbital mixtures, quarkonium system phenomenology in potential models 79−49496
charmonium mass spectrum using oscillator pot., Υ and Υ' masses 79−97595
charmonium model anal. 77−71490
charmonium model and the ψ and Υ families 80−47253
charmonium model of ψ family 78−78143
charmonium models, energy perturbation series from Schrodinger eqn. 79−6005
charmonium narrow states, hadronic and EM decays 78−70343
charmonium photoprod., ψ_c, η_c ang. distribs., non-Abelian gauge gluon exchange 77−57546
charmonium photoprod., gluon-exchange model 78−74214
charmonium potential, variation-iteration principle 78−54227
charmonium potential models, testing Q^2 duality 79−45082
charmonium psion states, confining pots. and inverse scatt. problem, Υ mass 80−4946
charmonium quark-antiquark pots., flavour independ., γ, γ', ψ and ψ' appls. 80−47254
charmonium resonances above open charm threshold, nonrelativistic quark model 80−78039
charmonium singlet state, possible resolution 78−74225
charmonium spectroscopy, explicit soln. of wave eqn. for arbitrary power pots. 80−403
charmonium spectroscopy, spin forces, obs. in $\psi'(3.68)$-$\psi''(3.77)$ struct. in e^+e^- annihilation 79−36047
charmonium spectrum, relativistic and nonrelativistic theory 78−50010
charmonium spin struct. and quark gluon effective interaction 77−13922
charmonium spin structure, and possible origin of quark spin depend. forces 79−30707
charmonium state decay, nonrelativistic and relativistic theory 78−58221
charmonium states, multimesonic decays, statistical quark model 78−82171
charmonium wave function, coloured glue effects using MIT bag model 79−75735
chromomagnetic and electromagnetic hyperfine interaction, charm meson spectrum 78−12879
classification in SU(4), quark-lepton analogy *(Norwegian)* 77−34137
conference on hadron struct. and lepton-hadron interactions, Cargese, France (July 1977) 80−4473
conference on particle physics, Honolulu, Hawaii (Aug. 1977) 79−49485
conserved vector current hypothesis, extension to gluons 77−71480
couplings and asymptotic scale factors 77−38202
D and F charmed meson decay and evidence for $(\bar{c}s)_R$ current 78−58167
d-wave $c\bar{c}$ in e^+e^- charm prod. 77−22749
debris of electron-positron annhihilations *(Polish)* 79−54345
decay, interference effects, 2nd order suppressed amplitudes 80−4987
decay constants, smoothness and spin-zero charm mesons in broken chiral SU(4)×SU(4) symmetry 79−58900

charm particles continued

decay obs. in high-energy neutrino interaction 77−13953
decay of short-lived particles in photoemulsion irradiated with 400 GeV/c protons *(Russian)* 79−3022
decay props. anal. 77−71507
decays, semileptonic, nonleptonic, isospin restrictions on charge distribs., branching ratios 77−54099
deep inelastic processes, charm prod., mass scales, parton model, generalised VDM 77−13930
deep inelastic production, sum rules in quark parton model 77−87981
deep inelastic quantum chromodynamic charm leptoproduction 79−54312
dilepton and trilepton production in neutrino experiments *(Polish)* 78−89704
dilepton charge production cross section for ν and $\bar{\nu}$, parton model 80−62966
discoveries during 1974-7, and associated theory *(Czech)* 78−86103
discrete charm of new resonances 77−34129
discussion and implication for unified theory of elementary particles *(French)* 79−67522
duality between resonances and free quark-antiquark pairs 79−63448
duality constraints on spectroscopy 78−21398
dynamical group selection for charmed baryons, SU(1.4) 78−37178
eight quark model, modified left-handed currents, charmed quark mixing 78−16982
elastic widths, from dynamics and finite energy sum rules duality 77−38139
elementary particle theories, properties *(Spanish)* 80−73681
EM mass difference using ρ-ω mixing and quark model 77−2834
EM mass differences in MIT bag model calcs., charm particles 77−49965
EM properties of charmed hadrons, $SU_6 \times U_c$ calcs., mag. moments, mass differences 78−70368
exotic charmed-strange mesons, quark model 77−87946
F meson masses, duality predictions 78−8619
flavour changing weak radiative decays, short and long distance effects 80−73712
flavour symmetry breaking and production processes in dual unitarisation, ϕ and ψ prod. 79−45080
four quark states and open charm production 79−63443
fragmentation function for charmed quarks from $\mu^+\mu^-$ and μ^-e^+ event data 78−62355
fragmentation function model, from neutrino data 80−37237
fragmentation functions of heavy quarks into hadrons, ν reactions, e^+e^- annihilation appls. 79−3013
Gargamelle, neutrino physics history, theory and expt. 78−50027
gauge theories, observable quantities 77−34099
Gelfand pattern, charmed hadrons and magnetic moment 80−398
gluon fusion model, hadronic charm prod. 78−66081
ground state, semileptonic decays 79−63473
hadron masses, five-quark model of ψ particles *(Russian)* 77−61263
hadron masses, from effective quark masses, sum rules 80−4965
hadron masses and EM mass differences in broken-SU(8) quark model 77−61256
hadron pair prod. rates in e^+e^- annihilation based on $c\bar{c}$ dominance 77−74703
hadron production and decay, book contrib. 78−82208
hadron spectroscopy, quark model explanation 79−30710
hadron-antihadron short distance pot., molecular charmonium P-wave bound states 79−328
hadron-hadron inclusive interactions, charmed particle production, η_c, ψ and other $c\bar{c}$ bound states 80−63036
hadronic charm prod. cross section and particle lifetimes, Monte Carlo anal. 78−89679
hadronic charmed particle decays, quark and particle helicities, charm changing current chirality 80−37256
hadronic coupling constants and the nonrelativistic quark model with charmonium potential 80−37207
hadronic multiparticle reactions, models, prod. of strangeness, baryon number, charm 78−74286
hadronic production of charmed particles, review 79−67610
hadronic props., superconvergence sum rules 80−78043
hadrons, $\Delta C = \Delta S$ decays 78−45912
hadrons, charmed, SU(4) mass-breaking, mass sum rules 80−62959
hadrons, mag. and transition moments, radiative decay widths 79−71724
hadrons, relation between spin, isospin, strangeness and charm 80−37183
hadrons $\Delta C = \Delta S$ decays, sum rules, internal symm. props. 77−30376
hadrons and quarks in high energy collisions, review 79−49482
heavy baryon spectroscopy in the QCD bag model 80−105866
heavy lepton and charm particle production by e^+e^- interactions, recent results, review 79−26337
heavy quark bound system, vibr. states 78−29300
heavy quark leptoproduction in QCD, characts. 79−17733
heavy quark semileptonic decay, gluon radiative corrections 79−75743
heavy quark semileptonic decays, gluon corrections 79−17688
heavy quarks, elementary particle physics developments, review book contrib. 79−22161
heavy quarks, elementary particle physics developments, review 79−22053
heavy quarks, widths of neutral vector mesons 78−8602
heavy triply charmed spin $3/2^+$ baryon, radial excitation spectrum 80−27482
hierarchical fermion masses from grand unification 80−105832
high energy neutrino physics, recent expt. results 80−4982
high-energy (>10 GeV) neutrino physics, review of development, book contrib. 78−82201
history of search for fundamental constituents of matter *(Polish)* 78−54588
inclusive nonleptonic and semileptonic decays of charmed hadrons, sum rules determ. 77−71514
inclusive semileptonic decay, struct. functions, scaling limits 78−82165
inverted charmed meson multiplets as a test for scalar quark confinement 78−70325
$J^P = 0^-$, 1^- and 2^+ multiplets, level shifts and chain mass, test of asymptotic planarity 77−38130
lepton+nucleon producing polarised baryon+anything, polarisation transfer charmed baryon prod. 77−82746
lepton-hadron scatt., charm changing charged current, chiral struct. anal. 77−13964
lepton-quark symmetry, theoretical ideas about charm and flavour mixing 79−49486

charm particles continued

lifetime measurement 80−73693
light-cone algebra anal. of inclusive charmed-particle prod. by neutrinos 77−18274
$m_{\eta c}^2 = m_\psi^2 - (m_\rho^2 - m_\pi^2) = (3000 \pm 20\ \text{MeV})^2$ after all 79−85288
$M_\psi - M_{\eta(c)}$ and $M_\Upsilon - M_{\eta(b)}$ lower bounds, concave and convex pots. 80−91057
magnetic dipole transitions in atomic and particle physics: ions and psions 79−9322
magnetic moments of charmed hadrons, additive-quark-model 77−82707
magntic moments and machinery of symmetry breaking 79−63477
mass formula for SU_4 charmed-hadron multiplets 78−37192
mass formulae, linear, quadratic appl. to vector and pseudoscalar meson 77−49935
mass spectra, SU(4) and SU(3)×SU(3)′ theories comparison *(Chinese)* 78−82127
mass splitting of charmed baryons, derivation using weight diagrams 80−27481
mass sum rules for hadrons with charm, beauty and taste 80−9152
masses of charmed mesons and baryons *(Russian)* 77−61258
masses of new mesons and effects of the fifth flavour 78−66098
meson, non-leptonic decay in SU(3) Bose quark model 79−85278
meson decay, simple symmetry breaking 78−21418
meson decays, soft hadron interaction effects on nonleptonic weak decays 80−86705
meson hadronic decay branching, $\bar{p}p \rightarrow n\pi$'s multiplicity 77−10288
meson lifetime radios and prod. in e^+e^- collisions 77−61307
meson mass, effect of u and d quark differences calc. 77−46019
meson mass calc. 77−10231
meson mass formulae in broken $SU(8)_w$ symmetry 78−37191
meson mass splitting in universal confining potential model 80−4967
meson mass via duality calc. 77−22697
meson non-leptonic decay, resonant struct., phenomenological calc. 77−49960
meson nonleptonic decay, massive quark model 78−33067
meson P-wave radial mixing, effect on E1 radiative decays, charmonium mass 80−37271
meson pair prod. in e^+e^- annihilation, quark model of broken SU(8) symm. 77−38182
meson prod. in e^+e^- annihilation, quark model 78−8680
meson production in hadronic and EM hadron interactions 79−13143
meson radiative decay, quark loop model, SU(3) splitting of quark masses 80−62990
meson semileptonic decay effects of hadron multiplicity on distribs. 78−4856
meson semileptonic decay inequalities for decay rates and lepton polarisations 79−89147
meson spectroscopy, a review using quark models 78−25010
meson threshold prod. by virtual photons, bound-state model, $e^+e^- \rightarrow D\bar{D}$ 77−10269
meson-baryon four body reaction amplitudes in exact SU(4) 77−18192
mesons, Cabibbo-suppressed nonleptonic decays 77−71509
mesons, dynamic SU(4,1) symmetry, mass spectra, anal. *(Russian)* 78−70350
mesons, nonleptonic decays, dual model current algebra relations and amplitudes 79−89132
mesons, nonleptonic decays of charmed mesons and chiral Lagrangians *(Russian)* 79−30732
mesons, production in e^+e annihilation 80−91106
mesons, props. determ. from two-step pot. model 77−74682
mesons, radiative decays, SU(4) and OZI violations 77−74688
mesons, review of three years e^+e^- research at SPEAR 79−63490
mesons, semileptonic decays, charged weak current struct. 80−102042
mesons, spectral function sum rule and onium 79−26329
mesons, three body decay, Dalitz plots quark line diagrams 79−30731
mesons, weak decay mechanism 79−93405
mesons and charmoniums, masses and mixing, OZI rule breaking 78−12889
mesons with non-zero charm, inclusive prod. in meson-nucleon and nucleon-nucleon interactions *(Russian)* 77−14008
MIT bag model, charmed and b-flavoured hadron mag. moments 80−95271
molecular charmonium, C-exotic mesons 77−71487
molecular charmonium prod. in e^+e^- annihilation into hadrons 77−30394
multimesonic decays of charmonium states in a constant matrix element quark model 79−26298
multimuon signal in deep inelastic μ-nucleus scatt. 77−71519
multparticle decay theoretical models for heavy hadrons containing charmed quarks 78−70344
neutral charmed particle, direct obs. of pair decay in 400 GeV/c proton interaction 79−85299
neutral charmed particle decay, direct observation in ν-emulsion interactions 80−9165
neutral currents, effect of quark-antiquark sea *(Russian)* 77−6078
neutrino interactions, charm particle prod. and subsequent decay into like-sign dimuons and trimuons 79−63469
neutrino interactions, leading particle effects in charm fragmentation 78−8650
neutron beam charm particle production and charmed particle lifetime 79−63465
new meson, possible semileptonic decay to K's in ν interactions 77−2819
'new particle' searches and discoveries, 'Review of Particle Properties' 1976 supplement 77−57515
nonleptonic charm decay and u-s symmetry 79−13078
nonleptonic decays of ordinary and charmed hadrons, vector-like model 78−41545
Okun-Zakharov-Pontecorvo model of CP nonconservation 77−67621
orto-charmonium spectrum, relativistic potential model, linear potential 79−58922
p+emulsion, 200 GeV, star event containing single electron, charmed particle generation, anal. 77−61414
pair prod. in muon deep inelastic scatt., event location in nucl. emulsion target 80−27906
para-charmonium spectrum, relativistic potential model, linear potential 79−58922
paracharmonium states, corrections to two-gluon annihilation rates 78−33039
parent-child relationship for prompt leptons and neutrinos produced in the forward direction 79−80824

charm particles continued
parity-violating amplitude of charmed-baryon nonleptonic decays 78—62398
PCAC and dual resonance amplitudes, old and new mesons, charm 78—45885
perturbative QCD, renormalisation improvement, charmonium decay and scaling violations 80—101993
photoprod., gluon-fusion model 78—45923
photoproduction, asymptotically free field theories 77—13934
photoproduction and electroproduction near threshold, Born approx. *(Russian)* 78—8675
photoproduction processes of charm particles with charm nonconservation *(Russian)* 78—74201
photoproduction total cross sections, quantum chromodynamics *(Russian)* 78—45880
pion-charmed baryon scatt. and coupling strengths, superconvergence sum rules 80—52532
production, expt. evidence reviewed 77—22823
production from e^+e^- and subsequent decay, complete ang. correl. calc. 77—49986
production from two-gluon annihilation in proton-proton collisions
charmed particle production from two-gluon annihilation in proton-proton collisions 79—347
production in νN and e^+e^- interactions, general survey *(German)* 77—22729
production in high energy ν-induced reaction, lifetime determ. 79—26426
production of charm-pairs in νN, μ^-N and pN 80—73748
production of charmed mesons by $\bar{p}$N and πN interactions 77—6176
proton interactions, beam dump expt. at CERN SPS 78—45979
pseudoscalar direct lepton production mechanism *(Russian)* 77—82738
pseudoscalar meson decay constants, Goldberger Treiman relations in charm sector, three point function Veneziano model 79—293
pseudoscalar mesons, muonic double β-decay, tree and box diagram approx., K and F 79—17717
pseudoscalar mesons in the c-$\bar{c}$ and b-$\bar{b}$ systems 79—93359
pseudoscalar mesons semileptonic decays, quark model 77—61281
QCD, 2-dimens., nonleptonic weak decays of charmed and storage mesons 79—40773
QCD, charm contrib. to electroprod. struct. functions 78—58170
QCD, charm photoprod., ψ, D, F etc. prod., sum rules, cross sections 78—58169
QCD, hadron interaction effective string lagrangian, Regge slope, charmonium pot. model 80—4939
QCD, hadronic charm production, cross section and charmed quark mass 79—36017
QCD, lifetime of $Q\bar{Q}$ states, pseudoscalar charmonium and upsilon states 80—68429
QCD, spin-dependent forces in heavy-quark systems 80—4937
QCD, two-dimens. extrapolation to four-dimens. 78—78081
QCD estimates for associated charm production by weak neutral currents 78—78169
QCD quark-gluon plasma, hadronic prod. of leptons, photons charm and ψ 78—89669
QCD test, prod. of heavy quark flavours in hadronic interactions 77—45957
quantum chromodynamics, electroprod. of charmed particles *(Russian)* 78—45878
quark, effective mass anal. 78—45991
quark exchange model, charmed meson prod. 78—8600
quark fusion model, strange and charmed quark numbers, vector meson description 78—58158
quark line rule, generalised, SU_4 symm. scheme, reaction of hadrons containing charm quarks 78—54614
quark mass differences in high energy collisions 78—45868
quark mass in asymptotically free gradient theory *(Russian)* 77—30333
quark model, mag. moments of charmed baryons 77—30332
quark model calculation of charmed meson mass spectrum 77—26491
quark semileptonic decay, gluon corrections to charged lepton spectrum 79—75765
quark-antiquark P-wave bound state, two-gluon annihilation rates 77—26492
quark-antiquark pot., charmonium model modifications, spin forces and instantons 78—93842
quark-parton model with charm for dimuon prod. in high energy νN and $\bar{\nu}$N interactions 77—57520
quarkonia from charmonium and renormalization group equations 79—22055
quarkonia states, heavy, strong decay into other heavy flavours, and triple-gluon vertex 80—47279
quarkonium, almost degenerate P-wave charmed-bottom meson multiplet, scalar confinement test 79—13052
quarks, three-component model extended, total cross sections 78—24999
radiative decay widths of charmonium states, superconvergent sum rules 78—21422
reciprocal effects and other quark theories, charm quarks, J/ψ discovery, gauge theories *(Danish)* 79—30698
Regge spectra of charmed baryons in dual resonance amplitudes 79—13088
Regge spectroscopy of charmed mesons 77—34138
relativistic quark models, $c\bar{c}$ and $b\bar{b}$ singlet triplet splitting, mass formulae *(Russian)* 80—37232
scaling, nonrelativistic Schrodinger eqn. charmonium 78—54613
scaling violations in deep inelastic lepton scatt., charm quark prod. 78—21436
semileptonic decay, effective chiral Lagrangian method 78—74254
semileptonic decay of charmed particles, formalism using helicity amplitudes 78—4852
semileptonic decay rate calc. 79—9366
semileptonic decay to K_s^0+e, obs. in e^+e^- 77—2853
semileptonic decays, DASP results on e^+e^- annihilation 80—42483
semileptonic decays of charmed baryons, SU(4) breaking, mag. moments, suppression factors 79—387
semileptonuc decay spectra of charmed mesons pairs produced in γN collisions 77—49952
semilocal duality constraints for mesons, on-shell particles, masses, couplings 78—58174
short lifetime charm particles from ν interactions detection in nuclear emulsion 79—22539
short lifetime particle detection system, bubble chamber technique 78—29716

charm particles continued
short lived charm particles observation in 400 GeV/c p+emulsion interactions *(Russian)* 79—22144
short lived particles search in high energy neutrino interactions 79—49510
single quark transition model, parity violating charmed hadron decays, current-current interaction 78—12907
spin structure of effective quark Hamiltonian, hyperfine splittings of charmonium 78—12871
stable charmed hyperfragments containing charmed baryon+nucleons, binding energies, lifetimes 78—89815
SU_3 subsectors of SU_4 and mass sum rules for charmed hadrons 79—35967
$SU_L(4)\times U(1)$ four-quark model, lepton quartets and W bosons 77—87934
SU(10) symmetry, charmed vector bosons mag. moments 78—17018
$SU(2)\times U(1)$ gauge model, right-handed charm current, CP violation 78—45795
SU(2) and SU(6) models, weak nonleptonic decays of charmed mesons 77—26521
$SU(3)\times U(1)$ gauge model of weak interactions, quark triplets, charmed hadron decay 77—2789
SU(3) quark sectors, weak hadronic and radiative decays of nonstrange charmed baryons 79—22092
SU(3) subalgebras of SU(4), generalised U-spin charmed baryon magnetic moment 79—36078
SU(3) symmetry in more than 3 quarks world, nonet struct., quark line rule 79—36022
SU(4,1) hadron dynamical symm. anal., charmed $1/2^+$ baryon and 0^- meson mass *(Russian)* 78—74237
$SU(4)\times SU(4)$ broken chiral symmetry, charmed hadron masses and decay consts. 79—40686
$SU(4)\times SU(4)$ chiral symmetry breaking, axial vector current divergences, kaon PCAC 79—45032
$SU(4)\times SU(4)$ current two point functions, meson decay consts. and bare quark masses from duality 78—8598
SU(4) symmetric 20-plet representation of charmed baryons, mass, EM splitting 78—54615
SU(4) symmetry breaking pattern and baryon masses 78—89690
SU(4) symmetry predicted ${}^1/{}_2{}^+$ charmed baryons, C_1^{++}, C_1^+, C_1^0, X_u^{++}, X_d^+, possible observation 79—40758
$SU(5)\times SU(5)$ chiral symm. breaking, Cabibbo angle, meson mass spectrum 77—74614
SU(8) symm. mag. moments of charmed vector bosons 78—4794
SU(8) symmetry and the baryon mass spectrum 79—80814
sum rules for charmonium and charmed mesons in QCD 77—30327
sum rules for four-body semi-leptonic decays 79—36067
supernuclei containing bound states of charmed baryons, existence, decay, phys. significance 77—79320
tensor force effects on ψ family in charmonium model 78—89675
trimuon production in higher energy ν interactions, rates and properties, $c\bar{c}$ prod. 79—49508
two-gluon annihilation of quark-antiquark pair *(Russian)* 78—45856
V+A currents coupling old quarks to new quarks 77—26486
weak and EM interactions at high energy [conf. Les Houches, France (July 1976)] 79—80785
weak and EM phenomenology, gauge theoretical prospective, charm and flavour conservation 80—4916
weak charmed current group struct., chiral $SU_4\times SU_4$ breaking 77—65118
weak charmed-baryon resonance prod., neutrino inclusive interactions, scaling behaviour 78—8645
weak decay processes in charm scheme of subhadronic constituents 78—25012
weak decays of charmed particles, generalised charge symm. 78—37184
weak interaction physics, present status and future prospects, review 79—67492
weak interaction scheme, charmed hadrons expt. data, four flavour model explanation 78—45860
weak interaction theory, review 78—4822
weak interactions with diagonal neutral currents *(Russian)* 77—74676
weak production of charmed baryons by neutrinos, relativistic quark model 78—41496
weak radiative decays in SU(4) and SU(8) 77—87977
weak semileptonic decays, free parton model 79—75766
X-particles and their backgrounds in 400 GeV/c proton interactions, emulsion chamber anal. 79—63548
$B^0\rightarrow D^+X(F^+X)$, W-exchange dominance, decay rates 80—86706
$B_c\rightarrow e^+e^-$+hadrons, decay due to weak neutral currents *(Russian)* 79—22146
$C\rightarrow\Lambda(K^0)$+hadrons, charm prod. cross section, new particle search *(Russian)* 78—89711
c-$\bar{c}$ associated prod., ν-induced multimuon prod. 79—17707
C_0^+(2260), lifetime estimates, free quark model anal. 79—67544
C_0^+ charmed baryon weak decays 79—9369
C_0^+ prod. and decay, test of charmed current struct. 77—61271
C^+(2.26) search in 45 GeV/c neutron beam, C^+ hadronic and semileptonic decay *(Russian)* 79—22145
$c\bar{c}$, fine-hyperfine splittings and Lorentz structure of confining potential with vacuum polarisation corrections 80—78041
$c\bar{c}$ bound states, e^+e^- decay processes, relativistic harmonic oscillator model 78—62393
$c\bar{c}$ prod. effects in $\nu(\bar{\nu})$-N dimuon same-sign prod. 77—49946
$\bar{c}c$ $\bar{q}q$ states, decay, hadronic and photo-prod., e^+e^- annihilation prod. 80—99092
$c\bar{c}$ spectrum, equaltime relativistic wave eqn. with confining potential 80—77977
$c\bar{c}g(c\bar{c}q\bar{q})$, exotic mesons, masses, decay widths, mixing matrix elements 80—62943
χ, charmed particles, particle multiplicity distribs. in hadronic decays 77—46044
χ(3.45), γ-transitions in charmonium system 78—78138
χ(3.45), radiative M1 transitions with charmonium model 79—13132
χ particles, radiative decay widths calc., broken SU(4) model 78—62395
$\chi\rightarrow\psi\gamma$, charmonium E1 radiative transitions and quark mag. moments 80—86721
$\chi/\varepsilon c(3.41)$ tensor meson dominance for $c\bar{c}$ states, $\psi'\rightarrow\varepsilon c\gamma$ and $\varepsilon c\rightarrow\psi\gamma$ 79—3019
χ_c production cross section in e^+e^- expts., two photon exchange mechanism 77—61306

charm particles continued

- $\chi_J \to \gamma\psi$, charmonium states radiative and hadronic widths, gluon spin 80−4998
- $\chi_J \to \gamma\psi$, upper and lower bounds using dipole sum rules 77−13958
- χ_J P-wave charmonium states, hadronic prod. cross section in K^-p, $\bar{p}p$, and π^-p 80−37292
- D, D* meson prod. in e^+e^- annihilation 77−2855
- D,D* mesons in algebraic approach to broken SU(4) 77−38097
- D(1.87) mesons semileptonic decay, multiplicity effects 77−49953
- D and F meson spectra, electromagnetic interactions effect 80−47293
- D charmed meson weak decays, tests via parity violation, strangeness violation and semileptonic decays 77−30368
- D meson, nonleptonic decay, matrix element computation and iteration 79−384
- D meson EM mass differences, bag model calcs 77−6124
- D meson states mixing 77−30374
- D-meson decay mechs., weak and leptonic two-body decays 78−41535
- D-meson prod. model, charmed particles 77−38124
- D^0, D^+, hadronic decay, branching ratios calc. 78−45913
- $D^+ \to \bar{K}^0\pi^+$, $D^0 \to K^-\pi^+$, two body decays of charmed mesons, quark recombination scheme 78−37207
- D^+-D^0, D^{*+}-D^{*0} mass differences using modified nonrelativistic Schrodinger eqn. 78−58186
- D^+-D^0 charmed mesons EM mass difference estimate, quark pair creation model 77−10250
- D^+-D^0 mass difference, Bethe-Salpeter eqn. calc. 77−26525
- D^+-D^0 mass difference, form factors, SU(4) coupling, vector meson dominance model 79−391
- $D^\pm$-D^0 mass difference, vac. isospin violations 77−26526
- $D^+ - D^0$ mass difference, EM effects 77−2833
- D** mass prediction from Regge slope factorisation 77−26503
- $D\bar{D}$ molecular charmonium from dual diagram and Schrodinger eqn. 80−86660
- $D\bar{D}$:DD^*:$D^*\bar{D}^*$ prod. ratio in e^+e^- collisions 77−6140
- $D\bar{D}^*$ production and decay, VDM, dual amplitude anal., e^+e^- annihilation 77−49992
- $e\bar{e}$, quark, diquark prod. thresholds, charm, colour excit. in 4-GeV region 77−79276
- e^-e^+ annihilation, >2 GeV, production of charmed particles and charged τ lepton, review 78−17006
- e^-e^+ annihilations, review of charmed particles 78−17035
- $e^-e^+ \to$charmed particles, contrib. of d-wave charmed quark pair 77−26534
- e^+e^- annihilation, 6 GeV, η_c existence, possible $c\bar{c}c\bar{c}$ state 77−82755
- e^+e^- annihilation, anomalous lepton prod., charmed mesons and heavy leptons 78−66134
- e^+e^- annihilation, axial vector meson prod. rate, non-relativistic quark model 77−38184
- e^+e^- annihilation, charmed axial vector meson prod., nonrelativistic quark model 78−25055
- e^+e^- annihilation, charmed baryon pair prod., symm. quark model, $c\bar{c}$ pair creation model 77−54111
- e^+e^- annihilation, charmed meson prod. at SPEAR 78−4865
- e^+e^- annihilation, energy bounds for charm and heavy lepton prod. 77−2810
- e^+e^- annihilation, Λ_c charmed baryon prod., branching ratio, inclusive cross sections 80−37280
- e^+e^- annihilation, prod. of orbitally charmed hadrons, free quark model anal. 79−22120
- e^+e^- annihilation, resonance decays above charm prod. threshold, single channel dominance 78−66133
- e^+e^- annihilation experiment review, ψ spectroscopy and charmed particles D and F 79−49533
- $e^+e^- \to$charmed mesons, decoupling of highly excited vector mesons 77−87986
- $e^+e^- \to D^0\bar{D}^0 + x\pi^0 + y\gamma$, mixing of neutral spinless charmed mesons, decay, CP, violation tests 77−46067
- $e^+e^- \to F^+$, SPEAR expt. results 79−93444
- $e^+e^- \to F\bar{F}(B\bar{B})$, $\tau\nu$ decay signature for F^+ and $B^\pm$ detection 80−91099
- $e^+e^- \to F^*\bar{F}^* \to F\gamma_1\bar{F}\gamma_2$, photon ang. correlations and prod. amplitudes 80−47319
- $e^+e^- \to$hadron jet, 3 to 17 GeV, including charm threshold and upsilon resonances, review 80−47321
- e^+e^- hadron production and new colour 77−87927
- $e^+e^- \to$hadrons, cross-section struct. in 0-8 GeV range, quark models and heavy leptons 77−30392
- e^+e^- inclusive electron prod., in multiprong events, charmed particle decay 78−66136
- e^+e^- inclusive prod. at 4.8 GeV, anomalous muon events, charm and heavy lepton explanations 77−247
- e^+e^- interactions, review 79−80833
- $e^+e^- \to p^-X$, charmed baryon pair prod. cross section, pole-dominated form factor 78−12922
- $e^+e^- \to$quarkonium state, D,F, Υ mesons, importance as experimental tool in new particle searches 80−42425
- e^+e^- resonance production above charm threshold 77−79275
- $e^+e^- \to U^+e^-$, SU(2)⊗U(1) gauge models 77−71502
- η, $c\bar{c}$ component, $\psi \to \eta\gamma$ and Okubo formula 77−6116
- η-$c\bar{c}$, η'-$c\bar{c}$ couplings from $\psi \to \eta'\gamma$, $\psi' \to \eta\gamma$ *(Russian)* 77−49962
- η_c, candidate evidence from SPEAR, crystal ball detector, recent results 80−74046
- η_C, coherent prod. and baryon-antibaryon pair decay 78−21421
- η_c, interpretation of X(2.88) obs. in $\pi^-p \to \gamma\gamma n$ 79−22150
- η_c, mass and other props, review from theoretical models 80−102025
- η_c, predictions of existence by extrapolation methods 78−93863
- η_c associated with gluon, hadronic prod. 80−105846
- $\eta_c \to \gamma +$anything, OZI rule violating decay in QCD 78−89709
- η_c mass determ. from QCD sum rules 78−74223
- η_c mass from dispersion sum rules in QCD, identification with X(2.83) *(Russian)* 78−89681
- η_c prod. and hadronic decay, charmonium model 78−41502
- F, F*, Schwinger phenomenological and dyon description 78−82109
- F, F* masses determ., inclusive η prod. by e^+e^- annihilation 77−87988
- F, nonleptonic decay rates and branching ratios, lifetimes 80−102047
- F, search in e^+e^- annihilation, preliminary results 78−78199
- $F(0^-)$, $F^*(1^-)$, charmed strange mesons, weak decays 78−74249
- F and F* from e^+e^- annihilation 78−78198
- F charmed meson prod. from ψ(4.0 to 4.5 GeV) decay 79−17719
- $F \to D\pi$ enhancement and the $\Delta I = 1/2$ rule 79−36069
- F meson nonleptonic weak decay modes 77−49961
- F meson prod. characts. from $e^+e^- \to \eta X$, $F \to \eta\pi$ 79−26338

charm particles continued

- F mesons, charm particle nonleptonic weak decays, pole dominance model 79−63475
- F mesons, semileptonic decay const., D and F decay const. ratio determ. 78−62392
- F parity violating nonleptonic decays, vector meson dominance model 80−78058
- $F \to \pi\pi\pi$, S_3 permutation group approach, charm model test 79−17723
- F-meson, decay mechs., weak and leptonic two-body decays 78−41535
- F-meson decay, hadronic, role of free-quark pairs 80−78059
- F-meson masses and leptonic decay consts. 78−66087
- F-meson production suppresion relative to D-meson 79−36100
- F-mesons, SU(3) rules for non- and semi-leptonic weak decays 78−45916
- F-mesons, weak selection rules in e^+e^- annihilation and ν scatt. 78−8679
- $F^- \to \tau^-\bar{\nu}_\tau$, charmed mesons, heavy lepton decays, ν_τ neutrino mass depend. *(Russian)* 78−62394
- F^+, hadronic decay, branching ratios calc. 78−45913
- F^+, weak nonleptonic decays, SU(3) symmetry and quark diagrams *(Russian)* 79−93411
- F^+(2030), lifetime estimates, free quark model anal. 79−67544
- F^+ decay, SU_4 20-plet dominance model, inclusive branching ratios 80−13299
- F^+ decay widths and branching ratios, quark recombination widths, free quark model 80−27500
- F^+ lifetime, 6 dominance and W^+ exchange dominance 80−37254
- $F^+ \to \mu^+\nu_\mu$, right handed currents 78−8662
- F^+ nonleptonic decay, quark annihilation hypothesis test 80−102044
- $F^+ \to p\bar{n}$, decay mode meas. for PCAC test 80−91018
- $F^+ \to \phi\pi^+(\eta\pi^+)$, heavy quark weak isospin, constraints from nonleptonic transitions 79−85257
- $F^+ \to \pi^+e^+e^-$, enhancement due to π^+ EM form factor, generalised PCAC applicability 78−82164
- $F^+ \to \tau^+\nu$, gluon enhancements in charmed-meson decays 80−95265
- $F^\pm$, weak decay constant from bag model extension 80−62967
- $F^\pm \to 3\pi$ or $K^\pm K_S^0$, charmed pseudoscalar meson nonleptonic decays, right handed $c+\lambda$ quark doublet 77−49958
- f_c(3.55) absolute γ-decay rates from tensor meson dominance and QCD pots. 79−9377
- F* meson and anomalous $e\mu$ events 78−66108
- F*-F, D*-D, pseudoscalar-vector mass differences, QCD nonrelativistic quark model 79−6339
- F*-F, mass difference calcs., scalar-exchange model 79−13124
- F**, charmed tensor meson, strong and EM decay modes 80−68451
- $\gamma N \to \psi(3.1) +$anything, cross section and N charmed quark composition 80−423
- $\gamma p \to$charmed mesons, photoprod. at CERN SPS and search for charmed mesons 79−26336
- γp total cross sections, 18 to 185 GeV, charm-anticharm contrib. 78−54635
- $\gamma\rho$ at threshold, source of charm production 78−70379
- J/ψ, inclusive production cross sections, correlating quark rearrangement model 79−54320
- J/ψ, radiative M1 transitions with charmonium model 79−13132
- J/ψ meson hadronic prod., role of ^3P charmonium states 77−22744
- Λ, charmed baryon mass in SU(1,4) dynamical group theory 80−62882
- Λ^+ decay, four body semileptonic decay rates of charmed baryons 78−8665
- $\Lambda_1{}^{/+}$, mag. moment from quark mass difference calcs. 80−37240
- Λ_c, structure of hadrons containing heavy quark, MIT bag model 80−86672
- $\Lambda_c{}^+$, confirmation of existence from neutrino experiments 79−75770
- $\Lambda_c{}^+$ lifetime, semileptonic branching fractions, nonspectator quark interactions 80−37260
- $\Lambda_c{}^+ \to p\bar{K}^0\pi^+\pi^-$, kaonic decay observation, prod. rates 79−26332
- $\Lambda_c{}^+ \to p\pi^+k^-$, lifetime of charged charm particles 79−67548
- $\mu^+\mu^-$ prod. from ν and $\bar{\nu}$ interactions, charm prod. and decay 77−74675
- μN, 270 GeV, multimuon final states, total cross section, associated charm prod. 80−13315
- μN inelastic scattering, dimuon events, charm particle prod. and semileptonic decay 77−10260
- $\mu N \to x\mu X$, $x=2$ or 3, charm muoprod. with small angle veto 80−47306
- μp deep inelastic scatt., charm effects, field theory anal. 78−21435
- ν, charmonium and strangeonium, linear+Coulomb pot. study, high αs regime 80−62935
- ν deep inelastic scatt., charmed quark prod. 78−45905
- ν inclusive prod. of charmed vector mesons 77−18273
- ν interaction, prod. and decay of short-living heavy neutral particle 77−87971
- $\nu(\bar{\nu})$ interactions, charm model of weak interactions, parton model anal. 77−6106
- $\nu(\bar{\nu})N$, high energy dimuon prod., consistency with charm particle prod. 78−89697
- $\nu(\bar{\nu})N \to \mu^-\mu^-X$, $E>30$ GeV, prompt like sign dimuon prod., Fe target, charm prod. 79−93395
- ν-nucleus reactions, multimuon events, QCD predictions for associated prod. of charm 78−25034
- $\nu_\mu(\bar{\nu}_\mu)N$, charm meson prod. and decay, lepton inclusive distrib., c-quark fragmentation function *(Russian)* 80−52493
- $\nu_\mu(\bar{\nu}_\mu)h \to \mu^\pm l^\pm + X$, charm contrib. to prod. of opposite sign dimuons 79−377
- $\nu_\mu + Ne \to \mu^- + e^+ + X$, possible charmed particle production 77−67645
- $\nu d \to \Lambda_c{}^+X$, high energy charmed baryon prod. obs. 80−105881
- νN, charm and strangeness production, role of gluons 79−13104
- νN, charmed particle prod. due to neutral weak currents *(Russian)* 80−68447
- $\bar{\nu}N$, neutral current charm particle prod. search 80−22600
- $\bar{\nu}N$, ratio of μ^+e^- events to μ^+ events, charmed particle prod. model 78−89702
- $\nu N \to$charmed hadron pairs, decay into $\mu^-\mu^-\mu^+$ or $\mu^\pm\mu^\pm$ 77−57527
- νN deep inelastic charm particle prod., breaking of scaling *(Russian)* 77−46043
- νN interactions, dimuon prod., quark-parton model, threshold effects of charm prod. 77−46041
- $\nu N \to \mu^-\mu^-X$, charm-pair production 80−22643
- $\nu N \to \mu +$charmed baryon, SU(4) breaking effects, quark parton model 79−40792
- $\nu N \to \mu e V^0$, Gargamelle results, charm search 77−26509
- νN scattering above 50 GeV, charge asymmetry rel. to charmed particle generation *(Russian)* 77−10241

charm particles continued
νN short-lived heavy neutral particle prod., possible heavy lepton or charmed meson *(Russian)* 77−74677
νN tetramuon prod. sources, heavy quark and lepton cascades, charm prod. 78−70356
ν_μN, charm pair prod. in QCD, trimuon rate 78−45907
ν_μN, F^+(2030) prod. and hadronic decay $F^+\rightarrow\pi^+\pi^+\pi^-\pi^0$, mass 80−91085
$\nu_\mu N\rightarrow\mu^-e^+$ hadrons, Gargamelle picture anal., strange particles and charm prod. 77−54097
νp interactions, charmed meson prod., Regge pole model, cross sections 78−33052
$\nu p\rightarrow\Lambda_c{}^+X$, evidence for $\Lambda_c{}^+$(2260) prod. 80−42442
$\nu p\rightarrow\mu^-D^+X$ or $\mu^-D^{*+}p$, cross sections estimation using V+A form of charm current 77−41839
$\nu p\rightarrow\mu^-\Lambda 3\pi^+\pi^-$, E>10 GeV, inclusive 79−376
$\nu p\rightarrow\mu^-pK^-\pi^+\pi^+\pi^0$, $\Sigma_c{}^+$ prod. and decay 80−86710
$\nu p\rightarrow\Sigma_c{}^{++}X$, evidence for $\Sigma_c{}^{++}$(2424) prod. 80−42442
p, intrinsic charm from non-negligible uudc$\bar{c}$ Fock component 80−86691
p+emulsion nuclei, 300, 400 GeV, search for short lived charmed particles 77−50023
pN, 400 GeV, prompt single muon prod., charm prod. cross section 79−80855
pN, charm-pair production 80−22643
pN 70 GeV collisions, search for prompt neutrinos 79−13160
pN→charm particles, obs. in high resolution streamer chamber 80−73742
pN interaction in nuclear emulsion with single electron emission, possible charm particle prod. *(Russian)* 77−252
pp, 63 GeV, $\Lambda_c{}^+$ diffractive prod. at CERN ISR, $\Lambda_c{}^+\rightarrow K^-p\pi^+$ decay mode 79−89204
pp, ISR energies, p fragmentation, D^+ prod. from $\Lambda_c{}^*$ and Λ_b decay 80−102080
pp, prompt lepton emission, 53 GeV, e/π ratio, charm particle total inclusive cross section 78−93914
pp, prompt μ and $\mu\mu$ prod. 400 GeV, possible charm prod. 78−89750
$\bar{p}$p 12 GeV/c search for D, D* and λ_c charmed particles, charmed pair prod. 79−426
$pp\rightarrow(K^-\pi^+p)X$, scalar field with isospin, IR asymptotic behaviour of one-fermion Green's function 79−89205
$pp\rightarrow(\Lambda^0\pi^+\pi^+\pi^-)X$, scalar field with isospin, IR asymptotic behaviour of one-fermion Green's function 79−89205
$pp\rightarrow e^\pm\mu^\mp+X$, charmed meson pair semileptonic decay, inclusive charm prod. cross section 78−89759
$pp\rightarrow eX$, origin of small p, direct electrons 78−21474
$pp\rightarrow\psi D\bar{D}X$, suppression and OZI rule 77−65185
$pp\rightarrow\psi X\rightarrow\mu^+\mu^-X$, Drell-Yan mechanism in colour quark model 77−6181
$\bar{p}$p resonant annihilation, η_c charmonium state prod. cross section 80−82991
$\pi C\rightarrow\pi C'$, constraints due to PCAC and charmed-baryon couplings 79−89082
$\pi^-N\rightarrow\mu^+\mu^-+$hadrons, 225 GeV, ψ and charm prod. 78−25092
π^-p, 340 GeV, associated charm prod. evidence, $D^\pm$ prod. 80−86767
π^-p, 70 GeV/c, direct electron prod. from charm particle pair decay, e/π ratio 80−105928
$\pi^-p\rightarrow D^0\bar{D}^0n$, 40 GeV, D^0 hadronic decay search for associated prod. of charmed particles 77−13990
$\pi^-p\rightarrow D^0\bar{D}^0n$, 40 GeV/c, search for associative prod. of charmed hadrons *(Russian)* 77−6178
$\pi^+p\rightarrow\bar{D}^0C_1{}^{++}$, 4.5 GeV, prod. cross sections, decay branching ratios 78−41576
$\pi^\pm p$, 18 GeV/c, charmed particle prod. limit 78−45967
ψ, charmonium state, decay modes, prod. mechs. 77−10247
$\psi\rightarrow 2\gamma(3\gamma)$, charmonium model calcs. 77−30387
$\psi(3684)\rightarrow D\bar{D}$ decay width from $e^+e^-\rightarrow$hadrons multistate approach anal. 77−71521
ψ(4.414), width anal. in quark model 78−17010
ψ (4.03), isospin and G-parity, model independent prediction 80−86689
ψ and ψ' (3684) hadronic production, charmed straton content of straton sea *(Chinese)* 79−63434
ψ and related particle decay, data anal. using quark model and VMD 77−54101
ψ family, charmed triplet and leptonic decays 77−67622
ψ meson, e^+e^- expts. (1975 and 1976) 77−87991
ψ meson, radiative decays, charmonium model 77−38174
ψ meson spectroscopy, charmonium model, quark-confining string 78−8625
ψ particles and charm, 1975 and 1976 expts. *(Czech)* 79−26288
ψ prod. in pp and πp inclusive interactions, quark energy distrib. 77−22813
ψ spectroscopy, quark-confining string model 77−6094
ψ to charm particles, 1975 and 1976, e^+e^- colliding beam technique *(Polish)* 78−74297
ψ/J, charmed particles, particle multiplicity, distribs. in hadronic decays 77−46044
ψ/J, expt. results and interpretation, review *(Russian)* 77−269
ψ/J and ψ' production in hadronic collisions, quark-antiquark annihilation, cascade process 78−25013
ψ/J discovery, expt. details, charm particles, review 77−54113
$\psi/J(3100)\rightarrow\eta'(958)\gamma$, e^+e^- storage rings expt., upper limit on partial decay width 77−49956
ψ-meson family, fourth quark, charm 77−57492
ψ', radiative M1 transitions with charmonium model 79−13132
$\psi'\rightarrow\chi\gamma$, charmonium E1 radiative transitions and quark mag. moments 80−86721
$\psi'\rightarrow\gamma\chi\rightarrow\gamma\gamma\psi$, radiative decay width in charmonium model 77−18283
$\psi'\rightarrow\psi\pi\pi$, charm model 78−74250
ψ'''(4.414) GeV, third radial excitation of $c\bar{c}\,{}^3S_1$, unorthodox branching ratios 79−17720
$\psi''(4.028)\rightarrow D\bar{D}$, or $\bar{D}D^*+\bar{D}D^*$ or $D^*\bar{D}D^*$, strong decay theory, radial excitation of charmonium 78−12909
Σ, charmed baryon mass in SU(1,4) dynamical group theory 80−62882
$\bar{\Sigma}^\pm$ prod., 4-7 GeV e^+e^- annihilation 79−9387
Σ_c, structure of hadrons containing heavy quark, MIT bag model 80−86672
$\Sigma_c{}^+$, mass and mean life from high energy cosmic ray data *(Chinese)* 80−102045
$\Sigma_c{}^+$, production and decay obs. 80−105894
$\Sigma_c{}^{++}$, confirmation of existence from neutrino experiments 79−75770

charm particles continued
Υ(9.54) and broken SU_3 in nonstrange quark sector, vector mesons 78−58166
Υ (9.5), heavy quark charge 78−37180
Υ and charmonium spectra, common pot. fit, Υ'''-Υ mass difference 80−86712
Υ observation, charmonium, c-quark and new elementary particles *(Danish)* 79−45048
Υ spectroscopy, asymptotic freedom 78−45865
X(2.82), γ-transitions in charmonium system 78−78138
X(2.83), radiative M1 transitions with charmonium model 79−13132
$X(2.8)\rightarrow 2\gamma$ decay width, possible determ. by Coulomb photoprod. *(Chinese)* 77−57541
X(3410), J^π possible expt. meas. from $\psi\rightarrow X+\gamma$ process *(Chinese)* 77−57581
X° pair production and decay in 400 GeV/c proton interactions 79−17768
Be+n, 250 GeV/c, search for charm prod. 78−41712
Be+n, 300 GeV/c, $\mu^\pm\mu^\mp$ and $\mu^{\pm\mp}$ events, upper limit for charmed particle prod. 78−37245
$C_0{}^+$ prod. and decay, test of charmed current struct. 77−61272
F^+, SU(3) predictions for decay using new weak mixing angles 79−97619
$F_1{}^{+*}$, weak decay modes, annihilation contribs. 79−93410
$Fe+\mu\rightarrow$multimuons+X, 150 GeV/c, charmed particle prod. 77−38177

charring *see combustion*

Chebyshev approximation
B-splines basis, Galerkin method for soln. of one-dimens. primitive eqns. 78−49650
celestial mechanics, planetary orbits computation using Chebychev polynomials *(French)* 80−61997
circular disc, stress intensity factors and crack energy 78−79260
circular plates subjected to transient loads, nonlinear dynamic response 78−16648
cracks, curvilinear, star-shaped array in infinite isotropic elastic medium 78−55609
double Chebyshev expansion technique, radial Coulomb eqn. 77−37768
edge crack pair in circular disc, polynomial series 78−46914
Fokker-Planck equation, numerical soln., Chebyshev polynomial approx., first passage time probability density functions 77−37744
Fredholm integral equations, with Cauchy type singular kernels, approx. solns. using Chebyshev series 79−2611
infinite range oscillatory integrals evaluation 77−5652
least-squares structure refinement, weighting scheme, using Chebyshev polynomial 79−73067
minor planet orbit determ. using Chebyshev's approx. *(French)* 80−94720
moment theory for weak Chebyshev systems, monosplines appl., quadrature formulae, one-sided L^1-approx. 77−67248
nonequilibrium heat conduction problem, Chebyshev approx. for roots of eqn. 77−11112
nonlinear shell theory, numerical method *(Russian)* 78−34006
planetary ephemeris, direct computation method *(French)* 78−7862
planetary satellites, ephemerides representation by Chebyshev polynomials *(Russian)* 79−16800
planets rectangular coordinates, approximation via Chebyshev polynomials *(Russian)* 80−62033
plate, elastic, under uniform twisting, periodic collinear cracks *(Japanese)* 78−67097
Poisson equation, accurate soln. by expansion in Chebyshev polynomials 79−49023
polynomial method for computing analytic solns. to eigenvalue problems, appl. to anharmonic oscillator 78−62058
polynomials, appl. of method of double application 78−81843
polynomials, application to nonlinear analysis of circular plates 77−49597
projections, reconstructions and orthogonal functions 77−41463
rare earth elements, atomic partition functions, Chebyshev approximations 80−67544
satellite navigation, Chebyshev approximations for compression of Ephemerides 80−61993
shifted Chebyshev polynomials, soln. of second kind operation eqns., convergence 78−62059
spectral densities, nonnegative, moment theory approx. 77−49563
ternary system compound formation, comp. and props. w.r.t. component electron struct., computer prediction 80−103444
thermoelastic stress in cylinders, Lanczos-Chebyshev method 80−33458
three-part contact problem, Chebyshev polynomials and elliptic integrals 80−33540
train, stability of unperturbed motion *(Russian)* 78−18160
viscous flow, downstream boundary layers finite-difference and Chebyshev approx. 80−33555
wavelength calculation, selected coord. method using Chebyshev integration formulae, tristimulus values *(German)* 77−82586

chelates *see coordination complexes*

chemical analysis
see also chemical analysis by nuclear reactions and scattering; chromatography; electrochemical analysis; electron probe analysis; ion microanalysis; mass spectroscopic chemical analysis; polarimetry; pollution detection and control; radioactive chemical analysis; spectrochemical analysis; thermal analysis; X-ray chemical analysis
AC arc, variable current, element concs. during interruption time depend. *(Russian)* 78−22597
accuracy and lower determ. limit 79−52818
acid-base titrations, logarithmic diagrams for pH value and error estimation 80−35619
acoustic gas analyser design and performance 78−11603
adhesion, surface chemistry studies, anal. appls. 80−88440
aerosol S compounds, techniques for chem. comp. determ. 78−95976
AES, anal. techniques 79−43691
AES, digital acquisition and processing 79−43698
AES, low beam current density, surface anal. 78−15748
AES depth profiling with $N_2{}^+$ ion sputtering 77−16889
air, polyurethane foam sampling system for organic compounds detect. 78−20080
air analyzer, automatic, calibration system, zero and span standardization 79−16107
air pollutant analysis and control instrumentation and organisation *(French)* 78−20549

chemical analysis continued
air pollution, gaseous, aerosol and particulate methods of chemical anal., review 80—7876
air pollution impurity concentration meas. methods survey *(Dutch)* 77—70826
air pollution measurement, particulates and gaseous pollutants anal. and calibration techniques 78—69531
air pollution monitoring system, minicomputer-based 77—66984
air-pollution gas analyzers, testing instrums. 79—8715
alloys, local composition determ., assessment of TEM direct lattice imaging technique 78—53294
alloys, surface segregation, atom-probe FIM quantification investig. 78—62263
alloys and mixed crystals, ellipsometric method of comp. determ. 80—35615
ambient air analysis, area survey and sampling mobile laboratory 80—104528
amine solutions, US analysis method 78—7277
amino acid analyser, LKB 400 automatic ninhydrin, new sampler loader 80—101916
amino and isothiocyanate groups on inorganic supports for immobilized enzymes 79—61920
analyser design impact of microprocessors *(German)* 78—61096
anodic film, automated interpretation of ellipsometer obs. 78—56902
aromatic acids, mixtures, quantitative anal. by ^{13}C NMR 78—31716
arteriovenous O_2 difference, noninvasive meas. method *(German)* 78—85441
asbestos, elemental intensity ratio variation used to identify fibres 80—3462
asbestos fibres concentration meas., in air and liquid, analytical methods review 80—72120
atmosphere, $NO/NO_2/O_3$ monitors intercalibration 78—69529
atmosphere, non-methane hydrocarbons monitoring via photoionisation 78—73549
atmosphere high acidity analysers, comparative tests near industrial installations in Fos-Etang de Berre region 78—81464
atmospheric aerosol, ground level meas. in Northern Greenland 78—85645
atmospheric aerosols, chemical characterisation, progress and problems 78—68969
atmospheric contaminants, detect. by laser absorptiometry 79—21004
atmospheric dust *(Dutch)* 79—16713
atmospheric NH_3 determ., method 80—56614
atmospheric particulates, chemical characterisation via light scatt. method 78—69533
atmospheric pollutants, gaseous, analytical control, review 80—101140
atmospheric pollution monitoring with mobile laboratory 79—83670
atmospheric precipitation, trace constituents chemical anal. in global baseline samples 79—16566
atmospheric pressure chemical species, stroboscopic extraction into regions of high vacuum 77—77858
atmospheric trace analysis, selection of calibration gas standards 77—91255
atmospheric trace gas IR monitor, airborne, nondispersive 79—8719
ATP determination, extracellular, in native platelet-rich plasma 77—25615
Auger digital scanning electron microscope 78—12797
Auger electron spectroscopy, quantitative analysis 77—85852
Auger electron spectroscopy blanking resistive heating cct. 77—29078
Auger microanalysis, high resolution, review 80—40792
Auger photoelectron spectrometer, high resolution 77—48704
Auger scanning microscopy, using beam brightness modulation 79—16097
automated multisample-stream chemical monitoring system 77—44531
automated rapid system for anal. of dissolved organic N in natural waters 78—93014
automatic gas analyser, meas. errors due to gas-water interaction *(German)* 78—44438
automatic gas/gaseous mixture thermal cond. analyser *(Spanish)* 78—76972
automatic system using microwave heating device 78—88666
automatic titrator, microcomputer controlled, for chem. anal. 78—27841
automation, appls. of bit-oriented I/O struct. 77—44532
Barnwell nuclear fuel reprocessing plant, remote sampling and on-line anal. system 79—13511
beta emitters, identification using absorpt. coeff. in Al, accuracy 77—57837
binary alloys, relative sensitivity factors by quantitative Auger analysis 77—60151
biological materials, electron energy loss spectroscopy anal. appl. 79—39269
biological samples, trace metals determ., microwave oven-based wet digestion technique 78—92542
biological specimens, ionising radiation damage at low temps., effects on microanal. 79—39453
biomedical instrumentation, status reports, appls. 77—25570
blood gas analysers, review 78—69238
blood gas analysis data processing system *(German)* 79—5419
blood gas monitor for extracorporeal procedures 79—100756
blood glucose monitoring technique for appl. in artificial endocrine pancreas 78—36062
blood plasma filtration, stagnant 77—48948
BOD values, short time determ. methods comparison *(Japanese)* 79—48192
boiler NO_x formation study during combustion 78—3434
bone mineral concentration estimation by beta-ray backscatt. *(German)* 78—69179
BULK: a computer program for calculating bulk-chemical analysis from mineral phases observed in thin section, FORTRAN IV program listed 79—2378
bytownite megacrysts., study of trapped basaltic melts, petrogenetic process study 78—95688
cellular mechanical and chemical analysis, recommendations of workshop on future of biomedical instrum. 80—81776
chalcogenide glass film, drift and thermal diffusion of Au electrodes, α-particle backscatt. meas. 79—4434
chalcogenide semiconductor amorphous film comp. monitoring by EPR 77—51940
channelling measurements, by Rutherford backscatt., resolution improvement 79—5209
characterisation and analytical techniques *(Japanese)* 77—84735

chemical analysis continued
chondritic meteorites, analytical scheme, appl. to Cocklebiddy 79—2483
chromatographic columns in parallel, equipment for measuring gas flow rate 80—21336
chromatography, liquid, detector characts. and use, book 78—15751
clay, thermobalance method of determ. and anal., modification 77—29073
clinical, using OLLI 4000 KLS microcomputer *(Swedish)* 77—44764
clinical analyser, customer serviceability design 78—44653
coal, ash content, determ. by forward-scattered γ-radiation, improved accuracy 78—7280
coal, mag. and Mossbauer characterisation 78—64903
coal analysis, Cl_2 content determ. using British Standard high temp. method 80—85252
coal gasification reactor atmospheres, industrial gaseous environment characterisation, Brinkley method 80—93817
colorimetric analysis, automatic, biological fluids, contamination study 77—25564
combustible gas and vapour monitoring, MOS sensors 79—16104
combustible gas detector, operational tests 79—16105
combustion sensor, Ca-Mg-Zr pipe-form ceramics appl. *(Japanese)* 80—55761
combustion system atmospheres, industrial gaseous environment characterisation, Brinkley method 80—93817
composition analysers, electronic self-balancing system, turbidity meter appl. 80—16754
composition meas., pneumatic process transmitter appl. 77—36854
composition variation determ. using electrolyte electroreflectance 78—80809
compound conductors, impulse heating, Cu vapour conc. determ. 80—75346
computer aided materials analysis 77—77843
concentration meas. by portable optoelectronic convertor 78—80820
concentration meas. kinetic reaction equation parameter determ. *(German)* 77—66782
concentration of poisonous and explosive gases, test tube indicator *(German)* 77—4950
condensation nuclei counter, particle conc. determ., particle size effects 79—20476
Conference, nuclear materials, safeguards and accountability meas., Williamsburg, USA (May 1978) 79—81045
conference on analysis instrumentation, Charleston, West Virginia, USA (May 1977) 79—16100
contamination in trace analysis 79—52842
contamination products from cinematographic film processing, in main drainage systems, anal. methods *(Russian)* 79—89023
coulometry, value of the Faraday 80—22320
crime prevention measures, metallic, explosive, and narcotic objects detect. *(Italian)* 79—100465
crystalline solids, electronic industry, chem. anal. instrumental methods progress 80—66903
Curie point pyrolysis system for hydrocarbon anal. 77—77854
cyclobutanone, absorpt. of pulsed IR radiation and decomp., joulemeter and opto-acoustic obs. 80—58328
cyclobutanone, IR laser photolysis sensitised by NH_3, and reaction temp. 79—47944
data acquisition, computer operational system *(German)* 78—27845
data factor analysis, reliability improvement 77—36802
depth profiles, ion scatt. technique, digital data collection 78—56942
depth profiling of light elements in materials with high-energy ion beams 77—59036
determination in organic cpds. and biological samples by combustion method with isotope exchange 79—57333
determination of minor impurities and alloying constituents in steel, appl. of inductively coupled plasma spectrometry 80—90903
dialysis expts., model, monitoring using chromatography refractive index detector 79—96724
digitizer for generating computer readable chem. data 79—74454
dihalogenated benzene derivatives, 77K, gamma radialysis radical pair formation, EPR 79—29334
dilatometric titration, pressure transducing instrum. appls. 77—36810
dilute solutions preconc. by nonboiling evap. 79—79327
N,N-dimethylcarbomoylchloride, chem. exchange rate by NMR method, temp. depend. 79—79243
dyestuffs in polymers, conc. distrib., microdensitometric determ., stops effect *(German)* 78—11598
EELS, filtered images 80—101062
EELS, in STEM, multi-channel averaging 80—101061
EELS, microanalysis, quantitative approach to inner shell losses 80—101059
EELS, standard for TEM, implanted Si 80—99017
electric insulating oils, composition, physical and chemical props. and determ. of free radicals *(Rumanian)* 80—97745
electrolyte concentration meas. instrum. using laser diode, optimsation of parameters 79—20488
electron capture detector, theoretical model 77—40620
electron energy loss spectroscopy, anal. appl., processing requirements 79—43692
electron energy loss spectroscopy for direct elemental analysis 80—71998
electron microscopy techniques, review, 1976-77 78—82077
electron spectrometer for microchemical anal. in 100 kV TEM 79—39251
electron spectroscopy, book 78—16896
electron spectroscopy, coincidence experiments, two-parameter 78—20135
electronic gas detection, Pellistor, VQ and TGS sensors *(Spanish)* 80—93832
electronic techniques appl. *(German)* 77—77841
electrophoretic ion focusing *(German)* 79—57334
ELISA and immunofluorescence, comparison 80—97749
ellipsometry of electrochem. surface layers 78—56874
energy loss spectroscopy, localised chemical characterisation *(French)* 77—77850
environmental analysis, recent advances, book 80—41961
environmental analytical chemistry developments 79—53006
environmental chemistry, anal. techniques, conf., Barcelona, Spain, (Nov. 1978) 80—88038
environmental microelements determining appl. of present ashing methods, critical anal. *(Bulgarian)* 79—88043
environmental radioactive pollution by U industry, monitoring using analytical chemistry 80—95488
environmental science, trace analysis *(Japanese)* 77—87116

chemical analysis continued
EPR sample cell for lossy samples 77–90664
error analysis of analytical results 80–21341
ESCA, appls. in industrial research 79–74462
estuarine waters, behaviour of trace chem. constituents 79–16512
ethyl cellosolve acetate on wafer surface, analysis of trace amounts 78–3433
ethylene, CW CO_2-laser irrad., low-press., chem. relax. 79–74404
ethylene furnace atmospheres, industrial gaseous environment characterisation, Brinkley method 80–93817
experimental data interpretation 78–77827
fast chemical separation procedures for short-lived nuclei 77–25351
ferrofluids, magnetic material conc. distrib. meas. device 78–16821
ferrographic particle separation technique for wear analysis 79–70395
ferronickel, thermoelec. determ. of Ni content 78–40096
Fisher moisture content determ., using titrimetric analyser with ammeter pick-up *(Russian)* 80–71984
fission reactor fuel and materials *(Japanese)* 79–26519
fission reactor safety, role of analytical chemistry in accident control, assessment and recovery 80–95389
fission reactor spent fuel γ-ray spectrometry and chemical analysis 78–54841
flow injection analysis, technique, appls. 80–55734
fluorescence immunoassays, review 79–79693
fluoropolymer adhesive joints, fracture and surface anal. by SEM and ESCA 77–55434
fossil fuels, appl. of cross-polarisation ^{13}C NMR with magic angle spinning 80–77819
gamma-scanning activation anal., optimal absorpt. thickness 79–70401
gas analyser, based on thermocouple vacuum gauge 80–61183
gas analyser, portable, 1920 to 1978 development 78–61124
gas analyser operation, uncontrolled component influence Wheatstone bridge appl. *(Russian)* 77–36845
gas analyser thermal, two-bridge, based on voltage ratios meas. 80–50907
gas analyser with acoustooptic detector and semiconducting generator based on Gunn diode *(Russian)* 80–101141
gas analysers improvement, thermomagnetic for use in power stations *(Russian)* 80–3445
gas analyzers, fast-response, dynamic characts. of primary measuring transducers 80–4697
gas and fluid analysis, continuous and quasicontinuous methods *(German)* 78–44437
gas composition and halogen concentration, solid electrolytic cell appl. *(Russian)* 77–40609
gas content analyser *(Russian)* 77–44557
gas microconcentrations in air determ., metrological certification of meas. methods 80–55972
gas mixture, using Krichevskii-Kazarnovskii equation, w.r.t. virial coeff. 77–11294
gas mixture production method, composition control 78–1765
gas mixtures, standard, SMES-2 system for metrological support 79–20487
gas mixtures preparation, (1 to 10^{-3})% molar range, installation for testing and calibration 80–99030
gas purity under measuring conditions, W-value determ. *(German)* 80–104489
gaseous emission from in situ sources, field experience 79–16660
gases, moisture content determ. using photocolorimeter 78–56936
gases, thermophysical props. tabulated for mixture composition certification 78–80818
Gay-Lussac, Joseph Louis, achievements in anal. chem. 79–49001
geometrical and chemical knowledge at high resolution, electron microscopy and inner shell excitations 80–79646
geothermal waste water, environmental effects on river system 79–29487
glass, Libyan Desert Glass, redox form. conditions, EPR obs. of as-received and irrad. samples 78–28228
glass, ultrapure, prep. for optical waveguides, review 78–3086
glass fibres, types E and A, surface composition, effect of ageing, reduction, exam. using X-ray photoelectron spectroscopy 79–20223
glass fragments discrimination, window, container glasses, forensic science appl. 79–11841
glass surfaces, corrosion, passivation and anal. 78–60854
gram atomic volume, density, atomic mass, packing factor, eqns. for calc. 79–95066
graphite furnace power supply control to allow interruption of analytical cycle 77–21432
graphite-AsF_5 intercalated species, fractional ionisation and identification 80–97397
gravimetric, pH titration system, computer controlled, for complex equilibria in soln. anal., appl. 79–87892
halofluorocarbons, in ambient air, background levels in situ quantification 78–69530
heavy ion deep inelastic processes fragments, element identification in ΔE-E telescope, computerised method 77–57839
heavy ion identification, using modified Zaidins empirical range-energy relationship, power law type algorithm anal. 77–57838
heavy metals, in aquatic systems, distrib. and speciation techniques 78–69390
hexamethyldisiloxane, polymer film, struct. determ., IR spectra, elemental anal. *(German)* 77–59224
high freq. induction melting and centrifugal casting, working curve sample prep. photoemission anal. *(Japanese)* 78–53050
high pressure preparation lock for surface analysis in ultrahigh vacuum chamber *(German)* 80–52261
high pressure pressure-jump apparatus for fast reactions in solution 80–62681
high resolution Rutherford backscatt. techniques, appl. to near surface anal. 79–5207
high temperature gas and vapour characterisation, conf., Gaithersburg, USA (Sept. 1978) 80–53910
high-temperature gases, equilibrium composition calculation *(Russian)* 79–20499
high-volume preparation of air to standard quality for zeroing analyzers 80–90829
holographic interferometric microscopy, appls. 77–34015
hot water springs in N.Spain, trace elements concs. *(Spanish)* 77–49097
hydro-chemical analysis of water routes flood gate of hydroelectric plant *(Croatian)* 80–12443
IC with Si substrate, new microanalytical method *(French)* 78–35760

chemical analysis continued
III-V semiconductor, and related cpds., low energy ion scattering spectrometry *(French)* 80–71551
impurity, Auger spectral analysis 77–15671
impurity profiling with 2.5 MeV van de Graaff accelerators 79–77626
industrial flare flames, smoke detection and control by electric fields 78–81360
industrial gaseous environment characterisation, Brinkley method 80–93817
industrial wastes, Mg recovering, use of sink-and-float test *(Japanese)* 80–55948
information theory applic. 78–3393
inorganic ions, adsorbed on porous SiO_2 glass in distilled water medium, determ. 79–24814
inorganic micro and trace analysis, historical perspectives 78–81784
inscribed jars found at Thebes, inconsistencies in comp. and provenance studies 79–26197
instrument use and planned acquisitions 78–88684
instrumentation, discussion of future under microcomputer advances 79–83536
instrumentation system, computerised, real-time 79–12786
intravascular O_2 saturation continuous meas. using fibre optic catheter *(German)* 78–85411
iodobenzene, soln., non-linear dielec. effect, comparison with fluoro, chloro and bromobenzene 80–60478
ion implantation, quantitative theoretical aspects 79–69140
ion-selective membrane electrodes development, Ag ion conduction ceramic systems *(Japanese)* 80–61203
IR gas analyser, non-dispersive, for industrial processes and environment protection *(Hungarian)* 80–55735
isotope dilution analysis, displacement and exchange reactions appl. 79–52834
kinetic and equilibrium assays, effect of reaction extent, uncertainty of rate parameters 79–34373
kinetic aspects, review 1975-1977 78–85216
kinetic method insensitive to variables affecting rate consts. 79–34374
labile species, electron photoejection, reaction kinetics characterisation 80–26089
laboratory computer networks 79–52797
laboratory methods, statistical evaluation, acceptability criterion 77–63977
laser interferometry in analytical ultracentrifuges, background suppression of multiplexer-gated modulatable laser 80–73430
light element chemistry of Apollo 12 site regolith samples 78–65515
linear parameter estimation, for chem. anal. 79–24843
lipids, modified iodometric method for peroxide conc. determ. in small samples *(German)* 79–52799
liquid, detection of impurities using moire patterns 78–8440
low-alloy steel, photometric anal. by time resolution of radiation *(Russian)* 78–23995
low-atomic-mass solids, high precision depth profiling of light isotopes 80–66902
lunar soils, volatile trace elements determ. by RNAA 79–44276
lung gas analysis using redox gas sensors *(German)* 78–85440
magnesite refractories, spinel bindal, with reduced thermal cond. 79–83162
magnetic susceptibility applications, review of literature 1975-1977 78–82006
marine atmosphere, SO_2 meas. at concs. lower than ppb 78–81340
marine minerals, anal. and exploration by Mobile Initial Condition Indicator 79–5687
Martin steel, thermoelectric determination of C content during melting 77–56276
medical laboratory automated procedures and equipment development *(Japanese)* 77–44766
medicine, paramag. O_2 analyser, for teaching 78–49622
membrane filters in air anal., review 79–79316
metal, microdetermination of C, purification of O_2 and flux selection *(Japanese)* 78–92571
metal interaction with gases and C, conf., Stuttgart, Germany (Sept 1977) *(Russian)* 79–57134
metals, group VA, O and N determ. from internal friction meas. 79–39246
methanol, chemisorption on Ni(111), methoxy species, electron energy-loss spectra 79–29391
microchemical techniques, conf., Davos, Switzerland, (May 1977) 78–85254
microchemistry, history *(German)* 78–81785
microcomputer system for automating analytical instrumentation 78–73127
microcomputer-based digital titrator 78–80805
microdensitometers, props. effect on photographic emulsion charact. curve 79–43673
microprocessors and millivoltmeters appl., 1978 exhibition in Munich *(German)* 79–20482
microscopy, use of squaric acid as reagent 77–21450
microscopy applications, review of literature 1976-1977 78–85221
mineral ores 77–41027
minicomputer appls., errors 78–92543
mixture chemical analysis, direct interferogram comparison of chromatography/Fourier transform IR spectra data 79–100458
mixtures, multicomponent, by method of additions 80–61187
mixtures of compounds, statistical analysis 77–52697
molecular configurational similarities, computer-assisted-examination of substructs. 79–81294
molecular configurations, augmented connectivity molecular formula 79–83542
molecular formulae and homologous series, inverted file structure for searching large data bases 78–35738
molecular ions, gas phase, spectroscopic props, review 78–33501
monitoring laboratory, installation 78–61123
moulding materials and mixtures, exam. of gases released 79–52817
multi-purpose instrument for biochemical and related undergraduate studies 78–73816
multicomponent analysis computations based on Kalman filtering 80–40772
N-nitroso compounds, estimation in environmental samples at parts-per-billion level 79–74448
natural and industrial objects, quality control, future programme, computer appls. 80–104484

chemical analysis continued
nematic liquid crystal material analysis in production quantities 77—76309
NMR and EPR appls., conf., Denver, CO, USA (Aug. 1979) 80—90598
NMR chemical shift, hidden partner analysis 79—43554
nomenclature for scales 79—66387
nonlinear calibration, theory 78—32784
nonspecificity coefficients of analytical methods 78—7305
nonspecificty coefficients of analytical methods, estimation and verification 78—7306
NQR short range remote spectrometer for anal. 80—55742
nuclear fuel reprocessing, conf., Gatlinburg, USA (Oct. 1977) 79—9847
nuclear fuel reprocessing, input analysis, verification *(German)* 78—70623
nuclear fuel reprocessing and refabrication, quality control 79—13506
nuclear fuel reprocessing plant, in-line monitors 79—13509
nuclear material accountability, analytical methods and laboratories, present and future 79—81047
nuclear materials, nondestructive assay instruments for DYMAC program 79—11875
nuclear materials safeguards, LASL analytical chemistry program 80—78380
nuclear materials safeguards and materials control, meas. tech. conf. Charleston, SC, USA (November 1979) 80—77544
nuclear oxide fuel anal., coulometry, emission anal., chromatography, X-ray anal. 80—18420
nuclear reactor atmosphere, helium cooled, industrial gaseous environment characterisation, Brinkley method 80—93817
nuclear safeguards, anal. chem. in nucl. fuel reprocessing 79—13505
nuclepore filters, clogging, cap form. model 79—20468
O_2 index test, measurement and appl. 79—79337
obsidian, hydration profiles meas. by sputter-induced optical emission, rel. to dating technique 79—24871
oil immersed transformers, dissolved gas causes and phenomena, anal. *(German)* 80—76570
optical fibres, ultratrace impurities determ., and behaviour during production by CVD process *(Japanese)* 80—87505
optical methods appl. possibilities *(German)* 77—36841
ore analysis by selective gamma-gamma method, elimination of geometrical effects 78—44425
organic C, dissolved in water, meas., new approach 79—74582
organic carbon analysis, automation 80—45592
organic compounds, trace analysis 78—85255
oxide phase identification, electron re-emission Mossbauer spectroscopy 77—16752
oxides, stoichiometry meas. and control 78—51694
oxidisability of water, determination using titrometric liquid analyser 79—79441
partial atomic vapour pressure, meas. by forward light scatt., transverse mag. field 79—16087
particle analysis, SIMS appl. 79—43695
pepperbush powder, a new standard reference material 79—39227
pesticides, organochlorine, determ. in soils 79—92098
pharmaceutical quality control, automation and filing system 79—52798
phase composition, quantitative anal. 77—52709
phosphosilicate films, deposited, P conc. meas. 79—69014
phosphosilicate glass, AES quantitative anal., electron irrad. induced surface comp. changes 77—48709
photochemical reaction temperature during laser photolysis, by use of cyclobutanone impurity 79—47944
physical adsorption, vacuum microbalance studies 80—76551
physiocochemical meas., modular equipment and microprocessor control *(French)* 80—30304
plastic sample containers, for trace element samples, selection, cleaning methods 78—35745
plastics identification by simple qualitative tests 79—5944
plating line Co concentration monitoring, by automatic colorimeter 80—105691
polarizing microscope components and applications 80—98973
pollutant particles, characterised by AES and XPS 79—43694
pollution control, polarisation and interference microscopy appls. 78—61544
pollution due to vehicle exhaust emissions, meas. and testing procedures survey and criticism *(German)* 77—56299
polychlorinated biphenyls, determ. in soils 79—92098
polycyclic aromatic hydrocarbons sorbed on fly ash, recovery for quantitative determ. 80—61177
polyethylene, low-density, mol. characterisation 79—52843
polyethylene terephthalate fibres, high freq. US effects on physical and chem. structs. *(Polish)* 78—51446
polymer systems, sedimentation field-flow fractionation in macromolecular characterization 80—66879
polymers, appl. of cross-polarisation ^{13}C NMR with magic angle spinning 80—77819
polystyrene lattice, emulsions-polymerised, particle size determ. by soap titration 80—40753
ponderomatic meas. for fluid detection in chem. anal. 78—68953
porphyrins, determ. in blood by phosphoresc. of porphinatocopper(II) 78—11574
portland cement concrete, determination of hydrated cement content by differential thermal analysis 79—79335
Portland cement-fly ash, physico-mech. props., SEM and X-ray diffr. anal. 79—74239
power transformers, electromagnetic testing of partial discharges for failure and breakdown prevention *(Russian)* 80—97743
preconcentration in inorganic trace analysis 78—85256
probe sampling rate, effect on sample composition, gas-phase combustion 77—52691
programmable pipette, microprocessor controlled stepping motor, repetitive dispenser appl. 80—42205
propane gas detector using SnO_2 doped with Nb, V, Ti, or Mo 79—29426
protein titrations by NMR, pH depend. of internal reference 77—86727
pseudobinary systems, internal calibration technique for quantitative analysis, AES 77—36834
pulse counter, high-speed DC coupled, sensitivity and performance 79—89524
pulse counting measurement systems, optimum parameters determ. 79—89523
pyrocarbon coatings, quantitative chemical method to determ. disordered C component 77—79462

chemical analysis continued
quantitative image analysis, applic. to mineralogy *(French)* 79—5631
quartz sand, pilot tests of acoustic device for dressing 78—7271
radiation chemistry instrumentation, in Inst. Nuclear Res., Warsaw 78—76888
radioactive particulates in gaseous effluents at nuclear fuel reprocessing facility 79—9848
representation space transform. to preserve chem. data struct. 79—74451
residual gas analyser, microprocessor-based 79—26175
rhodamine Zh, isomer separation, identification and emission efficiencies *(Russian)* 77—83871
rock, biotite gneiss and amphibolite mode estimation, using FISK (FORTRAN) program 77—86397
rubber, analysis and characterisation, literature review, 1974-76 77—77814
salt water analysis, Schales and mercuric nitrate methods *(French)* 77—78432
Savitsky-Golay convolution method, for least-squares fit smoothing and differentiation 79—16059
scanning Auger microanalysis, review 79—43699
scanning ESCA, operation and limitations 77—36818
scattering spectrometry, appl. with protons, 5 to 8 MeV, and heavy ions, 15 to 25 MeV, to special anal. problems 79—5210
schorl tourmaline, elastic const. 78—68718
scirpene toxins, in animal feeds, chem. anal. 78—48707
sea and beach persistent oil spill identification methods 80—90101
seawater, computerised high-precision titrations of major constituents 77—66926
seawater, excess ^{3}He and ^{4}He in Galapagos submarine hydrothermal water 78—40593
secondary electron emission ion detector, low noise, high voltage for polyatomic ions 77—40601
secondary ion yield, linear variation, quantitative anal. of mineral silicates *(French)* 80—108763
SEM, automation, quant. anal. of elementary images *(French)* 78—78045
SEM microanalysis techniques, review 80—71995
semiconductor characterisation and analytical techniques *(Japanese)* 77—84735
semiconductor devices, FETs, diodes and pyroelec. devices 77—52720
semiconductor impurities, trace element anal. 80—81399
semiconductor impurity anal. by photoelectric spectroscopy, review 77—24584
silica gel, skeletal struct. modification with alcohols and water vap., thermal analysis obs. 78—88659
silicates, ion bombardment, secondary positive mono-atomic ion emission, cation conc. depend and matrix effects *(French)* 80—50487
simplex optimisation calcs., high speed algorithms 80—40767
small particle identification, review 78—48739
smoke gas absorption by $MgSO_4$ nH_2O crystal *(Russian)* 77—52712
soil, ^{89}Sr and ^{90}Sr determ. using total sample decomp. 80—35808
solid surface, microgravimetric-IR study 80—76577
solid surface and thin film anal. methods, review 79—34410
solid-solid interface chemistry, characterisation, theory 80—75448
solids in water, measurement standard, macerated glass fibre filter paper, water analysis appl. 79—8454
spent THTR fuel, in-line and off-line destructive chem. anal. 79—13508
standard gas mixture preparation at high pressures certification 78—93718
standard sample homogeneity evaluation, optimal obs. planning 80—93721
Stark modulation for analytical microwave spectrometry 77—13802
static methods for certifying composition of binary gas mixtures 78—76961
steam reformer atmospheres, industrial gaseous environment characterisation, Brinkley method 80—93817
steel, austenitic→pearlitic transformation, partitioning, atom probe microanal. 80—3079
steel, austenitic type 304, temper embrittlement and surface segregation an AES and ionization loss spectroscopy study 79—43372
steel, corroded, Mossbauer effect anal. of corrosion products 78—19943
steel, Cr-Mo (2.25, 1 wt.%), decarburization, carbide effects in high temp. Na *(Japanese)* 78—15403
steel, Cr-Mo (9, 1 wt.%) appl. of electron energy loss spectrometry to precipitate morphology 78—48414
steel, Cr-Mo-V, low alloy, V effect on creep *(Czech)* 77—86088
steel, high alloy, instrumental anal., use of HF induction melting and centrifugal casting *(Japanese)* 77—56280
steel, high alloy, preparation for instrumented anal., HF induction melting, casting 78—48607
steel, high alloy, rapid anal., use of central laboratory computer *(German)* 77—48703
steel, industrial, surface, chem. characterisation by SIMS, glow discharge spectrometry and other techniques 80—66907
steel, Mn-Cr-V, structural changes during solution annealing *(Czech)* 78—84864
steel, nitride inclusions, identification by differential thermal anal. and evolved gas anal. 78—48721
steel, stainless, 316, surface analysis by SIMS, SEM AND ESCA 79—52825
steel, stainless, nitride phase determination method 78—7276
steel, stainless, vacuum transfer technique for Tokamak in situ surface anal. 79—2778
steel, stainless type 316, neutron irradiated, or themally aged diamond-cubic η phase formation, TEM study 79—99249
steel, thin sheets, C and N contents determ. by internal friction *(German)* 78—27715
steel, W content, rapid anal., scattered radiation recording using γ-absorpt. method 77—73489
steel 18 Gps, chemical composition effect on strength, statistical treatment of test data 79—57081
steel powder, high speed, S and O reduction in a H_2 gas stream 80—61015
steels, free-machining, fractography and X-ray photoelectron spectroscopy 80—7673
steels, nuclear reactor pressure vessel steels, optimum chem. comp. rel. to props. 80—93517
steroids, mixtures, quantitative anal. by ^{13}C NMR 78—31716
stopped-flow systems, automated, for fast react. rate anal. methods, review 78—95971

chemical analysis continued
- stratospheric ozonometer, using chemiluminescent reaction of ozone and olefins *(French)* 79−48574
- submersible liquid level alarm for evaporative concentration 79−74457
- sugars, detect. in HPLC systems using polarimetry, refractometry and optical rot. 78−48734
- sulphate aerosol, individual submicron particles detect. technique 78−69527
- superalloys, phase extraction, chemical and X-ray diffr. anal. 78−72951
- surface, single cryst., comp., and struct. analysis using low energy ion scatt., review 79−87547
- surface analysis, desorbed ions identification from high voltage pulse shapes 77−12502
- surface analysis, ion implantation and ion beam anal. in same UH vacuum sample chamber 77−4970
- surface analysis, quantitative, using ion-induced secondary ion and photon emission 77−86423
- surface analysis, review of AES technique and applications 78−68946
- surface analysis, review of ion scattering spectroscopy 78−68948
- surface analysis instruments for vacuum electronics *(Czech)* 77−18145
- surface analysis techniques and appls., symposium, Dayton, USA (Jun. 1979) 80−62363
- surface analysis techniques appl., electrification phenomena 80−80354
- surface analytical instruments, present status *(Japanese)* 78−80823
- surface characterisation, XPS and AES techniques 77−32495
- surface composition depth profiles, ion sputtering effects 80−35616
- surface contaminants analysis by plasma mass secspectroscopy 78−3433
- surface ionis. identification, adsorbed amines and hydrazines on ioxidised metal surfaces 77−21456
- surface potential changes meas. upon adsorption of gases using static capacitor method 80−62691
- surface reactivity investigation, techniques and appls., review *(French)* 79−92000
- surface-active agents, determ. in waste waters, review 79−53007
- surfaces, characterisation, literature review 1970-76 77−77816
- systematic analytical errors of multicomponent materials, exposing and calc. methods 78−7274
- TDPAC, appl. to chemistry and solid state physics, review 79−75665
- teaching, grading methods for quantitative analysis 79−48993
- teaching, problems 78−81736
- techniques for archaeological artefacts 80−89575
- TEM, quantitative elemental analysis 80−101060
- terrestrial minerals, volatile trace elements determ. by RNAA 79−44276
- thermal field-flow fractionation, peak broadening, plate height effects 78−20088
- thermo-plasma-chemical gas analyser appl. *(Russian)* 77−44560
- thermobalance for studying high-temp. sulphidation kinetics of metals 78−23876
- thermochemical analyser, continuous flow, high sensitivity 79−92022
- thermochemical gas analyzer, porous flame barrier, reagents, reaction products, conc. diffusion *(Russian)* 79−29359
- thermogravimetric analyser, low cost design 78−20116
- thermomagnetic gas analyser with internal convection, model simulation 77−56296
- thin film analysis and characterisation, conf., Les Arcs, France (Jan. 1978) *(French)* 79−8466
- thin film structures, chemical anal. by Auger spectroscopy *(Russian)* 78−92581
- thin films, chem. anal. by energy loss spectroscopy 80−104493
- thin films, thickness meas. anal. characterisation using proton-induced X-ray emission 80−35618
- thin films and interfaces, analytical techniques, review 80−80120
- thin foil, quantitative microanalysis, by energy loss spectroscopy *(French)* 80−50900
- thiorhodites, $M_xRh_{3-x}S_4$ (M=Cu,Co,Fe), thermal stability and thermochem. props. 79−86904
- thymine fragment damage retained in DNA polynucleotide chain after γ irrad. in aerated soln. 78−31773
- time sharing computers, data processing and optimisation appls. *(German)* 78−35750
- tinplate surfaces, Auger depth profiling and anal. 80−59768
- tissue lipid content analysis by photon absorpt. using ^{153}Gd 78−28041
- tissue-equivalent plastic A-150, density and composition uniformity 78−73252
- titration end-point, determ. using second derivative curves 79−84909
- titrator, microcomputer-controlled 79−74444
- titrator, microprocessor-controlled 79−74455
- titrimeters, reference materials for metrological certification using chromatometric reactions 79−34402
- total current spectroscopy 80−45185
- toxicity experiments, processing of automatic analyser data using trace reader and computer 78−24195
- toxicity studies, TOXIPAC-300 data processing system *(Japanese)* 79−25172
- trace analysis, state and development *(German)* 78−68956
- trace element analysis, pattern recognition techniques 77−40588
- trace element analysis, pH adjustment by gaseous reagents 78−73094
- trace element measurement, statistical evaluation 79−87921
- trace element profile of a California Redwood tree for environmental monitoring 80−97850
- trace elements in environmental materials, reliability aspects 78−40106
- trace gas analysis, microwave surface wave plasma production and appl. 79−19059
- trace impurity analyzer for He refrigerator systems 79−70388
- transformer testing, preventive, by analysis of gases dissolved in transformer oil *(German)* 80−71969
- transient species, form., quantitative anal. by extrapolation method 78−15685
- transition metal disilicides, powdered, determ. of free metals, oxides, photometric method 78−61101
- transition metal ferrocyanide selective sorbents for alkali metals, sorptive props. w.r.t. struct. 80−101051
- transuranic elements, in situ. conc. determ. using passive neutron monitoring 79−87933
- triboelectric charging technique for surface contamination analysis 80−11966
- trihalomethanes, determ. in water, comparison of dynamic and static head space and solvent extraction techniques 79−92114
- trihydroxybenzophenone on wafer surface, analysis of trace amounts 78−3433

chemical analysis continued
- turbulent dispersion concentration valves, system for wind tunnel meas. 79−5191
- ultra high vacuum technology developments *(Japanese)* 78−49845
- ultracentrifugation technique for direct meas. of DNA sedimentation consts. *(French)* 80−8004
- uracil, aq. soln., fast electron induced radical identification 79−24870
- urban plume particulates collected on Anderson 8-stage impactor stages, chemical anal. 78−69433
- user-oriented software Fourier spectrum display 78−64896
- vacuum instrumentation, specimen manipulator 79−63245
- vapour dynamic diffusion batcher with porous partition 78−79404
- vapours and gases, high-temp. characterisation, conf., Gaithersburg, USA (Sept. 1978) 79−40579
- Venus atmosphere, anal. by automatic interplanetary stations (Venera-4, 5, 6 and 8) 78−28520
- volatile trace organics, aqueous environmental samples, head space anal. 80−40763
- waste-water, use of total oxygen demand meter 79−96399
- wastewater treatment, instrumental anal. 79−74432
- water, dosing of vapour in vac. system to calibrate analysers 77−32850
- water, surface and effluent, analysis of nitrate content using potentiometric and colorimetric methods 79−100476
- water analysis, review 80−7877
- water concentration automatic chemi-luminescent meas. *(Russian)* 77−66784
- water sample, automated anal., pH, conductivity, alkalinity 79−12287
- wear debris anal., quantitative methods 78−64912
- X-ray energy dispersive spectrometry, applic. to mineralogy *(French)* 79−5630
- X-ray photoelectron spectrochem. quantitative analysis *(French)* 77−36836
- $Z>103$ transactinides, method for rapid separation and identification 77−26952
- β-$2CaO$-SiO_2, hydration mechanism and rate, SEM and chem. anal. 79−79218
- Ag films, electrodeposited and vac. deposited, AES depth profiling anal. 77−59232
- Ag-Cu-Pb coin chem. anal. by low energy γ-rays and neutron transmission meas. 80−35591
- $AgGaS_2$-$AgGaSe_2$ system, phase diagram, lattice consts., and IR spectra 80−60841
- Ag_5GaS_4, form. in Ag-Ga-S system 79−87618
- α-Ag_2S whiskers, growth in VLS system, SEM and X-ray diffr. anal. 79−46989
- Al alloys, H impurities, improving productivity and detection threshold, by removing moisture with light pulse 80−26076
- Al determ. in Bayer liquors by elect. cond. meas. 77−73493
- Al determination, Fe and Al alloys, in presence of V *(Polish)* 80−35605
- Al saponite, differential thermal anal., IR absorpt. spectra, chlorite-like mineral 78−88816
- Al sheet surfaces, chem. characterisation by SIMS, glow discharge spectrometry and other techniques 80−66907
- Al-Al_3Ni eutectic, Al_3Ni distribution along temp. gradient 80−84971
- Al-Mg (2.5wt.%) sheet, surface oxide state and weldability 80−59769
- AlF_3, single crysts., vapour phase chem. transport prep., chem. anal. *(French)* 79−69971
- Al_2O_3, adsorbed ethanol, acetic acid and acetaldehyde, inelastic electron tunnelling spectra, surface vibr. struct. determ. 80−35572
- Al_2O_3, high purity, sintering, impurity effects, analysis *(German)* 78−6881
- Al_2O_3-Dy_2O_3, phase diagram at high temps. *(Japanese)* 80−50619
- Al_2O_3-Eu_2O_3(Gd_2O_3), phase diagrams at high temps. exam. 78−44114
- Al_2O_3-SiO_2-CaO-B_2O_3(1,1,1 wt.%) chemical analysis by photocolorimetry and titration 79−20483
- Am metal, dilatometry and thermal anal., melting point, transformation regions 79−43241
- As determ. in ores of reduced heteropoly acids, photometric method 78−61103
- As_2S_3, determination of stoichiometric discontinuity, using US velocity 79−5242
- As(V), spectrophotometric determ. using haematoxylin 78−20104
- Au, adsorbed layer comp. anal., by ion-forwarded electron spectra 77−31850
- B, electron beam non-crucible zone remelting prep., anal. of gaseous inpurities 80−20785
- B modifications, exam. of physical props. and electron structure 79−94954
- B, tetragonal, X-ray diffr. and C doping obs. *(French)* 79−14731
- B-C system, free C determ. 79−87907
- B_4C, determ. of H_2O, Hz content by hot extraction methods *(German)* 79−49808
- BN, in steel, extraction, identification by IR anal. 80−85254
- BN, wurtzite, chem. comp. and processing props. in prep. of Geksanit-R sinterings 80−25632
- $BaNb_2O_6$, solid-phase formation reaction, thermographic, X-ray phase and chemical anal. 77−12783
- $BaTiO_3$, powder compacts, sintered, physical and chem. inhomogeneities 79−87594
- $Ba_2UO_2(HPO_3)_2$, synthesis and comp. 80−35516
- Bi_2O_3-$AlPO_4$, phase equilib. 80−35168
- C, determ. in UC_n-PuC_n refabricated fuel for breeder reactor 79−11877
- C microamount anal. in metals and alloys, by combustion nonaqueous titration *(Japanese)* 78−20120
- C, organic dissolved, determ. in methanol 80−16741
- C, surface groups, acidimetry, formation of derivatives 78−68918
- CO dose meter for working places exposed to extreme peaks of CO contamination 78−81096
- CO microconcentrations in air, metrological provisions for gas-analysing instruments 79−67248
- CO_2 analysis, amplifier and lineariser for Beckman LB-1 analyser 77−29215
- CO_2 expiratory concentration analysis by computer 78−57106
- CO_2 infra red gas analyser, calibration method 78−20115
- CO_2 lasers, CO_2-CO-N_2-He, ionisation wave, slow changes, dispersion curves 80−38822
- CO_2, new impurity analysis method 80−66908
- Ca, in phosphates 78−23976
- $CaAl_2O_4$ compounds and cements, quantitative thermogravimetry after hydrothermal treatment 80−16737

chemical analysis continued
$CaO-Al_2O_3$, molten binary slag, dissolved C study *(Japanese)* 78—60662
$CaO-SiO_2$ glass, trimethylsilylation method for silicate ion anal. *(Japanese)* 80—71975
$CaO-SiO_2$ slags, containing CaF_2 and B_2O_3, SO_2 capacity determ. by encapsulation method 80—11944
$CaO.3B_2O_3$, form. by dehydration of hydrated calcium borates *(Japanese)* 79—74378
$Ca_{10}(PO_4)_6(OH)_2$, hydroxyapatite, prep. by hydrotherm. recrystn., composition and props. study 79—33913
Cd, determ. in sea and fresh waters, interlaboratory comparison 78—81209
$Cd_xHg_{1-x}Te$, comp. determ. by electroreflection method 77—52708
$Cd_xHg_{1-x}Te$, comp. in successive layers determ. by chem. polishing etching of surface 77—7868
$Cd_3(PS_4)_2$, synthesis by roasting, and exam. of props. 79—4926
Ce, photometric determ. in cast Fe and steel *(German)* 78—68955
Cl disappearance meas. in seawater 79—88372
Co, trace element anal. in geological materials by atomic absorption *(Portuguese)* 79—66375
Co-CoAl eutectic, invariant composition redeterm. 78—3099
Cr (III), (VI), determ. in industrial wastes 78—61105
Cr surface reactive, field ion microscope and atom probe obs. 79—29410
Cr-Mo compound, susceptibility to thermal embrittlement 77—21458
$CsSn_2I_5$, surface props., Auger study, elec. cond. meas., photochem. study 80—66339
Cu, chem. aspects of corrosion inhibition by benztriazole 80—16545
Cu slip ring, Auger spectrosc. obs. of elemental surface composition as function of temp. 80—66901
Cu(I) complex, oxidation, fast reactions meas. by pulsed-flow instrument 80—66890
Eu-Te, chalcogenides, exam. of crystal-chemical characts. 79—1407
F atom conc. meas. via HCl titration 77—36830
F content in hot spring waters, Kohu City, Japan *(Japanese)* 79—70821
F content of seawater 78—32118
F, hot spring water content *(Japanese)* 79—8648
β-FEOOH, Mossbauer spectra obs., chemical and thermal anal., X-ray diffr., saturation magnetisation 80—88896
Fe, cast, white, high Cr, phase composition, B effect 80—104172
Fe, cast thermoelec. method of Si, Mn, C content monitoring, thermo EMF meas. 77—73490
Fe, desorption of $O_2(N_2)$, surface anal., XPS appl. 79—24875
Fe, determination in natural waters 79—84550
Fe determinations, effect of surface changes in Pt crucibles 80—61192
Fe, dissolved organic, determ. in seawater 78—81208
Fe III, high-spin, in cancer, EPR 78—53466
Fe ore, reduction degree, chemical anal. calcs. *(Russian)* 80—66769
Fe:C(N), small concs. determ., mag. and mech. relax. methods 80—7879
Fe^{3+}/Fe^{2+} ratio, quantitative Mossbauer spectra 80—7209
Fe-Al, sintered and worked alloy, nonmetallic inclusion identification by quantitative metallography 77—77701
Fe-Cu-Ti, improvement of irradiation-enhanced Cu embrittlement by Ti addition 79—43393
Fe-lanthanid-O systems, thermodynamic props., composition and lattice constants 78—31390
Fe-Si, mag. method for rapid analysis 77—44540
Fe-Si (3.1 wt.%), solubility product of BN 79—10955
Fe-Si alloy, Si content determ. from Seebeck coeff. 77—56269
Fe_3C melts, measuring C content using automatic device 79—39252
FeF_3, single crysts., vapour phase chem. transport prep., chem. anal. *(French)* 79—69971
Fe(II) determ., in Cu process metallurgical soln. by o-phenanthroline colorimetric method 78—7293
α-Fe_2O_3, analysis of car exhaust by Mossbauer spectroscopy 78—92963
γ-Fe_2O_3, small particles, vacancy sintering 77—65975
γ-Fe_2O_3:Fe_3O_4, magnetite impurity determ. by C_p calorimetry 78—2152
$Fe(OH)_3$ thin films, Mossbauer spectra obs., chemical and thermal anal., X-ray diffr., saturation magnetisation 80—88896
$Fe_2O(OH)_4$, Mossbauer spectra obs., chemical and thermal anal., X-ray diffr., saturation magnetisation 80—88896
Fe_2P, grown in liq. Cu medium, composition and mag. props. 79—11313
Ga selenites, binary, effect of nature of alkali metals on composition and props. of hydrothermal reaction products 77—24941
GaAs, concs. of C and O_2 in LEC grown cryst. determ. 77—39612
GaAs, epitaxial layer, C distrib., anal. by quasichem. reactions 77—11803
GaAs, impurity distribs. by chemical methods 77—43237
GaAs thin film, effect of O on thin film compositions obtained by secondary ion emission 80—26079
$GaAs_{1-x}P_x$, heterogeneous struct. obs. by anodisation-electrorefl. technique 78—84088
$GaAs_{1-x}P_x$:Zn, diffusion profile determ., $^{32}P/^{65}Zn$ double tracer technique 78—55888
GaP:Zn, diffusion profile determ., $^{32}P/^{65}Zn$ double tracer technique 78—55888
Ge-Si alloy, comp. determ. using ellipsometric method 80—35615
GeSi alloy, composition determ. by ellipsometry 79—83537
H, determs. in fast flow discharge systems, titration methods 79—34393
H, in metals, plasma-ion analyser 78—15746
H_2 concentration determ., based on contact potential meas. *(Czech)* 79—70386
H_2 detection using Pd gate MOS transistor, fabrication and elec. characts. *(French)* 78—2569
H_2 detector, based on H_2-sensitivity of Pd-ZnO Schottky barrier diode 80—11085
H_2 dissociator envelope degradation, AES characterisation rel. to appl. in atomic clock 77—61876
H_2 in plate subject to external stresses *(Russian)* 79—14836
H_2-sensitive Pd-gate MOS 78—2578
HC-NO_x photochemical smog, smog chamber simulation model *(Japanese)* 77—29087
HCl, detector for environmental monitoring 78—24366
HCl gas in ambient air, detection using coated piezoelec. quartz cryst. 78—92532
H_2O, composition, photometric determ. 80—27330
H_2O vapour, continuous detection during thermal decomposition reacts 80—3440
β-$H_2O.11Al_2O_3$, conversion from β-$Na_2O.11Al_2O_3$ and characterization 78—3069
H_2S, air pollution, new anal. method for remote areas 79—21028

chemical analysis continued
H_2S in air, preconc., determ. by flame photometric detection 78—92535
He in breath, determ. using acoustic analyser, for closing vol. meas 78—61223
He-N_2, de excitation rate consts., energy transfer, pulse radiolysis obs. 80—30303
Hg determ. in sea and fresh waters, interlaboratory comparison 78—81209
Hg vapour monitor, personal piezoelec. cryst. dosimeter 77—21672
Hg-vapour gas analysers testing using Zarzma equipment 78—76962
Hg_2Cl_2, surface composition, electron impact, mass spectrometry, AES and LEED meas. 79—60607
In, electrodiffusive conc. of impurities for analysis 78—22752
InP, concs. of C and O_2 in LEC grown cryst. determ. 77—39612
InSe thin film, sputter growth and chem. anal. by XPS/ESCA 80—80976
KCl cryst., Sr and Na impurities radial distrib., influence of form of crystn. front 80—107312
$KEuHP_3O_{10}$, synthesis of K_2CO_3, Eu_2O_3 and phosphoric acid, exam. of structure 79—1837
$KEu(PO_3)_4$, synthesis of K_2CO_3, Eu_2O_3 and phosphoric acid, exam. of structure 79—1837
$K_xPt(C_2O_4)_2.nH_2O$, chem. analysis and elec. cond. meas. 78—76060
$K_2UO_2(HPO_3)_2$, synthesis and comp. 80—35516
Li, surface characterization of film growth 80—81240
LiI UV photodissoc. cross section, reson. ionis. Li detection 80—63719
Li_xWO_3, Vegard relationships, lattice parameter versus composition, X-ray and chem. anal. 79—23582
$(Lu_{1-x}Sc_x)_2V_2O_7$, prep., cryst. chem. and chem. anal. 79—41986
$Lu_2V_2O_7$, prep., cryst. chem. and chem. anal. 79—41986
$(Lu_{1-x}Y_x)_2V_2O_7$, prep., cryst. chem. and chem. anal. 79—41986
Mg_2SiO_4, forsterite, ion scatt. spectrometry, atom shielding effect of O 80—50493
Mn (III), determ. in industrial wastes 78—61105
NH_3+Br_2, gas phase reaction, $NHBr_2$ identified by ESCA 79—31599
$NH_4Fe_3(SO_4)(OH)_5$, jarosite, decomposition 80—11624
$(NH_4)_2UO_2(HPO_3)_2$, synthesis and comp. 80—35516
NO, calibration standards, generated by gas phase titration 78—69507
NO measurement, photometric process analyser 80—57360
NO_2, calibration standards, generated by gas phase titration 78—69507
NO_2, quantitative detection N_2, CO laser mag. resonance 77—12855
Na, impurity conc. meas. by automatic plugging indicator 78—17283
Na ion, selective ion electrode technique 77—36855
Na, liq., thermodynamic activity of C, continuous method of determ. 77—56306
α-$NaFe_2O_3$:$Mg^{2+}(Co^{2+})(Zn^{2+})$, substitution of Fe^{2+} *(French)* 78—95034
$Na_2O-ZrO_2-SiO_2$ glass, treated with 2 N solns. of $NaCO_3$ and NaOH, surface layer comp. 80—35366
$NaPO_3-AlF_3(-NH_4HF_2)$ glasses, synthesis, chem. thermal and optical anal. *(French)* 79—100104
Nb_3(Ge,Si) A15 film, supercond. and structural props. 79—87177
NbN single crystal preparation, zone melting and nitriding techniques 80—60776
$NdTlO_3$, physicochem. props. 80—25625
Ni base superalloy, instrumental anal., use of HF induction melting and centrifugal casting *(Japanese)* 77—56280
Ni base superalloy, preparation for instrumented anal., HF induction melting, casting 78—48607
Ni based powders, determination of entrapped Ar content, using vacuum fusion tech. 79—5193
Ni-Cd sealed battery electrode performance meas. 80—66962
Ni-Cr(20 wt.%), oxidation in pure O_2, 800 to 1200°C, secondary ion emission exam. of oxide film *(French)* 77—59995
NiCr film deposition, gas phase analysis *(Polish)* 79—20492
NiO, lattice parameters, microstrains, non-stoichiometry, comparison between mosaic microcrysts. and quasi-perfect single microcrysts. 80—24414
$NiTiO_3$, synthesis from products of soln. spray drying, kinetics 77—16519
O_2 analyser, OTOX 90, operation, and multipoint monitoring 80—55736
O_2 analyser instrumentation and operation 78—69237
O_2 concentration, thermomagnetic gas analyser type MN5130 appl. *(Russian)* 77—44558
O_2 concentration determ. based on contact potential meas. *(Czech)* 79—70386
O_2 determination in liquids Na, manufacture and props. of ceramic probes 77—54308
O_2, gaseous and dissolved, direct readout instrument 77—40606
O_3, calibration standards, generated by gas phase titration 78—69507
O_3 concentration in water, chemiluminescent meas. method 77—60159
$O_2(^1\Delta)$ content determ. in chemical generator gaseous effluents, ratiometric system 78—76970
OH formation in H_2-NO flame, OH collisional broadening parameter, curve of growth method 80—53052
organohalogen analyser system, drinking water total organic halogen anal. 80—93830
P determ. in ores of reduced heteropoly acids, photometric method 78—61103
P, reactive, in natural waters, low concs. automated determ. in presence of As, Si and $HgCl_2$ 79—44277
PZT ceramics, PbO content estimation using analytical procedure *(German)* 78—53279
$PaCl_2$, thin films, reduction to Pd by Ne^+ ion irrad., 2 MeV He^+ ion backscatt. anal. 79—4493
Pb, determ. in blood, haematofluorometric method 78—53554
Pb salts, inorganic 80—77081
$PbO-SiO_2$ glass, trimethylsilylation method for silicate ion anal. *(Japanese)* 80—71975
$PbO-SiO_2$ glasses, constitution of silicate groupings 77—7676
Pd, catalyst on glass, used in electroless deposition, proton backscattering anal. 80—16749
Pt, catalysts, supported, characterisation, hydrogenation and H_2-D_1 equilib. 78—76910
Pu, analysis, in fuel fabrication facility 79—16115
Pu compounds, release from contaminated burning Na, LMFBR safety evaluation 77—23224
Pu contaminated soil, nondestructive anal. 79—11879
Pu, in Irish Sea, oxidation state 79—16516
Pu safeguarding, automated ion-exchange system for rapid Pu separation from impurities 80—78383

chemical analysis continued
- PuO_2, reactor grade, calorimetric assay 79—16116
- Re catalyst, supported, chem. anal. method 77—25332
- S compounds, water-soluble, anal. of atmospheric aerosols 78—96282
- S, determ. in submicrometric aerosols, SO_2-denuder appl. for continuous meas. 79—8699
- S, in organic compounds, (book) 79—11869
- SO_2, air pollution, high vol. sampling for isotopic studies 79—70500
- SO_2, air pollution, new anal. method for remote areas 79—21028
- SO_2, atmospheric, long-term monitoring method using permeation sampling, development 80—26189
- SO_4^{-} , quantitative determ. in aerosol particles 79—20474
- Sb thin film, pH sensitivity and electrode potential *(Japanese)* 79—39159
- Se gravimetric determ. by reduction of H_2SeO_3 77—90683
- Si (111) surface, anal. by ion-electron spectroscopy 78—72670
- Si, Czochralski cryst. growth, faceted and nonfaceted, Sb microsegregation 80—45227
- Si, EFG ribbon, characterisation by ion beam tech. 80—79833
- Si, impurity penetration depth, chemical-spectral determ. 80—19830
- Si, mechanically treated surface, chem. state *(Russian)* 80—11805
- Si, multigrained, grain boundary elec. and compositional props., surface anal. 80—76575
- Si, neutron transmutation doping, impurities 80—15134
- Si thin film, effect of O on thin film compositions obtained by secondary ion emission 80—26079
- Si/Al-Si systeym, vacuum deposition, rate controlling and composition anal. by electron impact emission spectroscopy 79—91591
- Si-Y-Al-O-N glasses, compositional anal., hardness depend. on N_2 content 79—34129
- SiC fibres obtained from polycarbosilane fibre 80—50582
- β-SiC, powder, synthesis by chemical vapour phase reaction from methylsilane, exam. of props. *(German)* 79—4938
- SiC, thin film, effect of O on thin film compositions obtained by secondary ion emission 80—26079
- SiC-Ni based superalloy reaction, at elevated temps. 80—3287
- Si_3N_4, reaction-bonded, internal oxidation processes role in high-temp. mech. props. 79—38915
- α,β-Si_3N_4+C, powders, high temp. reactions *(Japanese)* 77—48685
- SiO_2, film on Si, electron beam damage, obs. using scanning AES 80—2070
- SiO_2, surface characterisation by free radical spin labels 77—90701
- SiO_2-Al_2O_3-Fe_2O_3-CaO-MgO-Na_2O-B_2O_3-SO_3, exam. of white flaky inclusions, causes and formation time 79—29237
- SiO_2-Na_2O-CaO, electrochemically coloured, chemical composition and structure of surface layers 78—84758
- SiO_x thin films on Si, anal. by backscattering techniques 79—96385
- SmF, vaporisation, sublimation, Knudsen effusion method 80—6508
- Sn, monitoring breakthrough of ^{113}Sn in ^{113m}In eluates from ^{113}Sn-^{113}In generator 77—5078
- Sn, stannous ion, in ^{99m}Tc radiopharmaceutical kits, rapid colour spot test 77—86630
- Sn/graphite particulate composite, prep. using vacuum infiltration, microstruct., anal. 79—20005
- SnO_2, quantitative determ. by Mossbauer effect, using portable analyser 78—20131
- SnO_2 thin films, analytical characterisation 80—20053
- SnO_2:ThO_2, exposed to H_2, temp. depend. of resistivity 79—56219
- $Sr_2Co_2O_5$, characterisation and mag. props. *(French)* 79—90619
- Ta, film, CVD on silica, struct. and mech. props. 77—24965
- Ta, powdered, N_2 determ. by vacuum hot extraction with graphite addition *(Japanese)* 77—48683
- Tb-Sn-Se system, cross section Tb_2Se_3-$SnSe_2$ phase diagram, physicochem. anal. 79—87621
- Ti (III), (IV), simultaneous photometric determ. 78—61102
- Ti, cold worked, annealed, internal friction meas. of H degassing *(French)* 79—43304
- TiF_3, single crysts., vapour phase chem. transport prep., chem. anal. *(French)* 79—69971
- TiN, gaseous phase, crystallisation, effect of temp., vapour-gas mixture conc., and deposition time 79—33910
- TiN_2, ultrafine synthesis in RF plasma, X-ray diffr. chem. and electron microscopy anal. 79—70026
- TiO_2-P_2O_5 reduced glasses, prep., elec. transport, chem. anal., DC, AC cond., seebeck coeff. 78—30924
- $Tm_2V_2O_7$, prep., cryst. chem. and chem. anal., lattice const. determ. 79—41986
- $(U,Pu)O_2$ (30 wt.%), oxidation behaviour 79—66210
- $(U,Pu)O_2$, close coupled O-to-metal ratio anal., rapid thermogravimetric method 79—11878
- U accurate determ. of 5 to 25 mg using computer controlled redox titrimetry 79—87932
- U meas. safeguards materials, automated gravimetric titrator 80—622
- U meas. with automated gravimetric titrator 79—85609
- UO_2 fuel rod, Zircaloy clad, chemical activity determ. of fission product 79—49682
- V_2O_5 cathode, used in Li-V_2O_5 reserve cells, microstruct. optical reflectance, elec. cond. meas., chem. anal., SEM obs. 79—43752
- W-Ti(Zr)(Hf)-C, cubic solid soln., form. and props. 78—48348
- WC-Co hard metal, binder phase charact. by magnetic props. 79—29439
- Xe, retained in advanced nuclear fuels, meas. by microprobe anal. 79—40997
- $Y(OH)_3$-α-FeOOH, physicochem. props. rel. to growth of $Y_3Fe_5O_{12}$ 77—40418
- $Y_2Ti_2O_7$, precipitation from oxalates, carbonates, exam. 80—55641
- $Yb_2V_2O_7$, prep., cryst. chem. and chem. anal. 79—41986
- Zr, monitoring breakthrough in ^{113m}In eluates from ^{113}Sn-^{113m}In generator 77—5078
- Zr-Nb (1 at.%), high-temp. nitriding, chemical and metallographic anal., disintegration test 79—24668
- ZrB_2, impurity content, effect of synthesis conditions 80—21344

chemical analysis by mass spectrometry *see mass spectroscopic chemical analysis*

chemical analysis by nuclear reactions and scattering
- *see also chemical effects of nuclear reactions and scattering; neutron activation analysis*
- γ-adsorption analysis of a substance with allowance for effect of heavy impurities 79—61932
- activated samples, simultaneous two-sample meas. immune to detector intercalibration 77—57835

chemical analysis by nuclear reactions and scattering continued
- activation analysis, (α,n), (α,p) reacts. on B, C, N, Mg, Al, P 80—61206
- activation analysis, gamma-ray data automatic interpretation, computerised 77—44548
- activation analysis, new irrad. head design, electronic control system 80—66896
- activation analysis, photopeak integration, quality assurance of computer programs 79—1986
- activation analysis, photopeak integration methods rel. to multiplet anal. 78—11592
- activation analysis trends, conf., Munchen, Germany (Sept. 1976) 77—86405
- activation yield curves of photonuclear reactions for multielement photon activation analysis 79—20490
- activity evaluation and statistical accuracy in activation determ. of low element conc. 79—87928
- aerosol samples, simulated, Be content by proton scatt. anal. 79—5217
- aerosols, atm., instrumental anal. of light element comp. 78—69516
- aerosols, atmospheric, automatic time sequence filter sampler for proton induced X-ray emission anal. 77—60171
- air pollution monitoring, PIXE and NRA studies using lichen indicator 80—61744
- alloy, high temp. oxidation studies using $^{18}O(p,\alpha)^{15}N$, ^{18}O distrib. determ. 79—87912
- alpha-induced prompt gamma-ray spectrometry, developments in analytical uses 77—90686
- analysis using $^{14}N(p,n)^{14}O$ reaction 77—81769
- analysis using ion induced gamma rays 79—5220
- annihilation radiation measurement in activation analysis, specificity enhancement by triple coincidence 77—90687
- atmosphere dust, eval. using nuclear methods *(French)* 80—7993
- atmospheric particulate material, trace elements analysis by nucl. activation techniques 78—3991
- atmospheric sampling filters, charged particle induced X-ray fluorescence anal. *(French)* 78—27852
- Australian atmospheric contamination after 1974 French Pacific tests, cyclotron anal. by proton activation 79—57311
- backscattered gamma method, universal, based on computer interpretation of spectra, appl. to ores 79—1984
- barley seeds, N depth distrib., $^{14}N(d,p_0)$ reaction 79—5221
- biological materials, ion beam anal. in few MeV range 77—81768
- biological materials, radioactivation analysis, separation of U, Th, Cr, Mn and S *(French)* 77—90700
- biological samples, elemental retention during low temp. ashing, activation anal. method 78—11785
- biological samples, nondestructive proton and neutron activation analysis comparison 78—3691
- biomedical engineering textbook for undergraduates 80—8750
- bone C partial-body determ. by proton activation anal. 77—86605
- bone Ca activation anal., prod. of uniform ^{38}K yield using range modulator 77—40735
- borosilicate optical waveguide glass, B content determ. using nuclear track counting 80—95969
- brass, α- and β-phase, oxidation, prompt. nucl. reactions and reson. alpha scatt. study 80—66690
- cereal, proton-induced X-ray emission and nuclear reactions for determ. of protein quality 78—20321
- chalcogenide glass film, thermal diffusion of Au electrode layer, backscatt. anal. 78—10228
- characterisation by precision gamma scanning 79—49688
- charged particle activation, role in materials anal. 79—57310
- charged particle activation anal., are energy in ave. stopping power method 78—76963
- charged particle activation anal., average stopping power method 78—48724
- charged particle activation anal., determ. of Pb distrib. in human teeth 80—101303
- charged particle activation analysis, calibration 78—11587
- charged particle activator anal., method using target of defined thickness 79—34405
- charged particle chemical analysis, two reactions method 78—76964
- cigarette, density changes during burning as obs. by β-source attenuation 78—11792
- coal, meas. of specific energy ash and moisture by combined neutron and gamma-ray meas. 79—39255
- coal analysis by neutron-capture gamma-ray meas. in boreholes 79—52853
- coal calorific value determ., by neutron inelastic scattering *(Czech)* 80—101048
- coal slurry concentration, meas. in haulage pipelines by nucl. techniques 78—7301
- coatings and thin films, atomic composition depth distrib. by energetic ion anal. 80—35617
- complex materials, charged particle anal., range effect corrections, geological material appl. 77—48738
- computers in activation analysis and γ-ray spectroscopy, conference, Mayaguez, Puerto Rico (May 1978) 79—1983
- concentration profile meas. in thin layers using multiplier resonant nuclear reactions 77—56292
- concentration profile measurement using multiply resonant nuclear reactions 78—20108
- conference on ion beam anal., Washington, USA (June-July 1977) 79—5194
- counting rate effect elimination 79—5237
- cyclotron, small, applications *(Hungarian)* 78—70656
- depth selective Mossbauer effect spectroscopy empirical method of quantitative anal. using conversion electrons 78—20130
- development trends and appl. 78—55041
- diamond, ion beam analyses rel. to phys. props. 79—5219
- electrodeposited chrome black solar absorber surfaces, characterisation using $^{52}Cr(p,\gamma)$ 80—7878
- element analysis, using nuclear-physical methods *(German)* 77—25347
- elemental anal. using heavy ion collision-induced X-ray anal. 77—19041
- errors due to detector geometry, anal. *(Russian)* 79—70412
- film structure, low conc. ^{16}O depth profiling using $^{16}O(d,\alpha)$, α-particle energy anal. 79—5214
- films by elastic scatt. of ^{3}He 79—1975
- fission reactor fuel, nondestructive anal. using isotopic source assay system 79—11873
- fissionable isotopes, in aq. soln., pulsed neutron interrogation method assay 79—11874

chemical analysis by nuclear reactions and scattering continued
fissionable material, assay by neutron methods in presence of fission products 79−13513
fluorophosphate glasses, C determ. by deuteron activation analysis 78−68961
food samples, determ. of fluorine conc. using $^{19}F(p,p'\gamma)$ 79−5218
gamma counting, pulse pileup, random summing losses 80−58023
gamma spectrometry, Ge(Li) and HPGe detectors, coincident sum peaks 80−63447
gamma-gamma perturbed angular correl. to meas. appl. to chem. anal. *(Japanese)* 78−40098
gamma-photon activation technique for O trace levels determ. 79−87910
gamma-ray spectra, computer code for qualitative anal. 79−9943
gamma-ray spectra, computer methodology for spectral data reduction and anal. 79−1988
gamma-ray spectra, doublet resolving power and area determ. accuracy, comparison of computer programs 79−9944
gamma-ray spectra, for activation anal., computer programmes for anal. 78−7287
gamma-ray spectra, monoenergetic, mathematical model of spectra from Ge(Li) detector 78−13372
gas analysis, isotope technique appl., ionisation detectors, review 79−20481
geological materials, radioactivation analysis, separation of U, Th, Cr, Mn and S *(French)* 77−90700
geological samples, f/α particle track anal. for U, Th and isotropic disequilibria 78−7799
glass, float, low-Fe, weathered, surface, characterisation 80−93666
glass, Li depth distrib., meas. using $^{7}Li(p,n)^{8}Be$ 77−35582
grain legumes, proton-induced X-ray emission and nuclear reactions for determ. of protein quality 78−20321
graphite reinforced epoxy composites, moisture detection by nuclear reaction anal. 80−30306
graphite-epoxy composites, moisture profile meas. using nucl. reaction anal. 80−55760
heavy element superficial mass meas. by elastic α-particle scatt. *(French)* 79−61927
hepatic Cu measurement in vivo by nucl. reson. scatt. 77−9245
in situ capture gamma analysis of large mineral samples 80−61215
inversion probes in γ-γ methods, laminar medium, nuclear geophysics 79−34992
ion beam depth profiling of H and He 78−7300
ion beam material characterisation, conf., Aleria, Corsica (Sept. 1976) 79−96403
ion beams, use in material analysis by nuclear reactions and scatt. and ion-induced X-rays 77−4968
ion induced γ-rays, thick sample reaction yields, energies, appl. in prompt nuclear anal. 78−62502
light element profiles in heavy matrix materials, depth profiles and lattice locations using (n,p) and (n,α) 79−5205
light elements, simultaneous anal. using prompt nucl. reaction Γ-rays 78−7250
light ion diffusion in solids obs., using nuclear reaction depth profiling 79−5202
MAGNOX fuel canning material, corroded, F conc. profiles determ. using $^{19}F(p,\alpha\gamma)^{16}O$ reaction 79−92035
material analysis, 2 MeV $^{4}He^{+}$ ion backscatt. technique *(Chinese)* 80−35590
medical applications, review, book contrib. 80−11995
metallic materials, nucl. methods use, conc. gradients determ. *(French)* 79−43665
metals, airborne, in industrial districts, conc. rels., nuclear anal. technique 80−72107
metals, analysis of H ratios and profiling using nucl. techniques and Rutherford backscatt. 80−61202
metals, appl. of 30 MeV microtron for radioactivation anal. 77−66720
metals, ion beam analysis of light elements using nucl. reaction technique *(Japanese)* 78−31744
metastable isomer prod. via (γ, γ') at 6-8 MeV *(French)* 79−29433
meteoritic and lunar samples 80−62089
microanalysis by direct obs. of nucl. reactions, material characterisation, review 79−96409
molecular ion beams, effective beam energy spread, Al target, (p,γ) yield curves 79−3530
monazite sand, determ. of Th, U, and K from spectrometry of natural γ-activity 78−20408
multielement analysis of terrestrial and extraterrestrial materials by photon or neutron activation 78−12018
multielement quantitative analysis optimization method 79−16089
NBS reactor, summary of activities, (July 1976 to June 1977) 78−82435
NDT applics. 77−16884
near-surface microanalysis of solids using ion beam techniques 79−24868
neutron capture γ-spectroscopy, medical appl., Cd and N meas. in living human subjects 80−67241
neutron source density distribution and time variation in 14 MeV generator *(German)* 77−25349
non-crystalline solid, surface and thin film chem. anal. techniques *(French)* 77−73495
nonferrous metals, C, O, AND N content., microanal., surface treatment effects 78−11596
nozzle erosion, ion implantation effects, ion beam anal. 79−48011
nuclear fuels, elemental and isotopic conc. anal. using nondestructive assay 79−49691
nuclear ion microprobe at MeV energies, production and use, review 80−7883
nuclear medicine diagnostics, for teaching 78−49618
nuclear microprobe, two dimens. scanning, appl. to light element mapping 77−81447
nuclear microprobe anal. of stable isotope tracers spatial distrib. 80−50909
nuclear microprobe as analytical tool, review 79−87913
nuclear radiation as a probe of chemical bonding, review of theory and expt. techniques 79−79339
nuclear target composition determ. from α-scatt. and (p,γ) meas. 77−75019
nuclide activity measurement using γ-radiation, correlation factor for self-absorpt. 79−34401
organic binary system composition, determ. by γ-ray scatt. from low Z nuclei 79−87897

chemical analysis by nuclear reactions and scattering continued
organic materials, nuclear backscattering using cyclotron 78−80807
particle elastic scattering analysis, appl. to C, N and O determ. in size fractionated urban aerosols 78−81466
phosphosilicate glasses, P content determ. by Rutherford backscatt., PIXE, and activation anal. *(Hungarian)* 80−85233
photon activation anal., gamma-ray half-life vs. energy map 77−16883
photon activation anal., using electron linear accelerator, irrad. system 77−63992
photon activation analysis, appls. 78−11597
photon activation analysis, interference reactions producing identical radionuclides, quantitative evaluation 78−11588
photon activation analysis, low-energy photon and classical γ-ray spectroscopy 79−29428
photon activation analysis, nondestructive, X-ray spectroscopy applic. 77−90689
photon activation analysis of coins and art objects Au, Ag and Cu determ. 78−349
photon attenuation coeffs. in heterogeneous media, nuclear geophysics methods 79−39708
photopeak area computation methods 78−11593
PIXE, absorpt. edge method of charact. filters 79−8461
PIXE, appl. of protons from 3 MV Dynamitron accelerator 77−81453
PIXE, influence of matrix effects on absolute anal. 77−48721
polymethyl methacrylate, mol. wt. determ. by activation anal. of Cl in end group 79−66377
powders, composition, meas. by 60 keV γ backscatt. from ^{241}Am 77−52695
primary first-order interference in γ-activation anal. 79−16088
protein quality of leguminous plants, proton induced radiation anal. 77−48978
proton activation analysis, 11 MeV protons 78−88686
proton activation analysis for determ. of F_2 pollution from brick kiln 78−20504
proton activation analysis of environmental and ecological pollution determ. 78−3994
proton activiation analysis of B and Li local levels in minerals, rocks and ores 79−74477
proton beam trace element anal. at atmospheric press. 77−81454
proton elastic scatt. anal. of light elements 77−48729
proton scattering anal. of atmospheric particulate matter 77−25778
quartz, H concentration profiles by nuclear reaction method 79−60396
quartz sand from Lasko Polje, determ. of Th, U, and K from spectrometry of natural γ-activity 78−20408
reactor coolant, automated system for radioiodine anal. 78−35768
scalp hair as monitor of population exposure to environmental pollutants, nucl. activation analysis 78−3940
semiconductor materials, channelling-blocking measurements, (n,α) method for B-depth profiling 80−70276
serum, human, trace elements determ. by proton activation 80−81731
solutions, conc. changes, proton induced X-ray emission obs. 77−25325
spent reactor fuel, nondestructive burnup determ. calibration using destructive radiochem. anal. 79−89372
stable isotope tracer analysis by proton scattering 80−104487
steel, C and N conc. determ. by nuclear methods *(French)* 77−60160
steel, defective zones in cold rolling, activation analysis method 78−7278
steel, depth profiles of transition elements using (p,γ) react. 80−50910
steel, N determ. by track autoradiography 80−100979
steel cladding, B distrib., particle track etch technique 77−57719
steel melting, oxidation processes in jet refining unit 79−87898
steel surfaces, O and N profiles determ. using (d,p) reaction anal. 79−5216
superheavy elements in monazite crystals, proton induced X-ray spectra 77−17106
surface analysis using ^{6}Li and ^{35}Cl ion beams 79−5211
tapered corrosion sections, light element profiling using nucl. reaction analysis and scanned microbeam 79−92036
thin film, composition analysis, by ion beams *(French)* 79−8467
trace element, small proton accelerator suitability obs. for X-ray emission excitation *(German)* 77−25348
trace element analysis, by heavy ion induced X-ray emission 77−36808
trace elements in environmental materials, reliability aspects 78−40106
triton activation, 3.5 MeV, sensitivities for determ. of elements with $Z<34$ 77−90693
water pollution, arsenic in freshwater fish traced to fly ash leachate using neutron activation analysis 80−97827
water pollution, trace element detection by activation analysis *(French)* 77−41067
X-ray anal., role of automation 77−77863
X-ray emission induced by heavy charged particles, analytical appl. 77−4967
zircaloy, nuclear microprobe methods for investigating oxidative corrosion 80−71787
(γ, γ'), reaction activation anal. of elements using ^{16}N γ-rays 78−88689
γ-ray spectrometry with low-energy t and α particles, 0.1 to 100 ppm 79−8460
(n,p) and (n,α) reactions, and backscatt., appl. to fusion reactor materials, archeometry and nuclear spectroscopy 80−61200
Al, and Al-Cu(Pb) dil. alloys, pulsed ruby laser irrad., noncryst. phase form 80−35012
Al nuclear reactor fuel tubes, proton activation determ. of impurities 80−27741
Al-Nb superimposed metallic layers, ionic movements during anodization, Rutherford backscatt. and nuclear microanal. 80−71913
Al_2O_3 anodic films, H conc. profiles meas. 80−75261
$^{27}Al(p,\gamma)^{28}Si$, 992 keV, Al concentration determ. in GaAlAs 79−7760
Au-Ge-Si structure, O distrib. profile in Ge, from emitted α-particle energy anal. of $^{16}O(\alpha,\alpha)$ 79−5213
Au-Si structure, O distrib. profile in Au, from emitted α-particle energy anal. of $^{16}O(\alpha,\alpha)$ 79−5213
B concentration profiling in solids by neutron TOF 79−51131
B_1 neutron irradiated, quantitive anal. using cellulose nitrate solid state track detectors 78−56937
$^{10}B(n,^{4}He)^{7}Li$, determ. of B in complex matrices from ^{4}He and ^{7}Li tracks in plastic detectors 79−18080
$^{11}B(p, n)^{11}C$, steel B depth distrib. meas. using time of flight method 80−71986
Be depth profiling in alloys, simultaneous α and d detection in $^{9}Be(p,d)$ and $^{9}Be(p,\alpha)$ reactions 79−5203
Be distrib. in metals, using $^{9}Be(d,p)$ and $^{9}Be(\alpha,n)$ 79−5204

chemical analysis by nuclear reactions and scattering continued
BeO coating, on Cu-Be, atomic composition depth distrib. by energetic ion anal. 80−35617
Bi determ. by photon activation anal. 78−85273
Br, determ. in terrestrial, meteoritic and lunar samples, rel. to cosmochemical processes 78−12111
C, activation anal. by photon-nucleus reaction *(Japanese)* 78−76945
C depth profiling in solids using ^{12}C(d,p) 79−5212
C high sensitivy meas. using nuclear microprobe 80−50908
^{A}C(p,γ), A=12, 13, isotopic anal., estimation of ^{13}C/^{12}C conc. ratio 79−48014
^{17}C(d,p)^{13}C, high resolution depth profiling of C by spectral deconvolution 77−1966
CaO, C-content determ. of single crystals grown by arc fusion 79−8456
^{48}Ca stable isotope tracer analysed by proton activation 77−21622
CdSe film polycryst., thermal diffusion of Cr, 240-400°C 80−80001
^{252}Cf neutron sources, appls. of activation anal., review 80−18728
Cl, determ. in terrestrial, meteoritic and lunar samples, rel. to cosmochemical processes 78−12111
Cl, photoactivation analysis 79−61931
Cr steel, N depth distrib., ^{14}N(d,p_0) reaction, 3 MeV deuterons 79−5221
Cr-Ni-Nb steel, oxidation in CO_2, charged-particle nuclear techniques 80−61022
Cr_2O_3/Cr solar-absorber surfaces, chemical and struct. anal. 79−95283
Cs, trace identification in neutral-beam research 80−95401
D depth profiling with D(^{3}He,p), proton detection at backward angles 80−30309
D in stainless steel, depth distrib. determ. using D(^{3}He,p)^{4}He 79−4326
D(d,p)T spectroscopy for studying dynamic deuteron implant effects 79−51160
F density distrib. in human enamel, meas. with ^{19}F(p,$\alpha\gamma$) 77−56292
F determ. in atm. samples by ^{19}F(p,α)^{16}O react. using low energy accelerator 78−85239
F, determ. in terrestrial, meteoritic and lunar samples, rel. to cosmochemical processes 78−12111
F in microcracked Cr plate, microanalysis by ^{19}F(p,$\alpha\gamma$)^{16}O 79−79351
^{19}F(p,$\alpha\gamma$), analytic appl. of protons from 3 MV Dynamitron accelerator 77−81453
Fe ores, determinaton of Fe content, using ionisation effect of back β-scattering 79−52824
Fe:Yb,^{18}O, interaction between implants 77−27921
Fe-Cr (9 wt.%), oxidation studied using C^{18}O_2 and D_2O tracers 80−71784
Fe-Ni-Cr (44, 17 wt.%), nuclear microprobe methods for investigating oxidative corrosion 80−71787
FeO ultrathin homogeneous absorbing films, ellipsometric nucl. microanalysis data analysis, opt. consts. *(French)* 78−11011
Ge, single cryst., ^{18}F penetration, charged particle activation anal. 80−93828
Ge:H, amorphous, H content determ. by IR absorpt., gas evolution and nuclear reaction methods 80−44130
Ge(Li), well-type detectors for low-level radiochemical analysis 78−37119
H analysis in different materials problems, using ^{1}H(^{15}N, $\alpha\gamma$) and ^{1}H(^{19}F, $\alpha\gamma$) reactions 79−5196
H content of thin surface layers, nondestructive anal. by alpha-particle scatt. 77−56297
H depth profiling in materials, use of ^{1}H(^{15}N,$\alpha\gamma$) resonant reaction *(French)* 78−91357
H depth profiling in solids, using neutron TOF from H(t, n) 79−5198
H detection in metals by ^{1}H(^{15}N,$\alpha\gamma$) reaction 80−55767
H, determ. by simultaneous heavy-ion induced nuclear reacts. and at X-ray emission 78−85240
H determination by nuclear reactions *(Czech)* 80−3430
H isotopes, nuclear reaction anal. techniques, implantation studies, appls. 78−3422
H profiling using ^{15}N bombardment, method and appl. 79−5195
H surface layers anal., influence of ion beam bombardment 79−37731
^{1}H(^{19}F,$\alpha\gamma$)^{16}O, for meas. of H depth distrib. in solid 77−81435
^{2}H depth profiling with ^{2}H(^{3}He,p)^{4}He react. 80−49262
He concentration profiles meas., using ^{4}He(^{7}Li,γ)^{11}B reson. reaction at 1.68 MeV incident energy 79−5200
He depth profile meas. in thin metal foils 77−12858
^{3}He activation analysis, for determ. of elements with Z=12-47 78−11575
Hg, determ., in Pb, radioactivation and other methods 78−76952
Hg ores, determ. of Hg content using ^{57}Co isotope and scintillation counter 78−20539
I, determ. in terrestrial, meteoritic and lunar samples, rel. to cosmochemical processes 78−12111
^{129}I in bovine thyroid glands, activation anal. obs. 80−94380
K_2O-SrO-SiO_2, O_2 self diffusion exam. by proton activation anal. 79−65241
Li, determ. in terrestrial, meteoritic and lunar samples, rel. to cosmochemical processes 78−12111
Li isotope composition determ., α prod. by d bombardment 79−7029
Li isotopic comp. determ., using coincident meas. of complementary particles in ^{6}Li(p,α) and ^{7}Li(p,α) 79−5201
Li nuclear microprobe method, appl. to in situ anal. of H-related materials problems 78−7299
Li, quantitative location in brain tissue using nuclear Track Etch techniques 80−98133
^{6}Li induced reactions, depth distrib. of light elements in materials 77−16888
Mg alloy scales, F conc. profiles determ. using ^{19}F(p,$\alpha\gamma$) 78−88678
MgO, atomic C anal. by ^{12}C(d,p)^{13}C method 80−108766
MgO, C content determ. by ^{12}C(d,p)^{13}C 77−68991
^{53}Mn, in stony meteorites, determ. by activation anal. for cosmic ray effects investig. 78−12018
Mo, activation anal., charged particle prod. cross sections by 14 MeV neutrons 80−93829
Mo, D and ^{3}He trapping and mutual replacement 80−59493
N, activation anal. by photon-nucleus reaction *(Japanese)* 78−76945
N, determ. in metals, by deuteron irrad. nucl. microprobe anal. 78−7285
N determinaiton by track autoradiography 80−100979
^{14}N(p,γ)^{15}O, isotopic anal., estimation of ^{15}N/^{14}N conc. ratio 79−48014
^{15}N, anal. by proton scatt. 79−61926
^{15}N(p,$\alpha\gamma$)^{12}C, isotopic anal., estimation of ^{15}N/^{12}C conc. ratio 79−48014

chemical analysis by nuclear reactions and scattering continued
Na determ. by (p,γ) reacts., target excitation yields determ., appls. 77−44545
Na, trace identification in neutral-beam research 80−95401
Na_2O-CaO-SiO_2 glass, Na surface conc. determ., by ^{23}Na(p,α)^{20}Ne reaction 77−20171
Nb, activation anal., charged particle prod. cross sections by 14 MeV neutrons 80−93829
Nb, impurity conc. monitoring during single cryst. production 78−31337
Nb, lattice location measurements of O, using ^{3}He/^{16}O and ^{1}H/^{18}O prompt. nucl. reactions, ion irrad. effects 79−86813
Nb-Al superimposed metallic layers, ionic movements during anodization, Rutherford backscatt. and nuclear microanal. 80−71913
Nb-Ta superimposed metallic layers, ionic movements during anodization, Rutherford backscatt. and nuclear microanal. 80−71913
Nb-Ti, film, composition determ. by ^{3}He elastic scatt. 78−76974
NbTi, chemical comp., supercond. films and bulk surfaces 78−76973
Ni, deuteron diffusion obs. by D(d,p)T reaction *(German)* 77−59150
Ni-Cr thin film resistors, α-particle elastic scatt., and PIXE anal. 79−48022
O, activation anal. by photon-nucleus reaction *(Japanese)* 78−76945
O depth profiling in solids using ^{16}O(d,p) 79−5212
O_2 distrib. in metals determ. using nuclear microprobe, ^{16}O(d,p)^{17}O react. 77−36846
^{16}O(d,p)^{17}O, high resolution depth profiling of O by spectral deconvolution 77−1966
^{16}O(t,n)^{18}F, surface oxygen content of stainless steel *(French)* 77−29077
PbO-SiO_2 binary glasses, Pb depth profiles after acid etching, α-particle backscatt. 79−79343
Pt, adsorption of CO and D_2, absolute coverage meas. using nucl. microanal. 80−54511
^{238}Pu, alpha spectrometric determ. 80−81404
Si, determ. in metals, by deuteron irrad. nucl. microprobe anal. 78−7285
Si, displacement of group III, IV, V, and VI impurities in Si by He^+ and H^+ analysing beam 79−4330
Si, impurities of O, N, C, trace anal. by proton activation *(Chinese)* 80−81403
Si layers, epitaxially grown on sapphire substrates, Al conc. as a function of depth using ^{27}Al(p,α_0) reson. reaction 79−4328
Si, O content and depth profiling, ^{16}O(α, α)^{16}O reaction method obs. 79−34408
Si ribbon, EFG, C contaminant conc. determ. by nuclear techniques and SIMS 80−59506
Si surface, etched, O distrib. profile, from emitted α-particle energy anal. of ^{16}O(α,α) 79−5213
Si:Al epitaxial layers, nuclear microanalysis of Al impurities ^{27}Al(d,α)^{25}Mg 80−61193
Si:B, conc. profile of implanted cryst., by ^{11}B(p,α) chem. anal., annealing *(German)* 78−83843
Si:D, amorphous, thermal stability, comparison with Si:F 80−49542
Si:H, amorphous, H content determ. by IR absorpt., gas evolution and nuclear reaction methods 80−44130
Si:H amorphous film, H quantitative depth profiling by nuclear reactions and SIMS 78−14373
Si:Sb, dopant implantation, activation analysis errors due to isotope comp. *(German)* 80−34037
Si-Pt(Ni)(Pd), laser-induced reactions of metal films with Si, ^{4}He backscattering spectra 79−19471
Si_xB_{1-x} films, anal. of H ratios and profiling using nucl. techniques and Rutherford backscatt. 80−61202
$Si_{1-x}C_xH_z$ amorphous film, H content determ. by nuclear reaction analysis 80−59821
SiH_z, amorphous film, H content determ. by nuclear reaction analysis 80−59821
SiN_x, plasma deposited, H content meas. 78−63949
Si_3N_4, film, H_2 concentration profile, chem. bonding 79−33205
Si_3N_4 films on Si wafers, O determ. by ^{3}He activation anal. 80−71981
Si_xO_{1-x} films, anal. of H ratios and profiling using nucl. techniques and Rutherford backscatt. 80−61202
SiO_xN_y films on Si, ^{16}O conc. profiles anal., using (d,p) and (d,α) reactions with mag. spectrom. 79−5215
Ta, diffusion and surface distrib. of N, probed by (p,γ) resonance broadening method 78−38918
Ta film, determ. of thickness and O, N content 78−80824
Ta film on Corning glass, N and O content nondestructive determ. *(German)* 78−43272
Ta on Nb duplex layers, cation-transport processes during anodic oxidation, Rutherford backscatt. and nucl. microanal. 79−20264
Ta, thermally oxidised, ^{16}O conc. profiles anal., using (d,p) and (d,α) reactions with mag. spectrom. 79−5215
Ta-Nb superimposed metallic layers, ionic movements during anodization, Rutherford backscatt. and nuclear microanal. 80−71913
Ta_2O_5 film, atomic composition depth distrib. by energetic ion anal. 80−35617
α-Ti, O_2 diffusion from oxide surface layer, chem. anal. by nucl. reaction *(French)* 79−7710
Ti, thermally oxidised, ^{16}O conc. profiles anal., using (d,p) and (d,α) reactions with mag. spectrom. 79−5215
Ti:Pd, ion implanted, corrosion behaviour and Rutherford backscatt. anal. 80−71792
Ti:T, depth profiling by neutron TOF spectroscopy 77−73500
Ti-W/Au, metallisation on Al, temp. stability, barrier props., deuterium activation anal. 79−23868
U, determ. in environmental samples, neutron activation, neutron assay and fluorometric methods 78−61087
U, in porcelain dentures, rapid anal. by delayed fission neutron method 78−15907
U, mineral analysis using alpha particle absorption by cellulose nitrate *(Spanish)* 77−70358
U prospecting using microdistrib. anal. of Siwalik vertebrate fossils by nuclear Track Etch tech. 80−98489
V, anodised cryst., nucl. microanal. of oxide film for ^{16}O and ^{18}O profiles 79−52683
V-$D_{0.01}$, enrichment of D during the ion bombardment 80−54288
Zr, ion-implanted polycryst., thermal oxidation 80−71786
Zr, of C and N by photon and proton activation *(French)* 79−43666
Zr, use of nucl. reactions to trace source of O in anodisation 79−52683

chemical association *see association*

chemical batteries *see cells (electric)*

chemical bonding *see bonds (chemical)*

chemical bonds *see bonds (chemical)*

chemical composition *see chemical analysis*

chemical diffusion *see diffusion*

chemical effects of nuclear reactions and scattering
- *see also chemical analysis by nuclear reactions and scattering; radiation chemistry*
- cyclobutane-t, chemically activated by nuclear recoil, vibr. energy transfer 77—66763
- intratrajectory reacts. in radiolysis of aq. solns. by recoil particles from $^{10}B(n,\alpha)^{7}Li$ *(French)* 77—12812
- scanning proton microprobe in atmospheric environment 77—70394
- CN^- transformations by inner source based on $^{10}B(n,\alpha)^{7}Li$ 79—34341

chemical effects of radiation *see radiation chemistry*

chemical elements *see elements (chemical)*

chemical engineering *see chemical technology*

chemical engineering computing
- *see also computerised control; computerised instrumentation*
- bipolar cell stacks. leakage currents 80—76526
- combustion, turbulent premixed and diffusion, engineering flow modelling computation 78—1756
- compressible gas flow calc., programme 77—7410
- cryogenic refrigeration system, computer design and optimisation 79—71457
- equilibria prediction, vapour-liquid, Wilson and NRTL equations assessment 79—86883
- heavy water production plants, process simulation 79—22396
- liquid, cryogenic refrigeration system, computer design and optimization 79—58750
- nonlinear convective diffusion problem, application of stable explicit finite difference scheme 78—151
- OPTIMO code developments for techno-economic eval. of H production processes 80—45797
- petroleum industry automation 78—28327
- pharmaceutical dissolution testing, microprocessor controlled sampling system 80—86273
- polymerisation kinetics analogue simulation 77—36754
- porous catalyst, complex reactions, conc. and temp. profiles, computation method 79—86523
- pulsating overpotential Cu electrodeposition, appl. 77—81410
- separation processes simulation in H_2SO_4-Br cycle 79—74413
- turbulent friction factor, calc. by TI-57, binary-search method 80—83788

chemical equilibrium
- *see also chemical reactions; reaction kinetics*
- $A+A_n \rightleftarrows A_{n+1}^*$, cluster dynamics, classical trajectory study 80—3316
- acetone cation+ketene, proton transfer, CH_3CO^+ heat of form. 77—90592
- acetone vapour, mol. assoc., monomer-dimer equilib., thermal cond. meas., MO calcs. 79—52647
- acetylene+acetylene-$d_2(D_2O)$, H-D exchange, equilib. consts. 77—86299
- acetylene-N_2O flame, chem. equilib. rel. to AAS 77—4957
- acid, weak, ionisation in aq. soln., rate const. meas., elec. field jump method errors 79—43611
- acridine orange dye soln., dimerisation equilib., absorpt. spectra least squares anal. 79—50007
- alkali metal heteronuclear diat. mol. form., equilib. consts., enthalpy changes 78—25750
- anthracene anion radicals, enthalpy of disproportionation, calorimetric determ. technique 79—96296
- aqueous multicomponent multiphase equilibria, free energy minimisation method, comput. algorithm 80—40724
- aromatic compounds, oxidative bromination, chem. oscills. 80—3335
- arsenides, group III, chem. transport equilib. with I_2 *(French)* 77—55876
- arsenides, group III, chem. transport equilib. with I_2 *(French)* 77—55877
- Belousov-Zhabotinski reaction, chem. oscill. mechanisms 80—3304
- Belousov-Zhabotinski reaction, oscill., thermal props. 80—7762
- Belousov-Zhabotinsky reaction, chem. turbulence, strange attractor representation 80—85148
- Belousov-Zhabotruskii reaction, existence of solitary travelling wave solns. 80—35525
- benzene, and substituted forms, thermodynamic ionis. energy, rel. photoionis. energy 77—16858
- bimolecular diffusion-controlled reversible reactions, detailed equilib. principle 80—7770
- binary liquid mixtures, mol., intermol. props. from excess enthalpies 77—44503
- biochemical systems, temporal and spatial patterns 80—3340
- biomolecules+chloranil, charge transfer interaction, equilib. const., enthalpy and entropy determ., mol. polarisability 80—89708
- biopolymers, assoc.-dissoc. phenomena, review 79—11884
- Bray reaction, kinetics obs. *(French)* 80—7788
- Briggs-Rauscher reaction, chem. oscill. obs. 80—3336
- Brusselator, two-box model, multiple stable steady states, chem. hysteresis 79—100428
- carbocyanines, dye laser appls., soln. chem. 77—40568
- catalysis by polyelectrolytes 79—57217
- chemical instabilities, rel. to equilibrium phase transitions 78—65897
- chemical kinetics, connection to chemical thermodynamics *(Chinese)* 79—96352
- chemical waves, multiple, induced by electric field 79—92047
- chemical waves and the diffusive coupling of limit cycle oscillators 79—83454
- chemisorption kinetics, power adsorption isotherm, entropy correction 80—40734
- chemodynamics, far from equilibrium 77—32820
- combustion, NO_x and SO_2 form., oxidizing agent excess depend., thermodynamic anal. 78—15677
- complex ions, mobility and stability consts., counter-current ion migration determ. *(German)* 78—56900
- complexes, differentiation between poly-, mononuclear, stability consts., graphical method 79—87927
- computer calc. in single reaction or single moiety chemical networks 77—12820
- consistency between kinetics and thermodynamics 77—44460
- constants determination, projection map technique 78—53240
- Coordination equilibria in non-aqueous solvents. I 80—66860

chemical equilibrium continued
- cyanoacetylene, and isotopic forms, $^{13}C/^{12}C$ effects on partition function 79—29352
- cycling zone adsorption, travelling wave, continuous flow equilib. staged model 78—64874
- dilute solution, associated, lattice model, chem. equilib. laws 79—82139
- dimers, dissociating, in nonisothermal ideal gas phase, stationary state anal. 78—76848
- displacement, by elec. field *(French)* 77—25299
- dissipative structures, fluctuation effects, appearance of optically active states 79—83442
- dissipative structures, fluctuation effects on chem. oscill. systems 79—83441
- dissociation reaction, shift of chem. equilib. in laser reson. IR radiation field 77—56224
- divalent transition metal halides, Coordination equilibria in non-aqueous solvents. I 80—66860
- education, chemical, osmotic and electrochemical equilibrium, principle of virtual work 77—33767
- electric field effects and field chem. consequences 78—7224
- electrochemistry, equilibrium and nonequilibrium states, electron transfer and multiple electrode problems *(French)* 78—27777
- electron donor-acceptor complex formation, equilib. const. determ., reson. Raman spectroscopy 78—3329
- entropy differences and statistical effects, symmetry corrections and entropy of mixing 79—21480
- entropy gradient, heuristic approach 79—48991
- extraction equilibria of Cu, Ni, Co and Mn with versatic acid 911 79—43620
- extractive metallurgical processes, thermodynamic evaluations 80—11591
- far from equilibrium, concepts *(French)* 80—7761
- Field-Koros-Noyes chemical wave equation, asymptotic solutions 80—66857
- first-order kinetic model, optimal design of experiments to estimate parameters 78—15650
- fluctuation on dissipative structs., external constraints 80—71894
- gas flow, partial equilib. with reaction invariants *(French)* 79—52739
- gaseous mixtures, equilib. at high temp., Raman scatt. obs. 80—45619
- glasses, dielectric relax., order parameter model appl. 80—108151
- graph-like state of matter, LCGI schemes, expt. data statistical anal. 78—15696
- Hafke-Gilles reaction, oscill., thermal props. 80—7762
- homogeneous isothermal chemical mixture in closed vessel, equilib. distrib. 77—21413
- hydrides, first row, $AH_2(H_3)(H_4)$, and positive ions, chemical equilibria, correl., ab initio calc. 78—35714
- ilmenite, idealized, chlorination in presence of excess C 78—7226
- instability, chemical, role of diffusion in model 79—16027
- intramolecular H bond energy determination, by competing equilibria, IR spectra obs. *(Russian)* 78—29783
- ion+molecule, entropy change, enthalpy of form., equilib. consts., thermochemistry 80—30233
- ion-molecule equilibria in solvolysis, secondary β ^2H isotope effects, hyperconjugation 80—50874
- ionic surfactants, conductance stopped flow study of micellar equilibria 79—43642
- isothermal chemical thermodynamics, equilib. and nonequilib., stochastic basis 79—83496
- isotropic solid soln. cryst. surfaces, surface stress and chem. equilib. 80—107628
- lactam-lactim tautomeric equilibria, quantum chem. calcs. 80—50833
- Landau theory for chem. instabilities 78—16763
- lanthanide complex, struct. and equilib. by time resolved Eu(III) spectrosc. 80—78736
- lanthanide ion bound to macromol., struct. and equilib. by time resolved Eu(III) spectrosc. 80—78736
- laser specific and thermal reactions classifications 80—11919
- liquid, non-stoichiometric complex formation, thermodynamic equilib. consts. 77—21406
- liquid nuclear waste, simulated, ion exchange equilibration, radiotracer obs. 78—74444
- liquid phases, non-uniqueness in phase, chem. react. equilib. computations 79—43612
- liquid-vapour equilibrium in chemically irreversible systems *(Russian)* 78—3369
- liquid-vapour equilibrium in system with chem. reaction, thermodynamics *(Russian)* 77—63947
- liquids, dielectric relax., order parameter model appl. 80—108151
- local equilibrium, chemical affinity, theory 77—12823
- maser equation near nonequilibrium transition, stationary solns. 80—89466
- mass action equilibrium problem, numerical methods 77—9113
- metal complexes, solns., activity correction in thermodynamic stepwise stability constant expression 78—56912
- metals, electrocrystallisation and passivation kinetics, multiple stationary states and dissipative structs. theory *(French)* 80—7804
- methane-air flame, reactions, radical overshoot 79—34308
- methane-H_2 system in plasma reactor, exptl. and thermodynamic investig. *(French)* 78—15698
- methylene glycol(-d_A)$\rightleftharpoons$formaldeyhyde(-d_2)+$H_2O(D_2O)$ Raman spectra and normal vibr. 80—58271
- MHD generator, supersonic, working body thermodynamic props., chem. kinetics effect 78—91163
- micelle formation model, relaxation spectra 80—71934
- microemulsions, thermodynamic stability 78—95962
- molecular gases reacting mixture, chem. equilib. shift due to reson. laser radn. 79—43614
- molecular liquid, orientation dependent distrib. function from NMR relax. data 77—20737
- molecular thermodynamics appl. to phase separation and critical phenomena *(German)* 78—14447
- molecule+negative ion, thermochemical data, gas phase acidity scale, mass spectroscopic techniques 80—30234
- multiphase solids under stress, thermochemical equilibrium 79—1964
- multiple stationary states systems, meas. of stability and relative stability 80—3338
- multiple steady state system, fluctuations at chem. instabilities 79—11813
- multistable chemical reaction systems, separatrices calc. 79—16033
- multivalent binding to substrate, linear differential equations in chemical equilibrium calculations 80—30279

chemical equilibrium continued
- multivariate master equation for reaction-diffusion system 80—95045
- non-equilibrium, mol. dynamics studies of long range and short range fluctuations 80—21318
- non-rigid molecules in condensed phases, liquid struct. effects on chem. reactions and conform. changes 80—40725
- nonequilibrium chemical systems, transitions, fluctuations, stochastic simulation approach 79—24722
- nonequilibrium molecular system, time-depend. kinetic-thermodynamic description rel. to HF chem. laser 80—9877
- nonideal gas, dissociating, composition and thermodynamic props., initial at. method 78—40034
- nonrigid polyatomic fluid, chem. equilib., struct., statistical mech. calcs. 77—9111
- 1-octanol-H-bonding solute system, chain assoc., dipole correl. theory, dielec. const. anal 77—48675
- oil-water interface, chem. and hydrodynamic instabilities *(French)* 80—7789
- open chemical system, noise-induced transitions 80—3337
- oscillating Belousov-Zhabotinskii system, detection of BrO_2 *(German)* 79—29351
- oscillating reaction, homogeneous bifurcation phenomena obs. 77—48621
- oscillating reactions, thermal props. 80—7762
- oscillations, chemical and thermokinetic, feedback *(French)* 79—57205
- oscillators responding frequency switch 80—108837
- oscillatory chemical reaction systems, weak coupling 80—66775
- oxiphenol, radical transform. in aqueous solns., chem. equilib. *(Russian)* 79—39138
- phase space subdivision for chemically reacting system variational theory *(Russian)* 79—61895
- phase transitions, nonequilibrium transient behaviour 80—93732
- phthalocyanines, dye laser appls., soln. chem. 77—40568
- plasma, three-component, weakly-ionised, ionis. equilib. instability 80—10877
- polycaprolactam characteristics dependence, at equilibrium state, on polymerisation conditions, in closed system *(Japanese)* 78—95928
- polymer, synthetic, solns., assoc., quantitative evaluation, review 79—10773
- polyurethanes, vapour press. of solvent above swollen crosslinked networks rel. to rubber elasticity theory 80—45536
- potentiometric titration apparatus, microprocessor controlled, for equilib. studies 80—89579
- primitive solar nebula, equilib. chemistry thermodynamics calcs. 80—82231
- protein-ligand equilibrium binding, mathematical models 78—48688
- rare earth (III) complexes, cysteinates, thermodynamics of form. 80—89515
- rate coefficient derivation, using scatt. theory 78—15697
- reacting gas system, equilib. comp. determ. 77—9115
- reaction-diffusion system, instability of stationary solns. *(French)* 78—20055
- reactive flow in heated channel, criteria characterising approx. to chem. equilib. *(Russian)* 79—27712
- reversible photoredox system, thionine type and I_2 type, chem. equilibria *(German)* 77—90630
- reversible reactions, asymptotic expectation and variance of stationary probability distribution 79—11789
- rhodamine-B solutions, thermochromic and hyperchromic effects 79—91977
- Schlogl model, transition time statistics 80—89467
- seawater, acoustic attenuation due to chem. relax.-absorpt. 79—34851
- self-oscillating reaction system under periodic external force, thermal fluctuations 79—66338
- self-oscillatory reaction system, breakdown of synchronised state 79—39142
- sequential fast kinetics, relaxation methods obs. 79—43575
- silicate glasses, redox equilibria of multivalent ions 78—26447
- slags, application of activity concept to physical chemistry 78—53243
- solar thermochemical energy transfer system, reversible reactions screening 79—87999
- solid-gas reactions, existence of instabilities 80—7861
- solid-gas surface reaction, nonequilibrium thermodynamic anal. 79—79285
- sols, primary and secondary coagulation and heterocoagulation, role of surface chemistry 80—45551
- specific equilib. recombination rate coeffs., Laplace transform calcs. of temp. depend. 78—60989
- spin detonation, triple configurations, chemical equilib. 79—100379
- statistical basis, demonstration machine for teachers 79—40337
- steady states bifurcation in chemical systems, gravitation effects 80—11878
- stilbene, radiolysis, electron transfer and protonation, vis. spectra, isomer effects 77—60085
- synergetics, chemical processes far from equilib., conf. Bordeaux, France (Sept. 78) 80—3334
- system far from equilibrium, stochastic simulation 80—3339
- TCNE, K salt, in nematic liq. crystal solvent, ion pairing, EPR spectra 78—73020
- teaching, computer method using minimisation of free energy 79—30168
- teaching, double scales as visual representations 79—84908
- teaching, rate consts. rel. to equilib. consts., student demonstration 79—58501
- tetracene anion radicals, enthalpy of disproportionation, calorimetric determ. technique 79—96296
- thermal rate constants, quasiclassical trajectory calcs., detailed balance 79—87822
- thermodynamic theory of solvent-jump relax. method, coupled equilibria 79—39186
- thermodynamics, misconceptions in school 77—60865
- thermodynamics for calculating chem. equilibria, review for teachers 77—26108
- thermodynamics of chemical system in external fields 77—12818
- thymopoietin active fragment in H_2O, soln. conformation by DNMR spectroscopy 80—89710
- TNF-carbazolyl compound charge transfer complexes, equilib. consts. 78—64877
- transition metal compounds, $(M,M')Cr_2S_4$ and $(M,M')S$, where $M,M'=Mn,Co,Zn,Cd$, solid-state equilib. *(German)* 77—36486
- trifluoromethoxide gas phase ion reactions with carboxylic acids, ion cyclotron reson. obs. of competitive solvation 79—79227

chemical equilibrium continued
- two time correlation functions for Poisson representation, nonequilib. and equilib. chemical reactions 79—1936
- unsaturated two-component associated vapour, press., comp., thermodynamic calcs. *(Russian)* 80—64671
- variational principle 77—36780
- water, cavitation, gas supersaturation thresholds under high press. 77—16861
- water association, in superheated vap., equilib. consts., H bond vibr. 77—66750
- water vapour, dissociating, composition and thermodynamic props., initial at. method 78—40034
- zeolites, synthetic, thermal dehydration effect on physicochem. characts. 77—60120
- Zhabotinski system, ferroin catalysed, period of homogeneous oscills. 80—30225
- Zn-salt, molten system, separation of Hf and Zr 80—11884
- Ag complexes in fixing baths, math. model 77—34043
- $Ag_2S(Se)(Te)$, thermodynamic props., growth of single cryst. by chem. transport reaction 77—36380
- $AlN+Ni(Co)(Fe)$, reactions at sintering temps. 79—74377
- Am cpds., prep. and stability of highest oxidation states in phosphoric acid. soln. 77—29029
- $AmCl_3(s)+H_2O(g)\rightleftharpoons AmOCl(s)+2HCl(g)$, using ^{241}Am and ^{243}Am, equilibrium constant, heats of formation of AmOCl 77—29037
- Am(VI) formation in molten salts 77—29039
- $2Ar+Ar_2^+=Ar+Ar_3^+$, equilib. consts., mass spectrometric determ. 79—100347
- $Ar+Br_2$ collisions, dissociation reaction, trajectory study by ensemble method 80—66765
- $Ar+N_2(O_2, CO)$, molecular fluid mixtures, equilibrium props. 80—64867
- $Ar+Xe^+$, $XeAr^+$ form., dissoc. energy, reaction equilib. and rate consts. 80—61071
- As_2O_3, vapour phase equilibria over GaAs 79—66181
- B compound isotope exchange reactions, equilib. consts. 78—19999
- B_2H_6, equilib. with solid soln. of B in Si 80—97721
- $BaBr_2$-$BaCl_2$, vap. mixture, ion-mol. equilib., heat of form. of ions 80—26039
- $BaCl_2$-$BaBr_2$, vap. mixture, ion-mol. equilib., heat of form. of ions 80—26039
- Br_2 in Ar, solvent effects on equilibrium props. 80—61128
- BrF(Cl), rot. spectra in millimeter wave region, rot. transitions obs., equilib. const. determ. 80—78607
- C_n aggregates in equilib. C vapour, MINDO/2 calc., isomerism 78—29873
- $C_2H_2+OH^- \rightleftharpoons C_2H^- +H_2O$, equilib. consts., ab initio SCF and CEPA calcs. 78—3361
- Ca-S-O system, sulphide-sulphate equil., solid state EMF obs. 79—83492
- $CaCl_2.6H_2O$ heat of fusion system for solar energy storage 80—16846
- CaF_2, fluorite, solubility equilibria in geothermal waters 77—60368
- CaO-SiO_2 slags, containing CaF_2 and B_2O_3, SO_2 capacity determ. by encapsulation method 80—11944
- CdS films, chemically deposited, phase comp. and photoelec. props. 77—40394
- $Ce(BrO_3)_3$-malonic acid, multiple stationary states in oregonator 78—20061
- ClF, rot. spectra in millimeter wave region, rot. transitions obs., equilib. const. determ. 80—78607
- $Cl_2O+H_2O\rightarrow 2HOCl$, equilib. const., UV spectrum investig. 79—79238
- Cr_2O_3, reduction by H_2, reaction kinetics 80—11950
- Cs_2CO_3 and Cs_2SO_4, ionic equil., mass spectra obs., heats of reaction and form. of ions 79—87867
- Cu, extraction by Kelex 100, meas. and correl. of solvent extraction equilibria 77—29034
- Cu-KELEX 100 (alkyl β-hydroxy quinoline), distribution coeffs., model 78—53244
- Cu-LIX 65N (β-hydroxy benzophenone oxime) distribution coeffs., model 78—53244
- Cu_2O-CuO-$(\beta)Ga_2O_3$ system, thermodynamics and phase equilibria, 680-1000°C 77—36489
- Cu_2S-Fe S mattes equilibration with Fe-O-SiO_2 slags under controlled partial pressures of SiO_2 79—83152
- D_2-T_2-H_2, fusion reactor fuel, isotopic exchanges, equilib. consts., 4.2-300K 77—70331
- Fe, liquid, reactions of CO, CO_2, with dissolved O and C, equilibria 78—44397
- Fe^{3+} solutions, UV absorption spectrosc. obs. of equilib. 80—93812
- $FeCl_3$, nonaq. solns., solvent-solute interactions, Mossbauer investig. of equilib. consts. 79—1729
- $GdCl_3(s)+1.5L_2Cl_6(g)=GdL_3Cl_{12}(g)$, $(L=Al,Fe)$, entrainment, quenching, and chem. transport, rel. to appl. for GdIG CVD 80—24750
- GdS, vaporisation thermodynamics and dissoc. energy obs. 78—67822
- Ge-I, gas phase equilib. comp. 77—36776
- H-air, laminar diffusion flames, chem. nonequilib. effects model 78—48654
- $H_3CO^+ +H_2S\rightleftharpoons H_3S^+ +HCHO$, chemical equilib. consts., proton affinity of HCHO and H_2S 78—85189
- $H_3CO^+ +HCN\rightleftharpoons H_2CN^+ +HCHO$, chemical equilib. consts., proton affinity of HCHO and HCN 78—85189
- HF molecules, infinite linear chain, equilibrium structure and stabilisation energy 80—63856
- HF oligomers, Gibbs free energies, gas. equilib., ab initio calc. 79—20456
- $H_2O+Cl_2O=HOCl$, equilib. const., Fourier transform IR determ. 80—7765
- $H_2O+D_2O\rightleftharpoons 2HDO$, vibr. anharmonicity effect on equilib. 79—74410
- $H_2O+H^+\rightleftharpoons H_3O^+$, equilib., H_2O proton affinity calc. 78—92497
- $H_3S^+ +HCN\rightleftharpoons H_2CN^+ +H_2S$, equilib., rate coeffs. and proton affinity, flowing afterglow 78—56885
- $HfCl_4$-CsCl melt, equilib. phase diagram and vapour press., equilib. reaction 77—66764
- I partition equilibrium between air and NaOH aq, effect of CO_2 conc. 78—78474
- I_2 vapour, chemical composition at high temps. 77—36781
- ICl(Br), rot. spectra in millimeter wave region, rot. transitions obs., equilib. const. determ. 80—78607
- In_2Se_3, chem. transport reactions with I, single cryst. growth 77—16480
- K_2CO_3 and K_2SO_4, ionic equil., mass spectra obs., heats of reaction and form. of ions 79—87867

chemical equilibrium continued
$KF-BeF_2$, and $BaO-SiO_2$ systems complex ionic liquids, corresponding-state principle *(Japanese)* 77−56245
K_2SO_4, vaporisation thermodynamics, MHD generation appls. 77−9112
$LaMnO_3$, O_2 environment, phase stability and nonstoichiometric behaviour, 1200°C 78−43134
Li-LiH system, liquid Li, dilute solns., equilib. H press., solubility, heat of soln., CTR materials 77−14266
$Li+H_2O \rightleftharpoons LiOH+H$, equilib. consts., ab initio SCF and CEPA calcs. 78−3361
$LiF-BeF_2$, and $MgO-SiO_2$ systems, complex ionic liquids, corresponding-state principle *(Japanese)* 77−56245
LiH_2 and LiH_2^+ binding energies, LiH_2 ionis. pot. and form. heat 79−94042
Li_2O_2, gas, thermochem. props., mass spectra study 79−47957
Li_3O, gas, thermochem. props., mass spectra study 79−47957
Mn-S-O system, sulphate and sulphide reaction equilibria 77−52640
Mn-S-O system, sulphide-sulphate equil., solid state EMF obs. 79−83492
Mo-Fe-O-H system, thermodynamic equilib. 78−60657
MoF_5, gas, thermodynamic stability 80−26041
N_2-H_2O plasma state, partial equilib. with reaction invariants *(French)* 79−52739
$N_2+H_2+N_2H_4$, mixtures with nonthermal vibr. excitation of mol. N_2 80−76545
N_2+O_2, molecular fluid mixtures, equilibrium props. 80−64867
N_2+O_2+NO, mixtures with nonthermal vibr. excitation of mol. N_2, formula for calc. equilib. const. 80−76545
$NH_2^-+H_2 \rightleftharpoons NH_3+H^-$, chem. equilib., ab initio calcs. 79−34282
NH_4Cl, gas $^1A_1$ ground state, pot. surface 80−32626
$NH_4NO_3 \rightleftharpoons NH_3+HNO_3$ equilib. in atmosphere 79−88389
NO dimerisation, equilib. const. anal., trans-/cis-$(NO)_2$ zero pt. correlation energy difference 78−11509
$N_2O_4-NO-H_2O$, distrib. coeff. for N_2O_4 on liquid-vapour equilib. *(Russian)* 80−55699
$NO^+(NO)+SO_2$, cluster form., equilib. const. and rate coeffs., UV irrad. effects 77−60060
$N_2O_4 \rightleftharpoons 2NO_2$, chem. equilib., struct., statistical mech. calcs. 77−9111
$Na_2+Ar(Ne)(He)$, collision induced dissoc. rate, vibr. distrib. depend. 79−22791
$NaF-BeF_2$, and $CaO-SiO_2$ systems, complex ionic liquids, corresponding-state principle *(Japanese)* 77−56245
$NaF-ScF_3$ system, ionic equilib., mass spectra 78−7222
$Na_2O-Al_2O_3-B_2O_3$ glasses, kinetic study of Cu^+-Cu^{2+} equilib. 79−8448
$Na_2O-CaO-SiO_2-Cr_2O_3$ glass, redox equilibria of Cr ions, impurity effects 80−89477
Na_2O-SiO_2, aqueous solns., Raman and IR spectra, pH depend., species at equilib. identification 79−87866
Nb-Pt-O system, phase equilibria, diagram, unit cell parameters, supercond. 80−55352
$Np^{4+/3+}$ in fused salts, redox and chem. props. 77−29038
Np(VII) formation in molten salts 77−29039
$^{17}O+^{16}O$, fractionation by chemical equilib. 80−89513
$^{18}O+^{16}O$, fractionation by chemical equilib. 80−89513
Pb complex, $Pb(C_2O_4)_2^{2-}$, stoichiometry, form. const. determ., teaching appl. 79−84916
$PbSO_4-PbO.PbSO_4(PbS)(SO_2)$, solid, EMF determ. of O_2 equilib. press., 1000-1100K 78−48683
PbTe homogeneity region investig. in Pb-Te system, equil. consts. of quasichem. reactions 80−108405
$Pb(Zr,Ti)O_3$, thermodynamic properties and formation data 80−29939
PrP-I, heterogeneous equilib. 77−36777
$PtCl_2$, PtCl, decomposition equilibria by simultaneous torque Knudsen technique 77−29035
$Pu^{4+/3+}$ in fused salts, redox and chem. props. 77−29038
PuO_2, conversion to $PuC_{0.88}$, thermodynamic assessment 77−70293
Pu(VII) formation in molten salts 77−29039
$S_n+4H_2O \rightarrow 3H_2S+H_2SO_4$, chem. equilib. of aq. system, application to Venus and Io 80−50837
SF_6, equilibrium composition calc., in 20000 to 50000K range, in dependence on pressure 79−14511
$3SO_2+H_2O \rightarrow 2H_2SO_4+S_n$, chem. equilib. of aq. system, application to Venus and Io 80−50837
$Sc_2(SO_4)_3+Al_2(SO_4)_3$ aq. solns., complex form. reacts., kinetics, US relax. investig. 79−1942
$SeCl_4-SbCl_5$ systems, Raman spectra *(German)* 80−93324
SeS gas, thermodynamic props., quadrupole mass filter study 80−16716
$1/2S_2(g) \rightleftharpoons S(1)$ equil. reaction, improved ΔG^0 values calc. 77−32822
Si, Czochralski growth, equilib. of dissolved C and O with CO in ambient atm. 80−1949
Si, solid soln. of B, equilib. with B_2H_6 80−97721
Si-Ge-Br, heterogeneous system, equilib. gas phase composition, Si-Ge cryst. growth appl. 79−10820
Si-N-H gaseous system, deposition ranges of Si_3N_4 and Si *(French)* 77−36405
$SiC-H_2$ system, thermodynamic analysis 77−86347
Si_3N_4, low pressure CVD, thermochemical calcs. 80−108356
SiO_2, low pressure CVD, thermochemical calcs. 80−108356
$SiO_2-MgO-CaO-Al_2O_3$:Ce,Fe, redox equilib., expt. 80−85171
$SnSe_2$, sublimation, temp. depend. of equilib. constants 80−88312
TaF_x complex, with 4-(2 pyridylazo)-resorcinol, stability investig. by spectrophotometry 77−36782
Ti-O system, intermediate oxide thermodynamics under equilibrium press. 80−55351
$TiO_2-Ti-Cl_2$ system, thermodynamic analysis, gas phase equilibrium composition 80−21317
$TiO_2-Ti-HCl$, equilibrium composition of gaseous phase and TiO_x yield 78−27393
$TiO_3-Cl_2(SeCl_4)$, equilibrium composition of gaseous phase and TiO_x yield 78−27393
$TiO_{(g)}$, $TiO_{2(g)}$, thermochemistry, mass spectrometry 77−16857
TiS_2-I_2 system, thermodynamic considerations for layered dichalcogenide growth by vapour transport process 79−4903
U BCC alloys, solubility of H_2 and D_2 gas 79−96302
$U^{4+/3+}$ in fused salts, redox and chem. props. 77−29038
UF_5, thermochem., heat of formation, dissoc. energy, ionis. pot 77−70326
UH_4, thermochem., heat of formation, dissoc. energy, ionis. pot. 77−70326
V_2O_{5-x}, O_2 equilib. press. at 600°C 77−81421

chemical equilibrium continued
V_2O_{5-x}, O_2 equilib. press. as measure of O_2 binding energy in oxide system 79−16030
W-O-F system, gas phase, comp. and chem. transport reactions in discharge lamp *(German)* 77−32826
$ZrCl_4-CsCl$ melt, equilib. phase diagram and vapour press., equilib. reaction 77−66764

chemical exchanges
see also ion exchange; isotope exchanges
acetanilide, bromination, fast reaction kinetics, rot. Pt. electrode meas. 77−16821
acetate, OH abstraction, H· formation, CIDEP in pulse radiolysis 77−48656
acetic acid-methanol-tetrahydrofuran-d_8, superimposed intermolecular spin exchange reactions, NMR lineshape theory 80−32740
o,m-acetotoluidide, bromination, fast reaction kinetics, rot. Pt electrode meas. 77−16821
acetylacetonatobutyl halides, equilib. reacts. redistribution of −F, −Cl monofunctional groups *(French)* 78−64816
Acree relation, re-evaluation of its conceptual foundations *(French)* 78−7172
acridine, excited state proton transfer reactions, ns fluorometry obs. 79−5132
adsorbed molecules, NMR, effect of migration between physical and chem. adsorption sites 77−21422
alkali atom dimer polarisation transfer, atom-molecule-exchange reaction 78−13574
alkali ion pairs, intramolecular cation migration, freezing out by crown ether addition 77−58047
alkali metal indates and thioindates, prep., props. and struct. 80−35517
anthracene-aliphatic amine, photochemically induced H isotope exchange 79−11771
aromatic compounds, electrophilic substitution sites, perturbation theory calcs. 77−30800
aromatic substitution mechanisms 77−9056
atom+diatom, collinear exchange reaction rates and probabilities, threshold behaviour 78−27738
atom+diatom, collinear quantum mech. reactive scatt., hyperspherical coords. 80−108694
atom+diatom, transition states, trapped trajectories and classical bound states in continuum 78−88630
atom+diatomic molecule, exchange reaction, 3-dimens., natural coord. calcs. 80−26010
atom+molecule, collinear reactive scattering, generalised hyperbolic coords. 79−74363
atom+molecule, dissoc. and exchange, classical and near classical rates 79−11778
atom abstraction reactions, empirical correlation of activation energy and mol. polarisability 78−40038
atom transfer reaction in gas phase, reaction rate computing, tunnelling corrections 79−79237
atom transfer reactions, reaction rate computing, trajectory calcs. 79−74371
atomic and molecular collisions in intense light beams, quantum aspects *(Russian)* 79−6903
ATPase kinetics in E. coli cells, ^{31}P NMR meas. 78−77022
AX_3 type spin coupled system, two-position exchange, NMR line shape function 77−90600
basalt, hydrothermal alteration by seawater, chemical exchange exptl. results 79−20828
benzophenone-N,N-dimethylaniline, intramolecular exciplex systems, laser photolysis obs. 80−35550
bimolecular exchange reactions, dynamical-statistical method calcs. 80−104435
biradical, triplet state, $S-T_0$ CIDNP, biradical scavenging rate const. from mag. field depend. CIDNP 79−3461
boronising, powder, physicochem. characts. 80−61024
butyl boron halides, equilib. reacts., redistribution of −F, −Cl monofunctional groups *(French)* 78−64816
N-5-chlorosalicylideneaniline, $H^+-^{14}N$ double reson. NQR spectra temp. depend. thermochromism and tautomeric mech. 78−70849
cyclobutane derivs., nucleophilic substitution, mechanism 77−9057
cis-decalin, shift difference between chem. exchange sites using ^{13}C T_1 meas. 80−18945
5,5′-dichloro-1,1′-dianthraquinonyl synthesis by Ullman reaction *(Japanese)* 79−96304
2,5-dihydroxy-p-benzoquinone, proton tautomerism dynamics, ^{13}C NMR obs., CNDO calc. 79−52632
dimethyl sulphoxide, form. of $(CH_3SOCH_3)_2H^+$ and $CH_3.CH_3SOCH_3^+$ in ICR mass spectrometry, proton affinity 78−3319
N,N-dimethylacetamide, amide band rot., ^{13}C NMR using modified DEFT pulse sequence 79−93191
N,N-dimethylcarbomoylchloride, chem. exchange rate by NMR method, temp. depend. 79−79243
N,N-dimethyltrichloroacetamide, two-site exchange system, total line shape anal. 80−35519
direct reaction sequential impulse model 77−16808
disproportionation, ketone chemiluminescence during disproportionation, nonradiative transition processes 79−87846
ethyl radical proton exchange reaction with ethylene matrix, indirect ESR obs. 80−16700
exothermic exchange reaction, vibr. population inversion, quasiclassical model soln. 79−91924
exothermic triatomic exchange reactions, dynamics, anal. theory 78−3322
exothermic triatomic exchange reactions, prod. energy distrib., statistical dynamic model 78−92455
extended diffusion and ‘sticky’ collisions 78−86940
fast nucleus+molecule, atom capture, quantum calcs. 80−71911
force decomposition anal. along reaction coord. 78−27741
glyoxal-photoreduction-product-radicals, kinetics and intramol. dynamics 77−32808
granular porous media, resisto-capacitive model of gaseous exchange *(Polish)* 77−12831
imidazole, Z-irrad., EPR study of H exchange 80−40718
laser collision induced chemical reactions, collinear exchange model 79−66313
light atom exchange reactions quantum dynamics 80−101011
linear exchange reactions, dynamics, high-energy vibr. inversion, quasiclassical model 79−91923

chemical exchanges continued
- linear triatomic exchange reactions, quantum investig., computational method 79−91922
- lysine vasopressin, amide H exchange rates in aq. soln., ^1H NMR effects 79−83692
- lysozyme, tryptophan residues, H exchange for D, relax., proton NMR spectra 80−35846
- Mars, Viking gas exchange reaction simulation on UV irradiated MnO_2 substrate 80−72831
- mechanisms, dynamic NMR spectrosc. obs. book contrib. 79−30521
- meson transfer reactions, role of electron distrib. 79−55007
- methane, H abstraction by thermal H, 10-30K, ESR evidence 78−76839
- methane$+H^{-}\rightarrow H^{-}+$methane, force decomposition anal. along reaction coord. 78−27741
- methane+tritium reaction, reaction ergodography 77−21371
- methanol glass, H atom abstraction by methyl radicals, 15-100K, limiting rate const. rel. to tunnelling 77−60037
- methyl protons, NMR relax. in presence of chem. exchange 78−13515
- methyl transfer reactions, Marcus theory 80−21279
- methylene$+H_2\rightarrow CH_3+H$, triplet methylene abstraction, partial open shell FSGO calc. 78−80719
- minimum energy reaction paths, virial theory implications 80−97686
- NMR chemical shift between two sites in rapid exhange limit, Fourier transform method 79−24743
- NMR of solutions exhibiting chemical exchange, spin 5/2 and 7/2 nuclei 79−65750
- NMR spectral lineshape analysis of two-site exchange kinetics, student expt. 77−26118
- NMR spin echo, chemical exchange and T_2 relax., multiple sites 78−78727
- non-bonded spin-spin coupling of groups of nuclei 79−39143
- organometallic, fluxional, solid state chem. exchange, ^{13}C NMR magic angle spinning 80−7775
- oxytocin, amide H exchange rates in aq. soln., ^1H NMR effects 79−83692
- phenomenological rate equation model 79−87824
- proton relay model systems, reaction field theory of solvent effects 78−44346
- proton transfer photoreaction kinetics, in singlet excited state 78−48671
- proton transfer reactions, excited state, laser pH jump analysis method 79−47922
- PVC, chlorination reaction, X-ray photoelectron spectrosc. 80−3469
- pyridine+HCl, proton transfer interactions, NMR obs. 78−20007
- quantum reactive scatt. theory, nonorthogonal bases and coordinates 79−91909
- radionuclides in sample soil and water, distrib. coeff., environmental effects 77−13092
- rare earths, purification, laser methods 80−16712
- rate parameters, NMR determ. method using inhomogeneous mag. field *(French)* 77−21383
- semiconductor, prereduced surfaces, room temp. activity for oxygen isotopic exchange 79−91998
- statistical models characterisation, prior distribs., appl. to at.-diat. exchanges 77−66744
- steel melt, interaction with Al_2O_3:Zr ceramic 80−104305
- stilbene derivatives, electronic struct., frontier electron density, chem. reactivity *(Rumanian)* 79−72242
- sudden rotational approximation, reactive and inelastic, body-fixed frame, light-heavy-light systems 80−61073
- T_1 spin decoupling and chem. exchange on NMR lineshape 77−71818
- transition metal borohydrides, formation by reaction of transition metals with $NaBH_4$ or $CaBH_4$ in organic solvents 80−30223
- transition metal complexes, reaction mechanisms and solvent effects 80−26012
- triatomic exchange reactions, exothermic, semiclassical dynamics calcs. 80−25999
- tumour electrolyte exchange kinetics, meas. using fast neutrons 77−64125
- tunnelling in low-temperature atom transfer processes 79−66263
- two-dimensional NMR spectrosc. investig. 80−25218
- two-site exchange system, total line shape anal. 80−35519
- two-spin system with chemical exchange, amplitude-modulated DNMR 79−93194
- zeolites, synthetic, thermal dehydration effect on physicochem. characts. 77−60120
- Ag+SnTe, surface topotactic exchange 78−14640
- Al_2O_3:Zr ceramic, elec. props., additives effect, and interaction with steel melt 80−104305
- $Ar+Ar_2$, exchange and dissoc. interactions, three-body effects calcs. 77−9069
- BCl_3+H_2 laser induced chemistry, theory 78−76884
- BaF_2 crystal, selective etching and dissolution kinetics 80−71775
- BaO-$MMOo_4$, M=Cd,Pb, phase diag. cross sections and reactions 78−27487
- Bi_2Te_3, chemical bonding models, correctness test using mag. susceptibility, and chemical substitution 78−67680
- $Br+Br_2$, atom-exchange, rate and activation energy, trajectory model and pot. energy surface 78−64811
- $Br+HI\rightarrow HBr+I$, thermal rate const., 220-400K, H/D isotope effect 79−47906
- $C+CO_2$ reaction, kinetics at low press. and hydrogen inhibition 77−63950
- $C+CO_2$ reaction, Langmuir-Hinshelwood kinetics at intermed. press. 77−66766
- CF_x, exam. of graphite fluorination kinetics, meas. of activation energy, reaction rate 79−96284
- CH_2N_2+triplet $CH_2\rightarrow CH_3$, reaction rate constant determ. 77−36727
- $CO+CO_2$, exchange rates behind reflected shock waves for $C^{18}O$ and ^{13}CO 79−29363
- $CS+O\rightarrow CO+S$, rate const. temp. depend., ESR-mass spectrometer obs. 78−20013
- CaO:$MMoO_4$; M=Cd,Pb, phase diag. cross sections and reactions 78−27487
- $Ce(BH_4)_3$, synthesis from chloride salts and $NaBH_4$ in tetrahydrofuran 80−30222
- $Cl+DI\rightarrow DCl+I$, thermal rate const., 220-400K, H/D isotope effect 79−47906
- Cl+H(D)I, exothermic triatomic exchange reactions, prod. energy distrib., statistical dynamic model 78−92455
- $Cl'+HCl\rightarrow Cl'H+Cl$, barrier height, PNO-CEPA calculation 77−16795
- $CsCl+NaI\rightarrow CsI+NaCl$, solid-state displacement reaction 77−52635

chemical exchanges continued
- D exchange reaction between H_2 and water a hydrophobic catalyst supporting Pt 80−30208
- $D+D_2(\nu)$, vibr. relax. in at. exchange reactions, classical trajectory calcs. 77−44467
- $D+F_2(Cl_2)$, exothermic triatomic exchange reactions, prod. energy distrib., statistical dynamic model 78−92455
- $D+HCl\rightarrow DCl+H$, rate consts., EPR 77−9059
- D+HX(H=Cl,I), HX dissociative ionisation, H^+ signal origin, mol. beam obs. 80−66778
- D_2-T_2-H_2, fusion reactor fuel, isotopic exchanges, equilib. consts., 4.2-300K 77−70331
- DyB_6, form. mechanism, reduction of Dy_2O_3 by B, DTA appl. 80−55643
- $EuCl_3$-$NaPO_3$-H_2O system, Eu polyphosphates form. at 0°C 80−35515
- F+chlorobenzene→fluorobenzene+Cl, statistical theory, phase space theory 79−74369
- $F+H_2\rightarrow HF+H$ energy profile, minimal basis ab initio VB calcs. 78−50477
- F+HI, $^2P_{1/2}$-state excited I form. 78−23923
- F+muonium (H)(D)(T), exothermic triatomic exchange reactions, dynamics, anal. theory 78−3322
- F_2+Mu (H)(D)(T), exchange reaction, quasiclassical dynamics calcs. 79−91942
- Fe-C liquid alloys, Si and C transfer from SiO-CO gas phase 80−55655
- Fe-Zn, liquid-solid reaction in Zn bath, effect of Fe concentration, alloy layer growth, exam. *(Japanese)* 78−85037
- GaAs, gas-phase epitaxy, mass exchange during 79−78901
- H atom transfer reactions, activation energies from bond energies 78−40037
- H exchange reactions, low temp., tunnelling dynamics 79−29340
- H production by thermochemical cycles using fusion energy source 80−51010
- H release from fusion reactor wall materials 80−37579
- H+CN(NC)(NSi), bimolecular exchange reactions, dynamical-statistical method calcs. 80−104435
- $H+F_2(Cl_2)$, exothermic triatomic exchange reactions, prod. energy distrib., statistical dynamic model 78−92455
- $H+H_2$, 3-dimens. exchange reaction, surprisal theory, quantum dynamics 79−15964
- $H+H_2$, CI calc. of three dimens. pot. energy surface 78−56882
- $H+H_2$, collinear classical dynamics, chemically accurate pot. energy surface 77−48620
- $H+H_2$, collinear exchange reaction, quantum dynamics, surprisal theory 79−6988
- $H+H_2$, collinear exchange reaction, unified statistical model 79−34295
- $H+H_2$, collinear quantum mech. reactive scatt., hyperspherical coords. 80−108694
- $H+H_2$, collinear reactive scatt., Magnus approx. 77−16801
- $H+H_2$, exchange reaction, three-dimens., dynamical S matrix method 79−91930
- $H+H_2$, least squares fit to ab initio pot. energy function 78−56883
- $H+H_2$, planar reaction, cross section calcs., vibr. and rot. convergences 77−21376
- $H+H_2$, planar reaction, Schrodinger eqn., expansion as partial differential eqns. 77−21375
- $H+H_2$, three dimens. reaction, theory 77−21377
- $H+H_2$, three dimens. reaction, Porter-Karplus pot. energy surface, rot. distribs., rate consts. 77−21378
- $H+H_2(HD)(D_2)$, exchange reaction rate consts. meas., vibr. effects 79−5134
- $H+H_2(\nu_i=1)$, exchange reaction, integral and differential cross sections determ. 80−85153
- $H+H_2(\nu=1, j=0)$ exchange reaction, 0.9-1.1 eV, sudden rot. calcs. 79−79230
- $H+H_2(\nu=1)\rightarrow H_2+H$, exchange reaction, classical trajectory method, vibr. excitation, partial rate consts. 78−60993
- $H+H_2(\nu)$, vibr. relax. in at. exchange reactions, classical trajectory calcs. 77−44467
- H+HCl, barriers for abstraction and exchange reactions 77−48629
- $H+HR\rightarrow H_2+R$, (HR=hydrocarbon), tunnelling reaction, classical S-matrix calc. 77−29007
- H+methane, abstraction and exchange reactions, energy barriers, UHF-CI calcs. 78−11512
- $H+PH_3$, abstraction rate consts., 209-495K, time-resolved fluoresc. 77−16807
- $H^-+CH_4\rightleftharpoons CH_4+H^-$ intrinsic reaction coord., ab initio SCF calc. method 77−48626
- H^-+methane→methane$+H^-$, nucleophilic substitution, ab initio pot. energy classical trajectory anal. 78−68886
- H^++methane$\rightarrow H_2^++$methyl radical, quantum 80−71911
- H_2+alkali metal, exchange reactions and rot. transfer effects on transfer coeffs. 77−66749
- H_2+D_2, exchange reaction, steady-state, surface reaction effects *(French)* 78−85148
- H_2+D_2, exchange reaction, gas phase, heterogeneous initiation *(French)* 78−85149
- H_2+D_2 exchange reaction, on Pt(111) or (332) surface, mol. beam obs. 79−66269
- H_2+H, coplanar exchange reaction, 0-2 eV, reactivity bands, analytical method 78−35664
- H_2+H_2 exchange reaction mechanism, energy and geometry changes, H_4 FGSO calcs. 79−10025
- H_2+H(F), reaction products ang. distribs., Franck-Condon theory 79−87835
- H_2+H(F)(Cl), collision induced IR laser absorpt., rate enhancement, theory 79−66275
- $H_2^++He\rightarrow H+HeH^+$, endoergic exchange, DWBA calcs. 77−9055
- H_4, excited potential energy hypersurfaces, trapezoidal geometry, rel. to photochem. 2s+2s processes 77−30797
- $HD(v=5)+HD(v=0)\rightarrow H_2+D_2$, mol. H_2 exchange, reaction mechanism 80−85167
- HF+D, vibr. threshold energies, reagent energy effects 78−85145
- $HF+H'\rightarrow H+H'F$, transition state geometry, SCF CI calcs. 78−20009
- HI, H abstraction by thermal H, 10-30K, ESR evidence 78−76839
- H_2O, proton chemical exchange, proton spin-echo NMR 77−9053
- $H_3S^++HCN\rightleftharpoons H_2CN^++H_2S$, equilib., rate coeffs. and proton affinity, flowing afterglow 78−56885
- $H'+BrH\rightarrow H'Br+H$, collinear reaction, barrier height, PNO-CEPA cals. 78−3328

chemical exchanges continued
- $H'+XH \rightarrow H'X+X$, $X=H$, F, Cl,CH_3, collinear pot. energy barriers, PNO-CEPA calcs. 77−32777
- He_2, electronic and rot. energy relax., reactive collisions by isotope selective excitation 78−33541
- $HgH+NO \rightarrow HNO+Hg$, reaction rate temp. depend., chemiluminescence 78−68885
- IBr-benzene in n-decane soln., IR line broadening by chemical exchange 80−87111
- $K_4(MoCl_4)_2$+acetic acid, reaction kinetics and mechanism 77−86305
- $K_{0.3}MoO_3$, thermochemistry 77−77801
- $KrCl^*+Xe$, substitution efficiency during excitation in transverse AC electric discharge 80−50850
- $La(BH_4)_3$, synthesis from chloride salts and $NaBH_4$ in tetrahydrofuran 80−30222
- Li(D,T), prep. via exchange reaction 77−9109
- $LiInO_2$, prep., props. and struct. 80−35517
- $LiInS_2$, prep., props. and struct. 80−35517
- Mo, substitution and redox reactions in oxidation states III to VI, role in enzymes 77−86364
- $N^+ + H_2$ (hydrocarbons) rotational vibrational product excitations 79−47901
- NH_3, liq., vapour press., isotope effect, relevance to isotope exchange reaction calcs. 80−39272
- $NH_3+Hd \rightleftharpoons NH_2D+H_2$, deuterium separation factors, calc. 80−3310
- $NH_4^+ + LiH(H^-)$, substitution and abstraction reactions, ab initio calcs. 77−48624
- N_2H_2+ethylene reaction, H transfer, ab initio SCF GO calcs. 77−44469
- $N_2O_3 \rightleftarrows 2NO_2 \rightleftarrows 2NO+O_2$, heat exchange calc. *(Russian)* 77−84127
- Na^+-K^+-F^--SO_4^{2-}, asymmetrical reciprocal molten salt system, excess enthalpies 80−30268
- $Na+Na_2$, reaction probability, energy transfer 77−28998
- $Na+Na_2 \rightarrow Na_2+Na$, gas phase study 79−43568
- $Na+Na_2 \rightarrow Na_2+Na$, simple model study of exchange reactions 79−43569
- Na_2+Na, spin polarisation exchange via opt. pumping, NMR 77−14452
- $NaAsO_2$ aq. solns., O exchange between $AsO_2(OH_2)^-$, and water 78−92459
- $NaCl+KF \rightarrow NaF+KCl$, solid state reaction mechanism 79−61857
- α-$NaFe_2O_3$, Na-Ca substitution *(French)* 79−43576
- $NaInO_2$, prep., props. and struct. 80−35517
- $NaInS_2$, prep., props. and struct. 80−35517
- $NaK+Na$, spin polarisation exchange via opt. pumping, NMR 77−14452
- $NaMo_6O_{17}$, thermochemistry 77−77801
- $NaTaO_3$-$AgTaO_3$ system, synthesis by exchange reaction 79−47625
- $O(^3P)+CO(X^1\Sigma^+)$, vibr. deactivation and atom exchange, rate. consts., Monte Carlo anal. 77−48627
- $Pr(BH_4)_3$, synthesis from chloride salts and $NaBH_4$ in tetrahydrofuran 80−30222
- Pt, adsorption of water, H_2 and reaction between H_2 and adsorbed O 80−49514
- S-metal interactions 80−55710
- ScD_2, surface, interactions with reactive gases 78−23964
- $SiBr_4+H_2$, SiH_nBr_{4-n} heat of form., mass spectrometric determ. 79−20455
- Si_3N_4/Al_2O_3, powder compact, electron microprobe investigation of reactions *(French)* 80−26009
- SiO-CO gas phase, Si and C transfer to Fe-C liquid alloys 80−55655
- SiO_2, small amorphous particles, prop. by vapour-phase hydrolysis of $SiCl_4$; high resolution TEM 79−82157
- $Sm(BH_4)_3$, synthesis from chloride salts and $NaBH_4$ in tetrahydrofuran 80−30222
- SnTe substrate, Ag epitaxial growth and topostactic exchanges 78−14640
- SrO-$MMoO_4$, $M=Cd,Pb$, phase diag. cross sections and reactions 78−27487
- $T+HD$ hot atom exchange reactions, trajectory calcs. 80−26037
- TaS_2, kinetic study of NH_3/ND_3 exchange by neutron diffr. 79−29350
- TiN, from high-temp. reaction of NH_3 and $TiCl_4$, physicochem. props. 80−55334
- $TiO_{(g)}+AlO_{(g)}(BaO_{(g)})$, rel. to TiO dissoc. energy 77−16857
- $TlCl+KI$, solid state displacement reaction, kinetics and mechanism 79−11788
- $TlCl_3.(TlCl)_3$, labelled, exchange of Tl ats. rel. to γ-irrad., heat treatment, grinding 78−92470
- U isotope separation using ion exchange chromatography, U(IV)-U(VI) exchange isotope effects 79−36376
- UF_6+H_2, laser induced dielectric breakdown obs. 77−28992
- ^{235}U enrichment by chemical exchange process *(Japanese)* 79−26661
- $V_2O_{3-x}F_x$ $(0 \leq x < 0.3)$, preparation and physical props. 78−76619
- $XeCl^*+Kr$, substitution efficiency during excitation in transverse AC electric discharge 80−50850
- $YAl_3(BO_3)_4$-$NdAl_3(BO_3)_4$, substitution of Nd for Y in $YAl_3(BO_3)_4$, exam. 80−11551

chemical industry
- air monitoring anal. and instrum. technology *(German)* 77−21886
- air-pollution control, problems and solutions 77−9488
- ambient noise meas. *(German)* 77−68327
- benzolene gas and oil desulphuration by automatic gas-chromatographs and computers *(German)* 77−4965
- chlorocarbon industry impact on atmospheric O_3 layer 78−40648
- coal conversion, solvent refined, pilot plant experiences 79−52867
- coal liquefaction, Exxon donor solvent process development 79−48059
- distillation column control, FRACTRONIC system, appl. and development 77−39672
- distillation column control, material balance concept 77−43320
- distillation column control, process equipment influence 77−39671
- distillation column control, using analogue recursive computer 77−43321
- electrochemical processes, energy use analysis *(Dutch)* 80−72019
- electrochemical processes, energy use optimisation *(Dutch)* 80−72020
- electrolyser, low cost hydrogen production *(French)* 80−7803
- electrolysis cells, diaphragm type, voltage calcs. using adaptive algorithms 78−35700
- electrolytic hydrogen production, raw material of the future *(French)* 79−96328
- flow measurement, VDI and DIN 1952 standards and correction factors *(German)* 77−42946

chemical industry continued
- high-temperature power-technological industrial processes use of nuclear power, reviews 79−26729
- industrial organic chemicals production, electrical power applications development *(French)* 79−96327
- inorganic chemicals industry, water pollution and solid waste disposal 77−70704
- lasers for industrial chemistry 80−87427
- metal electrowinning, energy consumption reduction via anodic coal reaction 79−91965
- nuclear fuel reprocessing, on-line control *(Russian)* 78−74460
- olefines plants acoustic planning, technical and economic advantages 80−3561
- particle size measurement techniques, rapid response, online methods, pharmaceutical, agricultural products appl. 78−89429
- petro-chemical industrial plants, piping networks, noise abatement 80−28381
- petrochemical industry, prevention of water pollution 77−70705
- polyethylene process plants, low-density, high pressure compressor design 77−13764
- polymer manufacture, radiation treatment of waste-water, feasibility *(Russian)* 78−46181
- pump design, gas-lift type, <8 mm riser dia. 80−10324
- radiolytic H_2 production using laser, fusion system 77−25294
- reaction kinetics measurement and control using laser technology, free electron laser appl. 80−81349
- residence time measurement, magnetic recording and hybrid computers appl. 78−81953
- synthetic chemicals production, multiple digital differential thermal analysis instrumentation 78−77902
- H_2 production, very high temp. nuclear reactor, graphite moderated He cooled appl. 77−23247

chemical kinetics *see reaction kinetics*

chemical lasers
- activation and deactivation rates in high-power lasers 79−941
- alkali metal reson. line lasers based on photodissoc. 79−72560
- alkyl iodide photodissoc. laser, radn. field in plane cavity 77−19245
- amplifications of fundamental freq. and harmonics 77−38878
- atom+vibrationally excited molecule reactions, rel. to high power lasers 79−5155
- atomic and molecular lasers appl. to collision physics 80−63596
- atomic-transition lasers based on two-photon dissociation of metal-triiodide vapors 80−23679
- bimolecular reactions, classical dynamics, book contrib. 77−10909
- book 77−10901
- chain-reaction, for visible range 79−89899
- chemical laser, diluent effect on transition levels and population inversion *(Russian)* 78−25868
- chemical reaction control using chemical lasers 77−70312
- chemically reacting flow heterogeneous mixing, energy level population inversion 80−78848
- combustion driven nozzle, F_2 absorption meas. 78−79011
- CW, inhomogeneous broadening effects, two-level vibrational model 79−76679
- CW, small-signal gain meas., cavity scans by chem. probe laser 78−22119
- CW, unstable resonators effect on performance 79−41397
- CW diffusion chem. laser, quasi-one-dimensional flame-sheet model, energy parameters 77−10899
- CW diffusion type, simplified model extension 77−3573
- DF, pulsed, beam attenuation for spatial profiling of small focal spots 80−99780
- DF-CO_2 CW chemical transfer laser, comprehensive kinetics model 79−81422
- dye, electrochemical pumping 77−27287
- efficiency, in limits of fast and slow rot. relax. 77−14700
- efficiency under conditions of rotational equilib. 78−9376
- electrically assisted laser design 79−31947
- electrochemiluminescent laser configuration 80−33020
- electron beam excitation 77−711
- electronic chemical laser pot. systems, intracavity dye laser monitoring technique 78−62239
- electronic phototransition CW chemical laser with thermal initiation by shock wave 80−53283
- electronic transition laser development 79−946
- electronic transition lasers, conf., Snowmass Village, USA (Sept. 1976) 78−63076
- engineering aspects, colloquium, London, England (Nov. 1978) 79−31940
- flashtube-pumped photodissociation laser with improved characteristics 79−76712
- fluoride-H_2 system, F quantum yield in photodissociation, stimulated emission delay meas. 78−58753
- fluorinated alkyl iodides, stimulated emission, laser appls. 77−27285
- gas phase chemical reactions, laser obs. *(German)* 79−29365
- gas-phase reactions, spectral-kinetic investig. rel. to chemical laser development *(Russian)* 77−90604
- Group IV photolytic laser expts., for fusion research 78−63101
- group VI elements, auroral and transauroral transitions, high energy storage 77−10897
- Group VIA photolytic laser systems, for fusion research 78−59002
- heptafluoroiodopropane light amplifier, wave-front distortion due to photolysis-gas dynamic effects 79−18412
- HF laser, CW, with unstable telescopic resonator, radiation field structure 80−91786
- HF laser nanosecond pulse generation using Ar gas breakdown 79−81465
- high power lasers for practical appls., conference, Reston, Va., USA (Mar. 1976) 77−34895
- high-efficiency, high-power lasers for fusion appl. *(Japanese)* 78−5486
- high-power lasers and appls., conf., Munich, Germany (June 1977) 79−964
- highly viscous chemical laser nozzles flow, two dimens. Navier Stokes eqns., implicit marching method 78−63506
- hollow cathode gasdynamic jet carrying excited metal atoms as spectral light source and chemical reactor 79−46493
- inert gas hydrides, laser active media, feasibility, energy storage 78−79014
- inhomogeneous active medium, angular correction, telescopic systems 78−1276

chemical lasers continued

- iodomethane laser, photolysis wavelength, repetitive operation 79−3689
- ion-molecule reactions, thermal energy, book contrib. 77−50668
- IR laser cavities, rot. equilib. 80−1239
- lidar system, single-ended, for air pollution remote meas. 77−21910
- low pressure, line-shape flattening resulting from hypersonic nozzle wedge flow 80−91783
- mercuric halide dissociation lasers, discharge pumping 78−79009
- metal atom oxidation lasers, book contrib. 77−10913
- metal atom oxidation reactions, kinetics of chemilum. emitter form. and quenching 78−63107
- metal halide vapours, quantum efficiency of fluoresc. excited by photodissociation 79−81421
- metal oxide, temp. depend. of chemilum. reactions, activation energies for excited state form. 78−66818
- metal-atom resonance-line lasers using UV photodissoc. of alkali and group IIIA metal halides 80−58529
- metal-oxidiser reactions, intracavity dye laser spectroscopy 77−86293
- methane+O_2(NO), energy distrib. of HF 78−48644
- 3-methoxybenzanthrone in ethanol, photoprotolytic reactions, spectra, rate consts. and lasing thresholds 80−43327
- methyl isocyanide photodissoc., cyanide radical energy partitioning chemical laser determ. 78−73063
- molecular collisions in intense laser field, visible chem. laser possibility 78−62876
- molecular constraints implied by kinetic coupling schemes, maximal work 80−38010
- molecular diluent effect on transition levels and population inversion *(Russian)* 78−25868
- molecular laser, optical excitation by photodissoc. wave propag. in dense gas 80−74352
- molecular modern laser types, high output and efficiency *(German)* 77−7133
- molecule, collision-induced emission with laser irrad., cooperative chemical and optical pumping 78−22012
- multiline, master and slave oscillator among system 78−33741
- multiquantum deactivation reactions, simplified modelling 77−25266
- Navier-Stokes eqn., supersonic flow 77−42528
- nozzle, discharge coefficient 77−42529
- nozzle, effect of geometry and boundary layers on flowfield 77−27622
- nozzle, TRW CL XV, fluid mechanical and optical analysis, LAMP and BLAZER code calcs. 79−98350
- numerical modelling of pulse and CW lasers, book contrib. 77−10908
- optical diagnostics of CW chemical laser 79−36916
- optical inhomogeneity of laser medium, phase front meas. of output radiation 77−79841
- optical resonator design rel. to output beam quality, book contrib. 77−10964
- performance comparison, axisymmetric and two dimensional nozzles 78−9375
- photodissociation, switched, for inversion of atomic and molecular species 80−74206
- photodissociation laser, UV source for pumping 77−27295
- photodissociation pulsed laser with mag. field gain modulation 77−58343
- photorecombination laser, shock wave triggered, waveguide mode optical gain 80−5730
- photorecombination laser theory thermally induced behind a shock wavefront 79−76682
- photorecombination lasers, thermal pumping *(Russian)* 77−19242
- photorecombination reactions initiated by shock wave, light amplification *(Russian)* 78−63100
- photorecombination reactions initiated by shock wave, light amplification *(Russian)* 80−38011
- population inversion, statistical and dynamical models, book contrib. 77−10910
- power spectral performance, coupled fluid dynamic, kinetic and physical optics model 78−79040
- power-per-line analyser for real-time display of laser spectra on oscilloscope 80−58552
- pressure recovery, 1D flow model, comparison with DF laser results 77−71979
- pulsed, acoustic suppression, acoustic attenuator development 79−76680
- pulsed chemical laser amplifier, beam deflection 79−50331
- recombination gasdynamic streams, light amplification *(Russian)* 77−79814
- recombination processes, book contrib. 77−50663
- resonant electronic-vibrational energy transfer and use in pumping IR mol. lasers 80−9700
- resonator modelling, LAMP and BLAZER code calcs. comparison with CL XV meas. 79−36890
- review, reaction types and expt. techniques, book contrib. 77−10902
- review, recent progress *(Japanese)* 77−38876
- review 77−7099
- review of lasers oscillating on rot., vibr. and electronic transitions 80−102716
- review of lasers with wide-band optical pumping 79−31885
- steady state operating characts., numerical method 77−19241
- supersonic, flowfield, laser induced I_2 fluorescence meas. 80−38008
- supersonic mixing lasers, gas dynamics, book contrib. 77−10905
- surface spark discharges high current, light emission props. and appls., book contrib. 79−77449
- technology advances, conf., Washington, USA (Mar. 1978) 79−36911
- thermally initiated chem. lasers utilizing excited atoms, feasibility in visible 79−89898
- three body recombination processes for high power c.w. visible output 77−651
- threshold times, reaction product rot. distribs., ralax. rates 80−28222
- time-dependent kinetic-thermodynamic description of nonequil. mol. system 80−9877
- bis-trifluoromethyl phosphine iodide, stimulated emission, photodissoc. laser appls. 79−10295
- turbulent reactive gas flows, two-dimens., nonequil. processes analysis 77−51129
- vibrational interaction of diatomic and triatomic mols., theory 77−23670
- waxicons for high-power chemical lasers, interferogram analysis 80−14418
- window materials evaluation 77−46769
- ArF*, pumped by 150 keV electrons, dominant form., quenching processes 78−33730
- Ba-N_2O flame, candidate chem. laser reactions, intracavity dye laser absorpt. meas. 78−63108

chemical lasers continued

- BaO, ground state vibr. pop. distribs. from photoluminesc. in $Ba+O_2$ and $Ba+N_2O$ 77−34731
- Br, chem. pumped Br_2-CO_2 photodissociation laser, output energy increase by WF_6 addition 79−45939
- Br electronic transition chemical laser, stimulated emission at 3685 cm^{-1} 79−27249
- Br, IR laser action using pulsed microwave discharge, Br_2 source gas 80−48233
- C, IR laser action using pulsed microwave discharge, CO_2, CO and CF_4 source gases 80−48233
- CN ($A^2\Pi$), chem. prod., CN number densities for gain, emission and absorpt. meas. 78−63112
- CN photodissociation laser, IR stimulated emission due to BrCN photolysis 79−31888
- CN, radical fluoresc. excitation spectrum and laser emission from ICN photolysis 78−76892
- CN radicals, electronic transition laser, using C_3F_7CN and $(CN)_2C_4F_8$ photodissociation 78−50769
- CO, chem. form. from CS_2-O_2, laser dynamics and rot. relax. 77−10898
- CO, chemical CW laser with CS_2-air mixture, output power press. depend. 79−72594
- CO chemical laser, CS_2-O_2 mixtures in discharge 78−50766
- CO chemical laser, flash photolysis of time-resolved spectra and gain 79−86172
- CO chemical laser, high efficiency, CS/O_2 as fuel/oxidizer, chain reaction operation 80−23678
- CO, chemical laser, supersonic combustor driven 78−87047
- CO chemical laser using combustor-generated reactants 80−48288
- CO, discharge plasma, C combustion effect on vibr. excitation 77−50666
- CO, gain measurements in acetylene+O_2 detonation products 78−33729
- CO, high power combustor driven system 78−87065
- CO laser, CS_2-N_2O-O_2 continuous combustion, performance characts. *(Russian)* 78−55348
- CO, output spectra from CS_2-O_2-CO_2(N_2O) flame lasers 80−83601
- CO, pulsed and CW, book contrib. 77−10911
- CO, stimulated emission behind overdriven detonation wave front in CS_2-O_2 *(Russian)* 77−23668
- CO supersonically driven chem. laser, kinetics of physical processes 79−45937
- CO, thermochem. generation of CS 77−23666
- CO, thermochem. generation of CS and S 77−68207
- CO-N_2O gasdynamic laser, CO_2 vibr. level superequilibrium chem. pumping, mixture composition, He effects 79−76666
- $CO+H_2$ combustion in air, gasdynamic laser operating on combustion products, construction, amplification coeff. *(Russian)* 77−7075
- CO+O, vibr. deactivation 78−94305
- CO_2 00^01-10^00 transition in CO-N_2O reacting gas mixture, gain 80−74337
- CO_2, amplification factor in supersonic expanding stream of N_2O-CO-He mixture 77−10896
- CO_2, CO+0.5 O_2 oxidation reaction in supersonic stream 77−677
- CO_2, energy transfer from vibr. excited OD, mixing of $D+O_3+CO_2$ in supersonic streams 77−676
- CO_2, excitation by NO+N reaction, transverse flow, output power, intensity distrib. 77−79796
- CO_2, supersonic jet utilizing $D+O_3+CO_2$ mixture, gain meas. 79−89902
- CO_2-T_2-F_2, using energy transfer from TF to CO_2 77−58322
- $CS+O \rightarrow CO+S$, shock tube reaction, chemiluminescence and lasing 77−16824
- CS_2-O_2 pulsed chemical laser and pulsed CO TE laser, comparative study 79−31876
- CS_2+O_2, transitions gain coeff. maximal meas. method for cascade laser 77−31104
- CS_2+O_2, vibr. relax., effect of atomic O 79−66300
- Ca-N_2O-CO flame, Ca catalyzed, gain meas., emission band assignment 78−66815
- Ca-N_2O-CO flame, candidate chem. laser reactions, intracavity dye laser absorpt. meas. 78−63108
- Cl, IR laser action using pulsed microwave discharge, Cl_2, CH_3Cl, CH_2Cl_2 and CCl_4 source gases 80−48233
- Cl-HBr chemical laser, pulsed, computer simulation, effects of rot. nonequilib. 77−40547
- Cl+HI, chem. laser, energy distrib., spectrosc. obs. 78−71096
- Cl_2-HI-He chemical laser system, rot. nonequilibrium, kinetic modelling, three model comparison 80−53281
- Cl_2+HI, pulsed chem. laser, rot. distrib. time evolution, kinetic master eq. calc. 77−65593
- ClF-H_2, electron-beam initiation, energy parameters, stimulated emission from HF, HCl 79−89903
- ClF-H_2 chem. laser, HCl vibr. emission 80−97709
- ClF-H_2 chemical laser, HF rot. laser emission 79−98349
- ClF+H_2, reaction rate const. for $H+ClF \rightarrow HCl^*+F$ 77−71980
- $ClF_3(F_5)+H_2$ mixtures, stimulated emission rel. to reaction mechanism 77−50667
- Co_2 laser radiation amplification in reaction products of CO+N_2O, nonequilib. chem. pumping effects 77−83848
- $D^{79}Br$, $D^{81}Br$ IR laser line wavelengths 77−3360
- DF, antireflection coatings on window materials 79−64262
- DF, automated gain measurement system for high-energy chemical lasers 79−36914
- DF, CW, performance parameters and operating characts. 77−34885
- DF chemical laser, jet curtains for gas containment 78−63099
- DF chemical laser, small-scale CW, operation 80−58528
- DF chemical lasers, high-performance dichroic beam splitters 80−95932
- DF, combustor-driven cold-reaction laser, book contrib. 77−10905
- DF, discharge initiated lasers, design and operation 79−31946
- DF, F_2 absorption diagnostic, sensitive technique 78−74896
- DF, high energy, design and fabrication of shared aperture dichroic mirror 77−88885
- DF, IR laser spectra 79−45936
- DF laser, phase conjugation of 4 μm for single line and multiline radiation in Ge 80−83641
- DF laser, pulsed unstable resonator, mode control and performance studies 78−82995
- DF optically cascaded pulsed chem. laser 77−75497
- DF, optically pumped F_2-D_2-CO_2, optical inhomogeneities, interferometric meas. 77−674
- DF, photoinitiated chain reaction laser, high elec. efficiency 77−3574
- DF, pulsed, flow technology 79−36934

chemical lasers continued
DF, pulsed microwave discharge 78—58998
DF, pumping reactions in D_2-F_2 system, kinetics, book contrib. 77—10903
DF, refr. index changes during stimulated emission 78—17929
DF repetitively pulsed subsonic chem. laser, flameout using fluidic switching 78—29943
DF repetitively pulsed chem. laser, scalable fuel/diluent feed system 79—36935
DF small-scale CW, construction and performance 77—50682
DF TEA laser, He-free, with MW output 80—64060
DF, tunable, appl. to remote meas. of gases 77—87118
DF, unstable resonator, power meas. using calorimeter 77—7136
DF-CO_2, CW and pulsed chem. transfer lasers, book contrib. 77—10907
DF-CO_2, chem. amplifier of short light pulses, photolytic or fast electron initiation 78—13696
DF-CO_2, chem. laser utilising ClF_5, ClF_3, ClF and F_2, energy transfer characts. 79—94225
DF-CO_2, chem. transfer laser, efficient performance 77—34886
DF-CO_2, interaction between vibr. states, theory 77—23670
DF-CO_2, photolytic initiation, high performance laser characts. 77—34881
DF-CO_2, photostimulated D_2+F_2 reaction, vibr. energy transfer to CO_2 mols. 77—23669
DF-CO_2 CW chemical transfer laser, high pressure operating charact. 79—81449
DF-CO_2 chemical laser, possibility of increasing generation quantum yield and specific energy output 80—19025
DF-CO_2 chemical laser, photon branching in chain reactions, IR radiation initiation 80—91785
DF-CO_2 chemical laser, amplification of long and short pulses 80—95883
DF-CO_2 pulsed chemical transfer laser, analysis of calc. model 79—94226
DF-CO_2 pulsed photoinitiated chem. laser, characts. rel. to HF laser 79—64219
DF-HBr CW optical resonance transfer laser 80—64003
DF-HF CW lasers, performance, computer modelling 78—71094
$F+CH_4 \rightarrow HF+CH_3$, cross section and rate const. calc. using kinetic trajectory model 77—29010
$F+H_2$ chemical laser, vib. populations in $V \rightarrow V$, $V \rightarrow R,T$ energy transfer corrections 77—32794
$F+H_2(D_2)$, absolute rate coeffs. at 295-265K 80—81303
Ga stimulated emission obs. on 417.2 nm line, by GaI_3 photodissoc. 79—89897
Ge gas phase reactions with oxidisers, visible chem. laser development 79—948
Ge-N_2O, rate coeff. meas. for $Ge+N_2O \rightarrow GeO+N_2$ reaction 78—63110
GeF, use in chemical lasers 80—64004
GeO, population inversion of electronic levels by oxidation, visible emission 78—13697
GeO, produced in $Ge+N_2O$ reaction, kinetics of chemilum. emitter form. and quenching 78—63107
H halide, CW thermally driven and elec. discharge driven lasers, book contrib. 77—10904
H halide, pulsed, book contrib. 77—10906
H halide-CO_2, pulsed chem. transfer lasers, book contrib. 77—10906
H halides, $I^*(5^2P_{1/2})$ quenching, electronic-vibr. energy transfer 78—63114
H_2/F_2 laser, initiation using surface spark discharge UV light source 80—78923
H_2-F_2-He chemical CW laser, flows *(Russian)* 78—74895
H_2-F_2-O_2, chem. laser mixture, multiatm., spontaneous explosions 78—73044
HBr, CW laser, vibrationally excited molecules *(French)* 77—14699
HBr, electronic to vibr. energy transfer from excited halogen atoms, IR fluoresc. 78—63113
HBr, laser emission at 4 μm based on chem. generation of Br atoms 80—9878
HBr, pulsed, output performance, numerical anal. 80—1197
HBr, purely chemical laser 79—10294
HBr, sealed pulsed laser, extended use by Cl_2 activation 78—46622
HBr TEA pin laser 79—76711
HBr, vibrationally excited, chem. prod. for CW laser using CW supersonic mixing HF chem. laser 80—1196
HCN far IR laser, chem. pumping, 337 μm and 311 μm stimulated emission obs. 79—13958
HCl, 3.8 μm, 10.6 μm CW laser emission based upon Cl atom chem. generation 79—947
HCl cryosorption-pumped CW chemical laser 78—74894
HCl, electronic to vibr. energy transfer from excited halogen atoms, IR fluoresc. 78—63113
HCl flash initiated laser, Cl_2-HI reaction pumped 79—94224
HCl, helical TE laser, output power enhancement by CO_2 addition 79—98397
HCl, initiated by $NO+ClO_2$ reaction, performance and diagnostics 80—14333
HCl, isotopic transfer laser, intercavity cold gas isotope filter 78—46590
HCl laser, V=3 to V=2 band process, computer simulation 78—71095
HCl, pulsed, plane and helical electrode types, expt. study and modelling 80—32973
HCl, pumping reactions in H_2-Cl_2 system, kinetics, book contrib. 77—10903
HCl, purely chem. laser employing transverse flow 78—46591
HCl supersonic laser, visible chemiluminescence flow visualisation 79—76699
HCl TEA pin laser 79—76711
HCl, using ClO_2+NO chain reaction 77—71978
HCl, using H_2-ClF chain reaction, CW, performance 78—46593
HCl-Br_2-Ar, flash photolytically produced Br* to HCl electronic to vibr. and rot. energy transfer 80—48069
HD, spectral and time characts. 77—75499
HF, atm., pulsed chem. laser, model including rot. nonequilib. effects 79—55127
HF, atmospheric press., initiated by electron beam irradiated discharge 77—7076
HF, automated gain measurement system for high-energy chemical lasers 79—36914
HF, beam spectral anal. using near field holography 77—23680
HF, biased amplifier, amplified spontaneous emission and gain saturation nonlinearity 77—31087

chemical lasers continued
HF, CW, F atom prod. by SF_6 dissociation with microwave discharge 77—31099
HF, CW, freq. conversion in Ag_3AsS_3, $LiNbO_3$ and $LiIO_3$ 78—30023
HF, CW, freq. stabilisation by beat signals and anomalous dispersion 79—86187
HF, CW, longit. and transverse mode competition in stable, unstable resonators 80—95917
HF CW chemical laser, design of multipass telescopic amplifiers 79—27289
HF CW chemical laser, mode competition obs. 80—33040
HF CW chemical laser, spatial homogeneity of radiation improvement using telescopic resonator 80—106549
HF CW chemical laser amplifier with multiple pass telescope cavity, diffr. 80—19055
HF, CW chemical laser for remote pollution monitoring and process control, HF conc. in Al plant 79—48200
HF CW chemical laser with unstable telescopic resonator, diffr. effects 79—94265
HF CW chemical laser with cylindrical nozzle grid, excitation chain mechanism 80—28227
HF, CW diffusion type, arbitrary degree of F_2 dissoc., numerical anal. 77—34879
HF, CW diffusion type amplifier, efficiency 77—34878
HF CW laser, influence of mixing effects on energy characts. 80—9875
HF CW laser with cylindrical telescopic resonator, flame front model 78—59001
HF CW optically resonance-pumped laser 80—43356
HF, c.w., longitudinal mode beat intensities, tuning freq. depend. 77—671
HF chain reaction laser energetics, C_5F_{12} mol. addition and rot. nonequilib. *(Russian)* 77—42530
HF, chain reaction pulsed laser, simple rate eqn. model 77—3572
HF chemical laser, 10 kW CW arc-driven, diagnostic system for supersonic free jets 77—23667
HF chemical laser, flow anal. 79—81420
HF chemical laser, laminar flow pattern *(Russian)* 78—87048
HF chemical laser, pulsed, evolution, irreversible thermodynamic anal. 79—31887
HF chemical laser, pulsed, evolution, kinetic model, rot. nonequilib. 79—36888
HF chemical laser beam, phase fluctuation meas. 80—48317
HF chemical laser initiation by relativistic electron beam 80—64005
HF chemical laser phase control servo system 80—33063
HF chemical TE laser, 16 μm emission 80—83600
HF, combustor-driven cold-reaction laser, book contrib. 77—10905
HF, comparison of two microwave plasma sources for F atom prod. by SF_6 dissociation 78—22140
HF cryosorption-pumped CW chemical laser 78—74894
HF, cw chem. diffusion laser, amplifier operation 78—79015
HF, discharge initiated lasers, design and operation 79—31946
HF, discharge stabilisation using resistive electrodes in SF_6-C_3H_8 78—1251
HF, double-dishcarge, transitions in SF_6-C_3H_8 mixture, temporal characteristics 80—53282
HF efficient electron-beam-pumped chem. laser with high specific energy output 79—45963
HF, electron beam excited, energy characts. 77—75498
HF, electron beam initiation, efficiency up to 10% 77—34882
HF electron beam initiated chem. laser 79—13959
HF, emission due to mol. overtone, discharge initiated SF_6-H_2S-He mixture 78—17927
HF, F_2 absorption diagnostic, sensitive technique 78—74896
HF, $F+H_2$ threshold times, reaction product rot. distribs., relax. rates 80—28222
HF, flame propag. velocity in F_2-H_2 mixture 80—50855
HF, flowing TE laser using SF_6-H_2 mixture, operation at 10 kHz pulse repetition rates 78—17955
HF, fluoromethanols (mono and tri), decomposition activation of HF, non-statistical energy partitioning 79—945
HF, for fusion comparative review of Nd:glass, CO_2, HF and I lasers 77—7062
HF, H_2-F_2 mixture, pulsed, flame out 77—27284
HF, H_2+F_2 reaction, coherent emission efficiency 78—17928
HF, high press. radiation-chem. laser, electron beam initiation 77—75562
HF, high-energy laser, energy extraction, beam quality, for fusion ignition 78—63102
HF, IR laser spectra 79—45936
HF in absorption, anomalous dispersion meas. 80—95881
HF, initiation, H_2-F_2 mixture prep., F_2 handling and waste disposal *(Japanese)* 77—38876
HF large-volume laser amplifier, energy extraction 79—86174
HF laser, H_2+F_2 chain reaction, rotational nonequilibrium mech. vibr.-rotational energy exchange effect 80—48230
HF laser, Phoenix oscillator-amplifier system, laser-beam characts., rel. to plasma heating 79—76701
HF laser, pulsed unstable resonator, mode control and performance studies 78—82995
HF laser, spherical telescopic resonator, design 78—71120
HF laser conceptual design for laser fusion 79—86192
HF laser transitions, pure rotational, from exploding-wire metal atom oxidation lasers 77—14701
HF laser with resistive Ge electrodes, for optical studies of semiconductors 80—64061
HF, low-impedance Blumlein discharge initiated laser, efficient operation 79—36919
HF, master oscillator-amplifier system 79—22947
HF, modelling, Lorentz broadening 77—79813
HF multiline laser pulses, ns switching, amplification 77—38910
HF, nanosecond duration multiline laser pulse generation and amplification 77—38930
HF, numerical anal. of laser generation conditions 80—9872
HF, optically pumped F_2-H_2-CO_2, optical inhomogeneities, interferometric meas. 77—674
HF, output spectrum control using selective intracavity loss 77—3607
HF, phase control for coherent optical recomb. 79—72580
HF, photoinitiated chain reaction laser, high elec. efficiency 77—3574
HF, photoinitiated pulse H_2-F_2 system, parametric anal. 77—34880
HF, photopreionised atm. press. laser operation 79—967
HF, possible use as laser-fusion drivers 79—22979
HF premixed chain reaction CW laser, spectral output 80—95882

chemical lasers continued
- HF, pulsed, HI/SF_6 system 80—106514
- HF, pulsed, HI/SF_6 system 80—106515
- HF, pulsed, high energy prod. 77—34884
- HF, pulsed, rot. relax. rate effect on efficiency *(Russian)* 77—10900
- HF, pulsed, with spherical telescopic resonator, energy characts. calcs. 80—14367
- HF, pulsed chain and non-chain reaction lasers, book contrib. 77—10906
- HF pulsed chain reaction laser, scaling laws 80—32974
- HF pulsed chemical laser, operation at high press. of H_2-F_2 working mixture 79—89900
- HF, pulsed H_2+F_2 chain reaction laser, rot. nonequilib. mechanisms effect on performance 78—82958
- HF pulsed laser, appl. of CW X-ray preioniser 80—64037
- HF pulsed laser, Xe flashlamp efficiency for photoinitiation 80—69403
- HF pulsed laser initiated with CO_2 laser-produced plasma 80—38009
- HF, pulsed laser numerical modelling, rot. relax. 80—87388
- HF, pulsed microwave discharge 78—58998
- HF pulsed photoinitiated chem. laser, characts. rel. to DF-CO_2 laser 79—64219
- HF, pulsed-discharge initiated, H_2-F_2, comparison with nonchain H_2-SF_6 laser 80—28223
- HF, pumping reactions in H_2-F_2 system, kinetics, book contrib. 77—10903
- HF recirculating TE-laser, gas consumption characts. 79—68390
- HF repetitively pulsed subsonic chem. laser, flameout using fluidic switching 78—29943
- HF, rot. population transfer effect obs. 78—79013
- HF, rot. population transfer using IR-laser double-resonance expt. 79—55128
- HF, rotational nonequilibrium, efficient model 79—22945
- HF, short laser pulse generation possibility by cooled H_2-F_2 mixture photolysis 79—22946
- HF, simple high-power TEA laser operating in IR 79—94251
- HF, single-line CW, with unstable resonator, temporal stability 77—50690
- HF, small-scale CW, construction and performance 77—50682
- HF, stable discharges, with large electrode separation 78—55371
- HF TEA laser, He-free, with MW output 80—64060
- HF, time-depend. kinetic-thermodynamic description 80—9877
- HF, using F_2-H_2, ClF-H_2 mixtures, output energy, photoinitiating substances influence 79—89901
- HF, vibr. excited, laser design 79—31947
- HF, vibr.-rot. emission, from highly rot. excited states, in ClF_x-H_2 chem. laser 78—17926
- HF, window materials, absorption props. 77—46770
- HF, with flow-through chem. active medium, pulsed-periodic regime realisation 80—106513
- HF, with microwave excitation *(German)* 80—43326
- HF/DF, compact CW, using microwave discharge 79—72591
- HF/UF_6-H_2 nuclear pumped laser, characts. 80—78847
- HF-CO_2, interaction between vibr. states, theory 77—23670
- HF-DF, CW, freq. stability and stabilisation 78—22141
- HF-DF, CW laser, specie conc. and temp. by Raman spectra 78—58999
- HF-DF, pulsed, efficient excimer flashlamp initiation 77—88754
- HF-DF simultaneous laser excited by ferroelec. ceramic capacitatively coupled discharge 80—69413
- HF-HCl, utilising $ClF+H_2$ chain reaction, kinetic model 80—9874
- HF_2, electric discharge chem. laser, SF_6-H_2 mixture pumped by inductive storage unit 79—98409
- HF*, interaction with ClFx, relax. consts., stimulated emission delay 77—7077
- $HF(1\leq n\leq 7)+DF(0)$, vibr. deactivation calc., 300-3000K 79—31655
- HX, chemical laser performance isotope effects, computer simulation 78—29944
- He-CO_2-Cs mixture in rapidly circulating laser, interaction rate of Cs and CO_2, gasdynamic parameters 79—86173
- Hg halide electrically excited dissociation laser, kinetic processes 80—38013
- Hg halide lasers, efficiency of different pumping methods, review 79—36886
- Hg photodissociation laser, optically pumped 77—68206
- HgBr, 502 nm stimulated emission, prolonged optical pumping of $HgBr_2$ 79—18414
- HgBr dissociation laser is elec. discharge 78—50768
- HgBr, dissociation of $HgBr_2$, oscillator and oscillator-amplifier expts. 80—48232
- HgBr electrically excited dissociation laser, kinetic processes 80—38013
- HgBr, electrically excited dissoc. of $HgBr_2$, kinetic processes 80—48231
- HgBr, laser photolysis prep., laser induced fluoresc., collisional quenching processes 80—38014
- HgBr laser using dissociative excitation of $HgBr_2$, extraction efficiency increased by N_2 addition 80—38012
- HgBr radical, laser action by $HgBr_2$ photodissociation, ArF excimer laser pumping 78—13695
- HgCl photolytically pumped laser system, quantum chem. 80—32971
- $HgCl_2(Br_2)$, low lying excited state electronic struct. and photodissoc., appl. to lasers 80—63560
- I, $^2P_{1/2}$ state, relax. between hyperfine levels 80—18880
- I, $^2P_{1/2}(F=3)\rightarrow {}^2P_{3/2}(F'=4)$ transition, stimulated emission cross section determ. 79—13961
- I, 1 TW high power system, Asterix III 77—88765
- I, 100 ps pulse generation and amplification 77—19301
- I 1.315 μ laser, passive mode locking *(French)* 77—68203
- I, 1.315 μm, oscill. freq. selection hyperfine transition 77—10952
- I, 1.315 μm, transverse discharge excitation in $i=C_3F_7I$ 77—19243
- I, 1.315 μm, transverse discharge excitation in $i=C_3F_7I$, kinetic model 77—19244
- I 1.315 μm laser, Ni complex BDN II as saturable absorber 79—27297
- I, 1.315 μm laser wavelength, I saturable absorpt. cell 77—10985
- I, absolute quantum yields of ($^2P_{1/2}$), ($^2P_{3/2}$), photolysis of C_3F_7I, CF_3CFICF_3 and $CF_3OCF_2CF_2I$ 79—34339
- I, active medium refr. index change meas., delay method 77—58336
- I amplifier pumped by open high-current discharge radiation, physical parameters 79—89904
- I, angular spectrum form. of stimulated radiation, theory 77—14702
- I, Asterix III and German laser fusion programme 78—63136
- I atom laser, high power, developmental possibilities 79—975
- I chem. produced $^2P_{1/2}$ state, gain meas. 78—63115
- I, chemically pumped by $O_2(^1\Delta)$ 79—98348
- I, continuously pumped continuous flow photodissociation laser 78—59027
- I, continuously variable water filter for linearity testing of photoresistors 78—55397
- I, current design aspects, pumping system, optical arrangement and gas flow 79—31945
- I, direct solar-pumped 80—74353
- I, electronic transition chemical laser 78—55347
- I electronically excited atom prod., collisional release and photocomp. kinetics of I_2 78—66819
- I, energy profile meas. using hypersensitised photographic plates 78—5518
- I flashlamp pumped photodissociation laser characts., local optical inhomogeneities 80—53284
- I, for fusion, comparative review of Nd:glass, CO_2, HF and I lasers 77—7062
- I high power gas laser, operation, props. *(French)* 78—33731
- I, high power system, Asterix III, development 77—710
- I, high-power photodissociation laser, pulse propag. in amplifier 78—46592
- I, induced Mandelstam-Brillouin scatt., appl. of wave front reversal phenomenon *(Russian)* 79—59769
- I, iodoseptofluoropropane photodissoc. laser, refr. index distrib. fields, double exposure holography 80—9873
- I large-scale laser, implications of n-C_3F_7-I Raman spectrum and cross sections 79—23022
- I laser, Asterix III, light-plasma interaction expt. and light pulse props. 80—53349
- I laser, high-power, beam quality, gain saturation effect, for fusion ignition 78—63149
- I laser, high-power, pulse amplification 80—48234
- I laser, photodissociation, gain-switched, multi-atmospheric press. operation 79—76681
- I laser, photolytically pumped, chem. kinetics 80—48235
- I, laser, short pulse amplification, multilevel paraxial Maxwell-Bloch eqn. 79—36889
- I laser, smooth pulse oscillator for single mode operation 78—59057
- I laser medium, CF_3I, UV absorption modification, by vibr. excitation for fusion ignition 78—58717
- I laser of high efficiency, low-press. Hg lamp pumped 79—31929
- I, laser photolysis of perfluoroalkyl iodides 79—29382
- I, laser pumping reaction $O_2^*+I\rightarrow O_2+I^*$, model calcs. 79—86030
- I laser radiation, 2nd, 3rd and 4th harmonic generation 80—91844
- I laser radiation wavefront instability and optical inhomogeneity evolution dynamics 80—9876
- I laser with repeated use of regenerated mixture 80—28251
- I, methyl iodide photodissoc. laser, kinetic model, cross-section calcs. 80—58530
- I nanosecond single pulse laser, open electric discharge pumping 80—5763
- I, ns photodissoc. laser, 200 J output energy 77—27301
- I, optical pumping using high current plasmadynamic discharges 77—38923
- I, optically pumped, four-level model *(Korean)* 80—28224
- I, organic compounds usable as solvents in saturable absorber, nonlinear refr. index meas. 80—102758
- I, photochem., book contrib. 77—10912
- I, photochem., max. storable energy *(Japanese)* 77—38876
- I, photodissoc. laser, flashlamp reflector evaluation 77—79848
- I, photodissoc. of C_3F_7I with C_6F_{14}, energy of generation *(Russian)* 77—38877
- I, photodissoc. of C_3F_7I, CF_3I, CF_3CFICF_3, quantum yields 78—3355
- I photodissoc. ring laser, lasing regimes, emission and polarization characts. 80—48236
- I, photodissociated by nucl. induced excimer fluoresc. 80—78846
- I, photodissociation, active medium gain in mag. field 77—79816
- I, photodissociation, chem. changes in active media, IR spectrochem. analysis 77—14704
- I, photodissociation, high power system, nanosecond or shorter pulse prod. 77—38879
- I, photodissociation, pumped by high-current discharge with return current conductor 80—28225
- I, photodissociation, using I to group V element bonding mols., $(CF_3)_2AsI$ laser characts. 77—14703
- I photodissociation laser, short-pulse high-press., line broadening and saturation parameters 77—3575
- I, photodissociation laser, excited atom accumulation, kinetic eqns. 77—3576
- I, photodissociation laser, free oscill. conditions, kinetic model 77—3577
- I, photodissociation laser, quartz:Ti tube for C deposit elimination 77—10945
- I, photodissociation laser, I passive switch for 1.315 μm radiation 77—23685
- I photodissociation laser, pulse duration, mag. field control 77—75585
- I photodissociation laser, press. induced freq. shifts 78—37875
- I, photodissociation laser, 1.315 μm transition line struct. 78—59000
- I photodissociation laser, diffr. limited output beam 79—27286
- I photodissociation laser, tuning using Zeeman effect 79—50316
- I photodissociation laser, stimulated emission pulse temporal characts. with active-medium gain control 80—28226
- I photodissociation laser, characts. of new dye comps. for passive switches 80—91826
- I, photodissociation laser pumpband, UV spectral efficiencies of surface spark discharges 77—75496
- I photodissociation laser oscillator or amplifier, Faraday rot. in active medium 79—10296
- I photodissociation laser characts., reaction rate consts. of CF_3, n-C_3F_7 and i-C_3F_7 79—52671
- I photodissociation laser using CF_3I, n-C_3F_7I, optical inhomogeneity losses 79—55129
- I photodissociation Q-switched laser, optically thick active medium, chemical kinetics and gasdynamics 79—64218
- I, photolytic, atomic, system requirements for fusion appl. 77—46403
- I, possible use as laser-fusion drivers 79—22979
- I, pulse shaping 77—23691
- I, pulsed photodissociation laser, based on methyl iodide 78—50767
- I, pumping by inert gas halogen fluoresc. emission, C_3F_7I photolysis 77—34883
- I, Q-switched, emission at two frequencies 79—18413
- I, radial oscills. of medium, effect on laser output 78—5507

chemical lasers continued
  I, SAIL-I, performance characts. for laser fusion 77−88766
  I short-pulse laser, preamplifier stages characts. 79−94227
  I terawatt laser, ASTERIX III system 79−3713
  I, using ICF_2CN photodissociation 78−50769
  $I_2+O_2 \rightarrow 2IO$, flash photolysis, emission in 3400 Å band 77−3398
  IBr photodissociative laser, quenching by paramag. mols. 80−21263
  $IBr:CO_2$ photolysis, electron-vibr. pumping, 2.7 μm Br and 4.3, 10.6 μm CO_2 laser transitions 80−28196
  IF_2 pumping using F reactions with CH_3I, CF_3I and ICl 80−11915
  $I(^2P_{1/2})$ energy transfer and reactive collisions, laser pumping possibility 79−949
  In, photodissoc. of InI, lasing at 451 nm 77−14698
  KrF*, pumped by 150 keV electrons, dominant form., quenching processes 78−33730
  $La-F_2(ClF)(Cl_2)(SF_6)$, visible chem. laser development from reactions yielding visible chemilum. 78−63111
  $Mg-N_2O-CO$ flame, efficient chem. generation of $Mg(^3P)$ 78−63109
  $Mg-N_2O-CO$ flame, Mg catalyzed, gain meas., emission band assignment 78−66815
  N_2-CO_2 nonequilibrium aerosol flux mixing, inverse population of vibrational levels *(Russian)* 77−10743
  NF, $b^1\Sigma^+$ state, enhancement by I laser pumping, lasing potential 78−79012
  NF, chem. pumped electronic transition laser system, chem. and scale-up 78−63103
  NF, excited, lasing potential, prod. by $N+O_2F$ reaction 78−63106
  NF, lasing due to electronic transitions, H_2+NF_2 chain reaction kinetics 79−89899
  NF produced by $H+NF_2$ in subsonic CW laser device $a^1\Delta$ state scale up 77−79815
  $NF(a^1\Delta)+I(^2P_{1/2})$ system, electronic angular momentum transfer, chem. kinetic model 78−63104
  $NF(b^1\Sigma^+)$ enhancement by I laser pumping 78−63105
  NH, pure rot. lasing after flash photolysis of HN_3 79−86175
  NO, electronic to vibr. energy transfer from excited halogen atoms, IR fluoresc. 78−63113
  NO_2, $NO+O_3$, chemiluminescent reaction, theory of light amplification *(Russian)* 77−88717
  N_2O-CO flame, alkaline earth catalyzed chain reaction chemiluminesc. 77−40548
  N_2O-CO flame, Mg catalyzed chain reaction chemiluminesc. 77−36758
  N_2O_3 gas as possible photorecomb. laser medium 77−71981
  $Na-N_2O-CO$, photon yield, Na emission mechanism 77−63916
  NaN_3, solid, CO_2 laser radiation decomposition, for high-press. chem. laser 79−34326
  O_2, high energy pulsed laser feasibility at 1.27 μm, O_3 photolysis 78−63117
  O_2-I_2 100 W transverse-flow chem. laser 79−41374
  O_2-I_2 chemical laser, quenching of laser-excited O_2 by I_2 80−99515
  $O_3-Ar(CO)$, photorecombination laser, shock wave triggered, waveguide mode optical gain 80−5730
  OCS, high-intensity laser photolysis at 157 nm, $S(^1S)$ prod., photoionisation, and loss, laser appl. 80−21306
  OCS laser, two-quantum excitation, photolysis, energy transfer, for fusion expts. 78−59003
  $OCS-N_2-SF_6$ mixture laser, OCS photodissociation, electron dipole forbidden transition, absorpt. spectra 79−68389
  OD laser, pure rot. lasing intensity, pumping by collision induced energy transfer 78−74897
  $O_2(^1\Delta_g)+I(^2P_{3/2})$, possible electronic transition chem. laser 78−63116
  OH laser, pure rot. lasing intensity, pumping by collision induced energy transfer 78−74897
  Pb atomic photodissociation laser, 405.8, 368.3, 364.0 nm emission lines 80−87387
  $Pb+O_3$ reactions, chemiluminesc. 79−52673
  PbF, laser-induced fluoresc. of $A^2\Sigma$ state, chem. laser eval. 79−81222
  S, IR laser action using pulsed microwave discharge, SF_6 and CS_2 source gases 80−48233
  S_2, chem. pumped laser emitting visible radiation, construction possibility 79−13960
  SF_6+H_2 chemical laser, electron beam pumping 80−91784
  $Sc-F_2(ClF)(Cl_2)(SF_6)(Br_2)$, visible chem. laser development from reactions yielding visible chemilum. 78−63111
  ScF supersonic mixing flame, spontaneous emission, electronic transition chem. laser pot. 78−66817
  Se, laser action at 489 nm or 777 nm, OCSe photolysis 79−31889
  Se, OCSe photodissoc., forbidden at. transitions 78−79010
  Si, IR laser action using pulsed microwave discharge, SiH_4 source gas 80−48233
  SiF, chemilum. obs. of $A^2\Sigma^+$ and $a^4\Sigma^-$ states 78−66816
  SiF, use in chemical lasers 80−64004
  Sn gas phase reactions with oxidisers, visible chem. laser development 79−948
  $Sn+N_2O$, oxidation chemiluminesc., quenching kinetics 79−52672
  SnF, use in chemical lasers 80−64004
  SnO, population inversion of electronic levels by oxidation, visible emission 78−13697
  SnO, produced in $Sn+N_2O(O_2)(O)$ reactions, kinetics of chemilum. emitter form. and quenching 78−63107
  $Sr-N_2O-CO$ flame, candidate chem. laser reactions, intracavity dye laser absorpt. meas. 78−63108
  $Sr-N_2O-CO$ flame, Sr catalyzed, gain meas., emission band assignment 78−66815
  SrF, temp. depend. of chemilum. reactions, activation energies for excited state form. 78−66818
  SrO, gaseous chemiexcited mol., modulated transmission spectra 77−86316
  T_2+NF_3, chem. laser, TF spontaneous emission, Einstein coeffs. determ. 77−58073
  TF, meas. of $F+T_2 \rightarrow TF+T$ reaction rate 77−86291
  $TF-CO_2$, using NF_3+T_2 reaction, rate const. of energy transfer from $TF(\nu=1)$ to $CO_2(00^\circ0)$ 77−675
  Tl atomic laser pumped by TlI photodissociation 79−18411
  XeF, (B,C) state prod. and kinetics, XeF_2 photolysis with VUV radiation 80−32975
  XeF, from photodissoc. of XeF_2, $B(1/2)-X^2\Sigma^+$ transition, stimulated emission 78−71097
  XeF laser using XeF_2 photodissociation, fluoresc. and laser performance 80−32976

chemical lasers continued
  XeF molecule formed by XeF_2 photodissociation, laser action due to bound-free $C(3/2)-A(3/2)$ transition 80−14334
  XeO, luminesc. meas. of $O(^1S)$ absolute quantum yield in photolysis of CO_2, N_2O 80−35561
  XeO, photochem. laser performance, 0.54 μm stimulated emission 79−45938
  XeO photochemical laser, energy characts., kinetic model of physicochem. processes 80−28228
  $Y-F_2(ClF)(Cl_2)(SF_6)(Br_2)(IBr)$, visible chem. laser development from reactions yielding visible chemilum. 78−63111
  YCl supersonic mixing flame, spontaneous emission, electronic transition chem. laser pot. 78−66817
  YO, temp. depend. of chemilum. reactions, activation energies for excited state form. 78−66818

chemical reactions
  see also association; atom-atom collisions; atom-ion collisions; atom-molecule reactions; atomic inelastic collisions; catalysis; charge exchange; chemical exchanges; chemically reactive flow; chemiluminescence; chemisorption; CIDEP; CIDNP; corrosion; dissociation; electrolysis; free radical reactions; heat of reaction; ion-molecule reactions; isomerisation; molecule-molecule reactions; oxidation; photochemistry; polymerisation; pyrolysis; radiolysis; reaction kinetics; reduction (chemical); solvation
  $A+BC \rightarrow AB+C$, vibr. excitation, centrifugal effects calcs. 77−16791
  absorption, atmospheric NO_x removal, using MARTZCLEAN reagents based on $NaClO_3$ and K_2CO_3 *(Japanese)* 80−61147
  abstract 3-variable systems, toroidal oscills. 77−44462
  acetic acid, vapour, chem. reaction effect on speed of sound 80−103100
  acetic acid-pyridine, H-bonding, proton transfer, isolated system, solvent effect, MO calc. 80−55629
  cis-acetylene, triplet state, near IR electronic absorption spectrum, and form. 79−63997
  actinide lanthanide separation from high-level wastes by oxalate precipitation 79−49720
  activated complexes, exp. obs., bonding MO LCAO states 80−76506
  activated state of multidimensional planes of pot. energy of chem. reactions 77−90585
  activation of kinetic processes in condensed media 77−55368
  adiabatic reaction dynamics, quasiadiabatic treatment 77−60043
  aerodynamic levitation flow reactor and applics. 77−29046
  aerosol formation in reacting gases, relation of surface area to gas-to-particle conversion rate 78−48696
  air pollution control, venturi-jet scrubber, gas absorpt. with chem. reaction, performance study 78−81393
  Al_2O_3, high temperature interactions with Re 80−16665
  alkali atom+alkyl oxide cross-sections, hard-sphere model 78−7176
  alkali metal-rare earth oxides, $MLnO_2$, Ln=Y or Gd, synthesis and physicochem. props. 77−48216
  alkaline earth fluorides, thermodynamics and kinetics of O incorporation 77−84778
  alkaline phosphatase, slow reaction, vidicon-based spectrometer obs. 79−21817
  alkaline-earth-Os ternary oxide system, solid state prep. and reactions, cryst. struct., mag. and elec. props. 79−24739
  alkyl cyclobutane hydrocarbons, multiple initial vibr. state selection by chem. activation, relax. rate 77−40538
  alkyl fluorides, geometries, props. and protonation, ab initio mol. orbital study 79−22588
  α-aminoacids, stereoselective catalysed hydrolysis of esters *(French)* 79−66438
  angular momentum disposal, information theory anal. 78−80730
  aqueous solutions reactions on primitive Earth, energetics rel. to chemical evolution 77−33189
  Arrhenius equation and accel. testing 78−53182
  atoms, general adiabatic-diabatic transformation matrix, electronic non-adiabatic transitions 80−93751
  atoms, laser excited, reactive collisions 80−66793
  automatic detection of chemical reaction sites 78−92476
  azobilirubin, form., fast reaction vidicon-based spectrometer obs. 79−21817
  bases, K^+ affinities ab initio SCF calc. 78−58585
  Belousov Zhabotinskii reactions, model, computation of travelling wave solns. 79−70318
  Belousov-Zhabotinski reaction, chem. oscill. mechanisms 80−3304
  Belousov-Zhabotinski reaction, oscill., thermal props. 80−7762
  Belousov-Zhabotinskii reaction, analytic representation of oscills., excitability, travelling waves 77−36740
  Belousov-Zhabotinskii reaction, chaotic oscills. 79−5151
  Belousov-Zhabotinskii reactions, periodic and nonperiodic behaviour for different flow rates 79−100380
  Belousov-Zhabotinsky reaction, chem. turbulence, strange attractor representation 80−85148
  Belousov-Zhabotinsky reaction system, chem. turbulence 78−27752
  Belousov-Zhabotinsky system, limit cycle behaviour, modified Oregonator model 79−1266
  Belousov-Zhabotruskii reaction, existence of solitary travelling wave solns. 80−35525
  Belusov-Zaikin-Zhabotinsky reaction, chem. wave equation 78−15653
  Belusov-Zhabotinskii reaction, chaotic states obs. 78−20006
  benzene, monosubstituted, ring protonation and C_{1s} binding energies, STO-3G calc. 79−29336
  benzene, solid, ion implantation, chem. effects 80−55635
  benzene/cyclohexane reversible chemical reaction systems for thermal energy transport 80−67009
  benzenes, trisubstituted, dil. solns., relax. mech., Debye relax. times 78−80744
  benzonitrile, HCN elimination, ion kinetic energy spectrum peaks, collision gas sensitive 80−40679
  benzylidene t-butylamine N-oxide, amphiphilic liq. cryst. solvent effect on hydrolysis 79−100355
  bifurcation and stability of systems far from equilibrium 77−73461
  bimolecular autocatalytic reaction-diffusion system with Michaelis-Menten saturation law, multiple steady states 78−40045
  bimolecular endoergic reactions, threshold behaviour, statistical phase space approach 78−48615
  bimolecular gas phase reactions, collision theory, quantum corrections 79−8433
  bimolecular reactions, minimum state density criterion in transition state theory 79−52645

chemical reactions continued
binary liquid mixtures, excess internal press. and intermolecular interaction 78—35640
binary liquid systems with strong chem. interaction, spin echo obs. of self-diffusion *(Russian)* 79—95197
binary systems containing one chemical cmpd., reaction kinetics and diffusion *(Russian)* 79—87014
biochemical, catastrophe theory appl. 77—67232
biochemical fast reactions, in solns. membranes and cells, conf., Airlie, USA (Apr. 1978) 79—8485
biochemical systems, temporal and spatial patterns 80—3340
biochemical systems anal., mol. biology, book 77—21468
biological molecules, chem. reactions, Raman difference spectroscopic obs. 78—44368
biological processes, dense phase chem. reaction theory 80—3575
biological systems, perturbation spread in active media with auto-oscillatory props. 79—57562
biopolymer chains, intramol. reacts., enzyme catalysis appl., review 80—40953
biopolymer synthesis on solid supports 79—29397
bipolar trickle reactors, electric current versus potential plots 80—76521
bipolar trickle reactors, flow models for hydrodynamic characts. and reaction rate constants, 80—76522
bipolar trickle reactors, study using electrochemical tracer method 80—76523
bond rupture reactions in multiphoton dissoc. 79—47947
bonds in reactions, form. and breaking, partitioning anal. of electron reorganisation 80—104419
borides of group IV-VI transition metals, reaction with phosphoric acid 77—1946
branching ratios, information theory calcs. for known conditional probabilities 78—13406
Bray reaction, kinetics obs. *(French)* 80—7788
Briggs-Rauscher reaction, chem. oscill. obs. 80—3336
Brownian dynamics simulation in soln. 80—104422
butadiene-acrylonitrile copolymer, electronic struct., reactivity, SCF CNDO calc. 77—50580
butadiene-nitrile elastomers, high temp., and press. chem. transformations *(Russian)* 79—52659
n-butyl acetate, alkaline hydrolysis in water-alcohol mixture, solvent polarity effects 77—48639
cage reaction in solid state, model 79—87820
carbon tetrafluoride+methyl trichlorosilane, reaction, metastable C phase prod. 79—29341
carbonic anhydrase, active site substrate binding, environmental effects, CNDO and SCF LCAO calcs. 80—8002
cardiac chemical power, derivation of chem. power eqn. and determ. of eqn. consts. 80—16911
cast iron-steel mixture, interaction of Zr, formation reaction thermodynamics *(Russian)* 80—55645
catastrophe theory in chem. reactions, study and classification of propagating phenomena 78—7170
ceramics, chemical reactions, high temp., diffusion controlled 79—91935
chain molecule dynamics, intramolecular diffusion controlled reaction for pr. terminal reactive groups 78—9289
change kinetics, steady state approximation, validity 79—83439
Chapman-Enskog method for a multivelocity, multitemperature mixture of reacting gases *(Russian)* 79—15995
charge transfer ionisation reactions, review 77—60053
chelation study of aspartic acid with Zn(II), Cd(II) and Hg(II) 77—44464
chelatropic reaction, intrinsic single and dual mol. orbital symmetry conservation 80—102419
chemical energy conversion to mechanical and electrical energy *(French)* 79—52954
chemical power, appl. of power, work and efficiency eqns. to left ventricular energetics in man 80—16912
chemical waves and the diffusive coupling of limit cycle oscillators 79—83454
chemically reacting non-LTE plasma, elementary reactions 78—3337
chemonuclear fusion reactor, gamma-neutron, chem. reaction parameters 77—34466
chlorophyll a in benzene solns. and monolayers, chem. stability 79—47912
chlorophyll-a, photoinduced electron transfer to duroquinone in micellar soln., charge separation 78—23955
cholesteric liquid crysts., asymmetric synthesis failure using bimolecular reactions 80—44115
chromatographic reaction and separation in pulse-fed catalytic reactor 78—64880
circulation reactions, quasistationary circulation in liquids 79—15965
circulation reactions, stationary, self-oscillating mode 79—24721
clay, Al_2O_3 and SiC recovery by C reduction 80—108704
clay kaolinic, chlorination 78—6878
closed Friedmann cosmos, entropy prod. density for chem. reactions *(German)* 77—26101
coal, liquefaction by hydrogenation, developments 79—92051
coal gasification, in situ, kinetic model of char-steam reaction in Hanna subbituminous coal 80—30361
collinear asymmetric model reaction probabilities quantum and quasiclassical calcs. 80—85145
collision processes, dynamical and information theories, maximal entropy procedure 78—27740
colloid coagulation, 1st-order diffusion effects 79—39213
comet comae, gas-phase chemistry in one dimension 78—93154
complex chemical reaction network construction, appls. 78—11497
complex chemical reaction network construction definitions 78—11496
complex chemical systems, chemical process and rate models, computer simulation appls. 78—48620
complex formation consts., computer programs 80—26005
composite layered slab, solute diffusion, conc. depend., with/without chem. reactions 80—54427
composition centre waves, periodic chaotic, Pade approximant scheme 78—80716
compound formation in metal-semicond. interactions 79—28217
computer modelling, logarithmic formulations of parameters 78—48646
computer programs, math. model of chem. 79—52620
concentration fluctuations, use of master and Langevin eqns., diffusion effect 78—3313
concentration-dependent diffusion in a finite slab with and without chemical reaction 79—30389

chemical reactions continued
condensed phases, ternary diffusion with two moving boundaries 77—35760
conference, electronic and atomic collisions, Paris (July 1977) 78—58758
control using chemical lasers 77—70312
copolymers, cooperative reactions, sequential anal. of 2nd order Markovian chains 78—7204
copolymers, cooperative reactions, sequential anal. of binary copolymer with protecting monomer 78—7203
coupled, exact stochastic simulation, using digital computer algorithm 78—48625
coupled multistep chemical reactions, rate const. determ., relax. spectroscopy 80—66766
coupled oscillating chemical systems, phase-difference locking 79—11762
crossed beam studies, gas kinetics 79—74388
crystal growth and deposition, gaseous phase, chem. transport reaction 80—44161
cyanopolyynes, form. in gas discharges 79—5156
cybernetic prediction of chemical compound formation, in uninvestigated systems 79—11880
cyclobutane-t, chem. activated by nucl. recoil reaction, energy transfer interpret. 80—25985
π-cyclopentadienyl (carvone) iridium (I), synthesis and protonation 77—60062
decomposition driven convection of dissociating Navier Stokes fluid, instabilities 80—59128
decomposition theory transition matrices, var. calcs. 78—20005
dense plasma, coaxial acceleration and plasmochemistry *(Russian)* 78—92482
dextran, activation of acid hydrolysis by ultrasound, mech. stress effect on reactivity 79—74375
1,2-di(N-piperidyl)ethane-bis-N-oxide tetrahydrate, synthesis, cryst. and mol. struct. obs. 79—32985
diamond formation, hydrocarbon dissociation, Hugoniot data, high temp. and press. 79—47927
diatomic molecules, form. and dissoc. in interstellar medium 80—23471
dibromotetrafluoroethane, plasma quench reactions, electron attachment 77—90586
9,10-dichloro-m-carborane, electrophilic chlorination, B-trichloro-m-carborane, mol. and cryst. struct., X-ray diffr. 78—9268
differential geometrical analysis of chem. reacting systems 79—31434
diffusion controlled reaction kinetic studies by light scattering, one-step reaction case 78—35659
diffusion coupled reactor system, bifurcation diagram and nonhomogeneous steady states 80—16647
diffusion effects on reactions in solution, formulation 78—40031
diffusion processes, nonlinear, oscillations 77—73440
diffusion with chemical reaction, probabilistic interpretation 78—35645
diffusion-controlled, encounter-result probabilities, Onsager Monchick methods unification 79—87823
diffusion-reaction equations, semilinear parabolic systems, soln. existence and stability 79—47889
diffusion-reaction equations systems, existence, stability 79—20365
diffusion-reaction problem, nonlinear, dissipative structs., stability anal. 79—1938
dihydroxyanthraquinone, light-induced proton transfer, photochem. hole-burning obs. 80—76535
L-β-3,4-dihydroxyphenyl-α-alanine with L-glutamic acid, polymers and copolymers, synthesis and conform. 79—33996
direct chemical reactions in fast molecule collisions, eikonal approx. calcs. *(Russian)* 80—3332
discrete master equation, transition factor method, appl. to chem. reactions 78—36952
disperse reactive system, nonsteady heat exchange 80—26061
disproportionation, ketone chemiluminescence during disproportionation, nonradiative transition processes 79—87846
dissipative structures, fluctuation effects, appearance of optically active states 79—83442
dissipative structures, fluctuation effects on chem. oscill. systems 79—83441
dissipative structures in pseudo one-component systems 78—3309
double exchange reaction, representation of phase equilibria 79—66266
double potential wells, tunnelling and over-barrier decay rates, method of beats calcs. 78—44363
double well potential, transfer and tunnelling rates, density matrix calcs. 80—30209
DSeDTF, synthesis by trimethyl phosphite coupling of 1,3-thiaselenole-2-selone 78—10423
dual function catalysts, macroscopic distribution of components, selectivity effect 79—47967
dynamical correlations near instabilities in nonlinear chemical reaction systems 78—80715
dynamics, laser probe investigs. 79—43580
dynamics, mol. beam obs. 79—41233
dynamics, reactions with complex form., stochastic reduction 78—3315
dynamics evaluation via minicomputer 77—25246
Eckart barrier tunnelling, Arrhenius plot curvature 80—3298
EHF theory in chem. reactions, wave functions symmetry props. 78—92447
elastic chemically reacting non-simple mixture, accel. waves 77—75829
elastic scattering, in chem. reactive system, parametrised S-matrix models 79—79225
elastomer reinforcement, carbon black-polymer interaction 79—83171
electric discharge, non-self-sustained, NO and NO_2 produced in air 79—7502
electric discharge sintering, metal powder+punch electrode reactions 78—11148
electrical conductivity variation during solid state reaction *(German)* 80—34494
electrochemical reaction sequences, criteria for selective path promotion 80—26018
electrochemical reactor characterisation, marker pulse method improvements 80—76524
electrochemical reactors with three-dimensional electrodes, characterisation using electrochemical tracer method 80—76520
electrochemical voltage indicators, production, voltage response, resist. 77—1936
electron beam stimulation by relativistic beam collective effects *(Russian)* 77—77763
electron kinetics in nonpolar liquids 78—95918
electron pair mechanism, non-specialist teaching appl. 78—89279

chemical reactions continued
  electron pairs, destiny in chem. reactions 79—52652
  electron transfer, in rigid medium, exothermic rate restrictions 80—30224
  electron transfer reactions, free energy, anharmonic intramol. quantum mode depend. 77—12781
  with electronic isotopic substitution in flow and stopped flow NMR 77—25265
  electrons in fluids, conf., Banff, Alberta, Canada, (5-11 Sept. 1976) 77—89680
  electrostatic interactions in liquid state, effect on frontier orbitals and chem. reactivity 80—84046
  elementary reactions, cross-sections, hard-sphere model 78—7176
  elimination reaction, D kinetic isotope effects, tunnelling, zero-point energy effects 78—56889
  enamel, melted vitreous, for protective coating appls., gas generation in highly viscous phase *(Russian)* 77—73360
  endoergic reactions, reagent internal excitation effects on rates 80—93731
  endothermic, extreme mass combinations $LH+H \rightarrow L+HH$ and $HH+L \rightarrow H+HL$ 79—43570
  endothermic solid reaction, unsteady heat conduction, thermal conductivity change 80—76511
  energy barrier from overlap repulsion scheme 77—36734
  energy barrier location, sudden and gradual late barriers, classical trajectory method 78—92454
  energy requirements vibr. and translational energy depends. 79—57206
  enzyme, complexation, Mossbauer spectroscopy 77—12876
  enzyme catalyzed reactions with positive feedback, existence of stable limit stables 79—96289
  enzyme reaction systems, nonequilib. transitions, probability distrib. 79—12720
  enzyme-substrate reactions in differential scanning calorimeter, digital simulation 79—74794
  enzymic kinetics, rate constants estimation 79—70505
  epoxide resins, amine-hardened, heat distortion, glass transition temps., chem. cure 80—44302
  epoxy cure, autocatalytic reaction, kinetic parameter estimation 79—70327
  estuary and river sited power plants, water discharge and chlorination, simulation 78—96250
  ethanol+Al_2O_3, surface reaction, 295-575K, surface specieis study 79—100435
  ethyl cation, rearrangement pseudorotation modes, reaction mechanisms, permutation theoretic anal. 78—44369
  ethylene, chemistry in RF discharge, mass spectrometric obs. 77—9084
  ethylidene, rearrangement to ethylene, barriers, ab initio MO calcs. 80—104424
  exit problem, diffusion across pot. barriers, chemical reactions and crystal diffusion 79—80527
  exoergic collinear reactions, impulsive energy release model 77—90591
  exothermic, criticality, Frank-Kamenetzki parameter, upper and lower bounds 79—66335
  exothermic, energy disposal, information theory appl. 78—15658
  exothermic, Marcus eqn., Born approx., strong vibr. nonadiabatic transitions 77—56214
  far from equilibrium, concepts *(French)* 80—7761
  fast reactions in soln., nsec temp. jump technique with I_2 laser 78—31634
  fast reactions in soln. under high pressure, investigation using stopped-flow apparatus 80—86335
  ferrite spinels, normal and inverse, solid state chem. expts. for students 80—36815
  ferrogel, with $MnCl_2$ solution, production of MnMg ferrites 77—12582
  Field-Koros-Noyes chemical wave equation, asymptotic solutions 80—66857
  first order rate constant, evaluation method 79—1937
  fixed bed reactor catalyst decay, dynamic phenomena study *(German)* 78—7201
  fluctuation, equiv. of stochastic diffusion process with fluctuation dissipation theory 77—77734
  fluctuations, irreversible thermodynamics 77—52616
  fluctuations near nonequilibrium phase transitions to nonuniform states 80—45542
  fluid, dense, chem. reacting, Enskog theory 78—35667
  fluid, reacting spheres, kinetic theory 78—35668
  fluid-solid reactions, law of additive reaction times 79—83452
  fluorene and 9-allyl derivations, electronic struct. and reactivity 79—36523
  2-fluoroethyl to ethylene fluoronium ion interconversion, pot. energy surface, MNDO calc. 79—34296
  forced ionisation, appl. in secondary batteries 79—43755
  forced nonlinear oscillator system, stroboscopic phase portrait 79—57225
  formaldehyde, interstellar, prod. in diffuse clouds 79—40246
  Fourier sensitivity analysis, improved freq. sets 78—31628
  fracture, chemically-assisted, atomic modelling at crack tips 80—106754
  free atoms of metals [and their chemistry] *(French)* 80—21281
  gallic acid+BrO_3^-+H_2SO_4 system, uncatalysed oscillatory chemical reactions 78—61004
  garnierite, high-temp. reactions, spectrochem. anal. 77—70294
  gas absorption by liquid, exothermicity altering solubility and reaction rate 79—74341
  gas absorption with second-order irreversible chem. reaction, enhancement factors 78—80727
  gas mixture, reacting, atom conc. reson. absorb. meas., microwave discharge lamp calibration 79—92032
  gas mixture, reacting, Boltzmann kinetic eqns., Chapman-Enskog method 78—15656
  gas phase, laser obs. *(German)* 79—29365
  gas phase chemical reactions in IR laser field, collision-induced absorpt. spectra 80—76499
  gas-phase reactions, anal. using computer interfaced time-of-flight mass spectrometer 80—71967
  gas-solid, chem. equilib. of effusive beam source 80—52362
  gas-solid reaction, grain-cell model 79—66342
  gas-solid reactions, book 77—63958
  gas-solid reactions solid catalysed, effectiveness factors 79—47966
  gaseous electronics, conference, Pittsburgh, PA, USA (Oct. 1979) 80—22142
  gaseous mixtures, conc. fluctuation meas. using catalytic wire 77—26291
  generation in air-fed ozonisers 80—3323

chemical reactions continued
  glass reactions with aq. solns., influence of surface pot. on kinetics 80—108612
  glasses, alkali-silicate, chem. stability, cations coordination, leaching vacancy mechanism 80—35526
  glasses, alkali-silicate, chem. stability depend. on cation O_2 structs. 80—35527
  goethite, transformation to maghaemite in CsI discs 79—69259
  grain and phase boundaries between crystals, conf., Konigstein, Germany (Oct. 1977) 78—72762
  graphite fibres, elec. resist., mech. props. after nitration 77—32698
  graphite layers, C-C bond length increase on intercalation by metals *(French)* 77—28994
  graphite nitrate, charge transfer, ionic salt model 79—11780
  graphite-metal fluoride intercalation cpds., prep. and props. 80—40686
  Hafke-Gilles reaction, oscill., thermal props. 80—7762
  Hammett correlation, explanation of solvent effects by frontier orbital method *(French)* 78—11604
  hard sphere model of chemical reaction in condensed media 79—29349
  heat engines, chemically driven, finite time thermodynamics 80—76541
  heterogeneous nonideal chemically reacting system, comp., thermodynamic props. calcs. 80—76492
  heterogeneous reactions, modified entrainment method appls. 79—23551
  cis-2,trans-4-hexadiene, addition kinetics of HCl, Raman spectra meas. *(French)* 79—91940
  hexafluoroethane, chemical conversion and uniformity of etching SiO_2 in radial flow plasma reactor 80—76391
  hexafluoroethane, RF discharge chem., added acetylene effect, mechanistic model for fluorocarbon plasmas 80—84017
  hexamethylolmelamine, doped, and condensation resin, room temp. phosphoresc., thermal transforms. 80—45132
  high level liquid radioactive waste, denitration with formic acid, Pt group effects 79—36339
  high pressure boiler in-service scavenging by intermittent dosing with chelating agent 80—89485
  hollow cathode gasdynamic jet carrying excited metal atoms as spectral light source and chemical reactor 79—46493
  homotetrahedryl cation, rearrangement pseudorotation modes, reaction mechanisms, permutation theoretic anal. 78—44369
  hot atom reactions, nonequilib. vel. distrib. and reaction rate, Monte Carlo anal. 77—16855
  hot gas thermodynamics and diagnostics 78—76865
  hydration, hydrophobic, of nonpolar mols. in dilute aq. soln., Monte Carlo simulation 80—3314
  hydrationally active phases, electron structs. and props. of anions 77—44574
  hydrocarbon, conjugated, electrophilic substitution, graph theory 77—9076
  hydroxyl-terminated prepolymers, functionality determ. 79—31746
  8-hydroxyquinoline+phthalic anhydride, solid-state reaction kinetics 77—36746
  hypsorhodopsin, squid, form., picosec. spectrosc. obs. 79—39183
  inert gas halide ions, form., mass spectrosc. obs. 79—29346
  information retrieval, comparison of methods used by Wiswesser and Derwent 79—83541
  instability of evolving systems, elastic stability theory and catastrophe theory approaches 78—44442
  intermolecular energy transfer following kinetically controlled chem. activation, multistep deactivation processes 80—25985
  intermolecular reaction dynamics, pot. barrier crossing in high friction limit 79—29343
  interstellar C-H chemical system, mols. form. in diffuse cloud 77—26033
  interstellar catalytic reactions, effects of Fe grain temps. 77—71135
  interstellar chemistry, long-chain hydrocarbons, formation mechanism 80—46653
  interstellar cloud gas phase chemistry for C, N and O compounds 80—105319
  interstellar clouds gas phase chemistry, nonequilib. processes and temp. and activation energies effects 80—105298
  interstellar diffuse clouds, chemistry rel. to OH and HD column densities and temps. 78—93385
  interstellar molecule reactions, review 77—9790
  interstellar molecules, isotope effects on form. rates, appl. to DCN enrichment 77—82298
  interstellar plasmas, ion chemistry 80—62254
  interstellar surface reactions rel. to interstellar medium elemental depletions 78—36654
  intramolecular energy transfer, crit. energy calcs. 77—9046
  intramolecular interactions effect on transferability props. of localised description of chemical groups 80—102424
  intramolecular reaction, transient initial conditions for diffusive barrier crossing 79—29344
  intrinsic field theory, intrinsic reaction coordinate approach 80—11877
  intrinsic reaction coordinate ab initio SCF calc. method 77—48626
  ion+molecule reaction, equilib. consts., ion cyclotron reson. spectrometer meas. 77—56218
  ion lifetime distribution, following interaction with collision gas, determ. method 79—36732
  ion pairs, in dilute soln., Debye-Smoluchowski eqn. soln. 79—66259
  ion reactivity arising from different region of translational energy release distribution, need for ang. collimation 80—104483
  ion transport and chem. reactions in brown adipose tissue, network thermodynamics 78—92606
  ionic reactions, polyion effect, doubly charged counterions 78—31633
  ionic systems, chemical wave equation 78—15653
  irreversible chemical process, in elec. field, heat and mass transfer 78—11545
  jasmone and intermediate compound synthesis *(Japanese)* 79—8436
  kaolinite-mullite reaction sequence, interpretation from IR absorption spectra, comment 78—48720
  kaolinite-mullite reaction sequence, spectroscopic anal. of Al coordination changes 78—48719
  kinetic theory of reacting systems, transport processes, rate coeffs. 77—86284
  Kramers theory of friction and vel. in chemical kinetics 80—50826
  lacustrine sediments, selective chem. extraction of CO_3^{2-} associated metals 78—65406
  Lagrange-Hamilton formalism, concept of chemical inertia 80—7756
  large-angle elastic scattering, in reactive systems, interference effects, Regge pole anal. 77—58123
  laser applications to chemistry, overview 79—58800

chemical reactions continued
  laser chemistry 79—100415
  laser-chemical reaction kinetic mechanism *(Russian)* 80—101007
  laser-initiated chain reactions, rates, mechanisms, chemiluminesc. obs. 80—55651
  law of mass action, first order phase transition, chemical instability 78—80778
  limit cycle entrainment by periodic external excitation 77—61020
  liquid membranes, separation and reaction appls. 80—66871
  liquid phase, nonthermal laser excitation, reaction control *(Russian)* 77—9106
  liquid phase reaction systems, combination rates of steady state processes and transient phase process *(Chinese)* 77—77764
  liquid-solid reactions, shrinking core model application 79—47887
  liquid-vapour equilibrium in chemically irreversible systems *(Russian)* 78—3369
  liquid-vapour equilibrium in system with chem. reaction, thermodynamics *(Russian)* 77—63947
  liquids, reactive pair dynamics, kinetic theory 79—11761
  lithium formate monohydrate, dehydration, kinetic parameters from thermogravimetric data 79—61859
  localisation in ionized and excited states, conf. 77—30750
  loge theory and chemical reactivity 77—30758
  low temperature reactions, mechanisms and rates, review, book contrib. 77—40542
  LPE, molecular beam mass spectrometry, in situ anal. of minor gaseous species 80—52357
  lumped parameter system, with two parallel reactions, steady state multiplicity 77—60103
  macrocyclic receptor mols., chem. reactivity, mol. catalysis, transport processes 80—21280
  magnetic field effects, 1- and 3-dimens. models 78—19992
  magnetic field influence on chemical reactions *(French)* 79—47929
  master eqns., Poisson representation 78—35638
  master equations steady state soln., chem. react., two-photon laser appls. 77—9945
  materials synthesis at high press. 79—47645
  mechanism investigation using group frequencies 79—98057
  melt reacting with gas jet, heat and mass transfer, mathematical modeling 80—87819
  membrane process, coupled transport of electrons and metal cations 80—3403
  membrane transport, chemical reaction augmented, facilitation factors, prediction, appl. 79—91992
  metal atom reactions, cryogenic techniques and matrix isolation spectroscopy 77—9080
  metal gas reactions in arc plasma spraying 80—66427
  metal ions, in unusual valency states, reaction rate consts. 79—47921
  metal oxide-C mixtures, mathematical analysis of reactions 77—73469
  metal-gas system, ignition conditions with account of radiative heat loss *(Russian)* 77—32789
  metallic oxides reduction, mechanism and intrinsic rates 79—83153
  metals and alloys, sulphidation mechanism, review *(Polish)* 80—45413
  metastable decomposition, kinetic energy release distrib., mass spectroscopic determ. 77—44538
  methanation over polycrystalline Ni(Pt) foils, kinetic information 78—73081
  methane, conversion in H_2 plasma flow, Monte Carlo study 78—61010
  methane gas$\rightarrow$C(dissolved)$+2H_2$ (gas), kinetics on Fe and Fe-Ni surface 80—55712
  methane-d_3, activation, dissoc., internal energy distrib., trajectory calcs. 77—4899
  3-methoxybenzanthrone in ethanol, photoprotolytic reactions, spectra, rate consts. and lasing thresholds 80—43327
  methyl chloride-d_3, activation, dissoc., internal energy distrib., trajectory calcs. 77—4899
  MgO, high temperature interactions with Re 80—16665
  micellar system, photoinduced redox processes kinetics, intramicellar electron transfer 78—92603
  micelle formation model, relaxation spectra 80—71934
  micelle-confined molecules reaction, diffusion-controlled, luminesc. quenching, excimer form. 80—50890
  micelles, organic reaction kinetics 79—29416
  minimum energy reaction path, reference coord. approach 78—40025
  minimum energy reaction paths, reactive domains of energy hypersurfaces and stability 80—71893
  mode-mode coupling theory of chemical reaction in a dense fluid 79—57218
  model reaction bifurcation diagram, time-periodic soln. stability changes 79—47886
  modelling of dynamic phase memory in self-excited wave media 79—79505
  molecular beam, collisionless, high-resolution time-resolved laser spectroscopy 79—3501
  molecular beam reactions, transient complex form., product mol. translational energy distrib., theory 77—90602
  molecular chemical tunnelling, facts and hypotheses 79—59520
  molecular collisions, joint products' state distribs. 78—64807
  molecular dynamics simulation of chemical reactions in solution 80—40673
  molecular dynamics studies of the role of diffusion in chemical models with absorbing boundary states 79—8424
  molecular geometry, mass spectrometric investigation, using mol. rearrangement 78—86972
  molecular ions, cleavage and rearrangement, mass spectra 77—6944
  molecular ions, gas phase, spectroscopic props, review 78—33501
  molecular reactive collisions, product energy distrib., statistical-dynamic model 78—27736
  molecular systems, saddle points and min. energy paths, constrained simplex optimisation procedure 80—42943
  molecular tunnelling in chemical reactions *(Russian)* 77—52615
  molecule synthesis by ion implantation, laboratory simulation of interstellar process using photon emission 77—70297
  molten alloys, compound-forming, vol. of mixing, conc. depend. 80—103484
  in molten salts, acidity effects 78—73039
  montmorillonite, dehydration kinetics 78—76857
  multicomponent system with diffusion, nonlinear wave equations 78—19991
  multiphonon relaxation, statistical anal. 79—79223

chemical reactions continued
  multiple reactions, Cl isotope effects, mass spectrometric monitoring 79—39135
  multiple site reactivity, interaction field modified Hamiltonian method 78—11498
  multiple stationary states systems, meas. of stability and relative stability 80—3338
  muonium, H like atoms, phys., chem., review *(Russian)* 77—50566
  muonium, reaction with DNA and its constituents in water soln., rate constants 79—57210
  muonium$+Cl_2$, gas-phase reaction, muonium spin rot. rate meas. 77—58207
  naphthylamines, abnormal fluorimetric titration behaviour, kinetic anal., fluoresc. quantum yields and lifetime meas. 80—89560
  nascent products, vibr. state distrib., statistical thermodynamics calcs. 77—5782
  network thermodynamics with entropy stripping 78—7223
  Ni_2SiO_4, reaction with Fe to produce Ni gamma resonance spectroscopy *(Russian)* 78—15332
  nickel calcine, reactivity, contact I-V meas. 77—85975
  nickel oxalate, electronic struct. from Huckel calcs., optical props. and reactivity 77—89741
  nickeliferous limonites, pressure leaching for Ni extraction, using H_2SO_4 78—39717
  non-ionic reactions, temp. and press. effect on kinetic and thermodynamic parameters 80—3300
  non-rigid molecules in condensed phases, liquid struct. effects on chem. reactions and conform. changes 80—40725
  nonadiabatic cage reactions, relaxation hindrance 80—93740
  nonaqueous solutions, conf. Leeds, England (July 1976) 78—73036
  nonequilibrium chem. reaction wave probing of medium with varying energy level populations 79—76755
  nonequilibrium chemical phase transition, kinetic potential and Maxwell construction 77—87716
  nonequilibrium phase transitions and chemical reactions 79—79221
  nonequilibrium phase transitions in chemical systems 78—54325
  nonequilibrium reacting systems, critical bifurcations, scaling and Ginzburg criteria 80—81290
  nonequilibrium systems, with multiple stationary states, kinetic anal. 78—27735
  nonequilibrium systems, with multiple stationary states, stability, thermodynamic anal. 78—27734
  nonequilibrium thermodynamics, stochastic approach 79—52749
  nonlinear diffusion-reaction with autocatalysis and saturation law, single perturbation approach 80—35502
  nonlinear eqns. for reacting system with physical interactions 80—81288
  nonlinear reaction diffusion model, dissipative structures 79—66279
  nonlinear reaction diffusion systems, bifurcation anal., dissipative structs. in a sphere 79—11767
  nonlinear system, networks induced by symmetries of transformation groups 79—43556
  nonlinear system, spatial patterns as transform. group symmetries 78—27878
  nth-order reactions, reaction kinetics, DTA obs. 77—81386
  nuclear advanced MX fuels, Pu depletion by vapour-phase transport in carbothermic reduction processes 80—815
  nuclear fuel processing solutions, interactions 78—78487
  nuclear particle fuel prep. from U, Pu and Th nitrates, wet chem. process, for LWR, FBR and HTR *(German, English)* 77—65314
  nuclear reactor core meltdown, chemical reacts. between core melt and concrete 80—13588
  nucleoside anion + hydrocarbon cation, electrochemiluminescent electron transfer reaction 79—88046
  nucleotide anion + hydrocarbon cation, electrochemiluminescent electron transfer reaction 79—88046
  oil-water interface, chem. and hydrodynamic instabilities *(French)* 80—7789
  open chemical reaction system with exactly evaluable limit cycle oscillations 80—21260
  open chemical system, noise-induced transitions 80—3337
  open systems, arbitrary dynamic behaviour 77—73438
  orbital correspondence anal. in max. symm., appl. to spin-forbidden processes 78—78631
  orbital interaction and chemical bonds. Exchange repulsion and rehybridization in chemical reactions 78—85142
  organic chemistry, conf., York, England (Sept. 1978) 80—21259
  organic chemistry, isotopically modified compounds, nomenclature 80—3294
  organic chemistry, textbook, undergraduate level 78—57711
  organic glass, electron-cation recombination; charge distrib. simulation and luminesc. kinetics 80—2855
  organic reaction mechanisms, generalised mol. orbital theories, review 78—44366
  organic synthesis, computer simulation *(French)* 79—52653
  oscillating Belousov-Zhabotinskii system, detection of BrO_2 *(German)* 79—29351
  oscillating chemical reaction, periodic plane waves 77—48615
  oscillating reaction, homogeneous bifurcation phenomena obs. 77—48621
  oscillating reactions, thermal props. 80—7762
  oscillations, chemical and thermokinetic, feedback *(French)* 79—57205
  oscillations, reaction systems with exactly evaluable limit cycles 79—66262
  oscillations and runaway states in closed illuminated system 78—7188
  oscillatory, dynamical theory of pattern formation 77—9048
  oscillatory chemical reaction systems, weak coupling 80—66775
  oscillatory membrane reactions, focal nucleation size 79—92171
  oxoniomethylene cation, rearrangement to hydroxymethyl cation, barriers, ab initio MO calcs. 80—104424
  pairwise correlated generalised valence bond model, electron correl. model 78—41959
  particulate solid, reactions, viscous flow and Knudsen diffusion 77—4937
  pattern recognition in chem. dynamics 77—32768
  pentenes, in combustion of pentane, further reactions, isotopic tracer obs. 79—8438
  peptides, charge transfer, 1-electron reactions, pulse radiolysis obs. 80—45848
  pericyclic reaction path, spin-free quantum chem., particle-hole and pairing symmetries 79—6812
  petroleum spills on water, control using gellants 80—61496
  phenomenological eqns. for reacting fluids 78—3363
  phenomenological equations for reacting fluids 78—15649

chemical reactions continued
phenomenological relations, linear network thermodynamics 78—95905
photochromic glass, thermochemical effects 80—87448
photographic emulsion gelatin enzymic hydrolysis expts. 79—79311
photosynthetic carboxylation reactions, ^{13}C kinetic isotope effect 79—57566
photosynthetic redox conversions, electron transport, EPR obs. 79—92179
photosynthetically relevant mols., electronic structural props. 80—16902
physical-chemical solids with finite deformation, variational irreversible thermodynamics 79—6067
picosecond chemistry, review 77—5933
picosecond phenomena, conf., Hilton Head, USA (May 1978) 79—44940
pigment-antioxidant interaction, numerical analysis in polymers 79—39136
plasma, chemical reactions, rate coeffs., database creation, DATSTOR 80—48846
plasma, chemical species, number density variation with time, numerical model, PLASKEM 80—48845
plasma, diffusion fluxes, thermal cond., chem. reactive 77—47142
plasma, elementary processes and chem. reactions, review *(Czech)* 80—24126
plasma chemistry, conf., Rome, Italy (Sept. 1975) 78—3336
plasma chemistry, diagnostic techniques 78—3338
plasma chemistry, principles and problems 77—48644
plasma chemistry, status and trends 78—76864
plasma chemistry *(Czech)* 79—47924
plasma chemistry in gas, liq., or solid state 79—79241
plasma of given chemical content, chemical reactions, computer generation, REACS 80—48844
plasma reactions, transform energies from short-time pulsed probe analyser 77—15240
plasma reactor, double column, source of chemical reagents *(French)* 77—1023
plasmo-chemical reaction in electrical discharge, metal vapour prod. *(Russian)* 77—63913
plastic, reactive, structurisation kinetics, torsion cord method *(Russian)* 79—34304
polar solvent reorganisation energy in inner sphere complex charge redistrib. 80—40730
polarisation effects, orbital interaction and chem. bonds 78—31613
poly(N-vinylcarbazone), charge transport and struct., bromination effect 78—11516
poly(trans-1,4-butadiene), crystals in suspension, epoxidation kinetics 79—61861
polyacrylamide, conversion to poly-N-dimethylaminomethacrylate, Raman method meas. 79—74460
polyacrylonitrile, electronic struct., reactivity, SCF CNDO calcs. 77—50580
polyatomic molecules, unimol. decay, nonadiabatic interaction, selection and propensity rules 78—23932
polyatomic reaction dynamics, curvilinear natural coords. 77—77729
polybutadiene, electronic struct., reactivity, SCF CNDO calcs. 77—50580
polybutadiene, hydrogenation 80—26008
polyelectrolyte + physiologically active substance complexation, stability, kinetics *(Russian)* 80—8006
polyelectrolyte-counterion affinity, theory of Coulombic reactions 77—48648
polyethylene, chlorination, rate const. determ. using NMR spectra of chain sequence *(German)* 79—100366
polyethylene, electron microscopy with chlorosulphonation aid 77—89351
polyethylene, low-temp. relax., effects of chem.- and electron irrad.-crosslinking 79—4990
polyisocyanides, solns., struct. and acidification 80—19915
polyisoprene, electronic struct., reactivity, SCF CNDO calcs. 77—50580
polymer chains, intramolecular cross-linking reactions, Monte Carlo calcs. *(Russian)* 78—31636
polymer crosslinking in continuous flow stirred reactors 79—79246
polymer networks, creep during scission reactions 79—15738
polymer reactants in organic reactions, review 78—95923
polymer reactivity Mossbauer spectroscopy 77—12798
polymer transformation reactions, kinetics, statistics and mechanisms 79—43584
polymer-solvent interaction from gas-liquid chromatography, open tubular column expts. 78—35753
polymers, struct., bonding, reactivity by ESCA 78—53299
polyurethanes, linear, in physiological soln., in vivo, degradation by ester hydrolysis *(Russian)* 80—40690
polyvinyl acetate with iodine-iodide, reaction system, colour complex form., temp. effect 79—83457
porphyrin metallation, in monolayer films and assemblies 79—11817
porphyrins, dark transition of reduction products by disproportionation 79—53020
Portland cement, hydration mechanism 78—35349
positron + halide ion, competitive reaction in water, ang. correl. obs. 79—61846
potential energy barrier position between initial and final states 78—76831
potential energy surface, multidimens., topological stochastic approach 77—48638
potential energy surfaces, qualitative, from linear comb. of fragment configs. 78—44349
potential energy surfaces, use with algorithm to form reaction tree 77—70286
potential energy surfaces of chemical reactions, nonempirical calcs. 80—35505
powder reactions, isothermic kinetic eqn. *(Czech)* 79—70301
PQ developers, synergism 79—24732
prochiral, gravitational field effects 80—71899
product initial rot. state distrib., pump and probe laser obs. 80—85158
product state distribs., uniform phase space representation 77—28979
propan-1,3-dioic acid, H_2O_2, KIO_3, $MnSO_4$, $HClO_4$, I_2, periodic chem. reactions, bi- and tristability, rel. to biological mech. *(French)* 78—80726
n-propyl(n-butyl) tin dichloride, prep. and Lewis acid charact. 77—90597
proton transfer photoreaction kinetics, in singlet excited state 78—48671
proton transfer reactions, kinetic isotope effects, quantum theory 80—3301
proton-transfer reactions, potential energy curves and Bronsted exponents 77—32784

chemical reactions continued
PTFE + metal, fluoride prod., DSC and XPS anal., rel. to polymer wear 80—11889
PVC, chlorination reaction, X-ray photoelectron spectrosc. 80—3469
PVC, rigid plate, simultaneous diffusion and dechlorination in H_2SO_4 *(Japanese)* 77—52521
PVC, thermal stabilisation by triazine dithiols *(Japanese)* 80—108386
PVC + $Br_2(I_2)$, reaction in surface-modified film subject to thermal-radiative and photochem. action *(Russian)* 77—21385
pyrimidine, bi-exponential decay, methylation and vibr. excitation, proximity effects 80—78641
pyrochlore, high temperature chlorination 78—11180
quantum chemical methods appls. 80—93752
quantum chemistry, conf., Kyoto, Japan, 29 Oct.-3 Nov. 1979 80—101659
quantum mechanical kinetics problems, averaging principle, degenerate states and reson. effects 78—19996
quantum mechanical kinetics problems, averaging principle appls. 78—19995
quantum momentum decoupling approx. 77—12780
quantum statistical theory, formulation, lowest order results 77—60045
quantum tunnelling of proton and activated complex theory 78—17586
quartz, powdered, hydrothermal reactivity *(Japanese)* 78—23938
quasilinear parabolic system, chemical reaction study 80—7759
quinoline derivative, interaction with coenzyme Q_{10} 79—91948
radiative collisions 77—25255
rare earth metal + H_2O vapour, hydride form. 80—76504
rare earth orthophosphates, high-temp. treatment and formation of oxyphosphates *(French)* 77—44199
rare-earth ions in solns., radiationless energy transfer and complexation processes 79—10144
REACT program for computer-assisted simulation of chemical reaction sequences, structure elucidation applications 78—92477
reacting systems, sound wave attenuation, thermodynamic interpretation 80—43505
reaction mechanisms, models, computer method appls., conf., New Orleans, USA (1977) 78—48645
reaction paths, heat of formation, MINDO/2(3) forces method 78—9078
reaction-diffusion system, chemical turbulence 77—1913
reaction-diffusion systems, bifurcation theory, classification 80—108713
reaction-diffusion systems, dissipative struct., sphere bifurcation numerical determ. 80—76483
reactive diffusion in silicides with small homogeneity region, kinetics and mechanisms 77—35751
reactivity, reliability of quantum mechanical predictions, config. of reaction prod., H-bonded species 80—108691
reactivity with Y_2O_3, exam. by thermal anal. 78—85154
rear earth oxide, reaction with liq. Li and liq. Li-N 79—66276
rearrangement mechanisms, dynamic NMR spectrosc. obs. book contrib. 79—30521
recoil hot reactions, average energy of reaction rel. to system composition 77—73457
recombination probability, reactivity depend., scavenger effects 80—76494
recombination probability, reactivity dependence 80—45494
redox, using electrodes with covalently attached monolayers 80—45512
refractory compounds heat of formation determ. using self-propagating high-temp. synthesis 80—3392
refractory metals and oxides, reactions of liq. alkali metals, relevance to reactor technology 80—85173
renormalisation group approach to chemical instabiliites 78—15657
reversible, asymptotic expectation and variance of stationary probability distribution 79—11789
reversible reactions, first order, time depend. behaviour 80—97699
rhodamine 6G, aqueous soln., absorpt. spectra, ground and triplet state photoprotonation pH depend. 80—42961
rhodamine dyes in soln., bleaching, electronic and vibr. absorpt. spectra, fluoresc. 80—42960
RRKM complexes with centrifugal barrier, dissoc. prob., translational energy distrib. calc. 77—28997
ruthenium tris-bipyridyl, excited state electron transfer quenching, H_2O photoreduction mediators effects 80—102536
salicylamide, excited state proton transfer, kinetics, picosec. fluoresc. 79—59502
Schotten-Baumann esterification, teaching, use of positive photoresist 78—89284
self organisation mechanisms, synergetics, analogy with laser process 77—34867
self oscillating system with small periodic perturbations, perturbation theory 79—57224
self-oscillatory reaction system, breakdown of synchronised state 79—39142
semiclassical theory for near adiabatic photon assisted mol. collisions 79—5141
semiconductor metal interface, Schottky barrier, chemical reaction and charge redistrib. 78—95365
sequential fast kinetics, relaxation methods obs. 79—43575
L-serine, in aqueous solns., US spectra using automatic recording spectrometer 78—75735
serine proteases, enzymatic reaction mech. mol. orbital studies 77—60183
serine proteases, enzymatic reaction mechanism, CNDO/2 mol. orbital calcs. 78—27751
serum albumin, bovine, 2 types of soluble complexes with polyelectrolytes 79—92120
shock tube unsteady expansion wave technique, applic. 78—61011
sigmatropic reactions, mol. orbital symmetry conservation energy correl. diagrams *(Chinese)* 80—910
1,3-sigmatropic rearrangements, ab initio calcs., basis set and electron correl. effects 80—104428
silicate + $Ca(OH)_2$, (Portland cement), reaction rates 80—26006
silicate glass, hydration thermodynamics 80—81313
simulation, computer application 79—50158
soda-lime and reactor waste glasses, reaction with water, characterisation using ^{15}N H profiling method 79—54519
solar thermal energy storage by chemically driven heat pumps 79—57476
solar thermochemical electric power generation, reversible chemical reactions 80—61394
solid + liquid reactions, heat and mass transfer, with gas evolution 79—83443
solid phase chemical reactions, low temp. and fast, mol. motion effect 80—97681

chemical reactions continued
solid phase reactions, modelling using population balance approach 80—11874
solid state, elementary chemical step, activated complex theory 79—11763
solid state reaction monitoring by Mossbauer effect 77—12796
solid-fluid reactions, law of additive reaction times 79—83453
solid-gas surface reaction, nonequilibrium thermodynamic anal. 79—79285
solid-phase reaction kinetics, intercrystallite diffusion role 79—33106
solid-solid analysis and reactor developments, review 80—16648
solid-solid pellet systems, diffusion and reaction 78—85139
solid-state, control of reactivity, review 80—50853
solid-state reaction, excimer form. 79—47917
solid-state reaction, photoacoustic photocalorimetric obs. 80—61089
solid-state redox reaction, electron tunnelling rate, transfer model 78—76844
soluble non-linear reaction-diffusion system, dissipative structs. 77—44480
solvated electron + ion, in ethanol, reactivity, ion pairing effects 78—85147
solvated electron + phenanthrene, diffusion controlled reactions in polar solvents, reaction parameters 80—97687
solvated electrons, diffusion controlled reactions in polar solvents, reaction parameters 80—97687
solvation, classical mean space charge model 78—76841
solvent effects, semiempirical model 80—25986
sonochemical reactions, cavitation induced, rate dependence on US intensity 77—36732
spherical reaction diffusion systems, steady state spatial patterns, mitosis secondary bifurcation theory 80—40672
spin polarisation analysis using intermolecular interactions theory, chemical polarisation, exchange repulsion 80—76510
stability and relative stability in systems with multiple stationary states 79—79280
stacking reactions, temperature jump kinetics, Raman laser technique 79—2831
stationary states, pumped, model for mixing 80—71887
statistical mechanics models 80—27208
statistical models characterisation, prior distribs., appl. to at.-diat. exchanges 77—66744
statistical thermodynamics, nonlinear, mixing distance, steady state stability, appls. 77—9976
steady state spatial concentration profile, dissipative system, numerical algorithm 78—3310
steam plant, chemical washing, aqueous effluent neutralisation by use of ash 80—89486
steel, alloy, Fe-C-Si-S, liquid, desulphurisation with CaO, exam. of reaction mechanisms 78—80742
steel, austenitic, diffusion saturation with Cr in closed reaction space, kinetics and mechanism 79—52458
steel hydrogenation in HCl, influence of conc. depend. of anilines additives on time to fracture, principle of linearity of free energy *(Russian)* 79—15854
steel nitridation process, ionic, in glow discharge *(Russian)* 77—11412
stiff reactor model, exponential collocation using perturbation technique 78—40032
stimulated Raman scattering, appls. *(German)* 79—27320
stochastic analysis of chemical reaction with spatial and temporal structures 78—35639
stochastic model, with autocatalysis and saturation law 79—52623
stochastic process description, props. 78—60991
stopped-flow apparatus for rapid mixing and study of two fluids under high hydrostatic pressures 80—98929
strongly interacting systems, energy decomp. scheme 79—31431
strontium alumoborosilicate glass, effect of vaporous and liq. Cs 77—44509
submitochondrial particle membranes, interaction with paramagnetic probes 79—57604
superposition of reactive and nonreactive scattering amplitudes in the presence of a conical intersection 80—63733
supra antara cycloaddition, mol. orbital symmetry conservation, energy correl. diagrams *(Chinese)* 80—910
supra-antarafacial cycloaddition intrinsic single and dual mol. orbital symmetry conservation 80—102419
symmetry breaking, spatial struct. striation theory 77—12778
symmetry correl. and perturbation calcs. methods 80—104427
symmetry selection rules for ro-vibronic states 77—81385
synergetics, chemical processes far from equilib., conf. Bordeaux, France (Sept. 78) 80—3334
synthesis and process control, self directed, computer system 79—52628
synthesis computer design, interactive strategy 79—91945
synthetic organic reactions computer representation 77—25257
system far from equilibrium, stochastic simulation 80—3339
system with chemical reaction, thermodynamic stability, phase transitions 79—5174
TCNQ polycation salts, elec. cond. and chemical stability 79—83456
tertiarybutylisocyanide-borane, vibr., rot. consts., moment of inertia, microwave spectra obs. 80—32706
thermal chemistry as an exercise in photochem. 80—3379
thermal electrocyclic reactions, anal. using topological model 80—78512
thermal plasma, heat and mass transfer 78—1805
thermal stability of chemically reacting heat conductors 77—68369
thermal unimolecular reactions, transient phenomena, theory 79—15954
thermally-stimulated organic reactions in solid state 80—21309
thermochemical heat pump/refrigerator thermodynamic analysis 80—35716
thermodynamic perturbation theory for dense systems 77—70325
thermodynamically closed system, localised open systems 79—100357
TiO_2, high temperature interactions with Re 80—16665
topological model and orbital mapping for chemical systems 80—78512
transient diffusion with n-order irreversible chem. reaction, finite element method 78—85122
transition metal carbides, solid-phase reacts., effect of nonstoichiometry, thermodynamic evaluation 78—60632
transition metal oxide reactions with phosphoric acid melts, form. and analysis of phosphates 77—12517
transition state characterisation by struct.-reactivity coeffs. 78—40026
transparent polymers, laser-induced optical breakdown, chem. reactions effects *(Russian)* 78—35676

chemical reactions continued
transuranium oxide aerosol production, gas phase neutralisation of acidic droplets 80—26427
travelling waves for a model non-linear reaction-diffusion system 80—89476
trifluoracetic acid-water, molecular dynamics simulation of chemical reactions in solution 80—40673
trimoleuclar reaction, numerical simulation, rot. waves as asymptotic soln. 77—32772
truncated Kullback statistic, objective function for fitting partially known probability vectors 77—37737
TSeF, synthesis by trimethyl phosphite coupling of 1,3-diselanole-2-selone 78—10423
turbulence, steady state, theoretical anal. 77—56216
turbulence state, chem. reaction and diffusion, reduced model 77—4896
turbulent state in oscillator chem. reactions 77—4895
two component reacting fluid, density fluctuations, light scatt. spectrum, Rayleigh lines 80—25397
two time correlation functions for Poisson representation, nonequilib. and equilib. chemical reactions 79—1936
two-component bimolecular reaction system, stable limit cycles 79—47907
unimolecular decay, photoion-photoelectron spectroscopic obs. 79—30616
unimolecular decay dynamics, pole approx. calcs. 80—35501
unimolecular dynamics, classical trajectory calcs. 80—108692
unimolecular reaction, thermal, expressions for deriving rate const. 80—85164
unimolecular reaction theory, master eqn. basis 77—44457
unimolecular reaction theory, transition probabilities, relax. matrix, commutative properties 80—25991
unimolecular reactions, energy transfer effects, nonsteady state solns., weak collisions 79—74351
unimolecular reactions, in one dimension, theory 78—44364
unimolecular reactions, induced by monochromatic IR radiation 78—88645
unimolecular reactions, master eqn. solns. 77—70291
unimolecular reactions, nonequil. time-depend., model calc., single collision approx. 80—25987
unimolecular reactions, reformulation of theory 78—80712
unimolecular reactions, RRKM theory using effective strong collision freq. 78—44365
unimolecular reactions, strong collision rate consts. 77—73446
unimolecular reactions, temperature dependent A-factor 79—74347
unimolecular reactions, vibrational collisional energy transfer efficiencies 78—80714
uniqueness and multiplicity criteria for nth order chem. reaction 77—40528
unsteady heat conduction accompanied by an endothermic solid reaction *(Japanese)* 79—76939
van der Waals complex, formation, role of entropy 80—7840
variational methods, R- and S-matrix 77—60966
Venus, S chemistry of atmosphere/lithosphere system rel. to oxidation state of atmosphere and crust 80—98586
vibrational disequilibrium, in bulk reaction system 77—75119
vibrational distribution, rot. effects 78—80717
vibrational relax. of reactive mixture of viscous gases *(Russian)* 77—36735
vinyl fluoride, geometries, props. and protonation, ab initio mol. orbital study 79—22588
viscosity recorder with programmed dispensing unit 77—89212
wave propagation, coherent probe light pulse 80—61190
weakly coordinated molecular systems, mutual vibronic effects in chem. reactions and catalysis 78—64821
Wolff rearrangment, teaching, use of positive photoresist 78—89284
wood stabilisation, with ethylene glycol and isocyanate *(Japanese)* 80—2982
Zhabotinski system, ferroin catalysed, period of homogeneous oscills. 80—30225
Zn-salt, molten system, separation of Hf and Zr 80—11884
β-$2CaO$-SiO_2, hydration mechanism and rate, SEM and chem. anal. 79—79218
$AgReO_4$, solubilities and chem. reactions, comparison with $AgClO_4$ 79—15976
Al-SiO_2, Al-SiO_2(SiO)-Si, solid-state reaction mechanism 77—52623
AlB_{12} powder, nitriding, production of nitride materials 77—12560
Al_xCy, on diamond 77—72758
Al_2H_6, electron density distrib., reaction channels and bonding characts., electrostatic mol. pot. CNDO/2 calc. 80—23309
AlMg, high pressure nitriding 77—70336
AlN, epitaxial growth, by ammonolysis of $AlCl_3$, thermodynamics 77—8758
AlN powder, plasma synthesized, sintering behaviour, props. and struct. 79—100097
Al_2O_3, ion condensing metal plasma stream, coating microhardness, chemical reactions 79—42426
Al_2O_3:Ti^{3+}, corundum, point defect diffusion and interaction with impurity, Ti^{3+} to Ti^{4+} reaction 79—10985
Al_2O_3-Ta system, phase comp. of solid products formed in vacuum heating *(Russian)* 77—44185
$Al_2O_3+TiO_2$, reaction on sintering in reducing media 78—27457
$Al_2O_3(H_2O)_3$, gibbsite, synthetic, crystallinity and topotactic reactions, X-ray diffr. obs. 78—63851
$Al_2O_3(H_2O)_n$, uniform colloidal dispersion, prep. by chem. reactions in aerosols 80—97735
α-Al_2S_3, prep. by direct sulphidation, chem. vapour transport and AlI_3 flux growth 79—43118
$AmCl_3(s)+H_2O(g)\rightleftharpoons AmOCl(s)+2HCl(g)$, using ^{241}Am and ^{243}Am, equilibrium constant, heats of formation of AmOCl 77—29037
Ar-hexamethyldisiloxane, glow discharge positive column ion mass spectra identification 80—38834
$Ar+H_2{}^+$ endothermic charge transfer reaction, low energy crossed beam study 80—95720
$Ar(^3P_{2,0})$ + F-containing mols., rate consts. for ArF* formation 79—24731
As_2S_3-Tl_2S, As_2Se_3-Tl_2Se and As_2Te_3-Tl_2Te systems, vitrification and reaction characts. 77—15560
Au-Cl system, high temp. vaporisation chemistry incl. form. of vapour complex species 79—47963
$Au+Al_2O_3$, solid-state reaction, bonding, temp. depend. 78—48695
B, chem. props., reacts., review, book contrib. 78—48653

chemical reactions continued
B halide+metal halide, vapour deposition of Mo, W, Nb, and Ta borides *(French)* 77−36406
$BCl_3+N(CH_3)_3 \rightarrow BCl_3N(CH_3)_3$, complex formation, reaction product isotopic composition change *(Russian)* 80−81316
BN, high temp. compatibility with insulating oxides 77−24995
BN in contact with W, barrier layers for good high-temp. stability 79−70194
B_2O_3 containing glasses, wetting and reactions on Pt, effect of C and water 77−7951
Ba, silicates, solid state reactions, thermodynamics and kinetics *(German)* 80−76236
Ba-H_2 system, equilib. H_2 press. and enthalpy of forml of BaH_2 79−86893
$BaBr_2.H_2O$, dehydration, kinetic parameters from thermogravimetric data 79−61859
$BaBr_2.2H_2O$, dehydration kinetics, isothermal and nonisothermal kinetics 79−57227
$BaCO_3$-$SrCO_3$-$TiO_2(ZrO_2)$, ternary systems, solid-phase synthesis 78−52733
$BaHPO_4$, high temp. conversion to $Ba_2P_2O_7$, X-ray diffr. meas. 78−44371
$BaNb_2O_6$, solid-phase formation reaction, thermographic, X-ray phase and chemical anal. 77−12783
BaO-MoO_3, solid phase reaction, thermal analysis 80−55639
BaO-WO_3, solid phase reaction, thermal anal. 80−55639
$BaPO_3F$, prep. from $BaCO_3$, H_3PO_4 and NH_4HF_2, props. 79−52147
$BaPtO_3$, synthesis and struct. 77−80486
$BaTiO_3$ fibres synthesised from $Ba(OH)_2+2K_2O.11TiO_2.3H_2O$ fibre hydrothermal reaction *(Japanese)* 80−93527
$BaTiO_3$, synthesis by solid-solid reactions 79−38777
Be+graphite (Zr and Nb carbides)$\rightarrow Be_2C$, limiting stage investig. 77−36786
BeO, heated on W, thermal anal. using mass spectrometric, technique, vaporisation behaviour 80−79932
$BeO+SiO_2+V_2O_5$, reaction kinetics and mechanism, phenakite formation 78−23608
Bi_2O_3-CdO system, solid-state reaction, kinetics and mechanism 77−90303
C gases, position regulator for high-frequency heating 79−80612
$C_8{}^+AsF_6{}^-$, synthesis of first stage graphite salt, relationship to first stage graphite/AsF_5 intercalate 79−24738
$CH_2{}^+$, unimol. decay, nonadiabatic interaction, selection and propensity rules 78−23932
CN^-, electron propagator theory, mol. electron affinities calcs. 80−83521
CO, decomposition in corona discharge, qualitative chemical anal. of reaction products 78−60992
CO, methanation over Ni catalyst 77−56250
CO+chemisorbed O_2, on Pt surface, transient kinetics obs. 78−7229
CO+O, adsorbed on Ir (111), Langmuir-Hinshelwood reaction mechanism 79−29408
CO_2 glow discharge chemical processes and rate coefficients 78−63626
CO_2, proton affinity, cluster ion stability, mass spectrometer obs., appl. Martian ionosphere 77−77760
CO_2-methane reforming-methanation cycle for Solchem thermochemical solar energy transport 80−94096
CO_2+steam, H prod., plasmochem. cycle 80−45772
CS_2, proton affinity, cluster ion stability, mass spectrometer obs., appl. Martian ionosphere 77−77760
CS_2+O_2, vibr. relax., effect of atomic O 79−66300
$CaAl_2O_5$, form by interdiffusion of CaO and Al_2O_3 79−28998
$CaCO_3$, precipitation from Mg^{2+} containing soln. *(French)* 77−85915
$CaCl_2$, fused, exam. of hydrolysis at high temp. 79−11791
$CaEuAl_3O_7$, mechanism of solid-phase reactions of formation and physicochem. props. 77−52622
$CaEuGa_3O_7$, synthesis, mechanism and kinetics, cryst. props. 77−52268
$CaMg(CO_3)_2$, dolomite, reaction with ZrO_2, mineralisation during roasting 79−43180
CaO, heated on W, thermal anal. using mass spectrometric, technique, vaporisation behaviour 80−79932
CaO-Al_2O_3-H_2O system, chemical degradation under high gaseous pressure and temp. 79−20464
$CaO+CO_2 \rightarrow CaCO_3$, reaction kinetics, effect of temp. and CO_2 press. 80−45552
$CaO+MoO_3 \rightarrow CaMoO_4$, solid state reaction 79−43579
$CaO+WO_3 \rightarrow CaWO_4$, solid-state reaction mechanisms 77−36750
$Ca(OH)_2$, dehydration, unsteady heat conduction, thermal conductivity change 80−76511
$3CaO.Al_2O_3$-$CaSO_4.2H_2O$-CaO-H_2O, citric acid effect on reactions 78−27725
$3CaO.Al_2O_3+CaSO_4.2H_2O$, effects of prehydration on liq. hydration 79−100354
β-$2CaO.SiO_2$, carbonation reaction kinetics, with CO_2 and H_2O vap. 79−79219
$3CaO.SiO_2+H_2O+CO_2$, reaction conditions 80−26007
$12CaO.7Al_2O_3$, hydration in presence of $Ca(OH)_2$ *(Japanese)* 79−20364
$Ca_x(PO_4)_y(OH)_z$, nonstoichiometric, wet-process formation from α-$Ca_3(PO_4)_2$ *(Japanese)* 78−84752
$CaSO_4.1/2H_2O$, transition to gypsum, mechanism 77−48390
β-Ca_2SiO_4, hydrating, composition of soln. in contact 78−11138
Ca_3SiO_5, thermochem. effects on formation 80−16666
$3Ca.SiO_2$, carbonation reaction kinetics, with CO_2 and H_2O vap. 79 -79219
CdO-WO_3-H_2O, interconnection between kinetics of structure formation and chem. reactions 78−53198
CdS, crystallisation and stability in high-temp. alkaline solns. 77−52240
$CdTeMoO_6$, prep. and cryst. struct., X-ray diffr. obs. 79−1414
$CeNH_4P_4O_{12}$ and $Ce(NH_4)_2(PO_3)_5$, synthesis by solid-phase reaction, characts. 80−60778
Cl, interstellar chemistry as H ionisation source 79−40245
Cl^- soln. inhibition of o-Ps formation 80−1089
$Cl_2{}^-$, electron propagator theory, mol. electron affinities calcs. 80−83521
$CmCl_3$, vapour phase hydrolysis and ht. of formation of CmOCl 78−20062
Co, extraction with 2-(2-thiazolylazo)-4-methyl phenol by chelate form. 77−60063
Co_2-rare earths, H_2 reaction, thermal anal. 79−100434

chemical reactions continued
$CoAl_2O_4$, single crysts., pt. defects type determ. involved in reactions of form. and decomp. of inclusions 79−95003
$CoCl_4$ formation kinetics, in nonaqueous systems, rate constants and temp. change determ. *(German)* 79−70300
$CoFe_2O_4$ formation rate consts. meas. by Mossbauer effect 78−68875
$CoMoO_4$, formation and phase transition in CoO-MoO_3-Al_2O_3 system 79−61569
Co_2SiO_4, reaction with Fe to produce Co, gamma resonance spectroscopy *(Russian)* 78−15332
$Co_4TeMo_3O_{16}$, synthesis, mechanism and kinetics 77−32782
Cr complex, tetrakis (formamidinato) dimetal, formation 77−77753
Cr, thin film, chemical cpd. form. by $N_2{}^+$ and Ar^+ ion bombardment *(Russian)* 79−73225
Cr-Fe-Ni alloys, interface with Th carbide fuels, basic chemical compatibility, thermodynamic calcs. 79−93727
CrO_2, synthesis and morphology 79−24481
Cs-H_2 vapour, resonant character of laser induced formation of particles 80−89481
Cs-Sn alloy, peritectic reactions, phase diagram *(Russian)* 80−40784
CsA_3O_4, solid state reaction prep. between CsO_2 and As_2O_5 *(French)* 79−66280
$Cs_2As_2O_7$, solid-state synthesis, X-ray powder data *(French)* 80−15079
Cs_3AsO_4, solid state reaction prep. between CsO_2 and As_2O_5 *(French)* 79−66280
$CsPO_3$ formation, from dihydroorthophosphate dehydration, reaction thermodynamics 79−52643
$CsSbO_3$, solid state synthesis *(French)* 80−104438
Cu-Ga porous solid formed by shock compression 80−29905
Cu-Ni alloy prep. by sulphide-oxide reactions 77−48366
$Cu_{(5)}+Zn_{(1)}$, and chemical diffusion 77−9127
CuCl-Cl^- complex formation, UV absorpt. spectra 77−60064
$CuFeS_2$, exam. of dissolution kinetics, for dissolution in $FeCl_3$-HCl and $Fe_2(SO_4)_3$-H_2SO_4 solns. 79−11790
Cu(I) complex, oxidation, fast reactions meas. by pulsed-flow instrument 80−66890
Cu_2O, and CuO, reaction with solid K_2O and liq. K 79−66277
Cu_3RSe_3, R=rare earth, synthesis and form. mechanism 77−36736
CuS, covellite, dissolution in aq. NH_3 via hydrolysis of cupric amines 77−29004
CuS, S recovery by ammoniacal leaching 79−52618
$CuZr_2+H_2$, 550 to 850°C, absorption isotherms, thermodynamics 79−87841
Er, hydride form. by laser evaporation and condensation in H_2 79−10941
$Er_2O_3+VO_2$, high pressure, crystal structure and mag. props. of $ErVO_3$ 80−19773
F, with Ta, appl. of modulated mol. beam mass spectrometry anal. 78−56944
F_2+UO_2, reaction kinetics, molecular beam study 78−46157
^{18}F+hexafluoropropylene nonequilibrium effects in moderated nuclear recoil experiments 80−89509
^{18}F+methane, nonequilibrium effects in moderated nuclear recoil experiments 80−89509
α-Fe, carburisation and decarburisation kinetics in methane/H_2 mixture *(German)* 79−1949
Fe, commercial, diffusion saturation with Cr in closed reaction space, kinetics and mechanism 79−52458
Fe complex, $K_3[Fe(SCN)_6].4H_2O$, optical reflection spectrum, mag. suscept., permittivity, dehydration temp. 79−56809
Fe, liquid, reactions of CO, CO_2, with dissolved O and C, equilibria 78−44397
Fe:C, decarburisation by H_2, conversion electron Mossbauer obs. 78−85198
Fe/Cu_2O displacement reaction kinetics at temps. between 800 and 1050°C 80−21278
Fe-Mn powders, reactions with NH_4Cl and $(NH_4)_2CO_3$ 80−11597
Fe-Ni_3S_2 reaction couple solid-state displacement reactions 79−77841
Fe_2-rare earths, H_2 reaction, thermal anal. 79−100434
FeH and FeH_2 formation in interstellar clouds 80 -98704
Fe(III) salt soln., hydrolysis products, Mossbauer spectra 80−16671
$FeMoO_4+TeO_2$, solid state reaction 80−108709
$Fe(NH_4)_2(SO_4)_2.4H_2O$, rehydration kinetics, Mossbauer effect study 80 -61081
FeO based pigments, willemite struct., synthesis 80−20855
FeO surface, water-gas shift reaction kinetics 80−11949
FeO_2 nucleation, kinetics of formation of H_2O and C_2O 79−83449
$Fe_{0.925}O$, wustite, kinetics of reduction at moderate temps. 79−83154
Fe_2O_3 reaction with NiO, ZnO, and (Ni,Zn)O solid soln., microstruct. 79−87834
Fe_3O_4-$FeAl_2O_4$-$FeTiO_3$ titaniferous magnetite, chlorination, 1273 to 2273K 80−55752
FeOOH crysts., prep. by hydrolysis, struct. and reactions with silica 78−35678
α-FeOOH decomposition to α-Fe_2O_3 by heat treatment 80−2254
α-, γ-FeOOH, heats of form. of Fe_2O_3 by quantitative thermography 77−9110
$Fe_xV_{1-x}O_2$, $x \simeq 0.25$, synthesis and cryst. struct. *(French)* 79−55713
Ga-Te, alloys, liq., thermodynamic functions, struct. 78−40075
Ga+As reaction temp. determ. for GaAs synthesis 77−24978
$Ga+H_3PO_4$, interaction in aq. soln., ^{71}Ga and ^{31}P NMR obs. 79−22729
GaAs, epitaxial layer, C distrib., anal. by quasichem. reactions 77−11803
GaAs, nitridation, following oxidation, surface and contact props of GaN produced 77−20436
GaAs/HBr system, heterogeneous reactions, modified entrainment method appls. 79−23551
Ga_2O_3 reaction with K_2O and H_3PO_4, $KGaHP_3O_{10}$, $KGa(PO_3)_4$ and $Ga(PO_3)_3$ crystn. 79−52642
Ga_2O_3 solubility in H_3PO_4, $GaH_2P_3O_{10}$ and $Ga(PO_3)_3$ crystn. 79−52641
Ge, high purity melt, stability of oxide second phases 79−47898
Ge+S (vapour) reaction kinetics 78−35718
GeO formation from Ge-GeO_2 mixtures, gasification kinetics *(Russian)* 80 21273
H abstraction reactions, energies of activation calc. 78−31632
H atom cleavage from electronically excited mols., isotope effects 77−52620
H-atom abstraction kinetics in solids, free radical decay during accumulation 79−74352
$H+Br_2$, H+HBr, reaction props. dimensionality depend. 77−9050

chemical reactions continued
- $H+Cl_2 \rightarrow HCl+Cl$, translational and pot. relax., statistical calcs. 77—3435
- $H+H_2$, finite element methods for reactive scattering 78—92453
- $H+NO+H_2 \rightarrow HNO+H_2$, rate of reaction, temp. depend., third body efficiencies 78—23933
- H_2, field ionisation under nonequilibrium conditions 80—74244
- H_2-O_2-N_2 flame, K and P additives, electron attachment, compound form. 79—11794
- H_3BO_3-$B(OH)_4^-$ relaxation in ocean, rel. to pH depend. of low-freq. sound absorpt. 77—49072
- HCl flash initiated chemical laser, Cl_2-HI reaction pumped 79—94224
- HF, geometries, props. and protonation, ab initio mol. orbital study 79—22588
- $HO_2+NO \rightarrow OH+NO_2$, rate constant determination in Arrhenius form 79—47904
- $HOO+NO_2 \rightarrow HOONO_2$, FT IR spectral obs. 77—28993
- H_3PO_4, wet process, influence of high-intensity US 79—15993
- $HgBr_2+AgI$, solid state reaction, kinetics and mechanisms 77—16790
- ^{131}I+propane, U_3O_8 released radioiodine relative reactivity in O and He atmospheres 79—52644
- In complexes, formation in aq. solutions, perturbed γ-ray directional correlation 77—12847
- $In_2O_3+Sb_2O_3(Sb_2O_5.H_2O)$ reacts., complex oxide form., struct. 77—16516
- $InVO_4$, synthesis and thermal props. *(French)* 80—97443
- $K_3As^{III}{}_xAs^{V}{}_{4-x}O_{11.5-x}$, solid-state synthesis, crystalline phase *(French)* 80—15079
- $K_4As_2O_7$, solid-state synthesis, X-ray powder data *(French)* 80—15079
- K_2CO_3-SiO_2-As_2O_3, laser Raman spectrosc. study of ions in quenched reaction mixtures 80—25357
- $K_2(F,O)$-B_2O_3-SiO_2, effect of replacing B_2O_3 by Al_2O_3 or Ga_2O_3 78—63677
- K_2O glasses, partially leached, dehydrated surface reaction with water 80—3406
- K_2O-Ga_2O_3-P_2O_5-H_2O, reactions, 150-500°C 80—35514
- K_xO_y, thermodynamic props. 80—29184
- $K_4Sb_2O_7$, solid state synthesis *(French)* 80—104438
- $K_2Ti_6O_{13}$ fibre synthesis from melt reaction of TiO_2 and K_2CO_3 *(Japanese)* 78—44070
- $Kr+Cl_2$, $KrCl^+$ form., mass spectrosc. obs. 79—29346
- La-Ni-H compounds, prep. by gas absorpt. in La-Ni system, struct. 77—9078
- LaB_6 rods, chem. and electrolytic reaction in HNO_3 aq. soln. 79—87850
- $LaMnO_3$, solid phase synthesis mechanism 80—21268
- $LaNi_5+3H_2 \rightleftarrows LaNi_5H_6$ reaction, absorpt. capacity and reaction kinetics 79—43626
- $La_2O_3+NH_4H_2PO_4 \rightarrow La(PO_3)_3$, solid phase reaction 79—79235
- Li, reactions with dissolved salts in fusion reactor regime 80—32464
- Li/SO_2 cells, safety studies, kinetics of Li-organic solvent exothermic reactions 80—72030
- $Li+TiS_2$, intercalation chemistry and electrochemical energy storage 79—100541
- $LiPO_3$ formation, from dihydroorthophosphate dehydration, reaction thermodynamics 79—52643
- $Li(2^2P_{1/2,3/2})$, laser induced flame chemistry, saturated mode fluoresc. meas. 80—89491
- M_2O-MnO-B_2O_3 glasses, M=Li, Na, K, glass-forming region and physicochem. props. 78—63678
- Mg hydriding, Kirkendall marker movement 80—75385
- Mg-Al (25 wt.%) powder, reaction with high press. H_2, MgH_2 form. and decomposition *(Korean)* 78—11554
- $MgAl_2O_4$, spinel, epitaxial growth by solid-state reaction of MgO with molten Al 77—8751
- $Mg(NO_3)_2$-RNO_3 (R=Li, Na, K), thermogravimetric anal. of dehydration processes *(Japanese)* 80—66791
- MgO, heated on W, thermal anal. using mass spectrometric, technique, vaporisation behaviour 80—79932
- $MgTiO_2$, Mg_2TiO_4, $MgTi_2O_5$, formation mechanism 77—48373
- Mn^{2+}-oxalacetic acid-H_2SO_4-$KBrO_3$, chaos type reactions anal. 80—85165
- MnO based pigments, willemite struct., synthesis 80—20855
- Mo, borosilicate cladding compatibility *(Russian)* 77—66741
- Mo complex, tetrakis (formamidinato) dimetal, formation 77—77753
- Mo complexes, electron-rich bis(phosphine) dicarbonyl, chemistry and props. 77—77754
- Mo complexes organonitrogen derivs., chem. reactions, struct. 77—77752
- Mo cpds, chemistry and uses, conf., Oxford, Eng., Sep (1976) 77—77749
- Mo cpds., chemical structures, thermodynamic props., reactions 77—77750
- Mo film, carbonisation and oxidation, electron diffr. exam. *(Russian)* 77—44399
- Mo nitrido complex, with multiple Mo-N bonds, prep., struct. and reactivity 77—83758
- Mo, thin film, chemical cpd. form. by N_2^+ and Ar^+ ion bombardment *(Russian)* 79—73225
- Mo-Zr-C alloys, carburising and annealing effects *(Russian)* 77—59828
- $Mo+H_2S \rightarrow MoS_2$ 78—3078
- MoB_2, hexagonal, form. by plasma heating and props. 79—28996
- Mo_2C powders, prop. from vapour phase reaction of $MoCl_4$-methane-H_2 system 79—100068
- MoN_x, ion condensing metal plasma stream, coating microhardness, chemical reactions 79—42426
- MoSCl, thermal expansion and thermal transform. 78—26696
- $Mo_3S_4(Se_4)$, channel-type, topotactic redox reactions 77—90598
- $MoSi_2$, reactive diffusion of Si, kinetics and mechanism 77—35751
- N compounds, electroionisation synthesis 78—23937
- $N+H_2^+$, triplet state ab inito CI pot. energy surfaces 78—74729
- N_2 afterglow, chem. reactions rel. to plasma props, appl. to toluene polymerisation 80—3346
- $N_2+H_2+N_2H_4$, mixtures with nonthermal vibr. excitation of mol. N_2 80—76545
- N_2+O_2+NO, mixtures with nonthermal vibr. excitation of mol. N_2, formula for calc. equilib. const. 80—76545
- NH_3, inversion, transfer reaction theory calcs. 78—44364
- N_2H_4 production from NH_3 in atmospheric press. electron-beam controlled discharge 80—38799
- $^{14}N^{15}N+O$ plasma reaction system, isotope fractionation under simulated space conditions 78—73623
- NO, chemisorption on Ir, chemisorptive bonding and reaction 77—51596

chemical reactions continued
- NO+CO, on polycrystalline Pt surface at low press., reaction kinetics study *(German)* 79—15989
- NO+CO, on polycrystalline Pt at low press., reaction kinetics study *(German)* 79—15988
- NO^++metal atom reaction, obs. using magnetically confined afterglow 77—34750
- NO_x, plasma chemistry *(Russian)* 78—92482
- N_2O_4, dissociation, reaction with H_2O, HNO_3, N_2O_3 *(Russian)* 77—86313
- $NO_2^*+CO \rightarrow CO_2+NO$, laser-stimulated reaction 77—9075
- Na+water small-leak reaction in LMFBR steam generator, dissolution ratio of hydrogen 78—29545
- $Na_2CO_3+CaCO_3$ solid state reactions, Hedvall effect 79—96300
- $Na_{0.6}(D_2O)_2VX_2$, X=S,Se, struct., chem. reactions, and hydration/dehydration process 79—46616
- Na_2O glasses, partially leached, dehydrated surface reaction with water 80—3406
- Na_2O-Al_2O_3-SiO_2 glass, formation from alkoxides, phys. and chem. evolution 78—80503
- Na_2O-SiO_2 glasses, water reactions at elevated temps. and press. 80—81312
- β''-$Na_2O.Ga_2O_3$, reaction with water, particle size effect 77—21379
- $Na_{1+\alpha}(Ta_{1+\alpha}W_{1-\alpha})0_6$, synthesis by cation exchange, stability and struct. *(French)* 77—1110
- $Na_{3(1+x)}Yb_{(2-x)}(PO_4)_3$, single cryst. preparation and X-ray cryst. struct. determ. 79—42028
- $Na(3^2P_{1/2,3/2})$, laser induced flame chemistry, saturated mode fluoresc. meas. 80—89491
- Nb, borosilicate cladding compatibility *(Russian)* 77—66741
- Nb complex, prep. by halide reaction with tetramethylurea and tetramethylthiourea, and characterisation 79—15972
- NbN preparation, by precip. from gaseous NgF_5-N_2-H_2 mixture 80—20857
- NbO_x, phase comp. on heating 2000-4000K 80—21267
- Ni, B-containing diffusion layer formation *(Russian)* 77—48570
- Ni, B-containing multicomponent diffusion layer formation *(Russian)* 77—44400
- Ni, chemisorption of CO, carbonylation rate mag. field depend. 79—24828
- Ni, electroless plating application, brief report 77—70290
- Ni, thin film, chemical cpd. form. by N_2^+ and Ar^+ ion bombardment *(Russian)* 79—73225
- Ni-C melts, reaction with Al_2O_3, activation energy 79—83448
- Ni-Mo, discontinuous precipitation as internal sulphidation mode 77—8835
- Ni_2-rare earths, H_2 reaction, thermal anal. 79—100434
- $Ni(CO)_4$, form., ion migration, in NaCaX zeolite 79—33522
- $Ni(CO)_4$, form. reaction rate, substrate mag. phase depend. 80—108737
- $NiFe_2O_4$, solid state formation, exam. of kinetics for formation at 700 to 1400 degrees C 78—48648
- $NiMoO_4+TeO_2$, solid state reaction 80—108709
- NiO based pigments, willemite struct., synthesis 80—20855
- NiO:$Li^+(Na^+)$, finely divided catalyst, low-temp. doping 79—51128
- NiO-ZnO, solid solution, exam. of mechanism and kinetics of reaction with Fe_2O_3 ferrite formation 80—3309
- $NiO+Cr_2O_3 \rightarrow NiCr_2O_4$, kinetic parameters calcs. using anal. soln. of Fick's second law 78—34644
- No_3^--Cl^- soln., inhibition of o-Ps formation 80—1089
- O atom production and removal in DC glow discharge 79—77432
- O_2 $b^1\Sigma_g^+$ state prod. and deactivation following $O(^1D_2)$ quenching 80—76493
- O_2 discharge, O_3 production 80—38780
- O_2^+, symmetric charge transfer reactions, selected states, photo-ion, electron coincidence 78—73028
- O_2+metastable N_2, in upper atmosphere, rel. to NO 2150 Å auroral emission 77—9594
- O_3 form. in silent discharge, excited species reactions, discharge channel characts., numerical simulation 80—38813
- O_3 heterogeneous decomposition in stratosphere, lab. study 79—70850
- O_3, pot. energy surface analytical function, atmospheric reactions 78—7174
- O_3+cis-2-butene+formaldehyde$\rightarrow$propylene ozonide, gas phase reaction mechanism 77—33132
- $O(^1S)$ production in lower thermosphere, comparison of Chapman and Barth mechanisms 77—33235
- O_2—, electron transfer reactions, singlet O_2 form. and quenching 77—29002
- PH_3 conversion to P crysts. in Jupiter Great Red Spot, depend. on solar activity 79—101110
- PH_3, photolysis and abstraction reactions, rel. to Jovian atmosphere 79—66327
- Pb ceramic glaze, Cu^{2+} doped, Pb^{2+} release 80—49101
- Pb complex formation with oxyacids, IR and PMR study *(Russian)* 77—28582
- $Pb_5I_2Br_8$, form., cryst. symmetry, X-ray diffr. obs. 79—23570
- $Pb_5I_4Br_6$, form., cryst. symmetry, X-ray diffr. obs. 79—23570
- $Pb_2M_2{}^{III}Ge_2O_9$, (M^{III}=Fe,Mn,Sc,In), synthesis, X-ray diffr. and vibr. anal. 79—61360
- $Pb_2M^{II}M^{IV}Si_2O_9$, (M^{II}=Mg,Ni,Co,Cu for M^{IV}=Sn; M^{II}=Co, Ni for M^{IV}=Ti), synthesis, X-ray diffr. and vibr. anal. 79—61360
- Pb_2MoO_5, form. conditions 80—20853
- PbO-SiO_2 binary glasses, Pb depth profiles after acid etching, α-particle backscatt. 79—79343
- PbS, crystallisation and stability in high-temp. alkaline solns. 77—52240
- PbS, point defects and effect on decopperization of Pb with S 79—47918
- $Pb(Zr,Ti)O_3$, synthesis from cryochem. mixtures, chem. reacts. in sublimation drying 79—11538
- Pd complex, tetrabenzo tetra-azacyclohexadecine, I_2 oxidation product, synthesis and characterization 79—47900
- Pd-V, alloy and bilayer, silicide form. solid phase reaction with Si 80—6568
- $PuCl_3$, vapour phase hydrolysis and ht. of formation of PuOCl 78—20062
- rare earth oxide-Nb_2O_5 system, phase formation thermodynamics 77—86348
- $RbAsO_4$, solid state reaction prep. between RbO_2 and As_2O_5 *(French)* 79—66280
- Rb_3AsO_4, solid state reaction prep. between RbO_2 and As_2O_5 *(French)* 79—66280
- $Rb_4As_2O_7$, solid-state synthesis, X-ray powder data *(French)* 80—15079

chemical reactions continued
- $RbPO_3$ formation, from dihydroorthophosphate dehydration, reaction thermodynamics 79–52643
- $RbPO_3$-$Mn(PO_3)_2$ system, $Rb_2Mn(PO_3)_4$ and $RbMnP_3O_9$ form. 79–78943
- $Rb_4Sb_2O_7$, solid state synthesis *(French)* 80–104438
- Re-Hg-O system, solid state synthesis of 5 crystn. compounds, thermal and X-ray anal. *(French)* 79–66281
- Rh complex, h^5-indenylbis(ethylene)rhodium(I), ethylene displacement reactions 79–15975
- $S_n+4H_2O\rightarrow 3H_2S+H_2SO_4$, chem. equilib. of aq. system, application to Venus and Io 80–50837
- SF_6+H_2, interpretation of IR absorpt. spectrum at high intensity *(Russian)* 77–42327
- SO_2-lime plaster interaction *(German)* 77–86378
- $3SO_2+H_2O\rightarrow 2H_2SO_4+S_n$, chem. equilib. of aq. system, application to Venus and Io 80–50837
- Sb_2O_5 hydrated, preseparation stage in dehydration, phase transformation 80–35524
- Sc complex, $Sc(BH_4)_3$ with THF, synthesis and struct. 79–51068
- $ScCl_3$-NaCl-CsCl ternary system, cpd. form., thermographic investig. *(Russian)* 80–66490
- $Sc_2O_3+Sb(V)$ reaction, phase formation, structs. 77–84712
- Se-Bi bilayers, enthalpy of reactions obs. by differential scanning calorimetry 78–2398
- Si amorphous, film, hydrogenation by H diffusion, effect on elec. cond., band gap *(Korean)* 80–45326
- Si, commercial, nitridation, effect of BaF_2 80–81359
- Si, interstellar, chemistry in diffuse clouds 77–45507
- Si, nitridation, effect of Fe_2O_3 addition *(Japanese)* 77–60123
- Si, nitridation, effect of Fe alloy additions 78–48650
- Si, nitridation, effects of Fe and Al additions 77–16708
- Si nitridation, Fe-contaminant effects, mechanism 78–80496
- Si, nitridation, metal additives effects, comparative study 77–44511
- Si, nitridation by ion beam method 77–16705
- Si, powder, reaction with HF and $HF+H_2SO_4$ mixture 79–11821
- Si, powder compact, nitriding, growth of α and β phases 78–95717
- Si, reaction of rare earth impurities with carbon during cryst. growth 79–38733
- Si, reactivity with organic nitrogen compound, rel. to polishing *(Russian)* 79–70192
- Si-Ti-O-N system, formation of TiN and SiO_2 80–71617
- $Si+2XeF_2\rightarrow SiF_4+2Xe$, surface reaction, IR chemiluminesc. 79–83504
- Si+metal oxides, spray coated, IR investig. 79–39197
- $SiBr_x$, $x=1,2,4$, diffusive mass transfer of Si, calc. for closed system 77–44169
- SiC, form. from SiO_2 flour and coke breeze, kinetic and mechanistic study 79–15979
- $SiC+BaO+BaCO_3$ react., contact phenomena at SiC grain boundary 79–43193
- $SiC+CeO_2(Pd)$, high temp. chem. reactions, products obs. by X-ray diffr. 78–17312
- Si_3N_4, reaction-bonded, theoretical model of manufacture, effect of ambient reaction temp. and compact size 80–108379
- Si_3N_4, solid-solid reactions with Fe, Ni and Mo alloys 79–28151
- α,β-Si_3N_4+C, powders, high temp. reactions *(Japanese)* 77–48685
- Si_3N_4+MgO, hot pressing and effects 77–63614
- Si_3N_4+MgO, reaction during hot pressing 78–68658
- $Si_3N_4+ZrO_2$, X-ray diffr. phase anal. of reaction products 80–50613
- SiO_2 on Si, chem. stability of films produced by catalytic oxidation 77–86353
- SiO_2+ZrN, X-ray diffr. phase anal. of reaction products 80–50613
- Sn-Ni, equiatomic, metastable, transformation kinetics, Avrami parameters calc. method 78–92239
- SnO chlorination, Mossbauer and X-ray phase anal. 80–21266
- SnO, disproportionation, thermoEMF, Mossbauer spectroscopic, X-ray diffr. anals. 79–11776
- SnO_2 film, deposition from vapour phase, thermodynamic anal. 80–15418
- $Sn_xTi_{(1-x)}O_2$, solid soln., thermal reaction with V(V), Cr(III), Cr(VI), Mn(II), Fe(III), Co(II), NI(II), Cu(II), Sb(III) 80–16674
- $SrB_{0.5}B'_{0.5}O_4$, where B=Ln, Y, Sc, Fe, In, Rh and B'=Nb, Ta, synthesis and characterisation 79–69087
- $SrBi_8Ti_7O_{27}$, mixed-layer compound, synthesis and struct. 77–35530
- $SrFe_{12}O_{19}$, formation from α-Fe_2O_3 and $SrCO_3$ 77–8786
- Sr_2MNbO_6, (M=Ti, Zr, Nb), perovskite struct., synthesis, lattice constants and elec. props. 77–21369
- SrSn, Sr_2Sn, prep. by melting, characterisation *(French)* 77–70017
- $T+O_2$ high energy reaction, excitation function 78–68907
- Ta complex, prep. by halide reaction with tetramethylurea and tetramethylthiourea, and characterisation 79–15972
- Ta, nitridation by ionised glow-discharge to form FCC Ta_xN_y 77–52266
- $Ta+SF_6\rightarrow TaF_x$, $x=1$-5, thermochemical props. of TaF_x 79–100424
- TaC-TaB_2, phase diag., solubilities, reactions 77–63643
- TaS_2, 2H polytype, Li intercolation kinetics PAC hyperfine spectrosc. 79–87337
- TaS_2 (2H)+$NH_3(N_2H_4)$(pyridine)(O_2) gases, reacts., intercalation X-ray diffr. investig. 77–12828
- $^{99m}TcBr_6^{2-}$, preparation problems, decay const. 80–106020
- $^{99m}TcI_6^{2-}$, preparation problems, decay const. 80–106020
- Th complexes, O-donor complexes of cyclopentadienyl Th (IV) halides, prep. and characterisation 79–15974
- Th complexes, Th(IV) poly(pyrazol-1-yl)borate complexes, prep. and characterisation 79–15978
- Th nuclear fuel element reprocessing, avoidance of third phase *(German)* 79–6756
- Th-La(Y)(Ce)(Zr)(Bi)-H, hydride form. and supercond. 77–36007
- Ti alloy in Al alloy melt, raction zone formation, component interaction *(Russian)* 80–54377
- Ti complex, dichloro bis-cyclopentadienyl titanium+dialkoxy bis chelated titanium compounds reaction, IR spectra 79–79239
- Ti film, deuteriding inhibition by surface contamination, rel. to Ti sublimation pump operation 77–57335
- Ti, nitridation to form Ti_xN_y 77–44200
- Ti, nitriding, high temp., heat release kinetics *(Russian)* 77–66751
- Ti, nitriding kinetics at 1230 to 1500°C, diffusion and struct. investig. *(French)* 77–36683
- Ti, nitriding kinetics in RF discharge, surface hardening 77–36684
- Ti-Al-Cr-Mo alloy VT3-1, reactions with some refractory compounds 80–16585

chemical reactions continued
- Ti-Co(Ni) alloys, absorpt. of H_2, press.-composition-temp. relationships, enthalpy, entropy 80–2267
- Ti-Co(Ni) alloys, absorpt. of H_2, thermodynamic parameters calc 80–2268
- Ti-Mn, hydride form. *(Japanese)* 77–52629
- Ti-O alloys+Li melt, ternary solid soln. formation *(Russian)* 78–11396
- Ti-Si_3N_4 system, reactions under heating and plasma conditions 79–95988
- $Ti_{(5)}+P_{(V)}\rightarrow TiP$, direct two-temp. synthesis 77–81237
- TiC plasma-chemical synthesis, depend. on geometric and flow rate parameters *(Russian)* 80–40677
- TiC, production from tetrachloride and hydrocarbon, thermodynamic analysis *(Russian)* 80–7523
- TiH_2, nitridation to form Ti_xN_y 77–44200
- TiN-Al_2O_3, exam. of sintering and densification kinetics, and physical props. 79–95986
- TiN-VN alloys, synthesis in low-temp. plasma, phys.-chem. props. *(Russian)* 79–38761
- TiN_2, ultrafine synthesis in RF plasma, X-ray diffr. chem. and electron microscopy anal. 79–70026
- TiN_x, ion condensing metal plasma stream, coating microhardness, chemical reactions 79–42426
- $TiO+BaCO_3$, react., mechanism, effect of polymorphic transitions 79–11605
- TiO_2, obtained ions $Ti_2OCl\ (HCOO)_3(OH)_2$, by thermohydrolysis, exam. of crystallisation 80–2173
- TiO_2 reaction with C/Cl_2, high temperature chlorination 79–83450
- TiO_2 reaction with C/Cl_2, high temp. chlorination, volatile species 79–83451
- TiO_2-SiO_2 fibre, prep. from metal alcoholates, prep. of spinnable soln. *(Japanese)* 78–44071
- TiO_2+C+N_2, high-temp. reaction 77–90299
- TiS_2-$Na_2S(K_2S)$ systems, synthesis of Na_2TiS_3, K_2TiS_3, K_4TiS_3 and K_8TiS_6 *(French)* 79–52636
- Tl_2CO_3+8-hydroxyquinoline, solid state reaction 80–108708
- Tl_6TeO_6, solid, prep., thermal stability, cryst. parameters *(French)* 79–65037
- U, atom form. in chem. reaction, conc. determ. by laser fluoresc. excitation *(Russian)* 77–9156
- U complexes, tetranuclear halogenocomplexes, preparation, vibr. spectra *(French)* 77–83596
- U extraction, by underground leaching of ore-enclosing rock 77–61626
- U extraction by transfer between liq. phases, laser radiation effect 80–66795
- U isotope separation by selective laser photoexcitation in reactive two-phase flow 79–94109
- $U+O_2$, chemi-ionisation reaction involving laser excited atoms *(Japanese)* 79–13830
- $UAl_2+2Al\rightarrow UAl_4$, effect on Young's modulus and rupture strength in dispersion reactor fuel *(German)* 78–62596
- UF_4+F_2—UF_5, UF_6, IR matrix isolation spectra 77–12787
- UN form. by UO_2 reaction with C in NH_3 and N_2-H_2 mixture 79–47914
- UN formation, mechanism and kinetics, reaction of UO_2 with C and N_2 78–48649
- UO_2-zircaloy-4, reaction kinetics at high temps., O_2 diffusion 80–16667
- $(UO_2)_2Cl_3$, prep. and cryst. struct. 78–38674
- $U(g)+nC(graphite)\rightarrow UC_n(g)$ ($n=1$ to 6), enthalpy changes 80–7842
- $VOSb_2O_4$, synthesis and struct., stereochem. influence of lone pair *(French)* 77–15367
- $VOWO_4.3H_2O$, chemical behaviour and paramag. centre suitability 77–48670
- W, borosilicate cladding compatibility *(Russian)* 77–66741
- W filament, enhancement of field ionisation efficiency by carbide particle nucleation 77–90256
- W film, carbonisation and oxidation, electron diffr. exam. *(Russian)* 77–44399
- WF_6, mechanism of heterogeneous reduction by H_2 *(Russian)* 80–21265
- WO_2+NF_3, reaction product thermodynamic stability *(German)* 79–8449
- WO_3+CuO_- solid state reaction kinetics, $CuWO_{4\ x}$ formation study 80–66796
- $YCo_5(Ni_5)$, H_2 solubility *(Russian)* 78–15356
- $YMnO_3$, solid phase synthesis mechanism 80–21268
- Y_2O_3, U, C interactions, thermal anal. 78–85154
- Y_2O_3 with Cr surface, IR spectroscopy 79–100297
- Y_2O_3-Mn_2O_3, solid-phase reactions 77–48405
- Zn, extraction with 2-(2-thiazolylazo)-4-methyl phenol by chelate form. 77–60063
- ZnO nonohmic ceramic, formation mechanism 80–60813
- ZnO-Sb_2O_3-O_2 system, cpd. forming reactions 78–52699
- $Zn_3(PS_4)_2$ synthesis 77–24304
- ZnSe-HCl-H_2, vapour phase chemical kinetics in open tube horizontal furnace *(French)* 77–63909
- Zr, interaction kinetics with graphite, reactive diffusion 79–42318
- ZrC, prep. from $ZrCl_4+C$ *(Russian)* 78–19682
- $ZrC+CeO_2(UO_2)(SrO)$, high temp. reactions 80–3320
- $ZrCl_4$ with $POCl_3$ in O_2, for ZrP_2O_7 prep. 80–21272
- ZrN-Al_2O_3, exam. of sintering and densification kinetics, and physical props. 79–95986
- ZrN-NiO, solid-phase reactions 79–11774
- ZrN+W reaction, high-temp. compatibility 79–39132
- ZrO_2, crystallisation from $Zr(OH)_4$, effect of water vapour, heat treatment and grain size *(Japanese)* 79–19170
- ZrO_2, high temperature interactions with Re 80–16665
- ZrO_2-$Y_2O_3(Nd_2O_3)(Ce_2O_3)$, stabilised, reaction with Cr_2O_3 77–36438
- $ZrSiO_4$, zircon yellow pigment, synthesis *(Polish)* 80–66466
- $ZrTiO_4$, form. mechanism from spray drying of solns., precip., of hydroxides and reactions of hydrates and solns. 79–43182

chemical reactivity *see chemical reactions*

chemical relaxation
- activated processes in condensed phases, general kinetic models 80–81281
- alkyl cyclobutane hydrocarbons, multiple initial vibr. state selection by chem. activation, relax. rate 77–40538
- benzenes, trisubstituted, dil. solns., relax. mech., Debye relax. times 78–80744

chemical relaxation continued

- binary critical mixture, critical turbidity, kinetics, press. jump investig. 77—47548
- biomolecules, new electric field methods in spectrometry 79—8586
- cable temp. jump apparatus for chemical relaxation time meas. 77—12800
- chemically reacting systems, sound wave attenuation, thermodynamic interpretation 80—43505
- chemisorption of H_2 on graphite, substrate relax. effects 77—7962
- coupled multistep chemical reactions, rate const. determ., relax. spectroscopy 80—66766
- diatomic molecules, chem. relax. in dissoc. kinetics during laser excitation 79—31630
- diffusion limited and enzyme reactions, thermodynamics of chemical relaxation 79—43619
- 1,3-diphenylisobenzofuran, oxidation, dissoc. oxciplex relax., solute reencounter probabilities 79—34285
- gas, nonlinear waves propag., weak influence of relax. 77—55100
- gas dynamics with relaxation effects, acoustic waves, nonequilibrium atmosphere effects, review 78—79390
- glass melt, unified theory of chem. relaxation using light scattering or US absorption 79—16028
- high pressure pressure-jump apparatus for fast reactions in solution 80—62681
- initial slips and transient effects, theory 78—24729
- linear transport relaxation equations, matrices, variational principle 80—17785
- Liouville equation solution 78—44398
- micellar solutions, US absorpt. 80—45571
- micelle formation, in aq. solns., kinetics relax. process 78—76928
- nonadiabatic cage reactions, relaxation hindrance 80—93740
- polypeptides, in aq. poly(L-glutamic acid) soln., helix-coil transition, US relax. times 80—45849
- protein membranes, immobilised, H^+ ion transport, assoc.-dissoc. timescale factor 79—34529
- pulses and waves, lowest order mltiple time scale expsn. 78—68874
- pumped chemical system, stationary states, relative dynamic stability, model calc. 80—30211
- rarefied gas flow with chemical reaction, Monte Carlo simulation of homogeneous dissociating diatomic gas 77—51128
- reacting gas systems, relax. times calcs. *(Russian)* 77—70287
- reaction dynamics in liqs., generalised Langevin eqn. method, chemical relax. 79—91908
- reactors, chem., relaxation oscills. 79—39120
- repetitive pressure perturbation apparatus for studying rapid chemical relaxation kinetics 77—12801
- seawater, acoustic attenuation due to chem. relax.-absorpt. 79—34851
- sequential fast kinetics, relaxation methods obs. 79—43575
- sols, primary and secondary coagulation and heterocoagulation, role of surface chemistry 80—45551
- subpicosecond relax. time meas. using pulsed lasers *(Czech)* 78—78838
- systems with parallel reaction paths, relax. times 77—86285
- temperature jump and photochem. studies, fast flashlight appl. 78—22588
- tunnelling, Mossbauer emission spectroscopy studies 80—40683
- vibrational relaxation rate, thermal dissociation at high temps., ab initio calculations 79—74367
- H_2-Ar, relaxation rates, thermal dissociation, decomposition, master equation theory 79—74368
- H_3BO_3-$B(OH)_4^-$ relaxation in ocean, rel. to pH depend. of low-freq. sound absorpt. 77—49072
- $HNO_2+OH \rightarrow H_2O+NO_2$ react. kinetics, at high temps. behind shock waves 77—44477
- $MgCO_3^0$, in solution, ion-pair relaxation rel. to acoustic absorpt. 79—74914
- N_2, anharmonic molecules in disturbed thermosphere, vibr. relaxation rel. to NO conc. 79—12322
- NO_2, gas phase, chem. relax. times for dissoc. reactions *(Russian)* 77—70288
- N_2O_4 gas phase, chem. relax. times for dissoc. reactions *(Russian)* 77—70288
- O_2 dissociation relaxation behind regular reflected and stationary oblique shocks 78—85159
- Ru dimers, mixed-valence, electron transfer rate consts. calc. from intervalence transfer absorpt. bands 79—81164
- $Sc_2(SO_4)_3+Al_2(SO_4)_3$ aq. solns., complex form. reacts., kinetics, US relax. investig. 79—1942
- Zn-nucleotide, triphosphate complexes, ^{35}Cl NMR obs. 80—63661

chemical shift

- *see also isomer shift*
- acetic acid-H_2O, assoc. liq., struct. props., static and dynamic phys. props. meas. 79—70316
- acetone, ^{17}O chemical shift and NMR linewidth meas., self-association equilib. const. determ., mol. reorientations obs. 80—87148
- acetophenones, spectrosc. characts. using PPP SCF CI calcs. 80—102448
- adenine-uracil polynucleotides, alternating, premelting, melting, postmelting transitions 79—57574
- adsorbed layers, photoelectron spectra, review 79—52072
- L-alanine, ^{17}O NMR chemical shifts and linewidths, pH dependence 80—80625
- alcohol homologous series, $^1HT_1$-relax. time, paramagnetic, diamagnetic shift reagent effects *(German)* 78—43673
- alcohols, long chain conformations, ^{13}C pseudocontact shifts 79—13743
- alkali iodates, chem. shift, NMR obs. 80—48015
- alkali metal nitroprussides, Mossbauer spectra, dehydration effects 79—24237
- alkali metapenodates, chem. shift, NMR obs. 80—48015
- alkali silicate and borate glasses, appl. of XPS *(Japanese)* 79—34416
- alkaline earth zirconate perovskite type, X-ray K-absorpt. edge, chem. shift 79—91529
- alkanes, H^+ chemical shifts, extended Huckel calcs. with gauge in variant atomic orbitals 80—102449
- alkanes, linear, electronic struct., electronic relax. during photoemission *(French)* 78—5283
- n-alkyl amines, long chain conformations, ^{13}C pseudocontact shifts 79—13743
- alkyl benzenes, jet-cooled, intramol. vibr. relax., reson. fluoresc. and excitation obs. 80—14152
- 4-alkyl-3-phenyl-3 4-dihydrocoumarins cis- and trans-, ^{13}C NMR spectra 80—43067

chemical shift continued

- ammonium hydrogen oxalate hemihydrate, single cryst., DNMR obs., elec. field gradients, reorientation 77—85618
- amorphous materials, X-ray K-absorption edge chemical shifts 80—80904
- aromatic hydrocarbons, proton chem. shifts with ring currents, π-bond model 79—81215
- aromatic hydrocarbons, proton chemical shifts, localised π-bond model calcs. 80—43070
- arsonium salts, aq. soln., ^{75}As NMR spectra depend. on alkyl chain 77—69714
- atomic chemisorption, chemical trends, core-hole relax. effects, jellium model 78—76909
- atomic effective charge distrib. in cpds., chem. shift of electron levels 78—86785
- bacteria, yeast and leukaemic cells, dynamic struct. obs. by Overhauser enhanced ^{15}N NMR 77—90742
- benzaldehyde, electronic spectra, Cl and F substitution effects 80—23456
- benzene, ^{1}H chem. shift tensor, proton mag. shielding anisotropy 78—19348
- benzene, chem. shielding tensor obs. using proton-enhanced ^{13}C reson. in He-cooled probe 80—17978
- benzene, H^+ chemical shifts, extended Huckel calcs. with gauge in variant atomic orbitals 80—102449
- benzene, polycrystalline heteronuclear dipolar modulated chemical shift spectra, geometrical and orientational obs. 77—20750
- benzenes, 1,4-disubstituted, ^{13}C NMR spectra, chem. shift, substituent effects 77—14456
- benzenes, di- and mono-substituted, NMR spectral data, aromatic proton chemical shifts 77—79632
- benzenes, monosubstituted, ^{13}C NMR chem. shifts 79—42850
- benzenesenol, CCl_4 soln., PMR, barrier to internal rot. 78—1006
- benzenoid hydrocarbons, atom numerical code scheme for classification of chemical shifts 78—94205
- benzonitrile, field depend. ^{13}C NMR spin-lattice relax. and anisotropic mag. shielding 79—76450
- bis-methyldigermyl chalcogenide, ^{1}H and ^{13}C NMR study, chemical shifts 80—71201
- bis-methyldisilyl chalcogenide, ^{1}H and ^{13}C NMR study, chemical shifts 80—71201
- n-,t-butanol in alkanes, molecular relaxation processes studied by ^{13}C NMR 80—63654
- t-butanol-acetone-cyclohexane, complexation, thermodynamic parameters *(Russian)* 78—76905
- byotropic liquid crystals:Cs^+, ^{133}Cs NMR, chemical shift anisotropies 78—79525
- calcium formate, polycrystalline, heteronuclear dipolar modulated chemical shift spectra, geometrical and orientational obs. 77—20750
- calcium formate, selective high resolution ^{1}H NMR 79—61245
- camphene, plastic cryst., ^{13}C NMR obs. 79—95667
- d-camphor, high resolution ^{13}C NMR spectra, 275 to 343K 79—56621
- carbonyl compounds, ^{13}C chem. shifts, approximate SCF perturbation theory 77—6804
- carbonyl frequency correlation of aromatic derivatives with nonaromatic analogues 79—22709
- chloromethanes, Auger electron spectra and chem. shift 78—90231
- chlorophyll a-water interaction, NMR obs. in CCl_4 and trichloromethane 79—34501
- cholesteryl-m-fluorobenzoate, cholesteric liq. cryst., NMR, orientational order parameter 77—8429
- closed-shell system, harmonic oscillator model for mag. props., shielding tensor 79—81299
- CO_2 ferrite, crystal structure, X-ray absorpt. spectra, chemical shifts 80—88118
- copper chalcogen compounds, NMR chemical shifts 80—29636
- core replacement energy correlation with nonbonding s electron density 77—30921
- cyclic A_{2n}-systems, trans induction effect in NMR and ESR spectra 78—29799
- cyclododecane, force field, PMR of deuterated isotopomers 79—45695
- cyclohexane-d_0, -d_{11} ^{13}C-^{1}H coupling constant 78—13519
- cyclopropane, adsorption on Pt, NMR and PMR obs., chem. shift 77—51591
- cyclopropyl bromide, IR absorption, Raman scatt., assignments, thermodynamic functions 80—984
- cytochrome c, PMR, eight-ring current model heme ring, conformation depend. shifts 80—74185
- cis-decalin, shift difference between chem. exchange sites using $^{13}C\ T_1$ meas. 80—18945
- di-tert-butyl radical, ^{1}H NMR in organic solvents, press. depend. 79—31546
- diammonium oxalate monohydrate, NMR spectra, ^{13}C-^{13}C interaction, chemical shift effects 78—29800
- diatomic molecule, nucl. spin-rot. interaction const., electron spin current contrib. 80—23441
- dicarbaclosododecaboranes, icosahedral, electron transfer phenomena in isolated borane units 80—18871
- 2,3-dichloro-1,4-napthoquinone in EBBA, PMR obs., mol. struct., orientation and solute-solvent interactions 77—27806
- p-dichlorobenzene, charge transfer complexes, NQR shifts 78—55186
- 2,4-dichlorobromobenzene, UV absorpt. spectra of vap. phase, vibr. anal. 79—81211
- 2,2-dihalohexafluoropropane, IR and Raman spectra, gas, liq. and solid, normal coord. anal. 79—72314
- dihydromuconic acid, C=C bond, ^{13}C shielding tensor, NMR meas. 78—1005
- 2,6-dimethylbenzoic acid, ^{1}H chem. shift recovery from combined multiple pulse NMR and sample spinning 80—32738
- dipolar nuclear reservoir, spin-lattice relax. by chem. shielding tensor anisotropy 79—15372
- dipole NMR line width red. under magic angle conditions 80—60435
- DMSO-Tl^+, spin-lattice relax., chem. shift anisotropy 79—51870
- DOBAMBC, smectic A and ferroelec. smectic phases, ^{13}C NMR study 80—75153
- dynamic ^{13}C NMR spectroscopy, review 77—51971
- electron spectroscopy, shift of spectrum c.g. 77—27084
- ESCA chemical shift, indirect evaluation of Coulombic contribution to ionis. pots. for nonbonding electrons 78—92572
- ESCA chemical shifts and modified Sanderson electronegativity calcs. 77—83656
- ESCA shifts and effective charges 80—78648

chemical shift continued
ESCA studies of Ga, As, $GaAs,Ga_2O_3$, As_2O_3 and As_2O_5 78−92171
ESCA using X-ray photons >1500 eV, Au M_α X-rays (2123 eV) 78−72683
ethane, chem. shift, paramagnetic term, Pople formalism calcs. 78−21945
1,2-ethanediol, aq. soln., proton NMR study of H-bonding 79−78545
ethanol$_{(l)}$, hydroxyl proton chem. shift, density and temp. effects 77−1607
ethene, chem. shift, paramagnetic term, Pople formalism calcs. 78−21945
ethyl-trimethyl phosphines, $(C_2H_5)_{3-n}P\{E^{IVB}(CH_3)_3\}_n$, $(E^{IVB}=C;Si;Sn;$ $n=0,1,2,3)$, (^{1}H, ^{13}C, ^{29}Si, ^{31}P, ^{119}Sn) NMR 80−32744
ethylenic compounds, H^+ chemical shifts, extended Huckel calcs. with gauge in variant atomic orbitals 80−102449
ethyne, chem. shift, paramagnetic term, Pople formalism calcs. 78−21945
Fenske-Hall LCAO method, inner-shell binding energies and chem. shift calcs. 80−47871
ferrous porphyrins, 4-coordinated, PMR 77−58044
p-fluoranil, ^{19}F NMR and spin-lattice relax. meas., pot. profile calc., mole. reorientation 80−29634
fluorene conjugate bases, chem. shift, ring-current and excess-charge effects, semi-empirical calc. 78−33523
pfluorobenzaldehyde(-d_1), in smectic mesophase, mol. struct. and reorientation, NMR 77−27093
fluorobenzenes, substituted, cryst., ^{19}F NMR, chem. shift tensor meas. 78−10789
fluoromethanes, and perfluoroethane, NMR gas-to-liquid shifts, 2nd-virial coeff. of chem. shielding validity 79−85976
gelatin crosslinking by formaldehyde, ^{13}C NMR obs. 79−5187
glass, structure, NMR investig. techniques 78−23358
glycerol, aq. soln., proton NMR study of H-bonding 79−78545
1-glyceryl 1-octanoate-water-CsCl, Cs^+H_2O interaction in lamellar phase, NMR quadrupole splitting and chemical shift 80−50209
glycine, ^{17}O NMR chemical shifts and linewidths, pH dependence 80−80625
graphite intercalation compounds, magnetic resonance determ. of oxidation state 78−35051
graphite lamellar cpds., ^{13}C NMR studies 80−44936
group IV, V and VI elements, XPS, bond ionicity, struct. stability and charge transfer 77−44127
haloalkanes, ^{19}F chem. shielding, temp. depend., FT NMR obs. 78−86888
halomethanes, ^{13}C chem. shifts, trigonal additivity procedure 80−1002
halomethanes, ^{13}C chemical shifts, diamag. susceptibility, effect of non-bonded interactions 78−78726
hard X-ray lines, chemical shifts, applicability of Koopmans' theorem, HF calcs. 80−74145
heteronuclear dipolar modulated chemical shift spectra, double reson. multiple pulse NMR 77−20750
hexafluoride radicals, prep. and EPR spectra comparison, hyperfine splitting 78−68381
high-resolution NMR by double Fourier transform, chem. shift and spin echoes 77−57375
hormonal steroids, ^{13}C NMR spectra 80−81543
hydrocarbon, ^{13}C NMR shielding constants and tensors, finite perturbation calcs. 77−27092
hydrocarbons, ^{13}C chem. shifts, simplex optimised INDO calcs. 80−83284
hydrocarbons, α-substituent effects in ^{13}C NMR, quantum chem. calcs. 78−74680
hydrocarbons, conjugated, ^{1}H chem. shifts calc. 79−98121
hydrocarbons, proton NMR chem. shifts, mag. shielding effect of neighbouring C atoms 77−27094
hydrocarbons proximity and conform. effects, ^{13}C chem. shifts at γ position, INDO computations 77−50451
hydroxyl protons, temp. depend. of chem. shift, in R-OH cpds. 78−35054
ice, hexagonal single crystal, proton anisotropic chemical shift spectra 80−2650
ice, polycryst., natural abundance PMR, chem. shift meas. 79−67365
III-V phosphide semiconductors, ^{31}P nuclear mag. shielding 79−33549
III-V semiconductors, chemical shifts of NMR lines of Ga nuclei 78−88201
indenyl-Li ion pair in dimethoxyethane, ^{13}C NMR, temp. and counterion depend. 78−48062
indenyl-Na ion pair in dimethoxyethane, ^{13}C NMR, temp. and counterion depend. 78−48062
INDOR, pseudo, heteronuclear selective decoupling, automatic, using Fourier transform NMR spectrometer appl. 79−93185
inorganic compounds, chemical bonds using $K\alpha_1$ line chem. shifts, Mossbauer isomer shifts 77−27089
inorganic compounds, XPS chem. anal., chem. shift, core binding energy 78−20134
inorganic molecules, UV photoelectron spectroscopy, spectral assignment criteria, bonding 78−17717
insulating film, meas. by ESCA *(Japanese)* 79−4891
intermolecular interaction thermodynamic parameters determ. from chem. shifts of functional groups 79−64068
IV-VI compounds, XPS, bond ionicity, struct. stability and charge transfer 77−44127
keratin-NaCl, Na Auger electron spectra 78−53339
L_3 X-ray absorpt. discontinuity 77−85840
lanthanide ion complexes, lanthanide-induced NMR shifts, temp. depend. 77−68061
lanthanide shift reagents, pseudocontact shift, temp. depend. 79−95659
lecithin bilayer, ion-induced changes in head group conform, ^{31}P and ^{2}H NMR 78−3452
light elements, Z>10, K-LL Auger process, review 78−50523
liquid-vapour crit. pt. region, NMR freq. shift anomalous behaviour 80−44938
lithium perfluoro-octanoate-water, liquid crystal, ^{19}F multipulse NMR obs. 80−34795
2,6-lutidine, H bonding to iso- and tert-butyl alcohols, PMR obs. 79−27008
lyo-mesophases, induced chem. shift, NMR obs. 79−33548
macromolecule, microconformation by fast exchange NMR spectra 80−102593
macromolecule, NMR estimation of equilib. consts., intermediate exchange processes effect 80−1094

chemical shift continued
maleic acid, acid slats, melts, H_2 bonding, IR, NMR investigs. 79−65859
mesogen compounds, melting behaviour, proton NMR spectra 78−15044
metal-oxide system characterisation by high-resolution electron spectroscopy 77−40624
nido-metalloborane, high -resolution ^{11}B NMR obs. of $[(B_{10}H_{12})_2Ni]^{2-}$ 79−31553
metalloenzymes, ^{113}Cd as NMR active site probe 78−68999
metals and alloys, deposited on Au foil X-ray photoelectron spectroscopy 77−81196
methane, ^{13}C and proton medium shifts in gas phase and in soln. 77−88467
methane, NMR chem. shift., temp. depend., virial coeffs. 78−58722
methane+Kr(Xe), ^{13}C-mag. shielding density depend. 78−9173
methane-d_0,-d_1,-d_2,-d_3,-d_4, ^{13}C NMR chem. shifts, coupling consts. 78−37657
methanes, substituted, calculation of by INDO approximation 79−45657
methanol solns., IR spectroscopic detection of free lone-pair groups or terminal methanol mols., PMR 79−19869
methanol-β-quinol clathrate, orientation and reorientation dynamics, dielec. and NMR obs. 79−99783
methyl alcohol, intermol. interaction, thermodynamic parameters determ. from chem. shifts of functional groups 79−64068
methyl group, ^{13}C chemical shifts, H/H, H/Me and Me/Me interactions 80−95652
methyl group, NMR relax., spin rot. and chem. shift anisotropy effects 78−31117
methylfluoride, anomalous behaviour of proton chemical shift in gas-liquid crit. region 78−39419
1-methylimidazole complexes, with ferriporphyrins, PMR obs. 77−12214
methylmercuric halides, partially oriented, ^{1}H and ^{13}C NMR obs. 80−23437
mica, Fe^{2+} distrib. on octahedral sites, PMR investig. 78−15041
micellar solutions, micellar aggregation number, ^{13}C NMR chemical shift conc. depend. 80−48016
minerals, $K\alpha_{1,2}$ emission spectra, chem. shift, effective charges of Al,Si,Fe and O atoms 77−28659
molecular solid, effect of rigid-body vibrs. on NMR, quadrupole, chemical shift and dipole-dipole interactions 78−15056
molecular X-ray spectra, influence of inner level vacancy 77−27085
molecules, diamagnetic susceptibilties and NMR chemical shifts in terms of localised MO's 80−106256
molecules, Fenske-Hall LCAO method calcs. 80−47871
molecules, screening constant calcs., CNDO/S method *(French)* 79−94012
molecules containing 1st row atoms, K-shell binding energy shifts, NDDO MO calcs. 80−58413
molybdates, ^{95}Mo and ^{97}Mo Fourier transform NMR, chem. shifts and Larmor freqs. *(German)* 77−59473
monohalobenzenes, inner shell excitation and ionis., electron energy loss spectra, XPS, assignments 78−62934
mucopeptide N-acetylmuramoyl hydrolase, hen egg-white lysozyme, BC n.m.r., carboxyl group resonances 77−1978
multiple pulse zero-crossing NMR technique, rel. to ^{19}F chem. shift in solids 79−9230
naphthalene in EBBA, PMR obs., mol. struct., orientation and solute-solvent interactions 77−27806
1,4-naphthoquinone in EBBA, PMR obs., mol. struct., orientation and solute-solvent interactions 77−27806
neopentane adsorbed on graphite, quasi two-dimens. fluid, NMR 80−102525
p-nitrofluorobenzene, nematic phase NMR, ^{19}F shielding anisotropy 78−62824
nitroso and nitrosyl cpds., ^{14}N chem. shifts correl. with nuclear quadrupole coupling consts. 77−30888
NMR, cryst. spectra of quadrupole nuclei, separation of chem. shift and quadrupole interaction *(Russian)* 78−39440
NMR, double-quantum, cross-polarization, in solids, theory 80−100623
NMR, high resolution, automated anal., principles and computational strategy 80−58287
NMR, paramagnetic material effect on chem. shift and relax. times, mol. struct. effect 78−46373
NMR, quadrupole coupling const. and chem. shift, from single-cryst. data 78−91982
NMR, ring current theories 80−53020
NMR, rotating frame relax. time for spinning sample 79−47344
NMR, shift anisotropies removal using multiple pulse-magic angle spinning probe 78−12735
NMR chem. shift., temp. depend., virial coeffs. 78−58722
NMR chemical shift, nucl. other than protons, semi-empirical calcs., review 77−75188
NMR chemical shift between two sites in rapid exhange limit, Fourier transform method 79−24743
NMR exchange broadening in two-site system with unequal populations, limiting eqns. 79−76448
NMR line-shape anal. of peaks broadened by hidden exchange partner 79−43554
NMR lineshape fitting, iterative least-squares method, MNRCON program for chem. shifts 77−69715
NMR parameters, chem. shielding, ^{13}C chem. shifts 80−23435
NMR screening constants of O and N in molecules, INDOS/S parameterisation scheme 79−76449
nuclear magnetic shielding constants calc. by GIAO method using Gaussian functions 80−1001
nuclear magnetic shielding density 80−63559
octahedral paramagnetic complex ions, isotropic chem. shift, pseudocontact contrib. 80−91577
organic compounds, ^{13}C NMR, chem. shift, effective excitation energy calcs. 77−14457
organic compounds, electron donating, PMR spectra, paramag. shifts induced by N_2O_4 *(Russian)* 78−21946
organic polycyclic compounds, ^{13}C NMR, spin-lattice relaxation meas., rot. barriers in hindered methyl groups 77−10689
organic solids, proton chemical shifts, combined pulse NMR and magic-angle spinning 80−44934
organolead compounds, aliphatic and aromatic, ^{13}C and ^{207}Pb NMR 79−95657
organophosphorus compounds, liq., ^{31}P nucl. spin-lattice relax. and Overhauser effect 79−36666

chemical shift continued
organotin compounds, with remote substitutions, ^{119}Sn NMR constants 79—65748
oxalic acid dihydrate, NMR spectra, ^{13}C-^{13}C interaction, chemical shift effects 78—29800
oxalic and dihydrate, monocrystals, high resolution PMR 78—64283
oxide thickness measurements up to 120 Å on silicon and aluminium using the chemically shifted Auger spectra 78—23586
paramagnetic metal ions as structural probes for NMR investigation of inorganic and bioinorganic compounds 78—62828
paramagnetic systems, NMR shifts calc. using nonmultipole expansion method 80—2651
pentacoordinated ferrous porphyrins, ^{1}H and ^{19}F NMR, hyperfine shift, π electron binding 78—78719
peptide, NMR spectroscopy study 78—88694
phenols, substituted, proton NMR chem. shift in aprotic solvents 79—47342
phenylphosphines, and derivatives, ^{1}H, ^{13}C and ^{31}P NMR studies 80—87152
phosphates, cellular, heteronucl. two-dimens. NMR as conform. probe 80—3590
phospholipid bilayers, carbonyl groups dynamics, ^{13}C chem. shift anisotropy obs. 80—85326
photoelectron spectroscopy, biological appls., review 77—56558
pivalic acid, liq. and plastic crysts., ^{13}C NMR chem. shift, temp. depend. 80—2652
polar semiconductors, chemical shift of Zeeman masses 78—10338
poly(diallyldimethylammonium) chloride, struct., ^{13}C NMR 77—565
poly-L-ornithine solution, ^{15}N NMR, coil-helix transition, solvent effects and pH depend. 80—74275
polycrystalline solids, selective high resolution ^{1}H NMR 79—61245
polycrystalline solids, spin-one NMR, ^{14}N shift, elec. field gradient effects 77—77112
polyethylene, highly oriented fibres, 2-dimens. ^{13}C NMR 77—77114
polyethylene, homopolymers, copolymers and model systems, ^{13}C NMR chem. shifts and relax. times 79—72449
polyethylene, ultraoriented, ^{13}C-^{13}C dipolar satellites 77—28465
polyhedral A_{2n}-systems, trans induction effect in NMR and ESR spectra 78—29799
polymer primary structures ESCA and EHCO methods 78—52630
polymers containing main chain heteroatoms, struct., ^{13}C NMR investigs., review 79—55013
polymethinecyanines, symm. solvent effects on electronic struct., ^{1}H, ^{13}C NMR 78—13516
polyperfluorobutadiene, melts, solns., ^{19}F NMR, ^{13}C NMR spectra, microstruct., configurations 77—43894
polypropylene, isomeric, microconformation from slow exchange ^{13}C-NMR spectra of low mol. wt. cmpds. 80—102592
polysiloxane oligomers, ^{29}Si NMR, chem. shift effects of end groups 79—33550
polystyrene, chem. shift, conformational struct. *(Russian)* 80—5652
polyvynyilpyridines, atactic, chem. shift, conformational struct. *(Russian)* 80—5652
potassium hydrogen malonate, carboxylic proton chem. shift tensor 80—58280
powder pattern, homonuclear dipolar modulation in multiple pulse NMR 79—24224
1,2-propanediol, aq. soln., proton NMR study of H-bonding 79—78545
propionitriles (-O, NH, S), conformational investig., NMR, IR and semiempirical MO methods 80—95650
propylene-butene copolymers, PB centred tetrad ^{13}C NMR spectra assignment 80—58428
protein, NMR spectroscopy study 78—88694
protein titrations by NMR, pH depend. of internal reference 77—86727
proton magnetic shielding, chem. substitution effect on chem. shift, LCAO perturbation method 77—68064
pyridenes ^{15}N NMR chem. shifts, paramag. relax. reagent effect 78—15042
pyridil-benzo-X-azoles, NMR spectra, chemical shift and coupling const. data *(Italian)* 77—54566
pyridinium molten salts, ^{1}HNMR rel. to transport props. 77—73087
qauche NMR effect in ^{13}C, ^{19}F and ^{31}P chem. shifts and directly bonded coupling consts., bond angle effects 77—68056
quasilattice theory, complexation, thermodynamic parameters calcs., spectroscopic appls. *(Russian)* 78—76905
quasilattice theory of solutions, use in mol. spectroscopy, thermodynamic parameters determ. 79—96350
rare earth induced NMR shifts, temp. depend. 77—28464
rare earth tellurides, electron density distrib. from Mossbauer spectra 78—23374
rare earth-Pt intermetallics, L_3-absorpt. edge of Pt 79—78789
rare earths, compounds, K X-ray line shift associated with valency change and isomorphous phase transitions 79—47553
rare-earth oxides, R_2O_3, (R=Dy,Ho,Tm,Yb,Lu), EXAFS and chemical shift 77—81176
tRNA^{Phe}, yeast, in soln., H-bonded protons in tertiary struct., PMR, assignments 77—90728
semiconducting cpds., average valence-⟨4⟩ X-ray K-absorpt. edge shift and electronegativity 77—16424
semiconductor, polaron aspects of generalised Haynes' rules 78—18978
solid, H-bonded, NMR chem. shift tensors *(German)* 78—84489
solid state ^{2}H NMR, magic angle sample spinning to remove quadrupole broadening 79—97410
spin systems under multiple pulse NMR conditions, chem. shift relax. 80—34808
squaric acid, ^{13}C chemical shift tensor study of antiferroelec. second order phase transition 78—52462
squaric acid, antiferrodistortive phase transition, proton chemical shift tensor determ. 77—63300
steel, austenitic type 304, chem. shift obs. by ionization loss spectroscopy 79—43372
steroids, ^{13}C chemical shifts, β-, γ- and δ-substituent effects 77—23509
TCNQ-NMP, incomplete charge transfer, NMR relax. and line-shift meas. 80—20485
$TCNQF_4$, charge transfer complexes and salts, C(1s) and N(1s) XPS anal. of shake-up satellites 77—14492
ternary compounds, and complex systems, chemical shift in X-ray absorpt. spectra, effective changes 78—6811
tetrafluoro-1,3-dithioethane, ^{19}F chem. shift tensor multiple pulse NMR 77—77111

chemical shift continued
tetrafluoromethane, ^{19}F chem. shielding, depend. on internal coords. 78—5249
tetrafluoromethane, ^{19}F NMR, chem. shielding, intermol. interactions and rovibr. motion effects 78—9171
tetramethylammonium zinc tetrachloride, incommensurate phase transitions,^{13}C NMR study 80—75968
2,2,6,6-tetramethylpiperidine nitroxide radical.alcohol complex, NMR chem. shift 78—46366
1,1,3,5-tetramethylpiperidinium iodide, model cpd., struct., ^{13}NMR 77—565
1,1,3,4-tetramethylpyrrolidinium iodide, model cpd., struct., ^{13}C NMR 77—565
three-centre integrals, calc. method *(French)* 79—31550
titanocene, alkyl-substituted ^{13}C and ^{1}H NMR, chemical shifts prediction 80—63671
transition metal, chem. shifts of X-ray emission K-lines, free-atom approx. applic. 80—11513
transition metal carbides, charge transfer from XPS core level chem. shift anal. 77—72837
transition metal complexes, $M(CN)_5X^{n-}$, ^{13}C NMR, chem. shifts 79—51866
transition metal complexes, proton NMR chem. shift, covalency parameters calcs. 78—42098
transition metal nitroprussides, Mossbauer spectra, dehydration effects 79—24237
transition metal tetrahedral complex ions, F NMR chem. shifts, outer sphere cation effects 80—102527
tri(trifluoromethyl) germanium halides, gas, liq. and solid, IR and Raman spectra, normal coord. anal. 79—72316
trichloroacetic acid, proton chem. shift tensor 79—24224
trichloroacetic acid, proton chemical shift tensor 78—13520
1,2,3-trichlorobenzene, oriented mols., ^{13}C satellites use in proton spectra, r_α-structure 80—18872
triethylacetic acid, high resolution ^{1}H and ^{13}C NMR spectra at liquid-solid phase transition 80—11281
2,4,6-trifluoronitrobenzene, ^{19}F shielding anisotropies, nematic phase NMR 77—27090
trimethylacetic acid, high resolution ^{1}H and ^{13}C NMR spectra at liquid-solid phase transition 80—11281
trimethylphosphine, chem. shift anisotropy, struct., liq. cryst. NMR 77—61768
trimethylphosphonium oxide (sulphide) (selenide), chem. shift anisotropy, struct., liq. cryst. NMR 77—61768
tris(dimethylamino)phosphorus, ^{15}N and ^{31}P NMR aligned in liq. cryst., geom. struct. 78—82751
triscyclopentadienyl uranium chloride, ^{13}C NMR shifts, 160-320K 77—16190
two internal-vacancy atoms, Green function calcs. *(Russian)* 78—50451
two-centre integrals calculation method including ang. momentum *(French)* 80—32601
two-dimensional systems, order parameter from chemical shift anisotropy patterns 80—80624
urea-formaldehyde resins, ^{13}C Fourier transform NMR of chem. struct. 79—42849
UV photoelectron spectra at high temp., interpretation 78—17718
vanadyl triisopropylate, chem. shifts, NMR line widths, temp. and solvent depend. 78—70853
vinylidene fluoride-trifluorochloroethylene copolymers, ^{19}F NMR *(Russian)* 80—7181
X-ray, lineshifts in nonrelativistic and relativistic approxs. 78—951
X-ray absorption edge-shifts, empirical relations, effective ionic charge for isoelectronic series 78—55136
X-ray fluoresc. spectrometer system, automated, for chem. shift meas. 78—4750
X-ray K emission lines, chem. shifts, free-at. approximation interpretation 77—50395
X-ray spectroscopy, book 80—2899
XY_2 molecule, chem. perturbation of force field, Green's function appl. 79—76417
zeolite of transition metal, CO adsorpt., ^{13}C NMR study 79—52751
zirconocene dichlorides, alkyl-substituted, ^{13}C and ^{1}H NMR, chemical shifts prediction 80—63671
Ag and Ag_2O, X-ray absorption, discontinuities and limits, chem. combination effects 80—93435
Ag complexes in organic solns., ^{109}Ag NMR, solvent effects 77—16191
$AgBF_4$, ionic radii and chem. shifts, correl. with electronegativity 80—66054
$AgClO_3$, NQR of solid for mol. torsional vibr., comparison with $KClO_3$ 79—4743
AgF(AgI,AgBr,AgCl), NMR chemical shifts 80—74180
$AgIO_4$, chem. shift, NMR obs. 80—48015
AgO and Ag_2O, ESCA spectra, Auger effect, initial and final states effect 78—15280
Al, adsorption of O_2 and CO, interatomic Auger transition spectroscopy 80—11521
AlN, interatomic interactions from XPS 80—49171
AlN, X-ray Kα satellite struct., target chemical effects, 38 MeV F ion bombardment 77—24910
Al_2O_3, Kα X-ray satellite struct., target chemical effects, 38 MeV F ion bombardment 77—24910
Al_2S_3, X-ray Kα satellite struct., target chemical effects, 38 MeV F ion bombardment 77—24910
AsF_5 intercalation with graphite and benzenoid systems, EPR, NMR and X-ray diffr. obs. 80—19775
$As_2(Se,Te)_3$ glasses, X-ray absorption and photoelectron spectroscopy study 80—7463
As_2Se_3:X (X=Cu, Ag, Tl, I, Ge), effect of doping, NMR meas. 80—11282
Au and Au_2O_3, X-ray absorption, discontinuities and limits, chem. combination effects 80—93435
AuF_3, ^{19}F NMR chemical shift, crystal chemistry 78—87645
B and F chemical shifts, MINDO/3 in Pople's free electron model 79—93926
B compounds, ^{13}C NMR spectroscopy 79—89691
BF_3, ^{19}F chem. shielding, depend. on internal coords. 78—5249
BF_3, ^{19}F NMR, chem. shielding, intermol. interactions and rovibr. motion effects 78—9171
BN, interatomic interactions from XPS 80—49171
BaH_2, proton chemical shift tensor, heavy ion effects 79—19791

chemical shift continued

Bi and Bi_2O_3, X-ray absorption, discontinuities and limits, chem. combination effects 80—93435

Bi, chemical shift of X-ray L-absorption edge 79—52044

2,4-$C_2B_5H_7$, polyhedral, spin coupled ^{11}B-^{1}H systems, 2-dimens. correl. NMR 80—69166

CO, chemical shielding temp. depend. 78—5250

CO group, NMR chem. shift, solvent's dielectric const. effect, mag. anisotropy 79—42847

CO, solid, anisotropy of chem. shift tensor, ^{13}C NMR obs. 77—90054

CO_2, ^{13}C NMR, chem. shift., determ. of virial coeffs., rovibr. motion 78—58720

$CO_2+Kr(Xe)$, ^{13}C-mag. shielding density depend. 78—9173

^{13}C, 2D NMR spectra, off-resonance decoupling 80—74182

^{13}C chemical shifts, β-, γ- and δ-substituent effects 77—23509

^{13}C NMR, chem. shift, effective excitation energy calcs. 77—14457

^{13}C NMR, computer program chem. shift retrieval system 79—18206

^{13}C NMR, indenyl-Li(Na) ion pairs in dimethoxyethane, temp. and counterion depend. 78—48062

^{13}C NMR, RF amplitude effects in proton-spin decoupling 77—28463

^{13}C NMR chem. shifts, estimation by computer program based on additivity rules 78—13518

^{13}C NMR shielding constants and tensors in hydrocarbons, finite perturbation calcs. 77—27092

^{13}C NMR with off-reson. proton spin decoupling, proton chem. shift calc. methods 78—27101

^{13}C, natural abundance determ. in gas phase and extrapolation from liq. phase meas. 77—88470

^{13}C, shielding consts. and anisotropy of NMR shielding tensor, modified CNDO/S calcs. *(French)* 80—32610

^{13}C, slow-spinning magic-angle NMR for amorphous solid 77—48068

^{13}C, spin-echo spectral analysis 77—48086

C=C bond, ^{13}C shielding tensor, NMR meas. 78—1005

CaF_2, ^{19}F NMR chemical shift, press. depend. 0-4 kbar 77—20733

CaF_2, NMR direct observation in rotating frame *(Russian)* 78—39422

CaH_2, proton chemical shift tensor, heavy ion effects 79—19791

Cd, AES, $M_{4,5}N_{4,5}N_{4,5}$, vap. and solid, solid state effects 77—61857

Cd nitroprussides, Mossbauer spectra, dehydration effects 79—24237

CdF_2, high resolution NMR and chem. shifts of ^{111}Cd and ^{113}Cd, double reson. expt. 80—60460

CdO, ESCA spectra, Auger effect, initial and final states effect 78—15280

CdSe photoanodes, S substitution during operation and mech. of surface protection XPS study 80—107906

CdSe(Te), chemical shift and linewidth determ. 79—19792

Cl compounds, chemical shifts of X-ray electron and Auger lines 78—86912

ClF, chemical shielding temp. depend. 78—5250

ClF_3, ESCA chemical shift, energy levels, SCC-MO calcs. 79—64045

ClO_xF_y, ^{17}O NMR, chem. shifts, indirect coupling consts. 77—14453

^{35}Cl NMR, medium effects 77—1612

Co and its cpds., X-ray K-absorpt. edge shifts, plasmon energies correlation 80—20734

Co complex, with p-amino salicylic acid, X-ray K-absorpt. discontinuity, shape, chem. shifts 79—47545

Co complexes, Co(III) mixed complexes, orbital angular momentum reduction, ^{59}Co NMR chemical shift 80—58137

Co oxides, effective atomic charge rel. to chemical shifts in transition metal compound XAS 79—78788

Co ternary compounds, chemical shifts of K X-ray absorption discontinuities 78—19599

^{59}Co NMR, data compilation *(Japanese)* 79—68242

$CoCr_2X_4$ (X=O,S), K absorpt. discontinuity chem. shift, bonding parameters 77—77318

CoO, ESCA and Auger lines, chem. shifts 78—6817

Co_3O_4, ESCA and Auger lines, chem. shifts 78—6817

^{59}Co NMR line breadth and chemical shift data compilation *(Japanese)* 78—15045

$Co(ethylenediamine)_3(ClO_4)_3$, ESCA chem. shift meas., internal standards 78—50585

Cr and its cpds., X-ray K-absorpt. edge shifts, plasmon energies correlation 80—20734

Cr complexes, NMR study ^{31}P chemical shift, substituents electronegativity steric hindrance and π-bonding effect 80—95651

$CrMoO_4$, ESCA on H_2 reduction *(French)* 77—36365

Cs perfluoro-octanoate, amphiphilic liq. cryst., ^{19}F multipulse NMR study 78—76328

Cs_2 molecules, magnetic shielding studies by NMR 77—42341

$CsBF_4$, ionic radii and chem. shifts, correl. with electronegativity 80—66054

$Cs_3BiSbBr_9(Cl_9)$, ^{121}Sb Mossbauer chem. shifts, optical reflectance spectra, solid state band populations 77—40162

CsD_2PO_4, pseudo-one-dimensional ferroelectric transition, ^{31}P chemical shift and relaxation study 80—66123

$CsFeCl_3$, linear chain cryst., quadrupole and mag. reson., rel. to $RbFeCl_3$ 79—38403

$CsNiBr_3$, double ordering in mag. linear chain system, sp. ht. and NMR data 79—28545

$CsNiCl_3$, double ordering in mag. linear chain system, sp. ht. and NMR data 79—28545

$CsVO_3$, polycryst., quadrupole coupling const., asymmetry parameter, chem. shift, NMR computer calcs. 78—6584

^{133}Cs salts, powders, nucl. mag. shielding and quadrupole coupling 77—90056

Cu and Cu oxides, X-ray absorption, discontinuities and limits, chem. combination effects 80—93435

Cu and its cpds., X-ray K-absorpt. edge shifts, plasmon energies correlation 80—20734

Cu complexes, Cu(I)-P tetrahedral, ^{63}Cu FT-NMR 80—53021

Cu complexes, FT NMR, ^{63}Cu and ^{65}Cu chemical shifts and coupling constants 78—94260

Cu compounds, chemical shifts of X-ray electron and Auger lines 78—86912

Cu ternary compounds, chemical shifts of K X-ray absorption discontinuities 78—19599

Cu-Mn, dil., Kondo deviations of Mn electron spin relax. and g-factor, NMR meas. 79—51747

Cu-phthalocyanine, photoemission multielectron effects from quasi atomic Cu 80—93458

$CuAlS_2$, X-ray spectroscopic study 78—39626

$Cu_x(As_{0.4}Se_{0.6})_{1-x}$, amorphous, ^{77}Se NMR, comp. depend. 78—76329

chemical shift continued

CuBr, NMR chemical shifts, temp. depend. 78—68401

CuCl, NMR chemical shifts, temp. depend. 78—68401

$Cu_{0.5}Co_{0.5}Cr_{2-x}Rh_xS_4$, K absorpt. discontinuity chem. shift, bonding parameters 77—77318

$CuCr_2X_4$ (X=O,S,Se,Te), K absorpt. discontinuity chem. shift., bonding parameters 77—77318

$CuFeS_2$, X-ray spectroscopic study 78—39626

$CuGaS_2$, X-ray spectroscopic study 78—39626

CuI, NMR chemical shifts, temp. depend. 78—68401

$CuInS_2$, X-ray spectroscopic study 78—39626

CuO, on Cu, identification by electron spectroscopic methods 80—60747

Cu_2O, on Cu, identification by electron spectroscopic methods 80—60747

CuPd, chemical shift effects and origin of Pd 3d core level satellite 80—104039

Cu_2S-CdS heterojunction interface, depth distribution profiles, Auger spectra 80—88622

$DyCo_3$, X-ray absorpt. edge shifts 80—25483

ErF_3, single cryst. ^{19}F NMR, ligand hyperfine field interactions 77—48067

Eu compounds, X-ray L-absorption spectra, 'white line' absorpt. maximum, chem. shifts 77—58042

Eu-salt solutions, frozen, Mossbauer parameters depend. on pH and halide conc., Eu(III) complexes form. 78—3330

F in A_2MF_6 crystals and MF_2+AF melts, (A=alkali metal, M=transition metal) 79—56619

F_2, chemical shielding temp. depend. 78—5250

FSO_2OF, wide-line NMR anal. of mol. struct., chem. shielding tensor 77—83622

^{19}F, chem. shielding in isolated haloalkanes, temp. depend. 78—86888

^{19}F, in solids, multiple pulse zero crossing NMR technique 78—37041

^{19}F NMR chem. shifts in polar solvents, intermol. interactions 77—51975

^{19}F NMR solvent shifts, charge transfer contribs. 77—50454

$^{19}F^-$, in lyotropic liquid crystals, chemical shift anisotropy obs. 80—20478

Fe and compounds, X-ray absorpt. spectra, effective co-ordination charges, chem. shift 80—84805

Fe oxides, effective atomic charge rel. to chemical shifts in transition metal compound XAS 79—78788

Fe oxides, interatomic interaction by XPS 80—7474

Fe-Al(Si)(Ga)(Ge)(As)(Sn)(Sb), dil., XPS meas. 77—63538

Fe_3BO_6, Mossbauer exam. of electric field gradients 77—40163

$Fe(CO)_2(PF_3)_3$, ^{31}P and ^{19}F NMR, 25 to −100°C axial and equatorial ligand interchange 77—73091

$Fe(CO_3)(PF_3)_2$, ^{31}P and ^{19}F NMR, 25 to −100°C, axial and equatorial ligand interchange 77—73091

Fe_2O_3, core and valence level XPS spectra meas. 78—15290

Fe_3O_4, core and valence level XPS spectra meas. 78—15290

Fe_xO, core and valence level XPS spectra meas. 78—15290

FeOOH, core and valence level XPS spectra meas. 78—15290

$Ga+H_3PO_4$, interaction in aq. soln., ^{71}Ga and ^{31}P NMR obs. 79—22729

GaAs (110) surfaces, ordered and disordered, O_2 adsorption, XPS meas. 80—49498

GaAs (110)-Al(Ga) interface, interface states, photoemission study 78—95359

GaAs, transmutation doped, shallow donors, magneto-optical study, photocond. meas. 78—87996

GaAs, X-ray K absorpt. edge, effective ionic charge and bonding schemes 80—29827

GaAs:Fe, ordering of Fe impurity, NMR anomalous line shift obs. 78—27102

GaAs-Ga, (110) interface electron states, photoemission study, chemical shift, surface charge redistrib. 78—72259

GaN, interatomic interactions from XPS 80—49171

GaP, core levels, chem. shift and relaxation energy, temp. dependence 80—39520

$GdCo_3$, X-ray absorpt. edge shifts 80—25483

$Gd_xSm_{1-x}S$ K X-rays chem. shifts, electronic phase transition, semicond.-metal transition 77—28116

Ge:B(Al)(Ga)(In)(Tl), binding energy, excited state spectra, photolum., semi-empirical short range pot. 80—44534

H atoms, expectation values, GTO functions calcs. *(German)* 77—42340

H halides, spin-orbit coupling effect on proton mag. shielding 80—23440

H^+ chemical shifts, INDO calcs. 80—32743

H_2, harmonic oscillator model, elec. polarisability, mag. susceptibility and chem. shift tensor calcs. 79—81299

H_2 in organic solvents, proton chem. shift, Van der Waals solvent effect contrib. 77—68062

HBr, chemical shielding temp. depend. 78—5250

HBr, isotope chem. shift of μ^+ 79—55005

HCl, chemical shielding temp. depend. 78—5250

$H_{1.6}MoO_3$ bronze, proton shift tensors PMR meas. 80—71202

H_2O, liq., proton NMR chem. shift, press. depend. 77—8428

H_2O, liquid, diamagnetism, temp. dependence, NMR chemical shift calcs., molecular interactions data 80—75707

H_2O powder, PMR chem. shift anisotropy, nucl. mag. screening tensor 78—17687

$H_2O(D_2O)$ isotope effects, ^{17}O NMR 77—34663

$H_2Os_3(CO)_{10}$, and $H_4Os_4(CO)_{12}$, polycryst., PMR chem. shift 79—95655

$H_4Ru_4(CO)_{12}$, polycryst., PMR chem. shift 79—95655

H_2S, gaseous 1s binding energy and S $KL_2L_3(^1D_2)$Auger energy, XPS obs. 77—3416

H_2S, KLL Auger spectra of S, ab initio LCAO SCF calcs. 77—65515

H_2S, powder, PMR chem. shift anisotropy, nucl. mag. screening tensor 78—17687

H_2S, S K-LL Auger energies and chemical shifts 80—28069

H_2SO_2, S K-LL Auger energies and chemical shifts 80—28069

H_2SO_4, S K-LL Auger energies and chemical shifts 80—28069

H_4SO_2, S K-LL Auger energies and chemical shifts 80—28069

H_2SeO_4, NMR of ^{77}Se, chemical shift and screening tensors *(Russian)* 78—64285

He+CO, nuclear mag. shielding consts., interaction geometry depend., chemical shift, gauge invariant method 78—62866

HgSe(Te), chemical shift and linewidth determ. 79—19792

^{199}Hg nuclear shielding anisotropies rel. to isotropic chem. shifts in methyl mercury compounds 77—3384

I_2, anomalous visible band effects near B state dissoc. limit 77—6816

InCl, InBr, InI, UV photoelectron spectra of valence d shells, gas-phase 78—62845

$In_{1-x}I_x$, molten mixture, NMR, reson. shifts, relax. rates, quadrupole relax. 80—2654

chemical shift continued
KD_2PO_4, ferroelec. transition, ^{31}P chemical shift tensor meas. 77−28527
KD_2PO_4, ferroelec. transition, ^{31}P chem. shift obs. 78−76414
KD_2PO_4, ferroelectric transition obs. by ^{31}P chemical shift 77−59531
$KH_3(SeO_3)_2$, high-resolution PMR 78−35053
K_2TeO_3, D_2O soln., $^{123,125}Te$ Fourier transform NMR 78−15046
^{83}Kr, nucl. mag. relax. meas. in gas 80−43072
$^{138,139}La$, Fourier transform NMR 80−57354
Li^+-ligand complexes, NMR appl. ^7Li chemical shifts, expt. and ab initio studies 80−63670
Li_2CrO_4, electron irrad., reduced species form., XPS 79−11498
LiN_3, ionic nature, quadrupole splitting, mag. field depend., N^{3-} electron cloud deform., NMR 80−50210
$LiNO_3$, electron irrad. damage, XPS obs. 78−64444
Li_2SO_4, electron irrad. damage, XPS obs. 78−64444
$^7Li_2O$, β-radiation detected NMR of ^8Li obs., double freq. irradiation, $^{7,8}Li$ hyperfine struct. anomaly 78−91994
$^7Li_2S$, β-radiation detected NMR of ^8Li obs. double freq. irradiation, $^{7,8}Li$ hyperfine struct. anomaly 78−91994
$(MgAl_2O_4)_x(AMn_2O_4)_{1-x}$, A=Mg,Mn,Zn,Cd, $0<x<1$, mixed oxide spinels, chemical shifts of Mn K-absorpt. edge 80−29828
MgO, from $Mg+O_3$ matrix reaction, IR spectra, isotope shifts and blue matrix shift 78−80736
Mg_3P_2, ^{31}P multiple pulse NMR, chem. shift anisotropy 78−52369
Mn oxides, effective atomic charge rel. to chemical shifts in transition metal compound XAS 79−78788
MnO_4^-, aq. soln., O isotope substitution, ^{55}Mn NMR 77−30890
Mo, and oxides, AES expts., chem. shift and beam effects 79−15566
MoN, interatomic interactions from XPS 80−49171
MoO_3, ESCA on H_2 reduction *(French)* 77−36365
MoO_3, X-ray absorption, discontinuities and limits, chem. combination effects 80−93435
MoO_4^-, aq. soln., O isotope substitution, ^{95}Mo NMR 77−30890
MoO_x, AES expts., chem. shift and beam effects 79−15566
$MoO_{4-n}S_n^{2-}$ in aqueous soln., ^{95}Mo NMR identification 77−48069
$MoO_{4-n}Sn^{2-}$, (n=0-4), $^{17}O(^{33}S)(^{95}Mo)(^{97}Mo)$ NMR investig. 80−53022
MoS_4^{2-}, S isotope effect on ^{95}Mo nucl. mag. shielding 77−63301
N-containing cpds., ^{13}C chem. shift calcs. using approx. SCF perturbation theory 77−18945
N_2, solid, anisotropy of chem. shift tnesor, ^{15}N NMR obs. 77−90053
$(N(CH_3)_3H)_2SnF_6$, phase transition and temp. effects, Mossbauer and NMR spectra 78−88236
NF_3, nuclear resonance, effects of intermolecular interactions and intramolecular dynamics 80−63658
NH_4 perfluoro-octanoate, amphiphilic liq. cryst., ^{19}F multipulse NMR study 78−76328
NH_4BF_4, ionic radii and chem. shifts, correl. with electronegativity 80−66054
NH_4Br, ^{14}N NMR obs., rel. to structural transforms. 79−15368
$NH_4H_3(SeO_3)_2$, single crystal, ^{77}Se magnetic shielding, chemical shift tensors 80−71207
NH_4I, ^{14}N NMR obs., rel. to structural transformations 79−15368
NH_4IO_4, chem. shift, NMR obs. 80−48015
NH_4VO_3, polycryst., quadrupole coupling const., asymmetry parameter, chem. shift, NMR computer calcs. 78−6584
N_2O, ^{15}N NMR, chem. shift., determ. of virial coeffs., rovibr. motion 78 -58720
^{14}N NMR chemical shift, external neat nitromethane scale 78−24834
^{14}N screening, absolute scale 78−2762
^{15}N NMR chem. shift references evaluation 78−24835
^{15}N-$^1H^+$ NMR, coupling consts., double reson., difference proton Fourier transform spectroscopy 79−3467
Na_2 molecules, magnetic shielding studies by NMR 77−42341
NaBr, ^{23}Na NMR chem. shift meas. 77−71817
NaCl, ^{23}Na NMR chem. shift meas. 77−71817
NaF, ^{23}Na NMR chem. shift meas. 77−71817
NaI, ^{23}Na NMR chem. shift meas. 77−71817
Na_2O-TiO_2-SiO_2 glass, co-ordination of Ti, X-ray emission spectra study 80−84072
β-$Na_2O.Al_2O_3$, high-field ^{23}Na NMR 78−64284
Na_2TeO_3, D_2O soln., $^{123,125}Te$ Fourier transform NMR 78−15046
$NaVO_2$, polycryst., quadrupole coupling const., asymmetry parameter, chem. shift, NMR computer calcs. 78−6584
Nb complexes, F-containing, X-ray K absorption edges, chem. interpretation 78−74676
Nb, ESCA chemical shift *(French)* 77−44541
Nb films, oxidation, XPS study 80−80944
Nb, oxidation, ESCA *(French)* 77−36361
Nb, oxidation at high temp. and low O_2 pressure, ESCA study *(French)* 77−25179
Nb-Ti alloys, oxidation, ESCA *(French)* 77−36361
$(NbCl_nBr_{6-n})^-$ complexes in acetonitrile soln., ^{93}Nb spin relax. and mag. shielding 80−44944
NbN, interatomic interactions from XPS 80−49171
NbO, ESCA chemical shift *(French)* 77−44541
NbO_2, ESCA chemical shift *(French)* 77−44541
Nb_2O_5, ERCA chemical shift *(French)* 77−44541
$Nd_xSm_{1-x}S(Se)$, K X-rays chem. shifts, electronic phase transition, semicond.-metal transition 77−28116
Ni and its cpds., X-ray K-absorpt. edge shifts, plasmon energies correlation 80−20734
Ni intermetallics and oxide, interatomic interaction by XPS 80−7474
OF_2, core electron binding energies, XPS spectra 77−3417
OH, correlation between chem. shift and charge in organic cpds. 77−18946
OH proton, proton, rel. to coop. mol. orient. in soln. 78−1974
^{17}O, CNDO/S and INDO calculations relative to water 77−46576
P, amorphous, NMR studies 79−69740
P compounds, solid, ^{31}P NMR and π bond 79−4732
P-Se-Tl glasses, NMR of ^{31}P and ^{205}Tl 80−15812
$PBMoO_4$, ^{207}Pb mag. shielding anisotropy, Fourier transform NMR 77−90057
PF_3, nuclear resonance, effects of intermolecular interactions and intramolecular dynamics 80−63658
PF_5, ESCA chemical shift, energy levels, SCC-MO calcs. 79−64045
PF_5, nuclear resonance, effects of intermolecular interactions and intramolecular dynamics 80−63658
PF_3Br_2, spin systems under multiple pulse NMR conditions, chem. shift relax. 80−34808
PH_3, ^{31}P NMR chem. shift, virial coeff. determ. 78−58721

chemical shift continued
$PH_3(D_3)$, ^{31}P NMR, chemical shielding, centrifugal distortion, anharmonic vibr., cubic force consts. 78−82752
POF_3, nuclear resonance, effects of intermolecular interactions and intramolecular dynamics 80−63658
P_4S_{10}, ^{31}P multiple pulse NMR, chem. shift anisotropy 78−52369
P_4S_3, ^{31}P NMR spectrum and spin-lattice relax. time, 77 to 500K and 7 to 25 MHz 79−8064
P_4S_9, P_4S_{10}, ^{31}P NMR spectra, cf. related cpds. 77−8427
PSF_3, in orienting smectic solvent, ^{19}F and ^{31}P mag. shielding anisotropies, F-P-F bond angle 77−18942
^{31}P, in inorganic solids, multiple pulse NMR 78−52369
^{31}P, shielding consts. and anisotropy of NMR shielding tensor, modified CNDO/S calcs. *(French)* 80−32610
Pb and Pb oxides, X-ray absorption, discontinuities and limits, chem. combination effects 80−93435
Pb, chemical shift of X-ray L-absorption edge 79−52044
$PbCO_3$, ^{207}Pb mag. shielding anisotropy, Fourier transform NMR 77−90057
$PbCl_2$, $PbBr_2$, PbI_2, UV photoelectron spectra of valence d shells, gas-phase 78−62845
$PbCrO_4$, ^{207}Pb mag. shielding anisotropy, Fourier transform NMR 77−90057
$Pb(NO_3)_2$, ^{207}Pb mag. shielding anisotropy, Fourier transform NMR 77−90057
$Pb(NO_3)_2$, nucl. mag. shielding tensors of $^{207}Pb^{2+}$, NMR obs. 80−44939
PbSe(Te), chemical shift and linewidth determ. 79−19792
$PbWO_4$, ^{207}Pb mag. shielding anisotropy, Fourier transform NMR 77−90057
$PbZrO_3$, perovskite type, X-ray K-absorpt. edge, chem. shift 79−91529
Pd(II)-Gly-Tyr complexes, aq. soln., PMR obs., conform. 77−50450
Pt complex, chloro-bromo complexes of Pt (IV) and Pt (II), ^{195}NMR, cooperative shift effect 79−33547
^{195}Pt NMR shifts, referencing convention 79−33547
Rb and Rb compounds, X-ray K absorption edge, fine struct. 77−77319
RbF(Cl)(Br)(I), chem. shift in X-ray absorpt. spectra, correl. with ion contrib. to bond 78−76559
$RbFeCl_3$, linear chain cryst., quadrupole and mag. reson., rel. to $CsFeCl_3$ 79−38403
$RbNiCl_3$, cryst., ^{35}Cl and ^{87}Rb NMR down to 1.3K 79−42848
Ru complexes, $K_{\alpha 1}$ lines chem. shift, donor-acceptor capacity of ligands 79−33867
$Ru(NH_3)_6^{3+}$, isotropic chem. shift, pseudocontact contrib. 80−91577
SF_4, ESCA chemical shift, energy levels, SCC-MO calcs. 79−64045
SF_6, ^{19}F NMR, chem. shielding, intermol. interactions and rovibr. motion effects 78−9171
SF_6, gaseous 1s binding energy and S $KL_2L_3(^1D_2)$ Auger energy, XPS obs. 77−3416
SF_6, KLL spectra of S, ab initio LCAO SCF calcs. 77−65515
SO_2 80−28069
SO_2, gaseous 1s binding energy and S $KL_2L_3(^1D_2)$ Auger energy, XPS obs. 77−3416
SO_2, KLL Auger spectra of S, ab initio LCAO SCF calcs. 77−65515
$^{121}Sb_2O_3$ powder, NQR transverse chemical shift 77−28479
$ScVO_4$, ^{51}V NMR, nucl. quadrupole coupling const., chem. shift 77−90055
Se compounds, chemical shifts of X-ray electron and Auger lines 78−86912
Se, $L_2M_{4,5}M_{4,5}$ Auger spectrum following photoionisation, post collision interaction, chemical shifts 79−22678
Se, solid, chemical shift and nucl. spin-lattice relax., high temp behaviour 80−60445
Se, trigonal, NMR, tight-binding calc. 78−2759
^{77}Se, FT NMR in solns., chem. shift, I_1 relax. times, NOE enhancement 78−95528
Si (111), chemisorbed O_2 bonding geometry, electron yield EXAFS meas. 80−50461
Si (111), intermediate oxidation state, core photoelectron absorpt. vs. chemical shifts 80−81220
Si, chemisorption of XeF_2 and SiF_4, XPS and Auger spectra, surface chemistry 80−81358
Si compounds, free mol. chemical shift, binding energy and Auger spectra 80−32782
Si, core and valence electron excitations, AES, chemical shift and line shape 80−2365
Si, core levels, chem. shift and relaxation energy, temp. dependence 80−39520
Si, K_α X-ray emission spectra chemical shifts, linewidths and intensities in SiC, SiO_2, Si_3N_4 78−13461
Si, thermally oxidized, chemical shift meas. by ESCA *(Japanese)* 79−61761
Si:B(Al)(Ga)(In)(Tl), binding energy, excited state spectra, photolum., semi-empirical short range pot. 80−44534
Si:H, amorphous, 2p level shift, XPS obs. 80−97401
Si-SiO_2, angular-dependent X-ray photoelectron spectra 77−12485
Si-SiO_2 interface study by XPS 80−50507
SiF_4, ^{19}F chem. shielding, depend. on internal coords. 78−5249
SiF_4, ^{19}F NMR, chem. shielding, intermol. interactions and rovibr. motion effects 78−9171
SiN, interatomic interactions from XPS 80−49171
Si_3N_4 amorphous film, CVD, core and valence electron excitations, low energy electron loss spectroscopy and AES 80−2365
SiO_2 amorphous film, thermal, core and valence electron excitations, low energy electron loss spectroscopy and AES 80−2365
SiO_2, core levels, chem. shift and relaxation energy, temp. dependence 80−39520
SiO_2, quantity anal. of O ions, meas. of chemical shift in Si2p binding energy, using ESCA *(Japanese)* 78−48274
SiO_x, chem. shift of Si 2p core level, relax. contrib. 79−47141
SiO_x, core level shifts, nature of bonding 77−84698
SiX_4 (X=Cl,H,F), chemical shifts, relax., X-ray spectra, SCF Xalpha calcs. 80−27928
$SmCo_5$, X-ray K absorpt., chem. shift 79−91531
$SmCu_5$, X-ray K absorpt., chem. shift 79−91531
Sn, clean and oxidised, Auger spectra expt., fine structure anal. 80−29831
Sn organometallic cpds., chem. shifts in ESCA and Mossbauer spectra *(French)* 77−28685
$SnCl_2$, $SnBr_2$, UV photoelectron spectra of valence d shells, gas-phase 78−62845
SnF_2^{2-}, Mossbauer effect 77−85626

chemical shift continued
^{119}Sn NMR by pulse Fourier transform, T_1, T_2 and chem. shifts 77–55715
^{119}Sn-^{117}Sn primary isotope effect on mag. shielding, NMR of Sn cpds. 79–72338
SrH_2, proton chemical shift tensor, heavy ion effects 79–19791
TGS, ferroelectric phase transition, high resolution NMR study 80–97214
Ta film, photoemiss. from conduction band and core levels 77–16464
$TbCo_3$, X-ray absorpt. edge shifts 80–25483
Te compounds, dihalides, organometallics, ^{125}Te, ^{13}C, ^{1}H NMR spectra, nucl. coupling, exchange processes 79–95658
Te compounds, NMR orbital shift of ^{125}Te, depend. on ionicity and local struct. 77–32273
Te, NMR spectrum, electron paramagnetism and atomic self-diffusion mechanism 78–72426
Te, photoconductivity in strong mag. fields, doping effects, impurity levels 80–75602
Te, Te cpds., Auger spectra 78–58638
Te, trigonal, NMR, tight-binding calc. 78–2759
Ti, oxidation, ESCA *(French)* 77–36361
TiB_2 coatings, CVD, electron microprobe, SEM, X-ray diffr. characterisation *(French)* 78–43271
TiF_2, TiF_4, X-ray emission, core level chem. shift calcs. 80–53010
TiH_4, X-ray emission, core level chem. shift calcs. 80–53010
TiH_3F, X-ray emission, core level chem. shift calcs. 80–53010
TiN, interatomic interactions from XPS 80–49171
TiO_2-Ni, electronic props., struct., comp., chemical bonding 80–84499
Tl complex of lasalocid (X-537A), ^{205}Tl NMR study 80–58288
TlCl, TlBr, TlI, UV photoelectron spectra of valence d shells, gas-phase 78–62845
Tl_2O-B_2O_3, glass, ^{205}Tl NMR 77–59470
Tl_2O-GeO_2, glass, ^{205}Tl NMR 77–59470
Tl_2O-SiO_2, glass, ^{205}Tl NMR 77–59470
$TlPO_3$, vitreous and polycrystalline, NMR and IR exam. of cation motion 77–66041
^{205}Tl, solvated and adsorbed, NMR studies *(Rumanian)* 79–82888
$^{205}Tl^+$ adsorbed on hydrated silica, NMR relax. chem. shift 78–72427
$TmCo_5$, covalent electron number, from chem. shift of Co X-ray absorption spectra 77–59641
U, AES and loss spectra, changes on oxidation 77–20965
U complex, $U(acac)_4$, cryst. fields, mag. susceptibility, chem. shift *(French)* 78–84179
VB, nuclear quadrupole parameters 80–103896
VN, interatomic interactions from XPS 80–49171
Xe compounds, Xe chemical and isomer shifts, electron valence struct. *(Russian)* 80–53056
$Xe+CO(N_2)$, ^{129}Xe chem. shielding, second virial coeff. 78–66563
^{129}Xe, chem. shift in CH_4, CF_6 and SiF_4, chem. shielding 77–6707
^{129}Xe, chem. shift in NO gas, chem. shielding 77–6706
YCo_5, covalent electron number, from chem. shift of Co X-ray absorption spectra 77–59641
$Y_3Fe_{5-x}In_xO_{12}$, K absorpt. and Mossbauer spectra and other phys. props. *(Russian)* 77–32467
YVO_4, ^{51}V NMR, nucl. quadrupole coupling const., chem. shift 77–90055
^{89}Y in $Y(NO_3)_3$, YCl_3 and $Y(ClO_4)_3$ aqueous solns., NMR study 77–24754
^{89}Y spin-spin relaxation times, pH depend. 80–66059
Yb, 4f levels, hole lifetime and chemical shift, UHV study 80–20762
Yb complexes, lanthanide-induced NMR shifts, temp. depend. 77–68061
$YbVO_4$, ^{51}V NMR, nucl. quadrupole coupling const., chem. shift 77–90055
Zn and its cpds., X-ray K-absorpt. edge shifts, plasmon energies correlation 80–20734
Zn nitroprussides, Mossbauer spectra, dehydration effects 79–24237
Zn_3P_2, ^{31}P multiple pulse NMR, chem. shift anisotropy 78–52369
ZnS, ^{67}Zn and ^{33}S nuclear magnetic shielding, chemical shifts and linewidths 80–60434
ZnSe, ^{67}Zn nuclear magnetic shielding, chemical shifts and linewidths 80–60434
ZnSe(Te), chemical shift and linewidth determ. 79–19792
ZnTe, ^{67}Zn nuclear magnetic shielding, chemical shifts and linewidths 80–60434
$ZnTiF_6.6H_2O$ and $ZnTiF_6.6D_2O$, ^{19}F NMR, phase transition 79–19790
ZrO_2, perovskite type, X-ray K-absorpt. edge, chem. shift 79–91529

chemical structure
see also bonds (chemical); crystal atomic structure; crystal chemistry; molecular configurations
acrylonitrile-vinylacetate(styrene) copolymer films, gas permeation, chem. struct. effects *(Japanese)* 78–31691
alkali silicate glass, suitability of small angle neutron scatt. for struct. determ. 78–22663
alkyl halide, chem. struct. determ. using electron capture response 77–21428
artificial intelligence for chem. inference. automatic rule formation in mass spectroscopy, meta-DENDRAL 77–18775
asbestos, chrysotile, crushed, temp.-induced changes in struct. 77–24305
borides, refractory compounds, classification 79–94985
borides of Ib and IIb elements, interactions, product chem., phase, struct. anal., book contrib. 78–47305
chemistry, macromolecules, and the needs of man 78–95907
chromites, from India, struct. and comp. 78–44807
coke, anisotropic spheres obtained during needle coke form., struct. obs. 77 63573
colour, chemical origins 79–21479
computer representation, block-cutpoint tree method 80–63522
contribution of struct. groups to crit. vol. 79–91981
critical molar volumes, empirical calc. method 77–21405
crown ether-containing polymers, in alkali salt solns., complexation, viscosity obs. 80–64877
diffusive isothermal solute partitioning in layered medium, geologic appl. 77–16896
1,4-dihalonaphthalenes, binary solid solns. lattice stability, mol. motions 78–31182
electron beam curing, beam voltage effects on mech. props. and chem. struct. 77–70201
epoxy resin, low temp. thermal props., phonon states and crosslinked struct. *(German)* 78–75846

chemical structure continued
ethidium bromide E-DNA, intercalated birefringent fibres, microspectrophotometric investig. *(German)* 80–57392
exotic atoms, utilisation in chem. struct. studies, review 79–79277
ferrite spinels, normal and inverse, solid state chem. expts. for students 80–36815
fluorides, chem. formulae, advances in preparative chem. 79–47915
free atoms of metals [and their chemistry] *(French)* 80–21281
glass, nonuniformities and basic principles of struct. 79–41970
glass, surface struct. and reactivity influence of separation *(German)* 78–30817
glass comp., patent information, automated retrieval system 79–24715
graphite, acidic surface oxides, struct. investigation using diazomethane 79–52404
historical review *(Danish)* 79–9071
hydrationally active phases, electron structs. and props. of anions 77–44574
hydrocarbon ions, mass spectra, H atom scrambling, delocalisation 80–58135
7-hydroxycoumarin, absorpt. and emission spectra, ionic forms 78–21955
hydroxyl-terminated prepolymers, functionality determ. 79–31746
interfaces of nuclear and chemical physics, elementary particles and biochemistry 77–6284
ionene polymers, counterions and absorbed water influence on mech. relax. 77–40430
ionene polymers, ion conc. effect on mech. relax. 77–44284
kaolinite-mullite thermal sequence, structural analysis and transition phases 77–36484
Kevlar-49, chemical characterisation 78–95725
lithium oligopentadienyl and complexes, IR spectra *(Russian)* 80–71424
mica, North American, electrical cond. rel. to chem. composition 77–29285
Mossbauer effect appl., conference, Kyoto, Japan (Aug.-Sept. 78) 80–7199
muon capture probabilities of elements in ionic solids, chem. struct. factors 77–50550
NMR data bank, ^{13}C, DARC PLURIDATA system 80–30298
NMR in undergrad. instruction, general purpose microcomputers use for hypothetical spectra synthesis 80–42009
NMR spectra, computer-aided interpretation, minicomputer based file search system 80–62702
NMR spectra, computer-aided interpretation using artificial intelligence system 80–62701
novolac and novolac allyl ether electrets, thermal depolarisation, chem. struct. effect 80–71297
oxides, chem. formulae, advances in preparative chem. 79–47915
PAN fibre, pre-oxidised, IR absorpt. 77–28561
PAN fibres, SO_2 treatment 79–52403
pictorial reproduction, computer system 79–43708
PMMA, constancy of composition obs., dosimetry appls. 79–60286
poly(9-vinyl anthracene), struct. *(German)* 79–98256
poly(alkyl methacrylate) films, chemical characterisation from C Auger spectra, appl. of pattern recognition and factor anal. 79–79347
polyalkylmethacrylates, vitreous, thermal cond., press. and temp. depend. 78–2315
polyaromatics, elec. cond. correl. with chem. struct. and synthesis, charge transfer complexes *(German)* 80–15514
polyester fibres, thiuram and dithiocarbamate rubber accelerator degradation 79–78986
polyesters, linear aliphatic, chem. struct. rel. to viscoelastic props. 79–41977
polyethylene-propylene copolymers, branching effect on struct. and mech. props. *(Russian)* 79–52333
polymer, ageing and stabilisation, struct.-kinetic aspects *(Russian)* 79–52660
polymer, conjugated, synthesis and elec. props., review 80–15513
polymer, crosslinked *(German)* 78–75584
polymer, degradation, mol. mechanisms *(German)* 78–76860
polymer, glassy, elastic moduli, calc. method from chem. struct. *(Russian)* 78–75707
polymer crosslinking, rel. to azide photooxidation in polymer matrix 80–66832
polymer structure and optical behaviour 80–106583
polystyrene, constancy of composition obs., dosimetry appls. 79–60286
polyurethane, heat treatment, cross linking as function of structure and mechanical properties *(German)* 79–57229
pyridine, vibr. reson. lasing threshold, complex form. and solvent effects *(Russian)* 77–75507
quantum mechanics, replacement of chemical bond concept by loge theory 78–54243
quartz, creep and mechanism by which water accommodates dislocation glide 77–90414
rare earth double orthophosphates with alkali metals, spectroscopic obs., struct. and chem. nature 80–100674
rare-earth oxides, non stoichiometric phases in thin films 79–7755
REACT program for computer-assisted simulation of chemical reaction sequences, structure elucidation applications 78–92477
ring characterisation method 80–63853
sheet steels, carbonaceous residue, chemical characterisation from C Auger spectra, appl. of pattern recognition and factor anal. 79–79347
silane, coupling agent on E-glass fibre, structure, Fourier transform infrared spectroscopy 78–60643
silane, coupling agent on porous silica, Fourier transform infrared spectroscopy 78–60642
silicates, molten, stat. interpret. of Masson theory *(French)* 80–49078
silicates, molten, with high and medium Si contents, stat. theory *(French)* 80–49079
stereoisomer generation, algorithm and implementation 80–1080
stereoisomer generation, specification and enumeration, config. symmetry group appl. 80–1079
structural search codes for on-line compound registration 78–90319
styrene crosslinked polyester networks, low temp. γ relaxation, water and chem. struct. effects 78–44157
styrene-sodium methacrylate copolymers, linear expansion coeffs., ionic groups conc. depend 79–42284
tautomerism and alternating bonds, representation, Chemical Abstracts Systems 80–63851
TCNQ salts of ionene polymers containing triethylenediammonium or 4,4′-bipyridilium ring, chem. struct. correl. with cond. 79–91032

chemical structure continued
- technetium hexahalides, X_α-SW-calc. of chemically induced decay const. variation of ^{99m}Tc in TcO_4^- and hexahalides 79—54769
- thiourea, struct., hydration, ab initio SCF calcs. 80—58142
- transition metal phosphates, MH_2P_2O and $M_2P_4O_{12}$, formed by oxide reactions with phosphoric acid melts 77—12517
- urea-formaldehyde resins, ^{13}C Fourier transform NMR of chem. struct. 79—42849
- AgBr, photographic emulsions, adsorpt. of thiolic antifoggants, chem. struct., ESCA investig. 78—32907
- Al chalcogenate and chalcogenite double salts, form. laws and acid-base props. 80—101070
- β-Al_2O_3-Na_2O:Mg, with and without Co co-doping, ionic cond. and cryst. struct. 78—26723
- As-S-I system glasses, IR transmission spectra, structure-chem. comp. 79—42974
- As_xS_{1-x} glass, Raman spectra, chem. struct. *(Russian)* 78—76469
- $(As_2S_3)_x(AsI_3)_{1-x}$, glass, Raman spectra, chem. struct. *(Russian)* 78—76469
- $As_{1-x}S_x(Se_x)$, bulk-quenched glasses, opt. freq. dielec. const., chem. ordering effects 78—23472
- Au, Co-hardened, characterisation by Mossbauer spectroscopy, Co precip. formation 80—80108
- Au, electrodeposit, Co-hardened, state of Co in as-deposited material, Mossbauer obs. 80—15397
- Au-Co, electroplated, 'polymer' inclusions, chem. identity obs. 79—37931
- $Ba_x(Ba_{1-x}Al_x)Fe_2S_6[S_{1-y}(S_2)_y]$, cryst. struct., Mossbauer and mag. behaviour 77—55273
- C black, acidic surface oxides struct. investigation using diazomethane 79—52404
- C-bearing gases, K-shell X-ray yields, proton-induced, chem. effects 80—37820
- $Ca_{1+x}Ga_{1-x}N_y$, prep. *(French)* 77—44206
- $Cd_xHg_{1-x}Te$, comp. in successive layers determ. by chem. polishing etching of surface 77—7868
- CdS sprayed film, prep., optical props., struct. and comp. 79—78875
- CdSe $(11\bar{2}0)$, surface electronic struct. and chem. struct. 78—14788
- Fe_xN_y, prep. by reactive sputtering, struct. and props. *(Japanese)* 78—92190
- $Fe_{70}Ni_{30}$, short range order, diffuse elastic neutron scatt. study 78—52219
- Fe_xO_y, prep. by reactive sputtering, struct. and props. *(Japanese)* 78—92190
- $Fe_{1-x}Pd_x$ film, air-exposed, comp. profiles by AES, ESCA and ion sputtering 78—95245
- Ga chalcogenate and chalcogenite double salts, form. laws and acid-base props. 80—101070
- GaAs, anodic oxide layers, chem. depth profiles, XPS determ. 80—3222
- $GaAs_{1-x}P_x$, heterogeneous struct. obs. by anodisation-electrorefl. technique 78—84088
- GaP(As)(Sb) oxide, anodic, inferred from optical props., 1.5-6.0 eV 77—90209
- $(GaP)_x(ZnSe)_{1-x}$/GaP, epitaxial heterostructures, chem. microinhomogeneity 77—80831
- Gd-Co film, amorphous, Ar sputtered, struct. 78—63946
- Gd-Co-Mo film, amorphous, Ar sputtered, struct. 78—63946
- Ge-Si-Sb solid soln., distrib. of components in universal furnace expt. in Soyuz-Apollo programme *(Russian)* 78—31381
- GeS, GeS_2, SS 79—97683
- GeS_x glass, optical props., chem. struct. effects 77—63460
- $Ge_{1-x}S_x(Se_x)$, bulk-quenched glasses, opt. freq. dielec. const., chem. ordering effects 78—23472
- I_2 vapour, chemical composition at high temps. 77—36781
- In chalcogenate and chalcogenite double salts, form. laws and acid-base props. 80—101070
- $InVO_4.2H_2O$, $In_4(V_2O_7)_3.14H_2O$, physicochem. props. 77—85702
- $LaMn_{1-x}Cu_xO_{3-y}$, prep., struct., selected catalytic props. 77—36433
- $LaMn_{1-x}Cu_xO_{3+y}$, O_2 stoichiometry by thermogravimetry 77—36434
- Mn_xN_y, prep., rate of formation, chem. stability 78—11185
- Mo cpds., chemical structures, thermodynamic props., reactions 77—77750
- Na_3AlF_6, molten *(French)* 77—51297
- Na_2O-B_2O_3-Na_2SO_4, glass, exam. of chemical differentiation, using Cu ion segregation 78—87625
- Nb film, ion bombardment with N_2^+, Ar^+, struct. changes, chemical compound formation *(Russian)* 78—95084
- Nb-Ge-Si film, CVD, struct., comp., stability and homogeneity 80—15421
- $NbSe_3$, electronic struct., chem. interpret. of geom. deform., oxidation state formalism 80—107690
- $Nd_4Al_2O_3$ film, struct. characts., IR spectra 77—48157
- $NdCl_3$-$SnCl_4$-$POCl_3$, complex formation, struct. and comp. 77—89413
- Nd_3S_4 chem. and mag. structures, neutron diffr. obs., ferromag. long-range order *(German)* 78—10654
- Ni-Cr film, vac. deposition, elec. props. and comp. struct. 79—77966
- Ni-Cr-Mn alloy solidification, effects of Si, Mo and Co alloying 79—83193
- ^{18}O isotope shift in ^{13}C NMR, struct. depend. 80—69165
- PbO-SiO_2, based glasses, containing fluorides shear wave velocity rel. to chem. comp. *(Japanese)* 78—30702
- PbS, thin film comp. and struct. rel. to precip. by allyl thiourea 77—48356
- PbS-Si heterojunction, struct. and comp. 80—54530
- PbS-Si heterojunction, chem. struct., AES anal. 80—76115
- $Pb_xSn_{1-x}Te$, RF sputtered films, struct., lattice parameter, stoichiometric comp., RHEED 78—38975
- $(Sb_2F_4^{2+})[SbF_6^-]_2$ and $[Sb_3F_{14}^-]$ ion containing cpds., ^{121}Sb Mossbauer obs. of mixed oxidation state cpds. 79—28640
- Si-SiO_2 interface, chem. struct. of transitional region 78—95824
- Si-SiO_2 interface, ESCA and ellipsometric study 79—82678
- Si-SiO_2 interface, props. variation in SiO_x region 80—49548
- $Si_{1-x}C_xH$, amorphous film, H content determ. by nuclear reaction analysis 80—59821
- SiH, amorphous film, H content determ. by nuclear reaction analysis 80—59821
- Si_xN_y, film, chemical nonuniformity of films produced by ammonolysis of monosilane 77—1334
- SiO_2 film, on Si, SiOH and SiH groups, IR absorpt. results 78—26779
- SiO_2/Si interface, obs. of chem. struct. 78—27654
- SiO_x film, vacuum evaporated, phase comp., electron spectroscopy obs. 78—60042

chemical structure continued
- SiO_x, on Si exposed to O_2, phase comp., electron spectroscopy obs. 78—60042
- SiO_xN_y, low temp. films, comp., chem. bonding and contamination 78—47676
- $Si_xO_yN_2$ films, chemical struct. using AES 79—77945
- SiO_2 film, RF sputtered, stoichiometry and atomic defects obs. 79—90904
- SnF_2, α and γ modifications, elec. cond., $\alpha \rightarrow \gamma$ phase transitions, structs. 78—75867
- ^{113}Sn, chem. effect on electron capture probability and decay const. 79—54412
- Ta film, ion bombardment with N_2^+, Ar^+, struct. changes, chemical compound formation *(Russian)* 78—95084
- TcO_4^-, X_α-SW-calc. of chemically induced decay const. variation of ^{99m}Tc in TcO_4^- and hexahalides 79—54769
- $(Th,U)O_2$, burnup simulated, high O_2 pot., chem. state 80—91220
- $Th(NO_3)_4$-K_2HPO_3-H_2O, mixed phosphites formation and characterisation 77—52304
- Ti film, ion bombardment with N_2^+, Ar^+, struct. changes, chemical compound formation *(Russian)* 78—95084
- TiC_x, comp. determ. by neutron diffr. 77—40411
- TiO_x, surface film on plasma anodised Ti, comp. determ. 77—48591
- V_2O, γ-phase, struct., O at. position 79—10834
- V_2O_5, water in noncryst. solid, quenching of molten V_2O_5 *(French)* 78—42912
- WO_3 evaporated film composition and chem. structure rel. to electrocoloration 77—77175
- $Zn_2Fe(PO_4)_2.4H_2O$, phosphophyllite, chem., optical and X-ray data 77—15366
- ZnO-PbF_2-SiO_2, glass, shear wave velocity rel. to chem. comp. *(Japanese)* 78—30702
- ZnO-SiO_2 system, struct. and phase comp. of luminescent Zn orthosilicate 80—19951
- ZnS, RF sputtered film, stoichiometry, chem. comp. 78—34727
- $Zn_7Sb_2O_{12}$, $Zn_4Sb_2O_9$, and conditions of formation 78—52699
- $ZnSiP_2$, chem. inhomogeneities, X-ray lattice parameter meas. *(German)* 77—72693

chemical technology
- *see also chemical industry; chemical variables control; chemical variables measurement; oil refining*
- airborne contaminants monitoring in chem. labs., USA regulations 80—12869
- alkaline water electrolysis cells, development of inorganic membrane electrolyte 79—74396
- atoms, laser excited, reactive collisions 80—66793
- autocatalytic kinetic system, asymmetric multiple steady states 79—86527
- autoclave process for high-press. polymerisation of ethylene 79—24744
- autonomous and hybrid solar thermal electric plant energy storage requirements 79—57494
- biomass conversion to fuels and chemicals, Purdue Process 80—26149
- biomass gasification process, Garrett Energy Research 79—48040
- bipolar trickle reactors, electric current versus potential plots 80—76521
- bipolar trickle reactors, flow models for hydrodynamic characts. and reaction rate constants, 80—76522
- bipolar trickle reactors, study using electrochemical tracer method 80—76523
- blowing, gas jet-liquid bath interaction for different degrees of assimilation 80—43754
- CHISA international conference, Prague, Czechoslovakia (Aug. 1978) 80—62372
- coal, new catalysts for CO-H_2O induced liquefaction 80—30335
- coal combustion wastes processing, resource materials recovery, using combination sinter-dilute acid leach methods 79—48063
- coal conversion, by flash hydropyrolysis and hydrogasification 79—52868
- coal conversion, solvent refined, pilot plant experiences 79—52867
- coal conversion to hydrocarbons, underground, for industrial appl. 79—48052
- coal gasification, bituminous, in situ, linked vertical well concept 79—48051
- coal gasification, in situ, diagnostic and remote monitoring instrumentation development 79—48055
- coal gasification, Synthane process appl. 79—48057
- coal gasification, underground, US Department of Energy status 79—48054
- coal gasification system, fluidised-bed, low-Btu fuel gas production 79—48058
- coal hydrogeneration, direct appl. to power generation 79—48056
- coal liquefaction, 1978 status and development trends in US 79—48061
- coal liquefaction, Exxon donor solvent process development 79—48059
- coal liquefaction, low temp. chem. fractionation of H-rich components 80—30336
- coal liquefaction, up-grading of solvent refined coal by catalytic hydrogenation 80—30331
- coal liquefaction processes, research status 79—48060
- coal liquefaction residues gasification 79—52869
- coal pyrolysis, in entrained bed flow reactor, theoretical exam. with aid of physical models 79—48062
- combustible flow, stiff boundary valued problems in kinetics and diffusion, numerical methods 79—86525
- combustion, NO_x and SO_2 form., oxidizing agent excess depend., thermodynamic anal. 78—15677
- conference, Nice, France, (March 1980) 80—51941
- continuous flow stirred tank reactor, mixing model 78—63508
- direct flow plasma reactor, working of phosphate *(Russian)* 80—55663
- dispersion model, residence time distrib. calc. approx., Peclet no. depend. *(German)* 78—22421
- electrochemical electrodes, current distribution, network-type equivalent cct. investig. 78—35705
- electrochemical processes, energy use analysis *(Dutch)* 80—72019
- electrochemical reactor characterisation, marker pulse method improvements 80—76524
- electrochemical reactors with three-dimensional electrodes, characterisation using electrochemical tracer method 80—76520
- electronic techniques appl. *(German)* 77—77841
- enzyme particle, encapsulated, reactor systems, effects of mass transfer resistances 79—96522
- ethanol, industrial, production from municipal cellulosic waste 80—61502
- ethylene polymerisation plant, high-press. equipment design 79—24746

chemical technology continued
extraction columns, perforated plate, operation under jetting conditions, design 79−90299
falling film gas-liquid reactor anal. 79−86526
flow porous electrodes, axial dispersion determination 78−31650
fluidised bed, jet penetration depth of multiple vertical grid jets 80−38486
fluidised bed reactor, solid-circulation model, steady-state multiplicity 79−86524
fluidised system, heterogeneous, aerodynamic aspects of transfer processes, crit. state 80−79394
gas chromatography, prep-scale, high purity compound prep. for industry 77−1956
gas stripping column, periodically cycled, feedback control, simulations 79−1231
gas trace monitor, control of toxic gases 80−61499
GCFR with N_2O_4 coolant, power plant nuclear and chemical safety 79−30969
glass technology and applications, review of advances 77−66618
granular bed, aerosol filtration efficiency, triboelec. effects 80−38487
heat exchanger, mathematical models of processes *(Dutch)* 79−75525
heavy water, process simulation of production plants 79−22396
heavy water prod. plants, Girdler-Sulphide process, developments 79−22397
high-pressure apparatus, seals elastoplastic behaviour obs. *(German)* 78−21160
high-pressure laboratory for chem. engng. development 79−21507
hydrolysis of wood, ethanol production as alternative energy resource 79−48039
industrial gaseous environment characterisation, Brinkley method 80−93817
inert gas liberation in multiposition metallic reactor 78−59978
infinite dilution activity coeffs. determ. from total press. VLE data, eqn. of state influence 80−40727
ion chromatography appl., on-stream, impact on energy conservation 80−55737
laser beam appl., LASL developments 79−31719
linear parameter estimation, for chem. anal. 79−24843
liquid-liquid extraction column online control by modal control techniques 78−54865
metal extraction by adsorption, using low rank coals 79−11530
metallurgical wastes with heavy metals treatment, influence of heavy metal ions on flotation of $PbSO_4$ with sodium hexadecyl sulphate *(Japanese)* 80−55701
methanisation plant ADAM I, nuclear long-dist. energy circuit *(German)* 78−25335
methanol derivation from lignite, fuel appl. 80−61223
models of complex systems, based on network thermodynamics 78−20955
multistage vibr., rot. disc column, countercurrent liq.-liq. flow, axial mixing 77−3902
non-Newtonian fluids in jacketed agitated vessel, heat transfer, viscosity correl. 78−75143
nuclear chemical-bound energy system, short term market prospects *(German)* 78−82505
nuclear power generation fuel cycle factories, chemical technology development 79−31096
packed bed, hold-up profile, elec. cond. meas. 77−35201
packed column, liquid drop collisions with elements of packed column 77−15084
pH-neutralisation process, self-tuning control 80−30242
phase equlibria, molecular thermodynamics calculations, practical appls. *(German)* 78−18733
phosphate containing materials, technological prod. processes, review 80−97452
plasma chemistry, history, diagnostics, production, organic cmpd. synthesis 80−61099
plasma chemistry of heterogeneous systems 80−61100
plasma reactor, methane-H_2 system, exptl. and thermodynamic investig. *(French)* 78−15698
plasma source characteristics for chem. reactors *(French)* 78−11605
polymer fibres, ultra high modulus, prep. by soln. and melt spinning, review 79−11544
polymerisation of styrene, bulk, thermally initiated, batchwise, optimal temperature policies determ. 79−87845
porous catalyst, complex reactions, conc. and temp. profiles, computation method 79−86523
pulsed perforated plate column, mass transfer direction rel. to efficiency 78−71385
pulverised char feeder, laboratory scale 77−61058
radiation polymerisation control by dose rate regulation, expt. study 77−32787
radiation process control 77−67903
radioactive waste calcining facility, remote maintenance development facility installation 77−54342
radioactive waste calcining facility development 77−54341
radioactive waste vitrification system design 77−54340
reactors, chem., relaxation oscills. 79−39120
recycle reactors for catalyst evaluation 80−3402
shale oil extraction using nucl. heat sources, feasibility 77−34422
sieve plate column without downcomers, anal. and NH_3 stripping expt. 78−22430
solar chemical reactor theory and designs *(French)* 80−7916
solid-solid reactions, analysis and reaction development, review 80−16648
soluble fluids in laminar, turbulent flows, stretch model appls. to mixing, diffusion, react. 79−94736
Solvent Refined Coal process, trace element distrib., neutron activation analysis 78−3421
statically loaded structure design, limit load method *(German)* 79−50688
stirred tank reactor, homogeneous p-order reactions, mixing effects, two parameters model 80−14843
synthesis and process control, self directed, computer system 79−52628
transuranium processing plant, chem. process engng. 77−54338
transuranium processing plant, remote processing practices, equipment changing and modification facilities 77−54339
two-phase mixture flow in rotary mixer, optimal dimensions 78−63485
water electrolysis, development of medium temp. high press. concept for H_2 prod. 79−74398

chemical technology continued
water splitting thermochemical cycle for synthetic fuel prod. at fusion reactors 78−58458
wind powered brackish water purification by electrodialysis and reverse osmosis 80−35630
zone refiner, six sample, with built-in stirring, for organic materials 77−28715
BN production, powdered, in arc plasma *(Chinese)* 79−98999
Cu selective surfaces on Al-Cu alloy, chemical brightening and etching 79−62037
CuO selective surfaces on Al-Cu alloy, chemical brightening and etching 79−62037
D enrichment by CW vibr. photochem. of methane, economic aspects 80−11920
H plasmochemical prod. by H_2O decomposition in non-equilib. plasma 80−45773
H production, high efficiency alkaline electrolysis technology 80−30601
H production by ZnSe thermochem. cycle, chemical and process design studies 80−35782
H production from H_2O by two-stage plasmochemical cycle 80−45772
H, thermochem. prod. using SO_2-I_2 water splitting cycle 80−30600
H, thermochemical prod. using S-Br cycle, development of lab.-scale plant 80−35774
H_2 production, from high temperature electrolysis and fusion reactor 79−52915
H_2 production by KOH electrolysis, materials, geometry and characts. of electrolyser cell 79−74397
HI-H_2-I_2, H_2 separation in thermogravitational column 80−45561
NO measurement, photometric process analyser 80−57360
NbC production and superconductive props. *(Bulgarian)* 80−80467
NbN production and superconductive props. *(Bulgarian)* 80−80467
U extraction process for systems, with 2 extractable macrocomponents, graphical calc. 79−31098
Zn phosphating processes and additives 79−79147

chemical vapour deposited coatings *see CVD coatings*

chemical vapour deposition
see also vapour phase epitaxial growth
actinide dioxides, cryst. growth by chem. transport 80−16166
actinide pnictides, single cryst. and film growth by CVD 80−16165
arsenides, group III, chem. transport equilib. with I_2 *(French)* 77−55876
arsenides, group III, chem. transport equilib. with I_2 *(French)* 77−55877
boundary layer theory application, introduction 80−66431
brass diffused coating on steel from vapour-gas phase *(Russian)* 79−5080
chemical transport rate using flux function method 78−26469
closed system for B fibre prep. 79−83129
coatings, two-component from two sources, geometrical aspects of prod. *(Russian)* 79−38743
controlled nucleation thermochemical deposition, improvements over chemical vapour deposition 78−92387
crystal growth and deposition, gaseous phase, chem. transport reaction 80−44161
crystalline film growth reactor, gasdynamic problems 79−83130
diamond, synthesis on nondiamond substrate, electron diffr. and luminesc. exam. 77−76344
ellipsometric installation for semiconductor surface physicochemical process study 77−18071
ferrite, epilayers for bubble appl. 80−39829
fibre, optical, manufacturing technology 77−65632
fibres, graded index CVD fabricated fibres, dispersion with finite number of layers 79−3769
flow-graph model 79−78893
fluid dynamics and mass transport expts. 77−77398
fusion reactor first wall, feasibility of in situ regeneration by vapour deposition processes 77−18701
gas handling system for exacting crystal growth preparations 79−91593
glass, high silica content, isotopic CVD for low-loss optical waveguide prod. 77−72093
glass, ultrapure, prep. for optical waveguides, review 78−3086
glass CVD fibres with axial refractive index dip, dispersion meas. *(German)* 78−33857
glass fibre manufacture *(German)* 78−33933
glass fibreguides, for lighwave communication, fabrication and characteristion 80−50586
graded index fibres made by vapour phase axial deposition, refr. index profile 80−48477
graphite, pyrolytic C coating within pores 79−41035
growth, chem. transport, transfer inversion using Mo catalyst 79−11517
growth rates, consideration of effect of thermal boundary layer 80−54160
hardened metal, sintered, CVD of C rel. to atmosphere *(German)* 79−95966
heterostructures for integrated optics 77−39112
high deposition rate method using He gas, low loss optical fibres production appl. 77−11055
hydrodynamic descripion, two-component gas mixture with axisymm. stagnation flow geom. 77−40384
III-V compounds, crystal growth mechanisms *(French)* 79−33939
III-V compounds, vapour growth, using organometallic sources *(Japanese)* 80−16195
III-V semiconductor, vapour transport reactions and kinetics 79−28931
III-V semiconductor thin film prep. by low temp. CVD 80−60789
III-V semiconductors VPE using organometallics and hydrides *(French)* 79−33936
interface and vapour transport kinetics, interrel. in chem. vapour deposition 79−46583
interface morphology on profiled substrates, calc. of development 78−60040
isotope enrichment in CVD system 77−23301
isotope separation methods, by CVD and related processes 79−50148
IV-VI compound vapour growth and transport in microgravity 77−77400
kinetics, impurity capture 78−26468
laser applications in materials processing, seminar, San Diego, CA, USA (Aug. 79) 80−90609
laser deposition of film in active medium *(Russian)* 77−77394
light scattering, inelastic, as in situ probe of gas phase reaction 77−40383

chemical vapour deposition continued
lightguide fibre preform manufacture using modified CVD process 80−64228
low-loss graded-index fibre, 3 km and 10 km preform design and modified CVD method 80−58746
LPCVD-type plasma-enhanced deposition system [for semiconductor wafer processing] 80−60791
magnetic bubble materials, props. and preparation models, review *(Rumanian)* 80−93149
mass diffusion in two-dimens., perturbation method 79−2737
mass transport model, deposition rates 80−103599
mathematical modeling, chemical transport dynamical process *(Chinese)* 80−45232
MCVD optical fibres for transmission system field trial 80−43462
metal, plasma stream transport method, use of charge exchange plasma source 79−15613
metal halide layered materials, prep. and growth, book contrib. 78−19648
metal silicides, fabrication technique and characterisation, review *(Japanese)* 80−60779
metallurgical coatings, conf., San Francisco, USA (Apr 76) 77−31918
metallurgical coatings, conf., San Francisco (Apr. 1976) 77−40363
microgravity environment, benefits and constraints 79−83131
model, based on gas-phase diffusion and mass transfer at interface 77−59233
model, based on mass transport, rate limitation and reactant conc. effects 77−59234
monitoring of conditions, quick survey method 78−44019
morphological stability analysis 78−48323
morphological stability analysis 78−48324
morphological stability analysis 78−92200
multireaction chem. transport of solids, theoretical anal. 77−52236
optical fibre, doped deposited silica preform, CL drying simultaneous with consolidation 79−50466
optical fibre, fabrication, low OH content, vapour phase axial deposition method 78−83125
optical fibre, modified CVD prep., optical and mechanical props. reproducibility 80−69535
optical fibre, PCVD, dispersion measurement by mode-locked synchronously-pumped dye laser 80−64191
optical fibre construction, progress review 79−50459
optical fibre fabrication, computer-aided MCVD system *(Japanese)* 79−59852
optical fibre fabrication, reduction of OH-ion conc. 80−1310
optical fibre fabrication by improved CVD method 77−79976
optical fibre fabrication by improved CVD method 78−1448
optical fibre fabrication by isothermal plasma-activated CVD *(German)* 78−33928
optical fibre fabrication by vapour phase axial deposition, 1.3 μm, low-loss and wide bandwidth 80−38136
optical fibre fabrication in long lengths, improved deposition method 78−33922
optical fibre fabrication process, transmission properties 79−59806
optical fibre fabrication with medium numerical aperture and low-pulse-dispersion 77−79937
optical fibre manufacture, quartz, CVD process refractive index profile, liquid doping *(German)* 77−62050
optical fibre plasma activated CVD, influence of substrate temp. 80−48475
optical fibre preform, high-silica, OH-ion distribution 79−14121
optical fibre preform fabrication in axial direction by vapour phase axial deposition, continuous process 80−43473
optical fibre preform preparation, automatic diameter-control system 79−50463
optical fibre preforms produced at high rates by particulate-deposition methods 79−50461
optical fibre preparation, single-mode low birefr., polarisation characts. 79−7195
optical fibre preparation by Ar plasma augmented vapour deposition 80−48478
optical fibre refractive index change due to external forces 78−74971
optical fibres, bandwidth improvement due to modified CVD method *(German)* 77−54787
optical fibres, characteristic parameters and production methods, data transmission application *(French)* 79−90000
optical fibres, CVD fabricated, abrupt central dip in refractive index 78−22217
optical fibres, fabrication of synthetic silica tubing and fibres using SiO_2-B_2O_3 79−50462
optical fibres, graded index, fabrication techniques *(Japanese)* 79−59851
optical fibres, graded index, fabrication techniques using MCVD and refractive index profile control 79−59856
optical fibres, large-core high numerical aperture for data-link appls. 77−39028
optical fibres, low-loss single-mode, elliptical and circular core, laser gyro appl. 80−1344
optical fibres, MCVD fibre fabrication system design 79−55255
optical fibres, multimode graded index, modified process, reproducibility 78−90531
optical fibres, single-mode low-loss, fabrication with GeO_2-doped SiO_2 cores by CVD 77−39030
optical fibres, SiO_2, manufacture using modified CVD method *(Japanese)* 80−99864
optical fibres, vapour-phase axial deposition, simultaneous dehydration with consolidation 80−23780
optical fibres for data processing appls., outside vapour phase oxidation prep. 79−50426
optical fibres with refractive index dip on fibre axis 77−11004
optical glass fibre vapour phase axial deposition, OH content reduction by flame hydrolysis control 80−48474
optical graded-index fibre vapour-phase axial deposition method, fibre characteristics 80−58824
optical single mode CVD fibre, bend-induced birefringence obs. 80−58723
optical single mode fibres, homogeneous CVD fabrication and characterisation 80−69562
optical single mode fibres, ultra-low-loss, prep. of long lengths 79−76893
optical single-mode fibre with low attenuation, MCVD fabrication 80−53461
optical single-mode low-loss silica fibre prep., 10 km long 80−48476

chemical vapour deposition continued
passive components, fabrication for high temp. instrumentation 80−40266
phosphosilicate glass, CVD, P conc. meas. 77−80533
phosphosilicate glass cored fibre CVD production 77−39120
phosphosilicate glass flow mechanism, and appl. in MOS devices 77−77393
plasma activated, optical communications fibre manufacture appl. 80−23793
plasma CVD equipment, semiconductor IC production 80−25572
plasma deposition and plasma stream transport *(Japanese)* 78−92199
plasma stream transport method, use of charge exchange plasma source 79−15613
plasma stream transport method 78−52684
protective coatings for metals, chemically vapour deposited 78−44261
protective glassy layers at 500°C for Cu passivation 78−76785
pyrocarbon, deposition from gaseous hydrocarbons, kinetic model *(German)* 78−23851
quartz glass, Ge and B dopants, OH impurities, preform material and fibre optic waveguide struct. 80−64173
reactor, containing SiO_2 dispersed particulates, correlations with film characts. 80−76192
reactor improved design, with horizontally stacked quartz slabs 80−76195
refractory ceramic coatings, for high temp. use, current status *(Japanese)* 80−71619
refractory oxide layer growth by high-temp. electrochemical vapour deposition 78−23627
review 77−63561
rod-in-tube fabricated optical fibre characteristics 80−87574
semiconductor epitaxial films, book contrib. 77−12544
semiconductor fabrication trends, use of low-pressure hot-wall reactor, plasma systems and computer control 78−19670
semiconductor film growth, multilayer systems, spectroscopic ellipsometry, review 80−103603
Si, epitaxial film, kinetics of doping, gas-phase decomposition of SiH_4 77−16499
single-mode optical fibres with different B_2O_3-SiO_2 compositions 78−1392
solar absorber-reflectors, spectrally selective surfaces, CVD 79−79400
spectrally selective surfaces in photothermal solar energy conversion, tandem stack fabrication by CVD 80−45753
steel, C, carbide formation during chromising, exam. in terms of ternary phase diagrams 78−56818
steel, high alloy ledeburitic, wear and corrosion resistant coating by chemical vapour deposition 78−92403
steel, mild, Ta coating at atm. press. using CVD method 80−55591
steel, tool, TiC coated by CVD, wear resistance 79−34196
surface treatment by gas plasma *(Japanese)* 78−92386
techniques and appls. 80−25573
thin films, deposition techniques, review 80−80964
transparent conducting film prep. using reflecting high speed gas stream 80−11571
transport reactions, modified entrainment method 77−70002
vacuum creation problems *(French)* 80−101803
vaporizer for liq. organometallic compounds 77−77388
VLSI processing by low-pressure CVD, review 79−87581
wear resistant surface, review 78−72938
Ag, for appl, in high temp. photothermal conversion 79−79403
$AgIn_5S_8$, cryst. growth and props. 78−39677
$Ag_2S(Se)(Te)$, thermodynamic props., growth of single cryst. by chem. transport reaction 77−36380
Ag_2Te, growth by chem. transport *(Russian)* 79−38728
Al on Ni base alloys, transport agent comparison 78−11429
Al-Al_2O_3-SiO_2-Si capacitors, physical and elec. props. of RF plasma grown Al_2O_3 80−100530
Al-AlN-SiO_2-Si capacitors, physical and elec. props. of RF plasma grown AlN 80−100530
AlC_xN_y, refractory deposit, prep. by thermal decomp. of Al dialkylamides and characterisation 80−11572
AlF_3, single crysts., vapour phase chem. transport prep. *(French)* 79−69971
$Al_{0.5}Ga_{0.5}As$-GaAs heterojunction phototransistors, growth by metalorganic vapour deposition 79−67380
$Al_xGa_{1-x}As/Al_yGa_{1-y}As$ DH lasers grown by metalorganic CVD, CW operation in wavelength range 760-780 nm 80−64053
$Al_xGa_{1-x}As$-GaAs, p-n heterojunction laser, low temp. operation 80−1204
$Al_xGa_{1-x}As$-GaAs, p-n heterostruct. laser, tunnel injection and phonon-assisted recomb. 80−5733
$Al_xGa_{1-x}As$-GaAs, quantum-well heterostructure laser diode, temp. depend. of threshold current 80−87395
$Al_xGa_{1-x}As$-GaAs photopumped quantum-well heterostructure lasers grown by metalorganic CVD 79−98390
$Al_xGa_{1-x}As$-GaAs-$Al_xGa_{1-x}As$ photopumped quantum-well laser, room temp. CW operation 78−74908
AlN, CVD from $AlCl_3/NH_3$, calc. of equilibrium yields 79−52121
AlN, chemical and plasmachem. vapour deposition, optical and other props. 77−28727
AlN, crystn. from reactive pulse plasma 78−31308
AlN film, thermodynamics and kinetics of CVD 80−108354
Al_2O_3, alumina, whiskers growth by hydrolysis of AlF_3 79−28260
Al_2O_3, CVD, props. rel. to deposition parameters 78−92197
α-Al_2O_3 CVD and Czochralski grown crysts., imperfection anal. comparison 79−78868
Al_2O_3, CVD film on III-V semicond. substrate, ion beam etching, defect detection 80−89155
Al_2O_3, coating, wear characteristics, comparison or coated and uncoated WC hard metals 78−92365
γ-Al_2O_3, crystn. from reactive pulse plasma 78−31308
Al_2O_3, film, CVD on Si, chem., phys. and elec. props. 77−12543
Al_2O_3, film deposition from pyrolysis of Al acetylacetonate 77−85943
Al_2O_3 layer prep. by reduction by carbon in vacuum 77−8757
α-Al_2O_3, wear resistant coatings on cemented carbide machine tools *(German)* 79−74297
Al_xO_y supporting film prep. by Al evaporation 77−67538
Au film room-temp. plasma chemical transport deposition 79−78894
AuBr, I and P forms, growth by vap. transport, cryst. struct. 78−38676
B, β-rhombohedral, purification by electron beam melting and CVD 80−20781

chemical vapour deposition continued
B, CVD from BCl_3-H_2 and BBr_3-H_2 gas mixtures onto inert substrate, thermodynamic approach *(French)* 78−44020
B, CVD from BCl_3-H_2 mixture, on metallic substrate, thermodynamic exam. *(French)* 78−27412
B, CVD from impinging jets, mass transfer, equilib. and kinetics 78−27409
B, CVD on inert and metal substrates, Gibbs free energy minimisation 80−16201
B, chem. transport with I_2, BI_3 synthesis 78−52682
B, closed system CVD, deposition rate and rate-limiting steps 80−93492
B, closed system CVD, deposition rate, models for interpretation 80−97438
B deposition from BBr_3-H_2 mixtures, thermodynamic anal. 79−47634
B, deposition rate and supersaturation relationship using combined flux model 80−84856
B, deposition rate in closed systems, influence of HCl 80−84855
B fibre, prep. by closed CVD system, mech. props. and surface defects 79−52311
B fibre, prep. in closed CVD system 79−83129
B, filament CVD technology, book contrib. 78−48352
B filaments, CVD prep., elec. resist. 80−15523
B modifications, polymorphism, cryst. chem., struct., growth, book contrib. 78−47278
B, morphologies, influencing factors, temp. range 1390-1640K 80−89154
B, polymorphism rel. to CVD mechanics and deposit structs. 80−15403
α-B, rhombohedral, prep. methods, book contrib. 78−48295
B, structure of deposits-process relations 78−27410
B, tetragonal, phase I, prep. and struct., book contrib. 78−47277
B thermistor, pyrolitic, preparation and properties 77−12536
B-Si alloys, B-rich, prep., anal. and cryst. growth *(French)* 80−104091
B_4C, chem. erosion by H-plasma, first wall of fusion reactor 77−36676
$B_{50}C_x$, $x=1$ to 2, prep. and struct., book contrib. 78−47277
BN film, undoped and P-doped, effect of CVD parameters on props. 80−25571
BN, semicond. film, chemical deposition 80−71596
BN thick film, crystn. and semicrystn. CVD on C steel substrate 79−87586
$B_{50}N_x$, $x=1$ to 2, prep. and struct., book contrib. 78−47277
B_2O_3-SiO_2 low-loss single mode fibres, design, fabrication and transmission characts. 78−71199
BP:Ni pillar crystal growth from vapour 80−60758
B_xP_y, gas phase deposition from B-P-U-H systems, thermodynamics 79−11518
$B_{14}Si$ refractory thermoelectric material CVD and application 77−77411
C, amorphous, prepared by glow discharge method, elec. and optical props. 77−21036
C, columnar and laminar forms, deposition on polycrystalline Ni foils 78−63943
C fibre, vapour-grown, growth mechanism and props., review *(Japanese)* 77−66598
C, pyrolytic, spiral growth rel. to temp., press., flow conditions, dislocations, props. *(German)* 78−42931
C vapour deposition, feasibility of fusion reactor first wall regeneration in situ 77−18701
$CdCr_2S_4$ magnetic semiconductor crystal growth, structural defects, physical properties 80−60759
$CdCr_2Se_4$, single cryst. growth by chem. transport reactions 80−16163
$CdGu_2S_{4(1-x)}Se_{4x}$, opt. absorpt., elec. cond., spectral response, thermopower 77−72862
$CdIn_3Se_4$, cryst. growth, photoresponse and optical props. 78−39165
CdS films, from thermal decomp. of organometallics, growth kinetics and struct. 79−78895
CdS heterojunction solar cells by CVD method 80−45685
CdS, heterojunctions with InP and GaAs, prep. by CdS CVD and etching 78−52062
CdS:I single cryst., I detection by argentometric titration DEP 77−16875
CdS:I_2 system, interface kinetics and vapour phase mass transport 80−19732
$Cd_{1+y}(S_xSe_{1-x})$ single crysts., vapour phase transport and stoichiometry control 79−28940
CdSe film, effect of growth conditions on electrophysical properties 78−44024
CdTe, grown by chem. transport, morphology, struct. and microhardness *(Russian)* 78−22729
$CdTl_2Se_4$, single cryst., preparation, elec. cond. 77−24554
$Cd_{1-x}Zn_xSe$, epitaxial layer growth with Zn content from doping to solid soln. formation 77−85094
$CoCl_2(Br_2)(I_2)$, prep. using chem. transport via gas complexes *(German)* 79−15599
$CoCr_2S_4$, CVD grown, surface microstruct. 79−4905
$CoFe_2O_4$, epitaxial layer prod. by chem. transport 77−81224
$Co_{3-x}Mo_xO_4$ films, prep., struct. and elec. characteris. 80−108353
Co_xZrS_2, $(0<x\leq0.50)$, intercalation compounds, ordered phases obs. 80−33962
Cr, CVD on Ni, reaction mechanism, growth rate and struct. obs. 80−39476
Cr coatings, plasma-chemical deposition using transport reactions *(Russian)* 80−16191
Cr, preparation by decomp. of bis-arene cpds., struct. and phys. props. 80−60785
Cr_2S_3, single crystal, exam. of unit cell structures by interference contrast microscopy 78−67670
$CrWO_4$, cryst. growth and struct. *(French)* 77−43202
Cu and α-Cu-Zn alloy, whisker growth in Zn reduction, morphological change to dendrites 79−28261
$CuCl_2(Br_2)(I_2)$, prep. using chem. transport via gas complexes *(German)* 79−15599
$CuGa_xIn_{1-x}Se_2$, CVD, elec. and optical props., use as heterojunction solar cell absorber 79−52095
$CuIn_5S_8$, single crystn. phase, CVD prep., X-ray cryst. struct. determ. 79−65990
Cu_xMS_2, $(0<x\leq0.50)$ $(M=Zr, Hf)$, intercalation compounds, ordered phases obs. 80−33962
Cu_2O, CVD from Cu-O-H-Cl-N system, thermodynamic anal. 78−39676
Cu_2O, deposition by chem. transport using HU, HI *(German)* 78−31344
Fe whiskers grown from $FeCl_2.4H_2O$, exam. of growth morphology 78−72051

chemical vapour deposition continued
Fe-Cr-C, steel carbide formation during chromising, exam. in terms of ternary phase diagrams 78−56818
Fe-S system, chemical transport of non-stoichiometric phase 79−69972
Fe-Si layer, growth kinetics and morphology 78−95700
Fe_3BO_6, weak ferromag., growth of bulk single crysts. by vapour phase reaction 77−24939
$FeCl_2(Br_2)(I_2)$, prep. using chem. transport via gas complexes *(German)* 79−15599
$FeCr_2S_4$, pure and doped, CVD grown, surface struct., elec. props. and band struct. 79−4905
$FeCr_2S_4$, vapour grown, growth mechanism of multisteps on surface 78−75605
FeF_3, single crysts., vapour phase chem. transport prep. *(French)* 79−69971
β-Fe_2O_3 film, CVD and characterisation 77−44172
Fe_2TiO_5, pseudobrookite, single cryst. growth by chem. transport 78−80464
Fe_xZrS_2, $(0<x\leq0.50)$, intercalation compounds, ordered phases obs. 80−33962
(GaAl)As low-beam-divergence CW DH laser, grown by low press. metallorganic CVD 80−74376
GaAlAs-GaAs, high efficiency heterostruct. solar cell grown by metalorganic CVD 78−11118
$Ga_{1-x}Al_xAs$-GaAs DH lasers, very low threshold, grown by metalorganic CVD 78−55365
$Ga_{1-x}Al_xAs$-GaAs, abrupt quantum-well heterostruct. grown by metalorganic chemical vapour deposition 79−56933
$Ga_{1-x}Al_xAs$-GaAs DH lasers grown by metalorganic CVD, room temp. operation 78−1248
$Ga_{1-x}Al_xAs$-GaAs heterojunctions grown by metallorganic CVD 80−15599
$Ga_{1-x}Al_xAs$-GaAs laser, distributed Bragg confinement, room temp. operation 78−74907
$Ga_{1-x}Al_xAs$-GaAs low threshold room temp. DH lasers grown by metalorganic CVD 78−50804
$Ga_xAl_{1-x}Sb$, VPE with I_2 as transport agent 78−48325
GaAs, bulk purification by chemical vapour transport 79−24437
GaAs CVD for solar cell applications 77−77412
GaAs, CVD on W coated graphite, characterisation, and Schottky barrier solar cell characts. 79−28930
GaAs diode, high temp. and freq. characts., made by gas-transport method 79−19654
GaAs, epitaxial, polycryst., monocryst. layers and whiskers growth by CVD, SEM obs. electron diffr. study *(French)* 79−43150
GaAs, epitaxial layer growth by chloride process, μ and subμ thickness 78−23624
GaAs, film and solar cell on graphite, struct. and elec. props. 80−2286
GaAs film solar cell fabrication, substrate requirements 78−11125
GaAs growth dual-bubbler CVD system, characts., for MESFET applics. 78−6856
GaAs homojunction solar cells, large-grained, passivation method to improve open-circuit voltage 80−94070
GaAs multilayer with abrupt carrier conc. profile, vapour growth technique 78−11123
GaAs polycryst. film, for terrestrial photovoltaic energy conversion 79−15242
GaAs, polycrystalline, for solar cells 78−11124
GaAs polycrystalline film growth for solar cells 79−33941
GaAs, S doping behaviour during growth, electron conc. 78−26784
GaAs, VPE, review of growth techniques *(French)* 79−33935
GaAs, VPE, vapour-solid interface, expt. anal. *(French)* 79−33940
GaAs, VPE in Ga-$AsCl_3$-H_2 system at reduced temp. 79−11519
GaAs, whisker growth by thermal decomp. 77−55875
GaAs:Se(Zn) polycrystalline film, Hall effect, resistivity meas. 80−96911
GaAs-(GaAl)As DH stripe lasers, metal-organic CVD, life tests 79−98383
GaAs-Br_2(-Zn) system, filamentary cryst. prep. 78−52650
GaAs-HBr chemical vap. transport system, thermochem. data 78−6854
$GaAs_{1-x}P_x$, solid soln. comp. control during gas-phase heteroepitaxy 77−85091
GaInAs-InP, growth by low-pressure metalorganic CVD 80−71595
$Ga_xIn_{1-x}As_yP_{1-y}$, CVD by Ga-In-P-H-Cl system, 80−54159
$Ga_xIn_{1-x}As_yP_{1-y}$/Inp DH laser emitting at 1.15 micron grown by low-pressure CVD 80−64052
$Ga_{1-x}In_xSb$, vapour phase epitaxial growth by open tube method 78−84109
GaN, deposition from plasma reactor, organo-metallic and donor-acceptor complex exchange in HF plasma 80−38839
GaN, epitaxial growth kinetics in Ga-HCl-NH_3 77−80710
GaN film, deposition by pyrolysis of gallium trichloride and triiodide ammoniates 77−36402
GaN preparation in sealed fused silica ampoules 80−80982
GaN VPE for blue LEDs *(French)* 79−28928
GaN, VPE growth rate influence on elec. and luminesc. props. 80−100702
GaN:Zn epilayers, growth parameters effect on props., device struct. 78−26975
Ga_2O_3 film, growth by reactive vapour deposition, optical and elec. props. 77−48347
GaP, chem. vapour growth in closed system 78−35283
GaP, epitaxial layer prep. and elec. props. 77−85096
GaP, synthesis by gas chemical transport reactions, exam. of kinetics 79−95933
GaP-ZnS, solid solns., microstruct. investig. 78−2128
GdIG, expts. on chem. equilib. for possible appl. in CVD 80−24750
Ge, amorphous whisker growth 78−2400
Ge, epitaxial, in situ X-ray topography, misfit dislocations 78−47671
Ge, vapour transport rate, Ge-I_2 equilib. 700 to 1300K *(French)* 78−64476
GeAs$+Cl_2(Br_2)(I_2)$, high temp. Raman spectra, cryst. growth mechanism *(French)* 79−26999
GeC_x, amorphous, prepared by glow discharge method, elec. and optical props. 77−21035
Ge_3N_4 films, synthesis and principal props. 77−24960
GeO_2 doped silica, low loss single mode fibre, CVD *(Japanese)* 78−37979
GeO_2-P_2O_5-SiO_2 core for graded index fibre, prep. by modified CVD technique 77−88910

chemical vapour deposition continued
- GeO_2-P_2O_5-SiO_2 glass fibre, incorporation of OH in modified CVD process 80−50560
- GeO_2-P_2O_5-SiO_2 graded-index fibres, effect of deposition rate on spectral loss 80−87485
- GeO_2-SiO_2, pyrolytic film prep. 77−81223
- $GeSe_2$, single cryst. growth 77−52305
- HfO_2 film, CVD growth, struct., elec. and optical prop. characterisation 77−55891
- HfO_2 film, growth by thermal decomp. of β-diketonate complexes, characts. 79−100055
- $Hg_{1-x}Cd_xTe$, mixed crystals, crystn. by chemical transport 80−20775
- $HgCr_2Se_4$, vapour growth using $AlCl_3+Cl_2$ as transport components 78−35282
- $HgCr_2Se_4$-$CdIn_2S_4$ heterojunctions, prep. and photovoltaic prop. 78−34892
- HgS, cinnabar, chem. vapour growth in closed system 78−35283
- HgSe, CVD crysts., electrophys. characts. 77−85910
- $HoPo_4$, single crystal, conditions for transfer and formation 77−12507
- InAs, H_2O transport method, Hall element preparation 77−40377
- $In_{1.9}As_{0.1}Se_3$, growth by chem. vap. transport, characterisation as photoelectrode 78−43994
- n-$In_xGa_{1-x}As$ film, epitaxial growth on GaAs, using CVD system 77−1812
- In_2O_3 film prep. using reflecting high speed gas stream 80−11571
- In_2O_3 layers, chemically sprayed, prep. and intrinsic absorpt. in band edge 77−81169
- In_2O_3, transparent electrode deposition on PLZT ceramic 78−74848
- In_2O_3:Sn, transparent conducting films, prep. by $InCl_3$ thermal decomp., transmittance, resistivity 79−33944
- In_2O_3:Sn films, CVD prep. and elec. resist. meas. 79−52120
- p-InP film, CVD, growth characts. and CdS/InP solar cell efficiency 77−1813
- InP film, CVD on preferentially etched Mo, initial growth behaviour 78−51855
- p-InP film growth, by close space vapour transport 79−28944
- p-InP, prep. of single and bi-crysts., epitaxial layer and polycryst. films 77−81211
- InP, VPE 79−28927
- InP-SiO_2 interface, CVD problems, ESCA profiles 80−93497
- $In_{2/3}PSe_3$, cryst. growth and characterization 77−77357
- n-InSb MIS device interfaces, low-temp. CVD of SiO_2, characts. 80−16196
- LaB_6, chemical vapour growth of whiskers, and single crystals 78−72710
- $MgFe_2O_4$, epilayer, perpendicular anisotropy 80−39769
- $MnCl_2(Br_2)(I_2)$, prep. using chem. transport via gas complexes *(German)* 79−15599
- MnS(Se)(Te), CVD crystal growth, role of Mn-Al-Cl complexes 80−84840
- $Mn_{15}Si_{26}$, growth by Bridgman method and chemical transport, X-ray structural analysis 79−100043
- Mo borides, deposition from B halide+metal halide mixture *(French)* 77−36406
- Mo, CVD films of high IR reflectance 79−52119
- Mo, film, formation by reduction of $MoCl_5$, influence of electric field 80−93491
- Mo, for appl. in high temp. photothermal conversion 79−79403
- Mo, with high IR refl. and large solar absorpt., prep. and props. 80−26163
- Mo_2C, from $Mo(CO)_6$ pyrolysis, laser fusion target appls. 78−60861
- Mo_2C powder form. by CVD 77−12590
- MoO_2, MoO_3 and Mo_xO_{3x-1} single cryst. growth by chem. transport, elec. resist. meas. 77−59681
- MoO_2-I_2, heterogeneous equilib., vapour transport and cryst. growth 78−27405
- $MoSe_2$ lubricant, synthesis by Mo+Se vapour reaction, process kinetics 79−33942
- $MoSi_2$, diffusion grown layers, texture 79−74095
- $MoTe_2$, pure and V doped, single cryst. growth and vapour phase transport 79−28903
- NI dendrites on Al, CVD, selective solar photothermal absorber 78−52683
- Nb borides, deposition from B halide+metal halide mixture *(French)* 77−36406
- Nb, CVD, kinetics and microstruct., pressure and temp. depend. 80−11569
- Nb CVD coatings on graphite, grain struct. depend. on temp. 80−25574
- Nb, precipitation from gaseous phase, during H_2 reduction of $NbCl_5$ and $TaCl_5$, Ta behaviour *(Russian)* 78−44017
- Nb-Ga, A15 phase, chem. deposition on Hastelloy substrate, for superconducting tape *(German)* 80−104071
- Nb-Ge, compounds with A15 structure, films, TEM study *(French)* 80−80135
- Nb-Ge film, CVD and sputter deposited, critical current density and stability 77−28327
- Nb-Ge-Si, compounds with A15 structure, films, TEM study *(French)* 80−80135
- Nb-Ge(Si) and Nb-Ge-Si, A15 cpds., CVD prep. and supercond. crit. temp. 79−60949
- Nb-Si, compounds with A15 structure, films, TEM study *(French)* 80−80135
- Nb-Si compounds, CVD, struct. and supercond. props. 79−24447
- NbB_2, vapour transport in temp. gradient in presence of iodine 79−19997
- NbC coating on C steel and Armco Fe, deposition, struct. and props. 79−52462
- $Nb_xCr_{1-x}O_2$, $(x\geq0.5)$, cryst. growth by chem. transport and phase transitions 78−35281
- $Nb_xCr_{1-x}O_2$, cryst. prep. and struct., mag. props. 78−52198
- Nb_3Ga, thermodynamic and expt. study of CVD 79−24441
- $Nb_3(Ge,Si)$ A15 film, supercond. and structural props. 79−87177
- Nb_3Ge, CVD, AC losses, temp. depend., 4-20K 77−28311
- Nb_3Ge, CVD, hysteretic losses, precipitates and deposition temp. effects 77−28319
- Nb_3Ge composite filament, continuous, high-strength, prep. and supercond. props. 77−28765
- Nb_3Ge continuous supercond. tape, prep. by CVD 77−80893
- Nb_3Ge film, CVD fabrication of supercond. tape for high-field magnets 78−95698
- Nb_3Ge, supercond. film, prep. by chem. transport reaction, critical props. 79−47635

chemical vapour deposition continued
- Nb_3Ge tape, prepared continuously by CVD, props. 78−60257
- Nb_3Ge tape, supercond., prep. by continuous CVD process 78−11121
- NbN, Nb_4N_3-NbN, Nb_2N-Nb_4N_3, Nb_2N, cryst. growth parameters and morphology of chem. vapour deposition, X-ray diffr. and SEM study 79−23861
- $Nb_3Nb_{1-x}Si_x(Ge_x)$, impurity stabilised A15 supercond., transition temp., lattice consts., specific heat 80−93026
- NbO, single cryst. growth by chem. transport reactions 77−12508
- NbO_2, chemical transport with $TeCl_4$, exam. of deposition and crystal morphology 79−52093
- $NbO_{2.417}$, chemical transport with $TeCl_4$, exam. of deposition and crystal morphology 79−52093
- Nb_2O_5, single cryst. growth by chem. transport reactions involving $TeCl_4$ 77−36382
- $NbSbS_3$, synthesis and single cryst. growth and struct. 77−52234
- $NbSe_2$, I_2 vapour phase transport kinetics *(French)* 78−11092
- Nb_3Sn, critical currents, ang. depend., prep. conditions effects 77−43793
- Ni films, laser CVD 79−78897
- Ni-Cl boracite, chem. vapour transport, appl. of flux function method 79−52091
- $NiCl_2(Br_2)(I_2)$, prep. using chem. transport via gas complexes *(German)* 79−15599
- $NiFe_2O_4$, single cryst. prep. by chem. transport 78−23589
- Ni_2P, CVD on Mo plate, microhardness and resist. to chem. attack 79−66009
- Ni_2SiO_4, single crystals, chem. transport prod. mechanism and thermodynamics *(German)* 77−36383
- Ni_xZrS_2, $(0<x\leq0.50)$, intercalation compounds, ordered phases obs. 80−33962
- NpO_2, cryst. growth by chem. transport 80−16166
- P_2O_5-SiO_2 clad low-loss monomode fibres for 1.2 to 1.6 μm, modified CVD prep. 80−48479
- P_2O_5-SiO_2 glass, flow for integrated optical cct. fabrication 80−79005
- $PaAs_2$, Pa_3As_4, and PaAs, cryst. growth by chem. vapour transport, cryst. struct. 80−35066
- PbSe film, 50 μ, prep. in double quasiclosed volume 79−38745
- $Pb_{1-x}Sn_xSe$, single crystal and film, X-ray spectral investigation of solid solution 77−16477
- PbTe film, 50 μ, prep. in double quasiclosed volume 79−38745
- $PdCl_2(Br_2)(I_2)$, prep. using chem. transport via gas complexes *(German)* 79−15599
- Re, interaction with F_2 and fluorides at low temp. and high press. 78−39700
- Re, vapour deposited, hot burst strength 78−44021
- Sb_2O_3-SnO_2 film vapour deposition in conveyor furnaces *(French)* 78−15311
- Sc, CVD, open-tube technique 80−89128
- ScH_2, CVD 79−24420
- (Si,Al)N, vapour deposition, feasibility of fusion reactor first wall regeneration in situ 77−18701
- Si, amorphous, p-n junction preparation, by SiH_4 decomposition *(Czech)* 77−63560
- Si, amorphous film deposition from silane glow discharge plasma 77−44173
- Si amorphous film preparation, by SiH_4 decomposition 80−80956
- Si, amorphous film prepared by CVD, optical props. and struct., solar absorber appl. 79−52035
- Si, CVD, surface anal. during growth using RHEED and Auger spectroscopy 80−66433
- Si, CVD from SiH_4-HCl-H_2 system, rate-determining reactions and surface species 80−84405
- Si, CVD growth, high- and low-temp. models 78−6244
- Si, CVD growth and film morphology, rel. to model of mass transport 77−59233
- Si, CVD growth rate, temp. and conc. effects, mass transport model 77−59234
- Si CVD of polycrystal on liquid Sn layer 78−64479
- Si, CVD on liq. Sn layers in HCl presence, enhanced crystallinity 78−6853
- Si, CVD using CO_2 laser 78−56589
- Si, characterisation and morphology 79−33938
- Si, crystal growth mechanisms *(French)* 79−33939
- Si, crystallisation in Si-H-Cl system, adsorpt. layer comp. 77−15697
- Si deposition by SiH_4 pyrolysis at low temps. and atm. press. 79−91595
- Si, deposition on rotating disc, one-dimens. model 80−75461
- Si film, amorphous, formed by CVD, crystallisation 77−39746
- Si, film, chemically deposited on amorphous SiO_2, influence of substrate temp. and SiH_4 to N ratio on struct. 79−65346
- Si film, low press. techniques, IC fabrication process anal. 79−100058
- Si film, polycryst., electron microscopic investigation of initial stage of growth 79−23849
- Si film, polycryst., laser-induced CVD growth from $SiCl_4$ 80−84852
- Si film, polycrystalline, struct. thickness relationships 77−62779
- Si film, prep. by plasma-induced CVD from $SiCl_4$-H_2 79−83132
- Si, film deposition, growth kinetics under low H_2 press. 78−56586
- Si film deposition by CO_2 laser irrad. of SiH_4 80−16190
- Si film on SiO_2 substrate, CVD by pyrolysis of SiH_4 77−89678
- Si, for appl. in high temp. photothermal conversion 79−79403
- Si, gas phase diffusion and surface reactions 79−15614
- Si, high-purity, preparation by H_2 reduction of trichlorosilane *(Korean)* 77−21034
- Si MIS switch diode, charge storage effects, threshold depend. on driving voltage pulse freq. 80−49939
- Si on sapphire, deposition kinetics and interface characteris. 79−28234
- Si, on SiO_2 and Si_3N_4 substrates, nucleation in SiH_4-HCl-H_2 system at high temp. 80−49538
- Si optical fibres, advances in fabrication using MCVD process 80−99875
- Si, polycryst., deposition as example of pyrolytic CVD process 80−84407
- Si, polycryst., growth, props. and MIS appl. *(Slovak)* 78−92196
- Si, polycryst., growth kinetics in low press. CVD reactor 79−91594
- Si, polycryst., low press. CVD production processes 77−77395
- Si, polycryst. film doping during deposition and with diffusion 78−6088
- Si, polycryst. film from low. temp. pyrolysis of SiH_4 78−31342
- Si polycrystalline p-n junction deposition 78−10549
- Si, prod. of polySi vapour deposited coatings for solar cells, cost anal. 80−93495
- Si production, low-cost low-energy processes 78−11126
- Si, production by reduction of SiO_2 with C black in plasma reactor, feasibility 78−27426
- Si purification, using silicon fluoride as transport 78−35316

chemical vapour deposition continued
Si ribbons for solar cells, ultra high speed growth, elec. props. 80−89162
Si rich SiO_2-SiO_2-Si rich SiO_2 layers for dual electron injector struct. 80−96991
Si solar cells, growth of large grain polycryst. layers on graphite substrates by CVD on liquid layers 80−55849
Si, solar grade, by $SiHCl_3$ CVD process, low cost 79−62007
Si, using CO_2 laser for substrate heating 78−39698
Si, VPE, state of art 79−33937
Si, VPE growth mechanisms 79−28929
Si, whisker, growth by reduction of $SiCl_4$ in H_2 gas current 77−15726
Si:As, CVD, doping using SiH_4-H_2-AsH_3 system 80−79823
Si:B, highly-doped polycryst. thin film, growth kinetics and properties 78−44016
Si:H, amorphous, prod. by high temp. thermal decomp. of SiH_4, and photocond. 79−87585
Si:P, amorphous, substitutionally doped CVD, electrical props. 79−99566
Si:P, polycryst., growth in epitaxial reactor at 800°C, using PH_3 doping 77−1815
Si-Ge-Br, heterogeneous system, equilib. gas phase composition, Si-Ge cryst. growth appl. 79−10820
Si-N-H gaseous system, deposition ranges of Si_3N_4 and Si *(French)* 77−36405
Si-poly Si; growth rate effects, Hall mobility 77−76904
Si-SiO_2 interface in IGFETs, anal. of CVD SiO_2 on (100) and (111) surfaces, near-ideal structs. 80−100528
$SiAs+Cl_2(Br_2)(I_2)$, high temp. Raman spectra, cryst. growth mechanism *(French)* 79−26999
$SiBr_x$, x=1,2,4, diffusive mass transfer of Si, calc. for closed system 77−44169
SiC CVD substrate, Cu mirror vapour deposition, pulsed laser damage characts. 80−48314
SiC, chem. erosion by H-plasma, first wall of fusion reactor 77−36676
SiC coating on C fibre, chemical vapour deposition, relation between surface morphology and coating conditions *(Japanese)* 78−39704
SiC, controlled nucleation thermochemical deposition, charact. and props. 80−108355
β-SiC, growth kinetics by Van Arkel method 77−16479
SiC, microstruct. obs., optical and TEM 79−7560
β-SiC, powder, synthesis by chemical vapour phase reaction from methylsilane, exam. of props. *(German)* 79−4938
SiC pyrolytic coatings for HTGR fuel particles, props. rel. to deposition conditions 79−31088
SiC, Si_3N_4, (Si,Al)N, vapour deposition, feasibility of fusion reactor first wall regeneration in situ 77−18701
n-SiC, single cryst. layers deposition on charact. substrates, morphology *(German)* 79−28943
SiC, vapour deposition, thermodynamics of Si-C-Cl-H system *(German)* 79−11520
SiC_x, amorphous, prepared by glow discharge method, elec. and optical props. 77−21035
$SiCl_4$-$GeCl_4$-BCl_4 particulate layers consolidation, in fabrication of optical fibre preforms 80−60787
$SiCl_4+O_2$ in modified CVD process for optical fibre prod., reaction IR spectra 78−80472
$Si_xGe_{1-x}(H)$ amorphous alloys, from glow discharge, optical properties 78−19510
SiN_x films, plasma enhanced CVD, props. meas. and interpretations 80−80987
Si_3N_4, amorphous, CVD prep., struct. characts. by pulsed neutron diffr. 80−33891
Si_3N_4 amorphous films, CVD mech. and thermal props. *(Japanese)* 77−90280
Si_3N_4, CVD, struct., optical and mech. props. 77−1816
Si_3N_4, CVD anal. using hydrodynamics 77−40384
Si_3N_4 CVD films, microstruct. and MNS struct. characts. 79−65339
Si_3N_4, CVD from $SiCl_4$ and NH_3, mass spectroscopic anal. of intermediates 79−43149
Si_3N_4 coated fibres for high-strength and improved fatigue 79−50470
Si_3N_4, dielectric films made by NH_3-silane reaction, TEM study 80−84413
α-Si_3N_4, exam. of chemical vapour deposition, and IR transmission and reflectance 79−19993
Si_3N_4 film, deposition by pyrolysis of SiH_4-NH_3 mixture, struct. and props. of deposit *(French)* 77−40382
Si_3N_4 film, low press. techniques, IC fabrication process anal. 79−100058
Si_3N_4 film, plasma-activated CVD, optical prop. depend. on growth conditions 77−55892
Si_3N_4 film, prep. by reaction of active N with SiI_4 vapour 77−24963
Si_3N_4 film, synthesis mechanism 77−12538
Si_3N_4 film deposited from SiH_2Cl_2 and NH_3, characterisation 79−11521
Si_3N_4 film on Si substrate *(Korean)* 80−55300
Si_3N_4 films, amorphous, CVD, IR spectra 77−21031
Si_3N_4 for thin film passive components for high temp. instrumentation 80−40266
Si_3N_4, in hot-wall diffusion system 79−19996
Si_3N_4, intermediates in CVD, mass spectrometric detect. 78−27411
Si_3N_4, investigation of gas phase of CVD reaction 78−52681
Si_3N_4, kinetic model for RF plasma-activated CVD 78−27416
Si_3N_4 layers deposition, high-temperature, in resistance furnace, temperature gradient and nitrogen flow influence obs. *(Bulgarian)* 80−80981
Si_3N_4, low press CVD film, steady-state electron and hole space charge distrib. 80−29493
Si_3N_4, low press. CVD production processes 77−77395
Si_3N_4, low pressure CVD, thermochemical calcs. 80−108356
Si_3N_4, massive, Vickers microhardness effect of deposition parameters 77−56079
Si_3N_4, massive structural props., effect of deposition parameters 77−55272
Si_3N_4 noncrystalline layers, CVD growth, encapsulant layers for annealing GaAs 79−19994
Si_3N_4 on Si, optical waveguide, fabrication, propag. consts. 78−33826
Si_3N_4, plasma deposition, optical absorption as control test 78−35314
Si_3N_4, plasma stream transport method, use of charge exchange plasma source 79−15613
Si_3N_4, prep. by CVD, effect of raw gas flow rate *(Japanese)* 77−48348
Si_3N_4, pyrolytic, prep. by CVD, bulk and coatings, exam. of electrical, optical and physical props. 79−95935
Si_3N_4, pyrolytically-deposited, engng. significance 79−38746
Si_3N_4, rapid CVD, and struct. characts. 77−28767

chemical vapour deposition continued
Si_3N_4, room temp. CVD on InSb 80−71597
Si_3N_4, separation, effect of reactor geometry *(German)* 78−60583
Si_3N_4, Si rich, CVD film prep. and props. 78−76607
α-Si_3N_4 single crysts., growth, morphology, hardness and slip system 79−83112
Si_xN_y, amorphous, prepared by glow discharge method, elec. and optical props. 77−21035
$Si_xN_yH_z$, film, prep. from plasma-induced CVD from Si-NH_3 79−83132
Si_2NO_2, needle crystals, formation and growth rate, nitridation of Si-SiO_2 powder compacts *(Japanese)* 79−91574
SiO_2, CVD anal. using hydrodynamics 77−40384
SiO_2, dispersed SiO_2 particulates, size distrib. semi-in situ obs. by light scatt. 78−27406
SiO_2 film, CVD on GaAs using tetraethoxysilane oxidation 78−60582
SiO_2, film, formation from tetraalkoxysilanes in O_2 current, props. 77−44170
SiO_2 film, low press. techniques, IC fabrication process anal. 79−100058
SiO_2 film deposition by SiH_4 oxidation, kinetics and physicochemical model 79−42419
SiO_2 film deposition from SiH_2Cl_2 on Si 77−77407
SiO_2 film growth technology *(Japanese)* 77−40381
SiO_2 films, CVD at reduced press., optical props. 80−2957
SiO_2 films, prep. from tetraalkoxysilanes, by activation pyrolysis 79−87583
SiO_2, fused silica, isotopic CVD for low-loss optical waveguide prod. 77−72093
SiO_2, GeO_2 doped single-mode fibre with low loss at material-dispersion-free wavelength of 1.27 μm 77−68266
SiO_2 glass, high rate MCVD of optical fibres 80−83671
SiO_2 inversion layer in MIS solar cells, low-temp. process 80−12019
SiO_2 layers, passivating, deposition by plasma decomp. in planar reactor 78−88430
SiO_2, low press. CVD production processes 77−77395
SiO_2, low pressure CVD, thermochemical calcs. 80−108356
SiO_2, low temp. CVD on n-InSb, surface quality improvement and characterisation 80−49932
SiO_2, low-pressure deposition from tetraethylorthosilicate, modelling 79−87582
SiO_2 on InP, MIS struct. prod., resist., breakdown and interface states 77−15961
SiO_2, plasma stream transport method, use of charge exchange plasma source 79−15613
SiO_2 separation below 500°C, state and tendency of chemical gas phase separation *(German)* 80−100794
SiO_2, Si rich, CVD film prep. and props. 78−76607
SiO_2 silica glass fibre CVD manufacture and characteristics 80−28345
SiO_2, thermophoretic deposition of small particles in MCVD process 79−52123
SiO_2, thin film, obtained by oxidising SiH_4 in HF gas discharge plasma 77−11804
SiO_2, thin film, prep. from low-temp. oxidation of tetraisopropoxysilane, dielec. props. 77−8759
SiO_2, transfer in quartz capsule 79−4902
SiO_2, uniform film prep. by pyrolysis of tetraethoxysilane 77−40379
SiO_2:B(P) film, high temp. deposition and evaluation 79−69989
SiO_2:F fibre preform plasma chemical deposition *(German)* 78−33926
SiO_2:F fibre preparation by plasma-activated CVD *(German)* 78−33927
SiO_2:F layers, deposition from $SiCl_4$-SiF_4-O_2 gas mixture by plasma CVD method 78−95699
SiO_2:GeO_2 graded-index fibres, without index dip, fabrication by CVD method 78−9431
SiO_2-FeO_2 particulate mass transfer mechanism in modified CVD, thermophoresis 80−2955
SiO_2-GeO_2 particles, deposition props. in flame hydrolysis reaction for optical fibre fabrication 80−48470
SiO_2-P_2O_5-GeO_2 optical fibres, CVD, losses, reactant impurity effects 80−87522
SiO_xN_y, deposition kinetics in SiH_4-CO_2-NH_3-H_2 system 77−48346
SnO_2 CVD film form. mechanism 78−38977
SnO_2, cryst. growth by chem. transport method 78−3004
SnO_2, crystal growth habits *(Japanese)* 78−95686
SnO_2 film, CVD using $SnCl_4$-H_2O and $SnCl_4$-H_2O_2 systems, elec. and optical props. 78−52686
SnO_2 film, deposition from vapour phase, thermodynamic anal. 80−15418
SnO_2 film growth at room temp. 79−91592
SnO_2 film prep. using reflecting high speed gas stream 80−11571
SnO_2, transparent electrode deposition on PLZT ceramic 78−74848
SnO_2, VUV transparent electrode formation by chemical deposition and vacuum sputtering 79−56929
SnO_2:As film, prep. and elec. cond. 80−2959
SnO_2:Cr(Sb), cassiterite, gas phase growth on seed 77−24937
SnO_2/n^+-pSi heterojunction solar cells, fabrication by paint-on-diffusant method 80−94048
SnO_x:Sb,F film CVD for bistable storage CRT 77−77410
Sn_xO_y films, semiconducting, equipment for deposition on cylindrical objects 77−40378
SnS_2, cryst. growth, photoconductivity 77−85912
SnS_2-SnI_4, and SnS_2-I_2, systems, transport props. and thermodynamical calcs. 79−32928
SnS_xSe_{2-x}, growth by I_2 vap. transport, cryst. struct. 77−73223
SnTe film, 50 μ, prep. in double quasiclosed volume 79−38745
$Sn_xZr_{1-x}Se_2$, growth by I_2 vap. transport, cryst. struct. 77−73223
SrN, impurity activated whisker growth by CVD 79−66010
Ta borides, deposition from B halide+metal halide mixture *(French)* 77−36406
Ta, CVD, kinetics and microstruct., pressure and temp. depend. 80−11569
Ta coating of mild steel by CVD 78−15594
Ta, film, CVD on silica, struct. and mech. props. 77−24965
Ta, interaction with F_2 and fluorides at low temp. and high press. 78−39700
Ta, purification from Nb during precipitation from gaseous phase, during H_2 reduction of $NbCl_5$ and $TaCl_5$ *(Russian)* 78−44017
TaB_2, CVD on quartz substrate from gas mixture of $TaCl_5$-BCl_3-H_2-Ar 80−29880
TaB_2, vapour transport in temp. gradient in presence of iodine 79−19997
TaN film, growth by CVD, microhardness and corrosion resist. 77−36404

chemical vapour deposition continued
Ta_2O_5 film, for MIS device, CVD and characterisation 77−4742
Te, evaporated film epitaxial and amorphous-crystalline phase transition growth and struct. 79−51449
Th_3As_4-U_3As_4, cryst. growth by chem. vap. transport 78−23588
Th_3P_4, cryst. growth by chem. vap. transport 78−23588
$ThSb_2$, Th_3Sb_4, cryst. growth by chem. vap. transport 78−23588
Ti-B-N, CVD, lattice const. 79−74097
Ti-Zr-B system 78−60581
Ti(B,N), CVD coating on cutting tool 79−61802
TiB_2, CVD from $TiCl_4$, BCl_3 and H_2, equilib. thermodynamic anal. 77−59694
TiB_2, CVD from $TiCl_4$, BCl_3 and H_2, deposition kinetics modelling 77−59695
TiB_2, chemical vapour growth by modified hot wire method 78−60555
TiB_2 coating on graphite by CVD 80−21131
TiB_2 coatings, prep. by CVD and interaction with substrate 79−24680
TiB_2 thick film on low C steel substrate, CVD in US field, crystallite size 80−84854
TiC, CVD and activated reactive evaporation on WC-TiC-Ta(Nb)C-Co, substrate-layer interactions, AES obs. 79−24679
TiC, CVD effect of cemented carbide substrated 79−74096
TiC, CVD rate, depend. on gas composition 77−40386
TiC, coating, wear characteristics, comparison or coated and uncoated WC hard metals 78−92365
TiC, deposition from gas phase during pyrolysis of cyclopentadienyls 77−85944
TiC, deposition rate meas., rel. to mass transport model 80−103599
TiC, laser CVD, coating characterisation 80−93494
TiC whiskers, growth by CVD, catalytic effects of various metals and refractory oxides 79−33211
TiC whiskers, growth rate for CVD 77−47704
TiF_3, single crysts., vapour phase chem. transport prep. *(French)* 79−69971
Ti(N,C,O), wear resistant coating for cemented carbides and high speed steels 78−92406
TiN *(Japanese)* 77−63562
TiN, appl. of quick survey method for CVD conditions 78−44019
TiN, CVD growth in US field, effect on adherence and hardness 77−59696
TiN(C) whisker growth in CVD 80−59843
TiO_2, anatase, single cryst. growth by chem. transport reactions 77−36384
TiO_2, anatase film, intermittent CVD conditions rel. to struct. 78−11119
TiO_2 film, laser CVD 79−78897
TiO_2, rutile, film, CVD in $TiCl_4$-H_2O system 77−12541
TiO_x, thermodynamic of chem. transport systems 78−27393
Ti_2O_{2x-1}, prep. by chem. transport method, equilib. comp. of TiO_2-Ti-Cl_2 gas phase 80−21317
Ti_2O_3, cryst. growth by chem. transport and tri-arc methods, and characterisation 78−3003
Ti_4O_7, controlled growth by chem. transport reactions 77−90262
Ti_nO_{2n-1}, cryst. growth and characterisation 78−31311
TiP-I_2, exam. of equilibrium gas-transport reaction 79−95911
TiS_2, chem. transport rate effects on stoichiometry 77−90263
TiS_2, nonstoichiometric, chem. transport reaction mechanism 77−8735
TiS_2, V addition effect on chemical transport 79−24419
TiS_2-I_2 system, thermodynamic considerations for layered dichalcogenide growth by vapour transport process 79−4903
UAs, U_3A_5, cryst. growth by chem. vap. transport 78−23588
UO_2, cryst. growth by chem. transport 80−16166
UO_2, growth by chem. vapour transport, using $TeCl_4$+Ar 78−35284
USb, USb_2, U_3Sb_4, cryst. growth by chem. vap. transport 78−23588
USb_2, crystal growth by chemical vapour transport 80−15024
$U_{1-x}Th_xO_2$, solid solution, single crystal growth by chemical transport reactions 78−72708
V-O system, chemical transport of non-stoichiometric phase 79−69972
$(V_{1-x}Cr_x)_2O_3$, vapour phase transport, single cryst. growth *(French)* 77−24940
V_3Ga, single crystal prep. by iodine transport, supercond. T_c meas. 78−48294
VO_2, CVD behaviour *(German)* 78−23625
VO_2, chemical transport, mass spectrometric study 79−24860
VO_2, V_2O_3 and V_3O_5, film prep. under equil. conditions, struct. and elec. props. 80−108352
V_2O_3, vapour phase transport, single cryst. growth *(French)* 77−24940
V_2O_5 film, amorphous, CVD prep. method 80−55299
V_2O_5, low dislocation density cryst. growth, opt. props. 77−63551
V_nO_{2n-1}, cryst. growth and characterisation 78−31311
V_nO_{2n-1}, microsyntactic intergrowth 79−1402
V_nO_{2n-1}, V_6O_{13}, V_2O_5, Magneli phases, chem. transport using $TeCl_4$ *(German)* 78−31343
W borides, deposition from B halide+metal halide mixture *(French)* 77−36406
W, by reaction of WF_6 and H_2, kinetics 79−19995
W for thin film passive components for high temp. instrumentation 80−40266
W, high temp. strength and ductility 77−52406
W, interaction with F_2 and fluorides at low temp. and high press. 78−39700
W needle crystal growth, discharge-induced decomp. of hexacarbonyltungsten mols. 80−84414
W tube, CVD, study of preferred orientation *(Korean)* 77−8761
WC, sinterability of ultrafine powders obtained by CVD method 80−108378
W_2C, W_3C, wear resistant coatings, low temp. form., on steel substrate 78−92404
WO_2, cryst. growth, chem. transport conditions influence on morphology and quality 79−43114
WO_3, chem. transport, thermodynamic investigations *(Russian)* 79−69990
WO_3, close-spaced chem. transport rates *(Russian)* 80−11570
WSi_2, diffusion grown layers, texture 79−74095
YbSe, crystn. by chem. transport reaction with I_2 77−24935
Zn_3As_2, synthesis and layer growth 78−15312
$Zn_xCd_{1-x}S$ film, prep. and use as heterojunction optical energy converters 79−95488
$ZnFe_2O_4$, single cryst. prep. by chemical transport 77−16482
$ZnGeP_2$ layers, growth on Ge substrates, using chemical vapour deposition 79−52122
$Zn_xHg_{1-x}Se(Te,S)$ film preparation and props. *(Russian)* 78−11122

chemical vapour deposition continued
ZnO, c-direction cryst. growth and crystallographic polarity 79−28902
ZnO, CVD films on sapphire substrates, use as optical waveguide 78−90500
ZnO crystalline films, deposition techniques *(Japanese)* 79−74098
ZnS CVD window, IR lattice absorption, phonon assigments and image spoiling 80−33104
ZnS CVD windows for forward looking IR radar systems 78−46816
ZnS, epitaxy in quasiclosed volume 77−85093
ZnS film production, for luminophors, method and apparatus *(Bulgarian)* 80−7499
ZnS films, from thermal decomp. of organometallics, growth kinetics and struct. 79−78895
ZnS, single cryst. vap. growth by sublimation and chem. transport 78−27390
ZnS(Se) multispectral aircraft window materials, production processes 77−73237
ZnS(Se)(S_xSe_{1-x}), growth of cubic single crystal by I_2 transport 79−91572
ZnSe, single cryst. vap. growth by sublimation and chem. transport 78−27390
ZnSe-GaAs solid solns., chem. transport cryst. growth, struct. 78−43991
$ZnSiAs_2$, cryst. growth and elec. props. *(French)* 77−76815
$ZnSiAs_2$, synthesis and layer growth by CVD in open flow system 78−15312
Zn_2SnO_4, needle cryst. growth from ZnO-Sn mixture 77−12509
ZnTe, single cryst. vap. growth by sublimation and chem. transport 78−27390
ZnTe, vapour growth by closed tube method 78−39703
ZrC, CVD on reactor fuel elements 77−74941
ZrC, factors affecting CVD 77−8760
ZrC, single cryst. growth by modified hot-filament method, cryst. morphology and microhardness 79−19983
ZrC, whiskers, CVD on Ni, catalytic effect 78−51865
ZrC-C, CVD, microhardness and microstruct. 77−8916
ZrC-C mixtures, gas composition effect on CVD, bromide process 79−24448
ZrC_x whiskers, nonstoichiometric, synthesis by CVD 79−28941
ZrN(C) whisker growth in CVD 80−59843
ZrO_2 film, CVD from organometallic cpds. and characterisation 78−23626
ZrO_2 film, growth by thermal decomp. of β-diketonate complexes, characts. 79−100055
ZrO_2 powders, vapour phase reaction production 78−68660

chemical variables control
see also moisture control; pollution detection and control
air-pollution control, in chemical industry, problems and solutions 77−9488
alkali and sulphidity in kraft process black pulping liquor, computer appl. 77−29085
arterial O_2 tension, generation of variable amplitude sinusoidal changes for freq. response anal. 77−56563
artificial pancreas programmed control technology *(German)* 79−16346
Barnwell nuclear fuel reprocessing plant, remote sampling and on-line anal. system 79−13511
crystallisation process, controlled, from binary melt *(Polish)* 79−14708
crystallizer for growing single crystals from solutions with precision control of supersaturation 78−80465
dibutylphthalate, supersaturated vapour, aerosol form. by mixing of flows 79−39212
fine particulate emissions control electrostatic precipitation efficiency improvement 77−45140
gas chromatograph, on-stream, high-precision 79−16111
gas trace monitor, control of toxic gases 80−61499
glucoregulation in blood of diabetic dog 77−86652
incubator, portable, with radiant heating system and fine O_2 control 77−56511
industrial gaseous environment characterisation, Brinkley method 80−93817
irradiated nuclear fuel reprocessing streams, remote anal. techniques 79−13510
liquid mixture composition, using high-precision gas chromatograph 78−53283
multicomponent deposition processes, monitoring and controlling techniques, review 78−11113
paper mineral content, online methods 77−29086
particle size, rapid response, online method for continuous industrial processes 78−89429
refractometer, REMAT 20 process-control of photoelec. differential flow-through type 77−45885
respirator, servo control of end-tidal CO_2 in paralysed animals 79−39607
semiconductor alloy, for appl. in IR detector arrays, comp. control 80−31872
sludge systems, nitrifying activated, design and control 77−5243
wire samples, programmed control machine for corrosion testing 77−56172
C content in Fe_3C melt, measurement using automatic device 79−39252
CO_2 conc. regulation in climatic cabinets for corrosion testing *(German)* 78−53069
HCl production during radiation destruction of PVC *(Polish)* 77−29025
$Hg_{1-x}Cd_xTe$, for appl. in IR detector arrays, comp. control 80−31872
$Pb_xSn_{1-x}Te$, for appl. in IR detector arrays, comp. control 80−31872
Si, VPE growth, in process monitoring and control of doping gas conc. 79−24443
Si:H, amorphous, control and anal. of deposition, using plasma spectroscopy 80−45230

chemical variables measurement
see also chemical analysis; moisture measurement; pollution detection and control
activated sludge aeration, galvanic dissolved O_2 sensor improvement 77−70364
activity, species-selective electrochem. sensor, use of semi-permeable membranes, in book, for teachers 78−8200
adsorption measurement, dynamic characts. of adsorpt. calorimeter 78−24796
air pollution, Dutch airborne equipment appl. *(Dutch)* 78−20534
automobile exhaust emission meas. and testing procedures, error statistics, survey *(German)* 77−73839

chemical variables measurement continued
  blood O_2 level, optical continuous noninvasive meas. 77—2068
  cable temp. jump apparatus for chemical relaxation time meas. 77—12800
  cloud chamber, thermal diffusion, unsteady state, supersaturation profile 80—63449
  combustible gas and vapour monitoring, MOS sensors 79—16104
  combustible gas detector, operational tests 79—16105
  computerised for alkali and sulphidity meas. in kraft process black pulping liquor 77—29085
  concentration meas. kinetic reaction equation parameter determ. *(German)* 77—66782
  crystal nucleation growth rates, on-line meas., data reduction technique 79—38730
  electrochemical measurements on acid oxygen carbon electrodes, ESCA method appl. 78—31651
  enzyme reaction rate determ. by capacitance meas. 78—31997
  equipment for the measurement of ions in solution, review 80—71983
  exothermic fluid phase flow reacts., mechanisms, apparatus *(Russian)* 77—9042
  flame ionisation detector measures fluctuating concentrations hydrocarbon gases 77—57312
  flowing gas conc. fluctuation meas., laser schlieren technique 80—3444
  flue gases, extractive stack sampling system for cont. emission monitoring 79—96494
  gas chromatography, problems in use for on-line automatic control *(Spanish)* 77—32865
  gas monitoring, Fourier IR air monitor, description and appls. 79—16106
  gas monitoring system performance tests and specifications 79—16659
  gas monitors for in situ source emission, field experience 79—16660
  gas trace monitor, control of toxic gases 80—61499
  gaseous mixtures, conc. fluctuations meas. using catalytic wire 77—26291
  human serum, definitive meas. of constituents 80—93818
  hydrocarbon gas detector for dispersing vapour plumes 79—70400
  industrial furnace flue gas anal. using RF mass spectrometric method 77—71403
  metal, surface contamination detection by nondestructive test, surface potential difference meas. method 79—83424
  metal corrosion meas. specifications and quality assurance 77—12764
  O_2 index test, measurement and appl. 79—79337
  on-stream analysers development, w.r.t. speed and reliability 77—66778
  oxygen monitoring in process gas streams, sensor 80—52181
  oxyhaemoglobin dissociation curve analyser, devel. and improvement 77—13019
  paper mineral content, online methods 77—29086
  photosynthesis rate of wheat, using Geiger counters and IR analyser *(German)* 77—70436
  plating line Co concentration monitoring, by automatic colorimeter 80—105691
  pollutant estimation, meas. and sampling methods *(French)* 78—20506
  reaction rate consts., reliability criterion 79—8423
  refractometer, REMAT 20 process-control of photoelec. differential flow-through type 77—45885
  remote gas meas., using discretely tunable IR gas laser 77—49199
  repetitive pressure perturbation apparatus for studying rapid chemical relaxation kinetics 77—12801
  salinity and density from gamma-ray attenuation in seawater *(Russian)* 79—39897
  salinity in ocean, Kiel multi-purpose sea probe microprocessor-based data acquisition system *(German)* 78—85701
  salinity of seawater, microprocessor-based instrument 80—67440
  salinity/temperature sensor chain for estuarine meas. 79—5670
  semiconductor sensors, props. and appls. *(German)* 78—36991
  stearic acid homogeneous vapour phase nucleation, diffusion cloud chamber obs. 80—79923
  steel, mild, corrosion rate meas. in H_2SO_4 using microprocessor controlled potentiostat 80—71798
  sulphide melt, conc. EMF meas. using solid-electrolyte cell 77—40571
  supersaturated vapour, equilib. press. depend. on nucleating drop radius 80—69960
  trace analysis, state and development *(German)* 78—68956
  CO monitoring using automatic functional check *(German)* 77—53883
  Cl ion concentration in nuclear power station loop waters, potentiometric method improvements 79—85599
  Cl monitoring, TAGA 3000 mobile test unit 80—72114
  CoO, Co_3O_4, free enthalpy of formation, solid oxide electrolyte galvanic cell method 78—23959
  F content of hot spring waters, Japan *(Japanese)* 80—31074
  NO measurement, photometric process analyser 80—57360
  NO_x in flue gases, determination various methods, comparative evaluation 79—53014
  O_2 analysis, electrochemical sensors 80—93816
  O_2 concentration in water, continuous, in tubular columns, probes utilisation *(French)* 78—3836
  O_2 determination in flue gas of 200 MW plant, trial operation with Westinghouse probe *(Czech)* 80—89562
  O_2 meter, type 648, mains-free, features *(German)* 78—94858
  O_2 partial pressure and bioelectric potential simultaneous meas. in living tissue *(German)* 78—85453
  S meter, model XA-300, for laboratory use 80—26085
  SO_2 detection using thermal radiation at 53.53 GHz rot. reson. 77—78411

chemically reactive flow
  ablating plane (axisymmetric) body, turbulent boundary layer with neg. press. gradient 78—79389
  absorptive with chemical reaction in liq. film in laminar flow 77—42929
  accelerated flow, at permeable graphite burning surface, turbulent heat/mass transfer 78—38417
  active solute dispersion in rectilinear flow 79—60072
  admixtures, convective-diffusive transfer in cylindrical channel, soln. 77—7391
  aerodynamic eqns. and diffusion, boundary conditions *(Russian)* 77—55105
  air flows in triple point shock configurations, anal. thermodynamics *(Russian)* 79—32569
  air suspension homobaric flow in presence of physicochemical transform. 80—87820
  air wake, hypersonic, electron recomb., temp. depend. meas. 79—27834
  arc-heated gas flow, ion saturation current fluctuation probe 78—63574
  atom diffusivity meas., independence of wall reactivity 77—3909

chemically reactive flow continued
  autocatalytic kinetic system, asymmetric multiple steady states 79—86527
  axially irradiated cylindrical photoreactor, plug flow model 79—47942
  axisymmetric confined flame, aerodynamic and heat transfer, finite difference scheme, program 78—94689
  axisymmetric impinging jet, transfer characteristics at conical surfaces 77—3889
  axisymmetric laminar jet diffusion flame, split operator finite difference solns. 78—51252
  balance equations for chemically reacting mixtures 79—27710
  Belousov-Zhabotinsky reaction, chaotic output under stirred flow 79—77293
  Belousov-Zhabotinsky system, limit cycle behaviour, modified Oregonator model 79—1266
  binary mixture, turbulent flow, Reynolds eqns. and heat and mass transfer *(German)* 77—11281
  bipolar trickle reactors, flow models for hydrodynamic characts. and reaction rate constants, 80—76522
  bluff-body flame-stabiliser flow modelling 77—72367
  blunt body, boundary and wake, supersonic viscous gas flow, numerical soln. 80—38441
  boundary layer, thermodynamic coupling theory 77—72369
  boundary layer problems with relaxation processes, Enskog-Chapman method modification *(Russian)* 80—19523
  boundary layer stability of catalytically recombining gas 79—41768
  boundary layer theory, similarity soln. 78—30369
  buoyancy dominated wall diffusion flames, numerical model 77—68710
  burner with diffusive control, intermixing of gas streams with transverse swirled air flow 78—87418
  burning rate in engine cylinder, swirl and turbulence effects 80—89492
  carrier facilitated transport in heterogeneous media 77—39360
  carrier mediated transport theory, survey of applications 77—89113
  catalysts, heterogeneous, gas phase diffusion and reaction calcs., viscous flow importance 79—47970
  catalytic fluidised bed reactors, simulation by transient axial dispersion model 79—77289
  catalytic reaction in porous solid with boundary layer flow 78—31684
  catalytic reactive flow, normal velocity in laminar boundary layer *(French)* 77—75988
  catalytic surface boundary layer struct., kinetic, diffusion reaction phases 80—33706
  channel, distributed injection of gas or combustible gas mixture from walls 79—68810
  channel flow of reacting gas, momentum change due to heat injection 79—94741
  Chapman-Jouguet wave, gas flow near line of discontinuity of surface wave curvature 79—86462
  chemical laser nozzle, effect of geometry and boundary layers on flow-field 77—27622
  chemical laser nozzle, TRW CL XV, fluid mechanical and optical analysis, LAMP and BLAZER code calcs. 79—98350
  chemical laser resonator modelling, LAMP and BLAZER code calcs. comparison with CL XV meas. 79—36890
  chemical reactions, lattice model, coupling of translational and reactive dynamics 78—55696
  chemical reactors, annular, cylindrical, mass transfer in laminar flow 78—22429
  combustion, swirl flow, review 78—1755
  combustion, turbulent, implications of probability eqns. 78—14098
  combustion, turbulent premixed and diffusion, engineering flow modelling computation 78—1756
  combustion and fluid dynamics, possible space environment expts. 79—46402
  combustion flow, laser Doppler velocimetry 77—80255
  combustion front, laminar stability model 78—42680
  combustion front thermal propagation and thermodiffusional instability 80—7796
  combustion fronts in relativistic MHD *(French)* 77—47115
  combustion gas flow, spectroscopic temp. meas., cold boundary layer effects 77—31399
  combustion modelling, for large gas-fired furnaces 79—32710
  combustion zones, nonlinear acoustic phenomena 80—38156
  complex reacting gas flow, laser induced fluoresc. diagnostics 77—76011
  condensation, gas with chemically reacting noncondensable components 78—51258
  condensation on external surfaces, heat transfer data processing and correlation 77—42706
  confined burning jet, droplet vaporisation, expt. and theory 78—94855
  continuous flow stirred tank reactor, mixing model 78—63508
  continuum description of reactive mixtures *(French)* 79—41765
  convective combustion of disperse systems 80—53835
  convective diffusion, nonlinear surface reaction kinetics 80—106854
  convective diffusion to a particle in a fluid with linear kinetics 80—69943
  convective instability in horizontal porous bed 79—41769
  corundum-based refractory lining, wear resistance in combustion gas flow *(Russian)* 79—8370
  crystalline film growth reactor, gasdynamic problems 79—83130
  CVD fluid dynamics and mass transport expts. 77—77398
  CW supersonic chemical laser, porous nozzle, chemically reacting boundary layer 80—100022
  cylinder array, convective mass transfer with surface reaction 78—79369
  data acquisition system using stopped-flow spectrometry *(French)* 77—12779
  decane-air mixture, spontaneous ignition temp. limits determ. 77—52641
  detonation in wider tubes, theory 80—53887
  detonation sputtering, exp. determ. of dynamic characts. of two-phase flow *(Russian)* 78—94852
  detonation wave, gas-ionising, spatially-polarised struct., rel. to mag. viscosity *(Russian)* 77—39361
  diatomic gas, dissociation past strong shock waves 78—42683
  diffuse flame extinction conditions with two component gas mixture 79—91956
  diffusion boundary layers, with surface reactions, laminar or turbulent regimes, thermal simulation method 77—75912
  diffusion flame in turbulent boundary layer on liq. propellant surface behind shock wave 80—53763
  diffusion flames, laminar and planar, large activation energies, asymptotic development *(German)* 78—91035

chemically reactive flow continued
diffusion of chemically active additive in turbulent mixing zone, stat. characts. 77−35258
dispersion model, appl. to fluid flow 80−48784
dispersion model, residence time distrib. calc. approx., Peclet no. depend. *(German)* 78−22421
dispersion of chemically reacting solute in micropolar fluid in pipe 77−7478
dissociating air, non-equilibrium laminar boundary-layer 77−952
dissociating gas in pipe flow, heat transfer crisis, flow laminarisation 79−1265
dissociating gas in pipes, heat and mass transfer 80−24105
dissociating turbulent gas flow around triangular rod bundle, heat and mass transfer *(Russian)* 79−68822
disturbance wave-head amplification in homogeneous explosion in chem. reacting atm. 79−27658
Doppler velocimetry within turbulent phase boundaries 77−11289
drop, mass transfer accompanied by chem. reaction at surface 79−77290
drop formation hydrodynamics, macroencapsulation 80−64603
droplet evaporation in const. cross flow, with and without gas. chem. reaction 77−35214
droplet interactions, vaporisation effects 80−24106
droplet-vapour flow, burning, conservation eqns., mass transfer 77−39363
duct confined turbulent flames, laminar burning vel. effect on struct. and propagation 79−90351
dust clouds of solid fuels, ignition and flame quenching 80−28577
EHD flow, nonstationary, with charge diffusion, nonlinear and linear wave processes 80−59124
electrolyte, ionic mass transfer in narrow rectangular conduits 80−61105
with electronic isotopic substitution in flow and stopped flow NMR 77−25265
exothermic fluid phase flow reacts., mechanisms, apparatus *(Russian)* 77−9042
exothermic waves in gas flows 77−68709
falling film gas-liquid reactor anal. 79−86526
film growth by CVD with two-component gas mixture, hydrodynamic anal. 77−40384
finite-difference method for flow problems in highly irregular domains 80−6166
fire gas velocity measurement by cross correlation of random thermal fluctuations 77−58812
fire plume, turbulent, reaction rate, air entrainment, radiation 78−35682
fire whirl phenomenon, model 79−72958
first-order reaction, algebraic expression 79−94585
flame, atm. press., heat and mass transfer meas. using Ir/Ir-Rh alloy thermocouple 77−86314
flame, atm. press., ion sampling aerodynamic disturbance by sampling system 77−60142
flame, atm. press., supersonic sampling, boundary layer cooling 77−60143
flame, diffusion type, oppositely directed jets, elec. props. 78−56896
flame, laminar jet diffusion flame size prediction, Burke-Schumann theory extension 78−14096
flame, laminar jet diffusion flame size prediction from diffusion coeff. 78−14097
flame, laminar long wave stability, EHD problem anal. 80−53866
flame, laminar mixed-mode forced-free diffusion type, on vert. burning fuel slab 78−91033
flame, laminar premixed, two-dimens. elliptic partial differential eqns. soln. 79−94738
flame, laminar premixed gaseous, amplification of propagating acoustic signal 79−29357
flame, laser Raman diagnostics using coherent anti-Stokes scattering *(French)* 77−35280
flame, mass streamline, vel. and density fluctuations correlation *(Japanese)* 80−6164
flame, premixed, propag. in large-scale turbulence 79−50813
flame, premixed, propag. in supersonic airstream 77−84339
flame, premixed, turbulent, interaction effects 77−11279
flame, premixed laminar, multiplicity and stability, bifurcation theory applic. 80−16681
flame, round jet type, mass exchange between recirculation zone and outer flows, stabilisation 80−14842
flame, suppression of flow induced combustion noise using appl. of DC elec. field 80−38176
flame, turbulent, flow pulsation effect on chem. reaction 77−35260
flame, turbulent diffusing, analytic incorporation of probability density functions 78−75232
flame, turbulent diffusion, burning vel. *(Russian)* 77−7475
flame, turbulent diffusion, mass entrainment, momentum flux and temp. 79−32704
flame, turbulent diffusion, mean flow props. 78−1753
flame, turbulent mixed gases, thermal exchange effect on reaction rate 78−7205
flame, V-gutter stabilised, laser anemometry and schlieren photography meas. 77−35263
flame 79−64795
flame front, distorted, hydrodynamic discontinuity model 77−58802
flame front, laminar, hydrodynamic instability, nonlinear integro-differential eqn. 78−51253
flame front, laminar, hydrodynamic instability, numerical solns. 78−51254
flame front instability analysis in compressible ideal medium *(Russian)* 79−27711
flame gases, effect of EHD boundary layer on heat transfer 77−80228
flame induced flows propagating over condensed fuels, two-component LDV meas. 79−23380
flame jet, anal., pulsations of conc. and Archimedian forces *(Russian)* 77−51130
flame propag. in semi-open tube, mixture preheating effect 78−47067
flame propagation in flowing turbulent combustible mixture *(Russian)* 77−27624
flame propagation in long tubes, ducts investig., fibre optic technique 77−31404
flame propagation limits, mixture turbulence effects 80−16679
flame radiation, in IR porous perforated gas radiators 78−3335
flame stabilisation behind bluff-body flame holder *(Japanese)* 78−67284
flame stabilisation conditions, homogeneous reactor model anal. 79−86531

chemically reactive flow continued
flame stabilisation mechanism in two-phase fuel-air mixture flow 79−81996
flames, convection-diffusion coupling model 77−7481
flames, effects of finite reaction rate and molecular transport on premixed turbulent combustion 80−3348
flames, ignition and propagation, self-consistent 2-dimens. hydrocode 78−47066
flames, laminar and turbulent, normal vels. of propag. calc. 77−84342
flames, local turbulence props., Raman spectroscopy meas. 80−64648
flames, multiple turbulent, struct., operating conditions rel. to characts. *(Russian)* 77−7476
flames, premixed, laminar, time-depend. soln. determ. 78−67282
flames, unsteady, propagation, numerical modelling 79−64794
floating heat layer interaction with solid wall, computation, book contrib. 80−1642
flow regimes in long tubes 80−53886
flow through a slightly curved flame front 79−55430
flow velocity, field induced by flame spreading over fuel, laser velocimeter meas. 78−59529
fluid inhomogeneities as sources of noise 77−11181
fluidised bed, reaction near grid, two-phase model 78−67280
fluidised bed reactor, solid-circulation model, steady-state multiplicity 79−86524
fluidised bed reactor, steady states multiplicity 79−4086
fluidised bed reactors, mathematical modelling *(German)* 79−41767
forced convection with chemical reactions, turbulent shear flow mixing, numerical modelling 79−1272
free convection flow over plate induced by chemical diffusion and reaction 78−18358
fuel droplet, burning anal., quasisteady model *(Japanese)* 79−32712
fuel drops, liq., blast wave initiated detonation waves 79−64691
fuel mixture stream, regular reflection of shock wave from solid wall 79−77291
fuel self-ignition in homogeneous flow 80−53881
fuel-air mixtures, ignition and flame quenching 80−14847
fuel-vapour gas-phase diffusion flame ignition, stagnation point boundary layer 77−58803
fuel/air mixtures, conc. limits to initiation of unconfined detonation 80−38505
fundamentals of reactive fluid flows, book contrib. 77−84345
furnace heat transfer, 3-dimens. computer model predictions test 78−59504
gas, dissociating, relax. press. theory 79−81994
gas, ideal dissociating, differential effects of shock waves 77−15135
gas bubble motion in power-law fluid, heat and mass transfer with chemical reaction 79−77227
gas detonation wave, calculation of equilibrium flow *(Russian)* 78−1690
gas dynamics with relaxation effects, acoustic waves, nonequilibrium atmosphere effects, review 78−79390
gas flow, high-temp., heating of graphite body, numerical soln. 79−37318
gas flow in catalytic convertor, numerical soln. 78−67281
gas ignition in boundary layer on heated plate 79−64798
gas injected into shock layer flow, aerodynamic heating of blunt bodies 80−74998
gas mixture turbulent concurrent double pipe heat exchanger equilib. and nonequilib. reaction 78−94856
gas mixtures, chem. reactive, sound speed calc. *(Russian)* 77−35261
gas mixtures, detonating, symmetric piston motion 80−59073
gas phase catalytic reactions, periodic press. cycling, viscous flow effects 80−19521
gas-liquid cocurrent flow through packed beds, radial effective thermal conductivity 78−1723
gas-liquid flows with chemical reactions in hydraulic approx., mathematical modelling 79−18972
gas-liquid interaction in turbulent reacting flows, mathematical model 80−83862
gas-liquid reacting flow, interfacial area and liq.-side mass transfer 79−37420
gas-solid reactive flow near stagnation point, transient heat and mass exchange 79−77104
gasdynamic disturbance in chem. reacting gas mixture, shock wave formation 80−74999
gasdynamic equations, multiatomic gases with different elastic and inelastic rates 79−81993
gasdynamics of explosions, reactive systems, conf., Stockholm, Sweden (Aug. 1977) 79−64690
generalized ICE method for chemically reactive flows in combustion systems 79−10617
glassy material, destruction at critical point in radiative gas stream *(Russian)* 79−32910
heat and mass transfer, approx. theory 79−68821
heat and mass transfer, simultaneous, chemically reactive flow characts. *(Japanese)* 78−22431
heat engines, chemically driven, finite time thermodynamics 80−76541
heat exchange, of chemically reactive metals *(Russian)* 78−47068
n-heptane, cool flame stabilised by turbulence *(French)* 79−1952
heterogeneous catalytic reaction, natural convection 77−84341
heterogeneous chemical reaction, laminar flow past sphere, unsteady mass transfer 77−55102
heterogeneous mixing, energy level population inversion 80−78848
heterogeneous reaction kinetics, convective mass transfer of cone, in nonlinear viscous field 77−55103
n-hexane, tank flame, turbulence, holographic interferometric synchronous photography *(German)* 78−51255
highly viscous chemical laser nozzles flow, two dimens. Navier Stokes eqns., implicit marching method 78−63506
homogeneous fuel mixture, turbulent combustion theory 80−53883
homogeneous turbulence, chemical reactions, probability approach and particle models, comparison 80−14844
hydrocarbon diffusional combustion in air, finite activation energy anal. 78−95930
hypersonic boundary layer eqns. including chemical reactions, numerical error control, book contrib. 80−1699
hypersonic flow past blunt bodies, aerodynamic heating, effect of chemical reactions of injected gas *(Japanese)* 79−94739
ignition and flame quenching in flowing gaseous mixtures 77−80230
ignition of gas near heated plate *(Russian)* 78−9725

chemically reactive flow continued
- interface between immiscible liquids, convection induced by chem. react.-hydrodynamic coupling *(French)* 79—41682
- intraparticle ion exchange mass transfer, accompanied by instantaneous irreversible reaction 78—9722
- inverted flames, blowoff phenomena, explanation by area increase concept 80—14845
- ionic reaction rate increase in US cavitation, diffusion model 79—96312
- irreversible chemical process, in elec. field, heat and mass transfer 78—11545
- irreversible transport processes, noncoupled, nonstationary, classical variational principles 78—4567
- isobaric heating conditions, nonequilibrium flow, calculation of parameters *(Russian)* 80—19524
- isobaric turbulent reacting jet issuing into costream 78—63509
- jet, steady axisymmetric supersonic, approx. analytical soln. 77—55099
- jet diffusion flames, blowout and attachment mechanisms 79—72957
- jet flame, props. and mixing process in recirculation zone 78—91025
- jet flame, stabilisation using thick burner rim *(Japanese)* 77—68706
- jet flame stabilisation in subsonic and supersonic flows 78—34206
- kinetics, stiff ordinary differential eqns. numerical soln. 78—48631
- laminar chemically nonequilibrium mixture flow, characts. of combined heat and mass transfer *(Russian)* 79—59965
- laminar diffusion flames, struct. and extinction by suppressive agents 79—32705
- laminar flame front, diffusion-thermal stability *(Russian)* 77—7477
- laminar flow between parallel plates, reactant injection effects 78—34208
- laminar flow mass transfer with axial diffusion in pipe with chem. reaction 77—55101
- laminar heat transfer for boundary layers with mass injection and chemical reactions *(Chinese)* 80—59020
- laminar liquid film, falling, O_2 adsorpt. with zero order react. in entrance region 80—64652
- laminar liquid flow around plate, boundary-value problem soln. for generalised diffusion eqn. 77—7366
- laminar liquid flow in tube, props. varying with total conversion 78—42678
- laminar MHD flow with chem. reactions, solute dispersion 79—23378
- laser, chemical, pressure recovery, 1D flow model, comparison with DF laser results 77—71979
- laser Doppler anemometry of high-temp. industrial gas flow *(German)* 79—10618
- Laval nozzle, surface burning in two-phase flow, boundary layer interaction, Rakhmatulin model 78—83452
- liquid film, boiling, laminar, with chem. react. on catalyst surface, model 80—45553
- liquid film, laminar, stability, mass exchange and heterogeneous chem. reaction effects 77—75990
- liquid fuel droplets, transient heat flow in combustion gases, models 78—63507
- liquid fuel flames in open air, noise from jet and flames *(French)* 77—19476
- localized patterns in reaction-diffusion systems 80—59130
- low Mach number duct flows, combustion noise generation by chemical inhomogeneities 80—92237
- low speed shear layer, turbulent mixing of passive and reactive species 77—75989
- magnetogasdynamic medium, flow parameter distrib. near weak shock wave *(Italian)* 79—14494
- mass transfer, ionic, in open channels, electrolyte probe determ. 80—59110
- mass transfer for chemical reaction in both liq. phases 78—5825
- mass transfer in turbulent falling film with or without chem. reaction 79—41766
- mass transfer inside drop, influence of chemical volume reaction at large peclet numbers *(Russian)* 80—28508
- mass transfer rates at spheres, moving on circular path 77—3890
- mass transfer with axial diffusion and chem. reaction 79—23376
- mass transfer with chem. surface reaction on flat plate in flow *(German)* 79—72961
- melt reacting with gas jet, heat and mass transfer, mathematical modeling 80—87819
- methane, combustion, free turbulent jet form. 78—30329
- methane, jet, free turbulent flow, diffusion coeff. variation, mixing processs velocity 77—7480
- methane-air flame, Raman scattering diagnostics of turbulent flow field 78—18328
- MHD channel flow, effect of external circuit on dispersion of soluble matter 79—1267
- MHD flow near slender wing with supersonic leading edge *(Italian)* 79—14495
- microfluids, linear theory of mixtures 80—14777
- mixtures, phenomenological theory 79—1268
- multicomponent, turbulent boundary layer at flat plate 79—98822
- multicomponent nonequilibrium chemically reacting boundary layers, transport coupling theory 79—77294
- multicomponent systems, Langevin forces and noise correls. 77—16823
- multidimensional unsteady laminar flames, scaling transformations for numerical computations 80—19522
- near-wake phenomena, with and without external compression, axial and radial air injection effects 80—10273
- NMR meas. of transient species and effects at high resolution apparatus 77—150
- nonadiabatic flames, linear stability anal., diffusional-thermal model 80—14846
- nonbuoyant plume, advection of scalar quantities, stochastic props. 79—32471
- nonequilibrium boundary layer flow, exact and approx. solns. 80—79409
- nonequilibrium flow in channels, asymptotic method 79—86529
- nonequilibrium flows with transonic vel., second approx. 80—33622
- nonequilibrium isobaric chemically reactive flow, parameters for heating (cooling) *(Russian)* 80—59131
- nonequilibrium reactive flow over solid body, conjugate heat and mass exchange 77—42931
- nonequilibrium turbulent shear flow, prediction model *(German)* 79—18973
- nonisothermal turbulent jet, physiochemical processes, temp. and conc. effects 80—14849
- nonisothermal turbulent suction-controlled boundary layer, heat and mass transfer coeffs. at chemically-reactive surface 79—77102

chemically reactive flow continued
- nonlinear diffusion-reaction problems with time-dependent diffusion coefficient 79—98823
- nonuniform grids in finite difference approximations, application to fluid flow problems 80—105507
- nozzle flow, vibr. and chem. non-equilib. of multicomponent gas 79—7416
- oblating heat shield, Jupiter probe, C vaporisation into nonequilib. stagnation point boundary layer 79—1264
- one-dimensional compressible flow, math. model rel. to detonation 80—41985
- opposed gas-air jets, convective heat transfer in combustion 79—72960
- packed bed reactor, creeping flow, mass transfer 77—80227
- packed bed reactor, diffusion controlled mass transfer coeff. 79—43555
- parallel flows of unmixed reactants, temp. and conc. distrib. in reaction region 80—92236
- partial chemical equilibrium in fluid dynamics 80—69946
- particle in gas stream, convective, diffusion with nonlinear kinetics of heterogeneous chem. reaction 78—83499
- particles in a fluid, convective diffusion and mass transfer, wakes, chemical reactions 80—38394
- particles moving in reactive, dispersive system, mass transfer interaction 79—64738
- photosensitised reacts. in continuous chem. processes, scatt. effects 78—73057
- plane laminar relaxing gas jets, mixing with radiation accounted for, boundary layer eqns. 79—90349
- pollutant dispersion from point source with and without chem. reaction in semi-bounded waters 77—64329
- polyatomic chemically reacting gases, hydrodynamic eqns. 79—32711
- polyethylene oxide, dilute aqueous solution, effect of chemical additives on flow 80—83823
- polymerisation in flow-through reactor, low-temp. conditions 80—61092
- porous barrier flow, exit flux, composition depend. 77—31383
- porous body, highly dispersed, kinetic theory of transfer in heterogeneous chem. reactors 77—15136
- porous catalyst, complex reactions, conc. and temp. profiles, computation method 79—86523
- porous catalyst, simultaneous forced convection, diffusion and reaction 77—35254
- porous flow past solid undergoing pyrolysis, numerical solns. 80—43801
- porous media, heat and mass transfer during phase and chemical transformations 77—42917
- porous oxide pellet, spherical, reduction by gas flow *(French)* 79—27713
- premixed turbulent flame combustion, heat transfer obs. and calc. *(French)* 78—94688
- premixed turbulent flow, spectral interpretation of the propag. vel. *(French)* 79—4090
- pressure discontinuity system with 1 or 2 triplets, supersonic object, air equilib. physicochem. transforms. 79—90350
- pressure waves interaction with combustion field 78—63504
- propagation, natural convection effects 80—53882
- propane-air flame-generated turbulence, approach stream turbulence effects 79—64793
- propane-air mixture, turbulent combustion, model 79—64792
- pseudofluidised layer, hydrodynamical eqns. *(Russian)* 77—35233
- qualitative analysis of unsteady heat and mass transfer modes in a boundary layer with chemical reactions and intensive injections 80—69819
- quasi one-dimensional stationary flow in heated channel, criteria characterising approx. to chem. equilib. *(Russian)* 79—27712
- radiation-convection interaction 77—80231
- radiational flame propagation over gas suspension of solid combustible particles 80—53880
- radical species, tube electrode generation, laminar flow through EPR cavity, decomp., convection 77—24746
- random advection of chemically reacting species, probability density method 78—38418
- random choice method anal. of reacting gas flow, time-depend., one dimens. 78—9726
- random choice method for gas dynamics problems soln. 77—55106
- rarefied flow, boundary conditions for gasdynamic eqns. in presence of evap., condensation and chem. reactions 77—47042
- rarefied gas flow with chemical reaction, Monte Carlo simulation of homogeneous dissociating diatomic gas 77—51128
- Rayleigh-Benard instability, n-component reactive fluids 80—69945
- Rayleigh-Benard instability, reactive binary fluids 80—69944
- reaction-diffusion system, instability of stationary solns. *(French)* 78—20055
- reactors, chem., relaxation oscills. 79—39120
- real gas, blast wave, effects of compressibility, vibr. excitation, dissoc. and ionisation 77—68622
- recombination, in steady supersonic flow, in devices for laser isotope separation 79—31717
- reflection of detonation waves from a wall 80—53885
- relativistic thermodynamics of chemically reacting fluids 79—64801
- relaxing gas, nonlinear waves propag., weak influence of relax. 77—55100
- rotating propulsive nozzle flowfields for nonequilibrium chemically reacting supersonic flow 80—48764
- second-order reactions, in turbulent fluid, model, appl. to atm. plumes 79—20350
- second-order reactions, in turbulent fluid, model, formulation and validation 79—20349
- shock tube flow, laminar to turbulent boundary layer transitions 77—48642
- shock wave ignition of metal powders, pre-ignition processes 77—40546
- shock wave propag. across chemical deflagration 77—3846
- shock waves, completely dispersed, in relaxing mixtures, struct. obs. 80—59072
- show wave reflection from wall in stream of burning mixture *(Russian)* 79—14496
- simulation using Markov chains *(French)* 79—32706
- slow liquid combustion, evaporation and combustion front stability 80—53884
- solid propellant erosive burning, reacting turbulent boundary layer approach 79—32703
- solid-fluid turbulent mass transfer with instantaneous chem. react., appls. 77—3888
- solid-liquid mass transfer in concurrent two-phase flow through packed beds 79—4066

chemically reactive flow continued
soluble fluids in laminar, turbulent flows, stretch model appls. to mixing, diffusion, react. 79−94736
solute dispersion in non-Newtonian fluids, chemical reaction effects 80−38503
solute dispersion in porous medium in MHD flow between parallel plates, homo- and heterogeneous reaction effects 78−55697
space shuttle reentry, unsteady nonequilib. chemically reactive flow, parallel computation 78−47065
spatial propagation in vicinity of caustic *(Russian)* 77−58807
spherical drop, mass transfer and chemical reaction at transitional Reynolds number zone *(Russian)* 79−50814
stagnation flow at a heated curved wall, ignition condition 80−96242
stationary system, diffusion mixing model, approx. soln. 80−79410
steady state diffusion in red blood cell and model supspension 77−40644
stiff boundary valued problems in kinetics and diffusion, numerical methods 79−86525
stirred tank reactor, homogeneous p-order reactions, mixing effects, two parameters model 80−14843
stopped flow temperature jump apparatus with spectrophotometric detection of fast chem. reactions 77−3892
stopped-flow apparatus for rapid mixing and study of two fluids under high hydrostatic pressures 80−98929
supersonic combustion past a conical body with normal surface blowing 79−41770
supersonic mixing chem. lasers, gas dynamics, book contrib. 77−10905
supersonic nozzle, chem. nonequilib. flow, specific momentum losses 78−59505
supersonic stream of chemically reacting gas mixture, thermal crisis suppression by laser radiation 80−75000
surface reactions and mass transport, in Leveque's approx. 78−76907
swirl flow, combustion and non-combustion flow fields, numerical anal. 79−98821
swirled gas flame aerodynamics, empirical results 77−58804
tank reactor, continuously stirred, periodic regimes 79−4087
thermal diffusion flame, two dimens. cellular struct. formation 80−69947
thermal instability of vibr.-excited mol. gas, appl. to surface ignition *(Russian)* 78−56895
thermal kinetics meas. using modified commercial stopped flow apparatus 80−86291
thermal shock in chemically active medium *(Russian)* 79−32709
thermal-ignition analysis in boundary-layer flows 79−64800
thermoconducting gas, reaction tube under epitaxy of monocrystalline films *(Russian)* 80−55301
thin body, subsonic and supersonic flow of chemically reacting inviscid gas 79−98820
three-dimensional compressible mixing and reacting ducted flows, modelling 77−27621
transient coaxial entry tube flows, numerical program 77−15117
transonic flow, eqns. *(Russian)* 77−89208
transonic flow of relaxing mixtures 79−64797
transonic nozzle flow of vibr. relax. or chem. reacting gases 78−59506
transverse shocks in detonation waves, strength var. 78−26157
trickle bed, packed, gas-liq. reactions, extended crossflow model implications 79−46399
tubular flow reactors with first-order kinetics 79−4088
tubular reactor, effect of axial mixing on start-up time, with first order isothermal irreversible reaction 78−9723
tubular reactor with non-Newtonian laminar flow, diffusion and raction analysis 77−68703
turbomachine combustor, analysis and modelling of flow *(French)* 79−46401
turbulent, probability approach to modelling 77−42928
turbulent Ar-Ti powder two-phase jets, with Ti combustion, high temp. study 79−81934
turbulent boundary layer analysis for air and combustion products *(Russian)* 78−5732
turbulent boundary layer with suction under nonisothermal conditions, heat and mass transfer 80−92125
turbulent combustions, problems of bias on mean meas. *(French)* 80−53879
turbulent diffusion, flames, high Reynolds number, rocket exhaust appl., chem. processes theory 80−45504
turbulent flame, acoustic noise *(Russian)* 79−32708
turbulent flame, interaction of flow pulsation and chem. reaction 77−58801
turbulent flame, temp. and conc. calcs. *(Russian)* 79−32707
turbulent flame theory, probabilistic approach 77−24034
turbulent flames, laser Doppler vel. meas., using spark discharge particle generator 80−59139
turbulent flames and isothermal free jets, mathematical model *(German)* 79−74387
turbulent flows, steady and unsteady, computation in axi-symmetrical domains 80−1697
turbulent jet, light probe meas. 77−62310
turbulent liquid film, gas absorpt. accompanied by first order reactions 79−69327
turbulent mass transfer, $Pr \gg 1$ first order chemical reaction at wall 78−18357
turbulent mixing flow, simultaneous laser measurements of instantaneous vel. and conc. 77−35287
turbulent mixing with react. of miscible reactant streams, simulation 80−64651
turbulent pipe flow with heat transfer and chem. reaction 78−51257
turbulent pipe flow with heat transfer and chemical reaction 79−1271
turbulent premixed flame, theoretical predictions *(French)* 78−94853
turbulent premixed flame, variable density effects 78−5824
turbulent reacting flow, modelling, probability approach 79−72959
turbulent reacting flow, second-order closure anal. 77−39364
turbulent reactive gas flows, two-dimens., nonequil. processes analysis 77 51129
turbulent shear flow struct. 78−1754
turbulent shear layer between two streams obs. 80−6163
turbulent state, diffusion induced chaos 79−81995
turbulent stream, ignition *(Russian)* 77−80229
turbulent-jet-diffusion flame, effect of mol. gas radn. 77−80232
two phase chemically reactive flow, dynamic stability, numerical anal. *(Russian)* 79−68823
two phase fluid-gas mixtures, tubular reactor layout *(German)* 80−1698
two-phase, dynamic stability, mathematical model *(Russian)* 78−47069

chemically reactive flow continued
two-phase detonation front compression waves, solid particle oxidation reaction *(Russian)* 78−34207
two-phase reacting flow, heterogeneous, balance eqns. and soln., interior ballistic phenomena modelling 79−94737
two-phase reactive particle flow through normal shock waves 78−42676
two-phase upflow, vertical cocurrent, interfacial areas determ. for mass transfer 79−86528
unmixed fuel combustion, reaction-surface model, flow struct., gas dynamic parameters 80−35536
unsteady diffusion in wedge-shaped region with inhomogeneous boundary conditions, appl. of Sommerfeld-Malyuzhinets integral 77−89111
unsteady flow fields with detonation, num. modelling 77−55107
unsteady supersonic flow around wings with detached shock wave, numerical soln. 79−94647
variable property flow, in curvilinear orthogonal coords., numerical calc. 79−44746
velocimeter for fluctuating temp. and vel. meas. in combustion field 80−14856
vibrational relaxation, sudden-freezing 77−58806
viscoelastic reacting fluids flowing over flat plate, boundary layer anal. of surface deposition 78−42675
vortex ring, turbulent, acoustic emission accompanying burning 78−94676
wake of blunt body with chemical reaction, flow field meas. using laser Doppler anemometry 77−35262
wake structure of two-, three-dimensional flame holders 80−53786
wave head of gasdynamic disturbance, chem. amplification 77−62309
wave structures, kinetic theory of gases calcs. 79−94678
wavefronts in reaction-diffusion systems, instability and turbulence 80−106855
weak shock waves in chemically reacting gas *(Russian)* 78−42681
$2NO_2 \rightleftharpoons 2NO+O_2$, gas mixture turbulent concurrent double pipe heat exchanger equilib. and nonequilib. reaction 78−94856
Ar, ionising boundary layer in shock-tube side-wall flow 79−60144
Br_2, dissociating flow in supersonic nozzles, atomic recomb. and vibr. relax. effects 78−42677
Br_2 recombination in supersonic expansion in nozzle *(Russian)* 78−1757
Br_2+O_2, reaction with W surface, rate of reaction meas., gas flow experiment 78−92510
C particle combustion, diffusion and reaction in stagnant boundary layer 77−68705
CO-N_2O reacting gas mixture, gain due to CO_2 00^01-10^00 transition 80−74337
$CO+0.5\ O_2$, supersonic stream, oxidation reaction to produce chem. laser 77−677
CO_2-N, nonequilib. mixture convective and radiational heat exchange during flow past body 80−14850
CS_2-O_2 mixture, stimulated emission of CO behind overdriven detonation wave front *(Russian)* 77−23668
Cl, shock heated, radiative recombination under nonequilib. expansion in supersonic nozzle *(Ukrainian)* 79−37421
Cl_2-H_2 mixture, detonation initiation, nonequilib. physicochem. process simulation 80−38431
$D+O_3+CO_2$, mixing in supersonic streams to produce CO_2 chem. laser 77−676
DF pulsed chemical laser, flow technology 79−36934
DF repetitively pulsed chem. laser, scalable fuel/diluent feed system 79−36935
H supersonic flames, chemical kinetics and unmixedness effects on burning 80−64649
$H+NO_2 \rightarrow OH+NO$, $H+NOCl \rightarrow HCl+NO$, rate meas. by Lyman-$\alpha$ fluoresc. 77−21353
H_2, supersonic combustion in vitiated airstream, using transverse injection 78−14095
H_2-air jet diffusion flames with finite chemical reaction rates 79−81992
H_2-F_2-He chemical CW laser, flows *(Russian)* 78−74895
H_2-N_2-Na jet, ignition and extinguishment in simulated LMFBR accident conditions 78−8932
H_2-O_2 gas mixture in chem. equilib., elemental diffusional separation in nonisothermal flow 79−55429
H_2-O_2 reaction boundary layer, numerical anal. *(German)* 77−35253
HCl supersonic chemical laser, visible chemiluminescence flow visualisation 79−76699
HF chemical laser, flow anal. 79−81420
$N_2+N_2O_4 \rightarrow N_2+2NO_2$, turbulent mixing in shear layer 77−75989
NH_3 aqueous soln., stripping by sieve plate column without downcomers 78−22430
NH_3, flow in steel tubes, wall heat transfer with catalytic dissoc. 78−14099
$NO+N\,^4(S)$ state reaction rate, discharge flow and photolysis reson. fluoresc. method 79−5142
N_2O_4, dissoc. flow in tube, heat transfer and drag 78−71402
N_2O_4, dissoc. laminar gas flow, heat exchange with triangular bundle of rods 77−42930
N_2O_4, dissociating, nonsteady flow in steam-generating channel 79−37422
N_2O_4, dissociating, turbulent pipe flow, heat transfer, resistance 78−91026
N_2O_4 dissociating gas flow in channel, turbulent boundary layer *(Russian)* 79−60067
N_2O_4, dissociating turbulent convection on horizontal plate *(Russian)* 80−1587
N_2O_4, fission reactor coolant, heat transfer on condensation *(Russian)* 80−57860
N_2O_4, reactive turbulent flow, heat and mass transfer anal. *(Russian)* 77 42932
N_2O_4, reactor coolant, stability in two-phase flow *(Russian)* 80−609
N_2O_4, turbulent dissoc. flow, along heated tubes, heat transfer 80−63225
$(NO_2)_2 \rightleftarrows 2NO+O_2$, chemically unstable mixture laminar flow in channel, heat and mass transfer *(Russian)* 77−68707
$(NO_2)_2 \rightleftarrows 2NO_2+O_2$, nonequilibrium mixture laminar flow in channel, zone method anal. of heat and mass transfer *(Russian)* 77−72370
$N_2O_4 \rightleftharpoons 2NO_2$, gas mixture turbulent concurrent double pipe heat exchanger equilib. and nonequilib. reaction 78−94856
$N_2O_4 \rightleftharpoons 2NO_2 \rightleftharpoons 2NO+O_2$, quasi-equilib. and quasi-frozen flows, criteria and calc. formulae *(Russian)* 79−68824
$N_2 \rightleftharpoons 2N$ layer, hydrodynamic stability anal. 77−75993
O_3, decomposition flame, flat, laminar, vel., struct. 78−51256

chemically reactive flow continued
  $O_2^+.O_2$, reactions with CO_2, O_3 and methane in flowing afterglow, stratospheric appls. 79—2343
  $O_2^+.O_3$, reactions with H_2O and methane in flowing afterglow, stratospheric appls. 79—2343
  TiC plasma-chemical synthesis, depend. on geometric and flow rate parameters *(Russian)* 80—40677
  TiO_2:$TeCl_4$ system, chem. vapour transport, matrix isolation IR studies 80—93755
  U isotope separation by selective laser photoexcitation in reactive two-phase flow 79—94109
  UO_2 low temp. fluorination in 3-inch diam. fluoridised beds *(Japanese)* 79—81056

chemiluminescence
  aequorin, Ca^{2+}-induced luminesc., inhibition by anaesthetics 78—76985
  aequorin luminescence, light emission rel. to Ca^{2+} conc., Ca-independ. component 77—48750
  albumin, human serum, interaction with luminol. chemilum. and fluoresc. 77—21471
  albumin, human serum, kinetics of eosin-sensitised photochemilum. of solns. 78—68991
  alkali halide crystal, irrad., chemiluminesc. process during dissolution *(Russian)* 78—92133
  analyser, process industry appl., air pollutants monitoring 78—40094
  analytical, flow cell design 78—73090
  analytical applications, in soln. 79—24874
  9-anthracene-$(CH_2)_n$-N,N-dimethylaniline, electrogenerated chemiluminesc., intramol. exciplex form. 78—11503
  aromatic compounds in benzene polycrystalline host, active N_2 induced chemilum., 77K 80—60691
  aromatic hydrocarbon acceptor, energy-deficient, and tetrathiafulvalene donor systems, electrogenerated chemiluminesc. 79—20372
  associative ionisation mechanisms 77—32781
  ATP measurement in single red blood cells using firefly biolum. reaction 78—48951
  bacterial luminescence excitation by singlet O_2 79—39340
  beam-gas, kinetics of metastable excited state products 77—56231
  benzophenone-Eu complex, triplet-triplet energy transfer, viscosity and temp. depend. 79—87847
  bimolecular beam-gas single collision chemiluminesc., kinetics temp. depend., theory 77—63914
  bimolecular beam-gas single collision chemiluminesc., kinetics temp. depend., expt. 77—63915
  bone tissue preservation, effect of treatment on chemilum., rel. to bone fragment transplantation 77—86709
  bromomethane, VUV laser multiphoton dissoc., CH excited state branching ratio, chemiluminesc. 78—70884
  carbon steel, S determ., flame chemiluminesc. method 78—48711
  charge-pair recombination kinetics, nonGaussian diffusion 79—34312
  chemical laser nozzle, TRW CL XV, fluid mechanical and optical analysis, LAMP and BLAZER code calcs. 79—98350
  chemical laser systems, ion-molecule reactions, thermal energy, book contrib. 77—50668
  chemisorptive luminescence systems for surface reaction obs. 78—7236
  cyclopropane, IR laser photolysis, decomposition, flame reaction 77—66760
  detector for environmental HCl using luminol chemiluminesc. 78—24366
  digital integrator for chemiluminescent analysis 78—21196
  diphenyl styryl pyrazoline-active electrolyte system, electrochemiluminesc. spectral shift 77—20929
  9,10-diphenylanthracene, electrogenerated chemiluminescence, T_2 state emission 78—60524
  dosimetry, installation for luminescence meas. *(Russian)* 79—93202
  earthquake lights, proposed for study by chemiluminesc. NO air pollution apparatus 80—61906
  electrochemiluminescence, excimer-monomer emission ratio 78—31640
  electrochemiluminescence reactions, background electrolyte effects *(Russian)* 78—7209
  electrochemiluminescent cell, neuronal mechanism modelling *(Russian)* 77—40651
  electrochemiluminescent laser configuration 80—33020
  electrochemiluminescent organic dyes and new type of laser 77—678
  electrogenerated chemiluminescence, estimation of triplet energies, possibilites and restrictions 80—34992
  electrogenerated chemiluminescence, photo-induced, and up-conversion at semicond. electrodes 79—91510
  electron exchange initiated reacts., kinetics correl. with free energy changes 80—50856
  ethylene, multiphoton absorption, luminesc. and dissoc. in laser pulse field 78—1040
  firefly chemiluminescence emissions, time-resolved spectra 80—35822
  fluorocarbon solutions, dye-sensitized, spectroscopic obs. of 1.27 μm and 1.58 μm emission of single ($^1\Delta_g$) mol. O_2 80—85178
  fluoromethanols (mono and tri), decomposition activation of HF, non-statistical energy partitioning, laser emission 79—945
  formaldehyde, excited state photodecomp., rotationally resolved spectra 77—60088
  formaldehyde (A^1A_2) single vibronic level photolysis, H atom prod., HNO chemiluminescence 77—9108
  gas chromatography, selective detection by N_2 induced chemiluminesc. 80—89495
  gas phase chemical reactions, laser obs. *(German)* 79—29365
  gas-phase reactions, spectral-kinetic investig. rel. to chemical laser development *(Russian)* 77—90604
  gaseous chemiexcited mol., modulated transmission spectra 77—86316
  graphite intercalation by HNO_3, NO_2 evolution identification 79—43564
  halogen atoms produced in IR photodissoc., hydrogen halides form., IR chemiluminesc. 77—63932
  heavy particle shock-radiational recombination, chemiluminesc., kinetics, reversed predissoc. 77—1924
  heterogeneous excitation, ionisational mechanism 80—40173
  high temperature metallic species, absorpt. and fluoresc., high temp. fast flow reactor technique 80—42231
  high-temperature chemical processes, review, book contrib. 77—40545
  hydrodynamic electrochemiluminescence cell 80—45506
  5-hydroxy-2,3-dihydro-1,4-phthalazindione, electron beam excited chemiluminesc., chem. and light yields 78—53209
  3-hydroxyflavone, excited state proton transfer, luminesc. 80—35818
  infrared, detection, in ion-molecule reactions, vibrational product states appl. 78—88625

chemiluminescence continued
  ion-molecule reactions, anal. of spectra 78—64832
  IR, temp. and conc. non-uniformities effect in gas 78—48656
  IR laser photolysis of polyat. mols. photochem. appls. 80—66835
  KBr, γ-irradiated and additively coloured, chemiluminescence origin *(Russian)* 77—32453
  ketene, multiphoton laser-induced decomp. chemilum. and collision-assisted dissoc., rephotolysis 79—83491
  ketone chemiluminescence during disproportionation, nonradiative transition processes 79—87846
  laser vaporisation of metals, oxidation and chemiluminesc. kinetics 79—100385
  laser-induced chemical processes, optical selection of reagent orientation 80—11914
  laser-initiated chain reactions, rates, mechanisms, chemiluminesc. obs. 80—55651
  lipid systems, anti-oxidant action mechanism determ. by chemiluminesc. 77—56330
  luminol, electron beam excited chemiluminesc., chem. and light yields 78—53209
  luminol, quantum and excited state yields, pulse radiolysis 79—47930
  metal atom oxidation reactions, kinetics of chemilum. emitter form. and quenching 78—63107
  metal film, chemiluminescence associated with laser generation of atomic beams 80—5637
  metal halide (oxide) dissociation energies, calc. from chemiluminesc. reactions, temp. depend. rate const. correction 77—40524
  metal oxide, temp. depend. of chemilum. reactions, activation energies for excited state form. 78—66818
  metal-gas reactions, surface chemiluminesc. study 80—55708
  methane-air flame, reactions, radical overshoot 79—34308
  methanol multiphoton photolysis-produced radicals luminesc. 78—3358
  methyl radical + O(F), infrared chemiluminescence obs. 80—61080
  methylamine, $CH(X^2\Pi)$ and $OH(A^2\Sigma^+)$, production by multiphoton dissociation, rate constant, laser induced fluorescence and chemiluminescence study 79—98135
  4-methylumbelliferone, excited state reaction rate, fluoresc. and decay time 77—63919
  mild steel, S determ., flame chemiluminesc. method 78—48711
  molecular bond energies from time-of-flight chemiluminesc. 78—40051
  molecular vibronic states population inversion during chemiluminesc. 80—3351
  molecule-metal interaction and surface reactions, theoretical description 80—39652
  neuron inhibition simulation in electrochemiluminescence cell *(Russian)* 78—27925
  nucleoside anion + hydrocarbon cation, electrochemiluminescent electron transfer reaction 79—88046
  nucleotide anion + hydrocarbon cation, electrochemiluminescent electron transfer reaction 79—88046
  O_3, laser flash photolysis, $O(^1D)$ quantum yields in fall-off region, NO_2* monitor 80—45524
  organic compounds, electrochemiluminesc. excitation via generator producing bipolar voltage pulses 77—28629
  organic laser dyes, electrochemiluminescence, electrochem. oxidation, reduction 77—70304
  organic molecules in solution, electrochemiluminesc., US field effects 78—31260
  organic substances, electrochemiluminescence as possible source of coherent radiation, and role in biological processes *(Russian)* 80—76093
  oxalate esters, low intensity long duration chemilum., disposable lighting device appl. 80—11488
  ozone + olefins, in stratospheric ozonometer *(French)* 79—48574
  pea roots, circadian rhythms of ultra-weak chemiluminesc. 77—70432
  photoinduced recombination of atoms and radicals 79—5170
  photorecombination emission reaction mechs. during atomic collisions 80—18914
  photostimulated recombination of atoms after mol. photodissoc. 79—57263
  phthalamide derivative with aromatic amine, exciplex formation and fluoresc. quenching 79—87848
  piezochemiluminescent, piezochemomagnetic and piezochemovoltaic effects *(Russian)* 77—85820
  plant roots extracellular luminescence obs. 79—70534
  poly-N-vinylcarbazole film, triplet-triplet energy transfer, chemiluminesc. 78—43944
  polymers, stress-enhanced chemiluminesc. 80—40628
  prereaction effects on laser-initiated reaction rate meas. by chemilum. obs. 78—44386
  protein-lipid model systems, chemiluminesc. on exposure to formalin 77—56329
  PTFE, chemiluminescence, 25 to 172°C 77—55839
  PVC, ozonized, decomposition of peroxides, chemilum. meas. 78—68893
  pyrene, emission from triplet state in electrochemical at low temps. 77—77307
  quercetin, excited state proton transfer, luminesc. 80—35818
  reaction zone, electron transfer chemiluminescence, digital simulation 79—8200
  rubrene, electrochemilum. by DC, highly organised EHD convection obs. 80—71499
  rubrene, electrogenerated chemilum., production of excited states by direct heterogeneous electron transfer 79—20371
  rubrene, soln. in benzonitrite, electrochem. luminesc. 77—77776
  rubrene radical cation reduction at n-ZnO electrode, triplet state formation, luminesc. 77—16825
  rubrene thin layer and flow cells, steady DC electrogenerated chemilum. 80—55205
  semiconductor, narrow-band, heterogeneous chemiluminesc., ionisation mechanism of excitation 80—50438
  serum albumin, human, mechanism of eosin-sensitised photochemiluminescence 79—53044
  serum albumin solns., X-ray induced chemiluminesc. intensification by dye addition 79—79470
  sodium tetraphenylborate soln., electrolyte, steady state electrochemiluminesc. 79—57250
  sodium tetraphenylborate solns., stationary electrochemiluminesc. *(Russian)* 78—48243
  solutions, nonradiative energy transfer 79—11479
  step experiments, analytical treatment of diffusion and electron transfer 78—27763

chemiluminescence continued
trans-stilbenes, triplet energy, substituents effect, singlet-triplet absorpt. and electrochemilum. obs. 79−81225
tetracene anion+tetracene cation, electron transfer reaction, singlet fission 78−11502
tetramethyldioxetane, collisional dissoc. by supersonic Xe beam, chemiluminesc. 78−40029
tetramethyldioxetane, gas phase unimol. decomp. and chemiluminesc. initiated by TEA CO_2 laser 77−60068
tetramethyldioxetane, IR laser dissociation, chemilum. spectrum 79−5171
tetramethyldioxetane, multiphoton dissoc. time depend. 79−16020
TMPD, nonpolar photoionised soln., geminate pair quantum field, recombination fluoresc. elec. field quenching 79−20389
Al, chemisorption of O_2, photon and electron emission as indicators of intermediate states 80−39439
Al, galvanoluminescence during anodisation in non-dissolving electrolytes 79−52680
Al hydration, in vap. phase, rel. to upper atmosphere chemiluminesc. 79−29362
Al+halogen (SF_6) (NF_3) 77−9086
$Al+O_2$ reaction, surface chemiluminesc. study 80−55708
$Al+O_3 \rightarrow AlO+O_2$, chemiluminesc., $A^2\pi$-$X^2\Sigma^+$ transition obs. 78−31639
AlO, in $Al+O_3(N_2O)$ chemilum., perturbations and vibr. population anomalies obs., mechanism 77−63917
Al_2O_3 anode film, galvanoluminesc. during pulsed excitation 79−74006
$Ar+PCl_3$ reaction PCl emission spectra 78−21938
ArBr, emission spectrum and chemiluminesc. 80−45508
ArBr, pot. curves, population distribs. and chemiluminesc. for B(1/2) and C(3/2) electronic states 80−45509
$Ar^*+Fe(CO)_5$, chemiionisation and chemiluminescence reactions, Penning ionisation and fluoresc. obs. 80−97689
B+CsF(RbF)(KF)(NaF), gas phase chemiluminescence reaction 77−29013
$B+N_2O$, chemiluminesc. reaction, vibr. state distribs. 79−20354
$B+O_2$, chemiluminesc. reaction, vibr. state distribs. 79−20354
$B+O_2(NO_2)(N_2O)(O_3)(ClO_2)$, chemiluminesc. metal oxide formation 80−35509
Ba films, chemisorptive luminescence systems for surface reaction obs. 78−7236
Ba in $Ba+N_2O$ reaction, intracavity dye laser spectroscopy 77−86293
$Ba+Br_2(I_2) \rightarrow BaBr(BaI)+Br(I)$, time-of-flight chemiluminesc., mol. bond energies determ. 78−40051
$Ba+CCl_4 \rightarrow BaCl_2+CCl_2(\bar{A})$, chemiluminesc. spectrum and ang. distrib. obs. 79−15962
$Ba+CO(CO_2)$, flame spectra, 500-1150 nm mechanism 77−48646
$Ba+Cl_2$, 10^{-5} torr, dynamics, chemiluminesc. ang. depend., radiative lifetime 77−40539
$Ba+N_2O$, chemiluminescent flame, BaO states population 79−39153
$Ba+N_2O \rightarrow BaO+N_2$, chemiluminesc., ang. distrib. 78−44361
$Ba+N_2O \rightarrow BaO^*+N_2$, model electronically nonadiabatic reaction, large quantum effects 77−4897
$Ba+NO_3(N_2O)$, chemiluminesc., absolute photon yields determ. 77−86317
$Ba+O_2$ flame, chemilum. from three-body recombination reactions 77−77759
$Ba+S_2Cl_2 \rightarrow S_2^*+BaCl_2$, rearrangement reaction, crossed-beam chemiluminesc. 77−29009
BaO in $Ba+N_2O$ reaction, intracavity dye laser spectroscopy 77−86293
BaO^*, quenching of excited species formed by $Ba+NO_2$ chemiluminesc. reaction 77−58140
Br, and Br_2, luminesc. assignments in excimer laser photolysis of CBr_4 and CF_2Br_2 79−39184
$C+N_2O \rightarrow CN+NO$, chemiluminesc., CN $(A^2\Pi_i)$ vibr. distrib. 79−39152
$C+PbO \rightarrow CO+Pb$, chemiluminesc. from gas phase reaction 79−8426
$C^++H_2(D_2)$, $CH^+(D^+)$ $A^1\Pi$ rot.-vibr. population distribs. 80−23396
C_2, luminesc. assignments in excimer laser photolysis of CBr_4 and CF_2Br_2 79−39184
C_2+NO, laser-induced chemilum. reaction 80−61101
$C_2+NO(O_2)$, IR laser photolysis of polyat. mols. photochem. appls. 80−66835
$C_2+NO \rightarrow CN+CO$, chemiluminesc. reaction, crossed beam study 79−66299
$C_3+O_2 \rightarrow C_2^*+CO+O$, chemiluminesc., rate consts. 77−44466
$C_2(A^3\Pi_g$-$X^3\Pi_u)$, obs. in optically-pumped CO-Ar(-N_2) 80−16701
CF_2, luminesc. assignments in excimer laser photolysis of CBr_4 and CF_2Br_2 79−39184
CH, chemiluminesc. in flowing afterglow of Ar+methane 78−64839
CN $(A^2\Pi)$, chem. prod., CN number densities for gain, emission and absorpt. meas. 78−63112
CN, $A^2\Pi_i$ state vibr. distrib., chemiluminesc. 79−39152
CN, time resolved chemilum., in C_2+NO(vinyl cyanide)(ethylene), laser-generated radical kinetics 79−100352
$CN(B^2\Sigma^+$-$X^2\Sigma^+)$, obs. in optically-pumped CO-Ar(-N_2) 80−16701
CO, emission intensity, CS_2-O_2 flame, rate of population of CO vibr. levels 78−7186
$CS+O \rightarrow CO+S$, shock tube reaction, chemiluminescence and lasing 77−16824
Ca, flame luminesc., laser irrad. effects 77−77766
Ca, metastable, prod. in N_2O-CO flame, u.v. spectra 77−9081
Ca-N_2O-CO flame, Ca catalyzed, gain meas., emission band assignment 78−66815
$Ca+O_2$ reaction, chemiluminesc. absolute cross sections, photon yields and CaO dissoc. energy 80−97697
$Ca+S_2Cl_2 \rightarrow S_2^*+CaCl_2$, rearrangement reaction, crossed-beam chemiluminesc. 77−29009
CaO, chemisorption of O_2, adsorboluminescence from surface F-centres 80−20723
CaO in $Ca+N_2O+CO$ reaction, intracavity dye laser spectroscopy 77−86293
$Ca^*+Cl_2(HCl)$, luminesc. reactive collisions 77−16816
$Ca(4s4p\,^3P)+N_2O$, absolute chemiluminesc. cross-section and photon yield 78−53208
$Cl+H_2S \rightarrow HCl+HS$, laser-initiated chain reactions, rate consts., product energy distrib. 78−85144
$Cl+K_2 \rightarrow KCl+K^*$, chemiluminesc., electronic emission intensity 78−35689
$Cl+OH^* \rightarrow HCl^*+O$, reaction dynamics, vibr. excited reagent and product 77−81392
Cl+vinyl bromide-d_3 reaction, IR chemiluminesc. 80−102506

chemiluminescence continued
$Cl^-+HBr(HI) \rightarrow HCl+Br^-(I^-)$, vibr. product state distribs., IR chemiluminesc. obs. 80−81309
Cl_2 partially dissociated, recomb. reaction freezing in supersonic nozzle, chemiluminescence *(Russian)* 77−52644
$Cl_2+Ca(4s4p\,^3P) \rightarrow CaCl+Cl$, chemiluminescent reaction, state-to-state cross-section, beam-gas expt. 80−45510
$Cl_2+H_2(H_2S)$(methanethiol), laser-initiated chain reactions, rates, mechanisms, chemiluminesc. obs. 80−55651
$Cs+F_2$, electronic excited states, chemiluminesc. in flame, spectra 77−52643
$Cu+Cl_2(Br_2)(I_2)$, beam-gas chemiluminesc. reactions 80−85151
$Cu+F_2$, chemiluminesc. reactions, mol. beam study 80−97702
Cu+oxidant, chemiluminescence spectra and photon yields, population inversion 79−79255
CuF, from gas phase reaction, photon yields, chemi- and photo-luminesc., excitation spectra 79−5157
$D+F_2$, DF initial vibr. energy distrib., IR chemiluminesc. obs. 80−45497
DF, IR chemiluminesc. quenching, (V-V) and (V-T, R) energy transfer rates 78−20018
DF, IR chemiluminesc. quenching, (V-V) energy transfer rates 78−20019
$DF+CO_2$, vibr. relax. rate, chemiluminescence depletion method meas. 79−72399
DO_2+NO, reaction kinetics, near IR chemiluminesc. determ. 80−21261
$Dy^{3+}+O_3(SO_5{}^{2-})(SO_2)$, in H_2SO_4 soln., electrochemiluminesc. emitters quenching by electrolysis products 79−1794
F+carbonyl compounds, HF IR chemiluminesc., vibr. and rot. energy disposal 77−86318
F+ethylene (benzene) derivatives, deuterated, IR chemiluminesc. 80−102506
F+formic acid (formaldehyde), microscopic reaction dynamics, branching ratio, IR chemiluminesc. 78−73021
$F+H_2(D_2)$, rate consts., temp. depend. 80−81302
$F+HBr(HI) \rightarrow HF+Br(I)$, electronic and vibr. energy transfer 77−63899
$F+HCl \rightarrow HF+Cl$, time resolved vibr. chemiluminesc. and rate consts. 80−61069
F+hydrocarbon (substituted methane)(inorganic hydride), HF IR chemiluminesc., H abstraction rel. rate consts. 77−86319
$F+O_2+M \rightarrow FO_2+M$, flash photolysis IR chemiluminesc., rate const. 78−3311
$F_2+Mg(Ca)(Sr)(Ba)$, crossed beam chemilum., kinetics and mechanisms 80−21264
$F_2+TeH_2(TeD_2)$, TeF radical form., chemiluminescence obs. 80−43058
$Fe(CO)_5+Ar^*(^3P)$, chemiluminesc. 78−61014
$Fe(CO)_5$+inert gas, dissoc. energy transfer, chemiluminesc. 80−55647
$Fe(CO)_5+O_3$, modulated chemiluminesc. by CO addition 80−40692
$Ge+N_2O$, chemiluminesc. reaction, HTFFR kinetics study 80−76496
GeH_4+Cl_2, $HGeCl^*$ chemilum. obs., vibr. levels 77−81406
GeO, produced in $Ge+N_2O$ reaction, kinetics of chemilum. emitter form. and quenching 78−63107
$H+Br_2(HBr)$, H^* prod., IR chemiluminesc. meas. 79−100336
$H+Cl_2(SCl_2)(S_2Cl_2)(SOCl_2)(SO_2Cl_2)$, energy disposal, HCl IR chemiluminesc. obs. 78−92484
$H+Cl^- \rightarrow HCl+e$, associative reaction, product vibr. state distrib. 80−66794
$H+ClBr \rightarrow HCl+Br(HBr+Cl)$, product energy distrib., rate const., IR chemilum. obs. 77−81391
H+ClF reaction, IR chemilum., energy disposal and branching ratios 80−26017
$H+ICl \rightarrow HCl+I$, IR chemiluminesc., product energy distrib. 78−23926
$H+ICl \rightarrow HCl+I$, product energy distrib., rate const., IR chemilum. obs. 77−81391
$H+NO+M \rightarrow HNO+M$, $HgH+NO \rightarrow HNO+Hg$, rate consts. of photosensitised reactions 77−36757
$H+O_2$ system, production of $O_2(^1\Sigma_g{}^+)$ 77−63918
$H_2+H+NO \rightarrow HNO+H_2$, rate of reaction, temp. depend., third body efficiencies 78−23933
HBr, vibrationally excited, chem. prod. for CW laser using CW supersonic mixing HF chem. laser 80−1196
HCl laser, V=3 to V=2 band process, computer simulation 78−71095
HCl, vibr. emission from ClF-H_2 chem. laser 80−97709
HCl+Br, IR fluoresc. studies of state-selected energy transfer, photochemistry 77−77768
$HCl+CO_2$, vibr. relax. rate, chemiluminesc. depletion method meas. 79−72400
$HCl+Ca(4s3d\,^1D) \rightarrow CaCl+H$, chemiluminescent reaction, state-to-state cross-section, beam-gas expt. 80−45510
HF, IR chemiluminesc. quenching, (V-V) and (V-T, R) energy transfer rates 78−20018
HF, IR chemiluminesc. quenching, (V-V) energy transfer rates 78−20019
$HF+CO_2$, vibr. relax. rate, chemiluminescence depletion method meas. 79−72399
HF+D, vibr. threshold energies, reagent energy effects 78−85145
HN_3 IR multiphonon dissociation with electronic excitation 80−11934
HN_3+F, strong interactions in gas-phase reactions, arrested relax. IR chemilum. obs. 80−7773
HNO, low-lying states, pot. energy curves 80−9533
HNO, low-lying states, pot. energy surfaces calcs. 80−102460
HNO_3, atmospheric monitoring, chemiluminesc. method 79−16062
HNO^*, det. of H atom quantum yield in formaldehyde photodecomposition 79−96344
$HN_3{}^*+NH^*$, intermediate reaction of laser photolysis of HN_3 78−61037
HO_2+NO, reaction kinetics, near IR chemiluminesc. determ. 80−21261
H_2O^+, form. in Ar^++H_2O, kinetic and vibr. energy distrib. 80−16654
H_2S+NO_2, SO chemiluminesc. in Ar matrix 79−5146
$^2HN_3$ IR multiphonon dissociation with electronic excitation 80−11934
He+water (cyanomethane), afterglow, excitation and quenching reactions, optical pumping 78−35690
He^++SO_2, dissoc. charge transfer reaction, SO^+ $(A^2\Pi$-$X^2\Pi_r)$ emission 80−95659
$He(2^3S)+CS_2$, CS^+ and CS fluoresc. spectra assignments, vibr. populations, transition moments 77−14473
$Hg+2NH_3 \rightarrow HgNH_3+NH_3$, photosensitised, $HgNH_3$ complex lifetime 78−53193
$Hg+NH_3$, excited UV luminesc., low press., $HgNH_3{}^*$ form. 77−21388

chemiluminescence continued
HgCl, $B^2\Sigma^+$ state formed by photochemical reaction in $Hg/Cl_2/Ar$ 79−39154
$HgH+M\rightarrow Hg+H+M$, reaction rate temp. depend., chemiluminescence 78−68885
$HgH+NO\rightarrow HNO+Hg$, reaction rate temp. depend., chemiluminescence 78−68885
HgI_2, aq. soln., luminesc. after high energy electron pulse radiolysis 77−32793
$Hg(^3P_0)+Br_2\rightarrow HgBr(B)+Br$, crossed mol. beam chemiluminesc., cross section 78−31622
$Ho+N_2O\rightarrow HoO^*+N_2$ chemiluminesc. reaction, cross-section 78−76847
I chem. produced $^2P_{1/2}$ state, gain meas. 78−63115
$I+I\pm I_2$, termolecular chemiluminesc. reaction, rate const. for interaction with n-C_3F_7I 79−96291
$I^*(^2P_{1/2})+Br_2\rightarrow IBr+Br^*(^2P_{1/2})$, rate const., chemiluminesc. obs. 77−40520
$K+HgBr_2$, laser irrad., HgBr form., chemiluminescence 80−55658
$K_2+Cl(Br)\rightarrow KCl(KBr)+K^*$ product electronic state distrib., chemiluminesc. 77−40529
KrF^*, oscillatory bound-free emission spectra, semiclassical anal. method 80−7799
La-$F_2(ClF)(Cl_2)(SF_6)$, visible chem. laser development from reactions yielding visible chemilum. 78−63111
$La+OCS\rightarrow LaS$, chemiluminesc. vibr. analysis of $C^2\Pi\rightarrow X^2\Sigma^+$, D_0^0 determ. 77−48645
LaO resulting from bimolecular oxidation of La with O_2, NO_2, N_2O and O_3 77−29011
$Li+Cl_2$ (SF_6) (dichlorofluoromethane) *(German)* 78−92485
LiCa, laser chemiluminesc. 80−93759
LiF, γ-irradiated, chemilum. during dissolution *(Russian)* 78−80427
Mg films, chemisorptive luminescence systems for surface reaction obs. 78−7236
Mg, flame luminesc., laser irrad. effects 77−77766
Mg, metastable, prod. in N_2O-CO flame, UV spectra 77−9081
Mg-N_2O-CO flame, efficient chem. generation of $Mg(^3P)$ 78−63109
Mg-N_2O-CO flame, Mg catalyzed, gain meas., emission band assignment 78−66815
MgCl, spectra obs. in Mg^*-Cl_2 crossed beams, metastable Mg as new light source of forbidden lines 78−90112
MgO, chemisorption of O_2, adsorboluminescence from surface F-centres 80−20723
MgO, light emission during adsorpt. and desorpt. of O_2 78−38949
$Mg(^3P)+K(Ca)$, energy transfer and excimer form. in flowing afterglow 77−60049
$Mg^*+Cl_2\rightarrow MgCl^*+Cl$, chemiluminesc. studies 78−40030
$N+N\rightarrow N_2$, recombinational afterglow spectra, 10-300K 78−44355
N^++H_2 (hydrocarbons), rotational-vibrational product excitation 79−47901
N^++H(hydrocarbons), chemiluminescence, total reaction cross sections dependence on collision energy 79−47530
$ND^*+DN_3\rightarrow ND_2^*+N_3$, chemiluminesc. reaction of electronically excited species, rate const. 78−80771
NF^*+HF^*, microscopic vibrotational-electronic energy transfer, IR chemiluminesc. obs. 79−31662
$NF(a^1\Delta)+I(^2P_{1/2})$ system, electronic angular momentum transfer, chem. kinetic model 78−63104
$NF(b^1\Sigma^+)$ enhancement by I laser pumping 78−63105
NH, photofragment, energy distrib., chemiluminesc. reaction rates 77−90618
NH_3, IR multiphoton dissoc., laser fluoresc. and chemiluminesc. obs. 79−68276
N_2H_4-F_2 flame, chemiluminesc., HNF A-X emission spectrum 79−50033
$NH_2(A^2A_1)$, IR emission detection in UV laser photodissoc. of NH_3 80−11901
$NH(A^3\Pi, b^1\Sigma)$, two-photon generation in NH_3 UV laser photodissoc. 80−11901
$NH_3(ND_3)+Hg$, photosensitised luminesc., phase shift anal. 79−15966
NH^*+HCl(methane)(ethylene)(cyclopropane) (cyclohexane), rate const., time resolved chemiluminesc. 78−60982
$NH^*+HN_3\rightarrow NH_2^*+N_3^*$, rate const., time resolved chemiluminesc. 78−60982
NO chemiluminescent emission at 2.9 μm wavelength, auroral enhancement 80−12586
NO concentration meas. in gas mixtures, chemiluminescence method *(Russian)* 79−16094
NO γ-band chemiluminescence, obs. of N_3 form. in NaN_3 thermal decomp. 79−100351
NO, stratospheric growth before sunrise by photolysis 77−29356
$NO+C_2H_4$, HNO excitation by $O_2(^1\Delta_g)$ 79−52674
$NO+O$, absolute rate const., O_3 effect 80−45507
$NO+O$, chemiluminesc., rate const., optical comparison method meas. 77−90603
$NO+O$, in Ar matrix, chemiluminesc. 78−35688
$NO+O_3$, fs-states and rot. states, effect on reactivity 80−89473
$NO+O_3\rightarrow NO_2^*$, mol. beam chemiluminesc., kinetic and internal energy depend. 78−31638
$NO+O_3\rightarrow NO_2^*+O_2\rightarrow NO_2+h\nu+O_2$, chemiluminesc., translational and rot. energy effects 80−30218
$NO^++NO_2^-$ neutralisation reaction, spectroscopic study 79−13819
NO_2, cyclic chemiluminescent monitoring device, NO conc. effects 77−49177
NO_2 monitoring in stack gas, chemiluminescence appl. 79−57560
NO_2, $NO+O_3$, chemiluminescent reaction, theory of light amplification *(Russian)* 77−88717
NO_x, atmospheric monitoring, chemiluminesc. method 79−16062
NO_x source analysis, continuous, using diffusion interface module 78−40095
N_2O-CO flame, alkaline earth catalyzed chain reaction chemiluminesc. 77−40548
N_2O-CO flame, Mg catalyzed chain reaction chemiluminesc. 77−36758
N_2O+CO, Na catalysed, Na chemiluminesc., excitation mechanism, appl. chem. laser 77−63916
NO_2^* visible emission, formed in N_2O_4 UV-irrad., quantum yield 79−66298
$NO_2^*+CO\rightarrow NO+CO_2$, laser stimulated reaction, rate const. 78−40044
NS radical chemiluminescence produced by active $N+S(S_2Cl_2)$, kinetics study 79−39151
Na, chemisorption of halogens, surface chemiluminesc., MO description 79−43048

chemiluminescence continued
$Na+Cl_2$ reaction, surface chemiluminesc. study 80−55708
$Na+N_2O$, Na chemiluminesc., excitation mechanism, appl. chem. laser 77−63916
$Ne^*+Fe(CO)_5$, chemiionisation and chemiluminescence reactions, Penning ionisation and fluoresc. obs. 80−97689
$Ni(CO)_4$, ppb in air meas. by chemiluminesc. detector 80−40692
$Ni(Co)_4$+inert gas, dissoc. energy transfer, chemiluminesc. 80−55647
O source with improved long term stability for chemiluminescence reaction, mol. dissoc. and recombination 80−93758
O+acetylene reaction, kinetics, flash photolysis-reson. fluoresc. meas. 77−73439
O+chloroethylene reaction, kinetics, flash photolysis-reson. fluoresc. meas. 77−73439
$O+H_2S$, matrix reactions, IR spectra of products, chemiluminesc. 77−60057
O+NO binary reaction, crossed beams, NO_2 chemiluminesc. 78−64843
$O+O\rightarrow O_2$, matrix reaction, diffusion controlled, 8-20K 78−61013
$O^-+CO\rightarrow CO_2^++e^-$, vibr. chemiluminesc. 78−3340
O^++hydrocarbons, chemiluminescent reactions 79−96299
O_2, chemisorbed on metal films, active sites, chemiluminesc. and vacuum microbalance obs. 78−22950
O_2 singlet energy transfer in quenching, vibr. excited mols. 77−71828
$O_2+La(Y)(Sc)$, crossed beam chemiluminescence reaction, spectral simulation, hyperthermal energy meas. 78−80732
O_3 concentration in water, chemiluminescent meas. method 77−60159
O_3, photolysis, near UV, temp. depend. of $O(^1D)$ formation 78−15689
$O_3+H_2S(OCS)$, SO chemiluminesc. in Ar matrix 79−5146
OCS+Si(Ge), SiS and GeS multiple collision chemiluminesc., intercombination systems 80−45505
OH, chemiluminesc., form. from O+ethylene, mechanism, rate const., mathematical model calcs. 78−48655
$OH^{\cdot}+O$, $OH^{\cdot}+CO$, reaction rates, mechanism, flow discharge chemilum. obs. 77−52610
$O(^3P)$+alkenes, absolute reaction rate consts., 298-439K, photolysis-chemiluminesc. determ. 77−77747
$O(^3P)$+amines, rate consts. temp. depend., 298-440K 78−48616
$O(^3P)$+n-butane (NO(M=Ar)), reaction rate constants using flash photolysis-NO_2 chemiluminesc, method 77−44458
$O_2(^1\Sigma_g^+\rightarrow{}^3\Sigma_g^-)$, in O-COS-$O_2(^1\Delta_g)/O_2$ system, chemiluminescence 80−66806
O^*+H_2S, matrix reaction, diffusion controlled, 8-20K, $O(^3P)$ 78−61013
P_4, vap., oxidation, chemiluminesc., reduced press. system 77−32795
$P_4+H_2O(D_2O)$, vapour, chemiluminesc., transient emitting species 77−1926
Pb, chemiexcitation of ^3P metastable states, during combustion of acetylene and C_2H_2 78−3339
$Pb+F_2$, chemiluminesc. spectrum of PbF 79−24742
$Pb+N_2O\rightarrow PbO+N_2$, chemiluminesc. reaction, vel. depend. 78−27762
$Pb+O_3$ reactions, chemiluminesc. 79−52673
PbF, laser-induced fluoresc. of $A^2\Sigma$ state, chem. laser eval. 79−81222
PbO, chemiluminesc. spectra, Pb atom reactions, mol. consts. 77−9087
$Rb_2+Br\rightarrow RbBr+Rb^*$, product electronic state distrib., chemiluminesc. 77−40529
Ru complex, electrogenerated chemiluminesc., production of excited states by direct heterogeneous electron transfer 79−20371
$S+O_2\rightarrow SO_2$, matrix reaction, diffusion controlled, 8-20K 78−61013
$S+O_2\rightarrow SO_2(a^3B_1)$, in Ar:OCS:$O_2$ matrix thermoluminescence of SO_2 77−48647
$S+S\rightarrow S_2$, matrix reaction, diffusion controlled, 8-20K 78−61013
S_2, $^1\Delta_g$ and $^1\Sigma_g^+$ states, near IR emissions 80−18852
S_2, matrix isolated in solid Ar 79−47529
SF_6 mixtures, laser initiated explosions, chemilum. in near UV, visible and IR 78−48674
SF_6, multiple photon dissociation threshold behaviour, chemilum. obs. 78−42145
SF_6-methane, mixture, CO_2 laser induced multiphoton dissociation and chemilum., laser fluence depend. 79−57233
$SF_6+Ca(Sr)$, F_5S-F bond energy bounds from chemiluminesc. obs. 79−86081
SF_6+NO+O_3, laser sensitised reaction, time-resolved NO_2^* emission obs. 78−20017
SO, $(^1\Delta_g, {}^1\Sigma_g^+)$ chemiluminescence sensitised by metastable $O_2(^1\Delta_g)$, energy pooling 80−26016
SO_2, chemiluminescence at $(\mathbf{c}^1\Sigma^-\rightarrow\mathbf{a}^1\Delta)$ in Ar matrix, photolysis prod. and thermoluminesc. 79−5158
SO_2, IR photolysis, associated visible luminesc., 2-25 torr 79−29384
$SO(^1\Sigma^+\rightarrow{}^3\Sigma^-)$, in O-COS-$O_2(^1\Delta_g)/O_2$ system, chemiluminescence 80−66806
Sc-$F_2(ClF)(Cl_2)(SF_6)(Br_2)$, visible chem. laser development from reactions yielding visible chemilum. 78−63111
$Sc+NO_2$, chemiluminesc., nonequilib. product distrib. 80−101014
$Sc+O_2(NO_2)(N_2O)(O_3)$, oxidation, single collision chemiluminesc. 77−25267
$Sc+O_2\rightarrow ScO+O$, chemiluminescence, $A^2\Delta X^2\Sigma^+$ transition 77−1927
ScF supersonic mixing flame, spontaneous emission, electronic transition chem. laser pot. 78−66817
$Se+O\rightarrow SeO$, chemiluminescent reaction, $B^3\Sigma\rightarrow X^3\Sigma$ band emission 79−79254
$Si+2XeF_2\rightarrow SiF_4+2Xe$, surface reaction, IR chemiluminesc. 79−83504
$Si+N_2O$ flames, SiO emission, $A^1\Pi$, $b^3\Pi$ and $a^3\Sigma$ states 77−77767
SiF, chemilum. in $Si+F_2$, SiH_4+F_2 and SiD_4+F_2 80−3315
SiF, chemilum. obs. of $A^2\Sigma^+$ and $a^4\Sigma^-$ states 78−66816
SiF, use in chemical lasers 80−64004
SiS, chemiluminescent flame spectra, electronic states and rot. struct. obs., vibr. assignments, Franck-Condon factors determ. 80−85179
$Sm+F_2(N_2O)$, chemiluminesc., absolute photon yields determ. 77−86317
$Sm+N_2O$, mol. beam chemiluminescence, cross section energy depend. 77−32792
Sn, oxidation kinetics, in high-temp. fast flow reactor, chemiluminesc. titration meas. 77−48623
$Sn+N_2O$, chemiluminesc., high temp. fast flow reactor kinetics obs. 78−88636
$Sn+N_2O$, oxidation chemiluminesc., quenching kinetics 79−52672
$Sn+N_2O\rightarrow SnO(a^3\Sigma)+N_2$, chemiluminesc. high temp. fast flow reactor obs. 80−45493
$Sn+O_2(NO_2)$, chemiluminescence and photon yields 77−29012
SnF, use in chemical lasers 80−64004
SnO, produced in $Sn+N_2O(O_2)(O)$ reactions, kinetics of chemilum. emitter form. and quenching 78−63107

chemiluminescence continued

- Sr in $Sr+N_2O+CO$ reaction, intracavity dye laser spectroscopy 77—86293
- Sr, metastable, prod. in N_2O-CO 77—9081
- Sr-N_2O-CO flame, Sr catalyzed, gain meas., emission band assignment 78—66815
- $Sr+S_2Cl_2 \rightarrow S_2^*+SrCl_2$, rearrangement reaction, crossed-beam chemiluminesc. 77—29009
- SrF, temp. depend. of chemilum. reactions, activation energies for excited state form. 78—66818
- SrO in $Sr+N_2O+CO$ reaction, intracavity dye laser spectroscopy 77—86293
- $Sr^*+Cl_2 \rightarrow SrCl^*+Cl$, chemiluminesc. studies 78—40030
- $Sr^*+N_2O \rightarrow SrO^*+N_2$, visible chemiluminescence, absolute cross section and photon yields 78—92463
- 2-(stilbenyl-4)-5-phenyloxazole derivatives, electrolytic effects of substs. on electrochemiluminesc. intensity *(Russian)* 77—55834
- T_2+NF_3, chem. laser, TF spontaneous emission, Einstein coeffs. determ. 77—58073
- $Tb^{3+}+O_3(SO_5{}^{2-})(SO_2)$, in H_2SO_4 soln., electrochemiluminesc. emitters quenching by electrolysis products 79—1794
- $Te(^3P_1)$+inert gas, gas phase flash photolytic deexcitation obs., 1000K *(Russian)* 78—50626
- ThO_2, pure and Tb^{3+} doped, impurities effect in absorboluminesc. and photoluminesc. 79—38597
- $ThO_2{:}Pr^{3+}$, luminesc., calcination temp. and excitation process depend. 79—33749
- Ti, heat- mass- and charge transfer in high temp. oxidation 79—83369
- $Ti+O_2$ reaction, surface chemiluminesc. study 80—55708
- $Ti(^5F)+N_2O(O_2)(NO_2)$, chemiluminesc., TiO dissoc. mechanisms, confirmation of D°_0(TiO) 77—40534
- TiO, $(C^3\Delta\text{-}X^3\Delta)$ system, radiative lifetimes, oscillator strengths, flame spectroscopy 78—42136
- TiO, emission spectra in chemiluminesc. flames 77—38689
- TiO, photoluminesc. of $\alpha(C^3\Delta\text{-}X^3\Delta)$ system in chemiluminesc. flames 77—38690
- VO, from V oxidation, bandhead anal. 77—9077
- $Xe+Br_2 \rightarrow XeBr^*+Br$, rot. polaris. in chemiluminesc. 79—8432
- $Xe+Br(CCl_4)$, excitation functions and rotational polarisation, chemiluminesc., crossed beam study 80—76491
- $XeCl^*$ emission spectrum obs., in $Xe(6s,{}^3P_2)+RCl$ reactive quenching 79—100344
- $XeCl^*$ spectra, for $Xe(6s,{}^3P_2)+RCl$ vibr. energy disposal assignment 79—100345
- XeF_2+Si, surface reaction, IR chemiluminesc. 79—43633
- Y-$F_2(ClF)(Cl_2)(SF_6)(Br_2)(IBr)$, visible chem. laser development from reactions yielding visible chemilum. 78—63111
- $Y+O_2(NO_2)(N_2O)(O_3)$, oxidation, single collision chemiluminesc. 77—25267
- $Y+O_2 \rightarrow YO+O$, $A^2\Delta\text{-}X^2\Sigma^+$ transition 77—1927
- YCl supersonic mixing flame, spontaneous emission, electronic transition chem. laser pot. 78—66817
- YO, temp. depend. of chemilum. reactions, activation energies for excited state form. 78—66818
- YbCl, chemiluminesc., vibr. anal. 77—30917
- YbF, chemiluminesc., vibr. anal. 77—30917
- ZnS, decomposition in H_2 atmosphere, electron-hole mechanism *(Russian)* 77—16409
- Zr, heat- mass- and charge transfer in high temp. oxidation 79—83369

chemioception

- afferents from aortic and carotid bodies, relative latency of responses 80—101189
- amino acid taste and smell, catfish, electrophysiological distinctions 77—44694
- antennular chemosensitivity in the spiny lobster Panulirus argus, amino acids as feeding stimuli 78—53431
- bacterial chemotactic behaviour regu7tion by Ca^{2+} obs. 78—15851
- bacterial chemotaxis, change in membrane pot. 77—44695
- bacterial sensory electrophysiology, membrane pot. rel. to motility and chemotaxis in Bacillus subtilis 78—53373
- behavioral sensitisation in aplysia, presynaptic facilitation as a mechanism 77—36912
- behaviour patterns in cod released by elec. stimulation of olfactory tract bundlets 80—97951
- beta cell or artificial pancreas, technological challenge *(German)* 79—16346
- carotid body, a model for the chemoreceptive process *(German)* 77—29162
- chemoreception physics 78—15850
- chemotactic bateria, model for travelling bands 78—44516
- chemotactic bateria, steadily propagating rings, struct. 77—44693
- detectability index for characterisation of odour detection *(French)* 80—8072
- dynamic receptor pattern generation model 79—62207
- E. coli, migration chemotactic bands, quasi-elastic light scatt. obs. 78—77018
- EEG, differential arousal response to gustatory stimuli in the awake rabbit 80—12166
- EEG activity of the caiman olfactory bulb, computer anal. 77—81513
- EEG M-wave and CNV obs. in squirrel monkey 79—83805
- EEG monitor for free-swimming fish in olfactory system study 77—86718
- environmental odour emissions analysis, rbjective olfactometry *(German)* 78—7754
- evoked brain potentials, correl. anal. *(Japanese)* 80—97946
- file clam, mech. and chem. sensitivity at the mantle edge 78—53429
- gustatory function, radiation-induced changes, neutrons rel. to photons 80—12184
- hypercapnic stimuli, mathematical model of chemoreflex responses 79—34578
- insulin receptors on human platelets, ^{125}I-insulin binding meas. 79—92245
- leukacyte adhesion studied by spectroscopy for chemotaxis studies 77—56562
- lung, irritant receptors and afferent C-fibres, stimulation by prostaglandins 77—12939
- matching information to brain, problems 80—51114
- mouse sensitivity to curariform drug. 2.45 GHz irradiation effect *(French)* 80—3717

chemioception continued

- neuronal template-matching mechanism for sensory search with olfactory bulb, anal. 80—56069
- neutrophils rabbit, chemotactic factor-induced release of membrane Ca 79—88095
- odour identification, keys to 79—88096
- olfaction, new theory based on dispersion-induced optical activity 77—56393
- olfaction, possible binding site of Cu(I) 79—96060
- olfactometry, smell intensity meas. *(French)* 80—8073
- olfactory bulb, 55 counts/sec rhythm anal. and simulation 80—85422
- olfactory bulb, gain mediating cortical stimulus-response relations, nonlinear 80—12165
- olfactory bulb and cortex, spatial props. of an EEG event 79—16223
- olfactory bulb elec. responses to general and hunger arousal, rat. 79—79565
- olfactory bulb model, interactive neural masses, spatial and temporal charact. freqs. 77—25476
- olfactory bulb stimulation, inhibitory postsynaptic potentials in piriform cortex neurons 79—92244
- olfactory cortex, pig, maintained in vitro, effects of cooling 78—3525
- olfactory pattern recognition, modelling by an adaptive spatial filter 78—24080
- olfactory perception, neurophysiological correlates rel. to amygdalotomy 79—100637
- olfactory receptor sites location, inferences from latency meas. 80—56068
- olfactory sensitive neurons in lateral hypothalamus, response to gastric distension in rabbits 79—92243
- olfactory tubercle, unilateral lesions, modification of general arousal effects, rat 80—3652
- ovipositor receptor neurone sensitive to monovalent cation concentration, 77—77922
- Paramecium membrane potential changes during chemokinesis 80—26209
- radiation-induced changes in Na preference and fluid intake in the rat 80—35986
- respiratory control system simulation, state of the art 78—53441
- respiratory controller, development and evaluation of a model 77—44697
- respiratory plant dynamics under open control loop conditions 77—44705
- respiratory time series, cluster anal. 78—56959
- sensory measurements in connection with atmospheric odours *(Dutch)* 77—25775
- smell measurement methods, current status *(Japanese)* 78—92661
- sweet taste receptor, modelled by antibodies to thaumatin 78—27975
- synaptic facilitation and behavioral sensitisation in aplysia, possible role of serotonin and cyclic AMP 77—36913
- synaptosome opiate receptor, kinetics of stereospecific binding of spin labeled morphine 77—9215
- taste cells, insect, special purpose amplifier for spike train recording 80—72394
- taste hairs, insect, nonblocking AC preamplifier to tip recording 77—90971
- taste reception, physicochem. mechanism and chem. sensors development *(Japanese)* 80—85423
- telemetered EEG activity from the isolated olfactory bulb of rabbits 77—86516
- telemetered neurophysiological activity in the olfactory system of rabbits and pheromones 77—90816
- tongue receptors, dolphin, morphofunctional and bionic anal. *(Russian)* 79—43937
- trigeminal mesencephalic nucleus of rabbit, adjacent neuron identity of activation 79—92241
- Ca-dependent sensory-motor response of a marine dinoflagellate to Co_2 78—57026

chemisorption

- accommodation coefficient, in gas-surface scatt., classical model 77—25306
- acetylene, chemisorbed on metal surfaces, geometric and electronic struct., UPS obs. and HF LCAO calc. 79—86988
- acetylene, chemisorption on Pt (111), ethylidyne group form., LEED and ELS obs. 78—73075
- activated chemisorption, kinetics, adsorbate distrib., temp. and press. depend. 78—35720
- activated chemisorption kinetics, differential heat of adsorption meas. 78—84062
- adatom monolayer, on model transition metal surface, densities of states, chemisorption effects 78—26769
- alkali metal, on metallic surface, using density functional formalism 77—7975
- alloy, binary, atomic roughness and chemical adsorption at solid-liquid interface *(French)* 78—51787
- alloy, cleaved, electronic theory, off-diagonal disorder 79—4596
- Anderson model, correlation corrections to chemisorption energy 79—19538
- angle resolved secondary emission and electron energy loss study of electronic struct. 79—61477
- atom, chemisorbed on solid, diffusional motion, microscopic anal. 79—4467
- atom, coherent and diffusional motion on surface 77—1292
- atom, electronically adiabatic vibr. state lifetime 77—72768
- atom on metal, core electron binding energy 78—10280
- atomic chemisorption, chemical trends, core-hole relax. effects, jellium model 78—76909
- atomic chemisorption on simple metals, chem. trends, core-hole relax. 78—14586
- atoms on semi-infinite linear chain, chemisorption theory and superoperator formalism 80—93800
- Be clusters, of H_2, ab initio calcs. 80—3404
- binding energy of chemisorbed diatomic molecule, indirect coupling contrib. 77—1310
- bonding and surface structure, review 77—4252
- catalysis, chemisorption kinetics, determ. from substrate current fluctuations 80—84383
- catalyst, mag. characterisation, review 78—64881
- cellulose char, O_2 chemisorpt. kinetics 80—96730
- charge distribution resulting from localised phase density *(German)* 79—51434
- charge transfer processes, phys. significance and terminology 77—25307
- charge-density maps 79—19453
- chemisorbed atoms, theory of interactions *(German)* 78—31706

chemisorption continued
chemisorbed atoms and mols., vibrational motion dynamics, infrared absorpt. line shape 78—51814
chemisorption, of H(O), on electrode, volume of adsorbed species, temp. and press. effects 78—84060
chemisorptive luminescence systems for surface reaction obs. 78—7236
cluster Auger spectrum, SCF core-valence-valence calc. 80—48045
cluster chemisorption, book contrib. 80—107650
competitive, on metallic films, IR spectra, oil matrix technique 77—9118
complex chemisorption structures, interpretation 77—89652
conference, New York, USA (Oct. 79) 80—73093
conference on solid-vacuum interface, Amsterdam, Netherlands (June 78) 79—42342
conference on surface science, York, England (March 1977) 78—14540
'cubium' clusters, of H, size effects, embedding 77—59202
defective surface, theory 78—2362
diamond powders, of O_2, thermal desorpt. spectra 78—47661
dissociatively chemisorbed molecules, desorption kinetics 79—86977
electrochemical surface reacts. driven by linear pot. sweep, sequential reactions, kinetics 77—25276
electrolyte-solid interface, electrochemistry of surface 78—80798
electron beam damage in chemisorbed layers, tunnelling spectra 77—76672
electron spectroscopy and surface chemical bonding, book contrib. 80—24992
electron stimulated desorption data, chemisorbed systems, reinterpretation in Auger decay model 79—42375
electronegativity, spin-orbital, and catalytic activity 78—73078
electronic and ionic motion, exact unidimensional model 80—15369
electronic excitations of chemisorbed molecules, selection rule effects, EELS 78—76566
ellipsometry of clean surfaces, submonolayer and monolayer films, review 80—103546
embedding problem, SCFMO formalism 78—71977
energy levels, adsorbate, relax. shifts, line shapes and satellites in XPS and X-ray absorption spectra 77—90242
ethylene, chemisorbed on metal surfaces, geometric and electronic struct., UPS obs. and HF LCAO calc. 79—86988
ethylene, chemisorption on Pt (111), ethylidyne group form., LEED and ELS obs. 78—73075
extended Huckel theory, iterative method 79—87875
extraorbital screening charge around chemisorbed atoms, spatial variation 79—60886
fast thermal desorption, adatom-adatom interactions 79—95256
fixed molecule high energy photoelectron ang. distribs. 78—39667
gelatin layer, dry, aqueous soln. penetration 80—85221
graphite, adsorption and dissociation of O_2, CNDO/2 calcs. 79—28206
graphite, adsorption and migration of O_2, CNDO/2 calcs. 79—28205
graphite, chemisorption of CO, CNDO calc. using cluster model 80—54522
graphite, of atomic H, regular phases 78—38965
graphite, of H_2, substrate relax. effects 77—7962
graphite, of H, regular phase, CO-NDO approx. 77—15681
graphite, of H,cryst. orbital NDO calcs. 77—7965
graphite, of N periodic overlayers, CO-NDO calcs. 79—7745
graphite, of O_2, influence of Fe as impurity 80—96732
graphite, of O, CO-NDO calcs. 78—75937
graphite intercalation compound, interaction between one or two s orbitals *(French)* 80—65440
Green's function formalism appl. to chemisorption on real infinite systems 79—19461
Green's function methods for substrates with complex band. struct. 78—71961
heterogeneous atom recombination on surface sites, kinetics of Langmuir-Rideal mechanism 79—87876
heterogeneously catalysed reactions, kinetic instabilities, oscill. instabilities 79—24717
heterogeneously catalysed reactions, kinetic instabilities rate multiplicity 79—20341
1-hexene-water(-D_2O), field-induced surface reactions, field ionis. mass spectra obs. 78—95949
image charge effects, surface plasmons 80—84381
image charge effects on adsorbate valence spectra, perturbational study 80—84380
indirect interaction between chemisorbed atoms, theory 79—46923
interstellar oxide grains, mol. prod. 79—25690
interstellar oxide grains, S and Cl depletion 80—17635
interstellar transition metal grains, of H, rel. to H_2 catalytic form. 78—54005
ion electrostatic interaction at electrode surface, ion field penetration 80—81333
ionic crystal, of electropositive ion, polaris. effects 79—37923
IR spectral linewidth and sticking coeffs., non-adiabatic effects 80—39423
island formation and adatom interactions 79—46922
island formation and condensation of chemisorbed overlayer 80—49517
jellium, effective-medium theory of chem. binding 80—65367
jellium, of H_2, contraction of mol. band 79—28202
jellium, of H_2, interpreted by one-parameter analytic model 77—39735
jellium, of Li(H), simple model 79—60625
kinetics, heterogeneity effects *(German)* 78—85202
kinetics, heterogeneity effects *(German)* 79—51433
kinetics, power adsorption isotherm, entropy correction 80—40734
kinetics analysis using Ritchie's equation 79—90871
laser irradiation effects 80—84812
LEED crystallography of clean surfaces and chemisorbed species 77—24470
linuron, herbicide, interaction with soil, Fourier transform IR spectra 77—9142
lubrication mechanism, by surrounding gas molecules in adhesive wear 79—42143
lunar soil of water, alteration reaction in North Ray Crater soil (Apollo 16) 77—87287
magnetisation and chemisorption, book 77—25311
metal, BCC, of monolayer of atoms, charge in density of states determ. 77—47682
metal, chemisorbed O_2 and H_2O effect on surface props. 78—60187
metal, clean or oxidised, of amine, surface ionisation, mass spectra expts. 78—2360
metal, energetics of chemisorption, book contrib. 80—24740

chemisorption continued
metal, FCC, (100) surface, chemisorption-induced interaction between electronic levels of two-level adsorbate 80—39644
metal, interaction energy between two identical atoms 78—38964
metal, intra-adsorbate Coulomb correl., surface structure 77—15685
metal, intra-adsorbate Coulomb correl. and surface struct. roles 78—71979
metal, intra-adsorbate Coulomb correl. and surface struct. roles 78—71980
metal, narrow d-band, semiempirical theory, H and O chemisorpt. 78—75927
metal, of diatomic mol., competition between adsorbate-substrate bond and mol. bond. *(French)* 77—35810
metal, of H_2, interaction between gas atoms on approach to surface 78—14609
metal, of H, effect of surface on atomic H levels 77—35979
metal, of H, model, including image charge effects 79—73405
metal, of H, surface sp-conduction electrons, spin-density functional formalism 79—33321
metal, of hydrocarbons, correlation between energy levels and occupied molecular orbitals 79—19449
metal, review of chemisorption 79—42377
metal, simple, adatom geometry and chemisorption energies 77—66093
metal, vac. UV photoelectron spectrometer appl. *(Japanese)* 78—78044
metal catalysts, structural exam. of monometallic and bimetallic systems 79—95264
metal film, effect of chemisorption on supercond. 80—39703
metal films, evaporated, with BCl_3, HCl, interaction, adsorpt. 78—75945
metal films, of O_2, active sites, chemiluminesc. and vacuum microbalance obs. 78—22950
metal films, use of external mag. field, review 78—72003
metal oxidation, O Auger beak studies 77—1769
metal particles, small, characterisation and props., book contrib. 80—84417
metal surface, angle resolved Auger surface spectroscopy investig. 77—28694
metal surface, chemisorption, vac. UV photoelectron spectrometer for study *(Japanese)* 78—62264
metal surface, chemisorptive bonding anal. using PES 80—10791
metal surface, effect of gradient correction to exchange and correlation energies 77—11978
metal surface, electrochemical exam. of multiple states of chemisorbed atoms 77—44512
metal surface, electron correl. in chemisorbed H atom, friction coeff. 78—60026
metal surface, jellium, H chemisorption, linear response theory 78—91543
metal surface, jellium, H chemisorption, relax. energies in UPS 78—91544
metal surface, kinetics of adsorpt., desorpt. and migration, review 79—46921
metal surface, of molecule, self-consistent calc. 79—95260
metal surface, perturbative calc. of elec. field 80—45108
metal surface, tight-binding, dissociative chemisorption of molecule 78—2368
metal surface bonding, book contrib. 80—24990
metal surface chemisorption theory, electron localisation, surface interactions 80—84376
metal surface $H_2 \rightleftarrows H+H$ reaction rel. to catalysis, friction coeff. calc. 77—77807
metal surfaces, historical review 79—46920
metal surfaces, replacement phenomena of chemisorbed gases, review *(Japanese)* 77—72779
metal surfaces, theoretical models, chemical and solid state approaches 78—18911
metallic atom chemisorption, work function variations 79—46936
metallic surface, density functional calculations for atomic clusters 80—44699
metallic surface, self-consistent electron theory, review 80—88616
metals, adsorption of gases, review *(Japanese)* 79—46930
on metals, appl. of field emission techniques 78—35255
metals, liquid metal embrittlement, mechanism 79—43495
metals, of CO, electronic struct., vibr. spectra, and chem. 79—42390
metals, of gases, book 79—69370
metals, of H_2, quantum chem. model, valence band calcs. *(German)* 77—31909
metals, theoretical models, review *(Russian)* 78—84071
on metals, theory, appls. 77—35815
model chemisorbed systems, exact and approx. results for electron densities of states 79—42605
molecular, on crystal surface, calc. 77—81425
molecular metal clusters rel. to chemisorpt. and catalysis 77—76668
molecule-metal interaction and surface reactions, theoretical description 80—39652
molecules, IR line shape, dynamical theory 79—824
molecules, on metal surface, spectrosc., electron gas effects 80—54504
Monte Carlo simulation of two-point adsorpt. on binary metal alloy surfaces 79—46940
multiphoton processes, chemisorbed species on solid surfaces, desorption dynamics, quantum-stochastic approach 80—66864
nearly free electron metal surface, at. chemisorption 78—14588
neutron scattering by molecules, polymers and absorbed species, review 79—41911
neutron scattering from adsorbed mols., surfaces and intercalates, review, book contrib. 80—84394
NMR, effect of migration between physical and chem. absorpt. sites 77—21422
non-polar cpd. semiconductor surfaces, of O, π-bonding contrib. 80—6631
nondissociative, rel. to electron stimulated desorption 77—85060
order-disorder phase transition in chemisorbed layers, depend. of work function 79—19460
ordered adlayers, electronic struct. 79—38142
ordered overlayers, chemisorption energy, multiadatom effects 78—14581
ordered overlayers, on FCC metal surface, electronic struct. calcs. 79—60906
ordered solid surface, review of electronic struct. calcs. 77—28226
oxide semiconductor, gas adsorption effect on cond. *(Japanese)* 79—95408
pair interaction energies between chemisorbed atoms on metallic surface *(French)* 80—80076

chemisorption continued
particulate matter, of N_2O, decomposition 79—16014
perovskites, d-band, concepts of surface states and chemisorption, book contrib. 80—107651
phase transitions in chemisorbed systems 80—107656
photoelectron spectra, line shapes and relaxation effects 79—69956
photoelectron spectroscopy, solid-state, with synchroton radiation, review 80—71570
photographic stabilisers, of yellow colloidal Ag, semiconductor props. *(German)* 78—86369
plasmon effects in electron spectroscopies and chemisorption 79—33190
polar semiconductor, method for charge transfer process obs. 77—89824
polystyrene substrate, Cu vapour deposition, surface complex, XPS obs. 78—72026
powder catalyst, catalytic and sorption processes, calorimetric and adsorpt. kinetic methods 79—43629
Pt surface, chemisorbed CO, IR refl.-absorpt. spectra, absorbate island struct. 80—84385
quartz powder, of CaO soln. effect on lattice parameters, work function 79—37918
radioactive low level liquid wastes, chem. treatment, clay minerals, cation exchange capacity 78—33270
radionuclide absorption through damaged and undamaged skins of guinea pigs 80—26383
rare earth intermetallic, RNi_4Al, Hz absorpt. and cryst. struct. of hydride 78—34487
rate processes in condensed media, anharmonicity effects 79—19349
refractory materials, emission and adsorption props., rel. to electronic struct., review 77—76899
segregation in thin film, microscopic electronic theory 77—85112
semiconductor, of H_2, Anderson model of chemisorption including correlation and overlap effect 77—76662
semiconductor, of H_2, effect of surface states 78—51823
semiconductor, photodesorption, role of C 77—36787
semiconductor, surface and adsorbate states, charge injection into space charge layers 80—100496
semiconductor crystal surface, nonequilib. electron effects due to chem. excitation 78—72238
semiconductor crystal surface, nonequilib. electron effects due to chem. excitation 78—72239
semiconductor electrodes, charge distrib. and chemisorpt. processes *(German)* 79—52689
semiconductor surface, clean and with chemisorbed species, atomic and electronic struct. 78—72223
semiconductor surface, electronic struct. 78—14784
semiconductor surface, of mol. complexes, bond orbital model *(German)* 80—59807
semiconductor surfaces, review, book contrib. 80—107648
semiconductors, surface and interface electronic struct., book contrib. 79—42619
semiempirical calculations for chemisorpt. on transition metal 78—14611
shapes of islands of chemisorbed atoms as probe of long-range interadatom interactions 79—65320
silicates, core-level XPS peak intensity ratio ang. variations rel. to surface anal. and chemisorption 80—40225
simple metals, atomic chemisorption, atom-jellium model 78—84066
simple metals, density functional calcs. 80—108733
simple metals, density functional theory of chemisorption, book contrib. 80—107647
site geometry, detector integrated angular distrib., photoexcitation depend. on target orientation, anal. 78—56564
solid surfaces, surface processes, and solid/gas interactions 80—73125
solid-liquid metallic binary alloy, interfacial tension, chem. adsorption and temp. depend. 80—59777
solid/liquid adsorption equilib., kinetic studies using isotopic mol. exchange method 80—88427
Spheron 6, surface group obs. using gaseous reagents, surface acidity evolution during heat treatments *(French)* 77—66767
spin-fluctuation description 77—76666
stainless steel, austenitic, surface, interaction with O_2, and work function obs. 80—65364
steel, crack growth velocity in gaseous H_2 embrittlement, rel. to chemisorption 80—11831
steel ShKh15, high C, wear tests in fuel oil, O_2 conc. effect in oil *(Russian)* 77—16694
strength of solids modification 79—51423
superoperator formalism, appl. to Anderson-Newns model 80—26047
surface chemical bond, book 80—22147
surface contamination, anal. using mass spectrometer system with laser heating 79—87903
TCNQ-ϕ_4DTP, chemisorbed O_2 effects on mag. susceptibility 80—15679
TCNQ-TTF, chemisorbed O_2 effects on mag. susceptibility 80—15679
theoretical issues, book contrib. 80—107652
theory, book 80—105440
theory, by method of configuration interaction *(German)* 78—31707
theory, inverse matrix diagonal and off diagonal elements, self energy perturbation theory 78—82607
three-dimensional crystal, Hartree-Fock theory of surface states 80—44468
transition and noble metals, d-band metals, chemisorption, book contrib. 80—107649
transition and noble metals, of alkali metals, changes in work function due to charge transfer 78—18900
transition metal, chemisorbed acetylene and ethylene, UPS, and SCF-LCAO calcs. 79—19454
transition metal, chemisorption of H, effect of surface spin fluctuations 80—75613
transition metal, chemisorption of ordered overlayers with C(2×2) and (2×1) structs. 79—46925
transition metal, group VIII, O_2 chemisorption, UPS 79—7751
transition metal, group VIII, O_2 chemisorption, UPS 79—7752
transition metal, model Hamiltonian, specially parametrised 77—11785
transition metal, of CO, AES obs. 77—35818
transition metal, of H_2, Anderson model of chemisorption including correlation and overlap effects 77—76662
transition metal, of N_2-containing at high-pressure, XPS 77—20990
transition metal, of ordered atomic layers, HF Green's function formalism and phase shift technique 80—24733
transition metal, of single atom, relax. shifts and singular broadening in spectra 77—59203

chemisorption continued
on transition metal, semiempirical model calcs., extended basis set 77—72793
transition metal (001) surface, model, chemisorption, coverage depend. of adsorption behaviour 78—71976
transition metal clusters, alloying effects, model calc. 77—62751
transition metal compound surfaces, review 80—84349
transition metal ferrocyanides, crystal structures and ion-exchange props. 77—15362
transition metal surface, interaction energy between chemisorbed atoms, calc. 80—54507
transition metal surface, of H_2, Hartree-Fock-Slater model cluster calc. 78—26929
transition metals, core levels between surface and bulk atoms, variation of binding energy shifts, chemisorption effects 80—88615
transition metals, heat of chemisorption of H_2 calc. 78—38959
transition metals, of H_2 and O_2, chemisorpt. energy trends 80—107631
transition metals, of H, Hubbard-type surface mol. model binding energy calcs. 78—71990
transition metals, of H, O and CO, review 78—2378
transition metals, of light gas atoms, on (100) surface, model calcs. 77—11797
on transition metals, theoretical model, formalism 80—6651
transition metals on alumina, of CO, inelastic electron tunnelling spectra 77—31871
tunnelling spectra of chemisorbed atoms 78—47664
on two-band crystal, model calcs. 77—85072
two-dimensional colloidal state concept and role in activity of solids 80—55704
UPS, angle-resolved, chemisorption site determ. 78—71970
vacuum gauge, using depend. of elec. cond. of β-carotene on O_2 pressure *(Czech)* 77—139
vibrational frequencies of chemisorbed molecule rel. to interaction with surface 80—54519
water on metal surface, molecule struct., interband angle 80—59787
XPS of adsorbed atoms and molecules, many-body effects 80—55266
XPS of chemisorbed species core levels, shake-up and relax. effects 79—56910
zeolite of transition metal, CO adsorpt., ^{13}C NMR study 79—52751
zeolites, of Br_2 and I_2, Raman spectra 80—93301
Ag (001), of Cl, adatom bonding effects from coverage-depend. angle-resolved photoemission 79—82436
Ag (110), adsorption of O_2 and CO-O_2 interaction, ellipsometry-LEED expts. 78—91542
Ag (110), CN^- chemisorbed, Raman scatt. 80—45075
Ag (110), of Cl_2, XPS and UPS meas. 78—31293
Ag (110) surface, clean and Na dosed, of NO, surface reactivity 77—31882
Ag (111), adsorpt., coadsorpt., and reactivity of Na and NO 78—38948
Ag (111), chemisorbed Rb struct., and NO reactivity on Rb-dosed Ag 79—28207
Ag (111), clean or Na-covered, adsorpt.-desorpt. props. of Br_2 78—38944
Ag (331), adsorpt.-desorpt. props., coadsorpt. and surface struct. chem. of O_2 and Cl_2 78—34711
Ag, adsorption of O, surface species identification by XPS, high press. 79—28191
Ag clusters, of I, UPS obs. 80—84830
Ag film, chemisorption effects on optical reflectance and elec. resistance 79—33361
Ag film, evaporated, chemisorption effects on reflectance and elec. resist. 80—11495
Ag film, of O_2, modulated surface plasmon reson. method 79—82439
Ag, of CO, N_2, NO, semiempirical calcs. 78—14611
Ag, of Cl_2, on low index surfaces, energetics and structures 79—87000
Ag, of ethylene, IR refl. obs. 77—31903
Ag, of O, dielec. perm., plasma surface vibr., modulation spectroscopy 77—48198
Ag, of O_2, isosteric heat of adsorption determ. 77—55453
Ag, of O_2, surface-plasmon modulated reson. 79—83045
Ag surface, CO chemisorption, SIMS, XPS study 80—84382
Ag-Pd alloy, surface comp., AES expts., correl. with O_2 heat of chemisorpt. data 78—34684
AgNa mordenite, chemisorpt. of CO and H_2 80—2752
Ag(110), of ethanol, chemisorption and oxidation 78—61044
Ag(111), of S_2, surface layer struct. changes 79—42383
Al (100), of O, mol. orbital cluster calc. 78—14582
Al (100), of O, photoemission ang. depend., MO cluster model calc. 78—76576
Al (111), bonding of O, electronic struct. calcs., rel. to UPS data 80—59801
Al (111), of O, O-Al and O-O bond lengths, surface extended X-ray absorpt. fine struct. 80—29267
Al (111), of O, ordered overlayer, angular resolved photoemission 79—82462
Al (111), of O 78—14593
Al (111), of O_2, ordered O overlayer obs. 78—47665
Al (111), oxidation, initial stages, LEED anal. 80—80082
Al, clean and oxidised surfaces, secondary electron spectrum, EELS and AES, comparison 80—55237
Al film, polycryst., of O_2, synchrotron radiation photoemission expts., 70-150 eV 78—95228
Al, initial interaction of O with single cryst. faces, LEED, AES and work function study 80—84392
Al, initial oxidation, interatomic Auger transition spectroscopy 79—7746
Al, initial oxidation exam. by inter-atomic Auger yield spectroscopy 78—11419
Al, multiple oxidation states, obs. by photoelectron spectra of core level shifts 77—8720
Al, of CO, interatomic Auger transition spectroscopy 79—7747
Al, of dibenztetrathiafulvalene, ionisation and polarisation energies of mol., UPS meas. 78—79886
Al, of formic acid, electron tunnelling spectra study 78—84049
Al, of H_2, calc. of adsorption sites and binding energy 79—46953
Al, of O, (100) surface, overlayer electronic struct. 77—85058
Al, of O, site determ. by LEED 80—39421
Al, of O, unoccupied extrinsic surface resonances and site struct. determ. by soft X-ray absorpt. 79—73403
Al, of O_2, on (111) and (100) faces, AES and work function obs. 77—35822
Al, of O_2, orbital resons., Xα cluster model calcs. 77—72774

chemisorption continued
- Al, of O_2, photon and electron emission as indicators of intermediate states 80−39439
- Al, of O_2 (NO), 80 to 290K, 10^{-6} to 10^{-2} Pa, XPS study 78−95657
- Al oxidised surface, EXAFS in soft-X-ray region 79−37921
- Al surface, hydrasine and NH_3 adsorption and decomp., XPS obs. 80−92783
- Al surfaces, interaction with O_2, work function changes and ellipsometric parameters 79−47831
- Al-Al_2O_3-Pb, oxide-layer chemisorbed phenols, electron tunnelling spectra, 2K 77−62736
- Al_5, of Na, Si and Cl, core hole induced electronic relax. 79−90874
- η-Al_2O_3 of CO_2, IR and microgravimetric meas. 78−14578
- Al_2O_3, of ethanol, acetic acid and acetaldehyde, inelastic electron tunnelling spectra, surface vibr. struct. determ. 80−35572
- Al_2O_3, of ethylene glycol, inelastic electron tunnelling spectroscopic study rel. to lubrication 80−70302
- Al_2O_3, of formic acid, effect of formate ion conc. on conductance of MIM struct. 79−15233
- Al_2O_3, of formic acid, electron tunnelling spectra study 78−84049
- Al_2O_3, of isobutyl alcohol, gravimetry, IR investigs. 79−1546
- Al_2O_3, of linoleic acid, under carbon tetrachloride immersion, IR obs. 79−24822
- Al_2O_3, of monocarboxylic acids, tunnelling spectroscopy 78−91545
- η-Al_2O_3, of propylene, desorption and D exchange obs. 78−51827
- α-Al_2O_3, of water, electron binding energies, UPS, SCF-Xα-SW calcs. 77−69169
- Al(111), of O_2, SCF X_α scatt. wave MO calc. 79−42374
- Al(111), oxide layer amorphous to cryst. surface transition, slow positron obs. 80−75417
- Au (111), of O_2, AES investig. 77−55446
- Au, chemisorption of I, AES and LEED study 80−100405
- Au film, on W substrate, chemisorbed N_2 effect on crystallite growth, FEM obs. 79−46976
- Au, of CO, high resolution UPS 78−39666
- Au, of dibenztetrathiafulvalene, ionisation and polarisation energies of mol., UPS meas. 78−79886
- Au, of O_2, catalytic effect of Ca, AES study 79−15021
- Au/Ti thin films, effect of Cl_2 on elec. resistance, Ti atom migration and preferred orientation 80−34530
- Au-Pt (14 at.%) of CO, surface composition determ. 79−69328
- Ba films, chemisorptive luminescence systems for surface reaction obs. 78−7236
- BaB_6, thermionic emission, O_2 adsorption effects 77−8711
- Be, of H, on (0001) surface, mol. orbital cluster theory 79−15002
- Bi (0001), of O_2, LEED, AES and electron loss meas. 79−77908
- C, activated and impregnated, temp. depend. adsorption of HCN 80−89522
- C, chemisorbed oxygen surface complexes, thermal desorpt. analysis 78−56032
- C fibres, PAN-based, of O_2, surface characts. 78−35536
- C, from methanol-benzene solutions 78−14568
- C in steel, saturation kinetics for high-temp. carbonitriding *(Russian)* 79−52450
- C, of CO_2, surface area meas., temp. and chemisorption effects 78−95225
- CO, chemisorbed, CNDO calcs. of mol. struct. *(German)* 79−96368
- CO, on Ni(111), surface optical excitations, reflectance spectra, electron energy loss meas. 78−84064
- CU (001), of O, Ar^+ bombardment, angle resolved SIMS, surface struct. 79−77913
- $CaCl_2(Br_2)$, adsorption of NH_3 and ND_3, complex formation, IR and for IR spectra obs. 80−80063
- CaO, of O_2, adsorboluminescence from surface F-centres 80−20723
- CaO:Bi surface, O_2 chemisorpt., positive ion emission determ. 80−92785
- Cd, oxidation, chemisorption and oxide regimes, UPS and EELS study 80−81236
- Cd sorption and accumulation in sediment of Tama River 79−52972
- CdS, desorption of chemisorbed species, influence of surface states on absorption edge 77−16344
- CdS evaporated films, O chemisorpt. kinetics, effects on elec. cond. 78−6464
- Ce^{3+}, oxidation kinetics in X zeolite on O_2 adsorpt. 78−3373
- CeO_2, chemisorption of H_2, kinetics and characts. at different pressures and temps. 78−51821
- Cl, chemisorbed layer on Si (111), SCF LCAO calcs. of Si band struct. 78−88010
- Cl_2 absorption in acetic acid, kinetics in presence of homogeneous catalysts 80−11876
- Co (0001), of CO 78−6222
- Co (0001), of O_2, surface oxidation and CO oxidation 79−60631
- Co (0001) of NO, surface reactivity, LEED, AES, and thermal desorption study 80−80090
- Co (10$\bar{1}$2), struct. and CO chemisorption obs. 79−4474
- Co, of O, LEED anal. of Co{001}c(2×2)-O struct. 78−91546
- Co, polycryst. surface interaction with O_2, CO and CO_2 *(French)* 77−73219
- CoO, and CoO_4, surface reequilibration kinetics 77−55449
- ^{60}Co, sorption from water using fibrous ionites 77−56251
- Cr, of C, N and O, SXAPS obs. 79−52048
- Cr, of Cl_2, formation of $CrCl_2$ epitaxial layers *(French)* 78−22990
- ^{134}Cs, sorption from water using fibrous ionites 77−56251
- ^{137}Cs, study of absorpt. by Lemna minor 80−30677
- Cu (001), electronic struct. of $(M)_5CO$ clusters 78−95948
- Cu (001), O_2 chemisorption, Cu3d-O2p interaction study by angular-resolved photoemission using synchrotron radiation 80−84836
- Cu (001), of N atoms, electronic struct. of Cu_5N cluster, Xα scattered-wave calcs. 79−60902
- Cu (001), of S, thermodynamics, AES study 79−82452
- Cu (100), chemisorption and decomp. of formic acid, EELS study 80−16729
- Cu (100), interaction of CO and CO_2, molecular orbital calc. 77−31898
- Cu (100), of CO, vibr. excitations and struct., EELS and LEED study 80−39437
- Cu (100), surface state-surface resonance density 79−28392
- Cu (100), XPS of chemisorbed CO 79−15589
- Cu (100) surface, angle-resolved PES study, rel. to chemisorpt. of chalcogens 80−55273
- Cu (100) surface, interaction with O_2, AES, EELS, LEED and work function studies 80−24731
- Cu (100) surface, of N_2, electronically-activated 79−66348

chemisorption continued
- Cu (100) surface, of O_2, angularly resolved UPS meas. 78−71956
- Cu (100) surface of CO, vibr. spectrum 79−69347
- Cu (110) surface, interactions with O_2, N_2O, ellipsometry, AES, LEED study 80−6635
- Cu (111), dissociative chemisorption of O_2, AES, LEED and ellipsometric meas. 79−65317
- Cu (111), of CO, coverage depend. photoelectron spectra, adsorption sites 78−95647
- Cu (111), of CO, IR spectra, LEED, and surface pot. meas. 80−39438
- Cu (111), of CO, rel. to surface prep. 78−6223
- Cu (111), partially Cs covered, oxidation effect on UPS 79−78826
- Cu (111) of N_2O, kinetics using AES, LED and ellipsometry 79−65317
- Cu, adsorption and desorption of water vapour, relative humidity effects 80−49505
- Cu adsorption of O_2, N_2O on (100) surface, reaction with CO 80−103583
- Cu, chemisorpt. of CO, SIMS, AES, desorpt. meas. 78−87875
- Cu, chemisorption of H, density of states and chemisorption energy calc. 80−34315
- Cu, chemisorption on low-index and stepped surfaces, LEED, AES and UPS obs. 80−84391
- Cu, interaction with CO, Cu_nCO form., chemisorpt. bond 78−31631
- Cu, O-covered surface, ion-bombarded, molecular cluster ejection, model 79−87543
- Cu, of acetic acid, on (100) surface, acetate species struct. obs. 79−98232
- Cu, of CO, high resolution UPS 78−39666
- Cu, of CO, N_2, NO, semiempirical calcs. 78−14611
- Cu, of CO, on (100) surface, XPS shake-up satellites, Xα-SW cluster model calcs. 79−95899
- Cu, of H_2, dissoc. adsorption on stepped and unstepped surfaces, theory 77−89636
- Cu, of N_2, self- consistent electronic struct. calc. 78−2544
- Cu, of NO, photoelectron spectra 78−6830
- Cu, of O, S, Se, NO and O_2, cluster theory 80−29264
- Cu, of O_2, surface-plasmon modulated reson. 79−83045
- Cu, of P and P compounds, Auger spectra 78−43248
- Cu, oxidation, EXAFS obs. 80−71808
- Cu small particles, CO interaction, IR spectra obs. 77−20195
- Cu surface, (100), O chemisorption, angle-resolved UPS study 80−84384
- Cu surface, with chemisorbed CO, cluster calc. using SCF-Xα-scatt. wave method 77−62742
- Cu-Al, surface segregation during adsorption and low pressure oxidation *(French)* 78−75932
- Cu-Ni, chemisorpt. of CO, SIMS, AES, desorpt. meas. 78−87875
- Cu-Ni alloy surfaces, of CO, LEED, AES, thermal desorption, and work function meas. 79−90879
- Cu-O (0.05 to 0.1 wt.%) liquid alloy, deoxidation kinetics by rotating graphite cylinders 80−61084
- CuO-Cr_2O_3 based oxide, catalyst, adsorption of fluorobenzene, binding energy of F 1s electrons *(French)* 79−69346
- Cu_2O, adsorption and desorption of water vapour, relative humidity effects 80−49505
- Cu(100), N chemisorption, bonding, MO theory 77−76659
- Cu(100), of CO, angle resolved UV photoemission spectroscopy exam. 78−10284
- Cu(100) surface, of O_2, oxidation studied by angle-dispersive photoemission spectra 78−15585
- Cu(110), of ethanol, chemisorption and oxidation 78−61044
- Cu(110), of O_2, enhancement during Ne^+ bombard. 80−65070
- Fe (001) surface, initial reaction with water vap. 77−69173
- Fe (100), of O, molecular orbital theory of bonding 77−85059
- Fe (100) and (111) surfaces, of CO, CO_2, acetylene, ethylene, H_2 and NH_3 78−71996
- Fe (100) surface, of CO, chemisorptive bonding and dissociation 77−59212
- Fe (110), adsorption and decomposition of ammonia 79−69345
- Fe (110), complexes with PF_3, CO and cyanomethane, UV photoelectron obs. 78−19629
- Fe {001} surface, of S, determ. of c(2×2) structure of S, LEED 77−85063
- Fe, cryst. of $CO(H_2)(N_2)$, dissoc. chemisorpt. *(German)* 78−53257
- Fe, equilibration and replacement reactions between H_2 and D_2, anisotropies 77−24482
- Fe, ferromagnetic, of H, spin-spin interactions, UPS spectra calc. 80−6630
- Fe film, chemisorption induced mag. dead layers, ferromag. reson. obs. 79−91261
- Fe film, of O_2 and water vapour, XPS obs. 77−48587
- Fe, fine particles, chemisorption of CO, H_2, Mossbauer study 80−39415
- Fe, H_2 embrittlement and H_2 adsorption 80−89401
- Fe liquid, C saturated, decarburization by CO_2, effect of S 79−11726
- Fe, molecular adsorption and dissociative chemisorption of N_2, XPS obs. 79−99427
- α-Fe, of acetylene, (ethylene), struct., bonding, dissoc., UPS obs., MO calcs. 78−84050
- α-Fe, of benzene and methyl derivatives, MO LCAO calcs. 77−52674
- α-Fe, of CO, surface deactivation effects on molecular chemisorption 77−76669
- Fe, of CO and O_2 core level photoemission and LEED methods appl. 79−15003
- Fe, of Cl_2, formation of $FeCl_2$ epitaxial layers *(French)* 78−22990
- Fe, of N_2, dissoc. chemisorption during NH_3 catalytic synthesis, promoter action of K 79−29390
- Fe, of SO_2, X-ray photoelectron spectra 78−27370
- Fe, small particles, magnetisation-pressure isotherms for H_2 and SO_2 78−39949
- Fe surface, (111) and (100), adsorpt. and decomp. of NH_3 78−40077
- Fe surface, form. and decomp. of nitrides 79−24831
- Fe surface, H_2 chemisorption LEED, UPS, thermal desorption spectroscopy, work function meas. 78−14566
- Fe thin films, surface demagnetisation due to chemisorption, ferromagnetic reson. study 80−80616
- Fe+H_2O, clean surface oxidation and passivation by vapour, XPS, chemisorbed O 77−81424
- $Fe_{2\ x}M_xO_4$, M=Al,Cr, time dependence of oxidation, elec. cond. obs. *(French)* 77−66710
- FeTi, hydrogenation-dehydrogenation cycling, positronium form. 80−18947

chemisorption continued
α-Fe00H, of pyridine, acetic acid, CO_2, NO or trimethylchlorosilane, IR spectra 80—7855
Fe(111) clean single crystal surface, of N_2, NH_3, H_2, photoelectron spectroscopy, LEED studies 77—66087
α-Fe(111) single crystal surface, chemisorption of ethylene, halogeno-substituted alkenes, photoelectron spectroscopy study 77—62740
α-Fe(111) surface, chemisorbed CO, 300K, photoelectron spectroscopy study 77—62739
GaAs (100), of O and Al, ab initio theory 80—75612
GaAs (110), chemisorbed O_2, extrinsic surface states 78—91535
GaAs (110), chemisorption site geometry and interface electronic struct. of Al and Ga, photoelectron spectra 80—49843
GaAs (110), electronic states and initial steps in oxidation 78—91534
GaAs (110), of Al, electronic struct., tight binding calc. 80—49842
GaAs (110), of Al, XPS study of interface interaction, Al proximity effects and replacement reaction 79—100019
GaAs (110), of Cl, photoemission spectra and tight-binding calcs. 80—6629
GaAs (110), of O, surface EXAFS meas. 80—50460
GaAs (110), order-disorder interaction with O_2, LEED anal. 80—75445
GaAs (110), reconstruction and oxidation initial stages, ab initio calc. 80—49473
GaAs (110), with ultrathin Al and Cs overlayers, O_2 adsorption, comparative studies 80—50740
GaAs (110) surface, O_2 interaction, order-disorder effects, LEED, UPS anal. 80—6634
GaAs (110) surface, of 0_2, electronic struct. theory, oxidation, electron spectra interpretation 79—42376
GaAs, chemisorption and oxidation states of (110) surfaces 79—24049
GaAs, chemisorption of Li, charge injection into space charge layers 80—100496
GaAs, chemisorption of Ru, surface recombination rate reduction 80—49866
GaAs, cleaved (110) surface Cl chemisorption geometry 80—6659
GaAs, O_2 chemisorption 79—95466
GaAs, of Al, surface barrier formation, localised orbital theory 79—51671
GaAs, of Cs, isobars, LEED and loss spectroscopy meas. 77—4262
GaAs, of O, electronic struct., photoemission meas. 77—20385
GaAs, of O_2, effect of surface index and atomic disorder AES, LEED and optical ellipsometry 79—60638
n-GaAs, of O_2, valence band exam. 78—43298
GaAs, of O_2 on (110) surface, bonding sites 78—38938
GaAs surface, of O_2, Fermi level pinning by submonolayers of O 79—60637
n-GaAs/K_2Se-K_2Se_2-KOH/C solar cell, Ru (III) chemisorption on photoanode, effect on performance 80—3516
n-GaAs/K_2Se-K_2Se_2-KOH/C liq. junction cell, effect of Ru ion chemisorption on grain boundaries 80—55879
GaAs(110) surface, adsorption of water and methanol, UPS study 80—6632
GaAs(110), surface and interface states, effects of chemisorption, oxidation and passivation 77—85284
GaAs(111), O bonding, thermodesorption and ESCA meas. 77—86206
GaP (110), electronic surface states, initial steps of O_2 chemisorption 80—49844
GaSb (110), of Cl, photoemission spectra and tight-binding calcs. 80—6629
GaSb, chemisorption and oxidation states of (110) surfaces 79—24049
Ge (100), of H, expt. results compared with pairing model calcs. for Si (100) 78—34719
Ge (111), of CO, on cleaved surface, electron energy loss spectra 78—79885
Ge (111), of Cl, chemisorpt.-site geometry from polarised photoemission 77—15684
Ge (111), of H_2, calc. using Anderson Hamiltonian 77—55463
Ge (111) and (100), of O_2, CNDO calc. 77—55464
Ge (111) surface, chemisorption of O_2, surface-molecule model 79—90885
Ge (111) surface, of CO, UPS and ion-neutralisation spectroscopy 80—10785
Ge, of CO(Cl), surface photoemission, adsorption gate geometry 78—73079
Ge, of Cl, cluster model calc., iterative EHT 77—32062
Ge, of Cl_2, photoemission polarisation effects with synchrotron radiation 78—14580
Ge, of O(1s), XPS investigation 77—69170
Ge single cryst., of atomic H, highly efficient electron accommodation *(Russian)* 79—78818
Ge(111), of Cl, threefold co-ordinated site chemisorption, cluster model calc., extended Huckel theory 78—39178
H production on illuminated transition metal surfaces, tight binding model 80—45812
H_2 by $NdNi_5$ and $LaNi_4Cu$ intermetallics, cell volumes and desorption pressures correlation 78—22860
$H_2+D_2 \rightleftharpoons 2HD$ catalysis, MgO surface, SCF UHF calc. 77—9120
IR, chemisorption electron states for CO and O, electron field emission 78—84704
In, chemisorption of O_2, XPS and static SIM spectral study 80—80055
In-In_xO_y-Pb tunnel-junction barriers, evidence for chemical annealing effects 79—42701
InP, chemisorption and oxidation states of (110) surfaces 79—24049
InP, Fermi level pinning on exposure to O_2 79—60637
InSb (110), of Cl, photoemission spectra and tight-binding calcs. 80—6629
Ir (100), of acetylene, benzene and ethylene, geometric and electronic effects 77—55457
Ir, (100) and (111) surfaces, chemisorptive bonding and reaction of NO, UPS obs. 77—72786
Ir (100) surface, of CO, chemisorptive bonding and dissociation 77—59212
Ir (110), of CO, preexponential factor and desorption energy 78—71963
Ir (110), of O_2, AES, LEED, thermal desorption mass spectra, and contact pot. difference meas. 79—77901
Ir (110), of O_2, sorption and dissoc. kinetics 79—33186
Ir (111), of CO, coverage dependent chemisorption interaction, UPS 77—85897
Ir (111), of CO, UPS and XPS obs., comparison with Pt 78—38942
Ir (111), of NH_3, mol. adsorbate structs. from angular-resolved photoemission 80—76141

chemisorption continued
Ir (111) surface, electron beam induced desorption and dissociation of chemisorbed CO 78—56043
Ir (111) surface, of O_2, dynamics 77—59211
Ir, clean and adsorbate covered surfaces, field emission energy distrib. spectra 80—25535
Ir, clean normal and reconstructed (100) surfaces, multiplets role 77—15694
Ir, of CO, on (100) surface, photoemission investig. of bonding using synchrotron radiation 77—12498
Ir, of CO, on (111) surface, XPS and UPS 77—16450
Ir, of CO, on clean and oxidised (110) surfaces, kinetics obs. 79—11015
Ir, of H_2, adsorption and desorption kinetics, struct. of overlayer 80—84367
Ir, of H_2 and hydrocarbons, LEED, AES and thermal desorption meas. 77—1297
Ir, of NO, chemisorptive bonding and reaction 77—51596
Ir surface, of CO, mol. cluster calc. 80—100407
Ir(100), of acetylene, ethylene and benzene, geometric and electronic effects 77—21421
Ir(111), O_2 chemisorption, XPS obs. 77—20190
Ir(111), of O_2, LEED-Auger expts. 77—20191
KC_8 intercalation compound, of H_2 *(French)* 79—43624
KC_8 intercalation cpd., selective chemisorption of protium and deuterium *(French)* 77—32830
$KC_8H_{2/3}$, H_2 chemisorption *(French)* 78—27432
LaB_6 (100), of O_2, LEED, AES, work function meas. 78—71989
LaB_6 (100), of O_2, UPS and LEED study 80—49519
LaB_6 (210) surface, work function, struct. and chemisorpt. stability, XPS, UPS and LEED 80—65344
LaB_6, of H, N and O, time of flight atom-probe FIM study 80—6652
Li cluster, of H, ab initio HF calcs. 77—76670
Li clusters, of H_2, ab initio SCF-MO calcs. 79—77918
Li, of O_2, KVV Auger spectrum of oxidised Li 77—55454
Mg, clean annealed surface, exoelectron emission during O_2 and Cl_2 adsorption 78—39671
Mg film, polycryst., of O_2, synchrotron radiation photoemission expts., 70-150 eV 78—95228
Mg films, chemisorptive luminescence systems for surface reaction obs. 78—7236
Mg, of H_2, calc. of adsorption sites and binding energy 79—46953
$MgCr_2O_4$, of CO_2, O_2 and water vapour, mobility of chemisorbed molecules 77—51595
$MgCr_2O_4$, of CO_2, surface flow of CO_2 77—47083
MgO, adsorpt. of CO, IR spectra 80—2751
MgO, chemisorption on (100) surface, surface electronic struct. 79—11016
MgO, defect surface, chemisorption of mol. H_2, quantum mechanical approach 77—62761
MgO, light emission during adsorpt. and desorpt. of O_2 78—38949
MgO, of O_2, adsorboluminescence from surface F-centres 80—20723
MgO powder, decomp. of chemisorbed ethanol, propanol and acetic acid 78—92502
Mo (100), of H, phase changes, LEED obs. 79—77911
Mo (100), of O, Cs submonolayers effect on electron stimulated desorption of O^- 79—86991
Mo (100) surface, of O_2, electron energy loss spectra meas. 77—16440
Mo, coadsorption of CO_2 and O_2, AES and SIMS obs. 79—46928
Mo, of C, N, and O, SXAPS obs. 79—52048
Mo, of CO, low energy SIMS and electron impact desorption expts. 78—38941
Mo, of NH_3, and catalytic decomposition, field emission study 78—14596
Mo polycrystalline surface, of CO, substrate mediated C-O interaction, photoelectron spectra 79—34353
Mo(001), of H, atomic displacements, LEED obs. 80—70514
Mo(100), of O_2, low-energy SIMS, ion yields depend. on surface chem. and primary ion energy 78—73105
Mo(110), of CO, Auger yield attenuation interpret. *(French)* 77—85077
Mo(110), of CO, model *(French)* 77—85076
Mo(110), of Co, adsorption/desorpt. expt. obs. *(French)* 77—85075
Mo(111), of H_2S, growth of MoS_2 film 77—1329
N in steel, saturation kinetics for high-temp carbonitriding *(Russian)* 79—52450
N_2+methane, N_2 fixation, catalytic processes in non-equilibrium plasma chemical reactors *(French)* 80—89483
N_2+O_2, N_2 fixation, catalytic processes in non-equilibrium plasma chemical reactors *(French)* 80—89484
NO, adsorbed on Cu, species identification, struct., dissoc. chemisorption, desorption, UV photoelectron spectroscopy 78—52635
Na, chemisorption of H_2, calc. of adsorption sites and binding energy 79—46953
Na, of halogens, surface chemiluminesc., MO description 79—43048
NaCaX zeolite, ion migration and $Ni(CO)_n^+$ form., EPR obs. 79—33522
Nb (110) and (750), interaction with O_2, LEED, AES, SIMS, and EELS obs. 80—44408
Nb film, of SO_2, adsorpt., corrosion 78—79897
Nb, of H, photoemission studies 80—76145
Nb, of H, two-state model kinetics 80—75438
Nb, of O_2, electronic struct., UPS meas. 78—95682
Nb-O solid solution, interaction with O_2 at low press., segregation equilib. and chemisorpt. *(French)* 77—24483
Ni (001), chemisorption site determ. for S and CO, angle-resolved UPS 78—71970
Ni (001), electronic struct. of $(M)_5CO$ clusters 78—95948
Ni (001), of CO, angle-resolved polarisation-dependent photoemission, adsorbate orientation 77—4716
Ni (001), of CO, back donation in chemisorption bond, UPS study 80—107642
Ni (001), of CO and C_2H_2, final state mol. relax. 77—62752
Ni (001), of H, O and CO, localised orbital approach 77—69166
Ni (001), of O, electronic struct., KKR model calcs. 78—56200
Ni (001), of O and S, dynamical calc. of angle-resolved UV photoemission 77—85890
Ni (001), of O_2, $MSX\alpha$ total energy calcs. with non-muffin-tin corrections 77—72795
Ni (001), of O_2 overlayer struct. and theory of electron struct. 79—65319
Ni (001), of S, thermodynamics, AES study 79—82452

chemisorption continued

- Ni (001) surface, chemisorbed O_2, electronic struct. and overlayer struct. theory 79—28391
- Ni, (001) surface, chemisorption bonding c(2×2)O, self-consistent electronic struct. 79—78146
- Ni, (001) surface, localised orbital approach 78—14587
- Ni (100), bonding of chalcogen overlayers, photoemission expts. 77—35819
- Ni (100), chemisorption and decomp. of formic acid -d_1 79—34361
- Ni (100), dissociative chemisorption and mol. adsorption of NO 80—65373
- Ni (100), interaction with methane, diffusion of deposited C, AES-LEED study 79—99418
- Ni (100), of CO, Hartree-Fock-Slater mol. cluster calcs. 79—51650
- Ni (100), of CO, SIMS and XPS meas. 79—42378
- Ni (100), of ethylene and acetylene, angular resolved UPS exam. 78—72685
- Ni (100), of first row atoms, molecular cluster theory 77—1309
- Ni (100), of H_2, LEED, work function meas. and thermal desorpt. obs. 79—23843
- Ni (100), of H_2, possibility of reduced bond length 79—28202
- Ni (100), of H_2 and O_2, and their interaction, UPS investig. 77—51600
- Ni (100), of $H_2(D_2)(HD)$, vibr. excitation and struct., electron energy loss spectra 78—47660
- Ni (100), of NO, LEED, AES, UPS, and thermal desorption study 80—39449
- Ni (100), of O, bonding model 78—79889
- Ni, (100), of O, S and Se, struct. and energy levels calc. 77—47663
- Ni (100), of O and S, surface vibrs., electron energy loss spectra 79—33173
- Ni (100), of O_2, SIMS and XPS 79—15019
- Ni (100), of O(S), geometry of overlayers 78—2373
- Ni (100), with chemisorbed c(2×2)O, c(2×2)S and CO, photoemission angle-of-incidence depend. 77—32502
- Ni (100) and (110), reaction of acetylene, room temp., UPS expts. 80—61151
- Ni (100) and (110) surfaces, of S, UPS 77—32500
- Ni (100) and (111), of CO, C-O bond lengths, electronic struct. 78—6210
- Ni (100) and (111) surface, chemisorption of CO, tight-binding theory 77—20395
- Ni (100) and polycrystalline surfaces, CO chemisorption, low energy SIMS and AES 80—34309
- Ni, (100) surfaces, Si-, P- and Cl-chemisorbed, LEED and angle-resolved AES obs. 79—95258
- Ni (100)c(2×2)CO structure, dynamical LEED expts. 78—34710
- Ni, (100)p(2×2)O and (100)c(2×2)O surfaces, of CO, LEED and energy loss spectra 78—2375
- Ni (110), adsorbed H, adatom configuration, He diffr. study 80—103569
- Ni (110), chemisorption of O_2 and initial oxidation, AES, EELS, and work function meas. 80—54523
- Ni (110), effect of surface O on catalytic and chemisorptive behaviour, ligand effects and oxide states 77—85066
- Ni (110), of ethylene, adsorption and decomposition exam. 77—55459
- Ni (110), of H_2 and O_2, LEED 77—24470
- Ni (110), of N_2, mol. and dissociative mechanisms 80—39431
- Ni (110), of NO, LEED, AES and thermal desorption meas. 77—15695
- Ni (110), of O_2, initial stage kinetics, RHEED and X-ray emission 78—15588
- Ni (110) of O, 2D lattice gas model 79—69357
- Ni (110) surface, of H_2, demagnetisation, positive spin polarisation in electron field emission 78—52646
- Ni (111), chemisorption and reaction of NH_3, LEED, desorption and photoemission expts. 80—59799
- Ni (111), chemisorption bonding of H, UPS obs. 77—76671
- Ni (111), of CO, orientation of CO from angle resolved photoemission 77—8721
- Ni (111), of H, electronic struct. using angle-resolved photoemission 79—69573
- Ni (111), of H, surface geometry, LEED, thermal desorption, and work function meas. 80—39433
- Ni (111), of H_2, UPS obs. 77—1786
- Ni (111), of methanol, UPS and flash-desorption exam. 77—55455
- Ni (111), order-disorder transition of chemisorbed H, cluster-variation method 80—15372
- Ni (111) and (100), of benzene, vibr. EELS study 80—39436
- Ni (111) surface, acetylene chemisorbed, ind. vibrs., high resolution electron energy-loss meas. 79—90877
- Ni, Al_2O_3-supported, of S, thermodynamic parameters meas. 80—88424
- Ni catalyst, chemisorption of ethylene-(d), Raman and vibr. spectra 80—108747
- Ni catalysts, of $H_2(H_2O)$, dynamics, neutron spectrosc. obs. 80—59778
- Ni, chemisorpt. of CO, SIMS, AES, desorpt. meas. 78—87875
- Ni, chemisorption of S, ang. depend. of multicentre Auger matrix element for Ni (100)-c(2×2)S 78—92151
- Ni, chemisorption of S and Se, Xα cluster model calcs. 79—65313
- Ni, chemisorptive binding of O, CNDO calc. of potential energy curves *(German)* 80—44431
- Ni, clean, of S-containing alkanes, XPS and thermal desorpt. with mass spectrometric anal. 78—14595
- Ni cluster, of H, macroscopic props. 79—82445
- Ni clusters, electronic props. and implications for chemisorption 79—23886
- Ni, electron stimulated interaction of H_2O, AES obs. 77—31902
- Ni, ferromagnetic, of H, spin-spin interactions, UPS spectra calc. 80—6630
- Ni film, chemisorption induced mag. dead layers, ferromag. reson. obs. 79—91261
- Ni film, evaporated, of CO, ellipsometric investig. *(German)* 80—61156
- Ni film, of ethylene and acetylene, IR refl. study 79—69343
- Ni film, of H, influence on magnetism, ferromag. reson. spectroscopy 77—66395
- Ni film, of H_2, effect on ferromag. reson. 78—72375
- Ni film, of $H_2(CO)$, ferromag. reson. 78—15028
- Ni films, electronic struct. calc., effects of chemisorption; contact pot. and surface magnetisation 80—103734
- Ni films, of CO, effect on galvanomag. and mag. props. 79—33364
- Ni films, of CO, effect on galvanomag. and mag. props 79—33363
- Ni foil, of H_2, surface states 77—69399
- Ni foil, of H_2, surface states and thermo EMF 78—91674
- Ni, H adsorption, on (100)(110)(111) surfaces, inert model 80—50889

chemisorption continued

- Ni, methanol on (111) surface, methoxy species, electron energy-loss spectra 79—29391
- Ni microcrystals, H_2 chemisorption effect on superparamagnetic relax. time, Mossbauer meas. 79—61284
- Ni, of 0_2, angle resolved photoemission from chemisorption induced states and LEED spectra 77—85898
- Ni, of benzene, on (100) and (111) faces, LEED and high resoln. electron energy loss spectra 78—6224
- Ni, of CO, (100) surface, mol. cluster theory 77—69174
- Ni, of CO, ab initio LCAO MO SCF calc. for NiCO 78—62712
- Ni, of CO, CNDO calcs. *(German)* 78—29751
- Ni, of CO, carbonylation rate mag. field depend. 79—24828
- Ni, of CO, catalytic activity, SCF-Xα-SW calcs. 78—15711
- Ni, of CO, methanation 77—56250
- Ni, of CO, N_2, NO, semiempirical calcs. 78—14611
- Ni, of CO, on (100) surface, mol. levels, angle depend. calcs. 78—90069
- Ni, of CO, Raman spectra 80—2755
- Ni, of CO, vibr. spectra from electron energy loss spectra *(French)* 78—22951
- Ni, of I, bond nature 80—34297
- Ni, of H, cluster surface bonding energy, HF calc. 79—39204
- Ni, of H, embedded cluster model 80—39427
- Ni, of H, model, comparison with UPS data 79—46932
- Ni, of H, order-disorder transitions on (111) surface, LEED observation 78—47668
- Ni, of H, surface magnetism 78—95510
- Ni, of H, X_α cluster calcs. *(Japanese)* 78—72002
- Ni, of H_2, interaction between adsorbates, model Hamiltonian calc. 79—46964
- Ni, of H_2, isothermal desorption near Curie temp., rate meas. 80—29268
- Ni, of H_2, molecular complex model 77—1314
- Ni, of H_2, periodic surface model calc. 78—30822
- Ni, of H_2, photoemission spectrum, Anderson model parameterisation 77—40334
- Ni, of H_2, Raman spectra, vibr. bands 79—61368
- Ni, of hydrocarbons, C 2s levels, initial state shift 78—34703
- Ni, of hydrocarbons, C-H stretch vibration, broadened and softened, dehydrogenation 78—47666
- Ni, of NO, UPS, angle-resolved, in modified LEED system 78—15293
- Ni, of NO, XPES meas. 79—77922
- Ni, of O, effect on surface vibrs. 80—84361
- Ni, of O, S, Se, NO and O_2, cluster theory 80—29264
- Ni, of O_2 and CO, in bombard., particle ejection, SIMS obs. 79—78810
- Ni, of O(S)(Se)(Te), orbital energy spectrum of chemisorbed electrons 78—2542
- Ni, of S and CO, surface struct. from ang. resolved UPS 78—31303
- Ni, ordered overlayers of O and S, A-vector orientation depend. of angle-resolved photoemission 77—59671
- Ni, oxidation, chemisorption and oxide nucleation stages, low-energy SIMS and AES obs. 79—43083
- Ni, polycryst., of O_2, SIMS and flash desorption obs. 78—76568
- Ni, Raney, chemisorbed benzene struct., neutron inelastic spectroscopy study 80—101038
- Ni, Raney, of H_2, neutron inelastic spectroscopy investig. 77—48686
- Ni, SiO_2-supported, chemical of chemisorbed hydrocarbons *(German)* 79—92002
- Ni surface, (001), H_2 dissociative adsorption, calc. 80—101036
- Ni surface, (111), chemisorbed CO, bond energies 80—100398
- Ni surface, of CO, mol. cluster calc. 80—100407
- Ni surface, oxidation, structural changes, low energy ion scatt. study 80—35423
- Ni surface, polycryst., interaction with O_2, SIMS and flash filament meas. 79—47829
- Ni, surface of H_2O, neutron inelastic spectroscopy 79—69353
- Ni surfaces, of at., mol. H_2, semi-empirical CNDO MO calcs. *(German)* 79—95465
- Ni, surfaces (100), (110), and (111), interaction with O_2, 295 and 485K, photoemission obs. 77—72784
- Ni, thin films, surface demagnetisation due to chemisorption, ferromagnetic reson. study 80—80616
- Ni, with chemisorbed CO, ion-bombarded, molecular cluster ejection, model 79—87543
- Ni/SiO_2, of NO, desorpt. and IR expts. *(German)* 78—30835
- Ni-Co-Cr/Al_2O_3 catalyst, IR spectra of adsorption and interaction with pyridine 80—71946
- Ni-Cu alloy, of CO, inhibition by Cu *(French)* 77—1295
- Ni-Cu diffusion couple surface, epitaxial, of CO, AES 77—31891
- Ni-Fe, (100) surface, O interaction, LEED and XPS studies 79—82437
- Ni-Fe, electronic struct. calc., effects of chemisorption; contact pot. and surface magnetisation 80—103734
- Ni-SiO_2 supported catalysts, particle size, H_2 chemisorption, Mossbauer study 80—7219
- Ni-Th (1 at.%), surface comp., temp. and O_2 exposure effects, AES study 80—80914
- $Ni(Ni)_2$-ethylene cluster complex 78—82641
- NiO (001) surface, chemisorption of H, surface and second-layer defect effects 80—65369
- NiO, catalytic decomp. of methanol, mol. beam relax. spectrometry using surface temp. modulation 79—29401
- NiO, of H, cluster model, bonding 78—38939
- NiO perfect surface, of H, cation vacancies 79—69351
- NiO, prepared by thermal decomp. of $Ni(OH)_2$, microporosity and irreversible water vapour adsorption 80—80060
- NiO, undoped and Li_2O doped, surface reequilibration kinetics 77—55449
- Ni_3Sn, of CO, surface composition determ. 79—69328
- Ni(001) surface, p(2×2) and c(2×2) O superstructure, angle resolved photoemission from adsorbates 78—23585
- Ni(100) and (111), of H, preexponential factors 79—46918
- Ni(100), of unsaturated hydrocarbons, LEED and AES obs. 77—31904
- Ni(110), of ethylene and decomp. 77—85071
- Ni(111), adsorbed benzene, vibr. loss spectra 79—23838
- Ni(111), of CO, adsorption sites and long range order, vibr. spectra 79—46946
- Ni(111), of H, geometry, order and disorder 79—65311
- Ni(111), of H_2, geometry, LEED anal. 79—28200
- Ni{001}, of CO, LEED study of mol. orientation in c(2×2) struct. 79—86982
- PbS(Se)(Te), of O_2, room temp., UPS and XPS obs. 78—91529

chemisorption continued
PbSe surface, clean and O_2-exposed, XPS (UPS) obs., electronic struct. 78−52637
$Pb_{1-x}Sn_xTe$, MBE, O_2 uptake, AES, XPS and UPS expts. 78−95227
Pd (100), of acetylene, substrate effects on bonding, electronic spectrum 78−63933
Pd (100), of CO, adsorbate band formation, UPS expts. compared with calcs. 79−77916
Pd, (100) surface, benzene chemisorbed, angle-resolved photoemission symm. anal., polarisation depend. and lateral interactions 79−91568
Pd (111), chemisorption bonding of H, UPS obs. 77−76671
Pd (111), of acetylene, complex form., UPS 77−12826
Pd (111), of H_2, UPS obs. 77−1786
Pd (111), of NO, LEED, UPS, and thermal desorpt. expts. 77−69179
Pd (111), of O_2, EELS, AES and LEED obs. 79−86985
Pd (111), of O_2, UPS and thermal desorption spectra meas. 79−78833
Pd (111), of O_2 and NO, LEED, photoelectron spectra and thermal desorpt. expts. 77−69180
Pd (111), scattering, adsorption, and absorpt. of H_2 and D_2, mol. beam study 80−29277
Pd, chemisorbed O_2, reaction with CO, AES obs. 77−90640
Pd, chemisorption and decomp. reactions of O containing organic mols., UPS 77−63953
Pd, chemisorption of O_2 and CO, catalytic activity, SCF-$X\alpha$-SW calcs. 78−15711
Pd film, of ethylene and acetylene, IR refl. study 79−69343
Pd, H adsorption, on (111)(110) surfaces, inert model 80−50889
Pd layer, adsorption and absorption of H_2, kinetic analysis of models 77−47679
Pd, of CO, catalytic oxidation 77−70339
Pd, of CO, IR spectroscopic evidence for localised site adsorption 78−47669
Pd, of CO, N_2, NO, semiempirical calcs. 78−14611
Pd, of CO, Penning ionisation electron spectroscopy, metastable He impact, electron energy distrib. 79−52060
Pd, of CO, UPS investig. of nature of chemisorption bond 77−51598
Pd, of CO, ultra high vacuum technique 78−71960
Pd, of H, bond nature 80−34297
Pd, of H, embedded cluster model 80−39427
Pd, of H, model, comparison with UPS data 79−46932
Pd, of He(CO)(O_2), mol. beam study 78−79878
Pd surface, CO chemisorption, SIMS, XPS study 80−84382
Pd surface, of CO, mol. cluster calc. 80−100407
PdAg surface, CO chemisorption, SIMS, XPS study 80−84382
Pd(111), of H, bonding, photoemission spectra, SCF electronic struct. 79−33320
Pd(111), of H, preexponential factors 79−46918
Pt 6(111)×(100), of O_2, UPS studies 80−76151
Pt (001), of H, O and CO, localised orbital approach 77−69166
Pt, (001) surface, localised orbital approach 78−14587
Pt (100), of acetylene and benzene, LEED, AES, HPS and temp. programmed dehydrogenation exam. 77−55456
Pt (100), of H_2 and O_2, and their interaction, UPS investig. 77−51600
Pt (100), of O_2 and H_2, (1×1) and (5×20) configs. comparison 77−51599
Pt (100) surface, of acetylene and benzene 77−59216
Pt (100) unreconstructed surface, CO chemisorption 78−38962
Pt (111), chemisorption bonding of H, UPS obs. 77−76671
Pt (111), H adsorption, inert surface model 80−50889
Pt (111), of acetylene, complex form., UPS 77−12826
Pt (111), of acetylene, dissoc., EHT calcs. 79−39190
Pt (111), of CO, C-O bond lengths, electronic struct. 78−6210
Pt (111), of CO, orientation of CO from angle resolved photoemission 77−8721
Pt (111), of CO, weakly chemisorbed state at 77K 79−65322
Pt (111), of Cl_2, LEED, AES, thermal desorption, and work function meas. 80−75444
Pt (111), of mol. O_2, XPS, UPS, EELS, and work function meas. 80−76139
Pt (111) surface, chemisorption of acetylene, self-consistent EHT studies 79−61896
Pt (111) surface, chemisorption of ethylene, vibr. anal. of C_2H_3 species 80−61150
Pt (111) surface, of acetylene, EHT calcs. 77−62733
Pt (111) surface, of CO, LEED, desorption and work function meas. 77−72781
Pt {111}, of CO, refl.-absorpt. IR spectroscopy 77−1306
Pt {111}, of N_2, refl.-absorpt. IR spectroscopy 77−47676
Pt {111} surface, of CO, IR spectra, evidence for strong absorbate coupling interactions 78−14604
Pt catalyst, oxidation kinetics of CO, determ. using ^{13}C tracer 79−29400
Pt, chemisorbed O_2, reaction with CO, AES expts. 77−90639
Pt electrode, of H, entropy, temp. and press. effects 78−84059
Pt electrode, of H(O), volume of adsorbed species, temp. and press. effects 78−84060
Pt, electrode surface, of H, struct. and comp. exam. by LEED and AES 79−70342
Pt electrode surfaces, of H_2, electrochem. activity comparison 78−61015
Pt electrodes, of H, anion effects on multiple states, reflection spectra obs. 79−43634
Pt, of acetylene, characteristic loss spectrum and AES 77−55458
Pt, of acetylene or ethylene on Pt (111), ethylidyne form. 79−57291
Pt, of benzene, on (111) surface, LEED and Auger spectroscopy obs. 78−30823
Pt, of CO, effect of interactions on nature of chemisorption bond 77−51598
Pt, of CO, O_2, H_2, thermal desorpt. spectra 78−14607
Pt, of CO, O_2, H_2, UV photoemission spectra 78−14608
Pt, of CO, XPS obs. of dissoc. sorption 77−16863
Pt, of Co, photoemission meas. 77−63531
Pt, of ethylene, IR refl. obs. 77−31903
Pt, of ethylene and halogen substituted alkenes, photoelectron spectra 77−43429
Pt, of H, bond nature 80−34297
Pt, of H, embedded cluster model 80−39427
Pt, of H 79−46932
Pt, of H_2, incoherent inelastic neutron scatt. exam. 79−60642
Pt, of H_2 and O_2, on surfaces with variable kink concs. 80−35576
Pt, of hydrocarbons, C-H stretch vibration, broadened and softened, dehydrogenation 78−47666

chemisorption continued
Pt, of NO, effect of particle size of Pt supported on inorganic oxide carriers *(French)* 78−11552
Pt, of O_2, catalytic activity, SCF-$X\alpha$-SW calcs. 78−15711
Pt, of O_2, reaction with CO, transient kinetics obs. 78−7229
Pt, of O_2, thermomag. effect, temp. depend. *(Russian)* 78−60034
Pt, of O_2 and CO, SCF-$X\alpha$ cluster calcs. 80−65365
Pt, of substituted hydrocarbon monolayers, AES quantitative anal., calibration 78−31724
Pt, pot. energy function of two H atoms around Pt atom protruding from metallic Pt surface 80−10781
Pt, stability and struct. of high Miller index forces in vacuum and with adsorbed C and O 77−76651
Pt surface, of CO, mol. cluster calc. 80−100407
Pt surface, stepped or flat, H_2 chemisorption, calcs. 79−28208
Pt, surface struct. and electronic props., CO_2, O_2 and H_2 chemisorption, LEED, AES 77−1300
Pt surfaces, of H, field emission study 77−24477
Pt-Au, of H_2 and CO, effect of surface segregation 77−51601
Pt-Au (100), of H_2 and O_2, and their interaction, UPS investig. 77−51600
Pt-Pb fibre, CO adsorption and oxidation, AES and ESCA obs. 79−52469
Pt_3Sn, of Co, surface composition determ. 79−69328
Pt(100), of NO, vibr. spectra, electron energy loss, LEED and Auger investig. 79−90866
Pt(111), adsorbed benzene, vibr. loss spectra 79−23838
Pt(111), of acetylene, reaction at room temp., form. of vinyl-like species 79−46939
Pt(111), of ethylene, reaction at room temp., form. of vinyl-like species 79−46939
Pt(111), of H, preexponential factors 79−46918
Pt(111) plane and stepped surfaces, of H_2, bond breaking activity, model potential 80−108744
Pt(111) surface, of acetylene and ethylene, UPS meas. 77−52223
Rb, of methane, vibr. excitation and surface reactivity 79−73393
Re (0001), of CO, role of d-orbitals, angular resolved UPS and thermal desorption meas. 80−40232
Re, (0001) surface, nonuniform attenuation of d-bond photoemission, CO chemisorption 79−74060
Re, of alkali metal, bond, adatom valence energy level broadening *(French)* 79−33176
Re, of H, within wide temp. range 80−10778
Re surface, long range and temp.-depend. interaction with alkali metal atom, theory 80−59802
Re vicinal faces, of O_2, mirror electron microscopy, LEED and AES obs. 79−65323
Re-O_2, surface interactions and catalysis, 77 to 773K 79−79286
Rh (110), of CO and NO, LEED, AES, XPS, UPS, and desorption obs. 79−77899
Rh (111), dissociative chemisorption of CO_2, EELS and thermal desorption spectra meas. 80−6656
Rh (111), of acetylene and ethylene, EELS, LEED and thermal desorption mass spectrometry 80−80057
Rh (111), of CO, dissociation probability, isotopic exchange and AES meas. 80−40743
Rh (111), of CO, thermal desorption mass spectrometry and LEED meas. 79−77917
Rh (111), of CO and CO_2, high resolution EELS, thermal desorption, and LEED study 80−44419
Rh (111), of H_2, thermal desorption spectra and LEED obs. 79−86989
Rh (111), of methane, dissociative, vibr. activation 79−57292
Rh (111), of water, effect of adsorbed O, H, or CO, LEED and thermal desorption meas. 80−75435
Rh (111) and (100) surfaces, of H_2, O_2, CO, CO_2, NO, C, ethylene, acetylene, LEED, AES and thermal desorption meas. 78−38951
Rh, (111) surface, chemisorbed O_2, catalytic reaction between adsorbed O_2 and gaseous H_2 79−83503
Rh (111) surface, UPS meas. of chemisorbed and condensed CO using synchrotron radiation 79−33902
Rh (755), (331), of H_2, O_2, CO, CO_2, NO, C_2H_2, C_2H_4, and C, desorpt. temp. and decomp. characts. 79−65318
Rh, chemisorption of ethane, sticking coefficient per landing site 79−46941
Rh, chemisorption of N_2+H_2, (110), (111) and (100) planes 79−86979
Rh, dispersed on Al_2O_3, of CO, ^{13}C NMR obs. 80−1000
Rh, of CO, IR spectra, species identification 79−39198
Rh, of CO, on (110) face 78−6225
Rh, of formaldehyde, catalytic decomposition, transmission IR spectra 79−39199
Rh, of NO, reaction with CO, obs., reaction kinetics calcs. 78−61045
Rh supported surface, CO chemisorption, activated surface processes, IR spectra 80−16724
Rh/γ-Al_2O_3 disperse δ-phase, chemisorpt. of CO, IR spectra, site distrib., mol. mobility 78−72496
Rh-Cu catalyst, Al_2O_3 supported, chemisorbed CO, IR spectra *(French)* 80−60559
Rh(111), of CO, energy level shifts of CO 78−87865
Ru (0001), of acetylene, substrate effects on bonding, electronic spectrum 78−63933
Ru (001), dissociation of adsorbed H_2S, chemisorption and electronic struct. of S layer 79−79292
Ru (001), geometric struct. of chemisorbed CO, LEED obs. 79−51429
Ru (001), of CO, electron stimulated desorption ion ang. distribs. bonding geometry and bending vibrs. 79−33189
Ru (001), of O_2, uptake meas., thermal desorpt. spectroscopy and AES 80−108739
Ru (10$\bar{1}$O) of NO and CO, dissoc. 77−72783
Ru (10$\bar{1}$0) surface, interactions with N_2O 80−55713
Ru (10$\bar{1}$0) surface, oxide form., thermal desorption and ESCA obs. 79−82442
Ru (101), of O_2, CO+O_2 interaction 77−73471
Ru (110), methanol reaction, thermal desorpt. meas. 78−31685
Ru (∼001) stepped cryst., of O_2, 300K, LEED and AES obs. 80−11947
Ru catalysts, of O_2, EXAFS obs. 78−15708
Ru, dissociative chemisorption of CO, isotope exchange 79−34354
Ru, of NO and NO decomp. 78−18903
Ru, of O_2, on (001) surface, high resolution electron scatt. spectra 79−11013
Ru-Cu catalyst, of H, electron spectroscopy exam. 78−44405

chemisorption continued
Ru(001), of H_2O, conformation, electron stimulated desorption ion ang. distribs. 77—89637
Ru(001) surface, chemisorbed $CO+O_2$, and surface reaction 79—46924
Ru(101), of CO, surface structural chemistry and electron impact props. 77—1312
Ru(101), of NO, via mobile precursor state 78—43247
$^{35}SO_2$ interaction with atmospheric particulates 77—41137
Sd (111), of Cl_2, LEED, AES, thermal desorption, and work function meas. 80—75444
Si, (III) surface, of O_2 and H_2O, appl. of UPS ultrahigh vacuum apparatus *(Japanese)* 80—37125
Si (100), of H, new type of chemisorptive bond, theory 78—26930
Si (100), of H, pairing model calcs., compared with expt. 78—34719
Si (110), of H, kinetics of H generation and adsorption, UPS 77—55450
Si (110) surface, of H, UPS spectra meas. 77—20186
Si, (111), 7×7 and 1×1, chemisorption of Cl_2 , UPS obs. 78—34704
Si (111), chemisorbed O_2 electronic struct. tight-binding calc., XPS and UPS meas. 80—49845
Si (111), chemisorpt. of Cl, electronic states tight-binding method appl. 80—49564
Si (111), Cl_2 chemisorption, ang. resolved UPS and LEED meas. using Vidicon intensity processor 78—71972
Si (111), electronic states and initial steps in oxidation 78—91534
Si (111), H chemisorption, Auger surface spectroscopy 80—50472
Si (111), of CO, on cleaved surface, electron energy loss spectra 78—79885
Si (111), of Cl, chemisorpt.-site geometry from polarised photoemission 77—15684
Si (111), of Cl, LCAO calcs., Auger line shapes, localized density of states 78—56202
Si (111), of Cl, surface energy bands and atomic position of Cl 78—56041
Si (111), of H, localised model, ab initio HF-LCAO calc. 80—6930
Si (111), of H(Cl), conduction-band surface resonance 78—52051
Si (111), of O_2, low-energy electron loss spectroscopy obs. 77—1303
Si, (111), struct. depend. oxidation, high resolution photoemission yield spectroscopy 77—1305
Si (111), with chemisorbed Al, electronic struct., self-consistent pseudopotential calc. 78—34880
Si (111), with chemisorbed Cl and F, electronic energy struct. calcs. 79—78144
Si (111) 1×1, of Cl, in vacancies 79—77910
Si (111) 7×7 clean surface and O chemisorbed stage valence band density of states from $L_{23}VV$ Auger spectra 80—100717
Si (111) surface, clean and O_2-chemisorbed, electron states by AES 80—54747
Si, (111) surface, EXAFS of oxidation stage, O-Si bond length 79—95876
Si (111) surface, H chemisorbed, electronic struct. 78—39182
Si, (111) surface, of O, electronic density of states changes, AES obs. 79—65528
Si (111) surface, with Al overlayers, electronic states 80—11061
Si, acetone layer, CH radical production by sputtering, rot. and vibr. population distrib. 78—64436
Si, bonding states of adsorbed O_2, photoemission obs. 78—92170
Si, chemisorption of XeF_2 and SiF_4, XPS and Auger spectra, surface chemistry 80—81358
Si, epitaxial layer, growth mechanism from ion-molecular beams 80—2299
Si, H chemisorbed, relation of Si-H vibr. freq. to surface bonding geometry 80—49502
Si, of Ag, (111) surface AES 78—14589
Si, of Al, local density of states for monolayer on (111) surface 79—47142
Si, of CO(Cl), surface photoemission, adsorption gate geometry 78—73079
Si, of Cl, cluster model calc., iterative EHT 77—32062
Si, of Cl_2, photoemission polarisation effects with synchrotron radiation 78—14580
Si, of Ga on (111) surface, Ga-induced surface states 79—19644
Si, of H, electronic struct. calc. 78—14784
Si, of H, on (111) 77—62743
Si, of H_2, atom-probe FIM obs. 78—71968
Si, of H_2, local density of states method and bond orbital model calc. 77—8165
Si, of H_2, magnetic-sector atom-probe field ion microscopy exam. of hydride form. 77—80699
Si, of O_2, AES and photoelectron spectra exam. of early stages of oxidation 79—74272
Si, of O(1s), XPS investigation 77—69170
Si, of organic solvents *(Russian)* 78—91537
Si_3N_4 film, plasma etching, role of chemisorpt. of CF_4, CF_3H, CF_3Cl, CF_2Cl_2 and CCl_4 79—11714
SiO_2, of cetyl pyridinium bromide, adsorpt. pH depend., mechanism 79—20466
SiO_2, of diketons, under carbon tetrachloride immersion, IR obs. 79—24821
SiO_2 of pentan-3-one, under carbon tetrachloride immersion, IR obs. 79—24821
Si(111), of H, formation of monohydride and trihydride phases, LCAO model appl. 79—15004
Sn, O_2 precursor adsorption, chemisorption activation energy 78—71950
Sn, of O_2, AES and EELS study 79—46917
Sn, of O_2, appl. of electron energy loss struct. in Auger anal. 79—47559
SnO_2, hydrous, gel, of organic compounds, transmission IR spectroscopy 77—55465
SnO_2, O chemisorption, elec. cond. and EPR meas. correlation 80—84369
SnO_2 surface, interactions with O_2, H_2O and H_2, desorpt., ESR and cond. meas 80—10790
SnO_2 thin films, solid state gas sensor 80—40790
$SrFeO_{3-x}$, NO absorpt., IR spectroscopic study 79—78675
$SrTiO_3$ (111), O_2, H_2 and H_2O chemisorption, UPS and XPS studies, illum. effects 80—71572
$SrTiO_3$, of water, UPS meas. 78—10285
$SrTiO_3$ surface, oxidation and reduction by D_2O, $H_2{}^{18}O$, D_2, isotope exchange study 80—104461
Ta film, of SO_2, adsorpt., corrosion 78—79897
Th (111), struct., Debye temp., and oxidation, LEED and AES obs. 77—89625

chemisorption continued
Th, O_2 adsorpt., and oxidation, electron-induced luminesc. expts. 78—38946
ThO_2, pure and Tb^{3+} doped, impurities effect in absorboluminesc. and photoluminesc. 79—38597
Ti (0001), of CO, LEED struct. anal. 78—71964
Ti (0001), of CO, N_2 and O_2, valence band struct., XPS and UPS study 80—35062
Ti (10$\bar{1}$1), of CO, XPS, UPS, flash desorption mass spectra, and active ion bombard. obs. 79—11822
Ti film, ion stimulated N_2 sorption, TiN_x form., sorption ratio, capture coeff. anal. 80—39411
Ti film, of N_2, O_2, CO and CO_2, changes in work function 77—59221
Ti film, of O_2 and CO, quartz cryst. microbalance obs. of O/Ti and CO/Ti atom ratios 79—4475
Ti film, of SO_2, adsorpt., corrosion 78—79897
Ti, of H_2 and CO, flash desorpt. mass spectrometry obs. 77—89646
Ti, of N_2, O_2 and CO on polycryst. surfaces, secondary electron yield obs. 78—71971
Ti, of N_2, on {000}, at. underlayer form. 77—15693
Ti, polycryst., of N_2, O_2 and CO, secondary electron yield spectrum obs. 78—38933
TiC (001) surface, change in work function with chemisorption of O_2 and H_2O 80—29461
TiO_2 (100), of H_2, O_2, and H_2O, electron spectroscopy, evidence for Ti^{3+} photogeneration 78—38940
TiO_2, clean and hydrated, surface sites, XPS 80—35052
TiO_2, of H_2O, differential heat of chemisorption 78—84052
TiO_2, of O_2, phase investig. by UPS 78—72684
TiO_2, of O_2 and H_2O, electron stimulated desorption, AES and charact. loss spectra 78—22963
TiO_2, rutile, of acetic acid-d_4, IR obs. 78—30827
TiO_2, water, UPS meas. 78—10285
TiO_2, X-irrad., adsorpt. of O_2, EPR meas. 78—80211
TiO_3, water adsorpt. IR spectra 78—14577
U powder, hydriding kinetics, 13.3 and 26.6 kPa, 50-250°C 80—16725
V, oxidised in air during laser irradiation, switching effect *(Russian)* 80—24977
V surface, chemisorption of Br_2, struct., Na adsorption effects 80—101039
W (001), displacive transition, H adsorpt. effects, theoretical model 80—65352
W (001), of H, HF Green's function formalism and phase shift technique 80—24733
W (001), of H, surface phonons, lattice dynamical model 80—39405
W (001), of H_2, angle-resolved photoemission, symmetry-related polarisation effects 78—56566
W, (001) surface, localised orbital approach 78—14587
W (100), adsorbed H-induced lattice reconstruction, surface vibr. obs. 79—19445
W (100), adsorpt. of acetylene, room temp., electron spectroscopy obs. 79—7749
W (100), CO/H_2 surface complex, flash desorption and AES obs. 78—73083
W (100), of Ba, inelastic tunnelling spectra 78—47664
W (100), of H, D, ^{16}O, and ^{18}O, isotope effects obs. by SIMS 79—5234
W (100), of H, $H\nu$, vibrational mode, IR study 80—60582
W (100), of H, phase changes, LEED obs. 79—77911
W (100), of H, struct. determ. by surface vibr. modes anal., EELS obs. 80—39435
W (100), of Hg, AES, LEED, work function and thermal desorption expts. 78—34709
W (100), of O_2, LEED, electron energy loss, desorption and work function obs. 77—55451
W (100) substrate, of H_2 and halogens, adatom charge and binding energy, self-consistent calc. 77—62734
W (100) surface, of CO, mol. orbital study 78—71995
W (100) surface, of CO_2, NO, UPS studies 79—23841
W (110), adsorpt. of N_2, N_2O, and NO_2/N_2O_4, 300K and 100K, XPS, UPS, and XAES 79—28203
W (110), adsorpt. of NO, 300K and 100K, XPS, UPS and XAES 79—28204
W (110), chemisorption of O, Monte Carlo modelling of phase changes 78—71969
W (110), ionisation of hyperthermal Na atoms, temp. depend. 80—50504
W (110), O chemisorbed, island form. and condensation 80—49517
W (110), of CD, LEEO, XPS and Auger meas. 77—89647
W (110), of H_2, work function, Fowler-Nordheim studies 80—34501
W (110), of N, surface diffusion, scanning Auger spectroscopy exam. 77—55452
W (110), of O, displacement reconstruction model 79—46949
W (110), of O, three-adatom non-pairwise interaction, Monte Carlo simulations 79—82466
W (110), order-disorder transform. in chemisorbed O, theory compared with LEED data 79—7748
W (110), WO_2 and O_2 adsorption by LEED and AES 80—34317
W (110) surface, NO adsorption, chemical changes detected by AES 80—10787
W {001}, displacive surface phases formed by H_2 chemisorption, LEED study 80—49520
W {100}, of CO, electron beam effects, AES obs. 77—31897
W {110}, of β-N_2, underlayer mechanism 80—39432
W, chemisorbed H, surface cond. and intrinsic surface states, surface refl. spectra 80—15378
W, chemisorbed H_2, vibr. spectra characts., adsorption sites 80—70535
W, chemisorption of N_2+H_2, (110) plane 79—86979
W, clean and oxidised, mol. binding states of SiO 79—7750
W, direct inelastic and trapping-desorpt. scatt. of N_2, elementary steps in N_2 chemisorpt. 80—60737
W, hot filament, adsorpt. and decomp. of formaldehyde 77—90641
W, monolayer gas adsorption, relax., electron contrib. to chemisorption, Auger shift study 80—20738
W, of C, N, and O, SXAPS obs. 79—52048
W, of CO and acetylene, IR vibration spectroscopy using refl. inelastic electron scatt. 78—14603
W, of cyclic hydrocarbons, on (100) surface 80—59782
W, of ethylene, reaction with atomic H 77—36789
W, of H, angled resolved UPS exam. 77—55865
W, of H_2, HFS model cluster calcs. 77—51795
W, of H_2, vibr. states, electron energy loss spectra 77—31877
W, of halogens, UV photoelectron spectrosc. study 80—7854

chemisorption continued
W, of $NH_3(NH_3)$, decomposition mechanism, isotope effect 79–29409
W, of NO, 80K, FEM obs. 77–39733
W, of O, as (110) surface, adatom-adatom interaction energies determ. 78–67904
W, of O, atom interactions, Monte Carlo simulation 77–52667
W, of O, on (110) surface, phase transitions, coverage effects 78–79879
W, of O_2, initial oxidation, reaction probability 78–15700
W, of O_2, island form., adatom interactions 79–46922
W, of O_2, on (110) surface, low temp. precursor state 77–11794
W, of O_2, SIMS, hysteresis effect 77–72771
W, of O_3, energy accommodation and reactivity 77–86352
W surface, (110), chemisorpt. effects on dielec. function, refl. spectra 80–75616
WC, microcrystalline, mol. dynamics, motion of H_2O and H_2 mols. adsorbed on surface, catalytic activity 78–71941
W(100), chemical effects in electron loss spectrum 77–4705
W(100), of CO and N_2, AES and electron energy loss spectra 77–1313
W(100), of H, localised orbital approach 77–69165
W(100), of H, vibr. excitation of hydrogenic modes, angle dependent electron energy loss meas. 79–46914
W(100), of H_2, adsorbate-induced surface reconstruction 79–4472
W(100), of O_2, low-energy SIMS, ion yields depend. on surface chem. and primary ion energy 78–73105
W(100)-O chemisorption system, static mode SIMS 78–34712
W(110), of acetylene, rehybridization, electron energy loss spectra 78–31289
W(110), of CO and O_2, absolute coverage and work function meas. 100 and 300K 78–71986
W(110), of O, island dissolution phase transition 77–80698
W(111), of ethane, AES and LEED pattern exam. 79–15005
Zn surface, O_2 interaction, chemisorpt. and oxidation 78–64886
ZnO $10\bar{1}0$ surface, reaction of O_2, AES, LEED, EPR, desorpt., surface cond. and work function expts. 78–95950
ZnO, (0001) surface, of O, AES and refl. electron energy loss spectra 79–46927
ZnO dye sensitisation in electrostatic photography 79–67404
ZnO epitaxial film, nonuniform cond. due to H chemisorption *(Russian)* 80–65723
ZnO, nonpolar surface, chemisorption equilibria for CO and CO_2 79–65321
ZnO, of CO_2, NH_3, differential heat of chemisorpt. 79–52759
ZnO, of H, electrical cond. exam. adsorption centres 78–67913
ZnO, of H_2, effect on ESR and NMR *(Japanese)* 80–50186
ZnO, of H_2O, differential heat of chemisorption 78–84052
ZnO, of O_2, charge transfer, obs. by surface piezoelec. effect, contact pot., and surface photovoltage 77–89824
ZnO, of O_2, effect on conductivity of powder layers 78–43441
ZnO, of pyridine, acetone, dimethyl sulphoxide, UPS, mol. orbitals effect on bonding 78–72699
ZnO, of water, cond. and ESR meas. 79–56072
ZnO, powder, surface cond., effects of O_2 chemisorption and CO_2 photodesorption 77–11980
ZnO, prismatic surface, O_2 interaction obs. 77–31899
ZnO, with chemisorbed neutral red, photocond. meas. *(Japanese)* 79–42572
ZnS, of H_2, decomposition of H_2 atmosphere, electron-hole mechanism *(Russian)* 77–16409
ZnS, of O_2, after illumination and in presence of CO and O_2 78–87877
ZnTe (110) and (111) surfaces, O_2 adsorption, electron energy loss and Auger spectra 79–47568
Zr, adsorption and absorpt. of CO, NO, N_2, O_2, and D_2, dissoc. and diffusion 80–80085

chemistry
see also atmospheric chemistry
ACS Tenth Biennial Education Conference on Safety and Health in Academic Lab., recommendations 79–80387
Adams, Roger, his role in American chem. education and research 80–4497
advances in chemical physics 77–6806
in archaeology, nonscience undergraduate course 77–26104
biochemistry and biophysics horizons, book 78–68977
carbohydrate nomenclature, digital representation, chemistry education 80–62435
chemical research, appl. of physical instrumentation and computers, review 79–70295
compounds, complete set, chiral subset, algebraic props. 77–70282
computer-assisted learning in the University of Surrey Chemistry Department 79–30167
course for artists, art buffs 79–84880
education, computer usage, state-of-the-art 80–4488
education, physical sciences at Lanchester Polytechnic 79–44658
education, physics joint honours degree course at Manchester University 79–35456
eduction, paper-pencil inventory for cognitive functioning assessment 79–80386
formulae, historical development, review 78–73822
Gay-Lussac, biography 79–25815
Gay-Lussac, J.L., contribution to chemistry *(Russian)* 79–80407
glass *(Japanese)* 78–6885
group theory teaching, pedagogical approach to direct product represent. 80–17771
history, nineteenth century British atomism, A.W. Williamson and atomic theory 78–32637
kinetic molecular theory teaching, expt.-oriented approach 80–12868
laboratory course, for intellectual skills development 79–21484
lecture demonstration of meas. errors 80–17773
lecture demonstrations with student participation 79–84911
LMFBR Na/basalt concrete interactions following accident, chemical phenomenology 80–47639
molecular configurational similarities, computer-assisted-examination of substructs. 79–81294
organic, course for master's degree, Keller method 79–58461
organic chemistry, textbook, undergraduate level 78–57711
organic chemistry courses, unified approach to teaching of struct. and bonding 80–17732
particles of the same series operator representation, genetic relationships 77–66743
photographic process, latent image formation, Ag_6 cluster as quantum chemical model 79–24792

chemistry continued
plasma chemistry, electron-beam discharge regime anal. *(Russian)* 77–47272
post-graduate educational system in North America rel. to Muslim graduate student 78–65736
pure and applied chemistry, conf., Tokyo, Japan (Sept. 1977) 78–95906
quantum mechanical ideas development and use in chem. bonding in inorg. complexes 80–12878
quantum mechanical ideas development and use in chem. bonding in inorg. complexes 80–12879
relativistic corrections, anomalous chemical properties of elements due to high speeds of inner electrons *(French)* 80–93839
SI units applied to chemistry, consequences *(German)* 79–97339
theoretical chemistry, NMR, ESR and NQR, review 77–18943
transformation systems direct and inverse regulation control 78–11606
transplutonium element symposium, Baden-Baden, Germany (September 1975) 77–28974
undergraduate education, future changes 78–69929
$Z=106$, atomic and chemical props. by gas chromatography and aqueous chemistry, book contrib. 78–85121
Ha, (element 105), atomic and chemical props. by gas chromatography and aqueous chemistry, book contrib. 78–85121
Ir, recovery from laboratory residues 78–81957
Mo cpds, chemistry and uses, conf., Oxford, Eng., Sep (1976) 77–77749
Pb (II), solvent extraction by versatic acid 10 *(Japanese)* 79–4928
Rf, (element 104), atomic and chemical props. by gas chromatography and aqueous chemistry, book contrib. 78–85121

chemistry, physical *see physical chemistry*

chemistry computing
see also computerised instrumentation; spectroscopy computing
acid dissociation consts., computer programs 80–26005
activation analysis, optimisation, computer-selected conditions 78–15740
adsorption at soln.-electrode interface, AC polarographic data anal., computer program 80–3400
analogue computer applications in quantum chemistry training *(German)* 78–28903
analysis, instrumental, minicomputer appls., errors 78–92543
analysis, simplex optimisation calcs., high speed algorithms 80–40767
analytical chemistry, user-oriented software Fourier spectrum display 78–64896
analytical data acquisition, computer operational system *(German)* 78–27845
applications in organic struct. chem. and mol. spectroscopy in USSR 78–88624
aqueous multicomponent multiphase equilibria, free energy minimisation method, comput. algorithm 80–40724
archaeology, trace element neutron activation analysis, pattern recognition techniques 77–40588
Arrhenius A and E interconversion algorithms 79–15957
artificial intelligence for chem. inference, automatic rule formation in mass spectroscopy, meta-DENDRAL 77–18775
atmosphere, photochemical and kinetic data 80–4096
atom numerical code scheme for classification of chemical shifts 78–94205
automatic titrator, microcomputer controlled, for chem. anal. 78–27841
azetropic copolymerizations computer calc. *(Rumanian)* 78–23945
bases, mixtures, potentiometric titrations, computer-calc. curves, learning machine appl. 80–3426
binary mixtures, liquid-vapour equilib. data, internal consistency, automatic checking method 80–54364
binary solid-liquid equilibria, student experiment, phase diagram computer program 78–89285
B.I.P. An interactive graphic system for indexing energy bands of model polymers 79–59608
block-cutpoint tree representation of chemical structures for use in computers 80–63522
CAI, at Syracuse Univ. 77–23
CAI, current status 80–12867
canonical MO transformation to localized MO by Boys' method 77–88394
catalyst pellet, transient diffusion-react. eqns., approximation using Galerkin technique 79–96357
chain conformations and local motions, Brownian motion simulation 79–86098
characterisation of rings of a molecule 80–63853
chemical instability, mol. dynamics model, computer soln. 77–4892
chemical potential, computer simulation 78–31683
chemical research, appl. of physical instrumentation and computers, review 79–70295
chiral molecules, detection, identification by Cahn-Ingold-Prelog rules, computer program, for teaching 79–58499
chromatographic curves, machine treatment using statistical moments method 77–63981
chromatographic data processor, multistep calc. function *(Japanese)* 80–26091
chromatography, correlation type, noise sources eval. and practical considerations 80–40771
chromatography, multicomponent sorbents, composition, computer optimisation 78–27842
chromatography, nonlinear detector response quantification with lab. automation system 80–40775
coal chemical analysis, SEM images evaluation 80–71994
complex chemical systems, chemical process and rate models, computer simulation appls. 78–48620
complex formation consts., computer programs 80–26005
computer modelling of matter, conf., Anaheim, USA (March 1978) 80–51954
constrained variation of molecular geometry using FORMAC 79–10012
coupled chemical reactions, exact stochastic simulation, using digital computer algorithm 78–48625
coupled chemical reactions, stochastic time evolution, Monte Carlo simulation procedure 77–9047
crystal nucleation growth rates, on-line meas., data reduction technique 79–38730
crystal structure refinement with constraints, least squares refinement program 79–10744
crystalline compounds, computer identification techniques using X-ray powder diffr. file 77–70389
crystalline solutions, binary isostructural, thermodynamic mixing parameters computation, FORTRAN IV subroutines 77–86344

chemistry computing continued
cybernetic prediction of chemical compound formation, in uninvestigated systems 79—11880
cyclic tetrapeptides, potential energy minima 79—59527
data base, classification, comparison of pattern recognition methods 80—199
data base, error detect. by text searching 77—37678
data factor analysis, reliability improvement 77—36802
diamagnetic susceptibility calculation using Pascal's consts., BASIC program 80—37717
differential pulse voltammetry, stationary electrodes, computer based instrum. appls. 77—36809
digitizer for generating computer readable chem. data 79—74454
electroanalytical chemistry, recent appl. of digital computers, review 77—81451
electrochemical assay with instrument using ion-selective electrode technology and LSI technology 80—1116
electrochemical cell, convective diffusion eqn., computer soln., numerical methods 77—16830
electrochemical cell processes, geometrical and spatial orientational effects, computer calcs. 77—32804
electrochemical fast processes, use of high speed electronic memory for data acquisition *(Italian)* 77—9088
electrochemical surface processes, kinetics simulation 79—16004
electrochemical surface reacts. driven by linear pot. sweep, kinetics 77—25275
electrochemical surface reacts. driven by linear pot. sweep, sequential reactions, kinetics 77—25276
electrochemical system, LF impedance meas. technique using on-line computer 80—57339
electrochemistry, polarisation curve-fitting by computer modelling 79—96316
electrode reaction kinetic parameters, programs for computer retrieval, in FORTRAN 78—31654
electrolytic soln. conductivities, eqn. calcs., data anal., computer program *(German)* 77—32806
electron integrals transformation method, program in FORTRAN IV H 78—82603
element distributions obtained by ion microprobe, images quantification 78—73101
energy loss spectroscopy, quant. microanal. of thin foils *(French)* 80—50900
entropy calculation with computer simulation 77—22504
enzyme kinetics simulation 79—15961
ESR spectra, simulation by FFT 79—19763
estuary and river sited power plants, water discharge and chlorination, simulation 78—96250
ethanol, pulse radiolysis, solvated electrons decay kinetics 79—66319
ethylene, TEA laser induced multiphoton dissoc., model and expt. 79—16016
Faradaic impedance expt. meas. anal. prog. 80—11894
fluid binary mixtures at high press., phase equilibria, critical phenomena calcs. 77—35664
gas chromatography, data acquisition and use of microwave plasma detector as element analyser *(German)* 78—64895
gas chromatography, programmed temp., retention index calcs. by linear interpolation 78—27844
gel permeation, chromatography, minicomputer DP system 80—45591
Hartree-Fock-Roothaan equations, program for soln. by Roothaan's method 77—88395
heavy isotope labelled mols., isotopic distrib. calcs. 77—56265
HMO calculations, minicourse in HMO theory using small computers 78—25444
hydrocarbon combustion products, 1400-2600K, minimisation of NO, computer model 78—85161
information system 77—33978
interactive molecular analysis system, MOLY 80—63852
ion diffusion coefficients, meas., computer-assisted technique using Cottrell eqn. 80—3425
ion-selective electrode analysis use of microprocessor-based millivoltmeter 80—16752
ion-selective electrode measurements in flowing system, computer-controlled interference correction 78—92527
jj-coupling, one-particle matrix element calculation program 79—13624
kinetic rate equations, soln. by CAKE program 78—48630
kinetics computational processing, iterative optimisation techniques 77—32765
kinetics measurement over many orders of magnitude in time, using minicomputer 78—7200
large scale scientific computation via minicomputer 77—25246
liquid chromatography, computer-based bibliography update 78—31736
liquid chromatography, spectrometric detect., computer control of data acquisition, reduction and display 78—27850
macromolecule, simulation of Brownian motion of chains, chain dynamics 79—86099
macromolecules, quantum chemical characteristics, extended Huckel calcs. 79—45874
macromolecules in solution, US degradation simulation program 79—14148
mass action equilibrium problem, numerical methods 77—9113
mathematical model of chemistry, deductive soln. to problems 79—52620
MC-SCF computation scheme for large scale calculations on polyatomic systems 79—10039
metallic system, compound formation rel. to heat of mixing 80—55689
micellar diffusion-controlled reaction kinetics 80—30213
microelectronics, present and future review 80—55627
microhomogeneity studies by electron microprobe, computer program 80—21352
microphysics to macrochemistry, discrete simulations, review 80—54102
minerals electron microprobe data analysis, using FORTRAN IV programs 77—86878
MNDO calculations, total energy, anal. first derivatives 78—86763
molecular, graphs, search for self-avoiding paths 79—59336
molecular configurational similarities, computer-assisted-examination of substructs. 79—81294
molecular electronic structure theory, computer program for graduate instruction 77—78937
molecular formulae and homologous series, inverted file structure for searching large data bases 78—35738
molecular spatial models, Stuart-Briegleb type, computer construction 78—86970

chemistry computing continued
molecular structure, functional group discovery using central atoms concept 77—34537
molecular structure determination, computer applications 79—50158
molecular structure elucidation algorithm (ASSEMBLE), computer construction 79—18104
molecular structures, topological code, modified Morgan algorithm 80—58122
molecular systems including up to 232 orbitals, CNDO calcs., computer program 78—86788
multi-component one dimensional chemical kinetics calculations, new algorithm development 80—45479
multicomponent X-ray analysis, computer program using fundamental parameters and empirical coeffs. 78—44416
multiphase unknowns, identification by computer methods and quality of X-ray powder data 80—3452
neutron activation anal., cyclic instrumental, optimum timing parameters for determ. of short-lived nuclides, computer program 80—61211
neutron activation analysis program 77—21439
nuclear materials safeguards, computerised chemical modelling of deviations, from mass transfer equilib. 80—83171
organic compound structural elucidation, CHEMICS-F 79—18310
organic compounds, classification from voltammetric data, computerised pattern recognition 79—16057
organic compounds structure determ. from spectral data by CHEMICS-F computer program 79—36794
organic synthesis, computer simulation *(French)* 79—52653
oxidation kinetics, C by CO_2 in Fe-C melts *(Russian)* 80—40680
particle size measurement techniques, rapid response, online methods, continuous industrial processes appl. 78—89429
pattern recognition in chem. dynamics 77—32768
pH titration system, computer controlled, for complex equilibria in soln. anal., appl. 79—87892
pH-computations in terms of hyperbolic functions 77—25354
phenoformaldehyde thermosetting resin, computer stimulation of form *(Japanese)* 77—66619
photochemical smog, rate parameters and computer simulation 78—48677
pi systems representation, efficient computer manipulation 79—81148
polarography, differential pulse type, digital simulation with incremental time change 77—90662
polarography, pulse, chronoamperometric, chronocoulometric techniques, kinetic, mass transport effects 77—25334
polyatomic system, large, ALGOL-60 program for MO LCAO calcs. in Mulliken-Rudenberg approx. 77—88388
polymer chains in cubic lattice solvent, thermodynamic props., Monte Carlo method, computer simulation *(Russian)* 77—31787
polymer radiation chemistry, computer modelling 79—74382
polymer solution, concentrated, computer-aided simulation of individual chain conforms. *(Russian)* 77—42454
polymerisation, radiation-induced, solid state, computer modelling 79—66294
polypeptides, conformational analysis, empirical pot. energy algorithm 79—50174
polystyrene solutions, US degradation obs. 78—95989
potential energy surfaces, use with algorithm to form reaction tree 77—70286
potentiometric analyser, automated, with selective electrodes, microcomputer control 80—40773
potentiometric titration system, microcomputer controlled, for soln. equilib. obs. 78—92522
protein molecule, simulation of single mol. images combining computer and electron micrograph analysis 78—37781
proteins, conformational analysis, empirical pot. energy algorithm 79—50174
pulse polarography, microcomputer-controlled polarograph appls. 80—66895
pulse radiolysis system, computerised, using Biomation recorder and PDP 11/40 computer 77—40560
pyrene, laser-induced two-photon photoionisation, simulation, double pulse investig. 78—37690
quality control and chemical analysis of natural and industrial objects, future programme 80—104484
quasimolecules, electronic struct. calc., CNDO approx., computer program 78—86789
radiogas chromatography, software package for data collection and processing 78—20086
REACT program for computer-assisted simulation of chemical reaction sequences, structure elucidation applications 78—92477
reaction equilibria in single reaction or single moiety chemical networks 77—12820
reaction kinetics, discrete simulation methods, appl. 78—48627
reaction kinetics, interactive simulator, teaching appls. 79—48992
reaction mechanisms, deduction from rate laws, computer appls. 78—48623
reaction mechanisms, models, computer method appls., conf., New Orleans, USA (1977) 78—48645
reaction rate constants, computer modelling 79—74343
reaction rate eqn. integration, interactive computer program system 80—31469
reaction sites automatic detection 78—92476
reactions, computer modelling, logarithmic formulations of parameters 78—48646
reduction of SiO_2 using a plasma, thermodynamic computer anal. 77—40530
rock analysis, biotite gneiss and amphibolite mode estimation, using FISK (FORTRAN) program 77—86397
SCF calculations, simplified extrapolation procedure 78—82604
search system, one-dimensional, for GC and MS anal. 78—23977
semiempirical molecular quantum-chemical calculations, PARAMOL programs 77—88393
SISCOM, library search system for compound identification 79—49329
solutions, dilute, Monte Carlo free energy calcs. in isothermal-isobaric ensemble 78—92498
space filling molecular models 79—18309
space shuttle reentry, unsteady nonequilib. chemically reactive flow, parallel computation 78—47065
spectrochemical analysis, l-transformation, accuracy of transform. parameters *(German)* 79—43674
spectrochemical analysis, photographic emulsion calibration technique 79—79321

chemistry computing continued
spectroscopy, computer-assisted learning methods 79—84906
staircase voltammetry, microcomputer-controlled polarography appls. 80—66895
staircase voltammograms, synthesis, anal., convolution, devolution 77—25336
steel, high alloy, rapid anal., use of central laboratory computer *(German)* 77—48703
stereoisomer generation, algorithm and implementation 80—1080
steroids, mass spectra, computer-aided interpretation by pattern recognition methods 78—64898
structural chemistry interactive graphics display system 77—22536
structural formulae for chem. cpds., program for detecting presence or absence of struct. fragments 78—62941
structural search codes for on-line compound registration 78—90319
structural similarity in molecules, graph theory recognition 79—50157
structures, pictorial reproduction 79—43708
synthesis computer design, interactive strategy 79—91945
synthetic organic reactions 77—25257
TC-chromatograms online analysis by scanning system 77—40599
thermochemical data and calc. of phase diagrams, systems for storage and retrieval 78—31682
thermosetting resin, estimation of diff. co-eff. distrib. and mol. wt. distrib. by computer *(Japanese)* 77—66042
time sharing computers, data processing and optimisation appls. *(German)* 78—35750
titrator, microprocessor-controlled 79—74455
trimoleuclar reaction, numerical simulation, rot. waves as asymptotic soln. 77—32772
troposphere, photochemical mechanisms, computational methods 78—49084
troposphere, urban photochemistry, computer simulation 78—49085
turbulent diffusion, flames, high Reynolds number, rocket exhaust appl., chem. processes theory 80—45504
unimolecular reactions, master eqn. for rate coeff. Nesbet's algorithm 78—48612
X-ray chemical anal., equivalent wavelength representation and secondary fluoresc. calcs., minicomputer program 80—321
X-ray chemical analysis, computerised control 80—3453
X-ray crystallographic computations for students using programmable calculator 80—36811
X-ray diffr. anal., computer searching of JCPDS powder diffr. file 77—70390
X-ray diffr. anal., single cryst. automated technique, comparison with powder method 77—70386
X-ray diffr. powder phase identification, manual computer search techniques 77—70387
X-ray diffraction chem. anal., historical review 77—70383
X-ray fluorescence anal., interactive regression anal., computer program 80—3463
X-ray fluorescence anal., matrix corrections, minicomputer program 80—3458
X-ray fluorescence spectra, energy-dispersive, least-squares anal., detector response function approach 80—3457
X-ray fluorescence spectra, resolution by weighted least squares computer program 80—3459
X-ray powder diffr. anal., computer search/match methods evaluation, manual search comparison 77—70391
X-ray powder diffraction patterns, quantitative matching 77—70384
Ag_2Te, growth by chem. transport *(Russian)* 79—38728
^{81}Br isotope enrichment by laser photodissociation of HBr, computer model 80—1075
HONO+NO+NO_2+CO+air, UV irradiated, computer simulation, peroxynitric acid form., smog 77—63885
He-Cs mixture, Cs ion conc. determ. by radn. absorpt. 79—34395
I_2, photodissoc. cage effect, computer simulation 79—24771
U, determ. by computer-controlled titration system, evaluation 79—16113

Cherenkov counters
ψ(J) particle, discovery, props., experimental apparatus develop. *(Czech)* 78—78232
aerogel counter, increased photoelectron collection efficiency of photomultiplier 79—45568
atmosphere detectors for gamma-ray astronomy, sensitivity 77—3232
atmospheric electrons, MeV range registration instrument 79—5645
avalanche chamber, multistep gated 79—45536
beta emitter isotope pair counting using performance number criterion 77—83471
beta-emitter radioassay, prep. of plant samples 78—81088
beta-emitters, activity meas. of low radiators using Cherenkov radiation *(Czech)* 77—46450
biological sample ^{32}P and ^{45}Ca determ. by Cherenkov and liq. scintillation counting 80—98183
broad band focusing Cherenkov counter, design and performance 78—37510
calorimeter, separation of hadrons and EM particles 77—79523
CAMAC autonomous system for control of scintillation and Cerenkov counters 78—21833
charge to time convertor, gated seven channel 78—13388
chevron microchannel plate photomultiplier tube with 400 anodes for high energy appl. 79—45545
colour quenching of Cherenkov radiation effect of radioisotope maximum β energy *(Spanish)* 79—76268
cosmic neutrinos, detection and neutrino-nucleon interactions, 1-100 TeV 78—36413
cosmic ray individual showers direct obs. by method using Cherenkov light meas. 77—17309
cosmic ray muons and neutrinos, deep underwater detectors 80—8546
cosmic ray spectrometer, for study of 6 to 50 MeV electrons 78—45235
cosmic ray telescope of Sydney Univ., results 78—25388
Darmstadt linear accelerator, detector system and performance of elec. scatt. system 78—70680
deep water muon and neutrino detection using Cherenkov light gathering systems *(Russian)* 78—55109
differential Cherenkov counters with achromatic ring focus, hadron beam mass identification, CEDAR project 78—37522
differential counter in beam of secondary particles from H chamber 78—861
DUMAND array, study of ultrahigh energy neutrino interactions 79—80108
EAS, duration of atmospheric Cherenkov pulses 78—73595

Cherenkov counters continued
EAS Cherenkov radiation meas. by photomultiplier, cosmic ray induced noise 77—18735
eight-channel wide aperture, secondary particle identification 80—91371
electron scattering experiments, detection system, Saclay linear accelerator facility 80—52809
electron synchrotron-Cherenkov detectors 80—884
fast particles, separation of simultaneously produced scintillation and Cherenkov radn. 79—18076
fibre-optic data transmission systems for plasma diagnostics 80—79571
focusing, multiplexed, optical system 80—47819
gas, compact, high press., detection efficiency for electrons 77—6630
gas, large aperture with good rejection of slow particles 77—10545
gas Cherenkov counter with ionisation spectrometer, appl. to cosmic ray studies 80—94662
GFEU-30 hodoscopic photomultiplier 79—93869
high-speed pulse shaper/discriminator for scintillation and Cherenkov counters 78—86748
hodoscope Cherenkov spectrometer, particle identification 77—88343
hodoscope spectrum of TF-1 Pb glass, determ. of photon coords. 77—30707
imaging Cherenkov detector using gas-filled MWPC, photoionisation of triethylamine 80—91400
large acceptance threshold gas Cherenkov counter, design, efficiency 77—3226
large pressurised Cherenkov counter, design, construction, operation 77—3227
large solid angle counter for DELCO expt. at SPEAR 78—86729
large yield threshold counter 79—68149
light distribs. within light diffusion boxes, algorithm 79—49908
liquid differential counter, for proton and kaon, 2 to 9.5 GeV.c^{-1}, or kaon and pion, to 5 GeV.c^{-1}, separation 79—731
liquid H Cherenkov counter to distinguish pions from kaons at around 800 MeV/c 78—37509
liquid scintillation system ^{32}P Cherenkov effect detect. efficiency meas. using ^{60}Co external source 78—25387
liquid-filled, for gamma-ray counting of large samples 78—53491
magnetic detector, SPEAR, PbO-SiO_2 wall addition 78—37494
mirrors, ellipsoidal, fabrication and use 80—47818
multichannel gamma spectrom., energy reconstruction of events 79—76259
multineedle counter with cathodic focusing *(French)* 80—102392
multistep avalanche chamber, automatic scanning by TV digitiser 80—52822
multistep avalanche chamber, far UV Cherenkov photon detection appl. 80—58042
MWPC to defect vac. UV photons from Cherenkov radiation 79—18078
ninety channel, mass spectrometer, high energy electrons and gamma photons 80—91362
operation with UV photoionisation detector 79—26835
optical system evaluation program 77—34523
photographic detector appl. to search for Dirac monopole 78—70700
photomultiplier, sensitivity to gamma quanta 78—9032
photomultiplier and small size phototube evaluation for Cherenkov counter appl. 78—37511
photomultiplier gain stabilisation system for high counting rates 79—76277
photomultiplier wavelength shifter, coating technique 80—18760
photomultipliers for Cherenkov light, improved yield 79—22549
photomultipliers for low light level appl. 79—45547
plastic large area detector 79—741
relativistic collimated particle beam ave. particle energy meas., difference method 80—14049
relativistic particle av. energy determ. by double cone and combined methods 80—18763
ring imaging Cherenkov detection using multi-needle cathodic focusing detector 80—58040
ring imaging counter, single photon detectors 80—58036
scintillation counter, high refractive index organic liquids, ^{18}F, ^{14}C radioactivity meas. 79—26817
SF5 lead glass Cherenkov counter, high energy photon position determ. 80—58032
silica aerogel Cherenkov detector development 80—58037
silica aerogel counter 77—50329
silica aerogel counter test results from CERN PS 78—86731
silica aerogel counter with diffusing walls 80—27887
spectrometric channel control using blocks 78—866
spectrometric channels, optimum and conditions of 58AVP photomultipliers 78—9031
spot focusing detector 80—5440
superconducting mag. spectrom. for cosmic ray flux meas. 78—25383
swimming pool hadron calorimeter 78—37501
system for cosmic ray EAS research above 2×10^{14} eV 77—61649
tachyon detection, using Cherenkov and ToF detectors, book contrib. 79—45125
Teflon vials in assay of radioisotopes 78—858
telescope for α-particle and proton-spectroscopy on GOES and TIROS spacecraft 78—86734
total absorpt. spectrom., π^0 photoprod. on ^{4}He meas. 78—29694
total absorption Cherenkov spectrometer, characteristics for electrons and gamma quanta 78—5092
total absorption shower gamma spectrometer 77—46448
transition radiation effects on efficiency of particle detection 78—58893
Tyan Shan Cherenkov detector with conical reflector, electronics 80—102403
ultrarelativistic charge, X-ray prod., stack of plates with absorption and allowance for multiple scattering *(Russian)* 77—83450
vial design 77—18746
water Cherenkov neutrino detector, construction and performance 80—91397
water detector, use of di-potassium 2-amino-6, 8-naphthalene disulphonic acid as wavelength shifter 79—26834
Pb glass 480 channel detector, linearity, energy and spatial resolution 78—871
Pb glass counter, automated calibration system 80—106233
Pb glass EM shower detector, test results 78—70689
Pb glass large counter array, LED monitoring system 79—45565
Pb glass shower counters, optical filters to improve resolution 77—57818
Pb-glass detector for high-energy gamma rays 77—3222
Pb-glass hodoscope for 50 to 150 MeV photons 80—18758

Cherenkov detectors *see Cherenkov counters*

Cherenkov radiation
- *see also Cherenkov counters; electron radiation*
- alternating electric field effect 78—20984
- atmosphere, gravity waves generation by HF acoustic waves, Cherenkov radiation *(Russian)* 77—17265
- atmospheric Cherenkov pulse duration, depend. on cosmic ray shower parameters 78—89025
- atmospheric measurements, determ. of primary spectrum 10^{12} eV to 10^{15} eV 79—66895
- atmospheric showers, γ-ray initiated, computer simulations, Cherenkov radiation, geomag. field effects 77—49254
- atomic beam, arbitrary angle in uniaxial cryst., emission energy spectrum 77—57923
- boundary effect on radiation in alternating electric field 80—37940
- carcinotron, relativistic millimetre, electron beam in high current accelerator 79—68359
- channelled relativistic electrons and positrons, EM radiation, spectral and ang. distrib. 78—23549
- charge separated magnetic plasma, possible radio emission source in pulsars 77—47163
- charged particle beam, instability normal to beam *(Russian)* 79—13883
- charged particle moving in mag. cold plasma, pulsar magnetosphere appl. 79—62736
- charged particles internal forces, moving faster than light in a medium 80—78751
- Cherenkov type parametric optical oscillator, optical saturation 80—102771
- cholesteric liquid crystals, diffr. scatt. conditions, theory *(Russian)* 79—19151
- coherent hadron radiation at TeV energies *(Russian)* 79—92641
- coherent hadron radiation interpretation of cosmic ray anomalous events *(Russian)* 79—92642
- coherent microwave Cherenkov radiation generation, relativistic electron beam-dielectric loaded waveguide 77—58246
- coherent radiation novel sources, book 79—27231
- coherent submillimetric Cherenkov radiation generated by relativistic electron beam 77—38793
- color quenching, effect of radioisotope maximum β energy *(Spanish)* 79—76268
- colour attenuation, effect of refractive index of colouring solute *(Spanish)* 80—7432
- computer simulations of Cherenkov radiation from large cosmic-ray showers 79—66899
- conducting medium, Cherenkov and ohmic losses of relativistic charge, unified treatment 79—12998
- conductor, magnetodielectric material-coated, finite-length relativistic charge interaction 80—5666
- cosmic ray induced photomultiplier noise 77—33308
- cosmic ray large air showers, Cherenkov radiation image reconstruction 79—25420
- cosmic ray photons, effect on IR interferometric search for non-solar planets 80—98523
- cosmic rays, γ primaries meas., 10 to 100 GeV, using air showers Cherenkov light distrib., detector system 78—73597
- crystal, spherical integral reps. for cond. of abruptly activated current 80—42080
- crystal optics, relativistic phenomena 80—46839
- diffraction in spatially-periodic medium *(Russian)* 79—59623
- dipole Cherenkov effect in doubly anisotropic 77—38790
- Dirac particle in crystalline medium, semiphenomenological QED 77—32463
- Doppler effect in refracting medium, classical and quantum interpretations *(Russian)* 79—13002
- Doppler radiation associated with Cherenkov radiation in presence of alternating elec. field 79—59621
- E coli, photoreactivation following ionising irrad. rel. to Cherenkov emission 80—108969
- EAS, Akeno Air Shower project, e and μ obs., core energy flow, device description 79—72184
- EAS, atmospheric Cherenkov light, time struct. 77—33306
- EAS, Cherenkov pulse shapes obs. using improved Yakutsk apparatus 79—80169
- EAS, development, atm. Cherenkov study 79—84615
- EAS, high energy, Cherenkov light meas. 78—45169
- EAS Cherenkov radiation impulse shape *(Russian)* 78—49260
- EAS Cherenkov radiation meas. by photomultiplier, cosmic ray induced noise 77—18735
- EAS radio emission spectra, Cherenkov and synchrotron radiation mechanisms 77—64566
- EAS with $E_0>2\times10^{16}$ eV, position of maximum energy *(Russian)* 79—96870
- electron beam, Cherenkov modulation 78—5408
- electron beam, in bounded plasma, spectra of Cherenkov instabilities *(Russian)* 79—77402
- electron beam, relativistic, fields excited near plane magnetoedielectric slab 80—18986
- electron beam bunching at optical wavelengths; inverse Cherenkov effect 78—46497
- electron beam energy spread as result of Cherenkov diffr. 78—5407
- electron bunch coherent radiation, electron distrib. effects 78—66734
- electron showers, Cherenkov radiation from electron ang. distrib. function *(Russian)* 79—80861
- electrons in mica target, 140-250 keV, ang. distrib. of radiation at 4000 Å and 5000 Å *(Russian)* 78—55291
- emission probability of radiation from charged particles passing through crystals 79—99969
- energy loss spectra of keV electrons exciting EM radiation in thin films, calcs. *(German)* 77—90213
- ethene, optical synchrotron-Cherenkov radiation threshold effects 80—28154
- exploding black holes, search using atm. Cherenkov method 78—49473
- fast wave propag. along cylinder, Cherenkov amplification *(Russian)* 79—44759
- field interface of moving particles in statistically inhomogeneous medium 79—6063
- focusing, electric piston effect, appls. 79—55041
- free electron laser, Cherenkov-Smith-Purcell, collective and single electron interactions, book contrib. 79—27234

Cherenkov radiation continued
- free electron lasers, Cherenkov, Smith-Purcell, and TW amplifiers, operation regimes 79—919
- free electron lasers, mag. bremsstrahlung, Compton and Cherenkov, types *(Chinese)* 79—31851
- gamma rays in 10^{11}-10^{14} eV range using atmospheric Cherenkov technique 79—25422
- gamma-ray resonance frequency range *(Russian)* 78—80432
- generation and transition in cylinder 80—82653
- heavy ion Z^2 depend. of Cherenkov emission, expt. limits 80—78495
- of high-energy particles in EM excited medium 77—19147
- hybrid transition-Cherenkov radiation, props. 79—45897
- impulse of photon in medium with negative group velocity *(Russian)* 79—3670
- inhomogeneous medium, geometric optics description 78—66766
- intense field QED in continuous medium, appl. to Thomson scatt. and Cherenkov radiation 80—27435
- interference effects in transition radiation near Cherenkov radiation threshold 80—9454
- ionosphere, prod. by unstable plasma wave coupling 79—40003
- ionosphere, radiation from artificially injected electron beam 79—84571
- ionosphere low-latitude VLF emissions, prod. by incoherent Cerenkov process 79—75036
- large cosmic ray showers, Cherenkov radiation computer simulation using hadronic collisions models 78—57415
- laser theory 77—19228
- light source, intense, 60 nm to IR range 79—59784
- light sources, appl. in pulse radiolysis 80—42267
- liquid, photoelastic, EM wave-excited, radiation from uniformly moving charge 79—13882
- localised perturbation development in cold beam interaction in dielectric 79—89838
- mica, 210 keV electrons, Vavilov-Cherenkov radiation, ang. distrib. half width, spectral depend. *(Russian)* 80—71505
- mica, Vavilov-Cherenkov radiation ang. distribs. from 170 to 250 keV e^- *(Russian)* 79—22569
- momentum-energy Minkowski and Abraham tensors 78—45825
- monochromatization of beam of charged particles of Cherenkov interaction 79—36829
- multistep avalanche chamber, detection of far UV photons, Cherenkov light imaging 79—93871
- optical Cherenkov radiation, correl. with radiopulses in EAS 77—60560
- optical Cherenkov radiation, prod. with radiopulses in EAS 77—60559
- optical fibre transmission meas. technique using time dispersion of Cerenkov radiation 78—5557
- optical SHG by guided radiation mode coupling in thin film optical waveguide, aspects 80—106567
- optical synchrotron-Cherenkov radiation threshold effects 80—28154
- optical waveguides, low loss, transient radiation effects, Cherenkov radiation, absorpt., in fibres 78—30055
- oscillator at flight in homogeneous medium over plane boundary with periodically-inhomogeneous dielectric *(Russian)* 78—1138
- parametric resonance, in medium excited by external field 78—9308
- photographic sensitive material, short time exposure, expt. technique 80—86477
- plasma, Cherenkov adsorption of azimuthal EM travelling waves, magnetoactive heating and containment *(Russian)* 80—38675
- plasma, relativistic, longit. waves and beam instability *(Russian)* 79—60158
- plasma, three-dimens. vel. diffusion, in two-stream turbulence 78—59595
- plasma, weakly inhomogeneous, charge density wave transform. *(Russian)* 77—3924
- polarisation in Cherenkov radiation 77—79241
- QSOs, Cherenkov line radiation, emission line spectra *(Chinese)* 79—80366
- quantum theory of Cherenkov and Doppler effects, paradoxes 78—45824
- quasar emission-like spectra, H atom L_α line *(Chinese)* 80—105378
- quasars, amplification of cosmic Cherenkov radiation 77—41294
- quasilinear amplification, of longit. wave in plasma waveguide, by relativistic electron beam *(Russian)* 78—38506
- reactor core monitoring of boiling water and of steam content using Cherenkov radiation 80—73957
- rectangular waveguide, Cherenkov radiation source 80—99373
- relativistic charged particles, in field of EM plane waves 77—71913
- relativistic electron beam generated coherent submillimetre Cherenkov radiation 77—38788
- relativistic neutron in conducting medium 78—5410
- resonant frequency propagation in amplifying medium 79—22926
- resonant medium, coherent radiation generation by relativistic charged particle 79—33857
- ring imaging, single photon counting in multiwire proportional chambers 77—54448
- separation from simultaneously produced scintillation radiation 79—36489
- simultaneously-produced scintillation and Cherenkov radiation separation method 79—93893
- solar atmosphere, gravity waves generation by HF acoustic waves, Cherenkov radiation *(Russian)* 77—17265
- spatially dispersive media, Cherenkov effect 80—105516
- spent nuclear fuel inventory confirmation technique using Cherenkov light intensity meas. 80—78419
- stimulated and Cherenkov radiations, differential eqns. with respect to coupling constants, S-matrix 79—50278
- stimulated Cherenkov radiation, relativistic electron beams in dielec. resonators, book contrib. 79—27150
- stimulated EM shock radiation, book contrib. 79—27149
- superrelativistic oscillator model *(Russian)* 78—22077
- synchrotron-Cherenkov radiation, angular distribution 78—62998
- synchrotron-Cherenkov radiation, expt. aspects 77—19146
- tachyon + bradyon interactions, superluminal and subluminal EM fields 80—12902
- tachyons, thought expts. at superluminal relative velocities 77—57186
- TGS biaxial crystal, Cherenkov radiation from 660 MeV protons 77—16416
- thin surface layer, interactions between nondegenerate electrons, effect on cyclotron resonance, mag. cond. *(Russian)* 80—15802
- threshold behaviour of Vavilov-Cherenkov radiation 78—82895
- Tokamak, enhanced plasma-frequency radiation *(Chinese)* 80—59185
- transition and Cherenkov radiation interference at dielectric media interface 79—49429
- transition Cherenkov radiation in a dielectric slab 80—86099

Cherenkov radiation continued
- transition radiation from Cherenkov charge in nonstationary medium *(Russian)* 78—50694
- transition radiation from cylinder 80—48127
- ultrarelativistic charge, X-ray prod., stack of plates with absorption and allowance for multiple scattering *(Russian)* 77—83450
- ultrarelativistic charge in absorbing plate, radiation taking into account multiple scattering *(Russian)* 77—41792
- vacuum UV Cherenkov source as radiation standard *(Russian)* 78—63164
- vacuum-metal boundary, role of Cherenkov radiation in expts. on optical transition radiation 79—99243
- Vavilov-Cherenkov effect, radiator size depend. *(Russian)* 78—5405
- Vavilov-Cherenkov effect in motion of source with velocity exceeding velocity of light in vacuum *(Russian)* 78—12582
- visual phenomena induced by relativistic $^6C^+$ ions 79—24991
- waveguide, superluminal radiator theory *(Russian)* 80—64156
- wide atmospheric shower development, cascade curves restoration *(Russian)* 80—36463
- X-ray source *(Russian)* 77—5971
- $BaSO_4$, microscopic grains, optical Cherenkov radiation 79—56880
- Fe primaries, 10^{14} eV, proposed direct meas. 77—37490
- Ge, γ-electron-hole drop formation, time delay 77—31952
- K, atomic vapour, resonant interaction with laser, Vavilov-Cherenkov effect *(Russian)* 80—106573
- KOH-O_2-N_2O-t-butane pulse radiolysis, kinetics of transient O compound form. meas. from Cherenkov emission 77—70321
- ^{32}P radiation, counting efficiency improvement, wavelength-shifting compounds investigation 80—90893
- Pb-plexipop calorimeter module viewed by wavelength shifter bars 79—81127
- ^{89}Sr assay in aqueous solutions by Cerenkov radiation 79—87895

chilling *see cooling*

chiral symmetries
- *see also SU_n theory*
- γ_5 symmetry of massless fields, neutrino theory of photons 78—411
- $\eta \rightarrow \pi^+ \pi^- \gamma$, one-loop approx. in quantum chiral theory 78—25041
- σ model, $SU_2 \times SU_2$, modified Goldberger-Treiman relation, pseudoscalar form factor 80—27421
- σ model, SU(3) linear, renormalisation in one loop approx. 80—68368
- σ models, nonlinear, soft mass renormalisation of 1/N expansion 80—47164
- σ-model supersymmetric extensions, dynamical conservation laws, symmetric space valued fields 80—95227
- σ-models, non-linear, and universality in 3-D, scaling limit, and critical behaviour, chirality 80—62824
- $\sigma SU(2) \otimes SU(2)$ model, asymptotic chiral invariance 77—71431
- Abelian and non-Abelian gauge theories, mass generation, renormalisation, chiral and unified theories 80—4871
- Abelian gauge theories, (1+1) dimens., instanton effects 79—261
- Abelian gauge theories with dynamical symmetry breaking, effective pot., scale and chiral invariance *(Russian)* 80—57503
- algebraic structure of chiral $SU(4) \times SU(4)$ representation mixing 77—34102
- asymmetry in vectorlike weak SU(3), CP violation, one loop correction 79—287
- asymptotic chiral invariance, hadron elastic scatt. 78—4800
- axial currents in nuclei, chiral symmetry 78—46008
- axial superfield and the supergravity group *(Russian)* 79—17319
- axial vector matrix elements, chiral limit, renormalisation effects 79—17190
- axial-vector currents, chiral and gauge invariant regularisation 80—4956
- Bargmann-Wigner and Weyl spin-3/2 fields, spinors, chiral operator 80—31981
- bound states from instantons 78—78087
- BPHZL renormalisation and 1/N expansion and critical behaviour 80—52383
- breaking, connection with a quark model, unification of baryon and meson constraints 77—65116
- breaking, effect of distinction between current and constituent quarks 77—61210
- breaking in gauge theories involving massless fermions 77—38088
- broken chiral $SU_4 \times SU_4$ symmetry at infinite momentum, have quark mass ratios 79—80768
- broken isospin symmetry in chiral $SU(4) \otimes SU(4)$ and D^+-D^0 mass difference 78—89691
- Cabibbo angle and weak interaction invariant props. in chiral dynamics 79—71660
- canonical pseudoscalar-meson matrices, chiral $SU(n) \times SU(n)$ symm. of strong interactions 78—29266
- canonical $SU_4 \times SU_4$ pseudoscalar meson matrix, nonlinear chiral Lagrangian 78—397
- charmed meson decay, simple symm. breaking 78—21418
- charmed mesons, nonleptonic decays of charmed mesons and chiral Lagrangians *(Russian)* 79—30732
- charmed weak current group struct., chiral $SU_4 \times SU_4$ breaking 77—65118
- chiral field model diagram techniques for low temp. phase 79—58882
- chiral field theories with sophisticated topology 79—30650
- chiral Gross-Neveu model, antiparticle as bound states of particles, factorised S-matrix framework 79—49411
- chiral invariant SU(N) Thirring model, exact S-matrix 79—21911
- chiral models in three space dimens., finite energy static solns. 77—203
- chiral nonlinear field eqns., exact solns. 78—54527
- chiral rotations and the fermion-boson equivalence in the Schwinger model 80—101919
- chiral solutons and current algebra 79—40680
- chirality, self-duality, and supergravity counterterms, quantum corrections 79—75429
- chirality invariance and 'chiral' fields, book contrib. 79—58892
- classical Euclidean 2-D nonlinear σ-models, continuity eqns. 78—54210
- configuration mixing, harmonic oscill. covariant wavefunctions 77—49913
- confining theories, chiral symmetry breaking in gauge theories 80—95244
- conformal and chiral anomalies, anomalous Ward-Takahashi identities 80—86612
- conformal invariance in elementary particle physics, review *(Russian)* 79—21964
- conformally covariant spinor field equations 79—22004
- conserved chiral charge on Schwinger model 78—49961

chiral symmetries continued
- CP^{n-1} model with quarks, confinement and chiral symmetry breaking 79—54302
- CP(N) ($N \geq 2$) chiral theory, 2-dimens., non-selfdual instantons 80—86585
- CP symmetry spontaneous breaking in nonstationary isotropic metric 79—89079
- deep inelastic $F_2^n(x)/F_2^p(x)$ near $x=1$, chirality 77—10258
- dual chiral pion model, partially conserved axial-vector current 78—58175
- dynamical generation of effective degrees of freedom, flavours 79—22026
- dynamical quark mass generation and the mean instanton density 79—54305
- dynamically broken chiral symmetry and the gauge technique for Ward identities 80—47211
- extended PCAC hypothesis, soft-meson chiral symm. breaking 78—21353
- field theory, chiral symmetry and pion-nucleus interactions 79—80961
- gauge chiral spinor superfield as scalar multiplet 79—85241
- gauge chiral U(1) symmetry and CP invariance in presence of instantons 78—78075
- gauge field as chiral field on the path and its integrability 79—97492
- gauge fields, chiral fields on loop space, colour-electric flux rings 80—42327
- gauge invariant fermion theories, path-integral measure 79—54267
- gauge invariant Lagrangian, relationship to strong interactions *(Chinese)* 79—21968
- gauge model, dynamical symm. breaking, 4-fermion interaction 77—71442
- gauge symmetry without anomalies 77—6005
- gauge theory, renormalisation of ghost and Goldstone fields and ghost symmetries 80—90987
- gauging SU(n/m) 79—67467
- generalised chiral symmetry for all massless particles 77—6042
- gluon collective excitations, nonabelian gauge theories, effective chiral Lagrangian 79—22034
- gravitation, dynamical affine symmetries and covariant perturbation theory 77—49661
- Green's exponential functions, chiral and gravitational 79—97490
- Gross-Neveu chiral model, scatt. theory, 1/N expansion 80—348
- Gross-Neveu model, chiral invariant, S-matrix direct calc. 80—68362
- Gross-Neveu model embedded in U(1) gauge theory, fractional winding 80—86569
- hadron spectroscopy, quark models and SU(5) grand unification scheme 80—4958
- hadronic charmed particle decays, quark and particle helicities, charm changing current chirality 80—37256
- hadronic structure theory, derivation of static bag and bag constant estimation 79—58932
- harmonic confinement, relativistic approx. to meson spectrum 78—29303
- heavy lepton current chirality from $e^+e^- \rightarrow e^\pm \mu^\mp$ 77—74668
- homogeneous Lorentz group, chirality, Weyl spinors 78—93810
- hydrodynamic model, nonlinear pion+pion chiral Lagrangian, $e^+ + e^-$ and p+p collisions 78—32966
- hyperon non-leptonic decay in (8,8) model of broken chiral symmetry 79—36072
- hyperon nonleptonic decay, lightlike chiral struct. of hadrons 78—17014
- index theorem, axial-vector anomalies, in Schwarzschild and Taub-NUT spaces 78—93832
- induced second-class currents from isospin and chiral-symmetry breaking 79—97538
- instantons and Kahler manifolds 79—12925
- instantons and quark-mass generation—the how of spontaneous chiral symmetry breaking 80—4963
- isoscalar neutral current axial vector couplings and nucleon anomalous moments 80—27452
- isospin SU(3) symmetry, spontaneous breaking of chiral symmetry in QCD 79—93352
- K_l form factors and (8,8) model of chiral breaking, unitarisation 77—18286
- kink solns. of extended nonlinear model and particle interpretation 78—89612
- Kobayashi-Maskawa model, Cabibbo-like parameter and quark mass relation *(Chinese)* 80—42408
- large-N chromodynamics, chiral symmetry breakdown 80—91052
- lattice fermions, Dirac fields and Thirring fields, spontaneous breaking of chiral symm. 78—24962
- lattice Schwinger model, massive QED for fermions in 1+1 dimens. 78—78121
- lepton-hadron scatt., charm changing charged current, chiral struct. anal. 77—13964
- light quark mass spectrum in QCD 79—63427
- lightlike chiral structure of hadrons, nonleptonic hyperon decays 78—74253
- linear chiral $SU(4) \times SU(4)$ model, scalar meson decays 78—4801
- linear SU(4) meson σ-model, one-loop approx., spin zero mass spectrum and leptonic-decay 80—47278
- local conservation laws of principal chiral fields (d=1) 80—4888
- local supersymmetry, geometric interpretation 77—38096
- many-dimensional solitons, gauge invariant theory of nonlinear chiral field 77—34082
- mass generation for fermion field in absence of chiral symmetry breaking 80—347
- massless Rarita Schwinger field, axial current quantisation, chiral charge of ghosts 79—2918
- meson decay, tensor, current algebra approach, symmetry-breaking Hamiltonian, chiral $SU(3) \times SU(3)$ or $SU(4) \times SU(4)$ 80—68450
- meson dipion cascade decays, current algebra techniques, pole plus remainder model, chiral symmetry breaking and QCD 80—62972
- meson mass generation in chiral flavour $U(3) \times U(3)$ symmetry by instantons 79—89121
- meson mass hierarchy, quark flavours 78—429
- meson-baryon scatt. lengths in chiral Lagrangian model, πN coupling const. 77—88001
- mesonic octet decays, chiral QFT description using one loop approx. *(Russian)* 79—63471
- method of action-angle variables and the classical dynamics of a nonlinear Lagrangian 78—77702
- MIT bag model, chiral symmetry breaking 79—63408
- multicomponent chiral and gauge models, stationary solns. 79—85213
- N=1 supergravity, chiral invariance in four dimensions 79—40441

chiral symmetries continued

- N-flavour quark model, axial-vector current anomaly, decay constants and η-η'-η_c problem 79−13045
- neutral pseudoscalar meson radiative decays, K_{l4} decay in chiral quark model *(Russian)* 80−105900
- non-Abelian gauge theories, chiral U(1) current 79−85216
- nonAbelian gauge theory, light quarks and instantons, chiral symmetry breaking 79−63332
- nonleptonic hyperon decays and lightlike chiral struct. of hadrons 79−36074
- nonlinear 3-dimens. chiral field, phase transition, 1/N renormalised expansion 79−49365
- nonlinear chiral fields *(Russian)* 78−28968
- nonlinear realisations and local invariance 80−361
- nonlinear $SU(2)\times SU(2)$ and $SU(2)\times SU(1,1)$ chiral theories, exact finite energy solns. 79−54253
- nucleon chiral substructure, parton model 77−41787
- null-plane charges and Fourier transforms, broken symm. 77−2771
- $O(N)\times O(N)$ and $SU(N)\times SU(N)$ 2-dimens. models, conservation laws and S-matrices 80−68389
- $O(N)\psi^4$ interaction, strong coupling limit, rel. to renormalizability of chiral field 78−386
- O(N) invariant $(\phi^2)_3{}^2$ model, chiral field model and universality in 3-dimens. space 80−105796
- parity violation and the masslessness of the neutrino 79−85258
- partially conserved axial vector currents, corrections, light-plane commutators, sum rules, meson decay 79−304
- PCAC, chiral anomalies and quark masses 78−8556
- perturbative QCD, chiral symmetry using dimensionless regularisation 80−27476
- physical pion low energy electro- and photoprod., Ward identity, chiral symmetry breaking struct. 80−5003
- pion condensation, chiral symmetry, review, book contrib. 80−437
- pion photoproduction, weak interaction induced parity violating assymetries 79−71758
- precocious chiral grand unification based on $SU(8)_L\times SU(8)_R$ semi-simple gauge group *(Russian)* 80−42382
- principle chiral fields, Backlund transformations and local conservation laws 80−68388
- pseudoparticle, four-dimens., quantum effects calcs., SU(2) gauge theory, chiral symm. breakdown 77−30247
- pseudoparticle fields with massless excitations, Dirac eqn. equivalence for spinor with chirality 78−4788
- pseudoscalar meson decay, symm. breaking in chiral $SU(4)\times SU(4)$ model 78−21424
- pseudoscalar mesons, sum rule, symm. breaking of chiral $SU(4)\times SU(4)$, decay const., masses 78−33000
- pseudoscalar-meson decay constants, Goldberger-Treiman relations, and chiral $SU(4)\times SU(4)$ symmetry breaking 79−293
- QCD, dynamical chiral symmetry breaking and explicit breaking due to current quark masses 79−71717
- QCD, large N limit, pseudoscalar nonet chiral dynamics and low energy spectrum 80−101988
- QCD, neutron electric dipole moment, chiral estimate, current algebra, CP violating reactions 80−27471
- QCD, spontaneous breaking of chiral $SU(2)\times SU(2)$ symmetry 79−36013
- QCD, spontaneous breaking of chiral symmetry 79−71700
- QCD, strong interaction gauge theory, SU(3) colour gauge vector mesons, confinement 78−78136
- QCD, two colour, chiral props. of fermionic determinant, symm. breaking 78−25015
- QCD phase transitions, chiral symmetry breaking, confinement, as tunnelling through singular barriers 78−82145
- QCD spectrum, infinite number of colours at fixed coupling, interacting string model 79−2993
- QCD theory for the strong interaction 80−4962
- QCD vacuum in strong external gauge fields, spontaneously, broken chiral symmetries 80−57555
- QCD vacuum struct. in chiral $U(N)\otimes U(N)$ symmetry 79−93347
- QED, Ward identity, axial vector current divergence, chiral invariant regulator field 80−57526
- quantum chiral model, local polynomial current conservation in renormalised 1/N perturbation theory 80−13232
- quantum chirality, Wilson expansion for chiral field 79−71644
- quantum contour field equations, renormalisation and string like eqn. 80−86581
- quantum field theory with chiral Lagrangian for low-energy meson physics 77−65110
- quark and lepton masses, chiral charge space, statistical analysis 80−42428
- quark confining theories, chiral symmetry breaking 79−63423
- quark effective-bare mass distinction, pion in chiral limit 78−12866
- quark mass ratio, chiral perturbation in new key 80−37208
- quark model for symmetry breaking, current and constituent quarks 79−13033
- quark-mass generation by pseudoparticles, spontaneous breaking of chiral symm. 77−74646
- quaternionic multi $S^4\approx HP(1)$ gravitational and chiral instantons 80−31656
- relativistically invariant two-dimens. models, classification method *(Russian)* 78−70291
- renormalisation consts., by superpropagator method, nonlinear chiral theory 77−65112
- S-matrix, relativistic, factorised, in two-dimens. space-time with isotopic symmetry *(Russian)* 78−8547
- scalar field theory model analog 80−52415
- scale invariance in superspace 79−17313
- Schwinger mechanism for chiral breaking dynamical fermion mass generation 77−41789
- Schwinger model, $A=0$ gauge, breaking of chiral symm. 78−62307
- Schwinger model, canonical surface formalism, axial anomaly, chiral symm. breaking 78−12816
- Schwinger model, chiral symm. breaking and vac. struct. 78−89615
- Schwinger model, equivalent boson theory, anomaly-free Ward-Takahashi identities 80−82873
- Schwinger model, new and local Lorentz-covariant soln. for arbitrary gauge 79−40668
- Schwinger model, Ward identity, fermion axial vector current divergence, chiral invariant regulator field 80−57524
- self-duality and helicity in supergravity 80−46929

chiral symmetries continued

- Skyrme gauge model, topological solitons 80−9086
- $SL_{3,c}$ symmetry, vector meson covariant redefinition 77−54045
- SO(2) linearised supergravity, multiplets 79−80488
- soliton solns. of chiral $SU(3)\times SU(3)$ models 78−4761
- spin ± 1/2 polarised neutrons, differential scatt. by chiral systems, coupled oscill. model 80−102177
- spinor models, integrability in two-dimens. space-time 80−77935
- spontaneous breakdown in Nambu model, linearisation of theory 77−54043
- spontaneous breakdown of chiral $SU_N\times SU_N$ 79−9299
- spontaneous breaking, anal. of cold matter at super-nuclear densities including pion condensates 78−17128
- spontaneous breaking, using vacuum stability condition 79−35986
- spontaneous symmetry breaking in chiral quantum field theory, covariant formulation 78−21347
- spontaneously broken chiral SU_2 symm., equivalence to current algebra in field theoretic model 77−82688
- spontaneously broken chiral $SU(3)\otimes SU(3)$ symmetry, quark mass ratios, Goldstone pseudoscalar meson pairs 79−80770
- spontaneously broken chiral $U(1)_4$, weak-interaction singlet and strong CP invariance 79−80781
- spontaneously broken gauge theories with heavy Higgs bosons 80−1320o
- string representation of gauge fields, chiral field topological props. 80−52410
- string representations and hidden symmetries for gauge fields 79−49378
- strong interaction model with spontaneous symm. breaking, multiple particle prod. *(Russian)* 77−38120
- $SU_2\times SU_2$ mixing and decay widths of ρ and A_1 77−30369
- SU_2 nonlocal conserved currents for two-dimensional chiral theories 80−52413
- $SU_4\times SU_4$ breaking in nonlinear Lagrangian, pseudoscalar meson mass 77−57513
- $SU_4\times SU_4$ chiral breaking and Cabibbo angle 77−74641
- $SU_4\times SU_4$ chiral symmetry for pseudoscalar mesons 77−67583
- SU_7 grand unification model, two $(V-A)$ and one $(V+A)$ generations of quarks and leptons 80−57538
- $SU_L(2)\times SU_R(2)\times U(1)\times[SU(3)\times SU(3)]_c$ gauge model, chiral colour symmetry breaking 80−47234
- $SU_n\times SU_n$ representation mixing, group theoretic structure 77−82687
- $SU(2)_L\times SU(2)_R\times U(1)$, CP invariance, global chiral U(1) symmetry, axion-quark coupling 79−22009
- $SU(2)_L\times U(1)$, nonlinear realisation of Weinberg-Salem model for chiral $SU(4)\times SU(4)$ meson theory *(Russian)* 79−30693
- $SU(2)_L\times U(1)\times U(1)_R$ model, chiral symmetry and weak neutral currents 80−101980
- $SU(2)\times SU(1)\times SU(3)$ unifying mass scales without intermediate schiral colour symmetry 80−22555
- $SU(2)\times SU(2)$ chiral symmetric Lagrangian description of low energy πN and NN scatt. 79−26251
- $SU(2)\times SU(2)$ nonlinear theories, localised solns. 77−26451
- $SU(2)\times SU(2)$ pion and nucleon field theory, covariant perturbative expansion 77−5983
- $SU(2)\times U(1)$ gauge model, chiral $SU(2)\times SU(2)$ symmetry and electron mass 80−57542
- SU(2) supergroup for Yang-Mills fields, Baker-Campbell-Hausdorff formula 79−49414
- SU(2) supergroups, Yang-Mills, Lie groups, chiral coeffs., Baker-Campbell-Haussdorff formula 80−68355
- $SU(3)\times SU(3)$, ρ-meson as dormant Goldstone boson 80−368
- $SU(3)\times SU(3)$, combined models of symmetry breaking *(Russian)* 77−6051
- $SU(3)\times SU(3)$ chiral algebra, crossing matrix elements, Clebsch Gordan coeffs. 78−32998
- $SU(3)\times SU(3)$ chiral renormalisable gauge model, nonleptonic decays 78−24938
- $SU(3)\times SU(3)$ chiral symmetry breaking, BBS coupling constants, sum rules 79−35959
- $SU(3)\times SU(3)$ chiral symmetry breaking, Dashen mass formula, baryon mass differences, $\eta\rightarrow3\pi$ 79−289
- $SU(3)\times SU(3)$ dynamics, broken nonlinear chiral, and $\eta\rightarrow3\pi$ decay *(Russian)* 77−65117
- SU(3) breaking for pseudoscalar meson nonet 77−6046
- SU(3) colour gauge theory, effective scale depend. quark masses in chiral limit 77−18222
- $SU(4)\times SU(4)$ breaking scheme, vector mesons radiative decays 79−22099
- $SU(4)\times SU(4)$ broken chiral symm. 78−74176
- $SU(4)\times SU(4)$ broken chiral symmetry, charmed hadron masses and decay consts. 79−40686
- $SU(4)\times SU(4)$ broken chiral symmetry, decay constants, smoothness, and spin-zero charm particles 79−58900
- $SU(4)\times SU(4)$ broken symm. in quartet model, D- and F-meson masses and decay consts. 78−66087
- $SU(4)\times SU(4)$ chiral symmetry breaking, axial vector current divergences, kaon PCAC 79−45032
- $SU(4)\times SU(4)$ symmetry, broken chiral, mass spectra of D, F and η mesons 79−93312
- $SU(4)\times SU(4)$ symmetry breaking, Cabibbo angle, nonlinear hadronic Lagrangian, PCAC *(Russian)* 80−42360
- $SU(4)\times SU(4)$ symmetry breaking, quantitative meas. 79−93311
- $SU(4)\otimes SU(4)$, counting rules and determ. of quark masses 79−63437
- $SU(4)\otimes SU(4)$ broken chiral model, based on $SU(4)\supset SU(2)\otimes SU(2)$, Glashow-Weinberg model extension 78−12836
- $SU(4)\otimes SU(4)$ symmetry breaking parameter, meson mass 78−12838
- SU(4)xSU(4) symm., pseudoscalar mesons as Goldstone bosons 77−30278
- $SU(5)\times SU(5)$ chiral symm. breaking, Cabibbo angle, meson mass spectrum 77−74614
- SU(5) x SU(5) broken chiral symmetry, symmetry breaking parameters, limits 79−45026
- $SU(n+1)$ invariant chiral theory, duality eqns. soln. 79−9351
- $SU(N>5)$ chiral grand unification 80−91028
- $SU(N)\times SU(N)$ chiral symmetry, spontaneous breaking, instanton role 80−47219
- $SU(N)\times SU(N)$ symmetry breaking with extremum constraints 80−68385
- SU(N) chiral Gross-Neveu spectrum derivation 80−47176
- SU(N) Thirring model, S-matrix bound state poles fixing 80−360
- SU(N) Thirring model and 1/N expansion, chiral symmetry breaking 79−12977

chiral symmetries continued
superconformal unified field theory 78−12848
supergravity, auxiliary fields 79−17315
supergravity, chirally extended, Maxwell-Einstein, auxiliary field struct. 78−78126
supergravity, extended theories, algebraic props. 77−49875
supergravity, Hamiltonian formulation 78−24722
supergravity, superspace formulation, component formalism transform props. 79−12688
supergravity, symmetry breaking by instantons 79−21625
superspace, effective potential calc. 78−16944
superspace, explicit form for chiral multiplet tensor calculus 79−9302
superspace geometry and $N=1$ non-minimal supergravity 80−57155
supersymmetric chiral field, $1/N$ perturbation theory and quantum conservation laws 80−68373
supersymmetric chiral models, instanton type solns. *(Russian)* 79−58901
supersymmetric nonlinear σ model, S-matrix determ. 78−66052
supersymmetric nonlinear σ model, spontaneous breakdown of chiral symmetry 78−54549
supersymmetrical generalisation of classical chiral models in two-dimens. time-space *(Russian)* 79−12980
supersymmetry, OSp(1,4), superfield formulation in anti-de Sitter space 80−57508
symmetry breaking and extended PCAC 77−45986
tachyons, monopoles and related topics, book 79−44718
Thirring massive SU(N) model, factorisation 79−12951
Thirring model, chiral, CP^{n-1} and SU_n, exact S-matrix 80−90985
topological currents for chiral groups in three space dimens. 77−71451
transformation laws for chiral multiplet 77−71454
transverse pure gauge fields and nonlinear chiral solitons, Coulomb condition 78−78068
tumbling gauge theories with chiral fermion fields, symmetry breaking 80−99042
two-body equal-time wave eqn., quark-antiquark system 78−32992
two-dimensional σ-model semiclassical anal. of bound states 77−6028
two-dimensional chiral fields, hidden symm. 78−29243
two-dimensional classical field theory, nontrivial interaction between solitons *(Russian)* 78−32698
two-dimensional model, pseudoparticles and massless fermions 78−24974
$U_3 \times U_3$ symmetry spontaneous breaking 79−35957
$U_L(1) \times U_R(1) \times R_R$ group, mass ratio and symmetries of electron and muon, model 79−58917
U(1) chiral symmetry breaking from SU(1) gauge theory 80−86617
U(1) chirality invariance selection rules 78−8550
U(1) Goldstone boson, anal. of BRS invariance in nonAbelian gauge theories 79−80798
U(1) problem and zero-mass quarks 78−82124
U(1) problem in generalised θ-vacua, Goldstone boson and QCD 80−52399
unified field theory, axion, avoidance without massless quarks 79−63403
unified gauge model based on nonlinear chiral hadron Lagrangian 80−42378
up quark mass and chiral symmetry at infinite momentum 79−40685
weak quark and lepton chiral symmetries, dynamical breaking gauge interaction 80−47215
Weinberg sum rules, derivation of meson spectrum, duality unification with chiral symm. 78−29272
Wilson's lattice, local chiral symmetry for gauge theories 80−105774
A_1 and $\rho^1(1250)$ resonances, chiral symmetry scheme fit 79−284
A_1 meson in quark model and chiral symm. 78−12834
D^+-D^0 mass differences, chiral $SU(4) \times SU(4)$ model, broken isospin symm. 77−87917
$e^+e^- \to L^-L^+ \to$ pions, test for chirality of heavy-lepton current 77−18308
$\eta \to 3\pi^\circ$, chiral $SU(4) \times SU(4)$ breaking and tadpole term 80−22532
$\eta \to \pi^0 \gamma\gamma$ decay width and processes in chiral QFT *(Russian)* 80−32099
$\eta \to \pi^+ \pi^- \gamma$, quantum chiral theory, decay width determ. *(Russian)* 78−41544
η' assignment in SU(4) spectral function sum rules 77−38143
GpN and πK scattering, chiral dynamics and asymptotical restrictions, sum rules *(Russian)* 78−17047
$K \to \pi e(\mu)\nu$, form factors, SU(3) σ-model one loop calc., chiral symmetry breaking 80−52506
K_L, weak radiative decays in chiral theory using virtual π^0 and η pole diagrams *(Russian)* 78−78172
K_{l3} scalar form factor, chiral symmetry breaking model 77−71506
$K_{l4} \to \pi\pi\gamma$, form factors in chiral quantum field theory *(Russian)* 79−67550
KN σ-term, uncertainties in determ., K-matrix formalism 80−27522
NN interaction, chiral symmetry, book contrib. 79−97669
NN interactions and chiral symm., dispersion relation anal. 78−66048
NN scatt., nonlinear chiral dynamics, one-loop approx. *(Ukrainian)* 78−460
νN inelastic scattering, possible soln. with weak neutral currents to ρ-π puzzle 79−17714
$\nu_\mu N \to {}^- C_0{}^+$, $C_0{}^+ \to \Lambda^0 e^+ \nu_e$ Λ polarisation, chiral props. of charmed current 77−61272
$\nu_\mu N \to \mu^- C_0{}^+$, $C_0{}^+ \to \Lambda^0 e^+ \nu_e$, test of charmed current struct. 77−61271
$\phi \to \pi\gamma$, $SU(3) \times SU(3)$ algebra, appl. to ground state mesons, coupling constraints and decay rate 78−58183
(π,π), Weinberg chiral Lagrangian nonlinear terms, nuclear binding, optical pot. 80−78329
π condensed phase, σ-model, alternating-layer-spin struct. 80−83057
π decay constant, EM form factor, quark EM self-energy in QCD 80−37242
$\pi \to e\nu_e\gamma$, isospin-breaking, chiral limit, conserved-vector-current violation, σ model 80−62988
$\pi \to e\nu\gamma$ and $SU(3) \times SU(3)$ σ-model 80−78054
π field, nonlinear chiral models, many dimensional solitons 78−4792
π polarisabilities in chiral Lagrangian model, linear and nonlinear σ models, Compton scatt. 78−21323
π struct., gauge model, spontaneously broken chiral symmetry 78−45841
π^0 condensation in σ-model, chiral symmetry 79−80895
πK phase shifts, perturbation expansion about $SU(3) \times SU(3)$ symm. limit 79−58975
πK scattering amplitude, analytic continuation, chiral symmetry breaking 80−63027
πN s- and p-wave scatt., nonlinear chiral dynamics using superpropagators *(Russian)* 77−38198
πN scattering, low-energy, nonlinear chiral dynamics description *(Russian)* 78−17043
πN scattering, sigma term related to scatt. length, Altarelli-Cabibbo-Maiani relation derivation 80−57632
πN σ term in hybrid chiral bag model, PCAC and $SU(3) \times SU(3)$ symmetry violation 80−78096
$\pi N\sigma$ commutator, discussion using dynamical theory of πN amplitude 79−22134
$\pi^- p \to \pi^- \pi^+ n$, 203-357 MeV, integrated cross section, chiral symmetry breaking parameter 80−32125
$\pi^- p \to \pi^- \pi^+ n$, below 1400 MeV, PS11 contrib. threshold K-matrix, chiral symmetry breaking 80−32126
$\pi\pi$, ρ-meson contrib. in broken chiral symmetry model, phase shifts and lengths *(Russian)* 80−86756
$\pi\pi$ phase shifts, nonlinear σ model Pade calcs. 78−8695
$\pi\pi$ scattering, description in chiral symmetry *(Russian)* 79−93459
$\pi\Sigma$ scattering amplitude, sum rules for $\pi\Sigma$ reson. parameters *(Russian)* 79−22137
σ model, pion condensation, use of chiral symmetries, reply to comments 79−297
σ model, pion condensation, use of chiral symmetries 79−296
u-quark masslessness, consequences for SU(2) and SU(3) 79−22022
${}^2H(\pi,\pi)$, scatt. length, exchange current contrib. 80−78328

chlorine
see also nuclei with ......
absorption in acetic acid, kinetics in presence of homogeneous catalysts 80−11876
adsorbed, on Ag(111), props., struct., AES study 78−72024
adsorbed on metal-sapphire interface, effect on shear strength 80−49485
adsorption, on Ag low index surfaces, energetics and structures 79−82440
adsorption, on Al(Fe), thermal accommodation coeffs., translational (internal) gas-solid energy exchange 78−92506
adsorption and reaction with InP surface, electron spectroscopic obs. 78−56036
adsorption effects on Cu electrodeposition 79−20001
adsorption in Al-Al_2O_3-Au device rel. to press. depend. of current-voltage characts. 80−65704
adsorption on Ag, AgCl epitaxial layer form., RHEED 78−14642
adsorption on Ag low index surfaces, energetics and structures 79−87000
adsorption on clean annealed Mg surface, exoelectron emission 78−39671
adsorption on Fe (100), AES, LEED, work function, and thermal desorption meas. 79−82465
adsorption on flyash from coal combustion, cloud nuclei form. 77−21887
adsorption on Ni (111) surface 77−85069
adsorption on Si (111), electronic energy states, cluster-type calcs. 79−47149
adsorption on Si vacuum-crushed surface, EPR meas. 79−46957
adsorption on W (100), LEED and AES study 79−90878
adsorption-desorption props. and surface struct. chem. on Cu (111) and Ag (111) 77−89648
atom, $3p^5$, ${}^2P_{1/2} \leftarrow {}^2P_{3/2}$ fine struct., tunable IR diode laser detection 80−23348
atom, 3s subshell photoelectron ang. distrib. 77−65445
atom, and ions, two and three-electron Auger transition, with vacancies in 2p-shell 79−63972
atom, beam-foil populations, charge state distribs., independent electron model 77−19035
atom, chem. environent effect on Kα satellites intensity, heavy-ion collision 77−54527
atom, chem. generation for HCl laser, 3.8 μm, 10.6 μm CW laser emission 79−947
atom, electron affinity, variation-perturbation approach 77−54513
atom, foil excitation, K-vacancy bearing metastable states yield, 30-50 MeV 77−54600
atom, form. from HCl dissoc. excitation in afterglow, light emission 78−90115
atom, He (I) PES 78−37609
atom, initial state wave functions for photoionisation cross-sections, multi-configurational HF calcs. 80−47908
atom, K-fluorescence yield determ. using MWPC 79−18140
atom, K-shell ionisation by ultrarelativistic electrons, density effect 80−99576
atom, kinetic spectroscopy in far vacuum UV, oscillator strengths of transitions 78−13457
atom, L X-ray emitting levels, lifetimes 78−66493
atom, lifetimes of non-penetrating states, including core polarisation effects 79−89638
atom, metastable states, form. from Cl_2 dissoc. excitation, time of flight spectra 78−1094
atom, MINDO parameters 78−86786
atom, multiply-ionised, radiative electron capture on impact with Ca and Ni foils 77−6916
atom, oscillator strengths for Cl $4s$-$3p^5$ transitions and rate constants for specific product channels from $Ar({}^3P_{2,0})+Cl$ 77−46537
atom, photoelectron spectra, photoionisation cross-sections 78−90131
atom, photoionis. cross section of open 3p subshell 79−68213
atom, photoionis. cross sections, RPA with exchange method generalisation 79−10077
atom, photoionisation cross section, RPA with exchange 77−30838
atom, photoionisation cross section and reson. theory, many body perturbation theory, 3p and 3s subshells 80−69114
atom, photoionisation cross sections and ang. distribs., outer p subshell 80−9572
atom, Raffenetti-type atomic basis set calcs. 79−97974
atom, recomb., in presence of inert gas atoms and mols. 80−45496
atom, s-shell spin polarisation calcs. 77−75318
atom, SCF electron-gas local-spin-density model including correlation 80−9488
atom, static quadrupole polarisability and shielding factor, Hartree-Fock calc. 78−41950
atom, stripping in gaseous targets, equilib. charge state distrib., statistical anal. 80−5610
atom, X-ray and Auger transition probabilities to 2p level 78−17640
atom + highly charged ion, inner-shell charge transfer calcs. 77−50528
atom diffusion in Ar and He gas, diffusion const. 78−71417
atomic Kα X-ray satellite spectra, gas phase meas. 78−66496

chlorine continued
atomic VUV line emission from TFR-600 Tokamak 79—98987
atomospheric particulate distrib. in Houston-Galveston area 79—12252
atoms, photorecombination, rate constants determ., identification of spectral distribution of recombinative emission intensity 80—85195
atoms, radiative recomb., behind incident shock wave front *(Russian)* 77—65525
borate laser glasses, Cl^-coordinated, Tl^+, Mn^{2+} and Nd^{3+} impurities, absorpt. and X-ray obs. 79—38575
brine, routine anal. by X-ray fluoresc. spectrometry applying matrix corrections 78—88690
chemisorbed layer on Si (111), SCF LCAO calcs. of Si band struct. 78—88010
chemisorbed on Ni(100), LEED and angle-resolved AES obs. 79—95258
chemisorbed on Si (111), angle resolved secondary emission and electron energy loss study of electronic struct. 79—61477
chemisorbed on Si (111), electronic energy struct. calcs. 79—78144
chemisorbed on Si (111), electronic states, tight-binding method appl. 80—49564
chemisorbed on Si (111) surface, surface energy bands and atomic position of Cl 78—56041
chemisorption, and coadsorpt. with O_2 on Ag (331) 78—34711
chemisorption geometry, on GaAs cleaved (110) surface 80—6659
chemisorption in surface vacancies of Si (111) 1×1 79—77910
chemisorption on Ag (001), adatom bonding effects from coverage-depend. angle-resolved photoemission 79—82436
chemisorption on Ag (100), XPS and UPS meas. 78—31293
chemisorption on Al_5, core hole induced electronic relax. 79—90874
chemisorption on GaAs, GaSb, and InSb, photoemission spectra and tight-binding calcs. 80—6629
chemisorption on Ge, threefold co-ordinated site chemisorption, cluster model calc., extended Huckel theory 78—39178
chemisorption on Pd (111) and Pt (111), LEED, AES, thermal desorption, and work function meas. 80—75444
chemisorption on Si(111), conduction-band surface resonance 78—52051
chemisorption on Si(Ge), surface photoemission, adsorption gate geometry 78—73079
chemisorption on Si (111), ang. resolved UPS and LEED meas. using Vidicon intensity processor 78—71972
chemisorption on Si (111), LCAO calcs., Auger line shapes, localized density of states 78—56202
chemisorption on Si (111) 7×7 and 1×1, UPS obs. 78—34704
chemisorption on Si (111) and Ge (111), chemisorpt. site geometry from polarised photoemission 77—15684
chemisorption on Si and Ge, cluster model calc., iterative EHT 77—32062
chemisorption on Si and Ge, photoemission polarisation effects with synchrotron radiation 78—14580
chlorination of polyethylene, rate const. determ. using NMR spectra of chain sequence *(German)* 79—100366
corrosion of Cr and Cr_2O_3 78—15601
desorption from W, field ion microscope exam. 78—35270
determination, in coal, British Standard high temp. method 80—85252
determination, in Ir catalysts, by X-ray photoelectron spectroscopy 77—9146
determination, in refractory metals, spectrosc. method *(Russian)* 79—16095
determination, in water, by neutron activation and X-ray fluoresc. analyses 78—3428
determination by high press. liq. chromatography, Cl-specific detector *(German)* 79—87920
determination in small samples of healthy and burnt skin 79—5343
diffusion, in α-Ti, AES meas. 78—51735
difluorodichloromethane+^{38}Cl, reactions due to $^{37}Cl(n,\gamma)^{38}Cl$ 77—86342
effect of graphite-$FeCl_3$ intercalation compound formation *(German)* 79—52634
elastic scattering amplitudes, for high energy electron scattering, by ionised atoms, numerical calcs. 80—49057
energy straggling of Cl ions+Ar-methane, (isobutane) 78—58785
ethylene+Cl, nuclear recoil, addition and abstraction reactions, kinetics 77—86340
EXAFS amplitudes, wave function relaxation and chemical effects 78—46365
flowing afterglow, thermal electron dissoc. attachment rate consts. 77—10773
galactic abundance from Ar/Cl and Cl/O ratios in planetary nebulae 79—5887
gas, sparking pots., ionisation and electron attachment coeffs. 78—42705
geochemistry, Cl and Br degassing by volcanism along Reykjanes Ridge and Iceland 78—36136
hybridisation, bonding orbitals effects 79—36510
ileum epithelial cells and intercellular spaces, microprobe meas. of Na, K and Cl conc. profiles, rabbit 78—35819
impurity in Li aluminosilicate glasses, ESR spectra 80—66027
incorporation in SiO_2 prepared by Si oxidation in O_2-HCl ambients 78—11378
incorporation into SiO_2 on Si oxidation in trichloroethylene-O_2 79—91827
interaction with H_2SO_4 and water, surface reactions at low temps. 79—79288
interstellar abundance towards 20 stars, Copernicus obs. 78—36646
interstellar Cl, chemistry as H ionisation source 79—40245
interstellar Cl, depletion on oxide grains 80—17635
ion+target collisions, two-electron-one-photon transitions, X-ray spectra 77—19068
ion beam, metastable, collinear laser spectroscopy, isotope shift, fluoresc. detect. 80—37771
ion beam impact on Cu foil, K-shell X-ray yield 77—10623
ion concentration in nuclear power station loop waters, potentiometric method improvements 79—85599
ion implantation in Si, control of oxidation-induced stacking faults 79—46682
ion states with two intrinsic $L_{2,3}$ vacancies, single-photon decay *(Russian)* 77—6716
ion-foil interaction, K-shell vacancies and residual excitation 77—50519
ions, multiply-charged, beam-foil obs. of allowed L-shell transitions 80—14113
ions, two vacancies in K shell, 2 electron 1 photon, and hypersatellite transition probabilities 78—46294
isotope enrichment using laser photolysis of dichlorodifluoromethane 78—58859

chlorine continued
isotope separation, laser, isotope shift and absorption spectrum obs 77—34701
isotope separation, microwave reson., triplet state photochem. technique 77—32818
isotope separation, plasma ion cyclotron reson. 77—10787
isotope separation by liquid-phase thermal diffusion 79—89502
K-shell X-ray production, by 0.4 to 2.4 MeV ^4He and ^1H ions 79—47550
laser, atomic, pulsed microwave discharges of Cl_2, CH_3Cl, CH_2Cl_2 and CCl_4 source gases 80—48233
laser oscillation on 2580 Å band system, axial electron beam excitation of He-Cl_2 79—31879
laser UV transitions of ion, performance and spectroscopy 78—22111
lattice dynamics using simple bond charge model 78—55919
liquid, dynamics, depolarised Raman and Rayleigh scatt. 79—99867
liquid, entropy, computer simulation, Widom method 79—77486
liquid, mol. dynamics of '2-Lennard-Jones centres' pair pot. liq. 79—73082
liquid, mol. motion, Raman spectrum 78—5236
liquid, mol. reorientation, Raman spectra obs. *(French)* 78—31192
liquid, thermodynamic and struct. props., pair pots. calcs. 77—58939
liquid, transient stimulated vibr. Raman scatt. 78—71144
liquid-vapour surface, computer simulation 80—54478
marine aerosols, organic and inorganic Cl gas concs. and particulate Cl size distrib. 78—32187
marine atmosphere particulate Na and Cl vertical distrib. 77—37304
methane+Cl, rate const., discharge flow-reson. fluoresc. meas. 78—7178
methane-O_2-N_2Cl_2 mixture for CO_2 gasdynamic laser 77—50649
molecular crystal, bond charge model, for lattice dynamics 78—79692
molecular liquid, mean squared torque and mean squared force, interaction energy spherical harmonic expansion 80—54093
molecular static polarisability, ab initio SCF wave functions 80—74106
molecule, absorption in ultrasoft X-ray region 78—90187
molecule, and isotopic forms, $B^3\Pi(0_u^+)$ state, laser-induced fluoresc., collisional energy transfer rates 80—53038
molecule, Ar ion laser excited, normal and reson. Raman spectra 79—26993
molecule, Ar matrix, vibronic dephasing 80—6469
molecule, B-X transition, predissoc., laser-induced fluoresc. obs. 80—43093
molecule, B-X transition, rotationally resolved excitation spectra and predissociation in excited state 79—45754
molecule, bond order and Raman intensity, delta function eqn. 77—61693
molecule, dissoc. attachment by 0-8 eV electrons 78—74776
molecule, dissoc. electron attachment, negative ion prod. rates 80—18938
molecule, dissociation, weak bias and anharmonicity effects 78—82661
molecule, effective core potentials, all-electron calcs. 78—62704
molecule, electron impact dissoc. excitation, metastable fragment form. translational spectra 78—1094
molecule, electron impact total ionis. and electron attachment cross sections 79—3589
molecule, electron-attachment rate const., room temp. and 250°C, in $N_2(Ar)$ discharges 79—45841
molecule, fluoresc. quenching by collision-induced predissoc. 77—14472
molecule, geometry optimisation, ab initio MO calcs. 77—42232
molecule, ground and ionised states, Koopman's theorem and Mo relax. in ab initio calcs. 78—1035
molecule, ground state pot. energy curve, improved ab initio effective core pot. calc. 80—32625
molecule, Hartree-Fock-Slater calcs., using pseudopot. method 77—57859
molecule, inner shell excited states, X-ray absorpt. spectra, HF calcs. 80—78536
molecule, laser-induced fluoresc., excited $B^3\Pi(0_u^+)$ states, collision-free lifetimes of ro-vibr. levels 79—94029
molecule, matrix isolated, Zeeman effect and magnetically polarised luminesc. 78—46379
molecule, model potential SCF calcs. 80—95528
molecule, one electron props. and polarisability, SCF and CI calcs. 80—58159
molecule, partially dissociated, recomb. reaction freezing in supersonic nozzle, chemiluminesc. *(Russian)* 77—52644
molecule, photochemical reaction using Ar ion laser, Cl isotope enrichment 78—74780
molecule, potential curve calcs. 77—6881
molecule, pseudopot. calcs. 80—91446
molecule, pseudopot. theory calcs. of electronic struct. 77—42230
molecule, pseudopotential calcs., dissoc. energy, bond length, force const. 77—26964
molecule, quadrupole moment determ. by refr. index anisotropy meas. method 80—78722
molecule, reactive scatt. from clean and H_2 covered W surface 80—20743
molecule, resonance Raman spectrum, Q-branches of $^{35}Cl_2$ and $^{35}Cl^{37}Cl$ 78—25542
molecule, rot. relax. classical trajectory computation, using Lennard-Jones pot. 78—62880
molecule, semi-empirical INDO calc. of electronic struct. 80—32611
molecule, vac. UV absorpt. cross section 80—91574
molecule in Ar matrix, MCD, emission spectrum at 13600 cm^{-1}, Zeeman anisotropy 78—82057
monitoring of leaks using TAGA 3000 mobile test unit 80—72114
monolayer on Ag, enhanced Raman intensity 79—95766
multiple reactions, Cl isotope effects, mass spectrometric monitoring 79—39135
muonic atom, prod. by muon capture in Ar atom *(Russian)* 79—45869
muonium+Cl_2, gas-phase reaction, muonium spin rot. rate meas. 77—58207
neutron activation anal., 14 MeV neutron cross sections 79—52838
neutron activation anal. of short lived nucl. states in aerosols of Otto carburettor engine *(German)* 77—12860
neutron kerma, effect of isotopic abundance 78—29536
nuclear bombardment target prod. 80—9441
in oceans, Cl and Br origin 78—65342
opercular epithelium of killifish, isolated, membrane rich in Cl^- cells, active Cl^- transport 77—36882
Orion Nebula, Cl and Fe abundances from forbidden Cl II and Fe II near IR mapping 80—62217
overlayer on Cu (100), adatom bonding effects, photoemission study 80—104044

chlorine continued
photoactivation analysis 79−61931
planetary nebulae, abundances of He, Ne, Ar, N, and Cl 80−109532
propene$+{}^{38}\mathrm{Cl}\rightarrow\mathrm{CH_3CHCH_2{}^{38}Cl(CH_3CH^{38}ClCH_2)}$, thermal, terminal and central addition 77−86341
reaction with TiO_2, with C 79−83450
reactivity to ZnO $(000\bar{1})$ and $(10\bar{1}0)$ surfaces 79−61904
saline cooling waters, free and total residual Cl determ. via modified amperometric membrane probes 80−82112
seawater, Cl disappearance meas. 79−88372
simultaneous interactions with O_2 on Ta under low press. and high temp. 80−71938
solid, acoustic wave velocity calc. from phonon curves *(French)* 77−1180
solid, electron density distrib. using X-ray diffr. meas. 79−42006
solid, space group, anisotropic atom-atom forces 79−73127
steel, mild type ASTM A36, Cl embrittling effect on fatigue crack growth rate 79−74254
steels, austenitic stainless, Cl and H_2S effect on oxidation resist. 80−45418
stratosphere, acidic Cl vapour, midlatit. seasonal meas. 78−32142
stratosphere, Cl-ClO-Cl cycle, possible roles of ClO*, $ClNO_3$ and HOCl 77−17185
stratosphere, O_3 diurnal var. and scattering rel. to Cl concs. 78−7710
stratosphere atomic Cl, in situ obs., rel. to O_3 depletion 78−36241
stratosphere O_3-CO_2 coupling, photochemical radiative column model with Cl chemistry 80−85724
trifluorochloromethane$+{}^{38}\mathrm{Cl}$, reactions due to ${}^{37}\mathrm{Cl}(n,\gamma){}^{38}\mathrm{Cl}$ 77−86342
upper atmosphere, O_3 and Cl densities from OAO 3 stellar occultation meas. 77−9580
vapour pressure, 206 to 270K and 334 to 417K 80−19931
vapour-liquid interface, mol. orientation, theoretical and computer simulation 79−73377
X-ray emission spectra, detect. from Alcator-A Tokamak 80−92389
XPS in transition metal coordinate compounds, inner shell binding energies 78−21973
AgBr:Cl, exciton-phonon interaction, reson. Raman scatt. vs photolum. 80−29798
AgBr:Cl, impurity diffusion, vacancy pair and single vacancy contribs. 79−77830
Ar:Xe:Cl_2, photochem. XeCl prod., ESR 77−18947
Ar-Hg-Cl_2, elec. discharge, electron inelastic collision props. 80−79617
Ar-$N_2(Cl_2)(F_2)(H_2O)$ laser, energy pathways by proton excitation 78−5459
$Ar(4s\,{}^3P_{2,0})+Cl$, specific channel rate construction 77−46627
Au/Ti thin films, effect of Cl_2 on elec. resistance, Ti atom migration and preferred orientation 80−34530
B_2O_3-Li_2O-LiCl glass, X-irradiated, EPR of $Cl_2{}^-$ centres *(French)* 79−47333
$Ba+Cl_2$, 10^{-5} torr, dynamics, chemiluminesc. ang. depend., radiative lifetime 77−40539
$BaI_2+Cl_2(HCl)$(1,1-dichloroethane)(chloroethene), crossed beam metathesis, total cross sections 77−21354
$Br^*+I_2(Br_2)(Cl_2)(IBr)(ICl)(BrCl)$, deactivation rates of $Br^*({}^2P_{1/2})$, collision complex form model 78−42179
CaO:Cl, phosphon, luminesc., electron-hole recombination processes 79−65919
CaO:Cl, X-ray and UV luminesc., electron-hole recombination processes *(Russian)* 78−76528
$Ca^*+Cl_2(HCl)$, luminesc. reactive collisions 77−16816
CdS:Cl, $Cu^+(Cu^{2+})$, photoconductive sensitivity 77−43648
CdS:Cl, extrinsic, exciton absorption 78−72569
CdS:Cl, heavily doped, fluoresc. spectrum upper threshold calculated 78−52568
CdS:Cl, photoluminesc., conc. quenching mechanism 80−97336
CdS:Cl, resonant Raman scatt. exam. 78−39546
CdS:Cl, shallow donors electronic Raman scatt., reson. enhancement 80−45068
CdS:Cl, thin layer, electron pulse induced cond. relax. 80−2501
CdS:Cl thin films, surface and bulk photoconc. 80−88653
CdS:Cu, Cl films, photocond. growth and decay time 80−60041
CdS:Cu,Cl, film, photocond., applied voltage freq. effect on props. 80−39635
CdS:Cu,Cl film, photocond., use in laser-addressed electrolum. display screen 77−51777
CdSe:Cl, photoluminesc. props. near fund. absorpt. edge, impurity conc. effects 79−52003
CdSe:Cu,Cl film, induced impurity photocond., 0.6 to 1.2 eV 79−24012
CdTe:Cl, acceptor states study by donar acceptor pair excitation luminesc. 80−100683
CdTe:Cl, anomalous props., molecular centre with charge-state dependent config. 77−89728
CdTe:Cl, capacitance meas. and trapping, mol. centre model *(French)* 77−39872
CdTe:Cl, cryst., high resist., SCL currents, DC meas. 77−66170
p-CdTe:Cl, deep level characterisation, gamma-ray detector parameters 77−39802
CdTe:Cl, description of anomalous centres by non-purely electronic model 78−30886
CdTe:Cl, electroabsorption by impurities and defects, dichroism 77−40270
CdTe:Cl, electron irrad., defects 80−25460
CdTe:Cl, force variation due to charged defects 80−92634
CdTe:Cl, grown by travelling heater method, carrier homogeneity investig. 77−39848
CdTe:Cl, grown by travelling heater method, EPR defect charact. 77−40125
CdTe:Cl, heavily doped, elec. and photoluminesc. investig. of defect interactions 77−39603
p-CdTe:Cl, influence of gamma-irradiation on elec. props. 77−62951
CdTe:Cl, influence of lattice defects on electrical behaviour 78−2497
CdTe:Cl, interaction of impurities and lattice defects, changes in elec. props. and photoluminesc. 77−4685
CdTe:Cl, LPE from $CdCl_2$ soln., elec. props., defects 80−39689
CdTe:Cl, localisation of electrons, temp. depend. of cond. and Hall effect 78−14732
p-CdTe:Cl, mech. of electron recomb. 79−11176
CdTe:Cl, photoelectronic investig. of trap depths, TSC and SCL cond. 77−39893
CdTe:Cl, semi-insulating, Hall effect and cond. meas., carrier mobility 77−39849

chlorine continued
CdTe:Cl, semi-insulating, impurity photocond. spectra, local state distrib. in band gap 80−107865
CdTe:Cl, semiinsulating, Hall effect and elec. cond., impurity levels 77−55532
p-CdTe-Cl, compensated, hopping cond. 77−76818
CdTe-Cl compensated, Schottky diode, small signal capacitance 79−7899
Ce-Cl cycle for thermochemical H production 80−35783
Cl (IX-XV) allowed intra L-shell transitions, oscill. strengths and radiative lifetimes meas. 79−13676
Cl I, fine struct. splittings in some highly ionized $n=3$ doublets 80−43200
Cl I, isoelectronic sequence, multiconfiguration HF calc. of sp^6-s^2p^4d interaction 78−9072
Cl I, photoionisation cross section, calc. by many-body perturbation theory 78−62771
Cl I, wall-stabilised arc, absolute transition probabilities, 5300-6850 Å 78−9105
Cl I isoelectronic sequence, forbidden transition probabilities for ground terms 77−2376
Cl II in CuCl and $FeCl_2$ vapours, pulse generation at 5218 Å, 5221 Å 78−58990
Cl III, electron impact width of plasma lines, approximative semiclassical formula 80−43972
Cl III, Stark broadening of isolated lines by plasma 78−9116
Cl III lines, Stark broadening 77−27024
Cl VII, in laser heated plasma, emission intensity anomalies, 58-78 Å *(Russian)* 77−46521
Cl VII, transitions in laser heated plasma, intensity anomalies obs. 58 to 78 Å 78−1214
Cl VIII, Ne I like reson. and Na I-like satellite lines, relativistic HF calc., beam-foil spectra 78−94210
Cl XIII-XV, $\Delta n=0$ transitions, lifetime meas. beam-foil spectra 78−78798
Cl XIV, beam-foil obs. of oscillator strengths for E1 transitions 80−14112
Cl XIV, Rydberg electron-ionic core nonadiabatic long-range forces 80−23328
Cl, XVI, $1s2s\,{}^3S$-$1s2p\,{}^3P$ transitions, Lamb shift, VUV beam foil spectra obs. 80−52919
Cl XVI, intercomb. line obs., in laser-produced plasma 78−9106
Cl^- and Na^+, interdependence of transport in dog tracheal epithelium 80−61519
Cl^-, atomic core states, antishielding effects calcs. 80−83299
Cl^-, contracted Gaussian basis sets for mol. calcs. 80−83264
Cl^-, coupled transport in a liposome suspension 79−53069
Cl^- diffusion in marine sediments, hydrostatic press. effect, in situ expt. 78−44878
Cl^-, electron photodetachment cross-section determ., from CsCl dissoc. 77−3330
Cl^-, far UV spectra in solns. 78−94208
Cl^-, fluoresc. quenching of organic excited singlet states, rate meas., mechanism 77−38685
Cl^-, formation and destruction in ionospheric D-region 78−12049
Cl^-, formation by HCl dissociative electron attachment, differential cross section, Feshbach resons. 80−83508
Cl^- free-bound continuum radiation threshold broadening obs. in plasma 78−71579
Cl^-, free-ion polarisability, empirical values 77−20792
Cl^-, in aq. solns., limiting equiv. cond. rel. to water viscosity 77−1252
Cl^-, in Greenland snow and ice, natural and anthropogenic origins 79−70815
Cl^-, in He, ion reduced zero field mobilities and free diffusion coeffs. 77−47139
Cl^- interaction with Na^{2+} transport in canine tracheal mucosa 79−88060
Cl^- ion concentrations in river, spring waters in Okinawa Honto, origin *(Japanese)* 79−39324
Cl^- ion influence on Si anodic oxidation and Si-SiO_2 interface 79−15842
Cl^-, ion mobility in Ar, flow drift tube meas. 77−72405
Cl^- ion selective electrodes, appl. to biological materials 77−90974
Cl^- ions, labelled, adsorbed on Ag, surface diffusion 80−39413
Cl^- ions in nuclear reactor water coolant, determination by flow-type porous metallic Ag electrode 80−89577
Cl^-, pair polarisability, ab initio SCF MO energies 78−70741
Cl^-, plasma, broadening of free-bound radiation thresholds 80−53940
Cl^- radiative detachment threshold effect of plasma microfield 78−71580
Cl^-, role of Ca^{2+}-dependent regulator protein in intestinal secretion 79−66454
Cl^- soln. inhibition of o-Ps formation 80−1089
Cl^-, trace determ. by rate controlled coulometric titration 78−11576
Cl^-, X-ray microanal. of cultured skeletal muscle cells, calibration 79−100798
Cl^+, laser levels, radiative lifetimes meas. 78−42330
Cl^+, reson. line regularities in plasma Stark widths and shifts 80−43881
Cl^{16+}, Lamb shift meas. using beam-foil excitation, QED test 80−9551
${}^{36}Cl$, beta decay, K-shell electron ejection 77−18888
Cl^{5+}, static dipole quadrupole polarisabilities and shielding factors calc. using HF scheme 80−99450
Cl^{6+}, Cl^{7+}, excited state lifetimes, beam-foil meas. 77−10750
Cl-HBr chemical laser, pulsed, computer simulation, effects of rot. nonequilib. 77−40547
Cl^--$(H_2O)_n$, complex struct., coord. numbers 79−7049
Cl^--ionic crystal-metal system, charge transfer mechanism 78−11527
Cl^--$NO_3{}^-$ soln., inhibition of o-Ps formation 80−1089
Cl^--Ne(Ar)(Kr)(Xe), longitudinal diffusion coeff., generalised Einstein relation 79−86552
${}^{37}Cl$-${}^{35}Cl$ mass differences, for wide doublets, determ. with Manitoba II mass spectrometer 77−42432
Cl+Al, molecular K X-ray transitions, mol. radiative electron capture effect 78−58802
$Cl+Br_2\rightarrow BrCl+Br$, crossed mol. beam, translational energy depend. 78−25693
$Cl+C_2H_2$, reaction kinetics, stratospheric implication 78−31618
Cl+Cl collisions, impact parameter dependence of emitted noncharacteristic rad. 77−14563
$Cl+D_2\rightarrow DCl+Cl$, LEPS pot. energy surface, rate consts., isotope effect, quasiclassical trajectory calc. 78−56887

chlorine continued
Cl+DCl, vibr. relax. times, laser induced fluoresc. 77−27159
Cl+DI→DCl+I, thermal rate const., 220-400K, H/D isotope effect 79−47906
Cl+fluoromethane, photochlorination electron and oscill. energy 80−81320
Cl+formaldehyde, rate const. 78−85136
Cl+formaldehyde, rate const., 200-500K 79−39133
Cl+formaldehyde→HCl+HCO, stratospheric O$_3$ decreased sensitivity to Cl perturbations 79−12190
Cl+H$_2$, absolute reaction rate consts., 200-500K 78−15655
Cl+H$_2$, atom transfer reactions, reaction rate computing, trajectory calcs. 79−74371
Cl+H$_2$, atom transfer reaction in gas phase, reaction rate computing, tunnelling corrections 79−79237
Cl+H$_2$, reaction rate constants, Monte Carlo quasi-classical trajectory calcs. 79−74366
Cl+H$_2$O$_2$, absolute rate const., 265-400K 78−15652
Cl+H$_2$S→HCl+HS, laser-initiated chain reactions, rate consts., product energy distrib. 78−85144
Cl+H$_2$(HCl), relax. and chem. reaction, time resolved IR fluoresc. and mass spectrometry obs. 80−69177
Cl+H$_2$→HCl+H, quasiclassical trajectory calcs. 77−60040
Cl+HBr, rotated Morse curve-spline pot. function 78−80729
Cl+HCl, vibr. relaxation and reaction rates determ. 80−108698
Cl+HD, reactions, branching ratio, energy partitioning and ang. distrib. 79−70312
Cl+HI, chem. laser, energy distrib., spectrosc. obs. 78−71096
Cl+HI(HBr)→HCl+I(Br) 78−23929
Cl+HI→HCl+I, Monte Carlo quasiclassical trajectory anal., product distribs. 77−16783
Cl+HNO(H$_2$O$_2$)(HO$_2$), rate consts., stratospheric appl. 78−85125
Cl+HO$_2$ react. rate const. determ. at 298K *(French)* 78−64817
Cl+H(D)I, exothermic triatomic exchange reactions, prod. energy distrib., statistical dynamic model 78−92455
Cl+He(C)(O)(Ne), K-shell ionising collisions, average L-shell ionisation probability, K$_\alpha$ spectra 79−72408
Cl+inert gas, $3p^5(^2P_{1/2})$ state quenching 78−42192
Cl+K$_2$→KCl+K*, chemiluminesc., electronic emission intensity 78−35689
Cl+M+NO$_2$, reaction rate constants 79−100350
Cl+methane, reaction rate const., stratospheric modelling appl. 79−20345
Cl+methane-methane-d$_2$, free radical chain reaction, D isotope photochem. enrichment 79−36790
Cl+methane→HCl+CH$_3$, absolute reaction rate, flash photolysis-reson. fluoresc. obs. 77−56222
Cl+methanol (dimethyl ether), absolute rate consts., 200-500K, stratospheric chem. appl. 79−66271
Cl+methyl bromide→HCl+CH$_2$Br, IR laser isotope separation appls. 79−64113
Cl+NH$_3$, reaction rate consts., flash photolysis-reson. fluoresc. obs. 78−3327
Cl+NO$_2$, ClONO prod., FT IR obs. 79−8427
Cl+NO$_2$, matrix reactions, IR absorpt. obs. 78−15667
Cl+NOCl, primary and secondary photochemistry, vibrationally excited NO, IR fluoresc. obs. 80−48030
Cl+NO+N$_2$→NOCl+N$_2$, rate const. temp. depend. 78−76828
Cl+Na(K)(Cs), quasiclassical charge transfer cross section, rel. vel. depend. 77−19073
Cl+O$_3$(H$_2$O$_2$)(methane), reaction kinetics, temp. depend., reson. fluoresc. obs. 77−4903
Cl+O$_3$→ClO+O$_2$, rate consts. meas. 77−60059
Cl+OH*→HCl*+O, reaction dynamics, vibr. excited reagent and product 77−81392
Cl+SO$_2$, rate const. rel. to stratospheric Cl chemistry and Venus atm. 79−84353
Cl+T$_2$, atom transfer reaction in gas phase, reaction rate computing, tunnelling corrections 79−79237
Cl+vinyl bromide-d$_3$ reaction, IR chemiluminesc. 80−102506
Cl+Xe, coupled channel study, rel. to elastic approx. 79−81255
Cl+Xe, elastic scatt. for interaction pot., Cl(^{2}P)+Xe(^{1}S) 79−27059
Cl$^-$+Ar$^+$(Hg$^+$), in Ar, high press. ion-ion recomb. rate calcs. 78−31621
Cl$^-$+Ar→Cl+Ar+e, rate const., absolute total cross section, expt. results discrepancy 77−513
Cl$^-$+Ar→Cl+Ar+e, rate const., expt. discrepancy 77−514
Cl$^-$+chloromethane, S$_N$2 reaction, local orbital description ab initio FSGO method 78−76842
Cl$^-$+H$_2$, 4-11 eV, inelastic scatt. 79−98202
Cl$^-$+H$_2$(D$_2$)(O$_2$)(N$_2$)(CO)(CO$_2$)(methane), total electron detachment cross sections for energies around threshold 80−99550
Cl$^-$+H$_2$(He)(CO$_2$)(Ar)(Li)(Na)(Mg), negative ion stripping, at. beam form. 77−6926
Cl$^-$+HBr(HI)→HCl+Br$^-$(I$^-$), vibr. product state distribs., IR chemiluminesc. obs. 80−81309
Cl$^-$+H→HCl+e, associative reaction, product vibr. state distrib. 80−66794
Cl$^-$+He, term parameters, electron spectra and scatt. cross sections 77−27148
Cl$^-$+He(Ne)(Ar)(Kr), total electron detachment cross sections, near threshold energies 79−3555
Cl$^-$+inert gas atom, electron detachment and inelastic processes 78−42208
Cl$^-$+methane(fluoromethane), excitation functions, reactive scatt., eV region *(German)* 78−35677
Cl +Na(K), differential cross-section, small angle scatt. 79−98186
Cl$^-$+O$_2$, 0.2-100 eV, reaction differential cross sections energy depend. meas. 77−63902
Cl +Xe, elastic differential cross-section, 250-500 eV, well depth of 79−86027
Cl$^-$+Xe +Ne, three body ion-ion recombination probability, Monte Carlo simulation 80−85160
Cl$^+$+Ar, L-shell X-ray cross sections, 0.2-1.5 MeV, fluoresc. yield 78−1068
Cl$^+$+CO→O+CCl$^+$, reaction cross section, heat of form., mass spectrometric obs. 79−61843
Cl$^+$+D$_2$, inelastic and superelastic collisions, DCl$^+$ formation mechanisms 78−20011
Cl$^+$+He(Ne)(Ar), highly charged low vel. recoil ion time of flight spectra, cross section energy depend. 80−14222
chlorine continued
Cl^{13+}+Ne, Li-like Ne X-ray and Auger line intensities and populations 77−10625
^{38}Cl+ethane (methane)(vinyl bromide), rate consts., stratospheric temps., radiotracer meas. 77−48632
Cl^{4+}+Xe(Ar)(N$_2$), 20 MeV, electron loss cross sections, pot. model data anal. 79−27082
Cl^{5+}+Ca(Sc)(Ti) thick targets, 30 MeV, near symmetry collisions, double-K-vacancy sharing 79−3391
Cl^{n+}+Ar, K X-ray cross sections, 15 and 30 MeV, impact parameter depend. 77−19032
Cl^{n+}+Cl(Ar), branching ratio dependence on projectile velocity and nuclear charge 79−31475
Cl^{n+}+Cu, effect on projectile charact. X-rays and REC of target thickness 79−45662
Cl^{n+}+Cu film on C foil, X-ray production, radiative electron capture 77−19063
Cl^{n+}+Ne(SiH$_4$)(H$_2$S)(HCl)(Ar), K X-ray cross section, projectile charge depend. 77−19029
Cl^{n+}+S(Ar)(Al)(Cu), K-shell vacancy sharing ratio, foil or gas target 78−42198
Cl^{n+}+Ti(Ni), 35 MeV, K-shell vacancy sharing, impact parameter depend., X-ray obs. 77−71858
Cl^{q+}+Cu, K X-ray production and radiative electron capture, fluoresc. yield determ. 80−99553
Cl^{x+}+Au, differential single-scatt. cross sections at MeV energies 78−33570
Cl^{x+}+Cl(Ti)(Ni), K-shell ionization probability in energetic nearly symmetric heavy-ion collisions, 35 MeV 79−27078
Cl^{x+}+Sn(Sb)(Xe), vacancy sharing between K and L shells in 3dσ mol. orbital 79−22807
Cl^{x+}+X, (X=atom with Z=11-22), K-shell ionis. cross sections 78−13596
Cl$_-$, Thomas-Fermi-Amaldi eqn., approx. variational soln. 80−52870
Cl$_2$, electron dissoc. attachment peaks, 0−11.5 eV, Cl$_2$ pot. energy curves 77 75312
Cl$_2$, gas-liquid surface of mol. fluids, mol. dynamics computer simulations 80−39387
Cl$_2$ in Ar matrix, vibr. relax., stochastic classical trajectory approach 78−79707
Cl$_2$, molecular fluid, Rayleigh and Raman light scatt. props., orientational and collision induced effect 80−63644
Cl$_2$, resonance fluoresc. by Ar ion laser excitation 78−42122
Cl$_2$, electron propagator theory, mol. electron affinities calcs. 80−83521
Cl$_2^-$, gas phase photodissoc. spectrum 77−58098
Cl$_2^-$, in ion pairs with metals, ESR, in AR matrix, V-centre theory 77−16172
Cl$_2^-$, photodissoc. and photodetachment, pot. curves. 79−64060
Cl$_2^-$, pot. curve calc. 77−10596
Cl$_2^-$, vibrationally excited, reactions and photodestruction 77−60048
Cl$_2$-arc, low temp., visible and IR continuum radiation 80−38784
Cl$_2$-H$_2$ mixture, detonation initiation, nonequilib. physicochem. process simulation 80−38431
Cl$_2$-HI-He chemical laser system, rot. nonequilibrium, kinetic modelling, three model comparison 80−53281
Cl$_2$-Hg-Ar, photochem. reaction producing HgCl(B$^2\Sigma^+$), chemiluminesc. 79−39154
Cl$_2$-Kr(Xe), UV transient absorption following flash photolysis 79 61879
Cl$_2$-O$_3$ system photochemistry rel. to stratospheric composition 77−16849
Cl$_2$-O$_3$-H$_2$ dilute mixtures, photolysis products, Fourier Transform IR kinetic obs. 80−26033
Cl$_2$+2Br →Br$_2$+2Cl$^-$, aqueous soln., specific rate determ., competition technique 78−44348
Cl$_2$+Ar(He)(Cl$_2$), dissoc. in shock wave, density gradient meas. 77−83682
Cl$_2$+Ba→BaCl$^+$+Cl , chemi-ionis. reaction, mol. beam obs. 80−104434
Cl$_2$+Ca(4s4p^{3}P)→CaCl+Cl, chemiluminescent reaction, state-to-state cross-section, beam-gas expt. 80−45510
Cl$_2$+Cu(^{2}D), beam-gas chemiluminesc. reactions 80−85151
Cl$_2$+F, reaction kinetics, pot. energy surface and Franck-Condon integrals 79−61855
Cl$_2$+H, activation energy and trajectory calcs., temp. and isotope effects 78−76835
Cl$_2$+H, energy disposal, HCl IR chemiluminesc. obs. 78−92484
Cl$_2$+H, Faddeev equations and Franck-Condon models for chemical reactions 80−35507
Cl$_2$+H, nonreactive scatt., long range anisotropic pot. determ. 78−66626
Cl$_2$+H, reaction products ang. distribs., Franck-Condon theory 79−87835
Cl$_2$+H, reactivity-selectivity, bounds derivation 80−66763
Cl$_2$+H, stochastic-collision complex model theory 80−108696
Cl$_2$+H$_2$(H$_2$S)(methanethiol), laser-initiated chain reactions, rates, mechanisms, chemiluminesc. obs. 80−55651
Cl$_2$+HI, pulsed chem. laser, rot. distrib. time evolution, kinetic master eq. calc. 77−65593
Cl$_2$+HI reaction pumped flash initiated HCl laser 79 94224
Cl$_2$+H(D), exothermic triatomic exchange reactions, prod. energy distrib., statistical dynamic model 78−92455
Cl$_2$+H(D), uni- and bimodal product energy distribs. 79−57207
Cl$_2$+H→HCl+Cl, translational and pot. relax., statistical calcs. 77−3435
Cl$_2$+Hbr, four-centre reaction, quasiclassical trajectory study 79−57213
Cl$_2$+Hg+$\hbar\omega$→HgCl*+Cl, laser-induced harpooning reactions 80−83458
Cl$_2$+Hg→(HgCl$_2$)$_n$, surface catalysed reaction 79−100430
Cl$_2$+K$_2$(Cs$_2$), ionisation reactions, absolute cross sections 80−99565
Cl$_2$+Kr, KrCl$^+$ form., mass spectrosc. obs. 79−29346
Cl$_2$+Li, chemiluminescence spectra, excited Li *(German)* 78−92485
Cl$_2$+Mg*(Sr*)(Ca*), collision and reaction cross section meas. 79−59537
Cl$_2$+Mu, isotope effects and collision theory 79−57273
Cl$_2$+muonium (H)(D), pot. energy surfaces, inversion calcs. 80−93734
Cl$_2$+N$_2$ mixture, Raman laser optical excitation, electron phototransition theory *(Russian)* 80−99711
Cl$_2$+Na$_2$(K$_2$), collisional ionisation reactions 77−50508
Cl$_2$+Na(K)(Cs), at. negative ion prod. cross sections 77−531

chlorine continued

- Cl_2+Ne^*, quenching rate const. for metastable $Ne(^3P_2)$, flowing afterglow 78−46295
- Cl_2+O, reactive scatt., O atoms seeded in Ne supersonic nozzle beam 78−48637
- Cl_2+O, reactive scatt. in supersonic at. beam 79−36754
- Cl_2+OH, rate const. at 298K, rel. to stratospheric O_3 depletion 79−87831
- $Cl_2+SiAs(GeAs)$, high temp. Raman spectra, cryst. growth mechanism *(French)* 79−26999
- Cl_2+Si^*, collisional quenching, reson. line absorpt. expt. 78−46297
- $Cl_2+Si(SiO_2)(Si_3N_4)$, plasma etching, electron or ion bombardment, Ar^+ enhancement 79−82073
- Cl_2+Sn, reactive scatt., ang. distrib. and time-of-flight spectra 78−64842
- Cl_2+SnO, Mossbauer and X-ray phase anal. 80−21266
- Cl_2+Xe, classical trajectory calcs., energy threshold for collision induced dissoc. determ., 80−95709
- Cl_2+Xe, XeCl form., relax. and quenching 80−81314
- $Cl_2+Xe(6s,^3P_2)$, vibr. energy disposal from XCl^* spectrum 79−100345
- $Cl_2^-+HO_2$, reaction in pulse irrad. aq. soln. containing Fe^{2+} and Cl^- 78−20036
- $(Cl_2)_2$, binding, dispersion energy predominance 78−25421
- $(Cl_2)_2$, config., ab initio calc. 79−41098
- Cl_3^- energy surface, comparison of CNDO and ab initio results 77−23445
- Cl_3^-, photodissoc. and photodetachment, pot. curves. 79−64060
- Cl_3^-, VB pseudopot. calcs. on electronic states 77−26984
- $Cl_2^-(Cl^-)$, formed by electron impact from $SnCl_4$, ionis. efficiency curves 77−61865
- $Cl(^2P)$ isoelectronic series, Sternheimer valence shielding and antishielding factors 80−18807
- $Cl(^2P)+CH_4\rightarrow CH_3+HCl$, reaction rate const., laser flash photolysis-resonance fluoresc. kinetic study 80−45485
- $Cl(^2P)+ClONO_2$, rate consts., flash photolysis resonance fluoresc. meas. 77−60038
- $Cl(^2P)$+methane, absolute rate and temp. depend. 78−80731
- $Cl'+HCl\rightarrow Cl'H+Cl$, barrier height, PNO-CEPA calculation 77−16795
- ^{35}Cl, dosimetry, ion pair formation, depend. of average energy on atomic number 80−18695
- ^{35}Cl, nucl. mag. screening in ClH, pseudopot. calcs. 79−6879
- ^{35}Cl, surface anal. using ^{35}Cl ion beams 79−5211
- ^{35}Cl XVI, beam-foil excitation, Lamb shift and fine struct., QED test 80−9549
- ^{35}Cl XVI, n=2, Lamb shift, fine struct. 79−13675
- $^{35}Cl^-$, ion mobility in inert gas, drift tube mass spectrometric obs. 79−68896
- $^{35}Cl^{35}Cl$, $B^3\Pi(0^+)\rightarrow X^1\Sigma^+$, 6300 to 9900 Å, rot. anal., mol. consts., equilib. internuclear separation 78−42082
- $^{35}Cl^{37}Cl$, $B^3\Pi(0^+)\rightarrow X^1\Sigma^+$, 6300 to 9900 Å, rot. anal., mol. consts., equilib. internuclear separation 78−42082
- $^{35}Cl^{4+}$+atom (molecule), multiple electron loss cross sections meas. 79−45818
- ^{36}Cl in environmental water samples, anal. using electrostatic accelerator 79−20895
- $^{36}Cl^-$, self-diffusion in NaCl soln., β-active tracer, plastic capillary meas. method 77−50333
- ^{37}Cl, enrichment by ICl+acetylene selective photoaddition 77−60084
- $^{37}Cl_2$, pure rot. Raman spectrum 78−94252
- ^{38}Cl and ^{39}Cl in lower stratosphere, chemical form 78−44913
- $^{38}Cl+H_2(D_2)$ reactions, characterisation, effect of ethylene-I_2 scavenger 78−73071
- ^{38}Cl+ethylene+$HI(H_2S)$, thermal, mechanisms and rate consts., fluoroethane decomp. 77−86343
- $^{34m}Cl^-$ production, inorganic yields 80−23202
- $Cl(3p^5(^2P_{1/2}))$+carbon tetrachloride $(Cl_2)(He)$, VUV metastable state quenching, absolute rate const. 77−79641
- $Cl.+XHC=CH_2$, free radical reaction theory, ab initio calc. 77−52624
- Cs^+, 3d photoabsorpt. spectra, continuum and discrete states 79−81176
- CsBr:Cl, luminescence investig. of F_H-centre lifetime 77−20917
- $Cu+Cl^{q+}$, X-ray cross sections, projectile fluoresc. yields 78−74751
- CuBr(I):Cl, lattice-dynamical study of impurity modes 80−29129
- $D+Cl_2$, collinear reaction rate consts., quantum and semiclassical calcs. 77−12782
- $D+Cl_2$, reaction probabilities, information theoretic anal. 77−16799
- $DCl+Cl_2(DCl)$, vibr. relax., Monte Carlo quasiclassical trajectory calcs. 77−50502
- $F+Cl_2$, reaction rate consts. rel. to stimulated emission 78−3317
- Fe-Cl thermochem. cycle for H_2 prod. by H_2O pyrolysis 80−97811
- FeOOH:Cl, quadrupole interaction, Mossbauer spectra 80−15895
- $H+Cl_2$, collinear nonreactive collision, classical trajectory eqns. calcs. 77−57233
- $H+Cl_2$, collinear reaction rate consts., quantum and semiclassical calcs. 77−12782
- $H+Cl_2$, collinear reaction, quantal transition probabilities from classical trajectories 77−32773
- $H+Cl_2$, Franck-Condon factors for reactive collision processes 77−36741
- $H+Cl_2$, Franck-Condon factors in reactive collision dynamics, vib.-rot. distribs. 77−36742
- $H+Cl_2$, impulsive triatomic reaction, vibr. state distrib., impulsive energy release model 78−92456
- $H+Cl_2$ dynamics, Franck-Condon factors rel. to information theory for vib.-rot. distribs. and isotopic branching ratios 77−60041
- $H+Cl_2$(organic molecule), rate const., discharge flow-reson. fluoresc. meas. 78−7178
- $H+Cl_2\rightarrow HCl+Cl$, quantum mech. reaction coords., point transformation calcs. 77−36730
- $H+Cl_2\rightarrow HCl+Cl$, rate consts. meas., Lyman-α fluoresc. technique 77−16780
- $H+F_2(Cl_2)$, reaction probability, information theoretic anal. 77−16799
- H_2-Cl_2 cell, electrochemically regenerative, mass and heat balances 80−3503
- H_2-$H_2O(Cl_2)$, diffusion in stratified positive column, impurity effects 77 11320
- $H_2+H(F)(Cl)$, collision induced IR laser absorpt., rate enhancement, theory 79−66275
- HCl+Cl, vibr. energy transfer to oscilltory, rstricted rot. and translational motion 78−70908
- $HCl+Cl_2(DCl)(HCl)$, vibr. relax., Monte Carlo quasiclassical trajectory calcs. 77−50502

chlorine continued

- $HCl(\nu=1)+H(D)(Cl)(Br)$ reactions, selective vibr. excitation effects, kinetics *(German)* 77−21364
- ^3He-Cl, direct nuclear pumped lasers using $^3He(n,p)^3H$ reaction 79−31863
- ^3He-Cl, nucl. lasing, population inversion mechanism 80−63980
- ^3He-Cl volume pumped nuclear laser survey of lasing 80−63979
- $Hg(6^3P_0)+Cl_2$ reaction, reactive quenching metastable states 79−57208
- $K+Br_2$ (Cl_2), electron transfer crossed beam reaction, energy and ang. differential cross section 79−20358
- $K+Cl_2\rightarrow K^+(Cl+Cl^-)$, 5.5−14.0 eV, energy loss, spectrum maxima, mechanism 77−75286
- $K+Cl\rightleftarrows K^++Cl^-$, $KCl+M\rightleftarrows K^++Cl^-+M$, rate consts. in at. press. flames 77−60036
- $K+Cl\rightleftharpoons K^++Cl^-$, chemi-ionis. and recomb. cross sections 78−33583
- $K+I_2(IBr)(Br_2)(ICl)(Cl_2)$, ion-pair form., bond stretching effect on cross sections 78−1064
- $K_2+Cl(Br)\rightarrow KCl(KBr)+K^*$ product electronic state distrib., chemiluminesc. 77−40529
- $KBr:Cl^-$, diffusion traps for divalent ions, dielectric loss and ionic thermocurrent techniques 80−6566
- KI:Cl, dielec. relax. of impurity-vacancy complexes, ionic thermal current meas. 77−48124
- $KI:Cl^-$, lattice relaxation around tetragonal and rhombic defects 79−95110
- Kr-Cl_2 mixture, glow discharge positive column, electron energy distrib. and rates of inelastic processes, negative Cl ions form. 80−19632
- $Li+Cl_2$, product mag. deflection slotted disc velocity analysis 77−16806
- $Li+Cl_2(Br_2)$, ion pair form., double differential cross sections, 8-30 eV 78−11507
- $Li+F_2(Cl_2)(NO_2)$, $4^2S_{1/2}$ excited atom crossed beam collisional ionisation 79−64087
- $MgI_2+Cl_2(HCl)$, crossed beam metathesis, total cross sections 77−21354
- $MgO:Cl^-$, short-wave luminesc., V-centre electron recomb., impurity effects *(Russian)* 77−20921
- $Mg^*+Cl_2\rightarrow MgCl^*+Cl$, chemiluminesc. studies 78−40030
- $NH_4Br:Cl^-$, impurity mode, far IR transmission obs. 77−16308
- $NO^++X^-\rightarrow NO+X$ (X=Cl, Br, I), rate const. determ. in flames 78−48633
- $Na+Cl\rightleftharpoons Na^++Cl^-$, chemi-ionis. and recomb. cross sections 78−33583
- $Na_8Al_6O_{24}Cl_2$, radiolytic radiation damage, Cl voids and Cl gas bubble formation 79−7628
- $NaCl:Cl^-$, energy of migration of Cl^- 77−43380
- $NaI:Cl^-$, anharmonic effects on low-frequency impurity phonon resonances 78−75771
- Nb film, Cl impurity effects on supercond. transition temp. and transition width *(Russian)* 77−66222
- $Ne+Cl^{z+}$, many-electron stripping 77−75277
- $O+Cl_2(CS_2)$, reactive scatt. of beams, vel. distribs. 77−73443
- $O_2F+Cl+O_2$, $ClF^*(B^3\pi_0+)$ prods., B-X emission spectrum 79−57216
- $O(2^1D_2)+Cl_2$, reaction kinetics, vac. UV at. spectra 77−21365
- Re-O-Cl system, gas-transition metal interaction, kinetic model *(French)* 80−108740
- SO_4/Cl ratio in Ionian Sea coastal waters *(Italian)* 79−5499
- Se:Cl, trigonal, defect and impurity electron levels, surface photovoltage spectra 78−72108
- Se:O(Cl)(K) amorphous, elec. cond. increase on impurity addition 77−11920
- Si, thermal oxidation, role and effects of Cl 80−108622
- Si:Cl, amorphous, implantation effects on elec. props. 80−49716
- Si:H,Cl, amorphous, photocond., dark cond. and photoluminesc. 80−49802
- Si-SiO_2 interface, with Cl^- incorporated, characterisation by low temp. cond. meas. 78−60220
- Si-$SiO_2:Cl^-$, physics, electron and ion motion *(Dutch)* 80−60093
- SiO_2 MOS structure, Cl role in passivation 79−91150
- SiO_2:Cl, prepared in O_2-HCl and H_2O-HCl ambients, Cl conc. profiles using SIMS 79−65110
- SiO_2:Cl film, grown on Si surface in O_2-HCl mixture, Cl incorporation 79−70186
- $SrBr_2(SrI_2)+Cl_2$, crossed beam metathesis, total cross sections 77−21354
- $Sr^*+Cl_2\rightarrow SrCl^*+Cl$, chemiluminesc. studies 78−40030
- TiO_2 reaction with C/Cl_2, high temp. chlorination, volatile species 79−83451
- Xe-Cl_2 mixtures, low-press. excimer form. and quenching by e-beam excitation 79−50071
- (Zn, Hg)S:Cu, Cl, effect of superposition of two sinusoidal fields and freq. on electroluminesc. 78−39606
- $Zn_xCd_{1-x}S$:Cl, $Cu^+(Ag^+)$, high pressure luminesc. 78−19533
- $ZnO:Cl^-$, phosphors, emission spectra, impurity effects 77−32420
- ZnS:(Cu, Cl), electroluminesc., voltage effect on ageing rate 79−95848
- ZnS:Cl, deep traps, impurity electroabsorpt. and photocond. meas. 78−6707
- ZnS:Cl, self-activated, blue emission band 79−38633
- ZnS:Cl, shape of self-activated cathodoluminesc. band 80−34987
- ZnS:Cl, single cryst., deep centre study by impurity electroabsorpt., photocond. meas. 77−12411
- ZnS:Cl, spectral distrib. of photocond., effect of powerful UV illumination 78−14767
- $ZnS:Cl^-$, $Cu^+(Ag^+)$, interimpurity luminesc. at high press. 78−19532
- $ZnS:Cl^-$, $Cu^+(Ag^+)$, phosphor, high press. effect on thermoluminesc. 78−64419
- ZnS:Cu, Cl, I, anisotropy of blue Cu luminesc. centres 77−81137
- ZnS:Cu, Cl, Mn film, AC electrolum. 80−60680
- ZnS:Cu, Cl luminophor, photoluminesc. and struct. props. 77−32414
- ZnS:Cu,Cl, electrolum. brightness wave, effect of square pulses 77−52184
- ZnS:Cu,Cl, electrolum. voltmeter design, accurate high-voltage meas. 78−24813
- ZnS:Cu,Cl, exciton refl. spectra, hexagonal struct. 77−44021
- ZnS:Cu,Cl phosphor, effect of charged imperfections on electrolum. 77−32443
- ZnS:Cu,Er,Cl film, ageing and forming, DC electroluminesc., impact excitation 79−47522
- ZnS:Cu(Cl), electroluminesc. and photoluminesc. spectra, fine struct. *(Russian)* 78−84661
- ZnS:Mn, Cu, Cl films, AC electrolum. 80−60679
- ZnSe:Cu, Cl, high press. luminesc. 78−19532

chlorine continued
  ZnTe:Al,Cl, photolum., complex acceptor, ionization energy 80—20693
  ZnTe:Cl, ion implanted and annealed, photoluminesc. meas. 78—15208

chlorine compounds
  chloride solns., ice-water phase boundary, conc. depend. solute redistrib., spontaneous convection 78—26665
  chloride solution, acidic, Ti passivation and anodic dissolution 80—35541
  chlorides in wastewater, simultaneous automated determ. 77—29511
  chlorinated compounds, ^{13}C T$_1$ meas. and scalar coupling consts. 80—18945
  chlorine oxides in MOS structs., high-temp. annealing in N *(Russian)* 77—89858
  ClF$_6$, EPR of matrix, isolated radical 79—85977
  ClNO, unimolecular reactions, rate theory 79—74348
  ESCA chemical shift, indirect evaluation of Coulombic contribution to ionis. pots. for nonbonding electrons 78—92572
  ethylene+Cl$_2$(Br$_2$) complex, intermolecular interaction and struct. SCF-MO-LCAO CNDO/2 calc. 78—58763
  graphite, intercalation of chlorides in chlorosulphonic acid *(French)* 78—27436
  hydration complexes, gas phase, electrostatic calcs. 80—100055
  organic π-σ complexes, low freq. spectra 78—78713
  ozonosphere, ClX content rel. to temp. struct. and O$_3$ distrib. 78—57246
  solvents, intensity of US cavitation *(Polish)* 80—38464
  spectrometer of nuclear quadrupole resonance, superregenerative oscillator scheme *(Slovak)* 77—18059
  tetrachloroaurates and tetrachloroiodates, ^{35}Cl NQR freqs., correl. with crystallographic data 79—33559
  trichloroethylene additive for Si oxidation to eliminate oxidation induced stacking faults 80—39118
  volatile chlorides, adsorption isotherms meas. using radionuclides and chromatography 78—76902
  AgClO$_3$, ClO$_2$ spin Hamiltonian 78—60326
  Br+OClO, reaction rate consts., mass spectrometry meas. 78—3316
  BrCl+HBr, four-centre reaction, quasiclassical trajectory study 79—57213
  BrO+ClO, reaction rate consts., mass spectrometry meas. 78—3316
  Cl-containing systems, core Auger and core electron binding energy shifts, ab initio LCAO SCF MO UHF calcs. 77—30777
  Cl+H$_2$, gas phase H-atom transfer reactions, struct.-reactivity correl., pot. energy surfaces 80—104433
  Cl$_2$-CO$_2$ system, vapour-liquid equilib. *(Japanese)* 79—42258
  Cl$^-$Ar$_{N-1}$ small ionic clusters, thermodynamic behaviour 79—77769
  ClBS, form., photoelectron and microwave spectra 78—90214
  ClBr$^-$, pot. curve calc. 77—10596
  ClCF, radical in Ar matrix, vibr. relax., multiphonon processes, fluoresc. 77—65430
  ClCN, and isotopic derivatives, rot. depend. of Fermi resonance 78—94227
  ClCN, and isotopic species, force field calc., freqs., rot. consts. 79—22692
  ClCN, Cl and N quadrupole coupling, spectroscopic meas. 79—72337
  ClCN, general quartic force field, Machina-Overend parameters 78—50532
  ClCN, ground and first excited bending, vibr. state, props., mol. beam elec. reson. 80—37823
  ClCN, linear mol., Compton profile bond additivity, HF calc. 79—68268
  ClCN, vacuum UV photodissociation spectroscopy, quantum yield, fluoresc. polarisation 80—32736
  ClCN$^+$, fluoresc. quantum yields and lifetimes, meas. method, ion form. 77—6815
  ClCN+N$_2$*, vibr. energy transfer, α_3 vibr.-rot. const., microwave meas. 77—83578
  ClCO radical, struct. and props. calcs. 80—74112
  Cl$_2$CS, excitation, singlet and triplet states, two photon absorpt., singlet-singlet energy pooling, fluoresc. obs. 80—48032
  Cl$_2$CS, fluoresc. decay from second excited singlet state 78—25600
  Cl$_2$CS, forbidden transitions, laser optoacoustic spectroscopic obs. 77—61756
  Cl$_2$CS, potential energy surfaces and equilibrium geometries for ground and excited states 79—45634
  ClF, ^{19}F chem. shielding, temp. and internuclear distance depend. 77—75068
  ClF, chemical shielding temp. depend. 78—5250
  ClF, gas, rot. frame NMR, reorientational and ang. correl. times 78—78721
  ClF, geometry optimisation, ab initio MO calcs. 77—42232
  ClF, interhalogen UV laser on 285 nm band, fluoresc. and laser oscill. obs. 79—76674
  ClF, mol. beam Zeeman effect, dipole moment sign, coupling const. 77—75208
  ClF, rot. spectra in millimeter wave region, rot. transitions obs., equilib. const. determ. 80—78607
  ClF, total energy, MOs nonempirical minimum STO-4LGF calcs. 78—9074
  ClF UV laser system 80—83597
  ClF-H$_2$ chem. laser, HCl vibr. emission 80—97709
  ClF-H$_2$ chemical laser, electron-beam initiation, energy parameters, stimulated emission from HF, HCl 79—89903
  ClF-H$_2$ chemical laser, HF rot. laser emission 79—98349
  ClF+Ar, shock wave, vibr. relax., laser schlieren meas. 78—90267
  ClF+H reaction, IR chemilum., energy disposal and branching ratios 80—26017
  ClF+H$_2$, reaction rate const. for H+ClF$\rightarrow$HCl*+F 77—71980
  ClF+SF$_4$ (perfluoroethane) (Xe), thermal and photochem. reactions investig. 80—61117
  ClF$_2$, CNDO/2 calcs., mol. struct. and props. 77—79543
  (ClF)$_2$, mol. beam. elec. deflection obs. 80—53080
  ClF$_3$, ESCA chemical shift, energy levels, SCC-MO calcs. 79—64045
  ClF$_3$, interaction with thermal-energy electrons, cyclotron reson. obs. 77—19097
  ClF$_4$ radical, geom., ab initio MO calcs. 79—89610
  ClF$_5$, condensed phases, structural study by vibr. spectroscopy and X-ray and neutron diffr. 79—1405
  ClF$_5$, IR intensities, fundamental, overtone and combination band calcs. 78—29780
  ClF$_5$, microwave spectrum, rot. transitions, dipole moment, struct., nuclear quadrupole coupling consts. 77—14423
  ClF$_5$-IF$_5$, determ. of phase diagram, using DTA 79—4955
  ClF$_6$, EPR spectra, mol. symmetry, INDO calcs. 77—46580

chlorine compounds continued
  ^{35}ClF$_6$, radical, prep. and EPR comparison with other hexafluoride radicals 78—68381
  ClF$_n$-, ClF$_n{}^+$-, ClF$_n{}^-$-, inert gas cpds., n=1-6, localised MOs and bonding nature 78—9061
  ClF$_x$-H$_2$ chemical lasers (x=1,3,5), vibr.-rot. emission by HF 78—17926
  (Cl$_2$F)$^+$, structure, theoretical investigation 80—904
  ClFCS, potential energy surfaces and equilibrium geometries for ground and excited states 79—45634
  ClFCS, second excited singlet state fluoresc., spectra 79—6957
  ClFCS, second excited singlet state photophysics, laser excitation obs. 80—32758
  ClF(ClF$_2{}^-$)(ClF$_3$), ground and ionised states, Koopman's theorem and Mo relax. in ab initio calcs. 78—1035
  ClF(ClF$_2{}^-$)(ClF$_3$), localised MO ab initio calc., Gaussian orbital ab initio calc. 80—14083
  ClF$_3$(F$_5$)+H$_2$ chemical laser, stimulated emission rel. to reaction mechanism 77—50667
  ClFH$^+$, structure, theoretical investigation 80—904
  ClF*(B$^3\pi_0{}^+$), electronically excited, chem. generation, B$\rightarrow$X emission spectrum 79—57216
  ClF$_3$.xSbF$_5$, NQR anal. of complex ion struct. 77—12238
  ClF$_5$.xSbF$_5$, NQR anal. of complex ion struct. 77—12238
  ClH, nuclear mag. shielding of ^{35}Cl, pseudopot. calcs. 79—6879
  ClH-dimethyl ether, H bonded complex, IR and Raman spectra, mech. and elec. anharmonicity 79—89672
  ClH-dimethyl ether, vibr.-rot. IR spectra, quantum and classical mechanics 80—91561
  ClHCN$^-$, ClDCN$^-$, IR spectra, rel. to mol. geom. 79—22702
  ClHCl$^-$, deuteron quadrupole coupling const., nuclear mag. shielding, geometry depend. 78—58586
  Cl$_2$(H$_2$O)$_n$, mean vibr. amplitudes, Raman spectra, isotope effects 77—58014
  ClI$^-$, pot. curve calc. 77—10596
  ClN$_3$, VPS obs., comparison with ab initio and semi-empirical calcs. 80—53043
  ClNCO, VPS obs., comparison with ab initio and semi-empirical calcs. 80—53043
  ClNO, phys. and chem. data 78—27727
  ClNO+Cl$_2$O$\rightarrow$ClONO+Cl, reaction kinetics, IR spectra 78—35641
  ClNO+ClONO$_2$ react., gas phase, kinetics, mechanism, IR photometric investig. *(German)* 78—76834
  ClNO$_2$, catalysed by ClNO, thermal decomposition spectral photometric investig. *(German)* 78—95925
  ClNO$_2$, form. in matrix reaction, IR absorpt. obs. 78—15667
  ClNO$_2$, kinetics of thermal decomposition *(German)* 78—95924
  ClNO$_2$, phys. and chem. data 78—27727
  ClNO$_3$, far IR rot. and torsional spectra 77—79609
  ClNO$_3$, microwave spectrum 77—57984
  ClNO$_3$, phys. and chem. data 78—27727
  ClNO$_3$, standard enthalpies of form. determ. *(German)* 78—53235
  ClNSO, ground state geometry, ab initio calcs. 80—106259
  ClO, A$^2\Pi_i$-X$^2\Pi_i$ absorpt. cross-sections and oscill. strengths, f-values 77—38649
  ClO, A$^2\Pi$-X$^2\Pi$, UV absorpt. spectrum 78—74673
  ClO A$^2\Pi$-X$^2\Pi$ system, electronic transition moment and dissoc. cross-section meas. 77—38679
  ClO, A$^2\Pi$-X$^2\Pi$ system, photoabsorpt. cross sections 77—79624
  ClO, aircraft search for 3 mm emission in stratosphere 80—41510
  ClO, bandstrength determ. of fundamental vibr.-rot. spectrum 78—70872
  ClO composition of stratosphere, balloon borne in situ reson. fluoresc. obs. 80—90167
  ClO, dissoc. energy and bond length, CI calcs., bond function effects 80—102450
  ClO, free radical, Ar matrix absorpt. spectra, mol. vibronic states obs., spectroscopic const. determ. 80—83387
  ClO, fundamental vibr.-rot. spectrum, rel. to remote sensing 77—42317
  ClO, in stratosphere, conc. vars. at twilight rel. to interpetation of solar occultation meas. 80—85756
  ClO, laser excited fluoresc. 79—50077
  ClO, laser spectroscopy relevant to stratospheric photochemistry 78—88951
  ClO, MCSCF-CI electronic wavefunctions, dissoc. energy, dipole and transition moment 77—75052
  ClO, predissociation in stratosphere, cross sections and rate consts. 77—70763
  ClO radical, 2-0 vibrational overtone band, laser magnetic resonance spectroscopy study 80—48021
  ClO radical, IR vibr.-rot. spectra, background data for atm. meas. 78—58679
  ClO radical in stratosphere, in situ obs., rel. to O$_3$ depletion 78—36241
  ClO, remote meas. in stratosphere 79—58005
  ClO, rot. spectrum, mol. parameters in $\nu=0$, $\nu=1$ states 78—70821
  ClO, UV absorpt., lab. spectra rel. to atmos. identifications 77—34653
  ClO, UV spectra of $C^2\Sigma^- \leftarrow X^2\Pi$ system, rot. anal. 80—996
  ClO, vibr.-rot. bands, intensity parameters 78—17722
  ClO, Zeeman effect, relativistic corrections 77—83646
  ClO$^-$, electron affinity, formed in Cl$^-$+O$_2$ reaction 77—63902
  ClO$^-$ formation by ozonation of seawater 79—16518
  ClO$^-$, photodissoc. and photodetachment, pot. curves. 79—64060
  ^{35}ClO, microwave spectrum in excited vibr. state, centrifugal distortion const. 77—83580
  ClO+H$_2\rightarrow$HOCl+O$_2$, reaction rate consts. 79—5140
  ClO+HO$_2$, free radical reaction rate consts. and products at 298K, discharge flow mass spectra 80—67391
  ClO+HO$_2$, reaction product distrib. 80—72586
  ClO+NO$_2$+M, reaction rate constants 79—100350
  ClO+NO$_2\rightarrow$ClNO$_3$, reaction rate consts., stratospheric appl. 77—78306
  ClO+NO$_2\rightarrow$ClONO$_2$, fall-off curves, N inclusion effects 77—63910
  ClO+NO$_2\rightarrow$ClONO$_2$, reaction kinetics 77—86303
  ClO+OH, rate const. at 298K, rel. to stratospheric O$_3$ depletion 79—87831
  ClO+O(NO)$\rightarrow$Cl+O$_2$(NO$_2$) rate consts. meas. 77—60059
  ClO+O$\rightarrow$Cl+O$_2$, rate consts. calc. 220-1000K 79—79233
  ClO+O$\rightarrow$Cl+O$_2$, reaction kinetics, 220 to 426K, at. fluoresc. obs. 77—21380
  ClO$^-$+NO(NO$_2$)(SO$_2$)(CO$_2$), rate consts. at 300K 78—76829
  ClO$_2$, CW for IR mol. laser, optical pumping with ^{16}CO$_2$ and ^{18}CO$_2$ lasers 80—74343
  ClO$_2$, gas-phase electron g-tensor, magic doublet rot. Zeeman spectra 78—90212

chlorine compounds continued
ClO_2, ground state pot. calc. using orthogonal internal coords. definition 79—76479
ClO_2, inertia defects and dipole moments by kinetic consts. method 80 -928
ClO_2, laser mag. reson. spectra tuned by Zeeman level crossing avoidance, perp. spectra 79—68229
ClO_2, laser mag. reson. spectra tuned by Zeeman level crossing avoidance, high-field spectra 79—76424
ClO_2, laser-microwave double reson. of ν_1 band 80—48022
ClO_2, mol., analytical pot. functions, several surface minima 78—5158
ClO_2, predissoc. mechanism determ. from rot. level lifetimes 79—13732
ClO_2 radical, laser mag. reson., ν_1 band 78—94263
ClO_2, solns., reson. Raman spectra, appl. of Morse pots. 77—65485
ClO_2, solns., reson. Raman effect and absorption spectra 77—71807
ClO_2, standard enthalpies of form. determ. *(German)* 78—53235
ClO_2, waste water disinfection and oxidation appl. 80—12032
ClO_2 , Cl $L_{II,III}$ fluoresc. X-ray spectra, mol. orbital struct. 78—70848
$^{37}ClO_2$, $\nu_3=1$ state, laser-microwave double reson. obs. 80—95657
ClO_2-O_3 mixtures, photolysis quantum yields, atmos. chem. 79—52724
ClO_2+B, chemiluminesc. metal oxide formation 80—35509
ClO_2+NO reaction initiating HCl chemical laser 80—14333
ClO_3^-, Cl $L_{II,III}$ fluoresc. X-ray spectra, mol. orbital struct. 78—70848
ClO_3 , in $KClO_4$, detection by EPR of ClO_3 radicals created by X-irrad. 78—76311
ClO_3 , in $MClO_3$ and $MClO_4$ matrix, vibr. spectra, anion site asymmetry 77—27062
ClO_3 in $NaBrO_3$, Raman spectra, fundamental vibr. modes 78—78711
ClO_4 , Cl $L_{II,III}$ fluoresc. X-ray spectra, mol. orbital struct. 78—70848
ClO_4^-, dummy spheres in SCF Xalpha calcs. 80—69056
ClO_4 , ionisation energies, SCF-Xα transition state calcs. 80—74115
ClO_n^+, ClO_n and ClO_n^- (n=1 to 3), ab initio calcs., localised MO and nature of Cl-O bond 80—69070
ClO_x, reaction rate consts., atmospheric gas phase reactions, review 77—81390
Cl_2O, ab initio vertical ionis. pot., corrections to Koopmans' theorem 78—25749
Cl_2O, inertia defects and dipole moments by kinetic consts. method 80—928
Cl_2O, standard enthalpies of form. determ. *(German)* 78—53235
$Cl_2O+ClNO \rightarrow ClONO+Cl$, reaction kinetics, IR spectra 78—35641
$Cl_2O+H_2O=HOCl$, equilib. const., Fourier transform IR determ. 80—7765
$Cl_2O+H_2O \rightarrow 2HOCl$, equilib. const., UV spectrum investig. 79—79238
Cl_2O+OH, rate const. at 298K, rel. to stratospheric O_3 depletion 79—87831
ClO_2F, cryst. struct., X-ray and neutron diffr., Raman spectra *(French)* 78—83788
ClO_2F, pyramidal type mol., force field comput. using Green's function procedure 80—23407
ClO_3F, ^{19}F NMR line shape temp. depend. and spin-lattice relax. 78—91969
ClO_3F, ^{19}F spin-rot. tensors, appl. to liq.-phase rot. diffusion 80—43068
ClO_3F, heat capacity, permittivity, thermodynamic props., 2.7 to 160K 77—35713
ClO_3F, vap. phase Raman spectrum, single isotopic species bands 78—78712
ClO_xF_y, ^{17}O NMR, chem. shifts, indirect coupling consts. 77—14453
ClONO, form., reaction kinetics, IR spectra 78—35641
ClONO, form. in matrix reaction, IR absorpt. obs. 78—15667
cis-ClONO, microwave spectrum, rot. consts., inertial defects and config. 79—59439
ClONO, near UV absorpt. spectrum, rel. to atm. chem. 77—30881
ClONO, prod. via $Cl+NO_2$ react., FT IR obs. 79—8427
$ClONO_2$, chem. degradation in stratosphere 77—33134
$ClONO_2$ collection using impregnated filters, simulation 79—12257
$ClONO_2$, form., photolysis in stratosphere, photochem. absorpt. cross sections, UV spectra 77—33154
$ClONO_2$, form., reaction with OH, kinetics 77—86303
$ClONO_2$, gaseous, UV photolysis mechanism at 302.5 nm, stratosphere appls. 78—20031
$ClONO_2$, high resolution IR absorptivity 77—33184
$ClONO_2$, laboratory microwave spectrum, atm. chem. appl. 77—6760
$ClONO_2$, laser spectroscopy relevant to stratospheric photochemistry 78—88951
$ClONO_2$, photolysis products, very-low press. meas. 79—29376
$ClONO_2$, relative abundance among stratospheric Cl compounds 77 33155
$ClONO_2$, solar photodissoc. rates, current levels in stratosphere 79—53496
$ClONO_2$, stratospheric distrib. at sunset, balloon borne IR solar spectra obs. 80—41487
$ClONO_2+NO(ClNO)$ react., gas phase, kinetics, mechanism, IR photometric investig. *(German)* 78—76834
$ClONO_2+O(^3P)$, fast flow reaction, rate const. 77—12777
$ClONO_2+O(^3P)$, photolytic gas phase kinetics at 245K 79—52719
$ClONO_2+O(^3P)$, rate consts., flash photolysis-reson. fluoresc. obs. 77—77796
ClOO radical, struct. and props. calcs. 80—74112
ClOO, stratospheric chem., formation and loss reactions 78—16138
ClOO+NO, reaction in stratosphere 79—34889
$ClO(X^2\Pi_i)$ radical, first ionis. pot., photoelectron spectrosc., vibr. struct., bond length 77—14495
$ClO(X^2\Pi_i)$, radical, He(I) photoelectron spectrum, ΔSCF calcs. 79—72359
$ClO.O_2$ in stratosphere, possible existence and chemistry 80—77066
$Cl(^2P)+ClONO_2$, rate consts., flash photolysis resonance fluoresc. meas. 77—60038
$ClPF_4$, nonrigid mol., tunnelling mechanisms, spectrosc. theory 80—78605
$(Cl_3PNPCl_3)(PCl_6)$, X-ray cryst. struct. determ. 80—88095
$Cl_3PNPO(CCl_3)_2$, NQR spin-lattice relax. study of PCl_3 and CCl_3 group reorientation 78—2767
Cl_2S, inertia defects and dipole moments by kinetic consts. method 80—928
ClSN, force consts. and mean amplitudes of vibr. calc. 77—30855
Cl_2SO, A′-force consts., 4th-order secular eqn., L-matrix approx. vs. HLFS methods 79—36556
$ClSO_2OH$, superacid, props. and appls. *(French)* 79—74482
$Cl_nSi(CH_3)_{4-n}$, ^{35}Cl NQR, geminal and vicinal interactions on substituents electronic effect 80—63663

chlorine compounds continued
$Cl_nSi(OCH_3)_{4-n}$, ^{35}Cl NQR, geminal and vicinal interactions on substituents electronic effect 80—63663
$Cl_3SiOSiCl_3$, normal vibs. and force field, calcs. using electron diffr. struct. determ. *(Russian)* 78—46317
$^{35}ClF(^{37}ClF)+Kr$ potential, asymmetric, isotope substitution effect, Legendre expansion coord. transformation 78—70894
Cu compounds, chemical shifts of X-ray electron and Auger lines 78—86912
CuCl, pulse generation of Cl II at 5218 Å, 5221 Å 78—58990
$CuCl_xBr_{1-x}$, disorder-induced TA Raman lines 79—73929
$H+ClBr \rightarrow HCl+Br(HBr+Cl)$, product energy distrib., rate const., IR chemilum. obs. 77—81391
$H+ClO_2 \rightarrow OH+ClO$, primary energy disposal, laser-induced fluoresc. 79—24726
HF-ClF complex, and isotopic forms., mol. beam elec. reson. spectra, config., bonding, spectroscopic consts. 77—30860
Li+ICl, product mag. deflection slotted disc velocity analysis 77—16806
$O+Cl_2O$, reaction rate const. 79—20344

cholesteric liquid crystals
γ-irrad. induced colour transition, dosimetry appls. 77—48877
acceleration wave propag., theory 80—75154
acoustical activity 78—83880
additive colour properties and colour gamut 79—7546
alkyl-cyano-biphenyls (and p-terphenyls) and related cmpds., chiral, synthesis and liq. cryst. props. 77—27820
anisotropy fluctuations suppression by elec. field *(Russian)* 79—32900
3-arylcholest-2-enes and 3-arylcholest-3,5-dienes, synthesis and liq. cryst. props. 80—79689
asymmetric synthesis failure using bimolecular reactions 80—44115
binary mixtures, composition and temp. depend. of pitch 78—1984
binary mixtures, IR rotatory dispersion 77—36194
biphenyl mixtures with cholesteryl chloride, static and dynamic electro-optical props., cholesteric-nematic transition 80—100646
biphenyls, cholesteric blue phases, struct. and props. 80—103243
blue phase, BCC struct., theory 80—59380
blue phase, struct., Bragg diffr. of visible and UV light 80—59385
BMAOB-cholesteryl caprinate mixture, spiral pitch temp. depend. 78—79529
boojums, analogy with behaviour in superfluid ^3He-A 78—56014
boundary induced cholesteric-nematic phase transition 77—76533
Bragg diffraction, light Pendellosung fringes, theory 77—27830
Bragg light reflection induced by electric field *(Russian)* 79—51932
Bragg reflection *(Russian)* 79—4235
Bragg reflection of light, undergraduate expt. 77—60870
breast thermography, use of liq. cryst. sheets 80—41166
bubble domain texture, obs. of forming process 78—26431
bubble domains, mol. alignment, large pitch cholesteric 77—39534
bubble domains, struct. and props. in cholesteric-nematic mixture 77—89373
caprinate, spherulite growth rate and nucleation rate, optical method *(Polish)* 80—10652
capronate, proton spin-lattice relaxation in various phases *(Russian)* 80—97163
Cherenkov radiation, diffr. scatt. conditions, theory *(Russian)* 79—19151
chiral compound-MBAB mixture, helical screw sense and pitch determ., Grandjean-Cano method *(German)* 77—80609
chiral molecules, mol. biaxiality and temp. depend. of cholesteric pitch 77—7664
chirality determ. by circularly polarised light obs. *(Japanese)* 77—1078
cholesteric nonanoate, US attenuation near cholesteric to smectic A transition 79—28091
cholesteric-nematic liq. cryst. mixtures, electro-optic charact., light scatt. modes *(Japanese)* 78—79527
cholesteric-nematic mixtures, helix inversion 80—24358
cholesteric-nematic transition, helix stepped unwinding *(Russian)* 79—90548
cholesterilcinamate, low press. phase transition temp. change, relative transparency *(Russian)* 78—2242
cholesterin, synthesis and light refl. props *(German)* 80—10497
cholesterin ethers, dielec. absorption, heating/cooling and oxidation depth effects *(Russian)* 79—50984
cholesterol benzoates, intermolecular interaction, influence on optical props. *(Russian)* 79—77516
cholesterol cinnamates, intermolecular interaction, influence on optical props. *(Russian)* 79—77516
cholesterol derivatives, mol. packing coeffs. and thermal stabilities 80—100201
cholesterol pelargonate, liq. cryst., crystallisation rate const. and Avrami index 78—94994
cholesteryl 2-(2-ethoxy-ethoxy) ethyl carbonate, dynamics of isotropic-cholesteric transition, normal and blue phases 79—95134
cholesteryl 2-nitrobenzoate, mesophases, props. 77—11465
cholesteryl 4-chlorocinnamate, mesophase props. 77—11465
cholesteryl 4-nitrocinnamate, mesophases, props. 77—11465
cholesteryl acetate:cetyl alcohol, optical behaviour of spherulite texture 77—51314
cholesteryl acetate, phase transitions and solid polymorphs 78—2255
cholesteryl acetate-cholesteryl octanoate system, phase transitions, thermoanalytical microscopy obs. 79—55871
cholesteryl acrylate, mono- and polymer, liq. cryst. order 78—9942
cholesteryl alkanoates, mol. packing coeffs. 79—82195
cholesteryl azo dyes, prep., DSC , struct. props. 78—51412
cholesteryl benzoate, elec. drift mobility, 140 to 185°C *(Korean)* 79 65481
cholesteryl benzoate, orientational order, EPR study 78—75540
cholesteryl bromide, cryst. and mol. struct. 79—82194
cholesteryl caprilate, conduction mechanism 78—64046
cholesteryl caprinate, liq. cryst. mesophase electron emission 79—55664
cholesteryl caproate, isothermal crystn., spherulites growth rate, optical microscopy obs. 79—32892
cholesteryl caprynate, liq. cryst., DTA *(Russian)* 79—77496
cholesteryl capsylate and laurate, and their mixtures, elec. cond. *(Rumanian)* 79—64988
cholesteryl chloride, binary mixtures with cholesteryl benzoate and β-halogeno cholesteryl alkanoates, reciprocal helical pitch 79—90528
cholesteryl chloride, cryst. and mol. struct. 79—82194
cholesteryl chloride, depolarised light transmission, microstructural changes 78—22647

cholesteric liquid crystals continued
- cholesteryl chloride, optical rotatory power using multiple scaling 78—27176
- cholesteryl chloride+cholesteryl laurate, binary compensated, rhodamine 6G guest, electro-optical colour effect 80—71378
- cholesteryl chloride-cholesteryl crotonate, polarised light transmission, DC elec. field effect 77—77173
- cholesteryl chloride-cholesteryl crotonate (75:25% wt.) mixture, cholesteric-nematic transition field effect temp. depend. 78—75813
- cholesteryl chloride-cholesteryl nonanoate mixture, pitch, temp. and comp. depends. 77—39535
- cholesteryl chloride-cholesteryl pelargonate mixture, cholesteric-nematic transition 78—91244
- cholesteryl chloride-MBBA mixture, mol. orientation during mag. field induced cholesteric-nematic transition 79—28086
- cholesteryl chloride-myristate, mag. aligned, anisotropic US propag. 78—42895
- cholesteryl cimmanate, photoreaction in solid, mesomorphic, and isotropic phases 79—87863
- cholesteryl crotonate, depolarised light transmission, microstructural changes 78—22647
- cholesteryl decanoate, cholesteric pitch near smectic-A transition meas. 77—7856
- cholesteryl decanoate, NMR spectroscopy of blue phase 79—4236
- cholesteryl decanoate, optical activity in blue phase 80—100641
- cholesteryl decanoate organic solns., γ radiolysis, colour transition temp. 79—57266
- cholesteryl esters, blue phase, model 80—88030
- cholesteryl esters, isotropic mesophase, optical props. 79—65891
- cholesteryl esters, kinetics of cholesteric/blue phase transform. 79—95140
- cholesteryl esters, liq. crysts., P-T diagrams up to 5000 kg/cm^2 78—2003
- cholesteryl ethyl carbonate, long periods in sol. state, X-ray diffr. study 80—96503
- cholesteryl laurate, conduction mechanism 78—64046
- cholesteryl laurate, crystallisation kinetics and phase transitions, differential scanning dilatometric obs. 79—69230
- cholesteryl laurate, liq. cryst., DTA *(Russian)* 79—77496
- cholesteryl laurate-cholesteryl caprilate mixture, elec. cond. mechanism 79—10796
- cholesteryl laurate-cholesteryl caprylate (75 wt.%), polymorphic behaviour, optical, elec. and dielec. meas. 80—65208
- cholesteryl m-fluorobenzoate, NMR spectroscopy of blue phase 79—4236
- cholesteryl methacrylate, mono- and polymer, liq. cryst. order 78—9942
- cholesteryl methyl carbonate, liq. cryst., low-ang. X-ray diffr. obs., solid and liq. 80—49093
- cholesteryl myristate, cholesterogenic, blue phase, D NMR obs. 80—97151
- cholesteryl myristate, density of smectic, cholesteric, blue, isotropic phases 78—42897
- cholesteryl myristate, high press. mesomorphic and polymesomorphic transitions 78—18750
- cholesteryl myristate, polymorphism of blue phase, DTA and microscopy meas. 79—37819
- cholesteryl myristate, press. depend. of cholesteric pitch near cholesteric-smectic A phase transition 77—68918
- cholesteryl myristate, smectic A-cholesteric transition, tricritical behaviour, DTA and DSC study 80—65206
- cholesteryl myristate, two blue phases demonstrated by selective refl., 300-400 nm 79—90553
- cholesteryl nonanoate, cholesterogenic, blue phase, D NMR obs. 80—97151
- cholesteryl nonanoate, cyclohexanone admixture effect on mesophase order parameter, refr. index meas. 80—100165
- cholesteryl nonanoate, high press. mesomorphic and polymesomorphic transitions 78—18750
- cholesteryl nonanoate, liq. cryst.-isotropic transition at high press. 79—95135
- cholesteryl nonanoate, polymorphism of blue phase, circular dichroism at high-press. 79—37821
- cholesteryl nonanoate, polymorphism of blue phase, DTA and microscopy meas. 79—37819
- cholesteryl nonanoate, polymorphism of blue phase, optical rot. and refl. 79—37820
- cholesteryl nonanoate (decanoate), effect of cholesteryl alkanoyl esters on red-green transition temp. 80—19924
- cholesteryl nonanoate organic solns., γ radiolysis, colour transition temp. 79—57266
- cholesteryl nonanoate-MBBA, liq. cryst. mixture, two colour display device 80—70116
- cholesteryl oleate, thin film, disclination morphology *(Russian)* 77—62474
- cholesteryl oleate , isotropic phase, shear viscosity, logarithmic divergence 78—26668
- cholesteryl oleate-MBBA mixture, memory effect characts., crit. freq. rel. to erase voltage 78—94993
- cholesteryl oleyl carbonate, high-purity, prep. for thermal radiography 77—15311
- cholesteryl oleyl carbonate, isotropic phase, polarisation of scattered light 79—78691
- cholesteryl oleyl carbonate, isotropic phase, shear viscosity, logarithmic divergence 78—26668
- cholesteryl oleyl carbonate, optical rotatory power using multiple scaling 78—27176
- cholesteryl oleyl carbonate, press. depend. of cholesteric pitch near cholesteric-smectic A phase transition 77—68918
- cholesteryl p-acryloyloxybenzoate, mono- and polymer, liq. cryst. order 78—9942
- cholesteryl pelargonate, liq. cryst. phase transitions *(Russian)* 79—37818
- cholesteryl pelargonate, optical dispersion 79—64990
- cholesteryl propionate, liq. cryst., DTA *(Russian)* 79—77496
- cholesteryl propionate, struct. in characteristic phase, X-ray diffr. obs. 79—32891
- cholesteryl propionate-acetate mixture, light refl., twisting power 77—84641
- cholesteryl vinyl succinate (fumarate), polymer+monomer systems, liq. cryst. phase states 79—1494
- cholesteryl-m-fluorobenzoate, cholesteric liq. cryst., NMR, orientational order parameter 77—8429
- cholesterylalkanoates, liq. cryst., optical anisotropy and struct. ordering *(Russian)* 78—87616

cholesteric liquid crystals continued
- cholesterylpelargonate, cholesteric-smectic A transition, metal-supercond. analogue 79—23712
- cholestryl nonanoate-MBBA mixture, anomalous behaviour of electrical dissipative power 79—4237
- coatings, superimposed left- and right-handed, peak refl. and colour gamut 80—74472
- COC, cholesteric liq. cryst., positron lifetimes and phase transitions 80—59383
- COC, cholesteric-smectic-A transition, press. depend., optical meas. 77—47556
- COC, dynamics of isotropic-cholesteric transition, normal and blue phases 79—95134
- COC, prep., cryst. state, and mesophases 79—95143
- COC, shear flow, helix distortion, optical meas. 78—94982
- COC test of tricriticality 80—10648
- colour temperature characts. obs., using temperature wedge method 80—57359
- confocal cholesteric textures, optical and electro-optical props. *(Russian)* 77—80419
- continuous theory *(Russian)* 79—46568
- COOB-cholesteric liq. cryst. mixtures, helix pitch, temp. depend. 80—64895
- crystallisation, quasithermal, of cholesteric mixtures 80—92652
- cyanobiphenyl E-7 mixture, bistable cholesteric liquid crystal display 80—96437
- defect structure near smectic-A transition 79—46559
- differential calorimeter dosimeter for nonionising radiation 79—70649
- disclinations, generation process, matrix representation 78—59743
- disclinations, investig. by homotopic topology methods *(Russian)* 77—69140
- disinclinations, rotation defects, topology *(French)* 80—79679
- dispersion with rubber, prep. and props. 77—27821
- dispresed in polyurethane elastomers, optical props. 78—1986
- dissipation function theory 77—76303
- domain instabilities in elec. and mag. fields 79—94875
- dye activated CLC, distributed feedback, tunable radiation generation *(Russian)* 80—102720
- dye laser emission freq. tuning with cholesteric liq. cryst. Bragg mirror 79—89931
- EHD instability, phase diagram, for nematic-cholesteric binary mixture 78 - 1980
- EHD instability with isotropic mechanism *(Russian)* 78—87617
- electric field induced nematic to cholesteric transition, transient phenomena of relax. 78—75811
- electric field instability threshold and deform. period *(Russian)* 80—28914
- electro-optic cholesteric-nematic transition, and memory effect *(Russian)* 77—84911
- electro-optic effect, temp. independ. threshold voltage cholesteric-nematic phase change effect 79—91405
- electrodynamics, continuum theory 80—6356
- EM radiation in media with spatial dispersion, spatial coherence formation and polarisation increase 80—106442
- EM waves polarisation *(Russian)* 79—81333
- emissivity of liq. cryst. film on Al surface *(Japanese)* 77—35732
- enantiomers, discrimination using liq. crystalline solns., IR rot. dispersion meas. 79—16064
- esterification kinetic study by monitoring pitch changes in cholesteric liq. cryst. solvent 80—7786
- esters, effect of nature of organic solvent on gamma radiolysis 80—7835
- ferrofluid/lyotropic liq. cryst. combination, ferronematics and ferrocholesterics 80—59378
- fibreglass laminates, thermal NDT using liq. crysts. 80—93709
- field-induced nematic-cholesteric relax., hysteresis behaviour of texture 77—84900
- film, optical rotatory power near cholesteric to smectic A transitions 78—10865
- films, absorpt. and contrast in dichroic liq. cryst. displays 80—75155
- flow, Newtonian, capillary, shear, of oriented liq. cryst., effective viscosity 79—18957
- flow between two parallel hot plates in relative motion 80—49097
- flow between two parallel plates 78—18539
- flow normal to helical axis, steady, low shear rate 80—96443
- fluorescence of guest mols. in scatt. state 80—63698
- formiate, proton spin-lattice relaxation in various phases *(Russian)* 80—97163
- gamma irradiation of cholesteric products, effect of presence of organic solvents 79—24777
- gamma-ray radiation effects, dosimetry, thermography appl. *(Spanish)* 80—92457
- Grandjean lines, flow induced 78—71670
- Grandjean lines, optical study *(French)* 79—46560
- gyrotropy, depend. on thickness of layer 77—40204
- gyrotropy, region of electron absorption bands 78—10866
- heat-sensitive colour changes, visual display of EMF and eddy currents, for teaching 77—33804
- helical pitch rel. to temp. in induced cholesteric systems 79—64984
- helical sense and pitch from birefringence meas. 78—59744
- helix period, mag. field strength depend. near phase transition to smectic A *(Russian)* 78—59754
- imperfect, optical props. *(Russian)* 77—80420
- incompressible, static magnetic field effect on helical flow 78—6010
- intermolecular interaction 77—89378
- IR and UHF radiation visualisation instrum. 80—13071
- IR visualizer, cholesteric liq. cryst., wide dynamic range 77—79955
- isotropic phase, Brillouin scatt. 78—2867
- isotropic phase, pretransitional viscosity 80—84312
- Keating-Bottcher theory, of cholesteric systems with nonmesogenic additives 80—84057
- laser resonator for distrib. feedback dye laser, theory 79—31956
- Lehmann's effect, internal mol. rot. in time depend. temp. gradient 77—35478
- light reflection by crysts. with tilted molecular struct. 80—29713
- light reflection theory for crystals possessing a pitch gradient 79—91396
- light refraction, by a cholesteric prism under applied mag. field *(French)* 78—80319
- light scattering *(Russian)* 79—77517
- light transmission and reflection, incident angle dependence calc 78—43834

cholesteric liquid crystals continued
- lipid planar multibilayers, spin label study of nystatin and amphotericin B action 77—29108
- long pitch type, with homeotropic boundary alignment, elongated and spherulitic domain struct. 80—107047
- macroscopic helical structure origin 80—107043
- MBAB:cholesteryl chloride, thickness depend. of threshold elec. field for instabilities 79—32896
- MBBA, cholesteric struct. induced by chiral sulphoxides 79—86683
- MBBA, with chiral impurities, shear flow normal to helical axis 79—86689
- MBBA-BBCA-cholesteryl chloride, field induced nematic-cholesteric relax. processes, transient helical pitch 80—38906
- MBBA-cholesteryl chloride mixture, bubble domain texture, obs. of interference fringes 79—23520
- MBBA-CN mixed liquid crystal, dissipative structs. caused by EHD instability 77—80416
- MBBA/CC mixture, torsional shear flow in elec. and mag. fields 79—86697
- S-(+)-4-2′-methylbutyl phenol, cholesteric derivatives, appl. in display devices 79—19145
- microstructure rel. to optical props. 78—47240
- microwave thermophotoindicators, analysis of diffuse light spectra 80—73457
- mixture, molecular statistical theory with regard for steric repulsion forces *(Russian)* 78—34438
- mixture, optical activity *(Russian)* 78—71677
- mixture, storage effects 77—43972
- mixture, with positive dielectric anisotropy influence of external fields *(Rumanian)* 78—59751
- mixtures, electro-optical props., appl. to information storage *(Rumanian)* 79—78657
- mixtures, hysteresis, bistability effects under elec. fields 78—42907
- mixtures, optical props., temp. meas. *(German)* 77—44013
- molecular model, temp. depend. of pitch and elastic consts. 79—77510
- molecular order, determ. using birefringence 79—94902
- molecular ordering, small-angle X-ray scattering 79—60274
- molecular polarisability, arrangement order calc. *(Polish)* 80—10495
- molecular theory, intermol. pot., mixtures 77—76302
- molecular-optical, and structural anisotropy 80—84056
- molecular-statistical theory of temp. depend. pitch 77—15303
- multicomponent systems, optical props. 78—2002
- multiplexed liquid cryst. display, use of cholesteric-nematic phase change 80—107408
- NDT appls. 77—73395
- nematic to cholesteric transition, light induced *(Russian)* 78—14452
- nematic-chiral mixtures, viscosity and electrooptical characts.. 79—86682
- nematic-chiral-dye mixture, circular dichroism, selective light scatt. *(Russian)* 80—103944
- nematic-cholesteric field-induced relax. time, phase transition temp. depend. 79—86874
- nematic-cholesteric liq. cryst. mixture, NMR, reordering, nucleation and growth model 77—72546
- nematic-cholesteric mixture, helical pitch, depend. on composition 78—42899
- nematic-cholesteric mixture, spiral struct. formation *(Russian)* 77—58953
- nematic-cholesteric mixture, surface boundary conditions influence on transition *(Russian)* 79—23705
- nematic-cholesteric mixture, with positive dielec. anisotropy, light scatt. in elec. field 77—72548
- nematic-cholesteric mixture with positive dielectric anisotropy, light scatt. characts. 78—75537
- nematic-cholesteric mixtures, comp. depend. of helical pitch *(Japanese)* 77 72553
- nematic-cholesteric mixtures, spiral pitch temp. depend. *(Russian)* 80—19700
- nematic-cholesteric mixtures, ternary, comp. depend. of helical pitch *(Japanese)* 77—72554
- nematic-cholesteric soln., thermodynamic props. 79—32903
- network polymers, heterogeneous, from partially hydrolysed poly(methyl D-glutamate) and poly(oxyethylene glycol), mesophase struct. *(Japanese)* 78—95002
- 4-nitrophenyl-4-octyloxybenzoate/cholesteric liq. cryst. mixtures, helix pitch, temp. depend. 80—64895
- non-sterol, relationship between helical twist sense, absolute config. and mol. struct. 77—72552
- nonanoate, isothermic crystallisation, microscopic exam. *(Polish)* 80—10651
- nonlinear reversible hydrodynamics, external mag. field influence 80—75156
- nonmesomorphic solutes, effect on cholesteric pitch, max. refl. wavelength shift *(Russian)* 78—38620
- nonyloxybenzoic acid/cholesteric liq. cryst. mixtures, helix pitch, temp. depend. 80—64895
- nucleation of focal-ionic domains in field induced nematic texture 78—34430
- odd-even effect in helix of non-sterol cholesterogens 80—19701
- optical activity, polaris. azimuthal depend., helical chain model 77—11479
- optical activity light scatt., theory 77—36195
- optical properties, diffraction nature, review 80—70123
- optical properties, spatial dispersion effect 79—99844
- optical properties at normal incidence, boundaries effect 77—32345
- optical rotation and selective reflection, influence of orientational order 78—42900
- optical rotatory power using multiple scaling, De Vries model 78—27176
- optically absorbing, light refl. and transmission dynamical diffr. theory 77—58954
- optically active binary liquid crystal thermometry 79—42952
- ordering mechanism, helix pitch var. and deform. energy *(Russian)* 77—68921
- orientational order, spectral depend. of circular dichroism 78—26437
- orientational order parameter, comparison with nematic liquid cryst. 79—27917
- orienting effect of different substrates 79—46554
- oscillatory convective instabilities, caused by heating from below 80—103239
- panel, energetic sensitivity, as IR registrator *(Russian)* 79—89995
- PBLG, low freq. light scatt. modes revealed by Rayleigh scatt 78—19496

cholesteric liquid crystals continued
- phase IV, cholesteric struct. induced by chiral sulphoxides 79—86683
- phase transformations with temp. hysteresis 77—84902
- phase transitions, volumetric behaviour, dilatometric obs. 77—59106
- phase transitions and critical phenomena *(Russian)* 79—4407
- photographic plate, for images in IR, extreme characts. *(Russian)* 79—89994
- piezoelectric coeffs., Onsager theory, interparticle pot. and first moment vector 77—24264
- piezoelectric effect due to shear vibration 77—85656
- piezoelectric effects with vibration 78—6013
- pitch, temp. depend., mol. statistical theory 79—86703
- pitch, temp. depend. and relation to optical activity, mol. model 79—86706
- pitch observation, SEM freeze etching method 77—15316
- planar texture, field-induced square grid perturbation 79—90531
- planar texture, planar-finger print texture transform. around Cano disclinations 80—14999
- planar texture EHD distortion in crysts. with negative dielectric anisotropy 78—42894
- planar texture instability for cholesteric-nematic mixture with negative dielec. anisotropy 78—59739
- polarised light transmission 78—9946
- poly(γ-benzyl L-glutamate), soln. and film, light scattering study 79—66374
- poly(γ-benzyl-L-glutamate), in benzene soln., cholesteric liq. cryst. props. 79—94889
- poly(butyl acrylate), crosslinked, cholesteric liq. crystalline order 79—94893
- poly(glutamic acid)-poly(oxyethylene glycol), heterogeneous network film, polarising microscopic struct. obs. 78—9948
- poly(L-glutamic acid), texture in conc. soln. and solid films *(Japanese)* 79—90534
- poly(oxyethylene glycol), texture in conc. soln. and solid films *(Japanese)* 79—90534
- poly-γ-benzyl-L(D)-glutamate, soln., liq. cryst. and pretransitional regions, optical rot. 80—66145
- poly-γ-benzyl-L-glutamate, soln., liquid crystal transitions anal. 80—65207
- polymer liquid-crystalline solns., struct. 80—103235
- polymers, cholesterol containing, struct. and liq. cryst. props. *(Russian)* 78—38622
- polypeptides, electric field-induced phase transition 80—24571
- positive dielectric anisotropy mixture, helix pitch increase below 20 kHz 80—15997
- proton NMR spectra, angular depend. of second moment *(Russian)* 77—62478
- pseudoencapsulated film, selective light scatt. 77—16289
- radiation effect on cholesteric liquid crystals, gamma-ray dosimetry, thermography appl. *(Spanish)* 80—92457
- radiation monitoring appl., response charact. 79—2818
- refractive index meas. by cylindrical cell method 80—11358
- rotatory power *(French)* 80—50294
- Schiff base compounds, cholesteryl esters, mesomorphic behaviour 78—1994
- screw sense, form of spiral disclination lines calc. 78—67643
- screw sense determ. by droplet method 79—90544
- screw sense determ. by Grandjean-Cano wedge method, theory 80—84058
- selective reflection, temp. depend. γ-irrad. effects 77—43130
- semiconductor-liquid crystal interface props. *(Rumanian)* 78—83723
- shear electricity, symmetry considerations 78—60394
- shear flow induced propagating domains 80—54131
- shear flow induced propagating domains in cholesterics 80—64887
- sitosteryl esters, mesomorphic props. 79—90539
- smectic order in cholesteric mesophase *(Russian)* 79—95145
- solution, effect of γ-irradiation on colour transition temp. 77—47343
- solution of achiral mols., fluoresc. circular polarisation *(German)* 77—42350
- spherolites, of cholesterol liq. crysts., activation energy and growth rate 79—94900
- spiral twisting, orientational order effect *(Russian)* 78—42906
- stabilisation, multicomponent mixtures, refl. spectra, clarification temp. and melting point meas. 78—9951
- static strain waves, response to mag. and elec. fields 77—27813
- statistical hydrodynamics, microscopic theory 77—39540
- stearate, proton spin-lattice relaxation in various phases *(Russian)* 80—97163
- storage mode, director field and lifetime calcs. 77—55239
- striped domain structure in cholesteric-nematic mixture, refr. index distrib. 77—24261
- structural characts. from opt. circ. dichroism 77—62476
- surface, cholesteric helix, elec. field-induced high-order refl. 78—35115
- surface and bulk configurations, topology 80—59381
- texture, and electrohydrodynamic instability 79—90550
- thermal emissivity of semitransparent and opaque films 79—7703
- thermal field measurements, liq. cryst. improved technique 80—216
- thermal flow visualisation of film-cooling processes 79—186
- thermal fluctuations, spatial correl. function *(Russian)* 78—2005
- thermo-optical monitor, for nonionising radiation 78—11742
- thermoindicators, colour-temp. characts., time depend. 79—40567
- thermosensitive, appl. to study of temp. fields during plastic deform. of NaCl and AgCl 79—82278
- thermosensitive, props. *(Hungarian)* 78—59755
- thermosensitive film coating, dispersed liq. cryst. microdroplets in gelatin matrix, exam. of preps. 80—42220
- thermotropic, anomalous rheological responses, spectrometer study 80—6358
- thermotropic polymers, cholesteric with mesogenic moieties and flexible spacers in main chain, synthesis and light reflection 80—88028
- third harmonic generation, phase-matched, conversion efficiency 78—30021
- third harmonic generation 77—50728
- topological classification of distortions 78—79523
- total radiation monitoring using liquid crystals and thermoluminescence 80—3819
- transient electrodynamic instability, for system with positive anisotropic dielec. permeability *(Russian)* 78—51418
- twist, absolute sense, determ. by contact method *(French)* 77—27827
- twist waves, accel., effect of material nonlinearity 77—27816

cholesteric liquid crystals continued
- uncompensated system, increase in pitch of cholesteric helix with temp. 78−71676
- US attenuation, elec. field effects 77−15304
- US field visualisation by nematic-cholesteric mixed cell 78−1524
- US propagation, mesophases and phase transitions 78−79667
- US transducer characterisation 78−42512
- US velocity, temp. depend. 77−11637
- van der Waals interaction, influence of nonlocality effects *(Russian)* 77−81077
- viscosity coefficient measurements 79−77791
- visualisation of microwave fields 78−58031
- wedge layers, planar alignment, paired disclinations and disclinations of strength O 79−86696
- CsI, exam. of kinking process, using cholesteric liquid crystals 80−7629
- MBBA+optically active substance, pretransition optical rotation in isotropic phase *(Russian)* 80−92657
- SiO_2 glasses surface textures and defects, exam. using liq. crysts. 80−6364

chondrites *see meteorites*

choppers (circuits)
- DC microvoltmeter based on modem 80−31798
- fast electrostatic chopper of low power consumption 79−31284
- fusion reactor, Doublet III, plasma shape control, 1.5 Megawatt DC chopper power supply 80−102333
- gamma-resonance spectrometer, highly stable, simple circuit 77−65384
- low-power UV source, with electronic chopper 78−79087
- neutron Fourier TOF spectroscopy, influence of higher harmonics in chopper modulation function 77−6609
- PEP magnet power supply systems 77−83216
- preamplifier, strain gauge blood pressure transducer appl. 78−3659
- superconducting chopper amplifier, improved sensitivity 77−26306
- superconducting chopper amplifier for resistance meas., sensitivity and noise calc. 79−12817
- US pulse-echo system, chopping circuit 77−67162

chopping *see cutting*

chromatic aberration *see aberrations*

chromatography
- acetylene-NO-O_2, combustion products, 1400-2600K, minimisation of NO, computer model 78−85161
- acid-labile amino acid precursors in Murchison meteorite, chromatographic fractionation 77−64707
- acrylonitrile Na methallylsulphonate copolymer electrolytes in dimethylformamide, gel permeation chromatography appl. 80−21345
- acrylonitrile-styrene copolymers, compositional heterogeneities, determ. by thin-layer chromatography 79−24847
- adsorption isotherm determ. by step and pulse method, apparatus and data processing 78−6215
- affinity, calf lymph nodes, X-irrad. interaction between histone F2b and DNA 78−85346
- affinity chromatography, appls. and resin synthesis 78−11579
- air, low benzene cones, determ. by gas chromatographic method *(German)* 80−21429
- air and biological samples, chlorobenzenes determination by gas chromatography with photoionis. detection 80−35809
- air pollution, vertical diffusion study using airborne gas-chromatography and numerical modelling 78−69435
- air pollution samples anal., ion chromatography appls. 80−30625
- aliphatic amine mixtures, ionis. consts. determ. by gas-chromatographic anal. *(Russian)* 79−61921
- alkali metal polyphosphates, vitreous, mol. weight distrib. determ. by gel-chromatography 79−50173
- alkaline earths separation and identification by circular thin layer chromatography 79−66385
- N,N′-bis(p-alkoxybenzylidene)-α,α'-bi-p-toluidines, nematic phase, synthesis, thermodynamic props., gas-liq. chromatographic anal. 79−90763
- alkyl amines, plasma chromatography, reduced mobilities 79−74436
- alkyl halide, chem. struct. determ. using electron capture response 77−21428
- alkyl Pb compounds, in atmosphere, detect. via gas chromatograph-microwave plasma detector 78−68975
- alkyl Se compounds, in atmosphere, detect. via gas chromatograph-microwave plasma detector 78−68975
- aluminas, surface modified, DTA and TGA exam., gas chromatographic eval. 77−36785
- amino acid anal. by ion exchange chromatography 80−11986
- amino acid chromatographic instrument analysis and synthesis *(Hungarian)* 79−92030
- aminosilane stationary phase, for HPLC separation of polynuclear aromatic compounds 78−35747
- amplifier, programmable- or auto-gain, for gas chromatograph, spectrometer or polarograph 79−43644
- aqueous gel permeation chromatography review 77−36824
- aromatic hydrocarbons, in airborne particulates, gas chromatography/mass spectrometric, NMR analyses 77−13116
- atmosphere organic pollutants, determ. via gas chromatography after cryogenic sampling 78−81468
- atmospheric N_2O conc. meas. using electron capture-gas chromatography technique 77−9531
- atomic absorption detection, review 77−60138
- atomic absorption flow detector for gel chromatography, Mg-P_3 complexes determ. 79−87890
- autoionography of beta-emitting radionuclides distrib. on thin-layer chromatograms 78−20126
- automated HPLC instrumentation 80−40791
- automatic evaluation system using calculator *(Hungarian)* 77−56289
- automatic liquid sample injector for GC, syringe-type *(Japanese)* 80−50923
- azo dyes, UV-visible spectrophotometric 80−61207
- base line drift correction circuit, HPLC 80−45604
- benzene production, monitoring procedure for pure product 78−92583
- benzene-polybutadiene-cyclohexane system, vapour-liq. equilibria 79−95147
- benzo(a)-pyrene, separation and struct. resolution by thin layer chromatography-mass spectrometric meas. 78−7270
- benzo(a)pyrene, distrib. with respect to particle size in submicron atm. aerosols 79−74563
- benzolene gas and oil desulphuration using computer *(German)* 77−4965

chromatography continued
- biological fluorocarbon detection by gas chromatography *(German)* 78−96117
- block copolymers, chromatographic separation on porous adsorbents *(Russian)* 79−66392
- block-copolymer, mol. wt. distrib. and comp. determ., gel permeation chromatography method *(Russian)* 79−31755
- blood gas analysis in vivo using gas chromatography 78−40355
- blood gas chromatographic analysis, in vitro evaluation 77−81604
- blood gas sampler, for gas chromatography, design, construction and characteristics *(Japanese)* 78−85458
- breath anal. by gas chromatography, use of relative time programming 78−61268
- butyl rubber ethylene propylene ternary copolymer mixture, permeability, diffusion of gases and solvents 79−95217
- capacitor dielectric fluid test and anal., quality assurance 78−80272
- capillary column gas chromatography at nanogram resolution using dual beam Fourier transform IR spectroscopy 80−89554
- capillary columns for gas chromatography 79−83529
- capillary gas, mass spectroscopy and computer techniques, organic compound analysis in environmental samples appl. 78−80799
- capillary gas chromatography, review 78−44412
- carotenoid pigments, in geochem. systems, HPLC determ. 78−61078
- catalyst, diffusion in pores, gas chromatography obs. 79−70372
- catecholamines, HPLC and continuous flow anal. using flow cell based on rotating disk electrode 80−66894
- cellulose acetate butyrate, in soln., hydrodynamic behaviour 80−64876
- cellulose acetate polymer-solution interface props. from liq. chromatographic data 79−16039
- charcoal tube sampling technique, meas. accuracy 78−69508
- chlorofluoroethane, multiphoton dissoc. under CO_2 laser irrad., decomposing mol. energy distrib. 80−30251
- chloromethyl methyl ether, on-column reaction GC determ. in ambient air 78−20093
- chlorophyll a in benzene solns. and monolayers, chem. stability 79−47912
- chromatographic method of calibrating leaks 80−77800
- chrysotile, adsorpt. of organic micropollutants, XPS and gas solid elution chromatography exam. 78−80790
- Cibacron Blue F3GA affinity chromatography 77−78061
- circular thin-layer, ring-air technique alternative to ring-oven method 79−74478
- circulation, in steam, separation of isomers 79−16074
- coal, laser pyrolysis products exam. 79−20356
- coiled glass columns, for gas chromatography, rapid packing system 78−73095
- column, UV monitor, design, construction 79−1973
- column chromatography versus flameless atomic absorption spectrophotometry for As meas. in aquatic systems 80−55969
- column extraction, for Pu, U and Th separation 78−44421
- column switching technique for gas chromatographic analysis 78−92530
- complex gas mixture quantitative identification, automated system with dissimilar columns 80−55739
- complex mixtures, GC/MS profiles, HISLIB comparison method 78−7268
- composition determination, cc $LaS_{1.500}$-$LaS_{1.333}$, solid soln. region, density meas. 80−95075
- compound column, sensitivity regulation method 78−35752
- computer-controlled process chromatograph system 79−16102
- computerised monitoring of vinyl-chloride monomer for job safety 79−21727
- conference, Carlsbad, Czechoslovakia (April 79) 80−73097
- conference on analysis instrumentation, Charleston, West Virginia, USA (May 1977) 79−16100
- conversion factor of chromatographs, accuracy 79−74475
- coronene, distrib. with respect to particle size in submicron atm. aerosols 79−74563
- correlation type, noise sources eval. and practical considerations 80−40771
- crocidolite, adsorpt. of organic micropollutants, XPS and gas solid elution chromatography exam. 78−80790
- crude oil classification via computerised gas chromatograph mass spectrometry 77−81456
- cryocollector for IR spectrometer optical system 79−100467
- cytidine-5′-monophosphate, γ-irrad. aq. soln., spin-trapped radicals, liq. chromatography and EPR spectroscopy 78−53340
- data processor, microprocessor based, appls. to chromatography *(Japanese)* 78−61131
- data processor, multistep calc. function *(Japanese)* 80−26091
- data processor for automatic GC(LC) peaks anal. *(Japanese)* 80−50919
- data processor with thermal printer-plotter for GC and LC *(Japanese)* 80−50920
- dense gas chromatograph/mass spectrometer, interface design 79−34378
- density detector operation, mathematical modelling *(Russian)* 78−92580
- detector flow cells irradiation, varifocal compensated lens 79−27357
- di(alkylbenzylthio)ethane, oil additive, thermal stability determ. by chromatography, colorimetry 79−15969
- dichlorofluoromethane in atmosphere, gas chromatography-mass fragmentography anal. 79−62565
- dichloromethane, solidified, solubility in liq. N_2 at 77.4K 80−10673
- diepoxide-diamine network polymers, reaction mechanism investigation using gel permeation chromatography 80−40789
- differential chromatogram simulation and analytical feasibility *(Russian)* 78−35758
- diffuse reflect. spect., standards and calibration rel. to chromatography 77−56278
- diffuse reflectance spectroscopy, applics., standards and calibration 78−32848
- displacement chromatography, isotope separation appl., mathematical model 79−10219
- dry column chromatography 77−77837
- Du Pont DP-1, gas chromatograph/mass spectrometer, sub-picogram detection, wide dynamic range and automatic source rejuvenation 78−93782
- dual-phase column, gas chromatography, two GC columns arranged coaxially are inside the other 80−71962
- electrochemical detection and fraction collection system, for high performance liq. chromatography 78−35749
- electron capture detector measurement of ions using atm. press. ionis mass spectrometry 79−92017

chromatography continued
environmental air samples, gas chromatography-mass spectrometry anal. *(Japanese)* 79—79424
environmental sampling, gas chromatograph/mass spectrometer/data system and spectral search 77—77834
epoxy resins analysis, cured, combination of pyrolysis, gas chromatography and conventional analytical techniques *(Japanese)* 79—87914
1,2-epoxypropane, photopolymerisation by arenediazonium salts, obs. 79—24747
ethane-n-butane-n-hexane, vap.-liq. equilib. behaviour, visual cell, for 48.3-143.5°C, up to 7619 kPa 79—46790
ethylene deuterates, VP isotope effect in liq. and solid, chromatographic purification 77—43337
ethylene-vinylacetate-copolymers charact. by gel chromatography, viscometry, osmotic meas. *(German)* 78—14496
ethyleneterephthalate-ethylene glycol copolyester/15% polyglycol, semicryst. melting and glass transitions 80—49346
extraction, macroporous resins. use as supports for chelating liquid ion exchanger 77—90660
fast chemical separation procedures for short-lived nuclei 77—25351
ferrous alloy melting, chromatogravimetric equipment for redox studies 78—40097
fibre optics refractometers for liquid chromatographic use 77—2683
field flow fractionation, macromolecules appl. 78—90327
fission products in reactor coolant water, continuous radiochem. anal. 77—71652
flame-emission detector for LKhM-8MD gas-liquid chromatograph 77—52706
fluoromethane, deuterium separation at high press. by ns CO_2 laser multiple-photon dissoc. 80—91616
forced-flow, alkaline earth ions detected by photometric method 80—71965
Fourier transform gas chromatograph-IR system, trace organic pollutants detect. 78—68967
free radical copolymerisation kinetics, monomer reactivity ratios under high press. conditions, meas. methods 79—91950
frequency modulated correlation chromatography, mulitple injection technique 80—40764
gas, -solid, -liq., column preparation using graphitised thermal C black 77—77823
gas, adsorbents, modified geophitised C black 79—96358
gas, adsorption props. of transition metal hydroxides 79—66343
gas, appl. of photoionisation detector 77—21441
gas, automatic, vapour-liquid equilib. meas., appls. *(German)* 78—88667
gas, automatic purge and concentrator, volatile organic compounds in water determ. 80—97739
gas, CO_2 meas. in air using glass sample tubes 77—4959
gas, combined with mass spectrometry, forensic laboratory appl. 78—92556
gas, comparison of quenching effects in single-, dual-flame photometric detection 78—61072
gas, computerized testing of capillary column 79—16067
gas, conc. device 80—85235
gas, constant current electron capture detector, development, appls. *(Japanese)* 80—55764
gas, detectors, appl., development, sensitivity, response, operating conditions 77—1955
gas, digital system for cancer research 80—22469
gas, electrically heated metal tube for straightening ends of glass open tubular columns 79—6106
gas, electronics appl. in chemical technology *(German)* 77—77841
gas, errors made by non-specialists 80—55730
gas, experience with pneumatic process composition transmitter 77—44524
gas, flexible fused silica columns 80—45590
gas, for drug determ. in biological samples 79—34388
gas, Fourier transform IR detector system, programmable 78—92560
gas, graphitised C black packed columns, efficiency rel. to particle size 78—92536
gas, high-precision on-stream instrument, process control appl. 78—53283
gas, influence of temp. programming 78—68958
gas, infrared group specific detectors 78—92557
gas, injection port for ghost peak elimination *(Japanese)* 80—50918
gas, ionisation detector theory and performance, review 77—44564
gas, mass spectrometer anal. system, ion multiplier noise filter 78—92541
gas, mass spectrometer as detector appls. 77—77817
gas, method of trapping fractions for vibr. spectroscopic identification 77—4960
gas, multicolumn, multidetector chromatographic reactor, appls. 78—92590
gas, photoionsiation detector appl. 78—92561
gas, prep., use of as stationary phase *(German)* 79—29434
gas, prep-scale, high purity compound prep. for industry 77—1956
gas, problems in use for on-line automatic control *(Spanish)* 77—32865
gas, quantitative, errors, efficiency 78—92538
gas, quantitative, unrecognised systematic errors 78—92537
gas, self-monitoring high-performance chromatograph 77—36823
gas, small size chromatograph with novel temp. control *(Japanese)* 80—50922
gas, unit employing integral photoionisation detector 80—71963
gas, use of C-ray absorpt. detector, determ. of SO_2 in gas mixtures 77—29069
gas, using wall coated open tubular capillary columns, practical guide 80—21347
gas cell, suitable for chromatographic sampling after photolysis 77—70375
gas chromatogram, multidimens., design aspects 77—81436
gas chromatograms, reconstruction from interferometric GC/IR data 78—35737
gas chromatograph, N504 type, charact. 78—11599
gas chromatograph element-specific detection systems *(German)* 80—93837
gas chromatograph modification for capsule dosing system attachment 79—70407
gas chromatograph oven testing 77—77835
gas chromatograph radioactive effluent recycling timer 77—25326
gas chromatograph-mass spectrometer, dual EI/CI ion source *(Japanese)* 78—32919
gas chromatograph-mass spectrometer, field desorption ion source *(Japanese)* 78—32920

chromatography continued
gas chromatograph-mass spectrometer computer system, GCMS PAC-500 series *(Japanese)* 78—32918
gas chromatograph-mass spectrometer system, gas proportional counter detector 77—36815
gas chromatograph-second derivative UV spectrometer system 77—86394
gas chromatograph/mass spectrometer/calculator, low-cost bench-top system 77—4972
gas chromatographic air analyser fabricated on Si wafer 80—73343
gas chromatographic bipolar pulse differential electrolytic cond. detector 80—93814
gas chromatographic detectors, errors in operation 78—92554
gas chromatographic determination of residual monomers, extraction method of sample preparation 77—77845
gas chromatographic effluents, FT IR spectrometric identification 78—73091
gas chromatographic fractions, collection on activated charcoal, IR identification 79—79328
gas chromatographic fractions, on-line identification using multichannel Raman spectrometer 79—83524
gas chromatographic purge-and-trap concentrator with microprocessor control 80—93815
gas chromatography, atmospheric hydrocarbon concentrations meas. appl. *(Dutch)* 78—36300
gas chromatography, coated glass capillary columns 77—36814
gas chromatography, computerised instrumentation 77—77839
gas chromatography, data acquisition and use of microwave plasma detector as element analyser *(German)* 78—64895
gas chromatography, for determ. of halocarbons in air 78—85739
gas chromatography, laser optoacoustic spectroscopic detection 78—92521
gas chromatography, mass spectroscopy and mass spectrometry, current developments *(Japanese)* 78—35766
gas chromatography, programmed temp., retention index calcs. by linear interpolation 78—27844
gas chromatography, selective detection by N_2 induced chemiluminesc. 80—89495
gas chromatography, simultaneous element detection by microwave plasma detector unit 77—56288
gas chromatography—mass spectrometry, sample anal., review 78—3437
gas chromatography advances 79—52809
gas chromatography for volatile organic compounds determ. in city air 78—12003
gas chromatography interfaced with IR or PMR spectroscopy 77—52690
gas chromatography mass spectrometry technique 80—26094
gas chromatography peak identification by ^{13}C and ^{1}H Fourier transform NMR 77—77836
gas chromatography-IR spectroscopy interface, optimised sampling techniques 77—77831
gas chromatography-IR spectroscopy using Sadtler CIRA 101 analyser, vapour phase spectra of liqs. and solids 80—93809
gas chromatography-IR-PMR optimised method anal. 77—86392
gas chromatography-mass spectrometry, computer-based library system 77—44523
gas chromatography-mass spectrometry, computerised, data-blocking cross-correlation peak detection 80—62725
gas chromatography-mass spectrometry, integrated analytical systems, applics. in biomed. and related sciences, review 80—36200
gas chromatography-mass spectrometry, isotope labelled internal standard, isotopic distrib. calc. 77—56265
gas chromatography-mass spectrometry data system, research-oriented, principles and applics. 80—40770
gas chromatography-mass spectroscopy technique in environmental study *(Japanese)* 79—29496
gas chromatography-mass-spectrometry, ion counting operational characts. *(Japanese)* 77—60157
gas chromatography/chem. ionisation mass spectrometry, reactant ion monitoring detection technique 77—77821
gas chromatography/emission spectroscopy in environmental pollution studies 80—26070
gas chromatography/Fourier transform IR spectroscopy, review 80—55729
gas chromatography/IR spectroscopy, high resolution spectroscopy 78—20101
gas chromatography/mass spectrometry system with complete microprocessor control 77—44533
gas chromatography/mass spectroscopy analysis of volatile organic compounds in water supplies 79—12151
gas chromatography/mass spectroscopy system, computer-controlled, DP-102 80—22470
gas phase, developments, automation 77—25342
gas radiochromatography, nondestructive high-temp. method using proportional flow counter 78—44420
gas radiochromatography discharge flow counter for high temps. 79—24859
gas-chromatography, beta radio effluents, window flow counter 80—93824
gas-component analysis of laser fusion targets 79—8464
gas-liquid, computing integrator correction factor 78—76960
gas-liquid chromatography, quantitative anal., systematic errors 78—31722
gas-liquid system, phase equilib. determ. by gas chromatographic headspace anal. *(German)* 78—18753
gas-mass spectrometry integrated anal. systems, review 79—1972
gas-solid, using radiotracers, appl. to adsorption meas. of volatile chlorides 78—76902
gas-solid system, phase equilib. determ. by gas chromatographic headspace anal. *(German)* 78—18753
gas/photoionisation mass spectrometry, organic compds. anal. appl. 78—92531
gaseous fission products, continuous determ. of content in reactor loop 79—30905
gases in transformer oil, power transformer operating state determ. *(Czech)* 79—87894
GC, quantitation of unresolved peaks with similar mass spectra 79—20479
GC/MS integrated systems, review of current techniques 80—68289
GC/MS system for isotope ratio monitoring 79—22855
GC/MS/computer techniques for environmental anal. 79—57554
gel partition/permeation chromatography using n-alkane solutes 78—44429

chromatography continued
gel permeation, automated system using laboratory automation system 80—71961
gel permeation, behaviour of hydrophobic gel beads with double layer struct. 79—66386
gel permeation, combined with low angle laser light scatt., polymer molecular weight distrib. appl. 78—92230
gel permeation, minicomputer data system for polymer characterisation 80—45591
gel permeation, operating variables effect on peak shape 79—74433
gel permeation, polymer characterisation appl. 80—16740
gel permeation chromatography, calibration, appl. to polycarbonate 80—58424
gel permeation chromatography anal., data acquisition, computer control 80—97746
gel permeation chromatography of interacting multicomponent systems, protein isomerisation study 78—68950
gel permeation chromatography of interacting multicomponent systems, protein isomerisation kinetic consts. determ. 78—68951
gel permeation chromatography of polymers, using silicic sorbents *(Russian)* 79—52857
gel-chromatogram processing technique allowing for spreading, Friedholm eqn. soln. *(Russian)* 79—24880
gel-permeation, high-speed aq., mol. wt. determ. of polymers 79—61922
gel-permeation, mol. wt. distrib. of polymer films *(German)* 78—85252
glass bubble, gas anal. using chromatograph 77—52694
glass capillary columns and specification of dedicated instrument 78—80804
glass capillary gas chromatography, review 79—57319
glass capillary gas chromatography with on-column injection 80—11987
graphite, Fe-catalysed gasification, electron, microscopy 80—104358
graphite, laser pyrolysis products exam. 79—20356
halogen leak detection, reduction of background effects by means of chromatographic columns 78—70110
halogen specific detection for high press. liq. chromatography *(German)* 79—87920
heat of adsorption determ., expt. methods 79—42370
heat of adsorption determination, for teachers 79—35497
heterogeneous chromatography, meaning of chromatographic diffusion coefficient in isotope separation 79—50147
high molecular weight polyethylene for HV cables, characterisation using size exclusion chromatography 80—66897
high performance liquid, automatic system to monitor effluent tank contents 80—71982
high performance liquid, flow measurement, control system for reciprocating pumps, HPLC detectors appl. 78—92559
high performance liquid, sample introduction, syringe injection 80—66906
high performance liquid chromatography, automating preparatory techniques 77—52719
high performance liquid chromatography, automation 78—80806
high performance liquid chromatography, derivatisation techniques 77—44562
high performance liquid chromatography, developments 77—73491
high performance liquid chromatography, efficiency maximization 80—3438
high performance liquid chromatography, use for multicomponent serum analysis 79—79334
high performance liquid chromatography, UV discrete wavelength detector at 274 nm 79—75595
high performance liquid chromatography automation by microprocessor control 77—86422
high performance liquid chromatography with programmed runs 78—11583
high performance liquid chromatography/continuous flow anal. 78—11582
high performance low pressure liquid chromatography, laboratory appl. 78—80801
high pressure liquid, UV laser 2-photon excited fluoresc. detect. 78—7266
high pressure liquid chromatography, electrochem. detectors 77—36811
high temperature ALC/GPC equipment, Waters 150C, polymers appl. 79—10806
high-performance liquid chromatography, reversed-phase, hydrophobic effect 79—34385
high-pressure liquid chromatograph, operational principles and appl. *(German)* 77—12856
high-pressure liquid chromatography, microprocessor controlled 79—83528
high-sensitivity autoionography, detection of radioactive spots on thin-layer chromatograms 78—86960
HPLC, fluoresc. detect. method 78—48735
HPLC, fluoresc. spectrophotometric detect. method 78—48737
HPLC, high sensitivity UV detector 78—45709
HPLC, modular instrument 78—48736
HPLC, refr. index meas. detectors 78—45675
HPLC, two-pump gradient, accuracy and reproducibility 80—16742
HPLC, UV absorption detector 78—45707
HPLC, UV detection 78—45706
HPLC, UV variable wavelength monitor 78—45708
HPLC detection systems, review 78—48733
HPLC packing materials, comparison 79—24863
HPLCs, automated, with CRT display 79—57321
human disease study using mass spectrometry and metabolite profiling 80—51289
hybrid chromatographic system techniques for unique identification 79—70403
hydrocarbon resin, mol. wt., chem. constitution investigation by gel permeation chromatography *(German)* 78—64910
hydrocarbons, (C_2-C_9), determ. in rock samples by capillary gas chromatograph 79—39226
hydrocarbons, aromatic and aliphatic, gas chromatographic determ. in airborne matter 79—79434
hydrocarbons, volatile, detection and meas. in atm. review 77—64492
hydrocarbons chemisorbed on SiO_2-supported Ni, chem. composition *(German)* 79—92002
hydrodynamic, for colloidal particle size meas., mathematical modelling 77—1951
hydrodynamic, role of colloidal forces 78—48717
hydrodynamic chromatography technique for colloid particle size anal. 77 44530

chromatography continued
in-situ chemically-modified surfaces for normal-phase liquid chromatography 79—16056
indole decapeptide luteinising hormone, high-press. liq. chromatography, fluorometric detect. 78—20096
indolic compounds in pigmentary retinal epithelium of trout, chromatography detect. *(French)* 79—53115
industrial chromatograph dynamic error estimation 77—77853
industrial chromatograph static error determ. and correction 77—81446
information processing by computer 80—71970
inorganic gas chromatography for determ. of H_2O and CO_2 in rocks and minerals 80—85767
insulating oils, dissolved gas anal. for power transformer fault diagnosis 80—26097
integration TIM for GC-CI-MS system *(Japanese)* 77—90697
interferometric data from GC Fourier transform IR spectroscopy, functional group anal. 80—89548
ion, equipment for the measurement of ions in solution 80—71983
ion, historical and theoretical aspects, appls. 79—79336
ion, on-stream, appl., impact on energy conservation 80—55737
ion chromatography, inorganic ion analysis 79—83538
ion chromatography, method using conductimetric detection 79—16109
ion chromatography, new analytical technique for sulphate and nitrate assay in ambient aerosols 78—68974
ion exchange, appl. at NBS 80—7880
ion exchange, significance for chemical anal. and radiochem. 77—25343
ion exchange chromotography for Co and rare earth determ. in alloys for high energy magnets *(Polish)* 80—35606
ion exchange membrane detector for liquid chromatography, characterisation appls. 79—16055
ion exchange technique and appls. 78—3411
ion-exchange, enzymatic digestion of γ-irradiated DNA 78—85290
ionising radiation decomposition of chromatographic support materials *(German)* 78—92587
isotope separation, derivation of comprhensive expression for conc. profile 78—29856
Kevlar-49, chemical characterisation 78—95725
light pipe gas cell, Au coated internally, for gas chromatography/Fourier transform IR spectroscopy 80—89555
liquid, analogue differential wattmeter appl. *(Czech)* 78—23979
liquid, appl. to improvement of liquid crystal purity 79—14682
liquid, automatic fraction-separating system 80—45589
liquid, band broadening, in microcapillary tubes 78—61085
liquid, coupled with Raman spectroscopy for anal. of mixtures *(French)* 80—45595
liquid, detector characts. and use, book 78—15751
liquid, detector development 77—73492
liquid, differential deviation refractometer appl., high sensitivity and time response conditions *(Czech)* 78—80810
liquid, electrochemical detection by voltammetry 80—50906
liquid, electron capture detector 79—16091
liquid, high performance, amperometric and coulometric detectors 77—70347
liquid, high performance, direct-coupling to FT-NMR 79—34412
liquid, high performance, dual wavelength spectrophotometer detector use 79—92023
liquid, high performance, liq. sample loop geometry 78—92539
liquid, high performance, solute elution behaviour on porous polystyrene gel 78—92524
liquid, high performance, summary of the role of the mobile phase 79—11835
liquid, high performance, with CRT display, microprocessor-controlled 79—20478
liquid, high performance in-house slurry packing of columns, advantages 78—92555
liquid, high press., gravity flow, amberlite XAD copolymer packings 77—77822
liquid, high press., pulse dampening system 78—92540
liquid, microinstrumentation 77—12865
liquid, organic compound isolation from water 77—1957
liquid, packed microcapillary columns 78—61069
liquid, preparative, freely programmable fraction collector with automatic repetitive injection 79—79338
liquid, pump design review for HPLC apparatus 78—80800
liquid, radial compression separation system for improved column performance 80—76568
liquid, retention enhancement by ion pair form. in nonpolar stationary phase 78—35746
liquid, reverse phase, resolution change with column temp. 78—92525
liquid, Si target vidicon tube performance as multiwavelength detector 77—90658
liquid, sorption materials characteristics and development trends *(Czech)* 78—64904
liquid, thin-layer electrochem. detect. cell 77—25327
liquid, universal interactive controller for HPLC automation 80—55731
liquid, using volatile solvents, effluent detector 78—92529
liquid, UV detector suitable for preparative work, effluent flow over angled quartz plate 80—71960
liquid, variable wavelength UV photometer as detector 77—44535
liquid chromatograph, microprocessor-based, reproducibility 77—9152
liquid chromatograph for homogeneous mixture analysis 80—16757
liquid chromatography, computer-based bibliography update 78—31736
liquid chromatography, organic compound ionisation under atm. press. 80—86488
liquid chromatography, real time Fourier transform IR detector 78—86357
liquid chromatography, spectrometric detect., computer control of data acquisition, reduction and display 78—27850
liquid chromatography detector based on dielec. const. meas. 77—21436
liquid chromatography detectors, novel approaches 78—15747
liquid chromatography effluents on line anal., micro liq. chromatograph-interfaced Fourier transform IR spectrophotometer 80—73483
liquid chromatography/mass spectrometry combined analysis, appls. 78 31735
liquid column chromatography, scintillation counters, review *(Czech)* 80—27885
liquid or gaseous, principle, developments and appl. *(French)* 80—45596
liquid phase elution chromatography for determining solubilities of organic liqs. in H_2O 80—71958
liver support, using affinity chromatography systems 78—7538

chromatography continued
long-term reproducibility monitoring for chromatographic methods 79—70409
low-boiling compound separation by low-temp. gas chromatography 79—70397
lubricants, ester-type, thin-film test for meas. of oxidation and evaporation 80—40626
many component sample GC-MS anal. *(Japanese)* 78—35767
marine sample petroleum analysis by gas chromatography and mass spectrometry 77—4977
Mars Viking surface sampler subsystem, acquisition assembly 79—12380
metal species, identification and determ. by chromatographic-at. spectrosc. method 78—68972
methacrylic acid-N,N'-ethylenedimethacrylamide crosslinked copolymer soln., 3-dimens. struct. peculiarities *(Russian)* 79—55678
methane, machine treatment of chromatographic curves using statistical moments method 77—63981
methane diffusion in He, coeff. determ., gas chromatography method 77—11298
4,4′-methylenebis(2-chloroaniline), air sampling and anal. method 79—79420
α-methylstyrene-butadiene copolymers, chem. composition determ. by gel permeation chromatography 79—70410
microcomputer controlled GC with data processor and printer-plotter, appl. *(Japanese)* 80—50921
microconcentration meas., calibration characts. estimation 80—26084
Micronova computer interfacing scheme 80—93813
Microprobe Mole/plasma chromatograph system, for anal. of compounds on micron scale 80—101049
microprocessor based chromatographic system 80—71999
microprocessor based process gas chromatograph, System 9010 80—61205
microprocessor controlled liquid chromatograph 80—21351
microprocessor integrators for chromatography, development, operation, capabilities 77—56287
microprocessor-based chromatography data system 77—36826
microprocessor-based computing integrator 78—31737
microprocessor-controlled gas chromatograph, low temp. range extension 78—3395
microthin film chromatogram evaluation by scanning fluorimetry and digital image analysis *(German)* 79—5188
microwave-induced plasma in He, evaluation as element-selective detector in gas chromatography 77—81450
miniaturised systems, associated technical parameters 79—96391
mixture chemical analysis, direct interferogram comparison of chromatography/Fourier transform IR spectra data 79—100458
mixtures, determ. of number of compounds present 79—43657
mixtures, universal gas chromatographic system, based on frontal anal. 78—61114
monoalkylcyclohexanes, heats of vaporisation by gas chromatography-calorimetry method 79—34344
monoterpene hydrocarbons in rural atmospheres, gas chromatography/mass spectrometric anal. 80—17336
multicomponent sorbents, composition, computer optimisation 78—27842
multidimensional gas chromatography, advantages of pressure balancing 79—70408
multidimensional gas chromatography, pressure balancing techniques 80—89576
net repulsive van der Waals forces between different particles, macromolecular, or biological cells in liqs., appls. 80—34274
N-nitrosodimethylamine, trapping for GC/MS analysis 78—20094
nondisplacement chromatography for chromatographic isotope separation 79—50146
nonlinear, nonideal, computer simulation models 80—62639
nonlinear detector response quantification with lab. automation system 80—40775
nonrecursive, based on analogue delay device, for mass spectrometer ion multiplier 78—92541
nontechnical explanation for instrument technicians and operators 79—29431
nonvolatile materials, in-situ sampling system for thermal volatilisation anal. by GC/MS 77—77828
nuclear mixed oxide fuel, retained fission gas determ., new instrumental method 79—54477
nuclear oxide fuel anal., coulometry, emission anal., chromatography, X-ray anal. 80—18420
nucleic acid bases, anal. in photographic gelatins by liquid chromatography 79—20501
nylon 6,6, drawn fibre, selective degradation, gel permeation chromatography, TEM 78—71683
nylon 6,6, selective degradation, mol. wt. determ., gel permeation chromatography, TEM 78—71682
odour analyser, automatic, for atmospheric sulphide anal. *(Japanese)* 80—50924
odour detection, instrumental techniques *(Dutch)* 79—16658
oil pollution in marine sediments, rapid field detect. method 79—12143
oil spill analysis with gas chromatography 78—7294
on-stream analysers development, w.r.t. speed and reliability 77—66778
optical detectors for HPLC, conf., Loughborough, England (July 1977) 78—48732
organic residues, gas chromatogram quantitation, using algorithms for microprocessor based integrator 78—27839
organic solids, photoproduced in simulated Jovian atmosphere, mol. anal. 78—69740
papain inactivated by OH radicals and H_2O_2, optical density, amino acid composition and fluoresc. 78—53344
particle porosimetry by inverse gel permeation chromatography 77—90659
peak shape, dead volume and flow rate effects, exponentially modified Gaussian model 77—70351
pentane, combustion, isotopic tracer studies of the further reactions of pentenes 79—8438
perturbation chromatography theory, model independent aspects 79—8463
phenol (oestrogen) compounds, high-press. liq. chromatography, fluorometric detect. 78—20096
photographic emulsions, thin layer chromatographic anal. of dyes formed by development *(Japanese)* 77—26418
Pioneer Venus Sounder Probe gas chromatograph 80—67507
plasma chromatograph-mass spectrometer, H_2O determ. in electronic component packages 78—86379

chromatography continued
plasma chromatograph/mass spectrometer column overload prevention valve 80—16748
plasma chromatograph/mass spectrometer sample overload protection 79—39237
plasma chromatograph/mass spectrometer simultaneous electron impact/chem. ionisation carrier gas mixture 79—30600
plasma chromatography, baseline corrector for boxcar integrator instruments 77—52717
plasma chromatography, mobility and composition of hydrated positive reactant ions 79—74435
plasma chromatography, NH_4^+ reactant ion technique 78—44419
plasma chromatography and electron capture detector, comparison between two techniques 80—61176
plastics testing, automation 80—76443
PMMA, solvent cast, surface characts., chromatographic study 80—20020
poly(vinyl pyrrolidone), mol. wt. determ., high-speed aq. gel-permeation chromatography 79—61922
poly(vinylalcohol), mol. wt. determ., high-speed aq. gel-permeation chromatography 79—61922
poly [2-(p-azidobenzoyloxy)ethyl methacrylate], MW distrib. effects on photosensitivity *(Japanese)* 78—94418
poly-α-methylstyrene-polybutadiene, light beam and Curie point pyrolysis investigation *(German)* 79—57223
poly-ε-caprolactum, semicryst. melting and glass transitions 80—49346
polyacrylamide, mol. wt. determ., high-speed aq. gel-permeation chromatography 79—61922
polybutadienes, radiation chemically cross-linked, charact. by pyrolysis gas chromatography *(German)* 80—81348
polycarbonate, bisphenol-A, mol. wt. determ. using gel permeation chromatography 80—58424
polydisperse polymer, anal. of mol. mass. distrib. *(Russian)* 77—31038
polyelectrolyte+physiologically active substance complexation, stability, kinetics *(Russian)* 80—8006
polyethylene, crosslinked, from HV cables, high-pressure liquid chromatography and differential scanning calorimetry 79—100466
polyethylene, linear, bulk-crystallised, morphology study 79—32918
polyethylene, meas. of high chain extensions by gel permeation chromatography 77—88611
polyethylene glycol, mol. wt. determ., high-speed aq. gel-permeation chromatography 79—61922
polyethylene glycols, size exclusion chromatography, response correction of differential refractometer 79—34375
polyethylene terephthalate, mol. wt. determ. by GPC *(Chinese)* 79—55009
polyethylene wax characterisation by gel chromatography, osmotic meas. and scattered light meas. *(German)* 77—86420
polymer, gel permeation chromatography, data treatment 79—92037
polymer, volatile constituents anal. by thermal desorpt., gas chromatography and mass spectrometry 79—43664
polymer films, mol. wt. distrib. by gel-permeation chromatography *(German)* 78—85252
polymer molecular weight correlation with physical and rheological props. 77—51011
polymer-solvent interaction from gas-liquid chromatography, open tubular column expts. 78—35753
polymeric films, gas solubility, gas chromatographic determ. *(Russian)* 79—65205
polymers, gas chromatography meas. of struct. and interactions 77—90698
polymers, paints, testing, modern analytical methods appl. *(Polish)* 78—85253
polymers, pyrolysis-mol. wt. chromatography—vapour phase IR spectrophotometry, on-line system, reviews 80—55768
polymethylmethacrylate, denture base resin, residual monomer determ. 79—16077
polynuclear aromatic compounds, HPLC separation using aminosilane stationary phase 78—35747
polypeptide hormones, liquid chromatographic separation 79—74450
polypeptide hormones fragmentation anal. by chromatography 79—92448
polyphenylacetylene cis-trans isomers, rel. mol. wt. distrib., heating effect 80—106409
polypropylene, Halen and Daplen, semicryst. melting and glass transitions 80—49346
polystyrene, mechanical degradation, limiting degree of polymerisation 77—85985
polystyrene films, UV irrad., struct. changes, gel permeation chromatogram computer manipulation, substraction 79—96387
polystyrene lattice cleaning, dialysis, steam stripping and ion exchange effectiveness 80—3414
polystyrene solutions, US degradation obs. 78—95989
polystyrene-co-divinylbenzene microgels in dimethylformamide, diffusion coeff., viscosity and mol. wt. meas. 80—30286
polystyrene-polydivinylbenzene, interpenetrating network, IR, NMR and chromatographic anal. of intermediate regions 77—55711
polyurethane, interpenetrating network, IR, NMR and chromatographic anal. of intermediate regions 77—55711
polyvinylacetate solution, long-chain branching characterisation, molar masses 79—94122
porcelain raw material, ion exchange chromatography method, for separate determ. of Na_2O and K_2O 78—7272
porphyrin pigments, in geochem. systems, HPLC determ. 78—61078
positive pressure columns 78—73092
potential barrier, colloid particle separation 77—73474
powders, specific surface measurement, chromatographic method 77—77859
process chromatograph, on-stream gas, high-precision 79—16111
process gas chromatograph, microcomputer based 79—16101
process gas chromatograph H_2 flame ionisation detector air purifier and methanator 77—52696
process gas chromatographs, microprocessor based, calibration and data reduction 80—81402
process liquid, appl. for anal. of industrial streams 79—16110
propane, vapour-liquid and vapour-solid equilib. data, mass spectroscopic tracer pulse chromatography 80—37115
propanolol, (adrenergic blocking agent), high-press. liq. chromatography, fluorometric detect. 78—20096
propylene-alkyl acrylates alternating copolymers characterisation 79—51950
protein, amino acid composition determ. 79—44070

chromatography continued
proteins on diol-bonded SiO_2 gel stationary phase, high performance liquid chromatography 80—61174
pseudocontinuum mass transfer in media with spatially periodic boundaries 79—86500
pulse counting techniques, in organic mass spectroscopy-gas chromatography 78—31720
pulse gas chromatography meas. of mass transfer coeffs., internal diffusivity, and adsorption rate consts. in packed bed 79—48002
PVC chlorinated, mol. parameters determ. 79—41974
PVC soln., mol. wt. meas. by gel-permeation chromatography 79—7045
PVC-THF-H_2O, precipitation fractionation, influence of stereoregularity 79—7046
pyrochromatography of structurally related steroids 80—26050
pyrolysis gas, for analysis of tyre rubber blends, computer controlled 79—96396
pyrolysis gas chromatography for polymer quantitative anal., internal standard choice 80—61180
Quadmagnova, GC/MS system, computer scanning and control 78—76946
quadrupole mass spectrometer applics. to gas chromatography 77—25350
quaternary ammonium ions, detect. by liq. chromatography with ion-exchange membrane detector 79—16055
radial, high performance, apparatus and techniques 78—80802
radial chromatography, optimization of high performance thin layer chromatography 79—57320
radio-liquid chromatograph system, determ. of ^{14}C-labelled amino acids *(Japanese)* 80—104834
radio-scanning, continuous method, for ^{14}C-labelled compounds 77—70367
radioactive source leak testing under dynamic flow conditions 80—3432
radiochemical purity quality control by rapid feedback system 77—90900
radiochromatogram localisation detector for static direct meas. *(French)* 77—77842
radiochromatograms, thin-layer, anal. by proportional chamber 78—77174
radiochromatograms, ultra-low-level, multicounter system for scanning 77—88335
radiochromatographic gas purification equipment, adsorptive capacity of activated C for inert gases 77—52673
radiochromatography, beta-ray imaging using a multiwire proportional counter 80—102387
radiogas chromatography, software package for data collection and processing 78—20086
radiopharmaceutical purity determ., adaptation of multichannel scalar device for radiochromatogram scanning 78—48894
Raman spectroscopy, chemical species anal. in conjunction with liq. phase chromatography *(French)* 80—93823
rare-earth fission product isotopes, separation in thin-films chromatography *(German)* 80—37635
reaction and separation in pulse-fed catalytic reactor 78—64880
refractive index detector for monitoring model dialysis expts. 79—96724
11-cis-retinal prep. by irrad. of all-trans-retinal and high press. liq. chromatography 78—40453
reversed liquid phase chromatography, biochem. applic., review 79—34371
reversed phase, using non-aq. mobile phases, charact., appls. *(Japanese)* 80—50917
reversed phase chromatogaphy, sorbents and approaches 77—36825
rhodamine Zh, isomer separation, identification and emission efficiencies *(Russian)* 77—83871
rubber blend, computer controlled pyrolysis gas chromatography 79—20493
sample introduction automation 77—4949
scanning spectrofluorimeter-densitometer 80—31901
scirpene toxins, in animal feeds, chem. anal. 78—48707
search system, one-dimensional, for GC and MS anal. 78—23977
semiautomated thin-layer chromatography with scanning flame ionisation detector 79—74466
semiconductor gas detector, for gas chromatograph, electroadsorption phenomena *(Russian)* 78—7307
shape variation detection, two-component chromatographic peaks resolution 80—71971
silica gels, surface treatment, adsorption properties *(Japanese)* 78—95855
size exclusion, pore size matching, new method 80—3437
size exclusion chromatography in polymer characterisation 78—11580
solution adsorption, from liq. chromatography 78—84054
solvents and adsorbents classification, expanded solubility parameter treatment 79—74449
specific metal gas chromatographic detector, Ar plasma emission source 79—74438
spectroscopic element detector for gas chromatography 78—31721
stability criteria, appl. to gas chromatography 78—62049
standardised gas-chromatograph cells *(German)* 79—5243
stopcock batcher for gas withdrawal in chromatograph 79—52810
styrene-α-methylstyrene copolymers, prep., charact. by pyrolysis gas chromatography *(German)* 79—29355
styrene-butadiene copolymers, chem. composition determ. by gel permeation chromatography 79—70410
styrene-butadiene copolymers, struct. study by pyrolytic capillary gas chromatography *(German)* 78—18557
styrene-isoprene block copolymers, dilute soln., conform. obs. 79—10774
styrol batadiene polymers, light scattering and Curie point pyrolysis, pyrolysis gas chromatography *(German)* 79—96393
sugars, detect. in HPLC systems using polarimetry, refractometry and optical rot. 78—48734
supercritical fluid chromatograph, pneumatic amplifier pump 78—88665
surface contaminants analysis by plasma mass secspectroscopy 78—3433
TC, online analysis by scanning system 77—40599
teaching, mobile spectroscopy, chem. anal. laboratory 78—93502
technique and applications *(Dutch)* 80—93819
teflon-modified gas-liquid chromatography support 80—3429
tetrachlorodibenzo-p-dioxin determ. by low resolution gas chromatography-mass spectrometry 80—66893
thermochromatography, deposition zone position in temp. grad. tube 79—70402
thin layer, high performance, efficiency parameter terminology 78—20098
thin layer, high performance, programmed multiple development with small particle plates 77—77838

chromatography continued
thin layer, IR identification following programmed multiple development 78—15727
thin layer, luminesc. meas. methods 78—53305
thin layer, luminescence quantitation, solvent effects 78—53306
thin layer, prep. of sample application 77—70372
thin layer, quantitative, methodology, principles and appls. 80—16744
thin layer, quantitative photometric scanning, analysis of organic substances appl. 78—92558
thin layer and high performance thin layer chromatography, review of equipment 80—26082
thin layer chromatogram quantitative anal., computer controlled photometer 77—60326
thin layer chromatography-mass spectrometry, direct on-line coupling system 78—7270
thin-layer, amino acid and urea anal. of samples obtained by percutaneous electrophoresis 78—61237
thin-layer, precision zone determ. 79—74456
thin-layer, Programmed Multiple Development 77—4973
thin-layer fluorescence chromatograms, automatic meas. and data processing 79—29424
thin-layer gel apparatus for chromatography in organic solvent systems 78—27873
THTR fuel reprocessing Pu and Np separation from aqueous soln. *(German)* 77—83067
thymidine-5-monophosphate, γ-irrad. aq. soln., spin-trapped radicals, liq. chromatography and EPR spectroscopy 78—53340
trace organic pollutants in water, conc. and gas chromatographic determ. methods 79—52854
trans-Pu solvent extraction recovery and purification by trioctylphosphine oxide chromatography 80—93826
transactinides, gas phase separation methods 77—26954
transformer oil diagnosis, computerised evaluation of results *(Czech)* 80—97744
transition metal complex ions in aq. HCl, temp. gradient chromatography *(Japanese)* 78—61120
turbogenerators, H_2 cooled, heating-up detect. by gas stream chromatography and mass spectrography *(French)* 79—48024
two-dimensional chromatogram quantitative evaluation 79—84064
vacuum gas chromatography-mass spectrometry, using short gas capillary columns 78—95968
vacuum value for gas chromatograph/mass spectrometer system 79—39245
van Deemter equation modification, for organic liq. diffusion coeff. data interpretation 78—2277
vapour cell, single pass, for GC/IR spectrometer appls. 80—16743
Venus atmosphere, Pioneer gas chromatograph analyses, laboratory simulation 80—46362
Venus lower atmosphere composition, anal. by gas chromatography 79—48721
Viking lander gas chromatograph-mass spectrometer 78—77460
vinyl chloride, trace determ. in water by direct injection GC/MS 78—35739
water pollutants, trace analysis using automated HPLC 79—96384
waterborne oil fractional analysis by high-performance liquid chromatography *(Japanese)* 80—81936
Al_2O_3, alumina, adsorpt. of saturated hydrocarbons, gas-solid chromatography based on compensation effect 80—26053
Ar purifier, portable, 0.3 m^3/h, design and appl. *(Polish)* 79—12781
B_4C, kinetics of high temp. oxidation in oxygen, chromatography method 77—21305
^{10}B separation using anion exchange resin, isotopic plateau holding displacement chromatography *(Japanese)* 78—56886
Ba, detection by photometric method 80—71965
C black with pyrocarbon coating, surface props. *(French)* 78—68921
CHNS, simultaneous determ., combustion-gas chromatographic method, data processing 80—40762
CO_2, atmospheric, gas chromatographic meas. using electron capture detect. 79—57549
CO_2, vapour-liquid and vapour-solid equilib. data, mass spectroscopic tracer pulse chromatography 80—37115
Ca, detection by photometric method 80—71965
$Cs_2Ni_3(P_2O_7)_2.nH_2O$, thermal dehydration 80—35513
^{137}Cs-^{137m}Ba generator, for nucl. medicine, preparation by ion exchange chromatography 78—28071
Er, thin layer chromatography 78—20105
F_2, anal. with in-line gas chromatograph 77—63982
Gd, thin layer chromatography 78—20105
H_2, determ. in H_2O after photolysis, gas chromatography 78—61089
H_2SO_4, air pollution, new detector, aerosol mobility chromatograph 78—96297
He microwave detection system for gas chromatography 79—74447
^{129}I and organic compound determ. in LWR irradiated fuel solns. *(French)* 79—3230
^{131}I-4-iodoantipyrine preparation from ^{131}I-iodide 80—12256
$K_2Ni_3(P_2O_7)_2.nH_2O$, thermal dehydration 80—35513
La, thin layer chromatography 78—20105
Mg, detection by photometric method 80—71965
Mn pyrophosphates, physicochem. charact. 77—39562
Mo complexes, aquo ions in solutions, isolation, characterisation 77—77847
$(NH_4)_2Ni_3(P_2O_7)_2.nH_2O$, thermal dehydration 80—35513
NO_2, atmospheric, gas chromatographic meas. using electron capture detect. 79—57549
N_2O, determ. in water using electron capture detection gas chromatography, multiple equilib. 80—76566
$Na_2Ni_3(P_2O_7)_2.nH_2O$, thermal dehydration 80—35513
Nb, separation from fission products, fast chem. methods 77—16856
O_2, determ. in H_2O after photolysis, gas chromotography 78—61089
^{32}P-labelled compound, radiochromatographic scanning procedure 77—9151
PbO-SiO_2 glasses and crystal, silicate anion constitution 79—48023
$Rb_2Ni_3(P_2O_7)_2.nH_2O$, thermal dehydration 80—35513
Re compounds, formed during vaporisation-gas-chromatography, from filament 79—74465
Ru, neutron deficient isotopes, gas thermochromotographic separation from AgCl 79—865
S, SO_4^{2-} and related species, sampling and anal. of atm. aerosols 78—96283
SF_6 insulated switching installations and devices, gas chromatography appl. *(German)* 78—88668

chromatography continued
SF$_6$ tracer technique for near-stack reactor effluent dispersion studies 78—11992
SF$_6$ with gaseous contaminants, arc decomposition kinetics investigation by combined gas chromatograph-mass spectrometry methods 80—92250
^{35}S content of coolant gas in Windscale AGR, gas chromatographic and radiochemical anal. 78—73125
Sb separation from fission products, fast chem. methods 77—16856
Si gas-sensitive microtransducer, cond. variation with pulsed ethanol adsorption *(Russian)* 80—50915
Si, VPE layer props. control using boundary layer characts. 80—50561
SiO$_2$ gel, macroporous, modification of surface by adsorption of thin layer of polymer 80—6624
Sr, detection by photometric method 80—71965
Tc, separation from fission products, fast chem. methods 77—16856
^{99m}Tc, determination in bleomycin-^{99m}Tc preparations, thin layer and paper chromatography *(Russian)* 77—77855
^{99m}Tc radiopharmaceuticals, rapid miniaturised chromatographic quality control procedures 78—28070
^{99m}Tc-EDTA complex production method and renal retention obs. 80—12254
^{234}Th, isotope separation by extraction column chromatography using TnOA and filter paper 79—43659
U isotope separation by Redox chromatography 80—37565
U losses, at eluting agent interface in anion exchange chromatography, prevention 78—48706
UF$_6$ anal. with in-line gas chromatograph 77—63982
Zn plating electrolyte, ion-exchange chromatography of Zn, Cd and Al salts 77—16890
Zr, separation from fission products, fast chem. methods 77—16856

chromium
see also nuclei with ......
abundance in stars, Utrecht UV spectrophotometer obs. 78—69793
activators for cementation at Zr/graphite *(French)* 77—52552
adhesion layer, etching of deposited Au film, SEM anal. of abnormal undercutting 79—5075
adsorption of O$_2$ and initial oxidation on (100) surface 80—20034
adsorption of O, photoemission exam. 79—19976
AES meas. 77—36323
AES meas. of soft X-ray emission threshold potential *(Russian)* 79—33866
L-alanine:Cr^{3+}, X-irrad., thermoluminesc., ESR, UV photobleaching 77—9104
alkali halide:Cr^{+}, Szigeti charge and correl. with hyperfine coupling const. 80—96831
alkaline earth silicates, Cr^{2+} solid solubility 77—76564
alloying with rare earth metals, Ti, Zr, Hf, Nb, Ta 78—68651
alum:Cr^{3+}, forbidden EPR transitions, theory 78—31106
amorphous, elec. cond. calc., t-matrix approach 77—55510
Anderson model of 3d virtual states 77—72987
anodic behaviour in methanolic solns. 77—73368
antiferromagnetic, deformation waves and spin density waves, electron diffr. obs. *(Russian)* 79—19721
antiferromagnetic, elec. resist. near Neel temp. 79—33278
antiferromagnetic, electron interference oscills. and spin-density-wave energy gaps at Fermi surface 80—49574
antiferromagnetic, EM absorpt. 79—51925
antiferromagnetic, mag. and non-mag. impurities hyperfine interactions, ^{181}Ta and ^{100}Rh TDPAC meas. 78—43704
antiferromagnetic, mag. struct., phase transition, and magnon spectrum, random anisotropy effects 80—88722
antiferromagnetic, mag. susceptibility calc. two band model for electronic spectrum 78—10663
antiferromagnetic, magnetisation process *(Russian)* 78—15007
antiferromagnetic, mixed state, mag. torque and magnetostriction meas. 77—89909
antiferromagnetic, muon depolarisation, mag. anisotropy determ. *(Russian)* 79—61290
antiferromagnetic, muon diffusion, spin relax. and coherent motion 80—71281
antiferromagnetic, phase fixation, excitonic and spin superfluidity of electron-hole pairs 78—30872
antiferromagnetic, polarisation domain effects on US velocity 78—52329
antiferromagnetic, positive muons as light isotopes of H, book contrib. 79—82907
antiferromagnetic, pressure effect on Fermi surface by de Haas-van Alphen effect *(Russian)* 80—6701
antiferromagnetic, spin wave spectrum calc. 77—36063
antiferromagnetic, spin-flip transition 77—63186
antiferromagnetic, stress depend. of Fermi surface 77—11846
antiferromagnetic, stress depend. of spin density wave state 77—63257
antiferromagnetic, surface Raman scatt., calc. 80—45069
antiferromagnetic, transverse magnetoresist., electron interference oscills. 80—65534
antiferromagnetic, US attenuation and phase diagram 80—103831
antiferromagnetic spin density waves, mag. anisotropy 77—69540
antiferromagnetic spin-density-wave domain and size and behaviour, X-ray and neutron topography 79—42793
antiferromagnetic structure, mag. field effect, spin density wave model *(Russian)* 80—70953
antiferromagnetic transition, first order, crit. neutron scatt. obs. 79—33480
antiferromagnetic with nonmagnetic impurities, mag. susceptibility using two band model 80—2559
atom, $^7P_0^0$ state, radiative lifetime in matrices, meas. using laser ablation and selective excitation 80—71959
atom, double K-shell ionisation by electron impact, X-ray spectra 78—62928
atom, double K-shell ionisation by electron impact 78—62929
atom, excitations, comparison of gas-phase, plasma, sputtering and beam-foil 80—32820
atom, ionisation potential, term value, correlation energy by vertical anal. 78—41964
atom, Kα^h hypersatellite spectra and double photoionisation cross-section 79—85922
atom, Kα^h hypersatellite spectra and K-shell double photoionisation cross-section 78—21874
atom, Kα and Kβ X-ray spectra induced by 84 MeV N^{4+} 77—50517
atom, Kβ/Kα ratio anomalies, K-capture rel. to bremsstrahlung excitation 77—18825

chromium continued
atom, K-shell ionisation cross sections, proton induced 77—23556
atom, Koopmans' ionis. pot., relax. correction 79—18308
atom, multiphoton ionisation and absorpt. 80—95575
atom, O$^{2+,3+,4+,5+}$ induced K-shell X-ray production cross section, 7 to 24 MeV 77—61850
atom, radiative lifetimes, laser ablation and selective excitation spectroscopy 78—17824
atom, rel. at. transition probabilities, by flame at absorption spectroscopy 79—89642
atom, X-ray production by protons by 0.5 to 2.0 MeV energy 78—66646
atom, X-ray spectra, chemical bonding and multiple ionis. effects 78—50630
atom, X-ray spectra in Tokamak-10 facility plasma *(Russian)* 78—9837
atom, X-ray transitions in laser produced plasma 80—100093
atom in CO$_2$ hypersonic flow, excitation temp. meas., hook method 77—58200
atomic displacements in electron irrad. cryst. 79—46705
atomic fluorescence, intensity profile in acetylene-air flame 77—52680
atomic transition probabilities, oscill. strengths 78—74601
band electron momentum distributions calc. 78—18950
band structure, X-ray emission bands, self-consistent calc. 77—28104
band structure and Fermi suface of paramag. solid *(Russian)* 79—65375
black, coating on Cu substrate, selective solar energy absorpt., model calcs. 79—57440
black, electrolytic deposited, characterisation and thermal stability *(French)* 80—55898
black, electroplated solar collector coatings, high temp. optical and struct. degradation 80—66995
black, plating process for solar selective absorber 79—62031
black chrome, electroplated layer, field ion microscopy study 79—28246
black Cr and Ni electrodeposit spectral selective props. for solar absorbers 79—62036
black Cr coatings, optical props., using inhomogeneous medium theories 80—12026
black films, electrodeposited, visible and IR reflectance 77—81168
black solar selective absorbers, thermal degradation 80—61417
borate glass:Cr, Raman spectra of Cr^{VI} 77—52076
Bushveld Complex upper zone, magnetite Cr content vars. rel. to magma chambers heterogeneity and convection 80—56421
calcium tartrate tetrahydrate:Cr^{3+}, optical absorpt. spectrum, cryst. field parameters 80—16067
cast, B additions effect on struct. and props. *(Russian)* 78—19891
cathodic alloying on surface, for increased passivation and corrosion resist. 80—100940
cathodic dichromate treatment passivation of Sn plate, nature of Cr 77—56139
charged particle prod. cross sections for 14 MeV neutrons, Ti, V, Cr, Mn 80—42648
chemisorption of C, N, and O, SXAPS obs. 79—52048
coated Nb, prior thermal working effect on coating quality *(Russian)* 78—23820
coated steel Kh25N20S2, structural transformations, oxidation effect 79—57154
coating on Ti, effect on mech. props. *(Russian)* 77—44290
coating on Ti alloy, electrospark applied, friction and wear resistance obs. *(Russian)* 79—1916
coatings, electrodeposition, conditions rel. to H$_2$ conc., internal stresses 77—1933
coatings, plasma-chemical deposition using transport reactions *(Russian)* 80—16191
Compton X-ray scatt., electron binding energy effect 77—59639
concentration determ. in atm. and rainwater in Vizcaya, Spain *(Spanish)* 78—57264
concentration in atmospheric sedimentable powder, in Vizcaya, Spain *(Spanish)* 78—57265
condensates, lattice const., internal stresses *(Russian)* 80—107141
contact to GaAs, effect on minority carrier diffusion length 78—72260
corrosion, high-temp., in Cl$_2$ and Cl$_2$-O$_2$ mixtures 78—15601
corrosion at high temp. in Cl$_2$ and Cl$_2$-O$_2$ mixtures 77—77629
corrosion by O$_2$ containing H$_2$O and gaseous NaCl, volatile products 78—27674
corrosion due to V$_2$O$_5$ melts *(Japanese)* 80—93691
corrosion in SO$_2$, 700-1000°C 80—97642
corrosion resistance increase by Pd electrospark coating *(Russian)* 78—27669
corrosion resistant pure metal, passivity and pitting in chloride solutions 78—44258
corundum, Cr influence as impurity on thermochem. etching 80—88190
critical coeff. of resistivity near Neel temp. 77—59417
crystal equilibrium, lattice dynamical model 78—22811
crystal structure below Neel temp., X-ray diffr. study 78—83772
cubic fluoride lattice, π-electron spin density due to Cr^{3+} ion 80—49683
CVD of protective coating on steel, struct. and carbide form. 77—40387
CVD on Ni, reaction mechanism, growth rate and struct. obs. 80—39476
Debye-Waller factor, temp. variation, lattice dynamical calc. 78—55925
Debye-Waller factors, extended de Launay model calcs. 80—70352
Debye-Waller factors, temp. depend. calc. 78—22807
deposited by high rate sputtering, mech. props. 77—36630
determ. in water and organic materials, flameless atomic absorpt. spectrometry with wire loop atomiser 80—45586
determination, in biological materials, by NAA 78—27855
determination, in cement, by direct atomisation AAS *(Japanese)* 79—70413
determination, in Mg alloy, emission spectrographic DC arc-powder technique 78—48713
determination, in steels, by spectrographic method using combined discharge 79—57327
determination in urine by electrothermal atomic absorpt. spectrophotometry 80—61175
diffuse electron scatt. *(Russian)* 80—103438
diffusion characteristics in Ag, 1051 to 1220K 80—15308
diffusion chromising with sintering, effect on porous struct. of Fe-based powder PZh2K 79—66219
diffusion coating, carbide-free, on grey cast Fe 79—96205
diffusion coating of steel, fatigue fracture, microstruct. investigation *(Russian)* 79—52446
diffusion coating strengthening by plastic deformation, controlling physical factors *(Russian)* 77—25187
diffusion from GaAs substrates 80—10708

chromium continued
- diffusion in Au along grain boundaries, analytic and numerical solns. 77—4274
- diffusion in Cu 77—62674
- diffusion in Fe_3O_4, magnetite, as function of O partial press. 78—43183
- diffusion in Fe, and C diffusion, US effects *(Russian)* 77—59144
- diffusion in GaAs, interimpurity interaction effect on distrib. profiles of impurities diffusing simultaneously 77—76451
- diffusion in GaAs substrates, radiotracer profiles 80—24680
- diffusion in MgO crystal 77—35754
- diffusion saturation of commercial Fe and steel in closed reaction space, kinetics and mechanism 79—52458
- diffusion through Au films at low temp., Co effect 80—100361
- discontinuous thin film, AC equivalent circuit anal. 79—51690
- distribution in alloy steel welds, laser emission microanal. method 78—61110
- DMSO:Cr^{3+}, Nd^{3+}, energy transfer and migration, donor-acceptor interaction, phosphoresc. quenching conc. depend. 78—64403
- in early type peculiar stars, abundances 77—78803
- effect on carbon steel weld metal hot cracking resistance 79—79061
- elastic moduli meas. for paramagnetic Cr, comparison with Ti-V, V-Cr, rel. to bandstructure 80—7615
- electrochemical behaviour, in molten V_2O_5 *(Japanese)* 80—89498
- electrode reactions with molten glass 80—85186
- electrodeposit, formation of axial texture (111) [hkl], math. model *(Russian)* 78—84082
- electrodeposited chrome black solar absorber surfaces, characterisation using $^{52}Cr(p,\gamma)$ 80—7878
- electrodeposition, high purity 78—84724
- electrodeposition 80—16248
- electrodeposition mechanism 79—60648
- electrodeposits, BCC, on {100} Cu substrates, {211} twins obs. 77—47698
- electrodeposits, hardness estimation by X-ray diffraction method 77—36708
- electrodeposits, relation between preferred orientation and microstructure *(Korean)* 77—28733
- electrodes, arcing and breakdown meas. in vacuum 77—24238
- electrolytic, internal friction and bending modulus, −200 to 800°C *(Russian)* 77—39626
- electrolytic oxidation in SO_2 atmosphere, CrO_3 ionic defect effects *(Ukrainian)* 78—92504
- electron emission induced by low energy light ions 79—61482
- electron energy loss mechanism, surface and volume losses, anal. 79—91547
- electronic energy loss of protons (deuterons), 80-800 keV 79—23666
- electronic struct., spin-density functional calcs. 80—88476
- electronic structure model, Invar effect, antiferromagnetic-non mag. transitions 80—20370
- electroplate, protective coating, effect on props. of substrate 77—21330
- electroplated steel, laser treatment 80—21191
- electroplating, prod. experience with trivalent plating solns. 80—71606
- emissivitvy and reflectivity, oxide film thickness effect 79—82364
- enthalpy and specific heat, empirical eqn. *(Russian)* 80—92683
- etching, HF ion-plasma, cryst. surface layers treatment and study *(Russian)* 80—16517
- evaporated film, refl. and struct. 78—72021
- evaporated film, stratification phenomenon, interf. metrology *(French)* 77—59225
- fast reactor structural material, integral expts. 80—13612
- fast reactor structural materials, activation, (n,p), (n,α) cross sections 80—13624
- fast reactor structural materials, nuclear data 80—13611
- Fermi surface, stress depend., from quantum oscill. effects 78—91597
- Fermi surface under press., de Haas-van Alphen effect meas. 80—75499
- ferromagnetic surface layer on antiferromag. bulk, determ. by surface magnetoplasma wave detect. 78—68356
- film, 1/f type noise, spatial correlation 79—38194
- film, 3p-3d intershell interaction, photoemission 80—80934
- film, BCC, optical props. 79—78781
- film, beam splitter phase coatings, for producing phase quadrature interferometer outputs 78—77974
- film, contact reaction with amorphous Si 79—23846
- film, damping and vel. of longit. elastic waves at 9.4 GHz 80—10596
- film, defects and mechanical stability, different deposition methods *(Bulgarian)* 80—44438
- film, deposited by cylindrical magnetron sputtering, internal stresses 80—24773
- film, deposition on glass surface heated between room temp. and 300°C 77—90277
- film, EELS, anomalous L_3/L_2 white-line ratios 80—93444
- film, effect of substrate temp. on formation, electron microscope obs. 80—39469
- film, electron beam evaporator for in situ deposition studies in UHV electron microscope 80—40264
- film, evaporated, black selective solar absorbers 77—34956
- film, evaporated, concurrent ion bombard. effects 80—80142
- film, evaporated, on die-cast Zn , microstruct. and intrinsic stresses, substrate temp. effects 78—10304
- film, evaporated, optical props., rel. to struct. 80—55211
- film, obtained by thermo ionic precipitation, phase composition, lattice parameters *(Russian)* 80—96756
- film, on mild steel, hardness and protective props., rel. to grain size 78—11436
- film, on NaCl, preferential epitaxy induced by electron bombard. or elec. field 80—10824
- film, on polycryst. CdS, thermal diffusion, 240-400°C 80—80001
- film, on sapphire epitaxial relations 79—60649
- film, pattern generation by laser-induced oxidation 80—61009
- film, prep. by decomp. of bis-arene cpds., struct. and elec. props. 80—60785
- film, prep. by evap. and ion plating, AES determ. of comp. profiles 77—89675
- film, reversal etching in gas plasma, reaction mechanism, AES and XPS obs. 80—16564
- film, size effects on spin density waves, struct. and elec. props. 77—80973
- film, sputtering yields, proton-induced X-ray meas. 80—50488
- film, thickness meas., using nondestructive radioisotopic technique 80—68179

chromium continued
- film, trivalent, cathodic deposition, as bonding interface between Cu and polyethylene 80—76201
- film, vac. deposition onto low temp. substrate, cryostat *(Japanese)* 78—27403
- film, vacuum deposited, O^+ bombardment sputtering rates 78—88390
- film, vacuum deposited on Zn substrate cracking caused by intrinsic stresses 78—6238
- film, vacuum evaporated, particularities in growth on alkali halides with Pb colloids and F-centres 79—82496
- film, vacuum-deposited, quantitative mass anal. by colorimetry 77—69998
- film, vacuum-evaporated, with A-15 struct., prep. and characterisation 77—62768
- film, vapour deposited on low temp. KCl substrates, struct. obs. 80—10826
- film containing Cr_2O_3, struct., oxide percentage determ. and elec. props. 80—103607
- film for resistor appls., prep. and props. *(Hungarian)* 77—4737
- film on glass substrate with ZnS of MgF_2 underlayer thermal strength, recrystn. influence 79—87748
- film on Si, ion implanted, inert-gas-bubble form., TEM and Rutherford backscatt. anal. 79—90682
- film on steel, type AISI 316, thermal passivation in controlled vacuum 80—76276
- film sandwich structures Auger anal. 78—72030
- film vacuum deposition on glass display panels 78—39694
- films, photoresist film on reverse gas plasma etching 80—97634
- films, vac. deposited, defects *(Russian)* 79—33203
- films, vac. evaporated, optical cond. 80—76100
- fine particle solar absorber, effective medium theory 80—21396
- fine particles, δ- and BCC, mag. props. 78—52314
- fine particles formed by gas-evap. technique, cryst. struct. and habit 79—27935
- fission reactor structural material, resonance data eval. below 300 keV, Doppler effect calc. 80—13618
- fission reactor structural material data eval. for JENDL-1 80—13617
- floating zone-refining, activation anal. 80—29875
- foil, laser irradiated, low-angle X-ray scatt., angular block misalignment and hardness *(Russian)* 80—103413
- force field 79—33051
- fracture during electrospark cutting *(Russian)* 79—87719
- frictional behaviour, effect of mechanical properties 80—55548
- n-GaAs:Cr(Si), deep-level extrinsic photocond. response, decay at 4.2K 80—2420
- galactic cosmic rays, isotopic composition, balloon meas. 78—89024
- galvanic coating on steel 45, thickness determ. by profilography 80—85095
- gas phase, He I photoelectron spectra, photoionisation cross section meas. 79—98051
- glass:Cr^{3+}, absorpt. spectra, Fano antireson. and vibronic Lamb shift 80—71458
- guanidine aluminium sulphate hexahydrate:Cr^{3+}, ESR spectra fine struct. 80—93169
- guanidinium aluminium sulphate hexahydrate:Cr^{3+}, EPR, 295.5, 78.45, 1.61K, zero field splitting 78—68359
- guanidinium aluminium sulphate hexahydrate:Cr^{3+} pressure meas. from ESR 79—38375
- guanidinium aluminium sulphate hexahydrate:Cr, temp. depend. of zero field splitting parameter in EPR spectra 77—69679
- guanidinium gallium sulphate hexahydrate:Cr^{3+}, press. meas. from ESR 79—38375
- Hall coefficient, mag. field depend. at low temp. 77—20296
- hardfacing materials, friction characts. in high temp. Na *(Japanese)* 80—89356
- high purity, thermal cond., elec. resist., Seebeck coeff., 280-1000K 77—39816
- hyperfine interactions on ^{111}Cd-probe nuclei, TDPAC meas. 80—75904
- hyperfine particles, surface magnetisation, explanation of expt. work 78—23303
- II-VI semiconductor, Cr^{2+}-doped, Jahn-Teller interaction energy calc. 78—2455
- implantation in mild steel, annealing and rolling behaviour of conc. profile 78—75684
- implantation into Cu for corrosion protection 80—71789
- impurity concentrations on wall during Tokamak discharges, laser probing technique 80—49013
- incoherent neutron scatt. cross section, neutron polarisation anal. 79—24137
- Incoloy-800, creep-fatigue interaction 77—70113
- incommensurate antiferromagnetic crystal, inelastic neutron scatt. meas. 80—25088
- inelastic neutron scatt. expts., spin density waves 80—44818
- interaction with dense stream of N ions, metallography, microhardness, specific volume *(Russian)* 80—15169
- interatomic pair potential, phonon spectra 80—33927
- interface with polymer, electronic struct., XPS study 80—45204
- internal friction and segregation effects, cellular struct. *(Russian)* 77—66669
- internal magnetic pressure and compressibility anomalies, itinerant model 77—16034
- interstellar abundance and depletion models 80—46630
- ion beam milling, amomalous sputter yield behaviour 80—108624
- ion bombardment induced photon and secondary ion emission on O_2 atmosphere 77—90231
- ion-plated, deposition parameter influence on struct. and hardness 79—82485
- ions in Tokamak plasmas, spectroscopy and atomic physics 80—53938
- island film nonlinear I-V characteristics, 20 Hz to 15 GHz 79—7910
- island film photoconductivity obs. 78—95392
- island film real structure and electrical conductivity obs. 79—77948
- isotopic composition of primary cosmic rays 79—70937
- K shell prod. cross section of Ti, Cr, Fe, Ni, Cu, Zn for 75 to 150 keV p and e excitation 79—47552
- K-shell X-ray prod. by $^{14}N^+$ bombardment 80—91482
- kinetic friction re-examination using modified pin and disc machine 80—55547
- laser, near IR transitions in Cr vapour 80—99704
- lattice dimensions, difference between vacuum condensates and massive specimens *(Russian)* 77—31912
- lattice dynamics, and sp. ht., extended de Launay model 79—46762

chromium continued
lattice dynamics, improved Fielek model 80—59598
lattice dynamics, phonon dispersion and atomic force constants, phenomenological model 78—26640
lattice frequency spectra, sp. ht., Debye temp. 78—22799
lattice vibrations, Debye temp., freq. wave vector dispersion relations 78—63818
linear expansion coefficient, at low temp. 78—83977
liquid, multiple scatt. calcs. of resist. 78—76039
liquid, N_2 absorption at high temps., Cr-N phase diagram, solubility-temp. relation *(Japanese)* 79—43201
liquid, N activity coeff. 77—72699
localised moments, detection by electron energy loss spectra 77—69949
magnetic excitations of incommensurate spin density wave 80—11183
magnetic form factors, neutron diffr. study 79—47234
magnetic hysteresis of single cryst., neutron diffr. obs. 79—15327
magnetic phase diagram, near spin-flip temp. 80—60267
magnetic phase diagram in external mag. field, spin reorientation curve, critical point coordinates *(Russian)* 80—29548
magnetic phase transition at Neel temp. 78—2681
magnetic structure, effect of mag. field direction, neutron diffr. obs. 77—63121
magnetic superspace-group symmetry 80—79726
magnetic torque anal. in thermally activated domain model, near spin-flip temp. 77—63229
magnetic-atom cluster, spin Hamiltonian for direct exchange interaction 77—20519
magnetoresistance in antiferro- and paramag. states, meas. 15 to 80°C 77—85197
methylammonium aluminium sulphate dodecahydrate, single crysts., high-order EPR transitions of Cr^{3+} 80—108052
methylammonium aluminiumselenate:Cr^{3+}, EPR and linewidth anomaly 77—12191
methylammoniumgallium sulphate:Cr^{3+}, EPR and linewidth anomaly 77—12191
MgO:Cr^{3+}, single cryst., ESR linewidth 80—29605
muon probe, μ^+ depolarization and diffusion 77—59500
muon spin rotation meas. 79—56667
n=2-2 transitions in XUV spectra, anal. 80—102472
Neel temperature and Fermi energy, nonmag. impurity effects 80—65888
neutron activation analysis in water using preconc. on activated C 78—3993
neutron irradiated at 24.5K, elec. resist. exam. of radiation damage *(French)* 78—30671
nuclear material, neutron capture cross sections in intermed. energy region, method and exptl. facility 78—21637
optical absorption spectrum, 0.25-21 μm *(Russian)* 77—81118
optical constants 12 to 24 μm, anomalous skin effect region 77—20842
optical waveguide cladding, attenuation, mode props. 77—27351
oxidation, combination anal. using ESCA, AES and SIMS 78—72924
oxidation, combined AES and threshold potential spectroscopy 78—11026
oxidation, Cr-O bonding, high resolution AES *(French)* 79—100468
oxidation, electron microscope study *(Japanese)* 77—48577
oxidation, in air, CO_2 and H_2O vapour, kinetic peculiarities in formation of oxide films *(Russian)* 79—74303
oxidation, in hostile environment, in situ meas. method 78—44277
oxidation, reflectance IR study rel. to component of stainless steel 79—47811
oxidation in pure CO_2 77—86224
oxidation in TEM 77—48593
oxidation kinetics, 300 to 600°C, O_2 press. effects 77—59983
oxidation kinetics, 300 to 600°C, struct. and morphology of oxide film 77—59982
oxidation resistance, rare earth impurities effect 80—66703
oxidative vaporisation, thermochemical analysis 78—11447
oxide film form., combination anal. using ESCA, AES and SIMS 79—16092
oxide glass:Cr^{3+} absorption and emission 78—6774
paramagnetic, Hartree band struct., Fermi surface, nesting wave vector 80—49583
particle formation, ultrafine, via pulsed laser breakdown of $Cr(CO)_6$ 80—84881
particle nitrogenation, metallographic obs. *(Bulgarian)* 78—15712
particles, on reflecting substrate, selective absorpt. of solar energy, model calcs 79—79405
particles, ultrafine, for photothermal conversion of solar energy 78—71163
particulate layer on Cr_2O_3, high solar absorpt. characts., selective surface electroplating 78—87111
passivation, film form., stability and breakdown 78—19937
γ-phase Cr, new model, consistency with mixed-valency Cr chemistry 79—47995
phase transformation, low-temp., structural changes *(Russian)* 79—52202
phase transition at T_N 79—4676
phonon dispersion, Debye temp. and Debye-Waller factors, lattice dynamical model 78—55920
phonon dispersion curves, extended du Launay model 77—4162
phonon dispersion relations, modified tensor force model 80—103428
photon emission due to Ar^+ ion bombard., adsorbed and recoil-implanted O effect 80—80872
plasma, pulse hollow cathode discharge, time resolved high resolution spectroscopy 80—38759
plasma, Tokamak-produced, $2s^22p^k$-$2s2p^{k+1}$ transitions in F I to Be I isoelectronic sequences 80—37765
plasma impurity, flux on wall of DITE Tokamak 80—28688
plasma oscillations, Fermi level position effect on excitation energies for band transitions 79—99493
plasma produced by 250 ps laser pulse, X-ray spectra 77—19769
plate, microcracked, microanal. of F by $^{19}F(p,\alpha\gamma)^{16}O$ 79—79351
plated Cu crystal, const. strain rate tests, yield stress 79—83276
plated on steel, factors influencing durability 80—108643
plated steel, H_2 distrib., laser-mass spectrometer investig. 78—61113
plating thickness meas. with MIP-10 78—53144
polyethylene contact charging, electron transfer mechanism, PES characts. 80—35055
positron annihilation radiation angular correl., band struct. and Fermi surface study 78—6260
powder, plasma deposition for production of contact portions of cermet electric heating element 78—11364

chromium continued
powder, thermogravimetric exam. of nitridation rate *(Japanese)* 79—20292
powders (60 to 70%), spectral determination of Al and Fe 77—90679
protective coating on C steel, durability obs. using nuclear radiation excited X-ray fluoresc. 80—21206
purification, from bis(ethylbenzene)chromium *(Russian)* 80—35128
pyrolytic coating, effect of support metal mech. props. on formation *(Russian)* 80—7713
Q-state, single, antiferromag. phase, rel. to band struct. 77—15759
Q-vector locking, press. induced hardening 80—103870
radioactivation analysis, of biological and geological materials, separation methods *(French)* 77—90700
radionuclides prod. cross sections induced by 12-45 MeV protons 77—17310
reactions with Y_2O_3, IR spectroscopy 79—100297
reactor structural material s-wave resonance parameters from capture cross section data 80—13629
residual stress meas. by X-ray diffr. using $\sin^2\psi$ method 79—15059
ruby:Cr^{3+}, diffusion of localised optical excitations and trap emission 77—24887
ruby:Cr^{3+}, ESR saturation, dynamical mag. susceptibility increase in zero mag. field 77—40122
ruby:Cr^{3+}, exchange integral, pressure depend., test of theory 78—87741
ruby:Cr^{3+}, high mag. field spin-lattice relax. rates in ground state of ion 79—61407
ruby:Cr, lifetimes of laser-induced population density gratings, comparison with fluoresc. lifetimes 79—64276
ruby:Cr, relaxation behaviour, EPR study, environmental effects 80—66021
ruby, Cr^{3+} ESR transition influence on ^{27}Al, distant ENDOR and dynamic nucl. polarisation 80—2664
ruby, Cr content determ. *(Russian)* 77—48745
Saguenay fjord sediments, distrib. and partition of Co, Ni, Cr and V 77—33100
sapphire:Cr^{3+}, excess charge carriers, generation, transport and trapping 79—82646
secondary ion emission, energy spectra, 0-55 eV, contamination levels 79—15573
secondary negative ion emission, effect of adsorbed O_2 *(Russian)* 79—28881
self-diffusion activation energies, positron trapping meas. 79—74015
self-weldability in high temp Na *(Japanese)* 80—89392
silicate glass: Cr^{3+}, optical props., 88-273K, energy levels in crossing region 78—6709
silicate glass:Cr, Raman spectra of Cr^{VI} 77—52076
single modulation state, temp. limits of cryomagnetic method 78—72374
sliding charact., friction and wear *(Japanese)* 78—56778
solar abundance from photospheric spectra and oscillator strengths 78—69757
solubility in β-Na_2O-Al_2O_3 rel. to isomorphous replacement of Al^{3+} 77—85926
solubility in liq. Li, impurity effects of O_2, N_2 and C 79—77760
solution mechanism in fused KNCO 79—39271
source material, partial press. anal. 78—72731
spallogenic isotopes in Fe meteorites, radial distrib. 80—67488
specific heat of strained and annealed samples 79—38331
spin decay waves, appl. of interacting virtual bound state picture 77—69464
spin density wave, CDW and strain wave, effect of spin polarisation of reservoir and imperfect nesting 78—56284
spin density wave, Nambu-Eliashberg eqns. for k-state electron-hole pairing 80—97050
spin density wave, stress and impurity conc. depend. 77—73029
spin density wave, temp. depend. of second and third harmonics 77—12094
spin density wave phases, domains 80—103871
spin density wave Q vector, vel. depend. 79—4669
spin density wave Q-vector, temp. and press. depend. 80—11167
spin density wave state, phenomenological free energy density description 80—75720
spin density waves detected by Ta mag. hyperfine field meas. 78—60364
spin relaxation of μ^+-mesons *(Russian)* 79—8083
spin-density-wave antiferromagnet, uniaxial anisotropy 78—10640
spin-flip transition temperature, press. depend. from elastic const. meas. 80—65944
sputtered, growth struct., influence of substrate surface topography and ang. of adatom incidence 80—20058
sputtered film., internal stresses, effect of substrate orientation and rotation 79—77968
sputtered wafer, internal stresses 77—39753
steel, alloyed with Cr, Mo, Co, Mn, martensitic point position depend. on cooling rate *(Russian)* 79—70063
steel, maraging, 0Kh6N8M7S, effect of Cr, Ni and Mo on hardness 80—21093
steel, mild, conc. profile of implanted Ni and Cr 77—81339
Sternheimer valence shielding antishielding factor including exchange 77—85182
strain and spin-flip transition, Landau theory 78—39318
strain hardened metal and microalloys, low temp. brittleness 79—96140
strontium formate dihydrate:Cr^{3+}, optical absorption spectrum 80—50380
substrate for CdSe, thin film transistor, cryst. struct., substrate defect effects 80—70563
substrate for layered Co films, for digital mag. recording 79—83118
surface, (100), clean $(\sqrt{2}\times\sqrt{2})R45^\circ$ struct. 80—2255
surface, (111), acoustic phonons Brillouin scatt. data 78—95222
surface, (111), oxidation, LEED and RHEED meas. *(French)* 78—39955
surface, itinerant antiferromagnetism and density waves 79—82743
surface, X-ray prod. by 5 MeV/amu deuterons (oxygen ions), projectile Z depend. 80—42982
surface atom electron binding energy depend. on composition, Auger spectra, APS spectra 80—39655
surface electronic struct., tight-binding approx. calcs. 78—64090
surface reactive, field ion microscope and atom probe obs. 79—29410
target foil preparation by electrolysis 78—21110
TGS:Cr^{3+}, EPR and spontaneous polarisation stabilisation during annealing 77—4610
TGS:Cr^{3+}, EPR obs. of ferroelectric monocrystals, fine struct. EHT-SCCC-MO calcs. 79—19769

chromium continued
TGS:Cr^{3+}, EPR obs. of fluctuations near phase transition 78−43820
TGS:Cr^{3+}, polarisation reversal, static hysteresis loops, switching, EPR 78−43633
TGS:Cr single cryst., lattice defect influence on critical behaviour 80−25315
TGS-type crystals:Cr^{3+}, radiospectroscopic studies 79−15341
TGSe:Cr^{3+}, polarisation reversal and ageing mechanisms, EPR meas. 79−8044
thermal vacancies, energy of form. and conc. 80−29014
thin film, chemical cpd. form. by N_2^+ and Ar^+ ion bombardment *(Russian)* 79−73225
thin film resistor, rare earth alloying effects *(Russian)* 79−78211
thin films, electron-beam deposition on Al_2O_3, quartz and glass 80−7496
trace quantity analysis, based on laser ablation and selectively excited radiation 79−39228
transition metals, surface- or defect-induced magnetism, nearly half-filled bands 79−1671
transverse spin-density-wave phase, absence of neutron diffr. line broadening due to polarisation domains 77−24677
twin and stacking fault energies calc. 80−2038
ultrafine particle selective absorption of solar energy 79−62035
ultrafine particles, coatings for selective absorpt. of solar energy, efficiency 78−18060
ultrafine particles, selective solar energy absorption 78−18027
US velocity and damping in Neel temp. range, thermocyclic treatment effect *(Russian)* 79−91282
US vibrations, anomalous damping under hydrostatic press. 79−14890
vacuum-chromized Ti alloy VT3-1, fretting corrosion in couple with unprotected alloys *(Russian)* 78−56804
vapour deposited, struct., mech. props. 77−36400
vapour deposited on polystyrene, core-level spectra 79−56911
vapour deposition, columnar struct. rel. to deposition conditions 78−52675
vapour deposition by hollow cathode discharge, mass and energy anal. for incident ions on substrate 78−23630
vapour deposition on O-treated polystyrene, microscopic interactions 80−3407
vapour press. above different crystallographic planes *(Russian)* 78−18762
volt ampere characteristics during electron melting process *(Russian)* 80−75336
whisker crystal growth incorporated with field electron emission 80−44458
X-ray emission, plasmon satellite 77−28662
X-ray emission spectra, $K\beta_{1,3}$, low energy plasmon $K\beta'$ satellite 79−74020
X-ray emissive short-wave satellite lines in K-series, mech. of formation *(Russian)* 79−91538
X-ray fluorescence, $K\alpha$ hypersatellites 77−18830
X-ray K_β emission spectrum, unpaired electrons and plasmon correlation 78−88383
X-ray K absorpt. discontinuities 78−60532
X-ray K-absorpt. edge shifts, plasmon energies correlation 80−20734
X-ray K-emission satellites, quasi-stationary states and origin 80−80903
X-ray resonant Raman scatt. and fluoresc. near K-absorpt. edge 79−52042
XPS, valence bands 78−35249
XPS escape depths and relative photoionisation cross section for 3p subshell 77−73212
Zircaloy-4, ^{51}Cr bulk diffusion 79−73347
Al complex, Al urea$_6$(ClO_4)$_3$:Cr^{3+} structural phase transition, ESR meas. 77−20681
Al/Cr thin films, interdiffusion meas. 79−82391
Al-Cr, thin film metal contact, sheet resistance changes 80−80356
Al-Cr thin film interdigital transducers for SAW devices at GHz freqs. form. by electron beam lithography 80−4702
$Al_xGa_{1-x}As$:Cr, deep level props. 79−69465
$Al_xGa_{1-x}As$:Cr, exptl. verification of Cr^{2+} models of photoluminescent transitions 78−27320
$Al_xGa_{1-x}As$:Cr, high resist. film, photolum. and photocond. meas. 78−72596
$Al_{2x}Ga_{2(1-x)}O_3$:Cr^{3+}, luminesc., lifetime, 77 and 4K, struct., energy transfer 79−28798
$Al_{2x}Ga_{2(1-x)}O_3$:Cr^{3+}, luminesc., lifetimes 79−33784
$AlNH_4(SO_4)_2$:Cr^{3+}, optical spectral, crystal field, spin orbit and exciton interactions 80−34958
α-Al_2O_3:(Cr^{3+}), optical absorption spectra, DC and AC field effects 78−10925
α-Al_2O_3:Cr, crystal defects from X-ray irradiation, F-centres, X-ray luminesc. obs. 80−55176
Al_2O_3:Cr, electron irrad. induced cond., TSC and EPR study 80−80277
Al_2O_3:Cr, Mg, stabilisation of Cr^{5+}, thermal cond. meas. 78−22905
Al_2O_3:Cr, thermally detected EPR of Cr^{2+}, Cr^{3+} and Cr^{4+} meas. 77−63273
Al_2O_3:Cr photoexcited crystals, cooperative thermoluminescence quenching *(Russian)* 80−80881
Al_2O_3:Cr^{2+}, HF phonon spectroscopy using supercond. tunnel junctions 80−65178
Al_2O_3:Cr^{2+}, Jahn-Teller study, EPR data anal. 78−84172
Al_2O_3:Cr^{2+}, multiple-ion phonon absorpt. 79−82971
Al_2O_3:Cr^{3+}, impurity centre interaction with external elec. field 77−89727
Al_2O_3:Cr^{3+}, inhomogeneous spin system, time evolution towards saturated state 80−88869
Al_2O_3:Cr^{3+}, Jahn-Teller system, zero-phonon line broadening due to nonradiative transitions 80−108258
α-Al_2O_3:Cr^{3+}, local deform. due to uniaxial stress 80−34140
Al_2O_3:Cr^{3+}, new method for spin-lattice relax. time, inhomogeneously broadened ESR lines 79−15343
α-Al_2O_3:Cr^{3+}, Raman effect to probe dynamical processes of Cr^{3+} photoexcited states 80−2740
Al_2O_3:Cr^{3+}, ruby, reson. scatt. and trapping of 29 cm^{-1} acoustic phonons 80−93403
α-Al_2O_3:Cr^{3+}, solid soln. hardening, yield stress conc. depend. 77−28823
Al_2O_3:Cr^{3+}, solid-state nuclear spin-flip maser pumped by dynamic nuclear polarisation 77−31084
Al_2O_3:Cr^{3+}, spin-lattice relaxation time in Cr^{2+}, Mn^{3+} presence 79−99755
Al_2O_3:Cr^{3+}, standard reference material for EPR 79−12757

chromium continued
α-Al_2O_3:Cr^{3+}, stress-induced linear dichroism in $^3A_2(^3T_1)\rightarrow{}^3T_2$ transition, Jahn-Teller effect 80−34884
α-Al_2O_3:Cr^{4+}, ground state spin Hamiltonian parameters and electric field effect 77−15801
α-Al_2O_3:Cr(Ti)(V), impurities effect on thermoluminesc. 80−40170
Al_2O_3-Cr (III), radiationless relax., heat-pulse meas. technique 77−36277
Al_2O_3-Cr cermet, Ti effect on sinterability 79−61552
Al_2O_3-Fe_2O_3:Cr^{3+}, dil. paramag. system, Cr^{3+} conc., effect on cross relax. 79−15387
Al_2O_3-Fe_2O_3(:Cr^{3+}) paramag. system, cross relax. temp. and mag. field effects on Mossbauer spectra 79−33576
β-Al_2O_3-Na_2O:Cr, absorpt. and emission spectra, mag. susceptibility 79−15495
(Al_2O_3-Fe_2O_3):Cr^{3+}, (0.04 mol.% Fe_2O_3), paramag., cross relax., annealing temp. effect from Mossbauer meas. 80−44983
$Al_2(WO_4)_3$:Cr, and undoped crystals, luminesc. obs. 80−89047
Au/Pt/Cr films, diffusion of Si, depth anal., optical and Rutherford backscatt. meas. 79−10981
Au-Cr bifilm, resistivity and struct. changes under heat treatment, diffusion effects 77−1497
Au-Cr bilayer system, optical mechanical and corrosion properties 77−32707
$BaTiO_3$:Cr, annealed in H_2 and O_2, valence change in phase stability 80−20600
BaV_2O_6:Cr, EPR spectra temp. depend., paramagnetic ion point symm. 80−71166
$Be_3Al_2(SiO_3)_6$:Cr^{3+}, Raman effect to probe dynamical processes of Cr^{3+} photoexcited states 80−2740
$Be_3Al_2Si_6O_{18}$:Cr^{3+}, EPR spectra, exchange-coupled pairs 79−28596
$Be_3Al_2[Si_6O_{18}]$:Cr^{3+}, artificial emerald, distrib. of Cr^{3+} impurity 80−59505
$Bi_2Al_4O_9$:Cr^{3+}, luminesc. expts. 80−60656
$Bi_{12}GeO_{20}$:Cr^{3+}, level distrib. of Cr^{3+} ion, spectroscopic parameters, spin Hamiltonian, EPR spectrum 78−48030
$Bi_{12}GeO_{20}$:Mn, Cr, reversible photochromic effects, absorpt. spectra before and after illum. 79−91471
BiI_3:Cr^{3+}, ESR, spin-lattice relax., temp. depend. 78−88178
$Bi_{12}SiO_{20}$:Mn, Cr, reversible photochromic effects, absorpt. spectra before and after illum. 79−91471
CaO:Cr^{2+}, APR spectra 79−87313
CaO:Cr^{2+} Jahn-Teller system, APR spectrum, zero strain site energy level diagram 79−99756
$Ca_5(PO_4)_3F$: Cr^{5+}, spin-lattice relax. time and Debye temp., EPR obs. 79−28601
CaS:Cr^{3+}(Cr^+), EPR *(Russian)* 78−91946
CaV_2O_6:Cr, EPR spectra temp. depend., paramagnetic ion point symm. 80−71166
CdF_2:Cr^{2+}, orthorhombic Jahn-Teller distortion 78−19007
$CdIn_2$:Cr, photocond. and photoluminesc. spectra 77−28214
$CdIn_2S_4$:Cr, absorpt. and photoluminesc. spectra, Cr conc. depend. 79−78712
$CdIn_2S_4$:Cr, thermal cond., 1.8 to 200K, phonon scatt. by impurity ions 77−76627
$CdIn_2S_4$:Cr^{3+}, ESR and ENDOR 77−20692
CdSe:Cr far IR transmission and reflectance spectra 80−71429
CdTe:Cr, impurity photoionisation transitions, EPR meas. 80−39857
CdTe:Cr, introduction of elec. active defects 80−103647
CdTe:Cr, optical props. meas. 79−73969
CdTe:Cr^{2+}, absorpt. and luminesc. of $Cr^{2+}(d^4)$, cryst. field theory interpretation 79−83000
Co_3O_4:Cr, elec. cond. and thermo-EMF 80−20231
Cr (III), (VI), determ. in industrial wastes 78−61105
Cr electrodeposit on steel, stress meas., X-ray methods 79−29298
Cr I, discrepancies between theoretical and experimental oscillator strengths 77−83539
Cr I, inner shell absorpt. spectrum, 3d wavefunction collapse 77−23455
Cr I, vapour phase absorpt. spectrum, 30-400 Å, excitation of 3p-subshell 78−21866
Cr I excited levels, lifetime meas., oscill. strengths 77−71777
Cr I lines, 200-541 nm, oscillator strengths determ. from hook-method and absorpt. meas. 77−79582
Cr I to XXIV, energy levels, ionis. pots., g-factors, from spectral data review 77−79556
Cr II lines, A_{mn} transition probabilities 80−14099
Cr II-VI, struct. and transition probabilities, ab initio calc. using Thomas-Fermi central pot. 79−3360
Cr III, spectra obs. in low-voltage sliding-spark discharge 77−6710
Cr III complexes phosphoresc. risetime meas. in near IR by photon counting 77−41706
Cr IV, 3d and 4f energy level parametrisation, Slater parameters and correl. corrections 80−87041
Cr IV, semiempirical calc. of energy spectra 77−46499
Cr MIS solar cells on Si, proton radn. effects 79−92074
Cr, Nd:glass laser, enhanced performance due to double doping with Cr 79−31906
Cr V, used in construction of polarised proton filter for polarisation of slow neutrons 79−63238
Cr VII, autoionising transitions $ns^2np^6-nsnp^6mp$ 77−88419
Cr vacuum deposited coating on glass, strength 80−55505
Cr XIII, level struct. and predicted intercombination lines 80−14098
Cr XIV, wavelengths and energy levels, spectra obs. 77−428
Cr XV, mag. quadrupole lines, in TFR600 Tokamak plasma, 10-20 Å 79−13662
Cr XVIII, XIX, spectral energy levels, relativistic corrections, config. superposition method 80−32616
Cr XXI and XXII resonance lines in Tokamak discharges 79−68941
Cr XXII, X-ray spectra from laser plasma 78−17596
Cr XXIII, He-like ion resonance line satellites 79−10064
Cr^-, photodetachment cross-section meas., crossed beam expt. 77−61723
Cr^+ bombardment of stainless steels, effect on stress corrosion cracking and microhardness 80−85087
Cr^+, generation by laser ionis. source for ICR spectroscopy, chem. appls. 80−45597
Cr^{3+}, adsorption on SiO_2 zeolite surface, bonding, EPR, optical spectroscopy investig. *(German)* 79−95266
Cr^{3+} clusters in mol. complexes, interference effects in neutron scatt. 77−85544
Cr^{3+}, coupled in ionic crystals, optical spectra *(Rumanian)* 79−87474

chromium continued
Cr^{3+}, efficient cross pumping of Nd^{3+} in $Nd(Al,Cr)_3(BO_3)_4$ laser 78—59010
Cr^{3+}, electronic states interactions with crystal odd vibrs., R-lines vibr. recurrences 78—84639
Cr^{3+}, fluoresc. quenching of organic excited singlet states, rate meas., mechanism 77—38685
Cr^{3+} hydration model, external water interactions 78—78772
Cr^{3+}, impurity ion in frozen aq. solns., effect on Fe^{3+} spin-spin relax., Mossbauer obs. 79—33573
Cr^{3+} impurity spectra anal. with Trees' correction 78—68539
Cr^{3+}, in alums, resolution enhancement through multiple quantum transitions 78—19374
Cr^{3+} in crystals, radiationless relax., photoacoustic spectra 78—27264
Cr^{3+} in octahedral fluoride lattice, optical spectrum open shell SCF MO cluster CI calc. 78—19501
Cr^{3+} in ruby, B1, B2 absorpt. lines, double electron-nuclear resonance, optical detection *(Russian)* 80—7194
Cr^{6+}, in $(CrO_4)^{2-}$ ions, metal X-ray K absorption spectra, low energy maxima interpretation 79—74019
$Cr^{3+}:Al_2BeO_4$, Alexandrite, tunable laser sources development and appl. 80—48262
$Cr^{3+}:Be_3Al_2(Si_6O_{18})$, synthetic emerald crystal, quantum paramag. amplifier with resonator 79—89878
$Cr^{3+}:BeAl_2O_4$, alexandrite, potential laser material, stimulated emission and absorpt. spectrum 79—33734
$Cr^{3+}:BeAl_2O_4$, tunable laser performance, 701 to 794 nm, long-pulse and Q-switch operation 79—72573
$Cr^{3+}:BeAl_2O_4$ alexandrite laser, high gain performance 80—53299
$Cr^{3+}:BeAl_2O_4$ alexandrite laser, wavelength-tunable CW laser action 80—53300
Cr/Au layered films, microstruct. and interdiffusion during ageing, 423 to 573K 79—46965
Cr/Au metallisation system, corrosion inhibition using intermediary Pd layer 79—79155
Cr/Cr_2O_3, relative chemical potential of oxygen *(German)* 78—31642
Cr/Cu/Cr layer composite, influence of phase boundary on flow stress 78—60717
Cr/Mg ratio in achondrites and mesosiderite silicate fraction 80—51704
Cr/Pt/n-GaAs Schottky contact, barrier height change due to heat treatment 79—47165
Cr^{6+}/Cr^{3+} colloidal SiO_2 surface films on Al, TEM/XPS study 80—85090
Cr-(Pd_2Si)-Si, $CrSi_2$ form. kinetics 77—24492
Cr-Al_2O_3 heterophase film, elec. props. rel. to Al_2O_3 content 77—15969
Cr-Al_2O_3 powder targets for plasma-ion spray deposition of resistance films 80—84897
Cr-$Al_2O_3(Al_2O_3$-MgO) cermet selective surfaces for evacuated solar collectors 79—43785
Cr-Au film structure, on Si interdiffusion 77—39698
Cr-barium stearate-Cr structs., internal voltage work function meas. 79—82684
Cr-brass bilayer system, optical mechanical and corrosion properties 77—32707
Cr-covered objects, dispersion forces at 132-670 nm distances 79—42681
Cr-Cr_2O_3, black, solar selectivity at average temps. (100 to 250°C) *(French)* 80—55899
Cr-Cr_2O_3, black chrome films, surface microstruct. rel. to optical props. in solar absorbers 79—52036
Cr-Cr_2O_3, black chrome solar selective absorber, microstruct. 79—56875
Cr-Cr_2O_3, black chrome electroplating for solar energy photothermal conversion, prep. and struct. 79—74544
Cr-Cr_2O_3, black chrome electroplating for solar energy photothermal conversion, optical props. 79—74545
Cr-Cr_2O_3, chrome black, electroplated selective surface, thermal emittance, solar absorpt., refl., and roughness 79—79406
Cr-Cr_2O_3 black, selective coating, optical and topographical props. 80—26165
Cr-Cr_2O_3 black chrome, commercial, solar absorber coating characterisation 80—80111
Cr-Cr_2O_3 black solar absorber surfaces, microstruct. rel. to electroplating parameters 80—61418
Cr-Cr_2O_3 composite mixture, preferential sputtering, XPS expts. 79—87544
Cr-Cu bilayer system, optical mechanical and corrosion properties 77—32707
Cr-GaAs, metal-nn^+ Schottky diode, I-V characts., inverse branch, effect of dislocation defects *(Russian)* 79—15217
Cr-GaAs, Schottky-barrier diode, surface electron states 79—73578
Cr-Ge-Cr, study of metal contact resistance and microstruct. 77—89880
Cr-MIS solar cells, on polycryst. Si, grain boundary effect and conduction mech. 80—93894
Cr-N system, thermodynamic anal. 77—77461
Cr-$NdAlO_3$, dielectric films, phase composition and structure 80—39464
Cr-phthalocyanine-Cr sandwich, I-V and C-V characts. 80—60106
Cr-Pt thin film couple, diffusion, new Cr-Pt phases obs. 79—42319
Cr-Si, cleaved junction, interface states, capacitance meas. 79—91118
Cr-Si, metal-nn^+ Schottky diode, I-V characts., inverse branch, effect of dislocation defects *(Russian)* 79—15217
Cr-Si interfaces, metallurgical and electrical props. 80—60081
Cr-SiO, thin film, laser beam-treated, emission mode of SEM 79—28226
Cr-SiO cermet film, silicide form. during deposition 77—12535
Cr-SiO cermet thin films, thickness effect on density, resist., adhesion and annealing coeff. 77—69432
Cr-SiO film, elec. props., effect of P^+ and Ar^+ implantation 79—11239
Cr-SiO films, sputtered, elec. and struct. props. 80—39694
Cr-SiO_2 cermet film, deposition by RF sputtering of powder target, elec. resist. and TCR 79—78890
Cr-SiO_2 codeposited film, optical, elec., mechanical and corrosion props. 77—32708
Cr-SiO_2-Si structure, solid-phase interaction between Cr and SiO_2, X-ray spectral obs. 78—10560
Cr-SiO_2-n-Si tunnel diodes elec. characts. meas. and modelling 77—39955
Cr-SiO_x-Si MIS solar cell, current cond. 80—7936
Cr-SiO_x-Si MIS solar cells, photovoltaic performance and interface states, nucl. radiation effects 80—94004
Cr-Si(GaAs) Schottky barriers, interfacial structural defects effect on avalanche breakdown 79—42644
Cr-Y coatings, spectral determ. of Y content 77—90681

chromium continued
$Cr+F^{q+}$, (q=6, 8, 9), target and projectile cross-sections, X-ray prod. yields 79—81269
$Cr+H^+$, K X-ray production, 0.2-0.5 MeV, ionis. cross-section 79—31459
$Cr+N^+$, X-ray production cross section, $K\beta/K\alpha$ ratio, 0.5-2.5 MeV/amu 77—54526
Cr(II) lines, oscill. strengths in 2413-2718 Å wavelength range 80—106294
Cr_2O_3/Cr cermet film, RF sputtered, for selective black absorbers 78—30046
Cr_2O_3/Cr solar-absorber surfaces, chemical and struct. anal. 79—95283
Cr_2O_3-Cr, RF sputtered cermet film, selective black absorber 77—58399
Cr_2O_3-Cr black, electrodeposit on Ni, defects and their effect on props. 80—39474
Cr_2O_3-Cr black, solar collector coating, microstruct., FIM and SEM obs. 80—26166
Cr_2O_3-Cr film, electrodeposited, optical degradation rel. to surface morphology, SEM and AES obs. 79—79401
Cr_2O_3-Cr film, optical props., rel. to chemical/metallurgical constitution, appl. as solar absorber 78—56531
Cr(VI), biamperometric iodometric determ. using Pt-graphite electrode system 77—70359
^{35}Cr, ^7P states HFS, level crossing technique, core polarisation, spin orbit interaction, config. mixing 78—78668
^{48}Cr, production for life sciences appls. 80—94367
^{51}Cr, lung burdens of low-energy photon-emitters, interlaboratory comparison of meas. techniques 79—20671
^{51}Cr, whole-body counting of retention in man 79—62378
^{51}Cr-EDTA, limitations of single sample tracer method for determ. glomerular filtration rate 79—16271
^{51}Cr-labelled lymphocyte autoradiographic detection problems 79—29592
^{54}Cr, K_β/K_α intensity ratios, chem. effects 79—63949
$CsAl(SO_4)_2.12H_2O:Cr^{3+}$, ESR spectra 78—91944
$CsCdBr_3:Cr^{3+}(Cr^+)$, EPR of impurities, charge compensation, X-ray effects 80—60407
$CsCdF_3:Cr^{3+}$, ENDOR exam. of electron spin transfer 77—48089
$CsCdF_3:Cr^{3+}$, ligand polarisation and transferred hyperfine interactions 79—51535
$CsCl:Cr^{3+}$, ESR of Cr^{3+} centres, room temp. 78—91943
$CsMgCl:Cr^{3+},Mo^{3+}$, Cr^{3+}-Mo^{3+} exchange coupled pair, EPR study 79—42830
$CsMgCl_3(Br_3):Cr^{3+}(Cr^+)$, EPR of impurities, charge compensation, X-ray effects 80—60407
Cu:Cr, NMR satellite data rel. to impurity struct. 78—35052
emerald:Cr^{3+}, spin-lattice coupling consts. 79—99761
EuGaYIG:Cr, epitaxial garnet film, interaction pot. of domain walls with localised stress fields 80—44889
Fe, pure, Sn and Cr diffusion, effect of boundary struct., autoradiography study *(Japanese)* 80—49419
Fe-Cr diffusion couple, tracer diffusion meas. using tracer anal. 79—7716
Fe-Ni-C martensite morphology, butterfly-lenticular transition temp., Cr addition effect *(Japanese)* 80—81053
α-$Fe_2O_3:Cr^{3+}$, substitution effect on Morin transition, neutron diffr. study 80—44827
Ga complex, $Gaurea_6(ClO_4)_3:Cr^{3+}$ structural phase transition, ESR meas. 77—20681
GaAS:Cr, mag. field depend. of single carrier parameters, mixed cond. anal. 79—91043
GaAs: Cr, annealing with Si_3N_4, Cr profiles meas. 79—90693
GaAs: Cr, impurity levels charact. using dark capacitance and photocapacitance transient techniques 80—59920
GaAs:Cr, 0.84 eV no-phonon luminesc., fine struct. and origin 80—103980
GaAs:Cr, acceptor levels, photocapacitance meas. 79—95443
GaAs:Cr, Be, ion-implanted, semi-insulating, carrier mobility and conc. temp. depend. 77—76808
GaAs:Cr, Be^+ implantation, atomic conc. and defect density profiles after annealing 80—39123
GaAs:Cr, bulk and epitaxial, ion implanted, Cr conc., depth distrib. and diffusion coeff. 80—49243
GaAs:Cr, carrier equilibrium effects, impurity states, elec. resistivity 80—65488
GaAs:Cr, Cr distrib. and heat-treatment migration studies by SIMS 80—107305
GaAs:Cr, Cr^+ and Cr^{2+} centres, thermal treatment effects, EPR 80—65492
GaAs:Cr, current voltage characterisation, deep levels and Fermi level determ. 79—7823
GaAs:Cr, deep acceptor level, DLTS and optical DLTS study 80—92852
GaAs:Cr, deep impurity levels, AC photocond. meas. 78—19082
GaAs:Cr, deep levels, wavelength-modulated photocapacitance spectroscopy 80—76055
GaAs:Cr, deep trapping centre exam. by thermally stimulated discharge method and luminesc. 77—55495
GaAs:Cr, dislocation-free single crystals, point defects and rad. damage 80—88141
GaAs:Cr, dopant influence on hardness 77—84777
GaAs:Cr, EPR, annealing and IR excitation effect on Cr^+ signal, Cr content by colorimetry 77—69680
GaAs:Cr, effect of light on EPR centres 78—10767
GaAs:Cr, electroabsorption spectra obs., reduced effective mass determ. 80—50301
GaAs:Cr, epitaxial layers, MBE grown, Hall mobilities, substrate temps. 80—20335
GaAs:Cr, exptl. verification of Cr^{2+} models of photoluminescent transitions 78—27320
GaAs:Cr, FET, influence of Cr on mobility of electrons 80—92910
GaAs:Cr, far IR EPR spectroscopy, mag. field-modulation technique 80—15830
GaAs:Cr, fine structure in cathodoluminescence spectrum 78—56524
GaAs:Cr, gettering by back surface mech. damage 80—10759
GaAs:Cr, high resist., anomalously strong elec. field induced release of carriers from traps 78—6397
GaAs:Cr, high resistivity, specific resistance depend. determ. using impedance freq. depend. *(Czech)* 80—15536
GaAs:Cr, hole traps, ESR studies 80—75843
GaAs:Cr, hot electron relax. process and ionization of traps *(Russian)* 79—28354
GaAs:Cr, IR absorpt. determ., emissivity meas. 77—63421

chromium continued
GaAs:Cr, IR spectral detectivity 78—70184
GaAs:Cr, implantation depth profiles of S$^+$ and S_2^+ using AES, annealing effects 79—55774
GaAs:Cr, impurity conc. and segregation coeff., optical absorpt. meas. 79—56819
GaAs:Cr, impurity electron states by Xα scattered wave cluster method, electron-electron interactions 80—6767
GaAs:Cr, intracenter radiative transition in Cr^{2+} ions 79—11463
GaAs:Cr, ion implanted, implantation damage profiles, laser annealing, ellipsometry study 80—79819
GaAs:Cr, LPE, spiral growth patterns, dopant role 77—72800
GaAs:Cr, local level parameters from thermally stimulated excitation curves, influence of variations of rate of heating 80—6769
GaAs:Cr, low dose n-type ion implantation obs. 77—39608
GaAs:Cr, low temp. gettering 80—96549
GaAs:Cr, luminesc. stress splitting, 4.2K 78—84627
GaAs:Cr, luminescence and absorption spectra, temp. depend. of fine structure 80—6779
GaAs:Cr, mechanism of thermal quenching of luminesc. and photocurrent stimulation 77—55821
GaAs:Cr, Mg, ion implanted, elec. meas. and optical activation studies 79—86806
GaAs:Cr, n-GaAs interface, elec. props. 78—6438
GaAs:Cr, O, effect of O in photoluminesc. meas. 80—29799
GaAs:Cr, optical charging of paramag. centres, effect of potential relief 77—20694
GaAs:Cr, optical modulation study of proton bombardment 78—6720
GaAs:Cr, optical modulation spectra affected by 150 keV proton beam 78—10871
GaAs:Cr, optically excited, Hall effect meas. 77—20343
GaAs:Cr, optically induced transient EPR phenomena 80—50168
GaAs:Cr, origin of sharp near IR transitions 80—10913
GaAs:Cr, parameters determ. using cond., Hall effect and magnetoresist. meas. *(Slovak)* 78—47802
GaAs:Cr, photocapacitance of deep levels obs. 79—38021
GaAs:Cr, photoconductivity and photo Hall spectra 78—19091
GaAs:Cr, photoionisation transition Cr^{3+}$\rightarrow$Cr^{2+}, EPR studies 80—60638
GaAs:Cr, photoluminescence, YAG laser or krypton laser 80—60668
GaAs:Cr, photoluminescence in strong electric fields 80—108270
GaAs:Cr, plane-parallel plate subjected to laser illumination, photocond. meas., photodetector for far IR 79—93221
GaAs:Cr, redistrib. of Cr during laser annealing 80—88192
GaAs:Cr, relax. semicond., Dember effect meas. 79—28372
GaAs:Cr, S-type diodes, thermal quenching of injection currents and current-volage characts. 78—26942
GaAs:Cr, Schottky barrier, effect of trapping processes on photocapacitance 77—76866
GaAs:Cr, Se implantation, carrier conc. and mobility profiles depend. on dose and annealing temp. 77—47479
GaAs:Cr, Se layers, ion implanted, ohmic contact form., contact resist. meas. 79—91158
GaAs:Cr, semi-insulating, i.r. induced modulation of cathodoluminescence, and specimen current 77—1737
GaAs:Cr, semi-insulating, TSC, carrier recomb. and trapping 77—32014
p-GaAs:Cr, semi-insulating, illumination effect on mobilities 77—32043
GaAs:Cr, semi-insulating elec. compensation, Hall and resist. meas. 77—62855
GaAs:Cr, semi-insulating, complex permittivity, 2.5-36 GHz, 300-400K 77—69763
p-GaAs:Cr, semi-insulating photoelectronic analysis 77—80804
GaAs:Cr, semi-insulating, deep impurity level anal. 78—6332
n-GaAs:Cr, semi-insulating, contact effects, trapping levels 78—10465
GaAs:Cr, semi-insulating impurity photomagnetoelectric effect 78—34861
GaAs:Cr, semi-insulating, characterisation by photoelectronic data 78—68051
GaAs:Cr, semi-insulating, I-V characts. and surface currents 79—56234
GaAs:Cr, semi-insulating, I-V characts. and photocond. spectra dependencies on Fermi level 79—99576
GaAs:Cr, semi-insulating, defect chemistry, EPR study 79—99754
GaAs:Cr, semi-insulating, Cr charge states conc., EPR determ. 80—20450
GaAs:Cr, semi-insulating, thermal conversion suppression by arsine-controlled capless-anneal, ion implantation 80—49245
p-GaAs:Cr, semi-insulating, mobilities and carrier concentrations, temp. depend. 80—70702
GaAs:Cr, semi-insulating, Cr redistrib. during thermal annealing as function of encapsulant and implant fluence 80—84199
GaAs:Cr, semi-insulating, compensation mechanisms, Hall effect and optical absorpt. meas. 80—84477
GaAs:Cr, semi-insulating, Zeeman studies of 0.839 eV emission 80—103987
GaAs:Cr, semi-insulating, damage gettering of Cr during annealing of Cr and S implants 80—107304
GaAs:Cr, semiinsulating, hole recomb. domains, Hall mobility and photocond. 77—15867
GaAs:Cr, semiinsulating, LPE and elec. props. 77—44178
GaAs:Cr, semiinsulating, I-V characts., photocond., Fermi level, and deep levels 78—39118
GaAs:Cr, semiinsulating solid-state inductance, theory and expt. 78—56138
GaAs:Cr, Si, deep centre photoluminescence spectra 78—95601
GaAs:Cr, Si ion implantation and annealing, damage recovery, surface carrier profile 77—4119
GaAs:Cr, single cryst., optical quenching spectrum, disappearance of stationary high-field domain 78—47830
GaAs:Cr, site symmetry of Cr ions, ground-state splitting, ballistic phonon expts. 78—95273
GaAs:Cr, strong quenching of thermally stimulated conductivity by elec. field *(Russian)* 77—1434
GaAs:Cr, surface and bulk recombination parameter determ. from photoluminesc. spectra 77—55820
GaAs:Cr, Te implantation, electron conc. and mobility profiles depend. on dose and annealing temp. 77—39607
GaAs:Cr, thermally grown, DLTS study of Cr trap density 80—96815
GaAs:Cr, VPE grown, exam. of doping GaAs using Cr(CO)$_6$ 78—72737
GaAs:Cr, VPE growth, carrier conc. profiles, impurity level model 79—74099
GaAs:Cr, zero-phonon struct. in Cr^{2+} (3d^4) optical absorption 80—60640

chromium continued
GaAs:Cr, Zn(Se) shallow impurity implantation, elec. props. after annealing 80—24465
GaAs:Cr,O, semi-insulating, photocond. anal. of levels 80—20243
GaAs:Cr,O semi-insulating monocrystal development and four-level model 80—88191
GaAs:Cr,Se, ion-implanted, semi-insulating effects of Cr redistrib. on elec. characts. 80—59982
GaAs:Cr,Zn, implanted, doping profiles after laser annealing, elec. props. 80—2058
GaAs:Cr (Cr-Te), and undoped, transverse-acoustoelec.-voltage spectroscopy 79—99586
GaAs:Cr capless annealed, under As press., Cr redistrib., SIMS obs. 80—59503
GaAs:Cr diffusion profile meas. 80—6554
GaAs:Cr diode, high magnetosensitivity of negative resist. region 78—26946
GaAs:Cr excess electron lifetime determ. by US method *(Czech)* 77—20336
GaAs:Cr photoconductivity, large scale fluctuations of impurity electostatic potential 77—8145
GaAs:Cr photoluminesc. meas. 78—6761
GaAs:Cr plane-parallel photocond. plate, oscills. in current and light intensity in laser irradiation 80—49819
GaAs:Cr plate, illuminated, oscills. in V-I charact. 80—11038
GaAs:Cr pulsed electron beam induced recrystallisation and damage, amorphous layer formation 80—34052
GaAs:Cr semi-insulating substrate, photoluminescence obs. of surface degradation during LPE growth 78—6865
GaAs:Cr semi-insulating wafer, heat treatment technique for no thermal conversion 80—100857
GaAs:Cr substrates and LPE layers, Au film deposition and annealing, Cr redistrib. 80—15312
GaAs:Cr wafers, semi-insulating, surface degradation by heat treatment at 900°C 77—80820
GaAs:Cr^{2+}, cluster calcs. of Cr^2 electronic states 79—87064
GaAs:Cr^{2+}, dynamic Jahn-Teller effect, relaxation time for reorientation 80—6798
GaAs:Cr^{2+}, effect of uniaxial stress and temp. variation on Cr^{2+} centre, EPR expts. 79—95636
GaAs:Cr^{2+}, Jahn-Teller effect for ion impurities 80—107753
GaAs:Cr^{2+}, US attenuation meas. of Jahn-Teller distorted Cr^{2+} centres 79—28048
GaAs:Cr^{2+}(3d^4), Jahn-Teller distortion, photoinduced charge conversion, EPR 78—10758
GaAs:Cr^{3+} (3d^3), EPR, 5K, evidence for strong Jahn-Teller effects 77—43875
GaAs:Si, Cr, carrier concs. from Hall effect, microscopy, localised vibrational modes absorption meas. 78—56104
GaAs:Si,Cr, under layer of SiO$_2$, effect of annealing, on electron concentration and mobility, and impurity distrib. 79—4323
GaN:Cr, lattice parameters, variation with stoichiometry and doping 79—73153
β-Ga$_2$O$_3$:Cr, temp. depend. of luminesc. characts. *(Russian)* 77—28621
GaP:^{53}Cr, paramag. centres, identification from ESR and ENDOR spectra 80—80600
GaP:Cr, diffusion parameters and solubility and influence on elec. and optical props. 79—73343
GaP:Cr, ESR of doubly ionised Cr acceptor and IR luminesc. 78—56374
p-GaP:Cr, hole traps, ESR studies 80—75843
GaP:Cr, local level near valence band, photocapacitance 79—11080
GaP:Cr, origin of sharp near IR transitions 80—10913
GaP:Cr, photo-ESR of annealed crysts. 80—15795
GaP:Cr epitaxial layers, Cr conc. profile determ. 80—65029
GdAlO$_3$:Cr^{3+}, mag. field effects on fluoresc. 80—2850
GeO:Cr, dielectric thin film, transmission and EPR spectra 77—69676
GeO$_2$:Cr^{3+}, direct mechanism in supertransferred hyperfine interaction 79—23936
HIO$_3$:Cr, growth and struct. perfection, effect of impurity ions 77 12514
I$_2$:Cr, doping effect on elec. cond., semicond. props. 80—49732
n-InAs:Cr, Czochralski growth of high-resist. single crysts. 77—66587
InAs:Cr, high-resist., energy positions of deep levels, elec. and optical props. 79—7807
InP:Cr, electroabsorption spectra obs. 80—50301
InP:Cr, Hall and resistivity meas. 80—10990
InP:Cr, high-purity bulk, prep. from soln. 78—6839
n-InP:Cr, oscill. intrinsic photocond. 79—60871
n-InP:Cr, press. depend. of elec. resist. and Cr ionisation energy 80—80281
InP:Cr^{2+}, EPR, symm., spin Hamiltonian parameters 78—10759
InP:Cr^{2+}, Jahn-Teller effect for ion impurities 80—107753
n-InSb:Cr, deep impurities, elec. cond. and Hall coeff. meas., 4.2 to 120K 80—107791
InSb:Cr, electron and hole lifetimes, recomb. at trapping and acceptor levels 77—51760
InSb:Cr, press. effects on transport props. 78—56146
InSb:Cr, Zn impurity centre behaviour, impurity conc. and Hall coeff. meas. 80—65490
InSb:Cr,Zn, transport props. meas. 77—1424
InSb:Cr:Zn, magnetic freeze-out electrons at deep Cr level 79—15169
KAl(SO$_4$)$_2$.12H$_2$O:Cr^{3+}, ESR high-order transitions 79—11338
KCdF$_3$:Cr^{3+}, EPR, successive phase transitions 79—65717
KCr(SO$_4$)$_2$.12H$_2$O, phase transition associated fluctuations, Cr^{3+} EPR obs. 77—32247
KD$_2$AsO$_4$, Cr^{5+} EPR, line shape and elec. field effect 79—11336
KH$_2$AsO$_4$:Cr^{5+}, ferroelec. phase transition, EPR intensity and linewidth meas. 79—4721
KH$_2$AsO$_4$:Cr^{5+}, lateral proton config., ENDOR spectra 77—59483
KH$_2$(D$_2$)AsO$_4$(PO$_4$):Cr^{5+}, EPR, slow dynamics 78—15126
KH$_3$(SeO$_3$)$_2$:Cr^{3+}, EPR, ferroelectric phase transition 79—65716
KH$_3$(SeO$_3$)$_2$:Cr^{3+}, ferroelastic material, EPR, 77-300K 78—60331
KLiSO$_4$:Cr; optical activity characts. cryst.-chem. exam. 78—95569
KMgF$_3$:Cr^{2+}, 3d$\rightarrow$4d absorpt. band exam. 77—63435
KMgF$_3$:Cr^{2+}, dynamic Jahn-Teller effect 77—66416
KMgF$_3$:Cr^{2+}, HF phonon spectroscopy using supercond. tunnel junctions 80—65178
KMgF$_3$:Cr^{3+}, EPR spectrum, effect of external elec. field 78—68368
KMgF$_3$:Cr^{3+}, trigonal centres, EPR lines, pseudo-Stark splitting 78—68367
K$_2$NaAlF$_6$:Cr^{3+}, ^{2}E$_g$-^{4}A$_{2g}$ phosphoresc. spectrum, vibr. struct. 79—47494

chromium continued
$K_2NaGaF_6:Cr^{3+}$, mag. circular dichroism and absorption spectra 77−77254
$K_2NaGaF_6:Cr^{3+}$, magneto-optical study of $^2T_{1g}$, $^4T_{2g}$, ^2E_g-$^4A_{2g}$ transitions 80−71384
$KVO_3:Cr^{5+}$, study of ESR spectra 80−80601
$KZnF_3:Cr^{3+}$, ESR spectra of tetragonal Cr^{3+} centres, in external elec. field, 77K 77−24738
$LaAlO_3:Cr^{3+}$ enriched in ^{17}O isotope, flux growth 79−87573
$LaCrO_3$-Cr ceramic, prep., phase comp. and elec. cond. *(Polish)* 80−71621
$LaCrO_3$-Cr cermet, effect of explosive compacting on props. 77−12557
$LiAl_5O_8:Cr^{3+}$, fluoresc. and excitation spectra, zero phonon lines 79−33785
$LiAl_5O_8:Cr^{3+}$, primary and stimulated photon echo generation 79−10364
$LiAl_5O_8:Cr^{3+}$, self-induced transparency and light echo *(Russian)* 77−62016
$LiBaF_3:Cr^{3+}$, EPR, spin Hamiltonian parameters 79−65718
LiCl:Cr, electron transfer absorption bands 79−95810
$LiGa_5O_8:Cr^{3+}$, antisymmetric exchange interaction, EPR study 79−47331
$LiGa_5O_8:Cr^{3+}$, fluoresc. and excitation spectra, zero phonon lines 79−33785
α-$LiIO_3:Cr^{3+}$, absorption spectra, impurity environments 78−27275
α-$LiIO_3:Cr^{3+}$, EPR of impurity ion and radn. induced defects *(German)* 78−84480
α-$LiIO_3:Cr^{3+}$, hyperfine interactions, RF discrete saturation of EPR lines 78−48032
α-$LiIO_3:Cr^{3+}$, zero-field splitting const. calc. 77−51709
$LiNbO_3:Cr^{3+}$ glass, roller quenched, crystn. kinetics 80−44143
$LiNbO_3:Eu^{3+}$, Cr^{3+}, exciton migration, laser time-resolved spectra obs. 79−69861
$LiSO_4.H_2O:Cr^{3+}$, single cryst., EPR and optical absorpt. spectra 80−39855
$LiTaO_3$:Cr (III), radiationless relax., heat-pulse meas. technique 77−36277
$LiVO_3:Cr^{5+}$, study of ESR spectra 80−80601
$Lu_2(WO_4)_3$:Cr, and undoped crystals, luminesc. obs. 80−89047
$MgAlO_4:Cr^{3+}$, exchange parameters of Cr^{3+} pairs, optical and EPR meas. 77−69282
$MgAl_2O_4:Cr^{3+}$, exchange parameters determ. from emission and luminesc. excitation spectra 77−52160
$MgAl_2O_4:Cr^{3+}$, luminesc. spectrum, N-lines *(German)* 77−16382
$MgAl_2O_4:Cr^{3+}$, luminesc. spectra, N-lines and Cr^{3+} pairs 78−2896
$MgIn_2S_4$:Cr, EPR powder spectra 80−25197
MgO:Cr, elec. cond. at high temp. in oxidising atmosphere 77−69323
MgO:Cr, high resolution far IR spectroscopy of lower energy levels of Cr^{2+} 80−80822
MgO:Cr, optical and ESR studies 80−50175
MgO:Cr, X-ray stimulated luminesc. 79−28802
$MgO:Cr^{2+}$, APR spectra 79−87313
$MgO:Cr^{2+}$, critically coupled spin-phonon mode 78−67779
$MgO:Cr^{2+}$, dynamic Jahn-Teller effect, APR obs. 77−20693
$MgO:Cr^{2+}$, HF phonon spectroscopy using supercond. tunnel junctions 80−65178
$MgO:Cr^{2+}$, Jahn-Teller parameters determ. using heat pulses 77−62876
$MgO:Cr^{2+}$, paramag., spin-phonon coupling, inelastic neutron scatt. obs. 79−60441
$MgO:Cr^{2+}$, phonon spectroscopy using supercond. tunnel junctions 79−65157
$MgO:Cr^{2+}$, redox behaviour, ESR and X-ray diffr. 78−52341
$MgO:Cr^{2+}$, reson. relax. time for impurity electrons and localised phonons interaction, appl. to thermal cond. 80−59590
$MgO:Cr^{2+}$, reson. scatt. of phonons by ions 78−18716
$MgO:Cr^{2+}$, thermal magnetoresist. calc. 79−10994
$MgO:Cr^{3+}$, $^4A_{2g}\rightarrow{}^4T_{2g}$ spectra, new expt. results 80−11441
$MgO:Cr^{3+}$, $^4T_{2g}$ excited level of Cr^{3+} 78−43920
$MgO:Cr^{3+}$, axial centres, EPR and fluoresc. meas. 78−2731
$MgO:Cr^{3+}$, broad band luminesc., relaxed level and emission processes 78−31234
$MgO:Cr^{3+}$, coupling of T_{1u} and T_{2u} vibr. to $^2E_g\rightarrow{}^4A_{2g}$ transition 77−63453
$MgO:Cr^{3+}$, cubic centre, high resolution ESR, superhyperfine interaction 77−16162
$MgO:Cr^{3+}$, diffuse interstellar absorpt. bands origin 79−30101
$MgO:Cr^{3+}$, EPR obs., S=2 spin state D-tensor components 77−28433
$MgO:Cr^{3+}$, EPR spectra obtained at room temp. and 1200°C 80−68233
$MgO:Cr^{3+}$, emission and excitation spectra 80−93387
$MgO:Cr^{3+}$, no-phonon lines associated with broad band emission *(French)* 77−52163
$MgO:Cr^{3+}$, ODMR, octahedral and orthorhombic site symm. 80−71243
$MgO:Cr^{3+}$, ODMR study, Cr^{3+} ions in tetragonal symm. sites 80−88892
$MgO:Cr^{3+}$, optical excitation transfer 80−97325
$MgO:Cr^{3+}$, site symmetry of Cr^{3+}, polarised luminesc. meas. 77−12426
$MgO:Cr^{3+}$, spin Hamiltonian parameters, lattice expansion and vibr. effects 80−24851
$MgO:Cr^{3+}$, strain modulated ESR 78−88175
$MgO:Cr^{3+}$, valence conversion in single crysts., by UV irradiation *(German)* 78−84620
MgO:Cr(III), radiationless relax., heat-pulse meas. technique 77−36277
MgO:Li, Cr, charge compensation before and after ionising irrad. and light excitation 79−77598
$Mg_2SiO_4:Cr^{3+}$, elec. field gradients, asymmetry parameters 80−54660
$MgTe:Cr^{+}$, cryst. growth and EPR 78−39393
Mn_3O_4:Cr, elec. cond. and thermo-EMF 80−20231
Mo, arc, steady, vac., plasma ion mass and energy diagnostics 78−51385
on Mo, chromizing, formation of ordered solid soln. *(Russian)* 78−11402
$NH_4Al(SO_4)_2.12H_2O:Cr^{3+}$, zero-field fluctuations in Cr^{3+} near phase transition 77−28435
$NH_4Cl:Cr^{3+}$, ESR of Cr^{3+} centres, room temp. 78−91943
$NH_4H_2AsO_4:Cr^{5+}$, fast and slow dynamic reorientation 78−80306
$NH_4H_2AsO_4:Cr^{5+}$, ENDOR spectra 78−88224
$NH_4H_2AsO_4:Cr^{5+}$, antiferroelec. phase transition, EPR intensity and linewidth meas. 79−4721
$(NH_4)H_2PO_4:Cr^{5+}$, EPR exam. above and below T_c 78−68363
$(NH_4)_xRb_{1-x}Al(SO_4)_2.12H_2O:Cr^{3+}$ EPR study, effect of monovalent ions on trigonal distortion 80−11255
$(NH_4)_2SO_4:Cr^{5+}$, EPR study of ferroelec. phase transition 78−64337

chromium continued
$(NH_4)_2SO_4.Al_2(SO_4)_3.24H_2O:Cr^{3+}$, and deuterated derivative, structural transition studied by EPR 77−85553
$(NH_4)_xTl_{1-x}Al(SO_4)_2.12H_2O:Cr^{3+}$, zero field splitting, g-values, EPR spectra obs. 80−50169
$NaH_3(SeO_3)_2:Cr^{3+}$, deuterated, phase transitions, EPR 77−48135
$NaVO_3:Cr^{5+}$, study of ESR spectra 80−80601
Nd,Cr:Li-La phosphate glass, Nd luminesc. quantum efficiency meas., Nd-Cr nonradiative transfer 80−66296
Nd^{3+},Cr^{3+}:glass, nonradiative energy transfer from Cr to Nd, optical pumping efficiency improvement 80−33001
Ni/Cr multilayers, AES depth profiling by sputtering with $N_2{}^+$ ions 79−95881
Ni-Cr, movement and dislocations using SEM and diffr. contrast method *(Chinese)* 79−51110
Ni-Cr multilayer structs., sputter profiling, depth resolution and surface roughness effects, AES obs. 77−76694
NiO:Cr, effect of Cr additives on structure parameters *(Bulgarian)* 80−44319
Pb-(Sb)(Sn)(Ag) anodes, film behaviour for Cr electroplating 80−35115
PbTe:Cr, thermoelec. props., thermal and elec. cond. 79−82616
Pd/Ni/Cr layered catalyst for H_2-O_2 recombination in BWR coolant 80−18504
$PdH_{0.97}$:Cr, supercond. transition temp. depression, coexistent mag. behaviour 80−49976
Pt-Cr interface, low-temp. diffusion, ambient effects 80−100355
$RbAl(SO_4)_2.12H_2O:Cr^{3+}$, high order EPR transitions 79−22736
$RbCdF_3:Cr^{3+}$, EPR meas. of phase transition 79−61206
$RbVO_3:Cr^{5+}$, study of ESR spectra 80−80601
$Sc_2(WO_4)_3$:Cr, and undoped crystals, luminesc. obs. 80−89047
Si:Cr, EPR line intensity and widths, temp. depend. 79−28604
Si:Cr, impurity states, localised orbital approach 80−92851
Si:Cr, ion implanted, Cr conc., depth distrib. and diffusion coeff. 80−49243
Si:Cr, photoconductivity exam. 77−20361
Si:Cr, specific resistance, activation energy of deep levels, and carrier mobility *(Russian)* 78−72146
Si:Cr, spin-lattice relax. of Jahn-Teller Cr^0 centre *(Russian)* 78−72402
Si:Cr electronic states of impurities 77−43531
$Si:Cr^0$, spin-lattice relax. of Jahn-Teller centres, coexistence of minima with different symmetries 80−80602
n-Si-Cr, Schottky barrier IR detector 77−37985
SiO_2-Na_2O-CaO:Fe(As)(Cr) glasses, optical absorpt. changes on heat treatment 78−31224
$SnO_2:Cr^{3+}$, direct mechanism in supertransferred hyperfine interaction 79−23936
SnO_2:Cr(Sb), cassiterite, gas phase growth on seed 77−24937
$Sr_{0.5}Ba_{0.5}Nb_2O_6$:Cr, ceramic, additive effect on ferroelec. and pyroelec. props. 77−16256
$SrTiO_3:Cr^{5+}$, nonlinear Jahn-Teller coupling, local dynamics, near struct. transition 80−2625
$SrTiO_3:Cr^{5+}$ Jahn-Teller system, EPR, electric field effects 79−28599
TiC-steel composite, effect of method of Cr additions on props. 78−15341
TiO_2:Cr, anatase, single cryst., ESR of Cr^{5+} 79−28603
TiO_2:Cr, impurity levels, photocurrent and ESR meas. 80−29346
TiO_2:Cr, slightly doped, elec. cond. and defect struct., charge compensation, point defect model 80−75568
$TiO_2:Cr^{3+}$, maser, 8 mm, 15 MHz bandwidth, 15-18 dB gain at 4.2K *(Russian)* 78−25844
$TiO_2:Cr^{3+}$, rutile, temp. depend. of EPR 78−76299
TiO_2:Si(Fe)(Ni)(Mn)(Cr), anodes, performance in photoelectrolysis of water 79−74407
V_2O_3:Cr, anomalies in X-ray diffuse scatt. at high temp. metal-insulator transition 79−87042
V_2O_3:Cr, metal-insulator transition 79−37989
V_2O_3:Cr, metal-insulator transitions, XPS and UPS 79−33236
V_2O_3:Cr, pure and doped, sound vels. and elastic consts. from phonon dispersion curves 79−55844
V_2O_3:Cr, struct., props., rel. to V_2O_3:Al, X-ray diffr. and elec. resist. obs. 78−2531
W fibre reinforced, high temp. strength 79−70021
YAG:Cr, optical detection of phonons 80−92630
$YAG:Cr^{3+}$, absorption and luminesc., spectra, Cr conc. depend. 77−12435
$YAG:Cr^{3+}$, ESR absorption spectra, line broadening 78−91940
$YAG:Cr^{3+}$, optical absorption, cryst. field pot. expansion 77−36268
$YAG:Cr^{3+}$, radiation colour centres, absorpt. and thermolum. spectra 78−48206
$YAG:Cr^{3+}$ 80−2740
YAG:Nd,Ce,Cr, effect of γ-rays, fast electrons on optical props., annealing and colour centre destruction 77−8608
$YAlO_3:Cr^{3+}$, fluorescence R-lines anisotropy, effective Hamiltonian parameters 77−16368
$YCrO_3$-Cr (40 wt.%) cermet, effect of Cr preoxidation on props. 79−87603
Zn II complex, hexaimidazole-zinc(II) dichloride tetrahydrate:Cr(III), D-tensor orientation, charge-compensation vacancies 80−50172
$ZnAl_2O_4:Cr^{3+}$, luminesc. spectra, N-lines and Cr^{3+} pairs 78−2896
$ZnAl_2O_4:Cr^{3+}$, Raman effect to probe dynamical processes of Cr^{3+} photoexcited states 80−2740
$ZnGa_2O_4:Cr^{3+}$, weak exchange interaction determ., ESR study 80−93107
ZnS:Cr, anomalous temp. depend. of near IR absorption 79−28794
ZnS:Cr, vibr. modes of transition element impurities 78−76472
$ZnS:Cr^{+}$, Fe^{3+}, luminesc., cond. and paramag. centre conc. parameters 78−6724
$ZnS:Cr^{2+}$, Cr^{2+} $^5T_2$ and ^5E states, Jahn-Teller effect calcs. 80−39539
$ZnS:Cr^{2+}$, excitation spectrum of IR emission 77−12421
$ZnS:Cr^{2+}$, Jahn-Teller interaction energy calc. 78−2455
$ZnS:Cr^{2+}$, photoionisation, lattice relaxation energy 80−6778
$ZnS(Se)(Te):Cr^{2+}$, absorpt. and luminesc. of $Cr^{2+}(d^4)$, cryst. field theory interpretation 79−83000
$ZnS(Se)(Te):Cr^{2+}$, Jahn-Teller coupling 78−67997
ZnSe:Cr, piezodichroism due to reorientation of Jahn-Teller centres 80−11363
$ZnSe:Cr^{+}$, Fe^{3+}, luminesc. cond. and paramag. centre conc. parameters 78−6724
$ZnSe:Cr^{2+}$, Cr^{2+} $^5T_2$ and ^5E states, Jahn-Teller effect calcs. 80−39539
$ZnSe:Cr^{2+}$, excitation spectrum of IR emission 77−12421
$ZnSe:Cr^{2+}$, photoionisation, lattice relaxation energy 80−6778

chromium continued
ZnSe(Te):Cr^{2+}, spin Hamiltonian parameters and wave function coeffs., LCAO theory 77—39804
ZnTe:Cr, exciton refl. spectra 80—2806
ZnTe:Cr^{2+}, Cr^{2+} $^5T_2$ and ^5E states, Jahn-Teller effect calcs. 80—39539
β-Zr, Cr diffusion rates in temp. range 914 to 1240°C 80—15304
ZrF_4-ThF_4-BaF_2:Cr^{3+} glass, absorpt. spectra *(French)* 79—99918
$(ZrO_2)_{0.9}(Y_2O_3)_{0.1}$:Cr, Mn, stabilised single crystal, EPR of Mn^{2+} and Cr^{3+} obs. 80—66024

chromium alloys
see also chromium compounds
alloying with rare earth metals, Ti, Zr, Hf, Nb, Ta 78—68651
Brightray S, lattice contraction during ageing 80—3030
Carpenter 20 Cb-3 alloy, pitting resist. in low salinity geothermal brines 80—93681
cast iron, white, high Cr-Mo, fracture toughness 80—50726
chemically stabilised, sensitisation and corrosion resist., heat treatment depend., precipitation steel, stainless, Cr-Ni 79—38827
Chromel, thermocouple alloy, heat treatment effects on thermo EMF and mag. flux 77—63235
Chromel alloy, influence of elastic strain on oxidisability *(Russian)* 79—70116
chromel-alumel thermocouple readings, stability prediction 77—87760
chromel-alumel thermocouples, neutron irradiation effects *(Russian)* 77—82515
chromel-copel, thermocouples, neutron irradiation effects *(Russian)* 77—82515
chromindur, origin of coercivity, Lorentz microscopy, magnetisation and Mossbauer effect 78—64219
chromindur, phase separation, Mossbauer obs. 78—88116
Colmonoy, friction behavior in high temp. Na environment *(Japanese)* 80—40546
Colmonoy, self-weldability in high temp Na *(Japanese)* 80—89392
Colmonoy hardfacing materials, friction characts. in high temp. Na *(Japanese)* 80—89356
correl. between void swelling and thermodynamic stability 80—641
Cr-Au alloys, dil., elec. resist., 77-700K 78—64035
Cr-Mo-V steel turbine rotor, fatigue tests 78—39912
Cr-Re binary system, isomorphous transition region, phase diag. *(Russian)* 77—55945
cyclic oxidation, static and dynamic, high temp. alloys 78—88576
dilute alloys, amorphous, exhibiting Mossbauer effect, mean mag. props. *(French)* 80—80489
earth reentry exposure, simulated, effect on mech. props., oxidation of ThO_2 dispersion hardened alloys, Haynes 188 and Hastelloy X 79—5086
ESCA appl. to Ni-Cr resistor layers *(Hungarian)* 77—4951
Fe, cast, high Cr, hardfacing of roll, wear resistance and thermal durability 80—7686
Fe-Cr-Co-Si-Mo, plastic deform. influence on structure and mag. props. *(Russian)* 79—70176
ferritic alloy DT02, oxidation behaviour in CO_2 or Ar with H_2O and H_2, 823-123K 80—3249
Hastelloy, C-276, H transport rel. to ageing treatment 80—75384
Hastelloy, C-276, H-induced crack growth 80—71747
Hastelloy C-4, loaded at high temp., useful life 80—40523
Hastelloy N, Si additions, comp. of eta carbide after ageing 78—52816
Hastelloy X, corrosion behaviour in simulated HTGR He environment 79—54495
Hastelloy X, creep and creep rupture props. in air and helium at 900°C *(Japanese)* 77—52405
Hastelloy X, grain size effect. creep and creep-rupture *(Japanese)* 80—16382
Hastelloy X-R, reaction with sintered Li_2O pellets 79—39137
Hastelloy-X, fatigue crack propag, at elevated temps. in solid solution strengthened superalloys 78—39895
Hastelloy-X, low cycle fatigue crack propagation at 25°C and 760°C 80—104270
Hastelloy-X, Ni-Cr-Fe-Mo, cyclic oxidation resist. improvement by high temp. etching treatment 80—97627
Hayes alloy no.716, Fe-Cr-Ni-Co-W-Mo-Si-C-B (26, 22, 12, 3.5, 3, 1.2, 1.1, 0.4 wt.%), hardfacing alloy 80—100802
Haynes alloy 188, fatigue crack propag. at elevated temps. in solid solution strengthened superalloys 78—39895
Haynes alloy 188, H_2 permeability 77—46399
Haynes alloy 188, SEM exam. of fracture surface, due to low cycle fatigue at 700°C *(Japanese)* 78—52963
Haynes alloy 20 Mod, pitting resist. in low salinity geothermal brines 80—93681
Haynes Stellite 6B, Al_2O_3 particle erosion of surface, SEM obs 78—88545
Haynes Stellite 6B, particle erosion damage, TEM obs. 78—88546
Iconel, oxide film quantitative anal. by XPS and rastered ion bombardment 77—40604
In 519 high temp. low-cycle fatigue behaviour for nuclear process heat appl. 80—628
Incaloy 623, cold worked, factors affecting embrittlement in H_2S 78—31502
Incaloy 800, for LMFBR steam generators 77—3108
Inco 718, fatigued specimens, plastic zone size 77—25150
Incoloy, 800 and 807, heat resistant superalloys, for nuclear plants in He, creep props. *(Japanese)* 79—83263
Incoloy, alloy 800, $M_{23}C_6$/austenite phase boundary defect struct. resolution by weak beam microscopy 80—3046
Incoloy, evaluation for use in nuclear process heat appl. 78—13234
Incoloy, oxide-dispersion-strengthened, pulsed YAG laser welding 79—70075
Incoloy, stress corrosion cracking in high temp. caustic soln. 77—59964
Incoloy 600, H_2SO_4 vapour corrosion, in general atomic S-I thermochem. water-splitting cycle 80—45449
Incoloy 600 and 800, surface film in hot conc. NaOH, XPS study 80—11824
Incoloy 600 vacuum heat treatment for improved corrosion resistance of PWR steam generator tubing 80—5246
Incoloy 800, 600 and 718, press. vessel, fatigue design criteria 78—60758
Incoloy 800, and 800 H, low cycle fatigue behaviour comparison 79 —43438
Incoloy 800, and 800H, proposed specification changes 79—43298
Incoloy 800, appl. 79—43553
Incoloy 800, austenitic, creep fatigue interaction at 600°C 78—64672

chromium alloys continued
Incoloy 800, austenitic, fatigue at elevated temps., second phase form. effect 77—36637
Incoloy 800, cast, microstruct. evolution during creep, TEM obs. 79—43366
Incoloy 800, chem. behaviour and mech. performance in HTR He at high temps. 79—47842
Incoloy 800, clean and steam oxidised, T_2 permeation 80—88364
Incoloy 800, contamination and decontamination of samples from KFA experimental duct of DRAGON reactor 79—45600
Incoloy 800, corrosion and carburization in liquid Na up to 973K 79—47841
Incoloy 800, corrosion fatigue crack propagation in pure water at 85°C *(Japanese)* 79—43472
Incoloy 800, corrosion resist. props. in high temp. steam, review 79—47839
Incoloy 800, cracking in NH_3 at 600°C 79—70207
Incoloy 800, creep and fatigue props. in high temp. gas cooled reactor He environment 79—47776
Incoloy 800, creep crack growth, age hardening effect 79—43436
Incoloy 800, creep rupture, creep strength and tensile data, 500 to 800°C 79—43371
Incoloy 800, creep rupture ductility, 500 to 600°C, hardness and metallurgic exam. 79—43435
Incoloy 800, creep rupture props. at 525°C 79—43437
Incoloy 800, design codes and lifetime prediction aspects for nuclear and non nuclear appls. 79—47778
Incoloy 800, design problems in steam generators of high temp. reactors 79—45352
Incoloy 800, eddy current testing *(German)* 79—96257
Incoloy 800, effect of liquid Na on creep and rupture props. 79—47775
Incoloy 800, exam. of caustic stress corrosion cracking, comparison with type 304 stainless steel 79—29261
Incoloy 800, exam. of mech. and microstructural props. 79—5022
Incoloy 800, fatigue crack behaviour in bending and pull-push modes 77—81315
Incoloy 800, from KFA experimental duct at 700°C and 480 d in DRAGON reactor, mech. props. before and after contamination 79—47777
Incoloy 800, high temp. corrosion and mech. props. in Na environment 79—47840
Incoloy 800, high temp. gaseous corrosion in sulphidising environments 79—47838
Incoloy 800, high temp. oxidation in low O_2 pressures, SEM obs. of oxide morphologies 79—47844
Incoloy 800, intergranular precipitation, predicted behaviour 79—100148
Incoloy 800, mech. props. above 600°C 79—43370
Incoloy 800, mechanical props., heat treatment and appl., conf., Petten, Netherlands (March 1978) 79—43296
Incoloy 800, mechanisms of corrosion in He 79—47843
Incoloy 800, microstruct. effect on mech. props. 79—43367
Incoloy 800, oxidation resistance, alloy depletion effect 77—8989
Incoloy 800, pretreatment potential effect on pit generation *(Japanese)* 79—43474
Incoloy 800, reaction with sintered Li_2O pellets 79—39137
Incoloy 800, review of mech. props. up to 600°C 79—43368
Incoloy 800, review of structural charact., heat treatment and comp. effects 79—43297
Incoloy 800, review on high temp. gaseous corrosion in carburising and oxidising environments 79—47837
Incoloy 800, sensitisation and intergranular corrosion 79—47721
Incoloy 800, solution annealed, low and high cycle fatigue correlation 79—43439
Incoloy 800, steam oxidised, oxide coating anal. 80—89399
Incoloy 800, stress corrosion cracking and anodisation during straining in boiling NaOH soln. 80—30140
Incoloy 800, stress corrosion cracking in contaminated aq. media at high temp. *(French)* 79—20273
Incoloy 800, stress corrosion cracking in NaOH solns., electrochem. aspects, peening treatment 80—97618
Incoloy 800, thin wall tubing, creep-rupture testing in steam under constant and cyclic load 79—47774
Incoloy 800, use up to 550°C, creep ductility 79—43369
Incoloy 800 and 802, influence of carburisation on mech. props. 79—20254
Incoloy 800 Fe base heat resistant alloy oxidation 77—86231
Incoloy 800 for HTR appls., correlation of carburization behavior, mechanical property degradation, and exposure conditions 80—5244
Incoloy 800 H, 617, high temp. low-cycle fatigue behaviour for nuclear process heat appl. 80—628
Incoloy 800 in 50% NaOH, stress corrosion cracking, slow strain rate method *(Japanese)* 80—55575
Incoloy 800H, carburisation and dimens. stability in HTGR, He environment 80—45366
Incoloy 800H, H_2SO_4 vapour corrosion, in general atomic S-I thermochem. water-splitting cycle 80—45449
Incoloy 800H, high temp. low cycle fatigue, ageing and cold working effect 79—43277
Incoloy 800H, high temp.-low cycle fatigue, ageing and cold working effect on initial stress/strain curve 79—47720
Incoloy 825, corrosion resistance as structural material for denitrification vessel 77—36685
Incoloy 903, H_2 permeation and diffusion 78—26730
Incoloy 903, microstruct. and effect of H_2 charging 77—86143
Incoloy MA956E, mechanical alloying for high temp. appl. 78—44046
Incoloy-800, annealed, mech. behaviour anal. for elevated-temp. LMFBR appl. 80—18428
Incoloy-800, meas. of H and D permeation for reactor safety anal. 79—77822
Inconel, 617 and 625, heat resistant superalloys, for nuclear plants in He, creep props. *(Japanese)* 79—83263
Inconel, caustic stress corrosion cracking resistance, processing variables effect 80—71796
Inconel, chloride corrosion in hot acidic media 78—35552
Inconel, compact ductile fracture toughness specimens, load line displacement measurement method at elev. temps. 78—27700
Inconel, corrosion in acidic chloride soln. at 25°C 77—70202
Inconel, fatigue crack growth rate in high temp., high purity oxygenated water 80—40622
Inconel, ion plating using alumina 77—40476

chromium alloys continued
- Inconel, pressure vessel bottom, subcritical crack growth in ligament between instrumentation rods 79−22428
- Inconel, sputtering and blistering from H^+ and He^+ bombardment 78−79649
- Inconel, steam generator tubing, mag. probe inspection 80−85119
- Inconel, stress corrosion cracking in high temp. caustic soln. 77−59964
- Inconel, type 600, Li corrosion inhibitions by Al additions 80−108646
- Inconel, type 706, precipitation and creep rupture behaviour, optical and TEM study 79−74158
- Inconel 600, atomic S diffusion *(French)* 79−74307
- Inconel 600, corrosion fatigue crack propag. at 85°C in 50% NaOH, potential effect *(Japanese)* 80−11834
- Inconel 600, corrosion fatigue crack propagation in pure water at 85°C *(Japanese)* 79−43472
- Inconel 600, Cr diffusion 77−20110
- Inconel 600, effects of ageing and misorientation on intergranular corrosion *(Japanese)* 79−79158
- Inconel 600, equilibrium surface bombarded with high dose He^+ ions 78−95091
- Inconel 600, exam. of caustic stress corrosion cracking, comparison with type 304 stainless steel 79−29261
- Inconel 600, fusion reactor vac. vessel, air, N, adsorpt., thermal desorpt., heat treatment effects 78−54880
- Inconel 600, oxide layer, mechanical impedance meas. method 80−45444
- Inconel 600, PWR primary corrosion products 80−13578
- Inconel 600, reaction with sintered Li_2O pellets 79−39137
- Inconel 600, S penetration leading to sulphide form. *(French)* 79−74306
- Inconel 600, small bore tubing, crevice corrosion 80−60999
- Inconel 600, stress corrosion cracking and anodisation during straining in boiling NaOH soln. 80−30140
- Inconel 600, stress corrosion cracking in NaOH soln. 79−66196
- Inconel 600, stress corrosion cracking in NaOH solns., electrochem. aspects, peening treatment 80−97618
- Inconel 600, stress corrosion cracking in primary water 79−93728
- Inconel 600, surface composition depend. on H atom influx, AES 79−5192
- Inconel 600, thermal outgassing after various surface preparations 79−67952
- Inconel 600, thermal treatment, grain boundary microstruct. and SCC resistance 80−71675
- Inconel 600, XPS exam. of initial growth of oxide films 79−20240
- Inconel 600 alloys, stress corrosion cracking, prediction in 10% NaOH soln. at 315°C 80−97616
- Inconel 600 and 601, films deposited by cylindrical magnetron sputtering, internal stresses 80−24773
- Inconel 600 and 601, influence of carburisation on mech. props. 79−20254
- Inconel 600 and 718, gas desorption coeffs., electron- and ion-induced, bakeout temp. effect 79−65329
- Inconel 600 and 718 in liquid Na environment, fatigue crack propag. 80−40624
- Inconel 600 in 50% NaOH, stress corrosion cracking, slow strain rate method *(Japanese)* 80−55575
- Inconel 600 safe-end cracking failure at Duane Arnold reactor 80−104295
- Inconel 606, discontinuous creep process 79−66124
- Inconel 617, 800, corrosion behaviour in simulated HTGR He environment 79−54495
- Inconel 617, creep, morphological changes of carbides, affect on creep props. 80−108509
- Inconel 617, mass spectrometric study, high temp. reactor system appl. 79−43663
- Inconel 617, microstruct., mech. props., thermal ageing effect 77−36557
- Inconel 625, accelerated H_2 charging in aq. H_2SO_4 at 0.2% yield stress 80−30144
- Inconel 625, creep rupture behaviour in Ag environment 80−25853
- Inconel 625, creep rupture strength and corrosion in HTC in He *(German)* 77−77557
- Inconel 625, electron yields under ion bombardment for clean and oxidised surfaces 80−66368
- Inconel 625, nitriding in N_2-H_2 glow discharge 80−16590
- Inconel 625, organic contamination removal by plasma cleaning and etching 80−97645
- Inconel 625, plasma nitriding, hardness meas., Rutherford backscatt. surface anal. 80−45442
- Inconel 625, secondary ion emission due to H ion bombardment 79−8216
- Inconel 625, surface treatment of plane and hollow components in glow discharges 79−1923
- Inconel 675, wall and limiter material for Tokamaks, induced desorption diffusion and gas production by 100 eV electrons and ions 79−675
- Inconel 718, blistering by 2 MeV He^+ ions, optical microscopy and SEM obs. 79−42119
- Inconel 718, environment effect on high temp. fatigue crack growth 80−30090
- Inconel 718, grain growth during sintering 80−97449
- Inconel 718, H_2 permeation and diffusion 78−26730
- Inconel 718, H plasma effects on fusion device vacuum vessel 80−21111
- Inconel 718, heat capacity 313 to 1053K 79−10964
- Inconel 718, high temp. fretting fatigue, fatigue and fretting wear 80−3197
- Inconel 718, low cycle fatigue at 298 and 823K 77−86151
- Inconel 718, plastic deform., accelerated evolution of H_2 77−36594
- Inconel 718, superalloy, wear of superhard tool during cutting, SEM and metallographic obs. 78−64720
- Inconel 718, surface flawed tensile bars, utility in cyclic life studies 77−21342
- Inconel 738, SEM and electron beam analyser study *(German)* 79−20056
- Inconel 750, volatilisation of oxides during oxidation at 1200°C 78−23873
- Inconel 800, simulated, steam oxidation 80−76405
- Inconel 82, discontinuous creep process 79−66124
- Inconel alloy 600, precipitation effect on corrosion 77−25180
- Inconel alloy 600 in 10% NaOH soln. at 315°C, influence of thermal treatment 79−91841
- Inconel alloy 600 steam generator tubing, effect of C content and thermal treatment on SCC behaviour 79−91844

chromium alloys continued
- Inconel alloy 718, exam. of struct., properties and continuum synthesis of ductile fracture 78−76736
- Inconel hardfacing materials, friction characts. in high temp. Na *(Japanese)* 80−89356
- Inconel MA754, mechanical alloying for high temp. appl. 78−44046
- Inconel X750, positron annihilation study of ageing and creep 80−29824
- Inconel X750 springs, in-reactor stress relaxation 78−11256
- Inconel X, X-ray study of stress meas., elastic const. *(Japanese)* 79−66092
- Inconel X-750, deform. and fracture characts., 24-816°C 80−108551
- Inconel X-750 foil, surface pretreatment for improved coating adherence 79−15877
- Inconel-625, hydrogen permeation characts. 79−69295
- Inconel-718, blistering and exfoliation by 2 MeV He^+ beam 79−46722
- Inconel-sheathed MgO-insulated $Pt_{90}Rh_{10}$/Pt thermocouple, decalibrations during 1200°C use, ion microprobe obs. 78−57957
- Kh20N40 alloys, phase composition after quenching, tempering 78−60650
- localised magnetic moments in band antiferromagnets, impurity interactions *(Russian)* 80−54888
- mag. props. after isothermal thermomag. treatment *(Russian)* 80−25159
- Metglas 2826-A, anomalous magnetisation, critical effects, superparamagnetism 77−8328
- Metglas 2826A, direct meas. of decomp. on crystn. by X-ray microanal. in STEM 79−48025
- $Mn_{1.98-x}Cr_xFe_{0.02}Sb$, Mossbauer effect exam. 78−68432
- Multimet, fatigue crack propag. at elevated temps. in solid solution strengthened superalloys 78−39895
- Neel temperature of one dimens. electron gas in spin density wave state 80−65884
- Ni-Cr alloy Kh20N80, sintered sheet material, stopping power and pore size relationship 78−19693
- Nichrome, alloyed with refractory metal borides, mech. props., rel. to appl. as electrodes in electrospark machining 80−21174
- Nichrome, Kh20N80, varying porosity, effective thermal cond., 373-1400K, meas. method 78−75053
- Nichrome, oxidation resistant coating, electrophoretic deposition on Mo *(Japanese)* 79−20270
- nichrome, oxidised surface, adsorbed amines and hydrazines identification by surface ionis. 77−21456
- Nichrome, volatilisation of oxides during oxidation at 1200°C 78−23873
- Nichrome based dispersion hardened material, Ti, Y, Zr addition effects on crystallisation *(Russian)* 79−74143
- Nichrome wire, porous, strength charact. 78−6997
- Nichrome-silicate glass-CaF_2 multicomponent self-lubricating coating, prep. by plasma spraying, and props. 80−40604
- Nichrome/steel, porous metal-thread sheet materials, filteration, permeability and strength props. *(Russian)* 79−78915
- Nicrosil-Nisil, thermocouple appl. for digital furnace control system 78−49831
- Nimocast, diffusion of Cs, AES, SIMS depth profile study *(German)* 78−84008
- Nimonic, irradiated, void nucleation, numerical evaluation 80−70252
- Nimonic 105, quantitative STEM chem. anal. using standard and standardless programs 79−17578
- Nimonic 80A, lattice contraction during ageing 80−3030
- Nimonic 80A, order hardening, comparison between revised theory and expt. 80−93565
- Nimonic 80A, rapidly solidified, struct. and initial precipitation, field-ion and TEM study 79−78982
- Nimonic 80A, stress dip creep tests 79−74223
- Nimonic 90, creep rate stress exponents and friction stress, comparison with Lagneborg particle by-passing model 80−55481
- Nimonic alloy, effect of annealing on hardness, carbide phase strengthening *(Russian)* 79−34137
- Nimonic cylinder, stress redistribution obs. 77−4831
- Nimonic PE16, creep rupture props. in CO_2, air and vacuum environments at 700°C 79−74248
- Nimonic PE16, irradiation creep data obtained in fast and thermal neutron spectra correlation with displacement cross-sections 80−84993
- Nimonic PE16, neutron irradiated after heat treatment, solute segregation to pt.-defect sinks 79−78976
- Nimonic PE-16, electron irrad. in HVEM, void growth, vacuum environment influence 80−107323
- Nimonic type, elastic interphase strains on ageing effects on extinction *(Russian)* 77−66646
- nuclear microprobe methods for investigating oxidative corrosion 80−71787
- oxidation, ESCA characterisation 78−15584
- Permalloy, corrosion resist. and mag. props., effect of Cr addition 77−86219
- phase transformation, low-temp., structural changes *(Russian)* 79−52202
- Pt-Cr, (13-18 at.% Cr) resistivity and AC susceptibility, temp. 1.4−300K 78−2461
- rare earth ternary alloys, RT_6Al_6, T=Cr, Mn, Fe, Cu, cryst. struct. 80−107110
- Rene 41, Ni-Cr-Co-Mo-Ti-Al-Fe (18.96, 11.09, 9.65, 3.06, 1.59, 0.89 wt.%) formation of Cr_2O_3 monocrystals on heat treatment 79−52455
- Rene 41, volatilisation of oxides during oxidation at 1200°C 78−23873
- Sanicro 30, stress corrosion cracking in NaOH soln. 79−66196
- Sanicro 31, T permeation 80−88364
- saturation of Ti alloys with A and Cr, powder method 77−21052
- steel, 30KhG and 30KhN, carbide formation, Mo alloying effects *(Russian)* 78−48402
- steel, alloy, cluster formation susceptibility in 40 KhN, influence of isothermal working in H_2 *(Russian)* 78−56643
- steel, alloy, Cr-Cu-Mn-C, HT80, effect of grain size on sensitivity to reheat cracking *(German)* 78−72856
- steel, alloy, Cr-Mo, alloy SCM3, hydrogen embrittlement, delayed fracture, exam. *(Japanese)* 78−64620
- steel, alloy, Cr-Mo, pitting and crevice corrosion, exam. *(Japanese)* 78−64769
- steel, alloy, Cr-Mo-V, fatigue, failure probability based on residual strength 78−68797
- steel, alloy, Cr-Mo-V-P, quenched, temper brittleness in relation to V and P concs. 78−52986
- steel, alloy, Fe-Cr-Mo-Si-V, various steels, short rod stress intensity factor tests up to 700K, exam. 78−60815

chromium alloys continued
steel, alloy, Fe-Cr-Ni-Mo-Al, (13, 8, 2, 1, wt.%), H_2 effects on fracture, exam. 78—60809
steel, alloy, Fe-Ni-Cr-Mo-V-C, H_2S stress corrosion cracking, effects of overload, exam. 78—60886
steel, alloy, Fe-Ni-Cr-Mo-V-C, HY130, effect of H_2 and impurities on brittle fracture, review 78—60765
steel, alloy, Fe-Ni-Cr-Sb-C effect of Ni, Sb, on temper embrittlement 78—60813
steel, alloy, Fe-Ni-Mn-Si-Cr-Ni-Mo, effect of metallurgy on stress corrosion cracking, and hydrogen embrittlement 78—60885
steel, alloy, Mn-Cr-Cu, exam. of ductility when deformed, alloying addition effects 78—44175
steel, alloy, Mn-Si-C, exam. of fracture toughness for sheets, using linear elastic fracture mechanics 78—56762
steel, alloy, Ni-Cr-Mn, type 4340 intergranular brittle fracture, exam. by impact testing and Auger spectroscopy 78—52978
steel, alloy, Ni-Cr-Mo, alloys SNCM8, SAE 4161, heat treated, residual stress at fatigue fracture surface *(Japanese)* 78—64622
steel, alloy, Ni-Cr-Mo, SNCM8, mech. stre-ngth under combined alternating strength 78—64690
steel, alloy, Si-Mn-Cr, heat treated, exam. of microfractographic aspects of fatigue cracks *(Japanese)* 78—52959
steel, alloy, softening process in deformed type 15GYuT, metallographs *(Russian)* 78—52840
steel, alloy, V-W-Mo-Cr, exam. of carbide transformation 80—16299
steel, alloy, W-Mo-Cr-V, blanks welded to steel 45, optimal high temp. tempering 80—16351
steel, alloy low, Ni-Cr, tempered martensite embrittlement 80—7669
steel, austenitic, cold worked 10Kh11N23T3MR, structural transformations, aging effect, electron microscope obs. 80—40402
steel, austenitic, Cr-Mn, Kh4G18F, microstruct. and mech. props. during tensile deform. *(Russian)* 79—20114
steel, austenitic, Cr-Mn, martensitic transform. effect on hardening kinetics and fracture resist. of friction surface *(Russian)* 80—50727
steel, austenitic, Cr-Mn, metastable, plasticity, contrib. of martensitic transform. during deform. *(Russian)* 80—30018
steel, austenitic, Cr-Ni, anomalous stress-depend. of creep rate 80—11712
steel, austenitic, Cr-Ni, bulk and intergranular autodiffusion of ^{59}Fe *(French)* 79—55921
steel, austenitic, Cr-Ni, nonmetallic inclusions modification using rare earth metals *(Russian)* 80—40369
steel, austenitic, Cr-Ni (18,12 wt.%), containing coarse grain boundary precipitates, thermomechanical treatment 78—27545
steel, austenitic, Cr-Ni (18, 11 wt.%), creep rupture *(German)* 78—11297
steel, austenitic, Cr-Ni (18, 15 wt.%), oxidation resist., metallic alloying additions effect 79—52419
steel, austenitic, CrNi, high Mo, corrosion, effect of struct. *(German)* 77—90481
steel, austenitic, intercrystalline corrosion, N_2, C and Cr effects 79—83374
steel, austenitic, mechanical props. of DIN X8 CRNIMONB 1616 and DIN X2 CRNI 189, FBR safety anal. 78—60966
steel, austenitic, Mn-Ni-Cr, Mn effects on cracking *(German)* 77—59889
steel, austenitic, Ni-Cr, precipitation strengthened, anelasticity, plastic creep limit, 823K 79—1899
steel, austenitic, Ni-Cr high alloy, N_2, P and Ni effect on stress corrosion cracking and stacking fault energy *(Czech)* 78—60875
steel, austenitic (03KH18N10T), heat treatment for fission reactor appls. 80—66454
steel, austenitic Cr-Mn, $M_{23}C_6$ carbide precipitates comp., heat and thermomech. treatment influence *(Russian)* 80—40361
steel, austenitic Mn-Cr, thermal expansion *(German)* 77—59127
steel, austenitic stainless, biphase, ferritic, ageing and thermomech. treatment effects on struct. and props. 80—35226
steel, austenitic stainless, bulk and grain boundary diffusion of Fe, Cr, Ni, effect of Si content 78—38875
steel, austenitic stainless, Cr-Ni (18, 10 wt.%), ^{59}Fe self-diffusion in ferrite/austenite interface *(French)* 80—19975
steel, austenitic stainless, Cr-Ni-Mo (21,6,9 wt.%), N_2-strengthened, surface segregation of B, Auger and XPS spectra 79—90854
steel, austenitic stainless, Cr-Ni-Mo-Mn, Mo, Mn and ageing effects 78—35413
steel, austenitic stainless, Cr-Ni-Ti, creep deform. effects on intergranular TiC dispersion stability 78—84912
steel, austenitic stainless, friction in vac. at elevated temps. 80—55542
steel, austenitic stainless, hot plasticity, Y additions effect 79—83270
steel, austenitic stainless, influence of varying Cr, Mo, N contents on resist. to pitting corrosion 78—80668
steel, austenitic stainless, Ni free, corrosion obs. 79—24652
steel, austenitic stainless 12Kh18N10T and 15Kh17N2, corrosion cracking in chloride and alkaline solutions 80—55576
steel, austenitic stainless AISI 321, Cr tracer diffusion coeffs. 80—2193
steel, austenitic stainless Cr-Ni, ^{51}Cr tracer diffusion coeffs. 80—34225
steel, austenitic stainless Ni-Cr, heat resist. and comp. of non-metallic inclusions, effect of La, Nd, Pr and Ce 80—76315
steel, bearing, type AISI 52100, tricresyl phosphate treated, Auger anal. 79—52413
steel, brittleness onset during high-temp. tempering *(Russian)* 77—81276
steel, C-Cr (1.0, 1.5 wt.%), 52100 bearing steel, control of surface residual stress by heat treatment 80—97501
steel, C-Mn-Cr-Mo (0.4, 0.8, 1.1, 0.25 wt.%) C, Ni, Mo, Cr addition effects on toughness of bainite 78—11327
steel, CC Cr-Mo (2.25, 1 wt.%) effect of heat treatment on tensile props. 78—23745
steel, CC Cr-Ni, rock-like fracture *(Chinese)* 78—31497
steel, Co-Cr casting, fatigue at welds, hip replacement appl. 78—44697
steel, Co-Cr-Mo, maraging, age hardening, Mossbauer study 80—40002
steel, Co-Cr-Ni-Mo-Mn (39.65, 20.25, 15.33, 7.08, 1.9 wt.%) carbide formation during tempering after plastic deformation 80—16330
steel, complex alloy, Cr (12-18 wt.%), transformation behaviour *(German)* 80—40349
steel, Cr, 5KhGSVF and 0Kh16Mk, tempering resistance, mech. props., Cu addition effect 79—79012
steel, Cr, and Cr-Mo-Ni, austenite decomposition, deform. effects, ferrite reaction 79—1842

chromium alloys continued
steel, Cr, carbide form. depend. on Mn, Cr, V additions, cementite stabilisation, microstruct. *(Russian)* 80—55399
steel, Cr, carburising kinetics, in endothermal atm. 80—76410
steel, Cr, carburising with high-activity carburiser 80—76412
steel, Cr, coated with TiC, prep. and props. 80—76414
steel, Cr, Cr-Mo, Ni-Cr and Ni-Cr-Mo, quenched and tempered struct. effect on H diffusion coeff. and solubility *(Japanese)* 78—52857
steel, Cr, ferritic, corrosion morphology, electrochem. pot. and Mo additions effect *(French)* 80—45439
steel, Cr, H-dislocation interaction 79—8307
steel, Cr, high strength, hot dip galvanized delayed fracture *(Japanese)* 78—15512
steel, Cr, phase transform., effect of high temp. plastic deform. *(Slovak)* 78—19837
steel, Cr, tempering, initial stages of carbide form., electron diffr. *(Russian)* 78—19760
steel, Cr (12wt.%), mech. props, carbide phase struct. 79—15702
steel, Cr (13 wt.%), sintered, organometallic complex addition effects on mech. props. 80—25595
steel, Cr (13 wt.%), wear of Al bronze on steel in presence of aviation fuel 80—11781
steel, Cr (1 to 5 wt.%), effect on transform. of Cr content and all round press. of 25 kbar *(German)* 78—11219
steel, Cr (2%), austenite decomp., phase diagrams and struct. form. kinetics 80—76223
steel, CR (4 wt.%), Cr_7C_3 precipitate growth during tempering, effect of Cr diffusion *(Russian)* 79—52219
steel, Cr (9 wt.%), oxidation in CO_2, early stages study by AES 78—7080
steel, Cr (9 wt.%), SiO_2 vapour deposited coatings, exam. of corrosion protective props. 78—88563
steel, Cr and Ni-Cr, cyclic re-austenitizing 80—35222
steel, Cr bearing, carbide phase precipitation during tempering, Mossbauer, X-ray diffr. studies *(Russian)* 79—87636
steel, Cr ferritic stainless, meas. of alloy and impurity elemental distrib. using STEM 80—35601
steel, Cr ion implanted, corrosion behaviour 80—11840
steel, Cr maraging, internal friction, 120 to 700K *(Polish)* 79—96075
steel, Cr modified, heat resist. rel. to thermomech. treatment 79—20084
steel, Cr with metastable austenite, wear resist., temp. effect 80—76370
steel, Cr-C, (2.14, 1.08 at.%) tempered, resistance to small plastic deformation, strain relaxation *(Russian)* 78—56698
steel, Cr-C, carbide coating by CVD, interlayer form. 80—11574
steel, Cr-C (16.5, 3.65 wt.%) and (45.4, 2.15 wt.%), rapidly quenched, in situ carbide reactions during tempering *(Japanese)* 78—84862
steel, Cr-C (18, 0.9 wt.%), cavitation, abrasion resistance, effect of unstable austenitic struct. *(Russian)* 77—16695
steel, Cr-C (1, 1 wt.%), hot ductility and S segregation 80—66594
steel, Cr-Cu-Mn, fatigue crack propag. rate eval. by J integral method *(Japanese)* 79—8346
steel, Cr-Mn, annealing effect on mech. props. for cryogenic appl. *(Russian)* 78—19788
steel, Cr-Mn, metastable constitution diagram and phase transforms. *(Russian)* 80—50590
steel, Cr-Mn, powder forged, fracture processes and fracture toughness 78—72870
steel, Cr-Mn (13, 19 wt.%), elastic const. behaviour, anomalous, low temp. 80—97521
steel, Cr-Mn (13, 19 wt.%), liquefied natural gas appls., materials and weld props. 79—61735
steel, Cr-Mn-C-Si (20, 14, 0.2, 0 to 3 wt.%), high-temp. oxidation *(Russian)* 80—25904
steel, Cr-Mn-W(Mo), W and Mo addition effect on carbide form. in type 30 KhG *(Russian)* 79—87638
steel, Cr-Mo, annealed, creep and rupture, heat treatment effects 79—24548
steel, Cr-Mo, annealed, interaction solid soln. hardening, precipitation effects on creep 79—4974
steel, Cr-Mo, cast and forged, difference in mech. props. 77—48465
steel, Cr-Mo, creep resistant, creep, effect of carbide precipitation *(German)* 77—52398
steel, Cr-Mo, ferritic, grain boundary segregation, X-ray microanal. by STEM 80—66740
steel, Cr-Mo, grain size effect on ductile brittle transition 79—24615
steel, Cr-Mo, H embrittlement in H_2S environment, Mo effect 80—76415
steel, Cr-Mo, high-temp. props. and constitutive equations 79—34146
steel, Cr-Mo, kinematic hardening models, use in multi-axial cyclic plasticity 80—25717
steel, Cr-Mo, low alloy, stress corrosion cracking and corrosion fatigue 79—47806
steel, Cr-Mo, materials specifications for AGR steam generators 80—42772
steel, Cr-Mo, toughness of heat treated steels of equal tensile strength *(German)* 80—25727
steel, Cr-Mo, vacuum deposited Al film 79—70231
steel, Cr-Mo, X-ray elasticity constants at high specimen temp. *(German)* 80—35239
steel, Cr-Mo(2.25, 1 wt.%), corrosion behaviour in simulated HTGR He environment 79—54495
steel, Cr-Mo(-V), ductility and heat resistant prop. prediction rel. to fine struct. and solid soln. state 79—15751
steel, Cr-Mo (1.25, 0.5 wt.%), creep, fracture, Ti and Ti+B effects 77—36603
steel, Cr-Mo (1.25, 0.5 wt.%), creep and rupture, temp. and stress effects 77—86096
steel, Cr-Mo (1, 0.5 wt.%), heat treated creep failure, role of stress state 79—5047
steel, Cr-Mo (2.25.1 wt.%), exposed to H_2-H_2O-H_2S environment, fatigue crack growth 80—40623
steel, Cr-Mo (2.25, 1.0 wt.%), C transfer between structural steels and Na in LMFBR 79—97805
steel, Cr-Mo (2.25, 1.0 wt.%), thermally aged and Na decarburised, stress-rupture props. 80—21102
steel, Cr-Mo (2.25, 1 wt.%), annealed, heat treatment effect on tensile props. 78—11243
steel, Cr-Mo (2.25, 1 wt.%), creep-fatigue testing from thermal transient effects in CRBRP reactor 78—21660
steel, Cr-Mo (2.25, 1 wt.%), decarburization, carbide effects in high temp Na *(Japanese)* 78—15403

chromium alloys continued
- steel, Cr-Mo (2.25, 1 wt.%), in high temp. Na, heat treatment and metallurgical struct. effects 77—16619
- steel, Cr-Mo (2.25, 1 wt.%), relationship between minimum creep rate and time to fracture 78—56759
- steel, Cr-Mo (2.25, 1 wt.%), strain hardening shakedown load during bending 80—20958
- steel, Cr-Mo (2.25, 1 wt.%), weld metal, high temp. crack growth, effect of tempering, prestrain and grain refinement 78—27622
- steel, Cr-Mo (2.25, 1 wt.%) annealing, high strain rate tensile props. 77—25117
- steel, Cr-Mo (3 wt.%), temper embrittlement 77—36647
- steel, Cr-Mo (9,1 wt.%), austenitized in $\gamma+\delta$ phase field, secondary hardening and tempering 78—11247
- steel, Cr-Mo (9, 1 wt.%) appl. of electron energy loss spectrometry to precipitate morphology 78—48414
- steel, Cr-Mo (9, 1 wt.%) microstructural instability during creep, heat treatment effects 78—48472
- steel, Cr-Mo and Cr-Ni-Mo, V effects on recrystallisation *(Russian)* 77—66654
- steel, Cr-Mo and Ni-Cr-Mo-V low-alloy, additive remedy for temper brittleness 80—66659
- steel, Cr-Mo low alloy ferritic, meas. of alloy and impurity elemental distrib. using STEM 80—35601
- steel, Cr-Mo weld metal, reheat cracking, residual elements and microstruct. influence 80—66553
- steel, Cr-Mo weld metal, trace element embrittlement suppression by creep strength effects 80—66656
- steel, Cr-Mo-(V) austenitic, creep resist., high-temp. props. residuals effect 80—66600
- steel, Cr-Mo-V, 1% Cr, chem. comp. and struct. effect on deform. props. *(German)* 79—1888
- steel, Cr-Mo-V, austenite to bainite transformation under cooling conditions, effect on creep 80—3033
- steel, Cr-Mo-V, biaxial cyclic deformation behaviour 80—16431
- steel, Cr-Mo-V, brittle failure resistance obs. influence of cold plastic deform. 78—72858
- steel, Cr-Mo-V, cast, strain intensity approach of high temperature fatigue crack growth and failure 79—20175
- steel, Cr-Mo-V, combined Cr-Mn addition effects on hardenability 78—7046
- steel, Cr-Mo-V, creep, effect of microstruct., heat treatment, transform. temp. 78—11248
- steel, Cr-Mo-V, creep crack growth temp. depend., 525 to 600°C 78—64634
- steel, Cr-Mo-V, creep deform. under const. and cyclic temp. 79—38914
- steel, Cr-Mo-V, creep fatigue interaction 78—60841
- steel, Cr-Mo-V, creep fatigue interactions obs., strain controlled and load controlled tests 78—44214
- steel, Cr-Mo-V, creep fracture, microstruct. effects 78—64668
- steel, Cr-Mo-V, creep/fatigue interaction 78—64632
- steel, Cr-Mo-V, cyclic oxidation and crack growth during high strain fatigue 78—31586
- steel, Cr-Mo-V, environmental crack growth during isothermal high strain fatigue and temp. cycling 79—5082
- steel, Cr-Mo-V, fatigue crack growth rate and threshold under oxidising conditions 79—20272
- steel, Cr-Mo-V, fracture toughness data, comparison with equivalent energy and energy per unit area data 78—52965
- steel, Cr-Mo-V, high temp. main steam pipe, residual stresses in butt welds 80—21059
- steel, Cr-Mo-V, high temp. steam pipe weld, defect distrib. and growth 80—25979
- steel, Cr-Mo-V, high-temp. cumulative damage for stage I crack growth 78—19883
- steel, Cr-Mo-V, low alloy, creep fatigue interaction 78—64673
- steel, Cr-Mo-V, low alloy, V effect on creep *(Czech)* 77—86088
- steel, Cr-Mo-V, medium strength, correlation between crack initiation, propag. and microstruct. 78—60787
- steel, Cr-Mo-V, normalised and tempered, size and geometry effect on creep cracking behaviour 78—64630
- steel, Cr-Mo-V, press. vessel, fracture, effect of tempering 78—60799
- steel, Cr-Mo-V, rupture ductility rel. to cavitation, density and SEM obs. 79—34142
- steel, Cr-Mo-V, strength and ductility in creep, purity influence 80—66598
- steel, Cr-Mo-V, stress relief cracking mechanism 78—64669
- steel, Cr-Mo-V, stress rupture strength at high temps. *(German)* 80—40474
- steel, Cr-Mo-V, thermal fatigue and rupture strength 78—72857
- steel, Cr-Mo-V (0.5, 0.5, 0.25 wt.%), comparison of methods of correlating creep crack growth 78—60826
- steel, Cr-Mo-V (0.5, 0.5, 0.25 wt.%), creep crack growth, temp. effect 78—64667
- steel, Cr-Mo-V (0.5, 0.5, 0.25 wt.%), heat treated, microstructure effect on threshold region fatigue 78—56757
- steel, Cr-Mo-V (1, 0.5, 0.25 wt.%), long-time stress relaxation props. 77—12666
- steel, Cr-Mo-V (1 wt.%) oxidation assisted crack growth during high cycle fatigue at 550°C 77—16742
- steel, Cr-Mo-V alloy, crack growth during strain fatigue at 825K 78—39890
- steel, Cr-Mo-V creep crack growth, relation between engineering and metallurgical factors 78—11321
- steel, Cr-Mo-V low-alloy, high-temp. ductility and crack growth, impurities effect 80—66652
- steel, Cr-Mo-V low-alloy, mech. props. and stress relief cracking, effects of impurities and deoxidation practice 80—66599
- steel, Cr-Mo-V low-alloy, prior austenite grain boundary embrittlement by B 80—66657
- steel, Cr-Mo-V low-alloy, stress relief cracking, impurity and alloy content effects 80—66654
- steel, Cr-Mo-V low-alloy with high residual element content, cavitation control 80—66663
- steel, Cr-Mo-V press. vessel, crack growth under creep 78—60827
- steel, Cr-Mo-V-W, crack-growth and thermal-mech. fatigue 80—21072
- steel, Cr-Mo-W-V, long term creep rupture props., turbine blade *(Japanese)* 77—59909
- steel, Cr-Mo-W-V, long time stress relaxation props. *(Japanese)* 77—59841
- steel, Cr-Mu-W, carbide form., W effect 80—76259

chromium alloys continued
- steel, Cr-Ni, bainitic habit plane determ. 79—1927
- steel, Cr-Ni, martensite defect identification by positron annihilation 78—39867
- steel, Cr-Ni, microstructural distrib. of cathodic H_2, autoradiography *(French)* 79—99234
- steel, Cr-Ni, pendant drop melt extracted, struct. and props. 80—76242
- steel, Cr-Ni, soaking at forging temp., effect on struct. and mech. props. *(Czech)* 78—64628
- steel, Cr-Ni (14, 5 wt.%), 00Kh14N5M, tempering resistance, mech. props., Cu addition effect 79—79012
- steel, Cr-Ni (18,10 wt.%)-Ti stabilized, corrosion fatigue strength, inhibitor BA-6 effect *(Russian)* 77—16727
- steel, Cr-Ni (18%, 12(8)%), martensite formation and reversion, effect on void swelling 80—11641
- steel, Cr-Ni-(Mo) (25, 28, 2 wt.%), lattice dilation by N_2 77—16592
- steel, Cr-Ni-Cu (14, 5, 2 wt.%), phase transform. and props., preliminary heat treatment effect 79—79011
- steel, Cr-Ni-Mo, 'light spots', fractographic anal. 79—29204
- steel, Cr-Ni-Mo, dynamic and static softening behaviour at hot forming temp. *(German)* 80—25728
- steel, Cr-Ni-Mo, for boiler tubes, austenisation conditions effect obs., on structure and mechanical props. 80—3151
- steel, Cr-Ni-Mo, handbook data for type 34KhN1M 79—78960
- steel, Cr-Ni-Mo-Mn, wetting of TiC, expt. planning investigation 80—60822
- steel, Cr-Ni-Mo-V, magnetic induction, struct. dependence *(Czech)* 80—50141
- steel, Cr-Ni-Mo-V, Mossbauer austenitometry and mag. props. 80—40003
- steel, Cr-Ni-Mo-V-Nb (12,8,1,1.5,0.4 wt.%) Ce addition effects on strength and hardness *(Russian)* 78—15454
- steel, Cr-Ni-Nb, containing controlled particle dispersions, creep strength 77—52425
- steel, Cr-Ni-Ti-B, grain size effect on mech. and struct. props. *(French)* 80—45361
- steel, Cr-Ni-W(Mo), W and Mo addition effect on carbide form., X-ray obs. *(Russian)* 79—87639
- steel, Cr-Si, oxidation resist. in high pressure CO_2, Si effect 80—66704
- steel, Cr-V (1.5, 0.5 wt.%), ferritic, effect of temp. and microstruct. on creep damage 79—5023
- steel, Cr-W-Mo-Co, high-speed, from atomised powders, mech. and cutting props. 80—66556
- steel, Cr-W-V-Mo (3.9 to 4.5, 1.5 to 2, 0.9 to 1.2, 3.9 to 4.4 wt.%), heat resistant, type 8Kh4M4V2F1-Sh, mech. props. 80—16464
- steel, CrMo, cast, fatigue tests under varying stress amplitude and varying temp., amplitude damage *(Japanese)* 78—27605
- steel, CrMo, X-ray elastic consts. function of plastic strain *(German)* 78—31436
- steel, CrMoNi, cantilever beam method to determ. J_{Icc} and J_{Iscc} *(Chinese)* 78—15488
- steel, CrMoV, compact tension specimen, thickness effect 78—68764
- steel, CrMoV, creep and creep strength under alternate tension/compression *(Czech)* 77—63728
- steel, CrMoV, failure in post yield regime using single edge notched tension specimens 78—68765
- steel, CrMoV, low alloy, dispersed phase of VC, hardening mechanism *(Czech)* 78—60676
- steel, CrMoV (1 wt.%), high temp. creep and fracture 77—36598
- steel, CrNiMoV, weld metal, hot cracking resistance during electroslag welding, effects of Cr 79—87732
- steel, Croloy Cr-Mo, stress corrosion cracking in high temp. caustic soln. 77—59964
- steel, fatigue and tensile props., of heat resisting bars, type SUH 660-B and SUH 310-B at elevated temps. 79—38979
- steel, Fe-Cr-Al, sulphidation behaviour, 750°C, preoxidation effect *(French)* 78—15566
- steel, Fe-Cr-Ni (17.20, 7.34 wt.%), transform.-induced plasticity 78—23774
- steel, Fe-Mn-Cr-C (3,3,1 wt.%); intermediate phase form. during martensite form. 77—12626
- steel, Fe-Ni-Cr mag. susceptibility and magnetoresistance, temp. depend. *(Ukrainian)* 77—73004
- steel, ferritic, Cr-Mo (2.25, 1 wt.%), annealed, time depend. strain controlled fatigue, nuclear steam generator appl. 77—8915
- steel, high C, Cr addition effect on superplasticity 79—15729
- steel, high Cr, V additions effect on brittleness near 475°C *(Russian)* 78—19890
- steel, high speed, W-Mo-Cr-V, production by powder metallurgy 77—12574
- steel, high-strength, Cr (1 to 15 wt.%) effect on crack initiation stress *(Russian)* 77—16725
- steel, high-strength, fatigue, interaction effects between trace impurities and environment 80—66651
- steel, ledeburite, fracture during hot plastic deformation exam. 78—56755
- steel, low alloy Cr-Mo, heat fatigue, effect of technical factors 79—79058
- steel, low C, Cr-Ni (25, 25 wt.%), σ phase form., prestrain effects *(Japanese)* 78—92260
- steel, low C Cr-Ni, temper embrittlement by antimony, Ti addition effects 77—32683
- steel, low-alloy, case carburised, retained austenite effect on contact fatigue strength 80—30096
- steel, low-alloy, feasibility of electrochem. corrosion protection 79—70220
- steel, maraging, Cr-Ni-Ti, effect of Ti addition on hardness and energy scatt. 79—15687
- steel, maraging, investigation with lower Ni and Co contents *(Chinese)* 78—84812
- steel, maraging, Ni-Co-Mo (18,10,5 wt.%) precipitation *(Japanese)* 78—15402
- steel, martensitic, alloying element effect on coarsening behaviour of cementite particles in ferrite 80—66518
- steel, martensitic, Cr-Co-Ni-Mo, notch toughness, rel. to sensitivity to stress conc. 78—31532
- steel, martensitic, Cr-Ni, grain refining and phase transforms. effect on plasticity *(Russian)* 78—39837
- steel, martensitic, Cr-Ni deform., effect of phase composition and struct. *(Russian)* 77—25102
- steel, martensitic, Cr-Ni-Co-Mo-Ti, Kh12N8K5M3TYu, ageing of C free martensite *(Russian)* 79—1884

chromium alloys continued
  steel, martensitic, Ni-Cr-Mo, fatigue crack initiation and propag. in water 77—9000
  steel, martensitic 07Kh16N4B, corrosion cracking in chloride and alkaline solutions 80—55576
  steel, martensitic 12% Cr, temper embrittlement 80—66650
  steel, mild, and stainless, ferritic and austenitic, susceptibility of underclad cracking, rel. to chem. comp. 77—21280
  steel, mild Cr welding, 550°-850°C heating effects on structure and toughness 79—24540
  steel, Mn-Cr, blank hardened, shot peening effect on bending fatigue strength *(German)* 78—35402
  steel, Mn-Cr, normalised, shot peening effect on bending fatigue strength *(German)* 78—35401
  steel, Mn-Cr, tempered, case hardened, shot peening effect on bending fatigue strength *(German)* 79—24645
  steel, Mn-Cr-Ni-N, N effect on relaxation behaviour, internal friction temp. depend. *(Russian)* 78—52872
  steel, Mn-Cr-V, crack propag. resist. at hardness indentation, and fracture toughness *(German)* 79—29220
  steel, Mn-Cr-V, structural changes during solution annealing *(Czech)* 78—84864
  steel, Mn-Ni-Cr, diffusion of Fe, Mn, Si, V and W *(Czech)* 77—59148
  steel, MnCr (16, 5 wt.%), bending fatigue behaviour improvement by surface treatment *(German)* 78—84957
  steel, MnMoNiCr, pressure vessel, stress relief cracking 79—43404
  steel, Mo-Cr (3 wt.%), CrC formation in isochronal tempering, electron microscope study 80—7584
  steel, Ni-Co-Cr, high-strength medium C, Cr effect on props. 80—76339
  steel, Ni-Co-Cr-Mo-C (10,14,2,1,0.16 wt.%), stress corrosion cracking at 22°C in 3.5% NaCl 79—8390
  steel, Ni-Cr, (4,1, wt.%), isothermal embrittlement, AES exam. of grain boundary segregation 78—60814
  steel, Ni-Cr, anodic dissoln. in NaCl solns. at high current densities *(Russian)* 80—76396
  steel, Ni-Cr, case-hardened, surface durability in rolling contact fatigue testing 77—63684
  steel, Ni-Cr, corrosion on N_2O_4 flow 520-890K and 8-9 MPa *(Russian)* 80—3256
  steel, Ni-Cr, long-time exposure to N_2O_4, effect on mech. props. *(Russian)* 78—48573
  steel, Ni-Cr, P induced temper embrittlement, Mo effect 77—86148
  steel, Ni-Cr, temper embrittled, electron microscope and X-ray microstruct. obs. 79—38870
  steel, Ni-Cr, temper embrittlement by Sb, Ni, Cr effects 77—36628
  steel, Ni-Cr, temper embrittlement by Sn 77—86149
  steel, Ni-Cr temper embrittlement by P 77—40448
  steel, Ni-Cr-Mo, cleavage fracture toughness, temperature and notch sharpness influence *(German)* 80—35291
  steel, Ni-Cr-Mo, exam. of delayed fracture using fracture mechanics *(Japanese)* 78—52961
  steel, Ni-Cr-Mo, fracture toughness determ. from yield strength and cleavage fracture strength *(German)* 80—35292
  steel, Ni-Cr-Mo, Ni effect on fracture toughness, heat treatment effect *(Korean)* 79—91781
  steel, Ni-Cr-Mo, quenched and tempered, nothced bar tensile tests *(German)* 80—35247
  steel, Ni-Cr-Mo, weld, stress corrosion cracking, metallurgical effects 79—43468
  steel, Ni-Cr-Mo (11, 5, 3 wt.%), maraging, corrosion cracking in chloride and alkaline solutions 80—55576
  steel, Ni-Cr-Mo (2.5 wt.%), elevated temp. fatigue, effect of zero load rest period 77—8943
  steel, Ni-Cr-Mo and Ni-Cr, impact strength, effect of modified ausforming *(Japanese)* 79—11692
  steel, Ni-Cr-Mo increase of crack initiation time in delayed fracture by fatigue accumulation *(Japanese)* 78—11312
  steel, Ni-Cr-Mo-Ti-Al, quenching and ageing effects on props. of type 36NkhTYuM8 79—52275
  steel, Ni-Cr-Mo-V, stress corrosion cracking 77—52542
  steel, Ni-Cr-Mo-V, turbine rotor shaft, fracture toughness, validity criterion for K_{IC} 78—72861
  steel, Ni-Cr-P (0.06 wt.%), influence of intercritical heat treatment on temper embrittlement susceptibility 78—52863
  steel, Ni-Cr-Ti, thin bands, cold working, props. and struct. of 36NKhTYu 79—78994
  steel, Ni-Cr-Ti-P, Ti and P solubility effect on free surface segregation 79—11628
  steel, Ni-Mo-Cr, embrittling effects of residual elements 80—66655
  steel, NiCr, random load fatigue crack propag. 78—64692
  steel, NiCrMoV, stress corrosion cracking, cold work effects 78—11383
  steel, nonoriented, mag. props. texture, Cr addition effect 77—1880
  steel, pearlitic, Cr-Mo(-V), heat resist., Mo content rel. to mech. props. 79—20134
  steel, Si-Cr-Mo-W-V (2,4,1,3,2 wt.%), heat treatment and props. 80—16349
  steel, Si-Mn-Ni-Cr-Mo, acoustic emission during stress corrosion cracking appl. to materials testing 78—53042
  steel, sintered, Cr-Mo, CaF addition effects on struct. heterogeneity 78—60611
  steel, sintered, Ni-Cr-Mo additions, struct., props., thermomechanical treatment effects 77—12657
  steel, stainless, 12Kh13 and 15Kh11MF, austenite transform. kinetics 79—87612
  steel, stainless, 20Kh13, prep. by diffusion impregnation 80—60803
  steel, stainless, 304, weld decay, precip. of $M_{23}C_6$ during thermal cycles *(Japanese)* 79—52468
  steel, stainless, austenitic, Cr-Ni-Mn-Si-Mo-C alloy, 13Khi8N10G3S2M2, elastic moduli exam. after thermomechanical treatment *(Russian)* 79—24558
  steel, stainless, carbonisation and carburisation in high press. He environment *(Japanese)* 79—26516
  steel, stainless, cold plastic deform. effect on struct. and props. 80—29113
  steel, stainless, corrosion in nonisothermal Li flow 79—79177
  steel, stainless, Cr, Mo effects on passivation AES and electrochemical anal. 79—74292
  steel, stainless, Cr-Ni, low temp. plastic deformation, in mag. field 79—83256
  steel, stainless, Cr-Ni (18,10 wt.%) Ti stabilised, cavitation failure, relationship of corrosive and erosive factors *(Russian)* 77—16722

chromium alloys continued
  steel, stainless, Cr-Ni (18, 10 wt.%), long-term strength in H at high pressure 80—55485
  steel, stainless, Cr-Ni (18, 8 wt.%) average inclusion size and contents exam. measurements using optical microscopy and Br-Methanol methods *(Korean)* 79—66080
  steel, stainless, Cr-Ni (18, 9 wt.%), cold rolled, struct. 79—83214
  steel, stainless, Cr-Ni-Mn, N strengthened, low-temp. elastic props. 79—70109
  steel, stainless, Cr-Ni-Mo (16, 14, 3 wt.%), corrosion resist., vacuum heat treatment effect 79—87754
  steel, stainless, Cr-Ni-Mo-N, phase diagrams 80—35161
  steel, stainless, Cr-Ni-Nb stabilised, Te vapour effect on creep and tensile props. 79—24583
  steel, stainless, Cr-Ni-Ti, metallographic detection of $(Ti,Ni)_6C$ 80—66721
  steel, stainless, duplex alloy, Cr diffusion 77—20111
  steel, stainless, Fecralloy, creep-rupture props., 650-800°C 80—97535
  steel, stainless, ferritic, 18%Cr, stress/strain curve, H_2 charging influence, room temp. *(Japanese)* 78—39884
  steel, stainless, ferritic, Ni-free, effect of V, Ti addition on ductility 79—79048
  steel, stainless, Ni-Cr-Mo, two-phase, compositional charge of ferrite and austenite *(Japanese)* 79—4948
  steel, stainless, Ni-Cr-Mo-W (29, 13, 3, 2 wt.%), long-term strength in H at high pressure 80—55485
  steel, stainless, resulphurated, Cr-Mo (18,2 wt.%), Mo effect on corrosion resistance *(French)* 77—63830
  steel, stainless, stabilised with Cr-Ni-Nb, reaction with Te vapour 77—8986
  steel, stainless, surface cleaning by H^+ bombard., AES study 78—53022
  steel, stainless, type Kh17N13M2T, strengthening by plastic deformation and cold working *(Russian)* 78—52839
  steel, stainless complex alloy, hot ductility, B effect 80—30038
  steel, stainless ferritic, 10 to 30 wt.% Cr, ductile-brittle transition temp. 80—30095
  steel, stainless ferritic, Cr-Mo, corrosion behaviour, review 79—39018
  steel, stainless ferritic, drawability, mech. props., and grain boundaries in 08Kh16AMT and 08Kh18T1 80—35270
  steel, surface damage during friction, struct. effect 80—35339
  steel, type 1Kh17N2, alloying element redistrib. during friction *(Russian)* 77—81326
  steel, type 304, high C, low C, backscatter Mossbauer spectroscopy 80—40001
  steel, W-Cr (3 wt.%), CrC formation in isochronal tempering, electron microscope study 80—7584
  steel, W-Mo-Cr-V tool, laser surface melted, struct., heat treatment effect 80—76424
  steel, X5CrNiTi26.6, ferrite-austenitic struct., optical and electron microscopy 78—84848
  steel 23K2G2T, corrosion cracking susceptibility, C and Cr effects 78—19952
  steel 40 khNMS, high temp. thermomechanical treatment, Cr effects on props. 77—12651
  steel austenitic Cr-Ni-Be, cellular precipitation *(Japanese)* 78—11229
  steel austenitic stainless, Cr-Ni 316 type, electron irradiated, void swelling 79—42104
  steel Cr-Mn (13, 19 wt.%), for liquefied natural gas appls., material and weld props. 79—61736
  steel Cr-Mo (2.25, 1 wt.%), duplex LMFBR steam generator tubing, US equipment for NDT 78—11469
  steel Cr-Mo low-alloy, material selection for nuclear steam generator 78—54834
  steel Cr-V (1.5, 0.5 wt.%), cavitation effect of temp. and C content 78—64638
  steel electrode, erosion resist., influence of C and carbide-forming elements *(Russian)* 78—11389
  steel high strength, Cr, Cr-Mo, Ni-Cr, and Ni-Cr-Mo, diffusion of H_2, effect of quenching and tempering 77—90384
  steel Ni-Cr, Sb doped, temper embrittlement susceptibility, intercritical heat treatment effect 78—64570
  steel turbine casings, residual life determ. 80—93585
  Stellite, friction behavior in high temp. Na environment *(Japanese)* 80—40546
  Stellite, self-weldability in high temp Na *(Japanese)* 80—89392
  Stellite 6B, volatilisation of oxides during oxidation at 1200°C 78—23873
  stellite hardfacing materials, friction characts. in high temp. Na *(Japanese)* 80—89356
  Stellite-6, XPS obs. of aqueous oxidation, surface comp. and gaseous oxidation effect 80—81238
  strengthening by modified ausforming 78—76665
  stress corrosion cracking test machine, design and construction, appl. to Fe-Cr-Ni alloys 80—97649
  surface, itinerant antiferromagnetism and density waves 79—82743
  Ti-Al-Mo-Cr, etching as a functoon of struct. *(Russian)* 78—15568
  transition metals, surface- or defect-induced magnetism, nearly half-filled bands 79—1671
  Udimet 500, microstructural instability in industrial gas turbine engine vane 77—28833
  Udimet 520, Nicralloy-coated, microstruct. degradation, influence of corrosioin protective coating 80—40611
  Udimet 700, creep crack growth 78—48517
  Udimet 700, high temp. fatigue crack growth, fracture mech. approach 79—52340
  Udimet 700, Ni-Co-Cr-Al-Ti (18.8, 15.2, 4.5, 3.39 wt.%) exam. of high temp. creep 79—61684
  Udimet 700, Ni-Co-Cr-Al-Ti (18.8, 15.2, 4.5, 3.39 wt.%) exam. of high temp. creep, viscoplastic flow 79—61685
  Udimet 700, Ni-Co-Cr-Ti, hold time effects on high temp. fatigue crack growth 79—5036
  Vitallium, surgical implant, SCC and corrosion fatigue in Tyrode's soln. 79—29263
  Vitallium alloy, fretting corrosion of surgical implant material, electrochemical investigation 79—66197
  VT22, hot deform., microstruct. form. and mech. props. *(Russian)* 77—28830
  Zircaloy, H absorption, Sn(Fe)(Cr)(Ni) effect 80—49527
  Zircaloy cladding, stress corrosion cracking due to I and Cs redistrib. in LWR fuel rods 80—32343

chromium alloys continued
Zircaloy-2, neutron irradiated, inhomogeneous deformation behaviour 80—50679
Zircaloy-2, tritium diffusion 80—32341
Zircaloy-4, anomalous oxide growth during transient temp. oxidation 80—50773
Zircaloy-4, microstrain and particle size meas. by Warren-Averbach method 80—55420
Zircaloy-4, quenched and annealed, strain ageing 77—25071
Zircaloy-4 tubes, texture influence on anal. of thermoelastic/plastic anisotropy and initial yielding 80—35260
Ag-Cr, dil., elec. cond. meas., 1.5 to 30K 77—62914
Ag-Cr, dil., negative magnetoresist. in pulsed fields up to 35T 77—62899
AgCr, dil., specific heat, impurity contrib. Kondo temp. 80—65903
Al bronze, G, Si additions, corrosion resistance 77—16714
Al-Cr, Al-Cr-Mn, dil. alloys, Hall coeff. and elec. resist. 77—11898
Al-Cr, anisotropic electron scattering, Hall coefficient, path integral calc. 79—91027
Al-Cr, cold-worked and homogenised, precipt. kinetics, impurity resist. and TEM meas. 77—16596
Al-Cr, dil., electron irradiated, interaction of self interstitials with undersized solute atoms 78—63789
Al-Cr, dil., supercond., nucl. spin relax. and quasiparticle excitations 80—88680
Al-Cr, dil. alloys, single impurity and interaction effects in susceptibility 77—8269
Al-Cr, dilute, morphological stabilities of planar solid-liquid interfaces during unidirectional solidification 79—4960
Al-Cr, dilute, vacancy-impurity interaction investig. by tempering method *(French)* 77—68995
Al-Cr, Kondo alloys, spin and phonon resistivity independ. 78—47777
Al-Cr, liq., dissoln. and diffusion of alloying components, 700-1000°C *(Russian)* 80—15275
Al-Cr, magnetic susceptibility, single impurity and interaction effects 77—63093
Al-Cr, neutron irrad., Cr atom distribution NMR study 80—54957
Al-Cr, quench hardened, Cr effects on resoftening 77—66657
Al-Cr, quenched, thermal stability *(Russian)* 80—20976
Al-Cr, rapidly solidified, crystalline and amorphous structures 77—44274
Al-Cr, recrystallization texture 79—91679
Al-Cr, simultaneous recrystallisation and precipitation *(French)* 80—16313
Al-Cr, struct. form. and phase transform. kinetics *(Russian)* 78—15359
Al-Cr (0.1 wt.%), exam. of pre precip. behaviour, by elec. resistivity meas. and TEM exam. 78—48406
Al-Cr (3 to 11 at.%), cooling rate effect on solidification struct. and mech. props. *(Japanese)* 78—39755
Al-Cr alloys, anomalous sp. ht. and nuclear spin-lattice relax. 79—46814
Al-Cr alloys, corrosion inhibition by o-substituted phenols in NaOH soln. 78—44250
Al-Cr-Zn (2.5, 1.5 wt%), phase equilibrium, solubility *(Russian)* 78—19723
Al-Cr-Zr(Nb), calc. of phase equilibria 79—11569
Al-Cu-Mg-Mn-Zn-Cr, low temp. deformed, ageing and mech. props. 79—1881
Al-Fe (0.5 wt.%)-Ti-Cr, Ti, Cr addition effects on toughness/microstruct. relationship *(Japanese)* 77—48525
Al-Mg-Cr, tube drawing, tensile forces, plastic deformation *(French)* 79—70130
Al-Mg-Cu-Si-Cr (1,2.7,0.6,0.2wt.%), laser shock hardening of weld zones 78—39800
Al-Mg-Fe-Mg-Si-Cr, alloys, dendritic segregation with Fe, Mg, Si and Cr additions *(Polish)* 79—56980
Al-Mg-Mn-Cr (4, 0.45, 0.15 wt.%), laser shock hardening of weld zones, exam. 78—39800
Al-Si (35 wt.%), Cr, Co, Si addition effects on strength of powder 77—24983
Al-Zn-Mg-Cu-Cr, (5.6, 2.5, 1.6, 0.3 wt.%), laminates, 8 and 22 layers, adhesively bonded exam. of fatigue crack propag. 78—92345
Al-Zn-Mg-Cu-Cr, (5.6, 2.5, 1.6, 0.3 wt.%), alloy 7075, plates, adhesively bonded, exam. of fatigue crack growths 78—92348
Al-Zn-Mg-Cu-Cr, shot peened, positron annihilation meas. 77—63833
Al-Zn-Mg-Cu-Cr-Zr, high strength Cr and Zr addition effects 77—59820
Al_2O_3-NiCr composite, plasma sputtering of electroheating coatings, elec props. *(Russian)* 80—108350
Au- Cr, dil., spin glass state and Kondo effect, nucl. orientation of ^{54}Mn 78—6514
Au-Cr, conc. spin glasses, thermopower 80—65538
Au-Cr, cosputtered films, optical props. 0.2 to 6.1 eV 77—32454
Au-Cr, dil., conduction electron-local moment interactions using dHvA waveshape anal. 79—77981
Au-Cr, dil., elec. resist., generalised phase shift anal. of Kondo effect 80—75556
Au-Cr, dil., spin glass, elec. resist., press. and conc. effects 78—52278
Au-Cr, dil. alloys., elec. resist., deviations fro Matthiessen's rule 80—75541
Au-Cr, dil. spin glass elec. resist., press. and conc. depend. 80—24864
Au-Cr, spin glass, anomalous Hall effect 78—30908
Au-Cr, spin glass alloy, elec. resist. 77—8067
Au-Cr, UPS study, localised states 80—93449
Au-Cr alloy, quantitative Auger electron anal., sputter-yield ratio 77—44096
Au-Cr alloy pressure gauges, annealing effects 78—49854
Au-Cr alloys, Cr conc., quantitative Auger electron analysis 77—85852
Au-Cr Kondo alloy, effect of press. on resistivity 78—79978
Au-Cr pressure gauge, technological processing 77—49740
Au-Cr-GaAs Schottky-barrier diodes, effect of γ-radiation on current-voltage charact. *(Russian)* 80—2459
Au-Cu-Cr, thin layer, deposited on glass or Si substrate, X-ray microanalysis *(French)* 80—50902
Au-Mn-Cr, ferro- to non-magnetic transform. 77—12117
B fibre reinforced Al-Cr, calc. of thermodynamic interaction potential between B fibre and matrix 80—11627
B-Cr, diffusion coatings on alloy steel U8, wear resistance 78—56823
B_4C-Cr, contact reaction with liq. Ni 80—55707
CC Fe-Ni-Cr (35, 15 wt.%): Nb(Ti)(Mo), corrosion in HTGR He environment 80—61021
CU-Zr-(Cr), powder metallurgical alloys, thermomech. treatment effect on props. 80—50660

chromium alloys continued
Cd-Cr, dil., estimates of s-d interaction from supercond. transition temp. and mag. susceptibility 78—43561
Cd-Cr, dil., mag. and supercond. props. 79—38237
(Co,Cr,Ni)-TaC, eutectic alloy, directionally solidified, struct. defects, autoradiographic investig. *(Russian)* 77—25038
(Co,Cr)-$(Co,Cr)_7C_3$, eutectic creep model 77—36588
(Co,Cr)-$(Cr,Co)_7C_3$, eutectic alloy, directionally solidified, struct. defects, autoradiographic investig. *(Russian)* 77—25038
$(Co,Cr)(Co,Cr)_7C_3$ eutectic composite, creep anisotropy 78—19840
(Co,Ni)-$Cr_{23}C_6$ eutectic, microstruct. effect on fracture energy 80—7662
Co-Al-Cr, eutectic alloys, charact. by melting, oxidation resistance and composition 78—52768
Co-B-Mo-Cr, amorphous, Mo and Cr addition effect on corrosion behaviour 80—16568
Co-Cr, biolgoical implant, ion beam sputter of surface morphology, SEM obs. 77—44836
Co-Cr, containing dispersion oxides formed by internal oxidation, oxidation behaviour 78—19922
Co-Cr, fibrous eutectic, thermal stability 77—36547
Co-Cr, gas corrosion, in composite atmospheres *(Polish)* 79—79142
Co-Cr, high temp. sulphide corrosion 78—64775
Co-Cr, isothermal oxidation in 760 Torr O_2 at 1000°C 77—77639
Co-Cr (up to 25 wt.%), sulphidation and oxidation in Ar-SO_2, effects of increase in Cr content 80—11839
Co-Cr films, mag. props. in range of transition from thin-film to hypercritical state *(Russian)* 79—51824
Co-Cr mag. film, crystallographic texture formation effects on props. *(Russian)* 80—108471
Co-Cr orthopedic implants, surface oxide layer investigations using ESCA technique 79—25157
Co-Cr recording films, perpendicular mag. anisotropy, hysteresis loop, microstruct., TEM obs. 78—95491
Co-Cr superalloy, type MAR M509, high temp. fatigue behaviour 80—40485
Co-Cr system, phase diagram re-determ. from thermodynamic data 78—76631
Co-Cr-Al, eutectic alloy, unidirectional solidification, oxidation and tensile tests 78—52790
Co-Cr-Al, exam. of cyclic oxidation resistance at 1100 and 1200°C, comparison with Ni-Cr-Al system 78—88572
Co-Cr-Al, oxidation at 1000°C 77—59963
Co-Cr-Al, protective coating, exam. of interdiffusion kinetics, development of analysing procedure 79—5085
Co-Cr-Al, ternary system, interdiffusion, electron probe anal. 80—34256
Co-Cr-Al based coating, electron beam evaporation of low vapour press. elements 80—40613
Co-Cr-Al-C eutectic alloy, thermal cyclic loading, exam. 78—48496
Co-Cr-Al-Y, low temp. hot corrosion, Na_2SO_4-induced, mechanism, burner rig tests 80—40610
Co-Cr-Al-Y, turbine blade coating, hot corrosion by Na_2SO_4 and vaporous NaCl 78—19941
Co-Cr-Al-Y coated turbine airfoils, effect of electron beam deposition rate on struct. 79—23870
Co-Cr-Al-Y coating, Pt-modified, oxidation and hot corrosion resist. 78—11437
Co-Cr-Al-Y protective coating for combustion turbines, hot corrosion evaluation 80—40608
Co-Cr-Al-Y(Hf), high temp. oxidation 78—11432
Co-Cr-C, precipitation of $M_{23}C_6$, role of dislocations 78—44130
Co-Cr-C eutectic, creep and fatigue crack propag. 78—39859
Co-Cr-C eutectic alloy, thermal conductivity and electric resist. at high temp. 80—103668
Co-Cr-C-Al (39, 2.2, 2 wt.%), directionally solidified eutectic alloy, Larson Miller C const. 79—70162
Co-Cr-Mo (Zr)(Nb)(Ta), eutectic alloys, charact. by melting, oxidation resistance and composition 78—52768
Co-Cr-Mo shoulder prosthesis, wear and fatigue tests 80—26415
Co-Cr-Mo-Ni-Fe-Si-Mn-C, protective coatings by B diffusion, microstruct. and mech. props. 78—11427
Co-Cr-Ni alloy FSX 414, electrochemical corrosion meas. in molten sulphate 79—96178
Co-Cr-Ni superalloy Mar-M509 standard and Mo modified, phase anal. 77—63675
Co-Cr-Ni-Ta-Al-Y (25, 10, 5, 3, 0.5 wt%), exam. of hot corrosion 79—20251
Co-Cr-Ni-TaC, directionally solidified eutectic, mech. props. and sruct., thermal cycling effects *(Russian)* 78—92282
Co-Cr-Ni-W-Ta-C, alloy Mar M-509, TEM exam. of thermal fatigue crack propag. in cast alloy 78—76740
Co-Cr-Ni-W-TaC (15.7, 9.5, 3, 12.77 wt.%) alloy Co50B3W, temperature cycling effect on rupture strength 78—39898
Co-Cr-NiTaC eutectic, directionally solidified, microstructural stability 79—38815
Co-Cr-Nr-TaC eutectic alloys, fatigue, microstructure effects 78—23803
Co-Cr-Si alloy hot corrosion and oxidation expts. for ionic conducting scale 78—11446
Co-Cr-Ta(Al) alloy, high temperature wear resistant coatings, CrO_2 hardened 79—24677
Co-Cr-W-C, hardfaced coating for high temp. liquid Na service, deposition and wear 77—32724
Co-Cr-W-C, wear-resistant coating alloy, carbide form. and decomp. 77—32711
Co-Cr-WC, corrosion and corrosive wear in sea water 78—92408
Co-Cr-Zr, thermodynamically calculated phase diagram 79—91617
Co-Cr-Zr(Ni), phase diagram calc. 79—1848
Co-Cr(-Al-Y) coatings, hot corrosion resist., ductile-brittle transition 79—24674
Co-Fe-Cr-P-B sputtered amorphous films, mag. props. and corrosion resist. 79—28567
Co-Mo-Cr-Si, plasma and detonation coatings, Laves- and carbide-strengthened, comparative props. 78—15562
Co-Mo-Cr-Si Laves phase, sputter deposited, struct. and wear props. 77—40477
Co-Ni-Cr (20,20 wt.%), internal oxidation, improvement of mech. props. *(French)* 77—16521
Co-Ni-Cr superalloys, γ'-precipitation-strengthened, yielding 77—8894
Co-Ni-Cr-Al-Ta, S-57 alloy hot corrosion, cyclic oxidation, depth of attack determinations 80—11837
Co-Ni-Cr-B, centrifugally cast metallurgical coatings for wear resistance in plastics molding machines 79—29285

chromium alloys continued
- Co-Ni-Cr-B, X-306 centrifugally cast cylinder lining alloy, compatibility with hardfacing alloys 77—32726
- Co-Ni-Cr-C, carbide precipitation 79—29065
- Co-Ni-Cr-Mo, mech. props., effect of twinning and FCC to HCP transform. 77—4779
- Co-Ni-Cr-Mo (35, 20, 10 wt.%), MP35N, TEM study of phase transformations 80—81054
- Co-Ni-Cr-Nb, effect of Fe addition on precipitation behaviour 80—29962
- Co-Ni-Cr-Nb (40, 18, 1.8 wt.%), precipitation behaviour of NbC, effect of ageing temp. on morphology 80—89227
- Co-Ni-Cr-Nb FCC alloy, electron microscope obs. of deform. twins 79—60380
- Co-Ni-Cr-Ta-C (10, 10, 14, 1 wt.%), aligned eutectic, directionally solidified, fatigue crack propag. 78—27624
- Co-Ni-Cr-W-Fe, HA-188 alloy, hot corrosion, cyclic oxidation, depth of attack determinations 80—11837
- Co-W-Cr (15,20 wt.%), surgical implant ion beam textured, stress/strain relations, fatigue characts. 78—73297
- (Co-Ni)-$Cr_{23}C_6$ eutectic alloy, directionally soldified, microstruct. and crystallography 78—48390
- $(Co_{100-y}B_y)_{1-x}Cr_x$ thin film glasses, mag. props. and corrosion resist. 80—80576
- Co(Cr,Ni)-TaC fibrous eutectic, deformed, thermal stability of microstruct. *(Russian)* 79—1895
- CoCr, dil., low temp. specific heat and magnetisation 80—65925
- CoCrAl alloy, Al_2O_3 forming, oxidation resistance improvement by dispersed oxide addition 79—83379
- CoCrAl-Y(HF), Y and HF effects on oxidative behaviour 78—44275
- CoCrMo, artificial hip joints, fatigue strength 79—48375
- $(CoFeB)_{100-x}Cr_x$ thin films, magnetic props. and corrosion resist. 80—34709
- $(Co_{0.93}Fe_{0.07})_{75-x}Cr_xSi_{15}B_{10}$ amorphous alloy, thermal stability, Cr conc. effects, DTA expts. 80—59395
- $Co_2Ga_{2-x}Cr_x$, elec. resist. anomalies 79—38044
- $Co_2Ga_{2-x}Cr_x$, ferromag., local configurational studies, neutron scatt. and spin echo NMR 77—63114
- $Co_2Ga_{2-x}Cr_x$, ferromag., site selecting and moment distrib. 77—77031
- $Co_2Ga_{2-x}Cr_x$, mag. props. and order 77—12093
- CoNiCrMo, artificial hip joints, fatigue strength 79—48375
- $(Cr, Mn)_2As$, mag. props. and struct. 78—64190
- Cr binary substitutional solutions, thermodynamics 80—54410
- Cr bronze Sn, recrystn. props., hot rolling, annealing, polygonisation *(Russian)* 80—55419
- Cr/Ni_3Al-Ni_3Nb directional eutectic, oxidation and interaction with protective coating *(Russian)* 77—52526
- 25Cr-20Ni stainless steel dendritic solidification, growth morphology and solute redistrib. *(Japanese)* 80—81045
- Cr-$(Cr,Co)_7C_3$ eutectic, oxidation effect on toughness and strength 80—89404
- Cr-Al, abnormal thermal cond., 5 to 100K 79—19573
- Cr-Al, antiferromag., charge and spin density, neutron and X-ray diffr. 77—31971
- Cr-Al, antiferromag., transport props., anomalous crit. behaviour 79—61108
- Cr-Al, band struct. and density of states, KKR method and X-ray meas. 80—10863
- Cr-Al, couple phase diagrams and thermochemical data 79—66037
- Cr-Al, disordered alloy, effect of high press. on resistivity 78—95286
- Cr-Al, effect of Al concentration and hydrostatic press. on Neel temp. 79—33482
- Cr-Al, elementary excitations, exchange stiffness const., inelastic neutron scatt. study 79—47294
- Cr-Al, mag. excitation, neutron spectrometry 79—4654
- Cr-Al, spin density wave, neutron diffraction studies 79—1664
- Cr-Al, temp. depend. of Hall coeff. 79—33280
- Cr-Al alloy KH40NYu3, microplastic deform. *(Russian)* 77—66681
- Cr-Al-C, ternary system, phase relationships 80—76230
- Cr-AlN, dispersion hardened, erosion resistance 77—12637
- Cr-AlN, dispersion strengthened, hardness and oxidation rate, 1000 to 1500°C *(Russian)* 78—15574
- Cr-Au, matrix sensitive and insensitive factors evaluation using quantitative AES 79—24395
- Cr-B system, phase diagram, CrB_6 synthesis 79—78931
- Cr-C, binary alloy formation of nonequilib. Cr_3C in alloys quenched rapidly from melt 80—7581
- Cr-C, coupled phase diagrams and thermochemical data 79—66036
- Cr-C, hard coating preparation by ion beam methods 80—25579
- Cr-C facing alloys, effect of B on phase composition and facings props. during abrasive wear 80—21117
- Cr-Ce-N, Ce and N effects in ductile-brittle transition, microstruct., hardness, *(Russian)* 78—35497
- Cr-Co, dil., antiferromag., elec. resist. min., press. and impurity effects 80—59970
- Cr-Co, dil., Neel temp., impurity conc. depend. calc. 78—68232
- Cr-Co, dil., with local mag. moments, Neel temps. 79—73713
- Cr-Co, magnetic transformations, triple point *(Russian)* 80—88747
- Cr-Co, phase transformations and magnetostriction *(Russian)* 80—103869
- Cr-Co, spin density wave, neutron diffraction studies 79—1664
- Cr-Co (4 wt.%) alloy, antiferromag. transitions effect on opt. props. 77—12371
- Cr-Co (4.0 at.%) alloy, antiferromag., disappearance of resist. min. under press., and press. coeff. of T_N 80—10960
- Cr-Co (up to 8 at.%), antiferromagnetic, resist. minimum, Kondo effect by pairs of Co atoms 80—39566
- Cr-Co-Fe, chromindur alloy, field heat treatment, and mag. props. 80—35354
- Cr-Co-Fe, for telephone receiver mag. use 80—45318
- Cr-Co-Fe, low Co, phase separation, TEM and Mossbauer spectra obs. 80—71269
- Cr-Co-Fe cold formable mag. alloys for use in telephone receiver 79—52227
- Cr-Co-Fe permanent magnet anisotropic alloys, plastic deform., ageing, particle alignment temp. 80—35254
- Cr-Co-Ga systems, phase equilibria diagrams at 800 and 600°C *(Ukrainian)* 78—92236
- Cr-Co-Ni hard film on Mo substrate for magnetic recording 80—2608
- Cr-Co-V alloys, dil., elec. resist. min. 80—54680
- Cr-Cu(Al,Si,Zr,Ni,Mo,W) powder based composite, high temp. strength of W reinforcing fibres 79—70021

chromium alloys continued
- Cr-Fe, alloy with mixed types of order, uniform mag. phase diagram 79—78368
- Cr-Fe, antiferromag., elec. resistivity, Kondo effect 79—60812
- Cr-Fe, antiferromag. phase boundary, neutron diffr. meas. 78—95437
- Cr-Fe, antiferromag. sp.ht. around Neel point 79—73750
- Cr-Fe, antiferromagnetic, effect of press. on hyperfine mag. fields at Fe nuclei *(Russian)* 80—15936
- Cr-Fe, dil., antiferromag., mag. incoherent elastic neutron scatt. 79—73678
- Cr-Fe, dil., antiferromag., elec. resist. min., press. and impurity effects 80—59970
- Cr-Fe, dil., latent heat exam. of magnetic transitions 79—61156
- Cr-Fe, dil., magnetisation, Fe local moments 80—60215
- Cr-Fe, dil., Neel temp., impurity conc. depend. calc. 78—68232
- Cr-Fe, dil., spin correlations and neutron scatt. near crit. conc., theory 80—60327
- Cr-Fe, dilute, localised moment cluster model, ferromagnetic exchange coupling 80—39774
- Cr-Fe, disordered, polarised neutron diffuse scatt. meas., 4.6-110K 80—34592
- Cr-Fe, elastic moduli, electron conc., pulse echo overlap meas. 80—59550
- Cr-Fe, electronic struct., Mossbauer and positron annihilation study 79—82518
- Cr-Fe, low conc. alloys, coexistence of itinerant antiferromagnetism with paramagnetism 78—84386
- Cr-Fe, mag. moment of Fe, mag. suscept. meas. 79—61079
- Cr-Fe, mag. phase transition, sp. ht. meas. 77—12120
- Cr-Fe, magnetically insensitive Invar-type alloys *(Japanese)* 79—8034
- Cr-Fe, polycrystalline, antiferromag., elastic moduli and thermal expansion meas. 77—43860
- Cr-Fe, spin-glass phase, magnetisation curve test for mag. ordering 80—11201
- Cr-Fe, superparamagnetism and mag. order charact. near critical conc., neutron scatt. study 79—11293
- Cr-Fe, with Si and Ta additions, metallurgical and mechanical characterisation *(Italian)* 77—66674
- Cr-Fe (0.6 at.%), antiferromag., anomalous press. effect on resist. minimum 79—15138
- Cr-Fe (0.8-8 at.%), mag. phase transforms., sp. ht. obs. *(Russian)* 77—80941
- Cr-Fe (1 wt.%), fracture during electrospark cutting *(Russian)* 79—87719
- Cr-Fe (14 wt.%), spin density wave and spin glass ordering coexistence at low temps. 79—61059
- Cr-Fe (20 to 30 at.%), Mossbauer spectra temp. var. and ferromag. props. 77—81037
- Cr-Fe (30 wt.%) alloys, refined fine comminution 78—60598
- Cr-Fe (6.5 wt.%), atomic clustering and mag. defects, mag. moments 80—60246
- Cr-Fe alloy (up to 50%), hardness, oxidation and electronic constitution 80—30154
- Cr-Fe itinerant antiferromag. effect of mag impurities 77—32186
- Cr-Fe microstructural changes, heating and cooling cycles 79—78956
- Cr-Fe_x (x=0.5, 1.5 and 3.5 at.%), antiferromag., Kondo anomaly 80—11163
- Cr-Fe-C (28.4, 9.1 wt.%) prep. from $FeCr_2O_4$ chromite 80—100804
- Cr-Fe-Co dilute alloys, Neel temp., thermal expansion rel. to Co content 79—47281
- Cr-Fe-Ga system, phase obs. at 800 and 820°C *(Russian)* 78—23662
- Cr-Fe-Ni, cryst. struct. and defects, high resolution electron microscopy obs. 79—94961
- Cr-Fe-Ni, γ-solid soln., thermodynamic activity determ. at 1500K 80—108397
- Cr-Fe-Ni, phase diagram calc. 79—1848
- Cr-Fe-Ni alloys, claddings, chemical compatibility with UC nuclear fuels, thermodynamic model 80—63263
- Cr-Fe-Ni alloys, interface with Th carbide fuels, basic chemical compatibility, thermodynamic calcs. 79—93727
- Cr-Fe-Ni-Si, ternary phase equilibria for Cr-Fe-Ni rich portion, lattice stabilities 80—71628
- Cr-Fe-Si, mag. excitation, neutron spectrometry 79—4654
- Cr-Fe-Si, sp. ht., 1.4-4.2K 77—20079
- Cr-Fe-Si, spin density wave, neutron diffraction studies 79—1664
- Cr-Fe-V, calc. of phase equilibria using thermodynamic values from different models 78—60646
- Cr-Fe-V, dil., V effect on para- to incommensurate and commensurate transitions 78—68260
- Cr-Fe-V, effects of V on mag. transition, elec. and mag. props. 77—69554
- Cr-Fe(Cu), dil., exchange interactions 77—47986
- Cr-Fe(2.8 at%), antiferromag., meas. of incoherent elastic neutron scatt. cross section 79—19723
- Cr-Ga, dil., Neel temp., elec. resist. and thermal expansion meas. 79—51778
- Cr-Ge, dilute alloy, phase diagram of spin density wave states 79—24158
- Cr-Ge amorphous films, annealing effect on elec. resistance and struct. 80—54667
- Cr-Ge liquid and amorphous alloys, struct. props., cond., viscosity, surface tension *(Russian)* 80—54119
- Cr-Ge system, phase diagram, thermal anal., X-ray diffr., microhardness, and electron probe anal. *(French)* 80—97462
- Cr-Ge system, XPS, X-ray and neutron diffr. and mag. meas. to study chem. bonding and electronic struct. 80—60749
- Cr-Ir, magnetic transformations, triple point *(Russian)* 80—88747
- Cr-La, cast, B additions effect on struct. and props. *(Russian)* 78—19891
- Cr-La-V-Nb-Ta, La, V, Nb Ta effect on hardness and strength *(Russian)* 79—34050
- Cr-Mi-W-(-Mo), heat resistant weld seam metal, tensile strength, thermophysical characts. 79—91769
- Cr-Mn, order of mag. transitions in antiferromag. alloys 79—4677
- Cr-Mn, strain wave and spin density wave intensities, neutron diffr. 78—60266
- Cr-Mn (0.5 at.%), mag. phase transforms, sp. ht. obs. *(Russian)* 77—80941
- Cr-Mn alloys, antiferromag. and weak ferromag., elec. props. 79—56514
- Cr-Mn alloys, elec. resist. near T_N 77—69313
- Cr-Mn alloys, magnetisation process, magnetisation in 90-300K range *(Russian)* 78—15007
- Cr-Mo, behaviour of mag. impurities 79—4672

chromium alloys continued
Cr-Mo, binary continuous solid solution, elec. resist. and thermoelec. power behaviour 79−69492
Cr-Mo, elec. resist. and thermo-EMF, conc. depend., 4.2 to 1500K *(Russian)* 80−80247
Cr-Mo, electrical resistivity, spin density wave gap, Neel temp. 80−88534
Cr-Mo (2.25, 1 wt.%) steel, T permeation rate at 400 to 500°C, rel. to LMFBR conditions 78−17319
Cr-Mo low C steel forgings, material capabilities 77−42105
Cr-Mo pressure vessel steel, improvement through electroslag remelting 77−42104
Cr-Mo steel types JIS SCMV 2, SCMV 3 and SCMV 4, high-temp. high-cycle fatigue props., press. vessel appls. *(Japanese)* 80−93650
Cr-Mo-Fe (2, 14 wt.%), spin density wave and spin glass ordering coexistence at low temps. 79−61059
Cr-Mo-Ni-Ti alloy A-286, stress-rupture data correlation 77−44346
Cr-Mo-V, steamline bends, restorative heat treatment effects 78−68716
Cr-Mo-V steel, creep rupture tests on notched cylindrical specimens at 600°C 77−32670
Cr-Mo-V-Nb, supercooled austenite isothermal decomp., struct., strength and fracture characts. 80−60966
Cr-N system, thermodynamic anal. 77−77461
Cr-Nb, dislocation cell growth kinetics by TEM during annealing *(Russian)* 79−65084
Cr-Nb-Mo system, comp. and temp. depend. alterations in mech. props., phase diagram interpret. *(Russian)* 80−85045
Cr-Ni, blistering after 40 keV He ion bombard. 80−39175
Cr-Ni, fatigue, low cycle, test results, least square deviation method 77−63796
Cr-Ni, fusion reactor first wall materials, compatibility with impure He 80−32469
Cr-Ni, H_2 penetration from N_2-H_2 mixtures *(Russian)* 77−69117
Cr-Ni, high temp. strength, interatomic bonds ionic component correlation *(Russian)* 79−15761
Cr-Ni, Inconel, first wall material thermal response 80−32456
Cr-Ni, Inconel 718, fusion reactor blanket materials for Argonne Experimental Power Reactor 80−32450
Cr-Ni alloy, 01Kh18N40M5, blistering under high He^+ irradiation 80−29095
Cr-Ni alloy, He blistering at high irradiation doses 79−51167
Cr-Ni alloy NK40, thermal fatigue life *(Japanese)* 78−19880
Cr-Ni austenitic steel, Ti stabilised, nuclear reactor pipeline appl. *(Hungarian)* 77−18658
Cr-Ni compressor disk, surface plastic deform., optimal method 80−60924
Cr-Ni steel, austenitic, effect of Si on carburising mechanism at 930°C 77−56155
Cr-Ni steel, carburised, effect of atm. during heating to quenching temp. on austenite decomp. 77−56157
Cr-Ni steel, strengthening by elastic deform. at −196°C 77−55987
Cr-Ni VKh-4 alloy, deformation and fracture mechanism investigation *(Russian)* 80−11738
Cr-Ni-Fe, Inconel 625, plasma chamber material for power generating Tokamak, suitability tests 80−32449
Cr-Ni-Fe, ternary phase diagrams, interactive computer program 80−71629
Cr-Ni-Ga systems, phase equilibria diagrams at 800 and 600°C *(Ukrainian)* 78−92236
Cr-Ni-Mo-Cr_xC_y wear resistant coating prep. by laser beam melting, and props. 80−40607
Cr-Ni-Mo-Cu-Nb steel, martensitic precipitation hardenable, corrosion-resistant, heat treatment, structure and props. 79−74169
Cr-Ni-Nb steel, oxidation in CO_2, charged-particle nuclear techniques 80−61022
Cr-Ni-Ti alloy and steel, emissitivty and reflectivity, oxide film thickness effect 79−82364
Cr-Ni(Co)(Fe), liquid, N activity coeff. 77−72699
Cr-Ni(V), dil., mag. susceptibility, 77 to 400K *(Russian)* 80−50066
Cr-Os, magnetic transformations, triple point *(Russian)* 80−88747
Cr-Os, magnetic transition T-P-C diagram, triple points *(Russian)* 80−54895
Cr-Pd dilute alloys, itinerant antiferromag., neutron diffr. meas. 77−77032
Cr-Pt, dil., effect of Pt on itinerant antiferromagnetism 78−64191
Cr-Pt alloy, mag. props., effect of atomic environment 78−23247
Cr-Pt alloys, neutron diffraction study, (100) magnetic peak, magnetic structure transitions 79−56506
Cr-rare earth, dil., oxidation of Cr, effect of rare earth impurities 79−79160
Cr-rare earth alloy, calc. of phase diagrams, with immiscibility in liquid state, using thermodynamics *(Russian)* 79−20029
Cr-rare earth alloys, liquid phase, topology in diagrams of state *(Russian)* 80−54121
Cr-rare earth phase diagrams, model of ideal solns. *(Russian)* 77−55946
Cr-Re, dil. alloy, mag. susceptibility temp. depend., thermal expansion coeff. *(Russian)* 78−76225
Cr-Re, mag. excitation, neutron spectrometry 79−4654
Cr-Re, mag. excitations in commensurate antiferromag. phase 80−50079
Cr-Re, phase transformations and magnetostriction *(Russian)* 80−103869
Cr-Re, surface spin-density wave near T_N 79−91238
Cr-Re (0.18 wt.%), mag. excitations in longitudinal and transverse SDW phases 80−70946
Cr-Re(Ru)(Os)(Ta)(V)(Nb), Invar alloys, thermal expansion, plasticity *(Russian)* 79−55907
Cr-Rh, dil., hyperfine fields meas. 79−47056
Cr-Rh, magnetic transformations, triple point *(Russian)* 80−88747
Cr-Ru, dil. absence of mag. hyperfine field, TDPAC meas. 80−50237
Cr-Ru, magnetic transformations, triple point *(Russian)* 80−88747
Cr-Sb, dil., mag. phase diagram, elec. resist. and thermal expansion obs. 79−1669
Cr-Si, amorphous sputtered film, material for kilo-ohm sheet resistances, prep. and props 79−78227
Cr-Si, corrosion and failure mechanisms of coatings for gas turbine applications 79−29284
Cr-Si, dil., latent heat exam. of magnetic transitions 79−61156
Cr-Si, dilute alloy, mag. susceptibility and Neel temp. meas. 80−71017
Cr-Si, first order transition of spin density wave state, thermal expansivities meas. 77−85453

chromium alloys continued
Cr-Si, press. depend. of Neel temp. 77−69555
Cr-Si, thin films, deposition method, for controllable comp. with given elec. props. 80−35087
Cr-Si (1.37 at.%), thermal and elec. props. 79−78071
Cr-Si alloys, antiferromag.-ordering, neutton diffr. 77−69492
Cr-Si-Cu, struct. and supercond., Cu influence 80−50592
Cr-Si-Fe, mag. moment of Fe, mag. suscept. meas. 79−61079
Cr-Si-V, (2, 0.1 at.%), paramag. to commensurate spin density wave transition 80−65875
Cr-Si-V, dil., V effect on para- to incommensurate and commensurate transitions 78−68260
Cr-Sm-Pr, Sm and Pr additions and plastic deform. effects on texture *(Russian)* 77−55983
Cr-Ta, mixed SDW and Zeeman hyperfine interactions, TDPAC calc. 79−99797
Cr-Ti, cast, B additions effect on struct. and props. *(Russian)* 78−19891
Cr-Ti/MgO-NbC(TaC) dispersion-strengthened, high temp. wear and oxidation resist. 80−25877
Cr-Ti/NbC(TaC) dispersion-strengthened, high temp. wear and oxidation resist. 80−25877
Cr-V, binary continuous solid solution, elec. resist. and thermoelec. power behaviour 79−69492
Cr-V, cast, B additions effect on struct. and props. *(Russian)* 78−19891
Cr-V, disordered, extension of Taylor's theory of lattice vibr. 79−4387
Cr-V, itinerant electron antiferromag., spin fluctuations, low temp. specific heat 80−107439
Cr-V, strain wave and spin density wave intensities, neutron diffr. 78−60266
Cr-V-B-Y system, fatigue strength and fatigue fracture at 20 and 1100°C, SEM study 80−3194
Cr-V-Ce-N, (2.4 to 2.6, 1.7 to 2.3, 0.005 to 0.23 wt.%) V effect on hardness, and ductile to brittle transition temp. *(Russian)* 79−34138
Cr-V-Fe, mag. moment of Fe, mag. suscept. meas. 79−61079
Cr-V-Fe alloy, resistivity minimum, press. effect 79−38043
Cr-V(Mo), thermopower composition depend. 79−65445
Cr-W, anodic dissoln. at high current densities *(Russian)* 80−76395
Cr-W-O, phase relations, thermodynamic props. of $CrWO_4$ and Cr_2WO_6 80−104120
Cr-X-C amorphous alloys, (X=Fe, Co, Ni, Nb, Mo and Ta), crystn. temp. and hardness 79−73133
Cr-Y, cast, B additions effect on struct. and props. *(Russian)* 78−19891
Cr-Y_2O_3 dispersion hardened, oxidation and nitridation resistance, embrittlement 78−44267
Cr-Zr evaporation source improvement, diffusion barrier layer deposition for IC metallurgy 80−76163
CrAl coating on Ti alloy, electrospark applied, friction and wear resistance obs. *(Russian)* 79−1916
CrAl, semicond. solid solns., temp. depend. of elec. resist. at high temp. 78−67941
Cr_5Al_8, 26R cryst. struct., unit cell parameters 77−19904
γ-Cr_5Al_8, γ-brass, cryst. struct. redeterm. 77−47377
Cr_5Al_8, γ-phase, microstruct., transform. strains, TEM obs. 79−11614
$Cr_{99.94}Al_{00.6}$, thermal and elec. transport coeffs. near Neel temp. 79−78075
CrAs, anisotropy of compressibility 79−7648
CrC, wear mechanism in abrasive particle stream 77−12703
CrC-Ni alloys, exam. of activated sintering 80−16241
CrC-Ni-(P), hard alloys, sintered, fracture props., P addition effects 78−60610
Cr_3C_2 electrophoretic alloy coatings on C steel, sintered, struct. form., Ni-P undercoat effect 80−61027
Cr_3C_2/Ni-Cr, self-weldability in high temp Na *(Japanese)* 80−89392
Cr_3C_2/Ni-Cr hardfacing materials, friction characts. in high temp. Na *(Japanese)* 80−89356
Cr_3C_2-(WC)-Ni, sintered, cavitation erosion resistance *(Japanese)* 77−52500
Cr_3C_2-Ni, friction and wear, 20-1000°C 80−30112
Cr_3C_2-Ni alloys, electrophoretic deposition from conc. suspensions for P/M prep. of hard alloys 77−63575
γ-γ'-Cr_3C_2-Y eutectic, Y addition effect on oxidation during thermal cycling 79−74310
Cr_7C_3 fibre reinforced Cr alloy 73C, directionally solidified eutectic, fatigue crack propag. 77−36635
Cr_xC_y, enthalpy of form. and combustion 77−36784
Cr_xC_y-(Ni-Cr) sprayed coatings, for gas cooled reactor heat exchangers, factors affecting performance 80−40609
CrCo, dil., low temp. specific heat meas., 1.5 to 4K 80−60328
CrFe, mag. correls. and onset of ferromag., neutron scatt. study 80−50105
$Cr_{1-x}Fe_x$, Mossbauer spectra, mag. behaviour 80−20532
$(Cr_{1-x}Fe_x)_{1+\delta}Sb$, interstitial occupancy, Cr:Fe distrib., X-ray and neutron diffr. study 79−42012
$Cr_{11}Ge_8$, Cr_3Ge, thermodynamic functions 77−84948
$Cr_{11}Ge_8$, CrGe, and $Cr_{11}Ge_{19}$ amorphous films, short-range order, electron diffr. obs. *(Russian)* 78−56050
$Cr_{12}Ge_{19}$, CrGe, thermodynamic props. 77−36779
Cr_3Ge amorphous films, short range order struct. *(Russian)* 78−30841
Cr_3Ge, band theory, semiself-consistent band calcs. 78−2406
Cr_5Ge_3, amorphous film, short-range-order struct., electron diffr. meas. 79−15047
$Cr_{0.6}Mn_{0.4}$, mag. moment, neutron diffr. study 79−33459
$Cr_{0.98}Mn_{0.02}$, spin dynamics and spin wave form factor, neutron scatt. expt. 77−40047
$Cr_{995}Mn_{005}$, spin density wave Q vector, vel. depend. 79−4669
$Cr_{1-x}Mo_xCo$, $x \lesssim 0.25$, antiferromag., nucl. mag. relax. 78−6590
$(Cr_{98}Mo_2)_{90}Fe_{10}$, spin glass behaviour obs. 79−61157
CrN-MnN, synthesis and props. 77−40405
$CrNi_2$ type alloys, ordering, influence of static stresses *(Russian)* 78−56631
10CrNiCuP, suitability for power station chimney flue structural material, corrosion testing 80−108681
Cr_2O_3-Cr cermet films, for selective black absorbers 79−29483
Cr_2Os, σ phases, ordering, X-ray cryst. struct. determ. 80−107107
$Cr_xPd_{82-x}Ge_{18}$, amorphous, RF sputtered, elec. resist. and magnetoresist., Kondo type behaviour 78−76066
$Cr_xPd_{82-x}Ge_{18}$ amorphous alloys, magnetoresist., mag. susceptibility, magnetisation 78−80148
CrPt film, on sapphire, epitaxial relations 79−60649

chromium alloys continued
$Cr_{0.995}Pt_{0.005}$ alloy, mag. struct., neutron diffr. study 80—60198
Cr_2Ru, σ phases, ordering, X-ray cryst. struct. determ. 80—107107
CrSi, NMR and μSR, microscopic mag. props. *(Japanese)* 78—52368
$CrSi_2$ film, kinetics of growth 77—43454
Cr_3Si, band theory, semiself-consistent band calcs. 78—2406
Cr_3Si, charge distrib. X-ray diffr., rel. to supercond. V_3Si 77—68944
Cr_3Si, mag. susceptibility, 2 to 300K, rel. to electron energy spectrum 80—60185
Cr_3Si type phases, A-15, crystallographic interpretation of atomic volumes 79—10833
$Cr_3Si(Ga)(Ge)$, A15 cpds., self-consistent LMTO band calcs. 79—37954
Cr_5Te_6, magnetoresist. in region of mag. phase transforms. *(Russian)* 77—66299
$Cr_{1-x}V_x$, nucl. spin relax., spin fluctuation effect 80—34811
$Cr_{1-x}V_xCo$, localised mag. moment of Co impurity 78—27014
$Cr_{1-x}V_xCo$, mag. state of Co impurity, NMR exam. 78—27100
$Cr_{1-x}V_xCo$, $x \lesssim 0.05$, antiferromag., nucl. mag. relax. 78—6590
$Cr_{2.8}V_{0.7}Fe_{3.4}C_3$, stacking fault study, morphology, comp. and struct. 80—84190
$Cr_{1-x}W_x$, neutron scatt., selection rules for phonon mass operator 79—28065
Cu-Cd-Cr, precipitation hardened, low temp. elastic props. 77—73299
Cu-Cr, (1-1.3 at.%), elec. cond. exam. in solid and liquid phase *(Russian)* 77—62895
Cu-Cr, age hardened, fine precipitates struct., TEM study 80—3066
Cu-Cr, coating on Ti alloy VT9, plastic deform. and diffusion annealing effect on props. *(Russian)* 78—35425
Cu-Cr, dil., elec. cond. meas., 1.5 to 30K 77—62914
Cu-Cr, dil., in supercond. proximity, localised bands 78—10613
Cu-Cr, dil., mag. susceptibility 77—63092
Cu-Cr, dil., NMR data, ionic model and Kondo temp. 78—68399
Cu-Cr, dil., NMR satellite data, rel. to electronic struct. 78—68398
Cu-Cr, dil., negative magnetoresist. in pulsed fields up to 35T 77—62899
Cu-Cr, dil., spin glass, elec. resist., press. and conc. effects 78—52278
Cu-Cr, dil., spin-density magnetisation near Cr atoms, NMR study 80—80626
Cu-Cr, dil., thermal and elec. cond., deviations from Wiedemann-Franz law 77—66151
Cu-Cr, dil. alloy, Knight shift temp. depend., electronic struct. 78—84488
Cu-Cr, dil. alloy, Kondo resist. at 35 GHz 79—60814
Cu-Cr, dil. alloys, Frenkel defects, effects on anomalous resistivity and thermopower 77—8084
Cu-Cr, eutectic, effect of comp. and solidification conditions on microstruct. *(Russian)* 79—29037
Cu-Cr, formation of internal oxidation band 79—47820
Cu-Cr, formation of two phase microstructure, during volumetric and directional crystallisation *(Russian)* 79—29040
Cu-Cr, isothermal decomp. diagrams 79—38791
Cu-Cr, Kondo alloy, Josephson tunnelling effect 80—60145
Cu-Cr, Kondo alloy, NMR of Cu satellites, 1 to 4K 79—73837
Cu-Cr, microconductors, cast, struct. and physical props. exam 78—44232
Cu-Cr, precipitation hardened, wear 78—3234
Cu-Cr, vapour deposited, electron irrad., resistance behaviour *(German)* 78—47779
Cu-Cr (0.55 wt.%), crystallography of precipitates, strain field study 80—25699
Cu-Cr (0.6 wt.%), electron microscope obs. of shear bands *(German)* 77—48454
Cu-Cr (0.75 wt.%), deformation characts., fully reversed cyclic strain with fatigue cracks and dislocation struct. 80—81148
Cu-Cr (1 wt.%), exam. of low cycle fatigue props. at elevated temp. 78—64674
Cu-Cr (1.45 wt.%), unidirectionally solidified eutectic, cooperative growth 77—90341
Cu-Cr alloy, laser irrad., structural changes *(Russian)* 80—100247
Cu-Cr eutectic, thermal stability in temp. gradient 79—61611
Cu-Cr system, optimal mutual orientations between FCC and BCC phases *(French)* 78—15371
Cu-Cr-SiO_2 system, age and dispersion strengthened, dislocation struct. around SiO_2 particles 80—108468
Cu-Cr-Zr-Mg (0.5, 0.1, 0.03 wt.%), exam. of low cycle fatigue props. at elevated temp. 78—64674
Cu-Cr-Zr-Ti-B alloy system, solidification cracks formed during welding, reduction by microalloying with B 79—96148
Cu-Cr(-SiO_2), single crysts., yield and pre-yield behaviour rel. to aging time 80—81103
Cu-Ni-Cr, lattice imaging and optical microanalysis of spinodal decomp. 78—52754
Cu-Ni-Cr, microstruct. behaviour and mechanical hardening 78—47281
Cu-Ni-Cr (28, 2.8 wt.%), spinodal alloy, microstruct. and tensile props. 78—39858
Cu-Ni-Cr system, coarsening in the $(\gamma_1+\gamma_2)$ region, metallographic study 78—84762
Cu-Ti-Cr, internally oxidised, morphology, struct., particle precipitation singularities *(Russian)* 79—70067
CuCr alloys, supersaturated solid soln. dissociation *(Russian)* 79—52201
CuCr, dil., anisotropic hyperfine coupling, NMR study 80—65784
CuCr, dil., specific heat, impurity contrib. Kondo temp. 80—65903
CuCr-Pb, proximity effect, tunnelling conductance 78—52160
CuNiCr, IN838, heat treatment effect on fatigue and corrosion fatigue behaviour 80—20982
$Er_2Co_{17-x}Cr_x$, effect of substitution on mag. props. 79—78363
Fe, cast, high Cr, phase composition, mech. props. rel. to heat treatment 79—29108
Fe, cast, high Cr, wear resistance improvement 77—70186
Fe, cast, white, high Cr, phase composition, B effect 80—104172
Fe, cast, white Cr alloyed, wear resistance, effect on abrasive hardness 78—64722
Fe, cast white Cr 78—44124
Fe solid solution, substitution strengthening by Cr and Mo *(Czech)* 80—30080
Fe/Fe-Cr composite powder, X-ray diffr. exam. of densification during rolling 80—40289
Fe-Al-Cr (10, 5 to 10, wt.%), corrosion by coal char, SEM and X-ray diffr. exam. 78—88573
Fe-As-Cr, Cr additions to Fe-As melts, influence on surface tension and density *(Russian)* 80—15337

chromium alloys continued
Fe-As-Sn-Cr, melts, As and Sn distrib., Si, Cr, and Mn influence *(Russian)* 80—16274
Fe-B-Cr, metallic glasses, mag., struct., and elec. props. 80—88751
Fe-B-Mo-Cr, amorphous, Mo and Cr addition effect on corrosion behaviour 80—16568
Fe-C amorphous alloys, corrosion resistance improvement by Cr and/or Mo addition 79—66211
Fe-C-Cr, pearlite reaction kinetics 80—3006
Fe-C-Cr, thermodynamics and phase equilibria near eutectoid temp. 80—3005
Fe-C-Cr-Mn-Si-Ni (4.6, 38.7, 1.1, 2.0, 1.58 wt.%) alloy US-25, powder, compressibility and elec. resistivity in cold pressing under low press. 77—77444
Fe-C-Cr-Mo(Ni)(V), white cast, effect of abrasion on carbide microstructure *(German)* 78—88540
Fe-C-Ni-Cr, athermal alloy, exam. of martensite transformation kinetics 78—80545
Fe-CR, ion-etched, surface comp., effect of adsorbed CO, AES obs. 79—46896
Fe-CR (26 wt.%), role of C and N in brittle fracture 80—16456
Fe-C(graphite)-Ni-Cr, dynamically hot pressed mech. props., effect of Ni-Cr additions 78—60620
Fe-Co (25-35%), ordering, Cr addition effects, Mossbauer expts. *(Russian)* 78—19741
Fe-Co-Cr, 25KKh15 alloy, nuclear γ-reson. investig. of atomic redistrib. during annealing *(Russian)* 77—12640
Fe-Co-Cr, alloy K25Kh15, phase tranforms., nucl. gamma reson. and X-ray diffr. meas. *(Russian)* 77—44241
Fe-Co-Cr, atomic mag. moment, magnetisation, Mossbauer spectra and NMR spin echo spectra 77—63127
Fe-Co-Cr, Cr effect on struct. *(Russian)* 78—27535
Fe-Co-Cr, Cr effect on struct. of ordering 78—35407
Fe-Co-Cr, heats of form. adiabatic calorimeter determ. 78—35713
Fe-Co-Cr, mag. moment of Cr atoms, polarised neutron scattering 79—11290
Fe-Co-Cr, magnetic, phase transform. obs. *(French)* 79—47676
Fe-Co-Cr, solid state phase equilib., isothermal sections determ. 800-1300°C 79—91623
Fe-Co-Cr (27, 0.5 wt.%), internal stress and brittleness in ordered state *(Russian)* 79—61698
Fe-Co-Cr (50, 0.4 wt.%), ordering and recrystallisation 79—34029
Fe-Co-Cr film RF sputtering for magnetic recording 80—2947
Fe-Co-Cr-Mo (20, 15, 5 wt.%), maraging, stainless alloy fracture toughness 77—73326
Fe-Co-Cr-Si, structural transform. and mag. props. following heat treatment *(Russian)* 77—81274
Fe-Co-V-Cr alloys, struct. transform., appl. of mag., thermomag. methods *(French)* 79—20318
Fe-Cr, alloy, composition determination using secondary ion emission *(French)* 77—86409
Fe-Cr, amorphous alloy, effect of metalloidal impurities on corrosion resistance and electrochem. behaviour 78—72925
Fe-Cr, Ar ion bombard., O_2 flooded, secondary ion yield as function of original conc. *(French)* 78—39643
Fe-Cr, Auger electron and appearance pot. spectroscopic study of surfaces 80—11520
Fe-Cr, BCC, ferromag., spin wave stiffness constant 78—91851
Fe-Cr, BCC, local moments in Mossbauer study 80—108125
σ-Fe-Cr, brittle fracture stresses under high hydrostatic press. and high temp. *(Japanese)* 79—43397
Fe-Cr, compositional diffusionally bonded alloy, mass transfer investigation *(Russian)* 80—39342
Fe-Cr, corrosion in hot conc. caustic soda soln. *(Japanese)* 79—70225
Fe-Cr, crit. mag.-props. near ferromag. Curie points 77—63216
Fe-Cr, crystallisation temp., overcooling temp. *(Russian)* 80—97472
Fe-Cr, damping capacity *(Japanese)* 79—70104
Fe-Cr, decomposition Mossbauer study *(French)* 77—63678
Fe-Cr, diffusion of C 77—7907
Fe-Cr, dil., high freq. induction melting and centrifugal casting, working curve sample prep. photoemission anal. *(Japanese)* 78—53050
Fe-Cr, dil., local mag. moments, polarised neutron elastic diffuse scatt. 80—50088
Fe-Cr, dil., spin density wave under high press., neutron diffr. study 80—65798
Fe-Cr, dislocation mobility and internal friction, effect of alloying in α-Fe *(Russian)* 77—31671
Fe-Cr, disordered, mag. order, Mossbauer study 80—39992
Fe-Cr, effect of alloying additions on magnetoelastic effects 78—43624
Fe-Cr, electron state density and elec. resist. 80—39558
Fe-Cr, ellipsometric study of films formed in orthophosphoric acid 79—74290
Fe-Cr, Fe-Cr-Al(Si) film heaters, lifetimes for 800 to 1000°C temp. range 78—215
Fe-Cr, feasibility of electrochem. corrosion protection 79—70220
Fe-Cr, flow stress, effect of cathodic, H_2 charging *(Japanese)* 79—52313
Fe-Cr, friction and wear in controlled environment, effect of sliding mode and specimen geometry 78—15542
Fe-Cr, friction at elevated temps. 78—15548
Fe-Cr, friction behaviour in oxygen, development of wear-protective oxides and influence on sliding friction 80—30111
Fe-Cr, from ore reduction, metallographic investigation, optical miroscopy and SEM *(French)* 78—68648
Fe-Cr, gas corrosion, in composite atmospheres *(Polish)* 79—79142
Fe-Cr, grain-boundary segregation of carbon, electrochemical study 79—100147
Fe-Cr, hardness after nitriding, metallographic, electron microscopic and microprobe anal. 78—51608
Fe-Cr, high purity binary alloy, isothermal decomp. of austenite 78—64525
Fe-Cr, high temp oxidation studies using $^{18}O(p,\alpha)^{15}N$, ^{18}O distrib. determ. 79—87912
Fe-Cr, high temp. oxidation, internal stable nitride and oxide dispersion 79—39017
Fe-Cr, high-C, sulphide inclusion distrib. obs. 79—74168
Fe-Cr, high-temp. oxidation, borate inhibitors 80—66705
Fe-Cr, hyperfine magnetic fields, Mossbauer spectra 80—97165
Fe-Cr, impact strength, rel. to '475°C brittleness' *(Russian)* 78—92323
Fe-Cr, influence of annealing on hyperfine interaction parameters, Mossbauer effect 80—71263

chromium alloys continued
Fe-Cr, Invar, exchange interactions between ferromag. and antiferromag. components 80—29545
Fe-Cr, Invar alloy, explanation of phys. anomalies *(Russian)* 78—88112
Fe-Cr, ion-implanted, depth profile and diffusion coeff. 80—54277
Fe-Cr, irradiation induced void swelling, Cr additions effect 80—55408
Fe-Cr, lattice parameters, 293 to 1273K, α to γ phase transform., X-ray diffr. exam. *(Russian)* 80—50625
Fe-Cr, layers formed by reaction with molten Al, X-ray, EPMA and hardness meas. *(Japanese)* 78—72926
Fe-Cr, liquid diffusion of H_2 *(German)* 78—14487
Fe-Cr, mag. moments and Fe site hyperfine fields, magnetis. obs. 78—76276
Fe-Cr, mag. props. of Fe, local coupling with spin modulation of matrix 79—15299
Fe-Cr, mechanically polished, XPS determ. of comp. of surface and surface oxide 78—7074
Fe-Cr, microstructural study of oxidation, selective etching 78—44245
Fe-Cr, nondestructive in-depth surface anal. by XPS with different excitation X-ray energies 79—20328
Fe-Cr, oxidation, in H_2/H_2O vapour mixtures, epitaxial oxide phase formation, effect on oxidation 78—88568
Fe-Cr, oxidation, in hostile environment, in situ meas. method 78—44277
Fe-Cr, passivation films, modulation spectroscopy study 80—3244
Fe-Cr, passivity in H_2SO_4, XPS study 78—44256
Fe-Cr, random ferromag. alloys, local mag. moment calc. 80—70974
Fe-Cr, role of C in transform. by heating in $(\alpha+\gamma)$ phase *(French)* 78—52798
Fe-Cr, segregation of ^{121}Sb, Mossbauer spectroscopy 79—47698
Fe-Cr, single and two component, powder, compressibility and elec. resistivity in cold pressing under low press. 77—77444
Fe-Cr, specific heat enhancement and electron-phonon interaction 80—65242
Fe-Cr, spin waves by neutron spectrometry 80—44819
Fe-Cr, split bands evidence from sp. ht. and elec. transport data 77—24515
Fe-Cr, surface and bulk alloys, oxidation at 300°C 79—61792
Fe-Cr, surface atom electron binding energy depend. on composition, Auger spectra, APS spectra 80—39655
Fe-Cr, surface composition change caused by heating in high vacuum, XPS obs. 78—44254
Fe-Cr, surface covered with anodic oxide film, in-depth composition profiles 80—10763
Fe-Cr, surface segregation of impurities (C,N and S) *(French)* 77—56192
Fe-Cr, thermodynamics of chlorination *(Russian)* 79—52168
Fe-Cr, tracer diffusion meas. using tracer anal. 79—82376
Fe-Cr, unlimited component solubility, intercrystallite internal adsorption *(Russian)* 80—39294
Fe-Cr, use of electrochemistry in understanding $\alpha\rightleftarrows\gamma$ transform., interstitials role *(French)* 77—63662
Fe-Cr, X-ray exam. of dynamic characts. *(Russian)* 77—62608
Fe-Cr, XPS obs. of Fe 2p states 78—52625
Fe-Cr (10 to 70 at.%), ferromag. reson., anisotropy const., and saturation magnetisation *(Russian)* 77—81013
Fe-Cr (12 wt.%), corrosion in o-phosphoric acid 80—97622
Fe-Cr (13 wt.%)+polycarbosilane, powder metallurgy, characts. 77—85962
Fe-Cr (17.3 wt.%), oxidation at 1000°C, alloy grain growth effect 78—7075
Fe-Cr (1.20, 3.63, 7.98 wt.%), Mossbauer spectra shape depend. on deformations 79—61272
Fe-Cr (2 at.%), plastic flow enhancement during massive transformations 78—48468
Fe-Cr (20 wt.%), high temperature oxidation resistance, effect of rare earth and reactive element additions *(Japanese)* 79—20271
Fe-Cr (20 wt.%), role of rare earths and reactive elements in high-temp. oxidation 79—79178
Fe-Cr (20 wt.%) high temp. oxidation behaviour with small La additions (0 to 1.3 wt.%) *(Japanese)* 78—85039
Fe-Cr (24 wt.%), low temperature oxidation, kinetics, oxide morphology 80—11838
Fe-Cr (25 wt.%), vaporisation kinetics in vacuum *(Russian)* 77—72683
Fe-Cr (25wt.%), continuously cooled, embrittlement 77—36636
Fe-Cr (25wt.%), surface comp. rel. to passivation phenomena *(French)* 79—43479
Fe-Cr (26 wt.%) effect of Ni content and austenite phase, on low temp. toughness and embrittlement 78—60754
Fe-Cr (27.4 wt.%), oxidation, alloy depletion profiles resulting from preferential removal of less noble metals 79—11728
Fe-Cr (28 wt.%), intergranular corrosion and anodic polarization at grain boundary groove *(Japanese)* 79—15869
Fe-Cr (5, 10 and 20 wt.%), microcrack generation, healing of oxide scale 79—20280
Fe-Cr (5 to 30 wt.%), transpassive behaviour in acidic sulphate soln. 78—15565
Fe-Cr (5 to 40 wt.%), breakdown and healing of oxide scale during oxidation 77—63836
Fe-Cr (5 wt.%), friction and wear in controlled environments, oxide film effect 78—15546
Fe-Cr (70-92 at.%), coexistence of ferro- and antiferromagnetism *(Russian)* 78—47955
Fe-Cr (9 wt.%), extrinsic grain boundary dislocations, low C content influence 80—107273
Fe-Cr (9 wt.%), oxidation studied using $C^{18}O_2$ and D_2O tracers 80—71784
Fe-Cr alloy, Cr rich, solubility of S *(French)* 78—30761
Fe-Cr alloy, N solubility investigation *(Russian)* 80—92675
Fe-Cr alloy, sputter etching oxide film, comp. profile, quantitative AES 80—81383
Fe-Cr alloys, cold worked, internal friction due to H *(Japanese)* 80—70305
Fe-Cr alloys, corrosion, oxidation, combined ion-, electron-beam techniques appl. 79—43700
Fe-Cr alloys, damping capacity 79—100206
Fe-Cr alloys, in acid and neutral solns., thickness and optical constants of passive and transpassive films 80—66698
Fe-Cr alloys, M_s calcs. 77—8824
Fe-Cr alloys, mixed ferro-/antiferromag. interactions *(Russian)* 77—32173

chromium alloys continued
Fe-Cr alloys, $NaClO_3$ and NaCl effects on corrosion behaviour in hot NaOH soln. *(Japanese)* 80—35407
α-Fe-Cr alloys, recrystallised, C segreg. effects, TEM *(French)* 77—28828
Fe-Cr based coatings, hot corrosion resist. 79—24674
Fe-Cr film, sputtering yields, proton-induced X-ray meas. 80—50488
Fe-Cr melts, ultrasonic propag. and isothermal compressibility using pulse-phase method *(Russian)* 79—51202
α-Fe-Cr solid soln., thermodynamic activity of components 79—38797
Fe-Cr surface alloy formed by ion implantation, anodic polarisation 78—48561
Fe-Cr surface alloys, corrosion resistant, formation by ion implantation 79—28009
Fe-Cr-Al (14, up to 2 wt.%), Al effects on high temp. oxidations *(Japanese)* 79—15865
Fe-Cr-Al, Al addition effect on oxidation, 900 to 1200°C 79—66222
Fe-Cr-Al, Al effect on high temp. oxidation in wet O_2 79—66223
Fe-Cr-Al, attenuation and vel. of acoustic shock waves, amplitude depend. 78—63810
Fe-Cr-Al, blackness change in air, 1-8 micron, 1200°C, film props. depend. 77—66033
Fe-Cr-Al, elec. heating alloy, effect of rare earth additives on quality *(Chinese)* 78—84825
Fe-Cr-Al, electrical heating material, SEM obs. and surface analysis of oxide films formed at high temps. 77—16738
Fe-Cr-Al, HOS 875, oxidation, cyclic, role of thermal shock 80—97640
Fe-Cr-Al, Kanthal films, vac. deposited, evaporation characts., comp., struct. and elec. props. 80—88646
Fe-Cr-Al, kinetics and mechanism of high temp. S corrosion 80—25911
Fe-Cr-Al, scale and spalling resist. determ., appl. of cyclic oxidation method 77—77695
Fe-Cr-Al, scales, α-Al_2O_3, early stages development at high temp. 80—89413
Fe-Cr-Al, thermodynamic predictions in coal gasifier environment 79—38799
Fe-Cr-Al (0.3 wt.%), oxidation behaviour at high temps. *(Japanese)* 80—35404
Fe-Cr-Al (12, 3 wt.%), internal friction and rigidity modulus, strain amplitude depend. *(Japanese)* 80—92606
Fe-Cr-Al (14, 0.1 to 2 wt.%), oxidation at high temps. *(Japanese)* 78—60872
Fe-Cr-Al (17, 4 or 6 wt.%), high temp. corrosion in S vapour 80—40591
Fe-Cr-Al (7, 5 wt.%), expt. stainless alloys, phys. and mech. props. 80—97637
Fe-Cr-Al alloys, localised mag. moment determ. and electron struct. 77—66268
Fe-Cr-Al alloys, low temp. sp. ht., resistivity and coercive force 78—63866
Fe-Cr-Al-Ce, Ce effect on high temp. oxidation 79—100301
Fe-Cr-Al-Ce, high temp. oxidation *(Japanese)* 78—11413
Fe-Cr-Al-TaC (13.5, 3.7, 9 wt.%) eutectic alloy, directionally solidified, thermal cycling effects on microstruct. 77—32686
Fe-Cr-Al-Ti-Y_2O_3 (20, 4.5, 0.5, 0.5) type MA956, strain rate effect on fracture behaviour at 1366K 80—16458
Fe-Cr-Al-Y, high temp. corrosion depend. on Y, oxidation, stress growth *(Russian)* 80—40588
Fe-Cr-Al-Y, influence of Y additions on oxide-scale adhesion 77—8993
Fe-Cr-Al-Y, oxidation resistance, heat treatment and Al^+ ion implantation 80—71785
Fe-Cr-Al-Y, scales, α-Al_2O_3, early stages development at high temp. 80—89413
Fe-Cr-Al-Y (Y-Al_2O_3)(Y_2O_3), preparation and exam. of mech. props. 78—52720
Fe-Cr-Al-Y-C, GE-1541, volatilisation of oxides during oxidation at 1200°C 78—23873
Fe-Cr-Al(-Y), isothermal oxidation behaviour at 1200°C, SEM 80—50755
Fe-Cr-Al(-Y), oxide grain morphology and growth mechanism 80—3239
Fe-Cr-Al(-Y), thermal cycling influence on oxidation behaviour at 1200°C, SEM 80—50756
Fe-Cr-Al(Ni), corrosion by coal char at 871° and 982°C 80—3237
Fe-Cr-B, amorphous, Elinvar and Invar charact. *(Japanese)* 80—11832
Fe-Cr-B, B inhibition of oxidation, AES study 79—61785
Fe-Cr-B amorphous alloys, corrosion resistance, Invar and Elinvar characts. *(Japanese)* 79—96213
Fe-Cr-C, austenite to ferrite+precipitate reaction, TEM/STEM study 80—3075
Fe-Cr-C, crystallography of austenite-ferrite/carbide transformation 80—16303
γ-Fe-Cr-C, electromigration of C, effect of Cr addition 78—6184
Fe-Cr-C, electronic structure, thermodynamics of structure formation 79—99475
Fe-Cr-C, isothermal transformations 80—16302
Fe-Cr-C, lattice parameters of cementite, annealing effect 80—29007
Fe-Cr-C, lqiuid, reduction of Cr_2O_3 by dissolved C 78—6877
Fe-Cr-C, self-diffusion processes during homogenisation of heterogeneous systems *(Russian)* 79—60539
Fe-Cr-C, sintered, successive impregnation with C and Cr 79—95979
Fe-Cr-C, steel carbide formation during chromising, exam. in terms of ternary phase diagrams 78—56818
Fe-Cr-C (10,0.2 wt.%), isothermally transformed, precipitate orientations 80—50640
Fe-Cr-C (10,0.2 wt.%) isothermally transformed, carbide distrib., microstruct. development 80—3076
Fe-Cr-C alloy, bainitic struct. morphological changes, due to external stress, plastic deform. 78—44120
Fe-Cr-C alloys, equilibrium partition coeffs. for ferrite/liquid, austenite/liquid 78—39744
Fe-Cr-C solid solns., ordering and γ to α transforms, effect of heat treatment *(Russian)* 79—24520
Fe-Cr-C system, isothermal sections, 873 to 1373K, computer plotting 78—6894
Fe-Cr-C system at 870°C 77—28782
Fe-Cr-Co, anisotropic, spinel type permanent magnet, magnetic aftereffect 77—16118
Fe-Cr-Co, ductile magnet alloys, mech. props. 80—85001
Fe-Cr-Co, effect of heat treatment on strain gauge factor 78—72802
Fe-Cr-Co, elastic props. anisotropy at room temp. *(Russian)* 80—89279
Fe-Cr-Co, heat treatment effect on strain gauge factor *(Japanese)* 78—6954

chromium alloys continued
- Fe-Cr-Co, mag. alloys, Mossbauer spectra 78−19386
- Fe-Cr-Co, mag. props., heat treatment effects *(Russian)* 78−39365
- Fe-Cr-Co, mag. props. of ductile permanent ductile alloys *(Chinese)* 79−19746
- Fe-Cr-Co, magnetic domain walls, Lorentz microscopy 80−103854
- Fe-Cr-Co, mechanism of coercive force 80−34674
- Fe-Cr-Co, metallic magnets investigation, present state *(Polish)* 80−107987
- Fe-Cr-Co, permanent magnet, temp. effect 80−34701
- Fe-Cr-Co, spinodally decomposed magnetic alloy, magnetic flux temp. coeff. *(Japanese)* 78−35006
- Fe-Cr-Co (28, 10.5 wt.%) ductile magnet alloy, humidity-induced H$_2$ embrittlement 80−89406
- Fe-Cr-Co (31 wt.%, 23 wt.%), microstruct. and mag. props., ageing and thermomag. treatment effects 78−76769
- Fe-Cr-Co alloy, coercive force mechanism 80−71103
- Fe-Cr-Co alloy, Mossbauer exam. of spinodal decomposition 77−69742
- Fe-Cr-Co alloy, spinodally decomposed, micro-twinning 80−92537
- Fe-Cr-Co alloys, (5-9 wt.% Co), obtained by slow cooling under mag. field, permanent magnet props. 80−75797
- Fe-Cr-Co alloys, permanent magnet material development 78−91895
- Fe-Cr-Co alloys, permanent magnets, magnetic props. and heat treatment *(Russian)* 79−91809
- Fe-Cr-Co ductile magnet, with high (BH)$_{max}$, processing, mag. props., and microstruct. 77−8957
- Fe-Cr-Co ductile magnet alloys, phase diagram and mag. props., V or V+Ti addition effects 77−8959
- Fe-Cr-Co hard-mag. alloys, fine cryst. struct. *(Russian)* 77−66706
- Fe-Cr-Co martensite, ordering and segregation *(Russian)* 79−20052
- Fe-Cr-Co permanent magnet system, miscibility gap, microstruct. and mag. props. obs. 80−76228
- Fe-Cr-Co phase diagram, lamination region, resist. meas. *(Russian)* 78−27479
- Fe-Cr-Co-Al (27.5, 17.5, 0.5) alloy, magnetic props. and microstructure 78−72367
- Fe-Cr-Co-Al (27.5, 17.5, 0.5 wt.%) alloy, induced anisotropy 78−76239
- Fe-Cr-Co-Al(V)-(Nb)(Ti), phase equilib., X-ray diffr. meas. *(Russian)* 79−47658
- Fe-Cr-Co-Mo, melted in open induction furnace, microstruct. and magnetic props. 79−61626
- Fe-Cr-Co-Mo, microstruct., hardness, mag. props., influence of isothermal tempering and heat treatment 79−79129
- Fe-Cr-Co-Mo alloys, struct. transform. and mag. props. *(Russian)* 77−76543
- Fe-Cr-Co-Mo high energy permanent magnets, mag. props. 80−97119
- Fe-Cr-Co-Si alloy, interaction domains after heat treatment in mag. fields *(Russian)* 78−68286
- Fe-Cr-Co-V alloy, microstruct. and mag. props. 78−68221
- Fe-Cr-Co-V-(Ti) hard magnets, V and V-Ti effects on mag. and mech. props. 79−91810
- Fe-Cr-La(Y)-Al, La or Y with Al addition effect on high-temp. oxidation 79−100302
- Fe-Cr-Mn, Cr and Mn effect on N$_2$ solubility above 1000°C *(Bulgarian)* 79−65203
- Fe-Cr-Mn, influence of alloying with Ni, Mo, N on defect conc. energy *(Russian)* 80−54241
- Fe-Cr-Mn alloys, Mn content effect on Cr distrib. in suboxide layers *(Russian)* 77−12732
- Fe-Cr-Mn-C, high temp. oxidation, X-ray and weight gain meas. *(Russian)* 78−15571
- Fe-Cr-Mo, (30,2 wt.%) Bridgman-type, unexpected embrittlement phenomena, hydrostatic tensile test *(Japanese)* 80−55517
- Fe-Cr-Mo, grey cast, pearlitic, isothermal transform. of austenitic in bainitic range *(Rumanian)* 78−23698
- Fe-Cr-Mo, sputtering effect on surface comp., AES obs. 80−6601
- Fe-Cr-Mo, white cast, optimising fracture toughness and abrasion resist. 80−85042
- Fe-Cr-Mo (26, 1 wt.%), single crysts. and polycrysts. strain rate influence on low cycle fatigue props. 80−3126
- Fe-Cr-Mo alloy castings, thick-section, factors affecting 80−108374
- Fe-Cr-Mo and Fe-Cr-Mo-Si, amorphous films, corrosion resist. and ion plating use 80−89423
- Fe-Cr-Mo sintered, damping capacity and mech. props. 78−44161
- Fe-Cr-Mo-C, X-ray investigation after friction and oxidation 78−52997
- Fe-Cr-Mo-Ti (13, 1.5, 3.5 wt.%), equilibrium studies on chi-phase strengthening 79−24496
- Fe-Cr-Mo(Ni)(Mo-NI), AES using peak-to-peak value *(Japanese)* 79−20485
- Fe-Cr-N (5.9, 0.5 wt.%), martensitic, tempered, fine struct. 77−25079
- Fe-Cr-N system, distrib. of Er between austenite and ferrite at 1200°C 79−43205
- Fe-Cr-Nb-C, X-ray microanal. of carbide phases rel. to Nb conc. *(Russian)* 78−88467
- Fe-Cr-Ni, AES investigation of corrosion and growth nature of surface layers 77−77330
- Fe-Cr-Ni, analysis and synthesis of phase diagrams 79−11563
- Fe-Cr-Ni, appl. of computational techniques for treatment of thermodynamic data, phase diagram calc. 78−10172
- Fe-Cr-Ni, austenitic, oxidation behaviour on addition of Si 77−12740
- Fe-Cr-Ni, austenitic, self-diffusion and swelling under irradiation 80−39343
- Fe-Cr-Ni, α-particle induced precip. and phase instability 79−1470
- Fe-Cr-Ni, cold-rolled foils, dilatometric study 80−21033
- Fe-Cr-Ni, corrosion behaviour in hot conc. NaOH soln. *(Japanese)* 80−85082
- Fe-Cr-Ni, electron irradiated, resistivity during annealing, 4.2-1300K 78−87962
- Fe-Cr-Ni, Fe-rich, melting equilibria *(German)* 77−52282
- Fe-Cr-Ni, foil, in situ oxidation in HVEM 80−104354
- Fe-Cr-Ni, irradiated, Ni segregation to sinks 78−91472
- Fe-Cr-Ni, mag. state at low temps. *(Russian)* 78−56298
- Fe-Cr-Ni, melting and solidification *(French)* 77−66635
- Fe-Cr-Ni, neutron irradiated, rel. between irradiation induced swelling and shear modulus 80−15157
- Fe-Cr-Ni, shock loading effect on phase equilib. *(Russian)* 79−29017
- Fe-Cr-Ni, single crystal anomalies in curve of critical shear stress versus temp. at low temps. 77−16656
- Fe-Cr-Ni, solid soln. strengthened and precipitation hardened, in-reactor creep 79−43327
- Fe-Cr-Ni, spin system, relaxation props. at low temp. 79−82758

chromium alloys continued
- Fe-Cr-Ni, stable and metastable, thermal expansion, 4.2-290K *(Russian)* 78−47537
- Fe-Cr-Ni, stress corrosion cracking in high temp. caustic soln. 77−59964
- Fe-Cr-Ni, textured $(\alpha+\gamma)$ alloy, α' lath martensite formation 78−95749
- Fe-Cr-Ni, thermodynamic prediction in coal gasifier environment 79−43206
- Fe-Cr-Ni, two phase $(\alpha+\gamma)$ alloys, transformation-induced plasticity 77−63721
- Fe-Cr-Ni, two-phase $(\alpha+\gamma)$, and metastable austenitic, uniform elongation peak 77−77547
- Fe-Cr-Ni (12, 15 wt.%) austenitic alloy, Ni^{6+} irradiated, void swelling and phase stability, Si and Ti effects 80−65055
- Fe-Cr-Ni (18, 14 wt.%), single strain induced γ to α' cryst. transform. *(Japanese)* 78−11221
- Fe-Cr-Ni (18,14 wt.%), γ to ε to α martensitic transform., external stress effect, double tensile deform. exam. 80−108438
- Fe-Cr-Ni (19, 13 wt.%), austenitic, Ni$^+$ ion irradiated, multiple dislocation loops *(French)* 80−65064
- Fe-Cr-Ni (20,15 wt.%), low cycle fatigue life under hold time conditions, grain size effect 77−77577
- Fe-Cr-Ni (25, 20 wt.%), single crystal, stress corrosion cracking 78−35553
- Fe-Cr-Ni alloy, austenitic, Neel temp. and max. susceptibility predictions comp. effects 77−43833
- Fe-Cr-Ni alloy, deforming stresses anomalous temp. depend. *(Russian)* 77−81296
- Fe-Cr-Ni alloy, dual-ion-irradiated, swelling anal. 78−86600
- Fe-Cr-Ni alloy, quantitative anal. method based on ion bombardment induced secondary ion and photon emission 79−19963
- $\alpha+\gamma$Fe-Cr-Ni alloy, stress-induced α'-martensite occurrence 78−23704
- Fe-Cr-Ni alloy 800, sensitization times for intergranular corrosion 77−16746
- Fe-Cr-Ni alloys, linear expansion, 4.2-300K rel. to antiferromag. rearrangement 78−43146
- Fe-Cr-Ni alloys, oxidation-sulphidation in gas mixture, parabolic kinetics, thermochem. diagram 78−72932
- Fe-Cr-Ni and Fe-Cr-Co, BCC, atomic mag. moments determ. 77−59396
- Fe-Cr-Ni austenitic alloys, environment sensitive cracking, metallurgical variables effect 80−35391
- Fe-Cr-Ni austenitic alloy, cold deformed, α-γ transition, calorimetric study *(Russian)* 80−55390
- Fe-Cr-Ni based alloys, Ni$^+$ ion and neutron irradiated, γ' particle redistrib. and phase stability 79−78977
- Fe-Cr-Ni based alloys, surface oxides at high temps., backscattering Raman spectroscopy 80−93291
- Fe-Cr-Ni liquid alloy, N$_2$ soln. and TiN precipitation 78−6931
- Fe-Cr-Ni melts, S solubility and solid soln. precipitation *(Russian)* 80−15251
- Fe-Cr-Ni system, austenitic, energetic particle bombardment, thermodynamic and dimensional stability 77−27904
- Fe-Cr-Ni system, diffusion coeff. consts. calcs. for multi-component systems *(Russian)* 79−90815
- Fe-Cr-Ni system, isothermal diffusion *(Russian)* 79−69300
- Fe-Cr-Ni-Al alloys, 25 keV ion implanted, metallic corrosion behaviour 79−52447
- Fe-Cr-Ni-C (17.2, 7.34, 0.2 wt.%), twin related laths, fracture elongation, TEM study 79−29192
- Fe-Cr-Ni-C (23.19, 4.91, 0.025 wt.%), two phase alloy, effect of prestrain above Md temp. on Ms temp. 78−80543
- Fe-Cr-Ni-Cu-Sn, Cu and Sn effect on Cr and Ni segregation *(German)* 78−72777
- Fe-Cr-Ni-Mn-Mo, liquid, N$_2$ solubility 78−44087
- Fe-Cr-Ni-Mo-V, Mo and V effects on segregation *(German)* 77−55942
- Fe-Cr-Ni-P-C, amorphous, stress corrosion cracking 77−25123
- Fe-Cr-Ni-Si, sintered, carbide coated, crack propag. energy in impact bending 79−66162
- Fe-Cr-Ni-Ti-Al, superalloy, Ti, Ni, Al, H$_2$ variations effect on mech. props. 78−3188
- Fe-Cr-Ni(Mn)(Ni-Mn)-C alloy, carbide-austenite equilibria, 1173 to 1373K, microscopic and X-ray obs. 78−44085
- Fe-Cr-O system, phase relations at 1200°C using diffusion couple technique 80−89205
- Fe-Cr-O-C, stability diagrams, characteristics and calc. 79−10917
- Fe-Cr-P-C, amorphous, corrosion resist. in 1N HCl 78−80678
- Fe-Cr-P-C amorphous alloys, mag. props. 77−16055
- Fe-Cr-P-C sputtered amorphous films, mag. props. and corrosion resist. 79−28567
- Fe-Cr-Pd, electrospark coating on alloys, corrosion resist. increase *(Russian)* 78−27669
- Fe-Cr-Pd, Pd alloying effects on passivation 80−35373
- Fe-Cr-Si, heat resistive films prepared by sputtering, lifetime meas. 80−80132
- Fe-Cr-Si, oxidation resist. in high pressure CO$_2$, Si effect 80−66704
- Fe-Cr-SiC-B$_4$C powder mixture, compressibility and elec. cond. in cold pressing under low press. 78−60609
- Fe-Cr-Ta, eutectic alloy, exam. of eutectic temp., composition, and oxidation resistance 78−52767
- Fe-Cr-Ti (18, 0.1-0.9 wt.%), high temp. oxidation *(Japanese)* 80−71806
- Fe-Cr-Ti-Mo, sintered, mech. props. *(French)* 79−91726
- Fe-Cr-Ti-Mo ferritic alloy, annealed, cold rolled, fast reactor material, mech. props. 78−21646
- Fe-Cr-Ti-Mo-TiO$_2$ (13, 3.5, 1.5, 2 wt.%) dispersion hardened, void swelling 80−65046
- Fe-Cr-Ti-TiO$_2$ (13, 2.5, 2 wt.%), dispersion hardened, ferritic alloy DT02, oxidation, 823 to 1123K 79−61803
- Fe-Cr-Ti(Al) liquid alloy, thermodynamical anal. of O$_2$ solubility *(Russian)* 80−92676
- Fe-Cr-V-C, X-ray microanal. of carbide phases rel. to V conc. *(Russian)* 78−88467
- Fe-Cr-W-C, carbide/austenite equilibria, expt. and thermodynamic study 77−36459
- Fe-Cr-Y, Y addition effect on high temp. oxidation resistance *(Japanese)* 79−70223
- Fe-Cr-(C), oxidation, grain size and growth effects *(Japanese)* 77−48583
- Fe-Cr-(Co), decomposition of solid soln. in mag. field, neutron and X-ray diffr. study *(Russian)* 78−68694
- Fe-Cr-b amorphous Invar alloy, elastic props., Elinvar characts. and ΔE effect 79−56595

chromium alloys continued
Fe-Cr(-Mo), passivated single crystal, selective dissolution and surface enrichment 80–16543
Fe-Cr(Cr-Ni)(Cr-Ni-Mo)-Al, liquid, N solubility, AlN precipitation 79–11630
Fe-Cr(100) and (110) surfaces, lateral lattice spacings, simultaneous LEED and AES 77–20174
Fe-Cr(100) and (110) surfaces, initial oxidation stages, simultaneous LEED and AES obs. 77–20175
Fe-Cr(55 wt.%), phase decomp. early stages and clustering *(Japanese)* 80–55403
Fe-Cr(6 to 9 wt.%), transform. study during $(\alpha+\gamma)$ region reversion *(French)* 77–59780
Fe-Cu-Ni-Cr_3C_2-C based sintered friction material, wear, surface geometry and struct. effects 80–25875
Fe-Mn-Co-Ni-Cr, antiferromag. props., Neel temp. determ. 78–88124
Fe-Mn-Cr-C, twinning and strain induced FCC to HCP transform. 77–44248
Fe-Mo-Cr alloys, creep tests *(German)* 79–61648
Fe-Mo-Cr-C, carbide-austenite equilibria, 1173 to 1373K, microscopic and X-ray obs. 78–44085
Fe-Ni-Al-Co-Cr-Ti, YuNDK35T5BA, exam. of hypodissociation process *(Russian)* 79–11547
Fe-Ni-Cr, at. distrib. effect on mag. props. *(Russian)* 78–2657
Fe-Ni-Cr, austenitic, creep strength and ductility, effect of γ' precipitation 77–36597
Fe-Ni-Cr, austenitic, dispersion-hardened alloys, thermomechanical working *(Russian)* 77–66659
Fe-Ni-Cr, austenitic with dispersed phases, oxidation 80–16540
Fe-Ni-Cr, carbide form. by C diffusion, precip. distrib. and morphology 80–104164
Fe-Ni-Cr, compatibility with Li_2O pellets, mass spectrometric study of Li_5FeO_4 evaporation 79–8385
Fe-Ni-Cr, concentration ferromag. antiferromag. phase transition and mag. state diagram. *(Russian)* 80–20401
Fe-Ni-Cr, diffusion in Th at 500 to 800°C *(German)* 79–28157
Fe-Ni-Cr, heavy ion irrad., defect cluster obs. 80–107341
Fe-Ni-Cr, high Ni content, intergranular corrosion, effect of Cr *(French)* 80–7708
Fe-Ni-Cr, Invar alloy, ^{57}Fe effective field distrib., Mossbauer obs. *(Russian)* 78–19381
Fe-Ni-Cr, mag. and crystallographic transformation depend. on Cr, Ni addition *(Russian)* 79–83334
Fe-Ni-Cr, mag. props. in weak mag. fields *(Russian)* 80–75771
γ-Fe-Ni-Cr, mag. struct., neutron scatt. study *(Russian)* 78–68160
γ-Fe-Ni-Cr, magnetic phase diagram *(Russian)* 78–39292
Fe-Ni-Cr, oxide film form., combination anal. using ESCA, AES and SIMS 79–16092
Fe-Ni-Cr, preferential sputtering, XPS expts. 79–87544
Fe-Ni-Cr, pulsed HVEM irrad., effect on microstruct. evolution 80–34053
Fe-Ni-Cr, vapour-deposited film, effect of condensation temp. on form. of metastable phases and mag. props. 79–65700
Fe-Ni-Cr (10, 6 to 14 wt.%), electrochemical polarisation in high temp. water *(Japanese)* 79–15868
Fe-Ni-Cr (20, 15 wt.%), fusion reactor struct. alloys, dual-ion irrad, effects 79–45403
Fe-Ni-Cr (20, 15 wt.%), single and dual ion irrad., microstruct. studies 80–29077
Fe-Ni-Cr (23, 5 wt.%), martensite orientation formed under uniaxial stress alloy [001] 77–77475
Fe-Ni-Cr (25, 15 wt.%), high temp. creep, dispersed γ'-Ni_3(Al, Ti) effects *(Czech)* 78–64590
Fe-Ni-Cr (25, 15 wt.%), mobile dislocation density in steady state creep, strain transient dip test, TEM exam. 80–7650
Fe-Ni-Cr (30.6, 21.3 wt.%), Alloy 800, high temp. oxidation at low O_2 press., SEM, AES and electron probe microanal. study 80–93688
Fe-Ni-Cr (35, 15 wt.%), high temp. alloys, for HTR primary components, alloying additions for carburisation protection 80–5243
Fe-Ni-Cr (35, 15 wt.%) superalloy, stress rupture and tensile props., C and B additions effect *(Chinese)* 80–104244
Fe-Ni-Cr (40, 15.8 wt.%), precipitation and creep rupture behaviour, optical and TEM study 79–74158
Fe-Ni-Cr (45,25 wt.%), surface oxide layers, compar. study of comp. and struct. by secondary ion emission and electron microprobe *(French)* 77–56286
Fe-Ni-Cr alloy, cast, etching methods for determ. of primary struct. 78–23888
Fe-Ni-Cr alloy 800, creep ductility decline 77–48502
Fe-Ni-Cr alloy 800, minor alloying element effect on creep, ageing microstruct. 78–27572
Fe-Ni-Cr alloy electrodeposition from sulphate electrolyte with cystine and Na citrate additives *(Russian)* 78–48336
Fe-Ni-Cr alloys, stacking fault energies calc. 79–60387
Fe-Ni-Cr alloys, X-ray fluorescence anal., interelement correction, models, computer program 77–56315
Fe-Ni-Cr austenite, high N content, cryst. struct. electron diffr. and electron miscroscope anal. *(Russian)* 79–24490
Fe-Ni-Cr austenitic alloy, homogeneous and dispersion strengthened, internal stresses and high temp. creep 78–19841
Fe-Ni-Cr austenitic steel, martensitic transform. kinetics, metastability criterion *(French)* 78–68690
Fe-Ni-Cr base alloy, oxidation and hot corrosion *(Chinese)* 80–21149
Fe-Ni-Cr based alloy, KhN35VTYu, temp. depend. of energy of fracture, influence of γ' phase *(Russian)* 80–81147
Fe-Ni-Cr coating, electrodeposited, exam. of passivity 78–80655
Fe-Ni-Cr corrosion protective coating on steel 78–48572
Fe-Ni-Cr film, ferromag. reson. meas. *(Russian)* 77–1601
Fe-Ni-Cr melts, O solubility *(Russian)* 80–15250
γ-Fe-Ni-Cr solid soln., thermodynamic activities determ. in Ni rich corner at 1500K 77–32561
Fe-Ni-Cr system, absolute partial pressures and chem. activities of component metals 80–50600
Fe-Ni-Cr vapour deposited film metastable phase formation *(German)* 78–38984
Fe-Ni-Cr-Al-Ti-W-Mo (35, 15, 2.4, 2.3, 2.2 wt.%) wrought superalloy, freckles *(Chinese)* 80–104137
Fe-Ni-Cr-Al-Y, oxidation mechanism, Y addition effect on kinetics and oxide adherence 80–97623
Fe-Ni-Cr-B, X-101 centrifugally cast cylinder lining alloy, compatibility with hardfacing alloys 77–32726

chromium alloys continued
Fe-Ni-Cr-C, effect of austenite yield strength, stacking fault energy, on martensite morphology 78–80546
Fe-Ni-Cr-C, ferritic, P segregation to free surface, 723 to 823K, AES 78–48411
Fe-Ni-Cr-C, martensitic transform. effect of austenite prestrain above M_d temp. 78–15398
Fe-Ni-Cr-Mn-Al-Ti Incoloy 800, exam. of scale morphology, alloying element distrib. after oxidation 78–80677
Fe-Ni-Cr-Mo superalloy, mech. props., η-phase form. effect *(Chinese)* 80–20925
Fe-Ni-Cr-P-B, Metglas 2826A, TEM of shear bands 78–48483
Fe-Ni-Cr-P-B, Metglas 2826A, hardness, elastic moduli, density, cryst. temp., mech. props., for flywheel appl. *(Dutch)* 78–52878
Fe-Ni-Cr-P-B amorphous alloy, localized corrosion 80–16559
Fe-Ni-Cr-S, phase relations rel. to sulphidation of austenitic stainless steel 79–38800
Fe-Ni-Cr-Si, superalloy, Cr and Si effect on mech. props. and microstruct. *(Chinese)* 79–100207
Fe-Ni-Cr-Si (35, 18, 2 wt.%), heating element wire, failure and oxidation 79–83378
Fe-Ni-Cr-Si alloy 800, Si effect on creep and age hardening 77–48444
Fe-Ni-Cr-Ti, superalloy A286, powder, exam. of microstruct. and mech. properties 78–52979
Fe-Ni-Cr-Ti based alloy, 36 NKhTYu, high temp. deform. characts., superplastic behaviour *(Russian)* 77–63719
Fe-Ni-Cr-Ti-Al, ausaging alloy, cellular precipitate indentification *(Chinese)* 78–11225
Fe-Ni-Cr-Ti-Al, Ti and Al effect on microstruct. and mech. props. *(Chinese)* 79–74130
Fe-Ni-Cr-Ti-Al, with thermoelastic control coeff., comp. and heat treatment influence on props. *(French)* 80–81074
Fe-Ni-Cr-Ti-Al Elinvar alloys, dispersion-hardened, structural transform. *(Russian)* 79–1872
Fe-Ni-Cr-Ti-Mn-Mo, (25.8, 14.04, 2.17, 1.27, 1.30 wt.%), superalloy A-286, precipitation hardening, exam. of fracture toughness and mech. props. 78–92355
Fe-Ni-Cr-Y, oxidation at 800 to 1300°C, Y addition effects, comparison with Ni-Cr-Y alloy *(French)* 79–43481
Fe-Ni-Cr-Y, Y addition effect on selective oxidation/diffusion phenomena relationship *(French)* 80–108623
Fe-Ni-Cr-base superalloys, characterization for PNP components 80–5242
Fe-Ni-Si-Mn-Cr, effect of prolonged aging on mag. props. 80–16513
Fe-Sb-Cr, dil., interactions and precip., Mossbauer study 80–39997
Fe-Sb-Cr, dil., short range order, NMR study 80–71237
Fe-Sb-Cr, interactions and segregations, Mossbauer and X-ray diffr. study 80–70415
Fe-Si-Cr magnetic films, sputtered, corrosion reduction, effect of Cr obs. 80–80573
Fe-W-C-Cr, eta carbides at 1250°C 77–32581
Fe-W-Cr-Mo system, mag. and mech. props. rel. to production methods *(Japanese)* 80–71107
Fe-W-Cr-Mo-Co (18,12,3,x wt.%) magnetisation and hardness, cold working effect obs. *(Japanese)* 77–40428
Fe-W-Cr-Mo-Co with austenitic phase, magnetic and mech. props., cold working and ageing effects *(Japanese)* 78–60678
$(Fe_{100\ y}B_y)_{1-x}Cr_x$ thin film glasses, mag. props. and corrosion resist. 80–80576
$Fe_{0.5}Co_{0.5-x}Cr_x$ films, vacuum-deposited cryst. and mag. struct. *(Russian)* 80–93081
$(Fe_{0.07}Co_{0.93})_{75-x}Cr_xSi_{15}B_{10}$, amorphous, disaccommodation of mag. permeability and induced anisotropy 80–88741
$Fe_{1-x}Cr_x$, Mossbauer exam. 77–16222
$(Fe_{1-x}Cr_x)$-P-C, amorphous, mag. props. *(Japanese)* 77–85433
$Fe_{70}Cr_{30}$, disordered, X-ray spectra study of electronic struct. 77–77324
Fe_xCr_{1-x}, spin-wave evolution crossing from ferromag. to spin-glass regime 80–97080
$Fe_{65.4}Cr_{20.5}Al_{10.7}V_{3.4}$, effect of Al and V on form. of $L2_1$ superstructure and stratification 77–77474
$Fe_{85-x}Cr_xB_{15}$ metallic glass, Curie temp., crystn. temp. and room temp. elec. resist., Cr content effect 79–91229
$Fe_{36}Cr_{32}Ni_{14}B_{12}B_6$, amorphous X-ray absorpt. spectra, effective coordination charges 80–84805
$(Fe_{100\ -x}Cr_x)_{79}P_{13}B_8$ amorphous alloys, splat cooled mag. and transport props. 80–84593
$(Fe_{98}Cr_2)_{79}P_{13}B_8$ and $(Fe_{96}Cr_4)_{79}P_{13}B_8$, amorphous, low temp. sp. ht., mag. contribs. 80–80552
Fe_2CrSi, Heusler type material, mag. props. 77–40042
$Fe_{3-x}Cr_xSi$, limits of solubility, mag. props. and electron conc. 78–10670
$Fe_{36}Cr_{12}Ti_7Mo_3$, high temp. precipitation kinetics, internal friction study 79–43254
$Fe_{65}(Ni_{1-x}Cr_x)$, microhardness and specific heat, depend. on Cr content *(Russian)* 79–100240
$Fe_{65}(Ni_{1-x}Cr_x)_{35}$, low-temp. elec. and galvanomag. props. *(Russian)* 77–35910
$Fe_{65}(Ni_{1-x}Cr_x)_{35}$, mag. viscosity and anomalies near Curie temp. 79–73781
$Fe_{65}(Ni_{1-x}Cr_x)_{35}$, remanent magnetisation, temp. depend., anomalies near Curie temp. *(Russian)* 78–60310
FeNiCrAlLi alloy, γ' hardened, noncellular mech. for form of lamellar η phase morphology 77–28824
$Fe_{32}Ni_{36}Cr_{14}P_{12}B_6$, Metglas 2826 A, ferromag. reson. for g-values and relax. parameters, 77 to 430K 77–63289
$Fe_{32}Ni_{36}Cr_{14}P_{12}B_6$, metallic glass, changes in Curie temp., physical dimensions and mag. anisotropy during annealing 77–85446
$Fe_{32}Ni_{36}Cr_{14}P_{12}B_6$, Metglas 2826A, Hall resistivity, effect of thermal cycling and annealing 78–56125
$Fe_{32}Ni_{36}Cr_{14}P_{12}B_6$, shear band form. 78–68756
$Fe_{32}Ni_{36}Cr_{14}P_{12}B_6$, elastic, magnetoelastic and thermal props. 79–19759
$Fe_{32}Ni_{36}Cr_{14}P_{12}B_6$ metallic glass, dynamic mechanical props. 79–10894
$Fe_{32}Ni_{36}Cr_{14}P_{12}B_6$, glassy, ferromag. anisotropy of resistivity 79–23939
$Fe_{32}Ni_{36}Cr_{14}P_{12}B_6$, METGLAS 2826A, metastable crystallization phases, TEM obs. 79–55671
$Fe_{32}Ni_{36}Cr_{14}P_{12}B_6$, amorphous ferromagnet, long and short range exchange interactions, Mossbauer spectra and interpretation 79–56526
$Fe_{32}Ni_{36}Cr_{14}P_{12}B_6$, amorphous mag. solids, Mossbauer exam. 79–61281
$Fe_{32}Ni_{36}Cr_{14}P_{12}B_6$, Metglass 2826A, mag. props. under high press., Mossbauer meas. 79–73860
$Fe_{32}Ni_{36}Cr_{14}P_{12}B_6$, Metglas 2826A elec. resist. during crystn. 79–91014

chromium alloys continued

- $Fe_{32}Ni_{36}Cr_{14}P_{12}B_6$ glass, thermal expansion, glass transform. and crystn. temps. 80–2183
- $Fe_{32}Ni_{36}Cr_{14}P_{12}B_6$, metallic glass, high-resolution XPS study, electronic state struct. 80–29846
- $Fe_{32}Ni_{36}Cr_{14}P_{12}B_6$, metallic glass, Doppler broadening of positron annihilation γ-radiation and elec. resist. 80–66321
- $Fe_{32}Ni_{36}Cr_{14}P_{12}B_6$ metallic glass, crystn. kinetics by TEM 80–75186
- $Fe_{32}Ni_{36}Cr_{14}P_{12}B_6$, Metglas 2826A, EPR at 20 GHz 80–75848
- $Fe_{32}Ni_{36}Cr_{14}P_{12}B_6$ Metglas, bending deform., shear band form., high-speed cinematographic obs. 80–89322
- $Fe_{32}Ni_{36}Cr_{14}P_{12}B_6$, Metglas amorphous films, corrosion resist. and ion plating use 80–89423
- $Fe_{32}Ni_{36}Cr_{14}P_{12}B_6$ metallic glass, effect of pre-ageing on glass transition temp. 80–100326
- Gd-Cr amorphous films, spontaneous Hall effect and elec. resist. 80–80251
- Hf-Cr-Ga, X-ray microanalysis of phase equilibria *(Ukrainian)* 78–6898
- $Hg_{1-x}Zn_xCr_2Se_4$, magnetic struct., neutrongraphic and mag. investigation *(Russian)* 80–88726
- In-Cr film, electronic thermal cond., 1.5 to 3K 77–47934
- In-Cr films, supercond., sp. ht. discontinuity and transition temp. meas. 79–60969
- Ir_3Cr, yield stress and saturisation magnetisation 80–16389
- $LaNi_5$-H, with small Cr additions, NMR parameters *(Russian)* 80–29637
- $LaNi_{5-x}Cr_x$, Cr effect on hydride form. *(Japanese)* 79–43202
- Mg-Ni-W-Co-Al-Cr alloy KhN56VMKYu, Al effect on excess Mg phase 80–29926
- $Mg_3Cr_2Al_{18}$, pyrochlore struct. and its relatives 79–14773
- MgO/Ni-Cr (80, 20 wt.%) cermets, sintered, elec. resist. temp. effect 80–3206
- Mh-Rh-Cr, mag. transition, effect of press. 77–16077
- α-Mn-Cr, influence of Fe and Cr on Neel point *(Russian)* 77–1554
- Mn-Cr, spin fluctuations effect on sp. ht. 79–82788
- Mn-Cr-Mo-C, master alloys, development for low alloyed PM steel 80–50576
- Mn-Cr-Ti layers on low C steel, composite, residual stresses rel. to arc-spraying parameters *(German)* 80–104077
- $Mn_{1-x}Cr_xAs$, mag. props., phase diags. 77–66300
- $(Mn_{1-x}Cr_x)B$, Invar charact. 77–15602
- $Mn_{1.88}Cr_{0.12}Sb$, antiferromag.-ferrimag. transition, neutron crit. scatt. and crossover effect 80–71023
- $Mn_{1.88}Cr_{0.12}Sb$, magnon renormalisation 77–69520
- $Mn_{1.88}Cr_{0.12}Sb$, thermomagnetic props., antiferromag. to ferrimag. transition 77–63194
- $Mn_{2-x}Cr_xSb$, exchange-inversion interaction and acoustical magnon soft mode 77–40049
- $Mn_{2-x}Cr_xSb$ film, prep. and mag. props. 78–48009
- $(Mn_{0.95}Cr_{0.05})_3Si$, sp. ht. at low temps., mag. transitions *(Russian)* 77–32189
- Mo-Cr, cracking in NH_3 at 600°C 79–70207
- Mo-Cr, fusibility diagram *(Russian)* 80–20897
- Mo-Cr, powder mixture, activating effect of Group VIII metals on alloy .form. during sintering 77–59728
- Mo-Cr powder mixture, electric discharge sintering, struct. changes 77–77446
- Mo-Cr-V-P, load curves, structure states boundaries and strain hardening *(Russian)* 80–89241
- Nb-Cr, and Nb-V-Cr, supercond. crit. temp. and crit. field, Cr alloying effect 77–85375
- Nb-Cr, diffusion of N, effect of Cr and struct. defects 79–55938
- Nb-Cr, internal impurity adsorption effect on bond type of intercrystallite zones 77–16684
- Nb-Cr(-V), oxidation resist., Cr and V effects *(Russian)* 80–40585
- Nb-Mo-Al-(Cr) eutectic directionally crystallised alloy, heat resistance, alloy struct. *(Russian)* 80–40481
- Nb_3Al-Cr, mag. impurities effect on supercond. props. 77–1524
- $NbCr_2Si_2$, Mossbauer and magnetisation expts. 78–31138
- Ni base alloy IN792, carbide morphology 77–36508
- Ni based superalloys 713C and Mar-M200, Si effect on oxidation, hot corrosion and mech. behaviour 78–39950
- Ni superalloy Mar-M200, slow fatigue crack propagation rate meas. using high freq. resonant technique 78–52983
- Ni/Cr-Fe-C, Inconel, dislocation intersection and solution strengthening, effect of solute on obstacle profiles 80–7590
- Ni-(Co)-Cr, aluminide coating, microstruct. and chem. 80–76189
- Ni-(W,Cr)C, corrosion and corrosive wear in sea water 78–92408
- Ni-Al-Cr, ageing kinetics and γ'-phase particles spatial distrib. under applied load *(Russian)* 77–32598
- Ni-Al-Cr, heat resist., solidification range 80–35177
- Ni-Al-Cr, IN-100, growth geometry of carbides in dendritic monocrystals, solidification effects 79–11597
- Ni-Al-Cr, precipitation-strengthened, mechanical props. 78–84968
- Ni-Al-Cr, strain hardening, participation of various slip systems *(Russian)* 79–24536
- Ni-Al-Cr alloy Ehi 826 77–86120
- Ni-Al-Cr alloy IN 100 powder, rapidly solidified, effect of high melt superheat on microstructure 79–52195
- Ni-Al-Cr superalloy IN-100, crack retardation at elev. temp., hold time effect of single overload 79–79068
- Ni-Al-Cr_3C_2, eutectic, Al_2O_3 coatings for oxidation resist. 80–50776
- Ni-Al-Cr_3Cr_2, eutectic alloy, directionally solidified, oxidation resistance, influence of Y 80–89409
- Ni-Al-Cr-Co-Ti, Waspaloy, exam. of dislocation-precipitate interaction, cyclic stress-strain behaviour 78–84925
- Ni-Al-Cr-Mo-Ti-W-(Co) alloys EhI 826 and EhI 929, reverse elastic after effect under loading 78–39829
- Ni-Al-Cr-Ti-W-Mo, US vibration applied during solidification, improved strength, corrosion resistance *(Russian)* 78–15382
- Ni-B-Cr, composite, wear resistant coating on steel 45 78–11420
- Ni-base alloys, Nimonic PE-16, type 718 and type 625, neutron irrad. effects on fatigue crack propag. 80–29069
- Ni-based TaC eutectic, directionally solidified, elastic moduli 80–84984
- Ni-C-W-Cr(-Mo), Vickers hardness and crystallisation temp. 80–16361
- Ni-Ce-Fe-Ti (77, 20, 4, 2.5 wt.%), long-term strength in H at high pressure 80–55485
- Ni-Co-Cr alloys IN 738, Pt plated, aluminization 78–31583
- Ni-Co-Cr system, heats of formation and of transformation 80–50599
- Ni-Co-Cr TEM foils, white band contrast 80–75134

chromium alloys continued

- Ni-Co-Cr/Al_2O_3 catalyst, IR spectra of adsorption and interaction with pyridine 80–71946
- Ni-Co-Cr-Al-Ti-Mo superalloy IN738, casking porosity removal using hydrostatic press. sintering 80–55322
- Ni-Co-Cr-Al-Y, plasma-arc-sprayed, metallurgical characts. and oxidation behaviour 80–40618
- Ni-Co-Cr-Al-Y coating, electron beam evap., low press. gas scatt. 77–40474
- Ni-Co-Cr-Al-Y coating, electron beam deposited, for Ni-base superalloy, fatigue crack initiation and propag. 78–11438
- Ni-Co-Cr-Al-Y protective coating for combustion turbines, hot corrosion evaluation 80–40608
- Ni-Co-Cr-Mb-W-Ta, Cr, Mb, W, Ta effects on σ phase occurrence 77–36507
- Ni-Co-Cr-Mo-Al, Astroloy, extruded powder metallurgy superalloy, recrystallisation study 79–4976
- Ni-Co-Cr-Mo-Al-Ti (17.5, 15.1, 4.9, 4.15, 3.25 wt.%), creep and stress rupture behaviour in air and vacuum 80–60918
- Ni-Co-Cr-Mo-Ti-Al Nimonic 105, loading frequency and environmental effects on high temp. fatigue crack growth 78–64675
- Ni-Co-Cr-Ta-Al-W-Mo-Ti, cast, phase volume fraction determ. using manual point count practice 78–53052
- Ni-Co-Mo-Al-Cr, melt, effect of Al, Cr on O_2 activity, electrochemical determ. 79–11556
- Ni-Cr, (30 wt.%), collective dislocation movements, in situ study 80–100243
- Ni-Cr, alloy, composition determination using secondary ion emission *(French)* 77–86409
- Ni-Cr, anodic dissoln. in NaCl solns. at high current densities *(Russian)* 80–76396
- Ni-Cr, Ar ion bombard., O_2 flooded, secondary ion yield as function of original conc. *(French)* 78–39643
- Ni-Cr, austenitic alloy, oxidation mechanism, adhesion of Cr_2O_3 scale *(Polish)* 79–79143
- Ni-Cr, corrosion resistance of dental casting alloys 78–31561
- Ni-Cr, creep-fatigue failures, damage concept appl. 80–40535
- Ni-Cr, deformed, struct. form. during annealing, Ni_3Al type ordered phase precipitation *(Russian)* 80–45325
- Ni-Cr, degradation after exposure to 1% H_2S/H_2 gas mixture at 1000°C 80–89408
- Ni-Cr, dil. alloy paramag., μ^- relax. 77–24776
- Ni-Cr, dispersion strengthening, prep. from powder, mech. props. 79–91658
- Ni-Cr, ERNiCr-3 weld metal, strain-rate effects on high temp. behaviour 79–93726
- Ni-Cr, elementary excitations, exchange stiffness const., inelastic neutron scatt. study 79–47294
- Ni-Cr, film, quantitative anal. by DC arc optical emission spectroscopy 78–68940
- Ni-Cr, gas corrosion, in composite atmospheres *(Polish)* 79–79142
- Ni-Cr, heat resistant cast and wrought for petrochemical industry, creep rupture *(German)* 77–36618
- Ni-Cr, heat resisting, dispersion hardened, electrical resistance meas. *(Russian)* 77–66708
- Ni-Cr, heat-resist., high-temp. ductility and embrittlement 80–76314
- Ni-Cr, heavy ion irrad., defect cluster obs. 80–107341
- Ni-Cr, high temp. thermomech. treatment effect on tensile diagrams of KhN77TYuR *(Russian)* 80–60884
- Ni-Cr, high temp. wire resistance strain gauges 77–53896
- Ni-Cr, interband absorpt. and refractive index, photoconductivity dispersion function 77–36263
- Ni-Cr, ion irradiation induced void swelling and defect microstructs., TEM obs. 79–51164
- Ni-Cr, low short-term creep resist. at 700°C 80–76313
- Ni-Cr, low temp. sp. ht. near ferro-paramag. transition 77–63218
- Ni-Cr, mag. moment distrib. 77–32178
- Ni-Cr, matrix effect in SIMS anal. using O_2^+ primary beam 80–76576
- Ni-Cr, microstruct. effects in low-cycle fatigue tests 77–56108
- Ni-Cr, Ni rich, discontinuous precipitation *(German)* 79–91653
- Ni-Cr, ordering by nucleation and growth and by spinodal decomposition *(French)* 78–27471
- Ni-Cr, ordering in the vicinity of Ni_2Cr 79–38819
- Ni-Cr, oxidation effect on magnetic props. *(Russian)* 78–23868
- Ni-Cr, partial dislocation, stacking fault TEM study *(Chinese)* 80–84174
- Ni-Cr, phosphidation in P vapour, 700°C, phosphide layer struct. and kinetics 80–25906
- Ni-Cr, residual resist., CPA calc. to muffin tin pot. 77–62892
- Ni-Cr, self-weldability in high temp Na *(Japanese)* 80–89392
- Ni-Cr, solid soln., exam. of back stress role in creep behaviour of particle strengthened alloys 78–52889
- Ni-Cr, solid soln., lattice parameter meas. rel. to conc. and temp. depend. *(Czech)* 80–28949
- Ni-Cr, solid soln., US deform., electron microscope exam. *(Russian)* 78–35447
- Ni-Cr, solid soln., US effect on mech. props. *(Russian)* 78–23819
- Ni-Cr, solubility limit determ., X-ray method 79–43199
- Ni-Cr, solubility of H_2, 500 to 1000°C *(Japanese)* 78–38845
- Ni-Cr, spin polarised tunnelling expts. 78–39372
- Ni-Cr, spin wave stiffness consts., RPA CPA band model 79–61088
- Ni-Cr, surface oxide characterisation by Raman spectroscopy 80–50308
- Ni-Cr, variation in absolute thermoelec. power under heat/treatment *(Ukrainian)* 79–38051
- Ni-Cr, weak ferromag., stiffness const., low-temp. meas., rel. to RPA-CPA theories 78–31063
- Ni-Cr, wear tracks, TEM obs., tested in simulated face seal 77–52508
- Ni-Cr, wrought, fatigue at high temp., microstruct. assessment 79–29208
- Ni-Cr (0-35 at.%), neutron irrad. at 25K, damage, elec. resist. obs. *(French)* 80–54286
- Ni-Cr (2 wt.%), role of hydrostatic pressure on sintering of creep cavities 79–28980
- Ni-Cr (20 wt.%), Al and Ti containing, oxidation, effect of dispersal oxides 77–44404
- Ni-Cr (20 wt.%), CC W fibre reinforced, alloy by effect on struct. stability, mech. props., metallographic exam. 78–56600
- Ni-Cr (20 wt.%), high temp. frictional characts. 80–21118
- Ni-Cr (20 wt.%), Norton-Bailey parameters, from creep rupture data 80–30098

chromium alloys continued
- Ni-Cr (20 wt.%), oxidation, 800 to 1300°C, effect of volume and intergranular diffusion *(French)* 77—86228
- Ni-Cr (20 wt.%), oxidation, O_2 press. effects *(Japanese)* 78—15578
- Ni-Cr (20 wt.%), oxidation in humid air, 800 to 1250°C *(French)* 79—79165
- Ni-Cr (20 wt.%), plasma-sprayed coating, on steel 79—96222
- Ni-Cr (20 wt.%), reinforced by coated Mo filaments, effect of coating on composite strength 78—56710
- Ni-Cr (20 wt.%), surface oxide layers, compar. study of comp. and struct. by secondary ion emission and electron microprobe *(French)* 77—56286
- Ni-Cr (20 wt.%), volume and grain boundary diffusion of Ni and Cr, C effect *(French)* 79—95203
- Ni-Cr (20 wt.%) alloy LNKh, room-temp. friction characts. 80—25874
- Ni-Cr (20 wt.%) based composite, use of SiC fibres with protective Al_2O_3 coating, IR investigation 78—60623
- Ni-Cr (20wt.%), powder, nonspherical, mean pore size of sheet material 77—28757
- Ni-Cr (23 and 33 wt.%), kinetic and morphological study of sulphidation in S_2, H_2S and H_2S/H_2 79—52424
- Ni-Cr (25 to 40 wt.%), transport numbers of alloy components determ. 77—62667
- Ni-Cr (27.4 and 40.2 wt.%), compositional changes, in underlying alloy produced by oxidation 79—8395
- Ni-Cr (33 at.%), plastic deformation, HVEM study *(French)* 80—66605
- Ni-Cr (33 at.%), US deform. effect on short range order form. *(Russian)* 78—39839
- Ni-Cr (33.3 at.%) alloy, ordering after US deform., microhardness and elec. resist. meas. *(Russian)* 79—20113
- Ni-Cr (44 to 50 wt.%), oxidation 79—43483
- Ni-Cr (70 wt.%), oxidation behaviour, 1073-1473K 80—89416
- Ni-Cr alloy, cast, etching methods for determ. of primary struct. 78—23888
- Ni-Cr alloy, dispersion-hardened, prod. by mech. alloying 78—15345
- Ni-Cr alloy, EI 437B, vibrocreep at normal and high temps. 77—4824
- Ni-Cr alloy, KhN70VMTYu, gas turbine blades, thermocyclic strength characts., exam. 78—60743
- Ni-Cr alloy, Kh20N80, inclusions and plasticity, crystn. conditions influence *(Russian)* 80—20923
- Ni-Cr alloy, structural changes, during thermal stress cracking, X-ray and microhardness meas. *(Russian)* 78—35496
- Ni-Cr alloy EhI617, thermocyclic treatment effect on struct. and thermal fatigue resistance 78—7045
- Ni-Cr alloy Ehi 617, equation of condition for creep, expt. checking 77—86120
- Ni-Cr alloy KhN70MVYu wire, recrystn., optimum heat treatment 80—76278
- Ni-Cr alloy KhN70VMTYu, heat resistant, explosive loading effect on struct. and mech. props. *(Russian)* 78—39787
- Ni-Cr alloy submerged arc weld surfacing using metal powder filler additions 79—57157
- Ni-Cr alloys, creep crack growth, environmental sensitivity 80—85030
- Ni-Cr alloys, crystallisation anomalies *(Russian)* 78—19719
- Ni-Cr alloys, low temp. transform. mechanism, electrophys. props. obs. *(Russian)* 77—59777
- Ni-Cr alloys, method of etching in Br-methanol reagent 77—90516
- Ni-Cr austenitic alloy, oxidation mechanism, intergranular diffusion effect *(French)* 80—81229
- Ni-Cr base alloy, strain relaxation, effect of grain size, particle size, γ' vol. fraction 79—47741
- Ni-Cr based coatings, hot corrosion resist. 79—24674
- Ni-Cr coatings on steel, standardisation 79—57139
- Ni-Cr complex alloy with good creep resistance, friction stress/flow stress relation 79—8337
- Ni-Cr directional order anisotropy energy induced by neutron irradiation, temp. depend. 77—66294
- Ni-Cr electrochem shaping in nitrate and chlorate, hardening γ'-phase concentration influence *(Russian)* 77—8979
- Ni-Cr film, electrical props. rel. to AES conc. depth profile 77—32092
- Ni-Cr film, electron spin polarisation, meas. using supercond. tunnel junction 77—69637
- Ni-Cr film, long range order 79—60657
- Ni-Cr film, RF sputtered, Seebeck coeff. 77—63004
- Ni-Cr film, resistance stabilisation by surface oxide formation 79—78214
- Ni-Cr film, struct. transforms. induced during annealing, resist. obs. 79—77965
- Ni-Cr film, vac. deposition, elec. props. and comp. struct. 79—77966
- Ni-Cr films, vac. deposited, comp. and temp. coeff. of resist., AES obs. 79—91161
- Ni-Cr films implanted with N ions, electric properties *(Russian)* 80—107927
- Ni-Cr foldfoil strain gauge, for cryogenic anal. of supercond. structs. in high mag. fields, fusion reactors 78—54947
- Ni-Cr melt, N_2 diffusion *(Russian)* 78—18812
- Ni-Cr Nimonic alloys, mech. props., high-temp. irrad. effects 80—100885
- Ni-Cr plasma spray coated Ti substrate, interface interaction 77—21323
- Ni-Cr powder mixture, dispersion hardened, homogenisation 77—12638
- Ni-Cr resistor layers, ESCA meas., expt. *(Hungarian)* 77—4951
- Ni-Cr solid soln., Ni rich, thermodynamic activity of components 79—70043
- Ni-Cr superalloy, interactions between creep and low cycle fatigue *(Chinese)* 80—66572
- Ni-Cr surface, chemisorption, appl. of vac. UV photoelectron spectrometer *(Japanese)* 78—62264
- Ni-Cr thin film production by HF cathode sputtering *(Bulgarian)* 79—19992
- Ni-Cr thin film resistors, α-particle elastic scatt., and PIXE anal. 79—48022
- Ni-Cr thin film resistors using jumping electron beam, expt. *(Hungarian)* 77—4738
- Ni-Cr thin films, resistor appls., props. and prep. *(Hungarian)* 77—4737
- Ni-Cr type alloys, Co surface pretreatment to attain pore-free aluminised coatings 80—40612
- Ni-Cr wires, added metals effect on sublimation behaviour in vac. *(German)* 79—90775
- Ni-Cr/Au films, interdiffusion processes and oxidation phenomena 80—59735
- Ni-Cr/$MgSiO_3$, methanation catalysts, S resistant, XPS characterization 79—83506

chromium alloys continued
- Ni-Cr/ThO_2, adhesive energy, meas. techniques 80—50803
- Ni-Cr/ZrO_2-Y_2O_3 sputtered multilayered ceramic/metal coatings, props. 80—40620
- Ni-Cr-Al, hot corrosion resist. of Na_2SO_4 cooled specimens 78—44264
- Ni-Cr-Al, oxidation, NaCl vapour effects on microstruct. 78—44274
- Ni-Cr-Al, oxidation at 850°C in air containing HCl gas 79—8396
- Ni-Cr-Al, protective coating, exam. of interdiffusion kinetics, development of analysing procedure 79—5085
- Ni-Cr-Al, resist. to cyclic oxidation at 1100 and 1200°C 77—77641
- Ni-Cr-Al, shape of γ'-precipitates on surface after sublimation *(German)* 77—81266
- Ni-Cr-Al (15, 5 wt.%), oxide dispersion strengthened, effect of dispersoids on oxidation 78—80679
- Ni-Cr-Al (20, 4 wt.%), tensile stress effect on high temp. oxidation *(Japanese)* 80—89393
- Ni-Cr-Al (40, 4 wt.%), γ' and α-Cr duplex precipitation, TEM *(Japanese)* 77—25061
- Ni-Cr-Al alloy, Al_2O_3 adherence, improvement by addition of Pt and Rh 77—8995
- Ni-Cr-Al alloy, scale behaviour in carbonaceous gas atmos. 77—36693
- Ni-Cr-Al aluminised coating, diffusion paths for formation and degradation of oxidation resistant coatings 78—11431
- Ni-Cr-Al coatings, corrosion and thermal shock resist. in diesel engines 79—24675
- Ni-Cr-Al coatings Ni eutectic alloys in gas turbines, use of diffusion barrier 79—24673
- Ni-Cr-Al sintered alloy, hot vac. pressure, fracture and mech. characts. 80—66667
- Ni-Cr-Al_2O_3 powder targets for plasma-ion spray deposition of resistance films 80—84897
- Ni-Cr-Al-Cu, Evanohm, Kapitza conductance meas. using superconducting current comparator 77—41645
- Ni-Cr-Al-TaC, eutectic composite, microstructure, fatigue props. 80—85038
- Ni-Cr-Al-ThO_2, hot corrosion, cyclic oxidation depth of attack determinations 80—11837
- Ni-Cr-Al-Ti, KhN78TYu, heavily deformed, subgrain struct. due to discontinuous precipitation of γ' phase *(Russian)* 79—52218
- Ni-Cr-Al-Ti, stress corrosion cracking, factors influencing susceptibility 80—97617
- Ni-Cr-Al-Ti (Ti-Co), exam. of back stress role in creep behaviour of particle strengthened alloys 78—52889
- Ni-Cr-Al-Ti alloy type ZhS6U, effects of heat treatment in high vel. gas streams on props. 79—57025
- Ni-Cr-Al-Ti-Mo, low temp. mech. behaviour, precipitation 78—39860
- Ni-Cr-Al-W-Ti alloy MA 6000E, mechanical alloying for high temp. appl. 78—44046
- Ni-Cr-Al-Y coating for oxidation protection of Ni base TaC eutectics 77—40475
- Ni-Cr-Al-Y/ZrO_2-Y_2O_3, NASA two-layer thermal barrier coating, for gas turbine engines, test results 80—40617
- Ni-Cr-Al-Y_2O_3 superalloy, recrystn. and texture development 80—16328
- Ni-Cr-AlPt, exam. of phase diagram 79—8276
- Ni-Cr-B-Si, hard faced with WC, exam. of abrasion and wear props. 79—34202
- Ni-Cr-B-Si-Fe alloy, Cr content by X-ray fluoresc. 79—43654
- Ni-Cr-Ce, Ce effect on oxidation 79—43484
- Ni-Cr-Co, Mo, Ti, Y and R alloying additions influence on oxidation *(Russian)* 80—40587
- Ni-Cr-Co, Nimocast alloy 738, γ'' precipitate morphology and creep rupture, thermal stress crack effect 78—11318
- Ni-Cr-Co alloy IN738, electrochemical corrosion meas. in molten sulphate 79—96178
- Ni-Cr-Co alloys, relax. resist. exam. by bending and tension 79—24564
- Ni-Cr-Co base superalloy APK1, hot isostatically pressed, heat treatment, fracture props. 77—73251
- Ni-Cr-Co based alloy, IN-738 turbine blades, hot isostatically pressed investment castings, effect of heat treatment on grain boundary struct. 80—89270
- Ni-Cr-Co superalloy, combined TEM, FIM, atom probe microanalysis of precipitates and carbide phase comp. 80—100844
- Ni-Cr-Co superalloy, σ-phase effect on mech. props. *(Chinese)* 79—74229
- Ni-Cr-Co superalloy IN-792, crack growth resistance, metallurgical effects 77—36655
- Ni-Cr-Co-Al alloy IN-738, uniaxial damage accumulation law for time depend. loading with creep-fatigue interaction 79—83324
- Ni-Cr-Co-Al-Ti-W-Ta-Mo, IN 738 LC, loading frequency and environmental effects on high temp. fatigue crack growth 78—64675
- Ni-Cr-Co-Al-W-Mo-Ti-Ta, heat resist. and struct., Ta effect 80—76312
- Ni-Cr-Co-Mo, long-term corrosion stability rel. to use in joint endoprostheses 78—36059
- Ni-Cr-Co-Mo alloy MP35N alloys, cold worked, factors affecting embrittlement in H_2S environments 78—31502
- Ni-Cr-Co-Mo alloy MP35N, accelerated H_2 charging in aq. H_2SO_4 at 0.2% yield stress 80—30144
- Ni-Cr-Co-Mo-Al, IN-67 alloy, hot corrosion, cyclic oxidation, depth of attack determinations 80—11837
- Ni-Cr-Co-Mo-Al-Ti (10, 15, 3, 5.5, 4.5 wt.%), superalloy, exam. of creep and fracture behaviour 78—48464
- Ni-Cr-Co-Mo-Al-Ti alloys, Waspaloy, Astroloy, exam. of microstruct. effect on crack growth 78—52977
- Ni-Cr-Co-Mo-Ti-Al, powders, HCl surface treatment to prevent TiC precipitation, fracture props. 79—8397
- Ni-Cr-Co-Ti, superalloy sintering thermochemical surface treatment 80—25617
- Ni-Cr-Co-Ti-Mo-W-Al (14, 9.8, 5, 4, 3.9, 3 wt.%), low cycle fatigue, prior heat treatment effect 80—60962
- Ni-Cr-Co-W (47.5, 25, 12, 8.75 wt.%), vaporization of IN-643, high-temp. mass spectrometry 79—7685
- Ni-Cr-Co-(Se), oxidation resistance 77—21320
- Ni-Cr-Fe, high temp. corrosion and creep in carburizing and oxidising atmos. 79—11727
- Ni-Cr-Fe, Inconel, effects of heat treatment on surface segregation, Auger spectroscopic exam. 80—7602
- Ni-Cr-Fe, Nimonic-75, electroless siliconization 78—27679
- Ni-Cr-Fe, radiation enhanced precip. and dissolution of precipitates, point defect kinetics and dislocation obs. 80—108467
- Ni-Cr-Fe, stress corrosion cracking, factors influencing susceptibility 80—97617

chromium alloys continued
Ni-Cr-Fe (15.7, 7.63 wt.%), Inconel 600, anal. of pit generation by 3.5% NaCl, by stochastic theory *(Japanese)* 78—85038
Ni-Cr-Fe (75, 35, 12 wt.%), electron and α-particle irrad., positron annihilation and elec. resist. meas. 79—83054
Ni-Cr-Fe Alloy 600, acid intergranular corrosion rel. to caustic stress corrosion cracking stress relieving effect 77—66712
Ni-Cr-Fe Alloy 600, stress corrosion cracking in high purity water, effect of microstruct. 77—66713
Ni-Cr-Fe steam generator tubes, stress corrosion susceptibility, heat treatment effect 79—20258
Ni-Cr-Fe-Mo-Co (21.41, 19.28, 8.64, 2.16 wt.%), Hastelloy alloy X, exam. of thermal stability 78—84865
Ni-Cr-Fe-Si-B wear-resist. and corrosion-resist. coatings by furnace melting 80—35428
Ni-Cr-Fe-Ti alloy KhN77TYuR, long-term strength under in-pile irrad. conditions 78—6940
Ni-Cr-Fe-W, type EHI868, loading history effect on resist. to cyclic elastoplastic strain 80—16398
Ni-Cr-HfO_2, dispersion-strengthened, hot rolling effects on props. *(Russian)* 77—59797
Ni-Cr-M alloys, M=minor alloying addition Y, La, Ce, Sm, Th, U, Zr, V, corrosion rates 77—16750
Ni-Cr-Mg alloy, KhN70VMTYu, Mg effect on grain boundary struct., props. 79—19261
Ni-Cr-MgO system, elec. resist. variation with comp. and prep. method 78—60637
Ni-Cr-Mn alloy solidification, effects of Si, Mo and Co alloying 79—83193
Ni-Cr-Mn-Fe-Nb (20,3,3,2.5 wt.%), short-range order effects on tensile behaviour 80—25793
Ni-Cr-Mo (74, 20, 4 wt.%), long-term strength in H at high pressure 80—55485
Ni-Cr-Mo steel, corrosion and cavitation-erosion resist. *(Russian)* 78—11395
Ni-Cr-Mo-C hardfacing alloy, hardness and abrasive wear resistance 79—79117
Ni-Cr-Mo-Fe-Mn, Kh12M23, intermetallic phases exam. *(Russian)* 78—39740
Ni-Cr-Mo-Mn alloy 02KhN40MB, corrosion-resist, heat-resist., phys. and mech. props. 80—35411
Ni-Cr-Mo-Ti (19,11,3 wt.%) for TiC reactively sputtered coatings, adherence, XPES and wear study 80—25565
Ni-Cr-Mo-V steel disc, rolling contact fatigue and residual stress on contact surface 77—32671
Ni-Cr-Mo-W-Al-Ti, heat-resist., phase comp. 80—76250
Ni-Cr-Nb-Al eutectic alloys, sulphidation/oxidation at high temps., corrosion mechanism 78—72934
Ni-Cr-NbC eutectic composite, unidirectional solidification, thermal cycling, temp. range effect on microstructural degradation 80—89272
Ni-Cr-P, amorphous, corrosion behaviour, immersion tests and electrochem. meas. *(Japanese)* 80—85085
Ni-Cr-P thin films deposited by electroless plating, resist. characts. 79—4607
Ni-Cr-Si, corrosion and failure mechanisms of coatings for gas turbine applications 79—29284
Ni-Cr-Si, thermocouple alloy, props. and thermoelec. reference data 79—26057
Ni-Cr-Si (10, 1.8 wt.%), Zr, Hf, La or Sm alloying additions effect on oxidation resist. 77—63831
Ni-Cr-Si alloy system, oxidation resist. 79—24661
Ni-Cr-Ta alloy, precipitation hardening, 650 to 800°C 77—59798
Ni-Cr-Ta system, phase equilib. of Ni rich region at 1523 and 1273K 80—93541
Ni-Cr-Ta-Ti-Si, EP557 precipitation hardening alloy, mech. props., heat treatment effect 80—60877
Ni-Cr-TaC directional eutectic, high-strength, interphase boundaries *(Russian)* 79—38812
Ni-Cr-TaC eutectic-like composite, obs. of interfacial diffusion by high resolution TEM 79—4432
Ni-Cr-ThO_2 (20, 2 wt.%), dispersion hardened, model for high temp. deform. based on struct. obs. 78—19809
Ni-Cr-ThO_2(20, 2 wt.%), dislocation struct. after high temp. deform. 77—52393
Ni-Cr-Ti, type EHI698, loading history effect on resist. to cyclic elastoplastic strain 80—16398
Ni-Cr-Ti (19.51, 4.2 wt.%), quench-ageing and fracture *(German)* 77—70088
Ni-Cr-Ti rapidly solidified superalloys, surface segregation 80—76263
Ni-Cr-Ti-Al, precipitation of γ' phase during single and combined ageing treatment *(Russian)* 77—52328
Ni-Cr-Ti-Al/Au-Ni brazed joint, high temp., AE under elev. temp. and loading *(German)* 78—31597
Ni-Cr-Ti-Al-Fe-Co (19.65, 2.40, 1.37, 0.78, 0.52 wt.%), strength of γ' hardened alloy, ageing exam. 78—88501
Ni-Cr-Ti-Al-Mo-Nb-Fe (13-16, 2.35-2.75, 1.3-1.7, 2.8-3.2, 1.8-2.2, 2.0 wt%), heat resistant props, mech props. struct., stepwise ageing effects *(Russian)* 78—76666
Ni-Cr-Ti-Co-W-Al-Mo alloys AF-115 and AF2 1DA, superalloy powder compacts, fatigue origins 78—48521
Ni-Cr-Ti(Al), effect of ultrasound on crystallisation, dendritic structure, and plasticity *(Russian)* 80—11637
Ni-Cr-Ti(Nb)(Zr), eutectic alloy charact. by melting temp., composition and oxidation resistance 78—52771
Ni-Cr-W, oxidation behaviour in air at 1000-1250°C 80—89407
Ni-Cr-W (20, 10 to 40 wt.%), phase composition, struct. and props. 80—21034
Ni-Cr-W (20, 3 wt.%), high temp. creep, atmospheric effect on anomalous behaviour 78—80617
Ni-Cr-W-C(-Si), struct. and props. of corrosion and wear resistant alloys 79—24627
Ni-Cr-W-C(Si) hardness, corrosion resistance, wear resistance tests in 10% HCl *(German)* 78—92368
Ni-Cr-W-Co granules type ZhS6U, EP741, hot hydrostatic pressing 80—60796
Ni-Cr-W-Co-Ti, thermal fatigue, effects of inclusions 80—81183
Ni-Cr-W-Co-Ti heat resistant alloy ZhS6K, fatigue resistance, heat treatment and protective coating effects 77—81320
Ni-Cr-W-Co-(Al)(Ti)(Mo), high-temp. sulphide corrosion 80—76408
Ni-Cr-W-Mo-Al-Ti (15,6,3,2,2, wt.%), wrought, Si effect on transition brittleness *(Chinese)* 80—55491

chromium alloys continued
Ni-Cr-W-Mo-Ti-Al, heat-resist., recovery and recrystn. 80—76268
Ni-Cr-W-Mo-Ti-Al alloy KhN67MVTYu, heat treatment effect on mech. props. 77—70082
Ni-Cr-W(Mo)(Ti)(Al), long range ordering of matrix of complex heat resistant alloys *(Russian)* 77—77509
Ni-Cr-Y, oxidation at 800 to 1300°C, Y addition effects, comparison with Fe-Ni-Cr-Y alloy *(French)* 79—43481
Ni-Cr-Y, Y addition effect on intergranular and volumetric diffusion, oxidation reduction *(French)* 79—83382
Ni-Cr-Zr, degradation after exposure to 1% H_2S/H_2 gas mixture at 1000°C 80—89408
Ni-Cr-ZrO_2, dispersion hardened, sintered, rupture 77—21272
Ni-Cr-(Al), oxide dispersion strengthened, creep and tensile props. 77—86042
Ni-Cr-(Al), oxide dispersion strengthened materials, effect of prior creep at 1365K on room temp. tensile props. 78—39857
Ni-Cr-base superalloys, characterization for PNP components 80—5242
Ni-Cr-type alloys, theory of ordering, superstruct. form. *(Russian)* 77—81256
Ni-Cr(-Fe), blackness change in air, 1-8 micron, 1200°C, film props. depend. 77—66033
Ni-Cr(-Mo), creep parameters, high temp. 80—50685
Ni-Cr(-W), heat-resistant, integrated hemispherical degree of blackness, specific elec. resist., oxidised surfaces 79—86912
Ni-Cr(20 wt.%), oxidation at elevated temps., struct. effects *(French)* 77—59994
Ni-Cr(20 wt.%), oxidation in pure O_2, 800 to 1200°C, secondary ion emission exam. of oxide film *(French)* 77—59995
Ni-Fe-Cr, determ. of preferential locations of Mo or Cr on Fe and Ni sublattices, by X-ray intensity study 79—37662
Ni-Fe-Cr, extraordinary Hall effect, elec. and mag. meas. at 77 and 300K 80—34421
Ni-Fe-Cr, PE 16, thermally activated domain wall motion 79—95603
Ni-Fe-Cr (18, 18 wt.%) superalloy, mech. props., 4-295K 77—44327
Ni-Fe-Cr alloy, PE 16, coercivity of picture frame cryst. 78—14988
Ni-Fe-Cr base superalloy, addition effect on mech. props. *(Chinese)* 80—20998
Ni-Fe-Cr film, hysteresis loop meas. using magnetooptical system 79—69707
Ni-Fe-Cr soft magnetic film plating bath 79—43465
Ni-Fe-Cr superalloy type 718, heat treatment effect on room temp. and elevated temp. fracture toughness response 80—100922
Ni-Fe-Cr-Mo-Ti-Al, PE 16, thermally activated domain wall motion 80—88777
Ni-Fe-Cr-Nb-Ta-Mo alloy, fatigue crack growth, stress ratio and hold-time effects 80—40531
Ni-Mo-C-Cr, Vickers hardness and crystallisation temp. 80—16361
Ni-Mo-Cr-Si, plasma and detonation coatings, Laves- and carbide-strengthened, comparative props. 78—15562
Ni-Nb-Al-Cr, directionally solidified, exam. of growth and morphology 79—11601
Ni-Nb-Al-Cr (19.7, 2.5, 6.0 wt.%), eutectic, mech. props., high press. H_2 effect 77—63779
Ni-Nb-Cr-Al, directionally solidified eutectic superalloy, high temp. oxidation resistant coatings 78—39937
γ/γ'-δ-Ni-Nb-Cr-Al (20, 6, 2.5 wt.%), growth kinetics of γ' precipitates 77—40424
Ni-Nb-Cr-Al (20, 6, 2.5 wt. %), γ/γ'-δ type eutectic, fatigue, effect of composition and microstruct. 78—48520
Ni-Ni_3Al-Cr_3C_2 eutectic composite, creep 77—40431
Ni-W-Co-Cr, superalloy MAR 200, with Hf, cellular composite prod. by isothermal dendrite ripening 78—44150
NiAl-Cr, eutectic, directionally solidified, temp. behaviour of misfit dislocations *(German)* 78—3119
NiAl-Cr eutectic alloy, directional solidification singularities *(Russian)* 78—68678
Ni_3Al-Cr, powder, X-ray spectral analysis exam. 80—16239
(NiCo)-Cr-Al-Y/ZrO_2-Y_2O_3 plasma sprayed ceramic coating for turbine engine components 80—40616
NiCr film, resistive, electron beam deposition, evaporation, gas phase analysis *(Polish)* 79—20492
NiCr, hyperfine fields about μ^+ 79—56664
NiCr, sputtered, detection by electron probe microanal., substrate depend. 80—35607
NiCr thin film resistor, ‘clean vacuum’ deposition equipment suitability obs. *(Polish)* 79—15611
NiCr-AlY sintered fibre metal struct. abradable seal material, friction and wear 78—56785
NiCr-Ge, amorphous, junction, current-voltage charact. 80—44725
NiCr-MoAl-ThO_2 (13,3 wt.%), powder, mech. alloying 78—84744
$Ni_{0.89}Cr_{0.11}$, phonons with disorder caused by force consts., neutron diffr. obs. and CPA calc. 80—96602
Ni_2Cr, fine-domain ordered alloy, early deform. stages, dislocation struct. and motion *(Russian)* 77—81291
Ni_2Cr, neutron irrad., point defect prod. and annealing 78—87718
Ni_2Cr ordered alloy, mech. twinning *(French)* 77—72624
NiCrAlY, mechanically alloyed, maintaining elongated grain struct. after deform. 77—36534
Ni(Fe,Cr), electron states density model and mag. characts. calcs. *(Russian)* 80—92804
Ni_3(Fe,Cr), elec. resist., temp. depend. anomalies, Hall and Nernst-Ettinghausen effects *(Russian)* 80—10942
Ni_3(Fe,Cr), electron states density model and mag. characts. calc. *(Russian)* 80—92804
Ni_3(Fe,Cr), kinetic phenomena rel. to ordering and electron struct. *(Russian)* 78—76043
Ni_3Fe-Cr, transport props. and magnetisation, effect of Cr alloying *(Russian)* 78—39095
$Ni_xFe_yCr_{1-x}$, films, struct., mag. props., and corrosion resist. 80—34706
$Ni_{35}Fe_{30}Cr_{15}P_{14}B_6$, amorphous, anodic polarisation and localised corrosion 77—21310
$Ni_{36}Fe_{32}Cr_{14}P_{12}B_6$, metallic glass, crystallisation 79—77520
$Ni_{36}Fe_{32}Cr_{14}P_{12}B_6$, amorphous, electrochem. corrosion in chloride solns. 80—50763
$Ni_{36}Fe_{32}Cr_{14}P_{12}B_6$ metallic glass, mech. props. and thermal stability 80—76362
$Ni_2Mn_xCr_{1-x}Sn$, Heusler alloy, mag. moment exam. 77—24682
Nichrome, plasma spray coatings, relaxation phenomena 80—19876

chromium alloys continued
  Pd-Cr, dil., appearance of mag. order for Cr impurities in exchange enhanced hosts 79—4690
  Pd-Cr, dil., elec. resist., 7.4 to 300K, anomalous temp. depend. associated with cond. electron scatt. 79—73491
  Pd-Cr, dil., temp. dependent scatt. 80—59973
  Pd-Cr, liquid alloy, enthalpy of form. *(Russian)* 77—56244
  Pd-Cr (11-18 at.%), resistivity comparison with canonical spin glass system 78—10432
  Pd-Cr spin glass, magnetisation and magnetoresist. meas. 79—69680
  $Pd_{1-y}Cr_yH_x$, resistive Kondo behaviour as function of Cr and H conc. 80—59971
  $PdFe_{1-x}Cr_x$ ordering alloys, elec. resist., temp. depend. *(Russian)* 80—24866
  Pt-Cr, dil., appearance of mag. order for Cr impurities in exchange enhanced hosts 79—4690
  Pt-Cr, dil., elec. resist., 7.4 to 300K, anomalous temp. depend. associated with cond. electron scatt. 79—73491
  Pt-Cr, dil., surface segregation, equilib. surface composition, AES meas. 77—85039
  Pt-Cr, disordered, atomic order-disorder transform. effect on resist. min. 80—65911
  Pt-Cr, elec. resist. meas. through percolation limit, mag. order onset 77—69298
  Pt-Cr, grain boundary permeation 79—65253
  Pt-Cr, shallow silicide contact 80—70819
  Pt-Cr (0.3 and 0.5 at.%) anomalous resist. associated with conduction-electron scatt. from Cr impurities 79—99530
  Pt-Cr dil. alloy, 0.5 at.%, ^{195}Pt NMR for local mag. susceptibility 78—84484
  PtCr, AC susceptibility near percolation limit, ordered and disordered alloy 80—65900
  Pt_3Cr, ferrimag., magnetisation density, polarised neutron diffr. meas. 80—60204
  Pt_3Cr, Ll_2 ordered alloy, positive temp. depend. on strength, phase destabilization 80—81203
  $Pt_{0.75}(Cr_{1-x}Mn_x)_{0.25}$, pseudobinary, magnon energy derivation 80—107996
  $Pt_3Mn_xCr_{1-x}$ alloys, mag. props. 80—2562
  $Pt_3Mn_xCr_{1-x}$, electronic specific heat meas. comparison with band model calcs. 80—54400
  Rh-Pd-Cr, dil. alloy, mag. moment 78—95416
  Si-Cr, dil., spin density wave under high press., neutron diffr. study 80—65798
  Si-Ti-Cr system, plasma coating on Nb, alloy substrates, radiating power 79—60529
  $Sm_{1-u}Ce_u(Co_{1-x-y-w}Fe_xCu_yCr_w)_7$, permanent mag., improved mech. props. 79—87593
  $Sm_2(Co,Cr)_{17}$, exchange and crystal field parameters, anisotropy meas. 77—69535
  $Sm_2(Co_{1-x}Cr_x)_1$ 77—40054
  $Sm_2(Co_{1-x}Cr_x)_{17}$, bulk magnetisation and magnetocryst. anisotropy, interpretation 77—40055
  $Sm_2Co_{17-x}Cr_x$, effect of substitution on mag. props. 79—78363
  $Sm_2(Co_{0.8}Fe_{0.14}Mn_{0.04}Cr_{0.02})_{17}$, sintered, hard mag. props. 77—8340
  steel, austenitic stainless, 18 Cr-11 Ni, effect of boron on nucleation of $M_{23}C_6$ carbides *(Polish)* 78—84808
  steels, Cr-C-Mn(Ni), struct. prop. rel., design of struct. steels for high strength and toughness 80—97491
  Ta-Cr (15 wt.%), solid soln., discontinuous precipitation *(German)* 80—45314
  Ta-Cr-Si-Al, heat resistive films, prepared by sputtering, lifetime meas. 80—80132
  Te-Cr, dil. liq. alloy, elec. cond. at high temp. and press. 78—87959
  Th-Cr, supercond., press. meas. to 20 kbar 80—88667
  $(Ti,Cr)B_2$, sintering kinetics and props. 80—100811
  Ti alloy VT3-1, large forgings, heat treatment, struct. and mech. props. 78—52864
  Ti-Al-Cr, thermomechanical treatment effect on mech. props., strengthening mechanisms 80—55441
  Ti-Al-Cr-Fe-Si alloy AT6, and weldments, mech. and corrosion props. 77—90409
  Ti-Al-Cr-Mo (6, 2.0, 2.5 wt.%), microstructural changes and mech. props. 77—25080
  Ti-Al-Cr-Mo alloy VT3-1, reactions with some refractory compounds 80—16585
  Ti-Al-Cr-Mo system, VTZ-1 alloy, microstruct. influence on fatigue characts. 80—3195
  Ti-Al-Cr-Mo-Fe(V)(Zr), effect of structure and heat treatment on tensile strength, ductility, fatigue limit and notch sensitivity 78—56711
  Ti-Al-Cr-Mo-U, alloy VT22, phase composition and fatigue strength 78—3219
  Ti-Al-Cr-Mo-V, alloy VT22M, exam. of ageing and phase transitions *(Russian)* 79—11641
  Ti-Al-Cr-Mo-V, VT22 alloy, metastable β-phase decay under continuous heating, plastic strain effect *(Russian)* 80—71656
  Ti-Al-Cr-Mo-V alloy VT-22, effect of heating rate on phase recrystallisation *(Russian)* 79—34077
  Ti-Al-Cr-Mo-Zr hard alloy VK15, shot blasting in strength improvement 77—81272
  Ti-Al-Mo-Cr, weldment containing orthorhombic martensite, auto-tempering behaviour and alpha precip. strengthening 80—84976
  Ti-Al-Mo-Cr (4.5, 5, 1.5 wt.%), CORONA-5, effect of microstructure and heat treatment on fracture 78—60805
  Ti-Al-Mo-Cr (4.5, 5, 1.5 wt.%), weld metal, α/β interace sliding 80—108512
  Ti-Al-Mo-Cr-Fe, distrib. of Sn, Zr between phases, temp effect. 80—55357
  Ti-Al-Mo-Cr-Fe, effect of heating on thermal stability of phases, lattice constants and chem. comp. 78—56672
  Ti-Al-Mo-Cr-Fe (6.4, 2.7, 1.6, 0.4 wt.%), quenched VT3-1, decomposition kinetics of α'' and β in annealing *(Russian)* 77—66662
  $\alpha+\beta$-Ti-Al-Sn-Zr-Mo-Cr, low cycle fatigue crack nucleation and early growth 79—8354
  Ti-Al-V-Cr, electrochemical behaviour under tensile stress in boiling H_2SO_4 and acidic chloride solns. 78—95851
  Ti-Al-V-Cr-Mo-Zr (3,8,6,4,4 wt.%), beta-C, microstruct. effect on mech. props. 78—27577
  Ti-Al-V-Cr-Zr-Mo (3, 8, 6, 4, wt.%), phase transforms. 79—100113
  Ti-Al-V-Cr-Zr-Mo-Fe (3.4, 8.3, 5.8, 3.9, 4.2, 0.06 wt.%), shock loaded, residual strength 77—36589

chromium alloys continued
  Ti-Cr, diffuse electron scatt. *(Russian)* 80—103438
  Ti-Cr, dilute, superconducting transition temp. and mag. susceptibility 78—47899
  Ti-Cr, eutectoid decomposition 79—24491
  Ti-Cr, H_2 diffusion at room temp. *(Japanese)* 80—19987
  Ti-Cr, interaction with N_2 at elevated temp., nitridation behaviour 77—12742
  Ti-Cr, phase transformation, appl. of Philips STEM400 system 80—25689
  Ti-Cr, sintered, friction and wear, structural factors 78—60843
  Ti-Cr (15 at.%), aged omega phase, electron microscope exam. 78—72783
  Ti-Cr (6 wt.%), alpha precipitation kinetics 78—68697
  Ti-Cr disordered alloy, gap nature of electron spectrum in region of struct. instability *(Russian)* 78—18947
  Ti-Cr-B system, self-propagating high temp. synthesis, crystallochemical and mech. props. 80—20861
  Ti-Cr-Zr, martensite formation, chemical composition effect 80—50634
  Ti-M-V-Cr-Mo, RMI 38644, shock loaded, age hardening 79—29112
  β-Ti-Mo-Cr-Al (8, 4.5, 2.5 wt.%), metastable, tensile ductility, α-phase morphology and distrib. effect 77—86098
  Ti-Mo-Fe-Cr-Al, alloy VT3-1, influence of constitution on fracture toughness *(Russian)* 77—77559
  Ti-Mo-V-Al-Cr-Fe (4.8, 4.7, 5.2, 1.1, 1.0 wt.%), structural changes during heating up to 1000°C, DTA study *(Russian)* 80—93552
  Ti-V-Cr, BCC, press. derivatives of elastic moduli, Fermi surface topological changes, band struct. 79—61639
  Ti-V-Cr, electron-lifetime effects on props. 80—10951
  Ti-V-Cr, type Ti-15-333, irrad. induced creep 80—39163
  Ti-V-Cr-Al (13, 11, 3 wt.%) alloy spring wire, torsional fatigue props. 77—77649
  Ti-V-Cr-Al (13, 11, 3 wt.%), stress corrosion cracking in methanolic solutions 80—50752
  Ti-V-Cr-Mo, fracture resistance at low temps. 80—104284
  Ti-V-Mo-Cr system, β-phase stability 80—55353
  Ti-Zr-Cr-Mn/$LaNi_5$ hydriding alloy mixtures for H energy storage 80—45788
  $Ti(Al_xCr_{1-x})_2$, $0<x<0.4$, influence of Al on H sorption props. X-ray cryst. struct. determ. 79—28198
  TiC-(Mo-Cr-Ni-Mn) steel alloy, optimum comp. and manufacture conditions, Mn effect 80—84896
  TiC-Fe-Cr powder mixture, exam. of milling condition effects 80—16237
  TiC-Ni-Co-Cr, sintered, mech. props. effect of processing factors 78—11159
  TiC-Ni-Cr, hard alloy mixtures, pressing 77—63596
  TiC-steel composite, effect of method of Cr additions on props. 78—15341
  $TiCr_{1.8}$, H and D soln., enthalpy, solubility and mol. vibr. determ., comparison with soln. in metals and binary alloys 80—79951
  $TiCr_2$, mechanism of mixing and reactive diffusion 79—7706
  $Ti_{1-x}Zr_xCr_{2-y}Mn_y$, C14 type alloy, hydride form. *(Japanese)* 78—19944
  $Ti_{1-x}Zr_xMn_{2-y-2}Cr_yV_2$, hydrogen storage appl. *(Japanese)* 80—61443
  U-Cr, absolute thermoelec. power values 77—20303
  U-Cr metallic glasses, glass form. and thermal stability 80—75183
  U-Cr-Al (0.2, 0.1 at.%) fuel elements with high swelling resistance for KS-15O reactor 78—78471
  UO_2 pellets-graphite-Zircaloy cladding, evaluation of graphite lubrication 80—32342
  V-Cr, and V-Nb-Cr, supercond. crit. temp. and crit. field, Cr alloying effect 77—85375
  V-Cr, diffusion in H_2 *(Japanese)* 78—10221
  V-Cr, effect of alloying additive on thermoelectric props. 77—35927
  V-Cr, elastic moduli, comparison with paramag. Cr, Ti-V, rel. to band-structure 80—7615
  V-Cr, elastic moduli, US pulse echo meas. 78—84881
  V-Cr, electronic density of states, temp. depend. of elec. resist. and mag. susceptibility 77—11891
  V-Cr (15 wt.%), fusion reactor struct. alloys, dual-ion irrad. effects 79—45403
  V-Cr (15 wt.%), radiation-induced solute segregation 80—29086
  V-Cr (wt.%), 3.5 MeV $^{51}V^+$ irrad. induced void swelling and solute segregation 79—7637
  V-Cr alloys, absorption of H_2, thermodynamic parameters 78—87862
  V-Cr amorphous films, supercond. transition temp. 79—60953
  V-Cr-H system, electronic sp. ht. 80—49378
  V-Cr-Ti, fusion reactor first wall structural materials, prediction of life limiting props. 78—62605
  V-HfV_2-$HfCr_2$-Cr, phase diagram *(Russian)* 77—52288
  V-Mn-Cr, disordered BCC state, mag. phase diagram, mag. and elec. props. 77—63185
  V-Nb-Cr (20,5wt.%), corrosion in liquid Na, O_2 effects 77—8987
  $V_{3-x}Cr_xGa$, cryst. struct. and microhardness meas. 79—86740
  $V_{75-x}Cr_xGa_{25}$, supercond. transition temp. and electron-phonon coupling parameter 79—60952
  $(V_{1-x}Cr_x)_3Si$, elastic moduli, 4.2 to 290K, softening near supercond. transition *(Russian)* 80—92582
  $(V_{1-x}Cr_x)_3Si$, mag. susceptibility, 4.2 to 320K, density of states model 80—7035
  $(V_{1-x}Cr_x)_3Si$, single cryst., elec. resistivity, temp. depend. 79—56193
  $V_{3-x}Cr_xSi$, $x=0$ to 3, struct., supercond. and mag. props. 80—1962
  V_3Si-Cr solid soln., supercond. T_c and paramag. susceptibility *(Russian)* 77—59348
  Vitallium, orthopaedic implant material, metallurgical cond. effect on pitting resistance 79—70704
  W fibre reinforced Cr alloy, reactivity of Y_2O_3 protective film 79—100297
  W fibre reinforced Ni-Cr (20 wt.%), hot pressing kinetics 78—35334
  W-Cr alloys, segregation of Cr to gain boundaries, field ion microscope investigation 77—8816
  W-Cr powder alloys, sintering in presence of Cu-Ni liq. phase 80—16246
  W-Cr solid solution, precipitation behaviour, reaction front motion, lattice parameters *(German)* 80—55401
  W-Cr-Pd, Pd effects on diffusion 77—24445
  W-Ni-Cr, high-temp. phase diag. *(French)* 77—48393
  W-Ni-Cr, structural characterisation *(French)* 77—56074
  W-Re(Mo)(Cr), powder mixture, activating effect of Group VIII metals on alloy form. during sintering 77—59728
  $Y_2(Co_{1-x}Cr_x)_{17}$ 77—40054

chromium alloys continued
$Y_2(Co_{1-x}Cr_x)_{17}$, bulk magnetisation and magnetocryst. anisotropy, interpretation 77—40055
$Y_2(Co_{1-x}G_x)_{17}$, bulk magnetisation and magnetocryst. anisotropy, interpretation 77—40055
Zircaloy-4, deformation behaviour between 77 and 900K 80—71686
Zircaloy-4, vapour transport of Zr and Si 80—55437
Zn-Cr, dil., mag. anisotropy, 0.001 to 2K 78—68157
Zn-Cr, dil., mag. anisotropy, Hartree-Fock calcs. 80—11162
Zn-Cr, dil., mag. anisotropy below 1K, low field magnetisation meas. 80—20382
Zn-Cr, Kondo alloys, spin and phonon resistivity independ. 78—47777
Zr-Al-Cr H sorption props. for H storage, influence of Al 80—45794
Zr-Cr, role of oxide plasticity in oxidation behaviour 77—36680
Zr-Cr (1.9 wt.%), β-quenched and tempered, optical and TEM study 79—66061
Zr-Cr (1.9 wt.%), β-quenched and tempered, $ZrCr_2$ precipitation, TEM study 79—66062
β-Zr-Cr (1.9 wt.%), decomposition 79—87604
Zr-Cr-B system, self-propagating high temp. synthesis, crystallochemical and mech. props. 80—20861
Zr-Cr-Cu, phase diagram in Zr corner *(Russian)* 78—19721
Zr-Cr-Fe, irradiation damage, metallurgical struct. effect 77—51412
Zr-Cr-H, synthesis at high H pressure exam. of props. 80—29924
Zr-Nb-Cr (0.5, 0.5 wt.%), TEM study on intermetallics in Zr alloys 79—11622
Zr-W-Cr, Zr-rich corner of phase diag. *(Russian)* 78—80517
$Zr(Co_xCr_{1-x})_2$, H absorption and desorption props. 77—55448
$ZrCr_2$, $Zr(Cr_xFe_{1-x})_2$ and $Zr(Cr_xCo_{1-x})_2$, mag. props. H absorpt. effect 80—88821
$Zr(Cr_xCo_{1-x})_2$, Laves phase, phenomenological model for H_2 absorption capacity 77—84935
$ZrCr_2D_x$, site occupation modes and cryst. struct., neutron diffr. study 80—59440
$Zr(Cr_xFe_{1-x})_2$, Laves phase, phenomenological model for H_2 absorption capacity 77—84935
$Zr(Cr_xM_{1-x})_2$ (M=Fe, Co), H_2 absorpt. capacity 80—88433
$Zr(Fe_xCr_{1-x})_2$, H absorption and desorption props. 77—55448

chromium compounds
see also chromium alloys
acetylacetonate, Mrad range dosimeter appls. 77—16997
alkali halide:CrO_4^{2-}, frozen solns., absorption spectra, 4.2-300K 79—87467
alkali metal triple orthoarsenates, $KM^{II}Cr_2(AsO_4)_3$ and $NaM^{II}Cr_2(AsO_4)_3$, prep. by high temp. synthesis, and cryst. struct. 79—66028
trans-bis(N-1alkyliminodiacetato)-chromate(III) complexes, luminesc. spectra 80—1020
carbides, oxidation of H_2 80—104462
chalcogenide spinel, magnetic semiconductors, physical props. and possible applications 78—2474
chalcogenide spinels, $ACr_{1.9}Sn_{0.1}X_4$, Sn hyperfine interactions 80—15485
chalcogenide spinels, specific heats 79—11315
chalcogenide spinels, thermal stability, thermochemical, thermodynamic and crystallochemical props. 77—51519
chromate coatings, corrosion-protective, on Al, charact. 79—47798
chromite, carbothermic reduction 79—61900
chromites, reduction to ferrochromium in methane-H_2 gas mixtures 77—60109
chromium formate, mol., Hartree-Fock instability of SCF wavefunctions 80—9492
chromium phosphinate polymer, one-dimensional antiferromagnet, spin-flop 80—50131
chromocene, heat capacity meas., phase transitions 78—38853
$CoCr_2S_4$ films, galvanomagnetic and thermoelec. props. 80—54717
complex in borate glass, ESR study of effect of glass composition on symmetry 80—88052
complexes, NMR study ^{31}P chemical shift, substituents electronegativity steric hindrance and π-bonding effect 80—95651
Cr_20_3, pure, hydrothermal reactive sintering 77—36431
$Cr_2P_6O_{18}$, X-ray cryst. struct. determ. *(French)* 77—80452
$CrCl_2$:NO_2^-, aqueous solns., luminesc., absorpt. and Raman spectra *(Russian)* 77—36291
dibenzene chromium, heat capacity meas., phase transitions 78—38853
dibenzenechromium, cryst. and soln., dynamic struct., NMR expts. 77—15328
dichromate solutions for low-level dosimetry 79—29633
ferrites, polycryst., X-ray diffr. struct. anal., chem. anal. *(German)* 77—72598
intercalation cpd., NMR 77—90048
(iron, chromium) carboxylates, heteronuclear trimer exchange clusters, ESR spectra 80—80603
magnesite-chromite powder, exam. of rheological characts., compaction 78—60628
methylammonium alums, dielec. relax. near transition point 80—71301
methylammonium chromium alum, single cryst., Cr^{3+} EPR, g-factor, hyperfine splitting 78—2729
methylammonium chromium selenate, lattice consts. and ferroelec. props. 79—33641
methylammonium chromium selenate dodecahydrate crystals, dielectric relaxation 80—40043
$MgAl_2O_4$-Cr_2O_4, vaporization 79—99308
mol. consts. and mean vibr. amplitudes calcs. 80—106318
oxide, catalysis of graphitisable C graphitisation 80—89166
oxides, AES meas. 77—36323
oxides, XPS study, electron binding energies, spin orbit splittings, exchange splittings 79—78839
periclase-chromite blocks, produced from beneficiated starting materials, struct. and props. 79—87600
phosphates, $MCrTi(PO_4)_3$, M=Mg, Mn, Co, Ni, Zn, Cd, Pb, Ca, Sr, Ba, cryst. struct. *(French)* 77—84708
3p photoelectron spectra, light-inuced changed in multiplet satellites 80—80946
plasmon refl., 86 to 320K 80—50346
quartz ceramic, SiO_2-Cr_2O_3-TiO_2, creep and porosity, for ceramics with different structures 80—21011
refractory carbides, borides and nitrides, wetting by and interactions with liq metals 80—54473
spinelides, effect of cation distribution on Mossbauer spectra parameters 79—8082

chromium compounds continued
steel, stainless, Cr-Ni (18,10 wt.%) Ti stabilised, cavitation failure, relationship of corrosive and erosive factors *(Russian)* 77—16722
tetraphenylporphyrin, reson. Raman spectra, excitation profiles, nucl. distortion and Jahn-Teller effects 77—58018
triphenylphosphine compounds, $(C_6H_5)_3PM_xM'_{1\;x}(CO)_5$, M,M'=Cr, Mo, W, mixed cryst., CO vibr. spectra, modal anal. 78—35128
XPS and K-emission, multiplet struct. 77—63527
$AgCrX_2$, X=S, Se, EPR meas., g-factors, effective mag. moments, and dipolar shifts 79—8043
Al_2O_3:Cr_2O_3, dopant influence on struct. and mech. props. 80—24471
Al_2O_3:$CrCl_3$, calcination, mag. and optical studies of CrO_n 79—24736
Al_2O_3-Cr_2O_3, microstrain correction 78—59852
Al_2O_3-Cr_2O_3, solid soln., thermal expansion anisotropy, lattice consts. 80—54411
Al_2O_3-Cr_2O_3 melt, exam. of surface tension and density 79—1541
Al_2O_3-Cr_3, surface spark discharge, channel spreading and substrate vaporisation 77—89336
Al_2O_3-MgO-Cr_2O_3, effect of Cr_2O_3 on surface grain growth 79—23815
Al_2O_3-SiO_2-MnO-Cr_2O_3-B_2O_3 system, additive in sintering of high-alumina ceramic 79—61544
$AlPO_4$-Cr_2O_3, system, oxyorthophosphates form. 79—78942
B-C-Cr, paramagnetic centre struct. and defect form. 80—66034
$Ba_2MgCr(PO_4)_3$, cryst. data 77—39564
BaO-TiO_2-Cr_2O_3, new compound, phase relations *(Japanese)* 78—6911
C_2O_3:$^{125}Te^{6+}$, mag. hyperfine interactions, Mossbauer study *(French)* 79—24247
$CaCrO_4.H_2O$, cryst. struct. *(French)* 78—18593
CaO-MgO-Al_2O_3-Cr_2O_3-Fe-O_2-SiO_2 system, exptl. determ. of periclase and spinel comps. 78—6906
CaO-MgO-Cr_2O_3-Al_2O_3-ZrO_2-SiO_2 system, subsolidus region characts. 80 -97466
$Ca_5(PO_4)_3F$:Cr^{5+}, ESR, polymorphic transform., spin Hamiltonians 77—36117
Ca_3SiO_5-Cr_2O_3 solid solns., elec. cond., 800-1000°C, hydration 80—54683
$Cd_{1-x}Ag_xCr_2Se$, ferromag., magnetoresistance exam. *(Russian)* 78—84238
$CdCr_2S_4$, $CdCr_2Se_4$, variation of elec. props. with chalcogen content of gas phase, 500-700°C 77—20310
$CdCr_2S_4$, EPR line profiles in paramag. and ferromag. phases 79—28602
$CdCr_2S_4$, ferromagnetic semiconductor films, prep. and props. *(Japanese)* 79—47308
$CdCr_2S_4$, magnetic semicond., resonance Raman scatt., mag. circular polarisation props. 80—50341
$CdCr_2S_4$, phonon Raman scatt., mag. circular polarization effects 79—8134
$CdCr_2S_4$, polycrystalline films, mag. semicond., spinel-type, magneto-optical effects *(Japanese)* 79—47415
$CdCr_2S_4$, single cryst. prep. and elec. props. 79—38727
$CdCr_2S_4$:Ag, mag. semicond., ferromagnet resonance angular and temp. depend. 79—69730
$CdCr_2S_4(Se_4)$, ferromagnetic semiconductors, spinel-type, resonance Raman scattering and electronic structure *(Japanese)* 79—47421
$CdCr_2S_4(Se_4)$, spin depend. phonon Raman scatt., band struct. 78 68491
$CdCr_2S_4(Se_4)$, spontaneous magnetisation temp. depend., nuclear resonance freq. depend. *(French)* 80—80483
$CdCr_2S_{4-x}Se_x(O_x)$ X=0, 4, and solid solns., imperfect struct. model from cryst.-chem. investigs. 79—42053
$CdCrSe_4$, ferromag. semiconductor, mag. props. near Curie pt., doping effects 79—1670
$CdCr_2Se_4$, crit. behaviour near Curie point 78—31068
$CdCr_2Se_4$, crit. behaviour of optical absorption edge 78—35143
$CdCr_2Se_4$, deviation from Kittel's mag. resonance formula near T_c 79—87322
$CdCr_2Se_4$, energy band struct calc. by augmented plane wave method 80—103621
$CdCr_2Se_4$, energy structure, magnetooptic effects 80—71394
$CdCr_2Se_4$, ferromagnetic low anisotropy semicond., spontaneous magnetisation RF determ. 80—22396
$CdCr_2Se_4$ films, mag. hysteresis, domain struct., mag. viscosity 80—25169
$CdCr_2Se_4$, mag. semicond., domain struct. by IR Faraday effect 79—95604
$CdCr_2Se_4$, magnetic red shift origin, specular reflectivity, band struct. 80—40127
$CdCr_2Se_4$ magnetic semiconductor, photoinduced centre kinetics 80—71110
$CdCr_2Se_4$, modulated piezoreflection spectra 80—97237
$CdCr_2Se_4$, narrow conduction band, crit. behaviour of resistivity 79—78096
$CdCr_2Se_4$, optical reflectivity, dielectric const. by expt. data Kramers-Kronig anal., spinel struct. 79—99903
$CdCr_2Se_4$, photoferromag. effect quenching, photocond. 78—68488
$CdCr_2Se_4$, photoinduced infra-red optical absorption 78—23455
$CdCr_2Se_4$, reactor radiation influence on ferromagnetic phase transform. *(Russian)* 80—75760
$CdCr_2Se_4$, refr. index variation in strong alternating mag. field 80—23741
$CdCr_2Se_4$ single cryst., photocond. in air, vacuum, mechanism 77—8138
$CdCr_2Se_4$, single crysts., mag. semicond., spinel-type, magneto-optical effects *(Japanese)* 79—47415
$CdCr_2Se_4$, spin system heating by drifting current carriers, magnon-phonon system energy transfer *(Russian)* 80—29541
$CdCr_2Se_4$, velocity-field characts., above T_c 78—64049
$CdCr_2Se_4$:Ag, magneto-electrical props. temp. behaviour depend. on dopant conc. *(Russian)* 80—11006
p-$CdCr_2Se_4$:Ag, oscillatory magnetoresist., temp. and mag. field depend. 78—52011
$CdCr_2Se_4$:Ag(Gd), doping effects on exchange interaction 78—43579
$CdCr_2Se_4$:Cu, elec. props., temp. depend. *(Russian)* 78—72181
$CdCr_2Se_4$:Ga(In), photoconductivity, photomagnetoresistance near Curie point *(Russian)* 80—100485
$CdCr_2Se_4$:In(Ga), elec. resist. and magnetoresist., 2 to 200K 80—96876
$CdCr_2Se_4$:In(Ga), temp. driven metal-semiconductor transition, temp. and mag. field depend. *(Russian)* 78—88003
$CdCr_2Se_{4\;x}S_x$, influence of anion substitution on red shift of optical absorption band edge 77—32399
$CdCr_2Se_4(S_4)$, ESR line intensity near Curie point 78—64269

chromium compounds continued
CdCr$_2$Sr$_4$, press. depend. optical aborption edge shift and compressibility 79−28714
Cd$_{1-x}$Cu$_x$Cr$_2$Se$_4$ solid solution, spinel struct., X-ray investigation 79−78940
Cd$_{1-x}$Fe$_x$Cr$_2$S$_4$, single cryst., mag. semicond., spinel-type, magneto-optical effects *(Japanese)* 79−47415
(Co,Cr,Fe)$_3$O$_4$ film magnetooptical switch for synchronization of CO$_2$ and red laser beams 80−58615
Co complex, metal-metal bond, correl. effects, SCF calc. 77−65425
CoCr$_2$S$_4$, Faraday effect, appl. to CO$_2$ laser systems, radiation damage resist. 78−95579
CoCr$_2$Te$_4$, cryst. growth, struct., elec. props., Hall effect 78−43416
CoO-MgO-Al$_2$O$_3$-Cr$_2$O$_3$-TiO$_2$, form. and colour of spinel solid soln. *(Japanese)* 77−32550
CoO-MgO-Cr$_2$O$_3$-Fe$_2$O$_3$-TiO$_2$, form. and colour of spinel solid soln. *(Japanese)* 80−16059
CoO-ZnO-Al$_2$O$_3$-Cr$_2$O$_3$-TiO$_2$ system, form. and colour of spinel solid soln. *(Japanese)* 77−25001
(Cr,Al)$_2$O$_3$-ZrSiO$_4$ refractories, glass resist. and corrosion mechanism 79−61757
trans-Cr (III)(NH$_3$)$_4$XY complexes, d-d irradiation preferential labilisation, Adamson's rules, ang. method overlap 77−40557
Cr complex, $(-)_D$-tris(ethylenediamine) chromium (III), solid-state circular dichroism spectra, phase modulation spectrosc. obs. 80−93271
Cr complex, [Cr$_3$(CH$_3$COO)$_6$(OH)$_2$]Cl.8H$_2$O, mag. sp. ht. *(Japanese)* 79−33501
Cr complex, [Cr(NCS)$_{6-n}$(DMSO)$_n$]$^{n-3}$, phosphorescence spectra, decay times 78−10970
Cr complex, bis(ethylbenzene) chromium, thermal degradation, high purity Cr production *(Russian)* 80−35128
Cr complex, carboxylate-Cr (III), surface alignment of liq. cryst. 80−1924
Cr complex, Cr (III) acetyl acetonate, orientation in vitrified liq. cryst., ESR meas. 77−16152
Cr complex, Cr^V, doping agent for polarised targets 78−46198
Cr complex, Cr(V)-dimethylformamide, proton dynamic polaris. and relax. 78−91988
Cr complex, Cr(V)-fluoroorganics, proton and ^{19}F dynamic polaris. and relax. 78−91989
Cr complex, Cr(acac)$_3$, paramag. relax. reagent, effect on ^{15}N NMR chem. shifts in pyridenes 78−15042
Cr complex, dimer di-μ-diphenylphosphinatoacetylacetonatochromium(III), EPR of exchange coupled Cr^{3+} pairs 78−88172
Cr complex, dinuclear, exchange interactions, neutron inelastic scatt. obs. 77−55502
Cr complex, influence of anisotropy of spin-Hamiltonian parameters on EPR spectra *(Russian)* 77−28432
Cr complex, organic mol. singlet excited state energy transfer to complex quartet levels 77−25291
Cr complex, tetrakis (formamidinato) dimetal, formation 77−77753
Cr complex, trimeric clusters, low temp. mag. props. 78−76261
Cr complex, tris(2,2′-bipyridine)Cr(III), excited states, Raman spectra 80−97263
Cr complex, trivalent dimer, mol. electronic excitations, neutron inelastic scatt. 77−47985
Cr complexes, [Cr(H$_2$O)$_x$(NH$_3$)$_{6-x}$][Co(CN)$_6$], $x=1,2$, hydrogen bonding *(French)* 77−42437
Cr complexes, circ. dichroism of Cr(III) complex d-d transitions *(Japanese)* 78−13555
Cr complexes with glycilglycine, structure, optical, e.p.r. and mag. investig. 77−1103
Cr complexes with tissue, EPR detect. 77−9310
Cr spinellide, acid extracted, phase transform. on heating in air *(French)* 79−96003
Cr^{3+} complex ions, diffusion coeffs. meas., computer-assisted technique using Cottrell eqn. 80−3425
Cr/Cr$_2$O$_3$, relative chemical potential of oxygen *(German)* 78−31642
Cr-C, deposited by hollow cathode discharge, characterisation 78−11371
Cr-Co complex, [Cr(OCN$_2$H$_4$)$_6$][Co(NH$_3$)$_2$(NO$_2$)$_4$]$_3$.3H$_2$O, cryst. struct. 80−6392
Cr-Co-P, phase diagrams, lattice constants of phosphides 78−44099
Cr-Cr$_2$O$_3$, black, solar selectivity at average temps. (100 to 250°C) *(French)* 80−55899
Cr-Cr$_2$O$_3$, black chrome, solar absorptance of high temp. selective absorbers 80−101131
Cr-Cr$_2$O$_3$, black chrome films, surface microstruct. rel. to optical props. in solar absorbers 79−52036
Cr-Cr$_2$O$_3$, black chrome solar selective absorber, microstruct. 79−56875
Cr-Cr$_2$O$_3$, black chrome electroplating for solar energy photothermal conversion, prep. and struct. 79−74544
Cr-Cr$_2$O$_3$, black chrome electroplating for solar energy photothermal conversion, optical props. 79−74545
Cr-Cr$_2$O$_3$, black chrome electrolytic coatings for solar collectors 80−94100
Cr-Cr$_2$O$_3$, chrome black, electroplated selective surface, thermal emittance, solar absorpt., refl., and roughness 79−79406
Cr-Cr$_2$O$_3$ black, electroplated solar collector coatings, high temp. optical and struct. degradation 80−66995
Cr-Cr$_2$O$_3$ black chrome, commercial, solar absorber coating characterisation 80−80111
Cr-Cr$_2$O$_3$ black solar absorber surfaces, microstruct. rel. to electroplating parameters 80−61418
Cr-Fe-O, rutile type oxides, obtained from thermal decomp. of Cr$_{1-x}$Fe$_x$.OOH, Curie temp. and saturation magnetisation 79−24740
Cr-Ge, thermophysical props., at elevated temp. 80−103493
Cr-Ge system, phase anal. and physical props. 79−24160
Cr-Mo compound, susceptibility to thermal embrittlement 77−21458
Cr-Mo-N system, at high-pressure, temp., X-ray anal., phase diagram 80−50607
Cr-N, deposited by hollow cathode discharge, characterisation 78−11371
Cr-Ni-O, computer-assisted anal. and calcs. of phase diagrams 80−25667
Cr-S system, mag. props. *(Japanese)* 77−43825
Cr-S system, phase diagram exam. between 873 and 1364K 78−3105
Cr-Te system, NMR meas., effect of heat treatment 78−27112
Cr(AcAc)$_3$, use as relax. agent, in ^{13}C NMR intensity meas. 77−51981
CrAl$_3$Cl$_{12}$, gas, mol. struct., ligand field spectrum *(German)* 78−37762
α-Cr$_x$Al$_{2-x}$O$_3$ solid soln., catalysis of H-D exchange 77−52631
CrAl$_2$S$_4$, thermodynamic stability, enthalpy of form. 79−52737
CrAs, antiferromag.-paramag. transition up to 5 kbar 79−87256

chromium compounds continued
CrAs, heat capacity, enthalpy increments, thermodynamic props., 5 to 1280K 78−91450
CrAs, high press. paramag. antiferromag. transitions, elec. props., band model development *(Russian)* 80−60277
CrAs, mag. transition under press., volume striction mechanism 77−24696
(Cr$_3$AsO$_{13}$)$^{3-}$, condensed anion, obs. in (NH$_4$)$_2$HCr$_3$AsO$_{13}$ *(French)* 79−1415
CrAs$_{0.42}$Sb$_{0.58}$, mag. and struct. transitions under press., elec. resist. meas. 78−27038
CrB, crystallographic relationship with αMoB, UBC, ThBC 79−42025
CrB$_2$, CrB, and Cr$_5$B$_3$, mag. and thermal props. at low temps. 80−20385
CrB$_2$, crystal growth by floating-zone method, elec. and mag. props. 77−1801
CrB$_2$, electrodeposition mech., onto metal electrodeposit, cermet prop. 79−33992
CrB$_2$, helical mag. struct., neutron diffr. meas. 77−85425
CrB$_2$, itinerant antiferromag., sping fluctuations, NMR study 80−108119
CrB$_2$, NMR of ^{11}B meas. 78−56397
CrB$_2$, RF sputtered, comp. by XPS 78−51839
CrB$_2$, reactions with Ti-Al-Cr-Mo alloy VT3-1 80−16585
CrB$_3$, crit. spin-relax. in hard mag. direction 78−72390
Cr$_3$B$_7$O$_{13}$Cl, cubic, approx. nonlinear optical susceptibility 80−78904
Cr$_3$B$_7$O$_{13}$Cl, ferroelec. 43m-mm2 phase transition, molar heat capacity meas. 80−93249
Cr$_2$BeO$_4$, magnetoferroelectricity, weak pyroelectric effect 79−42914
CrBr$_2$, ferromag. domains, using liq. He mag. specimen stage 80−103855
CrBr$_3$, anisotropic, ferromag., temp. depend. of one-magnon light scatt. 77−90161
CrBr$_3$ anisotropic ferromagnet. crit. mag. relax., field and temp. depend. 79−1717
CrBr$_3$, Brillouin-Mandelstam scattering from thermal and excited magnons 80−70980
CrBr$_3$, HF spectra, susceptibility, spin waves in domain walls *(Russian)* 80−80909
CrBr$_3$, modulation of exchange integral, contrib. to temp. depend. of exchange interaction 77−69484
CrBr$_3$, parametric representation of the equation of state of a Heisenberg system in the critical region 78−79741
CrBr$_3$, reflectance and thermoreflectance meas. 77−24866
CrBr$_3$, reflectance and thermoreflectance spectra in paramag. and ferromag. phases 79−56770
CrBr$_3$, self consistent band struct., intersecting spheres model 79−37985
CrBr$_3$, thick crystal, magneto-optical imaging of domain struct., multiple diffr. 77−8552
CrBr$_3$, two-dimensional mag. insulator, cryst. field splitting, spectroscopic g-factors 79−47059
CrBr$_3$, two-dimensional mag. insulators, cryst. field spectra, mag. circular dichroism 79−47058
CrBr$_3$, XPS, satellite of Br 4s line 78−56556
CrBr$_4$, Raman spectra, struct. and thermodynamic functions 78−60443
CrC electrophoretic coating, electric field strength effect on deposition rate 78−19677
CrC, plasma sprayed coating 78−68835
CrC, precipitates in Ni-base superalloy, STEM microanal. 80−81067
CrC$_x$, electrophoretic coating deposition on coaxial surfaces 78−11528
Cr$_2$C$_3$, reactively sputtered solar selective absorbers for all-glass tubular evacuated collectors, absorptance and emittance 80−101132
Cr$_3$C$_2$ (Cr$_7$C$_3$) based coatings, detonation deposited, wear resist., 20-1000°C 80−11843
Cr$_3$C$_2$, bond energy and ionization efficiencies from SIMS 79−24400
Cr$_3$C$_2$, Cr$_{23}$C$_6$, plasma sprayed coatings for gas-cooled reactor appl. 79−24676
Cr$_3$C$_2$ fibre reinforced Ni-based composite, oxidation and creep, Y additions effect 80−66685
Cr$_3$C$_2$, final-state effects in C Auger spectra 78−6818
Cr$_3$C$_2$, form. from Cr$_2$O$_3$/graphite mixture in H$_2$ atmos. *(Japanese)* 78−92225
Cr$_3$C$_2$ formation in C surface during Cr$_2$O$_3$ dissociation in presence of C *(Russian)* 80−35570
Cr$_3$C$_2$, on Cr, mechanism of high-temp. oxidation, 1050 to 1100°C *(Russian)* 79−20226
Cr$_3$C$_2$, plasma sprayed wear resistance coating, exam. of wear behaviour 20 to 1000°C 80−16487
Cr$_3$C$_2$, reactions with Ti-Al-Cr-Mo alloy VT3-1 80−16585
Cr$_3$C$_2$/Ni-Cr hardfacing materials, friction characts. in high temp. Na *(Japanese)* 80−89356
Cr$_7$C$_3$ CVD coating on steel 79−83393
Cr$_7$C$_3$ dissolution in high and medium C steels *(Russian)* 80−103479
Cr$_7$C$_3$ electrophonetic coatings on steel, sintering 80−66707
Cr$_7$C$_3$, reactions with Ti-Al-Cr-Mo alloy VT3-1 80−16585
Cr$_p$C$_n$$^+$, $p=1$ to 4, CrC$_n$$^-$, clusters, electronic props., mass spectra obs. *(French)* 79−45877
Cr$_x$C, cathodic needle growth, at lower electric fields from Cr(CO)$_6$ vapour 80−76161
Cr$_x$C$_y$, diffusion coating on steel punch electrode, effect on elec. discharge sintering of metal powder 77−63598
Cr$_x$C$_y$, enthalpy of form. and combustion 77−36784
Cr$_x$C$_y$-Cr-Ni-Mo wear resistant coating prep. by laser beam melting, and props. 80−40607
Cr$_3$C$_2$(-Ni-Cr), self-weldability in high temp Na *(Japanese)* 80−89392
Cr(CO)$_3$, bond angles, hybrid bond orbital calcs. 78−94188
Cr(CO)$_5$, multiphoton ionisation, mol. cooling in pulsed supersonic beam 80−28070
Cr(CO)$_6$, bonding, IR intensity anal. 78−25526
Cr(CO)$_6$, electronic spectra following flash photolysis, intracavity laser technique 79−31538
Cr(CO)$_6$, electronic struct. and bonding, SCF-Xα-MSW calcs. 78−25431
Cr(CO)$_6$, LCAO-HFS-STO calc., basis set effects 80−52882
Cr(CO)$_6$, linear dichroism, distortion and local field contribs. 79−87415
Cr(CO)$_6$, MCD spectra, charge transfer transitions 80−95658
Cr(CO)$_6$, mol. vibrs. and reaction pathways, min. energy coords. and compliance consts. 77−57966
Cr(CO)$_6$, ν(CO) region, IR and Raman spectra in organic solvents 79−41169
Cr(CO)$_6$, photodissoc., Cr prod. 80−95575

chromium compounds continued

- $Cr(CO)_6$, photoionisation reson., 30 to 100 eV 79—76473
- $Cr(CO)_6$, relative intensities of ν(CO) and ν(MC) Raman bands 78—55176
- $Cr(CO)_6$, solid and matrix isolated, Raman spectra 79—28755
- $Cr(CO)_5(CS)$, cryst. struct. determ., Fourier method *(French)* 79—4282
- $CrCl_2$, epitaxial relationships studied by RHEED and Auger emission spectra *(French)* 78—22990
- $CrCl_2$, optical absorpt. spectra, spin-allowed transitions 78—52527
- $CrCl_3$, electronic struct. and struct. phase transition 80—59644
- $CrCl_3$, phonon dispersion curves 80—2130
- $CrCl_3$, reflectance and thermoreflectance meas. 77—24866
- $CrCl_3$, self consistent band struct., intersecting spheres model 79—37985
- $CrCl_3$, two-dimensional mag. insulators, cryst. field spectra, mag. circular dichroism 79—47058
- $CrCl_3$, two-dimensional mag. insulator, cryst. field splitting, spectroscopic g-factors 79—47059
- $CrCl_4$, ligand field states, multiple scatt. Xalpha calcs. 80—47891
- $CrCl_4$, mol. consts. and mean vibr. amplitudes calcs. 80—106318
- $CrCl_4$, Raman spectra, struct. and thermodynamic functions 78—60443
- $CrCl_2O_2$, electronic transition origin band identification with the van der Waals complex 78—5239
- $Cr_2(CrO_4)_3$, ferromagnet, ESR spectra near Curie temp. 79—8042
- Cr_xCy, magnetron-sputtered, solar selective absorbing surfaces 79—92079
- $CrEr_2S_4$, cryst. struct. *(French)* 77—15356
- $Cr_2Er_6S_{11}$, X-ray cryst. struct. determ. and refinement *(French)* 80—103298
- CrF_2, heat capacity, entropy, 10-300K, mag. ordering effects 79—87264
- CrF_2, thermodynamic props. meas., electrochem. method 77—7874
- CrF_3-BaF_2-NiF_2, X-ray crystallography study, phase identification at 700°C, cryst. symm. *(French)* 78—95733
- CrF_6^{3-}, electronic excitation energy calc. correl., energy correction 78—17576
- CrF_6^{3-}, multiple scatt. calcs. methods, comparative study 79—6865
- CrF_6^{3-}, spectra, cryst. field least squares fitting interpretation 80—44548
- CrF_2ZnF_2-NaF, solid-liquid equilib. diagram *(French)* 77—1216
- $(CrF_6)^{3-}$ 6a AR→AT complexes, electron densities, local orbital populations, polarised neutron diffraction 80—88725
- CrFeCN epoxy resin-based membrane studies, Ag sensitive electrode 80—16726
- $Cr_xFe_{2-x}CaO_4$ mag. phase transitions meas. *(Russian)* 79—75556
- $Cr_xFe_{3-x}O_4$, spin and charge density oscillations due to impurities *(Korean)* 80—20565
- $Cr_{1-x}Fe_xOOH$, $0 \leq x \leq 10$, prep., Mossbauer effect, Neel temp. 80—108134
- $Cr_{1-x}Fe_xS$, metal-dielec. transition, X-ray, thermal anal., elec. cond. temp. depend. 78—67942
- CrH (CrD), molecular vibration, IR spectra electron spin resonance, 4K 79—98084
- CrH, electronic props., H alloying effects, book contrib. 79—82522
- CrH_3 (CrHD)(CrD_2), molecular vibration, IR spectra, electron spin resonance, 4K 79—98084
- CrH_4, electronic structure, ab initio calcs. 79—89601
- CrH_6, Dirac-Fock one-centre calcs. 79—6837
- $(Cr(H_2O)_6)^{3+}$, ligand field spectroscopy, selection rules, intensity enhancement of forbidden transitions 80—45049
- $Cr(H_2O)_6Cl_3$, aq., solute structuring 77—15298
- $Cr(H_2PO_4)_3$-$Al(H_2PO_{43})$-H_2O system, IR spectra 79—87428
- $Cr_4H_2(SO_4)_7.24H_2O$, X-ray cryst. struct. determ., H bond study 80—92491
- $CrH(SO_4)_2.7H_2O$, X-ray struct. determ., hydrated proton complex and H bonding 77—80449
- CrI_2, Mossbauer spectrum, electronic and mag. props. 77—32302
- CrI_3, ferromagnetic, origin of magnetic hyperfine field transferred at iodine 78—92000
- $Cr_xMn_{1-x}As$, antiferromagnetic-ferromagnetic transition, mag. moment and elec. resist. meas. 80—15718
- $Cr_xMn_{1-x}As$, antiferromag. to ferromag. transitions, superexchange-double exchange mag. coupling, susceptibility and resist. obs. 80—50070
- $Cr_xMn_{1-x}As$, mag. susceptibility anomaly at displacive phase transition 80—93091
- $Cr_{1-x}Mn_xO_2$, hyperfine mag. fields at ^{119}Sn, Mossbauer study 80—71260
- $Cr_{1-x}Mn_xSi_2$, semicond. props. 78—79992
- CrMo molecule, electronic absorpt. spectrum from flash photolysis 77—6796
- $CrMoO_4$, ESCA on H_2 reduction *(French)* 77—36365
- $Cr_xMo_{1-x}O_2$ ($x \leq 0.5$), solid soln., trivalent Cr, X-ray powder diffr. anal. 80—70177
- CrN, antiferromagnetic EPR spectra, binding energy, isotropic exchange and ordering *(German)* 80—80604
- CrN, deposition by hollow cathode discharge process, and hardness 79—24452
- CrN, electron struct. calc. 80—49587
- CrN, mag. struct. and first-order antiferromag. transition 79—61132
- CrN-MN (M=Sc, Ti, V, Mn), rhombic distortion of cryst. lattice at low temp. 78—2253
- CrN-MnN, synthesis and props. 77—40405
- Cr_2N, AES investigation of corrosion and growth nature of surface layers 77—77330
- ε-Cr_2N phase, analysis of expt. results of Mills and Schwerdtfeger to yield partial enthalpy and entropy 78—52783
- Cr_2N-CrN, thermogravimetric exam. of equilibrium *(Japanese)* 79—20292
- $Cr(NH_3)_5ONOCl_2$, cryst. struct. determ. at 245K 78—75637
- $(Cr(NH_3)_6)[MnCl_5(H_2O)]$, X-ray cryst. struct. anal. 79—4285
- $Cr(NO_3)_3$, aq. soln., X-ray diffr. obs. 77—72541
- $Cr(NO_3)_3$, Cr $^7P_0^0$ state, radiative lifetime in matrices, meas. using laser ablation and selective excitation 80—71959
- $Cr(NO)_4$, bonding, shake-up intensities and shake-up energies, SCF Xα multiple scatt. calc. 80—74121
- $Cr(NO)_4$, XPS and UV photoelectron spectra, compared to NO data 80—58317
- $Cr_{11-x}Nb_xGe_8$, cryst. struct. *(French)* 78—38675
- $CrNbO_4$, elec. cond. meas. 80—100463
- $Cr_{1/3}NbS_2$, Hall coefficient and resistivity 80—39610
- $Cr_{1/3}NbS_2$, magnetic susceptibility, function of temp. 80—39756
- $Cr_{0.5}NbSe_2$, cryst. struct., metallic cond., mag. and phys. props. *(French)* 80—33956
- $Cr_{8-x}Nb(Ta)_{3+x}Si_8$, cryst. struct. *(French)* 78—38675
- CrO, A$^5\Pi$-X$^5\Pi$ transition, rot. anal. laser induced fluoresc. and discharge emission spectra 80—69173

chromium compounds continued

- CrO molecule, B$^5\pi$ and X$^5\pi$ states, potential energy curves 80—42962
- CrO, reduction by powdered graphite, mechanism 77—4748
- CrO_2 acicular particle suspensions, mag. props., optical meas. 80—44874
- CrO_2 amorphous thin films, Mossbauer and magnetisation data 80—34712
- CrO_2 and CrO(OH), fine particle obs. of cryst. morphology and topotaxy 80—65969
- CrO_2 and tetravalent Cr oxide derivatives, metallic, chem. and phys. props. review 78—31069
- CrO_2, epitaxial growth on rutile, possible appl. as bit oriented mag. material 77—16127
- CrO_2, epitaxial growth on sapphire in air 78—27414
- CrO_2, ferromag., new prep. method by high-pressure oxidation, SEM characterisation 79—43164
- CrO_2, ferromag. films, epitaxial growth in air, electron diffr. and SEM obs. 79—42410
- CrO_2, optical conductivities and dielec. functions in 0.2-6 eV range, rel. to band struct. 79—42938
- CrO_2, oxidative prep. method, mag. props. 80—44863
- CrO_2, particulate, proton donor adsorption effect on mag. moment, XPS anal. 80—71117
- CrO_2 powder, thermal-magnetic props. 79—51821
- CrO_2 powders, print through values and mag. characts. 80—44871
- CrO_2 semidry refractory, struct. and mech. props., surface-active agents effect 80—89304
- CrO_2, single mag. particle, remanent coercive force and remanent loop meas. 78—95480
- CrO_2, single particle material for tape and disc manufacture, prep., props., and appls. 78—52308
- CrO_2, synthesis and morphology 79—24481
- CrO_2, valence states of Cr, XPS obs. 80—40216
- CrO_3, ionic defects, influence of S during Cr electrolytic oxidation in SO_2 atmosphere *(Ukrainian)* 78—92504
- CrO_3, K$\beta_{1,3}$ X-ray emission spectra, low energy plasmon Kβ' satellite 79—74020
- CrO_3^- radical in K_2CrO_4 and $KCrO_3Cl$, g-factor anisotropy 78—67994
- CrO_3-PbO, acoustooptic props. from comp. and density 80—76000
- $(CrO_3)_4$, identification of polymer species by vapour phase electron diffraction 80—53135
- CrO_4^{2} , electronic struct. determ. from X-ray spectra 78—86885
- CrO_4^{2} , Franck-Condon effects in resonance Raman spectra and excitation profiles 80—14129
- CrO_4^{2-} in halide salt aqueous solution, absorpt. spectra, 4.2 to 290K *(Russian)* 78—60499
- CrO_4^{3-} substituted in $Ba_5(PO_4)_3Cl$, ESR study 80—2629
- CrO_n, mag. and optical obs., prep. by calcination of $CrCl_3$ 79—24736
- Cr_2O_3 addition effect on CaO sintering *(Czech)* 80—45258
- Cr_2O_3 addition to CdS_xSe_{1-x} photoresistors, extension of cutoff freq. *(Russian)* 78—84248
- Cr_2O_3 additive for $Pb(Mg_{1/3}Nb_{2/3})O_3$-$PbTiO_3$-$PbZrO_3$ ceramics, HF filters appl. *(Japanese)* 80—60507
- Cr_2O_3, adsorption of Cs, meas. of contamination using washing test 78—62597
- Cr_2O_3, antiferromag., muon spin rotation *(German)* 80—54877
- Cr_2O_3, antiferromag. reson. and mech. of parallel magnetoelectric effect 79—47337
- Cr_2O_3 barrier in WO_3 electrochromic cell 78—15147
- Cr_2O_3, carbothermic reduction to metallic Cr, effect of oxide additions (Al_2O_3, SiO_2, MgO, and CaO) *(Japanese)* 78—48651
- Cr_2O_3 carrier mobility temp. dependence 77—35958
- Cr_2O_3, catalytic graphitization of nongraphitizable C 80 97440
- Cr_2O_3, chemical strengthening of polycrystalline Al_2O_3 77—21302
- Cr_2O_3 coating on refractory fibre, effect on high-temp. strength *(Russian)* 77—52536
- Cr_2O_3 containing aluminosilicate glasses, paramagnetic defect formation, ESR study during crystn. 79—65739
- Cr_2O_3 corrosion, high-temp., in Cl_2 and Cl_2-O_2 mixtures 78—15601
- Cr_2O_3, corrosion product in LMFBR type mixed oxide fuel pins 78—70599
- Cr_2O_3, $Cr(OH)_2.0.4H_2O$, CrO_3, X-ray photoelectron spectra 77—73483
- Cr_2O_3, cryst. growth from decomposition of $K_2Cr_2O_7$ melt 79—43131
- Cr_2O_3 crystals, flux growth from $K_2Cr_2O_7$-K_2CrO_4-$K_2B_4O_7$ mixture *(Japanese)* 80—108339
- Cr_2O_3 crystals, growth by decomposition of $K_2Cr_3O_7$ melt *(Japanese)* 80—108338
- Cr_2O_3, decomp. of CaO-6Al_2O_3 80—92687
- Cr_2O_3, dielec. and thermophys. props. 77—52009
- Cr_2O_3, dielec. const. in mag. field, nonlinear magnetoelec. effect in Neel pt. region 80—66006
- Cr_2O_3, dielectric const. and loss, cond., 10^2-10^7 Hz, 30-450°C 77—59504
- Cr_2O_3, diffusion in NiO, spinel formation via solid state reaction, kinetic parameters calc. 78—34644
- Cr_2O_3 dissociation in presence of C in Ar, CO and vac. atm., Cr_3C_2 form. *(Russian)* 80—35570
- Cr_2O_3, EPR linewidth, near Neel temp. 78—23327
- Cr_2O_3 effect of addition on crystallisation of Na_2O-Al_2O_3-SiO_2-TiO glass 78—87626
- Cr_2O_3, effect of oxide additions on sintering in air and reducing atm. 77—59729
- Cr_2O_3, effect on oxidation of complex (Fe, Mn)-V spinels 79—43453
- α-Cr_2O_3, effect on props. of polycrystalline CdS *(Russian)* 79—65469
- Cr_2O_3, elastic consts., distance depend. of mag. interactions, US vel. meas. 77—4539
- Cr_2O_3, electron structures calc. using models, ESCA and X-ray spectral data 77—35863
- Cr_2O_3, electronic struct. study by XPS 80—25518
- Cr_2O_3, exchange parameters including temp. effects 79—24153
- Cr_2O_3, ferromagnetoelectric poling 77—16102
- Cr_2O_3 films, black, microstruct. depend. of optical props., SEM, XPS, and sputter depth-profiling 79—43049
- Cr_2O_3, fine struct. in elastic-electron-yield spectra at transition-metal core energies 79—69938
- Cr_2O_3 flux growth from $K_2Cr_2O_7$-K_2CrO_4-$K_2B_4O_7$ mixture 79—100037
- Cr_2O_3, grain growth during sintering *(Japanese)* 80—16261
- Cr_2O_3, high temp. corrosion in Cl_2 and Cl_2-O_2 mixtures 77—77629
- Cr_2O_3, hydrostatic compression, X-ray diffr. meas. 79—99269
- Cr_2O_3, IR active phonons 78—34578
- Cr_2O_3 in Cr film, struct., oxide percentage determ. and elec. props. 80 103607

chromium compounds continued
Cr_2O_3, influence of TiO_2 on sintering behaviour, densification as function of temp. 79—78919
Cr_2O_3, low energy X-ray emission satellite, unpaired election and plasmon effects 80—35007
Cr_2O_3, mag. phase boundaries near bicrit. and Neel points 78—34980
Cr_2O_3, magnetic susceptibility, near Neel temp. 79—56509
Cr_2O_3, magnetoelec. effect, SQUID magnetometer meas. 79—87302
Cr_2O_3, magnetoelectric effect mechanism, magnetoelec. susceptibility and antiferromag. reson. elec. shift meas. 80—44894
Cr_2O_3, magnetoelectric susceptibility meas. by SQUID, 1.6-4.2K 77—20664
Cr_2O_3, magnetostriction anomalies near mag. field induced transitions 77—66315
Cr_2O_3, magnon energy temp. renormalisation calc. 77—1531
Cr_2O_3, monocrysts. formed on heat treatment of Ni-Cr based alloy in air, struct. obs. 79—52455
Cr_2O_3, muon spin rotation expts. 80—71282
Cr_2O_3, muon states, local mag. fields 80—75911
Cr_2O_3, μSR meas. 79—56666
Cr_2O_3, O diffusion coeff. from creep meas. 78—18823
Cr_2O_3, optical generation of longit. phonon modes 77—43288
Cr_2O_3, paramagnetic-antiferromag. transition temp. increase in mag. field 77—12121
Cr_2O_3 polycrystalline powder, crystallite sizes and surface areas 77—66086
Cr_2O_3 powder, activation and sintering 77—21078
Cr_2O_3, RF sputtered coating for wear appls., on Inconel X-750 foil, prep. and props. 80—40605
Cr_2O_3, reaction with stabilised ZrO_2 77—36438
Cr_2O_3 reduction by C, mechanism, 7573-2073K *(Russian)* 80—45483
Cr_2O_3, reduction by H_2, reaction kinetics 80—11950
Cr_2O_3, reduction rate by C and C in liquid Fe-Cr-C 78—6877
Cr_2O_3, scale on austenitic Ni-Cr alloys, oxidation mechanism *(Polish)* 79—79143
Cr_2O_3, sintering behaviour, effect of TiO_2, C additions 80—66461
Cr_2O_3, slips and castings, rheological and technological props. 77—16779
Cr_2O_3, solid solubility in MgO 80—15247
Cr_2O_3, specific heat near. Neel temp. 77—63207
Cr_2O_3 substrate for CdS photoresistors, effect of heat treatment 78—80017
Cr_2O_3, thermal magnetoresist., 0.1 to 100K, magnon-phonon interactions 79—65266
Cr_2O_3, thin plate single crystal, vapour phase growth 78—64450
Cr_2O_3, US wave vel. near mag. transition 78—84263
Cr_2O_3, UV absorption spectra from reflectivity meas. 78—2879
Cr_2O_3, vacuum vaporisation, porosity and thermodynamic treatment effects *(Japanese)* 77—43436
Cr_2O_3 X-ray diffr. studies, crystallite size, phase transformation 77—21138
Cr_2O_3:$^{119}Sn^{4+}$, Mossbauer spectra *(French)* 79—24248
Cr_2O_3:Ga_2O_3 EPR, antiferromagnetic coupling energy temp. depend. *(German)* 78—10766
Cr_2O_3/Cr cermet film, RF sputtered, for selective black absorbers 78—30046
Cr_2O_3/Cr solar-absorber surfaces, chemical and struct. anal. 79—95283
Cr_2O_3/γ-Fe_2O_3/Pt electrode, two layer oxide surface film anal. by modulation spectroscopy *(Japanese)* 80—11491
Cr_2O_3-a-WO_3 electrochromic layer device, characts. 79—90009
Cr_2O_3-Al_2O_3, antiferromag. cluster stability, 300-5200K 77—20683
Cr_2O_3-Al_2O_3, crystalline soln., microstrain rel. to lattice energy and strain energy 77—24411
Cr_2O_3-Al_2O_3 solid solution, electrochemical determ. of activity 78—44391
Cr_2O_3-Al_2O_3 solid solns., effect of Cr on point of zero charge 78—61021
Cr_2O_3-Al_2O_3 solid soln., Vickers micro-hardness 80—66629
Cr_2O_3-Al_2O_3-$ZrSiO_4$, exam. of microstructure by optical microscopy 79—29073
Cr_2O_3-Al_2O_3-$ZrSiO_4$ system, electrosmelted refractories, phase comp., corrosion and glass resist. Cr^{3+} conc. depend. 79—33982
Cr_2O_3-aluminophosphate melt, resistivity, 800-1200°C 77—39903
Cr_2O_3-Cr, RF sputtered cermet film, selective black absorber 77—58399
Cr_2O_3-Cr black, electrodeposit on Ni, defects and their effect on props. 80—39474
Cr_2O_3-Cr black, selective coating, optical and topographical props. 80—26165
Cr_2O_3-Cr black, solar collector coating, microstruct., FIM and SEM obs. 80—26166
Cr_2O_3-Cr cermet films, for selective black absorbers 79—29483
Cr_2O_3-Cr composite mixture, preferential sputtering, XPS expts. 79—87544
Cr_2O_3-Cr film, electrodeposited, optical degradation rel. to surface morphology, SEM and AES obs. 79—79401
Cr_2O_3-Cr film, optical props., rel. to chemical/metallurgical constitution, appl. as solar absorber 78—56531
Cr_2O_3-CrO_3-ZrO_2.CrO_3H_2O, exam. of thermal transitions 79—100116
Cr_2O_3-doped $Ca_2(Al,Fe)O_5$, planar interfaces, TEM obs. 80—65008
Cr_2O_3-Fe_2O_3 solid soln., completely annealed, reclustering of Fe^{3+} ions 79—33578
Cr_2O_3-Ge, elec. props., molecular deposition method 80—34525
Cr_2O_3-H_2, interaction with surface, quantum chemical study 80—45549
Cr_2O_3-La_2O_3 mixtures, reactions with O_2 *(French)* 77—52524
Cr_2O_3-M_2CrO_4.MoO_3, phase diag. 77—86007
Cr_2O_3-MgO-TiO_2, phase relations in air at 1400°C *(Japanese)* 77—77465
Cr_2O_3-Mo_2O_3, catalyst, effect of Al_2O_3 additives on catalytic activity, in oxidation of methanol to formaldehyde *(Russian)* 79—66346
Cr_2O_3-MoO_3, physicochem. investig. of phase struct. 77—8807
Cr_2O_3-stainless steel system under fusion reactor first wall condition, oxide dispersoid stability 80—40374
Cr_2O_3-TiO_2 system, phase relations 78—80523
Cr_2O_3-V_2O_3-VO_2 system, phase equil. at 1273K *(French)* 77—35668
Cr_2O_3-WO_3, phase relations 78—92249
$(1-x)Cr_2O_3$-$x\alpha Fe_2O_3$, influence of Fe^{3+} on phase transition *(Russian)* 79—28522
$(1-x)Cr_2O_3$-$x\alpha Fe_2O_3$, mag. phase diagram, EPR method *(Russian)* 79—28521
Cr_2O_3-ZrO_2 granules, from spray drying of suspensions 80—104100
$Cr_2O_7^{2-}$ centre in lattice, optical props., mol. orbital calcs. 79—15491
$Cr_2O_7^{2-}$, triplet levels obs. by luminesc. meas. 79—69874

chromium compounds continued
$CrOCl_3$, electronic structure and valence ionisation energies, obs. by ab initio and SW-Xα methods 80—69073
$CrOCl_3$, ionisation energy, CI and ΔSCF methods 79—68194
CrO_2Cl_2, collisionless IR multiphoton production of electronically excited parent mols. 79—41211
CrO_2Cl_2, determ. of thermodynamic props. from vibrational freqs. and moments of inertia 77—31415
CrO_2Cl_2, electronically induced IR multiphoton absorpt., quasicontinuum states, excited singlet radiationless decay 80—48049
CrO_2Cl_2, fluoresc. excitation spectrum, free jet expansion cooling effects 79—3473
CrO_2Cl_2, inert gas matrices, IR spectra, emission spectra, photoselection 77—14443
CrO_2Cl_2, matrix isolation IR spectrum and force constants 79—3445
CrO_2Cl_2, multiphoton induced inverse electronic relax. 80—66836
CrO_2Cl_2, single vibronic level fluoresc. 77—3408
CrO_2Cl_2+carbon tetrachloride+acetone, intermediate complex form., electronic spectra 80—61075
CrO_2F_2, determ. of thermodynamic props. from vibrational freqs. and moments of inertia 77—31415
$Cr(OH)_3$, adsorption props. of surface, gas-chromatographic investigation 79—66343
$Cr(OH)_3$, coprecipitated with $Al(OH)_3$ gel, magnetic, optical studies, calcination 79—47995
$(Cr_4(OH)_6(NH_3)_{12})Cl_6.4H_2O$, exchange interactions in Cr^{3+} clusters, inelastic neutron scatt. obs. and Heisenberg Hamiltonian calc. 79—78359
$Cr_4(OH)_6(NH_3)_{12}Cl_6.4H_2O$, exchange coupled mol. Cr^{3+} tetramers, inelastic neutron scatt. 80—65792
β-CrOOH, neutron diffr. exam., cryst. and magnetic struct. *(French)* 78—2654
CrOOH(D), barrier to proton or deuteron tunnelling 80—70156
β-CrOOH(D), crystal struct., isotope effects on bond lengths 77—15371
α-CrOOH(D), isotope effects in bond lengths 77—80488
$Cr_2O_3(S_3)$, spectrally selective EM wave absorber, solar energy collector material, props. *(Dutch)* 78—50872
$Cr_2O_3.SH_2O$, heat-treated, narrow particle size distrib., surface props. 78—85210
CrP, valence electron energy spectrum, deduced from X-ray spectra and XPS 79—99984
$Cr_{12}P_7$, X-ray cryst. struct. redeterm. 79—19192
$CrPO_4$-Al_2O_3 system, oxyorthophosphates form. 79—78942
$CrPO_4$-Cr_2O_3 system, oxyorthophosphates form. 79—78942
$CrPO_4$-Y_2O_3, system, oxyorthophosphates form. 79—78942
$CrPS_4$, cryst. struct., X-ray diffr. *(French)* 77—19926
$CrPS_4$, cryst. struct. 77—47401
$CrPS_4$-Li intercalation cpd., phys. props. 79—19788
$CrPr_2S_4$, synthesis, single crystal growth, mag. and elec. props. 79—78857
$CrPr_2Se_4$, synthesis, single crystal growth, mag. and elec. props. 79—78857
$Cr_{1-x}Rh_xO_2$, ferromag., new prep. method by high-pressure oxidation, SEM characterisation 79—43164
$Cr_{1-x}Rh_xO_2$, oxidative prep. method, mag. props. 80—44863
CrS, magnetic struct. from neutron diffr. meas., Neel point 77—32164
CrS, X-ray diffr. obs., high press., diamond anvil camera method 77—4082
CrS-FeS, sulphorspinel, struct. and elec. props. 80—49834
Cr_2S_3, enthalpy and specific heat, temp. depend. 80—54406
Cr_2S_3, rhombohedral single cryst., AC cond., freq. and temp. depends. 77—76810
Cr_2S_3, single crystal, exam. of unit cell structures by interference contrast microscopy 78—67670
$Cr_2(SO_4)_3$, stability in atmosphere containing O_2 and S, 880 to 1040K 79—57222
CrS(Se), high press. semiconductor to metal transitions 78—26924
$CrS_{1-x}Se_x$, antiferromag. props., struct., variations near Neel temp. 78—64199
$CrS_2(Se_2)$, and alkali metal intercalates, phys. props. 80—44179
$Cr_2S_{3-x}Se_x$, elec. resist., thermal cond. and Seebeck coeff. meas. 80—24958
CrS_xTe_{1-x} (x=0 to 0.2), magnetic props. study 80—11194
CrSb, optical props., 0.05 to 5 eV 77—48194
$CrSb_2$, heat capacity and thermodynamic props., mag. transition, enthalpy of decomposition 78—43591
$CrSb_{1-x}As_x$, exchange striction and press. effect on Neel temp. 77—63189
$CrSb_{1-x}As_x$ press. effect on Neel point 80—71147
$CrSe_2$, layered, phys. and elec. props. 80—44594
$Cr_{3\pm x}Se_4$, struct., elec. and mag. props. 80—107160
Cr_3Se_4, mag. susceptibility and sp. ht. meas. *(French)* 79—56507
$Cr_3Se_xS_{4-x}$, mag. susceptibility and sp. ht. meas. *(French)* 79—56507
$Cr_2Se_{3-x}Te_x$, mag. props. and lattice parameters, comp. depend. 77—66263
Cr_3SeTe_3, anomalous Hall effect 77—69351
$CrSi_2$ based solid solns., prep., elec. cond. and thermoelec. props. 80—49697
$CrSi_2$ film formation kinetics on Si substrates with and without interposed Pd_2Si layer 77—24492
$CrSi_2$ formation on Pd_2Si and PtSi, radioactive Si tracer obs. 78—60578
$CrSi_2$, semicond. props. 78—79992
Cr_3Si phase structure, rel. between phase diagrams and superconductivity 80—88330
Cr_3Si, single cryst. growth by floating zone method, X-ray and neutron diffr. study 79—74084
Cr_3Si, specific heat at low temps., electron density of states, Debye temp. *(Russian)* 80—54398
$Cr_3Si_2(C_2)$, sputtered films, microstruct. and wear props. 78—64733
$Cr_{1/3}TaS_2$, Hall coefficient and resistivity 80—39610
$Cr_{1/3}TaS_2$, magnetic susceptibility, function of temp. 80—39756
CrTe, effect of high pressures on magnetic properties 78—52238
CrTe, film, attenuated total refl., magneto-optical effects 77—52196
CrTe, mag. ordering under high-press., ferromag. transition, ESR and neutron diffr. *(French)* 78—31053
CrTe, neutron diffr. at high press., mag. transition *(Russian)* 79—38326
$CrTe_{1+x}$, thermal expansion and spontaneous magnetostriction *(Russian)* 78—48017
Cr_5Te_6, high press. effects on magnetisation and mag. transitions, 77 to 360K 77—77057
Cr_7Te_8 film, optical and magneto-optical props., appl. as storage medium 78—23545

chromium compounds continued
Cr_2TeO_6, CC ^{57}Fe Mossbauer spectrum, hyperfine field, Neel temp. 79–56636
$CrTe_{1-x}Se_x$ (Sb_x), Curie temp., high press. and doping effects *(Russian)* 77–12125
$CrThS(Se)_3$, synthesis, cryst. characts. *(French)* 78–51517
$Cr_{1-x}Ti_xN$, cryst. and mag. struct., at low temps. *(French)* 80–29005
$CrTiNdO_5$, distrib. of Cr^{3+} and Ti^{4+} ions, Mossbauer spectrum 77–69747
Cr_2TiO_5, in Cr_2O_3-TiO_2 system, struct. determ. 79–60329
$CrTiRO_5$, R=Pr,Nd,Sm,Eu,Gd,covalency contribs. to Mossbauer spectra 78–10808
$(Cr_{1-x}Ti_x)_5S_6$, mag. props. 77–69548
$CrUSe_3$, mag. struct. and delocalized moments, powder neutron diffr. obs. 77–69496
Cr(V) complex, paramagnetic, dynamic polarisation of protons and deuterons 79–36453
$Cr_{1-x}V_xN$, solid soln., mag. struct. *(French)* 78–6519
$Cr_{1-x}V_xN$ solid solution, X-ray diffr. structure exam. at low temp., deformation study *(French)* 78–2069
$CrVO_4$, adsorption of methanol, IR spectra *(Russian)* 79–51435
$CrVO_4$, elec. cond. meas. 80–100463
$CrVO_4$, Neel temp., mag. susceptibility meas. 80–29550
$CrVO_4$, temp. depend. of heat capacity, 60-1080K, Debye temp. 77–7869
$(Cr_xV_{1-x})_2O_3$, impurity doping effects, elec. props. obs. 80–75609
$(Cr_{1-x}V_x)_5S_6$, mag. props. 77–69548
$CrWO_4$, cryst. growth and struct. *(French)* 77–43202
$Cr_{12-x}W_xP_7$, solid solns., prep., cryst. struct. *(French)* 78–63723
$^{51}Cr_2O_7{}^{2-}$ tracer solution preparation *(French)* 79–29385
Cs-Cr-O system, phase equilibrium 80–3012
$CsBr{:}CrO_4{}^{2-}$, coupling and fine struct., IR electronic and vibr. spectra obs. 80–45118
$CsCrCl_3$, co-operative Jahn-Teller distorted struct. determ. 78–63713
$Cs_3Cr_2Cl_9$, optical absorpt., MCD, exchange interactions 78–10917
$CsCrI_3$, Mossbauer spectra, struct., electronic and mag. props. 79–91320
$CsCrI_3$, Mossbauer spectra, struct., electronic and mag. props. 80–15908
$CsI{:}CrO_4{}^{2-}$, coupling and fine struct., IR electronic and vibr. spectra obs. 80–45118
$CuCr_{2-x}Fe_xO_4$, charge transfer, Mossbauer spectroscopy 80–15836
$CuCr_2O_4$-$MgCr_2O_4$, X-ray investig. 77–44224
$(CuCr_2S_4)_x$-$(Cu_{0.5}In_{0.5}Cr_2S_4)_{1-x}$ solid solution, piezoelectric effect, X-ray struct. anal. *(Russian)* 80–15978
$CuCrSe_2$, influence of excess Cu on physical props. 80–103836
$CuCr_2Se_4$, crit. behaviour near Curie point 78–31068
$CuCr_2Se_4$, cryst., preparation, elec. cond., thermo EMF 77–8125
$CuCr_2Se_4$ single crystal, magnetic props. *(Japanese)* 78–6520
$Cu_{1-x}Cr_2Se_4$, influence of excess Cu on physical props. 80–103836
$CuCr_2Se_{4-x}Br_x$, elec. resistance, Hall const., magnetoresistance singularities *(Russian)* 79–91078
$Cu_yCr_2Se_{4-x}Br_x$, ferromag. magneto-resistance exam. *(Russian)* 78–84238
$Cu_yCr_2Se_{4-x}Br_x$, ferromagnetic semicond., Hall effect 80–60012
$Cu_yCr_2Se_{4-z}Br_x$, degenerate ferromag. semicond., resist. minimum 79–73517
$Cu_yCr_2Se_{4-z}Br_x$, paramagnetic-ferromagnetic phase transition temp. depend. on element conc. 79–69672
$CuCr_2Se_4(S_4)(Te_4)$, binary and ternary solid solns., mag. and elec. props. 80–2407
CuFeCrMn spinel oxides, struct. determ., mag. states of Mn^{3+} ions *(Russian)* 78–19227
$Cu_{0.5}In_{0.5}Cr_2S_4$, piezoelectric effect, X-ray struct. anal. *(Russian)* 80–15978
CuO-Cr_2O_3 based oxide, catalyst, adsorption of fluorobenzene, binding energy of F 1s electrons *(French)* 79–69346
$DyCrS_3(Se_3)$, prep., elec. and thermal props. 78–43390
EuB_6-CrB_2 quasibinary cross section 77–86001
$(Fe,Cr)_3C$, reln. between bond energy and X-ray emission line shifts 78–50555
Fe-Cr oxide, quantitative depth profile, by AES *(Japanese)* 80–16751
Fe-Cr-O, computer-assisted anal. and calcs. of phase diagrams 80–25667
Fe-Ni-Cr-S-O compounds, occurrence in Allende chondrite *(French)* 78–32411
$FeAl_{2-x}Cr_xO_4$, spinel, elec. cond. behaviour during oxidation 79–19593
γ-$(Fe_{1/3}Al_{2/3-y}Cr_y)_2O_3$, lacunar spinels, elec. cond. behaviour during oxidation 79–19593
FeC_x-CrC_y-NiC_z, stainless steel carbide, solar selective surface, fabrication, magnetron sputtering system description 80–80967
FeC_x-CrC_y-NiC_z, stainless steel carbide, graded solar selective surface, magnetron sputtered 80–81485
FeC_x-CrC_y-NiC_z, stainless steel carbide, sputtered solar selective surface, grading profile 80–81486
$(Fe_2Cr_{4-y}Al_y)O_9$, IR spectra, lacunar γ-phase to corundum α-phase transform. 80–108199
$Fe_{1-x}Cr_xBO_3$, magnetisation, 4.2-600K 78–68187
$Fe_{1-x}Cr_xBO_3$, synthesis, cryst. chem. and mag. props. 78–31058
$(Fe_{1-x}Cr_x)_2O_3$, Mossbauer exam. of mag. struct. 77–24694
$(Fe_{1-x}Cr_x)_2O_3$, yH_2O crystal growth, characterisation by Mossbauer spectroscopy, mag. meas. and electron microscopy *(French)* 80–80655
$(Fe_{1-y}{}^{3+}Cr_y{}^{3+})_2O_3{}^{2-}$, γ to α transform. elec. cond. study, oxidation initial stage kinetics, lacunar spinel form. 78–92384
$Fe_{2-x}Cr_xO_3$, elec., optical and photocond. props. 79–56262
$Fe_{3-x}Cr_xO_4$, electron transfer and spin density distribs., Mossbauer spectra 79–24243
$Fe_{3-x}Cr_xO_4$, Mossbauer study above Verwey transition 78–43750
$(Fe_{6-y}Cr_y)O_9$, IR spectra, lacunar γ-phase to corundum α-phase transform. 80–108199
$(Fe_xCr_{1-x})_2O_3$ corundum-type solid solution single crystal growth, chem. vapour transport 80–93465
$Fe_{2-x}Cr_xP_{1-y}As_y$ mag. props., Mossbauer obs. 77–40156
$FeCr_2S_4$, vapour grown, growth mechanism of multisteps on surface 78–75605
$FeCr_2S_4$, vapour grown, struct. and stoichiometry, X-ray fluoresc. anal. 79–4263
$Fe^{2+}{}_{1+x}Cr_{2-2x}Ti_xO_4$ spinel, low temp. crystallographic transitions 77–15589
$Fe_{0.5}Cu_{0.5}Cr_2S_4$, ESR spectra, elec. and mag. props., Curie temp. 80–97137
$Fe_{1-x}Cu_xCr_2S_4$, Hall effect and magnetoresist. 79–78119

chromium compounds continued
$Fe_{1-x}Cu_xCr_2S_4$, mag. semicond., mag. props. and elec. cond. *(Japanese)* 79–47111
$Fe(Li_{0.5}Fe_{1.5-x/8}Mn_{x/8})O_4$ $0 \leq x \leq 2$ spinel system, X-ray diffr. anal. of loss of order on Cr substitution 79–73178
$(Fe_{1-x}M_x)_3P$, cryst. struct. and mag. props. 78–19222
FeO-Cr_2O_3, melt, exam. of viscosity and self-diffusion 79–95198
Fe_2O_3-Cr_2O_3, crystalline size and phase transform. study by X-ray diffr. 77–21138
α-Fe_2O_3-Cr_2O_3 solid solution, Mossbauer effect studies 80–71249
Fe_3O_4-Cr_2O_3-Ni_2O mixture, reduction by gases heated by electric arc discharge *(Russian)* 78–15704
$Fe(OH)_3$-Cr_2O_3 catalysts, for water-gas shift react., porous struct. 79–29407
γ-$FeOOH$-Cr_2O_3 catalysts, for water-gas shift react., porous struct. 79–29407
$FrCr_2S_4$, second-order phase transition, Mossbauer spectra 80–20569
$Ga_{0.67}Cr_2S_4$, semiconducting thiospinelide, spin glass type mag. ordering *(Russian)* 80–50123
$GaP{:}Cr_2O_3$, growth, dopant distribution, elec. resist. 78–34531
HfO_2-Cr_2O_3 system in Ar medium, phase equilibria, 1600-2500°C *(Russian)* 77–55953
$HgCr_{2-x}Al_xSe_4$ and $HgCr_{2-x}Ga_xSe_4$, temp. depend. of ESR linewidth, 105-300K 80–71161
$HgCr_2Se_4$, crit. behaviour near Curie point 78–31068
$HgCr_2Se_4$, cryst., preparation, elec. cond., thermo EMF 77–8125
$HgCr_2Se_4$, ESR line intensity near Curie point 78–64269
$HgCr_2Se_4$, electronic props. rel. to departure from stoichiometry 80–100472
$HgCr_2Se_4$, initial mag. permeab., 77 to 300K, domain wall motion and damped ferromag. reson. 79–28562
$HgCr_2Se_4$, Raman scattering, as function of temp. and incident photon energy 79–95781
$HgCr_2Se_4$, spontaneous magnetisation temp. depend., nuclear resonance freq. depend. *(French)* 80–80483
$HgCr_2Se_4$, thermorefl. near ferro- to paramagnetic transition 79–78660
$HgCr_2Se_4{:}Cd$, precipitations during growth by chem. transport method 80–55409
$HgCr_2Se_4$-$CdIn_2S_4$ heterojunctions, prep. and photovoltaic prop. 78–34892
$HoCrO_3$, cryst. field levels and mag. interactions, inelastic neutron scatt. study 77–69277
$KCl(Br){:}CrO_4{}^{2-}$, vibronic absorption spectra 78–10924
$KClO_4{:}CrO_4{}^{2-}$ AC elec. cond. and dielec. loss meas. 80–59699
KCr alum, relaxation behaviour, EPR study, environmental effects 80–66021
$KCr_xAl_{1-x}(SO_4)_2.12H_2O$, EPR of single crystals, zero-field splitting of Cr^{3+} 80–66015
K_2CrO_2, layer struct. elec. cond. props. *(French)* 78–26542
$KCr(SO_4)_2.12H_2O$, spin lattice relaxation, in liquid He and in vacuum 78–39434
$KCr(SO_4)_2.12H_2O$, ESR, spin-lattice relax., ambient gas atm. thermal cond. effect 79–8046
$K_2CrTi(PO_4)_3$, cryst. data 77–39564
$K_2HCr_2PO_{10}$, cryst. struct. data *(French)* 79–14756
$KH_2PO_4{:}CrO_4{}^{2-}$ $(CrO_7{}^{2-})$, electrical cond., thermal depolarisation studies 79–95212
$LaCr_3$ alloy development for thermoelec. appls. 80–35705
$LaCrO_3$, reactions with O_2 *(French)* 77–52524
$LaCrO_3$-Cr eutectics, prep. and microstruct. 80–108380
$LaCrS_3$, crystal atomic struct., X-ray diffr. analysis *(German)* 78–10003
$LaCrSe_3$ alloy development for thermoelec. appls. 80–35705
La_2O_3-Cr_2O_3-Y_2O_3 ceramics, fireproof, direct energy conversion appl. *(Czech)* 79–70455
La_2O_3-Mn_2O_3-Cr_2O_3, synthesis and properties of solid solutions 78–44038
$La_{0.84}Sr_{0.16}CrO_3$, sintering 77–77440
Li-Cr ferrite, $Fe(Li_{0.5}Fe_{0.25}Cr_{1.25})O_4$, one-magnon light scatt. with and without compensation temps. 78–31062
LiCr ferrite, elec. resist., thermoelec. power and Nernst-Ettingshausen meas. near compensation point 78–10487
$Li_xCr_yV_{1-y}S_2$, physical props., effect of metal substitution of Li intercalation 79–100395
$Li_{0.5}Ga_{0.85}Cr_{1.625}O_2$ spinel, tetrahedral coordination of Cr^{3+} ion, electronic spectra, X-ray and neutron diffr. *(French)* 79–65031
$LiMnCrF_6$, ferrimagnetic, magnetic props. *(French)* 79–1668
Li_2O-Al_2O_3-Cr_2O_3 system, subsolidus equilibria 80–60843
$MgCr_xFe_{2-x}O_4$, comp. effects on ferrite characts. 78–52305
$MgCr_2O_4$, vaporization 79–99308
$Mg(NH_4)_2(SO_4)_2.6H_2O{:}Cr_2O^{2-}$, optical absorption study, $Cr_2O_7{}^{-}$ and $CrO_4{}^{3-}$ centres 80–55128
MgO, Cr bearing basic refractory, prod. from brine MgO 79–83158
$MgO{:}CaO(SiO_2)(B_2O_3)(Cr_2O_3)$, effective of impurities on high temp. creep 80–40455
MgO-Al_2O_3-Cr_2O_3, vacuum vaporisation, Langmuir method 78–95149
MgO-Al_2O_3-Cr_2O_3 refractory system, phase conversion and props., X-ray anal. 77–90336
MgO-$CaMgSiO_4$-Cr_2O_3, spinel phase, phase equilibrium relations and spinel bonding 80–55376
MgO-CaO-FeO-Fe_2O_3-SiO_2-Cr_2O_3-Al_2O_3 spinel refractories, physicochem. prod. conditions 80–89185
MgO-Cr_2O_3, composition obs. by thermogravimetry 79–16081
MgO-Cr_2O_3, diffusion of Cr_2O_3 and Fe_2O_3 in gas phase during firing *(French)* 78–80495
MgO-Cr_2O_3, reaction sintering *(German)* 78–11174
MgO-Cr_2O_3, vacuum vaporisation 78–91434
MgO-Cr_2O_3, vaporisation rate, O_2 partial press. effect *(Japanese)* 78–63848
MgO-Cr_2O_3-CuO, phase relations and microstruct. 79–74140
MgO-Fe_3O_4-Cr_2O_3, isothermal sections, development of calculation data base 79–96006
MgO-NaCl refractory clinkers, Cr containing, densification, thermal treatment and phase composition effect *(French)* 80–76219
MgO-Nd_2O_3-$Al(Cr)_2O_3$, reactions kinetics in mixtures of components and phases 77–40523
$(MgO$-Fe_2O_3-Cr_2O_3-$TiO_2){:}Na_2O$, powder, prep., heat treatment, Na_2O impurity effect on props. 77–16528
$Mn_{1-y}Cr_yAs$, double exchange ferromag. coupling, magnetisation meas. 80–75751
$MnCrF_5$, antiferromag., mag. struct. *(French)* 78–52211

chromium compounds continued
$MnCrF_5$, cryst. struct. *(French)* 77—47403
$Mn_3Cr_2Ge_3O_{12}$ garnet, antiferromag. ordering *(Russian)* 78—80146
$Mn_{2.5}Cr_{0.5}O_4$, mag. struct., neutron diffr. obs. 79—33460
$Mn_xCr_{3-x}O_4$, cubic and tetragonal structs., neutron diffr. obs. 79—19369
$Mn_xCr_{3-x}O_4$, mag. struct. determ. by neutron diffr. 77—40035
$Mn_xCr_{3-x}O_4$ spinels, miscibility gap boundaries, annealing expts. 77—86012
$Mn_{1-x}Cr_xP$, mag. susceptibility and transitions 79—47256
$Mn_{1.88}Cr_{0.12}Sb$, magnetic phase transition effect on magnon renormalisation 77—59405
$Mn_{2-x}Cr_xSb$, sintered, intrinsic coercivity 77—89983
$MnCr_2Te_4$, elec. props., 100 to 650K *(Russian)* 79—11115
MnSb-CrSb, NiAs-type system, single crystals, neutron diffr. studies 80—60200
$MoSi_2$-$CrSi_2$, phase equilib., struct. and props. 80—50608
NH_4ClO_4:CrO_4^{2-}, thermal depolarisation, relax. parameters 78—43779
$NH_4H_2PO_4$:CrO_4^{2-}(CrO_7^{2-}), electrical cond., thermal depolarisation studies 79—95212
$(NaAl)_xSi_{2-x}O_6.H_2O$, analcite, polyhedral tilt transitions obs. at high press. 80—6515
NaCl-$AlCl_3$-$CrCl_3$, molten, electrochemical exam. of Cr 78—56939
NaCl-CsCl-$CrCl_3$ system, melting diagram determ. by DTA, phase comp. *(Russian)* 77—63645
NaCl-CsCl-$CrCl_3$ system, phase struct. anal. by X-ray method *(Russian)* 78—3112
Na_xCrO_2, layer struct. elec. cond. props. *(French)* 78—26542
$Na_3Cr_2(PO_4)_3$, crystallographic data, ionic conductivity *(French)* 80—88077
$Na_3Cr_2(PO_4)_3$, synthesis and cryst. struct. *(French)* 79—32964
$Na_3Cr_3(PO_4)_4$, crystallographic data, ionic conductivity *(French)* 80—88077
$NaCrS_2$, antiferromag. semicond., Raman and far-IR spectra 79—47454
$NaCrS_2$, intercalation cpd., NMR 77—90048
$Na_2Cr_2Ti_6O_{16}$, characterisation and mag. props., 90-800K, $Na_xTi_4O_8$ bronze isotypes *(French)* 80—39735
NaF-SrF_2-CrF_3, glass transition, crystn. and melting temps., optical transmission *(French)* 80—64910
$NaMnCrF_4$, cryst. struct. *(French)* 77—47402
$NaMnCrF_6$, ferrimagnetic, magnetic props. *(French)* 79—1668
Na_2O-BaO-Cr_2O_3-SiO_2 glass, ion-bombarded, optical line intensities 80—35037
Na_2O-CaO-SiO_2-Cr_2O_3 glass, redox equilibria of Cr ions, impurity effects 80—89477
Na_2O-Cr_2O_3-TiO_2 ternary systems, X-ray investigation 79—51067
NaOH:CrO_4^{2-}, electron tunnelling, pulse radiolysis 80—108722
$Nb_xCr_{1-x}O_2$, ($x\geq0.5$), cryst. growth by chem. transport and phase transitions 78—35281
$Nb_xCr_{1-x}O_2$, cryst. prep. and struct., mag. props. 78—52198
Nd-Cr-B system, phase equil. at 800°C, boride lattice parameters *(Russian)* 78—31388
$Nd(Al,Cr)_3(BO_3)_4$, CW laser action, CR^{3+} cross pumping, Nd^{3+} direct pumping 79—64231
$Nd(Mn_{1-x}Cr_x)_2Si_2$, mag. and structural props. 79—78342
$NiCr_2O_4$, plasma-sprayed coatings, props. 77—59999
$Ni_{1-x}Cr_xS$, elec. transport, mag. susceptibility and DTA meas. 80—96954
NiO-Cr_2O_3-$MgSiO_3$ methanation catalyst, S-resistant, IR and Raman spectra 80—93290
P_2O_5-GO_3-CaO(Nd_2O_3) systems, vitrification regions and physicochem. props. of glasses 77—11673
Pb-Cr-O system, equil. relationships, stability limits 77—59765
Pb_z-Sr_{1-z}(Zr_x-Ti_{1-x})O_3:Cr_2O_3, ferroelec. ceramic, reversible characts. and dielectric losses *(Russian)* 78—84517
$PbCrO_4$, paste, anomalous viscous flow 79—64617
$Pb_3Cr_2(PO_4)_2$, synthesis and cryst. struct. 79—19218
Pb(Zr,Ti)O_3:Cr_2O_3 ceramic, electrical cond. and dielectric const. meas. 80—2389
Pb(Zr,Ti)O_3:Cr_2O_3 ceramics, reson. freq. comp. and temp. depend. 80—70413
$Pb(Zr_{0.47}Ti_{0.43}Sn_{0.10})O_3$:$Cr_2O_3$, ferroelec. ceramic, reversible characts. and dielectric losses *(Russian)* 78—84517
Pr-Cr-B system, phase equil. at 800°C, boride lattice parameters *(Russian)* 78—31388
β-$RbCrCl_3$, co-operative Jahn-Teller distorted struct. determ. 78—63713
Rb_2CrCl_4, spin wave temp. depend. 79—4662
Rb_2CrCl_4, zone centre magnon gap determ., exciton-magnon combination band meas. 79—61082
Si-Cr_2O_3Al, current-voltage characts., oxide film effects 80—70841
SiO_2-Al_2O_3-Cr_2O_3 system, KT-11 type, chromia-containing material production based on high-silica glass fabric 80—45266
SiO_2-CaO-Na_2O-Cr_2O_3 system, water, alkali, acid resist., chem. durability 79—34162
Sm-Cr-B system, phase equil. at 800°C, boride lattice parameters *(Russian)* 78—31388
$Sm_8Cr_2Si_6N_2O_{24}$, apatite-like struct. study *(French)* 77—27854
$Sr_5(PO_4)_3Cl$:CrO_4^{3-}, EPR, cryst. field parameters 79—87309
$Sr_5(PO_4)_3Cl$:CrO_4^{3-}, polarised absorpt. spectra, visible and IR, ligand field transitions 79—95812
$TaSi_2$-$CrSi_2$, phase equilib., struct. and props. 80—50608
$TbCrSe_3$, prep., elec. and thermal props. 78—43390
TeO_2-Cr_2O_3 system, phase diagram and vitrification 79—83182
(Ti, Cr)B_2-based alloys, densification of powder mixtures by hot-pressing, elec. and mech. props. 80—20812
Ti-Cr_3C_2 composite, TiC and struct. form. during sintering 79—29011
TiC-Cr_3C_2(Cr_3C_2-WC), powder mixture, steel bonded, exam. of sintering behaviour 78—52712
$TiCrB_2$-Ni(Ni-Mo) systems, interphase reactions, electron probe anal., metallography and hardness exam. 80—2990
TiN-CrN system solid solns., electrophys. and galvanomag. props., energy spectra 77—15847
TiN-CrN systems, solid solns., mag. props. 77—12086
TiO_2-Cr_2O_3 rutile, Cr_2O_3 effects on O_2 tracer diffusivity, depth profile meas. by SIMS 80—24651
TiO_3:Cr_2O_3, dielec. consts., AC and DC resist. 80—20186
$TiSi_2$-$CrSi_2$, phase equilib., struct. and props. 80—50608
UO_2:Cr_2O_3, fission gas release and swelling 80—47567
$V_{1-x}Cr_xO_2$, VPE and elec. and optical characterisation 78—3053
$(V_{1-x}Cr_x)_2O_3$, Raman scatt. and phase transitions 80—71420
$(V_{1-x}Cr_x)_2O_3$, thermal props., rel. to phase transition 77—35709

chromium compounds continued
$(V_{1-x}Cr_x)_2O_3$, vapour phase transport, single cryst. growth *(French)* 77—24940
$(V_{1-x}Cr_x)_2O_{3+y}$, elec. props. and struct. 80—84494
$V_xCr_{3-x}S_4$, elec. and mag. props. 79—28523
VN-CrN solid solutions, thermal cond., Lorentz number 80—15317
VN-CrN system solid solns., electrophys. and galvanomag. props., 77 to 1300K 77—24567
VN-CrN systems, solid solns., mag. props. 77—12086
VO_2-$CrNbO_4$, solid solns., synthesis and phase diagram 80—35171
V_2O_3-Cr_2O_3, struct. and mag. props. 78—27041
V_2O_5-Cr_2O_3, phase diagram 77—70040
$YCrO_3$-Cr eutectics, prep. and microstruct. 80—108380
YPO_4-Cr_2O_3, system, oxyorthophosphates form. 79—78942
$ZnAl_2S_4$-$ZnCr_2S_4$, nonstoichiometric spinel solid solns., synthesis and cryst. chemistry 77—35526
$ZnCr_2Se_4$, magnetoelastic coupling, mag. suscept. meas. 78—76288
$ZnCr_2Se_4$:In, magnetoresist. and elec. resist. above and below Neel temp. *(Russian)* 80—88576
$ZnCr_2Se_4$:Mn, paramagnetic, giant cubic anisotropy 80—7073
$ZnMn_{1-x}Cr_xFeO_4$, Mossbauer effect, quadrupole splitting 80—29664
ZnO-Bi_2O_3-Sb_2O_3-Co_2O_3-MnO_2-Cr_2O_3, nonohmic ceramic, microstruct. exam. 78—47292
ZnO-Cr_2O_3, crystal structure, valence of chromium ion rel. to variation of Cr/Zn ratio *(Rumanian)* 79—65057
ZrO_2-Cr_2O_3 system, react., phase diagram 1600-2400°C 79—11580

chromosphere
5 min oscillation, possible heating mechanism for chromosphere and corona 77—17519
acoustic dissipation and H^- radiation, rel. to heating 78—96454
acoustic dissipation and H^- radiation 79—30029
acoustic wave refl. in transition region 80—36607
acoustic waves, radiatively damped, hydrodynamic code 77—13300
active region, 1978 April to May, chromospheric dark ribbon morphology *(Chinese)* 80—8613
active region, mag. and vel. fields config. and changes 77—17486
active region surges and coronal heating, Skylab X-ray images examination 78—12190
active regions, bidimensional spectroscopy obs. with birefringent filter *(Italian)* 80—98568
active regions, coronal and transition region temp. struct. 80—67692
active regions, currents sheets as heating source 78—28634
active regions on solar limb, 1175 to 1940 Å emission-line spectra 78—96446
activity from moving mag. feature in McMath region 12417 80—98642
activity in F- and G-type stellar chromospheres 77—53594
Balmer lines intensity fluctuations 79—53793
boundary layer structure influence on solar wind 79—53788
brightness distrib. at 3 mm wavelength, obs. at 1976 October 23 eclipse 79—30042
chromosphere-corona transition region, EUV obs. compared with filament-corona transition 78—28620
chromosphere-corona transition region, interpretation of C III and O V emission line ratios 78—28598
chromosphere-corona transition region, nonequilib. plasma density diagnostics via C III EUV Lines 78—53899
chromosphere-corona transition region, optically thin lines, OSO-8 obs. 77—9729
chromosphere-corona transition region, shock heating and emission lines form. 77—56889
chromosphere-corona transition region, thickness rel. to plasma flow along coronal sheared mag. arches 80—62092
chromosphere-corona transition zone, dynamics over sunspot, OSO-8 obs. 77—9728
continuum radiative losses, comparison with mechanical energy supply 80—72924
contrast profiles interpretation, embedded feature model 77—33443
convective instability of finitely conducting viscous model chromosphere 80—56790
convective noise waves, dissipation in mag. struct. rel. to chromosphere heating 78—65600
corona transition zone of solar active regions, non-thermal velocities *(French)* 80—77371
corona-chromosphere transition region, EUV models 78—69767
current sheet region during chromospheric flare development *(Russian)* 79—40159
downflow in supergranulation network rel. to transition region models 78—61838
dynamic response to soft X-rays from flares 78—65580
eclipse observations using plane grating as polar heliostat 79—84674
emission line profiles of inhomogeneous formations 77—37586
enhanced network, K-line obs. 77—78751
EUV and radio emission from chromosphere-corona transition 79—8894
EUV emission line nonthermal broadening near quiet solar limb 79—48748
EUV emission lines, profiles meas. near solar limb 79—16909
EUV line emission obscuration near limb 79—48762
EUV network in quiet regions 77—2386
Evershed flow in chromosphere-photosphere transition region 78—65593
faculae, initial growth phase and development 77—74030
faculae, mag., vel. and brightness struct. 79—25557
faculae, photoheliographic results, (1968 to 1971) 79—2487
fibril changes in small flare, high resolution obs. 79—44452
fibrils, lifetime and evolution 77—29760
fibrils evolution rel. to flare activity 77—17487
filaments and flare obs. 1967-9, Hα monochromatic light 78—61836
fine struct. and time var. of quiet Sun at 1.3 cm wavelength 79—30043
fine structures extending into corona, Hα obs. *(French)* 78—28607
five-minute oscillation, IR continuum obs. 77—78745
five-minute oscillations, horizontal energy flows struct. 80—62103
five-minute oscillations, influence of chromosphere and corona 77—91501
flare, 1973 June 15, Hα, magnetic and X-ray morphology 78—4173
flare, He I levels populations calc. 79—62809
flare soft X-ray radiation, chromospheric response 77—56885
flare spectrum, electron beam diagnostics 80—26827
flare transition region, thermal radioemission theory *(Russian)* 79—48763
flare upper chromosphere, semiempirical model 79—40148
flare/surge events, hydrodynamic simulation 80—12748

chromosphere continued
flares, ATM evidence for low nonthermal proton/electron energy flux ratio 79—8887
flares, chromosphere 3835 Å emission rel. to soft X-ray flux 78—89156
flares, effective time of observations *(Russian)* 78—40893
flares, effects of soft X-ray heating 79—40170
flares, energy transfer to chromosphere by soft X-ray photons 77—82210
flares, H Lyman α direct collisional excitation rel. to profile and polarisation 80—41780
flares, initial phase parameters determ. method 80—62104
flares, long-lived radioactive nuclei generation rel. to quiet Sun γ-ray emission *(Russian)* 77—45390
flares, Lyman continuum obs., energy transfer, chromospheric evaporation 79—21266
flares, O I 1355.6 Å and C I 1355.8 Å lines obs. 80—90381
flares, optical thickness and H ionization degree from Balmer line obs. 78—73694
flares, parameters and fine struct. determ. 78—24499
flares, plasma heating by energetic nonthermal electrons, theory 77—53505
flares, prod. of pulsed microwave bursts with quasithermal spectrum 77—78762
flares and associated radio emission *(Italian)* 78—96457
flares fast electrons scatt. in atm., X-ray spectrum 78—77542
flares nonthermal electron beams, reverse currents effects on chromospheric energy deposition 80—51711
flares occurrence rel. to sunspot mag. field oscills. 77—67084
flares X-ray emission, rel. to cosmic ray intensity preflare enhancements 78—45166
flares X-ray emission rel. to optical radiation 77—22188
flash spectrum, obs. at 1979 February 26 eclipse 80—67687
flows in magnetic flux tubes 78—16393
Fraunhofer line cores formation, empirical statistical model 78—7963
Fraunhofer line cores formation, empirical statistical model 79—12450
gas entry into non-spot magnetic tubes 77—78749
gravity waves generation by HF acoustic waves, Cherenkov radiation *(Russian)* 77—17265
Hα post-flare loops dynamics, 1973 July 29 flare 80—31286
heating by solar flares, charged particles beam collisional interaction with H target 78—93095
heating by sound waves 79—21246
heating processes, short period waves 77—74022
high-resolution observations, by LPSP expt. on (OSO-8) 77—64649
hydromagnetic structure near supergranule boundary, supersonic model 77—13298
impulsive flares, space-time relation to centimetre wavelength radioemission bursts *(Russian)* 79—16924
inhomogeneous model, for interpretation of data on quiet Sun mm wavelength emission 79—35231
K faculae as tracers of solar differential rotation 77—53501
limb flare, 1959 July 25, spectrum rel. to physical conditions 80—105227
limb spectra from Skylab, 2000-3000 Å region 77—45376
limb spicules, time evolution study of spectra 77—2387
line profiles calc. for inhomogeneous emission formations 79—25562
line profiles from OSO-8 spectrometer meas. 80—67690
linear hydrodynamical equations coupling with radiative transfer in non-isothermal atmosphere, method 78—20794
Lyman α filtergrams, high resolution, new transition region structs. obs. 80—82323
magnetic field above flocculus, determ. from radio obs. 80—98635
magnetic field strengths, lower limit 79—48746
magnetic fields of active regions, zero points 78—96465
magnetic neutral lines, assoc. with X-ray arches 77—17511
magnetic structures, models *(Italian)* 78—81603
magnetoacoustic wave propagation, resonance phenomena 77—13306
magnetoatmospheric waves conical propag. and spicule motions 77—49351
mass column density, rel. to Ca II line width Wilson-Bappu effect 79—12464
mass flow and ionization equilib. 80—36608
mechanical flux determ. from Ca II lines 80—67680
metallicity meas., chromospheric activity effects 79—53784
MHD shock waves, propag. in solar atmosphere 78—24503
MHD wave propagation in mag. flux sheath in presence of vel. field 79—62735
microwave brightness temperatures and circular polarisations from thermal regions, derivation 77—22172
microwave bursts, polarisation features interpretation 78—96468
model development for chromosphere and transition zone *(Russian)* 77—64726
modelling, hydrodynamic and mag. features *(Italian)* 78—81599
models, survey of last 30 years' research 78—69764
motions, EUV obs. by OSO-8 *(Italian)* 78—81602
network, evolution during active regions development *(Russian)* 78—57531
network, photospheric layers models from Mg II h and k line wings 78—57518
network, quiet 2.8 cm emission, small-scale sources 79—5794
network model 79—48747
network pattern, identification with 1.35 cm radiogranulation *(Russian)* 78—40897
network structure, from medium resolution EUV obs. 78—20801
observations and interpretation *(Italian)* 78—81604
observations and models, review of present knowledge 79—66976
oscillation mode and vel. amplitude of waves 79—21263
oscillations, power spectra, phase spectra and coherence spectra 79—8897
oscillations in mag. tubes, spectral line obs. 79—25564
oscillations obs. in C II 1336 Å line by OSO-8 78—28625
oscillations obs. with OSO-8, average phase spectra for Si II 79—62801
oscillations obs. with OSO-8, average power spectra for Si II 79—62800
oscillations obs. with OSO-8, basic meas. and analytical methods 79—62799
peak separation due to microturbulence 80—109407
periodic brightness fluctuations at 2.8 cm wavelength, rel. to photospheric vel. oscills. 79—35216
photosphere-chromosphere transition region, spectra during eclipse June 30 1973 80—8614
plage, absolute u.v. intensities meas. in 1750-2100 Å range 77—2405
plage development rel. to spectra and models *(Russian)* 77—64725
plage fragments, characts. assoc. with photosphere network props. 80—98634

chromosphere continued
plages, contrib. to Ca II lines vars. at solar minimum at cycle 21 onset 79—16907
plages, physical props. models based on Ca II and Mg II obs. 78—89153
plasma ejection during solar transients, rel. to He^+ obs. in interplanetary shock wave 80—72735
quiet and active, Lα spectra and models based on partial redistrib. diagnostics 79—75169
quiet disc, high resolution spectroscopy, space-time vars. 77—53498
quiet limb, emission measures, electron densities and nonthermal vels. from optically thin UV lines 77—17454
quiet solar chromosphere structure, form. *(Russian)* 79—48764
quiet Sun, activity, microspicules obs. in Hα and He I D_3 line 79—66983
quiet Sun, ubiquitous chromospheric structs. observed at mm and cm wavelengths 79—12456
radiation loss and mechanical heating 77—29784
radiative equilibrium departures, grey absorpt. 78—81531
radiative losses from solar and stellar chromospheres, empirical estimates 78—40915
radiative relaxation time 79—30040
radio brightness distrib. at 8.6 mm wavelength, interferometer obs. 77—2388
radio granulation, obs. by RATAN 600 telescope 77—78760
radio radiation, spectral polarisation obs. of local sources during March (1970) 77—53535
resonance line scatt. from optically thin structs. located above solar limb 78—65591
resonance line spectrum, polarisation in line cores 77—29744
rotation, obs. during 1972-73, years of declining activity 78—4186
rotation depend. on size of tracer features 80—12731
rotation rel. to chromospheric feature lifetime 79—44442
scaling laws, width-luminosity correls., Wilson-Bappu effect 79—40177
shock heating, methodological discussion 77—29745
shock waves and convection in flare region heated by electron stream 77—71079
short period acoustic heating theory appl. to chromospheric models *(Italian)* 78—85926
sinusoidal compressive waves radiative dissipation 79—84770
Skylab obs. of quiet and active solar events 77—56891
Skylab X-ray obs. and mag. field correls., computer solns. 77—82198
spectra, optically thick line formation, atmospheric dynamics 80—94767
spectra, spatial struct. in 3398 to 3560 Å region lines at extreme limb 79—12449
spectral line formation, C II reson. lines obs. rel. to temp. struct. 78—53896
spectroscopic Doppler rotation rates, 1966-1978 period 79—66977
spicule inclinations, statistical study 77—91508
spicules, contrib. to solar EUV line emission 80—4325
spicules, Heζ/H8 relative intensities in spectrum 78—40904
spicules, influence on brightness var. at extreme limb in centimetre radio waves 80—21969
spicules, influence on EUV limb brightening 77—22170
spicules, resonant response to granular buffeting 79—44444
spicules, simultaneous K and D3 line obs. *(French)* 77—29763
spicules and stability analysis of min. flux corona theory 80—41795
spicules generation, rel. to flare-assoc. mechanism for solar surges 80—21975
spikes, obs. during 1973 June 30 eclipse, photometric anal. 77—17520
structure compared with photospheric struct. 77—29777
structure from brightness distrib. at mm wavelengths 79—53799
sunspot, UV emission line spectrum obs. 77—13296
sunspot chromosphere, radial vel. and brightness oscills. regimes *(Russian)* 80—51727
sunspot mag. field motion rel. to proton flares 77—17488
sunspot umbrae, Ca II H, K and IR lines interpretation 78—53901
sunspot umbrae, Ca II H and K emission line shapes and centre to limb vars. 77—22178
sunspots, gases rot. motion *(Russian)* 77—64716
supergranulation, Mg I λ2582 line profile var. 79—40164
surge, EUV limb spectra obs. from Skylab 80—17560
synchrotron radiation from MHD shock wave front of magnetic field discontinuity, astrophysical appls. 77—25939
temperature and electron density above sunspot umbrae 78—53908
temperature at chromosphere photosphere boundary, from emission spectrum in far infrared *(German)* 80—51721
temperature distribution, acoustic wave heating 77—53508
temperature minimum, absolute brightness temp. meas. in far IR with balloon-borne interferometer 80—62095
temperature rise, acoustic waves effects 79—16911
transition region, Alfven wave reflection 77—29754
transition region, Bowen fluoresc. rel. to electron density determ. 78—93179
transition region, C V and O VII emission line ratios interpretation 80—98624
transition region, dielectronic recombination 77—36751
transition region, diffusion effects on comp. 80—46525
transition region, downflow of spicular material 77—33448
transition region, dynamic model rel. to coronal loops stability 79—101132
transition region, EUV line emission weakening short of 912 Å wavelength 80—21962
transition region, first-row elements excitation equilib. and line intensities 79—12401
transition region, line intensities from Si VI, VIII and XII excitation calcs. 80—31273
transition region, mass motions in impulsive flarelike brightenings, OSO-8 obs. 79—35217
transition region, Ni IX to Ni XII lines identifications from laboratory wavelengths 80—99474
transition region, origin for UV and radio fluctuations 80—90398
transition region, OSO 8 UV obs. of optically thick region 80—56788
transition region, relative chemical abundances in different solar regions 80—46518
transition region, shock wave dissipation 77—60740
transition region, Si V 1393 Å line in coronal hole and quiet Sun, OSO-8 obs. 77—91511
transition region, spectrum in vicinity of Si IV 1122 and 1128 Å 78—4170
transition region, temp. gradients from XUV He I, He II emission lines centre to limb behaviour 78—40888

chromosphere continued
transition region, theoretical network structure for coronal holes 80−85917
transition region, theoretical network structure for quiet Sun 80−85916
transition region and chromosphere, OSO-8 obs. of wave propag. 78−93183
transition region and inner corona, energy balance 80−90379
transition region and inner corona, temp. distrib. 79−75190
transition region compared with prominence-corona interface 77−29786
transition region downflow, evidence from Mg II core absorpt. wavelengths 79−12451
transition region emission, spectral obs. in Hα region 79−35233
transition region in quiet Sun, evidence for overlying EUV continuous absorpt. 79−92738
transition zone, area var. of supergranule network features with temp. 78−89152
transition zone, density diagnostics for EUV spectrum 77−60739
transition zone, energy balance and press. for network and active region features 80−21957
transition zone, EUV lines from limb brightening data in coronal hole 80−82333
transition zone, nonresonant heating mechanism *(Chinese)* 80−85921
transition zone, nonthermal effects assoc. with steep temp. gradients 79−84771
transition zone, search for turbulent free region 78−4174
transition zone, Si IV line profile vars., rel. to MHD disturbances 78−28626
transition zone, wave refl. and wave disorder 79−12453
transition zone dynamics 79−21247
transition zone instabilities rel. to preflare energy build-up, spectroscopic far UV obs. 77−17479
transition zone lines, quiet Sun, limb broadening, OSO-8 obs. 79−48752
transition zone plasma evolution during 1973 August 9 compact flare 79−5792
transition zone structure from Skylab NRL spectrograms 79−48744
transition-zone plasmas, electron densities and mass motions in flares 80−56804
UV and soft X-ray full-disc solar fluxes, rocket obs. 77−87360
UV spectra, preliminary results from OSO-8 LPSP instrument 78−49317
velocity fields, observations *(Italian)* 78−81601
velocity fields, theory *(Italian)* 78−81600
velocity gradients, rel. to Mg II line profiles 77−17460
velocity waves propag. in quiet chromosphere 77−22198
wave propagation in nonisothermal atmosphere, rel. to solar five minute oscills. 80−31276
wave propagation in the quiet chromosphere, near IR and Ca II line obs. 77−78746
waves, vertical propag., phase delay obs. 79−96981
waves in lower regions, energy transport 79−62804
X-ray and Hα flares comparison 78−7971
X-ray flare kernel, site, size, spatial stability and energetics 79−25555
XUV spectra of 1973 June 15 flare from Skylab, allowed transitions 77−78730
C I multiplets at 1560 and 1657 Å, overlapping emission peaks obs. and theory 78−93178
C III 1909 Å and Si III 1892 Å emission lines, echelle obs. 80−31277
C IV profiles at 1548 Å, OSO 8 time series 79−53785
C-like ions emission lines, density depend. 80−21963
CO emission lines in UV spectra of sunspots and flare 79−53795
Ca II H and K lines cores in integrated sunlight, rel. to solar activity 78−77535
Ca II K and Hα obs. during 1969 at Kodaikanal Obs. 78−61832
Ca II K line and Hα obs. of filaments, flocculi and prominences, during 1969 at Kodaikanal Obs. 78−61833
Ca II K line emission widths 77−41373
Ca II K-line emission, absolute fluxes rel. to H-R diagram 77−56937
Ca II lines, vel. and temp. disturbances, weighting functions 80−67679
Ca II network, differential rotation rel. to photospheric plasma 79−25585
Ca$^+$ network, giant cell circulations 79−8895
CaII K-line brightness fluctuations, statistical analysis *(Russian)* 79−21259
H I Balmer α line brightness fluctuations, statistical analysis *(Russian)* 79−21259
H I Lα/Hα ratio for flares, quasars and prominences 78−61826
H Lyman α and β lines, OSO 8 disc centre obs. compared with theoretical profiles 79−8888
H_2 emission in UV spectra of sunspots and flare 79−53794
Hα macrospicules, identification with EUV macrospicules and X-ray bright point flares 78−16361
Hα observations close to limb 78−28628
Hα off-band pre-flare activities 77−74025
Hα photography 78−40833
Hα plage formation after flare 79−44445
Hα, seven components form. rel. to 9873 MHz line appearance 78−89151
Hα spicules, dynamics at various heights, spectral obs. 80−90392
Hα spicules, spectra, props. 79−25563
He, $^3S \rightarrow 2^1S$ transition probability, electron collisions 78−5358
He I, D_3-line profile meas. with birefringent filter 78−4177
He I, He II XUV emission lines, intensity ratios and distrib. functions 78−57516
He I 10830 Å line obs. in undisturbed chromosphere 77−71102
He I 5876 Å line emission, height distrib. in middle chromopshere 77−17525
He I D_3 line obs. of spicules, photoionisation model 78−65592
He II 304 Å and He I 10830 Å spectroheliograms, comparison 78−20799
He II Balmer α line components 77−33436
Li production during white light flares 77−71092
Mg I and II, line profiles calc., comparison with expt. results 80−82320
Mg II h and k lines, Skylab high-resolution obs. 78−36544
N IV and Ne VII emission line ratios, electron density and temp. determ. 80−17559
Na distrib. and nonthermal motion vels. from D-line eclipse obs. 77−22200
Na I D-lines, formations beyond limb, filaments 79−96987
S I 1807 Å and 1900 Å lines, anal. of profiles 78−57517
Si I series in UV spectrum, 3000 to 1200 Å 77−56882
Si II, Si III, EUV emission line profiles, centre-to-limb vars. 78−28627

chromosphere continued
Si II, Si III lines, spectrum synthesis 78−36543
Si II 1816 Å line profiles and chromospheric vels., OSO-8 obs. 77−13301
Si II 1816.93 Å line profiles and persistent vel. fields, OSO-8 obs. 77−9730

chronographs *see chronometers*

chronometers
digital, 'Heathkit', operating instructions *(French)* 78−24765
digital chronometer with seven-function selector *(French)* 78−12677
digital event timer, liquid crystal display 77−5811
electronic quartz optically coupled chronometer 79−26036
horological microprocessor, design and circuit architecture, functions *(French)* 80−90822
marine chronometers, 1770-1920 79−39
quartz electronic watch, past and possible future developments 79−93102
shock wave velocity meas. unit 77−24039
Swiss watch and clock industry, microprogrammed counter logic *(French)* 80−8963
synchronisation circuit, for digital clock, using transmitted time code 79−67257
timekeeping clock synchronisation and comparison problems and equipment 77−71302
Re-Os nuclear chronometer, reliability, rel. to element rel. abundance 78−85919

CIDEP
acetate ion radicals, solns., pulse radiolysis, CIDEP, viscosity depend. 77−75189
acetate radical CIDEP, appl. of ns time-resolved EPR in pulse radiolysis 80−43075
benzophenone in isopropanol, submicrosecond time resolved EPR, lser photolysis, CIDEP polarisation mech. 78−80764
p-benzosemiquinone monoprotonated radical, submicrosecond time resolved EPR, lser photolysis, CIDEP polarisation mech. 78−80764
chemical reactions, spin-selective, radical pairs, density matrix description 77−12790
chemically induced dynamic spin polarisation, orientation depend. 80−63656
CIDNP/CIDEP, S−$T_{\pm 1}$ mixing in high mag. fields, theory 80−9619
conference, chemically induced mag. polaris., Sogesta, Italy, (April 1977) 78−13523
duro-semiquinone monoprotonated radical, submicrosecond time resolved EPR, lser photolysis, CIDEP polarisation mech. 78−80764
electron exchange effects, vector model 80−1004
enhancement factors meas. 79−50052
experiments, review 78−13528
finite element method, stochastic-Liouville eqn. 79−64018
infinite elements, in variational soln. of stochastic-Liouville eqn. 79−94014
intensities, time depend. 78−13536
light modulated expts., triplet and radical pair mechanisms 78−13538
low field effects, extension of Pedersen-Freed theory, $T_{\pm} \rightarrow S$ transitions 79−36664
micelle solns., aq., pulse radiolysis, CIDEP in time-resolved EPR 77−30891
photosystem I, of green plants and algae, CIDEP obs. 80−63679
potential forced diffusion 79−72339
pulse radiolysis study, examples of S-$T_{\pm 1}$ polarisation 78−86891
quinones, triplet quenching by organometal cpds., time resolved CIDEP and ESR obs. 80−95654
radical pair and triplet mechanisms 78−13524
radical pair mechanism 78−13527
radical pairs, electron spin motion, diamag.-paramag. exchange, mag. field effect 79−98123
radicals, radiolytically produced, CIDEP 78−13534
radicals prod. by flash photolysis, CIDEP 78−13535
in radiolysis, S-$T_{\pm 1}$ polarisation in H radical reactions 77−48656
secondary free radicals, primary reacting with substrate electron spin relax. time, theory 78−25573
surface diffusion and spin polarisation, 2-D CIDEP, asymptotic Green's function method appl. 80−91584
theory, radical-pair and triplet mechanisms 77−6809
theory, stochastic-Liouville vector model with asymptotic soln. 78−66567
transient radicals, EPR time profiles, CIDEP, electron spin-echo method 79−6953
triplet mechanism, vector model 80−48020
triplet mechanism 78−13537
two-dimensional fluid, and Heisenberg spin exchange 80−14157

CIDNP
benzoyl peroxide thermolysis, CIDNP obs. in low mag. fields 77−30885
biradical, triplet state, S-T_0 CIDNP, biradical scavenging rate const. from mag. field depend. CIDNP 79−3461
biradical magnetic field dependent ^{13}C and ^{1}H CIDNP, hyperfine coupling 79−3460
chemical reactions, spin-selective, radical pairs, density matrix description 77−12790
chemically induced dynamic spin polarisation, orientation depend. 80−63656
CIDNP/CIDEP, S−$T_{\pm 1}$ mixing in high mag. fields, theory 80−9619
conference, chemically induced mag. polaris., Sogesta, Italy, (April 1977) 78−13523
cyclododecanone, photolytic biradical anomalous CIDNP enhancement, pulse spin echo NMR obs. 78−46369
cycloheptanone, photolysis, CIDNP effects 80−18869
N,N-diethylaniline-pyrene, photochem. polarisation transfer, scalar paramagnetic exchange mechanism 78−25557
dispiro compound I, pyrolysis, CIDNP, S-T mixing, nuclear Overhauser effect 77−6803
finite element method, stochastic-Liouville eqn. 79−64018
free radical reaction, chemically induced dynamic polarisation in strong mag. field, radical rotation influence 80−76509
free radical reactions, spin-dependent reaction probabilities theory 78−20002
furil, photochem. reduction by pentachlorophenol, zero-field CIDNP study 77−90625
furil + pentachlorophenol, photochem. reduction, cross-relax. and CIDNP, PMR relax. obs. 79−52694
gas phase reactions, CIDNP effects 80−18869

CIDNP continued
  geminate recombination of radical ions in polar solvent, mag. field modulation, fluoresc. quenching 77—4912
  infinite elements, in variational soln. of stochastic-Liouville eqn. 79—94014
  intensities, time depend. 78—13525
  low field effects, extension of Pedersen-Freed theory, $T_{\pm}\rightarrow S$ transitions 79—36664
  magnetic field depend. in low fields 77—30885
  methanol, aq., radiolysis, CIDNP, methoxy radical involvement 78—53223
  nitroaromatic compound+anion radical, photo-CIDNP, acid-base equilib. effects 77—75185
  nuclear spin isotope effects 80—69167
  nuclear spin polarisation intensities, exciting light polarisation plane depend. 79—89688
  numerical methods, model depend. 78—13530
  pancreatic trypsin inhibitor tyrosine residues in soln., laser photo-CIDNP as surface probe 78—73138
  2-phenylcycloalkane, photolysis products studied by ^{13}C CIDNP and intersystem crossing 79—79275
  polarisation transfer, scalar paramagnetic exchange mechanism 78—25557
  polarisation transfer via nucl. dipolar relax. and spin-spin coupling 79—54867
  polymethylene chains, conformations, mag. field dependent biradical CIDNP 77—27097
  polymethylene flexible biradicals CIDNP and chain dynamics, field depend. 77—88473
  proteins in solution, laser photo-CIDNP as surface probe 78—73138
  pulse radiolysis applic. 77—32814
  pulse techniques applic. 78—1007
  radical ion reactions, photo-initiated, CIDNP 78—13526
  radical pair and triplet mechanisms 78—13524
  radical pair mechanism 78—13527
  spin dependent probability of reaction, radical pair theory 78—21943
  spin dependent reactivity in high mag. fields 78—13529
  trifluoroacetophenone+dimethoxy benzene. in acetonitrile photoreaction, nuclear spin polarisation, criterion for triplet-Overhauser mechanism 80—69168
  triplet Overhauser mechanism 78—13531
  two-dimensional fluid, and Heisenberg spin exchange 80—14157
  ^{13}C, CIDNP, obs. in reactions of organic and inorganic radicals during pulse radiolysis 80—63660
  Na_2+Na, spin polarisation exchange via opt. pumping, NMR 77—14452
  NaK+Na, spin polarisation exchange via opt. pumping, NMR 77—14452

cinefilming *see cinematography*

cinematography
  see also cameras; telefilming
  16 mm cine projection lens 79—72646
  16 mm projection installation, automatic, containing Ukraine-5 projector and ring bifilar magazine *(Russian)* 79—36980
  35 mm, effects of aspheric surfaces on optical performance and appl. to lenses 79—89021
  35 mm camera, necessity for production of number of apparatuses *(Russian)* 80—37111
  35 mm projectors, new projection lenses 80—87469
  acousto-optical light modulator for laser image recording on cinefilm *(Russian)* 79—89027
  additional meas. flashing technique *(Russian)* 78—54486
  additive film copying machine, modulator mechanodigital design *(German)* 78—65987
  angiography, physiological event marking using ECG R-wave triggering 77—52873
  animated cartoons, computer appl. *(Russian)* 80—105739
  Arriflex 35BP-II motion picture camera mounted with 350PF-1A zoom lens for wide-screen filming *(Russian)* 80—95176
  audio equipment development, Soviet cinema industry, survey *(Russian)* 78—29201
  automatic control system for high speed cine cameras *(Russian)* 80—285
  Beaulieu cine camera, 16 mm, time lapse apparatus 78—74089
  biomedical US images, cine display 80—108984
  bladder pressure noninvasive determ. from micturition cinecystourethrogram 79—92370
  brightness meter, 2Y aKP, using CdS photoresistor, optical system 77—10090
  camera automatic focusing mechanism principles and designs 79—30595
  camera development, interdisciplinary and international approach 80—81342
  camera spectrometer, for colour temperature meas. *(Russian)* 77—38050
  camera supply, control and synchronisation systems *(Russian)* 78—49936
  cameras, guide elements, use of powdered polymer coatings 78—78021
  cardiac scintigraphic cineangiography with ECG gating 77—9255
  cell flagella, laser damage, high speed cinematography 80—81785
  cell study, optical device for time lapse recording in vitro *(German)* 79—74813
  cellulose triacetate films, local loss of stability, expt. anal. using high speed cinefilming *(Russian)* 79—58822
  chemical photographic processing of colour positive motion picture films *(Russian)* 80—93780
  chemical-photographical processing influence on physical-mechanical props. of motion picture materials *(Russian)* 78—93778
  chip-formation process control 79—63319
  chromaticity analysis for automated TV complex 3 zonal objects registration process *(Russian)* 79—89026
  chromaticity of camera lenses, spectral transmission curves analysis 80—31925
  cine objectives quality evaluation, frequency transfer functions, measuring instruments *(Russian)* 77—41718
  cinefilm copying equipment using interference light filters, additive printing appl. *(Russian)* 80—62774
  cineholographic method for interferometry of fast processes 77—71958
  cineholography, investigation of high-speed events 78—37842
  cinema acoustics *(Russian)* 79—18609
  cinemicroscopic time-lapse unit circuit 79—67405

cinematography continued
  cinemicroscopy, beam deflection as alternative to light shuttering 78—21214
  cineroentgenography, quantitative biplane method, error propag. 78—73224
  cleaning negatives, internegatives by wet-buffing process 80—37101
  coherent illumination design aspects *(Russian)* 80—42280
  colour analyzer Tsvet-2 and printer OZX-A, changes and improvements *(Russian)* 80—22467
  colour and density table, film processing appl. *(German)* 79—49309
  colour atlas for colour organisation in film production *(Russian)* 78—93776
  colour duplication, Laboratory Aim Density control method 77—5953
  colour film copying techniques, lighting control *(German)* 80—62751
  colour film printer, rapid-acting light-setting mechanism *(Russian)* 79—35878
  colour film processes and cameras, review, 1894 to date *(German)* 78—93773
  colour motion picture using diffractive surface-relief structures 78—37089
  colour negative film Gevacolour type 682, 35 mm, 16 mm professional film making appl. 80—82838
  colour negative film LN-8, properties *(Russian)* 79—2861
  colour negative motion picture process, latensification representation *(Russian)* 78—86373
  colour photographic processing distortions *(Russian)* 79—17533
  colour positive cinefilm standardisation on sensiometric tests *(Russian)* 80—287
  colour reversal cinefilm, rapid processing technique, TV studio's appl. *(Russian)* 80—3385
  colour separation tests, computer appl. *(Russian)* 77—49796
  colour telecine camera KT 116 M *(Russian)* 78—29200
  computer simulation of photographic process, Syntha Vision 77—183
  computerised control of film production, automatic systems development *(Russian)* 80—42287
  contact print preparation of cine films using modified 16 mm cine projectors 79—6203
  continuous film copying equipment *(German)* 80—68281
  coronary artery disease, abnormal left ventricular contraction pattern cineangiography 79—83930
  densitometer measurement transformation into spectral density distrib. and colour coordinates *(Russian)* 80—77902
  digital photographic sound track recording optimisation *(Russian)* 78—89580
  digital rostrum controller, Pacesetter, computer control of animation filming process appl. 78—45743
  drops, fast-moving, interaction with liq. film surface *(Russian)* 79—64756
  dual language Super 8 sound system, airborne passenger entertainment appl. 80—4785
  dual track sound, picture recording and mixing system *(Russian)* 79—17532
  editing 16 mm film synchronised by time-code system 78—24875
  electron beam recording, film speed choice, TV image appl. *(Russian)* 77—38049
  electronic editing system *(Russian)* 79—89029
  environmental control processing wastes, industrial plants appl. *(Russian)* 79—44964
  equipment designs, Moscow design office *(Russian)* 80—62772
  equipment designs from Odessa design office over 25 years *(Russian)* 80—62771
  equipment development forecasting for 35 mm cameras *(Russian)* 80—284
  exposure control based on brightness measurement *(Russian)* 79—2862
  exposure measurements, quantitative study of additional measured exposure, continuous processing appl. *(Russian)* 80—62775
  exposure meter with photoresistor, semi-automatic, bridge circuit error calc. *(Russian)* 77—54008
  external synchronization of electric drive SA-120 when shooting combine pictures with TV images *(Russian)* 80—86484
  film, Fujicolour colour negative and positive 79—85191
  film camera construction impact of electronics *(German)* 77—79170
  film copying, automatic system for estimation of exposure conditions *(Russian)* 79—35877
  film copying, measurement of optical properties of film materials *(German)* 79—35867
  film copying, objective control of completeness *(Russian)* 77—54010
  film flicker effect caused by AC lighting source *(German)* 80—27363
  film grain multiplicative noise anal. 78—58932
  film processing, analysis of contamination products in main drainage systems *(Russian)* 79—89023
  film processing, effect of antifogging substances on Ag grain size *(Russian)* 79—67414
  film processing, use of microprocessor equipment 80—31915
  film processor, Russian 9P-55, with intensive solns. feed for cine-film negatives *(Russian)* 79—49324
  film production, use of different computer techniques 80—77887
  film production development and future *(Russian)* 80—9065
  film production technique and technology at Russian Mosfilm studio *(Russian)* 80—22462
  film production using address-time coding, 35 mm, electron image editing method *(Russian)* 79—17531
  film projection, sound track synchronisation, new system *(German)* 79—67402
  film slitting in the laboratory 78—93770
  film sound tracks, electronic cutting, thyristor appl. *(Russian)* 78—21252
  film soundtracks, low-cost pure, undistorted sound 79—27476
  film speed varying for repeated exposures at varying intervals *(Spanish)* 78—8459
  films, 16 mm Fujicolor reversal film RT 500 and RT125 80—106585
  films, new Gevacolor negative film type 682 80—106586
  films and processes, non-standard *(Russian)* 79—49326
  flow measurement, plane mixing layer vortex digital image processing 80—103095
  focused ultrasonic cleaning system, Covaral film protection, cinefilm appl. 80—31916
  frame count cueing system, Du Art, minicomputer appl. 78—37086
  frame position indicator in aperture during wide screen projection of films with latent covering *(Russian)* 80—37113

cinematography continued
  gait analysis, for daily orthopaedic practice, 2-D cinephotography, 6 component force measurement 77—48908
  hand position and forces during manual work, documentation method 79—74803
  high energy CO_2-laser pulse, interaction with liquid and solid targets, optical investigations 78—42829
  high resolution time lapse cinemicrography, use of improved air stream incubator 80—98196
  high speed, fluid flow and heat transfer visualisation *(German)* 79—86540
  high speed camera CKC-1M modifications and control *(Russian)* 80 105740
  high speed cine photography, in industrial engineering environment 78—37099
  high speed film processing solution management for ferricyanide bleach and fix, Rotex system 79—54206
  high speed movie recorders, human factor problems in artistic design 77—30212
  high-speed, high-intensity lighting 78—54483
  high-speed cineradiography, of projectiles 78—41395
  high-speed holocinematography of cavitation bubbles 78—37841
  high-speed intermittent cameras for research 77—49795
  high-speed motion picture photography and oscillography, synchronisation 80—8969
  high-speed movie camera, angle measuring reticle insertion into field of view 77—30213
  high-speed photography, increase in image quality using plate polyhedral compensator *(Russian)* 79—35879
  high-speed photography and photonic recording 78—86367
  high-speed with laser illumination *(Russian)* 80—279
  high-velocity gas jets, interaction, photographic study 78—42695
  holocinematography, high speed, acousto-optic beam deflection for spatial freq. multiplexing 78—74860
  holocinematography, high speed, spatial multiplexing for image separation 77—46704
  holographic, for cavitation bubble dynamics recording 79—86147
  holographic, principles 79—85192
  holographic, shooting parallax panoramogram and apparatus for stereo images *(Russian)* 80—22466
  holographic, three min film, ruby laser appl. *(Russian)* 78—29917
  holographic cinematograph systems for three-dimens. colour images *(Russian)* 79—26169
  holographic cinematography *(Russian)* 80—43295
  holographic cinematography in USSR 78—78976
  holographic cinematography system, integral photography with large aperture lens *(Russian)* 80—43296
  holographic interference fringes, real-time cine recording 80—23642
  holographic movie camera and projection system 80—78808
  holographic process for color motion-picture preservation using 3 lasers 79—17530
  holographic screens for colour flat image projection *(Russian)* 80—9066
  home movie sound track using stereo tape 78—16883
  home-made motion picture optics, development *(Russian)* 80—22463
  horse's hoof movement/load relationship camera and multicomponent force meas. panel *(German)* 79—16352
  illumination control of cine projectors, foreign equipment *(Russian)* 80—105741
  image evaluation with changing definition, grain, visual effect *(Russian)* 79—58814
  image information properties, highspeed vs. standard processing techniques *(Russian)* 79—58817
  image intensifiers for rapid filming, microchannel proximity tubes characts. *(French)* 78—49917
  image quality improvement, dependence of resolving power on lenses and filters *(Russian)* 80—27371
  image quality transfer 80—68279
  image sharpness index derivation, frequency transfer function, multistep cinematography *(Russian)* 77—34046
  Image Transform computerised videotape to cinefilm transfer system, signal improvement appl. 78—45742
  industrial cinefilm printer winder motor starting characteristics, motor with deep slip appl. *(Russian)* 78—29199
  information eval. of image quality for cinematographic systems *(Russian)* 78—54485
  information reflection systems automatic control *(Russian)* 77—74541
  instant cine film development and projection 78—78012
  instant high-speed colour, Polaroid system, scientific and engineering appls. 80—98993
  IR travelling matte system with electronic masking 79—75642
  laryngeal cinematography, high speed, optical/lighting system 80—17055
  laryngeal films, ultra high speed, automated anal. 78—36023
  laryngeal films, ultra high-speed, automated anal. 79—57746
  laser based, operation and applications 80—57405
  laser produced cavitation in water, behavioural study by holocinematography *(German)* 78—87371
  left ventricular cineangiograms, computing appl. for numerical information, wall movement obs. 77—90891
  lens performance meas. system, routine checking appl. 80—277
  lens-array photographic system, depth of sharp focusing, resolution 80—62763
  lenses, retrofocus type, design 78—37963
  lenses for photo-pattern production, Fabry-Perot interferometer appl. *(Russian)* 78—37959
  lenses with fixed and variable focal length, comparison of types *(Russian)* 80—27370
  light sources for Super 8 film projectors, short-arc lamp filled with rare earth halogens 80—62747
  lighting intensity ripple caused by metal halide lamps with alternating supply 79—75641
  lighting with metal-halide discharge lamps, luminance fluctuations assessment 80—4796
  lip synchronised recording technique for speech translation in cinefilms *(Russian)* 80—105737
  liquid cavitation technique for cleaning cinefilm 80—31918
  liquid crystal indicator of variable light-reading angle 78—57932
  liquid flow meas. *(Italian)* 78—14107
  liquid-waste, treatment in laboratories *(Japanese)* 79—54209
  Loch Ness and Morar Photographic Expedition (1979) 80—68280
  luminaire systems, statistical eval. *(Russian)* 79—89030

cinematography continued
  luminaires, development of techniques and technology *(Russian)* 80—27372
  MagnaScope 35 mm half-frame projection system 79—40637
  magnetic sound records release print KMP-23 *(Russian)* 80—90918
  magnetic stripe construction, coating techniques, sound reproduction quality 79—85188
  magnetic tapes, electroacoustic characteristics, multiple printing appl. *(Russian)* 77—38048
  magnetic tapes usage, ferromagnetic dispersions characteristics, structural and magnetic *(Russian)* 78—16886
  manual movie camera, Kinor 35P *(Russian)* 80—90917
  marksmanship training, moving target screen system with laser beam firing 78—54488
  materials sensitometric parameters automatic analysing instrument *(Russian)* 77—41720
  mechanical impulse testing techniques, computer evaluation, high-speed film recording 78—44343
  metal halide lighting parameters 78—21232
  metal plate high-gradient transverse deformation interferometry 78—82024
  microcinematographic analysis of cytotic processes of unicellular organisms 79—100800
  microscopic plankton, holographic motion pictures 78—48946
  mixing boxes for motion picture studios *(Russian)* 80—62773
  mixing complex at motion picture studio *(Russian)* 80—86483
  modular contact printer for high speed automatic additive colour film printing 80—42276
  monochrome, magnetic field effects on development process *(Russian)* 79—17534
  monochrome prints using two silent 16 mm projectors as contact printers, medical research lab. appl. 79—35865
  motion picture camera device for shooting in movement *(Russian)* 78—93777
  motion picture camera gyroscopic stabilisation system, anal. of dynamics and accuracy *(Russian)* 80—95173
  motion picture image brightness, time amplitude, sensitivity of visual analyser *(Russian)* 80—9063
  motion picture rerecording, warning system devices and electronic digital counter utilisation *(Russian)* 80—95177
  motion picture sound track, freq. distortion and two dimens. sound record scatt. *(Russian)* 80—95175
  motion picture studio management *(Russian)* 80—286
  movie camera, amateur, experience in developing company style 80—27369
  movie projector, 35-mm, VKF tooth drums *(Russian)* 80—9067
  movie projector 35KCA, unified type *(Russian)* 80—9062
  moving commutation station PKS-1 for Olympiad-80 *(Russian)* 80—22468
  neural unit activity rel. to movement, photographic technique for anal. 80—67310
  nuclear-medicine image display system, dynamic physiological function visualisation 79—5396
  object-related colour reproduction in film scanning [TV broadcasting], TV broadcasting appl. *(German)* 80—105726
  objective lenses testing by projection 80—9060
  ocular cinema photography 80—67186
  OMNIMAX system using Leitz wide-angle lens, domed roof in planetarium appl. 80—276
  optical component blank pressure shaping, semiautomatic apparatus 79—72731
  optical image immobiliser, Hollogon Skanner 78—37087
  optical sound track reproduction using photodiode as current source 79—10439
  photochromic tracer film, measurements using POLLY, film reading computer system 78—42696
  photographic sound track, KINTEK 7 channel system 80—28403
  photometric eval. of high speed cinematographic films, microprocessor control 79—21801
  picosecond X-ray cinematography, picosecond optical range gating 77—81549
  point light source, high-intensity, with adjustable light duration 78—42399
  Polavision, first instant colour movie system 78—24882
  polyester filmbase experience in motion picture industry, review 80—42278
  pool barbotage, heat transfer coeffs., high-speed cine-photography and oscillography 78—90982
  principles for indexing claws and maintenance characts. *(Russian)* 79—49325
  printing, wet, using variable speed step-optical printer 77—79175
  printing and processing conditions for dye transfer process materials, choice using automatic systems *(Russian)* 79—75643
  printing using new colour attenuation system 79—2859
  production association Ecran, 25 years of achievement *(Russian)* 80—62770
  professional technique development, 1978 *(Russian)* 79—89022
  projection brightness meter *(Russian)* 77—49797
  projection equipment for 16 mm films, perspectives *(Russian)* 80—77903
  projection systems, automation *(Russian)* 79—35876
  receiver for parallel operation of radiomicrophones *(German)* 80—4787
  recording equipment KZM-24, post-synchronization *(Russian)* 80—86482
  recording of fast processes, extension of meas. parameter ranges 80—57413
  recording techniques for video information transferred from magnetic tape 79—21835
  reflex cine camera Bolex H16, conditions for using ordinary lenses 79—26154
  renal diagnosis by blood circulation angiocinedensitometry *(German)* 79—2127
  rerecording panel 70K-21, modernisation of indicator desk *(Russian)* 80—37114
  retinal image cinematographic recording, accommodation microfluctuation appl. 80—81579
  reversal cinefilm development, effect of temperature, concentration factors on speed of process *(Russian)* 80—105735
  review of technical progress in 1977 in USSR *(Russian)* 78—89579
  rotating lens system for cine projection with continuous film transport 80—62766

cinematography continued
- running loop control systems, technical details *(Russian)* 80—289
- setting instrument for EBU/IRT time codes *(German)* 80—18029
- single-frame, automation *(Russian)* 78—86374
- small format anamorphic reduction printing using lateral maskings 80—281
- sound film production, cine film sizes, film transport mechanisms, tutorial series *(German)* 79—49310
- sound negative film, Eastman sound recording II film, 5373/7373 80—62768
- sound processing circuit diagrams *(German)* 80—18031
- sound quality monitoring, acoustic factors 78—33961
- sound reading systems for cine projectors, fibre optics appl. *(Russian)* 78—312
- sound recording, acoustoelectric data of 35 mm magnetic tapes, magnetic tracks on 70, 16 and S8 mm film prints *(Russian)* 79—18665
- sound recording and reproduction using a holographic method *(Russian)* 79—10273
- sound recording and reproduction using digital systems *(Russian)* 79—27487
- sound recording equipment *(Russian)* 77—74540
- sound reproduction improvement in cinemas *(Russian)* 79—10430
- sound reproduction in cinema, automatic control *(Russian)* 80—38212
- sound reproduction system Century, transistorised *(Russian)* 79—14194
- sound track films, appl. of computer program simulation of recording and reproducing system 80—62767
- sound track quality improvement *(Russian)* 80—288
- sound track quality increase using direct positive photographic sound tracks *(Russian)* 80—22464
- sound track recording, Dolby stereo procedure for optical sound prints *(German)* 80—18030
- sound track recording equipment, 35, 32 mm film appl. *(Russian)* 79—89024
- sound track stripe applicator, control system, colour release prints for both positive, reversal stocks appl. 80—42275
- sound-track cinefilms 3T-8, 3T-7, comparison *(Russian)* 80—105738
- spectral, colorimetric characteristics colour positive cine film dyes *(Russian)* 79—49323
- spectral characteristics of cine camera zoom lenses, measuring techniques *(Russian)* 79—49322
- starting tension reduction study, winding, unwinding cine film appl. *(Russian)* 79—58815
- stepper motor drives for use in synchronous interlock systems for cinematographic special effects 80—98991
- stereo film projection, in 3D motion picture theatre *(Russian)* 78—86371
- stereophonic film production using 4-channel photographic sound track, CCD, system Colortek *(Russian)* 79—58818
- stereophonic sound in anamorphic super-8 wide-screen prints 80—282
- studio lighting control, ring power supply system appl. *(Russian)* 79—2863
- Super 8 cinecameras, sound-recording unit *(German)* 79—80707
- Super-8 film, problems of printing from widescreen film, stereophonic soundtracks *(German)* 80—42279
- swimming parameters of aqueous organisms, determination by cine recording and computer processing *(Russian)* 77—32921
- synchronisation of film with EMG data by LED display device, rats appl. 77—81754
- synchronised with EMGs, function vastus, calf muscles in humans appl. 77—81468
- synchroniser cct. for image, sound in amateur cine films *(Russian)* 79—6210
- telecine, description of Thomson-CSF flying-spot twin format telecine *(French)* 80—37110
- telecine, digital storage techniques, colour film scanning appl. *(German)* 80—4786
- telecine FDL 60, CCD line scanning, digital frame store 80—278
- telecine projection machines, Telekino-75, optical-mechanical systems *(Russian)* 79—76800
- theatrical sound effect for cine films *(Spanish)* 79—41550
- thiosulphate processing technique, cinefilms appl. *(Russian)* 80—3386
- thunderstorm photography and lightning recording with modified cine sound camera 79—21058
- thyristor feeding device type TPU for light sources *(Russian)* 79—58816
- time control system, Q-Lock, for editing, dubbing 80—68278
- time lapse cinemicrographs of cultured cells, computer-aided analysis 78—92756
- time multiplier using thin mag. film, design and performance characts. *(Russian)* 80—299
- time-code system for synchronising 16 mm film, magnetic tape sound recording 78—24874
- time-lapse, time recording on 16 mm film 79—9252
- travelling Matte technique of optical trick cinematography 80—31917
- TV broadcasting appl. *(German)* 79—35866
- TV colour, electronic colour corrector for TV cameras, TV motion picture broadcasting appl. *(Russian)* 79—49321
- TV colour films, usable subject contrast range *(German)* 80—57408
- TV facilities, development and introduction *(Russian)* 80—22465
- TV microscopy and cinephotomicrography with Zeiss Axiomat 80—27343
- TV signals on cine film, electron beam recording *(Russian)* 78—21251
- two dimensional image scanning of movies using surface acousto-optic interaction 79—94352
- underwater filming, colour correction of illumination *(Russian)* 79—75645
- universal film copier *(German)* 80—18032
- UV-cured inks for edge numbering on all motion picture films 79—9254
- ventriculography, algorithm for automatic selection of end diastolic and end systolic cine frames 78—88757
- vibration of apparatus meas. by holographic interferometry *(Russian)* 80—37112
- videodensitometric camera and video disc system 77—40761
- videodensitometry and image analysis, minimum computer system 79—34664
- water throwing device for special effects *(Russian)* 79—89028
- wet printing systems development and future 79—21826
- X-ray, brazing mechanism obs. appl., high-temperature, kinetics of filling capillary gaps 77—5954
- X-ray cinematographic systems for ballistics diagnosis 80—13194
- X-ray obs. of gas injection into liquid metals 79—49360

cinematography continued
- X-rays, pulsed and continuous, motion picture filming of moving objects 78—57057
- zoom lens system design and manufacture 80—68288
- Cu, neutron irrad. cryst., slip band, growth rate, high-speed cinematographic recording 79—7607
- Xe lamp, electronic ignition *(Russian)* 77—41719

circuit analysis *see network analysis*

circuit analysis computing
- *see also circuit CAD*
- equivalent resistance program for teaching 77—5615
- fusion reactor, PHIBEX, poloidal field power supply for ignition, computer based cct. anal. 80—102329
- fusion reactor, Shiva Faraday rot. coils, circuit and mag. anal. 78—54951
- inductive transducer, technique for computing basic characts. 80—4696
- nonlinear network noise anal. using linear and nonlinear differential equats. *(German)* 77—88997
- Space Shuttle lightning current distrib., circuit modelling and exptl. verification 78—49293
- vertebrate retinal horizontal cells, spatial integration, computer analysis of network model 77—36920

circuit breakers
- *see also circuit breaking arcs; gas blast circuit breakers; oil circuit breakers*
- analogue safety data link, for Princeton Large Torus control room 78—54938
- arcs, HV, AC, switching, spectroscopic measurement of temp. distribution in constant pressure axial air flow *(Czech)* 80—86296
- ASDEX circuit breaker system, design, calcs. and tests 78—55032
- current measurement, using electron beam deflection tube 78—54393
- electric breakdown SF$_6$, contamination with metal particles theoretical model *(Italian)* 79—64937
- electronic, for biomedical recording and stimulation 79—34680
- exploding wire with inductive energy bank, quasistatic model, resistivity meas. 78—47199
- explosively actuated 100 kA switch, 70 μs opening time 78—8984
- fast circuit-breaker driven by magnetic pressure, fusion reactor appl. 80—13899
- fusion reactor, Doublet III, ohmic heating E-coil vacuum breaker system, function and operation 80—102323
- high current switch, fast closing, for fusion reactor field coils 78—74484
- high pressure gaseous flow in nozzles *(Spanish)* 79—98781
- HVDC interrupter test facility, dual 30 kA systems 78—55035
- interrupter and hybrid-switch testing for fusion devices 80—99289
- liquid metal plasma valve, 15 kA-30 kV, fusion reactor application 78—74488
- load coil, 1.5 MA, 10 MJ, for pulsed homopolar machine 78—13336
- oscillatory circuit with current breaker for discharge laser excitation 77—14759
- plasma science, conference, Monterey, CA, USA (May 1978) 79—37442
- plasma sheath breakdown to glow transition in plasma filled gap 80—100105
- toroidal field system on TEXT Tokamak, DC regulation 78—55038
- triggered vacuum gap, semicond. coated dielec., firing characts. 77—47286
- vacuum interrupter, for for high voltage DC current, for fusion reactors 78—74489
- Al, foil, elec. explosion, immersion medium effects 78—67389
- Cs-Ba discharge, grid-controlled switching element, spontaneous current cutoff 80—19626

circuit-breaking arcs
- *see also circuit breakers; sparks*
- AC arc, axially blown with N$_2$, field strength and energy balance eqn. 78—87523
- air blast arc, post-zero current and power loss meas. 79—19106
- air blast circuit breaking arcs, elec. grad. using plasma probe methods 78—87527
- breaking process, characts. calc. method *(German)* 77—76220
- current zero arc model based on forced convection 80—33831
- DC arc in blocked nozzle, boundary layer integral method anal. 80—6295
- deformation by narrow insulating slot *(Russian)* 80—28861
- electrode energy balance and arc column electrical conductivity meas. *(French)* 80—28864
- fuselink, high breaking capacity, arcing phenomena anal. 77—11425
- fusion switch vacuum arc development 78—13341
- gas blast arcs, very high current, elec. conductance of arc gap 78—87524
- gas blast circuit breakers, current zero period, boundary layer integral method 78—87522
- gas blast circuit breakers, radiative transfer investigation 79—27864
- gas blast circuit breakers, three nozzle arc models, review 79—27862
- gas blast circuit breaking arc, arc diameter, RF technique 78—87528
- gas blast circuit breaking arc, thermal disturbances in hot gas surround 78—87529
- gas blast circuit breaking arcs, air and SF$_6$, energy clogging 78—87531
- gas blast circuit breaking arcs, electron temp. at current zero, 3 kA arc 78—87526
- gas blast flow with arc heating 79—46502
- high current arc, turbulence 78—47197
- high current diffuse vac. arc, stable mode with ring array rod electrodes 78—9894
- high-current vacuum arc in a magnetic field 78—71572
- HV, AC, switching, spectroscopic measurement of temp. distribution in constant pressure axial air flow *(Czech)* 80—86296
- HV gas blast circuit breakers, arc mechanism and control 80—92409
- induction calc. using standard finite element software 79—41906
- laser-triggered breakdown in gases, basic processes responsible studies 80—38794
- plasma valve design with liq. metal cathodes, high-power conversion/switching appls. 78—9865
- quenching, plasma turbulence effects 79—27861
- radiative energy transfer 80—1416
- radiative transfer, magnetic stability, and turbulent heat exchange 78—75482
- slot, narrow insulating, cross-section current distrib. 77—72515
- speed high current of arc along flat electrode *(French)* 79—37572
- vacuum, anode spot and ion form., review 77—80382
- vacuum arc subjected to axial mag. field 80—6296
- weak mag. field driven arc velocity and configuration obs. 78—71596

circuit-breaking arcs continued
  SF_6, 20 kA arc, electrode vap. contamination, time depend. energy balance 78—87525
  SF_6 arc field distrib. and conductance in current-zero region 78—71590
  SF_6 breakdown at moderate temps., investigation 79—27863
  SF_6, gas blast circuit breaking arc, clogging transition 78—87530
  SF_6 high-current arc props., influence of electrode material 78—71592
  SF_6, high-temp. circuit-breaking arc, axial and radial heat transport 79—19105
  SF_6, optically thick, convection-loss dominated model 78—87519
  SF_6, plasma diagnostic techniques *(Japanese)* 78—55768
  SF_6 plasma thermodynamic props. at arc extinction temp. and pressures 80—79435
circuit CAD
  see also circuit analysis computing
  bandpass filters, SAW, withdrawal weighted CAD 78—66991
  digital bandpass filters instrumental realisation, operator parameters selection by computer modelling *(Russian)* 79—74984
  IEEE International Microwave Symposium, Orlando (1979) 79—68356
  International Microwave Symposium, San Diego, Calif., USA (June 1977) 78—5478
  SAW digital filter design using optimum pulse response techniques 77—46872
circuit design *see network synthesis*
circuit diagrams
  education, variable star, digitally synthesized, diagram 79—9067
  electrochemical recording of defect records in US inspection 79—66246
  polarimetry, balanced photorecording circuit compensation for laser illumination fluctuations 77—57379
  radioactive decay, electronic analogue, demonstration apparatus circuit 78—41122
  rapid heating attachment, for IMASh-5S installation 80—21230
  status monitor, for Elliot rotating-anode X-ray source 79—35908
  voltage follower, high impedance, for student lab. expt. on photoelec. effect 78—41109
circuit oscillations
  see also circuit resonance
  analogue circuits, dual mechanical and dual electrical, mutual energies and reciprocity law *(German)* 77—53772
  forced oscillations experiment for students 80—17780
  HF circuit, gas-discharge plasma excitation, operation anal. 77—39494
  Josephson junction, long, oscills., exact solns. of sine-Gordon eqn. 78—68115
  laser discharge, stimulated reactive oscills., laser-elec. circuit Q 77—58315
  magnetic film in elec. circuit during HF mag. reversals, coupled oscills. *(Russian)* 78—23307
  two coupled systems, reduction of effective noise temp. *(Russian)* 77—75790
circuit reliability
  see also quality control
  atrioventricular sequential demand pacemaker, R-wave sensing methods *(Japanese)* 79—5406
  cardiac pacemaker, high-reliability hybrid IC procurement 80—30942
  cardiac pacemaker semiconductor component reliability trends 80—30943
  IC, assessment using scanning electron microscope 78—24902
  optical semiconductor devices for fibre transmission systems, reliability tests 80—43464
  shift register, assessment using scanning electron microscope 78—29215
  VLSI processing by low-pressure CVD, review 79—87581
  Au conductor bonding performance and failure mechanisms 79—71436
circuit resonance
  see also circuit oscillations
  education, capacitor complete discharge time, thermal noise 80—17727
  passive resonant circuit detector for remote meas. of intracranial press. *(French)* 77—37074
  quartz crystal gravitational radiation antenna, Q factor 78—16715
  student experiment, dielectric consts. and capacitor dissipation meas., RLC ccts. 77—82339
circuit synthesis *see network synthesis*
circuit theory
  see also distributed parameter networks; filters; lumped parameter networks; network analysis; network parameters; network synthesis; network topology
  angular spectrum of EM field, elec. network equivalent 78—78867
  current in external circuit, induced by charged particle motion in device, for teachers 79—21503
  DC, teaching, approach using rectangle dissection 80—46757
  dissipative slowly modulated steady state, dQ=TdS far from equilib. 78—81934
  dual representation with field theory, Poynting's theorem 80—94963
  education, capacitor complete discharge time, thermal noise 80—17727
  education, elec. electric energy density in dissipative medium by cct. analogue 78—36759
  education, electrical circuit equivalent resistance and capacitance 78—69938
  elastic waveguide, appl. to YIG nonreciprocal thin film acoustic device design 77—85042
  mesh analysis using graph theory, generalised procedure, teaching 80—101681
  simple DC circuits, student concepts 80—77569
  thermodynamics, chemical and biological systems modelling appl. 78—20955
circuit topology *see network topology*
circuits *see networks (circuits)*
circular polarisation *see polarisation*
circular waveguides
  100 GHz bolometer mount efficiency meas. calorimeter *(Japanese)* 78—54460
  antenna array system, radioastronomy appl. 78—24465
  complex waves in a circular dielectric waveguide 79—81337
  cylindrical optical fibre transmission and guided mode behaviour 80—28348
  cylindrical waveguide filled with uniaxial, collisional, hot and moving plasma, dispersion for TE and TM modes 80—106934
  dielectric resonance method for determ. parameters of magnetodielec. materials 79—17449
  dielectric screened three-layer waveguide, cut-off characteristics and modal inversion 80—1303
circular waveguides continued
  elastic cylinder, end resonance under axisymmetric vibr. *(Ukrainian)* 80—23932
  electron beam in circ. waveguide electrostatic instability in rippled magnetic field 80—19588
  EM scattering by spherical shell with arbitrarily located circular aperture, anal. 78—62989
  EM wave propag. along rotating dielectric column in circular waveguide 78—1133
  far IR laser mode losses 77—38954
  flexible hollow waveguide, IR light propag., optical losses 77—19389
  hollow cylindrical anisotropic dielectric guide, propagation 79—32047
  inhomogeneous circular waveguide, asymptotic eigenvalues 80—53442
  laser, construction and operation characteristics *(Rumanian)* 78—59049
  light pipe coupling, design 77—7187
  linear travelling wave induction, long cond. cylinder, EM fields 78—46484
  microwave diathermy, circularly polarised direct contact applicator design and performance 78—7531
  microwave generation by relativistic electron beam propag. in circular waveguide 80—48128
  mm-wave, time-domain techniques for meas. and equalisation 77—18020
  optical, multilayer, negative dispersion and strong higher order filtering 78—13809
  optical, two-layer, light depolarisation, theory and expt. *(Russian)* 78—9454
  optical inhomogeneous circular waveguide, asymptotic eigenvalues of vector waves 80—96010
  optical modulator efficiency in thermal mode *(Russian)* 79—94345
  optical strip type, fabrication by Ag ion migration 80—96042
  optical wideband modulator, parameter optimisation *(Russian)* 79—94344
  partially filled plasma waveguide, dipolar modes, field and power density distributions 77—7555
  radially inhomogeneous waveguide modes, vector wave characts. 80—78960
  relativistic electron beam, radiation efficiency in periodically inhomogeneous mag. field 77—23608
  submillimetric waveguide laser for gas spectroscopy 80—33022
  TE_{0n}-mode filters for VLA radiotelescope circular waveguide system 79—66922
  Very Large Array waveguide transmission system for radiotelescope 77—5444
  X-ray transmission, curved Pb glass capillaries 78—86395

circulators (microwave)
  commutable circulator, with increased mean-power level 78—4637

citation analysis *see information analysis*

civil engineering
  see also architecture; building; dams
  aseismic bearing foundation system for power station earthquake protection 80—83206
  beams, eqn. of motion of large amplitude vibration of beams *(Japanese)* 80—33511
  Beck's rod, nonconservative flutter system, variational principle 79—1132
  bridges, dynamic interaction of moving vehicles and structures 80—64357
  building materials from reactor waste, γ-radiation dose rate calc. 79—18057
  circular arches with flexibly supported ends, spatial symmetrical vibrations and stability 79—3953
  clay layer, non-homogeneous, consolidation estimation method 79—58110
  column carrying concentrated mass, parametric reson. 79—1102
  continuous Timoshenko beam vibrations on Winkler Pasternak foundations 79—3955
  design to resist earthquake loading 80—81844
  Dnieper navigable lock, V.I. Lenin hydroelectric power station, problems *(Russian)* 77—86883
  earthquake engineering, amplification problem of elastic wave propag. in anomalous layers 79—44260
  earthquakes connected with human engineering activity, tectonic and tectonophysical conditions for occurrence 77—81802
  elastic structure buckling models for higher order catastrophes 79—1122
  elastic-plastic finite element analysis, interpolation vs. iterative soln. for Tresca yield condition 78—59312
  fibre reinforced composites, apparent fibre spacing 78—79222
  flood control planning 78—81245
  foundation engineering, soil consolidation due to shear loads distributed over rectangular area 79—57936
  FRC, reinforcement parameter 78—79223
  heat transfer through walls, harmonic temperature waves obs., thermoconductometer development and appl. 77—49720
  Krsko, construction, architecture and reactor system cooling *(Croatian)* 80—37416
  long span bridges, rational design and struct. safety *(Japanese)* 77—7303
  mechanical dished supports, oscillation and stability conditions based on mixed finite elements *(German)* 78—87299
  nuclear reactor containment structure design and service loads 80—106138
  offshore disposal of dredged material, sediment props. as tracers 77—5245
  plastic structures, dynamic adaptation to stochastic excitation 79—1116
  plate, optimal design under dead weight and surface loading 79—3915
  polymer-concrete composites, civil engineering appls., technical, processing, economic merits 79—11545
  PWR containment vessel optimisation 80—106137
  rectangular cylinders in heaving mode, aeroelastic instability 79—3954
  road construction, nondestructive testing principles, instruments and methods *(German)* 79—11742
  sediment research, society's needs and professional opportunities 77—64342
  seismic engineering, two-dimensional horizontal ground motions during earthquakes rel. to structs. design 79—48419
  seismic Rayleigh surface waves, interaction with structures 78—81109
  structural anal., soln. by orthogonal collocation 78—51063
  technical meteorology, technical and commercial appls. *(German)* 80—46231
  Timoshenko beam with axial force, vibration characts. 79—3956
  triangular slab on elastic foundations, thermally induced vibrations 79—3960

civil engineering continued
US fault detection, MatEval computerised test system *(French)* 79–52564
water run off at Syr Darya, aspects *(Russian)* 77–86942
wind effects, anal. of thunderstorm gusts in Australia 77–86996

civil engineering computing
see also architectural CAD; town and country planning
acoustic noise reduction system effectiveness study *(German)* 78–5612
anisotropic shells symmetry considerations 77–11123
anisotropic solid fluid flow with free or artesian surface analysis, finite element method appl. 78–92872
beam columns and frames incremental anal. 79–3925
bending circular plates nonuniform, finite element analysis 77–7316
boundary elements in potential and elasticity theory 79–35560
buckling of elliptic plate, simply supported, under uniform compression 77–42758
CG method generalisation, linear and nonlinear problem appl. 79–30243
coastal aquifer water flow analysis 80–26654
column, nonuniform, lower bound buckling load, finite difference scheme 78–18200
combined sewer system detention storage, real-time control algorithm 77–37281
concrete, unreinforced pavement slabs, environmentally induced stresses, computer experiments 78–35435
concrete creep, unified concepts of constitutive modelling and numerical soln. 77–25093
concrete slab, reinforcement optimisation by linear programming 77–89022
concrete splitting test, nonlinear numerical analysis 77–7339
crack growth in concrete, computer simulation using Monte Carlo method 78–76764
crack propagation based on fracture mechanics 77–35094
dam groundwater flow anal. by finite element method 78–92875
dam porous media unsteady flow calculation, combined finite element/characteristics methods appl. 78–91012
damsites preliminary hydrologic assessment, streamflow generation 77–21817
deflection of cables, cylindrical suspended roofs with complex loading, incremental algorithm 78–9558
dynamic stresses induced by moving cracks, numerical soln. 77–11146
dynamics of shells of revolution under axisymmetric load involving shear deformation 78–79210
earthquake wave analysis program WAVE, DEMOS-E library program 78–92800
elastic-plastic finite element analysis, direct soln. vs. quadratic programming 77–42740
elastic-plastic-creep-large strain analysis at elevated temperature by the finite element method 79–37185
elastoplastic anal. using ASKA program system, bending, isotropic/kinematic hardening, tunnel construction 78–63312
elastoplastic arches, shakedown anal. 78–51091
embedded foundations, soil-structure interaction problem, spring method 78–79216
finite element analysis, structural engineering problems 79–2607
flexure of composite laminates using thick finite strip method 77–42739
flood flows routeing in rivers, parameter optimisation 77–37263
fluid dynamics finite element method appls. 77–26158
free surface flow digital simulation by finite element method 78–90819
free vibrational analysis of frame structures 79–32329
frictionless tidal channel behaviour digital simulation by finite element and finite difference methods 78–92876
glass plate, stress analysis of large deflection by finite element method 77–7307
groundwater aquifer model *(German)* 79–53377
groundwater discrete kernel generator digital simulation using finite element method 78–92873
groundwater flow calc. by finite element Galerkin method 78–89320
groundwater flow model using finite element method 78–92874
groundwater two-dimensional flow digital simulation using finite element method 78–93018
high precision triangular laminated anisotropic cylindrical shell finite element 78–79206
hybrid river models software support 80–56499
hydraulic fracturing operations, material and structural simulations 78–31540
interactive buckling analysis of box sections using dynamic relaxation 79–7304
large deflection analysis of plates and shells by discrete energy method 79–3918
linear strain triangular element solns. 78–90719
metal sheeting, profiled, shear deformation, stressed-skin anal. 79–1121
modal anal., formulations for numerical calcs. 78–57767
multistorey frames with nonuniform columns, pocket calculator program for buckling 78–1580
nonlinear free surface flow digital simulation by boundary integral eqn. method 78–92850
nonlinear static and dynamic response finite element analysis 77–27469
optimal water distribution systems design 78–61457
pipeline nonlinear anal. by potential minimisation 77–68552
plastic buckling of structures 78–63342
plasticity, assumptions, models and computational methods 79–32285
plate, orthotropic, transient response to uniformly distributed transverse load, computer calcs. 77–68503
porous media one-dimensional unsteady drainage digital simulation, finite element method appl. 78–91011
potential landslide sites mapping, digital simulation 77–37204
rectangular plates, moderately thick, free flexural vibr., effect of geometric nonlinearity 79–3940
rivers, ungauged, distributed numerical model for estimating runoff and sediment discharge 77–91177
rivers, ungauged, runoff and sediment discharge estimation, distributed numerical method comparison 77–91179
rivers runoff and sediment discharge model, response to meteorological input 77–91178
sea surface waves loading of structures, diffraction and refraction computation, using finite and infinite elements 77–81910
seismic risk anal. of discrete system of sites in New England 77–86785
seismic structure yielding rate approx. 77–2522
shallow water with moving boundaries digital simulation by finite element method 78–92847

civil engineering computing continued
shear connector fatigue loading, computer reconstruction of response 79–43539
shells with internally attached structures, transient response 79–3941
soil-structure coupling. Nonlinear rheological relationships and boundary conditions in soil mechanics 79–7354
steel reinforced concrete, computer expt. on slender beam columns 79–70127
storm water and sediment hydrographs simulation from small watersheds 77–37264
strain hardening structures under repeated loading, deflection analysis 78–63313
stratified turbulent flow digital simulation using finite element method 78–90964
structural mechanics, computerised symbolic manipulation 79–32327
structural reliability and safety, probabilistic methods 78–39978
SUPERB general isoparametric finite element program 77–42682
symbolic generation of finite element stiffness matrices 79–32244
thermal problems, one-dimens., with phase change, efficient numerical technique 78–59270
time split finite element algorithm for environmental release prediction digital simulation 78–92880
two-dimensional flow with singularities digital simulation by finite element method 78–90822
two-dimensional hydrodynamics and water quality digital simulation by finite element method 78–92877
unsaturated soil simultaneous heat and moisture transport analysis by finite element method 78–92868
urbanisation effect on floods, predictive model 77–37276
variable domain finite element model for dam unsteady compressible fluid flow digital simulation 78–90820
water network anal. using node recording algorithms and admittance matrix 78–85613
water network anal. using sparse matrix and successive linearisation methods 78–85614
well flow anal. using finite element method 78–92870

cladding techniques
cracks under stainless steel cladding of pressure vessel, detection, causes, danger 80–52760
explosive coating technique for metals and alloys 78–3260
HTGR fuel particle coating, improved gas distributor 77–79455
optical single mode fibres, ultra-low-loss, prep. of long lengths 79–76893
pyrocarbon, quality control techniques 77–79461
pyrocarbon, X-ray anal. of porosity, effect on radiation stability 77–79464
pyrocarbon coatings, quantitative chemical method to determ. disordered C component 77–79462
silica optical fibre, low loss, silicone cladding 77–65619
Al_2O_3/Al clad powder prep. and physicomech. props. 79–29010
ZrO_2/Al clad powder prep. and physicomech. props. 79–29010

claddings
AGR fuel, material aspects 80–47577
AGR fuel cladding, development of high strength, ductile stainless steel alloys 80–45367
AGR fuel element design improvement 80–23112
AK4-1 alloy, sheet mat., fatigue and corrosion fatigue strengths, coatings effects *(Russian)* 78–11397
alkali lime germanosilicate GRIN fibre prep., losses and geometrical props. 80–69560
austenite cladding layers, damping of ultrasound 80–104390
biaxial creep behaviour, ribbed GCFR cladding at 650C 78–86597
breeder reactor, effect of cladding coating and internal pressurization on fuel-cladding interaction, rod overall length change 79–54581
breeder reactor fuel pin end closures, pulsed magnetic welding 79–93806
BWR Dresden-3 fuel rods, pellet/cladding interaction induced stress corrosion cracking 79–67899
BWR fuel preconditioning, initial pressurisation, fuel temps., fission product release 80–63357
BWR fuel rods, cladding, failure propensity, Studsvik Inter Ramp Project 80–13534
BWR with graphite channels, safety of nuclear power stations 79–26561
CANDU reactor core, materials and design criteria for fuel, cladding, and fuel channel 78–13238
Caramel fuel cladding rupture, development and detection at OSIRIS experimental reactor *(French)* 80–95371
cracks under stainless steel cladding of pressure vessel, detection, causes, danger 80–52760
D16 alloy, sheet mat., fatigue and corrosion fatigue strengths, coatings effects *(Russian)* 78–11397
degradation by fission products during irrad. in FBR 77–34396
diamond-based, fabrication and wear resist. 80–40576
EBR II, metallic driver fuel, irrad. perform. at high burn-up, fuel-cladding interactions 80–95348
EBR-II, fabrication of in-reactor creep capsules using previously irradiated cladding tubes 79–54478
EBR-II, mixed-oxide fuel pins, results from expt. F11A after cladding break 79–67861
EBR-II 80–13598
EBR-II breached fuel element experience, safe reactor operation 79–9736
EBR-II Mark II metallic driver fuel, performance to 10 at.% burnup, cladding breaches 79–67863
EBR-II preparation for breached-element operation, safety concerns 79–9792
EBR-II subassemblies, 61-pin wire-spaced, exptl. confirmation of design to minimize vibr. and wear 79–67825
fast reactor cladding material, transient burst tests 79–93770
fast reactor fuel rods, burnup-dependent heat transfer from fuel to cladding 79–36323
fast reactor safety, TREAT experiments, fuel pin failure, statistical analysis 79–97840
FBR cladding dilatation, effect of radial temp. gradient 80–68776
FBR fuel cladding alloys, phase instabilities and swelling behaviour 79–54500
FBR fuel development, international development programs 80–102248
FBR fuel pin failure, fuel porosity and crack effects on transient overpower analysis 80–71760
FBR fuel pins, cladding attack model 80–45446
FBR R and D programs in Europe, basic objectives 80–47566
fill-gas comp. and eccentric gap geometry effects 78–13284

claddings continued
- fission reactor, power ramp investigations, clad hoop strain and pellet clad interaction 80—16440
- fission reactor, strain ratcheting during power cycling 80—16442
- fission reactor fuel cladding, internally pressurised, instrument for strain meas. 77—65271
- fission reactor fuel performance modelling, pellet-cladding interaction 80—63264
- fission reactor fuel rod geometry changes, mech. interactions calcs. 79—40993
- fission reactor irradiated cladding, in-cell facility for mechanical testing 80—21244
- fission reactor materials, clad failure prediction during FBR overpower transiency, JANE code 80—78363
- fission reactor materials, irrad. behaviour, chemical process, densification, corrosion *(Japanese)* 77—83033
- fission reactor Zircaloy cladding, effects of stress biaxiality on ballooning behaviour 79—30919
- fuel element defects, loss of cladding tightness, anal. of fuel element exploitation *(Czech)* 80—52736
- fuel form and cladding carbide distrib. on fuel-clad interaction during irrad. 79—85618
- fuel pellet-cladding axial interactions, computer anal. of fuel pin performance 80—13605
- fuel pins, fast breeder, fuel-cladding mech. interaction, obs. and anal. 80—86959
- fuel-cladding chem. interactions at high burnup 78—86584
- fuel-pin failure threshold, effect of pellet density and axial restraint 78—17367
- fusion-welded optical fibre splice loss expts. 79—37023
- gas cooled fast breeder reactor core element fabrication technology 77—18682
- gas cooled reactors, internal insulation 80—47537
- gas core reactor, high temp., wall stabilisation, possible use of graphite 79—3190
- GCFR advanced alloy cladding, oxidation behaviour in the environment 80—104350
- GCFR claddings, neutron-induced He implantation, calc. of total flux 80—42773
- glass edge cladding-glass laser disc interface, reflection meas. 79—27300
- glass fibres, clad, thermal stresses 80—107360
- glass rods, compressively clad, residual stresses, comparison of optical and fractographic meas. 80—108539
- graded-index fibres, evanescent theory and perturbation theory comparison 79—32033
- HFEF/N irradiated fuel element eddy-current exam., cladding performance 79—9750
- HTGR, coated fuel particles, fabrication technology 77—79456
- HTGR coated particle development in UKAEA fuel element labs. 77—79457
- HTGR coated particles, failure rate prediction during neutron irradiation 77—79466
- Inconel 718 cladding possibility for gas-cooled fast breeder reactor fuel 77—18667
- irradiated fuel rod NDT using encircling and probe eddy-current systems 79—9751
- irradiation expt. 78—86587
- isotope induction at LAMPF, fabrication, cladding, handling of irrad. targets 80—23231
- kohlestein insulation for use in HTR systems, further investigations *(German)* 78—66346
- laser, double-current-confinement channelled-substrate struct., near-field and beam-waist position 80—106553
- laser glass cladding composition and design criteria 79—18450
- lightguide fibre preform manufacture using modified CVD process 80—64228
- LMFBR, cladding meltdown phase for loss-of-heat-sink event during shutdown 78—8923
- LMFBR, core-disruptive accidents, neutronic and fuel element behaviour 80—32357
- LMFBR, effective conduction mixing lengths for subchannel anal. of finite hexagonal bundles 78—13210
- LMFBR, molten cladding film relocation following HCDA, large wave dynamics 78—17365
- LMFBR, multichannel cladding relocation model for loss-of-flow accident 78—17366
- LMFBR claddings with axial fins, stress anal. including creep effects 77—88224
- LMFBR cores, performance of advanced alloys 77—42092
- LMFBR fuel rod cladding tubes, effect of rod bowing on measured local temp. distrib. 80—638
- LMFBR transient undercooling accident, molten cladding, wetting of UO$_2$ cracked fuel 78—4993
- lossy outer layers multimode step-index optical fibres, effect on optical links 79—18540
- LPWR fuel cladding temp. predictions for LOFT LOCE L1-5 79—89446
- LWR, fuel rod microstruct. changes associated with post-DNB operation during power-cooling-mismatch 78—21688
- LWR, post-LOCA γ-ray energy redistrib. and effects 78—13280
- LWR, stress conc. in cladding produced by cracked fuel pellets 78—50260
- LWR fuel, pellet clad interaction failures 80—16441
- LWR fuel-cladding gap, Cs-U-Zr-H-I-O system, chemical thermodynamics 78—82440
- Magnox AL 80, ion beam analysis of corrosion films 77—8978
- MAGNOX fuel canning material, corroded, F conc. profiles determ. using ^{19}F(p,$\alpha\gamma$)^{16}O reaction 79—92035
- magnox fuel cladding, surface struct. data acquisition and processing system 80—898
- melting clad temperature distribution in fission reactor, Pekeris-Slichter series expansion method 77—88238
- metal clad fibre reinforced composites, debonding risk 80—3132
- metal cladding on optical waveguide, effect on modes 77—7184
- mixed-oxide fuel, cladding breaches 78—82450
- mixed-oxide fuel pin, cladding breaches 78—82451
- mixed-oxide fuel-cladding interaction at high burnup effect of initial stoichiometry 79—67859
- monomode optical fibre dimensions, dispersion, and losses *(German)* 78—33866
- multichannel GaAs laser array output synchronisation 78—42417

claddings continued
- multimode fibres, cladding influence on light attenuation 79—76855
- nitrided stainless steel alloy for AGR 79—54496
- nuclear advanced reactors, materials and design 78—78452
- nuclear fuel cladding, three-regions rewetting model with decay heat generation and inlet subcooling 80—22965
- nuclear fuel cladding motion in 37 pin loss of flow expt. 80—18541
- nuclear fuel cladding strain meas., microprocessor-controlled microwave extensometer 78—33240
- nuclear fuel element cladding, corrosion product deposition, heat transfer model *(Bulgarian)* 80—71818
- nuclear fuel element codes, structural anal. 80—78362
- nuclear fuel element model for cladding performance during power changes, strain defects 78—58359
- nuclear fuel pellet-cladding interaction phenomenon investig. 77—46299
- nuclear fuel removal from irrad. cladding, eval. of methods 77—54306
- nuclear fuel rods steel-coated, effect of impurities on clad-corrosion *(German)* 79—49693
- nuclear fuel sheath deform. following fuel power transients, simulation 78—33258
- nuclear reactor fuel cladding tubes, 20/25/Nb stainless steel, biaxial creep meas. 78—82442
- nuclear reactor pressure vessel/cladding interface, residual gas analysis *(German)* 77—40603
- nuclear reactor structural materials, WR-1 irradiation facility 78—89945
- optical compound glass fibres, silicone and glass clad, medium loss 80—69533
- optical fibre, elliptically clad borosilicate single-mode, strain birefringence 80—33148
- optical fibre, power-law graded-index, core/cladding power distrib., propag. const. and group delay 80—48420
- optical fibre, power-law refractive index profile, scalar modal eigenvalues and group delays 80—28322
- optical fibre, single-polarisation single-mode, exposed cladding fabrication 80—58725
- optical fibre clad with Teflonlike plastic coating, press. sensitivity 80—33149
- optical fibre fracture stress and mirror size obs. 79—37020
- optical fibre refractive index profile distortion due to thermal stresses 80—58726
- optical parabolic index fibre, modal dispersion characteristics, lossy cladding effect 79—18515
- optical single mode fibres, homogeneous CVD fabrication and characterisation 80—69562
- optical single-mode fibre with low attenuation, MCVD fabrication 80—53461
- optical single-mode low-loss silica fibre prep., 10 km long 80—48476
- optical waveguide, semiconductor clad, attenuation and propagation coeffs. 80—79004
- optical waveguide fibre cladding composition effect on stress corrosion and fatigue 77—3664
- PBF, cladding temperature, deform., and failure threshold 78—13281
- PBF, irradiated fuel rods, behaviour following film boiling operation 78—13282
- PCI-induced cladding strain, effect of fuel density and fuel relocation, in-reactor meas. 80—104408
- pellet cladding interaction failures, stress corrosion of fission reactor cladding tubes 80—16526
- pellet-cladding interaction, irradiation tests 78—86588
- pellet-cladding interaction induced by radiation-induced dilation, mech. anal. 78—13302
- polymer cladding/glass core optical fibre waveguides, high numerical aperture 80—96024
- pulse dispersion in a clad lens-like medium 80—53445
- PWR, fuel monitoring, by delayed-neutron detectors 80—737
- PWR, peak cladding temp. sensitivity to LOCA reflood parameters 78—86639
- PWR core power manoeuvres, fuel duties and fuel preconditioning, FLAIR-CENSOR 80—63337
- PWR fuel assembly design, stress, temp., radiation and chem. environment effects on performance 78—13310
- PWR fuel cladding, long ballooning deformation following LOCA 80—660
- PWR fuel rod failure during film boiling, power cooling mismatch test 79—89445
- PWR hypothetical LOCA sensitivity to fuel rod material props. 79—89436
- PWR LOCA reflood, effect of low containment press. on peak cladding temp. 80—57897
- PWR rods subjected to simulated LOCA in PBF 79—89443
- pyrocarbon, agglomerate model 77—79458
- pyrocarbon, coating process and model 77—79459
- pyrocarbon cladding, gas permeability *(French)* 77—14234
- pyrocarbon coated fuel, neutron effects in range 1273-1773k 77—79434
- pyrocarbon coating deposition by gaseous hydrocarbon pyrolysis, theoretical anal. 77—40459
- pyrocarbon coating of Biso fuel, neutron effects on stress and strain 77—79437
- pyrocarbon coating of Biso fuel, neutron effects on stresses and strains 77 79436
- pyrocarbon coating permeability effect on U redistrib. in HTGR fuel 77—40460
- pyrocarbon coatings, mass spectrom. determ. of fission gas permeabilities 78—12785
- pyrocarbon coatings, TEM anal. 77—79463
- pyrocarbon coatings for Biso fuel, the permeability meas. 77—79433
- pyrocarbon coatings on HTGR fuel particles, Bacon anisotropy factors meas. technique 79—13418
- reactor cladding waste, spent fuel contamination, composition and amounts arising in EC 78—66360
- reactor fuel cladding, in-reactor creep testing 77—23211
- reactor fuel cladding dilatation, influence of radial temp. gradient 77—46287
- reactor fuel cladding failure under reactivity initiated accident conditions *(Japanese)* 79—30955
- reactor fuel pin claddings, fission gas driven creep calcs. 79—26531
- reactor fuel rods, cladded, thermo-irradiation induced creep, stress analysis 80—35275
- reactor materials, thermal and irradiation environment influences and material responses 80—52737
- rod-in-tube fabricated optical fibre characteristics 80—87574

claddings continued
- SGHWR fuel pins, fuel cladding ratchetting study 78—54855
- silicone resin clad fibre technology, optical and mech. props. 80—28349
- stability of fuel element for gas-cooled fast reactors *(Russian)* 77—83042
- stainless steel, cold-worked Type 316, transient mechanical behaviour 78—86598
- stainless steel, design fix for vibr. induced wear in fuel pin bundles 77—42094
- stainless steel, mixed oxide rods, high burnup irrad. performance 77—3099
- stainless steel, type 304, stress free swelling at high neutron fluences 77—42093
- stainless steel, type 316, clad fuel rods for GCFR, high temp. fast flux irrad. tests 77—18666
- stainless steel, type 316, deform. meas. on mixed oxide nuclear fuel 77—42088
- stainless steel, type 316, irradiated cladding, second-phase precipitation 79—54501
- stainless steel, type 316, updated temp. integrity limit for FFTF driver fuel pins 77—42089
- stainless steel clad Pu assembly, postirradiation examination 77—42090
- steel, alloy cladding, oxidation behaviour in GCFR He environment 80—16594
- steel, austenitic, alloy and stainless, fuel-element cans, deform., failure, rigid loading scheme 79—91765
- steel, brass clad plate/roll bonded Ni clad, fatigue crack growth behaviour 80—40484
- steel, Cu-Zn, brass clad, fatigue crack growth behaviour 80—40484
- steel, ferritic, underclad cracking mechanism, effects of residual strain and heat affected zone ductility 77—25158
- steel, for reactor fuel, B distrib. after Na exposure and high-temp. 77—57719
- steel, proposed mechanism for internal cladding corrosion in LMFBR mixed oxide fuel pins 79—8384
- steel, stainless, 316, nuclear fuel cladding, crack nucleation 78—72864
- steel, stainless, 316, oxidation behaviour in the environment, appl. to GCFR fuel claddings 80—104350
- steel, stainless, clad oxide fuel pin, thermodynamic model for attack 79—97807
- steel, stainless, cladding, irradiation enhanced creep 77—42074
- steel, stainless, cladding dimensional changes in FBR $(U,Pu)O_2$ fuel pins due to swelling and inelastic strain 80—104296
- steel, stainless, cracks under pressure vessel cladding, detection, causes, danger 80—52760
- steel, stainless, creep behavior of ribbed cladding in prototypic GCFR coolant environment 80—16480
- steel, stainless, dilation and bowing in EBR II ducts and cladding 80—625
- steel, stainless, EBR-II fuel pin cladding, obs. of in-reactor creep and swelling 80—13600
- steel, stainless, fast reactor cladding tubes subjected to thermal transients, rupture behaviour 80—37465
- steel, stainless, FBR cladding stress distrib., effect of irradiation-induced swelling 80—19850
- steel, stainless, FBR fuel pin cladding, burst strength eval. 79—89378
- steel, stainless, FBR fuel pin cladding, in-reactor endurance and rupture life 80—13599
- steel, stainless, FBR fuel pin cladding strain under transient testing 80—18425
- steel, stainless, FBR fuel rod cladding damage correl. for rod perform. predictions 80—18424
- steel, stainless, GCFR ribbed cladding, post-irradiation creep rupture tests 80—18430
- steel, stainless, in-reactor deformation and fracture behaviour of EBR-II driver fuel cladding 80—42769
- steel, stainless, interaction with $(U\text{-}Pu)O_2$ fuel, electron microprobe anal. 79—26524
- steel, stainless, LMFBR fuel pin cladding long-term in-reactor corrosion by liquid Na 80—16593
- steel, stainless, LWR fuel cladding material evaluation 80—99213
- steel, stainless, nuclear fuel-cladding chemical interaction, effect of O_2-metal ratio of $(U,Pu)O_2$ fuels 80—13763
- steel, stainless, phase instability effect on cladding deform. profile of LMFBR fuel elements 77—74921
- steel, stainless, tensile props. of GCFR ribbed claddings at 650°C 80—45364
- steel, stainless, type 316, cold worked effect of prior neutron induced creep on burst strength 78—62599
- steel, stainless, type 316 20% cold worked fission reactor fuel cladding, axial stress effects on transient mech. response 80—71743
- steel, stainless, type 316 cladding, Ti-modified, performance in mixed-oxide fuel pins 79—67865
- steel, stainless 316, cladding failure during thermal transients 79—8316
- steel, stainless FBR fuel pin cladding, failure stress and strain 811 to 1644K 79—89377
- steel, stainless type 316, irrad. induced nuclear cladding swelling, empirical development of design equation 80—59527
- steel, stainless type 316, temp. effects on swelling 80—32347
- steel antioxidation protective glass enamel cladding exam. of development 78—85031
- steel plates, explosively clad, fatigue crack propagation behaviour *(Japanese)* 80—104262
- steel-on-steel, creep-rupture strength in corrosive environment *(Russian)* 77—52533
- steels for PWRs, props. and development 77—38336
- stoichiometry effects on cladding attack on mixed oxide fuel 78—86583
- stresses in fuel rod cladding, effect of fuel-pellet chips 78—86589
- tear resistance, method of determ. 77—25211
- temperature dist. in cylindrical fuel pins with gap and cladding *(Italian)* 79—13397
- thermal stress analysis *(Russian)* 77—59952
- thermomechanical transient anal., strain-rate dependent plasticity 80—79864
- thin-film waveguide laser amplifier with lossy cladding 80—64074
- transient overpower accident, transient press. field of gas in MOX fuel porosity 79—36348
- waveguide, clad parabolic-index square-law dielectric, perturbation anal. 80—33190
- weldable clad metal interlayer growth kinetics model 79—24493

claddings continued
- wire/plane electrode air discharges in strong nonuniform field *(Rumanian)* 79—68964
- Zircaloy, deposits on inside surface in LWR cladding, SEM obs. 79—6741
- Zircaloy, irrad., tensile props., effects of temp., strain rate and annealing 77—48463
- Zircaloy, irradiated spent fuel cladding, annealing effects 79—89382
- Zircaloy, irradiation growth in annealed and cold worked samples 77—88225
- Zircaloy, LWR cladding, I_2 stress corrosion cracking 79—89380
- Zircaloy, LWR fuel rod cladding, damage accumulation during I_2-induced stress corrosion cracking 80—71810
- Zircaloy, PWR fuel induced cladding deformation, creep correl., in-pile meas. 80—97547
- Zircaloy clad defective fuel rods, behaviour under continued reactor operation 79—30915
- Zircaloy cladding, internally pressurized, effect of temp. nonuniformity on diametral expansion during transient heating in steam 79—30920
- Zircaloy cladding, stress corrosion cracking, inner surface texture effect 80—66695
- Zircaloy cladding, stresses due to pellet cladding interaction 80—42762
- Zircaloy cladding ballooning, analytical model for transient gas flow in LWR 80—18499
- Zircaloy cladding fabrication, review, characts. which impact fuel manufacture 79—59241
- Zircaloy cladding stress corrosion cracking due to I *(Japanese)* 80—78361
- Zircaloy cladding thermal failure and UO_2 fuel melting during LWR PCM transient 80—42834
- zircaloy cladding tubes of irrad. fuel, flattening test *(Japanese)* 77—42054
- Zircaloy claddings, PWR fuel assemblies, LOCA behaviour in multirod burst tests 80—27739
- Zircaloy for reactor fuel pin cladding, metallurgical processing, transient temperature distribution 80—47573
- Zircaloy fuel cladding, azimuthal temp. distrib. during LOCA 80—662
- Zircaloy fuel cladding, behaviour during loss of coolant accident in LWR *(Japanese)* 79—71889
- Zircaloy fuel cladding, irrad. capsule design for continuously monitoring creepdown 79—54513
- Zircaloy fuel cladding, irradiation-induced in-reactor corrosion in CANDU reactors 80—104352
- Zircaloy fuel cladding, O embrittlement obs. 78—89947
- zircaloy fuel cladding tubes, prod. and inspection *(Japanese)* 79—26518
- Zircaloy fuel claddings, multirod burst tests following PWR LOCA 80—777
- Zircaloy LWR cladding, modeling of deform. and fracture in SPEAR code system 79—93729
- Zircaloy PWR fuel cladding, balloon deformation during LOCA 80—659
- Zircaloy reactor fuel cladding tubes, high temp. deformation model with nonlinear temps. 80—661
- Zircaloy tubing, I_2 stress corrosion cracking, pellet cladding interaction mechanism *(German)* 80—16565
- Zircaloy-2, anodisation appl. 77—81341
- Zircaloy-2, effects of simulated fission products on mechanical props. 80—52740
- Zircaloy-2, elastic const. determ. 78—11257
- Zircaloy-2, hot-pressed, influence of diffused C on structure and oxidation 80—61016
- Zircaloy-2, irradiation creep under H^+ bombardment at 5.5 MeV 78—14392
- Zircaloy-2, irradiation induced creep in reactor claddings under biaxial stress conditions 79—30912
- Zircaloy-2, neutron irradiated, inhomogeneous deformation behaviour 80—50679
- Zircaloy-2, stress corrosion cracking in iodine vapour, 250-450°C 78—17313
- Zircaloy-2 cladding, beta-phase, creep and creep rupture props., 1000 to 1500°C 78—78470
- Zircaloy-2 cladding, bonding to UO_2 fuel, mechanisms determ. by SEM and EPMA 78—17317
- Zircaloy-2 cladding, fracture in iodine environment 78—31581
- zircaloy-2 cladding tube, fission cutting *(Japanese)* 77—67808
- zircaloy-2 cladding tubes, post neutron irrad. ring-tensile props. prehydriding effect 77—42053
- Zircaloy-2 claddings, oxidation reaction kinetics in steam environment in temp. range 1273-1673K 80—35401
- Zircaloy-2 tube, external pressure creep behaviour 79—57083
- Zircaloy-4, creep rupture at superimposed non-stationary stress and temp. loading 80—66630
- Zircaloy-4, elastic props., O additions effect 80—66565
- Zircaloy-4, irrad. growth prediction using crystallographic texture model 77—46300
- Zircaloy-4, microstrain and particle size meas. by Warren-Averbach method 80—55420
- zircaloy-4, Nb additions, corrosion behaviour 77—40469
- zircaloy-4, oxidation in high temp. steam atm. effect on cladding ductility 79—26515
- Zircaloy-4 cladding deformation under LOCA transient heating conditions, analytical modelling 80—104236
- Zircaloy-4 PWR cladding, effect of oxide coating on ductility 79—89381
- Zircaloy-4 spent fuel cladding, tensile props. and annealing characts. 79—22392
- Zircaloy-clad UO_2 fuel elements, stability during long-term storage 79—26588
- Zircaloy-UO_2 fuel rods, eddy-current testing of claddings using encircling and probe coils 80—21245
- zirconium alloys, cladding strain reduction by changing pellet configurations 79—81008
- Al-Zn alloy cladding materials, corrosion behaviour under vacuum heating *(Japanese)* 79—91845
- B_4C absorber pin in-reactor rupture test 79—93701
- BN-based, fabrication and wear resist. 80—40576
- $BaO\text{-}GeO_2\text{-}Na_2O$ borosilicate core glasses for high numerical aperture fibres 80—69534
- C, automatic image analysis, variables and errors, definition and quantitative description *(German)* 78—25296
- C transfer in nuclear fuel claddings *(German)* 77—50230
- Cr-Fe-Ni alloys, claddings, chemical compatibility with UC nuclear fuels, thermodynamic model 80—63263

claddings continued
- Cr-Fe-Ni alloys, interface with Th carbide fuels, basic chemical compatibility, thermodynamic calcs. 79–93727
- Cu/Cu single crystal, explosion clad bonding, TEM obs. 77–62763
- Cu/Cu system, explosive cladding, TEM obs. and thermomech. model 79–96041
- p-GaAs-$Al_{0.3}Ga_{0.7}As$, cladded dielec. waveguide, loss meas. using Raman scatt. 79–81539
- GeO_2-Na_2O borosilicate glass fibre prod. by phase separation and leaching 80–69558
- l stress corrosion failure of unirrad. tubes 77–3100
- InGaAsP-InP laser, LPE, 1.5 μm range, effects of double cladding struct. 80–48290
- Mo, borosilicate cladding compatibility *(Russian)* 77–66741
- Nb, borosilicate cladding compatibility *(Russian)* 77–66741
- Nb CVD coatings on graphite, grain struct. depend. on temp. 80–25574
- P_2O_5-SiO_2 clad low-loss monomode fibres for 1.2 to 1.6 μm, modified CVD prep. 80–48479
- Pt-Rh-W alloy corrosion by radioisotopic power system insulating and thermoelec. materials 78–7094
- SiC cladding possibility for gas-cooled fast breeder reactor fuel 77–18667
- SiC coatings, CVD on microspheres in fluidised bed, parametric investig. 77–40457
- SiC corrosion in HTGR fuel particles 77–67817
- SiC, pyrolitic coating for nuclear fuel particles 77–79465
- SiO_2-based single-mode doubly clad optical fibres, dispersion minimisation 80–9997
- SiO_2-P_2O_5 cladding vapour-phase axial deposition fibres at 1.3 μm and 1.6 μm 80–9996
- Th-U(20 wt.%) alloy fuel, compatibility performance of candidate cladding alloys 79–54509
- Ti, TiN, thermal stress analysis *(Russian)* 77–59952
- (U, Pu)C, LMFBR carbide fuel cladding damage anal. at TREAT 80–13602
- U-Si-Al fuel rods, Zr-Nb cladding, irradiation behaviour with peripheral voidage 78–54835
- UO_2 pellet, interaction between cladding in water reactor fuel pins 78–25286
- UO_2 pellets-graphite-Zircaloy cladding, evaluation of graphite lubrication 80–32342
- UO_2/Zircaloy pellet/cladding interaction, eval. of lubrication of graphite 79–67857
- UO_2-PuO_2 fuel pin, hyperstoichiometric, post irradiation examination 80–63258
- W, borosilicate cladding compatibility *(Russian)* 77–66741
- Zircaloy-2, effect of simulated fission products on mech. props. 80–73922
- ZnS, on ZnSe substrate, erosion-resistant composite window fabrication and evaluation 78–71211
- Zr alloy, cladding, new material development 77–50242
- Zr alloy, elastic props. of fuel cladding and press. tubing material 79–15711
- Zr, fuel element sheathing, reliability, including hydration process, probabilistic model *(Russian)* 80–52742
- Zr-Nb (2.5 wt.%), fuel cladding, anisotropy after creep and irradiaton 78–7001

classical algebra *see algebra*

classical field theory
- *see also classical mechanics; electromagnetic field theory; gravitation; special relativity*
- ϕ_2^4, coupled states of solitons *(Russian)* 77–6037
- ϕ^3 weak coupling model, s-channel cutting rules for 4-pomeron amplitude 77–38101
- ϕ^4 scalar field theory and exact solns. to classical SU(2) gauge theory 77–45949
- ϕ^4 theory exact soln., model of confinement 77–41811
- ϕ^4-theory, soliton soln., fluctuation renormalisation and extended particles 77–5996
- 't Hooft monopoles, interaction energy in Prasad-Sommerfield limit 79–12950
- 't Hooft-Polyakov monopole, fermion binding *(Russian)* 77–2548
- Abelian monopole equivalence to non-Abelian stringless counterpart by method of sections 77–49856
- acceleration through random classical radiation, thermal effects 80–73191
- action functional in distrib. spaces 78–54207
- affine motion in recurrent Finsler space 78–57797
- anisotropic media, scalar macroscopic field construction by method of images 78–32697
- Benney's long wave eqns., Hamiltonian formalism 80–31525
- bi-scale theory of gravitational and strong interactions 79–12696
- binding energy, two external sources, quark confinement anal. 80–4927
- black hole formation, effect of zero point fluctuations 78–12286
- canonical formalism in field theory, higher-order derivatives 78–16664
- canonical transformation for eqn. of form $\phi_{xt}=h(\phi)$ 77–33875
- carrier fields, multiple-interaction nonlocal formulations 77–52
- charge creation, advanced pot. *(Russian)* 78–12580
- charged particle system, virial theorem 80–86101
- chromodynamics, SU(n), classical noncommuting quark source charges 78–78144
- classical angular momentum of an electron-magnetic monopole *(Chinese)* 78–86460
- classical deflection in a central field 80–41993
- classical Lagrangian theory with radiative reaction, monopoles and positrons in Rohrlich formalism 79–72
- closed vortices and Hopf index in Abelian and non-Abelian Higgs model, and nonlinear σ model 79–12960
- composite media with complex geometry, pot. field problems 78–16663
- conformal invariance of multiple integral var. problem 77–71222
- constrained Hamiltonian formulation for interacting fields, stable particle-like solns. 79–49065
- continuum mechanics and field theory, role of Thomson and Maxwell 79–17179
- coupled field theory, classical perturbation theory appl. 78–57799
- coupled fields in one dimension: cross-over from a continuous symmetry to a discrete one 78–87758
- covariant representation of microscopic charge and current densities in terms of polarisation and magnetisation fields 79–71
- cross section generating solutions of field eqns. 79–97488

classical field theory continued
- curved space-time, neutrino fields with geodesic and shear-free rays, zero rest-mass fields 77–17890
- defect dynamics, gauge transforms. in vector field theory 79–27981
- deformable dielectrics, model of interactions 77–59521
- Dirac spinor field coupling to Klein-Gordon field, invariance prop. 78–4763
- Dirac strings, theory 77–22634
- Dirac-EM field interaction, localised soln. radius 77–79212
- Dirac-Schwinger covariance condition 77–78991
- discrete space-time, geometric formulation of electrodynamics and general relativity 77–26184
- dislocations and gauge invariance 79–27980
- dissipative and/or dispersive systems, perturbative and reductive method *(French)* 80–36868
- dyon solns. for classical Yang-Mills field eqn. 78–54560
- dyon-dyon nonrelativistic scatt., classical and quantum anal. 77–5985
- education, classical mechanics gauge invariance, derivation of Maxwell's eqns. 80–73131
- education, Lienard-Wiechert field expression, circulating charge in static mag. field 78–69933
- education, Lorentz theory for classical radiation reaction of accel. charged particle, dumbell model 78–49592
- Einstein Lagrangian as translational Yang-Mills Lagrangian 77–13660
- Einstein-Maxwell field, symplectic structure 78–29028
- elastic bodies, heat conduction, formulation removing paradox of infinite signal propag. speed 77–35014
- electrodynamics, classical, radiation reaction terms 80–48126
- electrodynamics, covariant formulation for charges of finite extension 78–77731
- electrodynamics, energy tensor definition for system of charged particles and EM fields 78–77734
- electrodynamics, nonlinear gauge approach, charged particle solns. 78–32695
- electrodynamics of point particles, energy tensor struct. 79–21566
- electromagnetism, nonlinear theory 79–5991
- electron acceleration in EM field, new field theory appl. *(Chinese)* 80–62494
- elementary length in nonlinear classical scalar field 77–45942
- elementary particle spin, reln. to universal props. of matter 78–21329
- EM wave scattering by inhomogeneous spherical particles, vector wave eqns. 79–27137
- embedding classical fields in QFT, electrodynamics, Yang-Mills theories, gravit. appls. 78–54223
- equilibrium states of charged particles in wave propagating along mag. field *(Russian)* 77–23601
- Euclidean 2-D nonlinear σ-models, continuity eqns. 78–54210
- Euclidean classical field eqns. with unique vacuua 80–32017
- Euclidean field theory, nonclassical configs. as minima of constrained systems 78–70256
- Euclidean field theory, nonlinear elliptic eqn., classical solns. 79–21569
- euclidean nonlinear classical field equations with unique vacuum 79–5989
- Euler-Lagrange eqns., generalised solns. 78–54206
- Euler-Lagrange hyperbolic systems of second order, relativistic strings 78–54209
- evolving 3-D vector fields, events 80–27148
- extended phase space, classical fields 80–86550
- f-g gravity theory, exact spherically symmetric solns. 79–319
- Fermion contribution to instantons 78–78079
- fermion-meron interactions in Minkowski space-time, classical Yang Mills fields 79–2913
- fermions on the hypertorus 78–74149
- ferromagnetic systems, crit. experiments, field theory, Borel transform. 80–80541
- field analysis computers, colloquium, London, England (March 1980) 80–94964
- field gradient directions normal to trajectory of a potential *(Russian)* 80–17818
- Finsler spaces, physico-geometrical remarks on theory of physical fields 77–22394
- flow fields and other vector field struct. and evolution 78–77733
- flux line collapse, invisible string 77–57451
- force concept in classical mech. and field theories 77–49
- force-free fields, Neumann's type boundary-value problem soln. 78–12585
- free electron laser, classical, semiclassical and quantum field theories 77–14684
- free relativistic particles, classical counterpart to Wigner's theory 77–65073
- frozen-in field condition, Lie derivative calcs. 79–2586
- gauge fields on coset spaces 78–45781
- gauge theories, non-Abelian, in space of reference frames 80–31977
- gauge theories for space-time symmetries 77–2723
- Gauss-Hertz principle 77–22415
- general relativity, classical fields with spin 78–8298
- general relativity, symplectic form, geometric construction 78–8289
- general relativity singularity-free extended particle model 78–54255
- general relativity spaces with Killing vectors, classical scalar and vector field evolution 80–4608
- general vector fields, classical theory, internal symmetries and conservation laws *(Russian)* 78–62328
- generalised forces, source strengths of Euler-Lagrange eqns. 77–2545
- generalised Fourier transforms 78–54205
- generalised Parseval eqn. 78–54204
- generalized Hamiltonian dynamics for fields 79–53989
- geometrisation, applied to Yang-Mills field theory 80–46841
- Gibbs random field, integral central limit theorem, equivalence of ensembles 77–53826
- global conformal transformations and dynamics 77–26460
- gravit. two-body spin-independ. system 77–17829
- gravitation, electromagnetic interpretation, contribution to classical theory *(Rumanian)* 80–68109
- gravitation, electrothermodynamical theory, gravitational field shielding *(Rumanian)* 80–68107
- gravitational field and force derivation using Faraday's and Maxwell's ideas of electromagnetic waves *(French)* 80–68106
- gravitationally coupled classical fields, decomposition method extension 78–127
- Hamilton-Dirac 3+1 anal., effect of gravit. interaction on classical field 77–82399

classical field theory continued
Hamilton-Jacobi eqn., generating function soln. for shocks in fields *(French)* 77—9890
Hamiltonian, completely integrable relativistic system 77—57450
harmonic fields in composite truncated wedge 77—5676
Heisenberg eqns. of motion for spin-3/2 field with interactions 78—370
Hellmann-Feynman theorems, hidden pots. 77—87654
higher order spaces, field theoretical aspects 78—21326
homogeneous massive scalar field model, existence of nonsingular isotropic cosmological soln. *(Russian)* 78—77635
induced potential problem in 3-D, functional analytic approach 78—58880
inequalities and symmetry breaking in classical lattice field theory 79—9131
inertial mass and potential energy 77—26225
instanton interactions and Riemannian geometry 77—71447
instanton solns. for coupled nonlinear scalar and fermion fields 77—79220
instantons, virial theorems, variational arguments 77—49857
instantons and antiinstanton forces in sigma model and Yang-Mills theory 77—26462
integrable field theories, as classical gases with generalised charges *(Russian)* 80—12922
interacting Dirac and Klein-Gordon fields, absence of solitary waves 77—30226
interdigital transducers, quasiacoustic wave propagation, field theory anal. 78—66998
invariant interaction Lagrangians, mathematical theory 79—30267
invariants of equivalent Lagrangians 79—40654
inverse scattering method for the classical massive Thirring model with anticommuting variables 79—12626
IR dynamics, classical current models 77—60947
Klein Gordon lattice field eqn. in 4-D space-time, Lorentz covariance 78—54184
Klein-Gordan equations with logarithmic nonlinearities, classical theory 79—5996
Lagrangian, exact solutions in field thory 79—75677
Lagrangian models of scalar fields, extended particles in two space dimens. 77—5995
Lie algebras associated with classical relativistic planar motion in axisymmetric EM fields 79—49064
Lie groups, associated observables 77—74249
Lie-admissible struct. 80—36880
limit theorems for random fields 78—81860
Lippmann-Schwinger type integral eqn. of motion, quantum corrections 78—62318
local class field theory, generalisation by K-groups 79—25875
Lorentz groups on skew symmetric tensor space, nonlinear realisations of direct product 78—62329
magnetic field of infinitely long conductor, DC current supplied, calc. *(Czech)* 77—19125
magnetic monopoles in classical field eqns. with a mag. charge 80—4872
many boson non-relativistic systems, classical field limit of scatt. theory 79—80501
massive free spin-3 field, local quadratic Lagrangian density absence 78—369
massive spin-3 fields, first order formalism 77—22638
massive Thirring model, localised solns. in presence of external electrostatic field 77—13864
massive Thirring model, localised solns. in presence of external electrostatic field 77—65095
massive Thirring model, quasiperiodic solns. of field eqn. 78—41418
massive Thirring model, renormalisation of higher conservation law 77—30020
massive Thirring model connection 79—12624
massless supersymmetric Wess-Zumino model and SU(2) gauge supermultiplet, classical solns. 78—8549
material symmetry transformation, density preservation 79—35552
Maxwell equations, homogenisation leading to relaxation phenomena *(French)* 79—21564
Maxwell equations, new invariance group 79—35575
Maxwell theory incurved spacetime stress-tensor trace anomaly 77—64983
meson fields, classical coherent component 78—78082
micropolar current and heat conducting magnetically-saturated solid, field eqns. 78—36845
microscopic charge and current densities in terms of polarisation and magnetisation fields 78—8251
monopole and dyon solns., stability, absolute minima of energy 77—30261
motion and radiation of a charge in a plane wave and a magnetic field *(Russian)* 79—21986
multi-terminal representations appl., graph theoretical field model 80—90689
multiple normal threshold discontinuities for 2 to 4 processes 77—60982
multipole matrix elements from classical field with sources 79—9504
N-particle systems, predictive relativistic mechanics *(French)* 77—45707
Newtonian connection, nontrivial extension of Galilei group *(French)* 78—36916
non-invariance symmetries and consts. of motion 79—75333
non-Lagrangian field equations, variational principles 79—21565
non-Lorentzian electromagnetic quadripotentials for the field of a classical point particle 79—71263
nonlinear, relativistic new solutions, charge barrier mechanism 78—54211
nonlinear σ model in two dimensions, geometry 77—41496
nonlinear σ-model, two dimens., scatt. of massless lumps, nonlocal charges 78—62300
nonlinear chiral fields *(Russian)* 78—28968
nonlinear classical field theory, dynamical charges and symm. 77—57211
nonlinear Dirac eqn. in four dimens., asymptotic solns. 77—6016
nonlinear evolution of three-wave interactions in inhomogeneous medium 77—74272
nonlinear field eqns. in Hamilton's canonical form, conservation and invariance 78—32693
nonlinear field theories, exact classical solutions 78—21327
nonlinear field theories equivalence to action-at-a-distance, three body forces 77—26181
nonlinear fields, one-dimens. 77—17830
nonlinear one-dimensional model with internal degrees of freedom 78—49684

classical field theory continued
nonlinear polynomial field, extended hadron bag model based on exact soln. 77—5997
nonlinear scalar field, time-dependent solns. 78—81865
nonlinear scalar field theory, localised solns. 78—32976
nonlinear scalar field theory in isotropic homogeneous space-time 79—2676
nonlinear spinor field, localised solns. 77—71223
nonlinear theory with positive mass square, static finite energy solns. 80—31984
nonlocal fields characterized by internal variables, geometrical theory 78—29014
nonperturbative techniques for QFT, topological props. of classical fields 77—82400
O(n+1) symmetric, nonlinear, symm. breaking, finite energy solns. 77—10172
O(n) nonlinear σ-model, field eqn. reduction 80—31979
one-dimensional field theories with odd-power self-interactions 79—254
orbital angular momentum of 'lumps' 80—86098
orbital symmetry conservation, chem. appl. of field theory *(Chinese)* 79—63884
ordered media containing defects, gauge-like variables 79—88889
ordered physical line structures, nonlinear local field theory, appl. to high polymers, supercond. flux line lattices 78—81859
oscillating irregular field, effective potential 79—75457
particle motion in classical gauge field, variational derivation and uniqueness of equations of motion 79—40658
particle-classical field interaction, appl. to linearised gravitation and symmetric electrodynamics 79—5992
particle-field interaction, classical vetsion of polaron-like models 80—46834
particle-like solns. of gauge theories 77—41779
partition of energy for uniformly propagating systems 77—67303
Pauli exclusion principle proof from self-consistent field theory of electrodynamics 78—49683
percolation theory at the critical dimension 79—152
periodic solns. to scale invariant classical field theories 77—67305
periodic solutions to classical field equations 80—46822
Planck's constant, numerical value, dynamic mechanism, classical/quantum physics borderline 79—21573
plane wave scatt. by lossless penetrable obstacles, low freq. expansions 77—26211
plane-symmetric cosmological model, Einstein eqn. solns. for dust 78—49733
polynomial conservation laws in (1+1) dimens. classical and quantum field theory, nonlinear Schrodinger eqn. 78—54224
pre- and post-processing techniques for complex analysis 80—94965
predictive relativistic mechanics, noninteraction theorem for interactions derived from classical field theory 79—40358
propagation operators, eigenfunction orthogonality *(Russian)* 77—49613
pseudoparticle configurations, conformal props. 77—41772
pulsons, two space-dimensional, dynamics of collisions in ϕ^4 field theory 78—8250
quantum aspects of classical and statistical fields 79—58585
quick-change fields in continua, regularisation 78—49663
radiating point charge, energy and ang. momentum splitting 78—69996
radiation field far arbitrary spin, U(2) theory 78—61
radiationless motion of classical electron 79—17247
radiationless motions of relativistically rigid classical electron 78—20983
random walks appl., using transmission line matrix, Monte Carlo approach 79—53991
real-time approach to instanton phenomena, multidimensional pots. with degenerate absolute minima 78—78067
reciprocity and conservation theorems, for fields with general time dependence 79—80452
reduction of dynamical systems 79—63011
relativistic, classical interacting fields, virial theorem and stability of localised solns. 78—21342
relativistic, strings and vortices with soliton solns. 77—5674
relativistic, symmetry mappings, particle number conservation, baryon number conservation 77—30063
relativistic bilocal model, subsidiary conditions, elimination of relative time 78—41174
relativistic classical nonlinear field eqns., virial theorem, solns. and nonlinear scatt. 79—97218
relativistic classical nonlinear field theory, PCT violation 77—65081
relativistic linear wave eqn., kinematical interpretation of subsidiary conditions 77—2737
relativistically invariant two-dimens. models, classification method *(Russian)* 78—70291
retarded self-interaction of classical point electron, divergences anal. 77—13620
rotators, multicomponent, Gaussian inequality 78—29058
scalar field, reln. of spin and orbital angular momenta 79—67170
scalar fields, relativistic time-depend. multipole anal., multipole moments definition 77—65087
scalar macroscopic fields in anisotropic stratified media, Green's functions 79—58544
Schwarzschild sphere and classical electron self-energy 78—49681
self-screening of classical Yang-Mills fields *(Russian)* 79—6289
set of point sources determ. 79—88816
sine Gordon equation, exact time depend. solns. in 2+1 and 3+1 dimens. 78—78074
sine Gordon theory, derivation based on infinite set of coupled pendula 79—92962
sine-Gordon equation, classical solns. of field eqns., moving t'Hooft-Polyakov monopole *(Russian)* 78—16935
sine-Gordon equation, exact mass spectrum, WKB approx. 77—33896
sine-Gordon equation, polynomial field theories, solitary wave solns. 77—2726
sine-Gordon equation, soliton solns. and appl. to solid state physics *(Japanese)* 77—30025
sine-Gordon interaction solitons and classical particles 77—74589
sine-Gordon supersymmetric theory, infinite set of bosonic conserved currents 78—62313
SO_4, $SL_{2,C}$ classical gauge field eqns., isotropic and solitary-wave solns. 78—93795
soliton models of hadrons, semiclassical approach to quantum field theory 77—5981
soliton quantisation, cancellation of zero-mode singularities 77—49838
solitons, nontopological, and appls. to hadrons 78—32968

classical field theory continued
- solitons, string like, 2-sphere range for variables 79—53988
- solitons in 2+1 dimens., Coleman's rules 77—82678
- solitons with particle properties, real scalar fields anal. 77—45936
- space of reference frames formalism, Einstein's gravit. theory, Maxwell's EM theory appls. 78—41173
- space-time inversion in gauge theory, classical approach 78—41416
- space-time model, classical *(Chinese)* 77—9889
- spin in kink-type classical field theories 78—81861
- spin-2 field theory of gravity, locally Lorentz invariant 77—5725
- spinning particle, Lagrangian formulation of classical and quantum dynamics 77—18173
- spinor field, indefinite charge 77—71221
- spinor field in Riemann space time, energy-momentum tensor symmetrisation *(Russian)* 77—82422
- spontaneous particle creation in strong gravitational field, semiclassical theory 78—54281
- spontaneous symmetry breaking, Eddington's no. cosmic variablity, inertia, and gravitation 79—80375
- stable limit cycles of vector fields, new negative criteria 78—57756
- statistical mechanics, classical, universal features for continuum-field nonlinear Hamiltonians 78—93543
- stimulated effects upon electron jarring in external EM field 77—79737
- string like solns., masses for monopole and dion *(Russian)* 77—5677
- structural defects in solids, 4-D geom. theory 79—84954
- supersymmetric relativistic harmonic oscillator, model 77—38086
- symmetry groups of field equations for spin 1/2 79—21568
- symplectic framework for field theories, book 80—22130
- sympletic geometry and second quantisation 77—45977
- tachyon classical field theory 77—64949
- teaching, curl operator when A.curl A≠0 78—62020
- tensor fields invariant under subgroups of the conformal group of space-time 79—2603
- thermoelastic solids, field-matter interactions, book 79—30270
- Thirring model, 2-D, complete integrability 78—49685
- Thomas precession, geometrical kinematical origin 79—6
- time dependent constraints in classical dynamics 80—57111
- topological theorem for bounded vector field, nematic liq. cryst. appl. 79—67171
- topology, propagation of surfaces of weak discontinuity, broken extremals in classical field theory 78—93541
- transient field initial-boundary value problems, hybrid simulation 77—41469
- twisted products for cotangent bundles of classical groups and Stiefel manifolds 78—49680
- twisted scalar field, vacuum solns. 78—93804
- two dimensional infinite particle systems, non-equilibrium dynamics with singular interactions 78—12579
- two-dimensional classical field theory, nontrivial interaction between solitons *(Russian)* 78—32698
- two-dimensional isoparametric Hermitian element for field problem soln. 77—60914
- two-dimensional massless Fermi field, symm. couplings 78—29228
- two-soliton soln. of coupled nonlinear evolution eqn. 77—79210
- two-tensor field theories for hadron-lepton gravit. interactions, interaction term 77—87932
- unified thoery of matter, derivation of fundamental physical law 78—20982
- variational principles on rth order jets of fibre bundles in field theory 78—86168
- vector field decomposition by scalar potentials 79—12625
- vector fields, eqns. for propagation of finite local disturbances 79—92961
- viscous fluid mixture with thermomolecular diffusion, new variational-Lagrangian thermodynamics 79—49185
- Werle type confining models, soliton-soliton interactions 79—85272
- WKBJ approx. for classical particles with spin in external field 78—32692
- wrinkled membranes with anisotropic and nonlinear elastic props., tension field theory 77—31220
- Yang Mills equations, nonzero temperature case, spherically symm. solns. 79—2941
- Yang Mills potentials, massless charged scalar fields, stability 77—34089
- Yang-Mills, exact multipseudoparticle solutions 77—22649
- Yang-Mills classical field classification using spinor methods 77—78990
- Yang-Mills eqn., multiple meron solns. 78—32987
- Yang-Mills equations, static spherically symm. solns., SU(2) gauge group 79—2914
- Yang-Mills field equations, with static external sources 79—21930
- zero frequency modes in perturbation expansion about classical field theory configs. 77—18169
- ν, classical, gravitational interactions 78—45833
- H atom, relativistic quantum mech. as weak-field limit of nonlinear theory 79—6878

classical mechanics
- *see also classical mechanics of continuous media; classical mechanics of discrete systems; classical theories of fluid structure*
- aerospace kinematic tools, vectorial mechanics and variational method 79—30218
- aircraft vertical manoeuvers 77—82385
- analogy with thermodynamics, symplectic struct. 79—71174
- arithmetic models formulation 78—86130
- autonomous Hamiltonian system near equilib. point, formal integrals 78—89047
- canonical formalism, Bose type classical Hamilton algebra, phase space variables 78—54170
- canonical formalism in field theory, higher-order derivatives 78—16664
- canonical mechanics, admissible forms 78—16691
- catastrophe theory appl. 77—67232
- cavity of entropy 80—27158
- combined algebra for classical and quantum mechanics 78—85
- conference, finite elements in nonlinear mechanics, Stuttgart, Germany (Aug.-Sept. 1978) 79—44727
- conserved densities, Hamiltonian systems 80—90682
- constants of motion and separable solns. in classical mechanics, group theoretical aspects 79—75332
- contact conformal transformations, finite, nonrelativistic 78—36815
- contact Lie algebras, contraction 78—36816
- contact stress problems, counterformal, improved numerical method and program 79—41632
- crossblow, by cone over thread, numerical solution *(Russian)* 78—55612

classical mechanics continued
- curvature statistics of some few-body Debye-Huckel and Lennard-Jones systems 80—42051
- deformation of symplectic structure and quantization 80—8853
- differential eqns. integrable in generalised hypergeometric functions *(Russian)* 79—12572
- digital model anal. using transient excitation 77—84209
- dimensional base selection in expt. design and planning 78—49636
- dynamic system, classical quantisation conditions with stochastic behaviour anal. 80—8922
- dynamical systems with many degrees-of-freedom, deterministic problem stochastic anal. 79—75455
- education, chimney breaking while falling 77—33768
- education, classical mechanics operator formulation, wave packets in config. space 80—73137
- education, dynamics of variable mass system, flexible inextensible rope 78—86071
- education, harmonic plane waves, particle displacement 80—73138
- education, Maxwell fish-eye pot. and Coulomb pot. from mechanics 78—49585
- eigenvalue problem for Lagrangian systems 77—49601
- entropy, nonequilib., Lyapunov variables, ergodic props. of classical systems 79—2739
- equilibrium correlation functions with various potentials, mol. dynamics expts. *(Spanish)* 79—90502
- Euler's theorem on rigid-body motion, matrix theoretic proof, for teaching 79—62964
- exchange energy diagrams of dynamic processes *(Russian)* 78—24658
- finite-differential element nets, topological props. 77—67247
- foundations, concepts of mass, weight, inertia *(German)* 79—67146
- fundamental laws and concepts, teaching *(Hungarian)* 77—37691
- fundamental mechanics, thermodynamics and gravitation (book) 80—41964
- generalised Poisson bracket and associated natural one-form 77—37719
- generating forms of K-generalised Lagrangian and Hamiltonian systems 78—4475
- goose chase, mechanics teaching 79—44665
- Grassmann variant of classical mechanics, particle spin dynamics 77—41495
- gravitational collapse, Oppenheimer-Snyder solution, Newtonian analogue 77—73945
- Green's function potential method appl. in mechanics 78—16634
- Hamilton equations, n distinct periodic solns. on each energy level *(French)* 79—44710
- Hamilton-Jacobi eqn., symm. and separation of variables 78—32666
- Hamilton-Jacobi eqn. and Lie group theory 77—57180
- Hamiltonian action of lagrangian, second variation extension *(French)* 77—82381
- Hamiltonian dynamics in symplectic phase space, Nambu's formulation 77—26168
- Hamiltonian dynamics of particles with gauge degrees of freedom 79—75330
- Hamiltonians, time depend. linear canonical transformations 77—74213
- Hemlholtz-Cartan theorem for simple integral of higher order *(French)* 79—71238
- Huygens' principle, formulation of quantum and classical mechanics *(French)* 78—36851
- implicit finite element algorithm for geometrically nonlinear problems of struct. dynamics, stability anal. 78—86157
- implicit finite element algorithms for geometrically nonlinear problems of struct. dynamics, accuracy anal. 78—86158
- inertial frames in classical space time 78—81826
- integration of mechanics eqns. with slowly varying coeffs. *(Italian)* 77—78968
- Lagrange's equations, invariance in form 80—82630
- Lagrange-Maxwell eqns., derivation and unified form *(Russian)* 79—84975
- Laplace operator in 2-D, coordinate transform., for teachers 78—61999
- Lie groups, associated observables 77—74249
- Lie-Backlund operators, exam. of isomorphic correspondence between classical and quantum-mech. invariants 80—90700
- linear nonconservative systems, exact Lagrangians 79—40355
- logical drawbacks 80—17799
- math. and phys. models, fundamental differences and future possibilities 79—25844
- mathematical models of dynamical processes and stability of motion *(Polish)* 79—63012
- measurement standards and structure of physical knowledge 77—74347
- mechanical system, geometry and stability theory 79—27558
- mixed boundary value problem in three dimens. 77—71184
- Moyal-Vey bracket, quantisation, quantum mech. as nontrivial deform. of classical mech. *(French)* 77—5685
- multiple parameter system vibrations and stability, book 78—93532
- Nambu's mechanics, rel. to quantisation of Dirac's singular theory *(Czech)* 77—30030
- Newton, particles and concepts of force, discussion for teachers 78—4437
- Newton's laws, simple demonstration 79—67129
- Newtonian Lie-admissible equations, struct. preserving transformations 79—53969
- Newtonian mechanics, inverse problem, Lagrangian computation method 78—89329
- Newtonian mechanics, linear connection and curvature 77—5733
- Newtonian mechanics, time-dependent transformation, relativity of force, geometrical viewpoint 77—57177
- Newtonian mechanics inverse problem, transition between second order and first order systems 79—53968
- nongradient systems, nonlinear instability behaviour 79—75331
- nonholonomic system, constrained perturbation procedures 78—16637
- nonlinear eigenvalue problem method 79—17208
- nonlinear oscillators, 1-D, intramolecular vibr. energy transfer, quantal, classical and statistical behaviour 80—91641
- nonlinear systems, asymptotic stability, geom. props. of Lyapunov functions *(German)* 78—87286
- nonlinear systems, parametric resonance phenomenon *(Russian)* 77—57182
- normal coordinates, rel. to natural coords., theory 77—22343
- null strings, free Nambu strings 78—12560
- oscillation-free transformations, periodic potential 78—16636
- perturbation expansion of classical one-dimens. Hamiltonian system 77—26167

classical mechanics continued
- phase space representation of quantum and classical mechanics *(Russian)* 79—25882
- physical analysis in factor analysis *(German)* 79—49024
- pipeline nonlinear anal. by potential minimisation 77—68552
- probability foundations, modal frequency interpretation 80—12885
- quadratic and cubic invariants in classical mechanics 80—90663
- quantum analogs, book 80—41969
- resonant classical Hamiltonians with two equal freq. 78—28936
- rotating components, design to probabilistic criteria 77—3716
- solid bodies, structural design computing, using 'moment schema' of finite elements *(German)* 80—14563
- statistical mechanics in classical physics, foundations 78—8334
- stochastic Hamiltonian classical and quantum, systems, Volta Memorial Conf. 80—8738
- swift rotation, appl. in beam choppers, turbine drives, etc., history 78—32643
- symmetric formulation, Jordan algebra 80—42050
- symmetries, first integrals, splittability of dynamical systems 78—36795
- symmetry of systems of differential eqns. 78—4465
- systems with non-integrable constraints, quantisation 80—36901
- time dependent Hamiltonian, scale gauge transforms., adiabatic approx. principle, suitability for teaching 78—45506
- time reversal in classical and quantum mechanics 80—42090
- time varying systems, stability anal. 78—37
- twisted products for cotangent bundles of classical groups and Stiefel manifolds 78—49680
- umbilic catastrophes, buckling mode 78—20945
- wind powered boat, demonstration of conservation laws 79—19

classical mechanics of continuous media
- *see also elasticity; fluid mechanics; mechanical contact; plasticity*
- ablating boundaries, algorithm for automatic tracking 79—32240
- Ahmad thick shell element, theoretically improved and easily implemented version 79—23205
- Airy functions, stress problem solns., teaching appl. 78—86063
- analytical and continuum mechanics, book 80—22163
- anelastic deformation, generalised representation by num. sol. of initial boundary value problems *(German)* 79—12610
- anelasticity, general linear response, anal. 79—10895
- anisotropic constitutive equations and Schur's lemma 78—89337
- anisotropic dissipative medium, σ-ε bond determ., scalar product maximum appl. *(Russian)* 79—12596
- anisotropic elastic medium reinforced with thin tapes, model 80—38276
- anisotropic layered medium, plane wave transmission 78—83150
- anisotropic media, natural oscills., partial differential eqn. system 80—57091
- anisotropic media, scalar macroscopic field construction by method of images 78—32697
- anisotropic micropolar fluid theory 80—31515
- anisotropic plate with curvilinear holes, plane elasticity problem, soln. approach *(Russian)* 80—33457
- anisotropic plate with curvilinear holes, plane elasticity problem, comment *(Russian)* 80—38260
- anisotropic plate with curvilinear holes, plane elasticity problem, basis of soln. *(Russian)* 80—38261
- anisotropic solids with magnetic symm., unified dynamic theory 78—77713
- anisotropic thermoelastic shells dynamical coupled problem, variational theorem *(Russian)* 79—14255
- annular dome subjected to uniform load over an eccentric circular area 79—46195
- applied mathematics, conf., Delft, Netherlands, Jan. 1978 79—2617
- arches, freely supported, reserve of resistance beyond limiting load *(Italian)* 79—18703
- array weakened by periodic system of round orifices, elastic-plastic problem *(Russian)* 79—50610
- atmosphere dynamics in quasistatic approximation, characterisation of approximation *(German)* 80—98383
- autonomous system instability, sufficient criteria, Lyapunov instability *(Russian)* 79—17210
- averaging in nonlinear mechanics 80—98796
- axisymmetric cylinder, experimental numerical hybrid method for stress anal. 80—48657
- axisymmetric shells, two noded straight element including shear deformation effects 78—47
- bar, elastic-plastic cylindrical, Lipschitz character of stress tensor during twisting 79—46221
- bar, homogeneous isotropic, shearing stress in Saint-Venant torsion, integral eqn. method 79—80445
- bar, stress changes and warping during heating *(Russian)* 79—59920
- bar with two natural freqs., minimum mass design 79—46246
- bars, rectangular, plastic flow during closed die cropping 79—37190
- beam, clamped, hinged, sudden change of boundary conditions, support failure vibrs. *(German)* 80—1456
- beam, conical viscoelastic, torsion, accumulated injury influence *(Russian)* 79—94512
- beam, fibre reinforced rigid plastic, impulsive loading 79—3928
- beam, hinged, large amplitude vibration 79—46258
- beam, impulsively loaded rigid plastic, additional support optimal location *(Polish)* 79—64498
- beam, large displacement-small strain anal., finite elements with rot. degrees of freedom 78—86161
- beam, out-of-plane vibr. including nonlinear inertia and nonlinear curvature effects 79—64558
- beam, rectangular cantilever, loaded by external force and own weight, optimum design *(Polish)* 79—64497
- beam, rigid plastic, stepped, impulsively loaded, optimal design for asymmetric mode motions 78—90723
- beam, simply supported on nonlinear elastic foundation, equilibrium paths and buckling 79—81747
- beam, straight rectangular, higher-order one-dimens. beam theory 80—48565
- beam, Timoshenko, non-stationary loaded, stress analysis, use of Laplace transformation and classical method 80—14564
- beam, two-span, with curved initial path contour, transverse vibrs. 80—38324
- beam column, axially creeping viscoelastic under initial axial compression, free lateral vibration 79—50639
- beam deflection under moving loads, finite element anal. *(German)* 79—23204

classical mechanics of continuous media continued
- beams, accuracy of elementary, and Timoshenko theory 77—80076
- beams, dynamic stiffness coefficients approx. determination 79—46186
- beams, elastic straight slender undergoing small strains and rots., nonlinear behaviour 79—64518
- beams, end loaded cantilever, lateral buckling 79—50617
- beams, fixed-free with support asymmetry, nonlinear, nonplanar, resonant oscillations 79—37212
- beams, frames, arches, axisymmetric shells, finite element anal., Newton Raphson method, nonlinear equilib. eqns. 78—22282
- beams, inextensional, nonlinear flexural-flexural-torsional dynamics, equations of motion 79—64494
- beams, inextensional, nonlinear flexural-flexural-torsional dynamics, forced motions 79—64495
- beams, isoparametric elements for cross sectional properties and stress anal. 79—44731
- beams, optimal layouts, allowance for cost of shear and bending 79—68566
- beams, plates and rings, refined finite element schemes based on moment scheme 79—53979
- beams, plates with varying thickness, fundamental freqs. 79—32324
- beams, rectangular, of arbitrary depth, free vibr. 79—98647
- beams, rigid plastic, quasimodel form solns. for dynamic response 79—90170
- beams, slender tapered with internal or external axial flow, dynamics theory 79—64499
- beams, slender tapered with internal or external axial flow, dynamics experiment 79—64500
- beams, thin walled elastic, as directed curves 80—1421
- beams flexural-torsional problem by series expansion in eigenfunctions 80—83732
- Beck's rod, nonconservative flutter system, variational principle 79—1132
- bending free toroidal shell shapes for Tokamak fusion reactors 79—64503
- Bernoulli-Euler beams, maximum stiffness, bending, transverse vibrs., singularities in design 79—81802
- biaxial plastic tension, instability calc. *(Russian)* 80—23920
- bifurcation from rotationally invariant states 78—77671
- biomaterial growth phenomena and behaviour, math. theory 77—81458
- blood vessel wall rheological props. *(Hungarian)* 78—35875
- bodies with binary material and kinematic-kinetic structure 78—73848
- bonded joints, adhesive nonlinearities, optimal length, performance 79—1103
- bone fixation screws for tibial fractures, anal. of forces 77—60300
- book, relativistic theories of materials 78—81907
- boundary-integral method, appl. to plates of arbitrary plan form 77—72155
- box beam anal. by finite strip method, performing element 79—80438
- buckling, two-mode, asymptotic anal., reln. to catastrophe theory 78—34042
- C^0 efficient finite element for simply supported rhombic plate 77—80065
- cable problems, finite element approach 79—49041
- cable-band membrane, axisymmetric, interdependence between geometry and forces 80—96185
- cantilever bars under axial load, parametric reson. by combined freqs. method 79—1131
- cantilever beam, minimum mass struct., axial vibrs., numerical determ. 79—10519
- cantilever beam shape optimisation *(Polish)* 78—79203
- cantilever beam with shear and longitudinal deformations, nonlinear bending 79—72822
- cantilever beams, free transverse bending vibrs., secondary effect influence *(French)* 79—18785
- cap, isotropic and orthotropic shallow spherical with hole, dynamic buckling 80—19258
- caps, thin elastic spherical, stability curves, boundary value problems 79—81745
- carrier field theories, multiple-interaction nonlocal formulations 77—52
- catastrophe geometry in physics 80—8786
- catastrophe theory, appl. to mech. of deformable bodies *(Polish)* 78—20966
- catastrophe theory, singularities, examples, Thom 80—8785
- catastrophe theory, symmetry and higher order cuspoids 78—62079
- cell collocation method in continuum mechanics 78—77711
- channel columns, optimum cross-section 79—50580
- chemically reactive mixtures, continuum description *(French)* 79—41765
- Cholesky factorisation method for mixed boundary conditions and discontinuous material prop. problems 79—81715
- circular arches, curved finite elements 78—5652
- circular cylindrical shells, 2- and 3-dimens. results for rotationally symmetric deformations 79—7286
- circular cylindrical shells under hydrostatic press., influence of boundary conditions on stability *(Chinese)* 79—32306
- circular plate, min. weight *(Russian)* 77—50951
- circular plate cantilever, calc. method *(German)* 80—83731
- circular plates, Ilyushin yield surface approx. 79—64505
- circumferentially travelling radial loads on rings and cylinders 78—1564
- clamped beams with two symmetric steps, nonlinear free vibrs. *(Japanese)* 79—14334
- clamped plate under transverse loading, strain energy minimisation, Timoshenko approx. soln. 79—46197
- clamped plate with ribs, nonconforming finite element method 77—22418
- closed cylindrical shells, crack propagation criteria 80—38341
- column buckling load problem, constrained minimum weight equivalence 79—7313
- column carrying concentrated mass, parametric reson. 79—1102
- column design, optimisation of support conditions and segmentation 78—51062
- complex system reliability under nonuniform random perturbation, asymptotic anal. *(Ukrainian)* 79—41589
- composite beams, vibration and buckling anal. 79—1123
- composite body homogenisation under action of large spatial freq. forces *(French)* 80—42061
- composite material, modelling as interpenetrating solid continua, plane wave solns. 78—13895
- composite materials with stochastic struct., complex dynamic moduli using conditional averaging technique *(Russian)* 79—27513
- composite media, Green's functions 78—77712
- compressed cylindrical shell, with random parameters optimisation model *(Russian)* 79—76966
- comressible circular block, bending into a spherical shell 80—1437

classical mechanics of continuous media continued
concrete structures, nonlinear deform. and ultimate load behaviour, finite element anal. 77—72163
condensation for mixed dynamic FE analysis of rotational shells 79—32231
condensed matter, phys. props. description using irreducible tensors 79—2627
cone-cylinder shell junction, boundary conditions 79—46196
conformal mappings for curved boundary finite-difference problems 79—3912
conic body torsion, double series method *(Russian)* 79—23206
conical sandwich shells, axisymmetric free vibrs. 79—37215
conjugate domains, eqns. of math. phys., soln. 78—20967
conjugate gradient solutions, finite element elastic problem with high Poisson ratio 78—90707
conservative loading 77—23867
consolidation theory, viscoelastic media, internal mobility effects, dual mechanics correlation 79—14280
constrained material continua, eqn. formation 79—40360
constrained material continua, functional formation of dynamics 79—40359
contact compression of circular cylinders with rough surfaces *(Ukrainian)* 79—50671
contact friction problems, associated and non-associated sliding rules 79—14351
contact with various frictional conditions, finite element anal. 79—32388
continuous beam resting on tensionless elastic foundation, soln. 79—46238
continuous system simulation by periodic structs. harmonic load response 79—18705
continuum mechanics, introduction, book 79—30234
continuum mechanics and field theory, role of Thomson and Maxwell 79—17179
continuum model of a particle system with three-point interactions 78—73852
continuum orbitals, used to describe and analyze radiationless processes 78—33549
continuum thermodynamics, existence of single temp., heat and entropy flux 77—13729
continuum with microstructure, general model 79—25848
contrinuous media, natural theory *(Russian)* 78—41157
Coserat surfaces 79—2629
Cosserat plate, Signorini problem, finite element anal. 80—1420
coupled fluid-structure systems, vibr. anal. by displacement method 79—7323
cracked plates, symmetric bending by reflected caustics method 80—19283
critical pressure of developing shells *(Ukrainian)* 77—68387
cross-spring hinge problem, 2-D, use of minimization methods in solving 78—18163
crystals, quasicontinuum theory 77—855
cumulative damage, continuum theory 77—31255
curved bar with linear elastic props., eqns. of motion *(French)* 79—94495
curved beam with viscous damping forced vibrations 79—50622
curved macro-element for cracks and corners 80—33448
curved plane slender bars and frames, geometrically nonlinear behaviour 78—13935
cyclic loading, elementary and classical rheological models, global behaviour *(French)* 80—22197
cylinder, hollow, calcs. using straight line method *(Russian)* 78—26027
cylinder, thick walled, thermal stress calc. taking nonlinear creep into account 79—46184
cylindrical envelope, stability under effect of axial contractive power and cross pressure *(Russian)* 78—42550
cylindrical non-axisymmetric wave propagation in laminated medium, continuum theories 79—14293
cylindrical shell, buckling investigation 80—19261
cylindrical shell, design for minimum wt. 78—9560
cylindrical shell, design optimisation under dynamic loading 79—59935
cylindrical shell, submerged 79—18715
cylindrical shell, vibration characts. *(Japanese)* 79—64565
cylindrical shell of elliptic section, stability *(Bulgarian)* 79—9108
cylindrical shell stability under external pressure *(Russian)* 77—54872
cylindrical shell with circumferential notch under axial compression, stability *(Polish)* 78—79239
cylindrical shell-filler system, natural and parametric vibrations, taking tangential interaction into account 78—67085
cylindrical shells, finite difference computation 78—9586
cylindrical shells, Ilyushin yield surface approx. 79—64505
cylindrical shells, inverse problems 80—99925
cylindrical shells, loading history, effect on plastic buckling *(Russian)* 79—14288
cylindrical shells, mildly sloped, with circular aperture, bending problem 79—18704
cylindrical shells, orthotropic, dynamics under axial impact 79—59936
cylindrical shells, orthotropic, noncircular, problem solubility *(Ukrainian)* 79—32255
cylindrical shells, stiffened, min. weight design for pure bending *(Japanese)* 80—64381
damped string, vibr. freq. depend. on kinematical nonlinearities 79—14296
deformable bodies, three-dimens., stability study 80—14596
deformable body three dimensional stability theory, variational principles 80—38300
deformable media, equivalence of force systems *(Russian)* 77—50886
deformable media, perturbation method in 3-D problems *(Russian)* 78—49660
deformable medium, rotational dynamics 78—20631
deformation processes, natural geometry *(German)* 79—86334
density determ. of body from given potential *(Russian)* 78—77710
developing shells, buckling elastic strain energy 79—86363
diaphragm supported cylindrical shells, static anal. using curved finite strip 79—27507
diatomic elastic solids, nonlocal continuum theory, kinematics, balance laws, wave propag. 78—9559
diatomic solids viewed as directed media, generalised continuum model 77—69051
dielectrics, hyperelastic, with saturated polarisation, variational and invariance principles 80—74730
differential geometry applic. 78—12566

classical mechanics of continuous media continued
differential type media with internal variables, thermodynamic theory 80—99923
diffusion itinerant oscillator model, Mori formalism calcs. 77—58634
Dini and trigonometric series summation *(Polish)* 79—63032
disc calc. by iterative method *(Polish)* 79—14252
disc with variable thickness, cross-section warping and corres. stress quantities *(German)* 78—18206
disclinations in continuum mechanics model, geometry and forces *(German)* 78—34511
discontinuity surface model, balance eqn. and phase transition 78—73850
discontinuous solutions, closed boundary condition systems 77—67286
disordered materials, bounds for effective elastic moduli 78—4486
dispersed medium freezing, origin of water aspiration 77—60130
displacement excitation of continuous systems 77—39254
dissipative and/or dispersive systems, perturbative and reductive method *(French)* 80—36868
dissipative processes, nonlinear theory *(Russian)* 79—30400
dissipative systems, limit cycles and constants of motion 79—35555
double curved membranes and thin shells, stress boundary problem solns. *(German)* 79—50585
double-layer lattice plate yield surfaces, anisotropic continuum treatment *(Japanese)* 78—22261
dual elastic continuum model, internal mobility induced consolidation 79—14352
dual elastic continuum model of media with quasicracks, tensional medium with mobility effects 77—72153
dual mechanics of tensional and fissional fields, appl. to continuum media 79—37156
Duffing's equation, steady and chaotic motions 80—77616
Duffing's equation, strange attractors, explosion, chaotic behaviour 80—77617
dynamic instability region, computation by finite element method 80—23927
dynamic plastic instabilities in stretching plates and shells 79—7302
dynamic problem of continua, reduction of stiffness, mass and damping matrices *(Polish)* 78—12565
dynamic substructure analyses with simplified computation 79—81716
edge notches, conformal transformations 80—27128
education, conservative discrete models, difference eqn. formulation, nonlinear solid, fluid phenomena, computer calc. 77—78924
effective implicit time integration in analysis of fluid-structure problems 80—92040
eight node solid element for pure bending 79—44734
elastic bar structures, exact anal. with nonlinear eqn. system, stresses 79—81731
elastic beam with steadily moving load resting on tensionless Winkler foundation 79—64519
elastic beams hung at both ends, lateral buckling, variational anal. methods 79—86361
elastic beams of various orders 79—76968
elastic circular cylinder, axisymmetric end-problem solns. 79—18700
elastic continua, discretised stress, strain, eqns. and theorems 77—49596
elastic continuum, two-diemsional, side effects of discrete methods 79—58
elastic cylinder under stress, biharmonic problem solution 80—4532
elastic discs, high frequency vibr. spectra, second order approx. theory potentiality *(Russian)* 79—10515
elastic fluid diffusion in elastic solid, mechanical theory 77—59136
elastic interface waves and sliding between two solids 79—18800
elastic materials, isotropic, in space of any dimension *(Japanese)* 78—41161
elastic materials, strongly anisotropic, wave propagation 79—14300
elastic medium, extremum problem for distributed parameter, and determ. of optimum props. 79—88811
elastic medium, surface concentrated loading, axisymmetric problem for homogeneous medium *(French)* 80—92041
elastic members, thin-walled, displacement theories for straight and circ. curved members *(Japanese)* 80—43615
elastic quadrilateral plates 79—46201
elastic shell, stable solutions of simplified problem *(French)* 79—5984
elastic shell revolution, transient motion in acoustic medium 79—7333
elastic shells, cylindrical, and of revolution, path independent integrals 80—87711
elastic strip pressing against elastic half plane, strain anal. 79—7345
elastic structure buckling models for higher order catastrophes 79—1122
elastic system, rotation effects on natural vibr. frequency *(Russian)* 79—7319
elastic thin shells of revolution, finite element anal. of dynamics, and response to Earth motion *(Chinese)* 79—76965
elastic tube, cylindrically symmetric vibr. *(German)* 79—7330
elastic-plastic frames, deformation anal. Monte Carlo technique 79—7295
elastic-plastic materials, dynamic behaviour *(German)* 79—14271
elasticity, linear theory of, shift function derivation 78—4484
elasticity, non-standard anal. methods 77—46
elasticity, non-standard anal. methods 77—47
elastodynamic stress intensity factors, ray theory approach 79—7339
elastoplastic circular plates, nonlinear behaviour equilibr. eqns. 79—14279
elastoplastic solid, fracture and yield conditions 79—14344
elastoplasticity finite element anal. for large strains, natural factor displacement method 80—14580
elastostatics, appl. of modified integral eqn. method 79—14254
electromechanics, investigation methods and techniques *(Polish)* 80—19296
elementary tensor analyses *(Japanese)* 79—30232
endochronic theories of material behaviour, uniqueness and stability 79—18752
energetically stable systems 79—2647
energy principles and finite element formulation *(Japanese)* 79—80437
error estimate for the approximation of Stokes problem by a conforming quadrilateral element *(French)* 79—49039
Euler column buckling, imperfect bifurcation in the presence of symmetry 79—72828
Eulerian computation technique for domains with moving boundaries 77—53779
evolving shells, postcritical deformations *(Ukrainian)* 79—32310
exterior Neumann problem, numerical soln. using double layer potl. 77—67287

- **classical mechanics of continuous media** continued
  - faceless linear cones, orders, gauge, and distance, appl. to continuum mechanics and special relativity 78—57753
  - fatigue crack propag. theory 78—5692
  - fibre composites, impetus of composite mechanics on test methods 80—11868
  - fibre reinforced composite, anelastic behaviour using continuum theory of internal separation 77—46907
  - fibre reinforced shell-type structures, strength estimation using limit state method 79—18820
  - filled polymer, mathematical model of strengthening *(German)* 78—63279
  - filler containing beam reinforced three layer plates *(Russian)* 80—43613
  - films as two-dimensional continua, dynamics, wave propagation and stability 79—68568
  - finite element analysis, natural mode technique, review 79—44728
  - finite element grids, optimal choice 78—77698
  - finite extension of an elastic strand with a central core 79—46217
  - finite incompressible elastic body, Hadamard theorem of integral inequality in bifurcation 77—41485
  - flat sheet, tensile deformation, strain rate sensitivity and necking 79—41590
  - flexibility matrix for skew-curved beams 79—98620
  - flexible bar, min. vol. design by dynamic programming *(Polish)* 78—13965
  - flexible long cylindrical shell with variable parameters, deformation anal. *(Ukrainian)* 77—68388
  - flexible thread in a stream, natural freq. *(Russian)* 79—90163
  - flexural vibration mode shape change by defects 79—7335
  - flow-induced oscillations, bifurcation to divergence and flutter, infinite dimensional anal. 78—89336
  - flows in dissipative materials, a priori estimates 78—16643
  - fluid coupled concentric cylindrical vessels, normal mode solution 79—37157
  - fluid saturated porous elastic cylinders, vibrations 79—10521
  - fluid systems, local equilib., discontinuity surface 79—84960
  - fluid-solid dynamic interactions and wave forces, numerical treatment 79—3944
  - fluid-structure coupling method in dynamic analysis of structs. 79—7322
  - fluid-structure systems, time integration, mixed methods 79—41568
  - fluid-structure systems, transient anal. 79—32232
  - foil bearing, deflection due to finite width bump, iterative methods 78—77691
  - follower forces and load stiffness, appl. to press., centrifugal load, frictional drag, cable load 79—64493
  - forces on sinusoidally oscillating cylinder, parametric study 79—32547
  - fracture mechanics, self-adaptive finite element capability 79—14345
  - frames, elastoplastic anal., uniqueness 79—7297
  - frameworks' stability analysis appl., w.r.t. sway excess of columns 78—51098
  - frameworks calc., composed of thin-walled open sections, with aid of computer 78—51059
  - fuel element spacers, structural anisotropic plates composed of cylindrical shells 78—89940
  - functional analysis applications *(French)* 77—67292
  - fundamental laws and constitutive equations, in space of any dimension *(Japanese)* 78—41160
  - fundamental laws of thermomechanics, constitutive eqns. *(German)* 78—24758
  - Galilean invariance of balance eqn. for singular surface in continuum 77—75792
  - gas-saturated porous media, deform. theory *(Russian)* 77—41483
  - Gauss principle appl. *(Polish)* 78—12564
  - Gauss-Hertz principle, extension of continuum form to time domain 78—73851
  - Gauss-Hertz principle 77—22415
  - Gauss-Hertz principle for fluid flow, Poisson eqn. and nonlinear flow 77—84212
  - general physics and heat, book 79—25814
  - general shell and axisymmetric shell elements, diagonal lumped mass matrix formulation 79—3911
  - generalised deformation minimum *(French)* 79—53977
  - generalised displacement functions, elastic continuum 79—7289
  - generalized simple materials 77—5666
  - geological media, hysteresis behavioural effects 80—21712
  - geometric field theory of finite deformation in continuum mechanics *(Chinese)* 79—71248
  - geometrical nonlinear shell theory, dual extremum and complementary stationary principles 80—4526
  - geometrical stiffness, appl. to beam and shell problems 77—33869
  - geometrical theory of structural defects *(German)* 80—88136
  - global element method for elliptic partial differential equations 80—46805
  - granular materials, influence of void compaction and material nonuniformity on acceleration waves 77—68472
  - granular materials, mechanics, continuum and statistical approach 79—59923
  - granular materials, void compaction and material nonuniformity, influence on acceleration waves, addendum 78—83280
  - granular materials flow, micropolar continuum theory 79—35565
  - gross variables, microdynamics and nonlinear stochastic processes 80—101754
  - gyroscopic problems in elasticity, orthogonality principle 79—17218
  - H-columns, local and member buckling finite strip method anal. 79—7306
  - half-space with cylindrical cavity, pure shear under tangential load 80—33464
  - Hamilton's principle for thermodynamic systems 79—88896
  - Hamilton mechanics, quasi-canonical eqns. of motion *(Ukrainian)* 80—31505
  - Hamiltonian continuum mechanics, differential geom. foundation 78—77708
  - Hamiltonian mechanics, differential geometric foundation 78—4483
  - hard rods and spheres, radial distrib. function, differential difference eqns. in Percus-Yevick approx. 79—18701
  - harmonic oscillator one-dimens. chain with friction, discrete-continuous transition 77—850
  - heat instability in thermoviscoelastic coupled dynamic problems *(Russian)* 79—10489
  - helically armoured cables, stiffness matrix derivation considering tension and torsion 79—46187

- **classical mechanics of continuous media** continued
  - hemispheres, thin elastic spherical, stability curves, boundary value problems 79—81745
  - heterogeneous materials, bulk prop. calc. models in Dyson eqn. formalism 80—1419
  - heterogeneous materials, generalised continuum theory derivation 77—853
  - heterogeneous solid media, statistical continuum theory, information theory approach, static field theory 80—22198
  - heteroolastic beam, progressive creep under loading *(French)* 79—7290
  - hexagonal continuum infinite half-space, elastic Green's function 79—63038
  - Hochschild cohomology within transitive Lie pseudogroups, appl. to deform. theory *(French)* 77—67227
  - holed plates, stress and deformation, finite quadrilateral elements technique *(Rumanian)* 79—18707
  - hollow shells, multi-layer with finite deflection, general theory *(Russian)* 79—81719
  - homogeneous isotropic bar, torsional stress anal. for variously shaped cross sections *(Russian)* 79—32269
  - homogenisation of a class of nonlinear problems *(French)* 79—71250
  - horizontally curved beam finite element including warping, nodal displacement degrees-of-freedom 79—44735
  - hydrocode convergence 78—36834
  - hyperbolic balance laws in continuum physics 80—4525
  - hyperbolic paraboloids elastic stability analysis, using reduced scale models 79—3910
  - ice domes, time dependent deformation 79—37152
  - ideal crystals, principles of satbility analysis 77—45697
  - imperfect shells, stability, numerical anal. *(Ukrainian)* 79—94514
  - imperfection sensitivity of N-degree-of-freedom system with coincident critical points, symm. effects, stability props. 78—79236
  - implicit-explicit finite elements in nonlinear transient analysis 79—44729
  - implicit-explicit finite elements in transient analysis: implementation and numerical examples 79—17216
  - implicit-explicit finite elements in transient analysis: stability theory 79—17215
  - incompressible materials, approx. in displacement method 79—72801
  - indeterminate beams, variable cross section, stress anal. using repeated integration 79—64510
  - infinite cylindrical shell, dispersion curves and distrib. coeff. of elastic waves *(Russian)* 77—46964
  - infinite dimensions and the fold catastrophe, particle modelling 80—8788
  - infinite finite elements 77—71196
  - infinite plane with crack in nonuniform steady field, stress intensity coeffs. 80—38343
  - infinite plate containing plane curved polygonal defects and cusps, stress anal. *(Chinese)* 79—72793
  - infinite plate with two holes, stress concentration reduction by interference fits 79—37158
  - infinitesimal operators of translation and rotation, conservation eqn. derivation, appl. to continuum mechanics 80—27127
  - inhomogeneous elastic material, antiplane crack problems 79—14343
  - inhomogeneous viscoelastic Voigt-Kelvin rod, stress propag. and harmonic vibrs. 79—94543
  - instability, post-, in class of smooth functions, mathematical model 80—69649
  - integro-differential type media, theory *(Ukrainian)* 79—49040
  - interdigital transducers, quasiacoustic wave propagation, field theory anal. 78—66998
  - internal coupling and fields of reaction *(Russian)* 78—16644
  - intrinsic parameters schematising shape and stress, Lagrangian formulation *(French)* 80—73173
  - isoparametric elements, stiffness matrix, stress intensity factors *(Chinese)* 79—92943
  - Kirchhoff plate, eigenvalues with nonlinear spline functions, matrix displacement method *(German)* 80—33446
  - Kirchhoff plates, matrix displacement method with parameter transformation by additional compatibility postulation *(German)* 78—79202
  - Kirchhoff shells, static and dynamic anal. based on mixed finite element formulation 79—32328
  - Koite's modified energy functional, appl. to cantilever circular cylinder shell freqs. 79—1130
  - Lagrangian formulation for continuous media 77—57192
  - laminated composite media, crack tip propagation, model by two-dimens. mixture theory 79—10528
  - laminated plates and shells, eqn. construction *(Russian)* 79—30254
  - large defection anal., hybrid finite element and finite difference approach 77—72201
  - large deflections of a plate sealing a liquid 79—27508
  - large strain applications of modified const. strain finite elements 79—2632
  - layered elastic materials, homogeneous continuum model 77—58546
  - layered shells, stress states, asymptotic approach *(Italian)* 79—10461
  - limit analysis, comparison of static and kinematic approaches *(French)* 78—86156
  - limit analysis, complete static solns., appl. to vertical cut *(French)* 79—18702
  - limit analysis in continuum mechanics, nonlinear optimisation problems, numerical methods 79—2628
  - linear elastic continua, variational principles, finite element techniques *(German)* 79—9113
  - linear mechanical boundary and eigenvalue problems with symmetries 77—72154
  - linear mixed problems, integral eqn. soln., two effective methods *(Russian)* 77—82388
  - linear shell theory, dual complementary variational principles generated from dual functionals *(German)* 79—97196
  - linear theory of elastic shells *(French)* 77—54883
  - liquid carrying pipe on elastic foundation, dynamic stability 79—90161
  - liquid-liquid mixing analysis, lamellar model 80—15246
  - liquid-saturated porous media theory with account of simultaneous deform. of structure and liq. *(Russian)* 77—41482
  - loaded construction, randomly loaded, crossing probabilities, numerical anal. *(German)* 80—96186
  - localized dynamic contact on structs. anal. by matched asymptotic expansions 79—7342
  - Lorentz invariant mech., adiabatic and reversible motions 77—35029
  - macrocontinuum model of a mixture and a discrete multi-constituent system 79—94482
  - macroscopic determinancy principle corollaries *(Russian)* 78—77714

classical mechanics of continuous media continued
- magnetisable and polarisable media, mech. and EM effects *(Russian)* 77—49611
- magneto-micropolar continua, spatial interaction 79—97198
- Marguerre's shallow shell theory 79—32239
- massive homogeneous elastic string, on rot. platform, deformation study, constitutive equations soln. 79—9107
- material symmetry transformation, density preservation 79—35552
- materials with memory, nonlinear integral representations 77—42732
- materials with variable bonding 79—1100
- Maxwell's initial boundary value problem, horizontal line (Rothe) method, convergence and error estimates 80—94957
- mechanics of vibr., introduction, book 79—80439
- membrane, fixed and of varying mass density, fundamental mode estimates 79—68564
- membrane, prestressed rectangular, forced vibration, near resonance response 79—68611
- membranes, arbitrarily shaped, vibrs. and dynamic response 79—7334
- membranes, excitable, nonlinear anal. for shaping threshold action 77—12871
- membranes, optimised dishes, strength and stability *(German)* 78—87256
- mesh analysis processes, convergence *(German)* 78—87257
- metal sheeting, profiled, shear deformation, stressed-skin anal. 79—1121
- metal targets, penetration by conical projectiles, ductile hole formation study 79—23220
- metallic column at elevated temp., parametric response 79—72829
- methodology and applications *(Russian)* 77—42733
- micromechanics, stochastic deformations of discrete systems 77—40
- micropolar continuum, isotropic, elastic fields of dislocations and disclinations 77—68971
- micropolar elastostatics, J-integral type conservation laws 79—18710
- micropolar thermoelasticity, radiation conditions, uniqueness theorems 79—12606
- microstructural EHD model of continuous medium, appl. to liquid crystals 77—42731
- microstructure with finite deformations, reciprocity theorem, stored energy function *(Italian)* 78—81836
- minimal normal modes, existence and bifurcation 79—72837
- minimum mass design of continuous structural members 77—80063
- minimum principle for the problem of torsional creep 79—75337
- mixed continuous mechanics problems, orthogonal functions *(Russian)* 78—49659
- mixed problems in theory of harmonic functions, Monte Carlo method appl. 79—10464
- mixtures of interacting continua, thermodynamics and nature of 2nd law 79—26016
- mixtures with diffusion, axiomatic theory of mech. behaviour 77—858
- modelling design process, finite element anal. appl. 80—28414
- momentum balance of continuous media, correction based on Ott's transformation 78—41249
- motion stability in neutral case *(Ukrainian)* 79—41594
- moving load in initially stressed thick plates attached together by a flexible core 79—81752
- multi-layer beam assembly bending, appl. to leaf spring *(Russian)* 79—81718
- multibar structure strength from heteroplasticity concept *(French)* 79—18742
- multicomponent continual system, dynamic processes, variational principle *(Russian)* 79—12595
- multicomponent random media, central momentum functions of material characteristics *(Russian)* 79—9188
- multicomponent solid body undergoing allotropic transform., fundamental deform. eqns. *(Russian)* 78—16645
- multilayered shells and directed surfaces 79—46185
- multiparametric elastic system, lower frequencies and crit. loadings *(Russian)* 79—44739
- multiperforated media submitted to tensile loading, overall behaviour *(French)* 79—76967
- multipolar equations derived from statistical mech., micropolar elasticity 77—45
- multistorey elastic frames, critical load numerical determ. *(French)* 79—14262
- muscle tissue, math. models 77—25358
- muscular organ mechanics 77—90836
- nematic liquid crystal, extensible, micropolar continuum theory 79—4244
- nematic liquid crystals subject to EM fields, continuum theory 80—33876
- net shells of revolution, equilib. eqns. under rotationally symmetric loads 79—14246
- nets, orthogonally woven, propagation fronts, from impulsive excitation 79—46199
- non-conservative systems, with ignorable coords. 79—25843
- non-local continuum mechanics, conservation laws 78—65770
- non-local continuum mechanics at atomic scale 78—12563
- non-self-adjoint problems and essential boundary conditions 79—44732
- non-stationary optimality conditions in structural design 79—72794
- nondissipative medium, boundary problem soln. with surface discontinuity *(Russian)* 80—101716
- nonholonomic systems, Hamilton-Jacobi integration method generalisation 79—12598
- nonhomogeneous cylinders and cylindrical shells, torsional oscillations anal. 79—18768
- nonideal realisations of constraints and loosenesses 78—73849
- nonisothermal rigid shell theory using fundamental laws of thermodynamics 80—87712
- nonlinear anal. of deep arches, using mixed curved-beam finite elements 78—18161
- nonlinear analysis, natural force approach 79—2631
- nonlinear continuum theories, generalised coordinate transformation 78—36828
- nonlinear dynamics, finite element anal., accuracy versus computational efficiency 79—40362
- nonlinear dynamics of tank containing fluid, direct method of soln. *(Ukrainian)* 79—35554
- nonlinear elastic cylinder, parametric biharmonic vibrs., reson. modes *(French)* 79—10522
- nonlinear elasticity incremental eqns., bifurcation of pressurised spherical shells 79—17225
- nonlinear elasticity incremental eqns., membrane theory 79—17224

classical mechanics of continuous media continued
- nonlinear elliptic problems for doubly connected domains, heuristic method *(Russian)* 78—86159
- nonlinear eqns. for structures with transverse shear *(French)* 77—82390
- nonlinear finite element analysis, review of soln. techniques 79—3914
- nonlinear first order evolution problem, MHD appl., of invariance principle 79—97197
- nonlinear isotropic body, plasticity theory determinantal ratios *(Russian)* 79—14274
- nonlinear physical media, boundary valve problem soln. by finite element anal. 79—17214
- nonlinear plate models, existence results *(French)* 80—31504
- nonlinear plate problems, unconditional stability of finite element scheme, nonlinear vibrs. *(Japanese)* 79—77004
- nonlinear second order system, eigenfunction expansion solutions of Fokker Planck eqn. 80—73172
- nonlinear shell equations, post buckling range, accuracy 78—22290
- nonlinear shell problems, hybrid stress finite element model 79—14251
- nonlinear shell theory, numerical method *(Russian)* 78—34006
- nonlinear structural dynamics, direct time integration methods 79—44730
- nonlinear structure stability problems, incremental displacement algorithms 79—81717
- nonlinear vibrating string eqn., unilateral problem 79—63031
- nonlinear vibrating system, combination reson. response amplitude calcs. *(German)* 79—10527
- nonlinear viscoplastic materials, upper yield points 79—10490
- nonlinear wave process in a finite dissipative region *(Russian)* 79—17240
- nonlinear wrinkling of nonlinear membranes of revolution 79—32242
- nonlocal continuum theory, using kinetic theory, stress, energy density *(Japanese)* 78—32677
- nonlocal media, boundary effects, gradient model anal. 79—90126
- nonlocal thin elastic plates, impact by cylindrical projectile, shearing stress anal. 79—10467
- nonstationary motion of particles in a liquid in a gravitational force field *(Russian)* 79—84955
- nonstationary multicomponent continuous systems, variational priciple, eqns. of motion *(Russian)* 79—27512
- nonuniform medium, model 80—38254
- normal dissipativity and concealed variables in eqns. of evolution *(French)* 79—25859
- Norton-Hoff material, limit anal. appl. *(French)* 79—23202
- nuclear power plant, aircraft impact, simplified derivation of reaction-time history 78—89958
- nuclear reactor upper internal structures, finite element structural model appl. 80—32362
- object shape rel. to physical description 79—42422
- objective and regular differentiation and integration, constitutive law and transport *(French)* 80—57090
- one-dimensional, in continua, non-propagative modes *(Japanese)* 80—4539
- optimal coordinate theory, appl. to physical problems 77—71211
- optimal design of bending elements 79—10470
- optimal rod and shell shape determ. using variational principle 80—5929
- orthogonal base functions and consistent diagonal mass matrices for two-dimensional elements 79—90125
- orthotropic annular plate, stability *(Polish)* 78—18209
- orthotropic annular plates, general nonsymmetric postbuckling anal. 79—7307
- orthotropic cylindrical shells, periodic problems, computer anal. *(Russian)* 80—23889
- orthotropic medium of revolution in plane deform. state, law of behaviour *(German)* 77—23866
- orthotropic plastic plate, optimal design under in-plane loading 79—7303
- orthotropic plate flexure, theoret. considerations, expt. investigations *(German)* 79—10463
- orthotropic plate with square hole and convective heat exchange, plane static thermoelasticity *(Russian)* 80—33456
- orthotropic sandwich plates, large deflection governing eqns. 79—7301
- orthotropic shells, heterogeneous, linear theory 77—67283
- orthotropic shells of revolution, free oscillations *(Russian)* 79—18796
- oscillating system, light damping, influence of eigenvalues *(German)* 80—31490
- oval cylindrical shells, free vibrs. modal method calcs. 79—7332
- panels, cylindrical, failure under gasdynamic periodic shock waves 80—14611
- panels with openings, stability loss and critical stresses 80—10219
- partial differential equation system integration in mechanics, comments 79—30233
- particle solids, computer generation 78—26026
- particle system to continuum model transition 77—854
- particulate material deformation mechanism as Markov process *(Japanese)* 80—14562
- pencil point breaking, stress anal., size and shape of points 79—84901
- pendent liquid drop, shape anal. 79—92936
- periodic solutions of systems with friction *(German)* 79—90199
- periodic structure averaging *(Russian)* 78—41158
- periodic structures, asymptotic anal., book 79—25851
- piezoelectric resonator, disturbances characterised by dissipative mech. parameters 79—28682
- pile, numerical soln. of beam eqn. with nonuniform foundation coeff. 80—64361
- pipe, use of dynamic absorber to control parametric instabilities 79—46198
- pipe conveying fluid, equilib. position stability 79—32319
- pipelines, installation, nonlinear finite element anal. 79—46183
- plane strain, spurious modes in two-dimensional isoparametric elements 80—52
- plastic structures, dynamic adaptation to stochastic excitation 79—1116
- plate, anisotropic, transcritical strength optimisation 78—30175
- plate, annular elliptic heated, const. thickness, buckling and stability criterion 80—28443
- plate, circ., large deflection anal., with nonuniform Jacobi polynomial load 79—37184
- plate, circular, flexural response on bilinear foundation 79—32238
- plate, circular, viscoelastic response to impulsive loading, expt. tests 79—81825
- plate, circular, with rigid inclusions, antisymmetrical carrying capacity 80—69650
- plate, circular impulsively loaded, finite viscoplastic deflections by mode approx. technique 79—81738

classical mechanics of continuous media continued
plate, circular thin hinged, bending, Hertz-Timoshenko hypothesis 80—33482
plate, circular thin nonhomogeneous, with circular hole, extensional vibr. 79—94546
plate, cylinder, sphere, temperature (one-dimensional) and thermal stress fields, inverse problems 80—79134
plate, eigenvalue problem, bidimensional approximation *(French)* 80—33445
plate, elastic, under tension stress conc. due to surface pit 78—83243
plate, elastic circular cylindrical, with arbitrary transference, stress-strain state *(Russian)* 80—23895
plate, elastic with rib, vibr. freq., Weierstrass condition *(Russian)* 79—81757
plate, flexural motion, effect of accelerometer mass 78—90741
plate, geometric imperfection meas. appl. 79—81713
plate, homogeneous, circular, prestressing effect evaluation 79—59
plate, laminated composite, notch tip stresses, experimental and numerical 79—77006
plate, linear elastic, classical boundary value problem 79—14261
plate, linearly elastic, free harmonic vibration fundamental frequency, approx. solution 79—46256
plate, nonlinear struct. response to sonic booms 79—32322
plate, optimal design under dead weight and surface loading 79—3915
plate, out of plane bending, steady state crack propagation, rotatory inertial effects 79—7340
plate, perforated, under axial loading, geometric discontinuities, in stress fields, optimization 79—37150
plate, prestressed simply supported rectangular, large deflections under uniform pressure 79—32235
plate, rate sensitive plastic, circular hole, dynamic expansion 79—10509
plate, rectangular viscoplastic under pressure impulse, deflection determination *(Polish)* 79—64533
plate, reinforced strip, 2-dimens. nonsteady temperature stresses 80—74734
plate, relationship between centres of flexure and twist 79—86335
plate, rib reinforced and supported, lying on a linearly deformable base, flexure 80—69651
plate, spinning nutating, resonant excitation 79—64504
plate, square, subcritical and supercritical behaviour when compressed by 2 concentrated forces *(Russian)* 79—59919
plate, stretched infinite, weakened by arbitrarily shaped hole, Gaursats functions 80—38249
plate, thick free circular, axisymmetric flexural vibrations 79—64575
plate, thick infinite, transversely isotropic, containing circ. hole, end effects 79—27510
plate, thin elastic, buckling problem, eigenvalue eqn. positive soln. appl. *(German)* 79—68610
plate, thin elastic, Chladni patterns in random vibration 79—81714
plate, thin stretched, with curvilinear holes, buckling and loss of stability *(Russian)* 79—68607
plate bending, curvilinear finite difference method for biharmonic equation 79—64539
plate deflection examination by moire optical contouring *(Polish)* 79—64607
plate deflection theory, discrete methods for boundary value problems 79—49045
plate deflection theory, dual extremum principles 80—31506
plate element, 2nd order *(German)* 79—10466
plate flexure with arbitrary boundary conditions, boundary integral formulation 79—25858
plate incompressible isotropic, stability under all-round compression *(Ukrainian)* 79—37149
plate infinite, oscill. in strong rarefied gas under constant force 79—10623
plate problems, biharmonic oscill., finite element discretisation, preconditioned conjugate grad. method 79—72795
plate structs., finite strip method for post-locally buckled anal. 79—30246
plate theory, justification of nonlinear model *(French)* 79—25852
plate theory, virtual work principle *(French)* 77—17817
plate thick, circular hole under axisymm. radial load, stress anal., displacements 78—79201
plate with bend interaction, numerical calc. method for stress and deflection *(Japanese)* 80—23919
plate with curvilinear elasticity, stress distrib. around hole, asymptotic method *(Russian)* 79—81726
plate with hole, contour reinforcement, plane stress state anal. *(Russian)* 80—33447
plate with rectilinear thin walled elastic inclusion, bending stress state *(Russian)* 79—81736
plate-spring struct., dynamic characteristic determ. by rigid finite element method *(Polish)* 78—18220
plates, annular, dynamic stability numerical soln. *(Polish)* 80—10173
plates, annular, of variable thickness, natural vibr. eigenfreq. Mindlin eqn. integration 80—38318
plates, buckling due to nearly homogeneous stresses *(German)* 79—81746
plates, clamped elliptical with concentrated mass, nonlinear vibration amplitude-freq. characts. 79—64561
plates, clamped impulsively loaded circular, membrane mode approx. solns. 79—64501
plates, clamped orthotropic rectangular, with varying thickness, natural frequencies 79—46253
plates, clamped regular curvilinear polygonal normally loaded over concentric circle, deflections 79—72803
plates, elastic, optimum bending and extension *(Russian)* 80—38259
plates, elastic homogeneous and isotropic, transient and time harmonic wave propagation 79—50633
plates, full-field numerical differentiation 79—59922
plates, isoparametric finite elements, variational formulation of plate equilib. problem *(French)* 80—43608
plates, isotropic and orthotropic annular, large deflection static and dynamic anal. 80—28413
plates, nonlinear vibrs., reson. phenomena under Duffing's eqn. 79—14305
plates, orthotropic circular, nonlinear dynamic anal. 80—64360
plates, orthotropic curved, bending behaviour, nonhomogeneity effects 80—23903
plates, orthotropic laminated, stress-strain state *(Russian)* 79—46189

classical mechanics of continuous media continued
plates, orthotropic rectangular, nonlinear vibrations by displacement formulation 79—64579
plates, polar orthotropic laminated annular, asymmetric vibrations 79—76993
plates, rectangular orthotropic, stress anal. and generalised orthogonality relations 80—38252
plates, rectangular with linearly varying thickness, deflection and surface stress formulae 79—30244
plates, ring sector, flexure under uniform and concentrated normal loads 79—72802
plates, sandwich, large amplitude vibration amplitude-frequency characteristics 79—64580
plates, simply supported, plastic buckling under edge thrusts 79—10510
plates, thermal stresses, temp. fields for butt-end narrow zone heating *(Russian)* 79—14248
plates, thick circular, axially symmetric vibration, elastodynamic deformation 79—37214
plates, thick orthotropic on elastic foundations, freq. anal. using triangular plate bending element 79—46273
plates, thin and thick circular, subjected to transverse pressure, lower bound limits 79—68565
plates, thin circular, modal anal. of transient asymmetric response 80—23931
plates, thin elastic, large amplitude vibrs. by conformal transformation method 80—19262
plates, thin rectangular elastic, bending, finite difference anal. 79—46181
plates, thin rectangular elastic, response using Greens functions 80—1424
plates, transversely isotropic rectangular, nonlinear vibrations 79—64559
plates, variable thickness annular, axisymmetric bending 79—46193
plates, vibrating elastic, transcendental equation solns. 79—53980
plates and shells, dynamic plastic anal. using stress resultant finite element formulation 79—37191
plates laminated, shear deformations and correction factors, plate and elasticity theory 79—76963
plates of arbitrary shape, limit anal. for plastic bending 80—14584
Poincare gauge invariance, conservation laws for particle, string and membrane systems 79—55
point defects, motion-dependent Burgers vector in elastic continuum 77—51371
point systems immersed in a continuum, calculus 77—49595
polar materials, restrictions on boundary conditions 78—54186
porous media, effect of fluid on mechanical props. 80—23883
porous media, elastic, variational theory 80—10146
porous media models using thermodynamics of mixtures 80—96184
portal frame, elastic-perfectly plastic behaviour under column axial force variations 79—7296
potential approach appl. 77—68429
pressure vessels, secondary creep problem, lower bound approx. soln. sequence 79—14284
prismatic beams, element stiffness matrix 78—5653
progressive waves in dissipative media, long range ray theory *(French)* 80—42070
pseudocontinuum theory, correspondence between representations 79—35553
quasi-Newtonian force 78—63765
quasi-steady motion stability in quasi-cyclic coord. system *(German)* 79—88806
quick-change fields in continua, regularisation 78—49663
radial ply motor tyres, deformation on road surface, anal. *(German)* 79—90201
rate sensitive materials, deformation mechanics, approx. anal. technique 79—23221
Rayleigh-Taylor instability, method of generalised coords. 78—65771
rectangular orthotropic plates, buckling strengths stress diagrams *(German)* 79—14289
rectangular plate, thick, general expression for exact soln. of dynamic anal. *(Chinese)* 79—37154
rectangular plate buckling, Von Karman eqns., generic bifurcation theory, symmetry props. 79—44748
rectangular vibrating plates separated by liquid filled gaps, viscosity friction calc. *(German)* 80—105504
reinforced concrete structures, nonlinear finite element anal. 79—41569
reinforced plate homogenisation by period system of curvilinear bars *(French)* 79—10462
reinforced rectangular plate, compressed in two directions in a manner conducive towards stability 78—22289
relativistic eqns., principle of objectivity, proper rigid frame 77—37757
research in the mechanics of deformable solids in the USSR *(Russian)* 79—27516
residual correction applied to a sequence of block tridiagonal matrices 79—72800
respiratory system, forced perturbation 79—100640
rheometric structure theory, convective differentiation and continuum electrodynamics 80—86087
rib-reinforced orthotropic cylindrical shell, structural design effect on stability 78—22288
ribbed-shell theory, inhomogeneous nonlinear problems 80—99924
right-angled ribbed plates, variable thickness calcs. *(Russian)* 79—27509
rigid body, moments and products of inertia, tensorial charact. 79—25847
rigid indentor sliding over power law viscoelastic layer, anal. 79—7346
rigid-plastic shells of revolution, optimisation *(Russian)* 77—68390
ring, under diametral compression, geometric discontinuities, in stress fields, optimization 79—37150
ring plates, stability under compressive stresses *(Russian)* 77—54873
ring shaped bodies, collapse *(German)* 78—87258
rod, composite, stress deformation state calc. *(Russian)* 79—64527
rod, naturally twisted curvilinear, asymptotic variational method anal. *(Russian)* 80—38251
rods, coupled thermoelastic wave propagation, asymptotic theory 79—12609
rods, elastic, large deflections and rots., asymptotic anal. 79—50584
rods, influence of mass distrib. on stability in presence of polygenic forces 79—81744
rods, large curvature, residual stresses determ. 79—41571
rods, optimality necessary conditions *(Russian)* 79—14249
rods, prismatic, torsion with internal constraints *(Russian)* 80—69647
rods, prismatic, torsion with internal constraints *(Russian)* 80—69648
rods, quasi-bifurcation within axial plastic compressive wave 79—10513

classical mechanics of continuous media continued
- rods with thin perforated walls, bending, finite element method *(German)* 80—14591
- rolling contact with dry friction, Duvorol computer code 79—90194
- rotating body, balancing on a string drive, eqn. of steady motion *(Russian)* 80—17800
- round bar, tensile deformation, mathematical description 79—10500
- rubber bonded cylinder, Lagrange anal. of dynamic props., conf., Haifa, Israel, (July 1977) 79—15683
- rubber bonded cylinder, Lagrange anal. of dynamic props. 79—14304
- rubber-like solids, biaxial deform. 80—1431
- Saint-Venant torsion problem, classical, integral and functional eqns. 78—57780
- sandwich panels, discrete field mechanics 77—62151
- sandwich shells and Cosserat surfaces, nonlinear compatibility equations 79—53976
- scalar macroscopic fields in anisotropic stratified media, Green's functions 79—58544
- semi-infinite plate, crack from triangular notch 79—41570
- semiclassical Green's function, energy-representation 80—90692
- semiinfinite plate, penetration into incompressible liquid, boundary value problem *(Russian)* 79—88804
- shakedown of deformable plastic structure, approx. methods, fatigue 77—54900
- shallow anisotropic shells of double curvature, weakened by hole, bending problem 79—90151
- shallow arches, natural structural shapes 77—80064
- shallow shells, arbitrarily oriented cracks, stress intensity factor 79—7341
- shallow shells, optimisation, formfinding, load bearing behaviour, stability *(German)* 79—27505
- shallow spherical shells, deflections and internal forces, finite element anal. *(Chinese)* 79—68583
- shallow spherical shells, stability under axisymmetric loading *(Russian)* 79—14287
- shallow thin shell finite element, stiffness matrix development 78—90705
- shape of planets and Sun due to rot., equipot. surface 77—13541
- sheet, plane elastic, containing circular hole or inclusion, radial deformation 79—41575
- sheet, stress changes and warping during heating *(Russian)* 79—59920
- sheet metal, limit strains, predictions from yield criterion 79—27539
- sheet metal stamping, finite element anal. 79—7344
- shell, aerohydroelastic opening of shell in nonstationary flow *(Ukrainian)* 79—32258
- shell, axially compressed cylindrical, axisymmetric imperfection effect on plastic buckling 79—64548
- shell, circular cylindrical with varying wall thickness, creep buckling, variational methods 80—14595
- shell, consistent second approx. to elastic strain energy 79—81732
- shell, cylindrical, cantilever, dynamic deforms. and stresses under impulsive loads 79—27504
- shell, cylindrical, elastoplastic plastic buckling in pure bending 80—19257
- shell, cylindrical, fibre reinforced, fluid conveying, vibr. characts., flow effects 80—14600
- shell, cylindrical, fibre-reinforced, axisymmetric damped vibrations calc. 79—14297
- shell, cylindrical, optimal natural freq. vibrs., rib eccentricity influence 80—38325
- shell, cylindrical, optimisation of strong loading modes, stress/strain state 80—10136
- shell, cylindrical, Rayleigh wave propag. using elasticity theory *(Russian)* 80—38307
- shell, cylindrical, semi-infinite, with end plate subjected to centrifugal force, large deflection analysis *(Japanese)* 79—1104
- shell, cylindrical, thin, circular, supercritical forms during axial compression *(Russian)* 80—74733
- shell, cylindrical, thin, tentative equation for vibrational analysis 80—5969
- shell, cylindrical, under axial shock, unsymmetrical bulging and buckling *(Russian)* 80—33492
- shell, cylindrical, viscous, explosive squeezing and effects 79—86378
- shell, cylindrical composite, with viscoelastic filler, parametric oscills., dynamic instability *(Russian)* 78—38221
- shell, elastic cylindrical, impact on surface of compressible fluid *(Russian)* 79—37181
- shell, elliptical cylindrical, nonlinear vibrs., freq.-amplitude characts. *(Russian)* 79—81753
- shell, geometric imperfection meas. appl. 79—81713
- shell, infinite cylindrical, in elastic medium, action of moving load, pressure waves *(Russian)* 79—81754
- shell, loaded thin walled truncated conical, dynamical stability, nonlinear material damping *(Polish)* 79—64496
- shell, plate and rod theories, simplified theories 80—52022
- shell, ring-stiffened, cylindrical and skew conical, under hydrostatic pressure, minimum-weight design *(Chinese)* 80—79135
- shell, round cylindrical with free edge, anal. under radial load *(Russian)* 79—76973
- shell, spherical, non-shallow, moderately thick, stresses and deform. 79—32241
- shell, spherical, non-shallow, torsional axisymmetric deform. subprogram 80—43607
- shell, spherical, subjected to external pressure, matching conditions 80—1447
- shell, spherical, with conical nozzle, thermal stress anal. 78—79204
- shell, spherical, with elliptical hole, stress state 80—33449
- shell, spherical, with rigid inclusions, antisymmetrical carrying capacity 80—69650
- shell, stretched cylindrical, with Z elliptical holes, stress concentration 79—46194
- shell, thin cylindrical, stiffened with viscoelastic rings, vibr. damping characts. 80—28452
- shell, thin elastic, containing liquid, free vibrs. *(Russian)* 80—33505
- shell, thin elastic, equilibrium state, existence and uniqueness theorem 79—94493
- shell, thin walled, shape accuracy, control technique *(Russian)* 80—23882
- shell, three-layer orthotropic cylindrical, with stiffening ribs, stability 80—74784
- shell, under concentrated loads, soln. *(Chinese)* 79—64492
- shell and surface rigidity, pseudobending, vibrs. and stability loss *(Russian)* 80—33470

classical mechanics of continuous media continued
- shell bending, static geometric analogy in classical shell theory *(Russian)* 79—37159
- shell of double curvature, bending in zone of elliptical loading area, stress anal. *(Russian)* 79—50593
- shell of revolution, structural anal. using ANTRAS program *(German)* 79—46192
- shell of revolution with internal press. subject to temp. field, optimum shape 78—22272
- shell of revolution with maximum torsional rigidity *(Russian)* 79—46188
- shell of variable thickness, inverse nonlinear stability *(Russian)* 77—50884
- shell stability under heating and loading 79—94518
- shell structures, appl. of new stress finite element 77—72157
- shell structures, hood-shaped, membrane solution *(German)* 78—46891
- shell structures, thin, curved finite element 78—79205
- shell structures with C_{nv} symmetry, anal. technique *(Chinese)* 79—72804
- shell subjected to centrifugal force, stress anal. *(German)* 80—23900
- shell wall anal., circular tanks under axisymmetrical pressure 79—46202
- shell wall on fluid, impact problems *(Ukrainian)* 80—38345
- shell with 6 reinforcing ribs, nonaxially symmetrical loading *(Russian)* 79—46190
- shells, angle ply laminated circular cylindrical, buckling closed form solutions 79—64552
- shells, axially compressed cylindrical and conical, post buckling behaviour, large elastic deflections 80—33490
- shells, axially loaded, prismatic and cylindrical, stability anal. *(Russian)* 77—19519
- shells, axisymmetrical, adaptional possibilities anal. after local buckling *(Polish)* 79—64543
- shells, conoid, parabolic, with vertical director line, stress analysis 78—51058
- shells, cylindrical, imperfect, closely-spaced, dynamics and failure criterion for axial impact 78—30207
- shells, cylindrical, layered, rotationally symmetric problems, isothermic solutions 80—77619
- shells, cylindrical, mixed finite element approx. convergence 80—33450
- shells, cylindrical, nonlinear parametric vibrations calcs., deflection *(Russian)* 79—46191
- shells, cylindrical homogeneous, nonlinear partial differential eqn. system, soln. existence and uniqueness 79—71249
- shells, double layered cylindrical, damped axisymmetric vibrs., refined theory 79—75338
- shells, flexible, self checking stepping calc. process 80—68044
- shells, free-form, nonlinear anal. by flat finite elements 79—14247
- shells, imperfect long cylindrical, lower critical hydrostatic press., stability 80—33491
- shells, Kirchhoff-Love, structural stability, mixed variational principles and non holonomeous constraints *(French)* 80—74779
- shells, metallic conical, failure under gasdynamic periodic shock waves 80—14611
- shells, nonconservative isometric buckling loads 79—81748
- shells, nonlinear geometrical anal. 78—77709
- shells, nonlinear Reissner-type theoretical relations *(Russian)* 79—55329
- shells, orthotropic cylindrical, under longitudinal line load 80—48566
- shells, parabolic, shallow, thin, elastic behaviour approximate calc. 79—57
- shells, simply supported circular sandwich, with opposite sets of loads, optical design *(Russian)* 79—50586
- shells, stiffened cylindrical under external load, vibration and buckling correlation 79—50629
- shells, thick cylindrical hyperelastic, large amplitude oscillations 79—64560
- shells, thin, stressed in axial compression, mass reduction, stress anal. 80—106716
- shells, thin, Timoshenko type, parametrisation and determination methods 80—28412
- shells, thin, torispherical and internally pressurised, plastic collapse 80—28440
- shells, thin circular cylindrical, stability problem soln. method *(Chinese)* 80—5928
- shells, thin elastic, recent advances in linear theory 79—59921
- shells, thin spherical, zonal winding pattern anal. 80—38253
- shells, three-layer cylindrical, axisymmetric free waves 80—5982
- shells, translational, load carrying characts. from positive to negative Gaussian curvature *(German)* 79—68567
- shells, two-layer cylindrical, stress-strain state, elasticity theory eqns. 80—33462
- shells for explosion containment 77—58594
- shells of revolution, bending, physical and geometrical nonlinearity, finite element method *(Russian)* 80—33471
- shells of revolution, finite element anal. of statics *(Chinese)* 79—76964
- shells of revolution, geom. characteristics, congruence of finite deform. *(Russian)* 78—86160
- shells of revolution, mixed finite element formulation for geom. nonlinear anal. 78—38189
- shells of revolution, rigid perfectly plastic, limit anal. program, plasticity criterion *(French)* 79—37155
- shells of revolution, rigid-plastic limit anal. under rotationally symmetric loading *(French)* 79—14276
- shells of revolution, ring type finite element method *(German)* 79—14250
- shells of revolution, Ritz-Galerkin method *(Russian)* 77—80062
- shells of revolution, stability *(Russian)* 80—43638
- shells of revolution, stability eqns., symmetry props. *(Russian)* 80—1450
- shells of revolution under nonaxisymmetric loading, elastic-plastic strain anal. 80—5958
- shells of revolution with variable geometry, optimisation of mass 78—67030
- shells of rotation, influence coeffs. calc. by Shtaerman-Hekkeler formula *(Russian)* 77—23865
- shells with large rectangular apertures, force and moment distribs. *(Russian)* 77—17813
- simply supported plate, obtuse corner, numerical modeling 79—32243
- simply supported plates, finite element anal. and Babuska paradox 79—81720
- skew plate, soln. of infinite matrix 78—75064
- skew plates, large amplitude vibrs., including shear and rotatory inertia effects 78—90743

classical mechanics of continuous media continued
skin wrinkling, human, using model of thin elastic shell on continuum foundation 77—52819
slab, transversely isotropic in plane strain, consolidation 79—64502
slabs, anisotropic skew ribbed, orthotropic plate theory anal. 79—37151
slender damped structures, vortex excited aeroelastic oscills., mathematical model *(German)* 78—94616
smooth interfacing of finite element models 79—72799
soil mechanics, classical numerical models *(French)* 77—72261
soil-structure systems, time integration, mixed methods 79—41568
solid, linear coupled fields 77—68391
solid body, motion about centre of mass under Newtonian force, stationary solns. *(Italian)* 79—9094
solid body motion, integrable case phase topology, bifurcation diagrams *(Russian)* 79—63033
solid body with vortex filling, canonical eqns. of motion *(Russian)* 79—63034
solid dynamics, SU(3) type configurations, global view *(Russian)* 79—25850
solid mechanics, continuum thermodynamics *(Japanese)* 79—75339
solid mechanics, elementary tensor anal. *(Japanese)* 79—40363
solid transient dynamic problems, finite element formulations using explicit time integration 78—18162
solid with cavity containing fluid, equilibrium position, optimal stabilisation 80—28442
solid-fluid mixtures, thermostatics 77—856
solid-fuel mixture, incompressible, equilibrium theory 77—857
solid-liquid system, connectedness of liquid and solid movements *(Ukrainian)* 79—50623
solids, classical and quantum scaling 79—35626
Somigliani dislocation containing medium, mechanics and kinematic props. *(Russian)* 80—38250
spacecraft, flexible, in gravitational field, stability 77—25906
spatial curved bars, kinematic elements of mechanisms, movement equations 80—46809
spatial structure stress analysis, continuum treatment method *(Japanese)* 78—22260
spherical cavity, variational anal. of stability *(Russian)* 77—50885
spherical elastic shell, thick walled, transient response, ray theory determ. 79—10484
spherical membranes, inflated nonlinear, dynamic snap out instability 79—32237
spherical shells, nonlinear state and dynamic response 79—32236
spinodal decomposition, near interface, continuum mechanics *(German)* 80—45272
spring, circular C-shaped, large deflection 79—50582
springs, stranded wire helical, static axial response 79—50581
square plates, laterally loaded, point supported, collocation soln. 79—18706
stability criteria, intrinsic, relative strengths 78—90738
stability criterion for feedback control of unstable waves 77—5671
stability of explicit-implicit mesh partitions in time integration 79—1101
stability problems, power method modification *(Russian)* 80—28444
static fields in inhomogeneous anisotropic medium *(Ukrainian)* 78—81837
statistical-kinematic analysis and limit equilibrium of systems with unilateral constraints 80—1451
steel bridges, higher order horizontally curved beam finite element 78—26028
stepped beams, nonlinear vibrations, transfer matrix method *(Japanese)* 79—64566
stiffened plate struct., nonlinear anal. by combined Rayleigh-Ritz-finite element method 77—72162
stiffness, exact straight line element calc. 80—79138
stiffness formulation of unbalanced anisotropic sandwich plates 77—84168
stiffness matrix for sandwich beams with thick anisotropic laminated faces 79—46182
stochastic boundary-value problems, solns. using digital simulation of space-random fields 79—41510
stochastic multi-component system, mean stress *(Polish)* 77—54874
Stokes fluids, in space of any dimension *(Japanese)* 78—41165
stratified media, Hamiltonian formalism for nonlinear wave propagation *(Russian)* 77—45705
stress tensor in nematic liquid crystals, micropolar continuum mechanics 78—67647
stress tensor in nematic liquid crystals, micropolar continuum theory 78—67648
stresses in mixtures 80—62469
stretched elastic sheet, punched hole, wave propagation 79—10524
stretched plate with noncircular hole, stability anal. *(Ukrainian)* 80—53661
string, nonlinear oscill., solns. sensitivity *(Russian)* 79—88805
string, nonlinear semi-infinite, initial value problem 79—49044
string, vibrating, motion above a concave obstacle, second order hyperbolic problem with unilateral constraints 80—57101
strings and membranes in external field 79—93341
strip weakened by identical circular transverse openings, stress state 80—43606
strong discontinuity wave in initially strained elastic medium 79—14301
structural anal., soln. by orthogonal collocation 78—51063
structural analysis, dynamic condensation method 79—3943
structural analysis, nonlinear theory of shells 79—30230
structural analysis constraint techniques for coupling of discrete axisymmetric and general structs. 77—3714
structural defects in solids, 4-D geom. theory 79—84954
structural dynamics, polynomials and variational methods 77—68393
structural dynamics, unconditionally stable explicit algorithm 78—48
structural optimisation problems, optimal archgrids 79—67160
structural panel, rectangular, with elastic edge constraints, dynamic response, Bolotin's asymptotic method 78—75091
structural problems, static and dynamic, combined finite element and transfer matrix anal. 80—53619
structural reliability under time varying multi-parameter loading 77—3715
structural stability in physics (conference, Tubingen, Germany, May and Dec. 1978) 80—8739
structurally inhomogeneous solid bodies, mechanics *(Russian)* 79—30231
structures of discontinuous shape, finite element analysis of bending behaviour *(Japanese)* 78—83238

classical mechanics of continuous media continued
structures with rotational degrees of freedom, large displacement-small strain anal. 78—89310
suction force, interpretation of Rice integral 78—49658
summed progressing wave formalism for initial value problem calcs. 80—92039
superposed rigid body motions, invariance 79—37153
surfaces, relativistic, classical theory *(Russian)* 78—69984
symmetry groups in crystals and elastic media 80—70147
symmetry in classical eigenvalue anal. 78—36827
symmetry of materials, transformation of coords. in constitutive eqn. 80—53621
synergetics, universal approach, bifurcation theory 80—8787
systems described by parabolic partial differential eqns., finite difference methods, comparison of accuracy 79—72796
systems described by parabolic partial differential eqns., finite element methods 79—72797
tank with fluid, variational anal. of dynamic reaction *(Ukrainian)* 79—32234
tapered cantilever columns, post buckling finite element anal. 79—1119
taut string, Chladni patterns in random vibration 79—81714
tensor equation $\mathbf{AX}+\mathbf{XA}=\mathbf{H}$, explicit son. *(French)* 78—86155
thermal stresses in cylindrical shell with circular hole or rigid inclusion 77—19518
thermodynamic functions, relations for irreversible processes 80—101715
thermodynamic fundamentals of continuum mechanics, equilibrium states 79—40373
thermodynamics of diffusing mixtures, constitutive eqns. for fluid-fluid and solid-fluid mixtures 79—88898
thermoelasticity theory with appl., book 78—79219
thermomechanics, introduction, book 78—54187
thermoviscous solids with microstructures, irreversible thermodynamics 78—34005
thick anisotropic shells, dynamic eqns. *(Russian)* 77—58547
thick cylinders, static and dynamic instability 80—23923
thick infinite plate with circular hole, axisymmetric stress and displacement boundary value problems 79—27511
thick plate with circular hole resting on smooth rigid bed, stresses, displacements 79—98602
thick plates and rods, under biharmonic loads, calculation model 79—14253
thin cylindrical shell, compression dynamics, nonlinear evolution of Rayleigh-Taylor instability 78—79243
thin cylindrical shells subjected to transient inner pressures, dynamic stress anal. 78—89344
thin layer surface inhomogeneity effect on dynamic surface response 79—7288
thin plate Semiloof element for structural anal. 79—3913
thin plates, treatment of boundary conditions on distinct boundary curves by integral eqns. *(German)* 79—49042
thin shell forming processes, geom. props. *(Russian)* 78—51061
thin shell structs. mixed elements, theory, criticism, examples *(German)* 79—27506
thin shell theory, stress boundary conditions 80—79137
thin shells, algebraic constraints for weak C^1 continuity 78—4458
thin shells anal., application oriented triangular elements *(German)* 79—84956
thin structures, finite element anal. of large displacements 79—27514
thin walled cylinder, minimum weight design, flexural and torsional stiffness constraints 80—79136
three-bar struct. under variable temp. 77—68389
time-dependent equations, multistep finite difference methods, boundary conditions 78—36829
time-evolution of the scattering kernels for half-space gas-solid systems 79—25849
Timoshenko arcs with variable cross section, in-plane vibr. 80—28453
Timoshenkos beam theory, natural frequency of continuous beam 78—83322
toroidal shells, branching solns. to nonlinear eqns. *(Russian)* 79—27557
torus, added-mass coefficients 78—32683
toy airplane catastrophe theory 79—58531
transient nonlinear mechanics problems, finite element anal., computational aspects 79—41565
transient response of continuous elastic structures with viscous damping 79—46254
transport processes, relativistic generalisation in continuum *(Hungarian)* 78—89383
triangular finite difference scheme for large deflection problems 79—32233
triangular plate elements, numerical investigation using variation principles with relaxed continuity conditions *(German)* 79—10465
tube, compressible hyperelastic, combined torsional and telescopic shear 79—64520
tube, micropolar elastic circular cylindrical, flexural rigidity 79—81724
tubes, pressurised elastoplastic, large strain solution 79—64537
tubes and tube systems with side constraints, lateral compression 79—50583
twisted stiff chain, spatial quadrupole correl. function 80—27130
two-component materials, thermo-viscoelastic theory 78—73854
undamped linear elastic systems, stability under follower forces, perturbation study 79—1110
unidirectional composites, two component finite element for determining transverse loads *(German)* 79—49043
unidirectional loaded rectangle disc with circular hole, estimation of error arising from Lagrange's reference system 79—50587
variable thickness, curved beam and shell stiffening element with shear deformations 79—44733
variational principle for spinning liquid-filled solid bodies 80—43609
vascular tonus model 77—25482
vibrating heterogeneous string *(French)* 79—7317
vibrating isotropic beams, Timoshenko's correction for shear 77—72226
vibrating string, acceleration discontinuity propagation due to solid friction *(French)* 80—22196
vibration analysis, of singly curved rectangular sandwich plates with clamped boundaries, iterative calc. using Kantorovich method *(Japanese)* 80—5970
vibrational brachistrone, curve of quickest descent anal., Coulomb friction *(Russian)* 79—67161
virtual work and differentiable manifolds, global and local model of material body 80—68043
viscoelastic Cosserat, thermomechanical behaviour 77—19539

classical mechanics of continuous media continued
- viscoelastic fluid behaviour, continuum model, allowing non-affine deform. 77—42793
- viscoplastic wave propagation, inversions for const. vel. case 79—12614
- viscous fluid mixture with thermomolecular diffusion, new variational-Lagrangian thermodynamics 79—49185
- wave diffraction theory appl. to free floating and moored rigid structs. 79—7321
- wave equations with dissipation, growth and instability theorems, appl. to continuum mechanics 78—36839
- wave fronts defined by eikonal equations, structural stability, elementary catastrophes 80—73187
- wave-power devices, Salter duck, two-pontoon system, operating efficiency comparison 78—94591
- weakly nonlinear systems, props., discussion 78—93535
- wind loaded structure, deterministic stability anal. 79—7314
- woven fabrics, partially set, finite axial extension, elastic deform. anal 80—19240
- ^{4}He, superfluid, continuum mechanics theory 77—69133

classical mechanics of discrete systems
- *see also N-body problems*
- 3-body unrestricted problem, distance lower bound estimates *(Russian)* 77—84137
- 3-D cable networks, finite element study of free vibration 79—23197
- accelerated reference frames, theory 80—41991
- acceleration dependent lagrangians, eqns. of motion 80—98795
- adaptive approaches and reliability estimations in finite element analysis 79—49026
- adiabatic invariant motion, charged particle in space periodic wave, variable length pendulum *(Russian)* 79—2623
- affine symplectic group, generating functions 78—41149
- analytical and continuum mechanics, book 80—22163
- angular velocity vector, attached to moving reference frame, time variation 80—41986
- anharmonic oscill., classical versus quantum case *(Spanish)* 80—73210
- anharmonic oscillator, Hamilton's principle appl. 79—84896
- anharmonic oscillator, perturbed, applics. of scaling transformations 77—82384
- approximately relativistic Lagrangians for classical interacting point particles 78—54179
- arbitrarily slow irreversibility, example 78—70083
- arithmetic models formulation 78—86130
- associative Hamiltonian algebras 78—69975
- asymptotic and total stability for generalized dynamical systems 79—17205
- asymptotic expansions in motion of two electrons in nuclear field 78—66459
- asymptotic stability of resonance systems 80—68031
- asymptotical level density of a physical system, Lanczos method 79—5977
- asymptotically stable movements, effect of vanishing constantly acting disturbances *(Russian)* 79—63020
- asymptotically uniform rotation of rigid body about fixed point *(Ukrainian)* 78—65761
- atom-oscillator scatt., classical mech. model for gas-surface accommodation coeff. 77—25306
- autonomous Hamiltonian system, gyroscopic forces, effect on stability *(Russian)* 80—17794
- autonomous Hamiltonian systems, orbital stability of periodic Lyapunov motions *(Russian)* 78—69664
- autoparametrically coupled systems, stochastic stability of stationary response 78—20961
- averaging in nonlinear mechanics 80—98796
- axially moving string on cylindrical guide surface, lateral motion 80—64358
- axially symmetrical solid body suspended on a string, stationary motions *(Russian)* 80—36839
- axisymmetric body under high dynamic press., integration of eqns. of motion *(Russian)* 77—50874
- axisymmetric rigid body in air, stability of unperturbed motion *(Russian)* 78—86146
- axisymmetric rotating mass, gyroscope precession 78—8238
- axisymmetric seismic response of thick circular plate supporting many rods, nuclear power plant appl. 80—1458
- ball, radius of gyration determ., using air track, undergrad. demonstration 78—49606
- ball and spring, elliptical motion 80—82613
- balls packing in rotating cylinder *(Ukrainian)* 79—41566
- bar under pure follower force, nonlinear static anal. 79—23199
- beam-truss gridworks, design formulae for exact elastic analysis 77—50870
- Bernstein's polynomials, differentiation and integration 78—40
- Bessel functions, zeros, for finite orders 78—36797
- bicycle dynamics, nongyroscopic aspects, lab. demonstration, for teaching 78—36769
- bifurcations in dynamical systems with internal resonance 79—46255
- billiard ball collisions, max. number of elastic collisions possible 80—12897
- billiards, nowhere dispersing in two dimens., ergodic props. 79—49025
- bipedal walking, linear stabilisation *(Russian)* 78—51055
- Boolean systems, atomicity and determinism 79—35518
- bouncing ball, student expt. 78—54122
- bowling ball path, rot. coord. system, for teaching 77—33788
- brachistochrone, arbitrary initial vel. object, for teachers 79—21500
- brachistochrones, tautochrones, evolutes, and tesselations, for teaching 79—25798
- brachistochronic motion of a dynamic system 79—67147
- cable-stayed cantilever beam dynamics 78—46889
- cam drives, geometric props. of applicable curves, constrained motion *(German)* 78—42525
- canonical formalism in distribution spaces 79—67219
- canonical transformations to imposed variables *(French)* 77—67268
- canonical transforms., time depend., effect on Hamiltonian 78—28940
- cantilever beam, pre-twisted, torsional vibr. 77—58583
- cantilever column under transient follower forces 78—1590
- centre of gravity, clothespin-belt demonstration, anal. of forces 77—5612
- centre of percussion demonstration, using physical pendulums 80—46752
- centrifugal buoyancy forces, particle in rotating fluid 78—12487
- charged particles in external fields, classical Dirac, Klein-Gordon eqns. 77—49829

classical mechanics of discrete systems continued
- circulant and near circulant systems, dynamics 79—12585
- classical Kepler problem in momentum space, education 78—36764
- classical machanics, freely moving balls on rotating discs, stable circular orbits 80—27074
- classical string problem, constants of motion 80—27113
- classical string problem, evolution eqn. 80—27114
- classical systems with regular or irregular motion, advances in understanding 78—93522
- clock escapement mechanisms, mathematical theory 78—41108
- closed cylindrical shell in moment state *(Polish)* 77—53774
- coefficient of restitution, bouncing ball expt. 77—33738
- collective angular momentum 80—4516
- collision processes, information theoretic maximal entropy theory, rel. to scatt. theory 78—81888
- collisions, elastic and inelastic, teaching expt. 77—57121
- column, free flying, asymptotic solns. to problem of lateral stability 79—14242
- combined dynamical systems, general props. 79—64490
- completely integrable classical systems connected with semisimple Lie algebras 77—17805
- completely integrable systems and symplectic actions 79—44712
- complex elastic systems, appl. of generalised functions to analytical methods of study *(Ukrainian)* 79—35537
- complex mechanical systems, small oscillation eqns. *(Russian)* 79—35539
- complex plane motions of a point *(Russian)* 78—86129
- composite mechanical systems dynamical flexibility, ficticious source method in polar coordinates *(Polish)* 79—32225
- conditional jointed structures, mechanical and mathematical models 79—23200
- conference proceedings, nonlinear dynamics, tribute to Sir Edward Bullard 78—93603
- conformal invariant model of localised spinning test particles 78—49729
- conformal pot. in N dimens. (N>1) 77—74271
- conservation law derivation using digital computers 78—12552
- conservation laws for particle collisions 77—33856
- conservation laws for particle collisions 77—33857
- conservation laws on dynamical systems via D'Alembert's principle 79—30217
- conservative and partially dissipative, equilibrium instability 77—5658
- conservative discrete system, upper and lower bound eigenvalues 77—89020
- conservative dynamic systems, search for cyclic coords. *(Russian)* 78—65764
- conservative dynamical systems, integrable by separation of variables, properties *(Italian)* 77—5656
- conservative finite dimensional system, stability of equilib. branching points *(Russian)* 78—86143
- conservative motion in phase space *(Spanish)* 78—36785
- conservative systems, perturbation expansion validity 79—12587
- constant of motion with discontinuities, Runge-Lenz vector 79—92932
- constraint formalism of classical mechanics, covariant relativistic quantisation, two-body problem 79—2622
- coordinate-free roation operator, for rotations in Euclidian space, for teachers 79—97145
- Coriolis effects in fixed frame, physical meaning 77—75788
- coupled large linear damped structures, eigenvalue anal. 78—1561
- coupled motion of rigid bodies about their center of mass 79—40065
- coupled oscillatory-reaction system exhibiting bifurcation scheme leading to a chaos 79—80517
- coupled response of a dynamic element riding on a continuously supported beam 79—46176
- crank-type four-bar function generators with transmission angle control 79—18699
- crawl swimmer, six-stroke, dynamics, mathematical model *(German)* 78—90702
- cylindrical shells, natural transverse vibr. *(Russian)* 77—58593
- damped harmonic oscill., action of retarded restoring force *(Italian)* 77—68381
- damped oscillator motion, expansion in normal modes 80—67951
- deformable gyroscope in non-Euclidean space, classical non-relativistic theory 77—30004
- differentiable dynamical systems, transformation frequency spectrum 80—77608
- differential geometry, appl. to mechanical systems, gyroscopic forces *(Russian)* 79—63016
- dipole interaction of an oscillator with scalar field 80—94
- distributed mechanical system with nonstationary boundaries, parametric pulse excitation 77—89021
- domains of possible motions with boundary, geom. *(Russian)* 78—28942
- driven oscillator motion with nondecreasing input vels., use in inertia actuated fuse 78—59293
- dry friction problems, graphical soln. for teaching 78—12511
- dynamic system behaviour near exist. boundary for periodic motions *(Russian)* 77—84138
- dynamic systems, equations of motion canonical transform 80—36843
- dynamic systems, numerical anal. of stable motions *(Russian)* 77—57181
- dynamical system, compactness of bounded trajectories in infinite dimensional Banach space 80—82636
- dynamical system, limit cycles and symmetries 80—62462
- dynamical system construction from pre-assigned family of solns. 80—39
- dynamical system subjected to a generalised force reducible to a canonical form *(Italian)* 80—22189
- dynamical systems, appl. of Gauss' principle of least constraint 77—17811
- dynamical systems, Clebsch potentials and variational principles 78—24657
- dynamical systems, connection between symmetries and first integrals 77—67269
- dynamical systems, conservation laws in Poincare-Cetaev variables 77—67267
- dynamical systems, dissipative, intermittent transition to turbulence 80—79132
- dynamical systems, equilib. configurations and small oscillations 79—25832
- dynamical systems, global first integrals, connections with critical phenomena 78—32667
- dynamical systems, homoclinic and heteroclinic points in Hemon mapping, analyticity 80—82634

classical mechanics of discrete systems continued
dynamical systems with SO(4) and SO(3,1) symmetry 80—22534
dynamics, fundamental principles generalisation, appl. to motion of disc on ice surface *(Russian)* 78—65762
dynamics of systems of solid bodies with combined control *(Russian)* 79—17209
dynamics systems, stochastic props., numerical methods reliability, time averages 78—41151
education, canonical transformation to the free particles 77—49521
education, cart wheels on inclined plane, theory and expt. 78—61977
education, circular motion with friction, numerical and analytical solns. 80—57029
education, classical mechanics, Hamilton's principle, variational formulation approx. solns., simple pendulum 77—33774
education, complementary Lagrange formalism 78—36745
education, Coriolis machine, inertial motion viewed from rot. reference frame, coordinate transformation 78—69934
education, mechanical mutual inertia in spring coupled system, mutual inductance analogue 78—49590
education, multiple scatt., elastic and inelastic, two particle system with fixed wall, air track expt. 80—73135
education, Newtonian mechanics, estimates of human body mechanical performance 78—40211
education, newtons laws of motion: some interpretations of the formalism 80—51984
education, Noether's theorem 77—45635
education, non-isochronous small oscills. 78—36749
education, oscill. and pendulum motion coupling of spring 78—36768
education, quantum mechanics, mechanical model 78—49591
education, rotating water sprinkler anal. 79—9064
education, rotation matrix formalism for rots. 77—82349
education, spiral spring, (nonhelical) simple harmonic motion, Bessel functions, closed form solns. 80—57026
education, spring-mass oscillator, parametric instability 77—78921
education, supernovae in binary systems: an application of classical mechanics 80—62428
educational film making, zero-g possibilities 78—12508
eikonal function for two classical relativistic particles 78—81828
Einstein relativistic two-particle systems 78—41152
elastic beams subjected to vertical and follower forces, lateral stability and eigencurves 77—68394
elastic collisions of N billiard balls in three dimens. space 79—30223
elastic collisions of three spheres in a line, eigenvalue and difference eqns. solns., for teaching 77—33786
elastic linear collisions, dynamic solns., for teaching 80—17769
elastic mechanical systems, design sensitivity analysis, adjoint variable methods 78—90706
elastic object in central force field, programmed motion control 80—17481
elastic structures, force method of anal. 79—18689
elastic structures, quadratic transformation of Gaussian process applied to stochastic dynamics *(French)* 77—54917
elastodynamics, appl. of Ritz theory to Hamilton eqn. 77—50977
elastoplastic structures, historical deform. analysis and parametric linear complementary problem 77—58563
electric oscillator, radiation damping const. statistical derivation *(Chinese)* 79—80427
electric power systems, interconnected, large-scale, derivability from Lagrangian 80—101707
electron trajectories, in homogeneous elec. fields, relativistic and classical 77—41436
elevator crash safety, teaching 77—41441
eliminability of masses and forces in Newtonian particle mechanics, Suppes theory 77—57176
ellipsoids of revolution, stationary movements, stability of orientations *(Russian)* 77—87646
equations of motion in phase space 80—17789
equivalent Lagrangians and quasicanonical transformations 77—33861
evaluation equations, nonlinear, canonical transforms. 77—87643
extended Delaunay method, appl. to disturbed hamiltonian dynamic system reson. *(French)* 79—21539
finite range and/or repulsive interaction systems 80—37
flexible damped satellites, Liapunov stability anal., comparative study 79—37148
flexible guideway, vibro-excitation under influence of crossing long train *(German)* 77—54870
flexible strings mechanism, variational principle in Euler representation *(Russian)* 78—54172
flotation of solid body on liquid surface, equilib. state *(Russian)* 78—67029
flutter-unstable dynamical system with gyroscopic (circulatory) forces, nonlinear behaviour 78—63276
follower load type systems, time invariant functionals 80—77609
force concept in classical mech. and field theories 77—49
forced oscillations, averaging and chaotic motions 80—73166
foundation of theoretical mechanics, inverse problem in Newtonian mech., book 79—25838
foundations of mechanics, book 79—25837
four rigid body system, transformation operator approach, spacecraft modelling appl. 79—25834
free rigid body stabilization by gyrocompass type frame *(Russian)* 77—84136
free vibrations in friction under parametric excitation *(Russian)* 80—43
fundamental constants introduction *(French)* 78—62071
Galilei invariance giving Newtonian point particle dynamics 77—87642
Galilei relativity in Newtonian mechanics, possible Lie admissible covering 78—73838
Galilei relativity in Newtonian mechanics, possible Lie admissible algebras, addendum 79—2619
Galileo's two bodies falling through air, numerical anal. for teaching 80—17755
Gauss and Mainardi-Codazzi eqns. generalisations, appls. to quantum and classical mechanics 78—62092
generalized Galilei groups in classical dynamics 79—30221
geometric formalisation of classical dynamics *(Russian)* 79—9105
geometric formulation of Hamilton's Principle, spin particles 78—45482
geometric quantisation, correl. between classical and quantum mech. in geometric language 79—25905
glider on inclined linear air track, viscous damping and restitation coeffs. 80—46768
golf clubhead speed coeff. 78—1563

classical mechanics of discrete systems continued
Goryachev-Chaplygin case, qualitative anal. *(Russian)* 77—65671
governing equations, elimination of singularities 77—17806
Grassmann variables, possible interpretation of theories 77—79001
gravity acceleration as a function of mass, for teachers 78—81766
Green function expansion into eigenfunction set 80—22205
gross variables, microdynamics and nonlinear stochastic processes 80—101754
group method of determining parameters *(Russian)* 77—71205
group theoretical foundations, elementary systems 79—30282
Gurney's ballistics calc. 80—67946
gyro-stabilisation platform, nonlinear loss of stability and trembling *(Chinese)* 80—62457
gyropendulum, aperiodic single rotor 80—14561
gyroplatform orientation in geographical meridan, effect of earth nonsphericity *(Russian)* 79—14240
gyroscope, reaction to impulsive torque, description for teaching 78—24604
gyroscope, stability of Staude's permanent rot. with damping 78—21126
gyroscope in Cardan suspension on rot. base, stability anal. *(Russian)* 77—852
gyroscopes, autonomous systems, invariance of kinetic and potential energy *(Ukrainian)* 79—50577
gyroscopic structure synthesis, Rayleigh-Ritz approach 79—18695
gyroscopic system, linear, damped, modal anal., appl. to satellite 78—63275
gyroscopic systems, instability *(Ukrainian)* 80—46788
gyroscopic systems, Levi-Civitas theorem extensions *(French)* 79—50579
gyroscopic systems, precessional equations, admissibility of passage *(Russian)* 79—30219
gyrostat, almost axial, almost symmetric, torque free spin near osculation condition 79—49029
gyrostat, nonregular precessions in a Newtonian central field *(Italian)* 78—81825
gyrostat, symmetric satellite, uniaxial stabilisation at libration points 80—14560
gyrostat with fixed point, lateral inertial imbalance effect on spin stability 79—32229
Hamel-Boltzmann eqns. of motion, variational principle involving conditional extremum 77—17801
Hamilton's principle for canonical equations of motion, teaching 80—105464
Hamilton's principle for nonholonomic systems *(Russian)* 79—9097
Hamilton function, conditionally periodic movement presentation 80—8915
Hamilton system, instability of equilib. position *(Russian)* 79—9100
Hamilton-Jacobi eqn. for non-conservative systems, separation of variables 77—37752
Hamilton-Jacobi generalised theories 79—2681
Hamilton-Jacobi generalised theory, phase space approach 80—36891
Hamiltonian autonomous system with 2 degrees of freedom, stability in 1st order reson. *(Russian)* 77—53776
Hamiltonian classical mechanics, gauge theory for long range fields 80—86077
Hamiltonian dynamics, for closed system of N particles in mutual interaction 78—62070
Hamiltonian dynamics, integrable and nearly integrable systems historical review 78—93521
Hamiltonian formalism, Lagrangian function, variational technique constraints *(German)* 79—88799
Hamiltonian formulation for an extended particle with interacting constituents 79—63022
Hamiltonian guiding centre problem 80—31533
Hamiltonian mechanics 80—82631
Hamiltonian system, ergodic components in the stochastic region 80—8918
Hamiltonian system, two-dimensional, stability of equilib. position in case of equal frequencies *(Russian)* 78—36814
Hamiltonian systems, additional integrals of motion 78—49711
Hamiltonian systems, integrability, Liouville theorem *(Russian)* 80—22191
Hamiltonian systems near point of equilibrium, periodic orbits *(French)* 77—13603
Hamiltonian with ergodic behaviour, classical quantisation 80—86148
Hamiltonians, quadratic, classes of quadratic invariants, interrelations and symmetries 80—31565
Hamiltonians linear in momenta, note 78—77468
harmonic oscill., time-depend., dynamical symmetries and constants of motion 77—64943
harmonic oscillations of single degree of freedom systems 80—33516
harmonic oscillator, time-depend., dynamical invariant, algebraic derivation 80—12898
harmonic oscillator, two dimens., q equivalent particle Hamiltonian 78—93525
harmonic oscillator one-dimens. chain with friction, discrete-continuous transition 77—849
harmonic oscillator one-dimens. chain with friction, discrete-continuous transition 77—850
harmonic oscillators, randomly disordered linear chain, normal frequencies 78—36818
harmonic oscillators, time-dependent, exact invariant determ., direct method 78—12597
heavy particle on rotating surface, stability of equilibrium, including damping 77—13604
heavy rigid body motion, Hill and Hadamard characteristics *(Russian)* 79—9103
heavy rigid body with fixed point, precession rel. to vertical *(Russian)* 77—62142
Heisenberg infinite classical and quantum models, intertwining, Trotter approx., coherent state formalism 79—44713
helical uniform structures, Hadamard stability *(French)* 77—68385
helicoidal spring, braking action and highest twisting moment 79—27502
Henon-Heiles Hamiltonian 80—36485
Hill's case of ave. three-body, problem, stability of plane orbits *(Russian)* 77—67271
hockey ball, collision theory, teaching approach 77—41435
hollow cylinder containing small oscillator, motion on inclined plane 77—19516
holonomic system, first integrals *(Russian)* 77—67272
homoclinic points and resonance in dynamical systems 80—4240

classical mechanics of discrete systems continued
horizon gyrocompass, stability of precessional motion, third order resonance *(Russian)* 79—46173
hyperbolic systems, high-order methods, dynamic problems 80—68033
ideal constraints, generalisation 78—65759
impact of rigid body on ice, hydrodynamic model *(Russian)* 77—20002
impact phenomena with elastically deformable stricker and solid obstacle 78—77703
impulse dynamical equations, nonholonomic system, solid on plane, rolling without slipping *(Italian)* 78—57769
inclined plane, sliding object, vel. determ. 77—5661
increasing weight of falling bodies, Aristotle's conclusion 80—46770
inertia ball demonstration, theory 78—73811
inertial properties of unidimensional dissipative systems *(Russian)* 78—16639
inextensible string, rectilinear motion 79—71240
infinite crystal, classical statistical mechanics 80—107067
infinite pendulum system, finite controllability 80—31494
infinitesimal operators of translation and rot., dynamic eqns. lineage 80—17788
inhomogeneous symplectic group, role in framework of Wigner isomorphism *(French)* 79—12589
instantaneous invariants in three-dimensional kinematics 79—18698
integrability in system with 1 quasi-cyclic coordinate 80—27110
integral of motion, semisimple Lie algebras 77—74215
interacting particles system, nonrelativistic classical and quantum mechanics conservation laws 78—89328
interconnected dynamical systems on Banach spaces, well posedness, instability, Lagrange stability 78—69976
intermediate-axis theorem, undergraduate demonstration expt. 78—61990
internal forces cancellation, for teaching 80—27079
invariance groups and Lagrangian theories for mech. systems 77—45689
invariant perturbation theory as alternative to Hamilton-Jacobi approach in classical mechanics 79—12588
invariant tori and cantori, variational principles 80—37666
invariant tori of fixed freq., Langrangian variational principle 79—25833
invariantive analytical mechanics of point-like bodies 79—5978
invariants, stability, in classical mechs., KAM theorem 78—41
inverse square law forces, problem soln. using 'unit radius' 77—60923
isoenergetic stability 77—49587
isotropic classical oscill. Lagrangian and Hamiltonian ambiguities, transform. props. 77—67270
iterative procedures for penalty function solns. of algebraic systems 78—57770
javelin dynamics including body interaction 78—38184
Kepler ellipse, symmetry prop. of vel. 80—101694
Kepler orbit, from initial conditions via Lenz vector 78—16602
Kepler oscillator problems, invariance groups *(German)* 79—67151
Kepler problem, anisotropic, Bernoulli sequences and trajectories 77—49609
Kepler problem, global symmetry anal. 77—5662
Kepler problem, Lorentz and anti-de Sitter group 78—36817
Kepler problem, time transformation stabilisation *(German)* 78—89333
kinematic equivalence of system of forces *(Polish)* 79—12590
KMS-states for quasi-free evolution, integral representations 78—4479
Kolmogorov eqn., separation of variables *(Russian)* 77—78970
Kubo-Martin-Schwinger states of classical dynamical systems with infinite phase space 80—44
Lagrange and Hamilton functions for non-quadratic expressions of kinetic energy *(German)* 79—88800
Lagrange formalism, direct and inverse variational characterisation of linear non conservative systems 78—93527
Lagrange mechanics, reln. between symmetry of dynamic eqns. and Noether's theorem 80—4515
Lagrange-Dirichlet theorem inversion in analytic potential case 79—71239
Lagrange-Ostrogradsky generalised mechanics, invariant fourth-order eqns. of motion *(Russian)* 80—42054
Lagrangian formalism for systems with general velocity depend. forces 80—27109
Lagrangian mechanics, consts. of motion anal. 78—81829
Lagrangian submanifolds and dynamics *(French)* 77—17803
lagrangian systems, second order differential eqns. 80—52015
Lagrangian systems with one degree of freedom, invariance and conservation laws 78—62067
Lagrangians and Hamiltonians, constructed from eqn. of motion, for teachers 78—62016
Lame's equation, Arnold-Moser-Russman criterion, elliptic stability 79—25836
Laplace (Runge-Lenz) vector, origins 77—13565
large structural systems with local nonlinearities, finite element dynamic anal. 79—44711
Levi-Civita theorem generalised to gyroscopic systems *(French)* 77—71202
Liapunov's periodic motions at heavy rigid body with fixed point *(Russian)* 80—22190
libration in systems of many degrees of freedom *(Russian)* 78—86141
Lie algebra, sl(2,R), integration of Hamiltonian systems 78—24660
lifting system cascade struct., signal flow graphs in modelling *(Polish)* 79—32224
limit cycles chaotic behaviour, self and mutual interaction 80—46789
linear elastic, effect of damping on vibration-stability reln. 77—19558
linear invariance and virial theorem in classical mechs. 77—74214
linear lumped-parameter systems, synthesis with prescribed mode shape 80—23881
linear motion, of glider on airtrack 78—12481
linear non-conservative systems, dynamics 77—2538
linear nonconservative systems with asymmetric parameters derivable from a Lagrangian 80—17790
linear oscillator, nonstationary narrow band response and first passage probability, stochastic process 80—62465
linear structures, complex, eigenvalues numerical bracketing *(French)* 80—42053
linear system, external parametric random perturbations, oscillations *(Russian)* 79—17207
linear system mean square response to nonstationary random excitation 80—57085
linear systems, damped free motion 79—64569
linear systems, multicoordinate problem *(Russian)* 79—9102
linear systems, stability of motion rel. to part of variables *(Russian)* 78—86144

classical mechanics of discrete systems continued
linearised spring pendulum system, stability anal. 77—64945
linked rigid body systems, nonlinear eqns. of motion *(German)* 78—87254
locally modified structs., derivatives of eigenvectors 78—5651
Lorentz-invariant Newtonian mechanics, kinematic const. nonexist. 77—74216
lumped-mass model with two degrees of freedom, equil. and stability 77—58543
Lyapunov stability in the presence of several resonances *(Russian)* 77—71203
magnetically levitated vehicles, dynamic behaviour, flexible guideways *(German)* 77—54869
many-body problems, orthogonal polynomials, asymptotic density of zeros 79—30286
many-dimensional oscillator problems, 'Arnold diffusion' instability 79—75334
marginal local instability of quasi-periodic motion, separation distance effects 80—82633
mass point displacement under effect of forcing conditions *(German)* 78—86149
masses of two bodies in dynamic interaction constituting an isolated system *(French)* 78—89326
matrix differential equation, rotations as solns., for teachers 78—62021
mechanical holonomic rheonomous systems with forces of generalised pot., stability *(Russian)* 78—28941
mechanical resonance, $J_0(x)$ obs. on reson. rot. vertical chain 80—42006
mechanical response and the initial value problem 79—2620
method of action-angle variables and the classical dynamics of a nonlinear Lagrangian 78—77702
micromechanics, stochastic deformations, material characts. 77—40
micromechanics of structured materials 77—67273
minimum weight disk design 78—36821
modified conservation laws in the classical Kepler problem 80—72755
molecular energy distribution in quasiperiodic and ergodic regimes 79—41227
moment problem, density functions, linear programming formulation 80—53620
momentum transfer in gravitation theory 80—4601
mooring cable in nonuniform stream, equilib. shape and tension *(French)* 78—63277
Morse oscillator, classical motion, calcs. 78—73796
motion in spherically symmetric force fields, vector consts. 78—85833
motion integral disappearance in multi-resonance conditions 78—77471
motion of solid body with elastic and dissipative elements *(Russian)* 78—65763
motion rigidity *(Russian)* 79—9099
mud thrown from wheel, critical speed, for teachers 78—12493
multi-degree of freedom mechanical systems, antiresonances *(Chinese)* 80—42049
multidegree of freedom system, response to nonstationary random excitation 79—32228
multidimensional infinite mechanical oscill. system, resonance and controllability 80—33444
multidimensional two particle problem with noncentral pot. 78—54174
multilink spatial mechanism structure and analysis *(German)* 79—21544
multimass undamped vibration system, decoupling from large struct. 78—57774
multiply charged periodic classical systems and random EM radiation, statistical equilib. 79—2621
multiply variable struct. systems, periodic regime anal. method *(Ukrainian)* 80—10134
multirigid body systems, equations of motion 79—46177
Nambu mechanics, particle-SU(2) monopole interaction 78—4478
Nambu mechanics, relation to generalised Hamiltonian mechanics 78—93526
Nambu mechanics, reln. to Lagrange, and Hamilton-Dirac mechanics 78—54180
network constructions, large strain anal., simplex membrane elements 79—32220
Newton's 2nd law, spatial translation symmetry, for teaching 78—54129
Newton's law, introduction of a repulsive force 78—73839
Newton's law, linear depend. of mass *(Italian)* 79—12706
Newton's laws, in rotating Cartesian frames 77—33751
Newton's laws of motion, planets and rocket dynamics 78—12509
Newton and Heisenberg eqns. of motion relation, harmonic and anharmonic oscill. 79—6018
Noether's theory for non-conservative generalised mechanical systems 80—31491
non-holonomic constraints, existence of potential function *(French)* 78—86128
non-invariance symmetries and consts. of motion 79—75333
non-Noether invariant origin, relation to Euler eqn. transformation props. 80—31493
non-stationary motion, stability anal. by linear approx. *(Russian)* 77—71212
nonconservative dynamical system mechanics, gradient method 80—46787
nonconservative dynamical systems, stationarity principle 79—30216
nonconservative mechanical systems, variational principles, finite element approach 79—49027
nonconservative systems, integration of motion eqns. *(Ukrainian)* 78—81827
nonconservative systems, simplified stability criterion from Lyapunov's method 80—46790
nondissipative system, universal properties, bifurcation phenomena and universal numbers 80—68035
nonhamiltonian systems with one degree of freedom, forced periodic motion *(Russian)* 78—20959
nonholonomic, with nonlinear constraint eqns., Lagrange type eqns. 77—5659
nonholonomic dynamical systems, generalized Hamilton-Jacobi method second form 79—30222
nonholonomic system, motion eqns. derivation *(Russian)* 78—20956
nonholonomic systems, generalised Hamilton-Jacobi method 77—71207
nonholonomic systems of higher order, Mangeron-Deleanu eqns. in Poincare-Chetaev variables 77—33853
nonholonomic systems under external influences, sledge on incline, gyroscope in cup *(Russian)* 80—52011
nonholonomous systems, degrees of freedom 77—30003

classical mechanics of discrete systems continued
- nonlinear, almost periodic systems, bounded solns. *(Ukrainian)* 79—92931
- nonlinear dissipative systems, oscillatory resistance forces *(Russian)* 77—80061
- nonlinear dynamic damper, subharmonic oscillation extinction 79—25835
- nonlinear dynamic problems, nonparametric identification technique 80—46792
- nonlinear dynamical systems, stability anal. by Newton-Raphson method 77—72150
- nonlinear interactive buckling, sensitivity and optimality 77—80086
- nonlinear mechanical system with time optimal condition, synthesis 78—54176
- nonlinear mechanical systems, constraint simulation 80—62461
- nonlinear mechanical systems of arbitrary order, stationary oscillations *(Russian)* 78—65765
- nonlinear mechanical systems with time optional condition 80—31492
- nonlinear mechanics, problem oriented software for asymptotic methods *(Ukrainian)* 79—49028
- nonlinear nonconservative systems, appl. of time depend. canonical transforms 80—17792
- nonlinear oscillations with parametric excitation, system with one degree of freedom *(Russian)* 77—89018
- nonlinear oscillator, stroboscopic phase portrait and strange attractors 78—54177
- nonlinear oscillators, Poincare scheme, assessment and validity range improvement 80—31489
- nonlinear oscillators, turning point approx. and appl. 80—67952
- nonlinear oscills. by Hamiltonian mechanics *(Russian)* 77—39215
- nonlinear resonances, asymptotic first approx. *(Russian)* 77—17808
- nonlinear string dynamics, rigid body motions, space curves, prolongation structures, fiber bundles, and solitons 79—97213
- nonlinear systems, asymptotic analysis by method of averaging 77—82382
- nonlinear systems, critical excitation anal. 77—78973
- nonlinear systems, estimates of perturbed motions *(Russian)* 77—54871
- nonlocal theories satisfying Bell's inequality 79—12642
- nonreactive scatt., classical differential cross sections in Legendre polynomials 79—836
- nonspherical top, rotational Brownian motion, and its appl. to dielec. relax. theory 78—21071
- normal modes in irreversible thermodynamics 80—52148
- numerical methods, Newtonian, Lagrangian and Hamiltonian mechanics, book 79—63024
- optimal control of moving bodies, use of Bulgakov normal coords. method *(Russian)* 79—9104
- optimal motion stabilisation *(Russian)* 78—86145
- optimum control theory, Hamilton-Jacobi theorem, canonical transforms 78—20962
- orbiting trajectories in noncentral fields 80—98794
- orientation of rigid bodies *(Russian)* 77—17810
- oscillating system, light damping, influence of eigenvalues *(German)* 80—31490
- oscillator, linear, excitation by stationary random force *(Russian)* 80—27116
- oscillator, linear parametrically excited, random vibration and stability 79—64491
- oscillator with bilinear hysteresis, response to stationary random excitation, stochastic averaging 79—46179
- oscillator with even non-linear damping 78—28938
- oscillators, coupled, stochasticity thresholds 80—46977
- oscillators, weakly nonlinear, system with slowly varying parameters, resonance 80—62463
- oscillators with nonlinear damping, stochastic anal. 79—41567
- overhung shaft-disc system with disc effect, critical speed determ. 79—46172
- overload cables, wave solns. of dynamics 77—35028
- pairs of focal curves in orthogonal planes and movable bar frames *(German)* 77—60927
- parachute influence on motion of axially symmetric air dropped object *(Polish)* 79—14243
- parametric excitation of linear systems having many degrees of freedom 77—84177
- parametric excitation system instability region determ. 79—23201
- parametric resonance, student expts. 79—58464
- parametric stabilisation of unstable equilibrium forms of mechanical systems *(Russian)* 79—46175
- particle heavy spring system, oscills., Stieltjes integral calcs. 79—71180
- particle in potential well, adiabatic invariants for varying mass, for teaching 77—33797
- particle in selfgravitating spherical dust shell, adiabatic invariance, education 80—105459
- particle motion in central force, without orbit precession 78—86057
- particle motion in cyclotron near reson., nonlinear behaviour *(Chinese)* 79—63828
- particle spin dynamics and supersymmetry 77—82690
- particle vibrational movement under impulse perturbation of an inclined plane *(Russian)* 80—17791
- particles with spin, Hamiltonian and Lagrangian formulation 80—86079
- passive vibr. isolation, shock absorber selection 78—55556
- pendulum, double with varying length, probabilistic characteristics of solns. *(Polish)* 80—8781
- pendulum, simple, with uniformly shortening string length, behaviour 80—27111
- pendulum-gyroscopic platform stabilised in inertial space, autonomous determ. of coords. *(Ukrainian)* 78—65760
- pendulums in orbiting spaceship, equilibrium and stability 79—44667
- periodic Hamiltonian flows, generalised Bertrand's problem 78—86131
- periodic motion of heavy rigid body about fixed point *(Russian)* 77—71204
- periodic orbits, simple time independent Hamiltonian system, general results 78—93523
- periodic systems, optimisation by analytic construction of control 79—21543
- perturbation expansion method, calcs. 77—33741
- perturbed Hamiltonian system, stability criterion 80—17793
- perturbed motion stability anal. *(Russian)* 78—16640
- phase space methods and the Hamilton-Jacobi form of dynamics 79—21542
- physical pendula, reconstructed 19th century expt. 80—82612
- plane four-bar linkages, synthesis *(German)* 78—42524

classical mechanics of discrete systems continued
- plane mechanisms, relative motion *(German)* 79—14245
- plane periodic motion of two rigid bodies *(Russian)* 78—73840
- Poincare canonical momenta and Nambu mechanics 78—77701
- Poincare gauge invariance, conservation laws for particle, string and membrane systems 79—55
- Poincare-Chetaev's equations, integration *(Russian)* 79—35547
- point mass systems, dynamically and kinematically controlled, motion *(Russian)* 77—33858
- point particle in viscous medium, Lagrangian for eqn. of motion 80—77610
- Poisson brackets, canonical invariance, for teaching 79—25810
- potential operators and the inverse problem of classical mechanics, differential eqns. 79—2618
- preloaded string, random vibrs. associate covariance function calc. *(German)* 80—28411
- prestressed cablenets, 3-D, finite element anal. 78—5650
- prestressed plane, cable structs., optimal design 77—80060
- principle of least action, minimal interpretation, variational calcs. 80—68039
- projectile acceleration meas. using stroboscopic picture, teaching demonstration 78—36779
- projectile fragmentation and momentum, teaching 77—45654
- projectile range formula for above ground level launch, teaching 78—8190
- proportionally damped dynamic systems, eigenvalues *(German)* 79—21540
- pseudoconservative systems, effect of damping on stability 78—81832
- pseudowork-energy principle nonrigid of rot. bodies, for teaching 78—49602
- quasi-linear nonautonomous systems, motion stability condition for periodic oscills. *(Russian)* 77—33855
- quasimodes associated with stable periodic orbits 77—17833
- quasistationary motions of mechanical systems *(Russian)* 78—62066
- railway vehicle motion on track of arbitrary curvature and twist *(Russian)* 77—17809
- random excitation of harmonic oscillations of single degree of freedom systems 78—54175
- random motion, roller device appls. 78—16600
- randomly excited systems, reciprocal theorem 77—41537
- Ray-Reid generalised systems, invariants derivation 80—101710
- Rayleigh's principle for simply supported beam, energy considerations 78—83322
- reaction of continuous dynamic systems with complex form under time-space random fields 78—65767
- rebound of elastic bodies in oblique impact 77—50873
- rectangular prismatic bodies, free motion, translatory and auto-rotating modes 80—43605
- relative motion versus motion of particle in pot. in predictive mechanics *(French)* 80—52006
- relative velocity problems concerned with boating, for teaching 78—12510
- relativistic classical and quantum dynamics 80—22192
- relativistic string with massive ends, classical and quantum theory 78—62073
- resonance, internal, of two damped oscillators 77—46905
- resonance between weakly coupled oscillatory systems 79—40357
- resonant motion, extremal props. 77—87246
- restricted three-body problem, perturbations of Lagrangian points 78—32327
- Riemann curvature of conservative systems 78—89332
- S-Riemann ellipsoids, stability conditions *(Russian)* 77—87645
- Riemannian manifold separability structs. *(French)* 77—13602
- rigid asymmetric body in Newtonian force field, motion *(Italian)* 78—81822
- rigid bodies, Euler-Poisson equations, reduction to obliquely symmetric form *(Russian)* 79—35548
- rigid bodies having inertia ellipsoid of revolution 79—32223
- rigid bodies interconnected by joints, differential eqns. of motion *(German)* 77—46906
- rigid body, class of integrals of eqns. of motion *(Russian)* 77—53769
- rigid body, perturbed motion about centre of mass, element formulation 78—41150
- rigid body, regular motions in gravit. field of sphere 80—62000
- rigid body, regular motions stability in Newtonian gravit. field 77—26165
- rigid body containing moveable mass, motion anal. *(Russian)* 79—32221
- rigid body dynamics, air table expt. 79—5941
- rigid body dynamics, nonexistence of single valued integrals and branching of solns. *(Russian)* 79—9098
- rigid body motion about fixed pt., order reduction of differential eqns. *(Russian)* 77—49590
- rigid body motion about fixed pt., perturbed Euler-Poinsot problem, splitting of separatrices *(Russian)* 77—49591
- rigid body orientation relative to rotating coord. system *(Russian)* 78—32668
- rigid body with discrete symmetry, conditionally-linear integration of eqns. of motion *(Russian)* 78—86135
- rigid body with fixed point, effect of viscous damping on spin stability 77—78974
- rigid body with fixed point, integration of eqns. of motion *(Russian)* 77—62146
- rigid body with fixed point, motion, variants of soln. *(Russian)* 77—62143
- rigid body with one fixed point, motion 77—78972
- rigid motion, canonical treatment for rigidly connected point systems 78—69972
- rigid shaft rotating in antifriction bearings, motion stability 80—68038
- ring, circular, force, displacement influence functions 79—18694
- ring of torsion coupled overdamped pendulums, nucleation theory of overdamped soliton motion 80—12899
- road vehicle stopping distance, weight transfer effect, for teaching 79—25800
- rods, generalised conjugate analogy for arbitrarily curved rods 77—49588
- rolling coin, computer anal. of motion *(Hungarian)* 78—73837
- rolling disc motion, new generalised Hamilton-Jacobi method 77—5663
- rolling missile, apsidal limits 79—3909
- rolling pendulum bob, conservation of energy and partitioning of kinetic energy 79—62956
- rotating chair, quantitative ang. momentum expt. 77—75789

classical mechanics of discrete systems continued
- rotation kinetics anal. with air cushion apparatus *(Hungarian)* 79—25811
- rotational Brownian motion of an asymmetric body 79—54062
- rotational symmetry in Hamiltonian dynamics 77—75791
- rotational-oscillatory system with many degrees of freedom, resonant motions *(Russian)* 77—33859
- rotations, nonlinear vector products calc. methods. 77—71201
- rotor, elastically supported, automatic balancing *(Polish)* 79—10458
- Rutherford scattering, positively charged particles interaction calc. 77—27468
- satellite in elliptic orbit, stability of cylindrical precession *(Russian)* 77—42729
- satellite orientation in a given direction, steady circular orbit *(Russian)* 79—46174
- satellite stabiliser system with 2-stage suspension, dynamics *(Russian)* 79—32222
- satellite with 2-degrees-of-freedom gyroscope, stability *(Russian)* 77—39212
- satellite with gyroscope in Newtonian field *(Russian)* 77—39211
- scattering cross-sections, two-asymptote approx. 77—7
- shape modes in damped systems 79—44715
- shell, rotating, conducting, in mag. field, forces and moments 78—37786
- Signorinis perturbation scheme for a general reference config. in finite elastostatics 78—83241
- simple harmonic motion, noncalculus derivation for introductory physics 77—17742
- simple harmonic motion demonstration on CRO 78—12518
- solid body rotation in Newtonian force field *(Russian)* 79—35546
- solid body with partly filled cavity, joint motion under total weightlessness 80—94952
- solid cylinder partially filled with fluid, translational motion *(French)* 77—65670
- solid viscoelastic body, motion relative to centre of mass *(Russian)* 80—53649
- soluble one particle models, point interactions with several centres 80—4518
- special relativistic theory with locally anisotropic space-time 77—67279
- spectral entropy method for distinguishing regular and irregular motion of Hamiltonian systems 80—4629
- speed-optimal control synthesis in near spherical symmetry problems *(Russian)* 79—9095
- sphere on imperfectly rough sloping plane 80—62464
- spherical pendulum in fluid flow, transverse vibrations *(Russian)* 77—87644
- spin axisymmetric high speed rotor, approx. anal. soln., coord. system linked to precession and nutation 77—17802
- spin-orbit coupling, classical derivation 79—53971
- spinning particle, Lagrangian function using variational formalism 79—40356
- spinning shell, Magnus instability 79—18693
- spinning top, on surface with friction, behaviour 79—58467
- spinning tops, mechanics *(German)* 78—87253
- spline function approximation in discrete mechanics 80—27112
- spring, energy changes, teaching expt. 80—46754
- spring-mass, base excited system with Coulomb and viscous friction, response determ. 80—19269
- spring-mass system, equivalence of horizontal and vertical systems, teaching 77—9841
- springs, helical, under compression and twist, stability, nonlinear Kirchhoff-Clebsch equations *(German)* 80—33443
- springs, static and dynamic effects, influence of mass 80—41990
- stabilisation of gyrostat in Newtonian force field *(Russian)* 77—851
- stability of continuous systems 77—2537
- stability of mechanical system with disturbed motion, n pairs of purely imaginary roots *(Russian)* 79—63021
- stability of motion on a ring *(Russian)* 80—42052
- stationary motion, stability, Lagrangian eqns. and Liapunov's direct method 80—69645
- stationary motions of material point in gravit. field of rot. body *(Russian)* 77—58545
- stationary response of a randomly parametric excited nonlinear system, truncation schemes 79—46178
- steady state response of systems with spatially localised non-linearity 77—84135
- steel rods, longit. impact on plate, contact time meas., student expt. 79—5939
- stiff frames construction, Tensegrity struct. and Maxwell's rules 78—28939
- stochastic transition, determination method 79—71366
- string, flexible elastic, simple wave interaction 77—68509
- string, partial elastic or anelastic impact against wall *(Italian)* 77—68380
- string response to accelerating mass 77—50875
- string vibr. against point shaped obstacle, energy theorem 78—81824
- string vibr. through moving ring 78—81823
- string vibrating against rigid wall, partially elastic or anelastic impact, energy calcs. 78—67028
- string with variable mass, nonlinear dynamics *(Polish)* 78—12553
- structural dynamics, time integration procedures, computational aspects, error propagation 79—32227
- structural dynamics, time integration processes, computational aspects, implementation 79—32226
- structural dynamics, vibrs., eigenrelations 78—1589
- structural optimisation problems, iterative methods 79—18690
- structural problems, static and dynamic, combined finite element and transfer matrix anal. 80—53619
- structural resonance, mechanical impedance and complex elasticity models, coupled systems *(German)* 80—99953
- structures dynamic problems, eigenvalue economisation, program *(Italian)* 79—35544
- SU(2) symmetry group generators for classical Calogero system 78—62332
- SU(3) broken symmetry group in central force problems 77—60960
- successive finite rotation of a rigid body 79—46180
- superlinear Hammerstein operators and nonoccurrence of secondary bifurcation 78—16641
- swing motion, example of parametric amplification 77—4
- symmetric gyroscope motion, differential eqns. stabilisation procedure including perturbing torques 80—4244
- symmetric structures, group representation theory appl. 80—74727

classical mechanics of discrete systems continued
- symmetric top on horizontal surface, computer program for initial value problem 79—44714
- symmetries of time-dependent Hamiltonians 80—101709
- symplectic manifolds, reduction through consts. of motion 79—49020
- synchrotrons, accelerated particle resonances, perturbation treatment in classical dynamics 79—22506
- teaching, torque and Newton's third law 78—12517
- tennis racket physics, teaching approach 79—71173
- test particles acceleration in one-dimens. random force fields 78—8237
- thick-walled cylinders, unloading after plastic deformation 77—42728
- third-order nonlinear systems with aperiodic excitations, Laplace transform technique 78—81830
- three dimensional mechanisms, position, velocity, acceleration function recurrence relations 79—14244
- three-support bearing shaft system, flexural amplitude determ. and reduction method 78—46890
- thrown string problem 78—89331
- time asymmetries and classical and quantum physics 80—22216
- time-dependent dynamical symmetry mappings, consts. of motion, classical particle systems 77—45688
- time-dependent three-dimensional harmonic oscillator, generalised invariants 77—49623
- top rising by friction, exact mathematical soln. 78—83343
- train, stability of unperturbed motion *(Russian)* 78—18160
- transient nonlinear mechanics problems, finite element anal., computational aspects 79—41565
- transient struct. response anal., matrix scaling technique 77—72148
- transitive dynamic systems, polhode concept generalisation *(French)* 78—62065
- translational symmetry of space and Newton's second law of motion 77—8
- translatory-rotary motion of gravitating spheroids *(Russian)* 78—73841
- transparent pots. in classical approx. 77—50872
- transverse pulse propagation along hanging chain, teaching 78—28898
- turbulent systems, transition to aperiodic behavior, recursive method 80—105493
- two body interactions, three particle final states, kinematics in relative coordinate system 79—67484
- two degree of freedom systems, approximate simulation 77—82383
- two dimensional infinite particle systems, non-equilibrium dynamics with singular interactions 78—12579
- two-mass system, free vibrs., damping factor optimisation *(Russian)* 80—42
- unified formalism for quantum and classical scattering theories 80—100
- uniform acceleration, student laboratory expt. 79—40326
- v=gt expression, origins of derivation 80—77593
- variational mechanics, new approach 77—71206
- vector laws of physics, reformulation 80—68036
- vibrating mechanical structures, realistic fatigue modelling 78—31517
- vibrating symmetric system under nonlinear forces, group representation theory 77—2536
- vibrating systems, nonlinear, multi-degree-of-freedom, harmonic excitation, instability 80—73162
- virtual work principle and integral laws of motion 79—67148
- walking apparatus, parametric optimisation *(Russian)* 77—50871
- weakly coupled geophysical systems, statistical anal. techniques 79—80428
- wheeled vehicle with nonholonomic couplings, eqns. of motion *(Russian)* 78—59292
- WKBJ approx. for classical particles with spin in external field 78—32692
- work hardening adaptation of discrete structures under dynamic loading 80—74726
- world-line invariance in predictive mechanics 80—31498

classical theories of fluid structure
see also kinetic theory; liquid theory
- (12-6-n) fluids, thermodynamic perturbation theory 78—26414
- adsorption, competitive, from binary liquid mixtures, adhesive hard sphere model 80—2265
- adsorption, Percus-Yevick and hypernetted chain theories, second and third virial coeffs. for hard-sphere gas 78—60031
- adsorption and wetting, unified theory using Percus-Yevick eqn. for hard spheres with surface adhesion 77—31879
- alloy, binary liq., viscosity coeffs. by Enskog theory 80—1920
- area of intersection of n equal circular discs, appl. to hard-disc fluid model 78—57755
- asymptotic form of structure factor of liquid 77—7651
- atomic fluid with repulsive pair pot., perturbation method 79—68997
- BBGKY hierarchy, the closure problem 79—14505
- BBGKY hierarchy for hard spheres in one dimens., uniqueness 78—29041
- biomolecular aqueous solution, attractive and repulsive dispersion forces 78—44447
- Brownian motion in fluid, repeated-ring kinetic theory 78—59729
- bulk distribution functions and fluctuation theorems for one phase fluid 78—8346
- n-butane, intermol. pair correls., RISM integral eqn. 78—63656
- linear Chapman-Enskog procedure, evolution equations of hydrodynamic variables 80—49075
- charged hard sphere dense classical fluid, equation of state and crit. point 80—64849
- charged hard spheres in neutralising background, radial distrib. function 77—33936
- charged hard spheres near charged hard wall, mean spherical approx. 79—23510
- charged hard spheres near charged hard wall, nonlinear Debye-Huckel theory rel. to HNC approx. 79—64970
- chloromethane, rot. dynamics, far IR spectra 77—19864
- coherent and incoherent scatt. functions, Maxwell relax. time 77—76283
- collective motion and effective potential 78—79513
- collective motions in classical liquids 79—55632
- correlation functions, perturbation theory for soft sphere systems 77—72536
- correlation functions, sum rules 77—76282
- Coulombic systems, charged hard sphere system, rel. to restricted primitive model 80—64854
- critical fluctuations, shear flow effects 77—20045
- critical maxima and minima of thermodynamic functions 77—27974

classical theories of fluid structure continued
critical opalescence, nonuniform fluid struct. factor calc., thermodynamical treatment 77—40198
critical viscosity of classical fluid, dynamic scaling 80—59689
dense, light scatt., point polarisability approx., local fields, interparticle pair correls. 77—55799
dense, non-spherical mol. polarised light scatt., local fields, interparticle pair correls. 77—55798
dense classical liquid, struct. factor, long range pot. 78—47224
dense dipolar hard sphere fluid, integral eqn. theory 77—76278
dense electrolytes, semiempirical analytic theory for pair correlation function 77—27800
dense fluid, depolarised light scatt. due to orientational fluctuations 77—47318
dense fluid, depolarised light scatt. due to orientational fluctuations 77—47319
dense fluids, HF kinetic sum rule 77—27803
dense gases and liqs., three-body nonadditive interactions, thermodynamics props., mol. dynamics simulation 79—7435
dense liquids, interface with solid wall, NVT Monte Carlo method 79—65310
dense simple fluid, equilib. props., 3-body forces effects 77—76273
dense simple fluid near wall, density profile calc., integral eqn.—Monte Carlo comparison 80—54083
density functional theory, direct correlation function-free energy relation 77—76285
diatomic molecular gas, atomic versus mol. description 77—7495
1,1-difluoroethylene, rot. dynamics far IR spectra 77—19864
dilute aqueous solutions, Monte Carlo studies of struct., review 80—54101
dilute gases, transport props., softness expansion for inverse power pot. 80—28589
dipolar fluids, boundary conditions for numerical simulation, book contrib. 79—60247
dipolar hard sphere fluid, dielec. const., pair distrib. function, Monte Carlo study 78—6001
dipole solvation, one polar mol. dissolved in 499 moderately polar particles 78—47221
direct correlation function of liq. from Ornstein-Zernicke eqn. 77—47314
disordered systems, mode softened unified theory 79—55637
dynamic correlation functions 78—26412
dynamical correlation functions of classical liquids 79—1381
dynamical fluctuations in simple fluids, kinetic theory 77—7652
electric double layer, primitive models, pot. difference and charge density 80—76515
electrolyte solution, primitive model, using modified BBGY integral eqn. 79—99049
electrolyte solutions, interionic radial distrib. function approx. scheme 77—32796
electrolytes, aq. soln., mol. dynamics simulation 80—54097
electrolytes, free energy, due to Coulombian and hard core pots. 79—23748
elementary modular theory, applic. to pure fluids 77—19859
Enskog equation, modified, approach to equilib. 78—94957
Enskog hard-sphere transport theory for dense fluids rel. to exptl. obs. 77—1254
equation of state, hard core fluid with two-Yukawa tail, appl. to Ar 80—59618
equation of state, hard-sphere fluid, Yukawa tail pot. 79—42211
equilibrium correlation functions with various potentials, mol. dynamics expts. *(Spanish)* 79—90502
equilibrium theories of simple liquids, review 80—38887
fluid-solid surface interaction, two-particle correlation function 78—79880
Fokker-Planck fluid, dilute, ang. and orientational correlation times 77—84380
Fokker-Planck fluid, orientational correl. time 79—23512
Fokker-Planck fluid of symmetric top mols. orientational relax. 78—5996
fourth virial coefficient and structural consistency, for inverse power pots. 79—99047
free energy theory, appl. to liq./vap. interface props. 80—10751
fused hard spheres eqn. of state near close packed limit 77—84881
generalised perturbation theory of classical fluids in crit. region 79—77474
Gibbs eqn., generalised, second-order fluids 80—24331
graph theoretic techniques 78—71662
H-theorem for the (modified) nonlinear Enskog equation 79—60242
halogenobenzenes, dipolar liquid, far IR absorpt. rel. to Mori continued fraction for autocorrel. function 78—2875
hard charged spheres, critical point 77—9974
hard core fluids, asymptotic behaviour of virial expansions 80—88010
hard core fluids, distrib. functions and equation of state, zero-separation theorem 80—44089
hard diatomic fluid mixtures, dense, orientational struct., Monte Carlo study 78—34415
hard disc fluid, infinite dilution solute chemical pot. by Monte Carlo simulation 80—88009
hard disc fluid, sixth and seventh virial coeffs. 78—91047
hard disc mixture, eqn. of state, compressibility and phase behaviour, mol. dynamics simulation 77—51291
hard dumb-bells, interaction site mol. statistical thermodynamics 77—55222
hard dumbbell molecules, reference pot., perturbation theories, spherical reference systems 80—28898
hard dumbbells, eqn. of state 77—30119
hard hetero/homonuclear diatomic mol. fluid, Monte-Carlo simulations 78—42873
hard ion mixtures, Ornstein-Zernike eqn. and Yukawa closure 80—107031
hard nonspherical molecule fluids, mixtures, conformal theory 79—94860
hard particle fluids, short range solvation forces 80—38885
hard prolate spherocylinders fluid, pair distrib. function expansion validity 80—24336
hard rod liquid, radial distrib. function 79—86663
hard sphere fluid, dielectric const., Monte Carlo simulations, mol. dynamics calcs. 80—28897
hard sphere fluid, generalised mean spherical approx. 77—11290
hard sphere fluid, impurity self-diffusion coeff., ring approx. 78—6167
hard sphere fluid, locally inhomogeneous, Percus-Yevick eqn. soln. 80—10474
hard sphere fluid, Ornstein-Zernike eqn. with Yukawa closure 79—99050

classical theories of fluid structure continued
hard sphere fluid, radial distrib. function, in semiclassical limit, integral eqn. theory 80—54089
hard sphere fluid, role of structure factor poles in prop. determ. 80—88011
hard sphere fluid, series expansion calcs. 80—44092
hard sphere fluid, soln. method for mean spherical approx. 80—1912
hard sphere fluid, y(r) function, Monte Carlo calc. 78—18523
hard sphere fluid contacting soft repulsive wall, Monte-Carlo method 78—67632
hard sphere fluid in small pores, mol. dynamics simulation 80—24333
hard sphere fluid mixture, density fluctuations 77—19657
hard sphere fluid near hard wall, diffusion coefficient, mol. dynamics simulation 80—64858
hard sphere fluid struct. near hard wall 79—23511
hard sphere fluid theory applic. to liq. particle dispersions 77—9129
hard sphere mixture, nonadditive dias., perturbation theory, double reference system 78—38597
hard sphere mixture, Ornstein-Zernike eqn. with Yukawa closure 78—18513
hard sphere system, high densities, Kirkwood eqn., variational principles 77—65942
hard sphere system, second-order perturbation theory 78—79516
hard sphere-spherocylinder equimolecular mixture, Monte Carlo simulation of fluids 80—44088
hard sphere/hard wall interaction, local density, adsorption theory *(German)* 79—77925
hard spheres, partition functions, Millet's method 78—71828
hard spheres in Percus-Yevick approximation used to derive sedimentation equilibrium eqns. 80—66884
hard spherocylinder fluid, Monte Carlo simulation, ang. correl. functions 80—75140
hard spherocylinders, Monte Carlo simulation 78—91046
hard- and soft-core equations of state 79—55635
hard-core fluid, with Yukawa tail, eqn. of state, Monte Carlo results 78—26410
hard-core particle system, zero separation theorem, virial coeff. 77—26261
hard-disc fluid, free volume props. 79—46534
hard-particle fluids, general scaled-particle-like descriptions 80—103231
hard-particle fluids, general y-expansion-like descriptions 80—107032
hard-rod fluid, anisotropic, correlation function, to 1st order in density 79—86675
hard-sphere dense fluid, equilib. props., semiclassical limit 77—76281
hard-sphere fluid, dense, polar, polarisable, Monte Carlo study 79—86665
hard-sphere fluid, density profile near container wall, mean spherical approx. 77—15149
hard-sphere fluid, direct correl. function 79—41918
hard-sphere fluid, liq.-solid instability, bifurcation anal. 79—27888
hard-sphere fluid, three particle interaction with wall 78—47223
hard-sphere fluid near hard wall, Monte Carlo calcs. 78—55795
hard-sphere fluid with dipoles and quadrupoles, integral eqns. approx. 80—24334
hard-sphere fluid/soft wall interface, nonuniform fluid in external field 78—34413
hard-sphere liq., Percus-Yevick eqn. perturbation soln., appl. to Ar and Xe 80—10483
hard-sphere liquid, pair pot. softness effect on liq., struct. factor 80—88012
hard-sphere mixtures, excess thermal cond. and viscosity 77—11292
Helmholtz free energy of triangular well fluid, Barker-Henderson perturbation theory 79—4218
heteronuclear dumb-bell fluid, local struct., reference interaction intersite model 77—11458
heteronuclear hard dumbbells, eqn. of state derivation 77—30085
high-density fluid-perturbation theory, based on inverse 12th power hard-sphere reference 79—99042
highly viscous liquids, nuclear magnetic spin relaxation, high-freq. translational jitter 79—51874
hydrodynamics, equations of motion and transport coefficients, using discrete formulation 79—90504
impurities, surface bound states, quantum and classical liquids 78—18859
inert gas mixture, dipole autocorrelation function, Lennard-Jones and exponential dipole pots., classical calc. 80—64665
inert gases, viscosity, expt. and derived from statistical models *(French)* 77—35302
infinite 1-D hard core system, selfadjointness of Liouville operator 78—29037
inhomogeneous fluid, pair and density correl. functions 79—27887
integral eqn. with approximation of direct correl. function in pot. rigid core region 77—84611
integral equations for liquids, systematic series formation 78—14264
intermolecular correlation effects on liquid props. determined by X-ray diffraction 77—27799
internal energy calcs. 77—28025
ionic fluid, equilib. props. using corresponding states concepts 79—27889
ionic solution, in mol. polar solvent, charged sphere model, statistical mechs. 78—71655
ionic solution theory, variational approach 77—7645
itinerant libration, two-dimens., simulation by 120 annuli 79—14662
itinerant oscillator model, mol. fluid, non-Markovian probability density function 78—47222
kinetic theory models of density fluctuations, memory functions 80—38886
lattice and continuous one-dimens. models, triple point 77—31571
Lennard Jones 6-12 fluid, Pade approximant for eqn. of state 77—3905
Lennard Jones 6-12 fluid, surface characts., density functional theory 77—24255
Lennard-Jones and Stockmayer pot. parameters, crit. evaluation, correl. methods 78—1966
Lennard-Jones chain, stochastic transition in classical nonlinear dynamical system 78—142
Lennard-Jones diatomics system, vel. autocorrelation functions 78—9931
Lennard-Jones fluid, 2-D, radial distrib. function, integral eqn. perturbation theory 78—26409
Lennard-Jones fluid, eqn. of state, Monte Carlo and perturbation theory 77—76519
Lennard-Jones fluid, hypernetted-chain eqn. of state 78—67800
Lennard-Jones liquid mixture, mol. dynamics, attractive term effects 77—11454

classical theories of fluid structure continued
Lennard-Jones two-dimens. fluid, Percus Yevick eqn., radial distrib. function, critical point 77−76272
Lennard-Jones type one-dimens. system, Van der Waals type eqn. of state 80−24562
light scattering, collision-induced and multiple, by simple fluids 80−53919
light scattering in fluid far from equilibrium 80−103965
liquid, fluctuating local structure, Fokker-Planck type eqns. 79−64966
liquid correl. function time-depend. struct. 77−1051
liquid film, mol. dynamics simulation of surface struct. 77−15666
liquid metal, eqn. of state and triplet and higher correlations in long wavelength limit 77−11453
liquid metal, polymer model, approx. eqn. for average distance between atoms calc. *(Russian)* 77−15293
liquid mixtures, local mole fractions consistency 78−83702
liquid-gas transition, hard sphere fluid, with Yukawa tail interaction 79−99304
liquid-vapour co-existence, dipolar hard sphere fluid, Monte Carlo method 79−99293
liquid-vapour interface nature, non uniform classical fluids statistical mechanics 79−77468
liquid-vapour interface struct. from uniformity of chemical pot. 79−60241
liquids, kinetic theory, dynamical struct. factor calc. 78−21050
Mayer function, delta-function expansion, virial coeffs. appls. 79−4221
mean spherical model, angular correlation functions 78−14261
memory function, dynamical struct. factor, current-current correl. function 78−26411
memory function, self-consistent theory, incoherent scatt. law. 77−89360
memory functions, microscopic theory, generalised Langevin equation 80−49076
methane, liq., mol. dynamics calcs. 77−19857
methane, liq., mol. dynamics simulation using singularity-free algorithm 80−54116
methane, liq. and gas, mol. dynamics simulation, thermodynamic props., struct. factors, etc. 79−50976
methyl iodide, liquid, rough sphere rot.-diff. model, relax. times 77−15294
microdynamics, book contrib. 79−60248
microphysics to macrochemistry, discrete simulations, review 80−54102
mixture, binary, of hard spheres with nonadditive diameters, Percus-Yevick eqn. approx. soln. 79−77471
mixture of dipolar hard spheres, dielec. props. 80−24335
mode coupling theory of simple classical liquids 79−55630
modified cell theory, eqn. of state for hard spheres 80−103445
molecular dynamics, fluctuation driven reson., hydrodynamic and kinetic theory simulation 77−55124
molecular dynamics, high speed computation of correl. functions 77−7648
molecular dynamics data, space-time Fourier transform 77−7647
molecular dynamics simulation of dense gases, test particle motion 78−9930
molecular dynamics simulations at constant pressure and/or temperature 80−64852
molecular fluid, spherical harmonic formalism, thermodynamic props. 79−27886
molecular fluid perturbation theory, Pople expansion third order term, anisotropic pot. 78−79510
molecular fluid site-site pair distrib. function, Ornstein-Zernike eqn. 78−22614
molecular fluids at equilibrium, integral equation derivation 80−64861
molecular liquid, mol. dynamics simulation, multiple time step methods and improved potential function 80−54098
molecular liquid, non-stoichiometric complex formation, thermodynamic equilib. consts. 77−21406
molecular liquid, orientation dependent distrib. function from NMR relax. data 77−20737
molecular liquid, thermodynamic functions, interaction site model calc. 78−71661
molecular reorientation in fluids, stochastic differential eqns. 79−82132
molten salt, hydrodynamic correlation functions 77−31577
molten salt, mol. dynamics simulation, of liquids with ionic interaction 80−54097
molten salts, density and charge fluctuations 79−55645
Monte Carlo calculations, optimisation of sampling algorithms 80−54099
Monte Carlo simulations, review, book contrib. 79−82140
nematogenic solutions, binary, Van der Waals theory 79−27916
nematogenic solutions, Van der Waals theory 79−27915
nonadditive hard spheres, scaled particle theory, positive nonadditive solns. 78−79515
nonpolar fluid, permittivity, comparison of Wertheim and Clausius Mossotti derivations, density depend. 77−77137
nonuniform fluid state, Van der Waals theory, thermodynamics, struct. and phase stability 79−77475
nonuniform one dimensional classical fluids, Lennard-Jones pot. interactions, Percus Yevick approx. and density functional calcs. 80−64864
one dimensional shouldered hard-sphere fluid, struct. factor 78−34417
one-dimensional fluid, triangular well pot., perturbation theory 77−35455
Onsager transition in hard plate fluid 77−48696
orientation autocorrelation functions of spherical Brownian particle 77−7646
Ornstein-Zernike and Percus-Yevick temperature dependent fluids, solvation forces 80−64862
Ornstein-Zernike eqn., rel. to pair pots. calc. 77−1054
Ornstein-Zernike theory, appl. in van der Waals model 78−26408
pair correlation function, self-consistent calcs. for simple fluids 77−1061
pair correlation function decay, Ornstein-Zernike eqn. numerical soln. 77−51148
pair correlation function of the liquid-vapour interface 79−55633
pair potential, self-consistent calcs. for simple fluids 77−1062
particle distrib. function, theoretical method 80−64856
Percus Yevick eqn. for square mound pot., perturbation soln. 78−22619
Percus-Yevick eqn. of state for sticky hard rod gas 78−9933
Percus-Yevick equation, nonequilibrium analogue 78−55797
Percus-Yevick equation, square-well pot., perturbation version 78−63648
Percus-Yevick integral eqn. perturbative soln. for of intermolecular pot. 79−30348
permittivity, dipolar hard sphere fluid, interaction-graph theory 79−51898

classical theories of fluid structure continued
perturbation theory for fluid of rod-like mols. interacting via Kihara potential 77−11291
polar fluid, equilib. theory, graph theoretical treatment 78−6002
polar fluid, long range and short range dipole correls., separation 79−1376
polar fluid, translationally invariant correlation function, thermodynamic and dielectric props. 77−35457
polar fluids, intermol. and thermodynamic potentials, angle-depend. pot. 78−22618
polar fluids, intermol. and thermodynamic potentials, preaveraged pot. 78−22617
polar liquid surface tension calcs. 77−31841
polarisable hard sphere fluid, thermodynamic props. 79−42277
poly(γ-benzyl-L-glutamate) solns., osmotic press. rel. to hard spherocylinder theories 79−94886
polyatomic fluids, generalised hydrodynamics 77−1055
polydisperse fluid, of hard or permeable spheres, scatt. function 79−86664
polyelectrolyte, 1-1 soln., excluded vol. theory, Khun statistical segment basis 78−83716
polymer chain dynamics, in soln., computer simulation 78−83718
polymer solution, conc., rheological props., rod-like mol. model 78−75114
polymer solutions, semi-dilute, field theoretic formalism 77−31575
radial distribution function, perturbation theory, three-body pot. 77−35456
radial distribution function of fluid, quantum corrections 77−3906
Raman isotropic polaris., dense fluid correlation function, kinetic eqn. 77−28567
real fluids, short range repulsions and long range attractions, simple pair pot. model 80−64850
renormalisation group anal. 80−17838
rigid particle fluid, statistical mech., general zero-separation theorem 79−46533
rigid spherocylinder fluid, virial eqn. of state 78−63836
rough sphere, rot. in bath of spheres, microscopic boundary layers 78−18521
rough sphere fluid, computer simulations 79−99041
rough sphere fluid, dynamical correlations, renormalised kinetic theory 77−19858
rough sphere fluid, kinetic theory, matrix elements 77−71262
rough sphere fluid, linear and ang. vel. correl. functions, kinetic theory 77−42951
rough sphere fluid, translational and rot. motion, particle roughness depend. 78−26403
scaled particle model for mixtures of hard spheres with nonadditive diameters *(German)* 79−10765
scaled particle theory for non-additive hard spheres 79−60252
scaled particle theory results for dense mixtures of convex shaped mols. 78−1969
semiclassical fluid, with square-well plus hard core potential, equilib. props. 80−10479
semiclassical statistical mechanics, nonperturbative incorporation of quantum effects 79−64819
short-range interparticle interaction potential, thermodynamic perturbation theory 77−43124
short-range structure universality, bridge functions 80−10478
silicates, molten, struct. and stat. interpret. of Masson theory *(French)* 80−49078
silicates, molten, with high and medium Si contents, stat. theory *(French)* 80−49079
simple classical fluid, new theory 79−99051
simple classical fluids theory, universality in short range struct. 80−75141
simple classical liquids, memory functions 79−55626
simple fluid, mol. dynamics simulation, including three-body interactions 80−54100
simple fluids, hard and soft-core eqns. of state, termination temps., Kihara pot. 80−70360
simple fluids, hard- and soft-core eqns. of state, characteristic curves 79−55861
simple fluids, hard-core equations of state, C_p extrema loci 79−60474
simple fluids, hard-core equations of state, characteristic curves 79−55862
simple fluids, order-parameter fluctuations near crit. point, Ornstein-Zernike theory 78−34416
simple liquid, dynamical structure factor and Green's functions 79−4228
Smoluchowski eqn., one-particle generalised, perturbation solution 77−27211
soft sphere viscosity, numerical calc. using discrete hydrodynamics 79−90505
solid substrate interaction, comparison of theories 78−63655
solvated ion dynamics, kinetic dielectric decrement, microscopic theory 80−7801
solvated ion dynamics, mol. theory, fluid struct. and ionic mobility 80−7800
solvent-rod mixture, two phase, interfacial free energies, quartic van der Waals theory 80−59377
solvophobic effect in simple fluid mixtures 77−31569
spherical particles, hydrodynamic interaction, translational, rot. and translational-rot. diffusion 78−26405
spinodal decomposition, of Lennard-Jones fluid, microscopic theory 79−99046
square well fluid, mean spherical approx. and optimized cluster theory 78−26407
square-well fluid, using corrected integral eqns. 78−79511
square-well fluid, very high density, Yvon-Born-Green eqn. solns. 77−1050
statistical mechanical models in X-ray and neutron diffraction data interpret 77−31551
statistical mechanics of nonequilib. steady states, dense fluid fluctuations, light scatt. 79−54035
statistical mechanics of nonequilib. steady states, microscopic theory 79−58623
statistical mechanics of nonspherical mols., hard-core models 77−51288
statistical mechanics of small chain mols. packing effect 78−71656
statistical mechanics of stationary states, appl. to low-density systems 79−58624
statistical thermodynamics, review 78--83703
sticky hard sphere fluid, eqn. of state, Percus-Yevick approx, 79−60240

- **classical theories of fluid structure** continued
  - sticky hard sphere pot., struct. function evaluation 80—33869
  - Stockmayer and Lennard-Jones pot. parameters, crit. evaluation, correl. methods 78—1966
  - Stockmayer fluid, mol. dynamics and thermodynamic perturbation theory, mol. polarisability effects 78—71419
  - Stockmayer molecules, two dimens. fluid, static props., dielec. const. mol. dynamics calcs. 80—54094
  - structure factor extrapolation into low-angle scatt. region 77—51289
  - structured fluid theory, appl. to substruct. redistrib. kinetics 78—13983
  - surface tension, hard-sphere fluid, interacting with wall, virial coeffs. 79—23808
  - surface tension of hard sphere fluid, wall 79—73081
  - thermodynamic behaviour near crit. point, book contrib. 79—60479
  - three-body correlation determ., heterodyne coincidence spectroscopy 77—10118
  - transition metal, electronic states densities from struct. and entropy data 77—1347
  - transport coefficients computation by cell hydrodynamics 78—38600
  - transport properties in mean spherical approx., appl. to inert gases 78—9927
  - tricritical phenomena, ternary, quaternary fluid mixtures, classical models 78—91416
  - tricritical points of model fluid mixture 77—31752
  - two dimensional radial distrib. function 78—67629
  - van der Waals forces, many-particle correl. attenuation *(Russian)* 77—27798
  - van Hove's dynamical structure factor for classical liquids 79—55631
  - variational optimization of truncated approximations 80—44097
  - velocity autocorrelation function, density depend. 79—14665
  - water, dielectric constant of bonded lattice model 78—23386
  - water, Ising lattice model with directional bonding, renormalisation group study 80—28894
  - water, liq., Monte Carlo studies of struct., review 80—54101
  - water, Monte Carlo simulation 80—54113
  - Widom-Rowlinson hard-sphere mixture model, transport props. 80—14981
  - X-ray critical multiple scatt., induced η 77—76525
  - Yukawa-tail fluid, semiclassical fluid struct. and thermodynamics props. 79—27895
  - Ar gas, thermally excited density fluctuations, neutron scatt. 79—23392
  - Ar, liq., depolarised scatt. lineshape correlation function theory 77—40253
  - Ar, liq., numerical anal. of density fluctuations 78—21051
  - Ar, liq., numerical anal. of transverse current correl. 78—21052
  - Ar, mode coupling theory of simple classical liquids 79—55630
  - Ar, mol. dynamics calc. 77—19857
  - Ar, van Hove's dynamical structure factor for classical liquids 79—55631
  - Br$_2$, mol. dynamics of '2-Lennard-Jones centres' pair pot. liq. 79—73082
  - t-butyl chloride, dipolar liquid, far IR absorpt. rel. to Mori continued fraction for autocorrel. function 78—2875
  - CO$_2$, mol. dynamics of '2-Lennard-Jones centres' pair pot. liq. 79—73082
  - CS$_2$, liq., light scatt. intensities, struct. models 78—60476
  - CS$_2$, X-ray scatt., reference-site-interaction model, intermol. pot. function 77—11459
  - Cl$_2$, mol. dynamics of '2-Lennard-Jones centres' pair pot. liq. 79—73082
  - F$_2$, mol. dynamics of '2-Lennard-Jones centres' pair pot. liq. 79—73082
  - F$_2$, viscosity coeffs., modified hard-sphere calcs. 77—11295
  - H$_2$, states velocity auto-correl. function, relax time, neutron scatt. obs. 80—58401
  - H$_2$-Ar, states velocity auto-correl. function, relax time, neutron scatt. obs. 80—58401
  - HCl, liq. struct. simulated by a Lennard-Jones pot. 80—1917
  - KCl, melt, mol. dynamics simulation 80—54097
  - N$_2$, liq., dephasing of mol. vibr. related to correl. functions 78—75523
  - Ne, higher order structure factors and their inverses 79—55646
  - Ne, mol. dynamics calc. 77—19857
  - O$_2$ viscosity coeffs., modified hard-sphere calcs. 77—11295
  - Pb, paracryst. struct., coordination statistics calcs. 77—1063
  - Pb$_x$Se$_{2-x}$ melts, viscosity and radial distrib. function for stoichiometric and peritectic comp. 80—1916
  - Rb, mode coupling theory of simple classical liquids 79—55630
  - Rb, van Hove's dynamical structure factor for classical liquids 79—55631
  - RbBr, molten, density and charge fluctuations 79—55645
  - SF$_6$-N$_2$O solution, IR and Raman rot. correl. functions, expt. and theory 79—46541

- **classification**
  - *see also indexing*
  - Ap and Am stars, numerical taxonomy 80—22015
  - astronomical images optimal classification into stars or galaxies, Bayesian approach 80—21920
  - astronomy, Be-stars, classification of faint objects 77—56993
  - astronomy, Shapley-Ames southern galaxies, Las Campanas survey and classifications 78—45409
  - composite materials, system for 80—7484
  - composite spectra stars, new classification scheme for bright stars of Hynek's (1938) list *(French)* 80—56876
  - contour maps classification problems 79—79999
  - data base, classification, comparison of pattern recognition methods 80—199
  - earthquake precursors, classification 79—88264
  - failure micromechanisms, classification according to failure type *(Russian)* 80—108557
  - galaxies, Hubble classification system, 50th anniversary 77—33657
  - galaxies, luminosity classifications, systematic and accidental errors 79—12510
  - galaxies of Magellanic type, classification system and struct. *(German)* 80—105348
  - geochemical data processing, Q-mode classification of large data sets, AGCL (FORTRAN IV) program 77—86941
  - geological appl. of statistical cluster analysis, using G-mode central method, FORTRAN V program 77—86879
  - griseofulvin tablets, tensile strength and disintegration times 77—60027
  - land use classification by thermal IR scanning imagery 77—26422
  - linear and angular dimensions, classification and symbols for means of meas. 79—6081
  - materials science, concept of system 80—101003
  - meteorites, ureilites, classification and elemental fractionation 77—41364
  - meteorology, macroprocess classification, statistical methods 78—16132

- **classification** continued
  - molecular structures, topological code, modified Morgan algorithm 80—58122
  - NGC 3928 C (Markarian 190), identification as miniature spiral galaxy 80—105347
  - powder compacts, active shrinkage theory and mechanism 77—63579
  - recurrent Lie group classification *(French)* 78—62047
  - rock cleavage, morphological classification 80—21736
  - Sb-type galaxies, luminosity classification rel. to Hubble const. local value 80—62339
  - seawater, optical classification using solar radiation spectral attenuation meas. 79—12127
  - sedimentary sea bottoms, machine classification 79—92626
  - statistical thermogram classifiers using coherent and incoherent light 79—96644
  - test instruments for magnetically hard materials *(Russian)* 77—67479
  - water usage regions in Lithuania, multi-image classification *(Russian)* 78—16069
  - Fe meteorites chemical classification, role of Ga, Ge and Sb nebular condensation 80—36594
- **classification, pattern** *see pattern recognition*
- **clathrates** *see molecules; organic compounds*
- **clay**
  - aeolian sedimentation of clay-sized particles on Earth and Mars, comparisons 80—31042
  - W. African continental shelf, suspended particle mineralogy and transport in water masses 77—81900
  - Al(1) clay of Frankische Alb, slope forms statistical investigation *(German)* 78—57211
  - atmospheric dust, imaginary refr. index rel. to particle size 78—7763
  - bedding dip and slope form correl., computer calc. *(German)* 77—64282
  - bentonite clay, Na enriched, buried radioactive waste isolation material appl. 79—81029
  - brown clay from North Pacific, ^{10}Be geochemistry and sedimentation 80—101356
  - calcining, particulate emission removal using electrostatic precipitator 79—24925
  - Canadian, neutron activation anal. 78—8487
  - Canadian quickclays and landslide process 77—44970
  - catalysts for peptide formation in prebiotic era 77—64435
  - clay, highly plastic, compaction and lime stabilization effect on pore size distrib. *(Japanese)* 78—31365
  - clay soil/sand mixtures, reflectance 80—56475
  - clay-Al floc, physical characts., density function 79—100454
  - clay-Al floc physical characts., floc strength determ. 79—100455
  - Cretaceous clay minerals from S.Atlantic DSDP cores *(French)* 79—84220
  - deep-lake clays from pluvial Lake Lahontan, palaeomagnetic record 80—101321
  - desert varnish, importance of clay minerals 77—86893
  - dispersion and swelling, effect on soil hydraulic cond. 78—53668
  - electroenforced sedimentation in consolidation region 80—26057
  - fault expt., seismic simulation 80—21734
  - fault gouge, mineralogy and physical nature 79—16454
  - floc, settling velocity, rel. to permeability 79—43636
  - fractionally charged particles conc. in large samples of matter *(Russian)* 79—88341
  - frozen sand-argillaceous rocks, elastic moduli 77—9406
  - gas-bearing water-saturated sediment, sound vel. as function of bubble distrib. 79—39703
  - glacial till landforms, fabric anal. 77—44989
  - greenalite, two-dimens. mag. order 79—61188
  - Grote Nete basin, Belgium, geomorphology *(Flemish)* 78—61452
  - groundwater flow anal. by finite element method 78—92875
  - halloysite, Al$_2$O$_3$(SiO$_2$)$_3$(H$_2$O)$_2$, NMR study of adsorbed water, molecular motions 78—95226
  - heat treatment, effect on rheological props. of enamel slips 80—60809
  - heavy metal ion removal in clay suspensions 77—86955
  - high resolution electron microscopy *(French)* 78—26396
  - ice-forming nuclei surfaces, elemental comp. 78—3881
  - Indian continental shelf, distrib. patterns of Al, Ti, Mn, Cu and Ni in sediments 79—25225
  - W.Indian Ocean, clay mineralogy and sedimentation 77—29279
  - E.Indian Ocean, clay minerals distrib. in sediments 79—44172
  - Indian Ocean, clay minerals in Cenozoic bottom sediments 79—53335
  - Indian Ocean, deep-sea sedimentation, lithologic and palaeomag. study 79—20810
  - isotropically consolidated sample prep. with random fibres 77—90531
  - kaolin, -flint mixtures, polyethylene oxide additive effect on plastic strength after tempering 79—24568
  - kaolin bodies, effect of mineralizers on firing shrinkage, microstruct. and strength 80—97488
  - kaolin grog particles, shape and density 80—97450
  - kaolinic, chlorination 78—6878
  - kaolinite, hydration, lattice deform., vol. expansion due to adsorbed H$_2$O 80—45555
  - kaolinite, sintering mechanism at 900 and 1050°C, influence of mineralizers 77—90305
  - landscapes, soils and erosion, Wither Hills, New Zealand 78—88864
  - Late Quaternary sedimentation on W.African continental margin 77--21753
  - marine sediments, underconsolidated, adhesive resistance 79—20814
  - Mars, clay minerals prod. by alteration of glass 78—89097
  - mechanical properties at high-press. 80—76966
  - metahalloysite, dehydration, lattice transformation mechanism 77—31780
  - micrometeorites contained in deep-sea sediments 80—46500
  - minerals, distrib. in sediments of Bay of Bengal 78—81146
  - minerals, symposium (New Delhi, 1972, October 10-12) 78—7617
  - montmorillonite, clay mineral, expanding type, surface props. rel. to heat treatment 79—29406
  - montmorillonite, dehydration kinetics 78—76857
  - montmorillonite, mech. props. at high press., rel. to fault behaviour 79—84234
  - montmorillonite, physicochemical and engineering props., k-fixation effect *(Japanese)* 78—31366
  - montmorillonite neoformation by post-depositional subsurface weathering in slope deposit 78—73367
  - mudboils nature and genesis, Keewatin, Canada 79—5478
  - natural clay permafrost, electrical props. 77—44967
  - NMR, substrate struct. and order on H$_2$O mol. relax. 78—7247

clay continued
non-homogeneous clay layer, consolidation estimation method 79—58110
nontronite, CO_2 adsorpt. and capillary condensation rel. to Mars volatile storage and atmospheric history 80—72833
Nottingham clay tobacco pipes, chronological groups, chemical analysis 79—29422
Okhotsk Sea, clay minerals distrib. in recent sediments 79—20804
palaeomagnetic intensity meas. of baked sediments, weathering effects 77—37135
pelagic sediments of NE tropical Pacific, metal content *(Japanese)* 80—8292
3T-phengite, existence in Xingyang metamorphic belt, tectonic significance *(Chinese)* 79—84264
Philippine Sea, clay sediments comp. and accumulation rates 79—2221
pianlintic clay, a new sedimentary rock *(Chinese)* 79—96759
plasticity determ. using drying process and shrinkage 79—20307
polygonal patterned ground in central New Jersey, origin during Wisconsin glaciation 79—25248
pottery manufacturing techniques, classification by X-ray anal. 78—354
radiative waste, long-lived, final disposal in underground clay formation, Belgium *(French)* 77—61572
radioactive low level liquid wastes, chem. treatment, clay minerals, cation exchange capacity 78—33270
radioactive waste, long-lived, disposal in Trisaia clay formation, Italy 77—61573
rare earth element separation, complexation method 80—3442
rectorite, stacking and ordered interstratification, high-resolution TEM obs. 80—109140
red clay, seawater ^{210}Pb scavenging rel. to particulate and soluble activities meas. 77—5223
remoulded, shear stress path, stress history rel. to shear strength characts. 78—77219
Rideau clay loam, moisture profiles during steady vertical flows in swelling soils 79—5524
rock joints filled with wet clay, shearing at high-press. 80—41438
Rother catchment, W.Sussex, fine sediment mineralogy of source rocks and suspended sediment 79—20827
lower Saint Lawrence estuary sediments, clay-sand sequence chronology in Rimouski shelf region 79—62530
sample preparation for X-ray diffr. anal. 80—97647
seawater-clay suspension, turbulent boundary layer 79—20858
sediment, artificial, const. vol. deform. effects on magnetisation 78—65265
sediments in S.E.Baltic, physical props. *(Russian)* 78—15990
seismic transverse waves propag., expts. 77—21682
silt-clay, fault creep and stress drops in saturated gouge 78—40547
sintering tendency, effect of basalt and chemical-mineralogical composition 78—11177
soft, increase in shear strength and rigidity due to Fe^{3+} addition *(Japanese)* 78—31463
soils, cracking and swelling dynamics 78—73359
soils, sandy and clay, microwave absorption *(Russian)* 78—81162
surface coating constituent mat., adsorpt. of Cs^+ 78—23843
suspension, Onsager transition 77—48696
suspensions with negative thixotropy, hysteresis loops, deflocculant addition effect 79—52789
terrigenous and volcanogenic deep sea bottom sediments chem. comp., Sea of Japan 77—21758
thermobalance method of determ. and anal. of clay mixtures, modification 77—29073
thermoluminescence dating of sediments baked by Chaine des Puys lava flows 78—92808
thermoremanent magnetisation, cooling-rate depend. 80—46174
thixotropy of clays subject to vibr., influence of various electrolytes *(French)* 77—41024
Triassic assemblages of Europe 79—12118
Turkish, neutron activation anal. 78—8487
Vulcano Island neighbourhood, clay minerals form. in volcanic and hydrothermal sediments *(French)* 79—62482
water suspended solid analysis by single-particle scatt. 79—79435
X-ray scattering from interstratified minerals 79—66685
Yolo light clay, moisture horizontal absorption, infiltration analysis 77—29345
Yolo light clay, water vertical infiltration analysis 77—29346
Al_2O_3 and SiC recovery by C reduction 80—108704
^{40}Ar-^{39}Ar stepheating analyses of clay concentrates in Irish orebodies 79—66684
$Fe_6Si_4O_{10}(OH)_8$, greenalite, metamag. clay mineral, mag. props. *(French)* 78—88817
H isotope exchange between clay minerals and seawater 78—69329
K-Ar dating method for argillaceous sediments 79—8716
Li, occurrence in flint clay and related rock types in United States, preliminary survey 79—48475
Mg removal from interstitial waters in reducing environments 79—66673

cleaning *see surface treatment*

cleanliness *see hygiene*

cleavage, crystal *see crystal cleavage*

Clebsch-Gordan coefficients
see also elementary particle theory
3-j symbols, derivation of recently discovered relations 77—60963
angular momentum, coupling coeffs. calc. method 77—9895
angular momentum theory, generalised equivalent operator products 79—49071
biatomic molecular gas, quantum kinetic theory *(Rumanian)* 78—91053
boost matrix elements of the homogeneous Lorentz group 79—92975
boson and fermion systems, eigenvalue spectra widths, symmetry, Wigner coeffs. 80—18213
caesium perfluoro-octanoate/D_2O system, ^{2}H NMR quantum orders, RF pulses 80—103892
calculation method for finite or compact continuous groups 80—4587
calculation program ANGMOM 78—89359
compact connected Lie groups, tensor product representation, decomposition 79—6021
constellations and projective classical groups, PO(n+1, C) and PSp(n+1, C), Lorentz and rotation subgroups 80—62869
coupling coeff., general theory 79—88829
coupling coefficients for cubic groups, $3j\Gamma\gamma$ symbols for double octahedral SU(2) group 79—21571
coupling coefficients for cubic groups, permutation symmetry 79—21572

Clebsch-Gordan coefficients continued
crossing invariant solution of baryon exchange degeneracy, reggeon F/D ratios in SU(4) 77—2766
crystal irreducible problems, use of Clebsch-Gordan reduction 78—2052
crystal point groups, extended integrity basis 79—69047
crystallographic double point groups, Clebsch-Gordan products and extended integrity bases 79—69048
crystallographic space groups 80—1955
D_{4h} symmetry, even and odd parity orbital combination 78—45514
De Sitter group SO (4.1), Wigner's coeffs. *(Russian)* 79—9134
De Sitter group SO (4,1) Wigner coeffs., most-degenerate representations *(Russian)* 80—8818
deformed nuclei, single particle matrix elements of radiative M2-transitions, Nilsson model 80—22753
double groups and projective representations, Clebsch-Gordan coeffs. calcs. 79—92977
double tetrahedral group, Wigner symbols, coupling effects 79—44760
extended integrity bases of finite groups 79—40349
finite groups, general theory 79—58570
finite magnetic groups 80—12930
fractional-parentage coefficients, reduced in quasi-spin space, submatrix elements of tensor operators 80—4578
functions on tableaux and frames of the symmetric group S_n, determined by computer program 78—86173
Gel'fand lattice polynomials and irreducible representations of U(n) 78—49700
generating invariants, nontrivial selection rules 77—82414
graded Lie algebras, Wigner Eckart theorem for tensor operators 77—45984
gradient formula for the $O(5)\supset O(3)$ chain of groups 78—78285
group SO_5, general expressions 77—13636
hidden couplings and relationships 78—88
holomorphic discrete series, Clebsch-Gordan coeff. determ. 80—8837
holomorphic discrete series, coeffs. of Clebsch-Gordan 79—71282
homogeneous Lorentz group SO(3,1), boost matrix elements and Clebsch-Gordan coeff. 78—4505
induced projective unitary-antiunitary representations, selection rules, Clebsch-Gordan series 78—54214
integral transformation describing Clebsch-Gordan coefficients, d-function SU(2) and their symmetry *(Russian)* 79—2665
intelligent states, computation of Clebsch Gordan coeff. 78—62101
ISO(n), explicit determ. of representation functions 80—31561
isoscalar factors, on noncanonical bases 78—81797
Koornwinder's polynomials and representations of the conformal group 79—63343
Kronecker products, decomposition into corepresentations of type I only 80—62517
Kronecker products, decomposition into corepresentations of type I and II 80—62518
Kronecker products, decomposition into corepresentations of type II 80—62519
Kronecker products, decomposition into corepresentations of type III 80—62520
Kronecker products, decomposition into corepresentations of type I and III 80—68066
Kronecker products, decomposition into corepresentations of type II and III 80—68067
Legendre moments calc. from partial waves 79—17273
Lie groups, semisimple, representation matrix elements and Clebisch-Gordan coeff. 79—97230
Lorentz group in n dimensions, tensor product decomposition 77—5626
Lorentz group O(2,1), coupling of continuous representations 79—49078
magnetic group, finite, irreducible tensor operators and Wigner-Eckart theorem 78—22678
magnetic monopole, appl. of summing of Clebsch-Gordan coefficients 77—41505
magnetic space groups, Clebsch-Gordan coeff. calcs. 80—79731
marcasite structure, space group selection rules 79—99099
meson sector in SO(8) model of elementary particles 78—58135
molecules, isolated, intersystem crossing, rot. motion effect 80—95669
multiplicities for space group representations 79—60291
multiplicity free 6-j symbols and Weyl coeff. of U(n) 78—65809
nonsymmorphic space group Pn3n 79—60293
nuclear microscopic collective Hamiltonian, spin-isospin part of the matrix element 79—63609
nuclear microscopic theory, coeffs. for SU_3-irreducible decomposition of operators and props. of basic interactions 79—63608
nuclear two-particle density matrix, for U(3(n−1)) states with $E_{min}+1$ in nuclei with $n\leq16$ 78—41624
nucleus, model density matrix, $U_{3(n-1)}$-irreducible decomposition 79—67692
partial wave analysis for supersymm. scatt. amplitudes 77—49872
phonons, coupled rotational band approach, zero-rank operators 80—47341
Pn3n, Clebsch-Gordan coupling coefficients 79—90585
polarisation in heavy ion reactions, Strutinsky model, asymptotic Clebsch-Gordan coeffs. 78—74391
projective Lie algebra of Lorentz group, homographic transform. 78—57739
pseudo-oscillators, group theory 80—22226
quantum chemistry, chain $SU(2)\supset D_\infty'\supset D_4'\supset D_2'$, mol. aggregates 78—17552
Racah algebra of Gln, generalised back coupling rules 80—47208
random walk and SU(2) Clebsch-Gordan coefficients 80—17822
recoupling coefficients, subgroup factorisation 78—66
relation to structural constants in classical algebras 77—13637
S_n group coeffs. generation by computer program 78—86172
selection rules for Pn3′n 80—98820
selection rules for type II Shubnikov space groups 80—98819
Shubnikov point groups, corepresentations 80—86121
SL(2,C) group, Clebsch-Gordan coeffs. 79—6022
Sn group coeffs. 77—74256
space groups, coupling coeff. 79—90584
space groups 79—60292
spl(2,1) superalgebra, irreducible representations, tensor product 80—82909
structural constants in symplectic and orthogonal algebras, explicit expressions 78—82
SU_3 group, biorthogonal system of isofactors 80—36906
SU_3 group, normalisation 79—106
SU_{mn} containing $SU_m\times SU_n$, irreducible bases *(Chinese)* 78—66049

Clebsch-Gordan coefficients continued

- SU_n C-G coeffs., contiguous relns., derivation method 78—74171
- SU_n group singlet factor, recursive formula for Clebsch-Gordan coefficients *(Chinese)* 79—58902
- SU_n groups, generating invariants in theory of representation of symmetrical group S_N 79—75700
- SU_n groups, irreducible representations of compact groups, tensor product decomp. and holomorphic induction 80—47205
- SU_n symmetry, method of generating invariants 78—16945
- SU_n theory, generating invariants of Clebsch-Gordan coeffs. 79—302
- SU(2), Clebsch-Gordan coeffs., bilinear relns., based on anal. of Poincare, Lorentz and rotation group SO(3) 80—57509
- $(SU(2)\times SU(2))sS_2$ group 77—17771
- SU(3)×SU(3) chiral algebra, crossing matrix elements, Clebsch Gordan coeffs. 78—32998
- SU(4), Clebsch-Gordan coeffs., matrix, elements and symm. props. 78—45803
- SU(4), Clebsch-Gordan series 78—16940
- SU(4), formation of baryonium and exotic baryons 79—75739
- SU(4) coeff. calc. 77—6045
- SU(5), Clebsch-Gordan series, quark model appl. 80—47256
- sums of products, for Clebsch-Gordan and Wigner coeffs., rel. between diagrams 78—81879
- symmetric group irreducible representations, tensor product decomposition 77—74255
- symmetries of 3j and 6j coeffs. 80—86621
- symmetry group, Clebsch-Gordan coeff. as eigenvectors of projection matrices 79—19175
- tensor properties of second-quantization operators and analysis of composite physical systems 79—25903
- three dimensional rotation group, realisation of kets 78—4522
- U(3) Wigner coeffs., canonical resolution of multiplicity problem, constructive soln. 77—17874
- unitary groups class II representations 77—41506
- universal generating function *(Russian)* 79—67188
- vector invariants method, use in anal. of physical symmetries 77—79003
- β-W, coeff. for $X\times X$ and $R\times R$ irreducible representations 79—14732
- Wigner's (2n+1) rule in MBPT 80—42095
- Wigner 12j symbols of first kind, calcs. 77—60953
- Wigner 12j symbols of second kind, calcs. 77—60954
- Wigner 3j-symbols, deriv. of props. by use of Lorentz group 77—33837
- Wigner function, parity operator expectation value appls. 77—45732
- Wigner scheme, Γ-decay of analogue states, β-decay 77—41930
- Wigner-Racuh orthogonal and symplectic groups, relationship 78—83
- N(1420), $SU(6)_w$ fits in baryon photo- and electroproduction 77—46057
- BH_3, electronic wave function determ., genealogical technique using Clebsch-Gordan coeff. 80—95529
- H atom, eigenfunctions in spherical and parabolic coords., relationship coeffs. 77—82409
- MnF_2 antiferromag., mag. space groups, Clebsch-Gordan coeff. calcs. 80—79731
- SU_{m+n} containing $SU_m \otimes SU_n$, irreducible bases *(Chinese)* 78—66049
- β-W structure Clebsch-Gordan coeffs. 79—37645

climatology

- *see also atmospheric humidity; atmospheric precipitation; sunlight; wind*
- 500 mb geopotential height in N.Hemisphere, climatological spectral study 77—5311
- 8000 yr. palaeoclimatic record of 'Double-Hale' 45 yr. solar cycle 77—78401
- Aberdeenshire, mesoclimate of Upper Don Basin 80—61889
- aerosol climatology in Europe, Project OPAQUE 79—66784
- aerosol layer in mesosphere, contrib. to polar albedo, rel. to climate 77—60467
- aerosols affecting temperature, zonal average climate model 80—77102
- aerosols and climate, study in Complex Atmospheric Energetics Experiment (CAENEX) 78—3904
- aerosols from Mount Agung eruption as test of global climatic perturbation 78—69440
- E.Africa, climate record in ice core from Lewis Glacier, Mt. Kenya 78—11931
- E.Africa, isotopic evidence for dramatic Pleistocene climatic changes 77—56723
- S.Africa, Late Cenozoic palaeoclimates, Gaap Escarpment, Kalahari margin 79—88471
- W.Africa, mean tropospheric conditions for 11-year period, climatological features 77—2221
- Afro-Asian monsoon, numerical index for monitoring during northern summers 77—78400
- air pollution climatic effects, review 78—28291
- Alaska, climate reconstruction from modern climate-tree ring relations 80—101425
- albedo changes of land surface affecting climate 80—98434
- albedo modification due to intensive solar energy production 78—85680
- N.America, climate vars. since 1602, reconstruction from tree rings 80—51528
- N America, late Pleistocene palaeoclimates inferred from speleothems stable isotope studies 78—57297
- N.America, palaeoclimatology (9500 to 22000 BP) from meteoric waters D/H ratios 77—60462
- N.America, Plio-Pleistocene continental glaciation rel. to Pleistocene stages terminology 79—62470
- N.America, Quaternary temps. and precip. for NW. coast region 80—98438
- S.America, southernmost part, glacial history 77—2188
- NW.America albedo increase following Pleistocene explosive eruptions, climatic effects 80—61789
- S.America and Antarctica, synoptic climatology and mountains 80—12532
- N. American glacial history extended to 75000 years ago 78—77284
- N.American high arctic climate change and glacier mass balance 78—36214
- American Southwest, evidence for cold, dry full-glacial climate 78—57296
- analogue prediction of short-term climate vars. using climate state vector 79—58019
- ancient Mesopotamia, barley harvest dates rel. to temp. 79—5597
- annual rainfall records, comparison methods for climatology 80—51587
- annual zonally averaged climatic model with diffuse cloudiness feedback 77—29416

climatology continued

- annual zonally averaged global climatic model with diffuse cloudiness feedback 77—87056
- Antarctic dry areas geochemical problems 79—79844
- Antarctic glaciation, Cenozoic evolution rel. to circum-Antarctic Ocean and global palaeoceanography 78—16063
- Antarctic Peninsula area, climatic vars. rel. to W. Antarctic ice sheet fluctuations 80—94549
- Antarctic Polar Front Zone, climatic characts. 79—2358
- Antarctic snow surface dust contamination, climatonomical modelling of temp. response 78—24354
- Antarctica, 30000 yr isotope climatic record from ice core 79—92586
- Antarctica, climatic record down to last ice age from ice cryst. size 80—94544
- Antarctica, Franco-American collaboration, automated weather monitoring stations *(French)* 79—66786
- anthropogenic climate change evidence from daily temps., Modena, Italy 80—41542
- anthropogenic effects, review 78—28293
- anthropogenic effects on UV radiation and climate 78—28289
- anthropogenic influences on climate, review 79—48565
- architectural design rel. to microclimate and energy conservation 78—3916
- Arctic, warm season affected by rainfall and temp. anomalies 80—98433
- Arctic Canada, ice-sheet initiation and climatic influences of expanded snow cover 79—66724
- Arctic ice cover evolution rel. to climatic changes 79—29781
- arid polar environments, characts. of tills deposited 77—91160
- artificial satellite, SEOCS, design 79—29965
- Asia, thermobaric field rel. to forecasting of data of breakup of Amur basin rivers *(Russian)* 77—53088
- Asiatic monsoon area, drought 77—53170
- Asiatic monsoon area, summer monsoon failures 77—53173
- astroclimate, influence on precision of photographic star positions obtained with wide-angle astrographs *(Russian)* 80—72748
- astronomical theory, teaching approach 79—84891
- astronomical theory of climatic change, supporting evidence 77—87058
- astronomical theory of climatic fluctuations geographical support 80—72509
- astronomical theory of climatic oscills. *(Russian)* 79—34937
- N.Atlantic, precipitation maps 80—51523
- NE.Atlantic circulation, climate and oceanic var., Little Ice Age 80—8422
- N.Atlantic climatic change rel. to volcanic dust veil index 77—78402
- N.Atlantic easterly gales, 1881-1970 period 80—77101
- N.Atlantic region, temp. trend 1970-77 period, warming *(German)* 79—16640
- atmosphere parameters relevant to helicopter icing problems, need for improved climatology 78—85657
- atmosphere particulate pollution, climatological effects 78—85678
- atmosphere precipitation, D-^{18}O relationship global climatic interpretation 80—17331
- atmosphere-ocean coupled model, ocean role in global climate 79—53507
- atmospheric dust rel. to planetary radiation balance, climatological consequences 78—36242
- atmospheric ionisation *(German)* 77—73905
- atmospheric research, introduction and current areas of interest 79—2351
- Australasia, Late Quaternary ice age climates 79—84470
- Australia, classification based on human thermal stress 80—31115
- Australia, variations in annual-mean max. temp., 1946-75 period 80—51526
- Australia and New Guinea, Late Quaternary climates 77—17209
- Austria, global radiation climate, 13 years records *(German)* 77—64412
- Baghdogra, India, thunder occurrence over airport 78—20499
- Bahrain, discomfort index based on wet-bulb temps. 79—20964
- Baikal-Amur region, climatic regionalization of estimated winter temps. 79—39842
- Baltic Ice Lake levels, dating rel. to S.Finland Salpausselka moraines 79—20872
- Baltic Sea region, aerological climatology rel. to atmospheric heat and moisture balance 77—87057
- Bangladesh, regional variations in seasonality of precipitation 77—53176
- Barents Ice Sheet as a relay regulator of glacial-interglacial alternation 79—2309
- baroclinic instability, critical temp. gradient, eddies, climate model 79—5562
- bioclimatic coefficients, change with respect to climatic zones *(Russian)* 77—53169
- bioclimatology, effective temperature and human comfort during hot spell of 1976 in British Isles 77—53166
- bioclimatology, wind chill in upland Britain 80—41546
- biosphere-albedo feedback and climate modeling 79—53508
- Birmingham, England, heat island synoptic climatology (1965-74) 80—85740
- Black Sea, Upper Quaternary deep-sea sediments stratigraphy 79—20811
- Bolivia, evidence for glaciation 3.27 Myr BP 79—34865
- Bombay (1848-1967), annual mean values rel. to sunspot nos. 80—81811
- Bombay Airport, urbanisation and industrial development effects on air temp. 77—53167
- boundary layer climates, book 79—8682
- NE Brazil, large scale circulation rel. to extreme drought and floods 77—45134
- N.E.Brazil, rainfall correl. with sea surface temp. 77—29398
- Britain, palaeoclimatic and geomorphic implications of ^{230}Th/^{234}U dates on speleothems 78—36128
- Britain, water balance, 50000 yr BP to present day 80—72566
- British Columbia, S central, late Pleistocene stratigraphy and climates 78—92804
- British Isles, abnormal weather pattern 79—80006
- British Isles, meteorological parameters affecting climate 78—7745
- British Isles, October weather recent trends 77—17210
- British Isles, tree-ring chronologies, proxy records of climate 78—44979
- British Isles, wet spell of September to October (1976) 77—45124
- British spring weather, survey (1950 to 1979) 80—98427
- British winters (1659 to 1979), study of temp. correl. with precipitation 80—98444
- Brunhes epoch δ^{18}O time scales and climate change 80—21817
- Brussels, urban climate modifications, first obs. *(French)* 79—2356
- Budyko model, stability 77—45130
- Budyko-Sellers climate models, variational formulation from temp. field 80—8420

climatology continued
Budyko-Sellers models, steady state solns. 79—16638
Budyko-Sellers zonal climate model, parameterisation 80—56597
Budyko-type models, nonlinear albedo-temp. coupling effects 77—45129
Burma during southwest monsoon, drought 77—53174
coastal California, late Quaternary climate and evidence for Ice Age refugium 78—57293
caloric insolation long-term vars. resulting from Earth orbital elements 78—73502
NW.Canada, freshwater shelled invertebrates as palaeoclimate indicators in late glacial times 78—20500
Canada, prairie cities increased sunshine due to natural gas use as fuel 77—17211
Canadian haze climatology 78—57304
causes of climatic change 78—73499
celestial chaos related to Earth's climatic and biological catastrophes 79—53509
early Cenozoic Atlantic Ocean, calcareous plankton palaeobiography and climatic fluctuations 78—16143
Cenozoic explosive volcanism recorded in deep sea cores, tectonic effects, climatic implications 77—49052
Cenozoic oceanic sedimentation rates rel. to climate and continental weathering 77—91107
change by cloudiness linked to circumarctic ocean temp. 77—29415
change in climate rel. to Earth orbital eccentricity fluctuations, mechanism, discussion 79—88466
Chile, Quaternary climatic changes 78—44980
China, agricultural growing season vars. in historical time *(Chinese)* 80—109246
China, effect of planetary motion on climatic changes 80—85741
N China, human climates 79—84468
NE.China, persistently low summer temp., causative circulation pattern *(Chinese)* 80—109235
Chinese chronicles, 2187 BC-AD 3 meteorological record 80—46213
cirque glaciations, Holocene and latest Pleistocene, in Shuswap Highland, British Columbia, ages 78—92856
climate, soil and vegetation, annual evapotranspiration value 79—79895
climate, soil and vegetation, annual precip. distrib. from storm sequences 79—84314
climate, soil and vegetation, annual water balance dynamics 79—79896
climate, soil and vegetation, annual water yield distrib. 79—84316
climate, soil and vegetation, soil moisture movement in liquid phase, model 79—79894
climate, soil and vegetation, storm surface runoff distrib. 79—84315
climate, soil and vegetation, water balance dynamics 79—79893
climate and weather, definitions 80—41540
climate change, study of upper air data 80—105045
climatic change, atm. feedback mechanisms with zonal climatology 77—33175
climatic change, computer modelling 79—92587
climatic change, influence of solar companion star 78—12198
climatic change, long-term, prod. by fossil fuel usage, proposed space obs. 79—29844
climatic change detect. and impact on hydrologic design 79—53396
climatic change effects on food production, statistical models limitations 78—57303
climatic change on terrestrial planets, review 79—53742
climatic evolution, review *(German)* 78—20503
climatic optimum, rel. to insular phosphorite form. on Ebon atoll, Micronesia 78—81121
climatic sensitivity, two-level atmospheric model 79—80004
climatic variations as random walk problem, appl. of two-timing methods 77—73879
cloud cover influence on atmos. top radiation budget 80—98398
cloud cover over surface types, climatological analysis 79—16596
cloudiness as climatic feedback mechanism, effects of cloud amounts on surface temp. changes 79—88467
clouds rel. to long-term stability of atm. and climate 79—74951
clounds, stratiform, modelling and effect on radiation balance *(French)* 80—82017
Clyde Foreland, Baffin Is., last interglacial-glacial cycle, stratigraphy, biostratigraphy and chronology 78—61536
composition perturbations and temp. feedback, climatic effects 80—41525
computer modelling of global climate and changes 80—46250
conference, on climatology, hydrology, atmospheric research and meteorology from space, Ajaccio, Corsica (1979 November 12 to 16) 80—62397
confusion in terminology *(German)* 78—65380
contemporary changes due to solar const. aerosols and radiative transfer *(Russian)* 77—41140
contemporary climate changes, natural and anthropogenic factors 79—34938
continental and regional heat meas., effects of climatically perturbed temp. gradient 77—81845
continental geoid fluctuations, effect on groundwater and environment 78—36215
continental ice sheet, stochastically driven with planetary wave feedback, model 80—77025
continental ice sheet model, spectral response to insolation vars. 79—2300
continental ice sheet model, stability to insolation periodic vars. 78—28251
continental ice sheet var., model for N. Hemisphere 77—21814
contour maps classification problems 79—79999
cooling since 1940, implications of atmospheric transmission meas. (1923 to 1957) 80—17374
coral reef, C and O isotope composition rel. to environmental factors 80—46202
correlations of changes in geomag. field, climate and weather 79—39648
Corsica (France), Quarternary alluvial deposits rel. to paleoclimates 78—57234
coupled ocean-atmosphere expt., ocean response, rel. to climate 80—12430
Cretaceous-Tertiary environment, effect of nearby supernova explosion 78—32499
Cretaceous-Tertiary extinctions, stratospheric aeronomy effects on climate 78—32215
critical parameters, Spacelab monitoring 77—21884
Cumberland Peninsula, Baffin Island, hornblende grain etching, age and palaeoclimate indicator 80—8307
data archiving and quality control by computer 80—61907
De Bilt, Netherlands, 1634-1977 average winter temps. 79—74949

climatology continued
deglaciation preservation spike in pteropods and foraminifera rel. to deep-sea carbonate 77—86853
dendrochronology, Japanese cedar record of air temp. 77—21880
Denton County, Texas, temp. data Fourier transform anal., cyclic behaviour 77—33179
Denver air quality, effects of meteorological and climatological factors 79—84350
Devon Island ice cap, arctic Canada, ^{18}O/^{16}O climatic record from snow cores 77—41141
Devon Island ice cap, core stratigraphy and palaeoclimate 77—53096
Devon Island ice cap, NWT, Canada, δ^{18}O vars. rel. to climatic change 80—4050
diabatic heating climatology of zonal atm. 79—53432
diffusive climatological models, branching structure 78—44976
diffusive nonlinear heat transport in simple climate model 78—81349
drought, classification and study of droughts at Kew 77—41121
drought definitions 80—105010
drought effects on agriculture in United Kingdom, 1975-76 period 78—57298
drought in semi-arid regions, effects of albedo change 78—32128
drought in streamflow series, statistical characts. 80—105009
drought in upper Midwest, USA, 1931 to 1969 period 79—70880
droughts, continental, study *(French)* 77—37344
dryness line localisation on all continents *(German)* 77—17179
Earth's evolution and paleoclimatology—a computational model 79—58080
Earth's orbital eccentricity correl. with palaeoclimate and palaeomagnetism 77—78093
Earth albedo, anthropogenic changes and effects on climate 80—81893
Earth global heat balance, annual var. 78—73300
Earth insolation, influence of orbital elements periodic vars. *(Russian)* 78—53605
Earth orbit and climate change relationship *(Chinese)* 80—67406
Earth rotation effects, contribution of space technology *(French)* 79—74827
Earth surface temperature, climatological significance of doubling of atmospheric CO_2 conc. 80—101426
Earth surface temperatures, implications of stratospheric aerosol modification by supersonic transports and space shuttle 80—98408
Earth zonal and global albedoes, depend. on reflectivity regional vars. 80—17377
East Midlands, England, monthly rainfall totals 1726-1975 period 77—64411
El Nino, climatic research project at Scripps Institution of Oceanography 78—69464
elm tree rings as rainfall record 78—65381
energy balance climate model response to parameter changes *(Russian)* 79—100938
energy balance climate models tests 80—77098
energy balance model, climate sensitivity to radiation flux calcs. 80—8421
energy balance model, sensitivity and role of cloudiness *(Russian)* 78—88902
energy balance model sensitivity to orbital parameter var. 80—12537
energy balance models, difference between seasonal and mean annual model calcs. of climate sensitivity 80—56595
energy balance models, global and one dimens., stability comparison 80—94596
energy balance models, stability expts. with improved albedo and IR emission 79—2357
energy consumption effects on climate 79—29848
energy contribution to anthropogenic climatic fluctuations, 21st century problem 78—57299
energy policy, climatic effects 78—61538
energy use and climatic changes 79—29846
energy-balance climate models, stability theorem 80—56594
England, air temp. variability (1660-1977) 80—98437
England, annual rainfall totals for 1725-1973 period 77—17207
England, decreasing wetness in 1969-77 period 78—65377
central England, monthly mean temps. for quintile distrib. 77—29418
England, spectral anal. of temp. data for 1659-1973 period 77—17208
England, summer weather pattern reliability w.r.t. future forecasting 79—84425
England's climate since 1830, increased October temp. 80—56599
England , summer index (1971-78) 80—85742
SE England dry years since 1698 77—29420
environmental conditions at 18000 yr BP, continental record initial evaluation 80—51529
environmental obs. from space based systems, present and future 79—5657
Eocene terminal event, formation of ring system around Earth 80—76890
erosion cycle and climatic change reversal 77—64338
NW.Europe, appl. of extended ^{14}C time scale by isotope enrichment 78—77314
Europe, climatic and human history rel. to Latin American comparison 79—2590
central Europe, Pleistocene climates and interglacials 78—40646
European agriculture rel. to climatic change 78—85679
European air temperature change patterns 78—92957
European Grosswetterlagen, temporal vars. and possible causes 79—58081
European potential climatological satellite missions 79—70886
evolution implications for Earth's early atmosphere 78—36285
evolution of atmosphere, climatic changes 79—34962
evolution of climate over last 250 million years, global heat balance 80—46252
experiments with general circulation models, statistical considerations 78—16141
extratropical storm tops, climatology rel. to stratospheric water vapour budget 77—87029
extreme wind speed probability, mixed wind climates 78—28295
falling snow, occurrence over United Kingdom 77—41124
feedback mechanisms in climate models, new modeling approach 80—98435
feedback systems, involving sea-ice, ocean temp. and CO_2 80—98443
Florida, USA, increased aridity since 1960 rel. to atmos. cooling 80—90214
fluctuations, relation of moistening to thermal regime 78—92937
fluctuations in 1870-1969 period, statistical study of likely causes 78—7751

climatology continued

- forecasting, climate prediction, problems 79—92570
- forecasting, review of major causative factors, economic and ecological effects *(French)* 79—48564
- fossil fuel use consequences, atmospheric CO_2 concentration increase 80—12041
- future energy strategies effects on atm. CO_2 conc., rel. to global climate 79—83640
- Gangetic West Bengal (India) drought incidence 77—53172
- general circulation model, climatic characts. response to solar radiation vars. 78—36260
- general circulation model, Earth rot. increased or decreased 5 times 80—56545
- Genoa, 1833 to 1900 meteorological obs. *(Italian)* 79—34936
- geomagnetic field reversals and climatic change, statistical correl. 78—61537
- geomagnetic intensity rel. to climate, historical records 79—39638
- geophysical timescales from absolute-dated ice cores from Greenland *(Danish)* 79—34776
- Germany, 1851-1975 precipitation changes *(German)* 77—33164
- glacial oscillations global mass and energy requirements, rel. to mean ocean temp. oscills. 77—78404
- glacial periods, implications of solar neutrino expts. 79—16918
- glacial sediments of English Lake District, pre-Devensian till 80—94523
- glaciation, causes 79—20961
- glaciation, influence of Earth albedo contrast to continental drift 79—74950
- glaciers-ocean-atmosphere global system, numerical modelling 79—84469
- global air pollution and climatic change, review 77—13120
- global air-sea interactions rel. to climate formation 78—16142
- global climate, mathematical model appl. to CO_2-climate sensitivity study 80—31117
- global climate, rel. of stratospheric sulphate aerosol layer 80—109212
- global climate, steady-state format 79—44244
- global climatic stability rel. to W. Antarctic ice streams 77—64321
- global January and July climate, numerical simulation with two-layer circulation model 77—56722
- global mass and energy requirements for glacial oscills. rel. to mean ocean temp. oscills. 78—81351
- global solar radiation in California, interpolation technique based on orthogonal functions 80—67402
- global warming due to CO_2 increase, temp. and precipitation changes 80—36389
- Gondwana Late Palaeozoic glaciation, nature from anal. of garnets and other heavy minerals 79—100874
- Gondwanan glaciation, cyclothems, continental positioning, and climate change 79—62526
- Gothenburg geomagnetic excursion, global climatic change 77—29251
- grassland surface temperature rel. to air temperature in summertime 77—78396
- greenhouse effect due to atm. N_2O, climatic implications 77—9460
- greenhouse effect rel. to trace gas transport and photochemistry *(Russian)* 80—81989
- greenhouse effects of some atmospheric constitutents 79—70882
- greenhouse effects rel. to trace gas perturbations 77—53179
- W.Greenland, glacier response to climate change 80—61820
- Greenland ice core records, 20 year climatic cycle 79—88470
- Greenland Ice Sheet impurities, past volcanism record 78—11855
- Greenland Sea area, climatic normals 80—77100
- growing season length as climatic indicator, fluctuations 80—61887
- NE. Gulf of Alaska, development of synoptic climatology 80—98405
- Hampshire, England, Butser Hill weather station, 1972-76, climatic data 79—58128
- heat from anthropogenic sources, affecting climate and general circulation 80—89694
- heat stress on man, parameter recording and processing, math. method *(German)* 80—82047
- N.hemisphere, aspects of climate (1950-1975) 77—70803
- N.Hemisphere, large scale climatic cooling 78—16145
- N.Hemisphere surface temp. anomalies, correl. with sunspot struct. vars. 80—31272
- hemispheric mean surface temp., nonequilib. model, pollution effects 77—49150
- high-latitude N Atlantic, Late Quaternary climatic change rel. to surface ocean kinematics 78—16026
- high-mountain regions, astronomical-climatic conditions evaluation for IR astron. obs. 79—62566
- Himalaya, summer weather and climate 80—72620
- historic climate correl. with wheat prices and wages 78—81346
- historical atm. comp. and climate from gas parameters meas. on Greenland ice cores 79—8681
- historical climatology 79—16641
- Holocene climatic change effects on tropical geomorphic processes 77—64418
- Holocene climatic fluctuations, evidence from rock glaciers in Jasper National Park, Alberta 78—77276
- Holocene glacial and tree-line vars. in White River valley and Skolai Pass, Alaska 77—78251
- Holocene palaeo-winds, evidence from palynology in Baffin Island 78—57262
- Hudson Bay rivers, climatological data from historical sources, content anal. 77—2224
- Hudson Valley, New York, tree ring-drought relationships 78—28299
- Hudson Valley, USA, periodicity of July Palmer Drought Severity index, tree rings 80—26606
- hurricane season activity analysis, N.Atlantic (1886-1974) 80—101427
- hydrologic cycle, climatic sensitivity, numerical model 79—8654
- ice age, CO_2 content of atmos. by polar ice core 80—61891
- Ice Age, maximum ice extent on island groups in Scotia Sea, Antarctica 78—20450
- ice age, relation to Sun interstellar dust accretion and neutrino prod. 79—12441
- ice age beginning, instantaneous glacierisation, albedo rate change and feedback effects 80—105006
- ice age climate and sea level at ~95000 BP 80—51444
- ice age climate numerical simulation with global general circulation model 77—33176
- ice age in northeast county Wicklow, climatic environment rel. to ice wedges form. 78—69379
- ice age origin in Antarctic ice-surge, O isotope and sea level study 80—51525

climatology continued

- ice ages, prod. by Earth albedo sudden change 79—44241
- ice ages, prod. by Earth encounter with interstellar cloud 78—57292
- ice ages, rel. to periods of heavy elements accretion by Sun *(Polish)* 79—58310
- ice ages and biological catastrophes rel. to solar system encounter with nearby supernova 77—29662
- ice ages and continental drift, theory 79—44209
- ice ages and Earth thermal equilib., comments and reply 77—21815
- ice ages and ecological catastrophes, prod. by Earth-comet close approach 78—53714
- ice ages and orbital vars., theory and numerical modelling 80—56598
- ice ages and thermal equilib. of Earth, comments 77—5313
- ice ages rel. to Earth's obliquity and eccentricity in orbit 78—53715
- ice ages rel. to solar radiation var. 78—12183
- ice albedo feedback on global sensitivity 80—109245
- ice cap-albedo feedback, effects on global climate, 2-D energy balance model 80—67407
- ice core records, from tropical Quelccaya Ice Cap 80—8345
- ice-albedo feedback effects on energy-balance climate models 78—7749
- SW Iceland, glacial chronology from palaeomagnetism of Esja, Eyrarfjall and Akrafjall mountains 80—89950
- Illinoian glaciation sea-level lowering, Bahama 'blue hole' 80—72557
- Illinois climate centre, review 80—77118
- impact of large solar energy systems 78—81358
- impact of nearby supernova 78—28297
- India, climatic water balance 77—64408
- India, periodicity of drought occurrence 78—32200
- N India, rainfall deficiency due to absence of tropical disturbances 77—53178
- India, summer monsoon, water vapour transport and vergence patterns 78—7727
- India, SW monsoon, normal period of large-scale break 77—53175
- Indian Ocean, ecologic and palaeoclimatic implications of vars. of O. universa 77—9445
- Indian Ocean, palaeotemps. during Brunhes epoch from sediment core study 80—12429
- Indian Ocean middle latitudes, Subtropical Convergence fluctuations and Quaternary climates 77—13087
- Indian summer monsoon, interaction with ocean 77—56650
- Indiana, divisional and state mean temperatures, correction for non-climatic trends 80—51524
- induced var. through stratosphere, magnetic field screening of cosmic rays 77—78398
- inland ice sheet thinning due to Holocene warmth 79—34873
- insolation rel. to climate, normal incidence solar intensity rel. to weather at Fort Hood, Texas 78—57240
- insolation rel. to climatological variables, solar energy availability estimation 78—81344
- insolation stability characterisation by stochastic time series 79—57396
- instantaneous rainfall rates, climatology 79—39841
- Institute of Meteorology and Climatology, Slovak Acad. Sci. (1964-74) *(Russian)* 78—88920
- interannual cloud-cover vars. in contiguous United States 78—92909
- interglacial chronology, Rocky and Mackenzie Mountains, ^{230}Th-^{234}U dating of calcite speleothems 78—36120
- interglacial episode termination and Wilson Antarctic surge hypothesis 78—53669
- interstadial sea level of −40 m at 30000 yr BP, ^{230}Th/^{234}U age support 79—16504
- IR cloud opacities averaging for climate modelling 79—8692
- IR cooling rates, effect of tropospheric aerosols 78—88886
- Iraq, duststorms, climatological and meterological study 77—73794
- Iraq, thunderstorms, climatological and meteorological study 77—73796
- Israeli coastal plain, weather year standardisation for solar heating simulations 79—84444
- Italy, vorticity generation and energy budget, 1961-65 period 78—81350
- Japan, late glacial age chronolgy from morainic features and Lake Biwa sedimentary sequence 79—34872
- Japan, Pinus pumila growth and climate fluctuation 77—33177
- Kalahari, evidence for widespread late Pleistocene humid period 79—58083
- karst landscapes, origin of labyrinth and tower styles, necessary climatic conditions 78—96208
- Labrador Shelf, early deglaciation 79—79891
- Lake Bosumtwi, Ghana, Holocene lake level variations, palaeoclimatological evidence 77—78249
- Lake Leman area, precipitation trends, evidence for 50 year cycle *(French)* 77—21824
- lake level fluctuations since 30000 yr BP, global maps 80—51447
- Lake Naivasha, Kenya, level changes rel. to equatorial westerlies over E.Africa 80—61819
- lake sediment sequences, pre-Pinedale, Yellowstone National Park, geology, palynology, climatology 79—66727
- large scale solar energy conversion effects, conf., Laxenburg, Austria, Dec. 1976 78—81352
- last (Eemian) interglacial, abrupt end in NE.France 80—21818
- last glaciation, rapid ice-sheet growth and glacial period initiation 80—51530
- Late Cenozoic climatic variations, rel. to Gulf Stream vel. fluctuations 80—12432
- Late Miocene Antarctic glaciation, correl. with phosphatic nodule beds in Victoria 79—12105
- late Pleistocene and Holocene climates, glacial retreat energy and dynamics and surface radiation 77—64416
- Late Pliocene global climatic cooling rel. to SW Atlantic abyssal circulation increase 78—40645
- Late Quaternary climatic changes, W.Africa, from deep sea sedimentation 78—73355
- Late Quaternary climatic variations in NW.Africa from E.Atlantic Sediment Cores 77—2223
- Late Quaternary deposits lithobiostratigraphic characteristics, Baltic Sea *(Russian)* 79—88332
- Late Quaternary glaciation of eastern Queen Elizabeth Islands, N.W.T., Canada 77—2189
- Late Quaternary lake levels in S.Afar and Ethiopian Rift 77—64337
- Latin America, climatic and human history rel. to European comparison 79—2590
- Laurentide Ice Sheet growth rate and sea level lowering 77—5214
- Liege, Belgium, sixteenth century weather record *(French)* 80—82029

climatology continued
Lisbon solar radiation climate, direct, diffuse and global intensities 80—36383
Lithuania and Kaliningrad region, river runoff dependence on climatic factors *(Russian)* 78—16067
Little Ice Age, N.Hemisphere average temp. obs. rel. to model calcs. 80—82050
Little Ice Age, palaeotemps. from high altitude tree growth in S. Norway 77—5312
local climatic anomalies, causes, rel. to precip. in Washington State 77—78399
local energy exchange dynamics and climatic boundary conditions, solar energy conversion effects, preliminary examination 78—81355
Loch Lomond Stadial in British Isles 79—79887
long-term climatic change, appls. to hydrometeorology 78—96240
long-term climatic change numerical modelling 78—77315
Madhya Pradesh (India), rainfall trends and periodicities 77—53177
Madrid, temp. in 1871-1975 period, Fourier series *(Spanish)* 77—9486
Mamontova Gora, Siberian nonglacial stratigraphy and radiocarbon dates rel. to glaciations 78—44819
man's impact on climate *(French)* 79—84360
man's influence on climate, conference, Manlo Park, California (1979 February 21 to 22) 80—62381
marine climate, appl. of model of ocean temp. annual var. 78—20433
measurement, use of automatic weather stations in United Kingdom observational network 79—80047
mechanisms and models of climatic change 79—12229
medieval European climate reconstruction using weather compilations, reliability 79—74929
W.Mediterranean, Middle Pliocene climate change 80—26605
Mediterranean Sea, heat and water budgets, dependence on climate and Atlantic waters 79—84291
Mediterranean Sea, hydrological regime during glacial periods *(French)* 80—4040
Mesozoic climate and global air-sea interactions 78—16142
Mesozoic greenhouse and climatic warming 79—20963
methane greenhouse effect in climate model 80—90211
Middle East, palaeoclimates evaluation from monthly temps./rainfall relation 80—31091
Middle Europe temp. averages in last 200 years *(German)* 77—2222
Milankovich model, review 77—9485
Milankovitch model of orbital changes affecting climate 78—44975
Milankovitch theory and ice ages, interactive climate feedback 80—46251
Milankovitch theory of ice ages, evidence from palaeomag. chronology of S.Australian beach ridges 80—98307
Milankovitch theory of ice ages, study using simple climate-ice sheet model 78—40644
Late Miocene, cooling event rel. to C isotope stratigraphy in New Zealand marine sediments 80—26479
Miocene glacial-eustatic changes in world ocean, rel. to Messinian salinity crisis 77—91151
model experiments, simulated changes in albedo, surface roughness, surface hydrology, solar energy conversion effects 78—81354
model of climate change, internal and external causes 79—16637
model with ice-sheet dynamics, stable periodic solns. 80—90210
modelling and prediction of climatic var. 77—21882
modelling using radiative-convective models 79—74954
models, effect of multiple reflections between clouds and surface 77—45131
models, forced noise level 78—44978
models, sensitivity to external forcing 80—82049
models, stability and extremal props. *(Russian)* 78—53716
Mohliner Feld (east of Basle), topoclimate investigations *(German)* 80—61890
monsoon circulations numerical simulation 80—21812
morphological method in research, appls. 79—71216
Nahal Yael, Israel, arid watershed, hillslope study 80—8342
natural disaster fallacies, Sahel drought example 78—57302
Negev rainfall diurnal variation, climatological and meteorological implications 80—17344
Netherlands, winter temps. rel. to solar cycle 79—5596
New England, 1816, snow and frost in year without summer rel. to Tambora volcano eruption 80—4089
S New Mexico, Holocene soils props. in semiarid region rel. to precip. 77—78184
New Orleans, synoptic climatology for environmental baseline analysis 77—64410
New York State, local climate trends in four cities 80—105044
New Zealand, last millennium, ^{13}C/^{12}C dating in kauri cellulose 80—21819
New Zealand, late-glacial chronology rel. to radiocarbon dating of Quaternary loess deposits 78—24271
New Zealand, temp. record, historical data and agricultural implications 80—61886
New Zealand, temps. and short-term climate change during last millennium 79—62574
Nile, climate variation affecting discharge 80—81946
Nile Cone, Lake Quaternary stratigraphy and sediment dispersal, climatic response 77—45040
nondeterministic theories of climatic change, comments 78—73503
nondeterministic theories of climatic change 77—64415
nonlinear quasi-geostrophic eqn., props. of thermally-forced and unforced flows 77—2191
W North America and N.Pacific regions, past climatic anomalies from tree ring data 77—64419
North Sea and Baltic pollution, natural and man-made influences *(German)* 79—5508
Northern Hemisphere, air temp. var. in 1881-1975 period 78—7737
northern hemisphere, temp. trend to year 2000, prediction 79—16646
northern hemisphere annual temperature approximation, simple method 78—81345
northern hemisphere climate vars. rel. to N.Atlantic tropical cyclones characts. 79—39843
Northern Hemisphere temp. changes rel. to dust from major volcanic eruptions 78—36258
Northern Hemisphere temperature, 1579-1880, reconstruction 80—12535
Norway Station/Sanae (Antarctica), surface temp. and sea-level press. 78—81324
numerical prediction, weather and climate, recent advances 78—96276
numerical simulation of climate and climatic change 79—16643

climatology continued
Observatorio Astronomico Nacional, Baja California, climatological and meteorological characts. 78—20635
ocean data and information services, appl. to climatic problems 78—69463
ocean surface mixed layer, climatological numerical models 77—2159
ocean-atmosphere climate model, large-scale long-term interactions 78—7750
ocean-atmosphere heat balance over northern hemisphere, annual cycle 77—41040
oceanic rainfall maps, global climatic features 78—65379
Ona, Norway, synoptic and climatological characteristics of fog 77—17176
Ontario, effect of Pleistocene climatic vars. on geothermal regime 79—57883
orbital changes of Earth in climate variation models 80—98441
Otway region, S.E.Australia 78—20501
S.Pacific, hydroclimatic anomalies 78—65335
N.Pacific, precipitation maps 80—51523
Pacific Pleistocenes palaeoclimatic stratigraphies, comparative anal. of results 78—57295
palaeoclimate during last 600000 years, pollen anal. of 200 m core sample from Lake Biwa, Japan 78—24356
palaeoclimate marine-continental correlation, 150000 yr O isotope-pollen record from N.Pacific 79—80008
palaeoclimate of S.Hemisphere since 80 Myr BP, causes for change *(Russian)* 80—98440
palaeoclimatic change, 230000 to 100000 BP, results from speleothems stable isotope geochemistry 79—2234
palaeoclimatic features, based on stable isotope compositions, Lake Biwa, central Japan 79—12230
palaeoclimatic inferences from former glaciers in Scotland and the Lake District 79—44243
palaeoclimatic research, status and opportunities 80—51527
palaeoclimatology, abrupt events time scales and causes 80—51531
palaeoclimatology, in world climate conference, Geneva (1979 February 11 to 23) 80—46727
palaeoclimatology, larval bivalve shell morphometry as temp. indicator 79—53510
palaeoclimatology, overview, and European air temp. trends *(German)* 79—16639
palaeoclimatology, record of E.Mediterranean Sea deep sea sediment core 78—57294
palaeoclimatology, role of tree-ring anal. in Indian region from preliminary survey 80—90212
palaeoclimatology and vegetation changes during 2000 years BP, from anal. of varved lake sediments 79—25279
palaeoclimatology and vegetation ecology *(French)* 78—88901
palaeoclimatology from tree rings, ^{12}C/^{13}C in cellulose and lignin as palaeothermometers 77—17253
palaeoclimatology of Okanagan Valley, British Columbia, from Holocene peat core palynology 77—5146
palaeotemperature series from last 700000 years, statistical study 79—5598
palaeotemperatures, effect of palaeoatmospheric O_3 concs. 79—96807
palaeotemperatures, from SiO_2 O isotopes in diatoms, 20000 yr record in deep-sea sediments 78—32247
palaeovariations rel. to almost intransitive Sun 79—21255
perturbed atmosphere thermal struct. and relaxation rates, photochemical radiative convective model 80—8408
Phanerozoic history and climatic instabilities 77—66981
physics of atmospheres, book 79—62568
pleistocene, southern trade winds and oceanic upwelling during last 75000 years 78—57217
Pleistocene deglaciation, influence on true polar wandering 79—44079
Pleistocene glacial vars. 79—66787
Late Pleistocene glaciology effects, study of Taylor Valley, Antarctica 80—8343
Pleistocene ice fluctuations rel. to Earth orbit vars. 77—37346
pleistocene volcanism and glacial initiation 77—91088
Pleistocene-Holocene transition, W.Pacific, from stable isotopes anal. in deep sea carbonates 78—73354
Pliocene and Pleistocene glaciations rel. to Barents Ice Sheet, evidence from Barents Sea 78—57227
Pliocene ocean climate in N. Atlantic, planktonic foraminifera record 77—17206
Pliocene/Pleistocene boundary age estimate and palaeoclimatology 77—91133
polar regions, climate rel. to ice sheets basal temps. 77—78250
potential evapotranspiration, continental maps based on Penman concept calcs. *(German)* 80—98368
power spectra computation technique 77—91305
Prairies, temp. trends and cycles 77—56724
Late Precambrian climate, effect of Earth rot. rate vars. 80—4097
Late Precambrian glaciation in Adelaide Geosyncline, palaeomag. evidence for low-latit. glaciation 80—101325
precipitation flux climatology of free atmosphere 77—78397
predictability of climate 79—16645
prediction 80—41539
prediction possibilities using sea surface temp. meas. 80—8377
present-day climatic change due to man's economic activity, future forecasting 77—78403
quartz distribution in Atlantic sediments, relation to climate, last glaciation 80—8308
quasi-cycles in meteorology, anal. of evidence 80—109239
Quaternary aridity in W. Australia 77—13113
Quaternary climatic change, physical evidence 77—64417
Quaternary climatic changes, insolation signature 79—74953
Quaternary climatic changes rel. to long-term insolation var. 79—88469
Quaternary glaciations and stratigraphical positions in China *(Chinese)* 79—79885
Quaternary period, climatic vars. rel. to sedimentation on N.Brazil continental margin 77—21748
NE Queensland, last interglacial-glacial cycle, dry land precipitation sequence 78—40598
radiation budget meas by satellite, climate appls. 80—109283
radiative forcing of atmosphere, sensitivity to variable cloud and moisture 80—56553
rainfall frequencies correl. with lunar phases 77—13112
rainfall short-period fluctuations for New Zealand 77—25746
rainfall variation in historical and contemporary epochs 80—36390

climatology continued
Rajasthan (India) drought and scarcity survey 77—53171
Rannoch Moor, radiocarbon dates and Loch Lomond Readvance deglaciation 77—13115
rapid glaciation in N.Hemisphere climatological conditions from oceanic evidence 80—90213
regional anomalies assoc. with hemisphere averaged temp. variation 80—77099
regional climatic effects of large-scale thermal pollution, simulation with NCAR general circulation model 79—53478
regional effects of power-plant heat rejection 77—25768
regional precipitation climatology, estimation of Fourier coeffs. for stochastic daily precip. models 79—53481
review of contemporary climate variation studies, performed outside of USSR 80—41545
river sands, climatic influence on petrology and chemistry 79—25274
Rumania, climatic conditions and electronic equipment operation *(Rumanian)* 79—44242
central Sahara, palaeoclimates during early Holocene 77—91252
central Sahel, Neolithic hyperarid period 78—73500
Sahel, West Africa drought conditions *(French)* 77—37345
Sahel region, general and regional circulation effects on climate *(French)* 79—20962
Salpausselka moraines, S.Finland, dating rel. to Baltic Ice Lake levels 79—20872
sand deserts, extent during glacial maximum and climatic optimum 78—36259
S.E.Scotland, potential moisture deficit, 200-year series 78—7746
Scotland, snowstorms from (1729 to 1830) 77—25757
Scotland, summers index (1881-1978) 80—85742
sea ice seasonal change model 77—17128
sea ice-ocean temp. oscillator model, nonlinear analysis 80—12413
sea-surface temperatures, satellite-determined, in tropical Pacific, climatological usefulness 80—31044
seasonal climate model on global scale 80—41544
seasonal snow accumulation, melt and water input, New England model 77—2187
seasonal temperature variations, subsurface energy storage influence 77—49122
seasonal zonal energy balance climate model with an interactive lower layer 79—80005
sediment climate record, diatomaceous sediments of Gulf of California 80—98351
seismic activity triggered by rapid climate change 80—81858
semi-arid region radio climate and tropospheric model 77—21844
short-period climatic fluctuations, effects on diatom biomass 77—49087
Siberian river diversion effects 80—41541
Sierra Leone, climatic regime rel. to surface and soil temps. seasonal vars. 80—109242
Silurian continental distributions, palaeogeography climatology and biogeography 77—66888
simple models, realistic modifications and climate stability 78—28294
simulation of geophysical fluid system rel. to climatic var. 78—81353
Sognefjord, Norway, local climates and growth climates, precipitation 77—21846
soil moisture, effect on circulation and rainfall in a tropical model 77—45133
solar activity, long-period vars. correl. with terrestrial climate *(French)* 78—73695
solar activity effects on weather and climate 79—16644
solar activity rel. to climate 78—28301
solar constant, Smithsonian Astrophysical Observatory program, (1902 to 1962) 80—36606
solar constant rel. to climate, conference, Big Bear City, Calif. (1975, May 19 to 21) 77—2380
solar cooling with increased sunspot activity rel. to climate 78—40896
solar energy availability concept, Canada 77—25762
solar energy conversion, possible effects 78—81356
solar energy conversion systems, chromatic impact. 80—30612
solar energy utilisation, climatic consequences *(French)* 77—73822
solar equatorial rotation, rel. to climatic changes 78—7960
solar far UV flux variations, rel. to climate *(French)* 78—40884
solar flare particles, possible cause of ancient climatic and biological catastrophes 77—78587
solar flux var. rel. to climate 77—21872
solar insolation prediction at Fort Hood, Texas, rel. to climatological variables 78—24333
solar intensity model year construction rel. to climate 78—57241
solar radiation, stochastic variation, effect on climate 79—21262
solar radiation intensity formula using climatological data 80—31108
solar radiation statistical estimate, in equatorial region (Singapore), power utilisation appl. 79—87972
solar thermal energy production, large scale, possible climatic effects 78—81357
solar UV vars. rel. to climatic changes 80—26607
solar variability and climate change, 1000-1980 AD, ^{14}C tree ring study 80—101424
South Africa, above and below normal rainfall periods estimation, 1972-2000 period 77—66980
South Pole, ^{210}Pb conc. or climatic changes 78—7748
Southern Hemisphere in 1928, explosive volcanic eruption effects 79—2204
space and time scales of climatic variability 77—64413
space observations of long-term climatic change, conf., Prague, Czechoslovakia (Sep. 1977) 79—29843
spectral analysis, rel. to astronomical theory of climatic change 77—13114
spectral soln. of stationary zonally symmetric global climate model 77—87055
stability of simple climate models, variational estimate *(Russian)* 78—69437
statistical methods *(French)* 78—32252
stochastic climate models, appl. to zonally averaged energy models 78—20502
stochastic model of climate var., theory 77—37347
stochastic models, appl. to sea surface temp. anomalies and thermocline variability 78—3918
storms and depressions over Arabian Sea, 1961-74 period 77—53168
storms secular variation in tropical N.Atlantic and E.Pacific Oceans 79—100929

climatology continued
stratosphere, dynamical climatology during late winter 1973 in southern hemisphere 77—25769
stratosphere, intense ionisation events, effects on NO_2, O_3 and climate, rel. to life extinction 78—96273
stratosphere, recent temp. trends 79—29845
stratosphere, seasonal climate, numerical simulation, energetics 79—5567
stratosphere, seasonal climate, numerical simulation, zonal temp. and wind 79—5566
stratosphere pollution, review of Climatic Impact Assessment Programme (CIAP) 78—16153
stratospheric aerosol layer and climatic effects 78—81331
stratospheric aerosol layer visible and IR optical props. influence on global climate 77—2240
stratospheric warmings, obs. and theory 79—74944
structural and stochastic anal. of zero-dimens. climate system 78—73501
Suess Wiggles and ^{14}C calibration curve for dendrochronology 79—74952
summer average vertical circulation over E.Asia and Pacific regions 80—12525
sunspots and volcanic dust effects on climate, statistical evidence from long-term temp. records 78—69439
sunspots occurrence rel. to climatic changes 79—58309
SURF storage ring calibrations for NASA stratosphere and climate programs 80—94721
surface flow in statistical climate model, parameterization of large-scale momentum fluxes 77—45104
surface flow over equatorial oceans, dynamics and climatology, 1911-70 period 79—58061
surface temp. trend in N. Hemisphere, 1969-73 extension 77—21883
surface temperature changes nonlinear response in climate model, ice-albedo, lapse-rate and cloud-top feedbacks 78—69438
Takoradi-khartoum air route, general synoptic climate 78—28300
Tasmania, vegetation and climate in postglacial times 80—41543
technological implications of weather and climate 77—45101
Tehran area, Ivan, precipitation climatology, 1894-1974 period 77—9483
Teletsk lake valley, limnoclimate *(Russian)* 77—21881
temperature and global rad. meas. for Israel's coastal plain (1967 to 1976) 79—80003
temperature and precipitation, temporal fluctuations averaging for continents Europe and N.America 78—92958
temperature changes since 1665, statistical study of likely influence of causative factors 79—8680
temperature measurement, time of observation vars. and apparent climatic change 77—81993
temperature variability, secular changes 80—21820
temperature vars. rel. to long term solar vars., solar activity and neutrino flux 78—45307
terrestrial heat flow palaeoclimatic and topographic corrections, erosion effects 79—34767
central Texas, Colorado River and Quaternary climatic change 77—91251
Texas High Plains, precipitation climatology 78—92959
thermal balance meas. by radiation pressure on satellite microaccelerometer 79—2380
thermal history, CO_2 content rel. to thermodynamic balance 79—29847
thermal pollution from fuel and energy consumption, effects on weather and climate 78—61539
thermodynamic systems of max. dissipation 79—70881
Tibetan plateau, preliminary anal. of climatic variation during last hundred years *(Chinese)* 79—62572
time series, linear trend analysis 77—49151
Tokyo, winter temps., spectral anal. of data for 1443-1970 period 77—45128
tornado activity rel. to precipitation, assessment 80—61882
tree ring, Greenland ice and tidal stresses rel. to climate periods 77—33178
tree ring width climatic interpretation, South Africa Widdingtonia cedarbergensis anal. 80—98439
tree rings, climatic information from $^{18}O/^{16}O$ in cellulose, lignin and whole wood 78—24355
tree-ring evidence of past climatic variability 79—16642
tropical climate anomalies and circulation modes 79—88468
tropical climate of ice age, simulation 78—16144
tropical storm freqs. rel. to sea surface temps. 77—91226
two-level primitive eqn. atm. model for climatic sensitivity expts. 78—81348
UK climatology network, significance of spatial variability of daily temps. and sunshine 78—3887
United Kingdom, 1975-6 drought, synoptic climatology 77—70802
United Kingdom, cloud freq. distrib. analysis 80—61892
United Kingdom, first cold snap of autumn mean date, 1871-1920 period 77—9484
United Kingdom Climatological Network, history and role of co-operating observers 79—5618
United States, 1896-1975 interannual temp. variability 80—61888
W.United States, climatic regionalization 77—29417
N.E.United States, precipitation patterns, 1941-70 period 80—31116
SW.United States deserts, holocene woodlands 78—28298
urban climate, model of aerosol effect 77—66978
urban microclimate of Alma-Ata, significant factors 80—101418
urbanization effects on climate, problem anal. 77—66979
US National Climate Program, beginnings 79—92598
SW.USA, climate and vegetation from packrat middens, 20000 BC to present 80—17370
USA during Holocene, depositional history of Pomme de Terre River 80—51446
USSR, information retrieval system 77—70838
Utah, Colorado, climatic/hydrologic regime rel. to rapids in canyon rivers 80—72564
Vancouver Island, Wisconsin stratigraphy, climate reconstruction 80—8267
variability, effects of volcanoes, pollution and CO_2 78—28292
variability, space and time scales 78—28290
variability and causal mechanisms 77—64414
variable Sun effects at beginning of Cainozoic era 79—75171
variation throughout Earth's history, causal mechanisms 80—82048
variations and temp. at Bergen, Norway *(Norwegian)* 79—39840
variations in climate models, forced or free variation 80—56596
volcanic activity causing climate change, ^{14}C and historical records 80—98442
volcanic activity triggered by rapid climate change 80—81858

climatology continued
Wales, summer index (1971-78) 80—85742
warming effect on W.Antarctic ice sheet 79—34864
water supply in United States, effects of climate and climatic changes 78—49044
watershed geomorphology, relative scales of time and effectiveness of climate 78—81229
weather and climate, solar-terrestrial influences, symposium/workshop proceedings (Columbus, Ohio, 1978 August 24-28) 80—27037
weather forecasting, finite element method *(Chinese)* 77—87024
Late Weichselian ice sheet of N.Eurasia 80—90109
wind, use of trees as local climatic indicator 80—82007
wind speed at sea, climatic comparisons of estimated and measured winds from ships 80—105020
wind velocity magnitude and persistence, probability models 79—5583
windchill maps of lowland Britain, calc. from instantaneous data 80—61893
winter temperatures in central England and Newfoundland, 1870 to 1970, anal. 79—80009
World Meteorological Organisation programme activity development 78—61531
world predicament and climatic change, need for interdisciplinary research 78—57300
late-Wurm Arctic Ice Sheet, rel. to N.Hemisphere glaciation 77—45132
SE Yukon, unique stratigraphic record of late Tertiary-Quaternary events 79—62499
Zaire Basin, climatic atlas *(French)* 79—39844
zero-dimensional climate model with ice-albedo and greenhouse feedback, catastrophes and resilience 79—80007
zonal asymmetry, in energy balance climate model, glacial transition 80—12536
zonal climate models, inclusion of meridional motion and large eddies 80—90138
zonal climatology, atmospheric feedback mechanisms, comments and reply 78—44977
zonally averaged climate model 78—81347
zoning criteria for climate features, for housing standardization 78—3917
C flux between biosphere and atmosphere, biomass burning 80—97838
CO_2, accumulation in atmosphere, effect on climate and harvests 80—40940
CO_2 and climate, model of geographically nonuniform effects 80—90143
CO_2, atmospheric content, climatological consequences *(Dutch)* 80—98411
CO_2, biosphere as source and/or sink 79—88030
CO_2 climate and society, IIASA conf. (Laxenburg, Austria, 1978 February 21-24) 79—8679
CO_2, climatic effects of increasing content 79—88029
CO_2 conc. increase problem, radiative-convective model 77—66977
CO_2 content of atmosphere, role of C storage by forests and oceans 78—53718
CO_2 content of atmosphere, response to deep-sea injections of fossil-fuel CO_2 80—31090
CO_2 effects on global surface temp. *(German)* 78—49121
CO_2, fossil fuel generated, models for ocean uptake 79—88031
CO_2 from fossil fuel burning, climatic effects, proposed CO_2 disposal in deep ocean 78—57301
CO_2, global problem of increasing levels 79—88032
CO_2, impact on climate 80—31118
CO_2, impact on snow and water surfaces cooling 79—92569
CO_2 increase effects, radiation energy balance and temp. 80—12498
CO_2 increase from fossil fuel burning, greenhouse effect, threat to W.Antarctic ice sheet 78—28296
CO_2 increase rel. to future climate, coupled atm.-ocean model 79—58082
CO_2 induced atmospheric temp. rise, Arctic sea ice decay 80—61802
CO_2 levels from combustion of fossil fuels, effects 79—2359
CO_2 levels rel. to agricultural expansion in late 19th century 78—53717
CO_2 model run in tandem with climate model, 1800-2100 AD 80—98381
CO_2, ozone and water vapour, atmospheric content, world climate effects *(Dutch)* 79—70838
CO_2, uncertainties associated with effect on global climate 79—88028
CO_2-climate problem developments 78—20460
$^{13}C/^{12}C$ from tree ring ^{13}C records, interpretation problems 79—62573
D/H climate indicator rel. to solar luminosity and sunspot cycle 79—75176
H_2O-CO_2, IR radiation transfer, CO_2 build-up effects on climate 79—80028
N_2O causing atmos. warming, fertilizer pollution 80—94579
N_2O greenhouse effect in climate model 80—90211
O isotope palaeotemperatures, from Tertiary period in North Sea area 78—88903
O_3 depletion by halocarbons, climate effects 80—98436
O_3, tropospheric, influence on climate 80—36365
O_3 vertical distrib. over Aspendale, Australia, climatology 78—20475
OCS, in atmosphere, contrib. to stratospheric aerosols and climate 80—41524
^{18}O palaeotemperature determs., effects of post-depositional alteration of rocks 77—29455
^{18}O stratigraphy in deep-sea sediments, evidence for deglacial meltwater effect 78—85530
$^{18}O/^{16}O$ palaeoclimatic, implications of subglacially precipitated calcite 79—20897

climb, dislocation *see dislocation climb*

clipping circuits *see limiters*

clock paradox *see special relativity*

clocks
see also atomic clocks; chronometers; time measurement
airborne clock synchronisation by minimum variance methods 77—37853
astronomical observatory clock, crystal-controlled, with computer-readable output, design 80—26746
Atkinson sundial at Indiana University 79—84678
automated time keeping system of Van Swinden Lab. 80—98891
circadian clocks, mathematical models 79—34470
crystal tuning fork development and biography of Jurgen Staudte *(German)* 79—30182
crystal-controlled, accuracy setting and control *(Czech)* 79—40541
digital, control by signals from standard freq. transmitter *(German)* 78—57902
digital, quartz controlled, techniques, problems 77—30133
digital, using thermal printer for time of day readings 80—42211
digital clock CADM for extension of standard freq. line 79—67288

clocks continued
digital clock using MM5315IC and CMOS ICs *(Spanish)* 79—8841
digital quartz clock, electronic corrector at astronomical observatory *(Polish)* 78—36462
digital timer, IC, high accuracy and repeatability, photographic appl. 79—35683
digital TTL, illumination timer for photographic darkroom appl. *(German)* 79—49315
Dodaira Station 91 cm. telescope clock system *(Japanese)* 77—73964
electrical stopwatch testing using semiautomatic device 79—30424
electronic programmable timers for industrial lab., Xanadu up-timer 79—9207
electronic timer using TTL or CMOS ICs, for programmed delays 79—35684
energy efficiency, mains and battery operated clocks, for teachers 78—81773
equipment and services, 1979 video yearbook 79—14197
escapement mechanisms, mathematical theory, for teaching 78—41108
global coordinate time scale, practical implications of relativity 80—47030
high precision, roles in gravitational expts. 77—74301
intercontinental clock synchronisation, ramp method 80—47034
isotopic generators appl. *(Spanish)* 78—15922
laboratory real-time clock, for computer, experiment and manual interaction 78—173
laboratory timer based on electronic clock module 79—67282
laser clocks, for psec. meas. review 78—12676
LASSO experiment on Spiro-2 spacecraft laser synchronisation from stationary orbit 80—82211
national time and frequency standards of Finland 80—47031
NBS-4, time dispersion 2.5 ns, long term clock development 77—45825
non-autonomous, classification and basic principles *(Czech)* 79—49208
non-autonomous (secondary), pulse and frequency controlled *(Czech)* 79—40540
oscillator period variation due to nonlinear feedback 77—68382
photon clocks 77—37801
portable quartz, accuracy in comparing time scales 80—101786
precision, synchronisation and time/frequency dissemination 78—49803
quartz, regulation by atomic time receiver of Rugby 60 kHz transmission 78—4597
quartz clock, accuracy, radio signal control *(French)* 80—95079
quasi-analogue display for electronic clocks *(German)* 79—49207
radio clock for reception and display of time code information 79—175
radio time signal coding and clocks for private and industrial use *(German)* 78—89445
radioluminous household clocks, population gamma-ray exposure 77—73586
random perturbations, absolute continuity theorem *(French)* 78—62150
rubidium, portable, time scale generating clock coordination appl. 78—36973
sand, historical development 80—22185
sapphire, single-crystal clocks and frequency standards 78—57915
satellite time system for utility companies 79—12774
sidereal digital clock 78—36464
simple darkroom timer design and construction 78—89577
stopwatch for automatic time keeping in undergraduate lab. 79—97158
sundials to atomic clocks for understanding time and freq., book 78—57904
synchronisation cct. for error monitoring, correction 78—73970
synchronisation experiment using Symphonie satellite 80—68184
synchronisation for VLBI, influence of relativity theory *(Russian)* 77—5664
synchronisation rules and transitivity 77—29982
time and freq. transmission, OMA 50 kHz Czechoslovak station *(Czech)* 79—30425
time transfer experiment, clock comparison by laser in the nanosecond range 80—47035
time transfer experiment using Nova satellite time signals 80—47036
time-code clock, date display, BST switch and alarm add on circuits 77—53866
time-code clock cct., slow code MSF transmission at 60 kHz, basis 79—67260
wristwatch balance period/oscill. amplitude meas., photoelec. method *(German)* 77—87755
Cs clocks made by Oscilloquartz Company, investigation of metrological characts. 80—101787
Li cells appl., 1979 state of art *(Spanish)* 79—96432
NH_3 special-purpose frequency standard and clock 78—57913
Si single-crystal clocks and frequency standards 78—57915

closed circuit television
Abbe's theory of imaging, lecture-room demonstration 78—41120
acoustic field schlieren visualization, using closed circuit TV system 78—46867
aerial survey image interactive hybrid optical/video processing system 77—53254
Benthic Untethered Multipurpose Platform for underwater acoustic TV 80—46319
colour single-tube camera, SICOLOR, appl. to endoscopy *(German)* 78—88758
electronic editing system for magnetic video recordings, ENG, cinefilm *(Russian)* 79—89029
eye tracking communication system feasibility for nonverbal cerebral palsy children 79—83981
holocamera for 3-D micrography of the alert human eye 80—98057
interactive, inservice training, in special education 79—48981
IR electropupillometer design *(Japanese)* 77—66870
LEED intensity measurement using modified CCTV system 80—31946
losses in TV transmission loops, TV camera operation, X-ray photograph transmission appl. *(Hungarian)* 78—21306
materials science, use of closed circuit TV as teaching aid 79—71209
neutron radiography edge enhancer 79—24706
ophthalmological research, training appl. *(German)* 78—24157
radioscopic system, for 400 kV X-rays, using microchannel plate image intensifier *(French)* 77—38071
reading aid, portable, for partially-sighted 79—29665
steam turbine flow holographic interferogram processing by minicomputer 77—19656
teacher training appl. 79—80388
teaching appl., preparation and installation in colleges *(German)* 78—12521

closed circuit television continued
thermal NDT system, production quality control appl. 79—11751
undersea stereoscopic television for offshore appls. 79—5677
vision aids, training and practice effects on performance 78—11770
X-ray image intensifier closed circuit TV system 80—3775
X-ray intensifier TV picture transfer 77—5077
X-ray intensifier viewing system, for biomedical applic. 77—9251

closed loop control systems *see closed loop systems*

closed loop systems
see also feedback
active optical systems, real-time control over optical wave fronts 78—71187
adaptive laser beam control process, optimal estimation techniques 77—88660
adaptive laser resonator, intracavity phase variations 77—88793
adaptive optics systems, target effects 77—88934
aneasthesia delivery system 78—40402
artificial heart, driven by automatic driving system 78—7541
beam pointing control system, visible to IR wavelengths 79—98426
blood pressure control in hypertensive crisis, closed loop control of sodium nitroprusside infusion 78—44688
blood pumps, pneumatic 77—52930
burn patient closed loop fluid resuscitation using microprocessor 78—36046
cloud chamber adaptive closed-loop expansion control system 79—93889
coherent optical adaptive Modal Wavefront Control System 77—19295
computer-controlled stimulator for ventricular myocardial function analysis 77—60267
deformable metal mirror characterisation techniques 79—59798
dimensional gauging using scanning laser beam 78—57898
eye long-term growth and shortsightedness model 79—83768
laser adaptive optical control with closed-loop estimation and predictive filtering 77—19298
light intensity control system *(French)* 77—83941
manual control operator performance, gain and vibration effects interaction 78—44756
mechanical prestressing, compensation of isolated muscle specimens *(German)* 80—36201
MINI-OTEC ocean thermal energy conversion plant test 80—45727
multichannel functional electrostimulator design for paretic gait correction 79—57810
multidither adaptive optics system operation 80—33141
muscle length reflex control, servosystem simulation 79—57639
nuclear reactor closed-loop control system synthesis 77—3117
nuclear research reactor ZED-2, two-phase control absorber development 79—85697
optical phase meas. receivers, direct detection 77—88661
optical wavefront distortion compensation in real time 77—17219
optical-sensing systems, with automatic light-intensity control, stabilisation 77—54784
phase-locked cavity used as electron model 79—63089
proportional counters, thin-window, rocket-borne, gas press. control system 78—17512
proton synchrotron booster RF accelerating system, dynamic closed loop control 77—83379
real time atmospheric compensation, active optical imaging 77—49307
seismographs, feedback-controlled wide-band, design, rel. to undesired side effects 79—39909
seismometers, wide-band feedback instrument 79—39907
Shuttle Orbiter re-entry, remote IR imagery and tracking 80—82171
solar thermal systems long-term performance predictions using closed-form solutions 80—30556
stochastic approx. procedures in continuous time 78—69969
stochastic systems theory, appl. to blood pressure control 80—81522
thermal-blooming compensation, using closed-loop adaptive single parameter system 78—94407
thermoregulatory system, human, engineering models, review 77—81471
two-phase thermosyphon feasibility for solar energy transport and storage 79—57491
US tumour irradiation, closed-loop energy and temp. control 79—83874
vacuum furnace, regulated particle-delivery system 78—21139
ventilation feedback control in small infants after open-heart surgery 79—70710
vibration system with PLL for measurement of dynamic shear modulus of cylindrical specimens 79—61827
wavefront meas. control, and conjugation, adaptive optical system aspects 79—59796
wavefront sensing systems compared 79—58766
wind energy conversion system control, on-line, performance in turbulent wind environment 79—48069

cloud chambers
adaptive closed-loop expansion control system 79—93889
charged particle hydrodynamic acoustic radiation in water *(Russian)* 77—54459
coronal discharge effect on cloud droplet growth 77—34514
discharge-diffusion chamber with working volume $60\times45\times18$ cm 80—47812
electrostatic paint and powder spray coating developments 79—83363
expansion and diffusion chambers, operational features and appl. 79—72192
expansion cloud chamber with thermoelectric cooling 78—90034
hybrid liquid-gas chamber, new combined track detector 77—83454
low level activity counting, factors affecting registration efficiency *(Russian)* 80—27875
low pressure, ionisation distrib. analysis 80—9461
low-pressure, anal. of ionisation distribs. 80—106236
low-pressure cloud chamber to study spatial distrib. of ionization 77—34513
muonic ionisation of He and Ar, restricted energy loss in range 3-200 GeV/c 77—88355
nonuniform vapour, nucleation model, cluster diffusion effects 77—4206
position sensitive detectors of high spatial resolution 79—76276
supersaturation profile in thermal diffusion cloud chamber in unsteady state 80—63449
thermal diffusion, continuous flow parallel plate type, analysis w.r.t. atm. water droplet growth 80—36416
time expansion chamber, relativistic rise meas. by cluster counting method 80—58030
tissue equiv. gas for α-particle tracks 80—9462
tube detectors, review *(Chinese)* 80—52830

cloud chambers continued
Yunan big cloud chamber set; momentum selector program *(Chinese)* 79—59308
NO_2 in nonane, supersaturated gas, photoinduced nucleation 78—80760
SO_2, gas, photooxidation, cloud chamber obs. 79—1961

cloud physics *see clouds*

clouds
see also atmospheric precipitation; sky
aerosol, scavenging of particles by cloud drops and small rain drops, elec. field effect 80—82001
aerosol capture by drops, effect of Brownian, thermo- and diffusiophoretic forces 77—16869
aerosol large particles ingestion by cloud, ice nucleation by freezing 77—37308
aerosol particle content study at cloud edges and in clear atmosphere *(Russian)* 80—21794
aerosol particles, precip. on evaporating droplet in turbulent gas flow 80—7870
aerosol particles, precip. on evaporating droplets 80—7869
aerosol particles scavenging by clouds and raindrops, elec. charge effect 79—53459
aerosols, characts. over India, role in warm rain process 79—92573
aerosols from coal-fired power plant plume, no detectable ice nuclei 77—21888
aerosols of marine air, submicron size distrib. and CCN supersaturation 80—77041
air entrainment, overestimates from aircraft temp. sensors in cloud 79—53483
air flows measurements via radar study 77—91243
aircraft contrail, iridescence 79—96797
airmasses over Asia in winter *(Japanese)* 79—66768
albedo and reflected radiance of horizontally inhomogeneous clouds 77—78417
altitude, satellite, radiosonde and lidar measurements 79—88444
altocumulus billows, example of large amplitude Kelvin-Helmholtz wave 80—72621
altocumulus clouds, contrast bow obs. from high flying aircraft 79—80029
altostratus mixed-phase cloud, lidar obs. 77—91220
American Meteorological Soc. Conf. (Issaquah, Wash., 1978 July-Aug.) 79—5551
analysis via space-derived pictures, appl. of photographic equidensity curve method *(Russian)* 77—53155
annual zonally averaged climatic model with diffuse cloudiness feedback 77—29416
annual zonally averaged global climatic model with diffuse cloudiness feedback 77—87056
anthelion, form. theory, light refl. in ice crysts. in cirrus clouds 79—62583
Arctic summertime stratus, form. and persistence 77—5290
Arctic summertime stratus clouds, solar radiation pyranometric meas. 78—32165
artificial clouds altitude determ. using IAS triangulation camera *(French)* 77—33192
artificial clouds form. possibilities and methods 79—29823
ash cloud trajectory, Mt. St. Augustine 1976 eruption 77—2234
astronomical clear sky occurrence determ. for Middle Asia *(Russian)* 79—88472
Atlantic Ocean, meteorological parameters changes and interaction with different-scale processes *(Russian)* 77—60447
atmosphere, fixed cloud-top temp. and fixed cloud-top altitude approximations for temp. profile 80—72616
atmosphere, radiation modulation of aerosol state by moving clouds *(Russian)* 78—88916
Atmospheric Cloud Physics Laboratory on Shuttle/Spacelab, droplets optical motion control appl. 80—12634
Atmospheric Cloud Physics Laboratory on Space Shuttle, image dissector for size and position of statically suspended particles 80—26616
attenuation of 1.25 and 2.0 mm waves, radiotelescopic obs. 79—34897
base height meas. with Mk3 CBR, potential accuracy limitation 78—45024
Bay of Bengal, unusual cloud feature assoc. with sea convection 77—53120
beam broadening in randomly inhomogeneous cloudy aerosol medium *(Russian)* 78—58911
Belgium, weather in 1975, review 77—25747
Belgium, weather in 1977 79—58049
Benguela Current, cloud cover anomalies rel. to high waves region 80—51434
boundary layer near water surface, diurnal characts., equatorial region, GATE meas. 78—61527
brightening of disperse media, role of laser fluctuations 79—41405
buoyant clouds, lateral interaction, numerical simulation 77—2197
California coast, marine fog form and fog-stratus systems development 80—77060
California stratus, $^{34}S/^{32}S$ ratios rel. to aerosol and cloud drop origin 77—29407
Canadian cumulus, turbulent characts. 77—64383
ceilometer using low-power laser radar 78—24390
cellular convection and assoc. cloud patterns 78—36249
charge separation, rel. to secondary ice crystal prod. 80—81998
cirrostratus clouds, IR emissivity meas. by remote sounding 80—82061
cirrostratus formed by lee wave, satellite photograph 79—84462
cirrus, backscatter and extinction coeffs. from laser radar obs. 77—60456
cirrus, falling ice particles survival distance in subsaturated air 77—33151
cirrus, influence on IR cooling rate 78—73455
cirrus, radiative transfer model for IR region 80—98397
cirrus, remote sensing of thickness, and composition from satellites 77—64461
cirrus and ice pellet shower clouds, lidar scattering, polarization characts. 77—64430
cirrus clouds, radiative props. in NOAA 4 VTPR channels rel. to satellite exploration 79—39853
cirrus outflow divergence determ. using ATS 1 pictures 77—53239
cirrus sunpillar form. from ice crysts., theory 80—85747
classification from visible and IR SMS-1 data 78—77309
classification techniques, comparative study 78—7809
clearing by laser beams, liq. water content and temp. fluctuations in clearance zone *(Russian)* 78—44999

clouds continued
climate and atmosphere long-term stability rel. to clouds 79—74951
climate model, sensitivity and role of cloudiness *(Russian)* 78—88902
climatic feedback mechanism, effects of cloud amounts on surface temp. changes 79—88467
cloudiness correl. with ozone vars. rel. to UV radiation protection 78—73456
coagulation processes, Monte Carlo simulation *(Russian)* 79—84377
cold front of midlatitude cyclone, cloud and precipitation struct. 80—109192
cold-frontal rainband, cellular struct. obs. 80—51512
colour guide, book 78—92952
composition analysis using continuous impactor-replicator 79—53544
condensation equations for turbulent cloud *(Russian)* 80—77039
condensation initiation by gravity waves 80—90159
condensation nuclei, balloonborne meas. using condensation nuclei counter 77—64460
condensation nuclei, meas. using horizontal thermal gradient spectrometer 80—77158
condensation nuclei, obs. over N.Atlantic 80—77074
condensation nuclei, size distribs. effects on cloud droplet sizes 77—87006
condensation nuclei counters, comparison of two instruments 78—61598
condensation nuclei counters using diffusion chambers 77—41224
condensation nuclei flux, continental surface meas. 79—53443
condensation nuclei from paper mill, calc. effects on rainfall 78—11970
condensation nuclei from paper mill, measured effects on clouds 78—7721
condensation nuclei obs., Barrow, Alaska 77—29386
condensation nuclei on USA Atlantic seaboard 77—5310
condensation nucleus counter, automatic light scatt. instrument 78—3980
condensation nucleus counter, dual-range performance 79—53543
condensation nucleus counters, comparisons, comments 77—56758
condensation nucleus spectrometer, new design 80—85765
condensation of monodisperse cloud regarded as isolated system 77—53150
condensation of water, thermodynamics of nucleation on charged centres 79—20955
conductivity charges in cloud due to lightning 80—61867
convection initiation and development in temperate latits. 78—20480
convective cloud activity, urban induced influences 77—78341
convective clouds, dry ice appls. for on-top seeding 78—73531
convective clouds, models of thermals 80—109228
convective clouds, one-dimensional models *(Polish)* 80—12466
convective clouds, three dimensional turbulent flow anal. 78—69395
convective clouds and rain showers form. over Indian Ocean 78—7735
convective clouds assoc. with severe thunderstorms, nature and effects on society 79—5560
convective day precipitation, correl. with atmos. parameters observed by radar 80—109205
convective dynamics, simulation of three-dimens. cloud model 79—16590
convective flux estimation over tropical ocean, sensitivity to model assumptions 80—90155
convective growth on subsynoptic scale, mathematical models *(French)* 79—70869
convective mesosystems, cloud cover and formation 78—16135
convective model, appl. to waste heat release from nuclear power plant 79—34452
convective parameterization, Arakawa-Schubert scheme appl. 79—16587
convective scale precipitation downdraughts in cumulus and synoptic scale interactions 77—33145
convective shallow cloud model, precip. mechanisms 78—81311
convective systems, life cycles, GATE data 79—53440
convective systems during Phase III of GATE 80—90153
cooling tower plumes from energy centres, predicted climatology 78—61541
cover effects over wheat acreage, LANDSAT data 77—78509
cover over surface types, climatological analysis 79—16596
coverage weather-satellite picture facsimile machine 77—9558
crystal collisions, secondary ice particle generation 79—79932
crystalline clouds, artificial, light scatt. matrices *(Russian)* 77—5317
cumuli, droplet size distrib. spectra *(Russian)* 80—81991
cumuli, measurement of horizontal eddy diffusivity by radar method *(Russian)* 79—88404
cumuli fields, space-time characts. *(Russian)* 77—91214
cumuli spacing and size, Hill computational stability, comments 77—41119
cumulonimbus, atmospheric dynamics problems 77—25729
cumulonimbus, unsaturated downdraft thermodynamics 80—51464
cumulonimbus, updraft-downdraft interaction, numerical model 80—98377
cumulonimbus anvils, protrusion into stratosphere, lifting of tropopause *(French)* 77—29357
cumulonimbus cloud top heights over Bombay, radar meas. 77—53127
cumulonimbus cloud top heights over Deccan Plateau and adjoining plains, radar obs. 79—48542
cumulonimbus clouds, elec. field strength and raindrop spectra, study from mobile ground station 78—92943
cumulonimbus convection, numerical modelling 79—84414
cumulonimbus convection, theoretical modelling 79—84405
cumulonimbus motion and splitting, role of downdraught, numerical simulation 79—44227
cumulus, air entrainment mech., obs. in Colorado, USA 80—90133
cumulus, aircraft meas. if ice, Florida 79—12213
cumulus, convection model response to radiative heating change 80—98396
cumulus, downward scatt. solar radiation 78—3876
cumulus, droplet distrib. broadened by turbulence 80—56582
cumulus, droplet evolution, theory 80—56556
cumulus, droplet size distrib. obs., 0.1-15 μm radius 80—51463
cumulus, finite cubic model, simulated radiance patterns 77—33187
cumulus, ice particle multiplication factors 79—58035
cumulus, large particles in supercooled regions 80—56564
cumulus, numerical simulation, of weak development *(French)* 79—16607
cumulus, one-dimens. time depend. model of small cloud 80—51506
cumulus, scattered and total solar radiation fluxes *(Russian)* 77—41169
cumulus, size and particles effects on satellite-observed reflected brightness 78—73510
cumulus, small fair-weather clouds, convective plume props. 78—16116

clouds continued
cumulus, three-dimens. microphysical model of evolution *(Russian)* 80—56531
cumulus, turbulence in boundary layer *(French)* 79—84412
cumulus and cumulonimbus forms and patterns 78—57289
cumulus cloud, vertical air vel. determ. using airborne meas. system 80—77159
cumulus cloud effects, representation in large-scale vorticity equation 79—88436
cumulus cloud statistics, satellite-derived, for W.Kansas 79—79955
cumulus cloud vorticity, determ. from GATE A/B scale pot. vorticity budget 80—90157
cumulus clouds, peculiarities of air entrainment mechanism *(Russian)* 78—24334
cumulus clouds, satellite tracking and derived mesoscale wind fields covariance anals. 80—82013
cumulus clouds, warm rain and salt seeding, numerical simulation 80—90201
cumulus congestus, NE Colorado, graupel particles characts. 78—81312
cumulus congestus, spatial heterogeneity of microphysical props. *(French)* 77—78342
cumulus congestus in Colorado, ice initiation 80—81997
cumulus convection, vorticity horizontal transport parameterisation 80—90158
cumulus convection and perturbation pressure, model 80—17325
cumulus convection in shear flow—three-dimensional numerical experiments 79—34915
cumulus convection in tropical depression, synoptic scale kinetic energy source 80—77088
cumulus convection initiation mechanisms and development 78—69410
cumulus convective transport rel. to easterly wave vorticity budget 77—56671
cumulus friction and moisture budget in tropical wave-CISK 79—16580
cumulus glaciation, rime-splintering hypothesis, field-of-flow cloud model 78—20476
cumulus life cycle effects on heat and moisture budget 77—56672
cumulus motion winds from ATS 6 images comparison with coinciding SMS 1 winds 79—79954
cumulus parametrization and wave-CISK hypothesis 77—45080
cumulus parametrization for 10-level atm. model 77—70782
cumulus scale convection, effects of seeding with C black dust 77—91223
cumulus seeding technique, preliminary tests 78—57352
cumulus transient ensemble, large-scale interactions 77—66954
cumulus transports in tropical wave composite during GATE 79—2336
cumulus updraft and downdraft rel. to GATE A/B-scale motion systems 78—16097
cyclonic storm, Arabian Sea, 1976 June, diurnal var. and secondary vortices form. 79—20915
cyclonic storm, rainbands, precip. cores and generating cells 78—81307
cyclonic storms, mesoscale and microscale organization and struct. of clouds and precip. 79—74946
depth, relation between Pasquill stability and Kazanski-Monin stability 80—17304
detrainment effects on properties of cumulus populations 77—70760
diffuse reflectance, semiempirical model 79—80014
diffuse solar radiation field in cloud layer *(Russian)* 79—29851
diffusion, tracking elec. charged air by ground level elec. field meas. 77—78450
diffusion chamber with continuous flow, improved design 77—2277
direct solar radiation rel. to cloudiness and solar altitude 79—58073
distribution, effect of local gravitational field of geological faults 78—32136
diurnal variation of rain and low cloud over Ozar airfield rel. to forecasting 79—100904
drop coalescence, collection efficiency of 81 μm drop falling in 20 μm drop cloud 80—90134
drop collision coalescence in presence of elec. field, simulation expts. 80—51516
drop collision in turbulent environment 80—56555
drop evaporation in diffusion regime of cloudy atmosphere, influence of optical consts. *(Russian)* 78—32145
drop growth by condensation, air parcel model 78—7729
drop growth in atmosphere by condensation, cloud physics appl. 79—44216
drop size distrib., Keily probe assessment for ground-based meas. 79—12317
drop size spectra, modification by urban pollution aerosol, physical demonstration 80—56571
drop spectrum evolution for condensed stage in turbulent atm. 78—81325
drop spectrum evolution rel. to collision efficiency 78—69415
droplet coalescence growth, fast computational method for Telford's theory 78—69486
droplet collision, numerical study of Stokes and Oseen flow approx. 78—16102
droplet collision efficiency enhanced by elec. field 80—61863
droplet collisions, satellite drop production expts. 80—12492
droplet condensation growth in turbulent medium, hygroscopicity and surface tension effects *(Russian)* 77—33142
droplet distribution evolution, supersaturation fluctuations, stochastic condensation theory 80—12490
droplet growth, effect of radiative transfer 80—8404
droplet growth and initial dew point temp. accuracy in cloud chamber on space shuttle 78—96268
droplet growth by condensation, parameterization 78—3869
droplet growth in presence of soluble gases, expts. 80—21807
droplet nucleation, expts. with monodisperse NaCl aerosols 80—82003
droplet size evolution and small-scale turbulence 80—56554
droplet size meas., comparison of electrostatic disdrometer with impactor slides 77—2278
droplet size spectrum evolution, effect of surfactants 77—78340
droplet spatial variability, cloud base meas. 80—12495
droplet spectra, effect of nuclei spectra 77—64364
droplet spectra evolution, effects of mixing, lab. expt. 77—70778
droplets, collisional problem in turbulent environment 77—5293
droplets, effect of electric charges and fields on collision freq. 80—8401
droplets, interception collection efficiencies 78—3381
droplets, light scatt. and mixed plate interference, blue Moon phenomenon 77—2244
droplets, size distrib. models, and visible and IR volume extinction coeffs. 77 25750
droplets, terminal vel. adjustment 78—16103

clouds continued
droplets size distrib. in cloud bases 78—73458
drops, 8-12 μm radiant energy transfer effects on mass and heat budget 79—5571
drops, crystallisation on CuS aerosol prepared by burning pyrotechnic mixture 78—96279
drops collision efficiency, elec. charges and vertical external elec. field effects 77—25738
dry air entrainment into cloud top, theory 80—90145
dynamic classification of messoscale cloud patterns 79—53476
dynamics and modelling, appl. to forecasting 80—8375
Earth cloud belts, latit. changes effects on zonal and global albedoes 80—17377
electric charge separation in thunderstorm, model 80—77076
electric field growth in finite cloud, comments and reply 77—78327
electric field measuring instruments, review 77—41226
electrical and microphysical meas. in maritime and urban clouds 79—12173
electrical charges fate in evaporating droplets 79—48559
electrification in axisymmetric time-dependent model 79—16594
EM pulse propagation in atmosphere with scatterers, diffusion theory 79—66775
EM pulsed beam wave propag. 78—12000
energy transfer in tropical subcloud layer, aircraft meas. during GATE 79—79989
entraining plume model, sensitivity analysis and appl. 79—20944
entrainment rate in hail-producing clouds *(French)* 77—53151
evaporation rate of particles, effects of nearest neighbour interactions 77—2209
explosion influencing development of convective cloud *(Chinese)* 80—82042
extinction coefficient, estimation from multiwavelength lidar backscatter meas. 80—98446
extinction coefficients, spectral correls., theory 79—96812
extinction meas. using electronic chopper for UV source 78—79087
F-region plasma clouds, high altitude limit of gradient drift instability 78—88984
F-region striated Ba clouds, electron density struct. meas. 78—88974
Florida Area Cumulus Experiment, rainfall results 1970-75 77—45113
Florida cumuli, seeded and nonseeded, precipitation Ag content 77—29387
Florida cumuli, Z-R rel. for seeded and nonseeded clouds 77—45099
flyash from coal combustion, S and Cl adsorpt., cloud nuclei form. 77—21887
formation and development, numerical convection model *(Russian)* 80—81987
formation and ice nucleation rel. to Chinese name for mica 77—91195
fractional cover, solar radiation transfer, two-stream approx. 80—51534
fractional coverage rel. to humidity and condensation in wave model 79—34911
frontal, size distrib. of precipitation particles 79—88437
frontal rainband, conditional symm. instability explanation 80—56584
frontogenesis caused by cumulonimbus convection 77—21845
fronts and depressions at middle latitudes, mesoscale struct. 80—26604
Fuego volcano eruption, aerosol emission, density temp. and particle content 80—90050
fuel drops, liq., blast wave initiated detonation waves 79—64691
funnel cloud, obs. in Glastonbury 79—66783
funnel cloud in Trinidad, West Indies 78—73498
funnel clouds, characts. from obs. during sailplane flights 78—69396
gasdynamics of explosions, reactive systems, conf., Stockholm, Sweden (Aug. 1977) 79—64690
GATE aircraft measurements, their value 80—82071
GATE cloud—subcloud layer interactions, 3-dimens. cumulus model 80—101400
Gaussian cloud model relations 77—70759
general circulation by GLAS model, cumulus friction and Jan. Hadly circulation 80—72588
general circulation model of atm. without clouds 78—49110
generating cell of precipitation trail with wind shear *(French)* 77—53152
global middle UV radiation meas. at ground, cloud effects 78—92882
glory formation, diffr. model 80—82053
granulometry, Knollenberg ASSP-100 performance *(French)* 77—53244
graupel, freely falling, wind tunnel study of hydrodynamic behaviour 78—49113
graupel development, numerical simulation 79—5573
graupel formation and growth, wind tunnel investigation 80—17324
hail cell detection, for cloud seeding criteria, radar method 80—90170
hail development during cumulus cloud seeding by ice particles *(Russian)* 77—81959
hail growth in supercell cloud, theory 80—98419
hail growth simulation, fresh and annealed accretions struct. 79—58034
hail growth simulation, rotation and mixed clouds effects 79—58033
hail nuclei determ. by radar and radiometric combined meas. *(Russian)* 79—12195
hail suppression paradox, stratification approach to statistical expt. 77—37312
hail-producing, N.E.Colorado, observed and computed microstruct. 78—7716
hailstone formation within cloud, microphys. recycling 80—90146
hailstorms, finger radar echoes form. mechanism *(Chinese)* 80—109234
hailstorms, numerical simulation using cloud model 78—28269
Hampstead storm, London, numerical simulation of quasistationary cumulonimbus system 78—77308
Hawaiian warm rain showers, aircraft obs. below cloud base 78—44932
height derivation using High Resolution IR sensor data 79—48539
heights from satellite imagery stereographic pairs 78—45017
N.Hemisphere, cloud cover correl. with middle troposphere organised vertical vels. 78—92939
high ice clouds, visible and LR optical props. from lidar and radiometer meas. 80—82060
hole-boring by high-intensity laser beams, theory 78—28319
horizontal funnel cloud over Shawnee, Oklahoma (1976 June 29) 79—66747
humid plume interaction *(French)* 79—16605
hurricane cloud system, model of cloud-group activity 80—26601
hurricane Debbie, 1969 August 13-19, cloud distrib. and development 78—20493
hurricane formation, tropical storm control by cloud seeding *(German)* 80—90207

clouds continued
hurricane modification expts. by cloud seeding, evaluation 78—85654
hydraulic jump in cloud assoc. with thunderstorm outflow 77—91194
hydrologic cycle, climatic sensitivity, numerical model 79—8654
hydrometeor clouds, thermal microwave radiances 78—85638
hydrometeors, size, conc. and struct. meas. with impactor and replicating devices 77—41218
ice, growth beneath water film, air bubble precipitation 78—83922
ice, two-step nucleation 78—49094
ice and water content from Nimbus 6 IR sounder data 78—92925
ice crystal growth in vapour at high saturation, thermodynamic anal. 77—1088
ice crystal habit discrimination using optical backscatt. depolarization technique 77—91309
ice crystal production, secondary, charge separation laboratory meas., thunderstorm electrification exam. 80—72623
ice crystals, producing concentric solar haloes 1974 April 14 77—2245
ice crystals, small sized freely falling, settling vels. determ. 77—78387
ice crystals in artificial cloud, anisotropic light scattering *(Russian)* 78—40658
ice deposition coefficient meas., appl. to cirrus cloud seeding 77—70779
ice depositional growth, parametrisation 77—70766
ice evolution within seeded and nonseeded Florida cumuli 79—100920
ice formation, possible role of O_3 *(Russian)* 77—29367
ice forming capabilities of Ag and Pb halide surfaces rel. to cloud modification 77—31872
ice nucleants at −1°C using bacteria 77—53221
ice nucleating materials 78—49093
ice nucleation, on natural and man-made particles 79—48530
ice nucleation by aerosol particles 80—61864
ice nucleation by fluid-breaking metaldehyde particles *(Chinese)* 80—12468
ice nucleation in atmosphere, natural nuclei origin 79—48531
ice nucleation on AgI aerosols at different supercooled fog temps. *(Russian)* 77—27983
ice nucleation on PbI_2, −10 to −25°C *(French)* 77—78301
ice nuclei, probability of form. in supercooled water 78—3909
ice nucleus concentration meas. with static vapour diffusion chamber 77—91308
ice nucleus counters 77—41225
ice particle counting in mixed-phase clouds by optical techniques 77—41221
ice particle shape meas. by imaging devices 77—41222
ice particle types in melting layer vicinity, determ. from Doppler radar meas. 77—78338
ice particle/water droplet discrimination with an optical ice particle counter 79—100973
ice particles, depolarisation of 19 and 28 GHz Earth-space signals 78—73492
ice particles, rapid changes in orientation and alignment along Earth-space radio propag. path 80—17330
ice splinter production during riming, NH_3 addition expts. 80—72585
ice splinter production during riming, possible mechanism 78—85662
ice-bearing cumulus evolution, numerical simulation and obs. 77—2216
identification against snow background, aircraft obs. *(Russian)* 77—29392
Indian Ocean, satellite-determined cloudiness rel. to weak monsoon over Kerala 77—56706
industrial cumulus, numerical simulation, comparison with obs. 79—12202
inhomogeneities in water props. 77—49135
insolation over tropical Pacific Ocean, cirrus cloud effects 78—92914
intense tropical convective system, mesoscale motion contrib. to convective fluxes 80—90156
interannual cloud-cover vars. in contiguous United States 78—92909
internal radiation field, cloud blackness determ. technique 79—58089
intertropical convergence zone cloud cluster, wind field behaviour 80—17322
intertropical convergence zone cloud clusters of Indian Ocean basin, features 79—29822
intracloud lightning discharge processes, radiation field wave forms 79—84386
intracloud lightning discharges, HF and VHF radiation temporal struct. 80—17337
ionosphere plasma clouds, deform. and striation, multilevel model with recomb. chemistry 77—25834
ionosphere plasma clouds, late time striation spectra 77—25836
IR cloud opacities averaging for climate modelling 79—8692
IR emissivity, in 10.5 to 12 μ band *(Russian)* 77—49167
IR fluxes in stratiform model clouds 79—84361
IR integral transmission function *(Russian)* 77—60466
IR long-wave (8 to 13 μm) radiation fluxes in free atmosphere, effects of clouds *(Russian)* 80—94598
IR radiation, cloud height, thickness and overlap effects 78—57252
IR radiation flux in atmosphere with cloud, approximation 79—39854
IR radiation transfer, radiative effects 79—100912
IR radiative cooling rate, theory 80—56565
IR radiative transfer, absorpt. in partial cloud cover model 80—12544
IR radiative transfer in cloudy sky, theoretical scheme 80—51540
IR radiative transfer in finite cloud layer 80—72629
IR remote sounding of atmosphere with multiple cloud formations 77—78319
IR remote sounding of cloudy atmosphere, CO_2 radiance data 77—78320
IR satellite data automatic segmentation and classification 79—5638
irradiance meas. from aircraft, computer simulation 77—70830
Israel and Jordan, rainfall fields, cloud seeding effects 78—73452
ITCZ, 13.9 GHz radar altimeter obs. of total attenuation 77—29355
Kelvin-Helmholtz billow cloud obs. 77—70730
Kenya, clouds microstruct. in high-freq. hail area 79—53484
Kitt Peak National Observatory, probability of clear daytime skies 80—12512
Landsat 2 cloud imagery rel. to future meteorological obs. systems 78—40626
LANDSAT-1 digital image registration and cloud effect rectification 77—78490
large transparent sphere effective extinction efficiencies using weakly collimated light 79—72487
laser backscattering from dense water-droplet clouds 79—53513
laser beam attenuation at mountain altitudes by fog and clouds *(Russian)* 79—48566
laser beam heating causing convection *(Russian)* 80—56529

clouds continued
laser echo-signal from cloud, calc. allowing for multiple scattering *(Russian)* 78—49137
laser evaporation of cloud medium, self-focusing possibility 79—27306
laser radiation intensity fluctuation in fine-droplet water aerosol at 630 nm 80—4109
lee wave clouds, S.W. airflow over Bank's Peninsula, New Zealand 80—85739
lenticular clouds, obs. rel. to Kelvin-Helmholtz waves under subtropical jetstream 79—66781
lidar backscatter from horizontal ice crystal plates 78—92984
lidar equation for inhomogeneous atm., double-scatt. approx. 79—29855
lidar measurements, by DFVLR mobile system 77—53248
lidar polarisation meas. for cloud phase discrimination 78—96269
lidar probing of fogs and clouds, double scatt. approx. 78—73512
lidar returns depolarization, scatt. from virga and source cloud 77—49169
lidar returns from clouds, double scatt. contrib. 79—5615
lidar scattering, four-component polarisation meas. 78—44996
lidar scattering from clouds at 347, 694 nm, polarisation props. 78—85689
light beam coherence through optically dense turbid layer 78—55300
light propag. through horizontally non-uniform scattering cloud layer *(Russian)* 79—25326
light pulse propagation through thick clouds, pulse width expression for scatt. slab 80—82059
light pulse reflection, height meas. *(Russian)* 80—82056
light reflection, path length difference and wavelength correl. *(Russian)* 78—69447
light scattering, directional scatt. coefficients meas. in droplet and cryst. clouds *(Russian)* 78—96292
light scattering, Mie formalism, optical communication appl. 77—88651
light scattering effects on satellite aurora and nightglow obs. 78—77385
lightning discharge, elec. field strength at ground level, calc. *(German)* 78—28254
liquid content measurement with ground based microwave instrument 80—94623
liquid water content, determ. from Nimbus 6 scanning microwave spectrometer data parameterisation 79—58047
liquid water content, organic aerosol effects 78—73465
liquid water content, retrieval from scanning multichannel microwave radiometer obs. 80—90261
liquid water content and extinction meas., droplet conc. and size determ. 80—51579
liquid water content meas. of lab. supercooled clouds, instrument design 78—96316
liquid water content measuring device 79—88489
liquid water content measuring devices 77—41223
liquid water content rel. to atm. visibility 78—81404
low cloud formation conditions in frontal zone, theory 80—41532
low cloudiness and advective fog formation, theory *(Russian)* 78—36228
low level over circumarctic ocean temp., climatic change study 77—29415
luminance field spatial structure 78—49140
mammatus over United Kingdom, 1975 April 7 obs. 78—24348
marine atmosphere, cloudiness rel. to ocean skin-layer thermal parameters *(Russian)* 78—36180
marine atmosphere, ranked interaction with ocean on sub-semidiurnal scales *(Russian)* 78—77260
marine stratocumulus convection, governing eqns. and horizontally homogeneous solns. 80—56542
marine stratocumulus convection, horizontally inhomogeneous solns. 80—56543
mass and heat flux determ. in GATE over tropical ocean 80—90154
mesoscale cloud patterns revealed by Apollo-Soyuz photographs 79—88395
mesoscale convergence affecting cloud convection, model 80—109201
mesoscale downdraughts, assoc. with cool ocean surface waters, GATE results 78—69365
mesoscale intense convective storm, Oklahoma, objective anal. 78—32168
mesoscale rainbands in extratropical cyclones, assoc. cloud microphysics and dynamics 80—82030
mesosphere, circulation and clouds rel. to thermosphere semi-annual temp. vars. 78—45061
mesosphere ice clouds production by Earth encounter with interstellar cloud, climatic effects 78—57292
meteorological parameters, feasibility of determination by microwave radiometric method 80—67435
meteorological physics, recent developments, review 79—25313
microphysical model, sensitivity to urban environment 80—82004
microphysical properties from lidar obs. 79—39811
microphysics, book 78—88896
microphysics anal. 79—16853
microwave absorption, rel. to pollutant gases monitoring from space using passive sensing techniques 80—76690
microwave radiation emission meas. 80—17351
microwave radiometric determ. of water content during BESEX 77—29479
microwave radiometry for precipitable water vap. and liq., dual-channel method 80—51564
microwave radiometry of liquid water content over Bering Sea 77—17158
microwave thermal emission, EM scattering effect 77—91211
mid latitude system enhancement due to Intertropical Convergence Zone *(French)* 80—31088
mixed-phase cumulus evolution, theoretical study 77—78325
modelling, isothermality 79—58076
modification by atmos. convection, axisymm. numerical model 80—26600
Mohliner Feld (east of Basle), cloud layer effects on topoclimate *(German)* 80—61890
moist adiabatic ascent in NE Colorado cumulus congestus clouds 79—53456
moist penetrative convection and incipient cloud form. 79—66755
moisture content of atmosphere determ., long-range, by thermal radioemission meas. *(Russian)* 79—5637
moisture excess, long distance meas. by radiometry 80—90196
momentum horizontal transport, cumulus-scale, in monsoon depression over India 78—44961
monochromatic radiation transfer in cloudy layers *(Russian)* 77—41168
monsoon, cloud genesis from digital simulation of evaporation phase 77—56712

clouds continued
monsoon, clouding rel. to droughts in quasi-geostrophic diabatic four level model 77—56713
monsoon airstream at metres height, temp. fluctuations 80—61845
monsoon clouds, aircraft meas. of elec. parameters 78—7792
monsoon clouds rel. to VLF atmospherics over Calcutta 79—88550
monsoon system oscillations, spectral anal. of obs. records 77—33148
morning and evening temp. differences of cloud tops over tropical continents and oceans 79—12219
Morning Glory, tropical Australian cloud formation 77—73818
motion estimates, aircraft verification expt. of wind vel. meas. 78—16113
motion estimation, Fourier phase difference technique 79—21046
motion of a large dusty buoyant thermal with a vortex ring 79—48561
motion vectors and moored buoy wind measurements, comparison 79—84394
motion wind data, meas. improvement 80—8386
motions, automatic tracking system using weather satellite picture sequences 78—45022
Mount Kenya, condensation nuclei and weather obs. 80—82012
mountainous terrain, numerical simulation of airflow and clouds 80—51450
multiburst cloud rise after nuclear explosion 78—94142
multimodal Doppler spectra in terms of sub-beam scale motions 77—29385
multiple light scattering, theory for dispersive media with spherical particles *(Russian)* 80—94599
multiple radiation scatt., stochastic approximation 79—80012
multiple reflections between clouds and surface, effect on climatic models 77—45131
natural illumination of Earth's surface in European USSR 77—78422
nimbostratus, rainfall evaporation, effect on mesoscale unsaturated downdraughts, numerical anal. 80—8400
Nimbus 6 high-resolution IR sounder channels, upwelling radiance sensitivity to clouds 78—32227
noctilucent, cine and television high-resolution obs. 79—39891
noctilucent, obs. in Poland during 1974 77—21826
noctilucent, particle sizes rel. to available mesospheric H_2O vapour 78—57248
noctilucent, photographic obs. from Skylab 77—60505
noctilucent, photographic obs. on 1976 June 18-19, Scotland 77—81982
noctilucent, related stratosphere and mesophere struct. 80—8412
noctilucent, visual observations from space 80—21825
noctilucent cloud formation, equilib. temps. of spherical ice particles 77—37302
noctilucent cloud obs. over western Europe and Atlantic during 1976 77—78346
noctilucent cloud particles, sunlight scattering rel. to characts. 78—11945
noctilucent cloud region, ion comp. 77—87011
noctilucent clouds, 1977 obs. over W.Europe and Atlantic 78—92929
noctilucent clouds, advances in space era, review 80—105095
noctilucent clouds, circularly polarised light detect. 79—48568
noctilucent clouds, elliptical polarization rel. to ice crystals 78—11946
noctilucent clouds, mesospheric structural parameters variations 77—49203
noctilucent clouds, spectral brightness in visible and near IR *(Russian)* 77—13098
noctilucent clouds, temp. of aerosol ice particles *(Russian)* 78—16093
noctilucent clouds, W.Europe during 1978, summary of obs. 80—12510
noctilucent clouds observed during 1976 in Poland 79—16559
noctilucent clouds over W.Europe (during 1979) 80—109289
nonconvective condensation, parameterization scheme, cloud water content prediction 79—12215
nonprecipitating models, subgrid-scale condensation 77—66955
nonspherical extinction and absorption efficiencies 79—7074
nucleation in clouds, minimum particle size 78—44939
nuclei concs., Robertson, New South Wales, Australia, 1968-1973 meas. 79—5569
numerical model to describe cloud evolution 80—56562
numerical models, methods of parametrisation of condensation process *(Russian)* 78—16091
observable optical horizon, theory, refraction, clouds and haze effects *(Russian)* 80—4107
Observatorio Astronomico Nacional, Baja California, cloudiness and climatological characts. 78—20635
ocean, effects of clouds on diurnal var. of underwater irradiances on horizontal surfaces 80—72549
ocean skin temperature, effects of clouds, hydrodynamic model *(Russian)* 78—65331
oceanic reflective clouds, correl. with precip. from Nimbus 5 microwave meas. 77—60455
Ondrejov laser satellite-tracking station, cloud cover data 78—36418
optical glory, theory, physical effects 77—60468
optical multiple backscatt. and depolarisation obs. using lidar 78—36292
optical props., similarity criteria *(Russian)* 80—85745
optically thick media, asymptotic radiance and polarisation 77—21776
organic material impact on fog and cloud processes 78—73467
orographic, air-truth lidar polarisation studies 78—73454
orographic, over Cascade Mountains, ice particle concs. 77—2210
orographic cloud seeding during Utah winter 80—41514
orographic clouds leeward of the Lesser Antilles *(French)* 80—94575
orographic disturbances over N Urals, lee wave clouds form. *(Russian)* 77—60448
overcast sky, ang. distrib. of diffuse solar radiation 80—85719
Pacific, equatorial waves in cloud vel. field 80—67395
tropical Pacific Ocean, cloud cover effects on satellite-determined sea-surface temps. 80—31044
NE.Pacific Ocean, clouds liq. water data rel. to United States west coast rainfall 80—82005
particle camera, aircraft-borne, for in situ photography of cloud particles 78—85750
particle size distribution from spaceborne line spectrum imagery, theory 79—5613
particle size distribution meas. by optical array probes 77—41220
particle size spectra evolution by condensation and coalescence, analytical soln. 80—109194
particle size spectrometer, computational technique for increasing effective sampling vol. 79—70863
Peak Terskol, climatic data, 1972-4 period *(Russian)* 77—70728
penetrative convection at top of growing boundary layer 80—12521
penetrative cumulus convection, assoc. with travelling disturbances in equatorial ionosphere 78—36361

clouds continued
photogrammetry from aircraft nose camera movies 79—53547
physics, course book 79—44239
physics of atmospheres, book 79—62568
physics rel. to atm. electricity, review 79—70842
planetary boundary layer, topped with cumulus, numerical model *(French)* 80—94574
polar and equatorial cloud bands interaction, GOES-1 imagery 79—39786
pollution from coal-fired power plants, effects on cloud and precip. processes 79—20933
precipitating continental convective clouds, microstruct. 78—7715
precipitation development and cloud growth, refined charge distrib. in stochastic elec. model 77—29374
precipitation from anvil clouds, melting and evaporation of hydrometeors 80—17323
precipitation initiation in updraughts, seeding 79—20924
pressure perturbations in deep convection, expt. study 79—53457
pulse diffusion in densely distributed scatterers 79—3632
pyrocumulus cloud over North Canterbury, New Zealand, 1878 April 10, obs. 80—109240
radar and satellite meas., comparison of simultaneous studies 79—58077
radar meas., passive, integral humidity and clouds drop phase characts. determ. 79—74991
radar measurement of clouds and precipitation, correl. and spectral anal. 80—12529
radar observation method, vertically pointing X- and K_a-band technique 80—46273
radar reflection from clouds and clutter target, broad-band noise technique 80—51454
radar reflectivity rel. to cloud dynamics and microphysics 80—61877
radiant energy density calc. and photon equiv. trajectories *(Russian)* 77—45149
radiation balance, sensitivity to cloud changes, zonal model 77—78419
radiation budget at top of atmos., influence of cloud cover 80—98398
radiation profiles in extended water clouds, obs. 79—79931
radiation profiles in extended water clouds, parameterization schemes 79—79930
radiation profiles in extended water clouds, theory 79—79929
radiative flux divergence effect on entrainment of saturated convective boundary layer 79—79979
radiative forcing of atmosphere, sensitivity to variable cloud and moisture 80—56553
radiative properties, parameterisation 80—56601
radiative transfer, cloud shape and mutual shading effects 80—101430
radiative transfer, mathematical modelling 80—90215
radiative transfer in cloudy atmosphere, model solar radiation and cloud struct. 79—21016
radio emission fluctuations of cloudy atmosphere at mm wavelengths *(Russian)* 77—21833
radiowave attenuation statistics at 15 and 35 GHz for very low elevation angles 79—8674
rain systems, large scale, vertical vels. and precipitation patterns, model 80—85727
rainband dynamics and cloud microphysics in occluded frontal system 77—33147
raindrop, single, growth by condensation and droplet capture, props. 79—12208
raindrop growth physics, for teaching 79—35502
raindrop interactions effect on drop size distrib. obs. at ground 78—44945
raindrop sise distributions parameterisation 78—77301
raindrop size distrib. with collision breakup in axisymmetric warm cloud model 79—34918
raindrop size spectra and growth in cumulus cells, model 80—21800
Raman rotational and double scatt., lidar meas. 78—77318
reflectance with laser beam illum., multiple scatt. contrib. 78—85686
reflected brightness, effects of cloud size and cloud particles, comments and reply 79—88425
remote measurement of water density and size distribs., using laser radar 77—91299
remote sensing, integral humidity, integral moisture temperature and height of drop cloud phase determ. *(Russian)* 79—5635
remote sensing, photography via Japanese weather satellite 78—49290
remove sensing in 0.35-3 μm range 80—77085
rime growth, splintering mechanism 79—39788
rolled stratocumulus, air circulation and precipitation formation *(French)* 77—9473
rotating thunderstorm, downdraught enhancement 80—8399
Sacramento Peak Observatory night sky conditions, cloud cover, seeing and precipitable water 80—51653
satellite cloud picture recorder for reception of APT pictures 78—81434
satellite derived cloud imagery, optical Fourier transform anal. 78—85749
satellite imagery distortion, removal by filtering 77—56744
satellite IR imagery, anal. at Central Forecasting Office 77—41123
satellite IR nephanalyses, techniques 77—41122
scavenging, in-cloud, rel. to aerosol particle size, mechanisms 78—16108
seeding, anal. of Florida Area Cumulus Expt. (FACE) rainfall results, natural variability effects 80—82002
seeding, Climax and Wolf Creek Pass expts. 80—82094
seeding, covariance anal. technique based on bivariate log-normal distrib. 77—70767
seeding, effectiveness of dry ice nucleation 79—84395
seeding, hygroscopic, in cumulus clouds, a model 79—88442
seeding, num. simulation technique 79—84519
seeding criteria, winter orographic clouds 79—84391
seeding effects on cloud-to-ground lightning 77—2218
seeding experiment, comparison of night-time and day-time seeding 79 -88441
seeding method for lightning triggering 78—3880
seeding of cloud, Wolf Creek Pass, USA, re-anal. of 1960 expts. 80—31100
seeding program in San Juan Mountains, Colorado 79—53468
seeding studies application of lidar remote sensing 80—109203
seeding with AgI, studies of ice-forming activity, verification of theory 80—101406
seeding with AgI and metaldehyde, Fujian province, China *(Chinese)* 80—46235
severe local storms, St. Louis region, urban effects 79—12199
shortwave albedo, pollution effects 78—7755

clouds continued
silver clouds, visible spectroscopic investig. from Salyut-4 orbit 80—82014
Skagit Cloud Seeding Project, Washington, effects on river annual runoff 79—79949
sky cover obs. for global solar radiation computation 77—25758
sky cover predictions, possible sunshine 79—16565
Skylab conical multispectral scanner IR data statistics 80—90223
small cumuli, updraft var. and water content 78—16105
smoke/dust cloud temporal analysis algorithm 80—98484
SMS images during GATE, wind field determ. accuracy 77—53147
SMS IR data appl. during GATE 80—31113
snow, epitaxial relationship during three dimensional dendrite form. 79—23875
snow, growth mechanism with specific grain boundary 79—23547
snow size spectra and snowflake aggregation efficiencies, theory and obs. 79—8660
snowflakes, vapour deposition and aggregation growth, analytical model 78—73433
solar insolation at Fort Hood, Texas, correl. with cloud cover and visibility 78—24333
solar irradiance three-dimens. transfer in clouds, finite geometry effect 79—58085
solar radiation absorption, cloud and aerosol effects on heating rate 78—57319
solar radiation absorption, effects of gases, aerosols and clouds 77—37407
solar radiation absorption, vertical and horiz. distrib. 80—72596
solar radiation budget in cloudy atm., modified two-stream approx. 79—58090
solar radiation distribution in cloudy atmosphere 78—3955
solar radiation input in tropical ocean regions, influence of clouds 78—3956
solar radiation scattering, cloud dimensions and orientation effects 77—33188
solar radiation transfer under cumulus cloud conditions, Monte Carlo method *(Russian)* 80—21793
sound attenuation obs. 77—34981
source thermodynamics rel. to snow crystalline forms *(Rumanian)* 77—33169
spiral bands in linear model of cyclonic vortex 77—25736
stability analysis of deep cloud streets 79—2335
stationary homogeneous shallow cumulus cloud field, statistical props. 78—73434
steady convection, two-dimens., in const. vertical shear, dynamical struct. 79—12209
stereophotogrammetric measurements of clouds in tropics, TROPEX data 79—29833
stochastic coagulation clouds, kinetic eqn. 78—92944
stochastic collection equation, computational instability in numerical soln. 77—2211
storm clouds, elec. field obs. *(French)* 80—85712
storm splitting leading to long-lived storms, numerical model 79—58032
stratiform, convection motions 79—53486
stratiform, microphysical model *(French)* 79—84410
stratiform, modelling and effect on radiation balance *(French)* 80—82017
stratiform cloud radar obs., spectral anal. 78—7686
stratiform clouds, horizontal dimensions 78—20490
stratiform clouds, results of meas. of local characts. *(Russian)* 77—53158
stratiform clouds, structure *(Russian)* 78—16088
stratiform ice clouds, precip. development, aircraft and Doppler radar meas. 77—70761
stratocumulus, cloud top entrainment of dry air and cloud breakup 80—90145
stratocumulus, diurnal evolution, radiative scheme in diffuse atmosphere *(French)* 79—84402
stratocumulus, finestructure of precipitation and temperature 79—88418
stratocumulus, IR absorption and liquid water content 77—21858
stratocumulus, supercooled, natural cloud seeding 78—20462
stratocumulus layer, entrainment affected by radiative cooling 80—94573
stratocumulus layer, entrainment leading to turbulence kinetic energy 80—90144
stratocumulus producing anticoronae, microphys. characts. *(French)* 79—53488
stratocumulus-capped planetary boundary layer, entrainment rate *(French)* 79—53489
stratocumulus-topped mixed layer, entrainment rate 77—21859
stratoform cloud dissipation and eddy formation over California coast 77—70732
stratosphere, nature of thin persistent very high clouds over Antarctica 78—36247
stratosphere cirrostratus, obs. over Scotland 79—16627
stratus, IR radiative cooling rate, theory 80—56565
stratus, shortwave radiative effects of unactivated aerosol particles 77—64382
stratus cloud, temp. profiles meas. using low-level atmospheric thermograph 80—105073
stratus cloud and radiative fog, form. and evolution in atmosphere boundary layer *(Russian)* 77—49104
structural effects on radiative divergence budget estimates, GATE 80—17319
subcloud layer over land, temp. and humidity struct. 77—91200
subcloud layer structure and interaction with shallow cumulus layer 77—45079
summer monsoon over S. Asia, break and active phases 78—3912
sunlight reflection by clouds, fast azimuthally dependent model 80—51532
supercooled, drop size distrib. influence on secondary ice particles prod. during graupel growth 78—73481
supercooled cloud, induced snowfall due to power plant plume 78—81284
supercooled water droplet surface effect on ice crystal kinetic formation *(Russian)* 77—13099
supercooled water drops, hydrodynamic behaviour, interaction with columnar ice crystals 78—32205
surface radiative flux, clear and cloudy conditions, parametrisation accuracy 78—77325
surface temperature changes nonlinear response in climate model, ice-albedo, lapse-rate and cloud-top feedbacks 78—69438
Tanggula region, global and net radiation *(Chinese)* 79—92568

clouds continued
temperature and humidity changes and overcloud inversion 80—77083
temperature fluctuation meas. by IR radiometry, feasibility study 80—56636
Thailand tropical atmospheric radiation and sky temp. calc. 79—58084
thermal control, Atmospheric Cloud Physics Laboratory on Spacelab 80—4090
thermal diffusion cloud chamber, continuous flow parallel plate type, analysis w.r.t. atm. water droplet growth 80—36416
thermal diffusion cloud chambers, aspect ratio. rel. to supersaturation distrib. 80—56631
thermal radiation fluxes calc. for cloudy atm. *(Russian)* 80—4103
three-dimensional cloud model, storm and boundary condition simulations 80—77049
thundercloud, positive streamer velocities meas., in quasi-uniform electric fields 80—72625
thundercloud electrification by precip. mechanism in presence of ion generation, model 79—84388
thundercloud structure and interactions in subcloud region 77—45094
thunderclouds, corona charging of frozen precip. 77—5295
thunderclouds, discharging using chaff, microwave radiometric detect. of corona 78—16106
thunderclouds, distrib. in conjugate area of low-latit. whistlers 77—2309
thunderclouds, effect of elec. forces on charge separation caused by combined precip. and convection 80—17333
thunderclouds, elec. field inclination effect on inductive charging mechanism 77—78315
thunderclouds, electrification rel. to sudden increases in shower intensity 78—20491
thunderclouds, infrasonic pulses detect. 77—29362
thunderstorm charging by polarization-induction mechanism 78—32166
thunderstorm electrification, airborne expts. 77—66970
thunderstorm top, ascent rate obs. 80—61861
thunderstorms, contribs. of cloud and precip. particles to elec. cond. and air relaxation time 80—17332
thunderstorms, elec. field growth, field struct. and charge distrib. 77—70777
thunderstorms, elec. fields, precip. elements charge and size, airborne obs. 78—73485
top heights determ. from satellite remote temp. sounding instruments 77—17256
topographic wave clouds in central and northern Urals, characts. 80—101413
tornado-producing cumulonimbus, 1973 June 4, Oklahoma, USA 77—17202
toronado clouds, expected lidar returns 77—21901
trace constituents in Indian west coast SW monsoon clouds 80—81967
trade wind cumuli, turbulence parameterization 78—44931
Transcaucasia, cloud field statistical struct. 78—92942
transfer processes, approx. analysis *(Russian)* 79—34902
tropical atmosphere, phase-lagged wave conditional instability of second kind 80—12513
tropical atmosphere, Taifun-75 data from equatorial Pacific area, typhoons 79—58052
tropical cloud bands, synoptic scale deform. 77—87002
tropical cloud cluster, struct. and evolution 80—12488
tropical cloud clusters, submillimetre radiation obs. from Cosmos 669 *(Russian)* 77—49165
tropical cloud clusters, temp., moisture and precipitation 77—29406
tropical cloud clusters, wind and dynamic fields 77—29405
tropical cumuli, props. and bulk thermodynamic effects 79—8657
tropical cyclone rainband microstructure 79—100927
tropical cyclones, photometric method for estimating cloud cover from satellite data 78—4007
tropical interaction with and modification of the subcloud region 79—34914
tropical iridescent cloud occurrence rel. to tropopause temp. 78—85675
tropical meteorology, review 77—64365
tropical troposphere, three-dimens. wind struct. around cumulus clouds over island 79—5588
tropospheric dynamics, influence of clouds *(Russian)* 79—8653
turbulent and radiative transport interaction in development of fog and low-level stratus 78—81313
turbulent atmosphere, pollution release, exposure freq. distrib. from multiple cloud sources 78—57255
two-dimensional model, incorporating eddy viscosity parameterisation 80—85708
type and amount, objective nephanalysis 79—53541
Typhoon Della, weather conditions in eye of storm 79—29828
Typhoon June (1975), water vapour and clouds liq. water meas. by scanning microwave spectrometer 78—73436
typhoon Ora, form. in intertropical convergence zone under influence of midlevel jets 80—12527
typhoons, intensity change with cloud-plume outflow aloft 77—45107
United Kingdom, cloud freq. distrib. analysis 80—61892
United States, recent increase in sunshine duration rel. to cloudiness 79—20930
urban effects on convective cloud heights, St. Louis region 79—16599
urban effects on precipitation initiation in convective clouds, radar first echoes appl. 79—16601
UV and integrated solar radiation received, influence of cloud layers 79—70883
vapour condensation, aerosol formation, size spectra model *(Russian)* 80—12483
vertically nonuniform stratocumulus water clouds, radiation transfer 77—45146
volcanic eruption clouds in Guatemala, atmospheric studies 80—41505
volcanic plume height, control by eruption energetics and dynamics 78—61381
vortex cloud street during AMTEX 75 79—79988
vortices, pressure from satellite obs. 80—26592
vorticity transport eqn. solns. for Atmospheric Cloud Physics Laboratory 80—94690
warm cloud electricity, shallow axisymmetric cloud model 80—81999
warm cloud microphys. calcs., momentum-conserving numerical techniques 79—58030
warm cloud microphys. calcs., momentum-conserving technique, model testing 79—58031
warm cloud showers, initiation, efficient nuclei mass range 79—58029
warm cumulus, elec. and microphys. meas. before and after seeding 77—56686
warm cumulus, three-dimens. numerical model with microphysical processes *(Russian)* 78—88884
warm fog and steam clouds, emission spectra variations, evidence for clusters in vapour phase 79—39849
warm frontal clouds in midlatitude cyclones, air motion and precipitation 80—109193
water droplet clouds, rate of evaporation, stability 79—52782
water droplet coalescence in turbulent clouds 77—45114
water droplet collision and coalescence for small Reynolds numbers 77—78326
water droplet spectrometry using light scatt. technique 77—41219
water droplet/ice crystal clouds, angular depolarisation and multiple scattering of polarised laser light 80—41549
water droplet/ice crystal clouds, angular scattering of polarised laser light 80—41548
water droplets acidity rel. to SO_4^{2-} prod. 79—5546
water droplets in mists, clouds, size, density distrib. meas., laser remote sensing technique *(Japanese)* 78—49175
water drops, coalescence, theoretical model of approaching drops 78—32207
water drops, coalescence problem, efficiency 78—32208
water drops, collisions, coalescence efficiency, expt. evaluation 78—32206
water drops accel. to terminal vel. 77—78334
water drops collision efficiency in atmosphere 77—29378
water drops crystallisation, kinetic parameters of AgI type reagents *(Russian)* 77—81963
water metastable states, phase diagram *(Russian)* 78—95129
water nucleation on ions, molecular model 77—1222
waterdrop interaction extps., review 78—11974
waterspout frequencies along USA East and Gulf Coasts 77—78329
waterspout in association with large cumulus congestus 80—41473
waterspout of 3 March 1977 at Iraklion, Crete *(German)* 78—16121
waterspout statistics for Nassau, Bahamas 78—92919
wave cloud obs. near Reno, Nevada 77—33121
wave clouds, central US (22 May 1973), comments and reply 79—88423
weather conditions for long gliding flights over England 79—58048
weather maps, for present weather, wind, and ceiling, examples, forecasting use *(German)* 80—4081
weather modification, three dimensional mesoscale models 77—25730
weather modification due to waste heat release from large dry cooling towers 79—84471
weather modification single area expts., confidence limits for seeding effect 79—79948
Wilson Cloud form. by low altitude nuclear explosions, water aerosol and droplets characts. 78—53704
wind derivation from cloud motion fully automated method, Meteostat data comparison with gradient winds 80—109244
wind vector calculation from cloud motion, Meteosat system 80—46270
wind velocity indicated by cumulus motion across sky 80—98418
winds in ocean regions, satellite obs. technique 80—85764
winter cloud systems over Sierra Nevada, liquid water content meas. 77—2213
winter orogaphic cloud seeding project, predictor control for evaluation 78—92922
winter thunderclouds of Hokuriku coast, Japan, elec. dipole struct. 78—73443
Ag cloud seeding of Florida cumuli, rainwater conc. obs. 80—56563
Ag seeding, trace analysis, neutron activation technique 77—17215
AgI pyrotechnic nucleant characts., use in Florida Area Cumulus Expt. 79—100919
AgI seeding review *(French)* 77—78343
Ba cloud striations rel. to bottomside equatorial spread-F 79—75022
CO_2 laser radiation influence on liquid drop cloud medium, dissipation 79—39858
HCl production mechanism, chemical model with trace gases 77—37325
H_2O vapour and cloud liquid determ. by dual freq. ground-based microwave radiometry 78—93007
SO_2 oxidation by O_3 in cloud droplets, HSO_3^- aerosols form. 78—44894
SO_2 oxidation in clouds and rain, O_2, O_3 and H_2O_2 role 79—84351
SO_2, vertical distrib., influence of clouds and rain, one-dimens. model 79—20982
SO_4^{2-} conc. in precip. 79—100915

Clusius-Dickel columns *see isotope separation*

cluster analysis *see pattern recognition*

cluster approximation
abrupt transformation, data partitioning, cluster anal. optimisation 78—36956
AC hopping conductivity, percolative approach, time dependent cluster approx. 80—39577
actinide oxides, chem. bonding, mol. cluster theory 80—10526
alkali halides, F-centre, cluster-Bethe lattice treatment 78—63762
alkali halides, U_2 centres, cluster-Bethe lattice calc. for electronic density of states 79—4531
alkali halides, U-centre, electronic struct., self-consistent model 79—65406
alloy, substitutional, analytic approximation for Herglotz property 79—37946
alloys, density of electronic states, dressed-cluster approx. 78—95249
alloys, disordered, residual resistivity due to clustering, ageing effects 80—65521
alloys, self-consistent cluster theories for diagonal and off-diagonal disorder 79—37950
amorphous Heisenberg ferromagnet, variational cluster method 80—39728
anthracene, isotopically mixed cryst., exciton dynamics 80—29329
antiferromagnet, cluster approximation, Neel temp. and specific heat calc. 80—54901
Ashkin-Teller-Potts model, magnetic indices for percolation problem, renormalisation group approach 79—63163
benzene, cryst., molecular exciton cluster states and spectra 77—66123
benzene-deuterate benzene cryst., triplet migration, cluster method 79—73510
Bethe lattice, bootstrap percolation 79—30376
binary alloy, one-dimens., embedded-cluster calcs. of phonon spectra 79—77703
binary alloys, disordered, electronic struct. 77—15755
binary alloys, electronic density of states, generalized cluster-Bethe-lattice approach 79—42432

cluster approximation continued
  - binary disordered system, effective-medium theories and augmented-space method 79—60668
  - binary lattice gas, crit. phenomena, cluster expansions and transcriptions 80—4670
  - bond percolation model, site-cluster distribs. and eqn. of state 77—74329
  - borate glasses, effects of clusetring and transition metal ions on electronic struct. 78—10347
  - boson gas, rigorous second-order cumulant expansion 79—44853
  - boundary free energy for phase interface, scalar-prod. expression, Ising model and cluster approx. 78—34591
  - charged particle moving in medium, electron density fluctuations, plasmons, wakes and clusters 79—47032
  - chemisorption, appl. of cluster techniques, book contrib. 80—107650
  - chemisorption of H on large cluster, bonding energy, HF calc. 79—39204
  - classical canonical ensemble 78—49752
  - cluster expansion formalism, independ. pair correlations 78—73922
  - cluster shapes at percolation threshold, effective cluster dimensionality, connection with percolation critical exponents 79—63166
  - cluster size and shape in random and correlated percolation 79—35633
  - covalent crystals., defect states, many-electron approach 78—67980
  - critical fluctuations, cluster dynamics 77—13725
  - crystal field theory, Hamiltonians of small perturbations, cluster model 77—24538
  - CSEM and CPA methods, comparison 77—4280
  - defect, energy of formation, Gibbs free energy 78—91332
  - diamond, cluster, electronic struct. of deep levels, LCAO, SCF method 79—82555
  - diamond, five-atom clusters, unrestricted Hartree-Fock calcs. 77—11866
  - diamond, neutral vacancy, generalised val. bond calc. 77—55493
  - dilute ferromagnet, slow neutron inelastic scatt. by spin excitations, cluster approx. 80—11168
  - dilute ferromagnetic systems, cluster theory, second-neighbour interaction 77—89965
  - dilute Heisenberg magnet, cluster expansion 80—15734
  - disordered alloy, self-consistent boundary site approx. in cluster theories 79—19500
  - disordered media, elec. transport theories, effective medium approx. improvement 79—47071
  - disordered system, ensemble averaged Green function, analytic approx. 77—11842
  - disordered system, low-freq. cond. due to variable range hopping, cluster approx. 80—92886
  - disordered systems, AC hopping cond., cluster approx., one-dimens. systems 79—95379
  - disordered systems, cluster approx. in theory of AC hopping cond. 80—2372
  - disordered systems, short-range order and off-diagonal randomness 78—75782
  - doped semiconductors, impurity states, cluster model 80—20117
  - electron correlation problems, lattice statistical aspects, Gutzwiller approx. 78—84160
  - electron correlations, ground state results in high density regime 78—72097
  - electron density of states, self consistent cluster-Bethe lattice calc. 78—67930
  - electron density of states of a crystal and infinite cluster 80—10850
  - electron gas, correlation energy, appl. of coupled cluster approx. 78—72102
  - electron gas, coupled-cluster expansion, inclusion of ring and exchange effects 77—76764
  - electron gas, Hubbard model at low temp., mag. props. *(Russian)* 78—43550
  - electronic structure of solids, appl. of fast self-consistent cluster calc. for large systems 79—82513
  - electronic transport in substitutionally disordered system, derivation of cluster approx. 78—84184
  - extrinsic semiconductors, impurity interaction and metal-nonmetal transition 80—29325
  - FCC clusters, size and shape depend., tight binding approximation 78—79920
  - FCC Ising ferromagnet., cluster variation approx. 78—68278
  - FCC lattices, ordered superstruct., phase diagrams, cluster variation calc. 80—39256
  - fermion clusters, many particle correlations, method of transition density operators 78—49763
  - ferromagnet with random anisotropy, Curie temp., constant coupling approx. 78—76264
  - ferromagnetic alloy, cluster-Bethe-lattice approximation of magnon states 77—32181
  - ferromagnetism, Bethe-Peierls-Weiss model, phase transition calc. 79—2585
  - finite disordered Hubbard cluster, thermodynamic and mag. props. 77—85409
  - fluctuations, wavevector depend. in cluster approx., appl. to one-dimens. Ising model 80—12999
  - generalised Mobius functions for rectangles on square lattice 78—36938
  - graphite, electronic props., self consistent LCAO calc., point vacancy in 2-dimens. cryst. 78—51932
  - graphite, Wannier functions and density matrix determ. in terms of localised orbitals 78—2408
  - graphite vacancy and substitutional impurities, moderately-large-embedded-cluster approach 80—49663
  - Heisenberg dilute systems, computer simulation, mag. conc. of clusters, linearised eqns. of motion 79—78409
  - Heisenberg ferromagnet, structural disorder effects on Curie temp. 79—78417
  - Heisenberg ferromagnet, structurally disordered, variational method for cluster model 78—91839
  - Heisenberg magnet, constant coupling approx., derivation 78—76213
  - Heisenberg model, random, thermodynamics 77—16032
  - Heisenberg random ferromag. 79—82807
  - HF approach, cluster-environment interaction 78—84117
  - homomorphic cluster coherent pot. approx., appl. to random systems 79 90930
  - homomorphic cluster CPA, rigorous proof for analyticity 79—19504
  - homomorphic cluster CPA analyticity 79—90929
  - Hubbard model, cluster-variation method in two-site approx. at high temp. 80—7071
  - Hubbard model, mag. field effect on Mott transition 78—34748

cluster approximation continued
  - Hubbard model, off-diagonal long-range order 77—28118
  - Hubbard model, single band, magnetic phase diagram, cluster variational calc. 80—60340
  - impurity cluster pairs, lattice localised modes 79—33058
  - impurity ion clusters in a two-dimensional lattice 78—23047
  - insulators, charge transfer processes influence on cryst. field 80—92865
  - interface modelling, Xα-scatt. wave cluster approach 80—49851
  - invariant Gibbs states, cluster props., surface tension 79—49172
  - irreducible cluster expansion for the logarithm of the s-particle density matrix of a many-boson system 79—21657
  - Ising cluster size and shape, Whitney polynomial 79—33080
  - Ising model, boundary free energy, natural iteration and cluster variation methods, critical points 77—17913
  - Ising model, cluster size and boundary distrib. near percolation limit threshold 77—20624
  - Ising model, cluster size and percolation 79—65630
  - Ising model, percolation points and critical point 77—20608
  - Ising model, quenched-bond disorder, cluster extension of effective-interaction approximation 80—93130
  - Ising model, relax. dynamics *(Russian)* 78—10635
  - Ising model, temp. depend. of domain wall parameters 79—69797
  - Ising model, two-dimensional renormalisation group approach 78—52261
  - Ising two-dimensional spin systems, decimation transforms. 77—77017
  - itinerant ferromagnet in disordered phase, energy band struct. 78—68141
  - largest cluster at two dimensional percolation threshold, Hausdorff dimens. and fluctuations 80—46982
  - lattice gas with finite range attractive potentials, cluster and percolation inequalities 77—61029
  - lattice system, distrib. of physical clusters 77—17916
  - Leman-Weaire-Thorpe theorem generalisation 79—95308
  - lightly doped, 1/f noise for hopping conduction, theory 80—44683
  - localised site cluster expansion, interacting paramagnetic sites, spin symmetry projection 79—7951
  - magnetic impurities and Kondo effect, theoretical model 79—33455
  - many body systems, Anderson model, localisation phenomena, state variable randomness, perturbation theory 80—29297
  - many-electron systems, ionis, pot., excitation energy, cluster expansion direct calcs. 79—26912
  - metal cluster, electronic spectrum fluctuations, appl. to Ni and Ti 79—19501
  - metal cluster, H site, SCF-Xα-MS calc. 78—47730
  - metal particles, small, characterisation and props., book contrib. 80—84417
  - metal-adsorbate system, appl. of cluster model theory, book contrib. 80—24991
  - microclusters, electric viewpoint of morphology, energy spectrum of single electron states 78—10327
  - microclusters, morphology, Hund and Jahn-Teller tendencies 79—46996
  - mixed diatomic system, cluster approx. for spectral density 79—51991
  - molecule, transition energy, direct calc., response function approach, multiple cluster expansion formalism 79—72293
  - muffin-tin orbitals and total energy of atomic clusters 77—47708
  - muffin-tin potential cluster calculations, scattering theory 78—18940
  - multiphonon relax., localised electron radiationless decay, continuum and cluster modes 77—52158
  - multiple scattering techniques 79—56105
  - multiple scattering X_α treatment, of scattering states of clusters 77—30747
  - multishell method, exact calc. of cluster in effective medium 78—10319
  - naphthalene, exciton migration, variable range cluster model 79—33762
  - naphthalene-h_8 and -d_8 mixed crystal, two-dimens. lattice, cluster-cluster interactions, model inhomogeneous distribs. 79—23922
  - narrow band systems, momentum distrib., cluster var. method 78—72060
  - nonideal system, thermodynamic variables, irreducible cluster integrals 77—67394
  - nonperturbative open shell theory, mol. ionisation pot. and excitation energies, HF multiple cluster expansion 79—22599
  - one dimensional fermion system, thermodynamics by cluster expansions 77—41535
  - one-dimensional Fermi system, mag. susceptibility, and dielec. function of two-dimensional Coulomb gas 78—10387
  - one-dimensional fermion system, cluster expansion methods and thermodynamics 78—6289
  - open-shell clusters, semiempirical LCAO-MO method of energy spectrum and electronic struct. calc. 80—54583
  - order-disorder transitions, cluster approach 79—94943
  - order-disorder transitions, relax. processes, under short range correl. conditions 79—73889
  - orthophosphates, dynamics of ferroactive cryst. 79—37801
  - percolation clusters density profiles, lattice animals 79—93075
  - percolation theory kinetic eqns., Bethe lattice in spin-glass limit 79—97309
  - permutation group irreducible representation 77—23416
  - plane wave set, orthogonalised, construction method, bound states 79—25894
  - plasma, weakly ionised, ion interaction through phonon exchange in neutral gas 79—27775
  - plasma, weakly ionised, ion interactions through acoustic field, plasmoid existence 79—27776
  - polymer chain, self interacting, Legendre transformation 80—15018
  - quantum single- and multi-component systems, modified cluster expansion method 77—2609
  - α-quartz, CNDO/2 calcs., electronic props. of perfect cluster, EPR parameters of O^- vacancy 80—107701
  - random alloy with short-range order, iterative calc. of energy levels 77—66104
  - random binary alloy with partial order, electronic struct., self-consistent approx. 77—62796
  - random Ising model, variational principle for distrib. function in the Bethe approx. 80—15674
  - random media, hopping transport simulation, cluster method 79—73510
  - random walk, self-avoiding, direct renormalisation group approach 78—73933
  - rare earth alloys, amorphous random anisotropy ferromagnetism in pair approx. 79—47276
  - rare gas clusters, small, structure, thermodynamic properties 80—88341
  - refractory metal compounds, electronic structure and chem. bonding 79—27948
  - renormalisation group for site and bond percolation, real space 77—45803

cluster approximation continued
  S-matrix formulation of cluster expansion in statistical mechanics *(German)* 78—41256
  scaling function in 2-D site percolation, cluster size distribution 78—24742
  semiconductor, cluster type effect on band struct. 77—28109
  semiconductor, covalent, molecular cluster model 78—43283
  semiconductor, deep transition metal impurity states, SCF CNDO cluster calcs. 80—100442
  semiconductor, with defects or impurities, local density of electron states 80—92857
  semiconductor amorphous, tetrahedrally bonded, electronic density of states calc. 77—8002
  semiconductors, doped, shallow impurity states, Hubbard bands and donor excitonic states, HF calc. 80—100443
  Si (111), surface relax., EHT and cluster calcs. *(Chinese)* 80—59762
  site random conductance networks, cluster approx. in effective medium model 78—19011
  solid electrolyte, mobility paths for MI_4^{-3} clusters, ab initio electronic struct. calcs. 80—70458
  solid solution theory, quasi-particles method 80—24560
  solids, local defects, moderately-large-embedded-cluster approach 80—49663
  spin glass, cluster mean field theory and evidence for spin clusters 79—78382
  spin glasses, Ising long and short ranged bond models in cluster approx. 80—20419
  spin glasses, thermodynamic props., cluster mean-field theory using Ising Hamiltonian 79—33499
  spin-glass, two-dimensional Ising model, low temp. dynamic props. 80—20425
  spinel solid solutions, $A_xB_{3-x}O_4$ type, quasichemical method of cluster components, electron exchange allowance 79—51475
  spinel systems, prop.-comp. relationship, electron exchange effect *(Russian)* 78—47524
  square lattice, appl. of real-space renormalisation group to site percolation 79—30377
  square lattice, percolation and cluster distrib. variable range interactions, exciton cluster model, layers 79—30379
  square lattice Potts model, corrections to series expansions 77—17917
  strongly coupled Jahn-Teller system, cluster model for optical absorption spectrum 80—89034
  substitutionally disordered systems, analytic extension of CPA to clusters 79—19503
  surface studies, cluster Bethe-lattice method appl. 80—49852
  symmetrical clusters, higher order isotropic exchange 77—51712
  symmetry-adapted-cluster expansion, variational determ., open-shell orbital theory applic. 78—54213
  tetrahedrally coordinated covalent semiconductor point defects, multiple scatt. Xα model 80—54636
  tetrahedrally coordinated semiconductors, electronic nature of vacancies 77—62863
  three-state Potts model variant, phase behaviour 78—68259
  tight binding model for clusters of arbitrary size, soln. of eigenvalue problem 77—43464
  transition metal, local densities of states and bonding props. 77—20401
  transition metal alloys, cluster model for sigma phase occurrence 77—59750
  transition metal alloys, ferromag. local ordering effect on spin wave stiffness const. 77—66282
  transition metal complexes, discrete variational Xα cluster calcs. 80—15444
  transition metal dichalcogenides, octahedral intercalate ordering study by electron diffr. 80—15076
  3d transition metal ions in crystals, Jahn-Teller coupling constants calcs. 80—49679
  transition metal surface, chemisorbed H_2, Hartree-Fock-Slater model cluster calc. 78—26929
  transition metal surface, electron states at steps, cluster-Bethe lattice approx. 78—52045
  transition metal surface clusters, Hartree-Fock-Slater model calcs. 77—72899
  transition metals, Fe series, interstitial H, cluster model for bonding mechanism 79—60753
  transition-metal compounds, effects of electron transfer on shake-up satellites, model calc. 78—95650
  two dimensional percolation, crit. amplitudes, universality test 77—13727
  two-dimensional Ising model, real space renormalisation transform. 78—2687
  two-dimensional lattice, cluster expansion method 78—34942
  two-dimensional percolation, cluster size distrib. 77—9967
  uniform cluster estimates for lattice models 79—25992
  variational, localised site cluster expansion, wave function higher ansatze, linear Heisenberg model 79—7959
  variational localised site cluster expansion, wave function ansatze, many body theory 79—6827
  variational localised-site cluster expansions, dimerisation in linear Heisenberg chains 79—60670
  variational localised-site cluster expansions, many-body VB theory 79—60669
  vibronically coupled systems 79—19540
  Ag (111) surface, adsorption of I, cluster calc. with Xα scattered wave method 77—31894
  Ag, electronic density of states, cluster approx., compared with photoemission spectra 79—60675
  Ag-Cu, surface segregation, electronic theory, density of states, cluster-Bethe-lattice approx. 80—49369
  Al, adsorption of O_2, relation between energy-band and cluster model 78—52048
  Al, SCF Xα scattered wave calc. for clusters up to 43 atoms 78—10323
  Al-Cu, disordered, electron energy struct. and X-ray emission bands, average t-matrix approx. *(Russian)* 80—24779
  AlZn, disordered, residual resistivity due to clustering, ageing effects 80—65521
  Al(111), chemisorption of O_2, SCF X_α scatt. wave MO calc. 79—42374
  AmO, and AmO_2, electronic struct. and chem. bonding and XPS line shape calcs. 79—33264
  As, amorphous, electronic struct. of defects using cluster-Bethe-lattice method 79—73471
  Au, electronic density of states, cluster approx., compared with photoemission spectra 79—60675

cluster approximation continued
  Au-Ag(Cu), surface segregation, electronic theory, density of states, cluster-Bethe-lattice approx. 80—49369
  BN, Wannier functions and density matrix determ. in terms of localised orbitals 78—2408
  $BaTiO_3$, cluster surface states, LCAO calc. 77—43686
  $BaTiO_3$, electronic props., SCF-MS-Xα calc. 80—54607
  BkO, and BkO_2, electronic struct. and chem. bonding and XPS line shape calcs. 79—33264
  C allotropes, diamond, graphite, gas-solid interface, electronic struct. HFR calc. 80—54745
  CO, chemisorbed on graphite, CNDO calc. using cluster model 80—54522
  CO chemisorption on Ni, Pd, Pt, Ir, mol. cluster calc. 80—100407
  CdS, amorphous antiferromag., mag. props. of dilute neutral donors 79—78367
  CmO, and CmO_2, electronic struct. and chem. bonding and XPS line shape calcs. 79—33264
  CoAl, electronic struct., cluster calc. 77—69209
  $Co_{1-p}Mg_pCl_2$, magnetic excitations, antiferromagnetic resonance spectra response simulation 79—99775
  CoO, unrestricted Hartree-Fock calc. for cluster model 80—2320
  $CsCoCl_3$, 1-D Ising antiferromag., mag. phase transitions 79—51779
  $CsMnFeF_6$, neutron scatt. and magnetisation meas. 77—66258
  $Cs_{11}O_3$, ionic clusters in alkali metal suboxide cryst., struct., vibr. freqs., Raman spectra 79—37772
  Cu, chemisorption of N atoms, electronic struct. of Cu_5N cluster, Xα scattered-wave calcs. 79—60902
  Cu, chemisorption of O, S, Se, NO and O_2, cluster theory 80—29264
  Cu, electronic density of states, cluster approx., compared with photoemission spectra 79—60675
  Cu, lattice and force consts., pairwise atomic repulsions in cluster model 79—32939
  Cu, lattice relaxation around μ^+ 79—56658
  Cu surface, with chemisorbed CO, cluster calc. using SCF-Xα-scatt. wave method 77—62742
  Cu-Ni alloys, density of states determ. by continued fraction method 78—47690
  Cu-Ni(Fe)(Mn)(V), dil., local mag. moments and Kondo effect, theoretical model 79—69651
  Cu_4 clusters, electronic structures, SCF-Xα-SW method 80—88468
  CuCl, electronic struct., ab initio HF SCF MO calcs. of $CuCl_4^{3-}$ cluster 78—95262
  $Cu_{75}Mn_{25}$, concentrated spin glass, changes in mag. cluster size 79—69685
  Cu_3Zn clusters, electronic structures, SCF-Xα-SW method 80—88468
  Fe, ferromagnetic, cluster method, environmental effects 78—95405
  α-Fe, lattice and force consts., pairwise atomic repulsions in cluster model 79—32939
  Fe, martensite, molecular cluster theory for electronic struct. 77—55497
  Fe-Al systems, band struct. and cluster calcs. 79—51480
  Fe-O compounds, MO cluster calc. of charge densities and elec. field gradients 77—76783
  FeAl, electronic struct., cluster calc. 77—69209
  $Fe(CN)_6$, Mossbauer isomer shift const., ab initio SCF calcs. 78—43751
  FeF_2, electronic struct., charge density and elec. field gradient, MO cluster calc. 77—51704
  FeF_6, Mossbauer isomer shift const., ab initio SCF calcs. 78—43751
  Fe_3O_4, doped, electron correls. above and below Verwey transition, Green function theory 77—51687
  GaAs (110), surface electronic struct. calcs. 80—80343
  GaAs, (110) surface structure, rotational relaxation, cluster model *(Chinese)* 80—107621
  GaAs, electronic struct., mol. cluster model, SCF multiple scatt. method 79—42446
  GaAs surface, cluster model approach for electronic struct. 78—56205
  GaAs, vacancies Xalpha cluster model, electronic dangling bond effect elimination 79—99504
  GaAs:Cr^{2+}, cluster calcs. of Cr^2 electronic states 79—87064
  GaAs:Cu, multiple scatt. Xalpha cluster model, impurity electronic states, dangling bond effect elimination 79—99504
  GaAs:Se, multiple scatt. Xalpha cluster model, impurity electronic states, dangling bond effect elimination 79—99504
  GaP(Sb)(As), (110) surface, trned in energy distribs. of Ga dangling orbital surface states 79—28397
  Ge surface, Cl chemisorption, cluster calc. by iterative EHT 77—32062
  Ge, surface, cluster model approach for electronic struct. 78—56205
  Ge:H, amorphous, H-states exam. 78—39059
  Ge(111), chemisorption of Cl, threefold co-ordinated site chemisorption, cluster model calc., extended Huckel theory 78—39178
  $Hg_{1-x}Mn_xTe$, mag. props., self-consistent two spin cluster model 80—54874
  KCl, F-centre first excited state radiationless decay, cluster model 77—52158
  KDP-type crystals, polarisation, dielec. const. thermodyn. props. 77—59527
  KD_2PO_4-type crysts., relax. processes in order-disorder transitions under short range correl. conditions 79—73889
  KH_2PO_4, press. and deuteration effects on static ferroelec. props., four-particle cluster approx. 80—34861
  KH_2PO_4-type cpds., collective vibr. of protons, cluster approx. 79—51210
  KH_2PO_4-type crystal, LF dynamics 80—10602
  $KNbO_3$, electronic props., SCF-MS-Xα calc. 80—54607
  $KNi_xMn_{1-x}F_3$, two-magnon Raman scatt. 77—66509
  $KTaO_3$, electronic props., SCF-MS-Xα calc. 80—54607
  $KZnF_3$:V^{2+}, calc. of t_{2g} antibonding mol. orbital in $|VF_6|^4$, rel. to ESR 80—50174
  $LaCl_3$:Pr^{3+}, crystal field parameters using multiple-scatt.-X_α method 78—95271
  Li (100), O adsorption, cluster models, ab initio HF LCAO theory 78—71978
  Li Al, electronic struct., mol. cluster calc. 78—14649
  Li, entropy and enthalpy of solution of H 78—51692
  Li_3AsO_4, electronic struct. of AsO_4^{3-} clusters 79—65417
  LiCl, aqueous soln., self consistent wavefunctions, HFS Xα pot. in cluster model, Compton profile calc. 79—78783
  LiCl:Cu^+, luminescent centre, cluster MO calculation of energy levels 78—64411
  LiCl:Cu^+, MO calc. of luminesc. Cu^+ centres 79—38609
  LiF, LCAO calc. of Compton profiles 79—95871
  LiH, cluster cryst., extended HMO calc. of defects 79—51521

cluster approximation continued
Li_2SeO_4, electronic struct. of SeO_4^{2-} clusters 79−65417
NH_4HSO_4-type crystal, ferroelectric phase transform. model, SO_4 group ordering 77−77156
Na entropy and enthalpy of solution of O(N)(C)(H) 78−51692
Na, metallic, Auger cross relaxation energy, SCF cluster model calc. 79−46945
NaCl, electronic struct., SCF cryst. cluster model 80−24792
NaV_6O_{15} monocrystal, electronic struct. and X-ray emission spectra anisotropy 80−84807
Na_xWO_4, cluster model 78−10351
Nb clusters, scattered wave $X\alpha$ calcs. 79−15068
Nb_6 clusters, electronic struct., scattered wave-$X\alpha$ calc. 79−11053
NbC, chemical bonding and X-ray emission spectral analysis 77−44088
NbC, electronic struct. of vacancies, effect on supercond. transition temp. 80−29347
NbC, valence band XPS meas., comparison with X-ray emission spectra and band struct. spectral calcs. 80−50535
NbN, chemical bonding and X-ray emission spectral analysis 77−44088
NbO chemical bonding and X-ray emission spectral analysis 77−44088
NbO, electronic struct. from photoelec.- and X-ray emission spectra and X_α calcs. of NbO_6^{-10} cluster 79−23892
Ni, adsorption of N_2, photoemission and electronic struct., cluster calcs. 80−97403
Ni, chemisorption of H, $X\alpha$ cluster calcs. *(Japanese)* 78−72002
Ni, chemisorption of O, S, Se, NO and O_2, cluster theory 80−29264
Ni, chemisorption of S and Se, $X\alpha$ cluster model calcs. 79−65313
Ni, cluster approach to single H atom in single crystal 78−47334
Ni clusters local densities of states 80−88466
Ni compound, $[Ni_3(CO)_6]_n^{2-}$, n=1,2, one-electron states in polynuclear carbonyls 79−95358
Ni, FCC, H-Ni_n self-consistent electronic screening charge density 79−33255
Ni, lattice and force consts., pairwise atomic repulsions in cluster model 79−32939
Ni, muon hyperfine field, cluster calc. 79−56661
Ni:He, defect props., quantum-chemical and lattice-defect hybrid approach 79−4528
Ni-Cu, ferromag., mag. moment, local environment effects, HF CPA cluster calc. 80−65817
Ni-H system, cluster calc. of electronic struct. of interstitital H 78−43326
NiAl, electronic struct. by cluster calc., comparison with self-consistent APW method 77−69209
β'-NiAl, self consistent embedded cluster model for Fe, Co, Ni mag. impurities 80−2549
β'-NiAl, self-consistent embedded-cluster model for mag. impurities 78−67973
NiO (001) surface, chemisorption of H, surface and second-layer defect effects 80−65369
NiO, bulk props., initial state MO Ni_4O_4 and $Ni_{13}O_{14}$, cluster model, lattice and force consts., photoemission and CT absorpt. spectra 80−84828
NiO, cluster model, unrestricted Hartree-Fock calcs. 77−85125
NiO, H chemisorption, cluster model, bonding 78−38939
NiO, H chemisorption, perfect surfaces, cation vacancies, self-consistent HF-VB calcs. 79−69351
Ni_3Ti, electronic struct., $X\alpha$ calc., photoelectron and AES spectra 80−20769
$NpAl_4$ clusters, band struct., variational $X\alpha$ calc. 79−4508
$NpAl_4$, clusters, X_α calculations *(Japanese)* 79−82519
NpO, and NpO_2, electronic struct. and chem. bonding and XPS line shape calcs. 79−33264
$PbHPO_4$-type crystals, ferroelec. transition, statistical model 80−25321
$PbMo_6S_8$, Chevrel-phase, electronic struct., LCAO calc. for idealised Mo_6S_8 cluster 77−43494
PbS, first-principles calc. of eqn. of states 80−49649
Pd-Er, fine struct. of Er^{3+}, dynamic Jahn-Teller effect of electronic Γ_8 quartet 77−35895
Pd-H system, cluster calc. of electronic struct. of interstitial H 78−43326
Pd-H sytem, electronic struct. of H, mol. cluster and pseudojellium models 80−24832
Pt compound, $[Pt_3(CO)_6]_n^{2-}$, n=1,2, one-electron states in polynuclear carbonyls 79−95358
$PuAl_4$ clusters, band struct., variational $X\alpha$ calc. 79−4508
$PuAl_4$, clusters, X_α calculations *(Japanese)* 79−82519
PuO, and PuO_2, electronic struct. and chem. bonding and XPS line shape calcs. 79−33264
Rb_2NiF_4, planar antiferromagnet, cluster-Bethe-lattice method 80−22306
Rb_9O_2, ionic clusters in alkali metal suboxide cryst., struct., vibr. freqs., Raman spectra 79−37772
Sb_2O_3, XPS, electronic struct. calcs. using scattered wave method 79−11502
Si (111), adsorption of Cl, electronic energy states, cluster-type calcs. 79−47149
Si (111) surface, relax. of surface atoms, Si_4H_9 clusters 77−35980
Si, deep level defects, struct. bonding, amphoteric centres 80−88506
Si, divacancy, positive, EHT calcs. 79−99184
Si, energy spectrum of Fe group impurities 79−23932
Si, neutral vacancy, generalised val. bond calc. 77−55493
Si, reconstructed surface physics, review 80 -10766
Si surface, Cl chemisorption, cluster calc. by iterative EHT 77−32062
Si, surface, cluster model approach for electronic struct. 78−56205
β-SiC, cubic, electronic props. of vacancies and divacancies 77−76767
Si_5H_{12} cluster, Si valence band Auger spectrum, cluster approach, comparison with experimental spectrum 80−40191
SiO_2, amorphous and α-cristobalite cryst., band struct., photoelectron and X-ray spectra interpret. 80−24787
SiO_2 clusters, CNDO/2 calc., appl. of cyclic boundary conditions 78−72110
SiO_2, g-tensor and ^{29}Si hyperfine tensors of E_1'-centre for model of O^- vacancy 79−19777
SiO_2, g-tensor of interstitial O and broken Si-O bond, MO model calc. 79−78520
SiO_2 polymorphs, CNDO/2 MO calc. 80−6386
SiO_x system, cluster plus effective medium tight-binding study 79−33216
$SrTiO_3$ (100) surface electronic structure, DV-$X\alpha$ cluster method 80−39646
$SrTiO_3$, cluster surface states, LCAO calc. 77−43686

cluster approximation continued
TaS_3(1T), inequivalent lattice sites in charge density distorted phases 80−15835
$ThAl_4$ clusters, X_α calculations *(Japanese)* 79−82519
ThO_2, electronic struct. and bonding, molecular cluster approx. 77−51657
Ti-H system, cluster calc. of electronic struct. of interstitial H 78−43326
TiC, electronic struct. and XPS, cluster method and band struct. 79−60710
TiC, TiC_6^{20-} cluster electron state, MS $X\alpha$ calculations 77−8037
TiC, X-ray emission spectra and chem. bonding 77−20958
TiN, X-ray emission spectra and chem. bonding 77−20958
TiO, X-ray emission spectra and chem. bonding 77−20958
TiO_2, cluster surface states, LCAO calc., electron energy loss peak interpretation 77−43686
TiO_2, clusters, surface electron struct. and defect states, DV-$X\alpha$ calc. 80−20268
TiO_2, OH^- adsorption on defect site, electronic struct. 79−47150
TiO_2, surface electronic struct. by discrete variational $X\alpha$ cluster calc. 78−43449
$Ti_xV_{1-x}C$, electronic struct. and X-ray emission spectra, cluster MO calc. 80−65444
UAl_4, clusters, band struct., variational $X\alpha$ calc. 79−4508
UAl_4, clusters, X_α calculations *(Japanese)* 79−82519
UO_2, electronic struct. and bonding, molecular cluster approx. 77−51657
$(UO_8)^{12-}$, electronic struct., variational Xalpha cluster calc. 80−39499
$(UX_6)^{n}$, X=N,O,S, electronic struct., variational Xalpha cluster calc. 80−39499
VN, electronic struct. of vacancies, effect on supercond. transition temp. 80−29347
VO, octahedral clusters, electronic struct., $X\alpha$ discrete variation and SW methods 78−63976
VO_2 clusters in metallic and semiconductor phases, electronic struct., $X\alpha$ calcs. 78−63977
V_2O_5, electronic and band struct. and spectra, CNDO CI cluster method 79−11091
V_3Si, electronic struct., charge distrib. and X-ray emission spectra 79−51481
W, chemisorption of H_2, HFS model cluster calcs. 77−51795
WC, small clusters, one-electron energy levels and charge densities determ. 77−59253
$W_xNb_yO_z$ ordering of atom string, cluster model 77−68959
YOF, electronic stuct. calcs. from XPS and X-ray emission spectra 80−35056
YVO_4, soft X-ray APS study of empty electron states, VO_4^{3} cluster model 80−25488
Zn_6 clusters, electronic structures, SCF-$X\alpha$-SW method 80−88468
ZnS:Mn^{2+}, $^4T_2$ level, Zeeman splittings, Jahn-Teller effect 80−40141
ZnSe, electronic struct. of charged Zn vacancy, cluster model 77−47764
Zr, charge-density anal. using cluster calc. 79−69958
ZrC, electronic struct. and XPS, cluster method and band struct. 79−60710
$ZrH_{1.65}$, charge-density anal. using cluster calc. 79−69958

cluster model (nuclear) *see nuclear cluster model*

clustering, impurity *see segregation*

clustering, solute *see segregation*

clusters, atomic *see atomic clusters*

clusters, globular (stellar) *see globular star clusters*

clusters, metal *see metal clusters*

clusters, molecular *see molecular clusters*

clusters, stellar *see stellar clusters and associations*

clusters of galaxies
see also galaxies; intergalactic matter
0915+320, wide-angle-tail radio source in group of galaxies, 4.9 GHz map 78−93441
A194, radial vels. 77−53691
Abel 1060 cluster, X-ray spectrum obs. by (HEAO A-2) 80−82518
Abel 2029, cD galaxy dynamics struct. 79−92850
Abel 2197, 2199, struct. of isophotes of elliptical galaxies 78−41058
Abell 1146, photometry, isophotal magnitudes and luminosity function 79−67105
Abell 1314, 1.4 GHz obs. of head-tail radiogalaxies IC 708 and 711 77−60833
Abell 1367, 17 W list from 610 and 1415 MHz obs. 79−35401
Abell 1367, H I deficient spiral galaxies 79−17072
Abell 1367, obs. rel. to galaxies redshift-magnitude bands and evolution 78−54033
Abell 1367 central region, peculiar radio sources Westerbork obs. 79−2574
Abell 1775, supermassive double VV 5-32-63/64 investigated 80−8693
Abell 1781, photometry of field galaxies 78−77609
Abell 1831, statistical and photometric study 80−51885
Abell 193, BV photometry of galaxies *(Russian)* 77−22319
Abell 193, list of 140 compact galaxies in neighbourhood 79−88736
Abell 193 and 2255, ellipticities of member galaxies *(Russian)* 79−8986
Abell 194, dynamical anal. using Multi Mass Model 80−98726
Abell 2029, radio and SAS 3 X-ray obs. 80−82519
Abell 2118 cluster, extent of hot intergalactic gas 78−86021
Abell 2142, spectroscopic obs. of X-ray cluster (40 1556+27) 79−48940
Abell 2197, 2199, giant galaxies optical extent rel. to clusters total masses 77−45557
Abell 2197 and 2199, Westerbork survey at 610 MHz, 18W catalogue 80−67883
Abell 2199, 3.5 and 4.0 mm obs. of central regions *(Russian)* 80−82525
Abell 2218, complex radiosource in centre, 2.7 GHz obs. 79−30137
Abell 2241, candidate X-ray cluster of galaxies, redshifts 77−17699
Abell 2255, red shifts of galaxies 79−40276
Abell 2256, X-ray cluster, steep-spectrum radiosource obs. 79−9016
Abell 2256, X-ray cluster of galaxies, radio props. 80−36726
Abell 2319, X-ray and radio obs. 77−53692
Abell 262, redshifts meas. 77−45579
Abell 2634, luminosity function *(Russian)* 78−28801
Abell 2634, radiosources around 3C 465, continuum maps 78−73764
Abell 2634, spectroscopic study and radial vels. 77−64857
Abell 2670, luminosity functions 78−16545
Abell 399/Abell 401, X-ray binary galaxy cluster, mass 80−90546
Abell 401, spectral obs. of halo of cD galaxy 78−32584

clusters of galaxies continued
- Abell 401, vel. dispersion meas. 77−26072
- Abell 401, X-ray cluster of galaxies, radio emission distrib. 80−98731
- Abell 401 and 2670, surface brightness distrib. of elliptical galaxies in cD clusters 79−97073
- Abell 426 and 1367, surface brightness and colour distribs. of elliptical galaxies 78−81681
- Abell 478, X-ray and radio obs. 78−8133
- Abell 478, X-ray cluster of galaxies, redshift and optical struct. 78−8134
- Abell 643, 1562, rich clusters with classical double radio sources, interferometric obs. 78−57662
- Abell 754, HEAO-1 pointed obs. 78−7856
- Abell 754, radio and optical obs. 79−25737
- Abell 754 (3U 0901-09), 2695 MHz radio obs. 77−26089
- Abell and Shane-Wirtanen catalogues, cross-correl. anal. 78−4118
- Abell cluster, lunar occultation obs. at 327 MHz, survey 80−73052
- Abell cluster radio sources, spectra and optical identification, SHF obs. 80−98729
- Abell clusters, 3-D nearest neighbours test 80−90545
- Abell clusters, 4C radio sources struct. and props. in declination ranges 10 to 20° and >50° 79−25743
- Abell clusters, 4C radiosources 79−88756
- Abell clusters, complex radio sources obs. at 2.7 GHz 79−92881
- Abell clusters, evidence against real existence 80−101643
- Abell clusters, galaxy distribs. in 10 groups 80−46682
- Abell clusters, interferometric obs. of radiosources 78−4380
- Abell clusters, mean mass from Hubble diagram scatter 77−13474
- Abell clusters, photometric study 78−4370
- Abell clusters, radio survey at 11.1 cm wavelength 79−58432
- Abell clusters, search for radio sources 78−12379
- Abell clusters, Westerbork aperture synthesis obs. of radio galaxies 78−12360
- Abell clusters, X-ray luminosity function 78−36704
- Abell clusters 401 and 399, possible gravitationally bound system, diffuse X-ray emission 79−25736
- Abell clusters and superclusters, search for X-ray emission 78−54091
- Abell clusters containing tailed radio galaxies, Westerbork synthesis obs. 80−56957
- Abell clusters fields, Westerbork obs. 78−96549
- Abell clusters of galaxies, Westerbork 610 MHz survey of extended radio emission 80−36727
- Abell rich clusters, possible nearby ring galaxies catalogue 77−33629
- accretion wake model of galactic and quasar jets in clusters 79−71135
- adiabatic density perturbations in early universe, evolution 79−25769
- angular size-red shift relation, test for deceleration parameter 78−12437
- angular size-redshift relation, sizes and shapes of nearby clusters of galaxies 78−4372
- anticorrelation rel. to dark intergalactic matter in galactic haloes 79−2567
- Ariel 5 clusters, optical morphology and galaxy density 78−8135
- Arp 205 (NGC 3448 and UGC 6016), aperture synthesis obs. of H I 79−53916
- aspherical clusters, dynamical friction effects 78−16547
- association with QSOs, radio source morphology appl. 78−93434
- AWM 4, poor galaxy cluster, extended X-ray emission detect. surrounding cD galaxy (NGC 6051) 80−51884
- AWM 4, redshifts for five galaxies in poor cluster 78−45415
- AWM 7, X-ray source identification by HEAO 1 80−90573
- Bautz-Morgan classes, distrib. rel. to clusters luminosity function and brightest galaxies 78−54057
- Big Bang model, galaxy cluster missing mass from massive leptons, additional ν species 78−81719
- binary galaxies, axis ratios and posn. angles for galaxies in pairs 78−93430
- binary galaxies, dynamics 78−4354
- binary galaxies, late type, mass-to-light ratios from luminosity-weighted averages 78−8113
- binding mass, contrib. of heavy stable neutral leptons 78−93091
- bright elliptical galaxies clustering props., implications of galaxy merging N-body simulations 80−56922
- bright galaxies membership, optical redshifts results 78−89252
- brightest galaxies luminosities, statistical model test 77−29938
- brightest members, statistical model and galaxy evolution 79−35405
- brightness spectrum, number-luminosity relation and cosmic luminosity 78−81696
- 3C 295, cluster, two-colour ISIT photometry rel. to galaxies evolution 78−24557
- 3C 303, QSO group in cluster, gravit. lens effect 77−78878
- CA 0340−538, core radius and mass segregation 79−35396
- CA 0340−538, photometric and structural study 80−26992
- CA 0340−538, X-ray emission, Ariel V sky survey obs. 77−5599
- CA 0340−538 (3U 0328−523), southern cluster of galaxies, vel. dispersion and global parameters 78−36705
- Cancer cluster, Westerbork survey at 610 MHz 80−67884
- Canes Venatici I galaxy group, neutral H obs. of NGC 4136, 4144, 4190, IC 4182 and (DDO 133) 79−84853
- Canes Venetici I group, H I obs. of barred Im galaxy (NGC 4214) 79−92862
- Carafe Group, spectroscopic and photographic obs. of peculiar galaxies 79−35387
- catalogue inhomogeneity, cluster props. distortion, statistical anal. method 80−67888
- catalogue of galaxies and clusters of galaxies in SMC direction 78−96410
- Catalogue of Southern Peculiar Galaxies and Associations, preliminary results 77−82129
- cD galaxies, ellipticity 80−22076
- cD galaxies in poor clusters, radial vel. meas. 79−8994
- Centaurus, (HMS 1247−-4102), galaxies redshifts meas. 77−45578
- Centaurus, Fe XXV and Fe XXVI line emission obs. in X-ray spectrum 77−45580
- Centaurus, spiral and elliptical galaxies distribs. rel. to Virgo cluster redshifts 78−54061
- Centaurus cluster, X-ray spectrum obs. by (HEAO A-2) 80−82518
- Centaurus galaxy group, distance 80−4434
- Centaurus I cluster, resolution into two velocity systems using new redshift data 80−77499
- chains, properties *(Russian)* 80−17676
- characteristic size, metric rod used for determ. of q_0 78−36703

clusters of galaxies continued
- Cl 0024+1654, two colour ISIT photometry rel. to cluster galaxies evolution 78−24557
- classical field component of galaxies, test 77−33658
- close binary galaxies, luminosity function 80−46683
- close pairs of galaxies, excess radio emission 78−57658
- clumps, formation and evolution in expanding Universe 78−93432
- cluster density, relation with Bautz-Morgan type 78−28804
- cluster effect on Hubble Modulus, numerical simulation test 79−2569
- clustering, statistical studies 80−105363
- clustering models, discrimination of statistical measures 79−35404
- clustering models discrimination, n-point galaxy correl. functions applicability test 80−8699
- clustering on large scale rel. to matter-radiation decoupling epoch of early Universe 80−62355
- clusters containing compact galaxies, redshifts of compact and normal galaxies 77−71143
- clusters with known galaxy number-density distrib., data compilation 79−80362
- collapse, disk galaxy gas envelopes ejection 80−82483
- collective relaxation in galaxy correlations 78−24579
- colour distribution of E and S0 galaxy clusters rel. to redshift 80−105361
- colour-absolute magnitude relation for elliptical and S0 galaxies 78−8108
- Coma, accurate positions of faint optical objects in fields of radiosources 79−9015
- Coma, anal. of supernovae light curves 78−32497
- Coma, calc. and obs. of peculiar galaxies 77−64859
- Coma, central regions struct. from equidensity diagrams 78−93435
- Coma, core radius and mass segregation 79−35396
- Coma, diffuse background light photographic meas. 77−91655
- Coma, distrib. of mean surface brightnesses of galaxies *(Russian)* 78−49543
- Coma, elliptical galaxies, surface brightness and colour distribs. 78−41063
- Coma, elliptical shape, quantitative examination 78−41061
- Coma, ellipticity profiles of elliptical galaxies 78−28785
- Coma, H I deficient spiral galaxies 79−17072
- Coma, intergalactic supernovae, limit on frequency 77−17604
- Coma, line of peculiar galaxies assoc. with cD galaxy NGC 4889 77−64860
- Coma, luminosity function and struct. 77−45574
- Coma, microwave emission from dust and hidden matter 78−4374
- Coma, new stellar standard sequence 78−93436
- Coma, nuclear radio emission upper limits for spiral galaxies 78−8107
- Coma, origin and transport of electrons in halo radio source 77−26073
- Coma, Perseus and Virgo, X-ray emitting intracluster gas models 77−45577
- Coma, photoelec. surface photometry, intergalactic gas luminosity upper limit 77−64858
- Coma, soft X-ray structure 79−62918
- Coma, spatial distrib. of Compton-produced X-ray flux, theory 77−33686
- Coma, two-dimens. struct., Zel'dovich disc model 78−41062
- Coma, Westerbork survey at 610 MHz, radio data and identifications 77−60628
- Coma, X-ray source, hydrostatic struct. of hot plasma 77−17697
- Coma Berenices cluster, soft X-ray spectra, constraints on models 78−36702
- Coma Berenices supercluster, appl. of nonisotropic Newtonian cosmological model *(Spanish)* 79−48978
- Coma cluster, 3.5 and 4.0 mm obs. of central regions *(Russian)* 80−82525
- Coma cluster, binary model 79−71133
- Coma cluster, diffuse radio emission obs. 79−88750
- Coma cluster, H I emission search, gas content determ. of elliptical galaxies 80−46657
- Coma cluster, halo radio source meas. by Westerbork survey 78−86027
- Coma cluster, intergalactic intracluster H I, improved limits 79−75276
- Coma cluster, low energy X-ray absorpt. obs. 78−86025
- Coma cluster, mass segregation and missing mass 77−45581
- Coma cluster, mass segregation and missing mass 80−98730
- Coma cluster, optical obs. of radio galaxy 78−12358
- Coma cluster, photometry of intergalactic optical surface brightness 77−87550
- Coma cluster, ratio of escape vel. to mean vel. *(German)* 78−53995
- Coma cluster, search for extended hot gas halo 80−56953
- Coma cluster, structure of diffuse X-ray emission 79−92874
- Coma cluster, X-ray emission monitoring by Ariel V Sky Survey 77−2491
- Coma Cluster galaxies, photometry 78−12381
- Coma cluster X-ray source, X-ray brightness distrib. prediction 79−92896
- Coma galaxy cluster, relativistic electrons streaming at speeds above Alfven vel. 79−40068
- Coma I galaxy cloud, redshifts and struct. 77−45575
- Coma/A1367 supercluster and environment 78−65700
- Coma/Abell 1367 supercluster, band theory appl. 79−92871
- compact galaxies, clusters, compact groups and pairs 80−17668
- compact group, dynamics and lifetimes 79−92870
- compact groups, distrib. of compact galaxies *(Russian)* 78−61926
- compact groups, galaxies anomalous luminosity function 80−82520
- compact groups, virial mass/light ratio 79−92872
- compact groups, X-ray emission obs. 80−90574
- compact groups of compact galaxies, distrib. *(Russian)* 78−28802
- compact groups of compact galaxies, eighth list, 32 objects *(Russian)* 78−93125
- compact groups of compact galaxies, morphology of 27 groups *(Russian)* 79−9008
- compact groups of compact galaxies, ninth list 79−88751
- compact groups of compact galaxies, seventh list *(Russian)* 77−22110
- compact groups of compact galaxies, tenth list 80−26991
- compact groups of compact galaxies 77−37656
- compact groups of galaxies, survey 77−22320
- core condensation in heavy haloes rel. to galaxy formation and clustering 78−54051
- core radii and mass segregation 79−35396
- Corona Borealis, vel. dispersion 77−49487
- correlation analysis of space and surface distribs. 78−16546

clusters of galaxies continued
correlation function, computer simulation of catalogue *(Russian)* 80—36729
correlation function evolution and density perturbations in expanding Universe 79—44646
correlation function for density perturbations in expanding universe, nonlinear theory 78—8173
correlation functions hierarchy rel. to galaxy clustering 79—30138
cosmological constant and data reduction 80—41923
cosmological deceleration parameter and Sunyaev-Zeldovich effect 79—62936
cosmological N-body simulation, rel. to galaxy clustering evolution 78—96550
covariance function, explanation for 9 Mpc break 78—65688
covariance function, Limber's relativistic formula, relativistic inversion 78—69891
Cygnus A cluster possible extended X-ray source 77—53700
de Vaucouleurs' groups of galaxies, type-redshift relation 77—17693
deep galaxy samples, correl. anals. rel. to clustering 79—67104
deep sample analysis 80—105362
dense groups, galaxy collisions 77—45573
density perturbations in expanding universe, three-point correl. function and higher order functions prediction 78—65730
density profiles 78—12382
discrepant redshifts in galaxy groups, examples 79—25722
distances from X-ray and microwave obs. 79—71134
distant cluster, photometric obs. and red shift 78—12377
distant clusters, brightest galaxies pseudo-pairs in Turner's (1976) sample 80—67849
distant clusters, LF gravitational radiation and redshift discrepancies 77—71148
distant galaxies clustering amplitudes, evolution effects 79—40260
distant richness class 4 clusters, cooling of microwave background by intergalactic hot gas 78—12369
distribution of galaxies, angular covariance function estimation 79—62920
distribution of galaxies round cluster from cluster-galaxy-galaxy three-point correlation function 80—94875
Doppler shift distributions in Universe, extragalactic peculiar motions 78—4416
double galaxies, observational data on well-defined sample 80—17674
double galaxies, redshift intervals periodicity 80—56923
double radiosources, compact hot-spots correl. with galaxy cluster membership 79—48947
dust, IR and radio radiation, upper limits *(Russian)* 79—21449
dynamical age determ., appl. to Virgo cluster 80—77498
dynamical effects in formation and evolution 78—41051
dynamical evolution 78—12384
dynamical evolution in clusters with LF radio emission 78—24558
dynamical evolution of hot intracluster gas from galaxies, Fe abundance in X-ray clusters 79—12530
dynamical model of rich clusters of galaxies 77—13477
dynamical models 79—9013
dynamical props. from nonlinear gravitational instability theory 77—87557
dynamically produced evolution of cluster luminosity functions 78—12380
dynamics, influence of long-wave primordial gravit. radiation interaction with galaxies 80—17661
dynamics and evolution of groups and clusters, galaxy collision effects 79—75282
dynamics of aggregates of galaxies, rel. to main galaxy dynamics 77—5577
E galaxies in Abell clusters, UR surface photometry 79—12525
elliptical and S0 field and cluster galaxies, photometry, colour distribs. 79—17071
Emden sphere model embedded in background supercluster, dynamical theory 80—62296
emission line galaxies, spatial distrib. rel. to clusters, visible spectra obs. 80—73046
emission-line galaxies in dense clusters 78—65703
enriched gas in clusters and dynamics of galaxies and clusters rel. to galaxy formation 78—77596
evolution evidence from ang. size-redshift relation 80—41903
evolution from correlation anal. of deep galaxy samples, techniques and appl. 78—41056
evolution of galaxies and intergalactic matter in clusters, model 80—85992
evolution of galaxies in clusters 79—71132
evolution of galaxy clustering, anal. from galaxy fields stochastic simulation 80—90530
expansion, rel. to gravidynamic theory for large cosmical masses *(Russian)* 77—17351
extended radiosources obs. in galaxy clusters 77—64861
extragalactic objects clustering in Universe *(Polish)* 78—96580
faint blue objects, distrib., clustering props. and nature 80—82476
faint galaxies apparent distrib. 79—21444
first brightest galaxy, multiplicity rel. to cluster Bautz-Morgan type 79—92873
formation, anisotropic gravit. collapse 78—4344
formation, density perturbations development after recomb. 78—49569
formation, role of small perturbations in inhomogeneous gas clouds one-dimensional collapse *(Russian)* 80—36497
formation, tenacious myths about cosmological perturbations larger than horizon size 80—105408
formation, violet gas dynamics 78—86018
formation and assoc. microwave background fluctuations 78—28865
formation in cold early universe, influence of black holes 78—16585
formation in expanding universe, new model 78—93489
formation in self-similar space-times, perturbation scheme 78—54099
formation of galaxies and gravit. clustering, efficiency 79—48903
Fornax, distance and local Hubble ratio 77—33661
Fornax cluster, bright members surface photometry 78—96548
Fornax cluster, membership determ. by photographic photometry 80—82523
four-point correlation function for Lick and Zwicky catalogues 78—45413
galaxies, Hubble's law as laboratory exercise in astronomy 78—65740
galaxies distribution determination, maximum likelihood method 80—56954

clusters of galaxies continued
galaxies number densities and radial cumulative distributions, in nine clusters 79—40278
galaxies radial velocities, interpretation of redshifts 80—4427
galaxies redshifts, angular anisotropy, effects of intervening clusters 77—2472
galaxies spatial density fluctuations, rel. to QSO-galaxy and QSO-QSO discrepant red shift assocs. 79—8999
galaxy clustering depend. on cosmological density parameter 79—48971
galaxy collisions in clusters, form. of elliptical galaxies by tidal interactions 77—78865
galaxy content 78—12383
galaxy correlation function evolution, N-body Monte Carlo model 80—62292
galaxy cosmogony based on spatial distrib. of matter 77—37652
galaxy covariance function, extension to small scales 79—101197
galaxy groups, mass-to-light ratios and crossing times 77—45572
galaxy number density, radial number density and radial cumulative galaxy distrib. 80—73050
gas content meas. by obs. of microwave background at 10.6 GHz 78—96551
gas replenishment rates in galaxies, stripping of spirals to form S0 galaxies 79—40253
gaseous halos rel. to evolution 80—17675
gaseous protoclusters spatial struct. and galaxy form. 78—93415
general problems 79—97068
geometric objects with fractional dimension, book contrib. 77—87640
giant galaxies in clusters, radioactive accretion flow 78—93433
gravitational binding energy, virial discrepancy explanation 77—49484
gravitational encounters in rich clusters of galaxies 79—17110
gravitational instability in early Universe, cluster-sized perturbations 78—93487
group of galaxies in Cetus with redshift discrepancy 78—36708
groups, radial vel. meas., membership, mass/light ratios and distances 77—33660
groups of galaxies, average ellipticity 80—12820
groups of galaxies, catalogue of 103 systems 77—17385
groups of galaxies, review 78—12385
groups of galaxies, virial props. 79—9010
halos, density and rel. distribs. as probe for expanding Universe primordial inhomogeneities 80—22122
head-tail galaxies in clusters, review *(French)* 78—41054
head-tail radio galaxies, galaxy counts in surrounding region rel. to tail orientation 78—54060
head-tail radio galaxies in clusters, radial vels. 79—9014
head-tail radio galaxies in poor clusters, radio and optical obs. 78—96530
head-tail radio galaxies velocities with respect to intracluster medium 78—49516
head-tail radio sources in clusters, role of hot gas in elliptical galaxies 80—36703
Hercules cluster, 3.5 and 4.0 mm obs. of central regions *(Russian)* 80—82525
Hercules cluster, disc galaxies sizes 79—75269
Hercules cluster, membership of galaxy (Markarian 295) 79—44608
Hercules cluster, Westerbork survey of NGC 6034 radio tail galaxy 78—36706
Hercules supercluster, Ariel V X-ray obs. 77—60832
Hercules supercluster, basic redshift data 80—36725
Hercules supercluster, cosmography 80—51883
Hercules supercluster, evidence for intracluster medium 80—22092
Hercules supercluster, galaxy distrib. in field 78—93437
Hercules supercluster, radio luminosity function at 610 MHz 79—44625
hierarchical clustering of nearby galaxy groups, appl. to Leo region 78—36707
hierarchical clustering pattern, stability 78—86026
hierarchical clusters as opposed to continuous clusters, determ. 80—73051
hierarchical model of clustering 79—35403
hierarchy of clustering 78—49546
high-order clusters of galaxies, existence 78—12386
hot gas in clusters of galaxies, review 78—12374
hot intracluster gas, Sunyaev-Zel'dovich effect in millimetric region 79—25765
Hubble constant determ., large turbulent Universe model 78—96578
Hubble constant determ., large turbulent Universe model 79—58453
Hubble constant value limits from obs. of galaxy clusters 79—67099
Hubble diagram as cosmological test, dynamics friction effects 77—9826
Hubble diagram curvature, from redshifts and photometry of distant galaxy clusters 78—49515
Hubble diagram scatter and Local Group motion 77—13475
Hubble modulus increase behind clusters 77—78872
Hubble ratio, local value, and extragalactic distance scale *(French)* 77—60826
Hydra, distance and local Hubble ratio 77—33661
Hydra I, photometric obs. of brightest galaxies 77—33659
Hydra I, ram-pressure sweeping, optical evidence 78—93429
Hydra I (Abell 1060) galaxies, UBV photoelectric photometry 80—51887
Hydra I cluster, study of extreme compact object 80—41898
hydrostatic struct. of hot plasma 77—17697
hypergalaxy, mass from Magellanic Stream kinematics 77—5573
Indus Supercluster galaxies, UBV photoelectric photometry and photometric parameters 80—67855
integrated Brandt masses for spiral and irregular galaxies in groups 78—93398
interacting galaxy pair, zero relative vel. surfaces in gravit. field 80—67881
interacting nonequilibrium systems near bright galaxies 78—36682
intergalactic abundances, gas loss from S0 galaxies 78—28784
intergalactic dust, evidence from Zel'dovich effect 78—54041
intergalactic H I clouds, search in NGC 1023 and Canes Venatici II 79—35389
intergalactic H I search in nearby groups of galaxies 79—30121
intergalactic hot gas in clusters of galaxies, distrib. 79—17089
intergalactic hot gas stability problem, role of massive photons *(Russian)* 79—44614
intergalactic matter, effects on evolution of galaxies 80—109543
intracluster Faraday rotation of radio sources, obs. 79—75285
intracluster Fe-enriched gas, origin and evolution 78—93390

clusters of galaxies continued
intracluster gas, origin and evolution, interaction with interstellar gas in cluster galaxies 78−45407
intracluster gas and galaxies dynamical interaction 77−13473
intracluster gas dynamical collapse and hot plasma form. 77−22322
intracluster gas flow patterns and X-ray emission 78−65705
intracluster gas in rich clusters, origin and distrib. rel. to cluster X-ray sources evolution 78−28770
intracluster hot gas, temp. and entropy 80−17660
intracluster medium, mass and metal abundance from elliptical galaxies chemical evolution 80−67843
intracluster medium, origin rel. to galactic coronae and quasar absorpt. lines 80−31355
ionised gas in clusters of galaxies, microwave search 80−82477
ionized gas in rich clusters of galaxies, angular broadening of distant compact radio sources 79−35380
IR luminosity/H I vel. width relation and distance scale 79−44596
isolated pairs of galaxies, radio continuum survey 78−57657
isothermal mass distribution, Coma cluster example 79−53918
Klemola 44, X-ray, optical and radio obs. 77−74150
Klemola 44, X-ray cluster of galaxies, redshifts and vels. 78−45414
large-scale distribution and motion, in adiabatic theory of form. 78−54056
large-scale structure in universe, formation and development 79−12526
Leo triplet (NGC 3623/7/8), H I distrib., 21 cm line obs. 79−44623
light neutral leptons, dynamical role in cosmology 79−35407
linear clustering in low-density universes 80−85993
linear clusters, member galaxy alignment, visible obs. 80−90516
local cluster, satellite galaxies and globular clusters, radial vels. and galactic mass 78−49522
Local Group, angular momentum of galaxies 78−93400
Local Group, colour-magnitude data, Virgo I cluster distance determ. 78−73763
Local Group, discovery of three new members, dwarf galaxies 79−5907
Local Group, distances for six nearest galaxies 78−89247
Local Group, H I 21 cm obs. of newly discovered dwarf galaxies 79−30133
Local Group, H I content of dwarf spheroidal galaxies, upper limit 78−57633
Local Group, H I obs. of Shostak high-velocity cloud 78−32575
local group, high sensitivity survey of high vel. H I clouds 78−65686
local group, high-velocity H I clouds map 80−26923
Local Group, motion from vel. anisotropy of distance Sc I galaxies, data 77−5560
Local Group, motion towards Virgo from galaxies distance scale and expansion rate outside Local Supercluster 80−105325
Local Group, motions of Sun, Galaxy and Andromeda nebula (M31) 77−91518
Local Group, new dwarf galaxy member discovery near (NGC 6822) 79−84852
Local Group, new Sculptor-type dwarf elliptical galaxy in Carina 77−82311
Local Group, peculiar motion rel. to Virgo cluster from bright nearby galaxies vel. field 80−36699
Local Group, peculiar vel. rel. to Virgo cluster, deceleration parameter determ. 80−62351
Local Group, peculiar vels. 80−62284
Local Group, planetary nebulae in NGC 147 and 185 77−33596
Local Group, possible new members from solar motion solns. 77−22321
Local Group, predominantly normal matter from primary cosmic rays antihelium abundance 78−73594
Local Group, secondary distance indicators 78−93402
Local Group, solar motion rel. to centroid 78−12376
Local Group, UKS 1927−177 and 2323−326, 21 cm. obs. of of new dwarf irregular galaxies 78−65697
Local Group, virial mass and mass-to-light ratio of Andromeda (M31) subgroup 80−12809
Local Group and the Galaxy, conf., Royal Greenwich Obs. (July 1975) 77−91631
Local Group galaxies, Cepheid variables freq.-period distribs. 78−28694
Local Group galaxies, H II regions morphology and distrib. 78−16541
Local Group galaxies, progression in Cepheid period-amplitude diagram characts. 78−53956
Local Group galaxies gravitational encounters, numerical expts. 77−57098
Local Group motion and Hubble diagram scatter 77−13475
Local Group motion from vel. anisotropy of distance Sc I galaxies, anal. 77−9796
local mean mass density and galaxy clustering 78−45436
local space density, of galaxy clusters, active nuclei and quasars 78−57676
Local Supercluster, Hubble flow anisotropy from galaxies relative luminosities and distances 80−31363
Local Supercluster, non-linear collapse in high density Universe 80−62330
Local Supercluster, redshift anisotropy, luminosity selection effects 77−74147
local supercluster and Hubble law isotropy test on quasars 79−97111
local supercluster and red shift anisotropy *(Russian)* 79−92875
Local Supercluster Hubble ratio and velocity-distance relation anisotropy 80−17698
Local Supercluster kinematics and aspherical structure growth in Universe 79−92899
low surface brightness galaxies in clusters and groups, comparisons *(Russian)* 79−80357
luminosity function of galaxy systems, from single galaxies and small groups to rich clusters 80−12808
luminosity functions, derivation 78−54058
inner M101 galaxy group, H I obs. 80−67885
M101 group, galaxies integral props. from H I meas. 78−49532
M81 group, M82 as field galaxy drifting through intergalactic dust 77−33632
M87 region, Fe XVII-XXIV X-ray line complex obs. 79−21425
M87/Virgo cluster X-ray source spectrum, 1.1 keV Fe line emission discovery 79−25758
M 101 group, reality questioned rel. to M 101 distance 80−67852
Magellanic Plane Group, membership of Sculptor dwarf galaxy 77−53429
Magellanic Stream and galactic wakes 79−48904
Markarian's chain in Virgo, inner structure and membership 77−71150
mass spectrum, low mass portion anal. 78−81695

clusters of galaxies continued
mass to light ratio using negative energy concept 80−86002
mass-loss hypothesis of virial mass discrepancy 80−22094
massive central systems effects on virial binding energy 77−78875
massive galactic haloes, form. and evolution, rel. to missing mass problem 78−28777
massive gas clouds, cooling, dynamics and fragmentation rel. to masses and radii of galaxies and clusters 77−60857
mean mass density assoc. with galaxies, estimation method 77−49486
member galaxies, morphology rel. to spiral galaxy evolution 80−90543
MFJG 18 and 19, dynamics of superclusters 80−105365
microwave background, cluster effects *(Russian)* 80−94899
microwave background obs. in direction of clusters of galaxies, cool ionized gas mass limit 78−41098
missing dark mass rel. to primordial star generation 78−61946
missing mass, N-body expts. 80−41904
missing mass problem, appl. of scale-covariant dynamics 80−26913
missing mass problem, evolutionary approach 77−37658
missing mass problem, implication of neutrino rest mass *(Russian)* 80−105414
MKW 11, identification with X-ray source 4U 1326+11 using HEAO 1 data 80−90574
MKW 3s, poor galaxy cluster, extended X-ray emission detect. surrounding cD galaxy (NGC 5920) 80−51884
MKW-AWM poor clusters, optical props. 80−94878
Morgan's poor clusters, optical props. 80−94878
morphological characteristics 79−17109
morphological evolution and galactic cannibalism 78−93404
morphology, positioned and photometric data anal. 80−67887
MR 2251−178, nearby QSO in cluster of galaxies 80−67900
multiplicity function rel. to spectrum of cluster sizes 78−8130
N-body computer simulations in expanding Universe 79−97114
N-body simulations, density profiles 79−35398
N-body simulations, set of separation vectors 79−35399
N-body simulations compared with galaxy clusters, masses and mass segregation 80−22091
N-body simulations of clustering, groups 79−44621
N-body simulations of clustering, initial conditions and galaxy collapse times 79−44620
N-body simulations of galaxy clustering, covariance function 80−31373
N-body simulations of galaxy clustering, fraction in groups as function of density enhancement 80−67879
nearby Abell clusters, associated bright galaxies position and magnitudes 80−67880
nearby cluster obs. at low galactic latit. 78−4373
nearby clusters, galaxy content and evolution 79−17108
nearby groups of clusters 80−17672
nearby groups of galaxies structure, quantitative membership probabilities 79−62919
nearby superclusters, X-ray source clustering rel. to hot gas 78−41065
nearest groups and field galaxies, distances from secondary indicators 79−8987
nests, origin, geometrical colour and morphological props. 80−67889
NGC2805, 2814, 2820 and IC2458, H I 21 cm obs. of close galaxy group 79−53917
NGC 1023 galaxy group, H I obs. and possible intergalactic H I cloud discovery 80−67886
NGC 1023 galaxy group, H I radial vels. rel. to group membership and mass/light ratio 80−82521
NGC 128 group, obs. 77−33631
NGC 337 and 6745, galaxy chain interpretation *(Russian)* 80−17658
NGC 3686 galaxy quartet, surface photometry, mass distribs. and group stability 80−62297
NGC 4631 group, tidal interactions model 78−54059
NGC 4631/NGC 4656 group, neutral H aperture synthesis obs. 78−54043
NGC 5128 group, eight UKS dwarf galaxies 79−25738
NGC 5416 cluster, redshifts, morphologies and photometry 79−58434
NGC 7331/Stephan's Quintet area, obs. at 1421 MHz 78−12392
nonlinear clustering development in expanding universe, BBGKY eqns. integration 78−8175
nonspherical, hydrostatic struct. of hot plasma and X-ray morphology, rel. to Perseus cluster rot. 79−35406
number density distribution for 10 clusters 77−82314
number density distribution of galaxy clusters 78−81693
number-density distrib. from red Palomer Sky Survey prints 78−57659
number-density distrib. of clusters near NGP 77−71149
orbit segregation in nonhomologously changing nonlinear gravitational field 78−4351
orientations of member galaxies, Monte-Carlo simulation 80−90528
origin, spontaneous prod. of cosmological fluctuations 80−94902
paired galaxies, classification into groups differing in phys. and kinematic props. 79−21443
pairs and triplets of galaxy clusters, list of 68 pairs and 21 triplets 79−35408
pairs of galaxies, tides rel. to H II regions distrib. 80−46664
pairs with Markarian components, spectroscopy *(Russian)* 77−37648
peculiar galaxy system in Hydra 79−58433
Perseus, accurate positions of faint optical objects in fields of radio-sources 79−12527
Perseus, compact and diffuse X-ray sources in core 78−49545
Perseus, energy-dependent map of X-ray emission, SAS 3 obs. 78−65702
Perseus, excess X-ray emission from NGC 1275, central giant galaxy 80−41907
Perseus, obs. rel. to galaxies redshift-magnitude bands and evolution 78−54033
Perseus, soft X-ray map 77−5579
Perseus cluster, hard X-ray obs. 77−13493
Perseus cluster, low energy X-ray absorpt. obs. 78−86025
Perseus cluster, search for extended hot gas halo 80−56953
Perseus cluster, soft X-ray spectra, contraints on models 78−36702
Perseus cluster, WSRT 610 MHz obs. and catalogue of sources 79−75283
Perseus cluster of galaxies, soft X-ray struct. 79−9009
Perseus galaxy cluster, low-resolution aperture synthesis map at 408 MHz 80−56958
Perseus X-ray cluster, form. of optical filaments in cooling gas round NGC 1275 galaxy 80−67862
PHL 957 (quasar) direction, limits on cluster H I emission 77−91659

clusters of galaxies continued
Phoenix group, example of plate processing via two-dimensional digital filtering 79—16835
photographic observations, image processing techniques 77—9664
photographic photometry method *(German)* 80—46681
photometry of remote clusters 80—105364
Pisces group, redshifts meas. 77—45579
poor clusters, 1400 MHz pencil beam obs. in direction of cD galaxies 80—62263
poor clusters, cD galaxies props. 79—48907
poor clusters, containing cD galaxies, catalogue 77—22111
poor clusters, D and cD galaxies obs. 78—32580
poor clusters containing cD and related galaxies, pencil beam obs. of radio emission at 6 cm 80—62293
position angles of galaxies in pairs and small clusters 78—8137
primaeval entropy fluctuations and gravit. clustering 78—28867
primeval galaxy clusters, appearance in X- and γ-ray regions, contrib. to background rad. 80—8692
primordial heavy leptons halos, annihilation contrib. to cosmic gamma-ray background 78—93479
primordial protoclusters, search for H I emission at $z=3.33$ and (4.92) 78—41066
protocluster, gaseous, vortex generation in protogalactic medium 80—62360
protoclusters, condensation as source of X-ray background 78—8168
protoclusters, initial conditions rel. to morphology 79—97089
protogalaxy interactions in newly formed clusters rel. to luminosities, colours and intergalactic gas 78—41060
Q 0957+561, double quasar, intervening galaxy as brightest member of rich cluster 80—27005
QSO-galaxy group assoc., 3C 273 field obs. 80—105385
quasars, clustering prediction from relation to giant elliptical galaxies 78—16564
quasars absorption lines, survey in QSOs of small and intermediate emission redshift 80—31218
quasistellar objects possible assoc. with radio galaxies and rich clusters of galaxies 78—8142
quintets of galaxies, statistical anal. of discrepant redshifts 78—65701
radial number-density distributions, of ten clusters of galaxies 80—8697
radial vel. meas. in clusters of galaxies 77—64856
radiative regulation of gas flow, X-ray source model 78—4371
radio and cD galaxies, optical props. 78—93413
radio galaxy luminosity and source size rel. to cluster membership 79—25729
radio halos, 610 MHz obs. 80—17673
radio sources, anal. of galaxy clustering 80—22103
radio sources in clusters, interferometer obs. 77—53693
radio sources in clusters of galaxies, props. 78—12398
radio sources in clusters of galaxies, review of obs. 78—12397
radio survey of Abell clusters at 11.1 cm wavelength 78—20897
radiogalaxies anomalous redshifts, prod. by foreground galaxy clusters 77—9798
radiogalaxies in clusters 78—28806
radiosources with complex morphology in galaxy clusters 78—93443
red shift of light traversing clusters of galaxies, photon prop. 77—29642
redshift determination using Image Dissector Scanner, visible spectra 80—90544
redshift discrete states, systems of galaxies 77—37643
redshift for southern cluster 0122—688, spectrographic obs. 80—41906
redshift-magnitude bands, internal struct. and galaxies morphological evolution 80—22070
redshift-magnitude bands and galaxies evolution, data anal. 78—57629
redshifts of radio tail galaxies in clusters 78—69889
relative velocities, missing mass problem 77—13478
relativistic electrons in intracluster space, hard X-ray spectra and gas heating 79—25735
relativistic interpretation of redshift related to light crossing clusters of galaxies 77—17685
relativistic spherically-symmetric inhomogeneities model rel. to struct. and kinematics 77—71147
relaxation effect on intergalactic gas and X-ray emission 80—46684
relaxation from aspherical initial conditions 78—96538
relaxation of inhomogeneous gravit. systems, delocalisation effect 79—62877
repulsive gravitational forces, possible clustering mechanism 77—37674
review 77—64862
rich Abell clusters, photometry and luminosity functions 79—88752
rich Abell clusters, survey at 408 and 1407 MHz 78—81694
rich cluster 0004.8—3450, bri photometry 80—46685
rich cluster at 00^h47^m, $-29°46'$, galaxies static props. using COSMOS meas. 79—40279
rich clusters, catalogue of galaxy morphological types 80—85872
rich clusters, Fe mass and distrib. in intracluster space 79—5895
rich clusters, form. times and gravit. const. var. 78—69892
rich clusters, galaxy density and vel. distribs. rel. to cosmological density 79—44644
rich clusters, galaxy morphology and implications for galaxies form. and evolution 80—62255
rich clusters, influence on disc galaxies evolution 79—92867
rich clusters, missing mass problem 78—8136
rich clusters, morphology and peculiar vels. of radiosources 78—77610
rich clusters, photometric technique and luminosity function 78—89264
rich clusters, study of 1889 clusters from Abell's catalogue 77—87556
rich clusters mean density and correl. function, theory and obs. 78—24559
rich southern clusters, bright galaxies photoelectric photometry 79—21436
rich X-ray emitting clusters, VHF obs. 80—62294
rotation, ang. moments mass depend. rel. to self-similarity 80—36490
rotation as opposed to transverse vel. 80—94876
SC 0627—544, Fe XXV and Fe XXVI emission lines in X-ray spectrum 79—48941
SC galaxies, space distrib., large-scale struct. 79—71106
scaling law for clustering 80—82522
scattering of microwave background, 9 mm obs. 80—105366
scattering of microwave background radiation 80—105367
Sculptor group, 21 cm obs. of dwarf irregular galaxy and possible intergalactic cloud 77—64843
Sculptor group, discovery of new dwarf irregular galaxy 77—22311
Sculptor group, search for intergalactic H I clouds 79—30122
secondary peak rel. to formation 80—77497

clusters of galaxies continued
self-similar gravitational clustering, theory 80—4447
separations, effects of neutrino rest mass on Universe density perturbations spectrum *(Russian)* 80—109576
sequences of galaxies in Virgo, Coma and Perseus clusters, evidence for galaxy populations 79—58415
Seyfert Sextet, membership of clumpy irregular galaxies (Markarian 296 and 297) 79—44608
Shahbazian 1 group of galaxies, dynamics from spectroscopic, obs. 80—67878
Shakhbazian 1, compact cluster, photometry of compact galaxies *(Russian)* 78—93428
Shakhbazian I, photoelectric V magnitudes 77—17700
Shakhbazian I, photographic photometry 77—33662
Shane-Wirtanen galaxies, two- and three-point correl. functions 78—8132
southern clusters, identifications with high galactic latit. X-ray sources 78—49553
southern groups and clusters of galaxies, catalogue 78—28539
southern groups and clusters of galaxies, redshift data 79—84861
southern radiosources with steep radio spectra, identification, assoc. with clusters of galaxies 78—32587
southern rich clusters, finding list for 474 objects 78—24470
space distribution, comparison with radio sources *(Chinese)* 79—17111
sparse groups, luminosity of first-ranked members 77—2473
spatial distrib., spatial pair-correl. function 78—4350
spatial distrib. in southern galactic hemisphere 79—12518
spatial distribution, statistical method of multiple binning 80—8698
spatial distribution of different types of galaxies 79—84862
spectral var. in brightest cluster galaxies 78—41030
spherical models at late times, general features 80—17697
spherical stellar systems, dynamical relaxation, tidal perturbations by external systems 77—49443
spherically symmetric accretion with self-gravitation, criteria for enhanced accretion 79—71098
spiral galaxies, membership of sparse groups rel. to number of companions 80—77481
stabilisation by subclustering 79—44624
stable heavy neutrinos, dynamical interactions and astrophys. effects 79—5743
statistical mechanics of gravitating systems 79—35311
statistical test for clustering, covariance function 80—56955
steep LF radio spectra search among quasars and clusters of galaxies 77—45583
Stephan's Quintet, early-type galaxies distances 80—4435
Stephan's Quintet, H I emission search 79—30136
Stephan's Quintet, radio continuum maps at 2695 MHz 77—57099
Stephan's Quintet, redshifted H I associations 80—67882
Stephen's Quintet, broadband 21 cm H I emission 80—109554
stochastic simulation of fields of galaxies 80—62295
structures and number-density distribs. 77—37655
subclustering, rel. to missing mass 77—45576
subsonic accretion of cooling gas 77—74151
Sunyaev-Zeldovich effect at 9 mm wavelength 80—41919
supercluster candidate 4U0134—11, no X-rays from hot gas 78—8164
supercluster dynamics 80—105365
supercluster membership rel. to Abell cluster richness 78—65704
superclustering, Universe large-scale inhomogeneity in spherically symmetric models 77—64889
superclusters, existence and role in cosmic hierarchy 77—71151
superclusters, X-ray emission, matter infall 79—67106
superclusters, X-ray emission, Uhuru meas., intergalactic gas 78—41064
superclusters and density profile secondary max. 80—98727
superclusters and galaxy formation 80—36728
superclusters reality, influence of intragalactic factors on external objects apparent distrib. 78—96552
supernova explosions, microwave pulsed emission upper limit 78—69890
test for superclustering, 2 D nearest neighbours test, appl. to Abell galactic clusters 80—41905
thermodynamics and galaxy clustering 80—51881
tidal effects and mass distrib. in Hypergalaxy *(Russian)* 78—4367
tidal forces, in inhomogeneous cosmological models 80—62338
tidal interaction of galaxies within cluster 79—35395
tidal interactions in expanding Universe, prolate systems form. 79—71164
tidal interactions in rich clusters, stochastic phenomena 80—105161
tidally interacting galaxies, evolution of mass and tidal radius 78—65699
triple close approaches effect on stellar system evolution, one-parameter family appl. 80—17618
Turner-Gott galaxy groups, virial mass/galaxy mass ratio from galaxy H I profiles 80—56937
two component Emden sphere model, theory 80—22045
two-point angular correlation function between quasars and rich clusters of galaxies 79—80364
3U 1247-41, Centaurus X-ray cluster, vel. dispersion 77—74148
unborn clusters, microwave and X-ray emission 78—8131
universal structural evolution 80—17700
Universe and general field clumpy structure 78—45443
universe inhomogeneities, power law relating mass fraction to density enhancement 78—57656
Ursa Major, distance from galaxies H I line profiles 77—29920
Ursa Major Cloud, probable membership of miniature spiral galaxy NGC 3928 (Markarian 190) 80—105347
velocity dispersion, radius depend. and comparison with elliptical galaxies 80—51876
velocity dispersion profiles 79—35397
velocity dispersion profiles of N-body simulations 80—21908
velocity dispersions in rich clusters 80—56956
velocity distrib. of galaxies in clusters 77—53690
velocity meas. rel. to microwave background 80—46686
velocity structure, galaxies radial vels. distortion by night sky spectrum 77—41406
very rich clusters of galaxies, comprehensive study, dynamics 79—21448
Virgo, Coma and Perseus clusters, soft X-ray morphology 77—2474
Virgo, distance and local Hubble ratio 77—33661
Virgo, distance from 21 cm line widths and optical methods, H_0 global value determ. 77—9827
Virgo, distance from galaxies H I line profiles 77—29920
Virgo, distance modulus from globular cluster photometry 77—74149
Virgo, ellipticity profiles of elliptical galaxies 78—28785
Virgo, excess X-ray emission from M87, central giant galaxy 80—41907
Virgo, foreground spiral galaxies identification 80—56926

clusters of galaxies continued
Virgo, galaxies photographic surface photometry 77—78870
Virgo, H I deficiency in spiral galaxies *(Russian)* 79—21438
Virgo, H I survey of early-type galaxies 79—30123
Virgo, large cluster area study from taxonomy *(French)* 79—35400
Virgo, M87 enormous mass rel. to cluster missing mass 78—28775
Virgo, obs. of NGC 4472, very weak radio galaxy 78—65708
Virgo, Perseus and Coma, X-ray obs., spectral evidence for hot evolved gas 77—17695
Virgo, Perseus and Coma clusters, Fe abundance from X-ray Fe line obs. 77—49485
Virgo, radio luminosity v volume emissivity diag. 77—17696
Virgo, redshift differences between spiral and elliptical components 77—17694
Virgo, structure of extended X-ray source 78—4410
Virgo, surface photometry of barred spiral galaxies 77—13453
Virgo, total magnitudes from Byurakan surface photometry 77—17698
Virgo, UBV sequences for bright galaxies 77—13476
Virgo area, Ames, Reiz and Zwicky catalogues reduction to B_T system of galaxy magnitudes 79—58411
Virgo cluster, 3.5 and 4.0 mm obs. of central regions *(Russian)* 80—82525
Virgo cluster, disc galaxies sizes 79—75269
Virgo cluster, distance and redshift rel. to Hubble's const. 78—89265
Virgo cluster, dynamical age determ. 80—77498
Virgo cluster, evidence for confining environment for Virgo A (M87) from 610 MHz map 80—62302
Virgo cluster, globular clusters luminosity distrib. 78—12308
Virgo cluster, highest energy cosmic rays diffusion 80—4208
Virgo cluster, intracluster gas interaction with hot interstellar gas in elliptical galaxy (M86) 80—90535
Virgo cluster, Local Group relative motion from bright nearby galaxies vel. field 80—36699
Virgo cluster, low energy X-ray absorpt. obs. 78—86025
Virgo cluster, luminosity-vel. width relation, distance and recession vel. 80—90542
Virgo cluster, optical jet assoc. with M89, discovery 79—25731
Virgo cluster, perturbation to Hubble flow rel. to elliptical galaxies mass to light ratios 80—98707
Virgo cluster, possible membership of compact blueshifted galaxy RMB 56 (1216+141) 78—16527
Virgo cluster, possible supernova discovery 80—90460
Virgo cluster, red shift and possible membership of Seyfert galaxy (NGC 4235) 78—49536
Virgo cluster, search for extended hot gas halo 80—56953
Virgo cluster, total mass-energy density in open Universe 80—62351
Virgo cluster, X-ray obs. of galaxies, rel. to dynamical evolution 80—26995
Virgo cluster, X-ray source struct. 78—54090
Virgo cluster and M87, X-ray emission, Ariel V SSI obs. 79—12528
Virgo cluster area, standard total magnitudes of 139 bright galaxies 78—65685
Virgo cluster core, membership and vel. distrib. 79—35402
Virgo cluster galaxies, 1.4 GHz continuum survey 80—98721
Virgo cluster galaxies, globular clusters 79—92902
Virgo cluster photometry, galaxies magnitudes reduction to standard B_T system 79—92852
Virgo cluster redshift controversy, evidence from Centaurus cluster 78—54061
Virgo cluster spiral galaxies, H I deficiency from 21 cm obs. 80—62277
Virgo cluster supernovae, gravit. waves detectability by reson. antennas 80—8545
Virgo I, distance modulus from colour-magnitude data of Local Group 78—73763
Virgo I distance and Hubble constant 79—62917
Virgo region, new velocities 78—86028
Virgo supercluster and mean mass density of Universe 80—94877
virial mass discrepancy in groups and clusters of galaxies 78—28803
virial mass for systems of galaxies estimation 80—17678
virial masses, scale covariant gravitation 80—98728
virial properties, analytical examination 80—17671
viscous heating of intracluster gas, theory 79—9011
VV 150, galaxy chain, photoelectric and spectroscopic study 80—98724
VV 493 (UGC 07910), possible galaxy chain, morphology and spectrum 80—98718
VV 644, compact 'nest' of galaxies *(Russian)* 80—94879
Weyl's geometry rel. to dynamical mass excess 78—69919
X-ray and microwave obs., cosmological deceleration parameter determ. 79—21476
X-ray and radio emission, intracluster gas heating by relativistic electrons 78—57655
X-ray brightness distrib. of cluster sources, gravitational potentials 79—12529
X-ray cluster found by Einstein Observatory, CCD camera study and redshift 80—62315
X-ray clusters, Compton scatt. of microwave background by intracluster gas 78—24575
X-ray clusters, energy spectra 77—13472
X-ray clusters, gas stripping from spirals 78—32586
X-ray clusters, optical and X-ray study 78—28805
X-ray clusters, radial distrib. of morphological types of galaxies 78—8129
X-ray clusters, radio limits on ionised gas 78—89243
X-ray clusters, spatial distrib. of Compton-produced X-ray flux 77—33686
X-ray clusters, structure and evolution 80—26994
X-ray clusters, vel. dispersions 77—9804
X-ray clusters, X-ray emitting gas evolution 79—40266
X-ray clusters, X-ray luminosity correl. with galactic content 78—32585
X-ray clusters evolution, subcluster collisions 79—53915
X-ray clusters observed by HEAO 1 scanning modulation collimator, X-ray locations and sizes 79—97090
X-ray clusters of galaxies, large-scale struct. 80—8700
X-ray clusters of galaxies, large-scale struct. 80—82524
X-ray emission, Compton and thermal models 78—12378
X-ray emission, origin 78—57660
X-ray emission detect. from distant clusters 80—26993
X-ray emission detectability, deep surveys predictions and strategies 78—96567
X-ray emission from rich clusters, clusters extended halos and superclusters, search 80—26988

clusters of galaxies continued
X-ray emitting clusters, radial vel. dispersions 80—8696
X-ray emitting clusters, spatial distrib. of heavy elements 77—91654
X-ray galaxy clusters, luminosity function 79—40277
X-ray halos, extended X-ray emission 79—5909
X-ray line emission from clusters of galaxies, numerical models 78—8149
X-ray line spectroscopy 78—36701
X-ray luminosity function, predictions from thermal bremsstrahlung model 79—101208
X-ray luminosity-richness relation 78—93431
X-ray observations of objects at cosmological distances from the 'Einstein' observatory 80—105171
X-ray source structure and spectra 79—58448
X-ray sources, evolution 79—17133
X-ray sources, luminosity function evolution 80—62314
X-ray sources, luminosity-temp. relation 79—44622
X-ray sources, props. 78—96565
X-ray sources, review *(Polish)* 79—101223
X-ray sources correl. with radiosources from 26.3 MHz survey 78—65707
X-ray spectra, obs. and relationship to other cluster props. 80—22093
X-ray spectra, OSO 8 data discussion 79—25734
X-ray spectra in 2-20 keV range, OSO 8 obs. 79—5908
X-ray spectral rel. to optical cluster props. 80—26996
X-ray survey of rich Abell clusters, HEAO 1 1-10 keV obs. 80—51882
X-ray temperatures, meas. rel. to other cluster props. 77—91668
X-rays from clusters of galaxies, sources struct. and spectra 78—12387
Yerkes poor cluster members, reshifts 80—51858
Zw 0335.1+0956, identification with X-ray source 2A 0335+096 using HEAO data 80—90574
Zw 1400+0949 cluster (NGC 5416 group), 21 cm obs. 80—22090
ZwCl 1122.3+6317, poor cluster with four bright Markarian galaxies 80—26989
ZwCl 1710.4+6401, BV photometry of member galaxies *(Russian)* 77—87555
Zwicky catalogue selection effects and intercluster dust tests 79—9012
Zwicky clusters, pencil beam and interferometer obs. of radiosources 79—9019
Zwicky clusters, radio sources detailed interferometer obs. and anal. 80—22099
Zwicky clusters and radio sources, statistical investigation of positional coincidences 78—4378
H I absorption in QSO spectra, search for cluster effects 78—93448
H I broad band emission, search 80—46667
H I content of intracluster medium 79—5896
H I search in galaxy clusters 78—49544
Si XIII and Si XIV line emission search with ANS crystal spectrometer 79—17131

clutches
see also brakes; drives
magnetic, for endoscopic carrier directional control 77—2066

clutter
see also radar clutter; radar displays; radar interference
Doppler phase meas. of interfering reflections from interfering objects 79—81340
IR background suppression algorithm 78—77985
optical matched filter correlator memory techniques and capacity 80—43280
quasi-staring IR sensor clutter rejection processor design 80—86417

CNDO calculations
AB system, molecular calcs., electric dipole moments and electronic valence population, CNDO study 80—37742
acetaldehyde, force consts., vibr. freqs., CNDO/2 and MINDO/2 calcs. 77—14607
acetaldehyde, optimum geometry, force fields, CNDO/force method 77—46498
acetylene, mean polarisability derivatives, variational calc. procedure 79—27108
acetylenes, substituted, CH wag group freqs., CNDO/2 calcs. 77—6745
acrylonitrile, semiempirical CNDO calcs. of electronic struct. and absorpt. spectra 78—995
adenine, hydroxy and methoxy derivatives, absorption UV spectroscopy and electronic struct. of ionic and tautomeric forms 80—74177
adenine, tautomers, polarisation, barriers and tunneling times calcs. 79—41114
AH_2 systems, $1b_1$ orbital effect on geometry, CNDO/2 calcs. 79—13640
AH system, molecular calcs., electric dipole moments and electronic valence population, CNDO study 80—37742
alcohol H-complexes interactions, H-bond vibr. freq., anharmonic calcs. 80—99453
alcohols, modified CNDO calcs., conformations, binding energies 77—6682
alcohols, saturated, bonded and nonbonded, quantum chem. calcs. 80—9514
alkanes, linear, electronic struct., electronic relax. during photoemission *(French)* 78—5283
n-alkanes, methane to n-tridecane, ESCA of core electron relax. and valance bands 77—18978
alkylbenzenes, electronic struct., photoelectron spectra rel. to semiempirical CNDO/S CI calcs. 79—54770
amines, modified CNDO calcs., conformations, binding energies 77—6682
amines, saturated, bonded and nonbonded, quantum chem. calcs. 80—9514
azobenzene, derivatives, photoelectron spectra, ionisation pot., electronic struct. determ. 80—1024
benzene, $^1B_{1u}$ state, vibronic mag. rot. strengths and oscill. strengths, CNDO/S calcs. 77—34670
benzene, d_3, $-d_6$, vibr. freqs, force consts., CNDO/2 calcs. 77—65449
benzene, mono-substituted, MCD, CNDO/S calcs. using capable ang. momentum operator 77—46587
benzene, photoelectron and optical spectra, occupied virtual orbital energies and eigenvalue ordering, CNDO/S calc. 77—61796
benzene, semiempirical CNDO calcs. of electronic struct. and absorpt. spectra 78—995
benzene, third-order nonlinear electric susceptibility, from CNDO wavefunction 78—37558
benzene, vibronic coupling and IR intensities, CNDO/S semiempirical calc. 79—36596
benzenes, substituted, CH wag group freqs., CNDO/2 calcs. 77—6745

CNDO calculations continued
benzophenone, metastable triplet state, SCF CI calcs. 79—54776
p-benzoquinone, electronic struct., CNDO/S calcs. 78—70754
1,1′binaphthyl, electronic struct., fluoresc. CNDO/S CI calcs. 78—90084
1,1′-binaphthyl, $T_n \leftarrow T_1$ absorption spectrum in rigid and fluid media, CNDO/A study 79—76355
biomolecules electrostatic model of solvation, SCF MO calc. 79—96305
bipyridines, torsional isomerisation of biologically active bicyclic molecules 80—27996
bond polarity parameters, IR intensities, molecular orbital study 79—63914
bonding parameters, semitheoretical method, appls. 78—912
bonding parameters calc., semitheoretical method 78—5142
bridging bond angle variations in siloxanes, silicates, Si nitrides and sulphides, mol. orbital calc. on model systems 78—55125
bromomethane-$d_{0,1,2,3}$, IR spectra intensities, dipole moment, bond charge, force consts. 77—83588
bromotrifluoromethane, mol. struct., electron diffr., microwave spectra, CNDO/2 calcs. 78—37766
s-cis-butadiene, natural orbitals, photochem. cyclisation 79—85900
butadiene-acrylonitrile copolymer, electronic struct., reactivity, SCF CNDO calc. 77—50580
canonically orthonormalised basis construction 77—50362
carbamides, electronic absorpt. spectra, expt. and CNDO calcs. *(Russian)* 78—37647
carbazole, CNDO/S and CI calcs., photoelectron spectrum assignment 77—67982
carbon tetrachloride, low-energy X-ray emission spectra, MO anal., ionis. pot., rel. to CH_4 and $CHCl_3$ 79—85975
carbonic anhydrase, active site substrate binding, environmental effects, CNDO and SCF LCAO calcs. 80—8002
carbonyl groups, intermol. interactions in H_2CO-H_2CO system, quantum chem., classical calcs. 78—86932
carboxylic acids, crystals, empirical interatomic potential functions 79—7567
charge transfer complexes, geometries, CNDO/2 and EHT calcs. 79—36530
charge-transfer and hydrogen-bonded complexes, electronic absorpt. spectra calc. *(Russian)* 78—37628
chemisorption, embedding problem, SCFMO formalism 78—71977
chemisorption, iterative extended Huckel theory, INDO and CNDO methods 79—87875
chemisorption of O on graphite CO-NDO calcs. 78—75937
chlorin, UV absorption and photoelectron spectra, CNDO/S3 calcs. 77—75210
chloroform, CNDO approx. 79—72240
chlorotrifluoromethane, mol. struct., electron diffr., microwave spectra, CNDO/2 calcs. 78—37766
cinnamaldehydes, electronic spectra, CNDO CI calcs. 78—29774
CNDO-CI method, parameterisation role 77—46497
CNDO/S-CI method, convergence problems 77—46496
computer program for calculating configuration interaction in CNDO approx. 77—50372
conjugated compounds, mol. polarisability additive scheme, CNDO approximation calcs. 77—50363
conjugated system, N-electron CNDO Hamiltonian, approach to exact soln. 77—26979
contact charge transfer complexes of organic molecules with O_2, CNDO/S calcs., absorpt. spectra obs. 80—69076
crystal structure, CNDO/2 calcs., unit cell polarity effects 78—22683
cyanine dyes, excited electronic states, CNDO/S CI calc., visual pigment spectra appl. 80—85333
cyclobutadiene, π face bonding with CO, HCN, benzene 79—98180
cyclohexane, conform. equilib., CNDO/2 calcs. on six-membered rings 80—23336
2-cyclohexenone, reduction by hydride ions, delocalised model, CNDO/2 calc. 79—79231
cyclopenta[h]cycl[4.2.2]azine, electronic struct., photoelectron data 78—5286
cyclopentene, ring puckering, semi-empirical and ab initio calcs. 78—9065
cyclopropane, IR band intensities, anal. using Coriolis interaction and CNDO/2 calcs. 79—41172
cyclopropane-d_0, d_6, absolute IR intensities, dipole moment derivatives and polar tensors 78—90165
cytosine, hydroxy and methoxy, derivatives, absorption UV spectroscopy and electronic struct. of ionic and tautomeric forms 80—74177
diamond:N(B)(Si)(O), substitutional impurities 79—87056
diamond, relaxation about the vacancy 78—71722
diamond, tetrahedrally bonded valence crystals, SCF perturbation theory appl. 79—37658
diatomic molecules vibr. consts. determ., IR spectroscopic, quantum chem. teaching project 79—84914
dibutyl-phenyl-benzoyloxy-benzoate, nematic liq. cryst., rot. barrier, PCILO and CNDO/2 calcs. 80—33874
dichloromethane, dielectric constant effect on nuclear spin-spin coupling constants, CNDO approx. 79—72240
difluoroacetaldehyde, optimum geometry, force fields, CNDO/force methods 77—46498
difluorodiazine, cis-trans isomerisation, mechanism and kinetics, CNDO/2 study 77—90589
diformamide, excited singlet and triplet states, CNDO-CI calcs. 77—26990
dihaleothanes, CNDO/2-type calc., FORCE method, relative stability, intramolecular atomic interaction energies 78—41957
dihaloethylene, CNDO/2-type calc., FORCE method, relative stability, intramolecular atomic interaction energies 78—41957
2,5-dihydroxy-p-benzoquinone, proton tautomerism dynamics, ^{13}C NMR obs., CNDO calc. 79—52632
dimethyl aluminium hydride dimer, electron density distrib., electrostatic mol. pot. anal. 80—52885
dimethyl cadmium, photoelectron spectra, 4d spin-orbit splitting, crystal field and band-broadening effects, CNDO calcs. 78—76577
dimethyl sulphide dimerisation, S lone pair nonbonded contacts, EH, MINDO/3, CNDO/2 calcs. 79—773
p-N,N-dimethylaminobenzonitrile, multiple fluoresc., mechanism 79—45742
dimethylketene, thermal dimerisation mechanism, CNDO/2-INDO calcs. *(German)* 79—54771
1,4-dioxane, conform. equilib., CNDO/2 calcs. on six-membered rings 80—23336

CNDO calculations continued
dioxodiazacycloalkanes, electronic struct., mol. orbital theory 77—14359
α,ω-diphenyl-trans-polyenes, 1st excited singlet valence states, CI and extended CNDO/S calcs. 78—74807
diphenylethylene, UV spectra, quantum-mechanical investigation of isomerisation pathways 80—43065
p,p′-diphenylsulphines, (He I) photoelectron spectra, assigned by perturbational mol. orbital and CNDO/2 calcs. 78—46396
discontinjous approx. mol. electronic wave functions, ab initio LCAO and VB ZDO appls. 77—50340
doublet with singlet ground state electronic system, long range interaction energy, CNDO approx. 80—53089
electronegativity of atoms, correl. of CNDO-bonding parameters 78—74577
electrostatic interactions in liquid state, effect on frontier orbitals and chem. reactivity 80—84046
ethane, mean polarisability derivatives, variational calc. procedure 79—27108
ethane, shift of electronic spectrum during dissoc., CNDO calc. 80—37759
ethane, two-stage diagonalisation of Hamiltonian in CNDO/2 method 80—42946
ethanol, conformational anal., barriers of internal rotation, electronic structure 79—63916
ethanol, conformational analysis and electronic structure 78—33429
ethers, modified CNDO calcs., conformations, binding energies 77—6682
ethers, saturated, bonded and nonbonded, quantum chem. calcs. 80—9514
ethyl cation, rearrangement pseudorotation modes, reaction mechanisms, permutation theoretic anal. 78—44369
ethylene, electronic struct., CNDO/S2 calc., photoelectron and UV absorpt. spectra 77—30783
ethylene, Raman intensities, CNDO approximation, polarization functions 79—93925
ethylene$+Cl_2(Br_2)$ complex, intermolecular interaction and struct. SCF-MO-LCAO CNDO/2 calc. 78—58763
ethylene dimer, intermot. pot., dissoc, energy, CNDO/2 calcs. 79—31641
ethylene mean polarisability derivatives, variational calc. procedure 79—27108
ethylene oxide derivatives, substituents effect on electronic state of epoxide ring, CNDO/2 calcs. 79—26891
ethylene-d_0,-d_4, IR band intensity and Coriolis interactions 79—54851
ethylene-O_2 complex, CI calcs., singlet-triplet transitions 79—63923
ethylenes, substituted, He I and He II photoelectron spectra, CNDO/S calcs. 78—55201
excited states, variable metric optimisation of mol. geometry 80—58178
fluorinated ethylenes, valence bond polar parameters, IR intensities, MO calc. 80—28013
fluorobenzene, singlet-singlet electron transitions, modified CNDO-CI method exam. 78—25552
fluorobenzenes, electronic struct., CNDO/S2 calc., photoelectron and UV absorpt. spectra 77—30783
fluorobenzenes, UV spectra calc., oscill. strengths 79—18203
fluoroethanes, mol. liqs., dielectric solvent effects, quantum chem. calcs. 77—14375
fluoromethanes, optimum geometries, force fields, CNDO/force method 77—46498
force constants, CNDO-2 calcs. *(French)* 77—14381
force constants, semiempirical quantum mechanical method 78—62947
formaldehyde, emission spectrum, forbidden n-π^* transition, electronic-vibr. struct., CNDO/2 calcs. 77—58035
formaldehyde, force consts., vibr. freqs., CNDO/2 and MINDO calcs. 77—14607
formaldehyde, ground and low lying excited states, CNDO/V^{N-1} method *(Russian)* 78—74576
formic acid dimer, vibr. spectra, CNDO/2 interpretation *(French)* 80—58155
formic acid-$d_0(-d_1)(-d_1)(-d_2)$, vibr. spectra, CNDO/2 interpretation *(French)* 80—58155
graphite, adsorption and dissociation of O_2, CNDO/2 calcs. 79—28206
graphite, adsorption and migration of O_2, CNDO/2 calcs. 79—28205
Green's function method for vertical ionis. pots. calc., CNDO adapted approx. 80—18799
Group IV-VI diatomic molecules, He(I) photoelectron spectra, calcs. 80—1023
haloalkane-aromatic complexes, ground and excited states, CNDO calcs. 80—69082
homotetrahedryl cation, rearrangement pseudorotation modes, reaction mechanisms, permutation theoretic anal. 78—44369
hydrazones, protonation energy and basic strength 80—37719
hydrocarbons, force constants, CNDO-2 calcs. *(French)* 77—14381
hydrocarbons, mol. geometry, CNDO/BW and MINDO/2 calcs. 79—41109
hydrocarbons, mol. Raman intensities calcs. 80—52993
hydrocarbons, saturated, bonded and nonbonded, quantum chem. calcs. 80—9514
hydrocarbons, saturated, modified CNDO calcs., conformations, binding energies 77—6682
hydrogen maleate ion, electronic spectra, CNDO/S CI calcs. 77—75128
hydroxyquinones, H-bonded, zero-phonon photochem., hole burning obs. 79—11802
ice, crystal structure, CNDO/2 calcs., unit cell polarity effects 78—22683
II-VI compounds with transition metal impurity, SCF LCAO MO formalism in CNDO and INDO approx. 79—38017
intramolecular electron transfer rate, purely electronic effects, simple model Hamiltonian 77—10592
invariance of CNDO/S method rel. to basis functions 80—74125
invariance requirements in approx. SCF MO theory 79—6824
iodotrifluoromethane, mol. struct., electron diffr., microwave spectra, CNDO/2 calcs. 78—37766
ionisation potential, SAMO-ZDO method 78—41947
IR band intensities and polar tensors, effective charge and dipole moment derivs. sign 77—34695
lactam-lactim tautomeric equilibria, quantum chem. calcs. 80—50833
large molecule, electronic struct., photoemission and optical absorpt. spectrum, CNDO/S3 model 80—53172
large unit cell semiempirical mol. orbital approach to props. of solids, general theory 79—87029
large unit cell semiempirical mol. orbital approach to props. of solids, Si and diamond appl. 79—87036

- **CNDO calculations** continued
  - large unit cell semiempirical mol. orbital approach to props. of solids, LiF and KCl appl. 79—87037
  - linear aggregates, small, polarisability determ., CNDO method and analytical models *(French)* 80—29298
  - liver alcohol dehydrogenase, proton relay system, SCRF PCE theory, CNDO/2 calcs. 80—85325
  - magnetic susceptibility and anisotropy, HF perturbation method *(French)* 78—37559
  - methane, force consts., vibr. freqs., CNDO/2 and MINDO calcs. 77—14607
  - methane, low-energy X-ray emission spectra, MO anal., ionis. pot., rel. to CCl_4 and $CHCl_3$ 79—85975
  - methane, mean polarisability derivatives, variational calc. procedure 79—27108
  - methanesulphonyl chloride, geom. struct., CNDO/2 calc., comparison with CF_3SO_2Cl 79—81295
  - methanol, and dimer, CNDO/2 calcs. of O-H stretching vib. freqs. and intensities 77—18927
  - methanol, conformational anal., barriers of internal rotation, electronic structure 79—63916
  - methanol-water, assoc. mixture, rot. barrier solvent effect, CNDO/2 calc. 78—29861
  - N-methyl acetamide, Na^+, Mg^{2+} binding to carbonyl O, lipid membrane permeation mechanisms 79—16134
  - N-methyl diformamide, excited singlet and triplet states, CNDO-CI calcs. 77—26990
  - methyl fluoroformate, isomer conformation, CNDO and ab initio STO calcs. 80—58151
  - methyl groups, electric dipole moment, perpendicular component, orbital calcs. 77—68138
  - methylene, triplet ground state, var. and perturbational calcs. 77—61680
  - methylene radical anion and dimer, semiempirical CNDO/2 and nonempirical SCF calcs. 77—79535
  - o-methylhydroxylamine, ionisation energies, He I photoelectron spectra, orbital calcs. 77—88497
  - 1-methylindan, circular dichroism, rot. strengths, CNDO/S calc. 79—3452
  - 12-methylsulphonyl-1-phenylethanol, S-O interactions, conform. anal. 79—31418
  - modified CNDO method using d-functions *(German)* 79—22603
  - molecular conformational props., internal rot. barriers, PCILO-CNDO calcs. 77—75056
  - molecular crystals, compositional disorder, approx. band struct., self consistent virtual crystal approx. 80—39486
  - molecular electronic absorption spectra, intramolecular hydrogen bond 80—42949
  - molecular electronic structure, semiempirical CNDO method, calc. progam 78—86782
  - molecular orbital methods, speed and accuracy, comparison of methods 79—41106
  - molecular polarisability, CNDO calcs. including polarisation functions in the basis set 79—6891
  - molecular polarisability, geometric approx., σ, π-contribs. 78—17819
  - molecular polarisability, ground and excited state, perturbation treatment 78—5144
  - molecular polarisability calc., CNDO/2 wavefunctions 78—913
  - molecular systems including up to 232 orbitals, CNDO calcs., computer program 78—86788
  - molecules, core electron binding energy shifts, σ- and π-relax. energies 78—29750
  - monochloroacetic acid, isolated molecules, internal rotation, CNDO/2 calcs., IR spectra 80—69254
  - $n \rightarrow \pi^*$ singlet-singlet transition probabilities 80—95689
  - 11-cis-N-methyl PRSB-benzene complexes, spectral props., CNDO/S calcs., bathochromic shift 78—31767
  - naphthalene, singlet-singlet transition, Born-Oppenheimer approx., CNDO/S calcs. 77—27045
  - naphthalene, triplet excimer conformation, σ-π interaction transitions 77—6701
  - naphthalene and fluoro derivations, CNDO calcs., σ core effect 79—41107
  - naphthalenes, substituted, CH wag group freqs., CNDO/2 calcs. 77—6745
  - p-nitroaniline, mol., second-order hyperpolarisability CNDO/S calc. 79—76358
  - nitroanilines electronic states, CNDO/s-CI correlative calcs. 78—58604
  - NMR, ^{13}C chem. shifts, screening constant calcs., CNDO/S method *(French)* 79—94012
  - NMR parameters, chem. shielding, ^{13}C chem. shifts 80—23435
  - NMR spin-spin coupling consts. calcs. 77—68060
  - nonbonded interactions, pot. energy curves, CNDO/2, INDO and extended Huckel calcs. 77—27140
  - nonrigid inorganic molecules, pot. surfaces, CNDO and ZDO calcs. 79—41112
  - nucleic acid components, pyrimidine and purine, electronic struct. 80—30654
  - nucleic acids, electronic absorpt. and emission spectra 80—55989
  - nucleic acids bases, excited state dipole moments and geometries 80—95738
  - nucleotide bases, electronic absorpt. and emission spectra 80—55989
  - occupied molecular orbitals, CNDO character orders, virtual pars orbitals contribs. 79—3373
  - octane, fragmental and molecular orbitals, CNDO/2 approx. calcs. 80—42947
  - one dimensional polymers, compositional disorder, approx. band struct., self consistent virtual crystal approx. 80—39486
  - one-dimensional molecular crystals, electronic struct., mol. orbital theory 80—54588
  - optical rotatory strength, CI role in CNDO/S calc. 77—83561
  - organic compounds, excitation energies, CNDO/S-CI method calc. appls. *(German)* 80—106275
  - organic molecules, Raman spectra intensities, electronic polarisabilities, quantum mech. calc. 79—27041
  - organic mols., relative Raman intensities, CNDO/2 INDO param. effect 80—95633
  - oxalyl chloride, rot. isomerism, CNDO and EHT-type methods 78—58591
  - PAA, effect of mol. struct. on nematic liq. cryst., phase 78—42901
  - PAA, nematic liq. cryst., rot. barrier, PCILO and CNDO/2 calcs. 80—33874

- **CNDO calculations** continued
  - parametrisation procedure for CNDO/S extension to transition metals and fourth row elements *(French)* 80—9511
  - PCILO method, modified, second-order energy using CNDO/2 and INDO Hamiltonian approxs. 79—36533
  - phenol, PMR in absence of intermol. proton exchange, long-range coupling and conformations 77—34660
  - phenol, singlet-singlet electron transitions, modified CNDO-CI method exam. 78—25552
  - phenol NH_3, intermolecular H-bond, semi-empirical CNDO/2 78—13427
  - phenol-formamide, intermol. H-bond, semiempirical CNDO/2, substituted derivatives 78—13427
  - phenol-methanol, dimers CNDO/2 calcs.. H-bond energy 78—13428
  - phlorin, UV adsorption and photoelectron spectra, CNDO/S3 calcs. 77—75210
  - phosphatidyl ethanolamine, charge distrib., dipole moment, CNDO calcs. 78—80840
  - phosphonatomethylene radical, EPR spectra and rot. barrier height, comparison CNDO calcs. 79—74409
  - phthalazine, excited states, protonation influence, semiempirical CNDO/S CI calc. 79—76353
  - phthalazine, fluoresc. and phosphoresc., expt. and CNDO/S CI calcs. 79—31585
  - phthalic acid derivatives, excitation energies, CNDO/S-CI method calc. appls. *(German)* 80—106275
  - 1,4-piperazine, conform. equilib., CNDO/2 calcs. on six-membered rings 80—23336
  - polyacenes, MCD, CNDO/S calcs. 77—79637
  - polyacetylene: AsF_5 X-ray and UV photoemission spectra, Auger spectra 79—98150
  - polyacetylene X-ray and UV photoemission spectra, Auger spectra 79—98150
  - polyacrylonitrile, electronic struct., reactivity, SCF CNDO calcs. 77—50580
  - polyatomic molecules, triplet states, var. and perturbational calcs. 77—61680
  - polybutadiene, electronic struct., reactivity, SCF CNDO calcs. 77—50580
  - trans-polyenes, 1st excited singlet valence states, CI and extended CNDO/S calcs. 78—74807
  - polyenes, electronic struct., spectra interpretation, CNDO/S2 calcs. 79—6870
  - polyenes, twisting force consts., CNDO theory potential energy surface 78—50474
  - polyethylene molecule, fractured, local electron level calc. 80—14263
  - polyisoprene, electronic struct., reactivity, SCF CNDO calcs. 77—50580
  - porphin, ground-state energies, force consts. and vibr. freqs., CNDO/2 calc. 79—18118
  - porphin, hypersurface of adiabatic pot. calc. by CNDO/2 method, vibr. freqs., absorpt. spectra calc. 80—95543
  - porphin, spin-spin coupling const., MO LCAO CNDO/2 calc. 79—41108
  - porphins, UV absorption and photoelectron spectra, CNDO/S3 calcs. 77—75210
  - positrons and positronium atoms bound to mols., approx. MO theory 77—23583
  - n-propanol, preferred conformers, PCILO study 80—95542
  - propion-aldehyde ion, fragment/mol. ion current ratio, field ionis. mass spectrum, CNDO/BW calc. 77—65544
  - propyne-d_0(-d_3), absolute and integrated IR intensities of fundamental modes 80—87179
  - pyrazine, intensity of intercombination transitions, influence of n-σ-type complex form. *(Russian)* 77—26980
  - pyrazine, $n\pi^*$ transitions, vibronic coupling 78—25501
  - pyridine(-d), force consts. and vibr. spectra by CNDO/2 force method 80—95540
  - pyridine and derivatives, CNDO/2 approx., unshared pairs of electrons 78—25443
  - 2-pyridyl phenyl sulphide, dipole moments, absorpt. spectra, meas. and calcs. 77—46574
  - 2-pyridyl phenyl sulphone, dipole moments, absorpt. spectra, meas. and calcs. 77—46574
  - pyrimidines, substituted analogues, absorption UV spectroscopy and electronic struct. of ionic and tautomeric forms 80—74177
  - pyrylium, substituted, electronic struct., CNDO/S calcs. 78—29749
  - α-quartz, CNDO/2 calcs., electronic props. of perfect cluster, EPR parameters of O^- vacancy 80—107701
  - quasi-relativistic SCF-MO-LCAO methods, CNDO and MWH appls. 78—41953
  - quasimolecules, electronic struct. calc., CNDO approx., computer program 78—86789
  - quinazolines, enzyme inhibitory, structure-activity quantitative study 80—78540
  - quinoxaline, excited states, protonation influence, semiempirical CNDO/S CI calc. 79—76353
  - radical doublet states, positive ion potential anal. in CNDO/BW calc. 80—91452
  - radical ions, conjugated, solvent effect in CNDO and INDO calcs. of electronic spectra by restricted methods 77—38624
  - radical ions and mols., solvent effect in π(PPP-like) and CNDO calcs. 77—38622
  - Raman intensities, CNDO approximation, polarization functions 79—93925
  - Raman intensity of molecules, modified CNDO/2/INDO method 79—825
  - Raman line intensities, modified CNDO/2/INDO calc. 78—25621
  - semi-empirical SCF-LCAO calc. including energy minimisation, GEOMO program 77—23428
  - semiconductor, deep transition metal impurity states, SCF CNDO cluster calcs. 80—100442
  - semiconductor, tetrahedral, bond orbital model on CNDO basis 77—47720
  - semiempirical theory for ground and excited states, Fock operator expansion, STO-3G and CNDO/S calcs. 80—58154
  - serine proteases, enzymatic reaction mech. mol. orbital studies 77—60183
  - serine proteases, enzymatic reaction mechanism, CNDO/2 mol. orbital calcs. 78—27751
  - singlet-singlet electron transitions, modified CNDO-CI method exam. 78—25552
  - solids, large unit cell calc. in CNDO approximation 77—28089
  - spin-orbit interaction, role of triplet-triplet transitions 79—63915

CNDO calculations continued
spin-spin coupling constant calculations in mol. by CNDO/SP methods 80—74126
TCNE, semiempirical CNDO calcs. of electronic struct. and absorpt. spectra 78—995
TCNQ, elec. struct. determ. 77—1350
TCNQ, electron-mol. vib. coupling 77—15782
TCNQ, semiempirical CNDO calcs. of electronic struct. and absorpt. spectra 78—995
TCNQ dimers, extended Huckel hamiltonian supermol. CNDOS calcs. 80—27953
11,11,12,12-tetracyanonaphthoquinodimethane, XPS anal. by CNDO/2 79—31593
tetrafluorobenzene, microwave spectra, dipole moment, centrifugal distortion consts. 77—75133
tetrafluoroethylene, electronic struct., CNDO/S2 calcs., photoelectron and UV absorpt. spectra 77—30783
tetrakis(trifluoromethyl)germane, gas phase electron diffr. struct., torsional force consts., CNDO/2 calc. 79—31687
thioacetamides, CNDO calcs., internal rot., ionisation pots., photoelectron spectra 78—5143
p,p′-thiobenzophenones, (He I) photoelectron spectra, assigned by perturbational mol. orbital and CNDO/2 calcs. 78—46396
thioformaldehyde, $\tilde{a}^3A_2 \leftarrow \tilde{X}^1A_1$ IR absorpt. spectra 80—83362
thymine, tautomers, polarisation, barriers and tunneling times calcs. 79—41114
toluene, singlet-singlet electron transitions, modified CNDO-CI method exam. 78—25552
transition metal complex, CNDO method for study of electronic struct. and props., review 77—88392
transition metal compounds, XPS, anal., approx. mol. orbital theories 77—18975
transition metal hydrate complexes, physico-chem. props. CNDO calcs. 79—41110
transiton metal hydrate complexes, struct., bond energies, CNDO cals. 79—41111
bis-triazolopyridazines, conformation calcs. by mol. mechanics and CNDO/2 method 80—69079
bis-triazolyls, conformation calcs. by mol mechanics and CNDO/2 method 80—69079
trichloromethane, low-energy X-ray emission spectra, MO anal., ionis. pot., rel. to CCl_4 and CH_4 79—85975
1,2,4-trifluorobenzene, microwave spectrum, dipole moment and centrifugal distortion constants 78—37630
trifluoromethane, quadratic CNDO force fields calcs., coord. effects 79—6877
trifluoromethylsulphonyl chloride, geom. struct., CNDO/2 calc., comparison with CH_3SO_2Cl 79—81295
TTF, atom-atom approx. and lattice energies 79—7568
TTF-TCNQ, mol. core excitons, high energy electron inelastic-scatt. spectra 77—69235
TTF-TCNQ, molecular coordination along stacking directions 79—47031
TTF-TCNQ, TCNQ and TTF bandwidths, extended Huckel and CNDO/2 calcs. 79—7771
two photon absorptivities, CNDO/S-CI calc. with second order time depend. perturbation eqns. 80—74122
two photon absorptivity, ion cyclotron reson. photodissoc. spectra, CNDO/S-CI-perturbation theory 80—74123
two-centred bonds, CNDO calcs. of electrostatic energy components, complexing effects 77—18791
two-photon spectra, dipole-forbidden transitions, CNDO-CI cross sections 79—81244
two-photon spectroscopy, dipole-forbidden transitions, double excited configurations, CNDO-CI methods 80—58332
unimolecular reactions, pot. energy surfaces, SCF perturbation theory 79—91918
uracil, aq. soln., fast electron induced radical identification 79—24870
urea, electro-optical coeffs. meas., rel. to nonlinear optics calcs. 80—34889
urea, force field for planar vibrs., CNDO/Force MO calcs. 79—76416
valence-nonbonded H atoms interaction and two-centre contrib. to total energy of mol. 80—32624
vibrational intensity calcs., CNDO/2 method with extended basis set 80—91445
water dimers, stability, CNDO/2 and STO-3G calcs. 79—760
xanthine, and biological methyl derivatives, electronic struct. from UV photoelectron spectra 79—24949
xanthoporphinogen, IR electronic excitation spectra, CNDO/S calcs. *(German)* 77—79617
y_t-base, ground and excited states, dipole moment, CNDO/S and INDO/S calcs. 79—36534
Ag cluster 78—33646
Ag clusters, charge distrib., density of states, CNDO calcs. 78—70995
Ag clusters, open-shell CNDO-MO calcs. 79—20397
Ag latent image particles, electronic effects 80—82840
Al_2H_6, electron density distrib., reaction channels and bonding characts., electrostatic mol. pot. CNDO/2 calc. 80—23309
AlN:O, deep impurity states, orbital spectra, CNDO/2 calcs. 78—6319
AsF_3 X-ray and UV photoemission spectra, Auger spectra 79—98150
AsFs X-ray and UV photoemission spectra, Auger spectra 79—98150
As_2O_3, electronic struct., X-ray emission, XPS, UPS obs., CNDO cluster calc. 78—52638
As_2O_3, X-ray emission spectrum and XPS, electronic struct. calcs. using scattered wave method 79—11502
BH_4^-, CNDO/2 calc. of chemical bonding 79—76345
$B_2H_5^+$, FSGO ab initio calc. of geometry, CNDO/2 calc. 78—41943
B_2H_6 and $B_2H_5NH_2$, electronic struct. and bonding, comparative calcs. 79—31397
BH_3F^-, CNDO/2 calc. of chemical bonding 79—76345
$(BH_2H)^-$ ion adduct, form., kinetic energy, interference charge density changes, CNDO/2 calc. 79—57211
BN tetrahedrally bonded valence crystals, SCF perturbation theory appl. 79—37658
BeO, tetrahedrally bonded valence crystals, SCF perturbation theory appl. 79—37658
Br_2CO and Br_2CS, signs of dipole moment derivatives, semiempirical CNDO calcs. 79—26890
$Br(H_2O)_n^-$, geometric and electronic struct., CNDO/2 calcs. 77—79542
$Br(H_2O)_n^-$, geometric and electronic struct., CNDO/2 calc. 79—41113
C, CNDO/S nucl. screening const. calcs. 78—86787

CNDO calculations continued
C-H bond containing molecules, correls. among bond lengths, stretching freqs. and bond order matrix elements 77—58192
CH_3, CH_2 and CH deformation vibration group frequencies and MO electron densities, interaction force const. 80—87101
CO, carbonyl group stretching freq. force const., CNDO/2 and localised orbitals calc. 77—30784
CO, chemisorbed, CNDO calcs. of mol. struct. *(German)* 79—96368
CO, chemisorbed on graphite, CNDO calc. using cluster model 80—54522
CO, chemisorption on Ni *(German)* 78—29751
CO_2, dimer struct. CNDO/2 and ab initio calcs. 77—71753
^{13}C, shielding consts. and anisotropy of NMR shielding tensor, modified CNDO/S calcs. *(French)* 80—32610
Cd, photoelectron spectra, 4d spin-orbit splitting, crystal field and band-broadening effects, CNDO calcs. 78—76577
2-chlorothiophene, σ^* anion radical, prod., ESR spectrum assignment 78—11539
Cl_3^- energy surface, comparison of CNDO and ab initio results 77—23445
ClF_2, CNDO/2 calcs., mol. struct. and props. 77—79543
$Cl_nSi(CH_3)_{4-n}$, ^{35}Cl NQR, geminal and vicinal interactions on substituents electronic effect 80—63663
$Cl_nSi(OCH_3)_{4-n}$, ^{35}Cl NQR, geminal and vicinal interactions on substituents electronic effect 80—63663
Co complex, O_2CoCl_4 and $O_2CoCl_4NH_3^{2-}$, struct. and bonding model, CNDO-UHF calcs. 80—95541
$Co(CO)_4^-$, extended CNDO calc. 80—918
$Co_2(CO)_8$, extended CNDO calc. 80—918
$Co_4(CO)_{12}$, extended CNDO calc. 80—918
Cu complex, β-diketonate complexes, CNDO calcs. 79—59358
Cu complex, $Cu(NH_3)_2(NCX)_2$, X=O, S, electronic struct., stereochem. 80—58156
N,N-dimethyloxamide, conform. anal., CNDO/2 energy optimisation, mol. props. 77—75328
$F_4S_4N_4$, SCF-Xα-CNDO/BW calcs., comparison 78—25435
Fe complexes, high spin ionic with halogen ligands, Mossbauer isomer shift calibration 77—16210
Ge, chemisorption of O_2 on (111) and (100) surfaces, CNDO calc. 77—55464
H-bonded complexes, geometries, CNDO/2 and EHT calcs. 79—36530
H_2 chain, infinite, lattice distortions, CNDO/2 calcs. 78—6018
HCS^+-CSH^+, struct. and stability, ab initio SCF calcs., CNDO calcs. 80—32608
HCl crystals, orthorhombic and cubic, CNDO calcs. 80—6383
HCl, solid, ferroelec., comparative calcs. 77—8529
HF, cryst., CNDO calcs., struct., binding energy, 4K 77—15338
HF, solid, ferroelec., comparative calcs. 77—8529
$HF+H_2O$(methanol)(ether), mol. electrostatic pot., H-bonds, CNDO/2 calc. 77—61822
HN_3+F, strong interactions in gas-phase reactions, arrested relax. IR chemilum. obs. 80—7773
H_2O, force consts., vibr. freqs., CNDO/2 and MINDO calcs. 77—14607
H_2O interaction with AgI surface clusters 77—4254
H_2O, semiempirical CNDO/2 wave functions, pair density anal., environmental effects 80—91451
H_2O-(HF)(F_2) complexes, CNDO/2 calcs. for electronic struct. and props. 78—25442
H_2O-H_2S complexes, equilib. config., H-bond energies and electron densities, CNDO/2 method 80—14084
(H_2O)-HF complexes, (x=1 or 2), geometry, CNDO/2 calc. 79—36531
$(H_2O)_2$, electrostatic mol. pot. curves, proton transfer and bridging pot., CNDO/2 calc. 79—94054
$(H_2O)_2$, struct. studied by CNDO/2 method 80—69081
$H_3O^+(H_2O)_n$, photodissoc. meas. and calc., rel. to atmospheric stability 79—86017
H_2SO_4 and $SO_3.H_2O$, CNDO/2 calc. of thermal stability 78—76840
I complexes, ICl.L (L=organic radical), charge transfer and quadrupole-interaction consts. calc. 77—10590
I-containing molecules, geom. struct. and dipole moments, CNDO/2 calc. 79—94103
$I(H_2O)_n^-$, geometric and electronic struct., CNDO/2 calcs. 77—79542
$I(H_2O)_n^-$, geometric and electronic struct., CNDO/2 calc. 79—41113
KCl, F- and H-centre production by nonradiative decay of self-trapped exciton 78—23042
$LiBH_4$, comparison of potential surfaces, calculated ab initio and semiempirical CNDO/2 scheme 79—41112
$Li(CO)_n$ (n=1,2,3,4,5,6,8), semiempirical CNDO calcs., solvation struct. 78—82649
$Mg(H_2O)_n^{2+}$, geometric and electronic struct., CNDO calc. 79—36532
$Mn_2(CO)_{10}$, extended CNDO calc. 80—918
N, CNDO/S nucl. screening const. calcs. 78—86787
N containing molecules, N NMR, nuclear mag. shielding, X-ray photoelectron spectra 78—17695
N-H bond containing molecules, correls. among bond lengths, stretching freqs. and bond order matrix elements 77—58192
NH_3, dipole moment derivatives, polar tensors, effective charges, CNDO calcs. 77—38613
NH_3, force consts., vibr. freqs., CNDO/2 and MINDO calcs. 77—14607
NH_3-(HF)(F_2) complexes, CNDO/2 calcs. for electronic struct. and props. 78—25442
NH_3-lithium halide complex, ab initio calcs., Li bond rel. to H bond 77—14343
NH_2OH, ionisation energies, He I photoelectron spectra, orbital calcs. 77—88497
NO_2^-, microwave transition probability in zero field, spin-orbit interaction 78—25518
NO_2^- triplet state lifetimes and fine structs., CNDO-CI calcs. 77—57897
NO_3^-, triplet state lifetimes and fine structs., CNDO-CI calcs. 77—57897
NO_x^--HNO_x-H_2O clusters, gas phase, thermodynamic quantities, mass spectra obs. 80—50875
N_2O_2, localised mol. orbitals from semiempirical CNDO calcs. 78—62726
N_2O_3, localised mol. orbitals from semiempirical CNDO calcs. 78—62726
N_2O_4, localised mol. orbitals from semiempirical CNDO calcs. 78—62726
Na zeolites, electronic struct., quantum chemical study 80—69058

CNDO calculations continued
NaCl crystals, electronic and hole centres and surface, quantum-chemical calcs. 80—65489
NaCl, electronic structure calculation, CNDO semi-empirical methods *(Russian)* 80—10909
NaCl, quantum-chem. calcs. of electronic and hole centres and surface 80—20118
Ni, chemisorptive binding of O, CNDO calc. of potential energy curves *(German)* 80—44431
Ni complex, β-diketonate complexes, CNDO calcs. 79—59358
Ni complexes, $Ni(PX_3)_4$ ($X=F$, OCH_3, Cl, CH_3, H), CNDO/2 calc. of magneto-optical props. and electronic content of metal-ligand bonds 77—23430
Ni surface, adsorbed CO, N_2, valence band photoemission, SCF MO CNDO calc. 80—100754
Ni surface, adsorption, chemisorption of at., mol. H_2, semi-empirical CNDO MO calcs. *(German)* 79—95465
O, CNDO/S nucl. screening const. calcs. 78—86787
OH, correlation between chem. shift and charge in organic cpds. 77—18946
$(OH)_2^{2-}$, electrostatic mol. pot. curves, proton transfer and bridging pot., CNDO/2 calc. 79—94054
^{17}O, screening constants by CNDO/S and INDO calculations 77—46576
PH_3, dipole moment derivatives, polar tensors, effective charges, CNDO calcs. 77—38613
$P_2O_4(OH)_4^{2-}$ group, electronic struct. calcs. 78—67971
^{31}P, shielding consts. and anisotropy of NMR shielding tensor, modified CNDO/S calcs. *(French)* 80—32610
$(PtCl_6)^{2-}$, quasi-relativistic SCF-MO-LCAO methods, CNDO and MWH appls. 78—41953
S containing small paramag. ions on MgO g-tensors and spin densities 78—46270
S cpds., electronic struct. of some 2-and 4-valence states *(French)* 77—10591
S-N system, inorganic, electronic struct. obs. by photoemission XPS and UPS, CNDO calcs. 80—78653
S_3^-, stabilized on MgO surface, CNDO calcs. of g-tensors and hyperfine coupling consts. 77—83625
SCl_2, electronic struct., group theoretical and CNDO/2 calcs. 78—33419
SCl_4, electronic struct., group theoretical and CNDO/2 calcs. 78—33419
S_2Cl_2, electronic struct., group theoretical and CNDO/2 calcs. 78—33419
S_2N_2, electronic struct. by CNDO/2 calcs. 78—62727
S_2N_2, semiempirical electronic struct. calcs., applicability testing, and for $(SN)_x$ 77—6681
S_4N_2, electronic struct. by CNDO/2 calcs. 78—62727
$S_4N_4H_4$, SCF-Xα-CNDO/BW calcs., comparison 78—25435
SO_2 PMDR, CNDO CI calcs. 79—72342
$SO_3+H_2O \rightarrow H_2SO_4$, gas phase kinetics, CNDO/2 calc. of H_2SO_4 and $SO_3.H_2O$ struct. 78—76840
SPF_3 band contours of E fundamentals, IR spectra 79—98089
Sb complexes, $SbCl_5.L$ (L=organic radical), charge transfer and quadrupole-interaction consts. calc. 77—10590
Sb compounds, Mossbauer effect, isomer shifts, quadrupole splitting, CNDO/II calcs. 77—24766
Sb halides, quadrupole-interaction consts., CNDO/2 calc. 77—10589
Sb_2O_3, electronic struct., X-ray emission, XPS, UPS obs., CNDO cluster calc. 78—52638
Se, amorphous film, highly disordered, UPS study 80—76148
Se_8, monoclinic, XPS and valence band struct., comparison with trigonal form and S_8 77—44124
Si compounds, free mol. chemical shift, binding energy and Auger spectra 80—32782
Si, semivacancy and pair of semivacancies calc. by CNDO/2 method 78—51537
Si-H bond containing molecules, correls. among bond lengths, stretching freqs. and bond order matrix elements 77—58192
Si_2H_6, tetrahedral edge sharing, distortions, MO calcs. 77—14380
SiO_2 clusters, CNDO/2 calc., appl. of cyclic boundary conditions 78—72110
SiO_2 crystal and amorphous modifications, structural defect model 80—38915
SiO_2 polymorphs, CNDO/2 MO calc. 80—6386
SiO_4 tetrahedra, semi-empirical molecular orbital model, radiation compaction application 79—73433
Si_2O_2, tetrahedral edge sharing, distortions, MO calcs. 77—14380
$Si_2O_6(OH)_2^{6-}$ group, electronic struct. calcs. 78—67971
Si_2S_2, tetrahedral edge sharing, distortions, MO calcs. 77—14380
Sn complexes, $SnCl_4.L$ (L=organic radical), charge transfer and quadrupole-interaction consts. calc. 77—10590
Sn compounds, Mossbauer effect, isomer shifts, quadrupole splitting, CNDO/II calcs. 77—24766
Sn halides, quadrupole-interaction consts., CNDO/2 calc. 77—10589
SnI_3 , vibr. intensities, forms and freqs. anal. SCF MO LCAO CNDO calcs. 78—9274
V-O coordination complexes, CNDO calcs. of stability and bonding *(German)* 79—31404
VO_2, semicond. phase, optical spectrum, CNDO CI calc. 78—27258
V_2O_5, electronic and band struct. and spectra, CNDO CI cluster method 79—11091
Zn complex, β-diketonate complexes, CNDO calcs. 79—59358

coagulation
aerosol, Brownian coagulation in transition regime 78—11571
aerosol, discrete coagulation eqn., approx. analytical soln. 80—55722
aerosol, high Knudsen number, coagulation rate measurement 80—71954
aerosol, kinematic coagulation calcs. in variable-speed gas stream 80—19491
aerosol, multicomponent, coagulation eqn., with/without particle growth 78—35727
aerosol, turbulent coagulation in pipe flow 79—37385
aerosol coagulation, simplified model 77—56254
aerosol coagulation and diffusion in turbulent jet 79—23355
aerosol particle coagulation by Brownian motion 79—96375
aerosol particle size distrib., dynamic behaviour, coagulation, condensation, nucleation and removal 78—35726
aerosol particles, microphysical processes 78—7709
aerosol particles in flow type chamber, coagulation, deposition 80—69908
aerosols, coagulation, initial size distrib. effect 80—104469
aerosols, coagulation, kinetics 79—39209
aerosols with broad initial size distributions 78—15717

coagulation continued
alloy, binary, theory for initial stage of grain growth and unmixing kinetics 78—19714
antithrombotic polymeric materials for artificial heart and devices for assisted blood circulation 78—36052
asymptotic analysis, systems with external source of particles 79—57300
atmosphere, steady-state coagulation eqns. and particle size spectrum model *(Russian)* 77—41115
atmospheric aerosols, particle size distribs. evolution via Brownian coagulation, num. simulation 80—41513
balance equations, homogeneous and nonhomogeneous, similarity solns. 77—9130
binary liquid system, colligative prop., composition diagram *(Russian)* 79—14663
binary system cluster dynamics, critical diffusion and phase separation kinetics 77—61042
biological tissue, coagulation by irradiation with laser light 80—41113
biomedical application, monitoring of mol. and cellular biological processes 77—48852
Bjerknes forces in viscous medium and acoustic coagulation of aerosols 77—68680
blood clotting, Fourier transform. IR obs. 78—68945
blood clotting characterisation by US digital fixed path interferometer 78—44670
blood coagulation and fibrinolysis under influence of direct elec. current 78—48766
blood coagulation parameter selection for automatic digital recording 77—21543
blood coagulation time, US meas. 79—83870
blood viscometers and anticoagulants compared 79—83834
Brownian coagulation 77—9133
Brownian coagulation in rarefied gases 77—36794
Brownian coagulation in transition regime 77—86383
Brownian particles, reversible adsorption and reversible coagulation, kinetic eqns. 79—16045
clouds, coagulation processes, Monte Carlo simulation *(Russian)* 79—84377
colloid, Brownian coagulation, with disintegration of aggregates 80—7864
colloid coagulation, 1st-order diffusion effects 79—39213
colloid stability, main affecting factors 78—11568
colloidal dispersions, stability in flow fields, trajectory anal. 78—5782
colloidal particles, Poiseuille flow, total particle conc. axial change 80—108752
colloidal solution, two-component, differential surface coagulation 79—79303
colloidal suspensions, coagulated, flow props., elastic floc model 77—939
colloidal suspensions, coagulated, flow props., energy dissipation in flow units 77—3862
colloids, amphoteric latex coagulation, reversibility and specific ion effects 80—45567
colloids, DLVO theory problems 80—45566
colloids, hydrophobic, coagulation mechanism 78—40085
disintegrating particles, steady-state distribution 79—57296
dispersion, coagulating, light scatt. data, Fourier inversion anal. 78—76932
dispersion, coagulating, light scatt. for close range struct. determ. 78—53273
droplets, statistical distrib. 79—74425
endoscopic Ar ion laser photocoagulator for bleeding digestive lesions 78—40287
endoscopic laser coagulator with recirculating gas-jet assist 78—48867
estuarine particle dynamics, math. model, phys. and chem. processes 77—21793
eutectic structure coarsening during and after unidirectional growth 78—35379
fibrinogen, bovine, high energy-induced aggregation, time resolved spectra 80—61655
fibrinolysis and coagulation, dynamic rheological studies 80—61614
fine particles clustering, experiment 80—26937
finite system 78—68933
flotation, noninertial, effect of particle aggregation 80—55719
glow-discharge polymer surface blood compatibility, Lindholm coagulation tests 77—81658
graphite grain surface reactions in interstellar and protostellar environments 78—4316
haemocoagulometer 79—39541
Hamaker functions, calc. from coagulation data, influence of Stern layers 78—48698
heparin assay in animal model of Pseudomonas sepsis, rheological approach 77—52953
immunoglobulin, human, high energy-induced aggregation, time resolved spectra 80—61655
integrodifferential equation, exact soln., breakdown effect 78—53272
interaction energy of two unequal spheres, heterocoagulation 79—29411
interstellar charged grains, thermal coagulation in dense clouds 79—53872
interstellar dust, grain growth by radiation pressure induced coagulation 80—94851
interstellar grains, large, towards ρ Ophiuchi, origin by coagulation 80—41870
invert emulsion, aggregation equilibrium 79—66356
laser photocoagulation in diabetic retinopathy therapy 79—79622
LMFBR maximum critical accident, assessment using theory of aerosols coagulation 77—3121
magnetic powder-liquid suspension, rel. to NDT by magnetic powder method 78—60942
metal-polymer deposit, simultaneous electrophoretic deposition and electrochemical precipitation 79—56938
metallic product migration in reactor oxide fuels 77—74926
mixed colloidal suspensions, selective coagulation 79—74426
model phospholipid membrane, structural changes, aggregation 79—66451
molten metal binary mixtures with wide immiscibility range, gravitational layering of components *(Russian)* 80—104092
monodisperse particles, Brownian coagulation and diffusive deposition 78—23967
monomer externally controlled coagulation, exactly solvable model 80—81368
pacemaker implantation surgery, intracardiac ECG derivation during electrocoagulation 78—40397

coagulation continued
- partial hepatecomy using high power CW and Q-switching ND:YAG laser *(German)* 77—44734
- particle masses, self-similar singular spectra in coagulating systems 79—70379
- particulate thermal coagulation and downstream transport from urban area source, math. model 78—44985
- planar micelles, structural changes, aggregation 79—66451
- PMMA aqueous colloid, coagulation kinetics, light scatt. determ. 79—39215
- pollutant mass density function multimodality 77—70807
- polydisperse system, turbulent coagulation in force field 79—57297
- polymer coatings, chemiphoretic deposition without electric current onto metal 78—64763
- polystyrene, sol, light scatt. data, Fourier inversion anal. 78—76932
- precipitation processes, study by particle site anal. 80—50883
- retinal photocoagulation by laser beam, temp. and bleaching dynamic meas. *(German)* 79—2098
- Schulze-Hardy rule, theory 80—89540
- sediments, agglomerated, in N.Chesapeake Bay estuary, microstruct. rel. to coagulation 79—53336
- serium albumin, bovine, high energy-induced aggregation, time resolved spectra 80—61655
- sheared coagulated sols, energy dissipation during sheared flow 78—63461
- sol, coagulated, viscoelastic props., elastic floc model 79—37270
- sols, primary and secondary coagulation and heterocoagulation, role of surface chemistry 80—45551
- solvated ion dynamics, mol. theory 78—35695
- stability ratio of primary and secondary minimum coagulation, kinetic theory model 80—3415
- steel, liquid, Stokes coagulation model, particle motion according to Boltzmann eqn. *(German)* 80—40357
- submicron particles, controlled generation *(Italian)* 77—48688
- suspension, flow equation 78—63487
- suspension, stirred, suspended particles absorpt. of solute molecules 78—30342
- theory, new aspects *(Russian)* 79—8453
- two-phase flow particle interaction, coagulation and rebound calc. 79—98789
- urban aerosols, size distrib. 78—3925
- Venus clouds, aerosol size distrib., coagulation sedimentation and turbulent mixing effects 77—71041
- Al-Mg alloy, creep rate, effect of dislocation pinning by impurity atoms *(Russian)* 78—38719
- Al-Mg-Mn alloy, disperse β-phase, kinetic laws of coagulation *(Russian)* 78—27519
- Au, colloidal, stability and Hamaker const. determ. 79—87883
- $CaCO_3$ aerosols, coagulation rate meas. 79—96374
- $Ca_x(PO_4)_y$, soln., coagulation effects on light scatt. obs., TEM, SEM 80—45090
- ^{60}Co, in radioactive waste water, improved removal using diethyldithiocarbamate 78—37415
- Cr-Mo (2.25, 1 wt.%), decarburization carbide effects in high temp. Na *(Japanese)* 78—15403
- CsI, mechanical props., effect of impurities 77—69034
- CuO, sol, mixtures with TiO_2 and α-FeOOH sols, differential surface coagulation 79—79303
- α-FeOOH, sol, mixtures with CuO and TiO_2 sols, differential surface coagulation 79—79303
- H_2SO_4 aerosol growth, kinetic model 77—37340
- H_2SO_4 secondary aerosol form. in urban atmosphere 77—33137
- KBr in contact with KCl, mutual diffusion, development of relief on contact surfaces 78—22964
- KCl, doped, elec. conductivity and optical absorpt., quenching from 750°C 78—2289
- Ni wire plasma sputtering with W particles, coagulation, struct. and particle size *(Russian)* 80—40260
- Ni-P-Al_2O_3 (SiC), composite deposit electrodeposition *(Russian)* 78—35326
- $PbCrO_4$, paste, anomalous viscous flow 79—64617
- Re hydrosols under action of US irradiation 80—58853
- Ti^{4+} hydroxide, coagulation struct. effects on particle size of TiO_2 78—52732
- TiO_2, sol, mixtures with CuO and α-FeOOH sols, differential surface coagulation 79—79303
- Zn_2SiO_4 ores, hydrometallurgical treatment for Zn recovery 77—52263

coal
- *see also mining*
- aerosol particle size classifier, parallel plate electrostatic device 80—95070
- Akabira coal mine, stress relief boring, monitoring programme 77—9423
- analysis, neutron activation, using standard reference materials as multielement irrad. standards 78—80815
- analytical assembly using capture gamma rays from accelerator neutrons 79—96401
- ash, radioactivity from stored radionuclides 79—89417
- ash characterisation with X-ray photoelectron spectroscopy 79—1977
- ash content, determ. by forward-scattered γ-radiation, improved accuracy 78—7280
- ash content measurement in moving wagons using neutron activation 80—3431
- automated multielement analysis using neutron-induced gamma spectrometry 79—48015
- baked C mixes, anthracite, petroleum, metallurgical and pitch cokes as fillers, chracteristics study 79—57052
- basins origin by salt solution 78—11899
- bituminous coal emulsification by ultrasonics 79—47997
- Bonnet Plume Basin, Yukon Territory, Canada, gravity profile anal. as aid to coal basin evaluation 80—76898
- borehole quantitative anal. method using neutron capture gamma-ray meas. 79—52853
- borehole radar exploration in seams 78—28235
- British coalfields, geological aspects, resources and reserves 79—57931
- brown, 60 years supply at Hambach open cast mine *(German)* 79—57352
- brown, pulverised, SO_2 emission reduction by limestone-additive process *(German)* 78—53724
- brown coal, adsorption and binding of U from seawater, IR spectroscopic obs. 78—82855

coal continued
- calorific value determ., by neutron inelastic scattering *(Czech)* 80—101048
- catalytic hydrogasification, effectiveness factor 79—47966
- caved faces of Appin Colliery, rock pressure distrib. 77—9420
- chemical analysis, computer evaluation of SEM images 80—71994
- chemical structure, NMR and IR obs. 77—40590
- cleaved surface, photoacoustic IR spectra 80—87104
- coke, shrinkage kinetics during calcination 80—93572
- combustion, NO_x and SO_2 form., oxidizing agent excess depend., thermodynamic anal. 78—15677
- combustion, operation of a centrifugal fluidized bed with continuous feed and removal of bed material 80—30349
- combustion, prod. of atm. N_2O 77—21890
- combustion, radiological aspects 80—61485
- combustion of coal particles, holographic meas. 79—76630
- combustion product recirculation, in combustion chamber of a steam generator, 200 MW *(Czech)* 78—27759
- combustion using stationary Stirling heat engines 80—30535
- combustion wastes, resource materials recovery, using combination sinter-dilute acid leach methods 79—48063
- composition determination by ^{252}Cf neutrons, flux level corrections 78—7303
- conversion, by flash hydropyrolysis and hydrogasification 79—52868
- conversion, underground, integrated fuel-generation and power-generation concept, using electrochemical engines 79—48053
- conversion, underground, US Department of Energy status 79—48054
- conversion demonstration plant, US DOE R and D program 80—40813
- conversion plants, exam. of corrosion and wear of steels, review 78—53012
- conversion processes, appl. of non-fossil-derives H_2 for synthetic fuel manufacture 79—74483
- conversion technologies, health and environmental effects 80—81493
- development possibilities of energy resources, review *(German)* 80—21355
- dewatered pipeline coal dust pollution model 77—37401
- dielectric relaxation and conductive impurities 79—82921
- dipping seams, seismic reflection method using Rayleigh channel waves 78—69471
- dispersion, solvent refined, elec. props., surface characts. 80—80333
- dissolution in organic solvents, fast-dump reactor apparatus for short reaction times 77—44575
- domestic coal, radiometric method for determ. of heating value, rel. to moisture content 78—20111
- dust mass flow meas. methods *(German)* 80—92242
- elastoplastic anal. of stresses, finite element method 79—66691
- electrical properties, meas. as function of freq., polarisation, EM wave direction and temp. 79—12113
- electrostatic precipitation technology development, stack gas ionisation by electron beams 78—57346
- elemental analysis by prompt neutron activation anal. 79—52848
- EM modelling of transmissions through in situ gasified coal seam 79—12298
- energy conversion, Conf., San Diego, CA, USA (Aug 1978) 79—48038
- energy conversion engineering, alternative energy sources *(Japanese)* 80—26105
- energy conversion systems, coal based, for electric power generation, performance and economic potential 80—16774
- energy demand and technology forecasting up to year 2000 *(French)* 79—92048
- energy utilisation technology in Japan overview 79—96413
- fast-neutron activation anal. 78—85742
- fault location in underground coal seams 80—94613
- fluid bed processing, mechanical energy relationships during deagglomeration of caking-coal-char 80—30353
- fluidised bed firing, technological state and economic chances *(German)* 79—92050
- fluidised-bed steam generating system to supply 100000 lb/h of saturated steam burning high S coal 80—108778
- flyash analysis for ^{222}Rn annual rate of release determ. in UK 80—17143
- flyash from coal combustion, S and Cl adsorpt., cloud nuclei form. 77—21887
- gamma-ray activity in bituminous, subbituminous and lignite coals 77—25684
- gamma-ray activity in coals, rel. to power station choice 78—11746
- gasification, acetylene prod. process, development and economics 80—30338
- gasification, alloys stress corrosion cracking testing 80—7726
- gasification, catalytic, predevelopment research 79—52870
- gasification, catalytic, preliminary research 79—52871
- gasification, demands made on materials used in process *(German)* 80—45438
- gasification, demonstration plant at Cool Water, California 79—100480
- gasification, fluidised-bed, low-BTU gas production, ash agglomeration process appl. 79—48065
- gasification, H production by H_2O photocatalysis on TiO_2 using solid C 80—26150
- gasification, in situ, instrumentation development 79—48055
- gasification, in situ, kinetic model of char-steam reaction in Hanna subbituminous coal 80—30361
- gasification, in situ, of eastern bituminous coals, linked vertical well concept 79—48051
- gasification, potential fuel source 80—93842
- gasification, Synthane process appl. 79—48057
- gasification, U-gas pilot plant developments 80—30343
- gasification by nuclear steam reforming of methane 80—55775
- gasification environment simulation 80—100831
- gasification for industrial scale H_2 production 80—61438
- gasification for industrial scale production of H 80—35791
- gasification of CaO catalyzed coal 80—30339
- gasification plant, high-temp. alloy evaluation for nucl. process heating 78—13237
- gasification plant using nuclear process heat, material corrosion 78—13348
- gasification system, Westinghouse fluidised-bed, low-Btu fuel gas production 79—48058
- gasification technology, environmental characterisation, equipment and strategy 80—30344
- gasification technology, US DOE R and D program 80—40810
- gasification using COGAS pyrolysis process 80—30342

coal continued
gasification using HTR 80—11996
gasification using steam for H production 80—35789
gasification/combined cycle power generation test facility, preview 80—16773
GEOLOG computerised technique for field observation recording and interpretation 78—7774
Greek lignites, burned in power plant, radioactivity of fly ash 79—62161
H-coal process, direct catalytic hydroliquefaction, developments 80—30332
hardness variations with maceral and orientation 79—24605
high-S coal, continuous sorbent regeneration in pressurized fluid bed combustion 80—30351
hydraulic coal trunk pipeline transport systems, methods of improving economic effectiveness 80—106837
hydrogasification by nuclear steam reforming of methane 80—30325
hydrogenation liquids, characterisation using dialysis 80—30334
hydrogeneration, direct appl. to power generation 79—48056
in situ gasification, EM modelling of refls. inside seam 77—41212
induction heating, underground coal gasification, technical and economic advantages 80—3476
Jharia Coalfield, India, seam mapping by elec. resist. methods 80—4133
KILnGAS coal conversion system for low BTU gas production 80—16776
laser pyrolysis in He or H_2, products exam. 79—20356
layer thickness meas., EM technique 78—53740
lignite deposit exploitation in W.Germany *(French)* 79—92054
liquefaction, 1978 status and development trends in US 79—48061
liquefaction, Exxon donor solvent process development 79—48059
liquefaction, heat transfer characts., modelling of preheaters and reactors 80—30337
liquefaction, low temp. chem. fractionation of H-rich components 80—30336
liquefaction, new catalysts for CO-H_2O induced liquefaction 80—30335
liquefaction, particle size distrib. as function degree of coal conversion 80—35626
liquefaction, potential for synthetic crude oil production, Canada 80—93841
liquefaction, up-grading of solvent refined coal by catalytic hydrogenation 80—30331
liquefaction, US DOE R and D program 80—40811
liquefaction by hydrogenation, developments 79—92051
liquefaction processes, research status 79—48060
liquefaction residues, Mag. separability enhancement, thermomagnetic anal. and Mossbauer study 79—83544
liquefaction residues gasification 79—52869
low rank, appl. to metal extraction from ammoniacal solution 79—11530
magnetic and Mossbauer characterisation 78—64903
magnetic susceptibility and Mossbauer meas. 80—60464
magnetic susceptibility anisotropy meas. as banding-plane indicator 78—77221
magnetic susceptibility anisotropy meas. of coal from S.Wales coalfield, coalification process indicator 79—53340
metamorphic rock as palaeo-geothermometer, appl. in Upper Rhine Graben 79—70800
methane gas interferometer for coal mine safety 78—44423
MHD generator, high-temp. plasma, mol. beam mass spectrometric sampling system 80—52358
MHD power systems, coal-fired, retrofitting to existing non-coal power stations 80—66983
microporosity, determ. from isotherm eqns. 79—51419
mineral content characterisation by Fourier transform IR spectroscopy 80—104474
mineral deposit evaluation with Metalog gamma-ray anal. technique 77—64446
mining, deep-level seams, bed rocks instability obs., by monitoring acoustic emission activity *(Japanese)* 80—10071
mining, processing and transportation, in Western US, impact 80—45621
multistage fluidised coal combustor 80—30345
National Coal Resources Data System of US Geological Survey 77—53208
neutron activation anal. 78—85265
neutron activation anal. 78—85740
neutron activation analysis of ^{16}O and ^{14}N 77—86430
neutron generator for ^{16}O analysis 77—86431
nuclear process steam for coal gasification 78—78488
nuclear techniques, characterisation of trace elements 78—85744
oxidation, for H_2 prod. for coal, water and electrons 79—61962
permeability to methane, influence of temp., geostatic and stratal press. *(Russian)* 79—66695
petrographic characterization using automatic image analysis 80—18002
plasma ashing technique for energy dispersive X-ray analysis of biological specimens in SEM 78—24199
PNP project, prototype HTR and coal gasification plant review 80—5393
polished section prep., structural anal. 79—15924
power generation, alternative processes development, IEA activities 79—48064
power station pollution, physics 79—44659
pressurised fluidised bed combustion, alkali emission and fixation 80—30352
pressurized fluidized bed combustor/steam generator design evaluation for combustion of high-S coals 80—30346
prompt-neutron activation anal., system optimisation 78—85743
prompt-neutron activation analysis for coal quality monitoring in elec. power generating plant 78—7302
prospecting, use of Ge(Li) and intrinsic Ge detectors in borehole sondes 77—37442
prospecting by seismic profiling, new technique testing 80—17404
pulverised, combustion, in combustion chambers of steam generators, digital simulation *(German)* 78—27758
pulverised low sulphur coals, US assisted drying in vacuum filtration 77—32539
PVC/coal blends, fluidized bed combustion of plastic waste with coal, removal of HCl 80—30347
pyrolysis, carbon isotope effects in gaseous products 79—84263
pyrolysis, in entrained bed flow reactor, theoretical exam. with aid of physical models 79—48062
quality, continuous nuclear analyzer development 79—52851
radioactivity, determ. of bulk α and β radioactivity *(Rumanian)* 79—88346
Raman scatt. and luminesc. 78—23460

coal continued
reflectance microscopy, considerations involved in automation 80—18001
reserves and resources, production and transport problems *(German)* 80—26102
resources, energy source, future prospects *(Russian)* 78—32099
reverse combustion along coal seam fissures, eng. model 80—30358
review of developments for efficient energy use *(Swedish)* 80—93845
Rosebud coal ash, elec. cond. 80—107476
seam acoustic imaging 79—53585
seam depth determ. by elec. method *(Spanish)* 78—45031
seam thickness meas. using resonant loop as EM sensor 78—57366
seams, synthetic seismogram calc. with reflectivity method 79—74844
seams with discontinuities, SH channel wave attenuation 78—69292
seismic imaging of faults in multi-moded coal seams 80—85778
seismic prospecting for coal, approx. diffr. theory for transparent half-planes 80—89974
seismic response of carboniferous rock, synthetic seismograms 78—69293
slurry concentration, meas. in haulage pipelines by nucl. techniques 78—7301
slurry diagnostics by US transmission 78—87216
solar coal gasification reactors, tech. and economic feasibility 80—76613
solvent refined, conversion to low-sulphur, ash-free boiler fuel, pilot plant experiences 79—52867
solvent refined coal, petroleum prod. via $ZnCl_2$ hydrocracking 80—30333
Solvent Refined Coal process, trace element distrib., neutron activation analysis 78—3421
specific energy ash and moisture by combined neutron and gamma-ray meas. 79—39255
steam gasification of Illinois coal and coke 80—30341
steam gasification using nucl. heat from GCHTR 77—83071
Stirling engine combustion and heat transport system design alternatives for stationary power generation 80—30536
stress meas. using borehole instrument with electrical strain gauges 77—9415
Sunagawa colliery, underground rock destruction seismic meas. method 77—9419
surface-mine inventory, LANDSAT imagery appl. 77—91320
synthetic, microsection prep. and struct. *(German, English)* 80—35458
tar and petroleum pitches, pyrolysis, press. effects on coke yield and microstruct. form. 77—70289
tar-pitch, production of C fibres *(German)* 78—44033
Texas lignite, economics of a carbonisation process plant 80—21358
thermal decomposition rel. to mud volcanoes, Copper River Basin, Alaska, composition of emitted gases 79—84308
thermal diffusivity and cond. meas. for in situ coal gasification appls. 80—30360
underground coal gasification, Netherlands *(Dutch)* 80—30322
underground coal gasification, potential impacts on groundwater quality 79—87949
underground coal gasification, US Dept. of Energy Program 79—87947
underground coal gasification in steeply dipping beds 79—87948
underground coal gasification program is eastern USA 79—87950
underground coal gasification project 79—87951
underground conversion to hydrocarbons, for industrial appl. 79—48052
underground gasification, field performance 80—30357
underground gasification, numerical model 80—30359
utilisation review and forecast (1950-2000) *(French, English)* 80—21363
vitrinite, in bituminous coal, microporosity and micromineralogy, small-angle X-ray scatt. study 79—12117
Al content, nuclear activation logging 79—80042
CO concentration meas. in coal pulverising plant, IR gas analysers 80—89572
Cl_2 content determ. using British Standard high temp. method 80—85252
Fe-containing minerals, in coals, mag. hyperfine fields meas. 78—88234
Fe-containing minerals in coals, magnetic hyperfine fields meas. 78—68427
Fe-Cr-Al(Ni) alloys, corrosion by coal char at 871° and 982°C 80—3237
FeS_2, pyrite, magnetic separation from coal, magnetokinetics of oxidation 77—12161
H content, total, neutron activation method 79—52852
H production by pressurised coal gasification 80—30609
H production from coal using steam-Fe process, development status 80—55942
H thermochemical production using air blown coal gasification, economics 80—35790
H_2 production from coal by centrifugal separation from gasification products 80—76643
^{226}Ra background levels in lower troposphere from coal burning 77—37361
S adsorption, content meas., using X-ray radiometric analysis 80—26077
SO_2 pollution electricity generation, policy options for control 80—51022

coating processes *see coating techniques*

coating techniques
see also anodisation; cladding techniques; coatings; electrodeposition; electrophoretic coating techniques; encapsulation; epitaxial growth; metallisation; spray coating techniques; vapour deposition
antireflection coating deposition from hydrolyzable soln. 77—58495
antireflection coatings applied from metal-organic derived liquid precursors 80—5847
automatic RF sputtering system for multicomponent film production 78—52672
boride coatings, technology, props., book contrib. 78—48574
boronising sintering of stainless steel 78—60594
ceramics coating by physical vapour deposition processes *(Japanese)* 80—55306
CVD, Mo on SiO_2 covered W-Re wire, for neurological electrode, elec. cond. and bending props. 78—11752
CVD, SiO_2 on W-Re wire, for neurological electrode, elec. cond. and bending props. 78—11752
developments 80—16534
diffusion coating of plate, residual stresses, with allowance for phase transform. *(Russian)* 78—11357
explosion, macroscopic and microscopic stresses, X-ray diffr. exam. 77—44407
Fe base alloy, with metallic coating, oxidation effects, wetting, adherence 78—7085
fibre, metallisation by continuous casting in Al and Al alloys *(Russian)* 78—35538

coating techniques continued
flat sheet withdrawn from wetting liqs., coating, meniscus shapes, flow model 77—29044
freeze and viscous coating of fibres 78—48350
geological samples, prep. for SEM 79—12785
glass fibre, continuous coating applicator 77—3659
glass shells, for laser fusion targets, plasma polymerisation coating method 78—60859
glass-ceramic, chemical plating with Ni and Cu 77—44379
glass-enamel coatings, effect of firing method on adhesion 79—24647
glow polymerisation, thin organic polymer coating technique *(German)* 77—12774
graphite, pyrolytic C coating within pores 79—41035
graphite tubes, for at. absorpt. spectroscopy, pyrolytic coating method optimisation 78—76940
hard overcoats in replicated optics 78—66968
inorganic thin layers, two-stage formation 79—27450
ion plating, surface treatment comparison *(French)* 79—57132
jet finishing for hot dip metallic coatings on strip, analytical description 77—28935
large optical component antireflection and protective coatings 79—72660
large scale functional film coating systems, selection 77—69985
laser applications in materials processing, seminar, San Diego, CA, USA (Aug. 79) 80—90609
laser fusion targets, plating methods 78—60862
local heating of powdered slip to produce silicide coatings on refractory metals 77—81335
metal coating, in situ deposition on ceramic powder particles, cermet form. 77—32713
metallurgical coatings, conf., San Diego, USA (23-27 Apr., 1979) 80—12848
metallurgical coatings, fabrication, struct., and appls., review 80—80121
multilayer beamsplitter coatings, accelerated fabrication method 80—102873
optical coatings, problems of application technology 78—83069
optical fibre, mechanical strength, fractographical analysis, review *(Japanese)* 80—35319
optical fibre coating concentricity improvement by tapered nozzles *(German)* 78—38095
optical fibre coating technique improvement 78—5593
optical fibre coating with conical shape applicator 80—58820
optical fibre high speed coating, forced convective cooling 80—23815
optical fibre processing techniques, review 79—50460
optical fibres, application using cylindrical bore dies, theoretical anal. of coating thickness and experimental comparison 79—46095
photoresist, negative, spin-coating technique for producing multilayer IR optical medium 80—74451
plastic powder coating, technique and appl. 79—38786
PMMA coated frit powder prep., corona-charging props. *(Japanese)* 80—25891
polymer coatings, chemiphoretic deposition without electric current onto metal 78—64763
polymer film coating of Al particles *(Russian)* 77—86232
polymer film coatings on metal electrodes, through electroinitiated polymerisation 77—77632
polymer film deposition onto steel, Pt and glassy C electrodes 78—76866
polypropylene, window of proportional counter, Lexan coating for eliminating UV sensitivity 79—74273
porous solid layer form. on viscose fibre, EM field effect *(Russian)* 77—66595
protective coating production, principles and technology of electron beam deposition 79—24439
pyrocarbon deposition in fluidised bed, qualitative model, investigation with Stromungsrohr 78—56595
pyrocarbon deposition on C black *(French)* 78—68921
refractory dielectric coatings appl. using electrodeless capacitor HF plasmotron 77—69984
roll coating, mass production of multilayer interference film *(Japanese)* 79—81577
sand, resin-coated, curing effects on physicomech. props. *(Korean)* 78—60855
silicone double-layer coating with double cone nozzle in-line with optical fibre drawing 80—53488
skin technology, industrial appl. of space processing 79—28991
solar-selective absorber, coating method for pipes *(Japanese)* 80—16834
solution deposition of inorganic glass, protective coating for anodized Al, solution deposited 79—34205
spin coating process, rheology and modelling 78—27655
spin-coating method for substrate coating with parting agent for self-supporting thin films 78—11112
sputter coating for SEM sample prep. conversion of vacuum coating units 77—34058
sputtering, effect of process parameters, on thickness distrib. *(Russian)* 78—31340
steel, C, siliciding in US field 79—39043
steel, low-C, bond form. between powder layer and dense basis during hot pressing 79—24669
strain-sensitive nontoxic brittle coating production 77—86197
surface coating technology, conference, London (1978) 79—83358
thickness monitoring by X-ray fluorescence during coating of steel with Sn or Zn 77—55884
thickness monitoring using bremsstrahlung from fast electron irrad. 77—77609
thin film coating techniques, for SEM and X-ray microanalysis 79—12783
thin film preparation and properties, symposium, Loughborough (1976) 77—77376
thin films, deposition techniques, review 80—80964
vacuum coater, automatic, using minicomputer or microprocessor, IC semiconductor industry appl. 78—48317
vacuum deposition, of graded-thickness film 80—76164
viscoplastic film entrained by moving surface, thickness calc. 79—72916
p-xylene, plasma polymerised films on glass, as laser fusion targets, deposition method 78—60860
Al on Ni base alloys, transport agent comparison 78—11429
Al, on steel, produced by thermal decomposition of alkyls 78—15590
Au deposition at high rates from organic plating baths *(French)* 80—66441
Au ion plating process 79—66186
B, fibre, metallisation by continuous casting in Al and Al alloys *(Russian)* 78—35538

coating techniques continued
C fibre, cementation technique for coating with metal 79—39000
C, pyrolytic film electrode, fabrication, electrochem. characterisation 78—92487
CaF_2 on glass, Na-resistant cell, coating apparatus 80—90874
Cr pyrolytic coating, effect of support metal mech. props. on formation *(Russian)* 80—7713
Cu-Al_2O_3, composite coatings, prep. by precip., props. 78—23841
Cu-coated TiO_2 particles, prep. for composites 80—89159
Cu-n-Si diodes, fabrication by electroless deposition method, characts. 80—100520
CuO solar selective black coatings for large area appls., prep. and props. 80—21411
CuS solar selective black coatings for large area appls., prep. and props. 80—21411
Fe, Fe-C, diffusion coating by Cr and Pb melt bath, kinetics *(Korean)* 78—60873
δ-Fe-Zn layer formed on hot dip galvanising, texture 77—9001
Mo, ionic siliciding, diffusion layer prod. 78—23855
Na_2O-B_2O_3-SiO_2 glass fibre, plastic coating influence on strength 80—58697
Nb alloy, oxidation protection from $MoSi_2$ coating, diffusion-slip casting appl. method 80—21187
NbC coating on C steel and Armco Fe, deposition, struct. and props. 79—52462
Ni aluminisation, soln. of binary multiphase diffusion problem allowing for variable diffusivity 77—16744
Ni coating, self lubricating containing oxides, carbides and borides on steel 80—21189
Ni electroless plating on Zn-Al alloys, baths and activating solns. *(Japanese)* 80—71604
Ni, pack aluminisation process kinetics 77—32718
Ni phase layer growth during aluminide coating 78—27682
Ni superalloy, electroless codeposition of Si and Ti 77—16513
Ni-B electroless-plated amorphous films, anomalous mag. temp. characts. 80—96757
Ni-Co-Cr alloys IN 738, Pt plated, aluminization 78—31583
PbS+CuS solar selective black coatings for large area appls., prep. and props. 80—21411
Pt, aluminization 78—31583
Pt coated Ni-Co-Cr alloy IN 738, aluminization 78—31583
Si on ceramics, coating with inverted meniscus (SCIM) technique, solar cell appl. 80—89163
Si, SOC (Si on ceramic) continuous coating for solar cells 80—93904
Si thick-film growth using contiguous capillary coating on porous C substrates 80—93507
SiC, fibre, metallisation by continuous casting in Al and Al alloys *(Russian)* 78—35538
U_3O_8, supported fission foils for laser excitation, preparation method 77—68218
Zn coating on continuous galvanising line, mass meas. and control 78—19960
Zn sherardising process development 79—78998
ZnS-Ag-ZnS for solar convertors 77—75642

coatings
see also anodised layers; antireflection coatings; claddings; decorative coatings; electrodeposits; electrophoretic coatings; epitaxial layers; insulating coatings; protective coatings; spray coatings; sputtered coatings; vapour deposited coatings; varnish
acoustic reflection-reduction coatings, evaluation procedure 78—9468
acrylate adhesive coating on glass substrate, mech. props. determ. using transfer functions of US oscillations *(Russian)* 79—87644
adhesion measurement, conf. Philadelphia, USA (Nov. 1976) 80—46729
adhesion measurement 80—50817
adhesion strength, meas. using microindentation method 80—40640
alloy, three component, conditions for mass transfer, diffusion processes 80—54445
anodic, and free anodic film on Al substrate, deform.-strength props. *(Russian)* 77—69203
atomic composition depth distrib. by energetic ion anal. 80—35617
bimetallic strip, interface struct., scanning Auger microprobe study 80—34322
boride coatings, diffusion-deposited on WC-Co, elemental and phase comp. 80—15402
boride coatings, high temp. resist. and struct. 79—39008
brittle, on graphite fibre reinforced epoxy, stress transfer to coating 79—96106
brittle coating analysis of orthotropic materials 79—27606
brittle coating technique of stress analysis in glass fibre reinforced plastic 80—35299
carbide coating formation by chromising C steels 78—88571
Carlite, on Fe-Si (3 wt.%), mag. props. rel. to stress coating 80—34727
ceramic glazes, Pb, Zn and added chromogenic ions release, as function of colouring oxide mill additions, voltammetric exam. 78—39920
ceramic-metal composite using metal-coated alumina powder 77—21081
coated inclusion in elastic medium 78—79215
compliant coating on panel, effects on transmission of free waves across rib 77—39248
composite, development and use in USSR *(Russian)* 78—52696
composite flat-belt-drive materials, testing of birefringent coatings 77—77652
cutting alloy detonation coating, struct. and friction *(Russian)* 78—15537
depth profiles, SIMS technique *(Japanese)* 78—85246
diamond indentation and draw tester, for meas. of ultra-adherence in films 78—72944
diazo compounds, continuous tone diazotype imaging films, model 78—32911
dielectric coatings, for laser mirrors, surface optoacoustic spectrometry 78—87085
diffusion coating of plate, residual stresses, with allowance for phase transform. *(Russian)* 78—11357
diffusion solution, relaxation of residual stresses *(Russian)* 77—70195
effectiveness rating of vibration-absorbing coatings 80—5870
elastic modulus meas., machine attachment for eliminating error in load-meas. device 77—25218
electrically conducting surface coating, of linear induction accelerator tube, beam losses and coating inhomogeneity 78—5066
electrode coating effects on elec. breakdown voltage hysteresis in air and SF_6 78—87553

coatings continued
electrode surface and coating effect on DC breakdown voltages in SF_6 78—87557
electrodes, electropolymerisation 80—50854
electroless Ni deposits from Ni/P and Ni/B plating solutions, solderability by contact angle meas. study 79—88910
electron backscattering by thin coatings on bulk materials w.r.t. thickness determ. *(German)* 77—10146
electron beam curing, beam voltage effects on mech. props. and chem. struct. 77—70201
electron-probe microanalysis of thin coatings, charact. fluoresc. correction 80—7881
EM coating thickness gauge calibration using air gap 77—57300
emissivity, low temp., calorimetric meas. technique 80—17941
enamel, rapid method for determining thermal expansion coefficient 79—20308
enamel (lacquer), integrated hemispherical emissivity, bulk expt. investig. 80—19970
enamel coating on metallic base standardization of estimation of impact strength 78—23768
enamel-metal interface, diffusion phenomena, spectroscopic investig. *(Russian)* 77—90508
ESCA examination 77—31919
ethylenic polymer films, highly fluorinated, exam. of wetting props. 78—60856
explosively formed coatings, macroscopic and microscopic stresses, X-ray diffr. exam. 77—44407
film thin, limits of observation of X-ray fluoresc. anal. 79—24857
fission reactor coated fuel particles, failure statistics 77—74945
fission reactor coated particle fuel, ^{137}Cs fission product conc., crack simulation, by YAG:Nd^{3+} laser 80—18416
fusion reactor, low Z coating development program 80—106182
fusion reactor coated heat sink materials, evaluation studies 80—32453
fusion reactors Doublet III neutral beam injector system, outgassing rate meas. and residual gas anal., coating props. 80—95457
fusion thermal tracers, thermophys. characts. investig. 77—5837
glass and ceramic developments for electrical industry appls. 79—78925
glass fibres, epoxy-acrylate coated, static and dynamic fatigue, tensile strength 79—1906
glass plastic coating, thick-walled, compressive strength evaluation method 79—15897
glyceryl dibenzoate, external plasticiser, for styrene-acrylic terpolymer, compatibility, surface tension meas. 79—15834
heat reflecting coatings, effect of thermal deformation depend. on heating rate 78—30169
heat sink materials for fusion appl., thermal shock testing 80—18651
heat-radiating coatings with variable degree of blackness, efficiency 77—28027
high-temperature materials, technological requirements, R and D, report 80—45222
HTGR fuel particles, inert gas intrusion as charact. procedure for pyrocarbon coatings 79—54512
HTGR fuel particles, influence of pyrocarbon props. on as-produced gas permeability of coatings 79—54511
hydrogel coatings, and impregnations in silastic, dacron and polyethylene 79—20719
lacquer, brittle, plasticizer *(Japanese)* 77—52479
lactose powder coated with fatty acids, tensile strength 77—21304
laminated coatings, for fuel confinement, fusion reactor target appls. 78—60883
layer build-up on contact materials *(German)* 80—7852
leads, solderability of external coatings after storage at 25-400°C 78—184
Lexan, on polypropylene window of soft X-ray proportional counters, for eliminating UV sensitivity 79—74273
macrostress calc., spontaneous stresses 77—36710
macrostress meas., spontaneous, dilatometric method 77—36709
macrostress meas., spontaneous, improved methods 77—35100
magnetic coated small dipole antenna, basic parameters *(Chinese)* 79—50193
magnetic fields, eddy current losses in thin conducting coatings *(Polish)* 79—98263
medullary implants with porous coating, stress distrib. 78—69256
melt-spread, contact reactions of Fe-group metals with Al base melts 78—60879
metal, brittle, ductility improvement by plating *(German)* 77—8954
metal, coated, heat resistance assessment at varying temps. *(Russian)* 77—25189
metal, polymer coated, wear and friction 77—21328
metal, resistance to plastic deform. under HF vibrs. rel. to surface treatment *(Russian)* 77—52400
metal coating stability, thermoelectric method of assessment *(Russian)* 78—11459
metal layered contacts, low temp. diffusion *(German)* 80—6538
metal surface, soot covered, refl. of slow electrons 77—36327
metallic, thickness depend. of wall heat transfer during nucleate N$_2$ boiling 79—32210
metallic channels on ferrite, installation 77—77626
metallic coatings, thickness meas., coulometric thickness gauge based on electrolysis laws 77—71293
metallurgical, conf., San Francisco (Apr. 1976) 77—40363
metallurgical coatings, conf., San Diego, USA (23-27 Apr., 1979) 80—12848
metallurgical coatings, conf., San Francisco, USA (Apr 76) 77—31918
metallurgical coatings, fabrication, struct., and appls., review 80—80121
metallurgical coatings conf., San Francisco (1977) 78—2394
metals, coated, IR surface wave interferometry 80—63913
metals, coating with H-transparent Pd layers, spot welding technique 79—47816
metals, surface layers, cross-sectional struct., appl. of cryogenic fracturing technique 77—30219
methacrylic polymer films, highly fluorinated, exam. of wetting props. 78—60856
nonconducting powder, temp. determ. in detonation deposition 80—226
nuclear fuel particles, mech. design concept 77—18670
on nuclear fuel particles, metallic fission product migration 77—50231
optical, for components of space laser communications system 79—86248
optical films with selective optical properties, for enhanced output and radiation spectrum correction, light sources appl. *(Russian)* 80—48372
optical modulator crystal coatings 77—19431
overlay coatings, electron beam deposition techniques 80—35100

coatings continued
oxide coating, thermal sprayed, AE study of porosity 80—25927
oxide film on metallic glass, removal using US oscill. energy *(Russian)* 78—72935
oxides, on Fe, Fe alloys, combined ion-, electron-beam techniques appl. 79—43700
paint coating directional emissivity, thickness and substrate effect, light scatt. theory 80—33437
paint coatings in radiation fields of reactors and accelerators, and after contamination by radionuclides 77—75006
paper, coating type and extent, attenuated total refl. spectrosc. obs. 79—79329
partially film coated crystal, strain field, deform. model and X-ray topography *(German)* 78—83653
Permalloy coated garnet films, bubble statics, dynamics *(Japanese)* 78—52326
phosphate containing materials, technological prod. processes, review 80—97452
photoactive catalyst used in light induced photocuring of coating systems 80—7820
photoelastic coating combined with moire method for strain meas. *(Japanese)* 79—32400
photoelastic coating method of meas. stress and strain 78—1614
photoelastic coatings, stress anal. technique 77—84201
photoelastic tests, construction of polariscope *(Polish)* 77—5887
plastic, review 79—96163
plastic surface coatings as alternative to standard thin section cover glass in microscopy 78—73974
plates, determ. of residual stresses using curvature gauging method *(Russian)* 79—98674
points, testing, modern analytical methods appl. *(Polish)* 78—85253
polyethylene coating on galvanized steel, thermal oxidation affect on adhesion *(German)* 80—35419
polymer, packing density investig. by mol. probe method *(Russian)* 77—44398
polymer coating, creep determ. by impression of rigid sphere 78—85084
polymer film coated steel, Pt and glassy C electrodes, prep., characts., stability 78—76866
polymeric coatings, on steel shot, mechanochem. degradation, substrate effects 79—79134
porcelain enamel layers on steel, H$_2$ induced fracture of layers 78—76752
porcelain enamel panels, TiO$_2$-opacified, quantitative X-ray diffr. anal. of anatase, rutile 79—32857
porosity determination by hydrostatic weighing 80—66714
powder coatings, in metal finishing, review 80—104330
pyrocarbon, fuel particle coating, strength and Young's modulus meas., brittle ring test 77—8868
pyrocarbon, gas permeable isotropic, fluidised bed prep. 77—46381
pyrocarbon coating, isotropic, gas permeability, neutron irradiation effect *(French)* 80—63260
pyrocarbon coating, isotropic, gas permeability meas. *(French)* 80—63259
pyrocarbon coatings, deposition in fluidized bed, TEM, changes by irradiation 80—34084
pyrocarbon coatings of nuclear fuel particles for HTR, production *(German)* 80—18585
pyrocarbon deposition on C black *(French)* 78—68921
pyrocarbon fuel coating, irradiation tests 78—86594
pyrocarbon nuclear fuel coating, props. and neutron irrad. behaviour *(German)* 77—67816
pyrolytic carbon HTGR coated-particle fuel performance charact. by fission gas pressure meas. 79—54584
quartz crystal microbalance with coatings of finite viscosity, transmission line analogy 80—17933
reflective coating for optical waveguides with abrupt turns 78—30059
refractory ceramic coatings, for high temp. use, current status *(Japanese)* 80—71619
residual stress meas. by improved ring-core method *(German)* 79—34272
resin-coated optical fibre, tensile strength tests *(German)* 78—33871
rheological characterisation with regard to appl. and film formation 79—77970
rotation curing using high dose electron beams 77—59958
saturation with Sb and As under glass fusion treatment *(Russian)* 78—35585
scattering layers, reflectance 79—99962
selective surface absorber coatings, technique for comparing effectiveness 80—30545
selective surface coatings, solar energy collector appl. *(Chinese)* 79—34439
selectively plated deposits, significant properties meas. 77—77615
semiconductor laser, electron beam pumping efficiency, coating effect 80—91795
solar collector, wavelength-selective surfaces for efficiency improvement 77—54812
solar collector glazings, effective beam rad. incidence angles for determ. of diffuse rad. transmittance 80—94112
solar energy collectors, black Ni electrochemical coatings, characts. investigation 80—95975
solar flat plate collector coatings, perf. comparison of flat black and selective coatings 80—61426
solar photothermal non-selective and energy control films coatings 80—26157
solar selective surfaces for thermal absorbers, review of basic physics and requirements 80—45752
sound absorbing viscoelastic coatings on submerged cylindrical shells, HF acoustic scatt. 78—1478
spectrally selective surfaces in photothermal solar energy conversion 80—45753
split birefringent coating on birefringent material, determ. of dynamic stress intensity factors 79—50684
spontaneous mactrostress calculation, from substrate deform. 80—15412
steel, aluminising by circulation method, thermodynamics 80—30163
steel, boride coatings, form. mechanism and struct. during crystn. of castings 80—35412
steel, boride coatings from induction heating microstruct. and props. 80—30165
steel, boriding in powdered mixture with high activity 80—30164
steel, fatigue fracture after Fe and Ce diffusion coating, microstruct. investigation *(Russian)* 79—52446

coatings continued

steel, galvanised, interface struct., scanning Auger microprobe study 80—34322
steel, galvanised coatings, thickness meas. using X-ray fluorescence radiation, apparatus design 80—21202
steel, low C, endurance limit, effect of coatings *(Russian)* 77—25145
steel, Si killed, effect of Al addition to Zn on phase composition and morphology of products of Fe-Zn reaction *(Polish)* 78—85021
steel, stainless, liquid phase bonding with Ni-P plating *(Japanese)* 78—7082
steel, X-ray fluorescence thickness meas. for Zn and Sn coatings 77—55884
steel, Zn coated strips, plastic deform. influence on struct. and quality *(Russian)* 80—40377
steel electrode, diffusion coating effect on electric discharge sintering of metal powders 77—63598
steel products, Zn coatings, thickness meas. by X-ray fluoresc. 77—54029
steel substrate, coating applied by explosive energy, adhesive strength 77—70235
steel/SiO_2-Al_2O_3 glaze, adhesive behaviour of metallic cation glaze exchanged on acid site struct. *(Japanese)* 79—66216
stresses in oriented transformer steel induced by coating layers *(German)* 79—28569
surface microgeometry meas. by stylus instrument 79—80575
textured, crystallites faces determ. 80—64846
thermal diffusivity of microsections, IR and X-ray electron-probe microanal. 78—2314
thermal insulation on metal backing, thermophys. characts., expt. determ. technique 80—4707
thermosensitive film coating, dispersed liq. cryst. microdroplets in gelatin matrix, exam. of preps. 80—42220
thermoset and coating technology, torsional braid and thermal anal. 80—55622
thickness inspection, correct. of errors of mounted eddy-current transducers 80—77775
thickness meas., beta backscatter method, meas. uncertainty prediction 77—56206
thickness meas., various methods, critical assessment 80—47018
thickness measurement, methods and instrumentation for measuring, review 78—73000
thickness measurement, metrological provisions 80—77749
thickness measurement using bremsstrahlung from fast electron irrad. 77—77609
thickness measurement using nuclear resonance methods 77—81334
thickness monitoring using slow-neutrons 77—71297
transparent film thickness and refr. index meas., polarisation-independ. reflectance matching 77—65052
tribopolymerized solid lubricating coatings, formation and behaviour 78—35528
trimethylamine.HCl coated piezoelec. quartz cryst. for HCl gas determ. in air 78—92532
triphenylamine coated piezoelec. quartz cryst. for HCl gas determ. in air 78—92532
two-phase diffusion, appl. of solvent-fixed coordinate system, constant surface flux of solute 78—26718
UV curing using electrodeless lamps 77—70199
varnish resin based on diacid prepared from 4,4′-oxydibenzoic aldehyde and dihydroxymethyl propionic acid *(Polish)* 77—28776
vibration absorbing coating, cut constraining layer effectiveness 79—32130
vibration-absorbing, detachable, investigation of energy losses 79—90078
vibration-absorbing coatings, geometry rel. to energy propag. 78—9596
viscoelastic (viscoplastic) fluid, free coating of vert. surface 78—42576
viscoelastic hollow cylinder, elastic coating, thermomech. responses 78—79230
vitreous enamel coating, method of quantitatively assessing blistered structure 78—53108
wood panel coatings, electron-beam curing 77—70200
X-ray fluorescence gamma-thickness meter based on NaI scintillation counters, improvement 79—35670
X-ray fluorescence thickness gauge, spectrometer channel with Si(Li) detector 79—35671
Ag on Cu, corrosion by thermal degradation products of chloroprene and silicone rubber 79—47801
Al castings, grain refinement by gas-generating mold coatings containing hexachloroethane 79—83355
Al coated steel, porosity evaluation, micro X-ray spectral anal. *(Russian)* 80—35389
Al coating reflectivity in vacuum UV, heating effect 80—95981
Al, coating thickness determ. H_2 generating method *(German)* 79—35660
Al, on steel, produced by thermal decomposition of alkyls 78—15590
Al-Mg alloys, overheating effects on microstruct. and props. 77—63698
Al_2O_3, detonation coating, porosity, electrical strength, phase anal. *(Russian)* 77—69204
Au coating for radioactive source backing, spontaneous resistance variations 77—54386
Au on Cu, corrosion by thermal degradation products of chloroprene and silicone rubber 79—47801
Au plated layer thickness meas., ^{195}Au nondestructive method 79—96244
Au-Pd coating for radioactive source backing, spontaneous resistance variations 77—54386
B fibres, plasticizing and wettability-enhancing coatings 79—29252
Be coatings, α-radiation meas. of thickness 78—82600
BeO, on Cu-Be atomic composition depth distrib. by energetic ion anal 80—35617
C black, graphitised thermal, coating for gas chromatography columns 77—77823
C fibre, metal-coated with Cu, Co or Ni, coating struct., SEM study 80—97605
C fibre, Ni coated, high-temp. compatibility 78—19829
C fibres, plasticizing and wettability-enhancing coatings 79—29252
C, isotropic pyrolytic, for biomedical devices, mech. props. 78—65150
C, paint type coating layer with spherical pigment, radiative transfer theory 80—61405
Cr black solar selective absorbers, thermal degradation 80—61417
Cr, diffusion coating strengthening by plastic deformation, controlling physical factors *(Russian)* 77—25187
Cr, on Nb, prior thermal working effect on coating quality *(Russian)* 78—23820

coatings continued

Cr^{6+}/Cr^{3+} colloidal SiO_2 surface films on Al, TEM/XPS study 80—85090
Cr-Cr_2O_3 black chrome, commercial, solar absorber coating characterisation 80—80111
Cr-Y coatings, spectral determ. of Y content 77—90681
Cu coated steel tube, segmental specimens, tensile testing 79—70255
Cu, fatigue behaviour effect of Zn, Au diffused coatings 78—72850
Cu-coated TiO_2 particles, prep. for composites 80—89159
Cu-rare earth oxide-Y composite coatings, oxide and Y effect on coating precipitation 80—55554
CuO, black Zn-dust pigmented solar selective coatings for solar photothermal conversion 80—66997
CuS, black Zn-dust pigmented solar selective coatings for solar photothermal conversion 80—66997
CuS-PbS, black Zn-dust pigmented solar selective coatings for solar photothermal conversion 80—66997
Eu_2O_3 ceramic powder, in situ deposition of metal coating, cermet form. 77—32713
Fe-Ni-Cr coating, electrodeposited, exam. of passivity 78—80655
Fe-Si (3 wt.%), domain wall spacing and core loss, forsterite and stress coatings effect 80—88780
Fe-Si (3 wt.%) grain-oriented transformer sheet, effect of phosphate coating containing Cr_2O_3 and CaO 77—16135
Fe-Zn, galvanised coating appl., metallurgy review 79—96199
Fe_2O_3, paint type coating layer with spherical pigment, radiative transfer theory 80—61405
Ga, spreading kinetics on thin Ag films, influence of melt-support interaction *(Russian)* 79—37903
GeS_x layers, formation on Ge surface in S vapour 79—7757
MnO_2 anode coating for enhanced O_2 evolution in seawater electrolysis 80—30435
Mo coated diamond powders, X-ray diffr. study 80—100936
Mo, coating, soldered to diamond surface, contact strength, device 78—60910
Mo-Zr-C (0.12, 0.002 wt.%), prep. of diffusion metal coating on alloy, oxidation rates *(Russian)* 78—56816
Mo_2C, phase and struct. transformations on heating 79—96206
MoS_2 on Mo, cryst. struct. and thermal stability 77—52539
$MoS_2(Se_2)(Te_2)$ coatings, growth kinetics and friction coeffs. 77—16731
$MoSe_2$ coating, on Mo, support annealing influence on orientation, texture and hardness *(Russian)* 80—20961
$MoSe_2$, lubricating coatings, texture, prep. by $Se_{(g)}$+Mo 78—53018
Mo_5Si_3 based coating, interaction with Mo alloy substrate *(Russian)* 80—21167
Na_2O-SiO_2 glass, coated with SnO coeff. of friction and fracture toughness 78—80657
Na_2O-SiO_2 glass, vitreous coating, adhesion to Fe-Ni alloy 79—20336
$NaPO_3$ coating on Fe_xO_y powders, coercivity increase 77—89980
Nb_3Sn, for RF cavities, props. 77—26891
Ni, binary alloy, irrad. with heavy ions, non-equilib. segregation phenomena 80—19950
Ni coating on mag. steel, thickness measurement of coating 78—76821
Ni coatings on Al alloy substrates, adhesion strength, meas. using microindentation method 80—40640
Ni solar selective black coatings, electrochem. deposition on Zn surfaces 80—29885
Ni-ceramic coating structure, influence of micropowder inclusion *(Russian)* 80—59820
Ni-Cr-W-Co-Ti heat resistant alloy ZhS6K, fatigue resistance, heat treatment and protective coating effects 77—81320
Ni-SiC coating adhesion to Al alloy, metal interdiffusion *(Russian)* 80—66697
Ni_2Al_3 layers, growth on Ni, NiAl substrates by cementation, kinetics, interdiffusion *(French)* 80—35127
PbS-CuS, black Zn-dust pigmented solar selective coatings for solar photothermal conversion 80—66997
RuO_2-TiO_2 coatings for Ti anodes, microstructural investigations 79 43469
Si, coating of mullite ceramic substrate, for solar cell appl. 79—34432
Si on ceramic, for developments using Si on ceramics and minute spherical cells low-cost photovoltaic solar cell fabrication 80—55839
SiC coated C fibres, effect on strength props. of C fibre reinforced plastics 80—104224
SiC coatings for HTR nuclear fuels, characterisation by small-angle X-ray scatt. 80—44451
SiC fibres, plasticizing and wettability-enhancing coatings 79—29252
SiC, for C fibres in glass composite, hot pressing production method *(German)* 78—95724
SiC, fuel particle, coating meas. of strength and Young's modulus, brittle ring test 77—8868
SiO, obliquely coated on In_2O_3 coated substrate, TEM exam. of surface topology 77—39726
SiO_2, sitall coating, control of phase composition, microstruct. and props. 77—32545
SiO_2, vitreous, strengthening by coating application 77—32636
SiO_2-Al_2O_3-CaO-MgO-Na_2O-K_2O-B_2O_3-ZrO_2, glaze, exam. of zircon crystallisation 79—19155
SiO_2-RO-Na_2O-Li_2O (RO=MgO, CaO, SrO) glass-ceramic coating, optimisation of props. by selective oxide action 80—55552
SiO_2-ZnO-Na_2O-Li_2O, glass-ceramic coating, optimisation of props. by selective oxide action 80—55552
Sn coatings on Fe particles, in mag. liqs., effects on long term stability 77—29051
ThO_2 microspheres, coated, coating permeability meas. 80—95343
Ti-Al on C steel, diffusion, struct. and props. 79—57156
Ti-C coating on steel, structural study, X-ray appl. *(Bulgarian)* 77—24242
TiB_2, coating, D^+ and $^4He^+$ irrad. effects 80—20753
TiC coating thickness meas. using X-ray diffr. 80—21243
TiO_2, paint type coating layer with spherical pigment, radiative transfer theory 80—61405
UO_2-UC microspheres, coated, coating permeability meas. 80—95343
U_3O_8, supported fission foils for laser excitation, preparation method 77—68218
WC-Co, composition and oxidation resistance of coatings deposited by thermal diffusion, using TiB_2 *(Bulgarian)* 80—45430
WSi_2 based silicide and borosilicide coatings on W substrate, serviceability at elevated temps. 79—87751
Zn fast reactions in hot galvanising rel. to props. 79—43486

coatings continued
Zn, phosphate coating, effect of grain size on film formation kinetics 79—34203
Zr diffusion in Cu, microstruct. and microanal. study of coating formed *(Rumanian)* 78—19917
ZrC formation on graphite via activated cementation *(French)* 77—52552
ZrO_2 coating on Zircaloy-4, effect on ductility 79—47819
ZrO_2 coating on Zircaloy-2, thermal cond. meas. 80—80009
ZrO_2-Y_2O_3 ceramic powder, in situ deposition of metal coating, cermet form. 77—32713
coatings, protective *see protective coatings*
coaxial cables
biological substances, dielectric props. meas. at RF and microwave freq. by coaxial line reflection methods 80—109065
capacitor loss measurement, using Q-bridges or resonant coaxial lines 77—34002
cryogenic vacuum feedthrough, with isolated shield, DC to 6.5 GHz 79—67324
electron beam autocorrelation by coaxial transmission line cavity 77—14652
EM field energy calc., using surface integral 78—5394
EM field theory, for structure with longitudinal inhomogeneity *(Russian)* 80—37936
enhanced radiation beams from three annular plasma layers coaxial line excitation 80—53996
fibre coaxial alignment system 79—37022
ionisation chamber cables, expt. investigation 80—78489
lumped-capacitance method for complex dielec. permitt. in polar liqs. 78—77936
magnetically insulated vacuum power transmission lines, pulse propag. 79—85765
permittivity determination of plastic samples using freq. variation *(German)* 79—26078
pipeline leak location by coaxial test cable characteristic impedance variation 77—57317
pulse forming network as rare gas halide laser pump 80—69424
RF-biased SQUID, with half-wavelength transmission line 80—22342
SHF power meter based on Hall effect in semiconductors 78—238
shielded cables, nonlinearities and multiple exposure anomalies at CASINO, MCCABE code verification 78—58502
standard signal transmission over long cables, using ESL ICs 78—5102
superconducting telecommunication, cryogenic envelope, determination of struct. and thermal insulation performance 79—58731
telephone, resistivity measurements on Cu conductors *(French)* 79—69487
transmission of 565 Mbit/s signals on coaxial cables and optical waveguides 80—43483
vacuum feedthrough to low-temp. apparatus 77—79101
coaxial lines *see coaxial cables*
cobalt
see also nuclei with ......
^{55}Co for nuclear medicine, production by ^{3}He bombardment of ^{55}Mn 80—36132
^{57}Co implantation in Si and Ge, Mossbauer spectra, dose dependence 79—82899
acoustic nuclear spin echo obs. at 4.2K *(Russian)* 78—6599
adsorption, of CO and O_2, XPS and UPS study 79—74050
adsorption and decomposition of water on pure surfaces *(German)* 80—26054
adsorption and reactivity of NO on (0001) face, LEED, AES, and thermal desorption study 80—80090
adsorption by Al_2O_3, radioactive waste storage 80—99240
adsorption by Mn and Fe oxides and soils and sediments 79—66422
adsorption of CO, AES obs. 77—35818
adsorption of O_2, CO and CO_2, XPS and UPS *(French)* 77—36362
AES meas. 77—36323
allotropic transformation, X-ray diffr. analysis exam. *(Russian)* 79—34027
amorphous, elec. cond. calc., t-matrix approach 77—55510
amorphous and liquid, density of electronic states 79—23881
amorphous and liquid states, electronic states and transport 79—99474
amorphous film, magnetoresist., in fields up to 80 kG 77—39823
Anderson-Gruneisen parameter, temp. depend., third-order elastic consts. calc. 79—46776
anodic dissolution into silicate glass melt, exam. 78—88582
anodic oxidation in neutral and basic soln. 79—39032
atom, electron bombard., 300 to 600 keV, K_α/K_β X-ray intensity ratios, K-shell ionis. cross sections 78—37747
atom, ionisation potential, term value, correlation energy by vertical anal. 78—41964
atom, $K\beta_{1,3}$ X-ray emission spectra, low energy plasmon satellites 80—19560
atom, $O^{2+,3+,4+,5+}$ induced K-shell X-ray production cross section, 7 to 24 MeV 77—61850
atom, rel. at. transition probabilities, by flame at absorption spectroscopy 79—89642
atom, X-ray spectra, chemical bonding and multiple ionis. effects 78—50630
atom, X-ray transitions in laser produced plasma 80—100093
atom$+H^+(D^+)$, K shell ionisation, nuclear Coulomb effect 80—91650
atomic and metallic 3p excitation 79—22633
atomic layers, Pauli paramagnetism to band ferromagnetism transition thickness depend. 78—72377
atomic magnetic moments comparison to values of ferromagnetic metal 78—52244
Auger effect, $K \rightarrow M^2$ radiative, low energy satellites meas. 80—45174
band model of high temp. magnetism 78—26809
band structure and X-ray emission spectra calcs. 77—28105
bulk modulus and thermal expansion coefficient, mag. contributions 79—8039
catalyst, magnetooptical investigation of mag. props. 79—69858
catalytic effect on W carburization 80—3255
cavitation erosion, role of twinning in single crystal 80—107272
chemisorption of CO on (0001) surface 78—6222
chemisorption of N_2-containing gases at high-press., XPS 77—20990
chemisorption of O, LEED anal. of Co{001}c(2×2)-O struct. 78—91546
coated C fibre, coating struct., SEM study 80—97605
coating, on Ni-Cr type alloys, surface pretreatment to attain pore-free aluminised coatings 80—40612
cobalt continued
coating onto $BaFe_{12}O_{19}$, $SrFe_{12}O_{19}$ and WC 80—25593
compact, on H_2 permeated backing, precipitation *(Russian)* 78—27520
concentration determ. in atm. and rainwater in Vizcaya, Spain *(Spanish)* 78—57264
concentration in atmospheric sedimentable powder, in Vizcaya, Spain *(Spanish)* 78—57265
corrosion, atmospheric, H_2O adsorption and chem. kinetics 80—11826
corrosion, indoor, rate meas. 80—76404
corrosion, model for cond. mechanism in oxide, rel. to basic atomic processes of metal corrosion 77—25198
corrosion by molten alkali metal hydroxides and liquid Li 77—44414
creep at low stresses of β-phase 79—79028
crystal field potential calc. 77—59366
crystal hyperfine fields and neutron scatt. 79—56172
DC reactive sputtering, glow discharge mass spectrometry and X-ray diffr. 79—38701
de Haas van Alphen oscill., effective mass 78—87900
Debye-Waller factor and Lindemann parameter, temp. depend., lattice dynamical model calcs. 80—59610
deformed, microstruct. singularities in pre-transform. temp. range *(Russian)* 80—45347
deformed and annealed, mechanism and kinetics of polymorphic transformation *(Russian)* 78—35381
deposition on primary coolant piping in BWR 80—13532
determination, in hydrodesulphurisation catalysts, by at. absorpt. spectroscopy 77—9145
determination, in NBS standard alloy steels, X-ray fluoresc. method 78—31734
diamond:Co-C, satellite phase, C content determ. *(German)* 77—72690
diffusing out of high current density plated Au, oxidation kinetics 78—92393
diffusion, in HgTe single crystals 79—77818
diffusion and electrotransport in Th, 965-1625°C 79—90828
diffusion coefficient in Al, resistometric determ. 79—51313
diffusion in Au, 700-1050°C *(Russian)* 77—80651
diffusion in Au, temp. depend. of isotope effect 78—47563
diffusion in Be, 1250 to 1493K, radioactive tracer method *(Russian)* 80—24668
diffusion in $LiNbO_3$, and its effect on acoustic velocity 77—84847
diffusion in molten Fe *(Japanese)* 77—51531
diffusion in Nb, radiotracer and electron microprobe meas. 77—76615
diffusion in Ni, and W diffusion, 1050 to 1400°C *(Russian)* 79—28147
diffusion in Pb, exam. by activation analysis 78—91488
diffusion in Pu, diffusion coeff. and mechanism 77—28046
diffusion in Si layers heavily diffusion-doped with P or B 78—59982
diffusion of Mn, 860-1246°C, mag. transform. effects 77—24427
dilute impurity hyperfine fields, comparison with model 78—14954
dipole field anisotropy, at interstitial sites, lattice-deformation effects 79—33584
dissolution kinetics and diffusion coefficients in molten Al 80—59666
dissolution kinetics in liq. Al, 700-900°C *(Russian)* 77—59119
electrical resistance temp. depend. near Curie point *(Russian)* 77—31989
electrical resistivity, effect of domain wall orientation at 4K 78—91662
electrical resistivity and specific heat meas., anomalies rel. to thermally excited states 80—6809
electrochemically prod. emitters, field ionis. props. 77—90254
electrode reactions with molten glass 80—85186
electrodeposited, influence of soln. pH on microstruct. 80—65399
electrodeposited coating, struct. and magnetic props. 79—46985
electrodeposited film, saturation magnetisation and perpendicular anisotropy meas. 78—76277
electrodeposition for solar selective surface *(French)* 79—52133
electrodeposition using insoluble anode 77—8772
electromigration and residual resistivity, in Au 78—71881
electron irradiated, low temp., elec. resist. recovery 77—35588
electron irradiated, mag. after-effect spectrum, 20-350K 77—1570
electropolishing in alcoholic soln. of H_2SO_4 77—16718
EM and acoustic energy attenuation in many-domain magnets 80—7140
energy band dispersion and mag. exchange splitting, angle-resolved photoemission meas. 80—71567
energy band dispersions and mag. exchange splitting 80—76146
entropy of fusion, local spin disorder 77—47601
epitaxial films, even magneto-optical effects 80—76007
evaporated film, X-ray diffr. study 80—6663
EXAFS and shape of K absorption discontinuity 77—20955
exploding wire, elec. resist. at high temp., submicrosec. pulse heating meas. 77—89747
extraction equilirbium, with versatic acid 911 79—43620
extraction with 2-(2-thiazolylazo)-4-methyl phenol 77—60063
Faraday rotation in X-ray region 79—82958
FCC, electrodeposition of HCP Co layer 79—11527
FCC, electron response and modified Bhatia model 79—37771
FCC, ferromag. domains of fine particles, Lorentz electron microscopy obs. 78—27053
FCC, itinerant ferromagnetism 78—23238
FCC, mag. props. of single-domain powders after plastic deform. *(Russian)* 78—6554
FCC, modified Krebs model, phonon dispersion relations 78—79682
FCC, selected area diffr. pattern indexing, graphical technique, for teaching 78—54132
Fermi surface under press., de Haas-van Alphen effect meas. 80—75499
ferromagnet, energy band struct. X-ray emission spectra *(Russian)* 79—15564
ferromagnetic, amorphous, normal Hall effect meas. 77—35924
ferromagnetic, anomalies in thermal expansion and heat capacity 79—73744
ferromagnetic, calc. hyperfine fields and their press. derivations 80—6796
ferromagnetic, EMF generation by pulsed laser irrad. 78—68021
ferromagnetic, HCP, electronic struct. calcs., band props. 78—39012
ferromagnetic, HCP, electronic struct. calcs., cohesive energy and exchange splitting 78—34791
ferromagnetic, HCP, electronic struct. calcs., mag. hyperfine field 78—39080
ferromagnetic, hyperfine fields at positive muons 78—43758
ferromagnetic, hyperfine mag. fields at ^{67}Ge, TDPAC meas. 78—43701
ferromagnetic, itinerant, Fermi surface and single particle excitations 80—34350
ferromagnetic, local mag. field at positive muon 77—12295

cobalt continued
  ferromagnetic, positive muons as light isotopes of H, book contrib. 79—82907
  ferromagnetic, spin subband level position determ. by de Haas-van Alphen meas. under press. *(Russian)* 79—90947
  ferromagnetic, temp. depend. of μ^+ hyperfine field 78—43761
  ferromagnetic domain struct., small-angle neutron scatt. 77—66382
  ferromagnetic film, ion plating prep., coercive force and magnetoresist. 77—12546
  ferromagnetic film, mag. anisotropy study using NMR spin echo method 80—60384
  ferromagnetic films, coercive force, ion plating prep. 77—28730
  ferromagnetic metals, spin fluctuation theory, Curie temp., mag. susceptibility 80—65937
  ferromagnetic micropowder, cryst. struct., coercivity, remanence, saturation 80—65967
  ferromagnetic properties, book contrib. 80—75724
  ferromagnetism, Stoner model, mol. field coeff., temp. and field depends. 77—72975
  ferromagnetism, theory 80—2541
  field emitted electrons, spin polarisation 77—40337
  film, electromigration exam. from structural changes and resistance increases 77—20213
  film, evaporated, adsorption of H_2, surface pot. meas. 77—31890
  film, evaporated, columnar struct. depend. on degree of texture 80—54567
  film, evaporated, texture and columnar struct. 80—54566
  film, evaporated, uniaxial mag. anisotropy 77—51929
  film, even magneto-optical transmission effects 77—32354
  film, ferromag., magnetoresistance parameter meas. *(Spanish)* 80—2485
  film, ferromagnetic, transverse Kerr magneto-optical, effect, thickness depend. 77—59559
  film, five atomic layers, electronic band struct. using linearised APW method 79—69393
  film, HCP, crystal struct. changes on ion bombard. 77—69018
  film, ion beam sputtering prep., struct. and mag. props. 80—35085
  film, Kerr magneto-optical consts. 78—76541
  film, linear mag. birefr. dispersion 77—69807
  film, low-angle grain boundary struct. *(Russian)* 79—42807
  film, mag. domain wall obs. by electron holography 80—80582
  film, magnetic domain wall width, shadow and interf. electron microscope exam. 79—11330
  film, on Cu, Mossbauer emission spectra 78—19387
  film, optical props. by self-consistent photometric technique 80—55217
  film, spin polarised photoemission, surface magnetism 79—52083
  film, texture and CO adsorption *(German)* 77—24485
  film, work function changes upon water contamination 80—44705
  film on Si substrate, laser irrad., cellular struct. and silicide form. 80—10710
  films, electromigration and Hall effect 77—62664
  films layered over Cr by DC sputtering for digital mag. recording 79—83118
  fine particles, prep. by gas evaporation technique, crystal habit 77—52239
  fine particles in Cu, interface magnetisation 80—88858
  fine powder, magnetic props., effects of electrolysis conditions in prep. 77—40091
  flameless atomisation, effect of interfering metals on absorption 77—90675
  flow stress, effect of mag. field 77—20673
  foil, naturally passivated, ESCA, sputter etching 77—70218
  foil, wall struct., bubble, plate domains, 1 MeV electron microscope study 78—84463
  fractionation of Co and Sc versus Fe content for crystalline phases of ultramafic nodules 78—65306
  glide ahead of terminating $\{10\bar{1}2\}$ twins 80—96545
  growth of single crysts. by electron-beam floating zone method 78—68624
  HCP, ferromag., anisotropic hyperfine interactions, NMR expt. 78—43658
  HCP, heavy-ion irrad., dislocation loops, TEM obs. 77—31667
  HCP, low energy interband absorption, electronic struct. exam. 79—73930
  HCP, NMR and nucl. relax. meas. in domain walls 77—36146
  HCP, positron annihilation meas. of electronic struct. 77—20224
  HCP, relationship of effects of systematic reflections to the crit. voltage 79—41916
  HCP film, uniaxial, mag. domain struct. 80—60385
  HCP to FCC transition, mag. domain nucleation 78—64218
  HCP-FCC transition, mag. domain behaviour, Lorentz electron microscopy 77—80958
  hyperfine field at positive muon 80—40029
  II-VI semiconductor:Co^{2+}, IR luminesc., local density of phonon states 79—33778
  implantation in Al, replacement collision probability at 4.2K 80—70237
  impurity, in Pd-H, Mossbauer study of local environment of substitutional impurities 80—60475
  impurity hyperfine fields 79—99518
  internal fields, positive muon investigation 78—68438
  internal friction anomalies in spin reorientation temp. range *(Russian)* 80—49299
  internal friction meas. during polymorphic transform. *(Russian)* 79—29049
  internal magnetic pressure and compressibility anomalies, itinerant model 77—16034
  internal strain rel. to strain tensor, group theory anal. 79—86835
  interstellar abundance and depletion models 80—46630
  interstitial site determ., μSR technique 80—71287
  ion bombardment, energy distrib. of positive secondary ions and sputtered atoms 77—32485
  ion in crystal, Racah parameter 78—56110
  itinerant electron ferromagnet, magnetovolume effects 80—60397
  itinerant electron ferromagnetism, press. effects on mag. props. 77—66241
  K-shell X-ray prod. by $^{14}N^+$ bombardment 80—91482
  Kerr equatorial effect freq. spectra anisotropy, dielectric permeability tensor *(Russian)* 80—55072
  laser, cataphoretic at. distrib. in chloride-He discharge 77—31092
  laser microprobe emission spectroscopy, matrix effects 77—16870
  lattice dynamics and compression curves 78—38793
  lattice sp. ht. calc. 79—69262

cobalt continued
  leaching, system geometry effects, mass transfer controlling case 79—61535
  levitation quenching 77—59711
  liquid, coordination numbers, calc. in microinhomogeneous struct. model *(Russian)* 80—38902
  liquid, density of states of d-band, heat of vaporisation 78—95253
  liquid, electrical transport 79—38040
  liquid, Hall effect, band struct. and exchange scatt. 80—80250
  liquid, multiple scatt. calcs. of resist. 78—76039
  liquid, N activity coeff. 77—72699
  liquid, N solubility depend. on added elements, mechanism *(Russian)* 80—65223
  liquid, soft X-ray band spectra 77—52199
  liquid, struct. factor and isothermal compressibility 77—11462
  liquid, struct. factor and radial distrib. curves, X-ray determ. *(Russian)* 77—31580
  liquid, thermoelec. power meas. 77—35928
  liquid, viscosity, up to 2100K, vibr. method 78—38866
  liquid, viscosity calc. using microinhomogeneous struct. model *(Russian)* 80—15284
  local magnetic fields probed by μ^+ 78—48103
  localised moments, detection by electron energy loss spectra 77—69949
  low-level transuranic storage, radwaste Sr, Cs, Co sorption meas. on soil sediment 80—95482
  lunar drill sample, neutron activation and radiochemical anal. *(German)* 80—51673
  magnetic aftereffects of H isotopes, book contrib. 79—82835
  magnetic anisotropy induced by mag. annealing and cold rolling, expt. 80—7695
  magnetic anisotropy induced by mag. annealing and cold rolling, calc. 80—7696
  magnetic anisotropy induced by magnetic and stress annealing 78—35010
  magnetic domain struct. temp. depend. 79—78436
  magnetic domain structure determ. high resolution colloid-SEM method 77—43846
  magnetic impurity in β'-NiAl, self consistent embedded cluster model 80—2549
  magnetic permeability, effect of ion implantation 77—28414
  magnetised to saturation, props., positive-muon study 78—6619
  magneto-volume effects calc., rel. to itinerant electron model 78—43621
  magnetocrystalline anisotropy consts. meas., 77-700K 78—43582
  martensitic HCP-FCC transition, neutron scatt. obs. 79—51252
  martensitically transforming, state of surface 78—43223
  melt, struct. charact. time depend. in X-ray studies *(Russian)* 80—24350
  metallic coated, produced by electrospark alloying, corrosion behaviour in Cl saturated NaCl solns. *(Russian)* 79—39026
  modulus defect due to internal strain 78—76286
  molten, contact reaction with graphite 80—15342
  molten, mag. small-angle scatt., persistent spin fluctuations 79—11288
  molten, near-order struct., X-ray scatt. meas. 77—55231
  monolayer, oxidation, quasisimultaneous SIMS, AES, XPS 78—72919
  muon resonance meas. of local mag. dipole field at interstitials 79—95699
  muon spin rotation; freqs., and relax. rates 80—55006
  n=2-2 transitions in XUV spectra, anal. 80—102472
  nearest-neighbour atom displacements derived from EXAFS spectra, temp. depend. 79—87524
  neutron sputtering yield determ. 77—36319
  NMR enhancement of modulating field due to anisotropic component of hyperfine field 77—55729
  NMR freq. depend. on interatomic distances for FCC single crysts. 79—69748
  NMR in paramagnetic and ferromagnetic states, crit. nucl. relax. 79—56622
  NMR of ^{59}Co in metal, temp. depend 78—52364
  NMR-ON meas., mag. hyperfine splitting const. of ^{60}Co, ^{52}Mn and ^{90}Nb 78—43651
  nuclear orientation on implanted ^{114m}In meas. 79—47345
  optical constants 12 to 24 μm, anomalous skin effect region 77—20842
  optical consts. and electronic characts., 20 to 1750°C 79—38516
  oxidation, use of SIMS for ^{18}O location 79—8394
  oxidation, XPS obs. of epitaxial CoO form. 80—66396
  oxidation at Curie temp. 79—29279
  oxidation at high temp. 78—23877
  oxidation at high temps., parabolic rate const. determ. 78—64779
  oxidation kinetics, effect of Curie temp. 77—48592
  oxidation mechanism in composite atmos. *(Polish)* 79—79142
  oxidation study using solid-state galvanic cell *(Japanese)* 77—56151
  oxide surface layer, TOF atom probe anal. 78—64766
  particle formation by evap., electron microscopy obs. of interaction processes 80—104053
  particles, single domain, randomly oriented easy axes and particle size distrib., coercivity 80—71119
  particles, vibrations associated with twins 80—100253
  passivation, film form., stability and breakdown 78—19937
  passivation films in neutral and alkalescent borate soln., modulation spectroscopic anal. *(Japanese)* 80—108628
  Permalloy-Co film, domain walls, magnetisation ripple *(Russian)* 79—47314
  permanent magnet material savings *(German)* 80—103851
  phase transformations and vacancy form. by positron annihilation 80—2155
  photoemission, exchange-split energy-band dispersions 80—35059
  plasticity, anomalous, near martensitic transform. temp. *(Russian)* 78—6971
  plated film, magnetisation and mag. interface anisotropy 77—85510
  plating γ-Fe_2O_3 powders, effect on mag. props. 79—69699
  plating line Co concentration monitoring, by automatic colorimeter 80—105691
  polyethylene oxide-Co^{2+} solution, complex struct., PMR *(Russian)* 77—40140
  positron trapping, monovacancy form energy 79—74016
  positronium form. in two-photon positron annihilation 79—61462
  powder, hot pressing on steel substrate, densification kinetics 80—40290
  powder, isostatic compaction *(French)* 80—40285
  powder, isostatic compression, elec. cond., densification models *(French)* 80—55321
  powders, rapidly solidified, nucleation, undercooling and homogeneous structs. 78—52708

cobalt continued
  production from reduction of $(Co_{1-x}Mg_x)_2SiO_2$ *(Russian)* 78—44043
  properties, review 79—95909
  purification from $CoCl_2$ and $CoCl_2$-NaCl by H_2 reduction *(Russian)* 79—28981
  PVC film, Co doping effect on chain vibrs. 79—95868
  radiative Auger effect, $K \rightarrow M^2$ 80—71522
  radioactive and stable, determ. in marine biological materials 80—36157
  radioactive release from reactor cooling water, fixation by sandy soil *(Japanese)* 78—74443
  radioactive waste, low-level, radionuclide migration in soil 79—54610
  radionuclide accumulation by oysters in reactor effluent, math. model 77—81589
  rare earth orthoaluminates: Co, Ti, effects of Co and Ti ions on cryst. growth 77—28711
  reaction, in Ar-SO_2 atmosphere, 500 to 900°C 78—39953
  reactive cathodic sputtering, X-ray diffr. exam. of chem. struct. *(French)* 77—63519
  rod, spontaneous vibr. modes excited by reversible magnetostriction 79—56587
  Saguenay fjord sediments, distrib. and partition of Co, Ni, Cr and V 77—33100
  seawater, predominance-area diags. and equilib. ratios for Co and Ni inorganic forms 78—3819
  secondary ion microanalysis, of Co ions, epilepsy study *(French)* 79—62414
  self-diffusion and isotope effect, influence of mag. order-disorder transition in FCC Co 80—29205
  self-powered flux detectors, response characts. in CANDU reactors 78—82594
  self-powered neutron flux detector response in mockup Bruce reactor core 78—58391
  single crystal, muon spin rotation expt. results 77—12294
  sintered with diamond, remanent magnetism 79—99731
  small angle critical neutron scatt. 78—31087
  small magnetic particles, anisotropy field, resonance meas. 78—64227
  solid solubility in Si, 1000-1270°C, radiotracer obs. 77—51500
  solutes in liquid Se-Te, mag. susceptibility meas. 77—51882
  spin fluctuations above Curie temp., diffuse mag. neutron scatt. obs. 80—50102
  sputtered film, high coercivity and high hysteresis loop squareness 79—91259
  sputtered film, mag. props. and microstructures 79—82837
  sputtering in inert atm., with uncooled cathode, oxidation of metallic coatings, X-ray diffr. obs. 78—3041
  steady creep rate, stress depend., exam. at phase transformation at 390°C 78—52923
  steady state creep rate, stress depend. rel. to FCC to HCP phase change 78—64598
  steel, alloyed with Cr, Mo, Co, Mn, martensitic point position depend. on cooling rate *(Russian)* 79—70063
  stopping power for 28 MeV α-particles, re-evaluation 78—79651
  stopping powers for 28.8 MeV α-particles 77—80556
  strontium tartrate tetrahydrate Co^{2+} electronic absorpt. spectrum 78—92098
  sublimation rate near Curie temp. 80—49351
  surface, {001}, LEED struct. anal. 78—47645
  surface, (0001), LEED and AES meas. 77—31857
  surface, (0001), LEED meas. 77—59188
  surface, CO adsorption-desorption kinetics, surface carbide form. effects 80—103574
  surface, electron spin polarisation, electron capture spectroscopy 78—95645
  surface, interaction with O_2 and air, XPS 77—16466
  surface, magnetic order 78—95439
  surface, O_2 layer thickness, reson. α-scatt. from ^{16}O 78—64778
  surface, polycryst., interaction with O_2, CO and CO_2, XPS, UPS *(French)* 77—73219
  surface (0001), chemisorption of O_2, surface oxidation and CO oxidation 79—60631
  surface (100), clean and C-covered, LEED-Auger expts. 78—38921
  surface $(10\bar{1}2)$, struct. and CO chemisorption obs. 79—4474
  surface roughness effects on backscatt. spectra 80—47016
  surface state on Co (0001), photoemission and synchrotron radiation obs., symmetry determ. 80—20771
  surface structure in HCP and FCC bulk phases 78—51807
  surfaces, Van der Waals forces computation 79—15204
  tensile strength, and elongation, influence of FCC phase retained at room temp. 79—47677
  thermal diffusivity meas., 300 to 1000K, Lorenz number determ. 80—29384
  thermal expansion and bulk modulus 77—31788
  thermomigration and electromigration in high-purity samples 79—55919
  thermophysical properties, 300-1700K 77—47790
  thin film, nuclear spin echo excitation on subharmonics, and multiple freq. *(Russian)* 80—60454
  thin films, optical and magneto-optical permittivities 80—66163
  trace element anal. by (pX,X) expt. 78—61128
  trace element anal. in geological materials by atomic absorption *(Portuguese)* 79—66375
  transient magnetic field discontinuity seen by O(F) ions 80—24515
  tunnelling electron spin polarisation rel. to band struct. 78—68095
  twins, $\{11\bar{2}1\}$, in single crystals., accommodation and form. 80—96540
  ultrafine particles prepared by vacuum evap. on running oil substrate, mag. behaviour 79—28565
  uniaxial magneto-crystalline anisotropy, temp. depend. 79—42753
  UPS, single cryst. and polycryst. film, electronic struct. 78—11081
  US damping temp. and mag. field depend. *(Russian)* 78—23313
  vacuum deposited coatings on metal substrates, cryst. struct. and stability 80—75481
  vacuum deposited on Ni (111), Mossbauer effect emission 79—80735
  X-ray diffraction investig. near FCC to HCP transform. *(Russian)* 77—47570
  X-ray K-absorpt. edge shifts, plasmon energies correlation 80—20734
  X-ray K-absorpt. edge shifts 77—4701
  X-ray K-absorpt. edges, plasma oscills. effects 77—59640
  X-ray K-absorption spectrum 80—97378
  X-ray K-emission satellites, quasi-stationary states and origin 80—80903
  X-ray L_{III} emission bands in α and β phases *(Russian)* 80—25491
  X-ray reflectivity, near $L_{2,3}$ absorpt. edge 80—71513

cobalt continued
  XPS escape depths and relative photoionisation cross section for 3p subshell 77—73212
  zinc formate dihydrate, Co^{2+}-doped, EPR spectrum, g-factor anisotropy for A- and B-sites 77—77089
  α-Al_2O_3:(Co^{3+}), optical absorption spectra, DC and AC field effects 78—10925
  βAl_2O_3:Co, absorpt. and emission spectra, mag. susceptibility 79—87471
  Al_2O_3:Co, gamma-irrad., low temp., induced absorpt. spectra 79—56820
  Al_2O_3:Co, spectra, heat treatment and irrad. effects 77—4659
  α-Al_2O_3:Co,H, Co and proton ENDOR, IR and optical spectra charge compensator nature and defect struct. 80—44956
  Al_2O_3:Co^{3+}, corundum, Jahn-Teller effect in trigonal symmetry 79—82563
  α-Al_2O_3:Co^{3+}, local deform. due to uniaxial stress 80—34140
  α-Al_2O_3:Co^{3+}(Co^{2+}), optically and thermally stimulated reactions, absorpt. spectra 80—80825
  β-Al_2O_3-Na_2O:Mg,Co, ionic cond. and cryst. struct. 78—26723
  Al_3O_3:^{57}Co, Mossbauer study of the charge state and symmetry of $^{57}Fe^m$ in diverse cobalt spinels *(Spanish)* 79—69754
  $BaTiO_3$:Co, annealed in H_2 and O_2, valence change in phase stability 80—20600
  $BaTiO_3$:Co, charact. behaviour of spontaneous polarisation and dielec. const. 78—60382
  $BaTiO_3$:Co, trap recomb. consts., photocurrents 78—43435
  $BaTiO_3$:Co, tricritical point, X-ray diffr. meas. 80—71341
  $BaTiO_3$:Co, voltaic current appearance on proton irrad. 80—104032
  C diffusion in β-phase, high-temp. vacuum metallography *(Russian)* 77—72718
  CaF_2:^{57}Co, γ-irradiated, Mossbauer spectra 77—81036
  CaF_2:Co, X-irrad., F-centre form., optical absorpt. spectra and dichroism obs. 79—42998
  CaF_2:Co, X-irrad., impurity effects on defect prod. 80—92525
  CaF_2:Co, X-irrad., luminesc. spectra 79—28801
  CaF_2:Co, X-irrad., thermolum. 80—60686
  CaF_2:Co, X-irradiated, optical absorption spectrum 78—35173
  CaF_2:Co^{2+}, designation of optical transitions near 5.40 nm, temp. evolution of absorption spectra meas. 77—55806
  CaF_2:Co^{2+}, elec. field effect on spectra induced by odd vibrs. 79—73973
  CaF_2:Co^{2+}, MCD spectra 77—28603
  CaF_2:Co^{2+}, parity-forbidden transitions, elec. field effect on electronic-vibr. spectrum 79—65905
  $CdBr_2$:Co, spectroscopic studies of interactions 80—29769
  $CdBr_2$:Co^{2+}, charge transfer near UV spectra, 4.2K, mag. circular dichroism 78—80378
  $CdBr_2$:Co^{2+}, exchange-coupled Co^{2+} pairs, optical absorpt. and Zeeman studies 80—66242
  $CdBr_2$:Co^{2+}, ground state g-value, EPR meas. 77—16159
  $CdBr_2$:Co^{2+}, polarised IR absorpt. spectra 77—40269
  Cd(Ca)F_2:Co^{2+}, Jahn-Teller split $^4A_{2g} \rightarrow {}^4T_{1g}(P)$ absorption band, elec. field effect 78—15202
  $CdCl_2$:Co, spectroscopic studies of interactions 80—29769
  $CdCl_2$:Co^{2+}, charge transfer near UV spectra, 4.2K 78—80378
  $CdCl_2$:Co^{2+}, ground state g-value, EPR meas. 77—16159
  $CdCl_2$:Co^{2+}, optical absorpt. spectra, Zeeman study 78—6712
  $CdCl_2$:Co^{2+}, polarised IR absorpt. spectra 77—40269
  CdF_2:Co^{2+}, MCD spectra 77—28603
  CdF_2:Co^{2+}, parity-forbidden transitions, elec. field effect on electronic-vibr. spectrum 79—65905
  CdI_2:CO^{2+}, EPR 78—68362
  $CdIn_2S_4$:CO^{2+}, site symmetry, spectral meas. 79—78729
  $CdIn_2S_4$:Co, optical absorption meas. 78—64384
  CdS:Mn(Co), intensity and spectral distrib. of luminescence *(Russian)* 77—16392
  CdS-Co^{2+}, IR spectrum, 4.2K, electron-phonon interaction effect on emission spectrum 78—27270
  CdS(Se)(Te):Co^{2+}, IR luminesc. quenching, Co^{2+} level position, ionisation energy 80—16079
  CdTe(Se):Co, impurity luminescence no phonon line depend. on temp., Debye temp. 80—66273
  (Co,Mo)/Al_2O_3, hydrodesulphurisation catalyst, prep., props. and appls. 77—86360
  (Co,Mo)/Al_2O_3 hydrodesulphurisation catalysts, physical props. and activities 77—86358
  (Co,Mo)/Al_2O_3(SiO_2), and unsupported, catalyst for hydrodesulphurisation 77—86355
  Co (VII), semiempirical investigation of spectra 78—33434
  Co alloys, determination of Ni and Co by flameless atomic absorption spectrophotometry 77—90674
  Co complex, circ. dichroism of Co(III) complex d-d transitions *(Japanese)* 78—13555
  Co, corrosion in Ar-SO_2 atmospheres, scale struct. obs. *(Japanese)* 80—55568
  β-Co, grain size independent viscous creep 80—40460
  Co I, excited level lifetime meas. 78—5178
  Co I, fine struct. splittings in some highly ionized n=3 doublets 80—43200
  Co I, multichannel anal. techniques, appl. to beam-foil spectroscopy, 3000-3950 Å, lifetimes 77—58206
  Co I, radiative lifetimes of atomic excited states, delayed coincidence technique 77—27030
  Co I and Co II, beam-foil obs. of lifetimes 80—14111
  Co I in solar photosphere, oscillator strength computation 78—40905
  Co II, unidentified lines in spectrum of HR 5049, southern Ap-star 80—82384
  Co II spectrum, wavelengths and estimated intensities 1020 to 9500 Å *(Spanish)* 80—52920
  β-Co superparamag. FCC particles, hyperfine interaction, relax. Mossbauer spectra 79—78573
  Co V spectrum analysis 79—72266
  Co XI-XVII solar $3s^23p^n$-$3s3p^{n+1}$ transition arrays, UV spectra classification 80—63570
  Co XVI, level struct. and predicted intercombination lines 80—14098
  Co XXIV, spectra calcs., fine struct., transition energies 77—42260
  Co^-, photoelectron spectra, electron affinity and fine-struct. interval 79—68212
  Co^+, Rayleigh and Compton scatt., differential cross section determ. 80—52912
  Co^{2+}, adsorption of SiO_2, zeolite surface, bonding, EPR, optical spectroscopy investig. *(German)* 79—95266

cobalt continued
Co^{2+}, complex formation with carboxylic acids in aqueous soln., thermodynamic parameters *(Italian)* 77–48669
Co^{2+} dopant in CaF$_2$, CdF$_2$, BaF$_2$, far IR absorpt. spectra peaks 78–27265
Co^{2+}, doped ion in divalent metal cpds., correl. between Szigeti charge and hyperfine coupling consts. 80–96832
Co^{2+}, fluoresc. quenching of organic excited singlet states, rate meas., mechanism 77–38685
Co^{2+}, impurity ion in frozen aq. solns., effect on Fe^{3+} spin-spin relax., Mossbauer obs. 79–33573
Co^{2+} in ionic crystals, exchange-coupled, optical spectra *(Rumanian)* 79–87474
Co^{2+} in zinc blende type hosts, Huang-Rhys number rel. to props. of host lattice 79–83018
Co^{2+} ion removal in high temp. water using TiO$_2$ 79–89376
Co^{2+}, mag. form factors, spherical and aspherical parts 79–78315
Co^{2+}, magnetostriction effects in garents and ferrimagnetic spinels 79–91277
Co^{2+} partitioning in olivine and silicate melts 79–66683
Co^{3+}, Sternheimer valence shielding antishielding factor including exchange 77–85182
^{59}Co NMR, chemical shift data compilation *(Japanese)* 79–68242
Co:^{129m}Xe, mag. hyperfine field determ. by Mossbauer effect 77–8460
Co:^{41}K, hyperfine field calc. by gamma ray ang. corr. method 78–6340
Co:Ga(Ge)(As), temp. anomalies of hyperfine fields 78–23265
Co:Lu, nuclear orientation meas., hyperfine field 77–32308
Co:MgF$_2$, laser, broadly tunable CW operation, output powers, optical pumping 80–32995
Co:MgF$_2$, tunable transition-metal-doped solid state lasers 80–58549
Co:Ra, hyperfine field determ. 77–85622
Co/CoO, relative chemical potential of oxygen *(German)* 78–31642
Co/γ-Al$_2$O$_3$ catalyst, ESCA and EPR meas. after hydrodesulphurization reaction *(French)* 79–52755
Co-Al$_2$O$_3$ catalysts, reducing and sulphiding treatments, XPS obs. 78–85196
Co-Al$_2$O$_3$-Al superconductor, spin polarisation of tunnelling electrons, band model 77–72947
Co-CoO films, evaporated, exchange anisotropy 80–88841
Co-Fe laminated mirror, with Ti-Gd sublayer, in polarising neutron guide 78–9012
Co-Fe(Ni) system, interdiffusion zone growths *(Czech)* 78–84009
Co-Ge planar interface, first phase to nucleate 77–62764
Co-like ions, multiply charged, laser plasmas, 1.5-15 Å 78–13462
Co-Mo, multilayer films, depth resolution determ. in Auger depth profiling meas. 79–78800
Co-Ni, interdiffusion coeffs. and conc. penetration curves, electron microprobe meas. 77–66047
Co-Ni interface, intrinsic interdiffusion coeffs. and activation enthalpies 77–84998
Co-Ni sandwich system, interdiffusion, Kirkendall effect 77–69121
Co-Si film system, diffusion marker expts. 78–79824
Co-Si film system, interaction kinetics 78–79823
Co-Si interface, glassy layer, ellipsometric charact. 80–103589
Co-Si interface, metal-semiconductor transition, rel. to first compound nucleation 80–24771
Co-WC, levitation quenching 77–59711
Co+F^{q+}, (q=6, 8, 9), target and projectile cross-sections, X-ray prod. yields 79–81269
Co+H^{+}, K-shell ionisation cross-sections calcs. 80–43165
Co+N^{+}, X-ray production cross section, Kβ/Kα ratio, 0.5-2.5 MeV/amu 77–54526
Co^{+}+H$_2$O, reaction rate consts., product distrib., ICR obs. 79–8428
CoCO$_3$, mag. props., microscopic level calcs. *(Russian)* 80–97078
Co(III) compounds, XPS exam., struct. of 2p lines 78–19631
CoSiF$_6$.6H$_2$O:Co^{2+}, spin Hamiltonians and pair interactions 77–36119
Co(VIII), resonance transitions, classification 80–42985
^{55}Co, carrier-free positron-emitting label for bleomycin from ^{56}Fe(p,2n)^{55}Co 79–79648
^{57}Co, disintigrating nucleus, energy absorpt. by mol. environment 78–80775
^{57}Co labelled bleomycin, Bayer map evaluation in lung scintigraphy *(Japanese)* 80–72319
^{57}Co labelled Co(acac)$_3$, diamag., ^{57}Fe(III) species prod. by electron capture decay, spin relax. 77–63329
^{57}Co, Mossbauer absorpt. and emission spectra, hyperfine struct. and relax. effects 80–71279
^{57}Co:Fe Mossbauer source linear polarisation rate meas. *(French)* 79–30633
^{58}Co dissolution control by H$_2$O$_2$ addition in PWRs 78–21657
^{58}Co dissolution during PWR refuelling shutdown, control with H$_2$O$_2$ 78–21698
^{58}Co dissolution in PWR coolant during PWR refuelling shutdown, control using H$_2$O$_2$ 80–23066
^{58}Co, uptake of gamma-emitting activation products in plants 80–30614
^{59}Co, excited states lifetimes, Doppler shift attenuation meas. 78–42009
^{59}Co, mag. hyperfine struct. analysis, spectral lines 4000 to 4300 Å 78–62752
^{59}Co NMR line breadth and chemical shift data compilation *(Japanese)* 78–15045
^{60}Co absorption through damaged and undamaged skins of guinea pigs 80–26383
^{60}Co beams, cylindrical ion chamber A$_c$ and A$_{eq}$ factors exam. 79–81121
^{60}Co behaviour in sediments in laboratory-scale aquatic ecosystem 78–3831
^{60}Co contamination of freshwater food chains, direct water borne contamination of organisms *(French)* 79–20688
^{60}Co, distrib. and behaviour in Urazoko Bay sediment 80–97825
^{60}Co, fixation on natural sorbents from phenol-polluted water 79–57506
^{60}Co gamma ray absorbed-dose standards comparison 78–74512
^{60}Co gamma rays effects obs., on polyethylene loss tangent variation *(German)* 80–75266
^{60}Co gamma-ray beam spectrometry, for instrument calibration 77–6608
^{60}Co γ-rays, dose assignment criteria, beagles, bilateral exposure 79–16305
^{60}Co in sample soil and water, distrib. coeff., environmental effects 77–13092
^{60}Co, inhaled, long-term clearance 79–79663
^{60}Co ion removal in waste water by oxine impregnated activated charcoal 79–26558

cobalt continued
^{60}Co leaching in cement composites 77–61508
^{60}Co long-lived γ-emitting aerosols, max. allowable emission rate from nuclear power station 80–32532
^{60}Co, long-term retention in Indian workers, dose commitment 78–35960
^{60}Co, management of radioactive waste produced on dismantling PWRs 80–27756
^{60}Co radiation therapy, eval. of dosimetric accuracy and uniformity 80–12269
^{60}Co, radioactive waste migration by complexing agent ethylenediaminetetraacetic acid 79–20687
^{60}Co radioecology in Urazoko Bay, levels in sargassoes and marine sediments 77–9448
^{60}Co, radionuclide leaching from hardened cement grout, container dimension depend. 79–13439
^{60}Co removal from waste water, adsorption on activated charcoal with oxine 78–58365
^{60}Co, sediment-bound, absorpt. through digestive tract of marine demersal fish 79–92400
^{60}Co source for radiographic inspection method 80–71861
^{60}Co source irradiation of 2 media, absorbed dose in vicinity of an interface 80–30894
^{60}Co sources for total body irrad., uniformity and standardisation 80–94338
^{60}Co teletherapy dosimetry survey of facilities 79–62367
^{60}Co teletherapy installations calibrations, US national evaluation 79–5360
^{60}Co teletherapy unit dose calibration, comparison of methods 80–30900
^{60}Co total body irradiation, dose distrib. meas. using thermoluminescent dosimeters 80–41245
^{60}Co-charging of γ-irradiation installation *(Bulgarian)* 78–82558
Co(10$\bar{1}$2), surface struct. of non-unique planes, LEED obs. 79–99402
CsCaCl$_3$:Co, EPR, 4.2 to 450K, ferroelec. transition 80–60414
CsCdCl$_3$:Co^{2+}, ground-state g-value, EPR meas. 77–16159
CsCdCl$_3$:Co^{2+}, Zeeman Raman scatt. and Zeeman IR absorpt. spectra 79–56782
CsMgCl$_3$:Co^{2+}, Zeeman Raman scatt. and Zeeman IR absorpt. spectra 79–56782
CsMnCl$_3$.2H$_2$O:Co, mag. impurity effect on Neel temp. and spin-flop field 79–61099
Cu, determination of Ni and Co by flameless atomic absorption spectrophotometry 77–90674
Cu:Co precipitates, mag. anisotropy, precipitate shape, coercive force 80–80500
Cu-Co, dil., impurity diffusion, mass depend. of energy factor of isotope effect 78–30795
Cu$_2$O:Co^{2+}, photomemory effect, EPR expts. 78–52353
Dy$_3$Al$_5$O$_{12}$:Ca^{2+}, optical absorpt. spectrum, strong crystal field of tetragonal symm. 77–32410
ErFeO$_3$:Co, Ti, effects of Co and Ti ions on cryst. growth 77–28711
F+Co(Fe) recoil, transient mag. field 78–29838
Fe-Co, bimetallic molecule, matrix isolated, Mossbauer spectrum 78–68425
Fe-Co, bimetallic molecule, matrix isolated, Mossbauer spectrum 78–88233
FeF$_2$:Co^{2+}, impurity-induced magnon, influence of localisation 80–11182
Fe(N$_2$H$_5$)$_2$(SO$_4$)$_2$:Co, Mossbauer effect and paramag. relax., superparamag. behaviour of correl. spin domains 77–69756
γ-Fe$_2$O$_3$:Co, impact-induced demagnetisation, magnetostriction and coercive force, appl. in mag. recording 77–16111
γ-Fe$_2$O$_3$:Co acicular powder epitaxially doped, coercivity increase, surface anisotropy *(Chinese)* 80–7130
γ- Fe$_2$O$_3$:Co powder, increased coercivity by epitaxial doping 79–82833
γ-Fe$_2$O$_3$:Cr, pure and doped, acicular particle suspensions, mag. props., optical meas. 80–44874
Fe$_3$O$_4$:Co, impact-induced demagnetisation, magnetostriction and coercive force, appl. in mag. recording 77–16111
GaAs:Co, effect of complex formation on impurity diffusion 77–11736
GaAs:Co, epitaxial layers and bulk, diffusion and elec. activity of Co 79–56333
GaAs:Co, intra d-shell excitations of acceptors 80–84757
GaAs:Co, neutral state of Co impurities, optical absorption and mag. susceptibility 78–39578
GaAs:Co, substitutional impurity elec. struct. 80–88513
GaAs:Co VPE layers, bound-exciton luminesc., Zeeman anal. 79–95818
GaAs:Co^{2+}, EPR assessment of 3d^7 transition metal impurity state 78–48031
GaAs:Co^{2+}, EPR expts., y-factor determ. 78–76301
GaAs:Co^{2+}, mag. and optical props. 78–10763
GaAs:Co^{2+}, piezoabsorption meas. tunnel splitting and Jahn Teller effect in ^{4}T$_1$(P) state 79–15494
GaP:Co, deep levels, IR photoluminesc., stress effects 80–55163
GaP:Co, optical spectra and Zeeman anal. of Co 3d^7 state 80–66247
GaP:Co, photolum. excitation spectroscopy 80–80841
GaP:Co, positron annihilation meas. rel. to deep levels study 80–60712
GaP:Co^{2+}, d→d luminesc. spectra 80–7414
GaP:Co^{2+}, EPR assessment of 3d^7 transition metal impurity state 78–48031
Ge:^{57}Co, ion-implanted, Mossbauer study, annealing effects 80–7231
InP:Co, diffusion, solubility and elec. activity of Co 77–43240
InP:Co, Hall and resistivity meas. 80–10990
InP:Co^{2+}, EPR assessment of 3d^7 transition metal impurity state 78–48031
KBr(I):Co, coloured and uncoloured, Mossbauer effect, inhomogeneous hyperfine fields 77–32307
KCdCl$_3$:Co^{2+}, Zeeman Raman scatt. and Zeeman IR absorpt. spectra 79–56782
K$_4$CdCl$_6$:Co^{2+}, ground-state g-value, EPR meas. 77–16159
K$_2$CoO$_3$.^{57}Co Mossbauer source 77–6592
KH$_2$PO$_4$:Co^{2+}, elec. cond. and diffusion, Co dopant effects 77–72716
KHSO$_4$:Co^{2+}, conduction and ^{3}H diffusion 77–15622
KHSO$_4$:Co^{2+}, impurity effect on growth habit from saturated soln. 77–4059
KHSO$_4$:Co(II), DC conductance, extrinsic and intrinsic regions 77–59141
KMgF$_3$:Co^{2+}, ^{4}T$_1$-^{4}T$_2$ transition, zero-phonon lines intensities 80–75529
KMgF$_3$:Co^{2+}, γ-irrad. single cryst., visible and IR absorption, MCD, annealing data 78–10926
KMgF$_3$:Co^{2+}, MCD and linear dichroism, 3d→4s transitions 79–56768
KMgF$_3$:Co^{2+} high energy absorption spectra interpretation 78–6716

cobalt continued

- $KMgF_3$:Ni, Co, emission from Ni-Ni and Ni-Co pairs, exchange coupling const. 79—33788
- K_2MnF_4:Co^{2+}, Raman spectra meas. 77—12389
- K_2SO_4-$ZnSO_4$ glass:Co^{2+}, visible spectra 79—51990
- $K_2Zn(ZrF_6)_2.6H_2O$:CO^{2+}, anisotropic exchange interactions between Co^{2+} ions, ESR spectra 79—95637
- $La_2Mg_3(NO_3)_{12}.24H_2O$:$Co^{2+}$, Ce^{3+}, relax. and ESR in magnetically cooled systems 78—88225
- $La_2Zn_3(NO_3)_{12}.24H_2O$:$CO^{2+}$, Mn^{2+}, Ni^{2+}, mag. exchange interactions, EPR 77—36118
- Li-Co ferrite, mag. anisotropy induced by thermomag. treatment, ionic order effect, magnetostriction meas. 80—103830
- $LiBaF_3$:Co^{2+} 79—65718
- LiCl:Co, electron transfer absorption bands 79—95810
- LiCl(Br):Co^{2+}, optical absorpt., charge transfer spectra 80—2797
- LiF:Co, flow stress changes during precipitation 80—92594
- LiF:Co, impurity effect on elec. cond. 79—7709
- LiF:Co, nucl. acoustic reson. 77—8445
- LiF:Co^{2+}, solid soln. decomp., precip. of new phase, electron microscope expt. 79—11619
- LiF:Co^{2+}, X-ray and electron microscope obs. of CoF_2 precip. morphology 77—31777
- LiF:Mg^{2+}(CO^{2+}), X-ray induced UV absorpt., band shapes, F- and Z-centers 77—20889
- $Li_{0.5}Fe_{2.17}Al_{0.33}O_4$:Co, single cryst., domain struct., mag. annealing effect depend. on induced anisotropy 78—68290
- $Li_{1-x}Fe_{5-x}O_8$:Co, single cryst., domain struct., mag. annealing effect depend. on induced anisotropy 78—68290
- $LiNbO_3$:Co, optical props. 78—64383
- $LiNbO_3$:Co, pure and doped, nonlinear excitation, multiphoton photorefractive process 79—36950
- $LiNbO_3$:Co^{2+}, Zr^{4+} films, LPE growth from Li_2O-V_2O_5 flux, X-ray and acoustic characterisation 80—15383
- $LiNbO_3$:Co^{2+}, Zr^{4+} film, improvement in temp. stability and SAW device appls. 80—75939
- $MgCl_2$:Co, spectroscopic studies of interactions 80—29769
- $MgCl_2$:Co^{2+}, ground-state g-value, EPR meas. 77—16159
- $MgCl_2$:Co^{2+}, Zeeman electronic Raman scatt. spectra 79—42962
- MgF_2:Co, photoluminesc. due to X-rays, colour centre thermal breakdown 79—24359
- MgF_2:Co, thermoluminesc. and TSC in activator band 79—24359
- MgF_2:Co^{2+}, Coulomb and exchange interaction const. optical spectra line assignment, new technique 80—45124
- MgF_2:Co^{2+}, MCD and linear dichroism, 3d$\rightarrow$4s transitions 79—56768
- $MgIn_4S_4$:Co, EPR powder spectra 80—25197
- MgO:Co, optical and ESR studies 80—50175
- MgO:Co, X-ray stimulated luminesc. 79—28802
- MgO:Co ions, impurity distrib. from EPR 77—51401
- MgO:Co^{2+}, ESR linewidths of Co^{2+} 80—80596
- MgO:Co^{2+}, electronic and impurity-induced Raman scatt. 80—100659
- MgO:Co^{2+}, next-nearest-neighbour ion effects on impurity 2p levels 77—20987
- MgO:Co^{2+}, strain modulated ESR, extensional and flexural modes 78—68365
- MgO:Co^{2+}, strain modulated ESR, extensional and flexural modes 78—68366
- MgO:Co^{2+}, weak dynamic Jahn-Teller coupling, neutron inelastic scatt. obs. 80—59934
- $MgSiF_6.6H_2O$:Co^{27}, spin Hamiltonians and pair interactions 77—36119
- $MnCl_2$:Co^{2+}, polarised IR absorpt. spectrum 77—40269
- $MnFeO_4$:^{57}Co, Mossbauer spectrum, 4s covalent bonding 80—20540
- Mo, determination of Ni and Co by flameless atomic absorption spectrophotometry 77—90674
- Mo, recrystallisation kinetics, deform. degree effects *(Russian)* 78—6943
- NH_4ClO_4:Co^{2+}, optical absorpt. spectra 77—66523
- $NH_4H_2PO_4$:Co^{2+}, elec. cond. and diffusion, Co dopant effects 77—72716
- NaCl:Co^{2+}, dynamic braking of dislocations *(Russian)* 78—6068
- Na_2O-CaO-P_2O_5:Co glass, bonding, symmetry meas. 79—46572
- in Ni, paramag. region, impurity effects on susceptibility, Faraday obs. *(Russian)* 80—88731
- Ni-Cr-Mn alloy solidification, effects of Si, Mo and Co alloying 79—83193
- NiS_2:Co, ferromag. props. 79—91227
- PbI_2:Co^{2+}, EPR 78—68362
- Pd:Co, doping, low temp. radiation induced impurity diffusion 77—15439
- PdH_x:Co, diffusion and interstitial site occupancy, Mossbauer spectra 80—20555
- PdH_x:Co^{57}, diffusion-induced reduction, Mossbauer study 80—108131
- RbCl:Co^{2+}, dielectric loss, impurity sites 79—91348
- $RbMnF_3$:Co, thermal cond., spin wave and mag. impurity contribs. 77—40046
- $RbMnF_3$:Co^{2+}, high-temperature EPR linewidth, impurity fast relax. effect 77—85556
- Si:^{57}Co, implanted, Mossbauer spectra, study of dose dependence 80—75900
- Si:^{57}Co, ion-implanted, Mossbauer study, annealing effects 80—7231
- Si:^{57}Co/^{57}Fe, Mossbauer spectra, deep level Co impurity study 80—29666
- Si:Co, diffused distrib. and state of Co atoms 77—1146
- Si:Co, diffusion coeff. of Co meas. 77—20126
- Si:Co, diode minority carrier lifetime, Lax method meas., effect of Co diffusion 79—69525
- Si:Co, electronic states of impurities 77—43531
- Si:Co, γ-irrad., interaction of deep-level impurity atoms with radiation defects 77—76457
- Si:Co, high-temp. ion-implanted and diffused samples, Mossbauer spectra of ^{57}Co 79—51891
- Si:Co, implanted or diffused, and annealed, localisation of Co atoms, Mossbauer obs. 80—39140
- Si:Co, influence of neutron irradiation on elec. props. 78—55895
- Si:Co, ion implanted, Co lattice location, channelling meas. 80—88201
- Si:Co, minority carrier lifetime investigation 80—80292
- Si:Co, study of impurity states 78—76020
- Si:Co, substitutional Co and Co precipitates, identification by Mossbauer spectroscopy 79—11631
- Si+Co(Fe) recoil, transient mag. field 78—29838
- SiO_2:Co(II), adsorption of H_2O, coord. lifetime, surface effect, NMR obs. 80—34299

cobalt continued

- $SrCl_2$:Fe^{2+}(Co^{2+}) electronic absorption spectra in far and middle infrared 78—68537
- $SrCl_2$:Mn^{2+}(Co^{2+}), cubic impurity EPR spectra, elec. field effect, mechanism 78—68361
- SrO:Co, noncentral and interstitial ion complexes, ESR obs. 80—71169
- SrO:Co^{2+}, EPR, optical, MCD absorpt. spectra 78—43692
- TiC-Co, grain growth kinetics *(French)* 77—44252
- W fibre reinforced, alloy by effect on struct. stability, mech. props., metallographic exam. 78—56600
- W fibre reinforced, high temp. strength 79—70021
- W-Mo-Co high-speed cutting steels, Co determ. 78—3416
- WC-Co, fracture mode determination, using Auger electron spectroscopy 80—7680
- WC-Co, grain growth kinetics *(French)* 77—44252
- WC-Co coating, sputter deposition, friction and wear characts. 77—44394
- WC-Co composite, surface anal. by quantitative AES 78—76622
- WC-Co composite chemical characterisation by AES and ISS 78—76621
- WC-Co DC and RF sputtered coatings, bias effect, struct., X-ray-Auger study 80—70565
- WC-Co particles electrophoretic deposition, on metal surfaces, wear resistant coatings preparation *(German)* 80—2969
- WC-Co sputter deposited film, struct. and comp. 78—72023
- WC-Co sputter deposited film, friction and wear 78—72918
- Xe: ^{57}Co, solid, ion implantation for rare gas matrix isolation, Mossbauer spectroscopy study 80—54271
- $YFeO_3$:Co, NMR of ^{57}Fe, spin echo 78—91987
- $YFeO_3$:Co^{2+}, weak ferromagnetism, single ion anisotropy contrib. 80—25126
- YIG:Co film, influence of stress induced anisotropy on domain struct. 80—100605
- YIG:Co LPE films, with rectangular bubble domains, prep. and props. 79—82848
- YIG:Co^{2+}, mag. permeability, illumination and impurity depend. *(Russian)* 78—64220
- $YbFeO_3$:Co, mag. struct. factors, neutron diffr. study 79—47248
- ZnO:Co ions, impurity distrib. from EPR 77—51401
- ZnO:Co varistors, microstructure-prop. relations 80—100249
- ZnO:Co^{2+}, polarised optical absorpt. spectrum, crystal field transitions 77—48206
- ZnO:Cu, O:Co, photocond., electron escape probabilities and trap depths 77—32041
- ZnS:^{57}Co Mossbauer sources, Fe^{1+} transient charge state 80—108128
- ZnS:Co, impurity-induced Raman scatt., central force const. reduction 77—32379
- ZnS:Co, Jahn-Teller interaction energy determ., piezospectroscopic expt. *(Russian)* 77—4623
- ZnS:Co Mossbauer source, Fe^{2+} abnormal populations and vibronic props. 80—15912
- ZnS:Co^{2+}, EPR and spin-lattice relax. of Co^{2+} centres *(Russian)* 79—1706
- ZnS:Co^{2+}, spin-lattice relax., phonon heating effect *(Russian)* 78—19317
- ZnS:Cu, Co, deep traps and stationary luminescence *(Russian)* 78—48227
- ZnS:Cu, O, Co, photocurrent spectral distrib., killer impurity effects 77—8135
- ZnS:Cu,O,Co photoconductors, killer impurities effect on electron escape probabilities and trap depths 77—4392
- ZnS:Lo, vibr. modes of transition element impurities 78—76472
- ZnS-CdS:Ag, Ni, Co, thermoluminesc. glow curves 78—95611
- ZnS-CdS:Ag, Ni, Co phosphor, thermoluminesc. 77—66547
- ZnS-CdS:Co, electron-irradiated phosphors, void formation mechanism 79—55780
- $ZnSO_4$ electrolytes containing Ge and Co, polarisation charact., exam. by cyclic voltammetry 80—104444
- ZnS(Se)(Te):Co, impurity luminescence no phonon line depend. on temp., Debye temp. 80—66273
- ZnS(Se)(Te):Co^{2+}, IR luminesc. quenching, Co^{2+} level position, ionisation energy 80—16079
- ZnSe:Co, effect of in-band position of states on photoelec. props. 78—23132
- ZnSe:Co, optical props. in near IR 78—43924
- ZnSe:Co^{2+}, depression of vibronic levels, transition of Jahn-Teller states from dynamic to static 78—43337
- $ZnSiF_6.6H_O$:Co^{2+}, spin Hamiltonians and pair interactions 77—36119
- $ZnSiF_6.6H_2O$:Co, influence of hydrostatic press. on Co^{2+} EPR spectrum 78—27084

cobalt alloys

see also cobalt compounds

- adhesive wear under unlubricated conditions 80—108593
- Alinco 5, thermal treatment in mag. field, mag. props. 78—91905
- Alnico, 5 and 8, spinel type permanent magnet, magnetic aftereffect 77—16118
- Alnico, domain struct., variation under influence of heat treatment *(Russian)* 78—23292
- Alnico, high-energy magnetic materials technology developments and props. *(Italian)* 80—54914
- Alnico 5 alloy, S and Ti additions effect rel. to non-metallic inclusions, coercive force and grindability 80—89375
- Alnico 5 and 8, spinodally decomposed magnetic alloy, magnetic flux temp. coeff. *(Japanese)* 78—35006
- Alnico alloy, C addition effects on struct. and mag. props. 78—23835
- Alnico alloys, effect of Ce addition on mag. props. 78—2699
- Alnico type YuNDK25DA alloy permanent magnets, thermal mag. hysteresis 80—75818
- amorphous, alloying elements influence on corrosion behaviour, XPS obs. 80—89422
- amorphous, effects of metalloids on mag. props. 80—75738
- amorphous, ferromag., sputter-deposited, soft mag. props., magnetostriction 80—34696
- amorphous alloys, effect of alloying additions on corrosion resistance *(Japanese)* 79—96215
- amorphous ribbon, saturation magnetostriction, and electronically controllable delay line 79—1700
- binary, and MAR-M322 type, influence of phase transform. on diffusion and mech. props. *(Russian)* 79—5000
- chromindur, origin of coercivity, Lorentz microscopy, magnetisation and Mossbauer effect 78—64219

cobalt alloys continued

chromindur, phase separation, Mossbauer obs. 78–88116
Cl $(Co_{100-x}Fe_x)_{83}B_{17}$, $1 \leq x \leq 30$, annealing embrittlement and crystn. 80–45329
composites, W fibre reinforced, reactions and recryst. 80–11603
corrosion resistance for long-term implants *(German)* 79–8565
creep-fatigue interaction in aligned eutectic and solid soln. 80–108554
Cu-Co, dil., rotational hysteresis of Co fine particles 78–23301
dilute, factors affecting high-temp. oxidation behaviour, alloying effects 77–77638
dilute, liquid, thermodynamics 77–20086
dilute alloys, amorphous, exhibiting Mossbauer effect, mean mag. props. *(French)* 80–80489
distillation deoxidation during electron beam melting *(Russian)* 79–70306
earth reentry exposure, simulated, effect on mech. props., oxidation of Haynes 188 79–5086
electrical resistivity and specific heat meas., anomalies rel. to thermally excited states 80–6809
$Fe_xCo_{1-x}Ti$, ferromag., high-field and high-press. mag. behaviour 78–91919
Fe-Cr-Co-Si-Mo, plastic deform. influence on structure and mag. props. *(Russian)* 79–70176
ferromagnetic, hyperfine fields of 4d and 5d impurities 78–31133
ferromagnetic films, coercive force, ion plating prep. 77–28730
ferromagnetism, Stoner model, mol. field coeff., temp. and field depends. 77–72975
films, deposition onto Cu, Ni surfaces, twinning 79–11527
GdCo amorphous film, magnetic compensation walls 77–8375
Hastelloy-X, fatigue crack propag. at elevated temps. in solid solution strengthened superalloys 78–39895
Hayes alloy no.716, Fe-Cr-Ni-Co-W-Mo-Si-C-B (26, 22, 12, 3.5, 3, 1.2, 1.1, 0.4 wt.%), hardfacing alloy 80–100802
Haynes alloy 188, fatigue crack propag. at elevated temps. in solid solution strengthened superalloys 78–39895
Haynes alloy 188, H_2 permeability 77–46399
Haynes alloy 188, SEM exam. of fracture surface, due to low cycle fatigue at 700°C *(Japanese)* 78–52963
Haynes Stellite 6B, Al_2O_3 particle erosion of surface, SEM obs. 78–88545
Haynes Stellite 6B, particle erosion damage, TEM obs. 78–88546
heat resistant, determ. of sub-ppm levels of Ag by graphite furnace atomic absorption spectrometry 78–48730
heat resistant alloys, atomic absorption spectrometry with heated graphite atomizer, Bi and Pb trace quantities 78–15749
Heusler alloys, hyperfine fields and mag. interactions, NMR spectra 78–88222
high heat resistant, industrial appl. and comp. *(Korean)* 79–24716
high-temperature materials, technological requirements, R and D, report 80–45222
In 519 high temp. low-cycle fatigue behaviour for nuclear process heat appl. 80–628
Incoloy 800, nuclear grade boiling tubing superalloy, Co and C content anal. 80–78397
Inconel 600, nuclear grade boiling tubing superalloy, Co and C content anal. 80–78397
Inconel 617, creep, morphological changes of carbides, affect on creep props. 80–108509
Inconel 617, microstruct., mech. props., thermal ageing effect 77–36557
intermetallic compounds, containing d-transition metal, hydrogenated, magnetism 80–34609
ion exchange chromotography for Co and rare earth determ. in alloys for high energy magnets *(Polish)* 80–35606
Kovar, thermostress treatment of thin-rolled sheets 79–52273
Kovar-silicon oxynitride-aluminium cathode, local electron emission and electroluminesc. patterns obs. 80–108327
mag. props. after isothermal thermomag. treatment *(Russian)* 80–25159
magnetic susceptibility and Knight shift meas., d-metal alloys 80–66055
Magnico alloy, with Si, Nb, Ti and La, low-temp. thermomag. treatment 77–63812
Magnico alloy, with Si, Nb, Ti effect of Ub on mag. props. and grindability 77–63811
metallic glasses, ductile-brittle transition 77–4847
metallic glasses, elastic const. 77–66671
metalloid-transition metal amorphous surface alloys formed by ion implantation, TEM study 78–67730
mischmetal-based magnets, $MM_{1-x}Sm_xCo_5$, demagnetisation, temp. depend., 175 to 425K 79–78440
mischmetal-Co system, thermomagnetic analysis of intermediate phases 80–93115
mischmetal-Co-Cu-Fe-Mg, mag. props. 80–35353
mischmetal-Co-Cu-Mg, mag. props. 80–35353
mischmetal-cobalt, $MMCo_5$, polished, domain wall grooving, optical microscopy and SEM obs. 77–8334
Mischmetall-Co_5, absorpt.-desorpt. characts. for H_2 77–89640
Mo Co_2, single crystal, polarised neutron diffraction, various temp. and applied fields 78–2650
Monel 400, stress corrosion cracking in high temp. caustic soln. 77–59964
Multimet, fatigue crack propag. at elevated temps. in solid solution strengthened superalloys 78–39895
$(Ni_{1-x}Co_x)_{0.98}Mn_{0.02}$, average mag. moment of Mn atoms 79–28509
Ni-Co, H_2 embrittlement, heat treatment and impurities effect 80–76331
Nimonic 105, quantitative STEM chem. anal. using standard and standardless programs 79–17578
NK, thermocouple alloy, heat treatment effects on thermoEMF and mag. flux 77–63235
Permendur, 50KF, magnetostrictive props., compression effcts 77–40109
Permendur 49, ordered and disordered, clean mild wear 80–16508
rare earth alloy, $R(Co,M)_5$, magnetisation reversal and high coercive force, domain boundary pinning *(Russian)* 77–8345
rare earth alloy, RCo_2, Invar props. 79–56593
rare earth alloys, RCo_2, elec. resistivity, thermopower, X-ray struct. meas. 80–24874
rare earth alloys, RCo_5, sintered magnets, texture determ. 79–100085
rare earth alloys, RCo_5, X-ray absorpt. spectra, electronic struct. 80–16122
rare earth alloys, RCoAl, mag. props. 78–2659

cobalt alloys continued

rare earth Co compounds, RCo_2, metamagnetic transitions in internal fields 80–60272
rare earth Co Laves phase cmpds., elastic props. rel. to temp., mag. field 79–51834
rare earth cobalt oriented materials as permanent multipole magnets 80–37925
rare earth cobaltide, RCo_2, 'as cast', fibre texture, neutron diffr. exam. 78–3117
rare earth cobaltides, R_2Co_{17}, ^{59}Co NMR obs. of hyperfine fields and mag. moments 77–20726
rare earth cobaltides, RCo_3 type, hydride phase synthesis, thermal stability and struct. 80–59438
rare earth intermetallic, permanent magnet, grain alignment, metallographic method using eutectoid transform. of Co_5R 77–9003
rare earth intermetallic $R_2Fe_{17-x}Co_x$, mag. anisotropy and hyperfine interactions 77–8298
rare earth intermetallic RCo_2, itinerant system, weak ferromagnetism 78–52191
rare earth intermetallics, permanent magnet material development 78–91895
rare earth intermetallics, permanent magnet production and props. 78–52309
rare earth intermetallics, $R(Co_{0.98}Fe_{0.02})_2$, magnetostrictive material, changes in vibr. modes near mag. phase transition 79–90736
rare earth intermetallics, RCo_2, elastic moduli, 4.2-300K 78–52332
rare earth intermetallics, RCo_2, itinerant metamagnetism, Van Vleck model 79–78297
rare earth intermetallics, $RCo_{5x}Cu_{5-5x}(Ni_{5,-5x})$, narrow Bloch walls, magnetisation, 4.2K 77–8333
rare earth intermetallics, RCo_5, magnetocryst. anisotropy 77–8299
rare earth systems, RCo_3-H_2 (R=Ce, Pr, Tb, Dy, Er), phase equilibria, from dissociation isotherms 80–50591
rare earth-$(Co_{1-x}Ni_x)_5$, single cryst., mag. props., mag. reversal 77–85489
rare earth-Co_{17}, mag. anisotropy 78–84414
rare earth-Co_2-Al, dil., nonmag. impurities effect on ordering temp. 78–84427
rare earth-$Co_{3.4}$, amorphous, mag. props. 77–72985
rare earth-Co, 2-17 comp., permanent magnet props. 77–8348
rare earth-Co, plastic magnet appl., anisotropic, based on moulding ferromagnetic powder material with plastics *(Japanese)* 80–60829
rare earth-Co, powdered, fine grinding in gastight attrition mill 79–33967
rare earth-Co, $R_{69}Co_{31}$, amorphous, mag. props. 80–84590
rare earth-Co, RCo_2:^{57}Fe, easy magnetisation directions, Mossbauer meas. and cryst. field calc. 77–63168
rare earth-Co. RCo_3 (R=Gd, Dy and Ho), effect of absorbed H_2 on mag. behaviour 79–33483
rare earth-Co, RCo_5, high anisotropy origin, cryst. field contrib. 77–73020
rare earth-Co, RCo_5, mag. moment orientation, anisotropic mol. field model 77–89950
rare earth-Co alloy, Curie temp. determ. 79–65672
rare earth-Co alloy, electron microscopy exam. 78–67722
rare earth-Co alloy, mag. anisotropy origin 79–38319
rare earth-Co alloys, ferromag., first and second order transitions 80–34631
rare earth-Co alloys, ferromagnetic intermetallic compounds, comminution charact. 77–12564
rare earth-Co alloys, spin wave spectra 78–56304
rare earth-Co amorphous alloys, mag. compensation temp. 77–66277
rare earth-Co permanent magnet EM acoustic transducer design 77–19508
rare earth-Co permanent magnets, generation mechanism of high coercive force *(Japanese)* 79–100269
rare earth-Co permanent magnets, microstruct., TEM obs., magnetisation 78–91901
rare earth-Co permanent magnets, processing and props., review *(Japanese)* 77–73049
rare earth-Co phases, fault struct. and shear transform., stacking sequence notation 77–35571
rare earth-Co system, spin reorientation and sp. ht. anomaly *(Japanese)* 79–47287
rare earth-Co systems, anomalous Hall effect and Kerr rotation obs. 77–11897
rare earth-Co-Ni alloys, $R(CoNi)_5$ type, mag. props. and mag. reversal phenomena *(Russian)* 77–51924
rare earth-Co-Si(Ge), $ThCu_2Si_2$ type, lattice parameters 78–51469
rare earth-cobalt intermetallic, RCo_2 79–19725
rare earth-cobalt intermetallics, RCo_2, spontaneous vol. magnetostriction and thermal expansion meas. 77–12183
rare earth-Sn-X, X=Rh, Ir, Ru, Co, cryst. growth and cryst.-chem. invest, supercond./mag. ternary cpds. 80–100777
rare-earth intermetallics, R_2Co_7, polymorphism of Ce subgroup alloys, eutectic decomposition *(Russian)* 80–66504
rare-earth-Co films, extraordinary Hall effect meas. 78–6459
Rene 41, Ni-Cr-Co-Mo-Ti-Al-Fe (18.96, 11.09, 9.65, 3.06, 1.59, 0.89 wt.%) formation of Cr_2O_3 monocrystals on heat treatment 79–52455
Rene 41, volatilisation of oxides during oxidation at 1200°C 78–23873
resistivity magnetoresistance, s,p impurities in ferromag. host 78–68008
satellite, hardness and erosion resistance to aqueous SiO_2 slurry 79–43441
sheet metal, deep-drawn, for implant device encapsulation, mech. and metallographic props. *(German)* 79–8564
$Sm_{1-x}R_xCo_5$ (R=Y, La, Ce, Nd), mag. props., domain boundary pinning on statistical conc. heterogeneities *(Russian)* 79–99728
solidification, method for evaluating influence of each element on microsegregation *(French)* 79–74159
steel, 18Kh2N4MA, Co effect on struct., and mech. props. 78–44147
steel, alloy, maraging, 250-grade, ductility and toughness of hot isostatically pressed powder 78–52925
steel, Co (2 wt.%), effect of Co on pearlite growth 77–90359
steel, Co-Cr casting, fatigue at welds, hip replacement appl. 78–44697
steel, Co-Cr-Mo, maraging, age hardening, Mossbauer study 80–40002
steel, Co-Cr-Ni-Mo-Mn (39.65, 20.25, 15.33, 7.08, 1.9 wt.%) carbide formation during tempering after plastic deformation 80–16330
steel, Cr-W-Mo-Co, high-speed, from atomised powders, mech. and cutting props. 80–66556
steel, high-speed cutting, struct. and props. Co addition effects *(Russian)* 77–21177

cobalt alloys continued
steel, maraging, grain refinement due to cyclic heat treatment 78–52971
steel, maraging, investigation with lower Ni and Co contents *(Chinese)* 78–84812
steel, maraging, solubility of Fe-Mo-Co (10, 0 to 20 wt.%) Laves phase, depend. on Co *(Russian)* 79–100145
steel, maraging, type 200, effect of freq. on cyclic crack growth in salt water environment 78–64680
steel, maraging 250-grade, fatigue crack growth model, notch analysis of fracture approach 78–52984
steel, maraging Ni-Co-Mo, precipitation, elec. resist. meas. *(Japanese)* 78–11228
steel, martensitic, Cr-Co-Ni-Mo, notch toughness, rel. to sensitivity to stress conc. 78–31532
steel, martensitic, Cr-Ni-Co-Mo-Ti, Kh12N8K5M3TYu, ageing of C free martensite *(Russian)* 79–1884
steel, martensitic, high C, Co addition effect on strength *(Korean)* 78–68736
steel, Ni-Co-C (9, 4, 0.2 wt.%) enthalpy, sp. ht. to 2000K 79–10960
steel, Ni-Co-Cr, high-strength medium C, Cr effect on props. 80–76339
steel, Ni-Co-Cr-Mo-C (10,14,2,1,0.16 wt.%), stress corrosion cracking at 22°C in 3.5% NaCl 79–8390
steel, Ni-Co-Mo-Ti, maraging, electron diffr. obs. of second phase *(Chinese)* 80–11655
steel, stainless, Cr-Ni, maraging, effect of Mo, Co additions on hardening 78–84835
steel, W-Mo-Co, high-speed tool, struct. and props., cooling rate effect at primary crystn. temp. 80–76241
Stellite, friction behavior in high temp. Na environment *(Japanese)* 80–40546
Stellite, ion plating of hard TiN decorative coatings 78–11441
Stellite, self-weldability in high temp Na *(Japanese)* 80–89392
Stellite 6B, volatilisation of oxides during oxidation at 1200°C 78–23873
stellite hardfacing materials, friction characts. in high temp. Na *(Japanese)* 80–89356
Stellite-6, XPS obs. of aqueous oxidation, surface comp. and gaseous oxidation effect 80–81238
super alloy X-40, creep-fatigue interaction at high-temp. 78–84958
superalloy, aluminite coating, improvement by sputtering *(French)* 79–29278
superalloy, attritious wear in grinding 77–32696
superalloy, machine thixocast, mech. prop. deficiencies 79–74244
superalloys, low temp. hot corrosion, Na_2SO_4-induced, mechanism, burner rig tests 80–40610
surgical implant materials, corrosion fatigue props. 79–39604
surgical implant materials, corrosion props. 79–39605
Ticonal, domain struct., variation under influence of heat treatment *(Russian)* 78–23292
Ticonal, effect of rare earth metals on mag. props., struct., and phase transformations 79–99732
ticonal, grindability improvement, thermomagnetic and heat treatments 77–16625
Ticonal, two- and one-dimens. modulated struct. after thermomag. treatment and water quenching *(Russian)* 80–29983
Ticonal strength, effect of thermal stresses and phase transforms. 79–87721
Ticonal with magnetic texture, struct. damages during ageing 77–16626
Ticonal with Sm, magnetic props., phase transform. after thermomagnetic treatment 78–3155
Ticonal-type alloys, struct. after quenching from 800-850°C *(Russian)* 77–59822
transition metal alloy, ferromag., H-impurity complex obs. by magnetic aftereffect 78–72373
transition metal alloys, AFe_2 and ACo_2, Invar effect, magnetovolume meas. 79–56592
twin-slip interaction in FCC crystal 77–51379
Udimet 500, microstructural instability in industrial gas turbine engine vane 77–28833
Udimet 520, Nicralloy-coated, microstruct. degradation, influence of corrosioin protective coating 80–40611
Udimet 700, creep crack growth 78–48517
Udimet 700, high temp. fatigue crack growth, fracture mech. approach 79–52340
Udimet 700, microstruct. of resolidified zones formed by laser melting single crysts. 79–78953
Udimet 700, Ni-Co-Cr-Al-Ti (18.8, 15.2, 4.5, 3.39 wt.%) exam. of high temp. creep 79–61684
Udimet 700, Ni-Co-Cr-Al-Ti (18.8, 15.2, 4.5, 3.39 wt.%) exam. of high temp. creep, viscoplastic flow 79–61685
Udimet 700, Ni-Co-Cr-Ti, hold time effects on high temp. fatigue crack growth 79–5036
Vicalloy 1, dilatometric anomalies and α to γ transform., effect of heating rates *(Russian)* 78–39762
vicalloy-2, high heating rate effect on mag. props. *(Russian)* 77–81328
Vitallium, surgical implant, SCC and corrosion fatigue in Tyrode's soln. 79–29263
Vitallium alloy, fretting corrosion of surgical implant material, electrochemical investigation 79–66197
wear resistance, struct. effect 79–29229
Ag-Co, dil., binding and caging of impurities and trapped interstitials 78–39462
Al-Co, composite, paramagnetic resonance and electron-positron annihilation *(Russian)* 79–87314
Al-Co, defect structs. introduced by electron irrad., Mossbauer study 80–7239
Al-Co, dil., binding and caging of impurities and trapped interstitials 78–39462
Al-Co, dil., electron and neutron irradiation, interstitital atom clustering at ^{57}Co impurity, Mossbauer meas. 78–30607
Al-Co, dil., electronic states, XPS meas. 77–44117
Al-Co, electron irradiated, self-interstitials trapped at Co impurities, Mossbauer line shape anal. 78–6615
Al-Co, electron irradiated, quadrupolar relaxation effect in Mossbauer effect 78–39459
Al-Co, liquid alloys, thermodynamic charact. calc. *(Russian)* 78–27475
Al-Co dil., fast neutron irradiation, Mossbauer spectra, interstitial atom trapping 77–27914
Al-$CoSi_2$-Si system, diffusion, compound form., and microstructure 80–34253
Al-$CoSi_2$-n-Si system, Schottky-barrier height 80–34520

cobalt alloys continued
Al-Mn-Co, permanent magnetic materials, grain struct. effect *(Rumanian)* 79–73773
Al-Ni-Co, directionally solidified ternary eutectic morphology *(Czech)* 77–59772
Al-Ni-Co, directionally solidified eutectic, morphological and mech. props. *(Russian)* 80–30057
Al-Si (35 wt.%), Cr, Co, Si addition effects on strength of powder 77–24983
Al-Zn-Mg-Cu-Co (6.5, 2.5, 1.5, 0.4 wt.%), fatigue crack propag. 80–55521
Al-Zn-Mg-Cu-Co-Fe-Si, powder alloy, fatigue crack tip plasticity, from load interactions 80–21066
AlCu-NiCo (5 at.%), Θ' hardened, creep mechanism 80–85013
$Al_4(Ni, Co)_3$ ternary phase in Al-Ni-Co system, cryst. struct., vacancy controlled phase *(Chinese)* 80–70164
$AmCo_2$, crystal structure and mag. props. of Laves phases 77–27851
Au-Co, dil, local moments, third harmonic de Haas-van Alphen wave shape anal. 78–84127
Au-Co, dil., conduction electron-local moment interactions using dHvA waveshape anal. 79–77981
Au-Co, dil., valence and core level spectra, XPS study 80–84838
Au-Co, dil. alloy, crystalline electric field and spin-orbit splitting, NMR results 77–32274
Au-Co, dil. alloy, de Haas-van Alphen obs. of spin dependent scatt. by mag. pairs 77–32007
Au-Co, electrodeposit, characterisation by ^{57}Co-^{57}Fe Mossbauer spectroscopy 80–39989
Au-Co, electrodeposit, Mossbauer meas. of Co chem. state 80–39990
Au-Co, electron scatt., spin-orbit effects 80–65533
Au-Co, electron scatt. by mag. impurity pairs, de Haas-van Alphen obs. 77–66162
Au-Co, electroplated, 'polymer' inclusions, chem. identity obs. 79–37931
Au-Co, liq. alloys, partial struct. factors 80–1919
Au-Co, liquid alloys, ^{59}Co NMR studies 79–95660
Au-Co, liquid alloys, struct. determ. by X-ray diffr. 78–6006
Au-Co, liquidus line determ. by mag. meas. 80–60250
Au-Co, spin glass, residual resistivity conc. depend. 80–2382
Au-Co, spin glass transition and anomalous Hall effect 79–61162
Au-Co, UPS study, localised states 80–93449
Au-Co electrodeposit, Co-hardened, state of Co in as-deposited material, Mossbauer obs. 80–15397
Au-Co electrodeposit, Co-hardened, characterisation by Mossbauer spectroscopy, Co precip. formation 80–80108
Au-Co electrodeposit, struct. and hardness characts. 79–28245
Au-Co electrodeposits, Co hardened, chemical state of Co, Mossbauer emission spectra 79–90897
Au-Co electrodeposits, Co hardened, high temp. film formation 79–91848
Au-Co electrodeposits, heating effect on microstruct. and surface topography 77–43456
Au-Co film, co-evaporated, struct. and ohmic behaviour 79–87021
Au-Co melts, struct., compressibility, X-ray and neutron diffr. 77–11614
Au-Co solid solution, mag. susceptibility 79–61081
Au-Co solid solution, mag. props., freq. depend. suscept. maximum 79–69655
Be-Co (0-50 at.%) alloys, thermal, metallographic and X-ray anal., phase diagram *(Russian)* 78–56611
Be-Co phase diagram *(German)* 77–59759
Be-Co-Ni, phase relations *(German)* 79–43209
C-Mo, dil., brute-force nucl. orientation meas. 77–59466
CaSb, resist., susceptibility and thermopower rel. to electronic struct. 78–67935
Cd-Co(-Mo), amorphous films, thermal stability of mag. props. *(Japanese)* 79–47307
Ce-Co, liq., charge transfer effect 78–94967
Ce-Co-Al (0-33.3 at.% Ce), isothermal section, X-ray study *(Ukrainian)* 80–39002
Ce-Co-Cu-Fe-Ti, sintered magnet, prep. and mag. props. 77–73043
Ce-Co-Si, thermoelectromotive force and electrocond. *(Ukrainian)* 80–54670
Ce-Co-Si system, mag. props. in 77-300K range *(Russian)* 78–56290
Ce-Mn-Co, cryst. struct. determ. 77–11508
Ce-Mn-Co, temp. conc. limits of homogeneous compounds *(Russian)* 78–23666
Ce-Sm-Co-Fe-Cu, permanent magnet props. 79–8013
$CeCo_2$, of Co, interdiffusion exam., growth kinetics of intermediate layers 78–2304
$CeCo_3$, and ternary hydride, mag. props. 80–108007
$CeCo_5$, adsorption and desorption charact. of H_2 *(Japanese)* 77–47667
$CeCo_5$ hard magnets, characteristics and appl. *(German)* 77–80966
$CeCo_5$, magnetisation and coercive strength 77–55688
$CeCo_{5+x}$, Cu and Fe modified, coercive force *(Czech)* 79–42805
$CeCo_x$, sorption at press. up to 1500 atm. 80–97819
Ce_2Co_7, and ternary hydride, mag. props. 80–108007
Ce_3Co, absorpt. of D, heats of reaction and equilib. press., T-getters for CTR 78–51683
$Ce_{5.3}Co$, absorpt. of D, heats of reaction and equilib. press., T-getters for CTR 78–51683
$CeCoAl_4$, X-ray anal. of crystal struct. *(Russian)* 77–55263
$Ce_2Co_5B_2$, crystal struct. *(Ukrainian)* 79–51050
$CeCo_{3.5}Cu_{1.5}$, and alloys of similar comp., cryst. structs., X-ray diffr. exam. 79–99120
$CeCo_{5-x}Cu_x$, $0\leq x\leq$ internal oxidation kinetics, oxide struct., X-ray study 80–104329
$CeCoSi_2$ film, Hall effect and magnetoresist. *(Russian)* 80–11109
$Ce_{1-x}Gd_xRu_2Zr_2Co$, spin-pairing state investig. via Josephson effect 77–47942
$CeMM_{0.8}Sm_{0.2}Co_5$, (MM = mischmetal), thermal props. *(German)* 77–8359
(Co,Cr,Ni)-TaC, eutectic alloy, directionally solidified, struct. defects, autoradiographic investig. *(Russian)* 77–25038
(Co,Cr)-$(Co,Cr)_7C_3$, eutectic creep model 77–36588
(Co,Cr)-$(Cr,Co)_7C_3$, eutectic alloy, directionally solidified, struct. defects, autoradiographic investig. *(Russian)* 77–25038
$(Co,Cr)(Co,Cr)_7C_3$ eutectic composite, creep anisotropy 78–19840
$(Co, Cu, Fe)_5Ce$, sintered permanent magnets, magnetic charact. 78–60608
$(Co,Cu,Fe)_5Ce$, sintered, mag. props. 78–68302
$(Co,Fe,M)_{78}Si_8B_{14}$ amorphous alloys (M = V,Nb,Ta,Cr,Mo,W,Mn or Ni), zero magnetostriction and low field mag. props. 80–34741

cobalt alloys continued
(Co,Fe)$_{0.75}$B$_{0.25}$ metallic glasses, annealed, equilib. crystalline phases 80—3019
(Co,Fe)$_{80}$B$_{20}$ glass, induced anisotropy and time changes of permeability 80—75815
(Co,Ni)-Cr$_{23}$C$_{6}$ eutectic, microstruct. effect on fracture energy 80—7662
Co base superalloy, rupture life, prior temperature cycling effect 78—60840
Co based amorphous alloy, mag. ordered, hyperfine field distribs., NMR meas. 78—68409
Co hard-alloy/U8 C alloy steel weld, local internal stress region boundaries 77—59846
Co-^{48}V, nucl. orientation of ^{48}V, γ-ray anisotropy obs. 80—97169
Co-3d transition metal alloys, hyperfine field and mag. perturbation distrib., NMR spectra meas. 79—61263
Co-(Cr,Co)$_{7}$C$_{3}$ eutectic, oxidation effect on toughness and strength 80—89404
Co-Al, band model of high temp. magnetism 78—26809
Co-Al, band struct. and density of states, KKR method and X-ray meas. 80—10863
Co-Al, couple phase diagrams and thermochemical data 79—66037
Co-Al, deformed, mag. props., positron annihilation *(Russian)* 77—85416
Co-Al, mag. struct. of Co rich intermetallic cpd., neutron scatt., cluster model 78—80130
Co-Al, multilayer martensite phases, illustration of polytype structures 80—84932
Co-Al, positron lifetime and angular correl. curves 79—47538
Co-Al, transition metal group VIII aluminide, NMR near equiatomic composition *(Russian)* 80—20479
Co-Al, X-ray K-absorption spectrum 80—97378
Co-Al coating, low temp. hot corrosion, Na$_{2}$SO$_{4}$-induced, mechanism, burner rig tests 80—40610
Co-Al solid soln., lamellar spacing in discontinuous precipitation, expt. proof of Gaussian distrib. *(German)* 77—36517
Co-Al system, nucl. spin relaxation exam. 79—19798
Co-Al-Cr(Nb)(Ta), eutectic alloys, charact. by melting, oxidation resistance and composition 78—52768
Co-Al-Nb, monovariant directionally solidified eutectics, struct. and mech. props. *(Russian)* 78—92254
Co-Al(Cr), gas corrosion, in composite atmospheres *(Polish)* 79—79142
Co-Ar film, struct., electron diffr. meas., rel. to metal-nonmetal transition 77—51626
Co-B, amorphous alloys, phase diagram 79—96002
Co-B (6.6 at.%), columnar alloys, metallographic obs. of eutectic struct. *(Russian)* 78—27469
Co-B alloys, amorphous, mag. moment and exchange stiffness constant 79—1662
Co-B alloys, amorphous, saturation magnetisation, mag. moments, X-ray diffr. obs. 79—4704
Co-B glass, X-ray obs. of struct. 79—1399
Co-B-Mo-Cr, amorphous, Mo and Cr addition effect on corrosion behaviour 80—16568
Co-B-Si, mag. props. different in amorphous and cryst. phases 77—69617
Co-B-Si amorphous alloy, liq. quenched, elec. resist. and cyclic deform. 80—59949
Co-B-Si ternary system, partial phase diagram, Co rich region 77—52293
Co-B(-Cr) thin film glasses, mag. props. and corrosion resist. 80—80576
Co-C, coupled phase diagrams and thermochemical data 79—66036
Co-C, dil., C segregation to single cryst. surfaces 80—39301
Co-C, dil., ferromag., electronic struct. of interstitials 77—62867
Co-C, ferromag., prep. by splat-quenching, obs. of electronic struct. of interstitial C 77—62868
Co-C, graphite nucleation on surface *(Russian)* 80—40360
Co-C interstitial alloys, electronic struct. and ordering of sp defects 78—91639
Co-C solid solns., surface graphite layer form., high-temp. metallography investig. 79—29306
Co-C supersat., solid soln. decomp. and graphite surface energy determ. *(Russian)* 77—15677
Co-C-TaC directional eutectic, high-strength, interphase boundaries *(Russian)* 79—38812
Co-Ca, liq. alloy form. kinetics *(French)* 80—96652
Co-Cd, dil. alloy, impurity hyperfine interactions 78—84416
Co-Ce Mischmetal powder, sintering 77—21055
Co-Co$_{2}$Sn, directionally crystallised eutectic, influence of prolonged annealing on microstructs. and props. *(Russian)* 79—74182
Co-CoAl, two phase, interaction between deform., fracture initiation and propag. 80—85006
Co-CoAl eutectic, invariant composition redeterm. 78—3099
Co-Cr, biolgoical implant, ion beam sputter of surface morphology, SEM obs. 77—44836
Co-Cr, containing dispersion oxides formed by internal oxidation, oxidation behaviour 78—19922
Co-Cr, high temp. sulphide corrosion 78—64775
Co-Cr, isothermal oxidation in 760 Torr O$_{2}$ at 1000°C 77—77639
Co-Cr (up to 25 wt.%), sulphidation and oxidation in Ar-SO$_{2}$, effects of increase in Cr content 80—11839
Co-Cr films, mag. props. in range of transition from thin-film to hypercritical state *(Russian)* 79—51824
Co-Cr mag. film, crystallographic texture formation effects on props. *(Russian)* 80—108471
Co-Cr orthopedic implants, surface oxide layer investigations using ESCA technique 79—25157
Co-Cr recording films, perpendicular mag. anisotropy, hysteresis loop, microstruct., TEM obs. 78—95491
Co-Cr superalloy, type MAR M509, high temperature fatigue behaviour 80—40485
Co-Cr system, phase diagram re-determ. from thermodynamic data 78—76631
Co-Cr-Al, exam. of cyclic oxidation resistance at 1100 and 1200°C, comparison with Ni-Cr-Al system 78—88572
Co-Cr-Al, oxidation at 1000°C 77—59963
Co-Cr-Al, protective coating, exam. of interdiffusion kinetics, development of analysing procedure 79—5085
Co-Cr-Al, ternary system, interdiffusion, electron probe anal. 80—34256
Co-Cr-Al based coating, electron beam evaporation of low vapour press. elements 80—40613
Co-Cr-Al-C eutectic alloy, thermal cyclic loading, exam. 78—48496

cobalt alloys continued
Co-Cr-Al-Y, low temp. hot corrosion, Na$_{2}$SO$_{4}$-induced, mechanism, burner rig tests 80—40610
Co-Cr-Al-Y, turbine blade coating, hot corrosion by Na$_{2}$SO$_{4}$ and vaporous NaCl 78—19941
Co-Cr-Al-Y coated turbine airfoils, effect of electron beam deposition rate on struct. 79—23870
Co-Cr-Al-Y coating, Pt-modified, oxidation and hot corrosion resist. 78—11437
Co-Cr-Al-Y protective coating for combustion turbines, hot corrosion evaluation 80—40608
Co-Cr-Al-Y(Hf), high temp. oxidation 78—11432
Co-Cr-C, precipitation of M$_{23}$C$_{6}$, role of dislocations 78—44130
Co-Cr-C eutectic, creep and fatigue crack propag. 78—39859
Co-Cr-C eutectic alloy, thermal conductivity and electric resist. at high temp. 80—103668
Co-Cr-C-Al (39, 2.2, 2 wt.%), directionally solidified eutectic alloy, Larson Miller C const. 79—70162
Co-Cr-Mo (Zr)(Nb)(Ta), eutectic alloys, charact. by melting, oxidation resistance and composition 78—52768
Co-Cr-Mo shoulder prosthesis, wear and fatigue tests 80—26415
Co-Cr-Mo-Ni-Fe-Si-Mn-C, protective coatings by B diffusion, microstruct. and mech. props. 78—11427
Co-Cr-Ni alloy FSX 414, electrochemical corrosion meas. in molten sulphate 79—96178
Co-Cr-Ni superalloy Mar-M509 standard and Mo modified, phase anal. 77—63675
Co-Cr-Ni-Ta-Al-Y (25, 10, 5, 3, 0.5 wt%), exam. of hot corrosion 79—20251
Co-Cr-Ni-TaC, directionally solidified eutectic, mech. props. and sruct., thermal cycling effects *(Russian)* 78—92282
Co-Cr-Ni-W-Ta-C, alloy Mar M-509, TEM exam. of thermal fatigue crack propag. in cast alloy 78—76740
Co-Cr-Ni-W-TaC (15.7, 9.5, 3, 12.77 wt.%) alloy Co50B3W, temperature cycling effect on rupture strength 78—39898
Co-Cr-NiTaC eutectic, directionally solidified, microstructural stability 79—38815
Co-Cr-Nr-TaC eutectic alloys, fatigue, microstructure effects 78—23803
Co-Cr-Si alloy hot corrosion and oxidation expts. for ionic conducting scale 78—11446
Co-Cr-Ta(Al) alloy, high temperature wear resistant coatings, CrO$_{2}$ hardened 79—24677
Co-Cr-W-C, hardfaced coating for high temp. liquid Na service, deposition and wear 77—32724
Co-Cr-W-C, wear-resistant coating alloy, carbide form. and decomp. 77—32711
Co-Cr-WC, corrosion and corrosive wear in sea water 78—92408
Co-Cr-Zr, thermodynamically calculated phase diagram 79—91617
Co-Cr-Zr(Ni), phase diagram calc. 79—1848
Co-Cr(-Al-Y) coatings, hot corrosion resist., ductile-brittle transition 79—24674
Co-Cr(VC)((Ti,V)C)-(Al), eutectic alloy, unidirectional solidification, oxidation and tensile tests 78—52790
Co-Cu, electrodeposited alloy, struct. and physicochem. props. 78—35327
Co-Cu, multilayer α'-phase form. during martensitic transform. *(Russian)* 77—59785
Co-Cu (8 wt.%), X-ray anal. of 126-layer rhombohedral martensite α'-phase 77—44251
Co-Cu-Fe-Ce, mag. characteristics of sintered permanent magnets 78—60312
Co-Cu-Fe-Ce alloys, sintered permanent magnets, mag. characts. 77—43855
Co-Cu-Fe-Sm magnet, microstruct. exam. after ageing, TEM meas. 77—48555
Co-Cu(Al,Si,Zr,Ni,Mo,W) powder based composite, high temp. strength of W reinforcing fibres 79—70021
Co-Cu(Ti)(Fe), neutron radiation stimulated diffusion, electrical resistivity exam. *(Russian)* 79—14959
Co-Fe, dil., effective mag. field at ^{59}Co, impurity conc. depend., spin echo expts. 78—48080
Co-Fe, dil., hyperfine mag. fields, press. effect, Mossbauer meas. 80—71277
Co-Fe, dil., magnetocrystalline anisotropy anomalous temp. depend. 80—71007
Co-Fe, double hexagonal alloys, crystalline and mag. props. *(Japanese)* 79—73132
Co-Fe, film, mag. and hyperfine field exam. of uniaxial anisotropy 77—66391
Co-Fe, internal friction anomalies in spin reorientation temp. range *(Russian)* 80—49299
Co-Fe, morphology and certain props. of α-and η-phase martensite *(Russian)* 77—1838
Co-Fe, soft mag. props. rel. to metallurgical aspects 80—88810
Co-Fe, temp. depend. of asphericity of mag. moment distrib. 77—20538
Co-Fe, transformation matrices, electron diffraction patterns 77—59779
Co-Fe (2.92 to 30.05 wt.%), determination of phase equilibrium diagram *(Japanese)* 78—48374
Co-Fe (30%) effect of annealing on magnetostrictive vibrs. 78—6558
Co-Fe (6 wt.%), magnetic properties, 850 to 1000°C range *(Slovak)* 79—4698
Co-Fe (6.25 wt.) FCC to HCP transform., model and expt. evidence 77—44243
Co-Fe alloy, HCP and DHCP, magnetostriction consts. determ. 78—80184
Co-Fe alloy, Invar characts. 77—1550
Co-Fe alloy, plastic deform. effects on phase comp. *(Russian)* 78—19743
Co-Fe alloy films, magnetostriction and orientation of easy magnetisation axes *(Russian)* 79—19756
Co-Fe alloys, FCC structure, average mag. moment, conc. depend. 78—88099
Co-Fe alloys, mag. anisotropy induced by mag. annealing through to double h.c.p. 77—1552
Co-Fe alloys, transformation induced microstructs. extended total dislocations, TEM study 79—42073
Co-Fe amorphous alloys, high permeability props. *(Japanese)* 77—51927
Co-Fe amorphous alloys, worked, perminvar type mag. hysteresis loop, longit. Kerr effect obs. 80—65958
Co-Fe epitaxial films, singularities of $\gamma \rightarrow \alpha$ transform., X-ray diffr. obs. *(Russian)* 79—52198
Co-Fe-B, amorphous, crystn. and thermal stability 80—107057

cobalt alloys continued
- Co-Fe-B films, amorphous, mag. annealing behaviour 79—73782
- Co-Fe-B sputtered amorphous films, mag. props. and corrosion resist. 79—28567
- Co-Fe-Cr-P-B sputtered amorphous films, mag. props. and corrosion resist. 79—28567
- Co-Fe-Mn, dil. ferromag. alloy, mag. moment, saturation magnetisation meas. 78—64195
- Co-Fe-Nb, heavily cold worked, magnetic hardening 79—20073
- Co-Fe-Nb (12, 3 wt.%), semihard magnetic alloy, relationship between precipitation and coercivity 77—8839
- Co-Fe-Nb alloy, mag. precipitation-hardening and Bloch wall pinning 78—80173
- Co-Fe-Nb alloys, effect of cold working on mag. props., and precipitation morphology 78—39803
- Co-Fe-Nb semihard mag. alloy, mag. precip. hardening 77—8960
- Co-Fe-Nb-Mo, semihard magnetic alloy, magnetic props. 78—95469
- Co-Fe-Ni semi-hard mag. alloy, 3-D Barkhausen effect meas. 77—69623
- Co-Fe-Ni semihard magnetic alloy, directional distrib. of magnetisation changes connected with Barkhausen effect 78—14985
- Co-Fe-Ni-Si-B glasses, soft mag. props. 79—73774
- Co-Fe-P film, ferromag., coercive force meas. 78—10737
- Co-Fe-Si-B, amorphous alloys, substitution effect on mag. props. 79—69695
- Co-Fe-Si-B, decomp. of amorphous state during annealing below recryst. temp., electron microscope study *(Russian)* 80—75164
- Co-Fe-Si-B, ferromag., magneto-optical spectra in amorphous and cryst. states *(Russian)* 80—84749
- Co-Fe-Si-B amorphous alloys, mag. props. 77—16055
- Co-Fe-Ti (12,6 wt.%), semihard permanent magnet, magnetic precipitation hardening 78—52830
- Co-Fe-Ti alloy, precipitation hardened, rel. between struct. and mag. props. 78—95470
- Co-Fe-V-Ni, mag. and mech. props., heat treatment and stress effects 80—60363
- Co-Fe(Ni), magnetic anisotropy induced by magnetic and stress annealing 78—35010
- Co-Fe(Ni)(Cr), liquid, N activity coefficient 77—72699
- Co-Fe(70 wt.%) alloy oxidation, diffusional scale growth at 1200°C 77—16748
- Co-Ga, band model of high temp. magnetism 78—26809
- Co-Ga, binary alloy, small-angle neutron scatt. from superparamag. behaviour 78—19217
- Co-Ga, β' phases, evidence of non-cubic lattice distortions around vacant sites 78—42956
- Co-Ga, ferromag., local configuration studies, neutron scatt. and spin echo NMR 77—63114
- Co-Ga, phase diagrams and cryst. struct., DTA, X-ray diffr. and microprobe anal. *(French)* 79—47660
- Co-Ga, spin glass materials, mag. field dependence of susceptibility peak 80—103840
- Co-Ga alloys, transition metal partially substituted, elec. resist. anomalies 79—38044
- Co-Ga binary system, lattice consts., phase transform *(Chinese)* 80—88108
- Co-Ga β' quenched single crystals, annealing-out of point defects 80—55426
- Co-Ga liquid and solid alloys, elec. resistivity at high temps., partial struct. factors 80—6806
- Co-Ga system, exam. of thermodynamics of α and β' phases 78—71870
- Co-Ga-B, phase diagram, metallographic, X-ray and electron probe anal. 78—92241
- Co-Ga-Mn, small-angle mag. neutron scatt., states of mag. order study rel. to Mn and Fe substitution 79—11292
- Co-Gd, dilute, magnetic annealing effect, induced anisotropy 77—73054
- Co-Gd amorphous film, struct., mag. anisotropy consts., saturation magnetisation *(Russian)* 79—99735
- Co-Gd film, amorphous, prep. conditions influence on supernetwork struct. 77—76709
- Co-Gd film, amorphous, stripe domains and mag. anisotropy by Lorentz microscopy 77—63243
- Co-Gd film, magneto-optic coeff. and refr. index, ellipsometric determ. 80—71501
- Co-Gd-B, rules of cmpd. form. in related systems 79—34010
- Co-Gd-Mo, amorphous film, mag. props., temp. depend. 78—10734
- Co-Gd-Mo amorphous films, resist. and extraordinary Hall effect, thermal annealing effect 80—70852
- Co-Gd-Mo films, sputtered, O effects on mag. props. during annealing 80—89374
- Co-Gd-Mo-Ar film, amorphous, mag. props. 78—80182
- Co-Gd-Mo(Au) film, amorphous Hall effect 77—85347
- Co-Ge, band model of high temp. magnetism 78—26809
- Co-Ge, liq., elec. resist. and thermoelec. power using t matrix approach 77—31988
- Co-Ge, liq. alloy, structure studied by X-ray diffr. *(Russian)* 79—77493
- Co-Ge binary system, phase diagram rel. to that of Ni-Ge *(French)* 80—97463
- Co-Ge eutectic alloys, X-ray spectral investig. of electron struct. 77—44087
- Co-Ge-B, Co rich, phase diagram 77—8800
- Co-H, system, melting temp., effect of H_2 *(Ukrainian)* 79—52153
- Co-Ho film, amorphous, stripe domains and mag. anisotropy by Lorentz microscopy 77—63243
- Co-mischmetall system, phase relations, microstruct., mag. props. 80—104118
- Co-mishmetal-rare earth alloys for high energy permanent magnets, manufacture technology *(Polish)* 80—35132
- Co-Mn, dil., hexagonal hyperfine field at ^{54}Mn, nucl. orientation meas. 79—8057
- Co-Mn, dil., NMR-ON meas., mag. hyperfine splitting const. of ^{52}Mn 78—43651
- Co-Mn, FCC, mictomagnetism, magnetisation and mag. susceptibility meas. 80—60310
- Co-Mn, interdiffusion 77—89595
- Co-Mn, permanent magnetic materials 78—8426
- Co-Mn (0 to 45 wt.%), high temp. oxidation 80—35371
- Co-Mn (10.24 at.%), Mn diffusion, 903-1148°C 77—24427
- Co-Mn (5.22 at.%), Mn diffusion, 868-1200°C, mag. transform. effects 77—24427
- Co-Mn alloys, FCC, mag. moments of Mn atoms 78—76226

cobalt alloys continued
- Co-Mn alloys, ferromagnetic, high field mag. susceptibility meas. 80—75729
- Co-Mn alloys, Nernst-Ettinghausen effect and electrical resistivity *(Russian)* 78—14714
- Co-Mn-Ni-Fe-Si-B amorphous alloys, mag. props., low magnetostriction 80—75832
- β-Co-Mn-Sn Heusler alloy, constitution and magnetic props. *(German)* 79—34009
- Co-Mn-Sn liquid alloy, magnetic props. *(German)* 79—87235
- Co-Mo, sintering, limited solid solubility, peritectic diagram 77—28754
- Co-Mo alloy electrodeposits, codeposited impurities rel. to H_2 permeation, props. 79—19493
- Co-Mo catalyst, Mossbauer spectra 80—7222
- Co-Mo-B metallic glass ribbons, tensile strength, crystn. temp. 80—89173
- Co-Mo-Cr-Si, plasma and detonation coatings, Laves- and carbide-strengthened, comparative props. 78—15562
- Co-Mo-Cr-Si Laves phase, sputter deposited, struct. and wear props. 77—40477
- Co-Nb, dil., NMR-ON meas., mag. hyperfine splitting const. of ^{90}Nb 78—43651
- Co-Nb alloys, segregation of Nb to stacking faults, field ion microscopy investigation 77—8816
- Co-Nb-C, obtained by liq. quenching, superconductivity 80—75699
- Co-Nb(W)(Mo)(Ti)-Si, directionally solidified eutectics 79—61575
- Co-Nd, dilute, magnetic annealing effect, induced anisotropy 77—73054
- Co-Ni, (10 at.%), magnetisation in high mag. field, Arrott-Noakes plot 80—54919
- Co-Ni, deformed and isochronally annealed, positron lifetimes, annihilation at dislocation trapped monovacancy 80—55221
- Co-Ni, dil., effective mag. field at ^{59}Co, impurity conc. depend., spin echo expts. 78—48080
- Co-Ni, electrodeposition, mag. props. *(French)* 78—64488
- Co-Ni, ferromag. film, ion plating prep., coercive force and magnetoresist. 77—12546
- Co-Ni, Hall effect, anomalous, residual coeff. calcs. using coherent pot. method *(Russian)* 80—80249
- Co-Ni, liq., thermoelec. power and elec. resist. meas. 77—51719
- Co-Ni, liquid, solubility of H, 1400 to 1800°C 77—1231
- Co-Ni, magnetic anisotropy induced by mag. annealing and cold rolling, expt. 80—7695
- Co-Ni, magnetic anisotropy induced by mag. annealing and cold rolling, calc. 80—7696
- Co-Ni, magnetocrystalline anisotropy consts. meas., 77-700K 78—43582
- Co-Ni, surface chemical comp. changes due to ionic bombardment *(Russian)* 77—1776
- Co-Ni, temp. depend. of asphericity of mag. moment distrib. 77—20538
- Co-Ni (0.45 to 7.23 wt.%) theoretical analysis of cation distrib. in (Co, Ni)O scale 77—12747
- Co-Ni (32 wt.%), FCC, rolling texture development 79—87657
- Co-Ni (33 wt.%), FCC deform. twinning kinetics, relationship to stress-strain behaviour 78—52887
- Co-Ni (5 to 95 at.%), paramag. props., 800-1800°C *(Russian)* 77—55660
- Co-Ni alloy, electrodeposition of cylindrical thin films 80—29886
- Co-Ni alloy, slip charact., and fatigue, FCC twinning and FCC to HCP martensite transform. effect 80—35182
- Co-Ni alloy surfaces, oxidation, APS 79—87755
- Co-Ni alloys, electrodeposited, struct., internal stress, and mag. props. 78—95471
- Co-Ni alloys, electropolishing in alcoholic soln. of H_2SO_4 77—16718
- Co-Ni fine particles, anhysteretic growth of exchange fixed remanent states 77—16116
- Co-Ni/steel/Co-Ni three layer composite, high strength with increased damping capacity 77—1850
- Co-Ni-Cr (20,20 wt.%), internal oxidation, improvement of mech. props. *(French)* 77—16521
- Co-Ni-Cr superalloys, γ'-precipitation-strengthened, yielding 77—8894
- Co-Ni-Cr-Al-Ta, S-57 alloy hot corrosion, cyclic oxidation, depth of attack determinations 80—11837
- Co-Ni-Cr-B, centrifugally cast metallurgical coatings for wear resistance in plastics molding machines 79—29285
- Co-Ni-Cr-B, X-306 centrifugally cast cylinder lining alloy, compatibility with hardfacing alloys 77—32726
- Co-Ni-Cr-C, carbide precipitation 79—29065
- Co-Ni-Cr-Mo, hip joint anchorage stem, superior fatigue strength, high corrosion resist. 79—29671
- Co-Ni-Cr-Mo, mech. props., effect of twinning and FCC to HCP transform. 77—4779
- Co-Ni-Cr-Mo (35, 20, 10 wt.%), MP35N, TEM study of phase transformations 80—81054
- Co-Ni-Cr-Nb, effect of Fe addition on precipitation behaviour 80—29962
- Co-Ni-Cr-Nb (40, 18, 1.8 wt.%), precipitation behaviour of NbC, effect of ageing temp. on morphology 80—89227
- Co-Ni-Cr-Nb FCC alloy, electron microscope obs. of deform. twins 79—60380
- Co-Ni-Cr-Ta-C (10, 10, 14, 1 wt.%), aligned eutectic, directionally solidified, fatigue crack propag. 78—27624
- Co-Ni-Cr-W-Fe, HA-188 alloy, hot corrosion, cyclic oxidation, depth of attack determinations 80—11837
- Co-Ni-Fe, metallic glasses, mag. props. *(German)* 79—51813
- Co-Ni-Fe, semi-hard magnet, irreversible magnetisation changes, directional distrib. 79—24196
- Co-Ni-Fe-Si(B), amorphous ribbon, magnetostriction meas. 80—15778
- Co-Ni-Mo-C, amorphous alloys, med. props. and thermal stability *(Japanese)* 80—85049
- Co-Ni-P, film, props. independent of mag. hysteretic and anhysteretic remanences *(French)* 80—2604
- Co-Ni-P electrolytic layers, partial anhysteretic remanent magnetisation, additivity prop. *(French)* 80—44882
- Co-Ni-Zn, diagram of state, crystalline lattice consts., microhardness *(Russian)* 80—66479
- Co-Ni(Ti)(Cu)(Mn), cryst. struct. and stacking fault influence on mag. props. *(Russian)* 80—25164
- Co-Os, short-range order parameters, ordering energy on first coordination sphere *(Russian)* 79—69058
- Co-P, amorphous, domain struct., mag. anisotropy origin 80—80554
- Co-P, amorphous, electrical transport 79—38040
- Co-P, amorphous, ferromag. antireson. 24 GHz microwave transmission, mag. props. 80—34778

cobalt alloys continued

- Co-P, amorphous, sound propagation 77—62586
- Co-P, amorphous alloy, domain struct., effect of annealing 78—60304
- Co-P, amorphous electrodeposited films, domain wall motion, Kerr effect 78—60322
- Co-P, amorphous electrodeposited foils, struct. characterisation by X-ray scatt. 79—77932
- Co-P, amorphous foil, complex permeability and eddy currents, annealing induced short-range order 77—8360
- Co-P, coating onto $BaFe_{12}O_{19}$, $SrFe_{12}O_{19}$ and WC 80—25593
- Co-P, cryst. and amorphous mag. films, ferromag. resonance line width *(Russian)* 78—88192
- Co-P, electrodeposited alloys, heat-induced structural changes *(Japanese)* 80—89263
- Co-P, electrodeposited amorphous alloy, mag. permeability 78—52310
- Co-P, electrodeposited amorphous alloys with high permeability, thermal treatment with and without field 80—89372
- Co-P, metallic glass, phonon propagation at low temp. 78—87756
- Co-P alloys, geometric struct. models and diffraction exam. techniques 80—79700
- Co-P amorphous alloy, domain struct. 78—10720
- Co-P amorphous alloy, ferromagnetic reson. exam. 79—28620
- Co-P amorphous alloy, mag. props. 78—10724
- Co-P amorphous alloy film, mag. domain struct. 77—69604
- Co-P amorphous alloys, electrodeposited, magnetic anisotropy 79—28568
- Co-P amorphous alloys, electrodeposited, mag. anisotropy 80—15713
- Co-P amorphous film, domain struct., influence of planar anisotropy 79—78472
- Co-P electroless film on Al base disc substrate, microstruct. rel. to mag. props. 78—68304
- Co-P film, amorphous, spin wave dispersion law, spin wave reson. obs. *(Russian)* 78—88196
- Co-P films, electrodeposited, magnetic recording media *(Japanese)* 80—29587
- Co-P films with various preferred orientations, mag. props. 80—100604
- Co-P grains, mag. props. *(French)* 79—33510
- Co-P metallic glasses, crystn. kinetics by differential scanning calorimetry 78—91257
- Co-Pd, transfer phenomena and association with electronic struct. *(Russian)* 79—91017
- Co-Pd alloys, 0-70 at.% Pd, conc. depend. of anomalous Hall field and resistivity *(Russian)* 78—14713
- Co-Pr, dilute, magnetic annealing effect, induced anisotropy 77—73054
- Co-Pt, amplitude depend. of internal friction *(Polish)* 79—95627
- Co-Pt, atomic ordering props. and domain growth in strong pulsed mag. field *(Russian)* 80—54918
- Co-Pt, films, electrolytic deposition conditions over large comp. range *(French)* 80—45242
- Co-Pt, mag. annealing, form. of ordered phase, study using X-ray scatt. *(Russian)* 80—81052
- Co-Pt, struct. and mag. props. rel. to degree of order 78—72368
- Co-Pt ferromagnetic alloy, 6 T ultrasonic study of magnetoelastic coupling 80—93154
- Co-Pt film, electrodeposited, saturation mag. induction, mag. anisotropy and coercive field meas. *(French)* 80—2610
- Co-Pt films, mag. and magneto-optic props., appl. to holographic and bit-by-bit storage 79—33512
- Co-Pu, metastable, high rate sputter deposition, annealing behaviour of deposits 77—21025
- Co-rare earth dilute alloys, mag. annealing, conc. depend. 78—35011
- Co-rare earth magnets testing method for mag. parameters 79—49260
- Co-Re, sputtered film, high coercivity and high hysteresis loop squareness 79—91259
- Co-Re sputtered films, mag. props. and microstructures 79—82837
- Co-Ru, dil., mag. hyperfine fields, TDPAC meas. 78—43702
- Co-Se, P-T diagram and structural study 78—56622
- Co-Si, band model of high temp. magnetism 78—26809
- Co-Si, directionally solidified eutectic composite alloy, form. and strength 77—90294
- Co-Si, liquid alloy, optical charact. *(Russian)* 77—24810
- Co-Si, surface physicochemical state, Auger electron spectroscopy study 80—100715
- Co-Si alloy, secondary ion mass spectrometry *(Dutch)* 79—1809
- Co-Si film system, diffusion marker expts. 78—79824
- Co-Si film system, interaction kinetics 78—79823
- Co-Si-B, amorphous ribbon, saturation magnetostriction meas. by small-angle magnetisation rot. 80—60391
- Co-Si-B, embrittlement by crystallisation *(Japanese)* 78—48513
- Co-Si-B amorphous alloys with metalloid elements, embrittlement/crystn. relationship *(Japanese)* 79—96134
- Co-Si-B-Fe alloy magnet, Al_2O_3 particle embedded surface, amorphous mag. anal. using electron diffr. 79—56568
- Co-Si-B-Fe amorphous alloy, electron diffr., mag. anal. *(German)* 79—61182
- Co-Si-Ge system, X-ray diffr. exam., band struct. *(Russian)* 78—56623
- Co-Si-Nb(Zr), eutectic alloys, charact. by melting, oxidation resistance and composition 78—52768
- Co-Sm, dilute, magnetic annealing effect, induced anisotropy 77—73054
- Co-Sm film, magneto-optic coeff. and refr. index, ellipsometric determ. 80—71501
- Co-Sm magnets, H_2 atm. sintering effect on mag. props. 77—85504
- Co-Sm permanent magnet, grain alignment determ., metallographic method using eutectoid transform. of Co_5Sm 77—9003
- Co-Sm-Cu, phase diagram 79—91632
- Co-Sm-Gd(Ho) magnets, prep. and characterisation 77—8351
- Co-Sm-Sn-$Co_{17}Sm_2$ eutectic fibre composite, coercive force 77—40084
- Co-Sn, dil., ferromag., temp. anomalies of Sn mag. hyperfine field and thermal expansion 79—33270
- Co-Sn, dil., hyperfine field, press. depend., Mossbauer spectra meas. 79—95375
- Co-Sn, electroplated, oxide films, XPS/AES expts. 79—15862
- Co-Sn (Sb), dilute ferromagnetic alloy, resistivity and magnetoresist. anisotropy 79—11106
- Co-Sn system, phase Co_3Sn obtained by splat cooling *(German)* 80—104147
- Co-Sn-M, n=Mg, Ca, Sr, Sc, Y, Zn, Cd, In or Th, cryst. growth and cryst.-chem. invest, supercond./mag. ternary cpds. 80—100777
- Co-Tb film, magneto-optic coeff. and refr. index, ellipsometric determ. 80—71501
- Co-Ti, dilute, internal oxidation 77—31810
- Co-Ti, multilayer and imperfect martensitic phases form. 78—19754

cobalt alloys continued

- Co-Ti (22 at.%), amorphous eutectic phase 80—55360
- Co-Ti (9 at.%), decomp. kinetics, elec. resist., hardness, and saturation magnetisation during ageing *(Russian)* 80—50587
- Co-Ti alloys, martensitic transformation depend. on ageing, cryst. struct. 79—91649
- Co-Ti-C, secondary precipitation and allotropic transform., TEM obs. 80—108453
- Co-Ti-Fe (3, 1 to 2 wt.%), spinodal decomposition 80—100839
- Co-Ti(Hf)(Ta)(Mo)(Zr)(Al)(Fe)(Ni), dendritic segregation 80—76260
- Co-transition metal, transition metal additives influence on struct., specific resistance, microhardness, mech. props., magnetic props. 79—29078
- Co-V, Co rich, ferromag. behaviour, mag. moments, Curie temp., and NMR spectrum 80—70964
- Co-V, ferromag. struct. in nucl. spin echoes 80—60453
- Co-V, solid and liq., mag. susceptibility and electronic struct. 80—39738
- Co-V (10 to 23 wt.%) system, phase constitution, X-ray and elec. resist. meas. 80—3007
- Co-V (12.4-18.7 at.%), ferromag. behaviour 79—24163
- Co-V (20.7 wt.%), cryst. struct., electron and X-ray diffr. study 80—44172
- Co-V alloy system, Co rich, low temp. phase, electron microscopy 77—84766
- Co-VC (12 wt.%), directionally solidified eutectic, oxidation 80—11821
- Co-W alloy electrodeposition, influence of $MgSO_4$ and gum arabic additives *(Russian)* 80—80991
- Co-W alloy electrolytic coatings, heat treatment effects on coercivity, hysteresis and structure *(Russian)* 80—60381
- Co-W-C system, η-carbide linear expansion coeff., X-ray diffr., 30-1500°C 77—25021
- Co-W-C system at 1150°C, phase equilibria, isothermal reactions and thermodynamic study 78—31385
- Co-W-Cr (15,20 wt.%), surgical implant ion beam textured, stress/strain relations, fatigue characts. 78—73297
- Co-WC, corrosion and corrosive wear in sea water 78—92408
- Co-WC, protective coatings by B diffusion, microstruct. and mech. props. 78—11427
- Co-WC dispersion hardened alloy, tensile deform., volume fraction of second phase effect, simulation *(Japanese)* 79—70122
- Co-WC hard alloys, rapidly quenched struct. 80—76233
- Co-W(Mo) magnetic alloys for high temp. appl. 77—85503
- Co-W(25 wt.%), cellular decomposition, third element effects *(Russian)* 77—1837
- Co-X-Co (X=Cr,Mo,W) systems, crystn. temp. and hardness 79—77529
- γ-Co-Zn, inversion antiphase domains, formation and stabilisation, electron conc. effect 78—14363
- Co-Zn, physical-chemical metallurgy *(German)* 80—108390
- γ-Co-Zn, struct. obs. 77—24290
- Co-Zn melt, Zn activity determ. *(German)* 78—19715
- Co-Zr, amorphous phase form. in Zr-poor region, hardness and fracture strength *(Japanese)* 80—84914
- Co-Zr, dil., mag. annealing effect, depend. of uniaxial mag. anisotropy on Zr conc. 80—39772
- Co-Zr-Er alloys, mag. annealing effect, effect of Er on induced uniaxial mag. anisotropy 80—39771
- Co_2-rare earths, H_2 reaction, thermal anal. 79—100434
- (Co-Ni)-$Cr_{23}C_6$ eutectic alloy, directionally soldified, microstruct. and crystallography 78—48390
- CoAl, bonding, self-consistent energy bands 78—91610
- CoAl, compositional depend. of oxidation rates 79—8393
- CoAl, electronic struct., cluster calc. 77—69209
- CoAl, X-ray spectra, electronic structure 79—78793
- $Co_{1-x}Al_x$, ordered β-phase, enthalpy of formation are defect struct. descript. 80—89519
- $Co_{49.6}Al_{50.4}$, Compton scatt., 59.54 keV γ-rays, charge transfer study 78—68578
- $Co_{1-x}Au_x$, amorphous, elec. resist., temp. depend., spin wave contrib. and resist. minimum 78—51961
- CoB and Co_2B, electrochem. behaviour in H_2SO_4 79—39030
- $Co_{0.8}B_{0.2}$ alloy amorphous thin films, anisotropic mag. and microstruct. props. 78—95487
- $Co_{1-x}B_x$ amorphous film, crystn., TEM obs. 79—87019
- $Co_{1-x}B_x$, polycrystalline and amorphous sputtered films, Brillouin spectra 80—2775
- $Co_{100-x}B_x$, amorphous, mag. struct., mag. susceptibility meas. 80—80485
- $Co_{100-x}B_x$, amorphous alloys, saturation magnetostriction and annealing behaviour 80—34739
- $Co_{100-x}B_x$ glassy alloys, mag. props. 79—73689
- Co_3B, crystalline, photoemission and electronic struct. 80—2926
- Co_3B, glassy and cryst., hyperfine field distrib., ^{59}Co spin echo spectra 80—80635
- $Co_{80}B_{20}$, amorphous metal ribbon, stresses, magnetoelastic anisotropy and zero-field mag. domain struct. 80—44896
- Co(Cr,Ni)-TaC fibrous eutectic, deformed, thermal stability of microstruct. *(Russian)* 79—1895
- CoCr, dil., low temp. specific heat and magnetisation 80—65925
- CoCrAl alloy, Al_2O_3 forming, oxidation resistance improvement by dispersed oxide addition 79—83379
- CoCrAl-Y(HF), Y and HF effects on oxidative behaviour 78—44275
- CoCrMo, artificial hip joints, fatigue strength 79—48375
- $(Co_{0.83}Cu_{0.17})_6Ce$, cryst. struct. and mag. props., decomp. during ageing *(Russian)* 79—37661
- Co_4CuCe, cryst. struct., mag. characts., ageing and decomposition *(Russian)* 79—4272
- $Co_4CuCe_{0.9}$, correl. of cryst. struct. and coercive force *(Russian)* 77—80962
- $Co_{35}Dy_{65}$, metallic glass, internal friction peaks 80—25753
- $Co_{67}Er_{33}$ amorphous alloy, sputtered, local order and amorphous struct. 80—88061
- $Co_{0.91}Fe_{0.09}$, X-ray scatt. factor 79—41907
- $Co_{0.92}Fe_{0.08}$, lattice dynamics by neutron scatt., FCC phase 77—51463
- $Co_{0.92}Fe_{0.08}$, phonon dispersion and Debye temp. temp. depend., neutron inelastic scatt. 79—33047
- $(Co_{1-x}Fe_x)$-B-Si, amorphous, mag. props. *(Japanese)* 77—85433
- $Co_{92}Fe_8$, FCC, electronic struct., ang. correlation of positron annihilation γ-quanta, meas. 80—10864
- Co_xFe_{1-x}, ferromagnetism and spatial long-range order 80—60159
- $Co_{74}Fe_6B_{20}$, metallic glass, zero magnetostriction, magnetisation characts. 77—12158
- $Co_{79}Fe_{6.5}B_{14.5}$ amorphous thin films, zero magnetostriction, high magnetisation 80—34708

cobalt alloys continued
- $(CoFeB)_{100-x}Cr_x$ thin films, magnetic props. and corrosion resist. 80−34709
- $(Co_{0.93}Fe_{0.07})_{75-x}Cr_xSi_{15}B_{10}$ amorphous alloy, thermal stability, Cr conc. effects, DTA expts. 80−59395
- Co_2FeGa, alloy, site preference of Co and Fe, Mossbauer and neutron study 79−78577
- $(Co_xFe_{1-x})_5Ge_3$, Mossbauer investig. of hyperfine field at Fe nuclei 77−20776
- $(Co_{0.89}Fe_{0.11})_{72}Mo_3Si_{15}B_{10}$, metallic glass, strain- and field-induced mag. anisotropy 80−108004
- $Co_{57}Fe_5Ni_{10}(Si,B)_{28}$, amorphous, soft mag. props., switched-mode power supply appls. 80−88850
- $(Co_{1-x}Fe_xNi_y)_{80}(Si_{1-z}B_z)_{20}$, amorphous films, spin wave spectra 80−34777
- $Co_{1-x}Fe_xSi$, solid solution, optical props. 78−72556
- $Co_{70}Fe_5Si_{15}B_{10}$, amorphous, crystn. and thermal stability 80−107057
- $Co_{70.4}Fe_{4.6}Si_{15}B_{10}$, amorphous, mag. aftereffect spectra and annealing props. 80−88831
- $Co_{75-x}Fe_xSi_{15}B_{10}$, quenched ferromag. ribbon, Brillouin spectra 80−2776
- $(Co_{1-x}Fe_x)_2Y$, substitutional Fe atoms effect on mag. and elec. props., paramagnon scatt. 77−36054
- β-CoGa, Cu addition effects on defect struct. *(German)* 77−11546
- CoGa, defect struct. model 79−46648
- CoGa, diffusion coeffs. of ^{60}Co, 800-1050°C 77−84966
- CoGa, onset of ferromag., diffuse mag. neutron scatt. meas. 77−63113
- CoGa, ordered electronic cpd., self-diffusion of ^{60}Co and ^{72}Ga 79−65238
- $Co_{0.54}Ga_{0.46}$, frequency depend. magnetisation, superparamagnetic behaviour 80−84624
- β-$Co_{52}Ga_{48}$, negative TCR obs. 80−75543
- $Co_{54}Ga_{46}$, superparamag. response to low DC fields 80−44860
- $Co_{56}Ga_{44}$, thermal release of injected He 77−31881
- Co_xGa_{1-x} alloys, cluster spin glass, host and impurity NMR and AC susceptibility 80−71194
- Co_xGa_{1-x}, β-phase, spin glass behaviour 80−44837
- Co_xGa_{1-x}, cluster spin glass, AC susceptibility in DC mag. fields, 77 to 500K 80−34670
- Co_xGa_{1-x}, NMR expts. interpretation 80−75870
- Co_xGa_{100-x}, electrical resistivity anomaly, spin cluster model 79−99531
- $Co_2Ga_{2-x}Cr_x$, ferromag., local configurational studies, neutron scatt. and spin echo NMR 77−63114
- $Co_2Ga_{2-x}Cr_x$, ferromag., site selecting and moment distrib. 77−77031
- $Co_2Ga_{2-x}Cu_x$, mag. and struct. phases from magnetisation, neutron, X-ray diffr. techniques 78−52253
- $Co_2Ga_{1.95}Fe_{0.05}$, mag. behaviour, Mossbauer effect and DC magnetisation meas. 80−50244
- $Co_2Ga_{2-x}Fe_x$, elec. resist., temp. and mag. field depend., mag. contrib. 80−96846
- $Co_2Ga_{2-x}Fe_x$, mag. field depend. of resist., 5.80K 80−70676
- $Co_2Ga_{2-x}M_x$ (M=V, Cr, Mn, Fe), mag. props. and order 77−12093
- $Co_2Ga_{2-x}Ni_x$, mag. and struct. phases from magnetisation, neutron, X-ray diffr. techniques 78−52253
- Co(GaTiV) alloys, ferromag. onset, electron conc. depend. 80−60203
- $Co_2Ga_{2-x}V_x$, ferromag., local configuration studies, neutron scatt. and spin echo NMR 77−63114
- $Co_2Ga_{2-x}V_x$, ferromag., site selectivity and moment distrib. 77−77031
- CoGd, H_2 and N_2 contaminated amorphous films, mag. props. 79−1690
- CoGe and TiCoGe, electronic struct., X-ray K- and L-spectra obs. *(Russian)* 78−11022
- CoGe, Co_2Ge and $CoGe_2$, X-ray spectrum analysis, energy band struct. *(Ukrainian)* 77−52200
- CoGe, vacancy conc. in B2 phase exhibiting triple defects 79−42058
- Co_2Ge_3, $CoGe_2$, amorphous film, annealing effects on struct. and elec. resist. 77−85099
- Co_5Ge_3 amorphous film, elec. resist., microstruct. and annealing 77−85188
- Co_5Ge_3, phase and struct. characts. 77−36450
- Co_5Ge_3, solid and liquid, physicochemical props. and structure 80−39548
- Co_2HfAl, Heusler alloy, paramag. state NMR and susceptibility meas. 79−65643
- Co_2HfAl, hyperfine fields of Fe impurities, Mossbauer spectra 80−71255
- Co_2HfSn-Fe, dil., Heusler alloy, Fe hyperfine fields, Mossbauer obs. 78−68424
- $Co_2HfSn(Al)$, ferromag., hyperfine fields meas. by NMR 77−63315
- $CoIn_3$, ordered phase, cryst. struct. determ. 78−2066
- CoIr, mag. susceptibility 77-500K *(Russian)* 77−80911
- $(Co_{1-x}M_x)B$, M=Mn or Fe, paramag., spin echo NMR spectra, ferromag. transition, spin-lattice relax. 80−29645
- $(Co_{1-x}M_x)B$, M=Mn or Fe, ferromag., internal fields meas. by NMR spin echo 80−29646
- Co_xMM, (MM+mischmetal), coercive force, effect of preparation conditions 78−95467
- $Co_{1-x}M_xSi$ (M=Fe, Ni), elec. field gradient, quadrupole splitting of ^{59}Co 80−29641
- CoMn, dil., low temp. specific heat and magnetisation 80−65925
- $CoMn_3$, mag. susceptibility, 77-500K *(Russian)* 77−80911
- $(Co_{1-x}Mn_x)_2B$, magnetocrystalline anisotropy meas., 4.2-300K 80−71006
- $Co_2Mn_xFe_{1-x}M$, (M=Ga,Ge,Si,Sn), hyperfine fields of Fe impurities, Mossbauer effect meas. 78−31130
- $Co_{50}Mn_xGa_{50-x}$, cryst. struct. transform. of B2 type *(German)* 79−91642
- $Co_{50}Mn_xGa_{50-x}$, ordering and disordering phenomena, mag. study 80−70154
- CoMnP, cryst. mag. struct., neutron diffr. study *(French)* 80−59439
- CoMnP, ferromagnetism and metamagnetism, polarized neutron diffr. study 80−44809
- CoMnSi, $CoMnSi_{0.85}Ge_{0.15}$, mag. props. 79−42758
- Co_2MnSi, ferromag. Heusler alloy, spin echo NMR meas. 77−63319
- $Co_3Mn_3Si_2$, Curie-Weiss law depend. of susceptibility, mag. props. *(Russian)* 79−65655
- $CoMnSi_{1-x}Ge_x$, amg. props. 80−60270
- $Co_{73}Mo_2Si_{15}B_{10}$, metallic glass, strain- and field-induced mag. anisotropy 80−108004
- Co_2Nb, mag. susceptibility, 77-500K *(Russian)* 77−80911
- Co_2NbSn, ferromag., hyperfine fields meas. by NMR 77−63315
- $Co_{2-x}(Ni,Fe)_xTiSn$, Heusler alloy, positive contribs. to hyperfine fields, magnetisation and NMR meas. 78−43654
- $Co_{0.65}Ni_{0.35}$, precursory phonon obs. of FCC to HCP transition 78−43082

cobalt alloys continued
- $Co_{20}Ni_{80}$, oxidation study by Auger electron spectroscopy *(Ukrainian)* 80−7711
- $Co_{1-x}Ni_xAl$, Knight shift and mag. susceptibility study, electron struct. peculiarities *(Russian)* 80−15814
- CoNiB, corrosion-resistant amorphous mag. thin films 80−54923
- $Co_{40}Ni_{40}B_{20}$, magnetostriction, temp. depend. 78−91921
- $Co_{40}Ni_{40}B_{20}$, spontaneous Hall effect and resistivity 79−19576
- CoNiCrMo, artificial hip joints, fatigue strength 79−48375
- $Co_{50}Ni_{20}Fe_6Si_{12}B_{12}$, amorphous, mag. props., effects mech. deform. 80−39840
- CoNiP, cylindrical amorphous electrodeposited layers, mag. props., torsion influence 80−88848
- CoNiP film, amorphous electrolytic, prep. and magnetic props. *(Slovak)* 79−51823
- $(Co_{1-x}Ni_x)_{75}(PBAl)_{25}$, amorphous, high-field magnetoresist. meas. 80−34423
- $Co_{1-x}Ni_xSi$, IR refl. spectra in plasma refl. region 78−27233
- $Co_{1-x}Ni_xSi$, solid solution optical props. 78−72556
- $Co_{2-x}Ni_xTiSn$, mag. ordering, ^{119}Sn Mossbauer spectroscopy and magnetisation meas. 78−43753
- CoP amorphous alloy, heat treatments influence on opt. props., struct. and DC resist. obs. 80−80892
- CoP, cylindrical amorphous electrodeposited layers, mag. props., torsion influence 80−88848
- CoP metallic glasses, elec. and optical props., annealing effects 79−38565
- $Co_{1-x}P_x$ amorphous alloy film, elec. resistance, temp. depend. *(Russian)* 80−103660
- $Co_{1-x}P_x$ glass, crystn., spin wave reson. 79−73104
- Co_2P, struct. comparison with Co_2Si, $PbCl_2$, and SbSI *(French)* 80−84155
- $Co_{35}P_{15}$, amorphous, strip domains, anisotropy const. effects 80−29571
- Co_4P, amorphous, mag. excitations and static struct., neutron scatt. obs. 78−68204
- Co_4P, amorphous ferromag., mag. excitations calc. in Heisenberg model 77−1546
- $Co_{80}P_{20}$, amorphous, sign and magnitude of ^{60}Co hyperfine field, nucl. orientation 78−48100
- $Co_{80}P_{20}$ glass, mag. props. 77−63125
- $Co_{82}P_{18}$, amorphous alloys, electronic struct., γ-ray Compton scatt. study *(Japanese)* 80−84422
- $Co_{78}P_{14}B_8$, amorphous, photoemission and electronic struct. 80−2926
- CoPd, single crysts., domain struct., temp. and field depend. 80−71085
- Co_3Pd epitaxial films, multiray dynamic theory of diffr. contrast to explain defects nature 79−64962
- Co_3Pd film, ordered, stacking fault obs. by TEM and interpret. using many-beam theory 80−107680
- $Co_xPd_{80-x}Si_{20}$, amorphous, low field susceptibility near transition temp. 77−66359
- $Co_xPd_{80-x}Si_{20}$, amorphous, structural and mag. heterogeneities 80−80484
- CoPr, coercive force variation as function of annealing temp. *(Japanese)* 79−47787
- CoPt film, on Al_2O_3, quantitative electron microprobe analysis 77−9150
- $CoPt_3$, electrolytic films, saturation mag. induction, coercive fields, thickness depend. *(French)* 80−44883
- $CoPt_3$, meas. of ordering instability 79−38818
- Co_5R-H(D) system, R=rare earth, mag. orientation aftereffect 80−50148
- CoSb alloys, sp. ht. and thermal expansion 77−47587
- CoSb, at. struct. and mag. susceptibility 77−39561
- CoSi, and TiCoSi, electronic struct., X-ray K- and L-spectra obs. *(Russian)* 78−11022
- CoSi, electronic struct. determ. by XPS and X-ray emission spectra 77−85147
- CoSi, IR refl. spectra in plasma refl. region 78−27233
- CoSi, NMR and μSR, microscopic mag. props. *(Japanese)* 78−52368
- CoSi, plasma refl., 80 to 300K, energy overlap of valence and conduction bands 79−28366
- CoSi solid solution, optical props. 78−72556
- CoSi, X-ray emission spectra obs. of valence band states *(Ukrainian)* 77−69935
- Co_2Si, struct. comparison with Co_2P, $PbCl_2$, and SbSI *(French)* 80−84155
- Co_2Si-Si, CoSi-Si, and $CoSi_2$-Si interfaces, chemical state, AES expts. 78−91767
- $Co_{74}Si_{10}B_{16}$ amorphous toroidal core, switching characts. and domain structs. 78−95477
- $Co_{74}Si_{10}B_{16}$, amorphous ferromagnetic alloy, isothermal annealing effect on static magnetic props. *(Japanese)* 79−52398
- $Co_{75}Si_{15}B_{10}$, amorphous, crystallisation study *(Japanese)* 78−9959
- $Co_{75}Si_{15}B_{10}$, amorphous, crystn. and thermal stability 80−107057
- $Co_{75}Si_{25-x}B_x$ glass, mag. moment, Curie temp., and microhardness, metalloid comp. depend. 77−55665
- Co_5Sm, coercive field of hard mag. materials, planar defect influence 77−24710
- Co_5Sm, coercive field temp. depend. 77−8358
- Co_5Sm, coercive force variation as function of annealing temp. *(Japanese)* 79−47787
- Co_5Sm crystals, microstruct., homogeneous precip. and nucleation 80−104160
- Co_5Sm, magnetic domains, nucleation and pinning, magneto-optical Kerr effect 80−39811
- Co_5Sm sintered magnet, effect of surface conditions on mag. props. 79−28556
- Co_2Sn, intermetallic phase, obtained by splat cooling *(German)* 80−104147
- Co_2Ta, mag. susceptibility, 77-500K *(Russian)* 77−80911
- $Co_2(Ti,Mn)Sn$, Heusler alloy, mag. meas. 79−47261
- CoTi, dil., low temp. specific heat and magnetisation 80−65925
- $Co_{1-x}Ti_x$, ferromag. props., Ti conc. effect 80−54872
- Co_2Ti, mag. susceptibility, 77-500K *(Russian)* 77−80911
- Co_3Ti, electron energy spectrum calcs. by supplementary plane wave method 80−6711
- $CoTi_{1-x}Al_x$, form. of mag. moment of Co atom, X-ray diffr., mag. meas. and NMR 77−43819
- $CoTi_{1-x}Al_x$, mag. and electronic props., ferromag. and paramag. state 80−65814
- Co_2TiAl, ^{59}Co NMR, above and below Curie temp. 78−2760

cobalt alloys continued
Co$_2$TiAl, Heusler alloy, paramag. state NMR and susceptibility meas. 79–65643
Co$_2$TiAl, hyperfine fields of Fe impurities, Mossbauer spectra 80–71255
Co$_2$TiSn, Heusler alloy, positive contribs. to hyperfine fields, magnetisation and NMR meas. 78–43654
Co$_2$TiSn-Fe, dil., Heusler alloy, Fe hyperfine fields, Mossbauer obs. 78–68424
Co$_2$TiSn(Al), ferromag., hyperfine fields meas. by NMR 77–63315
Co$_2$Ti(Y)(Zr)(Nb), Laves phase, elec. resist. rel. to mag. props. 77–59282
CoV, dil., low temp. specific heat and magnetisation 80–65925
CoV, phase dependent MNR spectra 80–108114
Co$_2$VAl, hyperfine fields of Fe impurities, Mossbauer spectra 80–71255
Co$_2$VAl(Ga), ferromag., hyperfine fields meas. by NMR 77–63315
Co$_2$VGa, ferromag. Heusler alloy, spin echo NMR meas. 77–63319
Co$_{35}$Y$_{65}$, metallic glass, internal friction peaks 80–25753
CoZn β- and γ-intermetallic compounds, thermodynamics *(German)* 78–92242
Co$_2$Zr, CoZr$_2$, and CoZr$_3$, mag. susceptibility 77-500K *(Russian)* 77–80911
Co$_{90}$Zr$_{10}$, ferromag. amorphous alloy, crystn. and domain struct. study 80–107056
Co$_2$ZrAl, Heusler alloy, paramag. state NMR and susceptibility meas. 79–65643
Co$_2$ZrSn-Fe, dil., Heusler alloy, Fe hyperfine fields, Mossbauer obs. 78–68424
Co$_2$ZrSn(Al), ferromag., hyperfine fields meas. by NMR 77–63315
Cr-Co, dil., antiferromag., elec. resist. min., press. and impurity effects 80–59970
Cr-Co, dil., exchange interactions 77–47986
Cr-Co, dil., Neel temp., impurity conc. depend. calc. 78–68232
Cr-Co, dil., with local mag. moments, Neel temps. 79–73713
Cr-Co, magnetic transformations, triple point *(Russian)* 80–88747
Cr-Co, phase transformations and magnetostriction *(Russian)* 80–103869
Cr-Co, spin density wave, neutron diffraction studies 79–1664
Cr-Co (4 wt.%) alloy, antiferromag. transitions effect on opt. props. 77–12371
Cr-Co (4.0 at.%) alloy, antiferromag., disappearance of resist. min. under press., and press. coeff. of T_N 80–10960
Cr-Co (up to 8 at.%), antiferromagnetic, resist. minimum, Kondo effect by pairs of Co atoms 80–39566
Cr-Co-Fe, chromindur alloy, field heat treatment, and mag. props. 80–35354
Cr-Co-Fe, for telephone receiver mag. use 80–45318
Cr-Co-Fe, low Co, phase separation, TEM and Mossbauer spectra obs. 80–71269
Cr-Co-Fe cold formable mag. alloys for use in telephone receiver 79–52227
Cr-Co-Fe permanent magnet anisotropic alloys, plastic deform., ageing, particle alignment temp. 80–35254
Cr-Co-Ga, phase equilibria diagrams at 800 and 600°C *(Ukrainian)* 78–92236
Cr-Co-Ni hard film on Mo substrate for magnetic recording 80–2608
Cr-Co-V alloys, dil., elec. resist. min. 80–54680
Cr-Fe-Co dilute alloys, Neel temp., thermal expansion rel. to Co content 79–47281
Cr-Mo-Co, dil., behaviour of mag. impurities 79–4672
CrCo, dil., low temp. specific heat meas., 1.5 to 4K 80–60328
Cr$_{1-x}$Mo$_x$Co, $x \lesssim 0.25$, antiferromag., nucl. mag. relax. 78–6590
Cr$_{1-x}$V$_x$Co, localised mag. moment of Co impurity 78–27014
Cr$_{1-x}$V$_x$Co, mag. state of Co impurity, NMR exam. 78–27100
Cr$_{1-x}$V$_x$Co, $x \lesssim 0.05$, antiferromag., nucl. mag. relax. 78–6590
Cu-Al-Co, precipitate-free zones near grain boundaries, growth kinetics, TEM obs. 80–40368
Cu-Al-Co liquid alloys, constant Co-content of 5 wt.%, mag. props. *(German)* 80–88720
Cu-Al-Si-Co (2.8, 1.8, 0.4 wt.%), superplastic phase, exam. of mech. props. 78–52891
Cu-Be-Co, cuboid (Co, Cu, Ni, Fe)Be inclusions, metallography, ageing effects 80–11645
Cu-Be-Co, discontinuous reaction, analytical TEM 80–100842
Cu-Be-Co (1.8, 0.2 wt.%), TEM obs. of precipitates, ageing charact. *(Korean)* 77–66648
Cu-Be-Co (2,0.3 wt.%) alloy, heat treatment, influence of tempering on hardness, tensile props. transform diagram *(French)* 78–31384
Cu-Be-Co(0.1,0.2 wt.%), discontinuous precipitation *(Japanese)* 80–55402
Cu-BeCo (1.85, 0.29 wt.%), type CA172 (TH04), strengthened by spinodal decomp., stress relax. in bending 80–7616
Cu-Co, (1-1.3 at.%), elec. cond. exam. in solid and liquid phase *(Russian)* 77–62895
Cu-Co, age hardenable single crystal., fatigue and fatigue cracks *(German)* 77–16689
Cu-Co, dil., binding and caging of impurities and trapped interstitials 78–39462
Cu-Co, dil., Kondo system, host NMR exam. 78–80246
Cu-Co, dil., valence and core level spectra, XPS study 80–84838
Cu-Co, dil. mag. alloy, NMR of ^{63}Cu around impurities 77–16187
Cu-Co, Kondo system, NMR, spin-lattice relax., impurity spin dynamics 77–69724
Cu-Co, liquid, surface tension *(Japanese)* 79–19431
Cu-Co, solid soln., mag. susceptibility near solubility boundary *(Russian)* 79–15281
Cu-Co, superparamagnetic, mag. aftereffects, dynamic neutron depolarisation study 80–50147
Cu-Co, thermoelectric power, precipitation effects *(German)* 77–85200
Cu-Co, time of flight atom probe, quantitative microanal., metallurgical appl. 80–86498
Cu-Co (1.5 and 4 wt.%), coherent Co-rich separations obs. by positron annihilation *(Russian)* 80–89082
Cu-Co (2 at.%), age hardened, stage I fatigue crack propag. 78–3203
Cu-Co (2 wt.%), single crysts., fatigued age-hardenable, dislocation structure *(German)* 80–54247
Cu-Co (2.48 wt.%), two-phase, surface meas. study of grain boundary sliding during creep 77–81299
Cu-Co alloy, ageing and reversion phenomena 79–91718
Cu-Co single cryst., precip. hardening *(German)* 80–84946
Cu-Co superparamagnetic particles, macrospin glass form. *(Russian)* 80–25165

cobalt alloys continued
Cu-Co-Fe, dil. alloy, low temp. resistivity maxima *(Russian)* 79–87091
Cu-Co-O system, distrib. of Co between Cu and Cu$_2$O *(Russian)* 77–16540
Cu-Co-S system, phase equilibria determ. by silica tube techniques 79 -60482
Cu-Co-Si (0.36, 0.11 wt.%), surface layer struct. on annealing, SIMS and AES exam. 80–88415
Cu-Ni-Co, alloy pre-form prep. through reduction of sintered oxides 80–40284
Cu-Ni-Co, mag. props. of system of disperse ferromag. particles, 73 to 673K *(Russian)* 80–65968
(Cu-Au)-Co, single crysts., solid soln. and particle strengthening, superposition 80–97495
Cu$_3$Au-Co, dil., LRO 78–18584
Cu$_3$Au-Co, single crystal, overaging mechanism 79–20081
Cu$_3$Au-Co, underaged, ordered and disordered single crystal, hardening mechanisms 78–3134
Cu$_3$Au-Co single cryst., precip. hardening *(German)* 80–84946
Dy-Co amorphous film, prep. by dual-source evaporation, mag. props. 77–89988
Dy(Co,Ni)$_2$, intrinsic mag. aftereffect obs. 77–63237
Dy(Co,Ni)$_2$, intrinsic mag. aftereffect meas., domain wall motion 80–71121
DyCo$_2$, field induced vol. magnetostriction 78–91920
DyCo$_2$, H$_2$ absorpt., Mossbauer study 80–44987
DyCo$_2$, magnetocryst. anisotropy props. by ^{57}Fe Mossbauer spectroscopy 77–63328
DyCo$_2$-DyAl$_2$ system, mag. and structural studies 80–108006
DyCo$_3$, amorphous, mag. struct. and moments 77–66260
DyCo$_3$, mag. and quad. interactions, Mossbauer spectra 77–12267
DyCo$_3$, X-ray absorpt. edge shifts 80–25483
DyCo$_{3.4}$, amorphous, mag. props. 77–32177
DyCo$_5$, rotational type spin reorientation, collinear to canted spin struct. change 77–63214
DyCo$_{5.3}$ noncollinear mag. struct. appearance in mag. fields, magnetostriction meas. *(Russian)* 80–100607
Dy$_{0.25}$Co$_{0.75}$ film, amorphous, displacement of mag. compensation temp. by elastic stress *(Russian)* 78–19284
Dy$_2$Co$_{17}$, and Y$_{2x}$Dy$_{2(1-x)}$Co$_{17}$, magnetocryst. anisotropy, 77-383K 77–89949
Dy$_2$Co$_{17}$, domain wall behaviour, TEM expts. 77–4524
Dy$_2$Co$_{17}$, hyperfine interactions and cryst. field effects, Mossbauer spectra 80–2369
Dy$_4$Co$_3$, cryst. field effect on mag. moment direction, neutron diffr. meas. 78–80132
DyCo$_2$Si$_2$, Mossbauer spectra 80–20558
Dy$_2$(Fe,Co)$_{17}$, mag. anisotropy fields by singular pt. detection 79–24156
Dy$_2$(Fe,Co)$_{17}$, magnetic anisotropy meas. by singular point detection method 77–63170
Dy$_2$(Fe$_{1-x}$Co$_x$)$_{17}$, hyperfine interactions, Mossbauer spectra 78–2780
Er-Co-Ni, cryst. struct. and H$_2$ capacity 77–89543
Er-Fe-Co, cryst. struct. and H$_2$ capacity 77–89543
ErCo$_2$, amorphous, mag. correlations, neutron exam. 79–73682
ErCo$_2$, amorphous, mag. correlations, neutron exam. 79–73683
ErCo$_2$, field induced vol. magnetostriction 78–91920
ErCo$_2$, mag. excitation spectrum, neutron inelastic scatt. obs. 79–78351
ErCo$_2$, mag. excitations, RPA theory 80–65830
ErCo$_2$, magnetocryst. anisotropy props. by ^{57}Fe Mossbauer spectroscopy 77–63328
ErCo$_3$, absorption of H$_2$, 77-300K 79–23737
ErCo$_3$, ErCo$_6$ and Er$_2$Co$_{17}$, Kerr effect determ. of domain structure, Bloch wall energy 80–39805
ErCo$_{5.6}$, easy magnetisation direction 78–84415
ErCo$_6$, domain wall grooving due to mech. polishing 79–70232
ErCo$_x$, sorption at press. up to 1500 atm. 80–97819
Er$_2$Co$_{17}$, domain wall grooving due to mech. polishing 79–70232
Er$_2$Co$_{17}$, magnetisation, magnetocryst. anisotropy and magnetostriction 77–8303
Er$_2$Co$_{17}$, single cryst., magnetostriction const. temp. depend., 78 to 300K 79–51836
Er$_4$Co$_3$, cryst. field effect on mag. moment direction, neutron diffr. meas. 78–80132
Er$_{65}$Co$_{35}$, amorphous, amg. ordering, susceptibility, magnetisation and hysteresis meas. 78–68190
ErCo$_3$B$_2$, ferromag. ordering and saturation moments 77–24711
(ErCo$_2$)$_x$(ErAl$_2$)$_{1-x}$, mag. and struct. investigations of intermetallic systems 78–95440
Er$_2$(Co$_{1-x}$Fe$_x$)$_{17}$, mag. anisotropy and intersublattice exchange interactions 78–31066
Er$_2$Co$_{17-x}$Fe$_x$(Mn$_x$)(Ni$_x$), saturation magnetisation, Curie temp., easy direction, and anisotropy field 77–8304
Er$_2$Co$_{17-x}$M, M=Fe, Mn, Ni, magnetisation, Curie temp., anisotropy 77–89947
Er$_2$Co$_{17-x}$M$_x$, M=Cr, Ni, effect of substitution on mag. props. 79–78363
ErCo$_{5-x}$Ni$_x$ ferrimagnetic series, magnetisation, coercive field meas. 78–91896
Er$_2$(Co$_{1-x}$Ni$_x$)$_{17}$, mag. anisotropy and intersublattice exchange interactions 78–31066
Er(Fe$_{1-x}$Co$_x$)$_3$, spin reorientation, easy axis of magnetisation 80–25144
Er$_2$Fe$_3$Co$_{14}$, Kerr effect determ. of domain structure, Bloch wall energy 80–39805
(Fe,Co,Ni)-Si(B), amorphous mag. alloy, magnetostriction rel. to soft mag. props. 80–84633
(Fe, Co, Ni)$_3$V, control of ordered struct. and ductility 80–21029
(Fe,Co)PBAl, metallic glass, viscous flow, alloying effect 78–79793
(Fe, Ni, Co)-Si-B, amorphous, compositional effect on struct. changes, after heating up to 700°C, exam. *(Japanese)* 78–48433
(Fe,Ni,Co)$_3$V, long-range ordered alloy for fusion reactor appl. 80–32481
Fe-Al-Co-Ni, Alnico alloys, irreversible remagnetisation processes in rotating fields *(Russian)* 79–8015
Fe-Al-Ni-Co-Cu alloys, Ti alloying and deoxidising addition *(Russian)* 78–80181
α-Fe-Be(P)(Mo)(W)-Co, effect of Co on solubility anomaly due to mag. transition *(Japanese)* 79–42257
Fe-C-Co, eutectoid alloy, Co addition effects on pearlite growth rate 77–16575
Fe-Ci, powder mixture, effect of granulometric distrib. on importance of Kirkendall effect during calcination *(French)* 77–11721

cobalt alloys continued
Fe-Co, 3d ferromagnet nuclear spin-lattice relaxation 80—80627
Fe-Co, amorphous alloy, stress effect on mag. domain struct. 79—33502
Fe-Co, annealing of point defects produced by plastic deform. *(French)* 78—72829
Fe-Co, atomic ordering phenomena, neutron diffr. obs. *(Russian)* 77—81254
Fe-Co, atomic valence states, ferromag. props. *(Ukrainian)* 78—2656
Fe-Co, BCC, ferromag., high-field susceptibility 80—7083
Fe-Co, BCC, ferromag., spin wave stiffness constant 78—91851
Fe-Co, compositional diffusionally bonded alloy, mass transfer investigation *(Russian)* 80—39342
Fe-Co, damping capacity of Gentalloy, internal friction meas., mech. and mag. depend. *(Japanese)* 78—52875
Fe-Co, determ. of chem. and magnetic interchange energies 77—80925
Fe-Co, dil., ensemble rotation concept in NMR on oriented nuclei 77—90061
Fe-Co, dil., film, NMR spin echo, rel. to struct. inhomogeneities *(Russian)* 80—29644
Fe-Co, dil., high freq. induction melting and centrifugal casting, working curve sample prep. photoemission anal. *(Japanese)* 78—53050
Fe-Co, dil., Mossbauer source, self-absorption effects *(French)* 79—24246
Fe-Co, electrodeposit, struct. *(Russian)* 79—56079
Fe-Co, electron energy spectrum calc. by Green function method *(Russian)* 77—35860
Fe-Co, electron state density and elec. resist. 80—39558
Fe-Co, equiatomic, atomic order, Mossbauer study *(French)* 78—27135
Fe-Co, ferromagnetic micropowder, cryst. struct., coercivity, remanence, saturation 80—65967
Fe-Co, film, magnetisation induced uniaxial anisotropy, dislocations effects 78—43618
Fe-Co, free enthalpy data, thermodynamic activity determ. at 1500K 77—59751
Fe-Co, Hall effect, anomalous, residual coeff. calcs. using coherent pot. method *(Russian)* 80—80249
Fe-Co, hyperfine field, variation with atomic order 79—7953
Fe-Co, hyperfine field distrib., temp. and press. depend. 78—91651
Fe-Co, isothermal compression and BCC→HCP phase transition, up to 300 kbar, at room temp. 77—90346
Fe-Co, liq., X-ray diffr., struct. determ. *(Russian)* 77—80409
Fe-Co, liquid, activity meas. by transportation method *(Japanese)* 79—4949
Fe-Co, local environment effect on atomic moments, itinerant model 78—68188
Fe-Co, local environment effect on at. mag. moment 79—82763
Fe-Co, long range order, neutron powder diffr. meas. 79—42243
Fe-Co, M_s calc. 77—8824
Fe-Co, mag. moment of Cr and Mn atoms, polarised neutron scattering 79—11290
Fe-Co, magnetised, circ. polarised γ-ray Rayleigh scatt., spin depend. 77—59637
Fe-Co, mech. behaviour in microplastic strain region *(Russian)* 78—39838
Fe-Co, Mossbauer investig. of order-disorder and α-γ transitions 77—48110
Fe-Co, order-disorder transformation, metallography, ordering kinetics 80—3026
Fe-Co, partially ordered, elec. cond. 78—91663
Fe-Co, solid and liq., paramag. susceptibility and electron struct., 800-1800°C *(Russian)* 80—25081
Fe-Co, surface comp. and surface segregation 80—34280
Fe-Co, surface excitations 80—25179
Fe-Co (25-35%), ordering, Cr addition effects, Mossbauer expts. *(Russian)* 78—19741
Fe-Co (30-70 at.%), order-disorder transition, comp. depend., neutron diffr. expts. 78—15393
Fe-Co (33 wt.%), oxidation and domain structure, electron microscope exam. *(Russian)* 79—1437
Fe-Co (35 wt.% and 52 wt.%), heat treated, decrease in sensitivity of mag. props. to mech. stresses *(Russian)* 78—56363
Fe-Co (46%) film, evaporated, uniaxial mag. anisotropy 77—51929
Fe-Co (5 to 25 wt.%), exam. of damping capacity of Gentalloy 78—72800
Fe-Co alloy, diffusion of H_2, diffusion coefficient and permeability *(Russian)* 78—79819
Fe-Co alloy, electrodeposited, comp. and struct. effects on H_2 diffusion and evolution overpot. 77—43377
Fe-Co alloy, optical characts., 0.073-4.92 eV, quantum absorption 79—56814
Fe-Co alloy, order-disorder and α-γ transitions 77—25042
Fe-Co alloy, V addition effect on atomic order parameters, dislocation struct., mechanical props. 79—91762
Fe-Co alloy particles for mag. tapes, mag. props. 78—95479
Fe-Co alloy ring samples, force fitting effect on mag. props. 77—40083
Fe-Co alloys, optical and spectrosc. props. *(Russian)* 78—72529
Fe-Co amorphous ribbon, mag. props. in low fields 79—73777
Fe-Co and Fe-Co-Ni, liquid, solubility of H, 1400 to 1800°C 77—1231
Fe-Co based alloys, redistrib. of elements, combined appl. of emission and absorption Mossbauer spectroscopy *(Russian)* 78—6031
Fe-Co based alloys (52KF, 35KKh, 35KFN), effect of heat treatment and mech. working, on sensitivity of mag. props. to mech. stresses *(Russian)* 79—34161
Fe-Co based amorphous alloys, mag. props. *(Japanese)* 79—95971
Fe-Co film, magnetisation induced uniaxial anisotropy 77—48016
Fe-Co films, optical props. order-disorder transformation influence, absorpt. band existence *(Russian)* 79—65942
Fe-Co films, ordered and disordered, Mossbauer study 79—24241
Fe-Co heterogeneous alloys, fabrication by powder metallurgy, tensile strength 77—63600
Fe-Co melt, volumetric characts., molar volume conc. depend. density *(Russian)* 80—33873
Fe-Co ordered alloys, enthalpy of form. 78—48376
Fe-Co-Al-Cu-Ti (40, 14, 7.5, 4.5 wt.%), metastable equilibrium, high coercive state *(Russian)* 80—66476
Fe-Co-B, amorphous, crystn. 80—79704
Fe-Co-B, metallic glass, Mossbauer investigation of electronic struct. 78—92009
Fe-Co-B powders, synthesis and mag. props., appl. to mag. recording 80—20432

cobalt alloys continued
Fe-Co-C (0.8 wt.%), unidirectional transformation process per struct. relationship, pearlite interlammellar spacing meas. 77—70045
Fe-Co-C-B, amorphous, room-temp. saturation induction 78—95476
Fe-Co-C(0.8 wt.%), unidirectional transformation, eutectoid reaction kinetics 77—70029
Fe-Co-Cd(Sn), mag. hyperfine fields at Fe, Cd and Sn sites, Mossbauer and TDPAC meas. 78—60363
Fe-Co-Cr, 25KKh15 alloy, nuclear γ-reson. investig. of atomic redistrib. during annealing *(Russian)* 77—12640
Fe-Co-Cr, alloy K25Kh15, phase tranforms., nucl. gamma reson. and X-ray diffr. meas. *(Russian)* 77—44241
Fe-Co-Cr, atomic mag. moment, magnetisation, Mossbauer spectra and NMR spin echo spectra 77—63127
Fe-Co-Cr, Cr effect on struct. *(Russian)* 78—27535
Fe-Co-Cr, Cr effect on struct. of ordering 78—35407
Fe-Co-Cr, heats of form. adiabatic calorimeter determ. 78—35713
Fe-Co-Cr, magnetic, phase transform. obs. *(French)* 79—47676
Fe-Co-Cr, solid state phase equilib., isothermal sections determ. 800-1300°C 79—91623
Fe-Co-Cr (27, 0.5 wt.%), internal stress and brittleness in ordered state *(Russian)* 79—61698
Fe-Co-Cr (50, 0.4 wt.%), ordering and recrystallisation 79—34029
Fe-Co-Cr film RF sputtering for magnetic recording 80—2947
Fe-Co-Cr-Mo (20, 15, 5 wt.%), maraging, stainless alloy fracture toughness 77—73326
Fe-Co-Cr-Si, structural transform. and mag. props. following heat treatment *(Russian)* 77—81274
Fe-Co-Mn, BCC, atomic mag. moment, magnetisation, Mossbauer spectra and NMR spin echo spectra 77—63127
Fe-Co-Mn, BCC, mag. state of Mn, NMR and saturation magnetisation meas. 78—39442
Fe-Co-Mn, dil. alloys, NMR freq. temp. depend., spin echo meas. 78—64296
Fe-Co-Mn and Fe-Cr-Co, BCC, atomic mag. moments determ. 77—59396
Fe-Co-Mo, phase relations in system at 1100°C 80—108392
Fe-Co-Mo ternary system, phase diagram *(Russian)* 80—16269
Fe-Co-Mo-C, amorphous alloys, med. props. and thermal stability *(Japanese)* 80—85049
Fe-Co-Mo-Nb(Ta) semihard mag. alloy, mag. props., thermal expansion, elec. resistivity and hardness *(Japanese)* 80—88789
Fe-Co-Ni, at. mag. moments, neutron scatt. and Mossbauer meas. 79—42744
Fe-Co-Ni Perminvar, mag. props. singularities in region of mag. anisotropy *(Russian)* 80—84614
Fe-Co-Ni powder, video recording appl. *(Russian)* 77—55910
Fe-Co-Ni-Al, Si alloying of mag. hard alloys *(Russian)* 79—73765
Fe-Co-Ni-Al (35, 14.5, 7.2 wt.%), high-coercivity, substructure and texture change during bending and upsetting 80—21037
Fe-Co-Ni-Al-Cu, polycryst. hard mag., C diffusion 79—77827
Fe-Co-Ni-Al-Nb (15-20, 14, 9, 0.1-5.5 at.%), Nb effect on magnetic props., lattice parameter *(Russian)* 77—55689
Fe-Co-Ni-Al-Zr magnetically hard alloys, reduction *(Russian)* 78—43614
Fe-Co-Ni-C, activity coeff. of C at 1273K 80—96667
Fe-Co-Ni-Si-B amorphous alloy, magnetostriction and permeability, effect of annealing 79—1701
Fe-Co-Ni-W alloy, 45KKhVN, plastic deform., electron microscope obs. *(Russian)* 78—80584
Fe-Co-P-C amorphous alloys, mag. props. 77—16055
Fe-Co-Si, BCC solid soln. interchange energies, high temp. neutron diffr. 80—29166
Fe-Co-Si (4,1.5 wt.%), textured, mag. props. 80—35200
Fe-Co-Si solid solutions, BCC, atomic configs., Mossbauer study 80—39006
Fe-Co-Si-B, amorphous, rapidly quenched, mag. heads appl. *(Japanese)* 80—54922
Fe-Co-Si-B, amorphous soft ferromagnet with high mag. induction 80—84619
Fe-Co-Si-B, zero magnetostrictive amorphous alloy with high saturation induction, mag. annealing 80—60362
Fe-Co-Si-B sputtered amorphous thin film, coercivity, galvanomagnetic props., resistivity 80—29578
Fe-Co-Si(B), amorphous ferromagnet, mag. after effect on soft mag. props. 80—84626
Fe-Co-Ta for semipermanent magnets *(French)* 79—47675
Fe-Co-Ti-Al alloy type YuNDK magnets, metallographic method of distinguishing cracks 80—85096
Fe-Co-Ti(V)(Cr)(Mn), sp. ht. in ordered and disordered phases 80—71061
Fe-Co-V, anelastic phenomena, related to atomic order, exam. of magnetostriction *(French)* 78—80579
Fe-Co-V, neutron irradiated, damage rates 79—77646
Fe-Co-V, ordered and disordered, dynamic ageing *(French)* 80—16355
Fe-Co-V, Vicalloy, $\alpha \rightarrow \gamma$ transform. under plastic deform., morphological singularities *(Russian)* 77—32576
Fe-Co-V, Vicalloy, magnetisation reversal by stretching and twisting 80—34733
Fe-Co-V, Vicalloy 1, γ-phase morphology and structural inheritance depend. on heating rate *(Russian)* 79—70059
Fe-Co-V (2 wt.%), gamma phase 77—36514
Fe-Co-V (2%), annealing of point defects produced by plastic deform. *(French)* 78—72829
Fe-Co-V (33, 33 at.%), BCC β phase, high temp. creep, existence of master curve 80—55473
Fe-Co-V alloy, Remendur, heat treatment effects on mech. and struct. props. 77—8846
Fe-Co-V alloys, effect of V on struct., electron diffr. and Mossbauer meas. *(Russian)* 77—77507
Fe-Co-V wire for high-speed matrix printers, wear resistivity obs. *(Japanese)* 80—55540
Fe-Co-V-Cr alloys, struct. transform., appl. of mag., thermomag. methods *(French)* 79—20318
Fe-Co-V(-Ni), annealing effect on microstruct. rel. to mag. and mech. props. 80—89267
Fe-Co-V(2%) alloy, correl. of resistivity with microstructure 78—72896
Fe-Co-W-C steel, M_6C carbide behaviour during ht. treatment *(Russian)* 77—66658
Fe-Co-X alloys, semihard wires, creeping magnetisation reversal 77—16106

cobalt alloys continued
Fe-Co-2 V, (49, 2 wt.%), solid soln., rheological study of crystallographic order on creep *(French)* 80—97548
Fe-Co(-V), neutron irradiated, influence of dislocation doping on recovery 79—46715
Fe-Co(-V), plastic flow, order-disorder transform. effect on creep, traction and relaxation *(French)* 80—35180
Fe-Cr-Ce, decomposition of solid soln. in mag. field, neutron and X-ray diffr. study *(Russian)* 78—68694
Fe-Cr-Co, anisotropic, spinel type permanent magnet, magnetic aftereffect 77—16118
Fe-Cr-Co, ductile magnet alloys, mech. props. 80—85001
Fe-Cr-Co, effect of heat treatment on strain gauge factor 78—72802
Fe-Cr-Co, elastic props. anisotropy at room temp. *(Russian)* 80—89279
Fe-Cr-Co, heat treatment effect on strain gauge factor *(Japanese)* 78—6954
Fe-Cr-Co, mag. alloys, Mossbauer spectra 78—19386
Fe-Cr-Co, mag. props., heat treatment effects *(Russian)* 78—39365
Fe-Cr-Co, mag. props. of ductile permanent ductile alloys *(Chinese)* 79—19746
Fe-Cr-Co, magnetic domain walls, Lorentz microscopy 80—103854
Fe-Cr-Co, mechanism of coercive force 80—34674
Fe-Cr-Co, metallic magnets investigation, present state *(Polish)* 80—107987
Fe-Cr-Co, permanent magnet, temp. effect 80—34701
Fe-Cr-Co, spinodally decomposed magnetic alloy, magnetic flux temp. coeff. *(Japanese)* 78—35006
Fe-Cr-Co (31 wt.%, 23 wt.%), microstruct. and mag. props., ageing and thermomag. treatment effects 78—76769
Fe-Cr-Co alloy, coercive force mechanism 80—71103
Fe-Cr-Co alloy, Mossbauer exam. of spinodal decomposition 77—69742
Fe-Cr-Co alloy, spinodally decomposed, micro-twinning 80—92537
Fe-Cr-Co alloys, (5-9 wt.% Co), obtained by slow cooling under mag. field, permanent magnet props. 80—75797
Fe-Cr-Co alloys, permanent magnet material development 78—91895
Fe-Cr-Co alloys, permanent magnets, magnetic props. and heat treatment *(Russian)* 79—91809
Fe-Cr-Co ductile magnet, with high $(BH)_{max}$, processing, mag. props., and microstruct. 77—8957
Fe-Cr-Co ductile magnet alloys, phase diagram and mag. props., V or V+Ti addition effects 77—8959
Fe-Cr-Co hard-mag. alloys, fine cryst. struct. *(Russian)* 77—66706
Fe-Cr-Co martensite, ordering and segregation *(Russian)* 79—20052
Fe-Cr-Co permanent magnet system, miscibility gap, microstruct. and mag. props. obs. 80—76228
Fe-Cr-Co phase diagram, lamination region, resist. meas. *(Russian)* 78—27479
Fe-Cr-Co-Al (27.5, 17.5, 0.5) alloy, magnetic props. and microstructure 78—72367
Fe-Cr-Co-Al (27.5, 17.5, 0.5 wt.%) alloy, induced anisotropy 78—76239
Fe-Cr-Co-Al(V)-(Nb)(Ti), phase equilib., X-ray diffr. meas. *(Russian)* 79—47658
Fe-Cr-Co-Mo, melted in open induction furnace, microstruct. and magnetic props. 79—61626
Fe-Cr-Co-Mo, microstruct., hardness, mag. props., influence of isothermal tempering and heat treatment 79—79129
Fe-Cr-Co-Mo alloys, struct. transform. and mag. props. *(Russian)* 77—76543
Fe-Cr-Co-Mo high energy permanent magnets, mag. props. 80—97119
Fe-Cr-Co-Si alloy, interaction domains after heat treatment in mag. fields *(Russian)* 78—68286
Fe-Cr-Co-V alloy, microstruct. and mag. props. 78—68221
Fe-Cr-Co-V-(Ti) hard magnets, V and V-Ti effects on mag. and mech. props. 79—91810
Fe-Mn-Co, mag. contribs. to $\gamma \to \varepsilon$ phase transforms 80—25694
Fe-Mn-Co-Ni-Cr, antiferromag. props., Neel temp. determ. 78—88124
Fe-Nb(Ta)-Co, Recalloys, semihard mag. alloys, mag. and elec. props., hardness, thermal expansion *(Japanese)* 79—5066
Fe-Ni-Al-Co-Cr-Ti, YuNDK35T5BA, exam. of hypodissociation process *(Russian)* 79—11547
Fe-Ni-Al-Co-Cu alloy, sintered single-crystal mag. prod., props. 77—66709
Fe-Ni-Al-Co-Cu-Sn alloy YuNDK35T5, Sn addition effects on physicomechanical and magnetic props. and workability *(Russian)* 77—70101
Fe-Ni-Al-Co-Cu-Ti, 38 to 40 wt.% Co, 8 to 8.5 wt.% Ti, alloy YuNDKT tempering and thermomagnetic treatments 78—3154
Fe-Ni-Al-Co-Cu-Ti alloy YuNDKT, nature of X-phase heat treatment effect on microstruct. 77—90380
Fe-Ni-Al-Co-Cu-Ti magnetic alloy electrolytic treatment with programmed pulse current *(Russian)* 79—100282
Fe-Ni-Al-Co-Cu-Ti YuNDK type, S effect on mech. props. 80—60927
Fe-Ni-Al-Co-Ti base alloys, highly coercive, phase comp., Mossbauer meas. 80—39996
Fe-Ni-Co, diffusion controlled phase growth 78—30782
Fe-Ni-Co, magnetic permeability, effect of ion implantation 77—28414
Fe-Ni-Co, phase diagram redeterm., Fe-rich portion 77—44219
Fe-Ni-Co, rel. between induced uniaxial anisotropy and coercive force 78—91904
Fe-Ni-Co, texture form. after cold working and annealing *(German)* 80—3089
Fe-Ni-Co alloy components, dynamics of arrival to arc discharge during roasting *(Russian)* 77—16895
Fe-Ni-Co alloys, struct., appl. of mag., thermomag. methods *(French)* 79—20318
Fe-Ni-Co base alloys, composition changes during electron radiation melting *(Russian)* 78—19718
Fe-Ni-Co coating electrodeposition optimum conditions *(Russian)* 79—83292
Fe-Ni-Co film, electron-nucl. mag. reson. 78—35063
Fe-Ni-Co foils, mag. reversals of mag. domains in low-coercivity channels *(Russian)* 79—42813
Fe-Ni-Co-B-C-Si, amorphous, room-temp. saturation induction 78—95476
Fe-Ni-Co-B-P soft magnetic metallic glasses, status report 78—64226
Fe-Ni-Co-C, substruct. effect in mech. props. 80—30086
Fe-Ni-Co-C (29.6, 10.7, 0.009 wt.%), thermal stabilisation role in martensitic transformations 80—25697
Fe-Ni-Co-Cu-Ti YuNDKT alloys, impaired mag. props. with C and S additions 80—60368
Fe-Ni-Co-Mo alloys, struct. transform. produced during tempering 77—86058

cobalt alloys continued
Fe-Ni-Co-Mo phase diagram and structure *(Russian)* 80—20899
Fe-Ni-Co-Mo-Ge alloy 40NKM, excess mag. noise after various thermomag. treatments *(Russian)* 80—29575
Fe-Ni-Co-Ta alloys, Co effect on martensite ageing at 300-600°C *(Russian)* 80—20972
Fe-Ni-Co-Ti, coherent particles effect inherited by martensite on $\alpha \dashrightarrow \gamma$ transformation *(Russian)* 80—108443
Fe-Ni-Co-Ti, martensite cryst. lattice tetragonality, $\gamma \rightleftharpoons \alpha$ transform. *(Russian)* 79—61587
Fe-Ni-Co-Ti, shape memory effect after appl. of bending moment *(Russian)* 80—45305
Fe-Ni-Co-V, effects on fusion reactor neutronics performance 80—47705
Fe-Ni-Co-W(Mo) (18.65, 8.99, 4.87 wt.%), ageing characts., 380-530°C 80—60876
Fe-Ni-Si-Mn-Co-Mo, effect of prolonged aging on mag. props. 80—16513
Fe-Ni-V-Co, Co influence on age hardening *(Russian)* 78—68703
Fe-Ni-V-Co, lattice parameter variation during ageing *(Russian)* 78—39812
Fe-Sb-Co, dil., interactions and precip., Mossbauer study 80—39997
Fe-Sb-Co, interactions and segregations, Mossbauer and X-ray diffr. study 80—70415
Fe-Si-Al sendust type alloys, Co preferred substitution sites, Mossbauer spectra 79—91328
Fe-W-Cr-Mo-Co (18,12,3,x wt.%) magnetisation and hardness, cold working effect obs. *(Japanese)* 77—40428
Fe-W-Cr-Mo-Co with austenitic phase, magnetic and mech. props., cold working and ageing effects *(Japanese)* 78—60678
$(Fe\text{-}Co\text{-}Ni)_{78}Si_8B_{14}$, amorphous, low coercivity and zero magnetostriction 78—23299
FeCo, BCC alloy, order-disorder transform., three-body interaction effects 80—39257
FeCo disordered alloys, Mossbauer spectra, hyperfine mag. field distrib., Curie temp. 80—7198
FeCo, electronic structures, order effect 79—90938
FeCo, ferromag., surface spin waves, cluster Bethe lattice approach 80—70983
FeCo, isothermal annealing effect on lattice const. *(Japanese)* 79—20076
FeCo molecules, matrix-isolation Mossbauer spectra 80—23448
FeCo, neutron irradiated, damage rates 79—77646
FeCo, ordered alloy, 550°C change, study through elec. cond. and specific heat meas. 78—56633
FeCo, ordered and disordered alloy, annealing of point defects created by neutron irrad. at 20K *(French)* 79—1467
FeCo, planar faults, faint electron microscopic image contrast obs. 80—107283
$(Fe_{0.06}Co_{0.94})$-B, amorphous, ferromag., mag. instability rel. to struct. 79—99729
$Fe_{50}Co_{50}$, disordering by laser irradiation, Mossbauer transmission spectroscopy and electron microscopy study *(French)* 79—23639
$Fe_{50}Co_{50}$, neutron irradiation, close pair recombination *(French)* 80—39162
$Fe_{68}Co_{32}$, ferromagnet, magnon heat cond. and lifetimes, 1-2 to 4.5K 77—16066
$Fe_{1-x}Co_xAl$, Knight shift and mag. susceptibility study, electron struct. peculiarities *(Russian)* 80—15814
$Fe_{3-x}Co_xAl$, site preference and local environment effects, Mossbauer and NMR meas. 80—71264
FeCoB, corrosion-resistant amorphous mag. thin films 80—54923
$(FeCo)_{80}B_{20}$, glass, elastic consts. 79—83249
$(FeCo)_{80}B_{20}$ glass, magnetisation, Curie and crystn. temps. 79—87289
$(FeCo)_{80}B_{20}$, metallic glass, saturation moments and Curie temp. 77—1542
$(Fe_{0.5}Co_{0.5})_{1-x}B_x$, amorphous, hyperfine fields and local mag. moments, Mossbauer study 80—75895
$(Fe_{0.65}Co_{0.35})B$, crystalline disordered, evaluation of complex Mossbauer spectra 78—43755
$Fe_{0.65}Co_{0.35}B$, crystalline disordered, evaluation of complex Mossbauer spectra 78—60370
$Fe_5Co_{75}B_{20}$, amorphous, magnetisation reversal and domain boundary configs. 80—88809
$Fe_{71}Co_9B_{20}$, glassy ribbon, magnetostatic effects 79—73790
$Fe_{73}Co_{10}B_{17}$, two amorphous phases form. and crystallisation 79—27924
$Fe_{80-x}Co_xB_{20}$, ferromag. metallic glass saturation magnetostriction meas. 77—36108
$Fe_{80-x}Co_xB_{20}$, spontaneous Hall effect and resistivity 79—19576
$Fe_xCo_{80-x}B_{20}$, amorphous, mag. after-effect 79—61189
$Fe_{35}Co_{32}B_{20}Si_{10}Al_3$, stress-induced variation in magnetisation and dynamic magnetostrictive charact. 80—88855
FeCoC, unidirectionally transformed eutectoid, crystallography of herringbone pearlite, TEM obs. 78—31399
$Fe_{0.5}Co_{0.5-x}Cr_x$ films, vacuum-deposited cryst. and mag. struct. *(Russian)* 80—93081
$(Fe_{0.07}Co_{0.93})_{75-x}Cr_xSi_{15}B_{10}$, amorphous, disaccommodation of mag. permeability and induced anisotropy 80—88741
Fe_2CoGa, alloy, site preference of Co and Fe, Mossbauer and neutron study 79—78577
$(FeCoNi)_8B_{20}$, glass, evidence supporting split-band model from magnetostriction 78—95509
$(Fe_xCo_yNi_{1-x-y})_{78}Si_8Bi_{14}$ amorphous ribbons, saturation magnetostriction and vol. magnetostriction 77—85538
$(Fe_{0.2}Co_{0.8})_{80}P_{17}Al_3$, Mossbauer spectra, isomer shift, mag. hyperfine field 80—11301
$(Fe_{100-x}Co_x)_{79}P_{13}B_8$, amorphous, hyperfine field distrib., ^{59}Co NMR spin-echo meas. 80—34818
$(Fe_{1-x}Co_x)_yPBAl$ metallic glasses, influence of composition and ageing on Curie temps. 77—85445
$(Fe_{1-x}Co_x)_{80}P_{13}C_7$ amorphous alloy, soft mag. material, props. 77—4533
$(Fe_{1-x}Co_x)_{78}S_{10}B_{12}$, amorphous, Hall effect and magnetoresist. *(Japanese)* 77—85199
$FeCo_2Si$, Heusler type materials, mag. props. 77—40042
$(Fe_{0.5}Co_{0.5})Si$, weak itinerant ferromag., polarised neutron scatt. exam. 77—4503
$Fe_{1-x}Co_xSi$, mag. props., sp. ht., n.m.r. and Mossbauer effect meas. 77—12129
Fe_2CoSi, Heusler type materials, mag. props. 77—40042
$Fe_{3-x}Co_xSi$, limits of solubility, mag. props. and electron conc 78—10670

cobalt alloys continued

$Fe_{3-x}Co_xSi$, structural, mag. moment, and hyperfine field behaviour, local environment model 79—65762
$Fe_xCo_{1-x}Si$ alloys, disordered, hydrostatic pressure effects on mag. props. 77—32175
$Fe_xCo_{1-x}Si$, mag. props., effect of hydrostatic press. 77—12101
$Fe_xCo_{1-x}Si$, mag. props. 79—56532
$(Fe_{0.05}Co_{0.95})_{78}Si_8B_{14}$ amorphous ribbon, anomalous mag. aftereffect 80—100602
$(Fe_{0.9}Co_{0.1})_xSi_yB_2$, $(Fe_{1-x}Co_x)_{78}Si_8B_{14}$ amorphous ribbons, magnetomech. coupling and saturation magnetostriction 78—68353
$(Fe_{1-x}Co_x)_{75}Si_{15}B_{10}$ amorphous alloy, soft mag. material, props. 77—4533
$(Fe_{1-x}Co_x)_{77}Si_{10}B_{13}$ alloys, amorphous, induced mag. anisotropy by mag. annealing 79—4671
$(Fe_{1-x}Co_x)_{77}Si_{10}B_{13}$, amorphous, mag. moments at 0K, Curie temp., mag. interactions 79—4670
$(Fe_{1-x}Co_x)_{77}Si_{10}B_{13}$, amorphous magnetic alloys, density meas. 80—1934
$(Fe_{1-x}Co_x)_{78}Si_{10}B_{12}$, amorphous alloys, magnetic anisotropy meas. 80—2570
$(Fe_{1-x}Co_x)_{78}Si_{10}B_{12}$, amorphous, roll mag. anisotropy 80—75757
$(Fe_{1-x}Co_x)_{78}Si_8B_{14}$ ribbon, magnetostriction exam. 79—73794
$Fe_{4.7}Co_{70.3}Si_{15}B_{10}$, amorphous ferromag., roll mag. anisotropy 79—51773
$Fe_5Co_{70}Si_{10}B_{15}$ amorphous magnetic alloy, decrease of permeability after demagnetisation, disaccommodation 80—39814
$Fe_5Co_{70}Si_{15}B_{10}$, amorphous ribbon, zero magnetostriction, low residual mag. loss 77—12157
$Fe_5Co_{70}Si_{15}B_{10}$, amorphous ribbon, HF mag. characts., magnetostriction role 77—66408
$Fe_5Co_{70}Si_{15}B_{10}$ amorphous ferromag. ribbons, change of permeability by heat treatment 77—85493
$Fe_5Co_{70}Si_{15}B_{10}$, amorphous, change of mag. props. by low temp. annealing 78—27058
$Fe_5Co_{70}Si_{15}B_{10}$, amorphous toroidal core, switching characts. and domain structs. 78—95477
$Fe_5Co_{70}Si_{15}B_{10}$, amorphous ferromagnetic alloy, isothermal annealing effect on static magnetic props. *(Japanese)* 79—52398
$Fe_5Co_{70}Si_{15}B_{10}$, amorphous, crystn. effect on mag. props. *(Russian)* 80—44858
$(Fe_xCo_{1-x})_{100-y}(Si_{0.4}B_{0.6})_y$ amorphous alloy zero magnetostrictive, mag. props. 79—99743
$(Fe_xCo_{1-x})_{78}Si_8B_{14}$, amorphous, saturation magnetostriction, strain modulated FMR obs. 80—75863
$(Fe_xCo_{100-x})_{100-(y+z)}Si_yB_z$ amorphous ribbon, mag. moment and Curie temp., comp. depend. 78—95421
$Fe_xCo_{1-x}Si(Ti)$, magnetic props., sp. ht. and resist. meas. 79—61120
$Fe_{1-x}Co_xSn$, transferred hyperfine fields at ^{119}Sn, Mossbauer spectroscopy 79—33582
$Fe_xCo_{1-x}Ti$, high press. mag. props. 78—23271
$Fe_xCo_{1-x}Ti$, mag. props. 79—56532
$Fe_{0.5}Co_{0.5}TiH_x$, transmission Mossbauer spectra 80—44964
$FeCo_2V$, ordered and disordered alloys, annealing of point defects created by neutron irrad. at 20K *(French)* 79—1467
$Fe_{49}Co_{49}V_2$, neutron irradiation, close pair recombination *(French)* 80—39162
$Fe_5(Fe_{1-y}Co_y)$, mag. and calorimetric props. 77—63083
$(Fe_{1-x}Mn_x)_3Si$, $(Fe_{1-x}Co_x)_3Si$, order distrib., hardening effect *(Russian)* 77—89410
$(Fe_{0.5}Ni_{0.5})$-Co, solid and liq., paramag. susceptibility and electron struct., 800-1800°C *(Russian)* 80—25081
$(Fe_{0.5}Ni_{0.5})_{1-x}Co_x$, paramag. susceptibility, solid and liq. phases 1000-1800°C *(Russian)* 77—16040
$Fe_{0.65}(Ni_{1-x}Co_x)_{0.35}$, Mossbauer spectra, ^{57}Fe hyperfine field distrib. 80—20533
Fe_3Si-Co, dil., cond. electron polarisation and moment perturbations 78—68224
$Fe_3Si_xAl_{1-x}$-Co, dil., site preference of ^{57}Co impurities, Mossbauer study 80—39999
Fo-Fe-Nb, cold-worked and aged, mag. props. and microstruct. 80—34690
$GDCo_2$, forced vol. magnetostriction and induced moment 77—36106
$Ga_{1-x}Co_x$, cluster spin glass system, host and impurity NMR studies 79—65745
Gd-Al-Co, H sorption props. for H storage, influence of Al 80—45794
Gd-Co, amorphous, mag. props. and ferromag. reson. 80—75862
Gd-Co, amorphous, RF sputtered, prep. and props. 79—1693
Gd-Co, amorphous, sputtered very thin film struct. 77—15707
Gd-Co, amorphous film, anisotropy due to resputtering effect 77—89989
Gd-Co, amorphous film, galvanomag. effects, Hall detector 77—89882
Gd-Co, amorphous film, Kerr and Hall effect meas. 77—24722
Gd-Co, amorphous film, RF sputtering, DC bias role 77—16494
Gd-Co, amorphous film, with cylindrical mag. domains, sputtering prep. *(Russian)* 77—12176
Gd-Co, amorphous films, mag. props. ferromag. reson. meas., 20-520°C *(Russian)* 80—97144
Gd-Co, and Gd-Co-Mo films, amorphous, mag. props., annealing effects 78—64235
Gd-Co, and Gd-Co-X (X=Mo, Cu, Au), sputter deposited amorphous alloy, substrate bias, magnetic anisotropy, annealing 78—48006
Gd-Co, CPA calcs., moments and transition temps. 78—52252
Gd-Co, disordered, saturation mag. moment calc., CPA 77—20515
Gd-Co, evap. amorphous film, mag. props. 77—24720
Gd-Co, evap. amorphous films, anisotropy, magnetisation and FMR meas. 77—66392
Gd-Co, evaporated amorphous film, perpendicular anisotropy by controlled O_2 contamination 77—89990
Gd-Co, LV multitarget sputtered film, substrate bias effect on anisotropy 77—16125
Gd-Co, sputter deposited amorphous alloy, substrate bias, magnetic anisotropy, annealing 78—48006
Gd-Co, sputtered film, growth induced anisotropy 77—16123
Gd-Co, thermally evap. amorphous film, mag. anisotropy 77—16122
Gd-Co, thin amorphous system, resistance and hardness, chemical comp. and temp. effect 80—15625
Gd-Co alloy, sputtered film, mag. props. determ. *(Chinese)* 78—2714
Gd-Co alloy amorphous thin films, anisotropic mag. and microstruct. props. 78—95487
Gd-Co alloy film, sputter yield ratio, combined ion deposition and etching 80—71594
Gd-Co amorphous film, DC or RF sputtered, mag. props., He$^+$-backscatt. investig. 77—20650

cobalt alloys continued

Gd-Co amorphous film, mag. anisotropy 77—20649
Gd-Co amorphous film, magnetisation processes near compensation point 77—69644
Gd-Co amorphous film, sputtered perpendicular mag. anisotropy 79—56576
Gd-Co amorphous film, sputtered, perpendicular anisotropy exam. 79—73707
Gd-Co amorphous film, sputtered, FMR spectra 79—73822
Gd-Co amorphous film 80—34725
Gd-Co amorphous films, annealed, short-range order and perpendicular mag. anisotropy 80—15765
Gd-Co amorphous films, correlation between struct. and mag. props. *(Chinese)* 80—54532
Gd-Co amorphous films, mag. anisotropy, static and ferromag. reson. expts. 79—33477
Gd-Co amorphous films, mag. struct., mag. bubbles, electron diffr. study *(Chinese)* 80—71126
Gd-Co amorphous films, model calculations for anisotropy formation induced by resputtering processes 78—64242
Gd-Co amorphous films, O_2 adsorption, effect on perpendicular anisotropy 80—34713
Gd-Co amorphous films, RF sputtered, magnetisation ripple effects 80—11232
Gd-Co amorphous films, struct. and mag. anisotropy 80—20438
Gd-Co amorphous films, uniaxial perp. anisotropy induced by resputtering effect, expt. *(Japanese)* 77—55885
Gd-Co amorphous films of rare earth transition metal system, preparation by co-sputtering 79—56928
Gd-Co amorphous ribbons, mag. props. and Invar effects 80—2574
Gd-Co amorphous sputtered films, magnetoelastic contrib. to perpendicular anisotropy, internal stress meas. 78—95490
Gd-Co amorphous sputtered film, magnetostriction and anisotropy 80—39821
Gd-Co amorphous thin film, mag. and optical props., conc. depend 79—19748
Gd-Co amorphous thin films, crystn. process and domain struct. *(Chinese)* 80—54533
Gd-Co based amorphous sputtered films, microstruct. variability and mag. anisotropy, implanted ion effects 80—88459
Gd-Co film, amorphous, Ar sputtered, struct. 78—63946
Gd-Co film, amorphous, ferrimagnet, mag. anisotropy, effect of ion bombard. during prep. 79—1692
Gd-Co film, amorphous, for bubble device appl., prep. and perpendicular anisotropy 77—69641
Gd-Co film, amorphous, inverted and biased loops 77—89996
Gd-Co film, amorphous, magnetisation and anisotropy meas. 77—8370
Gd-Co film, amorphous, magnetisation processes near compensation point 77—40101
Gd-Co film, amorphous, microstruct. and magnetism 78—64230
Gd-Co film, amorphous, perpendicular uniaxial anisotropy, dominant contrib. of preferential resputtering effect 77—36103
Gd-Co film, amorphous, phase separation as source of perpendicular anisotropy 78—64244
Gd-Co film, amorphous, preferential resputtering effect induced anisotropic distrib. of atomic pairs 78—63950
Gd-Co film, amorphous, selective resputtering-induced anisotropy 78—72376
Gd-Co film, amorphous, stability of small bits to temp. and mag. field changes 78—68314
Gd-Co film, amorphous ferrimagnet, anisotropic short range order effects on mag. props. 79—1691
Gd-Co film, bias-sputtered, dipolar mechanisms for mag. anisotropy 78—64233
Gd-Co film, evaporated and sputtered, struct. and mag. anistoropy, electron microscopy 79—56578
Gd-Co film, homogeneity of films prepared by bias sputtering 78—72379
Gd-Co film, sputtered, inert gas incorporation effect on uniaxial anisotropy 78—64232
Gd-Co film, sputtered from segment target, composition and mag. props. 78—27062
Gd-Co film, temp. depend. of mag. aftereffect *(Russian)* 79—8021
Gd-Co film, vapour quenched, amorphous, struct., electron diffr. meas. 77—28086
Gd-Co film, with layer struct., mag. torque and anisotropy 77—63246
Gd-Co films, amorphous, mag. anisotropy from torque meas. 77—47987
Gd-Co influence of gaseous phase on mag. props. *(Polish)* 80—39820
Gd-Co intermetallic compounds, magnetocrystalline anisotropy obs. *(Japanese)* 77—80926
Gd-Co sputtered amorphous films, resistivity anomalies, 42 to 300K *(Chinese)* 80—7001
Gd-Co sputtered films, preparation process, props. 77—59688
Gd-Co thin films sputtered from mosaic target, thickness and composition distrib. 80—6676
Gd-Co-Au amorphous magnetic films, domain wall obs. by Lorentz electron microscopy 77—80979
Gd-Co-B system, phase composition, struct., phase equilibria 78—35355
Gd-Co-Cu film, amorphous, influence of biased magnetron deposition parameters on props. 77—43856
Gd-Co-Fe film, amorphous, bias-sputtered, uniaxial perpendicular anisotropy 78—64234
Gd-Co-Mn, amorphous, ferrimag. props. and Hall effect 79—73692
Gd-Co-Mo, amorphous, sputtered very thin film struct. 77—15707
Gd-Co-Mo amorphous film, MCD, oxide surface layer effect 77—90132
Gd-Co-Mo film, amorphous, bubble and stripe domain wall vel. meas. 77—40094
Gd-Co-Mo film, amorphous, mag. props., ion implantation damage effects 77—89991
Gd-Co-Mo film, amorphous, mag. bubble dynamics 77—89997
Gd-Co-Mo film, amorphous, Ar sputtered, struct. 78—63946
Gd-Co-Mo film, amorphous, in-plane susceptibility near compensation point 78—64238
Gd-Co-Ni series intermetallics, induced moments, magnetisation meas. 77—63138
Gd-Co(-Au) amorphous film, domain wall dynamics near compensation point 79—1696
Gd-Co(-Au) film, ferrimag. amorphous, coated with Permalloy films, mag. props. 79—1695
Gd-Co(-Mo) films, amorphous, inhomogeneities of mangetization and anisotropy 79—65698
Gd-Mo-Mo amorphous film, domain drag effect obs. 78—91911

cobalt alloys continued
$Gd_2\ (Fe_{1-x}Co_x)_{17}$, hyperfine interactions, Mossbauer spectra 78—2780
$GdAl_2$-$GdCo_2$ system, EPR and mag. props. 79—33478
$GdCO_2$, lattice parameter determ. 79—14737
$Gd(CO_xNi_{1-x})_2$, mag. interactions, effects on moments *(Rumanian)* 79—15296
GdCo, amorphous film, MCD *(Japanese)* 78—39530
GdCo amorphous film, O_2 contaminated, TEM obs. of source of perpendicular anisotropy 78—14993
GdCo, amorphous film, XPS meas. 79—87295
GdCo amorphous sputtered film mag. props. from Mossbauer effect obs. *(Japanese)* 80—15933
GdCo, amorphous thin film, for thermomagnetic recording *(Japanese)* 80—11562
GdCo film, amorphous, sputtered, in-plane anisotropy induced by rare gas annealing 78—84458
a-GdCo film, magneto-optical Kerr effect spectra 77—12458
GdCo film, sputtered amorphous, incorporation of Ne, Ar and Kr 77—44163
GdCo film structure, dependent on substrate type *(Russian)* 80—24747
GdCo sputtered amorphous film, third elements effect on mag. anisotropy 79—91260
$GdCo_2$, ^{59}Co hyperfine field, temp. depend. splitting 77—8447
$GdCo_2$, adsorption of H_2, effect on mag. props. 77—20185
$GdCo_2$, amorphous alloys, atomic order, mag. behaviour 78—19221
$GdCo_2$, dilute ferromagnets, press. effect on Curie temp. 80—65873
$GdCo_2$, H_2 sorption props. 79—86980
$GdCo_2$, magnetovolume effects in itinerant electron ferromagnets 79—8038
$GdCo_3$, X-ray absorpt. edge shifts 80—25483
$GdCo_5$, domain wall grooving due to mech. polishing 79—70232
$GdCo_5$, Gd_2Co_{17}, Mossbauer effect 77—85635
$GdCo_5$, large Barkhausen discontinuities, effect of dynamic elastic stresses *(Russian)* 78—39364
$GdCo_5$, spin polarised energy band struct., APW calc. 78—10342
$GdCo_x$, mag. interactions, exchange fields, mol. field model 77—4498
$GdCo_x$, mag. interactions, effects on moments *(Rumanian)* 79—15296
$Gd_{1-x}Co_x$ amorphous thin film, magnetostriction 79—91281
$Gd_{1-x}Co_x$ film, amorphous, Curie and compensation temps., effect of O or Ar impurity 77—40093
$Gd_{1-x}Co_x$, film, resistivity, Hall effect, domain wall density 78—76169
$Gd_{1-x}Co_x$, temp. depend. of magnetisation 77—77043
Gd_2Co, amorphous ferromag. obtained by splat cooling, local and bulk mag. props. 79—1685
$Gd_{2+x}Co_{17-x}$, magnetocryst. anisotropy, stoichiometry and temp. effects 77—8296
Gd_2Co_{17}, NMR spin echo meas., dipolar field anisotropy 80—71236
$Gd_{65}Co_{35}$, amorphous, amg. ordering, susceptibility, magnetisation and hysteresis meas. 78—68190
$Gd_{67}Co_{33}$, amorphous, elec. resist. and magnetoresist. 80—49693
$Gd_{67}Co_{33}$, amorphous ferromag., mag. and transport meas. 77—89930
Gd_xCo_{1-x} amorphous films, microstruct. and mag. anisotropy 79—82838
Gd_xCo_{1-x} annealing amorphous film, ferromag. reson. 77—85580
$Gd_2Co_6Al_{11}$, NMR and mag. susceptibility 79—15367
$(Gd_xCo_{1-x})_{1-y}Ar_y$ amorphous films, effective anisotropy field, ferromag. reson. obs. 80—71123
GdCoAu amorphous film, bias field depend. of domain drag propagated bubble domains 79—78471
a-GdCoAu(Mo) films, perpendicular anisotropy temp. depend., Lorentz microscopy 77—28419
$GdCo_3B_2$, ferromag. ordering and saturation moments 77—24711
$Gd_{0.12}Co_{0.59}Cu_{0.29}$, sputtered film prep. for bubble device 77—16493
$Gd(Co_xFe_{1-x})_2$, mag. props., composition and temp. depend. 79—15289
Gd_3Co_3Ga, crystal struct., X-ray determ. *(Russian)* 79—27951
$Gd(Co_xIr_{1-x})_2$, C15 Laves phase struct., g shift, linewidth EPR meas., Fermi level movement interpretation 79—61210
$Gd(Co_xIr_{1-x})_2$, struct. and mag. moments, comp. depend. 79—86743
GdCoMo film, amorphous, sputtered, ferrimag., in-plane susceptibility near compensation point 78—64240
GdCoMo film, sputtered amorphous, incorporation of Ne, Ar and Kr 77—44163
$Gd_{6.9}Co_{74.0}Mo_{12.8}Ar_{6.3}$, amorphous film, spin wave reson. 79—73823
$Gd(Co_{1-x}Ni_x)_2$ compounds, NMR and thermal expansion 80—66070
$GdCo_{5c}Ni_{5-5c}$, intrinsic coercivity, anisotropy, exchange and cryst. field interactions 80—75806
$Gd(Co_xNi_{1-x})_2$, EPR exam. 79—28600
$Gd(Co_xNi_{1-x})_2$, mag. props., composition and temp. depend. 79—15289
$Gd(Co_xNi_{1-x})_2$, Mossbauer spectra, mag. props. 80—20563
$Gd_2(Fe,Co)_{17}$, mag. anisotropy fields by singular pt. detection 79—24156
$Gd_2(Fe,Co)_{17}$, magnetic anisotropy meas. by singular point detection method 77—63170
$Gd(Fe_xCo_{1-x})_2$, ferromag. reson. of pseudobinary cubic compounds 78—91961
$Gd(Fe_xCo_{1-x})_2$, Mossbauer effect at 78 and 300K, ^{57}Fe hyperfine fields 80—2677
$Gd(Fe_xCo_{1-x})_2$, paramag. behaviour, itineracy 78—39289
$Gd_x(Fe_{1-y}Co_y)_{1-x}$, evap. amorphous film, mag. anisotropy due to pair ordering 77—32219
$Gd_{0.1}La_{0.9}Co_5H_x$, ^{155}Gd Mossbauer spectra 77—63340
$(Gd_{1-x}R_x)(Co_{1-y}M_u)_5$, R=rare earth, M=Cu, Ni, Pt, origin of hyperfine fields acting on Gd, Mossbauer study 80—44967
$(Gd_xY_{1-x})Co_2$, mag. interactions, effects on moments *(Rumanian)* 79—15296
$Gd_xY_{1-x}Co_2$, transferred hyperfine interactions, ^{155}Gd Mossbauer effect and ^{165}Ho NMR expts. 77—63339
$(Gd_xY_{1-x})_4Co_3$, Curie temp. and resist.-temp. curves, comp. depend. 80—71020
$Gd[Co_xFe_{1-x}]$, NMR, hyperfine fields, conc. depend. 77—43902
Ge-Co, liq., enthalpy of formation meas. 80—30267
Ge_2FeGa, and Fe_2CoGa, site preference and local environment effects, Mossbauer and NMR expts. 78—43710
Hf-Co, amorphous, formation, decomposition and elec. transport props. 80—20143
Hf-Co, oxidation of intermetallic phases 79—100298
Hf-Co, phase diagram, X-ray diffr., thermal anal. and metallography obs. 78—60652
Hf-Co-Ga system, crystal atomic struct. and phase equilibria *(Ukrainian)* 78—84772
$HfCo_6$, saturation magnetisation, Co mag. moment and electron transfer 77—73005

cobalt alloys continued
$Hf(Fe_{1-x}Co_x)_2$, mag. props., Mossbauer spectra and magnetisation meas. 80—39948
$(Ho,Y)Co_2$, first order phase transitions 78—84426
$(Ho,Y)Co_2$, mag. props., elec. resist. and thermal expansion 78—76246
Ho-Co, amorphous film, Kerr and Hall effect meas. 77—24722
Ho-Co alloy amorphous thin films, anisotropic mag. and microstruct. props. 78—95487
Ho-Co amorphous film, anomalous Hall hysteresis loops near compensation point 78—19286
Ho-Co amorphous film, prep. by dual-source evaporation, mag. props. 77—89988
Ho-Co film, amorphous, microstruct. and magnetism 78—64230
Ho-Co film, evaporated, struct. and mag. anistoropy, electron microscopy 79—56578
Ho-Co film, vapour quenched, amorphous, struct., electron diffr. meas. 77—28086
HoCo film, amorphous, sputtered, in-plane anisotropy induced by rare gas annealing 78—84458
$HoCo_2$, cryst. field induced spin rot., Mossbauer meas. 77—16227
$HoCo_2$, easy direction of magnetisation, Mossbauer data, 4.2K 78—43584
$HoCo_2$, field induced vol. magnetostriction 78—91920
$HoCo_2$, ground state spin excitations, inelastic nneutron scatt. study 80—50077
$HoCo_2$, mag.excitations, neutron inelastic scatt. meas. 80—60231
$HoCo_2$, magnetisation reorientation 78—23300
$HoCo_2$, paramag. and ordered phases, Pauli type Co susceptibility, polarised neutron diffr. obs. 77—63077
$HoCo_2$, vol. magnetostriction, point charge cryst. field model 77—63254
$HoCo_2$:^{57}Fe, easy magnetisation directions, spin rotation like transitions 77—63168
$HoCo_3$, Ho_2Co_7, $HoCo_{5.5}$ and Ho_2Co_{17}, Kerr effect determ. of domain structure, Bloch wall energy 80—39806
Ho_2Co_{17}, magnetisation, magnetocryst. anisotropy and magnetostriction 77—8303
Ho_2Co_{17}, single cryst., magnetostriction const. temp. depend., 78 to 300K 79—51836
Ho_2Co_{17}, spin wave excitations, 4.8 and 78K 80—60230
Ho_4Co_3, cryst. field effect on mag. moment direction, neutron diffr. meas. 78—80132
Ho_xCo_{1-x} amorphous films, microstruct. and mag. anisotropy 79—82838
$HoCo_{5.5-x}Mn_x(Fe_x)(Ni_x)(Cu_x)$, cryst. struct. and mag. props. 80—75800
$HoCo_{5\ x}Ni_x(Cu_x)$, lattice parameters and mag. props. 79—82817
$Ho_2Fe_3Co_{14}$, Kerr effect determ. of domain structure, Bloch wall energy 80—39806
$Ho_xTb_{1-x}Co_2$ lave phase compounds, elastic props., temp. and magnetic field dependence 80—60393
$Ho_xY_{1-x}(Fe_{0.1}Co_{0.9})_2$, ^{57}Fe hyperfine interaction, mag. props., Mossbauer study 80—39951
La-Co-H, catalytic props. in hydrogenation of propylene, dehydrogenation of propane 80—30277
La-Ni-Co, H absorption for storage appls. 80—45790
$LaCo_x$, sorption at press. up to 1500 atm. 80—97819
$La_{1-x}Co_x$, amorphous, conc. depend. of Co moment 78—56300
La_2Co_7, mag. props. changes upon H_2 absorpt. 80—71270
La_2Co_7, mag. saturation and anisotropy, density, lattice parameters 77—85426
$LaCoAl_4$, X-ray anal. of crystal structure *(Russian)* 77—55263
$La(Co_{1\ x}Ni_x)_5$, distrib. of Co and Ni atoms, neutron diffr. obs. *(Russian)* 80—64954
$La_3Co_2Sn_7$, prep. and crystal structure *(German)* 80—84138
$LuCo_2$, anomalous high-field magnetisation 78—47958
$LuCo_2$, high-field magnetisation, Fermi liquid model 79—11303
$LuCo_2$, mag. interactions, effects on moments *(Rumanian)* 79—15296
$LuCo_2$, paramag., field induced mag. density localisation 77—72999
Lu_2Co_{17}, single cryst., magnetostriction const. temp. depend., 78 to 300K 79—51836
Mg-Ni-W-Co-Al-Cr alloy KhN56VMKYu, Al effect on excess Mg phase 80—29926
Mn-Co, spin fluctuations effect on sp. ht. 79—82788
$Mn_{46}Co_{54}$, amorphous alloy prep. by high-rate sputtering, struct. and prop. characteris. 79—24462
$Mn_{1-x}Co_xAs$, mag. props., phase diags. 77—66300
$Mn_{1-x}Co_xSb$, press. effect on saturation magnetisation *(Russian)* 77—80919
MnCoSi, effect of press on mag. transition temp. *(Russian)* 80—25137
MnCoSi, mag. struct. *(French)* 78—39323
MnSi-CoSi solid solution, mag. props. 78—56403
Mo-Co Kondo alloy, Co impurity susceptibilities, Knight shift 80—88721
Mo-Co-Al, phase diagram *(Russian)* 78—19722
Mo-Co-Si, cryst. struct. and defects, high resolution electron microscopy obs. 79—94961
Mo-Ni-Fe-Co-Zn alloys, Ni, Fe, Co and Zn distrib. using neutron-activation anal. 79—52531
$Mo_{1-x}Re_xCo$, mag. state of Co impurity, NMR exam. 78—27100
Nb-Co, alloying element influence on strength, ductility, surface and grain boundary energies *(Russian)* 79—74234
Nb-Co, X-ray emission spectra investigation of electron struct. of Laves phases *(Russian)* 78—23554
Nb_4CoP, new ternary phosphide with Nb_4CoSi type struct. *(Russian)* 77—55262
Nb_3Sn-Co, mag. impurities effect on supercond. props. 77—1524
Nd-Co alloys, NMR of ^{143}Nd and ^{145}Nd 78—19343
Nd-Co film, amorphous, exam. of domain struct. 78—68336
$NdCO_2$:^{57}Fe, easy magnetisation directions, spin rotation like transitions 77—63168
$NdCo_2$, cryst. field induced spin rot., Mossbauer meas. 77—16227
$NdCo_2$, magnetocrystalline anisotropic props., torque meas. 80—108003
$NdCo_5$, absorption of H_2, 77-300K 79—23737
$NdCo_5$, ferromag., thermomag. charact. in mag. field *(Russian)* 78—23273
$NdCo_5$, single ion anisotropy consts. temp. depend. effect of spatial variation of mag. moment 78—91864
$NdCo_5$, spin reorientation, magnetisation and torque curves, 77-925K 77—4532
$Nd_{0.35}Co_{0.65}$ film, vac. evaporated, magnetisation ripple struct., TEM and defocused Lorentz microscopy 80—7136
Nd_2Co_7, mag. saturation and anisotropy, density, lattice parameters 77—85426

cobalt alloys continued
$Nd_{64}Co_{36}$, amorphous, amg. ordering, susceptibility, magnetisation and hysteresis meas. 78—68190
Nd_xCo_{1-x} film, amorphous, mag. props. meas. 78—68312
$Nd_2Co_{17-x}Al_x$, magnetisation, Curie temp., anisotropy 77—89947
$Nd(Co_{1-x}Cu_x)_5$, coercive force temp. depend. 79—82823
Nd_3Co_3Ga, crystal struct., X-ray determ. *(Russian)* 79—27951
$Nd_{1-x}Dy_xCo_5$, rotational type spin reorientation, appl. to thermomagnetic generator 77—85451
$Nd_xPr_ySm_zCo_5$ permanent magnets, coercive force, low-temp. annealing influence *(Russian)* 80—39812
$(Nd_xSm_{(1-x)})_2(Co_{0.7}Fe_{0.3})_{17}$, mag. anisotropy 80—34622
$Nd_2Y_{1-x}Co_5$, saturation magnetisation and anisotropy, 4.2K-T_c 77—85427
$(Ni,Co)_3Ge$, Co effect on temp. depend. of yield stress 78—31487
$(Ni,Co)_3Ge$, single cryst., Co effects on temp. depend. of yield stress 77—4812
Ni base alloy IN792, carbide morphology 77—36508
Ni based Rene 80 superalloy, initial stages of pack aluminisation 80—76188
Ni superalloy Mar-M200, slow fatigue crack propagation rate meas. using high freq. resonant technique 78—52983
Ni-(Co)-Cr, aluminide coating, microstruct. and chem. 80—76189
Ni-Al-Co, electrical and mag. anomalies due to substitutional atoms 77—15839
Ni-Al-Co, heat resist., solidification range 80—35177
Ni-Al-Cr-Co-Ti, Waspaloy, exam. of dislocation-precipitate interaction, cyclic stress-strain behaviour 78—84925
Ni-Al-Cr-Mo-Ti-W-Co, heat resistant alloy EhI 929 reverse elastic after effect under loading 78—39829
Ni-based TaC eutectic, directionally solidified, elastic moduli 80—84984
Ni-Co, cryst. growth from melt, distrib. of growth directions 79—33924
Ni-Co, dil., optical absorpt., electronic struct. 80—108227
Ni-Co, dislocation intersection and solution strengthening, effect of solute on obstacle profiles 80—7590
Ni-Co, electrical resistance and H solubility at high press. *(Russian)* 79—91018
Ni-Co, elementary excitations, exchange stiffness const., inelastic neutron scatt. study 79—47294
Ni-Co, FCC, spin wave stiffness, inelastic neutron scatt. 77—63156
Ni-Co, FCC, spin wave stiffness const., neutron scatt. study 79—51769
Ni-Co, fatigued, struct. and cyclic stress strain, influence of stacking fault energy and atomic size-module-interactions *(German)* 79—42082
Ni-Co, ferromag. films, magnetoresistance effect, crystal struct. 78—68017
Ni-Co, ferromagnetic resonance, surface anisotropy 78—95526
Ni-Co, film, magnetisation induced uniaxial anisotropy, dislocations effects 78—43618
Ni-Co, high-field susceptibility, spin-wave spectrum, CPA calc. 80—65818
Ni-Co, liquid, activity meas. by transportation method *(Japanese)* 79—4949
Ni-Co, local mag. field on μ^+ 79—56665
Ni-Co, low temperature lattice parameter, Gruneisen parameter 77—76357
Ni-Co, mag. props. of single-domain powders after plastic deform. *(Russian)* 78—6554
Ni-Co, oxide scales, cation distrib. calc. by approx. analytical method 77—48594
Ni-Co, plasticity, athermal and thermal *(Russian)* 79—11685
Ni-Co, platelets, FMR field and linewidth, room temp. 77—4563
Ni-Co, recovery of single crystal after varying amounts of cold work 79—100162
Ni-Co, rolling texture development, dependent on relative stacking fault energy 79—52237
Ni-Co, solid and liq., paramag. susceptibility and electron struct., 800-1800°C *(Russian)* 80—25081
Ni-Co, spin wave stiffness consts., RPA CPA band model 79—61088
Ni-Co (10 wt.%), cast single phase, solidified from undercooled melt, mech. props. 77—48540
Ni-Co (25 at.%), polycrystalline, mech. damping 77—28850
Ni-Co (25 wt.%), short range order parameters from Mossbauer data 79—56645
Ni-Co (25 wt.%), single crysts., mag. annealing effect on magnetostriction and magnetisation *(Japanese)* 80—34744
Ni-Co (25 wt.%), single crysts., mag. annealing effect on magnetostriction and magnetisation at high temps. 80—108047
Ni-Co (5(66) wt.%), internal stresses during creep 80—3142
Ni-Co alloy, local ordering effect on spin wave stiffness const. 77—66282
Ni-Co alloy, stiffness const., interpretation within band model 79—42748
Ni-Co amorphous alloys, magnetostriction 80—34738
Ni-Co electrodeposit, strength, heat treatment and comp. var. effects 77—32660
Ni-Co film, anal. of main component by atomic absorpt. spectrophotometry 77—70381
Ni-Co film, magnetisation induced uniaxial anisotropy 77—48016
Ni-Co film, spin wave resonance 79—33542
Ni-Co film, spin-wave reson. exam. 78—2746
Ni-Co films, electron-beam evaporated, magnetoresist. anisotropy, deposition temp. effect 80—34528
Ni-Co plate, surface anisotropy from ferromagnetic reson. 78—48049
Ni-Co thin films, spin-wave reson. obs., exchange stiffness const. 80—44924
β-Ni-Co-Al, martensitic transform., metallographic, X-ray diffr., and elec. resist. obs. *(Russian)* 78—19748
Ni-Co-Al (1, 35.2 at.%), tempered martensite, new ordered phase 79—11560
Ni-Co-Al alloys, continuous precip., SEM, TEM, X-ray diffr. study 80—89220
Ni-Co-C solid solution, C precipitation, Ni_3Co ordering, Ni-Co lattice parameter meas. *(Czech)* 80—60867
Ni-Co-Cd alloys, electrodeposition from acetate bath 78—68637
Ni-Co-Cr alloys IN 738, Pt plated, aluminization 78—31583
Ni-Co-Cr system, heats of formation and of transformation 80—50599
Ni-Co-Cr TEM foils, white band contrast 80—75134
Ni-Co-Cr/Al_2O_3 catalyst, IR spectra of adsorption and interaction with pyridine 80—71946
Ni-Co-Cr-Al-Ti-Mo superalloy IN738, casking porosity removal using hydrostatic press. sintering 80—55322
Ni-Co-Cr-Al-Y, plasma-arc-sprayed, metallurgical characts. and oxidation behaviour 80—40618

cobalt alloys continued
Ni-Co-Cr-Al-Y coating, electron beam evap., low press. gas scatt. 77—40474
Ni-Co-Cr-Al-Y coating, electron beam deposited, for Ni-base superalloy, fatigue crack initiation and propag. 78—11438
Ni-Co-Cr-Al-Y protective coating for combustion turbines, hot corrosion evaluation 80—40608
Ni-Co-Cr-Mb-W-Ta, Cr, Mb, W, Ta effects on σ phase occurrence 77—36507
Ni-Co-Cr-Mo-Al, Astroloy, extruded powder metallurgy superalloy, recrystallisation study 79—4976
Ni-Co-Cr-Mo-Al-Ti (17.5, 15.1, 4.9, 4.15, 3.25 wt.%), creep and stress rupture behaviour in air and vacuum 80—60918
Ni-Co-Cr-Mo-Ti-Al Nimonic 105, loading frequency and environmental effects on high temp. fatigue crack growth 78—64675
Ni-Co-Cr-Ta-Al-W-Mo-Ti, cast, phase volume fraction determ. using manual point count practice 78—53052
Ni-Co-H, hydride formation in high press. range 80—65235
Ni-Co-H, solid soln., Curie points and spontaneous magnetisation behaviour 80—50093
Ni-Co-H system, phase transform. under high H_2 press., Co additive effects *(Russian)* 78—60645
Ni-Co-Mn, dil. alloys, NMR freq. temp. depend., spin echo meas. 78—64296
Ni-Co-Mn, dil. ferromag. alloy, mag. moment, saturation magnetisation meas. 78—64195
Ni-Co-Mo, phase relations in system at 1100°C 80—108392
Ni-Co-Mo alloys, electrodeposition, struct. 79—28970
Ni-Co-Mo-Al-Cr, melt, effect of Al, Cr on O_2 activity, electrochemical determ. 79—11556
Ni-Co-P, amorphous alloy, electrical and mag. props. 78—95281
Ni-Co-P, amorphous electrodeposited films, domain wall motion, Kerr effect 78—60322
Ni-Co-P, ferromag. film, amorphous to cryst. transition, diffr. and resistivity meas. 78—60587
Ni-Co-W, electrodeposition, surface morphology and cryst. struct. 80—71602
Ni-Cr-Al-Ti-Co, exam. of back stress role in creep behaviour of particle strengthened alloys 78—52889
Ni-Cr-Co, Mo, Ti, Y and R alloying additions influence on oxidation *(Russian)* 80—40587
Ni-Cr-Co, Nimocast alloy 738, γ″ precipitate morphology and creep rupture, thermal stress crack effect 78—11318
Ni-Cr-Co alloy IN738, electrochemical corrosion meas. in molten sulphate 79—96178
Ni-Cr-Co alloys, relax. resist. exam. by bending and tension 79—24564
Ni-Cr-Co base superalloy APK1, hot isostatically pressed, heat treatment, fracture props. 77—73251
Ni-Cr-Co based alloy, IN-738 turbine blades, hot isostatically pressed investment castings, effect of heat treatment on grain boundary struct. 80—89270
Ni-Cr-Co superalloy, combined TEM, FIM, atom probe microanalysis of precipitates and carbide phase comp. 80—100844
Ni-Cr-Co superalloy, σ-phase effect on mech. props. *(Chinese)* 79—74229
Ni-Cr-Co superalloy IN-792, crack growth resistance, metallurgical effects 77—36655
Ni-Cr-Co-Al alloy IN-738, uniaxial damage accumulation law for time depend. loading with creep-fatigue interaction 79—83324
Ni-Cr-Co-Al-Ti-W-Ta-Mo, IN 738 LC, loading frequency and environmental effects on high temp. fatigue crack growth 78—64675
Ni-Cr-Co-Al-W-Mo-Ti-Ta, heat resist. and struct., Ta effect 80—76312
Ni-Cr-Co-Mo, long-term corrosion stability rel. to use in joint endoprostheses 78—36059
Ni-Cr-Co-Mo alloy MP35N alloys, cold worked, factors affecting embrittlement in H_2S environments 78—31502
Ni-Cr-Co-Mo alloy MP35N, accelerated H_2 charging in aq. H_2SO_4 at 0.2% yield stress 80—30144
Ni-Cr-Co-Mo-Al, IN-67 alloy, hot corrosion, cyclic oxidation, depth of attack determinations 80—11837
Ni-Cr-Co-Mo-Al-Ti (10, 15, 3, 5.5, 4.5 wt.%), superalloy, exam. of creep and fracture behaviour 78—48464
Ni-Cr-Co-Mo-Al-Ti alloys, Waspaloy, Astroloy, exam. of microstruct. effect on crack growth 78—52977
Ni-Cr-Co-Mo-Ti-Al, powders, HCl surface treatment to prevent TiC precipitation, fracture props. 79—8397
Ni-Cr-Co-Ti, superalloy sintering thermochemical surface treatment 80—25617
Ni-Cr-Co-Ti-Mo-W-Al (14, 9.8, 5, 4, 3.9, 3 wt.%), low cycle fatigue, prior heat treatment effect 80—60962
Ni-Cr-Co-W (47.5, 25, 12, 8.75 wt.%), vaporization of IN-643, high-temp. mass spectrometry 79—7685
Ni-Cr-Co-(Se), oxidation resistance 77—21320
Ni-Cr-Fe-Mo-Co (21.41, 19.28, 8.64, 2.16 wt.%), Hastelloy alloy X, exam. of thermal stability 78—84865
Ni-Cr-Ti-Al-Fe-Co (19.65, 2.40, 1.37, 0.78, 0.52 wt.%), strength of γ′ hardened alloy, ageing exam. 78—88501
Ni-Cr-Ti-Co-W-Al-Mo alloys AF-115 and AF2 1DA, superalloy powder compacts, fatigue origins 78—48521
Ni-Cr-W-Co granules type ZhS6U, EP741, hot hydrostatic pressing 80—60796
Ni-Cr-W-Co-Ti, thermal fatigue, effects of inclusions 80—81183
Ni-Cr-W-Co-Ti heat resistant alloy ZhS6K, fatigue resistance, heat treatment and protective coating effects 77—81320
Ni-Cr-W-Co-(Al)(Ti)(Mo), high-temp. sulphide corrosion 80—76408
Ni-Fe-Co, alloy with step hysteresis loops *(German)* 79—42806
Ni-Fe-Co (17,3 wt.%), thin film ferromagnetic band, magnetisation under domain creep conditions *(Russian)* 79—91262
Ni-Fe-Co film, anal. of main component by atomic absorpt. spectrophotometry 77—70381
Ni-Fe-Co film, domain wall energy meas., by domain tip propag. method 77—55692
Ni-Fe-Co film, magnetoelastic vibr. generation during high freq. mag. reversals *(Russian)* 78—60320
Ni-Fe-Co film, nonmagnetostrictive, mag. props., effect of deposition parameters of Al underlayer 77—77078
Ni-Fe-Co films, for logic devices, mag. switching vel., anisotropy field and coercive force *(Korean)* 77—51930
Ni-Fe-Co films, nonmagnetostrictive, magnetoresistance effects 78—35013
Ni-Fe-Co films, saw tooth magnetic domains investigated 78—14994

cobalt alloys continued
Ni-Fe-Co-Ti, electron microscopy and mag. meas. 80—71097
Ni-Mn-Al-Si-Co, Alumel, Ettingshausen-Nernst coeff. and transport props. from 200 to 473K 80—44573
Ni-Mn-Co, low temp. anomalies of elec. resist. *(Russian)* 79—60788
Ni-Ti-Co, Co effect on martensitic transform. temp. and low temp. props. *(Korean)* 78—11224
Ni-W-Co-Cr, superalloy MAR 200, with Hf, cellular composite prod. by isothermal dendrite ripening 78—44150
$Ni_{1-x}Au_x$-Co, dil., hyperfine field and isomer shift, precip. process, Mossbauer expts. 80—25267
$Ni_{1-x}Au_x$-Co, dil., Mossbauer effect, mag. hyperfine field 80—20528
NiCo film, crit. angle meas., pinning mech. 79—1719
NiCo, itinerant electron model, spin wave stiffness const. calc. 80—34613
(NiCo)-Cr-Al-Y/ZrO_2-Y_2O_3 plasma sprayed ceramic coating for turbine engine components 80—40616
$Ni_{1-x}Co_xAl$, self-consistent embedded-cluster model for mag. impurities 78—67973
$Ni_{62}Co_4Al_{34}$, fine struct. of martensite, electron microscopy obs. *(Russian)* 79—46672
$(Ni_xCo_{1-x})_3Ge$ single crysts., $L1_2$ struct., cross-slip 80—40459
$(Ni_{1-c}Co_c)_{0.78}P_{0.14}B_{0.08}$, amorphous, mag. props., local environment model 77—12119
NiCoPd, anodic dissolution, SFE effect *(German)* 80—25924
No-Ni alloy, integral emissivity in range 1200 to 1700°C 77—43357
$NpCo_2Si_2$, itinerant magnetism obs. 77—28406
$NpCo_2Si_2$, mag. props., high press. studies with ^{237}Np(60)-resonance 80—39924
$NpCo_2Si_2$, mag. struct., neutron diffr. determ. 80—93084
$NpCo_2Si_2$, Mossbauer and magnetisation expts. 78—31138
$NpFe_{2-x}Co_xSi_2$, mag. and hyperfine props. 79—51887
$NpFe_{2-x}Co_xSi_2$, mag. and hyperfine props. 80—7247
Pd-Co, dil,. ferromag., magnetoresist. 78—91665
Pd-Co, dil., breakdown of ferromag. order, magnetoresist. obs. 80—71046
Pd-Co, dil., giant moment and Kondo-like coupling, nuclear orientation meas. 77—32160
Pd-Co, dil., local orbital moment evidence 77—20299
Pd-Co, dil., Mossbauer emission spectra, fast relaxation regime, ^{57}Co hyperfine field 78—60362
Pd-Co, dil., relax. of oriented ^{57}Co nuclei, Mossbauer meas. using ^{3}He-^{4}He refrigerator 78—24909
Pd-Co, dilute, extraordinary Hall effect meas., 2-250K 80—34420
Pd-Co, dilute, nuclear orientation expt., Co impurity in singlet Kondo state 77—63296
Pd-Co, dilute alloy, ferromag. ordering, depend. on Co impurity at low temp. 79—61055
Pd-Co, dilute ferromagnets, press. effect on Curie temp. 80—65873
Pd-Co, liquid alloys, enthalpy of form. *(Russian)* 77—56244
Pd-Co, Mossbauer effect under press. for ^{119}Sn impurity atoms and hyperfine mag. field model *(Russian)* 77—55742
Pd-Co, normal Hall effect *(Russian)* 80—103676
Pd-Co, pressure effect on Curie point, Debye temp. in ferromag. state *(Russian)* 77—32194
Pd-Co, very dil., Mossbauer emission spectra of ^{57}Co, relax. effects 80—29656
Pd-Co (0.1-45.7 at.%), thermo EMF at 4.2-300K *(Russian)* 80—92881
Pd-Co-P amorphous alloy, mag. an elec. props. 77—40043
$(Pd_{1-x}Au_x)_{0.99}Co_{0.01}$, mag. hyperfine interaction for impurity Co atoms *(Russian)* 80—7078
PdCo, dil., ferromag., nucl. mag. relax. 78—6590
PdCo, effect of hydrogenation on thermopower 80—39562
$(Pd_{0.996}Co_{0.004})_{1-x}Mn_x$ alloys, ferromag. and spin glass transition, NMR 79—65761
$Pd_{50}Fe_{37.5}Co_{12.5}$, elec. resist., cond. electron scatt. and heterogeneities of spin system *(Russian)* 79—56189
$Pd(M_nCo)$, giant moments, Mossbauer study of ^{57}Fe 80—44969
$(Pd_{95}Rh_5)Co$, exchange enhanced system, AC susceptibility meas. 77—16096
$PrCo_2$, magnetocryst. anisotropy props. by ^{57}Fe Mossbauer spectroscopy 77—63328
$PrCo_2$, strongly exchange-enhanced paramagnetism, susceptibility 80—60179
$PrCo_5$, EXAFS and shape of K absorption discontinuity of Co 77—20955
$PrCo_5$, uniaxial ferromag. cryst., irreversible rotation processes 80—39768
$PrCo_{5\pm x}$, high field first order transitions, role of K_3 anisotropy const. 80—65879
$PrCo_x$, sorption at press. up to 1500 atm. 80—97819
Pr_2Co_7, mag. saturation and anisotropy, density, lattice parameters 77—85426
$PrCoAl_4$, X-ray anal. of crystal struct. *(Russian)* 77—55263
$Pr(Co_{0.7}Cu_{0.3})_5$, anomalous magnetisation curves 80—15757
$Pr(Co_{1-x}Cu_x)_5$, coercive force temp. depend. 79—82823
$Pr(Co_{1-x}Cu_x)_5$, magnetocrystalline anisotropy exam. 78—39315
$Pr(Co_{1-x}Cu_x)_5$, saturation magnetisation anisotropy 78—47960
$Pr_2(Co_{1-x}Fe_x)_{17}$, hard direction magnetisation, 5-300K, and anisotropy field 77—12114
Pr_3Co_3Ga, crystal struct., X-ray determ. *(Russian)* 79—27951
$Pr_{0.75}Sm_{0.25}Co_5$ magnets, struct. and props. sintering temp. depend. *(Russian)* 79—82819
$Pr_xSm_{1-x}Co_5$, magnetisation and magnetocryst. anisotropy 78—68215
Pt-Co, dil, magnetopower, magnetoresistivity 78—68016
Pt-Co, dil., skew scatt. Hall effect, magnetoresist. and mag. anisotropy, orbital magnetism of impurity 80—70678
Pt-Co, dil., thermopower and magnetothermopower 79—65456
Pt-Co, dilute ferromagnets, press. effect on Curie temp. 80—65873
Pt-Co, magnetically hard, struct. and morphology, electron microscope study 79—82171
Pt-Co, magnetostatic and exchange interactions in composite magnets 77—69536
Pt-Co alloys, crit. neutron scatt. in crit. conc. region for onset of ferromagnetism 78—72347
Pt-Co melts, surface tension and density *(Russian)* 80—39388
Pt-Co multi-microelectrode system with independent penetration and structural reinforcement by mag. coupling, characts. *(Japanese)* 79—66586
Pt-Co resistance thermometer, for low temp. appl. 78—73994
Pt-Co system, low temp. susceptibility 80—65920
PtCo, absolute thermopower meas., 4-300K 78—10421
PtCo, ferromag. domain wall, freq. const. for thermal activation 77—89976

cobalt alloys continued
Pt_3Co, radiation damage profiles from low energy Ne^+, bombard. 80—70268
$Pt_{50}Fe_{12.5}Co_{37.5}$, elec. resist., cond. electron scatt. and heterogeneities of spin system *(Russian)* 79—56189
$Pt_{37.5}Pd_{12.5}Co_{50}$, elec. resist., cond. electron scatt. and heterogeneities of spin system *(Russian)* 79—56189
$R_{1-x}Co_x$, rare earth amorphous alloys, thermal stability, elec. cond. enthalpy 80—100172
Rh-Co (20 at.%), mag. virtual bound state alloys, XPS of core states 79—47588
Rh-Pd-Co, dil., local environment and mag. props. 78—64187
Rh-Pd-Co, dil., local moment formation 78—43562
Rh-Pd-Co, dil. alloy, mag. moment 78—95416
RhCo, disordered itinerant-electron system, spin-glass condensation 79—78424
Rh_2CoSn, ferromag., crit. exponent of ^{119}Sn hyperfine field, Mossbauer obs. 78—92008
Rh_2CoSn, ferromag., mag. hyperfine fields of ^{119}Sn, Mossbauer meas. 78—10816
Rh_2CoSn, ferromag. Heusler alloys, hyperfine fields, spin echo meas. 77—63314
Rh_2CoSn, hyperfine mag. fields at ^{119}Sn, under press., Mossbauer expts. 79—99812
Rh_2CoSn, metallic ferromagnet, hyperfine mag. field temp. depend. *(Russian)* 78—80265
Sc-Co, phase diagram determination, using X-ray diffr., metallography and DTA techniques *(Russian)* 79—34004
Sc-Co-Ga, phase equilibria, diagrams of state, X-ray, microstructural study *(Russian)* 80—55356
Sc-Co-Si, phase equil. and atomic struct. *(Russian)* 77—77462
Sc_3Co, new struct. type related to Fe_3C and Re_3B by periodic unit-cell twinning 79—4268
$ScCoC_{1-x}$, stabilising effect of C on alloying behaviour of Sc 77—36454
$Sc(Fe_{1-x}Co_x)_2$, magnetic saturation moment, Co conc. depend., NMR exam. 78—15037
Si-Co, liquid alloys, thermodynamic charact. calc. *(Russian)* 78—27475
Si-$CoSi_2$Si, double heteroepitaxy, solid phase and MBE 80—104063
$Si_{1-x}Co_x$ film, metastable impurity band, conductivity meas., semiconductor-metal transition 77—76884
Sm,$(Co,M)_{17}$, (M=Fe, Mn, Cr), exchange and crystal field parameters, anisotropy meas. 77—69535
Sm-Co, alloy powders and sintered magnets, effect of chem. treatment on mag. props. 78—60311
Sm-Co, amorphous, plasma-sprayed, role of Ar or H_2 atm. in mag. props. and crystn., rel. to H_2 storage 80—64898
Sm-Co, decomp. kinetics when aged, X-ray mag. props. and metallography study *(Russian)* 78—56644
Sm-Co, permanent mag., O ion impact, 5.5 keV, secondary Co ion emission, magnetisation depend. *(Russian)* 78—2967
Sm-Co alloy magnets, operational control of residual induction, maximum mag. energy 79—15324
Sm-Co base ternary alloy, mag. props. and cryst. struct. 77—8352
Sm-Co deposit, arc plasma sprayed, crystal and micro struct. exam. 79—28248
Sm-Co ring magnets for BWO, 110 to 170 GHz, design and appl. *(German)* 80—105684
Sm-Co-Cu, with Sm_2Co_{17} struct., aged, TEM high coercivity material, TEM obs. of microstruct. 77—77073
Sm-Co-Cu permanent magnets, phase diagram 77—21106
Sm-Co-Cu-Fe, single phase 2-17 sample, hard mag. props. 77—8349
Sm-Co-Cu-Fe-Ti magnets, comp. and sintering effects on coercivity 79—15326
Sm-Co-Cu-Fe-Zr, reversible changes in coercive force and struct. state during heat treatment 400-800°C *(Russian)* 80—29574
Sm-Co-Cu-Fe-Zr magnet, production and mag. props. 77—40085
Sm-Hf-Co alloy, rare-earth electron transfer 77—40028
Sm-Pr-Co, added Fe_2Sn, permanent magnets, demagnetisation curves, X-ray obs. 78—91900
Sm-Pr-Co, mag. props. and struct., comp. depend. *(Russian)* 80—20430
Sm(-Pr)-Co, sintered, cryst. phases *(Russian)* 80—39004
$SmCO_5$ based permanent magnets, props. and cryst. orientation *(Russian)* 80—20431
$SmCO_5$, etched microparticles, Barkhausen discontinuity, nucleation, and domain wall pinning 79—87288
$SmCO_5$ magnets, sintering time effect on props. 79—95977
$Sm_{1-u}Ce_u(Co_{1-x-y-w}Fe_xCu_yCr_w)_z$, permanent mag., improved mech. props. 79—87593
Sm_2(Co, Cu, Fe, M$)_{17}$, M=Nb, V, Ta, Zr, effect of M on mag. props. 77—89978
Sm(Co, Cu) alloys, coercivity mech. 80—44862
$Sm(Co,Cu)_5$, eutectoid transform. 77—8799
$Sm(Co,Cu)_z$, precip.-hardened, mag. and metallographic props. 77—8339
$SmCo_2$, hyperfine field exam. by NMR spin echo 78—23365
$SmCo_2$, hyperfine interactions and exchange fields acting on Eu^{3+}, Mossbauer obs. 77—63338
$SmCo_5$, adsorption and desorption charact. of H_2 *(Japanese)* 77—47667
$SmCo_5$, amorphous, supermag.-ferromag. transition and directional crystallisation 80—65891
$SmCo_5$, and related alloys, nucleation and pinning at 360° domain walls 77—73042
$SmCo_5$, and $SmCo_{3.5}Cu_{1.5}$, anisotropy and coercivity, Kerr effect, magnetisation and aftereffect expts. 77—8300
$SmCo_5$ based alloys, dissociation process *(Russian)* 78—27542
$SmCo_5$ based permanent magnets with low reversible temp. coeff. 79—51814
$SmCo_5$ based solid soln., X-ray diffr. obs. of decomp. *(Russian)* 77—81264
$SmCo_5$ based ternary and quaternary permanent mag. materials with low reversible temp. coeffs. 79—82822
$SmCo_5$, Bloch wall energy determ. *(German)* 78—19271
$SmCo_5$, coercivity, random substitution of Sm by Co *(Chinese)* 77—8343
$SmCo_5$, Cu-modified, magnetisation reversal mechanism 77—8350
$SmCo_5$, domain wall nucleation sites and magnetization reversal 79—56563
$SmCo_5$, domain wall pinning rel. to coercive force 77—1561
$SmCo_5$, EXAFS and shape of K absorption discontinuity of Co 77—20955
$SmCo_5$, electronic struct., X-ray photoelectron spectra 77—20992
$SmCo_5$, exchange and cryst. field effects 80—24857

cobalt alloys continued
$SmCo_5$ films, struct. transformations effect on coercive force and mag. reversal *(Russian)* 80–20436
$SmCo_5$, H_2 absorption in thin film hydriding alloys 80–65238
$SmCo_5$, hard mag. props., book contrib. 80–39759
$SmCo_5$, high coercivity isotropic plasma-sprayed magnet, eutectoid decomp. 80–80568
$SmCo_5$ hydride films, mag. props. 78–68306
$SmCo_5$, hyperfine field exam. by NMR spin echo 78–23365
$SmCo_5$, improvement of mag. domain contrast in SE-mode of SEM *(German)* 77–51920
$SmCo_5$, intrinsic coercivity losses, temp. depend. 78–95468
$SmCo_5$, intrinsic magnetic props. 79–82779
$SmCo_5$ isotropic plasma sprayed magnet, high coercivity 78–68295
$SmCo_5$, isotropic plasma-sprayed high coercivity magnet, eutectoid decomp. 80–75810
$SmCo_5$, mag. properties in low temp. range, obs. *(Russian)* 77–73050
$SmCo_5$, mag. props., effect of phase and struct. transforms. during liq.-phase sintering 79–100086
$SmCo_5$, magnetic aftereffect of H and D 79–56573
$SmCo_5$ magnetic alloys, pressed, sintering rel. to mag. props., cryst. struct. 78–60600
$SmCo_5$, magnetic anisotropy, Co contrib., ^{59}Co NMR Obs. 78–43583
$SmCo_5$, magnetic fastening for piezoelectric accelerometer 79–77035
$SmCo_5$ magnets, ageing at high temp. 80–7129
$SmCo_5$ magnets, effect of heat treatment on coercive force *(Russian)* 79–1684
$SmCo_5$ magnets, magnetisation and demagnetisation, heating effects 79–38357
$SmCo_5$, nucleation of reversed domains at Co_7Sm_2 precips. 80–75791
$SmCo_5$ permanent magnet, liq. phase sintered, hysteresis loops, ageing, temp. depend. *(Chinese)* 77–51921
$SmCo_5$, permanent magnet stability, during long-term ageing *(Chinese)* 80–55428
$SmCo_5$ permanent magnets, crystal texture effects on props. 80–100600
$SmCo_5$, polished, domain wall grooving, optical microscopy and SEM obs. 77–8334
$SmCo_5$, powder, comminution temp. effect on mag. props. 80–39819
$SmCo_5$, powder, exam. of protective preps. of organic media against oxidation 79–96220
$SmCo_5$ powder alloy, densification by cold working 77–4753
$SmCo_5$, powder prod. by electroerosion mag. props. 77–59718
$SmCo_5$ powders, orientability and texture, milling time effect 79–100168
$SmCo_5$, radial pulse magnetisation, magnetising and testing fixtures 77–8354
$SmCo_5$, remanence and energy product, X-ray method of planar orientation 77–8342
$SmCo_5$, single cryst., grown-in dislocations and stacking faults, TEM investigation 79–19253
$SmCo_5$, single cryst. and liq. phase sintered, magnetostriction, field depend. 77–63245
$SmCo_5$ single crystals subjected to shock waves, magnetisation, creation of high-coercivity state *(Russian)* 77–66384
$SmCo_5$, single crysts., mag. props. study and role of anisotropy *(French)* 79–38356
$SmCo_5$, single-cryst. and liq. phase sintered, elastic stiffness consts., US velocity obs. 77–73066
$SmCo_5$, sintered, anisotropic thermal expansion and fracture of radially oriented toroids *(Chinese)* 80–10686
$SmCo_5$, sintered, hard mag. material, magnetisation behaviour 80–75805
$SmCo_5$, sintered, high coercivity, microstruct. and mag. props. 77–69629
$SmCo_5$, sintered, mag. after-effect, expt. and model 80–75816
$SmCo_5$, sintered, mag. props. *(German)* 77–43852
$SmCo_5$, sintered, magnetic reversal processes *(German)* 77–32216
$SmCo_5$, sintered, orientation of particle easy axes, statistical model 77–8305
$SmCo_5$ sintered alloy magnetic properties *(Russian)* 78–72369
$SmCo_5$, sintered alloy permanent magnets, temp. depend. of domain struct. *(Russian)* 77–66380
$SmCo_5$ sintered magnets, periodic struct. and coercive force *(Russian)* 79–28554
$SmCo_5$ sintered magnets, struct. and magnetic characts., sintering temp. influence *(Russian)* 79–52397
$SmCo_5$ sintered magnets, eutectoid decomp. 80–89219
$SmCo_5$, sintered permanent magnet, mag. props., 4.2-300K, fields up to 100 kOe 77–8341
$SmCo_5$, sintered permanent magnet manufacture 80–20838
$SmCo_5$, Sm_2Co_{17}, magnetisation temp. depend., exchange and cryst. field effects 77–51890
$SmCo_5$, specific heat and kinetic props. at elevated temp. *(Russian)* 79–28530
$SmCo_5$ spheres, exam. of sintering in vacuum and Ar atmospheres 78–84738
$SmCo_5$, spin polarised energy band struct., APW calc. 78–10342
$SmCo_5$, sprayed magnet, microstruct. and mag. props. between 650°c and 800°C 79–82829
$SmCo_5$, substituted alloy, low reversible temp. coeff. 78–68178
$SmCo_5$, temp. depend. of Sm^{3+} magnetisation, exchange and cryst. field effects 77–8302
$SmCo_5$, temp. depend. of Sm mag. form factor, polarized neutron expts. 79–78329
$SmCo_5$ thin film, hydride form., kinetics, mag. monitoring 80–35571
$SmCo_5$, vacuum-deposited, eutectoid decomp. *(Russian)* 77–66621
$SmCo_5$, X-ray K absorpt., chem. shift 79–91531
$SmCo_{5+x}$, Cu and Fe modified, coercive force, demagnetization curves *(Czech)* 79–42805
$SmCo_x$-Fe composite permanent magnet material, mag. props. 77–40089
Sm_2Co_{17}, coercive force depend. on annealing temp. 80–65964
Sm_2Co_7 sintered magnets, coercive force and constitution, annealing temp. depend. *(Russian)* 80–88786
Sm_xCo_y, mag. and struct. investigations of intermetallic systems 78–95440
Sm_xCo_y, mag. props. 78–43568
$Sm_2(Co_{1-x}Al_x)_{17}$ *(Russian)* 78–64202
$Sm_2Co_{17-x}Al_x$, magnetisation, Curie temp., anisotropy 77–89947
$SmCo_3B_2$, high coercive forces, ferromag. ordering and saturation moments 77–24711
$Sm(Co_{0.65}Cu_{0.35})_{5.6}$, cryst. struct. and coercive force, heat treatment effects *(Russian)* 80–44170
$Sm(Co_{0.84}Cu_{0.16})_{6.9}$, microstruct. and domain struct., mag. reversal *(Russian)* 80–20429

cobalt alloys continued
$Sm(Co_{0.87}Cu_{0.13})_{7.8}$, coercivity and microstruct. 79–56569
$Sm(Co_{1-x}Cu_x)_{7.8}$ alloys, coercive fields, domain wall energies, mag. and metallographic exam. 78–91897
$SmCo_{3.5}Cu_{1.5}$, mag. aftereffects, coercive mechanism, magnetisation reversal 77–69634
$SmCo_{3.5}Cu_{1.5}$, single cryst., domain wall motion and domain form. 78–39359
$SmCo_{3.5}Cu_{1.5}$, single crysts., mag. props. study and role of anisotropy *(French)* 79–38356
$SmCo_{3.5}Cu_{1.5}$, time dependent magnetisation 78–80176
$SmCo_4Cu$, domain boundaries shift, mag. reversal processes 79–87286
$SmCo_4Cu$, nonuniform comp., domain struct. and mag. reversals process *(Russian)* 79–1681
$SmCo_{4.3}Cu_{0.7}$, highly anisotropic ferromag., mag. state after large Barkhausen jump *(Russian)* 79–4699
$SmCo_{5-x}Cu_x$, giant intrinsic mag. hardness obs. 77–59432
$SmCo_{5-x}Cu_x$, giant intrinsic mag. hardness 79–91255
$SmCo_{5-x}Cu_x$ magnet alloy, metallurgical study *(Korean)* 77–8853
$SmCo_{5-y}Cu_y$, giant intrinsic magnetic hardness, high field meas. 78–68289
$Sm(Co_{0.81}Cu_{0.15}Fe_{0.04})_{6.9}$ and $Sm(Co_{0.84}Cu_{0.16})_{6.9}$ powders, mag. props. *(Russian)* 80–20434
$Sm(Co_{0.86-x}Cu_{0.14}Fe_x)_7$, permanent magnet, sintering and heat treatment effects 80–39817
$Sm_2(Co_{1-x}Fe_x)_{17}$, anisotropy consts., conc. and temp. depend. *(Russian)* 78–64202
$Sm_2(Co_{1-x}Fe_x)_{17}$, magnetocryst. anisotropy, Tb, Mn or Cr substituent effects 77–8297
$Sm(Co_{0.85}Fe_{0.05}Cu_{0.10})_z$, coercive force meas. 77–4530
$Sm(CoFeCuMn)_7$, coercive force and anisotropy temp. depend. 78–68297
$Sm_2(Co_{0.8}Fe_{0.14}Mn_{0.04}Cr_{0.02})_{17}$, sintered, hard mag. props. 77–8340
Sm_3Co_3Ga, crystal struct., X-ray determ. *(Russian)* 79–27951
$Sm_2(Co_{1-x}M_x)_{17}$, bulk magnetisation and magnetocryst. anisotropy, interpretation 77–40055
$Sm_2(Co_{1-x}M_x)_{17}$, magnetocryst. anisotropy 77–40054
$Sm_2Co_{17-x}M_x$, M=Cr, Ni, effect of substitution on mag. props. 79–78363
$SmCo_2Ni_3$-Y(Pr)(Gd)(Tb)(Er), giant intrinsic magnetic hardness 78–56347
$SmCo_{2.5}Ni_{2.5}$, mag. after effect *(Russian)* 78–6544
$SmCo_{5-x}Ni_x$, giant intrinsic mag. hardness, temp. and time depend. 77–69627
$SmCo_{5-x}Ni_x$, giant intrinsic magnetic hardness, high field meas. 78–68289
$SmCo_{5-x}Ni_x$, giant intrinsic magnetic hardness analysis 78–88146
$SmCo_{5c}Ni_{5-5C}$, exchange fluctuations and giant intrinsic mag. hardness 78–56310
$Sm_2Co_{17-x}Ni_x$, effect of Ni on mag. props. 78–68296
$Sm_2Cu_{1.6}Zr_{0.16}Fe_{3.3}Co_{12}$, enhancement of mag. props. 79–82825
$Sm_xDy_{1-x}Co_5$, temp. compensated magnetic material, mag. and struct. characterisation 78–68177
$Sm_xEr_{1-x}Co_5$, temp. compensated magnetic material, mag. and struct. characterisation 78–68177
$Sm_{2-x}Gd_xCo_{17-y}Mn_y$, saturation magnetisation and anisotropy field temp. depend., suitability for microwave/millimetre wave TWT 79–82824
$Sm_{1-w}MM_w(Co_{1-x-y}Cu_xFe)_z$, (MM-mischmetal), mag. meas. and metallographic exam. 77–56119
$Sm_{1-x}Nd_xCo_5$ alloys, magnetisation, magnetocrystalline anisotropy, 4.2 to 280K 78–91863
$Sm_xNd_{1-x}Co_5$ powders, mag. props. *(Russian)* 79–51812
$Sm_{0.5}Pr_{0.5}Co_5$, sintered alloy permanent magnets, temp. depend. of domain struct. *(Russian)* 77–66380
$Sm_{0.5}Pr_{0.5}Co_5$ sintered magnets, periodic struct. and coercive force *(Russian)* 79–28554
$Sm_{1-x}Pr_xCo_5$ single crystals, magnetocryst. anisotropy and stepwise mag. reversals *(Russian)* 77–66291
$Sm_xTb_{1-x}Co_5$, temp. compensated magnetic material, mag. and struct. characterisation 78–68177
$Sm_{0.91}Zr_{0.09}(Co_{0.68}Cu_{0.10}Fe_{0.22})_{6.7}$, alloy permanent magnet, coercive force *(Russian)* 80–65966
Sn-Co alloy plating from sulphate electrolyte 80–16597
Sn-Co liq., elec. resist. and thermoelec. power using t matrix approach 77–31988
$SnCo_5$, magnetisation and cohesive strength 77–55688
$Sr_2(Co_{1-x}M_x)_{17}$, M=Mn, Ti, Zr, powders, influence of substitutes on mag. props. 80–100601
TC-Co, nearest-neighbour size correlation with grain size *(French)* 77–8843
Ta-Co amorphous metal films, struct. and elec. characterisation 79–87017
Tb-Co, amorphous film, Kerr and Hall effect meas. 77–24722
$TbCo_2$, magnetocryst. anisotropy props. by ^{57}Fe Mossbauer spectroscopy 77–63328
$TbCo_2$, magnetocrystalline anisotropy and spontaneous magnetostriction 80–75831
$TbCo_2$, origin of magnetostriction 79–78499
$TbCo_2$, polarised neutron diffr. exam. of mag. struct. 79–73681
$TbCo_2$, rhombohedral distortion at low temp. 80–34743
$TbCo_2$, spontaneous distortion, mag. props. due to cryst. field, exchange field, magnetoelastic energy 79–61096
$TbCo_2$, X-ray obs. of low temp. modifications of crystal struct. *(Russian)* 78–75632
$TbCo_3$, X-ray absorpt. edge shifts 80–25483
$TbCo_5$, mag. state of Tb sublattice neutron diffr. meas. *(Russian)* 77–80915
$TbCo_{5.1}$, singularities of mag. transition *(Russian)* 77–77053
$TbCo_{5.1}$, sublattice magnetisation, temp. depend., neutron diffr. anal. *(Russian)* 80–103815
Tb_2Co_{17}, magnetisation, magnetocryst. anisotropy and magnetostriction 77–8303
Tb_4Co_3, cryst. field effect on mag. moment direction, neutron diffr. meas. 78–80132
Tb_3Co_3Ga, crystal struct., X-ray determ. *(Russian)* 79–27951
$(Tb_{1-x}Gd_x)_3Co$, intermetallic cpd. mag. props., phase transform, and mag. hystersis *(Russian)* 80–93113
$(Tb_{1-x}Y_x)_3Co$, mag. props. and transitions, conc. depend. *(Russian)* 78–10671
Te-Co, dil. liq. alloy, elec. cond. at high temp. and press. 78–87959

cobalt alloys continued
$ThCo_5$ itinerant electron metamagnetism, polarised neutron study 80—39742
$ThCo_5$, lattice consts., magnetisation, and anisotropy fields 79—78364
$ThCo_5$, mag. transition due to Co moment change, metamagnetism of 3d-band 77—63184
Th_7Co_3, effect of absorbed H_2 on mag. behaviour 80—60184
Th_7Co_3, spin-pairing state investig. via Josephson current between weakly coupled superconductors 77—47942
$ThCo_{5-x}Al_x$, homogeneity regions, X-ray powder diffr. study 79—77554
$ThCo_{5-x}Mn_x$, struct. and magnetisation exam., temp. depend. 78—2662
$Th_{1-x}Y_xCo_{5-y}Fe_y$, lattice consts., magnetisation, and anisotropy fields 79—78364
(Ti,Al)Co, magnetovolume effects near crit. conc. for ferromag. 79—56591
Ti-Co, eutectoid decomposition 79—24491
Ti-Co, oxidation of intermetallic phases 79—100298
Ti-Co, radiation disorder model of phase stability 80—16297
Ti-Co, X-ray emission spectra investigation of electron struct. of Laves phases *(Russian)* 78—23554
Ti-Co alloys, absorpt. of H_2, press.-composition-temp. relationships, enthalpy, entropy 80—2267
Ti-Co alloys, absorpt. of H_2, thermodynamic parameters calc. 80—2268
Ti-Co-Al(Ga), Th_6Mn_{23} type struct., mag. susceptibility *(Russian)* 79—42736
Ti-Ni-Co, constitution diagram, isothermal section, interdiffusion coeffs. *(Russian)* 80—89200
Ti-Ni-Co, shape memory temp., alloying effect 79—38912
Ti-Ni-Co cubic B_2 alloys, phonon enhancement of electronic sp. ht. near martensitic transform. 79—60522
Ti-Ta-Co system, phase stability, X-ray anal. 79—61580
$Ti(Al_xCo_{1-x})_2$, $0<x<0.4$, influence of Al on H sorption props. X-ray cryst. struct. determ. 79—28198
TiC coated WC-Co cemented carbides, fracture toughness 80—85046
TiC-Ni-Co-Cr, sintered, mech. props. effect of processing factors 78—11159
$TiC-TiB_2-Co$ coatings, deposited by electron evaporation, struct. and props. 79—23871
TiCo, and TiCoSi(Ge), electronic struct., X-ray K- and L-spectra obs. *(Russian)* 78—11022
TiCo-H system, thermodynamic rels. and struct. transformations 80—49385
$TiCo_{2+x}$ ($x=-0.06$, 0.0, 0.13), stacking faults in cubic Laves phase 80—19816
$Ti_{1-x}Co_x$, electronic struct. and anomalies of elec. and mag. props. 80—6710
$Ti_{70}Co_{20}B_{10}$, amorphous alloys, crystn. behaviour, TEM study *(Japanese)* 80—84087
$TiCo_{1-x}Mn_x$, H absorption-desorption characteristics 80—96735
Ti(Fe, Co), itinerant ferromagnet, magneto-volume expts. 77—66404
Ti(Fe,Co), magnetovolume effects near crit. conc. for ferromag. 79—56591
Ti(Fe, Co), off-stoichiometric alloy, inverse mag. susceptibility rel. to defect conc. 80—60216
$Ti(Fe,Co)H_y$, mag. and ^{57}Fe Mossbauer studies 80—71272
$Ti(Fe-Co)_2$, itinerant electron ferromagnet, magnetovolume effects 80—60397
$Ti(Fe_{1-x}Co_x)$, density of states estimation from magnetisation and resistivity meas. 78—84119
$TiFe_{1-x}Co_x$, electronic struct. and mag. moment calcs. 80—65821
$Ti(Fe_{1-x}Co_x)$, ferro- to paramag. transition, press. depend. 77—73028
$TiFe_{1-x}Co_x$, mag. props., under high press. and in high mag. fields 78—95423
$TiFe_xCo_{1-x}$, thermal expansion and magnetoelastic effects 80—80585
$TmCo_2$, ^{169}Tm Mossbauer effect 80—71261
$TmCo_2$, paramag. and ordered phases, Pauli type, Co susceptibility, polarised neutron diffr. obs. 77—63077
$TmCo_5$, covalent electron number, from chem. shift of Co X-ray absorption spectra 77—59641
$TmCo_5$, easy magnetisation direction 78—84415
Tm_2Co_{17}, single cryst., magnetostriction const. temp. depend., 78 to 300K 79—51836
Tm_4Co_3, cryst. field effect on mag. moment direction, neutron diffr. meas. 78—80132
$Tm_2Fe_{17-x}Co_x$, and related cpds., easy magnetisation direction, Mossbauer spectra 77—63169
U-Co metallic glasses, glass form. and thermal stability 80—75183
U-Co-B, isothermal section of phase diagram, X-ray obs. 79—52157
UCo_2, cubic Laves phase, prep. and stoichiometry 79—24459
UCo_2, elec. resist. and mag. susceptibility meas., non-stoichiometry influence 77—63088
UCo_2 Laves phase, alloy systematics, rel. to the long periodic table 79—37649
UCo_2, mag. props., ferromag. transition *(Russian)* 78—68148
UCo_2, surface comp. and electronic struct., photoemission study 80—66382
$UCo_{5.3}$, mag. props., cryst. and domain struct. *(Russian)* 77—4529
$UCo_{5.3}$, mag. props. and cryst. struct. *(Russian)* 77—51925
$U(Co_{1-x}Fe_x)_2$, ferromag. onset, susceptibility and resist. meas. 80—70967
$U(Co_xNi_{1-x})_2$, cryst. struct. and mag. props. at 4.2K 80—54175
$U_{10}Co_{51}Si_{33}$, crystal struct., dimensions, space group and coord. *(Russian)* 80—88085
$U_2Co_3Si_5$, cryst. struct. 78—47285
$U_6Co_{30}Si_{19}$, X-ray cryst. struct. determ. 80—107111
UMn_2-UCo_2, mag. props., ferromag. transition *(Russian)* 78—68148
V-Co sigma phase alloys, NMR and electric-field gradients 80—108109
V-Fe, ^{57}Co Mossbauer spectra, diffusion mechanism of Fe 80—15292
V_3Co, nuclear spin-lattice relax. time, electronic density of states 77—59354
$V_{3-x}Co_xGa$, cryst. struct. and microhardness meas. 79—86740
$V_{75-x}Co_xGa_{25}$, supercond. transition temp. and electron-phonon coupling parameter 79—60952
V_3Si-Co solid soln., supercond. T_c and paramag. susceptibility *(Russian)* 77—59348
Vitallium, orthopaedic implant material, metallurgical cond. effect on pitting resistance 79—70704
W fibre reinforced, alloy by effect on struct. stability, mech. props., metallographic exam. 78—56600
W-Co, carburizing rate, Co effects *(Japanese)* 79—52453
W-Co, dil., excess resistivity, temp. depend., Kondo effect 78—68011
W-Co mixed powder, carburizing *(Japanese)* 79—52454

cobalt alloys continued
W-Cu contact materials with Ni and Co dopants, sintering 77—55908
W-Cu-Co, contact materials, activated sintering, Co effects 79—95967
W-Cu-Co, electrical contact material, comparison of Co and Ni effects *(Korean)* 78—10539
W-Fe-Co, sintering and mechanical props. *(Japanese)* 80—21086
W-Ni-Co, structural characterisation *(French)* 77—56074
W-Ni(Co) point-contact diodes as harmonic generators and mixers, DC bias dependence 80—75653
WC-Co, (3%), meas. of yield stress by compressive loading 79—54150
WC-Co, calc. of weakest link in struct. 80—11730
WC-Co, cemented carbide sintered, appl. of dihedral angle meas. to microstruct. 78—39716
WC-Co, cemented carbide, deformation, high temp., stress relaxation, and strain rate depend. 78—39854
WC-Co, comparison of indentation crack resistance, and fracture toughness 78—76739
WC-Co, composition and oxidation resistance of coatings deposited by thermal diffusion, using TiB_2 *(Bulgarian)* 80—45430
WC-Co, conditioned metal electrode, effect on electrical strength of vacuum gap 79—90489
WC-Co, contact reaction with BN at high pressures 80—61029
WC-Co, creep rupture strength meas. 78—31475
WC-Co, elastic and plastic charact. 80—35280
WC-Co, elastic moduli and their press. derivatives 79—83248
WC-Co, elemental and phase comp. of diffusion-deposited boride coatings 80—15402
WC-Co, evidence for H embrittlement 78—48530
WC-Co, exam. of effect of continuous carbide phase, on hardness, and deformation 78—52974
WC-Co, fracture toughness testing by double torsion bend test 78—27705
WC-Co, nearest-neighbour size correlation with grain size *(French)* 77—8843
WC-Co, on-line computer anal. of SEM obs. 79—87807
WC-Co, phase comp. and oxidation resist. of coatings deposited by thermal diffusion using TiB_2 80—21173
WC-Co, precursor derived powder, prep. 77—32541
WC-Co, prep. temp. effect on fine struct. of WC phase, X-ray obs. 79—33971
WC-Co, quantitative charact. of surface damage by electrochemical grinding 79—47836
WC-Co, rupture of bending specimens, use of quantitative metallography and stereology *(French)* 77—28899
WC-Co, rupture stress, microstructure and other effects 77—73343
WC-Co, STEM anal. of grain boundaries 80—79644
WC-Co, sintered, obs. of spinel particles by TEM 78—95714
WC-Co, sintered hard alloy, mechanism of penetration of liquid metals 78—60619
WC-Co, size factor effect on strength in complex stressed state 78—31483
WC-Co, TiC coated, TiC stoichiometry effects on mech. props. 77—66715
WC-Co, VK type hard alloy, influence of residual stresses on static strength 77—1862
WC-Co, various combinations, fracture characts. in bending, compression, and toughness tests 78—60808
WC-Co (10 to 30 wt.%) transverse rupture strength, residual stresses due to surface grinding effects 77—63789
WC-Co (10 wt.%), elevated temp. bend deform. and fracture, effect of C 77—59877
WC-Co (10 wt.%), high temp. transverse rupture strength 77—63790
WC-Co (10 wt.%), vacuum sintered, short-time bending creep rupture strength *(Japanese)* 78—15508
WC-Co (10%), cycle fatigue, optical microscopy and SEM obs. 77—52494
WC-Co (12 wt.%), sintering with various binding phases *(German)* 79—28984
WC-Co (15 wt.%), alloy VK15 coating on Ti-Al, detonation sprayed, antifriction props. 80—21188
WC-Co (15 wt.%), detonation spray deposited hard alloy coating, electrical conductivity 77—12025
WC-Co (15 wt.%) detonation spraying on to Cr-Ni steel with automatic powder feed 80—25558
WC-Co (5wt.%) hardmetal, η-phase precipitation effect on struct. and mech. props. 79—47696
WC-Co (6 to 20 wt.%), bend deform. and fracture up to 1000°C 77—48510
WC-Co alloy, hard metal, resistance of cavitation erosion *(Japanese)* 80—16575
WC-Co alloy, short-time creep rupture strength, C content effect 400° to 900°C *(Japanese)* 78—48487
WC-Co alloy, transverse rupture strength rel. to grain size and strain rate, 400° to 900°C *(Japanese)* 78—48486
WC-Co alloy time-depend. strength params. 78—31516
WC-Co alloys, brittle fracture, precision matching of mating fracture surfaces, by SEM fractographs 78—60807
WC-Co alloys, fracture toughness model 80—84243
WC-Co alloys, microstresses in two phases, mag. investig. 77—59879
WC-Co alloys, P additions, effect on hot pressing, hardness and wear resist. 78—11162
WC-Co alloys, single edge notched beams, exam. of fracture toughness 78—52975
WC-Co alloys fracture, spatially constrained crack tip opening displacement 77—77580
WC-Co and WC-Co-TaC-TiC-NbC cemented carbides, microstructure, high temp. deformation, uniaxial plastic compression 80—40451
WC-Co based cutting tools, temperature meas. method based on amount of W in binder 79—96264
WC-Co carbide, crack paths, SEM study *(Japanese)* 80—50710
WC-Co cemented carbide, bending strength, surface roughness effects *(German)* 77—8947
WC-Co cemented carbide, carbide grain size effect on strength rel. to structural defects 77—32689
WC-Co cemented carbide, relation between transverse rupture and tensile rupture *(Japanese)* 77—52473
WC-Co cemented carbide, indentation fracture, operative fracture mode survey 77—70183
WC-Co cemented carbide, fracture toughness meas., model for variation with microstruct. 78—60806

cobalt alloys continued
WC-Co cemented carbide, stress-strain curves using ultrahigh-pressure apparatus 79—43322
WC-Co cemented carbides, effect of Co form and distrib. in prep. starting mixture 78—44072
WC-Co cemented carbides, high temp. transverse rupture strength, effect of domain size of binder phase *(Japanese)* 78—92329
WC-Co cemented carbides, rel. between Palmqvist indentation toughness and fracture toughness 79—70155
WC-Co cemented carbides, transverse-rupture strength obs., w.r.t. domain size of binder phase *(Japanese)* 80—11741
WC-Co cermet, dynamic SEM wear obs. 77—36667
WC-Co compacts and sintered alloy, fine struct. of carbide phases, preforms re-pressing under high press. effect 79—28987
WC-Co composite, ion scatt. spectrometry and AES 77—60150
WC-Co cutting plates, hardness and struct. of TiB_2 coatings 80—21175
WC-Co from directionally carburized WO_3-C-Co_3O_4 mixtures, sinking *(Japanese)* 80—11589
WC-Co hard alloy, preheating influence on explosive shock hardening *(Russian)* 79—29083
WC-Co hard alloys, hot pressed, mech. props. 79—100260
WC-Co hard alloys, hot-pressed, wear resist. under abrasive friction, heat treatment effect 80—66555
WC-Co hard alloys, machined with polycryst. superhard materials, surface struct. using X-ray photoelectron spectroscopy 80—25919
WC-Co hard metal, binder phase charact. by magnetic props. 79—29439
WC-Co hard metal, stress conc. factor and stress intensity factor, rel. to wear *(German)* 78—11335
WC-Co hard-alloy cermets, strength, fatigue, static tests 79—29314
WC-Co hardmetal, defect initiated fracture and bond strength 78—11319
WC-Co hardmetals, β-SiC to turbostratic graphite transformation 79—74150
WC-Co hardmetals, heat-treated, single domain obs. 79—73771
WC-Co mixed powder prod. by rotary kiln, new continuous process 78—64502
WC-Co molten Zn reaction, lamellar struct. form. 79—33964
WC-Co particle-matrix composite, fracture and cleavage strength 77—73342
WC-Co powder, prep. by direct carburisation of WO_3 in presence of Co_3O_4 80—50573
WC-Co powder form. from Wo_3 and Co_3O_4 carburization, C behaviour *(Japanese)* 80—7517
WC-Co sintered carbide tips, microscopic stress anal. 78—5663
WC-Co sintered hard alloy, yield stress, internal thermal stress effect 79—100230
WC-Co sphere, erosion of Al by solid particle impingement at normal incidence 80—104304
WC-Co substrate, load-bearing capacities of TiC layers 80—40606
WC-Co-C, densification kinetics, in hot pressing of VK6 hard alloy 80—11600
WC-Co-Cu, interdiffusion up to 1120°C 78—11492
WC-Co-Ta, cemented carbide, deformation, high temp., stress relaxation, and strain rate depend. 78—39854
WC-Co(TiC-Co), powder compacts, effect of additional pressing at hydrostatic pressures on props. 78—56596
WC-NbC-Co, TiC and TiN coating by ion plating, and cutting tests 79—24678
WC-TaC-Co, cemented carbide, strength improvement by hot isostatic pressing 78—84969
WC-TiC-Co, powder for plasma arc sprayed coating 78—15591
WC-TiC-Co alloys, microstresses in two- and three-phases, mag. investig. 77—63758
WC-TiC-TaC-Co cemented carbides, transverse-rupture strength at 600 to 1000°C obs. *(Japanese)* 79—43374
WC-TiC-Ta(Nb)C-Co, CVD and activated reactive evaporation of TiC, AES obs. of substrate-layer interactions 79—24679
WC-TiC(TaC, NiC)-Co, hard, homogeneity and wear resistance estimation, by magnetic method 77—90558
W_6Co_6C cemented carbide, with CVD TiC coating, structure, composition and hardness exam. 78—11425
Y-Co, amorphous, thermal stability, crystn., DSC and elec. resist. study 80—107060
Y-Co, amorphous alloy film, spin reson. meas., exchange stiffness 78—68389
Y-Co, CPA calcs., moments and transition temps. 78—52252
Y-Co, Curie temp. determ. 79—65672
Y-Co, ferromagnet, first and second order transitions 80—34631
Y-Co, hyperfine fields, NMR spin echo 77—63318
Y-Co-Mn, amorphous, paramag. props. and Hall effect 79—73692
YCo_2, anomalous high-field magnetisation 78—47958
YCo_2, density of states, mag. props. 79—90936
YCo_3, amorphous ferromagnet, exchange dominated surface modes 78—52359
YCo_3 amorphous film, domain struct., influence of planar anisotropy 79—78472
YCo_3 amorphous films, ^{59}Co spin echo study 80—80636
YCo_3 film, amorphous, DC sputtered, easy axis and easy plane magnetisation 78—64237
YCo_3 film, amorphous, induced and surface anisotropies, ferromag. reson. and static meas. 77—85507
YCo_3 film, amorphous, impurity like relaxation mechanism 79—73820
YCo_3 film, amorphous, sputtered, in-plane anisotropy induced by rare gas annealing 78—84458
YCo_3, hydride phase synthesis, thermal stability and struct. 80—59438
YCo_5, coercivity, random substitution of Y by Co *(Chinese)* 77—8343
YCo_5, covalent electron number, from chem. shift of Co X-ray absorption spectra 77—59641
YCo_5, NMR enhancement of modulating field due to anisotropic component of hyperfine field 77—55729
YCo_5, solubility of H_2 *(Russian)* 78—15356
YCo_5, spin polarised energy band struct., APW calc. 78—10342
YCo_5, substituted, magnetocryst. anisotropy, different contribs. of two Co sites 77—8301
YCo_5, uniaxial intermetallic, large magnetisation anisotropy 80—71011
YCo_x, mag. interactions, exchange fields, mol. field model 77—4498
YCo_x, mag. interactions, effects on moments *(Rumanian)* 79—15296
$Y_{1-x}Co_x$, amorphous, conc. depend. of Co moment 78—56300
$Y_{1-x}Co_x$, amorphous, mag. props. 80—84590
$Y_{1-x}Co_x$, temp. depend. of magnetisation 77—77043
$Y_{2+x}Co_{17-2x}$ single crystal, magnetocrystalline anisotropy 79—38320

cobalt alloys continued
Y_2Co_{17}, and $Y_{2x}Dy_{2(1-x)}Co_{17}$, magnetocryst. anisotropy, 77-383K 77—89949
Y_2Co_{17}, NMR spin echo meas., dipolar field anisotropy 80—71236
Y_xCo_y, NMR meas. of ^{59}Co 77—85585
$Y_2(Co_{1-x}Al_x)_{17}$, low-temperature sp. ht. meas. 79—56541
$Y(Co_{1-x}Cu_x)_5$, neutron diffr., thermal expsn. *(French)* 80—19749
$Y(Co_{1-x}Cu_x)_5$, neutron diffraction study *(Chinese)* 80—39000
$Y_2(Co_{0.31}Fe_{0.69})_{19.2}$, statistical site occupancy deviations, neutron diffr. investig. 77—7717
$Y_2(Co_xFe_{1-x})_{17}$, mag. anisotropy assoc. with Fe substitution 78—76240
Y_3Co_3Ga, crystal struct., X-ray determ. *(Russian)* 79—27951
$Y_2(Co_{1-x}M_x)_{17}$, bulk magnetisation and magnetocryst. anisotropy interpretation 77—40055
$Y_2(Co_{1-x}M_x)_{17}$, M=Al, Cu, single crystal, mag. props. 77—47993
$Y_2(Co_{1-x}M_x)_{17}$, magnetocryst. anisotropy 77—40054
$Y(Co_{1-x}Ni_x)_5$, distrib. of Co and Ni atoms, neutron diffr. obs. *(Russian)* 80—64954
$Y(Co_{1-x}Ni_x)_5$, mag. heterogeneities and coercive force, neutron scatt. study 80—2553
$Y(Co_{1-x}Ni_x)_5$, spontaneous magnetisation mag. anisotropy, spin reorientation transformation *(Russian)* 80—7082
$Y_2Co_{17-x}Ni_x$, effect of Ni or mag. props. 78—68296
$Y_{1-x}Dy_xCo_5$, NMR meas. of ^{59}Co 77—85585
$Y_2(Fe,Co)_{17}$, mag. anisotropy fields by singular pt. detection 79—24156
$Y_2(Fe,Co)_{17}$, magnetic anisotropy meas. by singular point detection method 77—63170
$Y(Fe_xCO_{1-x})_2$ model, Co, mean mag. moment composition depend.; reciprocal susceptibility, thermal var. 78—47945
$Y(Fe_{0.022}Co_{0.978})_2$, ferromag. relax. model, Mossbauer spectra 80—15853
$Y(Fe_{0.022}Co_{0.978})_2$ mag. props., Mossbauer expts., 0.15-4.2K 78—43712
$Y(Fe_{1-x}Co_x)_2$, mag. hyperfine field, conc. depend., Mossbauer expts. 77—63337
$Y(Fe_{1-x}Co_x)_2$, mag. saturation moment, Co conc. depend., NMR exam. 78—15037
$Y(Fe_{1-x}Co_x)_2$, NMR study 80—75882
$Y(Fe_xCo_{1-x})_2$, $0.5 \geq x \geq 0.2$, Mossbauer effect meas., 5 to 300K *(German)* 77—24771
$Y(Fe_xCo_{1-x})_2$, compositional dependence of Co's mean mag. moment, local environment model anal. 78—43560
$Y(Fe_xCo_{1-x})_2$, ferromag. reson. of pseudobinary cubic compounds 78—91961
$Y(Fe_xCo_{1-x})_2$, Mossbauer effect at 78 and 300K, ^{57}Fe hyperfine fields 80—2677
$Y(Fe_xCo_{1-x})_2$, $x \leq 0.2$, mag. props. and Mossbauer meas. 80—75798
$Y_2(Fe_{1-x}Co_x)_{17}$, hyperfine interactions, Mossbauer spectra 78—2780
$Y(Fe_{1-}xCo_x)_2$, electronic sp. ht. meas., rel. to mag. props. 77—63197
$Y_{1-x}GdCo_5$, exchange interactions and magnetocrystalline anisotropy 80—34618
$Y_{1-x}Gd_xCo_2$, NMR meas. of ^{59}Co 77—85585
$Y_{1-x}Gd_xCo_2$, NMR of ^{59}Co 78—52376
$(Y_{1-x}Gd_x)Co_2$, spin echo NMR of mag. states 80—7190
$(Y_{1-x}Gd_x)_2Co_{17}$, ^{59}Co NMR, hyperfine fields and contrib. of 4f electrons 77—20727
$Y_{1-x}Ho_xCo_5$, NMR meas. of ^{59}Co 77—85585
$YMn_{2-x}Co_x$, mag. order in pseudobinary region 79—99689
$Y_{0.25}Nd_{0.75}Co_5$, basal plane anisotropy 77—8295
$Y_{1-x}Nd_xCo_5$, exchange interactions and magnetocrystalline anisotropy 80—34618
$Y_{1-x}R_xCo_5$, R=Gd,Tb,Nd, ferrimag., magnetisation, exchange interactions, mag. anisotropy 80—80565
$Y_{1-x}Tb_xCo_5$, spontaneous magnetisation anisotropy, spin reorientation transforms. *(Russian)* 80—7082
$(Y_{1-x}2Co_x)Co_5$, anisotropy fields, coercivities, annealing effects 78—91898
$Yb_2Co_{17-x}Fe_x$, magnetisation, Curie temp., anisotropy 77—89947
Zr-Al-(Fe,Co), H sorption props. for H storage, influence of Al 80—45794
Zr-Co, amorphous alloy film, spin reson. meas. 78—68389
Zr-Co, amorphous and crystalline, d-band struct., alloying effects 80—59862
Zr-Co, oxidation of intermetallic phases 79—100298
Zr-Co amorphous alloy, thermal stability and electronic props. 79—73487
Zr-Co metallic glasses, glass form. and thermal stability 80—75177
Zr-Co-Ga, mag. susceptibility in phases of structural type Th_6Mn_{23} *(Russian)* 79—24130
Zr-Co-H, catalytic props. 80—30274
Zr-Co-H, synthesis at high H pressure exam. of props. 80—29924
$Zr(Al_xCo_{1-x})_2$, Laves phase, H_2 absorption capacity meas. 78—87866
$Zr_{1-x}Co_x$, amorphous, conc. depend. of Co moment 78—56300
$Zr_{70}Co_{30}$ amorphous alloys, struct. factors and radial distrib. functions 80—84096
$Zr_{70}Co_{30}$, metallic glass, low temp. resist., supercond. T_c 79—38235
Zr_2CoGa_3, crystal struct. determ. by single crystal method *(Ukrainian)* 79—51049
$Zr(Co_xM_{1-x})_2$ (M=V,Cr,Mn) H absorption and desorption props. 77—55448
$Zr_3Co_{1-x}M_x$, M=Cu, Ni, Fe, Mn, Ag, and Ru, phase stability and supercond. T_c 78—80519
$Zr_{50}Co_{50-x}Ni_x$, transform. and deform. studies 79—1864
$Zr(Cr_xCo_{1-x})_2$, Laves phase, phenomenological model for H_2 absorption capacity 77—84935
$Zr(Cr_xCo_{1-x})_2$, mag. props. H absorpt. effect 80—88821
$Zr(Fe, Co)_2$, itinerant ferromagnet, magneto-volume expts. 77—66404
$Zr(Fe\text{-}Co)_2$, itinerant electron ferromagnet, magnetovolume effects 80—60397
$Zr(Fe_{1-x}Co_x)_2$, density of states estimation from magnetisation and resistivity meas. 78—84119
$Zr(Fe_{1-x}Co_x)_2$, ferromag. and mictomag., thermal expansion and forced volume magnetostriction 80—75830
$Zr(Fe_{1-x}Co_x)_2$, low temp. sp. ht. and mag. props. 79—61153
$Zr(Fe_{1-x}Co_x)_2$, mag. props. and Mossbauer effects 79—91322
$Zr(Fe_{1-x}Co_x)_2$, mag. saturation moment, Co conc. depend., NMR exam. 78—15037
$Zr(Fe_{1-x}Co_x)_2$, magnetovolume effects, thermal expansion and forced vol. magnetostriction meas. 80—29595
$Zr(Fe_{1-x}Co_x)_2$, mictomagnetism 80—15863
$Zr(Fe_{1-x}Co_x)_2$, NMR study 80—75882
$Zr(Fe_{1-x}Co_x)_2$, press. effects on ferromag. to paramag. transition 77—66302

cobalt alloys continued

- $Zr(Fe_{1-x}Co_x)_y$, transition region, spin glass or long range mag. order 80−44841
- $Zr(Fe_xCo_{1-x})_2$, mag. order in pseudobinary systems down to millikelvin temps. 78−19251
- $Zr(M_xCo_{1-x})_2$ ($M=V$, Cr, Mn), H_2 absorpt. capacity 80−88433
- $Zr(Mn_xCo_{1-x})_2$, Laves phase, phenomenological model for H_2 absorption capacity 77−84935
- $Zr(V_{1-x}Co_x)_2$, relation between electronic struct. and H_2 storing props. 80−76662
- $Zr(V_xCo_{1-x})_2$, Laves phase, phenomenological model for H_2 absorption capacity 77−84935

cobalt compounds

- *see also cobalt alloys*
- aluminosilicate glass:Co (14.3 wt.%), AC susceptibility meas. 80−88771
- bi-univalent cpds., soln., activity coeffs., osmotic coeffs., water activity, Gibbs energy, molality depend. 80−51963
- boranes, $OCH_3(B_9C_2H_{10})_2Co$ and $(C_2H_5)_2Co_2CB_9H_{10}^-$, cryst. struct. *(Czech)* 78−87649
- chalcogenide spinels, thermal stability, thermochemical, thermodynamic and crystallochemical props. 77−51519
- chloride layered compound with graphitised PAN fibre, struct. and elec. cond. 79−91600
- $Co_4Sb_4(CO)_{12}$, electronic struct. calc. *(Russian)* 80−58136
- fac- $(Co(NH_3)_3(NO_2)_3)$, X-ray cryst. struct. determ. 79−60311
- cobalt(III) complex, octahedrally-coordinated with monodentate ligands, optical activity 79−50090
- cobalt(III) complexes, mixed glycylglycinate, synthesis and config. *(French)* 80−2005
- cobalt formate dihydrate, mag. relax. phenomena near T_N 79−65656
- cobalt naphthalate electret, thermally stimulated discharge, 55-75°C 80−25279
- $CoCr_2S_4$ films, galvanomagnetic and thermoelec. props. 80−54717
- complexes, N-substituted salicylaldimine Co(II) and Co(III) complexes, struct. 77−58994
- cyanocobalamin-^{58}Co, whole body retention in rats, age effects 77−70559
- dimethyl glyoximate, molecular struct., cryst. structure 80−79769
- enamels, vitreous, objective colour evaluation rel. to firing parameters *(Czech)* 80−42252
- ferrite, crystal structure, X-ray absorpt. spectra, chemical shifts 80−88118
- ferrite, hot pressed, powders, influence of CoO and CuO alloying on physicomechanical characts. *(Russian)* 77−66600
- ferrite, spinel type catalytic oxidation of CO, role of mag. exchange interactions 78−56916
- ferrites, magnetostriction due to Co^{2+} ions, effect of excited states 80−65990
- formate dihydrate, mag. struct., antiferromag. mode 79−99678
- formate dihydrate, ordered state, paramag. cross relax. *(Japanese)* 77−43873
- intercalation, electron microscopy 80−84164
- myoglobins, Co-substituted, O_2 binding, thermodynamic investig. 80−67030
- oxalate, crystal growth in silicate gel, X-ray diffr. and i.r. spectrum 77−4724
- oxide surface layer, TOF atom probe anal. 78−64766
- oxides, AES meas. 77−36323
- oxides, effective atomic charge rel. to chemical shifts in transition metal compound XAS 79−78788
- phthalocyanide, thermal stability obs., by DTA *(German)* 80−11945
- phthalocyanine, electrochromism and oxidation 80−93768
- phthalocyanine film, sorption of O_2 and water, AES obs. 78−91531
- platino-oxalate, one-dimens. conductors, prep., struct. and elec. cond. 80−24900
- polyphosphinate, bulk compressibility meas. to 30 kbar 80−76306
- rare earth cobalt silicides, RCo_2Si_2, mag. props. 80−107988
- solid solns., determ. of degree of imperfection 77−80624
- spinels, ligand field stabilisation evaluation using Mossbauer determ. cation distrib. 78−31126
- stearate, monomolecular layer, electron escape depth, XPS *(Japanese)* 80−11532
- stearate, monomolecular multilayers, XPS escape length depend. on emission angle, elastic scatt. role *(Japanese)* 80−84833
- ternary compounds, chemical shifts of K X-ray absorption discontinuities 78−19599
- tetramethylammonium cobalt tetrachloride, Raman spectra near incommensurate phase transitions 80−76013
- tetramethylammonium tetrachlorocobaltate, ferroelectricity 78−76408
- trimethyl ammonium cobalt chloride, magnetisation temp. depend. 80−7128
- trimethyl ammonium cobalt chloride dihydrate, antiferromag., ^{59}Co NMR 77−77124
- trimethylammonium cobalt trichloride:CU, bound impurity effect, heat capacity meas. 79−61146
- trimethylammonium cobalt trichloride, mag. heat capacity and Neel temp. in mag. field 79−61147
- trimethylammonium cobalt trichloride, metamagnet, AC susceptibility and exchange consts. 80−70961
- triple orthoarsenates, $KCoCr_2(AsO_4)_3$ and $NaCoCr_2(AsO_4)_3$, prep. by high temp. synthesis, and cryst. struct. 79−66028
- tris (3-mercapto-1, 3-diphenyl-2-propen-1-onato) Co(III), multiple twinning 80−100250
- vanadates, elec. and mag. props., stoichiometry 78−51991
- X-ray K-absorpt. edge, effective nuclear charge 80−35006
- $AgCoPO_4$, crystalline struct. *(French)* 79−1422
- $B_2O_3.Fe_2O_3.2CoO$, mag. props. up to 1200K transitions and magnetisation curves 77−36069
- $BaCo_2(AsO_4)_2$, mag. model, 0K phase diagram, spin wave spectrum 79−87273
- $BaCo_2(AsO_4)_2$, magnetic field effect on mag. ordering neutron diffr. obs. 80−50053
- $BaCo_2(AsO_4)_2$, planar X-Y model, mag. ordering 77−66256
- $BaCo_2(AsO_4)_2$, quasi 2D XY helimag., sp. ht. meas. 79−61151
- $Ba_2Co_{1.65}Fe_{0.35}^{2+}Fe_{28}^{3+}O_{46}$, temp.-mag. field phase diagram, torque method 80−60276
- $BaCo_{1.5}Fe_{16.5}O_{27}$, type W ferrite, spin reorientation 78−60301
- $BaCo_{1.65}Fe_{16.35}O_{27}$, spin reorientation obs. using magneticaloric effect *(Russian)* 77−32195
- $BaCo_2(PO_4)_2$, quasi 2D XY helimag., sp. ht. meas. 79−61151

cobalt compounds continued

- Ba_2CoReO_6, new seignettomagnets and ferroelectrics 78−19425
- $Ba_2Co_{1.75}Zn_{0.25}Fe_{12}O_{22}$, trigonal ferrite, mag. anisotropy 79−73709
- $Ba_2Co_{2x}Zn_{2-2x}Fe_{12}O_{22}$, mechanically oriented, topotactic prod. technique, mag. props. 80−35140
- $BaMn_{0.99}Co_{0.01}F_4$, ferroelec. antiferromag., dielec. anomalies 80−71288
- $BaMn_{0.99}Co_{0.01}F_4$, magnetoelec. phenomena, dielec. behaviour near Neel temp. 80−71151
- $BaZn_{1.38}Co_{0.62}Fe_{16}O_{27}$, W-type hexaferrite cryst., first order magnetisation processes 78−95472
- Bi_2O_3-CoO system, X-ray diffr., thermal anal. and metallography obs. 80−24598
- CO complex, with 1,2,4-triazole, mag. susceptibility, 2-300K, struct. 77−77045
- CO III-EDTA solution, radiolysis by charged particles through $^6Li(n,\alpha)^3H$ reaction 80−93788
- $(CO(NO)_2CL)_2$, order-disorder struct., X-ray data 80−39037
- $CONa_6(SO_4)_4$, vanthoffite cryst. struct., lattice parameters and thermal behaviour 77−19929
- CO_4P, amorphous ferromag., spectral density functions calcs. 79−47269
- CaO-Al_2O_3-SiO_2 glass, remanent magnetisation, log t low 78−68300
- CdTe-Co system, reaction of components, DTA, microstruct. and microhardness obs. 79−38804
- $CeFe_2O_4$, prep. by double decomp. reaction, mag. characts. *(French)* 79−33463
- $(Co,Cd)Cr_2S_4$ and (Co,Cd)S solid soln., equilib. composition *(German)* 77−36486
- $(Co,Cr,Fe)_3O_4$, $(Co,Rh,Fe)_3O_4$ film magnetooptical switches, for laser beam synchronisation 80−58615
- $(Co,Mg)SiF_6.6H_2O$, phase transition at low temp., IR spectra 79−24302
- $(Co,Mn)SiF_6.6H_2O$, phase transition at low temp., IR spectra 79−24302
- $(Co,Mo)S_2$ hydrodesulphurisation catalyst, defect struct. and activity 77−86357
- $(Co,Zn)Cr_2S_4$ and (Co,Zn)S solid soln. equilib. composition *(German)* 77−36486
- $(Co,Zn)SiF_6.6H_2O$, phase transition at low temp., IR spectra 79−24302
- Co acetate, effect on colour attenuation in Cherenkov radiation *(Spanish)* 80−7432
- Co complex, ^{55}Co-bleomycin synthesis from cyclotron prod. ^{57}Ni 77−86629
- Co complex, 1-(2-thiazolylazo)-2-naphtholato Co (III), cryst. struct. 77−11536
- Co complex, 2,6-N,N-diacetyldiaminopyridine-Co(II) elec. cond., γ dose and temp. (303-363K) effects 80−103696
- Co complex, 2,6-N,N-dibenzoyldiaminopyridine-Co(II) elec. cond., γ dose and temp. (303-363K) effects 80−103696
- Co complex, $(NH_3C_6H_5)[Co(SO_3)DH_2(NH_2C_6H_5)](NH_3C_6H_5)ClO_4.H_2O$, cryst. and mol. struct. 80−33980
- Co complex, $[^{57}Co(1,10\text{-phenanthroline})_3](ClO_4)_2.2H_2O$, time differential Mossbauer spectra, aftereffects 78−27131
- Co complex, $[Co(NH_3)_6]I_3$, enantiotropic phase transition obs. 80−107412
- Co complex, bis-(β-diketonato) Co(II) dihydrate, Fe chem. states, Mossbauer emission 80−15917
- Co complex, bis(N-β-napthyl-salicylaldiminato) Co (II), space group, lattice consts., X-ray diffr. obs. 78−51496
- Co complex, bisdimethylglyoxime (thiosemicarbazide)-cobalt (III) nitrate, mol. and cryst. struct. of dihydrate 78−83803
- Co complex, $C0(l\text{-spartein})Cl_2$, IR circular dichroism spectra, vibr.-electronic interaction 80−55074
- Co complex, chemical shift in X-ray absorpt. spectra, effective changes 78−6811
- Co complex, Co II high spin binuclear species, magnetic exchange and anisotropic susceptibilities 78−39308
- Co complex, Co-thiourea compounds, X-ray K-absorpt. edge, effective nuclear charge 80−35006
- Co complex, $CoCl_2(indazole)_2$, linear chain ferromagnetism 79−56519
- Co complex, $CoCl_2(pyrazole)_2$, linear chain ferromagnetism 79−56519
- Co complex, $CoCl_2.2$ pyrazine, mag. sp. ht. below 2K 79−61152
- Co complex, $Co(C_3H_4N_2)_6(NO_3)_2$ and $Co(C_{11}H_{12}ON_2)_6(ClO_4)_2$, paramag., hyperfine sp. ht. 77−55683
- Co complex, $Co(C_5H_5NO)_6(ClO_4)_2$ and $Co(C_5H_5NO)_6(BF_4)_2$, $S={}^1/_2$ XY magnet, sp. ht. below 1K 77−55682
- Co complex, $Co(C_5H_5NO)_6(NO_3)_2$, simple cubic X-Y mag., specific heat, mag. exchange anisotropy meas. 78−39346
- Co complex, Co(III) diamine, ^{13}C NMR, spin-spin coupling const. *(Japanese)* 79−6952
- Co complex, Co(III) five coordinate, paramagnetic behaviour 79−15276
- Co complex, $Co(II)(1,2,4\text{-triazole})_2(NCS)_2$ quasi two-dimens. canted $S=1/2$ antiferromag. 80−70976
- Co complex, $Co(NH_3)_5FCl_2$, mol. motions, NMR 77−36145
- Co complex, $Co(NH_3)_6I_3$, phase transition investig. by NMR 77−1608
- Co complex, $Co(NO_2)_6^{4-}$, bond. props. and Jahn-Teller distortion, INDO-LCAO-MO calcs. 80−75532
- Co complex, $Co(acac)_3$, ^{57}Co labelled, $^{57}Fe(III)$ species prod. by electron capture decay, spin relax. 77−63329
- Co complex, cobalt pyridine chloride, EPR, effective g-values 79−42825
- Co complex, diimine complexes with ^{57}Co II, ^{57}Fe II anomalous spin states, Mossbauer spectroscopy 77−12261
- Co complex, diimine complexes with ^{57}Co (II), Mossbauer spectra, temp. depend. 77−12262
- Co complex, dipyridine chloride, single crystal metamagnetism 78−72345
- Co complex, dipyridyl chloride, metamag., mag. struct., NMR 77−85418
- Co complex, ligand-bridged binucl. complex anions, reson. Raman spectra 78−42067
- Co complex, $\Lambda(+)[Co(en)_3]^{3+}$, quadrupole transition circ. dichroism, production mechanism 79−3428
- Co complex, monofumaratotetraaquocobalt(II) monohydrate, cryst. struct. and cryst. binding 79−37681
- Co complex, O_2CoCl_4 and $O_2CoCl_4NH_3^{2-}$, struct. and bonding model, CNDO-UHF calcs. 80−95541
- Co complex, octaethylporphinato cobalt (II), electronic and reson. Raman spectra, simultaneous meas. 78−66554
- Co complex, oxygenated CoII amino acid-imdazole, XPS 78−21968
- Co complex, S_4N_4 with $CoCl_2$, mass and IR spectra, config. 78−13494
- Co complex, tetra-μ-benzoato-bis(4-methylquinoline)dicobalt II, triclinic cryst., antiferromag. exchange 78−39309
- Co complex, triazene-1-oxide complexes, EPR spectra in frozen nematic liq. cryst. glass 80−88871

cobalt compounds continued
Co complex, tris (ethylenediamine) cobalt (III) di-μ-chlorobis(trichlorocuprate) (II) dichloride, cryst. EPR 77—16157
Co complex, tris(ethylenediamine) cobalt(III) chloride, Raman scatt., interference effects 77—68047
Co complex, tris(ethylenediamine)cobalt(III) ion in complex anion solns., ^{59}Co NMR relax. obs. 80—25234
Co complex, Werner complexes, ^{57}Fe partial quadrupole splitting, emission Mossbauer spectra 80—15919
Co complex, with p-amino salicylic acid, X-ray K-absorpt. discontinuity, shape, chem. shifts 79—47545
Co complex, X-ray K-absorpt. edge, ligand field splitting, spectrochemical series 77—10688
Co complex $[Co(NH_3)_4CO_3]Br$, ^{14}N quadrupole interaction, $^1H/^{14}N$ double reson. 79—51882
Co complexes, 1,2-bis(diphenylphosphino)-ethane in-plane ligand ^{31}P hyperfine interaction, ESR obs. 77—77087
Co complexes, $[Co(H_2O)_x(NH_3)_{6-x}][Co(CN)_6]$, $x=1,2$, hydrogen bonding 77—42437
Co complexes, acetylacetonates, ^{57}Fe absorption and emission spectroscopy 80—40018
Co complexes, Co II tetraphenylporphyrins, constraint, ESR and optical detect. 80—83394
Co complexes, Co(III) mixed complexes, orbital angular momentum reduction, ^{59}Co NMR chemical shift 80—58137
Co complexes, $Co(en)_2Cl_2.Cl.HCl.2H_2O$, temp. dependence of NQR frequencies 80—66068
Co complexes, $K_3[Co(CN)_6]$, $Na_3[Co(NO_2)_6]$, and $(NH_4)_2[Co(NCS)_4]$, X-ray Co K absorpt. edge struct. 77—20956
Co complexes, NMR studies *(Japanese)* 79—8068
Co complexes, nitropentaammine and hexaammine Co(III) complexes, ion assoc. in aq. soln., conductance meas. *(Japanese)* 78—40059
Co complexes, tris(oxinato) Co(III) and tris(β-diketonato) Co(III), after effects of EC decay 80—15915
Co ferrite, crystalline anisotropy, FMR meas. 77—8408
Co ferrite, growth on fine acicular γ-Fe_2O_3 particles 80—29871
Co ferrite film prep. by vac. evaporation and annealing 77—85939
Co I, odd levels, hyperfine structure by level crossing and optical methods 77—83551
Co II acetylacetonate, XPS 80—74196
Co II complexes, with tetradentate Schiff bases, synthesis, struct. and ESR obs. 80—80598
Co III salen complexes, O binding, reson. Raman obs. 80—58267
Co oxide-based electrode, air hydrophobically treated, electrochem. characts. 79—61876
Co salts:M^{2+}, $M=Mn$, VO, EPR, spin-lattice relax. time meas., 180-380K 78—64268
Co Schiff base complex, N,N′-ethylene-bis (salicylideniminato)-Co II pyridine doped in Znsalenpy crystal, ENDOR, EPR studies 80—34819
Co Y zeolite, absorpt. spectra, Co^{2+} ions location upon dehydration 77—73152
Co^{2+} $[Fe(CN)_6]^{3-}$, time depend. phenomena caused by EC decay, Mossbauer study 80—44978
Co^{2+} complex, ammoniated zeolite, oxygenated product form., electronic spectrosc. obs. 80—991
Co^{3+} complex ions, diffusion coeffs. meas., computer-assisted technique using Cottrell eqn. 80—3425
Co^{3+} d^6-complexes and oxides, spin-state transitions, PES study 79—100014
^{58m}Co III complexes, stability rel. to internal conversion deexcitation, inner shell ionisation 77—42361
Co/CoO, relative chemical potential of oxygen *(German)* 78—31642
Co/Na zeolite, -A and -Y type, local coordination of Co(II) ions studied by X-ray absorpt. fine struct. spectroscopy 80—93434
Co-CoO films, evaporated, exchange anisotropy 80—88841
Co-complex, dichlorobis(pyridinium-2-thiolate)Co(II), cryst. and mol. struct. 80—28963
Co-Fe-O ferrite system, thermodynamic stability, dissociation and phase relations *(Japanese)* 80—55378
Co-Ge-Te system, phase equilib. 80—20908
Co-H, solid soln., magnetisation curve 78—84452
Co-Mo oxidic precursory state, supported on SiO_2 and γ-Al_2O_3 hydrotreating catalysts 79—61898
Co-O thin films, exam. of oxide phase reduction, by electron photographic analysis *(Russian)* 79—34359
Co-porphine, ab initio LCAO SCF MO calcs. 79—6860
Co-S, thermodynamic anal., phase diagram 79—43226
Co-Sb-Te ternary system, crystn., heat treatment and phase equilib. 79—52156
Co-W-O system, phase relations in dioxide-trioxide region, 1373K 78—11212
$Co_4\ (CO)_{12}$, heptane soln. Co-Co force consts., prereson. Raman spectra, rel. to solid IR spectra *(French)* 78—31193
$CoAl_{2-x}Fe_xO_4$, cation distrib., lattice parameter determ., X-ray diffr. exam. 79—69088
$CoAl_{2-x}Fe_xO_4$ system obs., using Mossbauer spectroscopy *(Rumanian)* 79—78575
$CoAl_tFe_{2-t}O_4$, Kerr effect, magneto-optical refl. spectra 79—82954
$CoAl_xGa_{2-x}O_4$, mag. interactions, susceptibility obs., 4.2 to 300K 79—15294
$CoAl_2O_4$, cation distribution, Mossbauer and X-ray diffr. obs. 78—95532
$CoAl_2O_4$, compatibility with containment metals 79—13534
$CoAl_2O_4$, cryst. growth by Verneuil method 77—1805
$CoAl_2O_4$, electron density distrib. 78—51481
$CoAl_2O_4$, single crysts., pt. defects type determ. involved in reactions of form. and decomp. of inclusions 79—95003
$CoAs_3$, prep. and characterisation 77—77356
$Co_3(AsO_4)_2$ polymorph, cryst. struct., closest packing 80—70174
$Co_3(AsO_4)_2$ X-ray K-absorpt. edge shifts of Co and As 77—4701
$Co_2(AsO_4)Cl$, cryst. struct., X-ray diffr. meas. 77—47380
$Co_2(AsO_4)Cl$, temp. depend. of mag. susceptibility 80—70962
$Co_3(AsO_4)_2.8H_2O$, optical absorpt. spectra, spin orbit splitting and cryst. field parameters 79—38560
CoB, diamag., nucl. spin-lattice relax. of ^{59}Co 77—59479
CoB, thermophysical props., 296-2000K 78—14477
CoB_{12}, growth from melt and phys. props. 80—20782
$Co_3B_7O_{13}Cl$, polydomain ferroelec., magnetoelec. effect below Neel temp. 78—10745
$Co_3B_7O_{13}Cl(I)$, boracite, single cryst. prep. and phys. props. 80—100763
$Co_3B_7O_{13}I$, intermediate phase between paraelectric and ferroelectric phase *(Russian)* 78—68465

cobalt compounds continued
$Co_3B_7O_{13}I$, neutron diffr. investig. of mag. and cryst. struct., ferro- and paraelec. phases 77—32170
$Co_3B_7O_{13}X$, $X=Cl$, Br, I, ferromag. ferroelectrics *(Japanese)* 79—65804
$Co_{1.8}BaFe_{0.2}Fe_{16}O_{27}$, influence of spin-reorientation on magnetoelastic props. *(Russian)* 79—8028
$Co_{1.8}BaFe_{0.2}{}^{2+}Fe_{16}{}^{3+}O_{27}(Co_{1.8}W)$, magnetoelastic props. under spin-reorientation conditions 79—69709
$CoBr_2,6[xD_2O(1-x)H_2O]$, mag. order investig. by neutron diffr. 77—66310
$CoBr_2$, lamellar, field depend. of uniform magnon. energies, antiferromag. reson. meas. 77—73086
$CoBr_2$, magnetic excitations, neutron scatt. investigation 80—39761
$CoBr_2$, magnon Raman scatt. 79—15462
$CoBr_2$, paramag. and antiferromag., Raman scatt. from electronic excitations and phonons 79—69826
$CoBr_2$, UV reflectivity spectra for band struct. calc. 77—20878
$CoBr_2$, XPS, satellite of Br 4s line 78—56556
$CoBr_2.2H_2O$, linear chain metamag. system, phonon and magnon widths 77—36065
$CoBr_2.2H_2O$, metamagnetic, relax. phenomena at phase transitions 79—24164
$CoBr_2.2H_2O$, phase transitions in ferrimag. state 77—63191
$CoBr_2.6D_2O$, crystallographic and mag. struct. determ. 77—8278
$CoBr_2.6(0.48D_2O, 0.52H_2O)$ spin-flop system, intermediate phase existence, sublattice magnetisation reorientation 80—80510
$CoBr_2.6[(D_2O)_{0.48}(H_2O)_{0.52}]$, antiferromag. ordering, quasi-elastic neutron scatt. study 79—61068
$CoBr_2.6[(1-x)H_2O.xD_2O]$, mag. intermediate phase, magnetisation and neutron scatt. meas. 80—60195
$Co(C_5H_5NO)_6(ClO_4)_2\ [(BF_4)_2]$, X-Y antiferromagnet, Neel temp., spin correlation functions 80—60345
$Co(CN)_6{}^{3-/4-}$, redox reaction on CdTe and ZnTe electrodes *(French)* 80—89482
$Co(CN)_6{}^{3-}$, electronic struct., ab initio LCAO SCF MO calcs. 79—18112
$Co(CN)_6{}^{3-}$, electronic struct., photochem. props., MS Xα calcs. 79—22600
$CoCO_3$, antiferromag., Raman spectra, 2-300K 77—32380
$CoCO_3$, birefringence of light *(Russian)* 78—56456
$Co(CO)_3$, bond angles, hybrid bond orbital calcs. 78—94188
$CoCO_3$, Brillouin-Mandelstam scattering from thermal and excited magnons 80—70980
$CoCO_3$, Brillouin-Mandelstam light scatt. obs. of spin wave spectra 80—93358
$CoCO_3$, exciton and magnon excitation spectra *(Russian)* 78—23467
$CoCO_3$ far IR spectrum, HF antiferromag. resonance and two-magnon absorption 77—40136
$CoCO_3$, LF exciton and Raman spectra, one-magnon and two-magnon scatt. 80—93333
$CoCO_3$, light interaction with spin system at antiferromag. reson. 77—69707
$CoCO_3$, light scatt. by thermal magnons and magnons excited by antiferromag. reson. 79—82965
$CoCO_3$ light scatt. from parametric magnons and phonons *(Russian)* 80—34937
$CoCO_3$, light scatt. from magnons and phonons excited by microwave pumping 80—66213
$CoCO_3$ light scattering on spin waves *(Russian)* 77—4650
$CoCO_3$, linear magneto-optical effect, birefr. 80—66155
$CoCO_3$, long wave IR spectrum, high freq. antiferromag. reson. *(Russian)* 78—31115
$CoCO_3$, monocryst. solubility under hydrothermal conditions 77—12512
$CoCO_3$, spherocobaltite, complexing during cryst. growth, electron diffr., neutron diffr. and spectroscopic obs. 77—44144
$CoCO_3$, spin excitation energies, quantum theory *(Russian)* 80—88735
$CoCO_3$, spin wave spectra light scatt. expts., review 80—50081
$CoCO_3$, two-sublattice noncollinear antiferromag., exciton-magnon light absorpt. mechanisms *(Russian)* 80—89017
$CoCO_3$, weak ferromag., antiferromag. reson., phenomenological theory 78—60339
$CoCO_3$, weak ferromagnet, optic study of spin wave spectrum *(Russian)* 79—47263
$CoCO_3$, weak ferromagnet, light absorpt. dichroism and mag. config. *(Russian)* 79—87457
$CoCO_3$, weak ferromagnet, antiferromag. reson. and two-magnon absorpt. *(Russian)* 80—29627
$CoCO_3$, weakly ferromagnetic, light scatt. accompanying spin system excitation by high microwave power *(Russian)* 78—2745
$CoCO_3$, weakly ferromag., light scatt. on spin waves *(Russian)* 78—72419
$CoCO_3$, weakly ferromag., light absorpt. dichroism and mag. config. 80—66223
$Co(CO)_4{}^-$, extended CNDO calc. 80—918
$Co_2(CO)_8$, extended CNDO calc. 80—918
$Co_4(CO)_{12}$, extended CNDO calc. 80—918
$Co(CO)_3(NO)$, appl. of HF and CI calcs. 80—9513
$CoCl_2$, acoustic phonon dispersion determ. from neutron scatt. 77—39645
$CoCl_2$, antiferromag., elec. field effect in NMR 77—28459
$CoCl_2$, antiferromag., elementary excitations 77—69519
$CoCl_2$, antiferromag., elementary excitations, electronic Raman scatt. meas. 77—80922
$CoCl_2$, antiferromag., mag. excitations, mag. neutron inelastic-scatt. meas. 77—85437
$CoCl_2$, antiferromag., phase diagram, heat capacity meas. 80—93126
$CoCl_2$, antiferromagnetic resonance, effect of hydrostatic pressure *(Russian)* 78—35042
$CoCl_2$, cryst., self-consistent band struct., intersecting spheres model 80—75505
$CoCl_2$, EXAFS amplitudes, many-body effects 80—97379
$CoCl_2$, electronic absorpt. spectra and coord. in cryst., soln. and melt 79—38570
$CoCl_2$, energy spectrum of valence electrons, X-ray emission spectra 77—16430
$CoCl_2$, interlayer force constants 78—14406
$CoCl_2$, lamellar, field depend. of uniform magnon. energies, antiferromag. reson. meas. 77—73086
$CoCl_2$, lattice dynamics, static displaced shell model 78—79689
$CoCl_2$, one-magnon Raman scatt. 78—43877
$CoCl_2$, polarised IR absorpt. spectra 77—40269

cobalt compounds continued

- $CoCl_2$, purification by H_2 reduction, of Co, exam. of conductivity *(Russian)* 79—28981
- $CoCl_2$, saturated soln., jet flow Raman spectroscopy for highly absorbing liq. systems 80—52323
- $CoCl_2$, solution, spin-lattice relax. time meas. using CW NMR spectrometer 77—57374
- $CoCl_2$, spin orientation of mag. impurity atom 77—59403
- $CoCl_2$, UV reflectivity spectra for band struct. calc. 77—20878
- $CoCl_2$, vapour pressure meas. 77—89534
- $^{60}CoCl_2$, whole-body retention in rats, age effect 77—70559
- $CoCl_2$-$Cd(NO_3)_2 4.1H_2O$, melt viscosity, equivalent conductivity, glass transition temp. 78—75855
- $CoCl_2$-He discharge, cataphoretic Co distrib. 77—31092
- $CoCl_2$-KCl-NaCl system, melting diagram investigation by thermographic anal. *(Russian)* 78—3111
- $CoCl_2$-LiCl-glycerin-water system, Co^{2+} ion coordination transition, spectral investig. 79—42953
- $CoCl_2$-NaCl purification by H_2 reduction, of Co, exam. of conductivity *(Russian)* 79—28981
- $CoCl_4^-$ formation kinetics, in nonaqueous systems, rate constants and temp. change determ. *(German)* 79—70300
- $CoCl_4^{2-}$, electronic energy levels calc. by conventional and X alpha Hartree-Fock methods 78—66470
- $(CoCl_4)^{2-}$, ligand field spectroscopy, selection rules, intensity enhancement of forbidden transitions 80—45049
- $CoCl_4^{2-}$, mol. orbital energy levels, semi-empirical calc. 77—3271
- $CoCl_n$, electronic struct., INDO theory 80—42948
- $CoCl_2(Br_2)$, polymorphic phase changes of adsorbed NO 77—31900
- $CoCl_2(Br_2)(I_2)$, prep. using chem. transport via gas complexes *(German)* 79—15599
- $CoCl_2 6H_2O$, g-tensor and exchange parameters, mag. reson. studies 79—87324
- $CoCl_2.2H_2O$, antiferromagnet, symm. of field-induced phases, mag. space groups 77—32166
- $CoCl_2.2H_2O$, antiferromag., light scatt. from phonons and magnons 80—40104
- $CoCl_2.2H_2O$, gamma-X-ray coincidence Mossbauer spectra 80—15913
- $CoCl_2.2H_2O$, Ising antiferromag., high field transverse magnetisation meas. 80—93143
- $CoCl_2.2H_2O$, linear chain metamag. system, phonon and magnon widths 77—36065
- $CoCl_2.2H_2O$, magnetisation temp. depend. 80—7128
- $CoCl_2.2H_2O$, magnon-phonon interactions and two-magnon Raman scatt., magnetoelastic waves and selection rules 80—34917
- $CoCl_2.2H_2O$, metamagnetic transition, microscopic dynamics 77—16073
- $CoCl_2.2H_2O$, metamagnetic, ^{55}Mn NMR of impurity spin 77—85613
- $CoCl_2.2H_2O$, phonons and electronic transitions, Raman spectra 79—28761
- $CoCl_2.2H_2O$, wagging and rocking band intensities of water 78—27200
- $CoCl_2.2H_2O$-$FeCl_2.2H_2O$, random mixture with competing spin anisotropies, tetracrit. transition, neutron diffr. obs. 80—2575
- $CoCl_2.2NC_5H_5$, 1-dimens. Ising ferromag., charact. EPR modes 79—91287
- $CoCl_2.2NC_5H_5$, magnetisation temp. depend. 80—7128
- $CoCl_2.6D_2O$, crystallographic and mag. struct. determ. 77—8278
- $CoCl_2.6D_2O$, neutron diffr. study, cryst. and mag. struct. *(French)* 78—42946
- $CoCl_2.6H_2O$ activated polyvinyl alcohol film, thermochromism *(Russian)* 79—91415
- $CoCl_2.6H_2O$, albrittonite, new mineral from Llano County, Texas 78—65286
- $CoCl_2.6H_2O$, antiferromag., spin flop and paramag. resons. at very low temp. 77—66426
- $CoCl_2.6H_2O$, paramag., PMR 78—91962
- $CoCl_2.6H_2O$ solution in ethanol, thin absorbing film, nonlinear optical props., Q-switch appl. 80—91836
- $CoCl_2.nH_2O$, cryst. struct. *(German)* 80—1987
- $CoCr_xFe_{2-x}O_4$, magneto-optical refl. spectra by equatorial Kerr effect *(Russian)* 77—32400
- $CoCr_2O_4$, Mossbauer spectra and cryst. struct. determ. 79—56637
- $CoCr_2O_4$, thermal expansion 79—73327
- $CoCr_2S_4$, CVD grown, surface microstruct. 79—4905
- $CoCr_2S_4$, excess entropy terms 79—86905
- $CoCr_2S_4$, Faraday effect, appl. to CO_2 laser systems, radiation damage resist. 78—95579
- $CoCr_2S_4$, ferrimag. semicond., magnetocrystalline anisotropy 80—71012
- $CoCr_2S_4$, specific heats 79—11315
- $CoCr_2Te_4$, cryst. growth, struct., elec. props., Hall effect 78—43416
- $CoCr_2X_4$ (X=O,S), K absorpt. discontinuity chem. shift, bonding parameters 77—77318
- $CoCs_2(SO_4)_2.6H_2O$, obs. of H^2T^7 Raman spin-lattice relax. process 77—51459
- $CoCs_2(SO_4)_2.6H_2O:Mn^{2+}$, EPR, 300K 79—51848
- $Co_{1-x}Cu_xCr_2S_4$, paramag. susceptibility 80—20373
- $Co_{0.7}Cu_{0.3}Cr_2S_{4-x}Se_x$, ferrimag. chalcospinel, paramag. susceptibility 80—15681
- CoF_2, 180-degree antiferromag. domain obs. by new magnetooptical effect 80—44855
- CoF_2, antiferromag. crit. props., neutron scatt. obs. 80—88749
- CoF_2, deformed, magnetoelastic interactions and single-domain antiferromag. state 77—43849
- CoF_2, domain formation in staggered field induced by uniaxial stress, neutron diffr. exam. 78—76289
- CoF_2, elastic constant determ. by US pulse echo overlap 79—14874
- CoF_2, linear and quadratic mag. birefr. 80—16005
- CoF_2, linear magneto-optical effect, birefr. 80—66155
- CoF_2, muon Coulomb capture ratio 78—62959
- CoF_2, phase transition in transverse mag. field, magnetoelastic interactions 79—65676
- CoF_2 plate, antiferromag. reson. in transverse mag. field 78—2749
- CoF_2, spin excitations in longitudinal mag. field 79—69657
- CoF_2, valence-electron density of states, XPS meas. 77—69963
- CoF_2, visual obs. of 180° antiferromag. domains, mag.-optical effect *(Russian)* 79—61349
- $CoF_2:MnSu^{2+}$, anisotropic antiferromagnet, spin impurity approx. *(Russian)* 79—87253
- $CoFeCN.xH_2O$, electron irrad., Mossbauer spectra 80—29652
- $Co_{(1-x)}Fe_xCl_2.2H_2O$, random mixture of anisotropic antiferromags., isotropic state obs. 78—84396
- $Co_xFe_{1-x}Cl_2.2H_2O$ solid soln., mag. props. and phase diagram 79—78346

cobalt compounds continued

- $Co_xFe_{3-x-y}Cr_yO_4$, epitaxial, magneto-optical props., effect of Cr^{3+} 78—52590
- $Co_{1-x}Fe_xCr_2S_4$, ferrimag. spinel semicond., Curie temp. variation with composition and elec. props. 77—15849
- $CoFeF_5.7H_2O$, thermal decomp. 77—81394
- $Co_x^{2+}Fe_{1-x}^{2+}Fe_2^{3+}O_4$ ferrites, effect of Fe^{2+} on Mossbauer parameters 78—76360
- $Co_x^{2+}Fe_{1-x}^{2+}Fe_2^{3+}O_4$, Mossbauer parameters, effect of Fe^{2+}, Zeeman patterns 79—28647
- $CoFe_{2-x}Ga_xO_4$, IR reflection spectra, permittivity spectra and effective ionic charges 79—69841
- $CoFe_2O_4$, cation self-diffusion, 1231 to 1390°C, vacancy migration mechanism 77—1260
- $CoFe_2O_4$, core line X-ray photoelectron spectra 78—7263
- $CoFe_2O_4$, epitaxial layer prod. by chem. transport 77—81224
- $CoFe_2O_4$ film, Faraday rot., birefr. 77—1663
- $CoFe_2O_4$, fine particles, surface effects on saturation magnetisation 77—69630
- $CoFe_2O_4$ formation rate consts. meas. by Mossbauer effect 78—68875
- $CoFe_2O_4$ mag. fluid particles, comp., struct., and mag. props. 80—60374
- $CoFe_2O_4$, mag. hyperfine fields, Mossbauer spectra 80—108139
- $CoFe_2O_4$, superexchange interactions, three-sublattice anal. 79—61095
- $CoFe_2O_4$ synthesis, chem., thermal histories rel. to fine cryst. struct. 79—43186
- $CoFe_2O_4$, thermally induced surface chemistry and struct., XPS 78—22939
- $CoFe_2O_4$ ultrafine particles, prep. and mag. props. 80—71116
- $Co_{1-x}Fe_{2+x}O_4$, prep. by wet and ceramic methods, struct., mag. and surface props. 78—52307
- $Co_{1-y}Fe_{2+y}O_4$, equilib. surface comp., cation comp. with stoichiometric oxygen content 78—79867
- $Co_{1-y}Fe_{2+y}O_4$ ferrite, $-0.1 \leq y \leq 0.1$, surface composition, AES 78—14557
- $Co_{1-y}Fe_{2+y}O_4$, role of vacant and chemisorbed O and charge transfer effect 78—79868
- $Co_xFe_{3-x}O_4$ film, magnetooptic recording material, mag. and magnetooptic props. 77—20832
- $Co_xFe_{3-x}O_4$, single cryst. mag. films, holograms recording and thermomagnetic writing 78—55324
- $Co_{2.94}Fe_{0.06}S_4$ Mossbauer ^{57}Fe spectrum, mag. transition, lattice atomic occupancy 77—48095
- $CoFe_2Se_4$, low-temp. thermal expansion anomalies and isothermal compressibility, mag. ordering and magnetorestriction 79—38363
- $Co_{1-x}Fe_xSi$, elec. and optical props. 80—49740
- $CoGa_{2-x}Fe_xO_4$, x=0.1—0.4, mag. susceptibility temp. depend. *(Russian)* 80—70957
- $CoGa_2O_4$, mag. props. 78—23254
- $CoGe_x$, Co X-ray emission spectra *(Russian)* 78—21942
- $CoGeO_3$, HP phase transform. 80—19941
- Co_2GeO_4, crystal growth by Czochralski method under 4 atm N_2 77—77368
- Co_2GeO_4, hydrothermal growth from CoO-GeO_2-H_2O 77—48329
- Co_2GeO_4-Mg_2GeO_4, solid solubility and cation distrib., free energy 77—35700
- $Co_2Ge_2Te_3$, struct., resist., and thermo-EMF 80—20908
- CoH_4, electronic structure, ab initio calcs. 79—89601
- $Co(H_2O)_6[SnF_3]_2$, crystal structure *(French)* 80—59441
- $Co^{II}(H_2PO_4)_2.2H_2O$, cryst. and powder diffr. data *(French)* 80—24419
- CoI_2, Mossbauer spectrum, electronic and mag. props. 77—32302
- CoI_2, polymorphic phase changes of adsorbed NO 77—31900
- Co(II) Schiff base complexes, structure and bonding, book contrib. 80—972
- Co(II)-containing aq. electrolyte soln., nucl. mag. relax., hydration shell *(Russian)* 80—54966
- CoIII salen complexes, O binding, reson. Raman obs. 80—58267
- $CoK_4(P_3O_9)_2.7H_2O$, cryst. data *(French)* 78—79568
- $CoK_2(SO_4)_2.6H_2O$, obs. of H^2T^7 Raman spin-lattice relax. process. 77—51459
- $CoK_2(SO_4)_2.6H_2O:Mn^{2+}$, EPR spectra, spin-Hamiltonian anal. 77—77088
- $CoK_2(SO_4)_2.6H_2O:VO^{2+}$, ESR, ion orientations 78—48029
- $CoK_2(SeO_4)_2.6H_2O:Mn^{2+}$, Tutton salt, EPR exam. of cryst. field parameters 78—39394
- CoM_2O_{4+x} (M=Rh,Mn), anomalous $^{57}Fe^m$ charge states, Mossbauer study 80—40017
- $Co_xMg_{1-x}Al_2O_4$, struct., catalytic activity, Co^{2+} ion distrib. 78—30595
- $Co_{1-p}Mg_pCl_2$, magnetic excitations, antiferromagnetic resonance spectra response simulation 79—99775
- $Co_{0.5}Mg_{0.5}O$, compatibility with containment metals 79—13534
- $Co_{0.5}Mg_{0.5}O$, sintered pellets, oxidation mechanism and kinetics, optical and SEM study 79—79137
- $Co_{1-x}Mg_xO$ ceramics as O_2 sensors, phase stability, elec. cond. and thermoelec. power meas. 78—3420
- $Co_xMg_{1-x}O$, solid solution, EPR of Co^{2+} *(Russian)* 80—11251
- $Co_xMg_{1-x}O$ system, thermodynamic investigation, 1100 to 1300K *(German)* 80—107430
- $(Co_{1-x}Mg_x)_2SiO_2$, reduction to Co *(Russian)* 78—44043
- $CoMgSnO_4$, paramagnetic props., and short-range ordering 77—32155
- $Co_{2-x}Mg_xTiO_4$, paramagnetic props. and short-range ordering 77—32155
- $(Co_{1-x}Mn_x)_2B$, $0 \leq x \leq 1$, magnetisation, lattice consts., press. depend. of Curie temp. 80—7137
- $Co_{1-c}Mn_cF_2$, antiferromagnet mag. impurities, spin excitation spectrum collective rearrangement in external mag. field 80—50199
- $Co_{0.25}Mn_{0.75}Fe_2O_4$, ferromag. reson. in frozen lattice model, anisotropy consts. 79—51859
- $^{57}CoMn_2O_4$, after effects of orbital electron capture 79—73870
- $Co_{3-x}Mn_xO_4$, solid soln., synthesis, effect of Bi_2O_3 admixture upon props., thermistor appl. 78—15325
- $CoMo/\gamma$-Al_2O_3 catalyst, ESCA and EPR meas. after hydrodesulphurization reaction *(French)* 79—52755
- $Co^{2+}Mo^{4+}O_3$, defect spinel struct., elec. and mag. props. 80—70176
- $CoMoO_4$, formation and phase transition in CoO-MoO_3-Al_2O_3 system 79 61569
- $CoMoO_4$, mag. susceptibility and electrical transport props. 79—56511
- $Co_{3-x}Mo_xO_4$ films, prep., struct. and elec. characteris. 80—108353
- CoMoP, X-ray cryst. struct. anal. *(French)* 79—4281
- $CoMo_2Re_2S_8$, cubic structure, mixed tetrahedral cluster *(French)* 77—15372
- $Co_2Mo_6S_6O_2$, O-containing Chevrel phases, synthesis and props. 80—108368

cobalt compounds continued
- $Co(NH_3)_5\ Br^{2+}$, aquation, polyelectrolyte catalysis, high pressure effect 80–55656
- $Co(NH_4)_2(BeF_4)_2.6H_2O$, cryst. struct. refinement by X-ray diffr., comparison with neutron diffr. *(French)* 77–47387
- $Co(NH_3)_5Br^{2+} + OH^-$, polyelectrolyte catalysis, high pressure effect 80–55657
- $Co(NH_3)_6Cl_3$, proton second moment meas., 96 to 404K 79–95652
- $Co(NH_3)_4Cl_2Cl$, cis and trans isomers, XPS, shake-up satellites 78–82783
- $Co(NH_3)_6(Cr(CN)_6)$, electron distrib., X-ray diffr. 77–19915
- $Co(NH_3)_6FeF_6$, anomalous Raman intensities, due to interionic coupling by H bonding 78–27230
- $Co(NH_3)_6(IO_4)_3.2H_2O$, dynamics of IO_4^- vibr. in lattice 79–42157
- $Co(NH_3)_5{}^{15}NH_3{}^{3+}$ complex prep. and Fourier transform NMR spectra *(Japanese)* 78–48060
- $Co(NH_3)_6(Pb_4Cl_{11})$, cryst. struct., and relationship with the chlorolead struct. moieties in $NH_4(Pb_2Cl_5)$ and $PbCl_2$ 79–32954
- $Co(N_2H_5)_2(SO_4)_2$:Co, Mossbauer effect and paramag. relax., superparamag. behaviour of correl. spin domains 77–69756
- $Co(NH_4)_2(SO_4)_2.6H_2O$, obs. of H^2T^7 Raman spin-lattice relax. process 77–51459
- $Co(NH_4)_2(SO_4)_2.6H_2O$, LF relax. meas. 78–15012
- $Co(NH_4)_2(SO_4)_2.6H_2O$ Tutton salt, low-temp. spin orientation, mag. props. 0-0.1K 79–15286
- $(Co(NH_3)_6)X_3$, (X=Cl, Br, I), internal and lattice vibr. normal coordinate anal. 79–69203
- CoNO, appl. of HF and CI calcs. 80–9513
- $Co(NO_3)_2$, aq. electrolyte, apparent molar heat capacity and volume, of 298.15K 79–65208
- $Co(NO_3)_2.6H_2O$ addition to molten salt heat transfer fluid, solar absorbing properties enhancement 78–87112
- $CoNb_2O_6$, bonding characterisation 78–38680
- $CoNb_2O_6$, Co^{2+}-Co^{2+} interaction, susceptibility and magnetisation, 3.3-300K 77–8282
- $CoNb_2O_6$, flux growth 77–21015
- $CoNb_2O_6$, magnetic struct., neutron diffr. and mag. susceptibility meas. 80–15693
- $CoNb_2O_6$, ordered state, field induced mag. transitions 77–16074
- $Co_{0.32}NbS_2$, intercalation compound, struct. and photoemission meas. 77–16453
- $Co_{1/3}NbS_2$, intercalate, metallic cond., Hall effect and mag. props. 77–76789
- $Co_{0.08}(Ni,Cu)_{0.92}Fe_2O_4$ sphere, rotational hysteresis, mag. field strength and orientation depend. *(Russian)* 77–16110
- $Co_xNi_{1-x}Cl_2.6H_2O$, calorimetry, γ-type transitions of sp. ht. 78–68256
- $Co_xNi_{1-x}Cl_2.6H_2O$, solid solution, mag. props. and phase diagram, calc. 80–7104
- $Co_x(Ni_{0.5}Cu_{0.5})_{1-x}Fe_2O_4$ ferrite, relation between elec. cond. and mag. anisotropy 80–75548
- $Co_xNi_{1-x}Fe_2O_4$, induced mag. anisotropy consts., conc. and temp. depend. 80–108001
- $(Co_{1-x}Ni_x)O$, single crysts., morphology change during compressive creep testing 79–29144
- Co_2NiO_4 powder prep. by freeze drying of solid solutions, solvent choice 80–11583
- $Co_{3-x}Ni_xO_4$, $0 \leq x \leq 1.1$, struct., semicond.-semimetal transition, Seebeck coeff. 78–87972
- $Co_xNi_{1-x}O$, antiferromagnet, neutron diffr. study of mag. struct. 80–34595
- $(Co_yNi_{1-y})_{1-x}O$ and O_2 prep. props., and reactions 77–12569
- CoNiZn ferrites, Fe excess, complex permeab. var. with annealing temp. 77–89979
- CoO (100), electron energy loss spectra exam. 78–72652
- CoO (100), surface struct., LEED anal. 80–15352
- CoO (100), surface struct., LEED study 80–39396
- CoO (111), surface relax., ionic model 80–6608
- CoO, ab initio SCF and CI calcs. on d-d transitions, $CoO_6{}^{10-}$ cluster d-electron localisation 77–35897
- CoO and Co_3O_4, XPS interpretation, valence band structure 77–12497
- CoO, antiferromag. mag. excitations, spin wave model, neutron scatt. study 79–51766
- CoO, antiferromagnetic, ^{59}Co NMR and hyperfine field 77–77109
- CoO as a spectrally selective material for solar collector appls. 80–26159
- CoO, Co_3O_4, form. by reactive cathodic sputtering of Co *(French)* 77–63519
- CoO, Co_3O_4, free enthalpy of formation, solid oxide electrolyte galvanic cell method 78–23959
- CoO, collinear antiferromag., equiv. type-II mag. struct. 78–56296
- CoO, compatibility with containment metals 79–13534
- CoO, cryst., Debye characteristic temp. calcs. 79–37796
- CoO, cubic NaCl-type cryst., Debye temp. 80–54333
- CoO, defect struct. and self-diffusion 78–63759
- CoO deposition on glass using laser beam 79–83364
- CoO, dielec. and thermophys. props. 77–52009
- CoO, dielec. behaviour, Dick and Overhauser shell model calcs. 80–45001
- CoO, ESCA and Auger lines, chem. shifts 78–6817
- CoO, electronic cond., rel. to basic processes of Co corrosion 77–25198
- CoO, electronic struct., XPS and UPS expts. *(French)* 79–38711
- CoO, electronic struct. calc. 78–43297
- CoO, electrotransport 80–2196
- CoO epitaxial layers, XPS obs. of formation on Co (0001) 80–66396
- CoO, evaporation curve struct. from AC arc electrodes *(Russian)* 78–3051
- CoO film, growth kinetics on high current density plated Au 78–92393
- CoO film, Poole Frenkel effect and elec. breakdown props. 77–85364
- CoO film on thermally aged Co hardened Au, mech. film breakdown and ESCA, expt. 77–4436
- CoO, for catalytic oxidation of CO 80–71945
- CoO, H_2 ortho$\rightleftharpoons$para conversion on mag. surface 79–47969
- CoO, high temperature physico-chemical interactions with oxygen under pressure *(French)* 78–31549
- CoO, hydrothermal growth from CoO-GeO_2-H_2O 77–48329
- CoO impurity in silicate melt, effect on elec. cond. *(Ukrainian)* 77–69104
- CoO, ionisation, electron density relax. effects. ab initio calcs. 78–50466
- CoO, isotope effects in CoO diffusion rel. to vacancies 80–84319
- CoO, mag. excitations, neutron scatt. expts., 13K 79–61092
- CoO, matrix isolated IR spectra, ground state vibr. freqs. 80–28015

cobalt compounds continued
- CoO, Mossbauer lines, quadrupole splitting due to defects 80–2670
- CoO, non-stoichiometry and temp.-depend. mag. susceptibility 79–82768
- CoO on Co_3O_4, oriented growth following Co_3O_4 pyrolysis 78–80739
- CoO, paramag. shifts of ^{19}F at O 78–43719
- CoO, phonon dispersion, calc. using extended three-body force shell model 77–27964
- CoO, plasma reduction melting *(Russian)* 78–31359
- CoO, polycrystalline, high temp. deform. 78–3174
- CoO, pressure sintering densification model, computer program 78–44040
- CoO, pure and Li doped, dislocation spacing effect on high-temp. creep 78–35444
- CoO, reduction, magnetic field effects 79–52764
- CoO, relax. valence averaging, Mossbauer spectra evidence 77–1626
- CoO, self consistent energy band calc. 78–23022
- CoO single crystal, compressive creep morphology 77–56034
- CoO single crystal, compressive creep 78–11275
- CoO, single crystal and polycryst., subgrain boundary form. and creep mechanism 77–39594
- CoO single crystals, strain rate deform. characts., yield stresses and work hardening 77 to 1400K 80–60939
- CoO, sintered pellets, oxidation mechanism and kinetics, optical and SEM study 79–79137
- CoO solar absorber surface spectral selectivity rel. to temp. and UV ageing 79–62027
- CoO, solubility of S at 1000°C 78–63858
- CoO, surface layer spacing relax., electrostatic argument 79–46901
- CoO, surface reequilibration kinetics 77–55449
- CoO, total conc. of point defects and deviation from stoichiometry 77–15407
- CoO, under controlled atmosphere, exam. of composition and temp. dependence, of lattice parameter *(French)* 79–19214
- CoO, unrestricted Hartree-Fock calc. for cluster model 80–2320
- CoO, valence band struct., cryst. field anal., photoelectron data 79–47007
- CoO, valence photoelectron spectrum, relative intensities, limited CI calcs. 79–63918
- CoO, vibr. IR absorption spectrum, mol. consts. 79–89666
- CoO, X-ray determ. of electron density distribs., atomic scatt. factors 80–15078
- $CoO:Ni^{2+}$, far IR absorpt. by impurities and collective antiferromag. reson. mode 77–8576
- CoO-Al_2O_3, isoelectric point meas. 80–88609
- CoO-Al_2O_3-SiO_2, amorphous, remanent magnetisation short time depend. 80–65919
- CoO-Al_2O_3-SiO_2, spin glasses, low-field susceptibility, freq. depend. 78–47981
- CoO-Al_2O_3-SiO_2, spin glass, magnetic aftereffects 79–61176
- CoO-Al_2O_3-SiO_2 glass, mag. ordering, Mossbauer exam. 77–24764
- CoO-Al_2O_3-SiO_2 spin glass, new state in very weak mag. field 79–78416
- CoO-aluminophosphate melt, resistivity, 800-1200°C 77–39903
- CoO-containing glass, effects of γ-rays, electron beam and neutron flux on transmissivity *(Japanese)* 77–73156
- CoO-Fe_2O_3, isoelectric point meas. 80–88609
- CoO-MgO, cryst. oxide demixing in O pot. gradient 79–37849
- CoO-MgO-Al_2O_3-Cr_2O_3-TiO_2, form. and colour of spinel solid soln. *(Japanese)* 77–32550
- CoO-MgO-Cr_2O_3-Fe_2O_3-TiO_2, form. and colour of spinel solid soln. *(Japanese)* 80–16059
- CoO-MoO_3, catalyst pellets, Raman spectra 77–40216
- CoO-SiO_2 systems high press. phases stability and MO-SiO_2 systems phase diagrams code 79–90779
- CoO-ZnO-Al_2O_3-Cr_2O_3-TiO_2 system, form. and colour of spinel solid soln. *(Japanese)* 77–25001
- CoO-ZnO-MgO ternary systems, solid solns., struct. charact. 80–60629
- $CoO + H_2S$, sulphurisation of (100) face, low-press. *(French)* 79–52754
- CoO_2, anodically formed, emission Mossbauer studies 79–61268
- $CoO_6{}^{10-}$ cluster, valence photoelectron spectrum, relative intensities, limited CI calcs. 79–63918
- $CoO_6{}^{10-}$, ionisation, electron density relax. effects. ab initio calcs. 78–50466
- $CoO_{(x)}$, black cobalt, solar absorptance of high temp. selective absorbers 80–101131
- CoO_x, O(1s), XPS energies, oxidised metal surfaces, powders 77–16457
- $Co_{1-x}O$, point defect struct., elec. cond. and Co tracer diffusion 79–10849
- $Co_{1-x}O$, single cryst. growth by skull melting 80–84844
- $Co_{1-x}O$ single crystal of controlled stoichiometry, ^{60}Co self-diffusion 77–43369
- $Co_{1-y}O$, self-diffusion and defect struct. 78–22889
- Co_3O_4 addition to molten salt heat transfer fluid, solar absorbing properties enhancement 78–87112
- Co_3O_4 anode, wear-resistant, use in applied electrochem. 80–40701
- Co_3O_4, catalyst for organic compounds oxidation in air 77–37353
- Co_3O_4 colloid, preparation and props. 79–100445
- Co_3O_4, crystal field calcs. for normal spinel struct., teaching approach 77–13554
- Co_3O_4, detector of CO, appl. in MOS device 78–76908
- Co_3O_4, ESCA and Auger lines, chem. shifts 78–6817
- Co_3O_4, electronic struct., XPS and UPS expts. *(French)* 79–38711
- Co_3O_4 film anode, electrochem. and corrosion processes in $HClO_4$ 79–61875
- Co_3O_4, in ZnO ceramics, non-ohmic props. 77–76833
- Co_3O_4, isoelectric point meas. 80–88609
- Co_3O_4, Mossbauer spectra and cryst. struct. determ. 79–56637
- Co_3O_4, surface reequilibration kinetics 77–55449
- $Co_3O_4{:}^{119}Sn$, hyperfine field exam., Mossbauer meas. 77–69753
- Co_3O_4:Li(Cr)(Al)(S), and pure Co_3O_4, elec. cond. and thermo-EMF 80–20231
- Co_3O_4:S, defect struct. and elec. props., electron, hole conc. 80–44601
- Co_3O_4-H_2, interaction with surface, quantum chemical study 80–45549
- Co_xO_y (x=1, 2 or 3, Y=1, 3, 4), conducting oxide prod. by amorphous citrate process 79–95985
- Co_xO_y, and $Co_x(OH)_y$ surfaces, chem. changes induced by Ar^+ bombardment, XPS obs. 79–83084
- Co_xO_y, anodic, comp. of layers formed by anodic oxidation of Co in neutral and basic soln. 79–39032
- CoO(:Li), dielec. dispersion and polarization 78–2803
- $Co(OH)_2$, adsorption props. of surface, gas-chromatographic investigation 79–66343

cobalt compounds continued
$Co(OH_2)$ effect on NiO electrode self-discharge during long term storage 80—21295
$Co(OH)_2$, hydrothermal growth from $CoO\text{-}GeO_2\text{-}H_2O$ 77—48329
$Co(OH_2)_6(SiF_6)$, phase transitions, spectrometric exam. *(French)* 78—88291
$CoOOH \rightarrow Co_3O_4$, morphology, topotaxy, comparison with $Co(OH)_2 \rightarrow CoOOH$ 77—16817
$(CoO)_nV_2O_5$, (n=1, 2, 3), elec. and mag. props. 79—78094
$CoO.Al_2O_3$, prep. from film forming soln. 80—60811
$CoO.Al_2O_3\text{-}Al_2O_3$, solid soln. *(Japanese)* 77—32567
CoP-NiCoP, composite ferromag. film, exchange coupling between soft and hard layers, FMR obs. 79—78448
CoP_3, prep. and characterisation 77—77356
$Co_{0.83}(Pt(C_2O_4)_2).6H_2O$, cond., dielec. const., microwave obs. 80—44636
$CoRb_2(SO_4)_2.6H_2O{:}Mn^{2+}$, EPR, 300K 79—51848
$CoRh_xGa_{2-x}O_4$, mag. interactions, susceptibility obs., 4.2-1000K 79—15293
$CoRh_2O_4$, Mossbauer spectra and cryst. struct. determ. 79—56637
Co_2RhS_4, mag. semicond., mag. and elec. props. 80—93121
$Co_xRh_{3-x}S_4$, thermal stability and thermochem. props. 79—86904
$Co(S, Se)_2$, metamagnetic transitions in external fields 80—60272
CoS, electrodeposition, using nonaqueous solvents 80—76200
CoS, X-ray L-emission spectra of S *(Japanese)* 78—15254
CoS-MnS(ZnS)(CdS), phase study by X-ray obs., lattice const. 79—1854
CoS_2, core-level and valence-band XPS 80—93450
CoS_2, ferromagnet, elec. resist. and thermal expansion anomalies 80—15542
CoS_2, galvanomagnetic effect of single cryst. 80—96912
CoS_2, hyperfine parameters and quadrupole splitting determ., ^{57}Fe Mossbauer spectra 77—77131
CoS_2, itinerant ferromagnet, ferromag. reson. and EPR meas. 80—66044
CoS_2, mag. props. rel. to Hubbard model 79—78373
CoS_2, microscopic mag. props., NMR meas. 79—91306
CoS_2, narrow-band ferromag., high press. effect on anomalous elec. resist. 80—70698
$CoS_2\text{-}FeS_2(NiS_2)$, ^{57}Fe isomer shift, quadrupole splitting, Mossbauer study 80—15832
$CoS_{(x)}$, black cobalt, solar absorptance of high temp. selective absorbers 80—101131
Co_3S_4, $Cu_{0.5}Co_{2.5}S_4$, $CuCo_2S_4$, spinels, ht. of formation 78—53237
Co_xS_y, exam. of thermodynamic activity, for several phases, using gas equilibration technique 78—52785
$\alpha\text{-}CoSO_4$, anhydrous, thermal decomposition, SO_3 evolution, gas equilib. and kinetic approach *(German)* 78—23943
$CoSO_4$, aq. soln., viscosity meas., viscous flow activation energy, entropy *(Japanese)* 77—43363
$CoSO_4$ soln. in H_2O, methanol-H_2O, US dispersion, 3-60 MHz *(German)* 78—59862
$CoSO_4.H_2O$, hydrate librational modes in IR spectra 78—48161
$CoSO_4.H_2O$, IR spectra, H_2O external modes temp. depend. 78—58683
$CoSO_4.6OC(NH_2)_2.H_2O$, cryst. struct. 78—34507
$CoSO_4.7H_2O$, electron capture aftereffects, time differential Mossbauer coincidence technique 80—39927
$CoSO_4.7H_2O{:}Mn^{2+}$, host spin-lattice relax. narrowing in single cryst. 78—27079
$CoS_{2-x}Se$, magnetism and metamagnetic transition, neutron diffr. and NMR meas. 80—15717
$CoS_{2-x}Se_x$, conc. and temp. effects on metamagnetic transition 80—15716
$CoS_2(Se_2)$, electronic struct., UPS and XPS study 80—80935
$Co(S_xSe_{1-x})_2$, $(0 \leq x \leq 1)$, mag. props. and elec. resist. 79—65657
$Co(S_xSe_{1-x})_2$, galvanomag. effects, obs. and interpretation 80—70726
$Co(S_xSe_{1-x})_2$, high field magnetisation, metamag. 79—91253
$Co(S_xSe_{1-x})_2$, metamagnetic transition, ^{59}Co NMR 79—38322
CoSb, cryst. growth from nonstoichiometric melt, and cryst. chem 78—35286
CoSb, electronic struct., XPS meas. 78—2990
$CoSb_3$, prep. and characterisation 77—77356
$CoSb_2O_6$, force fields rel. to cryst. struct. *(French)* 80—107104
γ-CoSe, d-electron deficit model, electrochem. meas. of free enthalpy *(French)* 78—30605
$CoSe_{1.95}$, NMR and susceptibility meas., absence of antiferromag. 77—16060
$CoSe_2$, ^{57}Fe isomer shift, quadrupole splitting, Mossbauer study 80—15832
$CoSe_2$, bulk mag. susceptibility, anomalous temp. depend., NMR and X-ray diffr. meas 79—87229
$CoSe_2$, core-level and valence-band XPS 80—93450
$CoSe_2$, electrocatalysts, reversible poisoning by CO, air pollution detection appl. 77—37363
$CoSe_2$, hyperfine parameters and quadrupole splitting determ., ^{57}Fe Mossbauer spectra 77—77131
$CoSe_2$, local mag. moments, spin fluctuation theory 79—65687
$CoSe_2$, mag. props. rel. to Hubbard model 79—78373
$CoSe_2$, paramag. metal, sp. ht., Mossbauer effect, absence of ordering 77—16036
$CoSeO_4$, electron capture and γ-radiolysis, radn. damage 80—16705
$CoSeO_4.4H_2O$, cryst. chemical and X-ray powder data 79—51073
CoSi, absorpt spectrum, phase correction in Kramers-Kronig anal. 79—56815
CoSi, thermoelectric and optical props. 78—91714
$CoSiF_6.6D_2O$, deuteron mag. reson. study 80—2646
$CoSiF_6.6D_2O$, phase transition, mag. anisotropy and IR absorption spectra 77—89537
$CoSiF_6.6H_2O$, anomalous thermal expansion near transition temp. 78—47516
$CoSiF_6.6H_2O$, effect of press. on struct. phase transition, 100 to 300K 77—80616
$CoSiF_6.6H_2O$, elec. resist. anomaly near struct. phase transition 79—95401
$CoSiF_6.6H_2O$, paramag., nucl. and electron spin lattice relax. 78—84494
$CoSiF_6.6H_2O{:}Co^{2+}$, spin Hamiltonians and pair interactions 77—36119
$CoSiF_6.6H_2O(.6D_2O)$, near IR spectrum, 80K, assignments 78—48164
Co_2SiO_4, cryst. growth from $PbO\text{-}SiO_2$ flux 77—16484
$\gamma\text{-}Co_2SiO_4$, electron density distrib. 77—35514
Co_2SiO_4, local in depth anal. by neutral beam SIMS 80—89565
Co_2SiO_4, reaction with Fe to produce Co, gamma resonance spectroscopy *(Russian)* 78—15332
Co_2SnO_4, paramagnetic props. and short-range ordering 77—32155

cobalt compounds continued
$CoSnTe_2$, thin films, metallic elec. props. 79—78212
$CoTa_2O_6$, force fields rel. to cryst. struct. *(French)* 80—107104
$Co_{1/3}TaS_2$, Hall coefficient and resistivity 80—39610
$Co_{1/3}TaS_2$, magnetic susceptibility, function of temp. 80—39756
B-CoTe phase, thermodynamic study by Galvanic cell meas. 80—29190
$CoTe_2\text{-}GeTe$, phase diagram, from thermal, X-ray, microstructural analyses 80—55367
$Co_{1-x}Te$, fluctuating localised mag. moments, d band motion, Mossbauer study 80—65768
$Co_4TeMo_3O_{16}$, synthesis, mechanism and kinetics 77—32782
$CoTiO_3$, antiferromag., mag. anisotropy, magnetisation meas. 80—65856
$CoTiO_3$, HP phase transform. 80—19941
$CoTiO_3$, prep. from film forming soln. 80—60811
$CoTl_2(SO_4)_2.6H_2O{:}Mn^{2+}$, EPR, 300K 79—51848
$Co(UO_2AsO_4)_2.8H_2O$, prep. cryst. struct. characterisation 78—30589
CoU_2S_5, mag. struct. and props. 80—11166
$CoV_2O_4{:}Fe$, spinel, prep. and Mossbauer spectra 79—28660
$Co_2V_2O_7$, V-O-V bridge stretching freq. correl. with bond angle 78—74636
$CoWO_4$, mag. struct. refinement, neutron diffr. meas. *(German)* 77—16049
$CoWO_4$, reduction in H_2 77—4931
$CoWO_4$, reduction in H_2 77—4932
$^{57}CoY_2O_4$, after effects of orbital electron capture 79—73870
Co_2Z ferroxplana form. process peculiarities 80—89368
CoZn, complex, $Co_pZn_{1-p}(C_5H_5NO)_6(CPO_4)_2$, dilute simple-cubic antiferromag., sp. ht. near crit. conc. 79—38336
CoZn ferrite, chemical shift in X-ray absorpt. spectra, effective changes 78—6811
$Co_{1-x}Zn_xF_2$, antiferromag. crit. props., neutron scatt. obs. 80—88749
$Co_cZn_{1-c}F_2$, Raman scatt. from Zeeman split levels 77—66243
$Co_{1-x}Zn_xFe_{2(1-y)}Cr_{2y}O_4$ spinels, solid solns., struct. 80—19764
$Co_xZn_{1-x}Fe_2O_4$, elastic behaviour, mag. field and temp. depend. 79—87301
$Co_xZn_{1-x}Fe_2O_4$, ferrite, DC cond., dielec. props., lattice consts. 80—80272
$Co_{0.0031}Zn_{0.5676}Ni_{0.4293}Fe_2O_4$, single phase ferrite powder, from solid solution of schoenite-type salt 77—16524
$(Co_{0.001}Zn_{0.189}Ni_{0.143}Fe_{0.667})SO_4.(NH_4)_2SO_4.6H_2O$, schoenite-type salt, formation of single phase ferrite powders 77—16524
$Co_xZn_{1-x}Rh_2O_4$, mag. props., EPR spectra, antiferromag. order 80—75736
$Co_xZn_{1-x}Rh_2O_4$ spinel, crit. conc. for long range mag. order, expt. evidence 79—47239
$CoZnSnO_4$, paramagnetic props. and short-range ordering 77—32155
$Co_{2-y}Zn_yTiO_4$, cation distrib. and mag. props. 78—14939
$Co_{2-y}Zn_yTiO_4$, spinel series, exchange integrals, mag. struct. and coercive force, magnetisation meas. 77—69507
$Co_{1-x}Zn_x$hexa(pyridine-N-oxide)$(ClO_4)_2$, dilute cubic S=1/2 XY antiferromag., sp. ht. data 77—66358
$CoZrD_3$, polycrystn., neutron and X-ray diffr. anal. of struct. 79—65061
$CoZrF_6.6H_2O$, effect of press. on struct. phase transition, 100 to 300K 77—80616
Co_xZrS_2, $(0 < x \leq 0.50)$, intercalation compounds, ordered phases obs. 80—33962
Co0, electronic polarisability of ions 77—40175
^{57}Co complexes, phenanthroline and ethylenediamine ligands, Auger processes, Mossbauer obs. 77—12277
$^{57}Co_3O_4$, Mossbauer study of the charge state and symmetry of $^{57}Fe^m$ in diverse cobalt spinels *(Spanish)* 79—69754
$^{57}CoCr_2O_4$, Mossbauer study of the charge state and symmetry of $^{57}Fe^m$ in diverse cobalt spinels *(Spanish)* 79—69754
^{57}CoO, compact single-line Mossbauer source preparation 77—10518
$^{57}CoRh_2O_4$, Mossbauer study of the charge state and symmetry of $^{57}Fe^m$ in diverse cobalt spinels *(Spanish)* 79—69754
$^{60}CoCl_2$, retention of tracer-level ^{60}Co in mouse, rat, monkey and dog 77—9271
$Co[Ag(SeCN)_2]_2$, and complexes, softness values and struct., IR spectra 79—59459
$Co^{2+}[Fe(CN)_6]^{3-}$, struct. determ. 80—15901
$Co^{2+}[Fe^{III}(CN)_6]^{3-}$, time depend. linewidth of Mossbauer spectrum 80—15911
$Co_2[Fe(CN)_6]$, and $Co_3[Fe(CN)_6]$, mag. susceptibility, reflectivity spectra and cryst. field 79—56808
$Co_{0.83}[Pt(C_2O_4)_2].6H_2O$, quasi-one-dimens. conductor, Peierls distortion and superlattice, X-ray study 80—29397
$Co[Pt(C_2O_4)_2].xH_2O$, Co deficient, displacive periodic antiphase model 78—30753
$Co(ethylenediamine)_3^{3+}$, charge distrib., ESCA, internal standards 78—50585
$Co(ethylenediamine)_3(ClO_4)_3$, ESCA chem. shift meas., internal standards 78—50585
$Co(urea)_2Cl_2.2H_2O$, two-dimens. mag. props., cryst. struct., specific heat 80—75777
Cr-Co complex, $[Cr(OCN_2H_4)_6][Co(NH_3)_2(NO_2)_4]_3.3H_2O$, cryst. struct. 80—6392
Cr-Co-P, phase diagrams, lattice constants of phosphides 78—44099
$Cr_{1-x}Co_xSi_2$, prep., elec. cond. and thermoelec. props. 80—49697
$CsCoCl_3$, 1-D Ising antiferromag., mag. phase transitions 79—51779
$CsCoCl_3$, anisotropic antiferromag., inelastic neutron scatt. study 78—60274
$CsCoCl_3$, antiferromag., spin wave spectrum 79—28514
$CsCoCl_3$, antiferromag., ^{59}Co NMR spectrum obs. by spin echo method 79—51881
$CsCoCl_3$, Ising antiferromagnet, electronic Raman scatt. on Co^{2+} 78—10878
$CsCoCl_3$, mag. struct., neutron diffr. meas. 78—43563
Cs_2CoCl_4, paramag. mag. exchange rel. to low temp. mag. characts. 77—55669
Cs_3CoI_5, cryst. struct. and thermal props. *(German)* 79—23578
$CsMn_{1-x}Co_xCl_32H_2O$, random mag. mixture, oblique-antiferromag. phase obs. 80—93142
$CsMn_{1-x}Co_xCl_3.2H_2O$, impure Heisenberg linear chain, EPR meas. 78—43634
Cu complexes, EXAFS obs. 80—998
Cu-Co heterobinuclear complex, cryst., mag. susceptibility of Cu-Co$(fsa)_2$ en, $3H_2O$ 80—2556
$Cu_{0.5}Co_{0.5}Cr_{2-x}Rh_xS_4$, K absorpt. discontinuity chem. shift, bonding parameters 77—77318
CuCoNi ferrite magnetoacoustic oscills. rel. to microstruct. 77—85536

cobalt compounds continued
- Cu_2O, meas. of standard molar free energy of form. by EMF method at high temp. *(Japanese)* 78-11546
- dibarium cobalt formate tetrahydrate Cu^{2+} doped, EPR of Cu-Co interactions 78-60334
- $(Fe,Co)O_4$, magnetostriction calcs. *(Dutch)* 80-2619
- Fe-Co-Ni-O, mag. powder prod. by reduction of oxalates 77-63582
- $FeCl_2.2H_2O$-$CoCl_2.2H_2O$ random mixture, phase diagram 79-73748
- $Fe_{1-x}Co_xCl_2$, mag. phase diagram 80-11198
- $Fe_xCo_{1-x}Cl_2$, metamagnet, mag. phase diagram by mag. induced light scatt. 80-65883
- $Fe_{1-x}Co_xCl_2.2H_2O$, random mixture with competing spin anisotropies, tetracrit. behaviour 80-60324
- $Fe_{(1-x)}Co_xCl_2.2H_2O$, antiferromag. random mixture, sp. ht. meas. 79-65678
- $FeCoCrO_4$, Mossbauer study, cation distrib. and Neel temp. determ. 79-33571
- $FeCoCrO_4$ spinel, elec. resistivity, temp. var. 79-38065
- $FeCoF_5.2H_2O$, ferrimag. props., suscept. and transitions, 3-296K 79-87240
- $Fe_{1-x}Co_xGe_2$ solid solns., mag. susceptibilities, multiple stages in mag. transitions, effective mag. moment 77-8286
- $Fe_{3-x}Co_xO_4$, charge transfer, ion distribs., Mossbauer effect 77-20767
- $Fe_{3-x}Co_xO_4$, effect of Fe^{2+} content on coercivity instability 79-51820
- $Fe_{3-x}Co_xO_4$, Mossbauer spectra, effect of Fe^{2+} conc. 77-69754
- $(Fe_{1-x}Co_x)_2P$, magnetisation, susceptibility, thermal expsn. 79-11302
- $(Fe_{1-x}Co_x)_3P$, cryst. struct. and mag. props. 78-19222
- $Fe_{2-x}Co_xP_{1-y}As$, mag. props., Mossbauer effect 77-40156
- $Fe_{2-x}Co_xP_{1-y}As_y$, band model of mag. props. 77-40029
- $Fe_xCo_{1-x}Rh_2S_4$, spinel struct., X-ray, mag., elec. and Mossbauer spectra meas. 77-12278
- $Fe_{0.2}Co_{0.8}S_2$, narrow-band ferromag., high press. effect on anomalous elec. resist. 80-70698
- $Fe_xCo_{1-x}S_2$, ferromagnetic solid soln., electronic props. 79-7990
- $Fe_{1-x}Co_xSi$ solid solution, semiconductor-metal transition 80-103627
- $Fe_xCo_{1-x}(1,10\text{-phenanthroline})_2(NCS)_2$, spin crossover, Mossbauer and magnetism study 80-44980
- Fe_2O_3-BaO-CoO system, phase comp. and mag. props., Bi_2O_3 additions effect 79-29032
- Fe_2O_3-NiO-ZnO-CoO (15.1, 17.6, 0.6 wt.%) ferrite, effect of electron beam machining on surface layer 79-34178
- Fe_3O_4-Co_3O_4 spinels, phase diagram anal., thermodynamic props. 80-3009
- FeS-CoS, melt viscosity 77-51536
- $Fe_{1+x}Sb$-CoSb solid soln., mag. props., Mossbauer spectra, solubility limits, and lattice consts. *(Russian)* 77-59394
- $(Gd_{1-x}Co_x)_{1-y}Ar_y$ amorphous mag. film, elec. and mag. prop. depend. on Ar 80-80410
- HCl-$CoCl_2$-H_2O, activity coeffs., 298.15K, electrostatic terms effects 79-24812
- $HCo(CO)_4$, mol. struct., gas phase electron diffr. expt. 78-13623
- $HgCo(NCS)_4$ calibration standard, low temp. molar mag. suscepts. meas. 78-65947
- $K_3Co(CN)_6$, NMR spin lattice relax. of ^{59}Co rel. to $Co(CN)_6$ octahedra vibr. modes 80-39885
- K_2CoCl_4, cryst. structs. of orthorhombic and monoclinic modifications 77-15358
- $KCoF_3$, antiferromag., ^{59}Co NMR exam. 78-76332
- $KCoF_3$, single crystal, mag. susceptibility, ^{19}F NMR and static measurements 79-11301
- K_2CoF_4, obs. of short range order by optical birefringence 79-11318
- K_2CoF_4, two-dimensional antiferromag., one- and two-magnon Raman scatt. 79-51945
- K_xCoO_2, layer struct. elec. cond. props. *(French)* 78-26542
- $K_2Co_2(SO_4)_3$, cubic langbeinite struct., low temp. mag. susceptibility 78-56299
- $K_2Co_2(SO_4)_3$ polycryst., growth and phase transitions 79-33918
- $KMn_{1-x}Co_xF_3$, Raman scatt. by mag. excitations 77-55775
- $K_2Mn_{1-x}CoF_4$, mag. and neutron scatt. exam. 79-33466
- $K_2Na[Co(NO4d2)_6]$, single cryst., X-ray deffrs. determ. of electron density distrib. 79-14746
- $K(Zn,Mn,Co)F_3$, crysts., Mn, Co distrib., as function of cryst. region *(German)* 78-14375
- $LaCO_{1-x}M_xO_3$, M = Mg, Ti, cryst. struct., elec. and mag. props. 79-86748
- $La_2Li_{0.5}Co_{0.5}O_4$ phase, intermediate electronic configuration 80-80226
- $LiCoO_2$, XPS of low spin Co (III) 78-31300
- $Mg_xCo_{1-x}(NO_3)_2.6H_2O$, crystal structure changes due to substitution of Mg^{2+} *(German)* 80-24428
- $MgFe_2O_4$-Co_3O_4 solid soln. spinels, domain wall formation inhibition, effect on bulk mag. props. 80-11220
- MgO-CoO, high surface area, O_2 adsorpt., EPR, volumetric investigs. 80-10782
- $(Mn,Co)Cr_2S_4$ and (Mn,Co)S solid soln., equilib. composition *(German)* 77-36486
- $(Mn,Co)O \rightleftharpoons (Mn,Co)Al_2O_4$, and $(Mn,Co)O \rightleftharpoons (Mn,Co)Cr_2O_4$, ion exchange equilib., 1100°C 77-32566
- $Mn_{0.27}Co_{0.73}Cl_2.6H_2O$, antiferromag., sp. ht. meas., phase transition obs. 79-78415
- $Mn_{1-x}Co_xF_2$, Raman scatt. by mag. excitations 77-55775
- $MnCo_2O_4$ DC sputtered films, struct. and elec. props. 80-54812
- $Mn_{1-x}Co_xSb$, ferromagnetic, NMR exam. 79-24228
- MnO, lattice dynamics using three body force shell model 77-76506
- MnO-CoO-O_2, semicond. solid solns., ageing effects on elec. cond. 78-23085
- Mn_3O_4-Co_3O_4 spinels, phase diagram anal., thermodynamic props. 80-3009
- $Mn_{1.18}Zn_{0.06}Co_{0.01}Fe_{1.75}O_4$, transport props. near Curie points 78-88100
- $(NH_4)_2Co(SO_4)_2.6H_2O$, sbumillimeter ESR meas., SH^3 term of effective spin Hamiltonian 78-64264
- $(NH_4)_2Co(SeO_4)_2.6H_2O:Mn^{2+}$, EPR 77-90017
- Na-Co strip-chain silicates, structural-composition inhomogeneities 80-88122
- $NaCo(CO)_4$, soln., ion sites, cryptand C221 doping effects 80-70102
- Na_2CoGeO_4, cryst. struct. determ. 79-90626
- Na_2CoGeO_4, hydrothermal growth from CoO-GeO_2-NaOH-H_2O 77-48329
- Na_2CoGeO_4, single cryst. growth and study of their piezoelec. and elastic props. 79-4906
- Na_xCoO_2, layer struct. elec. cond. props. *(French)* 78-26542

cobalt compounds continued
- $Na_2Co_2Ti_6O_{14}F_2$, characterisation and mag. props., 90-800K, $Na_xTi_4O_8$ bronze isotypes *(French)* 80-39735
- Na_2O-B_2O_3-CoO glass, Co^{2+} ion activated, magneto-opt. study 79-65844
- Na_2O-GeO_2-CoO glass, Co^{2+} ion activated, magneto-opt. study 79-65844
- Na_2O-SiO_2-CoO glass, Co^{2+} ion activated, magneto-opt. study 79-65844
- Na_2SO_4-$CoSO_4$-H_2O, phase equilib., activities, Pitzer eqn. calcs. *(Russian)* 80-65190
- $NdCo(BO_2)_5$, cryst. struct. 78-63735
- Ni-Co-Zn ferrite, exam. of electromag. characteristics 79-1409
- Ni-Zn-Co ferrites, synthesis from solid solns. of schoenite-type salts 80-93511
- NiCo ferrite, induced mag. anisotropy, hysteresis loops, Barkhausen effect *(Russian)* 78-64203
- $Ni_{2-x}Co_xBaFe_{16}O_{27}$, ferromagnetic reson., anisotropy and g-factor, spin-orbit interactions 77-24749
- $Ni_xCo_{1-x}Cl_2.6H_2O$, mixed uniaxial planar antiferromag., magnetisation process 80-88788
- $Ni_{1-x}Co_xF_2$, Raman scatt. by mag. excitations 77-55775
- $Ni_{1-x}Co_xO$, LF magnons, inelastic neutron scatt. exam. 77-66288
- $Ni_{1-x}Co_xO$ mixed crystal, lowest mag. excitation, antiferromag. reson. meas. 77-69704
- $Ni_xCo_{3-x}O$, composition depend antiferromagnetic-ferrimagnetic ordering, mag. susceptibility meas. 80-70973
- $Ni_{50}Co_{40}P_{10}$ amorphous film, spin wave excitation, ferromagnetic resonance study 80-50198
- $Ni_{1-x}Co_xS_2$, anomalous elec. props., polaron transport in highly correl. narrow bands 77-85222
- $Ni_{1-x}Co_xS_2$, elec. cond., thermoelec. power and optical meas. 80-59986
- $Ni_{1-x}Co_xS_2$, elec. transport and semicond.-metal transition 80-10985
- $Ni_{1-x}Co_xS_2$, Mott transitions, temperature induced, Hubbard model theory 80-29326
- $Ni_{0.5-x}Co_xZn_{0.5}Fe_2O_4$ ferrospinal solid solutions, cryst. lattice defects and props. 80-19796
- NiZnCo ferrite, excess Fe type, saturation magnetostriction meas., oxidation effects 79-82852
- NiZnCo ferrite, model of photomagnetic effect 77-43853
- NiZnCo ferrite, quantitative anal., using X-ray fluorescence 78-40090
- NiZnCo ferrites, switching time and coeff., hydrostatic press. effect 80-88802
- NiZnCo ferrites, temp. stability, effect of Fe content and processing conditions 79-28993
- NiZnCo ferrites, voltage response under sinusoidal and pulse magnetisation effected by hydrostatic press. 80-88846
- Pb-B_2O_3-SiO_2-Li_2O-ZrO_2-CoO, coloured, glass enamel, chemical durability and microstruct., CoO addition effect 79-29256
- $PbCo_2(PO_4)_2$, mag. susceptibility, elec. cond. and optical refl. 79-56495
- Pb_2CoReO_6, new seignettomagnets and ferroelectrics 78-19425
- PbO-CoO-SiO_2 system, melt, viscosity meas. in temp. range 950 to 1250°C *(Japanese)* 79-77663
- $PrCo_5$, heat treated, coercive force exam. 78-68298
- Pt complex, cobalt deficient dioxaloplatinate, orientational antiphase struct., X-ray scatt. determ. 80-24435
- $RbCl:CoCl_2$ system, precipitate form., ionic cond. meas. 80-96653
- Rb_2CoF_4, two dimens. Ising like antiferromag., spin wave excitations 78-72342
- $Rb_2Co_cMg_{1-c}F_4$, magnetic specific heat, dilution on a two-dimensional Ising-like antiferromagnet 78-91871
- $Rb_2Co_xMg_{1-x}F_4$, neutron scatt. exam., obs. of two dimens. mag. long range order 78-56295
- $RbMn_{1-x}Co_xF_3$, Raman scatt. by mag. excitations 77-55775
- $SbNbO_4:CoO$, growth, pyroelectric and ferroelectric props. 79-73886
- ScCoSi, X-ray determ. of struct., new representative of struct. type TiNiSi 78-79595
- $ScCo_{0.25}Si_{1.75}$, X-ray determ. of struct., new representative of struct. type $ZrSi_2$ 78-79595
- $SmCo_5$, heat treated, coercive force exam. 78-68298
- $SrCoO_{3-x}$, XPS spectra, shake-up satellite of Co2p 78-52617
- Sr_2CoReO_6, new seignettomagnets and ferroelectrics 78-19425
- TeO_2-CoO, phase diag. from thermographic analysis 78-23687
- TiC-Mo_2C-TiN-Co, fracture toughness, effect of microstructural defects *(Japanese)* 77-56087
- TiO-CiO solid soln., lattice thermal cond. 79-23791
- $TlCoF_3$ paramagnetic, nonmagnetic atomic nuclei spin density, NMR study 80-29633
- U(VI) peroxo complex ion precipitation with Co(III) complex cation 78-80728
- $^{57}CoV_2O_4$, after effects of orbital electron capture 79-73870
- V_xO-Co_yO, solid solutions, exam. of thermal conductivity 78-79827
- $YFe_{1-x}Co_xO_3$, reorientation transitions, neutron diffr., mag. behaviour *(Russian)* 77-24678
- $YFeO_3$, Co^{2+} substituted, reorientational transitions 77-59419
- $Zn_{1-x}Co_xF_2$, Raman scatt. by mag. excitations 77-55775
- ZnO-Bi_2O_3-CoO-MnO-Sb_2O_3 (97.5, 0.5, 0.5, 1.0 mole%), exam. of elec. props. at different annealing temps. 80-3099
- ZnO-Bi_2O_3-Sb_2O_3-Co_2O_3-MnO_2-Cr_2O_3, nonohmic ceramic, microstruct. exam. 78-47292
- ZnO-Co_3O_4, ceramics, impurity at. states, elec. cond. 79-11130
- $Zn_3[Co(CN_6)_6]_2.12H_2O$, X-ray cryst. struct. determ. 79-14751

cochlea *see ear*

Cockcroft Walton rectifiers *see voltage multipliers*

code convertors
- *see also codes; information theory*
- high speed decade counter, binary-decimal convertor, integrated circuitry 77-75028
- noise-tolerant continuously variable slope DM to linear predictive coding conversion 80-96141
- synchronous reversing decade counter, description of operation 77-71728
- transcoder, sequential with scale factor change facility *(Czech)* 77-21668

codes
- *see also encoding; error correction codes*
- criticality anal. using KENO and SU-HAMMER codes, for U-233 and U-235 solns. 78-89949
- digital coding of high-quality musical sound 80-5883
- electrotactile display stimulation codes for artificial sensory communication 78-36049

codes continued
- geological records, coding method based on data transmission theory *(Russian)* 80—17383
- Hierarchically Ordered Spherical Description of Environment, substructure code, spectra estimation 79—50001
- modular data based, nuclear reactor simulation appl. *(German)* 78—17445
- Moon surface features designation, numerical codes 77—53441
- neutron transport, anisotropic scattering treatment using improved comput. code *(Japanese)* 80—13526
- radio time-signal codes in Italy *(Italian)* 80—98888
- regenerative fibre-optic transmission system supervisory line codes *(German)* 78—33884
- sensory feedback code comparison using electrocutaneous tracking, for prosthetics 78—69255
- time codes, EBU/IRT, modified setting instrument, cinematography appl. *(German)* 80—18029
- Tokamak reactor modelling, time-depend. computer codes 77—34468

coding *see encoding*

coding errors
- *see also error correction; error detection*
- Hadamard transform optical instrument, systematic errors 78—94375

coefficient of thermal expansion *see thermal expansion*

coercive force
- *see also magnetic hysteresis*
- Alnico 5, thermal treatment in mag. field, mag. props. 78—91905
- Alnico 5 alloy, S and Ti additions effect rel. to non-metallic inclusions, coercive force and grindability 80—89375
- Alnico alloy, C addition effects on struct. and mag. props. 78—23835
- Alnico alloys, effect of Ce addition on mag. props. 78—2699
- Alnico type YuNDK25DA alloy permanent magnets, thermal mag. hysteresis 80—75818
- amorphous ferromagnet with random uniaxial anisotropy, hysteresis, magnetisation 77—80963
- amorphous ferromagnetic materials status and appls. *(Japanese)* 79—15325
- amorphous ribbons, twisted, magnetisation process, domain theory 80—71101
- amorphous thin films, struct. and mag. props., review 80—93148
- anisotropic materials, magnetisation reversal, 1/H law 78—84454
- attachable electromagnets of ferroprobe coercimeters, use of pole shoes 78—45662
- bubble domain film, growth induced order parameter, estimation from coercive force meas. 80—39828
- bubble film, quenching of coercive force by domain wall restoring forces, theory and expt. test 79—78460
- bubble materials characterisation using spatial filtering techniques 77—85528
- bubble peak vel., analytical method of determ. from overshoot data 79—33513
- bubble-domain materials, amorphous, Hall-effect hysteresigraph for coercivity measurement 79—73786
- chromindur, origin of coercivity, Lorentz microscopy, magnetisation and Mossbauer effect 78—64219
- chromindur, phase separation, Mossbauer obs. 78—88116
- coercimeter, electromagnetic, magnetising current amplitude and turn off speed effect 78—39997
- coercimeter, with cylindrical attachable electromagnet, exam. of design 78—76809
- coercimeter KIFM-1 with automatic measurement of the demagnetizing current 80—68229
- coercimeters with EM attachments 77—12765
- current threshold sensor, struct. and operational features 80—34689
- cylindrical magnetic domain material coercive force meas. 77—79130
- cylindrical magnetic domains, static and dynamic props. of isolated domain *(Russian)* 77—51915
- domain boundaries, pinning on defects with finite radius of interaction, random pot. form effect on mag. hysteresis *(Russian)* 80—84611
- domain boundary interacting with strongly localised pinning centres, influence on hysteresis *(Russian)* 80—65961
- domain wall motion, thermally activated, 77-423K 79—51804
- domain wall pinning by randomly distributed lattice defects 77—69611
- domain wall pinning simulation, coercive force, susceptibility, defect depend. 77—16103
- γ-Fe_2O_3 acicular particles, remanent coercive force 80—44872
- ferrimagnetic magnetisation theoretical models, for uniparametric materials 80—65960
- ferrite, connection between limiting hysteresis loops and number of easy magnetisation axes *(Russian)* 78—72364
- ferrite, coprecipitated, hot pressed, for appl. to mag. heads 77—85968
- ferrite, microwave mag. props., grain size effect 78—10722
- ferrite core, strength improvement method, SiO_2 and Bi_2O_3 additions, mag. characts. 79—24484
- ferrite film, prop. by plasma jet spraying microstruct. and magnetic props. 78—6546
- ferrite powders, mag. props., explosive shock treatment effects 79—52395
- ferrites, EM wave effects on mag. and optical props., lecture 78—27031
- ferrites, M type anisotropic, powder prep. and, sintered, effect of powder and pressing technology on alignment *(German)* 79—24472
- ferrites, sintering, strength and mag. props., vacuum effects 79—70028
- ferrites, soft and microwave, grain-size effects on mag. props., review 78—64222
- ferromagnet, domain wall cavity interaction energy, coercive field 77—8335
- ferromagnet, lattice coercivity of narrow domain walls 79—28552
- ferromagnet, precipitation-induced coercive field enhancement, analogy to precip. hardening 77—77490
- ferromagnet, random anisotropy amorphous, initial magnetisation, remanence and coercivity 77—80964
- ferromagnet, uniaxial, coercive force associated with domain boundary pinning on plane defects *(Russian)* 78—6543
- ferromagnet with narrow domain boundaries, magnetic reversal processes 79—87287
- ferromagnet with random anisotropy, spin correlation 79—73722
- ferromagnetic components comp. and struct. from coercive spectra of rock samples 79—62490
- ferromagnetic crystal, domain wall pinning effect and intrinsic coercivity, computer simulation 78—64217
- ferromagnetic domain wall dynamics, soliton theory appl. 79—82813

coercive force continued
- ferromagnetic domain wall dynamics and soliton theory, coercive force determ. 79—42796
- ferromagnetic domain wall pinning, planar defects, coercive force and correl. length, soliton theory 78—31092
- ferromagnetic domain wall pinning 77—1561
- ferromagnetic film, mag. props., rel. to struct. 79—91270
- ferromagnetic film, mag. props. meas. using planar magnetoresist. effect 78—21186
- ferromagnetic metals and alloys, coercive force, automatic meas. by remote means 79—24690
- ferromagnetic plate, magnetic hysteresis theory, singularities of magnetic reversals on industrial freq. *(Russian)* 78—39373
- ferromagnetic porous material, coercive field 78—14984
- ferromagnetic probe coercive force meter, different heads, for tubing inspection 78—60943
- ferromagnetic thin film, mag. domain wall energy determ. 79—95620
- ferromagnets, hardening by non-mag. inclusions, meas. of coercivity 79—38841
- film, with stripe domain structure, mechanism of mag. reversals *(Russian)* 77—80978
- fine particle system, coercivity and remanence, particle size distrib. effect 77—73053
- garnets, photomagnetic effects, irreversible 79—99719
- Gentalloy, in Fe-W system, damping capacity *(Japanese)* 79—20094
- giant intrinsic magnetic hardness, review 78—48004
- haematite, grain size and coercive force from high temp. AF demag. 77—37189
- hard ferrite particles, dependence on microscopic packing density, model *(German)* 77—20639
- hard magnetic material, coercive field, planar defect influence 77—24710
- hard magnetic material, micromagnetism, theory 78—52301
- high-coercivity, magnetisation characteristic linearity determ. using flux controlling technique *(Russian)* 80—100597
- highly anisotropic material, mag. aftereffects, coercive mechanism 77—69634
- hysteresis, local microscopic magnetisation intensity in presence of Shirobokov's domain struct. *(Russian)* 77—43851
- inhomogeneous model with competing anisotropies, coercivity value 77—69626
- magnetic, bubbly dynamics and jump probability 80—65977
- magnetic bubble materials, coercivity meas. method *(Chinese)* 79—71429
- magnetic domain boundary, interacting with localised defects, unidimensional flow of configs. *(Russian)* 80—65954
- magnetic domain drag effect in presence of variable mag. field or variable transport current 79—78433
- magnetic domain walls, thermal activation from planar pinning sites 79—87285
- magnetic hysteresis curve, multiple particle model *(German)* 78—80178
- magnetic particles, interacting, switching behaviour, dipole and Stoner-Wohlfarth models 80—44870
- magnetically soft cylinders, micromagnetics of curling configurations 79—82826
- magnetically-soft materials, mag. characts. determ. methods, review 79—40593
- magnetite, low stress effects on susceptibility and coercive force 78—16001
- measurement with superimposed sensor 78—88612
- metallic glass, micromag. calcs. and props. 80—80501
- metallic glasses, characts. and appls. *(French)* 80—39815
- metallic glasses, production and properties, technological appl. 80—71105
- meter attachment, with automatic current setting and recording for heat treatment monitoring 77—87795
- mischmetal-based magnets, $MM_{1-x}Sm_xCo_5$, demagnetisation, temp. depend., 175 to 425K 79—78440
- mischmetal-Co-Cu-Fe-Mg, mag. props. 80—35353
- mischmetal-Co-Cu-Mg, mag. props. 80—35353
- model with competing anisotropies 77—20643
- narrow magnetic domain wall material, theory of intrinsic coercivity 80—2597
- NDT coercivity meter with portable display system 78—53135
- Ni-Zn ferrites, mag. param. 78—35005
- orthoferrite cryst. films, local coercivity of domains boundaries *(Russian)* 80—80578
- pearlite, coercivity temp. depend., —196 to 770°C 77—20637
- pearlite in C steels (0.08 to 1.6 wt.%), exam. of temp. depend. of mag. coercivity 78—52304
- Permalloy, 50NP, and 79NM, magnetic properties and structure, environment effect during annealing 80—60366
- Permalloy, corrosion resist. and mag. props., effect of Cr addition 77—86219
- Permalloy, high-permeability, influence of grain struct. and non-mag. particles on mag. props. *(German)* 77—16112
- Permalloy film, coercive force associated with domain boundary displacement *(Russian)* 80—50151
- permalloy film, Fe-overcoated, optical and magneto-optical characts., mag. preps. 79—82956
- Permalloy film, M-H curve meas., magneto-optical instrument *(Japanese)* 77—37953
- Permalloy film preparation by RF sputtering 78—3044
- Permalloy films, RF sputtered on Au, coercivity 80—80575
- Permalloy RF sputtered films, O effects in mag. and elec. props. 80—100603
- Permalloy thick film coercivity control 80—15764
- permanent magnet ferrites, forming 78—64495
- permanent magnets props. improvement, by thermomechanical treatment, gyroscope-based guidance systems performance improvement 80—50144
- porous ferromagnet, with Bloch walls and self-consistent magnetisation, energy and coercive field 80—15760
- porous ferromagnet with Bloch walls, energy and coercive field 79—51818
- rare earth alloy, $R(Co,M)_5$, magnetisation reversal and high coercive force, domain boundary pinning *(Russian)* 77—8345
- rare earth alloys, amorphous, study of hysteresis effects using Monte Carlo technique 79—1686
- rare earth alloys, $R_{69}Ni_{31}$, amorphous, Curie temp., mag. susceptibility and coercive force, 4.2 to 300K 80—93092
- rare earth amorphous alloys, random mag. anisotropy, antiferromag., Monte Carlo calcs. 79—33471

coercive force continued
rare earth cobalt intermetallics, Cu or Ni-substituted, narrow Bloch walls, magnetisation, 4.2K 77−8333
rare earth garnet thin films, macroscopic magn. props., magneto-optical expts. 80−46764
rare earth intermetallics, $RFe_{5-x}Ni_x$, giant intrinsic mag. hardness 78−56354
rare earth intermetallics, RGa, mag. props., 4.2-350K 77−63230
rare earth iron alloy, amorphous film, cosputtered, struct. and mag. props. 78−60323
rare earth iron garnet single crystal films, synthesis and props., review 78−48013
rare earth orthoferrite, $RFeO_3$, spin reorientation and magneto-optical effects *(Japanese)* 79−47414
rare earth permanent magnets, physics and technology 80−20433
rare earth-$(Co_{1-x}Ni_x)_5$, single cryst., mag. props., mag. reversal 77−85489
rare earth-Co, 2-17 comp., permanent magnet props. 77−8348
rare earth-Co, $R_{69}Co_{31}$, amorphous, mag. props. 80−84590
rare earth-Co, RCo_5, high anisotropy origin, intrinsic coercive field 77−73020
rare earth-Co amorphous film, sputtered, in-plane anisotropy induced by rare gas annealing 78−84458
rare earth-Co permanent magnets, generation mechanism of high coercive force *(Japanese)* 79−100269
rare earth-Co-Ni alloys, $Pr(CoNi)_5$ type, mag. props. and mag. reversal phenomena *(Russian)* 77−51924
rare earth-Fe alloy, amorphous, random anisotropy model, generalised mol. field calcs. 77−28345
rare earth-Fe alloys, RFe_2, temp. depend of coercivity 79−61185
rare earth-transition metal intermetallics, struct. and props. review 78−10668
Rayleigh hysteresis, reexam. 78−48002
Recalloy, Fe-Nb, semihard magnetic alloy, magnetic props., hardness, microstruct. 78−56660
ring specimens, computer controlled mag. meas. system 80−86346
scaling relations in mag., mechanical and superconducting pinning theory 77−76403
semiautomatic digital coercimeter, exam. of design 78−76817
semiautomatic portable coercimeter 79−34250
$Sm_{1-x}R_xCo_5$ (R=Y, La, Ce, Nd), mag. props., domain boundary pinning on statistical conc. heterogeneities *(Russian)* 79−99728
soft magnetic materials, meas. via vibrating-coil magnetometer 77−41659
soft magnetic particles, coercive field strength meas. *(German)* 80−22395
steel, alloy, deep drawing sheet, annealing effect on coercive force *(German)* 80−29573
steel, alloy, YuNDK24, magnetisation direction in interaction domains *(Russian)* 79−99720
steel, C, cold rolled St3Kp, annealed, mag. nondestructive inspection of strip and ribbon 78−60913
steel, coercive force measurement method of quality inspection of heat and thermomechanically treated parts 79−5113
steel, cold-rolled sheet, St10 kp, St10 sp, mag. inspection of ferroprobe coercimeters 80−21234
steel, ELA, coercive force, differential meas. 77−71351
steel, high-speed, 30Kh2N2SMKt, deform. effects on physicomech. props. 78−23741
steel, induced anisotropy influence on mag. props., thermomagnetic working *(Russian)* 80−55549
steel, low alloy, type 3sp, effect of temp. at end of rolling on mech. props., and coercive force 78−72799
steel, low alloy and C, hardened and tempered parts, nondestructive magnetic inspection 78−95889
steel, low alloy and C, hardened and tempered parts, nondestructive magnetic inspection 79−1929
steel, low C, mech. props. determ., NDT methods 79−29176
steel, low C, quenched, struct. and props. after plastic deform. and tempering 78−23734
steel, low C and low alloy, rolled, nondestructive impact strength testing by coercive force meas. 79−52601
steel, low-C electric sheet, struct. and coercive force after second cold rolling 77−44270
steel, Mn, type 35SGM, magnetic, electrical, and mech. props. after tempering and hardening 79−66086
steel, Mn-Si, mag. method of NDT of mech. props. 80−21211
steel, stainless, plastic working of wires, high-density current appl. 79−57002
steel bearing parts, magnetic inspection of heat treatment quality 78−73007
steel case depth after quench hardening, inspection using coercimeters 80−104377
steel wire, magnetically hard Kh13N13M2-type, electroplastic drawing *(Russian)* 80−20967
steels, tool, type U10A and R6M5, phase comp. and phys. props. after hydrostatic extrusion 79−96053
superparamagnetism, coercive force as function of temp. 79−87292
TGS, deuterated, dielectric props., ageing 77−16257
TGS, spontaneous polarisation and coercive field from 30 to 1000 Hz 77−66464
TGSe, deuterated, dielectric props., ageing 77−16257
thermally activated domain wall motion and coercive field in materials with extremely narrow domain walls 80−25156
Ticonal, effect of rare earth metals on mag. props., struct., and phase transformations 79−99732
Ticonal with Sm, magnetic props., phase transform. after thermomagnetic treatment 78−3155
transition metal amorphous alloys, mag. props. 80−29576
transition metal ferromagnetic amorphous alloys, mag. props. 77−55690
trisarcosine calcium chloride crystals, ferroelec., electrooptic and ferroelastic props. 80−34865
twin crystals, magnetic reversals, role of magnetostatic interaction *(Russian)* 78−39361
uniaxial crystal, with narrow domain boundaries, coercive force *(Russian)* 80−50140
vicalloy-2, high heating rate effect on mag. props. *(Russian)* 77−81328
$(Ba,Sr)Fe_{12}O_{19}$, Ferroxdure, developments and research 78−84455
Ba ferrite powder, effect of lattice defects on coercivity *(German)* 79−24194

coercive force continued
$BaO-Fe_2O_3$, chemically coprecipitated, mag. props., orientation 80−15763
BaO.n Fe_2O_3, magnet, effect of SiO_2 on texture and densification behaviour *(German)* 79−24631
$BaTiO_3$ film, dielectric props. depend. on sinusoidal elec. field 80−71318
Bi-MnBi, directionally solidified composite, processing parameter role on mag. props. 80−35352
Bi-MnBi eutectic composites, microstructure and mag. props., annealing effect 79−82827
Ca ferrite magnets, anisotropic, BaO substitution effect on mag. props. *(Japanese)* 79−99697
$CdCr_2Se_4$, mag. semicond., domain struct. by IR Faraday effect 79−95604
Ce-Co-Cu-Fe-Ti, sintered magnet, prep. and mag. props. 77−73043
Ce-Sm-Co-Fe-Cu alloy, permanent magnet props. 79−8013
$CeCo_5$, magnetisation and coercive strength 77−55688
$CeCo_{5+x}$, Cu and Fe modified, coercive force *(Czech)* 79−42805
$CeMM_{0.8}Sm_{0.2}Co_5$, (MM=mischmetal), thermal props. *(German)* 77−8359
$(Co, Cu, Fe)_5Ce$, sintered permanent magnets, magnetic charact. 78−60608
$(Co,Cu,Fe)_5Ce$, sintered, mag. props. 78−68302
$(Co,Fe,M)_{78}Si_8B_{14}$ amorphous alloys (M=V,Nb,Ta,Cr,Mo,W,Mn or Ni), zero magnetostriction and low field mag. props. 80−34741
Co alloys, amorphous, effects of metalloids on mag. props. 80−75738
Co, and alloys, ferromag. films, coercive force, ion plating prep. 77−28730
Co, electrodeposited coating, struct. and magnetic props. 79−46985
Co, FCC, mag. props. of single-domain powders after plastic deform. *(Russian)* 78−6554
Co ferrite, growth on fine acicular γ-Fe_2O_3 particles 80−29871
Co ferrite film prep. by vac. evaporation and annealing 77−85939
Co, ferromag. film, ion plating prep., coercive force and magnetoresist. 77−12546
Co, ferromagnetic micropowder, cryst. struct., coercivity, remanence, saturation 80−65967
Co film, ion beam sputtering prep., struct. and mag. props. 80−35085
Co films layered over Cr by DC sputtering for digital mag. recording 79−83118
Co, fine powder, magnetic props., effects of electrolysis conditions in prep. 77−40091
Co single domain particles, randomly oriented easy axes and particle size distrib., coercivity 80−71119
Co, sputtered film, high coercivity and high hysteresis loop squareness 79−91259
Co-Cr films, mag. props. in range of transition from thin-film to hypercritical state *(Russian)* 79−51824
Co-Cr mag. film, crystallographic texture formation effects on props. *(Russian)* 80−108471
Co-Cu-Fe-Ce, mag. characteristics of sintered permanent magnets 78−60312
Co-Cu-Fe-Ce alloys, sintered permanent magnets, mag. characts. 77−43855
Co-Fe, soft mag. props. rel. to metallurgical aspects 80−88810
Co-Fe (6 wt.%) alloy magnetic properties, 850 to 1000°C range *(Slovak)* 79−4698
Co-Fe amorphous alloys, high permeability props. *(Japanese)* 77−51927
Co-Fe-B and Co-Fe-Cr-P-B sputtered amorphous films, mag. props. and corrosion resist. 79−28567
Co-Fe-Nb, heavily cold worked, magnetic hardening 79−20073
Co-Fe-Nb (12, 3 wt.%), semihard magnetic alloy, relationship between precipitation and coercivity 77−8839
Co-Fe-Nb alloy, mag. precipitation-hardening and Bloch wall pinning 78−80173
Co-Fe-Nb semihard mag. alloy, mag. precip. hardening 77−8960
Co-Fe-Nb-Mo, semihard magnetic alloy, magnetic props. 78−95469
Co-Fe-P film, ferromag., coercive force meas. 78−10737
Co-Fe-Si-B, amorphous alloys, substitution effect on mag. props. 79−69695
Co-Fe-Ti (12,6 wt.%), semihard permanent magnet, magnetic precipitation hardening 78−52830
Co-Fe-Ti alloy, precipitation hardened, rel. between struct. and mag. props. 78−95470
Co-Fe-V-Ni, mag. and mech. props., heat treatment and stress effects 80−60363
Co-Ni, ferromag. film, ion plating prep., coercive force and magnetoresist. 77−12546
Co-Ni alloys, electrodeposited, struct., internal stress, and mag. props. 78−95471
Co-Ni fine particles, anhysteretic growth of exchange fixed remanent states 77−16116
Co-Ni-Fe-Si(B), amorphous ribbon, magnetostriction meas. 80−15778
Co-Ni(Ti)(Cu)(Mn), cryst. struct. and stacking fault influence on mag. props. *(Russian)* 80−25164
Co-P, electrodeposited amorphous alloy, mag. permeability 78−52310
Co-P electroless film on Al base disc substrate, microstruct. rel. to mag. props. 78−68304
Co-P films, electrodeposited, magnetic recording media *(Japanese)* 80−29587
Co-P films with various preferred orientations, mag. props. 80−100604
Co-Pt, struct. and mag. props. rel. to degree of order 78−72368
Co-Pt film, electrodeposited, saturation mag. induction, mag. anisotropy and coercive field meas. *(French)* 80−2610
Co-Pt films, mag. and magneto-optic props., appl. to holographic and bit-by-bit storage 79−33512
Co-Re, sputtered film, high coercivity and high hysteresis loop squareness 79−91259
Co-Sm-Sn-$Co_{17}Sm_2$ eutectic fibre composite, coercive force 77−40084
Co-W alloy electrodeposition, influence of $MgSO_4$ and gum arabic additives *(Russian)* 80−80991
Co-W alloy electrolytic coatings, heat treatment effects on coercivity, hysteresis and structure *(Russian)* 80−60381
Co(-Re) sputtered films, mag. props. and microstructures 79−82837
$(Co_{0.83}Cu_{0.17})_6Ce$, cryst. struct. and mag. props., decomp. during ageing *(Russian)* 79−37661
Co_4CuCe, cryst. struct., mag. characts., ageing and decomposition *(Russian)* 79−4272
$Co_4CuCe_{0.9}$, correl. of cryst. struct. and coercive force *(Russian)* 77−80962

coercive force continued
- $Co_{74}Fe_6B_{20}$, metallic glass, zero magnetostriction, magnetisation characts. 77−12158
- $Co_{79}Fe_{6.5}B_{14.5}$ amorphous thin films, zero magnetostriction, high magnetisation 80−34708
- $(CoFeB)_{100-x}Cr_x$ thin films, magnetic props. and corrosion resist. 80−34709
- $Co_{57}Fe_5Ni_{10}(Si,B)_{28}$, amorphous, soft mag. props., switched-mode power supply appls. 80−88850
- Co_xMM, (MM+mischmetal), coercive force, effect of preparation conditions 78−95467
- CoNiB, corrosion-resistant amorphous mag. thin films 80−54923
- $Co_{50}Ni_{20}Fe_6Si_{12}B_{12}$, amorphous, mag. props., effects mech. deform. 80−39840
- CoNiP film, amorphous, electrolytic, prep. and props. *(Slovak)* 79−51823
- CoP, and CoNiP, cylindrical amorphous electrodeposited layers, mag. props., torsion influence 80−88848
- CoPr, coercive force variation as function of annealing temp. *(Japanese)* 79−47787
- $CoPt_3$, electrolytic films, saturation mag. induction, coercive fields, thickness depend. *(French)* 80−44883
- $Co_{74}Si_{10}B_{16}$, amorphous ferromagnetic alloy, isothermal annealing effect on static magnetic props. *(Japanese)* 79−52398
- Co_5Sm, coercive field temp. depend. 77−8358
- Co_5Sm, coercive force variation as function of annealing temp. *(Japanese)* 79−47787
- Co_5Sm crystals, microstruct., homogeneous precip. and nucleation 80−104160
- Co_2SnO_4, $CoMg(Zn)SnO_4$ and $Co_{2-x}Mg_2TiO_4$, magnetic props., short-range ordering 77−32155
- $Co_{2-y}Zn_yTiO_4$, spinel series, exchange integrals, mag. struct. and coercive force, magnetisation meas. 77−69507
- Cr-Co-Fe, chromindur alloy, field heat treatment, and mag. props. 80−35354
- Cr-Co-Ni hard film on Mo substrate for magnetic recording 80−2608
- CrO_2, epitaxial growth on rutile, possible appl. as bit oriented mag. material 77−16127
- CrO_2, oxidative prep. method, mag. props. 80−44863
- CrO_2 powders, print through values and mag. characts. 80−44871
- CrO_2, single mag. particle, remanent coercive force and remanent loop meas. 78−95480
- $Cr_{1-x}Rh_xO_2$, $(0<x<0.5)$, effect of x on coercive field 79−43164
- $Cr_{1-x}Rh_xO_2$, oxidative prep. method, mag. props. 80−44863
- Cu:Co precipitates, mag. anisotropy, precipitate shape, coercive force 80−80500
- Cu-Mn spin glass, hysteresis loops, temp. and field depend. 80−15742
- Cu-Mn-Al alloys, displaced hysteresis loop and microstructure obs. 80−84613
- Cu-Ni-Co, mag. props. of system of disperse ferromag. particles, 73 to 673K *(Russian)* 80−65968
- Cu-Ni-Fe, magnetic properties, heat treatment and compressive stress effects 80−60367
- Cu-Ni-Fe (14, 7 wt.%), solid soln., decomposed, magnetostatic interaction between ferromag. particles *(Russian)* 77−80967
- Dy, domain wall dynamics, NMR 77−69614
- $DyFe_2$ powders, mag. and hysteresis props. *(Russian)* 79−42800
- $Dy_xY_{1-x}Al_2$, domain wall dynamics, NMR 77−69614
- $(ErCo_2)_x(ErAl_2)_{1-x}$, mag. and struct. investigations of intermetallic systems 78−95440
- $Er_2Co_{17-x}M_x$, M=Cr, Ni, effect of substitution on mag. props. 79−78363
- $ErCo_{5-x}Ni_x$ ferrimagnetic series, magnetisation, coercive field meas. 78−91896
- $(ErEu)_3(FeGa)_5O_{12}$ film, for mag. writing and magneto-optical displays 78−6549
- $ErFe_2$ powders, mag. and hysteresis props. *(Russian)* 79−42800
- $(Er_{65}Fe_{35})_{100-x}B_x$ glasses, mag. props. 79−73693
- $(EuLu)_3Fe_5O_{12}$, Ga, Al or (Ca,Ge) substituted, mag. props. and growth of 2 μm bubbles 78−91910
- EuS films, mag. and elec. props. rel. to stoichiometry and defects 80−97122
- (Fe,Co,Ni)-Si(B), amorphous mag. alloy, magnetostriction rel. to soft mag. props. 80−84633
- $(Fe,Ni)_{83}B_{15}C_2$, amorphous alloy, mag. props., possible appl. to power transformers 79−28558
- $(Fe,Ni)_{80}P_{14}B_6$ amorphous alloy, mag. props., possible appl. to power transformers 79−28558
- Fe alloy YuNDK35T5BA, thermomag. treatment, post-decomp. processes 79−87668
- Fe alloys, amorphous, effects of metalloids on mag. props. 80−75738
- Fe alloys, anisotropic precipitation struct. in external mag. field *(German)* 78−72785
- Fe, and alloys, ferromag. films, coercive force, ion plating prep. 77−28730
- Fe, cast, grey, pearlitic relationship of magnetic props. to condition of C 78−56353
- Fe, coercive force measurement method of quality inspection of heat and thermomechanically treated parts 79−5113
- α-Fe, cyclically deformed, mag. props. 77−28412
- Fe, deformed, dislocation structure determ. from magnetic props. 78−55874
- Fe, ferromagnetic micropowder, cryst. struct., coercivity, remanence, saturation 80−65967
- Fe, film, ion beam sputtering prep., struct. and mag. props. 80−35085
- Fe, fine particle dispersions, shock induced mag. effects 79−82832
- Fe, nitrided wire, magnetic charact. and microstruct. *(Korean)* 78−19277
- Fe particles in Hg, ferromag. liquid, mag. props., ageing effects 77−12154
- Fe powder, BH_4 reduced, coercive force and remanence ang. variation 80−44879
- Fe powder, prep. by reducing iron phthalate in mag. field, mag. props. 77−40090
- Fe powder, sintered and hot pressed, effect of porosity, grain size on magnetic props. 79−96159
- Fe powders, Co- or Cu-plated, prep. by rad. and chem. plating, mag. props. 80−44867
- Fe powders, prep. by BH_4 process, comp. and stability 80−44878
- Fe-Al-Ni-Co-Cu alloys, Ti alloying and deoxidising addition *(Russian)* 78−80181

coercive force continued
- Fe-B, (16.3 at.%) amorphous, coercive force temp. depend. 80−25158
- Fe-B, amorphous alloy, mag. props. 80−84618
- Fe-B metallic ribbons, correl. between quenching temp. and mech. and mag. props. 80−89373
- Fe-B ribbon, microhardness, and static coercive force, melt overheating effect 80−84978
- Fe-B-C amorphous alloy, formation, mag. props., thermal stability and density 80−75796
- Fe-B-C amorphous alloys, room-temp. saturation induction over 17.5 kG 79−47300
- Fe-B-C amorphous alloys, effect of Si addition on mag. props. 80−34694
- Fe-B-C amorphous alloys for use in power transformers 80−88808
- Fe-B-C amorphous alloys with high saturation induction 80−84617
- Fe-B-Cr(Mo), metallic glasses, mag., struct., and elec. props. 80−88751
- Fe-B-Si amorphous alloys, crystallisation temp., Curie temps., saturation magnetisation 79−82820
- Fe-B-Si amorphous ribbon, strain induced anisotropy, and toroid diam. effect on mag. props. 80−34623
- Fe-c, Fe-Si-B, and Fe-Cr-P-C sputtered amorphous films, mag. props. and corrosion resist. 79−28567
- Fe-Co, ferromagnetic micropowder, cryst. struct., coercivity, remanence, saturation 80−65967
- Fe-Co alloy particles for mag. tapes, mag. props. 78−95479
- Fe-Co based amorphous alloys, mag. props. *(Japanese)* 79−95971
- Fe-Co-Al-Cu-Ti (40, 14, 7.5, 4.5 wt.%), metastable equilibrium, high coercive state *(Russian)* 80−66476 ,
- Fe-Co-B powders, synthesis and mag. props., appl. to mag. recording 80−20432
- Fe-Co-Cr, magnetic, phase transform. obs. *(French)* 79−47676
- Fe-Co-Cr-Si, structural transform. and mag. props. following heat treatment *(Russian)* 77−81274
- Fe-Co-Mo-Nb(Ta) semihard mag. alloy, mag. props., thermal expansion, elec. resistivity and hardness *(Japanese)* 80−88789
- Fe-Co-Ni-Al (35, 14.5, 7.2 wt.%), high-coercivity, substructure and texture change during bending and upsetting 80−21037
- Fe-Co-Ni-Al-Nb (15-20, 14, 9, 0.1-5.5 at.%), Nb effect on magnetic props., lattice parameter *(Russian)* 77−55689
- Fe-Co-Ni-Al-Zr magnetically hard alloys, reduction *(Russian)* 78−43614
- Fe-Co-Si-B, zero magnetostrictive amorphous alloy with high saturation induction, mag. annealing 80−60362
- Fe-Co-Si-B sputtered amorphous thin film, coercivity, galvanomagnetic props., resistivity 80−29578
- Fe-Cr-Al alloys, low temp. sp. ht., resistivity and coercive force 78−63866
- Fe-Cr-Co, mechanism of coercive force 80−34674
- Fe-Cr-Co alloy, coercive force mechanism 80−71103
- Fe-Cr-Co alloys, mag. props., heat treatment effects *(Russian)* 78−39365
- Fe-Cr-Co ductile magnet alloys, phase diagram and mag. props., V or V+Ti addition effects 77−8959
- Fe-Cr-Co hard-mag. alloys, fine cryst. struct. *(Russian)* 77−66706
- Fe-Cr-Co permanent magnet system, miscibility gap, microstruct. and mag. props. obs. 80−76228
- Fe-Cr-Co-Al (27.5, 17.5, 0.5) alloy, dependence on shape anisotropy and effective particle size 78−72367
- Fe-Cr-Co-Mo, microstruct., hardness, mag. props., influence of isothermal tempering and heat treatment 79−79129
- Fe-Cr-Co-Mo high energy permanent magnets, mag. props. 80−97119
- Fe-Cr-Co(-Mo), mag. props. after isothermal thermomag. treatment *(Russian)* 80−25159
- Fe-Cu, dilute, coercive field, initial permeability and relax. loss, non-mag. impurity effect 77−69628
- Fe-Mo(W), semihard magnetic alloys, magnetic, elec. mech. props. *(Japanese)* 79−70078
- Fe-Nb (3.1 wt.%), semihard mag. alloy, Recalloy, mag. props., elec. cond. *(Japanese)* 78−10723
- Fe-Ni, coercive force depend. on grain struct. and inclusions 77−20635
- Fe-Ni, electrolytic film, coercive force depend. on electroplating conditions *(French)* 77−55691
- Fe-Ni alloy, effect of thermomag. treatment in rotating field *(Russian)* 77−21294
- Fe-Ni film, mag. and struct. props., effect of O_2 partial press. during deposition 79−90903
- Fe-Ni-Al, type YuN14DK25BA, thermomag. treatment 80−16512
- Fe-Ni-Al alloy, metastable equilib. in its high-coercivity state *(Russian)* 79−52161
- Fe-Ni-Al alloys, phase diagram, miscibility gap, mag. props. 78−92237
- Fe-Ni-Al-Co-Cr-Ti, YuNDK35T5BA, exam. of hypodissociation process *(Russian)* 79−11547
- Fe-Ni-Al-Co-Cu-Sn alloy YuNDK35T5, Sn addition effects on physicomechanical and magnetic props. and workability *(Russian)* 77−70101
- Fe-Ni-Al-Co-Ti base alloys, highly coercive, phase comp., Mossbauer meas. 80−39996
- Fe-Ni-Al-Cu (25, 14, 4 wt.%), alloy YuND4, effect of Ti addition on structure, mag. props. 80−15714
- Fe-Ni-B-Si, amorphous, mag. props., heat treatment effects 80−89370
- Fe-Ni-Co, rel. between induced uniaxial anisotropy and coercive force 78−91904
- Fe-Ni-Co-B-P soft magnetic metallic glasses, status report 78−64226
- Fe-Ni-Co-Cu-Ti YuNDKT alloys, impaired mag. props. with C and S additions 80−60368
- Fe-Ni-Cr, vapour-deposited film, effect of condensation temp. on form. of metastable phases and mag. props. 79−65700
- Fe-Ni-Si-Mn-Cr(Co-Mo), effect of prolonged aging on mag. props. 80−16513
- Fe-Ni-Ti-Al-Nb, struct. mechanism for inverse $\alpha \rightarrow \gamma$ transform. *(Russian)* 80−40351
- Fe-Pd-Pt alloy powders, coercive force and specific remanence *(Russian)* 79−47302
- Fe-Pt films, mag. and magneto-optic props., appl. to holographic and bit-by-bit storage 79−33512
- Fe-Si (1-5 wt.%), optimum sintering conditions and mag. props. 77−85958
- Fe-Si (3 to 5 wt.%) sinters, mag. props., Si and Fe-Si additions effect 80−71104
- Fe-Si (3.25 wt.%), mag. props., influence of struct. and chemical composition of surface oxide layer 78−2700

coercive force continued
- Fe-Si (4 wt.%) alloy, coercive force, influence of stabilisation of domain struct. on temp. depend. *(Russian)* 77—52513
- Fe-Si (6.5 wt%) filament, formation by modified Taylor technique, and mag. props. 80—75795
- Fe-Si (6.5 wt.%), effect of ordering on mag. props. 79—51833
- Fe-Si (6.5 wt.%) ribbon, splat-cooled, mag. props. 80—88805
- Fe-Si amorphous films, mag. and magnetoelastic props. 79—99746
- Fe-Si-Al, Sendust, 12 μ thick film prep. by sputtering, mag. and other props. 77—55888
- Fe-Si-Al (6,4 wt.%), Sendust alloy, effect of Ni content on mag. props. 78—72897
- Fe-Si-Al Sendust alloy ribbon form, rapid quench prepared, elec. cond., coercive field, permeability 79—83151
- Fe-Si-Al-Ni alloy, Super Sendust, Ni content and thermomag. treatment effects 77—4861
- Fe-Si-B, magnetic metallic glasses, mag. props. 80—84620
- Fe-Si-B amorphous films, mag. props. 80—34710
- Fe-Si-B metallic glasses, mag. props., depend. on metalloid content 77—85485
- Fe-Si-Mn, effect of Mn addition on mag. props. and elec. resist. 78—91890
- Fe-Si(6.5 wt.%) ribbon, prep. by rapid quenching and mag. props. 80—45251
- Fe-Ta alloy, mech. drawn and aged, exam. of electrical resistivity, hardness, microstruct., and mag. props. *(Japanese)* 78—48545
- Fe-W system, damping capacity of Gentalloy, internal friction, mech. and mag. props. 79—77679
- Fe-W-Cr-Mo-Co (18,12,3,x wt.%) alloy, cold working effect obs. *(Japanese)* 77—40428
- Fe-Zn alloys, coercive force anisotropy after cold plastic deform. *(Bulgarian)* 80—75809
- $(Fe\text{-}Co\text{-}Ni)_{78}Si_8B_{14}$, amorphous, low coercivity and zero magnetostriction 78—23299
- $Fe_{1-x}B_x$ film, optical and magneto-optical characts., mag. preps. 79—82956
- $Fe_{100-x}B_x$, mag. and struct. props., comp. depend. 78—60314
- $Fe_{100-x}B_x$ ribbon, magnetostriction exam. 79—73794
- $Fe_{80}B_{20}$ amorphous alloy, low field magnetic props. 77—55690
- $Fe_{80}B_{20}$ glass, low-field mag. props. 77—8380
- $Fe_{80}B_{20}$, sputter deposited amorphous, low field mag. props. 78—68335
- $Fe_{83.4}B_{16.6}$, amorphous, mag. props. and microstruct., cooling rate and melt overheating effects 80—65965
- $Fe_{83.4}B_{16.6}$ amorphous, mag. props., melt overheating and cooling rate effects 80—89371
- $Fe_{80}B_{20-x}M_x$ (X=Al, Si, Ge, C, P) and $(FeCo)_{80}B_{20}$ glass, magnetisation, Curie and crystn. temps. 79—87289
- $Fe_{80}B_{15}Si_5$ metallic glass, large uniaxial magnetostrictive anisotropy, magnetisation reversal 80—34736
- Fe_xC_{1-x} amorphous sputtered film, mag. props. 78—68311
- FeCoB, corrosion-resistant amorphous mag. thin films 80—54923
- $Fe_{3-x}Co_xO_4$, effect of Fe^{2+} content on coercivity instability 79—51820
- $(Fe_{1-x}Co_x)_{78}Si_8B_{14}$ ribbon, magnetostriction exam. 79—73794
- $Fe_5Co_{70}Si_{15}B_{10}$, amorphous, change of mag. props. by low temp. annealing 78—27058
- $Fe_5Co_{70}Si_{15}B_{10}$, amorphous ferromagnetic alloy, isothermal annealing effect on static magnetic props. *(Japanese)* 79—52398
- $Fe_5Co_{70}Si_{15}B_{10}$, amorphous, crystn. effect on mag. props. *(Russian)* 80—44858
- $(Fe_xCo_{1-x})_{100-y}(Si_{0.4}B_{0.6})_y$ amorphous alloy zero magnetostrictive, mag. props. 79—99743
- FeN alloy, coercive force, effect of $Fe_{16}N_2$, anisotropic model 77—85501
- $Fe_{40}Ni_{38}\text{-}Mo_4B_{18}$ amorphous alloys, compatibility of DC and AC mag. props. 80—34695
- $Fe_{40}Ni_{40}B_{20}$, amorphous, processing conditions effect on mag. props. 79—73775
- $Fe_{40}Ni_{40}B_{20}$, amorphous, casting conditions effect on mag. props. *(Japanese)* 80—34698
- $Fe_{40}Ni_{40}B_{20}$, amorphous, mag. props., effects mech. deform. 80—39840
- $(Fe_xNi_{1-x})_{80}B_{20}$, amorphous alloys, engineering mag. props. 79—51832
- $Fe_{80-x}Ni_xB_{20-y}P_y$, amorphous, Rayleigh region and coercive force 80—88806
- $Fe_{40}Ni_{40}(Mo,Si,B)_{20}$, amorphous, soft mag. props., switched-mode power supply appls. 80—88850
- $Fe_{40}Ni_{38}Mo_4B_{18}$ glassy alloy, high permeability, low field mag. characts. 78—68301
- $Fe_{40}Ni_{40}P_{14}B_6$, amorhpous ribbon, influence of torsion on mag. props. 80—7138
- $Fe_{40}Ni_{40}P_{14}B_6$, amorphous ribbon, cold rolling, annealing mag. props. 77—8958
- $Fe_{40}Ni_{40}P_{14}B_6$, amorphous tape wound cores, mag. props. *(German)* 78—10727
- $Fe_{40}Ni_{40}P_{14}B_6$, amorphous, mag. props. 78—10728
- $Fe_{40}Ni_{40}P_{14}B_6$, amorphous ferromagnet, domain struct., Rayleigh region and coercive field 79—28559
- $Fe_{40}Ni_{40}P_{14}B_6$, amorphous, mag. props., effects mech. deform. 80—39840
- $\gamma\text{-}Fe_2O_3$ acicular particles, coercivity, magnetic recording tape appls. 78—14983
- $\gamma\text{-}Fe_2O_3$ acicular particles, coercivity increase by Co ferrite surface crystn. 80—44866
- $\gamma\text{-}Fe_2O_3$, clean and SiO_2 coated, reduction temp. influence on coercivities, coercivity factors and rheological props. 79—69698
- $\gamma\text{-}Fe_2O_3$, densified, rheological and mag. props. 80—44873
- $\alpha\text{-}Fe_2O_3$ film, prep. by reactive condensation and mag. props. 78—64241
- Fe_2O_3, haematite, single domain, defect moment components coercivities 79—16438
- $\gamma\text{-}Fe_2O_3$ particles, growing Fe-Co ferrite, coercivity increase 79—56571
- $\gamma\text{-}Fe_2O_3$ particles, mag. props. rel. to mag. tape appl. 80—15762
- $\gamma\text{-}Fe_2O_3$ powders, influence of densification on mag. props. 78—95481
- $\gamma\text{-}Fe_2O_3$ powders, mag. props., effect of Co plating 79—69699
- $\gamma\text{-}Fe_2O_3$, prep. from thermal decomp. of $[Fe_3(HCOO)_6(OH)_2]HCOO.4H_2O$ and characterisation 78—80741
- $\gamma\text{-}Fe_2O_3$, single mag. particle, remanent coercive force and remanent loop meas. 78—95480
- $\gamma\text{-}Fe_2O_3$:Co, impact-induced demagnetisation, magnetostriction and coercive force, appl. in mag. recording 77—16111
- $\gamma\text{-}Fe_2O_3$:Co acicular powder epitaxially doped, coercivity increase, surface anisotropy *(Chinese)* 80—7130
- $\gamma\text{-} Fe_2O_3$:Co powder, increased coercivity by epitaxial doping 79—82833
- $\gamma\text{-} Fe_2O_3\text{-}Fe_3O_4$, lodestone, microstructure and mag. props., source of mag. hardening 79—82828

coercive force continued
- $\gamma\text{-}Fe_2O_3$-organic interfaces, mag. struct., Mossbauer effect, IR absorpt., and magnetisation meas. 80—44869
- Fe_3O_4 film, prep. by reactive condensation and mag. props. 78—64241
- Fe_3O_4, magnetite, coercive force spectrum at high temps. rel. to thermal activation below blocking temp. 77—91111
- Fe_3O_4, magnetite film, coercive force and lattice const. 78—2707
- Fe_3O_4, magnetite particles, interaction fields effect on hysteretic props. 80—54921
- Fe_3O_4 particles, nonstoichiometric, morphology and enhanced coercivity, Mossbauer meas. 80—7132
- Fe_3O_4 powder, oxidation to $\gamma\text{-}Fe_2O_3$, coercivity changes 80—44864
- Fe_3O_4, spherulitic film growth, elec. and mag. props. 78—68627
- Fe_3O_4:Co, impact-induced demagnetisation, magnetostriction and coercive force, appl. in mag. recording 77—16111
- Fe_xO_y powder coated with $NaPO_3$, anomalous coercivity increase 77—89980
- $Fe_{80}P_{13}C_7$, amorphous ferromagnetic alloy, isothermal annealing effect on static magnetic props. *(Japanese)* 79—52398
- FePd epitaxial film, vacuum-deposited, for thermomag. recording, mag. and magneto-optical props. *(Russian)* 78—60319
- $FePd_{1-x}$ Pt_x, permanent magnet, coercive force increased by Pt 79—24157
- $Fe_{1-x}Pd_x$ films, vacuum deposited, mag. and corrosion props. 79—56574
- FePt epitaxial film, vacuum-deposited, for thermomag. recording, mag. and magneto-optical props. *(Russian)* 78—60319
- FeSi picture frame single cryst., domain wall motion and magnetisation reversal, time-depend. neutron depolarisation study 80—88782
- $Fe_{1-x}Si_x$ film, optical and magneto-optical characts., mag. preps. 79—82956
- $Fe_{100-x}Si_x$ ribbon, magnetostriction exam. 79—73794
- $Fe_xSi_yAl_z$ ribbon, magnetostriction exam. 79—73794
- $Fe_{75}Si_{15}B_{10}$, amorphous ferromagnetic alloy, isothermal annealing effect on static magnetic props. *(Japanese)* 79—52398
- $Fe_{75}Si_{15}B_{10}$, mag. behaviour rel. to magnetostatic interactions 80—11224
- $(Fe_{1-x}Si_x)_{1-y}By$, metallic glass, mag. props., crystallisation 80—65885
- $Fe_{2.6-x}Ti_{0.4}Al_x\ O_4$, $Fe_{2.4-x}Ti_{0.6}Al_xO_4$, titanomagnetite, monodomain, mag. props. 78—56346
- FeTiB, corrosion-resistant amorphous mag. thin films 80—54923
- $Fe_{3-x}Ti_xO_4$, $0.5 \leq x \leq 1$, mag. props. of antiferromag. phase 80—70960
- $(Gd,Bi)_3,(Fe,Al,Ga)_50_{12}$ LPE film, 180° Bloch wall pinning at etched nucl. tracks 78—39376
- $(Gd,Bi)_3(Fe,Ga)_5O_{12}$ magneto-optic film, ion irrad. effect on storage props. 78—52324
- $(Gd,Bi)_3(Fe,Ga)_5O_{12}$, LPE film, coercivity, influence of nuclear tracks 79—51829
- Gd-Al(C)(Cu)(Ga)(Ni)(Pd)(Rh) alloys, amorphous, mag. and elec. props. 80—80499
- Gd-Co, evaporated amorphous film, perpendicular anisotropy by controlled O_2 contamination 77—89990
- Gd-Co amorphous film, magnetisation processes near compensation point 77—69644
- Gd-Co amorphous thin film, mag. and optical props., conc. depend 79—19748
- Gd-Co film, amorphous, stability of small bits to temp. and mag. field changes 78—68314
- Gd-Co film, temp. depend. of mag. aftereffect *(Russian)* 79—8021
- Gd-Co(-Au) film, ferrimag. amorphous, coated with Permalloy films, mag. props. 79—1695
- Gd-Fe, DC bias RF sputtered film, mag. props. 77—16124
- $(Gd_{1-x}Co_x)_{1-y}Ar_y$ amorphous mag. film, elec. and mag. prop. depend. on Ar 80—80410
- $Gd_{0.12}Co_{0.59}Cu_{0.29}$, sputtered film prep. for bubble device 77—16493
- $GdCo_{5c}Ni_{5-5c}$, intrinsic coercivity, anisotropy, exchange and cryst. field interactions 80—75806
- $(Gd_{65}Fe_{35})_{100-x}B_x$ glasses, mag. props. 79—73693
- GdIG, thermal effect on re-entrant hysteresis loop and coercive force 78—2702
- $(GdMn_2)_x(GdAl_2)_{1-x}$, mag. and struct. investigations of intermetallic systems 78—95440
- $HoCo_{5-x}Ni_x(Cu_x)$, lattice parameters and mag. props. 79—82817
- $(LaLuSm)_3(GaFe)_5O_{12}$ bubble garnet film, coercivity 79—78459
- Li matrix ferrites, coercivity, synthesis, thermostability control 80—80569
- $Li_{0.5}$ $Fe_{2.5}O_4$, microwave material, mag. props., review 79—33504
- $LiFe_5O_8$, microstruct. and magnetic props., electron microscope obs. 79—87290
- $(Li_{0.5}Fe_{2.5}O_4)_{0.8}(CuFe_2O_4)_{0.2}$, struct., magnetic props., rectangular hysteresis loop 77—20645
- LiMnSc ferrites, role of intergranular microstresses in control of coercive force 77—20640
- $(MgFe_2O_4)_{1-\gamma}(Mn_3O_4)_\gamma$, polycrystalline, coercive forces 78—39366
- $MgIn_xFe_{2-x}O_4$ and $MgSc_xFe_{2-x}O_4$, Mossbauer spectra, elec. and mag. props. *(Russian)* 77—69737
- $MgM^{3+}{}_xFe_{2-x}O_4$, M=In,Al,Cr,Sc, comp. effects on ferrite characts. 78—52305
- Mn-Al-C, fine-grained cast struct., remanence and coercive force 80—60365
- Mn-Bi alloys, mag. props. improvement study *(Japanese)* 78—43617
- Mn-Ga, DO_{22} type alloys, magnetic props., crystal struct. *(Japanese)* 78—59784
- $Mn_{55}Al_{45}$ alloy, permanent mag. props., depend. on particle size 78—91899
- MnBi, domain boundaries shift, mag. reversal processes 79—87286
- MnBi particles, demagnetised, coercivity, remanence and magnetisation reversal 78—19281
- MnBi particles, effect of grinding on coercivity 77—36098
- MnBi, thin film, struct. and mag. props. 79—47315
- MnBi, two-phase coercive force for domain wall motion, mag. reversal nucleation mechanism *(Russian)* 77—48009
- $Mn_{2-x}Cr_xSb$ film, prep. and mag. props. 78—48009
- $Mn_{2-x}Cr_xSb$, sintered, intrinsic coercivity 77—89983
- $MnCu_{1-x}Dy_xBi_{0.86}$ film, mag. and magneto-optic props., appl. as storage medium 77—8550
- $Mn_xFe_{3-x}O_{4+y}$, prep., resist., hysteresis loop and mag. disaccommodation *(Spanish)* 77—73045
- $Mn_{3-x}Ni_xB_4$, with onset of spontaneous magnetisation below T_N, singularities of mag. props. *(Russian)* 77—59427
- $Nd(Co_{1-x}Cu_x)_5$, coercive force temp. depend. 79—82823
- $NdFe_2$, amorphous, magnetization and neutron scatt. meas. 79—78314
- $Nd_xPr_ySm_zCo_5$ permanent magnets, coercive force, low-temp. annealing influence *(Russian)* 80—39812

coercive force continued
- $(Nd_xSm_{(1-x)})_2(Co_{0.7}Fe_{0.3})_{17}$, mag. anisotropy 80—34622
- Ni, deformed, coercivity and remanence anisotropy 78—31093
- Ni, ferromag. film, ion plating prep., coercive force and magnetoresist. 77—12546
- Ni fibres, magnetisation reversal 77—69625
- Ni film, ion beam sputtering prep., struct. and mag. props. 80—35085
- Ni, mag. props. of single-domain powders after plastic deform. *(Russian)* 78—6554
- Ni wire in Ag matrix, coercivity meas. 77—20642
- Ni-Co, mag. props. of single-domain powders after plastic deform. *(Russian)* 78—6554
- Ni-Co-P, amorphous alloy, electrical and mag. props. 78—95281
- Ni-Co-Zn ferrite, exam. of electromag. characteristics 79—1409
- Ni-Fe, soft mag. props. rel. to metallurgical aspects 80—88810
- Ni-Fe alloys, high-permeability, development trends *(Slovak)* 79—4694
- Ni-Fe films, coercivity control for single-level masking bubble devices using surface modification and intermediate layers 79—51816
- Ni-Fe films, magnetisation reversal in narrow strips, TEM study 80—34720
- Ni-Fe multilayered films, mag. domain structures 79—82847
- Ni-Fe narrow stripes, mag. props. and domain struct. 79—82843
- Ni-Fe overlay, influence on bubble device performance 79—78466
- Ni-Fe-Co alloy films for logic devices, mag. switching vel., anisotropy field and coercive force *(Korean)* 77—51930
- Ni-Fe-Co film, nonmagnetostrictive, effect of deposition parameters of Al underlayer 77—77078
- Ni-Fe-Cr alloy, PE 16, coercivity of picture frame cryst. 78—14988
- Ni-Fe-Cr alloy, PE 16, thermally activated domain wall motion 79—95603
- Ni-Fe-Nb, hardperm alloy, effect of sheet thickness and heat treatment on magnetic props. *(Japanese)* 78—31095
- Ni-Fe-Nb, Hardperm alloy, sheets, effect of sheet thickness, and annealing, on mag. props. 78—76772
- Ni-Fe-Nb alloys, mag. permeability and struct. *(Chinese)* 78—84450
- Ni-Fe-Nb-Al alloys, mag. permeability and struct. *(Chinese)* 78—84450
- Ni-Fe-Nb-Mo-Al, head material for mag. recording, DC and AC mag. props. 80—88812
- Ni-Fe-Pd thin films, mag., surface and corrosion props. 80—34707
- Ni-Fe-Rh films, mag. and corrosion props. 80—34702
- Ni-Mn base polynary alloys, magnetic and elect. props. *(Japanese)* 78—15551
- Ni-P, amorphous alloys, low temp. mag. props., comp. depend. 77—66387
- Ni-P, amorphous magnetisation, NMR and coercive force meas. 77—32187
- Ni-P electrodeposit, magnetisation coercivity and magnetostriction 78—68338
- $Ni_{0.5-x}Co_xZn_{0.5}Fe_2O_4$ ferrospinal solid solutions, cryst. lattice defects and props. 80—19796
- NiFe film, sputtered, physical props. 79—77938
- NiFe, single and multilayer thin films, strip domains, inplane magnetisation 80—103866
- NiFe soft magnetic alloys, magnetic props., effect of annealing and fabrication *(German)* 78—53004
- NiFe stripes, mag. props. and domain struct. 80—44886
- $Ni_xFe_yCr_{1-x-y}$ films, struct., mag. props., and corrosion resist. 80—34706
- $NiFe_2O_4$, microstruct. and magnetic props., electron microscope obs. 79—87290
- $NiFe_2O_4$-Fe_2O_3, effects of excess Fe_2O_3 on mag. props. 77—85495
- NiO (111) platelets, antiferromag. S domains, optical obs., spin flop 80—54915
- $Ni_{1-x}P_x$, electrodeposited, amorphous, mag. and transport props. 78—52106
- NiS film, electrolytically deposited, S content influence 80—44884
- NiZn ferrite, magnetic props., porosity and grain size effects 77—36095
- Pb_z-$Sr_{1-z}(Zr_x$-$Ti_{1-x})O_3$:Cr_2O_3, ferroelec. ceramic, reversible characts. and dielectric losses *(Russian)* 78—84517
- $(Pb_{1-x}Ba_x)_5Ge_3O_{11}$, ferroelec. transition blurring, US relax., dielec. and opt. props. 78—95559
- $Pb(Zr,Ti)O_3$ film, ferroelec. and optical props. 77—85674
- $Pb(Zr_{0.47}Ti_{0.43}Sn_{0.10})O_3$:$Cr_2O_3$, ferroelec. ceramic, reversible characts. and dielectric losses *(Russian)* 78—84517
- $(Pd_xPt_{1-x})_3Fe$, magnetisation intensity and coercive force, antiferro- to ferromag. transition *(Russian)* 77—48008
- $PrCo_5$, heat treated, coercive force exam. 78—68298
- $Pr(Co_{1-x}Cu_x)_5$, coercive force temp. depend. 79—82823
- $Pr_{0.75}Sm_{0.25}Co_5$ magnets, struct. and props. sintering temp. depend. *(Russian)* 79—82819
- Pt-Co, magnetically hard, struct. and morphology, electron microscope study 79—82171
- $Pt_{0.7}Ni_{0.3}Fe$, magnetically hard, cryst. morphology and mag. domain struct. 77—69615
- RFeAl, scatter order cpds., mag. props. 77—51891
- SbSI, ferroelectric semiconductor, polarisation switching processes, effect of surface electron states 77—90115
- Si_xFe_{100-x} polycryst. ribbon, prep. by rapid quenching, and props. 80—75803
- Sm-Co, alloy powders and sintered magnets, effect of chem. treatment on mag. props. 78—60311
- Sm-Co, amorphous, plasma-sprayed, role of Ar or H_2 atm. in mag. props. and crystn., rel. to H_2 storage 80—64898
- Sm-Co base ternary alloy, mag. props. and cryst. struct. 77—8352
- Sm-Co-Cu, with Sm_2Co_{17} struct., aged, TEM high coercivity material, TEM obs. of microstruct. 77—77073
- Sm-Co-Cu-Fe, single phase 2-17 sample, hard mag. props. 77—8349
- Sm-Co-Cu-Fe-Ti magnets, comp. and sintering effects on coercivity 79—15326
- Sm-Co-Cu-Fe-Zr alloy, reversible changes in coercive force and struct. state during heat treatment 400-800°C *(Russian)* 80—29574
- Sm-Co-Cu-Fe-Zr magnet, production and mag. props. 77—40085
- Sm-Pr-Co, added Fe_2Sn, permanent magnets, demagnetisation curves, X-ray obs. 78—91900
- Sm-Pr-Co alloys, mag. props. and struct., comp. depend. *(Russian)* 80—20430
- $SmCO_5$, etched microparticles, Barkhausen discontinuity, nucleation, and domain wall pinning 79—87288
- $SmCO_5$ magnets, sintering time effect on props. 79—95977
- SmCaGe garnet LPE bubble film, coercivity, thickness depend. 78—68324

coercive force continued
- $Sm_2(Co, Cu, Fe, M)_{17}$, M=Nb, V, Ta, Zr, effect of M on mag. props. 77—89978
- Sm(Co, Cu) alloys, coercivity mech. 80—44862
- $Sm(Co,Cu)_z$, precip.-hardened, mag. and metallographic props. 77—8339
- $SmCo_5$, and related alloys, nucleation and pinning at 360° domain walls 77—73042
- $SmCo_5$, and $SmCo_{3.5}Cu_{1.5}$, anisotropy and coercivity, Kerr effect, magnetisation and aftereffect expts. 77—8300
- $SmCo_5$ based ternary and quaternary permanent mag. materials with low reversible temp. coeffs. 79—82822
- $SmCo_5$, coercivity, random substitution of Sm by Co *(Chinese)* 77—8343
- $SmCo_5$ films, struct. transformations effect on coercive force and mag. reversal *(Russian)* 80—20436
- $SmCo_5$, heat treated, coercive force exam. 78—68298
- $SmCo_5$, high coercivity isotropic plasma-sprayed magnet, eutectoid decomp. 80—80568
- $SmCo_5$, intrinsic coercivity losses, temp. depend. 78—95468
- $SmCo_5$ isotropic plasma sprayed magnet, high coercivity 78—68295
- $SmCo_5$, isotropic plasma-sprayed high coercivity magnet, eutectoid decomp. 80—75810
- $SmCo_5$ magnets, effect of heat treatment on coercive force *(Russian)* 79—1684
- $SmCo_5$, nucleation of reversed domains at Co_7Sm_2 precips. 80—75791
- $SmCo_5$ permanent magnet, liq. phase sintered, hysteresis loops, ageing, temp. depend. *(Chinese)* 77—51921
- $SmCo_5$, permanent magnet stability, during long-term ageing *(Chinese)* 80—55428
- $SmCo_5$, powder, comminution temp. effect on mag. props. 80—39819
- $SmCo_5$, powder prod. by electroerosion mag. props. 77—59718
- $SmCo_5$ single crystals subjected to shock waves, magnetisation, creation of high-coercivity state *(Russian)* 77—66384
- $SmCo_5$, single crysts., mag. props. study and role of anisotropy *(French)* 79—38356
- $SmCo_5$, sintered, hard mag. material, magnetisation behaviour 80—75805
- $SmCo_5$, sintered, high coercivity, microstruct. and mag. props. 77—69629
- $SmCo_5$, sintered, mag. props. *(German)* 77—43852
- $SmCo_5$ sintered magnets, periodic struct. and coercive force *(Russian)* 79—28554
- $SmCo_5$ sintered magnets, struct. and magnetic characts., sintering temp. influence *(Russian)* 79—52397
- $SmCo_5$, sintered permanent magnet, 4.2-300K, fields up to 100 kOe 77—8341
- $SmCo_{5+x}$, Cu and Fe modified, coercive force, demagnetization curves *(Czech)* 79—42805
- Sm_2Co_{17}, coercive force depend. on annealing temp. 80—65964
- Sm_2Co_7 sintered magnets, coercive force and constitution, annealing temp. depend. *(Russian)* 80—88786
- Sm_xCo_y, mag. and struct. investigations of intermetallic systems 78—95440
- Sm_xCo_y, mag. props. 78—43568
- $SmCo_3B_2$, high coercive forces, ferromag. ordering and saturation moments 77—24711
- $Sm(Co_{0.65}Cu_{0.35})_{5.6}$, cryst. struct. and coercive force, heat treatment effects *(Russian)* 80—44170
- $Sm(Co_{0.87}Cu_{0.13})_{7.8}$, coercivity and microstruct. 79—56569
- $Sm(Co_{1-x}Cu_x)_{7.8}$ alloys, coercive fields, domain wall energies, mag. and metallographic exam. 78—91897
- $SmCo_{3.5}Cu_{1.5}$, mag. aftereffects, coercive mechanism, magnetisation reversal 77—69634
- $SmCo_{3.5}Cu_{1.5}$, single crysts., mag. props. study and role of anisotropy *(French)* 79—38356
- $SmCo_{3.5}Cu_{1.5}$, time dependent magnetisation 78—80176
- $SmCo_{5-x}Cu_x$, giant intrinsic mag. hardness obs. 77—59432
- $SmCo_{5-x}Cu_x$, giant intrinsic mag. hardness 79—91255
- $Sm(Co_{0.86-x}Cu_{0.14}Fe_x)_7$, permanent magnet, sintering and heat treatment effects 80—39817
- $Sm(Co_{0.85}Fe_{0.05}Cu_{0.10})_z$, coercive force meas. 77—4530
- $Sm(CoFeCuMn)_7$, coercive force and anisotropy temp. depend. 78—68297
- $Sm_2Co_{17-x}M_x$, M=Cr, Ni, effect of substitution on mag. props. 79—78363
- $SmCo_2Ni_3$-Y(Pr)(Gd)(Tb)(Er), giant intrinsic magnetic hardness 78—56347
- $SmCo_{5-x}Ni_x$, giant intrinsic mag. hardness, temp. and time depend. 77—69627
- $SmCo_{5-x}Ni_x$, giant intrinsic magnetic hardness analysis 78—88146
- $Sm_2Cu_{1.6}Zr_{0.16}Fe_{3.3}Co_{12}$, enhancement of mag. props. 79—82825
- $SmFe_2$ powders, mag. and hysteresis props. *(Russian)* 79—42800
- Sm_2M_{17}, sintered magnet, hard mag. props. optimisation 77—8340
- $Sm_{1-w}MM_w(Co_{1-x-y}Cu_xFe)_z$, (MM-mischmetal), mag. meas. and metallographic exam. 77—56119
- $SmNi_4M$, M=Fe, Cu, Al, intrinsic mag. hardness 77—85506
- $Sm_{0.5}Pr_{0.5}Co_5$ sintered magnets, periodic struct. and coercive force *(Russian)* 79—28554
- $Sm_{0.91}Zr_{0.09}(Co_{0.68}Cu_{0.10}Fe_{0.22})_{6.7}$, alloy permanent magnet, coercive force *(Russian)* 80—65966
- $SnCo_5$, magnetisation and cohesive strength 77—55688
- $SnCo_2O_4$ spinel, mag. props. 77—1543
- $Sr_2(Co_{1-x}M_x)_{17}$, M=Mn, Ti, Zr, powders, influence of substitutes on mag. props. 80—100601
- $SrFe_{12}O_{19}$, hysteresis loops, formation processes 80—39813
- $SrFe_{12}O_{19}$ micropowder, high coercivity, obtained by extended wet milling, prep. and mag. props. 77—8776
- $SrFe_{12}O_{19}$, microstruct. and magnetic props., electron microscope obs. 79—87290
- $SrO.6Fe_2O_3$, ultrafine, microstruct. development during sintering, mag. props. 79—70022
- Tb-Fe, amorphous ferrimag. film, thermomag. writing using He-Ne laser 77—12163
- Tb-Fe, amorphous magnetism in bulk samples 77—66278
- Tb-Fe film, undoped and O-doped, amorphous, microstruct. and mag. props. 79—91273
- $Tb_{52}Ag_{48}$, amorphous, mag. after-effect meas. 79—24200
- $TbFe_2$ powders, mag. and hysteresis props. *(Russian)* 79—42800
- Tb_xFe_{1-x} film, amorphous, magnetostriction and magnetisation 78—68305
- $(Tb_{1-x}Gd_x)_3Co$, intermetallic cpd. mag. props., phase transform, and mag. hystersis *(Russian)* 80—93113

coercive force continued
  Ti-Permalloy thin film diffusion couples, low temp. interdiffusion interdiffusion 78—71889
  $Tm_{2.2}Bi_{0.8}Fe_{3.5}Ga_{1.5}O_{12}$ epitaxial film, Faraday effect and domain struct. near compensation point 77—20838
  UGa_2, cryst. struct., mag. and magnetoelastic props. *(Russian)* 79—38364
  US, low field mag. props. 77—73047
  WC-Co hard alloys, hot pressed, mech. props. 79—100260
  WC-Co hard metal, binder phase charact. by magnetic props. 79—29439
  WC-Co hardmetals, heat-treated, single domain obs. 79—73771
  $(Y,Eu,Tm,Ca)_3(Fe,Ge)_5O_{12}$ garnet film coercivity, new annealing method 78—84459
  $(Y,Sm,Ca)_3(Fe,Ge)_5O_{12}$ epitaxial films, mag. props., growth condition effects 80—97124
  $(Y, Sm, Lu, Ca)_3(Fe, Ge)_5O_{12}$:$Ne^+$, film, S=1 bubbles dynamic props., temp. depend. 77—20658
  $(Y,Sm,Lu,Ca)_3(Fe,Ge)_5O_{12}$ garnet film coercivity, new annealing method 78—84459
  $(Y,Sm,Lu,Ca)_3(Fe,Ge)_5O_{12}$ bubble magnetic garnet film, LPE grown, props., $CaCO_3/GeO_2$ molar ratio influence 80—50152
  $(Y, Sm, Lu, Ca)_3(FeGe)_5O_{12}$ LPE films, factors affecting coercivity 79—91267
  $(Y,Sm,Lu,Ca)_3(Ga,Ge,Fe)_5O_{12}$, film growth and mag. props. for bubble-memory appl. 79—87297
  $(Y, Sm, Tm)_3(FeGa)_5 O_{12}$ LPE films, factors affecting coercivity 79—91267
  YCo_5, coercivity, random substitution of Y by Co *(Chinese)* 77—8343
  $Y_{1-x}Co_x$, amorphous, mag. props. 80—84590
  $Y(Co_{1-x}Ni_x)_5$, mag. heterogeneities and coercive force, neutron scatt. study 80—2553
  $(YEuTmCa)_3(FeGe)_5$ bubble garnet films, ion-implanted, mag. susceptibility meas. 79—47311
  YFe_2 amorphous, spin-glass and mag. blocking transitions, low field DC susceptibility meas. 79—61141
  YFe_2, amorphous concentrated spin glass, susceptibility, Mossbauer and neutron scatt. meas. 80—39783
  $(Y_{65}Fe_{35})_{100-x}B_x$ glasses, mag. props. 79—73693
  $YFeO_3$ platelets, domain wall mobility, dynamic coercivity 78—91884
  $YFeO_3$, thermomag. recording in surface layer of orthoferrite 79—24165
  $Y_{3-3x-2z}Gd_{3x}Ca_{2z}Fe_{5-z-u}V_zSi_uCo_uO_{12}$, mag. props., effect of V substitution 77—20582
  $Y_{2.01}Gd_{0.99}Fe_{4.925-x}Mn_xO_{12}$, comp. depend. of mag. props., and stress sensitivity control 78—27057
  YIG, bulk, low mag. domain wall mobility 78—95463
  YIG, domain wall mobility and mass meas. method *(Russian)* 80—108033
  YIG, influence of X-ray radiation on mag. props. 77—8337
  YIG, plastic deform. and mag. props 77—40087
  $(YLuSmCa)_3(GeFe)_5O_{12}$ bubble garnet film, coercivity 79—78459
  $(YSmCa)_3(FeGe)_5O_{12}$ LPE films, optimum growth conditions for low coercivity 78—95499
  $(YSmCa)_3(FeGe)_5O_{12}$ LPE film, growth and coercivity 79—4707
  YSmLuCaFeGe garnets, growth and temp. characts. of small bubbles 78—80183
  $(YSmLuCa)_3(FeGe)_5O_{12}$, mag. props. and growth of 2 μm bubbles 78—91910
  $(Y_{1-x}2Co_x)Co_5$, anisotropy fields, coercivities, annealing effects 78—91898
  $Zr_{40}Cu_{60-x}Gd_x$, magnetically dil. glass, 4f moments, mag. susceptibility and magnetisation meas. 79—95575
  $Zr_{40}Cu_{60-x}Tb_x$, magnetically dil. glass, 4f moments, mag. susceptibility and magnetisation meas. 79—95575

coercivity *see coercive force*

cognitive systems
  see also adaptive systems; artificial intelligence; automata theory
  cognitron, feedback-type, self-organising neural network with associative memory 78—56962
  EEG patterns during cognitive tasks, controlled tasks anal. 80—67059
  EEG patterns during cognitive tasks, methodology and complex behaviours anal. 80—61531
  information processing and origin of pure geometry 77—44624
  neurological functional pattern description *(French)* 77—9186
  self-organising multilayered neural network study 77—40661

coherence
  see also light coherence
  acoustic signal coherence limits in random ocean environment 80—46193
  acoustic signals, matrix formulation of multiple and partial coherence 77—46831
  at-power reactor noise, second-order coherent functions 78—94070
  atom, coherent transients, spherical tensor treatment 79—26940
  atomic hyperfine struct. transitions, nonstationary RF coherence signals *(Russian)* 79—98011
  atomic ionisation by strong coherent EM field, nonperturbative calc. methods 80—5512
  atomic systems, coherent transients theorem 80—99808
  auroral infrasonic wave emission, multiplicity of wave forms 77—29534
  biological system, cooperative behaviour, Bose condensation, Frohlich model 78—35797
  blackbody radiation between parallel plates, coherence props. 79—85107
  cancerous cell culture, phonons, long-range coherence, microwave effects 78—35816
  cavity, optical, 1-dimens., with output coupling, thermal radiation, fluctuation-dissipation theorem 79—978
  channelled ions, reson. coherent excitation 79—51178
  channelling positron (electron), coherent radiation 77—76476
  charged particle beam, modulated, coherent EM radiation prod. 77—19149
  cinematic photography, design aspects *(Russian)* 80—42280
  coherent state, necessary condition to remain coherent 78—73879
  coherent states of an electron in a quantized electromagnetic wave 79—22000
  concert hall problem, coherence length and diffuse reflection formulation 80—91962
  condensed systems, with repulsive interactions, coherence effects 79—69624
  cosmic coherent avalanche catastrophies, gamma-freq. graviton radiation 78—85844
  curvature radiation 80—56704

coherence continued
  cyanomethane, multiple quantum coherence in dipolar relaxation measurements 79—73845
  cyclic X-ray monochromators, with perpendicular dispersion planes, emission coherence 80—90974
  cyclopentanone, excited triplet state, intramolecular tunnelling, optically detected electron spin coherence 77—61774
  Dicke-maser model dynamics, phase transition to the spontaneous coherent state 78—66792
  dispersive medium, envelope-soliton propagation for interacting coherent excitations 79—2639
  EEG coherence estimates, significance in determ. of central α and μ activities 80—61720
  electron diffraction line patterns, scattering model *(French)* 78—51397
  electron microscope image interpretation, instrumental, environmental conditions *(Polish)* 79—30623
  electron microscopy, axial high resolution, spatial coherence in 77—82654
  electron microscopy, partial coherence 77—71410
  electron optics, coherence, review 80—32900
  electron optics, isoplanatic image formation 78—9312
  electron optics, partially coherent sources, radiometric quantities 77—38797
  electron spin coherence in nonphosphoresc. triplet states, optical detect. meas., TADMR and FMDR 78—25578
  electron storage ring coherent microwave emission fine struct. 78—78875
  EM radiation in media with spatial dispersion, spatial coherence formation and polarisation increase 80—106442
  EM radiation intensity, produced by modulated electron/ion beams in gas 78—50686
  ensemble density matrix form., with off-diagonal (coherent) constraints 77—74314
  excitons, coupled coherent-incoherent motion, rel. to mean square displacement 79—19519
  extension of coherence function concept to quadratic models 79—72987
  field emission electron beams, two beam interference 78—63002
  frictional quantum mechanical system, one-dimens. scatt. model for coherence in stopping power problem 80—101736
  Frohlich brain wave model, limit cycle stability, enzyme-substrate reaction 78—44490
  impurity trapping of quasifree excitons and electrons, finite coherence effects 80—59880
  ionosphere S_q currents, spatial coherence scale of day to day variability over Europe 79—44299
  jet, axisymmetric, coherent struct. obs. using new optical technique 80—10282
  magnetosphere chorus and hiss observed by GEOS, coherence function appl. in automatic recognition technique 79—44307
  matter-photon interaction renormalisation, coherent states in matter-photon systems 77—68199
  metal vapour coherent two photon reson. third and fifth harmonic VUV generation 79—72627
  microwave Cherenkov radiation generation, relativistic electron beam-dielectric loaded waveguide 77—58246
  molecular system interacting with radiation field, equilib. mean values 79—27224
  Mossbauer effect, coherence and interference 78—27123
  Mossbauer freq. modulated γ-rays, phase coherence 80—7211
  multimolecular system, two-level mols., coherent trapping of single excitation 79—89875
  multiphoton excitation, collisionless, of large mol. kinetic eqns. 79—54914
  naphthalene-d_8:naphthalene, betamethylnaphthalene, $^1B_{2u}$ naphthalene exciton percolation kinetics, exciton coherency 79—33750
  ocean acoustics, two-point coherence function models with inhomogeneous background and anisotropy 80—81922
  one-mode fields, greatest lower bounds for degree of coherence of higher order 78—71068
  optical pumping with lasers, atomic polarisability, coherence between Zeeman sublevels 77—83549
  paramagnetic ions, spontaneous coherent state transition, susceptibility singularities 77—40119
  partially coherent radiation by charged particle beams in ionosphere 78—28407
  partially-coherent source imaging, speckle interferometry appl. 80—9032
  plane waves, difference between polarisation and coherence 80—8805
  pulsar coherent radiation, relativistic soliton model *(Russian)* 78—77568
  pulsar rotating magnetosphere, charge bunching mechanism for coherent curvature radiation 77—33538
  pulsars, narrowband versus broadband emission processes rel. to luminosities 80—51797
  pulse propagation and two-frequency mutual coherence function in random medium 77—10818
  quantum radiation inelastic scatt., correlation functions and higher order coherence 78—32721
  quantum theory, coherence and randomness, uncertainty relations 80—22231
  radiation source field in unbounded scatt. medium *(Russian)* 78—1160
  radio emission from pulsars 80—46596
  radio emission in nature, theory, solar system and pulsars appl. 80—46393
  radio waves, transionospheric, scintillation coherence time struct. 80—90281
  radioastronomy, mutual coherence function 79—75115
  radiometric recognition of coherence 77—74505
  radiometry, second order, radiant noise coherence 78—287
  relativistic electrons, channelling radiation, quantum beats 80—88226
  RF superradiance optical pulse generated under photon-echo conditions 80—95858
  shallow water horizontal spatial coherence meas. 78—5605
  solar diameter pulsations, phase coherence 79—92747
  STEM, partially coherent image form. 77—190
  stimulated EM shock radiation, by EM wave-fast electron interaction, freq. dispersive media 77—83796
  thermionic emission sources 77—22622
  time-frequency-space generalised coherence and scatt. functions 78—5603
  time-varying signal coherent detection using multiple obs. 80—43553
  transducer signals, flow noise rejection using coherence function method 77—84067
  two-level system in radiation field, dynamics, temp. depend. props. 78—66793

coherence continued
undersea acoustic signal coherence fluctuations 80—46191
underwater acoustic time delay estimation, cross-correl. and smoothed coherence transform methods compared 80—96086
underwater sound, cylindrically symm. formulation for spatial coherence loss 77—34985
underwater sound, freq. and time coherence in random multipath channels 77—84047
underwater sound, l.f. transverse to propag. direction 77—818
underwater sound in shallow water with rough boundaries, attenuation of coherent component 77—62091
undulator radiation, coherence, directional pattern, wavelength spread, polaris. 79—55043
undulator radiation theory, coherence, extension to short wavelengths 79—55042
unified wave propagation theory, tenuous random medium 78—4491
wave propagating in turbulent medium, four-point field coherence function 79—98279
white noise analysis, coherence improvement by use of repeated random sequence generator 80—36203
X-rays, crystallography appls. 78—26388
I_2, effusive collisionless beam, optical Rabi coherent transient damping, time resolved obs. 77—75231
Na, reson. two-photon ionis., photoelectron ang. distrib. and polaris., nucl. spin influence 79—10083

coherence distance *see coherence length*

coherence length
A15 compounds, coherence length and phonon softening 78—34587
EM coherence length in supercond. with mag. impurities 79—42696
film, nonequilibrium, inhomogeneous state onset 78—14875
granular microcylinder, flux quantisation phenomena above T_c *(Russian)* 80—70899
magnetic flux structures in superconductors, book 79—91199
spin susceptibility of conductivity electrons, spatial dispersion in superconductors *(Russian)* 79—51719
superconducting layered cpds., upper crit. fields and reduced dimensionality 80—70910
superconducting microbridges, props. in pure limit *(Russian)* 77—89903
superconductor resistive state, coherence length, penetration depth 80—97030
superconductor-normal metal interface in a finite geometry 79—33404
type II superconductors, correl. between flux-line lattice and cryst. lattice 77—1526
type II superconductors, crit. currents in non-transversal mag. fields 77—55646
type II superconductors, flux-line cutting 80—7055
type II superconductors, order parameter and mag. field of distorted vortex lattice 77—77014
Al superconducting films, precursor diamagnetism 77—32115
Al superconducting films, equilib. order parameter deviations from mean field theory 77—69453
Bi, amorphous films, supercond. fluctuation effects in perpendicular mag. fields 79—60980
$Cu_2Mo_6S_8$, normal state and superconducting property measurements 78—91660
In superconducting films, with implanted He particles crit. field anomalies *(Russian)* 77—69459
La-Al(Ge)(Au), amorphous, alloying effect on supercond. props. 79—60951
Nb films, supercond. props. and electronic density of states *(Russian)* 79—28439
Nb-Ti multifilamentary wires, crit. current degradation mechanism 77—28324
NbN, supercond. props., SQUID behaviour 78—72311
Nb_3Sn, coherence parameter, nonlinear high temp. supercond. elements with A-15 lattice *(Russian)* 80—60127
Nb_3Sn, fast neutron irradiation, effect on critical current density 78—19197
Nb_3Sn multifilamentary wires, crit. current degradation mechanism 77—28324
Nb_3Sn, superconducting props., appl. as coatings in RF cavities 77—26891
Pb-Sn, lamellar eutectic alloys, entropy, free energy, and transition temp. 77—51849
$PbMo_6S_8$, normal state and superconducting property measurements 78—91660
PdH_x, $x \simeq 1$, type I supercond. props. 79—56448
$(SN)_x$, fluctuation-induced cond. and dimensionality 77—28167
$(SN)_x$, supercond. props., review 78—6474
$Ta_{70}Nb_{30}$, Abrikosov vortex formation kinetics *(Russian)* 80—93055
TaS_2 intercalated with methylamine, supercond. layer cpd., crit. field enhancement and reduced dimensionality 80—60152
$V_3Si(Ga)$, coherence parameter, nonlinear high temp. supercond. elements with A-15 lattice *(Russian)* 80—60127

coherent accelerators *see collective accelerators*

coherent antiStokes Raman scattering
absolute Raman cross sections determ. by indirect meas. of stimulated Raman gain, technique 78—66864
acetylene, computer controlled CARS spectra of Q branches 78—62241
acetylene, Q-branch of CARS, form and width alteration due to press. *(Russian)* 78—29795
acetylene, Q-branches, high resolution pulsed CARS 78—17676
acridine dyes, resonance multiplex CARS spectra 79—13722
adjustable angle beam-crossing system 77—82613
air, atmospheric, pure rot. CARS obs. 80—99511
air, LF spectroscopy 79—13727
analytical capabilities, rel. to other methods 77—40589
angularly resolved coherent Raman spectroscopy, crossed beam config., 79—30570
anthracene, single cryst., CARS and CSRS, two-photon reson. effect 80—95946
applications 77—87844
augmented CARS spectroscopy linewidth parameter from laser mode structure 80—33083
bacteriorhodopsin, reson. CARS spectrosc. 80—8014
benzene, second order CARS, dispersion curves 78—58707
benzene liquid-filled waveguide, generation of enhanced CARS signals 79—89961
β-carotene, ν_1 line shape, CARS and CSRS 78—82727

coherent antiStokes Raman scattering continued
β-carotene, coherent anti-Stokes reson. Raman spectrum excitation profiles 77—56342
CARS, background suppression, polarisation techniques 77—5924
chemical analysis use, three-wave mixing phenomenon 80—40802
chrysene, excited electronic state, CARS obs. 79—31514
chrysene, excited singlet and triplet state, CARS obs. 80—83374
coherent anti-Stokes Raman scattering for local and continuous density meas. in gas flow *(French)* 77—35281
coherent anti-Stokes Raman spectroscopy, selection rules, depolarisation ratios, rot. struct. 77—34640
coherent Raman spectroscopy techniques, review 80—22440
combustion diagnostics, laser appls. 80—16688
combustion diagnostics, space- and time-resolved coherent anti-Stokes Raman spectroscopy 79—76757
combustion gases, CARS spectra 80—16682
condensed phases, perturbation theory of third-order nonlinear susceptibility 80—14393
crystals lacking symmetry centre, cancellation by nonresonant background 79—14039
density and temp. meas. *(German)* 79—27321
diphenylpolyenes, two-photon absorptivities via three wave mixing 79—68416
flame, bluff-body stabilised diffusion, CARS meas. 79—85964
flame diagnosis, CARS appls. 80—16689
flames, temp., specie conc. meas., CARS and laser induced saturation fluoresc. spectroscopy obs. 80—45617
flavin adenine dinucleotide, resonance CARS line shapes, excited state parameters 79—3448
four-photon spectroscopy of condensed media, nonlinear spectroscopy developments 80—91860
four-wave mixing spectroscopy in crysts., nonlinear spectroscopy developments 80—91861
gas, angularly resolved CARS config. 80—22453
gas, intensity pressure variation *(French)* 79—45998
gas quantitative analysis 78—68968
gases, review 79—27322
gases, vibr.-rot. transitions 79—18198
hexafluoride molecule selective excitation via Doppler free multiphoton process 78—55178
hollow dielec. waveguides 77—50721
homonuclear diatomic molecules, CARS spectral profiles, computer program 79—13723
integrated power, press. depend. 78—59081
internal combustion engine, CARS noninvasive temp. and species meas. 80—30293
isotropic liquid, polarisation props. 78—80334
lasers application in Raman spectroscopy, review 78—65979
lineshape, 3rd order nonlinear optical susceptibility 78—42378
linewidth determination by integrated power meas. 79—3744
liquid, dephasing of coherently excited mol. vibrs. *(Dutch)* 78—72505
liquid, surface CARS 80—1280
liquid, third-order nonlinear susceptibility ratio meas. by CARS Maker fringe technique 79—989
liquid media, comparison of inverse Raman scatt. and CARS 79—7178
methane, $\nu_1(a_1)$ vibrational state rotational structure, CARS obs. 79—98109
methane, concentration along line in jet, spatially resolved coherent anti-Stokes Raman spectra 79—74476
methane, CW coherent antiStokes Raman spectrum, ν_1 band, press. depend. 78—42377
methane, high-resolution CARS, press. depend. of intensity 80—9964
methane, intradoppler CARS saturation spectroscopy 80—43057
methane-d_0(-d_4) vibrational state rotational struct., CARS spectra *(Russian)* 80—99513
micro sampling cell 77—79169
molecular parameter meas. 77—57405
molecular resonant CARS, line shape and Doppler broadening 79—94002
molecular spectroscopy book 80—27051
molecule, homogeneous linewidth meas. 77—71810
molecule, resonance CARS intensity calc. 79—36959
molecules, excited, coherent anti-Stokes reson. Raman scatt. 79—59475
naphthalene, vibr. relax. studied by four wave mixing (CARS), spectral lineshapes obs. 80—80762
β-naphthol, preresonance enhancement in CARS 78—29786
β-naptholate ion, preresonance enhancement in CARS 78—29786
negative peak form. 77—75161
nickel-octaethylporphyrin, in benzene soln., reson. CARS and CSRS line shapes 80—74432
noncentrosymmetric crystals, anti-Stokes stimulated Raman scatt. by polaritons 79—36962
optical mixing spectra, real-time analysis system 79—67392
optically isotropic media, formed by randomly oriented elements, CARS study 80—14397
phase matching, three-dimensional, in four-wave mixing 80—83635
phase-matching geometry, three-laser, with counterpropagating beams 79—72626
polarisation sensitive spectroscopy 79—75605
polarised coherent active Raman spectroscopy and coherent Raman ellipsometry *(Russian)* 78—55414
polydiacetylene solutions, third-order nonlinear mixing (CARS) 79—10354
propane, diffusion flame, coherent spectral interference from C_2, CARS spectra 80—43404
pulse-sequenced CARS spectroscopy, method for nonreson. background suppression 80—53375
pulsed dye laser system, computer controlled 78—62241
quasiequilibrium sample, light scatt. and thermal radiation, phenomenological approach 80—91840
recent advances in Raman spectroscopy, review 78—41359
remote detection of CARS employing fibre optic guides 80—9984
resonance coherent anti-Stokes Raman spectroscopy conditions 77—65056
resonance conditions, lineshape 78—9415
resonance four-wave mixing spectroscopy, recent developments 80—53383
resonance spectroscopy, quasiresonant pumping 79—6190
resonance spectroscopy, results for β-carotene band 79—6189
resonance-enhanced CARS, and coherent anti-Stokes hyper-Raman spectroscopy 78—86980
resonant coherent Raman scatt. spectra of excited molecules 80—87129

- **coherent antiStokes Raman scattering** continued
  - review 79—16051
  - review 80—22443
  - rhodamine, CARS spectroscopy, vibr. spectra of electronic states 80—27964
  - rhodamine 6G, lasing, reson. CARS spectra in methanol, ethanol, acetonitrile, H_2O 78—74948
  - rhodamine B, 6G, resonance CARS line shape, scatt. processes in ground or excited states 80—48043
  - rotation relaxation in continuous media *(Russian)* 79—10186
  - rotational Raman studies, folded BOXCARS 80—101846
  - second order, mechanisms 78—58707
  - selection rules, polarisation, process description, book contrib. 78—22177
  - solvated electrons, Raman spectrum modification, polarisation CARS obs. 80—5549
  - sooty diffusion flame, CARS obs. 80—16690
  - spectral profile interpretation 79—83523
  - spectrometer for gases and flames 80—95154
  - spectrometer system for chemists, using freq. doubled Nd+YAG laser 78—64906
  - spectroscopy, laser linewidth effects 79—89012
  - spectroscopy technique fundamentals and instrumental aspects 78—32895
  - stilbene, two-photon absorptivities via three wave mixing 79—68416
  - supersonic mol. beam, CARS rot. temp. meas. 80—23423
  - techniques and applications 77—57404
  - s-tetrazine, vapour, reson. CARS spectrosc., radiationless relax. rate 80—78614
  - theory and applications 79—97444
  - theory and appls., review 77—71378
  - three laser coherent Raman scatt. 79—23016
  - two-photon resonant four-wave mixing with non-monochromatic waves 80—38066
  - very high resolution CARS spectroscopy in mol. beam 79—30568
  - water, coherent Raman ellipsometry, vibr. stretching region and liq. struct. obs. 80—93341
  - CO, detectability levels for CARS species sensitivity 80—43404
  - CO flame, background-free CARS technique 79—94288
  - CS_2, CARS with counterpropagating beams, three-laser phase matching geometry 79—72626
  - CS_2 in benzene, third-order nonlinear susceptibility ratio by CARS 78—46713
  - CS_2, pulse-sequenced CARS spectroscopy 80—53375
  - $CaCO_3$, calcite, coherent excitation of vibr., dephasing time meas. 78—35120
  - $CaCO_3$, calcite crystal, higher-order CARS spectra 79—14035
  - Cs vapour, coherent anti-Stokes Raman scatt. 78—71146
  - D_2, absolute Raman cross sections determ. by indirect meas. of stimulated Raman gain 78—66864
  - D_2, Q(2) line, absolute Raman freq. meas. using CW CARS 78—29794
  - GeH_4, vibrational state rotational struct., CARS spectra *(Russian)* 80—99513
  - $^{74}GeH_4$ mol. vibr., IR and CARS spectra *(Russian)* 80—102509
  - H_2, CARS, optical Stark effect on vibr., and rot. transitions 80—99512
  - H_2 gas, CARS due to rot. transition 77—10971
  - H_2, linewidth determ. by integrated power meas. 79—3744
  - H_2, solid, stimulated Raman scatt. and CARS 78—13752
  - p-H_2, solid, time-resolved CARS, disorder effects on coherent vibr. states 80—93342
  - H_2O in flames, CARS spectrum 79—36652
  - H_2O, liq., broad band vibr. struct., polarisation CARS obs. 79—85963
  - I_2, reson. CARS spectrum, electronic resonance enhancement 79—14033
  - I_2, vap., electronic reson. enhancement 78—29793
  - $LiIO_3$ crystal, polariton CARS spectra 79—36961
  - N_2, CARS, optical Stark effect on vibr., and rot. transitions 80—99512
  - N_2, computer controlled CARS spectra of Q branches 78—62241
  - N_2, crossed-beam phase-matched CARS generation 78—50850
  - N_2, discharge excited vibr.-rotation states meas. by CARS *(Russian)* 79—3429
  - N_2, flame temp., CARS spectra diagnostic investigation 80—43404
  - N_2, gas, picosec. pulse CARS obs. 79—6942
  - N_2 in nonequilibrium gas-dynamic current, vibr.-level populations determ. by Raman scatt. 80—99509
  - N_2, pure rot. CARS obs. 80—99511
  - N_2, Q-branches, high resolution pulsed CARS 78—17676
  - N_2, rot. temps. determ. in diffusion flames using CARS 79—29358
  - α-N_2, solid, coherent loss of vibr. and librational excitations 79—86852
  - N_2, solid, stimulated Raman scatt. and CARS 78—13752
  - α-N_2 solid, time-resolved CARS, disorder effects on coherent vibr. states 80—93342
  - N_2, supersonic mol. beam, CARS rot. temp. meas. 80—23423
  - N_2-Ar mixture, picosecond dephasing of coherently excited vibrations 78—22172
  - N_2-Ar(Kr)(O_2)(CO)(CH_4), liquid, high resolution CW CARS spectra 80—63635
  - N_2-CO, angularly resolved CARS 80—22453
  - NH_3, computer controlled CARS spectra of Q branches 78—62241
  - NO_2, discrete reson. CARS emission, temporal and spectral props. 80—95630
  - NO_2, reson. coherent antiStokes Raman and absorpt. spectra 79—54860
  - Nd:YAG pumped tunable sources, appl. to spectroscopy 80—58576
  - O_2, computer controlled CARS spectra of Q branches 78—62241
  - O_2, pure rot. CARS obs. 80—99511
  - O_2, Q-branches, high resolution pulsed CARS 78—17676
  - Si-O fibres, parametric excitation of anti-Stokes coherent stimulated scatt. *(Russian)* 80—58637
- **coherent optical transients** *see optical coherent transients*
- **coherent potential approximation** *see CPA calculations*
- **cohesive energy** *see binding energy*
- **coils**
  - *see also inductors; solenoids; windings*
  - AC loss measurement, in supercond., by coil simulation 80—37050
  - air coils, FFT calc. of mag. fields 80—74280
  - air coils, magnetostatic field FFT calcs., linear system theory 80—32868
  - ampere absolute value improved realisation 78—93737
  - Argonne/GA TNS Tokamak reactor supercond. ohmic heating coil design 79—31197
  - circular carrying AC, EM field produced in plane anisotropic cond. plates *(Rumanian)* 79—72456
  - circumferential stress in large high field magnet coils, thick-thin cylinder approach 80—95761
- **coils** continued
  - co-axial single layer circular coils, accurate computation of force 80—32877
  - coaxial, for signalling between surface and buried coils, max. induced voltage calc. 79—12299
  - coaxial loops, field config. at median surface, current ratio depend. 77—19127
  - conducting rectangular cylinder, losses due to finite length coils, exact analysis 77—10806
  - cryogenic rings, current induction and decay 80—106972
  - DC contactor magnet coil, electromagnetic field, transient states *(Polish)* 80—18962
  - design for magnet airgap EM field uniformity correction *(Russian)* 77—53959
  - eddy current induction calc., transient, in plate of finite thickness *(German)* 79—27129
  - eddy current magnetic field time constant calc *(Polish)* 77—83779
  - eddy currents force effects calc., induced in thin plate by cylindrical magnetic field 80—14269
  - eddy currents in conducting slab, electrodynamic forces on coil, anal. *(German)* 77—58226
  - eddy-current speed meter operating characteristic analysis 79—40543
  - electrically heated finite cylindrical coil, temp. distrib. calc. *(Polish)* 77—54865
  - ELMO Bumpy Torus Reactor toroidal magnet system design 79—31196
  - force between circular coil and parallel iron slab 79—76547
  - fusion, toroidal field superconducting coil cryogenic stability and field anal., design parameter 80—106200
  - fusion reactor, CC NbTi, pool cooling superconducting test coil, Japanese design 80—99340
  - fusion reactor, cluster test facility, design 80—90835
  - fusion reactor, DITE Tokamak bundle divertor, Mk.II design 80—91268
  - fusion reactor, Doublet III, neutral beam injection system, two-gap magnet design and performance 80—92379
  - fusion reactor, Doublet III, ohmic heating E-coil vacuum breaker system, function and operation 80—102323
  - fusion reactor, Doublet III, toroidal field coils, Cu alloy plate defect size restrictions 80—91257
  - fusion reactor, doublet Tokamak, parallel connected ohmic heating coil 78—54930
  - fusion reactor, FTR, equilib. field coils, electrical supply system, optimisation and computer aided performance anal. 80—91288
  - fusion reactor, Heliotron E, helical coil design, mag. field perturbations 80—99300
  - fusion reactor, high current density superconducting coils, cryostability 80—106201
  - fusion reactor, induction heating coils, 50 kA prototype superconducting cable, critical current 80—106196
  - fusion reactor, ISX-B, with bundle divertor, structural anal. 80—91254
  - fusion reactor, ISX-B toroidal field coil finger joints, fatigue life, structural evaluation 80—91253
  - fusion reactor, Large Coil Program, coil winding development support 80—106190
  - fusion reactor, Large Coil Program, General Dynamics Convair/IGC manufacturing engineering 80—106169
  - fusion reactor, Large Coil Program, Nb_3Sn forced flow superconducting test coil, Westinghouse design 80—99337
  - fusion reactor, Large Coil Program, NbTi superconducting test coil, General Electric design and manufacture program 80—102319
  - fusion reactor, Large Coil Program, test heater conceptual designs 80—91251
  - fusion reactor, Large Coil Program, Westinghouse superconducting mag. elec. design 80—91250
  - fusion reactor, Large Coil Task, CC NbTi forced flow superconducting test coil, Swiss design 80—99341
  - fusion reactor, Large Coil Test Facility test stand design description 80—102320
  - fusion reactor, large superconducting toroidal field coil program, progress report 80—99335
  - fusion reactor, maximum toroidal mag. field value by core constraint 80—102349
  - fusion reactor, MFTF, mag. cryostability 80—106198
  - fusion reactor, MFTF, superconducting mag. quench vent rate 80—106197
  - fusion reactor, multiple mirror, coil design and economic optimisation 80—99284
  - fusion reactor, multipole fusion confinement with 2 MA levitated superconducting coil 80—106191
  - fusion reactor, non-circular Tokamak field shaping coils, current optimisation 80—95426
  - fusion reactor, PDX, toroidal field coil and frame struct., anal., finite element anal. 80—106165
  - fusion reactor, PDX toroidal field coil joint fatigue testing 80—91252
  - fusion reactor, press. induced flow cooling, highly stable superconducting mag. systems 80—106192
  - fusion reactor, Princeton large torus 3-coil test 78—54945
  - fusion reactor, safety of superconducting fusion magnets: twelve problem areas 80—102348
  - fusion reactor, SLPX TF coil, stress anal. using COSMIC-NASTRAN 80—106168
  - fusion reactor, STARFIRE project, superconducting poloidal coils design study 80—106185
  - fusion reactor, STARFIRE project, toroidal field coil system preliminary assessment 80—106186
  - fusion reactor, superconducting toroidal system, force anal. for all fault conditions 80—91258
  - fusion reactor, superconductor optimisation for 12 Tesla toroidal field coils from Nb-Ti and Nb-Ti-Ta alloys 80—91272
  - fusion reactor, T-10M Tokamak, normal and supercond. inductive energy storage and switching 78—55018
  - fusion reactor, TEXT, toroidal field coil fabrication 80—91267
  - fusion reactor, TEXT, toroidal field coil power supply, thyristor controlled 80—91289
  - fusion reactor, TFTR, eddy current theory for structural materials 80—95427
  - fusion reactor, TFTR, large section water cooled Cu conductor, brazing joints 80—91260
  - fusion reactor, TFTR outer poloidal field coil insulation and mould design 80—91261
  - fusion reactor, TFTR poloidal field coils, tooling and manufacture 80—91262

coils continued
  fusion reactor, TFTR toroidal field coil support restraint struct. 80−95428
  fusion reactor, TMX, magnets, mech. design 78−58494
  fusion reactor, Tokamak constant tension D-shaped coils, lateral support struct. 78−55013
  fusion reactor, toroidal device with nonplanar mag. axis, magnet and coil engineering 78−55009
  fusion reactor, toroidal field coil in-plane bending stress, struct. support design 80−106164
  fusion reactor coil, multilayer structs., laminated beam theory anal. 78−55011
  fusion reactor coil design, cost anal., for neutral beam magnets 78−55005
  fusion reactor coil design codes 78−66367
  fusion reactor coil insulation and winding techniques 79−31210
  fusion reactor field coils, fabrication effects on structural behaviour 80−9406
  fusion reactor implosion heating coil, radially fed, design, fabrication 78−55006
  fusion reactor Large Coil Program, NbTi, superconducting test coil, General Dynamics Convair Division, Intermagnetics General Corp. design 80−99338
  fusion reactor magnet coil, 125 kG, 1 m, design, fabrication 78−55008
  fusion reactor RFC-XX, coil system, design, fabrication, testing 78−55007
  fusion reactor toroidal field coil finite element stress anal. 80−91256
  fusion reactors, Large Coil Program, low temp. stability, joints, design method 80−106195
  fusion reactors, Large Coil Program, pool boiling mag. quench press. calc. 80−106199
  fusion reactors, Large Coil Program, superconducting mag. coil struct. design status 80−106189
  fusion reactors, large Coil Program, Westinghouse coil cooldown and warmup 80−106193
  fusion reactors, Large Coil Program, Westinghouse coil stability testing, pulsed induction heating 80−106194
  fusion reactors, Large Coil Task, NbTi, forced flow superconducting test coil, EURATOM design 80−99339
  fusion reactors, Large Coil Test Facility, liq. He cooling system 80−102321
  fusion reactors, steady state resistive toroidal field coils 80−91264
  fusion reactors, TFTR mag. field coil electrical insulation system and test results 80−95429
  fusion reactors, TFTR poloidal field coil system, characts. 80−95430
  fusion-fission breeder reactor, supercond. poloidal field coil design 78−70640
  glass fibre reinforced epoxy prepreg, PDX TF coil insulation 78−62656
  heavy ion storage supercond. coil radial sector guiding field calc. 79−31262
  Helmholtz coil and fluxmeter system for magnetic saturation meas. 78−93738
  induction pacemaker with 100 kHz transmission during pulse intervals 77−81728
  JET Tokamak inner poloidal field coil design 79−31209
  JET Tokamak toroidal field coil design 79−31205
  JET Tokamak toroidal field coil manufacture 79−31206
  Large Coil Program, insulation system cryogenic elec. test 80−91263
  Large Coil Program, research and development activity 80−99336
  Large Coil Test Facility, instrumentation system design 80−95446
  load coil, 1.5 MA, 10 MJ, for pulsed homopolar machine 78−13336
  magnetic defectoscopes, nonsinusoidal periodic currents meas. 80−104386
  magnetic field induction vector remote meas. of 0.01 to 5 T, mag. induction Hall probe 78−93659
  magnetic field of toroidal ring in field of moving coil with currents, calc. 79−64149
  magnetic search coil, eye movement meas. system 79−74798
  magnetic search coils for eye position meas., implantation method 80−85548
  magnetic suspension densimeter, with single coil, for absolute density meas. 77−30132
  main field coil, D-shape, for ASDEX fusion expt., W.Germany 77−61601
  Marshall coil, epoxy-insulated, fabrication 78−66388
  Marshall implosion coil for shock heating of O-pinch plasma column 77−23267
  Meissner, in high-vacuum applications, anomalous behaviour 78−32826
  miniature coil wound systems protection, parylene (vacuum deposited polymeric coating) appl. 80−108607
  Mirror Fusion Test Facility, superconductor core manufacturing and quality 80−93521
  Mirror Fusion Test Facility supercond. coil development 79−31202
  morphognostic coil design for implanted nerve stimulator 79−84014
  mutual inductance on infinite cylinder 80−58443
  NMR flat crossed-coil detector, for blood flow meas. 78−40284
  nonuniform axial magnetic field generation, optimum design for coaxial circular coil systems 79−68348
  Oak Ridge National Laboratory superconducting coil fabrication development 78−50370
  plasma, high density, in mag. mirror, RF plugging coils 78−83604
  poloidal field coil design and development of JT-60 Tokamak 79−31204
  Princeton Large Torus, engineering tests on toroidal and internal poloidal field coils 77−23264
  pulsed NMR, anal. of homogeneous RF field delay line coils 77−49758
  pulsed superconducting coil, 1.5 MJ, and cryostat, performance tests 79−49259
  Q-factor measurement by damped oscillation method *(Japanese)* 78−89492
  rectangular field coil with split winding, uniformity condition 78−41335
  RF, design parameter effects on signal intensity of CW NMR or NQR spectrometer 77−49756
  RF field coils for Petula Tokamak compressional transit time mag. pumping heating 78−70634
  RF power supply cct. for implant telemetry, design 78−31926
  Rogowski coil for current and voltage meas. in pulsed X-ray devices *(Japanese)* 78−93788
  Rogowskii loop with ferrite core, precision meas. of high-power current pulse 78−4639
  shielded field coil as mag. induction meas. standard 77−74466
  stellarator toroidal field production by modular systems 80−10441

coils continued
  STEM zone-axis pattern formation using four sets of coils 80−70091
  superconducting, for Tokamak, active energy transfer rate control using inductor-convertor bridges 78−13338
  superconducting coil, buckling, vibr., lateral constraint and damping effects 78−63344
  superconducting for Fermilab doubler, design and fabrication techniques 79−36443
  superconducting wire, coil simulation, class and instability meas. 79−71487
  superconductive coil, appl. to mag. field modulation 77−18056
  TEXT iron core Tokamak, design formalism for OH and VF coil system 77−23259
  TEXT Tokamak, contacts for pulsed high currents 80−70029
  thick ellipsoidal coil and ferromagnetic ellipsoid system, vector potential 79−41269
  Tokamak fusion, Impurity Study Experiment, mag. field calcs. using GFUN-3D programme 78−66368
  Tokamak ohmic heating coil design and testing 79−32806
  Tokamak power reactor supercond. coil design, experimental 79−31198
  Tokamak power reactor supercond. poloidal magnet system design, experimental 79−31207
  Tokamak power reactor toroidal field coil design and manufacture 79−31201
  Tokamak superconducting toroidal field coil concept 79−31200
  Tokamak toroidal field coils, reduction of bending moments 80−47697
  Tokamak toroidal magnet supercond. cluster test design 79−31199
  toroidal field coil construction and appl. *(German)* 78−54877
  toroidal field coil design and development for JT-60 Tokamak 79−31203
  toroidal field coils, bending-free, for Tokamak reactor 78−55012
  toroidal field coils, EM parameters calcs. of current paths in homogeneous media *(Japanese)* 80−106155
  toroidal magnet coil design and testing 79−31195
  transducer induction moving coil null offset compensation method *(Polish)* 77−49718
  winding turns counting, using moire system 80−73428
  Fe core coils, mag. field dispersion 79−64139
  Nb_3Sn, multifilamentary coils for Lawrence Livermore Laboratory superconducting High Field Test Facility 80−90834
  $PbMo_6S_8$, supercond. wires prod. and characteris. 77−69462

coincidence circuits
  see also counters
  active well coincidence counters, expt. comparison with random drivers for U assay 80−78503
  anticoincidence gated scaler and live timer, counting loss correction for Geiger counter 78−86737
  avalanche transistor discriminator for low energy radiations 80−5450
  CAMAC, 2-D anal. of spectroscopic data, electronics 80−5460
  coincidence matrix, fast, programmable 79−97961
  coincidence selection element, tunnel diode, ICs, design 77−18755
  constant fraction differential discriminator for use in fast timing coincidence systems 79−45580
  dead time correction by the pulser method for single channel nuclear counting systems 79−13611
  dead time corrections in coincidence measurements by time-to-pulse-height converters or standard coincidence systems 80−9472
  digital multidiscriminator for use in gamma-gamma coincidence experiments 78−70707
  dissector one-electron current pulse timing, delayed self-coincidence method 79−26846
  double coincidence module with control channel, nanosec. range, priority discriminators 77−38569
  Euratom variable dead-time neutron counter, use for Pu passive assay 80−69042
  fast, smooth controlled- and high-stability-time resolution types 78−875
  fast-slow coincidence system construction, ortho-positronium lifetime meas. 77−38570
  four fold coincidence system, simultaneous counting of true and random events 79−81140
  high rate 4π β-γ coincidence counting system 79−45588
  high resolving-time, approx. 2 nsec, using ICs 78−874
  ion electron converter device, neutron decay weak interaction obs. 80−58100
  magnetic tape interfaces for a dual-parameter coincidence experiment 80−14055
  megachannel gamma-gamma coincidence system using PDP-8/E computer and moving-head discs 77−57834
  megachannel pulse height analyser for gamma-ray coincidence analysis 80−99430
  modular coincidence circuits and shapers, parameters 79−3320
  multidetector meas. of ang. correl. 79−41084
  MWPC, Bellcord—a multilevel fast preprocessor for 1024 ECL channels 79−45577
  MWPC, pressurised, for electron detection 77−14312
  neutron coincidence methods with thermal neutron, appl. limitations *(Bulgarian)* 79−85874
  neutron coincidence system without delay cycle *(Bulgarian)* 79−85873
  neutron thermal flux, absolute determ., $4\pi\alpha$-γ coincidence meas. 79−85576
  nuclear materials accountability, U and P NDA of crated waste by gamma-ray and neutron coincidence counting 80−83166
  nucleonic probe ccts with noise rejection, low-level activity meas. 80−52833
  portable neutron coincidence counter for assaying large Pu samples 80−69041
  positron spectrometer, low-background, many cryst. scintillation triple $\beta\gamma\gamma$ coincidence 77−54446
  pulse counting, high precision, limitations, optimal conditions 77−54463
  pulse height analyzer and D/A convertor appl. 80−22473
  pulses for adjustment of subnanosecond walk 79−76306
  scintillation hodoscope, track correlator as a fast trigger in the detection of π-μ Coulomb bound states 79−45574
  thermal neutron coincidence counting, correction for variable moderation and multiplication 80−69045
  three level coincidence-correlator detectors, underwater sound appls. 78−63245
  transceiver, inexpensive, use in cosmic ray time coincidence expts. with long baselines 80−52837
  X-ray coincidence intensity meas., tailing convections 79−81141

coincidence circuits continued
- X-ray intensity meas., twin channel method with one special counter, circuit *(German)* 77−6644
- X-ray-β particle coincidence technique to exam. β-decay of ^{252}Cf fission fragments 80−74094
- e-γ delayed coincidences using magnetic lens spectrometer and Ge(Li) detector 79−710
- $e^+e^- \rightarrow 2\gamma$, ang. correl. meas. device *(German)* 78−86726
- Ge(Li) coincidence detector system, meas. on ^{144}Ce decay 80−52605
- Ge(Li)-NaI(Tl) Compton suppression spectrometer for low level activity meas., rel. to Ge(Li) detector *(Slovak)* 78−21814
- Li isotopic comp. determ., using coincident meas. of complementary particles in ^{6}Li(p,α) and ^{7}Li(p,α) 79−5201
- Na(Tl), circular ring transaxial positron camera, coinc. electronics 78−31953

coincidence counters *see coincidence circuits; counters*

cold-cathode tubes
- *see also counting tubes; photomultipliers; phototubes*
- Antares CO$_2$ laser power amplifier, design 80−69423
- compact cold cathode electron beam gun, appl. CO$_2$ laser *(German)* 80−86501
- controlled gas discharge switch 78−86300
- electron beam production, μs, high-current, device design and characts. 77−82642
- encapsulated solid-state laser based on type-IMA tube 77−38915
- ion gun for sputter-etching, discharge characts. and improvements 80−105748
- ion source, floating potential of metal surface under ion bombardment 79−41057
- large-area cold-cathode grid-controlled electron gun for Antares CO$_2$ laser amplifier 80−68955
- laser triggered Krytron-Blumlein electro-optic switch 78−9450
- negative glow plasma, contact electrode charging time meas. 78−67525
- UV light source, miniature long lived cold cathode discharge 77−19375

cold rolling
- amorphous alloys, cold rolling 80−55423
- brass, 70:30, rolled, nucleation and annealing texture development 80−45320
- brass, cold rolling, inhomogeneous texture 80−89251
- α-β brass, cold-rolled, energy dispersive X-ray diffr. studies 80−40379
- brass, crystal structure and morphology of thin needle-like martensite 78−31425
- α-brass, drawability correlation with sheet metal texture 78−60683
- α-brass, FCC, fractographic obs. of SCC 78−64786
- brass, recovery and recrystallisation of plastically deformed α-phase, comparison of positron annihilation, elec. resist. and microhardness 79−52240
- brass, rolling and recrystallization texture as function of Zn-content 79−91676
- brass (70:30), cold rolled, optical, X-ray and TEM exam. of deformation struct., and textures 78−88500
- α-brass sheet, shear bands and recrystallisation 79−91680
- bronze, sintered, mech. props. 77−28839
- bronze P, heavily cold rolled, yield strength enhancement mech. 77−36539
- Co-Ni, magnetic anisotropy induced by mag. annealing and cold rolling, calc. 80−7696
- Duralumin 2017, superplasticity *(Korean)* 79−38902
- earing behaviour, and formability limits prediction from texture data 79−91703
- eutectoid thermomechanically treated, textural studies 80−29978
- FCC metal with cube orientation, texture variation during rolling 77−70065
- FCC metals and alloys, macroscopic shear band contrib. to rolling texture 77−86056
- Fe, Armco, electron microscope object prep. method 80−50789
- ferromagnetic single crystal, mag. anisotropy induced by cold rolling *(Russian)* 80−84595
- hard metals, roll deform. effect on separating forces in cold strip rolling 80−35212
- Invar, magnetisation, hyperfine field, elec. resist. and X-ray linewidth, effect of deform. by cold rolling 77−48556
- machine for cold rolling, deformed contrete reinforcing bars for model tests 78−60924
- materials texture, conf., Aachen, Germany, (March 1978) 79−83217
- metal, bulk deform. process 78−31459
- metal, cubic, heavily rolled, shear band occurrence 79−34058
- metal, friction and slip 78−64707
- metal, porous, stresses in deform. region during cold rolling 78−11241
- metal porous strip, metal pressure in cold rolling in elastic aftereffect zone 80−40421
- metal powders, deform. region stresses 79−61609
- metal strip, porous, elastic aftereffect in cold rolling 80−11689
- metal strip, sintered, algorithm for force and geometric parameters calc. 80−11727
- metallic glass, current exptl. data on struct., review 80−88058
- metallic glasses, mats. props. review 77−4043
- moments, calc. for longit. rolling periodically changing sections *(Polish)* 80−89239
- Nichrome/steel, porous metal-thread sheet materials, filteration, permeability and strength props. *(Russian)* 79−78915
- non-circular arc roll force model 78−48423
- Permalloy, FCC, mag. anisotropy induced by cold rolling 80−11188
- polycarbonate, glassy, rolled, craze initiation *(Japanese)* 77−8969
- polyethylene, oxidised, low-temp. dielectric spectrum 79−61304
- polyoxymethylene, rolled, prediction of yielding behaviour 77−73306
- recrystallisation, conf., Leeds, England (April 1978) 79−47706
- rolling force coefficient model, and its adaptive control *(Chinese)* 80−55418
- rolls, US monitoring of hardened thickness with low hardness gradient 78−60955
- shear band formation models, in rolling and extrusion 80−11666
- sheet, texture form., model *(French)* 78−68705
- sheet metal, roll bending on machine with elastic element, bending moment determ. 78−6948
- steel, 08Yu, annealing effect on texture, microstruct., and mech. props. 78−44138
- steel, 36NKhTYu, ageing to produce ultrafine grains, discontinuous precipitation *(Russian)* 77−81277

cold rolling continued
- steel, Al killed, cold rolled and recrystallised grain shape anisotropy 79−34064
- steel, Al-stabilised, texture formation in continuous annealing, effect of coiling temp. of hot strip 79−91688
- steel, alloy, low C, effects of pre-treatment on graphitisation behaviour *(Japanese)* 78−84860
- steel, austenitic, Cr-Ni (18,12 wt.%), containing coarse grain boundary precipitates, thermomechanical treatment 78−27545
- steel, austenitic stainless, cold worked, 20%, heat treatment effects on mech. state, load-relaxation expts. 77−52350
- steel, austenitic stainless, Cr-Ni, Mn and Mo effect on mech. props. rel. to treatment 79−96039
- steel, austenitic stainless, extrinsic grain boundary dislocation spreading 79−57004
- steel, austenitic stainless, FCC, fractographic obs. of SCC 78−64786
- steel, austenitic stainless, ferritic, prep. with fine grains by cold rolling and recrystallisation, superplasticity *(French)* 78−35406
- steel, austenitic stainless, matrix precipitation of Cr$_2$N, due to P addition, TEM exam. 79−4973
- steel, austenitic stainless, texture influence as through thickness strength 79−91771
- steel, austenitic stainless recrystallisation *(Japanese)* 77−52346
- steel, austenitic stainless type AISI 316, L sheet and LN plate surface comp. after different surface treatments 80−3253
- steel, C, cold rolled St3Kp, annealed, mag. nondestructive inspection of strip and ribbon 78−60913
- steel, C, thermomechanically treated, in situ composite material description 80−7649
- steel, C content effect on annealing texture, plastic anisotropy and mechanical props. 80−29976
- steel, C-Mn-(Cr), structural changes during stress cycling after heat treatment and cold rolling *(Russian)* 78−19787
- steel, cold rolled, deep drawing, continuous annealing effect on mech. props. *(German)* 77−90362
- steel, cold rolled, high strength, mech. props. 77−36527
- steel, cold rolled high strength sheet, with high drawability, fabrication process 77−73288
- steel, cold rolling, effect of transformations during quench hardening and tempering 77−55989
- steel, cold-rolled, recovery of lattice defects in cementite 77−90370
- steel, cold-rolled sheet, surface chemistry 80−61146
- steel, Cr, H-dislocation interaction 79−8307
- steel, Cr (17 wt.%), stainless, hot-rolled texture, effect on cold-rolled and annealed textures 80−55425
- steel, Cr-Ni (1.47, 1.48 wt.%), lath martensite microstruct. and props., cold rolling effect 80−55422
- steel, Cr-Ni (32,8), two phase austenite-ferrite alloy, fatigue behaviour *(Japanese)* 79−79091
- steel, deep drawing, texture control as affected by processing variables 79−91689
- steel, defective zones in cold rolling, activation analysis method 78−7278
- steel, eutectoid, mech. behaviour, thermomech. treatment effects 80−84970
- steel, high C, Burgers vector of dislocations in cementite crystal 77−27891
- steel, high C chrome type 9Kh2, cold rolling rolls, hardness determ. 79−87713
- steel, high strength, low alloy, response to cyclic plastic deform. 78−7035
- steel, KhVG, deformation ht. treatment on carbide precip. in KhVG 77−63700
- steel, low alloy, high strength, residual stresses during low cycle fatigue 79−29201
- steel, low alloy structural, pre-treatments to enhance graphitisation, dilatometric and optical microscopy study *(Japanese)* 79−78992
- steel, low C, Al-killed, effect of V on mag. props. 79−83339
- steel, low C, capped, cold rolled sheet, deep drawability, effect of carbide size, cold reduction annealing 78−64559
- steel, low C, cold rolled and recrystallised, containing Nb(CN) dispersion, struct. and textural aspect of deform. 79−47712
- steel, low C, cold rolled sheet, Cu effect on recrystallization texture *(Chinese)* 79−74173
- steel, low C, cold rolled sheet, strain rate effect on yield *(Japanese)* 79−96084
- steel, low C, containing P, Mg effect on annealing texture, mech. props. and plastic anisotropy 78−27536
- steel, low C, influence of cold rolling reduction on elastic stored energy 79−91731
- steel, low C, rolling deform., effect on NbC particle size distrib. 79−47717
- steel, low C, Ti-stabilized, recrystn. texture development 79−83231
- steel, low C, type En3, high strain deform., struct. and props. 80−89301
- steel, low C sheets, effect of N$_2$ content on recrystn. texture 79−83233
- steel, low-C electric sheet, struct. and coercive force after second cold rolling 77−44270
- steel, microalloy V-Nb, V, Nb effects on strength and formability of cold rolled sheets 77−55979
- steel, mild, cold rolled, texture and plastic anisotropy rel. to alloying and precipitation *(French)* 80−108475
- steel, mild, cold rolled sheets, microstruct. and strain path in deep-drawing 78−19775
- steel, mild, deformation texture *(French)* 79−70082
- steel, mild and type EN31, eval. of cold rolling oils and boundary lubrication characts. by SEM 80−85068
- steel, Mn-Cr-B (1.46, 1.03, 0.003 wt.%) 80−55422
- steel, Nb-V, cold rolled, HSLA, prod. by precipitation hardening, annealing 78−88471
- steel, Ni-Co-Mo (17.55, 8.02, 4.92 wt.%) maraging, lath martensite microstruct. and props., cold rolling effect 80−55422
- steel, Ni-Cr-Ti, thin bands, cold working, props. and struct. of 36NKhTYu 79−78994
- steel, non-alloy, work hardening due to shearing *(French)* 78−15423
- steel, non-oriented, texture and mag. props., effect of Mn and S content 77−86047
- steel, P, deep-drawing, spatial orientation distrib. of crystallites in cold-rolled and in annealed sheets 80−81079
- steel, plane C, nonstrain-ageing state 77−52349
- steel, rolls for cold-rolling mills, surface hardening, contact fatigue strength 79−24664

cold rolling continued
  steel, sheet, cold-rolled, US inspection for mech. prop. anisotropy 78—23750
  steel, sheet structural changes during rolling influence of lubricants on friction and wear 78—95815
  steel, Si, nonoriented sheet prod. with texture of {100} ⟨ovw⟩ 80—89246
  steel, Si (3 wt.%), textured, secondary recrystn., precip. annealing effect *(Japanese)* 80—71662
  steel, Si-P-C, low C, varying Si content, cold rolled annealing 80—3090
  steel, stainless, Cr (17 wt.%), recrystallisation texture, effect of N *(Japanese)* 79—4978
  steel, stainless, Cr-Cu (17, 0.6 to 1.1 wt.%), texture 80—84957
  steel, stainless, Cr-Ni (18, 9 wt.%), cold rolled, struct. 79—83214
  steel, stainless, ferritic Ti stabilised, changes in structure and mech. props., after alkali bath etching *(Russian)* 79—29271
  steel, stainless, hot rolled texture, effect on cold rolled and annealed textures *(Japanese)* 78—48425
  steel, stainless, Kh25T, impact strength and substructure produced by deform. during cold rolling *(Russian)* 79—24535
  steel, stainless, maraging, type 03Kh11N10M2T2, exam. of thermal embrittlement 78—84986
  steel, stainless, recrystallisation texture, effect of Cu, Ti additions on development *(Japanese)* 78—80558
  steel, stainless, surface morphology of H ion eroded samples 79—86968
  steel, stainless, type 304, description of deformation induced plastic anisotropy 79—43268
  steel, stainless, type 304, surface condition effects on IR absorptivity 79—56754
  steel, thread rolled, Moire fringe method for examining local deform. zones 80—21220
  steel, transformer, effect of uniaxial elastic stress on dynamic magnetostriction *(Russian)* 77—69651
  steel, transformer, inhibitory phase *(Russian)* 78—3139
  steel, transformer, textural barriers to grain growth after cold rolling and annealing *(Russian)* 78—39796
  steel, Zn coated, cold rolling influence on struct. and deform. of diffusional layer *(Russian)* 80—55465
  steel, Zn coated strips, plastic deform. influence on struct. and quality *(Russian)* 80—40377
  steel sheet, hot and cold rolled, cold formability, notched tensile test and stretch bend test *(German)* 80—61031
  steel stainless, Ti stabilised, intercrystalline corrosion, repeated cold deform. effect 79—57000
  steel transformer, Mossbauer atomic struct. anal., decarburising annealing, cold rolling *(Russian)* 80—11294
  steel tubing, cold rolled, nondestructive mag. method for determ. of mech. props. 78—23903
  steel with micro-duplex structure, rolling texture, neutron diffraction analysis 80—16327
  thin-wall cylinder cold rolling method 80—66535
  viscoelastic sheet thermomechanical deformations, numerical soln. 77—39236
  work roll spalling, prevention measures 77—55981
  Zircaloy-4, stress-relieved and cold-worked, stress relaxation in bending at 673K 80—93609
  Ag, (211)$[\bar{1}11]$ single crysts., shear band effects on rolling deformation 80—50651
  Ag, cold rolled, weak beam method appl. to dislocation obs. *(German)* 77—84757
  Ag, cold rolling, inhomogeneous texture 80—89251
  Ag, deformed bars, cold rolled, exam. of microstruct. by thin foil TEM 78—88502
  Ag, rolled single crystal with defined solute content, stored energy and recrystallization temp. 79—96037
  Ag-Ni, two ductile phase, exam. of rolling deformation 78—72819
  Ag-Ni, two ductile phase alloy, exam. of softening behaviour after cold rolling 78—72847
  Al, 1100 plates, substruct. development 80—108476
  Al and Al alloy 5022, plastic anisotropy of textured sheet *(Japanese)* 79—34103
  Al, cold rolled, annealed, fatigue crack propag. rate, temp. effect 78—39904
  Al, cold rolled, commercial purity, initial stages of recrystallisation, TEM obs. 79—56999
  Al, cold rolled, weak beam method appl. to dislocation obs. *(German)* 77—84757
  Al, cold rolled, X-ray diffr. and optical microscope exam. of fatigue damage *(Japanese)* 78—84976
  Al, cold rolled and annealed, substruct. near fatigue crack tip, X-ray microbeam technique exam. *(Japanese)* 78—64621
  Al, cold rolled bicrystal, plane grain growth anisotropy 79—91686
  Al, cold rolling, inhomogeneous texture 80—89251
  Al, cutting mechanism, anisotropy effects 79—11760
  Al, fatigue, effect of pre-existing subgrains 79—5041
  Al, orientation distribution function determ. using one pole figure *(German)* 77—25242
  Al, single crystal, deformation behaviour during cold rolling 79—47751
  Al, texture variation during rolling 77—70066
  Al/brass/Al bimetal, three layers, formed by cold rolling, exam. of formation of intermetallic phases at interface 78—56658
  Al-Ag, nonhomogeneity of deform. 78—84888
  γ'-Al-Ag (15 wt.%), dislocation splitting mechanism, cessation above critical temp. 78—26572
  Al-alloy plates, type VAD23, thermomech. parameters effect on struct. and props. 80—20988
  Al-Cu (4 wt.%), supersaturated and aged conditions, high strain deform. 80—60907
  Al-Cu-Mg, type D16T, thin-wall cylinder cold rolling method 80—66535
  Al-Cu-Mg-Mn(-Zn-Cr), low temp. deformed, ageing and mech. props. 79—1881
  Al-CuAl$_2$ eutectic, deformed, thermal stability 77—52348
  Al-Cu(Si)(Zn)(Mg)(Cr), recrystallization texture 79—91679
  Al-Mg (5 wt.%) deformed bars, cold rolled, exam. of microstruct. by thin foil TEM 78—88502
  Al-Mn (1 wt.%), single crysts., rolled to (123)$[41\bar{2}]$, recrystn. textures 80—104183
  Al-Mn(Cu)-Zr, particle stabilized structures, hot deform. 79—47733
  Al-Ni (6 wt.%) alloy, misorientation between subgrains, second-phase particles role, STEM microdiffr. obs. 80—104415
  Al-rare earth alloys, granules, rolling to form foil, exam. 80—20825
  Al-Sn dil. alloy, cube orientation texture development 79—96040

cold rolling continued
  Al-Zn, nonhomogeneity of deform. 78—84888
  Al-Zn-Mg, welded section stress in rolled plate edges, mechanical surface treatment and environment effects 80—21193
  Au, deformed bars, cold rolled, exam. of microstruct. by thin foil TEM 78—88502
  Au-Cu-Zn-Ni (13, 3.4, 8.5 wt.%), white gold, metallographic structure after cold rolling, effect of heat treatment, recrystallisation *(French)* 79—52238
  Au-Er, dil., cold-worked, EPR expts. 80—39864
  Au-Ni-Cu-Zn, white gold, metallographic struct., heat treatment and plastic working effect 80—40403
  α-brass, defect removal, obs. by positron annihilation 78—84677
  Cd, cold rolling texture development 80—25720
  Cd-Zn (Ag), annealed, work softened, exam. of crystallographic texture, hardness 78—80559
  Co, magnetic anisotropy induced by mag. annealing and cold rolling, expt. 80—7695
  Co, magnetic anisotropy induced by mag. annealing and cold rolling, calc. 80—7696
  Co-Fe, soft mag. props. rel. to metallurgical aspects 80—88810
  Co-Ni, magnetic anisotropy induced by mag. annealing and cold rolling, expt. 80—7695
  $Co_{50}Ni_{20}Fe_6Si_{12}B_{12}$, amorphous, mag. props., effects mech. deform. 80—39840
  Cr-Co-Fe, for telephone receiver mag. use 80—45318
  Cr-Ni steel, strengthening by elastic deform. at −196°C 77—55987
  Cu, anisothermal annealing, effect on props. of MOOB bands 78—23719
  Cu annealed and cold rolled, with bamboo structure, exam. of grain boundaries as vacancy sources in diffusional creep 78—88508
  Cu, cold rolled sheet, anisotropy of elastic and strength props. 80—81077
  Cu, cold rolling, mechanical props., ageing, annealing, recrystallisation, plastic strain *(Russian)* 80—35202
  Cu, cold-rolled, microstruct. 79—83216
  Cu crystals, two-phase, recrystn. retardation, particle size, spacing effects 80—89242
  Cu, defect removal, obs. by positron annihilation 78—84677
  Cu, recrystallisation of cold rolled samples *(French)* 79—43269
  Cu, rolled at room temp. and 200°C, variation in props., hardness and X-ray meas. *(Russian)* 77—73285
  Cu, rolled single crystal with defined solute content, stored energy and recrystallization temp. 79—96037
  Cu, strengthening by dislocation substructures 77—36538
  α-Cu-Al, FCC, fractographic obs. of SCC 78—64786
  Cu-Al$_2$O$_3$, dispersion-strengthened, vapour-deposited, effect on tensile creep 78—11115
  Cu-Al$_2$O$_3$ coatings, electrodeposited, dispersion hardened, exam. of props. 79—34181
  Cu-Al$_2$O$_3$ electrodeposits, dispersion hardened, props. 79—28258
  Cu-Ga, high dislocation density alloys and oxide precipitated struct., NMR, spin echo 80—39892
  Cu-Mn(Fe)(Ni)(Zn)(Ge), dilute solid soln., exam. of recrystallisation and stored energy 78—52836
  Cu-Ni (10 wt.%), deformed bars, cold rolled, exam. of microstruct. by thin foil TEM 78—88502
  Cu-Ni-Fe (26,8 wt.%), microduplex struct. form., recrystn. annealing *(Japanese)* 78—76659
  Cu-Ni-Sn, thermal decomposition after prior cold work 78—15427
  Cu-Si, high dislocation density alloys and oxide precipitated struct., NMR, spin echo 80—39892
  Cu-Sn-Mg, precipitation, effect of thermomechanical treatment *(Japanese)* 79—4970
  Cu-Sn(5 wt.%), electrical resistivity, annealing, cold rolling 77—8070
  Cu-Ti (Zr), strength improvement by thermomechanical treatment *(Japanese)* 78—48426
  CuZn32 bands, mechanical props. anisotropy after annealing at variable heating rates 77—90364
  Fe, (100) [001], texture development by recrystallisation and normal grain growth 78—27539
  Fe alloy, (110) [001] texture development by recrystallization and normal grain growth 77—32594
  γ-Fe alloy, supersat. solid soln., recrystn. inhibition by cold rolling 77—73286
  Fe alloy electrodes, rolled from powders, sintering problems 80—25608
  Fe, Armco, cold-rolling cavity formation, TEM study 78—6947
  Fe, Armco, dislocation struct. after hot and cold rolling *(Russian)* 77 8847
  Fe, Armco, flat-rolled and annealed, dislocation struct. and mech. props. *(Russian)* 79—20062
  Fe, Armco, rupture onset during cold rolling *(Russian)* 77—8904
  α-Fe, cold rolled, hydrostatic press. effect on microstructural changes during creep 78—39871
  Fe, cold rolled, struct., transmission Kossel patterns obs. 77—48451
  Fe, commercial, deformability, containing H$_2$ 77—90411
  Fe, creep at 77, 295K, formation of five struct. 80—60926
  Fe, high purity, boriding with cryst. B powder 80—84951
  Fe, isochronous annealing recovery, in cold rolled and explosively formed samples 79—100166
  Fe, powder preforms., hot consolidated rolled strip, mech. props. 78—15338
  Fe, pure, initial grain boundaries effect on cold-rolling and annealing textures *(Japanese)* 80—35205
  Fe, rolled sheet, magnetic film form. at metal/calamine interface after ferrous products cooling *(French)* 79—43274
  Fe, texture, recryst. annealing effect *(Czech)* 80—89249
  Fe, under US vibrs., initial struct. effect on C diffusion *(Russian)* 78—38876
  Fe-Al (4 wt.%) single crystals, rolling induced mag. anisotropy and its removal by annealing treatment *(Russian)* 79—61746
  Fe-Al(4 wt.%), ferromag. alloy, mag. anisotropy induced by cold rolling 80—30114
  Fe-C single crystals, effect of heat treatment prior to cold rolling on recrystn. texture 79—83232
  Fe-Co heterogeneous alloys, fabrication by powder metallurgy, tensile strength 77—63600
  Fe-Co-Cr-W-Ni-C, alloy KKhVN, transforms. during annealing and nature of hardening *(Russian)* 78—56653
  Fe-Co-Ni-W alloy, 45KKhVN, plastic deform., electron microscope obs. *(Russian)* 78—80584
  Fe-Co-Si (4,1.5 wt.%), textured, mag. props. 80—35200
  Fe-Co-V (2 wt.%), gamma phase 77—36514

cold rolling continued
α-Fe-Cr alloys, recrystallised, C segreg. effects, TEM *(French)* 77—28828
Fe-Cr-Co (28, 10.5 wt.%) ductile magnet alloy, humidity-induced H_2 embrittlement 80—89406
Fe-Cr-Ni, cold-rolled foils, dilatometric study 80—21033
Fe-Mn, γ to ε phase transform. induced by high press. and plastic deform. 78—68686
Fe-Mn-Ti-Al, magnetic texture rel. to annealing temp., Mossbauer investig. 77—28499
α-Fe-N solid soln., N precipitation kinetics, defects effect 77—59789
Fe-Ni (32.86, 30.65 wt.%), characts. of quenched struct. formed in textured sheets, TEM and optical microscopy study 79—34084
Fe-Ni alloys, graim growth texture 79—91687
Fe-Ni heterogeneous alloys, ferrite, martensite and austenite phase distrib., effect on mech. props. 80—45363
Fe-Ni-C, single crystal, form. and strength of strain-induced martensite 79—100225
Fe-Ni-C (24, 0.45 wt.%), single crystal, plastic deform. effect on martensitic burst transform. 79—15695
Fe-Ni-C (25, 0.2 wt.%), strain-induced martensite *(Korean)* 80—71646
Fe-Si (3 wt.%), anisotropy induced by rolling in (001) and (111) planes *(Russian)* 77—80931
Fe-Si (3 wt.%), cold rolled, effect of primary recrystallisation texture, on behaviour of secondary recrystallisation 78—39802
Fe-Si (3 wt.%), cube-on-edge oriented, high permeability, mill processing and mag. props. 77—86045
Fe-Si (3 wt.%), grain oriented, MnS-AlN-inhibited, precipitate morphology 77—12648
Fe-Si (3 wt.%), high induction grain oriented, metallurgical treatment and mag. props. 77—86044
Fe-Si (3 wt.%), hot rolled sheet steel, ductile-brittle transition temp. *(Chinese)* 78—31498
Fe-Si (3 wt.%), orientation distrib. in primary recrystallised textures, mag. permeability 77—12712
Fe-Si (3 wt.%), orientation development during secondary recrystallisation, primary matrix effect, magnetic props. *(Czech)* 78—60679
Fe-Si (3 wt.%), secondary recrystn., struct. inhibition, permeability improvement 77—12713
Fe-Si (3 wt.%), secondary recrystn., role of solutes 77—86043
Fe-Si (3 wt.%) (001) [100] single crystal, cold rolled texture *(Japanese)* 77—21169
Fe-Si (3 wt.%) high-permeability grain-oriented steel, quenching effect on primary recrystn. texture development 80—84956
Fe-Si (3 wt.%) single crysts., rolling-induced mag. anisotropy *(Russian)* 78—19243
Fe-Si (3.1 wt.%), solubility product of BN 79—10955
Fe-Si (6.5 wt.%), ductility and mag. props., Ni and Mn addition effects 78—76704
Fe-Si (6.5 wt.%), Ni, Al and Mn additions effect on mech. and mag. props. 77—12667
Fe-Si (6.5%) alloy, struct. and rolling texture 79—79006
Fe-Si steel, high permeability, processing effect on recrystn. and deform. 77—12716
Fe-Si-B, high induction alloy, improving mag. props. by adding B to coating 79—83338
Fe-Si(3 wt.%), ferromag. alloy, mag. anisotropy induced by cold rolling 80—30114
$Fe_{80}B_{20}$, amorphous, deform. and annealing effects on mag. and mech. props. 77—12717
$(Fe_{1-x}Co_x)_{78}Si_{10}B_{12}$, amorphous, roll mag. anisotropy 80—75757
$Fe_{4.7}Co_{70.3}Si_{15}B_{10}$, amorphous ferromag., roll mag. anisotropy 79—51773
$Fe_{40}Ni_{40}B_{20}$, and $Fe_{40}Ni_{40}P_{14}B_6$, amorphous, mag. props., effects mech. deform. 80—39840
$Fe_{40}Ni_{40}P_{14}B_6$, amorphous ribbon, cold rolling, annealing mag. props. 77—8958
$Fe_{40}Ni_{40}P_{14}B_6$, amorphous, deform. and annealing effects on mag. and mech. props. 77—12717
$Fe_{40}Ni_{40}P_{14}B_6$, amorphous alloy, small angle X-ray scattering 77—65953
$Fe_{40}Ni_{40}P_{14}B_6$ glass, positron lifetimes in as-received, cold-rolled, embrittled and crystallized samples 79—74177
$(Fe_{1-x}Ni_x)_{78}Si_{10}B_{12}$ amorphous alloys, cold rolled and as-quenched, mag. anisotropy 80—97089
Gd, texture formation during cold rolling *(Russian)* 78—92275
Mg cold rolling texture development 80—25720
Mg, recrystallisation after straining by rolling, −25 to 100°C *(French)* 77—59815
Mg, recrystallisation after cold rolling 78—72790
Mo, hardened sub-structure, high-temp. radiation resist. *(Russian)* 78—56654
Mo, irradiated with fission fragments, creep, 20-30K *(French)* 77—48493
Mo, orientation distrib. function depend. on deform. during cold rolling *(Russian)* 80—50647
Mo, orientation distribution function after longitudinal and cross cold rolling *(Russian)* 79—70076
Mo-B, Mo-B-Fe(Ni), microalloying influence on mechanical props., cold rolling, plasticity *(Russian)* 80—40502
Nb, cold-rolled, deform. zone geometry and texture gradients 77—48452
Nb, surface topography formation due to elec. transfer processes *(Russian)* 80—54482
Ni, cold rolled, influence of impurities on recovery and recrystallisation, positron annihilation meas. 79—15696
Ni, cold-rolled, anomalous effects during X-ray stress meas. *(German)* 80—104184
Ni, cold-worked, impurity-induced vacancy clustering 79—99972
Ni, creep at 77, 295K, formation of five struct. 80—60926
Ni, defect removal, obs. by positron annihilation 78—84677
Ni, deformed bars, cold rolled, exam. of microstruct. by thin foil TEM 78—88502
Ni, H diffusion in imperfect lattice, annealing and cold rolling effect 80—49425
Ni, Ni-Ti (1 wt.%), serrated yielding, 77 to 723K 77—32649
Ni, rolling texture, athermal softening *(Russian)* 77—66655
Ni-A-Ti (6,1 wt.%), γ′ phase precip., deform. effects *(Russian)* 78—48404
Ni-Fe, soft mag. props. rel. to metallurgical aspects 80—88810
Ni-Fe-Mo, K-effect, Mossbauer study 80—39998
Ni-P, struct. obs. by X-ray diffr., low temp. annealing and deform. effects 79—56995

cold rolling continued
Ni-ThO_2 (2.51 wt.%), dispersion hardened, high temp.-strength, deform. method and annealing effects 79—1882
Ni-thoria dispersed (2 vol.%), meas. and eval. of H_2 trapping by permeation technique 79—60555
Ni-ZrO_2, electron-beam-evaporated condensate, cold deform. and annealing effects on microstruct. 80—16331
Ni_3Al-B, $L1_2$ type intermetallic cpd. room temp. ductility improvement by B addition *(Japanese)* 80—35263
NiCrAlY, mechanically alloyed, maintaining elongated grain struct. after deform. 77—36534
$Ni_{35}Fe_{30}Cr_{15}P_{14}B_6$, amorphous, anodic polarisation and localised corrosion 77—21310
NiSb, dilute alloy, impurity-induced vacancy clustering 79—99972
$Ni_{78}Si_{10}B_{12}$, amorphous, struct. factor temp. depend., X-ray diffr. study *(Japanese)* 79—51005
Pb I-section beams, exptl. meas. 78—39845
Pd-Si, struct. obs. by X-ray diffr., low temp. annealing and deform. effects 79—56995
$Pd_{77}Si_{17}Cu_6$, amorphous, struct. changes due to cold rolling and low temp. annealing 79—66072
Re, metallo-ceramic, deform. and cold working by cold rolling *(Russian)* 78—56655
Sn plate, roll-force model 77—4788
steel, Cr-Ni, ferrite precip. *(Japanese)* 80—35187
Ta, rolled single crystal, recovery and recrystallization 80—3093
β-Ti alloy, rolling orientation pattern form. *(Russian)* 77—21161
α-Ti alloy, VT1-1, cold rolled, recrystn. texture and prop. anisotropy 78—52846
Ti alloys, texture strengthening 78—23724
Ti, cold rolled, transcrystalline SCC in methanol-bromine soln., crystallographic texture effect 79—15872
Ti, commercial, texture depend. stress corrosion cracking 80—104334
Ti, industrial grade structural changes during polygonization *(Russian)* 78—19779
α-Ti, plastically deformed by rolling, optical and electron microscope obs. 79—91666
α-Ti, primary recrystallization study by three dimensional anal. of textures and annealing, HVEM obs. 79—91677
α-Ti, primary recrystn., in situ investig. in HVEM 80—104185
Ti, rolling and recrystallisation texture formation *(Russian)* 77—59802
α-Ti sheet, texture dependent stress corrosion cracking in Br_2-methanol soln. 80—71803
Ti-Al-V (6, 4 wt.%), texture depend. stress corrosion cracking 80—104334
β-Ti-Mo, alloy, struct. changes during deformation and ageing *(Russian)* 78—39791
Ti-Mo, metastable β-phase, stress induced products formed by cold rolling *(Japanese)* 78—84843
β—Ti-Mo, thermal instability, hardness and tensile deform. *(Japanese)* 80—71703
Ti-Mo-Zr-Sn (11.5, 6.0, 4.5 wt.%) alloy, struct. as affected by processing history 80—84972
Ti-Nb-Zr-Fe-Mo-V, cold worked, struct. and phase transform. during ageing 78—3153
Ti-Ni, eutectoid decomposition, effect of interphase boundary struct. on mech. 79—4952
Ti-V, metastable β-phase, stress induced products formed by cold rolling *(Japanese)* 78—84843
Ti-V (15.5 wt.%), {332} deformation twins, optical microscopy study 79—79047
V, rolling textures, microstructure, micro orientation *(Russian)* 79—91663
V_2Hf base Laves phase compound tapes, supercond. props., prep. 77—40011
Y, texture formation during cold rolling *(Russian)* 78—92275
Zn, coating on steel strip, plastic deform. 77—90368
Zn, cold rolling texture development 80—25720
Zn, oriented polycrystals, tensile behaviour under hydrostatic press. *(Japanese)* 77—52417
Zn-Al eutectoid alloy, straining at elev. temp., whisker crystal 79—29087
Zn-Al(Mg) alloys, cold-rolled, texture formation rel. to Zn purity *(Russian)* 77—59804
Zn-Al(22 wt.%), alloy sheet, superplastic, cold-rolling effects on mech. props. and microstructure *(Japanese)* 80—71671
Zr, cold-rolled, textural transform. *(Russian)* 78—39790
Zr, rolling and recrystallisation texture formation *(Russian)* 77—59802

cold shortness *see brittleness*

cold working
see also bending; cold rolling; plastic deformation; slip; work hardening
Al alloy 7075-T6, fatigue crack propag. rate rel. to accumulated plastic strain rate, cold work effect *(Japanese)* 79—96115
alloy, cold worked, internal friction peak rel. to back reaction annealing kinetics 78—3161
alloy, cold-worked, particle size and strain determ. from X-ray diffr. profiles 78—88588
alloy, two-phase, deform. struct. and recrystallisation, review 79—34061
alloy, two-phase, recrystallisation mechanisms 79—47708
alloy V93, fatigue strength, effect of residual stresses and cold working 77—56101
annealing twins density, photoemission microscopy 80—35208
α-brass, 70:30, cold-worked, recrystallised grains nucleation on heating 80—29998
α-brass, polycrysts., deformed in tension or rolling, anneal hardening *(Japanese)* 80—93564
α-brasses, cold worked, atomic diffusion kinetics to stacking faults, Laplace transformation method 80—19977
cold-drawn sheet, texture changes in stamping *(Russian)* 77—90365
concrete, prestressed beam, fatigue strength of cold-worked non prestressed reinforcement 79—96123
corrosion resist. depend. on mech. and heat treatments 80—653
elastoplastic material, dynamic cold working, struct. modification *(French)* 78—52847
fastener hole, cold worked, residual strain 79—29088
fracture criterion for bulk cold working processes 78—56775
Hastelloy C-276, cold worked, annealed, surface segregation, Auger spectroscopy study 79—83204
hole, expt. study of fatigue crack initiation and growth 79—79063
Incoloy 800, mechanical props., heat treatment and appl., conf., Petten, Netherlands (March 1978) 79—43296

cold working continued
  Incoloy 800, review of mech. props. up to 600°C 79—43368
  Incoloy 800, review of structural charact., heat treatment and comp. effects 79—43297
  Incoloy 800, steam oxidised, oxide coating anal. 80—89399
  Incoloy 800H, high temp. low cycle fatigue, ageing and cold working effect 79—43277
  Incoloy 800H, high temp.-low cycle fatigue, ageing and cold working effect on initial stress/strain curve 79—47720
  internal friction meas. of thin wire U-shape specimens, electric circuitry modifications 80—59579
  latent cold work heat release kinetics meas. using adiabatic elec. heating 77—52344
  Lawsonite end plates for working spaces of liq. H_2 targets, prep. technique 77—67926
  metal, cold worked, grain size depend. of dislocation density 79—7614
  metal, cold-worked, particle size and strain determ. from X-ray diffr. profiles 78—88588
  metal, deformed struct. role in recrystallisation nucleation, review 79—34060
  metal, degree of deform. effect on thermophys. props. at high temps. 78—26694
  metal, recovered dislocation substructure, prod. and utility, review 77—84749
  metal deformability, flow curves mathematical description, thermal dependence *(German)* 78—15484
  metal working by pressure, full scale adaptive simulation applied to computer aided management 79—79055
  metal-liquid surface energy, effect of lubricants, plasticity during cold working stresses *(Russian)* 77—55419
  metals, cold forging, upset tests anal., stress-strain law determ. appl. *(French)* 79—20064
  metals, Snoek-Koster relaxation, theory 80—16369
  metals, tension methods in X-ray diffraction *(Italian)* 80—87984
  Nimonic PE16, abnormal grain growth after cold working and annealing 79—74176
  noble-metal tubes, cold-weld sealing 80—41556
  Nylon 6, small-angle X-ray scatt. struct. changes w.r.t. thermal and mech. history 79—41976
  plastic deformation incompatibilities, resulting from moderate cold drawing, X-ray line broadening determ. *(French)* 79—43265
  PMMA, mech. degradation in presence of metals, effect of low mol. wt. environment generated during mech. working *(Russian)* 78—31422
  polyethylene, γ-ray polymerised, cold compacted films, mech. relaxations, mechanism 77—16631
  polymer, fibrillation during cold drawing *(Russian)* 77—63691
  polypropylene, oriented, compressive elastic modulus and yield strength 80—16385
  porous metal, yield stress variation during cold deformation 80—16395
  positron studies of annealing in cold worked state, review 79—100163
  PVC, cold drawn, plastic fracture around cavities 79—56994
  Recalloy, Fe-Nb, semihard magnetic alloy, magnetic props., hardness, microstruct. 78—56660
  recovery recrystallisation and grain growth in materials, conf., Chicago, USA (Oct. 1977) 79—97122
  refractory composites, fibre reinforced, directionally solidified tensile tests, in HVEM, deform. and fracture *(French)* 78—68785
  sintered metal, cold forming with self aligning dies 78—11158
  SIPA irradiation creep, material with preferred direction for dislocation Burgers vector, cold worked 79—20118
  solid bodies, exam. of Rebinder effect in mech. working *(Russian)* 79—56992
  solid cylinder, annealed, dynamic forming by compression *(Japanese)* 77—70267
  stainles steel, type 316, irrad. in simulated environment, tensile props. 80—34076
  steel, 11YuA, cold worked, heat treated, electromagnetomech. props. NDT 79—4980
  steel, 45, EHI961, EHI437B, fatigue strength, effect of residual stresses and cold working 77—56101
  steel, alloy, carburized case parameters, effect on props. of 20Kh3MVFA and 12Kh2N4A 78—52989
  steel, alloying elements effect on cementite decomp. during plastic deform., Mossbauer study 79—82900
  steel, austenitic, 16H2NMB, struct., texture and mech. props. of product of transform. 78—92273
  steel, austenitic, 30KhGSA, heat treatment, preliminary, cold deform., elec. heating rel. to mech. props. 79—24554
  steel, austenitic, 800H, effect of hardening processes on initial stress-strain curve 78—84846
  steel, austenitic, cold worked, derivation of simple void-swelling equation 79—7631
  steel, austenitic, cold worked 10Kh11N23T3MR, structural transformations, aging effect, electron microscope obs. 80—40402
  steel, austenitic, Cr-Ni-Mo, Mo effect on lattice parameters and chem. comp. of σ-phase and $M_{23}C_6$ carbides 77—70072
  steel, austenitic, Ni-Ti, alloy N35T5, ageing, magnetisation and Curie temp. depend. on plastic deform., Mossbauer studies *(Russian)* 79—69669
  steel, austenitic stainless, 12Kh18N10T, deformed, phase comp. and props. after prolonged heating 80—30040
  steel, austenitic stainless, corrosion resistance in passive state, cold work effects *(Czech)* 77—59987
  steel, austenitic stainless, Cr-Ni (16, 16 wt.%), in-pile rupture strength, cold work and soln. annealing effects 77—63687
  steel, austenitic stainless, creep, performing effect under tensile and compressive load, rel. to Bauschinger effect 79—96103
  steel, austenitic stainless, electron beam welding effect, on mech. props. of steels 310L, 316, 21-6-9 78—48498
  steel, austenitic stainless, fusion reactor first-wall and blanket material, mech. props. 80—34074
  steel, austenitic stainless, irradiation induced creep, AISI 316, 20% cold worked effect of temp. change 78—72816
  steel, austenitic stainless, neutron irrad. effects on fatigue crack propag. 80—29069
  steel, austenitic stainless, struct. and mech. props. under low temp. deform. under linear and plane stress conditions 79—1902
  steel, austenitic stainless, type FV 548, 20% cold worked irradiated with 22 MeV C^{2+} ions or 46 MeV Ni^{6+} ions, study of void swelling 79—37744

cold working continued
  steel, austenitic stainless, types 304 and 316, environment effect on crack growth, under creep and fatigue conditions 80—85035
  steel, austenitic stainless, types 304L and 316L, work-hardened, electrochem. and corrosion behaviour in acid solns. 80—50757
  steel, austenitic stainless, welded joints, cold working effects on mech. and corrosion props. *(Hungarian)* 78—52838
  steel, austenitic stainless, X-ray line profile analysis 77—86048
  steel, austenitic stainless 304, stress corrosion cracking in $MgCl_2$ soln., cold working effect *(Japanese)* 80—104339
  steel, austenitic type 110G13L, preliminary strengthening inheritance, exam. 78—44137
  steel, austenitic-ferritic Ni-Cr, 12Kh21N5T, phase and struct. transform. *(Russian)* 78—95748
  steel, austenitic-martensitic, phase comp., struct. and mech. props. 80—29974
  steel, bars after drawing, mechanical characts. *(French)* 79—91662
  steel, C, cold strained, effect of rapid heating on strain ageing *(Russian)* 79—11642
  steel, C, ductile fracture under cold forming conditions, press. effect 78—52938
  steel, C, hardened, cold-drawn or shot-peened, residual stresses rel. to temp. *(French)* 77—77494
  steel, C, magnetomechanical acoustic emission for residual stress NDT 80—71149
  steel, C, transition from initiation to propagation of fatigue cracks 78—68802
  steel, C, type 1792AF 79—38966
  steel, C, wire, drawing effect on spheroidization *(Korean)* 77—66656
  steel, C, X-ray line fitting by Gram-Charlier distrib., appl. to tension test *(French)* 79—15689
  steel, C and alloy, cold formability *(French)* 78—60681
  steel, C and austenitic stainless, cold working effect on corrosion behaviour 79—74299
  steel, C type U10A, X-ray diffr. investig. of carbide residues after deform. and tempering *(Russian)* 77—81275
  steel, carbide formation, microscopic exam. aided by rating charts *(German)* 79—61805
  steel, Co-Cr-Ni-Mo-Mn (39.65, 20.25, 15.33, 7.08, 1.9 wt.%) carbide formation during tempering after plastic deformation 80—16330
  steel, cold deformation hardening, effect of C content and cementite shape 78—92277
  steel, cold drawn prestressing tendon, rational test for stress corrosion cracking 78—44246
  steel, cold drawn wire, anisotropic fracture *(Russian)* 77—1867
  steel, cold formed tubes, residual stresses 79—61605
  steel, cold strained, defects interaction with carbide strengthening phases, carbide decomp. degree *(Russian)* 80—84955
  steel, cold worked, AISI type 304 L and 316 L, pitting resistance in NaCl solns. 80—35393
  steel, cold worked, alloying additions effect on 200°C internal friction peak *(Russian)* 77—8867
  steel, cold worked, original struct. effect on softening during heating 80—60882
  steel, cold worked FV548, electron irradiated, void swelling after 10 ppm He preinjection 77—19989
  steel, cold-formed, low pearlite, Nb alloyed, Nb effects, precipitation, recrystallisation *(German)* 77—8832
  steel, cold-worked, Mossbauer obs. of cementite decomp. and restitution 78—64558
  steel, ductile fracture under cold metal forming conditions, metallurgical struct. influence 79—34125
  steel, eutectoid, U8, cold hydraulic press. forging effect on transform. and heat treatment *(Russian)* 79—52235
  steel, Fe-Mn, improvement of cryogenic mech. props. through thermal/mech. treatments 79—79098
  steel, ferritic, Cr-Mo (18, 2 wt.%), cold work effect on 885°F embrittlement 77—77499
  steel, ferritic, MA 956, oxide dispersion strengthened, mech. props. and damping behaviour 79—47702
  steel, ferritic, magnetomechanical acoustic emission for residual stress NDT 80—71149
  steel, Hadfield, containing Ni, carbide precipitation, heat and cold work effects *(Korean)* 77—77484
  steel, high Ni (19 wt.%), thermal stabilisation of austenite 78—15397
  steel, high strength, low alloy, low cycle fatigue, composition, thickness effects 79—57100
  steel, high strength, treatment effect on ductility and strength 80—60880
  steel, hypereutectoid, austenite dissociation depend. on strain at intercritical temps., pearlite transform. *(Russian)* 80—40362
  steel, inclusion effect on cold formability 80—29975
  steel, low alloy composite, ferrite-carbide struct., cold plastic deform. 77—90408
  steel, low C, hot rolled and cold deep drawn, nonmetallic inclusion distrib. in microcavitics *(Russian)* 79—52265
  steel, low-C, preliminary thermomech. treatment, cold deform. effect on struct. and props. 79—38847
  steel, low-temperature tempered, shock wave loading with combined treatment *(Russian)* 77—59857
  steel, maraging, plastic deform. effects on ageing kinetics *(Russian)* 77—77508
  steel, maraging Ni-Co-Mo, strengthening by repeated strain ageing *(Japanese)* 79—100157
  steel, mild, fatigue limit, effect of grain size, cold work, temp., loading frequency 77—32685
  steel, Mn-Cr, blank hardened, shot peening effect on bending fatigue strength *(German)* 78—35402
  steel, Mn-Cr, normalised, shot peening effect on bending fatigue strength *(German)* 78—35401
  steel, Mn-Cr-V, tool, quenched and tempered, fracture toughness *(German)* 80—25726
  steel, NiCrMoV, stress corrosion cracking, cold work effects 78—11383
  steel, prestrained pressure vessel, correl. between dynamical toughness characteristics 78—68816
  steel, railroad rail, effect of cold worked layer on Rayleigh wave dispersion 79—1014
  steel, Si(3 wt.%) grain oriented, high permeability obs. 77—1881
  steel, spring leaf retainer with variable ductility, processing error, cold working error *(German, English)* 79—70267
  steel, stainless, 0Kh12G14N4Yu2, effect of plastic deform. on biphase struct. 78—44176

cold working continued
steel, stainless, 20% cold worked type 316, creep deform. 77−66688
steel, stainless, 20% coldworked 316, irradiation creep, depend. on temp. and atom displacements 77−42075
steel, stainless, 304, shot peened, stress corrosion cracking, const. strain rate investig., cold work, sensitisation effect 79−20259
steel, stainless, 316, neutron irradiation embrittlement, pre-irradiation treatment and composition modification 80−3171
steel, stainless, cold plastic deform. effect on struct. and props. 80−29113
steel, stainless, cold worked, 316, prior stress history effect on irradiation creep 79−87648
steel, stainless, cold worked, pitting corrosion in NaCl soln. 78−44257
steel, stainless, cold-worked, 316, chem. comp. effects on rupture life, tensile props. 77−25152
steel, stainless, Cr-Ni, for cryogenic engineering, mech. props. 78−11240
steel, stainless, ferritic, high CR penny shaped central bursting defect in cold drawing 79−20071
steel, stainless, microduplex, austenite/ferrite, recrystallisation, annealing and cold work effects 79−47713
steel, stainless, neutron irrad., solution-annealed and cold-worked, swelling 78−13229
steel, stainless, neutron irradiated, stress effects on microstruct. 77−47490
steel, stainless, surface chem. rel. to metallurgical props., SIMS, XPS and AES *(French)* 80−80045
steel, stainless, type 304, effect of cold work as sensitization 79−66071
steel, stainless, type 316, 20% cold worked, exam. of creep 78−72817
steel, stainless, type 316, influence of preirrad. thermal-mechanical treatment on phase stability and swelling 79−55792
steel, stainless, type 316, neutron-irrad., void size reduction 78−79636
steel, stainless, type 316, stress-free swelling at high neutron fluence, rel. to LMFBR core environment 78−13239
steel, stainless, type Kh17N13M2T, strengthening by plastic deformation and cold working *(Russian)* 78−52839
steel, stainless, void swelling obs., electron beam effects *(Japanese)* 80−54218
steel, stainless 304, metallurgical factors on the corrosion and mass transfer in liq. Na *(Japanese)* 80−71804
steel, stainless 316, 20% cold worked, swelling increase due to inreactor temp. reduction 78−34547
steel, stainless Kh15N9Yu, elastic limit, effect of microstruct. and heat treatment 79−83251
steel, stainless type 316, neutron irradiated, or themally aged diamond-cubic η phase formation, TEM study 79−99249
steel, tool, maraging, based on N12M10, exam. of hardening, crack resistance and wear *(Russian)* 79−34047
steel, transformations, influence of type of cold plastic strain *(Russian)* 79−52232
steel, US wave velocity meas. rel. to cold working 80−99908
steel, wear characts. of burnished machined surfaces 80−108595
steel, X-ray and microhardness meas. at high strain rates *(German)* 78−3184
steel 12Kh18N10T, struct. and mech. props. after prolonged working at −183°C 77−55988
steel austenitic stainless, cold working type, heat treated, tool wear during cutting 79−47782
steel cold plastically deformed, exam. of structure of diffusion layers after borating *(Russian)* 79−34054
steel components, residual stress distrib. on surface cold working *(Russian)* 77−59975
steel high strength X 3 CrNiMoNbN 2317, Bauschinger effect and creep at room temp., effect of heat treatment *(German)* 77−36543
steel SS-41, plastic working with vibr., US hardness tester 78−53044
steel tube eversion, effect of material and geometrical parameters 79−15690
steels, C, cold worked and recrystallised, attenuation behaviour *(German)* 78−48445
steels, C, H_2 embrittlement after patenting and cold deform. *(Russian)* 79−29175
steels, C, quenched and tempered, struct.-prop. relationships 80−7599
steels, low alloy, particle coarsening reactions, effect of cold deform. 80−71664
steels, tool, cold hydrostatic extrusion rel. to struct., props. 79−20068
tensile, strain rate effect on stored and dissipated energies 77−86111
Zircaloy 4 tubing, cold-worked and annealed, stress relaxation behaviour 77−57717
Zircaloy-2, cold worked, temp. cycling effects on irradiation growth 80−2079
Zircaloy-2 cladding tubes, heat treatment influence on texture and mech. anisotropy 79−91694
Zircaloy-4, microstrain and particle size meas. by Warren-Averbach method 80−55420
Zircaloy-4, plain strain ductility dependent of struct. and texture 77−8885
Zircaloy-4 cold worked, strain ageing behaviour with varying O_2 content 77−48455
Ag-Ga solid soln., internally oxidised, hardness *(Japanese)* 78−60744
α-Ag-Ge, cold-worked, lattice imperfections, X-ray diffr. study 78−38732
Ag-Sb, cold-worked, lattice defects, convolution relations for X-ray line breadth calcs. 78−51394
Ag-Zn, cold-worked, lattice defects, convolution relations for X-ray line breadth calcs. 78−51394
Al alloy, recrystallisation during hot deform. and after cold working 79−47715
Al alloy 7075, fracture props., effect of thermomechanical treatment 78−60793
Al alloy 7075-Tb, coldworked fastener holes, elastic-plastic boundary layer determ. 79−34066
Al alloys, thermomech. treatments, effects on microstruct. 80−100858
Al and Al-Mn (1 wt.%), subgrain growth during annealing after cold work 78−56656
Al, α-particle bombarded, He bubble growth mech. 77−7774
Al, cold-worked, dislocation-pinning defects, US attenuation obs. 77−31673
Al, cold-worked, plastically deformed, internal friction spectrum, Hasiguti peaks associated with dislocations 80−7618
Al, cold-worked, transport props., 1.5-8.5K 78−7059
Al, deformed in uniaxial and equibiaxial tension, dislocation arrangements 80−108516

cold working continued
Al dilute alloys, cold worked, internal friction peaks 80−97520
Al, dislocation substructure formation under hydrostatic extrusion 78−56696
Al, effect of bias stress on US attenuation induced by geometrical kinks mobility *(French)* 77−31728
Al, fatigue crack propagation rates, stress intensity factors *(French)* 77−25154
Al, internal friction, strain amplitude dependent damping at 8.3×10^{-3} Hz 77−1172
Al, internal friction, strain amplitude dependent, hydrostatic press. effect 77−77520
Al, pure, cold worked, internal friction peaks 80−97520
Al, pure elec. cond. grade, substructural developments during recovery, Sandstrom's model validity 79−74187
Al, secondary recrystallization *(Czech)* 79−70080
Al, subgrain coalescence, grain boundary recrystallisation nucleation 80−3094
Al-Cr(Mn), cold-worked and homogenised, precip. kinetics, impurity resist. and TEM meas. 77−16596
Al-Cu, high temp. internal friction peaks 77−48470
Al-Cu (4 wt.%), stress corrosion cracking, effect of cold reduction *(Japanese)* 77−48580
Al-Cu (4.6 wt.%), cold work and ageing influence on ductility and fracture behaviour *(Japanese)* 80−89295
Al-Cu-Mg, cold plastic deformation, stress/strain relations 79−56991
Al-Cu-Mg-Si-Mn alloy AK8, fatigue strength, effect of residual stresses and cold working 77−56101
Al-Cu(Mg)(Zn), cold working causing preprecipitation, thermoelec. power *(French)* 79−8306
Al-Fe, dil., annealing after cold working, impurity-vacancy interactions, Mossbauer meas. 80−7236
Al-Ge alloy, Ge precip., ion irrad., dose rate and temp. depend. 78−79642
Al-Li, cold worked neutron irrad. alloys, He bubble behaviour, microstruct. changes 77−54359
Al-Mg, cold plastic deformation, stress/strain relations 79−56991
Al-Mg (2 wt%), high temp. creep, effect of cold working on mechanism 79−43351
Al-Mg alloys, cold-worked, transport props., 1.5-8.5K 78−7059
Al-Mg cold drawn wires with FCC lattice, texture and structure 77−70067
Al-Mg-Si rod, extruded and cold drawn, annealing *(German)* 78−39804
Al-Mg-Si-Cu, cold plastic deformation, stress/strain relations 79−56991
Al-Mn (1 wt.%), commercial, recrystallisation 79−47710
Al-Ni(Cd)(Fe)(Si), cold worked, struct. and props. 80−71666
Al-Zn, type 7075-T6, coldworked hole specimens, residual stresses, fracture mech. anal. 80−97587
Al-Zn-Mg (6,1.5%), influence of ageing and cold work on tensile and fracture props. *(Japanese)* 78−52842
Au-Cu(Ag)(Pt), cold worked, impurity conc. rel. to internal friction Bordoni peak, solid soln. hardening mech. 80−16363
B fibre reinforced Al, thermal degradation of tensile strength, due to fibre strength degradation 78−39861
B_4C rings, Al bonded, exam. of fabrication techniques 78−72748
Be-bronze BrB2, struct. and phase transform. during mechano-thermal treatment *(Russian)* 80−11667
Bi polycrystalline, plastic deform. and stored energy of cold work 79−43348
CU-Zr-(Cr), powder metallurgical alloys, thermomech. treatment effect on props. 80−50660
$Ca_{10}(PO_4)_6X_2$ (where X is F, Cl, OH or Co), influence of mech. treatment on struct. and reactivity *(German)* 79−43272
Cd-Ag, polycryst. wire, cold worked, resistivity changes 78−68827
Cd-Zn, polycryst. wire, cold worked, resistivity changes 78−68827
Ce, cold working, deform. induced struct. effects 80−25719
Co-Fe-Nb, heavily cold worked, magnetic hardening 79−20073
Co-Fe-Nb alloys, effect of cold working on mag. props., and precipitation morphology 78−39803
Co-Ni-Cr-Mo (35, 20, 10 wt.%), MP35N, TEM study of phase transformations 80−81054
Co-Ti alloys, martensitic transformation depend. on ageing, cryst. struct. 79−91649
Cr-Co-Fe cold formable mag. alloys for use in telephone receiver 79−52227
Cu, cold work, P effect on annealing 79−47707
Cu, cold worked, determ., of dislocation pinning and unpinning stages, using internal friction meas. 78−92278
Cu, cold worked, dislocation production 77−32597
Cu, cold worked, grain size effects on short-term strength *(Russian)* 78−56693
Cu, dislocation substructure formation under hydrostatic extrusion 78−56696
Cu, elastic modulus and internal friction during plastic deform., dislocation props. determ. 80−35244
Cu, electron-irradiation internal friction behaviour, shear modulus and damping meas. 80−55444
Cu, polycrystn., cold worked, calc. of dislocation density as function of plastic strain 79−38924
Cu, recrystallised, inhomogeneous deform. due to texture changes *(German)* 79−29158
Cu single crystal, large angle grain boundaries formed during cold work, TEM obs. of orientation relationships 79−90678
Cu, tough pitch wire, effect of oxygen and cold working on cupping development *(Japanese)* 79−79087
Cu, types MOb and M1, primary recrystallisation kinetics depend. on state of impurities *(Russian)* 79−66069
Cu, wire, recrystallisation *(German)* 77−86055
Cu, wires, effect of heat treatment during drawing 78−56659
Cu, X-ray and microhardness meas. at high strain rates *(German)* 78−3184
Cu-Ag (0.1 wt.%), cold-worked, internal friction peaks in kHz range 80−89276
Cu-Ag(Se)(Sn)(Ag-SeSn), Ag, Se, and Sn effects, singly and together, on recrystallisation 79−100164
Cu-Al, internally oxidised, structural, elec. and mech. characts. 78−60761
Cu-Al (3 wt.%), annealing twins density, photoemission microscopy 80−35208
Cu-Al-Fe, strength increase from intermediate annealing determ. of annealing temp. by recrystallisation 78−44136

cold working continued
- Cu-Al(Au)(Ga)(Ni)(Pd)(Rh)(Zn) (4 at.%), anneal hardening mechanism 80—60879
- Cu-Au, (0.02-5 at.%), cold worked, internal friction peaks 79—11652
- Cu-Au, cold worked solid solution, flow stress and activation volume 80—16393
- Cu-Au(Ni)(Zn), elastic modulus and internal friction during plastic deform., dislocation props. determ. 80—35244
- Cu-Be (2 wt.%), plastic deformation influence on ageing, granular microhardness *(Russian)* 80—55474
- Cu-Be-Ni-Ti-Mg bronze, alloying element influence on minimum thermo EMF, cold working *(Russian)* 80—34426
- Cu-Fe (2.46 wt.%), reversion phenomena and cold-working effect *(Japanese)* 80—35204
- Cu-Fe system, ageing and reversion phenomena study 80—89274
- α-Cu-Ga (3.4-15 at.%) cold-worked, lattice imperfections, X-ray obs. 77—55291
- Cu-Ni, cold worked solid solution, flow stress and activation volume 80—16393
- Cu-Ni (30-90 wt.%), elect. resist. rel. to cold working and heat treatment 80—71765
- Cu-Ni-P, precipitation hardening 77—12633
- Cu-Ni-Sn (15, 8 wt.%), prior deform. effect on spinodal age hardening 80—108465
- Cu-Ni-Zn alloy, FCC, cold-worked, microstruct., X-ray obs. 78—3143
- α-Cu-Ni-Zn-Pb, fire cracking and ordering *(German)* 78—60760
- α-Cu-Ni-Zn-Pb, fire cracking, effect of pores and impurities 79—29207
- Cu-Ni(Au), elastic modulus and internal friction during plastic deform., dislocation props. determ. 80—35244
- Cu-Sb, cold-worked, lattice defects, convolution relations for X-ray line breadth calcs. 78—51394
- Cu-Ti (4 wt.%), combined recrystallization and precipitation 79—29072
- Cu-Ti (5 wt.%), effect of cold work on ageing behaviour, TEM study *(Japanese)* 79—78991
- Cu-Zn, cold worked solid solution, flow stress and activation volume 80—16393
- Cu-Zn, cyclic stress/strain curves in monocrystalline and polycrystalline samples, cold work and Zn addition effects 78—95786
- Cu-Zn-Sn (24-34, 1.0 wt.%), cold-worked microstruct., X-ray diffr. obs. 80—3088
- α-Cu-Zn(Al), solid soln., intermediate temp. embrittlement *(Japanese)* 79—20158
- α-Fe, $(\bar{1}\bar{1}2)$ $[\bar{1}\bar{1}\bar{1}]$ anti-twinning slip system, low temp. strengthening, dislocation struct. 77—21164
- Fe, Armco, sleeve, deformed by cold drawing, exam. of surface and texture *(Russian)* 79—34057
- Fe, cast, increase in yield strength, after phase transformations 78—44125
- α-Fe, cold work aftereffects 80—88830
- Fe, cold work stored energy effects on mag. moment vs. temp. curve 78—95419
- Fe, magnetomechanical acoustic emission for residual stress NDT 80—71149
- Fe, penetration of H_2, influence of microstruct. changes induced by cold working *(Russian)* 77—20182
- Fe, single component, powder, compressibility and elec. resistivity in cold pressing under low press. 77—77444
- Fe-Al, hot- and cold-rolled, texture form., pole figures method *(Russian)* 80—45317
- Fe-Al (40 at.%), ordered, plastically deformed, neutron irrad. damage and recovery, resist. meas. 77—19993
- Fe-Al alloys, cold-worked, Mossbauer study of recovery 80—7593
- Fe-C (4 at.%), dislocation-C atom relax. 77—70074
- Fe-C alloy, oxidation at 500°C cold work and annealing effects 78—44276
- Fe-C-Cr-Mn-Si-Ni (4.6, 38.7, 1.1, 2.0, 1.58 wt.%) alloy US-25, powder, compressibility and elec. resistivity in cold pressing under low press. 77—77444
- Fe-Co-Cr, Cr effect on struct. *(Russian)* 78—27535
- Fe-Co-Cr, Cr effect on struct. of ordering 78—35407
- Fe-Co-Cr (50, 0.4 wt.%), ordering and recrystallisation 79—34029
- Fe-Co(-V) alloys, neutron irradiated, influence of dislocation doping on recovery 79—46715
- Fe-Co(Al), B_2 superlattices, point defect investigations 78—47357
- Fe-Cr, single and two component, powder, compressibility and elec. resistivity in cold pressing under low press. 77—77444
- Fe-Cr alloys, cold worked, internal friction due to H *(Japanese)* 80—70305
- Fe-Cr-Ni austenitic alloy, cold deformed, α-γ transition, calorimetric study *(Russian)* 80—55390
- Fe-H system, cold work internal friction peak, appl. of Schoeck's model 78—95771
- Fe-Mn (9 to 20 wt.%), ^{57}Fe Mossbauer spectroscopy in phase transformations 80—29948
- Fe-Mn alloys, high-purity, martensitic transform., heat treatment effect 79—56979
- Fe-Mn-Ti alloys, austenitic, precipitation strengthened 80—25714
- Fe-Mo(W), semihard magnetic alloys, magnetic, elec. mech. props. *(Japanese)* 79—70078
- Fe-Nb(Ta)-Co, Recalloys, semihard mag. alloys, mag. and elec. props., hardness, thermal expansion *(Japanese)* 79—5066
- Fe-Ni, austenite formed from martensite during annealing in $(\alpha+\gamma)$ region, crystallographic study 78—19782
- Fe-Ni, martensitic alloys, effect of cold working before ageing 79—47736
- Fe-Ni, secondary recrystallization *(Czech)* 79—70080
- Fe-Ni alloy, cold work stored energy effect on mag. moment vs. temp. curve 78—95419
- Fe-Ni-C, martensitic, internal friction 77—16633
- Fe-Ni-Co, texture form. after cold working and annealing *(German)* 80—3089
- Fe-Ni-Cr (30.6, 21.3 wt.%), Alloy 800, high temp. oxidation at low O_2 press., SEM, AES and electron probe microanal. study 80—93688
- Fe-Pd crystalline alloy, positive large linear magnetostriction 80—25173
- Fe-Si, grain oriented, with unique inhibition system for texture development 77—90366
- Fe-Si-B-S, grain-oriented, high induction, B and S addition effect on magnetic props. *(Slovak)* 79—4697
- Fe-Ta alloy, mech. drawn and aged, exam. of electrical resistivity, hardness, microstruct., and mag. props. *(Japanese)* 78—48545
- Fe-W-Cr-Mo system, mag. and mech. props. rel. to production methods *(Japanese)* 80—71107

cold working continued
- Fe-W-Cr-Mo-Co (18,12,3,x wt.%) alloy, effect on magnetisation and hardness obs. *(Japanese)* 77—40428
- Fe-W-Cr-Mo-Co with austenitic phase, magnetic and mech. props., cold working and ageing effects *(Japanese)* 78—60678
- Fo-Fe-Nb, cold-worked and aged, mag. props. and microstruct. 80—34690
- KCl:TlCl, lattice defects, X-ray line profile obs. 80—24455
- MgEu, dil. alloy, cold worked, valence transform. of Eu due to defect association, mag. suscept. and Mossbauer meas. 77—51404
- Mn-Ni-Ti (Zr) systems, and mech. props. thermal expansion for different heat treatments *(Japanese)* 79—29123
- Mn-Ni-Ti(Zr), non-ferromagnetic Elinvar-type alloys 79—24566
- Mn-Ni-V(Nb)(Ta), nonferromagnetic Elivar type, mech. props. meas. 77—48473
- MnZn ferrites, mag. domains on worked surfaces 79—99722
- Mo cold worked, dislocation struct. change during postdeform. at 493K 79—43271
- Mo, H and D trapping, enhancement due to He ion damage, annealing and cold work effects 77—31698
- Mo, single and polycrysts., struct. change during work softening, HVEM 80—103336
- Mo-Re, cold worked, strength 78—31426
- Mo-Ti-Zr (0.5, 0.7 wt.%) alloy TZM, props. and appl. *(German)* 80—21040
- Mo-Zr-C (0.063, 0.06 wt.%) alloys, ageing, effect of cold deform. by hydrostatic extrusion 79—57001
- Mo-Zr-C (0.63, 0.06 wt.%), quenched and deformed, structural changes during heating to ageing temp. *(Russian)* 79—1879
- Nb alloys, cold worked, chemicothermal strengthening, internal oxidation 80—35229
- Nb and Nb alloys, cold plastic deform., oriented microdistortions *(Russian)* 78—39840
- Nb, cold-worked, Snoek-Koster relaxation transient period, comparison with Schoeck's theory 79—34086
- Nb, dislocation damping, amplitude depend. 80—59469
- Nb, H_2 loaded, cold worked, plastic deformation, exam. of α internal friction peak 78—92307
- Nb, plastic deformation effects on superconducting specific heat transition 80—20352
- Nb-Ti multifilaments, effect of mech. and thermal treatments of supercond. props. 80—104197
- Nb-Ti superconducting alloy, critical current density, heat treatment effects *(Japanese)* 78—14909
- Nb-W-Mo-Zr (5, 2, 1 wt.%), surface-layer struct. and mech. props., effect of O_2 diffusion saturation 79—5087
- Nb_3Al, A-15 struct., converted from cold worked BCC struct., crit. currents 80—75697
- Nb_3Al, and $Nb_3Al_{0.76}Ge_{0.24}$, supercond. props. of cold worked core wires an basis of A15 phases 77—85369
- Nb_3Al, BCC struct., cold working and converting to A-15 struct. 78—64553
- Nb_3Al, mechanical and supercond. props. 79—38214
- Nb_3Sn, supercond. diffusion layer, Zr content and Nb cold working effects 77—16015
- Nb_3Sn, supercond. props. of cold worked core wires an basis of A15 phases 77—85369
- Nb_3Sn-Cu superconducting composites, produced by cold extrusion of fine powders 79—38767
- NbTi, supercond., crit. current densities and anisotropy factors, heat treatment effects 79—38285
- NbTi, supercond., processing parameter optimisation for high mag. field appls. 79—38290
- Ni, (99 wt.%), annealing twins density, photoemission microscopy 80—35208
- Ni alloys, recrystallised, grain boundary inheritance and props. 77—59816
- Ni and Ni-Co, recovery of single crystal after varying amounts of cold work 79—100162
- Ni, Bordoni peaks activation parameters 79—82282
- Ni, cold swaged, unidirectional recrystallisation over range of temp. gradients *(Japanese)* 78—48424
- Ni cold worked, annealed, exam. of anelastic relaxation at low temp. 78—84877
- Ni, dislocation substructure formation under hydrostatic extrusion 78—56696
- Ni, grain boundary migration during recrystallisation after cold drawing 77—73289
- Ni, irradiation-induced creep, mechanism for large transient strains 78—14391
- Ni-Al (6.3 at.%), influence of localised order on thermo-EMF and Hall-EMF *(Russian)* 78—6951
- Ni-Cr-W-Mo-Ti-Al, heat-resist., recovery and recrystn. 80—76268
- Ni-Cu (30 wt.%), cast cold- and warm-worked, recrystallization 79—29092
- Ni-HfO_2 (3 wt.%), dispersion hardened alloy VDU-2, thermal and mech. treatment 77—90376
- Pb-Sn, eutectic alloy, plastic deform., work hardening *(German)* 78—92279
- $PbMo_6S_6$, cold-worked core-wires, supercond. transition temp. and lattice instability 78—6469
- $Pd_{77.5}Cu_6Si_{16.5}$, cold drawn wires, surface markings, fracture stresses 79—56997
- Pt wire, cold worked, recovery of elec. resist. 77—12643
- δ-Pu alloys, at. vol. increase 77—19910
- $SmCo_5$ powder alloy, densification by cold working 77—4753
- Sn, acoustic emission rel. to effect of cold work on struct. transitions 77—63659
- Sn-Sb (0.57 at.%) solid soln., yield point for cold-worked and annealed specimens *(Russian)* 78—48448
- Sn-Zn (0.4 at.%) solid soln., yield point for cold-worked and annealed specimens *(Russian)* 78—48448
- Ta:H, recovery after cold working at 4.2K, resist. meas. 79—4977
- Ti alloys, metallurgical characterisation using thermoelec. power meas. *(French)* 80—45462
- Ti, cold worked, annealed, internal friction meas. of H degassing *(French)* 79—43304
- α-Ti, hydride precipitation, resistometric investigation, isothermal ageing effects *(Japanese)* 77—81265
- Ti, oxidation behaviour in high temp. steam after heat treatments *(Japanese)* 78—48565

cold working continued
Ti-Al-(V) (6,4 wt.%), hot salt stress corrosion susceptibility, microstruct. effects 77−36688
Ti-Al(Mo), swaged and recrystallized, grain growth 80−3092
αTi-Fe, plastically deformed, $\alpha \rightarrow \omega$ transform. 78−3095
Ti-Mo-Fe (3, 0.13 at.%), metastable phases, Mossbauer study 80−7243
Ti-Mo-Zr-Sn (11.5, 6, 4.5 wt.%), metastable beta III phase, recrystallization and grain growth 80−3091
Ti-Mo-Zr-Sn-Fe-C-Si alloy, β-III, cold deform. and annealing, effect on struct. and mech. props. *(Russian)* 79−24533
β-Ti-Mo-Zr-Sn(11.5, 6, 4.5 wt.%), metastable phase III, microstruct. and age hardening response 80−84945
Ti-Mo(Nb)(Ta), BCC struct., tetragonal phase form. by cold deform. *(Russian)* 78−88462
Ti-Nb, cold strained, exam. of ω and α phases, precipitated during ageing *(Russian)* 79−11620
Ti-Nb alloys, Fe, Mo, V, Ta alloying additions on microstruct. after combined treatment *(Russian)* 77−59826
Ti-Nb-Mo(V)(Ta)(Al)(Zr), BCC struct., tetragonal phase form. by cold deform. *(Russian)* 78−88462
$Ti_{55}Nb_{45}$, supercond., anomalous phonon thermal resist. 77−69451
γ-U alloys, at. vol. increase 77−19910
V, effect of cold working on diffusion of H, neutron radiography meas. 77−39696
W, structural defect recovery after irradiation and cold work 78−47429
W wire, cold drawn, dislocation processes occurring during tensile testing *(Hungarian)* 77−48450
Zn-Al-Mg alloy, annealed, recrystallised, influence of strain and purity on orientation *(Russian)* 79−52234
Zr alloys, reactor fuel sheath mat., thermophys. props. 77−46280
α-Zr and Zircaloy 2, fatigue, 20 to 700°C 77−70154
Zr base alloys, irradiation growth, dislocation model 78−51595
Zr, low temp. deformed, O_2 effect on production and recovery of defects, elect. resist. meas. 79−47705
Zr-Nb (1 wt.%), stress drop expt. during creep 79−29152
Zr-Nb (2.5 wt.%), annealed, irradiation growth at 353K 79−46710
Zr-Nb (2.5 wt.%), cold worked, in reactor oxidation of crevices and cracks 78−23865
Zr-Nb (2.5 wt.%), cold-worked, pressure tubing, metallography and mech. props. 80−89269
Zr-Nb (2.5 wt.%), heat treatment effects on slow crack growth, cold working effects 77−28836
Zr_3Al, cold worked, annealing effects 77−36535

collections of physical data
6 cm radio sources, data from Westerbork Synthesis Radio Telescope survey 79−88604
β-transitions, mixed Fermi and Gamow-Teller 79−54407
A=105, nuclear data sheets, levels, decays and J^π assignments 79−93486
A=111 nuclei, nuclear struct. data sheets to February 1979 80−9193
A=112, experimental nuclear structure data to January 1979 80−98763
A=117 nuclear struct. data sheets to June 1978 79−36130
A=119, nuclear data sheets, level and decay props. 79−71780
A=11, 12, energy levels, transitions and resonances, compilation 80−46743
A=121 nuclear data sheets, level schemes and decay properties 79−75818
A=123, experimental nuclear structure data to June 1979 80−94931
A=136 nuclear data sheets, level schemes and decay props. 79−75819
A=141 nuclei, data sheets 79−6371
A=142, nuclear struct. data sheets to Oct. 1977 79−30769
A=144 nuclear data sheets, levels, decays and J^π assignments 79−93487
A=145, experimental nuclear structure data to August 1979 80−94932
A=147 nuclear struct. data sheets to May 1978 79−30770
A=154, nuclear data sheets, levels, decay props., isomeric states, Nilsson orbitals 79−71781
A=159, nuclear data sheets, levels, decays, and J^π assignments 79−93488
A=163, nuclear data sheets to April 1979 80−98762
A=18-20, light nuclei, compilation of energy levels, nuclear struct. information 78−62478
A=195 nuclei, data sheets 79−6372
A=197 nuclei, review of nuclear struct. information 77−57585
A=198 nuclei, struct., level props., decay, review 78−17077
A=199, nuclear level scheme data sheets, decay scheme 79−13186
A=201 nuclear struct. data sheets to May 1978 79−30771
A=203, nuclear data sheets, level struct., decay schemes 79−13187
A=211, nuclear struct. data sheets to July 1978 79−36131
A=214 nuclei, struct. info., energy levels, spin, parity, decay 78−17078
A=215, nuclear data sheets, decay characteristics and level struct. 78−58224
A=218 nuclei, nuclear struct. info., energy levels, spin, parity, decay 78−17079
A=219, nuclear data sheets, decay characts. and level struct. 78−58225
A=222 nuclei, nuclear struct. info., energy levels, spin, parity, decay 78−17080
A=223, nuclear data sheets, decay characts. and level struct. 78−58226
A=226 nuclei, review of nuclear struct. information 77−57586
A=227, nuclear data sheets, decay characts. and level struct. 78−58227
A=230 nuclei, review of nuclear struct. information 77−57587
A=232, 236, 240 nuclei, review of nuclear struct. information 77−57588
A=234 nuclei, nuclear struct. info., energy levels, spin, parity, decay 78−17081
A=238 nuclei, nuclear struct. info., energy levels, spin, parity, decay 78−17082
A=242 nuclei, nuclear struct. info., energy levels, spin, parity, decay 78−17083
A=46, nuclear data sheets, level struct. and decay props. 79−13185
A=48, nuclear data sheets, to September 1977 78−82266
A=52 nuclear struct. data sheets to April 1978 79−36129
A=53 nuclei, struct., level props., ENSDF data 78−17076
A=54 nuclei, data sheets 79−6370
A=70, nuclear struct. data sheets to Oct. 1977 79−30768
A=84 nuclei, nuclear struct. data sheets to March 1979 80−9191
A=87 nuclei, nuclear struct. data sheets to January 1979 80−9192
A = 143, nuclear data sheets, level energies, J^π assignments 79−30775
A = 202 nuclear data sheets, levels and transitions 79−40831
A = 86, nuclear data sheets, level and decay schemes 79−30774
AB-type compounds, high press. and high temp. behaviour 78−22850

collections of physical data continued
absolute core-level binding energies for gaseous atoms and molecules 80−101670
absorption line lists for quasars, visible obs. 80−67899
acetic (ethanoic) acid, ideal gas thermodynamic props. 78−51275
acetic acid, PVT props., 448.15-603.15K, press. up to 10 MPa 78−14455
actinide aqueous ions, chemical thermodynamics, book 77−60108
actinide elements, chemical thermodynamics, book 77−60107
actinide sensitivities, analytic evaluation 78−82427
advanced reactor Centralised Reliability Data Organisation 79−13463
aerosol scattering, spectral-zonal functions *(Russian)* 80−21824
alkali isoelectronic series, transition probabilities, oscill. strengths, lifetimes, branching ratios 78−33470
alkali metal molten salts, physical props. data compilation rel. to energy storage 79−92090
alkaline earth halides, aq. solns., activity and osmotic coeffs. 78−53242
alkaline earth halides, refractive index, wavelength and temp. derivatives 80−88948
n-alkanes, vibr. data and force field consts., review 79−31750
alloy, multicomponent phase diagram calc., NPL alloy data bank 78−92243
asteroids, diameters for 396 objects and taxonomic system 79−2510
asteroids, magnitudes and phase relations compilation 79−88617
asteroids, new reduction and collection of meridian obs. of Ceres and Pallas 77−13277
asteroids, rotation rates, pole positions and shapes 80−17531
astronomical atmospheric extinction data, time trend and internal errors 77−49161
astronomical data, in observer's handbook of Royal Astronomical Society of Canada, (1979) 79−8796
astronomical data base standards, management and security 77−82282
astronomical ephemerides (1978) *(French)* 78−40802
atmosphere ozone content, July-Sept. 1978, Belgium 80−12484
atmospheric absorption line parameters, AFGL, compilation update 79−21013
atmospheric absorption line parameters compilation, AFCRL, updating 77−9495
atmospheric chemistry, reaction rates and photochemical data 78−77312
atmospheric trace gases and pollutants, data compilation on mag. tape 78−44995
atmospheric transmittance and radiance, high-resolution HITRAN and data compilation 79−66795
atmospheric transmittance and radiance, moderate-resolution, LOWTRAN code 79−66796
atom total energies, RHF calc., GTO basis sets for heavier elements 77−61686
atomic data handbook 77−23398
atomic electron binding energies, determ. from relaxed-orbital relativistic Hartree-Fock-Slater calcs. 77−42255
atomic electronic stopping power of ions, (ions C-Xe; targets H-Xe) 80−12859
atomic energy level and Grotrian diagrams, S I to Ti XXII, book 79−3387
atomic energy levels, calcs. one-electron atoms 77−79529
atomic form factors, relativistic Hartree-Fock, tables for Z=1-100 79−59381
atomic ground-state wavefunctions, optimised central pots. 80−32593
atomic ionisation of K-shell by Coulomb excitation 79−18272
atomic K and L X-ray line widths determ. 77−42265
atomic K- and L-shell ionis. by protons, plane-wave Born cross sections 80−12858
atomic mass evaluation, input values 78−70949
atomic mass evaluation 1977: mass table, mass excesses, total BEs, β-decay energies 78−4894
atomic polarisability tables in SI units 77−58191
atomic radiative and radiationless yields, K and L shell 79−76376
atomic spectral lines, 10000-40000 Å 78−50490
atomic weights 80−1076
atoms, natural line widths, K and L X-rays, XPS and KLL Auger lines 79−76383
ATS-6 electron content data presentation 78−61593
audiometric pure-tone threshold rel. to age, data tables 80−35918
audiometric thresholds, pure-time, relation to age, comparative anal. of data 79−5299
Auger electron energies, elements $10 \leq Z \leq 100$ 78−62774
auroras, catalogue from European sources, 450-1466 AD period 79−75010
benzene, tables of thermodynamic props. 77−24419
benzenes, di- and mono-substituted, NMR spectral data, aromatic proton chemical shifts 77−79632
binary alloys, thermal conductivity, data anal. and synthesis 78−95284
boron halides, diatomic isovalent sequence, free-mol. electronic transition intensity consts., systematics 78−42137
bright galaxies associated with nearby Abell clusters, position and magnitude 80−67880
bromides and mixtures, molten, elec. cond., density, viscosity, surface tension 77−80638
bromoethane, mol. parameters, vibr., pot. barrier height etc., data tables 79−76409
Canadian earthquakes, 1968 catalogue 77−49035
Canadian earthquakes, 1974 catalogue 78−40517
Canadian earthquakes, 1976, catalogue 79−44139
Canadian earthquakes, 1977 catalogue 79−84164
cavity resonators, natural frequencies of coaxial and concentric cavities *(French)* 79−31760
charge transfer cross sections of H, H^+ and H^- beams 80−32824
charged particle induced nuclear reactions, reaction list for atomic number 1-98 77−14099
chemical data base, error detect. by text searching 77−37678
chlorofluoromethanes, ideal gas thermodynamic props., mol. struct. 77−3912
collisional transition probabilities for alkali metal atoms in thermal plasmas from 1000 to 8000K 77−72406
compressible turbulent boundary layer data compilation 78−14035
contact binary stars, theoretical atlas of light curves and rot. broadening functions 80−17610
Copernicus UV spectral atlas for B3 IV type star ι Herculis 80−67583
cresols, ideal gas thermodynamic props. 78−75250
cross sections for charged particle prod. by 14 MeV neutrons for Fe, Co and Ni isotopes 80−9289

collections of physical data continued
'crystal data space-group tables', anal. of population freq. 77—80434
crystal sources, geometrical coeffs. for interpretation of γ-ray perturbed angular correl. with quadrupole interactions 80—73109
crystalline compounds, computer identification techniques using X-ray powder diffr. file 77—70389
cyanoacetylene, microwave spectrum, mol. consts. 78—74647
P Cygni type line profiles, theoretical, atlas 79—80297
deformed nuclei, single particle matrix elements of electric quadrupole γ-transitions 77—88072
diatomic molecule, intensity distrib. in branches of septet transitions 79—85944
dielectric relaxation, Williams-Watts type, normalised complex permittivity, num. table 80—7287
differential polarisation coefficients for (γ,X) reactions 80—73838
dimethyl ether, review of microwave spectrum, tabulated data 80—51965
Dirac-Fock Slater calculations of elements $Z=100$ to $Z=173$ 77—71739
dust, airborne, worldwide data on reduced visibility 78—40662
E2, M1 multipole mixing ratios in odd-mass nuclei, $A>150$ 77—30503
E2 transition probabilities between Nilsson states, odd-A nuclei 77—57622
Earth crust, in situ stress in N. America, compilation 79—29728
Earth crust in situ stresses, tabulation and depth depend. 79—29729
Earth Resources Observation System Data Center for Landsat data 78—36289
earthquakes, instrumentally determined, in China, catalogue 79—12081
earthquakes, US catalogue for 1568-1850 period 80—21643
earthquakes in Japan, 1885 to 1925, catalogue of $M\geq6$ earthquakes and smaller, damaging, earthquakes *(Japanese)* 80—67341
eclipsing binaries, linearised limb-darkening coeffs. for light curves anal. 78—49480
eclipsing binaries in Scutum-Vulpecula regions, visual minima obs., 1920-1950 period 77—33564
elastic electron scattering, by atoms and molecules, momentum-transfer cross sections 79—25777
elastic moduli, Kroner limits of technically important materials, function of temp. *(German)* 79—28032
electric breakdown of gases, H, He, CO_2 *(French, English)* 77—76221
electrical resistivity, data tables, 1-2000K 79—78072
electron affinities 77—27194
electron bremsstrahlung energy spectra, 1 to 2000 keV, neutral atoms $Z=2$ to 92 78—62920
electron impact, intermediate-coupling strengths for fine struct. transitions 80—32837
electron inelastic mean free paths of solids, data tables 78—84686
electron repulsion integrals for p-block ats., teaching appl. 78—93494
electron spectroscoy of surfaces, quantitative, electron inelastic mean free path 79—92041
elementary particle properties, leptons, mesons, baryons 80—67944
elementary particle properties review, leptons, mesons, baryons 78—66179
elements with $Z\leq30$, core electron binding energies in free and standard state 77—43168
EM cascades in air, Pb, Fe and Cu, caused by 10-100 GeV electrons and photons 79—21120
EM depth sounding interpretation, master tables, book 80—86043
empirical data tables, equivalent transformation *(Russian)* 79—9208
energy levels, wavelengths and transition probabilities of Cu-like ions 80—37780
environmental radioactivity, meas. of water, soil, and foodstuffs 79—5378
EPR of transition metal, rare earth and actinide ions in solids 80—51968
EPR saturation transfer data, tape library 79—51841
ES type galaxies, UBV photometry obs. 80—73053
even-even nuclei, internal conversion coeffs. of 2^+-0^+ E2 transitions 80—9268
ferroelectric, Debye temp., tabulation of calorimetric values 78—51639
fission prod. conc., sensitivity anal. 78—82428
fission product gamma-ray and half-life $29\leq A\leq69$, data collection 78—50134
fission track data reports standardisation 80—31436
flame calculations, list of rate coeffs. 78—85160
fluid density bibliography, temp. range exceeding 40K 80—51980
formic (methanoic) acid, ideal gas thermodynamic props. 78—51275
formic acid (-d), microwave spectra and rot. consts., astrophysical appl. 80—91550
fourth row element ions, relativistic Dirac-Fock-Slater orbital binding energies, one-electron transition energies 79—25778
free neutrinos investigations, research installations 77—50336
galactic globular clusters, basic parameters 77—91593
galaxies in Virgo area, reduction of magnitudes to standard B_T system 79—92852
galaxy, spherical, obeying $r^{1/4}$ law, tables of physical functions 77—13454
galaxy clusters with known galaxy number-density distrib., data compilation 79—80362
gamma reactions initiated by polarised particles, Legendre polynomial coeffs. 80—73107
gamma-ray internal conversion coeffs. for all at. shells, $30\leq Z\leq104$ 79—45206
gamma-ray transition strengths of $A=6$ to 44 nuclei, data tables 80—37345
gamma-rays, half-life vs. energy map, photon activation anal. appl. 77—16883
gas, binary mixtures, diffusion coeffs. lists 78—34254
gas laser submillimetre wavelength tables, 34 μm to 1.965 mm 77—7095
gas phase reaction consts. for electronically excited species, relax. processes, data tables 80—16644
gaseous ions transport props., data tables 80—12857
gases, thermophysical props. tabulated for mixture composition certification 78—80818
geochemical data bank design and use 77—9508
geological history computation from field survey and map data in FORTRAN 77—9522
geology, adequacy of non-metric data 78—81413
geophysical data series, linear trend analysis 77—49151
geophysics information system automation *(Slovak)* 77—56735
globular clusters, structural parameters and integrated magnitudes 80—46623
gravity, meas. in junction between Japanese and Bonin Islands 77—78085

collections of physical data continued
halogens, diatomic isovalent sequence, free-mol. electronic transition intensity consts., systematics 78—42137
halomethanes, ideal gas thermodynamics props. 79—32733
halomethanes, liquid densities, data tables 78—75703
halomethanes, vap. press. and boiling point data tables 79—77736
heat and mass transfer data, book 78—154
heat capacities, molar, correlation coeffs., data collection 78—85188
heavy elements, $Z=84$-103, at. electron binding energies 79—31735
high temperature species, JANAF thermochemical tables, thermodynamic properties evaluation and compilation 80—41959
high temperature system characterisation, models, phys. and chem. reference data sources 80—41958
high-temperature thermal transport props., work of CODATA task group 77—45818
hydrocarbons, 30.4 nm He(II) photoelectron spectra 80—82589
hydrocarbons, second virial coeff., empirical eqn. 77—58831
hydrologic data set distribution functions, extremes and confidence intervals 78—24313
impurity hyperfine fields for Fe, Co, Ni, and Gd 79—99518
indentation hardness number conversion table analysis 79—11736
inert gases, diatomic isovalent sequence, free-mol. electronic transition intensity consts., systematics 78—42137
injected ion drift tube mass spectrometer ionic mobility data in non-parent gas 78—87428
insulators, phonon dispersion relations, book, showing curves for over 100 cpds. 80—51970
internal conversion coefficients, $30\leq Z\leq104$, Hartree-Fock-Slater model calcs. 79—36199
internal conversion coeffs. for at. numbers $Z\leq30$ 77—46136
internal conversion coeffs. for E5, M5 transitions, $30\leq Z\leq104$ 79—26396
interstellar molecular transitions, rest freqs. 80—62218
interstellar molecules, identified before 1979 Sept. 80—51852
85 Io, astrometric obs., 1865-1977, and definitive orbit 80—4284
iodides and mixtures, molten, elec. cond., density, viscosity, surface tension 77—80638
iodoethane, mol. parameters, vibr., pot. barrier height etc., data tables 79—76409
ion+molecule reaction rate coeffs., ions containing C and H, review 77—25260
ion induced γ-rays, thick sample reaction yields, energies, appl. in prompt nuclear anal. 78—62502
ions, H-, He-like, $Z=4$ to 34, wavelengths, radiative transition probabilities, autoionisation rates 79—25776
isomer shift reference scales, Mossbauer Effect Data Centre 80—37147
JANAF thermochemical tables, 1978 supplement 78—93637
Japanese Evaluated Nuclear Data Library, first version evaluation *(Japanese)* 78—74428
Japanese Islands region, geophysical data compilation *(Japanese)* 80—67332
K-shell internal conversion coeffs. for pure E2 transitions compilation anal. 79—75910
K-shell ionisation, X-ray or Auger-electron prod. by ion impact, cross section tables 79—54947
L-shell Coster-Kronig energies for atoms $Z=11$ to 103 77—83524
libraries of nuclear data *(Spanish)* 79—36120
light noble gases in chondrites, achondrites and ureilites, anal. compilation 78—65574
light-diffusing glass catalogue and basic operational characteristics 79—46019
linear accelerators in research use, 1976 compendium 77—5609
linear polarisation mixing coeffs. for mixed dipole and quadrupole γ-radiations, Compton polarimeter 80—73110
liquid water, viscosity, −8°C to 150°C, anal. of data 78—95101
lunar normal albedo, digital file from photographic data 77—78684
magnetic null line tables for elements of astrophys. interest 77—70998
mass spectra, mol. wt. from 186-273, EPA/NIH mass spectral data base vol. 79—68329
mass spectra, mol. wt. from 273-381, EPA/NIH mass spectral data base vol. 79—64120
mass spectra, mol. wt. from 30-186, EPA/NIH mass spectral data base, vol.I 79—64119
mass spectra, mol. wt. from 381-1674, EPA/NIH mass spectral data base, vol.IV 79—64121
materials handbook, industrial 78—56571
materials review of mech., corrosion, thermal, elec. props., appl., economics, design considerations 79—1818
Mercury, transits in 1677-1973 period, collected obs. of internal contacts 77—25964
metal ions, in unusual valency states, reaction rate consts. 79—47921
metal monolayers, on metal cryst. surfaces, surface struct., review 80—80067
metals, elec. resist., temp. depend. data 80—51967
meteorological data from DB1 data buoy in North Sea 79—21079
methane, dense gaseous and liq., thermal cond.-viscosity correlation, up to 500 atm., 95-500 K 77—80657
methane+$H(HO)(O)(O_2)$, H abstraction, rate consts. calcs. 78—95921
methane-ethane liq. mixture, phase equilib., heat of mixing, vol. change, data evaluation 80—15233
methanol, and $-d_{1,3,4}$, thermodynamic props. struct. and spectroscopic data 77—39396
methyl formate, microwave spectra, rot. consts., moments and struct., radio astronomy appl., review 80—17637
mixed halide melts, elec. cond., surface tension, density and viscosity, tables 79—60531
molecular vibr. freq. tables, up to 13 atom mols., and Raman and IR values 77—79614
Mossbauer atoms, electron densities at nuclear centre and surface, calcs. using Dirac-Fock eqn. 80—74100
Mossbauer Effect Data Centre 80—37148
Mossbauer isomer shift, energy equivalents of one mm/sec, tabulation, book contrib. 79—87365
Mossbauer isomer shift expressions tabulation of consts., book contrib. 79—87367
Mossbauer isomer shift reference scales, book contrib. 79—87368
Mossbauer source preparation, tabulation, book contrib. 79—87366
Mossbauer transition characts. tabulation book contrib. 79—87364
motorway free-flow traffic noise obs. 78—90591
MSDC/EPA/NIH mass spectral search system 78—65912
muonic atoms, energy-level values, electrodynamic corrections 78—62956

collections of physical data continued
- naphthalene, and d_4 and d_8, vibr. anal. using best struct. and spectroscopic data 79—76410
- neutron effective resonance energy values for 96 isotopes 80—71978
- neutron induced fission prod. yields, tabulation 78—25253
- neutron induced reactions on $36\leq Z\leq 83$ targets, tables of cross sections and reaction rate factors 77—46162
- NMR, wide-line, investigation of inorganic and organic solids, reference list 79—19786
- noctilucent clouds, W.Europe during 1978, summary of obs. 80—12510
- noctilucent clouds over W.Europe (during 1979) 80—109289
- non-closed shell many-electron-theory at. charge wavefunctions, Be through Ne and Si 77—57849
- nonlinear crystals for frequency conversion of optical radiation, review *(Russian)* 80—38068
- nonlinear optical props. of uniaxial crystals 77—75615
- nuclear and atomic data sources 79—25081
- Nuclear Code Centre, Japan, history, activities *(Japanese)* 79—13618
- nuclear data files of UK Chemical Committee, summary of data, available in ENDF/B format 78—82425
- nuclear data for space technology 78—82407
- Nuclear Data Library KEDAK-3, reevaluations of ^{238}U, ^{239}Pu 77—23042
- nuclear data sheets, 1978 recent references cumulation 79—80862
- Nuclear Data Sheets, computer-readable form 77—22828
- nuclear data sheets, levels, J^π, transitions for $A=212$ 80—31430
- nuclear data sheets, levels, J^π, transitions for $A=221$ 80—31431
- nuclear data sheets, levels, J^π, transitions for $A=225$ 80—31432
- nuclear data sheets, levels, J^π and transitions for $A=204$ 80—31429
- nuclear data sheets, levels, J^π and transitions for $A=71$ 80—31428
- nuclear data sheets, levels, J^π and transitions for $A=73$ 80—101673
- nuclear data sheets, levels, J^π and transitions for $A=77$ 80—105439
- nuclear data sheets, levels and transitions for $A=140$ 80—31435
- nuclear data sheets, levels and transitions for $A=60$ 80—31433
- nuclear data sheets, levels and transitions for $A=64$ 80—31434
- nuclear data sheets, recent references, Jan. to April 1979 80—5039
- Nuclear Data Sheets, recent references 77—71551
- nuclear data sheets for $A=109$ nuclei 79—9441
- nuclear data sheets for $A=110$ 78—66189
- nuclear data sheets for $A=195$ to Jan. 1978 79—17781
- nuclear data sheets for $A=205$ nuclei 79—9442
- nuclear data sheets for $A=237$ to November 1977 78—82267
- nuclear data sheets for $A=241$ to November 1977 78—82268
- nuclear data sheets for $A=45$ 78—66187
- nuclear data sheets for $A=47$ 78—66188
- nuclear data sheets for $A=51$ nuclei 79—9440
- nuclear data table preparation 79—75812
- nuclear data tables, May to August 1979 references 80—41953
- nuclear data tables, recent references May-Aug 1978 79—30773
- nuclear decay data, ENDF/B file, applications 77—22978
- nuclear energy level transition probabilities for even-even nuclei 79—6406
- nuclear energy levels and structure in $A=16$, 17 nuclei 77—46116
- nuclear gamma-rays from energetic particle interactions 80—18219
- nuclear magnetic moments 79—54407
- nuclear medium energy data library 77—18765
- nuclear moments and moment ratios determ. by Mossbauer spectroscopy 77—22885
- nuclear physics recent references (May-August 1977) 79—441
- nuclear pion absorpt. data compilation 77—18619
- nuclear reaction and scatt. differential cross sections meas. by SPES I 79—75983
- nuclear separation and alpha- and beta-decay energies, 1977 at. mass evaluation tables 78—4895
- nuclear spin and moment data tables 77—22881
- nuclear structure, even-even nuclei, quasi-bands 78—82265
- nuclear structure data for $A=148$ nuclei, level props. 77—67697
- nuclear structure data for $A=56$ nuclei, level props., from ENSDF 77—74743
- nuclear structure data for $A=57$ nuclei, level props., from ENSDF 77—74744
- nuclear structure data sheets, 1979 recent references, cumulation 80—94930
- nuclear structure data sheets (July 1979) for $A=213$ 80—67942
- nuclear structure data sheets (July 1979) for $A=217$ 80—67943
- nuclear structure data sheets for $A=141$ to 01 Sept 1977 79—13184
- nuclear structure data sheets for $A=54$ to Dec. 1977 79—17780
- nuclear structure data sheets for $A=63$ (July 1979) 80—67941
- nuclear structure references 1975-7 79—30772
- nuclear-reaction and separation energies, 1977 at. mass evaluation 78—497
- nuclei, $A=32$ to 140, nuclear struct., binding energies, dipole moments *(French)* 77—46098
- nuclei, even-even, $58\leq A\leq 150$, E2, M1 multipole mixing ratios 78—50118
- nuclei with $A=194$, review of struct. information to July (1977) 78—89769
- nuclei with $A=207$, review of struct. information to August (1977) 78—89770
- nuclei with $A=209$, review of struct. information to September (1977) 78—89771
- nuclei with $A\leq 57$, E2, M1 multipole mixing ratios 80—22751
- nucleon-nucleon scattering, radiative corrections 79—26335
- OB-type stars, effective temps., ang. diameters, distances and linear radii 80—17584
- oceanographic data, global analysis 78—65316
- odd mass nuclei, $59\leq A\leq 149$, E2, M1 multipole mixing ratios 78—4911
- optical glass, laser induced destruction, table of data for 87 glasses *(German)* 77—75631
- optical glass, refr. index tables and calcs. for optical designer 80—83650
- organic compounds, crit. temps. correl. with boiling pts. 78—91421
- organic compounds, hydrolysis in water, rate consts. 78—76856
- organic liquids, optical anisotropy, tabulation for 25 liqs. *(French)* 77—59548
- organic molecules, UV photoelectron spectroscopy, systematic review 80—28057
- oscillator strengths for transitions in Be I, B I, C I, N I and O I isoelectronic series 80—37779
- oxide hydrides, oxide halides and hydroxide halides, cryst. struct. data tables, book *(German, English)* 80—51971

collections of physical data continued
- oxo-compounds of halogens and Xe, cryst. struct. data tables, book *(German, English)* 80—51971
- ozonograms, Oct.-Dec. 1978, Uccle, Belgium *(French, Flemish)* 80—21797
- palaeomagnetic directions and pole positions, pole nos. 15/1 to 15/232 78—28160
- palaeomagnetic directions and pole positions (pole numbers 14/1 to 14/574) 77—48993
- palaeomagnetic pole positions and palaeomag. directions, pole numbers (16/1 to 16/296) 80—72415
- palaeomagnetism, Cainozoic results, 1927-75 catalogue 77—52978
- Palaeozoic base maps, palaeogeography and plate tectonics 80—41441
- Pand S-phase data from local earthquakes, California, 1966-75 period 79—12088
- particle stopping power and range data compilation committee 80—9478
- phenol, ideal gas thermodynamic props. 78—75250
- photoabsorption cross sections for positive atomic ions with $Z\leq 30$ 80—26727
- photochemical data and kinetics of gas phase chemical reaction in atmosphere 80—101671
- photoelectric photometry obs. of globular star clusters 80—67800
- photoionisation and photoabsorption cross sections of He, O, N_2 and O_2 for aeronomic calcs., data tables 80—41599
- photonuclear data index 1973-1977 79—6568
- photonuclear reactions, differential polarisation coeffs. 78—4926
- physics fundamentals, 1973 CODATA-recommended values 77—57298
- pion-nucleon scattering, radiative corrections 79—26335
- plasma, radiative cooling rates, high-temp. low-density plasma $2\leq Z\leq 92$ 78—83534
- plastics and reinforced plastics, tabulated data as design guide 77—21087
- polyatomic chain molecules, vibr. freqs. 79—31731
- polyatomic mol. gas phase spectra, struct., review and tabulation 80—14136
- polyethylene, vibr. data and force field consts., review 79—31750
- positron-annihilation, Doppler broadened line shapes 79—19947
- practicing scientist's handbook 80—2
- propyne, microwave spectra and mol. consts., rot. anal. 79—76411
- pulsar radiation at 430 MHz, statistical summary of polarization 80—67760
- pulsars, obs. data for 147 known objects 77—9763
- radiation dosimetry, standardised radioactive decay data sets 80—13945
- radiation shielding benchmark experiments and sensitivity studies, neutron plus gamma library 77—26947
- radio sources, variable, data base of obs. (August 1966 to June 1972) 78—16552
- radioactive nuclides, quantum radiation, data handbook 80—94933
- radioisotope dosimetric data tables 80—105438
- raindrop induced forward and backward scattering amplitudes 79—34884
- rainfall and temp. anomalies, 1891-1975, for European USSR, N.Kazakhstan, and W.Siberia 79—39826
- rare earth elements, atomic energy levels, data tables 78—86805
- rare earth intermetallic compounds, ferromag. props., book contrib. 80—75726
- ratio of $\Delta\langle r^2\rangle$ for pairs of elements with analogous electronic structure, tabulation, book contrib. 79—85410
- ratios of $\Delta\langle r^2\rangle$ for two transitions in the same element or nuclide, tabulation, book contrib. 79—85409
- reactivity calc., cross-section library inadequacy 79—9697
- reactor design performance calc. improvement by data adjustment 79—9698
- relativistic electron transition operators, matrix elements 77—30822
- relativistic energy operator, matrix elements, complex electronic configs. 77—30792
- rocks and minerals, lattice conds. at mantle press. and temp. 78—69338
- row element ions 79—25778
- satellite data applications to marine activities 78—36439
- satellite data availability from Environmental Data Service 78—36288
- Saturn's satellites, surfaces and interiors present knowledge 80—4297
- seismicity of Central Asia, historical and modern data 80—36254
- selective information distribution system for international scientific cooperation *(Russian)* 79—179
- semileptonic weak and EM interactions, multipole operators, HO single particle matrix elements 80—73840
- sintering, 1958 to 1973 77—73245
- solar 810 MHz bursts in 1957-67 period, obs. data 77—33446
- solar abundance data for 67 elements 77—53542
- solar neighbourhood C and M-type stars 79—16946
- solar radiation data base for geographic distrib., USA 77—29413
- solar radiation data base using bright sunshine data approach 77—25763
- solar system, numerical values of consts. of IAU Commission 4 Working Groups Joint Report 78—40845
- solar UV continuum, absolute intensities, centre to limb vars. and Laplace inversion between 1400 and 2100 Å 79—62803
- solar weak Fraunhofer lines, effective form. depths tables *(Russian)* 79—44439
- space groups, tables of irreducible representations, construction and use 77—68938
- spectral classification of early type stars using UV line features 80—72927
- spectral lines in inductively coupled plasma-atomic emission spectroscopy 79—83519
- spectroscopic factors for single-nucleon transfer in $A=21$-44 region 77—71563
- stellar data, conf. (Strasbourg, France, 19-21 Aug. 1976) 77—78828
- Stellar Data Centre, Strasbourg, data surface distribs. on celestial sphere 77—2423
- stellar spectra, Fe lines equivalent widths in cool standard stars for spectral anal. 77—78771
- stopping powers of H in all elements, book 78—26607
- stratosphere, 1955-75 catalogue of perturbing influences on O_3 conc. 80—41502
- streamflow, empirical data, multivariate gamma distrib. fitting 78—81240
- streamflow data network design, economics of resource information systems 77—73893
- superconducting materials, table of props. 77—4460
- supernovae, type I, list of 44 objects, luminosity peak as secondary distance indicator *(French)* 78—4257
- surface tension, pure liqs., temp. depend. correl. 78—91512
- terrestrial meteorite impact structures, catalogue of 230 sites 77—73741

collections of physical data continued

- thermonuclear reaction rate data for intermediate mass nuclei 80–31427
- thermonuclear reaction rates, thick target meas. 80–73108
- thermophysical process ambiguous data gathering and processing optimisation *(Russian)* 80–73335
- toluene, tables of thermodynamic props. 77–24419
- transition metal, polynary oxocompounds, struct. data, book 78–51521
- TRIAD computer file, Tucson revised index of asteroid data 78–45261
- tropical winds, anal. and data listings 79–39787
- two-particle fractional parentage coeffs. 77–41905
- ultrasonic materials testing reference blocks and transducers, survey 78–68858
- underground nuclear explosions since 1963, in book 79–681
- US National Earthquake Information Service seismic data acquisition 77–29446
- US props of mammalian tissues 78–88727
- US vel. and atten. in mammalian tissues 78–57044
- US velocity and attenuation data in mammalian tissue, survey 80–46744
- USA Energy R&D Administration effluent date collection and reporting system 79–13545
- USSR-East German joint optical glass catalogue 79–76775
- vapour liquid critical pressures and volumes 79–99306
- vapour-liquid pipe flow, data bank of expt. data *(German)* 79–41739
- velocity parameters of atoms HF wavefunctions 77–71744
- vinyl cyanide, microwave spectra data tables 79–59445
- visibility var. over SW.United States, historical databases of pollution effects 80–21424
- water equation of state, between 350 and 1000°C (0 to 10 GPa) and between 100 to 350°C (200 MPa to melting curve) 80–15214
- water/steam systems, thermodynamic data tables 78–26679
- wind, speed and direction in Belgium, 1963-1972 obs. *(French, Flemish)* 77–87053
- work function of elements and its periodicity 78–19124
- X-ray diffr. powder phase identification, manual computer search techniques 77–70387
- $Z=95$ to 130, calc. of K- and L-X-rays binding energies 77–83525
- $K^{\pm}$ induced interactions, integrated cross sections, compilation 80–439
- π induced interactions, compilation of integrated cross sections 79–89187
- $\pi^- p \rightarrow \pi^0 n$, polarisation meas. 617 to 2267 MeV/c 79–9401
- $A=101$ nuclei, nuclear struct. data sheets to May 1979 80–41954
- $A=103$ nuclei, nuclear struct. data sheets to July 1979 80–41955
- $A=196$ nuclei, nuclear structure data sheets to Sept. 1978 80–41956
- $A=200$ nuclei, nuclear struct., data sheets to Nov. 1978 79–71778
- $A=206$ nuclei, nuclear struct. data sheets to July 1978 79–71779
- $A=229$ nuclei, nuclear struct. data sheets to March 1978 79–26361
- $A=233$ nuclei, nuclear struct. data sheets to March 1978 79–26362
- $A=49$ nuclei, nuclear struct. data sheets to Dec. 77 79–26360
- $A=62$ nuclei, nuclear data sheets to August 1978 79–71777
- Ag, projectile range for $Z=8$-20, 0.0125-12.0 MeV/nucleon 78–83856
- Al I to XIII, energy levels and ionisation energies, data compilation 80–14100
- Ar, absolute photoionis. cross sections for VUV regions 77–46547
- As VI, VII, spectra 100 to 300 and 500 to 1200 Å ranges 80–83307
- Au, projectile range for $Z=8$-20, 0.0125-12.0 MeV/nucleon 78–83856
- B, atomic spectra and energy level data tables 79–59386
- $^{10}B(n,\alpha)^7Li$, 10 keV to 1 MeV, review of cross section meas. 79–9587
- Ba, electrical resistivity; 1-1000K, data tables 79–78073
- $BaTiO_3$, thermodynamic props. 77–39680
- Be, atom, ground state, accurate CI wavefunction 77–42245
- Be, electrical resistivity; 1-1000K, data tables 79–78073
- Bk, emission spectrum, 2540-9800 Å, electrodeless lamp source 80–27970
- C_2, IR flame emission spectra, Ballik-Ramsay system 79–63999
- CO, fourth positive system in 1115-4759 Å range 77–49291
- ^{13}C-^{13}C spin-spin coupling consts., data compilation, meas. and appls. review 80–17725
- Ca, electrical resistivity; 1-1000K, data tables 79–78073
- Ca I to XX, energy levels and ionisation energies, data compilation 80–14101
- CaCl, aq., mean activity and osmotic coeffs., free energy, 298.15K 77–81411
- $^{139}Ce \rightarrow {}^{139}La$, internat. comparison of activity meas. March 1976 79–13613
- $ClNO_x(x=1,2,3)$, phys. and chem. data 78–27727
- ClO_x, reaction rate consts., atmospheric gas phase reactions, review 77–81390
- ^{244}Cm, emission spectrum, 2400-11200 Å, wavelengths, rel. intensities, Zeeman effect 77–46514
- C(n,n), total cross sections below 2 MeV, R-matrix fits to data 80–13466
- Co bi-univalent cpds., soln., activity coeffs., osmotic coeffs., water activity, Gibbs energy, molality depend. 80–51963
- ^{59}Co NMR line breadth and chemical shift data compilation *(Japanese)* 78–15045
- Cr, atomic transition probabilities, oscill. strengths 78–74601
- Cr I to XXIV, energy levels, ionis. pots., g-factors, from spectral data review 77–79556
- Cu and Cu alloys, diffusion in systems involving group VA elements, review 77–39697
- Cu bi-univalent cpds., soln., activity and osmotic coeffs., H_2O activity, Gibbs energy, molality depend. 80–51964
- Cu, γ-ray absorption cross-sections, 10-160 MeV 78–90136
- Cu, projectile range for $Z=8$-20, 0.0125-12.0 MeV/nucleon 78–83856
- Cu-Ag-X, X=metals, P, S, Se, phase diagrams and thermodynamic props., iso-activity coeff. curves 77–81249
- DT^+, adiabatic relativistic rot.-vibr. energy levels 77–57964
- Dy III lines in spectra of Ap and Bp stars 80–12764
- Fe II, oscill. strengths, astrophys. appl. 79–59398
- Fe III in astronomical sources, multiplet table 80–41732
- Fe, projectile range for $Z=8$-20, 0.0125-12.0 MeV/nucleon 78–83856
- Fe VIII to Fe XXVI, wavelength tables *(Japanese)* 79–13661
- $FeCl_2$, soln., activity coeffs., osmotic coeffs., water activity, Gibbs energy, molality depend. 80–51963
- FeVIII-XXVI energy level tables and Grotrian diagrams 80–74142
- H II regions, line intensity data compilation 79–88721
- H to Ca, leading atomic lines, solar spectra 79–25560
- H-like ions, departure coeffs. from thermodynamic equilib., rel. to radio-sources recomb. lines 79–76369
- H_2, photoionisation cross-sections, involving vibr. states, data tables 79–18242

collections of physical data continued

- HD^+, HT^+, adiabatic relativistic rot.-vibr. energy levels 77–57964
- HI 21 cm line survey of M31, contour maps, vel. profiles 80–73038
- H_2O^+, electronic spectrum, wavelengths and wave numbers of assigned levels 77–473
- He, absolute photoionis. cross sections for VUV region 77–46547
- He ion stopping powers and ranges in all elements 78–58565
- He isoelectronic sequences, screening constants, ground and excited states 78–62701
- He isoelectronic series, energy level and classifications of doubly-excited states 78–62736
- He, lifetimes of doubly excited states, autoionisation and radiative decay 79–18146
- $He+H^+$, electron ejection differential cross sections 77–46625
- ^4He, superfluid, steady state, at atm. press., practical data 79–60565
- ^4He, superfluid, thermodynamic props. 77–39708
- HfI, at spectrum, g-values, Zeeman effect, LS-coupling, ionisation pot. 77–3292
- I_2, molecular absorption spectra, line identification band atlas, 19000 to 18000 cm^{-1} 78–42079
- K I to K XIX, energy levels, tabulated data 80–51966
- Kr, absolute photoionis. cross sections for VUV region 77–46547
- Kr I spectra, transition probabilities and lifetimes 79–54793
- Li isoelectronic sequence, oscill. strengths 77–3309
- Li isoelectronic sequences, screening constants, ground and excited states 78–62701
- Li-like ions K...Fe, survey table of wavelengths in X-ray region 77–79569
- Mg, electrical resistivity; 1-1000K, data tables 79–78073
- Mg, I-XII, energy levels and optical spectra 80–87065
- Mn, atomic transition probabilities, oscill. strengths 78–74601
- Mn bi-univalent cpds., soln., activity and osmotic coeffs., H_2O activity, Gibbs energy, molality depend. 80–51964
- Mn, energy levels, Mn I to Mn XXV 78–21841
- N_2, N_3, spectroscopic data review 77–38680
- NH_3, thermodynamic props., anal. of data 78–93636
- Ne, absolute photoionis. cross sections for VUV region 77–46547
- Ni bi-univalent cpds., soln., activity coeffs., osmotic coeffs., water activity, Gibbs energy, molality depend. 80–51963
- Ni, projectile range for $Z=8$-20, 0.0125-12.0 MeV/nucleon 78–83856
- O VI, O VII, O VIII, energy levels and multiplet tables 80–930
- O_2, density of solid in equilib. with vapour 78–93656
- O_3, in lower atmos., Uccle, Belgium, April-June 1979 obs. *(French, Flemish)* 80–98385
- O_3, in lower atmos. Jan.-March 1979, obs. over Uccle, Belgium *(French, Flemish)* 80–94571
- OH radicals, microwave spectra data tables 78–50542
- Pb bi-univalent cpds., soln., activity and osmotic coeffs., H_2O activity, Gibbs energy, molality depend. 80–51964
- Pb, γ-ray absorption cross-sections, 10-160 MeV 78–90136
- Pt metals, lattice parameters, densities and atomic vols., tabulation 79–65033
- $(Pu,U)O_2$, <5 wt.% PuO_2, criticality data generated by SU-HAMMER 79–3198
- Ra, electrical resistivity; 1-1000K, data tables 79–78073
- Sc I to Sc XXI, energy level tables derived from atomic spectra anal. 80–101672
- $SiCl_4$ physical and thermodynamic properties, rel. to Si technology 79–65218
- SiS, and isotopes, microwave spectra and consts., review 77–23493
- Sn, γ-ray absorption cross-sections, 10-160 MeV 78–90136
- Sr, electrical resistivity; 1-1000K, data tables 79–78073
- $SrTiO_3$, thermodynamic props. 77–39680
- Ta, γ-ray absorption cross-sections, 10-160 MeV 78–90136
- Th II, oscillator strengths calc. 80–27982
- Ti alloys, data handbook of low temp. mech. and phys. props. 80–22153
- Ti, atomic energy level data tables, Ti I to Ti XXII 79–59385
- Ti, projectile range for $Z=8$-20, 0.0125-12.0 MeV/nucleon 78–83856
- U bi-univalent cpds., soln., activity and osmotic coeffs., H_2O activity, Gibbs energy, molality depend. 80–51964
- U II, oscillator strengths for calibration 77–42280
- UO_2-water tightly-packed lattices, ENDF/B-IV data evaluation 79–9805
- ^{233}U-Th fuel cycle, review of fast integral data 79–67834
- $^{233}UO_2/ThO_2$ water-moderated lattice analysis with ENDF/B-IV data 79–9800
- V, atomic energy levels in all stages of ionisation, data anal. 78–94207
- V, atomic transition probabilities, oscill. strengths 78–74601
- Xe I spectra, transition probabilities and lifetimes 79–54793
- YbI, first spectrum, wavelengths and intensities, Zeeman effect 79–3389
- Zn, elastic properties, compilation and review 78–27551

collective accelerators

- 5 MeV electron accelerator, modulator charging system upgrade 80–23182
- accel. of projectiles to hypervelocities using series of imploded annular plasma discharges 80–74042
- Auto-Resonant acceleration, computer simulation of linear and nonlinear wave growth phenomena 80–9439
- Auto-Resonant acceleration of ions, theoretical research program, review 80–5411
- Auto-Resonant accelerator, steady-state conceptual design, 30 to 1000 MeV, 1000 mA 80–5410
- Auto-Resonant accelerator electron beam generator, performance characts. 80–5413
- Auto-Resonant accelerator experimental program, review 80–5412
- autoacceleration process for generation of high current relativistic electron beams 80–14011
- autoacceleration via virtual cathode oscillation 79–72026
- autoaccelerator concept at NRL 79–72021
- autoaccelerator dynamics and stability 80–14012
- autoresonant acceleration, numerical simulation of cyclotron waves 79 72022
- autoresonant accelerator, lower bound for length 78–50419
- autoresonant accelerator, nonlinear characts. of cyclotron waves 80–13993
- autoresonant accelerator, slow cyclotron wave growth by periodic inductive structures 80–13994
- autoresonant collective ion accelerator, wave amplitude var. and energy flow 79–76176
- book 80–865

collective accelerators continued
- charged transmission line for pulsed high current accelerators, energy transfer 78—78519
- coaxial autoaccelerator, klystron instability of relativistic electron beam, stability criterion 78—82541
- coaxial autoaccelerator, resonant instabilities of relativistic electron beams 78—82540
- collective ion acceleration, by temporally modulated relativistic electron beam 78—50422
- collective ion acceleration and intense electron beam propagation within an evacuated dielectric guide 80—14002
- conference, Irvine, CA, USA (May 1978) 80—4479
- crystal, laser longit. polarisation wave, collimated charged particle accel. 80—32542
- current status 79—76161
- cyclotron resonance, Doppler effect, anomalous, amplification of slow waves in electron beam, obs. 80—78463
- dense plasma, coaxial acceleration and plasmochemistry *(Russian)* 78—92482
- dielectric guide controlled collective ion acceleration 80—14001
- electron accelerator, high-current, high pulse, inductive energy storage 78—46189
- electron accelerators, pulsed power technology for fusion expts. 78—50321
- electron and ion beam generation at high power, review 80—13988
- electron beam propagation in dielectric guide due to space charge neutralisation, surface flashover 80—18716
- electron beams, relativistic, striations in density distrib. rel. to plasma column instability 80—24154
- electron collective acceleration 79—76166
- electron guns, high-current, laminar beam formation 78—74516
- electron pulsed high current nanosecond accelerator 78—826
- electron-ion ring, stationary state 80—106217
- Experimental Test Accelerator, off-resonance transformer charging for 250-kV water Blumlein 80—23183
- field reversing E-layers, translation and compression in magnetically insulated diode 80—14017
- focusing ion accelerator based on HIPAC concept 80—14014
- foilless diodes, hollow relativistic electron beam generation 79—76170
- future technologies in high-energy physics, collective accelerators, laser accelerators, single-pass collecters 80—78466
- gyrating electrons, cylindrical layer, in open periodic struct., impedance 80—18719
- heavy ion acceleration, time-depend. study, fusion ignition appl. 80—86997
- heavy ion capture and accel. using relativistic electron beam and strong mag. field 80—9436
- heavy ion collective acceleration, ion beam front velocity 80—32539
- heavy ion collective acceleration, problems and prospects, review 80—14013
- heavy ion collective acceleration at Univ. of Maryland 79—76163
- heavy ion toroidal collective accelerator 78—33334
- helix controlled collective ion acceleration 80—14009
- high current medium energy ion accelerator with annular electron beam 79—97913
- high current short bremsstrahlung pulse sources 80—5400
- high-current pulsed linear ion accelerators, insulated drift tube 78—50417
- hollow-beam accelerator, with phase focusing, limiting current 79—18065
- induction accelerator charact. meas. instrument 78—5073
- induction accelerators made from pulse-line cavities with external pulse injection 79—76180
- induction linac, high power 79—49878
- induction linac for heavy ions, pellet-fusion appl., design/cost study 79—67982
- induction linear accelerators and their applications 79—67989
- intense relativistic electron beams for collective ion acceleration 80—13996
- ion acceleration and intense electron beam propag. in vacuum dielectric channels 80—14003
- ion acceleration controlled by a gas gradient 79—76169
- ion acceleration from rotating relativistic electron beam injection into neutral H 79—76167
- ion acceleration in a gas by high-current electron beam pinch 80—14000
- ion acceleration in diode with insulated anode 80—14005
- ion acceleration in vac. system with insulated anode 79—72025
- ion acceleration in vacuum by linear electron beam 79—85833
- ion acceleration with an intense REB in a periodic waveguide 79—72018
- ion acceleration with linear electron beams, book contrib. 80—866
- ion autoresonant acceleration, numerical simulation 78—21789
- ion beam production, high current in triode 80—99372
- ion beams from pulsed linear accelerator for inertial fusion 78—50325
- ion burst accel. and prefocusing using rel. electron beam interactions 80—14008
- ion collective acceleration, rel. to relativistic radially inhomogeneous electron beams 79—50201
- ion diode, dual current feed magnetically insulated for internal confinement fusion studies 79—93851
- ion source and injector for a heavy-ion cyclotron 79—54618
- ionisation front accelerator using intense relativistic electron beam, experimental feasibility program 80—13998
- ionised front accelerator, controlled beam front motion expts. 79—72019
- ions, collective acceleration in linear electron flow *(Russian)* 78—90001
- linear acceleration of ions using the collective interaction, theory 80—5402
- low acceleration in a gas gradient, ion energy dependence 80—18723
- Luce diode, acceleration mechanisms in single and multiple stage collective vacuum diodes 79—76168
- magnetically insulated diode, characts. of hollow electron beam 80—5398
- magnetically insulated diode, controlling hollow electron beam current with shielding beam 80—9437
- magnetically insulated diodes for prod. of intense proton beams 80—14004
- magnetostatic system of the collective electron ring accelerator 80—5407
- metallic ion collective accel. 80—74040
- multiple stage accelerator concept for rel. electron beam-powered collective ion acceleration 80—13999
- multiply charge of beams in linear accelerator with variable-phase focusing, general soln. 80—13992
- phase modulated collective ion accelerator 79—72017

collective accelerators continued
- plasma accelerator, linear rail type, plasma cluster ionised front vel., theory 79—46494
- power balance limit to intense relativistic electron beam front velocity 80—13997
- PR1590 Marx-Blumlein machine using dielectric anode 80—14006
- prepulse discharges in high current accelerator diodes with double shaping line 80—5399
- proton acceleration in system with insulated anode 79—31246
- proton collective acceleration using reflecting electron systems 80—14010
- 'Pulsed ferrite core tests for 50-ns linear induction accelerator' 79—690
- radiative collapse of a relativistic electron-positron plasma to ultrahigh densities 80—14929
- rectangular waveguide, Cherenkov radiation source 80—99373
- relativistic beam injection into drift cavity, pot. profile finite size particle calc. 80—18987
- relativistic electron beam, propag. in vac., ion accel. from anode plasma 80—47790
- relativistic electron beam accelerator, FX-75, 1-D coaxial transmission line model, FXPULSE program 78—58506
- relativistic electron beam interaction with apertured solid dielec. anode 80—14007
- relativistic electron beams, collective acceleration, beamfront velocity effects 80—75063
- relativistic electron beams with finite energy spread and improved emittance, development and investigation 80—91741
- relativistic stabilised electron beam in toroidal geometry 80—5401
- resonant transformer accelerators, beam instabilities 79—76174
- review of current status 80—5394
- space charge waves and collective ion acceleration 80—13995
- steady state autoresonant accelerator, 30 to 1000 MeV 79—49879
- superconducting resonators and solenoids, Q-values and field profiles 78—46188
- superconducting solenoids, resonators and cryogenic system 78—46187
- toroidal collective focusing accelerator for heavy ion acceleration 80—14015
- undulator linac, electron dynamics, coherent radiation source 78—82539
- vacuum diode, cathode plasma dispersion in transverse mag. field *(Russian)* 79—98997
- virtual cathode formation for collective-effect electron acceleration 80—14016
- waveguide containing relativistic electron beam, slow cyclotron wave 80—106983
- X-ray diagnostics on collective heavy ion electron ring accelerators 80—102358
- C ions, accel. to 170 MeV by electron beam 80—9433
- N ion acceleration expts. at JINR 80—5406

collective states, nuclear *see nuclear collective states and giant resonances*

collimators (optical) *see optical collimators*

collision processes
- *see also atom-surface impact; atomic inelastic collisions; charge exchange; chemical reactions; elastic scattering of atoms and molecules; elastic scattering of electrons by atoms and molecules; electron attachment; electron impact; elementary particle interactions; intermolecular mechanics; ion-surface impact; molecular inelastic collisions; molecule-surface impact; negative ions; Penning ionisation; plasma collision processes; potential energy surfaces for collision processes; quantum field theory; quasimolecules; radiation quenching*
- 1008—3814, southern ring galaxy in Vela, struct. rel. to collision with companion 79—58413
- achondrite meteorites, mag. effects of brecciation and shock 80—8603
- aerosol particle-small ion combination coeffs., size depend. 77—25320
- aerosols, highly dispersed, with elec., acoustic fields, collision rates 79—47986
- aerosols, particle-droplet inertial collisions 79—47989
- agglomeration, computer simulation *(Japanese)* 78—95706
- agglomeration, Monte Carlo simulation *(Japanese)* 78—95707
- aligned triple collision in celestial mechanics, new study *(French)* 78—85832
- angular entropy, information content of mol. scatt. ang. cross section 77—54583
- anharmonically coupled oscillators, semiclassical calcs. of eigenvalues 80—95514
- artificial satellites, collision freq. and debris belt creation 78—89035
- asteroidal belt, primaeval collisional process rel. to orbital characts. 79—8874
- asteroids, collisional disruption rel. to Fe meteorites cosmic ray exposure ages distribs. 79—30015
- atmospheric aerosol, particle collisions with cloud drops, effects of elec. fields and charges 77—25748
- atomic, and applications, book 77—27136
- atomic, two-state approximation in the adiabatic and sudden-perturbation limits 79—22780
- atomic collisions, post-adiabatic anal. 77—14515
- atomic four-body problems, Faddeev eqns. in momentum representation 79—59524
- atomic scattering computations, book contrib. 77—30946
- Bethe approximation 79—18249
- binary, approx. trajectories calc. 78—46413
- binary cascade models, up to 1 keV comparison of many body problems 78—29051
- bouncing ball experiment, theory of time of flight, for teachers 79—71196
- celestial mechanics, numerical simulation of systems of colliding bodies in gravit. field 77—29634
- celestial mechanics, statistical mechanics of Keplerian orbits in collisional systems 78—20625
- chemical reactions and reactive collision phenomena, props. of stochastic process description 78—60991
- classical deflection angle for 2 colliding particles, numerical calc. 77—58113
- classical theory, review 78—33563
- classical theory of collisional entropy production 79—10162
- classical trajectory calcs., empirical testing of nonrandom integration method 78—50607
- classical trajectory equations, integration by propagator method 77—57233
- classical trajectory model for electronically nonadiabatic collision phenomena 79—18248
- classical trajectory theory, choice of phase 77—50486

collision processes continued
cloud droplets, collisional problem in turbulent environment 77—5293
colliding bodies systems in gravit. field, effect of transversal viscosity 77—67026
Condon reflection principle in collision dynamics 78—46414
cosmic rays, applicability limits of quasilinear approximation to kinetic eqn. 77—91383
cosmology, bound condensations collisions rel. to struct. development in expanding model 78—93489
coupled attractive square well pots., exactly soluble model, multichannel calc. 77—42368
coupled space-time dependent scattering equations, semiclassical Magnus approx. 77—23529
curve-crossing collisions, scatt. matrx. 78—70891
diatomic mol. scatt., Schrodinger eqn. phase shift differences for some trigonometrical potentials 80—43132
dispersed flow, particle collisions in concurrent dispersed flows 77—15101
E-region of ionosphere, effective electron collision frequency 79—58153
Earth-comet close approach, rel. to ice ages and ecological catastrophes 78—53714
Earth/comet collision, rel. to Earth albedo sudden change and ice age onset 79—44241
Earth/comet collisions, rel. to origin of terrestrial life 78—73660
education, binary elastic collision in rel. space, isosceles trapezoid representation 78—61981
elastic bodies, nonlinear surface waves *(Ukrainian)* 79—32331
elastic collisions, theory 77—67264
elastic linear collisions, dynamic solns., for teaching 80—17769
elastic scattering of low energy neutrinos by atomic systems *(Russian)* 77—83754
elastic three-body linear collision, inverse scatt. problem, for teaching 79—35468
electron collision frequency in equatorial electrojet, comparison of models 78—36372
electron-molecular ion scatt., appl. of Schwinger variational principle 80—48086
electronic degrees of freedom, derivation of classical model via spin analogy 79—98192
energy transfer rate consts., reverse reaction effect 77—65520
entropy and chemical change, dynamical and information theories, maximal entropy procedure 78—27740
Faddeev equations, off-shell matrix elements evaluation 77—67336
fine particles clustering, experiment 80—26937
galaxies, collisions in dense groups 77—45573
galaxies, collisions rel. to form. of ring galaxies 77—33635
galaxies, collisions with intergalactic neutral clouds rel. to interstellar super 80—98717
galaxies, early-type, encounters with gas-rich dwarfs rel. to accretion phenomena 80—31349
galaxies, elliptical, form. by merging and to rot. props. 80—4444
galaxies, form. of ellipticals by tidal interactions 77—78865
galaxies, interactions rel. to spiral structs. origin 79—25714
galaxies, probability of ring structs., collisional form. rel. to ring galaxies relative abundance 79—92868
galaxies, tidal encounters rel. to Arp QSO-galaxy associations 80—90564
galaxies head-on collision, dynamical friction effects 79—44600
galaxies of Local Group, numerical expts. on gravit. encounters 77—57098
galaxies of unequal dimensions, collisions classifications 79—84850
galaxy mergers, stellar populations mixing processes 80—67860
galaxy merging, contrib. to galaxies rot. 80—4439
Galaxy-LMC encounter, warping of galactic plane 77—45540
gas, electron and hole drift velocity 80—57223
gas, weakly ionised, electron distrib. function, isotropic component, collision source 80—62599
gas, weakly ionised, electron distribution function, steady-state conditions and elastic collisions 80—57224
gas, weakly ionised, electron drift velocity and distrib. function 80—57225
gas, weakly ionised, electron transport quantities, divergences 80—57222
gas clouds in Seyfert galaxies and quasars, containment by particle flux 79—8820
gas phase NMR, kinetic theory, single relax. time approx. 77—14451
gravitational systems, inhomogeneous, delocalisation effect in encounters rel. to relaxation 79—62877
heavy particle elastic collisions, quantum effects *(Japanese)* 78—21015
heavy-ion collisions, QED, strong and supercritical fields, book contrib. 78—74193
ice crystal collisions, secondary 79—79932
impact craters, diameter to depth ratio dependence 80—94765
inelastic cross sections from microscopic optical model pots. 79—22792
inelastic scattering, R-matrix soln. of coupled eqns. 79—10163
information theoretic maximal entropy theory, rel. to scatt. theory 78—81888
interruption function in perturbation theory for molecular collisions 77—23528
interstellar C^+ ions, collisions with oxide grains rel. to formaldehyde prod. 79—40246
interstellar clouds collision and star form., suppression by interstellar gas heating 80—105349
interstellar grains, collisions in turbulent gas 80—77470
interstellar matter, collisional growth of giant mol. clouds 79—48877
ion cyclotron resonance spectrometry, collisionally damped ion motion 80—57419
ion-ion scattering, momentum dependence, in microscopic theory 78—41752
ion-molecule, ions energy distribution function, in homogenous medium *(French)* 77—19796
ionosphere, effective electron collision freq. vars. from multiple-freq. mas. of radiowave absorpt. 77—91347
ionosphere, electron collision freq. model and vertical incidence absorpt. during winter anomaly 79—21098
ionosphere, lower, electron impact ionisation rel. to electron distrib. function and ion concs. 77—78564
ionosphere photoelectrons, Coulomb-collision induced trapping by geomag. field 79—8739
ionospheric ions and electrons, collision cross-section 80—26666
JWKB phase shifts, using Gauss-Mehler quadrature formulas 78—46411
Keplerian orbits, statistical mechanics with collisional perturbations 77—49269

collision processes continued
Keplerian systems, numerical simulations of collisional evolution 80—109342
kinetic equation of gases 80—21914
kinetic theory, density effects expts. 78—12468
light scattering, moments of three-body portion 77—57961
lower ionosphere, collision freqs. for use in continuum momentum eqns. 77—87171
M31+M32, gravit. perturbations effects rel. to galaxies relative position 78—93394
M82, intergalactic cloud encounter model 79—75279
M82 with intergalactic dust cloud, dynamical evidence from Ne II 12.8 micron emission 79—17082
magnetosphere polar cusp, particle scatt. on waves rel. to low-freq. pulsations generation 79—53657
magnon elementary excitations damping *(Russian)* 79—28515
Manych meteorite, L-3 chondrite, impact remelting rel. to droplet chondrules comp. and origin 79—30014
meteorites collisions with planets, review 79—8884
meteorites parent bodies, collisions rel. to origin of polymict brecciated meteorites 78—57513
microscopic theory of collisions in atomic phys. survey of recent developments 78—46410
molecular collisions in a laser field: effect of the laser linewidth 79—6980
molecular interactions, source theory 78—46415
molecular relaxation, averaged j_z-conserving coupled states approx. 77—54585
molecular state, j_z CCS approx., partial wave parameters identification and differential cross section simplification 77—58112
Moon, early collisional heating 80—8563
Moon, Fahrenheit crater ejecta emplacement at Luna-24 site 80—8564
multiple scattering formalism, time depend. generalisation 78—86518
multitemperature gas mixtures, Maxwell-Grad moment method calcs. 77—47134
near-adiabatic collisions, theory, electron translation factor method 78—81889
near-adiabatic collisions, theory, scatt. coord. method 78—81890
Neptunee encounter with massive body rel. to chaotic satellite system and Pluto origin 79—84743
neutron flux, collision probability integrals, annular geometry, evaluation using analytic expansions 80—32317
NGC 4631 group of galaxies, tidal interactions model 78—54059
NGC 5128, peculiar galaxy, possible collision rel. to struct. and evolution 79—53913
NGC 6052, possible collision of two late type spiral galaxies, observational evidence 80—8681
NGC 6240, unusual radio galaxy, evidence for gas-rich galaxies collision 80—4440
NGC 7822 (W1), supernova remnant/H II region collision from kinematics studies 78—54028
nonadiabatic processes, rate const. temp. depend. 79—64064
nonadiabatic transitions, with pseudocrossing of a group of terms 77—65522
nonresonant, possible relax.-time comparisons failure for local thermodynamic equilib. 78—81935
novae, nonuniform stellar wind collision with main shell filaments rel. to light curves 80—62160
null event method in simulation, ion collision appl. 78—90262
one-dimensional gas, collision probability per unit time calcs. 77—60044
particle+two particle collisions, adiabatic approx. *(Russian)* 79—94052
particle adhesion upon impaction 79—52784
particle collisions, conservation of energy and conservation of vector momentum 80—101693
particle impacting wall diffusion layer, enhancement of mass transfer *(French)* 79—60050
particle passage through thin layers, Monte Carlo calc. 80—100708
particle scattering from target, spin-spin interaction calcs. 78—81730
particle stream, Keplerian, mutual collisions rel. to self-focusing, computer simulations 79—53704
particle transport theory, fluctuation problem, probability balance eqn. 77—37829
pattern recognition in chem. dynamics 77—32768
permutation operator, explicit representation, for teaching 79—35469
Phobos, dynamical evolution and time to collision with Mars 78—89104
planetesimal population, elastic and inelastic collisions rel. to equilib. vels. 80—31219
planetesimals, impact records rel. to late stage growth 79—96931
planetsimal aggregation during solar system system form., collisions rel. to jetstream configuration 78—69713
polyatomic gas, thermomagnetic phenomena at intermediate press. *(Russian)* 79—77329
potential scattering, cross sections and scatt. amplitudes 78—42152
potential scattering, refined Born approx. 80—77
pressure line shape in impact approx. with Debye screening, semiclassical and quantum calcs. 78—37591
principal value collision integrals, reduction scheme 77—57234
protogalaxies encounter, limiting radii of direct and retrograde satellite orbits 79—88572
pulsed laser-induced shattering of water drops 80—50471
quantum mechanical close coupling calcs. using averaged definite parity j_zCCS approx. 77—34710
R-matrix theories 78—58760
R-matrix theory 78—58761
rainbow scatt. props., semiclassical estimation 77—88523
reduced phase space approach calcs. 80—83438
relativistic Boltzmann kinetic eqn. derivation 80—68161
resonant energy transfer cross section, form factor formalism, 1st Born approx. appraisal 77—65519
Saturn ring particles, collision rel. to A-ring azimuthal brightness var. and particle size 78—32391
scattering length calc. with imprecise target wave function, variation principle 79—72375
scattering resonances, tunnelling decay, absorbing boundary layer 80—57121
Schrodinger equation, time-depend., explicit integration method 78—57805
semiconductor, electron and hole drift velocity 80—57223
semiconductor, intrinsic, electron distribution function, steady-state conditions and elastic collisions 80—57224

collision processes continued
- semiconductor, intrinsic, electron drift velocity and distrib. function 80—57225
- shock waves, astrophysical, post-collisional propag. and amplification *(Russian)* 79—44360
- solar nebula, particle-to-particle collisions rel. to chondrule form. 77—82178
- solar system, basaltic bodies destruction by high-vel. impact 77—64704
- solar system bodies, early collision history from early lunar chronology 77—60640
- solar system/interstellar cloud impending encounter, evidence 78—93352
- spectral line shape model with explicit parity consideration 77—58110
- spiral galaxies merging hypothesis for elliptical galaxies form., refutation 80—98723
- spiral galaxies of Virgo cluster, collisions rel. to H I deficiencies 80—62277
- stars in dense stellar systems, disruptive collisions and ultimate fate 79—25652
- stars in galactic nucleus, collisions rel. to black hole sustenance 78—57632
- statistical mechanics, nonequilibrium, review 80—12983
- stellar collisions, post-Newtonian gravit. radiation 77—13226
- surface integrals for triple collision integrals in kinetic theory of gases 77—84381
- symposium, Florida, USA (March 1979) 80—51946
- terrestrial planets accretion, shock degassing rel. to atmospheres origin *(Russian)* 79—101099
- thermosphere, minor species collisions rel. to response to gravity waves 79—58140
- three-body problem, stability of interplay motions 77—60583
- three-level system, stimulated Raman scatt. and stimulated collision induced fluoresc. 78—87103
- three-particle collision processes, kinetic eqns. 78—1044
- time dependent methods 78—33561
- time-dependent, adiabatic perturbation approx., semiclassical theory 77—71242
- total cross section, semiclassical limit, fast oscills. 77—83672
- transfer collision frequencies for inelastic collision 79—71357
- Tunguska event, comet collision with Earth 78—49390
- two Coulomb centres problem at small inter-centre separations 78—70892
- ureilite meteorites, mag. effects of brecciation and shock rel. to strong nebular mag. fields 80—8602
- white dwarf with main sequence star, physical processes and consequences 77—64758
- VII Zw 466, ring galaxy, UBVR photometry rel. to form. by collision 79—8991
- Zwanzig-Feshbach projection method and Landau-Zener approx., time-depend. approach 80—31553
- NN collisions around 10 TeV, nucleon fragmentation by diffr. rel. to high-energy γ-quantum prod. 79—80174
- Cu exploding, wire accelerated evaporation of fast drops colliding with target *(Russian)* 77—15570

collision sequences, focused *see sputtering*

colloid chemistry *see colloids*

colloids
- *see also Brownian motion; coagulation; electrophoresis; electroviscous effect; emulsions; gels; magnetic fluids; thixotropy*
- adhesion of particles, effect of elastic contact deformation 77—29048
- aerocolloidal suspension of solid particles, shock wave entering aerocolloid domain 78—51227
- aerosol OT-n-heptane-water, reversed micellar solution; addition of electrolyte, neutron small angle scattering 80—104468
- Agave cantala natural fibre, small-angle X-ray scatt. of densely packed colloidal system, scatt. inhomogeneities 80—76565
- aggregation, powdered Pt electrode 79—11830
- alcohol-water solutions, containing radioisotopes, radiochemical purification *(Russian)* 77—86432
- alkali metal-iron sulphides colloid, produced by reaction of iron salts with alkali sulphides 79—43635
- p-alkylbenzenesulphonate mixed micelles, dimens. determ., small angle X-ray scatt. *(French)* 77—29053
- amino acid residues, form. of mixed micelles and relative compatibility at interface 80—71951
- amphoteric latex coagulation, reversibility and specific ion effects 80—45567
- anisaldazine, colloidal particles in water, elec. polarisability anisotropy 79—39208
- anisylidenebenzidine, particle size distrib. function, electrooptical diffusion method for determ. 80—8956
- anthracene, fluorescence spectra in aq. and surfactant solns. 77—83639
- aqueous suspensions of spherical colloid particles, phase transitions 77—4938
- arene, photophysics, functionalised micellar assembly, phosphoresc. and triplet Ag^{+} enhancement 78—95598
- aromatic hydrocarbon-dicyanobenzene, aq. micellar soln., fluoresc. quenching mechanism 79—50063
- aromatic hydrocarbon-N,N-dimethylaniline, aq. micellar soln., fluoresc. quenching mechanism 79—50063
- benzophenone ketyl radical, in micelle, decay rate in mag. field, photolysis meas. 80—85154
- bile salt micelles as liquid membranes 80—21327
- birefringence in Rayleigh and anomalous diffr. approximations 80—29710
- bitter technique, model calc. for colloid accumulation on surface in mag. field *(German)* 77—9139
- Brownian coagulation, with disintegration of aggregates 80—7864
- capillary-porous body, mass transfer parameters, adsorpt., osmotic moisture 78—11563
- n-caproic acid, colloidal dissolution in water 79—66358
- cetyltrimethylammonium bromide, aq. soln., mol. conform., laser Raman spectra 78—21934
- cetyltrimethylammonium bromide, micelles, solubilised nitroxide spin probes, ESR 78—21950
- cetyltrimethylammonium bromide and chloride aqueous micelle, fluoresc. showing coexistence of rod-like and globular struct. 79—61910
- cetyltrimethylammonium bromide-1-butanol system, micellar conc. meas. using fluoresc. probe study 80—85217
- chain molecules with polar head, scaling description of adsorption 78—3378

colloids continued
- chlorophyll, colloidal solns., elec. charge of particles 80—94438
- chlorophyll-a, photoinduced electron transfer to duroquinone in micellar soln., charge separation 78—23955
- cholesterol + water, interaction in organic media, dielec. and NMR spectroscopy 78—76979
- chromatography, hydrodynamic, role of colloidal forces 78—48717
- CIDEP, examples of S-T$_{\pm 1}$ polarisation 78—86891
- coagulated colloidal suspensions, couette flow, viscosity effect 79—90317
- coagulated colloidal suspensions, expt. props. of flow curve parameters 77—938
- coagulated colloidal suspensions, flow props., elastic floc model 77—939
- coagulated colloidal suspensions, flow props, energy dissipation in flow units 77—3862
- coagulation, 1st-order diffusion effects 79—39213
- coagulation, DLVO theory problems 80—45566
- coagulation, stability ratio of primary and secondary minimum coagulation, kinetic theory model 80—3415
- coal dispersions, solvent refined, elec. props., surface characts. 80—80333
- colloid, electrostatically stabilised, very dilute, struct. and ordering, Monte Carlo method 77—36795
- colloid suspensions in a polymer solution *(French)* 79—87879
- colloidal plates, parallel, polymer adsorption, excluded volume effects, polymer-solvent interactions 80—45568
- concentrated, appl. of modern concepts in liquid state theory 80—40750
- concentrated dispersions, dynamic light scattering 79—15469
- concentrated hexagonal close packed dispersions, disjoining pressures calcs. 78—23971
- conference, Budapest, Hungary (Sept. 1975) 78—11567
- conference, San Juan, Puerto Rico (June 1976) 77—25318
- copolymer, graft or block, multiphase composite systems, struct., colloidal behaviour *(Chinese)* 78—73088
- copolymer micelles in solution, review 77—21424
- correlation and responsè functions 80—22286
- corrosion products model, prep. and charact. 80—16561
- counter-ion quenching of organic compound fluoresc. in micellar aq. solns. of surface-active substs. *(Russian)* 77—54573
- critical binary liq. mixture, wall phenomena *(French)* 79—16041
- crystal latex, colloidal, nonlinear electro-optical props. 79—61337
- crystals, colloidal, ordered suspensions of charged latex spheres, acoustic shear waves 80—6466
- DBS micelle solution, hydrophobe molecule solubility, NMR 79—83517
- decylammonium chloride micelles, ^{13}C longitudinal relax. times and nuclear Overhauser enhancement anal. 80—83390
- dense Lennard-Jones fluids, solvent struct. and solvation forces between rigid particles 80—30287
- depletion stabilisation and depletion flocculation, theory 80—89534
- deposition of colloidal particles onto surface of rotating disc 77—48690
- detergent micelle microviscosity, rel. to photochem. activity of chlorophyll 77—21478
- diamond, colloidal particles in water, elec. polarisability anisotropy 79—39208
- dibenzylketone, photolysis in micellar soln., quantum yield and ^{13}C enrichment 80—97711
- dichroic colloidal particles, size distrib. determ. by electro-optical method 79—6087
- dichroism in homogeneous elec. field 79—8122
- dichromated colloid layer holographic diffraction grating characteristics 79—27424
- 3,3′-diethylthiacarbocyanine iodine-rhodamine 6G, energy transfer with increased local conc., Forster mechanism 80—69220
- diffuse double layer, modified nonlinearised Poisson-Boltzmann equation 79—79305
- dilute colloidal suspension, Krishnan effect, theory 77—34824
- 1,5-dimethylnaphthalene, fluoresc. quenching by cyclic azoalkanes, micelle system probe 80—35578
- diphenylanthracene in 2,2,4-trimethylpentane, light scatt. and fluoresc. standard by monochromator 80—57247
- dipolophoresis and electrophoresis, in presence of linear grating of cylinders 79—57234
- Disjoining pressure of thin layers of binary solutions 78—15716
- dispersed colloids, electrokinetic pot. determ., streaming pot. meas. 77—16868
- dispersion, coagulating, light scatt. for close range struct. determ. 78—53273
- dispersions, colloidal, microrheology, Brownian diffusion of doublets of spheres 77—4942
- double-layer structure, electrohydrodynamical determination 78—95960
- dye solutions, in micellar media, rot. diffusion, transient absorpt. meas. 79—92005
- dye-detergent model systems, degree of fluoresc. polarisation 78—27287
- dynamics of colloidal dispersions, review 80—71956
- dynamics of colloidal systems: time-dependent structure factors 80—93803
- electrical double layer theory, through Born-Green-Yvon eqn. 80—35539
- electro-optic studies, electric polarisability, stability 80—85222
- electro-optical characterisation of polarisation processes 77—24821
- electro-optical phenomena, induced dichroism rel. to elec. field calc. 78—50699
- electro-optics and dielectrics, conf., Uxbridge, England (Apr. 1978) 80—82577
- electroconcentration effect, gap between nonconductive fibres 80—11895
- Electrokinetic measurements with submicron particles and pores by the resistive pulse technique 77—86384
- electrolyte solution containing spherical particles, appln. of hypernetted chain approximation to particle interaction 80—85185
- electrolyte solutions, overlapping electrical double layers, repulsive interface forces 78—44382
- electrophoresis, mass transport, apparatus 78—85168
- electrophoresis, nonlinear, of dielectric and conducting ideally polarisable particles 77—25270
- electrophoresis of particles with adsorbed polyelectrolyte 79—47991
- electrostabilisation effect in elec. field 79—39210
- electrostatic interaction between spherical colloidal particles 80—55724
- emulsion polymerisation, ideal, first-stage kinetics calcs. *(Russian)* 79—66295
- Escherichia coli, aq. colloid suspension, electrophoretic mobility and elec. polarisability 78—35813
- excess pressures 77—86386
- excimer formation in micellar surfactant solns., distributional effects 78—64855

colloids continued
ferritin particle visibility in SEM with field emission gun 79—25174
ferrofluid, convective stability of horizontal layer in mag. field *(Russian)* 77—3885
ferrofluid constitution examination by rotating test tube method 80—33693
ferrofluids, exptl. obs. of agglomeration in presence of mag. field *(French)* 78—92514
ferromagnetic colloid, natural convection, mag. field effects *(Russian)* 77—62307
ferromagnetic colloids, helical flow in mag. field *(Russian)* 78—75213
field separation with hydrodynamic amplification 78—27779
Floc density, porosity and void ratio in colloidal systems and aerosols 78—3383
flocculation, book 78—92520
flow alignment, transition from isotopic to nematic phase 80—84060
fluorescence, apparatus for meas. electrically induced polarization changes 77—46662
fluoroanthene in micelles soln., fluoresc., halide ion induced quenching and enhancement 80—95672
fluorocarbon emulsions, colloidal props. 78—48703
forces between dissimilar colloidal plates for various surface conditions 77—60135
fractionation and size analysis using flow field-flow fractionation 78—61062
freeze-fracture, for electron microscopy 78—337
geomagnetic field effects on charged particles in ocean *(Russian)* 77—60416
graphite, in mag. field, optical transmission meas., polarisation depend. 78—31712
Graphon, colloidal dispersion in butanol, stability ratio 79—29413
Graphon, in butan-1-ol, colloidal particles, dispersion force interactions calcs. 79—24842
haemoglobin reactions as interfacial phenomena, hydrophilic colloid model 77—9167
Hamaker consts. and combining rules for model oil-water systems 78—68934
Hamaker functions, calc. from coagulation data, influence of Stern layers 78—48698
hard sphere solvent struct. effects on particle interactions 78—7237
Helmholtz eqn. soln. for interactions between particles of arbitrary shape 79—100453
hexadecyltrimethyl-ammonium bromide, micelle form. in aq. soln., laser light scatt. 78—27825
hexadecyltrimethylammonium bromide, micelle shape and aggregation, conc. depend. 79—24833
n-hexane, colloidal dissolution in water 79—66358
n-hexyl alcohol colloidal dissolution in water 79—66358
hydrophobic colloids, coagulation mechanism 78—40085
hydrophobic particle interactions, stability, dynamic theory 80—89544
interacting Brownian spheres, depolarised light scattering 79—34370
interaction force, calc. of electronic component 79—11829
interfaces, elec. double layer struct. 78—40088
interfacial electric polarisability, and interactions 80—108751
interference colours associated with mag. domains 80—2598
intermicellar kinetics theory, stochastic approach, master equation for, irreversible reactions 80—76561
intervesicular lipid transfer, direct fusion of phospholipid vesicles, kinetic basis comparison 78—96034
ionic direct micellar phase, local order determ. by neutron scatt. *(French)* 79—92013
ionic micelles, form., equilib. and relax. kinetics, theory 78—35723
ionic surfactants, conductance stopped flow study of micellar equilibria 79—43642
isoprene-styrene copolymer latexes, film-forming properties 78—53266
latex, colloidal concentrated dispersions, dynamic light scattering 79—15469
latex, colloidal cryst., optical props. near MP 78—11562
latex, monodisperse, Kirkwood-Alder transition press. meas. 78—7239
latex, monodisperse, mechanical props. 78—48701
latex, shear waves, elastic modulus determ., light scatt. 80—58956
latex colloidal crystal, melting, particle packing fraction depend. 77—73475
latex globules, monodisperse, obs. of crystalline superstruct. 80—35582
latex polymer, electrodeposition on metal 78—53015
lecithin, inelastic light scattering at second micellar formation 77—21492
lecithin, rheology and structure in conc. solns. and liquid crystalline state 77—64007
light scattering, Percus-Yevick approx., for spherical particles 78—94368
linear elasticity, soft contact problems 80—48653
liquid crystal, colloid and surface chemical aspects 78—9950
liquid film, free, squeezing mode relax., laser scatt. rel. to colloid interaction 78—87354
lyotropic mesophases as defects in binary mixtures 77—31586
macromolecular colloids, electrokinetic pot. determ., streaming pot. meas. 77—16868
magnetically induced linear optical birefringence and dichroism in colloidal dispersions 78—8431
Manoxol OT-cyclohexane-water reversed micellar system, singlet-singlet energy transfer 80—9531
materials with ionisable surface groups, colloidal behaviour 80—89543
Maxwell-Wagner dielectric dispersions, vol. ion polarisations 80—97188
metal, annealing, irradiation-induced defects in alkali halide crystals 80—107316
metal colloids in ionic cryst., preparation, optical, mag. resonance, elec. props. 80—59459
metal-filled epoxy polyester, PE-933, elec. cond., theory and expt. 80—60057
metal-filled polymer, elec. cond., theory and expt. 80—60057
metals and alloys, corrosion, colloid chem. appls. 80—89541
1-methylpyrene, fluoresc. quenching by Cu^{2+} in micellar system, general kinetic model 80—32753
micellar aggregate, solubilisation parameters and dynamics, photoluminescence obs. 79—79297
micellar diffusion-controlled reaction kinetics 80—30213
micellar dye soln., energy transfer 80—45581
micellar interface, reaction kinetics, rotamer population, fast proton transfer 80—26050
micellar phase dissoc.-recombination kinetics, stochastic model 80—55628
micellar solns., small angle neutron diffr., micellar struct. *(French)* 78—11564

colloids continued
micellar solutions, cluster size distribution for the Ornstein-Zernike correlation 80—97734
micellar solutions, crit. behaviour 80—105601
micellar solutions, crit. concs. 77—4943
micellar solutions, fluoresc. quenching rel. to aggregation numbers 79—34364
micellar solutions, micellar aggregation number, ^{13}C NMR chemical shift conc. depend. 80—48016
micellar solutions, US absorpt. 80—45571
micellar solutions vs. microemulsions 77—60131
micellar system, naphthalene as fluoresc. probe 78—95599
micellar systems, aqueous, thermochemistry 80—61133
micellar systems, solubilisation 80—89546
micelle, definition 78—48699
micelle dissociation-recombination kinetics, stochastic model 80—30291
micelle formation, in aq. solns., kinetics relax. process 78—76928
micelle formation model, relaxation spectra 80—71934
micelle formation of cationic surfactants, influence of perfluorinated counter-ions *(German)* 79—74423
micelle forming detergent solutions, fluoresc. quenching by O$_2$, dynamic parameters and solubility characts. 79—83513
micelle solns., aq., pulse radiolysis, CIDEP in time-resolved EPR 77—30891
micelle systems, relax. and size distrib., kinetics 77—25316
micelle-confined molecules reaction, diffusion-controlled, luminesc. quenching, excimer form. 80—50890
micelles, distrib. of solubilised mols., for teaching 79—58497
micelles, highly charged hard sphere model, HNC approx. 78—23969
micelles, inverted containing water, hydrodynamic vol. determ. by fluoresc. polarisation 80—50892
micelles, Laplace pressure 80—7865
micelles, organic reaction kinetics 79—29416
micelles, reversed, solubilisation and catalysis, review 80—45545
micelles, surfactant assoc. and physical chem. 79—57306
micelles formation, considered as polycritical phenomena *(French)* 77—63968
micellisation kinetics, pressure-jump and stopped-flow methods 80—45564
microemulsion, border between lyophobic and lyophilic colloids, thermodynamic stability 80—40747
microemulsions, quasi-elastic light scatt. 80—108755
microemulsions, stability, thermodynamic approach 78—95959
microemulsions of micelles, interpretation of second virial coeff. of osmotic press. *(French)* 78—64891
microparacrystals in physics, review *(German)* 79—27933
microrheology, chains of spheres in shear flow 77—7354
microrheology, pairs of interacting spheres in shear flow 77—7352
microrheology, primary and secondary doublets of spheres in shear flow 77—7353
minerals with small specific surface, heat of wetting determ. 77—29050
mixed colloidal suspensions, selective coagulation 79—74426
mixed sterically-stabilised dispersions, equilib. aspects of heteroflocculation 80—45570
model, elastic moduli, Monte Carlo methods 80—108754
molecular attraction forces between solids, effect of EM lag 80—71949
molecular forces, theory 78—40087
monodisperse latex, simulation study of eqn. of state of simple liquid 77—63964
myristyltrimethylammonium bromide, micelle size, press. dependence, photon correlation spectrosc. 80—11953
neutron scattering techniques in applied research, medium-flux research reactors 79—13514
nonlinear rheological behaviour and shear dependent struct. 79—7358
oil in water microemulsion, added NaCl, light beating spectroscopy of micelles mutual diffusion coefficient 78—80793
optical anisotropy, intrinsic, anomalous diffr. approx. 80—53213
ordered colloidal dispersion, electrostatically stabilised, polydispersity and osmotic press. 79—74428
ordering, statistical mech., theory 78—23968
Ostwald ripening and its application to precipitates and colloids in ionic crystals and glasses [Review] 78—80548
particle growth rate, effects of convection and Brownian motion 79—52778
particle separation by potential barrier chromatography 77—73474
particle size analysis using hydrodynamic chromatography technique 77—44530
particle size distrib. change kinetics, statistical approach 78—7241
particle size distribution, reduced electric dipole moments, polarisabilities using electric birefringence 78—95958
particle size distribution function, electrooptical diffusion method for determ. 80—8956
particle size measurement, hydrodynamic chromatography, mathematical modelling 77—1951
particle size measurement, submicron, ultrasonically induced birefringence technique 80—30290
particles, in a flowing solution, SAXS 80—61163
particles in colloidal state, refr. index, theory 78—95567
petroleum, study of colloidal nature using automated Bonse-Hart X-ray small-angle scatt. unit 79—16044
phase transformation, small cluster formation, fifth state of matter 80—39304
phase transitions, statistical mechanics approach 80—40749
phospholipid vesicles, conform. change and fusion phenomenon, dynamic light scatt. obs. 78—11615
photochromic dyes, quasi-crystals produced in applied electric field 80—85225
photosensitive glass, full-colour polychromatic, subcolloidal Ag precipitation 79—47953
planar micelles, structural changes, aggregation 79—66451
PMMA aqueous colloid, coagulation kinetics, light scatt. determ. 79—39215
Poiseuille flow, total particle conc. axial change 80—108752
poly-L-glutamic acid-poly-L-leucine block copolymers, association colloids 80—26064
polymer adsorption on small spheres, scaling approach 78—3377
polymer flocculation and stabilisation, concentration effects 80—45569
polymer soln., colloid stability near repulsive wall 80—21326
polymer spheres colloidal suspension, steady state shear flow coupled to conc. fluctuations 80—61170

colloids continued
- polymers, blend, interphase phenomena, form., thermodynamic, colloidal and morphology props. *(Russian)* 78–40089
- Polymers at interfaces and the interactions in colloidal dispersions 78–11572
- polystyrene, colloidal dispersion in butanol, stability ratio 79–29413
- polystyrene, in butan-1-ol, colloidal particles, dispersion force interactions calcs. 79–24842
- polystyrene, in butanol, electrophoretic mobility, charge origin 78–85211
- polystyrene interfacial colloidal crysts., microscopic obs. 80–97737
- polystyrene latex, colloidal crystal, grain boundary struct. and boundary diffusion obs. *(Japanese)* 78–15721
- polystyrene latex particles, swollen, aggregation studied by photon correlation spectrosc. 80–66886
- polystyrene latexes, edge dislocations 79–96370
- polystyrene latexes, monodisperse, model colloid systems 80–89545
- polystyrene lattice cleaning, dialysis, steam stripping and ion exchange effectiveness 80–3414
- polystyrene particle colloidal suspension in KCl(LiCl) aq. solns., dielectric loss 78–35728
- polystyrene particles flocculation, light scatt. for close range struct. determ. 78–53273
- polystyrene-polydimethylsiloxane, block copolymer micelles, small angle X-ray scatt. 79–69003
- polystyrene-polyethylene/propylene block copolymer, micelle form. in lubricating oil 80–61171
- polystyrene-polyisoprene, block copolymers, association colloids 80–26064
- polyvinyl alcohol, in water-ethanol mixture, processes of structure formation 80–10482
- polyvinyl alcohol/vinyl acetate copolymer, in water-ethanol mixture, processes of structure formation 80–10482
- preparation 80–71953
- PTFE, in butan-1-ol, colloidal particles, dispersion force interactions calcs. 79–24842
- PTFE, in butanol, electrophoretic mobility, charge origin 78–85211
- pyrene, fluorescence spectra in aq. and surfactant solns. 77–83639
- pyrene, in aq. micelle system, fluoresc. quenching by inorganic ion 77–10697
- pyrene, in micellar environments, fluoresc. quenching by nitroxyl radical 79–13754
- pyrene, micellar solns., fluoresc. quenching 78–25588
- pyrene, micellar system, fluoresc., solubilisate distrib. statistics, kinetic model 79–34366
- pyrene derivatives, micelle-embedded, rot. relax., time-resolved fluoresc. depolaris. obs. 80–58300
- pyrene excimer formation in micellar surfactant solns., distributional effects 78–64855
- pyrene excimer formation in micelle, time-resolved spectra 79–79298
- pyrene-3-sodium sulphonate solubilised in didodecyldimethylammonium bromide-benzene inverted micelles 80–3417
- pyrene-N,N-dimethylaniline heteroexcimer systems, micellar solns., fluoresc., photoinduced electron transfer 78–25590
- pyrene-sodium 5-[1-pyrenyl]pentanoate intramicellar excimer formation in CTAC and SDS micelles, fluoresc. probe 80–16733
- 1-pyrene-sodium sulphonate, excimer form. in inverse micelles, fluoresc. probe 77–88491
- radiation therapy, intracavitary uses of colloids 80–36110
- radioactive particles, size and charge distribs. nuclear medicine appls. 80–30853
- radiocolloids and pseudoradiocolloidal states or uranyl acetate solns. 78–44390
- rheological props., terminology and symbols 80–26065
- rheology of concentrated dispersions, review 77–19578
- rhodamine 6G, micellar soln., aq., fluoresc. decay for rot. diffusion const. 79–11826
- rhodamine R derivatives, water (heavy water) detergent solns., luminesc., lasing 79–56836
- rhodamine-6G-3,3'-diethylthiacarbocyanine iodide-sodium lauryl sulphate, soln., premicellar region, energy transfer 80–20685
- sedimentation, rapid, under gravity, basic theory and experimental demonstrations 80–66885
- sedimentation equilibrium eqns. derivation using hard spheres in Percus-Yevick approximation 80–66884
- sedimentation hydrodynamic interaction between spherical particles, effect of repulsive interparticle forces 80–45577
- sedimentation through polyethylene oxide semidilute aq. soln. 78–95965
- sepiolite, electric polarisability, anisotropy, length depend. of ionic contrib. 80–85224
- sepiolite, size distributions, transient electric birefringence 80–85223
- silica, fractionation and size analysis using flow field-flow fractionation 78–61062
- simple shear flow of dilute fluid suspension, orthokinetic collisions of hard spheres 77–35199
- single colloidal crystals, prod. technique 79–99097
- size distrib., photon correl. spectroscopy, methods of cumulants, histogram and Laplace transform 79–58801
- size distributions, transient electric birefringence 80–85223
- sodium 10-undecanoate, γ-ray induced polymerisation in aq. micelle solns. 80–61093
- sodium decyl sulphate/water/decanol/Na_2SO_4, lyotropic mesophase, mag.-oriented, X-ray diffr. obs. 80–1921
- sodium dodecyl sulfate, micelle form. in aq. soln., laser light scatt. 78–27825
- sodium dodecyl sulphate: Gd^{3+}, micellar system, chain folding, ^{13}C NMR obs. 80–61158
- sodium dodecyl sulphate, micelle shape and aggregation, conc. depend. 79–24833
- sodium dodecyl sulphate, polydisperse micellar solns., light scatt., size, shape and aggregation number calcs. 80–89531
- sodium dodecyl sulphate, solution, micellar, quasielastic light scattering, at low conc. limit 79–79307
- sodium dodecyl sulphate micelles, diarylalkane intramolecular excimer formation, microfluidity and fluoresc. meas. 78–80791
- sodium dodecyl sulphate micelles-ω-(α-naphthyl) dodecanoic acid soln. fluoresc. decay obs. 80–61158
- sodium dodecyl sulphate NaCl aq. soln., micellar props., laser light scatt. exam. 78–92513
- sodium dodecylsulfate, micellar solution, critical micelle concentraion for thermalized positronium formation 79–96345

colloids continued
- sodium dodecylsulphate micelle, intramicellar fluorescence quenching of $[1\text{-pyrenyl-}(CH_2)_n\text{-}N(CH_3)_3]^+Cl^-$ by cationic surfactant nitroxyl radical 80–9627
- sodium octyl benzene sulphonate, micellar aq. soln., Cotton-Mouton effect in mag. field 79–16047
- sodium p-octylbenzenesulphonate ionic micellar solns., neutron diffr. meas. *(French)* 78–44409
- solute hydrophobic interaction, mol. aggregation, free energy, entropy and enthalpy, scaled particle theory 77–84609
- solution droplets, solid, particle form., heat and mass transfer 78–95967
- solvation force between particles, Monte Carlo calc. 80–21328
- spherical particle, electrophoretic mobility 79–34316
- spherical particle, nonlinear polarisation of diffusion part of thin double layer 77–25315
- spherical particle, zeta-pot. determ. from electrophoretic mobility, double-layer polarisation 77–29015
- spherical particle dispersion, optical turbidity and refr., particle size and relative refr. index meas. 79–92012
- spherical particles, light refr. theory 80–23622
- spherical particles numerical method for electrophoretic mobility determ. allowing for polarisation 77–25269
- spheroidal particles, colloidal dispersions, refractive index 80–106454
- stabilisation by polymers, excluded volume effects 77–60129
- stability, dynamic theory 80–89544
- stability, interaction forces between colloidal particles 77–32842
- stability, main affecting factors 78–11568
- stability against coagulation 77–32843
- stability in flow fields, trajectory anal. 78–5782
- stability theory, direct operational determ. of disjoining pressure 80–40752
- stimulated resonance between electrical and shear fields by a colloid system 79–1971
- stochastic transport eqns. 78–93609
- strongly interacting small particle dispersions, struct. factors, radial distrib. 79–74427
- structure determ. by neutron diffr. and small angle scatt. 80–40748
- structuring dispersions, meas. device for dynamic dielectric behaviour 78–31710
- submicroscopic struct. determ. using very-slow neutron transmission 77–62448
- superheated supercond. colloid as a total absorption detector preliminary calcs. 78–78579
- superheated supercond. colloid neutron detector, detection and background rejection tests 78–78580
- surface and colloid science, conf., Stockholm, Sweden (Aug. 1979) 80–86035
- surface forces, direct meas., elastic deform. effect 80–93805
- surfactant addition to flowing liquid, effect on hydrodynamic resist. 77–7438
- surfactant micelles, hydration 80–89518
- surfactant micelles 80–45572
- surfactant solutions, aggregation, micelle and microemulsion form. 80–89547
- suspension, electrophoretic clarification 77–60127
- suspension concentrates, physical stability criteria, review 80–45562
- suspension technology for coatings production purposes 77–73476
- suspensions, colloidal, radiometric method for particulate processes characterisation, theory 80–45578
- suspensions, colloidal, radiometric method for particulate processes characterisation, expt. 80–45579
- suspensions, rheology, colloidal forces role, review 80–103063
- Syton determination of size distribution of submicron particles in colloidal suspension, FODA 78–61057
- 1,2,4,5-tetracyanobenzene, CT complex in micellar soln., fluoresc. and photolysis study 79–61911
- tetraethylene glycol dodecyl ether-H_2O, binary micellar solns. and emulsions, dielec. behaviour 80–44994
- tetraethylene glycol dodecyl ether-H_2O-heptane, binary micellar solns. and emulsions, dielec. behaviour 80–44994
- thermodynamic stabilisation, theory 80–81369
- thionine in sodium lauryl sulphate micellar solns., absorpt. spectra and fluoresc. yield, local dye conc. depend. 80–106343
- two-component solution, differential surface coagulation 79–79303
- two-dimensional colloidal state concept and role in activity of solids 80–55704
- van der Waals attraction, many-body, between two equal spheres, easily calculable approx. 77–9134
- Van der Waals attraction between two spheres 79–24837
- water-cetyltrimethylammonium bromide-haxanol system, ^{13}C NMR, catalysis in micellar and liq. cryst. phases 79–61909
- water-polystyrene spheres (highly charged), solid- and liq.-like phases, soft core liq. theory 77–63963
- Ag, adsorpt. of acetonitrile, surface enhanced Raman spectra obs. 80–97251
- Ag, adsorpt. of benzene (deuterobenzene), surface enhanced Raman spectra obs. 80–97251
- Ag, adsorpt. of N,N-dimethyl aniline, adsorpt. on Ag colloids, surface enhanced Raman spectra obs. 80–97251
- Ag, adsorpt. of pyridine, surface enhanced Raman spectra obs. 80–97251
- Ag, colloidal, reaction with photographic stabilisers, equilib. conditions *(German)* 78–61067
- Ag, granules and colloidal particles on Cs_2O film in Ag-O-Cs photocathode *(Chinese)* 80–2279
- Ag halide, fine grain, colloidal stability 79–20443
- AgBr colloidal suspension radiolytic reduction obs. 79–91979
- AgBr, photographic emulsions, weakening of colloid protection by gelatin 78–32906
- AgCl, luminescence fatigue, adsorbed Ag atoms 80–66281
- AgCl, surface crystallisation, due to colloid adsorption 80–54544
- AgI hydrosols, kinetics and mechanics of colloid systems formation 80–101045
- AgI, stability, dynamic theory 80–89544
- Al_2O_3 gel, prep. of ultra-fine particles, from $Al(OH)_3$ colloidal soln. 79–74431
- Al_2O_3, porous, anodic, growth, physical model 78–48662
- Al_2O_3, porous, anodic, growth, ionic cond. 78–48663
- $Al_2O_3(H_2O)_n$, uniform colloidal dispersion, prep. by chem. reactions in aerosols 80–97735
- Au sol, grain boundary struct. obs. and boundary diffusion 78–51552

colloids continued
- Au sols, solutions of large colloidal particles acoustically induced birefringence 80−93274
- Au, stability and Hamaker const. determ. 79−87883
- C blacks, in butanol, electrophoretic mobility, charge origin 78−85211
- C, refractive index determ. 79−66363
- Co particles, ferromagnetic colloids in toluene, small-angle X-ray scatt., interparticle correlations 79−11831
- Co_3O_4 colloid, preparation and props. 79−100445
- copper phthalocyanine, size distributions, transient electric birefringence 80−85223
- Cr^{6+}/Cr^{3+} colloidal SiO_2 surface films on Al, TEM/XPS study 80−85090
- Cu, metal cluster, optical spectroscopy, atom to bulk 78−95591
- Cu^{2+}-1,5-dimethyl-2,4-hexadiene, fluoresc. quenching method for determ. binding const. 80−89530
- Fe-bearing colloids in river water, mechanism of removal in estuaries 78−20437
- $\alpha-Fe_2O_3$ colloids, absorpt. index and colour 79−92009
- Fe_xO_y, prep., thermal decomposition of metal chelates 80−71953
- β-FeOOH, colloidal suspension, ionic spin relax. theory for Mossbauer spectra 78−19384
- H_2O-organic aerosol-n-heptane reverse-type micellar soln., neutron small-angle scatt. *(French)* 80−26059
- KAg_4I_5, superionic film, elec. ionic cond. and electron spectra 80−6543
- KCl, additively coloured, colloid size distrib., replica microscopy, absorpt. spectra 77−47449
- KCl, additively coloured, colloid nucleation and growth, TEM 77−62526
- KCl, colloidal suspension, radiowave dielec. dispersion 80−11311
- LiCl, colloidal suspension, radiowave dielec. dispersion 80−11311
- MnO_2 submicron particle collection, by H_2 bubbles 78−11560
- NH_3-$AlCl_3$ solution, Al_2O_3 ultrafine gel particle form. 80−93807
- Na-bentonite, electrokinetic pot. determ., electrophoresis meas. 77−16868
- $Na_2SO_4.12H_2O$ aq. soln., dodecanol additive effect near critical micelle conc. 77−73472
- ^{23}Na in heterogeneous system, nuclear mag. relaxation time determ., rel. with dimensions of colloidal particles 80−75876
- O_2, lifetimes and reactivity in aq. micellar system 78−46398
- O_2, singlet state lifetime in D_2O soln., decay of micellar system 78−46301
- P, colouring of glasses 77−8961
- PbS, colloidal, light scatt. and electron microscopy 78−3379
- SiO_2 colloid, Brillouin scatt., particle size and density depend. 77−32844
- SiO_2 colloidal sol, particle size distrib., small-angle X-ray scatt. obs. 77−44516
- TiO_2 in non-aqueous liquids, effects of mol. architecture of long chain fatty acids on dispersion props. 80−40751
- V_2O_5, amorphous semicond., solubility and fibrous texture 80−75162

colorimeters
- *see also colorimetry*
- automatic, plating line Co concentration monitoring 80−105691
- colour difference effects on tristimulus values *(Hungarian)* 79−88994
- DCM 26 colour measuring instrument, design, components and operating system 79−93203
- digital, A/D convertor cct. *(Russian)* 77−37963
- digital colour integrator 78−29138
- display colour meas. appl. 79−40605
- integrated semicond. transducer suitable for colour distinction 77−10086
- multisample rotating disc, microcomputer, control 79−80663
- photocolorimeter, automation of measurements *(Russian)* 80−68238
- photoelectric colorimeter reconditioning methods 79−39618
- reflectance spectrophotometers, old geometry problems *(German)* 78−54431
- reproducibility for industrial measurement *(German)* 77−57377
- review of modern instrums. 78−93747
- scanning, computerised, for meas. of white uniformity on colour TV picture tube 79−26098
- self-calibrating automatic ranging spectrophotometer/colorimeter 79−30574
- single-beam photoelectric colorimeter (KFO), meas. transmission coeffs. in visible spectrum 78−77963
- spectral masks, refl. sample colour meas. 77−34013
- spectrocolorimeter, SPEKOL, meas. of surface fluorescence 79−80664
- spectrophotometer, ACS Spectra Sensor 78−54429
- spectrophotometer, Zeiss DMC 25 automatic recording instrument errors 78−54430
- spectrophotometer for colour measurement, flexible instrument with microprocessor 78−54428
- spectrophotometer with pulsed Xe flashtube and parallel wavelength sensing 78−54427
- Technicon Autoanalyzer II, systematic absorbance errors 79−21802
- thermochromism, Gardner standards behaviour obs. *(Hungarian)* 78−24842
- three-colour photoelectric, with spectral masks, calibration 77−30196
- tristimulus, metrological qualification *(Hungarian)* 78−24841
- tristimulus, with Si photovoltaic cells *(German)* 80−17994
- tristimulus colorimeter MOMCOLOR *(Hungarian)* 77−18067
- tristimulus for PVC system plate-out testing *(Hungarian)* 78−93751
- Zeiss Automatic Colorimeter RFC-3, colour-meas. performance 78−54426
- Zeiss DMC 26 universal model *(German)* 78−54432

colorimetry
- *see also colorimeters; spectrochemical analysis; spectrophotometry*
- biomembrane potentials meas. using the dye safranine 79−48386
- cholesteric liquid crystals, investigation of colour-temp. characts. 80−57359
- chromaticity fluctuations anal. *(Russian)* 80−42249
- CIE-UCS system, determ. of most similar temp. *(German)* 78−54433
- CIELAB and CIELUV colour spaces, colour difference evaluation *(Hungarian)* 78−29135
- colour colorimetry, new system basis 80−4751
- colour image evaluation from tristimulus values transfer functions measurements 80−87333
- colour matching, review of basic laws and progress during the last 15 years 78−65955
- colour negative films (high speed), testing 78−86364
- colour reproduction, of images obtainable by two-primary colour projections 80−12125
- colour reversal films, colorimetrical investigations *(German)* 79−44961

colorimetry continued
- colour sicence contributions, collection of papers by D.B. Judd 80−98761
- colour vision testing, colorimetric assessment of Holmgren wool test 78−53409
- computerised colour matching, spectrophotometry 80−17995
- conference, Troy, NY, USA (July 1977) 78−49882
- constancy limits, colour, and colour perception 80−41025
- consumer product quality assurance, colorimetric theory and equipment *(German)* 80−86372
- contrast meas., haze method and apparatus 79−71508
- correlated colour temp. determ. *(Hungarian)* 78−93749
- correlated colour temp. determ. from isotemperature lines 78−8433
- correlated colour temperature and colour-difference formula 78−54424
- D65 source, reproduction accuracy 79−32016
- di(alkylbenzylthio)ethane, oil additive, thermal stability determ. by chromatography, colorimetry 79−15969
- diacetylenes, photopolymerisation, solid-state reaction, photoacoustic photocalorimetric obs. 80−61089
- distortion visual and objective assessment *(Hungarian)* 79−63291
- educational colorimetric laboratory, calibration of set of surface colour standards 78−49625
- electrochemistry, optical experimental methods 78−20022
- emission spectra and excitation meas. using fluorescent samples *(Hungarian)* 77−26380
- fluorescent dye colour coords., spectroradiometric meas. *(Spanish)* 78−49880
- fluorescent material colour meas. *(Spanish)* 78−49879
- fluorescent materials, reflective radiance factor meas. by two-monochromator method *(Japanese)* 80−68237
- fluorescent source UV assessment using metameric pairs classification *(Japanese)* 77−87806
- four-colour reproduction, colorimetric anal. by photomechanical means 79−75635
- Fraunhofer diffraction, white-light, theoretical determ. of chromaticity inform. 79−72477
- glass, boric acid content, differential-photometric determ. using SPEKOL spectrocolorimeter 78−23984
- glass, white-surface, spectral reflection coeffs. and colour coordinate comparison 77−71358
- glass filters for reproducing radiation of B and C sources 77−88947
- grating type monochromators, errors caused by polarisation of meas. system *(Japanese)* 80−101815
- hardness measurement, colorimetric method for high frequency treated bandsaw blades 79−74325
- heterogeneous reaction kinetics, microcalorimetric and thermogravimetric curve comparison 77−21359
- hydrographic charting by multispectral and ocean colour scanners 77−5368
- Judd's contributions to colour metrics and eval. of colour differences 80−94945
- laser heated surface colour temp. meas. pyrometer 78−57956
- leading in glazed caramics, colorimetric method *(Spanish)* 80−73414
- light source, D65, for colour meas. 79−32018
- light source brightness measurement, standard photometric system errors 78−58005
- lunar colorimetric map, absorpt. strip intensity distrib. at 0.95 μm *(Russian)* 79−44381
- mathematical determination of colour contrast, uniform chromaticity scale construction 78−49881
- matrix techniques in colorimetry 80−105690
- metameric object-colour stimuli counting using freq. limited spectral refl. functions 78−8432
- metameric white samples for testing relative UV content of light sources and daylight 79−58767
- metrics, facts and formulae 80−97900
- microcomputer appl., description *(French)* 77−5882
- microprocessor controlled spectrophotometric colorimeters *(Hungarian)* 80−101851
- microprocessor-based system, features 79−58770
- microscopical stain colour rendition by dyes produced in reversal colour films *(German)* 80−12318
- multicolour image storage on black and white film, using crossed grating 79−31813
- Munsell renotations for samples of OSA uniform colour scales 79−12833
- nematic liquid crystal cell, with pretilt angle, electro-optical properties *(Japanese)* 78−43837
- ocean surface chlorophyll concentration obs. from high altitude 77−4976
- online shade monitor, strip materials 79−30526
- optimum colour appearance anal using spectrophotometers in quality assurance laboratories 80−90877
- photoelectric tristimulus colorimeter design, CTE system of colour measurement 80−9018
- photographic films, high speed, colorimetric testiing of Boots 400 and Agfa CNS 400 80−18026
- photographic materials, colour component triads, colorimetric determ. for positive materials *(Russian)* 80−95178
- photographic papers, colorimetric evaluation of colour separation *(Russian)* 78−49926
- photographic parameter estimation, colour and density table *(German)* 79−49309
- photometric analysers, automatic reactive, H_2O composition checking 80−27330
- Polaroid photography colour reproduction 78−54490
- polychromatic line apread function colour meas., colorimetric MTF 78−50712
- polyvinyl acetate with iodine-iodide, reaction system, colour complex form., temp. effect 79−83457
- proton radiography, solid state detectors 78−92424
- PVC near-colourless transparent film, colorimetric determ. of colour 78−49884
- quality control appl., theory and practice *(German)* 79−80665
- reflecting sample, apparatus with spectral masks 77−34013
- reflective glass colour standards 80−90878
- reflectometer, spherical, calibration of lustrous colour standards appl. *(German)* 77−18066
- repeatability *(Hungarian)* 78−93748
- reproductions, colorimetric comparison 80−95119
- retroreflecting material metrology, errors in luminous refl., chromaticity meas. 80−68235

colorimetry continued
- retroreflective material chromaticity meas. under nighttime geometry 80—73411
- rose tinted instrument, features 79—218
- saturation of coloured samples at various levels of reflectance 77—67487
- scintillation counter appl., liquid, use of miniature ^{14}C and ^{3}H standards 80—21346
- sensitometry characteristic curves corresponding to visual impression 80—82803
- sensitometry system based on spectral densitometer 80—82804
- sensitometry using densitometer with more than 3 channels, dye specific densities 80—82802
- solid-state reaction, photoacoustic photocalorimetric obs. 80—61089
- sorbitol, crystallisation, thermal investig. 78—47257
- spectral sensitivities of colour-reproduction systems 78—49883
- spectral transmission and reflection coeffs., USSR special standard 77—30195
- spectrocolorimeter, SPEKOL, meas. of diffuse reflectance spectra, of differently matted polyamide fibres 80—77836
- spectrofluorimetry, colorimetric calcs. rel. to monochromator bandpass intensity spectrum 77—29071
- spectrophotometric for 0° illumination/diffuse observation measuring geometry *(Hungarian)* 78—93750
- spectrophotometric random errors effect on color difference meas. 78—12741
- standards, colour matching and adaptation exam., using Japanese observers *(Japanese)* 79—6163
- standards, prep. of OSA Uniform Colour Scales Committee samples 79—2807
- steel, C, corrosion inhibition by 2-ethylamino-ethanol in aerated 3% NaCl soln., pH effect 80—21160
- thermochromism appl. *(Hungarian)* 77—18068
- thiospinels, thermodynamic stability, enthalpy of form. 79—52737
- toxic micro-concentration, photo-colorimetric lens technique *(Russian)* 77—40610
- tristimulus colorimeter to MOMCOLOR *(Hungarian)* 77—26381
- ultramarine pigments, instrum. for colour measurement and control 80—62711
- uniform colour scales, Optical Society of America 80—12134
- uniform colour scales, space lattice used to sample colour space 79—26100
- uniform colour scales of OSA samples, colorimetric specification 78—65952
- wavelength calculation, selected coord. method using Chebyshev integration formulae, tristimulus values *(German)* 77—82586
- whiteness, visual impression and colorimetric definition 80—81597
- whiteness formulae 79—58768
- whiteness perception, individual differences and common trends 79—100612
- Al film, energy losses of electrons, microcalorimetric meas. · 80—59543
- Al_2O_3-SiO_2-CaO-B_2O_3(1,1,1 wt.%) chemical analysis by photocolorimetry and titration 79—20483
- B, dissolved, in water, determ. via azomethine H colorimetric method 79—92115
- C thin layers, thickness determ. by objective colorimetry 78—77844
- Co enamel, vitreous, objective colour evaluation, rel. to firing parameters *(Czech)* 80—42252
- Cr film, vacuum-deposited, quantitative mass anal. by colorimetry 77—69998
- $CrAl_2S_4$, thermodynamic stability, enthalpy of form. 79—52737
- Fe(II) determ., in Cu process metallurgical soln. by o-phenanthroline colorimetric method 78—7293
- GaAs:Cr, EPR, annealing and IR excitation effect on Cr^{+} signal, Cr content by colorimetry 77—69680
- Mn VI, colorimetric determ., appl. to Egyptian Mn ores 78—53285
- PbO, stoichiometric deviations on heating in vacuum 77—25035
- $ZnAl_2S_4$ and $ZnCr_2S_4$, thermodynamic stability, enthalpy of form. 79—52737

colour
- *see also colour vision*
- alkali phosphate glasses, colour and absorption spectra of Fe 77—85752
- 3-nalkyl-6-(4-n-alkyloxy-phenyl)-1,2,4,5-tetrazines, stable dyestuffs with liq. cryst. props. 80—19693
- alloy colour and colour stability as alloy design criteria 80—101005
- asteroid families, obs. evidence for common origins 77—91468
- benzyl viologen, mechanism of electrochromism *(Japanese)* 80—34893
- beryl, channel constituents, electronic absorption spectra of Fe^{2+} 79—69863
- borate glass:S, (boro-ultramarine), blue chromophore identification 77—20888
- camera lens photographic chromaticity, spectral transmission curves analysis 80—31925
- ceramic glazes, Pb, Zn and added chromogenic ions release, as function of colouring oxide mill additions, voltammetric exam. 78—39920
- chemical analysis of coloured cpds. by reson. Raman spectroscopy *(Japanese)* 79—48017
- chemical origins 79—21479
- cholesteric liquid cryst. soln., effect of γ-irradiation on colour transition temp. 77—47343
- cholesteric liquid crystal coatings, superimposed left- and right-handed, peak refl. and colour gamut 80—74472
- cholesteric liquid crystals, additive colour properties and colour gamut 79—7546
- cholesteryl nonanoate (decanoate), effect of cholesteryl alkanoyl esters on red-green transition temp. 80—19924
- cholesteryl nonanoate organic solns., γ radiolysis, colour transition temp. 79—57266
- chrome yellow, crystal lattice deform. effect on colour *(Rumanian)* 78—23422
- clay soil/sand mixtures, colour and reflectance rel. to sand content 80—56475
- colour matching, review of basic laws and progress during the last 15 years 78—65955
- colour sicence contributions, collection of papers by D.B. Judd 80—98761
- colour space and mathematical structure *(Spanish)* 79—80666
- computer colour measuring instruments 79—67372
- conference, Troy, NY, USA (July 1977) 78—49882
- daylight, chromaticity locus *(Japanese)* 77—78355

colour continued
- demonstration of continuous spectrum, optical filters to audiences, students 77—45649
- demonstrations for polytech. students 77—49533
- dichroic dyes, guest-host interactions in liquid cryst. devices, colour switching 77—51312
- electrochemical voltage indicators, production, voltage response, resist. 77—1936
- encoding with coherent optical processing system 77—7020
- feature space mapping, linear transformation for improved colour image interpretability 77—78499
- film, interference colours produced by white light refl. teaching paper 80—8754
- flame emission anal., apparatus for teaching 77—29976
- fluorite, use of proton irrad. to reveal growth and deform. features 80—84216
- gems and minerals 77—37182
- glass, colouring by colloidal P 77—8961
- glass, photochromatic, induced colour by optical/thermal treatment 80—34954
- halosodalites, synthesis, cathodochromism, reflectivity spectra 77—40399
- holographic pseudocolor encoding, spatial filtered imaging technique 79—18370
- hydroxypropyl cellulose in conc. aq. soln., mesophase struct., colour 77—19870
- imaging multispectral optoelectronic system effectiveness evaluation 79—81553
- LANDSAT data digital chromaticity mapping for water quality anal. 79—29872
- liquid crystal display, with dichroic dye guest, field-induced colour switching 80—1327
- liquid crystal dyes, field-induced colour changes 80—25340
- luminous colour control methods in pulsed arc discharges in Ne-Hg lamps *(Japanese)* 80—103214
- minerals, physical theories for origin of colour 78—69323
- mixing demonstration, teaching 79—58505
- Moon, Mare Crisium spectrally distinct units correl. with radar-detected subsurface interface 79—16848
- multiquark hadrons in two dimens. QCD, asymptotic solns. with Regge trajectory spectra 78—66085
- nematic liquid crystal display device, generation of arbitrary colour 80—5815
- ocean, Monte Carlo model including atm. and ocean scatt., absorpt. 78—61421
- ocean, remote sensing 77—78460
- optical pseudocolouring through contrast reversal filtering 79—81378
- optimum colour rendering of holographic images *(Russian)* 77—7035
- paste, direct tensile tests and tied crack model 78—11178
- phase imaging systems, chromaticity, luminous efficiency 78—33824
- photographic materials, colour component triads, colorimetric determ. for positive materials *(Russian)* 80—95178
- picture colour component detection in SAW scanning 78—59149
- pigments, willemite struct., NiO, MnO, and FeO based, synthesis 80—20855
- polyarylenealkyls, colour, EPR, electron density delocalisation degree determ. *(Russian)* 80—7152
- polycarbonate, colour appearance during oxidation *(Russian)* 79—24643
- polycarbonate, turning yellow during oxidation, kinetic regularities *(Russian)* 79—24644
- polyethylene, with various antioxidant, stabilized and TiO_2 pigment additions, photo-yellowing and oxidation 79—16015
- polypropylene, stability under radiation sterilisation 77—60245
- primary colours used in physics and art, for teaching 79—35464
- proteins, EPR absorption of tissue constituents, colour correlation, using mouse liver 77—90727
- pseudocolour encoding of holographic images using single wavelength 78—87025
- pseudocolour encoding of spatial frequency information 78—87018
- psychometric measures for specifying colour appearance 80—76747
- quartz, rose, charge transfer mechanism for origin of colour, EPR and optical expts. 78—52537
- rainbow hologram colour blur 79—13922
- rare earth oxyhalides and oxysulphides, thermochromic luminescent mats. *(Russian)* 78—48230
- reflection nebula, optical colours, polarisation, composite and mixture of nebula grains 78—16502
- rocks and minerals, colour values from diffuse reflectance spectra *(French)* 78—11881
- sapphire, natural, origin of colour 79—70794
- schlieren image colorisation using electro-optical technique 78—33904
- schlieren system, colour images of inhomogeneous transparent media 78—33905
- seawater off Ireland west coast, surface waters colour, UV absorbance and salinity 78—85603
- secondary colour aberration limited system performance estimation 79—23041
- segmentation method of detecting cellular images using colour information *(Japanese)* 78—11783
- space, formal props., metric and vectorial character *(Spanish)* 77—68284
- spiral galaxies, colours rel. to morphological type in stochastic star form. model 80—12818
- standards, prep. of OSA Uniform Colour Scales Committee samples 79—2807
- textiles, uniformity meas., appl. of microdensitometry *(Czech)* 79—30524
- time dependent physical spectrum 78—9317
- two-colour laser Doppler velocimeter *(German)* 80—10326
- uniform colour scales, space lattice used to sample colour space 79—26100
- visible spectrum vision-related partitioning 79—92222
- water quality monitoring, modular system *(German)* 80—26186
- Al_2O_3 anodic oxide film colour and structure obs. 78—11450
- $BaCuO_2$, prep. and props. *(French)* 77—43201
- C films, diamond-like, on Si, colour chart 80—97366
- C materials, optical microscopy, reflection, interference colours, terminology 78—42871
- CdO film, chromatic changes on heat treatment *(Russian)* 77—55843
- CoO-MgO-Al_2O_3-Cr_2O_3-TiO_2, form. and colour of spinel solid soln. *(Japanese)* 77—32550

colour continued
- $CoO-MgO-Cr_2O_3-Fe_2O_3-TiO_2$, form. and colour of spinel solid soln. *(Japanese)* 80—16059
- $CoO-ZnO-Al_2O_3-Cr_2O_3-TiO_2$ system, form. and colour of spinel solid soln. *(Japanese)* 77—25001
- $\alpha-Fe_2O_3$ colloids, absorpt. index and colour 79—92009
- $He-I_2$ laser, sequential separate multicolour output operation *(Japanese)* 80—28205
- $InSb/Pb_{0.79}Sn_{0.21}Te$ photodiodes, two-colour sandwich detector 77—82602
- $La_2O_3-Y_2O_3-Al_2O_3-SiO_2$, coloration by transition metal oxides, absorpt. bands *(Japanese)* 80—55148
- $Na_2S-B_2O_3-GeO_2$, darkening and fading in UV irradiation *(Japanese)* 77—36270
- Na_2S-GeO, darkening and fading in UV irradiation *(Japanese)* 77—36270
- Nb_2O_5, single cryst. growth by chem. transport reactions involving $TeCl_4$ 77—36382
- NiC, colour change on replacement of PbO in glaze *(German)* 79—91813
- NiO samples, colour difference, X-ray line broadening study 80—100206
- NiO-MgO-ZnO, solid soln. form and colour *(Japanese)* 77—63647
- $PbMoO_4$, colour origin 77—85921
- $Pb_2Ta_{2-x}M_{2x}O_{7-x}$, (M=Ti, Sn Zr), oxygen deficient, form., IR spectra, dielec. const. *(Japanese)* 77—48171
- Si, ion implanted, colour generation model 77—85868
- Si_2N_4 powders, synthesis, charact. 79—33977
- SnO_2:Cr(Sb), cassiterite, gas phase growth on seed 77—24937
- $Sn_xTi_{(1-x)}O_2$, solid soln., thermal reaction with V(V), Cr(III), Cr(VI), Mn(II), Fe(III), Co(II), NI(II), Cu(II), Sb(III) 80—16674
- $Ta(OR)_2Cl_3.L$, halo-alkoxide complex, prep. and props. 78—18605
- Tl_2WO_4, solid-state prep., cryst. struct. and props. 78—38673
- V_xO_y, FTIROS thermochromic materials, colour and visual contrast 80—33100
- WO_3, amorphous coloured film, charge transfer, XPS 77—12491
- $ZrSiO_4-Fe_2O_3$, pink colour form. kinetics 79—60360

colour blindness *see colour vision*

colour cameras, television *see colour television cameras*

colour centres
- *see also F-centres; OH^--centres; paramagnetic resonance of colour centres; U-centres; V-centres*
- absorption wavelength, finite-pot. well models 78—12463
- alkali, borate glass:S, blue and green coloration, absorpt. spectra 79—87470
- alkali halide: $Ge^{2+}(Sn^{2+})(Pb^{2+})$, T-centres, absorpt. spectra, energy level diagram 77—73157
- alkali halide, chalcogen^{2-} vacancy centres, absorpt. and fluoresc. spectra 78—48204
- alkali halide, irrad., colloidal centre growth, model 77—19946
- alkali halide, thermal annealing, monomolecular and bimolecular sequence of kinetics 78—47373
- alkali halides, electron irradiated depth distrib. profiles of colour centres 79—27977
- alkali halides, polarization, photoinduced, rel. to exchange between vacancy and impurity 80—59914
- alkali halides, positively charged long-lived excited states and spontaneous tunnel transitions 79—82552
- alkali halides, positron annihilation, expt. techniques, positron states, book contrib. 80—2894
- alkali halides, radiolysis, growth of colloidal metal inclusions 78—92493
- alkali silicate glass, photochromism 77—43955
- alkaline earth fluoride crystals, colour centre thermal stability 78—83811
- alkaline earth oxides, point defect props., band struct., lattice simulation calc. 80—19797
- amethyst, Fe^{3+} diffusion, associated phenomena 77—36269
- diamond, dynamic Jahn-Teller distortions at trigonal optical centres 79—87069
- diamond, electron radiation damage 77—84798
- diamond, irradiated, optical study of TR12 and 3H defects 77—85772
- diamond, N9 and ND1 energy levels, electron irrad. photocond. obs., thermolum. 78—6324
- diamond, natural, impurity complexes, shape and dimens., diffuse X-ray scatt. obs. 78—47398
- diamond, natural, thermoluminescence, phosphorescence, defects, low temp. 78—11000
- diamond, optically active centre effect on strength props. 80—40462
- diamond, optically active defects, anomalous X-ray scatt. 77—89434
- diamond, type-I, electron irrad., annealing at 800-1500°C 80—24500
- diffusion-controlled defect recombination, incorporating Coulomb interaction and annihilation 78—23044
- education, electrochromism in WO_3, advanced lab. expt., colour centres, proton diffusion 80—17738
- electron irradiation, energies greater than 1 MeV, defect form. and secondary electron emission *(Russian)* 77—55304
- fluorites, natural colour centres and associated rare earth ions 79—61408
- fluorochloroapatite, synthetic, defect struct. and colour centres obs. *(Russian)* 78—30612
- fluorphlogopite, valence transition of Ti impurity, ESR and optical absorption data 77—16155
- glass, colour centre form. by UV irrad., afterglow, thermolum. and EPR obs. 78—10047
- glass, electron irrad., colour centre depth distrib. 79—73217
- glass, photochromic, spectral characts. control 80—16073
- glass, surface layers diffusion containing Pb and Cu 77—36677
- glass film compositions, electrochromism *(Russian)* 79—28721
- halide photochromic centres, isothermal relaxation kinetics 80—16072
- III-V semiconductor, localised defects, one-electron pseudopot. 77—24533
- ion implantation, appls. to colour centre research, review 79—19272
- ionic crystal, positron annihilation decay kinetics *(Russian)* 78—6805
- ionic crystals, electronic and vibr. props. of point defects, book 80—51962
- KBr, thermally processed cryst., optical absorption bands *(Russian)* 78—76513
- laser with superfluid He cooling 80—48282
- luminescence, nonuniform broadening profile, optical excitation migration effects 78—48215
- luminescence band, deform. and shift, impurity centres, migration of excitations, math. modelling 78—48225
- magnetic semiconductor, mag. colour centre continuum model 79—28321

colour centres continued
- metal colloids in ionic cryst., preparation, optical, mag. resonance, elec. props. 80—59459
- metal oxides, Mollwo-Ivey relation between peak-colour absorption energy and average O ion spacing 77—90179
- minerals, physical theories for origin of colour 78—69323
- mixed fluoride crystals, nucl. radiation effects 80—80831
- multiphonon tunnel processes in homogeneous elec. field *(Russian)* 78—39607
- non-rigid impurity centre, symmetry group *(Russian)* 80—29019
- nonmetal, impurity optical absorption and emission, anharmonic effects 78—56503
- nonmetallic crystals, ENDOR of impurity centres 80—25249
- optical fibres, UV radiation-induced losses rel. to colour centre form. 80—87517
- optical glass, coloured, laser damage threshold, optical absorpt. influence 80—91830
- optical glass, radiation coloration due to fast electron irradiation 79—98452
- optical isolation mechanisms 77—19288
- phonon many-mode interaction, absorption band shape, adiabatic approx. 78—2883
- phosphate glasses, fading mechanisms 79—95851
- phosphate glasses, $P_2O_5-Al_2O_3-Mg(Ba)(Sr)(Ca)O$, struct. energetics and charging under irrad. *(Russian)* 77—84791
- photodichroic materials as coherent optical computing elements 77—71962
- photographic emulsions, ultra-fine grained, nature of produced colour centres during photolysis *(Russian)* 80—73517
- α-quartz:Al, γ-irrad., thermal cond. below 10K 79—51320
- quartz:Cu, glassy and cryst., luminesc. centres 77—4679
- quartz, comparison of different radiation effects 78—26596
- quartz, E_1' centre formation and regeneration, α and γ radiation efficiency 79—32992
- quartz, electron irradiated, optical and anelastic absorptions and resonator freq. 78—64385
- quartz, electron irradiation effects on optical, dielec., elastic props. 80—59521
- quartz, electron pulse irrad. effect on defect formation 80—15155
- α-quartz, EPR of E'_4-centre 79—73810
- quartz, irradiated, fused, crystalline, absorpt. spectra, colour centres 80—7384
- quartz, pulse electron irrad., temp. effect on colour bleaching 79—1779
- quartz, radiation induced, rel. to diffuse interstellar bands origin 77—13432
- quartz, smoky, HF US relax. 78—71796
- quartz, synthetic, connection between lattice deform. and coloration pattern 78—10930
- quartz, synthetic, discoloration rel. to lattice deform. 77—24872
- quartz, synthetic, fading rel. to lattice deformation *(German)* 78—63760
- α-quartz, uncompensated Ti^{3+} centre, annealing, X-irrad., EPR meas. 79—65731
- quartz resonator, electron irrad., rel. to optical absorpt. 77—8609
- radiation damage, mechanisms, in semiconductors and insulators, review 80—107315
- review, fifty years of colour centre physics 80—105487
- review of colour and symm. in imperfect crystals 78—72562
- ruby, induced absorpt., radioluminesc., thermoluminesc., Cr^{3+} conc. depend. *(Russian)* 77—90206
- ruby, radiation-induced optical processes, impurity effects 80—66310
- sapphire, radiation-coloured, vacuum UV spectra 78—84605
- semiconductor, optical absorption by impurities, phonon-electron interaction 78—56502
- semiconductor, Raman scattering from impurities 78—56468
- semiconductor, Raman scattering from impurities 78—56469
- silicate Fe activated glass, diffraction trating recording by UV laser 80—5842
- silicate glass, dangling bond states 80—24846
- silicate glass, nonactivated, far UV image recording, colour centre formation *(Russian)* 77—5950
- silicate glass darkening due to UV radiation from laser produced plasma jet 78—52598
- silicate glasses:Cu^+, effect of UV irrad., absorption bands 78—31222
- silicate glasses, radiation coloured, photoinduced dichroism 79—69808
- silicates, radiation induced, rel. to diffuse interstellar bands origin 77—13432
- spinel transparent glass ceramics, colour centre form. due to alkali metal vapour and X-ray irradiation 79—87316
- α-quartz:Ge, Ge^{3+} centres, dynamic interchange, EPR obs. 79—19776
- Ag halide, glass, kinetics of photochromic processes 80—103930
- Ag halide photochromic glass, darkening mechanisms under pulsed laser excitation 78—25938
- Ag halide photochromic glasses, colour centres struct. 80—66254
- AgBr, pure and doped, identification of shallow electron centres 77—59267
- $AgBr:Cu^+(Cu^{2+})$, luminesc., ion interactions 77—66534
- AgCl, colloid bands induced by reactor irradiation at low temps. 78—26567
- AgCl, colloid centres induced by reactor neutrons at 20K 78—72560
- AgCl photochromic glass, additional absorpt. spectrum, ellipsoidal model of colour centres 80—40142
- AgCl, pure and dopded, identification of shallow electron centres 77—59267
- $AgCl:Cu^+(Cu^{2+})$, luminesc., ion interactions 77—66534
- $Al_{2x}Ga_{2(1-x)}O_3:Cr^{3+}$, luminesc., lifetime, 77 and 4K, struct., energy transfer 79—28798
- AlH_3, photo-and thermochem. reactions, 200-350K, UV Induced local states 78—31667
- AlH_3, photoelectric effect spectra and kinetics, photochem. mechanism colour centres 78—56506
- $\alpha-Al_2O_3$, AES, electron energy loss, and optical spectroscopy obs. 78—35176
- Al_2O_3, anodic oxide films, luminesc., breakdown and colouring 78—19528
- Al_2O_3, corundum, γ-irrad., colour centres, growth method effect 77—1710
- $\alpha-Al_2O_3$, defects in unirradiated cryst., optical absorpt. spectra 79—61409
- Al_2O_3:Co, spectra, heat treatment and irrad. effects 77—4659
- Al_2O_3:Ti(Si), annealing, electron irrad., absorpt. spectra 77—20890

colour centres continued
β-Al_2O_3-Na_2O, AES, electron energy loss, and optical spectroscopy obs. 78—35176
β-Al_2O_3-Na_2O, ENDOR meas. of defects 80—66074
β-Al_2O_3-Na_2O, tunnelling states, electron spin relax. 79—78518
As_2S_3, D-centres, microscopic model *(Russian)* 79—46654
As_2S_3, glassy, optical absorption spectra after 4.5 MeV electron bombardment *(Russian)* 77—32408
As_2Se_3, D-centres, microscopic model *(Russian)* 79—46654
As_2Se_3, glassy, optical absorption spectra after 4.5 MeV electron bombardment *(Russian)* 77—32408
As_2Te_3, D-centres, microscopic model *(Russian)* 79—46654
B_2O_3 glasses, thermolum., additives effect 78—27337
B_2O_3-Li_2O-LiCl glass, X-irradiated, EPR of Cl_2^- centres *(French)* 79—47333
$[(100\text{-}x)B_2O_3.xLi_2O]_{98}.2CdO$, glass, X-ray irrad., EPR study of Cd^+ centres *(French)* 78—43638
BaF_2:Er^{3+}, single-site multiphonon and energy transfer relax. 78—52547
$BaSO_4$, with small retrapping factor, thermolum. glow curve 77—52188
$CaCO_3$, γ-irrad. defects, absorpt. spectra obs. 77—63447
CaF_2, additively coloured, Ca colloid form. and size evolution during annealing 77—20895
CaF_2, bleaching characteristics of crystals coloured by low energy electrons 78—76497
CaF_2, doped, colour centre form. by UV irrad., afterglow, thermolum. and EPR obs. 78—10047
CaF_2, natural fluorite colouring, effect of impurities on absorpt. spectra 79—56822
CaF_2:Dy, colour centres, antiresonance-type phenomenon in external fields 78—68529
CaF_2:Dy^{3+}, fluoresc. spectra, A-centres and B-centres, Stark levels 80—25428
CaF_2:Na, single cryst., X-irrad., optical absorpt. and thermoluminesc. 80—34952
CaF_2:O^-, Jahn-Teller distortion, electronic struct., MS Xα calc. 78—23057
CaF_2:RF_3, colour centre prod. by γ-irrad., absorpt. spectra obs. 78—72565
CaF_2:U(Th), and pure, electron microscopy study of lattice deformation due to electron irrad. 79—65077
$CaFPO_3$, colour centre form., X-ray and electron bombardment *(Russian)* 77—19948
$Ca_5F(PO_4)_3$, colour centre accumulation deformation effects 77—84743
CaO, absorpt. band identification of colour centres 77—40271
CaO, electron irradiated, symmetry assignment of new point defect 78—31261
CaO, neutron irrad., MCD, optical absorpt. lines 77—77255
$Ca_2P_2O_7$:Sb, (Sb,Mn), luminesc., activation, colour centres *(Russian)* 78—92123
$Ca_2P_2O_7$:Sb(,Mn), luminesc., colouration 80—2828
$Ca_3(PO_4)_2$:Sb,(Sb,Mn), luminesc., activation, colour centres *(Russian)* 78—92123
β-$Ca_3(PO_4)_2$:Sb(,Mn), luminesc., colouration 80—2828
$Ca_{10}(PO_4)_6Cl_2$, nonstoichiometry effect on X-irrad. induced electron-excess centres 77—62525
CaS, absorpt. band identification of colour centres 77—40271
CaS, colour centres and photoluminesc., flash stimulation bands *(Russian)* 77—20923
CaS:Cu, colour centres, optical and thermal depths determ. 80—66275
CaS:Cu, colour centres and photoluminesc., flash stimulation bands *(Russian)* 77—20923
$CaSO_4$, γ-irradiated, ESR and bleaching studies of radical ion centres 80—2637
$CaSO_4$:Dy, photo-stimulated thermolum., for high-exposure dosimetry 77—9262
CdF_2, colour centres, IR absorpt. and photocond. after UV irrad. 80—79784
CdF_2:NaF(AgF), colour centres, IR absorpt. and photocond. after UV irrad. 80—79784
CdO, point defect props., band struct., lattice simulation calc. 80—19797
CdS, local cathodolum. of single crysts. under colour contrast conditions in SEM 79—8191
CdS:Mn(Co), intensity and spectral distrib. of luminescence *(Russian)* 77—16392
CdTe, Yb^{3+} implantation, nonstoichiometry effect 77—15440
CoO-containing glass, effects of γ-rays, electron beam and neutron flux on transmissivity *(Japanese)* 77—73156
CsBr, impurity absorpt. spectra after γ-irrad., aggregated colour centres 79—4829
CsBr, temp. depend. of Cs colloids absorption bands 80—40145
CsBr:Cl(F), luminescence investig. of F_H-centre lifetime 77—20917
CsBr:NO_2^-, luminesc. centre polarisation and reorientation *(Russian)* 78—76529
$CsCaCl_3$:Pb, and undoped crystals, photolum. and thermolum. meas. *(Russian)* 77—85767
CsI, temp. depend. of Cs colloids absorption bands 80—40145
CsI:NO_2^-, luminesc. centre polarisation and reorientation *(Russian)* 78—76529
Cu halide based photochromic glasses, spectral props. 80—29708
$CuGaS_2$, coloration, pure and Fe doped, EPR and optical absorpt. obs. 78—88336
GaAs:Mg ion implanted, photoluminesc. and annealing characts. 77—16361
n-GaAs:Si LEC crystal, carrier conc., B acceptor centres, Hall meas. and IR spectra 78—6717
GaN, photoluminesc. characts. for 35 implanted elements 77—24884
GaP crystals, radiation defects, TSC obs. 80—65588
GaP:Cu, deep levels, photoluminesc. and optical cross sections 79—38653
GaP:Zn,O, Auger coeff. from luminesc. decay and Hall effect 77—48226
GaP:Zn,O, Auger coeff. from luminesc. efficiency and Hall effect 77—48227
HfO_2:M^{n+}, M=Ce, Pr, Tb, Eu impurity valence transitions 77—51694
Hg_2Cl_2, single cryst., luminesc. 397 nm band props. 77—66529
In_2Se_3, absorpt. spectra, 77 and 300K, freezing of absorpt. centres 77—24417
KBr, additively coloured, self-enhancement of amplitude hologram *(Russian)* 80—9828
KBr and KBr:Sr X-irradiated, optical investig. of Br_3^- centres 77—16348
KBr bicrystal, rel. to Ag^+ injection transport and grain boundary mobility, electrodecoration obs. 80—2214

colour centres continued
KBr, colour centres isothermal decay 79—51975
KBr, defect accumulation under electron irrad. at 4K 80—107233
KBr, efficiency of creation of X_3^- centres in X-rayed alkali halides *(Russian)* 78—71731
KBr, electrolytic coloration effect on dislocation density 77—4106
KBr, excitation of thermolum. near liq. He temp. 80—40171
KBr, interaction between F- and α-centres, luminesc. meas. 79—73988
KBr, m-crocryst. powders coloured in electrodeless discharge, reflectance spectra, thermolum. 78—15238
KBr, optical conversion, luminesc. and colour centre formation 79—24354
KBr, S centres, luminesc. and photochemistry *(German)* 77—44055
KBr, substrate, with colloidal centre vacuum deposition of Au particles *(Rumanian)* 78—60579
KBr, X-irrad., I-centre activation energy and thermal diffusion 78—72606
KBr:Au^-, optical absorpt. bands and MCD, electron-lattice interaction 80—108236
KBr:KI, microcrystalline powder, isothermal decay of colour centres 79—42995
KBr:P, colour centre fine struct., ODMR 78—6604
KBr:S^-, Jahn-Teller model of S^- ion centre 79—82567
KBr:Tl, nonradiative transitions in colour centres, WKB approximation 77—85803
KBr(Cl)(I):O_2^- centres, luminesc., polarisation temp. depend. 78—87943
KBr(I):Co, coloured and uncoloured, Mossbauer effect, inhomogeneous hyperfine fields 77—32307
KCl, additively coloured, colloid size distrib., replica microscopy, absorpt. spectra 77—47449
KCl, additively coloured, colloid nucleation and growth, TEM 77—62526
KCl and KCl:KBr, colour centres isothermal decay 79—51975
KCl, colour centres laser spectra, induced F' band absorpt. 80—2779
KCl, cryst., two-layer colloidal K and Cu colour centre light absorption 77—12408
KCl, efficiency of creation of X_3^- centres in X-rayed alkali halides *(Russian)* 78—71731
KCl, electrolytic coloration effect on dislocation density 77—4106
KCl, electron impact, colour centre distrib., channelling 79—14866
KCl, electron irrad., secondary electrons and radiation defects 79—55782
KCl, H_2O-related centres 78—67711
KCl, m-crocryst. powders coloured in electrodeless discharge, reflectance spectra, thermolum. 78—15238
KCl, phonon scattering on small radius colloids 78—38798
KCl, positively charged long-lived excited states and spontaneous tunnel transitions 79—82552
KCl, positron annihilation in colour centres 77—73185
KCl, S centres, luminesc. and photochemistry *(German)* 77—44055
KCl, substrate, with colloidal centre vacuum deposition of Au particles *(Rumanian)* 78—60579
KCl, thermal and photothermal conversion of colour centres, after high-dose electronic interaction *(Russian)* 80—39156
KCl, with divalent impurity, reorientation of impurity-vacancy complexes, thermally stimulated depolarisation 77—65977
KCl, X-centres thermal decay process, activation energy *(Russian)* 79—90651
KCl, X-irrad., I-centre activation energy and thermal diffusion 78—72606
KCl, X-irrad. induced deform. effects, glow curves *(Russian)* 79—52022
KCl, X-irradiated, formation of cation defects 78—91359
KCl:Ag, formation of Ag atoms and self-localised holes by illumination, EPR meas. 78—31108
KCl:Ca, Z_4 centres, thermal and optical bleaching 80—19802
KCl:$CaCl_2$, KOH, complex form., U-centre influence, optical absorpt. bands 77—80502
KCl:Eu^{2+}, γ-irrad., photostimulated low temp. recomb. luminesc. 80—11435
KCl:Na, electron trapping from α_A and F_A-centres, low temp. depend. 80—11444
KCl:P, colour centre fine struct., ODMR 78—6604
KCl:PO_2^-, phosphoresc. and PMDR spectra, electronic and vibr. states 79—65768
KCl:Pb^{2+}, origin of 420 nm emission band 77—40279
KCl:S^-, Jahn-Teller model of S^- ion centre 79—82567
KCl:$SnCl_2$, electronic struct. of Sn^+ centres, model 77—43530
KCl:Tl^+, absorpt. spectra, electrolytic coloration, migration in electric field, heat treatment 78—23504
KCl:Tl^{2+}, Na, X-irrad., activator-impurity association *(Russian)* 77—85761
KCl-KBr:Tl^+, cryst., luminesc. and excitation spectra 77—66535
KCl-Mg, X-irrad. and F-bleached, optical and ESR spectra 77—48052
KCl-$SrCl_2$, photoluminescence of Z_4-centre and associated Z type colour centre *(Russian)* 79—4851
KCl-Tl^+,Ca^{2+}(Sr^{2+}), electrolytic colouring, colour centre form., optical absorpt. spectra 79—15497
KCl(:LiF), radiative Q-centres, opt. absorpt. and thermal conductivity 77—47450
KF, deformation coloration 77—76397
KF:Hg^{2+}, electrolytic colouration 78—75665
KI, efficiency of creation of X_3^- centres in X-rayed alkali halides *(Russian)* 78—71731
KI, quenched, absorpt. and emission spectra, α-centres 80—11442
KI:S_2^- centres, luminesc., polarisation temp. depend. 78—87943
KI:Tl, nonradiative transitions in colour centres, WKB approximation 77—85803
K_2O-B_2O_3 glass, γ- and UV- irrad., thermodecolorisation and thermolum. 80—20721
K_2O-B_2O_3 glass, laser decolorisation of colour centres 79—43008
KI:Tl^+, X-irrad., absorpt. spectra investig. of Tl_2^+ centres 77—20887
LiD:Mg^{2+}, X-irrad., dielec. loss 80—55024
LiF, γ-irrad. induced defects, positron capture and annealing obs. 80—60707
LiF, γ-irrad. pure and Mg-doped, phonon scatt. and interstitial clusters 80—70254
LiF, thermally stimulated exoemission, radiation defects and adsorpt. centres 78—11087
LiF with stable F_2 centres, F_2^+ colour centre generation accumulation, tunable laser production *(Russian)* 80—28238
LiF:Hg^{2+}, electrolytic colouration 78—75665
LiF:Mg cryst., Mg electron colour centers 80—100229
LiF:U, X-ray and γ-ray irrad., EPR of U^{5+} centres 79—91295

colour centres continued
- $LiF:U_3O_8$, X- and γ-irrad., U^{5+} luminesc. molecular centres, optical and ESR expts. 77–48224
- LiF-OH, γ-irrad., colour centre lasing at 0.84-1.13 μ at 300K 80–5739
- LiI crystal, irradiated at low temps., optical absorption spectra 80–45123
- LiI, reactor irrad., absorpt. spectra 79–65902
- LiI:Tl, absorpt. spectrum obs. 80–50378
- $LiNbO_3$ crystals, polaron character of colour centres 80–2013
- $LiNbO_3$, optical absorption of hole centres, polaron model 80–97314
- $LiNbO_3$, optically active centres, form. by electron and γ-irrad. 78–18642
- $LiNbO_3$, pure, two-photon photorefractive recording 78–31220
- $(Li_2O\text{-}Al_2O_3\text{-}SiO_2):Fe_2O_3$, glass, pyroceramic form., colour centres, magnetochem. investig. 77–16537
- $LiTaO_3$, picosecond study of colour centre translocation 80–40144
- $LiTaO_3:M$, optical damage of transition-metal-doped ferroelectric 78–95571
- $LiYO_2:Nd^{3+}$, absorption and luminesc. spectra, γ-irrad. induced colour centre form. 77–63441
- $MgF_2:Mn$, X-ray luminesc., activator flash 79–65958
- $MgF_2:Mn(Co)$, photoluminesc. due to X-rays, colour centre thermal breakdown 79–24359
- MgO, implanted K aggregates, TEM and optical spectra obs. 78–83838
- MgO, neutron irrad., MCD, optical absorpt. lines 77–77255
- $MgO:Fe^{3+}$, Mn^{2+}, X-irrad. induced anion Frenkel defects, stabilisation by Fe^{3+}, optical and ESR obs. 77–68969
- MgO:Li, mech. deformed crysts., imprinting of slip bands using Li impurities 80–59473
- MgO:Li, thermally generated $[Li]^0$ defects, valence compensation 79–77598
- MoO_3, film, colour centre studies, optical absorpt. spectra 78–71724
- NH_4ClO_4, formation of colour center by X-irradiation, optical absorption spectra 79–19247
- $Na_8(Al_6Si_6O_{24})Cl_2$, sodalite, photochromism, ESR and optical spectra obs. 77–32407
- $Na_6Al_6Si_6O_{24}(NaX)_{2n}$, X=Cl, Br or I, sodalites, thermal destruction of colour centres *(Russian)* 80–84169
- NaBr powder coloured in electrodeless discharge, reflectance spectra, thermoluminescence props. 78–6796
- NaBr, thermally processed cryst., optical absorption bands *(Russian)* 78–76513
- $NaBr:Eu^{2+},Ho^{3+}$, single cryst., cluster luminesc. centres *(Russian)* 77–20922
- NaBr:Pb, absorpt. and emission spectra of Pb centres 79–78717
- NaCl, additively coloured, sensitised with O, photochromic props. 79–28792
- NaCl, additively coloured, SHG 80–1274
- NaCl crystal, radiation coloured by electron beam, holographic lattice recorded by He-Ne laser 78–58950
- NaCl crystal with aggregate colour centres, photocond. kinetics 78–19100
- NaCl crystals irrad. by high electron doses, annealing, colour centre prod. 80–2074
- NaCl, efficiency of creation of X_3^- centres in X-rayed alkali halides *(Russian)* 78–71731
- NaCl, electron impact, colour centre distrib., channelling 79–14866
- NaCl, electron irrad., secondary electrons and radiation defects 79–55782
- NaCl, formation during fast electron beam irrad. *(Russian)* 77–7716
- NaCl, gamma irradiated, optical bleaching of colour centres, F-aggregate centre form. 79–95813
- NaCl, γ-irrad., C-centres, position ang. correl. obs. 78–22712
- NaCl, influence of coloration on intrinsic luminesc. 78–80399
- NaCl, m-crocryst. powders coloured in electrodeless discharge, reflectance spectra, thermolum. 78–15238
- NaCl, microcryst. powder, isothermal stability of colour centres, thermolum. glow curve 79–15535
- NaCl, optical conversion, luminesc. and colour centre formation 79–24354
- NaCl, optically bleached and X-irrad., relation between F- and C-centres 77–72613
- NaCl, positron annihilation in colour centres 77–73185
- NaCl, substrate with colloidal centre, vacuum deposition of Au particles *(Rumanian)* 78–60579
- NaCl, X-centres thermal decay process, activation energy *(Russian)* 79–90651
- NaCl:Ag, formation of Ag atoms and self-localised holes by illumination, EPR meas. 78–31108
- $NaCl:Ag^+$, X-irrad., B-centres, thermal annealing, monomolecular and bimolecular sequence of kinetics 78–47373
- NaCl:Cu, UV absorpt., emission, excitation spectra, Cu^- centres 77–81127
- $NaCl:Mn^{2+}$, X-irrad., thermoluminesc. and EPR 79–61444
- NaCl:NaOH, $NaNO_3$, oxygen-colour centres, thermo-optical transform. 77–69862
- NaCl:O, photographic recording in far-UV, colour-centre formation 79–23035
- $NaCl:OH^-$, additively coloured, form. and decay of defect clusters and elec. double layers, Au decoration obs. 79–10850
- NaCl-CdO heterojunction form. in cathode-plasma dyeing, temp. depend. *(Russian)* 78–67710
- NaCl(:Ca) cryst., radiation colouring, amplitude-phase hologram appls., diffraction efficiency 77–68191
- NaCl(:Ca), irrad. at room temp., stored energy rel. to thermolum. 80–10574
- NaF, gamma irrad., colour centre stimulated emission, threshold pump power, tuning range 79–73971
- NaF, two-photon absorpt. cross sections of N_1 and F_3^+ centres 79–73991
- $NaF:Hg^{2+}$, electrolytic colouration 78–75665
- NaF:LiF, γ-irrad., colour centre form., reflectance and thermolum. meas. 79–55739
- NaI, X- or γ-irrad., colour centre formation and accumulation *(Russian)* 77–65978
- $Na_2O\text{-}3SiO_2$ glass, high-temp. thermolum., colour centre absorpt. 80–16110
- $Na_2O\text{-}Al_2O_3\text{-}B_2O_3\text{-}SiO_2\text{-}AgCl(Br)$, photochromic glass, kinetics of thermal decolorisation 80–103931
- $Na_2O\text{-}B_2O_3$ glass, γ- or UV-irrad., laser and thermal bleaching of colour centre, absorpt. spectra 79–33744

colour centres continued
- $Na_2O\text{-}CaO\text{-}SiO_2$, glass, formation of colour centres, linear absorption of UV radiation 80–103328
- $Na_2O\text{-}SiO_2$ glasses, elementary electronic excitations, refl., luminesc., and photoemission meas. 80–84778
- $NdGa_3(BO_3)_4$ crystal structure by X-ray spectral microanalysis 79–46621
- $Nd_xLa_{1-x}TaO_4$, polycryst. optical centres, thermodynamic equilib., 1600-1700K *(Russian)* 77–68970
- $PbMoO_4$, colour study from absorption, fluorescence and thermoluminesc. exam. 78–31245
- $PbMoO_4$, defect electron centres after X-irrad. 79–55738
- $PbMoO_4$, optical absorption of hole centres, polaron model 80–97314
- $PbO\text{-}SiO_2$ and $Na_2O\text{-}PbO\text{-}SiO_2$ system glasses, radiative paramag. and optical absorpt. centres 77–8402
- $RbBr:O_2^-$ centres, luminesc. polarisation temp. depend. 78–87943
- RbCl, with divalent impurity, reorientation of impurity-vacancy complexes, thermally stimulated depolarisation 77–65977
- $RbCl:Au^-$, optical absorpt. bands and MCD, electron-lattice interaction 80–108236
- RbCl:Sn, Sn-centres study, X-ray and coloration effects 78–76500
- Si, A-centres, electron irrad., influence on positron annihilation spectra 78–76552
- Si, diffusion of P, excess vacancy generation by E-centre dissociation 77–72720
- n-Si, efficiency of radiation defect generation by electron bombardment, influence of Fermi energy 77–11596
- Si, electron irrad. induced defect form., carrier density, mobility and lifetime changes 77–43250
- Si, electron irradiated, photolum. due to interstitial complex 77–44048
- Si, surface, etched and heat-treated, optically stimulated ESR investigation 80–11245
- Si:B, photoconductivity, impact neutralisation of H^--like centres 77–69377
- Si:P, diffusivity, strain-induced band gap narrowing, E-centres 80–29228
- Si:P, E-centre formation mechanism 77–72614
- SiC, radiation damage, review 77–80553
- SiO_2, dangling bond states 80–24846
- SiO_2, g-tensor and ^{29}Si hyperfine tensors of E_1'-centre for model of O^- vacancy 79–19777
- SiO_2 glass, optical props. of colour centres, intrinsic and modified defect states 79–60756
- SiO_2, vitreous, colour centres, dangling bond defects, radiation effects 78–71732
- SiO_2, vitreous, exam. of electron excitations and intrinsic defects 78–87905
- $SiO_2:Ag$, fused, crystalline, props. 78–10954
- $SiO_2:Al$ gel, gamma rad. effects, depend. of H_2 adsorption and colour centre form. on Al content 79–69156
- $SiO_2\text{-}Al_2O_3\text{-}Li_2O:TiO_2(ZrO_2),Fe_2O_3$, pyroceramic glass, coloration, absorpt. spectra obs. 77–8615
- SiO_{2-x}, paramagnetic E centre, reply to comment on new concept of model 80–24445
- SiO_{2-x}, paramagnetic E′-centre, comment on new concept of model 80–24444
- SiO_{2-x} system, model for paramagnetic E′-centre 78–35034
- $SrCl_2:S$, S_2^- and S_3^- mol. paramag. centres, investigation using EPR, Raman and optical spectroscopy 79–51855
- $SrF_2:Na$, γ-irrad. cryst., spontaneous and induced colour centre emission 79–7131
- $SrSO_4$, celestite, colouring mechanisms 79–82998
- $SrTiO_3\text{-}Ni$, electrochromism, optical and elec. meas. 79–95732
- TiO_2, anatase single crystals, switching, coloration and memory effect 78–72216
- TiO_2, rutile, deuteron and alpha-particle implantation, chemical effects, optical and cond. meas. 78–67755
- V_2O_5 amorphous film, photochromism and thermochromism 80–93254
- WO_3 electrochromic amorphous films, colouring and bleaching, expt. and anal. 77–20829
- WO_3 films on Si, sapphire, glass and metal substrates, colour intensity dependence obs. *(Russian)* 80–2430
- WO_3-electrolyte electrochromic cells, proton injection phenomena 80–71448
- WO_{3-y} thin films, charge storage and types of colour centre, expt. 77–20830
- WO_5 film, amorphous, band structure and colour-centre band, fast electron energy loss spectrum 77–55478
- $WO_3(WO_3\text{-}UF)(WO_3\text{-}MoO_3)$ glass film compositions, electrochromism *(Russian)* 79–28721
- YAG, colour centres conceived as bound polarons 78–63990
- YAG, optical absorption of hole centres, polaron model 80–97314
- YAG, transient colour centres caused by UV radiation 77–84744
- $YAG:Cr^{3+}$, radiation colour centres, absorpt. and thermolum. spectra 78–48206
- YAG:Mn, impurity-induced O^- colour centres, absorpt. and fluoresc. spectra 77–1709
- YAG:Nd,Ce,Cr, effect of γ-rays, fast electrons on optical props., annealing and colour centre destruction 77–8608
- YAG:Ti, crysts., colour centres, optical absorpt. spectra 79–65080
- $YAlO_3$, $YAlO_3:Nd$, colour centre form. rel. to growth conditions, absorpt. spectra 79–90652
- Y_2O_3 sintered body, blackness study thermoluminescence anal. *(Japanese)* 78–23541
- ZnO, red, electronic and opt. props., electrophotographic props. 77–57419
- ZnS:Au, phosphor, 'blue' and 'green' centre form. *(German)* 79–38665
- ZnSe, electron irrad., short-lived optical absorpt. 79–51989
- ZnSe:Ga, P, optically detected mag. reson. of P_{Se}-centre 79–33566
- ZnTe:Cu, red centre, electric and optical props. 80–20239
- ZrO_2, cubic single crystal, colour centres 77–15410

colour display tubes, television *see colour television picture tubes*

colour filters *see optical filters*

colour model
- $\Delta I=1/2$ rule in QCD, higher order gluon corrections, diagrammatic anal. 80–4945
- η' meson as pseudoscalar gluon, current sum rule saturation in QCD *(Russian)* 79–71718
- θ-vacua and confinement in two-dimensional models 80–77990
- θ-vacua in two-dimensional quantum chromodynamics 79–67499

colour model continued

σ_L/σ_T electroprod. data, colour excitation, proposed direct inclusive leptoprod. tests 80−52514
σ models, nonlinear, perturbative approach to symmetry restoration 80−37163
σ SU(3) model, quark-loop contrib., low-energy meson dynamics 78−12869
't Hooft transformation, explicit solns. 80−345
ACD off light-cone, transverse momentum cut-off 78−381
Adler's chromostatics, quark colour algebra 80−18120
Adler's classical algebraic chromodynamics, construction method 79−26295
Adler chromodynamics, colour charge algebras 79−22040
algebra of colour 78−62354
algebraic QCD, quantum theory of quarks and gluons, field values from noncommutative Jordan algebra 79−71714
asymptotic catastrophe, temporary freedom in lepton and quark interactions 79−85253
asymptotic fields, colour confinement in QFT 78−70331
asymptotic freedom, for teaching 80−17761
asymptotic freedom and dense baryonic matter 79−62738
asymptotic freedom infrared instability 80−73678
asymptotic scattering states of colored classical particles 80−397
asymptotically free colour gauge theory, electroprod. local duality and precocious scaling 77−22630
axial gauge, QCD, differential identities and soft-gluon singularities 77−74585
axial-vector currents, chiral and gauge invariant regularisation 80−4956
axion mass in extended $SU(2)\times U(1)$ colour gauge theory 78−78080
axions, astrophys. constraints on axion mass and number of quark flavours 79−36009
b quark, a possible member of a colour sextet 79−71712
B-L as fourth colour in an $SU(2)_L\times U(1)_R\times U(1)$ model 79−97589
b-mesons, mass splitting, SU_3 nonet of SU_6 80−47288
b-quark, horizontal gauge symmetry, Cabibbo universality and fermion masses 80−22583
bag model, spectroscopic appls., baryonium, gluonium, quark phase of matter, review 78−50008
bag model, string like solns., baryon-antibaryon states mass formulae *(Russian)* 79−93369
bag model, variational principle description *(Russian)* 79−40757
bag model of hadrons, review 79−75736
bag model of quark confinement 77−79248
bag model of quarks *(Hungarian)* 79−13032
bag theory, excited states of confined quarks 77−6080
bare Pomeron in four-dimensional quantum chromodynamics 79−336
baryon couplings and 'missing resonance' in quark model with chromodynamics 80−57558
baryon decay, QCD model for internal structure, pseudoscalar-meson and photon emission 80−68452
baryon dynamics description in dual and gauge theories 77−65138
baryon spectroscopy and photoproduction couplings using new baryon wavefunctions 80−102016
baryon-quark phase transition, asymptotic freedom studied using renormalised coupling constant 78−4830
baryonium, review of QCD, duality, string models and bag models 78−78135
baryonium and dibaryon, quark shell model 78−41479
baryonium and nonexotic hadron trajectories from a color-dependent potential 80−13286
baryonium model from $qq\bar{q}\bar{q}$ hadron spectrum, T- and M-diquonium 78−58172
baryonium muliquark system model of fireball, high energy pion production 79−97603
baryonium spectroscopy based on duality and unitarity 79−58947
baryonium states in QCD, review 80−102001
baryoniums coupled directly to photon 79−17694
baryons, multiquark, masses and decay modes 79−89119
baryons and mesons, parton distribs. consistent with naive quark model and QCD 80−62937
beauty and charm photoprod. in QCD, $q\bar{q}\rightarrow b\bar{b}$ or $c\bar{c}$ mechanism 80−32079
bilocal gauge field theory 80−31986
Bjorken scaling violation, QCD and models of quarks with substructure 80−105851
bootstrap theory, topological colour and disc mating unitarity as the source of zero triality 79−49492
bound colour-octet states of liberated quarks, deep inelastic processes 80−52475
bremsstrahlung contrib. to $q\bar{q}$ sea polarisation 79−67507
bremsstrahlung model of Brodsky and Gunion, comments 79−93362
bremsstrahlung production of high-energy lepton pairs in QCD, gauge invariance effects 77−74650
broken colour gauge theories, effective weak vertex, colour contrib. 79−40750
broken colour symmetry model, status 77−34119
broken QCD $(N)_2$, operator soln. for massless quarks 79−13055
broken supersymmetry, existence of massless colour octet quarks and unstable hadrons 78−89631
broken-SU(8) model, determ. of charged hadron masses and EM mass differences 77−61256
CERN School of Physics, Austerlitz-Zeist, Holland (June 1978) 79−30857
charge confinement, Schwinger model compared with $(QED)_4$ 80−62902
charge invariance, QCD, renormalisation group, confining and asymptotically free soln. 80−62881
charged spin-1 gluons, integer charged quarks, e- and ν- prod. 77−49894
charges of quarks, η-problem of meson masses, $\eta\rightarrow 2\gamma$, colour model 77−57542
charges on quarks developed by spontaneous breaking of colour symm. 78−21387
charm, elementary particle theories, properties *(Spanish)* 80−73681
charm particle nonleptonic weak decays, pole dominance model 79−63475
charm particle photoproduction total cross sections, quantum chromodynamics *(Russian)* 78−45880
charm photoprod. with linearly pol. photons, QCD calcs., gluons 80−68464
charmed baryon mass and F/D ratio, colour magnetic interaction 80−62957

colour model continued

charmed baryons in a quark model with hyperfine interactions 79−97601
charmonium, C-even, decay sum rules in QCD 77−54081
charmonium, mass in QCD 80−105867
charmonium, rel. to gluons, quantum chromodynamics theory 78−62362
charmonium and asymptotic freedom in QCD 79−6327
charmonium and QCD, review 78−82157
charmonium and similar two fermion systems, effective Hamiltonian 78−21381
charmonium model of ψ family 78−78143
charmonium photoprod., gluon-exchange model 78−74214
charmonium wave function, coloured glue effects using MIT bag model 79−75735
chiral properties of fermionic determinant in two-colour QCD, symm. breaking 78−25015
chiral $SU(4)\times SU(4)$ symmetry, broken chiral, mass spectrum of D, F and η mesons 79−93312
chromelectric-flux-tube model, finite time corrections 80−32083
chromodynamics, SU(n), classical noncommuting quark source charges 78−78144
chromomagnetic and electromagnetic hyperfine interaction, charm meson spectrum 78−12879
classical quark statics, $q\bar{q}$ pot. in Prasad-Sommerfield background, colour flux line focusing 79−49467
classical solutions of quark confinement model 79−13084
Clifford algebra based unified theory for quarks and leptons 80−47228
color embeddings, charge assignments, and proton stability in unified gauge theories 79−6309
colour confinement, possible mechanism gauge invariance 79−54311
colour confining pot., upper bound, Yang-Mills theory and lattice QCD 79−2992
colour gauge gluons and fermions in strong coupling field theories 77−6009
colour octet weak current induced by quark mixing, consequences of possible existence 78−58161
colour spin and path ordered phase factor, path integrals 80−4932
colour zitterbewegung, non-Abelian Wilson loop integral evaluation 79−36007
colour-flavour symm., renormalisation effects in guage theories 78−33018
coloured dual diagrams 79−22072
coloured quarks and octonions, book contrib. 79−58937
composite quarks and leptons, mag. moments 80−91056
compound quarks, gluons and parton confinement 79−22017
Compton effect in QCD 77−74656
Compton effects, quark and gluon jets 80−32101
Compton scattering, deep-inelastic, manifestation of colour effects 78−37215
conference, lepton-hadron physics, Karlsruhe, Germany (Sep. 1978) 80−73098
conference, quarks and leptons as fundamental particles, Schlamding, Austria, (Feb.-Mar. 1978) 80−17709
conference on hadron struct. and lepton-hadron interactions, Cargese, France (July 1977) 80−4473
confinement, ferroelectric mechanism analogue *(Russian)* 80−13274
confinement, spin depend. forces, semiclassical model 79−67500
confinement in colour SU(N) gauge theory 78−8592
confinement with regular cutoff via SU_n colour gauge group 77−6083
convergence properties of the Pade approximants on a lattice 79−17615
Cottingham formula renormalisation, hadron mass EM contrib., np mass difference in QCD 79−36053
coupling parameter trajectories 78−8519
coupling strengths and renormalization scale parameter in QCD by dimensional transmutation 79−6316
covariance problems in two-dimens. QCD 80−22575
CP^{N-1} model, instanton and large-N methods, QCD similarity 80−77963
CP^{N-1} model, QCD toy model, instantons θ vacua and confinement 80−9138
CP^{n-1} model with quarks, confinement and chiral symmetry breaking 79−54302
CP invariance, QCD confinement of colour, modification of axion scheme 80−73663
CP nonconserving effects in QCD 79−63430
CP violation in weak interaction, renormalization of QCD vacuum parameter θ 79−40683
currents, quarks and gluons 77−71482
currents in Su(5) and E_7 unified gauge theories 78−54600
cylindrical gauge field configurations, confinement in QCD 78−12870
decay function without phenomenological input 80−47247
deep inelastic ν prod., QCD and hadronic energy ang. distribs. 80−390
deep inelastic lepton-hadron scatt., semiinclusive hadron prod., quark fragmentation function corrections, QCD 80−63013
deep inelastic lepton-hadron scatt. in massive vector gauge models 78−74262
deep inelastic leptoprod., ang. energy flow, perturbative QCD predictions 80−9176
deep inelastic leptoproduction, normalising the renormalisation group anal., QCD twist effects 80−86690
deep inelastic muon scatt. at large Q^2, inconsistency with QCD 79−93374
deep inelastic quantum chromodynamic charm leptoproduction 79−54312
deep inelastic scatt., field theoretical description, QCD, quark-parton, and light cone algebra *(Russian)* 80−42388
deep inelastic scatt., incusive observables and hard gluon emission 80−99094
deep inelastic scattering, struct. functions, 2nd order corrections, theoretical calcs. in QCD 79−71688
deep inelastic struct. function behaviour near physical region endpoints, QCD anal. 80−99101
deep inelastic struct. functions, direct method for QCD predictions of scaling violations 79−80800
deep inelastic structure function moments, QCD expt. test 80−22610
deep inelastic structure function suggested by saddle points of the anomalous dimension 79−13127
deep inelastic structure functions, QCD tests, Bernstein moments 80−101983
deep processes in non-relativistic confining potentials 79−9329

colour model continued
- degrees of freedom of color in hadron physics, survey *(Russian)* 78—16979
- dense neutron star matter eqn. of state, QCD instanton effects 79—92796
- dense quark gas, colour magnetic stability 79—71709
- dihyperon, possible stable particle in 6-quark colour gauge theory 77—22691
- dilepton angular correlations, test for two body QCD subprocesses 80—387
- dilute gas approximation, higher order corrections, appl. to gluon propagator and static quark pot. 79—49400
- dimuon production, QCD and high transverse momentum data reconciliation 79—49478
- dipole ghost, taming, four dimens. field theory 79—22019
- diquark colour excitation and narrow reson. 77—18234
- diquark contribs. to scaling violation and deep inelastic σ_L/σ_T, structure functions, QCD 80—22573
- diquark spectrum in two-dimens. chromodynamics 79—71719
- diquark-antidiquark states, mass difference in lattice gauge theory 79—2985
- diquonium decay into mesons, exact selection rules for chromo-harmonic potl. 79—13054
- Dirac equation in a linear potential 80—27392
- Dirac particle+two Klein-Gordon particles, relativistic three-body wave equation, preon model 80—73574
- direct lepton generation in strong interactions, unified model, colour quark state *(Russian)* 80—82933
- discrete charm of new resonances 77—34129
- discrete finite nilpotent Lie analogs: new models for unified gauge field theory 78—66025
- discrete symmetries, natural flavor conservation and weak mixing angles 79—49438
- discriminative deep inelastic tests of strong interaction field theories, QCD scaling violations 79—89105
- divergences, IR and collinear, cancellation in one-loop corrections to QCD cross sections 79—40730
- double-logarithmic quark and form factors and the evolution of parton jets 80—68421
- Drell-Yan conjecture in asymptotically free theories 79—17689
- Drell-Yan formula in QCD, lepton pair prod. 78—33025
- Drell-Yan model at measured Q_T: asymptotic smallness of the one-loop corrections 80—105847
- Drell-Yan muon prod., QCD correction uniqueness 80—78032
- Drell-Yan process as a probe of color excitation 79—36021
- Drell-Yan process higher order corrections, QCD and parton model sum rules 80—95251
- Drell-Yan processes, asymptotic freedom corrections, Q^2-dependence 80—62933
- Drell-Yan processes, perturbative QCD corrections 79—22035
- Drell-Yan processes, perturbative versus asymptotic freedom convections 79—63446
- dual string models with non-abelian colour and flavour symm. 77—2804
- dual topological unitarization, correspondence with quark-parton model and QCD 79—93361
- dynamical preon model from primordial QCD 80—105840
- dynamical pseudo Goldstone bosons, production and decay characts., colour interactions 80—22557
- dynamical quark mass generation and the mean instanton density 79—54305
- dynamical symmetry breakings in quantum chromodynamics *(Chinese)* 79—22050
- dynamically broken-gauge theories, P and T violation in QCD 80—9093
- echo hadrons, colour confinement and fractionally charged states 79—67506
- effective hamiltonian for $\Delta C=1$ nonleptonic interactions in the Kobayashi-Maskawa model 80—86667
- effective Lagrangian due to heavy quarks in quantum chromodynamics 80—99090
- effective Lagrangian with two color-singlet gluon fields 80—86680
- electric and magnetic confinement schemes for mesons and baryons 80—4960
- electric confinement and magnetic superconductors, appl. of QCD 78—58157
- electron-meson deep inelastic scatt., sea quark contrib. in 1/N 2-dimens. QCD 80—47307
- electroproduction, polarised, flavour singlet coefficient functions, QCD corrections, sum rules 80—47301
- energy momentum sum rule beyond the leading order in QCD 80—78024
- equipartitioned jets, new tests of QCD 79—71697
- Euclidean light cone gauge, 1/N expansions with non-isoscalar gluons 80—47169
- exceptional Lie groups, basic props. 77—74611
- exclusive processes in QCD, baryon form factors at large momentum transfer 79—89153
- exotic four-quark states in two-dimensional quantum chromodynamics 79—45055
- exotic meson $(Q^2\bar{Q}^2)$ spectroscopy, instanton effects 79—89140
- exotic new quarks and dynamical symmetry breaking 80—73669
- exotic NN resonances, joined spring model, Bose quark model anal. 79—89120
- factorization breaking in deep inelastic neutrino hadron production in perturbative QCD 79—80820
- Faddeev-Popov procedure and Gribov copies in gauge theories, QCD appl. 78—32979
- Fermi-Bose couple of coloured preons, primordial QCD, leptons and quarks 80—52461
- fermion mass, unified gauge model based on E6 80—32053
- fermion-pseudoparticle interactions, non-generation of quark masses 78—37175
- Feynman diagrams, colour group indices, IR divergences in Yang-Mills theories 78—54547
- Feynman rules of QCD inside hadron 79—63425
- flavour and colour quark groups, unitary symmetry links 80—9151
- flavour changing weak radiative decays, short and long distance effects 80—73712
- flavour nonsinglet structure function, $F_3^{\nu N}$, strong interaction field theory discrimination, QCD 79—75774
- flavour singlet Wilson operators and coeff. functions in asymptotically free gauge theories 79—67501

colour model continued
- flavour state production in pp and $\bar{p}p$ interactions, QCD estimates 79—54301
- flavour symmetry breaking and isovector parity-violating potentials 79—80780
- Fock space description of $1/N_c$ QCD expansion 80—4955
- forbidden states in collisions between clusters of parafermions 79—22025
- forces in QCD *(Polish)* 80—4933
- form factor, exclusive quark, leading IR behaviour in QCD 77—54074
- four flavour $SU(2)_L \times U(1)$, gauge model with unconfined colour, $\Delta I=1/2$ rule, GIM currents 77—82708
- fragmentation functions beyond leading order in QCD 80—13282
- gauge field propagator and the number of fermion fields 80—62928
- gauge fields, chiral fields on loop space, colour-electric flux rings 80—42327
- gauge groups, quark line rule 78—29305
- gauge invariance and the quark-antiquark static potential 79—97587
- gauge symmetry, spontaneous breakdown, grand unification of QCD and $SU(2) \times U(1)$ 79—49380
- gauge theories, an introduction for experimental particle physicists 78—82119
- gauge theories, facts and prospects, conf., Schladming, Austria (Feb.-Mar. 1978) 79—26203
- gauge theories, high energy scatt. of quarks, QCD IR struct. 77—74649
- gauge theories and strong gravity 79—58869
- gauge theories of weak, EM and strong interactions 77—13835
- gauge theory, quark elastic scatt. and large transverse mom. hadron prod. 78—8610
- gauge theory aspects 80—91011
- gauge theory in two-dimens., high-energy scatt. anal. 77—13933
- generalised ferrion chromodynamics, eqns. of motion and lagrangian density 79—93358
- geometrodynamics, eightfold way, review 80—95243
- glueball pomeron singularity cancellation 80—73687
- glueball spectra, prod. and decay for QCD and SU(n) gauge theories 80—62941
- gluon, soft, radiation in QCD 77—13921
- gluon and quark jets in a recursive model motivated by quantum chromodynamics, Υ decay 80—62936
- gluon and quark observation, QCD interactions and confinement 79—2981
- gluon and quark population evolution in QCD jets, numerical estimates 80—101987
- gluon bremsstrahlung, nucleon structure functions in QCD 79—49469
- gluon bremsstrahlung and multiperipheral cluster models 79—22082
- gluon chain model in QCD 77—26487
- gluon chains and multiquark hadrons 79—93337
- gluon collective excitations, nonabelian gauge theories, effective chiral Lagrangian 79—22034
- gluon colour charge measurement 79—22028
- gluon condensation and QCD 80—102007
- gluon distrib. function, tests of QCD 78—45796
- gluon distribution in hadrons, colour cancellations and coherence effects 79—40746
- gluon distributions in QCD, definitions 80—37227
- gluon exchange diagrams, effect on parity violating weak interactions 79—97565
- gluon field condensation, instability of Yang-Mills level *(Russian)* 78—70289
- gluon fragmentation functions from quark jets 79—49453
- gluon jets from QCD, jet ang. radius and energy depend. 78—89662
- gluon mass shell Ward identities verification in axial gauge 79—13037
- gluon momentum fraction, colour elec. tube and linear potential model anal. 79—17679
- gluon operator coefficients in electroproduction 79—58926
- gluonic decay of heavy quarkonium states, QCD test, three jet struct. 78—62365
- gluonic long-range forces between hadrons 79—9339
- gluonium, scalar, J/ψ radiative decay as gluon source, QCD sum rules 80—47296
- gluons in e^+e^- annihilation, QCD anal. of strong interaction dynamics 79—9386
- gravitationally induced CP effects, quantum gravidynamics, QCD quark sector 80—86616
- ground-state baryons in a quark model with hyperfine interactions, masses 80—4944
- hadron+hadron, jet production, large transverse momentum 80—42503
- hadron+hadron$\rightarrow\mu^+\mu^-X$, QCD anal. jet recoil on large ρ_T muon pair 79—9416
- hadron+hadron inclusive cross section of symmetric hadron pairs produced, hard scatt., parton model and QCD 80—63052
- hadron calorimeter expts., asymptotic power laws, QCD and parton model predictions 80—57560
- hadron collisions, theory and phenomenology of lepton pair production, review 78—82159
- hadron form factors in quantum chromodynamics, asymptotic form *(Russian)* 78—17021
- hadron inelastic scatt., secondary hadron multiplicity distribution, Regge like parton model *(Russian)* 80—78100
- hadron interactions, inclusive, large momentum transfer, quark counting, EM form factors 80—68498
- hadron jets, rapid parton and hadron distribution 80—86693
- hadron jets from quantum chromodynamics 78—25056
- hadron leptoproduction, QCD perturbation theory and final-state jet measures 79—89117
- hadron mag. moments, colour mag. moments and transition M1-moments, quark mass parameter 79—97596
- hadron masses, behaviour of constituent quarks 80—57557
- hadron masses, soliton model and QCD 79—13083
- hadron plasma theory *(Russian)* 78—37148
- hadron production, quark colour correlations *(Russian)* 79—93382
- hadron scatt. mediated by qg→qg and gg→gg 80—82988
- hadron spectroscopy with covariant Coulomb and confining interactions 80—32090
- hadron states, quark sea and non-Abelian gauge field contrib. 79—327
- hadron total cross sections in quark parton model 78—45859
- hadron-hadron, in H, AL, inclusive particle distribs., QCD predictions 80—99112
- hadron-hadron 3-jet collisions, charge conjugation asymmetries and trilinear gluon coupling 80—105934

colour model continued

- hadron-hadron collisions, dilepton ang. distribs., QCD and quark model anal. 79−80801
- hadron-hadron inclusive interactions, charmed particle production, η_c, ψ and other $c\bar{c}$ bound states 80−63036
- hadron-hadron scatt., colour distribution in high p_T qq scatt., colour singlets 80−4940
- hadron-hadron weak interactions, right handed currents effects in QCD 79−13016
- hadronic μ-pair prod., hadron mass corrections and parton transverse momentum 79−36034
- hadronic cascades between $Q\bar{Q}$ bound states, QCD anal. 79−85261
- hadronic collisions, production of D- and ψ-mesons, QCD calc. *(Russian)* 79−9348
- hadronic colour induced Van der Waals force consequences 78−45863
- hadronic colour singlets systematics, narrow quark states with baryon number one 79−13039
- hadronic decays of quark-antiquark resonances, suppression 80−9163
- hadronic form factor asymptotics in QCD *(Russian)* 80−62983
- hadronic large p_T phenomena, effect of parton transverse momenta, QCD Born terms 79−30716
- hadronic lepton pair production, QCD jets 80−62994
- hadronic massive lepton pair prod., theory review, Drell-Yan model, QCD predictions 78−89752
- hadronic muon pair prod. QCD radiation and mean scaling, longitudinal and transverse momentum 80−42405
- hadronic production of charmed particles, review 79−67610
- hadronic reactions, trajectory slopes in gauge-dual-topological approach, jet multiplicity 80−18142
- hadronic structure functions and form factors in low-order QCD with Migdal regularization 79−30720
- hadronic structure theory, derivation of static bag and bag constant estimation 79−58932
- hadronic transitions between $q\bar{q}$ bound states, colour gauge field theory 78−37181
- hadronic wave functions at short distances and the operator product expansion, QCD tests 80−57564
- hadrons, existence of long-range forces, magnitude of coupling constants 80−13272
- hadrons, QCD model, asymptotically free field theory, anomalous dimensions of composite particles 80−73665
- hadrons, Yang-Mills pots., Van der Waals force and fermion motion 80−52465
- hadrons collective model based on quantum chromodynamics 77−13926
- hard processes, parton model and QCD, review 80−47258
- hard QCD processes, relations through mass singularity universality 79−22054
- hard scattering processes, hadronic jets and QCD 79−71727
- heavy 1^{--}-onia, two-jet cross section in perturbative QCD 79−93357
- heavy baryon spectroscopy in the QCD bag model 80−105866
- heavy charged quark system decays, CP noninvariance, six-quark model/QCD anal. 79−80826
- heavy flavour multiplicities at very high energies 79−75744
- heavy flavour prod. in e^+e^- annihilation, QCD contrib., inclusive quarkonium prod. 79−85267
- heavy meson hadroproduction, QCD effect on scale breaking 80−37239
- heavy meson weak decays, heavy quark decay, QCD corrections, real gluon role 80−57586
- heavy quark bound states of top quark and antiquark pairs, QCD test 80−68430
- heavy quark dynamics in non perturbative QCD vacuum 79−80795
- heavy quark leptoproduction in QCD, characts. 79−17733
- heavy quark potential, non-perturbative contrib., appl. to QCD 79−13025
- heavy quark prod., nonperturbative gluoprod. versus perturbative QCD fusion models, B and ψ 80−91058
- heavy quark prod. in photoproduction, QCD model, possible large p_T process connection 78−78137
- heavy quark semileptonic decays, gluon corrections 79−17688
- heavy quark system prod. in QCD, duality predictions 79−13074
- heavy quark systems, spin dependent interactions, QCD perturbation theory anal. 79−36019
- heavy quarkonium states, hadronic transitions, QCD anomalies for Υ'' and ψ' 80−105888
- heavy quarkonium states decay, three jet structures 78−45846
- heavy quarks, widths of neutral vector mesons 78−8602
- heavy quarks in QCD *(French)* 80−78017
- hidden colour and the isobar content of the deuteron 80−102024
- Higgs boson decay, QED and QCD radiative corrections 80−95275
- Higgs bosons photoproduction in QCD 80−22558
- Higgs self coupling effects on asymptotic freedom 79−266
- high mass dilepton prod., comparison with Drell-Yan formula in asymptotically free theories 80−4942
- high p_T hadronic jet photoprod., QCD anal., quark and gluon jets 80−42474
- high p_T processes, parton transverse momentum effects, QCD description 79−17774
- high P_T theory, use of polarised beams and targets, QCD tests 79−63409
- high-transverse-momentum symmetric-particle-pair spectra and correlations 80−95250
- higher order QCD jets in photoproduction 80−99087
- higher-twist effects in QCD, deep inelastic scattering and the Drell-Yan process 80−102020
- hypercomplex quark fields and quantum chromodynamics 79−93344
- hyperon non-leptonic decay in quartet model 78−12910
- impulse approximation in QCD, partons p_t distrib., appl. to deep inelastic electron scatt. 78−62368
- inclusive electroproduction, local duality and precocious scaling, quantum chromodynamics 77−2842
- inclusive lepton pair prod., P violation, quark-parton model in Weinberg-Salam theory, QCD 80−37217
- inclusive leptoproductions, scaling violation, colour-octet model effect 79−13077
- inelastic Compton scatt., hadronic contrib., two-dimens. QCD calcs. 79−45062
- infrared properties of quark gas 80−395
- infrared regularizations in a model gauge theory 79−30700
- infrared struct. of QCD, quark confinement, perturbation theory 77−71443
- instantaneous Coulomb interaction in SU(2) Yang-Mills QCD 80−396

colour model continued

- instantaneous Coulomb interaction in SU(2) Yang-Mills QCD 80−22574
- instanton correction to vac. energy densities and bag const. 80−37211
- instanton density in a theory with massless quarks 80−37210
- instanton effective size estimate from gluon field strength tensor vacuum expectation value 78−70326
- instanton effects in finite density and temperature OCD 80−9139
- instanton effects on quark-antiquark potential 78−93847
- instanton statistical mechanics in QCD 80−57567
- instanton suppression as origin of quark confinement 79−9338
- instanton system weakly interacting with anti-instanton system, external electric fields, structure and stability 80−77956
- instanton-anti-instanton interaction effects on current correlation functions in QCD 80−102010
- instantons, dynamical role in quarkless chromodynamics, bag model test 80−47246
- instantons, gravitational, flavour currents of QCD, Green's functions, foam-like structure of space-time 80−62825
- instantons, relationship to confinement, one-dimens. quantum mech. model anal. 79−12962
- instantons, the quark model, and the 1/N expansion 79−36005
- instantons and infrared divergences 78−70284
- instantons and quark-mass generation—the how of spontaneous chiral symmetry breaking 80−4963
- instantons and the 1/N expansion 80−400
- instantons as link between weak and strong coupling in QCD 80−42403
- instantons in non-perturbative QCD vacuum 80−47243
- instantons in nonAbelian gauge theories and QCD mesons 80−105777
- integer quark charge model, enhanced flavour charge 79−49457
- interacting instanton-antiinstanton system under external colour mag. fields in SU(2) gauge 80−101920
- interaction potentials for multiquark states from instantons and other background gauge field configurations 80−101995
- intermediate vector boson, hadron-hadron collisions, Weinberg-Salam model 80−9186
- intermediate vector boson decay, QED and QCD radiative corrections, hadronic jets 80−73759
- inverted charmed meson multiplets as a test for scalar quark confinement 78−70325
- IR singularities, spin $^1/_2$ quark confinement in three dimens. 79−337
- IR singularity quark confinement model, coloured bound state absence 79−338
- isospin SU(3) symmetry, spontaneous breaking of chiral symmetry in QCD 79−93352
- isospin violating mass differences and mixing angles, quark mass and QCD 80−52505
- isospin violation, induced by current quark mass 80−32069
- jet analysis, QCD calcs. and phenomenological models 80−52523
- jet and lepton-pair production in high-energy lepton-hadron and hadron-hadron scattering 79−17729
- jet asymmetry in polarized proton collisions *(Russian)* 79−17685
- jet cross sections and quark form factor, high energy asymptotics 80−32112
- jet fragmentation axis 79−93350
- jet processes in QCD 78−82104
- jet prod., exponentiation of leading logarithmic cross sections 79−63445
- jet production by a gluon source in QCD 79−22056
- jet production in e^+e^- collisions to order α^3 and α^4 and including QCD corrections 80−13322
- jet struct. in hadronic lepton pair prod. ang. energy cross section, QCD 79−75806
- jet structure in e^+e^- annihilation, deviation variable, QCD calc. 79−9388
- jet structures of leptons, quarks and gluons, perturbative QCD, process dependence 80−68470
- jet time development in perturbative QCD 79−93356
- jets, angular distrib. of energy, QCD transverse ang. momentum distrib. 79−71726
- jets from coherent states 80−13266
- jets of quarks and gluons, leading logarithmic approx., parton interpretation 80−68433
- Judek effect and nuclear hidden colour excitations in heavy cosmic ray-nucleus reactions 80−27567
- Klein-Gordon particles+Dirac particle, relativistic three-body wave equation, preon model 80−73574
- Kobayashi Maskawa model, QCD effects and CP violation 80−42427
- ladder model of QCD, hadron struct. 80−37213
- large p_T hadron prod. off nuclei, QCD parton model, nucleus as gluon filter 79−89110
- large p_T hadronic collisions, QCD sensitive test, quark and gluon jets 80−57647
- large p_T jet prod. in hadronic collisions, QCD calc. for inclusive cross section 78−86439
- large Q_T transverse momentum lepton pairs and hadron jets prod., reaction mech., perturbative QCD 79−2999
- large transverse momentum particle and jet prod., QCD approach 79−17761
- large-N chromodynamics, chiral symmetry breakdown 80−91052
- lattice gauge theories, chiral symmetry dynamical breaking 80−99061
- lattice gauge theories, strong coupling phase large space-time dimension, Ising model 80−27397
- lattice gauge theory, coupling consts. and meson two-body decay amplitudes 77−34126
- lattice gauge theory, map between corner and link operators, QCD relation 79−35926
- lattice gauge theory *(Chinese)* 79−63336
- lattice QCD_2, Wilson's loop eqn. soln. for large N limit 80−78030
- lattice QCD, hadron mass spectrum, effective Hamiltonians, degenerate perturbation theory 80−102003
- lattice QCD, mass levels of boxiton (glueball) states 79−54259
- lattice SU(N) gauge theory, vacuum structure, large-scale 80−57470
- leading IR divergences in quantum chromodynamics, behaviour in axial gauge 77−13924
- lepton+hadron, deep inelastic scatt., QCD event states, 3-jet events 80−52515
- lepton+nucleon, quark and gluon jets, Breit frame, QCD 80−62995
- lepton pair prod., nonfactorisability of inclusive distribs. in nonperturbative QCD 79−13085
- lepton pair prod. struct. functions, QCD improved quark-parton model 80−73671

colour model continued
lepton pair production, QCD and hard-scatt. model, spin-spin asymmetries 80—63014
lepton pair production in two-dimens. QCD 77—74644
lepton structure model 80—91063
lepton-hadron deep inelastic scatt., higher order QCD corrections 79—97629
lepton-hadron deep inelastic scatt., massive vector gauge model *(Russian)* 78—89720
lepton-hadron deep inelastic scattering, QCD and model-independ. theory *(German)* 79—58965
lepton-hadron inclusive interactions, quark and target mass effects, colour SU$_3$ theory 77—6090
leptonic colour model, expt. evidence 78—62350
leptoproduction, $\mu N \to \mu X$, broken colour gauge theory of integer charge quarks 80—13313
leptoquark bosons, confinement in SU$_4$ theory 79—45052
light cone gauge theories, singlet gauge operator nonconservation, QCD flavour charge operators 80—52462
light quark mass and low energy η meson interactions *(Russian)* 79—67513
light quark mass spectrum in QCD 79—63427
light quark spectroscopy, review 80—42424
light quarks and QCD Boson representation, dynamical symmetry breaking 80—52472
light-cone gauge, QCD calcs., non-singlet quark struct. function 80—57464
lorentz invariance of two-dimensional quantum chromodynamics 79—67504
Lorentz structure of confining quark-quark interaction, asymptotic freedom, new particle spectroscopy 78—66077
low p_T fragmentation, short distance counting rules, QCD diagrams 80—22572
M1 radiative meson decays, QCD corrections 79—17718
magntic moments and machinery of symmetry breaking 79—63477
many-body interactions from quark exchanges, nuclear tetrahedral struct. and props. 79—6459
Markov branching processes 80—27463
mass differences of up and down quarks, grand unification 80—62978
mass singularities and coherent states in gauge theories, QED and QCD results 79—12948
mass singularities factorisation for polarised parton legs in low order QCD perturbation theory 79—40737
mass singularities in QCD, double cut diagram method 80—37215
mass splittings of heavy mesons and baryons *(Chinese)* 78—78146
masses in scalar dynamics, gluon theories compared with QCD 80—57553
massive gauge-invariant QCD, quark confinement and vortices 80—384
massive gluinos 79—2987
massive lepton pair hadroproduction, QCD and parton model anal. 80—42421
massive lepton pair prod. by polarised p, constituent spin prop. test, QCD 79—89201
massive lepton pair production at large q_T, large p_T jet props. 79—54326
massive lepton pair transverse momentum distrib. in hadron collisions, QCD predictions 79—9391
massive propagators in instanton fields, Green's functions, quantum chromodynamics 79—49390
massive QCD, asymptotic freedom with infinitely many quarks 79—71699
massive quark pot. scatt., cancellation of infrared divergences 79—71707
massive Schwinger model, decay of metastable vacs. 78—24989
massless chromodynamics, vacuum rearrangement 78—70327
massless fermion effective action with instantons perturbation theory vacuum for QCD 79—71608
massless field theory observables, infrared finiteness proof for all perturbation theory orders 79—21917
massless non-abelian gluon confinement and rising total cross sections 80—13264
massless QCD$_2$, non-Abelian travelling wave solns., SU(2) subalgebra 80—57563
massless QCD, instanton contribs. to fermion Green's functions 79—22037
massless QCD 78—78093
massless quarks in QCD, dynamical symmetry breakdown 80—52471
massless scalar QED, colour confinement model 78—33027
meron and meron pair analogs in XY model 80—32010
meron configurations in two dimens. O(3) σ model 78—32983
meson+meson cross sections in QCD *(Russian)* 80—4968
meson and baryon mass formula, chromodynamics consideration *(Russian)* 80—91071
meson dipion cascade decays, current algebra techniques, pole plus remainder model, chiral symmetry breaking and QCD 80—62972
meson mass generation in chiral flavour U(3)×U(3) symmetry by instantons 79—89121
meson masses in gauge theory with harmonic oscillator pot., coloured quark-gluon model 79—350
meson spectroscopy, quark mixing and quantum chromodynamics *(Russian)* 79—54329
meson spectroscopy, spin struct., effective scale quark confinement in QCD 79—17684
meson wave functions in 1+1 dimens. QCD 78—54559
meson-mass generation by instantons in coloured gauge field theory 79—54321
meson-meson quantum chromodynamic two-dimens. anal., high-energy behaviour 77—65140
metastable multiquark states, colour chemistry 78—74212
MIT bag, 2-dimens., force between two point colour charges 79—334
MIT bag model, approx. QCD lower bound for bag constant B 79—17681
MIT bag model, coloured quark and gluon constituents of mesons 80—4929
Moufang plane and octonionic quantum mechanics 78—69999
multi-jet structure of hadronic final states and trajectory slope 78—93843
multibaryon resonances, coloured quark-cluster model, possible 3-baryon state 79—6318
multicolour QCD, loop average, exact eqn., lattice regularisation 80—22570
multicolour QCD as dual resonance theory, mesons on rising Regge trajectories 78—16987

colour model continued
multilegged propagators in strong-coupling expansions 80—4861
multiparticle production in chromoelectric flux tube model in 1+1 dimens. field theory 80—73666
multiparticle production on nuclei, role of colour 78—93981
multiquark dibaryon resonances 79—67518
multiquark hadron states, colour manifestations 80—18124
multiquark states as verification of colour 79—13067
N-flavour quark model, axial-vector current anomaly, decay constants and η-η'-η_c problem 79—13045
Nachtmann moments of $F_2^{\nu N}(x,Q^2)$ and energy momentum sum rule 80—57580
negative parity baryons, spectrum and mixing angles, QCD type quark model 79—26307
neutral current scattering expt., test of nonconfinement, gauge theory of physical colour 77—46017
neutral light vector boson, possible exist., quark model construction 77—49898
neutrino charged current, new phenomena colour-scheme interpretation 77—2817
neutron matter-quark matter phase transition, QCD and extended Higgs model, instantons 80—91062
new physics from experiments above 100 TeV, appl. to QCD, weak interaction, and gauge theory 79—63564
non leptonic hyperon decay amplitudes, calc. without arbitrary parameters 80—13300
non-Abelian Block-Nordsiech conjecture, counter-example 80—78021
non-Abelian gauge theories, coupling constant IR props., colour confinement 79—93293
non-Abelian gauge theories, high energy behaviour, reggeon field theory, QCD 80—62822
non-Abelian gauge theories, local covariant operator formation, quark confinement 80—47190
non-Abelian gauge theory, colour model, high-energy hadron interactions 77—45973
non-Abelian gauge theory, colour-singlet quark form factor anal. 77—65084
non-Abelian gauge theory of quarks and gluons in two dimens. 79—30654
non-Abelian two-dimens. theories, novel inconsistency, quantum chromodynamics 77—65097
nonabelian gauge theories, coherent state approach to IR behaviour 78—82107
nonAbelian gauge theories, Faddeev-Popov ghost decoupling, QCD gauges and gluons 80—52406
nonAbelian gauge theories, low energy quanta emission, coloured gluons 77—79223
nonleptonic 20+15 dimens. weak interactions 79—71746
nonleptonic hyperon decays, QCD corrections 80—91087
nonlinear Dirac equation with SU(3) colour symmetry, vanishing soliton solns. 79—71693
nonperturbative QCD, large N$_c$, QCD bag model, instantons and η' mass 80—57559
nonperturbative QCD effects at large momentum transfers, e^+e^- annihilation to hadrons 78—82226
nonrelativistic colour quark model, meson and baryon masses 78—50014
nonrelativistic pot. models for heavy quark systems, Υ and ψ hadronic decay 78—89688
nonrelativistic QCD, short range NN interaction 80—32200
nonrelativistic quark model with one gluon exchange pot., baryon spectroscopy in $SU(6)\otimes O(3)$ 78—78147
nuclear EM form factors asymptotic behaviour 77—10301
nuclear force, strong short-range repulsion 78—12880
nuclear forces in saturated nuclei 79—13211
nucleon-nucleon interaction as derived from the De Rujula, Georgi, Glashow phenomenological quark-quark potential 80—78172
O(10), SU(4) colour subgroup, fractional charged gauge boson, proton half-life 80—73644
octonionic Hilbert space, Poincare group at SU(3) 77—2791
octonionic Hilbert space description of elementary particles 79—9306
octonionic structures in particle physics 80—9147
octonions in quantum mechanics 80—27479
off-shell particle scattering, total cross sections, QCD 80—68418
opposite-side angular correlation of high-p_T particles as a probe of gluons 79—71703
OZI rule, justification in QCD 80—62924
OZI rule violation model due to spinless bosons 79—89107
P and T invariance in colour gauge theory of strong interactions 78—37153
P and T violating electromagnetic interaction of the quark in the instanton field 80—52430
pairing theory of Yang-Mills field and string phase 79—13047
parton distrib. in rel. to transverse impulse in quantum chromodynamics *(Russian)* 79—63433
parton distribution functions, Q^2 depend., QCD parameterisation 80—82937
parton model, asymptotically-free, $W^\pm$, Z^0, μ-pair prod. 78—12865
path group appl. to gauge theory and quarks 80—31985
path-depend. approach to coloured mag. monopoles 78—37127
path-integral in collective fields and its application to nuclear and hadron physics *(Russian)* 79—93277
perturbation theory and QCD, quark binding 77—71444
perturbative appl. of QCD 79—97571
perturbative aspects of QCD, an introduction 79—30714
perturbative field theory effects and Regge pole representation, QCD, dual topological unitarisation 80—42434
perturbative QCD, $\alpha_s(q^2)$ meas. in deep inelastic scatt. 80—4949
perturbative QCD, chiral symmetry using dimensionless regularisation 80—27476
perturbative QCD, gluon bremsstrahlung by confined sources 79—45067
perturbative QCD, hard hadronic processes, e^+e^- annihilation, lepton-hadron deep inelastic scatt. 80—52477
perturbative QCD, jets, inelastic distribs., colourless clusters, scaling, multiplicity and tree evolution 80—52459
perturbative QCD, large p_T hadronic collision jet struct. 79—75721
perturbative QCD, parton primordial transverse momentum 79—40728
perturbative QCD, recent progress 80—42418
perturbative QCD, renormalisation improvement, charmonium decay and scaling violations 80—101993
perturbative QCD and exptl. signatures of weak bosons 78—93916
perturbative QCD and hard scattering processes, review 79—45075

colour model continued
- perturbative QCD corrections in inelastic Compton scattering 79—93342
- perturbative QCD in a covariant gauge, moments of struct. functions 80—32073
- photon and lepton hadroproduction, QCD test 79—17745
- photon distribution functions, QCD predictions using Altarelli-Parisi eqns. 80—78019
- photon production by gluon jets in QCD 79—75732
- photon structure functions, anomalous components, using Altarelli-Parisi eqns. for QCD scale breaking 79—63479
- photon structure functions, QCD predictions in asymptotically free gauge theory 79—30736
- photon structure functions parametrisation 80—37267
- photoproduced pion inclusive distrib. in QCD, recombination model 79—85303
- planar model electrodynamics, phase diagram, continuum limit, and mass spectrum 79—63426
- polarised deep inelastic electroprod., QCD higher order effects, sum rule correction 79—93428
- polarised deep inelastic scatt., parton transverse momenta role, struct. function, QCD evolution 80—78034
- polarised electroproduction, target mass effects 80—78072
- Pomeranchuk singularity in QCD *(Russian)* 79—22078
- Pomeron two-gluon exchange model, quark counting, hadron-size effects for total cross sections 77—57495
- positive parity excited baryons in quark model with hyperfine interactions 78—82161
- potential model of meson mass 78—45874
- potentially CP violating phase in QCD, alleged axion mass, PCAC quark masses 78—66080
- power corrections at short distances, hadronisation, smearing, higher twist 80—105844
- power law confinement potentials, bound states 80—18123
- preconfinement as a property of perturbative QCD 79—54310
- prompt lepton prod., QCD anal. 79—9346
- proton fragmentation functions, Q^2 depend., lowest order QCD calcs. 78—62359
- protons, flavour symmetry breaking in antiquark distribs. 79—36006
- pseudomesoniums, spectroscopy, prod. and decay props. 79—45058
- Q^2 dependence for quark and gluon fragmentation functions, QCD predictions, Altarelli-Parisi eqns. 80—78018
- Q^2 dependence of quark and gluon fragmentation functions in a parton picture based on QCD 79—9336
- Q^2 dependent parton distribution function on QCD 78—93857
- $Q^2\bar{Q}^2$ resonances in baryon-antibaryon systems, $N\bar{N}$ scattering and $N\bar{N} \rightarrow \pi^+\pi^-$ 78—58171
- QCD_2, fermionic Green function and functional determinant, closed representation 80—13269
- QCD_2, massless, fermionic Green's function and determinant 80—22560
- QCD_2, $q\bar{q}$ bound state spectrum in leading 1/N approx. 80—78031
- QCD, 1+1 dimens., dynamical symmetry breakdown 80—82949
- QCD, 2-D, evidence against colour confinement 79—26293
- QCD, 2-dimens., Bose form, SU(N) confining phase 80—52463
- QCD, 2-dimens., confinement effects on analyticity meson inelastic form factor, scatt. amplitude 79—333
- QCD, 2-dimens., IR structure, EM form factors and inelastic struct. functions *(Chinese)* 79—58935
- QCD, 2-dimens., nonleptonic weak decays of charmed and storage mesons 79—40773
- QCD, 2-dimens. multiflavour, local colour symmetry breakdown, massive gluons and quarks 80—82942
- QCD, $\mu^+\mu^-$ prod. total cross section from Drell-Yan process, large perturbative corrections 80—385
- QCD, μ pair transverse momentum distrib. in Drell-Yan processes 78—62374
- QCD, π structure function and scaling phenomena in Drell-Yan lepton pair prod. processes 80—405
- QCD, a non-perturbative approach 80—22588
- QCD, ang. energy flow beyond lowest order in deep inelastic reactions 79—93351
- QCD, anomalous dimensions of gauge-invariant three-fermion local operators of twist three 80—86662
- QCD, asymptotic freedom, energy levels J/ψ and Υ mass difference *(Chinese)* 80—52480
- QCD, asymptotic precictions for exclusive processes, form factors, struct. functions, and low-mass jets 79—71701
- QCD, axial gauge, mass shell behaviour 78—49966
- QCD, baryons in 1/N expansion, mesons and glue states 80—13267
- QCD, Bjorken scaling violations 79—22033
- QCD, bound on MIT bag constant and Nielsen-Olesen unstable mode 79—89100
- QCD, charm contrib. to electroprod. struct. functions 78—58170
- QCD, charm photoprod., ψ, D, F etc. prod., sum rules, cross sections 78—58169
- QCD, colour ferromag. vacuum states, two loop energy densities, MIT bag constant 80—99085
- QCD, coloured cuts and mass gaps 79—9335
- QCD, confinement and long range gauge fields 80—73668
- QCD, confinement and quark theory, introductory review 79—67502
- QCD, decays of heavy leptons and intermediate weak bosons 78—8524
- QCD, dimension-5 Lorentz invariant operator system 79—89104
- QCD, direct γ prod. beyond leading order, $qq \rightarrow qq\gamma$ process 80—86664
- QCD, dynamical chiral symmetry breaking and explicit breaking due to current quark masses 79—71717
- QCD, dynamical props. 78—70332
- QCD, E_7 model, quark and lepton assignments 78—8590
- QCD, e^+e^- annihilation energy, asymptotically free perturbation theory 78—66045
- QCD, effective Lagrangian, possible σ-model 80—86679
- QCD, effective lagrangian with no U(1) current problem 79—89066
- QCD, effective low energy Lagrangian 79—40731
- QCD, electric field representation without gauge field constraints 78—93846
- QCD, energy of classical sources, finite confinement from Pade approximants 78—41478
- QCD, equation for dual chords *(Russian)* 79—58936
- QCD, equations of motion for n-loop averages 80—82935
- QCD, expt. test 78—8601
- QCD, factorisation and the parton model 78—93848
- QCD, failure of U(12) 77—67576
- QCD, field strength and action copies in any axial-like gauge 78—82143

colour model continued
- QCD, field theoretical aspects, perturbative effects 79—26286
- QCD, gauge independ. approach to hard processes, structure functions, gluons 80—86665
- QCD, gauge independence of IR cancellation, fermion-fermion scatt. 78—50006
- QCD, gauge invariance and perturbative calcs. 79—63417
- QCD, gauge invariant quantum variables, $SU(N)_1 \otimes SU(N)_2 \otimes SU(N)_3$ algebra 79—30705
- QCD, Gell-Mann-Low function in 3 loop approx., nonAbelian gauge theory with fermions 80—86675
- QCD, generalized Lipatov-Altarelli-Parisi equations and jet calculus rules 79—71704
- QCD, ghost gluon bound state and pseudoscalar mixing 80—86685
- QCD, gluon colour screening by Higgs mechanism 78—93861
- QCD, Green's functions for composite particles 79—85262
- QCD, hadron interaction effective string lagrangian, Regge slope, charmonium pot. model 80—4939
- QCD, hadron prod., large-transverse-momentum correl. 79—63438
- QCD, hadron struct. theory, expt. tests 79—93367
- QCD, hadronic and supersymm. string states 79—75724
- QCD, hadronic charm production, cross section and charmed quark mass 79—36017
- QCD, hadronic semi-inclusive processes, calc. of scaling props. 79—13027
- QCD, hadroprod. of heavy quark flavours 79—22062
- QCD, hard processes, universality of mass singularities 78—82101
- QCD, hard semi-inclusive processes 78—93862
- QCD, heavy quark semileptonic decay, gluon radiative corrections 79—75743
- QCD, heavy quark-antiquark bound systems, effective potential 79—49477
- QCD, heavy-vector meson-nucleon scatt., cross section suppression, Υ and ψ 80—22564
- QCD, high energy behaviour of inclusive differential cross sections 78—45862
- QCD, high P_T hadron prod. in pionisation region and vacuum singularity *(Russian)* 80—86772
- QCD, high transverse momentum meson prod., hadron-hadron collisions 78—45861
- QCD, higher order, charge conjugation asymmetries from two gluon exchange 80—4935
- QCD, improved evolution eqns. based on probabilistic interpretation 80—86673
- QCD, impulse approx. and scaling phenomena 79—22043
- QCD, in 2-dimens., bound states and asymptotic limits 79—71716
- QCD, inclusion of parton transverse momentum 79—26290
- QCD, inclusive deep-inelastic scatt., asymptotic freedom, review 80—32084
- QCD, inclusive distributions in extended leading logarithms 79—13066
- QCD, inclusive hadronic annihilation of heavy quark-antiquark bound states, Υ, ψ decays 78—45866
- QCD, inclusive production at large transverse momentum, cross section 78—62369
- QCD, infinite-mass limit determ. 78—66039
- QCD, infrared, near-mass-shell, behaviour of non-Abelian gauge theories 78—24947
- QCD, infrared behaviour, colour-singlet quark form factor 78—24948
- QCD, infrared behaviour of effective coupling 80—42393
- QCD, instanton induced interactions 79—71698
- QCD, IR behaviour of higher order derivative field theories 79—30699
- QCD, IR struct. of quark-antiquark scatt. kernel, quark binding pot. 78—8588
- QCD, jet anal. in lepton-hadron deep inelastic scatt. 79—40785
- QCD, jet invariant mass in e^+e^- annihilation 79—85307
- QCD, jets, deep inelastic scatt., renormalisation group 79—26287
- QCD, jets in high energy collisions 79—45114
- QCD, large N limit, pseudoscalar nonet chiral dynamics and low energy spectrum 80—101988
- QCD, lattice and continuum, Λ parameters connections 80—82945
- QCD, lattice-gauge theory calc. of π and ρ-meson decay consts. 78—74154
- QCD, leptoprod. and Drell-Yan processes beyond leading approx., Bjorken scaling 79—6323
- QCD, lifetime of $Q\bar{Q}$ states, pseudoscalar charmonium and upsilon states 80—68429
- QCD, long range parton correlations at large Q^2 *(Russian)* 80—68428
- QCD, long-range correl. in forward quark-quark scatt. 78—4779
- QCD, massless, two dimens., bound states 78—62371
- QCD, massless two-dimens. model, operator soln., local colour SU(n) symm. 78—41480
- QCD, Migdal's regularisation scheme, hadron struct. 78—4782
- QCD, Migdal approx. and 1/N expansion, string tension 80—101992
- QCD, modified, exact global colour SU(3) symm., asymptotic freedom 78—41493
- QCD, multicolour, series expansion for meson masses 78—21315
- QCD, neutron electric dipole moment, chiral estimate, current algebra, CP violating reactions 80—27471
- QCD, new quarks and hadrons 78—8591
- QCD, nonperturbative, fundamental scale of strong interactions 79—36002
- QCD, OZI rule violating radiative decays of heavy pseudoscalars 78—89709
- QCD, particle transversal momenta, parton distribs. in hadrons *(Russian)* 79—93370
- QCD, parton and dimuon intrinsic transverse momenta 79—13038
- QCD, parton and gluon distribs. 78—16981
- QCD, parton cross sections, infrared and mass singularity regularisation 80—32075
- QCD, parton distrib. function, transverse momenta, axial gauge ladder model 80—27467
- QCD, parton jet and shower model 80—86663
- QCD, parton transverse mass distrib. 78—8587
- QCD, parton transverse momentum distribution 78—29301
- QCD, perturbation theoretic parameter Λ 78—89667
- QCD, perturbative, colour singlet distribs. and mass damping 79—63418
- QCD, perturbative contributions to quark masses 80—47249
- QCD, photoprod. of heavy quark flavours 78—21384
- QCD, positive-parity excited baryons in a quark model with hyperfine interactions 79—67511

colour model continued

- QCD, positivity constraints on quark and gluon momentum distribs. 78—74205
- QCD, quantised electric flux tubes 78—45844
- QCD, quark and gluon fragmentation functions, quarkonium decay inclusive hadron spectrum 79—97584
- QCD, quark and gluon propagators 80—52469
- QCD, quark confinement, background theory 80—18113
- QCD, quark liberation and finite temp. renormalisation group, hadron-quark phase transition *(Russian)* 79—67515
- QCD, renormalisation group calcs., cancellation of ambiguities *(Russian)* 80—62930
- QCD, renormalisation group invariant charge and confinement 78—45791
- QCD, resonance props. from sum rules 79—26301
- QCD, review 78—37146
- QCD, scaling violation pattern, higher order terms 80—27468
- QCD, Schrodinger equation scaling props. 79—67496
- QCD, slope of leading Regge trajectory 80—42391
- QCD, spectral function sum rules in charged current sector 79—80796
- QCD, spin depend. quark-antiquark forces 79—49476
- QCD, spin-dependent forces in heavy-quark systems 80—4937
- QCD, spontaneous breaking of chiral SU(2)×SU(2) symmetry 79—36013
- QCD, spontaneous breaking of chiral symmetry 79—71700
- QCD, stagnant gauge for gluon propagator 80—57554
- QCD, string constant, Regge slope and Λ parameter, empirical quarkonium approach 80—91053
- QCD, strong interaction gauge theory, SU(3) colour gauge vector mesons, confinement 78—78136
- QCD, struct. functions, perturbation theory *(Russian)* 78—8595
- QCD, summing large perturbative corrections near kinematical boundaries 80—47251
- QCD, testing of gluons by energy-energy correlations in heavy quarkonium decay 79—71690
- QCD, three gluon jets as test 78—25001
- QCD, three gluon vertex 79—49454
- QCD, transverse momentum distribs. of μ pairs from pN interactions, p-nucleus study 78—62375
- QCD, transverse momentum of jets in electroprod. of hadrons 78—62367
- QCD, transverse quark polaris. in large-p_T reactions, e^+e^- jets, and leptoproduction 79—17741
- QCD, two dimens., bound state eqns. on null planes, Hamiltonian approach 78—37137
- QCD, two dimens., hadron scatt., leading order calcs., meson-meson scatt. 78—4831
- QCD, two dimens., hadron scatt., multi-Regge and inclusive reactions 78—4884
- QCD, two dimens., multiparticle amplitudes 79—36029
- QCD, two dimens., renormalisation group functions 78—29242
- QCD, two dimens., soln. of Bars-Durgut model for baryons 79—75741
- QCD, two dimens., with SU(N) gauge symm., $N \to \infty$ limit 78—41489
- QCD, two dimens. light-like gauge formulation, hadronic reactions 78—21388
- QCD, two jet process noncollinearity in first order perturbation theory 80—22567
- QCD, two-dimens., bare pomeron graph 78—4824
- QCD, two-dimens. extrapolation to four-dimens. 78—78081
- QCD, two-dimens. with massless fermions in 1-1 dimensions 80—62926
- QCD, two-photon scatt. amplitudes, leading order behaviour 80—52458
- QCD, unconfined quarks and gluons 78—45850
- QCD, universal multiplicity hypothesis, bounds on quark gluon coupling, quark mass, and confinement region 78—74213
- QCD, universal multiplicity hypothesis, quark-gluon coupling constant 79—6319
- QCD, vector gluon propagator using gauge technique 79—45049
- QCD, weak coupling approx. Schwinger-Dyson eqn. *(Chinese)* 80—52476
- QCD anal. of p_T^2 behaviour observed in semi-inclusive neutrino data 79—36015
- QCD anal. of the low energy behaviour of hadrons 79—80813
- QCD analysis of charged-current structure functions 79—49462
- QCD and ψ parameters, charmed quark current in quark-gluon coupling *(Russian)* 80—13277
- QCD and dual resonance model vertices, string prod. operators, singlet colour states *(Russian)* 80—42410
- QCD and Feynman-x depend. of lepton pairs produced in hadron collisions 79—36036
- QCD and hadron dynamics 79—97593
- QCD and hadronic structure 80—42416
- QCD and heavy quarks *(German)* 80—37214
- QCD and jets in leptoproduction 79—45059
- QCD and large momentum transfer processes 80—42419
- QCD and particle-string variables 78—24939
- QCD and polarised quarks *(Russian)* 78—74217
- QCD and QED IR equivalence in non-perturbative solns. 77—74579
- QCD and resonance physics, appl. of sum rules to ρ-ω mixing 79—22060
- QCD and resonance physics, appl. of sum rules to reson. props. of mesons 79—22059
- QCD and resonance physics, general technique for deriving sum rules 79—22058
- QCD and short range nuclear phenomena 80—91060
- QCD and the spin dependent forces in quarkonium 79—63421
- QCD approx. for nucl.-quark matter phase transition in neutron star cores 80—67771
- QCD asymptotics and kinematic thresholds in deep inelastic scattering, structure functions 79—54315
- QCD at high temp., MIT bag model and thermodynamic pot. 79—30706
- QCD at low Q^2, structure function moments, correspondence relation 80—73673
- QCD axial gauge, $O(\alpha_s)$ infra-red divergences, deep inelastic quark struct. function 80—86676
- QCD black body radiation, big bang universe hadron era 80—62341
- QCD calc. of structure function moments, renormalisation prescription depend. 80—4948
- QCD calc. of three-jet processes in leptoprod. and hadronic μ-pair prod. 78—21338
- QCD conf. La Jolla, CA, USA, 1978 79—97592
- QCD constituent-interchange to p_T^{-4} dominance transition at high transverse momentum 79—40744
- QCD contributions to vacuum polarization 80—91059

colour model continued

- QCD contributions to vacuum polarization 80—105834
- QCD corrections at Z_0 for hadron initiated lepton pair prod., renormalisation appl. 80—86678
- QCD corrections for Higgs-boson production 80—68419
- QCD correl. functions, multipole expansion and Casimir-Polder effect 79—80797
- QCD coupling const., renormalisation prescription depend. 80—4954
- QCD development from classical Yang Mills theory, a qualitative critique 79—80804
- QCD diagrammatic structure, deep inelastic scatt. in asymptotically free theories 79—2996
- QCD effects, parton transverse momenta, large-p_T hadron prod. 78—66083
- QCD estimates for associated charm production by weak neutral currents 78—78169
- QCD estimates for heavy-particle prod. 78—82108
- QCD exclusive processes, π, K, ρ form factors, hadronic wavefunction evolution eqns. 80—18135
- QCD expansion parameter choice 80—78025
- QCD extended leading logarithm approx. for inclusive distribs. and lepton pair prod. 80—379
- QCD gauge field strength and dual variable formulations 79—35946
- QCD gluon contribs. to large p_T reactions 78—41504
- QCD ground state wave function, model 80—73662
- QCD hadron jets, branching processes, multiplicity distrib., KNO scaling *(Russian)* 80—101998
- QCD hadronic μ pair prod., gluon gauge depend., struct. func. calc. 79—80810
- QCD hadronic spectrum, α-expansion method extraction, harmonic oscillator test 79—3009
- QCD hard scatt. off nuclear targets 79—63444
- QCD high energy predictions for elementary particle interactions using methods of cut vertices 79—89128
- QCD higher order effects in spin-dependent deep inelastic electroproduction 80—13281
- QCD higher order effects of structure function moments 80—62979
- QCD higher order prediction ambiguities, nonleading log corrections 80—392
- QCD in 2-D quark confinement and parton model 79—17670
- QCD in axial gauge, boundary terms and Poincare invariance, asymptotic gauge pots. 79—329
- QCD in two colours, virtual quark-quark scatt. in pseudoparticle background 78—12823
- QCD infrared regularisation ambiguities 79—71705
- QCD interactions, perturbation theory and the parton model 79—58927
- QCD invariant charge, study of gauge theory by Lipatov's method *(Russian)* 78—74220
- QCD IR divergences exponentiation 78—41492
- QCD jet calculus, inclusive p_T distrib. with exclusive form factors consistency 80—391
- QCD jet calculus, simple algorithm for quark and gluon jets 79—93346
- QCD jet calculus and tests 79—67516
- QCD jet dynamics, hadron and photon prod. at large transverse momentum 79—45077
- QCD jet fragmentation functions in leading log approx. 80—101981
- QCD jet simulation, cutoff choice effects 80—102015
- QCD jets, algorithm for parton spectra 78—89680
- QCD jets, algorithm to determ. multiparton distribs. 79—45064
- QCD jets, hadron prod. dynamical ansatz 79—71702
- QCD jets, multiparton distribs. 79—13065
- QCD jets, resolution algorithm 79—63455
- QCD jets, transverse momentum struct. 79—22031
- QCD jets, transverse spread 79—22032
- QCD jets in neutrino deep inelastic scattering, kinematics, thrust and spherocity distrib. 79—75762
- QCD lattice gauge theory, matrix Pade approximants, ratio of hadron to nucleon mass 80—4928
- QCD low energy tests, gluon non-zero effective mass, ψ decays 80—91054
- QCD model for gluon jet fragmentation, oblate transverse momentum struct. 79—9340
- QCD multijet model, universal quark-jet fragmentation in soft hadronic reactions 80—13285
- QCD multiplicity generating functions, quark and gluon jets 79—71720
- QCD observables in higher order calcs. 79—9334
- QCD of hadron struct. 78—93849
- QCD of quark matrer to nuclear matter transition at neutron star density 78—54608
- QCD on mass shell, Ward identities 78—16913
- QCD opposite two hadron correl., scale violations in quark/gluon fragmentation functions 79—54299
- QCD perturbation expansions in coupling const. renormalisation by momentum space subtraction 79—63416
- QCD perturbation theory, asymmetries in inclusive hadron prod. 78—50057
- QCD perturbation theory, high energy behaviour of jet and lepton-pair prod. 79—2932
- QCD perturbation theory, nonperturbative effects on factorisation in high momentum processes 79—36016
- QCD perturbation theory, quark decay functions, heavy hadron prod. 78—62364
- QCD perturbation theory calc. of transverse momentum distrib. in lepton-hadron scatt. 79—89163
- QCD perturbation theory for confined quarks and gluons, p glue content 80—52460
- QCD perturbation theory for confined quarks and gluons 80—401
- QCD perturbation theory of hard processes in asymptotically free field theory, ϕ^3 80—13263
- QCD perturbation theory predictions, applications and expt. verification, review 79—13026
- QCD perturbation theory test for various processes, review 79—326
- QCD phase transitions, chiral symmetry breaking, confinement, as tunnelling through singular barriers 78—82145
- QCD phenomenological model of high- and low-energy behaviour 79—63439
- QCD phenomenology, quarks and gluons in medium energy nuclear physics 80—42563
- QCD phenomenology of deep-inelastic scattering 80—73660
- QCD polarisation operator at finite temps. and densities, one loop approx., gluons *(Russian)* 80—68427

- **colour model** continued
  - QCD prediction for ang. distrib. of dileptons in hadron collisions 79—26300
  - QCD predictions, high p_T processes subject to sum rules, SU(3) symmetry constraints 79—354
  - QCD predictions, parton and gluon transverse momenta for large p_T particle prod. 79—40723
  - QCD predictions, subtraction scheme depend., struct. function scaling 79—49450
  - QCD predictions for e^+e^- annihilation jets, ang. correlations and asymmetries 79—9389
  - QCD predictions for inclusive and semi-inclusive leptoprod., hadron ang. distribs. 79—13041
  - QCD predictions for jet transverse momentum in leptoproduction 79—63442
  - QCD predictions for large momentum transfer baryon prod. 79—89125
  - QCD predictions for large p_T hadron prod. by polarised hadrons 78—82148
  - QCD predictions for processes involving real photons 79—6330
  - QCD predictions of deep inelastic scaling violations, non-perturbative effects 79—40732
  - QCD processes, large IR corrections, soft gluon emission 80—78028
  - QCD $q\bar{q}$ running coupling constant, β-function from string model, Pade approx. 79—343
  - QCD quark-gluon plasma, hadronic prod. of leptons, photons and ψ *(Russian)* 78—89672
  - QCD quark-gluon plasma, hadronic prod. of leptons, photons charm and ψ 78—89669
  - QCD renormalisation in two loop approx. in arbitrary gauge 80—102002
  - QCD running coupling const., nonperturbative determ., N struct. functions 79—75726
  - QCD scale parameter from quark matter phase transition 79—89112
  - qCD scattering processes with hard gluon emission, jet prod. 80—62939
  - QCD screening discussion from QED massless scalar problem 77—79237
  - QCD spectral function sum rules, EM current flavour components 80—99084
  - QCD spectrum, infinite number of colours at fixed coupling, interacting string model 79—2993
  - QCD spectrum calcs. in lattice gauge theory using Wilson's fermion method 79—367
  - QCD structure function relation between deep inelastic ν reactions and polarised electroprod. 80—37221
  - QCD systematic description of heavy quark systems 79—9341
  - QCD test, prod. of heavy quark flavours in hadronic interactions 77—45957
  - QCD tests and singlet struct. function moments 80—82941
  - QCD tests in γ-γ collisions and high p_T photon production 79—89129
  - QCD tests in τ-lepton decay and e^+e^- annihilation 80—102006
  - QCD theories of interactions, CP conservation, in presence of pseudoparticles 78—16923
  - QCD theory for the strong interaction 80—4962
  - QCD theory of three-jet prod. in large momentum transfer reactions 79—93373
  - QCD theory prediction of jet structure in $e^+e^- \rightarrow$ hadrons 78—12920
  - QCD three jet prod. in large P_T processes, two particle inclusive distribs. 79—9342
  - QCD transverse lattice theory, confinement and hadron bound states 80—4961
  - QCD two virtual gluon exchange force, using quark van der Waals force 78—82152
  - QCD two-dimens. 't Hooft Hamiltonian spectrum 77—65106
  - QCD vacuum, asymptotic freedom, quark confinement, Yang-Mills theory for strong interactions 80—73638
  - QCD vacuum, effects on hadronic currents, instantons, e^+e^- annihilation and precocious scaling 79—332
  - QCD vacuum, quantum liq. model, gauge and rotational invariances of colour fields 80—13283
  - QCD vacuum in strong external gauge fields, spontaneously, broken chiral symmetries 80—57555
  - QCD vacuum nonperturbative fluctuations, bag effect in low P_T hadronic spectra 80—37218
  - QCD vacuum props., strong interaction theory 79—26233
  - QCD vacuum struct. in chiral $U(N)\otimes U(N)$ symmetry 79—93347
  - QCD with heavy quarks, effective qauge theories 80—52467
  - QCD with N colours, approx. solns. 80—91051
  - QDD, quantum dath dynamics, SU(3) model for composite quarks and leptons 80—91055
  - $Q\bar{Q}$ bound states, hadronic decay, azimuthal correlations 79—93442
  - quantised strings and chromodynamic IR behaviour, Yang-Mills electric flux lines 77—30316
  - quantum chromodynamics, ξ scaling in lepton-hadron inclusive interactions 77—61298
  - quantum chromodynamics, electroprod. of charmed particles *(Russian)* 78—45878
  - quantum chromodynamics, field strength formulation 78—16924
  - quantum chromodynamics, hadroprod. of lepton pairs and real photons 78—50056
  - quantum chromodynamics, introduction *(Chinese)* 79—63412
  - quantum chromodynamics, IR asymptotics of quark form factors *(Russian)* 78—45882
  - quantum chromodynamics, IR struct. perturbation theory calcs. 77—74577
  - quantum chromodynamics, low-energy spectrum 77—2793
  - quantum chromodynamics, of coloured quarks, asymptotic freedom, zero charge, point charges in quantum electrodynamics *(Polish)* 78—45822
  - quantum chromodynamics, scale violation in presence of instantons 77—61196
  - quantum chromodynamics, short distance Regge singularities, renormalised gluon ladder 77—49909
  - quantum chromodynamics, strong interaction theory, review 79—67498
  - quantum chromodynamics, two dimens., confinement form factors, deep inelastic scatt. 77—30322
  - quantum chromodynamics, two dimens. U(N) invariant, 't Hooft bound state eqn. 77—26495
  - quantum chromodynamics, unified approach to gauge, dual, Gribov theories 77—18223
  - quantum chromodynamics in two dimens. 77—74590
  - quantum chromodynamics in two-dimens., Lorentz invariance 79—93339
  - quantum chromodynamics psi-spectroscopy model *(Hungarian)* 79—13068
- **colour model** continued
  - quantum effects of pseudoparticle size, non-Abelian gauge theories 77 22648
  - quantum number correlations at large transverse momentum and QCD 79—9337
  - quantum-chromodynamic β function at intermediate and strong coupling 79—89108
  - quantum-chromodynamic phenomenology of gluon jets 80—4941
  - quantum-chromodynamic predictions for inclusive spin-spin asymmetries at large transverse momentum 79—49472
  - quark and gluon jet longitudinal momenta, QCD anal. 80—22571
  - quark and parton phys., introduction, book 79—85276
  - quark antiquark pot. in QCD 78—4825
  - quark charge, fractional and integral models, effect of colour oscillations 79—75725
  - quark charge below colour threshold, rigorous theorems and parton model 79—85266
  - quark charges in QCD 79—97575
  - quark cluster, model of ordinary and exotic hadrons 79—40759
  - quark condensation in QCD 80—42401
  - quark confinement, analyticity of parton model, QCD_2 calc. 78—41484
  - quark confinement, infinite momentum frame formulation 79—36026
  - quark confinement and field theory, conf., Rochester, USA, (June, 1976) 77—71440
  - quark confinement and lattice calculation, by Monte Carlo methods 79—13023
  - quark confinement for gluon generation 78—25008
  - quark confinement in condensate of non-Abelian vortices 78—70328
  - quark decay lifetimes in Pati-Salam model 77—79243
  - quark decay patterns, liberated QCD and confined QCD theory 79—9328
  - quark distributions and quark jets from the CERN bubble chamber neutrino experiments 79—45085
  - quark distributions in QCD, Q^2 dependence parametrisation 79—58938
  - quark electrostatic forces, Lagrangian model with colour brightening 77—6079
  - quark form factor, non leading contribs. to asymptotic behaviour 78—8586
  - quark fragmentation: some simple tests for quantum chromodyanmics 79—49470
  - quark fragmentation into mesons, statistical model, vector meson contrib. 78—54639
  - quark fragmentation jets in QCD, cascade model 80—78045
  - quark gas, nonAbelian gauge field theory 78—21341
  - quark gas at finite temp. and density, QCD effects 80—95248
  - quark hyperfine interactions in negative parity baryons, QCD 78—16984
  - quark jet, $q\bar{q}$ pair production mechanism, average transverse momenta 80—18118
  - quark jet fragmentation, semiclassical model 79—45071
  - quark lattice and QCD in nuclei 80—5101
  - quark liberation from chromodynamical confinement, possibilities 79—30708
  - quark mass, electroweak contrib. 80—101990
  - quark mass dependence on QCD parameters 79—17675
  - quark mass effects as isospin and SU(3) violations in radiative decays of vector mesons 79—22091
  - quark mass shell gauge in Kondo-Yang-Mills theory 77—30309
  - quark masses from Weinberg-Salam model renormalisation group eqns. 80—42377
  - quark masses in QCD, one loop approx. calc. in axial gauge 79—58925
  - quark pair condensation and confinement 79—17677
  - quark sea, nonleptonic processes and $\Delta I=1/2$ rule 77—79255
  - quark stars, possible existence, 2nd order perturbation theory 80—26889
  - quark structure model 80—91063
  - quark-diquark model with broken colour symmetry, hadron spectrum 78—12874
  - quark-gluon field coupling const., meson mass differences *(Russian)* 80—105898
  - quark-line rule for hadron nonets, review 79—26304
  - quark-nucleon phase diagram and quantum chromodynamics 80—105855
  - quarkonia, S- and P-wave, gluon jets, perturbative QCD anal. 80—32070
  - quarkonia, spectra, decays, levels, jets, sum rules 80—18112
  - quarkonia states, heavy, strong decay into other heavy flavours, and triple-gluon vertex 80—47279
  - quarkonium decay, gluon jets and gluonic resonances, QCD test 78—93841
  - quarkonium decay into heavy quark flavours, ψ (J) energy distrib., QCD perturbation theory 78—82146
  - quarkonium decays into heavy quarks 79—58943
  - quarkonium radiative transition amplitudes, QCD dispersion sum rules 80—52511
  - quarks as quasiparticles of bound states *(Russian)* 78—25009
  - quarks with more than three colors in a class of asymptotically free gauge theories 80—394
  - quasi-confinement of quarks 77—13923
  - quasiconfinement in colour gauge symmetry, unconfined quarks and gluons 80—86686
  - quaternionic Hilbert space and colour confinement, admissible symmetry groups 80—27458
  - quaternionic Hilbert space and colour confinement 80—27457
  - radiative corrections in gauge theories, QCD current algebra formulation, weak interaction universality 78—93883
  - radiative transitions and gluon-exchange contributions in QCD 79—45074
  - random colour magnetic quantum liquid formation in QCD 80—99088
  - relativistic many-body theory, quantum chromodynamics and neutron stars/supernova 79—40752
  - relativistic string quantized in four-dimensional space, supersymmetrical Lagrangian in QCD principles *(Russian)* 80—13276
  - renormalisation group and infrared behaviour 79—58931
  - renormalisation of four dimensional operators 78—16929
  - renormalization of Yang-Mills theory developed around an instanton 79—45009
  - rest frame proton, colour gluon content, bag model and QCD calcs. 79—335
  - restricted theory as subset of nonAbelian gauge theory 80—62851
  - review of evidence for three-valued colour degree of freedom 77—82702
  - review of quark model with SU(n) symmetry, 3 colours and 5 flavours 79—9343
  - right handed colour octet currents for charm and colour excitation in $\nu(\bar{\nu})$ reactions 78—93874

colour model continued
S-wave colour singlet states, multiquark configurations, determ. and systematic labelling 78−58155
saturation of colour confining forces and effects 80−73672
scalar U(N) QCD in the large-N limit, hamiltonian method 80−37212
scale breaking for quark and gluon distribs., diagrammatic anal. 79−71706
scale dependent quark mass in colour gauge theory, $e^+e^-\rightarrow$hadrons anal. 77−30320
scale-invariant gauge theories, instanton role in QCD, QED and $CP^{(N-1)}$ 80−27400
scattering, deep inelastic, energy flow and energy correlations, perturbative QCD, infrared safety 80−27465
Schwinger model, canonical surface formalism, axial anomaly, chiral symm. breaking 78−12816
semi-inclusive deep inelastic neutrino scatt. QCD effects 79−30724
semiclassical methods, hadron struct. theory 79−97594
semiclassical QCD, regularisation and renormalisation 80−4925
semiempirical mass formula for hadrons in quark model and QCD 78−74236
singlet condensation, flux squeezing in QCD 80−52470
singular gauge instanton field, gauge zero modes, instanton determinants, and quantum-chromodynamic calculations 79−71635
six quark s-wave states, props., depend. on number of quark flavours 79−45060
SO(8)×SO(8) phenomenological symmetry, synthesis for leptons and hadrons 79−13035
soft gluon resummation formulae for hard parton processes in QCD 80−105842
soliton, bag-like solns. of coloured quark model 78−8609
solutions of Yang-Mills eqns. with external sources, colour charged particles 78−89624
source charge constraint integration in QCD with fixed sources 80−42402
spin-$^1/_2$ particle, energy in constant coloured mag. field 79−80742
stable dibaryon in QCD, Λc^0 bound state 79−67519
static colour change screening in classical gauge theories 79−45050
static potential energy of a heavy quark and anti-quark 79−13028
static potential $Q\bar{Q}$ model in weak coupling expansion 77−74647
static quark forces in classical chromodyanamics, bag models, SU(2) Yang-Mills field 79−2990
stellar evolution, terminal stages in QCD 77−78773
Sterman-Weinberg improved jet formula 79−63447
Sterman-Weinberg jet formula 79−6325
Sterman-Weinberg jet formula corrections for e^+e^- annihilation from QCD perturbation theory 79−36086
Sterman-Weinberg jets, leading log derivation 79−63413
string dynamics in external field 78−8585
string interactions in quantum chromodynamics, string lagrangian construction *(Russian)* 79−63432
string operator eqns. of motion in QCD 80−4953
string state, WKB-like wave functional and path-dependent phase factor, colour flux 80−52481
strong coupling QCD, variational approach, Schrodinger eqn. and effective Hamiltonian 80−95245
strong CP problems, soln. in Weinberg-Salam model, colour group extension 79−75699
strong-coupling calcs. of hadron spectrum in QCD, lattice Hamiltonian 77−41819
structure function in deep inelastic scatt., QCD predictions for singlet case 80−73707
structure functions, bounds for the ratio of anomalous dimensions, scalar gluon theories 80−57595
structure functions, nonsinglet, parton distributions, QCD parametrisation, leading and next-to-leading order corrections 80−68456
structure functions and masses of current quarks 80−22585
structure functions for quarks, gluons, hadrons in QCD 79−54318
structure functions in deep inelastic scatt., second-order contributions, ep and μp scatt. 80−13314
structure functions moments prediction 80−42460
$SU_L(2)\times SU_R(2)\times U(1)\times[SU(3)\times SU(3)]_c$ gauge model, chiral colour symmetry breaking 80−47234
SU_N gauge group uniqueness in grand unified model, U_1 color, proton stability 79−316
$SU(2)_L\times U(1)$, strong CP-violating phase, one-loop corrections, Higgs particles 80−62910
SU(2)×U(1) gauge theories, successes and current issues 80−18064
SU(2) colour Yang-Mills theory, quark source charge screening, confinement 80−22565
SU(2) symmetry, classical quark confining solns. incorporating colour 79−339
SU(2) Yang-Mills field equation instability, removal by (1+1) dimens. Higgs mechanism, SU(N) generalisation 79−58924
$SU(3)_{colour}\times SU(2)\times U(1)$ gauge, full operator structure of the non-leptonic $|\Delta S|=1$ weak Hamiltonian 80−99089
SU(3)×U(1) electroweak model, strong extension, flavour and colour gauge exchange symmetries *(Chinese)* 80−101975
SU(3)′×SU(3)″ scheme of three triplet model, colour symm. ψ-mesons descript. 78−78151
SU(3) colour gauge group, coloured monopoles 80−68360
SU(3) colour gauge theory, effective scale depend. quark masses in chiral limit 77−18222
SU(3) gauge fields, colour screening 78−82102
SU(3) rule for weak decays of charmed and strange mesons, colour struct. of currents 78−45916
SU(3) scheme of three quark binding in baryons mass formulae 78−12876
$SU(4)_F\times SU(4)_C$ synthesis of strong, weak, and electromagnetic interactions 80−13255
$SU(4)\times S_3^\alpha$, straton model, meson classification *(Chinese)* 78−78145
$SU(4)\times S_3^\alpha$ scheme, straton model, ϒ (9.5) props. *(Chinese)* 79−9347
SU(4)⊗SU(3)′ model, ϒ particles and SU(3)′ colour space *(Chinese)* 80−42409
SU(4) broken lattice gauge theory spectrum 79−49474
SU(4) spectroscopy 79−80808
SU(4) spin-isospin quark model explanation of nucleon-nucleon repulsive core 78−12984
SU(5), unification of weak, EM and strong interactions, review 80−105814
SU(5) electroweak-strong interaction model, broken colour symmetry and gluon mass 80−73650

colour model continued
SU(5) grand unification, heavy coloured Higgs scalars, b-quark mass 80−57543
SU(6) breaking of baryon wave functions, chromodynamic spin-spin force 79−340
SU(6) unified gauge group, neutral current coupling to ν_μm and ν_e 78−54626
SU(6) unified gauge model, based on SU(3)×U(1) and colour SU(3) subgroups 78−12847
SU(7) grand unified theory with heavy colour 80−42380
SU(N) colour groups, $N>3$, quark content 80−4938
SU(N) scalar QCD in two dimens., and the parton model 78−93856
subcomponent models of quarks and leptons in SU(3) subcolour, proton decay 80−78035
sum rules and moments of dimuon prod., valence quark transverse moments 78−54660
sum rules for charmonium and charmed mesons in QCD 77−30327
sum rules forlight quarks in QCD *(Russian)* 78−45812
superalgebra generalisation, 3-colour extension of OSP (4,1) de Sitter and SU(2,2;1) Wess-Zumino superalgebras 79−330
superconducting quark matter, asymptotically high density 78−12863
superconductivity unified model of weak, EM and strong interactions 77−49888
superdense matter, quark and gluon plasma, hadronic structure, neutron stars, hadron collisions, review 80−73683
superoperator generalisation of dual model with coloured quarks, three reggeon vertex *(Russian)* 78−74234
supersymmetric new hadronic states, production, decay and detection 78−70302
symmetry breaking and asymptotic freedom in colour SU(3) gauge models 77−13917
't Hooft's eigenvalue problem in two-dimens. QCD 80−4920
tachyons, monopoles and related topics, book 79−44718
tensor product of the octonionic Hilbert spaces and colour confinement 79−2982
thermodynamic pot. at finite temp. and density, QED and QCD 78−8535
three gluon coupling hadronic signature, η' in gluon jets, QCD vertex 79−75727
three gluon exchange contribution to forward high energy scattering 79−26310
three gluon integral equation and odd C singlet Regge singularities in QCD 80−101991
three large p_T jets, hadronic prod., perturbative QCD anal., processes and formalism 80−42508
three quark Hamiltonian from $q\bar{q}$ interaction, pairwise interactions in colour hypothesis 80−86670
three quark sources, colour algebra 80−52468
three triplet quark model with observable colour, hadron weak current, $\Delta T=1/2$ rule *(Russian)* 78−74219
three-triplet model, SU(2)⊗U(1) theory of weak interactions, spiral chromatic currents *(Russian)* 77−221
topological bootstrap prediction for three coloured, eight flavoured quarks 80−86694
topological expansion for baryons and mesons, reaction diagrams using coloured quark lines 77−82700
totally inclusive leptoprod., scaling anal., target mass corrections in QCD parton model 80−102052
transverse lattice QCD, hadron mass spectrum 80−57568
transverse momentum of massive muon pairs in QCD 78−45867
transverse quark polarization in large P_T reactions and e^+e^- jets 79−63410
triple gluon vertex meas. 79−71695
two jet model, large p_T hadronic multiplicity, colour octet exchange 78−62377
two particle inelastic scatt., mass divergences, QCD and parton model 79−22049
two photon processes, manifestation strength of colour below and above colour threshold 80−381
two-dimensional QCD, Lorentz invariance 80−37216
U(1) colour symm., Higgs coupling, proton stability 78−29290
U(1) Goldstone boson, anal. of BRS invariance in nonAbelian gauge theories 79−80798
U(1) problem in generalised θ-vacua, Goldstone boson and QCD 80−52399
U(1) without instantons 80−13265
U(N) lattice gauge QCD, complete integration in large-N limit 80−42338
unconfined colour gluons, possible existence in mass range 1.1 to 1.8 GeV 77−30324
unconfined colour quark models, weak interactions and neutral currents *(Russian)* 80−105841
unconfined quarks and gluons, quasiconfinement model, confining and nonconfining phase transition 80−86687
unconfined unstable quark, unified gauge theory predictions, selection rules 77−61253
unification of fundamental forces in nature, elementary particle constituents $SU(3)_c$ gauge symmetry, review 80−27448
unified description of quarks and leptons using colour and flavour degrees of freedom 80−27445
unified gauge theories, grand, asymptotic freedom constraints 80−62914
unified gauge theory, improved Pati-Salam model for strong+EM+weak interactions 79−318
unified gauge theory with Abelian massless gluons, binding of fractionally charged quarks 78−29296
unified theories, mass scales, alternatives to SU(5) 80−27441
unified theories, quantised Grassmann variables, colour and flavour degrees of freedom 77−49891
unified theories with spontaneously broken colour symmetry, QCD scalar parton effects 79−80783
unified theory of elementary-particle forces 80−105827
unifying mass scales without intermediate schiral colour symmetry, $[SU(2n)]^4$ unified model 80−22555
unitary spin, colour and unified theory, consideration of many-dimensional space-time 78−8570
universal Regge slope α' from the QCD gluon propagator 80−78026
unpolarised lepton-lepton collisions, photon 3rd struct. function, QCD implications 80−73708
vacuum, QCD, colour mag. permeability 80−78023
vacuum behaviour in QCD 80−62923
vacuum dynamic props. in QCD 80−4931

colour model continued
vacuum polarization about instantons 79−21928
vacuum structure in calibration theories, CP violation, cosmology *(Russian)* 80−27478
valence quark clusters in nucleon structure functions from neutrino scatt. 80−95252
valence quark-parton transverse momentum distrib. 78−12862
van der Waals forces in QCD colour singlets 78−86441
Van der Waals-like forces between hadrons induced by color confining potentials 79−49460
vector meson leptonic width, duality between vector mesons and perturbative QCD 80−57589
vector meson mass spectrum, radiative decay, QCD nonrelativistic potential model 79−36046
vortex string picture and large p_T reactions 79−63415
weak and EM interactions at high energy [conf. Les Houches, France (July 1976)] 79−80785
weak current colour-octet component, lepton-hadron correspondence 77−6077
weak hadronic current in coloured quark model 77−18236
weak hadronic currents in colour $SU(3)\times SU(3)$ model, diagonal neutral currents *(Russian)* 77−49902
weak nonleptonic decays, $\Delta S=1$, six-quark model 80−22582
Wilson loop formula for static $Q\bar{Q}$ potential in QCD 80−42399
Wilson operator formalism, generalised parton model equivalence 78−93855
Yang heavy axion, contradiction of muon anomalous mag. moment data *(Russian)* 79−49484
Yang-Mills fields, ambiguous relationship for dual models 79−49495
Yang-Mills gauge theory, classical soln. in colour meson model 78−45780
Yang-Mills instability, colour-screening 77−45951
Yang-Mills theories, infra-red struct., QCD mag. mom. anal. 77−13859
Yang-Mills theory, conserved flux, elimination of colour charge from gauge field 78−89659
Yang-Mills theory, covariant canonical formalism, quark confinement, absence of localised coloured/charged physical states 80−57573
Yang-Mills theory, non-Abelian structure, IR finite asymptotic states 79−265
Yang-Mills theory, nonleading IR divergences in QCD, renormalisation group function 77−71422
Yang-Mills theory, quark confinement and observables in covariant canonical formalism 79−6322
Yang-Mills theory developed around instanton, renormalisation 80−32027
Z(N) topological excitations in Yang-Mills theories: duality and confinement 79−12938
Zweig rule in two-dimensional QCD, ψ and Υ decays 80−52479
Zweig suppressed decay of heavy 1^{--} vector mesons, two gluon exchange 78−54616
b quark$\to\psi(\eta_c)+X$, B branching ratios assuring colour suppression 80−37259
B-meson decays, Cabibbo patterns, QCD effects, Kobayashi-Maskawa model 80−42451
$B\bar{B}$ narrow states in QCD 77−57494
$c\bar{c}g(c\bar{c}q\bar{q})$, exotic mesons, masses, decay widths, mixing matrix elements 80−62943
$\chi(3.45)$, radiative M1 transitions with charmonium model 79−13132
D charm decay, 20-dominance model validity from QCD 79−71747
D-meson decay, hadronic, six-quark model, quark-mass dependence, final state interactions, mixing angle effects 80−62973
D^0, $\bar{D}^0$, decays, charm changing neutral current limits, QCD depend., mass differences 80−32062
$D^0\to K^+K^-$, $\pi^+\pi^-$, branching ratio, $\Delta I={}^1/_2$ rule violation, colour radius interactions calc. 79−93412
D^+, D^0 nonleptonic decays, vectorial colour octet $q\bar{q}$ annihilation 80−52500
$D_{15}\to\rho\gamma$, SU(6) selection rule violation from quark hyperfine interactions 79−6329
D^{*+}-D^{*0}, QCD relation between EM mass differences 79−71750
ed, deep inelastic scatt., nucleon struct. function moments anal., asymptotic freedom critical tests 79−54344
ed scatt., P-violation calc. in weak interaction theory 80−42469
$e\bar{e}$, quark, diquark prod. thresholds, charm, colour excit. in 4-GeV region 77−79276
$e^-e^+\to$hadrons, finite energy sum rules in QCD 79−40754
e^+e^-, annihilation, polarised gluon bremsstrahlung as QCD test 80−32077
e^+e^-, vector and axial vector gluon prod., as signatures for axial chromodynamics 79−40729
e^+e^- 80−63010
$e^+e^-\to$ jets, on-shell QCD quark form factor from two particle correlations 80−86740
$e^+e^-\to3$ jets, three gluon coupling in perturbative QCD 80−105913
$e^+e^-\to4$ jets, differential 4-jet acoplanarity distribs., QCD predictions, heavy quark prod. 80−78083
e^+e^- annihilation, charge current asymmetry as QCD test, neutral gluons 80−57616
e^+e^- annihilation, energy correlations in perturbative QCD 79−85310
e^+e^- annihilation, energy correlations, sensitivity of QCD tests to gluon spin 79−89113
e^+e^- annihilation, event shapes, QCD perturbation theory calcs. 79−36056
e^+e^- annihilation, gg and qg coupling equality on resonance, QCD calcs., expt. tests 80−389
e^+e^- annihilation, gluon jets and heavy quarkonium prod., QCD test, ψ prod. 80−42479
e^+e^- annihilation, gluon jets, multiplicity and ang. distribs. asymmetries 80−91105
e^+e^- annihilation, hadron jets transverse momentum and ang. distribs. from QCD 79−40793
e^+e^- annihilation, hadron multiplicity distribution, Regge like parton model *(Russian)* 80−78100
e^+e^- annihilation, hadronic jet structs., QCD tests, max. directed momentum parameter 78−25057
e^+e^- annihilation, hadronic final state charge current asymmetry, QCD test, neutral gluons 80−37289
e^+e^- annihilation, hard gluon bremsstrahlung from heavy quarks, jet cross section 80−32078
e^+e^- annihilation, heavy quark jet ang. distribs., quark mass, QCD anal. 80−42481

colour model continued
e^+e^- annihilation, high energy, secondary hadron transverse momentum, QCD anal. 80−37285
e^+e^- annihilation, high energy, QCD tests 80−42420
e^+e^- annihilation, higher order QCD corrections 80−47316
e^+e^- annihilation, is there a QCD test at available energies? 79−40748
e^+e^- annihilation, jet ang. distrib., QCD correction 80−42482
e^+e^- annihilation, jet azimuthal ang. correlations in QCD 80−9179
e^+e^- annihilation, jet struct., test of QCD and quark-confining string 78−33040
e^+e^- annihilation, jets, colour-singlet subsystems, large rapidity gaps 80−68469
e^+e^- annihilation, opposite side quantum number correlations 80−105863
e^+e^- annihilation, QCD and semilocal duality (hadrons/$\mu^+\mu^-$) cross section ratio 80−78085
e^+e^- annihilation, QCD and jet acollinearity, quark-gluon coupling 80−105914
e^+e^- annihilation, quark fragmentation in field-theoretic model of composite hadrons 80−82986
e^+e^- annihilation, sphericity like distribs., testable QCD predictions 80−37284
e^+e^- annihilation, sum rules for Υ-family formation, QCD anal. *(Russian)* 79−54347
e^+e^- annihilation, tensor anal., QCD test 80−42396
e^+e^- annihilation, zero mass limit for class of jet-related cross sections 79−71736
e^+e^- annihilation and other processes, event shape anal., QCD perturbation theory 79−13140
e^+e^- annihilation channel, differential dispersive theory of ψ/J 78−45933
e^+e^- annihilation cross section, fourth-order QCD contribs. 80−82987
e^+e^- annihilation energy correlations, QCD test 79−13141
e^+e^- annihilation into hadrons, non-perturbative effects in QCD 79−89173
e^+e^- calorimetric experiments, $\gamma\gamma$ processes, tests of QCD 80−22628
$e^+e^-\to e^+X$, QCD predictions for deep inelastic scattering on an electron 79−63493
$e^+e^-\to e^+e^-+2$ gluon jets from $\gamma\gamma$ interactions cross section, gluon role in QCD 80−4976
$e^+e^-\to e^+e^-+2$ jets, $\gamma\gamma\to q\bar{q}$ contrib. to cross section, QCD corrections 80−78106
$e^+e^-\to e^+e^-+$gluons, gluon jet production, quark models 80−22576
$e^+e^-\to e^+e^-gg$, gluon jet polarisation in photon-photon scatt., QCD test 80−52550
$e^+e^-\to e^+e^-\gamma\gamma\to e^+e^-\bar{q}q\to e^+e^-h$, 100 GeV, QCD tests 80−18141
$e^+e^-\to e^+e^-qg(q\bar{q})+$ jet, $\gamma\gamma$ initiated 3 jet events in QCD 80−102057
e^+e^- final states, $q\bar{q}$ decay, semiclassical model, vacuum polarisation by colour field 80−63011
$e^+e^-\to\gamma+$hadrons, γ-spectra and QCD anal. 78−8678
$e^+e^-\to\gamma^*\to\gamma+$hadrons, QCD predictions 80−63009
$e^+e^-\to\gamma^*\to$hadrons, hadron calorimetric meas., QCD predictions, gluon emission 80−91102
$e^+e^-\to\gamma\to q\bar{q}g$, charge distrib., Sterman-Weinberg criterion, QCD test 79−71694
$e^+e\to$HX, associated production of gluonic jets and heavy mesons 78−93892
$e^+e^-\to$hX, high energy predictions from perturbative QCD 80−42417
$e^+e\to$hadron jets, 30 GeV, strong coupling constant and QCD test 80−37283
$e^+e^-\to$hadron jets, QCD, Monte Carlo model 80−27514
$e^+e^-\to$hadron jets, test for planar events in QCD 79−40794
e^+e^- hadron production and new colour 77−87927
$e^+e^-\to$hadrons, 12, 30 GeV, jets, quark fragmentation and coupling constant, QCD comparison 80−105915
$e^+e^-\to$hadrons, asymptotically free QCD perturbation theory for multijet final states 78−74267
$e^+e^-\to$hadrons, azimuthal correlations, quantum chromodynamics anal. 78−70382
$e^+e^-\to$hadrons, below 2 GeV, comparison of QCD sum rules with expt. 79−49458
$e^+e^-\to$hadrons, energy correls. in QCD, asymptotically free perturbation theory 79−63497
$e^+e^-\to$hadrons, finite energy sum rules, cross section, QCD calcs. 78−62413
$e^+e^-\to$hadrons, higher order QCD corrections 80−95280
$e^+e^-\to$hadrons, inclusive distribs., jets, $1+1$ dimens. QCD 78−66137
$e^+e^-\to$hadrons, jets from heavy quarks, QCD perturbation theory 80−63012
$e^+e^-\to$hadrons, non-perturbative QCD vacuum, total cross section corrections 80−86735
$e^+e^-\to$hadrons, parton model and QCD 80−105860
$e^+e^-\to$hadrons, QCD perturbation theory sum rule, ρ, ω and ϕ mesons 79−85268
$e^+e^-\to$hadrons, R problem, QED and QCD corrections, quarks and leptons 80−95281
$e^+e^-\to$hadrons, semiinclusive hadron prod., quark fragmentation function corrections, QCD 80−63013
$e^+e^-\to$hadrons, three-jet events and QCD test at PETRA 79−97631
$e^+e^-\to$hadrons, total cross section, QCD higher order corrections 79−85309
$e^+e^-\to$hadrons, two and three point energy correlations, QCD struct. 80−102019
e^+e^- high energy data from PETRA, QCD anal., QCD coupling constants 80−82985
e^+e^- inclusive annihilation, leading logarithm sum for struct. functions in QCD 79−71735
$e^+e^-\to$jets, energy cone distrib. around jet axis, QCD anal. 80−86732
$e^+e^-\to$jets, exclusive calcs. for QCD jets, Monte Carlo approach 80−105911
$e^+e^-\to$jets, jet ang. momentum, ang. distrib., oblateness and invariant mass, QCD calcs. 80−73722
e^+e^- jets, two-particle distribs. from single-particle fragmentation functions, effects of heavy quark flavours 80−68468
e^+e^- narrow angular jets, QCD and hadron phenomenology, cones or tubes 80−13320
$e^+e^-\to\psi X$, estimate of inclusive ψ and $\psi\eta_c$ prod., QCD anal. of cross section 79−85308
$e^+e^-\to q\bar{q}$ chromoelectric-flux-tube model of particle production 79−89176
$e^+e^-\to q\bar{q}g$, (3g), jet-mass spectra, perturbative QCD 80−63006

colour model continued

$e^+e^-\to q\bar{q}g$, energy-momentum distrib. 79—71696
$e^+e^-\to q\bar{q}g$, gluon fragmentation, polarised 80—82988
$e^+e^-\to q\bar{q}g$, long. polarised beams, beam-event asymmetry, massless QCD null result 80—91104
$e^+e^-\to q\bar{q}gg$, 4-jet prod. in lowest order QCD perturbation theory 79—49459
$e^+e^-\to q\bar{q}q\to$jets, ang. energy flow in perturbative QCD 79—49455
$e^+e^-\to q\bar{q}q\bar{q}$, 4-jet prod. in lowest order QCD perturbation theory 79—49459
$e^+e^-\to$quark jet, dimensionally regularised box graphs, zero mass case 80—102005
$e^+e^-\to$quark jet, two particle correlations in QCD 80—105858
e^+e^- resonance decay modes in Han-Nambu colour model 77—18307
$e^+e^-\to\Upsilon$, suggested search for gluon hadronic states in collinear gluon jets 78—89663
$e^+e^-\to$vector mesons, colour quark model for new reson. above 4 GeV 78—17033
eN, deep inelastic scattering and asymptotic freedom, Q^2 dependence of moments 80—82978
eN, scaling violation, Callan-Gross relation, colour excitation 77—65159
eN deep inelastic polarised scatt., QCD corrections 80—52517
eN deep inelastic scatt., QCD anal. 80—95276
ep, deep inelastic scatt., higher order asymptotic freedom corrections 80—105903
ep, deep inelastic scatt., nucleon struct. function moments anal., asymptotic freedom critical tests 79—54344
ep, high Q^2, QCD corrections to parity-violating asymmetries 80—22618
ep deep inelast. scatt., QCD perturbative corrections 78—74263
ep deep inelastic scatt., scaling violations and QCD parametrisations, struct. functions *(Russian)* 80—37277
$e^\pm p\to e^\pm\gamma+X$, deep-inelastic bremsstrahlung, quark charges, colour gluon mass 78—74216
$eq\to eqg$, gluon fragmentation, polarised 80—82988
η, η' and η_c, mixing and decays in nonrelativistic quark model for QCD idea 78—82166
η, vacuum symmetry, decay consts., mixing consts. in SU(3)×SU(1) QCD 80—27483
η Dalitz decays, excitable colour gluons 78—58181
η decays of ψ's, VMD and colour model coupling const. calcs. 77—26516
η_c and η_c', mass prediction using QCD 80—22590
η_c mass determ. from QCD sum rules 78—74223
η_c mass from dispersion sum rules in QCD, identification with X(2.83) *(Russian)* 78—89681
η', QCD sum rules for mass, possible pseudoscalar gluonium, instanton effects 80—388
$f_c(3.55)$ absolute γ-decay rates from tensor meson dominance and QCD pots. 79—9377
F*-F, D*-D, pseudoscalar-vector mass differences, QCD nonrelativistic quark model 79—6339
γ-γ scatt., QCD higher-order asymptotic freedom, corrections, γ struct. function calc. 79—89130
$\gamma+$hadron$\to$lepton pair, perturbative QCD, twist-2 photon operator, parton subprocesses 80—73716
$\gamma^*\gamma^*\to 2$ jets in e^+e^-, parton model QCD corrections for doubly deep processes 80—73758
γe collisions, jet production, QCD study 79—89142
$\gamma\gamma$, jet and single particle prod. at large p_T 79—49565
$\gamma\gamma$, jet production, QCD study 79—89151
$\gamma\gamma\to$hadrons, energy pattern for two and three jets, colour corrections, calorimetric expts. 79—71774
γN, deep inelastic scatt., QCD phenomenology 80—42443
$\gamma N\to$jet$+X$, QCD cross sections 80—73715
$\gamma N\to\pi^+X$, QCD cross sections 80—73715
$\Gamma_{pol}N\to\pi^\pm N$, weak neutral interactions, QCD renormalisation 79—93433
γp, heavy quark particle photoprod., QCD model, vector dominance implications 80—86730
γp cross-section observed increase, jets as source, QCD and vector-meson dominance model 80—22620
$\gamma p\to\gamma+$jet$+X$, perturbative QCD predictions large p_T real photon in final state 79—89165
$\gamma p\to h^\pm X$, large p_T photoprod., perturbative QCD test 80—37276
$\gamma p\to p\pi^0$, quantum chromodynamics and P-odd effects *(Russian)* 79—89172
$\gamma p\to\pi^0+$jet$+X$, perturbative QCD predictions 79—89165
$\gamma p\to\pi X$, large p_T, perturbative QCD 80—86723
$\gamma p\to q\bar{q}p$, quark-antiquark jet diffractive photoprod. in perturbative QCD 80—73714
$hh\to\mu^+\mu^-+$jet$+X$, QCD anal. of recoiling jets and angular effects in large q_T pair prod. 79—45078
in deep inelastic scattering, quark jet as trigger for gluon jet 80—62996
J/ψ, radiative M1 transitions with charmonium model 79—13132
$J/\psi\to\eta(\eta')\gamma$ decay rate, QCD sum rules 80—52497
K charge radius, coloured quark field theory 80—62945
K hadronic decays, $1/N_c$ expansion 78—25042
K^0-$\bar{K}^0$ mixing, strong interaction corrections in six quark model, QCD calcs. 80—82957
$K^+\to\pi^+e^+e^-$, quantum chromodynamics *(Russian)* 77—2822
K^+n scatt., QCD, one-gluon-exchange, resonating group method, soft-core approx. 80—63025
K^+p scatt., QCD, one-gluon-exchange, resonating group method, soft-core approx. 80—63025
$K^\pm p$, 130, 200 GeV, jet prod. cross sections, QCD anal. and scale breaking 80—99111
$K^\pm p$, 200 GeV/c, high p_T jet prod., QCD expt. test 79—89200
$K^+\pi$ scatt., QCD, one-gluon-exchange, resonating group method, soft-core approx. 80—63025
lh deep inelastic processes, QCD predictions 80—73677
LN scattering, structure and fragmentation function moments, meas. and QCD predictions 80—37274
Λ-hypernuclei, QCD and spin-orbit splitting, spin-orbit pots. 79—85398
M(1.86) as possible coloured kaons, Han-Nambu weak interaction theory 77—2799
μ pair prod., QCD ang. correl. 78—49976
μ pair production in hadron-hadron collisions, gluon effects, QCD predictions 78—78148
μd, deep inelastic scatt., nucleon struct. function moments anal., asymptotic freedom critical tests 79—54344
$\mu^+\mu^+$ production in hadron-hadron collisions, small transverse momentum distrib., QCD soft gluon bremsstrahlung effects 79—75723

colour model continued

μN, deep inelastic scattering and asymptotic freedom, Q^2 dependence of moments 80—82978
μN, deep inelastic struct. function, Nachtmann moments in QCD 80—27510
$\mu N\to\mu X$, colour model explanation of νW_2 rise 79—45092
$\mu N\to\mu\psi X$, diffractive and non-diffractive ψ leptoprod. in QCD 80—424
μp, deep inelastic scatt., higher order asymptotic freedom corrections 80—105903
μp, deep inelastic scatt., nucleon struct. function moments anal., asymptotic freedom critical tests 79—54344
μp, hadron prod. ang. distribs. and transverse momentum, QCD test 80—82980
μp, semi-inclusive, ang. correl. tests of QCD 79—17735
μp, semi-inclusive scatt., quantum chromodynamic predictions 78—29324
μp high energy data, QCD energy momentum sum rule, gluon fraction of proton 77—49971
n, structure function nonsinglet moments from deep inelastic lepton scatt., QCD 80—62980
N form factors, weak, asymptotic behaviour within QCD dipole and triplepole formulae 80—62987
NN elastic scatt. constituent description, spin-correl. meas., reaction mechanisms, QCD instanton effects 79—89180
NN large angle elastic scatt., spin correlation asymmetries, partons and coloured quarks 79—63411
$NN\to NN$, large momentum transfer, spin effects, QCD quark and gluon interactions 80—22577
NN short range interaction, six quark symmetry props., nucleon colour mag. attraction *(Russian)* 80—42411
NN system, mag. colour attraction, quark configurations 80—27472
NN two body systems, polarisation phenomena, 6 MeV/c to 150 GeV/c, QCD anal. 79—80840
$NN\pi$ amplitudes, parity violating, QCD calc. in Weinberg-Salam model and SU(4) flavour symmetry breaking 79—67520
$NN\rho$ couplings, parity-violating, QCD and MIT bag model, $1/2^-$ resonance contribs., $SU(6)_w$ symmetry 80—57540
$\bar{\nu}$ anomaly at >50 GeV, anal. using right handed colour octet current scheme 77—30360
ν deep inelastic scatt., energy flow, test of perturbative QCD 79—67534
$\nu(\bar{\nu})$ deep inelastic scattering, scaling violations of struct. function moments and perturbative QCD 79—40736
$\nu(\bar{\nu})N$, 2-200 GeV, q and $\bar{q}$ distribs. Nachtmann moments, gluon distribs. 79—392
$\nu(\bar{\nu})N$ inclusive scatt., scaling violation evidence, QCD test 78—89701
$\nu_\mu(\bar{\nu}_\mu)N\to\mu\mp X$, colour excitation in deep inelastic scatt. 79—13099
νFe scattering, comparison of moments from valence struct. function with QCD predictions 79—49521
νN, above W prod. threshold energy, QCD effects, cross sections and neutral currents *(Russian)* 79—67537
νN, charm and strangeness production, role of gluons 79—13104
νN, deep inelastic scattering and asymptotic freedom, Q^2 dependence of moments 80—82978
νN, semi inclusive π prod., angular asymmetries in QCD 79—9360
νN, structure functions of deep inelastic scatt., QCD test, high-twist contribs. 80—57579
νN, two gluon mechanisms, quarkonia, glueballs and Higgs scalars 80—78077
νN and $\bar{\nu}N$ reactions, dimuon prod. mechanism, coloured quark model 77—22725
νN reactions, field theory phenomenology 79—54304
νN scatt., QCD effects above W prod. threshold, structure functions 79—71738
νN scatt. with charge exchange, quark-parton model and QCD description *(German)* 79—26324
νN single- and di-muon prod., colour excitation, weak interaction model anal. 78—45906
$\nu_\mu N$, charm pair prod. in QCD, trimuon rate 78—45907
$\Omega\to\Lambda K$, QCD and valence quark approx. 80—105893
Ω^- nonleptonic decay branching ratios from Weinberg-Salam and MIT bag models 80—37261
$\Omega^-\to\Xi^*\pi(\Xi^0 l^-\nu_l)$, nonleptonic hyperon decays, QCD description, PCAC anal. 80—95269
p, structure function nonsinglet moments from deep inelastic lepton scatt., QCD 80—62980
p Dirac form factor and QCD 78—45864
$p(\bar{p})p\to\gamma X$, large angle real photon prod. at large p_T, QCD anal. 80—22644
$p(\bar{p}p)\to W^\pm X$, QCD perturbative predictions 79—40812
p-n mass difference, anal. of expt. data, scaling violation and renormalised struct. functions 79—97628
$p+N\to\mu^-\mu^+X$, 400 GeV, charged gluon effects, broken colour gauge model study 79—49473
pd, 70 GeV, $\pi^\pm$, $K^\pm$, p, $\bar{p}$ prod. with 0.5-2.2 GeV/c transverse momenta, yield ratio, QCD *(Russian)* 80—83012
pN, μ pair prod., QCD predictions for zero and nonzero rapidities 78—89674
pp, 70 GeV, $\pi^\pm$, $K^\pm$, p, $\bar{p}$ prod. cross sections, QCD-parton model anal. *(Russian)* 80—63044
pp, D, B, K prod., QCD model for heavy flavour prod., two gluon annihilation 80—86744
$p\bar{p}$, hadronic jets, possible intermediate bosons 80—18149
pp, jet thrust spectrum, 3-jet structure, QCD calc. 80—47333
$\bar{p}p$, pp, 130, 200 GeV, jet prod. cross sections, QCD anal. and scale breaking 80—99111
pp, $\bar{p}p$, 200 GeV/c, high p_T jet prod., QCD expt. test 79—89200
$\bar{p}p$, pp, 540 GeV, Υ and ψ transverse momenta from QCD $2\to 3$ processes, gluon subprocesses 80—52546
$\bar{p}p$, pp, beauty prod. total cross section from perturbative QCD 80—32080
$\bar{p}p$, pp, lepton pair prod., transverse momentum distrib., QCD calcs. to leading logarithms 80—42486
$\bar{p}p$, pp, pol. and unpol. beams, hadronic jets, vector bosons, QCD and weak interference 80—57648
pp, transverse momentum fluctuations and high p_T processes in QCD 79—36014
pp, Υ production cross sections, colour excited states in Han-Nambu model *(Chinese)* 79—49480
pp and $p\bar{p}$, Higgs-boson production at large transverse momentum in quantum chromodynamics 79—40745
pp collisions, real photon prod. at large p_T, cross section calc. 79—13149
$\bar{p}p\to\gamma$, Z^0+X, charge asymmetry, QCD-parton model study 79—93349

colour model continued
- $pp \to \gamma X$, large p_T direct photon prod., QCD scale violation effects 79−71772
- $pp \to \gamma X$, perturbative QCD anal. 80−63042
- pp high p_T polarised elastic scatt., QCD explanation of asymmetries 80−13323
- pp interactions, effects of hard gluon bremsstrahlung in dimuon and Υ prod., QCD anal. 79−13058
- $pp \to jet + X$, P-violating weak effects in high transverse momentum collisions, QCD anal. 79−63559
- $pp \to l^+l^-X$, QCD quark-quark correction for Drell-Yan formalism 79−75731
- $pp \to l^+l^-x$, QCD corrections to Drell-Yan formula 80−22578
- $pp \to meson + lepton$ pair, transverse momentum distrib. and branching ratios, proton gluon distribution 80−52537
- $pp \to \mu^+\mu^-X$, gluon corrections to Drell-Yan model 79−36037
- $pp \to \mu^+\mu^-X$, muon pair ang. distrib., QCD model study 79−36035
- $pp \to \mu^+\mu^-X$, spontaneously broken colour gauge theory effects in Drell-Yan process 79−26344
- $pp \to \mu^+\mu^- +$anything, Drell-Yan formalism 78−78229
- $pp \to pX$, diquark fragments, large transverse momentum baryon production 80−47330
- $pp \to pX$, high p_T, spin-spin asymmetries, polarisation, hard scatt model with QCD 80−13339
- $pp(\bar{p}) \to W^{\pm}(Z^0)X$, QCD perturbation theory struct. function predictions 80−42505
- pp polarisation asymmetry in high p_T inclusive prod., QCD and gluon models 79−40819
- $pp \to pp$, large momentum transfer, multiple-scattering model, three-quark proton 80−63031
- $pp(p\bar{p})$, heavy flavoured states, assoc. prod. QCD calcs. 79−85274
- $pp \to \pi^0$, large transverse momentum jets investig. at 52.4, 62.7 GeV 80−18151
- $pp \to \pi^0X$, intermediate $p_\perp$ distribution through a QCD resummation mechanism 80−83010
- $pp \to \pi^+X$, P-violating weak effects in high transverse momentum collisions, QCD anal. 79−63559
- $pp \to \pi X$, crucial spin tests of QCD approaches to large transverse momentum processes 79−63558
- $pp \to \pi X$, large P_T, transversely polarised beam and target, QCD predictions 79−49553
- $pp \to \pi X$, large-P_T reactions in broken color gauge theory 80−95292
- $pp \to \pi + X$, high p_T jet prod., QCD perturbation theory 79−89209
- $pp \to \psi X \to \mu^+\mu^-X$, Drell-Yan mechanism in colour quark model 77−6181
- $p\bar{p} \to W^{\pm}X$, front back asymmetry in QCD and Weinberg-Salam model 79−97579
- $pp \to x\pi X$, QCD radiation and mean scaling, longitudinal and transverse momentum 80−42405
- $pp.\bar{p}p$, polarised and unpolarised, jet cross sections vector boson signals, QCD-weak interference 80−5026
- π charge radius, coloured quark field theory 80−62945
- π decay constant, EM form factor, quark EM self-energy in QCD 80−37242
- π EM form factor asymptotics in QCD perturbation theory, partonic interpretation *(Russian)* 80−62984
- π EM form factor factorisation and asymptotic behaviour in QCD 80−91090
- $\pi \to e\nu\gamma$, vector form factor, quark masses and isospin breaking 79−13111
- π form factor, ϕ peak, unitarity and gluonic corrections 80−22615
- π form factors, in QCD, light cone Bethe-Salpeter eqn. soln. 79−80827
- $\pi^0,\pi^{\pm}$ EM polarisabilities, sum rules, coloured quark field theory 80−57561
- πN coupling, parity violating, weak and EM interaction model anal. 79−67599
- π^-N, 16, 22 GeV, dimuon prod. parton intrinsic transverse momentum, QCD perturbation 80−63037
- π^-N in Be, 150, 175 GeV/c, high mass muon pair prod., Drell-Yan QCD corrections 80−13343
- $\pi^+n \to p\pi^0$, quantum chromodynamics and P-odd effects *(Russian)* 79−89172
- πp, beauty prod. total cross section from perturbative QCD 80−32080
- πp, quark-diquark elastic scatt., diquark fragments, large transverse momentum baryon production 80−47330
- πp, real photon prod. at large p_T, QCD and CIM anals., jets 79−89185
- $\pi p \to \pi X$, high p_T π^0 prod., leading particle contrib., QCD calcs. 80−73746
- $\pi p \to \pi p$, large momentum transfer, multiple-scattering model, three-quark proton 80−63031
- $\pi^-p \to \gamma X$, large angle real photon prod. at large p_T, QCD anal. 80−22644
- $\pi^{\pm}p$, 130, 200 GeV, jet prod. cross sections, QCD anal. and scale breaking 80−99111
- $\pi^{\pm}p$, 200 GeV/c, high p_T jet prod., QCD expt. test 79−89200
- $\pi^+\pi$ scatt., QCD, one-gluon-exchange, resonating group method, soft-core approx. 80−63025
- $\psi(3.1)$ and $\psi(3.7)$, colour symmetry breaking model 77−18233
- $\psi(4.1) \to \psi(3.1) + \pi + \pi$, coloron model, quark composite struct. 78−29332
- ψ decay, high energy direct photons, γ, π^0 momentum distribs., QCD calcs. 80−32098
- $\Psi \to \eta'\gamma$, QCD, width, exclusive OZI violating radiative decay 80−68458
- ψ hadronic production, gluon contrib. in QCD framework 78−78139
- ψ particles and colour symm. 77−57493
- ψ', radiative M1 transitions with charmonium model 79−13132
- $\psi' \to \psi + \eta$, two gluon mechanism, Υ dynamics test 78−89665
- QCD, $\bar{q}$ polarisation in quark sea of proton 78−12867
- $qg \to l^{\gamma}$, high P_T photon polarisation as QCD test 80−4934
- $q\bar{q} \to 3$ gluons$\to 3$ jets, jet kinematics and observability 79−45070
- $(\bar{q}q) \to (\bar{q}'q')\gamma$, width, exclusive OZI violating radiative decay 80−68458
- $Q\bar{Q}$ annihilations in QCD, strong radiative corrections 79−80809
- $q\bar{q} \to g\mu^+\mu^-$, large q_T muon pairs ang. distribs. in perturbative QCD 79−85275
- $Q\bar{Q}$ mass, approx. scheme is QCD 80−42398
- $q\bar{q}$ non Abelian gluon interactions, long distance behaviour of chromostatic potential 79−17676
- $q\bar{q}$ pair energy modification in Wilson loop formalism 80−18122
- $q\bar{q}$ resonance energy spectrum, leptonic and radiative decay widths, QCD pot. calcs. 80−52491
- $q\bar{q}$ states, decay with large mass in 2-D QCD, appl. to meson decay anal. 79−89126
- $q\bar{q}$ systems, nonperturbative potential model 80−78040
- $q\bar{q} + l^+l^- +$ hadrons, probe of OZI suppression 79−17680
- ρ form factors ratio, high momentum transfer behaviour in QCD 78−70340
- $SU(8) \times SL(3,R)$ colour quark model, vector states in e^+e^- annihilation at 3.9-4.5 GeV 77−41850
- Σ-hypernuclei, QCD and spin-orbit splitting, spin-orbit pots. 79−85398
- $\Sigma^- \to \Lambda K$, QCD and valence quark approx. 80−105893
- $\Sigma^+ \to p\gamma$, $1/2^-$ resonance poles to parity-violating amplitude, two-quark weak transitions 80−78062
- Σ^{*-}-Σ^{*+}, QCD relation between EM mass differences 79−71750
- τ particle properties, QCD type gauge theories, absence of $\tau^+\tau^-$ resonance in e^+e^- annihilation 78−37144
- τ semihadronic decay rate and branching ratio, QCD calc. 79−36119
- Υ, interpretation as coloured particle, masses and leptonic decay widths 79−54322
- Υ, leptonic decay width, mass depend. in QCD 79−49488
- Υ, pot. model, heavy quarks 78−45875
- Υ, quixotic interpretation as $Q\bar{Q}$ bound state 80−13280
- $\Upsilon(9.46) \to$ hadrons, gluon spin and colour, QCD nontrivial test 80−82971
- $\Upsilon(9.4)$ family, gauge theory mass anal., harmonic oscillator pot. 78−82186
- $\Upsilon(9.5)$ hadronic prod., parton distrib. and QCD 78−78142
- Υ (9.5), possible colour-excited states *(Chinese)* 78−82169
- Υ decay, multiplicity decrease due to charm prod. suppression 79−49518
- $\Upsilon \to e^+e^-$, harmonic oscillator model, QCD gluon-bottom quark coupling 79−3016
- Υ spectroscopy, asymptotic freedom 78−45865
- Υ', lepton heavy width QCD radiative corrections 79−49515
- $\Upsilon' \to \gamma 2^{++}(\bar{b}b)$, photonic decay widths in tensor meson dominance 79−75754
- $\Upsilon' \to \Upsilon + \eta$, two gluon mechanism, Υ dynamics test 78−89665
- $V \to \gamma h$, use of QCD in OZI-violating radiative decays 79−26302
- X(2.83), radiative M1 transitions with charmonium model 79−13132
- $\bar{b}b2^{++} \to \gamma\Upsilon$, photonic decay widths in tensor meson dominance 79−75754
- $\gamma N \to \mu\bar{\mu}X$, QCD cross sections 80−73715
- ^2H nucleus wave function momentum contribution from QCD diagrams *(Russian)* 80−68562
- $pp \to \pi^+\pi^-X$, QCD testing by high energy hadroprod. of lepton pairs 79−26343
- $\pi^-N \to \mu^+\mu^-X$, lepton ang. distrib. calc. by QCD 79−26303
- $Y \to 3g$, angular patterns and front-back moments, QCD 80−73702

colour perception *see colour vision*

colour photography
- aerial photography, multispectral, soil survey in New Zealand 78−85728
- aerial photography maps, colour maps made from B & W negative 80−109270
- archival storage of colour films by rainbow holographic technique 79−18373
- astronomy, galaxy image picture processing system for colour 77−49303
- camera and instant film development, interdisciplinary and international approach 80−81342
- cassette film camera for automatic and rapid prod. of colour pictures *(Russian)* 78−93780
- cine film colour duplication, Laboratory Aim Density control method 77−5953
- cinematography, colour film processes and cameras, review, 1894 to date *(German)* 78−93773
- colorimetric comparison of colour reproductions 80−95119
- colorimetric evaluation of colour separation *(Russian)* 78−49926
- colour atlas for colour organisation in film production *(Russian)* 78−93776
- colour correction requirements, dependence on original 78−21239
- colour mixing and colour films *(German)* 78−93774
- colour rendering evaluation, extension of CIE colorimetric system, in film and television 78−310
- colour rendering index role *(Hungarian)* 77−18116
- colour reproduction index, CIE, theoretical basis *(German)* 78−4718
- colour TV faults recorded using 35 mm Kennedy monobar camera 79−21824
- colour-IR photographic filters 77−71396
- crop canopy complex aerial photographic images, analysis and electronic area meas. 79−26159
- developing agents in processing solns., polarographic determ. 78−4726
- digital colour recording system for digital-analogue hybrid image processing 78−16880
- digital processing techniques applied to astronomical images 77−60626
- distortions due to inaccurate modelling of process, cinematography appl. *(Russian)* 79−17533
- disulfides as antisilvering compounds in fixing developers 79−24795
- dye-releasing compounds, colour imaging technology for instant photography 78−62247
- ecosystem succession detection by aerial IR photography 78−81459
- electronic masking techniques, telefilming appl. 78−32902
- electrophotographic process for colour slide film *(Japanese)* 77−71394
- exposure meter errors during colour photographic printing 80−101818
- exposure meters for colour positive process, review 78−12781
- film archival storage, white light processing technique 80−99637
- film densitometer with Si photodetector 80−4791
- film material sensitivity, copier technology appl. *(German)* 79−26156
- film spectral sensitivity meas. by Hadamard spectrosensitometry 77−26414
- flood-plain delineation by multispectral data analysis 77−73885
- fluorescence angiography, colour and black and white, use of interference filters 78−48856
- fluorescent brightening agents effects on reproduction of halftone prints *(Japanese)* 77−26417
- fluorescent lamp suitability evaluation by image psychophysical and subjective estimations 79−71555
- fluorescent lamps for light sources, evaluation of suitability *(Japanese)* 77−26415
- fogging effects diagnosis, use of granularity meas. 79−47952
- four-colour reproduction, colorimetric anal. by photomechanical means 79−75635
- four-colour thin apochromat design 79−27364
- high-speed scanning colour printer 79−93246
- holographic schlieren photography and interferometry, coloured patterns appl. *(Russian)* 77−34852

colour photography continued
- holography, emulsion VRE-52, determining characts. 77—634
- image amplification by redox couple reaction 79—24802
- image archival storage using Fourier multicolour holograms 80—102674
- image form., optical transfer functions for tristimulus values 78—33685
- image interpretation, RADC's research 77—74534
- image processing, using graphic arts scanner and off-line digital processing 77—79191
- image sharpness rel. to spatial freq. for Ag and dye *(Russian)* 78—49933
- image stability and dye fading mechanisms 80—62754
- instant colour-discrimination shadowgraphic technique and film 80—9057
- IR film for mapping and multispectral photointerpretation 79—25356
- Kodak instant-print colour film cameras *(German)* 78—21233
- lens transmittance 78—62250
- Lichtenberg figures at cryogenic temperatures *(German)* 77—82536
- magenta pyrozolone azomethine dye, electrochemistry of fading mechanism 79—24761
- Maxwell, discoveries relevant to wireless and colour reconstruction 80—27093
- mountain aerial photography, colour film types compared 77—29500
- multispectral aerial photography, Khomas Trough region gossaniferous outcrop identification 77—5346
- multispectral aerial photography, rock type identification in NW Cape Province, S.Africa 77—5345
- multispectral computer anal. for thermal burn depth diagnosis 78—3648
- multispectral photography appl. using MKF-6 camera and MSP-4 projector 80—56633
- multispectral scanner data principal-axis transformation to colour composite picture 79—29879
- negative film, rapid access processing 78—21240
- negative films (high speed), colorimetric testing 78—86364
- non-mechanical dispergation of color couplers 79—24799
- objective colour correcting coatings 79—75631
- optical laboratory experiments *(Spanish)* 79—21510
- optical printers, electronically controlled additive lamp house 80—105732
- opto-electronic device for aerial colour photograph interpretation *(Russian)* 80—61920
- paper, *(Russian)* 79—67409
- photoelastic optical retardation determ. 79—72865
- photofinishing printer response customisation 80—4793
- photographic light sources, characteristics and parameter definition using graphical method for correct choice of compensating filters *(German)* 80—52342
- photomicrography with colour films, colour reproduction *(German)* 78—20338
- photosensitive glass, full-colour polychromatic, subcolloidal Ag precipitation 79—47953
- planetary obs. from space probe *(German)* 77—53445
- Polaroid photography colour reproduction 78—54490
- Polavision, first instant colour movie system 78—24882
- polychromatic processing technique for colour image transparencies 80—86473
- prediction model for multispectral imagery 77—71395
- printer quality and productivity improvements 79—93245
- printing and processing efficiency improvement for motion pictures 78—78023
- processing monobath with high pH 77—41712
- real time laser recording, plastic versus metal coatings 77—74536
- reversal film, method for increasing resolution during processing *(Russian)* 79—75644
- reversal films, accelerated development process, activating substances *(Russian)* 77—34047
- review of colour reproduction by photography 78—309
- SEM and TEM temporal event representation by colour microphotography 79—17566
- slides preparation, using heat shrinkable material 79—6202
- spectral sensitivities of colour-reproduction systems 78—49883
- spectrozonal light source factors in exterior photography *(Russian)* 79—40638
- subtractive colour photographic printing, exposure parameter calc. 79—26167
- subtractive photographic colour printing, correcting light filter selection 80—62764
- surface texture colour reproduction visual qualities 78—16881
- thermoluminescence spectra estimation using colour transparency film 77—86646
- thin layer chromatographic anal. of dyes formed by development *(Japanese)* 77—26418
- transparency projector/scanner and printer 80—52343
- TTL spot exposure meter, applications and description 78—12782
- vegetation resources interpretability for various space acquired image types 79—26160
- zero order diffraction microimage reproduction from surface relief gratings 79—17518
- Ag, graining, comparison with colour image *(German)* 79—29380

colour picture tubes, television *see colour television picture tubes*

colour receivers, television *see colour television receivers*

colour television
- acoustooptic FM and freq. shifted heterodyne CO_2 laser system 78—5568
- astronomy, galaxy image picture processing system for colour 77—49303
- colour images, composition and decomposition 79—50233
- colour measurement, CIE system, photoelectric tristimulus colorimeter 80—9018
- colour rendering evaluation, extension of CIE colorimetric system, in film and television 78—310
- edge detection, choice of coordinates 77—79775
- holographic colour video memories, recording and playback technique 80—9833
- holographic recording of digital colour TV signals on photographic film *(German)* 78—22101
- image coloration psychophysics 78—65025
- image feedback processor, ghost image elimination from TV display 78—46519
- image recording on monochrome film by carrier frequency photography *(Japanese)* 77—41711
- imaging computer peripheral 79—20667
- imaging system, real time Doppler, colour TV display of particle size or density 77—62038

colour television continued
- liquid crystal light valve operation and appls. 78—46826
- megnetic deflection yokes, mag., integral eqn. method for anal. 79—50183
- meteorology, thunderstorm development on colour TV display, of METEOSAT data 79—100936
- microneurology, appl. of colour TV as surgery teaching aid 78—40396
- microscopy, applications 80—98972
- photography of colour TV faults 79—21824
- planetary satellite Io, brightness increase after eclipse, colour TV obs. 77—87318
- pulse interval modulation semiconductor laser communication system 78—9331
- secondary frequency standard, using colour TV burst signal 78—24826
- seismic data colour TV display system 79—74995
- Skylab colour TV as primary data recording system 77—60569
- spectral sensitivities of colour-reproduction systems 78—49883
- subjective colours under monochrome flickering obs., using subjective modulation transfer functions *(Japanese)* 78—3490
- telecine scanning, digital storage techniques *(German)* 80—4786
- three dimensional video images formed by parallax panoramagrams, real-time transmission 79—31807
- undersea stereoscopic television for offshore appls. 79—5677
- underwater TV, wide angle correcting lens 80—91883
- visual perception of chromatic blur, effect of luminance contrast 79—39419
- X-ray colour TV system with soft X-ray preferred display 80—56186

colour television cameras
- C-CD, marine life forms obs. appl. 80—51301
- electronic colour corrector, TV motion picture broadcasting appl. *(Russian)* 79—49321
- electronic masking techniques, colour film reproduction appl. 78—32902
- lens testing, meas. of spectral transmission and modulation transfer function 78—94456
- lined interference filter cementing technique 79—72729
- single tube SICOLOR, appl. to endoscopy *(German)* 78—88758
- three colour channel hybrid system to synthesize complex point spread functions 79—41347
- underwater TV, wide angle correcting lens 80—91883

colour television picture tubes
- corrector lens for color television tube 79—86243
- design, human eye characteristics exploitation 77—56372
- electron microscope video monitor with colour-coded CRT display 79—80729
- large-screen colour projection TV system, using electron-beam-scanned semicond. laser quantoscope 80—99783
- laser electron-beam tubes for projection TV 79—59743
- white uniformity meas. using computerised scanning colorimeter 79—26098

colour television receivers
- SAW filter design for nonlinear phase response, building-block method 77—27433

colour tv *see colour television*

colour tv receivers *see colour television receivers*

colour vision
- *see also eye*
- 100-Hue response, scotopic axis 80—26236
- 100-hue test, validity of Pinckers' version of Panel D-15 78—3493
- accommodation response, effects of colour 78—69042
- acuity deterioration in acquired colour vision deficiencies 80—56040
- acuity with short exposure times 80—81603
- adaptation to coloured gratings, aftereffects *(Japanese)* 79—79547
- adaption, additive effect, unambiguous evidence 80—89760
- adaption curiosity, expt. obs. 80—89757
- afferent visual systems of cat and rhesus monkey, responses to wavelength contrast 80—56030
- aftereffects, spatial frequency contingent range 79—2071
- afterimages, interactions with simultaneous contrast 79—2069
- anarchic versus random 100-hue responses of colour-vision-defective patients 79—62257
- anisometropic amblyopia, increment threshold spectral sensitivity 77—44670
- anomaloscope, portable filter type, for colour vision genetics study 77—5004
- anomalous trichromacy, single pigment shift model 78—11654
- appearence specification, terms and formulae 78—56995
- Bezold-Brucke hue shift meas., effects of psychophys. procedure and stimulus duration 77—32901
- Bezold-Brucke hue shifts, short-flash obs. 80—72170
- Bezold-Brucke phenomena of extrafoveal retina 80—45898
- Bezold-Brucke phenomenon for purple colours 80—108898
- binocular colour fusion, wavelength difference limit 80—101182
- binocular colour fusion limit 79—57659
- binocular image perceived direction 79—43923
- blue adaption, use in study of Drosophila behaviour and visual receptor mechanisms 80—8224
- blue cone signals in red-green opponent-colour ganglion cells, macaque retina 79—79549
- blue receptor distrib. in primates revealed by spectral photic damage and histochem. response expts. 80—12130
- blue-sensitive cones, apparent saturation at colour-opponent stage 79—57661
- blue-sensitive cones, non-contribution to luminance 80—51098
- brightness generation, chromatic signals contribution, cybernetic model 77 90795
- brightness generation, colour-brightness, contrib. of cortical colour channels to brightness sensation 78—11657
- brightness under contrast, psychophys. functions 78—57000
- cat, domestic, neural basis for colour discrimination 78—48800
- cat, effect of stimulus size 78—69076
- cat, trichromatic vision 78—35858
- cell stimulation in insect eyes, using blue SiC LED *(German)* 79—39623
- chromatic aberration, effect of yellow ocular filter, fish eye 80—8046
- chromatic aberration meas. with chromoretinoscopy 80—81581
- chromatic aberration rel. to accommodation, meas. using dynamic laser speckle pattern 80—81582
- chromatic adaptation, review 78—53403
- chromatic adaptation effect anal. by linkage model 77—70467

colour vision continued
chromatic adaptation effects and colour appearance at various illum. levels *(Japanese)* 78—92628
chromatic adaption effects on colour discrimination and colour appearance 80—41026
chromatic backgrounds, dual role in colour perception 79—53126
chromatic border perception, by R and G cones in trichromatic eye 79—57658
chromatic border perception, role of red- and green-sensitive cones 78—69091
chromatic Craik-O'Brien effect for equiluminous stimulus, discontinuous chromaticity edge 80—45901
chromatic induction, no background additive effect 80—41030
chromatic input to stereopsis, calcs. 80—16948
chromatic mechanisms exposed by colour substitution pupil response 79—92221
chromatic modulation sensitivity functions, colour difference scaling 79—53121
chromatic opponent-response functions of anomalous trichromats 79—53123
chromatic stereopsis, opposition of photometric and dioptric factors *(Italian)* 78—56986
chromatic stimuli, duration thresholds 79—57657
chromatic temporal freq. response in humans 80—108902
chromaticity coordinates for spectrum colours of extrafoveal cones 78—7360
chromaticity diagram showing cone excitation by stimuli of equal luminance 79—100613
chromatostereopsis, 28 annotated references covering 166 years 79—5290
chromoretinoscopy and its instrumentation 80—94201
coding properties of sustained and transient channels, human 77—25440
colour matching at moderate to high levels of retinal illuminance 78—56981
colour navigation light judgement by colour defective men 79—53119
colour sicence contributions, collection of papers by D.B. Judd 80—98761
colour TV images, effect of luminance contrast on chromatic blur 79—39419
coloured surrounds, effects on colour naming and luminosity 80—56054
colourfulness, new concept 78—56996
complementary colours, composition and efficiency in prod. whites 79—29529
complementary colours, efficiency of optimum colour stimuli 80—51101
complex stimuli viewed in light and dark surrounds, perceived saturation 77—70468
cone activity, correl. with horizontal cell morphology, goldfish retina 80—45900
cone afterimages, interchangeable background obs. 80—45902
cone interactions at high flicker frequencies 78—35857
cone light adaption, frog, receptor rel. to ganglion sensitivity changes 79—48253
cone outer segments, light-induced changes in membrane current, tiger salamander and turtle 80—108899
cone pigments, intraretinal distrib. in certain teleost fish 79—74667
cone receptor, inhomogeneous waveguide model and Stiles-Crawford effect 77—90797
cone saturation in humans, rel. to cone signal eqn. 77—44663
cone sensitivity to flicker, primate, during light and dark adaptation, ERG obs. 79—43900
cone spectral mechanisms, ERG and psychophysical obs. 80—61565
cones, evidence for equivalent-background hypothesis 80—16931
cones, post-receptoral adaption obs. 79—79548
conference, Troy, NY, USA (July 1977) 78—49882
congenital colour defectives, colour discrimination obs. for different illuminants 79—79544
congenital colour defectives across young Sardinian population 79—62255
congenitally defective, increment thresholds for white and spectral lights on white background 77—90792
constancy limits, colour, and colour perception 80—41025
contrast sensitivity, achromatic and colour, instrument for testing 78—73275
counter colour difference and anti-colour, work of human visual system 77—86499
countercolour system and colour vision eqns. for arbitrary colour *(German)* 78—57007
CRT-observer interaction 77—77901
crustacea with scotopic eyes, screening pigment effects on spectral sensitivity 78—65009
cyanine dyes, excited electronic states, CNDO/S CI calc., visual pigment spectra appl. 80—85333
demonstrations for polytech. students 77—49533
depth of field, wavelength dependence obs. and calc. 79—62240
desaturating blue increases only chromatic brightness 77—44666
detection of coloured stimuli by independent linear systems 80—16942
detection threshold for lights of varying purity 79—74665
deuteranomalous trichromats, locus if unique green 78—53400
diabetic retinopathy, impairment of colour discrimination 78—15841
dichoptic colour and brightness combinations 78—53407
dichromat, large-field colour naming with rods bleached 80—12126
dichromat long-wavelength-sensitive photoreceptor spectral sensitivity determ. by border percept elimination 78—69092
dichromats, large-field substitution Rayleigh matches 80—101173
difference discrimination, chromatic spatial frequency characteristics obs., using TV techniques *(Japanese)* 78—3489
differential thresholds representation 78—27953
discrimination, chromatic and achromatic, field separation, gap effect 77—25446
discrimination, report on 30 ophthalmologically normal old people 79—5287
discrimination ability in the white region, evaluation 80—16941
discrimination by Bering Sea spotted seal 78—69077
discrimination in the cat, effect of stimulus size, shape and viewing distance 79—74668
discriminations that depend on blue cones 80—12131
distant light visibility calc., colour and flash time corrections 79—83781
distinctness of borderline rel. to Natural Colour System 78—57002
dyschromatopsias, hazards in aviation 79—11934
edge and colour discriminations, retinal neurons network 79—48256
electro-oculographic ratio, rod and cone contribution 79—11925

colour vision continued
electro-oculography, on-line system for quantitative study of ocular kinetics 79—34699
electroretinogram, frog, rod and cone generation of wavelets 78—48799
electroretinogram, increment spectral sensitivities of primate late receptor pot. and b-wave 77—70461
endoparietal eye of Limulus polyphemus, spectral sensitivity 80—41029
equal saturation contours for surface colours 78—57001
evoked potential amplitude and coloured pattern displacement 79—79546
evoked potential in man, detect. of luminosity response *(Japanese)* 77—56374
evoked potentials, luminosity and chromatic responses in man, subjective hue estimates 80—97903
evoked potentials and latent chromatic response, reproducibility *(Japanese)* 78—92629
exchange threshold method of anal. in humans 80—12129
extrafoveal vision, vernier acuity and apparent depth for targets of different hues 79—39420
eye strain and chromatic asthenopia rel. to affectations of optic pathways *(Italian)* 80—56041
far peripheral retina, spectral sensitivity 80—104586
Farnsworth-Munsell 100-hue test, electronically scored instrumentation 77—52895
Fechner-Benham colour effect, hue reversal following white light adaption 80—51112
Fechner-Benham subjective colour 77—44685
field-additive pathway detection of brief-duration, long-wavelength incremental flashes 80—89758
figure recognition, small-size, comparison of halftone and colour scales 78—48785
flashes, incremental, long-duration, long-wavelength, detect. by chromatically coded pathway 80—89759
flicker, lateral interactions and rod intrusion 77—81503
flicker and chromatic adaptation 79—74669
flicker visibility, spectrally mixed adapting fields 79—43901
fly photoreceptor sensitising pigment 77—90796
FM 100-Hue test, normal response 77—90793
focus on retina, best value for various fixation distances, phakic and aphakic eyes 80—108882
foveal colour thresholds, quantum fluctuation model 77—44669
foveal tritan vision, colour naming evidence 79—83780
foveally viewed yellow target, chromatic uncertainty effect on detectability 78—65005
functional similarity with polarisation vision 78—3497
ganglion cell response to far violet light, macaque 78—11656
general zone theory of colour and brightness vision, formulation 79—29527
general zone theory of colour and brightness vision, space-time field 79—29528
goldfish, absolute visual sensitivity 79—48258
goldfish spectral sensitivity, conditioned heart ratio meas. in restrained or curarised fish 77—48805
grating duration perception, effects of colour specific adaptation 77—21529
gratings, coloured, perceived duration, interocular effects of adaption 80—56051
grey toad, colour perception constancy, role of background in recognition of blue stimuli 78—15844
habituation, dishabituation and generalisation induced in visual centres by colour flashes 77—12918
haploscopic apparatus for study of colour perception under different adaptation conditions 78—56997
heterochromatic flicker, two band model 78—7357
Holmgren wool test, colorimetric assessment 78—53409
hue change with eccentricity, rod and cone contribs. 80—45904
hue change with rod intrusion during dark-adaptation 80—51104
hue response recovery following chromatic adaptation 78—53404
hue substitution, wavelength latency effects 77—44684
human, 3-D homomorphic model and digital colour image processing 79—88077
human system, integration of adequate visual stimulus expression 77—21525
hummingbird, near UV light perception 80—97914
hypermetropia rel. to chromatic aberration in small animals 78—40140
illuminance dependence of 100-Hue response for normal subjects of different ages 77—90794
image coloration psychophysics 78—65025
images, model of local spectral description 79—79545
incremental and decremental light stimuli, colour signals 77—21526
inductive colour contrast, expt. investigation of model *(Russian)* 80—76739
inductive colour contrast, math. modelling *(Russian)* 77—52793
infant, search for short-wavelength-sensitive mechs. by chromatic adaption obs. 80—85397
infants, human, 2 months old, discrimination of chromatic from white light 78—40164
infants, human, white-adapted photopic spectral sensitivity 78—40165
insect colour vision, effected by one visual pigment and filters 80—94212
insect eye slow cell resonses, colour adaptation 78—64988
interocular light adaptation effect on Lie specific threshold 78—69079
interocular transfer of colour-contingent motion positive aftereffects 78—69100
isorhodopsin, physiological activity in rat rods 77—60204
Judd's contributions to colour metrics and eval. of colour differences 80—94945
large-aperture holographic visual simulator 80—102679
lemon shark retina, spectral sensitivity and Purkinje shift 77—70469
luminance and opponent colour contribs. to visual detect., temporal and spatial integration 79—8510
luminance and opponent colour contribs. to visual detect., temporal and spatial integration 79—8509
luminance flicker enhancement by colour-opponent mechanisms, monkey obs. 80—61549
luminescent material choice, psychophys. considerations, in book contrib. 77—73172
luminosity-type cells in the turtle retina, short-wavelength input 80—41012
luminous efficiency in the red-green region of the spectrum 80—61563
Mach bands, definitions 78—69096
macular pigmentation density and short-wave cone sensitivity variations with eccentricity 80—97912

colour vision continued
- matching functions obs. using Japanese observers, rel. to photometry and colorimetry standards *(Japanese)* 79—6163
- McCollough aftereffects, calorimetric matches 78—65026
- McCollough effect, classical conditioning model 77—36937
- McCollough effect, right hemispheric sensitivity 77—16934
- McCollough effect, role of test pattern background hue; 80—41036
- McCollough effect, synaptic modification associative learning model 77—21531
- McCollough effect retention in darkness, storage vs. enhanced read-out 77—36936
- McCollough effects, binocular interactions during establishment 79—48271
- medical display system perceived dynamic range evaluation from receiver operating charact. curves 78—44662
- metacontrast masking, interactions between blue- and red-sensitive colour mechanisms 80—41027
- metacontrast masking rel. to luminance transients 77—81506
- metameric white samples for testing relative UV content of light sources and daylight 79—58767
- metrics, facts and formulae 80—97900
- minimally distinct borders, distinctness and fading 78—11653
- model simulating luminous-signal processing 80—81604
- modulation sensitivity, differences in red and green characts. 77—32896
- modulation sensitivity, differences in red and green characts. 77—32897
- motion perception, role of colour 78—85312
- movement aftereffect, colour-contingent, interocular transfer obs. 80—61578
- movement detection mechanism spatial characts., abnormal visual pathways 80—89756
- movement detection mechanism spatial characts., chromatic stimuli 80—89755
- multicoloured images, rod contrib. conditions, rod and long-wave cone interactions 77—32899
- multidimensional scaling 78—64979
- multispectral image visual interpretation aided by colouring 77—58281
- Munsell colour space geometry, colour difference determ. 80—51100
- Munsell colours, principal hue components 78—56999
- negative colour afterimage and McCollough effect, comparable retention times 79—53146
- neural networks, colour sensitive, reaction to intensity and colour steps *(German)* 80—76737
- neuronal network in retina to identify interactions between photoreceptors and horizontal cells 78—11648
- night myopia, night presbyopia and colour discrimination 80—81602
- occipital EEG, feedback delay, amplitude threshold and control 80—21465
- ontogenetic change in human colour vision, developmental pseudocyananopsia 78—35854
- opponent chromatic mechanisms, relation to photopigments and hue naming 79—62258
- opponent chromatic mechanisms predict hue naming 80—12132
- opponent processes, psychophysical and electrophysiological studies 78—53402
- opponent-colour channel spectral sensitivity 78—7359
- opponent-colours theory and colour blindness 80—12133
- opposite colour difference and anti-colour, humans 77—70471
- opposite colour difference and anti-colour, humans 78—20180
- opposite colour difference and anti-colour in human visual system 78—65004
- optic tectum movement detecting cell response to change of wavelength, pigeon 78—7348
- optic tract and lateral geniculate neurons, spectral responsiveness and temporal freq. response 77—36923
- optoelectronic device, colour sensing, neural mechanism modelling 80—12128
- orientation detector colour inputs, human visual system 77—25435
- orientation selectivity in detection of chromatic gratings 79—96562
- orthogonal combination of three visual channels 78—3491
- orthogonal systems generating hypersensitivity, colour and depth 78—80881
- owl monkey, Aotus trivirgatus, spectral sensitivity and colour vision 77—70470
- pair of heterochromatic light pulses, mixture and resolution 79—34565
- parafoveal stimuli, spectrally different, psychophysical tests of equiv. luminance 78—53414
- pattern induced flicker colours, effect of time delays 77—48808
- perceived colour differences, two dimensional fluctuation effects 79—29531
- perception, colour changes due to distance and lighting, direct assessment using Natural Colour System 78—57004
- perception, human, graphic model *(German)* 78—57005
- perception, of surface blacks and whites 79—74673
- perception, rate distortion coding simulation for colour images 78—7361
- perception and Stiles' π mechanisms, humans 77—44683
- perception fundamentals 78—77054
- perception in Greek literature 80—22184
- perception of coloured field, effect of subtense and surround luminance 78—57003
- peripheral retina, hue and saturation of spectral lights 77—52788
- peripheral retina spectral sensitivity functions 77—52787
- peripheral vision, absence of rod activity 77—9194
- photochromatic interval estimation for peripheral vision 78—27954
- photocoagulation using ruby laser, colour discrimination time variability 78—53401
- photographic fluorescent lamp suitability evaluation by image psychophysical and subjective estimations 79—71555
- photopic spectral sensitivity, development in human infants 80—45905
- photoreceptor function, rel. to prolonged depolarising afterpot. 78—15832
- photoreceptor signals at visual threshold, turtle obs. 80—56042
- photoreceptor spectral sensitivity on-line computation using programmable pocket calculator 78—69264
- photoreceptor survival in light-damaged eye of albino rat, ERG 77—36927
- photoreceptor transduction process, reversible events 80—51102
- photoreceptors, arthropod, prolonged light-induced cond. change on recovery from anoxia 77—12915
- physiological basis of trichromatic to tetrachromatic colour scheme transition 78—53406
- physiological measurement facility, monkey detected responses *(Japanese)* 78—92752

colour vision continued
- physiological models and line elements 80—97910
- pigeon, Columba livia, spectral sensitivity of red and yellow oil droplet fields 78—80876
- pigeon near-field acuity, effects of scotopic adaptation and wavelength 77—44664
- pigeon visual pigments, oil droplets and spectral sensitivity 78—11655
- pigments in isolated retina of chicken and pigeon 77—44667
- pigments of Gekko, ionochromic behaviour 77—36928
- pineal organ, frog, change of threshold after light-adaptation of chromatic response 80—72164
- pineal photoreceptors, evidence for vertebrate visual pigment with two physiologically active states 78—44504
- polarised light retinal photography of monkey eye 78—40163
- polychromatic imagery, optical system aberration influence 77—7014
- prediction model for multispectral imagery 77—71395
- prime colour theory of human vision 78—53410
- psychometric measures for specifying colour appearance 80—76747
- pupil responses, human, instrumentation for automated study 80—36164
- pupil responses to foveal exchange of monochromatic lights 80—97911
- Purkinje's arcs, explanation for blue colour 77—44665
- quality control and appearance, CIE Standard Observer colour specification 80—61539
- Rayleigh Match, spatio-temporal characts. 77—32900
- reaction time as measure of temporal summation at suprathreshold levels 77—32898
- reading addition determination, comparison of 3 methods 80—36198
- receptor adaptation, spectral sensitivities and photopigments, fly 77—29149
- red ang green colour cone mechanisms, human, relative modulation sensitivities 79—53124
- red-absorbing visual pigment of butterflies, rhodopsin 80—3646
- red-green dichromats, wavelength variation in directional sensitivity obs. 80—45903
- red-green opponent channel, short-wave cone input obs. 80—41028
- red-green opponent spectral sensitivity, meas. methods disparity, perceptual basis 79—53120
- red-sensitive colour mechanism spectral sensitivity, small blue adapting field effect 79—74666
- reflected light common and relative components as information about illum., colour and 3-dimens. form 78—56982
- reproduction of images, obtainable by two-primary colour projections 80—12125
- response time to peripheral retina stimuli, binocular summation 78—24073
- retina, chicken, visual pigments and oil droplets 77—73530
- retina, teleost, enhancement of hyperpolarising S-potentials of surround illumination 79—2051
- retina, turtle, modes of chromatic interactions 78—7347
- retina chromaticity horizontal cells of turtle, synapse mechanisms 80—51079
- retina neural networks between cone and photopic L-type horizontal cells 79—83782
- retina of carp, colour coded S-potentials, latency measurement 79—53097
- retina outer plexiform layer lateral interactions after atropine block of horizontal cells, turtle 77—70457
- retinal class IV ganglion cell luminance and chrominance processing in frog 78—40148
- retinal cone chromatic organisation, baboon, using light-stimulated NBT reduction 77—64031
- retinal cone mechanism saturation, blue-sensitive receptors 77—29151
- retinal cone pigments, human spectrophotometry, annotated bibliography *(Italian)* 79—62256
- retinal ganglion cell activity in ground squirrel under halothane anaesthesia 78—40147
- retinal ganglion cells, macaque, macular pigmentation and spectral sensitivity 79—43877
- retinal horizontal cells, amplification of graded pots. 77—32889
- retinal hue signal generation, optoelectronic robot model 80—3647
- retinal image motion, effect on vision in coloured light 80—51105
- retinal sensitivity, monochromatic stimuli, large eccentricities 79—5285
- retinal site of transient tritanopia 79—88078
- retinal spectral sensitivity to light it has scattered, human 77—9193
- retinal spectral-response characteristics model, light propag. through human eye 79—92215
- retinal suprathreshold time integrative props. studied using pairs of pulses of different hues 80—81600
- retinex systems' role 80—81598
- retinex theory 78—40162
- retinula peripheral cells within Drosophila visual mutants, response to monochromatic white-noise 78—69078
- review, recent studies *(Japanese)* 80—12127
- rhabdom spectral absorption, crayfish visual pigment, photoproduct and pH sensitivity 78—65008
- rhodopsin, conformeric states, spectrophotometry 77—90725
- rhodopsin in digitonin, isolation of 3 isochromic forms 77—52951
- rhodopsin kinetics at room temp. meas. by picosec. spectroscopy 77—64036
- rod contribution to colour information, using scotopic luminosity function and colour mixture data 78—35855
- rod sensitivity, effect of cones 77—44668
- rod-cone interaction in human scotopic vision, cone increment thresholds 77—60218
- rod-cone interaction in human scotopic vision, rod increment thresholds 77—60217
- rod-cone interactions, variegated colour sensations, flicker fusion expts. 77—40673
- rods, role in iconic storage 79—24987
- Roth 28-hue test 78—3494
- saturation enhancement in coloured Hermann grids varying only in chroma 80—72168
- scaling data analysis 80—97901
- schematic eyes, reduced, for vertebrates, table including computed longitudinal chromatic aberrations 80—51074
- scotopic axis in 100-Hue response of congenital defectives under high press. Na illum. 80—16940
- scotopic hues of simultaneous contrast 79—53122
- selective chromatic adaptation at different spatial freqs. 78—65006
- senile macular degeneration, colour discrimination rel. to visual acuity 80 108897

colour vision continued
sensation space in human visual system 77–25432
sensitivity, resolution and Rayleigh matches following monocular occlusion for one week 80–104585
sensitivity, within-species vars. in squirrel monkey 78–7358
sensitivity during successive chromatic contrast, interactions between photopic mechanisms 77–25449
serous retinopathy, monolateral central, colour discrimination in 23 patients 79–5286
short-wavelength cone pathways, response saturation, colour opponent mechanisms control 80–41017
signal transmission by visual pathways, distortions of retinal images 80–85400
simultaneous colour contrast, deviations of induced colours from directions of complementary colours 78–56998
spatial adaptation of short-wavelength pathways in humans 80–97913
spatial frequency channel interactions in human visual system 80–12140
spectral response of human eye, rhodopsin thermal activation energy 78–92630
spectral sensitivity, direct readout system for clinical and research purposes 78–3488
spectral sensitivity analysis, math. techniques 77–52786
spectral sensitivity in goldfish, photochem. and neural correlates 80–81599
spectral sensitivity of human eye, colour coordinates number triple *(Russian)* 80–76741
spectral sensitivity of human eye, deductive derivation of mathematical model *(Russian)* 80–76740
spectral sensitivity of light-adapted goldfish, relfex obs. 79–48263
spectral sensitivity of the goldfish, cone mechanisms identification 80–56043
statistical study of colour matching functions 78–53408
stereopsis, role of colour contours 79–74677
Stiles' $\pi_1(\mu)$ mechanism, wavelength variation of directional sensitivity obs. 80–51103
Stiles's Π_5 colour mechanism, field displacement and field additivity props. 80–45899
Stiles Π_1 and Π_3 colour mechanisms, theory 79–62259
Stiles Π-mechanisms candidacy for colour-matching fundamentals 78–56980
Stiles-Crawford function at 35° in temporal field, foveal peak stability 79–62262
Stiles-Crawford function peak shift with wavelength 78–92631
Stiles-Crawford hue shift following photopigment depletion 79–57660
subjective colours under monochrome flickering obs., using subjective modulation transfer functions *(Japanese)* 78–3490
tawny owl, visual pigments and colour vision in a nocturnal bird 79–48262
temporal brightness enhancement determ. by luminance 79–74672
temporal coding, psychophys. results 77–81504
temporal resolution of chromatic stimuli, with or without luminance transients, exam. 78–35856
tetrachromatic matches, Maxwell spot and additivity 79–29530
tetrachromatic matching, additivity and Maxwell spot 78–53405
tilt after-effect magnitude, colour and contour rivalry influence 78–69098
transient tritanopia, expts. in blue cone monochromacy 79–16209
transient tritanopia at the level of the ERG b-wave 79–100614
trichromacy, large-field, in protanopes and deuteranopes 77–56379
trichromatic colour matching, high-level, rel. to pigment-bleaching hypothesis 80–35891
trichromatic theory and time vector in relativity theory *(French)* 78–57006
tritanomaly detection, optimisation of a Rayleigh-type equation 80–56044
tritanopic purity difference function for minimally distinct borders 78–15842
TV colour measurement CIE system 80–9018
TV picture quality and coding limitation 77–12923
uniform colour scales, Optical Society of America 80–12134
unique hues, lack of invariance with brief stimulus duration obs. 80–56045
vector algebra description of operations with colour, human visual system 78–96047
vector magnitude operation in colour vision models, derivation from signal detect. theory 80–101174
vectour model for normal and dichromatic color vision 80–51099
vernier-horopter and colour 78–65007
violet effect, strongly saturated subjective colour induced by flicker light *(German)* 79–53125
visible spectrum vision-related partitioning 79–92222
visual masking, action of red sensitive colour mechanism on blue sensitive colour mechanism 79–8511
visual pigments of bioluminescent and nonbioluminescent deep-sea fishes 79–74670
visual processor, human colour-vision discrimination, statistical-communications approach 79–5288
visual target discrimination rel. to colour of illumination 79–53135
wavelength discrimination near absolute visual threshold, goldfish 79–48264
wavelength discrimination of peripheral cones and change with rod intrusion 77–44662
wavelength-specific brightness contrast as a function of surround luminance 80–61564
whiteness, visual impression and colorimetric definition 80–81597
whiteness perception, individual differences and common trends 79–100612
zone fluctuation model, nonlinear processing at receptor level 80–81601

columbium *see niobium*

COM *see computer output to microfilm*

coma *see aberrations*

combination scattering spectra *see Raman spectra*

combinational circuits *see combinatorial circuits*

combinational mathematics *see combinatorial mathematics*

combinatorial circuits
batteries, combinatorial rules, for teaching 79–62962
binary tree-based image processor architecture 79–72524
particle detectors, combinatorial logic trigger system 77–54465
programmable trigger logic 78–17533

combinatorial mathematics
see also graph theory; sorting; trees (mathematics)
cation-deficient close-packed structures, combinatorics 79–23558
composite next nearest neighbour degeneracy, one-dimens. lattice space 77–65002
dimer config. enumeration, n-dimensional theory, graph paths 78–54315
education, Fibonacci numbers, recurrence relation soln., combinatorics function anal. 80–51988
finite element anal., combinatorial approach to flexibility method 77–2528
Gel'fand lattices, exponential of, and irreducible representations of U(n) 77–60897
graph complexity, measure 77–71176
isomers, enumeration by combinatorics, Polya's theorem 78–93501
multiterm linear recursion relations 77–29992
porphyrins, isomers, enumeration by combinatorics, Polya's theorem 78–93501
spacecraft trajectory optimal correction with constraint on pulse count 77–64598
statistical thermodynamics, partitions, for teaching 79–58496

combustion
see also explosions; flames; heat of combustion; reaction kinetics
100 MW fluidised bed combustion district heating plant burning high S content residual oils 80–108777
200 MW atmospheric fluidised-bed combustion steam generator, comparison of three designs 80–108776
accelerated flow, at permeable graphite burning surface, turbulent heat/mass transfer 78–38417
acetylene-NO-O_2, combustion products, 1400-2600K, minimisation of NO, computer model 78–85161
acoustic mode excitation by vortex shedding in combustion chamber 80–19150
acoustic noise generation, spectrum using Fourier transform techniques 78–1500
aerosols, particle size distrib., health hazards 78–81394
air, plasma, slow burning gasdynamics, due to Nd laser beam *(Russian)* 80–108715
air pollution source inventory for Tehran, methodology and approach 79–52996
air suspension homobaric flow in presence of physicochemical transform. 80–87820
alkaline impurity, source function in combustion products flow *(Russian)* 77–56301
anthropogenic combustion, as source of polycyclic aromatic hydrocarbons in recent sediments 78–57192
atmospheric fluidised-bed combustion boiler development facility, first year of operation 80–108775
atmospheric rate chemistry calculations, algorithmic approach 77–13095
atmospheric turbulent puff combustion *(Japanese)* 80–12470
automatic gas analyser, meas. errors due to gas-water interaction *(German)* 78–44438
ball lightning explanation by water electrolysis and combustion 78–69436
benzene-air combustion products for CW gasdynamic laser, gain values 77–75494
bioenergy conversion systems, efficiency improvements 80–30511
biological samples, elemental retention during low temp. ashing, activation anal. method 78–11785
bluff-body flame-stabiliser flow modelling 77–72367
boiler convective heating surface fouling with ash, NO_x formation dependence 79–83678
boiler NO_x formation study 78–3434
boilers, air pollution reduction measures, 1974-76 results for Zagreb *(Croatian)* 77–37362
brown coal, in combustion chamber of a steam generator, 200 MW *(Czech)* 78–27759
burner with diffusive control, intermixing of gas streams with transverse swirled air flow 78–87418
burning rate in engine cylinder, swirl and turbulence effects 80–89492
calorimetry, use of DC comparator apparatus 79–75529
chamber of TPP 210 A steam generator, radiant heat flux distrib., light model simulation 78–94567
chemical and physical processes study *(Italian)* 77–66756
cigarette, density changes during burning as obs. by β-source attenuation 78–11792
coal, ash content, determ. by forward-scattered γ-radiation, improved accuracy 78–7280
coal, fluidised bed firing, technological state and economic chances *(German)* 79–92050
coal, fluidised bed gasification, power generation fuel gas manufacture for combined cycle gas turbines 80–26104
coal, NO_x and SO_2 form., oxidizing agent excess depend., thermodynamic anal. 78–15677
coal, radiological aspects 80–61485
coal and fuel oil, prod. of atm. N_2O 77–21890
coal particles, holographic meas. 79–76630
coherent Raman spectrosc. obs. 80–16691
combustion diagnostics, space- and time-resolved coherent anti-Stokes Raman spectroscopy 79–76757
combustion front thermal propagation and thermodiffusional instability 80–7796
combustion-driven oscillations in small tube 79–52664
complex systems, pyrolysis and combustion charact., Fourier transform IR spectroscopy 80–86462
computation of diffusion flare 80–10276
concentration fluctuations in turbulent gas flows, by Fourier analysis of Raman signals, nonintrusive measurement technique 78–92564
concentric hyperdetonation on consideration of combustion kinetics 79–68748
condensed fuel, combustion and extinction in stagnation pt. boundary layer 79–29356
condensed systems, IR spectro-pyrometer obs. *(Russian)* 77–36756
convective combustion of disperse systems 80–53835
convex nonlinear boundary value problems, iterative bounds for stable solns. 78–54167
corundum-based refractory lining, wear resistance in combustion gas flow *(Russian)* 79–8370
critical heat fluxes in internally heated annular channels 78–31637
deflagration waves, heterogeneous, flame model for gas phase, nonlinear differential eqn. 80–81326

combustion continued
deflagration waves, heterogeneous, flame model for gas phase, partial differential eqn. 80—85177
deflection mapping, speckle superposition techniques 78—44379
determination in organic cpds. and biological samples by combustion method with isotope exchange 79—57333
detonation of unmixed liq.-gas mixture with surface evap., fluid dynamical characts. *(Russian)* 78—55630
detonation wave magnification by pulsation energy 80—59075
diagnostics, laser appls. 80—16688
diagnostics, laser Raman and fluoresc. techniques 78—88635
diffuse flame extinction conditions with two component gas mixture 79—91956
driven acoustic oscillators, plane wave theory anal. 80—102951
droplet, finite reaction rate model rel. to flame sheet model 79—34306
droplet combustion, unsteady temp. modelling criteria 78—38179
droplet-vapour flow, burning, conservation eqns., mass transfer 77—39363
EHD flow, nonstationary, with charge diffusion, nonlinear and linear wave processes 80—59124
ethylene-O_2-N_2-Al particle mixture, two-phase detonation and combustion *(French)* 80—61097
exhaust gases, from internal combustion engine, Raman scatt., fluoresc. interference 78—15728
filtration displacement reactor theory 80—7795
flame, combustion model and calc. 78—35684
flame, free-jet diffusion type, ionis. meas. and combustion progress 80—30238
flame, premixed, turbulent, interaction effects 77—11279
flame, V-gutter stabilised, laser anemometry and schlieren photography meas. 77—35263
flame diagnostics using multichannel pulsed Raman spectroscopy 80—30237
flame noise, flow induced, suppression using appl. of DC elec. field 80—38176
flame propag. in semi-open tube, mixture preheating effect 78—47067
flame propagation in flowing turbulent combustible mixture *(Russian)* 77—27624
flame temperature meas., using nonlinear inversion techniques 79—85140
flames, effects of finite reaction rate and molecular transport on premixed turbulent combustion 80—3348
flames, IR radiation 77—19513
flow fields, combustive and non-combustive, with swirl numerical anal. 79—98821
fluid, combustion, vaporisation and heat transfer under elec. field 80—7798
fluid, electric field induced promotion of combustion, vaporisation, and heat transfer 79—20370
fluidised beds, combustion facility, radiation heat transfer, particle size and flow parameter effects 80—69641
fluidised-bed, development for HTGR fuel reprocessing pilot plant 79—45397
fluidised-bed steam generating system to supply 100000 lb/h of saturated steam burning high S coal 80—108778
flyash analysis for ^{222}Rn annual rate of release determ. in UK 80—17143
flyash from coal combustion, S and Cl adsorpt., cloud nuclei form. 77—21887
fossil fuel, combustion in atm., effect of CO_2 on climate 79—2359
fossil fuel, effect of global radiative heat balance, model 78—3863
fuel, liq. droplet, combustion, quasi-steady analytical model predictions 78—35681
fuel drop, surface eqn., burning rate vs. Damkohler number 80—81327
fuel droplet, deflagration and extinction in weakly reactive atoms. 78—64840
fuel droplets, mathematical models of transient heat flow 79—18673
fuel oil, NO_x and SO_2 form., oxidizing agent excess depend., thermodynamic anal. 78—15677
furnaces, heat transfer and pollution *(French)* 79—16001
furnaces, large, gas-fired, combustion modelling 79—32710
gas, boundary layer combustion, combined heat transfer 78—91029
gas flow, spectroscopic temp. meas., cold boundary layer effects 77—31399
gas ignition in boundary layer on heated plate 79—64798
gas jets, laminar homogeneous, combustion process *(Russian)* 78—94850
gas phase, probe sampling rate effect on sample composition 77—52691
gas turbine chamber flow three-dimens. calc. 80—79405
gas turbine combustion chamber, isothermal model, bluff body, recirculation phenomena in primary zone 79—47925
gas turbine wideband combustion noise obs. *(Japanese)* 80—11890
gas turbines, jet mixing, secondary zone characteristics *(Russian)* 77—84292
gas turbines, perturbations produced by unsteady combustion and heat addition 80—53764
gasdynamics of explosions, reactive systems, conf., Stockholm, Sweden (Aug. 1977) 79—64690
gaseous medium, fast chemistry and diffusion interaction 80—16678
gases, CARS spectra 80—16682
gasless systems, heat losses effect on ignition by combustion wave 79—100371
generalized ICE method for chemically reactive flows in combustion systems 79—10617
graphite, combustion product radial distrib., electric field effects 79—100374
graphite fuel element and C fluidised bed combustion for HTGR U recovery 78—13314
heat exchangers, combustion 78—27761
heavy oil droplet with simultaneous cracking inside, combustion mechanism 79—74385
Helmholtz pulsating combustion system, prediction of pressure and frequency 79—43585
hexane, liq., burning rate in small vessel, convection effect 78—35680
homogeneous fuel mixture, turbulent combustion theory 80—53883
HTGR containment, layering and combustion following depressurization accident 78—13277
hydrocarbon combustion products, 1400-2600K, minimisation of NO, computer model 78—85161
hydrocarbon fuels, universal formula for elec. cond. of combustion-products plasma 79—19004
hydrocarbon fuels combustion prod. plasma with alkali impurity, elec. cond. 79—55466

combustion continued
hydrocarbons, in combustion engines, CO_2 laser action 79—45924
ignition and flame quenching in flowing gaseous mixtures 77—80230
industrial gaseous environment characterisation, Brinkley method 80—93817
internal combustion engine, conc. fluctuation meas. 80—71973
isothermal flame problem, 2-dimens., combustion limits and rates 79—100369
jet, free, heated, turbulent, high temp., eddy diffusion, methane combustion obs. 78—30329
kerosene, combustion in air rel. to press. 3-15 kgf.cm^{-2} 79—66297
kerosene combustion products, porous evaporative cooling of construction elements 79—55372
Kevlar 49, fibre, mech. props., environmental effects incl. sunlight, ionising rad. 77—36560
kinetics at high temperature, model *(Russian)* 79—29360
laminar diffusion boundary layers, ignition and extinction 78—64838
laminar flame front, diffusion-thermal stability *(Russian)* 77—7477
laminar flame propagation, asymptotic anal., review and extension 79—47926
laminar flames, premixed, non-adiabatic, nonlinear theory 80—93757
laser Doppler velocimeter with variable frequency shift for combustion flow meas. *(Japanese)* 78—67294
laser induced fluorescence spectroscopy, saturation effects 77—44526
light scattering diagnostics for combustion gases 77—47124
liquefied petroleum gas, burning velocity, gas comp. and air/fuel ratio effects 80—66804
liquefied petroleum gas, combustion products, seeded, elec. cond. meas. 77—58835
liquid fuel droplets, transient heat flow in combustion gases, models 78—63507
liquid fuel film, combustion behind shock wave, heat and mass transfer in turbulent boundary layer *(Russian)* 78—71401
liquid scintillation wastings, combustion system *(Japanese)* 80—63503
LMFBR, Clinch River, humidity effect on burning rate of Na droplets, Fick's eqn. anal. 78—13297
metal, laser initiated combustion, time-resolved spectroscopy 78—7207
metal combustion, laser-initiated, time-resolved spectroscopy 77—77765
metal combustion under CW CO_2 laser radiation action 80—30241
methane, combustion, appl. of sensitivity analysis, numerical Green's function procedure 79—100334
methane, concentration along line in jet, spatially resolved coherent anti-Stokes Raman spectra 79—74476
methane-air combustion product, electron-neutral energy exchange in AC field 77—42519
methane-O_2 mixture, laser initiated combustion 80—55661
methane-O_2-N_2Cl_2 mixture for CO_2 gasdynamic laser 77—50649
methanol-O_2 flame, combustion and ionisation 79—20357
methyl radical+O_2 (NO), mass spectra, absence of reaction in combustion system 78—53195
MHD convertors, combustion products, O_2 effects 78—18388
MHD generator, combustion stability 79—32827
MHD generator, electrothermal instability in the seeded combustion gas boundary layer near cold electrodes 78—71547
MHD generator, turbulence of combustion products in channel 79—64866
MHD generator combustion products plasma with mixed alkali impurities, elec. cond. calc. 79—86621
MHD plant, coal-fired, thermal modelling of components 79—52946
MHD power generators, combustion products plasma characterisation, generator channel flow, diagnostic techniques 80—43993
MHD process, coal-fired, NO_x control, expt. results 79—52947
microwave heating of flame plasma for enhanced combustion 79—20369
mixture burning in Soundhaus' tube, radial self excited vibr. regimes *(Ukrainian)* 78—68892
model optimization of detonation-wave description on consideration of combustion kinetics 79—91955
modelling, turbulent premixed and diffusion combustion, engineering flow computation 78—1756
monopropellant drop, surface eqn., burning rate vs. Damkohler number 80—81327
multifuel fluidised bed combustion packaged boiler to supply 10000 lb/h saturated steam at 100 psig 80—108779
natural gas, NO_x and SO_2 form., oxidizing agent excess depend., thermodynamic anal. 78—15677
Nomex, fibre, mech. props., environmental effects, incl. sunlight and ionising rad. effs. 77—36560
nonlinear acoustic phenomena related to combustion zones 80—38156
nonlinear medium is form of complex structures, burning 79—18688
oil recovery from Utah tar sand deposit, by in situ combustion 79—48046
oil-fired burners, particle size distrib. characterisation using Beta distrib. 78—81384
opposed gas-air jets, convective heat transfer 79—72960
organic compounds, ^{14}C-labelled, gaseous, anal., radioactivity meas. using piston type counter tube, automated 77—56281
organic specimens, calcination methods, for spectrochem. anal. *(Russian)* 78—23997
oxy-acetylene combustion products, seeded, elec. cond. rel. to MHD power generation 77—3922
passive optical diagnostics of combustion flow 77—44527
PBI fibre, mech. props., environmental effects, incl. sunlight and ionising rad. effs. 77—36560
pentane, combustion, form. and destruction of pentenes 79—1953
pentane, combustion, isotopic tracer studies of the further reactions of pentenes 79—8438
perfect fluid, combustion fronts in relativistic MHD *(French)* 77—47115
petroleum-acetylene-O_2 combustion products, seeded, elec. cond., for MHD power plant 78—34256
photographic recording of combustion processes, thermograms of flames *(Russian)* 80—62779
photon correl. velocimetry, turbomachinery and industrial burner velocity and turbulence profiles 79—60083
plasma, combustion product plasma, near-electrode contraction conditions 78—94946
plasma ashing technique for energy dispersive X-ray analysis of biological specimens in SEM 78—24199
plasma heat conductivity, nonlinear, self-similarity waves of combustion *(Russian)* 80—24141
plasma of combustion products, discharge on cooled Cu electrodes, rel. to erosion damage in MHD channels 78—1925

combustion continued
- plasma of combustion products, electron conc. and mobility determ. by HCN laser submillimetric interferometry 78—1889
- plasma of combustion products, noise temp. meas. using contactless capacitive convertor 78—9830
- PMMA, spreading of two-phase film of melt, heat and mass exchange, ignition and combustion *(Russian)* 78—76861
- PMMA fuel, combustion and extinction in stagnation pt. boundary layer 79—29356
- pollution monitoring in fossil-fuel flames 77—41149
- polymer, flammability, heat transfer meas., moving wire technique 80—3347
- powder combustion theory, Stefan problem *(Russian)* 77—56230
- premixed burning in diffusion flames, Libby Economos flame zone model 79—60093
- premixed turbulent flow, spectral interpretation of the propag. vel. *(French)* 79—4090
- pressure waves interaction with combustion field 78—63504
- process admittance measurement, acoustic impedance tube technique 80—64320
- process hazard modelling and logic theory 79—91953
- propane, ignition by small sparks 79—55587
- propane, vibr. combustion, modulation in injection-vibr. apparatus *(Russian)* 77—9083
- propane flame, wake stabilized, response to sudden accel. or deceleration of free stream 80—61096
- propane-air laminar flame plasmas interaction with microwave TM_{010} mode in combustion bomb cavity 80—53939
- propane-air mixture, turbulent combustion, model 79—64792
- propane-air mixture, turbulent combustion zone, initial temp. fluctuations influence on reaction evolution *(French)* 79—15998
- propane-air mixtures, combustion limits in large vols. 79—100368
- propane-O_2 mixture, combustion to detonation transition, stochastic aspects 79—100381
- pulverised coal, in combustion chambers of steam generators *(German)* 78—27758
- pulverised coal reactors, cold flow mixing rates with recirculation 79—50762
- quiescent fuel mists, ignition and flame quenching 79—8437
- radiative heat transfer, Milne-Eddington absorpt. coeff. 78—90680
- Raman spectroscopy, remote spontaneous, new trends in recording of signals 80—73485
- reaction zone propagation, combustion wave structure inversion in porous media 80—89494
- reactive solid exposed to step in surface temp., ignition 79—83458
- scramjet combustor, modelling of three-dimensional compressible mixing and reacting ducted flows 77—27621
- sensor, Ca-Mg-Zr pipe-form ceramics appl. *(Japanese)* 80—55761
- shock tube, combustion driving technique improvement 79—37350
- shock wave ignition of metal powders, pre-ignition processes 77—40546
- shock waves, starvation kinetics 78—64841
- show wave reflection from wall in stream of burning mixture *(Russian)* 79—14496
- simulated MHD combustion chamber working on natural gas and O^2 enriched air, NO formation, investigation 80—106984
- slow liquid combustion, evaporation and combustion front stability 80—53884
- solid propellant erosive burning, reacting turbulent boundary layer approach 79—32703
- solid propellent burning in three coord. systems, anal. 78—1558
- solid rocket propellant combustion, holographic recording 78—82935
- sooting flame, absorpt. spectrosc. using tunable diode laser 80—55660
- space environment, expt. possibilities in combustion and fluid dynamics 79—46402
- spherical drops, asymptotic combustion, drop shrinkage and flame movement, heat and mass transfer 77—81405
- spin combustion, mathematical model 79—29364
- steady combustion wave, degeneration conditions 80—7794
- steam-gas power station with multi-stage high-sulphur residual fuel oil combustion 77—9487
- stiff boundary valued problems in kinetics and diffusion, numerical methods 79—86525
- submicrometre particle detector and size analyzer 79—75672
- supersonic combustion past a conical body with normal surface blowing 79—41770
- supersonic flow, nonequilibrium physicochemical processes, open-cycle MHD generator 80—103196
- supersonic flow around circular cone, shock and combustion waves 78—26154
- swirl flows in combustion, review 78—1755
- swirling recirculating reacting turbulent jets passing through diffusers 79—50764
- technology, IR applications 80—86431
- temperature, specie conc. meas., CARS and laser induced saturation fluoresc. spectroscopy obs. 80—45617
- thermal instability of vibr.-excited mol. gas, appl. to surface ignition *(Russian)* 78—56895
- thermal-ignition analysis in boundary-layer flows 79—64800
- thermionic diodes, flame-heated, ceramic and alloy materials suitability evaluation 79—48157
- tubular reactor, model calc. with longitudinal transfer and heat losses through sides *(Russian)* 78—73043
- turbomachine combustor, analysis and modelling of flow *(French)* 79—46401
- turbulent, averaging of pulsed laser Raman signals 78—70839
- turbulent, implications of probability eqns. 78—14098
- turbulent, model for molecular mixing of unmixed gases *(Russian)* 78—94849
- turbulent boundary layer analysis for air and combustion products *(Russian)* 78—5732
- turbulent combustions, problems of bias on mean meas. *(French)* 80—53879
- turbulent diffusion flame, burning vel. *(Russian)* 77—7475
- turbulent flame theory, probabilistic approach 77—24034
- turbulent premixed flame, variable density effects 78—5824
- turbulent-jet-diffusion flame, effect of mol. gas radn. 77—80232
- unmixed fuels, reaction-surface model, flow struct., gas dynamic parameters 80—35536
- urban aerosols, optically absorbing component identification as graphitic C 79—34939

combustion continued
- velocimeter for fluctuating temp. and vel. meas. in combustion field 80—14856
- vibrational, rel. to initial impedance of resonator at end of tube. *(Russian)* 77—9082
- vortex ring, turbulent, acoustic emission accompanying burning 78—94676
- wood energy in W.Virginia 80—72006
- Al combustion in water vapour thermodynamic calc. 0.1 to 40 MPa *(Russian)* 79—39148
- Al particulate combustion process model *(Russian)* 78—85164
- B ignition and burning *(Russian)* 80—45502
- C particle combustion, diffusion and reaction in stagnant boundary layer 77—68705
- C, porous particle, internal combustion, model 78—92481
- CC CO_2-gas dynamic laser, combustion-type, effect of residual CO on performance 79—68378
- CHNS, simultaneous determ., combustion-gas chromatographic method, data processing 80—40762
- CO chemical laser using combustor-generated reactants 80—48288
- $CO+0.5\ O_2$, supersonic stream, oxidation reaction to produce chem. laser 77—677
- $CO+H_2$ combustion in air, gasdynamic laser operating on combustion products, construction, amplification coeff. *(Russian)* 77—7075
- CO_2, combustion gasdynamic laser, working cpds. simulation *(Russian)* 79—27239
- CO_2, combustion-driven gasdynamic laser, effect of N_2 preheat 77—38854
- CO_2 gasdynamic laser, operating on combustion products, gain coeffs. of complex working media 80—58506
- CO_2 gasdynamic lasers, amplifying characteristics, combustion product utilisation 79—27240
- $CS_3+N_2O+O_2$ combustion, CO laser performance characts. *(Russian)* 78—55348
- F, 2-compartment bomb calorimeter 80—57300
- $H+O_2 \rightarrow OH+O$, combustion, quasiclassical trajectory calcs. 78—53201
- H_2, heat transfer in furnaces calc. *(French)* 80—19218
- H_2, supersonic combustion in vitiated airstream, using transverse injection 78—14095
- H_2-N_2-Na jet, ignition and extinguishment in simulated LMFBR accident conditions 78—8932
- H_2-N_2O-CO-Ar, conc.-time data for O and CO_2, 2000-2850K 78—85162
- H_2-O_2-CO-Ar, conc.-time data for O and CO_2, 2000-2850K 78—85162
- H_2+O_2, combustion, kinetic modeling and sensitivity anal. 80—89490
- hydrocarbon-water, emulsions, superheated, bubble nucleation 78—61056
- Mg, ignition, critical conditions 79—100372
- Mg particles in air at high pressures *(Russian)* 77—70302
- NH_3-NO mixtures, combustion emission spectra, identification of NH_2, NH, OH, NO by rapid scanning spectra *(French)* 79—52665
- NO formation in constant volume combustion, prediction *(Japanese)* 79—16002
- NO_x to NO_2 conversion in metallic materials, expts. *(German)* 80—55716
- $N_2O+H \rightarrow N_2+OH$, rate const., 2000-2850K, combustion of $H_2/N_2O/CO/Ar$ 78—85162
- Na burning, aerosol release, temp., O conc. depend., LMFBR safety anal. 77—83049
- Na, large pool combustion in LMFBR, determ. of burning rate and flame struct. 80—47644
- Na liquid, contaminated, release of Pu compounds during burning, LMFBR safety evaluation 77—23224
- Na, reson. line, laser excitation, combustion Rayleigh scatt., at. flame fluoresc. spectroscopy 80—42972
- $OH^{\cdot}+CO$, rate consts. 77—16781
- Pb, chemiexcitation of ^3P metastable states, during combustion of acetylene and C_2H_2 78—3339
- Pu fumes, aerodynamic and dissolution behaviour of laser-ignited droplets 79—13438
- ^{239}Pu and ^{233}U droplets burning in air, aerosol generation investig. rel. to inhalation hazards 79—67959
- SF_6+H_2 mixture, equilib. composition and transport props., 300 to 15000K 77—24051
- Ti+C(B)(Si) self-propagating, high-temp. synthesis wave, radiating power 79—100377
- W/Cu powder with varying W particle size, burning behaviour and crack form. tests *(German)* 78—7005

comets
- 1577, motion rel. to Kepler's rejection of solid celestial spheres 80—36830
- 1974 observations, discoveries and recoveries 78—73682
- 1975, new periodic comets 77—91487
- 1975 observations, discoveries and recoveries 78—73683
- 1976 perihelion passage deisgnations 78—36523
- 1977, perihelion passage designations on Minor Planet Circulars 4583-4622 79—16871
- active long-period comets intrinsic number density in inner solar system 79—53772
- airglow emissions from inner comas 78—45282
- P/Arend-Rigaux, orbital elements, ephemeris for 1977 Apr. 7-Dec. 3 77—25986
- P/Arend-Rigaux (1977k), position and tail obs. (1978 March 5) 78—40874
- P/Arend-Rigaux (1977k), positions, appearance and spectrum 78—12157
- P/Arend-Rigaux (1977k), precise positions 1977 Aug. 77—91477
- P/Arend-Rigaux (1977k), precise positions 1977 Oct.-1978 Jan., total visual magnitude estimates 78—36517
- P/Arend-Rigaux (1977k), precise positions for 1977 Nov.-Dec. 78—20745
- P/Arend-Rigaux (1977k), precise positions for 1977 Oct.-1978 Mar. 78—65548
- P/Arend-Rigaux (1977k), recovery and ephemeris continuation 77—74013
- P/Arend-Rigaux (1977k), recovery and positions 77—82172
- Arend-Roland (1957 III), visible and UV spectra anal. *(Chinese)* 80—12709
- artificial comet, solar radiation interaction, proposed expt. 79—16887
- P/Ashbrook-Jackson, ephemeris for 1977, Feb.-Oct. 77—17440
- P/Ashbrook-Jackson, orbital elements from 1948-70 obs. 77—37573
- P/Ashbrook-Jackson, orbital evolution in 1660-2060 period *(Russian)* 78—49377

comets continued
P/Ashbrook-Jackson (1977g), 1978 April precise posns. from ESO La Silla *(French)* 79—101117
P/Ashbrook-Jackson (1977g), ephemeris for 1978 Mar.-1979 Mar. 78—24486
P/ Ashbrook-Jackson (1977g), magnitude estimates (1978 Aug.-Sept.) 78—85912
P/Ashbrook-Jackson (1977g), precise position (1977 Oct. 13) 78—20749
P/Ashbrook-Jackson (1977g), precise position for 1978 Apr. 5 78—53887
P/Ashbrook-Jackson (1977g), precise positions (1977 May and Sept.) 77—91485
P/Ashbrook-Jackson (1977g), recovery, appearance and positions 77—49334
P/Ashbrook-Jackson (1977g), spectroscopic obs. 78—96437
P/Ashbrook-Jackson (1977g), total visual magnitude estimate for 1978 July 1 78—73679
P/Ashbrook-Jackson (1977g), total visual magnitude estimates 78—93169
P/Ashbrook-Jackson (1977g), total visual magnitude estimates 1978 July 78—77519
P/Ashbrook-Jackson (1977g), total visual magnitude estimates for 1978 Oct.-Nov. 79—5787
P/Ashbrook-Jackson (1977g), visual magnitude estimates (1978 September 7 and 10) 78—89128
P/Ashbrook-Jackson (1978 XIV), photoelectric BV photometry rel. to opposition effect 80—31258
P Ashbrook-Jackson (1978 XIV), precise positions (Sept.-Oct. 1978) *(German)* 80—46453
P/ Ashbrook-Jackson (1978 XIV), precise posns. (1978 April) *(French)* 80—41767
atmospheres, interplanetary shock waves interaction 77—22032
P/Barnard 1 (1884 II), orbit recalc. and motion *(Russian)* 80—46487
P/Barnard 2 (1889 III), orbit of one apparition object *(Russian)* 79—92727
Bennett (1970 II), CN (0-0) band brightness profile obs. rel. to CN prod. 80—82303
Bennett (1970 II), emission features, coma comp. 79—16884
Bennett (1970 II), O(^1D) and H_2O^+ brightness profiles 79—35192
Bennett (1970 II), production rate and possible origin of H_2O^+ 77—5497
Bennett (1970 II), production rate and possible origin of O(^{2}D) 77—5496
binding energy average value in cometary dynamics theory 80—41770
biological evolution, origin of terrestrial life 80—51672
P/Boethin (1975 I), libration around 1/1 resonance with Jupiter 80—72883
P/Borrelly, rotating nucleus model and fan-shaped coma 79—44414
P/Borrelly (1980i), recovery and approximate positions, (1980 July 9 and 21) 80—94755
Bowell (1980b), discovery posns., elements and ephemeris 80—51695
Bowell (1980b), precise positions, elements and ephemeris (1980 March-July) 80—62075
Bowell (1980b), precise posn. and orbital evolution 80—56770
Bradfield (1974 III), nuclear brightness meas. using deconvolution technique 79—84745
Bradfield (1974 III), precise position determ. 80—46494
Bradfield (1974 III), precise positions 1974 April 7-May 12 period 77—91473
Bradfield (1974 III), strip photometry 77—33412
Bradfield (1975p), anti-tail photographic obs. 77—33410
Bradfield (1975p), precise positions for 1976 Jan. 31-Feb. 1 77—17446
Bradfield (1976a), precise position for 1976, Mar. 77—2371
Bradfield (1976d), precise positions 1976 Mar. 27, 28 77—22140
Bradfield (1978c), discovery positions and appearance 78—32397
Bradfield (1978c), emissions from head 79—96971
Bradfield (1978c), IR and total visual magnitudes (1978 March) 78—45283
Bradfield (1978c), positions, elements and ephemeris 78—32401
Bradfield (1978c), positions, improved elements and ephemeris 78—36514
Bradfield (1978c), positions, magnitudes and UBV photometry 78—36521
Bradfield (1978c), positions, orbital elements and ephemeris 78—40875
Bradfield (1978c), positions and appearance (1978 February) 78—32405
Bradfield (1978c), positions and visual magnitude estimates 78—40873
Bradfield (1978c), precise position, spectroscopic obs., total visual magnitude estimates 78—40879
Bradfield (1978c), precise positions, parabolic elements and ephemeris 78—65551
Bradfield (1978c), precise positions 1978 Feb.-Mar., total visual magnitude estimates 78—45288
Bradfield (1978c), precise positions and magnitudes (1978 Feb.) 78—32404
Bradfield (1978c), search for mm wave emission from HCN, CO and methyl cyanide 79—75157
Bradfield (1978c), semiaccurate position 1978 March 8, IR obs. 78—36529
Bradfield (1978o), discovery and positions 78—93165
Bradfield (1978o), parabolic orbital elements and ephemeris, (1978 October 29 to 1979 January 27) 79—2524
Bradfield (1978o), precise position for 1978 Oct. 18 78—96439
Bradfield (1978o), precise positions for 1978 Oct., parabolic elements, ephemeris 78—96433
Bradfield (1979 l), parabolic orbital elements and ephemeris (1979 December 25 to 1980 January 14) 80—26812
Bradfield (1979c), discovery, approx. positions 79—75158
Bradfield (1979c), ephemeris and total visual magnitude estimates 79—92721
Bradfield (1979c), obs. of diffuse object (1979 September) 79—101120
Bradfield (1979c), precise position for 1979 August 18 79—84751
Bradfield (1979c), precise positions for 1979 Aug., parabolic orbital elements, ephemeris for 1979 Sept.-Oct. 79—88624
Bradfield (1979c), precise positions for 1979 Jun.-Jul., parabolic orbital elements, ephemeris 79—80271
Bradfield (1979c), precise positions for 1979 Jun.-Jul., parabolic orbital elements 79—84746
Bradfield (1979c), precise posns., elements and ephemeris (1979 June-July) 79—75159
Bradfield (1979c), precise posns. (1979 June 25) 79—70999

comets continued
Bradfield (1979c), total visual magnitude and coma diameter (1979 August 3) 79—80274
Bradfield (1979c), total visual magnitude estimates, (1979 August 4 to 12) 79—88623
Bradfield (1979l), 1980 March 4 magnitude and coma diameter 80—51696
Bradfield (1979l), discovery posns. (1979 December) 80—31254
Bradfield (1979l), ephemeris and IR mags. (1980 Jan.-May) 80—41769
Bradfield (1979l), extension ephemeris (1980 Jan.-Mar.) 80—31257
Bradfield (1979l), obs. of precise position in 1980, 8th to 22nd Jan. 80—36572
Bradfield (1979l), photographic obs. and spectra 80—51693
Bradfield (1979l), photographic obs. in 1980 23-4 Jan. 80—36574
Bradfield (1979l), posns., elements and ephemeris (1980 Jan. 5-26) 80—31256
Bradfield (1979l), precise positions (1979 December 28 to 30) 80—31255
Bradfield (1979l), precise props., orbital elements and ephemeris (1979 Dec.-1980 Feb.) 80—26813
Bradfield (1979l), spectra and visual obs. (1980 Jan.-Feb.) 80—41768
Bradfield (1979l), spectroscopic and photographic obs. in near IR 80—105205
Bradfield (1979l), UV spectrum, IUE obs. 80—90371
Bradfield (1979l), visual obs. (1979 February 8 to 20) 80—46489
brightness prediction 79—75164
brightness variation and nuleus struct. 79—2521
P/Brooks 1 (1886 IV), orbit recalc. and motion *(Russian)* 80—46487
P/Brooks 2 (1980f), recovery, positions and perihelion passage correction 80—85899
capture by Laplace scheme, orbital elements statistical consequences 78—53888
capture by Neptune, lower bound on duration 79—2475
capture by planets, Laplace hypothesis 78—28592
capture problem in celestial mechanics 78—77477
capture theory, orbits examination *(Swedish)* 79—40138
catalogue of ancient and naked-eye objects (2314 BC-AD 1970) 80—105181
Cernis-Petrauska (1980k), antitail, precise posns., parabolic elements and ephemeris 80—105206
Cernis-Petrauskas (1980k), positions, (1980 August 10 and 17) 80—101556
Cernis-Petrauskas (1980k), positions, parabolic orbital elements and ephemeris 80—98614
Cernis-Petrauskas (1980k), total visual mag. and coma dia. (1980 Aug.-Sept.) 80—101561
chemical analysis by neutron-gamma techniques 79—53728
chemistry, organic mols. rel. to origin of life and transfer to Earth 78—73660
P/Chernykh, precise positions and magnitudes (1977 Sept.-Oct.) 78—7926
P/Chernykh (1977l), approx. positions (1977 Sept. 1-2) 77—82169
P Chernykh (1977l), definitive orbit at first apparition (1977 to 1978) 80—62079
P/Chernykh (1977l), discovery obs. and appearance 77—82168
P/Chernykh (1977l), precise positions, improved elements and magnitudes 78—7932
P/Chernykh (1977l), precise positions, orbital elements, ephemeris 77—87333
P/Chernykh (1977l), precise positions 1977, Sept. 77—91475
P/Chernykh (1977l), precise positions 1977, Sept. and Oct., ephemeris to 1978 Apr. 78—7941
P/Chernykh (1977l), precise positions 1977 Aug.-1978 Mar. 78—53886
P/Chernykh (1977l), precise positions 1977 Dec.-1978 Jan. 78—49379
P/Chernykh (1977l), precise positions 1977 Sept.-Dec. 78—24490
P/Chernykh (1977l), precise positions (1977 November 17 to 1978 January 8) 78—32400
P/Chernykh (1977l), precise positions and ephemeris for 1977 Aug.-Oct. 77—82170
P/Chernykh (1977l), precise positions and visual magnitudes 1977, Aug. and Sept. 77—87330
P/Chernykh (1977l), precise positions for 1977 Oct.-Dec., total visual magnitude estimates 78—20755
P/Chernykh (1977l), precise positions for 1977 Sept. 79—25546
P Chernykh (1977l), precise positions for 1977 September 77—82173
P/ Chernykh (1977l), precise posns., improved elements and ephemeris 78—69747
P/Chernykh (1977l), precise posns. (1977 Sept.-Nov.) 78—16351
Chernykh-Petrauskas, discovery posn. (1980 July) 80—94756
chondrites and C1 carbonaceous chondrites origin, rel. to solar gases in meteorites 79—71008
P/Clark (1973 V), orbital elements, ephemeris for 1978 Feb.-Sept. 78—20744
P/Clark (1978g), recovery on 1978 Apr. 13, positions Apr. 13-30 78—49388
close approaches to Earth, list of events 78—73621
close encounters with Jupiter, mass distrib. throughout Solar System implications 80—77329
collision with Mercury and Moon, swirl pattern production 80—51675
comae, effect of solar photodissociative ionisation 80—90370
comae model, gas-phase chemistry in one dimension 78—93154
comas, positive molecular ions prod. 77—87327
P/Comas Sola, ephemeris for 1977/78 Jul. to Feb. 77—53482
p/Comas Sola (1977n), ephemeris for 1978 July-1979 June period 78—69749
P/Comas Sola (1977n), recovery obs. 1977, Sept. 77—87332
p/Comas Sola (1977n), tentative obs. (1978, November 29) 79—16889
P/Comas Sola (1977n), total visual magnitude estimate, (1978, October 8) 78—96435
composition and struct., observational techniques 77—78717
computer generated pictures 80—17549
convolution of cometary brightness profiles by circular diaphragms 79—12433
cosmic dust, book 78—57498
cosmic rays, anomalous component, source material from comets 79—71003
Cretaceous species extinction explained by cometary impact 80—76977
P/d'Arrest (1976 XI), meteoroids characts. 78—53876
P/d'Arrest (1976 XI), nucleus light curve and rotation 78—53877
P/d'Arrest (1976e), precise positions, 1976, Aug.-Nov. 77—5503
P/d'Arrest (1976e), precise positions 1976, July-Oct. 77—17441

comets continued
  P/d'Arrest (1976e), precise positions 1976 Aug. 14-23 period *(French)* 77−91474
  P/d'Arrest (1976e), precise positions (1976, July-August) 77−37571
  P/d'Arrest (1976e), precise positions and antitail 77−37580
  P/d'Arrest (1976e), precise positions for 1976 Oct. 15, Nov. 14, Dec. 23 77−22151
  P/d'Arrest (1976e), radio OH lines obs. 77−49333
  P/d'Arrest (1976e) precise positions 1976 June.-Aug. and total visual magnitudes 77−2372
  P/Daniel, predicted orbital elements 78−53883
  P/Daniel (1979b), recovery on 1979 Feb. 2, precise position, ephemeris 79−30013
  P/Denning 1 (1881 V), orbit recalc. and motion *(Russian)* 80−46487
  P/Denning-Fujikawa (1978n), precise positions, orbital elements 79−5780
  diffuse moving object, discovery and precise positions for (July 1, 1976) 77−33423
  digital image enhancement 78−81556
  discovering machine hoax, hydrocarbon bond detection 80−13
  discovery and positions for 1977 July 18-19 78−77518
  discovery probability, selection effects 78−7939
  discovery probability, vel. to reality of concentration of perihelia 80−67660
  Donati (1858 VI), rot. period of nucleus 78−57506
  P/Du Toit 1 (1944 III), movement of one-apparition short-period object *(Russian)* 79−92725
  P/du Toit-Neujmin-Delporte, predicted orbital elements 77−17444
  P/Dubiago (1921 I), orbit of one apparition object *(Russian)* 79−92727
  dust, low vel. particle meas. during cometary fly-by mission using capacity type detector 78−93113
  dust and cold-cloud aggregates theory 80−105210
  dust composition rel. to primeval solar nebula 77−41404
  dust grains, effects of solar radiation on orbits 77−5493
  dust grains, simulation *(Russian)* 78−36532
  dust grains in coma, rel. to IR continuum interpretation 78−7923
  dust particles, impact mass spectrometer for chemical analysis on fly-by mission 78−93112
  dust release and mantle development 79−44412
  dynamic processes on Earth, extraterrestrial causes, rel. to extinction of life 78−92820
  dynamics, exact solns. of diffusion eqn. 80−82304
  dynamics and evolution, review 80−82260
  Earth close approach, rel. to ice ages and ecological catastrophes 78−53714
  Earth impact, rel. to Earth albedo sudden change and ice age onset 79−44241
  electric current and mag. field struct. 79−40141
  P/Encke, 1977, August obs. possibilities *(French)* 77−45359
  P/Encke, changes in orbital period due to rotation of nucleus 80−62078
  P/Encke, ephemeris, (1978 June 1 to November 8) 78−49380
  P/Encke, ephemeris (1980 Oct.-Dec.) 80−105209
  P/Encke, ephemeris and total magnitude predictions 77−49336
  P/Encke, position for 1977 July 14, visual magnitude estimate, coma diameter 77−78719
  P/Encke, postperihelion interference filter photometry 79−2519
  P/Encke, precise positions, 1977, Aug. to Oct. 78−7942
  P/Encke, precise positions, 1977, Jul. 77−71061
  P/Encke, precise positions, 1977, Sept. 77−91476
  P/Encke, precise posn. for 1980 Oct. 8 and perihelion passage correction 80−109398
  p/Encke, rotating nucleus model, and fan-shaped coma 79−44414
  P/Encke, semiaccurate position, CN production rate and ephemeris correction 77−67070
  P/Encke, semiaccurate posn. and appearance (1980 August 8) 80−94758
  P/Encke, spin axis precession, nongravitational motion and sublimation 80−46483
  P/Encke, suggested search for ejected meteoric debris 77−78719
  P/Encke, total magnitude estimates (1977 September) 78−7925
  P/Encke dust, large grains in short supply 78−85908
  P/Encke fragment as possible Tunguska object 78−89120
  ephemerides on minor planet circulars 4425-4482 for four objects 78−85886
  equations of motion, recurrent power series integration 80−72882
  erosion by interplanetary plasma, lab. simulation 77−87323
  evolution to asteroids, Monte Carlo orbit evolution simulations 80−82261
  P/Faye (1976i), precise position, total visual magnitude estimates and coma diameters 77−22150
  P/Faye (1976i), precise position for 1977 Feb. 19 77−82166
  P/Faye (1976i), precise positions (1976, September-1977, January) 77−45362
  P/Faye (1976i) precise positions 1976, Jul.-Oct. 77−13289
  P/Forbes (1980a), recovery obs. and corrected ephemeris 80−46490
  formation and primitive solar nebula evolution rel. to solar accretion disk 78−81566
  Fujikawa (1978n), discovery and positions (1978, October 9 and 10) 78−96431
  Fujikawa (1978n), precise position, (1978, October 10) 78−93166
  Fujikawa (1978n), precise position for 1978 Oct. 11 78−96434
  Fujikawa (1978n), precise positions, (1978, October 11 to 16) 79−5779
  Fujikawa (1978n), precise positions, orbital elements and ephemeris 78−93168
  P/Gehrels 3 (1975o), 1976, Oct.-Dec. precise positions 77−25982
  P/Gehrels 3 (1975o), orbital elements, ephemeris for 1977 Oct. 4-1978 Aug. 20 period 77−82165
  P/Gehrels 3 (1975o), precise positions 77−60726
  P/Gehrels 3 (1975o), precise positions for 1978 Feb.-Mar. 78−73677
  P/Gehrels 3 (1975o), precise posns. for 1978 March-April period 78−49385
  P/Gehrels 3 (1975o) precise positions, (1977 November 18 to 1978 March 5) 78−40876
  P/Giacobini (1896 V), movement of one-apparition short-period object *(Russian)* 79−92725
  P/Giacobini-Zinner, assoc. Draconid meteors prediction for (1979 October 9) 79−92728
  P/Giacobini-Zinner, brightness during June to August 1972 rel. to solar flares 77−25983

comets continued
  P/Giacobini-Zinner, ephemeris for 1978 April-November period 78−28588
  P/Giacobini-Zinner (1972 VI), brightness rel. to 1972 August solar flares 78−57534
  P/Giacobini-Zinner (1978h), recovery, positions for 1978 Apr. 30 and May 1 78−49389
  Giclas (1978k), discovery report 78−85915
  P/Giclas (1978k), precise position and improved orbital elements 78−85916
  Giclas (1978k), precise positions, orbital elements and ephemeris 78−89122
  P/Giclas (1978k), precise positions 1978 Sept., elliptical elements, ephemeris 78−93162
  P/Giclas (1978k), spectroscopic obs. 78−96437
  Great Comet of 1577, Tycho Brahe's obs. and deductions 78−32407
  P/Griff-Skjellerup (1977b) assoc. meteors, Florida results 77−53484
  P/Grigg-Skjellerup, 1977, April obs. possibilities *(French)* 77−45359
  P/Grigg-Skjellerup, ephemeris for close Earth approach in 1977 April 77−13286
  P/Grigg-Skjellerup (1977b), precise positions, magnitudes and coma diameters (1977, March-April) 77−49339
  P/Grigg-Skjellerup (1977b), precise positions, total visual mag. estimates, coma diameters 77−60729
  P/Grigg-Skjellerup (1977b), precise positions 1977, Apr.-May and meteor activity 77−71064
  P/Grigg-Skjellerup (1977b), precise positions 1977 Jan. 21-26 77−22143
  P/Grigg-Skjellerup (1977b), precise positions (1977 Jan.-Aug.) 78−7928
  P/Grigg-Skjellerup (1977b), precise positions and appearance (1977, April) 77−45360
  P/Grigg-Skjellerup (1977b), precise positions and ephemeris, 1977, Mar.-Apr. 77−33414
  P/Grigg-Skjellerup (1977b), visual mag. and meteor shower 77−33418
  groups and pairs, statistical theory 77−41357
  P/Gunn, ephemeris continuation for 1978 July-1979 April period 78−61805
  P/Gunn, position, osculating elements and ephemeris for 1977/8 77−33420
  P/Gunn, precise positions, 1976, Jul.-Oct. 77−17432
  P/Gunn, precise positions, Aug., Sept. and Oct. 78−12155
  P/Gunn, precise positions for 1977 Oct. and Dec. 78−69750
  P/Halley, cometary micrometeoroid hazard workshop proceedings (Noordwijk, Netherlands, 18-19 April 1979) 80−36782
  P/Halley, joint NASA-ESA mission 80−82168
  P/Halley, navigation capability for ion drive rendezvous 79−35096
  P/Halley, orbit parameters and ephemeris, 1759-2024 period 80−62076
  P/Halley, orbital evolution, 1000 BC to present 80−12710
  P/Halley, orbital evolution tendency and ancient history *(Chinese)* 79−16886
  P1 Halley, orbital motion, 837-2061 AD 77−74011
  P/Halley, rotation period from halo diameter meas. 80−51694
  P/Halley, space mission *(Polish)* 80−67516
  P/Halley, US space agency plans for 1980 research 80−46492
  P/Halley, visibility, prospects for 1986 apparition 80−4303
  P/Halley 1986 apparition, student lab. expt. 77−45652
  Haneda-Campos (1978j), discovery and initial posns. 78−85911
  P/Haneda-Campos (1978j), precise position for 1978 Sept. 29 78−93167
  P/Haneda-Campos (1978j), precise positions, (1978 September 2 and September 8) 78−89124
  Haneda-Campos (1978j), precise positions, magnitude, orbital elements, ephemeris for 1978 Sept. 78−85913
  P/Haneda-Campos (1978j), precise positions, orbital elements and ephemeris 78−89121
  P/Haneda-Campos (1978j), precise positions 1978 Aug.-Sept., ephemeris for 1978 Sept.Oct. 78−89131
  P/Haneda-Campos (1978j), precise positions (1978, September 6 and 8) 78−85914
  P/Haneda-Campos (1978j), precise positions and orbital elements 78−89127
  Harlan (1976g), elliptical orbital elements and ephemeris for 1977 Apr. 7-Oct. 24 77−22148
  Harlan (1976g), precise positions 1976, Jun.-Oct. 77−5506
  Harlan (1976g), precise positions 1976 Jul. 19, Sept. 18, Oct. 24 77−22139
  P/Harrington (1980m), recovery and precise positions (1980 September 4 to 9) 80−101558
  P/Harrington-Wilson (1951 IX), not identical to Periodic Comet Taylor (1916 I) *(Russian)* 79−92724
  Helin (1977e), discovery, positions and appearance (April 16-18) 77−41359
  Helin (1977e), positions, appearance, parabolic elements and ephemeris 77−49335
  Helin (1977e), precise positions, elements and ephemeris (April-May 1977) 77−45364
  Helin (1977e), precise positions, orbital elements, ephemeris for 1977 Jul.-Nov. 77−64700
  Helin (1977e), precise positions (1977, May) 77−49338
  Helin (1977e), precise positions (1977 April 18-29) 78−7935
  Helin (1977e), precise positions for 1977 April 18-22 period 77−41360
  historical comets, Latin terminology 80−62437
  historical records, comets obs. in Greek and Roman sources before 410 AD 78−77658
  historical records, possible supernovae amongst comet and nova descriptions 77−2448
  P/Holmes, elements and ephemeris for 1978 Apr.-1979 Jan. period 78−36525
  P/Holmes (1979f) recovery and precise position (1979 July 20) 79−80272
  P/Honda-Mrkos-Pajdusakova (1980c), independent recovery 80−67658
  P/Honda-Mrkos-Pajdusakova (1980c), recovery and positions (1980 May 1 and 6) 80−67656
  hydrodynamic forces in splitting comets 80−46491
  Ikeya-Seki (1965 VIII), polarization reversal, grain segregation due to radiation press. 79−8881
  image enhancement by digital processing 79−25516
  International Comet Mission, proposed fast flyby of P/Halley P/Tempel 2 rendezvous 80−82166
  interplanetary submicron dust, cometary origin 79−30008
  interstellar medium interaction, effects of solar system encounters with dense interstellar clouds *(German)* 80−109500
  interstellar origin hypothesis 77−37569

comets continued
inverse-square orbits; A geometric approach 79—44662
ionospheres and plasma tails 77—64703
IR spectral features, laboratory simulation 80—26728
isophotometric atlas, pt. II 80—109377
P/Jackson-Neujmin, ephemeris for 1978 June 21-1979 January 7 period 78—53878
P/ Jackson-Neujmin (1978q), recovery, and ephemeris for 1978 Nov.-1979 Feb. period 79—12435
P/Johnson (1976h), continued ephemeris (1977, May-December) 77—45361
P/Kearns-Kwee (1963 VIII, 1972 XI), orbit determ. for 1963-73 period 77—78721
P/Kearns-Kwee (1963 VIII), orbit evolution, influence of Jupiter 78—7938
P/Klemola (1976j), positions for 1976 Aug. 25-1977 Jan. 21 period 77—78718
P/Klemola (1976j), precise positions 1976, Aug. and Sept. 77—2370
P/Klemola (1976j), precise positions 1976, Oct. 77—17431
P/Klemola (1976j), precise positions for 1976 Sept. 16-19 77—17445
Kobayashi-Berger-Milon (1975 IX), Irish amateur obs. (1975 July-Aug.) 79—75165
Kobayashi-Berger-Milon (1975 IX), Lyman-α obs. 80—4301
Kobayashi-Berger-Milon (1975 IX), precise position determ. 80—46494
Kobayashi-Berger-Milon (1975 IX), precise positions 1975 Aug. 4-14 period 77—91473
Kobayashi-Berger-Milon (1975h), positions 77—13287
Kobayashi-Berger-Milon (1975h), visual spectroscopic obs. 77—33424
Kobayashi-Berger-Milon (1975IX), Swann band profiles 78—85909
Kohler (1977 XIV), precise positions (1977 Oct.) *(German)* 80—46453
Kohler (1977 XIV), precise positions for 1977 Sept.-Dec. from photographic obs. 80—4302
Kohler (1977m), discovery obs. and position 77—82171
Kohler (1977m), occultation of 70 Ophiuchi, prediction 78—7930
Kohler (1977m), OH 1667 MHz line absorption detection 78—4152
Kohler (1977m), positions, elements, ephemeris and magnitude estimates 77—91484
Kohler (1977m), positions, spectral emissions and magnitudes 78—7924
Kohler (1977m), precise positions, (1977 October 4 to 1978 April 8) 78—73680
Kohler (1977m), precise positions, (1977 October 5 to 19) 80—105203
Kohler (1977m), precise positions, magnitudes, elements and ephemeris 77—87328
Kohler (1977m), precise positions, orbital elements, ephemeris, total visual magnitude estimates 78—45286
Kohler (1977m), precise positions, parabolic elements, ephemeris 77—87334
Kohler (1977m), precise positions 1977 Sept.-1978 Jan., total visual magnitude estimate 78—36518
Kohler (1977m), precise positions (1977 Oct.-Nov.) 78—16355
Kohler (1977m), precise positions (1977 September-October) 78—4155
Kohler (1977m), precise positions and magnitudes 1977, Sept. 77—87331
Kohler (1977m), precise positions and total magnitudes 1977, Sept. 77—87335
Kohler (1977m), precise positions for 1977, Oct. to Dec. 78—20751
Kohler (1977m), precise positions for 1977 Oct.-Dec. period 78—28590
Kohler (1977m), precise positions for 1977 Oct.-Nov., total visual magnitude estimates 78—20743
Kohler (1977m), precise positions for 1977 Sept.-Dec., total visual magnitude estimates 78—20753
Kohler (1977m), precise posns. for 1977 October-1978 March period 78—61806
Kohler (1977m), total visual magnitude estimates, 1977 September 77—87329
Kohler (1977m) precise positions (1977 October 13 to November 10) 78—7937
Kohoutek (1972 XII), Swan Cloud, 1974 January 11, rel. to cometary plasma tails general morphology 80—98612
Kohoutek (1973 XII=f), HF obs. 79—8883
Kohoutek (1973 XII), analysis of IR continuum 79—62792
Kohoutek (1973 XII), C and O prod. rates 77—49331
Kohoutek (1973 XII), CN and C_2 spectrophotometry 78—20738
Kohoutek (1973 XII), CN violet (0,0) spectra 80—82308
Kohoutek (1973 XII), ion tail dynamical response to solar wind interaction 80—85897
Kohoutek (1973 XII), ion tail interaction with compression region of solar wind corotating stream 78—49267
Kohoutek (1973 XII), Mariner 10 UV obs. of Lyman-α line 79—96970
Kohoutek (1973 XII), Mariner 10 UV spectrometry 77—45337
Kohoutek (1973 XII), origin of high speed HCN jets 77—49332
Kohoutek (1973 XII), photographic obs. from Skylab 77—60505
Kohoutek (1973 XII), plasma irregularities in tail 77—13285
Kohoutek (1973 XII), precise position determ. 80—46494
Kohoutek (1973 XII), precise posns. (1974 Jan. 17-20) *(French)* 78—81577
Kohoutek (1973 XII), spectrum interpretation by means of Franck-Condon factors, Rydberg-Klein-Rees method calc. *(French)* 77—17428
Kohoutek (1973 XII), strip photometry 77—33412
Kohoutek (1973 XII), tail shape and orientation 77—67069
Kohoutek (1973 XII), visible spectra, band intensity var., electrospectrophotometer meas. 80—8588
Kohoutek (1973XII), Swann band profiles 78—85909
P/Kohoutek (1980j), recovery and approximate positions (1980 August 6 and 7) 80—94757
P/Kojima (1970 XII), ephemeris for 1977/78, Aug.-Jul. 77—71066
P/Kojima (1977r), precise positions 1977 Dec.-1978 Jan. 78—36519
P/Kojima (1977r), precise positions (1977 Dec. 5, 20) 78—20748
P/Kojima (1977r), precise positions for 1978 Jan. and Mar. 78—65549
P/Kojima (1977r), recovery posns. and earlier obs. 78—20739
P/Kopff (1976b), ephemeris for 1977 Feb. 6-1978 Jan. 12 period 77—13290
P/Kopff (1976b), precise positions 1977 June, July, Sept. 77—91478
P/Kopff (1976b), precise posns. (1977 June-Oct.) 78—16356
P/Kopff (1976b), precise posns. (1977 Oct. and Dec.) 78—28587
Kowal, two probable comets, discovery posns. and ephemerides 79—96973
P/Kowal 2 (1979a), precise positions, elliptical elements and ephemeris 79—40140
P/Kowal 2 (1979a), precise positions, improved orbital elements and ephemeris 79—48739
Kowal (1977f), discovery positions 77—45365

comets continued
Kowal (1977f), positions, orbital elements, ephemeris 77—53479
P/Kowal (1977f), positions, orbital elements, ephemeris for 1977 Jun.-Oct. 77—64699
P/Kowal (1977f), precise position for 1977 June 13 77—82164
Kowal (1977f), precise positions 1977, May and orbital elements 77—53481
Kowal (1977f), precise positions and possible ephemerides (1977, April-May) 77—53476
Kowal (1979a), discovery report and positions, (1979, January 27 to 29) 79—25548
Kowal (1979a), precise positions, orbital elements and ephemeris 79—35195
Kowal (1979a), precise positions 1979 Jan., orbital elements, ephemeris 79—25549
Kowal (1979h), discovery and approx. posns. (1979 July) 79—92718
Kowal (1979h), ephemerides for parabolic and elliptical orbits (1979 May-Oct.) 79—96972
Kowal (1979h), precise positions for 1979 Jul., parabolic elements, ephemeris for 1979 Aug.-Sept. 79—88625
P/Kowel (1977f) ephemeris continuation (1978 Jan-Aug) 78—12160
P/Lexell (1770 I), orbit evolution, influence of Jupiter 78—7938
long-period, statistical study of orbits evolution 79—53775
long-period comets, distribs. of inclination of perihelion dynamical implications 80—101563
long-period comets, nongravit. perturbations 79—70998
long-period comets nature, implications of solar system origin 79—8856
long-period comets perihelion points distrib ., statistical tests 80—4304
Loras (1976k), precise positions 1976, Dec., ephemeris for 1977, Jan.-Jun. 77—17442
loss of long-period objects, planetary collisions 80—77358
Lovas (1974c), precise positions, 1976, Aug.-Oct. 77—5501
Lovas (1974c), precise positions 1976, July 26-Sept. 18 77—17435
Lovas (1974c), precise positions 1976, Oct.-Nov. and orbital elements 77—22145
Lovas (1975 VIII), precise positions and ephemeris for (1977 May 17 to December 23) 77—37578
Lovas (1975 VIII), precise posns. (1977 Aug. and Sept.) 78—12159
Lovas (1976 XII), precise posn. (1978 February 4) 78—49386
Lovas (1976k), discovery obs. 77—5500
Lovas (1976k), precise position, orbital elements, ephemeris for 1977 Aug.-1978 Mar. 77—64701
Lovas (1976k), precise position 1976, Dec. 77—33421
Lovas (1976k), precise positions 1976, Nov. 77—5505
Lovas (1976k), precise positions 1976, Nov. and Dec. and improved elements 77—9709
Lovas (1976k), precise positions 1976, Nov. and Dec. and improved elements 77—17434
Lovas (1976k), precise positions 1976, Nov. and ephemeris for 1976/77 Nov.-Feb. 77—17433
Lovas (1976k), precise positions 1976 Dec. 26-30 77—22141
Lovas (1976k), precise positions 1976/77 and ephemeris for 1978 Mar.-Jun. 78—24491
Lovas (1976k), precise positions (1976 November 23) 77—9708
Lovas (1976k), precise positions (1977, January) 77—29726
Lovas (1976k), precise positions for 1977 Feb. 11, 19 and Mar. 14 77—53480
Lovas (1977c), approx. position 1977, Feb. 77—33413
Lovas (1977c), discovery confirmed, 1977 February 23 obs. 77—25981
Lovas (1977c), discovery report 77—29724
Lovas (1977c), precise position, improved elements and ephemeris 77—82174
Lovas (1977c), precise position (1977, March 12) 77—33417
Lovas (1977c), precise positions, orbital elements and ephemeris 77—41358
Lovas (1977c), precise positions, parabolic elements, ephemeris, correction 77—33416
Lovas (1977c), precise positions (1977, March-April) 77—49337
Lovas (1977c), precise positions and corrected ephemeris 77—33415
Lovas (1977c), precise positions for 1977 Feb. 28 and Mar. 19 77—37577
Lovas (1977t), approx. positions for 1978, Jan. 78—24488
Lovas (1977t), approx. posn. and stellar appearance 78—28591
Lovas (1977t), asteroid-like appearance and orbit 78—28582
Lovas (1977t) designated as asteroid 1977 YA 78—36485
Machholz (1978l), discovery report 78—89123
Machholz (1978l), elliptical elements and total visual magnitude estimate 78—89129
Machholz (1978l), orbital elements and ephemeris (1978, September 19 to October 9) 78—89126
Machholz (1978l), positional obs., (1978, September 14 and 15) 78—89125
Machholz (1978l), precise positions, total visual magnitude estimates, 1978 Sept. 78—89130
Machholz (1978l), precise positions 1978 Sept.-Oct., magnitudes, parabolic orbital elements, ephemeris 78—93163
Machholz (1978l), total visual magnitude estimates for 1978 Oct. 79—5785
Machholz (1978l), total visual mags. and ephemeris continuation 78—93159
magnetic field determ. from polarization by atomic fluorescence 77—25938
magnetic tail, laboratory simulation 79—62793
magnitude distrib. 80—72886
Meier (1978 XXI), photoelectric BV photometry rel. to opposition effect 80—31258
Meier (1978 XXI), position from 1979 April 21 to 30, meas. and reduction *(French)* 80—72884
Meier (1978f), discovery position, appearance and motion 78—49384
Meier (1978f), OH emission at 1665 and 1667 MHz 78—61800
Meier (1978f), positions, elements, ephemeris, magnitudes and spectrum 78--53881
Meier (1978f), posns., elements, ephemeris and magnitudes 78—61801
Meier (1978f), precise position, orbital elements, ephemeris and magnitude law 79—5781
Meier (1978f), precise position, total visual magnitude estimate, 1978 Nov. 79—5789
Meier (1978f), precise positions, (1978, May 2 to June 9) 78—69751
Meier (1978f), precise positions, orbital elements and ephemeris 78—53884
Meier (1978f), precise positions 1978 Apr., spectroscopic obs. 78—49387

comets continued
  Meier (1978f), precise positions and magnitude estimates (1978 May-June) 78—69748
  Meier (1978f), precise positions for 1978 Apr.-May, total visual magnitude estimates 78—57505
  Meier (1978f), precise positions meas. at ESO, La Silla, in (April 1979) 80—105204
  Meier (1978f), precise posn. and visual mag. estimate (1978 Nov.) 79—5784
  Meier (1978f), precise posns. (1978 May-July) 78—77520
  Meier (1978f), precise posns. and total visual mag. estimates (1978 Aug.-May) 78—57504
  Meier (1978f), total visual magnitude estimates for 1978 July 78—85910
  Meier (1979i), discovery report and positions (1979 September 20 and 21) 79—92722
  Meier (1979i), ephemeris continuation (1979 December 3 to January 2) 80—26815
  Meier (1979i), non-parabolic orbit, ephemeris with elliptical elements (1980 January 2 to March 22) 80—31259
  Meier (1979i), precise positions, parabolic orbital elements and ephemeris 80—4306
  Meier (1979i), precise posns., orbital elements, ephemeris and magnitudes (1979 Sep.-Oct.) 79—101118
  Meier (1979i) total visual mag. estimates (1979 Sept.-Oct.) 80—8590
  P/Metcalf (1906 VI), movement of one-apparition short-period object *(Russian)* 79—92725
  meteors (comet debris) studies, video techniques appl. 79—80241
  MHD model 79—2522
  molecular Λ-doublets transitions 80—14132
  monochromatic brightness var. 78—81590
  monochromatic brightness variations, appl. of core-mantle model 78—81589
  Morehouse (1908 III), tail helical waves 80—4305
  Mori-Sato-Fujikawa (1975 XII), precise positions 1975, May and June 77—53483
  Mori-Sato-Fujikawa (1975j), improved orbital elements, ephemeris for 1977 Feb. 6-Aug. 5 77—17443
  Mori-Sato-Fujikawa (1975j), positions, 1975 Dec. 4-10 period 77—74012
  Mori-Sato-Fujikawa (1975j), precise position (1976, October) 77—29728
  Mori-Sato-Fujikawa (1975j), precise positions 1976, Mar.-Sept. 77—17438
  Mrkos (1957 V), CN (0,0) vibr. band anal. 78—20734
  near-Sun comets, twilight visibility function 77—5321
  neutral cometary atmospheres, average random walk model for mol. phot. dissociation 80—77351
  neutral cometary atmospheres, CN production 80—82303
  new and old comets, differences 78—36513
  nineteenth century comets, new orbits 80—56771
  nongravitational effects in orbital motion, comparison of correction methods 78—61811
  nonperiodic comets, cosmic snowball model *(German)* 79—80275
  nuclei, comp. of volatiles 78—12154
  nuclei, dust layer models 80—77350
  nuclei, ejection of matter, meteor streams form. and evolution theory 77—67074
  nuclei, gas kinetic eqn. for layer surface *(Russian)* 78—20737
  nuclei origin in presolar nebula, dust gravit. instability 79—2523
  nuclei rocky component, composition and rel. to Trojan asteroids 80—56751
  nuclei vaporisation, effects on light curves and life times 80—56772
  nucleus, definition and lack of theory 77—87336
  P/Olbers, orbit parameters and ephemeris, 1759-2024 period 80—62076
  Oort cloud, existence, review 77—87326
  Oort cloud, form. from mass removed from early solar system by outer planets 78—53841
  Oort cloud, origin 78—57502
  orbit determ. by Lambert 80—42024
  orbit evolution, influence of Jupiter 78—7938
  orbital accelerations caused by solar companion star 78—81567
  orbital elements distrib., effect of galactic forces *(Russian)* 80—77353
  orbital elements on Minor Planet Circulars 4583-4622 for 24 objects 79—16871
  orbital evolution of short-period comets treated as a Markov process 80—46484
  orbital evolution of short-period objects, Monte Carlo simulations 80—62073
  orbital inclinations distrib. of original comets, anomalies rel. to origin of comets 80—98615
  orbital motion, data processing for comparison of obs. and theory 77—41307
  orbital speed, in Kepler ellipse, theory 77—70984
  orbits, dynamic charact. based on orbital elements phase distance 80—56774
  orbits, evolution under perturbing influence of giant planets and nearby stars 80—98613
  orbits, influence of solar companion 80—31260
  orbits, of ancient and medieval comets 80—62077
  orbits, perihelion distrib. asymmetry 78—96429
  orbits, perturbations by solar companion star 78—12198
  orbits, reciprocal semimajor axes accuracy 80—62074
  orbits, three-dimens. model construction 78—61808
  orbits catalogue, third edition 79—40092
  orbits determination, method for study of error propag. 77—25914
  orbits for one-appearance objects in 1840-94 period 79—96975
  orbits of nearly parabolic comets, distrib. of nodes and perihelia 80—67661
  organic compounds in nuclei, simulation of UV effects *(Russian)* 78—32406
  origin, celestial mechanical aspects of planetary ejection hypothesis 80—62080
  origin and contrib. to planets 79—58300
  origin from former asteroidal planet 79—16888
  origin in interstellar gas cloud 79—8882
  origin of intense meteor showers 78—16358
  origins, research and interplanetary relationships 78—57507
  osculating orbits and anal. of original orbits 78—32395
  P/Schwassmann-Wachmann 1, obs. on 21st and 22nd Jan. 1980 of coma dimensions 80—36573
  Palomar Sky Survey comet, discovery and semi-accurate position 80—77352

comets continued
  Palomar Sky Survey record of probable comet, posn. and daily motion 78—69752
  perihelia distribution for long-and short-period comets 78—20756
  perihelion passage designations for 1978 period 80—31241
  periodic, missing objects, uncertain orbits and Jupiter effects 77—67072
  periodic comets, major semi-axis less than 30 AU, catalogue 80—72791
  periodic comets, recent, gas and dust props. 79—70997
  photoelectron fluxes in atmospheres 79—2520
  physical processes, review 77—25985
  planetary atmospheres interactions, rel. to 1908 Tunguska event 78—49378
  in planetary science conference (Boston, MA, 28 October 1977) 79—53740
  plasma, acceleration in solar wind, rel. to ion-acoustic turbulence *(Russian)* 80—106923
  plasma acceleration, role of mag. structs. 80—46486
  plasma motion of solar wind through coma 78—49391
  plasma tail disconnection events, mag. field line reconnection at interplanetary sector boundaries 78—93155
  plasma tail disconnection events, rel. to sector boundary crossings and high-speed stream encounters 80—46482
  plasma tails disruption, triggering by flute instability 78—93156
  plasma tails electron density deduced from refr. of occulted radiosources 79—53773
  plasma tails fine structure 79—12432
  plasma/solar wind viscous boundary layer 80—56769
  P/Pons-Winnecke, movement in 1858-1909 period *(Russian)* 79—92723
  P/Pons-Winnecke, possible age of assoc. 1916 meteor shower *(Russian)* 79—92729
  P/Pons-Winnecke (1976f), continued ephemeris (1977 Apr.-Nov.) 77—37575
  population in circumterrestrial space 78—73599
  positive ions bimolecular reactions, laboratory studies 77—63896
  possible comet, discovery 77—17436
  possible comet, discovery 78—20747
  precise posns. on Minor Planet Circular 5333-5390 for eight objects 80—77325
  precise posns. on Minor Planet Circulars 4391-4424 for 15 objects 78—81578
  precise posns. on minor planet circulars 4425-4482 for eight objects 78—85886
  precise posns. on Minor Planet Circulars 4483-4520 for 13 objects 78—93140
  precise posns. on minor planet circulars 4521-4548 for 16 objects 79—2514
  precise posns. on minor planet circulars 4549-4582 for five objects 79—12421
  precise posns. on Minor Planet Circulars 4583-4622 for 14 objects 79—16871
  precise posns. on Minor Planet Circulars 4623-4648 for three objects 79—25538
  precise posns. on Minor Planet Circulars 4649-4688 for 11 objects 79—35178
  precise posns. on Minor Planet Circulars 4689-4722 for 23 objects 79—53754
  precise posns. on Minor Planet Circulars 4723-4746 for 14 objects 79—66953
  precise posns. on Minor Planet Circulars 4747-4788 for five objects 79—75136
  precise posns. on Minor planet circulars 4789-4844 for 14 objects 79—84729
  precise posns. on Minor Planet Circulars 4845-4936 for ten objects 79—101107
  precise posns. on Minor Planet Circulars 4937-5016 for 16 objects 80—8580
  precise posns. on Minor planet circulars 5017-5066 for 11 objects 80—17533
  precise posns. on Minor Planet Circulars 5137-5188 for seven objects 80—46459
  precise posns. on Minor Planet Circulars 5189-5248 for 13 objects 80—67631
  precise posns. on Minor Planet Circulars 5249-5286 for six objects 80—67632
  precise posns. on Minor Planet Circulars 5287-5332 for eight objects 80—67633
  precise posns. on Minor Planet Circulars 5391-5422 for eight objects 80—85884
  precise posns. on Minor Planet Circulars 5423-5454 for seven objects 80—98599
  precise posns. on Minor Planet Circulars for eight objects 80—31241
  primordial comets, interiors radiogenic melting 80—67659
  probable comet on Palomar Sky Survey prints, 1954 Feb. 11 position 79—80270
  probable discovery trail in Phoenix (1978 November 30) 79—25547
  protocometary cloud, relation of solar apex 77—25984
  protoplanetary eruptive evolution and comets 79—70969
  recent UV and IR obs. and prospects for Spacelab 77—33425
  P/Reinmuth 1 (1979j), recovery obs. 80—8589
  P/Reinmuth 2 (1980n), recovery posns. and appearance (1980 Sept.) 80—101560
  roman numeral designations for 1975 77—33422
  rotating nucleus model for comets with fan-shaped comae 79—44414
  Russell (1979d), discovery posns. (1979 June) 79—71000
  Russell (1979d), precise posns., elements and ephemeris (1-79 June-July) 79—71002
  p Russell (1979d), precise posns. (1979 June-July) and improved elements 79—84748
  Russell (1979d), semiaccurate positions and ephemeris continuation 79—80273
  Russell (1980l), discovery posns. and ephemeris (1980 September) 80—101557
  Russell (1980l), ephemeris (1980 Sept.-Dec.) 80—105207
  Russell (1980l), precise positions, parabolic orbital elements and ephemeris 80—101559
  Sanguin (1977p), discovery, appearance and positions 77—91482
  Sanguin (1977p), positions, elements and ephemeris 77—91486
  P/Sanguin (1977p), positions, improved elements and ephemeris 78—16352
  P/Sanguin (1977p), precise positions 1977, Oct. to Dec. 78—20752

comets continued
P/Sanguin (1977p), precise positions (1977 October 11 and 19) 78−7936
Sanguin (1977p), precise positions for 1977 October 78−4151
P/Sanguin (1977p), precise posns. (1977 Nov.-1978 Jan.) 78−73685
P/Sanguin (1977p), prediscovery position, elliptical elements, and ephemeris 78−4153
P/Schorr (1918 III), movement of one-apparition short-period object *(Russian)* 79−92725
Schuster (1975 II), precise positions, 1977, February 12 to 25, and orbital elements 77−37579
Schuster (1975 II), precise positions 1977 Feb. and May 77−71065
Schuster (1975 II), precise positions 1978 Jan., ephemeris for 1978 Apr.-1979 Mar. 78−40880
Schuster (1975 II), precise posns. (1977 June) 78−12158
Schuster (1976c), precise position and tail obs. (1977, January) 77−29727
Schuster (1976c), precise positions, ephemeris for 1977 Feb. 6-1978 Apr. 22 period 77−17437
Schuster (1976c), precise positions for 1976 Mar. 25 and Jun. 2 77−22147
P/Schuster (1977o), confirmation and semiaccurate posns. (1977 Oct.) 78−7929
P/Schuster (1977o), discovery and positions (1977 October) 78−7927
P/Schuster (1977o), found during survey for high-inclination minor planets 79−75156
P/Schuster (1977o), positions , orbital elements and ephemeris 77−91481
P/Schuster (1977o), precise positions, 1977 October 16 and (1978 January 2) 78−65550
P/Schuster (1977o), precise positions 1977, Nov. 78−12156
P/Schuster (1977o), precise positions (1977, October 9-17) 77−91483
P/Schuster (1977o), precise positions (1977 September) 78−7933
P/Schuster (1977o), precise positions and ephemeris for 1977/78, Dec. to May 78−7940
P/Schuster (1977o), precise positions for 1977 Sept.-Dec. 78−20754
P/ Schuster (1977o), precise posns. (1977 Dec.-1978 Jan.) 78−36524
P/Schuster (1977o), precise posns. (1977 Nov. and Dec.) 78−20741
P/Schwassmann-Wachmann 1, 1976 Nov. 17 outburst obs. 77−5502
P/Schwassmann-Wachmann 1, 1978 September 13-14 magnitude 78−93160
P/Schwassmann-Wachmann 1, 1978-9 ephemeris 78−77521
P/Schwassmann-Wachmann 1, appearance (1978 Nov.-Dec.) 79−12436
P/Schwassmann-Wachmann 1, appearance and total magnitude (1979) December 80−36571
P/Schwassmann-Wachmann 1, CO$^+$ obs. near minimum brightness 80−82305
P/ Schwassmann-Wachmann 1, coma obs. (1979 October 31) 80−8591
P/Schwassmann-Wachmann 1, compact condensation obs. 79−25550
P/Schwassmann-Wachmann 1, ephemeris for 1977 Aug. 5-1978 April 12 period 77−60727
P/Schwassmann-Wachmann 1, magnitudes (1979 February) 79−40139
P/Schwassmann-Wachmann 1, new outburst, spectrum and visual magnitude estimates 79−53774
P/Schwassmann-Wachmann 1, outburst, total visual magnitude estimates, 1978 March 6-8 78−36527
P/Schwassmann-Wachmann 1, photometric and polarimetric obs. during 1976-77 outbursts *(Russian)* 79−80276
P/Schwassmann-Wachmann 1, precise positions, 1978 January 1 to 16, and outburst date 78−32399
P/Schwassmann-Wachmann 1, precise positions, (1978 February 27 to March 12) 78−49381
P/Schwassmann-Wachmann 1, precise positions 1976, Oct. and magnitudes for Dec. 77−17439
P/Schwassmann-Wachmann 1, precise positions 1976 Oct. 30-Dec. 27, visual magnitudes 77−22138
P/Schwassmann-Wachmann 1, precise positions 1977 Dec.-1978 Feb., total visual magnitude estimates 78−36520
P/Schwassmann-Wachmann 1, precise positions (1976, Sept.-Nov.) 77−29725
P/Schwassmann-Wachmann 1, precise positions and magnitudes 1976/77 Nov.-Feb. 77−37574
p/Schwassmann-Wachmann 1, precise positions and magnitudes (1976 Oct.-Nov.) 77−5498
P/ Schwassmann-Wachmann 1, precise posns. (1977 Dec.-1978 March) 78−69746
P/Schwassmann-Wachmann 1, precise posns. (1977 March and Aug.) 78−16354
P/Schwassmann-Wachmann 1, precise posns. and magnitudes (1977-8) 78−28585
P/Schwassmann-Wachmann 1, rotation and outbursts 80−67655
P/Schwassmann-Wachmann 1, total visual magnitude estimate, (1979 February 4) 79−30011
P/Schwassmann-Wachmann 1, total visual magnitude estimates for 1978 Oct. 79−5788
P/Schwassmann-Wachmann 1 (1974 II), outburst and CO$^+$ detect. spectrophotometric obs. 80−72881
P/Schwassmann-Wachmann 2 (1979k), recovery posns. and ephemeris 80−26811
P/Schwassmann-Wachmann 3, rotating nucleus model and fan-shaped coma 79−44414
P/Schwassmann-Wachmann 3 (1979), discovery report and precise positions 79−88622
P/Schwassmann-Wachmann 3 (1979g), precise position, orbital elements, ephemeris for 1979 Aug.-Sept. 79−84750
P/Schwassmann-Wachmann 3 (1979g), precise position (1979 August 22) 79−92719
P/Schwassmann-Wachmann 3 (1979g), precise positions, orbital elements and ephemeris 79−92720
P/Schwassmann-Wachmann (1), brightness during June to August 1972 rel. to solar flares 77−25983
Seargent (1978m), continuation ephemeris for 1978 Nov.-Dec. period 79−5782
Seargent (1978m), discovery, posns. and appearance 78−93158
Seargent (1978m), ephemeris extension and magnitude estimate 79−44416
Seargent (1978m), positions 1978 Oct. 78−93161
Seargent (1978m), precise positions, 1978, October 6, and parabolic orbital elements 78−96432
Seargent (1978m), precise positions, parabolic orbital elements and ephemeris 78−93164

comets continued
Seargent (1978m), precise positions for 1978 Oct., parabolic elements, ephemeris, UV spectra 78−96436
Seargent (1978m), precise positions for 1978 Oct. 78−96438
Seargent (1978m), total visual magnitude estimates for 1978 Oct. 79−5786
Seargent (1978m), UV spectrum 79−44413
P/Shajn-Schaldach, ephemeris for 1978 June-1979 March period 78−53879
P/Shajn-Schaldach (1978i), recovery positions 78−73678
short-period, distrib. of Jovian perturbs. on orbital elements 78−40871
short-period, with large perihelion distances, search, unidentified asteroids obs. 78−85907
short-period comets origin, comet belt beyond Neptune model 80−94759
P/Smirnova-Chernykh (1975 VII), ephemeris for 1978, Feb.-Dec. 78−20750
P/Smirnova-Chernykh (1975e), ephemeris for 1977, Jan.-Nov. 77−5504
P/Smirnova-Chernykh (1975e), precise position 1976 June 4 77−33426
P/Smirnova-Chernykh (1975e), precise positions (1976, May-June) 77−37572
solar wind interaction with non-magnetic bodies 78−49270
solar wind interaction with type-1 tails 78−49393
solar wind-comet interactions 78−49392
space probe missions for direct investigation 77−37494
split comets, relative motions of fragments 77−37570
split comets, separation vels. and differential decelerations 78−28581
splitting test and comets with multiple nuclei 79−66961
Star of Bethlehem, role of comets/novae in 5 and 4 BC 79−67136
P/Stephan-Oterma (1980g), recovery, positions, elements and emphemeris 80−82307
P/Stephan-Oterma (1980g), total visual magnitudes and coma diameters, (1980 September 7 to 11) 80−109397
Tago-Sato-Kosaka (1969 IX), H and OH prod. rates 78−28580
Tago-Sato-Kosaka (1969 IX), tail structure (1969 Dec.-1970 Jan.) 79−44415
tail magnetic field, size 79−88626
tail magnetic field magnitude estimation 78−93157
tails, H$_2$O$^+$ surface brightness rel. to CO$^+$ 80−72880
tails, hydromagnetic models 80−56773
tails, small-scale turbulence theory 79−44411
tails of type-1 comets, Kelvin-Helmholtz instability 80−46493
P/Taylor (1916 I), movement of lost comet rel. to possible recovery *(Russian)* 79−92724
P/Taylor (1916 I), nuclei separation vels. during disintegration 78−61812
P/Taylor (1916 I = 1977a), precise positions, orbital elements, ephemeris 77−22142
P/Taylor (1977a), precise and prerecovery positions 77−45363
P/Taylor (1977a), precise position 1977, Jan. 77−22144
P/Taylor (1977a), precise positions (1977, February-March) 77−49340
P/Taylor (1977a), precise positions (1977, March-April) 77−64702
P/Taylor (1977a), precise positions and prediscovery obs. (1976 Nov.-1977 Feb.) 77−33419
P/Taylor (1977a), precise positions for 1977 Jan. 14 77−22146
P/Tempel 1, ephemeris for 1977, Jan.-Jul. 77−17430
P/Tempel 1 (1977i), ephemeris for 1978 Feb.-Nov. 78−20742
P/Tempel 1 (1977i), precise position 1977, June 77−71062
P/Tempel 1 (1977i), recovery on 1977 April 12, precise positions 77−60728
P/Tempel 2, 1976 December-1977 September ephemeris 77−5499
P/Tempel 2, joint NASA-ESA mission 80−82168
P/ Tempel 2, optical spectrophotometry at 3 AU distance, albedo, nucleus radius 80−26814
P/Tempel 2, rotating nucleus model and fan shaped coma 79−44414
P/Tempel 2, US space agency plans for 1980 research 80−46492
P/Tempel 2 (1977d), BV photometry, (1979, January 28 and 31) 79−30012
P/ Tempel 2 (1977d), ephemeris (1978 June 1 to 1979 February 16) 78−49382
P/Tempel 2 (1977d), precise position 1977, April 77−71063
P/Tempel 2 (1977d), recovery obs. (1977, March 27) 77−37576
theories and observations 78−69753
Torres, discovery and positions, 1980 June 13 and 14 80−82306
Torres (1979e), discovery and approx. posns. 79−71001
Torres (1979e), precise position, parabolic orbital elements and ephemeris 79−84749
Torres (1979e), precise positions, (1979 July 3) 79−75161
Torres (1979e), precise positions for 1979 Jun.-Jul. 79−84747
Torres (1979e), precise posns., elements and ephemeris (1979 June-Aug.) 79−75160
Torres (1980e), 1980 June 17 semi-accurate posn. 80−85898
Torres (1980e), precise posns., elements and ephemeris (1980 June-July) 80−85900
Tritton (1978d), discovery, appearance and positions (1978 Feb.) 78−32403
P/ Tritton (1978d), positions, elements and ephemeris 78−36531
Tritton (1978d), positions, elliptical elements, ephemeris and magnitude law 78−36522
P/Tritton (1978d), precise positions 1978 March 78−40877
P/Tsuchinshan 1, ephemeris for 1977 Oct.-1978 July period 77−82167
P/Tsuchinshan 1 (1978e), precise position (1978 March 8) 78−45285
P/Tsuchinshan 1 (1978e), recovery, precise position 1978 Feb. 4 78−36526
P/Tsuchinshan 1 and 2, orbital elements, ephemerides for 1977-79 *(Chinese)* 77−22137
P/Tsuchinshan 2, ephemeris for 1977 Nov.-1978 Apr. period 77−91480
Tsuchinshan (1977 X), osculating orbital elements, hyperbolic orbit determ. *(Chinese)* 79−80269
Tsuchinshan (1977q), 1977 November 8 precise positions and appearance 78−4154
Tsuchinshan (1977q), discovery positions 78−7934
Tsuchinshan (1977q), positions, elements, and ephemeris 78−16350
Tsuchinshan (1977q), precise positions, elements and ephemeris 78−16353
Tsuchinshan (1977q), precise positions, improved parabolic elements and ephemeris 78−45284
Tsuchinshan (1977q), precise positions (1977 December) 78−28584
Tsuchinshan (1977q), precise positions for 1977 Nov.-Dec. 78−20746
Tsuchinshan (1977q), precise posns. (1977 Nov.-1978 Jan.) 78−61804
P/ Tsuchinshan (1978p), recovery and semiaccurate posns. 79−5783

comets continued
Tunguska, 1908, catastrophe, cosmochemical anomaly in silicate microspherules comp. 78−96430
Tunguska catastrophe, motion of low-density gaseous bodies in the atmosphere 79−84554
Tunguska cosmic body, chemical comp. and nature 78−61810
Tunguska event, 1908, new egregious theory 79−21229
Tunguska event, comet collision with Earth 78−49390
Tunguska event, comet impact theories confirmed 78−7642
Tunguska event, comet impact with Earth's atm., nonthermal ^{14}C prod. 77−78720
Tunguska event, thermal explosion of porous meteoroid, model 78−61813
Tunguska meteorite, collision between Earth and comet 78−32396
P/Tuttle, 1858-1967 motion *(Russian)* 79−92726
P/Tuttle (1980h), ephemeris (1980 Oct.-1981 Feb.) 80−105208
P/Tuttle (1980h), recovery and precise position (1980 July 14) 80−85901
P/Tuttle-Giacobini-Kresak, 1978-9 ephemeris 78−73684
P/Tuttle-Giacobini-Kresak (1978r), recovery and semi-accurate positions 79−12434
type 1 tails, helical plasma waves 77−78716
type 1 tails, magnetic field origin 77−49341
type 1 tails, origin of mag. fields 77−13288
type I tails, ray struct. and electrodynamical forces *(Russian)* 79−101119
unidentified object on Palomar Sky Survey (prints no.1267) 79−96974
P/Van Biesbroeck, ephemeris continuation (1977 Nov.-1978 Nov.) 77−91479
van Biesbroeck, orbital elements and ephemeris for 1977 Feb-Aug. 77−9710
P/Van Biesbroeck (1977s), precise positions 1977 Dec. and 1978 Mar. 78−45289
P/Van Biesbroeck (1977s), precise posns. (1978 April-May) 78−73686
P/Van Biesbroeck (1977s), precise posns. (1978 Jan.-May) 78−61802
P/Van Biesbroeck (1977s), recovery position 78−20740
van den Bergh (1974 XII), precise position (1976, October 31) 77−29729
volatile gases rel. to solar nebula NH_3 synthesis, kinetic model 80−62041
West (1975n), Belgian obs. 77−41356
West (1975n), edge-on nucleus configuration obs. 77−33409
West (1975n), ices evaporation rates 77−87325
West (1975n), Lyman α obs. 77−82163
West (1975n), microwave continuum radiation obs. 78−16349
West (1975n), nucleus A precise positions, nuclei B and D separations and position angles 77−53478
West (1975n), nucleus splitting, photography and narrow-band photometry 78−36512
West (1975n), photography and narrow-band photometry 77−17429
West (1975n), positions from photographic obs. 77−33411
West (1975n), precise positions 1976 Apr. 1 and Jun. 2, orbital elements 77−17447
West (1975n), precise positions of nuclei, 1976 May and September 77−9707
West (1975n), scatt. phase function of cometary dust, 0.5 to 18 μ 77−29731
West (1975n), search for CH RF emission 78−20735
West (1975n), spectrographic obs. 77−29730
West (1975n), tail components orientation and struct. *(French)* 77−53475
West (1976 VI), CN (0-0) band brightness profile obs. rel. to CN prod. 80−82303
West (1976 VI), coma mols. and dust distrib., visible emission profiles 80−101562
West (1976 VI), dust bursts, split nucleus, flare-ups, particle evaporation 79−30010
West (1976 VI), dust tail striae, propagating inhomogeneities 78−61809
West (1976 VI), emission bands and continuum flux heliocentric depend. 80−36575
West (1976 VI), ionosphere CO^+ brightness profile 80−85896
West (1976 VI), IR obs., dust model 78−81592
West (1976 VI), IR obs., results 78−81591
West (1976 VI), Lyman α isophotes 80−46485
West (1976 VI), photographic photometry near perihelion passage 79−35193
West (1976 VI), polarisation of head 80−8587
West (1976 VI), precise position determ. 80−46494
West (1976 VI), radiation polarisation obs. 79−62794
West (1976 VI), spectrophotometry, emission bands and lines obs. 80−56768
West (1976 VI), spectrophotometry after perihelion passage, emission features vars. 78−57503
West (1976 VI), striated tail study 79−35194
West (1978a), discovery, positions and spectral obs. 78−24489
West (1978a), ephemeris, (1978, June 11 to September 9) 78−61807
West (1978a), positions, parabolic elements and ephemeris 78−28583
West (1978a), positions and ephemeris extension (1978 Jan.-July) 78−36516
West (1978a), precise positions 1978 Jan., Mar. 78−49383
West (1978a), precise positions for 1978 Jan.-May 78−61799
West (1978a), precise posns. (1978 February-March) 78−40872
West (1978a), precise prediscovery positions, hyperbolic elements 78−40878
West (1978a), semiaccurate positions 1978, Jan. 78−24492
P/Whipple, ephemeris for 1977 Apr. 7-1978 Feb. 1 77−22149
p/ Whipple (1977h), confirmed recovery and positions (1977, May) 77−56876
P/Whipple (1977h), ephemeris (1978 June 21 to 1979 April 17) 78−53882
P/Whipple (1977h), precise positions 1977, Jul. and Aug. 78−24487
P/Wild 2, (1978b), precise positions, (1978 February 8 to April 12) 78−53885
P/Wild 2 (1978b), discovery and precise posns. (1978 January) 78−28586
P/ Wild 2 (1978b), positions, appearance and magnitudes (1978 Jan.-Mch.) 78−36530
P/Wild 2 (1978b), positions, elements, ephemeris and magnitude estimates 78−36515
P/Wild 2 (1978b), positions, elements and ephemeris 78−28589

comets continued
P/Wild 2 (1978b), precise positions 1978 Feb.-Mar., total visual magnitude estimates 78−45287
P/Wild 2 (1978b), precise positions (1978 Feb.-Apr.) 78−53880
P/Wild 2 (1978b), precise positions (1978 January 27) 78−32398
P/Wild 2 (1978b), precise positions for 1978 Jan.-Feb. 78−32402
P/Wild 2 (1978b), precise positions for 1978 Mar.-May, ephemeris 78−73676
P/Wild 2 (1978b), precise posns. (1978 February-April) 78−73681
p/Wild 2 (1978b), precise posns. and magnitudes (1978 Jan.-May) 78−61803
P/Wild 3 (1980d), discovery posns., orbital elements and ephemeris (1980 April-June) 80−67657
p/Wild 3 (1980d), precise positions, improved orbital elements and ephemeris 80−72885
P/Wolf (1884 III), motion in interval 1925-1967, and precalc. of 1975-1976 apparition 78−24493
P/Wolf-Harrington, orbital elements, ephemeris for 1977 June 6-1978 June 1 period 77−53477
P/Wolf-Harrington (1977j), precise position 1978 Jan. 3 78−36528
P/Wolf-Harrington (1977j), precise positions (1977, July-August) 78−7931
P/Wolf-Harrington (1977j), recovery and positions 77−67071
P/Wolfe-Harrington (1977j), independent recovery in Japan 77−71067
C II line excitation by C I photoionisation 80−58223
C isotope ratio 79−5766
C production in cometary coma, model 79−16885
C_2, reson. fluoresc. statistical equilib. calc., appl. to comets 78−1016
C_2 Swan/Phillips band ratio, statistical equilib. 79−96969
C_2 Swann band strengths calc. 77−61810
C_2, synthetic spectra calcs. 78−28579
CN abundance from radiance of violet CN spectral bands 78−16348
CN radicals, newly created, possible detect. in spectra 78−61798
CO and CO^+ bands intensities, reson. fluoresc. calc. 79−35191
CO rich comets, struct. of ionospheres 77−29723
$^{13}C^{16}O^+$ (2,0) band, comet-tail system, rot. anal. 80−74157
H atmosphere dynamics, dissociative heating effects *(Russian)* 78−20736
H_2O^+, electronic spectrum, predicted IR and microwave lines, comet tail bands 77−473
O I 7990 Å and 11287 Å branching ratios, astron. appl. 79−41134
OH radical lifetime at 1 AU 80−46488
TaC-Ni(-W) alloys, oxidation resistance 77−60000

command and control systems
aerospace systems and electronics, IEEE conference, Washington D.C., USA, 26-29 Sept (1976) 77−5420
environmental satellite telemetering service, NOAA 80−56592
Ionospheric Sounding Satellite, command system *(Japanese)* 77−78609
simulated underwater partial launch system, photogrammetric data reduction system 77−79075
small submersible, command and control acoustic communications system design 79−5666
UK-6 satellite, computer command system 79−25440

commerce
see also marketing
British trade weights and measures activities 80−27267
exponential function, growth and compound interest 77−5637
geophysical prospecting equipment for Hungary, aspects 78−7787
LWRs, 150 to 500 MWe, market in developing countries *(German)* 80−32423
mankind's future needs and aspirations in space, conf., Washington USA, 1976 Oct. 78−4078
nuclear power, U enrichment, market survey *(German)* 78−4999
OTEC ocean thermal energy conversion, commercialisation in USA 79−61957

commissioning
see also installation
4150 MW nuclear power station with PWRs, at Bugey, in France, commissioning report *(French)* 80−37571
AEI MS702 mass spectrometer, setting-up and commissioning 79−63323
AGR, fossil-fired steam conditions, commissioning experience 78−17406
BWR, TVO I, startup principles 80−9372
Calcutta variable energy cyclotron vacuum system design, testing and commissioning 78−86707
CANDU nuclear stations, decommissioning 77−74973
Hinkley Point B AGR commissioning and three years' operational experience 80−23107
LMFBR, decommissioning of Na reactor expt. 78−8942
LWR plant, decommisioning 78−29603
mine concentrator X-ray on stream anal. system 78−35778
nuclear reactors, decommissioning, main problems 80−676
nuclear reactors, decommissioning, state-of-the-art handbook 80−824
PWR reactors, start-up procedures *(Slovak)* 79−36346
PWRs, 900 MW, in France, construction report *(French)* 79−63801

communication channels
see also channel capacity
atmospheric scatter channel for ELOS optical communications system 79−29862
multichannel IR receiver performance 79−76596
optical channel conditioning against intersymbol interference and timing errors *(Italian)* 77−23622
optical communication, channel displacement and diffusion coefficient determ. *(Russian)* 79−98303
optical communication channel and photodetector array, computer simulation 77−71944
quantum statistical model, asymptotic relations 78−33687
sea surface scattering channel and undersea communications, modelling 79−1022
supervisory/service channel for fibre optic transmission systems 80−95803
time-varying shallow water channel weighting function meas. 78−5606
troposphere, energy spectrum of delays *(Russian)* 79−2329
troposphere communication channel, energy spectrum of delays 79−84442
VLF signals propagation, multi-mode, statistical anal. *(Russian)* 79−5702
wideband subcarrier PFM analogue optical communications channel 77−27378

communication networks
  see also computer networks; radio networks; telegraph networks; telephone networks
  air pollution meas., French local networks, examples and software *(French)* 77—37459
  biomedical broadband communication network combining satellite link and TV broadcast techniques 77—64145
  conference, EUROCON, Venice, 1977, May 78—53552
  fibre optics and role in public telecommunication 80—43484
  hierarchical control system, simple communication network 79—45610
  Italian local digital network applicability of optical cables *(German)* 78—33886
  microwave transmission characteristics survey *(Norwegian)* 79—29834
  UK Post Office junction and trunk network applications for optical fibre systems *(German)* 78—38016

communication systems *see telecommunication systems*

communication theory *see information theory*

communication transmission lines
  see also telephone lines
  optical fibres, low-OH-content, transmission-loss characts. over 0.5 to 2.5 μm range 79—59830

communications applications of computing *see communications computing*

communications applications of control
  see also communications computer control; telephony
  light beams propagation, thermal self-action and compensation methods 80—106579
  medical communications using pre-existing statewide microwave network 77—48899
  optical communication conference, Munich (1977) *(German)* 78—33854

communications computer control
  see also communications computing; electronic switching systems
  automated meteorological data transmission from commercial aircraft via satellite 78—57327
  nonvocal communication aid improvement by microprocessor technology 80—8217
  ocean surface currents mapped by coastal HF radar system 78—28351
  rehabilitation of severely disabled, microcomputer environmental control and communication system 80—8216
  semantically accessible communication aid development trends 80—8218
  surface meteorological buoy and aircraft VHF link 80—46298

communications computing
  see also communications computer control
  acoustic measurement and anal. system *(Japanese)* 79—68522
  acoustic radar systems, microcomputer appl. 80—106685
  acoustic transmission system, impulse response meas. with digital computer processing *(German)* 80—91999
  antennas and propagation, symposium, Stanford (1977) 77—75378
  broadcasting and recording studios, computer-aided method for acoustical design 79—64402
  EM pulse propagation, in weakly nonlinear plasma, numerical calc. 77—58863
  EM scatt. from surfaces, nonrectangular patch model, program availability and appls. 79—81332
  EM wave scattering, by complex shaped bodies, effective scattering area *(Russian)* 78—13647
  eye tracking communication system feasibility for nonverbal cerebral palsy children 79—83981
  geosynchronous satellite orbit determination using VLBI and computer program *(Japanese)* 80—21925
  HF max. usable freq. prediction along foF2 line, MINIMUF-3 algorithm 79—25372
  IEEE International EMC Symposium, Atlanta (1978) 78—82876
  ionospheric propagation, ray tracing calc. through Bradley/Dudeney ionospheric model 78—7826
  linear array, far-field directivity patterns, electrical analogue simulation 77—804
  microcomputer-based speech synthesis system 79—94421
  nuclear reactor accident management, automated notification of reactor data to off-site personnel 80—95388
  ocean receivers for acoustic signals from moving radiating sources 79—59859
  optical communication, light scatt. by clouds 77—88651
  optical communication channel and photodetector array, computer simulation 77—71944
  optical fibre propagation modes, with non-circular cross sections 79—76874
  optical signal receivers, optimal and nonoptimal, logical structs. efficiency comparison, simulation *(Russian)* 78—71041
  propagation data, radiosonde utilisation 79—2350
  radar symposium, London (Oct. 1977) 78—24395
  radiowave scattering signals, incoherent, spectral analysis *(Russian)* 79—5621
  solar power satellite, computer modelling of power transmission system 80—40866
  sonar, digital phase shift beamformer, design and implementation 79—1034
  speaker verification device, microprocessor based 80—102936
  speech coding, parametric coding of speech spectra, computer studies 80—96137
  speech recognition, computer-aided, for Polish vowels in continuous speech 80—33380
  troposphere, radio propag. characts. prediction using FORTRAN computer programs *(Italian)* 78—85666
  verbal communication aid for nonvocal patients 79—57816
  vowel identification using piecewise separation technique 79—46123
  waveguide, optical perturbed, propagation constants calc. *(Japanese)* 78—42423
  Yugoslav soil medium-wave conductivity chart computation *(Slovenian)* 79—39718

community antenna television
  fibre optics market in Japan 79—32044

community planning *see town and country planning*

commutation
  see also commutators
  arc quenching system for transient and statistical flashover, fusion reactor systems 78—75455
  ionospheric plasma probe measurements, commutable source of ref. voltages 80—31192

commutation continued
  six-channel MOSFET commutator, monopolar mass spectrometer appls. *(Russian)* 78—74099
  transformer-rectifier flux pump power supplies, current commutation 78—12703

commutators
  see also commutation
  electric machines, volts-per-bar and flashover, causal mechanisms and preventive measures 80—92408
  electrophysiological recording from behaving animals, 10-channel commutator 79—84050
  explosive-magnetic generators, energy take-off to inductive load using circuit breaking 80—59323
  Kalousek commutator, appl. to electrochem. stripping anal. 78—53290
  magnetocumulative generator, megampere pulse shaping, explosively compressed plasma column *(Russian)* 78—1912
  multichannel, for nanosecond generators, Torus accelerator investigation appl. 77—71708
  multichannel commutator for thermal analysis data transfer to single recording instrument 79—52821

compacting *see densification*

comparators (circuits)
  see also phase comparators
  AC unit, 40 Hz to 100 kHz, USSR special standard 77—30179
  AC-DC, for AF current and voltage meas. 77—18024
  auto reference level comparator, used in physiological research 78—31992
  betatron energy varying and stabilisation, tunnel diode based circuit 77—6581
  capacitance testing 78—16811
  cryocurrent comparators, ring cavity elements, field attenuation 77—144
  cryogenic current comparators, double constant current source, appl. 79—21775
  cryogenic voltage comparator, for Josephson voltage standard 77—18030
  DC comparator apparatus for resistance thermometry and combustion calorimetry 79—75529
  detector produces unambiguous output 78—4627
  digital latency meter for evoked potentials 77—60322
  double constant current source for cryogenic current comparators, standard resistor calibration appl. 78—93731
  frequency comparator based on delay line technique 79—6144
  gated constant-fraction discriminator for use with fast-focused photomultiplier tubes 78—58063
  laser diode life testing, with constant light output current 80—1215
  least or greatest interval timer 78—62183
  liquid N_2 two-level controller 80—52241
  microwave moisture content-attenuation-voltage convertor with time-domain attenuation comparisons *(Polish)* 78—70131
  monochromator drive, using high-speed digital servo 78—36992
  photographic enlarger exposure meter 79—89018
  photon count cct. using high-speed comparator in discriminator 78—77979
  Q-meter, digital, automatic, design procedure 78—70155
  solid state ionisation current comparator 77—23383
  superconducting current comparator, appl. to meas. of Kapitza conductance of Evanohm 77—41645
  timer, touch controlled, photography appls. *(Spanish)* 80—86478
  US beam power meas. calorimeter bridge for 1 to 15 MHz 77—27446
  voltage ratio meter for low-freq. AC 79—17440
  wideband current and voltage comparators 77—57356

compasses
  see also navigation
  corrected gyrocompass asympotic stability *(Russian)* 79—10457
  floating-core flux-gate compass design and operation 77—71354
  gyro-horizon compass, stability conditions *(Ukrainian)* 77—72144
  gyrooptical compass, signal measurement time *(Russian)* 80—33007
  marine, Lord Kelvin's involvement 79—58759
  orientation compass of VEB Carl Zeiss JENA 77—82578
  ships, adjustment in fog using atmosphere polarised sunlight, cct. 78—24831
  single-rotor corrected gyrocompass motion subject to random parametric disturbance *(Russian)* 79—10456
  theodolite, THEO 080 A, with attachable circular compass 80—56634

compensation
  see also error compensation
  acoustic field formed by rigid scatterers in field of harmonic point sound source, compensation 78—18112
  active acoustic suppression systems with finite number of couplings, approximation and stability aspects 78—18111
  active vibration suppression systems, effectiveness of critiera for placement of compensating sources 78—18099
  active vibration-suppression systems, automation 78—18098
  active vibration-suppression techniques for mechanical systems with many degrees of freedom 78—18101
  active wavefront compensation device image degradation and post-processing 77—58283
  anemometers using thermally compensated thermistors, math. models *(French)* 80—90227
  automatic thermo-compensator for viscosity meter, cct. *(Russian)* 77—55114
  Babinet-Soleil modified compensator 77—74485
  chromatic-aberration-free microscope optics 80—86395
  crystal parabolic frequency/temp. characteristic compensation 79—55294
  DC microvoltmeter based on modem 80—31798
  density meter using radioisotopes, temp. compensation *(Russian)* 77—49713
  digital thermocouple cold junction compensation methods *(Italian)* 78—37002
  double-beam Fourier spectroscopy with interferometric background compensation 77—38038
  dynamically tuned gyrosope drift *(Russian)* 77—53890
  electrolyte electrical conductivity meas., voltage amp. for temp. compensation *(German)* 78—54399
  electrometer operation in ionizing photon radiation fields by compensation method 77—79110
  flow meas., hot wire and hot film temperature compensating circuits, temp. probe appl. 78—59510
  flowmeter, linear and nonlinear specific gravity digital compensation 78—34242
  flowmeter, viscosity change influence on reading *(Russian)* 77—65823

compensation continued
- frequency response, instrum. for joint operation with broadband amplifier 77—45862
- galvanomagnetic semiconductor voltage and current transducers, Gauss effect compensation 78—77892
- high-speed pulse shaper/discriminator for scintillation and Cherenkov counters 78—86748
- hot-wire anemometer temp. compensation errors estimation *(Russian)* 78—57345
- IC temperature sensors used in thermocouple cold junction compensation circuits 80—77777
- injection laser longitudinal mode stabilisation by temp. compensation 79—45964
- ion cyclotron double resonance expts., oscillator coupling elimination 77—67530
- Kelvin bridge, link resistance compensation 78—86292
- laser interferometric system, double-freq., with automatic compensation *(Chinese)* 80—27340
- light divider phase distortion compensation improvement 78—58073
- light scanners, compensated moving-coil mirror galvanometer 77—58479
- linear rotary potentiometer nonlinearities, guidelines 78—45646
- load cell design and development for materials testing 80—105628
- magnetic airgap EM field gradient by coil correct design *(Russian)* 77—53959
- magnetic induction, stabilised source 78—94360
- mechanical prestressing, compensation of isolated muscle specimens *(German)* 80—36201
- multichannel temperature recorder, Thermodac II with 24 channels, thermocouples 0 degree C compensation 78—65930
- multimode waveguide sound fields, active suppression system 78—18113
- near IR absorption analysis, differential compensation method 78—80819
- noise in Fourier spectrometer, improved InSb photodiode preamplifier circuit 80—73474
- optical systems, high-precision compensated levels, geodetic appl. 80—101813
- optical wave, phase distortion compensation efficiency 78—1177
- optomechanical properties determ., polarisation device application, by compensation method 80—40643
- optotransducers, electronic compensation for dirty lenses 80—68189
- phase meter, digital, using delayed pulse train 77—49742
- photomultiplier external compensation networks for improved impulse response *(German)* 77—41682
- photomultiplier modulating cct. with spurious signal compensation 78—58033
- photomultiplier output, background and dark current automatic compensator 77—87851
- plasma potential function during electron energy distrib. function measurement by probe, voltage follower cct. 80—54041
- plate radiation compensation at subcritical freqs., coupling of sound and vibr. fields 78—18110
- platinorhodium-Pt thermocouples, 1000-1300°C range, cold junction electrode compensation 78—216
- polarography, DC, charging current compensation, in situ methods 77—25337
- potentiostat, double probe compensation system, resist. characts., slope optimisation 77—44568
- pressure transducer, miniature implantable, biomedical appl. IC fabrication techniques 80—76849
- pressure transducer temperature coefficient sensitivity, compensated using positive feedback 80—17928
- radiometer, absolute differential, compensation cct., features 78—65956
- reference source radiation, temp. instability and compensation methods 79—14071
- resistance thermometer, conductor resistance effect compensation using hexagonal bridge *(German)* 78—77910
- resistance thermometer thermal inertia *(Russian)* 80—62667
- river system, robust decentralised control of water quality 79—57522
- rotational symmetric aspheric in compensated interferometers, computer-generated-holography testing 80—33128
- saturated flux density measurement using compensation technique, for cores with square hysteresis loop *(Russian)* 79—54158
- semiconductor junction laser module for optical fibre communications 80—5757
- semiconductor magnetophonon oscillations, separation by low-pass-filtering autocompensation 78—2499
- shading effects and countermeasures 78—78922
- spatially-varying image degradation compensation by linear programming 77—58275
- step-stare spaceborne optical system image motion compensation 80—90322
- step-stare spaceborne optical system smear compensation by focal plane manipulation 80—82172
- strain gauge transducers temperature compensation methods 77—22541
- strain gauges, compensation of temp. curve of modulus of elasticity *(German)* 80—31734
- stress measurement, polarisation device application, by compensation method 80—40643
- temp. in hydrostatic density meter, design *(Russian)* 77—41573
- temperature, in optical modulator, feedback control method 77—42611
- temperature, pure water electrical conductivity meas. *(Czech)* 80—62684
- temperature compensation techniques for SAW devices 80—74614
- temperature compensation with metallic overlay films on quartz 80—79043
- temperature during illumination measurement using photoresistors, digital linearisation using microprocessors *(German)* 78—77961
- temperature meas. by compensated thermocouples *(German)* 78—41304
- thermal compensator for diode laser closed-cycle refrigerator stabilisation 78—50797
- thermal losses in heat capacity meas. at high temp. by modulation method 79—85144
- thermal-blooming compensation, using closed-loop adaptive single parameter system 78—94407
- thermocouple cold junction compensation method for portable instruments 79—2768
- thermoelectric thermometer cold junction thermo-EMF compensation, parameter optimisation *(Russian)* 78—86270
- thermoelectric thermometers, automatic compensation of thermal EMF of free ends 79—6123
- thermoresistive transduction of nonelectric variables, compensation for thermal inertia *(Russian)* 77—53885

compensation continued
- transducer moving coil null offset using coupled RLC circuit *(Polish)* 77—49718
- turbulence-degraded image compensation, computer simulation techniques 77—60625
- vacuum gauge thermal compensation for accuracy improvement 79—67332
- vibration isolation system, correcting forces appl. 78—18100
- vibrations of inhomogeneous elastic structs., active compensation 78—18103
- wavefront optimal estimation for compensated imaging system 77—46691
- wavefront reconstruction for compensated imaging 77—46690
- wavelength-scanning ellipsometer signal level regulation and dark current compensation 79—26105
- wedge compensator, operating nonlinearity elimination 79—32065
- wedge compensator for automatic control system 78—13808
- wideband AC electronic voltmeter *(Spanish)* 78—86304
- X-ray tube anode voltage compensation under dropping power condition, digital compensation system *(Bulgarian)* 79—35902
- $\mathrm{K^2H_2PO_4}$ electro-optic shutter natural birefringence compensation by β-$\mathrm{LiIO_3}$ monocrystal 79—55247
- Se photocells, temp. coeff. of sensitivity 78—82033
- Si resistors, both p-type and n-type 78—91698

compensation, charge *see charge compensation*

compilers (program) *see program compilers*

compiling programs *see program compilers*

complementarity
- coherence and randomness in quantum theory, uncertainty relations 80—22231
- Galois construction and subject construction, holistic methods in quantum logic 80—27177
- geometric quantisation and general relativity 78—8288
- quantum mechanics, development and Heisenberg's role *(Polish)* 78—89291

complete computer programs
- *see also subroutines*
- ADIF, a FORTRAN IV program for solving the shallow-water equations 79—84493
- airborne noise, personal calculator program for A-weighted sound pressure level and noise ratings 80—23828
- alloy phase stability, program for calc. using modified pair potentials, in FORTRAN 78—35352
- astronomical period-finding technique, Fortran IV computer program 79—21195
- atmospheric sound absorpt., personal computer program 80—96065
- ballistics, max. range at elevated launch height, expt. and BASIC program 79—97156
- BKWAVE, calculation of 1-dimensional shock wave propagation 80—38448
- BULK: a computer program for calculating bulk-chemical analysis from mineral phases observed in thin section, FORTRAN IV program listed 79—2378
- CRI waveform display, Fourier analysis using SR56 calculator 78—36986
- curve fitting program on KIM-1 using FOCAL 79—35693
- cylindrical demagnetisation matrix computation, FORTRAN IV program 78—76274
- DEC-SIM program, for finite breadth light pulse excited decay curve simulation *(Hungarian)* 80—11473
- dendrogram association analysis, FORTRAN IV program 77—5326
- dosimetry calculations due to radionuclides in aquatic food chains, NEPTUN interactive code in FORTRAN 80—109039
- drill hole or sample area-of-influence determ., FORTRAN IV program 77—5327
- Easter date determ. for any year, program for HP 29C 80—77268
- education, recursive method for partition function calc., average energy calc., APL program 79—9050
- EEG bispectra computation computer program, in FORTRAN 78—92727
- electrode reaction kinetic parameters, programs for computer retrieval, in FORTRAN 78—31654
- equation of state variables calculation using TI-59 80—77738
- exploratory drilling exhaustion sequence plot program in FORTRAN 78—57334
- FLYSCH, geologic strata simulation listing 77—18
- FORTRAN, for analysis of variance and means 80—98792
- FORTRAN 336 statement program for prismatic plate assembly anal. 78—90737
- FORTRAN least-squares approx. for lateral absorbed dose distrib. for 25 MeV electrons appl. *(Japanese)* 78—74505
- Fresnel rhomb design, TI 58/59 program 79—32040
- geological history computation from field survey and map data in FORTRAN 77—9522
- geomagnetic anomaly of thin dike, curve fit by calculator program 80—98228
- geophysics regression program in FORTRAN 79—84495
- Hankel transforms, related, of orders 0 and 1, numerical integration by adaptive digital filtering, FORTRAN IV algorithms 79—92599
- heat transfer calc. in FORTRAN 77—7289
- heavy water production, Girdler-sulphide process phys. props., in FORTRAN 78—25300
- interferometers performance computing, Fabry-Perot, program for TI-59 calculator 79—35816
- jet noise, geometric acoustics model, computer prediction program 78—34118
- Lagrange's interpolation formula program for Texas Instruments SR-56 78—77699
- landform erosion simulation program in FORTRAN 80—85650
- lateral training of time stratigraphic units in FORTRAN 79—62510
- LEED surface struct. determ., multiple scatt. based programs, in FORTRAN, book 79—86971
- light interferometry, 3D orthographic projection plotting program 79—85172
- linear prediction in least-squares scheme for max. entropy spectra, Fortran subroutines 80—98465
- lithostratigraphic correl. of subsurface sequences in FORTRAN IV 79—62509
- logical searching of the lunar data, FORTRAN program incorporating Boolean search capabilities 79—2491
- magnetic field reduction to pole, fast Fourier series algorithm 77—5333

complete computer programs continued
magnox fuel cladding, surface struct. data acquisition and processing system 80—898
mathematics teaching by computer, long-division practice program in BASIC 80—98775
MTF calculation in radioisotope scanning, improved FORTRAN II program 77—21612
Muskingum constants evaluation, FORTRAN IV 80—31077
nuclear power stations, accumulation ponds cooling possibility analysis *(Slovenian)* 80—91208
physics teaching using SWTP 6800 system in BASIC 80—98776
plasma diagnostics, Abel inversion program for emissivity, in FORTRAN, book contrib. 77—51242
power spectrum analysis, nested variance technique, space physics, appl. in FORTRAN 77—87275
radioactivity, decay product radioactive accumulation, FORTRAN program 80—68611
sedimentology, ellipsoidal grain thin sections, Monte Carlo simulation in FORTRAN 77—5332
seismic refr. survey depth determination, program for pocket calculator 80—82088
seismic waves refl. coeffs. for layered media, in FORTRAN 77—49186
seismology, Zoeppritz's amplitude eqns. and Knott's energy eqns., in FORTRAN 77—40988
selenide thermoelectrics, analytical model for performance and degradation predictions 80—108805
self consistent FORTRAN subroutines for Earth motion determ. 80—85845
single crystals, growth simulation in FORTRAN 80—88069
solid state detectors spectra, fast analysis, LIZA program 80—37706
SPEED 2, computer program for data reduction from automatic data acquisition systems in FORTRAN 80—27279
speed and displacement relations for tire skids for PET in BASIC 80—57038
TEM convergent beam pattern anal., for Zr foil thickness determ., FORTRAN program 79—4215
terrain analysis FORTRAN program 77—9509
texture, calc., library program, in FORTRAN IV 78—22598
thermophysical properties of ethane from 90 to 600 at press. up to 700 bar, in FORTRAN 77—84940
thylakoid membrane of green plants, simulation of electron transport in primary photosynthesis reaction, in PL/1 *(German)* 77—86468
toroidal pinch systems, numerical anal. using programs in FORTRAN-D *(Japanese)* 78—5910
traverse point location in stack sampling, for HP calculator program 80—94139
volcanic rocks classification using Irvine and Baragar classification scheme, FORTRAN IV program 78—57203
X-ray diffraction data collection on macromolecules, FORTRAN program 77—51279
X-ray fluoresc. anal., data reduction, anal. using QUAN computer program 77—56267
X-ray scattering curve desmearing, FORTRAN program 77—84587
XLFRAC: a program for the interactive testing of magmatic differentiation models, in FORTRAN IV 79—2377

complex angular momentum plane
see also angular momentum theory; Pomeranchuk poles and trajectories; Regge poles and trajectories
$\pi\pi$ scattering at high complex energies, amplitudes with isospin 1 or 2 77—67631
analytic pole extrapolations, accurate tests 78—24976
asymptotic behaviour of quasipot. scatt. amplitude in plane of a complex orbital momentum *(Russian)* 79—75701
complex momenta eikonal approx., hadron-nucleus collisions at asymptotically high energies *(Russian)* 78—74294
Coulomb amplitude, integral representations 78—78118
Coulomb functions with complex angular momenta, calculation subroutine 79—85245
deuteron, eight quark model, ang. momentum group anal. 79—89098
eigenfunction expansion involving resonant states for complex poles residues of outgoing Green function 77—82885
elastic scattering, Sommerfeld poles and backward peaks 78—21357
Faddeev eqns., pole approx. *(Russian)* 78—49986
froissaron exchange theory 77—67632
hadron scatt. amplitude, axiomatic restrictions 78—32967
hadron-proton amplitudes, real parts from 3-universality 77—49926
Hermite polynomials, zeros and the algebra related matrices 79—49421
inclusive cross sections in scatt. angle, anal. props., ladder models with dynamical symmetry 79—93390
isobar model for $ab \to jkl$, overlap integrals 77—46032
K_L^0-K_S^0 transmission regeneration in H, comparison of expt. data and theoretical prediction *(Russian)* 77—49955
kinematics free ang. momentum trajectories, theory and phenomenology 79—89134
kinematics-free ang. momentum trajectories, Yukawa pot. numerical examples 79—89135
nucleus-alpha back-angle anomalies, S-matrix continuation to complex l-plane 77—30613
operator addition 80—86622
Oxford Rutherford type model, semianalytic treatment, dual unitarisation scheme, trajectory parameters 78—16996
P-wave isovector $\pi\pi$ phase shift, pion form factor left hand cut contrib. 80—27504
Pade approximants in Wick Cutkosky model 77—18162
production amplitudes in fifth order perturbation theory, pion and nucleon reactions 77—54088
pseudoresonance Argand loops *(Russian)* 79—9354
resonance multipoles, complexity, appl. to π^+p scatt. *(Russian)* 79—26346
scattering amplitude, quasipotential, analytic props. in complex planes of rapidity and angular momentum 80—68399
sequential pole model of vector meson Zweig rule violations, glueball possible identification 77—26520
t-channel exchange model with s-channel absorptive effects, high energy polarisation data interpretation 77—30435
T-matrix, perturbation formalism for complex poles and widths, appl. to intermediate struct. 78—66255
$e^+e^- \to$hadrons, asymptotically free quark model predictions in complex plane 77—71522

complex angular momentum plane continued
$\gamma p \to N\pi$, position and residue of the pole in the $M_{1+}^{(3/2)}$ amplitude *(Russian)* 79—22112
$\bar{p}p$ elastic scatt. complex zeros, 2.0 to 2.6 GeV, evidence for 3^{--}, 4^{++}, 5^{--} resonances 77—74712
$\pi^{\pm}p$ forward elastic scattering, differential cross section anal. outside Coulomb interference region 77—67678
$\pi\pi$ P-wave anal., ρ pole parameters 77—46079
$\pi\pi$ S-wave phase shift, lower bounds, ε° and ρ poles 78—45953
$\pi\pi$ system resonance poles positions 77—6096
$^4He(\pi,\pi)^4He$, eikonal and quasi-eikonal models in complex ang. momentum plane *(Russian)* 77—50160

compliance constants *see elastic constants*

composite insulating materials
binary dielectric mixture relative permittivity formulae compared 80—15939
electric field behaviour near singular points 79—31763
epoxy resin based composites, superconducting magnet insulators, gamma-ray radiation effects 80—24495
epoxy resin composite containing mica flakes, thermal depolarisation current, 20-190°C 77—90091
epoxy resin insulation, adapted models selection problems for electric ageing *(German)* 80—89365
epoxy resin-ferroelectric $Pb(Zr,Ti)O_3$ composite, dielec., elastic and piezoelec. consts. 77—8515
epoxy-Al composite, thermal conductivity 77—76630
epoxy-Al composite, thermal conductivity model 77—76629
fatigue behaviour, influence of superposition of elec., mech. and environmental stresses 80—97590
fatigue damage monitoring of processes damaging elec. insulating materials 80—97673
glass fibre reinforced epoxy, as electrical insulation for Tokamak toroidal field coils, mech. props. 78—64610
glass fibre reinforced epoxy prepreg, PDX TF coil insulation 78—62656
glass fibre reinforced epoxy resin, mech. props. 78—64582
glass-epoxy laminate, superconducting magnet insulators, gamma-ray radiation effects 80—24495
glass-fibre epoxy resin composite, thermal cond. and diffusivity, 2-15K 77—24457
ice-silica compound system, electrical breakdown at cryogenic temps. 80—45007
polymer film and liq. N_2 at cryogenic temperatures, partial discharge 78—1920
polymer-TiO_2 composite, dielec. props. *(Japanese)* 78—95540
polypropylene-polyurethane laminates, meas. of dielectric losses at cryogenic temps. 80—25301
rubber, C-black loaded SBR, elec. cond., effect of milling and thermal-oxidative ageing 77—55529
space shuttle insulation coating, combined load testing at 1100°C 79—34261
thermosetting polymers, fibre-reinforced, mech. props., 4.2-300K 77—25160
$Pb(Zr,Ti)O_3$ ceramic-polyvinylidene fluoride composite film, complex piezoelec. props. 78—64323
TiO_2-polycarbonate laminate, impulse surface flashover in vacuum, effect of normal elec. stress 79—4199

composite materials
see also cermets; composite insulating materials; composite superconductors; concrete; eutectic alloys; fibre reinforced composites; fibres; filled polymers; laminates
acrylic bone cement containing second phase dispersions, strength 77—81663
acrylic bone cement-stainless steel interface, shear strength 77—86706
adhesion between two crystals, theory 80—104417
adhesive, reinforced, fatigue resistance 77—4834
advanced, design, applications and test methods 80—77550
aggregate, polycrystalline, deform. 77—4816
aggregate, polycrystalline, grain boundary sliding contrib. to total strain 77—25114
aggregate particles, concept and test method for unified charact. of geometric irregularity 77—28954
aggregate phase contents, sampling in quantitative image analysis *(French)* 77—28961
aggregates, influence of particle size ratio on continuity 78—39712
aligned composites, in-situ growth by disproportionation of amorphous metal systems 78—72755
alkali-aggregate reaction particle size effect on expansion *(Japanese)* 78—31374
alloy, disperse state formation *(Russian)* 78—52757
alloys, two-phase systems, deformation textures 79—83219
alumina-acrylic composite bone cement 79—79689
anisotropic axisymmetric solids, asymmetric stress anal. 78—26033
anisotropic composite cantilever, bending and torsion, mathematical formulation 79—18708
anisotropic composites, bounds and self consistent estimates for overall props. 78—5654
aramid/epoxy composite, tensile test 80—11778
asbestos-reinforced friction materials, wear and thermal processes 80—40559
asbestos-rubber, classification 80—7484
average bulk props. calc., bounds 77—16237
B-epoxy composite, elastic moduli, effect of particle shape 78—15444
beam, vibr. and buckling anal. 79—1123
beams, exam. of contact problem, using boundary value problem soln. 78—42532
beams, shearing stresses distrib. under three point flexure, fracture due to surface peeling 78—44183
bearing capacity of designs, subject to intense surface heating 78—67057
bi-material, elastic composite, Southwell's analogues for plane and bending problems 78—87265
biaxial analogs of triaxial stresses 79—55345
bimaterial composite, influence on elasto-dynamic stress intensity factors of crack straddling interface 77—68532
bimaterial full-plane with crack at any angle to interface 77—14965
bimaterial plate, cracked, finite element anal. of stress distribution 78—75104
binary composites, percolation effects and sum rules in optical props. 79—69801
binary mixture theory for thermal diffusion in unidirectional fibrous composites 78—87230

composite materials continued
bitumen-filler systems, selective sorption 79—100437
bitumen-silica composites, dynamical mechanical props. 80—58996
bituminous mixes, fatigue strength, effect of mix and test variables 77—63881
bituminous mixture, aggregate surface area determ. 77—77689
bonded composite hollow circular cylinder, asymmetrical transient thermoelastic problems 78—30181
bonded composite hollow circular cylinder, transient thermal stresses under symm. temp. distrib. 77—54887
bonded elastic half-plane, intersecting crack anal. 77—14953
bonded elastic half-planes, interface crack 77—14952
bonded sector plates, stress anal., soln. of elastostatic boundary value problems 80—1425
bonded wedges, plane problem *(Russian)* 79—23284
bone, compact, fatigue damage, residual strength and stiffness 77—90834
bone tissue, compact, destruction 80—67135
bone-prosthetic material composites, fracture toughness 77—37108
brittle composite, local crack-driving force, elastic and thermal mismatch 78—7017
brittle failure prediction 77—89072
brittle microheterogeneous bodies, crit. equilib. diag. *(Russian)* 77—54930
brittle plate containing stochastically distributed rigid rod like inclusions, strength *(Russian)* 77—23917
calcified tissue, role of collagen in elastic props. 78—3539
carbographite mats., elec. cond. temp. depend. 77—43592
carbons, artificial, graphitisation shrinkage kinetics 77—48385
catalyst pellet, transient diffusion-react. eqns., approximation using Galerkin technique 79—96357
cellulose, fibres, membranes and composites, polystyrene used for modification of props. 78—95727
cement and ion-exchange resin composite for radioactive waste solidification, ^{137}Cs leaching 77—65275
cement based on Ca(OH)$_2$ and polymethylphenylsiloxane, high-temperature high-strength props. 77—36439
cement mortar-epoxy resin mortar, durability of jointing of successive pours with epoxy resin adhesive *(Japanese)* 77—8793
cemented carbides, wear resistant coating of Ti(N,C,O), CVD 78—92406
ceramic, quartz glass based, organosilicon binder, spalling-resistant, prod. 80—40313
ceramic composite, mech. props. *(Polish)* 78—31481
ceramic composite, toughening by oriented nucleation of microcracks 77—8921
ceramic filled with polymer, ZrO$_2$ stabilised, fracture mechanism *(Russian)* 80—100895
ceramic-glass-glass composites, crack growth, elec.-mech. analogue 80—85022
clad sheet metal, optimum combination of composing sheets for deep drawing 77—81241
classification system 79—61508
classification system 80—7484
coalescence in two-phase multicomponent system, theory 77—81248
complex dielectric const., bounds 80—108170
complex dielectric constant, exactly solvable microscopic geometries and rigorous bounds, for two-component dielec. material 80—75918
component bonding strength, apparatus, results 77—4887
composite body homogenisation under action of large spatial freq. forces *(French)* 80—42061
composite glass shells, bonded joint efficiency during external hydrostatic pressure cyclic loading 79—57079
composite glasses, high strength, prod. by overlayering 80—89193
composite material, cubic arrangements of spherical particles in isotropic matrix, effective conductivities 78—55547
composite medium, two-component residually stressed, elastoplastic crack model *(German)* 78—90790
compound arbitrary anisotropic body, stress singularity, composites appl. *(Russian)* 80—33455
compressed laminar structures, stability *(Russian)* 79—18759
compression testing fixture, new 77—77688
concrete, prestressed, low-temp. tensile strength and linear expansion coeff. of reinforcing steel 80—30051
concrete, prestressed beam, fatigue strength of cold-worked non prestressed reinforcement 79—96123
concrete, reinforced, failed slabs, nonlinear analysis by finite element method *(Japanese)* 77—42785
concrete, ribbed compression reinforcement, ultimate strength anal. of lapped joint 79—96086
concrete-polymer modifications, unsolved materials properties problems 77—4763
conference, nonmetallic materials and composites at low temps., Munich, Germany, July 1978 80—22139
connectivity and piezoelectric-pyroelectric composites 78—80290
constant temperature front advancement in composite bodies 77—14884
constrained viscoelastic damping composites, noise and vibration insulation 80—83743
constrained zones at singular pts. of inclusion contours, method of caustics 77—51003
contact problem involving a linearly deformable base reinforced with finitely large cover plates 80—14631
copolymer, graft or block, multiphase composite systems, struct., colloidal behaviour *(Chinese)* 78—73088
crack eminating from circular hole, mixed-mode crack anal. using conservation laws of elasticity 80—84239
crack extension micromechanism 80—108566
crack growth, 3-D geometric effects, implications for composite material structures 80—10204
crack growth, conc. criterion 80—65146
crack stress singularities for crack meeting interface 77—3776
crack tip fatigue behaviour and stress state study *(Japanese)* 80—28470
cracked composite full-planes, stress singularities 78—34077
cracked composite materials, finite element stress anal. 78—34083
cracked elastic surface layer bonded to half-space, fracture anal. 79—27586
cracks, Griffith, at interface of two bonded dissimilar elastic wedges, stress field, inverse Mellin transforms 80—53718
with cracks, periodic problem *(Russian)* 77—50987
cryogenic structural materials 77—17989
cubic arrays of spheres in dielectric matrix, permittivity 78—56415
cylinder, circular, transversely isotropic, concentrated loads, 3-D anisotropic elasticity theory 80—83734

composite materials continued
cylinder, circular transient thermal stress anal. 78—79217
cylinder, composite of compressible elastic materials, second order torsion 79—72808
cylinder, mechanical loading, photoelastic stress anal. 78—26031
cylindrical rod, approx. one-dimens. thermal conduction 77—11117
cylindrical rod, periodic structure, torsional vibrations, interfacial elastic parameters 80—96215
cylindrical shell, stiffened and stable, rational design using elasticity 80—5954
cylindrical shells, probability anal. of stability, mass minimisation 78—42553
cylindrical shells, reinforced, stability loss under isotropic external pressure 78—42554
cylindrical shells of viscoelastic material, natural transverse vibrations 80—43660
cylindrical tubes, compressible, wire-layer reinforced, inflation and extension 79—3922
cylindrical wound shell with viscoelastic core in axial compression, optimisation 77—4821
damage studying by NDT 80—66735
Debonding of circular second phase particles 78—5688
deformability surfaces 78—23792
delamination visualisation, US pulsed schlieren method 79—70289
deposition by electrolysis *(French)* 77—73375
development and use in USSR *(Russian)* 78—52696
diamond composite with Cu-Ti matrix, microstresses, X-ray diffr. exam. 78—56679
diamond-metal strip, strength props. 79—61678
diaphragm for loudspeaker, B-Ti, preparation by physical vapour deposition *(Japanese)* 80—58883
dielectric, elastic, containing 2 rigid spherical conductors, electrostrictive stress conc. 77—23883
dielectric and optical props., electrostatic polarisability calc. 79—51507
dielectric-loss meas., interfacial polarisation and loading factor effects 80—2693
diffusion theory of medium theory 78—22884
Dislocation creep in particle-strength systems 78—3182
disordered two-phase, site percolation approach to transport props., effective medium theory 77—61032
dispersed material, thermal diffusivity 79—55943
dispersion hardened, soln. method of synthesis and crystn. 78—3076
dispersion hardened metallic matrix composite, powder metallurgically produced effective interparticle distance effects *(German)* 78—52727
dissolution of precipitate plates, one-phase diffusion controlled, in planar composites 80—15244
double-skinned composite circular cylindrical shells failure under external press. 78—75078
double-skinned composite circular cylindrical shells under external press., experimental behaviour 78—75077
dough moulding compound, exam. of tensile and fatigue props. 79—20152
dynamic anal., review and computer programmes 77—50946
dynamic stabilization of multiphase media subjected to vibrations under low gravitation conditions 80—7511
effective bulk dielec. const., analytical props. 78—56414
elastic, with periodic structure, homogenisation, functional and appl. *(French)* 77—67292
elastic characts. by vibr. tests and discrete conservative model calcs. *(French)* 80—45337
elastic constant estimation, elastic wave scatt. theory 80—34114
elastic inclusions in anisotropic solids, generalised plane problems 77—17823
elastic interface waves involving separation 77—80100
elastic laminated composites, mixture theory for dynamic response 79—49049
elastic laminated composites, transient wave propagation 79—50630
elastic longitudinal waves, diffr. at elastic circular inclusions (fibres) *(Russian)* 78—63368
elastic media, crack retardation at boundary *(Russian)* 79—23275
elastic medium with arbitrarily shaped inclusions, effective moduli 77—72172
elastic mixtures with long range spatial interaction 79—12600
elastic moduli of two-component systems, comment 80—23896
elastic modulus and expansion coeff., approx. method *(Russian)* 77—39681
elastic multilayers systems, elastic fluid motion *(Russian)* 79—46211
elastic nonlinear media, effective characteristics *(Russian)* 77—58553
elastic properties, self-consistent field approx. 78—51078
elastic properties determ. methods, review 77—42746
elasticity parameters, meas. reliability establ. 77—52574
electrical contact material, sintered, corrosion under tropical marine climate 78—11366
electrolytic Fe based composite metal-powder coating structure *(Russian)* 79—83170
electrophotographic two-component developer discharge and contact interaction *(German)* 78—62258
electroplated diamond-composite abrasion-resistant coatings 79—61737
electrostrictive resonators, finite element simulation 78—59237
EM wave propagation, self-consistent theory 78—56442
endosseous implant material, radiation processed alumina-polyacrylic acid composite 77—60308
epichlorohydrin/bisphenol A epoxy polymer concrete, viscoelastic props. 80—45340
epoxy, Ag powder filled, thermal cond. below 3K 78—51757
epoxy, reinforced, outgassing rate in vacuum, control by pretreatment 79—40583
epoxy composites, dynamic crack propag. 80—40497
epoxy impregnated superconducting composites, mech. props., strain effect at 4K 80—25822
epoxy resin cured with composite curing agents, arc resistance *(Japanese)* 78—92371
epoxy-rubber particulate composite, toughness and fracture mech. 80—71727
epoxy/graphite composite and cured epoxy resin, thermal expansion and swelling 80—92450
equivalence conditions from thermodynamical ratios *(Russian)* 79—9197
failure analysis of composites with stress gradients 80—10199
failure criteria, for complex loading 80—81206
failure prediction, macroscopic anal. 80—10200
fatigue and fracture, lecture *(Japanese)* 77—8928

composite materials continued
- fatigue life and static strength testing, sample size estimation 79−91867
- fatigue strength determ. under plane stress state condition 80−16475
- fatigue testing, critical factors for frequency dependent processes 77−8903
- ferroelectric phase formation energy in inhomogeneous inclusion under press. 77−12338
- ferroelectric-nonferroelectric composite, permittivity calcs. 77−85659
- fibre reinforced, applicability of generalised continuum theories 77−859
- fibre reinforced plastics, exam. of strength criteria 78−75105
- fibreboard, made from Asplund pulp-PMMA composite, props. *(Japanese)* 80−7664
- fibrous composites, stationary transfer, effective heat conduction coeffs. 80−64337
- fibrous heat treated composites, thermal stress anal. 77−46943
- filler containing beam reinforced three layer plates *(Russian)* 80−43613
- finite element anal., computer simulation, stress and strain props. 77−3717
- flat belt drive material, tension relaxation under simulated drive conditions 78−56688
- flat rectangular anisotropy plates, supersonic flutter 77−62196
- flat-belt-drive materials, bonding of birefringent coatings 77−77652
- flexible spherical shell, dynamic and static loss in stability 77−52439
- flow through porous medium, Rayleigh-Taylor instability 80−69912
- fluid impregnated solids, elastic and dynamic response regimes 78−90713
- flywheels, filament wound composite materials, characterisation 80−81097
- forced vibrs. shell, viscoelastically damped, filled with pressurised liq., forced vibrs. 78−9584
- fracture, appl. of exptl. methods 80−11869
- fracture, elastic mismatch and interfacial bonding influence 80−40506
- fracture and fatigue, review 78−68781
- fracture behaviour estimation using simulation model and finite element method 77−42777
- fracture mechanics 80−10202
- fracture time under tensile loading 78−88521
- friction and bearing materials, development, friction and wear theory, review 80−60979
- fusion reactor, three-dimens. solid finite element anal. for simulating composite windings 78−55003
- fusion reactor liners, thermal fatigue tests 80−32460
- generalised continuum theory derivation 77−853
- glass and ceramic developments for electrical industry appls. 79−78925
- glass bead epoxy resin, direct obs. of debonding at crack tips 80−3167
- glass bead-reinforced epoxy resin composite, bulk and shear elastic props. 78−6959
- glass ceramic, machinable, elastic moduli press. and temp. derivatives, specific heat 78−52873
- glass ceramic, second-order microstresses 78−27468
- glass filament reinforced, water solvent effects on S-glass 77−4889
- glass microsphere reinforced, composite, mech. charact. calc. 78−64578
- glass reinforced plastic orthotropic shell and filler system, compactile performance 78−5659
- glass shells with metallic inserts, structural strength 80−35283
- glass transition model 77−84901
- glass-ceramic, aligned, hot extrusion method for prep. 77−32552
- glass-epoxy composite, elastic moduli, effect of particle shape 78−15444
- glass-epoxy plate, twisting in large deflection regime 77−23870
- glass-metal composites, elec. cond. 80−10970
- glass-sintered metal, fracture energy, direct meas. *(French)* 80−104376
- glass/Cu-polymer compound powders, prep. and corona charging props. *(Japanese)* 78−19679
- glued members, low frequency acoustic flaw detector inspection 78−60954
- grain and phase boundaries between crystals, conf., Konigstein, Germany (Oct. 1977) 78−72762
- graphite, ATJ-S, strain response to mixed tension and compression loading 78−26032
- graphite based composite material, with ZrB$_2$ and SiC additions, prep., props., struct. 77−28775
- graphite composite aircraft structures, flaw detection by US methods 78−44288
- graphite composites containing refractory carbides, electrochem. etching for microscope section preparation 77−28949
- graphite dispersed Al-Si, wear characts. *(Korean)* 80−93658
- graphite filled PTFE, carbon aspect ratio effect on friction and wear characts. 77−59945
- graphite particle-Al alloy composite, improved damping capacity and machinability 77−4786
- graphite particle-Al alloy composite, prod. by pellet method, and mech. props. 78−27454
- graphite-based, survey 78−56609
- graphite-epoxy, for spacecraft communication antenna fabrication 78−4063
- graphite-epoxy, Saint-Venant's principle and end effects 78−38198
- graphite-epoxy composite, hydrothermal ageing 77−21189
- graphite-epoxy composite, open-section stiffened compression panel, buckling and struct. efficiency 77−35061
- graphite-epoxy plate, twisting in large deflection regime 77−23870
- graphite-SiC-FeSi crucible mat., oxidation loss and wettability of inorganic fluxing materials *(Japanese)* 78−84755
- Green's functions 78−77712
- Griffith crack, interface of layer bonded to half plane, approx. method 78−79258
- gum and C black filled vulcanisates, rubber, natural and styrene/butadiene, unixial and equibiaxial fatigue 79−8363
- harmonic waves in 3-D elastic composites 77−891
- heat conductance, combined numerical method 78−63261
- heat conduction, prismatic rod with concentric heat generating core 79−32183
- heat conduction in composites, Sturm-Liouville problem eigenvalue bounds 79−50568
- heat conduction lattice model 79−81682
- heat exchange during rupture *(Russian)* 77−48517
- heat transfer on layered composites 78−71264
- heat-resistant, creation of matrices with operating temp. of 1100°C *(Russian)* 77−55913
- heterogeneous, mechanical properties analysis, influence of prestress and limited deformation 78−38205
- heterogeneous matrix system, thermal cond. 78−9555

composite materials continued
- heterogeneous matrix systems, calc. of thermal cond. coeff. *(Russian)* 77−24455
- high precision triangular laminated anisotropic cylindrical shell finite element 78−79206
- high-temperature materials, technological requirements, R and D, report 80−45222
- holographic, nondestructive testing of brazed, and epoxy bonded honeycomb panels 78−40017
- Homalite-epoxy duplex specimens, crack arrest study via dynamic photoelasticity 78−31515
- honeycomb based composite, deform. theory 80−35250
- HTGR fuel rods, carbon-carbon composites designed for high weight and low strength 77−71684
- in situ composites, crystallographic relation determ. by texture goniometry 79−86654
- in-plane shear charact. 80−35251
- information service, Soviet 78−8182
- inhomogeneous anisotropic body, stress singularity near rib *(Russian)* 80−19243
- inhomogeneous systems, hysteresis of phase transitions, general soln. 78−59926
- inorganic particle reinforced thermosetting resins, chem. bonding, mech. bonding and compression tests 77−59735
- insulating and conducting particles mixture, percolation problem 78−60097
- interface crack, singularity anal. 80−10201
- IR segmented composite window design 80−106621
- isotropic composite material containing spherical inclusions at nondilute concs., effective elastic moduli 78−67037
- Kevlar-epoxy, for spacecraft communication antenna fabrication 78−4063
- lamellar, strain hardening of matrix, mechanism *(Russian)* 77−59801
- laminated composite media, crack tip propagation, model by two-dimens. mixture theory 79−10528
- laminated half space under influence of vibrations *(Russian)* 78−63370
- laminated plates, dynamic response variational method, general functional 77−3770
- laser beam determination, of elasticity-compressibility modulus, during compaction 79−43542
- layered, continuum modelling of dynamic behaviour 77−887
- layered composite containing a crack, impact response 77−50991
- layered composites, heat conduction eigenvalue problems 80−74702
- layered composites, US spectrum anal. rel. to NDT 77−81357
- layered elastic composites, harmonic wave frequency estimation, eigenfrequency bounds 79−46252
- layered elastic quarter space, transient contact shear stress under anti-plane loads 77−14936
- layered half-space, transient response under reciprocating anti-plane shear load 77−14935
- linear reinforced composite material with anisotropic structural components *(Russian)* 79−30250
- linearized theory of elastic wave propagation in initially stressed bodies *(Russian)* 78−83318
- macromolecules, epitaxial crystallisation, review 79−42409
- magnetic susceptibility, inhomogeneously random composite 78−19200
- magnetoelectric composite, growth from melt, gas bubble form. ahead of solidification front 79−29044
- manufacture by explosive welding *(German)* 79−43171
- martensitic memory alloy composite, for prefabricated constructions *(Russian)* 77−21059
- matrix impurity distrib. in melt crystallisation *(Russian)* 80−100277
- mechanical behaviour, book 80−94935
- mechanical properties, theory, review 80−64392
- mechanical strength, density depend. *(German)* 78−94592
- mechanical strength, internal stress depend. on density gradients *(German)* 79−1105
- melt infiltration of porous materials, math. model 79−100089
- membrane, rectangular, consisting of strips, free vibr. anal. 77−39252
- membranes, composite, relaxation time, network thermodynamics formalism 78−68926
- metal fibre materials, thermal and elec. conductivities 78−10419
- metal gauze reinforced porous permeable mats. with prearranged struct., prep. 78−68652
- metal matrix, state of the art review, book 78−72706
- metal particle composite, physical and optical props. 78−56528
- metal reinforced, thermal activity, diffusivity, cond. meas. method 79−37141
- metal sheet/composite material bonded, finite element anal. of patched cracks 80−10192
- metal spheres in dielec. medium, optical props. using effective medium theory 77−24811
- metal systems, high-temp., conf., Helsinki, Finland (June 1975) 77−52295
- metal wire reinforcing rolled glass 80−104107
- metal-composite shell, three-layer, stochastic formulation of optimisation using heuristic methods 80−38268
- metal-containing plasma polymerised fluorocarbon films, deposition, struct., and polymerisation mechanism 79−78928
- metal-glass mats. alloyed with Cu, powder prep. and props. 78−72912
- metal-insulator composite films, optical props., rel. to solar collector appls. 78−72622
- metallic, thermal fatigue, effects of inclusions 80−81183
- metallopolymer composite with var. elec. cond. 77−43676
- MgO-ZrO$_2$ ceramic reinforced with filamentary crystals, mech. and thermal props. 80−45262
- micaceous-crystalline material, cast, prep. and props. 77−12591
- micro- and macro cracks 80−11767
- microballoon reinforced plastics, acoustic and mech. props. rel. to hydrophone applic. *(Japanese)* 77−7793
- microcrack enlargement in heterogeneous materials, conc. criterion 80−11769
- microwave absorbing ferrite-dielectric composite 77−7880
- mineral filled plastics, US meas. 77−40482
- modelling as interpenetrating solid continua, plane wave solns. 78−13895
- moduli of 2-phase linearly elastic composite by differential scheme 77−39227
- molten metal binary mixtures with wide immiscibility range, gravitational layering of components *(Russian)* 80−104092
- mortar specimens, repeated impact bending load study *(Japanese)* 80−93622

composite materials continued
mullite single crystal reinforced refractory with phosphate binder, compressive strength *(Russian)* 77—44293
multicomponent polymer homopolymer blends, macroscopic phase separation 80—45289
multilayer cylindrical shell, elastic filler, strength and stability under combined loading, mass minimising 77—65699
multimodulus material, apparent flexural modulus and strength 77—28845
multipoint moments meas. by optical struct. anal. 79—15910
NDT methods 80—11867
nonlinear elasticity, extremum principles, appl. to composites 78—51072
nonlinear multimodulus orthotropic material, nonsymmetric compliance matrix theory 78—26032
nonlocality and size effect, composite mechanics 77—65675
nonuniform medium, model 80—38254
nuclear fusion reactor materials development trends 77—46401
nylon-quartz fibre support for low temp. mag. suscept. meas. 78—65947
optical and dielectric properties, theory 79—56753
optical properties, review 78—56496
orthotropic composite model materials, photoelastic calibration 80—87715
orthotropic materials design for stress optimisation 78—63291
orthotropic plate, twisting in large deflection regime 77—23870
orthotropic plates, large deflection behaviour anal. 79—98605
orthotropic sandwich plate containing part-through crack under mixed mode deform., stress intensity factors 78—34068
orthotropic sandwich plates, simply supported, forced vibrs. 77—46861
overall elastic moduli prediction 80—75285
particle dispersed composite, fatigue life anal., reliability concept *(Japanese)* 79—29200
particle-filled polyurethane resin, tensile strength, particle size effect 77—73305
particulate, mechanical model 78—51105
particulate brittle composite, fracture, theoretical aspects 79—70156
particulate reinforced epoxy resin model specimens, Young's modulus, expt. study *(Japanese)* 78—56683
paste-like composite with polymer binding, rheological props., wall effect 77—47072
penetrant, new, for composite and adhesively bonded struct. 77—32739
percolation, in a thin ply of unidirectional composite 79—42511
perfectly disordered, linear elasticity theory 77—862
permanent magnet, magnetostatic and exchange interactions 77—69536
permanent magnets, elastic, parameter anal. *(Russian)* 78—29132
phenolic novolac resin-rubber mixture, glass transition, mixing ratio effect *(German)* 79—77732
phosphate containing materials, technological prod. processes, review 80—97452
physical nature of fracture 78—80653
physical properties, review 77—4720
piezoceramic multielectrode bar, equivalent elec. cct. 77—46877
piezoelectric medium, integral parameters at longit. shear *(Russian)* 78—30232
piping conveying swirling liquid, free harmonic wave propagation 77—84187
plane deformation for composite with longitudinal cracks 78—67096
plasma spraying, coatings and composite materials 78—3247
plasticity, field theory, integral presentations of second-rank tensors 80—69690
plastics, filled and reinforced, optical const. determ. 78—19472
plate, composite layered, loads and stresses 79—94570
plate, natural vibration investigation using finite element anal. 77—68495
plate, optimal laminate design for max. fundamental freq. 77—50956
plate like inclusions, plastic props., sintered Al-Al_2O_3 results *(Russian)* 80—58923
platelet reinforced media, effective moduli and isotropic props. 80—40422
plates and shells, construction elements, review of physical props. 78—67056
Plexiglas 80—66592
plexiglass composite, long term strength and durability 80—75294
PMMA based composite (acrylic bone cement), effect of $BaSO_4$ and glass particle dispersions, on fracture behaviour 78—76753
PMMA-metal oxide composite powder, prep. and props. *(Japanese)* 78—95708
PMMA-mortar, thermocatalytically polymerised, fracture morphology and mech. props. 78—27595
PMMA-wood polymer composite, dielec. prop. at low temp. *(Japanese)* 78—31545
PMMA/PVC, cracking in layered composites 78—95808
Poisson coefficients, allowable values 80—64370
polyamide 6, glass fibre reinforced, fatigue fracture types under circular flexural loading *(German)* 79—70170
polycarbonate blends, yield and deform. behaviour, impact modification 77—36572
polyester polymer concrete, longitudinal deform. modulus study is creep conditions *(Bulgarian)* 80—71685
polyester resin concrete, effects of styrene-unsaturated polyester ratio on props. *(Japanese)* 80—89299
polyester-polyurethane semi-interpenetrating networks, mech. props., morphology 80—45362
polyethylene, ultraoriented, fibrillar struct. 77—89389
polyethylene and ion-exchange resin composite for radioactive waste solidification, ^{137}Cs leaching 77—65275
polyethylene implant-bone composite interfacial strength, porous high density polyethylene 78—31979
polyethylene-Fe, wear resistance on steel counterbody, exam. 78—68826
polyhedral sandwich domes, elastic behaviour, failure, practical investigation and numerical simulation 78—59309
polymer based composite propellants, solid 79—43431
polymer blends and composites, behaviour, review 78—76626
polymer composite anisotropic plates, stress conc. around holes with shear strain taken into account 80—43618
polymer impregnated concrete, computer simulation 78—31375
polymer impregnated coral, by-product of commercial gamma irrad. plant 77—59794
polymer impregnated gypsum cast, mech. props. 79—100107
polymer latex film composite, glass transition temp. determ. using thermomech. curves 80—75342
polymer matrix composites, component interaction mass spectrometry investigation *(Russian)* 80—35511

composite materials continued
polymer-cement composite, review 79—70039
polymer-concrete composites, civil engineering appls., technical, processing, economic merits 79—11545
polymer-containing metal-filled lubricant, tribological study on steel 80—104301
polymeric, thin-wall tubes, rupture time determ. 80—64473
polymeric composites, sliding wear mechanisms at metal surfaces, microscope obs. 79—87742
polymeric interphase, physico-chemical problems 80—16262
polyorganosiloxane-asbestos composites, high-temp. transitions 79—38802
polystyrene composite with mica flakes, TDC meas., interfacial polarisation 78—64316
polystyrene-polybutadiene block copolymer, oriented microlattice obs. 78—2025
polystyrene-wood, polymer composite, dielec. props. at low temperature range *(Japanese)* 78—95541
polystyrene/polyethylene blend, particle dimension as function of melt viscosity added graft copolymer conc. 77—52279
post buckling analysis of composite plates 77—42756
powder metallurgical parts, development, and manufacture of semifinished products 80—50578
powder metallurgy *(German)* 80—20849
powder reinforced metal composite with glass microsphere filler prod. in space 78—52726
powder strip shaping device, deform. zone configuration effects 77—24979
prealloyed powder blending, composite materials fatigue and tensile props. *(French)* 80—20850
preparation under microgravity conditions, stability during melting, thermal soak, solidification *(German)* 80—7521
pressure vessel, holographic exam. 77—28957
pressure vessels with hardening metal liners 80—7655
prism under partial compression, photoelastic anal. 79—18852
propag. of cracks, effect of humidity 77—86133
propergol, rheological props. during polymerisation *(French)* 78—23762
PTFE impregnated porous bronze, coeff. of friction, temp. effect 78—64737
PTFE-C black composite form. monitoring by electrochem. method 77—36446
PTFE-metal composites, polymer mol. diffusion, polymer-metal reaction 80—11889
PVC, asbestos reinforced, CIR/Palram process preparation, mechanical and thermal properties measurements 79—66106
PVC composite, MBS type multifunctional impact modifier effect on mech. and rheological props. *(Polish)* 78—52751
PVC metal particle composite, effect of size, shape, and oxide content of metal particles, on segregated network form. 79—20021
PVC-Cu composite, annealing effects on elec. resist. 78—68060
PVC-Cu composites with chemically deposited ultrafine copper particles 80—93534
quartz dental composites, acrylic acid grafted on particles by gamma-radiation 80—66840
radioactive waste, high-level, evaluation of products for solidification 77—61555
random elastic sphere distrib. in elastic matrix, effective bulk and shear moduli 80—99927
random functions theory appl. to microinhomogeneous media *(Russian)* 78—63280
random particulate composite, US wave propagation, velocity as function of frequency and volume fraction of inclusions 80—59583
refractory, ultra-lightweight, thermophys. characts., moisture effects *(Russian)* 77—55921
refractory wear-resistant coatings, composite struct. develop., props. 77—63618
reinforced, semi-microscopic theory of plastic deformation *(Russian)* 77—23893
reinforced composite pull-out forces, effect of matrix stresses 77—21334
reinforced concrete structs., initial stress approach to nonlinear dynamic anal. 77—83036
reinforced cylindrical shell, nonuniform thickness, optimisation 77—68465
reinforced open cylindrical shells, bending stability 79—41581
reinforced organic composite, graphite, or C-C, ablation, mathematical modelling 79—41564
reinforced plastic cylindrical shells, optimal design under dynamic constraints 80—102996
reinforced plastics, design guide 77—21087
reinforced plastics, failure subject to short-term tensioning 79—61725
reinforced plastics, load-bearing capacity, effect of one-sided heating 80—81135
reinforced plastics, low frequency acoustic flaw detector inspection 78—60954
reinforced plates, heat conduction and thermoelasticity eqns. *(Russian)* 77—75795
reinforced rectangular plate, compressed in two directions in a manner conducive towards stability 78—22289
reinforced shell, in plane stressed state, strength characts. 79—14264
reinforced shell of revolution, failure in bending 79—90185
reinforced tube, bending and flexure 78—51076
reliability exam. of mech. strengths and fatigue characts., review 80—11762
residual stresses in shells of revolution, cut-out element method glass-plastic composite, thermoelastic residual stresses in shells of revolution, cut-out element method 80—38271
resin, Langmuir type model for anomalous moisture diffusion 78—67867
resin impregnated glass tape, friction and rheological props. 77—63806
resin mortar, strength anal. by reliability concept *(Japanese)* 78—31466
rib stiffened constructions, design criteria 80—102977
ribbed cylindrical casings, stressed-deformed condition under external hydrostatic press. 78—6996
ribbed multilayer cylindrical shells, stability and optimal design 80—58949
ring under one sided heating, strength testing assembly 79—96260
ring-stiffened filled cylindrical shell, loaded, stress-strain state 79—41582
rod, composite, stress deformation state calc. *(Russian)* 79—64527
rod, semi-infinite, wave propagation 80—10180
rod, small deformations, initial stresses effect 78—63284
rods, strongly anisotropic, dispersion of longit. waves *(French)* 78—12573

composite materials continued
rotating composite inhomogeneous disc of variable thickness with axial hole, stresses 79—94484
rubber-epoxy resins, heterogeneity analysis, light scatt. and statistical methods 78—2024
rubber-modified glassy polymers, thermal stresses 77—77567
S glass-Ni sphere composite, exam. of crack shape and fracture toughness 78—72886
sandwich composite beams, stress distrib. meas. under four-point bonding, multilayer builtup theory 80—96190
sandwich plates, simply supported in shear, critical stresses *(Polish)* 79—32247
semi-infinite medium with periodic surface temp., contact resistance, heat cond. using Heaviside operational method 78—9549
separation failure 78—9610
shear modulus, determ. by twisting tests on circular specimens 80—25752
shell, cylindrical, composite with viscoelastic filler, optimisation w.r.t. long-term stability 79—18760
shell, cylindrical, torsional vibr. in mag. field 80—48624
shell, cylindrical composite, with viscoelastic filler, parametric oscills., dynamic instability *(Russian)* 78—38221
shell, multilayer composite, optimisation, buckling under stability and vibr. conditions *(Russian)* 80—53667
shell, optimization model including statistical parameters 78—22271
shell, orthogonally stiffened, buckling eqns. 78—26063
shell, orthotropic, cylindrical, with elastic core, stability 77—65701
shell, rotation under axisymmetrical strain, elastoplastic edge effect 79—94509
shell, stiffened, buckling under destabilizing loads including torsion 78—26062
shell, thick walled, composite radial bonding efficiency 80—99926
shell of revolution high modulus material shape of wound membrane rationalization 77—27473
shell with multiple stiffener sizes, minimum weight design 78—38218
shells, cylindricals, composite, buckling and vibrational response to axial compression 80—64423
shock compression at 30 kbar, expansion adiabats 80—66592
short sandwich beams, vibrs. 77—75842
Si-SiC-Ni based superalloy reaction, at elevated temps. 80—3287
silica paricle filled epoxy resin, mech. props., fracture by slow crack growth 77—40443
simulation of tensile behaviour and fracture void initiation *(Japanese)* 78—52948
sintered, microstrained state, opt. polarisation investig. 78—11476
sintered composite-liq. metal interaction, mass transfer eqn. approx. soln. 78—67262
sitall base composites, antifriction props. 77—77591
Sitall-based composite mat., grinding 77—63822
skin technology, industrial appl. of space processing 79—28991
slab, spatially reinforced, optimisation in stability problem 80—102978
small particle composite, optical properties from periodic multiple scatt. theory 78—56444
small particle composites, optical props. 78—56445
small-particle metal-insulator composites, anomalous far IR absorption 80—71427
soil-cement mixture for earthfill dam embankment *(Japanese)* 78—39729
solid propellants, fracture criterion, fracture time computation 78—75106
spacecraft polymer composite matrix materials, space radiation effects evaluation 80—70263
spatially reinforced, viscoelastic props. determ. using averaging methods 80—102973
spectral selectivity of composite materials, optical props. and fabrication of composite solar absorbers, review 79—74520
sphere, composite elastic nonhomogeneous, with concentric spherical inclusion, opposite couple stress, displacement 79—94494
spherulite, two-phase, ht. cond. anisotropy 78—2316
stability of multilayer composites under inelastic deformations 80—99944
stability of viscoelastic rods and shells under loads that decrease with time 80—69700
steel, austenitic, heat-resisting, deformation and fracture rel. to grain-boundary reaction nodules 78—80591
steel, martensitic, welded composite vessels, glass fibre reinforced plastic wound, struct. strength 80—97552
steel, stainless, reinforced glass matrix, vibr. damping anal. rel. to internal friction 80—40413
steel, stainless, two-phase $(\alpha+\gamma)$, twin-related lath occurrence rel. to fracture elongation 77—90443
steel, stainless-glass composite, sintered, corrosion resistance 77—77608
steel (alloy)-TiC (70, 30 wt.%) composite, sintered, wear resist. 80—100815
steel base composite, sintering, mech. props. 77—21061
steel core/sheath tube system, non-fracturing core, stress transfer mechanism 77—52454
steel matrix-bronze surface, water lubricated bearing material, manufacture, friction, corrosion and erosion 78—11341
steel-based, corrosion behaviour of composite materials in N_2O_4 oxidising atmospheres *(Russian)* 80—76421
steel-concrete composite T-beam, third point loading tests, ultimate flexural strength determ. 77—86252
steels, self lubricating composite, frictional props., Ag-Cu-Zn-Cd lubricant 78—11340
stochastic fracture models, and strength test results statistical anal. 80—64470
stochastic fracture models, appl. to composites and polymers 80—10198
stochastic struct., complex dynamic moduli using conditional averaging technique *(Russian)* 79—27513
stratification of composite materials in regions of compression *(Russian)* 77—36613
strength, review *(Japanese)* 78—39850
strength and deformation anisotropy, numerical characts. 80—38285
strength criteria, appl. to glass plastics 80—10208
strength criteria, stress, anal. *(Russian)* 80—1482
strength design *(Japanese)* 77—9039
stretching, stress distribs. 80—58931
stretching, zone of disturbed stress state calc. 80—39206
structural anisotropy in viscoelasticity 77—86073
structural design and appl. *(Japanese)* 77—8796
styrene polymers, elastomer toughening, grafting techniques 78—35347

composite materials continued
styrene-butadiene block polymers, multiphase systems, struct., props. 77—31600
styrene-butadiene-styrene triblock copolymer, US relax. 77—89502
superplastic flow, role of interphase-boundary dislocations, ledges and diffusion 78—11295
surface, flame propagation velocity rel. to thermal props. *(Russian)* 80—7797
surface charact., combined ion scattering spectrocopy, SIMS, SEM, energy dispersive X-ray techniques 79—43702
surface thermoelastic waves in the regular layered half space *(Ukrainian)* 79—50625
symposium, USA-USSR, 1978, on composite materials fracture 80—11766
T-beams, repeated loading effects 77—86253
temperature field on periodic heating *(Russian)* 77—42715
tensile strength eval. under uniaxial tension under pressure 78—19828
testing with fluctuating components using monoenergetic electrons, sensitivity 79—79209
tetrafluoroethylene-vinylidene fluoride mixture, in epoxide-diphenylene propane resin, exam. of temp. depend. of stress relaxation, viscoelasticity 80—11688
thermal conduction processes, nonstationary, numerical simulation *(Russian)* 80—92016
thermal conductivity, calc. for material with spheroidal inclusions 77—28055
thermal conductivity, effective 80—54447
thermal conductivity and thermal expansion, conference, Chicago, USA (Nov. 79) 80—31425
thermal conductivity range, knowing ranges for components 78—2313
thermal plasma engineering in metallurgy, inorganic materials technology 78—3070
thermal properties, effective, bounds determ. 79—23745
thermal stresses investigation, using polymer models 80—40639
thermoelastic condition of a body containing a heat-evolving inclusion *(Russian)* 78—9563
thermoelectric heterophase material with artificial anisotropy of thermo EMF 77—89781
thermoelectric materials, thermoelec. props. degraded by strengthening additive 79—47114
thermographic technique, for examining damage extent 79—43540
thermography, NDI method for damage detection 80—35445
thermoplastic based composites, mean stiffness 80—11693
thick walled composite tube manufactured by polymerisation of inner cylinder 78—46916
thick walled rings, calc. taking into account deformation nonlinearity 77—58565
three phase including void phase, phase relationship 77—25036
three phase sphere and cylinder models soln. for effective shear props. 80—25749
three-layer cylindrical shells, initial stressed and deformed state 80—102974
three-layer structure, axisymmetrically driven, acoustic radiation 78—1507
three-layer structures, calc. of antisymmetric modes 77—50975
Timoshenko type shells of composite material, nonlinear theory *(Russian)* 78—63283
transient hygrothermal stresses, coupled diffusion of heat and moisture 80—33451
transport properties of arrays of spheres, exact solns. 78—56120
transversely isotropic composite with penny shaped crack, stress intensity, crack energy 79—98660
tube, collapse under external press. and surface tension forces 77—58572
two component granular composites, pole spectrum calc. 79—69764
two phase, depend. of texture and microstruct. on yield stresses of components 79—91697
two phase diffusion model 79—55936
two-component materials, thermo-viscoelastic theory 78—73854
two-component media, macrocrack problem *(Ukrainian)* 79—98666
two-phase elastic isotropic bodies, dynamics eqns. for composites 80—33461
underwater acoustic reflection props. 79—94394
unidirectional, three-dimens. fracture 80—64471
unidirectional composites, two component finite element for determining transverse loads *(German)* 79—49043
uniform thickness, analysis of determ. methods of shear moduli 77—63873
urea-formaldehyde resin/wood materials, book 80—73114
US inspection system for aircraft materials 80—81274
US velocity rel. to mineral content 80—45962
US waves, scatt. coeff. and uel. dispersion 79—86844
viscoelastic creep, self-consistent estimates 78—13921
viscoelastic layered composites, wave propag., dispersion and dissipation effects 80—102982
viscoelastic properties modelling 78—75082
viscous composite, steady creep bending stresses 78—71280
vitroceramic-metal, development, Spacelab appl., mech. props. *(French)* 78—92229
Washington degradation test, aggregate behaviour 77—28955
wax-graphite composite, electrical cond. 79—24044
wax-graphite composite, specific capacitance, temp. and grain size depend. 80—50286
wear of water-lubricated composite materials 80—60984
wedge, composite, plane elasticity stress singularities 80—38262
wedge, plane composite, singular eigenfunctions for plane harmonic problems 80—79206
wedge, stress state anal. near vertex *(Russian)* 80—19242
windmill blades materials and design 79—43719
wood dimensional stabilisation, with 2-hydroxyethyl methacrylate and MMA *(Japanese)* 80—7532
wood stabilisation, with ethylene glycol and isocyanate *(Japanese)* 80—2982
wood-PMMA composites, temp. depend. of viscoelastic behaviour *(Japanese)* 77—77541
wood-polymer composite, dynamic viscoelasticity and modulus *(Japanese)* 78—59356
X-ray determ. of elastic moduli *(German)* 79—91876
yarns, multi-filament, twisted, tensile props. calc., modified Platt's equation *(Japanese)* 80—5985
zircon bricks, thermal conductivity meas. up to 1200°C *(Japanese)* 78—95193

composite materials continued
- Ag particles embedded in dielec. KCl medium, search for maximum metallic resist. 80—107756
- Ag-Cu composite wires, size effect and interface contribution to diamagnetism 77—69490
- Ag-polystyrene powder mixture, hot-pressed, elec. resist. 77—32556
- Ag-SiO_2, film, optical props., appls. 77—754
- Al alloy matrix, reinforced with fibrous and particulate nonmetals, wear, friction 77—4758
- Al smelting cathodes, comp. and props. 77—28740
- Al/Sn, kinetics of adsorption softening of solid interface *(Russian)* 79—61619
- Al-Al_2Cu, eutectic composite, abrasive fragmentation *(Czech)* 80—30110
- Al-Al_3Ni, eutectic composite, abrasive fragmentation *(Czech)* 80—30110
- Al-Al_3Ni eutectic composite, structural response to shape variations 79—83190
- Al-AlN, disperse system prep. by heterogeneous reaction in molten metal *(Czech)* 77—85964
- Al-Co(Ni)(Ru)(Rh)(Pd)(Ir), composite, paramagnetic resonance and electron-positron annihilation *(Russian)* 79—87314
- Al-Cu-Mg/mica particulate composite mech. props. 80—100919
- Al-$CuAl_2$ lamellar composite, creep, microstruct. obs. 79—8331
- Al-$Fe_{78}Mo_2B_{20}$ wire composite, mech. props. 80—40441
- Al-graphite particulate composite, exam. of friction, wear and tensile props. 78—72890
- Al-powder based composite, hydrostatic pressing 77—63593
- Al-SiC cermet elasticity, porosity meas. by US means 80—81101
- Al-Si(9.3, 12) with graphite particles seizure resistance study using Hohman wear tester 80—89360
- Al-steel profiled composite, pulling from melt, mech. props. 78—3075
- Al-W composite, mixtures theory, physical constants determ. from experimental dispersion curves 80—45338
- AlB_2 flake reinforced composites, prep., props. rel. to aspect ratio, book contrib. 78—48366
- AlN thread-like crystals reinforced mullite-corundum ceramics, props. 80—108525
- AlN-Al_2O_3, phys. and mech. props. of hot-pressed 77—52275
- Al_2O_3, composite base ceramic coating, hot pressed, H_2 permeability 77—56164
- Al_2O_3, Mo-refined single crysts., fabrication 80—16250
- α-Al_2O_3 thread-like crystals reinforced mullite-corundum ceramics, props. 80—108525
- Al_2O_3-Cu composite, dispersion-strengthened, hardness, tensile strength and struct. 77—70063
- Al_2O_3-Cu composite, vapour deposition, microstruct., texture and surface topography 77—70001
- Al_2O_3-$MoSi_2$, for use as heating element, fabrication method and prop. *(Japanese)* 79—95989
- Al_2O_3-Nb composites, influence of gas impurities on solid-state bonding on annealing 80—11739
- Al_2O_3-NiCr composite, plasma sputtering of electroheating coatings, elec props. *(Russian)* 80—108350
- Al_2O_3-polymethylsiloxane composite, thermoreactive compaction 80—20879
- Al_2O_3-TiC, composite, fracture behaviour in three-point bending 80—60951
- Al_2O_3-TiO_2 (1 wt.%), with and without α-Al_2O_3 laminar crystals, bend tests 77—16531
- Al_2O_3-TiO_2 (1 wt.%), with and without α-Al_2O_3 laminar crystals, heat resistance 77—16532
- Al_2O_3-ZrO_2 composite, fracture toughness increase by microcracking in energy dissipative zone near crack tip 79—20156
- $3Al_2O_3.2SiO_2$-ZrO_2 composites, sintered, in situ-reacted, fracture props. 80—81158
- $Al_2O_3.3P_2O_5.5H_2O$-SiO_2 composite, binding and struct. 79—66030
- Au solar black, optical props., microstruct. influence 79—42937
- B-epoxy plate, twisting in large deflection regime 77—23870
- B_4C-Al composite moderator rods, production and props. *(Russian)* 79—18006
- BN composites, polymer impregnated 80—7526
- BN-SiO_2, sintered, oxidation kinetics 79—96171
- B_2O_3-Na_2O-SiO_2-Al_2O_3, effect of alumina dispersions on the thermal cond./diffusivity/stress resist. 80—39368
- B_2O_3-PbO(ZnO) glass-ceramic-cement composites, review 79—38783
- $BaTiO_3$, doped-undoped ceramic composites, sintering behaviour 79—100094
- $BaTiO_3$-Ni ferrite, piezoelectric-piezomagnetic sintered two-phase composite, magnetoelec. conversion 77—12181
- Bi_2Te_3-Sb_2Te_3 composite billet, diffusion during plastic deformation *(Russian)* 79—23767
- C, baked mix, optimum binder content estimation 77—73253
- C fibre reinforced plastic pressure vessel, immersion technique for acoustic emission detection 77—1902
- C reinforced metal sintered composite materials, form of C present *(German)* 79—95978
- C/C composite with S-modified pitch binder precursor, carbonisation and mech. props. *(German)* 77—44183
- C-C composite, oxidised, SEM study 77—52522
- C-C composite, structure model, Rosen model with fractional matrix 80—11719
- C-C composite material, syntactic-foam type properties 78—44169
- C-C composites, existence diagram and properties *(French)* 78—64517
- C-PVC composite, fluctuation induced tunnelling conduction 78—52044
- C-PVC composite, transport props. 79—38073
- CaO-Al_2O_3-SiO_2 glass-$MoSi_2$ filler, vitreous composite prod. 77—90313
- Cd-B(W) particulate composite, dispersion hardening, grain size and texture strengthening 77—8840
- Co-Ni-Cr (20,20 wt.%), internal oxidation, improvement of mech. props. *(French)* 77—16521
- Co-W-C system, η-carbide linear expansion coeff., X-ray diffr., 30-1500°C 77—25021
- Cr_2O_3-Cr film, optical props., rel. to chemical/metallurgical constitution, appl. as solar absorber 78—56531
- Cu and Cu alloy, unidirectionally solidified, morphology of solid liquid interface and solute redistribution *(Japanese)* 77—21133
- Cu/graphite-SbF_5 wire composites, synthesis and elec. props. 80—70781
- Cu-Al composite, simulation of tensile behaviour and fracture void initiation *(Japanese)* 78—52948
- Cu-Al composites, laminar, polycryst., electron diffr. proportional anal. 77—44444

composite materials continued
- Cu-Al_2O_3 composite coating, codeposition kinetics from $CuSO_4$ plating bath 78—15555
- Cu-Al_2O_3 disperse phase alloy oxidation kinetics 77—48584
- Cu-Al_2O_3 dispersed composite, electron beam deposition, struct. characterisation 77—44197
- Cu-Al_2O_3 dispersed system, electron beam evaporated thick film, struct./prop. relations 77—44198
- Cu-BN composite electromachining tools, dynamic hot pressing 80—84889
- Cu-coated TiO_2 particles, prep. for composites 80—89159
- Cu-Fe, composite, simulation of tensile behaviour and fracture void initiation *(Japanese)* 78—52948
- Cu-$Fe_{78}Mo_2B_{20}$ wire composite, mech. props. 80—40441
- Cu-ferrous alloy, hard inclusion composite exam. of wear resistance props. 79—34153
- Cu-Nb multifilamentary composite, dislocation resistivity 80—70671
- Cu-Ni composite formation by electric discharge sintering 77—63594
- Cu-plated C fabric, plasma sputtering influence on strength and elec. cond. *(Russian)* 80—21008
- Cu-rare earth oxide-Y composite coatings, oxide and Y effect on coating precipitation 80—55554
- Cu-SiO_2, low-temp. recovery creep, Orowan loop accumulation 80—81126
- Cu-W composite powder, prod. by H_2 reduction of $CuWO_4$ 79—20006
- Er_2O_3-Ta, oxide grain growth at interface 77—81245
- Fe alloy granule reinforced Cu M2 wear resistance in rubbing with lubrication 80—16490
- Fe alloy granule reinforced Cu, friction in vacuum 80—25880
- Fe alloy granules in Cu binder, exam. of wear characteristics without lubrication 79—96154
- Fe base composite, sintering, damping props. 77—21061
- Fe based dispersion strengthened thick condensates, struct., mech. props. 77—90361
- Fe powder-plastic composite, soft mag. material, mag. and mech. props. 80—75812
- Fe/Cu composite, prop. of fatigue crack crossing interface under residual thermal stress effect 80—45371
- Fe-(Cr)-C alloys, sintered, successive impregnation with C and Cr 79—95979
- Fe-Al alloys, powdered composites, metastable gamma-phase decomp. *(Russian)* 77—59741
- Fe-Al powder composite, phase composition, produced in low-temp. plasma 77—90295
- Fe-Al_2O_3 granular films, superparamagnetism and relax. effects 80—71118
- Fe-B alloy reinforced polysulphone exam. of tensile and flexure props. 78—72823
- Fe-Cr (13 wt.%)+polycarbosilane, powder metallurgy, characts. 77—85962
- Fe-Cr-Ni, two phase ($\alpha+\gamma$) alloys, transformation-induced plasticity 77—63721
- Fe-Cu composite plates, vol. fraction and residual stress, effect on fatigue strength *(Japanese)* 79—8349
- Fe-Cu-glass ternary multiphase composite, microstruct. and props. *(German)* 77—90314
- Fe-Fe_2O_3 composite films, structural props., microhardness, 250 to 700K 78—84095
- Fe-glass porous material, wear resist. under dry friction 80—25876
- Fe-glass-Cu sintered material, Cu effects on strength 77—77443
- Fe-graphite porous sintered, determ. of impregnation depth with polycaprolactam-finely divided Cu metallic polymer 79—70272
- Fe-Mo-CaF_2 sintered composite, struct. and mech. props., heat treatment effect 80—66526
- Fe-Ni heterogeneous alloys, ferrite, martensite and austenite phase distrib., effect on mech. props. 80—45363
- Fe-P-Cu-SiO_2-$FeAl_3$-asbestos, thermal and elec. conds., temp. and composition depends. 77—66609
- Fe-P-S composite sintered bearing materials manufacture, wear intensities 80—20881
- Fe-refractory compound condensate, struct. and mech. props., disperse particle content depend. *(Russian)* 78—19772
- Fe-TiC pseudofused composite magnetoabrasive powders, props. 80—100926
- ε-FeAl, eutectoid, directional decomp. rate rel. to lamellar period 77—4773
- ε-FeAl, eutectoid, directional decomp. rate, reply to comments 77—4775
- ε-FeAl, eutectoid directional decomp. rate, comment 77—4774
- γ-Fe_2O_3, small particle composite, preparation methods, superparamagnetism, optical transparency 78—60315
- GaAs-polyethylene mixture, optical transmission spectra, IR filter prep. using computer appl. 80—2763
- Ge-Al_2O_3, film, optical props., appls. 77—754
- H_2 production from coal by centrifugal separation from gasification products, high strength composite materials appl. 80—76643
- KCl-Al composite, optical and IR reflectance 78—56465
- KCl-Al(Pd) composite, far IR absorption 78—56466
- $Li_{0.5}Fe_{2.5}O_4$-LiNb(Ta)O_3, in situ composite growth, phase diag., melting relns. 77—21132
- Li_2O-SiO_2 glass ceramic, aligned, prep. by hot extrusion and microstruct. 77—32552
- Mn_2SiO_4-MnO eutectic composite, EFG die-top geom. effect on solidification interface shape 77—48420
- MoS_2 containing sintered Mo composite, friction and wear props. 80—11786
- NaCl polycryst. containing Al_2O_3 dispersion, diffusive creep 80—97531
- Na_2O-B_2O_3-SiO_2 glass-Ni compact, indented, strength and fracture toughness 80—93636
- Na_2O-CaO glass phlogopite mica powders, composite fabrication, cellular struct. 80—84902
- Na_2O-PbO-SiO_2 glass-ceramic composite, directionally crystallised 80—107058
- Ni spheres in glass matrix, brittle composites, fracture 79—66141
- Ni-Al_2O_3 composite film, selectively absorbing, optical props. 78—6798
- Ni-Cr-Al-TaC, eutectic composite, microstructure, fatigue props. 80—85038
- Ni-Eu_2O_3, specific resistivity and emissivity, 1000 to 1500K 77—43675
- Ni-Mo-MoS_2 composite, Mo alloying effect on physicochem. interactions 80—7692
- Ni-P-Al_2O_3 (SiC), composite deposit electrodeposition *(Russian)* 78—35326

composite materials continued
- Ni-pigmented anodic Al_2O_3, for selective absorpt. of solar energy, optical and struct. props. 80−55892
- Ni-SiO composite film, acoustic damping capacity and struct. *(Russian)* 77−59070
- Ni-Ti/Cu composite, plastic deform. influence on internal friction *(Russian)* 80−100871
- Ni-TiO_2 electrochem. composite coating phase composition and microhardness factors *(Russian)* 79−91598
- Ni-ZrO_2, dispersion-strengthened condensate, density and mech. props. 77−44196
- $NiFe_2O_4$-$BuTiO_3$, in situ composite growth, phase diag., melting relns. 77−21132
- PVC-Cu, particulate composite, mech. props. effect of particle size 78−95799
- PZT-polymer flexible composite transducer 78−80291
- Pb impregnated porous Ni, porous, internal friction and effective elasticity modulus, temp. depend. *(Russian)* 79−29118
- Pb-Al_2O_3 composites, mech. alloyed, hot hardness meas. *(Japanese)* 78−84830
- p-PbTe based composite material thermoelec. props. degraded by strengthening additive 79−47114
- Pb(Zr,Ri)O_3:Ni-silicon rubber flexible composite pyroelectric, dielectric props. 80−80704
- Pb(Zr, Ti)O_3-epoxy resin composite piezoelec. relax. due to ionic cond. 77−36179
- S-based composite, engineering props. 77−86093
- $Sb_2O_5.nH_2O$ acid membranes, synthesis and characterisation 80−81027
- Si particle reinforced Al, internal stresses, X-ray diffr. meas. *(Russian)* 78−23765
- Si/SiC ceramic composite, room temp. props., effect of SiC content and orientation 78−27599
- Si-Al, composite, simulation of tensile behaviour and fracture void initiation *(Japanese)* 78−52948
- Si-Al-O-N composites, dense direct prep. from naturally occurring SiO_2 and Al powder 78−11187
- Si-based, survey 78−56609
- Si-SiC, film, optical props., appls. 77−754
- SiC thread-like crystals reinforced mullite-corundum ceramics, props. 80−108525
- β-SiC/Si abrasive resistant material, prep. and props. 80−20878
- SiC-Bn composite, polymorphic transforms. 77−81259
- SiC-Si, bulk resist. of technical SiC powders 79−28350
- SiC-Si, wear resist., props. under abrasion and corrosion 80−100927
- SiO_2 powder filled epoxy resin, flow props. during curing *(Japanese)* 78−59355
- SiO_2-Al_2O_3-Cr_2O_3 system, KT-11 type, chromia-containing material production based on high-silica glass fabric 80−45266
- SiO_2-Na_2O-K_2O water glass with polyethylene filler, thermogravimetric and thermomechanical anal. 79−20020
- SiO_2-Ni granular metal films, minimum metallic cond. 78−56241
- $SmCo_x$-Fe composite permanent magnet material, mag. props. 77−40089
- Sn/graphite particulate composite, prep. using vacuum infiltration, microstruct., anal. 79−20005
- TaB_2-ZnS:Ag(Ag,Ni)-glass binder, thermally stable, comp. 77−63617
- (Ti, Cr)B_2-based alloys, densification of powder mixtures by hot-pressing, elec. and mech. props. 80−20812
- Ti base sintered bearing materials, metallic solid lubricant infiltrated, antifriction props. 80−60981
- Ti-Mn, superplastic, microduplex grain struct. stabilisation 78−44058
- Ti-TiC composite, X-ray struct. anal. 77−28825
- TiB_2-Al_2O_3, thermal stability of composite materials 78−60638
- TiB_2-Al_2O_3 system-based composites 77−85979
- TiB_2-CaO, thermal stability of composite materials 78−60638
- TiB_2-MgO, thermal stability of composite materials 78−60638
- TiB_2-$TiSi_2$ composites, high-temp. oxidation, scale comp. 78−15561
- TiB_2-Y_2O_3, thermal stability of composite materials 78−60638
- TiC-(Mo-Cr-Ni-Mn) steel alloy, optimum comp. and manufacture conditions, Mn effect 80−84896
- TiC-Au film, prep. by activated reactive evaporation, struct. and mech. props. *(Japanese)* 78−3252
- TiC-C composites, hot pressed, thermophys. props. at high temps. 80−59675
- TiC-Co(Ni), grain growth kinetics *(French)* 77−44252
- TiC-Ni composite coating, activated reactive evaporation prep., structure 77−44393
- TiC-Ni composite coatings, form. and wear resistant props. 77−63602
- TiC-steel composite, effect of method of Cr additions on props. 78−15341
- TiN-AlN, composite, erosion resist. in electron stream 78−11365
- TiN-AlN composites, struct. and props. 77−40413
- TiN-Nb(Ta)N, microcomposite film prod. for radio resistors 78−3052
- U extraction from seawater using composite absorbents 80−24730
- W reinforced Al, melting under weightlessness *(Russian)* 78−23691
- W wires monolayer tapes, mixtures theory, physical constants determ. from experimental dispersion curves 80−45338
- W-Al fibrous heat treated composites, thermal stress anal. 77−46943
- W-Cu composite materials, vel. dispersion and scatt. of transverse US waves 78−91383
- W-PVC material, fabrication and performance, acoustic properties 80−76218
- W-ThO_2 composite, struct., lamination tendency, effects of method of manuf. 78−68653
- WC-Co, calc. of weakest link in struct. 80−11730
- WC-Co, grain growth kinetics *(French)* 77−44252
- WC-Co, sintered hard alloy, mechanism of penetration of liquid metals 78−60619
- WC-Co alloys, P additions, effect on hot pressing, hardness and wear resist. 78−11162
- WC-Co cemented composites, abrasion by quartz 80−16495
- WC-Co composite, ion scatt. spectrometry and AES 77−60150
- WC-Co composite, surface anal. by quantitative AES 78−76622
- WC-Co composite chemical characterisation by AES and ISS 78−76621
- WC-Co hardmetals, heat-treated, single domain obs. 79−73771
- WC-Co molten Zn reaction, lamellar struct. form. 79−33964
- WC-Ni hard alloy composite, sintered, void healing 80−60821
- WCuB prep. by infiltration of W skeleton by CuB, hardness meas. *(German)* 78−64508
- Y_2O_3-TiB_2, ceramic, production by sintering in vacuo, or hot moulding at 1500°C 78−60629

composite materials continued
- Zn particulate composite, mech. props., microstruct. correlation, at low and high temps. 77−32624
- Zn-Cd liquid/Fe-Ni-Al mag. powder, effective viscosity of composites *(Russian)* 80−54424
- Zn-Pb, production under conditions when gravity forces are balanced out by EM forces 78−31363
- ZnO-B_2O_3-SiO_2 glass-ceramic-cement composites, review 79−38783
- Zr-ZrO_{2-x} composite, wetting charact. 77−44207
- ZrB_2-Ta composite, vacuum hot-press sintering and microstruct. *(Japanese)* 78−23649
- ZrC-C, disordered, Hall const. anomalies 79−56277
- ZrC-C composite system, electrical resist. meas., percolation theory anal. 78−84269
- ZrC-C composite system, negative magnetoresist. 80−60008
- ZrC-C composites, hot pressed, thermophys. props. at high temps. 80−59675
- ZrC-NbC-MoC_{1-x} system, thermal expansion coeff. up to 2500°C 79−69267
- ZrN-Al_2O_3 composites, strength rel. to solid-, liquid-phase sintering 80−100823
- ZrN-AlN, composite, erosion resist. in electron stream 78−11365
- ZrN-AlN composites, struct. and props. 77−40413
- ZrO_2-Y_2O_3(Nd_2O_3)(Ce_2O_3), stabilised, reaction with Cr_2O_3 77−36438

composite models of hadrons
- *see also parton model; quark models*
- 1/N expansion and the theory of composite particles 80−73604
- Bethe-Salpeter wave function divergence at origin 78−74147
- bilocal fields, ϕ^3 vertex, unitary S-matrix 78−62323
- constituent rearrangement model, nonleptonic hyperon decay 78−62357
- constituent rearrangement model and hadron reactions review 79−26294
- constituent-interchange model, pp and $\bar{p}p$ elastic scatt. 77−2856
- deep inelastic electroproduction struct. funct., Abelian gauge field effects 79−71754
- deep inelstic pp, πN, eN scatt., lepton-hadron relation, multiparticle prod. phenomena, average multiplicities 78−37247
- Dirac model of extended particles, physical aspect of interactions 80−9142
- double scattering in hadron-deuteron collisions, hadron struct. probe 77−74732
- dual topological unitarisation, review of S-matrix developments for hadron bootstrap theory 78−62381
- dynamical groups for the motion of relativistic composite systems 80−9115
- dyonic models of hadrons, quark mag. charge allowed values *(Russian)* 80−13275
- dyonium Hamiltonian on S^3 sphere, gauge invariant formalism 80−27460
- dyons, spatial volume integral of Tr F(tilde) F, Yang-Mills theory 80−77943
- extended hadron model and ϕ^4-field theory fluctuation renormalisation 77−5996
- extended hadron model based on exact soln. of nonlinear field eqn. 77−5997
- extended hadrons, functional eqns. soln. by stochastic methods 78−21376
- extended hadrons in geometrically formulated gauge dynamics with fibre bundles 80−9141
- extended technicolour scalarless theories 80−78001
- fermion+vector gluon systems, Bethe-Salpeter eqn. 77−13868
- fixed angle and Regge behaviour, hard scatt., fragment x-distrib. 78−78154
- four particle representation from Dirac's electron theory 79−36031
- hadron constituent model discrimination using large transverse momentum data 78−12881
- hadronic resonance props., consideration as compound of bradyons and tachyons 78−58163
- hadrons as compounds of bradyons and tachyons, ground state and decay anal. 78−58156
- heavy leptons as hadron constituents 77−30319
- large transverse momentum hadronic reactions, hard scatt. model of urbaryons with two-jet struct. 77−41813
- leading particle absorpt. in nucl. matter 77−88067
- lepton bound states of sub-hadronic dimens., quark lepton relation 78−54609
- lepton-hadron relation, νp interactions, globality prop. of charged multiplicity, pion prod. 77−2813
- lepton-hadron relation, e production in small-p_T pp interactions at 2800 GeV^2 77−2868
- lepton-hadron relation and the nucleon-nucleon potential 79−22207
- leptons bounds to strongly interacting matter 78−41485
- Lie group framework for composite particles and mass spectrum 79−97608
- magnetic monopole model, partial wave dispersion relations, strong van der Waals force 80−105849
- magnetic monopole model of hadrons, low energy pp scatt. 78−41563
- magnetically bound monopole pair, possible fermion struct. 80−86661
- mass spectrum in relativistic extended models 77−34116
- meson, gluon model, calc. of mass in MIT bag model *(Russian)* 77−74657
- meson bound state eqn. and solutions 78−78101
- meson resonances, EM decays and props. of stratons *(Chinese)* 78−29336
- meson structure wave functions, instantaneous interaction approx. straton+antistraton pair *(Chinese)* 77−10216
- meson structure wave functions in relativistic straton model, Bethe-Salpeter eqn. *(Chinese)* 78−50011
- MIT bag model for vector meson and baryon radiative decays 78−66110
- multiparticle production description by Chapman-Kolmogorov eqns. 78−12882
- muon model *(Russian)* 77−30312
- neutrino decay of hadrons and quantum number conservation laws *(Russian)* 79−348
- nonrelativistic many-body theory, foundations and statistical mechanics 80−82947
- number operators for composite particles in nonrelativistic many-body theory 80−94982
- overlap function in high energy collisions of composite objects 77−6087
- pairing vibration model of meson states, supercond. model of hadrons *(Chinese)* 77−10217
- partons, ancient Greek theory 77−64910

composite models of hadrons continued
- perturbation expansion of quantised composite field theory, gauge invariance *(Chinese)* 78—82156
- phenomenological two-component model for hadron constituents, large p_T spectra, pp inclusive reactions 78—25086
- preon model for hadron and lepton struct. 78—78124
- progress and current state of theory *(Chinese)* 79—97591
- quantised theory, UV and IR divergences, renormalisation *(Chinese)* 78—24997
- quark structure, weak interactions model 77—30313
- relativistic composite system, light-front wave functions 80—73592
- relativistic harmonic-oscillator model for extended particles with SO(3,2) internal symmetry 80—18121
- relativistic string theory in external field 79—97574
- relativistic two-particle system and spin-mass relations of meson 79—67505
- rest-mass level density, statistical model of hadrons, non-interacting pions 78—62353
- scaling violation and hadronic constituents with size and excited states 78—29299
- spinning tachyons as particle constituents, free spinning point particle theory 78—41155
- straton model, $\Delta(1236)$ prod. by high energy neutrinos *(Chinese)* 78—12900
- straton model, bound states of mesons, average radii, pion appl. *(Chinese)* 78—78150
- straton model, meson wave functions, Bethe-Salpeter eqn., SU_6 symm. *(Chinese)* 77—34125
- straton model, near-flat-bottom interaction pot., wave function of pseudoscalar meson *(Chinese)* 78—82167
- straton model, SU(5) extension, descript. of new Υ particles near 9.5 GeV *(Chinese)* 78—82168
- straton model of $1/2^+$ baryon semileptonic decays and high energy neutrino-nucleon reactions *(Chinese)* 78—12873
- straton model theory, extension to SU_5 *(Chinese)* 78—24996
- string type solns., in classical gauge field theories, broken gauge symmetry 78—62317
- $SU_4 \otimes SU_3'$ structural model of straton with integral charges *(Chinese)* 78—12860
- $SU(4) \times S_3^{\alpha}$, straton model, meson classification *(Chinese)* 78—78145
- SU(5) model, dyons and monopoles 80—82931
- subnuclear physics, review 77—67623
- tachyon and bradyon compound system model based on conformal relativity 79—93343
- three particle bound state, $Z=0$ condition 78—41481
- triple spinor model 79—13044
- twistor theory, particle models 80—13278
- two neutral vector gluon model, explanation of psi-mesons 77—226
- unified coupling scheme, world of composite nucleons 78—25000
- unitary relativistic wave equation exhibiting extended particle structure 80—9102
- unitary space of particle internal states 79—30712
- unitary space of particle internal states 80—18119
- urbaryon model, single-particle distribution function structure 77—18343
- urbaryon rearrangement model, transverse momentum in multiple prod. processes 77—57487
- urbaryon rearrangement model, two-jet production cross section at large p_T 77—2884
- wave eqns. for extended hadrons, de Sitter fibre bundle 77—18189
- Weyl Lie algebra representations as elementary particle models 79—2949
- Yang-Mills dyons, mag. charge and Pontryagin index equality in SU(2) 80—57562
- $\Delta(1232)$ isobar in nuclei, one-boson-exchange and straton model anal. *(Chinese)* 78—78275
- $K^{\pm}p \rightarrow hyperon + X$, 4-16 GeV/c, unified descript. of $\Lambda, \bar{\Lambda}, \Sigma^+, \Xi^-$ prod., urbaryon model 78—66173
- p struct. anal. from high-energy pp expts. 78—62457
- pp scatt., high energy, impact picture for polarisation and rotation parameter 78—70341
- pp scattering, charged secondary particles average multiplicities, total cross sections, lepton-hadron relation 78—33100
- π, wave function renormalisation const., upper bounds 78—74215
- π compositeness from wave function renormalisation constant 80—101997
- $\pi^{\pm}$, π^0, Santilli's model for hadron constituents number, computation simple approach 80—42389
- Υ, bound state of unconfined integer charge spin-$^1/_2$ fermions, theory 79—93375

composite particles
- *see also alpha-particles; deuterons; nuclei with mass number 1 to 5; tritons*
- nuclear cluster theory of composite-particle interactions, computational procedures 79—13225

composite superconductors
- A15 compound, deform. processing, rel. to multifilament conductor manufacture 78—39864
- A15 multifilamentary high-field superconductors, status of development 79—61004
- A15 superconductors, effects of material parameters on H_{c2} 79—61005
- AC losses, mag. field depend. of loss-freq. charact. 79—33384
- applied superconductivity, conf., Pittsburgh, USA (Sept. 1978) 79—33374
- barrier resistance meas. in multifilamentary composite superconductor 79—30506
- bronze process, metallurgy 80—3004
- continuous resistive transition self-field instability depend. 78—50369
- critical state stability anal. 77—89907
- current distribution, magnetisation and losses, fusion magnet material 77—28331
- design, problems associated with use of high-purity Al in elasto-plastic region 77—28851
- eddy current losses 78—62636
- effect of axial conduction and metal-helium heat transfer 78—91832
- endurance in mixed state, fatigue failure *(Russian)* 80—44778
- energy dissipation, expt. and theory 77—85386
- filamentary superconductor, Ginzburg-Landau theory of upper crit. field 79—78276
- flux jump nucleation theory, critical state stability 77—28290
- flux jumps and training 80—70911
- forced flow cooled, normal zone propagation velocity 79—82732

composite superconductors continued
- granular, Ginzburg-Landau theory, props. 80—88673
- granular metal-semiconductor system, exciton enhancement of supercond. transition temp. 79—7921
- granulated, superconducting transition, influence of particle size 79—69619
- inhomogeneous combined superconductor, normal zone equilibrium 80—75675
- inhomogeneous superconductivity, Ginzburg-Landau theory 80—88672
- integrated composite conductor for fusion program 78—62631
- Kirkendall void elimination by solution anneals 80—7520
- layered composite, Josephson current, effect of lattice defects and localised mag. moments *(Russian)* 77—80879
- longitudinal field losses, freq. depend. for twisted multifilament supercond. 77—63037
- losses under high rate pulsed transverse field 79—33385
- losses under nonisothermal conditions, cooling effects 79—87218
- magnet stability, critical current margin design criterion 80—31807
- magnet wound with composite supercond., stability in typical coil configs. 77—26350
- magnetic instabilities 77—80889
- magnetic properties, effect on losses in variable mag. field 80—34549
- magnetoresistance and Hall coeff., classical theory 80—84547
- maximum persistent current, in AC magnetic fields 78—31024
- multifilament, AC loss meas. apparatus 77—22576
- multifilament, longit. and transverse field losses 77—28308
- multifilament, transverse resistivity 77—72956
- multifilament superconductors, effect of local heat dissipation on stability 80—60156
- multifilament type, AC losses reduced below level of filament hysteresis losses by field screening 78—27000
- multifilament type, scaling law for AC losses 78—27001
- multifilamentary, AC losses in transverse AC mag. field 80—34568
- multifilamentary, asymmetry of normal zone propagation velocity with respect to current 79—33415
- multifilamentary, carrying DC transport currents, transient field losses 80—84551
- multifilamentary, current distrib., external field effects 77—28338
- multifilamentary, current transfer, expt. results for NbTi and Nb_3Sn 78—72316
- multifilamentary, current transfer, theory 78—72315
- multifilamentary, flexibility and elec. characts. 77—24990
- multifilamentary, losses in coil 78—62637
- multifilamentary, mag. props. effect on losses in variable mag. field 80—60136
- multifilamentary, magnetization effect on central field of supercond. magnets 79—65599
- multifilamentary, production and crit. currents 77—28766
- multifilamentary, self-field losses 77—28315
- multifilamentary, twisted, for Tokamak toroidal field coils 77—26871
- multifilamentary, voids growth obs., via hot stage SEM 80—70089
- multifilamentary, with alternating twist, coupling losses in transverse pulsed field 78—10602
- multifilamentary coil, hysteresis losses 77—26363
- multifilamentary composite, coupling losses in outer normal layers 79—99667
- multifilamentary composite superconductor power losses 79—30507
- multifilamentary composite superconductor transport current distrib. 79—30505
- multifilamentary composites, transverse elec. cond. 77—24648
- multifilamentary superconducting wires, in situ, anal. of continuity proximity effect conductivity 79—60997
- multifilamentary superconductor, current distrib. close to input leads 78—84363
- multifilamentary wire, transverse resistance effect on volt-ampere characts. 80—70897
- normal zone evolution, dynamic simulation 77—89914
- normal zone propag. calcs. 77—43778
- partial quench and recovery, simulation, transient heat transfer expt. 78—83219
- power increase at current close to crit. current, expt. meas. 77—28314
- propagation velocity expressions 80—60155
- proximity effect, McMillan tunnelling model 79—73639
- standards for practical superconductors, development 79—33442
- stress-induced heating, finite element calc. 77—28342
- stress-induced heating, influence on mag. performance 77—26357
- technical superconductors, preparation velocity of normal-conducting zone 79—24096
- technical superconductors, requirements and basic properties *(Slovak)* 78—88069
- threads of mixed materials containing many filaments, stability and transverse conductivity meas. *(French)* 79—73629
- transient loss analysis and measurements using equivalent circuit technique 79—60978
- transport current, interaction with transient external field 79—33393
- triple-phase phenomena, during quenching by pressurised superfluid ^4He 80—20364
- wire critical current density rel. to tensile stress at 4.2K, obs. 79—33439
- Ag-Nb-Ga, phase relations, A15 phase diffusion layer formation 78—52764
- $Al\text{-}Al_2O_3$, supercond. granular film, mag. penetration depth, depend. on normal state resist. and temp. 79—56378
- CdS-In, photosensitive granular superconductor 79—78246
- Cu alloy-Nb composite wires, resist.-temp. meas., percolation theory 79—28490
- Cu, electrical conductivity, effect of cyclic strains and work hardening at 4.2K 78—91655
- Cu normal metal in composite superconductor, neutron irradiation effects 79—38049
- $Cu\text{-}Gd_2O_3$ matrix, high sp. ht. material for improved adiabatic stability 77—40404
- Cu-Nb (17 wt.%) multifilamentary wires, fabrication and supercond. characts. 79—56476
- Cu-Nb (7 wt.%), solidification microstruct., SEM 77—12611
- Cu-Nb alloy, prep. for multifilamentary Nb_3Sn supercond. wire 80—84879
- Cu-Nb alloys for superconducting wire, casting of dendritic structure 80—2976
- Cu-Nb composite superconductor produced by rapid quenching 78—48351

composite superconductors continued
Cu-Nb filamentary composites, powder metallurgy prod., supercond. props. 79—56477
Cu-Nb multifilamentary composites, in situ formed, anomalous strength increase 79—43323
Cu-Nb$_2$Sr, multifilamentary supercond. composites, in situ formed, critical currents 79—65625
Cu-Nb$_3$Sn, in situ formed multifilamentary composite, supercond. and mech. props. 78—39279
Cu-Nb$_3$Sn composite wires, powder metallurgically produced, supercond. props. 78—31026
Cu-Nb$_3$Sn multifilamentary tapes, in situ formed, crit. current density anisotropy 80—84576
Cu-Nb$_3$Sn superconducting composite, crit. props., AC hysteretic losses 80—50014
Cu-Nb-Sn composites, cold-powder-metallurgy processed, supercond. critical currents 79—78279
Cu-Nb-Sn dil. alloys containing Nb$_3$Sn precipitates, superconductivity 78—43507
Cu-NbTi, composite conductor, acoustic emission 80—97032
Cu-Nb(Nb$_3$-Sn) composite wires, powder metallurgy prod., supercond. props. and annealing 79—33428
Cu-Sn-Nb multifilamentary alloy, high field crit. current density 78—27004
Cu-V$_3$Ga, supercond. in situ composites, stress effects on crit. props. 80—65757
Cu-V-Ga dil. alloys with V$_3$Ga particles, supercond. props. and microstruct. 78—39278
Cu(Sn)/Nb(Al), composite superconductor fabrication and characts. 77—81242
Ga-insulator compound, obtained by impact compression method, superconducting properties *(Russian)* 79—7919
In-Bi (22 at.%), directionally grown eutectic two phase superconductors, magnetisation behaviour 77—28293
In$_2$Bi-In, thin lamellar eutectic strips, unidirectionally solidified, morphologic and crystallographic study *(French)* 77—55264
Mo$_5$PbS$_8$ embedded in resin, composite supercond., high transition temp. 80—88660
Nb alloys, for appl. in magnets, technology *(Dutch)* 78—49871
Nb wire, Cu clad, proximity effect, Meissner screening length meas. 79—60996
Nb wire, Cu clad, supercond., Meissner effect in Cu meas. 78—64166
Nb/In composite superconductor, transport props. 80—88658
Nb-Nb$_3$Al, fabrication by quench-age method 77—40403
Nb-Sn, diffusion couple, phase equilibria, effect on T_c and H_{c2} 79—56462
Nb-Sn, filamentary, crit. current and temp., as function of reaction conditions 77—28330
Nb-Ti, crit. current changes and fatigue damage after 4.2K strain cycling 77—28323
Nb-Ti, Cu clad, Meissner effect in Cu Meas. 78—64166
Nb-Ti, multi-filamentary superconducting wires, mag. field dependence of AC losses 78—60256
Nb-Ti, multifilament composite technical superconductors, development and manufacture 79—19707
Nb-Ti, multifilament superconductor, metallurgical design 79—33434
Nb-Ti, multifilamentary, Mirror Fusion Test Facility, superconductor core manufacturing and quality 80—93521
Nb-Ti, pinning curves, high field J_c and scaling behaviour 80—93064
Nb-Ti, wire drawn and hydrostatically extruded supercond., crit. current density 79—38275
Nb-Ti (46%) dual matrix, fabrication 77—24989
Nb-Ti filamentary superconductor critical current density rel. to thermal treatment 79—33440
Nb-Ti in Cu, composite supercond. field replication and flux shielding 77—28286
Nb-Ti in Cu matrix, cyclic stress effects on transport props. 77—28336
Nb-Ti multifilamentary cable magnet, quench development 77—26351
Nb-Ti multifilamentary composites, high current, effect of nature and struct. of matrix on losses 77—24649
Nb-Ti multifilamentary composites, high current, crit. current degradation 77—24659
Nb-Ti multifilamentary supercond., commercial, crit. current density 79—38274
Nb-Ti multifilamentary superconducting composite, subjected to rotating mag. induction, losses 79—33386
Nb-Ti multifilamentary wires, high B losses 77—24650
Nb-Ti superconducting multifilamentary wires, mechanisms for crit. current degradation 77—28324
Nb-Ti/Cu composite disc, crit. state model for crit. current determ. 79—99665
Nb-Ti/Cu sheet composite, flux trapping and shielding capabilities in transverse fields 80—15667
Nb-Ti-Ta, pinning curves, high field J_c and scaling behaviour 80—93064
Nb$_3$/Sn-Cu composites, in situ processed, supercond. props. 80—75698
Nb$_3$(Al,Ge) wire, improved fabrication method 77—28763
Nb$_3$Al core wires and pressed powder compacts, supercond. transition 80—34541
Nb$_3$Al, multifilamentary, metallurgy, fabrication and supercond. props. 77—28764
Nb$_3$Ge composite filament, continuous, high-strength, prep. and supercond. props. 77—28765
Nb$_3$Ge, supercond. tape, growth technique via amorphous state 78—84708
NbN embedded in resin, composite supercond., high transition temp. 80—88660
NbSn multifilamentary superconducting composites, micromechanics 79—38878
Nb$_2$Sn, filamentary segments, flux pinning, proximity effects, percolation thresholds 78—56269
Nb$_3$Sn A15 composite superconductors, hydrostatic extrusion *(French)* 80—104090
Nb$_3$Sn composite processes with Cu-Sn-Zn matrix, superconducting props. 78—84370
Nb$_3$Sn, composite supercond., powder metallurgical prep. 80—2981
Nb$_3$Sn, composite superconducting wire, critical current-bend strain relationships 80—93063
Nb$_3$Sn, composite wire, boundary resistance and cryogenic stability 79—69629
Nb$_3$Sn composite wires, supercond., degradation mech. under tensile strain at 4.2K 79—38284

composite superconductors continued
Nb$_3$Sn composites, crit. currents and microstruct. 79—38280
Nb$_3$Sn conductor, bronze-process fine-filament, development and props. 79—33426
Nb$_3$Sn, current carrying capacity increase by Hf addition 80—7056
Nb$_3$Sn, current transfer, theory 78—72315
Nb$_3$Sn, current transfer, expt. results 78—72316
Nb$_3$Sn, diffusion-processed layer, texture meas. 79—82726
Nb$_3$Sn, effect of diffusion couple Sn content on superconductivity 79—61009
Nb$_3$Sn fatigue effects in unidirectional composites, computer simulated model 80—35289
Nb$_3$Sn, filamentary, fatigue tests on small coils 78—64652
Nb$_3$Sn filamentary composite conductor design 79—30515
Nb$_3$Sn, filamentary conductors, type-II, low temp. 30 GeV proton effects on critical props. 78—52178
Nb$_3$Sn, filamentary superconducting composite, TEM 77—80887
Nb$_3$Sn filamentary superconducting composites, mechanical properties and microstructure 79—57054
Nb$_3$Sn filamentary wires, fabricated by infiltration method, supercond. props. 77—28761
Nb$_3$Sn, filaments in Cu matrix, thermal strain effects on superconducting critical temp. 80—93032
Nb$_3$Sn, grain size in A15 reaction layers 78—14911
Nb$_3$Sn, high-current A-15 microcomposite material 80—44781
Nb$_3$Sn in bronze, supercond. props. thermally induced matrix stresses 77—32134
Nb$_3$Sn in Cu matrix, cyclic stress effects on transport props. 77—28336
Nb$_3$Sn monofilament wires, supercond. props., effect of Be alloying additions to bronze matrix 79—87222
Nb$_3$Sn monofilamentary composite conductors, tensile stress influence on critical current 80—97046
Nb$_3$Sn, monofilaments, radiation-enhanced diffusion growth, crit. current density 80—65758
Nb$_3$Sn, multifilament composite technical superconductors, development and manufacture 79—19707
Nb$_3$Sn, multifilament conductors, strain-crit. current meas. 78—64174
Nb$_3$Sn multifilament conductors, strain effect on crit. props. 78—80108
Nb$_3$Sn multifilament conductor critical current rel. to mech. strain 79—31215
Nb$_3$Sn multifilament conductors, fabrication and props. 79—33427
Nb$_3$Sn multifilament superconductors produced by ECN technique, prep. and props. 79—33975
Nb$_3$Sn, multifilament superconductor, metallurgical design 79—33434
Nb$_3$Sn multifilament superconducting composites, alternative technologies for fabrication 79—38756
Nb$_3$Sn multifilament superconductors, designed for high B appl., losses 79—33414
Nb$_3$Sn multifilament superconductors, AC losses 79—60979
Nb$_3$Sn, multifilament superconductor, pulsed mag. field losses and critical current densities 80—54853
Nb$_3$Sn, multifilamentary, flexibility and elec. characts. 77—24990
Nb$_3$Sn, multifilamentary, prod. by ECN powder metallurgy method, and supercond. props. 77—28762
Nb$_3$Sn, multifilamentary, optimization of high field crit. current density 79—38288
Nb$_3$Sn, multifilamentary and cabled superconductors, cryogenic stability anal. 79—59260
Nb$_3$Sn, multifilamentary composite wires, critical current strain depend. 77—20511
Nb$_3$Sn multifilamentary conductor, crit. current, tensile stress effects 77—28329
Nb$_3$Sn multifilamentary conductor, for fusion research magnets, manufacture and props. 77—28760
Nb$_3$Sn multifilamentary conductors, crit. current under tensile stress 77—89912
Nb$_3$Sn multifilamentary conductors, enhancement of supercond. crit. current by tensile stress 78—6490
Nb$_3$Sn multifilamentary conductor for fusion research 79—35797
Nb$_3$Sn multifilamentary composite superconductor, reaction treatment, crit. current, transition temp. and bend props. 79—33430
Nb$_3$Sn multifilamentary composite superconductor, effect of heat treatment on supercond. props. 79—33376
Nb$_3$Sn multifilamentary conductors for large-scale magnets, crit. currents, stability, and stress effects 79—38291
Nb$_3$Sn multifilamentary composite wires, supercond. crit. current density, temp. and mag. field depend. 79—33425
Nb$_3$Sn, multifilamentary conductors, production using solid state diffusion technique 79—56454
Nb$_3$Sn multifilamentary composites, supercond. destruction by current, long N-S interfaces 79—56480
Nb$_3$Sn, multifilamentary conductors, effect of bronze on compression 79—61012
Nb$_3$Sn, multifilamentary conductors, stress-induced enhancement of critical currents 79—69644
Nb$_3$Sn multifilamentary composites, crit. currents, flux pinning, and crit. field 79—78280
Nb$_3$Sn, multifilamentary coils for Lawrence Livermore Laboratory superconducting High Field Test Facility 80—90834
Nb$_3$Sn multifilamentary composite supercond. wires, transverse sections prep., ion milling, TEM obs. of grain size 80—101000
Nb$_3$Sn multifilamentary dipole magnet, construction and performance 77—28758
Nb$_3$Sn multifilamentary hollow superconductor and magnet, fabrication and crit. currents 79—38289
Nb$_3$Sn, multifilamentary high-field superconductor, status of development 79—61004
Nb$_3$Sn, multifilamentary supercond., crit. current, bend tests 77—28335
Nb$_3$Sn multifilamentary supercond., Cu-stabilised, recent developments 77—28759
Nb$_3$Sn, multifilamentary supercond., stress effects 77—32133
Nb$_3$Sn multifilamentary superconductors crit. current up to 18 T 77—47950
Nb$_3$Sn multifilamentary stranded compd. supercond., design, processing, mech., supercond. props. 77—76999
Nb$_3$Sn multifilamentary superconducting wires, crit. current density in high mag. field 79—38281
Nb$_3$Sn multifilamentary superconductor, stress induced normal⇄supercond. transition 79—33377
Nb$_3$Sn multifilamentary superconducting wires, improved high-field props. 79—47215

composite superconductors continued
Nb_3Sn multifilamentary supercond. composites, crystallographic texturing 80—71669
Nb_3Sn, multifilamentary superconductor preparation by 'in situ' and cold powder methods, review 80—93522
Nb_3Sn multilayered supercond. power line conductors, elec. props. and growth morphology 77—28325
Nb_3Sn, neutron irrad. effect on upper crit. field and crit. current 77—72954
Nb_3Sn, neutron irrad. effect on supercond. fusion magnet props. 78—52128
Nb_3Sn, sp. ht., 4-24K, calorimetry 77—32116
Nb_3Sn, stabilized multifilamentary superconductor, internal Sn diffusion process 79—61749
Nb_3Sn, supercond. composite, residual stress state, crit. currents 80—80468
Nb_3Sn, supercond. props. and appls., state-of-the-art 79—33413
Nb_3Sn, supercond. tape, crit. current, effect of Sn-Nb phase, annealing 79—24119
Nb_3Sn supercond. tape substrate structural changes 79—33373
Nb_3Sn, superconducting, formed from Cu-Sn alloy, props. 79—42709
Nb_3Sn superconducting multifilamentary wires, mechanisms for crit.current degradation 77—28324
Nb_3Sn superconducting multifilamentary composites, strain depend. of crit. current and crit. field 79—33432
Nb_3Sn superconducting multifilamentary conductors, AC losses 79—33394
Nb_3Sn superconducting multifilamentary wire, stress effects 79—33431
Nb_3Sn superconducting multifilamentary conductors, localisation of defects by inductive procedure 79—33433
Nb_3Sn superconducting wires, in situ multifilamentary, mech. props. 79—47746
Nb_3Sn superconductor, bronze processed, effect of third element additions 77—28333
Nb_3Sn superconductors, Kirkendall voids, effects on mech. and supercond. props. 79—33429
Nb_3Sn-Al_2O_3 composite, electron beam deposited, microstruct., rel. to supercond. props. 79—37935
Nb_3Sn-Cu, high-current A-15 microcomposite material 80—44781
Nb_3Sn-Cu composite superconductors, in-situ, AC losses 79—38283
Nb_3Sn-Cu multifilamentary wires, in situ prep., supercond. and mech. props. 79—38768
Nb_3Sn-Cu multifilamentary composite wire, Nb_3Sn filament morphology and grain size 80—100855
Nb_3Sn-Cu superconducting composite, electron beam co-evaporated, TEM study 79—28247
Nb_3Sn-Cu superconducting composites, produced by cold extrusion of fine powders 79—38767
Nb_3Sn-Cu superconducting composite with submicrometer filaments, fabrication and props. 79—38282
Nb_3Su-Cu supercond. composites, fabrication, magnet appl. 80—11602
NbTi cabled and soldered superconds. with low losses, for fusion research magnets, development 79—35796
NbTi, composite wire, boundary resistance and cryogenic stability 79—69629
NbTi composites, cryogenic stability due to boundary resistance between filament and matrix 79—58748
NbTi, current transfer, theory 78—72315
NbTi, current transfer, expt. results 78—72316
NbTi filament reinforced Cu, superconducting composite, elastic const., temp. depend. 78—68717
NbTi, filamentary conductors, type-II, low temp. 30 GeV proton effects on critical props. 78—52178
NbTi in Al, AC losses and crit. current 77—28310
NbTi, monocore and filament conductors, crit. current densities and anisotropy factors, heat treatment effects 79—38285
NbTi multifilament superconductor, AC loss reduction by low twist rates 77 12057
NbTi, multifilamentary, production samples, performance meas. 77—40012
NbTi, multifilamentary composite wires, critical current strain depend. 77—20511
NbTi multifilamentary composite, appl. of method for continuous meas. of crit. current 77—24656
NbTi multifilamentary composite wires, supercond. crit. current density, temp. and mag. field depend. 79—33425
NbTi, neutron irrad. effect on supercond. fusion magnet props. 78—52128
NbTi, solid soln. supercond., crit. current anisotropy 79—38273
NbTi supercond. threads in Cu matrix, struct. composition and props. *(French)* 79—73649
NbTi, superconducting multifilamentary conductors, crit. current density, bending effects *(German)* 80—39727
NbTi superconducting wire, Cu clad, proximity effect, Meissner screening length meas. 79—60996
NbTi/Cu, room temp. elastic consts., US determ. 77—59839
NbTi/In composite superconductor, transport props. 80—88658
NbTi/In granular composite, resistivity mag. field depend. 80—15654
NbTi-Al-(Cu-Ni) multifilamentary composite supercond. wire, stability, AC losses 77—76998
NbTi-Cu, acoustic emission 80—84546
NbTi-Cu, cryostatic influence of formvar coatings on sizing of stabilizer 79—61633
NbTi-Cu, supercond. composite, use in temp. and heat transfer coeff. meas. 80—77780
NbTi-In granular supercond. composites, mag. field-induced dissipation 80—84545
Ni-Nb(-Cu)-C, NbC dispersed supercond. tapes, fabrication and characts. 78—19773
Pb-Bi (12 at.%), Sn fibre reinforced type II superconductor, flux pinning *(German)* 77—85397
Pb-Cd, oriented lamellar superconductor-normal composite, supercond. 79—1650
Pb-Cd eutectic composite, mag. flux entry in proximity effect regime 79—33418
Pb-Cd lamellar eutectic composite, pair potential meas. 79—33396
Pb-Cd-Pb junctions, pair pot., mag. field depend., crit. currents meas. 80—84555
Sn-KCl granular superconductors, far IR absorpt. 80—84548
Ti-Nb superconducting composite in Cu matrix, low temp. effects in ductility 79—57119

composite superconductors continued
V/Cu-Ga, V_3Ga phase form., TEM obs. *(Russian)* 80—84933
V-Al/Cu-Ge, transition temp. and upper crit. field, heat treatment effects 79—38268
V-Al/Cu-Ge composite tape, transition temp., upper crit. field 78—68126
V-Hf-Nb(Zr), multifilamentary, superconducting props. improvement 79—38267
V_3G_3Ga multifilamentary wires, effect of low temp. neutron irrad. 77—32132
V_3Ga composite prep. and testing for high-field supercond. magnet 79—30513
V_3Ga, composite-processed, with improved current carrying capacities in high mag. fields 79—38272
V_3Ga, crit. temp. and field, prep. from V-Al and Cu-Ga 78—43506
V_3Ga, development by diffusion processes and use in 17.5 T supercond. magnet 79—61015
V_3Ga, diffusion-processed layer, texture meas. 79—82726
V_3Ga, filamentary conductors, type-II, low temp. 30 GeV proton effects on critical props. 78—52178
V_3Ga, grain size in A-15 reaction layers 78—14911
V_3Ga, high current density multifilament wire, neutron effects on equilibrium and transport props. 78—52126
V_3Ga, high-current A-15 microcomposite material 80—44781
V_3Ga multifilament superconductors, AC losses 79—60979
V_3Ga, multifilament superconductor, pulsed mag. field losses and critical current densities 80—54853
V_3Ga multifilament wire, crit. current props. above 4.2K 77—32135
V_3Ga, multifilamentary, prod. by ECN powder metallurgy method, and supercond. props. 77—28762
V_3Ga, multifilamentary high-field superconductor, status of development 79—61004
V_3Ga multifilamentary stranded compd. supercond., design, processing, mech., supercond. props. 77—76999
V_3Ga multifilamentary supercond. wire, fabrication and props., crit. review 79—38271
V_3Ga, multifilamentary wire, stress effect on critical currents 77—80891
V_3Ga, multifilamentary wire, crit. current props. with third element additions 79—61013
V_3Ga multifilamentary wires, critical current densities 79—69645
V_3Ga-Cu, high-current A-15 microcomposite material 80—44781
V_3Ga-Cu composites, supercond. props. 79—95557
V_3Ge, bronze-processed, stress-induced enhancement of supercond. T_c 78—64159
V_3Ge, formation by composition diffusion process, and crit. temp. determ. 77—85959
V_2Hf base Laves phase compound tapes, supercond. props., prep. 77—40011
V_2HfZr, C-15 cryst. struct. supercond. props. 78—64173
V_3Si embedded in resin, composite supercond., high transition temp. 80—88660
V_3Si, grain size in A-15 reaction layers 78—14911
V_3Si, supercond. tape, growth technique via amorphous state 78—84708

composition measurement *see chemical analysis*

compressibility
see also compressibility of gases; compressibility of liquids; compressive strength
alkali halide, Anderson-Gruneisen parameter evaluation 80—24617
alkali halide, interaction potential, Gruneisen parameter, compressibility 78—14304
alkali halide, overlap repulsion and pot. energy function for Bohr-like atoms 77—15344
alkali halide crystal, struct. stability and repulsion 79—65028
alkali halide crystals, compressibility, force const. and IR absorpt. freq. 77—27955
alkali halides, cryst., pot. parameters, Hellman function calcs. 80—2181
alkali halides, isothermal compressibility calc., 0-1000K 77—7784
alkali halides, softness parameter, additivity rule 80—1959
alkali hydride, repulsion interaction 78—26488
alkali hydrides, bulk props. prediction from molecular behaviour 78—51468
alkali hydrides, crystal binding anal., interatomic force model, Debye temp. 79—65030
alkali hydrides, lattice props. from interacton pot. energy function 80—100199
alkali hydrides, thermodynamic props. calc. using ionic pots. 78—10155
alkali metal, model potential calculation of binding energy and compressibility 78—91632
alkali metal alloys, dil., binary, equilib. at. vol. and compressibility 80—70295
alkali metal halides, crystal properties, cohesive energy, bulk modulus and press. depend., interionic force model 80—15035
alkali metals, compressibility and binding energy, Shaw's optimised model pot. 78—26620
alkali metals, contrib. of John Bardeen 80—57057
alkali metals, effective ion-ion potential, compressibility and force consts. 80—70158
alkali metals, equation of state and vol. depend. of thermodynamic props., pseudopot. theory 78—18738
alkali metals, phonon dispersion binding energy, compressibility, elastic consts. electron screening and Ashcroft pot. calcs. 80—65174
alkali metals, pseudopotential calcs. of binding energy, compressibility and resistivity 79—65025
almandine, synthetic, hydrostatic compression, isothermal bulk modulus 78—40545
bar (tube), compressible, combined loading, elastic-plastic problem 78—63311
binary system, A^NB^{8-N}, ground state of electron subsystem, quasimolecular model 79—69055
bone tissue crystals, effect of compression 77—25492
Born model, electrostriction rel. to dielec. and thermoelastic props. 80—71322
bovine hip bone, compression tests, effect of specimen shape and size on mech. props. and fracture mode 78—69132
brittle rod, optimum specimen shape for compression tests, gluing technique effects 80—50797
brittle rod, optimum specimen shape for compression tests, struct. and technological parameters 80—50798
bronze powder, granulated, effects on sintering kinetics 77—63599
calcite rock, compression wave studies 78—81151

compressibility continued
capillary piezometer with opticomech. readout, for compressibility meas. 77—39264
chalcogenide crystals with FCC structure, Moelwyn-Hughes parameter appl. to calcs. 77—80437
charged two-dimensional isotropic Fermi liq., static and dynamical props. 79—19532
chlorite, cryst. struct. and compressibility at high press. 78—63717
compressibility, finite element displacement model 77—867
consolidation in compressible mixtures 79—46271
corundum, hydrostatic compression, X-ray diffr. meas. 79—99269
critical compressibility factor correlation in three-parameter eqn. of state 78—2226
cross-rolling and compression textures, numerical prediction 80—40382
cubic materials, isothermal compressibility 79—99262
diamond, compressibility, appl. of Murnaghan eqn. of state, Morse pot. 80—79861
dielectric function, degenerate electron gas at metallic densities, nonlocal interactions, compressibility and dispersion 80—107730
dispersed media, shock compressibility, brittle destruction 80—49303
Earth mantle elements compounds and modifications, high press. and temp. thermodynamics 80—81874
elastic solids, finite plane strain problems, analytic soln., volume changes 77—68452
electron gas, quasi-one-dimensional, pair correl. function and plasmon dispersion curve 77—62851
electron-hole liquids, relation between bulk compressibility and surface energy 80—65465
fatty acid monolayers, light scatt. meas. 80—89011
FCC cryst., theory of response to [110] uniaxial loading 79—19310
fibre reinforced plastic, props., implications for structural design 80—81174
fibre reinforced thermoelastic materials, nonlinear thermodynamic continuum theory 80—14579
filled polymers, cumulative internal damage, US assessment 79—57180
fusible-metal deformation, effect on contact-melting kinetics 80—49339
fusion target implosion, laser compression efficiency, wavelength depend. calcs. 77—35369
Gibbs equilibrium thermodynamic pot. second derivatives, discontinuity surfaces rel. to phase boundaries of q-component systems 79—82304
granular medium, compressibility and force transmission, discrete probabilistic model 78—15448
graphite⇄diamond equilib. transition press. 78—34617
hard disc mixture, eqn. of state, compressibility and phase behaviour, mol. dynamics simulation 77—51291
hard dumbbells, eqn. of state 77—30119
hard-alloy powder mixtures, compressibility in hydrostatic working 78—68645
heterophase systems, pressure-induced elastic fields, effective inclusion method 79—10502
hot gas plasma, building up compression rings by dielectric spark discharge in layers of liquid 78—38493
hydrogels, two-component, elasticity theory and compress. meas. 80—44246
III-V semiconductor, heavily doped, pressure volume characts. nonlinearity, intervalley electron redistrib. 77—8012
inert gas solids, isotherms 77—20041
inorganic solids, Tait eqn., appl. to press. depend. of melting temp. 77—24381
interfaces separating compressible bulk phases, stability 80—107610
intermetallic phases with $L1_2$ and $D0_{19}$ struct., atom incompressibility, lattice parameter approach 78—91294
Invar, volume magnetostriction 79—56590
ionic compressibilities and radii 80—24397
ionic crystal, compressibility rel. to interionic repulsive force 77—11500
ionic crystals, migration volumes calc. 80—103324
ionic solids, lattice and defect props., modified electron gas approx. 79—42054
Ising double chain, compressible, mag. susceptibility and thermodynamic props. 79—15320
isotropic material, modified stress deviator for plastic compressibility *(German)* 78—13914
isotropic solid, temperature depend. of modulus of compression *(Russian)* 77—32661
itinerant electron ferromagnetism, press. effects on mag. props. 77—66241
itinerant electron ferromagnets, magneto-volume effects 80—60397
Kaprolon, compressibility, elec. cond., sound vel. behind shock front 78—95105
lung parenchyma described as prestressed compressible material 77—90837
measurement of solids, optical method *(Slovak)* 80—37023
membrane system, closed, vesicular, mechano-chemistry 77—60189
metal, BCC, neutron irradiated, spontaneous recombination volumes of Frenkel defects, rel. to compressibility 78—71765
metal, cavity growth in irrad. sample under stress 79—73211
metal, criterion for supercond. rel. to compressibility *(Russian)* 78—23200
metal, semistatistical calcs. 77—35879
metal, work-hardening, plastic, sintered, porous, irreversible deform. 78—35459
metal polyphosphinates, bulk compressibility meas. to 30 kbar 80—76306
metal powder, milling conditions effect on densification during pressing and sintering 78—11149
metal powder explosive pressing, shock compression parameters *(Russian)* 77—52260
metal-composite rods, compressed, delamination 80—64396
metals, compressiblities, general pseudopotential approach 80—54631
metals, eqns. of state based on free energy expressions, isothermal compression moduli *(Russian)* 79—90753
metals, ground state of solids, spin density functional method, binding energy, compressibility 80—65477
metals, lattice dynamics model *(Hungarian)* 77—27952
metals, local pseudopot. approach 80—65129
metals, simple, binding energy, compressibility, interionic pot. and transition temp. using pseudopot. method 79—46598
methane, solid, thermodynamic props. from US velocity obs. 79—46753
minerals, bulk modulus-volume relationship, for cation-anion polyhedra 80—41434
mixtures containing polar substances, corresponding states principle use in crit. states calc. 80—39196

compressibility continued
modelling by steel spheres, packing density coeff. 78—84916
Mohr-Coulomb material, axisymmetric compression around circular hole 79—57914
natural rubber vulcanisate, network changes during physical testing 80—60936
nuclear matter, incompressibility rel. to superdense celestial bodies theory 80—67773
optical fibre clad with Teflonlike plastic coating, press. sensitivity 80—33149
optimisation of geometrically imperfect stiffened cylindrical shells under axial compression 79—3916
orthorhombic crystals, finite strain theory appl. to evaluation of compression curves *(French)* 77—69028
orthotic material characterisation by mech. impedance method 78—36066
partially ionised fluid, thermal instability, compressibility and collisional effects 78—55693
particles, small, impossibility of comminution by compression 78—52709
perovskite structure crystals, appl. of repulsion parameters of ions and radicals 79—32943
phlogopite, cryst. struct. and compressibility at high press. 78—63717
plasma column, influence of external mag. axial field on an autocompression, review *(Rumanian)* 80—24148
plastometer, electronically controlled, for tensile and compression tests *(German)* 80—3273
plate incompressible isotropic, stability under all-round compression *(Ukrainian)* 79—37149
polyacetylene, pristine and doped, press. effects on resist. 80—103698
polydimethylsiloxane, crosslinked, stress/strain relations from large compression to high elongation 80—66589
polyethylene, doubly oriented, low density, deformation and structure, exam. 80—11705
polyethylene, orthorhombic and triclinic lattices, eqns. of state 79—28069
polyethylene, X-ray diffr. at press. up to 14000 kg cm^{-2}, 298K 77—35492
polyethylene cryst., unit cell variations with temp. and high press. 78—47250
polyethylene high press. phase, struct., phase diagram and compressibility 78—9961
polyethylene terephthalate, solid and molten, press. effects on compressibility and crystn., thermodynamic interpret. 80—84102
polymer crystal, hydrostatic compressibility, H_2 bonding effect on anisotropy 80—25782
polymer materials volume compressibility, meas. equipment 77—77674
polymers, equation of state *(German)* 79—82309
polymethylsiloxane-toluene gels, light scatt., compression moduli, cooperative diffusion 78—23970
polystyrene, expanded, dynamic compressibility 78—48476
polystyrene spheres, crystallised suspension, gravitational compression 78—23975
polyvinyl-pyrrolidone/polyethylene glycol oligmers, elasticity theory, and compression meas. 80—44246
polyvinylidene fluoride, equation of state, compression ratios, theory 80—10634
polyvinylidene fluoride, X-ray high press. study 80—6369
porous materials, expression relating porosity and compressibility 79—100069
porous metal gauze materials, struct. and hydraulic characts. 80—11729
porous structure, shrinkage kinetics, boundary slip and superplasticity 77—36611
PTFE and filled PTFE, nonlinear creep, compression bulk modulus 80—66593
Pyrex glass, isothermal compressibility to 20 kbar, inductance coil method 80—49302
pyrope, synthetic, hydrostatic compression, isothermal bulk modulus 78—40545
α-quartz, compression to 120 kbar 77—15493
quartz, finite strain theory appl. to evaluation of compression curves *(French)* 77—69028
quartz, isentropic compression by ultrastrong mag. field *(Russian)* 78—47468
rare earth Co Laves phase cmpds., elastic props. rel. to temp., mag. field 79—51834
Rayleigh-Taylor instability, thermal cond. and compressibility effects 80—79262
red cell membrane elastic area compressibility meas., osmotic correction 78—20147
rock compressibility, nonelliptical crack effects 79—2227
rocks, compressional and shear wave velocities under high press., effect of high-low quartz transition 80—12380
rocks, new model for analysing effect of fractures 80—8300
rocks, P-V meas., 5 to 45 kb *(Chinese)* 79—23676
rubber-like solids, anisotropy of compressibility 79—43302
ruby, cryst. struct. and compression up to 46 kbar 79—37682
sandy soil, mech. characts. under static loadings 79—88345
semiconductor, diamond-like, adiabatic pot. in quasi mol. model 78—2063
shock compression of solids, review 80—24534
shock compression-pulse heating working process, apparatus design 80—16357
simple metals, compressibility, Harrison pot. calcs. 80—96460
simple metals, model pseudopot. appl. to various props. 80—59845
small particles, cause of reduction in lattice spacing *(Russian)* 80—38967
soil, sandy moist, compressibility and plasticity during repeated shock loading 78—11885
solid bodies, hydrostatic compression eqn., geophys. appl. 79—62489
solids under press., simple model for Gruneisen parameter and adiabatic compressibility 77—11706
spatial elastica theory with centreline compressibility 78—79211
spherical laser target hydrodynamic compression stability *(Russian)* 80—106159
springs, helical, under compression and twist, stability, nonlinear Kirchhoff-Clebsch equations *(German)* 80—33443
steel, alloy, low, dual phase, high strength, exam. of energy absorption by structual collapse 80—7640
steel, stainless, atomised powder, effect of ultasonic refining on processing preps. 79—33972
structural and electronic changes under 200 kbar press. and above 80—24588

compressibility continued
Tait equation of state, high press. and isothermal bulk modulus 77—84882
thulium ethyl sulphate, Van Vleck paramag., mag. reson. on uniaxial and uniform compression *(Russian)* 79—61243
transition metal, 3d, giant internal mag. press. and compressibility anomalies, itinerant model 77—16034
transition metal, BCC isothermal compression to 100 kbar 78—43069
transition metalloids, t-matrix theory of thermal and nonstoichiometric softening 79—86788
transparent dielectric, optical stimulation of compression pulses, absorbing layer effects *(Russian)* 77—1174
TTF-TCNQ, deuterated, compressibility under hydrostatic press., neutron diffr. meas. 78—2197
uniaxial stress component, effect on eqns. of state determ. with opposed-anvil X-ray apparatus 80—49301
vacancy formation energy, correl. with compressibility 78—2112
valinomycin monolayers, struct., area and compressibility determ. 78—44461
zincblende structure group IVA covalent crystals, Murnaghan parameter estimates from Morse pot. 78—95014
Ag, isothermal compression curves to 120 kbar, X-ray diffr. study 78—83876
Ag, phonon dispersion, binding energy, compressibility, pseudopot. calc. 77—4164
Ag-Ni alloy, composite powder mixtures, compressibility and sinterability 77—63592
AgBr(Cl), formation vol. of Frenkel defect 78—79606
Al 6061-T6 alloy, shock-compressed, reshock and release 77—32732
Al alloy with different props. in tension and compression, creep 80—81129
Al, compression, effect of press. on lattice defects up to 90 kbar *(Japanese)* 77—72654
Al, isothermal compression curves to 120 kbar, X-ray diffr. study 78—83876
Al, metallic, phonon freq., binding energy, compressibility, elastic const. and energy band gap calcs., linear pot. 80—88284
Al, model pot. calc., binding energy and compressibility 79—99650
Al, shock compression at high press. *(Russian)* 80—92608
Al-Si alloy, compression, effect of press. on lattice defects up to 90 kbar *(Japanese)* 77—72654
Al_2O_3-SiO_2-Fe_2O_3-CaO-MgO-TiO_2, refractory, corrosion and mech. behaviour correlations 80—40563
$Al(PO_3)_3$-LiF system glasses, microhardness and US vel. 79—99274
$Al(PO_3)_3$-NaF system glasses, microhardness and US vel. 79—99274
Ar, monolayer, adsorbed on graphite, lattice spacing and isosteric heat below 50K, LEED obs. 80—34303
Ar monolayers, on graphite, condensation and compression, high resolution LEED obs. 79—77906
As, band structure and cryst. energy, pseudopot. calc. 79—90954
Au, phonon dispersion, binding energy, compressibility, pseudopot. calc. 77—4164
BN, structural changes at high pressures and temps. 80—40345
BN, structural changes occurring during shock compression in presence of H_2O 80—16301
BP, sp. ht., Debye temp., compressibility and Gruneisen coeff. meas. 78—63865
Bi island films, effect of surface press. on lattice spacings 79—11045
C blacks, powders, resistivity rel. to compression *(French)* 80—35349
C, glassy, prep. from liq. phenolformaldehyde resin, TEM obs. 79—83145
C shock compression, diamond production 80—11613
CF, X-ray diffr., high press. effect 78—83766
$Ca_3Al_2Si_3O_{12}$, grossular, cryst. struct. and compressibility to 60 kbar 78—63718
CaO, electronic structure 80—2332
Cd, compressibilities, temp. depend. *(French)* 79—65135
$CdB^4C^5{}_2$, chalcopyrite struct., surface energy and compressibility, rel. to glass form. 79—51417
$CdCr_2S_4$, thermodyn. props. 78—51703
$CdCr_2Sr_4$, press. depend. optical aborption edge shift and compressibility 79—28714
$CdGa_2Se_4$, linear expansion anisotropy 79—86910
$CdTl_2Te_4$, single and polycryst. samples, linear expansion, heat capacity and thermodynamic props. 80—103489
Ce binary and pseudobinary intermetallics, struct. and mag. data 80—20129
Ce, polymorphic $\gamma \rightleftarrows \alpha$ transform. and volume anomalies under press. 80—34189
CeP(As)(Sb), room temp. from neutron diffr. meas. of lattice parameter variation up to 41 kbar 77—27940
$CeSn_3$, low temp. mag. behaviour, press. induced valence change 77—63078
$CoFe_2Se_4$, low-temp. thermal expansion anomalies and isothermal compressibility, mag. ordering and magnetorestriction 79—38363
CrAs, anisotropy of compressibility 79—7648
Cr_2O_3, hydrostatic compression, X-ray diffr. meas. 79—99269
Cs, absolute zero isotherms and polymorphic transition 79—73310
Cs, volume and compressibility meas. for liq. and solid phases up to 22 kbar 77—47541
Cu, cohesion, electron statistical model 77—27846
Cu crystal, cohesion and vacancy form., electron statistical model 80—54169
Cu, crystal lattice behaviour under intense unidimensional compression *(Russian)* 78—6123
Cu-Ni-Fe, magnetic properties, heat treatment and compressive stress effects 80—60367
CuCl, defect and impurity bands, lattice consts. 80—54638
CuCl, pressure depend. of structural, chemical, elec. and mag. props. 80—96596
$CuCl_2.2D_2O$, cryst. struct., mag. and reson. props. 80—60424
$CuCl_2.2H_2O$, magnetoelastic props. under press., antiferromagnetic resonance, lattice parameters 80—29598
D_2, solid, melting curve, meas. of P, V, T and longitudinal sound velocity 79—37814
Fe and related compounds, hydrostatic compression expts. 78—83862
Fe, atomised powder compacts for mag. cores, oxidation, compressibility, heat treatment *(Japanese)* 78—72752
Fe, BCC, neutron-irradiated, Frenkel defect spontaneous recomb. volumes 79—60355
Fe base amorphous alloys, Invar and Elinvar characts. 80—29592

compressibility continued
Fe based porous metals, exam. of volume change under high pressure 78—52906
Fe powders from Fe-C melts, atomisation, props. 79—70013
Fe, single component, powder, compressibility and elec. resistivity in cold pressing under low press. 77—77444
Fe-Ag (50 wt.%), plastic behaviour in compression, deform. rate effect *(French)* 80—71711
Fe-C-Cr-Mn-Si-Ni (4.6, 38.7, 1.1, 2.0, 1.58 wt.%) alloy US-25, powder, compressibility and elec. resistivity in cold pressing under low press. 77—77444
Fe-Co alloy, isothermal compression and BCC→HCP phase transition, up to 300 kbar, at room temp. 77—90346
Fe-Cr, single and two component, powder, compressibility and elec. resistivity in cold pressing under low press. 77—77444
Fe-Ni Invar, magnetovolume coupling enhancement factor, temp. depend. 80—88851
FeF_2, EXAFS at high press., bond compressibility, at. spacings 78—39628
$(Fe_{1-x}Mn_x)Si$, US vel. rel. to mag. struct. and phase transforms *(Russian)* 77—47976
α-Fe_2O_3 (haematite), X-ray diffr. compression studies under hydrostatic isothermal conditions 78—85539
α-Fe_2O_3, hydrostatic compression, X-ray diffr. meas. 79—99269
Fe_3O_4, magnetite, isothermal compression up to 70 kbar under hydrostatic conditions 78—30698
FeS_2, EXAFS at high press., bond compressibility, at. spacings 78—39628
Fe_3Se_4, thermal expansion, compressibility, magnetisation, susceptibility and magnetostriction 77—66318
Fe_2SiO_4, spinel, isothermal compression up to 75 kbar hydrostatic press. 77—43280
Ga-Sn alloys, compressibility, US velocity meas. *(Russian)* 77—59060
GaS, elastic prop. anisotropy, Debye temp. *(Russian)* 80—88244
Ge, carrier relaxation rate temp. depend. and pair density in large electron-hole drop 80—75509
GeO_2, α-quartz structure, compression mechanism 79—23673
H_2, solid, installation for isothermal compression up to 25 kbar, 60 to 130K 79—35769
H_2, solid, melting curve, meas. of P, V, T and longitudinal sound velocity 79—37814
H_2, solid, metallic, high density, thermodynamic props. 80—88337
^3He, solid, ordering obs. at melting press. in high mag. fields 80—84341
$Ho_xTb_{1-x}Co_2$ lave phase compounds, elastic props., temp. and magnetic field dependence 80—60393
InSb, sputtered NaCl-type compression 79—46751
K, absolute zero isotherms and polymorphic transition 79—73310
K, electron-ion interaction model pseudopot. calcs. 78—26486
K, volume and compressibility meas. for liq. and solid phases up to 14 kbar 77—47541
KBr, analysis using density functional formalism 79—90592
KCN, crystal props., log potential model calc. 78—63829
KCl, thermal expansion, compressibility and melting calcs. 79—33069
KM_gF_3, bond energy, equilib. distances and compressibility calcs. 80—70159
$K_2Pt(CN)_4Br_{0.3}.2.7D_2O$, under hydrostatic press., compressibility, neutron diffr. 79—46742
LiF, cohesion energy, compressibility and density, ab initio calc. 77—72648
$LiTmF_4$, Van Vleck paramag., mag. reson. on uniaxial and uniform compression *(Russian)* 79—61243
$(Mg,Fe)_2SiO_4$, shock deform. expts., Hugoniot data implications 80—94497
Mg, finite strain theory appl. to evaluation of compression curves *(French)* 77—69028
$Mg_3Al_2Si_3O_{12}$, pyrope, cryst. struct. and compressibility to 60 kbar 78—63718
Mg_3Cd, effect on order, of compression deformation 78—52924
MgIn, X-ray diffr. exam. of compressibility 78—51610
MgO, electronic struct. calc., lattice const., cohesive energy and compressibility 79—78003
Mn_5Si_3, elastic moduli, phase transitions, ultrasonic velocity 80—92589
Mo, BCC, neutron-irradiated, Frenkel defect spontaneous recomb. volumes 79—60355
Mo selenides, ternary, Chevrel phase supercond., compressibility and vol. depend. of Tc 78—31008
Mo sulphides, ternary, Chevrel phase supercond., compressibility and vol. depend. of Tc 78—31008
MoS_2(2H), elastic consts., from dispersion curve and linear compressibility data 77—11618
NH_3-H_2 mixture, rel. to possible existence of metallic ammonium 80—24567
Na, electron-ion model pseudopot. calcs. 78—26486
Na, linear potential and phonons 79—82293
Na, volume and compressibility meas. for liq. and solid phases up to 22 kbar 77—47541
NaBr, analysis using density functional formalism 79—90592
NaCN, crystal props., log potential model calc. 78—63829
NaCl, thermal expansion, compressibility and melting calcs. 79—33069
NaF, ab-initio calc. of cohesion energy, compressibility and density 78—71782
NaF, isothermal compression at 673K, up to 10 GPa, X-ray diffr. study 80—59565
$NaNO_2(NO_3)$, linear compressibility to 27 kbar, X-ray diffr. obs. 80—34125
Nb_3As, structural and supercond. props. press. effects 80—39700
α-NbD_x, under hydrostatic press., γ ray diffr., Bragg refls. 78—75726
Nb_3Ge, and $Nb_{0.82}$, structural and supercond. props. press. effects 80—39700
$NbSe_2$(2H), elastic consts., from dispersion curve and linear compressibility data 77—11618
Nb_3Si, structural and supercond. props. press. effects 80—39700
Nb_3Sn, multifilamentary conductors, effect of bronze on compression 79—61012
Ni based porous metals, exam. of volume change under high pressure 78—52906
Ni, dislocation intersection and solution strengthening, effect of solute on obstacle profiles 80—7590
Ni, single crysts., strengthening, tested under compression at 293 and 77K *(German)* 80—50689

compressibility continued
Ni/Cr-Fe-C, Inconel, dislocation intersection and solution strengthening, effect of solute on obstacle profiles 80—7590
Ni-Co, dislocation intersection and solution strengthening, effect of solute on obstacle profiles 80—7590
NiS, antiferromag., press. effect on metal-nonmetal transition 77—69229
Pb, model pot. calc., binding energy and compressibility 79—99650
Pb, P-V meas., 5 to 45 kb *(Chinese)* 79—23676
Pb, shock compression at high press. *(Russian)* 80—92608
Pd-Zn, $L1_0$ type intermetallic phase, X-ray diffr. study of lattic compression 80—49182
PrAs, room temp. compressibility 77—85595
PrN, compressibility, mag. susceptibility and NMR freq. shift meas. 77—85595
PrS, isothermal compressibility 79—99262
PrSb, compressibility and NMR freq. shift 77—85595
PrSe, isothermal compressibility 79—99262
Rb, absolute zero isotherms and polymorphic transition 79—73310
RbCN, crystal props., log potential model calc. 78—63829
Re, Anderson-Gruneisen parameter, bulk modulus and compression curves 78—30690
ReO_3, compressibility collapse phase transition, NQR study 80—39282
ReO_3, Fermi surface, pressure induced anomaly 79—19505
$(SN)_x$, linear compressibilities, X-ray determ. 78—34565
$SbGe_xSe_y$ glasses with const. Sb content, heat capacity, thermal expansion, US vel. and elastic moduli 77—76574
Se, vitreous, mech. props. at temps. <300K, uniaxial compression tests *(French)* 78—55908
Si, compression, effect of press. on lattice defects up to 90 kbar *(Japanese)* 77—72654
Si rubber as electro-optic material for optical hydrophones 80—43412
α-Si_3N_4, lattice and atomic position parameters, neutron diffr. study 79—42040
Si_3N_4-Mg_2SiO_4-Si_2N_2O, compressive creep, composition effect 80—50674
Si_3N_4-MgO, compressive creep, source of viscoelastic effect 80—50675
Si_3N_4-MgO, compressive creep, oxidation induced compositional change 80—50676
SiO_2, α-quartz structure, compression mechanism 79—23673
SiO_2, fused, isothermal compressibility to 20 kbar, inductance coil method 80—49302
SiO_2, shock compression at high press. *(Russian)* 80—92608
SmS, metallic phase, compressibility anomalous behaviour 80—29114
SmS, vol. changes at press. up to 20 kbar 78—71791
α-Sn, lattice dynamics 80—107389
Sn, tetragonal β-phase, neutron-irradiated, Frenkel defect spontaneous recomb. volumes 79—60355
SnS_2 berndtite, cryst. struct. and compressibility at high press. 78—67685
SrF_2:Er, activation vol. for interstitial motion, dielec. const. meas. 80—49412
SrF_2:La, type-I dipole reorientation, activation vol. determ. from dielec. const. 80—88916
Ta, BCC, neutron-irradiated, Frenkel defect spontaneous recomb. volumes 79—60355
$TaSe_2$ (2H), thermal and elastic props., X-ray diffr. exam. 79—37754
TiC, deform. at high temps. 80—104239
TiN, synthesised in SHF discharge plasma, exam. of props. *(Russian)* 80—7524
TiO_2, rutile, isothermal compression under hydrostatic press. to 106 kbar 80—31035
TiO_2, rutile, single cryst., high temp. compression in O_2 atmosphere *(French)* 79—51194
TiO_2, rutile phase, shock induced phase transition anisotropic behaviour 80—103475
TlCl, ground-state props., Wannier functions, and electronic struct., ab initio self-consistent calc. 80—80178
TlCl, self-consistent electronic struct. and ground state props. 80—15451
TmSe, mixed valence cpd., thermal, mag., and transport props. 79—61074
UAl_2, high field, high press. mag. props. 80—11172
UO_2 powder, precompaction effect on compressibility 78—41846
V_2O_3, hydrostatic compression, X-ray diffr. meas. 79—99269
V_3Si, static compressibility, up to 20 kbar 77—43281
W (110) mobility and two-dimens. compressibility of adsorbed Xe, field emission current fluctuation method 80—80089
W, BCC, neutron-irradiated, Frenkel defect spontaneous recomb. volumes 79—60355
W, P-V meas., 5 to 45 kb *(Chinese)* 79—23676
W powder, hydrostatic pressing 78—11161
WC-Co, elastic moduli and their press. derivatives 79—83248
WC-Co, various combinations, fracture characts. in bending, compression, and toughness tests 78—60808
Xe, monolayer adsorption on Ag (111), statistical mech. 80—34306
$Y_3Fe_{5-x}Al_xO_{12}$, $Y_{3-x}Gd_xFe_5O_{12}$, linear expansion 77—48024
Y_2O_3, effect of roasting temp. of $Y_2(C_2O_4)_3$ on crushing, compressibility, sintering props. 77—8790
Yb, structural and electronic changes under 200 kbar press. and above 80—24588
Zn, creep, compression anisotropy effects 79—83275
Zn-Cd alloys, liq. and solid, ultrasound speed and compressibility meas. 80—102941
$ZnB^4C^5_2$, chalcopyrite struct., surface energy and compressibility, rel. to glass form. 79—51417
ZnS, cubic, compression 80—107358
$ZnSiF_6.6H_2O$, spin-phonon interaction between Ni^{2+} ions, phonon bottleneck effects, splitting parameters *(Russian)* 80—15796
Zr, HCP, neutron-irradiated, Frenkel defect spontaneous recomb. volumes 79—60355
β-Zr-Mo oxidised alloys, high temp. deformation, X-ray study 79—79045
$ZrSiO_4$, zircon, cryst. struct. and compressibilty at high press. 79—82184

compressibility of gases
see also high pressure phenomena and effects
air compression, pneumatic-freq. method for volume determ. of complex shape bodies *(Polish)* 79—49199
Burnett data reduction, fast least-squares method 78—47082
chlorotrifluoromethane, compressibility, 298 to 348K, Burnett expansion obs. 79—27733
cool flame explosion, during piston compression, time predicted by Livengood-Wu integral method 78—15675

compressibility of gases continued
equation of state, nonanalytic, modification for low density limit, appl. to ethylene 79—46779
Eulers eqns. soln. for expansion of sphere at constant velocity *(French)* 80—33719
hard-sphere fluid, direct correl. function 79—41918
high pressure physics and technology, conf., Moscow, Russia (May 1975) 78—51611
large-volume gas mixture preparation, compressibility ratio 80—59165
liquid-vapour interface, surface tension-compressibility relation 80—44397
mixtures, thermodynamic props. prediction 78—83512
mixtures, vapour-liq., equilibria, fugacity coeff. calc., pseudocritical method 77—27972
piezometer deformation errors in gas and liquid compressibility meas. 78—5646
Pitzer correlation extension for compressibility factor calcs. 79—86557
propane, compressibility, virial coeffs., Burnett method 78—47083
propane-propene mixtures, compressibility, virial coeffs., Burnett method 78—47083
propene, compressibility, virial coeffs., Burnett method 78—47083
real gas, blast wave, effects of compressibility, vibr. excitation, dissoc. and ionisation 77—68622
Redlich-Kwong equation of state, modification to polar gases 78—9742
spherically centralized compression wave *(Russian)* 79—10622
steam, low and moderate density, compressibility factor and viscosity coeff. eqn. 80—33722
subharmonic nonlinear acoustic resonances in open tubes 77—72404
thermal-diffusion coupled appl. to gas compression and decompression with porous material 78—94882
thermodynamics of compression, fundamentals review 77—39390
thermophysical props. tabulated for mixture composition certification 78—80818
trifluoromethane, PVT study by Burnett method 77—42949
unit compressibility law *(German)* 79—77325
Ar, adiabatic compression to 25 kbar 79—86549
Ar, compressed gas, PVT meas. at high press. 80—98927
Ar, second virial coeffs. from compressibility meas., mol. pot. parameters calc. *(Spanish)* 77—47133
CO_2, fugacity at high temps. and press. from exptl. decarbonation reactions 79—16439
H, spin-polarised, density, magnetisation, compression and thermal leakage 80—44391
He, dense, semi-empirical eqn. of state and compressibility factors 77—7499
Kr, second virial coeffs. from compressibility meas., mol. pot. parameters calc. *(Spanish)* 77—47133
N_2, thermodynamic and transport props., consistent correlation using Lennard-Jones (12-6) and Buckingham (exp-6) pots. 78—91045
Ne, molar volumes and thermodynamic props., 25 to 150C, up to 7 kbar 77—42957
SF_6, second virial coeffs. from compressibility meas., mol. pot. parameters calc. *(Spanish)* 77—47133

compressibility of liquids
acetone-methanol, acetone-CCl_4, methanol-CCl_4 and acetone-methanol-CCl_4 mixtures, acoustic and physicochem. obs. 79—96347
acetonitrile-carbon tetrachloride-n-butanol, mixtures, compressibility, free length, molar and available vol., US meas. 78—2200
acetonitrile-methanol, excess vol. and isentropic compressibility, from density and US vel. meas. 78—79776
acetonitrile-toluene-n-butanol, mixtures, compressibility, free length, molar and available vol., US meas. 78—2200
acrylamide aqueous solution, ultrasonic investigation *(Chinese)* 80—107371
air-water interface, modified technique for dynamic surface press. and relax. meas. 78—6201
alcohols, dil. aqueous solns., isentropic compressibility behaviour from sound vel. meas., dissolution mechanism 80—30269
alkali halides, molten, rigid sphere model 77—7946
alkali nitrates, molten, pVT data, thermal press. coeffs., compressibilities 78—43097
alkali nitrates, molten, thermodynamic study *(French)* 77—31781
n-alkanes, isothermal compressibility 78—47461
aniline, determ. from US velocity meas. *(Japanese)* 77—59068
aniline-phenol, liq., US vel., adiabatic compressibility, H-bonded complex form. 77—35635
aqueous non-electrolytes, solution structure, adiabatic compressibility studies 78—87605
benzene binary liquid mixtures, adiabatic compressibility and mol. interaction 77—15494
benzene-cyclohexane(carbon tetrachloride), binary liq. mixtures, molar heat capacity isothermal compressibility 79—66328
benzene-ethanol, excess vol. and isentropic compressibility, from density and US vel. meas. 78—79776
benzene-n-heptane, excess vol. and isentropic compressibility, from density and US vel. meas. 78—79776
benzene-tetrahydrofuran, soln., excess thermodynamic props. and interactions, US vel. and density meas. 80—39288
benzene-toluene and benzene-o-xylene mixtures, US vels., compressibility, expsn. coeff. 79—33038
benzyl alcohol-n-butanol, excess vol. and isentropic compressibility, from density and US vel. meas. 78—79776
binary liquid alloys, surface tension, compressibility and surface segregation 78—67889
binary mixtures near critical state, gravitational distrib. of thermodynamic props. *(Russian)* 80—88241
borate glass melts, struct. determ. using graph theory 79—64980
bromobenzene+m-xylene, US vel. and adiabatic compressibility 78—51614
butanol-methylethyl ketone, soln., excess thermodynamic props. and interactions, US vel. and density meas. 80—39288
t-butyl alcohol, aq. soln. 80—88237
n-butyl alcohol, dil. aq. soln., US vel., 4.04 MHz 78—67770
carbon tetrachloride-benzene(cyclohexane), binary liq. mixtures, molar heat capacity isothermal compressibility 79—66328
CBOOA, liq. cryst.-isotropic transition at high press., P-V-T eqn. of state 79—95135
o-chlorophenol-acetone (ethyl methyl ketone), thermodynamic and transport props. 80—92686

compressibility of liquids continued
cholesteryl nonanoate, liq. cryst.-isotropic transition at high press. 79-95135
colloidal dispersions, conc., hexagonal close packed, disjoining pressures calcs. 78-23971
cryogenic binary mixture, ultrasonic velocity, compressibility, heat capacity, at 298.15K 79-10898
cryogenic liquids, Jacobson's const. and intermolecular free-length eval. w.r.t. pressure and temp. 80-15176
4-cyano-4'-octylbiphenyl, smectic-A phase, layer compressibility coeff. 79-73297
cyclohexane, determ. from US velocity meas. *(Japanese)* 77-59068
dioxan(-oxalic acid)(-benzoic acid), solns., compressibility, internal press., US vol., H-bonding 79-82272
dioxan-cyclohexane-chloroform, mixtures, compressibility, free length, molar and available vol., US meas. 78-2200
dioxan-methanol system, US vel., compressibility, complex form. 79-82283
p-dioxane-water mixtures, adiabatic compressibilities and sound vels., temp. depend. 79-28044
diphenyl hexachloride, liq., imaginary compressional modulus (compressional viscosity) 77-76480
electrolyte solutions, light scatt., conc. depend. of compressibility and activity coeffs. *(Russian)* 77-1758
electrolytes, US determ. of adiabatic compressibility, and hydration numbers 78-20027
electrolytic aqueous solution, US study of apparent molar compressibility 78-10125
emulsion, osmotic compressibility, hard sphere fluid calcs. 77-9129
equation of state, modified Redlich-Kwong-Soave, liq. state representation 77-27968
ethane, fluid, saturated, compressed, sound velocity meas., compressibility, sp. ht. determ. 77-76488
ethanol-water mixtures, specific volume, compressibility, viscosity, up to 3200 bar, 15, 25°C 78-10113
ethyl alcohol, dil. aq. soln., US vel., 4.04 MHz 78-67770
ethylene-propylene copolymer, solution in hydrocarbon solvents, adiabatic compressibility 77-51425
glycerol, influence of electrolytes on acoustic props. 78-75728
haemoglobin, in salt soln., diffusion rel. to intermol. interactions, light scatt. investig. 77-44585
hard hetero/homonuclear diatomic mol. fluid, Monte-Carlo simulations 78-42873
hard sphere, surface tension, compressibility, bulk modulus press. coeffs. and Rao's acoustical parameter 80-80027
hard-sphere fluid, direct correl. function 79-41918
hard-sphere liquids, equations of state and evaluation of isothermal compressibility 79-73285
4-4'-di-heptyloxyazoxybenzene, liq. cryst.-isotropic transition at high press. 79-95135
n-hexane, superheated liq., US wave vel., adiabatic compressibility, heat capacity 78-2198
hexantriol-1,2,6, influence of electrolytes on acoustic props. 78-75728
hydrocarbons, saturated open-chain, transport behaviour of excess electrons and props. 80-39643
hydrocarbons, shock compression, dynamic high press. eqns. of state 80-6450
Isopar-M, pressure-volume isotherms determ., use in deep-sea instrument float 77-25786
isothermal, meas. over wide temp. range 77-43265
isothermal bulk modulus and compressibility, intermol. interaction *(Russian)* 77-35658
isothermal compressibility 78-47461
liquid crystal, isotropic phase, compressibility and thermal expansion anomalies, appl. to MBBA 77-43138
liquid metal, isothermal compressibility, harmonic pot. model calc. 79-14870
liquid-vapour interface, surface tension-compressibility relation 80-44397
lysozyme-salt water soln., critical mixing point, turbidity and viscosity meas. 77-86437
MBBA, liq. cryst.-isotropic transition at high press., P-V-T eqn. of state 79-95135
MBBA, nematic-isotropic transition, isothermal compressibility and thermal expansion coeff. meas. 79-99301
MBBA, volume meas. and phase transitions at high press. 79-90764
metal, electronic theory of thermodynamics and struct., summer school lecture series 80-6353
metal, long wavelength limit of liquid struct. factor, compressibility 78-67633
metals, compressibility calc. by struct. factor *(Russian)* 78-59847
metals, isothermal compressibility and eqn. of state at m.p. 80-79673
metals, liq., compressibilities, surface tension at melting temp. 78-91370
methane, liq., mol. dynamics calcs. 77-19857
methane+N_2(Ar), compressed-liquid dielectric const., derived excess vol. 79-11377
methyl alcohol, dil. aq. soln., US vel., 4.04 MHz 78-67770
methylethyl ketone-butanol, soln., excess thermodynamic props. and interactions, US vel. and density meas. 80-39288
micellar solutions, crit. behaviour 80-105601
mixtures, binary, excess isentropic compressibilities and isochoric heat capacities 80-21313
molecular dynamics simulation, sp. ht., thermal press. coeffs., compressibilities 77-28013
molten metal, relation between surface energy melting temp. and Fermi wavelength 77-51571
molten salts, compressibility hard sphere calcs. 77-51295
molten salts, isothermal compressibility obtained from adiabatic thermal press. coefficients 79-95065
multicomponent alloys, partial struct. factors in the long wavelength limit 78-22633
nitrobenzene-aniline, US vel., sp. ht. and compressibility 79-33037
nonelectrolyte aqueous solutions, temp. of max. density rel. to partial compressibility, struct. strengthening 80-30270
one-dimensional fluid, triangular well pot., perturbation theory 77-35455
organic ternary liq. mixtures, intermolecular interaction study, US vel. meas. 80-79879
phenol-aniline (quinoline) (pyridine), liq., US vel., adiabatic compressibility, H-bonded complex form. 77-35635

compressibility of liquids continued
piezometer deformation errors in gas and liquid compressibility meas. 78-5646
Pitzer correlation extension for compressibility factor calcs. 79-86557
polarisable hard sphere fluid, thermodynamic props. 79-42277
polarity parameters correlation with compressibilities 79-19305
polyacrylamide aqueous solution, ultrasonic investigation *(Chinese)* 80-107371
polyethylene glycol solns., US vels. and adiabatic compressibility 77-72655
polyethylene terephthalate, solid and molten, press. effects on compressibility and crystn., thermodynamic interpret. 80-84102
polymer solution, partially deuterated, osmotic compressibility from elastic neutron scatt., general formulation 79-90517
polymer solutions, dynamic compressibility study via press. transient technique 77-86256
polystyrene, diethyl malonate soln., near-crit., osmotic compressibility, correlation length, scaled functions 80-11422
polystyrene, swollen network in benzene, pendent chains, influence on thermodynamic and viscoelastic props. 80-28481
polystyrene melt, viscosity, thermodynamic props. *(Russian)* 79-51295
polystyrene solution, in toluene and cyclohexane, acoustic absorption and dynamic compressibility 77-55321
polythene melts of high density, viscosity meas., entropy and compressibility *(German)* 78-67162
polyvalent electrolyte apparent molal adiabatic compressibility and US vel. obs. 78-61028
n-propyl alcohol, dil. aq. soln., US vel., 4.04 MHz 78-67770
proteins, globular, compressibility in water at 25°C 80-40951
quantum liquid mixture, stability and stratification 80-59754
Rao's acoustical constant, temp. depend., from C_1-parameter 80-6462
rare gases, liquid, long wavelength limit of liquid struct. factor, compressibility 78-67633
seawater, differential isothermal compressibility meas., hydration and ion-water interactions 77-73761
semiconducting liquid alloys, anomalous thermodynamic props., theory 80-49287
simple fluids, hard- and soft-core eqns. of state, characteristic curves 79-55861
simple fluids, hard-core equations of state, characteristic curves 79-55862
simple liquids, thermodynamic props. and solubility parameters 78-2265
simple metal, entropies and struct. factors 77-7656
smectic-A liquid crystal, layer rigidity, stress relax. 78-18545
solutions in alcohols, ultrasonic vel. and density meas. used to calc. compressibility, intermol. free length and salvation no. 80-96150
square-well fluid, eqn. of state and thermodynamic props. 77-7834
structural relaxation times, smoothed cell potential model 77-27796
temperature dependence, eqn. 79-90710
ternary liquid mixtures, molecular interaction and thermodynamic props. 78-59861
ternary liquid mixtures, nonlinear effects with high amplitude US prop. 78-51613
ternary liquid mixtures, physical props., determ. by density and US vol. meas. 79-37751
tetrahydrofuran-benzene, soln., excess thermodynamic props. and interactions, US vel. and density meas. 80-39288
thermally induced surface fluctuations on simple fluids 80-88403
thermodynamic results for simple fluids with various pots. *(Spanish)* 77-72533
thermophysical properties rel. to compressibility 78-83964
triangular-potential fluid, Zwanzig's perturbation theory, appl. to thermodynamic props. 79-41920
triple point surface tension and bulk modulus, theoretical relationship 78-47638
two-dimensional square well fluid, anal. eqns. for compressibility factor 79-77664
unassociated liquids, estimate of props. 79-51232
water, anomalous compressibility to 1-9 kbar, correl. with supercoding 79-65134
water, compressibility modulus 78-75701
water, determ. of adiabatic compressibility on basis of Schaaffs' molecular kinetic theory, 25 to 80°C 80-88265
water, eqn. of state determ. from sound speed eqn., sp. vol. and compressibility 77-47538
water, physical props., two-state model approach 80-75144
water, Rayleigh-Brillouin scattering and compressibility 79-91455
water, relax. compressibility and heat capacity 80-92580
water, shock compression at press. approaching 1 Mbar *(Russian)* 80-79851
water and saturated monatomic alcohol mixtures, effects of chlorides on struct. 79-86840
water-dioxane mixtures, compressibility, density, US vel. rel. to temp., conc., struct. *(German)* 77-43263
water-urea-valeric acid systems, sound vel. and liquid structure *(Japanese)* 77-1177
weakly associated liquid, US wave reson. absorpt. 80-34141
Al, liquid, dynamical struct. factor 78-71667
Al-Si, compressibility and struct. factors at zero wavevector 79-23515
$Al_2(SO_4)_3$ soln., adiabatic and apparent molal compressibility determ. from US vel. meas. 78-63797
AlSb, molten, temp. depend. of vel. of sound and adiabatic compressibility 77-27944
Ar, hole theory, compressional viscosity and vibrational relaxation 80-70311
Ar, liq., shock wave compression, 400 to 910 kbar 80-29101
Ar, mol. dynamics calc. 77-19857
Au-Co alloys, molten, US vel. meas., compressibility and partial struct. factors determ. 77-69045
Au-Co melts, struct., compressibility, X-ray and neutron diffr. 77-11614
$BiCl_3$-Bi molten solution, US velocity and compressibility 77-84845
$CaCl_2 \times 5.99,5.33H_2O$, molar cond., compressibility, expansivity 78-51712
$Ca(NO_3)_2.nH_2O$, aq. soln., conc., compressibility, elec. cond. 77-69024
Cd-$CdCl_2(Br_2)(I_2)$ molten solution, US velocity and compressibility 77-84844
$CdCl_2$-NaCl, KCl molten salt mixtures, US velocity and adiabatic compressibility obs. 78-75730
$Ce_2(SO_4)_3$ soln., adiabatic and apparent molal compressibility determ. from US vel. meas. 78-63797
Co, struct. factor and isothermal compressibility 77-11462

compressibility of liquids continued
  Cs, volume and compressibility up to 22 kbar, eqn. of state 77–47541
  CsCl, aq. soln., density, isothermal compressibility, 293.15K, up to 200 MPa 80–44243
  D_2O, compressibilities and sound speed rel. to normal water as function of temp. and press. 78–2201
  D_2O, heat capacity, compressibility and speed of sound 79–82284
  D_2O-H_2O mixtures, US vel. at 298.15K, adiabatic compressibility 78–10127
  F, hard sphere model with attractive interactions 80–96434
  Fe, struct. factor and isothermal compressibility 77–11462
  Fe-Cr melts, ultrasonic propag. and isothermal compressibility using pulse-phase method *(Russian)* 79–51202
  Ga, liq., effective pair pot. and thermodynamical props. 77–47600
  Ga-Sn alloys, compressibility, US velocity meas. *(Russian)* 77–59060
  Ga-Te alloys, liq., compressibility and US velocity meas. 77–51426
  GaSb, molten, temp. depend. of vel. of sound and adiabatic compressibility 77–27944
  Ge, temp. depend., MP to 1400K 77–15498
  H_2, liquid, effect of ortho-para composition *(Russian)* 78–34419
  H_2, liquid, shock compression obs., various geometries 77–58732
  H_2, perturbation theory and quantum effects, thermodynamic props. and quantum stat. corrections *(Russian)* 78–22867
  $HClO_4$, aq. soln., anomalous u.s. props. 77–1176
  H_2O, shock compression at high press. *(Russian)* 80–92608
  ^{3}He, equation of state and crit. exponents near liq.-vapour crit. point 80–24707
  ^{3}He-^{4}He mixture, equation of state and crit. exponents near liq.-vapour crit. point 80–24707
  ^{4}He, superfluid, thermodynamic props. determ. from sound velocity data 77–15649
  ^{4}He, superfluid, thermodynamic properties, at very low temps., rel. to interacting boson systems 78–2320
  Hg, electrical and thermodynamic props. in metal-semicond. transition range 80–20144
  Hg, expanded liq., thermodynamic and electron transport props. 79–23938
  Hg, P-V-T relations for temperatures of 40 to 240°C and press. up to 1400 kg cm^{-2} 78–6140
  Hg-In (3 at.%), amalgam, thermodynamic and electron transport props. 79–23938
  Hg-Na (3 at.%), amalgam, thermodynamic and electron transport props. 79–23938
  InSb, molten, temp. depend. of vel. of sound and adiabatic compressibility 77–27944
  K, isothermal compressibility calc. at 400 to 1800K from density data 78–2186
  K, volume and compressibility up to 14 kbar, eqn. of state 77–47541
  KI, soln. in organic solvents, elec. cond., shock compression effects 79–46822
  Li-Ag, liq. alloy, density, compressibility and diffr. data 77–47336
  LiCl, aq. soln., density, isothermal compressibility, 293.15K, up to 200 MPa 80–44243
  LiCl, aqueous solution at 298.15K, isentropic compressibility 78–22783
  MBBA, nematic-isotropic transition, compressibility-press. relations obs. 77–51481
  N_2-Ar(methane)(ethane) binary and ternary mixtures, dielec. const., excess vol. 80–7254
  Na, volume and compressibility up to 22 kbar, eqn. of state 77–47541
  NaCl, aq. soln., isothermal compressibility, hydration parameters, up to 350°C and 10^3 kg cm^{-2} 78–10112
  Ne, mol. dynamics calc. 77–19857
  Ne-H_2 mixture, liquid vapour phase equilib., sound vel., compressibility, thermodynamic perturbation theory obs. *(Russian)* 80–39306
  Ni, struct. factor and isothermal compressibility 77–11462
  $NiCl_2$, aq. soln., viscosity meas., struct. props. 78–75863
  Pb, thermodynamic characterisation, by isobaric expansion meas. 80–103494
  Pu, hard-sphere model, phys. prop. meas. interpret., adjacent solid phase implications 77–19866
  S liquid, compressibility 77–65997
  Se liquid, compressibility 77–65997
  Se, US rel. temp. depend., melting effects 78–38782
  Tb, struct. factor and compressibility, rel. to metal-nonmetal transition 78–2529
  Te liquid, compressibility 77–65997
  Te, US rel. temp. depend., melting effects 78–38782
  Te-Se liquid mixtures, sound vel. meas., adiabatic compressibility determ. 80–65161
  U, hard-sphere model, phys. prop. meas. interpret., adjacent solid phase implications 77–19866
  Zn-Cd alloys, liq. and solid, ultrasound speed and compressibility meas. 80–102941
  $ZnCl_2$-LiCl(NaCl)(KCl)(CsCl), molten, US velocity, thermodynamic quantities and struct. *(Japanese)* 80–88270

compressible flow
  see also compressibility
  acoustic gravity waves travelling wave solns. 80–48721
  acoustic noise of compressible fluid flow in pipes and valves *(French)* 77–19477
  acoustic resonance in vaneless radial diffusers with swirling flows 79–18882
  acoustic velocity, compressible liquid flow with heat transfer 79–14131
  acoustic wave propag. in waveguides with moving medium, energy transport 77–46837
  acoustic wave propagation, pressure field soln. 80–6077
  adaptive-wall wind tunnel, iterative anal. of subsonic flow 78–22364
  Aerodynamic investigation of a planar multi-channel subsonic venturi tube *(Russian)* 79–50796
  air, damp, working characteristics of vortex tubes *(Russian)* 80–74903
  air, dry, through pipe, kinetic tenecity calc., with aid of nomogram *(German)* 77–35244
  air jet, heated, turbulent, discharged downward, temp. profiles 79–27677
  aircraft engine intake flow distortions leading to acoustic fatigue failure of inlet guide vanes 80–53542
  Alfven-acoustic-gravity wave propag. and reflection, compressible, inviscid, perfectly conducting isothermal fluid 77–51124
  anti-dynamo theories, compressible flow effect 80–56361
  approximate solution in gasdynamics 80–92174
  atmosphere, gravitational convection with compressibility 79–58051

compressible flow continued
  atmosphere, MHD wave propag. in presence of rot. and variable mag. field 79–40024
  atmospheric air, shock formation distance 79–37351
  axial-flow compressor cascade flows computer simulation 78–79333
  axisymmetric confined flame, aerodynamic and heat transfer, finite difference scheme, program 78–94689
  axisymmetric steady flow, slightly conducting gas in mag. field 77–15128
  blast loading on three-dimensional structures, transient, computational simulation 77–68624
  blunt body in supersonic flow, Navier-Stokes eqns. numerical computation 80–10263
  blunt-based axisymmetric body, subsonic turbulent near-wake 78–94740
  boundary layer, 3D, stagnation pt., compressible, large injection rate 77–89139
  boundary layer, near oscillating porous plate 77–84268
  boundary layer, nonstationary, with self-induced press. 78–34164
  boundary layer, refractive index meas. by light refl. 78–8438
  boundary layer, Reynolds number effects on turbulence field 80–19434
  boundary layer, stagnation point, discontinuous solns. for three-dimens. flow 77–42856
  boundary layer, unsteady, similarity problems 78–1633
  boundary layer flow, laminar, thermal response behaviour 78–75136
  boundary layer flow, unsteady, compressible, 3-D, near axisymmetric stagnation point 80–103011
  boundary layer flow past profile set between permeable walls 79–46335
  boundary layer flow singular nonlinear differential eqns. 78–63413
  boundary layer turbulence at high subsonic speed, coherent structures 80–19422
  boundary layer with hard suction 78–26097
  boundary layers, laminar, compressible, Prandtl=0.72, sharp pressure rise effect 80–83782
  boundary layers, laminar and turbulent, two-point finite difference method 77–19617
  boundary layers on expanding cylinder and sphere 77–35158
  boundray layer, oscill., numerical anal. 77–89140
  branched converging compressible flows, separation and blockage 79–37337
  bubble cavitation in inviscid compressible liq. 80–28553
  bubble in liquid subject to tension pulse, model 79–55406
  canal, converging, unsteady 2-D compressible boundary layer flow 79–20885
  cascades with different trailing edge thicknesses, vortex shedding freq. determ. 78–75152
  cavitating fluid model *(Russian)* 78–55668
  cavity flow, compressibility effects in channel for wedge shaped obstacle 79–77256
  channel, friction, with a pseudoshock 77–27546
  channel flow, unsteady, of compressible gas with shock waves, appl. to gasdynamic laser 77–72327
  chemically reacting flows, turbulent, steady and unsteady, computation in axi-symmetrical domains 80–1697
  circular plane parallel flow around cylinder *(Russian)* 77–68618
  complex aerofoils, compressible flows, isoparametric Hermite cubic element 80–1617
  compressible flow fields, two-dimensional, computation by modified local stability scheme 78–1681
  compressible supersonic turbulent boundary layers, compressible press. gradient effects 79–60001
  compressible turbulent boundary layer, improved Van Driest skin-friction formula 77–58712
  compression shock stability in streams of spontaneously condensing vapour 80–28563
  conical diffuser, with suction, compressible boundary layer swirling flow 78–38360
  conical nozzle and diffuser, laminar compressible boundary layer swirling flow 80–48768
  conservation equations, characteristic method of lines soln. 80–59064
  conservative difference scheme, second order sequel to Godunov's method 79–72907
  convection, natural, in spherical layer of viscous compressible gas 78–9640
  convection in compressible fluid with infinite Prandtl number 80–38398
  critical flow, choking, finite difference calcs. *(French)* 77–19616
  curved wall, turbulent boundary layer detachment by perpendicular compressive thrust *(German)* 78–94661
  curved wall flow turbulence, integral method calc. *(French)* 77–54984
  cylinders, optimum stepped piston 77–42860
  cylinders and airfoils, primitive variable least-squares finite element formulation 80–33623
  detonation sputtering, gas flow parameters calc. *(Russian)* 80–16181
  detonation sputtering, interaction between detonation waves and gas and powder flows *(Russian)* 80–16182
  difference schemes from fluid mechanical integral theorems 78–14032
  diffusive instabilities in rotating elec. conducting compressible layers 80–38379
  dispersive compressible fluid, steady two-dimens. jet flow 80–64598
  dispersive compressible fluid, transonic nozzle flows 80–69895
  duct, curved transition type, three-dimens. turbulent subsonic flow calc. 80–38498
  duct flow, 2-D viscous and compressible, momentum and energy transport, streamwise computation 80–53858
  duct flow, base press. oscills. 79–46386
  duct flow, compressible laminar flow, superimposed sound field effect 77–75933
  duct flow, laminar, numerical method 79–4030
  duct of arbitrary cross section, parabolic procedure for three-dimens. compressible viscous flow prediction 79–94716
  ducts, 3-dimens. viscous compressible flow, inviscid flow considerations for 90° elbow 80–64639
  ducts, steady 2-dimens. axisymmetrical turbulent boundary layer, compressible fluid *(Chinese)* 80–59109
  dust trajectory photography for compressible flow velocity meas. 79–82008
  Ekman layer, mechanically induced unsteady compressible, theory 80–24033
  elastic compressible spheres, flow in tubes 80–24097
  elastic porous media, transient compressible liq. flow, linearisation of non linear partial differential eqn. 78–63490
  elastic shells, excitation and stress field in compressible fluid 78–51183

compressible flow continued
elastic tube conveying compressible flow, 2-dimens. model nonlinear stability anal. 79—64547
elastico-viscous fluid, compressible, nonperiodic wave propag. 80—43724
elementary gasdynamics of real fluids, similarity principle 77—75876
Euler equation for compressible flow, integration scheme 79—81913
Eulerian and Lagrangian computer codes, pressure iteration, multigrid method 80—53738
Eulers eqns. soln. for expansion of sphere at constant velocity *(French)* 80—33719
expansion of compressible fluid in venturi, critical rate determ. *(French)* 78—55659
finite element methods, book contrib. 79—32446
finite shrouded disc, laminar boundary layer in rot. compressible isothermal flow 80—43727
flat bodies with blunt tail sections, subsonic flow and wake obs. 77—68616
flow around lattice, calc. by successive approxs. *(Russian)* 78—63443
fluid, perfect, 3-dimens. rot. flow, Lagrangian invariants appl. 80—43720
fluid channels indirect design using global variational method with trial functions 77—27595
fluid force on oscillating disc in a still fluid 80—14724
forced convection flow and heat transfer of compressible fluid in porous medium *(French)* 78—30354
free boundary motion and nonsteady flow 80—6078
free shear layer, compressibility effect on stability 80—33562
fusion reactors, divergent impulsive crossflow over packed columnar arrays 80—47702
gas, calc. 77—7410
gas, conducting, stream flow in orthogonal mag. and mass forces fields *(Russian)* 77—27618
gas, dissociating, relativistic flows, growth and decay of weak waves, shock wave formation 80—69949
gas, fluid mechanics eqns. invariant solns. 79—90272
gas, heat exchange in free convection condition *(Russian)* 80—28502
gas, perfect, vortex sheet, separation from smooth body at large Reynolds number *(French)* 80—74908
gas, rot. in mass-transfer equipment, eddy contact element radial press. distrib. 78—26126
gas, Stewartson 1/3 layer in countercurrent centrifuge *(French)* 77—928
gas centriguge, effect of compressible flow on max. separating power 78—70644
gas compression in heavy piston, hypersonic speed, shock waves 80—69869
gas flow in catalytic convertor, numerical soln. 78—67281
gas flow in non-uniform pipe, gas-line model, acoustic wave anal. 80—14726
gas flow into duct, self-excited oscillations 80—33647
gas flow past surface, interaction of radiation with convection *(Russian)* 80—99994
gas flow through cracks, surface roughness influence 80—69929
gas flow through exhaust valve, analytical calc. using flux analysis method *(Japanese)* 80—69896
gas jet, wall impact model, subsonic 78—34176
gas jet transport system, steady state, radioactive distrib. in compressible stream tube *(German)* 78—90007
gas with fluctuating pressures and temperatures, meas. by transit time of spark charged plasma cloud determ. *(German)* 80—14861
gas-liquid laminar flow, numerical investigation *(German)* 77—15111
gas-particle flow in shock tube, finite difference calc. *(Japanese)* 80—79390
gases with molecular viscosity, flow calc. in large particles method *(Russian)* 80—74826
Goethert's rule with improved boundary condition 78—26138
gravitational compression of a body within the approximation of the special theory of relativity 80—4611
gravitational instability in presence of suspended particles and rot. 79—64633
gravity wave, internal, propag. in shear layer, discontinuity form. 79—32543
Hartmann-Sprenger tube, gas temperature calc., using Lagrange equations *(Japanese)* 79—4041
heat and momentum transfer to axisymmetric bodies, free stream turbulence 77—11216
heat exchange, unsteady, between semiinfinite plate with heat sources and gas stream 77—75918
heat pipe, gas-loaded, near ideal, analytical model 80—53615
high Reynolds number supersonic flow, compression corner flowfields, turbulent boundary layer separation 80—14735
high subsonic Mach number boundary layer, turbulence effects on artificial thickening 77—27545
hodograph eqn., numerical soln. 78—51179
holonomic formulation of boundary layer eqns., use of tensors 79—1153
horizontal pipes, isothermal compressive gas flow with imperfect gas 79—77258
hot wire anemometry of turbulent compressible gas flows 79—46408
hydrodynamics computer codes, limited compressibility 80—53803
hypersonic turbulent compression corner flow, numerical simulation 77—62276
ideal electrically conducting gas, weak discontinuities in singular surface theory 80—43736
ideal gas, polytropic soln. to problem of spherically symmetric flow 80—106810
ideal gas flow, choked and supercritical, through orifices and convergent conical nozzles, numerical soln. 80—38474
implicit finite difference method, Romb, for numerical solution of hydrodynamic flow and heat conduction *(Russian)* 80—14725
incompressible viscous Navier-Stokes eqn., numerical soln. by finite element of penalisation type 79—50747
integral momentum eqn. for flows with entropy gradients across inviscid streamlines 77—11214
inviscid, rotating, compressible fluid, linear stability 80—92161
inviscid fluid, profile of isogradient vaneless diffusor with swirl flow 79—86445
inviscid ideal gas flow, direct simulation methods 80—48733
inviscid linearly-sheared parallel flow, characterisation of acoustic disturbances 80—69848
jet, circ., controlled perturbation, smoke visualisation 78—90956
jet, circ., free shear layer transition wave development 78—94643
jet, coaxial, initial swirl of inner and outer flows effect on aerodynamics 77—68652

compressible flow continued
jet, hodograph eqn., numerical soln. 79—60042
jet, hypersonic liq., moving into gas, shock layer anal. 78—26177
jet, supersonic, flowing onto infinite perpendicular barrier, limiting expansion ratio 78—59439
jet, turbulent, plane, impinging on plane surface, RMS boundary press. pulsations 78—59438
jet exhaust noise, role of shear-layer instability waves 77—47054
Lagrangian and Hamiltonian formulations of compressible hydrodynamics 79—94581
laminar boundary layer, acoustic field effect for compressible liquid *(Russian)* 77—68617
laminar boundary layer, with adverse press. gradient, development and separation 78—26144
laminar boundary layer with large acceleration and cooling 77—11213
laminar boundary layers, at large Prandtl numbers, pressure gradient effects 80—19321
laminar boundary layers, stagnation point flow with continuous moving surfaces 77—15054
laminar boundary-layer flows with swirl and large suction 80—1519
laminar compressible boundary layer, with vectored mass transfer 77—23974
laminar compressible boundary layer flow at stagnation pt., vectored mass transfer 79—27661
laminar compressible boundary layer flow at stagnation pt. 79—10583
laminar compressible boundary layer on rot. sphere with heat transfer, buoyancy and viscous dissipation effects 77—15053
laminar compressible boundary layer swirling flow in nozzle, flow and heat tranfer 78—94795
laminar compressible boundary layers, Taylor-Gortler instability 78—26140
laminar compressible boundary-layer, 2D eqn., near separation, numerical soln. 77—46989
laminar compressible MHD boundary layer flow, effect on heat transfer 79—14489
laminar to turbulent boundary layer transition prediction, linear stability theory 78—38279
laminar trailing edge stall, triple-deck eqns. num. soln. 77—55020
laminar wall jet 80—28542
laser heated nozzle flow with swirl, axisymmetric comp. boundary layer 80—14775
Laval nozzle, reflection of acoustic waves from subcritical inner parts 77—27574
lifting, asymptotic estimate of trancative error *(French)* 80—19419
around lifting profiles near permeable walls *(French)* 77—68614
liquid layer adjacent to gas stream, surface waves, subsonic and supersonic disturbances 79—23336
liquid metal flow in heat pipe, low temp. region, effect of compressibility, friction and evaporation 77—47066
low Mach number flow in presence of isolated obstacle *(French)* 80—53806
Mach line flow, two-dimens., equivalence conditions, physical interpretation *(German)* 80—1634
magneto-acoustic waves, generation and radn. in compressible fluid 77—68699
magnetogasdynamics, reciprocal type transformations 80—48804
mass gas flow stabiliser, expt. 77—75960
meridional flow of compressible fluid in a rapidly rotating short cylinder 80—106812
metals, compressibility in presence of anharmonic interaction *(Russian)* 78—23763
MHD, in transverse mag. field, streamline orthogonal-net anal. 79—37417
MHD flow, compressible, subsonic, use of Pitot tube probe 77—84347
MHD generator, compressible laminar boundary layer separation from segmented electrode wall 77—27598
MHD shear flow stability 78—51244
MHD slip flow regime over porous plate, skin friction and heat transfer 77—31392
MHD streams, interaction of bounded subsonic and unbounded supersonic MHD streams 79—37419
MHD-gravity waves, over-reflection in stratified flow 77—11207
mixed compressible flow, type-independ. soln. 79—4035
molecule, moving in compressible viscous fluid, hydrodynamic drag 79—27732
Mott-Smith method for shock waves in supersonic compressible flow, modification 79—50754
Navier-Stokes eqns. similarity solns. for large Prandtl number 77—3801
Navier-Stokes equation, limiting form at high Reynolds number *(French)* 80—74823
Navier-Stokes equations, Lighthill's theory to non-adiabatic cases 78—83372
Navier-Stokes equations, mixed explicit-implicit splitting method 77—58715
Navier-Stokes equations, num. soln. at high Reynolds no., blunt body problems applic. 77—55019
Navier-Stokes equations, num. soln. method for hyperbolic systems of eqns. 77—58716
Navier-Stokes solutions using Stetter's method 79—32551
Newtonian fluid, laminar flow between rotating discs 77—31320
non-isothermal disc rot. in quiescent compressible gas, heat transfer 80—14704
non-uniform pipe gas flow simulation model 80—33682
non-viscous barotropic fluid flow in bounded domain, existence theorem *(French)* 80—42068
nonadiabatic compressible gas flow in tube, eqns. system numerical integration *(Russian)* 78—83427
nonaxisymmetric flow problems, computational technique 79—55419
nonequilibrium adverse pressure gradient flow, turbulence model 77—58660
nonequilibrium gas flow, growth of discontinuities 80—48734
nonlinear differential eqns. of plane, vortex-free flow, integration *(German)* 77—11218
nonlinear near-sonic potential flow with viscosity, solns. *(German)* 80—1646
nonlinear one-dimensional waves in near-sonic flows 79—41701
nonsteady flow of dropping compressible liquid in pipes, effect of friction laws 77—55091
nonthermally conducting gas, monotonic difference scheme of open calculation *(Russian)* 80—103039

compressible flow continued
nonuniform grids in finite difference approximations, application to fluid flow problems 80—105507
not-so-slender wing theory 77—58717
nozzle, convergent-divergent, compressible turbulent boundary-layer heat transfer *(German)* 78—22399
nozzle, critical air flow, heat transfer, numerical study 79—98778
nozzle, heat transfer of transonic air flow 79—1230
nozzle, subsonic and supersonic, turbulent boundary layer heat transfer 79—1229
nozzle and diffuser flow, laser heated, laminar compressible boundary layers 80—53831
nozzle of rocket, compressible turbulent boundary layers, heat transfer and skin-friction 79—14451
nucleation homogeneous, gasdynamics of supersonic flow with condensation 77—62292
numerical convection, upstream-centred scheme 77—27548
numerical integration of the gasdynamic equations 80—92175
obstacle in potential flow, vortical and entropic distortions 79—32532
one-dimensional flow with heat addition theory 77—916
orifice flow, computer-aided numerical anal. 80—87806
orifices, rectangular square edge 79—77161
parallel compressible flows, stability inviscid theory 77—72277
parallel viscous flow, linearised disturbances, asymptotic solns. 77—35161
perfect fluid, irrotional stationary flows, unicity condition *(French)* 78—87356
permeable boundaries in multidimensional unsteady flow 80—38490
permeable capillaries under deform., press. loss model 78—26141
permeable plate gas screen region, heat transfer and friction laws 79—1250
perturbation potential for unsteady near-sonic flows *(German)* 80—1635
pipe flow of ideal gas analysis, numerical methods comparison *(German)* 80—33621
pipeline compressible flow and heat transfer simulation program 77—19638
planar gas flows with weak energy supply 79—90273
plane, calc. using equipotential equation 79—90274
plane parallel elec. charge fluid, Lyapunov functionals 77—14990
plane periodic waves, nonlinear propagation in relaxing gas, numerical anal. 80—92170
plane plastic flow of compressible solids 78—55575
plane steady flow, variational anal. 80—92173
plane subsonic flow with circulation, generalised indirect calc. method *(German)* 79—86452
plate, flat, attached subsonic and transonic turbulent boundary layers, press. fluctuations effect 79—94642
plate falling upon surface of compressible liq. *(Russian)* 77—929
polymer solution, compressible flow about spherical polymer mol. 79—10595
polytropic medium layer on linear elastic substrate, mass-impact generated shock waves 80—69870
porous medium, laminar isothermal flow of two immiscible compressible fluid phases 80—69919
porous plate skin friction, injection or removal from boundary layer due to turbulent wall jet 78—47029
Prandtl-Meyer expansion with access of heat *(German)* 79—86484
pressure relief valves, maximum isentropic flow of dry saturated steam 79—81978
pulsating laminar compressible flow in cylindrical pipe with through flow 77—80216
quasi-one dimensional steady compressible flow, time marching finite area calc. 79—81912
radiating gases, sonic wave propag., wave front curvature effects, shocks 80—87784
radiative gas dynamics, radiation transfer eqn. *(Russian)* 80—64653
Rankine-Hugoniot jump conditions, viscous and thermal effects 78—59418
reattaching laminar and turbulent separated flow, three-dimens. heat and mass transfer 77—65759
recent theoretical and expt. developments, book 80—1620
recovery temperature data for cylinders in compressible flow 77—47036
over rectangular cavities, induced tones and press. oscills. meas. 79—32493
rectangular elbow, 3-dimens. turbulent compressible duct flow, stagnation pressure losses, vortices 80—64640
rectangular surface embedded in uniform subsonic flow, stability 77—80178
relativistic gas dynamics in two dimens. 80—83863
relaxing gas flow, discontinuity growth 80—28525
Reynolds equation at very low spacing, compressible, numerical soln., factored implicit scheme, mag. recording appl. 80—92183
rotating Bernoulli surfaces in compressible inviscid flow, vorticity transport 80—19403
rotating cylinder, linearsed anal., appl. to gas centrifuges 78—71345
rotating gas, perfectly conducting compressible in mag field under gravity, wave dispersion relations *(Chinese)* 80—77276
rough surface boundary layer calculation methods 80—1595
self-modelling discharge of compressible fluid in bulk machines, initial parameter determ. *(Russian)* 79—77026
semibounded compressible stream, optimal suction at heat-cond. porous surface *(Russian)* 80—79346
shear layer instability of compressible fluid 77—80177
shell, cylindrical, impact on surface of compressible fluid, numerical method *(Russian)* 80—87746
shell, spherical, impact on surface of compressible fluid, numerical method *(Russian)* 80—87747
shock free flow around a convex angle 80—1625
shock layer, hypersonic, vibr. nonequilib., near stagnation streamline, low Reynolds no. flow 78—87417
shock wave, quasilinear hyperbolic system of gas dynamics *(Russian)* 80—33629
shock wave interaction with turbulent boundary layer disturbed by injection 80—74916
single particle drag coeff. in still air 80—33620
sink-vortex flow in compressible medium, book contrib. *(German)* 80—1603
slim profile relaxation drag minimisation in near solidified subsonic flow *(German)* 79—81916
solid particle suspension in compressible fluid, wave propag. 80—69858
sonic conditions prediction 77—65754

compressible flow continued
sonic nozzles, expt. study using gas flow dimensionless characts. 79—81945
sound amplification in nonuniform flow 78—83158
sound attenuation in low Mach no. nozzle flow 79—50721
sound wave transmission through nonuniform circular ducts 80—74900
spherical gas bubble in compressible liquid, nonlinear free oscillation, asymptotic method *(German)* 80—48773
spherical oscillating gas bubbles, nonlinear forced vibrs. in compressible liquid *(German)* 79—98793
spherical piston flow, approx. anaytical soln. *(French)* 79—27660
spheroids, harmonically oscillating, unsteady airload prediction, analytical soln. 78—51184
square, transonic flow, 3-dimens. density field meas., holographic technique 78—47080
stability of aligned, stratified, compressible magnetoatmospheric shear flow 78—26197
stagnation point boundary layers, unsteady, three dimensional, compressible, numerical soln. 79—37335
stagnation pt. boundary layers for laser heated flows 77—89141
stagnation-point boundary layer with hot wall, mag. field effect 77—72359
stationary disc in rotating cylinder, laminar compressible flow 80—43728
stationary supersonic flow of compressible fluid, distrib. eqns. *(French)* 77—62278
steady homenergic compressible flow with finite shocks, variational principle 80—69874
steady stratified flows over a long obstacle 79—90306
Stirling cycle compressible flow anal. using computer modelling 80—35717
stratified compressible flow, inhomogeneous acoustic-gravity wave eqn. 77—80174
study, gas dynamics method based on iterative techniques *(Hungarian)* 78—94757
sub and transonic flow over wing, flow separation, vortex struct., shock wave shape *(French)* 80—14733
subcritical flows past lifting profile *(French)* 77—72322
subcritical steady plane flow past profile with sharp trailing edge, smoothness and circulation *(French)* 78—18312
subsonic, density function approximation *(Hungarian)* 79—14421
subsonic, finite element anal., numerical approx. *(French)* 77—47037
subsonic, flow separation downstream of stepped rod in wind tunnel 77—58718
subsonic, past symmetric profile, num. soln. method *(French)* 77—58720
subsonic, three dimensional flow transverse to circular cylinder 77—58719
subsonic, two-dimens., finite elements soln. by streamline perturbation 77—51077
subsonic aerodynamics, finite element approach 79—55399
subsonic aerodynamics, finite element method appl. 77—47038
subsonic base pressure fluctuations on axisymmetric blunt-based body, Mach no. depend. 80—19423
subsonic flow visualisation, water fog generation system 77—24037
subsonic plane pot. flows, least squares finite element anal. *(Chinese)* 80—59063
subsonic rotationally symmetric flow density and absolute velocity *(Hungarian)* 79—81914
subsonic streamwise corner, laminar-turbulent transition 77—62269
subsonic turbulent boundary-layer flow, compressibility effects 77—62268
subsonic viscous flow, 3-D unsteady actuator disc theory 79—27615
suction effects on shock wave-boundary layer interaction, numerical Navier-Stokes soln. 79—1243
suction from boundary layer on thermally insulated porous surface, optimal absorption rate distribution 77—35123
supersonic compressed boundary layer on two-dimens. plate, unstable localised disturbance characts. 77—55031
supersonic corner flow, boundary region 79—32559
supersonic corner flow, viscous-inviscid interaction 79—32563
supersonic flow, viscous, past corner, energy eqn., asymptotic solns., heat transfer 79—32564
supersonic flow, wake of axisymmetric body, ideal gas, numerical anal. 78—59420
supersonic laminar boundary layers in three dimens. 77—31277
supersonic separated turbulent boundary layer, laser velocimetry meas. 77—35274
supersonic turbulent compression corner flow, numerical simulation 77—62276
supersonic two-phase flow, phase separation 79—23358
surface friction dependence on compressible fluid injection and removal by suction from wall jet 77—47052
swirl flow with closed streamlines, high Reynolds no. 77—84269
temperature gradient effects on sound propag., thin shear layer expansion 77—14826
thermal instability in presence of mag. field and rotation 77—89204
thermal pipes, sonic restriction on power at high temp. 80—103023
thermoconducting gas, reaction tube under epitaxy of monocrystalline films *(Russian)* 80—55301
thermoconvective waves in stratified compressible fluid, stability criterion contradiction 80—19414
thermodynamic consistency, finite difference scheme 80—48732
thermodynamics of compression, fundamentals review 77—39390
three dimensional gasdynamic flow, variational principle for *(Russian)* 77—35157
three-dimensional compressible mixing and reacting ducted flows, modelling 77—27621
time depend. flow, numerical soln., first order local stability scheme 77—72318
transient coaxial entry tube flows, numerical program 77—15117
transient gas flows with vibr. relaxation, acceleration wave growth and decay 80—1610
transonic axisymmetric pot. flow around inlets, Cartesian mesh soln. 77—72323
transonic boundary layers, freely interacting, compressive and expansive flow 77—89145
transonic flow, shock wave interaction with turbulent boundary layer, pressure distrib. 80—74918
transonic flow, shock wave interaction with turbulent boundary layer, wall shear stress 80—74919
transonic flow, unsteady, turbulence modelling, compression waves developing into shock wave 80—74909
transonic flow around spheres, orthogonal collocation soln. 77—39307

- **compressible flow** continued
  - transonic flow of perfect gas around uniformly expanding sphere 80—28528
  - transonic flow problems, modified FLIC method, finite element anal. 80—74911
  - transonic flow round aerofoil or cascade 78—22365
  - turbine cascade flow, surface-oriented coords. in num. simulation 77—55018
  - turbulence excitation and spectrum *(Russian)* 77—3837
  - turbulent boundary layer, compressible, extended mixing length appls. 78—94655
  - turbulent boundary layer, data compilation 78—14035
  - turbulent boundary layer, nominally steady, two-dimens., vel. and temp. profile prediction method 80—1624
  - turbulent boundary layer, supersonic, wall temp. effect 78—94765
  - turbulent boundary layer flow on insulated flat plate, anal. 77—51045
  - turbulent boundary layer generation in unsteady flow 78—90828
  - turbulent boundary layer on permeable plate 79—1169
  - turbulent boundary layer with heat transfer, surface roughness 78—90931
  - turbulent boundary layer with injection, eddy viscosity and turbulence energy methods 77—62267
  - turbulent boundary layers, local anal. soln. 77—75895
  - turbulent compressible boundary layer on permeable rough surface with heat transfer 79—1176
  - turbulent compressible boundary layer with heat-transfer effects on conditions at the sublayer 80—14672
  - turbulent compressible flow, kinetic theory, comparison with classical theory 77—3814
  - turbulent mixing at gases interface 78—1683
  - turbulent mixing coefficient correlations for compressible coaxial submerged and coflowing jets 77—42883
  - turbulent separation criterion for axially symm. flow at tail of body of revolution 78—22340
  - turbulent shear layers, review, book contrib. 77—47034
  - turbulent shear stresses in compressible boundary layers 80—14736
  - turbulent tube flow, heat transfer 78—71314
  - turbulent vel. profiles at transonic vels., local skin friction coeff. 78—67214
  - two-dimensional gas flow model, comparison of two methods of computation *(Russian)* 78—59413
  - two-dimensional jet flow in ideal compressible gas, calc. method 78—83448
  - two-dimensional supersonic viscous in reactions near walls, prediction method 77—58726
  - two-parameter skin friction formula for adiabatic compressible flow, shocked relaxing boundary layer 78—51188
  - two-phase blowdown from horizontal pipe, unequal phase vel. and temp. theory appl. 77—39335
  - two-phase flow, compressibility effect on hydrodynamics, resistance coeff. 78—55684
  - two-phase flow dynamics, distributed parameter model 80—24086
  - uniformly expanding sphere and cylinder, compressible flow, expansion vels. 79—77173
  - unsteady boundary layer coupled to non-uniform flow, num. determ., shock tube appl. *(French)* 77—65752
  - unsteady comp. laminar boundary layer flow, num. anal. 79—94586
  - unsteady compressible flow, dissipative thermodynamic effects 78—26136
  - unsteady compressible flow in ducts, modified governing eqns. 79—46392
  - unsteady flow analysis in duct with junction, FLIC method 78—18340
  - unsteady heat transfer from rotating disc or cone with large suction 77—47025
  - unsteady motion on transversely sheared mean flows, scatt. and distortion 79—59997
  - unsteady transversely sheared mean flow characts., gusts 78—26142
  - unsteady two-dimensional and axisymmetric compressible boundary layers 79—27616
  - unsteady two-dimensional subsonic, transonic and supersonic flow calcs. by method of characts. 77—55021
  - upsteam-centred finite-difference scheme for ideal compressible flow 77—27547
  - variable density turbulent subsonic flow, pressure pulsation and vel. divergence correlations 80—100008
  - variable domain finite element model for dam unsteady compressible fluid flow digital simulation 78—90820
  - variational principle and finite element method 79—46336
  - variational principle for compressible heavy fluid 78—83426
  - velocity measurements inside a rotating cylindrical cavity with a radial outflow of fluid 80—96275
  - viscous compressible flow, hybrid integration scheme, shock tube problem 80—69868
  - viscous compressible flow at high Reynolds number, global approach and coupling approach 80—48742
  - viscous compressible flows at high Reynolds number, book contrib., review 80—19424
  - viscous compressible fluid, wave perturbations *(Russian)* 78—75161
  - viscous compressible fluid motion in unbounded domain, weight function approach 80—79345
  - viscous drop, almost spherical, in arbitrary flow of compressible fluid, Faxen's theorem 80—87786
  - viscous flows in unbounded domains, weight function approach to uniqueness 79—46334
  - viscous fluid, eqns. of motion, initial value problem 80—62477
  - viscous gas equations, numerical solution, difference schemes, moving grids 80—48730
  - viscous heat-conducting gas, numerical simulation methods 80—38449
  - viscous heat-conducting gas, numerical solns. *(German)* 77—11217
  - volume flow measurement, integrating pressure tubes, theory, method and experimental results *(German)* 80—33712
  - vortex flow, boundary-value problem 78—26139
  - vortex shedding from smooth and roughened cylinders in crossflow near plane surface 79—81911
  - vortex tube, gas separation calc. and obs. *(Japanese)* 79—4021
  - vortex tube, soln. for vel. profile and state of gas *(German)* 77—89138
  - wake of aerofoil with sinusoidal vibration *(Japanese)* 77—15031
  - wall jet, three-dimens., press. and vel. meas. 80—19456
  - water vapour, wet, boundary layer in compressible flow 80—10295
  - water-entrained gas flow, force on moving body 78—63480
  - wave linear propagation in rotating fluid, critical level absorption and valve effects 80—106805
- **compressible flow** continued
  - waves on axisymm. mean flows in compressible atms., generalised Eliassen-Palm and Charney-Drazin theorems 78—81306
  - weak nonlinear waves in compressible fluid, higher order approx. 80—92165
  - weakly compressible gas flow, stability in pipe of model roughness 80—28562
  - wood chip disc refiner, steam flow anal. 79—50787
  - yawed cone, anal. of compressible laminar boundary layer 77—23973
  - ^{4}He, superfluid, cable-in-conduit conductor, heating-induced flows 80—38229
  - Li/He heat pipe, start-up power, heat transport, thermal regulation 80—53615
  - N_2, cryogenic, shock wave-boundary layer interaction *(German)* 78—71370
  - Rn concentration variation, temporal (spatial), rel. to Earth crust 80—33671
- **compression, bandwidth** *see bandwidth compression*
- **compressive strength**
  - *see also compressibility*
  - acrylic cements for fixation of orthopaedic implants 79—84000
  - adhesive materials 77—16638
  - Al alloy 6061, energy absorption during uniaxial tension and axial compression, geometric and heat treatment effects 77—73312
  - alloy, heat resistance under one sided loading 77—1872
  - alloy hard, binary carbide with Ni-Mo binder, physicomech. props. 77—90461
  - alumina, polycryst., strain rate depend. rel. to microplasticity 77—36620
  - anisotropic plasticity, theory development, expt. results 79—27553
  - anvil, truncated, compressive strength, high press. apparatus appl. 78 84906
  - baked C mixes, anthracite, petroleum, metallurgical and pitch cokes as fillers, chracteristics study 79—57052
  - balsa wood, cryogenic insulation, exam. of strength specifications, props. 80—25819
  - bone, human vertebrae, depend. on age and density 77—36985
  - bone, rel. to density and strain rate 77—36976
  - bone compressive strength quantitation and effects on bone remodelling 78—31836
  - bone strength, rel. to mineral supplemental diet in young rabbits 77—36986
  - brass, M63, yield stress decrease in compression, rel. to previous elongation *(Polish)* 80—50665
  - brittle material, statistical and micromech. theory 78—64618
  - brittle material, uniaxially compressed, failure mechanism, theory 78—26624
  - brittle material 77—44358
  - brittle materials, diametral compression tests, tensile strength meas., appl. to biaxial stress fracture *(Japanese)* 78—72840
  - brittle materials, diametral compressive stress considering Hertzian contact, fracture and tensile strength meas. *(Japanese)* 78—72946
  - brittle materials, load-transmitting medium to measure strength 80—40652
  - brittle materials, strength in nonuniform triaxial compression 78—76725
  - brittle materials, ultimate tensile strength determ. by radial compression testing 78—7132
  - brittle materials under complex loading systems, design parameters 79—38917
  - buckling strength of orthogonally stiffened plates under uniaxial compression 80—5964
  - calcite, anisotropic elastic const. meas. by uniaxial compression test *(Japanese)* 79—79822
  - cement, hot pressed, type III, role of admixtures on pastes and H_2O cured cement, exam. 78—44073
  - cement, hot-pressed paste, strength, X-ray diffr., DTA, Ir spectra, microstruct. exam. 77—8864
  - cement, regulated set, sulphate resistance and long term strength 78—35438
  - cement based on $Ca(OH)_2$ and polymethylphenylsiloxane, high-temperature high-strength props. 77—36439
  - cement in concrete cured by accelerated methods, gypsum content effect on compressive strength 77—63615
  - cement mortar, deform. charact., expt. study *(Japanese)* 78—56704
  - centering device for specimens in compression tests 80—61033
  - ceramic, fine powder, compaction during pressing and green strength, absorbed layer effect *(German)* 77—77450
  - ceramic nuclear fuels, mech. props. at compressive deformation 80—651
  - ceramics, mech. props. meas., apparatus for up to 1700°C *(French)* 80—104374
  - ceramics, mech. test apparatus for up to 2200°C *(French)* 80—104372
  - ceramics, microstructure dependence of mechanical behaviour 78—88533
  - chamotte concretes, phosphate binder based, strength props. 80—89305
  - circular ring, inner boundary shapes, optimised, diametral compression 80—38369
  - clay, highly plastic, compaction and lime stabilization effect on pore size distrib. *(Japanese)* 78—31365
  - compact bone, empirical strength theory, biaxial stress characts. 78—77081
  - composite, biaxial analogs of triaxial stresses 79—55345
  - composite material, compression testing fixture, new 77—77688
  - composite shell, orthotropic, cylindrical, with elastic core, stability 77—65701
  - compression, high strain rate, 1023 steel 79—34099
  - compression failure anal., glassy materials investigation 78—55608
  - concrete, compressive fatigue life, estimate of distrib., statistical method *(Japanese)* 78—11328
  - concrete, compressive strength and ultimate strain under impact loading 79—70128
  - concrete, compressive strength determ. using small-diameter cores 80—25784
  - concrete, crack propagation, uniaxial compressive stress *(Japanese)* 78—11330
  - concrete, creep, elasticity and strength in tension and compression 78—11287
  - concrete, creep, time dependent behaviour under high tensile stress *(Japanese)* 78—31465
  - concrete, creep during drying and wetting 79—52319
  - concrete, elasticity modulus and strength, aggregate conc. effect 80—66591
  - concrete, flowing, expt. studies *(Japanese)* 80—89298

compressive strength continued
- concrete, high strength, made with a special cement admixture, mech. props. *(Japanese)* 80—89297
- concrete, microcrack phenomena, geometric probability calcs. 79—57091
- concrete, porosity determ. from combined US and gamma absorption meas., mech. props. 79—29295
- concrete, prestressed beams without web reinforcement 79—52318
- concrete, relayed addition of admixture and flowing concrete, props. *(Japanese)* 80—89461
- concrete, rich mix, thermal props., expt. study *(Japanese)* 77—77536
- concrete, strain rate effect on strength and deform. during hardening process *(Japanese)* 80—93616
- concrete, strength, shrinkage strain and deterioration down to −160°C *(Japanese)* 80—100886
- concrete, strength properties under generalised stress, mathematical description 80—20941
- concrete, uniaxial compression, finite element failure anal. *(Japanese)* 80—35265
- concrete, US testing of compressive strength *(German)* 78—68847
- concrete cylinder, failed, compressive props. enhancement by polymer impregnation 77—77542
- concrete masonry units, mixed with pelletised slag 78—52707
- concrete pressure vessel, uniaxial compressive strength, 450-1033K 78—44299
- concrete sandwich composites, behaviour under compressive and tensile loads 77—8877
- creep in circular specimen subject to pure bend, ultimate tensile and compressive strength *(Russian)* 80—74768
- cylinder, at small elastico-plastic deformations *(Russian)* 79—10497
- cylinder, short, visioelastic, expt. and theoretical investigation of heat evolution in cyclic compression 78—13929
- cylindrical shell containing elastic filler subject to axial compression and external press., weight minimization 79—86352
- cylindrical wound shell with viscoelastic core in axial compression, optimisation 77—4821
- diamond, compressive strength for [111] loading 79—79036
- diamond, high press. appl. by spherical diamond indentor, plastic deform. obs. method 78—35619
- diamond, mechanical strength depend. on thermal working parameters, microcracks *(Russian)* 80—55501
- diamond, yield stress from Hugoniot elastic limit and elastic consts., compressive yield strength 79—83261
- dispersion hardened alloy, load type effect on yield stress 78—35458
- Duraluminium rings, stress/strain relations, compression and tension tests, rigid plastic theory 79—34098
- elastic springback in beams and plates, bending 80—38256
- endosseous implant material, radiation processed alumina-polyacrylic acid composite 77—60308
- epoxide resin, tensile, compressive and shear yield strengths, pyramidal criteria 77—8884
- epoxy, Al_2O_3-filled, shock-wave compression, 0.4-3.7 GPa 78—59856
- epoxy resin, deform. rate depend. of mech. props. at cryogenic temps. 80—55456
- epoxy resin, low temp. irradiation effects on mechanical props., use in superconducting magnets 78—60737
- epoxy resin, powder filled, exam. of mech. props., thermal contraction 80—25821
- epoxy resin adhesives, crack propag. and mech. props. 78—68783
- epoxy resin composite, powder-filled, of adjustable thermal contraction, mech. props., for construction of superconducting magnets 79—61691
- epoxy resin systems, synthesis review, phys. and mech. props. at low temps. 80—25650
- epoxy-polyglycol elastomers, fracture strength under compression 79—38929
- equine long bone forces and moments, in vivo and anal. studies 78—40216
- ethylene-propylene-diene terpolymer, sulphonated, ionically cross-linked, foam elastomer, thermo-mech. props. 78—48362
- Fe alloy YuNDK35, magnetic, brittle, strength in three axial stress state 79—66134
- femur, canine, in-depth mech. props. anal. 80—16979
- femur, rat, influence of hypergravity on compressive strength 80—3690
- femur intracondylar cancellous bone, compressive strength rel. to loading rate 78—40219
- fibre, inorganic, refractory behaviour testing 77—25204
- fibre reinforced plastic, tensile and compressive strengths, structural theory 77—52435
- fibreglasses, long-term strength evaluation, parametric methods efficiency 80—40662
- fibrous composite materials, models for composites with different props. in tension and compression 78—35417
- fibrous structure, low-density, centrifugal method for mech. prop. obs. 80—71823
- filament wound material, lamination theory for failure envelope prediction under biaxial loading 79—38931
- foam plastic, device for compression tests at different temps. 80—25947
- furan resin, effect of silica fillers *(Polish)* 78—68740
- furfuralacetone resin, filled, elastic modulus calc. 79—57030
- genesis problem, approx. soln. of initial states and properties 77—14927
- GFRP, unidirectional, compressive fracture mode 77—21251
- glass, compressive testing 77—16773
- glass, diffusion strengthening technique 78—31418
- glass, engineering type 13v, strength under static and cyclic loads 79—43356
- glass, industrial cylindrical tubular elements under internal and external press., deform. and failure resistance 78—35460
- glass, K-8, dynamic compression and unloading 77—9029
- glass, strength under linear tension, bending, torsion and compression of type K8 79—14062
- glass, stress in working zone under biaxial compression, Moire-band method 77—81369
- glass, technical, STL10, A-1, A-3, A-6, 13V, statistical features of strength characts. 79—43353
- glass fabric reinforced phenol resin, effect of thermal loading on physicomech. props. 79—24622
- glass fibre bricks, synthesis, strength 80—40304
- glass fibre reinforced epoxy, as electrical insulation for Tokamak toroidal field coils, mech. props. 78—64610
- glass fibre reinforced epoxy, struts for superconductive storage magnets, mech. props. 80—25824

compressive strength continued
- glass fibre reinforced epoxy, transverse shear effect on compressive strength 80—40439
- glass fibre reinforced epoxy, unidirectional, buckling 78—44166
- glass fibre reinforced epoxy resin, cryogenic tensile, compressive and shear props. 78—6983
- glass fibre reinforced epoxy-phenolic binder, exam. of short cycle fatigue strength under compression 80—11759
- glass fibre reinforced plastic, failure under compression, tension and bending 79—96142
- glass fibre reinforced plastic laminates, failure in compression 80—11755
- glass fibre reinforced plastic shell with rubber filler, stability under axial compression 80—7643
- glass fibre reinforced plastics, cyclic strength in complex stressed state 80—3181
- glass fibre reinforced plastics, cylindrical shells, compressive and flexural strength *(Japanese)* 80—81115
- glass fibre reinforced plastics, laminated ring with extra steel pin radial reinforcement, mech. props. 80—11714
- glass fibre reinforced plastics, relation between matrix vol. changes and mech. props. 80—11715
- glass fibre reinforced plastics, under compressive load *(Japanese)* 78—92301
- glass fibre reinforced polyester, compressive fatigue tests at cryogenic temps. 80—25870
- glass fibre reinforced polyester, struts for superconductive storage magnets, mech. props. 80—25824
- glass fibre reinforced polyester tube, strength under biaxial loading 79—38892
- glass fibre reinforced polymer matrix laminates, compressive strength 78—64609
- glass microsphere reinforced, composite, mech. charact. calc. 78—64578
- glass plastic coating, thick-walled, compressive strength evaluation method 79—15897
- glass plates, thermally tempered, strength degradation 78—48505
- glass reinforced plastics, strength in biaxial compression in three planes of symmetry 77—59874
- glass rod, optimum sample shape for compression testing, failure 80—71756
- glass shell, built-up, local strengthening influence on supporting capacity 80—71714
- glass shell, cylindrical, bearing capacity under axial compression 80—76323
- glassy materials, compression cracking theory and failure 80—7677
- granite, exam. of fracture mech. under dynamic loading 79—29218
- granite, weathered, bearing capacity determined by graphical soln. of pole trail method *(Japanese)* 78—56706
- granodiorite, fracture under uniaxial compression, mech. and AE meas. *(Japanese)* 78—56748
- granular material, particle crushing under high triaxial stresses *(Japanese)* 78—15466
- granular material crushing strength determ. apparatus 79—70260
- graphite, deform. and fracture mech., high temp. effects 77—63763
- graphite, diametral compressive strength, comparison with uniaxial tensile strength *(Japanese)* 78—72947
- graphite, irradiated ultimate tensile bending and compressive strength charact. 78—15479
- graphite, microhardness changes, effect of annealing and neutron irradiation 77—8861
- graphite, pyrolytic commercial, high-temp. thermal and mech. props. 80—75372
- graphite, structural, impact toughness, reln. to compressive strength 78—88605
- graphite fibre filled polyimide composite laminates, space environment, phys. and mech. response 80—81140
- graphite fibre reinforced epoxy laminate tension-compression fatigue loading, fatigue residual strength degradation model, comparison with expt. results for 78—35491
- graphite fibre reinforced epoxy resin, cryogenic tensile, compressive and shear props. 78—6983
- graphite reinforced epoxy, scale effect in fatigue 79—91780
- graphite reinforced epoxy laminate with arbitrarily symmetrical struct., stability 79—61649
- graphite-epoxy laminates, AS/3501-5, compressive fracture strength 79—43396
- graphite/epoxy laminates fatigue characts. under compression loading 78—84971
- gypsum, strength changes on setting *(Japanese)* 77—36619
- gypsum casts, improvement in impregnation method, exam. of mech. props. 78—48503
- HTGR graphites, irradiation effect on thermal shock resist. and mech. props. *(Japanese)* 80—66622
- human intervertebral discs, strength changes under compression 78—11690
- ice, Antarctic deep core, mech. tests under hydrostatic pressure *(Japanese)* 79—79890
- ice, columnar grained, rheology 79—57044
- ice strength meas., in situ tests 77—37423
- inorganic particle reinforced thermosetting resins, chem. bonding, mech. bonding and compression tests 77—59735
- jointed rocks, strength and deformation characteristics in true triaxial compression 79—84235
- Kevlar aramid fibre reinforced composites, flexural strength 79—11671
- laminates, damage zone failure analysis 80—85059
- Ll_2 ordered alloys, positive temp. depend. of strength, phase destabilization 80—81203
- magnesial refractory concretes, cast. props. 80—89306
- magnesite artifacts, roasted, props., filler porosity effect 80—104099
- mandibular bone, compressive strength rel. to microstruct. and strain rate 79—57689
- marble, Italian Ondagata, diametral compressive strength, comparison with uniaxial tensile strength *(Japanese)* 78—72947
- materials under complex stress, with local dynamic loading, strength 79—91768
- metallurgical coke, mech. behaviour charact. *(French)* 80—104371
- methane, crystalline, deform. under hydrostatic press. 77—70136
- MgO-ZrO_2 ceramic reinforced with filamentary crystals, mech. and thermal props. 80—45262
- Mo, slip line study of pure single crystal compressively deformed at low temps. 79—43361
- mullite, high temp. mech. props. in compression 77—56033

compressive strength continued
mullite ceramic rollers, heat treatment effects 79—61616
mullite single crystal reinforced refractory with phosphate binder, compressive strength *(Russian)* 77—44293
multilayer shells with fillers, exam. of stability under axial compression comparison to theory 80—7643
noncircular prismatic block between parallel frictional platens, press. distrib. and bulging profiles during compression 78—18207
nonmetallic material, mech. props., testing installation, +600 to −190°C 78—15633
nylon, oriented, transverse compression 78—68728
Nylon 6, unidirectionally reinforced, mech. props. and fracture 77—21252
oil shales, review of thermophysical properties 79—100479
optical fibre cables with spacers, transmission characts. and mech. props. 79—46070
optical fibres, surface compressive strength, increase after ageing under load 79—46065
organoplastics, fracture characts., effect on strength 80—66642
organotextolite, in plane state of stress, temp. depend. variant of strength 80—40449
paper strip reinforced paraffin, model composite, optimum reinforced plates, tension/compression tests 77—86124
piezoceramic, compression tests, fracture stress distrib. at various loading rates 78—15529
piezoelectric ceramic, bend and compressive strength, stressing rate effect 77—52409
plastic, fibre-glass reinforced, flat stressed state, strength and deformation props. function of reinforcement struct. 80—19866
plastic, static strength determ. from elasticity and internal friction 77—70094
plastic laminates, glass- and fibre-reinforced, strength anisotropy comparative anal. 80—19872
plastic specimens under compression, multiposition device for creep exam. 80—25946
plastics and reinforced plastics, tabulated data as design guide 77—21087
plate, obliquely stiffened, subjected to uniform compression, buckling strength *(Japanese)* 78—67067
plate, orthotropic, rotationally retrained, buckling under uniaxial compression 77—84169
plexiglas, strength in biaxial compression, testing machine 79—15899
Plexiglas 80—66592
PMMA glasses, crosslinked, strips, sheets, compression, tensile testing, mech. props., plasticiser effects *(Russian)* 77—32621
PMMA with stress-raising flaw, deform. 80—25799
PMMA-mortar composite, thermocatalytically polymerised, fracture morphology and mech. props. 78—27595
polyacetal, stress-strain relations, effect of strain rate and static outer press. *(Japanese)* 77—52418
polyamide, Al_2O_3 filled, low temp. thermal and mech. props. 80—25816
polycaproamide, deformability props. in cyclic extension-compression 79—20183
polycarbonate, compressive recovery behaviour 79—38919
polycarbonate, particles, critical stress 77—28869
polycarbonate, stress-strain relations, effect of strain rate and static outer press. *(Japanese)* 77—52418
polydimethylsiloxane, rubber elasticity in uniaxial tension, compression 79—15714
polyester resin concrete, effects of styrene-unsaturated polyester ratio on props. *(Japanese)* 80—89299
polyethylene, high density, crystalline, flat stressed state, yield point time-temp. factors 78—64601
polyethylene, high density, strength props. *(German)* 79—100219
polyethylene, increase in strength on compression *(Russian)* 79—34119
polyethylene, orientated, var. of yield stress with orientation, yield criteria exam. 78—52900
polyethylene extrudate, transverse compression 78—68728
polyethylene-glass fibre composites, gamma-irradiated filler 80—66840
polymer, hollow spherical particle filled, strength criterion 79—11682
polymer concretes, hydrothermally stable, hydraulic cement-type fillers 80—85144
polymer impregnated gypsum cast, mech. props. 79—100107
polypropylene, increase in strength on compression *(Russian)* 79—34119
polypropylene, mech. behaviour rel. to combined press.-temp. effects 77—16648
polystyrene, cryogenic foam insulators, low temp. props. 80—25818
polystyrene, glassy, thermally activated deform. 79—20126
polystyrene, impact resisting *(German)* 79—100219
polystyrene, particles, critical stress 77—28869
polyurethane, cryogenic foam insulators, low temp. props. 80—25818
polyurethane foam, rigid integral, effect on flexural and compressive strength, due to tall oil oligoether 78—68743
porcelain, elec., comparative assessment of methods of determ. strength 80—40429
porcelain, elec., high-strength, development from ceramic raw materials, mech., elec. props. 79—24630
porcelain, electrotechnical, compressive strength 80—100882
portland cement, doped with ZnO, struct. and props. 80—60914
powder, tensile and compressive strength meas. *(Japanese)* 80—25780
PVA carbonisation process and carbonised block props., high temp. resistant materials *(Russian)* 79—8268
PVC, fatigue life, influence of cyclic loading conditions 80—76350
pyroceramic, stress in working zone under biaxial compression, Moire-band method 77—81369
quartz ceramic, physicomech. props., influence of surfactant incorporated during synthesis 80—20856
quartz dental composites, acrylic acid grafted on particles by gamma-radiation 80—66840
rare earths, elastic and mechanical properties, review 79—70132
rectangular plate, stability, mechanical props. dependent on strained condition *(Russian)* 79—10494
refractories, high-temp. installation for thermomech. testing 79—83425
refractories, hot compressive strength 77—12677
refractory, ultra-lightweight, thermophys. characts., moisture effects *(Russian)* 77—55921
refractory ceramic creep meas. in tension and compression 78—31486
reinforced concrete deep beams, optimal force transmission 78—34009
rings, bearing capacity under compression 78—83256
rings, circular optimal plastic, stress/strain relations for rigid plastic material 79—34098

compressive strength continued
rock, deformation and fracture under general triaxial stress states, anisotropic dilatancy *(Japanese)* 78—56750
rock, mech. props. rel. to cooling *(Japanese)* 80—31036
rock half-space, impact of steel cylinder and effects 80—85649
rock like material, anisotropic elastic const. meas. by uniaxial compression test *(Japanese)* 79—79822
rock materials, strength determ. in triaxial compression, suggested methods 78—81432
rock parameters, drillability *(German)* 79—74888
rocks, failure processes and AE under compression *(Japanese)* 78—56749
rocks, in situ strength from triaxial testing 77—44975
rotationally restrained orthotropic plates under uniaxial compression, buckling 78—67065
rubber, creep processes associated with uniaxial compression 78—68734
ruled shell exposed to internal load pulses, compact strength 79—3929
sandstone, mech. props. rel. to water content *(Japanese)* 77—44980
sea ice, and stress relax. meas. *(Japanese)* 77—81916
sea ice, failure by compression *(Japanese)* 78—88841
shallow cylinder subject to axial compression, max. stress computation 77—14909
sital, structural glass component, strength in complex stress state 79—91763
sital, technical, compressive and bending strength 77—70131
slab, semi-infinte, stress amplitudes and fatigue damage resulting from cyclic Hertzian compression 77—19567
snow cover, cohesion strength and compression resistance 80—26560
sodium tartrate tetrahydrate, gel-grown single crysts., charact. 77—90261
soft elastic material bonded to rigid end plates, compression moduli 79—90134
soil stabilisation with granulated slag, increased compressive strength *(Japanese)* 78—31464
solids weakened (strengthened) by inhomogeneity, tensile and compressive strength 78—42571
spheroplastic, spherical shells, supporting capacity 80—87723
steel, alloy, static and fatigue strength, tension and compression test results 78—95810
steel, austenitic, high tensile X 3 CrNiMoNbN 23 17, creep at room temp., effect of Bauschinger effect *(German)* 77—1852
steel, austenitic stainless, porous fibre, sintered and compacted, mech. props. 79—15623
steel, CrMoV, creep and creep strength under alternate tension/compression *(Czech)* 77—63728
steel, energy absorption during uniaxial tension and axial compression, geometric and heat treatment effects 77—73312
steel, fatigue life, influence of cyclic loading conditions 80—76350
steel, fatigue strength with stress concentrator, mean compressive stress effect 77—21264
steel, ferrite-pearlite, ductile fracture, pearlite colony morphology and hydrostatic press. effect *(Japanese)* 78—15510
steel, high strength, press. depend. yield and plastic vol. change 78—19810
steel, high strength sheet, absorbed energy during compression and crushing 77—36593
steel, high-speed, quenched and tempered notch toughness, ultimate and yield strength in tension and compression 78—95782
steel, intermediate class Kh16N6, structural aspects of work hardening 77—90369
steel, low C, instability obs. by large strain compression 80—35253
steel, mild, tubes between rigid plates, lateral compression, strain hardening effect 78—48422
steel, process induced matrix inclusion separation 77—28818
steel, quenched and tempered 52100 bearing, plastic deform. in compression 77—40437
steel, shell, circ. integrally stringer-stiffened, buckling under axial compression 78—63346
steel, stainless, laminated with Cu interlayers, mech. props. 77—48506
steel, stainless/Al laminate, sandwich sheet material, plane strain compression and rolling 79—57062
steel, two-phase austenitic-ferritic, plastic deformation under hot working conditions 77—48466
steel, type 4130, high strain rate compression, plastic flow 79—34099
steel, U8A, 5KhNM and 12KhNZA, superplasticity under compression 77—86086
steel, ultrahigh C, heat treated, mechanical properties and microstructure 79—57012
steel 45, fracture surface obs. during fatigue failure 77—86185
steel 52100, compressive strain induced austenite transform. 77—86027
steel high strength X 3 CrNiMoNbN 2317, Bauschinger effect and creep at room temp., effect of heat treatment *(German)* 77—36543
steel plate, thin, in compression, initial deflection and postbuckling behaviour analysis 80—50666
steel plate collapse, anal. by live energy minimisation 78—52910
steel rod reinforced concrete, laterized columns, random axial loading, compressive strength to failure 78—27614
Ta, single crystals, microyielding, high amplitude damping 77—52396
tensile/compressive strength test machine calibration *(German)* 77—77654
testing of hard alloys by mag. loss on polarity reversal 77—59879
Textolite 80—66592
thermoplastic materials, flexure testing 77—86087
thick-walled tubes, compression by external pressure, expt. data, modified plasticity theory 78—59316
thick-walled vessel, of brittle material, strength under external press. 78—30182
thin metal strip, effects of hardening and anisotropy on plane strain compression 77—80083
thin walled tubes, inextensional collapse 78—18193
thin-walled sections, secondary local buckling 79—98644
Thornel 300/Fiberite 1034 graphite epoxy composite, elastic moduli, environmental effects 77—86068
three layer cylindrical shell having low stiffness filler, resistance to axial compression 79—86353
tobacco shreds, compressive charact. curve *(Japanese)* 79—61656
tubular sample, state of stress 80—23899
tuff, deform. charact., expt. study *(Japanese)* 78—56704
viscoelastic shell, thick-walled, deform. in post critical stage 77—58566
W, static deform., removal of surface layer effect on mech. props. in single crystal 79—43359
Westerly granite, failure under triaxial compression 78—11884

compressive strength continued
- wood stud walls, rel. between maximum compressive load and width *(Japanese)* 80—3124
- ALN, O_2 effects on sintering 77—77451
- Al 7039 alloy, high strain rate compression 79—29137
- Al alloy, 51S, modified by misch metal, for space appl. 80—55466
- Al alloy, cast AL15V, brittle, strength in three axial stress state 79—66134
- Al alloy, mechanical properties, correlation with elect. cond. 79—34114
- Al alloy 2024-T3, fatigue crack propag., load interaction effects 77—56055
- Al alloy 7075-T6, buckling under axial compression on circ. integrally stringer-stiffened shell 78—63346
- Al alloy AMg6, preliminary plastic deform., effect on stability of compressed rods 77—81305
- Al alloy with different props. in tension and compression, creep 80—81129
- Al alloy-mica particle composite, cast prep. and mech. props., bearing appl. 80—71613
- Al bronze, creep forging 77—59848
- Al, circular tube, forming limit of free bulge-forming *(Japanese)* 80—55477
- Al, fatigue life, influence of cyclic loading conditions 80—76350
- Al, longitudinal compressive impact test, comparison of expt. and calc. results *(Japanese)* 79—96119
- Al single crystal, Bauschinger effect, orientation depend. 77—21237
- Al-Cu (4 wt.%), single crystal, anisotropy in plane strain compression 77—36599
- Al-Cu (4 wt.%) alloy, precipitation hardened, single crystal, directional plastic behaviour, exam. 78—39788
- Al-Cu-Mg/mica particulate composite mech. props. 80—100919
- Al-$CuAl_2$ eutectic, superplastic behaviour during compressive deform. 77—52429
- Al-Mg-Mn alloy AMG-6M, endurance determ. by dimensionless damageability curves 79—96141
- Al-Si eutectic alloy, hardness rel. to tensile and compressive strength 79—52354
- AlB_2 flake reinforced composites, prep., props. rel. to aspect ratio, book contrib. 78—48366
- AlCu, electron microscope spot prep. of deform. bands 79—15922
- AlCuMgPb, microstruct. and flow stress during deform. at 573K 77—81307
- AlN, polycrystalline, stress-strain data up to 1.25 GPa 80—100899
- AlN-Mo cermets, ZrO_2 and mullite whisker reinforced, strength var. with temp. 80—104232
- Al_2O_3, ceramic Sinoksal, strength variation dependence on type of loading and temperature 79—57080
- Al_2O_3, compressive stress state strength determ. in brittle material 77—16757
- α-Al_2O_3 fibre FP reinforced Al and Mg composites, fabrication and props. 80—81004
- Al_2O_3, hot pressing characts. 78—27456
- Al_2O_3, polycrystalline, stress-strain data up to 1.25 GPa 80—100899
- Al_2O_3, spalling and cracking by compression 77—81313
- Al_2O_3-Mo cermets, ZrO_2 and mullite whisker reinforced, strength var. with temp. 80—104232
- Al_2O_3-Si_3N_4 preparation, compressive strength 80—25634
- Al_2O_3-SiO_2 glasses, thermally toughened, residual compressive stresses evaluation 78—31523
- Al_2O_3-W cermet, sintered pressed compact, compressive and transverse rupture strength 78—19850
- B fibre reinforced Al, tensile and compressive strength, prior thermal treatment effect 78—11264
- B fibre reinforced Al, X-ray investigation of internal stresses *(Russian)* 77—73290
- B fibre reinforced epoxy and Al, cryogenic tensile, compressive and shear props. 78—6983
- B_4 C, mech. and thermal props. 80—21083
- BN, polycryst. cubic, props. 80—21013
- BN, polycrystalline cubic, compressive strength and thermal stability 78—44170
- BN, wurtzite-type, lattice distortions 77—11636
- B_6O, mech. and thermal props. 80—21083
- $BaAl_2O_4$-Ba_2SiO_4-$BaZrO_3$, fusibility diagram 79—83184
- Ba_2SiO_4 cement, hardened, H_2SO_4 resistance *(Japanese)* 77—77602
- BeO, polycrystalline, stress-strain data up to 1.25 GPa 80—100899
- β-brass, effective Young's modulus, in isoaxial bi- and tri-axial crystals 77—90391
- C adsorbent, granules and artifacts, strength, mech. characts. 78—23771
- C, baked mix, optimum binder content estimation 77—73253
- C, dense hard-type solids prep. from petroleum coke powder by grinding 79—20002
- C fabric reinforced plastic laminates, tensile and compressive strength determ., 20-1500°C 80—100880
- C fibre reinforced CuO-H_3PO_4 effect of C fibre on props. 79—43192
- C fibre reinforced epoxy, fatigue strength 78—15495
- C fibre reinforced phenol resin, karbovoloknits, improving transverse tensile, interlaminar shear and compressive strengths 79—87691
- C fibre reinforced plastics, angle ply specimen, calc. of strength and elastic response 79—20108
- C fibre reinforced plastics, failure under compression, tension and bending 79—96142
- C fibre reinforced plastic multilayer laminate, strength and deform. *(Russian)* 80—30019
- C fibre reinforced plastics, strength props., effect of SiC coating on fibre 80—104224
- C glass fibre hybrid plastics, review of mech. props 79—20107
- C-C composite material, syntactic-foam type properties 78—44169
- CaO-SiO_2, cements, effect of additives on compressive strength, carbonisation shrinkage, frost resistance 79—1897
- β-$Ca_3(PO_4)_2$, synthesis and fabrication, prosthetic appl. 79—24479
- $Ca_{10}(PO_4)_6(OH)_2$, synthesis and characterisation in dense polycryst. form 77—4749
- $Ca_5(PO_4)_3OH$ bioceramic, material props. 80—93523
- β-Ca_2SiO_4-CaO-SiO_2 paste, hydration, compression strength and composition 80—50584
- Cd-B(W) particulate composite, dispersion hardening, grain size and texture strengthening 77—8840
- Cd-Ge broken lamellar eutectic composite, tensile and compressive props. 80—71694

compressive strength continued
- CdTe, single crystals, plastic deformation and dislocation struct. 79—8321
- $(Co_{1-x}Ni_x)O$, single crysts., morphology change during compressive creep testing 79—29144
- CoO single crystal, compressive creep morphology 77—56034
- CoO single crystal, compressive creep 78—11275
- Cr-Ni compressor disk, surface plastic deform., optimal method 80—60924
- Cu, bicrystal, $\{110\}$ $\langle 112 \rangle$, deform. *(German)* 77—48513
- Cu, M1E, yield stress decrease in compression, rel. to previous elongation *(Polish)* 80—50665
- Cu, mechanical twinning in $(110)[\bar{1}12]$ single crystal under plane strain compression *(German)* 77—36616
- Cu, powder, compression and stress relaxation *(Japanese)* 79—96060
- Cu powder compacts, yield curve comparison, different loading paths *(Japanese)* 80—93621
- Cu-Al-Ni (14.5, 3 wt.%), polycrystalline, pseudoelastic, cyclic stress strain response 77—86144
- Cu_3Au-Co, single crystal, overaging mechanism 79—20081
- Cu_2MnAl, Heusler alloy, single crystal, plastic deform. 77—44308
- Cu_2O, creep substruct. under compression, X-ray diffr. study 78—95785
- Cu_2O, creep tests, exam. of a creep machine mech. ability *(French)* 79—20325
- Dy_2O_3-based ceramic, preparation, mech. props. 77—24998
- Fe, cast, grey, brittle, strength in three axial stress state 79—66134
- Fe, cast, pearlitic, residual compressivel stress distrib. effect on resultant stress conc. in notched samples 78—92336
- Fe, high purity large single crystal sheet prep. method *(French)* 77—77375
- Fe-Al, single crystal, twinning and pseudoelasticity 79—15718
- Fe-CaF (6 and 9 wt.%), sintered, elevated temp. mech. props. 77—28878
- Fe-Mo-CaF (15, 9 and 6 wt.%), sintered, elevated temp. mech. props. 77—28878
- Fe-Ni (15, 25 at.%), longitudinal forces in the hot torsion test *(German)* 79—38889
- Fe-Ni single crystals, stress induced martensite 77—8827
- Fe-Ni-C (21, 0.6 wt.%), stress assited and strain induced martensite morphologies 78—3187
- FeAl single crystal, compressed, dislocation arrangement 78—14354
- Ge, high press. appl. by spherical diamond indentor, plastic deform. obs. method 78—35619
- Ge, yield stress from Hugoniot elastic limit and elastic consts., compressive yield strength 79—83261
- HfC-$HfBr_2$, preparation and high temp. antifriction props. 79—1918
- LiF, dynamic strength, cryst. orientation effects 78—39846
- LiF, US attenuation, 4.2 to 300K 77—47513
- $Li_2O.2SiO_2$, ceramic, prep. of oriented microstructure by unidirectional solidification of melts 80—71614
- $Li_2O.2SiO_2$, directionally solidified, thermal and mech. props. *(Japanese)* 80—16295
- $100(Li_2O.2SiO_2).3B_2O_3(3Na_2O)(3MgO)(3Al_2O_3)(3SiO_2)(3P_2O_5)$, directionally solidified, thermal and mech. props. *(Japanese)* 80—16295
- Mg, plastic anisotropy of extruded bars *(German)* 77—86126
- MgO, compressive stress-strain behaviour at high temps. 80—25774
- MgO, MgO-CaO (58 wt.%), comparison of high temp. creep and fracture 77—16658
- MgO, strength under confining press. of 250 kbar, brittle-ductile transition 77—47510
- MgO, ultrafine grained Fe doped, high temp. creep 79—15727
- Mo, polycrystalline, fracture and ductile-brittle transition, hydrostatic press. effects 78—60735
- Mo-Ti-Zr alloy TZM, fatigue and plastic flow, irradiation effects 77—52466
- Mo-TiC lamellar eutectic composite, deformation and strength, room temp. to 2073K *(Japanese)* 80—71702
- Mo-Zr-C (0.08, 0.02 wt.%), struct. and banding tendency, thermomechanical treatment effects 77—86063
- NaCl, halite, dynamic recrystn. during compression creep, geophys. appl. 80—25772
- NaCl, strength under confining press. of 250 kbar, brittle-ductile transition 77—47510
- Na_2O-CaO glass phlogopite mica powders, composite fabrication, cellular struct. 80—84902
- Nb, stress differential in surface oxide softening of single crystals 77—86116
- Nb-N (0.3 to 300 at. ppm), deform. 77—48477
- Nb_3Sn, filamentary, fatigue tests on small coils 78—64652
- Nb_3Sn, hot isostatically pressed, plastic deform. 80—108510
- $(Ni,Co)_3Ge$, Co effect on temp. depend. of yield stress 78—31487
- Ni alloy, heat resistant, fatigue limit comparison in torsion and tension-compression 80—81181
- Ni single crystal, compressed, strengthening and dislocation cells *(German)* 80—66536
- Ni/Ni_3Al-Ni_3Nb, directionally solidified lamellar eutectic alloy, deform. anisotropy and fracture 77—36604
- Ni-base superalloy, $\langle 111 \rangle$ monocrystals under compression, inhomogeneous deformation 77—63736
- Ni-TaC, eutectic alloy, fibre reinforced, directionally solidified, anisotropic yielding behaviour 79—11675
- Ni-Ti mech. memory alloys, tensile props. *(Korean)* 77—63724
- Ni-Zn ferrites, polycrystalline, grain boundary slip *(Japanese)* 77—63764
- $Ni_3(Al,W)$, yield stress, orientation depend. 78—39830
- Ni_3Al, ductility, tensile and compressive tests *(Japanese)* 77—52414
- Ni_3Al, ductility in poly- and single crystals, compressive and tensile tests 78—56715
- NiO, doped and pure single crystals, plastic deform. 77—36578
- NiO-CaF_2, hot-pressed, mech. props., thermal expansion rel. to CaF_2 additive 79—43321
- Ni_3V, ordered, domain size effect on mech. props. 79—79027
- Pb, anomalous grain growth 77—8855
- PbO, sintered, pure, prep. and props. 77—48361
- $Pb(ZrTi)O_3$ type piezoelectric ceramics, compressive properties 79—33612
- Pd-Cd eutectic, unidirectionally solidified, tensile and compressive props. 78—27567
- 239PuO_2, stoichiometric, high-temp. deformation 80—81111
- S, S mortars, S Concretes, effect of H_2S 77—4818
- S-based composite, engineering props. 77—86093
- $(SN)_x$ single crystal, mech. props. 79—24580

compressive strength continued
Sb, compressive stress-strain curves in single crystals device *(French)* 79—47852
Sb, deformed in compression, secondary slip system *(French)* 79—66120
Sb-Ge, unidirectionally solidified, exam. of compressive props. and struct. 78—68730
Sc, strength and plasticity 77—90429
Sc_2O_3, hot pressing characts. 78—27456
Si, compressed, polycrystalline, deform. and recrystallisation texture 78—27538
Si, high press. appl. by spherical diamond indentor, plastic deform. obs. method 78—35619
Si, yield stress from Hugoniot elastic limit and elastic consts., compressive yield strength 79—83261
Si-Al-O-N, compression creep, comparison with SiC and Si_3N_4 79—15728
Si-Al(Ti)C, sintered, exam. of props. 80—25644
SiB_4, mech. and thermal props. 80—21083
SiC coated B fibre Al-V-Ti, tensile and compressive strength, prior thermal treatment effect 78—11264
SiC, compression creep, comparison with Si_3N_4 and sialon 79—15728
SiC pyrolytic coatings for HTGR fuel particles, props. rel. to deposition conditions 79—31088
α-SiC, uniaxial compressive damage at low homologous temps., AE and SEM obs. 79—91736
Si_3N_4, hot pressed, high temp. compressive cracking, optical and electron microscopy exam. 78—76733
Si_3N_4, reaction bonded and hot pressed, compression creep, comparison with sialon and SiC 79—15728
SiO_2 glass, strengthened by ion exchange and quenching brittle destruction theory 80—45398
SiO_2 glass, stressed state investigation by NDT using UHF waves 78—11460
SiO_2-Al_2O_3-CaO-MgO-Na_2O (1.58, 7.16, 3.59, 14.9 mole.%), polished sheet, strength in commercial state and after strengthening by ion exchange 79—1904
SiO_2-Na_2O-K_2O water glass with polyethylene filler, thermogravimetric and thermomechanical anal. 79—20020
Ta, single crystal, microyielding microflow parameters 77—52395
$(Ti,Cr)B_2$, sintering kinetics and props. 80—100811
$(Ti, Cr)B_2$-based alloys, densification of powder mixtures by hot-pressing, elec. and mech. props. 80—20812
Ti, plastic anisotropy of extruded bars *(German)* 77—86126
Ti-Al-Mo-Zr, compressor disk, surface plastic deform., optimal method 80—60924
TiB_2, preparation method rel. to compressive strength 80—55327
TiC-B, struct. and mech. props. 80—55461
TiC-steel composite, effect of method of Cr additions on props. 78—15341
TiC-TiB_2, preparation and high temp. antifriction props. 79—1918
TiC-TiB_2, strength and antifriction props. over wider range of concs. 80—50673
TiO_2 based construction ceramics, fibre-like cryst. reinforced, mech. props. 80—55341
TiO_2-Al_2O_3-SiO_2 system, ternary glass-forming region and phys. props. 80—84919
α-U, polycrystalline, compressive deform. at low temps. 77—28856
$UC_{1.5}$, creep behaviour and phase change under compression stress 78—35432
UO_2, superplastic creep 79—15730
V, high purity crystals, anomalous slip under compressive deform. 77—63737
V, impact deform., influence of previous static loading *(Russian)* 78—6972
V-Ti-O single crystal alloy, mech. props. 77—25112
W, polygonisation critical stage in single crystals deformed in compression 79—4979
W, porous, physicomechanical props. sintering effects 77—12575
W-WC, activated sintering, mech. props. *(Korean)* 78—60622
WC-Co, elastic and plastic charact. 80—35280
WC-Co, rupture stress, microstructure and other effects 77—73343
WC-Co, size factor effect on strength in complex stressed state 78—31483
WC-Co(TiC-Co), powder compacts, effect of additional pressing at hydrostatic pressures on props. 78—56596
WSe_2, lubricant, prep. by self-propagating high-temp. synthesis, technological characts. 78—35338
YH_x, mech. props. 77—44333
Y_2O_3, hot pressing characts. 78—27456
Yb_2O_3-based ceramic, preparation, mech. props. 77—24998
Zn, plastic anisotropy of extruded bars *(German)* 77—86126
Zn polycryst., compressive strength, temp. and strain rate effects 80—16616
Zn, polycryst., temp. and strain rate effects 80—16616
Zn, pyramidal edge and screw dislocation mobility, compressional stress pulse technique 77—19957
Zn, thermal recovery and stress-strain relations 78—11266
Zr-Dy dil. alloys, plastically deformed, mech. props. and microstruct. *(Russian)* 79—20112
ZrC based cermets, strength and gas-abrasive wear resistance 77—25163
ZrC-ZrB_2, preparation and high temp. antifriction props. 79—1918
ZrC-ZrB_2, strength and antifriction props. over wider range of concs. 80—50673
ZrH_x, mech. props. 77—44333
ZrO_2, stabilized porous refractory, mech. strength 80—35322
ZrV_2, anomalous softening at martensitic transform. 80—93630

compressors
air compressor, reciprocating, capacity control system 80—90859
annular axial, nonaxisymmetric flow anal. 79—32679
axial, end-wall boundary layer calc. method 79—98702
axial flow, stator blade wake guidevane mean velocity and decay characts. anal. 80—95085
axial flow stator blade, boundary layer development 79—4002
axial-flow compressor cascade flows computer simulation 78—79333
boundary layer charact., influence of external flow turbulence 80—87811
cascade deviation, prediction and measurement 80—24049
cryogenics of Sulzer, Switzerland 80—82769
cryosurgical apparatus coolant supply system 77—81637
discharge system interactions, mathematical modelling 79—80447

compressors continued
ELMO-G quiet running vacuum pumps and compressors for plant noise reduction 80—5872
fluid machinery manifold impedance meas. 78—42501
high-pressure, 6-piston device for elastoplastic media, 100 kbar 79—35774
high-pressure, for low-density polyethylene process, design 77—13764
hydraulic, for compressed air energy storage power system, performance analysis 79—83639
infra-sound reduction from auxiliary compressors of large wind tunnels 79—81628
isothermal compression installation, for solid H_2 up to 25 kbar, 60 to 130K 79—35769
jet injector, operation mode, biomedical appl. 78—7524
low temperature He compressor *(Japanese)* 77—53918
manifold, fluid induced damping 78—83164
membrane compressor for inert gas and mixtures 78—86286
noise emission of fans, blowers, dynamic compressors, acoustic test methods *(French)* 77—19478
nuclear power stations containment structures testing, for pressure tightness *(Spanish)* 80—13775
photon correl. velocimetry, turbomachinery and industrial burner velocity and turbulence profiles 79—60083
pneumopress, for extracting interstitial water from marine sediments 80—26643
Rankine cycle, Stirling engine powered heat pump appl. 79—48164
sound level meas. methods *(German)* 80—14520
sound power estimation in free field above refl. plane 77—39154
sound power meas. indoors by two-surface method 77—39152
supercritical, transonic flow computation 80—96276
three-dimension transonic flow prediction, characteristic method appl. 80—96277
transonic axial rotor, flow field anal. by laser velocimetry 79—4009
vaneless radio diffusers with swirling flows, acoustic resonance study 79—18882
vapour compression distillation unit, compressor and flow system matching 78—83931
zero mechanical work thermal compressor or pump, in high speed rotating frame 78—57962

Compton effect
γ-ray sources for Compton profile meas. 79—35907
acetic acid and isomeric methyl formate, Compton profiles 77—30928
acetylenic compounds, linear mol., Compton profile bond additivity, HF calc. 79—68268
active galactic nuclei, X-rays from inverse Compton refl. 79—48920
adjoint photon transport, Monte Carlo biasing scheme, Compton scatt. and absorpt. 78—77819
alkali fluorides mol. Compton profiles, parallel-perpendicular anisotropies 79—94038
alkali halide molecules, zero point Compton profile anisotropy rel. to nucl. charge 79—64054
alkali halides, anisotropies in Compton profiles 80—20730
alkali halides, electron momentum distrib. and Compton profiles 79—13631
alkali metal halide molecules, zero point Compton profile anisotropies and bond polarities, correl. 80—78659
anisotropic momentum densities from Compton profiles 77—48268
annihilation radiation from point isotropic photon sources, numerical calc. 79—85096
astronomical, X-ray sources, emission mechanisms, detection techniques 77—22061
astrophysical sources, Compton emission models, constraints from gamma-ray data 80—67902
astrophysical spectra, Compton effect and resonance scattering 79—58242
astrophysics, relativistic electron spectra inference from meas. of inverse Compton radiation 80—90339
atmosphere, γ-radn. EM effects, Compton electron currents 78—93020
atmosphere MeV gamma radiation, Compton scatt. rel. to theoretical zenith angle distrib. 77—45208
atom, As to Yb, Compton profiles from HF wavefunctions 77—14393
atom, Compton K-electron line contour *(Russian)* 79—93959
atom, K-shell electrons, Compton scatt. of 1.12 MeV gamma-rays 77—68016
atom, profile asymmetry obs., Al, Ti, Fe, Cu, using Kα fluoresc. 77—57937
atoms, Compton profile, Fourier anal. 79—89588
atoms, light, Compton scatt. 77—83546
atoms, off-mass-shell and binding effects, Compton profile depend. 79—18154
atoms, X-ray Compton and photo-effect in laser field 79—13688
atoms and molecules, X-ray and electron scatt., Compton defect, Compton shift 77—88428
band structure, optical cond., Compton profile, self consistent calcs. 80—65435
benzene, mol., directional Compton profile, ab initio SCF LCAO MO calc. 78—62857
black hole accretion discs, Compton scatt. rel. to Lightman-Eardley instabilities and disc thickening 80—31324
black holes, accreting, Compton gamma ray emission spectrum 78—32504
black holes, electron-positron pair production in hot unsaturated Compton accretion models 80—36658
black holes, supermassive, unsaturated Compton accretion discs models for hard X-ray spectra 80—22033
bonds, AH and AB (A, B=Li-F), linear momentum operator expectation values calcs. in molecules 79—7566
bone, osteoporosis early detection by Compton gamma-ray spectroscopy 78—11729
bone density determination, effective attenuation coeff. of soft tissue 80—101220
bound and free electron Compton scatt. in coherent EM field 78—94225
bound electron state scatt., binding and off-mass shell effects, relativistic anal. 78—17637
bound state Compton cross section, depend. and IR behaviour on binding and off-mass shell effects 79—63967
cis- and trans-2-butene, Compton profiles, theory and expt. 78—50597
C, valence electron radial and momentum distribs., X-ray form factors and Compton profiles 79—65956

Compton effect continued
- 3C 273, quasar, second-order Compton interpretation of X-rays and γ-radiation 80—22106
- cancellous bone, densitometry meas. 79—39489
- α Carinae (Canopus), generalised Compton effect in spectrum 78—53938
- causality props. of form-factors of one particle matrix elements of current commutator 77—30385
- charged vector mesons, Compton scatt. cross section meas. 79—22102
- chiral Lagrangian model, linear and nonlinear σ models, pion polarisabilities, Compton scatt. 78—21323
- circularly polarised photons on polarised electrons, Compton scatt. cross sections 77—18260
- clusters of galaxies, Compton-produced X-ray emission, spatial distrib. 77—33686
- clusters of galaxies, intracluster relativistic electrons hard X-ray spectra and gas heating 79—25735
- coherent radiation novel sources, book 79—27231
- compact X-ray sources, Comptonisation of Fe X-ray spectral features 78—20908
- Compton currents, historical aspects and recollections 78—80018
- computerised emission transaxial tomography, effect of Compton scatt. photons 79—66530
- cosmic γ-ray bursts, balloon obs., effect of multiple Compton scatt. in atmosphere 78—28352
- cosmic diffuse γ-ray background from galactic halo 77—53711
- cosmic microwave background, inverse Compton scatt. by ionised gas in clusters of galaxies, microwave search 80—82477
- cosmic microwave background radiation, Compton scatt. by gas in galaxy clusters 78—24575
- cosmic radiosources, Compton effect and relativistic electrons spectra in plasma turbulent reactor *(Russian)* 77—19760
- cosmic spherically-symmetric nonthermal sources, Compton and synchrotron processes 79—88583
- cosmic X-ray and γ-ray background radiations origin 77—33703
- cosmic X-ray sources, spectra, rel. to Comptonization of X-rays by low-temperature electrons 79—35108
- critical angles in total reflection of, Compton, X-ray and fluoresc. scatt. 80—59343
- crystal, Fourier transforms of Compton profiles, LCAO calc. 79—83050
- crystal, X-ray scatt., electron binding energy effect 77—59639
- cyclopropane, γ-ray Compton profile meas., MO calcs., rel. to propene 77—10706
- Cygnus X-3, gamma radiation from inverse Compton scatt. during radio outburst 77—64884
- Cygnus X-3, inverse Compton γ rays 77—41421
- deep-inelastic Compton scatt., manifestation of colour effects 78—37215
- deposition profiles of irradiated materials interfaces, Monte Carlo calcs., photo Compton current 79—24383
- detector energy resolution and angular broadening effects on Compton profile anisotropy 77—20949
- diamond, C-C bonding, Compton profile calcs. 77—75232
- diamond, Compton profiles, X-ray struct. factors, band struct., LCAO calc. 78—51889
- diamond, directional Compton profiles, X-ray scattering factors and 1-electron density matrix 80—10458
- diamond, five-atom clusters, unrestricted Hartree-Fock calcs. 77—11866
- diamond, ground-state, electronic properties, ground-state in local-density formalism 77—69223
- diamond, momentum density, Compton profile 77—20235
- diamond-structure semiconductor, Compton profile interpretation 80—29820
- diatomic mol., directional Compton profiles for mol. simulation of crysts. 77—30931
- differential Compton scatt. cross-sections meas. 77—30731
- dopplertrons and gyrotrons, coherent radiation from magneto-resonant relativistic electron beams, book contrib. 79—27227
- education, Compton collision formula and Klein-Nishina formula ang. depend. verification, undergraduate expt. 78—62010
- effective Compton wavelength, high energy QED approach 78—37213
- electron beam, relativistic, unmagnetised, stimulated scatt. anal. of HF incident pump wave 79—77345
- electron beam polarisation in storage ring by laser beam interaction 79—93860
- electron binding effect, inelastic scatt. cross section of 279 keV photons by K-shell electrons in Th 77—54537
- electron energy states, Compton profiles *(Japanese)* 77—36306
- electron gas, relax. of induced Compton scatt. during propag. of radiation flux *(Russian)* 77—27231
- electron gas-radiation field interactions, instability development, interstellar case 80—77274
- electron mass operator in plane wave field, near cyclotron reson. region *(Russian)* 78—86432
- electron momentum densities, expt. determ., review 77—76776
- electron momentum distribution, study by means of Compton effect *(Polish)* 78—48252
- electron plasma, partially degenerate, at high temp., Compton scatt. opacity 77—11322
- electron plasma in mag. field, photon absorpt. quantum mechanical treatment 79—1296
- electron rest-mass, student laboratory expt. 78—16607
- electron wavelength, determ. by cryogenic metrological technique 78—37165
- electron-photon cascade simulation by Monte Carlo programs 79—54330
- electron-photon cascades, Monte Carlo simulation of cascade development 79—44322
- electron-photon collision, relativistic variance of cross section *(French)* 78—45924
- electronic potential energy and X-ray scatt., relationship 79—28311
- electrons, inverse Compton effect on starlight 80—26702
- electrons, ultrahigh energy, traversing cosmic blackbody photon gas, effective penetration distance 79—5742
- EM total pulse, nature of extracted signal 78—42268
- EM wave refl. by relativistic electron bunch, freq. conversion efficiency 78—1143
- energy-momentum relation for electron, for teachers 79—40322
- ethanol, liq., Compton profile at 60 keV 79—47535
- ethanol-H_2O, liq., Compton profile at 60 keV 79—47535
- extragalactic compact X-ray sources, observational consequences of synchrotron self-Compton models 77—29961
- Fermi surface mapping from one-dimens. Fourier transform of Compton profile 77—39764

Compton effect continued
- Fermi surface parameter determ. from Fourier anal. of Compton profiles 77—4285
- ferromagnet, spin dependent electron momentum distrib. by double Compton scatt. 78—35218
- flare stars, fast electrons inverse Compton effect rel. to flare emission spectrum 80—67731
- form factors, off-shell, use of Ward identity for Compton scatt. polarisability 78—66120
- forward Compton amplitude of stationary composite system, low-energy theorem, additive external EM interaction 78—17024
- Fourier transform, one dimens., of Compton profiles 77—73187
- free electron Compton scatt. of spectrally narrow radiation flux 80—20731
- free electron laser basic mechanisms, stimulated Raman and Compton backscattering 79—7106
- free electron lasers, mag. bremsstrahlung, Compton and Cherenkov, types *(Chinese)* 79—31851
- free-free transitions in quantum electronics 80—28183
- galactic cosmic rays, contrib. to diffuse X-ray flux in 2 to 7 keV range 80—98745
- galaxies active X-ray sources, hard X-ray emission mechanism 79—97080
- gamma camera, 3-D particle track chamber 77—86622
- gamma Compton experiment, with annular ^{241}Am source, momentum resolution and reliability meas. 80—312
- gamma photon detection processes, statistics of radiation 77—65010
- gamma ray spectrometer, collimator system, intensity profile meas., construction 78—90013
- gamma-ray backscatter peak shape *(Czech)* 77—50303
- gamma-ray camera appl. 78—10087
- gamma-ray Compton scatt. studies and spectrometers 79—74014
- gamma-ray elastic and Compton scatt. through small angles, Ge(Li) meas. 79—718
- gamma-ray penetration in heterogeneous systems 79—18050
- gamma-ray source properties, electron momentum density studies 80—14028
- gamma-ray-detector, form of high energy interaction, effect on spectral peak centroid determ. 79—36468
- geometrical considerations in Compton scatter densitometry 80—30869
- graphite, Compton profiles, momentum densities, comparison with glassy C 80—2895
- ground state electron momentum density, Compton scatt. meas. 77—81172
- hadronic targets, spin-$^1/_2$, Compton scatt., optimal sum-rule inequalities 80—105815
- hadrons, multipole polarisabilities from Compton scatt. amplitudes 80—13311
- Hercules X-1, Compton scatt. rel. to X-ray continuum and Fe line emission during X-ray low state 80—105393
- Hercules X-1, reson. Compton cyclotron scatt. rel. to cyclotron line form. 80—8711
- hydrocarbons, Compton profiles, deviations from bond additivity, rel. to strain energy 79—81240
- hydrocarbons, liq., Compton profiles, bond additivity 80—93423
- hydrogenic atoms, Compton profile and X-ray scatt. factors, elec. field and elec. field gradient effects 79—31458
- hydrogenic orbitals, Compton shift *(French)* 78—42012
- II-VI and III-V compounds, Compton line shapes of atoms 77—44080
- incoherent scattering of gamma rays, spectrometer for electronic momentum distribs. investigation *(German)* 77—41741
- induced Compton scatt. from nonlinear charges, nonlinear classical theory 77—68857
- induced Compton scattering by relativistic electrons *(Russian)* 77—10826
- induced Compton scattering in pulsar winds 78—96497
- inelastic scatt. of X-rays and synchrotron radiation in crystals, review 78—39625
- intermediate-Z elements, γ-ray scatt. from K-shell electrons, Compton scatt. cross-sections 78—58643
- interstellar maser lines intensity vars. due to induced Compton scatt. 78—4319
- inverse Compton reflection, steady-state theory 80—67533
- inverse Compton reflection, time-depend. theory, X-ray sources appl. 80—12652
- inverse-Compton emission from radiosource electrons and microwave background photons, prospects for X-ray detect. 79—71144
- ionic crystals, scatt. spectra with synchrotron radiation 78—23547
- isovector Compton scattering, low energy expansion of two current amplitudes 78—16946
- kinetic energy in Compton profiles 78—72628
- laser, scatt. stimulation by decelerated EM waves, semiclassical theory 78—29926
- laser-plasma interaction, stimulated Brillouin to stimulated ion Compton scatt. evolution 78—42762
- liver fat content determ. by photon scatt. technique 78—24124
- low energy e^6 Compton scatt. 78—45925
- low energy parameters, bound computation, conjecture proof 80—27507
- low energy photon scatt., exchange currents and relativistic corrections 78—21433
- low energy proton Compton scattering, p polarisabilities 78—93886
- lung density, Compton scatt. meas., multiple photon interactions 80—67146
- M87 halo, 3K background photons Compton scatt. contrib. to X-ray emission from Faraday rot. 80—67844
- metallic crystals, scatt. spectra with synchrotron radiation 78—23547
- methane, γ-ray Compton profile meas. 78—25623
- methane, Compton profiles, high energy electrons impact spectroscopy 77—27188
- methanol, Compton profile meas., non-additivity of elastic and inelastic X-ray scatt. 78—43953
- methanol, liq., Compton profile at 60 keV 79—47535
- methanol-H_2O, liq., Compton profile at 60 keV 79—47535
- methyl formate and isomeric acetic acid, Compton profiles 77—30928
- microwave background radiation spectrum, evidence for Compton distortions 78—86039
- mole,cule, Compton profile single- and double-gaussian FSGO model 77—88504
- molecular isoelectronic series, Compton profile, empirical correlation with energy 78—78758
- molecule, anisotropic Compton profile, LCAO calcs. 77—6863

Compton effect continued
- molecule, profile calcs. by FSGO 77—30933
- molecule electron impact spectroscopy, high energy, Compton defect 77—88578
- molecules, Compton profile, Fourier anal. 79—89588
- molecules, light, Compton scatt. 77—83546
- monochromatic photon beam generation by high energy electron beam *(Japanese)* 78—74821
- monochromatic polarised photon source from Compton backscattered laser light on electrons 80—52800
- monochromatisation of gamma photons *(Russian)* 79—89516
- Monte Carlo scatt. simulation including γ-ray polarisation 77—34476
- moving mirror reflection analogy to the Compton effect 78—82218
- moving poles in the scale-dimension plane and scaling violation 79—12983
- multiphoton stimulated Compton scattering of relativistic electrons 80—48198
- multiple Compton effect, cross sections, γ spectra and number *(Russian)* 79—370
- multiple scattering, energy profiles, anal. and numerical calcs. 77—93
- multiple scattering, error bounds of multiple scatt. corrections 78—16959
- multiple scattering, Monte Carlo calcs. 77—94
- multiple scattering, operator formalism for nonstationary electrons 78—12846
- multiple scattering effects in Compton profile meas., correction using semi-empirical methods 80—91093
- neopentane, spherical Compton profile, rel. to diamond C-C bond, SCF calcs. 77—75232
- neutrino Comptonisation in high-temp. nuclear matter, neutral current theory 80—21905
- nonlinear inverse Compton radiation spectrum, deepest descents method 78—85840
- nonrelativistic form factors for γ-rays off bound electrons, Fortran program 77—10252
- NP 0532, Crab pulsar, model, X-ray, optical and radio emission 78—4265
- NP 0532, Crab pulsar, optical and X-ray pulses, Compton effect 79—53849
- nuclear, Compton scattering, diffractive behaviour, meson exchange effects 78—33165
- nuclear energy level excitation, Compton mechanism, cross section estimation *(Russian)* 79—49620
- nuclear resonance scattering of gamma rays, line inversion 80—39919
- nucleon magnetic moments and fine struct. const., upper bounds in terms of Compton scattering cross sections 77—2836
- one-dimensional pot. arrays, ordered and disordered, electron states, one-electron density matrix, Fourier-transformed Compton profile 79—69385
- origin of Compton defect at high momentum transfer 78—15247
- parity violating part of amplitude, weak interaction effects 77—2840
- particles accelerated by Alfven waves, distrib. function self-similar solns. 79—32757
- Penrose Compton scattering in black holes in Centaurus A, 3C 273 and NGC 4151, rel. to gamma-ray emission 80—56925
- perturbative QCD corrections in inelastic Compton scattering 79—93342
- photo-Compton deposition profiles, anal. approach, QUICKE4 code 77—20948
- photon beams, high energy, depth of max. dose var. with fluid size 77—70555
- photon model for X-ray coherent scatt. by cryst. 80—24309
- photon scattering by weakly bound electron 77—65442
- photon splitting into three components by electron in quantised plane EM field 80—18101
- pion polarisability 78—456
- PKS 0548—322, BL Lacertae object, synchrotron self-Compton model for X-ray spectrum 80—17654
- plasma, EM wave stimulated Compton scatt. from ion bunches 77—51192
- plasma, ion temp. meas. using stimulated Brillouin and Compton scatt. 77—58892
- plasma, photon soliton and fine structure due to nonlinear Compton scattering 80—10363
- plasma, relativistic particles, Compton effect and pair production *(Russian)* 77—24052
- plasma, stimulated Compton scatt., Bose condensation and onset of final equilib. state 77—51193
- plasma, stimulated Compton scatt., density inhomogeneity effects 78—30446
- plasma, stimulated Compton scatt., wave spectrum and electron temp. evolution 77—62347
- plasma, stimulated Raman and induced Compton scatt., nonlinear kinetics 77—35328
- plasma-laser refl., Compton-induced effect 77—993
- polyethylene, Compton defect 77—73183
- pomeron-photon analogy, current-current model 77—87984
- positronium determination in matter, Compton profile comparison to γ-annihilation radiation ang. correlation *(Russian)* 77—55845
- positrons, planar channelled, Compton scatt. anal. 79—7639
- profile calculation, two-electron theory 79—86012
- profile interpretation to give ionic deform. and bonding 77—40301
- profiles, information theoretic calcs. 80—23290
- propene, γ-ray Compton profile meas., MO calcs., rel. to cyclopropane 77—10706
- proton Compton effect, γp elastic scatt., <450 MeV, dispersive anal. 79—396
- proton differential cross sections, 450 to 950 MeV 78—93885
- proton electric polarisability 79—49524
- protons, Compton scatt., Regge pole model 78—93884
- pulsar synchro-Compton radiation damping of linearly polarised plasma waves 78—61877
- pulsed ruby laser, apparatus for registration of gamma secondary radiation 79—76303
- QCD Compton effects, quark and gluon jets 80—32101
- QSOs and BL Lacertae type objects, physical problems 78—57649
- quasar-like objects, inverse Compton scatt. rel. to IR and optical emission 78—20905
- quasars, Comptonised spectrum, Monte Carlo simulation 80—90566
- quasars and active galactic nuclei, magnetic flare model, magnetised accretion disc around massive black hole 80—22113
- quasipotential approach to deep inelastic scatt. at bound state *(Russian)* 77—49972

Compton effect continued
- radial distribution function, derivation from exptl. Compton profiles 78—15244
- radial electric fields from air polarisation due to Compton electrons excited by γ-quanta pulse 80—21805
- radiation and relativistic electrons spectra form. by Compton scatt. at nonzero particle fluxes 79—8825
- radiative transitions, classical theory appl. 78—74597
- radio sources, Compton-limited sources fuelling in expanding synchrotron sources theory 80—12821
- radio sources, form. of universal and diffusion regions of relativistic electrons non-linear spectra 80—109555
- radio sources, superluminal, inverse Compton scatt. in mag. dipole model 80—56959
- radiography, Hounsfield number definition and computerised tomography number conversion 78—35952
- reflection and catching of electrons in field of opposite EM waves 77—10824
- reflection and elastic scatt., Compton scatt. and special relativity 80—46756
- relativistic charged particles, in field of EM plane waves 77—71913
- relativistic Compton laser, power potentiality *(Russian)* 78—90405
- relativistic electron+laser photon scatt., angular and energy distrib. *(Russian)* 79—3029
- relativistic electron beam, stimulated Compton scatt. *(Russian)* 79—86122
- relativistic electron ring, Compton scatt. of laser radiation, photon-electron interaction optimisation *(Russian)* 77—30356
- relativistic invariance as gauge invariance, high intensity Compton scatt. 78—41201
- relativistic Maxwellian electrons, moment generated radiative transfer functions 78—24747
- renormalisation and mass singularities in Compton scatt. of massless electrons 77—30237
- resonance Compton scattering in intense EM wave field 77—34803
- resonant X-ray Raman scattering, IR divergence of Compton effect 78—21873
- scattering amplitude constraints, below photoprod. threshold 80—32102
- scattering by interfering EM fields from independ. sources. 80—43241
- scattering of laser photons on relativistic electrons, energy spectrum *(Japanese)* 77—13908
- scintigraphy, multichannel, collimated, Compton effect on spatial resolution, digital spatial filtering 78—69182
- scintillation counter NE213, organic liquid, Monte Carlo calcs. of electron energy loss spectrum for incident gamma-rays 77—6613
- secondary bremsstrahlung, contrib. in gamma quanta transport problems 79—40782
- semiconductors, Fourier transformed X-ray Compton profiles 80—35004
- simulation by reflection from moving mirror, comment 79—67561
- simulation by reflection from moving mirror, reply to comment 79—67562
- small-angle scatt. of 5 and 6 GeV photons on ^{1}H and ^{2}H 77—46052
- soft-photon emission effects and radiative corrections for electromagnetic processes at very high energies 79—71752
- solar spectra, wavelength shift 77—53495
- solvated electrons, Compton profile evaluation 79—29339
- solvated electrons, dipole polarisability, Compton profiles 78—27877
- stimulated backscattering from relativistic unmagnetized electron beams, book contrib. 79—27334
- stimulated Compton scatt., X-ray regime, growth time limitation 77—7049
- stimulated Compton scattering and collisionless Landau damping 77—34802
- stimulated Compton scattering and related phenomena, book contrib. 78—82219
- stimulated EM shock radiation, book contrib. 79—27149
- structure dependence, ordered and disordered solids 78—35223
- sum rule for directional Compton profiles 80—2889
- superconductirg thin films Cooper pains, photon scatt. on plasmons, Landau-Ginzburg theory 80—65738
- supernova models, Fermi statistics effects on neutrino transport 77—26019
- synchrotron reabsorption sources, Compton scatt., rel. to quasars 80—72761
- teaching, from Compton effect to quarks, at., proton, and nucl. struct. 78—24596
- tetrahedrally coordinated semiconductors, electronic struct. and Fourier transformed Compton profiles 79—38689
- thermodynamic data determ. by X-ray and neutron scatt. 78—83974
- three Ge(Li) Compton polarimeter with kinematic selection, for γ polarisation meas. 77—83456
- tissue, imaging of transverse sections, corrections for multiple scatt. and attenuations 77—40742
- tissue densitometry, calc. of single and multiple scatter photon fluences 78—28048
- tissue sample mass determ. for energy-dispersive X-ray fluoresc. anal. 77—48971
- tomography, emission computed, Compton scatter correction, integral transport method 80—61683
- transition metal, 3d, paramag., energy band calcs. 78—91608
- turbulent plasma, nonlinear Compton scatt. rel. to emission lines broadening and displacement *(Russian)* 77—91418
- two photon processes, manifestation strength of colour below and above colour threshold 80—381
- two-electron atom, momentum distrib. and Compton profiles, Fourier integral calcs. 77—3276
- urea, single crystal Compton profiles, H-bonding and dimer config. effects, calc. and meas. 78—80431
- vacuum polarisation effects on Compton scatt., unmagnetised electrons, ambient mag. field, astron. appls. 80—86631
- vector boson elast. scatt., Lorentz covariant scatt. amplitude and Compton scatt. 77—2776
- vector meson photoproduction and Compton scatt. by nucleons 79—22114
- vector particle, differential cross section, calc. by Feynman's method *(Russian)* 78—12916
- virtual Compton amplitude, anal. model 77—22739
- virtual Compton amplitude, high-energy deep-inelastic scatt. 78—41550
- virtual Compton amplitudes, duality props. 77—30388
- water, Compton profile meas., non-additivity of elastic and inelastic X-ray scatt. 78—43953

Compton effect continued
water, profile correction for multiple scatt. 77—32460
water irradiated by photons up to 2 MeV, initial energies of Compton electrons and photoelectrons 80—108320
wave and particle descriptions of light, equivalence, rel. to radar freq. shift 80—101692
Xα wavefunctions, Compton profile as criterion for choice of local exchange parameter α 78—33410
X-ray computerised tomography, energy-dependent reconstruction 77—12991
X-ray emission spectrum, multiple Compton scatts. effect, Monte Carlo calcs. 78—96389
X-ray sources, compact, optically thick radiative transfer rel. to X-ray spectra form. 80—22115
X-ray sources, Compton scattering effects 79—84869
X-ray sources, Comptonization and radiation spectra, Monte Carlo calc. *(Russian)* 79—80372
X-ray sources, time-dependent Comptonisation and X-ray reverberations rel. to rapid time variability 80—86013
X-ray spectral lines profile evolution due to Comptonisation, Monte Carlo computations 79—66916
X-ray spectroscopy by Compton-scatter method, for diagnostic X-rays 77—2044
X-rays Comptonization by low-temp. electrons, Monte Carlo calc. 80—12653
XX Ce, γ-α phase transition, study by Compton scattering 80—59650
eγ scatt., coherent states and quantum nonperturbing measurements 79—315
γe Compton and Thomson scatt. in strong magnetic fields, differential cross sections, neutron star appl. 79—67530
$\gamma e \to \gamma\gamma e$, polarised photon splitting on unpolarised electron *(Russian)* 79—371
γN, inelastic virtual Compton scatt., quark struct. 79—89164
γN, $\pi^0 \to 2\gamma$, $\eta^0 \to 2\gamma$ and N EM polarisabilities 77—18289
$\gamma p \to \gamma p$, 2 to 6 GeV, differential cross section meas., parton model anal. of energy depend. 79—63485
$\gamma p \to \gamma p$, differential cross sections in 240 to 440 MeV range, $\Delta(1232)$ region 77—10255
$\gamma p \to \gamma p$, differential cross sections at large angles, 2-6 GeV 78—37214
$\gamma\pi$, hadron photoprod. and saturation of sum rules *(Russian)* 79—49529
pγ, Compton scattering, 375 to 1150 MeV, differential cross section 80—57604
π^0 decay, Compton electron scatt., 0.1 to 5.0 GeV 79—397
Ag, integral K-shell Compton scattering, cross-section, for 1250 keV photons 78—90128
Al, Compton defect calcs. in Born impulse approx. 77—88427
Al, Compton profile, multiple scatt. correction 79—61456
Al, Compton profile from 662 keV γ-ray spectroscopy 78—56539
Al, Compton profile from X-ray Ag K_α fluorescence radiation 78—48257
Al, Compton profiles for liq. and solid phases 79—91519
Al, Fermi momentum, for solid and liq. phases, temp. variation, Compton scatt. obs. 80—50451
Al, γ-ray Compton profile, asymmetry 79—91520
Al, incoherent scatt. factors calc. by direct integration over impulse approx. Compton profiles 80—102475
Al, multiple scattering, relativistic cross section for double scatt. 79—69898
Al, polycryst., X-ray attenuation and photoelec. coeffs. in range 0.3 to 1.3 Å 79—99979
AlN, effect of valence states on X-ray Compton line shapes 77—8682
^{241}Am spectrometer for Compton scatt. studies 79—2899
Ar, Compton profile, local density approx., Kohn-Sham self consistent scheme 78—94193
Ar, Compton profiles, Xalpha wavefunctions 80—106265
Ar, Compton profiles using Gaussian expansion of at. orbitals 80—945
Ar electron energy loss spectra, Compton defect characterised by shift and asymmetry parameters 80—95723
Ar, impulse Compton profiles, atomic optimised pot. model 78—74618
Ar, incoherent scatt. factors calc. by direct integration over impulse approx. Compton profiles 80—102475
Au, K-shell electrons, 1.12 MeV γ-ray scatt. 77—54539
Au, K-shell electrons, Compton scatt. of 1.12 MeV gamma-rays 77—68016
Au, K-shell electrons, Compton scatt. of 1.12 MeV gamma-rays, energy distrib. meas. 77—68017
Au, relativistic 1s wavefunctions test, using exptl. Compton profiles 80—32600
^{198}Au, 412 keV γ-radiation, Compton scattering and Bragg diffraction, study of electron densities in solids 80—18059
B, 1st order Compton profiles, momentum distribs., correlation effects 77—88429
BH_4^-, electron momentum distribution and Compton profiles, FSGO calcs. 80—87032
B_2H_6, electron momentum distribution and Compton profiles, FSGO calcs. 80—87032
$B_3H_8^-$, electron momentum distribution and Compton profiles, FSGO calcs. 80—87032
B_4H_{10}, electron momentum distribution and Compton profiles, FSGO calcs. 80—87032
Be, anisotropy, theoretical investigation by K-emission, APS, and Compton profiles 78—63970
Be, Compton profile, electronic energy calc. 80—37822
Be, core electron distribution, X-ray diffr. and γ-ray Compton profile obs. 80—1958
Be metal, electron distribution and momentum density, Compton scatt. 80—11502
C, 1st order Compton profiles, momentum distribs., correlation effects 77—88429
C, glassy, Compton profiles, momentum densities, comparison with graphite 80—2895
CO_2, electron impact spectra, 35 keV electrons, Bethe surface and Compton profile 79—27091
Cd, integral K-shell Compton scattering, cross-section, for 1250 keV photons 78—90128
Ce, Compton profile study of γ-α phase transition 80—11503
Ce, electronic structure, Compton profile meas. 80—10867
ClCN, linear mol., Compton profile bond additivity, HF calc. 79—68268
Co^+, Rayleigh and Compton scatt., differential cross section determ. 80—52912
$Co_{49.6}Al_{50.4}$, Compton scatt., 59.54 keV γ-rays, charge transfer study 78—68578

Compton effect continued
$Co_{82}P_{18}$, amorphous alloys, electronic struct., γ-ray Compton scatt. study *(Japanese)* 80—84422
Cr, single cryst., Compton X-ray scatt., electron binding energy effect 77—59639
D_2, Compton profile determ. by high energy electron impact spectroscopy 77—68083
F, 1st order Compton profiles, momentum distribs., correlation effects 77—88429
F_2, Compton scatt. profile, SCF MO theory calcs. 78—58577
FCN, linear mol., Compton profile bond additivity, HF calc. 79—68268
Fe, $3d^64s^2$ and $3d^74s$ configs., Rayleigh and Compton scatt., differential cross sections 80—52912
Fe, Compton profile from 662 keV γ-ray spectroscopy 78—56539
Fe, Compton profile of mag. electrons meas. 77—32461
Fe, effect of valance state on X-ray Compton line shape 77—8682
Fe, ferromag., Compton profile meas. with circularly polarised gamma rays from oriented nuclei *(Japanese)* 78—23548
Fe, spin dependent momentum distrib., APW calc. 78—2416
Fe-Al, directional Compton profiles, self-consistent APW band struct. calc. 80—25476
$Fe_{49.7}Al_{50.3}$, Compton scatt., 59.54 keV γ-rays, charge transfer study 78—68578
$Fe^+(Fe^{2+})$, Rayleigh and Compton scatt., differential cross section determ. 80—52912
Fe_3O_4, magnetite, Compton profile, 100 and 300K 78—35219
Ge, Compton profile anisotropy, pseudopot. calc. 79—28854
Ge, Compton scatter, spatial spread meas., imaging with position-sensitive detectors 78—46214
Ge, directional Compton profile meas., strúctural information 79—28855
Ge, directional Compton profiles, X-ray scattering factors and 1-electron density matrix 80—10458
Ge, effect of valence state on X-ray Compton line shape 77—8682
Ge, inelastic X-ray scatt. cross section accompanied by intermediate momentum transfer 79—24387
Ge, inelastic X-ray scattering cross sections, in case of small momentum transfer 77—27786
Ge, valence electron radial and momentum distribs., X-ray form factors and Compton profiles 79—65956
Ge(Li)-NaI(Tl) Compton suppression spectrom. for low-level activity meas. 78—9022
H_2, anisotropic Compton profile, LCAO calcs. 77—6863
H_2, Compton defect, high energy electron impact spectroscopy 77—71876
H_2, Compton profile, electronic energy calc. 80—37822
H_2, Compton profile and momentum distribution, impulse approx. 78—25626
H_2, Compton profile determ. by high energy electron impact spectroscopy 77—68083
H_2, correl. Gaussian wave function calc. 79—81241
H_2, electron impact spectroscopy for Compton profile meas. 78—90299
H_2, $X^1\sigma_g^+$, momentum distrib., electron correl. and mol. vibr. effects, theory 77—88557
H_2^+, Compton profile and momentum distribution, impulse approx. 78—25626
HCN, linear mol., Compton profile bond additivity, HF calc. 79—68268
$H_2(D_2)$, Compton profile, impulse approx., electron correl., vibr. and rot. effects 78—17585
HNC, linear mol., Compton profile bond additivity, HF calc. 79—68268
H_2O, Compton profile, electronic energy calc. 80—37822
H_2O, H-bond contrib. to Compton profile, HFS Xα model 78—17726
H_2O, liq., Compton profile at 60 keV 79—47535
H_2O, mol., Compton profile, directional, polarisation functions 79—36706
He, Compton profile asymmetry, high momentum transfer, calc. *(French)* 78—42013
He, Compton profile determ. by high energy electron impact spectroscopy 77—68083
He, Compton profiles using Gaussian expansion of at. orbitals 80—945
He, electron impact spectroscopy for Compton profile meas. 78—90299
HeH^+, electronic momentum distribution, Coulomb shift and correl. coeffs. 80—83266
In, integral K-shell Compton scattering, cross-section, for 1250 keV photons 78—90128
inert gases, solid, Compton profiles, APW-Xα calc. 80—80894
K, Compton profiles using Gaussian expansion of at. orbitals 80—945
KBr, Compton profile, 59.54 keV γ-rays 78—64426
KCl, Compton profile, 59.54 keV γ-rays 78—64426
KCl, Compton profile anisotropies, charge and momentum distrib., LCAO-SCF-MO calc. 79—3500
KF, Compton profile, 59.54 keV γ-rays 78—64426
Kr, Compton profile, local density approx., Kohn-Sham self consistent scheme 78—94193
Kr, Compton profiles using Gaussian expansion of at. orbitals 80—945
Kr, impulse Compton profiles, atomic optimised pot. model 78—74618
Kr, incoherent scatt. factors calc. by direct integration over impulse approx. Compton profiles 80—102475
Li, Compton defect 77—73183
Li, Compton profiles in liq. and solid states 79—87520
Li, liq. and solid states, γ-ray Compton profiles 77—48269
Li-Mg alloy, X-ray Compton scatt. 77—16421
LiBr, Compton profile anisotropies 79—27044
LiCl aqueous soln., ion-water clusters, electronic struct., Compton profile 78—47227
LiCl, aqueous soln., self consistent wavefunctions, HFS Xα pot. in cluster model, Compton profile calc. 79—78783
LiCl, Compton profile anisotropies, charge and momentum distrib., LCAO-SCF-MO calc. 79—3500
LiF, anisotropic Compton scattering using synchrotron radiation 80—60703
LiF, Compton profile interpretation to give ionic deform. and bonding 77—40301
LiF, effect of valence state on X-ray Compton line shapes 77—8682
LiF, LCAO calc. of Compton profiles 79—95871
LiH, cryst., Compton profile, position space anal. 79—47536
LiH, directional Compton profiles 79—4867
LiH, Fourier transforms of Compton profiles 79—83050
Li_3N, electron density study using Compton scattering 80—79750
Lu, Compton profiles, electronic configurations 80—11501
$LuH_{2.05}$, Compton profiles, electronic configurations 80—11501

- **Compton effect** continued
  - methanol-water mixture, Compton profile meas., non-additivity of elastic and inelastic X-ray scatt. 78—43953
  - MgO, effect of valence state on X-ray Compton line shape 77—8682
  - Mo, integral K-shell Compton scattering, cross-section, for 1250 keV photons 78—90128
  - N, 1st order Compton profiles, momentum distribs., correlation effects 77—88429
  - N_2, electron Compton profiles from energy loss spectra 79—7013
  - NH_3, electron impact, 35 keV, Bethe surface and Compton profile 80—87235
  - NH_3, electron scatt., 35 keV, Compton defect 79—27092
  - NH_3, experimental electronic Compton profile beyond impulse approx. *(French)* 80—53057
  - NH_3, expt. electron Compton profile beyond impulse approx. 80—87083
  - NH_3 molecule, Compton profile asymmetry, 35 keV electron impact spectroscopy 79—7025
  - NNO, linear mol., Compton profile bond additivity, HF calc. 79—68268
  - Na, Compton profiles in liq. and solid states 79—87520
  - Na, Compton profiles using Gaussian expansion of at. orbitals 80—945
  - Na, incoherent scatt. factors calc. by direct integration over impulse approx. Compton profiles 80—102475
  - Na, liq. and solid states, γ-ray Compton profiles 77—48269
  - NaBr, Compton profile, 59.54 keV γ-rays 78—64426
  - NaBr, Compton profile anisotropies 79—27044
  - NaCl, Compton profile, 59.54 keV γ-rays 78—64426
  - NaCl, Compton profile anisotropies, charge and momentum distrib., LCAO-SCF-MO calc. 79—3500
  - NaF, Compton profile, 59.54 keV γ-rays 78—64426
  - NaI:Tl scintillation crysts., analytic calc. of photofractions to monoenergetic γ-rays 79—52038
  - Nb, Compton profile meas. 77—4698
  - Nb, integral K-shell Compton scattering, cross-section, for 1250 keV photons 78—90128
  - Nb, $NbH_{0.76}$, profile anisotropy, electronic struct. of hydride 77—73182
  - $NbD_{0.6}$, Compton profile meas. 77—4698
  - $NbH_{0.29}$, Compton profile and electron momentum distrib. anisotropy 77—44079
  - NbO_2, rutile phase, energy levels, momentum density, and Compton profile, embedded cluster model 80—50453
  - Ne, 1st order Compton profiles, momentum distribs., correlation effects 77—88429
  - Ne, Compton profile, local density approx., Kohn-Sham self consistent scheme 78—94193
  - Ne, Compton profiles, Xalpha wavefunctions 80—106265
  - Ne, Compton profiles using Gaussian expansion of at. orbitals 80—945
  - Ne, electron energy loss spectra, Compton defect characterised by shift and asymmetry parameters 80—95723
  - Ne, experimental electronic Compton profile beyond impulse approx. *(French)* 80—53057
  - Ne, expt. electron Compton profile beyond impulse approx. 80—87083
  - Ne, impulse Compton profiles, atomic optimised pot. model 78—74618
  - Ni, multiple scattering, relativistic cross section for double scatt. 79—69898
  - Ni^{2+}, Rayleigh and Compton scatt., differential cross section determ. 80—52912
  - Ni-P amorphous alloys, electrodeposited and melt-quenched atomic and electronic structures 80—88062
  - $Ni_{81}P_{19}$, amorphous alloys, electronic struct., γ-ray Compton scatt. study *(Japanese)* 80—84422
  - O (O^+) (O^{2+}), Rayleigh and Compton X-ray scatt. cross sections in plasma 80—43884
  - O, first order Compton profiles, momentum distribs., correlation effects 77—88429
  - OCN^-, linear mol., Compton profile bond additivity, HF calc. 79—68268
  - Pb, K-shell electrons, 1.12 MeV γ-ray scatt. 77—54539
  - Pb, K-shell electrons, Compton scatt. of 1.12 MeV gamma-rays 77—68016
  - Pb, K-shell electrons, Compton scatt. of 1.12 MeV gamma-rays, energy distrib. meas. 77—68017
  - Pb, relativistic 1s wavefunctions test, using exptl. Compton profiles 80—32600
  - Pd, Compton profiles, comparison with band struct. calcs. 78—84675
  - Pd, electronic structre, Compton scatt., soft X-ray emission and X-ray photoelectron spectra 79—77999
  - $PdH_{0.72}$, Compton profiles, comparison with band struct. calcs. 78—84675
  - $PdH_{0.72}$, Compton profile, electronic struct. *(German)* 78—92140
  - polycryst., X-ray attenuation and photoelec. coeffs. in range 0.3 to 1.3 Å 79—99979
  - Pt, atomic Compton cross sections 79—18152
  - Pt, Compton cross-sections due to K-shell electrons, ang. variation 78—21883
  - SCN^-, linear mol., Compton profile bond additivity, HF calc. 79—68268
  - SCO, linear mol., Compton profile bond additivity, HF calc. 79—68268
  - SE, Compton profile, charge density and momentum density determ. 77—63480
  - Sb, integral K-shell Compton scattering, cross-section, for 1250 keV photons 78—90128
  - Sc, electron momentum distrib., renormalised free atom model 77—1756
  - Se, Compton profile, charge and momentum density 80—55220
  - Se, Fourier-transformed Compton profile as microstruct. probe 77—59636
  - Se, trigonal and amorphous, Compton profiles 77—32464
  - Se, valence electron Compton profile, self-consistent OPW calcs. 77—36307
  - Si, Compton profile anisotropy, pseudopot. calc. 79—28854
  - Si, directional Compton profile meas., structural information 79—28855
  - Si, directional Compton profiles, X-ray scattering factors and 1-electron density matrix 80—10458
  - Si, inelastic X-ray scatt. cross section accompanied by intermediate momentum transfer 79—24387
  - Si, inelastic X-ray scattering cross sections, in case of small momentum transfer 77—27786
  - Si, momentum density, Compton profile 77—20235
  - Si, three-dimensional electron-positron pair momentum density from positron annihilation meas. 79—43059
  - Si, valence electron radial and momentum distribs., X-ray form factors and Compton profiles 79—65956
  - SiC, momentum density, Compton profile 77—20235
- **Compton effect** continued
  - Si_3N_4, CVD, chem. bond nature, Compton scatt. expts. 80—49539
  - SiO_2, amorphous and cryst., Compton profile study 78—88378
  - Sn, integral K-shell Compton scattering, cross-section, for 1250 keV photons 78—90128
  - Ta, K-shell electrons, Compton scatt. of 1.12 MeV gamma-rays 77—68016
  - Te, Compton profile, charge and momentum density 80—55220
  - Th, ang. variation of Compton cross-sections due to L-shell electrons 77—3322
  - Th, Compton spectrum due to L-shell electrons 77—34593
  - Th, incoherent scatt. of gamma rays 77—79585
  - Th, K-shell electrons, 1.12 MeV γ-ray scatt. 77—54539
  - Th, K-shell electrons, Compton scatt. of 1.12 MeV gamma-rays 77—68016
  - Th, K-shell electrons, Compton scatt. of 1.12 MeV gamma-rays, energy distrib. meas. 77—68017
  - TiC, calcs. of 2γ-ang. correlations and Compton profiles 78—39624
  - TiC, LCAO band struct., Compton profile 77—85138
  - U ore, U content determ., radioisotopic X-ray technique using Compton scatt. 77—70357
  - V, and $VD_{0.68}$, anisotropic Compton profiles 80—97368
  - V, Compton profiles, comparison with band struct. calcs. 78—84675
  - V deuteride, Compton profiles 79—8206
  - V, effect of valence state on X-ray Compton line shape 77—8682
  - V, energy bands, calcs. using LCGO method 78—91608
  - V, energy bands, Compton profile, optical cond., SCF LCAO calcs. Gaussian orbitals 78—47698
  - $VD_{0.77}$, Compton profile, electronic struct. *(German)* 78—92140
  - $VD_{0.77}$, Compton profiles, comparison with band struct. calcs. 78—84675
  - $VH_{0.71}$, Compton profile, electronic struct. *(German)* 78—92140
  - $VH_{0.71}$, Compton profiles, comparison with band struct. calcs. 78—84675
  - ZnO, valence electron states, X-ray Compton profile 79—65955
  - ZnS, Compton profile, state of valence electrons 78—11018
  - ZnS, valence electron states, X-ray Compton profile 79—65955
- **Compton profile** *see Compton effect*
- **Compton scattering** *see Compton effect*
- **computation** *see calculation*
- **computational complexity**
  - algorithm design 77—17959
  - field theory problems, alternating continuity principle in piecewise solutions 79—84959
  - hydrocarbon crystal structure calc. by molecular packing analysis 78—14303
  - image generation system for nonplanar projection modelling 80—99667
  - laser resonator standing wave simultaneous forward and backward integration 79—94258
  - neutron transport, probability table method extension 79—584
  - novel Monte Carlo binning technique 79—160
  - nuclear fuel rod modelling complexities 77—46231
  - transonic potential flow, finite element method programme, optimal control theory anal. 80—24045
- **computational linguistics**
  - automatic spoken word recognition using linguistic information 79—55274
  - speech and nonspeech category boundary adaption, case against features detectors 79—72763
- **computer-aided analysis**
  - *see also analogue simulation; CAD; circuit analysis computing; control system analysis computing; digital simulation; electric machine analysis computing; hybrid simulation; power system analysis computing*
  - acoustic design of concert halls, preference tests for simulated acoustic fields 80—23838
  - acoustic field in finite cuboidal spaces, computer-aided geometrical field analysis of directional props. 80—19157
  - acoustical design of broadcasting and recording studios 79—64402
  - advanced reactor cycles, total core analysis 79—9782
  - air pollution, housing estate heat supply methods comparison *(Hungarian)* 79—2366
  - airbase noise contours, prediction via NOISEMAP program 79—1025
  - ambulatory ECG computer anal., YALECG 79—70661
  - amorphous metals, computer simulations of tensile deformation and radiation damage *(Japanese)* 79—42137
  - analytical chemistry, user-oriented software Fourier spectrum display 78—64896
  - angiocardiogram objective quantitative processing, Cardiac Image Analysis System 79—70629
  - aperture-type light conductor, photometric charact., computerised calc. by Monte Carlo method *(Russian)* 80—1339
  - auditory nervous system activity analysis 80—30921
  - axially symmetric hollow collectors for high temp. solar installations, radiative heat transfer computation 78—79093
  - axisymmetric transducers, with various boundary conditions, single integral computer method for Green's function 80—87591
  - bioelectric signal waveform analysis, computerized method for electronystagmogram anal. *(Croatian)* 79—20697
  - biological signals, harmonic analysis, aorta blood pressure 77—52899
  - breath volume and time components, computer aided meas. using magnetometers 79—16332
  - bubble chamber, projection graphic display for computer aided image anal. 80—27895
  - Cambridge crystallographic data centre: computer-based search, retrieval, analysis and display of information 80—1877
  - cardiac acoustic model for computer-aided surface acceleration mapping 78—35791
  - cataract formation in rabbits and monkeys by acute microwave irradiation, computer thermal model 79—5326
  - computerised tomography, computer assisted determ. of OTF 80—46030
  - concrete, reinforced cross-section, reponse to short-term and sustained loads 79—52358
  - crack propagation based on fracture mechanics 77—35094
  - crystal atomic structures, computer-aided graphical representation of projections onto planes 79—60217
  - crystal structural fragment, automatic construction, taking account of attainable chem. bond lengths 80—92419
  - cultured cells time lapse cinemicrographs 78—92756
  - current flow in corona discharges with arbitrary outer-conductor geometries 77—62418
  - dielectric parts, stress patterns and deformation characts., computer anal. 80—17787

- **computer-aided analysis** continued
  - district heating power station chemical water treatment pH value calc. *(Russian)* 79—43572
  - DNA thermal transition midpoint, CAA 79—74593
  - ECG, automated Holter anal., shape oriented system 79—70662
  - ECG, random access mass storage anal., RAMSES, for quantitative anal. of long-term ECGs 79—70663
  - echocardigram, automatic anal. and VTR recording 80—8112
  - echocardiograms, left ventricular anal. *(German)* 80—81667
  - EEG, multivariate pattern recognition technique, cerebral abnormality localisation 79—16327
  - EEG alternations, power spectral analysis 80—30924
  - EEG field plotting method for isopotential maps 79—39542
  - EEG sleep state analysis, automatic real-time practical method 80—67263
  - elastic coefficients, independent 4th-order for all cryst. classes, numerical methods anal. 79—69219
  - elastic deformation, critical equilibrium states of nonlinear elastic systems, unified method of computation 79—98610
  - elastic wave propagation in nonlinear elastic half-space, 2-D 77—48
  - electric field, permittivity meas. through ponderomotive forces determ. 79—215
  - electrical conductivity and threshold switching in non-cryst. semiconds. of computer simulation 78—88002
  - electrocardiogram, computer anal. *(Chinese)* 79—57787
  - electromagnetic field anal., computer methods, MHD and finite elements method 80—32879
  - electron micrographs, computer simulated in defect identification 79—69101
  - electron-image calculation system, interactive, for use in electron microscopy 80—24325
  - electrostatic fields in complex periodic structures *(Russian)* 78—33648
  - electrostatic lens systems, non-rotationally symmetric 77—79740
  - EMG, single motor unit action pots. identification by computerised anal. 80—72343
  - engineering design, numerical, vital role of expt. stress anal. 79—32418
  - ESCA spectra automatic analysis by top down method *(Japanese)* 77—40598
  - excitable membrane analysis 80—56004
  - extrusion process using orthotropy concept of Hill, kinematically determined problems in rigid-ideal plastic *(German)* 80—1445
  - field analysis computers, colloquium, London, England (March 1980) 80—94964
  - films, deposition profile with shadow effect, theoretical model 79—82473
  - flow cytometric data, computerised display and anal., review, book contrib. 80—109082
  - Frevel ZRD-SEARCH-MATCH program, for powder diffr. anal., generalisation 80—59341
  - gas turbines, temperature gradient along cooling channel surface, heat transfer in initial hydrodynamic section, computation 79—18892
  - gastrointestinal signals, quantitative analysis 80—41339
  - graphic analysis using microprocessor-based system 79—70665
  - heating of single family dwellings, heat pump appl. 79—43784
  - human gait, representation by 4 dimens. vectors *(German)* 78—88723
  - image analysis, production control of precision components *(German)* 80—42193
  - incompressible flow, losses due to direction change 79—18896
  - incremental compiler for data acquisition 79—89550
  - interactive graphics system developed for NDT 80—66729
  - interferometer, double-beam, computer analysis program 79—71520
  - inverse pole figures, calc. method on digital computer 80—20950
  - ischaemic episode, computerised continuous beat by beat anal. and rational plots 79—62394
  - Japanese kinki dialect, anal. and perception of two-mora word accent types *(Japanese)* 78—92659
  - Kolmogorov statistical model, monolayer, for cryst. vaporisation kinetics pt.II 79—95152
  - laboratory test interpretation using computer 79—74770
  - laryngeal films, ultra high-speed, automated anal. 79—57746
  - laser calorimetric data, automated anal. 80—4714
  - lattice parameter program, least squares method 79—64958
  - leg loading components correlation in snow skiing 79—96608
  - loudspeaker driver parameters, time domain measurement implemented with digital computer 79—59901
  - MAGIC, multisoln. direct methods procedure 79—73062
  - medical radioactivity, absolute meas. technique using a gamma camera 79—25087
  - memory function, transverse current correlations in classical one component plasma 78—94892
  - MHD steam power plant, coal-fired, economic optimisation 79—52942
  - MIS structure non-stationary processes *(German)* 77—39952
  - molecular crystals, optimum packing in atom-atom approx., algorithm and computer program 80—1960
  - molecular packing arrangement drawings, plot of packing program POP1 79—94839
  - molecular topological symmetry 79—41251
  - multicircuit shells of revolution, computer anal. by field method 77—3729
  - multielement atomic emission/fluoresc. spectrometer system, computer-controlled 80—45587
  - nuclear containment vessel response to impact using PISCES finite difference codes 77—3097
  - nuclear event analysis program using EVAL language 79—89561
  - nuclear reactor risk 77—38373
  - nuclear tracks, etched, statistical distribs. using computer image anal. 80—83235
  - nystagmus, automatic on-line anal. *(German)* 80—76846
  - ocean receivers for acoustic signals from moving radiating sources 79—59859
  - oculomotor function analysis 80—46092
  - optical fibre connector, using resilient alignment method, finite element program 78—71230
  - optokinetic stimulus pattern by computer graphics for study of optokinetic nystagmus 79—44008
  - paraboloidal mirrors, image formation determ., solar concentrator appl. 77—46780
  - photon correlation in nanosecond range using programmable digital counter, photomultiplier evaluation 78—54464
  - planar channelling effects for relativistic protons and π^- mesons, deflection effects 79—77656

- **computer-aided analysis** continued
  - polyethylene, crystalline, twist disclination formation and longitudinal motion of defects 80—19810
  - pre- and post-processing techniques for complex analysis 80—94965
  - pressure vessels, axisymmetric, with structural discontinuities, elastic stress analysis *(Japanese)* 80—38265
  - prosthetic aortic heart valve dysfunction computer-assisted detection 77—40922
  - pump pipeline pressure surges calc. *(Spanish)* 79—23364
  - quantitative analysis software package for use with the APD 3500 79—50947
  - radiographic film quality appl. 80—8158
  - radiographic screen-film system, determination of charact. curve and its gradient 79—5362
  - radiographs, hardware configurations, software strategies 79—16290
  - radionuclide cardiac output determination, automated computer program 80—56196
  - radiotherapy, computer assistance in planning seed implants 79—100711
  - radiowave propag., direct attenuation function and field strength calc. 79—25373
  - radiowave scattering signals, incoherent, spectral analysis *(Russian)* 79—5621
  - rapid eye movements, computerised anal. method, REM sleep period appl. *(Japanese)* 80—41273
  - refinement of initial parameters in overlapping spectral bands resolution 79—41198
  - relaxation data anal., superimposed exponentially decaying signals, computer technique 78—23360
  - respiratory tracer gas nonlinear computer anal., non-invasive meas. method 79—62395
  - RFIT, data evaluation program, theoretical background 78—29562
  - river pollution distribution determination by remote sensing, computer aided analysis 80—81512
  - rock fracture in uniaxial compression *(Japanese)* 80—12379
  - secondary cells, Pb-acid, cell design analysis computing for optimal electrical performance characterisitics 80—55832
  - seismic analysis and discrimination 78—20530
  - seismology, computer-aided anal. and discrimination, bibliography 77—81832
  - semiconductor-insulator interface, microcomputer-aided interface-state analysis 80—80383
  - shock waves in bubbly liquids *(French)* 78—26183
  - Shubnikov-de Haas quasi-periodic oscill. curves, harmonic analysis, computer method *(Russian)* 78—39132
  - solar building, using Cal-ERDA programs 79—57456
  - solar concentrator performance, parabolic dish, pointing errors effects on receiver performance 79—48097
  - solar plant composite heliostat, computer anal. and optimisation 79—39283
  - solar radiation, numerical model based on standard meteorological observations 79—34929
  - solar space heating systems, load optimisation algorithms 80—45643
  - steel, Fe-Si (3 wt.%), Bauschinger effect, computerised evaluation method 80—93625
  - steel, Nb-Mn, Molytor 53, Bauschinger effect, computerised evaluation method 80—93625
  - steel, standard, energy dispersive X-ray fluoresc. spectrometry, computer directed optimisation 80—45585
  - steels, high-strength low-alloy, Bauschinger effect, computerised evaluation method 80—93625
  - stress relieving notches, expt. and computer aided study, and optimisation 79—59926
  - structural analysis constraint techniques for coupling of discrete axisymmetric and general structs. 77—3714
  - structural dynamics analyser development, microcomputer-based 80—53733
  - structures dynamic problems, eigenvalue economisation, program *(Italian)* 79—35544
  - sunlight reflected from polygonal heliostat, optical simulation 79—29452
  - sunlight transmission through uniform waterdrop atmosphere 78—36244
  - surface roughness three-dimensional anal. problems *(Polish)* 77—67411
  - Telemed programme for serial comparison fo ECGs 80—26395
  - TEM convergent beam pattern anal., for Zr foil thickness determ. 79—4215
  - ternary molten salt phase diagrams, computation 79—100118
  - thermoelasticity in solid symmetrical bodies of revolution, thermal transients calc. *(Spanish)* 79—23208
  - tibia fractures, ^{99m}Tc-pyrophosphate scans, algorithm for automatic computer anal. 79—88171
  - turbulent boundary layer on turbine blade 79—64647
  - two dimensional electrostatic field shape investigation *(Czech)* 79—27126
  - two-phase cryst. structures, orientational electron microdiffr. anal. with aid of OMEGA program 80—103218
  - US test procedure, for detection of fatigue damage 80—71848
  - VVER-440 reactors, emergency operating conditions following main circulation pipe failure 79—9823
  - walking, computer animation of gait 79—11957
  - wind turbines variable pitch vertical axis 80—61265
  - X-ray data, computer-aided anal. 77—67416
  - X-ray stress meas., computer-aided system *(Japanese)* 80—104366
  - YZARC, multisoln. direct methods procedure 79—73062
  - Al alloys, energy dispersive X-ray fluoresc. spectrometry, computer directed optimisation 80—45585
  - $Cd_xHg_{1-x}Te$, flameless atomic absorpt. anal. using interactive computer processing 79—66380
  - Fe, Armco, Bauschinger effect, computerised evaluation method 80—93625
  - Fe laminated cores, eddy currents calc. in arbitrarily shaped three-dimens. cores, appls. *(German)* 79—45886
  - Na_2XO_4, (X=S, Cr, Mo, W), anal. and calc. of binary and ternary phase diagrams 80—88299
  - Si ribbon growth, technology assessment 1978-1986, computer anal. using PECAN 79—8244
  - TiS, vaporisation chemistry and thermodynamics, computer-automated simultaneous Knudsen-torsion effusion 80—48837

computer-aided circuit analysis *see circuit analysis computing*

computer-aided circuit design *see circuit CAD*

computer-aided design *see CAD*

computer-aided instruction
- *see also education*
- acceptability, costs and developments 80—9
- analogue computer applications in quantum chemistry training *(German)* 78—28903
- atomic orbitals, hydrogen-like, shape, teaching appl. 78—93496
- audible, use of audio or video recordings 80—42008
- audio-visual aid, for teaching and examinations, microprocessor appl. *(Hungarian)* 77—53723
- automated simulation of direct school/society interaction 79—35487
- ballistics, max. range at elevated launch height, expt. and BASIC program 79—97156
- binary solid-liquid equilibria, student experiment, phase diagram computer program 78—89285
- biomechanics film data reduction and anal. using PLATO system 79—35873
- biomedical engineering instruction, microprocessor-based instrumentation system 77—22361
- biophysics, physiology, pharmacology CAI 77—25
- biophysics, teaching appls. of analogue computers 79—84890
- calculus teaching, discrete approach using computer 79—80398
- celestial mechanics, diurnal motion of Sun seen from Mercury, computer aided soln. 78—61969
- chemical education, state-of-the-art 80—4488
- chemical equilibrium teaching, computer method using minimisation of free energy 79—30168
- chemical reaction kinetics, teaching, Monte Carlo method, computer program 77—24
- chemical spectroscopy, computer-simulated laboratory experiments for students 79—40339
- chemistry, at Syracuse Univ. 77—23
- chemistry, CAI using microcomputer, systems, appls. 80—57042
- chemistry, current status 80—12867
- chemistry at University of Surrey 79—30167
- chemistry education, binary system for carbohydrate nomenclature 80—62435
- children's pocket calculators, educational pot. and teacher reactions 80—22178
- clinical experiences, computer simulated patients 79—17162
- comparative evaluation of instructional systems, survival principle 79—92906
- computer augmented video education, project status report 80—22174
- computer physics, elementary concentrated one-week course 78—73799
- conservative discrete models, difference eqn. formulation, nonlinear solid, fluid phenomena, computer calc. 77—78924
- didactic microcomputer *(German)* 79—80396
- differential eqn. teaching with interdisciplinary models 78—77640
- ecology, CAL approach to population dynamics 79—30166
- education, minicourse in HMO theory using small computers 78—25444
- educational computing, minicomputer, microcomputer 79—48989
- educational technology and the computer 78—49615
- electromagnetic field theory teaching for University of Iowa undergraduate students 77—9835
- engineering design curricula, computer appls. 80—27065
- equivalent resistance program in APL 77—5615
- field effect transistors, computer simulation, student lab expt. 79—44673
- fluid mechanics and heat transfer, course for final year B.Sc. students 77—60877
- frontiers in education, conference, Urbana-Champaign (1977) 78—81779
- geology, computer simulation of geologic processes, 77—17
- geology, computer simulation of geologic strata 77—18
- geology, conf., Syracuse, USA (Nov. 1975) 77—15
- geology, interactive CRT display of Bouguer gravity models 77—22
- geology, PETROS data bank, igneous rock major element analyses 77—2249
- geology, PLATO system 77—20
- geology 77—16
- geophysics and geology, interactive computing with graphic display 77—21
- Glasgow University, computer-aided learning project in maths 77—71168
- graphics and electromagnetic fields 77—33781
- graphics for numerical analysis tuition 78—81817
- historical development outline 78—12502
- HMO theory, student use, computerised visual aids 78—77649
- human factor studies, conf., San Francisco, USA (Oct. 1977) 78—48742
- individualised nursing programme adaption of Classroom Teacher Support System 80—22175
- individualised testing, support system 79—92914
- individualized instruction, computer managed self-paced course 77—26113
- integrated problem sets, generation and reproduction using computer program 79—58479
- interactive computer assistance with calculations arising in undergraduate laboratory experiments 79—35493
- interactive computer terminal as 'lab. assistant' in introductory physics expt. 78—36761
- interactive graphical displays for physics undergraduates 77—13558
- interactive learning, the Millikan Lecture 78, educational uses of computers 79—25785
- kinetic theory of gases, computer modelling of mol. vel. distribs. 79—30169
- lesson design for computer-based instructional systems 79—35490
- mathematics teaching by computer, long-division practice program in BASIC 80—98775
- mathematics teaching by computer-assisted learning 79—80401
- microcomputer applications in physics teaching, review 79—30171
- microcomputer systems, comparative eval. 79—30173
- microcomputer use at University of Michigan 80—62431
- microcomputer use in high school physics 79—30172
- microcomputer-based multiboard communication system for nonverbal handicapped children 78—57126
- microcomputers in schools, software and equipment choice 80—98772
- microprogrammed intoned speech synthesizer system 79—64442
- musical keyboard fingering characteristics, CAI *(Japanese)* 78—28889
- NMR in undergrad. instruction, general purpose microcomputers use for hypothetical spectra synthesis 80—42009
- nuclear engineering, computer assisted learning 77—13557

computer-aided instruction continued
- nuclear engineering course, incorporation of commercial reactor codes 78—4448
- nuclear engineering laboratory, computer modules for calculation of prompt-neutron generation time 78—4447
- nuclear fuel management analysis core, computer code for teaching assistance 78—4449
- nuclear in-core fuel management computer system 80—36826
- nuclear medicine computers 79—25096
- nuclear reactor thermal hydraulics, computer graphics 80—36824
- nuclear scattering simulation in one-dimens. 77—33780
- numerical analysis, interactive teaching package 80—86058
- numerical electronic technique, in physics education 80—46777
- palaeontology, statistically oriented teaching approach 77—19
- pendulum motion, computer simulation, undergraduate teaching aid *(German)* 77—67166
- Personalised System of Instruction, feedback with computer generated tests 78—69950
- PET 2001, multidisciplinary summer course for schoolchildren 80—98774
- photogrammetric model deformation, interactive demonstration program 77—74183
- physical pendulum, computer-aided laboratory exercise 80—67985
- physics, A-level, computer managed independent learning 79—62948
- physics, student response to comput. phys. teaching lab. project at Surrey Univ. 77—53724
- physics CAL packages at Univ. of Surrey 78—81756
- physics computer assisted learning using microcomputers 79—62972
- physics computer-aided teaching, hinted finding scheme, simulation appls. *(French)* 80—98777
- physics teachers and students guide to calculator choice 80—4494
- physics teaching using SWTP 6800 system in BASIC 80—98776
- physics tutoring, personal computer feasibility 79—30174
- PLATO, programmed logic for automatic teaching operations, student assessment 79—35486
- point group symmetry, derivation and recognition schemes, computer assisted learning programmes 77—29973
- pressure transducer design, for biomedical instrumentation students 77—45656
- programmable calculators for elementary physics teaching 78—12506
- programs for high-school expts. 78—86094
- project development recommendations 80—22176
- quantum measurements, interactive computer program, for teaching 78—41113
- quantum mechanics, computer graphic presentation for non-physical science students 77—49526
- quantum mechanics CAI via graphics 77—67164
- reactor kinetics, computer assisted learning package 77—33809
- recursive method for partition function calc., average energy calc., APL program 79—9050
- relativity, appearance of objects moving at relativistic speeds, computer programs 78—12484
- Rutherford scatt., electron deflection, inverse 1st, 2nd and 3rd power field, program 77—87594
- science teaching, undergraduate, computer assisted learning system 77—37695
- SEM Plato IV network teaching 80—68003
- ship structural design for diploma and undergraduate courses 79—35494
- simulated laboratory exercises, validity of graphic approach 78—81780
- speech training aid, SIRENE, computerized 79—70701
- speed and displacement relations for tire skids, program for PET 80—57038
- staffing needs and position in vertical organisational struct. of educational institution of computer-assisted-learning agency 80—42007
- stochastic processes computer simulation in science teaching 77—17739
- student computer aided laboratory instruction Karlsruhe Univ. 79—12556
- teacher/administrator training, educational computer use 79—35489
- teaching, Newtonian motion anal. using micro-computer simulations *(Japanese)* 80—31462
- teaching, two-dimens. Brownian motion simulation on micro-computer *(Japanese)* 80—31461
- teaching machines and conversation theory 78—49614
- transient fields graphics 77—10805
- TRS-80, teaching at Keene High School 80—98773
- undergraduate EM field problems, numerical method computer programs 77—10804
- visual simulation techniques in military training devices 79—50413
- voice synthesis machines, principle and appl. 79—98564
- X-ray crystallographic computations for students using programmable calculator 80—36811

computer-aided logic design *see logic CAD*

computer applications
- *see also administrative data processing; CAD; complete computer programs; computer-aided analysis; computerised control; computerised instrumentation; computerised signal processing; engineering computing; information science; military computing; natural sciences computing; social and behavioural sciences computing; subroutines*
- electronics appl., conf., Portland, Ore., USA, May, 1977 77—81598
- lighting, effectiveness, ESI meter application 80—22417
- mathematical model, for hydraulic calc. of steam boilers 79—68816
- radionuclide pathway anal., RAMM system of programs 77—13015
- resource management, conf., Alamogordo, NM, USA, 1978 78—69541
- saturated steam parameters in reactor containments with escape of coolant, equations of state, integration by computer 80—68764
- weather forecasts with computer wording, description of input and useage 80—17310

computer architecture
- *see also logic design*
- chemistry and microelectronics, present and future, review 80—55627
- FASTBUS—details of addressing and bus mastership 79—89554
- on-line alarm analysis in the hierarchical control system of the WWR-SM research reactor 79—76104
- parallel computers, appls. in University research 79—54114
- reactor trip system, design of internal architecture for Westinghouse microprocessor-based [nuclear reactor] integrated protection system 79—76100
- single-chip microcomputer in instrument design and meas. techniques *(German)* 80—27276
- tomography, high speed, special purpose digital processor architectures and numerical approx. methods 80—30878

computer-controlled phototypesetting *see computer-controlled typesetting*

computer-controlled typesetting
- electron beam laser technology and applications 77—19262

computer evaluation *see computer selection and evaluation*

computer facilities
- computer-assisted-learning agency, staffing needs and position in vertical organisational struct. of educational institution 80—42007
- laboratory computer system for routine, plant and environmental radiation monitoring appl. 79—9912
- microelectronics and microprocessor impact on metals prod. and NDT 79—74320
- R20 computer centre, noise level meas. *(Hungarian)* 79—41513
- STAR-100 system for weather prediction, experience 79—70879
- TELEMED system user support organisation and program library 78—7491

computer-generated holography
- aberrated diffraction pattern obs. 80—102681
- acoustic hologram correction for nonuniform relative motion 79—46119
- acoustical holography, digital reconstruction and computer graphics display 80—23842
- algorithm for synthetic Fourier transform hologram, variable magnification imaging system 79—3655
- aspheric, testing in reflected light using blazed synthetic holograms 80—91881
- aspheric testing, in-line and carrier freq. holograms, comparison 80—87349
- binary coding mask Fourier transforms using computer *(Russian)* 78—37831
- binary data, holographic coding methods investig. 77—68192
- binary digital hologram as matched filter, Fourier domain quantization effect 77—3544
- binary digital hologram synthesis, PCM method 78—17876
- binary Fourier holograms, wavefront coding by Lee method 77—75441
- binary Fourier transform holograms 80—19004
- binary Fresnel zone plate construction 80—78809
- binary holograms 80—9841
- binary phase digital refl. holograms, fabrication and appls. 77—34840
- chalcogenide glass films, kinoform optical elements and integrated optics elements prod. 77—75634
- coherent image deblurring using computer generated holographic filters 77—14669
- n-colour complex kinoform, distortions in reconstructed image *(Russian)* 78—66790
- detour-phase holograms, comparative study and error models 79—98311
- diffraction patterns, third and fifth order aberrations, computer generated hologram 80—9829
- digital holography applied to borehole electromagnetic wave exploration *(Chinese)* 80—82080
- digitally generated hologram, deterministic phase coding 77—7027
- digitally simulated and optically produced holograms compared 77—75456
- displayed by line printer, phase coding effects 78—25819
- distorted image convolution deblurring by Fourier-Bessel transform holograms *(Russian)* 79—22897
- double-phase holograms, Fourier transform subcells and phase coding 79—27200
- dual computer-generated holograms, interferometric testing of aspherical surfaces 80—9830
- fast Fourier transform holography method 78—71064
- Fermat number transform for microwave holography data processing 80—43298
- filter synthesis for coherent optical image deblurring 79—3646
- Fourier hologram machine synthesis *(Czech)* 78—66784
- Fourier transform holograms, computer-generated, generalisation *(Japanese)* 77—34847
- generalized sampling theorem with application to computer-generated transparencies 79—41343
- gratings, prod. of two-dimens. laser beam deflections 78—58956
- grey level on axis computer holograms for incoherent image processing 77—34848
- hologram construction from X-ray views or acoustic views, using iterative technique 80—69339
- hologram matrix US imaging method 79—46120
- image reconstruction from kinoforms and distorted holograms *(Russian)* 78—13664
- image reconstruction from three-dimensional computer-generated holograms, using line printer 77—42506
- incoherent polychromatic imaging with holographic optical elements 80—69349
- information display using the methods of digital holography 79—72529
- IR holographic elements, laser materials processing appl. 80—37964
- IR optical components and aspherics, 10.6 μm interferometric testing 80—74523
- kinoform lens production and optical testing *(Russian)* 79—98310
- kinoform method, for filtering and image synthesis 77—58295
- kinoform synthesis by Fresnel transform evaluation, least squared error method *(Russian)* 79—22913
- laser beam deflector using computer-generated holograms 77—38979
- lens recording techniques for IR wavelengths 80—95847
- line printer displayed binary hologram generation by phase reference method 78—9344
- Lohmann hologram, detour phase error 79—41351
- mapping and remote sensing by optical filtering 80—101458
- Mellin transform hologram scale invariance obs. *(Russian)* 79—94183
- Mellin transform using computer generated hologram 77—10850
- microwave holography using quadratically spaced linear antenna array, microcomputer processing 80—32938
- multispectral size-averaged incoherent spatial filtering 80—33146
- numerical, appl. for brain-computed hologram, image restoration and pattern recognition 78—33692
- one-dimensional kinoform preparation using photographic template *(Russian)* 79—22914
- one-image-only digital holography 79—41352
- optimum quantization and relative information content of holographic magnitude and phase 80—43286
- phase coding with high quality computer holograms 77—628
- phase determination of amplitude modulated complex wavefront 78—55305
- phase error reduction 78—74863
- phase profiles generation, recent advances, book contrib. 79—76644

computer-generated holography continued
- phase-frequency signal intensity characteristics *(Russian)* 79—94176
- photoresist, large size, distortion free 77—79777
- polarisation, improvements of writing and reading algorithm 78—46538
- polarisation hologram, expt. using NaF 77—61923
- polarisation holography system and reconstructed image quality 80—102677
- pure binary hologram analysis and expt. 79—55092
- quantisation error minimisation method 77—83836
- radio data aperture synthesis reconstruction 79—21191
- real-time kinoform synthesis using chalcogenide glass films *(Russian)* 78—13669
- reference wavefront for aspheric component testing 80—14495
- reflection holograms, computer-generated IR image construction 78—25814
- reflection kinoform prod. on stainless steel, for use with CO_2 laser 77—79780
- review, coding schemes and discrete Fourier transform holography 80—9827
- rotational symmetric aspheric in compensated interferometers, computer-generated-holography testing 80—33128
- scale and rotation invariant optical pattern recognition and classification 80—99655
- scanner, computer produced hologram, with auxiliary reflector 78—71054
- scanner, computer-generated hologram, for laser materials processing 79—18367
- single-step continuous-tone computer-generated holograms 80—48181
- space multiplexing 78—17874
- space-variant holographic systems using phase-coded reference beams 78—74868
- space-variant optical elements 78—37856
- spatial filter for large object formats, interpolation 78—22099
- spatial filters CAD, optimisation method *(Russian)* 80—28171
- spatial filters for large objects 77—23753
- spectrum shaping, iterative computer method 80—102634
- spectrum shaping and image reconstruction, iterative method 80—106475
- stereoscopic approach 77—7025
- synthetic ternary-complex Fourier holograms *(German)* 77—58293
- techniques and appls., book contrib. 79—76645
- three-dimensional reconstructed images from computer generated hologram, characts. 80—43297
- transparencies, generalised sampling theorem for Dirac Δ functions 78—42284
- Two-stage holographic rejector filter *(Russian)* 77—75675
- visualization of 3-D objects using computer-synthesized holograms 80—1154
- volume holograms constructed from computer-generated masks 78—87026
- wave field three-dimensional energy distrib. 78—71009
- x-y plotter display 79—55088
- As-Se-S-Ge chalcogenide amorphous film, computer-generated holograms using electron beam irrad. 80—95846
- CO_2 laser beam shaping 77—14726

computer graphic equipment
see also interactive terminals; plotters; remote consoles
- astronomy, graphic processor for pseudo-colour images representation *(Italian)* 80—98562
- CAI for physics undergraduates 77—13558
- calculator system using X-Y recorder and computer as digitiser 80—13046
- cardiac graphic analysis using microprocessor-based system 79—70665
- cardiology, computer graphic techniques for heart damage quantification 79—29654
- chart recorders, pen control 77—79121
- colour plotter system for computer graphics output, appls. in geoscience 80—98467
- cursor, aided-track, for improving digitising accuracy 79—29899
- ECG 22 78—81027
- EEG topographic display, brain lesion localisation *(Japanese)* 77—5100
- Kanji character memory and display system 78—9351
- large-area plasma display high-speed low cost selection circuitry 78—38556
- oceanographic space-time data series anal. 78—3998
- patient contour plotter, for use in radiotherapy treatment planning 77—70567
- raster graphics device, picture processing, psychology 80—41330
- spectral data analysis using graphics display terminal 78—54473
- STEM image analysis techniques 80—73539
- video-sync mixer for cassette videotape recording of computer images 79—29604

computer graphics
see also curve fitting; interactive systems
- 21-channel EEG monitor with real-time result colour display 80—72364
- acoustical holography, digital reconstruction and computer graphics display 80—23842
- aerodynamics appl., parachute opening flowfield computation, using He bubble technique 78—30374
- air pollution data analysis using combined interactive graphic presentation and clustering technique 79—83656
- angiograms, augmentation of computed tomograms 80—8150
- astronomical appls. of graphic routines for interactive Tektronix video unit and Printronix printer *(Italian)* 80—8553
- astronomical stellar data base, retrieval techniques and graphics display 77—78652
- astronomy, graphic processor for pseudo-colour images representation *(Italian)* 80—98562
- atmospheric refraction, interactive computer graphics applied to visual image transmission 79—8689
- base metal exploration with rapid pyroclastic mapping 77—53052
- biological macromolecule conformations 77—36865
- biostereochemical modelling, interactive computer graphics, appl. to DNA-protein interaction 78—88693
- B.I.P. An interactive graphic system for indexing energy bands of model polymers 79—59608
- Bouguer gravity model, interactive CRT display, for geology CAI 77—22
- brightness perception nonlinearities, computer plotted luminance profiles 77—56380
- bubble chamber, projection graphic display for computer aided image anal. 80—27895

computer graphics continued
CAD of windows as passive solar collectors, using interactive program 79—62146
CAI, geophysics and geology, interactive computing with graphic display 77—21
cardiac, wall motion abnormality detect. using regional changes in ventricular shape and vol. 79—70633
cardiac arrhythmia monitoring, joint interval histogram and correlation coeff. scatter diagram techniques 77—25572
chemical structures, pictorial reproduction 79—43708
comets, computer generated pictures 80—17549
computer films for research, review 79—21512
constant value curve tracing technique, nuclear medicine, EEG appl. 77—70510
contour map production for electrophysiology 80—72340
cranial computerised tomography scans, picture processing and image anal. appls. 80—8183
crystal atomic structures, computer-aided graphical representation of projections onto planes 79—60217
cutaneous receptors, on-line receptive field mapping technique 79—74797
data bank model, appl. to geological data 77—53199
designer work station link for ES computers 79—30442
display of three-dimensional information in computed tomography 79—70606
distributed computing system THESEUS for mag. field analysis 79—41293
dynamic electric and magnetic field evolutions, visualisation using computer graphics display 80—46776
dynamic field teaching, algorithm 77—10805
echocardiographic, graphic representation of 2-dimens. structs. in motion 79—70597
echocardiography and pulsed Doppler, off-line data processing of left ventricle performance 79—62323
education, computer graphics and electromagnetic fields 77—33781
education quantum mechanics, computer graphic presentation for non-physical science students 77—49526
electromagnet GFUN program with interactive graphics 77—18053
electron-image calculation system, interactive, for use in electron microscopy 80—24325
epicardial mapping of ventricular arrhythmia onset by digital computer 79—70672
fusion reactor, PDX Tokamak, finite element anal. using computer graphics 80—95424
geological data automatic contouring techniques 78—7820
graphics interface package for the HBOOK histogramming routine; subroutine package HPLOT 78—89465
gravity studies using the facilities of UMRCC and the Computer Graphics Unit 78—77878
high speed biological cell sorter, data acquisition and display 78—44622
hologram generation, quantisation error minimisation method 77—83836
hologram x-y plotter display 79—55088
human body planar motion in free fall, interactive computer graphics 78—40221
image generation system for nonplanar projection modelling 80—99667
image generation with efficient storage, modified ray tracing method 80—43278
image processing microprogrammed video display 80—72366
infography in automated graphical design *(French)* 77—87747
information display using the methods of digital holography 79—72529
interactive curve-fitting program, for science students 77—60913
interactive film anal. system 80—3876
interactive graphics system developed for NDT 80—66729
interpretation system for resistivity soundings over horizontal strata 78—45014
LANDSAT colour image digital data display using matrix printer 78—12024
Landsat imagery geometrical correction *(French)* 80—81889
large-scale hydrodynamic system simulation programs 77—21799
lung volume determination, interactive graphics 77—77985
macromolecules, graphics model building and refinement system 78—75505
mass spectra, graphic display, dynamically refreshable controller with vertical line generator 78—314
medical images, computer definition of regions of interest, double-cursor method 79—29612
meteorology, data editing and validation using interactive graphics 78—77330
meteorology, isoline printing method *(Russian)* 77—53245
micrographics, computer, using electron beam film recording equipment 77—10120
minicomputer-based interactive graphics biology film anal. system 78—44744
Mirror Fusion Test Facility, neutral beam injection, optimisation by computer graphics 78—66376
molecular graphics appl. to struct. determ. of snake venom neurotoxin 78—27892
molecular packing plotter program 77—15272
molecular spatial models, Stuart-Briegleb type, computer construction 78—86970
musculoskeletal complex shape cross-sectional props., interactive graphics software package 79—79595
musculoskeletal system modelling, interactive computing and graphical display techniques 77—40685
neuronal structures reconstruction and display, three-dimensional 78—11624
neurophysiology, computer assisted unit data acquisition/reduction 78—61266
NMR, knob-controlled CRT display expansion algorithm 77—22578
nuclear fuel cycle cost sensitivity to data uncertainties, interactive graphic computation 79—9837
nuclear reactor thermal hydraulics teaching 80—36824
nucleic acids studies, at. coords. of helices, by computer program 79—86095
numerical anal. tuition, computer-aided 78—81817
oceanography, acoustic reflection profile display using dot matrix plotter with minicomputer 77—9548
ocular motility test in strabismus and amblyopia evaluation, computer administration and analysis via PAL8 program 78—48784
optical design, optimisation and interactive graphics improvements 80—78933

computer graphics continued
optical spatial filters from binary computer generated holograms 77—50774
optical-rose diagrams, geological data 77—9505
optokinetic stimulus pattern for study of optokinetic nystagmus 79—44008
orbital motion on an interactive-graphics terminal, teaching appl. 80—73152
organs, dynamic display system 80—8177
particle track data in plastics, rapid anal. using interactive programming and graphic displays 78—66456
PDP-15 interactive graphics, appl. to seismic surface waves anal. 78—81427
periodic satellite coverage pattern generation computer graphic system 77—37496
phase diagrams, computer generated for ethylene and propylene 78—83928
photograph simulations, on storage display, appls. to X-ray topography and TEM 79—14637
physics laboratory experiments, graphic computer simulations 80—105470
plotter using linear step motors 79—93127
plotting, 3-dimens., irregular to regular grid data conversion 77—5328
polarcardiography, triaxicardiometry and other displays 79—39581
polymers, adsorbed molecules, configurational behaviour, computerised dynamic display 79—874
potential flow 2-D bodies synthesis with limited interactive graphics 77—11166
pressure transducer design, CAI for biomedical instrumentation students 77—45656
pulsatile flow in arteries simulation, utilitarian approach 80—3669
quadrupole mass filter, computer simulation of ion trajectories in quadrupole field 80—52349
quantum mechanics CAI via graphics 77—67164
rectangular and triangular diagram printer-plotting FORTRAN routines 77—5325
red cell anal. 80—21597
rocks, activation anal., gamma-ray spectra processing with computer graphics 79—2228
scintigraphy, longitudinal tomographic reconstruction using a calligraphic CRT graphics system 80—8173
sea ice, airborne laser profiles, interactive correction and anal. system 79—25338
seismic surface wave processing using PDP-15 interactive graphics 77—81818
shear modulus of superplastically formed sandwich cores 79—32286
simulated laboratory exercises, validity of graphic approach 78—81780
space filling molecular models 79—18309
spatial derivatives mapping 77—40965
spot diagram automatic computation and plotting program 79—72645
structural chemistry interactive graphics display system 77—22536
surveying and cartography, interactive graphical systems appl. *(German)* 79—21023
TEM multistrip component design appl. 79—30630
three-dimensional, for electron microscopy computational morphology appl. 78—28132
tomography system 78—3578
TRIPLOT, APL program for plotting triangular diagrams 78—57335
US imaging system appl. 80—99905
USA National Weather Service graphic display network 79—12320
video interferogram analysis by TV camera-microprocessor system 80—73440
video monitor, large screen, for computer output display 80—77597
virology laboratory minicomputer appls. 77—44856
visual fields, computer appls. 80—45892
visual simulation and image realism, seminar, San Diego, USA (Aug. 1978) 80—3639
walking, computer animation of gait 79—11957
wrist, human, kinematic and kinetic analysis by stereoscopic instrumentation 79—92274
X-ray tomography dynamic boundary surface detection 78—53479
PLZT electro-optic shutter stereoscopic display applications 80—90826

computer installation
see also computer maintenance; distributed processing
criteria for selecting and interconnecting micro-, mini-, midi- and maxi-computers 77—17961
nuclear lab. computing facilities 79—89527

computer interfaces
see also CAMAC; computer peripheral equipment; data communication equipment; program processors
asynchronous serial computer interfaces 77—17958
automatic acoustic emission analysis system with programmed control *(Russian)* 78—46866
automatic microdensitometer with Electronika-100 computer 77—45908
Barkhausen effect, mag. thin films, statistical anal., instrumentation, computer interfacing 78—82008
Biomation 8100 recorder interfaced to remote computer, data acquisition in photolysis expts. 78—21107
bit-oriented I/O structure applications to laboratory automation 77—44532
brain autoradiographs, rapid quantification, data recording via microprocessor interface 80—41332
Bruel and Kjaer acoustic level recorder type 2306, interfacing to a digital computer for a graphical output 80—53572
bulk holographic store controller *(Russian)* 79—22915
Cary 118C spectrophotometer, universal computer interface 78—73972
chromatographic Micronova computer interfacing scheme 80—93813
Coulter S blood analyser and IBM 1800 computer, minimum-interrupt digital interface 80—3849
CROs, plug-in type used for spectrum and logic analysis, timers, computer interfaces 77—41648
data acquisition, Event Handler II 79—89542
device coupler for interactive systems 78—24767
digital drift chamber digitizer system 79—45602
echocardiogram, M-mode, automatic computer anal. *(Japanese)* 80—72274
echocardiogram processing, microprocessor-based system 77—40726
Electrophysiological Data Interface 79—79677
FASTBUS, medium energy physics appls. 80—42912

computer interfaces continued
FASTBUS, molecular data bus system for high energy physics 80—42911
fibre optics for computing system interfaces 77—68278
fibre-optic processor serial interconnect system 78—1426
gamma camera/computer pulse-stretching interface 78—40380
GB-IB interface system, automatic meas. in solid state physics *(Japanese)* 79—75509
High Density Connector Interface, fibre optic link 80—91901
IBIS, geographic information system based on digital processing and image raster data type 77—56747
IEEE 488-1975 interface bus, high speed ADC and addressable trigger generation 80—41283
IEEE-488 bus compatible DVM variations and advanced features 80—86279
instrument simulator, design and use 80—4490
interface for serial computer terminals plotter 80—98904
interferometry, far IR, interface for computer control 77—82590
Ionospheric Sounding Satellite, interface equipment for telemetry receiving system *(Japanese)* 77—78610
IR spectrophotometer data processing system applications 80—90912
laboratory automation using computer control 79—49213
laboratory experiments, computer interfacing methods, undergraduate course 77—13524
laboratory interface system for general purposes, appl. to LSI-11 minicomputer 80—77763
laboratory microcomputer and A/D convertor interfacing 80—22337
magnetic tape interfaces for a dual-parameter coincidence experiment 80—14055
mass spectrometer to multichannel analyzer interface 80—27916
MBNIM, modular approach to fast trigger logic for high energy physics expts. 79—49920
MDS-501 DMA channel controller, interface between Biomation 8100 and Intel MDS-800 microcomputer system 80—203
measured value preprocessing and direct sample identification *(German)* 79—5418
microcomputer-based data acquisition system for NMR spectrometer interfacing 78—74042
microdensitometer computer interface design and construction, for X-ray image anal. 77—44821
microdensitometer with computer-controlled scanning table *(Russian)* 79—6197
microdensitometer with minicomputer for semiautomatic interpret. of spectral plates 78—21199
microprocessor based control of RF linac cavities 79—71996
microprocessor based interface/controller for desktop programmable calculator 79—35690
microprocessor multichannel analyzer laboratory project 80—101685
microprocessor triac interface, used to control kiln temperature 78—45632
microprocessor-based experiment controller/interface 79—80590
microprocessor-minicomputer combination for instrumental flexibility 77—54483
multichannel analyser to computer interface 79—93904
multichannel spectrometer, quantometer, design trends for computerised control 79—80694
NMR spectrometer interfacing 79—12828
NMR spectrometer-computer interface, demonstration expt., signal averaging influences on S/N ratio 80—36813
position sensitive 2-D detector for blocking expts., electronics and computer interface *(German)* 77—38551
PQR line shape, digital-analogue interface for data processing 79—45615
pressure meter interfacing to supervisory computer 78—8409
repeater gyrocompass angular digitiser construction principle *(Russian)* 80—73311
scintillation camera interface to scintigraphic data and computer 77—21613
SNOOP module CAMAC interface to 168/E microprocessor, bubble chamber pictures 80—58103
solid-state, for nuclear power station data acquisition, use of fast analogue scanner 77—6656
spectrometer user interface to computer systems 79—9986
television data compression, for cytology and chromosome anal. 77—86683
terminal to audiovisual device interface 80—67986
tide gauging network, automated, microcomputer interface and telemetry 79—5692
transthoracic impedance curve processing, patient-computer interface 79—34686
TRIUMF data interface 77—88304
US flowmeter automation 78—38426
Varian EM-360 NMR spectrometer interface with Altair 8800B microcomputer 78—89519
visual stimulator for electrophysiology expts. 78—69230
weather forecaster console for satellite data handling system 80—90205
X-buses, appl. to CESR control system, interface hardware 79—72069
X-Y recorder for Auger spectrometer using pulse height analyser 78—49942

computer internal arrangement *see computer architecture*

computer maintenance
wear problem, review 79—20210

computer networks
see also distributed processing
data analysis at LAMPF: a hierarchical approach 79—89562
data communications 79—89576
distributed, solar thermal test facility control 80—72075
distributed microcomputer control system for high-energy gas-laser facility 77—61975
Fermilab control system, computerized network of distributed processors 77—83302
geology appls., teleconferencing 77—53202
health care deliverty data processing course 79—80394
hierarchical computer networks for processing data base generated by X-ray CT scanner 80—81732
ISABELLE ISR, computer based control and monitoring system 78—46191
King Faisal Specialist Hospital (Saudi Arabia) information system 78—57105
laboratory computer networks 79—52797

computer networks continued
multi-microprocessor network, for sonar signal processing algorithms soln. 78—45044
nuclear instrumentation on line data processing 78—37529
optical moving target indication, multi-minicomputer network 77—5445
seismic data teleprocessing global network 77—29255
Shiva laser fibre-optic digital links 79—85804
terrain data production using distributed processing 77—37413
USA National Weather Service graphic display network 79—12320

computer operator training *see training*

computer output to microfilm
development trends *(Czech)* 77—18114
electron beam laser technology and applications 77—19262
holographic document retrieval and conversion to photographic microforms 79—76643
laser alphanumeric character generator for line printer and COM 80—33067
laser imaging dry process development film *(German)* 79—9253
laser microfilm system recording module 77—18120

computer peripheral equipment
see also character recognition equipment; computer graphic equipment; computer output to microfilm; data communication equipment; data preparation equipment; interactive terminals; keyboards; magnetic tape equipment; mark scanning equipment; printers; punched tape equipment
coupling device for small computers to external devices, physical expts. automation 80—31722
EEG data acquisition and data processing system, peripheral equipment 80—41270
electrically erasable and programmable read only memory writer *(Japanese)* 79—101072
GB-IB interface system, automatic meas. in solid state physics *(Japanese)* 79—75509
node module allowing independent systems to share peripherals 77—57305
optical link transfer cardiological data to hybrid computer system 77—86677
pressure transducer calibration and metrological servicing 77—57314
rehabilitation of severely disabled, microcomputer environmental control and communication system 80—8216
voice synthesis, principle and appl. 79—98564

computer peripherals *see computer peripheral equipment*

computer printers *see printers*

computer programming *see programming*

computer programs, complete *see complete computer programs*

computer programs (listings) *see complete computer programs*

computer science education
biophysics, teaching appls. of analogue computers 79—84890
calculus teaching, discrete approach using computer 79—80398
chemical kinetics simulation 77—13555
computer physics, elementary concentrated one-week course 78—73799
gravitational problems, programmable pocket calculator appl. 78—4438
laboratory experiments, computer interfacing methods, undergraduate course 77—13524
parallel computers and University research 79—54114
physics joint honours degree course at Manchester University 79—35456

computer selection *see computer selection and evaluation*

computer selection and evaluation
arrhythmia monitoring systems evaluation criteria 78—11765
criteria for selecting and interconnecting micro-, mini-, midi- and maxi-computers 77—17961
critically ill patient monitoring by integrated computer systems 78—35998
ECG interpretation sytems, user's experiences 78—7496
high energy physics computing, CERN conf. Jadwisin, Poland (June 1978) 79—89570
large computer systems and new architectures 79—89578
METEOSAT data processing system *(Italian)* 80—109275
microcomputer selection for materials testing appl. *(German)* 77—32744
microcomputer systems 79—30173
nuclear medicine, buyer's guide to current performance and future promise 78—48883
online vectorcardiographic analysis microprocessors and instrumentation 78—36020
system performance optimization 79—89579
theodolite microprocessor selection, development, and programming 78—24218

computer software
not used for applications software for which see specific applications
see also programming; software engineering; systems software
electron beam fusion accelerators, data acquisition and processing 78—37469
GEC Elliott CAMAC interface on PDP-11 computer running RSX-11M executive, software driver module 77—38590
hologram memory control system and software *(Russian)* 77—58262
IFECS interactive software, thermal stress modelling appl. 79—80440
Ionospheric Sounding Satellite control, software for automated system *(Japanese)* 77—78607
IR Astronomical Satellite (IRAS), on board computer software 79—80192
microprocessor-based experiment controller/interface 79—80590
microprocessor-controlled pulse sequencer for pulsed NMR experiments 80—68231
multichannel AutoAnalyzer automation 77—41686
optical software survey for digital image processing 77—75431
reliability and maintainability symposium, Los Angeles (1978) 78—50250
toroidal fusion reactor, common problems in control system software design 77—23282

computer storage devices *see storage devices*

computer subroutines *see subroutines*

computer testing
aerospace guidance computer coverseal particle detection using X-ray 78—21313
CAMAC module for testing data acquisition systems 79—89568
CAMAC test system based on S-100 bus 78—36984

computer typesetting *see computer-controlled typesetting*

computerised communications control *see communications computer control*

computerised control
see also chemical engineering computing; command and control systems; communications computer control; computer-controlled typesetting; computerised materials handling; control engineering computing; direct digital control; electrical engineering computing; industrial computer control; mechanical engineering computing; nuclear engineering computing; power system computer control
21-channel EEG monitor with real-time result colour display 80—72364
above-knee prosthesis simulator system in eval. of proposed damping torque control schemes 77—44854
acoustic beam steering and focusing, with variable frequency array transducers 80—38191
acoustic data buoy, microprocessor controlled, underwater signals processing 79—21024
air pollution control, online, two level prediction method 77—21952
air pollution monitoring system, minicomputer-based 77—66984
aircraft noise monitoring systems, requirements 80—23849
animation filming, digital rostrum controller 78—45743
annealing of electron field emitters and multiple multichannel analyser, precision temp. regulator 78—86384
application node system image manager subsystem within distributed function laboratory computer system 79—45606
arterial blood pressure, indirect noninvasive automatic meas. device 77—44771
artificial leg with 6800 microprocessor *(French)* 79—100792
atom probe time-of-flight field-ion microscope, for metal defects study 77—82645
biomedical applications of microprocessors 78—57095
blood pressure control in hypertensive crisis, closed loop control of sodium nitroprusside infusion 78—44688
Bonn isochronous cyclotron, beam stabilisation and automatic energy variation 79—54705
BWR, block-monitoring index for diagnosis of power station operating characts. 79—59185
CAMAC and microprocessor appl. to target room control 78—37468
CAMAC control of π^- biomedical beam line 77—90886
capacitor fed fusion expts., computer based control system 80—13912
CERN, Intel 8080 microprocessor development system 77—83314
CERN ISR, control system, addition of local intelligence to CAMAC 79—72212
CERN ISR, on-line Q meas. during phase displacement acceleration 79—72076
CERN ISR control scheme for acceleration by phase displacement 79—72213
CERN linac, computer control system 77—38480
CERN proton synchrotron, automatic procedures 79—72074
CERN proton synchrotron, improvement project for computer assisted controls 79—72209
CERN proton synchrotron, stand alone control system for continuous transfer ejection to SPS 78—82552
CERN PS, computer controlled beam local radial perturbation and rotation 79—72072
CERN PS booster, microprocessors in control and beam obs. 77—88302
CERN SPS, control systems operating experience, suggested principles for future accelerators 79—72211
CESR computer control system, description 79—72210
CESR control system, distributed microprocessors appls. 79—72217
cinematography, automatic control systems for film production *(Russian)* 80—42287
cinematography, Du Art frame count cueing system, minicomputer appl. 78—37086
climatic test chambers, automation using microprocessor programmers 80—21430
CODAS, Joint European Torus, control and acquisition system 78—36982
computer-based instrument using SK.2 cylindrical coordinator *(Russian)* 80—76856
conference on cyclotrons and their appl., Bloomington, USA (Sept. 1978) 79—54626
Cornell electron ring, high resolution digital time base 79—76215
Culham fusion expts., distributed control systems using microcomputers 80—13909
Culham fusion expts., integrated data network for microcomputer based diagnostics 80—13910
Culham fusion studies, appl. of microcomputer to data acquisition and control 80—13908
cyclotron at MSU, computer control 79—54704
cyclotron corporation bus-oriented computer control system 79—54703
dielectric const. measurements, complex, wide-range dynamic measurements using microcomputer control techniques 80—22383
digital thermal field analysers 78—82034
distributed parameter nuclear reactor three-point model, neutron and delayed-neutron emitter behaviour, distributed control appls. *(Spanish)* 80—22889
doubler tevatron microprocessor quench protection system 79—72088
drip feed unit microprocessor control development 78—53563
electrostatic generator 78—29666
EOSCOR: A light weight, microprocessor controlled solar neutron detector 79—101063
Euratom Data Acquisition Co-ordinating Committee activities 80—13904
Fermilab 1000 GeV switchyard, microprocessor control of He refrigerator system 79—68006
Fermilab booster beam damper, logic and control module 77—83313
Fermilab control system, computerized network of distributed processors 77—83302
Fermilab linac, microprocessor-based preaccelerator control system 77—38481
Fermilab main ring power supply, minicomputers control system 77—83303
file management for experiment control parameters in distributed function computer network 77—57306
film processing, use of microprocessor equipment 80—31915
fission reactor safety system, microcomputer based 77—67845
fusion experimental facilities, computerised control and data acquisition 80—13890
fusion experiments, fibre optic signalling in control 80—13919
fusion experiments, microprocessor applications in data acquisition and control 80—13918

computerised control continued
fusion reactor, 2XIIB, neutral beam injector system, automated control 78—62620
fusion reactor, Doublet III, computer control system 80—99321
fusion reactor, Doublet III, neutral beam injector system, instrumentation and control 80—99322
fusion reactor, MFTF, supervisory control and diagnostics system software 80—99324
fusion reactor, MFTF, supervisory control and diagnostics system, database management system 80—99326
fusion reactor, MFTF, supervisory control and diagnostics system, database management system, data structs. 80—99327
fusion reactor, pulsed expts., computer-based control systems 78—62624
fusion reactor, TFTR, energy conversion and storage systems, fault detection and protection 80—95431
fusion reactor Ingra injector, control and data acquisition system 80—13913
glucoregulation in blood of diabetic dog 77—86652
heart, artificial, microcomputer based automatic controls 80—67289
Heidelburg postaccelerator, computer control system 79—72214
high-energy gas-laser facility, distrib. microcomputer control system 77—61975
HV pulse controller and temp. monitor microcomputer-based, Kerr effect study appl. 79—6103
hydrological system, state space modelling and identification 79—79908
inertial surveyor for automatic position, azimuth and gravity disturbance meas. 77—5353
inhalation exposure system, microprocessor-controlled for repeated exposure of animals to aerosols 79—70726
insulin delivery to diabetics, by pulsed insulin infusion 77—37099
intra-aortic balloon timing, microprocessor control 78—44725
ISABELLE half-cell control system 77—88303
ISABELLE ISR, computer based control and monitoring system 78—46191
isolated heart preparation appl. for biomedical research 78—53603
IUCF control system 79—54702
JET, control and data acquisition system, CODAS 78—62619
JET, control and data acquisition system 80—13905
JET, control system, communications, diagnostics, data storage and anal., NORD computers 80—68943
JT-60, control system 80—13906
Karlsruhe cyclotron, computerised diagnostics, control and extended beam optimization 79—54709
KEK 12 GeV proton synchrotron, computer control system of main ring magnet power supply 79—72071
KEK beam line magnets control by CAMAC serial highway 79—68007
knee locking, sensor-controlled external system, exptl. study 78—40406
laboratory automation, interfacing system 79—49213
laser automated alignment, CO_2 10 kJ laser for fusion research 79—76703
laser fusion project, Shiva, control and alignment systems, development trends 79—85764
laser fusion reactor, NOVA, pulsed power control system, fibre-optic multi-tapped computer bus 80—95443
left ventricular assist system microprocessor controlled electromechanical convertor 78—15928
LEP storage ring, control system design 79—72050
limbs, using microcomputer, motion analysis using goniometers 80—51138
LMFBR Na loop computer control system based upon TOSBAC-40 multicomputer 80—47662
LSI-11 based auxiliary crate controller for beam line and experiment control 79—89565
Lucke goniometer control appl. 78—18500
machining, conference New Delhi, India (1977) 78—4590
magnet power supply for mass spectrometer, programmable 80—37121
manipulator, computer controlled, for use as remotely controlled arm 78—81083
mass spectrometer, mag. scanning, ion current meas., computer controlled electronics 78—8464
medical counterpulsation assist pumping, optimum performance determ. under computer control 78—24181
microcomputer control for solar energy applications 80—50945
microcomputer-aided arm prosthesis using myoelectric pattern recognition 78—53576
microcomputer-based blood-pressure recorder *(Japanese)* 80—67139
microcomputer-controlled instrument for electrochemical studies 78—73128
microprocessor applications in upgrading accelerator controls 77—83173
microprocessor control systems for nuclear power plants, program reliability *(Spanish)* 78—58369
microprocessor for mirror sight stabilisation 79—27369
microprocessor-based tilting bed for blood pressure control 80—26412
microprocessor-controlled tape drive 79—93123
microscope-spectrophotometer, computer processed, for measurement of absorption spectra of rock-forming minerals 80—18010
minicomputer appls. *(German)* 77—90702
minicomputer assisted function generator for the dynamic control of chromaticity correction sextupoles 79—68009
minicomputer controlled SEM for image and microtopography anal. 78—29214
monochromator accessory module, microcomputer-controlled for dual wavelength operation 79—74440
multichannel functional electrostimulator design for paretic gait correction 79—57810
multidither adaptive optical system, 69-channel hybrid controller 80—33136
multiple projector presentation, slide projection control using microprocessor 78—55425
National Synchrotron Light Source, distributed computerised control system 79—72086
neutral beam systems, computerised, development and operation 79—93849
neutron activation anal., control software for high throughput system 79—11849
neutron detector, expt. control and data acquisition system 79—45589
neutron spectrometer, triple-axis, computer-control system with CAMAC interface, program functions 77—19840
neutron TOF expts., control and data processing system 78—25385
NMR spectrometers, time-sharing control by minicomputer 79—93192
NODAL interactive language for synchrotron control 79—9987

computerised control continued
  nuclear demagnetisation refrigerator, microprocessor controller 80—37043
  nuclear facilities entry control system design 79—85688
  nuclear fuel reprocessing facilities continuous criticality control, dynamic approach 78—50291
  nuclear medicine measurements, quality assurance 77—40764
  nuclear power station advanced control concept, computer-based system design 77—67909
  nuclear reactor constrained feedback control system design 77—88257
  nuclear reactor protection system design using microcomputers 77—67823
  nuclear steam generator tubes testing and evaluation using CIS/DASIO system *(Czech)* 80—63301
  oceanographic monitoring stations in Arabian Gulf, computer control and data acquisition 79—8728
  on-line ECIL TDC-312 computer-controlled four-circle neutron diffractometer 78—55787
  optical stimulator for vision expts. 80—26423
  orthotic-prosthetic and manipulator system uses of microprocessors *(Croatian)* 78—44694
  paraplegics' multitask exoskeleton computer control 78—53580
  particle size meas. by laser beam expt. 78—70098
  patient position monitoring during radiation treatment using transmitted X-ray beam 77—40894
  PEP storage ring, computer control systems, design and performance 79—72208
  PETRA storage ring, serial data acquisition system 79—72085
  PETRA storage ring control system, applications and future developments 79—72083
  PETRA storage ring control system, control console for man machine communication 79—72084
  photochemical smog, minicomputer based prediction system for reducing acute damage 79—57541
  photoelectric photometry system at Trieste, data acquisition and processing software *(Italian)* 79—58258
  pion range shifter for clinical therapy, microprocessor control 77—32953
  PLT, neutral beam test stand, data acquisition system 78—62622
  polariscope interactive control system to evaluate stresses 80—19299
  polisher, controlled, for optical fabrication 78—75006
  pollution meas. network, Baden-Wurtemberg *(German)* 79—52977
  pool boiling expt., computer controlled temp.-controlled operation 79—14238
  Portable Automated Mesonet, design, performance and operation, for meteorology 77—78426
  power reactor operational control algorithms 79—67896
  prostheses development, myoelectric and multifunctional arms 77—25594
  proton accelerator, target and collimator precision position control and monitoring via CAMAC 77—67927
  PWR control, computer program *(German)* 79—59249
  radiation therapy, comprehensive computer system, design and development 79—25078
  radiation therapy 79—25099
  radiation therapy 79—92367
  reactor neutron density microprocessor-based flux wire evaluation and anal. system 80—63353
  RF linac cavities, microprocessor based control 79—71996
  rigid-vane artificial heart development 79—84025
  robots and manipulators, symposium, Warsaw (Sept., 1976) 78—53574
  Saclay linac, flexible dialogue using computer control room 77—38499
  Saturne II, beam liner computerised control system, organisation, function, hardware 77—83400
  scanning laser beam system for surface inspection with defined flaw analysis *(German)* 80—3278
  scintillation counter arrays, testing with computer controlled LED flashing system 77—57802
  Scylla IV-P, computer-based control and data acquisition system for CTR 78—62621
  self-scanning silicon photodiode array with microcomputer control 80—35612
  SIN meson factory, computer control strategies 79—54701
  single crate CAMAC control system for negative ion source test facility 79—72216
  SLAC, control and monitoring system, use of microprocessors, cost 77—83177
  SLAC accelerator, automatic phasing using microprocessor controller 77—88305
  SLAC beam, feedback system for steering and energy correction in beam switchyard 79—93852
  solar battery, charging networks and stepping motors, microcomputer mechanical proportional control 80—50987
  solar energy management system 80—66951
  solar energy system control, 16 channel data logger and serial data link 80—50947
  solar heating equipment, for building, community and agricultural appl., use of heat tube 79—57412
  solar thermal, test facility, 5 MW, real-time computer control 80—72075
  sonar, fibre optic system, geological and hydrographic survey applications 78—88947
  spectrometer, anti-Stokes Raman 80—24111
  spinal injury, μP controlled stimulation of paralysed muscle, exp. study, positive control, dynamic movement appl. 79—83883
  SPS computer control system, operational experience 77—83292
  stepping motor microprocessor controller for 100 kJ CO$_2$ laser beam alignment system 77—54035
  storage ring, CESR control system, interface hardware 79—72069
  superconducting dipole magnet system, for MHD facility 79—52948
  superconducting heavy-ion resonator, microprocessor based feedback system 77—88292
  superconducting solenoid, control of field-changing tasks by microcomputer 79—216
  tactile hearing aid, portable with microprocessor control 79—84029
  tetraplegics' jointed manipulator with joystick control 78—53581
  tetraplegics manipulator, microcomputer control 80—41314
  TEXTOR, computerised control system design 80—13907
  thermonuclear fusion research, user-engineered command language 80—27819
  thyroid function radioimmunoassay, quality control, computer program *(French)* 80—94348
  titrator, microcomputer-controlled 79—74444
  Tokamak plasma equilibrium, feedback control 78—55738

computerised control continued
  TRIUMF cyclotron, meas. and corrections to beam props. 79—54710
  TRIUMF data interface 77—88304
  underwater robot/manipulator, development and remote control 78—77356
  upper limb prostheses multifunctional control via EMG signal identification 78—3683
  upper-limb prostheses multifunctional control microprocessor system, myoelectric signal identification method 78—88766
  US flaw detector, microprocessor controlled, for flaw classification in welded plates 80—100992
  US flowmeter 80—24111
  US plate testing equipment, computer controlled, working experience *(German)* 80—93720
  VICKSI accelerator, computer aided control system 79—54697
  VICKSI computer control system, operating experience 79—72215
  VICKSI cyclotron, automatic isochronisation and computer aided centering 79—54706
  visual stimulator for eye movement and visual evoked pots. study, microcomputer-controlled 80—41350
  voice command of a six-degree-of-freedom manipulator, robotic arm appl. 80—12313
  Volta Lake, hydrological models, data bases and computerised control 80—4057
  wastewater treatment, distributed digital processing and closed loop computer control 80—45824
  Wyoming Infrared Telescope (Jelm Mountain), computer control 78—85848
  X-ray images processing, CALTIX system description *(French)* 77—4872
  X-ray powder diffraction film scanning system 80—22492
  XRF and emission spectrometry, equipment developments 79—20486
  ZGS 500 MeV booster synchrotron, data acquisition and control, sequential logic and minicomputer 77—83304
  GaAs, vapour phase epitaxy using computer control 79—38744
  H$_2$O vapour under point corona discharge, microprocessor control for vapour generator and EHD phenomena 80—106852
  TeO$_2$ acousto-optical tunable filter with microcomputer control 80—102833

computerised industrial control *see industrial computer control*

computerised instrumentation
  see also astronomy computing; astrophysics computing; automatic test equipment; biology computing; chemical engineering computing; chemistry computing; computerised monitoring; computerised spectroscopy; computerised tomography; electrical engineering computing; electronic engineering computing; geophysics computing; nuclear engineering computing; physics computing
  2D acoustic velocity field meas. in solid samples 80—35462
  8-channel digital speech synthesizer based on linear predictive coding techniques 79—64439
  23rd International Aerospace Instrumentation Symposium tutorial, Las Vegas (1977) 78—12074
  200 W power supply, series-regulated, programmable, 0-50 V range 77—82543
  8450A spectrophotometer, microcomputer system based on MC5 SOS processor 80—68272
  A/D data acquisition module for microprocessor systems, high-speed, multiple channel 77—57304
  abrasive surface quantitative charact. profile meas. system, on-line computer controlled 77—52603
  absorption spectrometer for gas phase samples, computer controlled 80—86459
  AC calorimetry technique *(Japanese)* 80—27306
  accelerator lab. system 79—89529
  acoustic beam steering and focusing, with variable frequency array transducers 80—38191
  acoustic coupling between rooms, meas. system using decrease in sound level method *(French)* 80—69611
  acoustic emission system for monitoring components and struct. in severe fatigue noise environment 77—63869
  acoustic excitation impulse generator 78—90618
  acoustic telescope, transport noise, meas. appl. 79—94426
  admittance bridge, microcomputer controlled, for passive network testing 77—18037
  aerosol particle sizing by laser beam Mie scatt., computer program 77—37457
  aerospace instrumentation, conference, Las Vegas, Nev., USA, (May 1977) 78—12075
  aerospace test meas. symposium, San Diego (1976) 77—41284
  ambient air monitoring, microprocessor appls. 79—48201
  anaesthesia delivery system, microprocessor controlled 77—44832
  analogue recorder, guide to different techniques 77—41583
  analytical plotters, photogrammetric appl., future prospects 78—40708
  analytical plotters, props. and software aspects, photogrammetric appl. 78—40709
  analytical stereoplotter, OMI AP/C4, photogrammetric appl., features 78—40715
  analytical stereoplotter, TRASTER 77, photogrammetric appl., features 78—40712
  analytical stereoplotting system, C-100 PLANICOMP, features 78—40711
  aneasthesia delivery system, closed loop design 78—40402
  anemometry, laser-Doppler, microprocessor-based signal processing system 77—89218
  Anger camera/computer system using seven pinhole collimator for myocardial perfusion tomography 80—61663
  Anglo-Australian 3.9 m telescope, computer-controlled slewing, setting and tracking 77—17371
  Anglo-Australian Telescope, computer control system 77—91434
  anodic oxidation, open-cct. transient method for overpotential anal. 78—27776
  antibiotic concentration assay, computer-aided method *(German)* 79—5414
  aortic ejection click and first heart sound description 80—30827
  APD 3600 automatic X-ray powder diffractometer, sophisticated derivative method appls., JCPDS data base 80—107017
  appliance acoustic emission determ. facility development 77—58507
  arterial blood pressure, indirect noninvasive automatic meas. device 77—44771
  arterial tonometer, microprocessor based 78—31955

computerised instrumentation continued
artificial satellite attitude determ. system, Taiyo (1975-014A) *(Japanese)* 77—17319
asbestos fibre counting by automatic image analysis 80—73538
aspheric surface contour meas. machine and computer system 80—14494
astronomical automated spectrum scanner, 3000-11000 Å region 79—53724
astronomical laser ranging equipment, computer system *(Japanese)* 78—89080
astronomical photoelectric photometer, multifunction, system design 77—73949
astronomical telescope, 3.9 m, Anglo-Australian 78—16291
asynchronous serial computer interfaces 77—17958
atmosphere optical props. obs., by sounding with laser 80—36412
audiometer, pure-tone and speech *(Japanese)* 79—74774
audiometer, screening, and real-time computer techniques 78—81009
audiometry system for canine evoked response, in dental instrument noise studies 77—29226
auditory, visual, and somatosensory evoked potentials in pediatric diagnosis 80—26407
auditory evoked responses, computer driven bipolar stimulator 78—57011
Auger microprobe, scanning, with advanced image processing 80—68304
Auger scanning electron microprobe, analytical techniques, and computer control 79—79359
Auto-Field II$^{\mathrm{TM}}$: an automated and manually-controlled visual perimeter 80—46087
autocollimator, photo-electric, calibration with laser interferometer system and microcomputer 80—1304
autodensitometer, flatbed, for biophys. appl., error analysis 77—52937
automated counting system, design philosophy 79—88923
automated gain measurement system for high-energy chemical lasers 79—36914
automated measurement of noisy voltages with preset confidence level 77—37906
Automated Meteorological Data Acquisition System 77—87077
automated microprobe *(French)* 79—6237
automated multichannel meas. systems, microcircuit program device for analog signal switching 79—26042
automated nondestructive assay system for Pu samples 77—61512
automated shipboard acquisition and processing of offshore geophys. data *(Russian)* 78—53750
automated visual edge match system for image quality assessment 78—62218
automated X-ray microanalysis with electron microprobe and SEM 78—27840
automatic astrometric and photometric meas. appl. *(Russian)* 78—24467
automatic calorimeter system for bolometer mount effective efficiency meas. in 35 GHz band 78—86272
automatic evaluation of isotope anal. of nuclear fuels, isotope dilution, mass and α spectrometry 78—55120
automatic microimage analyser, MORPHOQUANT 78—37053
automatic network analyser, EM reflection coeff. meas., calibration 78—89463
automatic potentiometer, microprocessor-controlled for nanovolt meas. 79—21771
automatic sprayer with programmable dose for serial expts. *(Hungarian)* 80—104822
automatic titrator, microcomputer controlled, for chem. anal. 78—27841
axial tomography, abdominal area appl. 77—44782
balance, microprocessor based, capabilities 80—13067
balance, precision, read-off automation using Michelson interferometer 77—5809
Baylor visual fields programmer 80—46085
beamforming array, linear adaptive algorithm 80—21834
BEBC, on-line control system for RF separated hadron beams 77—38530
Bermuda Eleuthera Acoustic Range environmental meas. buoy 77—41229
bioengineering and medical instrumentation, symposium, Laramie, USA, (May '76) 77—25571
biofeedback training device for speech therapy, portable, microprocessor-based 80—104808
biological research, computer-assisted mapping with the light microscope 80—67308
biological samples, multichannel analyser spectroscopy using XRF, minicomputer appls. 78—20106
biological STEM, low-dose, using digital data processing system 78—24203
biological STEM, on-line data processing system 78—24202
biomechanical spatial motion, data collection method using sonic digitiser 79—39441
biomedical, present and future trends 80—26405
biomedical applications of microprocessors 78—57095
biomedical engineering instruction, microprocessor-based instrumentation system 77—22361
biomedical rotating laminar radionuclide camera 80—3796
biosciences, microprocessor appls. 80—21557
bit-slice microprocessor appl. 79—89566
blind mobility aid, mechanical position sensing, evaluation 79—12045
blink comparator, semi-automated, for large photographic plates *(Japanese)* 78—89081
blood cell computerised counting and sizing system 78—31932
blood cells, spectral meas. 79—25058
blood flow detection in human heart, US pulsed Doppler flowmeter system, microcomputer based 80—104690
blood flow meas. from US Doppler signals, on-line computer system decoding 78—3570
blood flow plethysmograph microprocessor control 79—62402
blood gas analysis data processing system *(German)* 79—5419
blood pressure direct measurement for intensive care and operations, computerised correction system 78—44635
blood pulse measuring by computer *(German)* 80—104823
body motion computer-aided tracking using CCD image sensor 78—61269
body radioactivity measurement, SABRE 3 computer system 78—85425
body surface and epicardial activity, computer-aided meas. system 79—39551
body surface ECG potential mapping, data acquisition system 79—29653
body surface potential mapping, microcomputer processing system *(Japanese)* 80—72347
bone mineral analyser, microcomputer based 79—53218
brain impedograph 78—77139

computerised instrumentation continued
breath by breath anal. of ventilation and pulmonary gas exchange, minicomputer system 79—62393
Bruel and Kjaer acoustic level recorder type 2306, interfacing to a digital computer for a graphical output 80—53572
bubble and spark chamber photographs analysis with PA-BESM-4 system, exchange apparatus 78—9045
bubble chamber, H MIRABELLE, monitoring by minicomputer *(French)* 77—10531
bubble chamber film analysis, semiautomatic measuring system 80—58105
bubble chamber film scanning and digitising system based on Intel 8080 microprocessor 78—29714
bubble chamber photographs digitising machines, distributed computer system 78—5110
burn patient closed loop fluid resuscitation using microprocessor 78—36046
BWR systems 80—83211
calculator for chromatography automatic evaluation system *(Hungarian)* 77—56289
calligraphic projection display resolution and contrast photometer and X-Y plotter 80—86373
calorimeter, low temperature investigations, simple off-line arrangement 80—90850
calorimeter for temp. range 4-380K 80—98915
calorimetric system for recording plasma blowoff and scattered light distributions from laser plasmas 80—59287
calorimetric system for temp. range 3-300K, with on-line computer 78—4620
CAMAC automated nucl. chem. laboratory 78—17542
CAMAC autonomous system for control of scintillation and Cerenkov counters 78—21833
CAMAC expt. for precise meas. of ^{235}U(n,f) cross section 80—52702
CAMAC I/O module based on Signetics 8X300 microcontroller 80—47835
CAMAC instrumentation in European labs. 77—54482
CAMAC module for testing data acquisition systems 79—89568
CAMAC standard 160-MHz decade counter with digital readout 78—9041
CAMAC test system based on S-100 bus 78—36984
CAMAC to GPIB interface 78—36985
CAMAC-controlled calibration system for nucl. reactor systems 78—37532
cancer therapy facility, microprocessor based control system 78—40398
capacitance meters, direct reading using auto-ranging 78—32835
capillary column gas chromatography at nanogram resolution using dual beam Fourier transform IR spectroscopy 80—89554
cardiac arrhythmia, pill electrode, system 79—39566
cardiac arrhythmias, automatic detection in long term ECG monitoring 80—3850
cardiac fields online body surface potential mapping 79—83992
cardiac hybrid computer for dye-dilution curves 78—40365
cardiac intracellular transmembrane action pots., automated anal. 79—70729
cardiac output estimation during exercise by rebreathing technique, automated system 77—37090
cardiac output measurement, in vitro comparison of six commercially available thermodilution systems 78—77135
cardiac radionuclide cineangiography, clinical utility of real-time computer-based system 78—80957
cardiac rhythms, computer diagnosis of abnormalities using P-wave detector for interval measurement 78—44663
cardiac stimulator, microprocessor-controlled dual-channel 80—56279
cardiac strength interval curve rapid generation 78—40456
cardiogram cart under microcomputer control 78—31942
cardiograph processing and display, online *(Italian)* 79—25135
cardiology, conf., Rotterdam, Netherlands, (Sep.-Oct. 1977) 78—81013
cardiology, pressure meas. anal. *(Swedish)* 77—44779
cardiology applications, conf., Stanford, USA, (Sept. 1978) 79—62387
cardiopulmonary resuscitator, programmable, for evaluation of standards 80—72374
cardiopulmonary stress test data acquisition and control systems 79—79673
cardiopulmonary stress testing in children 80—30911
carotid artery imager, CW Doppler US and spectrum analyser 79—57731
catheter pressure meas., transducer smearing correction using microprocessor based discrete deconvolution 80—67275
cerebral blood flow noninvasive regional meas. and computer analysis 78—35948
cerebral blood flow system using H_2 clearance method 78—40457
charge injection device as stellar tracking sensor 80—85861
chemical, analyser design impact of microprocessors *(German)* 78—61096
chemical analysis, 1978 exhibition in Munich *(German)* 79—20482
chemical analysis, instrumentation, discussion of future under microcomputer advances 79—83536
chemical analysis laboratory automation 77—77843
chemical synthesis optimisation system 79—52628
chromatograph, microcomputer controlled GC with data processor and printer-plotter *(Japanese)* 80—50921
chromatographic Micronova computer interfacing scheme 80—93813
chromatography, automatic liquid sample injector for GC, syringe-type *(Japanese)* 80—50923
chromatography, microprocessor based low cost data processor *(Japanese)* 78—61131
chromatography, microprocessor-based data system 77—36826
chromatography, nonlinear detector response quantification with lab. automation system 80—40775
clinical, human motor units EMG spikes and twitch waveforms anal. 77—73519
clinical chemical anal. appl. *(Swedish)* 77—44764
cloud chamber adaptive closed-loop expansion control system 79—93889
co-ordinate reader, using X-Y plotter and HP 9830A calculator *(French)* 78—77886
colorimeter, multisample rotating disc, microcomputer control 79—80663
colorimeter, Zeiss DMC 26 universal model *(German)* 78—54432
colorimetry using microcomputers *(French)* 77—5882
colour measurement, computer aided 79—67372
Compton scatter imaging of transverse sections, corrections for multiple scatt. and attenuations 77—40742

computerised instrumentation continued
Computed Tomography radiological method for non-invasive examination 77—77979
computer data input/output control panel, for thermophysical experimentation 79—17401
computer-based instrument using SK.2 cylindrical coordinator *(Russian)* 80—76856
computerised tomographic scanner acceptance testing 77—73569
cone, computer-driven hardware model, response obs. 80—72402
conference, Gaithensburg, MD, USA (1978) 78—70104
conference on analysis instrumentation, Charleston, West Virginia, USA (May 1977) 79—16100
contactless metrology with image dissector tube and computer *(French)* 77—33975
Contouromat hardwired left ventricular angio processing system 79—16326
Contouromat hardwired left ventricular angio processing system 79—16325
control of Joyce-Loebl microdensitometer for objective-prism spectra meas. 80—105173
coordinate meas. uncertainty computation program *(German)* 80—86256
coordinate measurement, computerised, problem oriented language MAUS *(German)* 78—89432
coordinate measurement, mating simulation *(German)* 78—77846
coronary sinus blood flow on-line computerised assessment by thermodilution 78—81024
correlation spectrometer, computer assisted, for remote sensing of air pollution 78—4002
coulopotentiograph system, automatically controlled, for trace analysis of metal ions 79—92026
coulopotentiograph system for trace analysis of metal ions 79—92026
Coulter S blood analyser and IBM 1800 computer, minimum-interrupt digital interface 80—3849
CRO design using modular system 78—93671
cryoelectronics appls. 80—98920
Crystal Ball data acquisition system 79—89531
crystallography, modern techniques and apparatus survey 77—4019
cytogenetics microscope for automatic metaphase spread finding 77—56550
Daresbury Laboratory automated magnet field meas. facility 79—30509
data acquisition system designing for accelerator development facility 77—57307
data analysis at LAMPF: a hierarchical approach 79—89562
data compression in microprocessor-based data acquisition systems 79—12270
data logger, YODAC-8, microprocessor controlled, for temp. data acquisition 78—49813
data logger for recording slow sea oscillations 80—36414
data logger mean square error minimisation *(Russian)* 77—9994
data loggers 80—73337
data recording system for KSC 60 cm reflecting telescope, microcomputer control *(Japanese)* 80—94717
data transfer in on-line systems 79—89571
defect radiographs, method and apparatus for automatic decoding 78—40002
deformable mirror figure sensor control 77—19384
deformable-mirror system, computer-aided, using differential angle control 79—27356
Delta Scan, computerised entire body transverse scanner, technical description 77—44781
demodulation system, microprocessor based 78—44627
densitometer, automated for radiograph interpretation, ^{252}Cf wire anal. appl. 77—61643
dielectric loss meas., on-line calculator based system 78—54397
differential capacitance measurement by desk calculator controlled system for semiconductor-liquid junctions . 79—78170
differential photometer, 6800 microprocessor control, astronomical appl. *(French)* 79—58253
differential pulse voltammetry at dropping Hg electrode, computerised instrumentation 79—79326
diffractometer, two-circle SSD, microcomputer control, appls. in angle dispersive mode 79—14641
digital data logger, microprocessor-based, for radiation detectors 79—26848
digital measuring system for recording nonstationary temp. fields 77—53912
digital memory recorder, electromyography and nerve conduction appls. 78—43999
digital microdensitometer, for automatic astronomical photographic wavelength meas. 77—64655
digital speech voltmeter using microprocessor 79—72768
digital system for measuring probabilistic and statistical characteristics of infralow-frequency processes 79—71431
digital transient recorders, enhancement of signal averaging using microcomputer 78—57930
digital voltmeter, self-calibrating high-resolution 77—57346
digitizer and image analyzer, microcomputer-controlled 80—86270
direct-reading photometry system with automatic instability correction 79—26099
distributed processing data acquisition system at Brookhaven National Laboratory 79—89532
dosimeter for pulsed neutron dose rate meas., portable, microcomputer-based 80—86991
dosimetry, automated data acquisition and anal. system at LAMPF pion therapy facility 78—53506
dosimetry, the computer as an active element 79—67961
double-beam scanning microspectrophotometry for rapid microscopic image reconstructions 80—18008
drift chamber data acquisition, microprocessor based system 80—58066
drift tubes, ion time of arrival spectra determ., using CAMAC crate interfaced to microcomputer 78—93661
dye laser wavelength scanning with microcomputer control 79—94248
dynamically focused electronic sector scanner based on CCDs 80—98042
ECG, His bundle activity noninvasive recording 77—13023
ECG, long-term recordings, rapid computer analysis system Argus/H 78—36002
ECG, microprocessor based ambulatory monitor 77—48918
ECG analysis system, application to hypoxic rat ECGs 78—57088
ECG cassette recording and automatic processing microprocessor system 78—36021
ECG interpretation system in ambulatory health service 79—79669

computerised instrumentation continued
ECG microcomputer-based evaluation system, improving diagnostic capabilities 78—88761
ECG S-T segment elevation meas. instrument, programmable 78—31956
ECG systems, current status and future trends *(Japanese)* 79—44013
echocardiographic and systolic time interval processor 79—83869
echocardiographic tracking system, microprocessor-controlled 80—67169
echocardiography, automatic range gate tracker 79—83868
echocardiography, real-time, using burst analogue sampling 77—9234
echosonography, real-time, computer controlled bidirectional phasing 79—12023
eddy current probe, thickness measurement of plating layers *(German)* 79—85112
EEG, real-time detection of brain events, expt. 77—44793
EEG delta rhythm during sleep, computerised anal. system 80—12285
EEG frequency analyser, real-time, microprocessor monitored 78—57092
EEG period and amplitude anal. system, microcomputer-based 80—72353
EEG phasic event detection by microprocessor 78—57091
EEG signal averager, flexible and low cost 79—43998
effective annealing time determ. using analogue computer 78—88475
eight-channel scanning electromyograph 79—29674
eight-sensor low-energy γ topograph *(Russian)* 78—35932
electric impedance meas., microprocessor-based, advantages 78—89501
electrical resistivity expts. in He II environment using computerised facility 80—31799
electro oculography, computerised diagnostic system 80—21566
electro-optical gauging system, microcomputer-controlled 79—86271
electrochemical analysis, programmable charge transfer analyser 78—3406
electrochemical apparatus, multi-purpose microprocessor based 79—43592
electrochemical data interpolation, fast Fourier transform method 79—16061
electrocutaneous tracking, evaluation of sensory feedback codes 79—25004
electroencephalograms, online real time analysis 79—100773
electromanometer, appl. for nuclear materials safeguarding 80—99211
electromedical, microprocessors appl., development trends *(Italian)* 80—17173
electromedical equipment, computer controlled systems *(German)* 79—62421
electrometer, for apparent power meas., analogue simulation *(Czech)* 77—5859
electron image processing, and improvement 78—24890
electron microprobe, automated, evolution of quantitative elementary point anal. in geosciences *(French)* 78—78046
electron microscope-microprobe systems, automated, for quantitative metallography 78—35631
electron microscopy, image processing system for micrographs based on minicomputer 80—73549
electron microscopy, isolated atoms visualisation *(French)* 78—24892
electron spectroscopy, features 78—86390
electron test accelerator, Chalk River, control computer 78—90004
electron test accelerator, computer control of beam transport system 78—25359
electronic balance with integral microprocessor 79—67255
electronic microbalance and precision balance design *(German)* 78—57935
electronic thermometer, microprocessor based linearisation of thermocouple temp. charact. 80—221
electronics in nuclear science and technology 80—9347
Electrophysiological Data Interface 79—79677
electrophysiological stimulator, microprocessor based 78—44748
elementary particle interaction event recording and analysis by computer *(French)* 80—63496
ellipsometer, calculator-coupled, for film thickness meas. 77—82490
EMG activated spatial morse code general purpose communication device 80—30946
ENDOR spectrometer, computer-controlled 79—80654
energy dispersive X-ray particle analysis system using beam blanking and digital scan-stop 78—24004
Enraf-Nonius CAD-4 diffractometer, mechanical design, computer control and system performance 80—24318
epicardial mapping, computerised display system *(Japanese)* 80—101279
EPMA, computer-controlled, CAMEBAX system, operating experience 78—35779
ERASMUS Tokamak data acquisition system, program struct. 80—49012
error reduction, using microprocessors *(Czech)* 78—8398
errors sources and reduction *(German)* 77—5791
estuarine current meter data acquisition microcomputer system 80—46265
evoked potential multi-channel data acquisition system, microprocessor controlled 78—11750
exercise cardiopulmonary response analysis, breath-by-breath computer system 78—35995
exercise ECG computer-assisted anal., implementation and clinical anal. 78—81051
eye autorefractor, optical subsystems 79—25127
eye examination, evaluation of Refractor III system for subjective exam. 78—3622
eye long-term growth and shortsightedness model 79—83768
eye refractor, automatic, optical system 78—61274
Fabry-Perot interferometer, microcomputer stabilisation 78—74055
faradaic admittance, rapid drop time on-line FFT meas. 78—92544
faradaic admittance, SYDAGES system for on-line FFT meas. 78—20090
FAS-II system, new dimensions in automatic image anal. 79—58678
FASTBUS, high speed nucl. data acquisition 78—46251
FASTBUS, project evaluation 79—89555
Fermilab, multi-user control and data acquisition systems 77—54480
Fermilab main accelerator quadrupole transistorised regulators 77—83243
fibre fabrication, computer-aided MCVD system *(Japanese)* 79—59852
fibre optics transmission characts. meas. by computerised signal processing system 79—76876
field emitter electron beam exposure system for semiconductor fabrication 79—30624
field ionisation kinetic data acquisition and processing, computer controlled 78—2999

computerised instrumentation continued
file management for experiment control parameters in distributed function computer network 77—57306
film, large format, for use with laser scanning system 78—62260
film thickness measurement, microprocessor based instrumentation *(German)* 80—57260
Finnish seismic array, data transmission, recording and handling 79—39917
Fizeau wavelength meter, laser and other monochromatic sources, digital display 78—89450
flow injection analyser for viscosity measurement 80—33713
flowmeter reference installations, development prospects for meas. computer complexes 80—96320
flowmeter system for calibrating transducers, with steady and pulsating flows 80—79416
fluctuating noise measurement system *(French)* 80—64316
fluorescence marker concentration dynamics, as probe of mobility 77—9303
fluorometer, automated, for U analysis 79—11871
fluoroscopy for non-invasive cardiovascular imaging 80—17121
foot function assessment system, normal and pathological feet 79—100760
foot load dynamic distrib., quantification system 80—94388
foot load static distrib., quantification using the PET computer 80—94387
foot/floor contact temporal patterns during walking, automated on-line meas. system 78—77128
force distribution under human foot, online meas. system 78—96110
FORTRAN software, for mini-computers to control four-circle neutron diffractometer 80—38876
forward scattered light system for optical fibre diameter meas. 78—62176
fraction collector, freely programmable, with automatic repetitive injection, for preparative liquid chromatography 79—79338
fracture surface SEM analysis, microtopography 80—68312
frequency counter, 100 MHz microprocessor controlled, Hewlett Packard (5315A) *(French)* 79—88938
frequency tracker for laser Doppler anemometry 79—72968
full photon counting Rayleigh spectrometer, minicomputer system using autocorrelation or FFT 78—41351
fusion reactor ignition, eight-beam CO_2 laser system, minicomputer-CAMAC control system 78—58493
gain stabilized NaI(Tl) γ-ray detector, electronics, disc-based minicomputer, power shape in LWR core 78—33284
gait, human, limb segment inertia influence on joint loading 79—92270
gait analog tracings and computerized analysis through a PDP-11/45 79—29643
gait analysis automated accelerometry system 77—90934.
gait measuring system for treatment evaluation, microprocessor controlled 80—61731
gallstone vol. meas. system 79—62348
gamma camera, computer controlled, nuclear cardiology appl. 80—61682
gamma camera low loss data acquisition with subsequent computer anal. 79—49358
gamma cameras for medical diagnosis *(Swedish)* 79—70607
gas chromatogram, multidimens., design aspects 77—81436
gas chromatogram quantitation, using microprocessor-based integrator, algorithms 78—27839
gas chromatographic purge-and-trap concentrator with microprocessor control 80—93815
gas chromatography, computerised instrumentation 77—77839
gas flow meas. with vortex meter and microcomputer *(German)* 80—92241
gas turbine annular vortex shedding acoustic resonance analysis *(Japanese)* 80—14526
gated regional spirometry (GRS) 79—25097
GB-IB interface system, automatic meas. in solid state physics *(Japanese)* 79—75509
GC/MS/computer techniques for environmental anal. 79—57554
gel permeation chromatography, automated system using laboratory automation system 80—71961
gel permeation chromatography anal., data acquisition, computer control 80—97746
general purpose automated meas. system based on synchronous waveform digitisation under computer control *(Portuguese)* 80—82753
GenRad 2512 portable digital spectrum analyser, simplicity of operation due to interactive display, technical specifications 80—64326
geophysical prospecting, γ-γ well-logging for density, computerised instrumentation *(Hungarian)* 80—21843
glassware dimensional and sidewall inspection using digital camera and computer 78—16890
graphic display system for computerised tomography 78—3578
grating generating by microcomputer, appls. to human visual system 79—2172
grating monochromators, servocontrolled and automated scanning system, using microcomputers. 78—33852
gravity sedimentation anal. of human blood leukocytes 80—98197
gross and segmental motion analysis in dynamic cardiac imagery 79—25093
growing bubbles on heated plate, meas. using computerised image anal. system 80—22322
haploscope, automated miniaturised device for testing binocular visual function 77—2004
hardwired image analyser software control 78—57917
Harris data memory, operation and educational uses 80—17779
heliometric station operating data 79—58069
HELIOS-1, HELIOS-2, onboard shock identification computer 79—92679
heterodyne interferometer for index gradient meas. 80—13131
heterogeneous charge transfer kinetic effects, deconvolution by FFT faradaic admittance meas. 78—20091
Hewlett-Packard 8450A UV/Vis spectrophotometer, user interface 80—68268
high energy physics CAMAC hardware 79—13617
high energy physics data acquisition packages 79—89535
high energy physics detectors—limits to growth 79—89537
high energy physics expts., computer technology effects 79—89536
high performance liquid chromatography, automation 78—80806
high performance liquid chromatography, SLIC-1400 universal interactive controller 80—55731

computerised instrumentation continued
high performance liquid chromatography, with CRT display, microprocessor-controlled 79—20478
high performance liquid chromatography automation by microprocessor control 77—86422
high performance liquid chromatography with programmed runs 78—11583
high-performance data-acquisition and data-analysis computer system 79—93899
high-performance multimeters and voltmeters with microprocessors *(French)* 79—67349
high-power glass laser users' facility with computer control 77—19341
high-pressure liquid chromatography, microprocessor controlled 79—83528
high-speed blood cell anal., software system 78—44671
high-speed dual-lag photon-correlation signal processor development 77—18095
Holifield Heavy Ion Research Facility 79—93900
holographic droplet image analysis by TV camera and table calculator via IEC-Bus 78—36337
holographic interferograms evaluation, of thermal boundary layers *(Czech)* 78—62220
HTGR nuclear fuel microspheres, automatic particle size analyser 79—12921
human locomotion evaluation equipment clinical practice appl. 77—86676
hybrid computer for chemical reaction residence time meas. 78—81953
hydrometeorological data, shipboard automated information processing system 80—41553
hysteresisgraph with discontinuous sweep mode 80—86351
IL 282 CO-Oximeter for measurements on whole blood 80—56159
illumination measurement using photoresistors, digital linearisation using microprocessors *(German)* 78—77961
image analyser control, diode matrix replacement by PROMs 77—22539
image analysing computer, Quantimet, device for automatic scanning of irregular areas 77—5906
image dissector tube with minicomputer control suitable for IC mask inspection 79—55065
image intensification of X-ray diffr. patterns from biological structures 77—66878
image sensor, minicomputer controlled, fluctuating image time averaging and coherence function detect. 79—41341
in-core movable neutron flux mapping computerised console development 78—13308
INI-3 measuring system for nanosecond pulses 79—35793
insect optical cells anal. using microcomputer *(German)* 77—86724
instantaneous frequency measurement system for microwave signals *(Japanese)* 80—73327
integrated surface physics and chemistry laboratory planning for automation 79—67269
intelligent microscopes, recent and near-future advances 80—98166
intensive care, instrumentation and control, conf., London, England (May 1979) 79—70702
intensive care ventilator, microcomputer-controlled 80—51292
interactive computer program for measurement of data obtained using the extra-stimulus technique during electrode-catheter studies 78—24156
interferogram fringe pattern reduction, automated system 80—47097
interferometer, computer-controlled Fabry-Perot, for Brillouin spectroscopy 79—40622
interferometer, far IR 77—82590
interferometer, large aperture AC, for optical testing 79—27446
interferometer, microprocessor based, heterodyne 80—9030
interferometer for precision linear displacement meas. 80—27285
interferometer phase detection using LSI-11 microcomputer and high-speed digital techniques 78—71545
interferometer signals processing, far IR, use of microcomputer 77—2689
interferometry seminar, San Diego, CA, USA (Aug. 1979) 80—73096
intra-aortic balloon pump controller, within computerised evaluation system 77—56538
intraocular fluid dynamics meas. by minicomputer-based system 78—24130
intravenous antiarrhythmic drug infusion, automated delivery 78—81058
ion microprobe mass analyser and SEM combined depth profiling 79—74481
ionising radiation metrological work automation 77—75033
IPNS time of flight neutron scattering instruments system 79—89558
isochronous cyclotron mag. field automatic meas. system 78—82547
isotachophoretic analysis, development of data processing system *(Japanese)* 79—24873
isotope record monitoring system 79—70652
jet engine noise meas., flowing duct sound separation probe 78—13878
Kalousek polarography 79—52792
KEK proton synchrotron, control computer system 77—88301
keyboard-programmable sample processing and analysing system 78—24769
knee locking, sensor-controlled external system, exptl. study 78—40406
Knudsen cell quadrupole mass spectrometer, high temp., control and data acquisition, system 79—26171
laboratory automation approaches 79—12777
laboratory automation using computer control, interfacing system 79—49213
laboratory computer systems, minicomputers, microprocessors, uses 77—79072
laboratory instrumentation system, computerised, real-time 79—12786
laboratory microcomputer and A/D convertor interfacing 80—22337
laboratory multimeter with microprocessor, precision *(French)* 79—6139
laboratory vehicle for air-pollution measurements with computer-controlled data acquisition and navigation system *(German)* 79—39327
LAMPF standard data-acquisition system 79—89534
Large Azimuthal Telescope program control system 79—16829
Large Coil Test Facility, instrumentation system design 80—95446
large-aperture interferometer with low-resolution holographic corrector plate 80—74315
laser absorption calorimeter, computer-controlled, for small absorpt. coeff. meas. 78—45680
laser beam deflecting system, electro-optic, using Kerr cell and birefringent calcite prism 77—7103
laser beam deflector using computer-generated holograms 77—38979
laser data acquisition/analysis system for Si vidicon optical detector 78—58041
laser interferometer, computer controlled 80—56294

computerised instrumentation continued
- laser interferometer for routine aspheric surface testing 80—14495
- laser polarimeter for active spill detection 77—21938
- laser radar system, mobile computerised meteorological phenomena observation 80—56644
- laser sliding reference interferometer for two-dimensional phase meas. 77—19280
- laser transit anemometer system, for measurements in supersonic flow 80—10332
- laser unequal path interferometer with electro-optical camera and minicomputer, fabrication/test appl. 80—77847
- laser wavemeter, inexpensive broadband optics and minicomputer interface 78—89448
- LEED beam intensity measurement by photographic method, use of Vidicon camera 77—7638
- liquid chromatograph, microprocessor controlled 80—21351
- liquid chromatograph, microprocessor-based, reproducibility 77—9152
- liquid chromatography, automatic high temp., Waters GPC 150C equipment, polymer appl. 79—10806
- liquid chromatography, high performance, with CRT display 79—57321
- liquid flowmeter calibration automated secondary standard 77—37841
- liquid scintillation counting, single and double labels, absolute activity analyser vs. on-line computer 77—83470
- liquid scintillation counting, single and double labels, quench correction with on-line computer 77—79520
- liquid-scintillation counting, one-button, using microprocessor 77—14308
- LLL, microprocessors appl. 77—54481
- LMFBR core instrumentation, approach based on IR television, on-line computing, pattern recognition 77—54310
- local circulatory system characterisation by CW Doppler US flow meas. 78—57109
- long bone mechanics study under microprocessor control 80—76851
- LSI-11 based auxiliary crate controller for beam line and experiment control 79—89565
- lunar occultations observations, microprocessor-controlled data acquisition system 77—49311
- lung function meas. system, mobile *(German)* 78—3630
- lung volume, online calc. by digital computer 80—72351
- machine tool industry, angle measurement, automatic testing of precision dividing heads *(German)* 80—82740
- magnetic meas. system for ring specimens 80—86346
- magnetic torque curve analysis, online microprocessor system 78—254
- magnox fuel cladding, surface struct. data acquisition and processing system 80—898
- main program and overlay manager subsystem within distrib. function lab. computer system 78—36980
- mandibular movements diagnosis, system for meas. and processing *(Japanese)* 80—101249
- marine digital gravity meter, computing unit design *(Russian)* 79—39936
- marine sediment analysis and pollutant detection by X-ray fluorescence 77—5361
- marine seismic data acquisition, minicomputer based system 77—82072
- mass spectrometer, microcomputer-based controller for temp. programming direct inlet probe 78—16893
- mass spectrometer solid state magnet control unit 79—12879
- mass spectrometry, features, book 79—26179
- MDS computer systems, improvement of pulse-mode photographic images 80—30862
- measured value preprocessing and direct sample identification *(German)* 79—5418
- measurement data processing system error analysis 78—41288
- measurement data processing system error expressions 78—41287
- measurement data processing system vector optimization 78—41289
- measurement error charact. improvements, using microprocessors *(German)* 78—24773
- measurement technique, congress, Moscow (1979) *(German)* 80—36964
- measurement-computation complexes, general principles, introduction to the USSR 80—52177
- mechanics expts., model for computer based data acquisition and control 77—63844
- medical, laboratory equipment and procedures development *(Japanese)* 77—44766
- medical microscopy, advent of intelligent microscopes 80—81678
- medical technological developments, 1977 trends 78—48902
- medical US diagnosis, F mode images for any diagnostic plane utilising microcomputer and light pen 80—41147
- medical US imaging, digital scan convertor system using microprocessor 78—96082
- megachannel gamma-gamma coincidence system using PDP-8/E computer and moving-head discs 77—57834
- meteor radar system, Illinois University, data processing algorithm 77—41205
- meteor wind automatic meas. set, drift obs. accuracy *(Russian)* 77—41248
- meteor wind automatic meas. set, programming and systems interaction *(Russian)* 77—41247
- meteorological data acquisition and processing, computerised data collection system *(German)* 80—37007
- meteorological data acquisition system, microprogrammable microprocessor-based 77—64496
- meteorological instruments development in Finland, by Vaisala Oy manufacturer 79—12310
- Meteosat sea-surface temperature DP, analysis of first results 80—76985
- methyl group meas. in plastic industry, computer-infrared method 77—27073
- metrological support to computer-aided process control, design and upgrading 80—185
- MGH positron camera, medical transverse section imaging 79—66516
- MHD combustor and channel temp. meas. 80—73364
- microcomputer based laser interferometer for angular displacement in instrument graduation *(Polish)* 80—90816
- microcomputer based nuclear data acquisition system 80—63500
- microcomputer controlled haploscope for binocular experiments 80—46091
- microcomputer controlled UV ozone calibrator 80—13149
- microcomputer system for automating analytical instrumentation 78—73127
- microcomputer-aided data-processor for mag. susceptibility *(Japanese)* 79—63283

computerised instrumentation continued
- microcomputer-based data acquisition and analysis system for CO_2 rebreathing studies 80—36161
- microcomputer-based data acquisition system for NMR spectrometer interfacing 78—74042
- microcomputer-based digital titrator 78—80805
- microcomputer-based neurophysiological stimulator, design of and impact on clinical procedures 80—26393
- microcomputer-based pulmonary wedge pressure measurements 80—26391
- microcomputer-based system for rat locomotor activities meas. 79—20722
- microcomputers in biomedical and clinical applications 78—73283
- microdensitometer computer interface design and construction, for X-ray image anal. 77—44821
- microphotometer, automated, SAMB, for morphometric and densitometric analysis *(French)* 77—10085
- microprocessor—based unit data acquisition and reducing system 80—21598
- microprocessor based chromatographic system 80—71999
- microprocessor based data acquisition and exptl. control system 78—36086
- microprocessor based digital scan generator, interface to image processing computer 79—12902
- microprocessor based instrument, Dinamap, for arterial press. automatic determ. 78—96108
- microprocessor based real-time speech processor 79—64437
- microprocessor based system for ECG analysis, design and development 78—73287
- microprocessor based telemetry demodulation system 79—20738
- microprocessor controlled reactivity meter for real time monitoring of reactors 78—33263
- microprocessor for biomedical meas. 79—44065
- microprocessor for optical processing system noise analogue signals 78—81955
- microprocessor in real-time Fourier analysis *(German)* 79—67266
- microprocessor multichannel analyzer laboratory project 80—101685
- microprocessor multiple arrays, operating systems for nuclear diagnostic system 79—49918
- microprocessor-assisted high-precision viscometry 79—50816
- microprocessor-based, characts. 80—67440
- microprocessor-based, programmable laboratory equipment controller and data acquisition system 79—6104
- microprocessor-based anemometer, features 79—60087
- microprocessor-based blood gas analyser 78—40356
- microprocessor-based blood gas analyser computational algorithms 79—57805
- microprocessor-based colorimetry system 79—58770
- microprocessor-based data acquisition system for the Goldmann perimeter 80—46086
- microprocessor-based diffractometer 80—70082
- microprocessor-based EEG 79—62403
- microprocessor-based experiment controller/interface 79—80590
- microprocessor-based instruments 80—21559
- microprocessor-based interferometric data reduction system versatility 80—73439
- microprocessor-based optical multichannel analyser 80—33167
- microprocessor-based teleradiology system 80—26343
- microprocessor-based timer interval meter *(Russian)* 80—52172
- microprocessor-controlled 64-cell pulsed optical receiver for crosswind sensing 77—18096
- microprocessor-controlled contrast sensitivity measurements 79—92327
- microprocessor-controlled digital compound scan system 79—57735
- microprocessor-controlled gas chromatograph, low temp. range extension 78—3395
- microprocessor-controlled target polarization monitor 79—88990
- microprocessor-minicomputer combination for instrumental flexibility 77—54483
- microprogrammable integrated meteorological data acquisition system 78—77374
- microscope, computerised focusing technique 77—22596
- microscope photometry, on-line data collection and processing for solids, fossils and organic matter *(German)* 79—26101
- microscopic image semi-automatic anal. device 79—79705
- microwave instrumentation review 79—212
- miniature endplate potential amplitude online meas., programmable calculator conversion 79—84051
- minicomputer based, reflection spectra measurement 79—61402
- minicomputer controlled instrument for US vel. and attenuation meas. 79—86312
- minicomputer coupled to rapid-scanning spectrometer, monitoring of optical filter 80—23774
- minicomputer coupled to rapid-scanning spectrometer, monitoring of optical filters 80—28309
- minicomputer for condenser capacitance and loss tangent meas. *(Russian)* 78—70159
- minicomputer general purpose system 79—89543
- minicomputer high-level languages and real-time operating systems for scientific instrumentation 79—12778
- minicomputer system, automatic visual stimuli, hand and eye movement monitoring *(French)* 79—34682
- minicomputer-aided ECG diagnostic system 79—44024
- minicomputer-based interactive graphics biology film anal. system 78—44744
- minicomputer-based scheme for turbulence measurements with pulsed Doppler ultrasound 80—26435
- minicomputer-controlled diagnostic and display system for high-energy lasers 79—36915
- minicomputer-controlled high-speed transient recording system *(Russian)* 77—9992
- minicomputerised pressure transducer data logging system *(Russian)* 79—6102
- minicomputerized automatic radiocardiogram analysis *(Japanese)* 79—29614
- minority carrier lifetime mapping by SEM 80—96903
- MINUS3—a general purpose data acquisition system at LBL's 88″-cyclotron and superHILAC 79—93901
- MIRABELLE hydrogen bubble chamber, control by minicomputer *(French)* 77—3225
- mirror electron microscope, microprocessor system 80—62798
- mobile gamma camera with remote image processing computer system, for nuclear medicine 78—92700

computerised instrumentation continued
modular system, standardised, for space scientific instruments 77—71005
moire fringe biostereometry using parallel light beam 79—100701
moire fringe data handling system, industrial lab. appl. 79—30523
moire stress analysis interferometer with microprocessor 80—31858
monochromator, high-intensity, automation using wavelength-scan and intensity-control system 80—86366
MORPHOQUANT automatic microscope image analyser, universal program system 80—56160
mosaic sensor test and calibration facility for focal plane arrays 80—86425
motion analyser system for 3-dimens. location of body parts 77—40820
motor unit recruitment and firing freq. control in elec. stimulated muscles of cat 78—81092
multi-faceted data gathering and analysing system 78—37530
multi-scale system for photon meas. *(French)* 79—63882
multiaxis neutron diffractometer automation 80—102417
multichannel analogue detector system for star/planetary nebulae spectroscopic obs. 78—36461
multichannel analyser, microprocessor-controlled, transfer of blood pressures and neural activities for computer anal. 80—72356
multichannel data logging minicomputer switching program synthesis *(Russian)* 77—9993
multichannel electrometer data-acquisition system 79—89564
multichannel instrum. for measuring energy of pulsed laser radiation 79—76731
multichannel polarimeter, data acquisition and control system *(Japanese)* 80—77842
multichannel precision temperature measuring device, minicomputer, Pt 100 resistance thermometer appl. *(German)* 78—77914
multichannel radiometer, programmable, for Earth remote sensing 80—77253
multichannel system for radioastronomical data recording and processing in real time *(Russian)* 78—65507
multielement trace analysis, neutron activation programme using absolute counting 77—77862
multimeter, control functions performed using 4 bit, microprocessor chip *(Slovenian)* 79—181
multimeter, microprocessor controlled *(French)* 77—74433
multimode optical fibre bandwidth computation from refractive index profiles 79—76815
multiple data streams, dynamically configured software system 79—89548
multiple fuel failure resolution with gas tagging, barycentric coordinate technique 79—13485
Multiple Mirror Telescope guide alignment system 79—75107
multiple response parameters meas. 78—57136
multiplexer, microcomputer-based, for performing depth profiling with Auger spectrometer 79—67435
multiprocessor based data acquisition system, design 79—89556
multipurpose data acquisition and processing system based on Mir-2 computer 78—32799
multiunit spike train sampling control by peak discriminator 79—34717
multiuser particle track photograph meas. computer programs *(Russian)* 77—38591
multivariate discrete information analyser, particle recording appl. 78—78601
muscle contraction, time resolved studies using small angle X-ray diffr., design of data collection system 79—12052
muscle contraction, time-resolved X-ray diffr., data-collection system *(Japanese)* 80—46108
MWPC readout system 78—17505
myocardial contractility, real time meas. by analogue computer with digital displays *(Japanese)* 79—44015
narrow band optical filters for solar astronomy *(Russian)* 78—16292
NBS automatic pulse measurement system, capabilities 77—18018
NDT, microprocessor and microcomputer appl. 79—91891
NDT instrument for grain size and anisotropy meas. 79—11753
neural histological section, computer-assisted mapping with the light microscope 80—30963
neural pulse wave analysis, microprocessor-based instrument 80—104791
neural spikes amplitude discrimination system 77—52778
neuromuscular miniature endplate potential online acquisition microcomputer system 78—36015
neuronal interconnection meas., semiautomatic system design 78—44742
neuronal response analyser with microprocessor *(French)* 79—20730
neurophysiological clinical laboratory appl. *(Swedish)* 77—44625
neurophysiological spike unit data acquisition and reduction system 79—79713
neurophysiology, real-time display techniques 77—2071
neutral beam system, 120 keV, for fusion reactor ignition 78—66377
neutral beam systems, computerised, development and operation 79—93849
neutron activation analysis of rock samples, automatic instrument 78—3769
neutron diffractometer, computer-controlled CAMAC system *(German, English)* 77—19843
neutron expts., data processing system 79—81143
neutron scatt., automatic data processing *(Russian)* 80—54079
neutron TOF expts., control and data processing system 78—25385
Niels Bohr Institute on line data acquisition system 79—89557
night vision system testing image scanner 77—39102
NMR computerised tomography, human whole-body line scan imaging system 79—66502
NMR zeugmatographic imaging, gradient control device using microprocessor 80—89822
noise analysers, microprocessor based 79—18654
noncontact microprocessor-based ocular pulse monitoring system 80—46089
nonexponential nuclear relaxation data acquisition and processing system using Nairi-2 computer 78—32800
noninvasive His bundle and sinoatrial node activity recording system 79—39560
nonlinear optics, digital data acquisition and on-line processing at Moscow State University 78—46709
nonlinear temp.-time program for DTA *(German)* 78—8406
NPL voltage standard, Weston cells meas. system 77—82572
NQR spectrometer, fast pocket computer frequency-controlled 79—80655
nuclear, LMFBR subassembly fault detection, microprocessor-based distributed system appl. *(Japanese)* 79—41002

computerised instrumentation continued
nuclear, multichannel analyzer data processing by minicomputer systems 79—36497
nuclear energy level lifetime measurement using on-line computer and registration time shift compensation 80—68577
nuclear engineering computer instrumentation, laboratory instructional programs 80—31472
nuclear fuel cladding strain meas., microprocessor-controlled microwave extensometer 78—33240
nuclear fuel reprocessing, destructive chem. anal. system 79—13508
nuclear instrumentation, computer-based data acquisition system for multi-station teaching laboratory 78—4446
nuclear instrumentation computer network for on-line data processing 78—37529
nuclear instrumentation laboratory course, computer based data acquisition and anal. 80—36820
nuclear lab. computing facilities 79—89527
nuclear laboratory instruction with multichannel analyser/microcomputer system 80—31471
nuclear materials accounting and control system 79—13507
nuclear medicine, computers and quality control 79—16295
nuclear medicine, precision computer display techniques 80—109011
nuclear medicine, sequential method for high 3D resolution imaging 78—53489
nuclear medicine diagnostics, for teaching 78—49618
nuclear physics, impact of changing computer technology 79—89538
nuclear physics, impact of changing computer technology 79—89539
nuclear physics data acquisition with UNIX time-sharing system 79—41085
nuclear physics GSI data acquisition system 79—89533
nuclear power plant diagnostic instrumentation experience 79—3218
nuclear pulse height analyser, microprocessor based digital controller 79—3335
nuclear radiation detection lab., desk top calculators 80—36821
nuclear reaction thresholds and half-life meas., computer controlled system 78—55114
nuclear reactor, microprocessor appl. 80—83147
nuclear reactor fuel consumption determ., automated techniques *(German)* 77—14236
nuclear reactor in-core meas. *(Czech)* 78—86637
nuclear reactor multivariable parameter meas. and display microprocessor solution 79—72221
nuclear science, nuclear power systems, confs., San Francisco, USA, 19-21 Oct. 1977 78—33304
nuclear ventriculograms 77—86627
nystagmus analysis system using microprocessor 77—48917
object dimension meas. by computer-controlled laser beam scanning 79—98431
object dimension meas. by computer-controlled laser beams 80—31715
ocean internal wave obs. temperature measurement array 77—5380
ocean observation system, microcomputer based 79—16677
ocean-bottom seismometer capsule, operationally optimized 79—39911
oceanographic, Kiel multi-purpose sea probe microprocessor-based data acquisition system *(German)* 78—85701
oceanographic data system, microprocessor based 79—16676
oceanographic integrated research ship, with data acquisition and processing systems 79—34969
oceanography, microcomputer applications 78—36322
oceanography, microprocessor-based particle data collection system 78—36323
oil prospecting, new seismic reflection techniques 78—73541
on-line and real-time processing in radio astronomy 79—16838
on-line ECIL TDC-312 computer-controlled four-circle neutron diffractometer 78—55787
on-line monitor for α-emitting aerosols 78—46236
online analysis of large bubble chamber pictures, data acquisition system, CDC 1700 computer *(French)* 77—42223
online measurement of fluid reabsorption in renal tubules 79—92442
online topographical analysis in SEM 80—68310
online vectorcardiographic analysis microprocessors and instrumentation 78—36020
optical analysis system for agar-cultured micro-organism colonies, microcomputer-based 80—56304
in optical astronomy 78—4111
optical fibre birefringence measurement system 79—64352
optical fibre characts. meas. using digital methods *(French)* 79—90011
optical fibre diameter meas. 78—1443
optical fibre impulse response measurement system, time to freq. domain transform. by minicomputer 77—19406
optical image restoration using computer-controlled microdensitometer 77—23628
optical plotter, computer controlled, for filter generation *(French)* 78—90538
optical scanner, automated, for blood agglutination reactions 77—52861
optical shop computer-controlled interferometry, in-process production tool 80—74531
optical surface measurement technique, 3-D, using computerised electro-optical instrument 79—86272
optical system test interference pattern analysis program and error elimination method 79—76894
optical system testing, interferogram analysis, point spread function and OTF determ. 79—76616
optical systems conf. San Diego, CA, USA (Aug. 1978) 79—76356
optimal statistical conversion of instrument signals, for measurement accuracy increase 77—5795
optoelectronic device transfer function meas. and digital data processing apparatus 79—50399
optokinetic stimulus pattern by computer graphics for study of optokinetic nystagmus 79—44008
organ Boehm Professional 2000, programmable *(German)* 79—37096
orthodontic appliance mechanical behaviour determ., computer-controlled device 78—44727
oscillograms processing, in exploding wires expts., with aid of microcomputer and main-frame computer *(Russian)* 80—28854
oscilloscopes, microprocessor equipped, self-test facilities 79—88935
pacemaker automated test system developments 80—30944
paediatric radioluscent bone length meas. 78—48891
paper, rubber and plastics industries, conf., Brussels, Belgium (1976) 77—27638
parallel processor for real-time speech signal processing 79—64436

computerised instrumentation continued
paralysis treatment, microprocessor based stimulator *(Slovenian)* 80—104809
particle and nuclear physics, conference, Santa Fe, NM, USA (1979) 79—88779
particle beam profile monitor providing multiple profile during beam spill, Fermilab 77—57784
particle counter, programmable command data acquisition equipment *(French)* 77—54464
particle detectors, microprocessor-controlled data acquisition system for temporal/angular correl. between β- and γ-ray emission *(Spanish)* 80—106238
particle size analysis by automatic sieves 80—52380
particle size distribution measurement apparatus, rel. time 79—17390
patient contour drawing using US compound B-scanner 79—83865
patient topology, optical process for three dimensional assessment 79—20692
pattern generator for E-beam lithography 80—13188
PDP 11 and MBD branch driver for data acquisition 79—89567
PDP 11/40 minicomputer dynamic analysis system, noise analysis of fluid power equipment, graphical presentation of results 80—64327
peripheral nerve, single unit detection by real time correlation 79—12047
peripheral node module allowing independent systems to share peripherals 77—57305
permittivity meas. apparatus for VLF high-field meas. on insulating materials *(French)* 80—98933
personnel dosimetry, automatic film-badge reading system 78—40335
PET appls. in laboratory 80—27278
PETRA storage ring, control system 77—83315
phase noise meas. with high-resolution counter and online calculator 77—37945
phase tracking meteor radar ambiguity elimination algorithm *(Russian)* 77—41311
phase-locked interferometry 78—58022
phoneme recognition system based on human audition, psychophysical expts. 78—69115
photochromic tracer film, measurements using POLLY, film reading computer system 78—42696
photoelastic method, automated system for treating expt. data 79—15929
photoelectric pulse signals, precision loss meas. using microcomputer 80—13142
photogrammetric automation 'Zenit' automatic processing of line images *(Russian)* 78—21106
photogrammetric automaton 'Zenit', program-control module for interference coordinate measuring system *(Russian)* 78—21103
photogrammetric instrum. applic. of incremental and parallel computing 77—10121
photogrammetric system, cancer diagnosis appl., cytographs automatic analysis *(Russian)* 78—24161
photogrammetric system 'Zenit', read-out procedures design, for images with convex boundaries *(Russian)* 78—21105
photographic zenith tube obs., automatic control using minicomputer *(Japanese)* 79—101083
photomapping, Gestalt computer-controlled system features 78—40714
photometer, computer-controlled, for meas. of Raman spectra on photographic plates 77—65051
photometer, computer-controlled, for quantitative anal. of thin layer chromatograms 77—60326
photometer, twin-beam multiband computer-controlled, URSULA 78—49334
photometer data evaluation, photoelectric high speed *(Japanese)* 78—32345
photometer for rapid stellar light variation, microprocessor controlled *(Spanish)* 80—82222
photometers, automatic for luminaire studies 80—4752
photometric analyser, titrations 79—49267
photometric analyser for crystallographic orientations in rock thin sections, microprocessor controlled 80—41560
photometry for astronomical appl., data collection with aid of microcomputer *(Czech)* 80—67570
photometry system, high-speed, using dynamic compensation 77—18112
photon counter, microprocessor-controlled, ODMR appl. 79—88992
photon counting microspectrophotometer for study of single vertebrate photoreceptor cells 80—12323
photoscanner, for prod. of hard copies of medical images 78—40370
physical measurement and standardisation requirements *(Italian)* 79—93845
physical objects measurement, data assessment appl. *(German)* 77—75702
physiological stimulator, programmable, real-time numerical simulation appl. to laboratory instrumentation 77—44873
Picker FACS-I diffractometer, microprocessor-controlled optical incremental angle encoder system 80—18058
picosecond streak camera, nearly online, for diagnostics for CW mode-locked Nd:YAG laser radiation 79—49314
pion$^-$ radiotherapy, dynamic rangeshifter for modifying depth-dose distribs. 78—3595
pipette, programmable, appls. 80—42205
plant trace element anal. by X-ray fluoresc. for environmental pollution study 78—3690
plasma cross section reconstruction, Farey dissection optimization, computer anal. 77—84523
plasma electron temp. and density meas., semiautomatic system for double probe anal. 78—87490
plethysmography, whole-body, automated real-time anal. system 78—28112
plotter/printer, HP-IB 7245A model, microprocessor-controlled 79—35689
polarimeter, elliptical, for astronomy and atm. sciences 78—61745
polarography, DC wave automatic anal., minicomputer appl. 77—25333
polarography, microprocessor controlled polarograph for determ. of species with overlapping waves 77—12844
pole figures, automatic determ., review 79—87819
polyisobutane, relax. times, self diffusion, devel. and appl. of NMR data acquisition system 80—34807
polymer, physically nonlinear, stress relaxation during stretching 78—23754
polymer contact electrification measuring apparatus, computer-controlled 80—86341
portable neutron spectrometer/kerma-rate meter, design, performance 78—33361

computerised instrumentation continued
positron camera-computer system for various section images 79—66528
positron emission tomography, engineering aspects of PETT V 79—66517
positron emission transverse tomograph, PETT IV 78—40299
potentiometer, microprocessor-controlled, for nanovolt meas. 78—89502
potentiometric analyser, automated, with selective electrodes, microcomputer control 80—40773
potentiometric analysis with ion-selective electrodes, computer automation 80—3424
potentiometric stripping analysis, micro-computer system 79—52793
potentiometric titration apparatus, microprocessor controlled, for equilib. studies 80—89579
potentiometric titration system, microcomputer controlled, for soln. equilib. obs. 78—92522
potentiometric titrations with ion-selective electrodes, automated, equivalence pt. determ. method 78—3391
potentiostat, computer interfaceable 78—57976
potentiostat, microprocessor controlled, for electrochem. meas. 79—85133
power spectral density signature analysis, statistical algorithm 79—624
precision optical element testing by phase meas. interferometry 80—74520
pressure meter interfacing to supervisory computer 78—8409
primary pressure transducer dynamic charact. meas., automatic system 79—80589
process chromatograph system, minicomputer-based, computer controlled 79—16102
process gas chromatograph, microcomputer based 79—16101
process gas chromatograph, System 9010, microprocessor based 80—61205
process gas chromatographs, microprocessor based, calibration and data reduction 80—81402
programmable, intelligent instruments, using microprocessors 77—33998
programmable PRP 8 computer photometer, design, uses 77—74483
proton synchrotron, CERN, online function generation optimisation 78—834
proton synchrotron slow extraction beam parameter monitoring and control system in CAMAC standard online with ES 1010 computer 78—29674
Proton-Electron Tandem Ring Accelerator magnet field meas. 79—31271
psychrometer, microprocessor-based, for determ. of relative humidity and dew point *(German)* 79—29875
pulmonary blood flow, noninvasive meas. using PDP 12 digital computer 79—70685
pulmonary conductance, elastic recoil, on-line meas. system 79—16317
pulmonary gas exchange data online acquisition system 78—28100
pulmonary vascular response to hypoxia, online impedance analysis system 77—52943
pulse generator, digital, for proton enhanced ^{13}C high-resolution NMR spectrometers 79—58762
pulse height analysers, CAMAC data acquisition interface 79—3336
pulse radiolysis system 78—64862
pulse radiolysis system using Biomation recorder and PDP 11/40 computer 77—40560
pupilometry, instrumentation for stimulating and monitoring human pupil 78—48911
pupilometry equipment, pupil response as indicator of visual function 78—40154
pyrolysis gas chromatography, for analysis of tyre rubber blends 79—96396
pyrometry in solar furnace *(Japanese)* 78—32821
Q system: an experiment in software standardization for data acquisition 79—89549
quadrupole CAMAC universal timer 78—9040
quadrupole gas analyser with integral microprocessor 78—73109
radar, airborne, for oceanographic remote sensing 79—80063
radar reflection factor data, cartesian interpolation and display 80—31136
radiation absorption measuring instrument characts. evaluation with reference to information theory *(German)* 78—86753
radiation monitoring, multi-channel analyser, portable microprocessor controlled, accessories, data acquisition 80—63474
radiation monitoring system, digital communication techniques 79—49866
radiation protection networks for nuclear plants, minicomputer-based 80—855
radiation therapy, computer controlled 79—92367
radiation therapy, dose distributions, wedge-shaped, computer-controlled collimator motion 79—5358
radioactive waste surveillance, using real-time unfolding algorithm 79—85679
radioastronomical data reduction, via digital electronic integrator *(Russian)* 78—57465
radiochemical purity quality control by rapid feedback system 77—90900
radiograph scanning using computerised microdensitometer, for bone distrib. profile determ. 78—15890
radiography, computerised tomography, equipment operation 77—86617
radiography, computerised tomography using EMI general purpose scanner 77—5060
radiography, fan beam tomography scatter effects 77—5097
radiography, micro-dose system 80—51233
radiography, sampling tomography multi-sectional reconstruction method using computer *(Japanese)* 78—31896
radiography, X-ray tomography, review 77—5073
radioheliograph control system, 8 cm instrument at Toyokawa, Japan 80—98549
radioimmunassay, plasma renin activity estimation 80—46023
radioimmunoassay, automated on-line system, Gammaflow 77—9247
radioimmunoassay, instrumentation developments 77—86614
radioimmunoassay anal. system 79—25100
radioisotope imaging, rapid dynamic studies 79—16297
radioisotope scanning system 77—9254
radiology appls. 80—8142
radionuclide analyser system for nuclear power stations 79—81100
radionuclide cardiography, hardware and software techniques 79—57806
radionuclide cardiology, off-line viewing using videotape 78—65119
radionuclide emission tomography of head with ^{99m}Tc and scintillation camera 77—52866
radiotelescope RT-22, automatic obs. by computer 80—109359
radiotherapy, automatic var. of field size and dose rate in rot. therapy 78—11720
radiotherapy afterloading applicator, dose distrib. around 79—53249

- **computerised instrumentation** continued
  - radiotherapy treatment planning, use of computed tomography 77—12996
  - radiotherapy treatment verification and recording using small computer 77—81554
  - radiowave propagation, maximum usable frequency predictions, real-time updating 79—58179
  - Random-Access Memory-Interval Timer and buffered storage system 79—84066
  - rapid temperature change measurement, computerised thermistor cct. 78—49829
  - reactimeter, microprocessor based, nucl. engineering lab. class enhancement 80—36825
  - reactor coolant, automated system for radioiodine anal. 78—35768
  - real time moire topography equipment controlled by microcomputer 78—89441
  - real time online data processing system for EEG and body movement, mouse 79—92443
  - real time recorder and display for reconnaissance sensor data 79—32081
  - real time wavefront anal. automatic method for interferograms 79—75585
  - real-time ECG contour anal. program using microprocessor system 78—73288
  - recorder, six colour, six channel, synchronised by a microprocessor *(French)* 78—77885
  - redox titrimetry for accurate determ. of 5 to 25 mg of U 79—87932
  - reference averaging radiometer using microprocessor 78—70176
  - Refractor III system, computer-assisted eye examination 79—34698
  - refractory ceramic, deform. test apparatus and method *(Russian)* 78—35613
  - remote multiplexing for nuclear reactor instrumentation and control circuits 80—57885
  - remote platform data acquisition and control by minicomputer 77—5330
  - remote radioactivity working level monitor, microprocessor assisted calibration 77—61616
  - remote sensing technology, Canadian advances 78—16170
  - remotely controlled computer-guided preparation facility for X-ray fluoresc. anal. at fuel reprocessing plant *(German, English)* 78—17399
  - renal, thyroid and hepatic clearance, automatic meas. 79—34644
  - renography, role of midi-maxi computer interaction 78—7476
  - repeater gyrocompass angular digitiser construction principle *(Russian)* 80—73311
  - resistance thermometer automatic calibration oven 80—98914
  - resistivity variation meas. in Si slices, automated photovoltaic system 80—52274
  - respiratory gas analyser utilising glow discharge selective spectral emission, microprocessor based 79—100772
  - respiratory gas monitoring instrument using microprocessor *(Japanese)* 80—72358
  - respiratory pattern monitor for premature infants, apnoea detection 77—81635
  - respiratory response to exercise, on-line anal. 78—7458
  - respiratory tracer gas nonlinear computer anal., non-invasive meas. method 79—62395
  - retarding potential difference system for ionis. efficiency meas. 77—41724
  - retino-tectal mapping using microprocessor controller 78—31995
  - reverberation room ANS qualification for discrete frequency sound power level meas. 77—62122
  - reverberation room qualification with computer-controlled instrumentation system 77—58516
  - ring detector positron camera system for brain reconstruction tomography 78—40306
  - Ritchey Chretien telescope, microprocessor control system *(German)* 79—53726
  - Rome road traffic noise, 24-hour obs. and statistical analysis *(Italian)* 80—87651
  - room acoustics analyser using public telephone line and computer 77—35004
  - Royco aerosol particle counter 225, data processing system and modified system props. 80—37005
  - sample control and identification system, computer operated, for neutron activation anal. of soil 79—96402
  - SAR: a fast computer for CAMAC data acquisition 79—89569
  - scanning colorimeter, for meas. of white uniformity on colour TV picture tube 79—26098
  - scanning device, for 'Zenit' photogrammetric automaton *(Russian)* 78—21102
  - scanning microscope stage for microdensitometry, computer-controlled 79—26117
  - scanning system, microobjects dimensions determining, adaptive tracking algorithm appl. *(Russian)* 78—21094
  - scintigraphy, real-time system for multi-image gated cardiac studies 77—21611
  - scintigraphy and angiography, equipment for quant. evaluation and off-line operation *(German)* 78—88736
  - scintillation camera, multidetector design with 254 channels 77—40739
  - scintillation camera control, Pilotix module *(French)* 77—37040
  - scintillation camera transaxial tomograph, Humongotron 77—52867
  - scintillation counter, microprocessor-controlled, with programming facilities 79—26831
  - SCRIBE, system to help the badly handicapped, using a microprocessor *(French)* 80—56282
  - sea surface contour airborne radar as remote sensing instrument 80—51562
  - seafloor instrumentation systems, multifunctional, USA's offshore instrumentation program 79—53584
  - SeaTrak Data Processor, surface data reduction system for current meter 78—45042
  - seawater, computerised high-precision titrations of major constituents 77—66926
  - seismic broadband recording and data processing system 77—49173
  - seismic field recorder, dedication of micro-computer to signal selection 77—82073
  - seismic instrumentation and data analysis, conf., Durham, England (Aug. 1977) 79—39905
  - seismoacoustic station ASS-1, construction, operation principles *(Polish)* 78—24377
  - self-scanning silicon photodiode array with microcomputer control 80—35612
  - SEM, automatic quantitative anal. of images 79—6229
- **computerised instrumentation** continued
  - SEM, automation, quant. anal. of elementary images *(French)* 78—78045
  - SEM, focusing and stigmating system using minicomputer 78—37113
  - SEM, gradient image processing using on-line digital computer 78—21288
  - SEM, on-line stereo processing technique using minicomputer 78—37114
  - SEM, ultra high resolution, with electron optical system and microprocessor control 80—99002
  - SEM computer-aided topographical analysis 80—70094
  - SEM diffractogram online computation 80—70095
  - SEM images evaluation, coal chemical analysis 80—71994
  - semi-automatic universal test machine *(German)* 77—81346
  - semiconductor wafer defects, study by ASLEEP, SEM and scanning AES 79—19256
  - semiconductor-insulator interface, microcomputer-aided interface-state analysis 80—80383
  - sequence controller for Harwell 6000 series modular instrumentation 78—24784
  - serum samples, trace element anal., automatic data acquisition, on-line method 78—48726
  - shipboard meteorological data system 80—46299
  - Shuttle/Spacelab mission, instrumentation requirements and provisions 77—70972
  - Shuttle/Spacelab missions, low power CAMAC and NIM modular system for spaceflight use 77—70973
  - SIN 600 MeV cyclotron, therapy controllers for patient irradiation by pions 79—57754
  - single-chip microcomputer in instrument design and meas. techniques *(German)* 80—27276
  - single-crystal diffractometry, peak searching, crystal setting and determining automatic cell constants 80—6319
  - skeletal maturity determination system *(French)* 80—41209
  - skeletal radiographic imaging, computer/scanner approach 77—77989
  - sleep EEG activity and hormonal change correlation 77—9314
  - solar acousto-optical radio spectrograph, data correction and calibration 78—73631
  - solar data collection system using microprocessors 78—69542
  - Solar Maximum Mission satellite, hard X-ray imaging spectrometer control 79—80194
  - solar power measurement, microcomputer-controlled photodiode light meter and thermistors 80—50946
  - Solar Thermal Test Facility, 5 MW, heliostat focus and alignment system 78—50894
  - solid state nuclear track detectors, real time automatic evaluation with on-line television system 78—17496
  - SOLO, an interactive minicomputer based bedside monitor 80—26392
  - Soviet 6 metre reflecting telescope, position control via computer *(Norwegian)* 78—36456
  - Spar Buoy Oceanographic Telemetry System software engineering 80—46308
  - spectrophotometer for colour measurement, flexible instrument with microprocessor 78—54428
  - spectrophotometers, microprocessor based data acquisition and control system 80—22335
  - spectrophotometric colorimeters *(Hungarian)* 80—101851
  - spectrophotometry, computerised colour matching 80—17995
  - spectroradiometer for reflectance measurement 80—56658
  - spectrum microphotometer connection to PDP 11 digital processor for astronomical photographic plate meas. *(Italian)* 80—8550
  - speech analysis, computer-controlled method for articulatory activities meas. 77—56391
  - speech trainer for multihandicapped children, display method and control program *(Japanese)* 80—108922
  - spiral galaxies surface photometry, computerised data reduction system, (appl. to NGC 157) 79—40264
  - SPS beam instrumentation, closed orbit correction 77—83305
  - SQUID fluxgate magnetometers, magnetopneumographic meas. 80—104711
  - ST-segment response in exercise ECG, accurate automatic measurements 78—77140
  - static campimeter with CRT display 77—90941
  - steam turbine flow holographic interferogram processing by minicomputer 77—19656
  - steel, non metallic inclusion eval. using Quantinet systems 79—15923
  - steel, stainless, ferritic, 430, precipitate study using ion microprobe mass analyser 79—15678
  - steel, tubes, helical welded, computerised US quality control 78—35601
  - STEM, computer graphics analysis of images 80—73539
  - STEM, data recording and replay with aid of minicomputer 80—57440
  - STEM, image registration 80—104838
  - STEM coupling to small computer 79—54235
  - stimulator for ventricular myocardial function analysis 77—60267
  - stopped-flow apparatus, data acquisition and processing using minicomputer *(German)* 78—53190
  - stopped-flow system, computer controlled, for fundamental studies of reaction kinetics 79—15953
  - stopped-flow systems, automated, for fast react. rate anal. methods, review 78—95971
  - strain meas. speckle photography with hybrid optical/electronic image processing 80—106768
  - stress exercise facility automation using microcomputer system 79—70682
  - subnanosecond EM pulse data acquisition and processing system 78—32801
  - surface microgeometry meas. by stylus instrument 79—80575
  - surface roughness meas. using microcomputer 80—47014
  - synchrophasotron, Dubna, drift chamber system, characts., on line operation 77—6627
  - synchrotron radiation facility expts., distributed computing system for data acquisition and control 77—38513
  - systolic time interval meas. microprocessor system for heart malfunction detect 79—79681
  - tachycardia termination system, microcomputer-based 80—56280
  - tachystoscope, computer-controlled, for eye accommodation time and rest position meas. *(German)* 79—2143
  - tactile senses pattern discrimination power meas. 79—83971
  - telescope control, zenithal blind spot of altazimuth-mounted equipment 78—53823
  - TEM multistrip components using computer graphics 79—30630

computerised instrumentation continued
temperature and humidity monitor for biological exposure chambers, microprocessor-controlled 79—49239
temperature biotelemetry system for free-swimming fish 77—25624
temperature changes precise meas., microprocessor-controlled system 80—22361
temperature-jump apparatus, data acquisition and processing using minicomputer *(German)* 78—53190
terminal to audiovisual device interface 80—67986
test and meas. instrumentation microprocessor development 77—37864
test facility for far IR focal plane array testing 79—5755
theodolite microprocessor selection, development, and programming 78—24218
theodolites, electrooptical and microprocessor-based *(Czech)* 78—77860
Therac 6 linear accelerator, computer controlled evaluation for X-ray therapy 79—5363
thermal analysis system, Du Pont 1090, microcomputer-controlled 80—16613
thermal diffusivity meas. system using microprocessor *(French)* 80—14559
thermogravimetric data acquisition and reduction program 78—64901
thermoluminescent dosimetry system for automated radiological monitoring 80—27827
thermometer, resistance, TI calculator program *(Czech)* 80—13078
thermometers, high precision using MPUs 79—54130
thermometers development trends, thermocouple and resistance temperature detector 79—85135
thermophysical experiment, automatic information-processing system 78—196
thin dust layers, particle size effects automatic correction, computer appls. in spectrometry 79—83539
thin film fabrication and simultaneous computer-controlled measurement equipment, automatic 79—69984
thin-layer fluorescence chromatograms, automatic meas. and data processing 79—29424
three-coordinate workshop meas. machines 80—27280
three-dimensional cellular tree structure meas. semiautomatic system 79—70720
thunderstorm classification, automated data acquisition and analysis 78—7772
tide gauging network, automated, microcomputer interface and telemetry 79—5692
time digitiser for laser ranging, ps. resolution, built in CAMAC minicrate 78—36301
time keeping system of Van Swinden Lab. 80—98891
time-freq. secondary standards automatic recording/processing system 77—87738
time-of-flight analysis cross-correlation, for molecular beam scattering 79—55000
time-resolved X-ray diffraction data collection by position sensitive detector 77—51269
time-to-number convertor, wide-range high-resolution 78—9039
timer program controller, automatically controlled coulopotentiograph system 79—92026
titrator, microprocessor-controlled 79—74455
TLD processing using desk-top computer 77—81580
Tokamak data processing, no. of computers required 80—59252
tomographic radiography, Siretom 2000 head unit 78—28037
tomographic radiography, Somatom whole-body scanner with image reproduction 78—28036
tomographic scanner image quality evaluation phantom 77—73573
tomographic scanning, engineering status 77—73571
tomographic X-ray imaging *(Japanese)* 77—66845
tomography, axial, transmission and emission techniques, review 77—77973
tomography, computer assisted axial, equipment and technique *(Danish)* 77—52862
tomography, computerised, axial, for teaching 78—49619
tomography, cylindrical, appl. to intact circulatory system 77—77971
tomography, dynamic 3D imaging system for cardiac structures and functions 78—44600
tomography, electron density and at no. determ. 77—81553
tomography, operating principles, image construction, appls. 78—28047
tomography, principles and development 78—31945
tomography, two-component spectral analysis 77—25548
tomography, value in radiotherapeutic management of juxtasellar tumours 77—56450
tomography, whole body, automatic determ. of isodoses in human radiotherapy *(German)* 77—9236
tomography appl. 77—48859
tomography equipment for intracranial diagnosis, Japan 77—53877
tomography for detection of intra-orbital foreign bodies 78—3577
tomography scanner commissioning 77—73570
tomography with X-ray beams *(German)* 78—53480
tomography with X-ray transmission pencil beam scanner 77—44741
tomography X-ray photography appl. 78—44588
torque magnetometer, automatic rotating-head, microcomputer control 78—21183
torsional oscillation test instrument with process computer control *(German)* 77—21344
toxicity studies, TOXIPAC-300 data processing system *(Japanese)* 79—25172
transient data systems, state of the art and trends 79—89546
transient phenomena recording, microcomputer controlled, student experiment 79—84919
transient recorder for signal averaging 80—31723
transient-flow parameter meas. and computing set, features 77—72389
TRIUMF biomedical pion beam automated dose mapping system 78—73254
troposphere, meas. using microprocessor controlled lidar 79—58137
turbine blade surface temperature meas. IR pyrometer 77—17983
TV detector, for stellar radial vel. determ. 78—16305
TV-computer interface system for human body sway study 77—81526
two-phase flow meas., real-time, digital signal processor 77—80235
two-string balance microprocessor operation *(German)* 78—57936
ulna bending stiffness, microprocessor-automated noninvasive meas. 79—92275
ultrasonic open channel flowmeter with microprocessor 79—68877
UNISOR ISOL data aquisition system 77—14324
universal stereoplotter, US-1, photogrammetric appl., features 78—40713

computerised instrumentation continued
urethral pressure profiles, meas., microcomputer system *(Slovenian)* 79—2154
US diagnostic system, real-time, for dynamic and still images 79—92309
US dynamic imaging, high resolution 80—17042
US echocardiographic system, two-and three-dimensional, computerised, atrial septal defect detection appl. 78—20237
US flowmeter, interface development 78—38426
US histopathology, A-scan pattern recognition, use in signal processing 77—64108
US phased array diagnostic instrument with microcomputer *(Japanese)* 79—88146
US synthetic aperture imaging resolution 77—25530
US system for left ventricular function quantitative evaluation 80—85457
US time-of-flight tomography breast pathology appl. 78—24107
US tissue characterisation by angle scan and freq.-swept scatt. technique 80—45958
US velocity and absorption measurement, minicomputer program control *(Japanese)* 80—53587
UTR-2 radiotelescope northern sky survey, expt. techniques and data processing 78—57461
vapour pressure computer-automated meas. by simultaneous Knudsen torsion-effusion method 80—73334
variable iris photometer as automation example *(French)* 79—62748
vascular laboratory instrum. management using computer 78—7460
vector ECG meas., bandwidth limitation effects 78—36001
ventricle volume characts., nuclear medical determ., appl. of computer system *(German)* 78—88737
ventricular functionanalyser, microprocessor-based 80—26402
versatile oceanographic data-logger 80—46264
very low frequency counters, use digital time interval conversion with microprocessor control 77—74430
vestibular postural control evaluation in humans using computer-TV interface system 77—44773
vibration-acoustic diagnostics, random signal patterns recognition *(Slovak)* 79—18612
VICKSI beam line instrumentation and control system 77—83401
video interferogram analysis by TV camera-microprocessor system 80—73440
video stereophotogrammetry, interactive computerised, for Mars Viking 1975 Lander data 78—81557
video-tracking of micro-circulation, appl. of bit-slice processors *(German)* 78—88749
videodensitometric camera and video disc system 77—40761
vidicon, Si target, and minicomputer system, for laser intensity profiles meas. 79—27267
virology laboratory minicomputer appls. 77—44856
viscometer, absolute oscillating cylinder, with digital data acquisition system 79—82003
visual acuity meas. computer-aided system *(German)* 79—2144
visual evoked potential on-line evaluation by sliding average form. *(German)* 78—85402
visual evoked response meas. using computerised rapid random flash 79—83776
visual stimulator for electrophysiology expts. 78—69230
visual stimulator for eye movement and visual evoked pots. study, microcomputer-controlled 80—41350
visually evoked response test goggle system using liquid crystal shutters 79—79676
vocal synthesiser using programmable filter *(French)* 80—48524
voltammetry, cyclic differential pulse, computerised instrumentation 78—85235
voltammetry, linear sweep anodic stripping time, real time anal., recursive estimation 80—26067
voltmeter, digital, microprocessor controlled, calibration and averaging 79—40550
voltmeter, LF, fast response, for true RMS 2 mV-10 V range 79—21770
voltmeter, LF, fast response, microprocessor-based, for true RMS value 78—89503
water organic spill detector, development and appl. 77—41070
water quality monitoring, portable laboratory 80—61472
wave data analyser system for buoys 77—5362
weak X-ray scatt. interpretation by automated diffractometer 79—68977
whistler routine observation control with microprocessor *(Japanese)* 80—31144
wind pressure data acquisition system, microprocessor based 79—70888
wind profile determ. X-band solid-state radar system 78—12028
wind tunnel testing, conference, Rhode-St-Genese (1976) 77—27634
wind velocity meas. system 77—56742
wrist, human, kinematic and kinetic analysis by stereoscopic instrumentation 79—92274
writing aid for motor handicapped, microprocessor-based device, LOGOS 78—81077
X-ray crystallography using automatic flat-bed microdensitometer 77—35438
X-ray diagnostic table, computer controlled, multidirectional, CASSETTELESS spotfilm device *(Japanese)* 78—61278
X-ray diffraction, time-resolved, muscle contraction kinetics obs. *(Japanese)* 80—56291
X-ray diffraction and fluorescence anal. using RSX-11M operating system 80—322
X-ray diffraction expts., SPADE software package 79—63195
X-ray diffractometer, automatic triple-crystal, precision meas. of Bragg and Huang intensity distribs. 78—18491
X-ray diffractometer, HAG 4/A universal instrument, applic. versatility of basic software 80—52375
X-ray diffractometer, state-of-art 77—19833
X-ray diffractometer controlled by laboratory automation module 80—317
X-ray diffractometer data, automatic attachment for punching to tape 78—34385
X-ray diffractometer PW1100, computer controlled slit unit 80—37135
X-ray gauging system, semi-automatic 77—10156
X-ray powder diffraction, computer automation 80—1899
X-ray powder diffraction anal., Guinier camera, film densitometry and search match procedures 80—3454
X-ray powder diffraction film scanning system 80—22492
X-ray powder diffraction system, computer-controlled, with automatic sample changer 77—84577
X-ray powder diffractometer, APD3600, file searching techniques 80—24319

computerised instrumentation continued
X-ray spectrometer, basic oxygen furnace, process monitoring 79−17586
X-ray tomography, principles *(German)* 78−3601
X-ray tomography, selective I imaging using K-edge energies 78−24131
X-ray tomography by image reconstruction *(French)* 77−37037
X-ray transmission computerised tomography, review 77−48860
X-ray TV-computer unit for measuring defect parameters in weld seams 79−67451
xerographic copy line profile meas. using microcomputer/microdensitometer system 78−74088
ZGS, mini-computer based digital RF control system 77−83310
Al alloys, contamination, automated nondestructive inspection 80−16629
CO uptake in respiration, computer aided measuring system *(German)* 80−3875
Ge detectors array, collimated, computer-driven scanning bed, clinical appls., tomography 78−40309
H meters, on-line, calibration system 78−86236
$LiNbO_3$, IR parametric oscillator source for remote air pollution monitoring 77−21936
NaCl 46 cm window optical evaluation facility 80−74526
Pu, determ. by automated coulometric method, apparatus 79−16114
Rn-Th monitor for earthquake prediction research 78−73532
S meter, model XA-300, for laboratory use 80−26085
Si ribbon grown by capillary action shaping technique, electron channelling analysis 77−76418
WC-Co, on-line computer anal. of SEM obs. 79−87807

computerised manufacturing control *see manufacturing computer control*

computerised materials handling
see also stock control data processing
automated sintering and hot pressing system 79−33961
CANDU fuel pellet stacking, mathematical model of automatic assembler 80−37464
dynamic materials accounting for LWR fuel cycle 79−36325
dynamic safeguards accounting and material control via modern estimation methods 77−34417
fissile material inventory and criticality control system, on-line, INMACS 79−89486
fluidised bed combustor, control and instrumentation 80−30350
Mars Viking surface sampler subsystem, acquisition assembly 79−12380
nuclear fuel, simulator program MHSS 77−38337
nuclear fuel accountability and control, use of novel data collection and processing techniques 79−85749
nuclear fuel fabrication control system for remote operation 80−18571
nuclear materials control system, generalised concept 79−89449
nuclear reactor fuel reprocessing, in-process inventory dynamic measurement 77−38371

computerised monitoring
60 Hz half-cycle sinusoid defibrillating waveforms for low-energy application 78−3664
aerosol electrical analyser, microcomputer-modified, for particle size anal. 80−40756
AGS, microprocessor based beam loss monitor system 79−72070
air monitoring, minicomputer data processing system 77−64439
air pollutant analysis and control instrumentation and organisation *(French)* 78−20549
air pollution, CO_2 laser long-path absorption system, automation 78−92971
air pollution, CO_2-laser long-path absorption system, error anal. 79−25340
air pollution, French local networks, examples and software *(French)* 77−37459
air pollution, on-site automatic analysers review *(French)* 78−81451
air pollution detection and control, current status in India 77−41144
air pollution detector sampling by minicomputer and multicomponent chemical unit *(French)* 77−37452
air pollution monitoring by pulsed dye laser 79−48204
air pollution monitoring system, program system *(Japanese)* 78−81414
ambulatory arrhythmia monitoring, automated family classification 79−66566
ambulatory ECG monitoring problems 78−11763
ambulatory EKG recording using several computers in parallel 79−62389
ambulatory rhythm 78−85431
antischistosomal drug screening in vitro by multichannel US activity monitor 79−20604
application of microprocessors to continuous heart rate monitoring of high risk infants 79−62401
Arabian Gulf, comprehensive oceanographic monitoring programme 79−8728
Argus ECG monitoring system reappraisal 78−7479
arrhythmia ambulatory anal. in real-time with minicomputer 80−85523
arrhythmia detection, edit and recall system, microprocessor-based 80−89891
arrhythmia detection program comparison data bank 78−15921
arrhythmia detection using a low-power, CMOS processor 78−73276
arrhythmia detection with a multi-microprocessor system for distributed and parallel processing 80−85524
arrhythmia identification and verification by 3-channel eval. of long-term ECG records 80−85518
arrhythmia monitoring, ARGUS/RT microcomputer system 78−81014
arrhythmia monitoring, multimorphology computerised system 79−70676
arrhythmia monitoring, single scan algorithm for QRS-detect. and feature extraction 80−85520
arrhythmia monitoring systems evaluation criteria 78−11765
arrhythmia monitoring using interactive computer system, clinical evaluation 78−81028
arrhythmia quantification, template matching algorithm evaluation 80−85519
artificial heart, non-invasive determ. of instantaneous cardiac output and dynamic performance 77−44845
attenuator monitoring, computational tables and computers for efficiency improvement 77−79073
automated multichannel data and meas. system type MIIS-1, for transducer data 79−2754
automated vapour deposition apparatus based on programmable calculator 78−44022
automatic monitor of effluents from nuclear facilities 77−61615
automatic weather stations, network in Switzerland, appl. *(German)* 80−17356

computerised monitoring continued
benzolene gas and oil desulphuration by automatic gas-chromatographs *(German)* 77−4965
biomembranes, excited, automatic meas. of ionic current electrophysiological characts. *(Russian)* 80−76865
blood pressure ambulatory recordings, minicomputer processing 80−89887
blood pressure automatic monitoring, long-term, minicomputer system 80−101276
blood pressure continuous recording in ambulant hypertensives, computer anal. 79−62390
BWR plant diagnosis system, on line process computer appl. 78−46146
calorimetric dosimeters, automation of calorimetric measurements evaluation 79−67965
CAMAC diagnostic module for on-line monitoring of CAMAC integrity 80−5459
CANDU distributed computer control systems 79−76105
cardiac arrhythmia monitoring, Aztec replacement by correl. for VPB detect. 79−62388
cardiac arrhythmias management, automated feedback control of drug therapy 80−41307
cardiac left ventricle function, nucl. medicine equilib. meas. 79−62357
cardiac output, by transthoracic admittance plethysmography *(Japanese)* 77−86693
cardiac output and shunt calc. from dye dilution curves using automated catheterisation system 78−81023
cardiac output automatic determ. by indicator dilution in computerised monitoring system 78−81022
cardiac output on-line determ. by thermodilution in coronary care unit 78−81021
cardiac probe, microprocessor-based, for gated equilib. and beat-by-beat left ventricle function 79−62396
cardiac surgical patient postoperative management, computerised intensive care 77−40918
Cardiac Surveillance Unit experience with Argus ECG monitoring system 78−11762
cardiocirculatory computer-aided monitoring after open-heart surgery, appl. to adrenaline effects meas. 78−81059
cardiopulmonary function automated testing system 79−70673
cardiopulmonary monitoring in respiratory intensive care unit 78−20306
cardiopulmonary monitoring of high-risk infants using microprocessor-controlled memory 78−31962
cardiovascular computerised monitoring in medical intensive care unit 78−20304
cardiovascular monitoring in the coronary care unit 78−20308
chemical analysis, automated multisample-stream monitoring system 77−44531
chemical variables, on-stream analysers development, w.r.t. speed and reliability 77−66778
Cherenkov light photograms, automatic scanning by TV digitiser 80−52822
clinical vectorcardiographic microprocessor system *(Bulgarian)* 80−61722
computer-processed ECG trends, conference, Amsterdam (1976) 78−7477
computerised reactor safety systems, design, specification and implementation 79−63783
coronary care unit interactive ECG monitoring 78−7481
critically ill patient monitoring by integrated computer systems 78−35998
crude oil classification via computerised gas chromatograph mass spectrometry 77−81456
deep tissue temp. monitoring by ultraminiature thermistors 80−3761
digital radiation monitoring system, signal processing by distributed microcomputer data modules 79−59279
directional interplanetary charged particle flux meas. in space, digital onboard processor 77−64610
ECG, 24 hr, automatic analysis on minicomputer-based system 80−89889
ECG, ambulatory, computer processing system 80−89897
ECG, Argus algorithm development 79−70680
ECG, automated Holter anal., shape oriented system 79−70662
ECG, Frank xyz signal interpretation by unmodified 12-lead computer system 80−94400
ECG, Holter recording anal. using Argus/2H 79−70679
ECG, Holter recordings, low cost arrhythmia analyser, GRETA 80−94403
ECG, Holter tape high speed digital anal. with full editing capability 80−89896
ECG, interactive analysis techniques with Random Access Mass Storage ECG Analysis System 78−81034
ECG, long-term, flexible data presentation in DCG processing 79−70681
ECG, monitoring abnormal QRS events, sequential improvements in on-line algorithm 78−81026
ECG, multiform ventricular complex identification, 2-dimens. clustering technique 79−66570
ECG, QRS detector/delineator devel. and eval. 80−89892
ECG, random access mass storage anal., RAMSES, for quantitative anal. of long-term ECGs 79−70663
ECG 24 hr recording, anal. using operator-controlled computer system 80−89888
ECG ambulatory monitoring, adaptive algorithm for noise rejection 79−66571
ECG ambulatory monitoring, detect. algorithm for multiform premature ventricular contractions 79−66572
ECG arrhythmia analysis, dual-processor computer 79−66569
ECG arrhythmia classification in context, extension of single-beat algorithm 78−85426
ECG automated monitoring, new electrode system 80−89898
ECG frequency-domain analysis 80−85521
ECG monitoring, automated cardiac dysrhythmia anal. 80−17164
ECG monitoring, state of art 78−11766
ECG monitoring in ambulatory patients 78−20309
ECG monitoring system features *(Swedish)* 79−44005
ECG signal parameter trend anal. 78−15920
ECG ventricualr arrhythmia monitor, performance standards and trends 78−7478
EEG, automated monitoring of long-term implanted electrodes *(Russian)* 80−76857
EEG, automatic recognition of inter-ictal epileptic activity in prolonged recordings 80−3838

computerised monitoring continued
EEG, cable telemetry, siezure monitoring 77—5090
EEG, computerised statistical monitoring 77—40917
EEG, peak-detection algorithm for anal. 79—74772
EEG automatic pattern recognition, patients under general anaesthesia during operations 80—17154
EEG brain function monitoring, microcomputer based system 77—73611
EEG cable telemetry seizure-monitoring system 78—3640
EEG monitor using Walsh transform on standard microprocessor 80—26399
EEG waveform detection by microprocessor 77—73610
effluent sampling programme data statistical evaluation 79—13547
electronic system of power-station control with modules and distributed software based on controbloc elements *(French)* 79—76110
ethylene, air pollution monitoring, computer controlled CO_2 laser absorpt. system 80—89699
exercise ECG anal. using microcomputer 79—70683
expendable bathythermograph digital recording and display system 80—46318
exposure to vinyl chloride monomer, gas chromatograph system 79—21727
fast solid-state camera for high-speed event diagnostics 80—78985
fission reactor cores, improved instrumentation and computer control systems 78—29601
foetal heart rate on-line data management during labour, prediction of one-minute Apgar scores 78—44655
foetal heart rate variability monitoring by digital filtering 79—48353
Holter ECG high-speed anal. 79—66568
Holter tape processing, 60× computer system 79—66567
HP 5600A patient monitoring system 79—25152
HTGR fuel rod length meas. and control microcomputer system 79—71942
HV pulse controller and temp. monitor microcomputer-based, Kerr effect study appl. 79—6103
hybrid focal plane detectors for heavy ions 79—68163
hysteresigraph with data printout 79—58760
in plane strain displacement near crack tip at high temp., optical meas. 79—32412
in situ coal gasification using EM remote sensing, reconstruction algorithms for geophysical applications in noisy environments 80—77168
industrial health service automated ECG analysis results 79—39563
intensive care in paediatrics *(German)* 78—88754
intensive care instrumentation, book 77—17006
intensive care unit, use and acceptance of automated monitoring systems 78—81057
intensive monitoring computer system, SOLO, one-patient multiparameter bedside monitor 78—81053
interactive lake survey programme for water resource surveillance 78—81257
intra-auricular P wave monitor, experience, performance evaluation 78—11764
intravenous antiarrhythmic drug infusion, automated delivery 78—81058
ischaemic episode, computerised continuous beat by beat anal. and rational plots 79—62394
labour ward information and monitoring system *(German)* 78—88750
laser absorption system, computer-controlled, for air pollution monitoring 78—49182
late pregnancy toxaemia, ongoing medical surveillance system 77—81602
LMFBR data multiplexing system 79—76102
LMFBR-subassembly outlet computerised temp. monitoring based on estimation theory 78—8948
medical systems, automatic diagnosis systems 77—40841
micro-computer based system for the management of the critically ill 79—25153
microcomputer system for on-line analysis of electroencephalographic data 78—73277
microcomputer-based data acquisition and analysis system for CO_2 rebreathing studies 80—36161
microcomputer-based pulmonary wedge pressure measurements 80—26391
microcomputers for bedside monitoring of patients *(German)* 78—88751
microcomputers in biomedical and clinical applications 78—73283
motion online detection in digital video images, mice identification in labyrinth expts. *(German)* 78—92754
movement-activated recording monitor for motor activity 77—25565
multicomponent, multipoint infrared ambient air monitor, microcomputer-controlled 80—40945
multiple microprocessors for continuous patient monitoring 80—26389
myocardial ischaemia and necrosis monitoring in acute myocardial infarction 80—85525
NDT, conveyor belts with steel reinforcing cables, computer-aided magnetic defectoscopy 77—73417
neonatal intensive care unit, surveillance aid *(French)* 77—44831
neonate cardiorespiratory monitoring, automatic system with microprocessor 80—94399
neurological intensive care facility requirements 79—92420
neurology monitoring system for stroke patients 80—26394
neurosurgical intensive care, non-invasive monitoring techniques 80—81757
neurosurgical patient monitoring computer system 79—88206
neutrino channel monitoring system, acquisition of digital information 77—3199
neutron irradiation system, computer controlled 80—19851
nuclear, materials, containment and surveillance techniques for the IAEA 79—85645
nuclear instrumentation computer-controlled pulser system 80—52841
nuclear material, VACOSS electronic sealing system appl. 79—85687
nuclear materials safeguards, nondestructive, energy-dispersive, X-ray fluorescence analysis of product-stream concentrations from reprocessed nuclear fuels 80—83163
nuclear medicine appl. 78—7466
nuclear power plant loose parts monitoring techniques and experience 79—3211
nuclear power plant machinery surveillance and diagnostics automation 79—641
nuclear power plant operational diagnostics and control computerisation 79—3233
nuclear power plants, diagnostic system using noise anal. 78—50279
nuclear power station, use of fast analogue scanner 77—6656
nuclear power station advanced control concept, computer-based system design 77—67909

computerised monitoring continued
nuclear power station radiation monitoring, decentralised system using microprocessors *(Spanish)* 80—47727
nuclear radiation at power plants 78—816
nuclear reactor, power measurement by continuous calorimetry, automated system 78—17336
nuclear reactor core protection and surveillance system 79—9811
nuclear reactor microcomputer-based parameter monitoring system *(Hungarian)* 80—18451
nuclear reactor pump coolant tests 78—70585
nuclear reactors, computer modules appl. *(German)* 79—49788
nuclear reactors, online, computer applications, information processing, control, monitoring, data acquisition and evaluation 80—47595
obstetric computer-aided monitoring system *(German)* 80—41300
obstetrics monitoring, microprocessor data acquisition and preprocessing with minicomputer signal processing 77—44775
oil spills remote monitoring, computer controlled laser radar system *(Japanese)* 78—92994
on-line alarm analysis in the hierarchical control system of the WWR-SM research reactor 79—76104
online Reactor Noise, Vibration and Loose Parts Monitor 79—3212
optical film, monitoring of props. during deposition, wide band monitoring system 79—81582
optical multilayer coating production with continuous thickness reoptimisation 79—76890
oxyhaemoglobin dissociation curve direct obs. in man in vivo, computer investigation 78—85433
pacemaker centre and follow-up network 77—81691
pacemaker tracking system based on microprocessor, hardware considerations 78—36070
partial discharges, on-line computerised system for meas. in insulation structures 77—5863
particle beam profile monitor providing multiple profile during beam spill, Fermilab 77—57784
particle size distrib., on-line measurement techniques, instruments *(German)* 78—60895
patient critical care fluid balance monitoring 79—25151
patient fluid management records system 79—25150
patient intensive care appl., signal interference problems *(German)* 78—3628
patient monitoring, multi-microprocessor system *(German)* 78—88752
patient monitoring and pulmonary function testing using self-diagnosing microcomputer-based cart 78—31943
patient monitoring in operating room, inexpensive general purpose computer 78—36045
personnel dosimetry and access monitoring by process computers in nucl. power station *(German, English)* 78—17440
personnel dosimetry monitoring, use of evaluation device for rod and process computer at power station *(German, English)* 78—17441
physiologic profiling, automated, in acute ill patients 80—30914
pollution, air, in Mexico City, minicomputer based system 77—66984
pollution monitoring chart data processing equipment [pollution monitoring] *(Japanese)* 79—100555
Portable Automated Mesonet, design, performance and operation, for meteorology 77—78426
postoperative cardiac surgical patient care, automation of meas. and interventions 78—20310
power plant machinery monitoring and online diagnostic systems 79—9810
proton storage ring, NAP-M, supervising system using ODRA-1325 digital computer 77—65365
pulmonary artery blood press. anal. algorithm 78—40376
PWR, computerised axial power distrib. monitoring system 77—65279
radiation monitoring, computer software for digital count rate estimation 80—18689
radiation monitoring, digital data collection and display 79—59278
radiation monitoring, distributed processor-based system for large scale power plant monitoring 79—59280
radiation monitoring, microprocessor based systems 77—67897
radiation monitoring of nuclear power stations, on-line computer appl. 80—5391
radiation safety monitoring instrumentation complex at the USSR nuclear power plants *(Russian)* 79—76108
radioactive effluent monitoring, symposium, Portoroz (1977) 78—89985
radiotherapy accuracy, errors in patient set-up 78—11726
rapid eye movement automatic detect. system and normative data 79—74771
reactor logic protection system using a redundant computer struct., self-checking procedures *(French)* 79—76103
Reactor Noise, Vibration and Loose Parts Monitor 79—3212
reactor protection systems, treatment, analysis and presentation of information on component faults and [nuclear power] plant disturbances 79—76098
reactor trip system, design of internal architecture for Westinghouse microprocessor-based [nuclear reactor] integrated protection system 79—76100
remote diagnostic techniques used in Viking lander operations 78—57426
remote multiplexing control and safety systems evaluation 79—76109
respiratory data management subsystem 79—83980
respiratory monitor and histogram computer for rodent studies 77—52944
RF environmental field intensity automated meas. system 77—37947
rheocardiography, 4-electrode, in computer-aided cardiac output determ. 80—61718
rod dosimeters, automatic evaluation of staff dosimeters during reactor shut down *(German)* 79—67960
second-generation ECG monitoring system development 78—7480
seismic recording network at Campotosto reservoir *(Italian)* 80—101446
sick sinus syndrome 24-hour Holter ECG monitoring 79—39562
sinus node autonomic control in man, quantitative assessment 79—70684
sleep research, microprocessor appl. 79—96693
solar cells, output monitoring, design and utilization of a microprocessor-controlled absolute spectral response system 80—81476
solar-terrestrial environment monitoring and forecasting system, SELDADS, for radiocommunication appls. 79—58097
SOLO, an interactive minicomputer based bedside monitor 80—26392
SOLO monitor, microcomputer bedside monitor 80—94404
spectrometer, semiconductor mosaic type, amplification-conversion tract meas./monitoring automation 78—78547
spike-wave EEG patterns, quantification method clinical evaluation 78—11754

computerised monitoring continued
- steel weld fatigue life estimation, multichannel NDT monitor 78—56846
- stellar objects, using TV-type photon counter *(Russian)* 80—31212
- stroke patient monitoring system, regional cerebral blood flow meas. 79—79626
- Super-Phenix FBR, data processing and collection *(French)* 79—76107
- Super-Phenix FBR control system evaluation *(French)* 79—76106
- supraventricular arrhythmia rapid anal. from long-term oesophageal recordings, drug assessment 80—89904
- surgery, microprocessor-based patient monitoring system 78—44681
- systolic time interval processing system, STIPS 78—81029
- telemetric human movement correction using computer and electrostimulating device 77—86656
- temperature of radiotelescope structure, error correction computation *(German)* 79—84669
- thin films, vac. deposited, mass change, optical transmittance, and reflectance, simultaneous meas. apparatus 79—75501
- three dimensional human motion employing optoelectronic means 77—48886
- Tokamak Fusion Test Reactor, conceptual digital computer control systems 77—23281
- total cardiac monitoring integrated microcomputer/minicomputer system 78—35997
- toxic gas monitor based on laser photoacoustic spectrometer *(German)* 80—12046
- transcutaneous pO_2 measurement in computer-assisted monitoring of infants 78—85432
- transthoracic impedance curve processing, patient-computer interface 79—34686
- underground explosions, using Gauribidanur seismic array 79—39913
- Unibed patient monitoring system based on microcomputer and LSI technology 78—20305
- USA Energy R&D Administration effluent date collection and reporting system 79—13545
- uterine contraction waveform online processing system 78—15916
- vascular interface system for automation of haemodynamic monitoring and therapy 78—81054
- ventricular arrhythmia model 80—89893
- ventricular arrhythmia on-line study 78—81060
- ventricular arrhythmia quantification, minicomputer system 79—70677
- ventricular ectopic activity, semiautomated data reduction 79—66573
- ventricular fibrillation detect. by computer 79—70675
- ventricular fibrillation recognition using ECG power spectrum 78—81032
- vertebrate cornea, transparent layered structure thickness monitor 78—92737
- vibration, rotating laser light beam appl. *(Russian)* 78—71299
- vinyl chloride, air pollution monitoring, computer controlled CO_2 laser absorpt. system 80—89699
- visual system neuron response to light stimulus determ. 77—86725
- water monitoring system, Finland 80—67026
- water quality monitoring system CAD 77—41100
- weld flaws, by acoustic emission monitoring 80—11866
- West German LWR primary system online surveillance 79—3217
- world's natural resources, by satellite, Conf. on Earth resources electronics Rome, Italy (Mar.77) *(Italian)* 77—82056
- ZGS, computerised meas. of injection betatron tunes 77—83312
- ZGS, low level beam diagnostics for polarised proton operation 77—83311
- Ge on-line, hyperpure detector, radiation monitoring system 78—37493
- H maser, field-operable design improvements 79—55099
- O_2-CO_2 transport real-time and interactive control in mechanically ventilated patients in ICU 79—62404
- Pu laboratory stack monitoring, computerised system 79—3256
- Zn, corrosion rate monitoring, automatic, in near-neutral soln., using a microcomputer 80—50749

computerised navigation
- artificial satellites autonomous navigation problems, shoreline information 78—53732
- Geological Undersea Surveyor, Acoustically-Navigated, for Mid-Atlantic Ridge appl. 80—4120
- laboratory vehicle for air-pollution measurements with computer-controlled data acquisition and navigation system *(German)* 79—39327
- Navy navigation satellite system TRANSIT, on-board computer 79—29978
- oceanographic robot submarine with computer control 77—5375
- spacecraft final descent vel. control autonomous algorithm 77—29620
- submersibles, acoustic navigation for precise underwater surveys 79—5683

computerised numerical control
- diamond turning, Honeywell Corporation facilities 80—5852
- reactor protection system, development of integrated numerical protection system *(French)* 79—76097

computerised pattern recognition
- acoustic emission signal sorting 77—40516
- acoustics, speech and signal processing, IEEE international conf., Washington, DC, USA, 1979 Apr. 79—55275
- adenocarcinoma cell clump feature extraction methods in automated uterine cancer cytology *(Japanese)* 80—72362
- aerial photographic analysis and stereographic mapping with electro-optical pattern recognition 77—19186
- aerial photography rapid screening by optical power spectrum analysis 78—63033
- aerosol observation using laser radar *(Japanese)* 80—51028
- air pollution data analysis using combined interactive graphic presentation and clustering technique 79—83656
- algae recognition by coherent spatial filtering with simulated input 79—79696
- ambulatory arrhythmia monitoring, automated family classification 79—66566
- ambulatory EKG recording using several computers in parallel 79—62389
- arrhythmia ambulatory anal. in real-time with minicomputer 80—85523
- arrhythmia detection, edit and recall system, microprocessor-based 80—89891
- arrhythmia detection with a multi-microprocessor system for distributed and parallel processing 80—85524
- arrhythmia detector evaluation, ECG database development 78—81018
- arrhythmia identification and verification by 3-channel eval. of long-term ECG records 80—85518
- arrhythmia monitoring, multimorphology computerised system 79—70676

computerised pattern recognition continued
- arrhythmia monitoring, single scan algorithm for QRS-detect. and feature extraction 80—85520
- arrhythmia monitoring using interactive computer system, clinical evaluation 78—81028
- arrhythmia quantification, template matching algorithm evaluation 80—85519
- arrhythmia sorting, oesophageal electrode for atrial electrogram 79—39574
- artifical vision machine for blind people *(Korean)* 79—66583
- astronomical digitized images, use of interactive structural instruments *(Italian)* 80—98554
- automated pattern recognition with hybrid optical/digital systems 78—63037
- automatic pattern processor for simple and complex interference patterns 80—13129
- automatic speech recognition, speaker authentication and data entry 79—94419
- automatic speech recognition by zero-crossing analysis methods 79—94420
- biological specimen pattern recognition via matched spatial filtering 78—69261
- biomedical image acquisition and processing system design and implementation 77—37086
- blood cell differential counter, ADC 500, pattern recognition based image processing system 78—73282
- body surface mapping of cardiac field 79—39553
- brain scanning utility, patterns of diagnostic clues 77—77988
- breast thermography vein-finding algorithm 78—40393
- bubble chamber film, track rescue system 78—70728
- bubble chamber tracks, signal processing procedure for interimage identification 78—70727
- cardiac arrhythmia monitoring, Aztec replacement by correl. for VPB detect. 79—62388
- cardiac arrhythmias diagnosis, online real-time pattern recognition *(Italian)* 78—85439
- cardiac dynamic imagery, gross and segmental motion anal. 79—70632
- cardiac image description and analysis, interactive knowledge-based systems approach 78—81031
- cell analysis in haematology, LARC system overview 78—31931
- cell recognition and counting using adaptive coherent optical processor 78—77120
- cell type recognition by multiangle laser beam scattering flow system 77—21595
- cervical smear screening with coherent optical processing 77—21653
- chemical dynamics applics. 77—32768
- chest photofluorograms, recognition of vessel shadows *(Japanese)* 79—57761
- chest photofluorograms, recognition of vessel shadows for automated meas. and classification 77—81566
- chest photofluorograms automated interpretation using AISCR-V3 software system 79—88183
- chest radiograph nodule detection system 80—8140
- chest radiographs, algorithms for finding rib cage 77—44804
- chest radiographs, processing of large numbers, problems 80—8138
- chest X-ray automated anal. 80—98098
- chest X-ray lung region subimage automated extraction for pneumoconiosis opacities detection 79—88182
- chest X-ray rib extraction algorithm for pneumoconiosis detect. 78—31904
- chest X-rays automated screening, image segmentation and cardiac silhouette anal. 79—88178
- chromatograms, two-dimensional, quantitative evaluation 79—84064
- chromosome analysis, automatic, specialised image treatment equipment *(French)* 77—37111
- chromosome analysis by automatic image recognition *(French)* 77—37110
- chromosome spread automated detect. and classification 77—60328
- chromosomes, irradiated, identification by pattern classification system 77—37114
- cloud motions, automatic tracking system using weather satellite picture sequences 78—45022
- composite bioelectric potential analysis, online hybrid system 77—9313
- computer-aided seismic analysis and discrimination 78—20530
- computerised tomographic scan data format 78—73243
- conditioning EEG activity, computerised laboratory 80—30912
- continuous ECG processing program 78—92725
- coronary artery bypass graft patient recovery trajectory classification algorithm 80—94411
- cross correl, quantum noise limited electron micrographs 77—67546
- crude oil classification via computerised gas chromatograph mass spectrometry 77—81456
- crystalline compounds, computer identification techniques using X-ray powder diffr. file 77—70389
- crystallography appl. *(Japanese)* 77—55208
- data base, classification, comparison of pattern recognition methods 80—199
- data extraction and classification from film, conf., San Diego, USA (Aug. 1977) 78—63023
- diagnostic cytogenetics, automatic system 77—78021
- digital image registration with automatic microscope, appl. to cell analysis 77—29239
- Earth resources satellite picture web grammar model applic. 77—37466
- ECG, ambulatory arrhythmia quantification by correl. technique 78—81020
- ECG, Argus algorithm development 79—70680
- ECG, computerised Holter tape processing systems for drug testing, validation technique 78—81017
- ECG, Holter recording anal. using Argus/2H 79—70679
- ECG, Holter recording processing, computer system 78—81015
- ECG, Holter recordings, low cost arrhythmia analyser, GRETA 80—94403
- ECG, Holter tape dual-channel anal. system, ARGUS/2H 78—81016
- ECG, long-term, efficient data compression and arrhythmia detect. 79—70678
- ECG, monitoring abnormal QRS events, sequential improvements in on-line algorithm 78—81026
- ECG, multiform ventricular complex identification, 2-dimens. clustering technique 79—66570
- ECG, QRS detector/delineator devel. and eval. 80—89892

computerised pattern recognition continued
ECG, real-time microcomputer system for intra-aortic balloon pump control 78—36067
ECG 24 hr recording, anal. using operator-controlled computer system 80—89888
ECG ambulatory monitoring, detect. algorithm for multiform premature ventricular contractions 79—66572
ECG and VCG, wave recognition algorithms for automatic QRS meas. *(German)* 78—69225
ECG arrhythmia analysis, dual-processor computer 79—66569
ECG arrhythmia classification in context, extension of single-beat algorithm 78—85426
ECG arrhythmias high speed pattern recognition 78—36004
ECG classification by linear multiple regression analysis 77—13027
ECG diagnosis improvement by nonlinear feature extraction methods 80—85530
ECG diagnostic information from HF notches 79—39570
ECG diagnostic interactive minicomputer system 78—36022
ECG frequency-domain analysis 80—85521
ECG Holter analysis, appls. of Dyna-Gram IIIB system 78—81019
ECG pattern classification from complete computer descriptions 80—56265
ECG rhythm analysis, syntactic approach 80—89900
ECG wave, automatic recognition method *(Japanese)* 79—57794
ECG/VCG, rhythm diagnosis using statistical signal anal., identification of transient rhythms 78—77142
ECG/VCG rhythm diagnosis using statistical signal anal., identification of persistent rhythms 78—77141
echocardiogram analysis in a pattern recognition framework 79—83864
echocardiography, US, picture processing of 2-dimens. data 77—77958
EEG, automatic recognition of inter-ictal epileptic activity in prolonged recordings 80—3838
EEG, interictal epileptic activity, comparison of traditional reading and automatic recognition 78—48913
EEG, multivariate pattern recognition technique, cerebral abnormality localisation 79—16327
EEG, peak-detection algorithm for anal. 79—74772
EEG automatic pattern recognition, patients under general anaesthesia during operations 80—17154
EEG automatic segmentation based on autocorrelation function 79—96673
EEG classification, parametric pattern recognition model 79—79665
EEG epileptic transient detect. 78—53542
EEG pattern classification using logic windows in time domain *(Japanese)* 77—70563
EEG sleep pattern feature extraction and recognition by real-time anal. *(Japanese)* 78—73271
EEG spike detection and quantification, microprocessor-based system 80—36173
EEG standardised classification, sequential epoch method 78—57101
electro-oculographic activity, computerised meas. during sleep 79—74781
electrocardiograms, using finite Haar transforms 78—3654
electrocorticography, clinically effective spike recognition program 79—44000
electromyography, clinical, computer anal. 78—80985
electrophoresis and ultracentrifugation pattern analysis, FORTRAN program DIANA 2 77—40549
electrophoretic waveform analysis for blood serum protein composition determ. 78—64928
epileptic spike pattern determ. by point spectrum 77—9294
epithelial tissue pattern recognition 79—25145
exercise ECG analysis, noise-impervious pattern recognition approach 78—7515
exercise ECG processing reproducibility rel. to waveform recognition and lead system 78—7513
fish stock discrimination, X-ray fluoresc. tissue anal., pattern recognition technique 77—60330
functional imaging, appls. in three radiological modalities 80—8139
gait analysis in humans using pattern recognition 78—40374
gastric Ba-filled X-ray films, computer screening *(Japanese)* 78—73211
GEOS-1, magnetosphere plasma resons. on-line tracking for electron density small-scale struct. 79—35073
gradient pattern coding—an application to the measurement of pneumoconiosis in chest X-rays 79—34632
gross and segmental motion analysis in dynamic cardiac imagery 79—25093
Hewlett-Packard ECG analysis program 78—7490
HG ECG, computer methods for anal. 80—72352
His bundle ECG pattern recognition program for drug evaluation 78—35999
histology appl. of interactive pattern recognition system PEEP/DECIDE/GRAPH 78—73291
Holter ECG high-speed anal. 79—66568
Holter tape processing, 60× computer system 79—66567
human body tomography appl. *(Japanese)* 78—3603
hybrid method, suboptimal statistical transform *(French)* 77—46703
hybrid optical-digital image processing, appl. to handwriting and aerial photos 77—68178
hybrid optical-digital radiography system for lung disease detection 78—11753
image anal. in cytology/cytogenetics, using Golay transform processor 78—61152
image analyser and algorithm for pattern discrimination 79—18362
image analyser control, diode matrix replacement by PROMs 77—22539
image analysing computer, Quantimet, device for automatic scanning of irregular areas 77—5906
image analysis of individual features, adapted image process 77—61052
image dissector tube with minicomputer control suitable for IC mask inspection 79—55065
interictal epileptic EEG transient morphological discrimination algorithm 79—100758
IR pattern recognition for breast cancer screening 77—21652
IR spectra, binary coded, feature selection for automated interpretation 80—3428
IR spectra, feature selection, using numerical taxonomy and information theory 79—50012
Japanese reactor noise pattern library 79—3338
labial muscle EMG analysis and feature extraction by Hanning Cosine Modulated wave function 77—81605
LANDSAT images segmentation, spectral, spatial and semantic constraints exploitation 79—25336

computerised pattern recognition continued
line detection algorithm, for Landsat data 80—77150
liver scintigraphy, pattern recognition 80—8157
lung tissue micrograph computer processing approach 80—8123
lung tissue stereological parameter computer anal. 78—73280
lung ventilation and perfusion scintigrams, computer aided diagnosis 79—88181
lymphoblast automated morphological anal., subclassification of acute leukaemia 77—81620
mass spectral analysis by simplex pattern recognition 77—21429
matched spatial filter optimisation for diatom recognition 80—48180
medical diagnosis and treatments evaluation via expected outcome loss 77—25587
medical image structural analysis, fast feature extraction *(German)* 79—5393
medical images, computer-aided diagnosis, conf., Coronado, USA, (Nov. 1976) 77—78018
medical imaging techniques implemented on pipeline minis and array processor, nerve fibre counting appl. 80—98165
medical scintigraphic images and lesion detectability 79—62354
MICRO-VIDEOMAT, use in light microscopic liver diagnosis 77—78013
microcomputer-aided arm prosthesis using myoelectric pattern recognition 78—53576
microscopic cell image scene segmentation technique 77—78073
Minnesota code ECG classification program 78—7506
molecular dynamics, dilute gas simulation, pattern recognition algorithm for mol. formation 77—75249
morphometric cytology pictorial pattern recognition 80—81796
morphometric cytology pictorial pattern recognition appl. 79—25179
multiform PVC detect. using time-domain and freq.-domain anal. 79—70674
multivariate and conventional ECG analysis programs compared 78—7492
myocardial ischaemia and necrosis monitoring in acute myocardial infarction 80—85525
nerve cell unitary discharge automatic recognition *(French)* 77—37072
nerve fibre counting by pipeline multiminicomputer image processing 80—109013
neural spike recognition and on-line classification by unsupervised learning system 79—57789
nuclear reactor abnormal behaviour monitoring system 78—698
nuclear reactor core instrumentation, approach based on IR television, on-line computing, pattern recognition 77—54310
optical computer pattern processing and texture analysis 77—10855
optical power spectrum sampling and nonparametric pattern recognition algorithms 78—63032
optical processor, real-time, for pattern recognition of biological specimens 78—40454
optical-digital system for pattern recognition of coal-workers' pneumoconiosis 78—40389
optical/digital pattern recognition automated system 80—48175
organic compounds, classification from voltammetric data, computerised pattern recognition 79—16057
P-wave, a new method of detect. in electrocardiograms 79—48360
pancreatic cell moving granules anal. by digital moving image processing 79—84063
piecewise-linear approximated ECG waveform recognition 78—57119
Pipberger program QRS onset and offset determ. algorithm parametrisation 79—39559
pneumoconiosis, small lesions, computer aided identification 80—30887
polar reference texture in radiocolloid liver images 78—73241
poly(alkyl methacrylate) films, chemical characterisation from C Auger spectra, appl. of pattern recognition and factor anal. 79—79347
polyatomic molecules, structure recognition, from IR, UV, NMR and mass spectra, computer method 78—25737
pre-partitioning and zone setting, nonlinear, and pattern space 77—21953
prostate tumour diagnosis by pattern recognition in US sectional pictures 79—83866
prostate US sectional pictures, pattern recognition for tumour diagnosis 80—51194
pulmonary infiltration interactive analysis 77—21625
pulmonary oedema, quantitative diagnosis from chest X-rays using computer controlled optical system 77—77981
radiograph feature extraction via least squares fit to model 77—14229
radiographic feature enhancement via TEXAC image processing computer 80—12251
radiographic image texture anal. appl. 77—21643
radioisotope lung scan automatic classification 77—29201
rapid eye movement analysis during sleep 80—76870
rapid eye movement automatic detect. system and normative data 79—74771
real-time multispectral feature classification by analogue CCD 78—24438
satellite onboard feature classification by CCD analogue signal processing 77—70980
scale and rotation invariant optical pattern recognition and classification 80—99655
segmentation method of detecting cellular images using colour information *(Japanese)* 78—11783
seismic analysis, appl. of PAL, highly tutorial interactive pattern recognition program 77—81833
seismic events, pattern automatic recognition 77—81831
severe weather forecasting system 78—20498
sheet steels, carbonaceous residue, chemical characterisation from C Auger spectra, appl. of pattern recognition and factor anal. 79—79347
Siemens program for ECG analysis 78—7489
sinters, texture anal. of sinter struct., appl. to Ca ferrites in sinters of rich Fe ores 80—18009
skeletal muscle disease, Fourier optical evaluation of histopathologic findings 77—37091
sleep EEG data classification by autoregressive model 79—57628
sleep telemetry in rat, automatic identification and recording of vigilance states 78—48948
speech, connected, pitch period analysis using digital computer algorithm 79—59878
speech patterns, computer interpretation based on formant trajectories 79—59877
speech recognition, linguistically oriented system for word spotting in conversational speech 79—64424
speech trainer for multihandicapped children, display method and control program *(Japanese)* 80—108922

computerised pattern recognition continued
statistical pattern recognition for early diagnosis of heart attacks 77—25584
steroids, mass spectra, computer-aided interpretation by pattern recognition methods 78—64898
stomach radiograms, pattern anal. system *(Japanese)* 79—39481
stomach radiograms image anal. 79—88176
structure extraction, search-free technique, appl. to M-mode echocardiogram and chromosome image 78—81025
TELEMED system user support organisation and program library 78—7491
textural pattern recognition, comparison of optical-digital and all-digital techniques 80—99638
thermography of breast, feature extraction for mass screening 77—60237
tomography image processing and evaluation using PDP-10 computer 78—44587
tomography images, object location using global local segmentation 80—12249
two-dimensional pattern distortion analysis, biproportional matrix projection method 79—88229
two-dimensional random field model for image structural analysis *(Russian)* 80—63932
ultrasonics symposium, Annapolis (1976) 77—19469
US histopathology, A-scan pattern recognition, use in signal processing 77—64108
vectorcardiogram computer interpretation method, prototype system 77—90954
ventricular arrhythmia model 80—89893
ventricular arrhythmia on-line study 78—81060
ventricular arrhythmia quantification, minicomputer system 79—70677
ventricular ectopic activity, semiautomated data reduction 79—66573
ventricular fibrillation detect. by computer 79—70675
ventricular fibrillation recognition using ECG power spectrum 78—81032
visual and nervous systems, straight line recognition algorithm 79—34562
weather pattern classification and machine recognition 77—21879
X-ray image series encoding and analysis 79—83928
X-ray powder diffraction patterns, quantitative matching 77—70384
X-rays with spatial modulation 78—45761
zero crossing and FFT speech recognition systems compared 79—76917
Ni-Cd cell lifetime prediction, computerised pattern recognition 80—3504
α-U, autoionic images of dislocation struct., computer interpretation 77—62453
U prospecting, pattern recognition appl. 77—66999

computerised picture processing
see also computer-generated holography
acoustic attenuation reconstruction from back-scatt. US 80—30821
acoustic holographic image reconstruction for moving objects 78—75019
acoustic image improvement using statistical estimation theory 79—46115
adaptive binarisation using hybrid image processing system 78—87019
adenocarcinoma cell clump feature extraction methods in automated uterine cancer cytology *(Japanese)* 80—72362
adrenal uptake measurements, operator-independ. background subtraction method 78—7429
analytical video stereoscopy, extended images, real-time photogrammetry 78—88926
Anger camera image digital filtering 77—9256
angiocardiogram objective quantitative processing, Cardiac Image Analysis System 79—70629
angiocardiographic image computer quantitation 80—36118
angiocardiography, digital multiprocessor system 80—94362
angiograms, digital, comparison of methods of meas. blood flow *(German)* 79—39468
angiographic computerised evaluation of left ventricular wall motion 79—70634
angiographic definition and quantification of regional left ventricular contraction 79—70637
angiographic images of left ventricle, system for off-line anal. using minicomputer 78—80964
angiography, computerised, anal. and visualisation of blood dynamics and motion of organs 80—8170
angiography, new tool for X-ray functional diagnostics 79—79640
antibiotic concentration assay, computer-aided method *(German)* 79—5414
artificial stereo created by digital processing 79—31806
astrometry, photography against stellar background, iterative trajectory search algorithm *(Russian)* 77—17376
astronomical digital image processing, interactive system for computer reduction and display of two-dimensional data 79—58257
astronomical digitized image presentation and evaluation, software package 79—58267
astronomical image anal. system 78—7886
astronomical image processing at Trieste Observatory *(Italian)* 79—58270
astronomical image processing digital techniques 78—81555
astronomical images, interactive program for digital display *(Italian)* 80—98559
astronomical IR photographs, processing techniques for revealing faint objects *(Russian)* 77—13250
astronomical photographs reduction by method of dependences 80—4237
astronomical plate analysis, interactive imaging technique appls. 79—58266
astronomical plate processing, two-dimensional digital filtering techniques 79—16835
astronomical telescope speckle interferometry, online digital autocorrelator 78—81548
astronomy, digitised images anal. via interactive data processing system (CIPS) *(Italian)* 80—98560
astronomy, photon counting and analogue TV systems with digital real time image processing 78—96402
atmospheric and oceanographic information processing system 77—78519
atmospheric research system 79—39873
Auger microprobe, scanning 80—68304
automatic computerised transverse axial tomographic scanner system 77—12985
automatic film scanner KAMA using CRT with double deflection scheme 77—38552
axial tomogram digital enhancement 79—70630
BASIC interactive image processing for landuse anal., teaching appl. 77—74176
binary image analysis, distance and region association algorithms 79—72523
binary tree-based image processor architecture 79—72524
biological data processing and synthesis 79—25180
biological structure electron micrograph processing computer programs 79—57835
biomechanics film data reduction and anal. using PLATO system 79—35873
biomedical image optical differential operation processor 77—52911
biomedical image processing, identification of human chromosomes 79—62418
biomedical image processing fundamentals 79—25144
biomedical pictures, digital processing and enchancement techniques 77—40815
blood cell differential counter, ADC 500, pattern recognition based image processing system 78—73282
blood cell motion dynamics tracking and quantification method 79—53074
body organ moulded picture representation from computerised tomography scans 78—35951
body surface potential distribution map recording and processing 78—57116
body surface potential image recording and processing methods 79—20704
bone, disease diagnosis, automatic texture anal. methods 80—8156
boundary trace transform: an edge and region enhancement transform 79—70713
breast parenchymal patterns meas. 80—8155
C-filter: a method for filtering of biomedical specimens 79—20736
cardiac, wall motion abnormality detect. using regional changes in ventricular shape and vol. 79—70633
cardiac function scintigraphy using Bonn System III 78—73198
cardiac graphic analysis using microprocessor-based system 79—70665
cardiac left ventricular wall motion assessment from computer-processed fluoroscopy 79—62358
cardiac nuclear medicine, left ventricular edges detect. methods 80—98132
cardiac radiographic image sequence analysis and recording 78—57069
cardiac radionuclide cineangiography, clinical utility of real-time computer-based system 78—80957
cardiac right ventricular angiogram computer quantification 79—62360
cardiac scintigrams, time gated, analysis by digital boundary detect. techniques 80—98081
cardiac scintigraphic image handling using microprocessor system 80—85489
cardiograms, image processing, cardiac function meas. *(Japanese)* 80—94354
cardiology, nuclear, automated chest parsing algorithm 80—61678
cardiology, varifocal imaging 79—70631
cardiovascular radiopaque marker tracking algorithm 78—40329
cartography radar image interpretation, line detection technique 78—61630
cell analysis in haematology, LARC system overview 78—31931
cell image analysis on PDP-12, software system for information from scanning microphotometer *(German)* 78—20333
cell membrane particle diameters meas. by computer from electron micrographs 80—101307
cell membrane particles diameter meas. method 79—84065
cell microscopic images *(Japanese)* 79—39373
cellular logic techniques in radiological image analysis 80—8171
cerebral blood flow, linear computer model 79—92288
chest photofluorograms, computer anal. and appl. to automated screening 80—72282
chest photofluorograms automated interpretation using AISCR-V3 software system 79—88183
chest radiograph nodule detection system 80—8140
chest radiograph optoelectronic processing for pulmonary venous hypertension detect. 79—74754
chest radiographs, model-directed detection of ribs 79—88179
chest radiographs, processing of large numbers, problems 80—8138
chest X-ray automated anal. 80—98098
chest X-ray images, recognition of feature points, by sequential decision process model *(Japanese)* 79—39480
chest X-ray lung region subimage automated extraction for pneumoconiosis opacities detection 79—88182
chest X-ray rib extraction algorithm for pneumoconiosis detect. 78—31904
chest X-rays, coal miners, small opacities computer anal. 78—40324
chest X-rays automated screening, image segmentation and cardiac silhouette anal. 79—88178
chromatograms, two-dimensional, quantitative evaluation 79—84064
chromosome autoradiograph analysis by computer 78—57071
chromosome metaphase spread, automatic finding, prep. and eval. of object spectra 80—98168
cineangiocardiography, accuracy of ventricular models and localisation of contraction anomalies 80—89845
cineangiograms, anal. system 80—72284
cineangiography, automatic detect. of apex of heart 80—89847
cineangiography, left ventricular contour segmentation from anatomical landmark trajectories and its application to wall motion analysis 80—94363
cineanigiocardiogram of left ventricle, automatic processing and cardiac function display techniques *(Japanese)* 80—72311
circular ring transverse axial positron camera system efficiency optimisation 77—12994
clinical nuclear cardiology computer system 79—25094
close-range photogrammetry problems solved by analytical plotter 77—71397
coded aperture tomography, one-dimens., ODCAT 80—17126
coded image obtained with nonredundant pinhole array, digital deconvolution 77—61919
coding without point by point sampling 78—33678
colour photograph image processing, using graphic arts scanner and off-line digital processing 77—79191
colour photography of accidental thermal burns, diagnosis appl. 78—3648
colour scanner imager for colour picture reproduction 78—42415
colour TV display of blood flow in brain *(Swedish)* 77—44780
colour TV imaging computer peripheral 79—20667
comets, computer generated pictures 80—17549

computerised picture processing continued
Compton scatter imaging of transverse sections, corrections for multiple scatt. and attenuations 77—40742
computerised tomographic scan data format 78—73243
computerised tomography, incomplete measurement data preprocessing procedures 80—3803
computerised tomography, non-linear smoothing filters and noise struct. 80—17118
computerised tomography image reconstruction, interpolation effect 78—77110
conference, Bonas, France (June 1976) 78—58927
constant variance enhancement, digital processing technique 77—61920
convolution reconstruction technique for divergent beams 77—12987
coronary angiogram computer quantitation 80—41233
coronary artery quantitation using digital image processing techniques 80—85517
cranial computerised tomography scans, image anal. and computer graphics appls. 80—8183
CRT half-tone image display system using MIR-2 computer 80—62641
CRT screen image distortion corrections in R7912 transient digitiser, FORTRAN programs 79—30440
Cytocomputer biomedical image analysis 79—92419
cytofluorometer, imaging system for correlating fluoresc. cell meas. in flow 78—61240
cytology, digital picture analysis 77—21650
dark-field imaging, computer simulation 80—100151
data extraction and classification from film, conf., San Diego, USA (Aug. 1977) 78—63023
data extraction from film using optical and/or digital and/or electronic devices 78—63024
deblurring of coherent optical image using digital computer 79—3646
defocused grainy photographs, digital restoration by noise cheating and Fourier techniques 77—50626
diagnostic radiological digital image processing facility 80—36127
diatom photography characterisation by Fourier transform differences 79—79697
digital data compositon for satellite and radar imagery 80—67413
digital image enhancement by median masking technique 80—106483
digital image processing, architectural breakthroughs 80—63939
digital image processing, book 79—910
digital image processing applications, conference, San Diego (1977) 78—81528
digital image processing applications, seminar, San Diego, CA, USA (Aug. 79) 80—105424
digital image processing developments 80—14287
digital image-enhancement, used for human anatomy scanning 80—94408
digital map revision 80—17422
digital picture analysis, book 77—17962
digital scan resolution enhancement, processing algorithm 78—15887
digital system for image processing *(Italian)* 80—98558
digital thermal field analysers 78—82034
diploid fibroblasts, human, nuclear morphometry 79—43831
display of three-dimensional information in computed tomography 79—70606
display system using computer generated integral photograph 78—87021
dose reduction in X-ray computed tomography using a generalized filter 79—83946
double-beam scanning microspectrophotometry for rapid microscopic image reconstructions 80—18008
dynamic boundary surface detect. algorithm, appl. to X-ray tomography 77—78019
dynamic processes represented by chains of maps, analysis 77—37062
dynamic random-dot stereograms, computer generated, binocular depth perception 78—80879
Earth resource surveying and interpretation 78—24391
ECG, surface isopotential and gradient maps 79—70670
ECG data processing development, status, and trends 79—39558
ECG gated acquisition cardiac imaging, quantification of left ventricular function 79—70638
ECG gated radionuclide cardiac imaging system 79—70639
ECG map reconstruction computer system 79—39561
ECG surface potential map reconstruction from limited no. of leads 78—57117
echocardiogram, M-mode, automatic computer anal. *(Japanese)* 80—72274
echocardiogram computer-assisted interactive interpretation 78—80938
echocardiograms, 1D and 2D *(German)* 80—81665
echocardiographic, graphic representation of 2-dimens. structs. in motion 79—70597
echocardiographic images, video recorded, interactive segmentation 80—89817
echocardiographic images enhancement by lateral filtering 79—70592
echocardiography, two-dimens., wall motion and thickening quantification by computer-aided contouring 78—80937
echocardiography, US, picture processing of 2-dimens. data 77—77958
edge gradient preferential enhancement, median-window filter algorithm 77—50629
edge operator evaluation test procedure 79—75646
electrical parameters imaging inside a patient, CT technique 80—8117
electron image processing, and improvement 78—24890
electron image processing 79—30613
electron micrograph, 500 kV, atomic resolution 80—100149
electron micrograph, image processing systems, random noise removal 78—12791
electron micrograph, optical vs. computerised 77—67541
electron micrograph images, HV, man-machine interactive digital image processing 79—17568
electron micrograph quantitative interpretation, image processing techniques 79—82128
electron micrographs, error sensitivity, resolution limit 79—71570
electron micrographs preprocessing of nucleic acid molecules for automatic computer anal. 79—70711
electron microprobe analysis, computer controlled beam-scanning and camera cct. 79—43706
electron microscope image real-time processing 79—25181
electron microscope images, automatic investigation 80—92425
electron microscopy, bright field images, signal-to-noise enhancement in incoherent superposition 80—101906
electron microscopy, cell ultrastructure anal. 80—85555

computerised picture processing continued
electron microscopy, image reconstruction of low and high dose micrographs of neg. stained glutamine synthetase 80—85551
electron microscopy, imaging and diffraction from localised defects and disorder 80—100152
electron microscopy, many-beam structure images, optimal comput. techniques 80—95203
electron microscopy, microdensitometer—computer correlation analysis of ultrastructural periodicity 80—85553
electron microscopy, phase contrast simulation, of Au cluster atoms on W support film 80—100150
electron microscopy, simulation of digital image restoration 77—57431
electronic radiography, computerised, for early detect. of vacular disease 80—41226
electronic radiography 80—8162
elemental concentration maps, determ. from digital secondary ion images, algorithm development 80—40761
environmental change detection in digitally registered aerial photographs 80—106477
enzymes, molecular struct. reconstruction from electron microscopy images 80—89715
epithelial tissue pattern recognition 79—25145
FAS-II system, new dimensions in automatic image anal. 79—58678
fast convolution of large arrays, using number theoretic transforms 78—22092
feature subset selection in remote sensing 79—25337
film-grain noise, low-contrast image detection 78—94370
flow measurement, plane mixing layer vortex digital image processing 80—103095
fluoroscopic cardiac imaging, real-time computerised system 80—36123
fluoroscopy for non-invasive cardiovascular imaging 80—17121
Fourier transform image reconstruction, polar sampling theorems in computerised tomography 79—92373
functional imaging, appls. in three radiological modalities 80—8139
galaxy photographs, image processing techniques 77—9664
gamma camera image processing *(French)* 77—37038
gamma camera-computer systems for rapid dynamic imaging studies 78—44598
gamma-angio-encephalographs, enhancement, reduction of statistical fluctuations *(French)* 79—5345
Ganymede image restoration by maximum entropy method 77—60624
gated cardiac scintigram anal., digital boundary detect. techniques 80—98106
gated cardiac studies, data processing system 79—25091
gated regional spirometry (GRS) 79—25097
geometrical anal. of image parts, CLIP parallel processor, algorithm implementation 78—58936
geothermal research by IR scanning, image processing 77—64458
glaucoma diagnosis by digital processing of optic nerve head images 78—81043
Graphic Interactive System for Processing of Electrocardiographic Maps 79 39552
grey-differentiation in black and white pictures, displaced using arbitrary colours *(French)* 79—81370
halftone images, spatial resolution and tone reproduction 78—63016
heart wall motion cine display using ^{99}Tc^{m}-labelled red blood cells 80—17129
heart wall motion quantification using computerised US technique 78—40279
high-speed digital image processing 78—12680
high-speed X-ray cylindrical scanning multiaxial computerised tomography unit 78—80956
high-temperature reactor structural displacement and strain analysis *(Japanese)* 80—78352
histology appl. of interactive pattern recognition system PEEP/DECIDE/GRAPH 78—73291
histopathological information obtained from US tissue signatures and microscopy of biopsy samples 80—51195
hologram synthesis, simulation of highlights on diffuse surface 78—46546
holographic, image digital reconstruction with limited-length arithmetic register *(Russian)* 79—22910
holographic contour fringe computer-aided analysis 77—49766
holographic image reconstruction, unconditionally stable algorithms *(Russian)* 79—22909
holography, computer-generated polarisation, improvements of writing and reading algorithm 78—46538
hospital integral picture processing and communication system 78—57104
HPD-SHP-IBM 360/44 system for anal. of meson diffraction dissoc. experiments 79—22573
hybrid image processing 78—25810
hybrid optical corelator system for automated stereo compilation 78—63035
IBIS, geographic information system based on digital processing and image raster data type 77—56747
image analysis by LEITZ-TAS with process computer 80—68773
image analysis of individual features, adapted image process 77—61052
image analysis system for Earth resources surveys 79—5644
image digitising system for computer input of crystallographic structure models 79—50939
image digitizer system design considerations 80—10025
image display, medically significant features 77—78020
image feedback computer contrast control expts. *(Japanese)* 79—22903
image generation system for nonplanar projection modelling 80—99667
image generation with efficient storage, modified ray tracing method 80—43278
image matching using struct. information, edge vector correlation 78—63036
Image mensuration by maximum a posteriori probability estimation 78—63015
image processing and eigen representation 78—55312
image processing applications at IBM Madrid Scientific Center 80—102657
image processing in high-energy physics 77—18769
image reconstruction, computerized, fragment size choice 80—78785
image reconstruction from kinoforms and distorted holograms *(Russian)* 78—13664
image reconstruction from projections, book 80—51961
image reconstruction from projections, freq. domain techniques 78—58935
image reconstruction quadratic optimisation 77—16981
image reconstruction with limited angle projection data 79—66508

computerised picture processing continued
image rectification system, for Landsat digital data 77—56734
image resolution through atmospheric turbulence 79—36855
image restoration, a posteriori method, OTF phase and magnitude estimation 79—72502
image restoration, use of computerised microdensitometry 79—55066
image restoration and synthesis, Japanese activities 77—58273
image segmentation and feature extraction, overview 78—58937
image semi-automatic anal. device 79—79705
image statistics, computed tomography appl. 80—8159
image transmission techniques, conference, San Diego, USA (Aug. 1976) 77—79773
image-convertor camera, high-speed, computer treatment of images 78—42295
images degraded by spatially varying pointspread functions, 2D digital restoration 78—78920
imaging system, 3D, based on serial tomograms, processing system 79—83859
imaging system, new, in computed radiography 80—8147
interactive image digital/optical processing system development problems 78—74855
interactive software, structure and design philosophy 78—58940
International UV Explorer (IUE), image processing 79—80234
intravenous angiography, digital video subtraction system 80—41234
intravenous angiography, digital video subtraction system 80—98089
intravenous contrast angiography, improved digital real-time processing and storage 79—70624
IR aerial colour photographs of citrus orchards, automatic analyser 77—56749
IR staring mosaic sensor background suppression and tracking 80—86415
iterative ρ-filter reconstruction from incomplete projections 77—25582
Jovian centre location in Voyager image transformation 80—101534
karyotyping automatic image processor *(French)* 77—40953
kidney membrane conformational changes anal. after renal ischemia 78—73142
land-use mapping, evaluation of LANDSAT image data 80—101443
Landsat, satellite-aided evaluation of population exposure to air pollution 79—92116
LANDSAT data anal. for geological structure research *(Italian)* 80—109281
LANDSAT data correction for haze, Sun angle and background reflectance effects 77—78491
LANDSAT data digital chromaticity mapping for water quality anal. 79—29872
LANDSAT data for geological studies in India, digital anal. 77—78511
LANDSAT geoexploration, digital mosaicking and lineament enhancement *(Japanese)* 80—82169
LANDSAT image anal. for terrain investigations in Florida 77—78530
LANDSAT image and digital terrain elevation data processing with parallax 77—29501
LANDSAT image photointerpretation/classification using negative spectral bands 77—78498
LANDSAT imagery, computer aided and air-photo interpretation techniques 79—74976
Landsat imagery for terrain analysis, computer analysis and picture processing programs 78—40691
LANDSAT imagery geologic processing software 78—20521
Landsat imagery laser film recorder and processor 80—105084
LANDSAT imagery processing and enhancement 78—69545
Landsat images, digital differential rectification 80—41570
LANDSAT images and appls. 78—65404
LANDSAT images segmentation, spectral, spatial and semantic constraints exploitation 79—25336
LANDSAT large area classifier MAXL4X 77—78534
LANDSAT multispectral data classification algorithms 78—61629
LANDSAT ratio image dynamic range reduction technique 78—69547
LANDSAT satellite images; low-cost enhancement of multispectral data 78—20559
LANDSAT scene- and map-corrected images using mini computer 78—7806
LANDSAT-1 digital image registration and cloud effect rectification 77—78490
landuse imagery anal., change detection metrics and MIXELS 77—82070
Large Area Crop Inventory Experiment, LANDSAT image registration accuracy meas. 77—26421
laryngeal films, ultra high speed, automated anal. 78—36023
laryngeal films, ultra high-speed, automated anal. 79—57746
laser spatial profile meas. by pyroelectric vidicon camera 80—87425
LEED intensity measurement by photographic method with digital image processing appl. to Si (111) surface 79—60234
left ventricular boundary extraction from radioisotope angiocardiogram *(Japanese)* 77—81562
left ventricular function, effects of intracoronary nitroglycerin, computer anal. 79—70575
left ventricular images digital processing *(Japanese)* 80—12224
left ventricular localised wall motion abnormality assessment, usefulness of quantitative parameters 80—89848
leg long bone growth meas. in children from radiogram, error reduction using computer processing 78—77103
leukaemia cells locomotion analysis 80—40983
linearly degraded images, iterative image restoration 80—95807
linearly degraded images, iterative restoration, reblurring procedure 80—99640
liver gamma camera scans, clinical evaluation of computer processing 79—29579
liver mass estimation from γ-camera images 79—83908
liver scintigraphy, intercomparison of image processing and display methods 79—53234
living cell volumetric changes in freezing and thawing, thermodynamic model and expt. 79—92192
long-wavelength hologram image reconstruction microcomputer system 78—1196
lung tissue micrograph computer processing approach 80—8123
lung tissue stereological parameter computer anal. 78—73280
mammogram inspection, computer-assisted microcalcification outlining 79 16291
mammogram inspection by computer 79—57757
man-machine conversational image processing system 79—13916

computerised picture processing continued
mandible X-ray image changes, desmodontal gap evaluation with data-processing system 79—62337
marine photography and side-scan sonar image processing 77—5357
mass density evaluation in vivo from computerised tomographic scans 77—12992
mast cell automatic counting using image analysing computer Quantimet 720 78—20335
medical, flashing tomosynthesis: three-dimensional X-ray imaging 80—26325
medical computerised tomography, streak artifact reduction method 80—98067
medical diagnostics problems of computer applications *(German)* 79—20696
medical image processing, subjects and objectives 77—52898
medical image processing in diagnostic radiology 80—81690
medical image structural analysis, fast feature extraction *(German)* 79—5393
medical images, computer-aided diagnosis, conf., Coronado, USA, (Nov. 1976) 77—78018
medical images, edge coincidence segmentation 80—109012
medical imaging system evaluation by contrast-detail-dose analysis 80—98140
medical imaging techniques, developments, review 80—26324
medical imaging techniques implemented on pipeline minis and array processor, nerve fibre counting appl. 80—98165
medical laboratories appl., isotope dispersion within organism obs. *(Hungarian)* 78—35933
medical scintigraphic images, use of pattern recognition for lesion detectability 79—62354
medical tomography, convolution reconstruction algorithms comparison, fan beam *(Japanese)* 79—57760
medical tomography, ultra-fast convolution approximations 79—66511
medical tomography workshop, conf., Newport Beach, USA (Jan 1979) 79—66507
medicine, nuclear, digital filtering and edge detection 80—58065
medicine, nuclear, microprocessor systems for data acquisition, image processing, RIA anal., patient data retrieval 80—61670
medicine, tomography and US, conf., Haifa, Israel, (Aug. 78) 80—27035
membrane fracture faces obtained by freeze fracturing, complementary struct., digital image processing 79—62205
meteorological satellite data *(Japanese)* 78—7711
meteorological satellite visible and IR image data, computer processing 79—29864
METEOSAT project, interactive image system 80—109330
Meteosat project MISS IDA, interactive image system 80—36404
microdensitometer with computer-controlled scanning table *(Russian)* 79—6197
microphotometer, automated, SAMB, for morphometric and densitometric analysis *(French)* 77—10085
microprocessor based digital scan generator, interface to image processing computer 79—12902
microprocessor based interactive radiographic image display 79—25092
microprocessor-based optical/digital processor 78—63027
microprocessor-based radioisotope system for liver disease diagnosis 79—83925
microprocessor-controlled hologram interferometry analysis using intelligent TV system 79—76648
microprogrammed video display 80—72366
microscope automatic image analyser, performance, appls. *(German)* 78—4691
microthin film chromatogram evaluation by scanning fluorimetry and digital image analysis *(German)* 79—5188
molecule images, simulation by point models and kinematical struct. amplitudes 80—103223
MORPHOQUANT automatic microscope image analyser, universal program system 80—56160
Muehllehner's tomographic camera, quantitative evaluation of depth effect 77—86609
multiplane γ source image reconstruction using Fresnel zone plate aperture 77—52874
multiple analysis at JPL's Image Processing Laboratory 80—82219
multiple image object detection techniques 77—37087
multiply-exposed radiograph digital image restoration improvement 78—78054
multispectral remote sensing ratio image digital processing and interpretation 78—81461
multispectral scanner data processing mechanisation 77—56778
multispectral scanner imagery, two-dimensional digital filters appl. 80—31152
myocardial ^{201}Tl perfusion images 80—30860
myocardial infarct size computerised quantification from ^{201}Tl scintigrams 78—44601
myocardial infarction, topographic relation between myocardial ^{201}Tl uptake and left ventricular kinetics 78—61243
myocardial perfusion images using ^{201}Tl, quantitative evaluation methods 79—39479
myocardial perfusion imaging using ^{201}Tl, computer processing 79—62356
myocardial perfusion scan interpretation 78—80960
myocardial scintigraphy, computerised extraction of organ contours *(German)* 78—88735
nerve axon automatic counting 78—31994
nerve fibre automatic counting using an array processor in a multi-mini computer system 79—79710
nerve fibre counting by pipeline multiminicomputer image processing 80—109013
new means for picture formation in computer tomography 80—26326
NGC 5195 (M51 comparison), appl. of negatives superposition method, processing of obs. *(Russian)* 77—13251
noisy image local segmentation, statistical segmentation algorithm construction 79—55074
noninvasive numerical dissection and display of anatomic structure using computerized X-ray tomography 80—17117
nonlinear image processing methods for nuclear medicine 78—48874
nonlinear image restoration with signal-dependent noise, decomposed local algorithm 78—78951
nuclear angiocardiography, computerised, ECG-gated, automatically generated LV regions of interest 79—70626
nuclear angiocardiography, first pass technique, automation during anal. 79—70625

computerised picture processing continued
nuclear events picture anal. multiprocessor system *(Italian)* 80—69047
nuclear imaging 80—3801
nuclear medicine, coded aperture imaging, qualitative and quantitative 80—89843
nuclear medicine, composite video output signal from GAMMA-11 computing system 79—29610
nuclear medicine, Fourier multiaperture emission tomography 80—41188
nuclear medicine, image processing, tracer kinetics, cardiology appls. 78—48873
nuclear medicine, precision computer display techniques 80—98100
nuclear medicine, sequential method for high 3D resolution imaging 78—53489
nuclear medicine, static gamma camera image processing 80—36095
nuclear medicine clinical image processing 79—92371
nuclear medicine imagery data smoothing with digital filter 79—25070
nuclear medicine images greyshade scale improvement 77—21609
nuclear ventriculograms, scintigraphic data 77—86627
OCR picture enhancement and stroke-width standardisation algorithm 77—38822
oncology, radiation, use of computers review 79—25098
ophthalmological diagnosis images 80—46083
optical computing for image bandwidth compression, analysis and simulation 78—94373
optical image restoration, digital 77—23628
optical microscopy, automatic image analyzer appls., densitometric and geometric studies 80—98974
optical moving target indication, multi-minicomputer network 77—5445
optical power spectrum sampling and nonparametric pattern recognition algorithms 78—63032
pancreatic cell moving granules anal. by digital moving image processing 79—84063
parallel array processors 77—38816
parallel logic device and half-adder circuit for digital optical processing 80—10027
particle size distribution meas., online stroboscopic microscope apparatus 80—101783
phased array US imaging, real-time digital scan conversion and multidimensional processing 79—48363
phosphorylase A crystals, automated struct. determ., from micrographs 80—92425
photoelastic fringes, automatic stress analysis method 80—14639
photogrammetric automation 'Zenit' automatic processing of line images *(Russian)* 78—21106
photogrammetric online processing, general sequential algorithm 77—78463
photographic plate digitalised image, object detect. using FINDER program *(Italian)* 80—98575
photokeratoscopic technique for corneal image study 77—1993
photomapping, Gestalt computer-controlled system features 78—40714
physics of computer assisted tomography 78—24173
platelet aggregation studies using TEXAC whole picture analysis 79—25133
pockels readout optical modulator, for optical/digital processing systems 78—79125
polar reference texture in radiocolloid liver images 78—73241
positron camera, 3-dimens. imaging using Fourier techniques 77—32951
positron computerised transaxial tomography, physical aspects 77—12993
precision image isocon X-ray TV camera 80—101263
precision SEM image analysis system with full-feature EDXA characterization 80—68311
profile digitised diffractographic data processing 77—58276
proportional multidetector for lung function study *(French)* 77—37035
pseudo-colour images, microprocessor controlled method for electronic image processing *(German)* 78—92724
psychology applications, eye tracking experiments, raster graphics device 80—41330
pulmonary vascularity computerised texture features rel. to catherisation parameters 80—8154
quality improvement by computer, electron animation, satellite pictures, X-ray appl. *(Russian)* 79—6105
radar and optical imaging, three-dimensional density function reconstruction, inverse problem 79—27197
radar image simulation, point scatt. model, remote sensing appl. 79—12296
radioangiography, cerebral perfusion image processing, minicomputer system 77—29200
radioastronomical aperture synthesis imagery data optical reconstruction 78—69702
radioastronomy image reconstruction 80—56718
radiocardiography, equilibrium left ventricular ejection fraction determ., background noise estimation 80—94365
radiogram, stomach contour extraction *(Japanese)* 78—53482
radiographic feature enhancement via TEXAC image processing computer 80—12251
radiographic image anal., patient diagnosis appl. 78—61256
radiographic image anal. 80—8163
radiographic image analogue processing by photographic spatial filtering 78—57070
radiographic image analysis 77—21624
radiographic image computer-controlled subtraction procedures 80—109014
radiographic image enhancement and anal. system, digital computer eval. 78—27708
radiographic image smoothing and edge enhancement 80—109015
radiographic imaging, digital video acquisition system for extraction of subvisual information 78—69208
radiographs, hardware configurations, software strategies 79—16290
radiography, computed, image processing techniques and comparison with standard radiography 80—12250
radiography, computed, low-dose X-ray imaging system 80—98092
radiography, contrast in computerised transverse axial tomography of brain 77—86608
radiography, digital processing appls. 80—98103
radiography, interactive meas. in computerised tomographic imagery 77—77984
radiography, micro-dose system 80—51233
radiography, tomography using video techniques 77—73568
radiography, transaxial scanning X-ray tomography, coronal or sagittal plane reconstruction 77—77986
radiography, video subtraction procedures 80—98102

computerised picture processing continued
radioisotope angiocardiograms, image enhancement and left ventricular contour extraction techniques appl. 80—72283
radioisotope cardiac scan computer-aided anal., using ECG gate 78—40328
radioisotope emission computed tomography, review 78—44599
radioisotope image correction and computer-aided processing 77—9253
radioisotope imaging, 3-dimens., with circular ring transverse axial positron camera 77—77982
radioisotope imaging, digital images, math. models and physiological parameters 80—98107
radioisotope lung scan automatic classification 77—29201
radioisotope scintigraphy, intercomparison of processing and display methods using math. tumours 78—15886
radioisotope scintigraphy, zero summation filter optimisation 77—16963
radioisotope subtraction technique in diagnosis of abdominal abscesses 78—73212
radioisotope three-dimensional imaging using source-depend. time-modulated apertures 77—29202
radiological imaging at Bureau of Radiological Health 80—8160
radionuclide angiography, gated, use of computer-generated functional images to define ventricular boundaries 80—85487
radionuclide angiography determ. of left-ventricular ejection fraction and segmental wall motion 78—61246
radionuclide angiography technique for assessment of regional wall motion abnormalities 80—85488
radionuclide cardiac motion study, computer-processed, ECG gating device 78—73210
radionuclide computed tomography, method for γ attenuation correction, reconstruction algorithm 78—40307
radionuclide emission tomography of head with ^{99m}Tc and scintillation camera 77—52866
radionuclide images, digital image superposition algorithm, accuracy and reproducibility 78—73209
radionuclide tomographic section, synthesis, and enhancement 80—109003
radionuclide tomographic section synthesis and enhancement 79—25103
radionuclide tomography, 3-dimens., with circular ring positron camera 77—73566
radionuclide ventriculography, computerised, assessment of LV wall motion and regional kinetics 80—89850
Radon inversion formula for diverging X-rays 77—37088
random nucleated halftone screen 78—62192
random objects max. likelihood reconstruction from noisy objects 77—37089
real-time adaptive contrast enhancement for imaging sensors 79—32079
real-time image contrast enhancement, local area histogram equalisation and gain control 77—50636
real-time satellite data acquisition, analysis and display system—a practical application of the GOES network 80—17382
real-time spatial modulators for optical/digital processing systems 78—63025
reconstruction formulae, computer implementation 80—52179
reconstruction from projections 80—52178
reconstruction of 3-D objects from cone beam projections 79—34665
reconstruction spots for digital sampled images 78—63034
recursive digital filtering method, two-dimensional, problems 78—58933
regional myocardial function quantitative parameters 79—25095
remote sensing, image processing and information extraction 77—64438
remote sensing system specification using computer image simulation 80—48439
remote sensor automatic image processing 77—21931
remote-sensed data texture anal. 78—61628
remote-sensing data, computer elaboration and image processing 78—40690
renal histopathological section image dissection and analysis 79—79679
renal tubulus, digital picture anal. 79—70712
restoring with maximum entropy, Poisson sources and backgrounds 78—66769
retinal nerve fibre atrophy development evaluation 77—40856
review of digital image processing research, Osaka University 80—9820
review of methods 80—83562
rI image processing with a microprocess 80—8175
ring detector positron camera system for brain reconstruction tomography 78—40306
ring pseudorandom aperture for transverse section radioisotope tomography 77—64129
rotated image correlation by gradient vector sum histograms 79—75647
satellite imagery, filtering to remove cloud cover 77—56744
satellite IR pictures, automatic digital techniques for oceanic features enhancement and extraction 79—5682
SAW device for optical image processing 78—71051
scintigram change obs. by crosscorrelation 78—80961
scintigram preprocessing and display by microcomputer *(Hungarian)* 78—15881
scintigraphic image adaptive restoration 80—27914
scintigraphic restoring filter, appl. of constrained optimization 79—39494
scintigraphic scans, computerised reconstruct. 80—30846
scintigraphy, digitised images display, minimisation of data transfer losses 80—56206
scintigraphy, image processing and display methods, multicentre comparison 79—53233
scintigraphy, medical, digital image processing methods 78—80947
scintigraphy, nontraumatic assessment of ventricular wall motion and stroke vol. after myocardial infarction 77—52865
scintillation camera transaxial tomograph, Humongotron 77—52867
scintillation cameras, automatic field uniformity corrections 80—17128
sea ice/lake SAR L-band imagery 78—36311
seismic imaging by holography, techniques and appls. 79—66831
SEM diffractogram online computation 80—70095
SEM images evaluation, coal chemical analysis 80—71994
shape descriptors, Fourier-Walsh, radiographic image processing appls. 80—8153
side scan sonar system capability improvements 80—43574
signal detection methods, optical/digital components evaluation in hybrid processor 78—63026
SIMS ion images, multifeature mass analysis utilising digital image processing, Fe anal. appl. 79—43684
Skylab S-192 conical scanner data digital processing 77—82046
smoke/dust cloud temporal analysis algorithm 80—98484
smoothing and image noise 78—69190

computerised picture processing continued
soil pattern data from aircraft/LANDSAT scanners delineation by digital anal., Indiana 77—78496
solar corona, global-scale 3-D reconstruction 80—56719
solar corona and comet details enhancement, digital image processing 79—25516
solar corona and comet digital image enhancement 78—81556
solar granulation, digital enhancement of balloon-borne imagery rel. to photometric props. 78—7956
sonar, side looking, picture improvement 79—84516
SonoChromascope, US B-scan image acquisition, display and recording 80—30818
soot particles in flue systems, computerised image digitisation *(French)* 79—83675
spatial image, research projects at IROE Institute (Firenze) *(Italian)* 80—56668
spatially-varying image degradation compensation by linear programming 77—58275
speckle imaging phase estimation, FFT-based algorithm 79—76605
spline functions for image restoration 78—42280
square-field scanned image construction time optimisation *(Russian)* 80—63933
stenosis densitometric analysis from remote terminal 79—83900
stereo image digitiser for automatic feature extraction 80—106614
stereo image processing, control system 78—4728
stereophotogrammetry, automatic, using structural pattern recognition techniques 78—61632
stress ^{201}Tl scintigram anal. methods comparison 80—89851
structure model, photograph to digital convertor 79—60213
submarine periscope optical test equipment 80—78943
synthetic focus digital acoustic imaging for nondestructive evaluation 79—52611
television ophthalmoscope image processor/graphics system 77—81633
TEM 80—82852
TEM image recording and processing TV system 79—58851
TEM micrograph image restoration, of weak-phase object using computer *(Japanese)* 79—71571
TEM three-dimensional image reconstruction from projections under limited view angle 80—9078
texture analysis and EPQ of radiographic images 79—34643
texture analysis by hybrid optical/digital system 80—78787
thermal IR scanner analogue data digital processing 77—82045
thermographic image digitisation and anal., for skin temp. applic. 77—16960
three-dimensional computer graphics for electron microscopy, computational morphology appl. 78—28132
three-dimensional image reconstruction, direct Fourier transform techniques 77—12986
three-dimensional image reconstruction for cone-beam X-ray sources 78—77111
three-dimensional objects machine visualisation via skeletal transformations 77—40674
three-dimensional scintigram processing algorithm 78—7446
time of flight tomography, reconstruction of US vel. distribs. in soft tissue 77—48850
tissue section electron microscope image texture discrimination and automated meas. 78—57099
tissue US backscatter and attenuation distrib. mapping, digital reconstruction 80—51188
tomographic image boundary detect. 78—40326
tomographic image boundary finding and complex object localisation 80—109016
tomographic image correction, with simulation 80—85470
tomographic image enhancement techniques 79—25102
tomographic image processing 78—35950
tomographic image reconstruction using two-dimens. kernels formed by simple back-projection,, ramp filter realisation *(Korean)* 80—72275
tomographic radiography, Siretom 2000 head unit 78—28037
tomographic radiography, Somatom whole-body scanner with image reproduction 78—28036
tomographic reconstruction, detective quantum efficiency in detection of small objects 80—46046
tomographic reconstruction noise, effect on detectability 78—40296
tomographic scan edge position uncertainty reduction by density derivative processing 80—109017
tomographic scanner image quality evaluation phantom 77—73573
tomographic scans, sigma scan 80—17111
tomographic system error propagation, hybrid anal. 78—40327
tomographic X-ray imaging *(Japanese)* 77—66845
tomography, axial, transmission and emission techniques, review 77—77973
tomography, basic physics, mathematics and data reconstruction 78—73218
tomography, boundary-finding scheme and complex object location 80—98104
tomography, computer system architecture 77—25549
tomography, cylindrical, appl. to intact circulatory system 77—77971
tomography, display requirements, review 77—81571
tomography, dynamic and ECG-gated, reflection technique for improved temporal resolution 80—98094
tomography, edge position uncertainty reduction 80—98105
tomography, fan-beam geometry, consistent projection sets 80—30884
tomography, fan-beam reconstruction methods 80—26337
tomography, global local edge coincidence segmentation 80—98101
tomography, high speed, special purpose digital processor architectures and numerical approx. methods 80—30878
tomography, image enhancement techniques 77—77987
tomography, limited data, image reconstruction using polar pixel Kalman filter 80—98095
tomography, multiple window display techniques 80—98099
tomography, offset detector, interleaving vs. separate processing 80—30877
tomography, operating principles, image construction, appls. 78—28047
tomography, patient scanning time and picture quality improvements 77—25550
tomography, three dimensional, imaging and image processing systems, developments *(Korean)* 79—62398
tomography, using video recorded fluoroscopic images 77—37082
tomography image processing and evaluation using PDP-10 computer 78—44587
tomography images, display processing, digital enhancement 78—48875

computerised picture processing continued
tomography images, object location using global local segmentation 80—12249
tomography reconstructions with limited data using estimation theory 80—30883
tomography spectral artifact correction 78—35953
tomography with diverging X-ray beam, reconstruction algorithm 77—70535
tomography with X-ray beams *(German)* 78—53480
tomography X-ray photography appl. 78—44588
tomosynthesis, flashing system, using simultaneously 25 X-ray tubes 80—81768
tomosynthesis, serioscopy, and coded scan tomography, theory 78—35920
transaxial image reconstruction and processor architecture 79—34633
transaxial tomography, quantum-statistical limitations 77—12990
transaxial X-ray tomography reconstruction using convolution methods, digital simulation *(Japanese)* 78—35931
transverse section picture reconstruction, correction functions and statistical noise 77—12989
tumour detection by microwave enhanced thermography and computer-aided image analysis 79—70604
TV image anal. system, software based 79—40559
TV-microprocessor system, for high speed image counting and sizing 78—94377
two-dimensional random field model for image structural analysis *(Russian)* 80—63932
US 3D imaging and vol. from series of arbitrary sector scans 80—8109
US and radiographic images 79—79195
US attenuation reconstructive tomography 80—30822
US computed tomography, cancer detect. appl. 80—30820
US echo and reconstruction imaging via adaptive ray tracing 79—83867
US image feature enhancement via digital processing 78—73183
US image sequences, logical neighbour operations appl. 80—8113
US images corrected for refr. and attenuation, comparison of high resolution methods 80—30817
US imaging, digital focusing in near field of sampled acoustic aperture 77—60232
US impediography, quantitative characterisation of lesions in vivo 80—17039
US ophthalmological signal acquisition and image enhancement 78—57045
US real-time diagnostic system 80—30819
US real-time image computerised anal. 79—70598
US tissue analysis, comprehensive system 80—51189
US tomography techniques survey 80—30823
US two-dimensional images, extraction of cardiac parameters 77—25533
vectorcardiography, 3-dimens. 80—94405
ventilation studies, ^{127}Xe distrib. in lungs 78—44606
ventricle, left, cineangiographic images automatic processing 79—83927
ventriculography, left ventricular wall motion anal., externally referenced polar coord. system 80—89846
videodensitometry and image analysis, minimum computer system 79—34664
videodensitometry via an S-100 bus microcomputer angiocardiograms appl. 80—26434
Viking experiment, basic techniques 77—91403
Viking Orbiter and Lander stereo image processing 78—81554
weather maps, structural description of contour maps 80—101419
weighted line-finding algorithm for digitised picture 80—99660
white blood cell images boundary finding 79—12021
X-ray automated screening image processing laboratory 77—13004
X-ray computed tomographic image optimal processing 78—80955
X-ray computed tomography, aspects 78—53481
X-ray computed tomography, computation-intensive reconstruction algorithms implementation 80—8206
X-ray computerised tomography, energy-dependent reconstruction 77—12991
X-ray image processing techniques for Ariel 5 rot. modulation collimator 79—80236
X-ray image series encoding and analysis 79—83928
X-ray images processing, CALTIX system description *(French)* 77—4872
X-ray microbeam scan system with interactive display terminal *(Japanese)* 77—81563
X-ray real-time subtraction imaging, digital video image processor 79—25080
X-ray tomography, iterative reconstruction algorithms 77—12988
X-ray tomography, noise power spectrum 78—53492
X-ray tomography, selective I imaging using K-edge energies 78—24131
X-ray tomography by image reconstruction *(French)* 77—37037
zone plate camera longit. tomogram digital processing, computer simulation 78—40311
Ge detectors array, collimated, computer-driven scanning bed, clinical appls., tomography 78—40309

computerised power station control *see power station computer control*

computerised power system control *see power system computer control*

computerised process control *see process computer control*

computerised signal processing
see also biology computing; computerised pattern recognition; computerised picture processing; medical diagnostic computing
acoustic attenuation coefficient slope for liver tissue, statistical estimation from refl. US signals 80—46000
acoustic data buoy, microprocessor controlled, underwater signals processing 79—21024
acoustic emission, random signal parameters, computer calc. 77—44454
acoustical data anal. using digital techniques 78—83193
AES/APS self-convolution inversion, FFT and digital signal processing 79—71430
airborne dust pollution monitor 80—55971
ambulatory ECG computer anal., YALECG 79—70661
analytical chemistry, user-oriented software Fourier spectrum display 78—64896
anemometry, laser-Doppler, microprocessor-based signal processing system 77—89218
arrhythmia detection with a multi-microprocessor system for distributed and parallel processing 80—85524
arterial blood pressure preprocessor 79—83979
atmosphere echo sounding, Doppler shift extraction hy adaptive linear-prediction filtering 77—64453

computerised signal processing continued
atmosphere radar signal processing, for SOUSY-VHF-radar, using preprocessor 80—85774
auditory evoked potential data acquisition, dual-processor system 79—79712
auditory nonlinear distortion in sound perception 77—5010
automatic acoustic emission analysis system with programmed control *(Russian)* 78—46866
avian heart rate meas. using autocorrel. techniques 78—31989
bioelectric signal processing using an extended desk computer *(German)* 80—26387
biological signal processing, minicomputer, rat experiments example 77—37119
biomedical frequency-time domain signal processing system 80—81760
biomedical signal processing and telemetry, digital bandpass analysis 78—57107
biomedical signal processing microcomputer development 78—81012
biomedical US signals in diffuse liver disease 80—67173
blood flow measurement by US Doppler method, computer-aided determ. of angles *(German)* 78—80931
blood pressure long-term recordings, fast data reduction, hybrid system 80—41278
blood pressure measurement, noninvasive techniques 80—41298
body surface potential mapping, automated acquisition and processing system 78—81033
brain imaging positron camera output processing *(Swedish)* 78—28032
brain potential comparison, average evoked, on spectral and coherency function basis 77—2072
Bryn processor, acoustic array gain, sampling error effect 78—66975
burst correlator processor, for laser Doppler velocimeter 79—50827
cardiac blood flow meas., computerised system 80—36051
cardiac catheterisation, automated processing and storage system 79—70694
cardiac catheterisation computer system 79—70695
cardiac intracellular transmembrane action pots., automated anal. 79—70729
cardiac strength interval curve rapid generation 78—40456
cardiology data processing system 80—56236
cardiovascular and other physiological signals, 7-channel data averager/printer 78—40366
cerebral blood flow, atraumatic meas. by ^{133}Xe *(French)* 77—37039
cerebral regional blood flow and vol. meas., intravenous isotope method 77—86610
chromosome spread automated detect. and classification 77—60328
clinical EEG in perspective 79—70655
conference on analysis instrumentation, Charleston, West Virginia, USA (May 1977) 79—16100
data manipulation and handling, for teachers 80—4489
digital correlator signal preprocessing 80—83556
digital EMG processor and three-state myoelectric control design 79—53283
digital radiation monitoring system, signal processing by distributed microcomputer data modules 79—59279
digital techniques for beamforming and signal processing 79—18619
Doppler sonar controller 80—43575
ECG, 24 hr, automatic analysis on minicomputer-based system 80—89889
ECG, ambulatory, computer processing system 80—89897
ECG, Argus algorithm development 79—70680
ECG, automated Holter anal., shape oriented system 79—70662
ECG, computer assisted interpretation, critical appraisal 80—17151
ECG, digital filters, implemented on microprocessor 78—85428
ECG, flexible signal-averaging system 80—67270
ECG, Holter recording anal. using Argus/2H 79—70679
ECG, Karhunen-Loeve expansion, automatic phase alignment 79—48356
ECG, long-term, efficient data compression and arrhythmia detect. 79—70678
ECG, long-term, flexible data presentation in DCG processing 79—70681
ECG, measurement error determ. 80—94401
ECG, microprocessor signal averaging for recording μV activity from cond. system of heart 77—44820
ECG, microprocessor-based evaluation system for conventional leads 80—89894
ECG, multiform ventricular complex identification, 2-dimens. clustering technique 79—66570
ECG, period analysis using minicomputer 77—13024
ECG, random access mass storage anal., RAMSES, for quantitative anal. of long-term ECGs 79—70663
ECG, T-wave location by computer, R-T interval 80—76854
ECG, time-selective filtering 80—89895
ECG ambulatory monitoring, adaptive algorithm for noise rejection 79—66571
ECG ambulatory monitoring, detect. algorithm for multiform premature ventricular contractions 79—66572
ECG analysis system as part of regional cardiovascular information system 78—81049
ECG analysis system oriented toward polarcardiology 78—85447
ECG and VCG data analysis appl. *(Swedish)* 78—24163
ECG arrhythmia analysis, dual-processor computer 79—66569
ECG artifact in referential EEG recordings, minimisation by computer subtract 80—94390
ECG baseline estimation and removal using cubic splines and state-space computation 77—44808
ECG contour analysis system utilising decision tables, real-time, microprocessor-based 80—89880
ECG interpretation system in ambulatory health service 79—79669
ECG microcomputer-based evaluation system, improving diagnostic capabilities 78—88761
ECG monitoring by contour comparison, QRS triggering with real-time correlator *(German)* 78—92715
ECG processing A/D convertor control by microprocessor *(Bulgarian)* 79—25123
ECG processing optimisation, conf., Halifax, Nova Scotia, Canada (Jan. '79) 80—76850
ECG R-waves, microprocessor detect. 79—96685
ECG real-time analyser with digital readout, portable device 80—56234
ECG signal quality assessment during acquisition 79—70666
ECG signals, random noise influence quantitative assessment of program accuracy *(Slovenian)* 79—25143
ECG waveform automatic processing using syntactic methods 79—44006
ECG/VCG minicomputer digitising and preprocessing system 77—40863

computerised signal processing continued
echocardiogram, M-mode, computer-assisted anal. 78—80942
echocardiogram on-line computer anal. 78—80941
echocardiogram processing, microprocessor-based system 77—40726
echocardiography, high-resolution 80—76814
echographic information related to left ventricle and mitral valve in diastole, anal. by small computer 78—80939
EEG, cerebral potential sources location for visual field impairment assessment in humans 80—30922
EEG, dynamic anal. of event-related vars. *(German)* 78—85400
EEG, event-related, sequential freq. anal., hybrid method 77—81759
EEG, frequency domain and time domain anal. 79—34676
EEG, microcomputer-based period and amplitude anal. system 80—72353
EEG, on-line artifact rejection 77—40833
EEG, quantification of computer analysed serial EEGs from stroke patients 77—5096
EEG, using short epoch Fourier transforms, automated system 77—44824
EEG analysis, real-time programming system 79—100767
EEG analysis methods and activation techniques *(Croatian)* 78—44666
EEG and electrooculograms, sleep research anal. 79—62377
EEG artifact automatic detect. during sleep 79—100759
EEG artifact detection technique for automated anal. 78—31941
EEG artifact rejection, contamination by drowsiness 77—90932
EEG data, low cost microcomputer system 77—40881
EEG delta rhythm during sleep, computerised anal. system 80—12285
EEG dynamic evolutionary spectral analysis 78—57102
EEG epileptic transient detect., pattern recognition techniques 78—53542
EEG eye movement artefact removal, by correlation methods 77—44826
EEG nonstationary point automatic detect. *(French)* 78—57112
EEG signal averager, flexible and low cost 79—43998
EEG signal averaging, S/N relationships 79—83977
EEG signal processing, frequency-domain instrumentation 79—83743
EEG slope descriptor computation, time and frequency domain comparison 78—57115
EEG spectrum analysis, LF activity isolation by autoregressive filter 79—96672
EEG wave duration anal., microcomputer implementation 80—21558
electro-oculographic activity, computerised meas. during sleep 79—74781
electro-oculography, on-line system for quantitative study of ocular kinetics 79—34699
electrocardiograms, automatic processing using syntactic methods 79—62386
electrocardiographic data processing, filtering and sampling 78—24162
electrocardiography technological development and clinical appl. *(Italian)* 79—25136
electronystagmography signal processing *(French)* 77—37078
electronystagmography system for vestibular testing, microprocessor-based 4-channel 80—41293
electrophysiological signal processing system *(French)* 77—37112
EMG, dynamic arm movements data, acquisition and anal. 80—36179
EMG, filter bank analyser for automatic anal. 80—98162
EMG, quantitative, value of automatic anal. 80—8203
EMG, surface, muscle fibre conduction vel., direct on-line estimation 79—100765
EMG activity in extraocular muscles, visual display 77—40834
EMG digital processor design and performance 79—96712
EMG electrode array for muscle fibre activity, output analysis *(Swedish)* 78—24193
EMG of Vastus medialis for graded isometric torque tensions, power spectrum distrib. 78—44673
EMG signal onset and termination establishment method 79—83761
emission spectroscopy signal-to-noise ratio improvement and data processing *(Japanese)* 77—21448
exercise ECG, reproducibility 79—70667
exercise ECG anal. using microcomputer 79—70683
exercise ECG testing in diagnosis of coronary lesions of left anterior descending artery 79—70692
far IR, digital processing using microcomputer 77—2689
fast signal averager based on sampling oscilloscope interfaced to minicomputer 77—57308
flow rate measurement, using laser Doppler anemometer-computer system 79—68881
foetal biophysical signal analysis 77—77999
Fourier analyser system for vibrs., shock and noise 77—68335
gamma camera in rat renal function studies, appl. to radiation effects monitoring 77—56454
gamma emitting organs, 2 and 3-dimens. digital Fourier reconstruction 80—101705
geophysics, digital signal processing appls. to seismology 79—29915
haemodynamic and cineangiographic data treatment, computer system SYSCORMORAM 78—81030
heart block computer detect. by correl. of surface and endocardiac ECG 80—94410
high energy physics, optical computing introduction 79—89581
high energy physics computing, CERN conf. Jadwisin, Poland (June 1978) 79—89570
histopathological information obtained from US tissue signatures and microscopy of biopsy samples 80—51195
holograms, double exposure, automatic meas. of 3D displacements by scanning technique 78—37844
Holter ECG high-speed anal. 79—66568
Holter tape processing, 60× computer system 79—66567
hydrophones, calibration system using pseudo-Gaussian noise signals 77—84045
image data processing system, Skylab X-ray solar obs. appl. 77—60619
image from inline hologram, interfering output suppression using digital processing technique 79—50248
INI-3 measuring system for nanosecond pulses 79—35793
interplanetary shocks identification, by computer on board HELIOS-1 and (HELIOS-2) 79—92679
intestinal motility study by computerised anal. of sounds and EMG wall pots. *(German)* 78—31944
intracardiac electrograms processing 80—21553
LANDSAT data high-level computer processing 78—69546
laser doppler anemometer, microprocessor-based autocorrelator 77—72396
left ventricle ejection fraction meas., scintillation camera deadtime 79—62355

computerised signal processing continued
left ventricular diameter-time curve shape from M-mode echocardiogram, automated anal. 78—80940
long-term spectra, computerised meas. method, English and Finnish data comparative study 80—104688
magnetic torque curve analysis, online microprocessor system 78—254
medicine, microcomputer based signal averaging system 80—36159
metal adhesive bond quality meas., digital US signal analysis 79—47863
meteor wind automatic meas. set, drift obs. accuracy *(Russian)* 77—41248
microcomputer based biomedical signal processor 80—26390
microprocessor for optical processing system noise analogue signals 78—81955
microprocessor speech synthesiser terminal 79—81660
microwave holography using quadratically spaced linear antenna array, microcomputer processing 80—32938
microwave radiometers, microprocessor-based unit 80—77874
microwave spectrum analysis, using microcomputer 78—41329
multichannel analyser, microprocessor-controlled, transfer of blood pressures and neural activities for computer anal. 80—72356
multidither adaptive optical system, 69-channel hybrid controller 80—33136
multiform PVC detect. using time-domain and freq.-domain anal. 79—70674
multiple-input algorithmic processor for multistage decimation and filtering 77—78069
multivariate EEG automatic classification 77—73607
myocardial ischaemia and necrosis monitoring in acute myocardial infarction 80—85525
neural pulse wave analysis, microprocessor-based instrument 80—104791
neuronal spike train sampling, implementation of French-Holden algorithm 78—40440
neurophysiological spike train processing, data reduction program 77—44861
NMR spectroscopy, Fourier, S/N ratio optimisation, influence of receiver circuit and digital processing *(Czech)* 79—17461
noisy blood flow meas. pulsed US spectral analysis 79—57705
nondestructive eval., internal friction technique, computer-assisted digital processing system 79—43537
nuclear power plant diagnostic system using noise anal. 78—50279
obstetrics monitoring, microprocessor data acquisition and preprocessing with minicomputer signal processing 77—44775
online filtering 79—89574
ophthalmological tissue differentiation, digitisation of HF US signals 78—80935
optical scan system for encoding and tabulation of visually scored sleep data 80—8197
P-wave detection in noise, consecutive vectorcardiogram external product technique 77—9289
particle track data in plastics, rapid anal. using interactive programming and graphic displays 78—66456
phase invariant signature algorithm (PISA) processing of ECG and phonocardiogram for cardiac anomaly detect. 78—40395
phonocardiogram quantitative anal. for murmur detect. 80—56270
phonothyreogram and phonocardiogram frequency spectrum analysis by minicomputer, ECG reference time signal 79—83966
photometer, computer-controlled, for quantitative anal. of thin layer chromatograms 77—60326
photon correlation spectroscopy, automatic processing device, microprocessor, laboratory appl. *(German)* 77—40938
physiological signal pre-forming system for automatic freq. anal. 78—3621
Picker FACS-I diffractometer, microprocessor-controlled optical incremental angle encoder system 80—18058
polygraphic sleep recordings, computerised scoring method 80—109049
power spectral density signature analysis, statistical algorithm 79—624
Proteus, advanced signal processor system 77—65648
pulmonary artery blood press. anal. algorithm 78—40376
pulmonary function using ^{133}Xe, camera-computer system *(German)* 77—21600
pulse rate, blood press. and rate-press. product automatic meas. during rest and exercise *(German)* 78—35974
radar, passive detection system for wide class of illuminator signals 79—64408
radar and sonar coherent optical processing techniques 78—75018
radio beacon position calc. from satellite Doppler data using microcomputer 79—12271
radiocardiography, noninvasive meas. in clinical cardiology 77—40754
radiography, bone Ca level meas. using computerised tomography, correl. with ACTA numbers 77—40756
radiography, computerised tomography, equipment operation 77—86617
radiography, computerised tomography, MTF meas. method appl. to EMI head scanner 77—48864
radiography, sampling tomography multi-sectional reconstruction method using computer *(Japanese)* 78—31896
radiography, tomographic scanning, reprocessing X-ray transmission data 77—73565
radiography, X-ray tomography, review 77—5073
radionuclide axial tomography by half back-projection 78—28056
real-time, appl. to underwater acoustic imaging 79—90089
real-time kinoform synthesis using chalcogenide glass films *(Russian)* 78—13669
real-time speech high-performance processor design 80—96144
renogram, comparison of techniques for filtering of noise 77—32952
representation of gait by 4-dimensional vectors *(German)* 78—88723
respiratory muscle EMG anal. by digital computer technique 78—28102
respiratory resistance measurement, modified forced oscill. technique using computer 77—86692
scintigram improvement by computer processing 79—16296
scintillation camera interface to scintigraphic data and computer 77—21613
scintillation probe detector in assessment of cardiovascular disease 80—3800
SEASAT radar altimeter 80—56613
seismic recordings, dynamic range compression *(Russian)* 79—39930
SEM, gradient image processing using on-line digital computer 78—21288
signal analysis and simulation program 79—79678
sinus node autonomic control in man, quantitative assessment 79—70684
sleep EEG, digital filtering for estimation of alpha-delta 78—44652

computerised signal processing continued
solar spectrometric research, automation system for on-line signal processing *(Russian)* 80—12659
sonar, signal processing algorithms soln. with multi-microprocessor network 78—45044
sonar appl., fifth generation concept 77—88995
sonar signal processing by chip slice microcomputer 79—94408
sonar signal processor, 36-channel, programmable 78—66976
spectrum analyser, real-time, with on-line definition of confidence levels 77—73959
speech research, computer aided signal handling 77—56389
speech signals, data reduction, methods and results 79—81648
steel, hot rolled strip and plate shape meas. device 80—35498
surface profile digitization for stylus instruments 80—36993
surface profile filtering using digital filters 80—36994
synthetic aperture radar underwater mapping, array processing 78—69549
systolic time interval, off-line processing of exercise data 77—40868
systolic time interval processing system, STIPS 78—81029
systolic time intervals during exercise 79—70668
thermal-description kinetics, processing of experimental data with Promin-2 computer 79—67267
time-domain wave-shaping filter weights computation 78—77351
tissue characterisation by computer-aided US method *(German)* 78—80932
tissue characterisation by computer-aided US method *(German)* 78—80933
tissue parameter identification by digital processing of real-time US clinical cardiac data 80—51191
tomographic scanning, engineering status 77—73571
tomography, focal-plane, image reconstruction using digital computer 80—61674
tomography, image construction, restoration and enhancement 77—44743
tomography, meas. of mass density distrib. of human body in vivo 77—29198
tomography, meas. of mass density distrib. of human body in vivo 77—29199
tomography simulator, emission computed, design 80—61672
ultrasonics symposium, Cherry Hill (1978) 79—50472
upper-limb prostheses multifunctional control microprocessor system, myoelectric signal identification method 78—88766
US, reconstruction of tissue refr. index and attenuation distrib. 77—64113
US A-mode echo computer spectral anal. 80—51193
US computerised tomography scanner evaluation 79—48301
US crack detect. system 77—19490
US echoes from kidney, computer anal. 78—35901
US FM blood vol. flowmeter processing technique 78—31878
US tissue signature analysis, cepstral signal processing 80—46002
Varian EM-360 NMR spectrometer interface with Altair 8800B microcomputer 78—89519
vectorcardiogram information enhancement, automatic pre-processing 80—94402
vectorcardiogram parameter sensitivity to digital filtering 79—39576
vectorcardiography, microcomputer system 79—70669
ventricular fibrillation signal anal. 80—85522
video-angiocardiographic image series storage improvement by digital signal processing *(German)* 78—92723
visual evoked potential on-line evaluation by sliding average form. *(German)* 78—85402
voice production, analysis synthesis, computer appl. *(Dutch)* 77—12938
wavelength modulation spectrometry, computer modelling 77—63974
X-ray transmission computerised tomography, review 77—48860

computerised spectroscopy
see also spectroscopy computing
100 GHz to 1 THz atmospheric emission and absorption meas. 79—34980
AAS, microcomputer based, 2-channel spectrometer 79—24864
acousto-optic spectrograph, for radioastronomy *(Russian)* 79—25506
acousto-optical tunable filter spectrometer development 80—101848
AES, digital acquisition and processing 79—43698
analytical chemistry, computers and optimisation, conf., Amsterdam, Netherlands (April, 1978) 79—52791
anti-Stokes Raman spectrometer, microcomputer-controlled 80—24111
astronomical spectroscopy, appl. of general image anal. system 78—53834
atmospheric, neutron activation anal. system appl. 77—81442
atomic absorption spectrometer control by microcomputer system 77—1958
atomic absorption spectrometry 79—52794
atomic absorption spectrophotometer, microcomputer control and data reduction 78—35762
atomic absorption spectrophotometer, two-channel, microcomputer-based, appls. 78—56926
atomic fluoresc. spectroscopy using inductively couple plasma, computerised 77—12839
Auger electron spectrometer, control using HP 9845 desktop computer 79—21726
Auger microprobe, microcomputer controlled 80—81414
Auger spectrometer, digital methods for film anal. 77—56268
automated correlation spectrometer with two Ge(Li) detectors 78—82562
automated X-ray microanalysis with electron microprobe and SEM 78—27840
automatic precision wavelength comparator for spectrograms 78—82042
automatic scanning system for grazing-incidence spectrometer 80—14250
beam-foil spectroscopy facility at University of Liege, computer controlled system 79—45866
bit-oriented I/O structure applications 77—44532
blood alcohol determ., spectrophotometric method *(German)* 79—5415
Brillouin spectrometer with high contrast and resolution, fully stabilized 80—57386
burnup meter for fast reactor fuels using γ-ray spectrometer with minicomputer *(Japanese)* 77—50206
CAMAC, 2-D anal. of spectroscopic data, electronics 80—5460
CAMAC spectroscopic data anal., programming techniques 80—5461
Cary 118C spectrophotometer, universal computer interface 78—73972
circuit breaking arc column electrical conductivity meas. *(French)* 80—28864
circular dichroism spectrophotometer, near IR, microprocessor controlled 80—22454

computerised spectroscopy continued
- compilation of computer-readable spectroscopic reference data 78−64894
- computer compatible conversion for printing multichannel analysers 78−90036
- computer controlled gain stabilizing system for scintillation spectrometer using LED, processor in feedback 78−17473
- control of spectrometers in microanalysis lab. *(German)* 77−52686
- conversational data processing system for instrumental analysis *(Japanese)* 77−82496
- cooled and intensified array detectors 78−65983
- correlation NMR spectroscopy and appls. 79−49262
- crude oil classification, GC-MS-COM output pattern recognition 77−81456
- CW dye laser spectrometer with computer control 79−75618
- Darmstadt linear accelerator, detector system and performance of elec. scatt. system 78−70680
- Darmstadt linear accelerator electron scatt. facility, data processing 78−70681
- deconvolution method for use in small computers 79−76321
- deconvolution of spectra by least-squares fitting 78−64897
- deep-level transient spectroscopy, capacitance and conductance, using HP desk-top computer semiconductor processes and devices testing appl. 80−37091
- densitometer system for photographic spectral sensitivity meas. 78−29190
- desktop-computer controlled apparatus for measurements of optical spectra 80−31879
- digital interval synthesiser, computer-controlled 78−8386
- digital lock-in amplifier simulation 77−151
- digital modulator and synchronous demodulator system: an alternative to the analog phase detector 78−70107
- digital multidiscriminator for use in gamma-gamma coincidence experiments 78−70707
- digital phase-shifter for multiple quantum NMR 80−17974
- digitised EPR system, appln. to saturation transfer 80−77825
- discharge simulation, interactive programme, adaptation to disc supported microcomputer 80−24269
- dispersive IR spectrophotometry, on-line minicomputer system, design, appls. 77−63975
- dispersive IR spectroscopy 79−54205
- dispersive systems, IR spectroscopic data processing 79−49304
- diver-operable multiwavelength spectroradiometer 80−90251
- dual wavelength spectrophotometer, computer-controlled, for UV-vis. mol. absorpt. meas. 79−40620
- dual-grating direct-reading spectrograph mirror system design and performance 80−81397
- dye CW laser, on-line computer control, laser isotope separation appl. 78−70948
- dye laser spectrometer, computer controlled, time averaging to improve sensitivity 80−101850
- ELDOR spectrometer with computer-controlled scanning 77−1619
- electron energy loss spectroscopy, anal. appl., processing requirements 79−43692
- electron impact spectrometer, low energy, computer controlled, for mol. energy loss spectra 78−25756
- electron microprobe, automation using microcomputer system, anal. appl. 79−43703
- electron microprobe anal. using energy dispersive spectrometry 80−55765
- electron microprobe analysis, computer controlled beam-scanning and camera cct. 79−43706
- electron microscopy, scanning, high voltage computerised particulate charact. 79−48036
- electron probe anal., energy dispersive/wavelength dispersive combined X-ray system, automated control 79−43705
- electron probe analysis, electron beam positioning, computer automated 79−43704
- electron-probe computerisation development 79−11859
- emission quantum yield spectrometer and program system *(Japanese)* 79−89008
- emission spectrophotometry, review of data processing systems *(Japanese)* 78−88685
- emission spectroscopy signal-to-noise ratio improvement and data processing *(Japanese)* 77−21448
- ENDOR spectrometer, computer-controlled 79−80654
- energy loss spectroscopy, quant. microanal. of thin foils *(French)* 80−50900
- environmental sampling, gas chromatograph/mass spectrometer/data system and spectral search 77−77834
- EPR and ST-EPR spectra of nitroxide spin labels in rigid-lattice limit, rapid computer simulation 79−93189
- ESCA 36 spectrometer, advanced data anal. 77−90684
- ESCA for nondestructive charact. using TV type position sensitive detector 78−76969
- ESCA spectra automatic analysis by top down method *(Japanese)* 77−40598
- ESCA spectrometer, sample probe microcomputer automation 79−58846
- Fabry-Perot spectrograph, self-scanned photodiode array for image detect. *(French)* 80−73465
- far IR complex reflectivity meas., automated asymmetric interferometer 79−30534
- far IR Fourier spectrometer automation *(Russian)* 79−6192
- Febry-Perot interferometer, with automated data acquisition and stabilisation system 78−70180
- flood-plain delineation by multispectral data analysis 77−73885
- flow microfluorometry instrumentation, rapid data collection, analysis and graphics 78−86348
- fluorescence anal., computerised correction for excitation beam absorpt. 77−77818
- fluorescence decay times determ. in nanosec. and subnanosec. range 80−5443
- Fourier NMR spectroscopy, computer programmable digital pulse generator 80−98959
- Fourier spectrometer, 0.010 cm^{-1} working resolution, 20 to 1200 cm^{-1} 79−75603
- Fourier transform spectrometer, rapid scanning, very high resolution, data processing aspects 80−95150
- furnace at. absorpt. anal., computer-assisted, turnkey data system, natural water anal. appl. 77−77829
- gamma spectrometer, single-channel, transform. into computer controlled multichannel analyser 79−57765

computerised spectroscopy continued
- gamma spectrometer system for meas. isotopic and total Pu conc. in solns. 80−63363
- gamma spectroscopy on-line system, automatic sequencing using microprocessor controller 77−54393
- gamma spectroscopy system control., appl. of CAMAC system 78−37531
- gamma-gamma coincidence 2-D analysis 77−18733
- gamma-ray four-detector counting system, computer controlled 79−9957
- gamma-ray spectra, mobile computerised analysis and data processing system 79−9959
- gamma-ray spectra from Ge detectors, automatic anal. 77−3246
- gamma-ray spectra from heavy ion-nucleus reactions, interactive computerised system 79−9509
- gamma-ray spectrometer, remote computer-controlled, for nuclear power plant monitoring 79−9916
- gamma-ray spectrometry, original version of neutron activation analysis 79−11861
- gamma-ray spectrometry appl. in radiological protection meas., small computer system 79−9917
- gas analysis by computer-controlled microwave rotational spectrometry 78−85227
- gas chromatograph-mass spectrometer computer system, GCMS PAC-500 series *(Japanese)* 78−32918
- gas chromatograph/mass spectrometer/calculator, low-cost bench-top system 77−4972
- gas chromatography-mass spectrometry, computerised, data-blocking cross-correlation peak detection 80−62725
- gas chromatography-mass spectrometry data system, research-oriented, principles and applics. 80−40770
- gas chromatography-mass spectrometry integrated anal. systems, review 79−1972
- gas chromatography/mass spectrometry system with complete microprocessor control 77−44533
- gas chromatography/mass spectroscopy system, DP-102 80−22470
- GC/MS integrated systems, review of current techniques 80−68289
- graphics display terminal for spectral data analysis 78−54473
- high data rate spectrometers, computer coupling system *(German)* 79−49212
- high resolution scanning resonant Raman spectrometer 79−6185
- HISS computer facility 79−89559
- HP 8450A, UV/visible computerised spectrophotometer 80−31883
- INDOR, pseudo, heteronuclear selective decoupling, automatic, using Fourier transform NMR spectrometer appl. 79−93185
- inductively coupled plasma spectrometer, data processing using APL 79−17501
- internal reflection spectroscopy of biological samples *(German)* 79−5417
- IR, computerised dispersion system as alternative to Fourier transform method 77−82631
- IR, dispersive, industrial applications, for analysis in soln. 79−49305
- IR, microwave and Raman spectral data, simultaneous computer acquisition *(Japanese)* 80−4776
- IR absorption spectra, on-line processing system 78−4711
- IR analyser, microcomputer controlled, for multicomponent anal. 77−36822
- IR diffuse reflectance, Fourier transform spectrophotometer 77−5929
- IR microscopy coupled with scanning photoluminescence spectrophotometry 80−73447
- IR quantitative analysis, advancements and appl. 80−16746
- IR spectrophotometer, digital data acquisition/analysis system 80−73482
- IR spectrophotometer data processing system applications 80−90912
- IR spectroscopic equipment developments, review 79−67398
- IR spectroscopy, computerised, noise props. 80−86466
- laboratory-based computer, minis, midis and desk-top calculation 79−9984
- Leuven isotope separator on-line at CYCLONE cyclotron 78−70682
- light source development support spectroradiometric system *(Japanese)* 78−45733
- magnetic double focusing mass spectrometer, microprocessor controller for linked scans 80−101870
- magnetic spectrometers data acquisition and anal. 79−89530
- mass spectrometer, data acquisition and processing system, gas chromatograph input 80−13181
- mass spectrometer, mag. scanning, ion current meas., computer controlled electronics 78−8464
- mass spectrometer electron multiplier three-state time delay switch 80−37116
- mass spectrometer for isotopic solids anal. 78−78026
- mass spectrometer ion multiplier noise filter based on analogue delay device, anal. appl. 78−92541
- mass spectrometer to multichannel analyzer interface 80−27916
- mass spectrometers, selected fragment scans in direct mixture analysis, active computer monitoring and control 80−35597
- mass spectrometry, computerised data acquisition and interpretation, review 78−321
- mass spectrometry, technical aspects including data reduction and analysis 80−57417
- mass spectroscopy, smoothing of experimental ion kinetic energy data by digital computer 79−93112
- mass-analysed ion kinetic energy spectrometer, computer-controlled system 79−35884
- medium energy physics, data analysis, array processor appl. 79−89560
- megachannel gamma-gamma coincidence system using PDP-8/E computer and moving-head discs 77−57834
- Michelson Fourier transform stellar spectrometer 80−98552
- microbeam anal., conf., Ann Arbor, MI, USA (June 1978) 79−39258
- microcomputer based scanning instrument controller, for optical spectroscopy 78−93764
- microcomputer interfaced spectrophotometer for kinetic studies 80−62726
- microcomputer scanning system for respiratory mass spectrometer 78−88756
- microcomputer techniques *(Japanese)* 78−16855
- microcomputer-controlled microwave-optical spectrometer 80−86448
- microcomputer-controlled multichannel analyser for spectral measurement of short light pulses 79−93890
- microcomputer-controlled Raman spectrometer 80−27352
- microdensitometer with minicomputer connecting facilities 78−21198
- microdensitometer with minicomputer for semiautomatic interpret. of spectral plates 78−21199

computerised spectroscopy continued
microprocessor controlled data acquisition system, for pulsed laser spectroscopy 78—86341
microprocessor controlled optical spectrophotometer operational principle 79—26104
microprocessor-based spectroscopic instrumentation 80—9047
microprocessor-controlled apparatus for pulsed spectra meas. 80—68261
microprocessor-controlled pulse sequencer for pulsed NMR experiments 80—68231
microspectrofluorometry of biogenic amines, automatic correction of excitation spectra, on-line system 77—9308
microwave spectrometers, modern aspects, book contrib. 80—52328
minicomputer driven microprobe *(French)* 78—74111
minicomputer-based gamma spectrum analysis system SAMPO78 80—14043
minicomputer-operated optical spectroscopy laboratory and programming 77—74526
mixed n-γ field portable scintillation spectrometer with pulse shape discrimination 77—77992
modular minicomputer multiparameter data system, neutron spectrometer 77—23396
monochromator, minicomputer controlled, with repetitive optical scanner 78—27843
monochromator accessory module, microcomputer-controlled for dual wavelength operation 79—74440
monochromator scanning control system using microprocessor, spectral line shift correction *(Japanese)* 80—57384
Mossbauer CAMAC data acquisition system 79—30439
Mossbauer data acquisition system using minicomputer 78—90050
Mossbauer diffractometer using microcomputer 80—7210
Mossbauer microprocessor controlled spectrom. 79—97931
Mossbauer spectrom. system with data processing capability 77—30699
Mossbauer spectrometer, microcomputerised 79—67447
Mossbauer spectrometer, piezoelec., with fast channel advance rates, coupled to PDP8e computer 78—24904
Mossbauer spectrometer based on Motorola MEK 6800D1 microprocessor 78—37120
Mossbauer spectroscopy, automated complex, information retrieval and processing *(Russian)* 78—82091
Mossbauer systems, synchronous digital triangle generator and servo loop pre-amp 77—88351
multichannel analyser, built from microcomputer 79—58490
multichannel analyser to computer interface 79—93904
multichannel apparatus for material analysis using atomic spectra 80—76586
multichannel AutoAnalyzer automation 77—41686
multichannel Cerenkov mass spectrometer, automatic meas. of electronic apparatus characts. 79—26173
multichannel Cerenkov mass spectrometer, electronic recording apparatus 79—26174
multichannel scaling using 8-bit microcomputer 78—82595
multichannel spectrometer, quantometer, design trends for computerised control 79—80694
multilayer optical film thickness analyser 78—32785
neutron activation anal., absolute, computer-based system 79—11846
neutron activation anal., comparative, computer system 79—11855
neutron activation anal., control software for high throughput system 79—11849
neutron activation anal. instrumental, in US Geological Survey (Reston) 79—11850
neutron activation anal. of soils, computerised 77—44546
neutron activation analysis, instrumentation and software developments 77—90690
neutron activation analysis, multi-user computer system 79—11854
neutron diffractometer, reflection centring algorithm 78—75503
neutron irradiation short-lived products, rapid anal. using minicomputer based pulse height analyser 79—11866
neutron portable spectrom./kerma-rate meter, microprocessor system 77—54485
neutron spectrometer, triple-axis, computer-control system with CAMAC interface, program functions 77—19840
neutron spectrometer control using microprocessors *(German)* 79—49363
NMR, appl. of computers 80—54958
NMR, appl. of microcomputer system *(Japanese)* 79—75564
NMR, automated spin-lattice relax. time meas., pulse optimisation 77—21437
NMR, automatic system, for recording, processing and summation 80—27327
NMR, Fourier, S/N ratio optimisation, influence of receiver circuit and digital processing *(Czech)* 79—17461
NMR, multipurpose 7T, with superconducting magnet 79—97411
NMR, pulse type, programmable pulse sequence generator 80—17979
NMR Fourier transform spectroscopy *(Czech)* 80—17984
NMR frequency-ratio spectrometer for investigating isotopic effects of light nuclei 79—21793
NMR in undergrad. instruction, general purpose microcomputers use for hypothetical spectra synthesis 80—42009
NMR relaxation times, computer-assisted meas. method 77—22586
NMR spectrometer, for quantitative analysis, microprocessor-controlled digital integrator 80—11971
NMR spectrometer, FT, multipurpose, design and computer interfaces 80—86362
NMR spectrometer, pulse, controlled by programmable digital unit *(Czech)* 78—77952
NMR spectrometer interfacing 79—12828
NMR spectrometer-computer interface, demonstration expt., signal averaging influences on S/N ratio 80—36813
NMR spectrometers, time-sharing control by minicomputer 79—93192
nonflame atomiser, programmed unit for at. absorpt. anal. 78—54462
NQR, electronics appls. 80—63668
nuclear instrumentation, standard microprocessor based 80—36822
ODMR spectrometer system, use of signal averager with minicomputer facilities for control, data recording and evaluation 80—31825
Omega spectrometer, CERN, modular trigger basic techniques 80—58104
one-arm magnetic spectrometer, Alfa facility, description and characts. 79—26809
optical constant calculation from frustrated total internal reflection meas. 79—33658
optical instrument appls. 79—54192

computerised spectroscopy continued
optical multichannel spectrometric detectors, vidicon, online data handling capability 78—74077
optical spectra, direct encoding using computer interfaced vidicon TV camera 77—10114
optical systems conf. San Siego, CA, USA (Aug. 1978) 79—76356
phosphate and alkaline phosphate activity determ. by dual microcomputer-controlled stopped-flow spectrometer 80—57379
photoelectron spectrometer for valence shell electrons ang. distrib. meas. 77—58202
photographically recorded spark source mass spectra 79—43658
photoionisation mass spectrometer 80—77905
photon correlation in nanosecond range using programmable digital counter, photomultiplier evaluation 78—54464
photon counting spectrometer, computer controlled, rapid scanning of low light level spectra 78—86338
photon flare centre determ., online optoelectronic convertor *(Russian)* 79—75111
photosensor spectral responsivity calibration microprocessor system 80—86409
physiocochemical meas., modular equipment and microprocessor control *(French)* 80—30304
plasma diagnostics, automatic system for addition at. conc. meas. in MHD generator 79—50892
PLT Tokamak cyclotron radiation Fourier transform spectral analysis 79—32815
polymer film, formation, time-lapse IR spectroscopic obs. 79—74458
PQR line shape, digital-analogue interface for data processing 79—45615
programmable multielement atomic absorption system 78—80803
programmable timer for pulsed NMR spectrometers 79—40598
Pu nondestructive assay, gamma-spectrometric method 79—81068
pulse height analyser data, on-line method for peak area determ. 79—755
pulse height analysers, windowless stabilisation scheme 79—9976
pulse height analysis computer system 79—9975
pulsed FT NQR, automation for Zeeman studies of single crystals 80—66066
pulsed NMR relaxation, computer controlled, general programme 78—4669
Quadmagnova, GC/MS system, computer scanning and control 78—76946
quadrupole analyser, automatic operation using microprocessor systems *(French)* 79—54212
quadrupole mass filter, computer simulation of ion trajectories in quadrupole field 80—52349
radiative decay curve anal., computer applications *(Hungarian)* 79—45617
radioactive waste, control and accountability by gamma scan assay 79—9913
radiotelescope spectrometer, computer controlled receiver *(Russian)* 77—9674
Raman spectra, digital processing 77—61131
Raman spectrometer, digital control system, appl. to soft mode spectroscopy 78—86345
Raman spectrometer, scanning and computer controlled, for study of gases 79—26148
rapid-scan spectroscopy, at NAVWPNSUPPCEN Crane 78—41362
reaction products, weak excitation spectra, automatic recording of laser-induced fluorescence signal 80—76574
residual gas analyser, microprocessor-based 79—26175
rocks, minerals, anal. of small samples using X-ray quantometer 78—61112
rocks, multielement analysis with DFS-36 quantometer and ES-1020 computer 79—70392
scanning dye laser, microprocessor controlled, for spectrometric anal. systems 78—20081
scintillation spectrometer, photomultiplier gain stabilization, computer control software 78—13369
scintillation spectroscopy, organic, use of logarithmic pulse height and energy scales 80—37690
SHG, computer controlled intracavity, in CW ring dye laser 80—91841
sickle cell anaemia sickling kinetics, multiangle laser scatt. spectrophotometer 79—79494
SIMS, computerised system for energy spectra determ. 80—3423
small-spot scanning IR spectrophotometer head 78—29133
specimen heating and cooling installation, programmed, for MKh 1303 spectrometer 79—93253
spectrochemical analysis, photographic emulsion calibration technique 79—79321
spectrochemical analysis in hydrocarbon flames, computer processed laser Raman spectra 79—43652
Spectronic 2000 spectrophotometer, interactive microprocessor-controlled instrument 80—105716
spectrophotometer, automated clinical/analytical system 77—52687
spectrophotometer, high-energy, 0.25-2.4 μm, for rapid food constituent anal. 79—17508
spectrophotometric measurement, dual wavelength, precision optimisation 79—92019
spectroradiometry automation and applications 78—12740
SPEKOL 20 routine spectrophotometer 79—54167
standard spectrometric source conversion peak half-width determ. 77—79499
steelworks computerised spectrometric analysis and management information system 80—89574
stopped-flow spectrophotometry, fully automated, with hierarchical computer controlled system 77—21426
super modified simplex, appl. to flame spectrophotometry 78—3397
thermal desorption mass spectroscopy, computer control, data acquisition, appls. 80—61181
thermal ionisation spectrometry with automatic data eval. for isotopic comp. determ. of U and Pu 80—66913
time domain spectrometer system, on-line 80—271
time resolved spectroscopy, techniques with image detector (OMA 2) 79—75614
time-of-flight analysis cross-correlation, for molecular beam scattering 79—55000
time-of-flight mass spectrometer, computer interfaced, gas-phase reactions anal. 80—71967
time-resolved X-ray diffraction counter and data acquisition system 78—45758

computerised spectroscopy continued
- TOF spectrum, computer interaction through direct memory access and with buffer memory 78—70685
- toxic gas monitor based on laser photoacoustic spectrometer *(German)* 80—12046
- toxic substances identification using online infrared system 77—90709
- tunable acoustooptic narrow band optical filters, appl. computer-controlled spectroscopy 77—75705
- tunable diode laser spectrometer, rapid-scanning computer-controlled 80—101854
- TV camera and microcomputer appl. to instantaneous spectra meas. *(Japanese)* 80—31888
- two-photon spectrometer for organic crystals 78—58064
- US Doppler spectragrams refreshed display and haemodynamic parameter meas. 80—41152
- UV spectrometers, on OSO-8, computer-controlled, mission operations 80—41723
- UV-visible spectrophotometer, rapid scanning, computerised, automatic absorbance calibration method 77—67509
- UV/vis spectrophotometry, use of automation in achieving improved accuracy 80—27356
- vibrational transducer anal. from piezoelectric polymer transducers 78—29105
- video fluorometer, computer-controlled, multichannel, features 79—20495
- vidicon spectrograph for multichannel detection of Raman spectra 77—74518
- vidicon-camera parallel-detection system for angle-resolved electron spectroscopy 80—4817
- vocal pitch extraction and visual display using computer 77—52807
- voltammetry, cyclic, AC, on-line digital FFT faradaic admittance data acquisition 78—61118
- Wang type 720C for remelting process anal. 78—23560
- X-ray analysis, high-speed, profile fitting method 78—75492
- X-ray double crystal spectrometer, microcomputer automatic control *(Polish)* 80—32563
- X-ray fluoresc. anal. system for small medical samples, computerised target changer 77—60249
- X-ray fluoresc. spectrograph, automatic computerised, for rock trace elemnt anal. 77—56320
- X-ray fluoresc. spectrometer, multichannel, computerised, for air particulate anal. 77—60170
- X-ray fluoresc. spectrometer system, automated, for chem. shift meas. 78—4750
- X-ray fluorescence analyser, computer-controlled 78—23982
- X-ray fluorescence analyser with minicomputer *(German)* 78—88677
- X-ray fluorescence in vitro, medical applications, automated system 77—5063
- X-ray fluorescence spectrometer system, PW1400, microprocessor controlled *(German)* 80—16758
- X-ray fluorescence spectrometry, single and multielement anal., optimum excitation conditions, automated determ. 80—323
- X-ray photoelectron spectroscopy, quantitative, parameters, appls. 79—43697
- X-ray residual stress anal., computer controlled, software, precision 78—5712
- X-ray spectra, nonlinear least squares anal. of full-energy peaks 77—88328
- X-ray spectrometer, automated, qualitative anal. 80—22497
- X-ray spectrometer, computer controlled, for steel alloying element determs. 77—56318
- X-ray spectrometer, full automation of Philips 1220 model 77—196
- X-ray spectrometer control, interactive program for data collection, manipulation chem. anal. appl. 78—7312
- X-ray spectrometry, data interpretation, online system using multivariate statistical anal. and pattern recognition 80—3461
- X-ray spectrometry, quantitative, comparison of mathematical models 79—17587
- CO$_2$ laser Helios fusion system beam diagnostics 80—78882
- ^{252}Cf-^{235}U subcritical multiplier, computer-controlled cyclic activation anal. 79—11865
- Cl monitoring using TAGA mass spectrometer-based instrumentation and minicomputer system 80—72114
- ^{57}Fe Mossbauer spectroscopy, added precision 77—88327
- Ge(Li), automatic anal. of complex γ-ray spectra 78—33370
- LiNbO$_3$ computer-controlled IR parametric oscillator source 77—19365
- LiNbO$_3$ computer-controlled Nd:YAG-pumped parametric oscillator 77—54758
- NaI(Tl) scintillation detectors, microprocessor-based multichannel analyser 80—91378
- Si detectors, automatic anal. of complex charged particle spectra 78—33370
- Si, polycrystalline, film thickness meas., visible spectral reflectance analysis 78—32786
- Si(Li) electron spectrometer on-line with an automatic irradiation apparatus 78—90014
- Si(Li) energy dispersive X-ray spectra 79—1981
- U, mass analysis for accountability in nucl. fuel processing 79—16112
- U resource survey, NURAB system for processing neutron activated samples 79—11847
- X-ray fluorescence analysis energy-dispersive, for nondestructive assay of nuclear materials 80—83163

computerised test equipment *see automatic test equipment*

computerised tomography
- 3D imaging with a restricted view angle 80—17066
- 3D real time display diagnosis 80—51182
- γ attenuation correction, reconstruction algorithm 78—40307
- abdominal abscesses detection, role of ^{67}Ga-scintigraphy, ultrasonography and CT 80—17096
- abdominal aortic aneurisms, US and X-ray CT diagnostics *(German)* 79—79616
- abdominal aortic aneurysms, comparative study with ultrasonography 79—29586
- abdominal diseases diagnosis and management 78—88739
- abdominal examination, increased diagnostic capabilities with fan beam unit 79—66550
- abdominal infection evaluation, complementary role of ^{67}Ga-citrate imaging and computed tomography 78—73207
- abdominal organs, in vitro, effect of preservation on attenuation coeff. 77—56449
- abdominal tomodensitometry with opacification *(French)* 79—66551

computerised tomography continued
- abdominal tumours, CT biopsy, aids for lesion localisation 79—92365
- accurate fan-beam reconstruction 78—78931
- acoustic attenuation reconstruction from back-scatt. US 80—30821
- acoustical imaging, US visualization and characterization, conf., vol.8, Key Biscayne, FL, USA (May-June 1978) 80—83720
- ACTA 77—60259
- adrenal gland CT 79—92364
- air pollution remote monitoring, two-dimens., via computerised tomography 79—39330
- Algebraic Reconstruction Techniques, modifications 80—3774
- algorithms for reconstruction 80—17114
- aliasing artifacts with filtered-backprojection algorithm reconstruction 80—26329
- analogue optical method of information processing *(French)* 80—94349
- anatomical cross-section determ. using radiotherapy simulator, for treatment planning 78—61244
- anatomical cross-sectional geometry and density distribution data base 80—101287
- anatomical feature or lesion volume estimation algorithm 80—98080
- angio-tomographic device, posterior fossa midline visualisation 79—34642
- angiograms, augmentation of computed tomograms 80—8150
- artefact and error considerations 80—36099
- artifacts, nonlinear, partial vol., correct. algorithms 80—76829
- attenuation coefficient absolute values 79—83918
- automated scene analysis of CT scans 80—41175
- autoradiography, coating of slides with nuclear emulsions, new semiautomatic device 77—70574
- autoradiography, study of renal localisation of ^{99m}Tc labelled pharmaceuticals, rat 77—56463
- autoradiography of diffusible substances using electron microscope and ultrathin frozen sections 77—60314
- axial, complementary role with radionuclide brain imaging 77—77975
- axial, computerised, abdominal area appl. 77—44782
- axial, equipment and technique *(Danish)* 77—52862
- axial, for teaching 78—49619
- axial, half back-projection 78—28056
- axial, impact of EMI scanning on meningioma diagnosis 77—5061
- axial, transmission and emission techniques review 77—77973
- beam analysis tomography, current density and transverse/longit. emittance reconstruction 79—49336
- beam hardening, post-reconstruction method for correction 79—39491
- beam hardening artifact explanation 79—83931
- beam hardening correction, polyenergetic X-ray beam 79—25082
- beam hardening correction 78—65125
- beam hardening reduction, calc. method 78—80951
- beam-hardening correction method illustration 80—46042
- beam-hardening corrections, uncertainties 80—46041
- Bevalac, computed tomographic radiotherapy beam profile reconstruction with multiwire proportional chamber 79—79631
- biliary ductal system, status demonstating ability of ultrasonography and body CT scanning 79—92310
- biliary tract disorders, evaluation by cholescintigraphy, ultrasonography and CT 80—17093
- biomedical, Siretom 2000 initial clinical experience 78—28038
- biomedical, Somatom fast whole body computer tomograph with direct image reproduction 78—28036
- biomedical head unit, Siretom 2000, operation 78—28037
- bladder cancer management, value of CT 79—88160
- blood pump human fitting 78—40432
- body, brain scanning, economic, medical justification 79—57766
- body organ moulded picture representation 78—35951
- body scanners, comparison of translate-rotate, pure rotary types 78—69211
- body scanning by longitudino-axial sectioning 80—41177
- body spine visualisation program development 79—88212
- body tomography, single photon emission, nuclear medicine computer interfaced to Anger multiplane scanner 80—61665
- bolus material of shredded-gel for use with EMI CT 1010 brain scanner 80—41173
- bone Ca level meas. using computerised tomography, correl. with ACTA numbers 77—40756
- bone mineral measurement using EMI scanner vs. densitometry 78—24119
- bone tumour evaluation, contribution of CT 79—66552
- boundary-finding scheme and complex object location 80—98104
- brain, anatomic and pathologic correls. 79—34636
- brain, baboon, ^{11}C-flunitrazepam displacement visualisation 79—83730
- brain, clinical interest of coronal and sagittal sections 79—29587
- brain, contrast 77—86608
- brain, CT scanning, traumatic and emergency patients 79—34639
- brain, experimental oedema, serial meas. of specific gravity and CT attenuation 80—98005
- brain, imaging, comparative study with γ-camera, single-photon emission CT, and transmission CT 80—109004
- brain, irrad. quantitative assess. by CT scan anal. 80—72306
- brain, neurodiagnostic studies and head injury management 79—39470
- brain, positron imaging device for dynamic studies 79—48327
- brain, sella and parasella lesions, sagittal and coronal reconstructs. 79—39471
- brain, Xe regional kinetics meas., imaging methods in transmission CT 80—98131
- brain abscess, electroencephalographic computerised tomographic correls. 79 -83899
- brain and body imaging, review 79—34659
- brain and spine appls. 80—30886
- brain CT, dose to thyroid and eye 79—92389
- brain diagnosis, comparative study of radionuclides and CT 80—72320
- brain imager, transverse-section, for single-gamma emitters 80—3794
- brain images, automated anal. 80—8151
- brain imaging, role and relation of CT to radionuclide imaging 79—34637
- brain lesions, isodense, shape anal. 80—8152
- brain metastasis, clinical symptomatology 79—29584
- brain tumours contribs. of histograms to CT study 79—66548
- brain US imaging through skull 80—51185
- breast calcifications, tomographic visualization by US scatt. 79—66497
- breast tissue characterisation in vivo by US TOF computed tomography 80—51186
- Buddha sculpture survey using X-ray computed tomography *(Japanese)* 80—101915

computerised tomography continued
cardiac blood pool, ECG-gated emission CT 80—98117
cardiac imaging, ECG-coated, motion phantom 80—98115
cardiac imaging with ^{11}C-palmitate and PETT IV system 80—89849
cardiac insufficiency, criteria in X-radiology *(German)* 79—53237
cardiac muscle stress/strain relationship determ. 79—92262
cardiac studies 80—98088
cardiotomography, methods and results of morphological anal. 79—34647
cardiovascular dynamics instrumentation evolution (1940-80) 79—83983
cardiovascular imaging by transmission computed tomography 80—36121
cardiovascular measurements, conf., Bellingham, USA (Sept. '78) 80—31419
cerebral angiotomography, simultaneous multisection method 80—98127
cerebral blood flow, confidence limits with positron emission system 79—11994
cerebral blood volume meas. by ^{11}C-labelled carboxyhaemoglobin 80—8134
cerebral regional blood volume, meas. with EMI 1010 scanner 79—53212
cerebral regional blood volume, variations meas. 79—29583
cerebral vascular disease, experience with radionuclide imaging and computed tomography 77—77977
cerebrovascular disorders, CT diagnosis, review 79—34638
chest and abdomen exploration 78—7433
circulatory system visualisation, 250 simultaneous scans by new CT system 79—79625
cisterna magna, unusually large, plain film, angiographic and CT indications 79—66549
coded aperture imaging, analogical deconvolution *(French)* 78—35943
coded aperture imaging, qualitative and quantitative 80—89843
coded aperture tomography, one-dimens., ODCAT 80—17126
coding sequences for classical tomographic imagery reconstruction 79—8530
colour TV imaging computer peripheral 79—20667
computer assisted ring detector positron camera system for brain reconstruction tomography 78—40306
computer tomography, radionuclide imaging and ultrasonography in hepatic mass lesions 79—88211
computerised scintillation camera transaxial tomograph, Humongotron 77—52867
computerised tomography, image enhancement techniques 77—77987
computerised tomography, patient scanning time and picture quality improvements 77—25550
computerised tomography, resource sharing computer hierarchy for 3D image reconstruct. 80—26345
computerised tomography of head with ^{99m}Tc and scintillation camera 77—52866
conference, Haifa, Israel, (Aug. 78) 80—27035
conference, international congress of radiology, Rio de Janeiro, Brazil (Oct. 1977) 79—16284
conference on nuclear power systems, Washington, USA (1978) 79—41045
congenital intracranial vascular malformation detect., scintigraphy vs. tomography and angiography 78—77104
contrast dose for enhancement of brain CTs 79—88193
contrast enhancement, quantitative aspects in cranial CT 79—92360
convolution approximations, ultra-fast 79—66511
convolution kernels, breast scans 80—41216
convolution method for image reconstruction from projections 80—46043
convolution reconstruction algorithms comparison, fan beam *(Japanese)* 79—57760
convolution reconstruction technique for divergent beams 77—12987
convolutional techniques in three-dimensional image reconstruction, generalised correction functions 79—25085
convolving kernels, high speed, for CT with triangular spectra and/or binary values 79—66515
cost-effectiveness considerations in evaluation of new technology 78—69192
cranial, vs. radionuclide brain scan, clinical efficacy and cost anal. 77—77974
cranial CT, valve and limitations in spreading process diagnosis *(German)* 80—36105
cranial CT scans, picture processing, image anal. and computer graphics appl. 80—8183
cranial scintigraphy, value of adding emission CT sections to conventional pertechnetate images 80—56187
craniocerebral CT scanning in the neonate, review 79—34640
craniofacial anomaly assessment, computerised versus conventional tomography 78—73239
cross-sectional reconstruction, correction for spectral artifacts 77—21621
curvelinear view generation from CAT scanned data 80—8149
cylindrical, appl. to intact circulatory system 77—77971
cylindrical scanning, high temporal resolution, appls. to physiology and medicine 80—30885
data acquisition and reconstruction algorithm 77—77979
data treatment in transaxial tomography, optical improvement 79—34666
definition and scientific basis, health care needs, appls. and costs 80—36115
Delta Scan, computerised entire body transverse scanner, technical description 77—44781
density function for diverging X-ray beams, fast digital convolution technique 78—58099
density reconstruction using arbitrary ray-sampling schemes 78—80954
depth-dose distribution, effect of slice thickness 80—46038
detectability in CT images 80—3806
detector vibr. sensitivity 78—35955
development and prospects, three generations equipments survey *(Italian)* 79—25061
digital enhancement of axial tomograms 79—70630
digital image processing applications, seminar, San Diego, CA, USA (Aug. 79) 80—105424
digital image-enhancement, used for human anatomy scanning 80—94408
digital processing appls. 80—98103
digital video image processor for real-time X-ray subtraction imaging 79—25080
display instrumentation *(Japanese)* 79—70688
display of three-dimensional information in computed tomography 79—70606
displays, review 77—81571
distortion problems in secondary-scan reconstruction in CAT 80—104729
divergent beam reconstruction algorithms compared 79—83932

computerised tomography continued
divergent beam X-ray transform, math. theory 78—96088
divergent beams, reconstruction, comparison of algorithms with and without rebinning 80—98066
diverging X-ray beam, reconstruction algorithm 77—70535
dose determination method 80—21542
dose from CT scan, meas. using pencil shaped ionisation chamber 79—20683
dose rate as ultimate limit for spatial and density resolution 79—83935
dose reduction in X-ray computed tomography using a generalized filter 79—83946
dose reduction using a generalised filter 79—66557
dose specification philosophy 79—16309
dosimetry, exposure meas. techniques 78—69212
dual energy scanning, noise considerations 80—3804
dual-energy, optimum energies 80—56205
dual-energy scans, data processing 78—69215
dynamic 3D imaging system for cardiac structures and functions 78—44600
dynamic boundary surface detect. algorithm 77—78019
dynamic emission computed tomography, quantitative pots. 78—77105
dynamic spatial reconstructor, high temporal resolution scanner 80—51235
ECG synchronised, time cutting methods using special X-ray generator 79—66538
edge coincidence segmentation for medical images 80—109012
edge position uncertainty reduction 80—98105
effective photon energy and linearity meas. 80—30841
electric impedance CT, a new imaging technique 79—66500
electrical conductivity and permittivity imaging 80—98055
electrical parameters imaging inside a patient, CT technique 80—8117
electron density and at. no. determ. 77—81553
electronic file for X-ray pictures 80—101288
elemental anal., usefulness of photon mass attenuation coeff. 78—77108
EMI brain scanner, collimation effects on performance characts. 78—53484
EMI brain scanner, patient dose 78—28080
EMI first generation scanner, dose rel. to collimator geometry 79—74760
EMI general purpose scanner 77—5060
EMI scanner picture automatic outlining, for radio therapy treatment planning 80—41206
emission, double-tracer, multiple-organ, transaxial, radiotracer distribs. localisation and characterisation 80—98128
emission, review 80—56213
emission axial CT from multiple γ-camera views using freq. filtering 80—94321
emission computed tomography, appls. of nuclear medicine, review, review *(Japanese)* 79—70610
emission computed tomography, CCA system 78—73285
emission computed tomography, Compton scatter correction, integral transport method 80—61683
emission computed tomography stimulator, design 80—61672
emission CT, single photon, current status 79—66526
emission CT system, expt. meas. of impulse response and noise 80—56182
emission tomographic system design 79—53276
emission tomography, attenuation correction and incomplete projection 79—66532
emission tomography, comparison of scanner and camera systems 79—66529
emission tomography, improved coded-aperture system 79—66534
emission tomography, simultaneous calcs. of attenuation and activity coeffs. 79—66531
emission tomography, single-photon, physical attributes 80—109007
emission transaxial tomography, effect of Compton scatt. photons 79—66530
encephalic exploration, clinical value of single photon emission CT 80—51216
energy selective and conventional systems, noise and dose comparisons 79—66540
engineering status 77—73571
equipment, for intracranial diagnosis 78—31884
equipment and reconstructive methods, review 80—30849
evaluation of CT scanning, cost containment 80—36117
evolution and current status of CT X-ray scanners 79—53225
eye socket, X-ray computerised tomography for medical diagnosis *(German)* 79—100727
facial bone scanning by emission tomography 78—31892
fan beam systems, scatter effects 77—5097
fan-beam geometry, consistent projection sets 80—30884
fan-beam reconstruction methods 80—26337
fan-beam scanners, circular artefacts reduction 78—35924
fan-beam scanners, suppression of ring artefacts by software algorithm 79—5394
fan-beam to parallel-beam conversion by rubber sheet transformation 80—109009
fast edge detection, 3-D clinical appl. 80—8181
fast multiwire proportional chamber data encoding system for proton tomography 79—92337
field measurement utilising the partial vol. effect 80—89865
filter function technique for tomographic reconstruction 80—61729
filter gain in reconstruction tomography 79—83919
filtered neutron-beam computed axial tomography 80—101258
first image reconstruction based on Radon inversion formula 78—77109
flashing tomosynthesis: three-dimensional X-ray imaging 80—26325
flashing tomosynthesis system, using simultaneously 25 X-ray tubes 80—81768
fluid characterisation by US and CT 80—98045
fluoroscopic image as input data 79—66518
focal spot intensity distrib. and collimator width effects 79—70622
focal-plane tomography, image reconstruction using digital computer 80—61674
Fourier transform image reconstruction, polar sampling theorems 79—92373
Fourier transform reconstruction in CAT by exact interpolation 80—21538
functional principles and applications *(French)* 79—70691
gamma camera, computer controlled 80—61682
gamma camera, electronically collimated, for single gamma emission computed tomography 78—44603
gamma transaxial tomography, focused collimator scanner 79—66519

computerised tomography continued
  gamma-ray camera using Compton effect 78—10087
  gantry geometry rel. to aliasing and other geometry dependent errors 80—81695
  generalized image synthesis from projections 80—67579
  geometrical enlargement in CT scanning 80—41200
  geophysical EM remote sensing, appl. 80—77169
  geophysical techniques 80—82114
  glioblastoma tumour volume monitoring, autopsy rel. to CT meas. 80—21526
  global local edge coincidence segmentation 80—98101
  global Local edge coincidence segmentation for computer tomography images 80—8180
  graphic display system 78—3578
  grey matter calcification secondary to radiation therapy 77—56424
  grey-scale image recording systems, comparison of 9 different types 79—16319
  head and neck 3-D mapping derived from computed tomographic serial scans 80—8148
  head CT, new scanning method 79—66542
  head CT using ^{99M}Tc 77—52866
  head scanner, dose distrib. 79—83940
  head scanner, translate-rotate type with Xe detectors, performance characts. 80—46036
  health risks due to radiation exposure 80—61654
  heart, CT of normal and infarcted patients 80—30859
  heart and circulation, dynamic spatial reconstruction system 79—66520
  heart imaging, new design for high speed CT 79—66544
  heart imaging from computerized tomography 78—88741
  heavy ion therapy, treatment planning programme 80—72295
  heavy particle computed tomography 80—8146
  hepatic mass evaluation, relationship of ultrasonography, nuclear medicine and CT 80—17092
  hierarchical computer networks for processing data base generated by X-ray CT scanner 80—81732
  high speed, special purpose digital processor architectures and numerical approx. methods 80—30878
  high temporal resolution, appls. to physiology and medicine 80—56214
  high-speed X-ray cylindrical scanning multiaxial computerised tomography unit 78—80956
  hip joint clinical investigations *(German)* 79—83921
  history, early 2D reconstruction and recent topics stemming from it 80—86029
  Hounsfield, G.N., Nobel Award Address 80—86030
  Hounsfield number definition and computerised tomography number conversion 78—35952
  human body in vivo, mass density distrib. meas. 77—12992
  human body in vivo, mass density distrib. meas. 77—29198
  human body in vivo, mass density distrib. meas. 77—29199
  hybrid system for X-ray transmission and positron tomography using $Bi_4Ge_3O_{12}$ scintillators 78—48876
  hydrocephalus, role of computed cranial tomography and radionuclide cisternography 77—77978
  hyperthermia, nonintrusive meas. by US temperature tomography 79—53282
  IEEE statement on technology development 80—41199
  image algorithm improved for CT scanners 79—20664
  image artifacts due to nonlinear shadows, classification 79—66539
  image boundary detect. 78—40326
  image boundary finding and complex object localisation 80—109016
  image construction, restoration and enhancement 77—44743
  image correction with simulation 80—85470
  image discrepancies due to object-time depend. in several geometries 80—46044
  image display by TV and photography 80—8129
  image display system 80—46039
  image documentation, state of the art and outlook 79—62338
  image enhancement techniques 77—77987
  image enhancement techniques 79—25102
  image formation using fan-beam scanning and noncircular source motion 80—101913
  image function reconstruction from noisy data in low-dose case, algorithm based on Wiener filter *(Korean)* 80—76824
  image noise and smoothing in scanners 78—85368
  image processing 78—35950
  image processing and evaluation using PDP-10 computer 78—44587
  image processing appl. of multiple bandpass filters 80—109002
  image processing of scans, sigma scan 80—17111
  image processing techniques and comparison with standard radiography 80—12250
  image quality evaluation phantom 77—73573
  image quality in photon imaging 80—81687
  image reconstruction, basic physics and maths. 78—73218
  image reconstruction, Fourier techniques evaluation in relation to number of X-ray sums 78—77112
  image reconstruction, interpolation effect 78—77110
  image reconstruction, linear and modified cubic spline interpolation 79—83929
  image reconstruction, linear rel. to modified cubic spline interpolation 79—66545
  image reconstruction, projection completion methods 78—42285
  image reconstruction, quadratic optimisation 77—16981
  image reconstruction *(French)* 77—37037
  image reconstruction by projection, review *(Italian)* 79—53207
  image reconstruction filters, Fourier convolution algorithm for three-dimensional density function, critical review of previous filters *(Korean)* 80—72313
  image reconstruction formulae, computer implementation 80—52179
  image reconstruction from divergent ray, 3D 79—98299
  image reconstruction from hollow and truncated projections, theory 78—24912
  image reconstruction from projections, blurring due to object movement 80—78784
  image reconstruction from projections, book 80—51961
  image reconstruction from projections 80—52178
  image reconstruction principles in X-ray tomography 78—88745
  image reconstruction processor 79—100738
  image reconstruction using polar sampling theorems 79—81366
  image reconstruction using two-dimens. kernels formed by simple back-projection,, ramp filter realisation *(Korean)* 80—72275
  image reconstruction with limited angle projection data 79—66508

computerised tomography continued
  image restoration and enhancement, conf., London, England (Dec. 1978) 79—25101
  image second-order statistics, information and artifacts 80—46040
  image statistics, information and artifact 80—81713
  image statistics 80—8159
  image understanding systems, seminar, San Diego, CA, USA (Aug. 79) 80—94918
  imaged distribution, continuous time-dependence 79—20662
  imagery, interactive meas. 77—77984
  images, display processing, digital enhancement 78—48875
  imaging system, 3D, based on serial tomograms, processing system 79—83859
  imaging techniques, book 80—12861
  imaging techniques, developments, review 80—26324
  incomplete geometries in fast X-ray scanner 78—80952
  incomplete measurement data preprocessing procedures 80—3803
  industrial NDT computed transverse axial tomography system 80—89430
  information extraction at different energies 79—39488
  interstitial dosimetry, utilisation of the CT scanner 80—104770
  intra-orbital foreign bodies detection 78—3577
  intracavity radiotherapy, interactive treatment planning using CT 80—8145
  intracerebral spontaneous haematoma diagnosis and prognosis 78—73195
  intracranial cystic abnormalities, children, CT diagnosis, review 79—34641
  intracranial mass lesion detection, computerised cranial tomography and radionuclide imaging 77—77976
  intracranial meningioma diagnosis, use of CT 80—17058
  intracranial vascular malformations, use of CT in diagnosis 80—21525
  intrathoracic space demands, CT representation *(German)* 80—109018
  iodinated contrast studies, optimum energy study 80—81685
  ion exchange membranes, ion diffusion studied by autoradiography 77—90637
  isodoses in human radiotherapy, automatic determ. using whole body computer tomography *(German)* 77—9236
  iterative reconstruction algorithms 77—12988
  iterative three dimensional reconstruct. from twin cone beam projections, simulation study 78—80949
  Japan, devel. of computerised tomography and US technology 80—30879
  kidney diseases, value of CT *(German)* 80—76832
  limited data, image reconstruction using polar pixel Kalman filter 80—98095
  liver, comparison of radionuclide imaging, computer tomography and grey-scale US 77—52864
  liver, comparison of scintigraphy, US and computerised tomography scanning 80—17105
  liver, comparison with nucl. medicine scans 80—17109
  liver, nuclear imaging, comparison of conventional rectilinear and multiplane tomographic scanning 80—17106
  liver and biliary tract 80—17108
  liver carcinoma, VX2, improved detectability in the rabbit with contrast enhancement 80—98118
  liver hepatoma, dog, evaluation of 3 imaging instruments 80—17074
  liver volume measurement by emission CT 80—12230
  longitudinal, bilateral collimator, gamma camera and minicomputer 80—61666
  longitudinal radioisotope tomograph 77—81556
  lung dose in half body radiotherapy, determ. by CT 80—104763
  machines, back projection speed improvement for 3-D reconstruction 78—4742
  machines generalised $|\omega|$ filter for 3-D reconstruction 78—4741
  maximum entropy reconstruction from cone-beam projection data 79—39469
  mediastinum diseases diagnosis appl. *(French)* 80—85473
  medical appl. *(Japanese)* 79—5355
  medical diagnostics problems of computer applications *(German)* 79—20696
  medical imaging, conf., San Diego, USA, (Aug 1978) 80—17025
  medical imaging, conference, San Diego, USA (Aug. 1979) 80—94919
  medical imaging overview 80—98082
  medical imaging systems, information capacity considerations 80—98090
  medical microprocessor applications and costs 79—44011
  medical physics conf., Atlanta, USA (July-Aug. 1979) 79—83858
  medical physics conference, Ottawa, Canada (Jul. 1976) 77—16897
  merits rel. to US and radionuclide imaging 79—48324
  metals, autoradiographic study of H distrib., exptl. difficulties 77—52586
  microbeam X-ray scan system using interactive display terminal *(Japanese)* 77—81563
  microprocessor based interactive radiographic image display 79—25092
  microwave CT, 10.5 GHz 80—104719
  microwave scanner for soft tissue tumour detect. 80—17054
  motion blur recovery technique, system resolution recovery, appl. to X-ray computerised tomography 80—105756
  MTF determination from edge response function, single step calc. 78—35938
  MTF meas. method appl. to EMI head scanner 77—48864
  Muehllehner's tomographic camera, quantitative evaluation of depth effect 77—86609
  multichannel semiconductor detectors for X-ray transmission computed tomography 80—58058
  multidimensional space and time signal processing in biology and medicine 80—85493
  multiplanar emission tomography, new method using a 7 pinhole collimator and Anger scintillation camera 79—16281
  multiplane tomographic scintillation camera image quality improvement 79—92338
  multiple window display techniques 80—98099
  multiple window display techniques 80—109010
  multiple-energy scans, increased tissue differentation using colour display 80—98125
  multislice reconstruction from twin-cone beam scanning 79—66546
  multispectral X-ray computed tomography and its evaluation by principal component analysis 80—8182
  myocardial ^{201}Tl scintigram anal., nonredundant coded aperture tomographic method 80—94364
  myocardial ^{201}Tl scintigram anal. by coded aperture imaging 79—79647
  myocardial infarction, acute, ^{99m}Tc imaging in dogs, emission-computed tomography appl. 79—79638
  myocardial perfusion imaging with ^{201}Tl, single photon emission CT *(Japanese)* 80—98114

computerised tomography continued
myocardial perfusion tomography, Anger camera/computer system using seven pinhole collimator 80—61663
myocardium, transverse CAT with ^{201}Tl 80—67222
NDT applications *(German)* 80—76439
nerve fibre counting by pipeline multiminicomputer image processing 80—109013
neural diseases, quantitative EOG and CT obs. 80—36070
neuroradiology, radiation dose to critical organs of staff and patients 80—8184
neutron radiography for nucl. fuel 78—82529
new means for picture formation in computer tomography 80—26326
NMR, human whole-body line scan imaging system 79—66502
NMR zeugmatography 79—66501
noise factor of a polyenergetic X-ray beam 80—56204
noise power spectrum 78—53492
non-linear smoothing filters and noise struct. 80—17118
noninvasive numerical dissection and display of anatomic structure using computerized X-ray tomography 80—17117
nuclear fuel element inspection 80—73927
nuclear fuel pin bundle reconstruction, maximum entropy method 79—63883
nuclear images, enhancement techniques 77—77987
nuclear imaging, positron emission tomograph, design and performance characts. 79—48328
nuclear imaging, single photon ring system 79—53220
nuclear imaging, single photon system, initial performance of SPRINT 79—66523
nuclear imaging, time-coded, appl. of algebraic reconstruction technique 79—92348
nuclear imaging 80—3801
nuclear imaging using multi-slice fan beam collimators 79—44993
nuclear medicine, computer appls. in image and data processing 79—16294
nuclear medicine, computers and quality control 79—16295
nuclear medicine, new imaging methods, conf., London, England (Feb. 1979) 79—83897
nuclear medicine, trends *(French)* 80—26327
nuclear medicine computers 79—25096
nuclear reactor 80—99268
object location in computed tomography images using global local segmentation 80—12249
object reconstruction, 3-D, emission and transmission tomography 79—66535
object reconstruction from projections, influence of detector arrays fixed errors 78—4743
offset detector, interleaving vs. separate processing 80—30877
operating principles, image construction, appls. 78—28047
optical instrumentation in medicine, conf., Toronto, Canada, (Mar. '79) 80—36777
optical inverse radon transform, for image construction systems 78—42288
optical reconstruction from projections via circular harmonic expansion 78—42286
orbit, direct coronal CT by using a dedicated head scanner 80—56177
orbital disease, appl. obs. CT scanning 80—56174
orbital mass lesion patients, advantages of a fourth generation CT scanner 80—56176
orbital trauma evaluation by CT 80—56175
organs, dynamic display system 80—8177
OTF computer assisted determ. 80—46030
outline, physics aspects in medical engineering *(German)* 78—92735
pancreas, ^{11}C-labelled amino acids for rectilinear and positron tomographic imaging 80—12258
pancreas imaging experience 79—88210
pancreatic disease, study by multiple imaging modalities 80—17094
pancreatic scanning with ^{11}C methionine positron emission CT 80—30861
partial volume phenomenon effects on linear attenuation coeffs. 80—41176
particles and radiation therapy, conference, Berkeley, USA (1976) 79—20619
patient care, cost of technically improved diagnostic images 80—17084
patient diagnosis appl. 78—44588
pattern recognition and 3-D construction 79—83924
pencil chamber for direct beam CT meas., evaluation 80—46056
performance and applications 80—98085
performance risk measures, concepts 80—8165
performance risk measures, information theoretic approach 80—8166
phantom for imaging biological fluids by US and CT scanning 80—104692
phantom optimisation 78—48892
physics 78—24173
physics and engineering workshop, conf., Newport Beach, USA (Jan 1979) 79—66507
physiologic tomography, noninvasive meas. of myocardial metabolism, blood flow and function 80—104730
picture documentation and filing 79—66554
picture formation, new method 80—46031
picture quality, artefacts in CT pictures 79—16286
pion beam treatment planning, deep seated tumours, CT scans 80—41180
planar positron cameras, 3-D reconstruction using Fourier deconvolution of generalised tomograms 78—40295
planning issues (in 1975 and 1976) 80—17103
positron annihilation detectors ring, wobbling mathematics 79—63867
positron camera, 3-D image reconstruction, Fourier deconvolution method 80—61669
positron camera, cylindrical, multilayer hybrid computed tomographic system, $Bi_4Ge_3O_{12}$ scintillation crysts. 78—48876
positron camera proportional chamber, Fourier deconvolution technique 78—40297
positron camera system, ring detector, brain research, computed transaxial tomography 80—61739
positron camera using ring detector system, for emission tomography of brain 80—30880
positron camera-computer system for various section images 79—66528
positron circular ring camera tomographic system, resolution improvement anal. *(Korean)* 80—72312
positron circular ring cameras, trends and prospects 79—66524

computerised tomography continued
positron computerised tomographic scanning, radionuclide conc. determ. 78—3587
positron CT, data acquisition and processing electronics 80—61690
positron CT, system design considerations 79—66525
positron emission computed tomograph, POSITOLOGICA 80—104753
positron emission computer-assisted tomographic scanner 80—36116
positron emission CT, detect. system 79—66522
positron emission CT crystal size optimisation 80—61681
positron emission CT device with continuously rotating detector ring 80—81697
positron emission CT optimisation of system design parameters 80—26347
positron emission tomography, appl. to meas. of cerebral metabolic rate 80—3799
positron emission tomography, engineering aspects of PETT V 79—66517
positron emission tomography, fully 3D considerations 80—36098
positron emission tomography, sampling requirements and detector motion 79—66527
positron emission tomography and its applications 79—11996
positron emission tomography for assessment of myocardial integrity 80—36120
positron emission transaxial tomograph, PETT IV and computer system 78—80959
positron emission transaxial tomography, ring detector, attenuation, scatt. radiation and random coincidences 80—61684
positron emission transverse tomograph, PETT IV 78—40299
positron emission-computed tomography, multi-slice, design criteria, shielding 80—61673
positron emitters, high resolution computed tomography 77—66837
positron imaging *(Japanese)* 80—94347
positron imaging instrumentation 77—44745
positron ring cameras for emission computed tomography 77—44742
positron tomograph, Donner 280-crystal, data acquisition, image reconstruct. and display 80—61671
positron tomography, ^{52m}Mn, new short-lived, generator produced radionuclide 80—109006
positron tomography, Donner 280-crystal high resolution system 79—66533
positron transaxial, physical aspects 77—12993
positron-emitting radiopharmaceuticals, new imaging system 79—16280
posterior fossa tumours of childhood, use of CT 79—100702
precision image isocon X-ray TV camera 80—101263
present state and technical perspective, review *(French)* 77—16974
principle, development and specific equipment realisation *(Slovak)* 79—70690
principles, general reviews 79—96662
principles, realisation and results interpretation *(Czech)* 80—36085
principles, reconstruction, equipment and dose 78—53481
principles 77—48859
principles *(German)* 78—3601
principles *(German)* 78—53480
principles and development 78—31945
principles and methods for medical and industrial appl. 79—74755
projection reconstruction *(Japanese)* 80—81700
prostatic carcinoma treatment planning, US imaging rel. to CT 80—3786
proton beams computed reconstruction 78—48870
proton computed tomography, evaluation study expt. results 79—53223
proton density reconstructions at LAMPF 79—53216
protons, comparison with X-rays 80—30881
pulmonary arterial occlusion, comparison of methods in detect., dog expts. 80—56191
pulmonary nodule diagnosis 80—17110
pulmonary nodules, noninvasive diagnosis 79—29582
quality assurance, computer assisted slice thickness determ. 80—46027
quantitative CT, progress toward 80—81696
quantitative US attenuation tomography, effects of phase cancellation, reflection and refraction 79—48302
radiation protection requirements for patients and accompanying parent 77—70524
radiation therapy, compensation for inhomogeneities 79—25065
radiation therapy, dose calcs. from CT data 79—25062
radiation therapy, external, use of axial CT in treatment planning *(French)* 79—66553
radiation therapy, interstitial, dosimetric localisation, use of CT scanner 80—21540
radiation therapy, treatment planning, depth dose scaling using CT scans 80—30899
radiation therapy, treatment planning system, clinical application 79—29588
radiation therapy, use of CT scanning 79—20660
radiation therapy, utility of CT, estimate of outcome 80—67229
radiation therapy treatment planning, absorbed dose calcs. method 79—92386
radiation therapy treatment planning, aids for use with EMI CT5005 scanner 79—100704
radiation therapy treatment planning, value of CT scanning 80—72294
radiation therapy treatment planning 79—88174
radiation therapy treatment planning *(German)* 80—17090
radiation therapy treatment planning and the distortion of CT images 80—76830
radiation therapy treatment planning in coronal and saggital sections, feasbilitiy study 79—62344
radiation therapy treatment planning of bladder carcinomas 79—88159
radiographic contrast agent techniques applied to computerised tomography examination 78—65105
radiographic imaging, 3-dimens. 80—85486
radiological images, conf. Newport Beach, CA, USA (June 1979) 80—8141
radiology conference, London, England (Apr. 1979) 80—30838
radionuclide CT of the body, clinical appls. 79—83906
radionuclide CT of the body using routine radiopharmaceuticals 79—83905
radionuclide imaging, fundamental limitations 80—30882
radionuclide scanner, potential resolution using ^{137}Cs, radiotherapy planning 79—48323
radionuclide tomographic section, synthesis, and enhancement 80—109003
radionuclide tomographic section synthesis and enhancement 79—25103
radiotherapeutic management of juxtasellar tumours 77—56450

computerised tomography continued
radiotherapy, dose calculation, based on computed tomography images use of scatt. radiation meas. 80—51265
radiotherapy dosage calculations for inhomogeneous media, direct use of CT numbers 79—83943
radiotherapy planning, childhood craniofacial sarcoma management 80—12221
radiotherapy planning appl. 80—94334
radiotherapy program development by means of CT *(French)* 80—85472
radiotherapy treatment planning 77—12996
radiotherapy treatment planning appl. 80—51232
radiotherapy treatment planning using the ACTA-scanner 78—65104
rebinning algorithm for fan-beam X-ray scanners 80—26346
reconstructed anatomic morphology, 3-D, visual enhancement and display 80—8176
reconstruction, detective quantum efficiency in detection of small objects 80—46046
reconstruction, energy-dependent 77—12991
reconstruction, three-dimensional, from planar projections 80—99639
reconstruction algorithm, smoothed, clinical and expt. investigation 80—98122
reconstruction angles optimisation 80—8178
reconstruction from projections, uniqueness and resolution, book 79—43989
reconstruction in desired plane 80—41340
reconstruction method for limited field of view 79—48325
reconstruction noise, effect on detectability 78—40296
reconstruction noise rel. to detectability 78—69213
reconstruction of 3-D objects from cone beam projections 79—34665
reconstruction of objects from incomplete projections 80—41211
reconstruction of random objects from noisy objects, max. likelihood 77—37089
reconstruction simulation, no. of rays versus no. of views 78—69214
reconstruction using convolution methods, digital simulation *(Japanese)* 78—35931
reconstructions from restricted region scan data 79—66543
reconstructions with limited data using estimation theory 80—30883
reconstructive tomography and applications to ultrasonics 79—66578
reflection technique for improved temporal resolution with dynamic and ECG-gated imaging 80—98094
region-of-interest X-ray tomography 80—98093
regularization in Fourier-synthesis 2-D image reconstruction 79—74748
relevance and accuracy for radiotherapy planning 79—20627
renal imaging with radionuclides, US and CT 80—17095
reprocessing X-ray transmission data 77—73565
resolution, comparative studies with spiral and elliptical blurring patterns 80—104728
resolution loss, arbitrary symmetrical focal spot intensity distribs. 80—46025
review, principles, development and situation in Sweden *(Swedish)* 78—65106
review 78—44599
review and comparison with classical X-ray diagnostic technique *(German)* 80—67239
review of computed tomography using X-ray, emission and ultrasonic sources 80—17083
review of state of the art and introduction to CT *(German)* 80—101251
rigorous error bounds 79—66514
Roentgen-video computed tomography for 3D dynamic imaging by heart lungs and circulation 80—17112
rotating fan-beam scanner, exptl. bench design 80—51230
sampling theorems in polar coordinates 80—28169
sampling tomography multi-sectional reconstruction method using computer *(Japanese)* 78—31896
scan data format considerations 78—73243
scan edge position uncertainty reduction by density derivative processing 80—109017
scanner, fourth-generation, performance evaluation 80—46035
scanner acceptance testing 77—73569
scanner commissioning 77—73570
scanner development for head and neck diagnosis *(Japanese)* 78—61277
scanner evaluation and selection 80—46065
scanner for early detect. and evaluation of heart disease 79—66521
scanner geometry optimisation 80—46037
scanner principles and problems 79—20625
scanner resolution, geometrical limitations 78—73237
scanner slice thickness meas. *(Japanese)* 79—92353
scanner X-ray tubes 79—66537
scanners, effect of X-ray source filtration on dose and image perform. 80—30865
scanners, fast, incomplete scan geometries 80—26330
scanners, radiation beam and image slice parameter evaluation technique 79—39487
scanners, specification and evaluation of performance 80—89832
scanners, status in 1979 79—66536
scanners, survey of noise, dose and contrast detectability and resolution 80—104750
scanning, general principles, review 77—16973
scanning methods and reconstruction algorithms 80—17115
scanogram, technique and appls. 80—104748
scatter reduction in nuclear medicine and computed axial tomography 79—5368
scintigraphy, longitudinal tomographic reconstruction using a calligraphic CRT graphics system 80—8173
scintillation camera single-photon computed tomography, optimised collimator 78—77106
scintillation camera transaxial tomograph, Humongotron 77—52867
scintillation camera whole-body single-photon emission CT system 80—17086
secondary sections for radiotherapy plane section *(German)* 80—89841
section images, three-dimensional display *(Japanese)* 80—81701
selective I imaging using K-edge energies 78—24131
SEM autoradiography for location and study of microscopic β-active particles 77—57425
sensitometry, definitions and practical techniques 78—69194
short-scan fan-beam algorithms for CT 80—85469
simulated neutron tomography for nondestructive assays 80—99218
single photon emission CT, review 80—81698
single photon emission tomography, camera configs., performance anal. 80—61686

computerised tomography continued
single-photon emission tomography, imaging capabilities of Ge camera 80—61668
skeletal system CT examination 78—88740
skull, diagnostic advantages of tilting investigation unit *(German)* 80—94351
skull, struct. changes due to Recklinghausen's disease, X-ray and nuclear medicine diagnosis *(German)* 80—76831
smoothing and image noise 78—69190
software balancing of multiple detectors during CT scanning 80—46026
Somatom, rapid image reconstruction and examination speed 78—92693
spectral artefact correction and determ. of electron density and at. no. 80—51231
spectral artifact correction 78—35953
spectral effects on transmission values, mathematical model 79—16287
spinal cord, X-ray reconstruct. using bone suppression 80—76822
spine, double exposure technique in CT 80—21524
spine, upper cervical, pathology evaluation 79—29585
spleen radiotherapy and computed tomography in treatment planning 80—56180
statistical limitations, attenuation coeff. variance derivation 79—8537
steel, stainless, C heterogeneities demonstration by high-resolution autoradiography *(French)* 77—66729
stochastic filter for transverse section reconstruction 79—66513
streak artifact reduction, computational method 80—98067
streaking artifacts, edge-induced evaluation 80—81711
strobe-sequenced device to facilitate 3D viewing of cross-sectional images 80—104720
structural material analysis 80—101001
system architecture 77—25549
system error propagation, hybrid anal. 78—40327
technical review of CT scanning 79—34635
TGM-1 multidirectional tomograph, operating characts. 80—104726
theoretical design of system, 4-mm resolution example 80—8179
thermography, numerical simulation 79—83889
thoracic region, diagnostic capability of CT *(German)* 79—39498
thorax 3D reconstruction, ultra-high speed, parallel processing computers appl. 79—48338
thorax and abdomen, clinical study 80—17107
three dimensional, imaging and image processing systems developments *(Korean)* 79—62398
three-dimensional emission tomography using scattered photon information 80—98134
three-dimensional fast scanning system using limited tilting angle 77—73556
three-dimensional image reconstruction, direct Fourier transform techniques 77—12986
three-dimensional image reconstruction for cone-beam X-ray sources 78—77111
three-dimensional imaging using source depend. time-modulated apertures 77—29202
three-dimensional imaging with circular ring transverse axial positron camera 77—77982
three-dimensional phantom and cone-beam X-ray projection computer generation 80—46045
three-dimensional scintigram processing algorithm 78—7446
three-dimensional visualisation of anatomic sites and radiation dosimetry contours 78—77113
tissue heterodensity meas. for charged particle radiotherapy 79—20623
tissue US parameters, quantitative cross-sectional imaging 79—53277
TOMAX autostereoscopic display, three-dimens. viewing of tomographic data 78—85446
tomography machine uses radioisotopes for patient diagnosis 77—56464
tomosynthesis, serioscopy, and coded scan tomography, reconstruction 78—35920
tomosynthesis and computer tomography: a continuous description with examples 80—99020
trabecular bone density, increased in children with chronic renal failure 79—20612
trabecular bone density and other parameters, normal values in adults and children 79—20611
transaxial, equipment operation 77—86617
transaxial image reconstruction and processor architecture 79—34633
transaxial scanners for reconstructing objects from their X-ray projections, review 80—102632
transaxial scanning X-ray tomography, coronal or sagittal plane reconstruction 77—77986
transaxial scanning X-ray tomography, oblique viewing plane reconstruction 78—77114
transaxial tomography, quantum-statistical limitations 77—12990
transmission, review 77—48860
transmission and emission computed tomography, review *(Japanese)* 78—81042
transverse analogue tomography, cross-sectional imaging of X-rays 80—56201
transverse axial scanner system 77—12985
transverse section imaging with the MGH positron camera 79—66516
transverse section picture reconstruction, correction functions and statistical noise 77—12989
transverse tomography with incoherent optical reconstruction 78—28052
treatment planning, three dimensional model for CT radiotherapy 80—8192
trunk CT, body and gonad doses 79—66559
tuberculous thoracic aortic aneurysm, early diagnosis 79—34634
tumour location by CT, use of masking lattice *(German)* 80—41213
twin-cone beam projections, 3D reconstruction by algebraic reconstruction technique 79—2155
two phase flow, computerised tomography meas. technique 80—59135
two-component spectral analysis 77—25548
two-dimensional US attenuation coefficients, computerised tomographic reconstruction 79—57733
two-phase flow, isotopic computerised tomography meas. 80—59136
ultrafast scanners, picture reconstruct. techniques for incomplete data 78—80950
ultrasonic tomography based on perturbation solns. of wave eqn. 79—70593
upper abdomen and retroperitoneum exam., CT rel. to ultrasonography 80—21506
urological diagnosis, possibilities and limitations *(German)* 78—85369
US, data acquisition system 80—26310
US, of breast, progress 80—51196

computerised tomography continued

- US, phase incoherent and other signal processing obs. 80—26312
- US, refractive index field reconstruction for strongly refractive asymmetric fields 80—4760
- US, transmission tomography by reconstruction compared with pulse-echo imaging, tissue-equiv. test objects 80—51154
- US, var. of acoustic speed with temp. in excised human tissues 80—51150
- US and related techniques, new imaging methods 79—66496
- US attenuation reconstructive tomography 80—30822
- US breast tumour diagnosis, computer aided 3D display system 80—45988
- US computed tomography, cancer detect. appl. 80—30820
- US computerised tomography scanner evaluation 79—48301
- US CT, improvements in data acquisition and pre-processing 80—26309
- US diagnosis, role of computer 80—8111
- US imgaging, digital data acquisition system 79—39454
- US medical image digital processing methods *(Chinese)* 80—30805
- US reflectivity imaging, reconstruction with spherical transducer arrays 80—38203
- US refr. index and attenuation images rel. to breast tissue types 80—17036
- US resolution improvement techniques and C-mode scan 79—25052
- US tissue characteristion, static and moving, high spatial resolution US meas. techniques 80—51187
- US tomography in cardiology 80—30824
- US tomography techniques survey 80—30823
- USA government regulation of use 80—17104
- video image analysis *(Japanese)* 79—29599
- video photography in computed tomography and US imaging, film selection 80—41224
- video recorded fluoroscopic images 77—37082
- video techniques 77—73568
- visual pathway CT 80—56178
- volume estimation, computer algorithm 80—98043
- volume estimation algorithm based on polyhedral approx., using US or CT data 80—104790
- whole-body, appl. to radiation therapy *(German)* 78—35945
- whole-body NMR imaging machine 80—101285
- wholebody autoradiography, B-radioluminescence method for tritium detection 77—52945
- wiener filtering of successive overlapping sections of an X-ray reconstruction 80—51214
- X-radiation therapy, computer simulation of central axis dose distributions 79—8531
- X-ray, annotated bibliography 80—30876
- X-ray, axial, principle and medical diagnosis appl. *(Spanish)* 79—20698
- X-ray, dynamic boundary surface detection 78—53479
- X-ray, Rotate/Rotate type whole body scanner using direct magnification 80—21565
- X-ray attenuation meas., elemental anal., tomography appl. 80—50912
- X-ray beam calibration, determ. of effective energies 79—20666
- X-ray computed tomographic image optimal processing 78—80955
- X-ray computed tomography, 3-dimens., of heart, lungs, and circulation 79—53224
- X-ray computed tomography, computation-intensive reconstruction algorithms implementation 80—8206
- X-ray computed tomography *(Japanese)* 80—41181
- X-ray filtration, noise and artifacts 80—17119
- X-ray imaging *(Japanese)* 77—66845
- X-ray source without moving parts, for ultra high speed tomography 79—66541
- X-ray tomography, dose, detectivity and information content 79—25141
- X-ray tomography, non-computed, using coherent light reconstruction 80—17116
- X-ray tomography, transaxial simple rotational photographic method 79—93242
- X-ray tomography 77—5073
- X-ray transmission pencil beam scanner 77—44741
- X-ray tube, heavy-duty rotating anode type 80—73568
- zone plate camera longit. tomogram digital processing, computer simulation 78—40311
- ^{137}Cs source 77—60239
- Fe and steel, macrosegregation of S and form. of equiaxed crystals, autoradiographic study, cast struct. effect 77—63658
- FeTi ferrite, H trapping study by high resolution autoradiography and degassing *(French)* 77—81368
- ^{153}Gd sources for computerised tomography scanners, radiation therapy planning 79—20626
- HgI$_2$ detectors for X-ray CT, evaluation 80—89837
- Ni sheet, surface, adsorbed ^{3}H, ethylene-^{14}C determ., autoradiography method 77—63989
- Xe detectors, dual, experimental, for quantitative CT and spectral artifact correct. 80—76825

computerised traffic control *see traffic computer control*

computing applications to accounting *see accounts data processing*

computing applications to aerospace engineering *see aerospace computing*

computing applications to architectural design *see architectural CAD*

computing applications to art *see art*

computing applications to astronomy *see astronomy computing*

computing applications to astrophysics *see astrophysics computing*

computing applications to billing *see accounts data processing*

computing applications to biology *see biology computing*

computing applications to biomedical engineering *see medical computing*

computing applications to business *see administrative data processing*

computing applications to chemical engineering *see chemical engineering computing*

computing applications to chemistry *see chemistry computing*

computing applications to circuit analysis *see circuit analysis computing*

computing applications to circuit design *see circuit CAD*

computing applications to civil engineering *see civil engineering computing*

computing applications to command and control systems *see command and control systems*

computing applications to communications engineering *see communications computing*

computing applications to control engineering *see control engineering computing*

computing applications to control system analysis *see control system analysis computing*

computing applications to control system design *see control system CAD*

computing applications to distribution *see distributive data processing*

computing applications to education *see educational computing*

computing applications to educational administration *see educational administrative data processing*

computing applications to electric machine analysis *see electric machine analysis computing*

computing applications to electric machine design *see electric machine CAD*

computing applications to electrical engineering *see electrical engineering computing*

computing applications to electronic engineering *see electronic engineering computing*

computing applications to engineering *see engineering computing*

computing applications to finance *see financial data processing*

computing applications to geophysics *see geophysics computing*

computing applications to history *see history*

computing applications to information science *see information science*

computing applications to language translation *see language translation*

computing applications to linguistics *see linguistics*

computing applications to literature *see literature*

computing applications to logic design *see logic CAD*

computing applications to manufacturing *see manufacturing data processing*

computing applications to mathematics *see numerical analysis*

computing applications to mechanical engineering *see mechanical engineering computing*

computing applications to medical administration *see medical administrative data processing*

computing applications to medical diagnostics *see medical diagnostic computing*

computing applications to medicine *see medical computing*

computing applications to music *see music*

computing applications to natural sciences *see natural sciences computing*

computing applications to nuclear engineering *see nuclear engineering computing*

computing applications to physics *see physics computing*

computing applications to police *see police data processing*

computing applications to power system analysis *see power system analysis computing*

computing applications to power system design *see power system CAD*

computing applications to psychology *see psychology*

computing applications to social and behavioural sciences *see social and behavioural sciences computing*

computing applications to stock control *see stock control data processing*

computing applications to town and country planning *see town and country planning*

computing military applications *see military computing*

concrete

see also cement industry

- acceptance tests comparability for separation charact., quality control *(German)* 78—68848
- acoustic emission at prior loading meas. method 78—27703
- admixture, appl. to retempering, producing flowing concrete *(Japanese)* 78—31373
- aggregate, shape and texture anal. by modified Fourier method, orientation effects 77—77691
- albedo for low energy γ-radiation 80—32534
- albedo number meas. using ^{60}Co, ^{137}Cs sources 79—26768
- autoclaved, polymer impregnated and water cured, chemical resistance *(Japanese)* 78—31554
- automatic testing installation *(German)* 77—48604
- bamboo-reinforced columns, behaviour when subjected to eccentric loads 79—52320
- barytes concrete, gamma ray buildup factors 80—27823
- beam, unbonded partially prestress reinforced, ultimate moment of resistance 77—25107
- beam with mixed type of reinforcement, shear and bending strength 79—20124
- bearing with steel inserts in precast column to beam connections, load capacity determ. 77—73427
- Berger coeffs. for Eisenhauer-Simmons γ-ray buildup factors in concrete 78—78510
- bituminous, thermal stresses and brittle point, automatic installation for meas. 80—55605
- borated concrete use in Hanford N-reactor spent fuel basin 77—42128
- BWR containment vessels of prestressed concrete, pressure tests 80—81254
- CANDU irradiated fuel storage, concrete canister programme, heat transfer and shielding effectiveness 78—58388
- cathodic protection using lightning conductors connected with diodes 79—52418
- chamotte concrete, alumina-based cement, thermomech. props. 78—35455
- chamotte concretes, phosphate binder based, strength props. 80—89305
- compression tests, device for centering specimens 80—61033
- compressive fatigue life, estimate of distrib., statistical method *(Japanese)* 78—11328
- compressive strength and ultimate strain under impact loading 79—70128
- compressive strength determ. using small-diameter cores 80—25784
- concrete, fresh, behaviour under a vibr. action, large particle segregation *(Japanese)* 80—88329
- concrete, impact bending capacity *(Japanese)* 80—89341
- concrete-paraffin shielding, fast neutron leakage, use of Monte Carlo method 77—23309
- concretes, further development of 2 point test for workability and extension of its range 80—66728
- continuous damage parameter for non-ageing materials 80—16418
- core strength, effect of length of diameter ratio 77—63861
- crack growth, computer simulation using Monte Carlo method 78—76764
- crack propagation, uniaxial compressive stress *(Japanese)* 78—11330
- cracking along anchored deformed reinforcing bars 79—96122
- cracking in seawater due to embedded metal corrosion 80—30116

concrete continued
  - creep, elasticity and strength in tension and compression 78—11287
  - creep, long term prediction and shrinkage from short term tests 79—20122
  - creep, time dependent behaviour under high tensile stress *(Japanese)* 78—31465
  - creep activation energy under short-term static and cyclic stresses 77—63730
  - creep during drying and wetting 79—52319
  - creep problems, unified concepts of constitutive modelling and numerical soln. 77—25093
  - creep rig, low cost 78—11466
  - creep rupture *(Japanese)* 78—31519
  - creep theory *(Chinese)* 79—74196
  - creep under combined shear and compression stresses *(Japanese)* 77—40511
  - creep under nonuniform temp. distrib., linear viscoelastic analysis 77—62172
  - cylinders, fracture, fluid pressure testing using H_2O and N_2 gas 78—60750
  - dam construction elements, appl. of fracture mechanics to thermal stress cracking 78—76766
  - damping meas., expanded hysteresis loop method 77—12665
  - deformation under complex loading, mathematic description 80—25783
  - density meas. by back-scattered gamma radiation 77—36699
  - drying shrinkage due to wind action *(Japanese)* 79—61838
  - durability study in temp. cycles and water resistance of S concrete and mortars 78—27613
  - dynamic loading due to steam condensation, in BWR pressure suppression system 79—97754
  - elastic modulus variations, gauge meas. by embeddable-strain-units 78—84878
  - elasticity modulus and strength, aggregate conc. effect 80—66591
  - electrical conductance of concrete meas., automatic instrument 77—77659
  - electrical properties of lossy dielectric material containing short randomly distributed metal fibres 80—20584
  - endochronic model for nonlinear triaxial behaviour 78—51095
  - epichlorohydrin/bisphenol A epoxy polymer concrete, viscoelastic props. 80—45340
  - fast neutron albedo for Fe, concrete and Fe-covered concrete radiation shields 79—76151
  - fatigue, applicability of Palmgren Miner partial damage hypothesis 78—11316
  - fatigue, load-deform. behaviour *(German)* 79—11693
  - fatigue strength obs., of unreinforced concrete, cyclic loads testing *(Dutch)* 78—52945
  - fatigue strength rel. to static strength *(Japanese)* 78—11329
  - fatigue test, determ. of loading-deform. charact. and internal damping *(German)* 77—25229
  - FBR HCDA, one-dimensional penetration of molten UO_2 into substrate limestone concrete [following FBR HCDA] 80—47640
  - ferroconcrete, cracked, strain meas. *(German)* 79—34275
  - fibre and polymer reinforced, commercial prospects 77—12592
  - fibre reinforced, glass or steel, mechanical props. and drying shrinkage obs. 79—87706
  - fibre reinforced concrete, strength calc. 78—11286
  - fibre reinforced concrete beam, load-deflection curves in flexure 78—35437
  - fission reactor pressure vessels, containment material, development of different types to overcome various problems 80—52738
  - fission reactor shielding, sorption and diffusion of fission product I 79—67898
  - floors, structure-borne noise 77—42665
  - flowing concrete, expt. studies *(Japanese)* 80—89298
  - fracture, role of aggregate 79—79076
  - FRC, reinforcement parameter 78—79223
  - fresh concrete, props., relayed addition of admixture and flowing concrete *(Japanese)* 80—89461
  - fusion reactor shields, neutron activation props. 80—13787
  - gamma photons penetration, 6 MeV, expt. benchmark data and computed data comparison 80—5256
  - gamma-ray build-up factors of Eisenhauer-Simmons Taylor coeffs. 77—34394
  - gamma-ray buildup factors, Tchebycheff-fitted Berger coeffs. 79—31226
  - gamma-ray linear attenuation coeff., radiation protection at γ-irradiation installation, GOU-1 *(Bulgarian)* 78—82530
  - gamma-ray spectra, high resolution 77—50309
  - glass fibre reinforced concrete, flexural strength 78—11288
  - hardening of materials, plastic and viscous, steady and cyclic loading 77—4793
  - heat resisting, exam. of deform. behaviour, description of testing rig and operation *(French)* 79—15720
  - heat storage in passive solar heated building using concrete block under concrete slab 80—55922
  - high alumina cement concrete, quality, thermal anal. investig. 79—15912
  - high density, radiation shielding below 1 MeV 79—13535
  - high strength, made with special cement admixture, mech. props. *(Japanese)* 80—89297
  - holographic interferometry study of chemical bond of concrete to smooth steel rods 78—88593
  - hydrofracture grout containing radioactive waste, leaching 77—10478
  - ilmenite concretes, fast neutron attenuation 79—76048
  - internal strains by nine-gauge devices 77—51008
  - joints glued with reaction resinous mortar, photoelastic exam. *(German)* 78—76825
  - large-scale steel melt/concrete interactions test for meltdown accident 78—17387
  - leachability determ., radioactive tracer method 78—61135
  - LMFBR, liquid Na-limestone concrete interaction following HCDA, US meas. 80—78412
  - LMFBR, pool-type, dried hot concrete vessel design 78—50248
  - LMFBR, post-accident containment, high-temp. behaviour of concrete 79—31000
  - LMFBR accident, large scale Na/concrete reactions 79—30999
  - LMFBR concrete containment struct., exptl. anal. of dynamic loading 78—41867
  - LMFBR post-accident containment, time-resolved penetration of liquid Na into limestone concrete 79—93787
  - LMFBR prestressed concrete reactor vessels, analytical model and code applications 78—74448

concrete continued
  - loaded concrete and reinforced concrete structs., US testing 77—36707
  - LWR, HCDA, behaviour of concrete in contact with molten corium 80—13584
  - LWR concrete shielding, ANS coupled cross-section standards 79—59281
  - LWR core meltdown risk anal., penetration of hot melts into concrete structures 80—750
  - magnesial refractory concretes, cast. props. 80—89306
  - marine structures for energy conversion 79—43712
  - masonry units, splitting tensile test 78—53061
  - masonry units, use and production of pelletised slag, mech. props. 78—52707
  - mathematical models for stress relaxation and deformation 77—14923
  - membranes, rectangular reinforced, torsional stiffness 80—65131
  - microcracking, geometric probability calcs. 79—57091
  - moisture content meas. by 4 electrodes *(German)* 78—60929
  - Na-concrete interactions, high-temp. nuclear materials consideration 77—50243
  - NDT *(Japanese)* 80—30188
  - neutron activation field anal. of plastic state, two source method 77—25352
  - neutron attenuation, normal and ilmenite concretes 77—23308
  - neutron number and dose albedo 79—93681
  - neutron reflection characteristics 77—71633
  - North Sea oil production platforms, use of steel and concrete in construction 79—78985
  - nuclear power station, full scale tornado-missile impact tests 78—41876
  - nuclear reactor containment vessels, cement selection criteria *(Polish)* 79—49876
  - nuclear reactor core debris interaction with concrete, LMFBR, HCDA anal. 77—71676
  - nuclear reactor core meltdown, chemical reacts. between core melt and concrete 80—13588
  - nuclear reactor prestressed concrete safety containments, calc. and constructional problems *(Russian)* 79—30961
  - nuclear reactor shield, effect of liner on heat and mass transfer characts. 78—17388
  - nuclear reactor shield, interaction with molten core material, heat flux determ. 78—17385
  - nuclear reinforced concrete structures, under missile loading, finite difference code 80—13956
  - penetration of molten metallic pool from reactor meltdown, acoustic technique 80—13544
  - piezoelectric transducers, prep. method problems for UF-90PTs instrument, for US testing of concrete 78—90622
  - plain, deform. and fracture 79—70167
  - plastic-brittle behaviour, hardening and softening constitutive eqns. 77—21270
  - plasticity theory anal. of shear 78—83270
  - plates, cracked, and beams existence of critical strain energy release rate 78—76765
  - polyester resin concrete, effects of styrene-unsaturated polyester ratio on props. *(Japanese)* 80—89299
  - polymer concrete, fracture toughness meas. 79—70168
  - polymer concrete, longitudinal deformation modulus investigation in creep conditions *(Bulgarian)* 80—71685
  - polymer concretes, hydrothermally stable, hydraulic cement-type fillers 80—85144
  - polymer impregnated, incorporation of low and medium level radioactive wastes 77—61564
  - polymer impregnated, polymerised by accelerated electrons, fabrication and strength *(Japanese)* 77—77456
  - polymer impregnated cylinder, failed, compressive props. enhancement 77—77542
  - polymer-cement composite, review 79—70039
  - polymer-concrete composites, civil engineering appls., technical, processing, economic merits 79—11545
  - polymer-modified, unsolved problems 77—4763
  - porosity determ. from combined US and gamma absorption meas., mech. props. 79—29295
  - portland cement concrete, determination of hydrated cement content by differential thermal analysis 79—79335
  - pressure vessel, reinforced concrete, stress anal. of cracked shell 78—44213
  - pressure vessel, uniaxial compressive strength, 450-1033K 78—44299
  - pressure vessels, finite element creep anal. 78—41813
  - pressure vessels, multicavity PCRV, design and anal. for ultimate strength calc. 78—44182
  - prestressed, comparison of tension testing instruments for reinforcement rods 79—8410
  - prestressed, cooling pipes anal. for reactor vessels 80—32370
  - prestressed, low-temp. tensile strength and linear expansion coeff. of reinforcing steel 80—30051
  - prestressed beam, fatigue strength of cold-worked non prestressed reinforcement 79—96123
  - prestressed beams without web reinforcement, shear strength 79—52318
  - prestressed concrete reactor vessels, perforated plate ligaments, time varying stress 79—49679
  - prestressed hollow beams in combined torsion and bending 79—96087
  - prestressed members, creep fracture during manufacture 78—76767
  - quality assessment, US pulse vel. meas. practical use 80—100991
  - quality control, construction of operating charact. curves *(German)* 77—28960
  - quartzite, vitrified, and quartzite based refractory concretes, prep. and props. 80—89188
  - radioactive, CANDU spent fuel, containment in concrete canisters, UO_2 oxidation 77—6539
  - radioactive spent ion exchange resins from power plants, bituminisation and cementation 77—61565
  - radioactive waste, medium-level, cementation and bituminisation methods of solidification 77—65313
  - radioactive waste solidification, leaching behaviour of ^{90}Sr 78—37416
  - radioactive waste solidification in concrete, polymer impregnation 77—6537
  - rare reinforced concrete structures, failure, expt. determ. and calc. methods *(Chinese)* 79—74243
  - reactor shielding thermal stress cracking anal. *(German)* 80—5232
  - reactor vessels, behaviour of perforated slabs under temp. and external load 79—30917

concrete continued
refractory, fracture strength meas., test apparatus simulating usage conditions 80—71824
refractory, high temp. mech. props. *(French)* 77—56019
refractory concretes, review of new developments *(French)* 79—15636
reinforced, elasto-plastic anal. of plane frame *(Chinese)* 80—5950
reinforced, failed slabs, nonlinear analysis by finite element method *(Japanese)* 77—42785
reinforced, finite element anal., convergence of iterative methods 78—38186
reinforced beams, shear strength calc. 80—99942
reinforced concrete, cracking strength and max. rack width *(Chinese)* 80—5988
reinforced concrete, lower bound anal. for torsion 78—35436
reinforced concrete containment model behaviour under thermal gradients and internal pressure 80—42837
reinforced concrete deep beams, optimal force transmission 78—34009
reinforced concrete slabs, generalised yield lines 79—83265
reinforced concrete structs., initial stress approach to nonlinear dynamic anal. 77—83036
reinforced concrete structs., missile impact loading, nuclear power plant appl. 79—31237
reinforced concrete structural integrity assessment, NDT method 78—56847
reinforced cross-sections, response to short-term and sustained loads 79—52358
reinforced curved beam, expt. investigation of collapse 77—90404
reinforced deep beams, with web opening, structural idealization 79—20125
reinforced slabs, nonlinear statical props. anal. 80—25809
reinforced slabs, punching shear strength under in-plane biaxial tension 80—100876
reinforced slabs optimum design, subjected to biaxial moments, using analytical and graphical methods 80—50664
reinforced walls, local behaviour under missile impact *(French)* 78—44180
reinforced walls, local response to missile impact 78—44181
reinforced with mild steel rods, random axial loading, compressive strength to failure 78—27614
restrained stress and thermal cracking of thick walls 79—100264
review, physics and chemistry 78—73013
ribbed compression reinforcement, ultimate strength anal. of lapped joint 79—96086
rich mix, thermal props., expt. study *(Japanese)* 77—77536
sandwich composites, behaviour under compressive and tensile loads 77—8877
shield design for variable energy cyclotron 77—61622
shielding, dose transmission factors, for 14 MeV neutron generator 77—71702
shielding for thermoluminescent dosimeter monitoring post 78—817
shields containing iron, two dimens. cross section sensitivity anal. of Fe 77—23311
short steel wire reinforced (polymer impregnated) concretes, cracking and toughening 78—80626
slab, explosive shock resist., tensile fracture 80—85065
slab reinforcement optimisation by linear programming 77—89022
splitting test, nonlinear numerical analysis 77—7339
steel bar reinforced concrete member, effect of steel bars on US testing 78—60923
steel fibre reinforced concrete, strength problems 77—4844
steel fibre reinforced concrete, tensile strength and ultimate strain *(Polish)* 80—21027
steel fibre reinforced concrete, vibr. compaction, pressure compaction and curing *(Japanese)* 80—89179
steel fibre reinforced concrete *(Japanese)* 77—4762
steel reinforced concrete, computer expt. on slender beam columns 79—70127
steel reinforced concrete, local bond-stress/slip relationships under repeated loading 79—20123
steel reinforced concrete beams, mech. strength determ. under combined bending and tension 78—60749
steel reinforced concrete slabs, connected via shear connectors, exam. of fatigue in shear connectors, exam. of method 79—43539
steel-concrete composite T-beam, third point loading tests, ultimate flexural strength determ. 77—86252
strain rate effect, on strength and deform. during hardening process *(Japanese)* 80—93616
strength, NDT standardization 79—91902
strength, shrinkage strain and deterioration down to −160°C *(Japanese)* 80—100886
strength estimation by US pulse velocity method, aggregate variation effects 77—63867
strength properties under generalised stress, mathematical description 80—20941
stress determ. by holographic and speckle techniques *(French)* 79—27603
stress distribs. under splitting loads *(Japanese)* 78—35495
stress-strain diagrams, anal. and classification of low deforming materials by their behaviour under stress 79—15753
stress-strain relationships, applicable to biaxial tension and compression 80—65133
structural systems, time-varying stresses calc. by variational principle 77—3732
surface crack width meas. by light-dependent resistor 79—96250
tensile strength determ. under impulse loading *(German)* 79—15919
tensile testing apparatus 79—96241
tensile testing device, axial 80—61054
testing accelerated, using accelerated curing procedures 79—5091
thermal decomposition, empirical model for kinetics and stoichiometry 78—17386
thermal decomposition in interaction with molten nuclear core materials 80—22946
thermal performance of double hollow wall/roof 80—19222
Thermocrete heat storage material development 79—57483
transducer, viscoelastic, in-situ, Duomorph, appl. to polymeric materials 79—30463
two dimensional, reinforced, finite element analysis of structures taking account of nonlinear physical behaviour and discrete crack development 79—57121
ultrasonic analyser, pulse velocity method 80—45472
ultrasonic wave velocities and density, calc. and meas. 79—52545

concrete continued
unbonded, prestressed, review *(Japanese)* 78—6884
uniaxial compression, finite element failure anal. *(Japanese)* 80—35265
unreinforced pavement slabs, environmentally induced stresses, computer experiments 78—35435
unsaturated, dynamic props. of impulsive-type loading 79—70106
US assessment, of strength at early ages 77—25225
US testing of compressive strength *(German)* 78—68847
US testing of deep foundations 78—88585
US wave propagation and microcracking *(French)* 80—39225
water transport, neutron radiography study, results review 78—59961
workability, predictions from viscosity-elasticity analogy, effect of aggregate volume conc. 77—25087
Al_2O_3-SiO_2 refractory concrete, elastic props. 80—89280
C fibre reinforced CuO-H_3PO_4 effect of C fibre on props. 79—43192
MgO-spinel concrete, cast, hardening by elec. heating 80—21258
Pu, reactivity effects of reflecting and interspersed concrete, composition effects 79—63788
S concrete, mech. strength, effect of H_2S 77—4818
SiO_2 concrete, elastic moduli meas. during heating and cooling 80—55451

concurrency (computers) *see multiprocessing systems*

condensation
see also clouds; drops; fog
accommodation coefficients, effects on evaporation and condensation *(Japanese)* 78—81933
acetic acid vapour, homogeneous nucleation, assoc. clusters, crit. supersaturation temp. depend. 77—31762
acetone, condensation in presence of instabilities, photographic study 78—10180
acoustic reflection from liquid surface, influence of condensation and evaporation 79—46097
aerosol, coagulation and condensation, dynamic behaviour 77—25312
aerosol, heteromolecular nucleation and condensation, multi-dimens. theory 78—92518
aerosol, polydisperse, growth in adiabatic condensation nuclei counter, finite expansion time 79—79306
aerosol cluster, mol., sticking probability to solid surface 77—12833
aerosol formation, growth, general dynamic eqn., H_2SO_4/H_2O aerosol simulation appl. 79—47990
aerosol growth by condensation, general dynamic eqn., exact solns. 79—39218
aerosol particle size distrib., dynamic behaviour, coagulation, condensation, nucleation and removal 78—35726
aerosols, condensation nucleus counters, comparisons, comments 77—56758
air-steam mixtures, heat transfer to moving droplets 78—90997
air-stream mixture, direct contact dondensation on single droplet 77—68370
alkali halide, molecular processes of condensation and evaporation 79—69237
alkali metal vapour condensation from gas flow (He,Ar,N_2) heat and mass transfer 78—75192
annular flow condensation, of steam inside tubes, heat transfer 78—14003
atmospheric gases condensation on cold metal surfaces, nucleation barrier 78—22838
atomic absorption spectrometry, graphite furnace, electrothermal atomisation 79—24852
benzene, benzene-d_6, vibrational anharmonicity, condensation effect, vap. press. isotope effect 78—58657
benzene aqueous hetero-azeotrope mixture, condensation heat transfer coeff. *(German)* 80—33425
benzothiazoline products, bicondensed, for thermographic recording 79—24767
binary alloys, kinetic nucleation model 77—85118
binary mixture flow in vertical channel, film condensation 78—75139
binary mixture supersaturated vapour condensation, homogeneous nucleation 78—2247
binary mixture vapour condensation, forced-free convection, finite difference treatment 78—5741
binary mixtures, condensation on finned surfaces, heat transfer 77—39198
binary vapour in inert gas, heat and mass transfer 79—59916
binary vapour mixture condensation into immiscible liquids *(German)* 78—18760
binary vapour mixture in presence of inert gas 77—80051
bubble collapse in liquid, pressure wave, nonequilib. vapour condensation effects 80—59060
bubble condensation, in subcooled liquid, high-speed photographic study 78—42654
bubble motion and bubble-droplets in immiscible liq., photographic obs. method *(German)* 79—72931
butane, condensation in porous bulk media 78—47510
butane drops, nucleation in flowing water 79—1099
BWR steam condensation pressure variations 78—46134
capillary condensation, Kelvin eqn. direct exptl. verification 79—33159
capillary condensation and absorption processes 79—28175
capillary condensation and adsorption, adsorptive pot. boundary layer approx. 78—2366
capillary condensation and adsorption, Gibbs free energy, unitary approach 77—76643
capillary condensation theory, adsorbates liq. or gaseous props. 80—80028
carbon tetrachloride aqueous hetero-azeotrope mixture, condensation heat transfer coeff. *(German)* 80—33425
channel, local (total) heat transfer coeffs., friction factors 78—51045
chemical potentials, use in condensation of pure vapour, imperfect gas case 79—86880
chemical states at surfaces exposed to high-temp. vapours 78—11559
chemically reacting gas, chemically reacting noncondensable components 78—51258
chladone 21 film condensation on vertical tubes, heat exchange 80—24577
circular tube under centrifugal accel. field, condensation heat transfer 80—74713
cloud, warm cumulus, three-dimens. numerical model with microphysical processes *(Russian)* 78—88884
cloud condensation nuclei, effects of urban pollution aerosol on drop size spectra 80—56571

condensation continued
  cloud condensation nuclei, meas. using horizontal thermal gradient spectrometer 80—77158
  cloud condensation nuclei on USA Atlantic seaboard 77—5310
  cloud drop growth by condensation, air parcel model 78—7729
  cloud droplet distribution evolution, supersaturation fluctuations, stochastic condensation theory 80—12490
  cloud droplet growth by condensation, parameterization 78—3869
  cloud nucleus counter, dual-range performance 79—53543
  clouds numerical models, methods of parametrisation of condensation process *(Russian)* 78—16091
  cluster formation, in rarefied nozzle flowfield 80—5639
  cluster model, excluded volume effect 79—10932
  compression shock stability in streams of spontaneously condensing vapour 80—28563
  condensation heat transfer, effect of surface thermal conductivity 78—22252
  condensation on AgI aerosol particles, implications for ice-forming activity 80—101406
  condensation-driven fluid motions, nuclear reactor safety 80—63228
  contact angle and solid surface prop. effects 79—77867
  contact angle hysteresis, dropwise condensation heat transfer 78—71273
  convection, augmented, bubble pumped, in submerged condenser system 78—94535
  cooled pipe, droplets from vapour condensation, size distrib., laminar flow 80—79111
  cosmic dust condensation onset, role of association reactions 80—26931
  cryogens, porous solids, gradientless heat transfer, metallic thermal cond. theory 79—59902
  crystal rough surface smoothing, during evaporation or condensation 80—103470
  cyclohexane aqueous hetero-azeotrope mixture, condensation heat transfer coeff. *(German)* 80—33425
  dew formation on cooled glass surface, surface resist. changes 77—11777
  dew point calc., iteration scheme 79—19359
  dew-point hygrometers, automatic, condensate phase state determ. 78—8408
  dibutylphthalate, supersaturated vapour, aerosol form. by mixing of flows 79—39212
  dielectric fluids vapours, freon-113 and diethyl ether, heat exchange obs. *(Russian)* 79—1055
  dielectric liquid, film condensation, heat transfer enhancement in elec. field 78—55551
  disc, rotating, condensation in presence of const. axial suction 77—42839
  drop electrification by evaporation or vapour condensation *(French)* 78—61511
  drop growth in atmosphere by condensation, cloud physics appl. 79—44216
  droplet, nonequilibrium evaporation and condensation, quasisteady theory 79—99394
  droplet growth, method for condensation eqn. soln. 78—7795
  droplet growth and initial dew point temp. accuracy in cloud chamber on space shuttle 78—96268
  droplets nucleation in finite systems, theory and computer simulation 80—26038
  drops, noncirculating, direct contact condensation 78—94548
  dropwise, heat transfer 77—58531
  dropwise condensation, condensing surface thickness effects 78—22250
  dropwise condensation, heat flux and drop size distrib. 79—50573
  dropwise condensation, max. drop size rel. to heat transfer coeff. 78—94559
  dropwise condensation and nucleation heat transfer rate, mechanism 77—4193
  dropwise condensation of Hg, heat transfer meas. 78—94560
  dropwise condensation theory 77—7858
  dropwise theory, further developments 80—38245
  dust condensation processes investigation, expt. techniques 80—26940
  dust formation in space medium thermodynamics and kinetics, workshop, Houston, Texas (1978 September 6 to 8) 80—22131
  electron irradiation effects on surface prop. of solids 80—70261
  enhanced film condensation by surface forces, optimum condenser tube fin geometry 78—75039
  ethane, condensation in porous bulk media 78—47510
  ethane, flow continuity in arterial capillary systems in cryogenic heat pipes 80—64536
  ethylene, condensation, zero point energy shift, isotope effects 78—95147
  excess component concentration, appl. to conc. determ. in nonstoichiometric appls. 78—43131
  extended surface heat transfer with condensation on to fin 78—94551
  external condensation problem, with suction (blowing), self-similar soln. 79—94705
  film, along vertical plate in enclosed chamber, effect of noncondensable gas 77—80703
  film, condensation of moving vapour on horizontal cylinder, exptl. dependences 80—58892
  film, flow down vertical surface, effect cooling conditions on heat exchange *(Russian)* 78—46934
  film condensation in three dimens. flows 78—94692
  film condensation inside pipes, heat transfer, general correlation 79—46312
  film condensation of steam in vertical Cu tube, heat transfer coeff. 78—94553
  film condensation of vapour in elec. field, heat exchange intensification 79—86331
  film flow, of condensate on finned surfaces, heat exchanger design 78—75038
  film type, data correlation using method of thermodynamic similitude 79—90250
  filmwise condensation, onto vertical fluted plate, numerical anal. 78—94552
  Fisher's droplet model, pure filled vap.-liq. nucleation theory 77—62626
  Fisher's droplet model for gas above T_c and the metastable phase 80—49348
  fission reactor ECCS, flooding phenomena with condensation 79—89429
  fission reactor LOCA containment anal., new condensation mass removal model 79—89423
  flow, transient, two-phase, flow reversal prediction LOCA conditions 78—94811
  flow of vapour over horizontal cylinder, two-phase boundary layer eqns. 79—46306

condensation continued
  flowing vapour, on horizontal melting surface, laminar film condensation 77—15661
  fluoromethanes, condensation, zero point energy shift, isotope effects 78—95147
  fluted tube, condensation heat transfer, Gregorig model 78—87236
  fluted tubes, condensation heat transfer coeffs., valley flow and gravitation effects 80—19368
  fog-containing vapour-gas mixture, mass transfer in vapour condensation 77—58772
  forced convection condensation in the presence of noncondensables, boundary values *(Japanese)* 80—92151
  forced flow laminar filmwise condensation of vapour in vertical tube 80—43762
  free jet, homogeneous nucleation of clusters, noncryst. struct. *(French)* 78—79760
  free molecular vapour flow, mass transfer during condensation in channel 78—51198
  gas, in contact with condensed phase, hydrodynamic eqn. and slip boundary condition 80—14791
  gas bubble nucleation, exptl. data use in flow boiling bubble population prediction 78—90696
  gas exchange in closed volume during vapour condensation, residual gss density change 77—59692
  gas mixture, binary, condensation in boundary layer flow, numerical method 79—1236
  gas-liquid droplet system, phase transition kinetics and kinetic eqns. 78—83933
  gas-porous electrode, mass exchange in transport zones 77—32801
  gas-vapour droplets, nonuniform mixture, acoustic wave attenuation 78—83154
  gases, high velocity flows, nonequilib. homogeneous condensation, determ. of maximal supercooling 80—6086
  glass, bubbles, form., condensate trace quantities determ., spectral anal. techniques *(Russian)* 77—36852
  grain formation by nucleation, astrophysical environment 78—16501
  grooved horizontal conduit, film mass transfer enhancement 79—72947
  heat and mass transfer with condensation from turbulent nonuniform boundary layer, analysis 77—89124
  heat pipe, low-temp., evaporator-condenser interrelation effect on thermal resistance 77—89003
  heat transfer, condensate pattern for condensation of immiscible liquid binary vapour 78—94558
  heat transfer, nonequilib. temp. profiles, mass transfer engineering calc. 80—63227
  heat transfer augmentation, in horizontal tube condensation, using twisted-tape inserts and internal fins 78—71265
  heat transfer by condensation of gas-vap. mixture, in high-press. pipe 78—94589
  heat transfer data processing and correlation 77—42706
  heat transfer in horizontal tube, effect of in-line static mixer 77—41626
  heat transfer with steam condensation, theory, problems of interest 78—30161
  heterogeneous, in cylindrical channel and on aerosol particles 79—57298
  heterogeneous condensation in Lavale nozzle *(Russian)* 77—89007
  heterogeneous photocondensation process initiation by laser radiation 80—67410
  homogeneous, cluster size distrib., stochastic model 80—22311
  homogeneous condensation, from supersaturated vapour, stochastic simulation 78—51657
  homogeneous vapour nucleation, in carrier gas, hydrodynamic theory 79—69236
  horizontal elliptical conduits, turbulent film evaporation and condensation 79—1182
  horizontal tube, heat transfer with filmwise condensation, vapour vel. influence 80—33598
  hydrocarbon vapour, spontaneous condensation in submerged turbulent jet 79—64721
  ice, electrical effects during condensation and phase transitions 78—67821
  imperfect gas, generalised theory of condensing systems 79—35653
  in tube appl. to dynamic model of reboiler 77—7298
  inert gas adlayer, on graphite, cleavage face, 2-dimens. condensation, crit. temps. 80—20032
  inert gas adsorbed monolayer, Percus Yevick theory 77—7968
  intense evaporation and condensation, molecular kinetics anal. 79—86330
  interaction force between droplet and condensating vapour 80—79113
  interface kinetics of condensing vapour region 79—69321
  interfacial heat transfer coeff. for vapours in direct contact condensation 77—58530
  interstellar dust condensation in clouds, importance of reaction kinetics 80—26939
  interstellar space, disequilib. condensation environments as frontier in thermodynamics 80—26942
  interstellar volatiles condensation on dust grains, role of grain growth by radiation pressure induced coagulation 80—94851
  Ising cluster size and shape, Whitney polynomial 79—33080
  isobutane, condensation in porous bulk media 78—47510
  isotope separation, using nonequilib. condensation with selective laser photoexcitation, mathematical model 79—31720
  kinetic analysis, BGK eqn. 77—11683
  kinetic theory, evaporation, condensation, linear, nonlinear problems 78—75802
  kinetic theory, hydrodynamic eqn. and slip boundary condition 78—63903
  kinetic theory, physical-mathematical problems *(Italian)* 79—40505
  kinetic theory, stochastic approach *(Russian)* 77—72676
  kinetic theory of one-dimensional evaporation and condensation problem *(Japanese)* 78—81932
  kinetic theory treatment of nonlinear half-space 79—27500
  kinetics of crystalline surfaces *(Russian)* 77—43424
  laminar condensation, intermittent charact. 78—94555
  laminar condensation heat and mass transfer at stagnation point of droplet in ternary mixture 79—14227
  laminar film, condensation on underside of inclined flat plate 79—50700
  laminar film condensation, non-condensing gas in tube 78—94554
  laminar film condensation, on vertical plate, surface tension effects 78—95148
  laminar film condensation from moving vapour, with suction 78—59459
  laminar film condensation inside tubes, with noncondensable gas 79—14234

condensation continued
laminar film condensation of mixed vapours, combined body force and forced convection 78—51162
laminar film condensation on helical elliptical cylinders, governing eqns. soln. 78—9689
laminar film condensation on vertical surface with heat generation 79—72786
lattice gas, one-dimens., for teachers 79—18
lattice gas, two-dimens., thermodynamic pot. for homogeneous nucleation 79—82326
Laval nozzle, supercritical steam supersonic discharge 80—48765
Laval nozzle, two-dimens. two-phase flows with nonequil. phase transition 77—51101
liquid film condensation on vertical wall, linearised stability anal. 79—55381
liquid metal vapour, laminar film condensation under effect of electromotive force 79—1258
liquid-gas interface, Stefan flow of binary mixture, with evap. or condensation 79—37381
liquids, impurity separation, laser thermal method *(Russian)* 77—7859
LMFBR, condensation from large HCDA vapour-gas bubble onto structures 79—93774
LOCA, counter-current flow limiting phenomena with vapour condensation, model 77—61519
LWR post-accident aerosol removal, steam condensation expt. 79—13456
LWR safety, condensation heat transfer in stably stratified systems 80—63311
mass transfer in cylindrical channel with evaporation and condensation at walls 80—6101
matrix isolation of aggregated species, cluster form. 77—62630
metal condensation on alkali halide, nucleus saturation density and epitaxy 78—18928
metal films, nucleation on alkali halide crystals, effect of ionisation of condensing flux 80—107675
metal vapour condensing ejector thermal design 77—61062
metals, expansion, isentropic, vaporisation and condensation kinetics anal. 77—66623
meteoric matter, evaporated, mass spectrum of particles formed in condensation 79—71005
methane, condensation, zero point energy shift, isotope effects 78—95147
MHD convertor, phase transition in condenser *(Russian)* 79—1350
mixed 2-D flows of supersaturated and two-phase medium with nonequilib. phase transitions 79—77224
mixed vapours, suction effects heat and mass transfer *(German)* 80—33609
monodisperse cloud regarded as isolated system, drop growth and supersaturation 77—53150
multicomponent condensation, simplified mass transfer anal. 80—10675
multicomponent mixtures condensation *(German)* 79—55323
multidroplet system, condensation-evaporation by kinetic theory 80—7873
non-condensing gas on flat plate and horizontal tube, forced convection condensation 80—64553
non-isothermal condensation, temp. distrib. 79—27501
nonequilibrium heterogeneous-homogeneous condensation in supersonic nozzle *(Russian)* 77—51096
nonequilibrium two phase flow, voids fraction and vapour phase condensation 79—90310
nonsteady flow in nozzles with spontaneous condensation 78—47011
nucleation, homogeneous in vap., microcluster metastable equilib. conc. 77—62627
nucleation, microscopic theory *(Russian)* 78—67801
nucleation, microscopic theory *(Russian)* 78—67802
nucleation homogeneous, gasdynamics of supersonic flow with condensation 77—62292
nucleation of liq. droplet, stat. mech. treatment trans.-rot. paradox 77—62625
nucleation process kinetics, diatomic clusters role *(Russian)* 77—31750
nucleation processes, computer simulation, single spin flip kinetic Ising model 77—62613
nucleation theory, atomistic models of microclusters, exact free energy barrier 77—62612
nucleation theory, role of replacement free energy, review 77—62611
nucleation theory, time depend., supersaturated cooling gas 78—6151
nucleation theory with Maxwell demons 77—85054
on falling laminar liq. sheet 77—42815
one-dimensional system, Bose-Einstein condensation at const. press. 80—22276
organic compound, two-dimensional condensation with adsorbed mol. reorient. 78—61051
organic fluids, liquefaction shock wave obs. 77—51484
parallel-flow and counter-flow condensation on an internally cooled vertical tube 80—64555
paramagnetic vapours and condensing materials, apparatus for susceptibility meas., 300-1600K *(Russian)* 79—93178
particle, spherical, transient heat-mass exchange 79—7276
pendular ring condensation on spherical adsorbent, surface tension curvature depend. 79—46926
perturbed flow, moisture form. kinetics 80—79387
phase transformations, second order, critical phenomena, space environment applications 79—46783
photocondensation, molecular compounds behaviour in strong light beams *(Russian)* 77—49798
physical clusters, modified Mayer theory for homogeneous condensation from small nuclei 80—79924
pipes, two-phase stream, stratified flow, condensation calc. 79—23349
plate condenser with grid pattern slotlike channels, low-press. steam condensation, heat transfer 78—75040
polymer films, vertical development, from gas phase, computer simulation *(German)* 77—27839
powder condensation growth, math. model of jet-plasma treatment process *(Russian)* 80—7513
processes, mechanism, using kinetic theory of gases 78—30746
propane, condensation in porous bulk media 78—47510
pulsed condensation of matrix mixture for spectroscopic investigations 79—36799
quantum statistical mechanics 79—42232
raindrop, single, growth by condensation and droplet capture, props. 79—12208
raindrop growth physics, for teaching 79—35502
raindrop size spectra and growth in cumulus cells, model 80—21800

condensation continued
rarefied flow, boundary conditions for gasdynamic eqns. in presence of evap., condensation and chem. reactions 77—47042
rarefied gas 2-D flow in presence of condensation 79—32577
rate of formation of condensation nuclei in two component metastable media 80—79930
retrograde vapour, shock wave induced condensation 80—34177
rotating heat pipes, condensation heat transfer, external boundary condition effects 79—94612
rotating heat pipes, condensation heat transfer, noncondensable gas effects 78—51167
rough surfaces, adsorpt., capillary condensation 79—1544
saturated vapour, slightly nonequilib. condensation on liquid surface 80—19930
semi-microscopic description of evaporation and condensation 80—39254
separation, partial condensation methods, thermodynamics *(German)* 78—20054
shape of drop on inclined plane, solar still aspects 78—79856
shock compression of condensing media, relax. processes kinetics 78—94610
slowly moving vapour, film condensation heat transfer 80—19376
snow, rel. to grain growth 80—26553
solar nebula, condensation rel. to lunar element correls. and bulk comp. 77—60637
solar nebula, Ga, Ge and Sb condensation rel. to Fe meteorites chemical classification 80—36594
solar nebula, gaseous matter condensation rel. to planetary system form. 79—8857
solar nebula, Th, U, Pu and Cm condensation and fractionation 79—35154
solids, amorphous and crystalline, condensing from gas phase, nucleation, growth and transform. 80—24745
spherical condensed phase, rel. to motion in uniform vapour gas flow, kinetic theory 78—1725
spherical droplet, evaporation and condensational growth, mass transport calcs. 80—97736
spherical liquid droplets, nonlinear condensation and evaporation 78—63902
spontaneous condensation processes, classification 80—6500
statistical mechanical theory of the kinetics of phase transitions, review, book contrib. 80—73270
steam, annular duct flow, heat transfer to condensate film 78—94709
steam, condensation, heat transfer 77—62297
steam, condensation inside vertical straight and coiled pipes, heat transfer 79—90244
steam, dropwise condensation, effect of condenser tube material on heat transfer 78—75059
steam, dropwise condensation, moving picture study 80—74863
steam, dropwise condensation on electroplated Au layer, thickness depend. 79—46791
steam, film condensation in tube, heat transfer, vibr. effect 78—51044
steam, horizontal flow on cylinder, condensation 78—94550
steam, method for calculating expansion 77—27573
steam, tube condensation, augmented internal geom., and press. drop 78—94556
steam bubbles, condensation, influence of noncondensable gases *(French)* 79—23717
steam bubbles direct contact condensation in water at high press. 77—39202
steam condensation heat transfer on below-freezing pt. surface 78—75042
steam condensation in capillaries 79—1066
steam condensation in moving two-phase film, heat transfer, volumetric coefficient 80—48696
steam condensation on bundle of smooth horizontal tubes, heat transfer effects 78—30164
steam condensation on external entrance length of cooled rot. tube 77—75906
steam condensation on PTFE coated surface, heat transfer 77—89012
steam condensation on turbulent water surface 79—64748
steam droplets growth in Laval nozzle 79—32648
steam dropwise condensation, heat transfer coeff., surface shape, orientation, coolant flow rate 77—27528
steam jet condensation, dynamical pressure pulse effects 78—94549
steam jet condensation in turbulent liquid flow, heat transfer 80—33599
steam-air mixture, condensation, transport and thermodynamic props. *(Japanese)* 78—34251
steam-inert gas, uncondensable gas content effect on steam condensation heat transfer in vert. tube 78—75041
steam-water mixture, intensive drop condensation, flow boundaries 77—35204
stearic acid homogeneous vapour phase nucleation, diffusion cloud chamber obs. 80—79923
subcooled boiling flow, vapour bubble growth and recondensation 79—93692
sublimation-condensation in annular gap, heat and mass transfer 77—35141
sulphate aerosol, stratospheric, kinetics of growth by condensation in homogeneous medium *(Russian)* 80—94566
sulphate particle formation by heteromol. nucleation and condensation in cavities 80—26183
superheated vapour in horizontal tube, condensation, local convective heat transfer coeff. 80—19927
superheated vapour in vertical tube 78—87783
supersaturated gas condensation kinetic model, cluster nucleation assoc. and dissoc. 78—85151
supersaturated vapour, nucleating centre nonstationary formation rate calc. 80—34178
supersaturation during heat and mass exchange in stationary gas medium 79—94480
supersonic nozzle flows of condensible vapour, near-equil. heterogeneous nucleation and similarity rules 77—58759
supersonic two-phase flow, nonequilib. condensation, boundary condition numerical anal. 80—64565
surface suction effect on condensation in presence of noncondensable gas 78—90691
thermal plumes development, effect of condensation *(French)* 79—23192
thermal stability of condensed systems containing stabilized atoms *(Russian)* 77—89536
thermodynamic function singularities, vapour fluctuations 77—41558
thermodynamics of nucleation on charged centres 79—20955

condensation continued
  thermostatic control, rot. conical (spherical) jacket radiatively heated from side 77—42710
  thin films, kinetics under complete condensation conditions 80—88453
  thin films, precipitation and nuclei form. in presence of condensation centres, thermodynamic model 80—103594
  transonic unsteady-state flow of supersaturated vapour, in presence of condensation 77—35162
  trichloroethylene aqueous hetero-azeotrope mixture, condensation heat transfer coeff. *(German)* 80—33425
  triplet excitons, condensation in mag. field 80—2341
  tube, vertical, heat transfer upon steam condensation 80—48547
  tube flow, laminar film condensation 79—46388
  tubes with in-line static mixers, surface renewal model 78—75060
  turbulence model of condensation, in circ. tube, boundary layer with suction approx. *(Russian)* 79—59971
  turbulent annular-mist flow, wall and interfacial shear stress 78—94812
  turbulent film condensation of vapour on rough surface, heat transfer 77—39285
  turbulent filmwise condensation heat transfer coeffs. 78—63429
  turbulent jet, quasi-two-dimensional description of rapid-type nucleation 77—35190
  two dimensional system, melting and condensation theory 80—57231
  two-electron level with quasidegenerate levels, local phase transitions and temp. effects in lattice dynamics 80—10666
  two-phase condensing flow, thermally governed transient flow surges 78—30346
  two-phase countercurrent flow, turbulent steam condensation in a horizontal channel 80—106800
  two-phase evaporating and condensing flows, system mean void fraction model 78—42520
  two-phase flow, mixing and condensation in high-speed flow, review 78—47014
  two-phase flow with condensed liq. particles, heat transfer to wall with solid condensate layer 79—86426
  two-phase fluid, 2-D supersonic flow, condensation effects calcs. *(French)* 77—84272
  two-phase laminar boundary layer, forced convection condensation *(Japanese)* 78—34191
  two-phase stream, heterogeneous condensation 79—64488
  two-phase turbulent flows, condensed phase formation, anal. 79—81853
  two-surface problem of evaporation and condensation, in presence of noncondensable gas 80—6169
  vacancy theory, cell model calcs. 77—55224
  vacuum metallisation chamber condensate removal system 79—58752
  Van der Waals gas, percolation and clustering 77—61019
  vapour, kinetic theory of evaporation and condensation between concentric cylinders and spheres 77—62629
  vapour bubble, in immiscible liquid, collapse 78—94547
  vapour bubbles, oscillating, evaporation-condensation resonance frequency 80—19488
  vapour condensation on vertical surface, laminar flow in film condensate 78—75057
  vapour deposited coatings, two-component from two sources, geometrical aspects of prod. *(Russian)* 79—38743
  vapour distribution between parallel plates, condensation, evaporation 77—3847
  vapour flows with condensation 80—48794
  vapour mixtures, with or without inert gas, condensation, heat transfer coeff. calc. *(German)* 77—39724
  vapour of high-boiling mixture, condensation on evaporating bubbles of low-boiling liq. 80—59021
  vapour-gas mixture, condensation, effect of thermal resist. of drops on heat and mass transfer 77—15015
  vapour-gas mixture, liq. drop growth rate on surface during vapour condensation 77—11779
  vapour-liquid-solid growth mechanism *(Russian)* 80—107074
  vapour-noncondensible gas mixture, body force convection condensation *(Japanese)* 79—50574
  vertical fin, film condensation on extended surface 80—6505
  vertical flat plate, generalised soln. 80—59028
  vibrational anharmonicity, condensation effect, vap. press. isotope effect 78—58657
  water, characteristic IR emission due to latent heat of transform. 77—31754
  water, droplet growth rel. to condensation coeff. *(Russian)* 79—34901
  water, thermodynamics of nucleation on charged centres 79—20955
  water condensation number, from micron size drop evaporation and growth rate determ. 79—90774
  water condensation on charged centres 78—51791
  water drops, evaporation and condensation in air, quasi-steady approximation 77—21854
  water in early solar system, low-temp. condensation rel. to meteorites H and O isotope study 80—36518
  water vapour, condensation from moist air in curved channels, mass and heat transfer 79—90251
  water vapour, condensation in presence of H_2SO_4 and HNO_3 pollutants 78—81343
  water vapour, desublimation in vacuum, heat and mass transfer and duration 77—11687
  water vapour, in rarefaction waves, heterogeneous nucleation 77—58731
  water vapour, photoinduced nucleation 79—10934
  water vapour condensation, electric field influence 80—14268
  water vapour condensation in rarefaction waves, homogeneous nucleation case 77—42869
  water vapour expansion with condensation, nozzle flow at high pressure 80—106828
  water vapour in rectangular channel, partially cooled perimeter, heat transfer 78—94557
  water vapour nucleation and condensation on AgI, mol. beam investig. 77—52212
  water vapour-Ar mixture, rarefaction waves 79—46796
  water vapour-N_2, nonstationary rarefaction wave, nonequilib. condensation obs. 77—75937
  water vapour-N_3 mixture, rarefaction waves 79—46796
  wind energy generator system, tornado-type, latent heat from moist air, effect on vortex 80—30365
  Ag, condensation on glass, temp. depend. *(Russian)* 77—32525
  AgBr, evaporated layers, use as registrating system *(Bulgarian)* 80—52344

condensation continued
  Al film, condensation from partially ionised vapour flow, peculiarities of form. and struct. 79—28252
  AlN, condensates, growth from vapour, morphological comparison with, ZnO, MgO 78—34450
  Ar, cluster formation and homogeneous nucleation, comparison of expt. and theory 80—79925
  Ar, clusters in supersonic beam, electron diffr. study 80—5655
  Ar, monolayer, condensation and compression on graphite 79—65316
  Ar, nonequilibrium condensation and surface tension in supersonic jet flow *(Russian)* 80—65210
  Ar nucleation, Ar in He carrier gas, supersonic nozzle flow 78—94871
  Ar on $CdCl_2$ cleavage face, two-dimens. condensation of second adlayer 79—99413
  Au vacuum condensation on KCl, spatial distribution of nuclei 78—18931
  BF_3, boiling/condensation heat transfer props., cryogenic appls. 78—79192
  Bi adsorption, and condensation on W 79—73394
  C fine particle formation by C vapour condensation 79—52781
  C particle formation,C_2+C_3 as possible first step 78—68876
  CO, boiling/condensation heat transfer props., cryogenic appls. 78—79192
  CO_2, adsorption and capillary condensation on clays rel. to Mars volatile storage and atmospheric history 80—72833
  CO_2, free expsn. of jet, nonequilib. effect 79—27676
  CO_2 free jet, rarefied flow, homogeneous condensation scaling law 80—6121
  CO_2 jets, homogeneous condensation, similarity law 79—42229
  CO_2, mol. beam; interaction with cooled surface, AC excitation effects *(Russian)* 77—62744
  CO_2, nonequilib. expansion, retardation temps. $\leq$1200K, vibr. relax. and condensation influences 78—5777
  CO_2-N_2-H_2O gasdynamic laser, water vapour condensation and mol. relax. processes 79—13946
  CS_2, condensation vibr. shift, intermol. interaction, vap. press. isotope effect 77—61742
  CdSe, film, vacuum condensation thermodynamics, starting powder comp. effects 77—81220
  Cs, vapour in Ar, fog condensation in MHD generator, heat and mass transfer 80—1410
  Cu on Mo and steel, substrate limiting temp. during vaporisation and condensation coating in vacuum *(Russian)* 80—100787
  DyI_3/CsI/Hg arc, time varying arc constrictions due to periodic metal iodide condensation-evaporation discussion 79—60205
  Er, laser evaporation and condensation in H_2 and Ar atmospheres 79—10941
  Fe, adsorption and condensation on W foil, meas. by thermal desorption in pulse time-of-flight mass spectra 79—15023
  Fe, condensation in planetary nebulae rel. to form. models 79—40238
  Fe-Ni-Si planetary cores, condensation from solar nebula 78—12112
  Fe(111), hydrazine multilayer condensation 79—46956
  H isotopes condensation in laser fusion targets 77—42190
  H_2O, condensation onto ice, deposition coeffs. 80—6507
  H_2O, condensation via rarefaction wave 78—71847
  H_2O droplet growth in presence of soluble gases, expts. 80—21807
  H_2SO_4 aerosol growth, kinetic model 77—37340
  HTO, atmospheric condensation-evaporation model 77—29326
  He condensation forevacuum pump 78—86282
  He, condensing on positron, Monte Carlo lifetime spectra, temp. and elec. field effects 78—55263
  ^{3}He-^{4}He mixture systems, evaporation and condensation 79—65283
  ^{3}He-^{4}He mixtures, evaporation and condensation meas., weak coupling model anal. 79—51366
  ^{3}He-^{4}He system, evaporation and condensation mechanism 79—77858
  ^{4}He charged drops in cryogenic vap., He^+ mobility, 1.3-2.0K 79—32734
  ^{4}He, superfluid, interface conditions between liq. and vapour 80—10723
  ^{4}He, superfluid, sound pulse amplitude meas. method sound transform. at free surface 80—54451
  ^{4}He, superfluid film third sound meas. as capillary condensation probe in probe material 80—20005
  Hg, dropwise condensation, at Cu surface, heat-transfer meas. 77—75781
  Hg, two-dimensional, on W 80—107666
  $Hg_{3-\delta}AsF_6$, theory of phase transitions 80—6486
  ^{115}In aerosol generation technique for atm. tracer obs. 80—26190
  Ir-C, adsorption and initial stages of condensation of Sm 79—69366
  Kr monolayer, on graphite, phase transition from localised to nonlocalised solid 77—11787
  LiF, condensation and evaporation in monomers, dimers and trimers, mol. beam method *(German)* 77—85052
  MgO, condensates, growth from vapour, morphological comparison with, ZnO, AlN 78—34450
  Mo(100), condensation of Cu and Ag, early stage 80—80072
  N_2 (-CO_2 mixture), jet, molecular rot. level population during condensation 79—86481
  N_2, capillary condensation and evap., apparatus and calc. method 80—2150
  N_2, capillary condensation and evap., scanning curves within B-type hysteresis loops 80—2151
  N_2, hypersonic nozzle flow, supercooling and spontaneous condensation 78—1549
  N_2, liq., impurity separation, laser thermal method *(Russian)* 77—7859
  N_2-He mixture, film condensation, appls. to condensers for cryogenic installations 78—59941
  N_2-O_2-Ar saturated air vapour mixture, film mixed condensation, comparison with water vapour 77—11780
  NH_3, condensation by homogeneous nucleation in supersonic nozzles 77—11230
  $(NH_4)_{10}[W_{12}O_{40}(OH)_2].H_2O$, thermal polycondensation 79—14924
  NO, boiling/condensation heat transfer props., cryogenic appls. 78—79192
  NO_2 in nonane, supersaturated gas, photoinduced nucleation 78—80760
  N_2O_4, fission reactor coolant, heat transfer on condensation *(Russian)* 80—57860
  $2NO_2 \rightleftarrows N_2O_4$, condensation, heat transfer and aerodynamics *(Russian)* 80—19932
  $N_2O_4 \rightleftarrows 2NO_2$ equilib. system, condensation heat transfer on horizontal tube bundle *(Russian)* 78—46970
  Na vapour condensation from rising bubble, effects of internal circulation velocity and noncondensable gas 78—50258
  NaCl aerosols, density rel. to formation by condensation 78—7244

condensation continued
  Ni (111), C monolayer phase condensation, LEED and AES obs. 79—46960
  Ni-W (2%), Mg diffusion meas., 970-1330K, appl. of vapour collect and AES method 78—75876
  O_2 bidimensional condensation on lamellar halide *(French)* 78—75941
  Pb, at. beam, interaction with low-temp. glass condensation surface 78—19626
  Pb vapour, diffusion-limited condensation meas. rel. to vacuum processing of metallurgical melts 77—8775
  ^{212}Pb atoms and ions, attachment coeffs. on monodisperse aerosols 79—66367
  Re tip, condensation remoulding, field emission microscopy 78—2995
  SF_6, condensation in supersonic nozzle flow 78—34611
  SF_6 condensation in supersonic nozzle expansions, trimerscritical model derivation 79—77211
  SF_6, inhibition of homogeneous condensation by vibr. excitation, isotope separation appl. 78—37688
  SF_6, supersonic jet, condensation and gasdynamic cooling 80—6089
  SF_6, supersonic jet expanding into vac., interaction with CO_2 laser beam 80—5584
  SF_6-Ar, condensing flow, gasdynamic and IR meas. 80—6501
  $SO_2+H_2O+O_2(N_2)(Ar)$, condensation nuclei form., ion polarity and age depend. 79—39220
  Si, electron-hole droplet condensation, phase diagram and surface tension 79 19521
  SiO vapour, refractory silicates nonequilib. phases condensation 79—60497
  Ti-N_2, condensate formed by plasma flow precipitation in vacuum, cryst. and surface props. *(Russian)* 80—100788
  U enrichment by photochemical laser, two-phase flow with condensation, mathematical model *(French)* 80—74029
  U isotope separation by selective laser photoexcitation in reactive two-phase flow 79—94109
  UF_6, non-equilibr. condensation calcs. for laser isotope separation 80—10132
  UO_2, closed boiling system, effect of condensation on dispersion following LMFBR HCDA 78—8936
  UO_2, condensate solidification onto steel struct. in above-core region of LMFBR after HCDA 78—17364
  UO_2, condensed vapour following core disruptive accident, particle-size distribs. using first-generation model 78—13295
  UO_2 fuel vapour, condensation on vertical steel substrate 77—46330
  UO_2 vapour condensation from rising bubble, effects of internal circulation velocity and noncondensable gas 78—50258
  W (100), condensation of Cu and Ag, early stage comparison with Mi(100) 80—80072
  W, LEED and electron microscopic investigs., review *(Hungarian)* 77—47654
  W tip, condensation remoulding, field emission microscopy 78—2995
  Xe monolayer on graphite, phase transition from localised to nonlocalised solid 77—11787
  Zn aerosol, prismatic and spherical particle form. 77—9135
  Zn vapour, diffusion-limited condensation meas. rel. to vacuum processing of metallurgical melts 77—8775
  ZnO, condensates, growth from vapour, morphological comparison with, MgO, AlN 78—34450
  Zr-N_2, condensate formed by plasma flow precipitation in vacuum, cryst. and surface props. *(Russian)* 80—100788
condensers (electric) *see capacitors*
condensers (steam plant)
  Arizona Nuclear Power Project waste water reclamation for cooling 79—9861
  coolant contamination control using atomic absorption spectrophotometer method 77—373
  enhanced film condensation by surface forces, optimum condenser tube fin geometry 78—75039
  heat transfer in tubular condenser apparatus *(Russian)* 80—1411
  LWR, condenser tube failures 78—21715
  plate condenser with grid pattern slotlike channels, low-press. steam condensation, heat transfer 78—75040
  steam turbine condensates, ion-exchange polishing analysis *(Russian)* 80—89487
  supersonic nozzle discharge, heat transfer and gas dynamics 78—55671
  tube corrosion resistance performance review 79—39046
  turbulent flat jet condenser, nozzle hydraulic and heat transfer characts. 78—94793
condensing *see condensation*
conductance, electric *see electric admittance*
conductance, electric, measurement *see electric admittance measurement*
conductance measurement, electric *see electrical conductivity measurement*
conducting materials
  see also bimetals; electrolytes; metals; semiconductor materials; superconducting materials
  ESCA, X-ray type, C 1s contaminant buildup on conductors and insulators 78—95981
  Au plated Ni powder for electroplating conductive pastes 79—95957
conduction, heat *see heat conduction*
conduction bands
  see also Fermi level; semiconductor materials
  actinide alloy, resistivity temp. depend. due to localised spin fluctuations 77—8083
  actinide compounds, conduction electron polarisation, model density of states 79—37949
  actinide metals and intermetallics, localised versus itinerant character of 5f electron states 77—28138
  alkali graphite intercalation compound, evidence for alkalilike cond. bands 80—45201
  alkali graphite intercalation compounds, evidence for alkali-like conduction band, UPS study 80—45208
  alkali metal alloy, cond. electron density depletion by charge transfer state 79—95372
  n-alkanes, conduction band struct., LEED, secondary electron emission and UPS study 80—70601
  alloy, disordered, energy band struct. and elec. cond., effect of short-range order 80—10860
  Anderson model, asymmetric, t-matrix approx., ground state 80—20061
  Anderson model, perturbation expansion in infinite conduction bandwidth limit, Kondo temp. 79—28506
conduction bands continued
  Auger XVV spectra, many body effects in incompletely filled bands, theory 80—7448
  n- $(Bi_{1-x}Sb_x)_2Te_3$, magnetoresist. in quantising mag. field 80—24953
  Cain model, two-band, dispersion and iso-energy surfaces of valence and conduction bands *(Russian)* 80—24783
  charge-density-wave metal, mag. susceptibility of cond. electrons 80—44523
  crystal with narrow allowed band, elec. field ionisation of deep impurity level 79—15118
  deformation potential screening by free electrons in multivalley cond. band 77—76756
  degenerate semiconductor, band nonparabolicity effects on behaviour of Debye screening length 78—2438
  degenerate semiconductor, with nonparabolic energy bands, magnetic quantisation, Fermi energies 78—30864
  diamond, (100) surface states, SCF extended tight-binding method 77—47881
  diamond, natural, anisotropy and saturation of hot carrier drift velocity 80—6867
  dielectric liquid, drift mobility and conduction band energy of excess electrons 77—4348
  dielectric liquids, cond. band minima, rel. to electron mobility maxima 78—80029
  dielectric solids, laser damage, conduction-band electron interaction theory 80—35017
  electrode and volume controlled photocurrents 80—6908
  electron gas, ang. correl. in positron annihilation 80—24821
  electron gas, degenerate, collective props. using electron knock-out processes 80—6758
  electronic phase transition accompanied by valence change, effect of damping and hybridisation of f-electrons 77—24520
  ethane, dense fluid, cond. band energy determ. 79—87136
  ethylene, conduction band struct., LEED, secondary electron emission and UPS study 80—70601
  excitons, Wannier and Frenkel, simple model for unified treatment 79—69422
  extrinsic semiconductors, carrier concs. and Fermi levels 77—66112
  ferroelectric transition, conductivity band theory rel. to vibronic theory of ferroelectricity 79—19854
  ferromagnetic semiconductor, absorpt. edge and cond. band width, temp. and mag. field depend. 77—36267
  ferromagnetic semiconductor, doped, electron spin polarisation and conduction band struct. 80—65449
  ferromagnetic semiconductor, electronic excitation spectrum 80—11149
  ferromagnetic semiconductor, spectral density approach for s-f model quasiparticle concept 80—80173
  ferromagnetic semiconductors, dielectric function depend. on magnetisation, light absorpt. coeff. *(Russian)* 80—15467
  ferromagnetic semiconductors, electronic quasiparticle spectrum 80—97051
  ferromagnetic semiconductors, s-f interaction on conduction band, red shift effect theory 80—59872
  p-GaAs, spin relaxation of photoelectrons 77—85207
  glasses and amorphous semiconductors, band struct. and forbidden gap, review 78—75987
  graphite, diamagnetism with quasilinear dispersion law, orbital susceptibility, valence bands *(Russian)* 80—80475
  graphite, high energy cond. and valence band states, XPS 78—39664
  graphite, X-ray emission and absorption, XPS, electronic struct. 77—16431
  graphite intercalation compound, interaction between one or two s orbitals *(French)* 80—65440
  group IV semiconductors, acoustic deform. pot., pseudopot. calc. 77—1363
  heavily doped, Raman phonons, interband excitation effects 78—52501
  hexaborides of Ba, La, Ce and Sm, rel. to work functions 79—65537
  hybridised conduction band, intrinsic upper limit of electron-phonon coupling *(Chinese)* 80—54589
  hybridization effect on phase transitions in the Falicov-Kimball model 78—91617
  II-VI semicondcutors acoustic deform. pot., pseudopot. calc. 77—1363
  III-V semiconductor, deform. effects, theory 78—34761
  III-V semiconductor, heavily doped, pressure volume characts. nonlinearity, intervalley electron redistrib. 77—8012
  III-V semiconductors, acoustic deform. pot., pseudopot. calc. 77—1363
  III-V semiconductors, conduction-band struct. from reflectivity meas. when subject to mechanical strain 79—42449
  indirect exchange interaction through narrow conduction zones *(Russian)* 79—4538
  n-InSb, intraband processes exam. by stimulated spin-flip Raman scatt. 77—19362
  intermediate valence, three-site, six-electron, even-parity model 80—20125
  Kondo lattice, phase diagram 80—7077
  laser diode, spontaneous emission linewidth, calcs. 77—10927
  layer materials, SXAPS interpret., cond. band self-convolution model, cryst. field splitting 78—23558
  many-valley semiconductors, antiferromagnetic or atomic ordering effects on conduction electrons 80—2329
  metal, antiferromag., thermoelec. power in mag. field 80—70686
  metal conduction electron photoemission spectrum, effect of recoil on shake-up spectra, infinite summation method 80—50526
  metal surface, disordered, multiple scatt. of cond. electrons 80—10959
  metals, conduction band widths 80—103619
  metals, hybrid, exchange interaction of localised moments rel. to Fermi surface 77—28381
  metals, X-ray photoelectron and absorpt. spectra, edge singularities in spin-depend. final-state interactions 78—6810
  metals, X-ray photoemission, intrinsic plasmons effects 78—39661
  MIM heterojunction, theory of reson. tunnelling through insulator cond. band. 77—59336
  mixed valence state, electronic structure 79—11092
  molecular crystal, band structure, excitonic processes, trap distrib. 80—6720
  Multiphonon effects in the theory of electron tunelling between deep impurity levels and the conduction band in strong electric fields 78—2447
  multivalley semicond., biexciton props. 77—66120
  narrow-band solids, electronic correlations 79—56112
  optical joint density of states, oscillator strength effects 77—11838

conduction bands continued
OPW method, instability rel. to error in core eigenvalues 78—63963
orientational metal-insulator phase transitions in quadrupolar strands with itinerant electrons 80—15455
p-n heterojunctions, forward-biased, charge accumulation 80—107902
parametric wave excitation in semiconductor electron plasma *(Russian)* 79—33252
passive layer, on Fe electrode, semiconductor model, appl. to electrochem. reactions, review 80—26022
polyethylene, one-, three-dimensional, energy band struct., ab initio calcs. 79—95330
polyethylene film, soln.-cast, low energy electron scatt. obs. of band struct. 80—16131
polypeptide chains, struct. of conduction and valence band 80—76700
polypeptides, electronic struct., side-chain disorder effect 80—76706
pyrene, band structure, excitonic processes, trap distrib. 80—6720
rare earth compounds, mixed valence state, conduction band struct. 80—103624
rare earth intermetallic, cubic, direct coulombic contrib. of cond. electrons to cryst. elec. field 79—91005
rare earth intermetallics, cubic, exchange coulombic contrib. of cond. electrons to cryst. elec. field 79—95376
rare earth intermetallics, RAl_2, exchange modification of cond. bands 79—82568
rare earth metals, EFG produced by conduction electrons, mag. ordering effects 77—40020
rare earth superconductors, spin splitting of cond. bands and spin-orbit scatt. 79—56461
rare earth tellurides, electron density distrib. from Mossbauer spectra 78—23374
rare earth-Al_2 (Zn), mag. coupling mechanism 79—4655
semiconducting binary alloy, cond. band edge shift near precip. point, order fluctuations 77—24517
semiconductor, carrier number and effective bandwidths *(Spanish)* 78—18954
semiconductor, covalent, non-orthogonal tight-binding approach 80—2442
semiconductor, electron-donor recombination, Monte Carlo studies of transitions between excited donor states 79—38093
semiconductor, ferromag., band edge energy anomalous carrier density mag. field depend. 80—49774
semiconductor, homogeneously doped, intervalley junction 77—4433
semiconductor, hot electrons, photoexcited in quantizing mag. field, energy distrib. calcs. 79—42586
semiconductor, narrow gap, mag. quantum oscills. of Auger transition rate 77—69340
semiconductor, Wannier excitons, fine structure, lineshape and dispersion, review 80—44520
semiconductor, zinc blende struct., cond. band nonparabolicity and cyclotron reson. linewidth *(German)* 78—75993
semiconductor isotype heterojunction barriers, cond. band discontinuity, C-V profiling meas. method 80—70801
semiconductor thin films, degenerate one-valley and many-valley, photogalvanic effect calcs. 80—34487
semiconductors with superstructure, weakly bound states of elementary excitations 79—60733
solid, linear combination of Gaussian orbital basis sets 78—6258
substitutional alloys of intermediate valence systems, static mag. susceptibility con. and temp. depend. 80—84586
superconducting transition temp. enhancement by localised states, band struct., electron-phonon interaction 78—47902
TCNQ, electron- and phonon-polaron effects in valence and cond. bands 77—76757
TCNQ, infinite stacks, all valence electron band struct. 78—39001
tight binding calc., overlap and next-nearest-neighbour interaction effects 78—72059
transition metal, dichalcogenide layer cpds., bonding and phase transitions 80—34186
transition metal based alloy, resistivity temp. depend. due to localised spin fluctuations 77—8083
transition metal dichalcogenides, layer type cpd., reflectivity meas., 6-40 eV 77—55801
TTF, infinite stacks, all valence electron band struct. 78—39001
TTF-TCNQ, Madelung energy, electronic struct. *(Russian)* 78—6253
tunnelling MIS structures photovoltaic energy conversion, band struct. 80—92995
x-ray edge singularities of relaxed-out bound states and relaxed-in band states 78—92173
Ag halides, tetrahedrally coordinated, semiempirical band struct. model 77—51655
Ag halides, valence and cond. states, UPS, temp. depend. 77—20997
$AgAsS_2$, cryst. and amorphous, band struct., photoemission and refl. spectra obs. 77—66581
AgBr, photographic emulsions, dye spectral sensitization, latent image form., subcond. band events 78—32905
Al, positron annihilation, ang. correl. meas., electronic momentum density calcs. 77—4284
AlGaAs p-n diodes, I-V characts., tunnelling 80—100510
$Al_{0.35}Ga_{0.65}As$-GaAs N-p heterojunction diodes, current suppression by cond. band discontinuity 80—80362
$Al_xGa_{1-x}As$, lower conduction band struct. 78—6270
$Al_xGa_{1-x}As$:Cr, deep level props. 79—69465
α-Al_2O_3, additively coloured single crystal, luminescence *(Russian)* 80—55169
Ar, solid gaseous, valence and inner shell excitonic band struct. 80—6735
As-Se chalcogenide glass, optical const. photoinduced changes mechanism 80—7321
Au, conduction electron g-factor meas. 77—35859
Au, core-electron excitation edges 80—66345
B, evaporated, electronic struct., XPS, SXS and isochromat investig. 80—76143
B_2O_3-CaO-Fe_2O_3 glasses, semicond., cond. models, electronic props., 77-800K 80—54688
BaO, single cryst. on Ir, electron affinity, conduction band edge position, low energy electron reflection spectra 78—14790
BaO, surface pot. meas., cond. band edge, electron affinity, LEER 77—24606
$BaTiO_3$, K-edge X-ray absorpt., cond. band states 80—97382
Be, noncubic crystal, temp. depend. of elec. field gradient 79—99515
Bi, dispersion reln. for electrons near bottom of band 77—15742
Bi electron properties, carrier spectrum 78—84137

conduction bands continued
Bi, film, oxidation, UPS, valence band, cond. band and 5d core states 77—20995
Bi film, oxidation kinetics and interfacial bonding using final states 77—56127
Bi, oxidation, charge transfer obs. from final state changes 77—51703
BiI_3, excitonic shifts of quasiatomic optical core to cond. band transitions, UPS obs. 78—11079
n-Bi_2Se_3, cryst. nonparabolic cond. band., IR refl. and Hall voltage meas. 77—31940
n-Bi_2Se_3, nonparabolicity of cond. band and anisotropy of electron effective mass 79—60692
Bi_2Se_3:Sn(Pb), dopant influence on elec. cond. 79—51569
Cd, noncubic crystal, temp. depend. of elec. field gradient 79—99515
Cd_3As_2, electron conc. temp. depend. heavy hole-cond. band energy gap 79—69410
Cd_3As_2, low-temp. energy band struct. and depend. of direct gap on press. and temp. 77—62822
n-$CdCr_2Se_4$:In, electrical props., 93-168K 80—49713
$CdGa_2S_4(Se_4)$, band struct., pseudopot. method 80—92816
n-$Cd_xHg_{1-x}Te$, conduction band struct., IR refl. spectra obs. 80—39502
$CdI_2(Br_2)(Cl_2)$, dielec. function and band struct., EELS meas. 80—40195
CdS, band structure calcs. by modified orthogonalised plane wave (MOPW) method 80—54609
CdS, photoanode, difference between Fermi level and bottom of cond. band 79—62013
CdS, photocond. cryst. characterisation of electron-trap responsible for acoustic holographic echoes *(French)* 79—19544
CdS, spin flip Raman scatt. linear k term 78—19475
CdSe-Si n-p heterojunction, vacuum deposition, photovoltaic effects *(Korean)* 77—28243
$CdSiP_2$, pseudodirect bandgap semiconductor, natural birefringence 79—65834
n-$CdSnAs_2$, optical absorption rel. to energy spectra *(Russian)* 78—75994
n-$CdSnP_2$, Hall coeff. and elec. cond. meas., 24-900K 80—54721
CoSi, plasma refl., 80 to 300K, energy overlap of valence and conduction bands 79—28366
Cr_3Si, specific heat at low temps., electron density of states, Debye temp. *(Russian)* 80—54398
CsI, cond. band density of states, rel. to secondary electron spectra 77—12473
$CsSnBI_3$, electronic struct., XPES and band theory calc. semimetallic behaviour 79—78837
$CsSnCl_3$, electronic struct., XPES and band theory calc. semimetallic behaviour 79—78837
Cu (100), three-layer film, work function and density of states, self-consistent calc. 77—35978
Cu, Bloch states, photoelectron spectra, angle resolved 78—92175
Cu, conduction band, high momentum components determ. from annihilation radn. ang. correlation 79—19508
Cu, core-electron excitation edges 80—66345
Cu, energy band dispersions and lifetimes using angle-resolved photoemission 79—77998
Cu halides, tetrahedrally coordinated, semiempirical band struct. model 77—51655
Cu, multipole wave functions, singular points in band struct. and Wannier function tails 79—37956
CuBr, density of states of cond. band calc. 77—62819
CuCl, density of states of cond. band calc. 77—62819
CuCl, UPS meas., electronic struct. 80—50529
CuI, thermoreflectance spectrum, 4-7 eV region 79—19904
D_2O, effect of phase density on ionisation process and electron localisation 77—89731
Eu chalcogenides, cond. band spin struct. 80—71577
EuO, magnetic semiconductor, piezoresistance effect, 4.2 to 300K 80—34450
EuS, conduction band density of states, redistrib. near ferromag. saturation 78—67939
EuS, spin polarised tunnelling and mixed spin states in conduction band 79—52085
EuTe, exchange and superlattice band splittings, magneto-optical meas. in high mag. fields 79—61342
Fe-Al (8 at.%), XPS investig. of cond. band region 77—16456
Fe-Al alloys, conduction band states, X-ray spectra obs. *(Russian)* 80—29317
Fe-based alloy, effect of sp-3d impurity interactions in resistivity 79—46696
FeF_3, thin film, optical absorpt. meas., lack of F to delocalised states in cond. band 79—15546
$FeSb_2$, quasi-magnetic semicond., mag. susceptibility 80—39757
$Ga_{1-x}Al_xAs$ electrodes, interface capacitance meas., flatband pot., conduction and valence band boundaries *(French)* 79—33339
$Ga_{1-x}Al_xAs$, non-shallow levels and cond. band struct. from Hall carrier conc. meas. 80—39607
$Ga_{1-x}Al_xAs$, velocity saturation and cond. band struct. under press. 78—26863
GaAs anodic oxide, states, electrochemical meas. 80—80176
GaAs, conduction band effective mass, influence of high uniaxial stress 80—80162
GaAs, conduction band mapping by angle-resolved photoemission 79—83105
n-GaAs, conduction band nonparabolicity and coupled plasmon-phonon modes, IR refl. spectra 80—55110
GaAs, DC biased, filamentation of laser radiation 80—74428
GaAs, diffusion coeff. of hot electrons 79—15156
GaAs, effective mass, Raman spectrum determ. 80—24797
GaAs, electron transient vel. characts., Γ-L-X cond. band ordering 78—79997
GaAs, free-carrier impact ionisation, orientation depend. rel. to cond. band 77—76836
GaAs, $\Gamma_6{}^c$-$L_6{}^c$-$X_6{}^c$ cond. band ordering, velocity field characts., Monte Carlo calcs. 78—18957
GaAs, heavily doped, electron effective mass, Kane equation calcs. 79—77989
n-GaAs, heavily doped, test of cond. band edge random fluctuations by MCD 77—63438
n-GaAs, high temp. mobility anal. in three-valley ($\Gamma_6{}^c$-$L_6{}^c$-$X_6{}^c$) model 79—99544

conduction bands continued
GaAs, impact ionisation, electron band struct. effects obs. by temp. tuning 77—85232
GaAs, lower cond. band struct. 78—6271
GaAs, lower conduction band minima, ordering and props. 77—28114
GaAs, piezoresistance and conduction band minima 78—51993
GaAs, resonance Raman scattering by 2 TO phonons and cond. band minima ordering 77—20854
GaAs, three level cond. band struct., uniaxial stress effects, resist. and Gunn effect threshold meas. 77—85137
GaAs, three-level struct., from high-stress and high-field obs. 77—15764
GaAs:Cr, carrier equilibrium effects, impurity states, elec. resistivity 80—65488
GaAs:Sn, doping characts. during LPE 79—10866
GaAs-$Al_{0.3}Ga_{0.7}As$ n-N heterojunction, LPE grown, cond. band discontinuity, C-V profiling meas. 80—70801
GaAs-$Ga_{1-x}Al_xAs$, superlattice umklapp processes in resonant Raman scattering 78—64362
GaAs-Ge heterojunction, band discontinuities, angle-resolved UPS obs. 79—7878
$GaAs_{1-x}P_x$ based structs., carrier conc., mobility calcs. from Hall effect meas. 78—60138
$GaAs_{1-x}P_x$ electrodes, interface capacitance meas., flatband pot., conduction and valence band boundaries *(French)* 79—33339
$Ga_xIn_{1-x}As_yP_{1-y}$, conduction band and phonons, Shubnikov-de Haas effect, magnetophonon resonance, Raman scattering 80—24795
$Ga_zIn_{1-x}P$, piezomodulation spectra of cond. band struct. 77—48191
$Ga_{1-x}In_xP_{1-y}As_y$, electron transient drift vel., influence of effective mass in gamma cond. band 80—2384
GaP, camel's back excitons, rel. to band structure 78—47707
GaP, Cs(Cs-O) activated, with negative electron affinity, near UV photoemission and secondary emission 78—11074
GaP, density of states effective mass and cond. band energy minima 77—28101
GaP, effective mass anisotropy at X_{1c} and X_{3c} minima of conduction band, optical absorpt. spectra 77—8021
GaP, electron-hole drops, self-consistent surface calculation 80—65464
GaP, fine struct. of indirect exciton 78—19509
GaP, line shape and symmetry analysis of core-level electroreflectance spectra 77—8600
GaP, luminesc. from electron-hole drops, 2 to 77K 79—11454
GaP, proton implanted, thermally stimulated current meas. 80—24943
GaP, stress-induced X_{1c}-X_{3c} conduction band mixing 79—19515
GaP:Si(s)(O)(Ta), donor centre struct. and conduction band nonparabolicity 78—14695
GaP-liq. NH_3 soln. junctions, elec. characts. *(French)* 80—2460
GaS, layered, conduction band photoelectron spectroscopy 77—52217
GaS, valence and conduction bands, synchrotron radiation photoemission spectra 77—63536
GaSb, inversion of Γ and L conduction bands under uniaxial stress, photoluminescence meas. 79—33229
GaSb, L-states, uniaxial stress effect on i.r. free carrier absorption 77—1674
GaSb, photolum. spectra under hydrostatic press., energy shift of direct gap and L-conduction band 79—19930
GaSb, solid solns., impact ionisation, cond. and valence band effects 80—65583
n-GaSb:Te, elec. transport mechanism in cond. band from Hall mobility and transverse mangetoresist. meas. 79—73531
GaSe, layered, conduction band, photoelectron spectroscopy 77—52217
GaSe, valence and conduction bands, synchrotron radiation photoemission spectra 77—63536
Ge, cyclotron reson. in strong elec. fields, classical theory 80—7172
n-Ge cyclotron resonance line shape at 337 μm, obs. 77—39770
Ge, deep donor character of muons and protons 80—10911
Ge, direct gap recombination, at high excitation level and low temp. 79—38650
n-Ge, direct identification of $L_3' \rightarrow L_1$ transition, electroreflectance 77—1689
n-Ge, effect of non-parabolicity in quantum mechanical treatment of cyclotron reson. 77—31937
Ge, electron-hole drop freq. depend. damping 80—88482
Ge, energy-gap narrowing and state filling under laser irrad. 79—42441
Ge, ion implanted, cond. and valence bands study by X-ray bremsstrahlung and photoelectron spectra 80—2360
n-Ge, line shape cyclotron reson., 337 μm, 15-80K 78—6577
n-Ge, piezoresistance under mechanical stress, rel. to cond. band minima 80—6836
H, Wannier functions, variational calc. 77—15740
H_2 crystal, exciton states, intermediately bound-exciton theory 77—69234
H_xWO_3 bronzes, Anderson transition, XPS 80—107705
$HfS_2(Se_2)$, vacuum UV reflectivity spectra, cond. band model 77—44012
$Hg_{0.77}Cd_{0.23}Te$, spin-flip, Raman laser,, cond. band nonparabolicity effect 77—79832
$Hg_{1-x}Cd_xTe$ films, Tamm surface states, Kane model 79—28395
n-$Hg_{1-x}Cd_xTe$, optical phase conjugation 80—83644
$Hg_{0.98}Mn_{0.02}Te$, resonance acceptor level 78—23048
HgTe, contrib. of resonant states to conductivity 79—51577
HgTe, mag. sub-band struct. under uniaxial stress 77—11883
HgTe, zero gap semiconductor, resonant acceptor states 80—6772
II-VI semiconductor-electrolyte boundaries, electrolyte boundaries, photo e.m.f. meas., semicond. energy bands 77—1481
InAs, longitudinal magnetoresistance in extreme quantum limit *(Russian)* 80—11008
N-InAs, Moss-Burstein effect, S, Sn, Te dopants 78—64389
InAs, photoluminescence exam. 79—28809
n-InAs, Shubnikov-de Haas oscills., conduction electron density, phonon scatt. 77—15768
$In_{1-x}Ga_xAs$-$GaSb_{1-y}As_y$, new heterostruct. characts. 78—72247
n-$In_{1-x}Ga_xAs_yP_{1-y}$, cyclotron reson., cond. band nonparabolicity 80—29311
In_2O_3-SnO_2-Si heterojunctions, elec. and photovoltaic characts. 78—52070
InP, deep level trap interaction with lowest and upper cond. minima 80—49654
InP, deep-level traps and cond.-band struct. 79—19542
InP, Kramers-Kronig electroreflection spectra 77—4655
InP:Te, mag. props. of conduction electrons 78—6510
InSb, conduction and valence band effective mass parameters 79—60689
n-InSb, conduction band effective mass anisotropy and nonsphericity 79—69414

conduction bands continued
n-InSb, conduction-band struct. from reflectivity meas. when subject to mechanical strain 79—42450
n-InSb, convective instability in crossed mag. and elec. fields 77—62939
InSb, cyclotron harmonic transitions, warping and inversion asymm. effects 78—68383
n-InSb, elec. cond., press. dependence 80—6830
InSb, film, E_0, E_1 absorption edge size quantisation, optical and electroreflectance spectra 80—34998
InSb, intraband photocond. in mag. fields 79—47123
InSb, inversion asymm. splitting of cond. band, Shubnikov-de Haas meas. 78—10348
n-InSb, longitudinal magnetoresistance in extreme quantum limit *(Russian)* 80—11008
InSb, magnetic freeze out *(Japanese)* 78—39130
InSb n-type, heavily doped, effects of hydrostatic pressure on electron mobility and conc. 77—4390
n-InSb, photoluminescence exam. 79—28809
InSb, pinning struct. of cyclotron-phonon reson., effect of nonequidistant Landau levels 77—11881
InSb, polar semiconductor, impact ionisation in crossed elec. and mag. fields 79—28355
InSb:Cr:Zn, cond. band, change in electron density with mag. field 79—15169
InSe, optical props. from 2-25 eV 80—29760
InSe, valence and conduction bands, synchrotron radiation photoemission spectra 77—63536
KBr, electronic states at (100) surface, accounting for spin-orbit interaction *(Russian)* 78—91750
KCl, electronic states at (100) surface, accounting for spin-orbit interaction *(Russian)* 78—91750
KI, cond. band density of states, rel. to secondary electron spectra 77—12473
KI, electronic states at (100) surface, accounting for spin-orbit interaction *(Russian)* 78—91750
n-$KTaO_3$, light and heavy cond. electrons at zone centre 79—73426
$KTaO_3$, Shubnikov-de Haas effect, cond. band struct. 80—10875
LiF, evaporated film, UPS, valence and cond. band struct. 77—63528
ND_3, effect of phase density on ionisation process and electron localisation 77—89731
NaCl, conduction band struct. from first principles 79—65379
Na_xWO_3, vacuum UPS exam. 78—84700
Nb, BCC lattice, optical props., energy band calc. of combined density of electron states 79—15075
Nb-Mo, electronic struct., thermoreflectance meas. 0.5-5.0 eV 80—45050
$NbH_{0.29}$, Compton profile and electron momentum distrib. anisotropy 77—44079
$NbSe_3$, electronic struct., chem. interpret. of geom. deform., oxidation state formalism 80—107690
Ne, solid, cond. band calcs., use of electron atom scatt., phase shifts 77—85139
Ni clusters, electronic props. and implications for chemisorption 79—23886
Ni, core-electron excitation edges 80—66345
Ni-Fe, IR spectra, cond. electron characts. *(Russian)* 77—48173
PbI_2, excitonic shifts of quasiatomic optical core to cond. band transitions, UPS obs. 78—11079
PbI_2 intercalated with organic mols., energy band splitting *(Russian)* 78—76027
PbS, conduction band nonparabolicity and carrier scattering mechanism 79—11065
PbS-Ge heterojunction, influence of conduction band discontinuity on lux-ampere characts. 78—39200
$PbSe_{1-x}Te_x$, p-n junction, inversion of conduction level 78—47856
$PbSe_{1-x}Te_x$, symmetry change in cond. levels, photovoltaic effect and reflectivity obs. 78—34766
$Pb_{1-x}Sn_xSe$, valence zone struct. effect on mobility/inherent conc. ratio *(Russian)* 79—73437
$Pb_{1-x}Sn_xTe$, DH laser, gain-freq.-current relation, k.p band model 77—61951
$Pb_{1-x}Sn_xTe$:In, Hall effect and photoconductivity *(Russian)* 80—103720
Pd (111), energy dispersions for valence and conduction bands 79—38719
Pd, hydride and alloys, electronic band struct., comparative study of electric and mag. props. 78—95259
Pt, core-electron excitation edges 80—66345
ReO_3, cubic lattice stability, screening effect on vibrs. 80—75356
$(SN)_x$, quantum chem. calcs. of electronic struct. 78—6257
Se, amorphous, trigonal and monoclinic, 2p photoabsorpt. spectra 78—23551
Se, trigonal, luminesc. identification of indirect transition 80—55189
Si (111), chemisorption of H_2(Cl), conduction-band surface resonance 78—52051
Si, amorphous, clean and O_2 adsorbed, light sensitive electron laser meas. 79—24396
Si, deep donor character of muons and protons 80—10911
Si, doped, basis functions for studying intervalley effects 79—69442
Si, exchange and correlation pot., band struct. calc. 78—56068
n-Si, impurity-assoc. magnetophonon reson. 80—20221
Si on sapphire, residual strain effect on elec. props. *(Japanese)* 80—84522
Si, pseudopotential calculation of phonon dispersion curves 80—10620
Si, stressed, at high mag. field, submillimeter cyclotron res. of electrons 77—81012
Si, with non-spherical pots. for two basis atoms, electronic struct. 78—72069
Si:F(,H), amorphous, electronic struct., orthogonalised LCAO calc. 80—44486
Si:Pt, elec. props., deep-level transient spectroscopy and thermal emission meas. 79—82542
Si:Se, impurity states, A- and B-centres, electron, hole thermionic emission rates 80—96813
n-SiC, 6H polytype, expitaxially grown, electronic props. meas. 77—39975
β-SiC, cubic, conduction band minima location and shape determ. 77—85141
SiC polytypes, localisation of cond. band minima in Brillouin zone 80—20082
Si(111), conduction-band surface resonance 78—52051
SmS, semicond. phase, cond. band model, elec. and thermal cond. meas. 77—39854

conduction bands continued
SmS, semicond. thin film, absorpt. and refl. spectra, fine struct., cond. band extremum 79—69897
SmS, semicond.-metal transition, cond. band type, deform. pot. determ. 79—69417
SmZn, ferromag., cond. band antiparallel polarisation exceeding 4f moment 80—60207
SnI_2, single crysts. and film, optical props. 77—32437
SnS_2, conduction and valence band density of states 77—62817
SnS_2, Sn4d photoionisation, second threshold 80—40222
$SrTiO_3$, K-edge X-ray absorpt., cond. band states 80—97382
$SrTiO_3$:Nb, Fermi surface meas., oscillatory magnetothermal effect study 79—65357
Ta, density of unoccupied electronic states, UV isochromat spectra and SXAPS 79—77977
Ta film, photoemiss. from conduction band and core levels 77—16464
Te conduction band parameters, interband magnetoabsorption meas. in Faraday configuration 77—89695
Te, cyclotron reson. in pulsed high mag. fields, cond. band struct. 80—59867
Te, existence of allowed states in forbidden band, low temp. photocond. spectrum *(Russian)* 77—11960
Te, inversion layer, single sub-band, splitting due to sheet separation in cond band 79—15207
Te, optical activity, de Haas-van Alphen oscillations and cond. band parameters 80—54605
Te, photo-excited carriers, far IR magneto-spectroscopy 80—50343
Te, trigonal, self-consistent ground state, X_α calcs. 80—54604
TiO_{1+x}, conduction band determ. 78—60055
TiO_2, cond. and valence band struct., gap anisotropy 77—47729
TiO_2, rutile, K-edge X-ray absorpt., cond. band states 80—97382
$TiS_2(Se_2)$, vacuum UV reflectivity spectra, cond. band model 77—44012
Tl_xTe_{1-x}, amorphous, bonding and electrical conduction 79—90951
UO_2, U_3O_8, U_2O_5, shake-up satellites and band struct. 77—55861
$UP_{1-x}S_x$, sp.ht. and electronic struct. 79—91240
V-Al alloys, conduction band states, X-ray spectra obs. *(Russian)* 80—29317
V_2O_5, energy band structure, tight-binding method 80—70602
W, conduction electron g-factor, US vel. quantum oscills. 77—28100
W, optically polarised conduction-band electrons, spin-polarised photoemission obs. 79—74055
Yb, film, amorphous and cryst., transport props. rel. to band struct. *(Russian)* 77—12026
Zn, noncubic crystal, temp. depend. of elec. field gradient 79—99515
$ZnGa_2S_4$, band struct., pseudopot. method 80—92816
$ZnGeP_2$, pseudodirect bandgap semiconductor, natural birefringence 79—65834
$Zn_{0.1}Hg_{0.9}Se$ type alloy, dispersion law of cond. band *(Russian)* 77—1366
ZnO (0001), (000$\bar{1}$) and (10$\bar{1}$0), UPS rel. to elec. struct. 78—15288
ZnO (10$\bar{1}$0) surface bias voltage effect on hardness, charge exchange near dislocations 78—52078
ZnS, band structure calcs. by modified orthogonalised plane wave (MOPW) method 80—54609
ZnS-metal interface in MIM struct., photoexcitation level assignment *(French)* 80—15622
ZnSe:Co, effect of in-band position of states on photoelec. props. 78—23132
$ZnSiAs_2$, pseudodirect bandgap semiconductor, natural birefringence 79—65834
n-$ZnSiP_2$, IR absorption 77—12377
$ZnSiP_2$, pseudodirect bandgap semiconductor, natural birefringence 79—65834
$ZrS_2(Se_2)$, vacuum UV reflectivity spectra, cond. band model 77—44012

conduction electron spin resonance *see CESR*

conduction in solids, ionic *see ionic conduction in solids*

conductivity, electrical *see electrical conductivity*

conductivity, thermal *see thermal conductivity*

conductors (electric)
see also bimetals; overhead line conductors; wires (electric)
1/f, conductance noise, with four arbitrarily shaped and placed electrodes 77—85275
1/f noise in electrical conductors, survey 80—107878
AC forces acting on conductors of bifilar lead *(German)* 79—41281
conducting bodies, capacity and energy calcs., for rotational symmetry *(Polish)* 79—875
curved rectangular conductor magnetic field calc. 77—61895
cylinder in harmonically variable transverse mag. field, EM wave penetration 79—81328
cylindrical, carrying elec. current, magnetothermoelastic interactions, mechanocaloric effects 79—72815
cylindrical conductor, exact surface-impedance matrix expression 79—98266
cylindrical conductor carrying AC, temp. and stresses 78—82875
cylindrical conductor with surface crack, eddy currents calc. 80—23601
eddy current testing of tubes, rods and wires, non-destructive *(German)* 80—25971
EM field penetration, mean time constants calc. *(German)* 79—3613
explosion in water obs., for varying cross section/length ratio *(Russian)* 77—7612
film conductor, pulse nonlinearity meas. 78—56242
force between circular coil and parallel iron slab 79—76547
force between current carrying conductors, arbitrary shape, error anal. *(Slovak)* 78—22065
gas filled, internal heat transfer calc. 78—1656
geomagnetic influences on man-made systems 80—12887
heterogeneous, planar nonstationary EM field anal. in transient state *(Polish)* 78—71000
hollow conductors for force-cooled superconducting magnets, fabrication and properties *(Japanese)* 80—90868
MHD kink instability 80—6307
moving, parallel to infinite conducting slab, EM field calc. 80—18959
multiparallel system of conductors losses in thin nonmagnetic plate calc. 80—78743
noise, four-probe investigation, theory 77—85276
nonmagnetic conductors, three-dimensional eddy current calc. *(French)* 80—14270
plate surface element models 79—41290
skin effect calc. by Leontovitch boundary condition *(Russian)* 78—2508

conductors continued
skin effect in current carrying conductors, finite element analysis 77—83785
skin effect transients on hollow sphere in plane field of system of conductors *(German)* 80—37927
sphere, dielectric-coated, modal and near field characts. 80—28144
two-dimensional regions with rotational antisymmetry, coeffs. of potential matrix 77—33830
Au film, surface resistivity at 337 μm 77—39913
Au film, whisker growth due to high current densities 77—69191
Cu, high-conductivity, treatment technique for low temp. applics. 78—27650

confinement, plasma *see plasma confinement*

connecting *see joining processes*

connectors (electric) *see electric connectors*

conservation laws
see also C invariance; CP invariance; CPT invariance; elementary particle symmetry; P invariance; T invariance
σ-model supersymmetric extensions, dynamical conservation laws, symmetric space valued fields 80—95227
σ-models, conservation laws, infinite series, differential geometric content 80—62841
acoustic wave number, freq. modulation at a moving material interface 77—7231
anomalies of quantum conserved currents in exactly solvable models 78—387
anomalous muon capture and lepton number conservation 80—68654
artificial compression method for shocks and contact discontinuities 78—70298
asymmetric creation of matter and antimatter in the expanding Universe 79—75302
baryon asymmetry of the Universe, quantum black hole evaporation *(Russian)* 80—109577
baryon asymmetry of the Universe, unitarity and possible origins, comments 79—88589
baryon charge nonconservation, strong gravit. interaction, nuclear decay time *(Russian)* 77—26470
baryon nonconservation in grand unified theories, rel. to Universe isotropy and homogeneity 80—22125
baryon number generation, examples unitary and CPT invariance 79—35960
baryon number generation in grand unified theories 79—26279
baryon number nonconservation limits, grand unified theory nucleon decay modes 80—411
baryon- and lepton-nonconserving processes in grand unified theories 80—13253
Benjamin-Ono eqn. 80—31524
beta decay, gauge invariance and Coulomb interaction 78—46031
bilocal quantum field theories, conservation laws 79—12931
bimetric gravitational theory 80—4616
Bohr's correspondence principle *(Russian)* 79—17627
Born-Infeld equation, two-dimensional system of conservation laws *(Russian)* 80—42365
causal structure and four-momenta conservation law *(Rumanian)* 80—46887
chiral field, supersymmetric, 1/N perturbation theory and quantum conservation laws 80—68373
chiral O(N)×O(N) and SU(N)×SU(N) 2-dimens. models, conservation laws and S-matrices 80—68389
classical Maxwell-Dirac and Klein-Gordon 79—49066
classical systems with infinite set of conservation laws 80—86102
collective excitations in nuclei, microscopic model of giant dipole resonance 77—54135
collisions, classical and relativistic 77—33856
collisions, classical and relativistic 77—33857
conformal conservation laws in action-at-a-distance theory 80—42335
conformal invariance in quantum field theory 79—63377
conformal invariance of world lines of particles with non-zero rest mass *(Russian)* 77—2575
conservation laws in media with freq. dispersion 78—5597
continuum mechanics, discontinuity surface model, balance eqn. and phase transition 78—73850
cosmological baryon number domain structure, from symmetry breaking in grand unified field theories 79—84876
cosmological baryon production, expanding Universe, baryon to entropy ratio, number nonconservation 79—44652
coupled nonlinear evolution eqns., infinite sequence of conservation laws 77—57156
CP^{N-1} two-dimens. model, infinitely many conserved local charges 80—47179
CP^N σ-models, 2-dimens., local conserved currents, conservation laws 80—86579
current definition and nonconservation, geometrodynamics for quarks and hadrons 78—45809
current nonconservation in light-cone quantisation of scalar field 80—47220
de Sitter space, conservation laws from action principles in five-space 77—22451
deuterons, current conservation and off-shell effects with arbitrary interaction 79—45183
diatomic molecular spectra, space and time parity nonconservation *(Russian)* 79—50098
dielectrics, hyperelastic, with saturated polarisation, variational and invariance principles 80—74730
differential equations, first-order, symm. and first integrals, algebra and conservation laws *(Russian)* 77—30034
dual symmetry and magnetic charge conservation *(Chinese)* 79—80766
dynamical symmetries and conserved quantities 79—71651
dynamical topology for the space of states 80—27418
early Universe, baryon number generation due to CP- and B-violating interactions 80—109571
elastic stress intensity factor calcs. using elastostatics M-integral conservation law, plane cracks 78—46913
elastic string, Riemann problem 80—42059
elasticity, of J-integral type 77—49598
electrodynamics, classical, field, conservation principle, history, review *(Russian)* 78—36849
electromagnetism in non-Riemannian space, Maxwell's equations as conservation laws 78—77737
electron- and muon-number nonconservation, new interaction 77—65128

conservation laws continued
  elementary particle symmetry, rel. to conservation law, Noether theorem 79—45034
  elementary particle systematization, conservation and symmetry principles 79—9295
  elliptic sine eqns., Backlund transformations and Bianchi identities 78—8553
  EM wave absorption/scatt. in moving layer, energy and momentum conservation 78—25775
  energy conservation and the principle of equivalence 79—54018
  energy momentum tensor for vector-tensor theory of gravity and electromagnetism, charge conservation 78—12633
  energy momentum tensor symmetries, concomitant conservation laws, Einstein massless scalar meson field appl. 78—86205
  energy problem, struct. of gravitational field *(Russian)* 79—21598
  Euclidean invariance, spontaneous breaking, long range ordered media, defect, config. classification 78—59748
  evolution equations, nonlinear, and their conservation laws, spectral transform method 80—62488
  factorisation of classical and quantum S-matrix, rel. to conservation laws 77—30277
  fermion number conservation spontaneous breakdown in two dimens. 77—67584
  fermion number nonconservation in cosmological models, Big Bang theory 79—80381
  fermion number nonconservation in the presence of instantons *(Russian)* 79—49408
  Fermion number violation in the presence of instantons 79—12949
  field theory, Lie-Backlund operators props. from variational derivatives 80—37159
  flat space time, conservation laws based on traceless energy momentum tensors 80—52085
  flavour conservation in superheavy quark models 77—49893
  fluid dynamic hyperbolic system soln. decay, conservation laws with convex extension 77—49599
  G conjugate invariance of current matrix elements in $\nu(\bar{\nu})N$ elastic scatt. 78—54627
  gauge groups in local field theory and superselection rules 77—18190
  general realtivity weak conservation law covariant formulation 80—73224
  general relativistic plasma MHD conservation laws, black hole rot. energy 79—2685
  general relativity, conserved quantities for self gravitating system 79—63098
  general relativity, differential conservation laws *(Bulgarian)* 78—32735
  general relativity, gravit. gauge group $SL_{2,C}$ 77—22456
  general theory, violation and spontaneous phenomena 79—54275
  general vector fields, classical theory, internal symmetries and conservation laws *(Russian)* 78—62328
  generalised gravitation theory, with electromagnetism, derivation of conservation laws 79—49146
  geometrised gravitational theory, energy-momentum tensor 79—25958
  geometrized theories of gravitation 79—21636
  Glashow-Iliopoulos-Maiani mechanism, horizontal and vertical quark flavour mixing 79—67512
  Goldstone theorem generalisation, scalar fields, conserved current and mass spectra struct. 80—68339
  grand unification, neutron oscillations and massive neutral Majorana leptons, baryon number 80—91033
  gravitation, gauge theory, special relativistic limit, angular momentum conservation 80—22256
  gravitational field with absolute parallelism struct., integrable covariant energy-momentum conservation law 80—8873
  gravitational radiation, total stress-momentum definition 77—79014
  group theoretical construction of two-dimensional models with infinite sets of conservation laws 80—99056
  hadron decay neutrino prod., and quantum number conservation laws *(Russian)* 79—348
  Hamiltonian eqns., infinite-dimens., integrable 78—57744
  heavy leptons weak doublet, prod. and decay, lepton mixing, lepton number nonconservation 77—54094
  heavy quarks, possible exotic charge or baryon number 80—47245
  Higgs induced neutral currents, natural flavour conservation and quark mixing angles 80—42392
  Higgs meson prod., muon-number violation 78—41422
  hydrodynamics, quantum relativistic, nonlinear generalised equations 80—68380
  hyperbolic conservation laws; initial and initial-boundary value problems, large-time behaviour 77—74233
  hyperbolic laws, Glimm scheme for solving, a deterministic version 78—20972
  hyperbolic system, first order, supplementary conservation law 79—9077
  hyperon nonleptonic decays, $\Delta I={}^{1}/_{2}$ rule violation 79—45087
  ideal vortex motion, two dimens., symms., conservation laws 78—87349
  impulse conservation, appl. to elastic rod collisions *(German)* 78—22274
  infinite conservation laws for EM and asymptotic gravitational fields 79—21613
  interacting particles system, nonrelativistic classical and quantum mechanics conservation laws 78—89328
  internal gravity waves, conservation law 77—15047
  internal waves with finite fluid depth, inverse scatt. problem, Backlund transformation 80—31517
  inverse Noether theorem, general formalism for symmetry and conservation 80—46850
  inverse scattering problem, N-soliton of eqn. $\sigma_{xt}=e^{\sigma}$ 78—8269
  isolated systems, integral conservation laws, privileged vector fields method, general relativity, external Kerr metric *(German)* 78—16698
  Korteweg-de Vries eqn., generalised, conserved quantities 80—68054
  Korteweg-de Vries equation, invariances and conservation laws 79—26244
  Korteweg-de Vries system, Lax representation, conservation laws 80—82893
  Kortweg de Vries (Burgers) nonlinear long waves, mathematical modelling 80—8791
  Lagrangian mechanics, consts. of motion anal. 78—81829
  Lagrangian systems with one degree of freedom, invariance and conservation laws 78—62067
  Landau-Fokker-Planck eqn., for arbitrary statistics, relativistic and nonrelativistic case 80—36935
  lepton flavours conservation laws, unified gauge theories, new neutral lepton 77—54095
  lepton number conservation, $\mu^{+}\rightarrow e^{+}+\gamma$, brief review 77—57516

conservation laws continued
  lepton number conservation, double beta decay 78—58256
  lepton number non-conservation in Weinberg model with two Higgs doublets 77—67585
  lepton number nonconservation with scalar bosons 78—4798
  linear field theories, conservation of source strength, superpotentials 77—5726
  linear invariance and virial theorem in classical mechs. 77—74214
  local conservation laws of principal chiral fields (d=1) 80—4888
  local relativistic quantum field theory, additive conservation laws 80—22507
  macroscopic electrodynamics, forces and energy-momentum tensor 77—5675
  magnetic current conservation, EM duality, secondary symmetry, magnetic current conservation 80—27431
  magnon elementary excitations damping *(Russian)* 79—28515
  massive Thirring model, conservation laws in quantum ($\cos\phi-1$) theory *(Russian)* 77—200
  massive Thirring model, four fermion interaction, conservation laws 77—41777
  massive Thirring model, renormalisation of higher conservation law 77—30020
  matrix theory of elastic wave scatt., conservation law 78—63217
  matter field spacetimes, symm. mappings satisfying vanishing contraction of Lie deform. of Ricci tensor 79—113
  mechanical systems, follower load type, time invariant functionals 80—77609
  mechanics conservation law derivation using digital computers 78—12552
  micrononcausal Euclidean wave functions for baryons by assuming 'Yukawa type' couplings and G′-parity 79—45030
  minimal gauge theory of leptons, new heavy lepton, associated neutrino, muon number nonconservation 77—54096
  molecular liquids and solids, dissipation functions, conservation laws 77—45817
  Moller scatt., high intensity, scatt. energies 80—22541
  multiplicative baryon number conservation, $H\rightarrow\bar{H}$ oscill. upper limit, baryon to lepton transform. 79—298
  muon number conservation spontaneous breakdown, off-diagonal neutral currents 77—49889
  muon number nonconservation in gauge model with heavy lepton 77—61239
  muon number nonconservation in lepton structure model 77—61250
  muon number nonconservation postulation 77—87916
  muon number nonconserving processes, models with doubly charged leptons 77—74613
  muon number violation, Weinberg model extension 77—67610
  muonic number nonconservation in $\mu\rightarrow e\gamma\gamma$, $\mu e\rightarrow\gamma\gamma$, and $\gamma e\rightarrow\gamma\mu$, pole model anal. *(Russian)* 79—80817
  neutron-antineutron oscills., proton instability *(Russian)* 80—101948
  Newton's 2nd law, spatial translation symmetry, for teaching 78—54129
  Noether's theory for non-conservative generalised mechanical systems 80—31491
  non-invariance symmetries and consts. of motion 79—75333
  non-local continuum mechanics, conservation laws 78—65770
  nonequilibrium expressions for entropy, thermodynamic quantities, using density series expansion 78—8371
  nonlinear difference-difference equations, derivation of infinite number of conservation laws 78—89324
  nonlinear evolution eqns., conservation laws, group theoretical derivation 80—57520
  nonlinear evolution eqns., inverse scatt. method, conservation laws *(Russian)* 80—105804
  nonlinear evolution equation soln. by spectral transform, conservation laws, cylindrical KdV eqn. 79—2658
  nonlinear evolution equations, conservation laws by spectral transform 79—5985
  nonlinear field eqns. in Hamilton's canonical form, conservation and invariance 78—32693
  nonlinear waves, modified conservation laws *(Russian)* 77—45706
  nonsymmetric unified field theory, conservation laws, Bianchi type identities 78—73910
  particle collisions, conservation of energy and conservation of vector momentum 80—101693
  photoproduction processes of charm particles with charm nonconservation *(Russian)* 78—74201
  physical system, model of space-time from set theory concepts 80—82660
  physical systems, principle of stability of invariance 77—26164
  planet formation process, conservation laws and mass distrib. 78—81565
  Poincare gauge invariance, conservation laws for particle, string and membrane systems 79—55
  polynomial conservation laws in (1+1) dimens. classical and quantum field theory, nonlinear Schrodinger eqn. 78—54224
  principle chiral fields, Backlund transformations and local conservation laws 80—68388
  pseudospherical surfaces in soliton eqns., conservation laws, Backlund and scale transformations 79—75688
  quantum field theory, Lagrangian formulation, conservation laws, relativistic gravitation *(Russian)* 80—68337
  quantum theory consequences of more general theory of symmetries, conservation laws 78—49718
  quark flavour conservation in neutral currents 77—49899
  reciprocity and conservation theorems, for fields with general time dependence 79—80452
  relativistic magnetofluids and symmetry mappings 79—23379
  relativistic magnetofluids and symmetry mappings. II 79—27701
  relativistic QFT, quantum microsystem evolution, nonconservation effects 80—22515
  relativistic quantum theory with correct conservation laws 80—82677
  Robertson-Walker metric and symmetries belonging to contracted Ricci collineations 78—24580
  rotational covariance and Yang-Mills monopole 77—13870
  s-channel helicity conservation at $\gamma V,\gamma\gamma$ and NN vertices, vanishing of spin-zero covariant coupling 79—40691
  scale and conformal invariance, scalar currents, theory with continous mass spectrum 78—62335
  Schnurs, combinatorial hierarchy, spin dichotomy and conservation of quantum numbers 80—68383
  Schwinger model, new and local Lorentz-covariant soln. for arbitrary gauge 79—40668
  self consistent cranking model with RPA corrections, high spin states, conservation laws 77—14047

conservation laws continued
- self-consistency conditions for a symmetry violating external field *(Russian)* 80−42361
- shock formation and decay for conservation law in several dimens. 77−53788
- shock waves, global structure anal. 80−8800
- sine-Gordon supersymmetric model, higher local quantum conserved currents 80−52435
- sine-Gordon supersymmetric model, quantisation of conservation laws and superrenormalisation 79−89058
- sine-Gordon supersymmetric theory, infinite set of bosonic conserved currents 78−62313
- sine-Gordon system, Lax representation, conservation laws 80−82893
- soliton solutions, nontopological, conservation laws 79−45022
- solitons, multidimens., additive topological laws of conservation *(Russian)* 77−74601
- solitons, theory and applications 78−36811
- sound waves in media with freq. dispersion conservation laws 78−5597
- sourceless Yang-Mills eqns., eqns. of motion, holonomy functional formulation *(Chinese)* 79−80760
- space-time property of fermion number *(Chinese)* 79−49418
- stationary Einstein-Maxwell space-times, conserved quantities determ. 78−49737
- string in static field, conservation laws 79−21969
- strong P and T noninvariances in a superweak theory 78−82123
- SU(2)$\times$U(1) unified gauge theory, mech. for nonconservation of muon number, $\mu \rightarrow e+\gamma$ appl. 77−30303
- SU(2n) principle models for integrable nonlinear systems, current constraints, conservation laws 80−86619
- SU(4)$\times$U(1) unified gauge theory, muon number conservation 79−71655
- SU(5) invariant theory, B-L nonconservation and neutron oscillation 80−78005
- SU(5) without symmetry constraints, unified model of quarks and leptons, conservation laws 80−101968
- SU(s) grand unification, neutrino mass and oscillations, B-L nonconservation 80−52449
- superconductivity and elementary particles theory, review 80−4911
- superconformal confinement 77−65134
- supersymmetric Sine-Gordon model, infinite set of local quantum conservation laws 80−47207
- supersymmetry, spontaneous breaking through dimensional reduction 79−40441
- symmetries of energy momentum tensor, concomitant conservation laws 78−57831
- symmetry and conservation, for teachers 79−26
- symmetry mappings, particle number conservation, baryon number conservation 77−30063
- test particles, with internal struct., conservation laws 77−67338
- Thirring model, massive and quantum sine Gordon model, infinite set of conservation laws 78−29226
- time dependent flow area problems, conservation eqns. in control vol. form. 77−72264
- translational symmetry of space and Newton's second law of motion 77−8
- two dimensional field theories with infinite number of conservation laws and Backlund transformations 80−9095
- unified models of quarks and leptons, B-L conservation and B nonconservation 80−95229
- unified thoery of matter, derivation of fundamental physical law 78−20982
- unitarity violation in $\pi^- p$ elastic scatt. at 100 GeV 79−71764
- Volterra and nonlinear self-dual network eqns., conservation laws generation 77−53749
- wave eqn., new conservation law *(Russian)* 77−78989
- weak hadronic $\Delta S=0$ baryon-π amplitudes, Melosh transformation 78−12857
- Yang equations, invariance props. 80−62836
- Yang-Mills field, conservation-law violation at high energy by anomalies 80−62855
- eν interaction, local conservation law from neutrino massless, gauge invariance 80−42355
- $\gamma \rightarrow e^- e^+$ generalised conservation laws of physics, electron energy spectra theory 79−85246
- $\gamma \rightarrow e^- e^+$ generalised conservation laws of physics, electron energy spectra theory 79−85247
- $\mu \rightarrow e\gamma$ or 3e, heavy leptons, CP violation 77−82727
- μ number nonconservation, gauge model with left-handed lepton doublets 78−8542
- μ number nonconservation 78−45806
- μ-number non-conservation in gauge theories of weak interactions 77−74630
- $\mu^+ \rightarrow e^+ \bar{\nu}_{ee} \nu_\mu$, $\bar{\nu}$l search for muon number conservation test, neutrino expt. 80−47270
- $\mu^+ \rightarrow e^+ \nu\bar{\nu}$, e^+ polarisation, weak interactions and lepton number conservation 80−42444
- $\mu^+ \rightarrow e^+ \nu\bar{\nu}$, μe universality and μ number nonconservation in rare decays 80−42445
- np$\rightarrow$dπ^0, 795 MeV, test of isospin invariance 79−75786
- ν_μ mass limit in absence of muon-lepton-number conservation, unified gauge theories 78−21368
- $\nu \leftrightarrows \bar{\nu}$ oscillations, conditions for observation 79−17636
- $\bar{\nu}_\mu e^- \rightarrow \nu_e \mu^-$, exotic lepton number violation and neutrino Majorana masses, Higgs sector 80−86615
- νN interactions, quasielastic scatt., book contrib. 78−78171
- P decay, baryon number-lepton number conservation or violation, grand unification implications 80−27425
- $\bar{p}$ decay and baryon number of universe 77−49964
- $\pi^0 \rightarrow \gamma\gamma$, μe universality and μ number nonconservation in rare decays 80−42445
- $\pi^+ \rightarrow \mu^+ \nu$, muon momentum, weak interactions and lepton number conservation 80−42444
- $\pi^+ \rightarrow \mu^+ \nu$, μe universality and μ number nonconservation in rare decays 80−42445
- $\pi^- p \rightarrow \delta^- p$, near production threshold, nonobs. of $\delta^- \rightarrow \pi^+ \pi^- \pi^-$ enhancement 79−13113
- $(\bar{\psi}\psi)^2$ two dimensional model, equivalence to sine Gordon systems, conservation laws 79−2917

consoles, remote *see remote consoles*

constant current modulation *see amplitude modulation*

constant current sources
- calibrated current sources with direct radioactivity collection in vacuo 77−74449
- cryogenic current standard based on AC Josephson effect 77−82557
- DC source (10^{-16} to 10^{-6} A) for electrometer testing 77−79112
- DC supply for Hg-Ar arc discharge lamps 78−12722
- DC therapeutic transistorised apparatus *(Bulgarian)* 78−24175
- double, for cryogenic current comparators, appls. 79−21775
- double, for cryogenic current comparators, standard resistor calibration appl. 78−93731
- GaAs laser diode power supply control cct. *(German)* 80−78852
- glow discharge electrolysis, power supply unit, current regulator 77−39489
- high stability constant current source *(Chinese)* 79−44991
- highly stable, resettable const. current supply, SQUID appl. 79−67289
- ionisation current sources for electrometer calibration 77−79111
- iontophoresis, gated HV system with accurate current monitoring 78−69259
- magnet winding supply, regulated source based on industrial thyristor convertors 77−37921
- mass spectrometer magnetic analyser constant current solid-state power unit 80−86499
- precision voltage and current source [for thermoelectric transducer calibration] for thermoelectric primary transducer calibration 79−80605
- programmable, for automated controlled-current coulometry 77−70353
- pulsed low current, at acoustic freq., using LED and photomultiplier 78−93724
- stimulator for electrophysiological expts. 77−21663
- Tietze-Schenk, for resistance meas. *(German)* 79−88974
- Wheatstone bridge fed from a bilateral constant current source 80−57338
- wide-range current generator for Hall meas. appl. 77−82545

constant voltage diodes *see avalanche diodes; Zener diodes*

constants
- *see also elastic constants; gravitational constant; lattice constants; optical constants*
- astronomy, tracking data processing and mass determ. *(Russian)* 78−49297
- blackbody radiation constant, determ., teaching expt. 77−67160
- Boltzmann's const. determ. by elec. noise thermometry 78−36767
- calculations of fundamental consts. in various theories 77−30354
- CGS to SI conversion for electromagnetism 78−16592
- conference on metrology and fundamental constants, Varenna, Italy (July 1976) 80−105603
- cosmological const. and Einstein eqns. Kerr-Schild soln. 77−30059
- cosmological constant and supergravity 77−74171
- Dirac's large number hypothesis, fundamental const. variability 77−67153
- e/m ratio measurement apparatus, power supply 77−60873
- electric fractional charge, $^1/_3$e, expt. determ. on Nb sphere 79−21694
- electrical standards progress and fund. consts. role *(Japanese)* 78−24760
- electron and proton charge equality, test via meas. of electric neutrality of matter 77−57579
- electron rest-mass, student laboratory expt. 78−16607
- elementary particle constants and cosmic object size, empirical relation 77−82338
- evapotranspiration, psychometric constant γ, pressure depend. 77−53149
- Faraday, coulometric meas. 80−22320
- fine-struct.-const. calculated value, gravit. charge quantisation 77−26524
- fine-structure const. value from EM field as 42 state superposition 77−30293
- finite-struct. and gravit. const. in unified theories 77−41802
- fractionally charged ions, search in He gas 80−8954
- fundamental, indirect determ. theory *(German)* 77−41565
- fundamental constants, self-consistent values *(German)* 79−12758
- fundamental nuclear constants, direct test of constancy 77−2889
- fundamental physical and astrophys. consts., review, dimensional and dimensionless combinations *(Russian)* 77−49706
- fundamental physical constants rel. to SI base units 77−87724
- gas constant, value determ. of 8314.48 JK^{-1} kmol^{-1} by accoustic method 79−93094
- gas constant. determ., low freq. acoustic thermometry, 4.2 to 20K 79−30477
- gravitational acceleration, absolute determ. method 79−71187
- interactions with realizations of ampere and kilogram, suggestion of systematic effect in weighing measurements 79−85127
- International Astronomical Union 1976 system of constants *(Russian)* 78−73611
- man's size in terms of fundamental constants 80−105489
- molecular size and Avogadro's number, determ., student expt. 78−81741
- philosophical investig. of physical consts. 80−12884
- photon rest mass upper limits from astrophysical data 77−34200
- physical constants, conceptual nature 77−67167
- Planck's const. time variation on cosmological scales 77−57113
- Planck's constant, and finite struct. const. calc. 78−82135
- Planck's constant, time invariance 78−93556
- Planck's constant cosmological var. upper limit from microwave background radiation spectrum 78−12434
- Planck constant, upper limit determ. to freq. dispersion by nonlinear spectroscopy 77−79050
- precession change, revision of IAU System of Astronomical Constants 77−17331
- precession matrix based on IAU (1976) system of astronomical constants 79−48653
- Rydberg const., determ. using H_α polaris. spectroscopy 79−9202
- Rydberg constant, determ. from Hα line fine struct. meas. 79−54093
- speed of light from CO$_2$ laser freq. and wavelength 77−49708
- speed of light via CO$_2$ laser freq. and wavelength meas. 77−45822
- Stephan's constant determ., student expt. 78−69948
- variation of fundamental constants, summary of obs. evidence 79−12759
- $e^- p$ mass ratio, direct determ. using cyclotron resonance technique 78−70093
- H , Rydberg consts., saturated absorpt., spectroscopy meas. 80−105604

constitution diagrams *see phase diagrams*

constraint theory
- *see also operations research*
- bodies with binary material and kinematic-kinetic structure 78−73848

constraint theory continued
continuum mechanics, nonideal realisations of constraints and loosenesses 78−73849
nuclear power stations, optimal size and location in energy parks 80−95489
optimal control, problems with constraints, transformation methods of an exponential function type 78−12541
optimisation of energy storage systems, compressed air, w.r.t. economics 80−26167
potential energy surfaces, analytical expressions from constrained optimisation 77−6698

construction *see building*

construction industry
see also civil engineering
materials evaluation using high temp. thermal analysis 78−80687
noise abatement, legal considerations, statutory law 78−87197
reinforced concrete structural integrity assessment, NDT method 78−56847
solar energy Implementation Centre proposals 79−57394

constructional engineering *see civil engineering*

contact (mechanical) *see mechanical contact*

contact angle
see also capillarity; surface tension; wetting
adhesion, interfacial energy-contact angle relation 79−91904
adhesion, of liq. to solid surface, contact angle rel. to dielectric constant 80−10741
adhesive energy measurement techniques 80−50803
albumin, adsorbed layers on polystyrene 80−61508
black lipid film stability, interfacial props. effects 78−15798
brass, contact angs. meas., aq. ethanol (glycerine) solns., 20-70°C 78−56025
bubble enclosed between parallel flat horizontal walls *(German)* 77−66071
cadmium arachidate monolayer transfer from air-water interface to solid, contact angles 77−55424
capillary flow, initial stage analysis, relax. model 80−74977
Computer simulation of the liquid-solid-vapour contact angle 78−2340
condensation and evaporation, contact angle and solid surface prop. effect 79−77867
creeping flow over surface, angle of contact, viscous liq. 78−51149
decane on Teflon FEP, effect of drop size on contact angle 80−2245
drop on fibre systems, contact angle, phase contact areas, drop vol. and Laplace excess press. meas. 77−7950
drop size measurement, spherical mirror method 79−64806
drop spreading on solid surface, initial stage charact. 80−59761
dropwise condensation and nucleation heat transfer rate, mechanism 77−4193
Duralumin, contact angs. meas., aq. ethanol (glycerine) solns., 20-70°C 78−56025
dynamic contact angle correlation 79−46889
Dynamic contact angles and contact angle hysteresis 78−10258
Dynamic fluid interface displacement and prediction of air entrainment 78−2337
elastically deformable bodies, wetting, influence of vol. deform. of solid 79−11008
elastically deformable bodies, wetting, reduction of effects of deformation to line tension 79−11007
electrolyte solutions, aq., wetting angle rel. to rate of meniscus movement capillary rise 79−65292
emulsion, creamed, vol. fraction, effect of film thickness and contact angle 80−81370
ethanol, aq. solns., contact angs. with metals, 20-70°C 78−56025
ethylene glycol on Teflon FEP, effect of drop size on contact angle 80−2245
fibrinogen, adsorbed layers on polystyrene 80−61508
finely grooved solid surface, apparent contact angle of liquids, SEM study 77−51573
fingerprint/surface, contact angle meas. 78−78056
glass, surface props. and contact angle after treatment with glow discharge and heating 80−21139
glass/Hg drop interface, contact angle meas. technique 77−55421
glycerine, aq. solns., contact angs. with metals, 20-70°C 78−56025
graphite fibres, HM, surface comp. and energetics 80−54480
hexatriacontane, contact angle data with many liquids, interaction parameter calc. 77−55423
homogeneous surface, hysteresis of contact angle 78−51793
hydrodynamics at finite visible contact angles, interface motion, drop spreading, solns. *(Russian)* 77−27640
hysteresis, dropwise condensation heat transfer 78−71273
hysteresis, mol. interpretations 80−88400
liquid drop on solid substrate, deviations from Young's equation 77−66075
liquid film, hydrodynamics, three-phase contact, perimeter expansion rate, theory 78−22937
liquid meniscus steady movement in capillary tube 77−69146
liquid spreading, edge effect for zero contact angle 78−84032
liquid surface shape near stripwise heterogeneous wall, analytical soln. of Laplace eqn. 78−67890
low melting, metals, on Cu surface, spreading kinetics 80−10742
MBBA, nematic liq. cryst., surface alignment using lecithin monolayers, contact angle meas. 79−4247
measurement, for sessile drop on horizontal surface, projected image magnification 77−55421
meniscus profile, differential interference method 79−56039
meniscus-film-vapour equilibrium, generalised Young equation at low or zero contact angle 79−65298
metal-liquid insulator interface, in presence and absence of applied elec. field 79−19429
mica, surface free energy dispersive component, adhesion to water and n-alkanes 77−55435
mica, surface free energy nondispersive component, adhesion to polar liq. 77−55436
microdrop, two-dimensional, on solid body surface, stability dynamics 78−51790
mixture, binary, nucleate boiling heat transfer, conc. depend. 78−87249
nematic liquid cryst., surface alignment using lecithin monolayers, contact angle meas. 79−4247
Newton black film, line tension, determ. by cnt. bubble method 80−88406

contact angle continued
Newton black films, line tension determ. by diminishing bubble method 80−88407
Newton black soap film, interaction forces, contact angles 79−77870
nitrobenzene, contact angle on pretreated polyethylene, H_2O environment *(Japanese)* 78−79858
organic polymer surface energy anal. comparison of one- and two-liq. methods 77−59181
plane pendent drops, instability 80−29247
PMMA, surface energy anal., comparison of one- and two-liq.-contact-angle methods 77−59181
poly(dihydroxypropyl methacrylate), surface charact. 80−61140
poly(ethylene terephthalate), surface props. rel. to UV irrad. *(Japanese)* 78−79859
poly(hydroxyethyl methacrylate), surface charact. 80−61140
poly(methoxyethyl methacrylate), surface charact. 80−61140
polyethylene, contact angle data with many liquids, interaction parameter calc. 77−55423
polyethylene terephthalate film, surface modification by corona discharge, adsorption and wettability 77−86212
polymer, surface electric charge, effect on interaction with liq. medium 79−56036
polymer-water interfaces 80−20010
polystyrene, crosslined, swollen, surface energy, contact angles 79−73379
porous media wetting, capillary rise, contact angle effect *(German)* 78−84033
PTFE, contact angle data with many liquids, interaction parameter calc. 77−55423
PTFR, surface energy anal., comparison of one- and two-liq., contact-angle methods 77−59181
PVC, surface energy anal., comparison of one- and two-liq.-contact-angle methods 77−59181
quartz, dynamic wetting angle of dry lyophilic surface 80−88405
random sphere packing, contact angle and film jumps 77−66076
ring tensiometry, effect of contact angle 78−60011
rivulets, flowing down vertical solid surface, contact angles, roughness effect 79−27731
rotationally symmetric fluid bodies in gravit. field, thermodynamic treatment of capillary phenomena 78−10262
rotationally symmetric fluid bodies with one asymptote, holms, capillary props. 77−66077
Sessile liquid drops, meas. of small contact angles 80−10749
silicate glass, high temp. microscopy investigation of softening temp., viscous flow, angle of contact *(Polish)* 77−55242
silicate glasses, surface energy calc. from wettability data 77−35804
soap film, contact angles, thermodynamic description 78−47639
soap film, Newton black, contact angle meas. 78−47640
soda-lime glass, chemically modified, water contact angle, adhesional wetting 77−55426
solid bodies, capillary interaction 78−51792
solid or liquid, surface free energy theory, thermodynamics, mol. forces and struct. 77−55437
solid/melt interfacial tension and contact angles of small particles, determ. from crit. vel. of engulfing 80−79915
spherical particle with a droplet, approx. eqn. 79−60604
spreading phenomenon in dry powder electrophotography 78−63904
static drop on inclined plate, shape, finite element method anal. 80−29245
steel, contact angs. meas., aq. ethanol (glycerine) solns., 20-70°C 78−56025
steel/water drop interface, contact angle meas. technique 77−55421
surface energy, theory and appls., symposium, New York, USA (Apr. 1976) 77−55422
surface forces, interfacial press. and zero contact angle systems 77−55425
surface polarisation from sessile drop contact angle meas. 77−85365
surface problems with prescribed contact angle, max. and min. principles 79−37907
surface roughness effects, contact angle hysteresis *(German)* 77−62710
surface roughness effects on wetting 77−59178
surface tension, review of theory 79−77866
surface tension measurement method, max. force exerted by meniscus formed by cone on free liq. surface 80−39390
sytrene-tetrahydrofuran block copolymer, H_2O contact angle and surface struct. *(Japanese)* 78−79861
Teflon, surface modification, contact angle meas. 77−51574
thin films, lens formation, alternating elec. field effect 80−12060
thin liquid films in emulsions, contact angles 80−92761
viscous liquid creeping on surface, asymptote to free surface and vel. depend. of contact angle 80−6600
wall effect in surface tension determ. using Wilhelmy plate 80−2246
water, adsorbed multilayers on quartz, surface forces 80−6597
water on PMMA, effect of drop size on contact angle 80−2245
water on semiconductor substrate surfaces, measurement of contact angle *(German)* 80−34276
wet particulate systems, pendular band strength between unequal-sized spherical particles 80−104418
wetting, exam. of accompanying size effect *(Russian)* 80−6596
wetting, ionic crystal surfaces 80−10746
wetting, of rigid solid, by simple fluid, statistical mech. treatment 77−89618
wetting angle determ. method for adhesive and material to be joined *(German)* 77−62709
wetting of a vertical plate by a liquid, model 78−22319
wetting tension depend. on meniscus curvature, adjacent liquid film disjoining press. isotherm 80−2247
Young equilibrium 78−14541
Al-graphite adhesion and contact angle, effects of metal additives *(Japanese)* 78−60008
Al_2O_3 surface energy measurement by const. temp. method data for liquid Cu-Sn and Au-Ag 78−6208
Al_2O_3, surface energy meas. by temp. variant method for liquid metals 78−6209
Au surface, clean, hydrophilic nature 80−80029
Be, contact angs. meas., aq. ethanol (glycerine) solns., 20-70°C 78−56025
Cu, Aq. ethanol (glycerine) solns. contact angs., 20-70°C 78−56025
Cu, meas. of contact angle between melt and cryst. during Czochralski growth 77−28708
Cu-Sn binary system, wettability and interaction between solids and liqs. *(Japanese)* 80−92760

contact angle continued
- Fe-C (graphite), adhesion and wettability of graphite *(Russian)* 80—20008
- Ga, contact angle meas. between melt and crystal during Czochralski growth 78—64461
- Ga liquid, contact angle with Nb and Zr substrates 79—77864
- Ge, contact angle meas. between melt and crystal during Czochralski growth 78—64461
- H_2O, contact angle measurement, effect of acoustic energy 78—95207
- H_2O, contact angle on polystyrene, cause of hysteresis 78—95206
- ^4He, superfluid against solid ^4He, surface tension and contact angle 79—42339
- In liquid, contact angle with Nb and Zr substrates 79—77864
- Ni, contact angs. meas., aq. ethanol (glycerine) solns., 20-70°C 78—56025
- PbSe-flux, interfacial tension at boundary of fused systems 77—35797
- PbTe-flux, interfacial tension at boundary of fused systems 77—35797
- Pd-C (graphite), adhesion and wettability of graphite *(Russian)* 80—20008
- Pt-C (graphite), adhesion and wettability of graphite *(Russian)* 80—20008
- Rh-C (graphite), adhesion and wettability of graphite *(Russian)* 80—20008
- Si film, critical surface tension, aligning props. of nematic MBBA mols. 79—90846
- Si, surface doped with metal impurities, water adhesion energy *(Russian)* 77—89620
- A-SiC, self-bonded polycryst., wetting by Si, base plate surface roughness effect 79—23809
- SiO_x thin films, deposition and characterisation study 80—80133
- Sn liquid, contact angle with Nb and Zr substrates 79—77864
- Ti-molten glass system, interactions and wetting, EPR anal. 78—14542
- WC-Co, cemented carbide sintered, appl. of dihedral angle meas. to microstruct. 78—39716

contact e.m.f. *see contact potential*

contact lenses
- back surface aspheric, inspection 80—66711
- base curve radius selection of a soft lens, sagittal depth consideration 80—46096
- chemistry, properties, advantages and disadvantages of various types 80—3872
- circular, tear film dynamics and O_2 tension 78—48929
- corneal, for use in holographic diagnosis of human eye 80—12209
- corneal edema with contact lenses under closed-eye conditions 79—96553
- corneal environment, osmotic responses to contact lenses 80—12078
- corneal oedema, effect of peripheral fenestration 78—3470
- corneal pressures due to soft contact lenses and corneal asymmetry 80—104621
- corneal scatt., border-enhancement spread, subjective monitoring method 79—29641
- corneal sensitivity and thickness after wearing PMMA and gas-permeable contact lenses 80—61544
- diagnostic testing of wearer 80—12312
- DuraSoft, evaluation and control when fitted to refractive astigmats 79—34706
- fabrication, spincasting using polyhydroxyethyl methacrylate 77—795
- fabrication and fitting, state of art and science 80—12311
- gel materials for extended wear, water flow cond. 78—81062
- gonioscopic lens *(Italian)* 80—21573
- hard, dimens. stability of different materials 78—77150
- hard gas-permeable type, O_2 tension underneath 78—3473
- hydrogel, change in lens power due to flexure 79—11917
- hydrogel, light transmission 79—11918
- hydrogel contact lenses, red spot phenomenon 78—77151
- hydrogel lens power changes due to flexure 80—67286
- hydrogel lenses, accuracy of manufacturers stated centre thickness 79—92425
- hydrogel of high water content as a material for the soft contact lens *(Japanese)* 80—12300
- hydrogel Soflens, radii and thickness meas. by interferometry 80—8118
- hydrophilic contact lenses, meas. and laboratory-stated parameters 78—77149
- longitudinal spherical aberration and its effect on visual acuity 80—99816
- mathematical model for dioptric effects of eye optical parameter changes 78—3477
- ophthalmolscopic and vision function meas. instruments 79—96689
- performance evaluation by border contrast enhancement 78—3492
- peripheral curve design, factors affecting 80—8208
- peripheral curve design, specifying for reproducible performance 80—61733
- poly(vinyl pyrrolidone), silicone grafted, for contact lenses, surface props. and stability of thin tear film 80—17194
- refractive error stability of contact lens wearers 80—108879
- rigid and flexible, myope accommodation 78—48787
- rotation on toric corneas, nonprism and prism-ballast hydrogel lenses 78—3474
- simple photokeratoscope for corneal curvature meas. 78—3624
- soft, apparatus for longit. spherical aberration meas. 79—79684
- soft, back radius changes on flexure 80—61732
- soft, in-office meas. 78—7339
- soft, meas. of O_2 flux into cornea 79—34705
- soft, O_2 flux into human cornea 79—34549
- soft contact lenses, future developments 80—12310
- squeeze forces in contact lenses with a steep base curve radius 80—108926
- thickness of a lens, definition 80—46094
- toric soft lens rotation, indication by prism-ballasted and truncated spherical trial lenses 80—8209
- ultra-thin, corneal-edema response 79—34552
- X-chrom lens for people with colour defective vision *(Italian)* 80—17186

contact potential
- *see also contact resistance*
- compression couplings, pot. simulation using polarisation optical method *(Russian)* 79—78156
- eye, retina injuries, magnetoretinographic meas. using SQUID magnetometer 80—104702
- heat of adsorption, isosteric, determ. using contact pot. difference meas. 79—66347
- Kelvin method contact PD meas. manipulator 78—57979

contact potential continued
- meas., H_2 and O_2 concentration determ. appl. *(Czech)* 79—70386
- measurement of local variations on solid surface, device with high spatial resolution 77—39921
- metal, surface pot. drop and contact pot. difference in terms of orbital electronegativity 78—2546
- metal and supercond. at transition temp., cryostat for pot. difference changes meas. 77—22573
- metal junctions, diffusion of interstitial H, interface pot. 80—44368
- metal-to-metal meas., surface pot. jump effect of spots, coatings and cryst. surfaces 77—51805
- meter, IC, for meas. work function of electrons 79—35780
- multilayer thin film struct. thermoelec. props. 80—92964
- physics course demonstration *(Russian)* 79—21508
- polymer, molecular charge states, contact charge exchange 78—14822
- precise diode method for recording contact potential changes caused by gas adsorption 79—88982
- rare earth metals, electron work function by contact pot. difference method *(Russian)* 79—60913
- Schottky, non-degenerate diode, current-voltage characts., analytical approx. 79—95494
- semiconductor, disordered, electroabsorption, contact excitons influence 80—10882
- semiconductor contact potential and conductivity simultaneous automatic meas. 78—21118
- semiconductor contact potential difference and surface cond., combined meas. method 77—18042
- semiconductor-conductor interface, book contrib. 79—1621
- surface films, thermodynamics of Volta effect 77—51604
- thermoelectric effects and contact pots., general theory for teachers 78—4440
- work function measurement method for use in inert medium 79—49250
- Al (111) adsorption of O_2, possible ordered struct. 80—44412
- Al-dimethyl terephthalate contacts, effect of elec. field on contact electrification 79—19660
- As_2Se_3 amorphous thin films, illumination-induced change in contact pot. 80—20251
- Au-Ag, electron interferometric meas. of contact PD 77—32069
- Bi-Sb alloys, electron work function determ., contact pot. difference method 77—39920
- C, black, surface acidity effects on work function 78—2548
- Cd-Bi alloys, electron work function determ., contact pot. difference method 77—39920
- CdS-Au structure, work function of {0001} faces of CdS, contact pot. difference meas. 78—23164
- Cu-Cd(In)(Sb), electron work function, contact pot. difference meas. 78—80041
- Cu-dimethyl terephthalate contacts, effect of elec. field on contact electrification 79—19660
- Fe microspheres, impact on mech. polished electrodes, contact pot. influence on charge transfer *(French)* 78—47198
- Ga, electron work function meas., dynamic capacitor method 77—39919
- GaAs (110), struct., elec. props., effects of illumination, O_2 absorpt., electron bombard. *(French)* 78—34690
- n-GaAs (110) surface, Cs adsorption, work function meas., contact pot. difference vs. coverage curves 79—23839
- GaAs, MBE (001) layers, work function meas. 80—49870
- GaAs surface, contact pot. difference meas. 77—20403
- p-GaAs/electrolyte soln., electrode photoemission, energy diagram, Volta pot. 77—62990
- GaAs-GaSe n-p heterojunction, elec. props., interface states 80—65670
- GaP (110), electronic surface states, initial steps of O_2 chemisorption 80—49844
- GaP, cleaved (110) surface, electron surface props. 80—11067
- GaP, surface, contact pot. difference meas. 77—20403
- GaP(As)(Sb), electronic surface props., contact potential difference and photoemission expts. 77—47884
- GaP(As)(Sb), surface states, contact pot. difference, photoemission, and low energy loss spectra expts. 77—85285
- p-Ge (111) surface, Cs adsorption, work function meas., contact pot. difference vs. coverage curves 79—23839
- Ge powder/Au electrode contact pot. difference, grain size depend. 80—44723
- Ge/electrolyte soln., photoemission, energy diagram, Volta pot. 77—62990
- Hg-polymer interface, contact potential and charge exchange meas. 80—75642
- InAs, electron surface props., contact potential difference and photoemission expts. 77—47884
- InAs surface, contact pot. difference meas. 77—20403
- InP(As), surface states, contact pot. difference, photoemission, and low energy loss spectra expts. 77—85285
- Ir (110), chemisorption of O_2, sorption and dissoc. kinetics 79—33186
- Ir (110), chemisorption of O_2, AES, LEED, thermal desorption mass spectra, and contact pot. difference meas. 79—77901
- Ir (111) surface, chemisorption of O_2, dynamics, contact pot. difference meas. 77—59211
- Ir, chemisorption of CO on clean and oxidised (110) surfaces 79—11015
- Ir, chemisorption of H_2, adsorption and desorption kinetics, struct. of overlayer 80—84367
- Ir, work function changes rel. to O_2 adsorption, continuous meas. method 79—33328
- Ir, work function meas. rel. to O_2, H_2 adsorpt. 77—66094
- k, adsorption on Re (10$\bar{1}$0) surface, electron-adsorption props. 79—33192
- La, adsorbed monolayer on W (112) face, LEED and contact pot. difference meas. *(Russian)* 77—1316
- Mo (110), of Cs and O_2, common adsorption, work function and thermal stability by contact pot. method 80—44427
- Mo (110), oxidation exam. of LEED 78—92402
- Mo (110), oxidation of adsorbed C, electron diffr., contact pot. difference, and AES obs. *(Russian)* 79—52430
- Mo, coadsorption of O_2 and Cs, struct., emission props., thermal stability 80—66878
- Mo-dimethyl terephthalate contacts, effect of elec. field on contact electrification 79—19660
- $Na_2SO_4.10H_2O$, solid-liq. transform., solar energy conversion applicability 78—60155
- $Na_2S_2O_3.5H_2O$, solid-liq. transform., solar energy conversion applicability 78—60155
- Nb, supercond. point contacts, freq. and voltage depend. in noise background 79—58796

contact potential continued
- Nb-H, electron work function, 300 to 600 degrees C, contact potential difference meas. 80—29462
- $NbC_{0.86}$, single crystal work function, thermionic emission and contact pot., microhardness and binding 79—19649
- Nd film, on W(100), struct., electronic and dynamic props. *(Russian)* 77—76702
- PbS film surface with oxysulphate layer, photoelec. memory effect 77—55584
- Pt and Au threads in air, pull-off force, influence of electric charge 79—11196
- Re:C, work function, graphitic layer formation 80—96966
- Sb-In, electronic work function, contact pot. difference meas. 77—85299
- Sb-Sn, electronic work function, contact pot. difference meas. 77—85299
- Sb-Zn, electronic work function, contact pot. difference meas. 77—85299
- Se, amorphous film-metal system, contact pot. distrib. and photo-EMF, work function 77—76925
- Si-GaSe n-p heterojunction, elec. characts., interface states 80—70812
- Si-insulator structures, contact pot. meas., vibr. condensor method *(German)* 79—11232
- α-SiC:Al diodes, ion implanted, transient characts. of electrolum. 79 24369
- SiO_2-Si stratified system surface charges, adsorption and desorption effects *(Russian)* 80—49942
- Sn-Cu, chem. potential change at supercond. transition temp. of Sn 77—28301
- Sn-Pb alloys, electron work function determ., contact pot. difference method 77—39920
- Sr submonolayers adsorbed on Mo crystal, LEED and contact pot. study 80—2271
- Ta-H, electron work function, 300 to 600 degrees C, contact potential difference meas. 80—29462
- V-H, electron work function, 300 to 600 degrees C, contact potential difference meas. 80—29462
- W (100), adsorbed La, depend. of work function, heat of adsorpt. on surface coverage, contact potential study 78—67912
- W (110), (112), of Cs and O_2, common adsorption, work function and thermal stability by contact pot. method 80—44427
- W (112), adsorption of La, contact pot. difference meas. *(Russian)* 78—14618
- W-dimethyl terephthalate contacts, effect of elec. field on contact electrification 79—19660
- Zn- and ZnO-electrolyte contacts, characts. 77—1482
- ZnO, chemisorption of O_2, charge transfer obs. by contact pot. difference 77—89824
- ZnO, dye adsorption, contact pot. difference 80—27365
- ZnO, electron beam induced decomposition and desorption, AES and contact pot. difference meas. 78—79893
- ZnS, chemisorption of O_2 after illumination and in presence of CO and O_2 78—87877
- $ZrC_{0.84}$, single crystal work function, thermionic emission and contact pot., microhardness and binding 79—19649

contact resistance
- *see also contact potential*
- analyser system 79—99605
- brass, in contact with metals, for high compressive stress and high current density 77—59324
- conductive filler-polymer composite conductivity theory *(Japanese)* 78—11351
- constricted conducting cylinder, potential distrib. 77—88617
- Duralumin, in contact with metals, for high compressive stress and high current density 77—59324
- four-terminal meas. circuit stray-impedance errors 78—77940
- III-V multilayer structs., contact resistance profiling method 78—56213
- impedance meter, AC, battery-operated, for contact resist. determ. before patient monitoring 78—81006
- insulating mechanical supports, appl. to meas. thermal conductance 80—82772
- low temperature characts. 78—68072
- metal-metal, effect of surface roughness and surface films 78—10540
- metal-semiconductor interface, meas. method 80—105672
- metal-semiconductor ohmic contact props., factors affecting contact resistance of semiconductors, theoretical model 80—60076
- metal-semiconductor thermoelectric coolers, effects of contact resist. and dopant conc. 80—81481
- metal-semiconductor-metal junction, tunnelling phenomena in terms of exact method and WKBJ approx. 80—20329
- metallic foil contact resistance transducers, thermochemical method of oxide film formation 78—89466
- metallic point contacts, nonlinear resist. rel. to phonon emission and background effects 78—68074
- metallic sliding contact, resistance at single point, friction force *(Japanese)* 78—11343
- microscopic point contact resistance, size depend. 79—69582
- Ni, oxidation in air, 50-150°C, film growth obs. using AES and contact resist. 80—3242
- ohmic contact 1/f noise intensity and contact resistance analysis 77—62982
- ohmic contacts to semiconductor, meas. of contact resistance using transmission line model 80—70826
- planar devices, contact resistance derivation 78—60205
- probing and Auger analysis of contaminants, combined technique 80—39662
- rough surface modelling and online monitoring 79—80576
- semiconductor-metal contacts, contact resist. and bulk resist. of semicond. samples, pulse method 78—52083
- semiconductor-metal systems, method for analysing influence of extrinsic parameters 80—25007
- solids in vacuum, contact adhesion, single asperity experiments 77—11149
- spheres at high pressure, contact stresses and spreading resistance 78—71296
- steel, mild, two sandblasted interfaces, tangential displacement, contact press. and lubricating film distrib. effect 80—16484
- steel, mild or stainless, in contact with metals, for high compressive stress and high current density 77—59324
- steel mild, ground/sandblasted interfaces, tangential displacement, contact press. and lubricating film distrib. effect 80—16484
- transducers using electrically conductive paper 77—13747

contact resistance continued
- Ag-Pd and Ag-Ag, effect of surface roughness and surface films 78—10540
- Ag-Pd-Cu, contact-spring props., fatigue and spring limit *(Japanese)* 79—29117
- Ag-Zn, internally oxidized, elec. contact characts., alloying additions effect *(Japanese)* 80—88619
- $Ag_7I_4PO_4$, solid electrolyte, ionic cond. meas., 4-79°C 80—54433
- Al, in contact with metals, for high compressive stress and high current density 77—59324
- Al/Cu thin film couples, interfacial reactions, low temp. contact resist. meas. 80—44709
- Al-Au couple, electroformed, nonohmic characts. and electron emission 80—60066
- Al-Cr, thin film metal contact, sheet resistance changes 80—80356
- Al-Si, contact resist. response surface of sintered Al film on Si (100) 79 - 78175
- Al-Si contacts, effect of vacuum ambience 77—43718
- (AlGa)As CW injection laser, contact thermal resistance increase after lifetests, reliability statistical study 79—76687
- Au electrodeposited coating properties obs., Cu diffusion under high temperature *(Czech)* 78—91486
- Au, immersion plating on Al, adhesion and contact resist. 79—39033
- Au surface, lubrication by plasma-deposited thin films of fluorocarbon polymer 80—89157
- Au-Al_2O_3-Al system, influence of mech. modulation on elec. transport 80—2481
- Au-Cu, oxidation kinetics of Cu out of Au soln. at 50-150°C 80—21171
- Au-Fe-Ni layer coating, Fe and Ni conc. meas. by X-ray diffr. *(German, English)* 80—34330
- $CdGa_2S_4$ double surface-barrier diodes, current-voltage characts. 80—92972
- $CdSnAs_2$-Au(Al), surface barrier junction, elec. props., temp. depend. 80—65686
- Cu, cold-drawn, in contact with metals, for high compressive stress and high current density 77—59324
- Cu, oxidation in controlled clean air and standard laboratory air, 50-150°C, contact resist. and AES meas. 79—70202
- Cu, sintering, contact resist. determ. of neck growth rate and mass transport mechanism 77—55899
- Cu-Ni thin film couples, interfacial reactions, contact resistance meas. 78—63882
- Cu_2O and CuO powders, contact resistance, temp. and pressure dependence, obs. *(German)* 79—4555
- GaAs, circuit effects in time-of-flight diffusivity meas., Monte Carlo method 80—88563
- n-GaAs epitaxial layers, alloyed in As_2 beam, metal-Ga contacts 79—95495
- n-GaAs nonalloyed ohmic contacts of TiPtAu by pulse-electron-beam annealed Se implants 80—2466
- GaAs, ohmic contact form. to n- and p-type samples by MBE, characts. 79—47159
- n-GaAs, study of ohmic contacts 80—60083
- GaAs transferred electron devices, ohmic contacts 78—52082
- GaAs:Cr, Se layers, ion implanted, ohmic contact form., contact resist. meas. 79—91158
- n-GaAs:Sn, heavily doped, nonalloyed ohmic contact form. by MBE and metallisation 79—7895
- GaAs:Te-implanted by laser-annealing, ohmic contacts 79—19658
- GaAs/Ni-Ge-Au cathode struct., with enhanced injection efficiency, contact resist. 77—20431
- n-$GaAs_{0.6}P_{0.4}$, reproducible ohmic contacts 79—73587
- GaInAsP, rectifying and ohmic contacts 80—80376
- p-$Ga_xIn_{1-x}PyAs_{1-y}$/Au-Zn, specific contact resist. 80—84509
- GaN-In(Sn)(Sb)(Te), using GaN made by oxidation and subsequent nitridation of GaAs, I-V characts. 77—20436
- GaP, comparison of contact resistances of Au-Zn, Au-Zn-Sb, Au-Ge-Ni and Au-Ge-Ni-Sb alloyed contacts 80—70825
- Ge amorphous evaporated film, to metal contact resist. diffusion and microstruct. 77—89880
- a-Ge-Si crystal interface, low resist. elec. behaviour 77—89843
- $HfPt_3$, corrosion resist. and elec. cond., bulk and film samples 78—72285
- Hg/hard metal, investigation *(Bulgarian)* 77—62983
- p-InP, ohmic contact using Be-Au metallisation, low contact resist. 80—65677
- p-InP-Cd(Zn), ohmic contact formation on InP by laser photochemical doping 80—80369
- Mo-Si sputtered contacts, contact resistance 80—92970
- Nb-Ge, A15 struct. superconductor, high field transport props. TEM study 80—34574
- Nb-Ge-Si, A15 struct. superconductor, high field transport props. TEM study 80—34574
- Ni/Au-Ge/GaAs alloyed contacts, prep. by LPE of GaAs from Au-Ge-Ni melts 77—77437
- Ni/Au-Ge/nGaP system, specific contact resistance calc. 78—43474
- Ni-Au alloy, oxidation in air, 50-150°C, film growth obs. using AES and contact resist. 80—3242
- Ni-W surfaces in contact, deform. and adhesion at very low loads 80—39457
- $PbS_{1-x}Se_x$ diode laser, contact degradation due to diffusion 80—102734
- $Pb_{1-x}Sn_xTe$ diode laser, contact degradation due to diffusion 80—102734
- Pt-Ir, Au covered, spectral characts. of VLF noise, allowing for logarithmic creep *(Russian)* 77—85301
- Ru, as elec. contact material, environmental interactions and prep. 80—29463
- RuO_2, as elec. contact material, environmental interactions and prep. 80—29463
- Sn-Ni electrodeposit, contact resist. corrosion effect 78—47847
- Te-CdS-Te contacts, ohmic nature, monitoring method 77—39935
- Ti metal-metal interface, adhesion energy, surface treatment and ion implantation effects 80—107660
- ZnO-NiO:Li_2O n-p heterojunction, contact resist., effects of water vapour 80—34506
- ZnS, low resistivity, ohmic contact noise characts. and contact resistance 78—14827
- $ZrPt_3$, corrosion resist. and elec. cond., bulk and film samples 78—72285

contactors
see also relays
DC contactor magnet coil, electromagnetic field, transient states *(Polish)* 80—18962
high current switch, fast closing, fusion reactor fast discharge expt. 78—74483
contacts, electrical *see electrical contacts*
content-addressable storage
hologram memory control system and software *(Russian)* 77—58262
holographic index memory system *(Russian)* 77—58259
memory system principles and descriptions *(German)* 78—29910
optical memory systems *(Russian)* 77—58257
continuous creation hypothesis *see cosmology*
continuum hypothesis *see set theory*
continuum mechanics *see classical mechanics of continuous media*
contours, surface *see surface contours*
contrast transfer function *see optical transfer function*
control devices, electric *see electric final control devices*
control engineering applications of computing *see control engineering computing*
control engineering computing
see also computerised control; control system analysis computing; control system CAD
CANDU, digital computer control 77—54324
mechanical actuator, stepper motor, appl. to control of scientific apparatus 78—62683
nuclear reactor, one dimens. slab, optimal control of Xe oscills., computer program *(German)* 77—61529
optimal control initial states conversion, using gradient restoration algorithms, hypersonic flow with axisymmetric body appl. 78—4474
SEM system, computer controlled for quantitative three-dimens. characters. of particulate materials 77—2714
control equipment
see also actuators; controllers; electric control equipment; mechanical control equipment; nonelectric final control devices; relays; telecontrol equipment; thermostats; valves; variable speed gear
abrasive particle shape control and quantitative eval. apparatus 78—4586
modular instrumentation system for nuclear industry 77—67780
photographic film copying, control mechanism to reduce waste quota *(German)* 78—93772
pollution control equipment operation and maintenance 78—61615
single channel pulse height analyser, control and meas. system contruction appl. 79—93891
wire spark erosion machine for hard metals, control cct. 79—35695
control facilities
CRT man-machine communication system in nuclear power stations 79—45364
Fermilab, multi-user control and data acquisition systems 77—54480
LLL, microprocessors appl. 77—54481
nuclear power station, design of advanced control room 79—45362
nuclear power stations, control rooms, human factors design approaches, improvement of man-machine interface, error reduction 80—63327
control gear, electric *see electric control equipment*
control nonlinearities
see also bang-bang control; hysteresis; nonlinear systems
intracranial pressure regulation, nonlinear parametric feedback model 79—96599
reactor nonlinear control system, relative stability anal. 77—3116
control rooms, radio *see radio studios*
control system analysis
see also Bode diagrams; correlation methods; describing functions; frequency response; linearisation techniques; perturbation techniques; phase space methods; piecewise-linear techniques; poles and zeros; sensitivity analysis; stability; state-space methods; step response; three term control; transfer functions
artificial heart, control system, anal. of effectiveness of algorithm using aortic blood press. as regulated parameter 80—3864
differential games, control systems with aftereffect 80—68025
nuclear power reactor, neutron-field control system, stability anal. 77—3086
on-off fission reactor zonal control systems, analysis 77—71680
reactor nonlinear control system, relative stability anal. 77—3116
respiratory ventilator model and design optimisation 79—20713
Tokamak plasma equilibrium, feedback control 78—55738
tracking Michelson interferometer stability improvement *(Russian)* 78—29149
control system analysis computing
laboratory computer system for routine, plant and environmental radiation monitoring appl. 79—9912
thermonuclear device self-adjusting system automatic feedback parameter search 78—26336
wind energy conversion system control, on-line, performance in turbulent wind environment 79—48069
control system CAD
nuclear channel reactors, automatic control system design for energy distrib. 78—82475
PWR power plant self-tuning control and simulation 79—9827
thermal regenerator, with variable mass flow rate, computer model 78—75047
control system computer aided design *see control system CAD*
control system synthesis
see also Bode diagrams; correlation methods; describing functions; frequency-domain synthesis; frequency response; linearisation techniques; perturbation techniques; phase space methods; piecewise-linear techniques; poles and zeros; sensitivity analysis; stability; state-space methods; step response; three term control; transfer functions
astronaut transfer in weightlessness, biomechanical model 78—96106
attitude control of space vehicle descent to surface of atmosphere-less planet 78—16265
BWR load following plant, low sensitivity design fo controller 78—78473
dynamic systems, elements of statistical energy anal. 77—75740
fission reactor suboptimal control param. inbedding method appl. 77—34421
gyrostat motion time-optimal damping under random perturbations 77—68379
HTGR Core Auxiliary Cooling System mathematical simulation 78—29570
HWR dynamics modelling for digital control system design 79—9829
control system synthesis continued
Large Space Telescope optimal fine pointing control using Annular Momentum Control Device 77—73934
nuclear power station model validation and automatic control 77—88261
nuclear reactor closed-loop control system synthesis 77—3117
nuclear reactor distributed parameter optimal control methods 78—54858
nuclear research reactor ZED-2, two-phase control absorber development 79—85697
oculomotor control system feedback, photoelectric matrix method *(Korean)* 77—90779
plasma flute oscillation suppression, regulator synthesis *(Russian)* 80—24212
plasma frequency response investigation as automatic control problem 79—10649
plasma instabilities, feedback controller development 79—50853
probkotron plasma stabilisation system, automatic, against flute oscills. *(Russian)* 80—24211
PWR steam supply control system optimisation 78—50251
PWR system model 77—88262
reactor spatial control during nuclear station load cycling, multivariable control algorithm 79—13490
signal amplitude digital auotmatic control system, instrumental realisation algorithm *(Russian)* 79—39924
speed-optimal control synthesis in near spherical symmetry problems *(Russian)* 79—9095
stationary system impulse response function, Cauchy problem reduction 77—37729
stochastic object, suboptimal adaptive control 79—30371
stream pollution controller design via pole assignment 77—60434
superheated steam, control system using an adaptive regulator, synthesis *(Polish)* 79—75518
Tokamak, ISX, dynamics and feedback control 78—71528
Tokamak power reactor, position control and sensor requirements 78—5035
toroidal plasma, ion temp. control by neutral injection 79—37514
HF chemical laser, phase control for coherent optical recomb. 79—72580
control systems
see also adaptive systems; closed loop systems; delay-differential systems; discrete time systems; distributed parameter systems; integrated control systems; multidimensional systems; multivariable control systems; nonlinear control systems; optimal control; physical instrumentation control; sampled data systems; time-varying systems; traffic control systems
ambient noise indices, control instruments and systems *(French)* 79—76913
communication/control systems for motor impaired people, standardisation 80—17198
hot-film anemometers, freq. optimisation theory 78—26218
instrumentation and control technology, decentralisation, past developments and future trends 80—4701
LMFBR inherent shutdown system, expts. and analyses 79—31041
on-line system for RF separated hadron beams at BEBC 77—38530
plasma instability, suppression by feedback method automatic control, stabilisation methods 78—63564
prosthesis, sensory feedback system for above knee prosthesis *(Japanese)* 80—72372
random signal analysis, conf., London (April 1977) 77—44822
seismic recording equipment, digital automatic amplitude control unit parameters choice *(Russian)* 79—39964
USSR State Bureau of Standards, metrological resource programmes 80—90809
control theory
see also control system analysis; control system synthesis; optimal control; stability; two-term control
differential encounter-evasion game, nonstationary, theorem on the alternative 80—68026
dynamics of systems of solid bodies with combined control *(Russian)* 79—17209
irreversible energy conversion processes, information model *(Ukrainian)* 78—89419
nuclear plant mix with minimum natural fuel requirement, optimum theory 79—26469
nuclear reactor Xe oscillation control problem 80—674
observability for regular processes 77—67211
porous media, miscible or immiscible displacements, identification and modelling 78—69392
variational approximations to renormalization groups 79—63169
controllability
see also stability
biological compartmental systems, multi-input and multi-output, controllability, observability and structural identifiability 78—76978
biological compartmental systems analysis, computer program 77—40625
biped locomotion dynamics, control theoretic study *(Japanese)* 79—11963
CANDU advanced BLWR with enriched fuel 77—71683
multidimensional infinite mechanical oscill. system, resonance and controllability 80—33444
pendulum inverted, design and stabilisation control *(Japanese)* 80—73167
quantum systems control, pure states and mean values 80—22210
controllers
see also cryostats; instruments; servomechanisms; thermostats
AC power, Veritron, thermal equipment temperature regulation, automated manufacturing processes *(German)* 79—80598
annealing of electron field emitters and multiple multichannel analyser, precision temp. regulator 78—86384
artificial leg, EMG operated, for locking/unlocking of knee joint 78—7545
astronomical laser ranging equipment, system controller *(Japanese)* 78—89079
automated variable pressure controller design and error analysis 77—57315
betatron redundant solid-state controller 79—88163
cardiac assist devices, in-series, digital afterload phase angle controller 77—44843
cardiac-assist in-series devices, controller 78—81075
cell freeze conservation control unit *(German)* 79—5410
cryogenic, for temps. 78 to 300K 77—22555
cryogenic pressure regulator 78—57963
crystal oven pilot-lamp stability controller 78—54374

controllers continued
current regulator based on industrial thyristor convertors, for magnet winding supply 77—37921
DC proportional heater/cooler temperature controller for physiological research 78—7553
Doppler sonar controller 80—43575
driven oscillator motion with nondecreasing input vels., use in inertia actuated fuse 78—59293
electric furnace, muffle type, automation of temp. regime 77—61068
electric heating regulator using a FET amplifier and Schmitt trigger convertor *(French)* 79—58681
electron microscope stabilisers, Hg-Zn battery as reference voltage source 79—9262
EPR spectrometer, simple temp. controller, 85-400K *(German)* 78—45663
eye continuous movement monitoring, proportional-integral adaptive system *(German)* 79—16320
fusion reactors switching and regulating elements, high-power tetrodes appl. 79—54592
gas flow control, automated, transducer 78—59508
gas flow rate meas. up to 2.8 m^3/sec, dynamic volumetric method 77—72380
gyrostabilizer, nonlinear suspension bearing, dynamic error *(Russian)* 78—75063
heart, artificial, microcomputer based automatic controls 80—67289
heavy ion electrostatic analyser control system *(French)* 77—42211
holographic system path length difference controller *(Russian)* 79—22916
HV pulse controller and temp. monitor microcomputer-based, Kerr effect study appl. 79—6103
hydraulic, heart power supply and control modules, implantable 78—31978
hydrophones, towed, location system, shipboard microcomputer controller 79—2401
intra-aortic balloon pump controller, within computerised evaluation system 77—56538
knee locking, sensor-controlled external system, exptl. study 78—40406
knee-torque, electrohydraulic, for prosthesis simulator 78—11779
laboratory temperature regulation cct. 77—45836
liquid He transfer controller, semiautomatic 79—17428
liquid N_2 two-level controller 80—52241
liquid nitrogen level control, sensing diode and Norton amplifier 78—29121
LSI-11 based auxiliary crate controller for beam line and experiment control 79—89565
luminous flux, controllable regulator for KIM-9-75 source 77—39010
machine tools, conference New Delhi, India (1977) 78—4590
magnet-current regulator for RE1301 microwave spectrometer 79—21779
magnetic flux, resonance conditions stabilisation in NMR radiospectrometers 80—52286
manostat, stable automatic pressure controller, use of thin polyester film 79—35700
microcomputer based scanning instrument controller, for optical spectroscopy 78—93764
microprocessor based interface/controller for desktop programmable calculator 79—35690
microprocessor-based, programmable laboratory equipment controller and data acquisition system 79—6104
microprocessor-based experiment controller/interface 79—80590
multichannel acousto-optical modulator control system *(Russian)* 79—72525
multidither adaptive optical system, 69-channel hybrid controller 80—33136
neutral beam filament supply, 15 V 10^3 A, programmable, regulated, for fusion reactor 78—70630
noise reduction in steam power, chemical, petrochemical industries 78—51002
nuclear pulse height analyser, microprocessor based digital controller 79—3335
panoramic pulsed NQR spectrometer programmer, design, basic functions 77—61100
plasma, flute oscills. suppression by regulator with cross feedback *(Russian)* 78—26262
plasma flute oscillation suppression, regulator synthesis *(Russian)* 80—24212
pneumatic amplifier pump, for supercritical fluid chromatography, control and programming 78—88665
precision DC stabiliser based on P-136 stabiliser 78—8411
pressure regulator device, behaviour anal. 78—93668
pressure regulator for proportional regulation of two gas pressures, anaesthetic appl. 78—53560
probkotron plasma stabilisation system, automatic, against flute oscills. *(Russian)* 80—24211
prosthesis, above-knee, knee control, finite sensor state anal. 77—40935
prosthesis, EMG operated 77—48954
rapid-scan spectrometer control unit 78—74067
resistance furnace programmed temperature regulator 78—86256
roller pump for pulsatile blood flow 78—44721
rostrum controller Pacesetter, digital, computer control of animation filming process appl. 78—45743
scanning cytophotometer appl., design method 78—31920
sequence controller for Harwell 6000 series modular instrumentation 78—24784
SLAC accelerator, automatic phasing using microprocessor controller 77—88305
solar energy management system 80—66951
temp., dynamic type, 60 to 900K within 0.05K 77—10009
temp. rise, sensitive, for furnace 77—17980
temperature, at cryogenic temps. 80—90856
temperature, filament heating for gas adsorpt. state study *(Japanese)* 77—51603
temperature, for range 77-300K 77—33995
temperature, of He cryostat, using digital voltmeter *(Czech)* 78—29120
temperature, two-point, for inductive loads *(German)* 79—26051
temperature control of electrometer varactor-bridge amplifiers 79—9219
temperature controller with improved set-point setting, construct. *(German)* 78—45606
temperature controllers, time-linear, used in analysis of thermoluminescence glow curves 79—63202
temperature regulator, contact, analytical and experimental study 79—185

controllers continued
temperature regulator and controller selection and specification 79—71439
temperature regulator circuits, using thyristors and triacs *(Spanish)* 79—6115
temperature regulator for 77 to 340K range, Ge transistors use as heating elements 77—67442
temperature regulator for heating units and cryostats 77—37880
temperature regulators, on-off control, accuracy improvement 79—75527
temperature regulators using Darlington cct. as sensor and controller *(German)* 79—30467
thermocouple temperature controller for field emitter 78—24898
thyristor temp. regulator for pulsed NMR spectrometer 80—105687
thyristor thermostabiliser use in atomic absorpt. spectroscopy with non-flame sample atomisation 79—96388
time-lapse apparatus for 16 mm Beaulieu cine camera 78—74089
vacuum press., for RF sputtering apparatus 77—28720
vehicle speed, using Pb-acid battery, response to chopper-controlled discharge 79—48120
voltammetric analysis, automatic controller, design 80—71968
water quality, observer-based, polluted river stream appl. 77—81938
X-ray studies of phase transitions at low temp., automatic system 77—15281
Cu-constantan cryogenic thermometer and temp. controller *(Czech)* 79—26056
D ion source, pressure regulation by regulating electrolyser 78—842
O_2 flow regulator, solid-state, high-temperature 80—57301
SiC thin-film thermistors with high thermal response *(Japanese)* 80—105629

convection
see also convection in liquids
14-variable convection model, chaotic response to periodic modulation of model 79—98728
A-type stars, He convection zone rel. to rot. and variability 77—87397
ablating body shape, numerical soln. method *(Russian)* 78—75134
absorbing-scattering infinite slab, combined conductive and radiative heat transfer 78—71269
acetylene-air flame, eddy entrainment and combustion in depth process, three-region model 79—100384
admixtures, convective-diffusive transfer in cylindrical channel, soln. 77—7391
advection processes, finite difference method, balanced expansion technique 78—77719
aerosol enclosures under convective stirring conditions, quiescent boundary layer thickness 79—66364
aerosol flows in finite tubes in random orientation, sedimentation 79—50778
aerosol precipitation from laminar gas stream, free convection effect 78—83459
air, heat transfer in laminar natural convection in cubical cavity 80—24022
air, in wall cavity, slot filtration, temp. distrib. 77—65662
air flow and heat transfer, in horizontal pipe, thermogravit. effects 77—31305
air jet, heated, turbulent, discharged downward, temp. profiles 79—27677
air jet, vertical axisymmetric buoyant, profile meas. 78—90906
air pollutants dispersion from area sources in convective turbulence, model 78—28303
air suspension homobaric flow in presence of physicochemical transform. 80—87820
air-water interface, combined heat and mass transfer coeff. 78—30166
alloy melt, temperature distribution during cryst. growth by Czochralski method *(Russian)* 80—75192
analog solution of free convection mass transfer from downward-facing horizontal plates 80—43706
annulus, forced convection, experimental study *(Italian)* 79—81977
annulus, tall, vertical, conduction regime of natural convection stability 80—99987
annulus with inner rot. tube, heat transfer 79—1204
annulus with permeable insulator, radiative and free convective transfer 78—94575
aortic tissue, rabbit, convective and diffusive transport of ^{125}I-serum albumin 78—44482
aquifer, temp. field due to hydrothermal convection, numerical calcs. 80—90105
arc, DC low voltage, anode energy balance investig. at reduced press. 80—19637
arc, high press., convection 78—59701
Archaean crust, geothermal heating rel. to vertical tectonism in greenstone belts 80—81861
Arctic fjord waters, saline convection and mixing 79—48504
artificial membrane lung, fluid vortices and mass transfer 77—52919
asthenosphere, convection rel. to magmas and volatile components 80—41418
asthenosphere, convection rel. to radial and lateral temp. vars. 77—5141
asymptotic free convection from an insulated vertical flat plate at high Prandtl number 80—24014
asymptotic laminar thermal convection, unified treatment *(Italian)* 79—18883
atmosphere, 10-level model, parametrization 77—70782
atmosphere, African wave disturbances, convection role, linear primitive eqn. model 80—77043
atmosphere, cellular convection and assoc. cloud patterns 78—36249
atmosphere, circulation associated with cold front, moist case 79—2334
atmosphere, convection development over inhomogeneous heated surface *(Russian)* 77—29365
atmosphere, convection enhancement in extratropical cyclone after separation from polar front *(French)* 80—56517
atmosphere, convection in thin layer above water surface *(Russian)* 77—45073
atmosphere, convection rel. to submillimetre radiation from tropical cloud clusters *(Russian)* 77—49165
atmosphere, convective boundary layer, temperature variance profile parameterisation *(French)* 80—56518
atmosphere, convective breaking localisation in perturbed stratified layer 77—70716
atmosphere, convective vortex model, unsteady two-cell similarity soln. 79—16626
atmosphere, critical evaluation of mixed-layer model with penetrative convection 80—51483

convection continued
  atmosphere, digital simulation of monsoon evaporation phase, moisture eqn. development 77—56712
  atmosphere, double diffusive convection during 1975 hurricane Eloise 77—70738
  atmosphere, dry penetrative convection 78—92889
  atmosphere, estimation of convection efficiency and vel. in general circulation via laboratory models *(Russian)* 77—81961
  atmosphere, forward air flow effect on evolution of convection 80—90116
  atmosphere, free convection structure in surface layer 77—37294
  atmosphere, freely convecting, above water surface, oscills. natural freq. *(Russian)* 78—11964
  atmosphere, gravitational convection with compressibility 79—58051
  atmosphere, initiation and development in temperate latits. 78—20480
  atmosphere, internal gravity waves generated by penetrative convection 77—2196
  atmosphere, lapse rate depiction for clear-air convection 77—53145
  atmosphere, Lorenz system, 14-D generalization 78—75131
  atmosphere, mean thermodynamic instability in N tropics 77—25751
  atmosphere, meas. of heat flux and struct. functions of temp. fluctuations with acoustic Doppler sodar 80—105023
  atmosphere, models of thermals 80—109228
  atmosphere, moving thermals rel. to hydrodynamical accelerator in upper atmosphere *(Russian)* 78—16225
  atmosphere, obs. of smoke plume assoc. with intense local fire 77—49148
  atmosphere, parametrisation, conditional instability of second kind hypothesis appl. 78—61530
  atmosphere, penetrative convection linear stability 77—33146
  atmosphere, penetrative cumulus convection assoc. with travelling disturbances in equatorial ionosphere 78—36361
  atmosphere, perturbed, photochemical radiative convective model for thermal struct. and relaxation rates 80—8408
  atmosphere, similarity theory for viscous fluid convection anal., use of Soviet work *(Russian)* 78—16174
  atmosphere, turbulence characts. under convective conditions *(Russian)* 79—16577
  atmosphere, unstably stratified theory of turbulent convective plume *(Russian)* 77—49108
  atmosphere, vertical eddy heat flux in northern hemisphere 77—33133
  atmosphere, vertical heat flux determ. on basis of semiempirical turbulence theory 78—3907
  atmosphere, vertical heat flux in boundary layer 78—20487
  atmosphere, wave generation and frontal collapse 78—77300
  atmosphere boundary layer, boundary layer, appl. of mixed-layer similarity scaling to observed dispersion from ground-level source 80—105021
  atmosphere boundary layer dynamics, IR radiation effects 79—39815
  atmosphere convection dynamics equations, non-Archimedean approach 80—77048
  atmosphere convective precipitation, mechanical effect of urban area 78—81338
  atmosphere dynamical meteorology, trough-ridge systems as slantwise convection 79—79993
  atmosphere in astronomical observatories convection rel. to dome seeing 80—12657
  atmosphere surface layer, convection speed of features of organised motion 80—72602
  atmosphere-ocean, penetrative convection regime, entrainment rate *(Russian)* 78—69401
  atmospheric, fixed cloud-top temp. and fixed cloud-top altitude approximations for temp. profile 80—72616
  atmospheric boundary layer, convective matching layer 78—81310
  atmospheric boundary layer, temperature-humidity covariance budget 78—73430
  atmospheric boundary layer, three-dimens. model rel. to expt. data 78—73428
  atmospheric boundary layer, turbulent penetrative-convection planforms, laboratory obs. 79—48550
  atmospheric convective diffusion from nuclear power station spray cooling 78—94078
  atmospheric transport problems, contaminant movement, Galerkin finite element method 80—74902
  atomiser, absorption zone atom distrib. convection effects calcs. *(Russian)* 77—68730
  atomiser chamber electrode-diffusion flame, atoms distrib. in absorpt. zone, convection currents role *(Russian)* 79—34420
  auto-oscillations and instability phenomena in the simplest model of convection *(Russian)* 79—32504
  axial wall conduction, with var. prop. convection, axial temp. distrib. calcs. 77—15010
  axisymmetric convection, stability, solar granulation appl 79—77093
  axisymmetric convection in prescence of mag. field, solar granulation and sunspots appl. 80—12724
  axisymmetric convection in rotating sphere, non-slip surface effects 79—64657
  axisymmetric convection in shallow rotating cylinder, centrifugal acceleration effects 80—96260
  axisymmetric heat exchange, variational method *(Ukrainian)* 78—1547
  axisymmetric jets, coherent structs. using optical technique, convection vel. 80—69888
  baroclinic atmosphere, two dimensional, zonal flows convective instability *(Russian)* 80—94564
  Basin and Range province, tectonic extension rel. to convective heat transport and heat flow 79—70763
  bed of inductively-heated particles, water-cooled, natural convection heat transfer 78—71396
  Benard, generalised problem with viscosity variations 78—71329
  Benard convection, in heat conducting media *(German)* 78—79308
  Benard convection, initial and boundary condition effects, book contrib. 80—1591
  Benard convection, mean field equations 80—83798
  Benard convection, pretransitional induced, two-dimens. numerical anal. 79—68703
  Benard convection, transient, laser speckle photography obs. 79—32508
  Benard convection, very viscous fluid, theory 80—10236
  Benard convection in a finite box, secondary and imperfect bifurcations 79—50725
  Benard convection in rot. fluid, DuFort-Frankel difference scheme 77—51035
  Benard convective instability, anomalies in sound propag. 77—34975
  Benard convective instability threshold, seed particle motion 77—11172

convection continued
  Benard phenomenon, asymptotic behaviour of differential systems rel. to competition of species *(French)* 77—67197
  Benard problem, R^2 class of mappings, invariant Cantor sets and strange attractors 80—59037
  Benard problem, two dimens. nonlinear temp. and vel. distribs. 78—34134
  Benard system, convective instability, hydrodynamic fluctuations 77—35143
  Benard type, distant sidewalls effect on transition to finite amplitude convection 78—22348
  Benard-Rayleigh problem, nonlinear evolution of 2D perturbation continuous spectrum 78—14013
  benzene, free convection heat transfer in tube at supercrit. press. 78—42518
  bibliography of heat transfer 78—63425
  binary gas mixtures, convective instabilities in closed vertical cylinder heated from below 79—72880
  binary gas mixtures, mass transfer analysis using model of convective diffusion for turbulent flow in tube 77—7454
  binary isotopic gas mixture, convection-diffusion eqn. soln. for centrifuge axisymm. vel. field 78—17434
  binary mixture vapour condensation, forced-free convection, finite difference treatment 78—5741
  Bingham fluid, forced convection of polymeric and disperse systems in ultradeep boreholes 79—68762
  blood oxygenator, convective-diffusion model 78—44711
  boiling, forced convection in uniformly heated annular channel, generalised correlations 79—46171
  boiling, nucleate, subcooled, latent heat transport contrib. 78—75046
  boiling, subcooled, nucleate, mechanistic model 78—90697
  boiling, sustained and transient, inlet subcooling effect on flow instabilities 78—94809
  boiling, transition type, in forced convective flow, boundaries meas. 79—27499
  boiling and bubbling heat transfer under the conditions of free and forced convection 78—90637
  α Bootis (Arcturus), giant convective elements hypothesis rel. to variable mass loss 77—22213
  boundary layer, transitional, natural convection instabilities effect *(French)* 78—38333
  boundary layer flow, viscous dissipation effects on combined forced and free convection 77—54995
  boundary layer turbulence, at vertical plate 79—32501
  boundary layer with blowing, numerical exponential box scheme 79—1240
  boundary layers, heat transfer, variational description 77—68581
  bounded coaxial jets, convective heat transfer in turbulent mixing, swirling 80—64541
  Boussinesq convection in deep rotating spherical shell, temp. boundary effects 79—64655
  Boussinesq convection in deep rotating spherical shell, vel. boundary effects 79—64656
  Boussinesq eqns. with Catteneo-Fox modification, uniqueness theorem *(Italian)* 79—94606
  Boussinesq equation, finite element anal. 78—79292
  Boussinesq fluid, porous media, convective instabilities 77—80213
  Boussinesq fluid, Rayleigh-Benard instability in nonreactive binary fluids, results 79—90226
  Boussinesq fluids, Rayleigh-Benard instability in nonreactive binary fluids, theory 79—90225
  Boussinesq fluids, viscosity, conductivity and power spectrum of turbulent convection 80—98543
  Boussinesq turbulence, statistical theory 80—48713
  Brownian particle diffusion in shear induced convection, Poiseuille flow 80—33591
  bubble in power-law liq., convective heat and mass exchange, $Pe \leq 1000$ 78—55683
  bubble Reynolds number effect on heat transfer of forced convection subcooled boiling *(Japanese)* 80—19365
  building, thermal energy balance, method for including environmental modulation *(French)* 79—3900
  buoyancy cross-flow effects on longitudinal boundary layer flow 77—58687
  buoyancy effects in entraining turbulent boundary layers: a second-order closure study 80—21815
  buoyancy-thermocapillary convection layers with free surface, energy stability theory 80—87768
  buoyant atmospheric plumes, critical thermal power during atmosphere penetration *(French)* 80—33585
  buried convective heat source, in semiinfinite solid, steady temp. distrib., surface temp. 77—58534
  buried cylindrical heat source, transient temp. distrib., upper and lower bounds 78—75048
  n- butanol, natural convection from temp. fields in spherical partially filled vessel 80—1561
  calculations, quasisteady approach 78—34131
  camphene-coated surface, convective local mass-transfer coeffs., holographic interferometry method 78—75234
  casting in space environment, dendrite remelting and macrosegregation in low-gravity 79—47669
  cataclysmic binaries accretion discs, convection as viscosity source 78—93307
  catalyst granular bed, static, flow transfer processes 80—45554
  cavernous aquifer, thermal convection currents 77—64340
  cavities, advanced numerical anal. of 2-D time depend. free convection 80—43704
  cavity, horizontal, laminar natural convection heat transfer 79—55383
  cellular conv. in liquid heated below rel. to surface deformation and active agents *(Russian)* 77—54973
  cellular convection in a stratified atmosphere 80—98652
  cellular convection in rot. fluid annulus steady linear theory 78—38339
  cellular flow wavelength selection, convection and turbulence 80—38380
  central difference approximations to the heat transport equation 79—3885
  centrifugally driven thermal convection in rot. cylinder 78—51172
  β Cephei stars, effects of convection and mass loss on instability strip 80—90436
  Cepheid variables, double-mode and bump, rot. and convection effects on period ratios 78—93249

convection continued
channel, vertical, round, in nonuniform mag. field, steady-state MHD convection 80—33696
channel, with diverging walls, blood streaming viscous-convected inertia effect 77—52828
channel flows of high temp. gases, heat transfer 78—94722
channel with porous walls, convective diffusion and mass transfer *(French)* 80—79305
channels, buoyancy induced flow, general correl. eqn. 77—58790
channels, radiant heat transfer problems commonly encountered in convective heat transfer analysis 80—48562
channels of non-circular section, transient convective heat transfer calc. *(Russian)* 78—38176
channels of various cross-sections, convective heat transfer 77—11262
chemically driven convection of dissociating Navier Stokes fluid, instabilities 80—59128
chimney, thermally isolated, convective heat outflow, mathematical model soln. *(German)* 78—90887
circular channel with laminar flow, convective heat transfer *(French)* 78—63424
circular cylinders and spheres, fluid flow and convective heat transfer *(German)* 79—94624
circular fins with triangular profile, convective efficiency 78—67007
circular tube thermal entrance region, laminar droplet flow convective heat transfer 80—6049
closed gas centrifuge, eigenvector soln. of linearised eqns. of thermal convection 80—83797
cloud, warm cumulus, three-dimens. numerical model with microphysical processes *(Russian)* 78—88884
cloud development, effects of explosion *(Chinese)* 80—82042
cloud model, shallow convective, precip. mechanisms 78—81311
clouds, stability anal. of deep streets 79—2335
clouds, three dimensional turbulent flow anal. 78—69395
coarse-grained soil, free thermal convection, effective thermal cond. 77—25705
coaxial radiative and convective heat transfer in gray and nongray gases 80—102963
cold electron plasma waves, parametric decay, convective loss effect 80—38634
collectors with absorbent selective surfaces, theoretical performance, convection aspects 79—29482
colloidal dispersion, particle growth rate, effects of convection and Brownian motion 79—52778
columns convecting over linear heat sources, interaction, wind effect *(Russian)* 78—55637
combined convection flow along vertical surface, fluctuating boundary layers 80—96254
combined convection heat transfer in rod arrays, numerical anal. 78—90898
combined convective flow through circular pipe, viscous dissipation effects 79—68803
combined convective laminar boundary flow, vertical cylinder in horizontal flow, finite difference approx. 78—90893
combined forced and free convection in horizontal tubes with temp. depend. viscosity 77—15023
combined free and forced convection, periodic vortex formation 80—74878
combined free and forced convection heat transfer in closed spaces 80—1564
combined heat transfer, state of the art review 80—79119
combustion of opposed gas-air jets, convective heat transfer 79—72960
complex heat exchange, radiant and convective components meas. method 78—32809
complex heat exchange in model of direct heating furnace 78—5631
complex unsteady flow, convective modelling procedure based on quadratic upstream interpolation 79—68694
compressible convection in stellar interiors 78—89183
compressible fluid layer through porous medium, thermal instability 80—92114
compressible fluid with infinite Prandtl number 80—38398
compressible fluids, thermal instability in presence of mag. field and rotation 77—89204
compressible gas, heat exchange in free convection condition *(Russian)* 80—28502
condensation of chemically reacting gases, chemically reacting noncondensable components 78—51258
condenser system, submerged, buble pumped augmented natural convection 78—94535
conducting fluid, finite amplitude overstable convection, stability *(German)* 79—41751
conducting fluid, heated below, stability in parallel mag. and gravit. fields 77—7472
conducting fluid in porous box, thermohydromag. stability and onset of convection 77—62308
conduction-convection problems, error growth for explicit difference schemes 80—92017
conductive-convective transient heat transfer, finite-element method 79—3888
cone, convective mass transfer, in nonlinear viscous field, rel. to heterogeneous reaction kinetics 77—55103
confined thermal convection driven by non-uniform heating from below, boundary layers 80—87769
conservation eqns., skew upstream differencing schemes 77—3822
contact binary stars, possibility of convective energy transfer between components *(Russian)* 77—17615
convection in numerical fluid dynamics, tensor viscosity method 79—72888
convection-rolls, two-dimens., stability, temp. depend. viscosity 79—32507
convective combustion of disperse systems 80—53835
convective difference schemes and Hermite interpolation 77—68368
convective diffusion problems, finite element solns., Navier-Stokes eqns. 80—1583
convective dynamo, models for planetary and solar magnetism 78—89090
convective flow, numerical modelling 79—68695
convective heat transfer, with conjugate boundary conditions *(Russian)* 77—23956
convective instability, review 77—84226
convective plume in uniform isothermal atmosphere *(Russian)* 78—5738
convective-dispersion eqn., non-self-adjoint, finite element solns. 77—27529

convection continued
cooling efficiency in flow around wall, initial turbulence effects 80—79315
corona wind cooling of flat surface, convective heat transfer coeffs. 78—87234
cosmic rays, radially outward convection rel. to large amplitude wavetrains of neutron intensity 80—94660
Couette flow, permeable wall layer, heat transfer and temp. distrib. 78—51165
coupled conduction-turbulent convection in a circular tube 78—94691
creeping, finite-element thermal-mechanical model 77—7290
critical heat flux for forced convection boiling in heated round tubes, generalised correlation 79—68697
critical point hydrodynamics 78—59361
critical radius effect with a variable heat transfer coefficient 78—83205
cross flow field and loop recuperator with heat losses *(Polish)* 78—13888
crystal growth and materials processing, future fluid flow research, space environment possibilities 79—47622
crystalline film growth reactor, gasdynamic problems 79—83130
cumulus scale convection, effects of seeding with C black dust 77—91223
cumulus transports in tropical wave composite during GATE 79—2336
curly-viscous fluids, free convection under boundary conditions of second kind 77—75942
curly-viscous fluids, three-dimens. free convection about slender bodies of revolution 77—75943
CVD, RF plasma activated, kinetic model 78—27416
cylinder, circ., inclined, laminar 3-dimens. free convection, stability *(French)* 79—18884
cylinder, forced convective heat transfer, sound wave effects 80—43699
cylinder, heat transfer by free convection and radiation 79—14209
cylinder array, convective mass transfer with surface reaction 78—79369
cylinder array, wall attached and with tip clearance, heat transfer and press. drop 79—14394
cylinder in pulsating air-water spray, forced convective heat transfer *(French)* 79—7274
cylinder under hyperbaric conditions, rel. to diver safety 77—48760
cylinders, vertical and coaxial, theory of convection, velocity profile and heat transfer 80—59036
cylinders in crossflow, forced convection heat transfer, aspect ratio effects 80—64546
cylinders of limited dimensions in cylindrical housings, heat transfer 78—67008
cylindrical annuli, concentric, eccentric horizontal, natural convection heat transfer 79—55382
cylindrical cavity, thermal convection with uniform volumetric energy generation 78—94541
cylindrical porous medium, free convection boundary conditions, mean heat transfer 80—79302
cylindrical slab of fluid, in weightlessness condition, surface-tension driven convection *(Russian)* 78—90872
Czochralski crystal growth, heat, mass and fluid flow, computer simulation 80—104055
density stratified reservoir, selective withdrawal from line sink 77—14980
dialysis efficiency prediction using convective field theory 77—48945
diatomic gas, transient flow, temp. and conc. profiles, by rot. Raman scatt. 77—75995
diatomic gas, weak nonlinear wave propag., effect of convection, vibr. relax. 77—27623
difference schemes and Hermite interpolation 78—63268
differentially heated inclined cavity, 2-D, convective loss determ. by finite difference methods *(French)* 79—24906
diffusion and convection in parallelogram cross-section pipe with plug flow *(German)* 80—100000
diffusion flame, radiation-convection interaction 77—80231
diffusion-convection const. coeff. eqn., centred differencing, box scheme, mesh size, errors 77—7386
diffusion-convection eqn. anal. with explicit difference methods 78—62165
diffusion-convection eqn. soln. 78—90888
diffusion-convection equation, 1-D, finite elements method, weighted residuals 80—53775
diffusion-convection equation, stability of finite difference approximations 80—82730
diffusion-convection equations, finite difference scheme 78—42596
diffusion-convection partial differential equations, finite element method soln. 78—90889
diffusive instabilities in rotating elec. conducting compressible layers 80—38379
diffusively induced convection in tilted square cavity, finite difference method 77—7385
dioctyl phthalate, polydisperse, spectronephelometer studies 79—21797
discharge under transverse convection conditions 80—24272
discharging gas reservoir, thermal instability obs. 77—15016
disperse media thermal insulation, heat cond. anal. *(Hungarian)* 79—1056
distilled water, transition boiling curve on Inconel surface under forced convective conditions 80—10653
double diffusive convection, influence of third diffusing component, stability anal. 79—72889
double-diffuse convection, diffuse interface model, high Rayleigh nos. 78—90963
double-diffusive system between infinite horizontal planes, heat and salt transfer 77—39298
drill holes, vertical, natural convection effect on temp. 77—78135
drop, asymptotic evaporation, convection and Jakob number 77—59108
drop evaporation rate in forced convective flow with transverse sound fields 78—51224
drop in uniform (shear) stream, convective heat and mass exchange, $Pe \leq 1000$ 78—55683
droplet aerosol optical bleaching, influence of free convection 80—9924
droplet convection vaporization with unsteady heat transfer in circulating liq. phase 80—53771
droplets of concentrated cloud, approx. eqn. for mass and heat flux in constrained flow 77—47073
drying, heat and mass transfer, optimal control 78—67006
dryout characts. of steam generator 78—90990
duct, thermal entrance region, laminar forced convection, finite-element soln. 80—10118
duct, vertical, laminar steady flow, combined forced-free convection, finite element anal. 79—27637

convection continued
  duct flow, turbulent convective heat transfer 78—94719
  duct wall cavities, heated bottom surface, forced convection heat transfer 80—6048
  ducts, non-circular, forced convection heat transfer problems 80—64557
  ducts and pipes intricately shaped cross section, heat transfer, Laplace and structural method 78—83477
  Dufour's effect and hydrodynamic stability *(French)* 78—30284
  dust laden gas in channel, combined heat transfer 78—91031
  dust-liquid channel flow, with varying inlet temp., transient forced convection soln. 78—87375
  Earth, convective stability of upper mantle, viscosity jump effect 77—70620
  Earth's crust, fault zone model, convection fluid dynamics 79—34778
  Earth core, Gruneisen parameter reevaluation rel. to adiabatic circulation 79—39685
  Earth deep mantle convection and lithosphere basal shear stress, roles in plate tectonics 78—57188
  Earth interior, convection models having multiplicity of large horizontal scales 79—16430
  Earth interior, convective stability with radioactive heat sources 77—9381
  Earth lower mantle, convection rel. to geoid 80—31023
  Earth lower mantle, lithospheric slab penetration beneath Sea of Okhotsk 77—73700
  Earth mantle, Benard problem with viscosity depend. on temp. and press. 78—69317
  Earth mantle, convection and subcrustal stresses under Australia 80—72484
  Earth mantle, convection pattern and stress system under African plate 77—81859
  Earth mantle, convection shaping by tidal bulge, rel. to global tectonics 78—32048
  Earth mantle, convective instability of many-layered models 79—25216
  Earth mantle, creep laws 78—69305
  Earth mantle, creep rate, influence of natural radioactivity 79—92520
  Earth mantle, flow pattern and thermal structs. evolution beneath subduction zone 80—56440
  Earth mantle, geodynamic consequences of Nd-Sr isotopic correl. 79—92512
  Earth mantle, nonNewtonian theory *(German)* 77—70631
  Earth mantle, parametrised convection model rel. to Earth thermal history 79—16429
  Earth mantle, radiogenic heating in convecting mantle rel. to oceanic bathymetry flattening 80—85642
  Earth mantle, roll cell convection under Pacific plate 78—73345
  Earth mantle, simple tectonic plate model 79—25221
  Earth mantle, single-cell convection rel. to geoid 77—60362
  Earth mantle, solid-state convection rel. to Earth thermal evolution 80—89988
  Earth mantle, spin-symmetric convection rel. to Phanerozoic plate tectonics 78—92812
  Earth mantle, two-dimensional flow beneath rigid accreting, lithosphere 79—12102
  Earth mantle, two-scale convection rel. to global gravity anomalies 78—85528
  Earth mantle, two-scale flow model rel. to plate tectonics 78—73348
  Earth mantle, viscoplastic convection with phase transitions and shearing processes 78—3738
  earth mantle connection, numerical anal. 80—51371
  Earth mantle convection, countercurrent accompanying descending Pacific lithosphere beneath Japan *(Japanese)* 80—94514
  Earth mantle convection, influence of moving lithospheric plates 79—74880
  Earth mantle convection, seismic focal mechanisms and thermal boundary layer 77—17070
  Earth mantle convection and stress field under Pacific plate, from geopot. harmonics 77—9393
  Earth mantle convection model, plate tectonics mechanism 77—81860
  Earth mantle convection models, laboratory expt. 77—9396
  Earth mantle discrete plumes, formation of discrete islands in linear island chains 78—44796
  Earth mantle plume, fluid-dynamic model of ascending flow 80—12370
  Earth mantle subsolidus convection and cooling, lower mantle viscosity constraint 77—9384
  Earth mantle two-scale convection and global gravity anomalies 77—17067
  Earth mantle vertical and horizontal motions, polymorphic phase boundaries effects 77—9395
  Earth plasma sheet, magnetised plasma slow convection theory 80—109312
  Earth thermal history model with parameterized convection 80—26470
  Earth upper mantle, finite deformation during fluid flow 79—92519
  Earth whole mantle convection rel. to plate tectonics 77—44957
  EHD, convective instability in dielectric fluid between two coaxial cylinders 80—74994
  EHD augmented baking, corona wind impingement effects 78—87235
  n-eicosane, freezing, control by natural convection 80—39262
  electrically conducting fluid, laminar flow mass transfer at high Peclet numbers 80—43784
  electrically conducting fluid, MHD natural convection flows, buoyancy effects 78—18351
  electrically conducting rarefied gas, oscill. flow, past vertical porous plate, free convection 78—90830
  electro-osmotic enhancement of the neutral tracer transfer through a capillary membrane 78—3371
  electrochemical cell, convective diffusion eqn., computer soln., numerical methods 77—16830
  electrodiffusion problem solution for arbitrary system of singly charged ions 80—21300
  electrohydrodynamics, inversely normalised frequency, rel. to Prandtl number 79—23369
  electrolytic cells, gas sparged, mass transport anal. 80—24004
  electrostatically assisted, steel plate cooling meas. 80—69628
  electroviscous effects on convective heat transfer in coaxial horizontal channel 79—77100
  emissivity meas. by thermoreceiver/gas heat exchange 77—22552
  energy stability of a natural convective flow in a horizontal annular space 79—68815
  enhancement of heat transfer, review 79—1196

convection continued
  entrainment from body surface under convective aerodynamic heating, numerical soln. 79—81949
  entrance region flow in a vertical cooled pipe with variable viscosity 79—7409
  ethyl alcohol, free convection on turbulent horizontal layer, effect of thermocapillary forces 79—98722
  Eulerian and Lagrangian renormalization in turbulence theory 78—9629
  evolution systems and convection-diffusion, stiffness and stability, Gershgorin theory 80—77626
  external noise effect on transition to turbulent convection 80—96263
  extrudate swell, thermally induced, Galerkin method 80—79312
  F-region, convection and scintillation rel. to aurora 77—87158
  F-region, convection vortices rel. to neutral wind southward midnight surge 77—33233
  F-type star, main sequence, convection and photospheric granulation 80—90417
  farmhouse heating solar energy collection and thermal storage system 79—57482
  ferromagnetic colloid, natural convection, mag. field effects *(Russian)* 77—62307
  ferromagnetic convection in crossflow over a cylinder, heat transfer rate 80—1558
  ferromagnetic fluid in inhomogeneous mag. field, thermal convection 80—1559
  ferromagnetic fluids, convective heat transfer 79—98725
  ferromagnetic suspensions, convective heat transfer and thermophysical props., mag. field effects 79—77264
  film boiling on sphere, in forced convection 79—32211
  film condensation, along vertical plate in enclosed chamber, effect of non-condensable gas 77—80703
  fin array, shrouded, with, without tip clearance, laminar heat transfer 79—55376
  fin heat loss, temp. depend. thermal cond. and tip heat loss 79—72780
  fin in boiling water, convection and heat transfer coeffs. 80—19219
  fin thickness for an optimized natural convection array of rectangular fins 80—5915
  fin with internal heat generation, convective loss, temp.-depend. cond., perturbation approx. soln. 78—5633
  finite amplitude Benard convection in cylindrical container, radius effects 79—81877
  finite amplitude Benard convection in shallow cylindrical container 78—38325
  finite amplitude three-dimensional, in cubic box of fluid-saturated porous material 79—55373
  finite amplitude two dimensional Benard convection, in finite rot. system, weakly nonlinear theory 78—83394
  finite element anal. 77—89115
  finite element analysis, book contrib. 79—32523
  finite element method anal. 78—18148
  finite element method in fluid mechanics, book contrib. 79—32521
  finite element methods, book contrib. 79—32522
  finite medium freezing (melting), variational anal., radiation and convection effects 80—38244
  finite-amplitude convection in compressible medium, appl. to solar supergranulation 79—88637
  finite-amplitude thermal convection and geostrophic flow in a rotating magnetic system 80—87813
  finned assemblies, dimensions effects on heat flowrate, free convection to condensation 80—74714
  fins, convective, heat transfer *(German)* 79—76945
  fins, nonlinear problems, 1-D conduction, initial value problem 80—83726
  fins optimisation, circular, with heat generation, using variational technique 77—65658
  fire in polytropic atmosphere, gas flow in convection plume *(Russian)* 78—96262
  fire plume, turbulent, reaction rate, air entrainment, radiation 78—35682
  fission reactor HCDA, natural convection heat transfer in fuel debris bed cooled at top and bottom 79—93785
  flame, laminar mixed-mode forced-free diffusion type, on vert. burning fuel slab 78—91033
  flame propagation, natural convection effects 80—53882
  flames, convection-diffusion coupling model 77—7481
  flames, convective mass transfer, appl. to air pollutants distrib. *(German)* 79—52662
  flat plate, in forced flow, approx. method for heat transfer calc. 78—94682
  flat plate boundary layer in porous medium, free convection, similarity solns. 78—75199
  flat vertical plate, transient and steady state numerical solns. in natural convection 80—14701
  flat vertical plate, transient natural convection in air 80—64556
  flow stabilisation in vertical layer by permeable partition 80—14699
  flow-through reservoir, vel. and temp. fields, num. simulation 77—17152
  flows in spherical shell, bifurcation and stability 80—28507
  fluctuating boundary layer, at horizontal plate, free and forced convection 78—30277
  fluctuating flow over semiinfinite plate, buoyancy effects 77—80152
  fluid, in porous sintered metal, heat transfer in forced convection 77—55084
  fluid dynamics, truncation error estimation due to upstream differencing, consistency check 79—23294
  fluid heated from below, Bernard problem with perturbed lower wall 80—79320
  fluid in inclined slender slot, stability depend. on rad. and convective boundary conditions 79—86513
  fluid layer, selection mechanisms for convective motion pattern form. 78 54316
  fluid layer, turbulence from Rayleigh-Bernard instability 78—42605
  fluid layer, two-component, Soret effect on thermal instability 77—11185
  fluid layer between co-axial cylinders, instability of natural convection 80—64558
  fluid layer heated from below, thermal disturbance propag. 79—32464
  fluid layer overlying layer of porous medium 77—68587
  fluid layer stability, under general convective boundary conditions 78—94683
  fluid layer stability to convection with non-volumetric energy sources 80—38406
  fluid layer with internal heat sources 78—38319
  fluid motion stability, book, part II 77—3811

convection continued
- fluid saturated porous media, 3-dimens. and multicellular steady and unsteady convection 79—94615
- fluid-saturated porous layer with heat source, thermal convection onset 79—13406
- fluidised bed, high-temperature, radiant, conductive-convective components of external heat exchange 80—43709
- fluidised bed, rate of heat transfer from freely-rising slug of hot gas 80—96307
- fluids with internal rotation, microconvective heat, mass transfer processes 79—86435
- forced, from gases and liquids to circular cylinder in crossflow, correlating equation 77—80160
- forced, heat propagation eqn. *(Italian)* 78—83375
- forced, laminar, wedge flow with separation use of perturbation method 80—1523
- forced, rot. bodies with non-uniform surface temp. 79—23315
- forced, turbulent, in square cavity, shear effect 79—1180
- forced and free convection in laminar flow over plate 80—24005
- forced and free convective flow past a semi-infinite vertical plate 79—37286
- forced and free convective heat and mass transfer *(French)* 80—48689
- forced and natural convection in pipe entrance region 77—42814
- forced convection, over horizontal plate, buoyancy-induced streamwise press. gradient effects 77—58681
- forced convection along vertical cylinder with uniform surface heat flux, buoyancy effects 77—15026
- forced convection boiling, heat transfer correlations *(German)* 80—53781
- forced convection boiling heat transfer, Dengler and Addoms concept 78—1546
- forced convection flow and heat transfer of compressible fluid in porous medium *(French)* 78—30354
- forced convection heat propagation eqn., singularity theory *(Italian)* 79—18670
- forced convection heat transfer at inclined plates, solar collector appl. 78—30285
- forced convection heat transfer from cylinder in cross flow, turbulence intensities 79—1190
- forced convection heat transfer in horizontal layers, buoyancy effects 78—90901
- forced convection heat transfer in porous medium with Joule-Thomson effect 77—89198
- forced convection in a plane channel with recesses 80—19392
- forced convection in annuli, experimental study *(Italian)* 79—37322
- forced convection in annuli and rod bundles with variable heat flux distribution 78—94082
- forced convection in channel flows, turbulence, review 79—1195
- forced convection in flows through rows of surface protrusions 78—94732
- forced convection in HF EM fields 77—39354
- forced convection in presence of external mag. field, similarity soln. group theoretic approach 79—77266
- forced convection in two-phase flow from jets, mass transfer near interface *(German)* 80—53782
- forced convection quench data rel. to steady-state nucleate boiling data 78—90995
- forced convection with chemical reactions, turbulent shear flow mixing, numerical modelling 79—1272
- forced convection within straight noncircular ducts 78—90878
- forced convective flow from spheres 79—1189
- forced convective laminar heat transfer in annulus 80—48688
- forced laminar convection flow on inclined surfaces, buoyancy force effects 80—6046
- forced- and free-laminar joint flow past flat plate 77—47002
- forced-convection boiling upflow system, instabilities in parallel channel, nonlinear model 77—57724
- forced-convection heat transfer from irregular melting wavy boundaries 80—38389
- free, between two long vertical thin plates moving in opposite directions 80—28503
- free, from sphere in slightly thermally stratified fluid, streamlines 78—5781
- free, horizontal cylinder heat transfer to air, water and Si oils, correlation eqns., viscous dissipation 78—5632
- free, in horizontal eccentric annular channel 78—38310
- free, in vert. rectangular enclosure, Gill's soln. consts. determ. 79—50728
- free, transient and steady-state, negligible effects of temp.-depend. props. 78—5634
- free air/water convective flow confined by 2 parallel vertical walls, variable fluid props. 79—55369
- free and forced convection, heat and momentum transfer with opposing flow 80—6061
- free and forced convection flow in rot. channel bounded by permeable bed 79—23366
- free atmospheric convection, rigorous formulation using matched asymptotic expansions *(French)* 77—65740
- free connection heat transfer from isothermal spheroids, thick boundary layer and turbulence effects 77—15022
- free convection, fluctuating boundary layer flow 77—11183
- free convection, vertical and horiz. temp. gradients, oscill. modes and Prandtl number 77—89122
- free convection 2D flow, steady state, finite element anal. method 77—75910
- free convection about rectangular prismatic cryst. growing in soln. 80—19382
- free convection across inclined air layers with one surface V-corrugated 79—32198
- free convection along nonisothermal vertical flat plate, soln. technique 77—58682
- free convection and heat transfer from inclined isothermal plate, local nonsimilarity soln. 80—38403
- free convection and radiative transfer, at vertical plane surface 78—55645
- free convection at low Rayleigh number in two-dimensional cavities 79—64660
- free convection between horizontal concentric cylinders in a slightly-thermally stratified fluid 79—59972
- free convection boundary layer flow and heat transfer, variational technique 80—106796
- free convection boundary layer on arbitrary shaped bodies in saturated porous media 80—24009

convection continued
- free convection boundary layer on flat plate due to small temp. fluctuations 79—64663
- free convection boundary layers on cylinders of elliptic cross section 78—90877
- free convection effect on Stokes problem for vertical plate in elasto-viscous fluid 78—67226
- free convection effects on MHD accel. flow past vertical porous limiting surface 80—23996
- free convection effects on oscillatory flow past infinite porous vertical limiting surface 79—92751
- free convection effects on the Stokes problem for an infinite vertical plate 78—90879
- free convection flow, spectral energy distrib. in transition region *(French)* 79—64651
- free convection flow between heated vertical parallel plates, quasilinearization 80—92148
- free convection flow between two containers at different temperature *(German)* 79—81984
- free convection flow from horiz. circ. cylinder with harmonically oscillating temp. 79—23323
- free convection flow in circular pipe, correction to previous paper 80—28504
- free convection flow over plate induced by chemical diffusion and reaction 78—18358
- free convection flow past vertical porous plate set in impulsive motion 80—69818
- free convection from instantaneous heat source in viscous fluid 79—14210
- free convection heat and mass transfer on finned tubes 77—39284
- free convection heat transfer from vertical thin wire to air, laminar-turbulent transitions *(Japanese)* 80—92152
- free convection in an enclosure 77—80162
- free convection in bounded vol. with heating from above 79—14211
- free convection in inclined air layers heated from below 80—38396
- free convection in laminar boundary layer along rot. plate, nonsimilarity solns. 77—31307
- free convection in photoabsorption in liqs., gases and plasmas 77—11191
- free convection in rectangular enclosures filled with fluid and with porous media, review 80—79115
- free convection in Stokes' problem for infinite vertical limiting surface, mass transfer effects 80—28501
- free convection laminar flow, viscous dissipation and pressure stress effects importance 78—63428
- free convection loop embedded in heat conducting solid, heat transfer 80—96257
- free convection loops, dissipation effects in laminar and turbulent flow 80—19372
- free convection melting, Prandtl no. power exponent 77—89116
- free convection near wires in supercritical press. of CO_2 77—68584
- free convection past circular cylinder, curvature effects 77—31308
- free convection suppression, inclined air honeycomb, radiative coupling 77—58684
- free convection suppression, rectangular honeycomb, tilt and horizontal aspect ratio effects 77—58686
- free convective flow around cylinders near rigid walls, finite difference soln. 77—51053
- free convective flow in porous medium, longit. vortices, onset, linear stability anal. 78—94813
- free convective heat tranfser at a vertical semiinfinite plate 78—79318
- free convective heat transfer, external surface of vertical isothermal cylinder 78—83390
- free convective heat transfer from inclined cylinders, mean rates and buoyancy force components 77—42837
- free convective heat transfer in fluid confined by wavy wall 78—55642
- free convective heat transfer in liq. saturated porous bed at high Rayleigh number *(German)* 80—33605
- free convective heat transfer in near-critical region from vertical surfaces 79—23314
- free convective laminar flow, non-uniform gravity effects, finite difference soln. 80—33604
- free laminar convection, three-dimens., about surface, numerical anal., visualisation *(French)* 78—87343
- free MHD convection, near plane and axisymmetric bodies, approx. soln. *(Russian)* 78—94832
- free MHD convection, near plane and axisymmetric bodies 79—94728
- free thermal convection in a vibrational field under conditions of weightlessness 80—87773
- free-convection boundary layer on an isothermal horizontal cylinder 79—41688
- free-convection flow past an accelerated vertical infinite plate 80—92154
- free-forced convection from a heated cone, cross flow transition, similarity soln. 78—90892
- free-forced convection from a heated longitudinal horizontal cylinder 80—10244
- Free-forced convection in the entry region of a heated straight pipe 78—90883
- freestream turbulence statistical characts., convective heat transfer calc., boundary layer eddy viscosity 78—83366
- freeze-drying of food models, heat and mass transfer 79—1098
- Freon-11, forced convection boiling heat transfer in vertical annular passage 79—32509
- frontogenesis caused by cumulonimbus convection 77—21845
- frost formation, under forced convection, heat transfer and mass transfer *(Japanese)* 77—58533
- frustum of cone, laminar natural convection flow 80—53768
- fully developed laminar flow with internal heat generation between horizontal parallel plates, thermal instability 78—90899
- fully turbulent free convection heat transfer, surface renewal approach 80—14697
- fundamental convective heat transfer, entropy generation 80—38411
- gas, boundary layer combustion, combined heat transfer 78—91029
- gas, circulating, forced convection through porous cavity, solar heating *(French)* 80—69626
- gas, horizontal layer, oscillatory instability of convective motion 77—54974
- gas, rotating, convective instability in gravitational field 79—27642
- gas bubble dissolution (growth), convective transport effect 80—87792
- gas bubble motion in power-law fluid, heat and mass transfer with chemical reaction 79—77227
- gas filled porous media, free convection heat transfer 79—98796

convection continued
gas flow past surface, interaction of radiation with convection *(Russian)* 80—99994
gas flow patterns in furnaces, composite heat transfer 78—90677
gas injection through loose layered material, heat transfer, free convection effects *(Russian)* 79—18953
gas phase transport, definition of hydrodynamic regime acquired during crystn. 79—51029
gas pipe flow, turbulent Graetz problem, Joule-Thomson effect 78—75204
gas plane flows in presence of weak supply of energy *(Russian)* 79—32498
gas tube flow, radiative and convective transfer 78—94576
gas-filled cavities with baffles, free convection 78—94702
gas-liquid flow, hydrodynamics and transport processes, electrodiffusion modelling method 79—90309
gas-porous electrode, mass exchange in transport zones 77—32801
gas-solid dispersions, heat exchange in uniform elec. field 77—11273
gas-solid suspension flow through packed beds, convective heat transfer 79—4075
gaseous configuration of star under convective equilibrium, generalised integrals involving elliptic functions 77—71107
gases, stresses produced by temp. and conc. inhomogeneities 77—31419
GCFR radial blanket velocity and temp. distrib., buoyancy effect 79—9678
geothermal reservoir, effect of magma dike intrusion on free convection 78—7599
giant stars, late type, nonlinear coupling between pulsation and convection 77—13356
glacial ice, melting in sea water, heat and mass transfer *(German)* 80—33606
glass, melting in fire-heated tanks, modelling *(Polish)* 80—96633
glow discharge with convective cooling, plasma column thermal instability 77—24232
glycerol, natural convection from temp. fields in spherical partially filled vessel 80—1561
Graetz problem in horizontal isothermal tube, natural convection effects 77—75911
granitic magma of Bushveld Complex, convective mixing rel. to crystallisation history and trace element abundances 80—109145
gravity wave system, induced by convection 79—88423
grey bodies system, closed combined radiation convection heat transfer, two-layer gas model 78—75052
groundwater, thermal convection in porous medium 77—33109
groundwater vertical movement, correction to terrestrial heat flow meas. 80—3969
central Gulf of California, thermal waters discharges rel. to terrestrial heat flow meas. 80—3968
Haley-Shaw cell, convective motions, theory and expt. 78—42607
Hall and ion slip currents effect on heat transfer in MHD fluid in channel 79—27702
heat and mass transfer in porous media subject to fires 79—86507
heat and mass transfer interaction, around vertical flat plate 77—58669
heat and moisture transfers with const. heat flux *(French)* 80—33582
heat convection in channel flow, temp. distrib., variational soln. 79—72886
heat exchange, convective, in fibrous materials at elevated press. of gaseous medium 80—19217
heat exchanger, tubular bundle type, with longit. drive, forced turbulent convection *(French)* 79—86333
heat island, numerical results, truncation errors 79—10447
heat loss meas. from solid surface to airstream 79—37140
heat pipe, high temp., subsonic vapour flux, heat exchange and friction 77—75779
heat pipe, spectroscopic, operation 80—106708
heat source driven turbulent convection between 2 rigid plates at arbitrary Prandtl number 80—69829
heat storage, periodic, heat-carrying fluid and storage material transport kinetics 79—3901
heat transfer, local, cross flow, free convection and free stream turbulence effects 77—15009
heat transfer, through boundary layer, nonisothermal surface 78—46965
heat transfer, transient, during natural convection *(Russian)* 77—68367
heat transfer and flow instability of natural convection over upward-facing horizontal surfaces 78—94698
heat transfer augmentation, convective, effect of mech.-produced unsteady boundary layer flow 78—71261
heat transfer augocentation thermal entrance regions using thermal instability 79—81887
heat transfer bibliography, Japanese works 79—23317
heat transfer coeff. from gas to thermocouple meas. 78—18149
heat transfer coefficient measurement using heat-flux sensor, error anal. 79—94463
heat transfer conference, Aug. 78, Toronto, Canada 78—90624
heat transfer crisis in annuli with hot spots 77—39283
heat transfer from cylinder submerged in non-Newtonian fluid 79—1221
heat transfer from cylinders in vertical cyclone chambers 78—90870
heat transfer from porous sphere in low Reynolds number flow 78—59482
heat transfer from vertical surface to CO_2 at supercritical press. 77—68585
heat transfer in laminar region, horizontal and inclined cylinders 80—99915
heat transfer meas. using local heat flux sensor, appl. to heat transfer in supersonic flow 79—82015
heat transfer with diffusion, finite element anal. 79—4011
heated air, ascending bubbles, interaction with ambient cold air 79—84362
heated body in perfect incompressible fluid, convective heat and mass transfer 80—43698
heated curved wire, free convective heat transfer, numerical study 80—69835
heated cylinder in radial elec. field, corona characts. power freq. variation effects 78—87538
heated disc with impinging jet, saturated forced convection boiling, CHF upper limit 79—81891
heated wires, liquid surrounded, surface thermal state under boiling, from large applied heat flux 79—81690
heating surfaces, furring, mass transfer, convective heat transfer, mathematical model *(German)* 77—23854

convection continued
Hele-Shaw cell, permeability determ., geothermal modelling appl. 78—59466
Hele-Shaw cell, supercritical convective motions, equilib. stability boundary, porous flow simulation 80—33583
helical coiled tubes, laminar convective heat transfer 78—94678
helically rib-roughened tubes, forced convection heat transfer and friction characts. 80—96258
heterogeneous liquid stream, stress diffusion effect, molar diffusion coeff. 78—79338
HGTR core, multiregional coupled conduction-convection model 78—94083
high Prandtl number convection, geophs. appl. 79—81875
high Prandtl number convection, thymol blue visualisation method 80—6182
high subsonic nozzle flows, pressure waves from convection of temp. disturbances 80—6125
homeotropic nematic films heated from below, overstability and inverted bifurcation 79—77501
homogeneous isotropic turbulence, inertial convective region, scalar fluctuation spectrum *(German)* 80—92120
horizontal channel, unsteady natural convection 79—41554
horizontal channel with differentially heated ends, forced and free convection heat transfer 80—6045
horizontal circular cylinder, mixed convection, boundary layer effects 77—15011
horizontal concentric annuli, free and forced convection heat transfer for fully developed laminar flow *(Japanese)* 78—30150
horizontal cylinder, laminar free convective heat transfer 78—75130
horizontal cylinder, suddenly heated, onset of manifest convection *(German)* 80—53780
horizontal cylinder with different end temps., natural convection, jets 80—99996
horizontal cylinders with asymmetric boundary conditions, natural convection numerical anal. 77—39282
horizontal cylindrical surface, free convection, local nonsimilarity anal. 78—75120
horizontal fluid layer, internally heated, heat transfer and stability props. of convection rolls 78—14015
horizontal fluid layer in porous medium, convective instability, critical Rayleigh number 80—64564
horizontal layer, crit. slowing near Rayleigh-Benard convective instability 79—18889
horizontal pipe subjected to external convection and radiation, laminar forced convection 80—79307
horizontal porous layer, with internal heat sources, thermal convection 77—84247
horizontal porous layer of two different media flow patterns and convection 80—10303
horizontal porous layer with timewise periodic boundary conditions, stability and convection 79—81965
horizontal ribbon growth from melt, forced convection heat flow effects 80—107079
horizontal rotating fluid layer, heated from below, convection rolls nonlinear props. 80—6066
horizontal tube, fully developed laminar flow, combined free and forced convection, expt. 78—87391
horizontal tube turbulent flow secondary current struct., thermogravitation effects 78—90902
horizontal wire, heated, heat transfer expts. 79—32190
hot film probe in reversing flow, forced convection, finite difference soln. 80—14702
hot gases, convective heat transfer coeffs. to solid surface, moving thermocouple meas. 80—42230
HTGR piping, heat transfer characts. of horizontal annular insulation layer *(Japanese)* 79—26520
human body; convective heat loss 77—48759
human body, rel. to diver safety, evaluation of meas. under hyperbaric conditions 77—48760
human convective heat loss assessment in cold water 78—81093
humid atmosphere, water droplet vaporis. model with natural convection 78—33999
humidity stratification, effect on conditions for free convection *(Russian)* 79—10562
hydrodynamic fluctuations near threshold of Benard convection 78—26099
hydrodynamic instabilities and turbulence, flow states, examples and meas. methods 80—92116
hydrodynamic instability at onset of convection, stochastic treatment 77—19590
hydromagnetic convection, thermally driven, in rapidly rotating sphere 80—14548
hydromagnetic convection post marginal state, amplitude determ., Landau's conjecture 79—77286
hydromagnetic free convection flow, similarity solutions 79—27639
hydromagnetic free convection flow in Stokes problem, for porous vertical limiting surface with const. suction 80—90328
hydromagnetic thermal convection instability, effect of suspended particles 79—53709
hydrothermal convection, theoretical study rel. to Cyprus ophiolitic sulphide ore deposits origin 79—29761
hydrothermal flows, two-phase, in permeable media, struct. 80—85693
hydrothermal systems, convective heat fluxes from cooling plutons 78—36206
hypersonic laminar near wake of blunted cone, convective heat and mass transfer 79—98752
hypersonic shock layer, screening of selective heat radiation in boundary layer *(Russian)* 79—32497
ice layer profile on const. temp. plate in forced convection, laminar to turbulence transition regime 80—24007
immiscible liquid horizontal layer, convective stability 77—7392
impulsively started vertical plate, mass transfer and free convection currents 80—64567
impurity diffusion coeff. in convecting fluid 78—5747
inclined flat plate with isothermally heated surface downwards, natural convection heat transfer investigation 79—10563
inclined fluid layer, conduction and natural convection regimes *(French)* 78—42514
inclined fluid layer, double diffusive instability, secondary convecting layers 80—92112

convection continued
- inclined surfaces, wave instability of laminar mixed convection flow 80—69837
- incompressible laminar transient forced convection heat transfer in circular pipe 79—50798
- incompressible viscous oscill. flow past porous sucking vertical plate 78—30283
- Indian Ocean floor, geothermal convection through oceanic crust and sediments 79—79812
- induced turbulent flow and natural convection, combined effect heat transfer rates 79—90243
- inert gas mixtures, internal forced convection, numerical calcs. 77—47005
- infinite Prandtl number thermal convection in a spherical shell, Earth mantle 80—59033
- infinite vertical limiting surface with suction, Stokes free convection effects 80—19364
- infinite vertical porous plate, unsteady free convective elastica-viscous flow, viscous dissipation heat 80—24012
- inhomogeneous medium, two-dimens., light propag. problems rel. to thermogasdynamic waveguide development 80—32914
- injection of hot-fluid against plate, laminar flow 79—32502
- instability, crit. slowing, config. inversion acoustic obs. 78—34133
- instability and convection in fluid layers: a report on Euromech 106 79—68783
- instability in thermal entrance region of heated channel 77—42812
- instability of convection rolls in inclined layer 77—58674
- instability of self-similar spherical expansion into vacuum 80—28490
- interfacial boundary layer in water tank, heat transport, thermal struct. 78—9638
- interfacial cellular convection, effect on mass transfer enhancement 80—14690
- interferometric measurement of convective heat transfer coeffs., errors 77—71315
- interstellar medium, absolute and convective instabilities 80—98539
- ion-selective membrane, flicker noise and turbulent convection in depleted layer 78—48692
- ionosphere, auroral convection over 60°≤Λ≤75° from Millstone Hill incoherent scatter 80—67454
- ionosphere, elec. fields and plasma convection in dayside auroral oval 80—98501
- ionosphere, latit. struct. of convection flow on November 21, 1975, Chatanika obs. 77—87160
- ionosphere, polar cap connection during Tordo 1 polar cusp Ba plasma injection expt. 78—77402
- ionosphere, rapid subauroral ion drifts obs. by Atmosphere Explorer C 80—4188
- ionosphere, rocket-borne meas. of ion convection in dayside aurora 78—77391
- ionosphere polar F-region, plasma convection, drifts and winds 77 33274
- irreversible transport processes, noncoupled, nonstationary, classical variational principles 78—4567
- isothermal circular cylinder, unsteady combined convection in viscous incompressible flow 79—55391
- isothermal concentric spheres, natural convective heat exchange 80—64340
- isothermal horizontal circular cylinder, laminar free convection, thick boundary layer 80—64566
- isothermal vertical plate, natural convection, leading edge geometry effects, expt. 78—87346
- isotope centrifuge, effect of thermal convection on separative power, numerical anal. 78—58500
- jet, aerodynamically generated noise *(French)* 77—75951
- jet, buoyant, turbulent in cross flow, finite difference method 78—90907
- jet, confined in centrifugal force field 79—98720
- jet, noise radiated from convecting quadrupoles, flight effects 79—32601
- jet array impinging surface, convective heat transfer 78—90953
- jet incident on plate, convective diffusion in boundary layer 78—67242
- Jharia Gondwana sedimentary basin, India, groundwater movement rel. to geothermal meas. 80—98276
- Jupiter, CO thermochemistry, implications for atm. convection 78—36500
- kinetic theory, convective diffusion to a particle in a fluid with linear kinetics 80—69943
- Krogh tissue cylinder, transient convective mass transfer 80—3598
- laminar, combined free and forced, in internally finned square ducts 77—51060
- laminar assisting forced and free convection, comprehensive correlating equation 77—51051
- laminar boundary layer, transient ccnvective heat transfer 78—30286
- laminar boundary layer flow convection anal. by integral and characts. methods 78—34137
- laminar boundary layer on moving surface under combined action of free and forced convection *(Ukrainian)* 79—50695
- laminar channel flow, heat transfer 78—79317
- laminar circular jets, friction heat effect on temp. distrib., anal., forced convection 80—10279
- laminar combined free and forced convection across horizontal cylinder, flow and heat transfer characts. 77—84245
- laminar convection, heated vertical surface, boundary-layer thickness and Prandtl number 78—51161
- laminar convection in forced upflow, with radiative transfer 78—47064
- laminar cyclone, free and forced convection 78—55548
- laminar eddy motion, in flat horizontal fluid layers, resulting from thermal lift *(German)* 77—11171
- laminar film boiling heat transfer, thermal conductivity and convection effects 80—74864
- laminar film condensation of mixed vapours, combined body force and forced convection 78—51162
- laminar flow, within Trombe wall channel 79—86397
- laminar flow between coaxial cylinders *(French)* 78—38314
- laminar flow in flat channel, conjugate steady heat exchange 77—75919
- laminar flow in internally finned tubes 78—94724
- laminar flow in vertical tubes, buoyancy effects 78—5722
- laminar flow over plate, convective heat transfer 77—39290
- laminar flow pattern, press., enthalpy, vel. from point source of heat 78—79316
- laminar flow structure, in vertical free convective cavities 78—34125
- laminar forced convection between concentric spheres, num. soln. 77—42831

convection continued
- laminar forced convection to turbulent free convection transition over heated plate 79—32516
- laminar free convection, boundary layers, similar solns. 77—27524
- laminar free convection boundary layer heat transfer, series solution predictive capability 78—71335
- laminar free convection duct connecting fluid reservoirs 79—55421
- laminar free convection flat plate problems, new formulation *(Italian)* 79—46302
- laminar free convection flow between two parallel vertical walls 77—47010
- laminar free convection flow with and without heat sources through coaxial circular pipes 79—86431
- laminar free convection from upward-facing inclined flat plate 77—7395
- laminar free convection in 1-D solar induced flows, theory 80—3495
- laminar free convection in small aspect ratio rectangular enclosures with isothermal boundary conditions 80—6060
- laminar free convection past heated vertical plate, leading and trailing edge and discontinuous temp. effects 77—15028
- laminar free convection with uniform heat flux on vertical plate *(French)* 77—39292
- laminar free convective flow, three-dimens., num. soln. 77—42826
- laminar free convention boundary-layer in three-dimensional systems 80—33587
- laminar gas flow, heat exchange to selectively emitting liq. in radn. field 77—84343
- laminar heat transfer from perforated surfaces 78—94727
- laminar heat transfer in noncircular ducts, Schwarz-Neumann technique 77—80161
- laminar natural convection along cylinder, stability 78—1663
- laminar natural convection boundary layers on horizontal circular discs 79—77067
- laminar natural convection boundary layers on horizontal heated plates 77—7396
- laminar natural convection heat transfer from an inclined cylinder 80—33586
- laminar natural convection heat transfer to a viscoelastic fluid 78—83436
- laminar natural convection on horizontal surface 77—80159
- laminar natural convection over a slender vertical frustum of a cone *(German)* 79—77116
- laminar plume above a line heat source in a transverse magnetic field 78—67269
- laminar pulsating channel flow 77—31297
- large particle fluidised beds, gas convection model of heat transfer 80—14801
- large Prandtl number fluid, convection at Rayleigh numbers up to 760000 78—42597
- large wavelength convection rolls low Prandtl number fluids 79—27643
- laser-beam induced heat and mass transfer 78—93635
- latent heat-of-fusion energy storage: experiments on heat transfer from cylinders during melting 80—6492
- layer, dense, large Biot no., heat exchange *(Russian)* 78—83400
- layer heated from below through layer of finite thermal cond. 79—68696
- layer with nonlinear density temp. relation 78—94697
- layered porous medium heated from below, onset of convection 80—33593
- leading edge effect on free-convection heat transfer 78—79319
- line thermal numerical model, initial conditions influence 78—92932
- linear convective stability, Soret effect, horizontal quiescent layer of two-component fluid 80—92144
- linear penetrative convection, boundary conditions imposed by stratified fluid 79—55404
- liquid, in vertical cylindrical cavity, sudden ambient temp. change *(French)* 77—47009
- liquid in vertical slot under turbulent flow, thermal free convection 79—98721
- liquid interfacial instability, mass transfer under high press. 79—94601
- liquid metals, flow at high temperatures through circular pipes, connection mechanism *(Spanish)* 79—37315
- LMFBR finite hexagonal bundles, laminar mixed-convection heat transfer 79—607
- local mass-transfer coeffs. meas. by holographic interferometry, vortex instability effect 78—75234
- local thermal currents on boundary surface, meas. method 77—10014
- local transfer coeffs. augmentation, in channel downstream of constriction 78—5800
- longitudinal convective fins, internal heat generation, optimization 80—9333
- Lorentz model of convective instabilities, 1-D dynamics of particle in pot. well 79—4007
- Lorenz attractor, origin and struct., appl. to specific model systems 78—29054
- Lorenz model, periodic solns. and bifurcation struct. at high R 79—81692
- Lorenz model dynamics for convective instability 80—59007
- low Prandtl number fluid, nearly insulating boundaries, two-dimensional convection rolls 80—74883
- low pressure plasma, two-dimens. turbulent convection 80—28676
- low quality flow boiling, turbulent forced convection and nucleate boiling heat transfer 80—14696
- low thermal cond. materials, anal. of optimum method of inspecting by active thermal method 78—72996
- low-finned staggered tube bank, flow and heat transfer, high Re *(German)* 78—33996
- low-velocity heat transfer to flat plate in presence of corona discharge in air 79—77112
- lunar thermal history and convection 79—84690
- lung, analytic model, Green's function for convection-diffusion eqn. 78—11684
- lung gas concentrations during air breathing, influence of gas exchange 77—12942
- RR Lyrae stars models, convection effects on radial pulsations 80—26863
- magma chambers, evidence from Cr content vars. in magnetite from upper zone of Bushveld Complex 80—56421
- magmas convective mixing, implications of density var. among mid-ocean ridge basalts 80—56460
- magnetic field effect *(Russian)* 78—26201
- magnetic field influence on convective heat transfer in feebly ionised air 79—23370

convection continued
- magnetic fluid, heat transfer, in coaxial cylinder system, numerical calcs. *(Russian)* 77—47015
- magnetic fluid, in current-carrying plate field, free vertical convection *(Russian)* 77—65806
- magnetic fluids, heat and mass transfer 80—59123
- magnetic fluids, instabilities, leading to rupture of continuity 80—59003
- magnetic flux ropes and convection 78—71399
- magnetic stars, field connection by internal circulation rel. to oblique rotator model 77—45407
- magneto-active plasma convection, two velocity hydrodynamic eqn. solution *(Russian)* 80—79459
- magnetoelectrolytic convection, accuracy of estimation method 80—14691
- magnetosphere, adiabatic plasma convection in tail plasma sheet 79—25408
- magnetosphere, connection elec. fields rel. to global distrib. of electron density in F_2-layer 77—64514
- magnetosphere, convection and empirical models of high-latit. elec. fields 77—45255
- magnetosphere, convection and field-aligned currents during weak global mag. disturbances 79—53660
- magnetosphere, high-latit. convection field, parallel elec. fields and inverted-V precip. events 77—33297
- magnetosphere, influence of convection on lower ionosphere current and wind systems 77—5386
- magnetosphere, nonstationary convection and high-energy particle prod. 77—53312
- magnetosphere, plasma convection dynamics rel. to macroscopic elec. fields 78—49238
- magnetosphere, plasma convection rel. to model current system for high-latit. mag. activity 79—92636
- magnetosphere, plasma dynamics in mag. field laboratory simulation 79—16757
- magnetosphere, plasma mantle dynamics rel. to plasma sheet form. 79—40022
- magnetosphere, polar cap convection after interplanetary mag. field becomes northward 80—94658
- magnetosphere, polar cap convection rel. to boundary mag. fields, laboratory simulation 78—57396
- magnetosphere, solar wind induced convection rel. to plasmapause struct. 77—53285
- magnetosphere convection, development of stratified precip. struct. 78—28377
- magnetosphere convection, one-dimensional gasdynamical model 78—81508
- magnetosphere convection, rel. to upper atmosphere dynamics 77—29525
- magnetosphere convection, role in global scale electrodynamic coupling of ionosphere high and low latit. regions 80—77194
- magnetosphere convection, role of particle precip. 79—25400
- magnetosphere convection, variability of S_q vars. field magnetically conjugate structs. 79—58191
- magnetosphere convection electric field, divergence rel. to auroral currents and elec. pots. and precip. generation 80—67453
- magnetosphere convection role of hot plasma 78—32297
- magnetosphere convection vel. fields, dynamics and interrelations with polar ionosphere struct. 80—4176
- magnetosphere dayside cleft, convection direction rel. to mag. field perturbations 79—40023
- magnetosphere electric convection field, model 78—89004
- magnetosphere midlatitude convection elec. fields, rel. to ring current development 78—57395
- magnetosphere plasma convection, rel. to elec. current system over auroral arc 77—33296
- magnetosphere polar cusp, convection patterns rel. to dayside magnetopause mag. merging 79—66884
- mantle convection, depth extent from seismic energy release of deep and intermediate earthquakes 80—41404
- Marangoni convection 80—66425
- marginal convection in a large rigid box 79—90257
- marine stratocumulus convection, governing eqns. and horizontally homogeneous solns. 80—56542
- marine stratocumulus convection, horizontally inhomogeneous solns. 80—56543
- Mars atmosphere, effects of suspended dust particles on radiative convective model 79—84717
- mass transfer, stationary, convective, inside drop, influence of chemical volume reaction at large peclet numbers *(Russian)* 80—28508
- mass transfer in laminar flow between two plane parallel plates 79—37321
- mass transfer measurement methods, review *(German)* 78—46959
- mass transfer with axial diffusion and chem. reaction 79—23376
- massive spherical particle, heating by radiation and convection 77—50866
- measurement, Moire pattern appl. *(Japanese)* 77—26295
- measurement by differential light interferometer with achromatic $\lambda/2$ compensation 78—87419
- medium containing heavy particles, convective stability 77—80203
- medium convection velocity vector using heat wave method 79—23183
- melting surface, air bubble evolution effect on boundary layer separation 78—67015
- Mercury, internal convection 78—12127
- mesoscale convective systems, inertial instability 80—90131
- metals, unidirectional solidification, heat flow model 80—79914
- metastable chaos, transition to sustained chaotic behavior in Lorentz turbulent convection model 80—4643
- meteorology, aspects relevant to astrophysics 78—88898
- MHD, entrance flow, vertical channel, thermal convection, linear anal. 78—38410
- MHD, nonstationary convection in plane vertical channel *(Russian)* 77—27615
- MHD, unsteady convection in vertical cylinder 79—77271
- MHD, unsteady free convective flow past infinite plate with time depend. suction 79—27704
- MHD boundary layer eqns. soln., natural convection 77—11276
- MHD channel flow, fluid with variable viscosity, free convection effects 78—14090
- MHD convection, forced horizontal flow between moving porous walls 77—68695
- MHD convection in boundary layer, overplane and axisymm. bodies, theory 79—77270
- MHD convection in horiz. layer *(Russian)* 78—26202

convection continued
- MHD convection in infinite channel 77—72361
- MHD convection with rot. spatial heat source, stability 79—4085
- MHD convective flow through porous channel with Hall and wall conductance effects 80—74993
- MHD dynamo, convectively-driven models, solar dynamo appl. 78—42668
- MHD forced convection, with transverse mag. field, surface curvature effect 77—35245
- MHD free and forced convective flow between porous plates with Hall effect 79—41763
- MHD free convection about semi-infinite plate in strong cross field, skin friction, heat transfer 77—15134
- MHD free convection effects on oscill. flow of viscous incompressible fluid past porous limiting surface 79—81985
- MHD instability-convective instability analogy, AC and DC fields *(Russian)* 77—65807
- MHD Stokes problem for vertical plate, free convection 79—18970
- MHD unsteady free convection past a hot vertical plate 78—87396
- MHD viscoelastic free convection boundary layer flow past porous plate 80—10317
- micropolar fluid flow in channels, convective heat transfer *(Russian)* 79—18920
- micropolar fluid layer between rigid boundaries, thermal instability, numerical soln. 79—68692
- micropolar fluid with stretch, convection, appl. to Earth mantle 78—51202
- midocean ridge hydrothermal systems, hot water egress thermal constraints 79—39700
- mist formation in turbulent convection field, critical supersaturation model 80—64611
- mixed, on vertical plate with unheated starting length, num. soln. 77—42827
- mixed, over semi-infinite vertical flat plate 78—55646
- mixed boundary value problem, analytic soln. 80—5909
- mixed convection, numerical anal. 78—42604
- mixed convection about a sphere with uniform surface heat flux 79—32519
- mixed convection across horiz. cylinder with uniform surface heat flux 78—30295
- mixed convection for gas mixture above flat plate 78—5636
- mixed convection from plates, flow direction effects 80—38222
- mixed convection heat transfer rates in vertical tubes, expt. 78—90897
- mixed convection on a horizontal plate with uniform surface heat flux 78—90903
- mixed convection to air in a vertical pipe 78—90896
- mixed convection universal profile 77—62255
- mixed convective flow, laminar, over horizontal plate, wave instability 79—32499
- mixed forced/free, from horizontal plate, in porous medium 77—75908
- mixed forced/free laminar convection about sphere, buoyancy effects 77—75907
- mixed free/forced convection about inclined surfaces in porous medium 77—75973
- mixed layer growth, penetrative convection in stratified fluid 78—44908
- mixed-convection heat transfer around an isothermal flat surface of finite length 78—90891
- moist convection over heated island, two-scale model 80—41492
- molecular lasers with gas pumping, temp. field calc. 79—76673
- molten materials with internal heat sources and consolidated boundaries, free convection *(German)* 80—59019
- molten reactor core debris pool, hydrodynamic instabilities and convective mixing 78—8931
- monocomponent gases, convective instabilities in closed vertical cylinder heated from below 79—77072
- monotone difference schemes for diffusion-convection problems 80—8801
- monsoon circulation dynamics 79—5559
- Moon, distortion due to convection unlikely 78—61761
- motile particles, two dimensional numerical study 77—56399
- moving horizontal flat plate, laminar boundary layer, buoyancy effects 80—74877
- moving layer, heat exchange, numerical-anal. soln. 77—7291
- multidimensional body, radiative-convective heating, unsteady temp. calc. method 78—90640
- multireaction chem. transport of solids, theoretical anal. 77—52236
- natural, between circular cylinders, with internal heat generation *(Russian)* 79—27490
- natural, from corrugated plates to air 78—38321
- natural, from vert. DC current-heated plate, linear stability anal. 78—90873
- natural, heat transfer in enclosed cavity 77—51056
- natural, in closed container, numerical simulation 78—46969
- natural, in confined region between two concentric square ducts 79—23320
- natural, in confined region between two horizontal ducts for variable fluid properties 79—23321
- natural, in porous medium, singular perturbation problem 79—94715
- natural, in presence of transverse mag. field similarity soln. 78—67197
- natural, in slightly inclined rectangular box heated from above 79—59976
- natural, in square box, by multi-point finite differences 77—89083
- natural, in turbulent vertical layer 78—42599
- natural, in volumetrically heated fluid layer, at high Rayleigh numbers 77—47006
- natural, Navier-Stokes eqn. soln. numerical stability 80—92147
- natural, nonuniform alternating electric field, influence 77—50860
- natural, on vertical heated surface, expt. *(Japanese)* 80—5912
- natural, over uniform heat flux vertical surface, higher-order approx. 78—59388
- natural, three dimens. numerical anal. in inclined channel with square cross section 80—14546
- natural, transient and steady-state numerical solns. 80—10119
- natural, unsteady, vertical plate with time depend. temp. or heat flux 77—75777
- natural convection, between nonuniformly heated plates, stability 77—58668
- natural convection, heat transfer in rectangular cavity with vertical walls of different temps. 78—67195
- natural convection, vertical isothermal surface, K-ϵ turbulence model 77—58683
- natural convection air flows, vel. meas. using laser velocimeter 79—82016

convection continued
- natural convection at a heated semiinfinite vertical plate with internal heat generation 80—23995
- natural convection boundary layer, laminar to turbulent transition, critical values for air *(Japanese)* 80—14657
- natural convection boundary layer turbulence next to heated vertical surfaces 79—68684
- natural convection film boiling, from spheres to saturated liquids, integral calcs. 78—34129
- natural convection flow, nonisothermal flat plate, numerical soln. 78—67194
- natural convection flow above heat source, instability 79—90252
- natural convection flow adjacent to vertical surface, leading edge effect 79—55389
- natural convection flow interaction over heated body 77—51059
- natural convection flows, hot wire measurements, fluid temp. and mixed convection effects 79—64817
- natural convection for three dimens. flows 78—94692
- natural convection from heated submerged cylinder 78—94704
- natural convection from line thermal source, buoyancy-induced flow 77—19603
- natural convection from spheres and cylinders immersed in a thermally stratified fluid 80—6059
- natural convection from vertical surface in thermally stratified fluid 77—15021
- natural convection heat transfer characteristics of flat plate enclosures 79—76944
- natural convection heat transfer from isothermal horiz. plates 77—7384
- natural convection heat transfer in closed gas-filled tubes 78—94703
- natural convection heat transfer in moderate aspect ratio enclosures 80—38405
- natural convection heat transfer on inclined flat plate *(Chinese)* 78—18298
- natural convection in a shallow annular cavity with differential heated walls 80—79295
- natural convection in a slightly slanted rectangular box filled with a porous medium *(French)* 80—19378
- natural convection in a vertical cylindrical well filled with porous medium 80—79297
- natural convection in air layer enclosed within cylindrical cavities 78—38317
- natural convection in air-filled enclosure 78—94707
- natural convection in closed cavity, numerical technique 79—10446
- natural convection in doubly inclined rectangular boxes 78—94708
- natural convection in enclosed cavities, finite element numerical soln. 80—1557
- natural convection in enclosure, ventilation effect on temp. 78—94705
- natural convection in enclosures, review 79—1193
- natural convection in horizontal cylindrical annulus 79—81880
- natural convection in horizontal space bounded by two concentric cylinders with different temperatures 79—68698
- natural convection in inclined hemispherical cavities 77—80150
- natural convection in open rectangular cavities with adiabatic sidewalls 77—39297
- natural convection in porous layer with permeable boundary *(Russian)* 79—18941
- natural convection in porous media and geothermal systems, r eview 79—1194
- natural convection in porous media bounded by concentric spheres and horizontal cylinders 79—68699
- natural convection in presence of heterogeneous catalytic reaction 77—84341
- natural convection in region between concentric cylinders *(French)* 78—94700
- natural convection in vertical open tube, analytical treatment 77—39289
- natural convection instability 78—14007
- natural convection loop, transient behaviour, two vert. branches with point heat source and sink 79—46163
- natural convection mass transfer along porous vertical plate 78—90876
- natural convection of air over a heated plate with forward-facing step 78—90875
- natural convection over confined horizontal plate heated from below *(German)* 77—72134
- natural convection plume above horiz. line heat source, vel. field 78—30292
- natural convection through high L/D rectangular cells, correlations 80—33603
- natural convection transport to air above heated ridge, expt. 78—94680
- natural convective flow through duct with restricted entry 79—14393
- natural convective heat transfer in vertical wavy channels 80—53774
- natural convective oscillatory flow from heated wire on axis of horizontal cylinder 77—72295
- natural convective wall plume, boundary layer eqns., higher order anal. 80—64550
- natural in spherical layer of viscous compressible gas 78—9640
- natural laminar and turbulent convection, from isothermal spheres, correlation eqn. *(German)* 80—33607
- natural laminar convection, side wall effects on heat transfer through vertical air layer 80—19377
- natural laminar convection about isothermal cylinder, Navier-Stokes eqn. soln. 80—92143
- natural laminar convection in open vertical pipe, numerical soln. method 78—5799
- natural laminar convection over cone with const. wall heat flux *(German)* 80—38414
- natural laminar convective heat transfer in triangular enclosures 80—38404
- natural thermoconvectional filtration in circular porous interlayers 78—94817
- natural three-dimensional convection, strongly implicit algorithms 80—33422
- needles, nonisothermal, forced convective heat transfer 78—90636
- nematic liquid, oscillatory convective instability *(French)* 79—1279
- nematic liquid crystal, flow in flat channel, heat transfer anal. *(Russian)* 77 72397
- nematic liquid crystal, obliquely oriented, thermal convection *(French)* 78—22643
- nematic liquid crystals, coherent neutron scatt. studies, review 79—41956
- Neptune, convective vortices rel. to equatorial flow 80—67653
- Neptune thermal evolution, convective cooling model and comparison with Uranus 78—85903

convection continued
- non-condensing gas on flat plate and horizontal tube, forced convection condensation 80—64553
- non-Newtonian fluid, forced convection, on circular cylinder, suction and slip velocity effects 78—34169
- non-Newtonian fluid, free convection from vertical plate, variable gravity force effect 77—42878
- non-Newtonian fluid, laminar forced convection heat transfer in square duct, numerical solns. 78—18318
- non-Newtonian fluid, thermal convection 78—22376
- non-Newtonian fluid duct flow, heat transfer 79—1219
- non-Newtonian fluid mixing, convective heat transfer theory 79—77094
- non-Newtonian liquid mixture separation by thermal diffusion in parasitic convection 80—64587
- nonisothermal magnetisable fluid, thermal convective stability, modulated mag. field effects 80—64646
- nonlinear, stable explicit finite difference scheme 78—151
- nonlinear convection, in Hele-Shaw cell, stability 79—41685
- nonlinear convection in a layer with nearly insulating boundaries 80—33592
- nonlinear convection in elasticoviscous layer heated from below 77—68634
- nonlinear dissipative system, successive bifurcation leading to stochastic behaviour 77—14975
- nonlinear double-diffusive convection 77—19607
- nonlinear heat transfer on boundary, difference method of solving conjugate nonstationary convection problem 80—92020
- nonlinear interactions in turbulent and convective flows, barotropic and baroclinic instability 79—98706
- nonNewtonian duct flow, wall heat transfer in entrance region 79—4049
- nonresonant second-order interaction of waves, generation of deeply penetrating gravity-like oscill. 78—28508
- nonsimilar laminar free convection flow along a nonisothermal vertical plate, finite difference method 78—75119
- nonstationary, in cylindrical layers of gases, and liqs., hot-wire acoustic method 78—45617
- nonstationary convection in a rotating system, book contrib. 80—1593
- nonstationary MHD convection, in vertical circular channel *(Russian)* 78—94833
- nonstationary one-dimensional diffusion under forced convection, Omega functions as auxiliary functions 78—93631
- nonsteady, finite difference scheme numerical anal. 78—46884
- nonuniformly heated horizontal surface, convection and Rayleigh-Benard instability 77—39296
- nozzle, heat transfer, turbulent boundary layer regime 78—9670
- nuclear reactor, BWR rod bundles, combined radiation and convection under emergency cooling conditions 77—14249
- numerical convection, upstream-centred scheme 77—27548
- numerical fluid dynamics, tensor viscosity method 79—72888
- numerical methods in convection theory 78—89058
- numerical prediction of recirculation flows with free convection encountered in gas-agitated reactors 79—10602
- ocean, stably stratified, convective instability 77—86913
- ocean gyre, poleward heat flux 80—85668
- ocean layered thermohaline convection, multiple components transport through diffusive interfaces 80—12396
- mid-ocean ridges, convective heat transport by ridge crest hot springs 80—98304
- ocean surface mixed layer, heat transport during catastrophic mixing events 79—16503
- oceanic crust, topographically driven subcritical hydrothermal convection 80—101345
- onset with spatially periodic heating, nonreson. wavelength excitation 78—94699
- open systems, definitions of heat, internal energy transfer by convection 80—69644
- open wind tunnel jet flow, convection and refraction of acoustic waves *(French)* 77—24007
- open-loop thermosyphons with geological applications 80—38407
- optimisation of convective annular/circular fin of minimum mass 80—79109
- organic fluids, natural convection and boiling heat transfer, electric field freq. effects 80—1560
- orthotropic plate with square hole and convective heat exchange, plane static thermoelasticity *(Russian)* 80—33456
- oscillators in convective biperiodic regime, velocity oscills. 80—53759
- oscillatory convective flow, double boundary layers 79—81874
- oscillatory flow, line heat source in horizontal rectangular chamber 78—90868
- oscillatory flow of electrically conducting fluid past porous plate, free convection currents 79—55428
- oscillatory flow past infinite, porous plate, free convection current effects 78—14079
- oscillatory flow past infinite vertical plate with variable suction and constant heat flux 78—38324
- oscillatory flow past vertical porous plate with constant suction, free convection effect, correction to earlier paper 77—27594
- oscillatory MHD boundary layer flow, free convection effects 78—91018
- osicllatory, in porous medium heated from below 78—79320
- overstable convection in horizontally treated rotating fluid 78—67202
- oxygenator efficiency prediction using convective field theory 77—48945
- E.Pacific Rise—Galapagos Rise system, seawater circulation rel. to convective heat loss 78—73331
- parallel channel forced convection boiling upflow system, instabilities 80—9327
- parallel plate channel, combined forced and free convective laminar flow, solute disperison 79—98801
- parallel plate channel, convective-radiative interaction, air-operated solar collectors appl. 80—96259
- parasitic convection effects in thermal diffusion column in sampling mode 80—19386
- partial spectral expansions 79—32193
- particle convective diffusion to rot. disc surface 78—18334
- particle deposition, onto rot. disc, convective diffusion, external force field 78—40081
- particle in gas stream, convective, diffusion with nonlinear kinetics of heterogeneous chem. reaction 78—83499
- particle transport to rotating disc surface under external force field 78—15718
- particles in a fluid, convective diffusion and mass transfer, wakes, chemical reactions 80—38394

convection continued
- particles moving in reactive, dispersive system, mass transfer interaction 79—64738
- penetrative, appl. of clipping approx. for inhomogeneous turbulence simulation 80—19331
- penetrative convection in rotating fluid, finite difference method 79—81902
- penetrative convection model, appls. to atmopshere, ocean and laboratory expts. *(Russian)* 78—24335
- periodic heat transfer in directly opposed free and forced convection flow 77—27522
- permeable cylinder, numerical anal. of free convection heat transfer 79—98723
- phase changes subject to convection and radiation, perturbation solns. 79—76962
- photoabsorption convection in horizontal tube, unsteady-state convection, num. investig. 80—33594
- photoabsorptive convection, steady states in field of continuous laser radiation 79—14212
- photosphere, convection rel. to Fraunhofer lines asymmetry 78—4175
- photospheric convective vels. from granule contrast profiles in Fe I 6569.2 A line 77—17507
- pipe, heated, vertical, gas buoyancy effect on downward flow and heat transfer 78—74427
- pipe, rotating, curved, convection heat transfer, appl. to spacecraft spin system 78—94737
- pipe, with nonuniform heat source, convective heat transfer 77—31298
- plane channel of variable cross-section, conjugate heat transfer *(French)* 78—59386
- plane parallel flow, free convection in Couette and Poiseuille flows, numerical simulation 80—99995
- plane thermal boundary layer, temp. distrib. determ. by var. formulation 77—23947
- planetary atmosphere, convective instability of fluid layers 80—56754
- planetary satellites, convection in ice crusts, effect on surface relief 79—84730
- planets, convection mode effects on thermal evolution of small bodies 80—26764
- plasma convection in force-free mag. field, mechanism for chem. separation in cosmic plasmas 79—35125
- plasma convective cells, nonlinear excitation by interchange modes and spectrum cascade processes 80—69997
- plasma sheet, adiabatic accel. of ions induced by convection 78—88997
- plasmasphere, heavy ions convection and magnetospheric circulation 77—64533
- plate, downward-facing, flat, heat transfer augmentation by nonuniform elec. field corona 78—94873
- plate, flat, optically thin boundary layer, of grey medium near leading edge, radiative-convective heat transfer 78—91027
- plate, flat, transparent, non-absorbing, natural convection due to solar radiation, buoyancy-driven flow 80—69826
- plate, heated, semiinfinite, vertical, with heat sources and sinks natural convection 80—59035
- plate, multiply connected, convective heat exchange, small parameter method for thermoelastic equilib. problems. *(Russian)* 78—63301
- plate, upward-facing inclined, measurements of heat transfer 79—23327
- plate, vertical, free convection boundary layers and heat transfer 80—59002
- plate, vertical, heat transfer coeff., interpolating eqns. between two limiting cases 79—37309
- plate and laminar slug flow with periodically changing temp., transient heat transfer 80—74872
- plate in combined convection, vel. profiles 78—18301
- plate melting in free convection flow 78—94531
- plate oscillation effect on horizontal free convection flow 77—75904
- plate temp. oscillations, response of horizontal free convection boundary layer 78—59391
- plate with cylinder in turbulent boundary layer, forced convection heat transfer 80—64540
- plate with impinging hot gas jet with low Re, convective heat transfer 80—96256
- plates, vertical and inclined, mixed convection combined, heat and mass transfer 80—64552
- plume, above vert. heated plate, development of wall and free types 78—90881
- plume, axisymmetric, buoyant, turbulence meas. 78—9637
- plume, buoyant, turbulent, pl./line heat sources, temp. and vel. distribs. 77—84254
- plume, round, due to falling source of heat 78—14016
- plume, turbulent, thermal, along vert. wall, struct. and heat transfer 78—90880
- plumes in inversion conditions, cross-sectional asymmetry, pollution 80—30619
- point heat source, natural convection in rotating environment 79—10445
- point sources buoyant convection phenomena 80—28506
- Poiseuille flow, convective instability and heat transfer, viscous dissipation effects, vortex onset 77—31295
- Poiseuille flow, horizontal plane, heated from below, axial heat cond. effects on thermal instability 77—42825
- polar troposphere, convection as source of medium scale thermospheric gravity waves 79—21088
- polyacrylamide solution, tube flow, friction and convective heat transfer, rheological changes effect 79—1220
- porous catalyst, simultaneous forced convection, diffusion and reaction 77—35254
- porous cavity, Darcy medium, 2-dimens. solns. 78—91007
- porous cylinder, vertical, shape ratio and lateral boundary conditions effect on onset of natural convection *(French)* 77—50861
- porous elastic matrix, onset of convection, variable prop. effects 77—84321
- porous insulation filled cavity wall, forced and free convective heat loss 77—75909
- porous interlayers between horizontal coaxial cylinders, flow field, natural convection and heat transfer 80—28558
- porous layer flow, surface heat flux 77—39343
- porous layers, convective heat transfer by integral methods 79—7408
- porous media, convective heat transfer 80—6053
- porous media, infinite, compact heat source 79—32659
- porous media, saturated, natural convection with heat generation 77—51114

convection continued
- porous media filled vertical enclosure, convective heat transfer, boundary layer 79—59908
- porous medium, anisotropic, nonlinear thermal convection 79—55414
- porous medium, deep evaporation characterisation, of water *(French)* 78—59468
- porous medium, effect of temp. depend. viscosity and thermal expansion 79—32662
- porous medium, horizontal, subjected to end-to-end temp. difference, natural convection 78—91010
- porous medium, saturated, mixed convection boundary layer flow on vertical surface 80—106798
- porous tubes and flat plates, with wall resistance, laminar mass transfer 79—60053
- positive surface tension gradients, Rayleigh-Benard convection *(French)* 80—75404
- potential flow over bodies, convective heat transfer 78—59395
- power-law fluid, free convection around thin bodies of revolution under second kind boundary conditions 77—7422
- propane-air flame, eddy entrainment and combustion in depth process, three-region model 79—100384
- propane-air flame, premixed turbulent, three region model 79—100383
- protoplanetary cloud, convection rel. to ang. momentum transfer by meridional currents 77—53436
- pseudocontinuum mass transfer in media with spatially periodic boundaries 79—86500
- pulsating stars, mixing length theory of convection 77—49367
- Puna geothermal area, Hawaii, thermally driven ground gas convection system discovery from Rn survey 80—85657
- pyrocumulus cloud over North Canterbury, New Zealand, 1878 April 10, obs. 80—109240
- quadratic finite element schemes for 2-D convective transport 78—21084
- radial heat transfer, conduction, convection and heat of phase change 78—90700
- radiant-convective heat exchange problems, nonstationary, analytical soln. method 80—33432
- radiative convective heat transfer of thermally thin body 80—79110
- radiative heat transfer between isothermal parallel plates, flow models, numerical analysis 80—14547
- radiative transfer, transient temp. of body, surface radiation, quasi-linearisation approach 77—80054
- radiative-convective heat transfer, numerical methods 78—94577
- radiative-convective heat transfer from extended surface, Monte Carlo method 78—67005
- radioactive gas, convective diffusion and adsorption in porous media, inverse problem 79—90322
- radioactive gas adsorpt. in porous medium, convective diffusion *(Russian)* 78—87387
- radioactive material storage, thermodynamics of free-convection air-cooled storages 80—5282
- rapidly rotating flows in geophysical fluid dynamics 77—45102
- rarefied gas, convective heat transfer coeff. and surface emissivity, effect of degree of vac. 78—1693
- rarefied gas, high speed, convective heating of concave bodies 79—1214
- Rayleigh-Benard convection, crit. effects 78—71328
- Rayleigh-Benard convection, flux ropes, dynamic effects 79—46166
- Rayleigh-Benard convection, one free and one rigid boundary 80—10237
- Rayleigh-Benard convection, periodic thermal perturbation, chaotic response 78—94685
- Rayleigh-Benard convection, wave number selection, sidewalls effect 80—106799
- Rayleigh-Benard inertial convection at low Prandtl number, in circular geometry 77—75917
- Rayleigh-Benard instability, vel. field, transition to turbulence 80—6029
- Rayleigh-Benard velocity field meas. 78—46966
- Rayleigh-Bernard convection, forced phase diffusion 80—103019
- reaction zone propagation, combustion wave structure inversion in porous media 80—89494
- reactor fuel element surface roughness, turbulent convective heat transfer 77—46208
- real gas, slug flow, radiative and convective transfer interaction 77—58529
- rectangular body in forced convection, heat transfer study, flow separation 80—74874
- rectangular cavity packed with porous media, heat transfer 78—71392
- rectangular cavity with porous filling, steady convection and boundary layers 80—79309
- rectangular channels, turbulent forced convection, momentum and heat transfer, secondary flows *(German)* 79—77259
- rectangular ducts, fully developed laminar forced convection, general inequality theorem 80—43780
- recuperative heat exchanger, convective heat transfer, nonNewtonian carrier, conjugated problem 79—1086
- refrigeration, heat transfer by natural convection with simultaneous frosting on horizontal cylinders in a vertical array *(Japanese)* 80—58890
- reverse osmosis system, combined forced and free convection system 79—52750
- RI fluctuation spectrum in region of convection above heated surface *(Russian)* 77—9497
- river/atmosphere time dependent, single dimensional heat exchange, analysis *(Bulgarian)* 78—57221
- rod cluster assembly, forced convection heat transfer, Poisson eqn. by finite difference scheme 78—79189
- roll cells, 3-dimens., within rigid boundaries, temp. and vel. fields 79—81888
- rotating annulus interior, influence of geometry *(Russian)* 77—91212
- rotating annulus with negative radial temp. gradient 78—90912
- rotating Benard convection, asymptotic sidewall effects 78—14014
- rotating disc, convective mass transfer 80—43707
- rotating fluid, layer heated, turbulent convection 80—100003
- rotating fluid, nonlinear convection 77—68597
- rotating fluid subject to horizontal temp. gradient, baroclinic waves 77—84251
- rotating fluids, convective modes and convective stability 79—16818
- rotating isothermal disc, heat transfer meas. using Mach Zehnder interferometer 80—38223
- rotating layer, convective wave motion, turbulence *(Russian)* 77—58670
- rotating self-gravitating fluid sphere with uniform distrib. of heat sources, MHD convective instability 77—29264
- rotating viscoelastic fluid layer heated from below, MHD convective instability 77—58800

convection continued
roughened rod in smooth channel, turbulent convective heat transfer 78−51241
rubrene, electrochemilum. by DC, highly organised EHD convection obs. 80−71499
saturated porous layer, sudden temp. rise, stability, linear and energy methods, convection 80−74972
saturated porous material in box, three-dimens. convection 78−71393
saturated porous medium, free convection boundary layers, lateral mass flux effects 77−27592
sea water, haline connection induced by freezing *(Japanese)* 78−88843
second moment turbulence closure to heat and mass transport in two-dimens. thin shear flow 80−24010
second order fluid, natural convection flow from porous plate, suction and injection effects 80−59029
second order fluid, oscillatory convection flow from vertical plate 77−7423
secondary convective flows in plane inclined layer *(Russian)* 77−80153
self-gravitating fluids, convection rel. to definition of g-modes and p-modes 77−41291
self-gravitating fluids in perturbed configurations, normal modes rel. to convection 78−32337
semi-infinite porous medium bounded by horizontal surface, mixed convective flow, vortex instability 80−79304
semicircular cross section tube, nonsteady convective heat transfer 80−99999
semiconvection in stars, semitheory 78−69787
separated air flow, surface orientation effects 79−98709
shear flow, stratified, free-turbulent, buoyancy effects on large scale struct. 78−90849
shear turbulence, acoustic field, convective amplification, jet noise appl. 77−23943
shrouded parallel disc system, rot. and coolant throughflow effect on heat transfer and temp. field 77−15017
simple body melting time with convection boundary condition 80−99914
simultaneous boiling and forced convection heat transfer from horizontal cylinder to water in crossflow 77−15018
single-mode equations, numerical solns. 77−27530
singular perturbation problem with nearly resonant operator 78−22352
sinusoidal thermal perturbation transmission through wall, heat conduction and convection *(French)* 77−15007
slab with temp. depend. thermal cond., convective boundary, transient cond., finite difference method 78−75031
slat solar collector natural convection obs. 79−62055
small particles suspended in turbulent fluid, convection, mass transfer 80−87793
snow, dry, heat and mass flux 79−57980
in soils, convective-dispersive solute transport with combined equilib. and kinetic adsorption model 77−64356
solar, granulation, convection models, book contrib. 80−4329
solar atmosphere, convective efficiency rel. to solar const. time var. 79−21262
solar atmosphere, dynamo action in thin slab 79−44430
solar atmosphere, penetrative instabilities theory in presence of thermal dissipation 80−109406
solar collector, heat loss characts. analysis and obs. 79−88004
solar collector 79−62056
solar collector honeycomb cell heat transfer interferometric meas. 79−62053
solar collectors, free convective heat transfer 80−45748
solar convection zone, depth rel. to high solar latits. rot. model calcs. 79−101129
solar convection zone, large scale circulation rel. to Sun differential rot. 77−22164
solar convection zone, solar cycle driven by dynamo action of global convection 77−56903
solar convection zone, struct. adjustments rel. to solar luminosity short term fluctuations 80−82321
solar convective zone, dynamical struct. rel. to general mag. fields 77−22166
solar convective zone, non-stationary mechanisms rel. to non-uniform ang. vel. distrib. maintenance *(Russian)* 79−96985
solar corona, mag. loops, downflows and convection 78−93175
solar cosmic ray propagation, anisotropic diffusion-convection eqn., dimensional soln. 80−17453
solar cosmic rays propag., diffusion in mag. fields, convection in solar wind, dimens. method soln. *(Chinese)* 78−81511
solar drying of agricultural crops, using no-glass flat plate collectors, analytical model 79−70465
solar energy collection, double glass, convection in vertical rectangular channels *(French)* 80−85300
solar energy collection, heat losses by conduction and convection, reduction techniques 79−79409
solar energy collection and storage, latent heat diode walls, space heating *(French)* 80−61298
solar energy compound parabolic concentrator, natural convection, finite element soln. 78−90634
solar envelope, convection efficiency of Opik's cellular convection theory 80−12732
solar flare region heated by electron stream 77−71079
solar granular convection, effects in response of C I 5380 Å response to solar luminosity vars. 80−85910
solar granulation, Benard cell convection model rel. to spatial power spectrum 78−65581
solar granulation, lines convective blue shift rel. to limb shift 79−12448
solar granulation, one-dimensional speckle interferometry rel. to convective model 78−45299
solar granulation motions, effects on photosphere mag. fields fine struct. 80−98646
solar granulation structure, vertical motion models 80−90375
solar granulation structure, vertical motions spatial and temporal behaviour obs. 80−85912
solar heating, air movement control 80−66946
solar intense magnetic flux tube, convective instability 79−30038
solar interior, convective mixing rel. to interstellar dust accretion and neutrinos prod. 79−12441
solar low photosphere, horizontal temp. var. rel. to convective flux 77−22163
solar magnetic fields and convection, primordial field theory, review 77−56902

convection continued
solar models, convective mixing length and He content rel. to H-R diagram fits 80−26835
solar nebula, primordial, influence of convection on struct. and evolution 80−62042
solar photosphere, convective correction to spectral lines measured wavelengths 78−93181
solar photosphere, small-scale mag. fields and convection 78−53906
solar photosphere, two-dimensional spectral anal. of disc centre granulation 77−53520
solar photosphere, waves and convective motions determ. from spectral lines asymmetry *(Russian)* 80−72901
solar receiver convective losses determ., using cryogenic heat transfer tunnel 79−83636
solar regenerator buoyancy effects, study 79−68709
solar regenerator of hygroscopic solutions, for air dehumidification 79−57464
solar water heater, natural circulation, with linear and nonlinear temp. distribs. 77−75778
solid laser planar active element convective cooling *(Russian)* 78−82978
solid reacting particles, ordered system at high Peclet numbers, mass transfer, convection 80−69830
solid with liquid inclusions, convective effects 80−23868
solid-state convection in planetary interiors, numerical methods 79−84693
solidifying liquid metals, flow in two-phase zone 79−81953
solidifying melt, two phase zone formation, convection *(Russian)* 80−93547
Soret driven convective instability, mass diffusion and boundary effects 80−53776
Soret driven instability, secondary effects 80−6062
Soret-driven convective instability in two-component liq. layer heated from below, phase transition picture 79−77110
space environment, transport processes in fluids 79−46825
spatially periodic convective flow, stability and fluctuations 80−19394
spent fuel pool natural convection, multichannel analysis 79−9786
sphere, convective heat transfer coeff. 79−32511
sphere in power-law fluid, convective heat transfer 78−87340
spheres, concentric, cooling by forced convection, at low Reynolds no. 79−1183
spherical closed space, gas compressibility effects on thermal convection 80−1562
spherical drop combustion, asymptotic, drop shrinkage and flame movement, heat and mass transfer 77−81405
spherical gas layer, heat transfer by natural convection 77−51058
spherical laser target hydrodynamic compression stability *(Russian)* 80−106159
spherical porous layer, multicellular free convection flow *(French)* 79−46375
squall lines, radar obs. during GATE 78−20474
square cavity, steady free convection, mixed-interpolation finite elements comparison 78−45486
square duct entrance region, Laminar flow and heat transfer to non-Newtonian fluid 80−10243
stability of convective motion in two-dimens. vertical fluid layer with permeable boundaries 77−55086
stability of motion due to nonuniformly distributed heat sources *(Russian)* 77−80154
stable finite element simulation of convective transport 79−46317
stable salinity gradient heated from below, convection and layers 80−24016
stably stratified medium, plane free convection from local heat source 80−96253
stars, adiabatic stability of rotating gaseous masses 77−91516
stars, compressible convection onset in model atmospheres 78−65605
stars, convection and magnetic fields 78−89185
stars, convection as cause of forced mixing 80−56818
stars, convection in rotating spheres and spherical shells 78−89184
stars, convective elements fluctuations rel. to stochastic evolution 80−31293
stars, convective zone boundaries 78−89187
stars, equilib. problem in rotating convection zone 77−56917
stars, fundamental hit correctable inconsistency of local mixing-length theory 80−26841
stars, late-type, convection rel. to acoustic energy generation and chromospheres 78−7986
stars, magnetic, convective stability 80−94781
stars, main sequence intermediate and late differential rot. models 80−105238
stars, massive, convective and semiconvective mixing 80−90405
stars, mixing length parameter rel. to Hertzsprung-Russell diagram age and mass calibrations 80−51744
stars, penetrative convection 78−89186
stars, pure perturbation spectra of convectively neutral fluids 77−41292
stars, URCA convection 78−89189
stars of about 1 $M_{\odot}$, semiconvection and vibr. stability 77−22204
statically stressed fluid, transition to turbulence, inverted bifurcation 77−7370
stationary cellular convection, rotation effects *(German)* 79−81904
steady, past marginal state, amplitude determ., Landau's conjecture 79−55311
steady and time dependent convection in a rectangular box 78−94706
steady and transient, fluid layer with volumetric energy sources 78−9639
steady convection, two-dimens., in const. vertical shear, dynamical struct. 79−12209
steady Rayleigh Benard convection in horizontal fluid layer 79−55368
steady state convection-diffusion eqn., quadratic finite element solns. 80−92019
steady State stefan problem with convection 80−69625
steam-water mixture, with high vap. content, annular flow, heat transfer, press. loss 78−75193
Stefan axisymmetric single phase problem *(Russian)* 79−59905
Stefan problem simulation and control, associated variational inequality 78−67009
stellar accretion discs, steady, optically thick, convective vertical energy transport 80−62112
stellar and planetary atms., thermal convection approximations 79−35127
stellar atmosphere, thermal-convective instability, finite Larmor radius effect 78−32438

convection continued
- stellar atmosphere, thermal-convective instability, radiative transfer effects 78—53929
- stellar atmospheres, free convection effects on unsteady laminar boundary-layer flow 79—35237
- stellar C-O degenerate core, convective energy transfer during C-burning flash 77—78774
- stellar convection, energy transport 78—89180
- stellar convection, hydrodynamics rel. to solar obs. 78—89182
- stellar convection, IAU Colloquium 38 (Nice, France, 1976 August 16-20) 78—89176
- stellar convection, mixing-length theory rel. to physical models 78—89179
- stellar convection, modal eqns. in spheres and spherical shells 79—101137
- stellar convection, value of mixing length 80—77379
- stellar convection 78—89194
- stellar convection in rot. magnetic star, toroidal field effect 80—41816
- stellar convection parameters, meas. technique 79—21273
- stellar convection phenomena numerical simulations 77—29789
- stellar convection theory (1930-1945) 78—89177
- stellar convection zones dynamics, effect of rot. on turbulent viscosity and cond. 80—36612
- stellar convective envelopes, non-local convection, statistical theory *(Chinese)* 80—85933
- stellar cores, He flash and convection 78—89191
- stellar degenerate core, convection effects on C burning 80—41810
- stellar degenerate cores, URCA process rel. to convection 77—22203
- stellar dynamical instabilities at start of convection 78—89181
- stellar envelopes, convective overshoot effects on He shell flashes 77—56909
- stellar interior, semiconvection as occasional breaking of weakly amplified internal waves 79—48778
- stellar interiors, core He flash models with two-dimensional convection 80—105230
- stellar interiors, degenerate C burning front convective propag. rel. to core implosion 80—77390
- stellar mixing-length theory 78—89178
- stellar penetrative atmosphere, convective, gravity and acoustic instabilities 79—84783
- stellar photoconvection 78—89190
- stellar structure models, convection theory including turbulent kinetic energy flux 78—57543
- stellar turbulence, conference, London, Ontario, Canada (1979 August 27 to 30) 80—73102
- stellar turbulent convection equations, ensemble averaging 80—67698
- stochastic perturbation of convective motion, truncated spectral model 80—92146
- Stokes' problem, mass transfer effects of MHD free convective flow 80—62003
- Stokes flow, free convection effects, finite difference anal. 80—14695
- Stokes problem, effects of free convection on oscillatory flow past infinite porous vertical limiting surface 80—109348
- Stokes problem, free convection effects, rarefied gas flow past plate 79—32581
- stratified Boussinesq fluid, in rotating spherical annuli, small Reynolds number convection 80—6047
- stratified fluid, duct, equilibrium breakdown, thermosiphon work *(French)* 80—59114
- stratified fluid, rectangular enclosures, stabilising thermal gradient effects on natural convection 79—81889
- stratified fluid flow along heated inclined wall, double diffusive instability 79—55405
- stratified horizontal porous layer, onset of natural convection *(French)* 77—89002
- stratified incompressible fluid, convective flow, Euler-Poisson eqns. *(Russian)* 77—31300
- stratified layers, form. and merging in differentially heated slot 79—59982
- subcooled forced convection boiling heat transfer at subatmospheric pressure 78—94525
- submerged jet closed vessel recirculation flow, temp. distrib. and buoyancy 78—90958
- subsea permafrost, heat and mass transport by interstitial water convection 79—2302
- subterrestrial fluid convection, appl. to Rn long-distance migration 77—37246
- Sun, ang. momentum outward transport by gas convection rel. to equatorial accel. 77—53531
- Sun, anisotropic convective elements rel. to differential rot. mechanism 79—25556
- Sun, areodynamic lift on cylindrical mag. flux tube in convective flows 79—101126
- Sun, axisymmetric convection with a magnetic field 78—89165
- Sun, convection and mag. fields, basic props. of mag. flux tubes 77—13297
- Sun, convection in deep rotating spherical shell 77—53562
- Sun, convection in dirty solar models contaminated by accretions 79—44436
- Sun, convection in rotating deep compressible spherical shell 78—20795
- Sun, convection patterns 77—56897
- Sun, convection rel. to polar vortex, spectroscopic search 79—5801
- Sun, convection zone and angular vel., Boussinesq model 77—56898
- Sun, convective element intrinsic mag. field 80—101583
- Sun, convective noise waves dissipation in solar upper atmosphere mag. struct. 78—65600
- Sun, convective zone cophasal regions model 78—96469
- Sun, differential rot. effect on convection struct., Maunder minimum nature 80—101573
- Sun, differential rot./global convection system modulation by nonlinear dynamo 78—40889
- Sun, heat flow near obstacles in convection zone 78—28609
- Sun, mag. field transfer by two-dimensional convection and solar semi-dynamo 77—49349
- Sun, mag. fields and convection rel. to meridional motions 77—53493
- Sun, meridional circulation and heat redistrib. in convective envelope 79—40150
- Sun, surface appearance of disturbances in heat flow assoc. with differential rotation 77—29751
- Sun, two-dimensional stochastic motions rel. to differential rot. problem 77—53518

convection continued
- sunspot umbrae, material motions obs. and convective energy flux 77—45374
- sunspots, convective inhibition rel. to thermal struct. 77—5517
- sunspots, convective overstability in mag. field in downdraft 80—21960
- sunspots, running penumbral waves origin 78—93188
- sunspots, spectroscopic search for convective vels. 79—92745
- sunspots magnetic flux tubes physics, longitudinal overstability rel. to umbral dots 80—26825
- superheated vapour in horizontal tube, condensation, local convective heat transfer coeff. 80—19927
- superheating-convective instability, effect of boundaries 77—35137
- supernova core, Rayleigh-Taylor convective overturn rel. to explosion 80—77429
- supernovae, explosive core overturn and mass ejection 80—72988
- supernovae, lepton-driven convection 79—84811
- surface mass transfer interaction with transverse curvature in natural convection boundary layers 80—24008
- surface with sharp boundary condition change, laminar flow, concentration distrib., convective diffusion *(Russian)* 79—94590
- suspension, solid separation at wall, heat transfer 78—9685
- swirling convective boundary layer, vorticity dynamics 80—59048
- temperature distrib. in microwave-irradiated cylinders simulating living tissues 80—3760
- ternary gas mixture, natural convection, naphthalene sublimation appl. 80—6511
- terrestrial planets, solid convection, conf., Moffett Field, California, USA (Dec 1977) 79—84691
- terrestrial planets, solid-state convection, obs. evidence 79—84692
- terrestrial planets, subsolidus convective cooling histories 79—66939
- thermal, temp. field meas., buoyant vortex bubbles and turbulent thermals 78—34232
- thermal analysis, finite element method for temp. depend. parameters 79—32184
- thermal convection, two-phase, in porous layer, flow visualisation study 79—72930
- thermal convection at high Rayleigh number, variation of Nusselt number 80—79300
- thermal convection in a large box with imperfectly insulated sidewalls 78—59399
- thermal convection in Hele-Shaw cell 77—31301
- thermal convection in porous media, dispersion effects 80—103027
- thermal convection in saturated heat generating porous layer 79—77113
- thermal convection onset under const. flux boundary conditions, mag. field effect 78—69676
- thermal convection with spatially periodic boundary conditions: resonant wavelength excitation 78—59392
- thermal diffusion and convective stability, role of rotating container 79—68725
- thermal energy storage material cylinders, heat transfer during melting 79—3894
- thermal fluids of Abano region, N.Italy, forced convection circulation paths 79—20883
- thermal instability of stochastically modulated flow 78—14011
- thermal perturbations in moving nonlinear media, convective spatial localisation, cond. coeff. depend. 80—106706
- thermal plume, vel. meas. by electrochem. probe *(French)* 78—9728
- thermal plume modelling, review 79—4056
- thermal-convective instability of partially ionized plasma, radiative transfer, medium porosity and collisional effects 80—67538
- thermal-ignition analysis in boundary-layer flows 79—64800
- thermally driven shear flow heated from below, stability 78—67177
- thermally stratified enclosures with localised heating from below, natural convection 80—24017
- thermocapillarity-induced creeping in rectangular enclosure, low Marangoni no. 80—10116
- thermoconvective instabilities of confined fluids, review 80—38399
- thermoconvective motion of low Prandtl no. fluid in annulus 78—30290
- thermoconvective waves in a conducting and radiating fluid 80—19415
- thermoconvective waves in horizontal gas layer 77—7407
- thermoconvective waves in stratified compressible fluid, stability criterion contradiction 80—19414
- thermoelectric coolers, heat load estimation curves 78—45613
- thermogravitational convection asymmetry, finite difference method 78—59267
- thermohaline convection, past marginal state, determ. amplitude and freq., Landau's conjecture 79—55312
- thermomolecular fluid flow effects in low-g, crystal growth from vapour 79—73117
- thermosiphon, inverse, thermo-hydraulic design 78—94534
- thermosolutal convection rel. to stellar convection 78—89188
- three dimensional free convection flow and heat transfer along a porous vertical plate 78—90866
- three-dimensional, natural, in box 78—5743
- three-dimensional laminar stream tube network, convective mixing 80—14815
- three-dimensional natural convection in a confined porous medium heated from below 79—72937
- thunderclouds, effect of elec. forces on charge separation caused by combined precip. and convection 80—17333
- time dependent, double diffusive, stability in inclined slot 78—5744
- time scale of convection of fluid cooling from surface *(Russian)* 80—1582
- tissue, microwave heating, effect of surface cooling and blood flow 78—57038
- tissue, perfused, macroscopic temp. distrib. 78—64944
- tmosphere boundary layer, similarity theory for turbulence and convection *(Polish)* 77—25753
- toluene, free convection heat transfer in tube at supercrit. press. 78—42518
- toroidal thermosyphon, transient and stability behaviour 80—38408
- transient combined heat cond. and convection problem, explicit numerical soln. method 79—81869
- transient combined laminar free convection and radiation in rectangular enclosure 77—7388
- transient convective turbulent heat transfer in tubes, thermal and hydrodynamic instability 78—83485
- transient free convection flow around two-dimensional or axisymmetric bodies 80—69817
- transient free convection from a suddenly heated horizontal wire 79—32515

convection continued
transient free convection from an isothermal horizontal circular cylinder *(German)* 79—77115
transient free convection on isothermal vertical flat plate 78—22345
transient heat exchange between a radiating plate and a high-temperature gas flow 79—94609
transient natural convection in curly viscous fluids, boundary layer approx. 79—77096
transient natural convection in horizontal cylinder with constant cooling rate 77—42841
transient natural convection in rectangular enclosures, numerical anal. 79—77111
transient natural convection in vertical enclosures 77—42822
transient thermal convection in horizontal rectangular spaces heated from below, waves 80—1566
transient turbulent convective heat transfer in concentric annuli *(German)* 77—7399
transpiration-cooled system, thermal response in radiative and convective environment 78—32323
transport eqn., 2-D, upwind finite element scheme 77—13713
transport eqn., unsteady convective diffusive, upwind finite element scheme 79—97320
transport eqns., modified upwind scheme and conjugate gradient method 79—77107
trench with radiative wall conditions, free convection 80—79324
tropical depression, synoptic scale kinetic energy source, cumulus cloud convection 80—77088
trough-ridge systems as slantwise convection 79—84456
tube, horizontal, laminar combined convection, circumferentially nonuniform heating effect 78—71331
tube, vertical, laminar and turbulent heat transfer, air and Ar 78—71332
tube bundle in asymmetric flow 79—98710
tube bundles in cross flow at critical Reynolds nos., heat transfer efficiency 79—98708
tube turbulent convection, effective power dependence of heat transfer coeff. 79—4006
tubes, entry length heat transfer by combined laminar convection, computation methods 78—38312
turbomachines heat transfer, unsteady 78—67198
turbulence, vortex shedding influence on noise generation 77—3830
turbulence creation, review *(Hungarian)* 79—23312
turbulence effects heat transfer from cylinders in crossflow at critical Reynolds no. 79—98707
turbulence theory, review 80—4536
turbulent, numerical models based on unsteady Navier-Stokes eqns. 80—38415
turbulent advection, scalar spectrum model 79—32474
turbulent boundary layer, vel. profile 78—94693
turbulent boundary layer, wall capacity and resistance effects 79—1192
turbulent boundary layer on plate, convective heat transfer 77—7387
turbulent buoyancy convection heat transfer, two-dimens., with internal heat sources 78—94540
turbulent buoyant convection from source in confined region 79—59983
turbulent channel flow transport, inequalities, variational principles 79—60063
turbulent convection in fluid layer with internal and external heating, reactor safety anal. 79—32514
turbulent convection in vertical layer, numerical modelling *(Russian)* 78—9636
turbulent convection mode numerical modelling 79—64653
turbulent convection within rapidly rotating superadiabatic fluids with horizontal temperature gradients 78—90913
turbulent convective heat transfer from rough surfaces 79—27638
turbulent convective transport, surface renewal and interfacial conditions 77—913
turbulent flow with polymeric additives, convective heat transfer 79—77098
turbulent flow with subcritical and supercritical press., natural convection effect on heat transfer 78—5739
turbulent forced convection, heat and mass transfer, analogeous relationship *(Japanese)* 79—14396
turbulent free and forced convective flow in vertical channels 80—19391
turbulent free convection from rough surface, heat transfer 79—55388
turbulent free convection heat transfer from flat vertical plate to power law fluid 78—67225
turbulent free convection in mag. field, statistical characts., vortices 80—79310
turbulent jet, heat transfer to flat plate 79—1226
turbulent jet, signal transit velocities 77—35192
turbulent mass transfer to wall, fluctuations, Schmidt no. effect 77—58659
turbulent medium with density gradient, MHD effects, appl. solar convection *(Russian)* 78—47055
turbulent scalar fields, transport eqn. for probability density function, closure 80—1585
turbulent suspension, combined radiative and convective heat transfer 78—9724
turbulent thermal boundary layer, integral approach 79—55390
turbulent thermal convection in presence of rot. and mag. field, stellar and planetary dynamos appl. 80—6042
turbulent vertical buoyant jet decay in uniform environment, unified scaling law 78—90905
two dimensional convective transport, vorticity at wall with suction, finite difference representation 80—10255
two phase natural convection in permeable medium adjacent to vertical heated surface 79—68790
two temperature fluid layer heated from below, stability 77—65741
two temperature theory of heat cond. fluids 78—26017
two-dimensional box, heated from below, smooth transition to convective regime 78—18304
two-fluid system, in horizontal layer, with internal heat sources, natural convection 78—94539
two-phase convection in a sandbox rel. to geological porblems 77—64238
two-phase flow, dryout region of forced convection evaporation, heat transfer coeff. 78—90988
two-phase flow, interface of spherical particles, unsteady state mass transfer 78—47018
two-phase flow instability in parallel channels 78—94810
two-phase laminar boundary layer, forced convection condensation *(Japanese)* 78—34191
two-phase Stefan problem solns. 80—43594

convection continued
underground optical waveguide beam distortion by air convection 77—62063
unified similarity theory, turbulent convection at vertical surface 78—90890
uniformly heated horizontal circular cylinder banks, natural convection heat transfer 80—64538
unstable heat transfer conditions, free convection-film boiling transition 78—14006
unsteady buoyant plumes in neutral surroundings, time similarity anal. 79—81870
unsteady combined forced and natural convection from circular and elliptic cylinders *(Japanese)* 79—32510
unsteady combined free and forced convection in flow in narrow channel 79—60061
unsteady compressible flow, dissipative thermodynamic effects 78—26136
unsteady convective heat transfer in fluid tube flows *(Russian)* 79—18961
unsteady forced convection heat transfer from impulsively started circ. cylinder 79—27633
unsteady free convection flow past an infinite plate with constant suction and heat sources 79—81868
unsteady laminar, in uniformly heated vertical pipes 78—38323
unsteady laminar heat transfer in circular duct flow in receiver tubes in solar collectors *(Japanese)* 79—77058
unsteady MDH convective diffusion, exact anal. 79—72953
unsteady mixed convection heat transfer from a horizontal circular cylinder 79—81879
upper atmosphere, ion convection momentum sources in thermosphere neutral comp. 78—77380
upsteam-centred finite-difference scheme for ideal compressible flow 77—27547
upstream differences critical evaluation 77—900
upward turbulent free convection, adjacent to horizontal surfaces 79—59977
upwindings of high order Galerkin methods in conduction-convection problems 79—3886
Uranus, convective vortices rel. to equatorial flow 80—67653
Uranus magnetosphere, plasma dynamics in mag. field laboratory simulation 79—16757
Uranus thermal evolution, convective cooling model and comparison with Neptune 78—85903
W Ursae Majoris stars, role of photospheric convection 78—49478
vapour-noncondensible gas mixture, body force convection condensation *(Japanese)* 79—50574
variable viscosity fluid, convective heat transport 78—55641
velocity field amplitude, convection rolls, wavenumber dependence 78—71327
Venus atmosphere, dynamics rel. to Earth-synchronous rot. 79—25531
Venus atmosphere, vertical convection rel. to strong horizontal winds 77—29682
vertical circular channel, convective stability relative to periodical disturbances *(Russian)* 80—43711
vertical cones in laminar free convection, integral method 79—81881
vertical cylinder, combined heat and mass transfer in natural convection 80—59027
vertical flat plate, wave instability of liminar mixed convection flow 80—10245
vertical fluid layers, heat transfer by natural convection 77—80158
vertical internally heated annulus entry region, mixed convection in water 80—24015
vertical layer, steady convective flow stability, boundary thermal props. effect 78—55644
vertical layer with space-modulated temp. distrib. on boundaries, convective motions 79—90240
vertical natural flow, adjacent to surface transition limits 79—50726
vertical plate, infinite, const. suction and mass transfer, unsteady free convection 78—18290
vertical plate, infinite, variable suction and mass transfer, unsteady free convection 78—18291
vertical plate, laminar natural convection heat transfer, supercritical CO_2 and He 80—64544
vertical plate, longit. and transverse vel. of free convection *(French)* 79—1177
vertical plate in free convection, temp. profiles meas. 77—915
vertical plate with uniform blowing, laminar combined forced and free convection 80—74876
vertical porous stratum, natural convection, modified Poiseuille flow distrib. 78—5794
vertical surface against stably stratified fluid, heat transfer 78—90885
vertical surface melting, heat transfer interferometric meas., convection effects 80—64339
vertical tubes with zero inlet subcooling, forced convection boiling, critical heat flux 80—64549
vertical uniformly heated tubes, forced convection boiling, critical heat flux, inlet subcooling 80—19374
vertical wall heat transfer with combined forced and free convection *(Russian)* 79—94618
vertically staggered patterns in free convective flow, book contrib. 80—1592
vibrating fluid layer heated from above, stability limit *(Russian)* 78—46960
vibrating layer of fluid heated from above 79—86424
viscoelastic fluid, free convection flow past a vertical wall 80—10239
viscoelastic fluid layer, convective instability, boundary thermal cond. independence 78—9659
viscoelastic fluid layer, thermal instability, lift and thermocapillary forces effect 79—86434
viscoelastic fluid layer heated from below, vertical periodic oscillations, convection, overstability 80—48755
viscoelastic free convection boundary layer flow past infinite plate with constant suction 78—90936
viscoplastic liquid, steady free convection 77—35175
viscous flow, 2nd order upwind scheme critique 78—94744
viscous fluid, convection energy, theory 79—86436
viscous fluid, convection rates, Earth upper mantle and continental drift appl. *(Russian)* 80—1581
viscous fluid, stability of steady vertical flow 80—64520
viscous gas, with internal heat sources, thermoconvective stability *(Ukrainian)* 79—32495

convection continued
viscous heat generating fluid, convective flow and heat transfer near moving porous plate 80—14703
viscous incompressible flow problems, two-dimens., Navier-Stokes eqns. soln. and contaminant effects 77—58638
visualisation, in environmental and technical systems *(German)* 79—86540
volatile binary solution, theory of evaporation, of large drops 79—10931
volumetrically heated fluid layer, combined natural turbulent convection and radiation 80—74871
vortex filament form. from ascending flows over evap. liquid 78—63440
wake of step, with pulsating jet, thermal convection *(French)* 80—10240
wall, perforated, relative effects of external and internal convection *(French)* 79—1248
wall conductance effects on convective horizontal channel flow 79—23374
wall temperature distributions, in regions of deteriorated heat transfer 78—83377
wall temperature with internal cond. and external convection, calc. method *(French)* 80—19215
walls, permeable, cooling characts., heat exchange, rad. emitter design 80—64535
water, boiling critical heat flux density, free motion conditions, 1-205 bar *(Russian)* 79—68560
water, boiling curves, subcooled and forced convective conditions 79—14230
water, convection rel. to fine structure of thermal boundary layer near air-water interface *(Russian)* 78—22332
water, cooling, boundary layer thermal state during transition from free to forced convection *(Russian)* 78—81192
water, free-convection boiling, critical heat flux density 80—48691
water, layer, semiinfinite, cooled (heated) from below, convection onset, density anomaly influence *(German)* 78—22350
water, on melting ice layer, heated, free convection onset criterion, density anomaly effect *(German)* 78—22351
water, simple theoretical and expt. study, geophysical appl. and analogies 80—24018
water droplet forced convection and heat transfer rel. to vapour conc. *(Chinese)* 79—23185
wave-transition spectra and vacillation in open rotating cylinder 78—14020
weakly amplified modes, interaction in nonlinear convectible instability *(French)* 79—64650
weather, severe convective event numerical simulation and prediction, Navier-Stokes eqns. initialisation 80—31111
weather modification due to waste heat release from large dry cooling towers 79—84471
whirlwind, ring-shaped, onset caused by rising air in stratified atmosphere *(Russian)* 78—77298
white dwarfs external layers, convection rel. to interpretation of spectra 79—62824
with volumetric heat sources, fluid layer in spherical segment 79—614
CO_2, heat transfer at critical point, heat transmission coeff. determ. *(German)* 77—35133
CO_2, laminar free convection at supercrit. press. under cooling conditions, heat transfer analysis 79—86428
CO_2 laser, convective-cooled, fast-flow, pulse discharge stability 78—94389
CO_2 pulse-periodic laser, gas stream gasdynamic perturbations, heated gas convective removal 79—94207
CO_2, supercritical, natural convection to cooled horizontal cylinder 79—98724
CO_2-air, heat transfer from cylindrical anemometer probe 77—84256
CO_2-N, nonequilib. mixture convective and radiational heat exchange during flow past body 80—14850
Fe_2O_3, hematite, reduction, exam. of role of convective mass transfer 78—52724
H-He fluid planets, dynamics and He distrib. 78—28555
H_2-CO_2, turbulent flow heat transfer, expt. and numerical anal. 78—94690
H_2-He gas mixtures, 1000-25000K, transport property correlations 80—75029
He, in confined region between two horizontal ducts for variable fluid properties 79—23321
He, liq., ht. transfer in centrifugal acceleration fields, free convection and boiling regimes 77—89604
He, sound transmission at liq. solid interface, probe of melting kinetics 80—92734
He, supercrit., forced convective heat transfer meas. 77—27523
He, supercritical, natural convection heat transfer 78—94694
He-I in capillary channels, forced convection boiling heat transfer 80—48707
^{4}He gas lasers, horizontal, heated from below, Nusselt and Rayleigh numbers 80—79311
N_2 cryogenic vapour columns, improved natural convection heat transfer 79—59986
N_2 vapour columns, cryogenic, complex flow 78—34119
N_2-Ar corona dishcharge, convection and mixing, atm. press., mass spectra obs. 80—1853
N_2O_4, dissociating turbulent convection on horizontal plate *(Russian)* 80—1587
Na boiling in tubes, heat transfer and pressure drop 80—28408
O_2 gas, magnetically enhanced thermal convection 79—50802
O_2, magnetothermal convection in nonuniform mag. field 78—1746
SF_6, long-range correlation length near liquid-vapour transition, Rayleigh scatt. 77—8593
SF_6-N_2, horizontal cylindrical power cable, convective heat transfer, simulation *(Russian)* 77—58676
Ti, heat- mass- and charge-transfer in high temp. oxidation 79—83369
Zr, heat- mass- and charge-transfer in high temp. oxidation 79—83369

convection in liquids
absorbing-emitting, natural convection boundary layer flow 77—58808
Alad'ev wall superheat correl., expt. validity test 78—83393
alternating circulation heat transfer, mathematical model *(Rumanian)* 79—14208
annuli, spherical rot., stratified convection of viscous Boussinesq fluid 79—27635
annulus, spherical, rot., forced thermal convection of viscous fluid 79—27634
arterial bifurcation, steady convective diffusion model 77—21546

convection in liquids continued
Benard convection, stability of horizontal layer of fluid heated from below 80—87767
Benard instability, critical fluctuation, slowing, optical and acoustic study 79—77075
Benard-Rayleigh convection, finite amplitude, nonlinear stability anal. 79—46311
Bernard convection, and linear fluctuation theory, Markovian processes and irreversibility 80—87766
binary alloy indirectional solidification, convective and interfacial instabilities 80—60851
binary fluid system, Onsager coeffs., steady state soln. for Benard convection 80—64851
binary liq. layer, microgravity, thermoconvective stability 80—74866
binary liquid mixture heated from above, convective instability, optical meas. 77—42823
binary melt, crystallising, thermoconcentrational convection in liq., core 80—6043
binary melt, thermoconcentration convection in solidification, influence on impurity distrib. *(Russian)* 79—73292
boiling, mechanism model based on rotating vortex model with spatial heating 80—14694
boundary layer, heated, stability 78—38332
bubble boiling in large volume at cylindrical and spherical surfaces, max. crit. heat flux 77—11188
buoyancy induced flow adjacent to vertical uniform flux surface in cold water 80—69834
buoyancy induced flow in water 79—23316
capacitor oil, electrical and gravitational convection *(Russian)* 79—27630
carrier mediated transport theory, survey of applications 77—89113
casting solidification, impurity distrib., effect of thermal-gravitational convection, numerical study *(Russian)* 78—19734
cathodic diffusion boundary layer, free convective flow obs. with shadow Schlieren method 78—68894
cavity flows, two and three dimens., multistep technique with implicit difference schemes 79—37398
cellular, numerical simulation *(Russian)* 78—34120
cellular convection with liq. film flow 77—68588
channel, local heat flux *(Russian)* 78—38330
channel, rectangular, laminar forced convective heat transfer for 3rd kind temp. boundary conditions 78—87341
chemically active liquid in horizontal porous bed, convective instability 79—41769
cholesteric liquid crystals, oscillatory convective instabilities, caused by heating from below 80—103239
combined convective heat transfer along vertical plate with uniform blowing *(Japanese)* 80—74867
combined convective heat transfer with opposing flow around an isothermal wedge *(Japanese)* 80—69838
complex domain heat exchange, new soln. techniques 78—94509
conducting liq., heated layer in mag. field, convection stability numerical calc. *(Russian)* 78—47053
conducting liq. in mag. field, convective flow stability *(Russian)* 78—47052
conducting liq. layer, surface tension effects, MHD convection stability and thermocapillarity *(Russian)* 78—47054
cone/plate system in fluid, friction heating and convection 78—87238
convective cells, stochastic oscill. spatial-time spectra *(Russian)* 80—103029
convective diffusion to surfaces of poorly streamlined bodies 80—6041
corrosion pit, convective diffusion 80—40601
Couette flow, instability of longitudinal convection rolls 78—26122
critical heat flux of saturated natural convection boiling with heating from below 80—10114
critical heat transfer to flowing cooling water 77—74910
cryogenic fluids stored in closed vessels, free convection heat transfer 80—1565
crystal growth by travelling solvent method, heat flow, diffusion and convection 77—39549
crystal growth from melts, hydrodynamic behaviour under large intertial accelerations 80—66421
crystal growth from solution, convection effects, holographic interferometic obs. 80—77565
crystal rotation in crucible, melt forced convection, computational results 80—84116
crystallisation on cooled wall with forced convection in melt 78—26022
crystallisation on vertical wall with thermal convection in melt 78—26021
cylindrical spaces, liquid filled, natural convection development, transients 80—1563
dielectric liquids, electrical convection and jet flow 80—1692
dielectric organic liquid, concentric annuli, heat and momentum transfer, electric field effects 80—96315
diffusion to drop, convective, large Peclet no., finite Reynolds no., asymptotic soln. 79—41742
diffusive convection, fluids with gradients of two properties, low Prandtl number, boundary layer method 80—69816
dissociating fluid layer, heated, effect of rot. on Benard convection 79—4020
drop in viscous fluid stream, nonstationary mass transfer *(Russian)* 79—10561
drops in liquid, diffusional interaction 79—81947
duct, circ., laminar convective MHD heat transfer for 3rd kind temp. boundary conditions 78—87342
Earth core, convection rel. to geomag. field generation and surface heat flow 77—73638
Earth core, example of nonlinear geomag. dynamo action 77—73637
Earth core, mean-field electrodynamics and dynamo theory of geomag. field 77—73636
elastoviscous liquid, combined free and forced convection flow through porous channel 80—103073
electric field, influence in dielectric fluid *(Japanese)* 78—5805
electrochemical cell, AC component effect on convective diff. processes, characts. 77—63929
electrochemical pit growth, convective diffusion in pits, ionic components conc. calc. 80—45409
electrochemical processes with free convection, numerical simulation 79—52681
electroconvection in weakly conducting liquids 78—18297
electroconvective instabilities overstable 79—27706

convection in liquids continued
electrodes, sheet, mass transfer to continuous moving surface 80—69821
electrodiffusion method for convective heat transfer characts. in various liquids 79—94746
electrolysing cells, hydrodynamic flow, free convective mass trans. 77—81407
electrolyte, ionic mass transfer in narrow rectangular conduits 80—61105
electrolyte, layer, convection onset condition 79—14492
electropolishing of horizontal surfaces kinetics, role of natural convection mass transfer 79—57143
electroviscous effect, AC characteristics, pressure-drop fluctuations 80—107457
embedded heater in solid, melting and natural convection 78—90646
enclosure between horizontal cylinders, steady and transient convection 79—41553
enclosure with heat source and sink on horiz. boundary, laminar natural convection 78—90882
energy stability of the Eulerian-mean motion in the upper ocean to three-dimensional perturbations 80—92149
ethyl alcohol, free fluid surface, thermo-capillary forces on transport process, turbulent gravitational heat convection 77—75920
evaporation with natural convection, simultaneous heat and mass transfer in laminar boundary layer, numerical anal. *(French)* 80—53778
ferrofluid, convective stability of horizontal layer in mag. field *(Russian)* 77—3885
ferromagnetic fluid rotating about vertical axis, convective instability of layer 79—27698
ferrosuspensions, internal rotations and the other transport phenomena 80—28573
film boiling under natural convection conditions, heat transfer 78—83231
filtration, plane, of underground waters, convective mass transfer, boundary problems *(Russian)* 80—83793
fine particle deposition, on rotating disc surface, convective diffusion under elec. double layer forces 78—61060
finned plate surface, convective heat transfer, vortex flow and turbulence intensity 77—72296
flat plate, gradual acceleration in variable viscosity fluid 78—30281
flat-plate solar collectors, laminar mixed convection in fully developed flow *(French)* 80—61411
floating zone melting, microgravity simulation of Marangoni convection 79—28911
flow in porous media, diphasic incompressible, diffusion-convection eqn., mixed finite element method, water flooding 80—74969
flow induced by a torsionally oscillating wavy cylinder 79—64772
fluctuating free convection flow on horizontally magnetised plate 80—33683
forced convection boiling, critical heat flux, Fe_2O_3 scale effects 80—64344
forced convection condensation in the presence of noncondensables, boundary values *(Japanese)* 80—92151
forced convection film boiling on plate with varying heat flux 78—5737
forced convection heat transfer near forward stagnation pt. of cylinder, variational method 79—98726
forced convection of supercritical press. water in heated small bore tubes 77—65739
forced convection with rheological systems, review 79—1222
forced convective film boiling, math. model 79—18686
forced convective transition boiling, prediction methods, literature review 77—3825
forced heat convection of linear flow of non-Newtonian fluids through rectangular channels 80—92141
free, in saturated porous medium boundary layer with lateral mass flux 79—27689
free convection, from downward facing inclined flat plate 78—34123
free convection boiling, critical heat fluxes generalised eqn. 77—62138
free convection effects in flow past accelerated plate in dissipative liquid 80—10246
free convection effects on the flow past an infinite vertical oscillating plate 79—94605
free convection heat transfer from heated cylinders immersed in a shallow water layer 80—38413
free convection heat transfer on a magnetic cylinder in a uniform magnetic field 80—83852
free convection in finite vertical channel, magnetic field effects 78—67270
free convection mass transfer from horizontal surface, electrochemical and holographic interferometric obs. 78—87344
free convective heat transfer, from inclined plate in water, effect of US vibr. 77—51055
free convective heat transfer from horizontal tube to fluid near critical state *(German)* 77—7397
free convective heat transfer from horizontal tube to refrigerants near crit. state *(German)* 77—11192
free convective motion, solution method 77—51057
free laminar convection for liquid in ribbed slot 80—96261
free turbulent heat exchange surface, free convection liquid flow 80—64543
Freon-11, pool-boiling, heat transfer from inclined plate 78—51046
fully developed free convection flow in a circular pipe 79—64766
geothermal energy extraction problem, thermal convection in shattered rock zones 77—78162
glacial ice free convection melting in saline water 78—3835
Gorter-Mellink convection in He II, axial heat slow eqn. and dimens. anal. 80—64545
groundwater singly dispersive convection, finite-difference simulation 77—37265
groundwater with convective dispersion, finite element anal., book contrib. 79—34877
heat exchanger, heat transfer coefficient, iteration-free calculation 78—1655
heat exchangers, high temp. thermal storage using latent heat method *(French)* 80—40912
heat exchangers, intermediate, effectiveness in three-loop nuclear power stations determ. 80—608
heat transfer with phase change, finite element anal. 79—3887
heating surface during boiling, temp. distrib. for a sudden increase in power *(Russian)* 77—84114
hexane, liq., burning rate in small vessel, convection effect 78—35680
high Prandtl number fluid with strongly temp. depend. viscosity 77—3823

convection in liquids continued
horizontal flat plate, heat transfer in natural convection flow *(Japanese)* 79—64658
horizontal layer, heat transfer meas. 79—41555
horizontal liquid layer, convective instabilities dynamics 79—4008
horizontally heated rotating fluid, spatial oscillations 77—55004
hot layer, hydromagnetic stability, effect of non-uniform elec. cond. 79—14485
hot-film probe, in reversing flow, forced convection, finite difference soln. 80—12177
hydrodynamic stability open disc theorem, thermal and thermohaline convection 78—59370
hydromagnetic convection in vertical annular pipe, rad. mag. field 79—60068
hydromagnetic flow, stability in temp. field 80—92231
hydromagnetic free convection past infinite porous flat plate in rot. system, slip effects 79—81989
hydromagnetic thermal instability of rotating fluid layer, Hall current effects 79—27699
ice, crystal growth rate in subcooled pure water 77—80431
ice-water interface, local temp. meas. and convective flow 79—73293
ice-water phase boundary, conc. depend. solute redistrib., spontaneous convection, chloride solns. 78—26665
immiscible incompressible fluids, interfacial convective instability, diffusional exchanges, adsorption-desorption processes 80—70504
in-stream settling basin sediment routeing, convective dispersion model 77—37272
incipient boiling, transition to film boiling 78—90660
inclined surface, natural convection flow, transition, vortex system, meas. method 79—27632
incompressible viscous flow, finite element-anal. by penalty function formulation 79—41651
instability, natural convection in vertical fluid layer, anal. by linear stability theory 78—34180
instability of convection rolls in moderate Prandtl no. fluid 79—50727
insulants, elec. stressed, bulk electroconvection 80—87814
interface, stability problem, diffusion, reaction and convection 80—33567
interface between immiscible liquids, convection induced by chem. react.-hydrodynamic coupling *(French)* 79—41682
ionic mass transport, at inclined circular disc electrode 78—26117
laminar boundary layer, along a heated horizontal hollow cylinder, buoyancy and variable viscosity 78—46964
laminar dispersion in circular tubes, approx. anal. 77—46986
laminar dispersion in rectangular conduits, side wall effects, convection 78—94636
laminar film, convective coupled heat transfer, Nusselt no. computation 78—59398
laminar flow in circular tubes, forced and combined convection, finite difference anal. 80—48711
laminar forced convection, multiple finite spheroidal transform and its application 80—12910
laminar free convection due to point source of buoyancy 77—15029
laminar heat convection, liq. flowing in annular channel with const. heat flux, numerical soln. 78—83392
laminar unsteady free convection flow past vertical flat plate, effects of suction 78—18296
linearly-stratified horizontal layer, onset of thermohaline convection 77—42897
liquid, dielectrophoretic heat transfer 78—94874
liquid crystal, nematic, oscill. convective instabilities 78—9943
liquid fuel droplet heating with internal circulation 78—75194
liquid insulants, stressed bulk electroconvection, preliminary obs. electrically stressed 80—53873
liquid layers, superposed, boiling, convection heat transfer 78—30159
liquid metal continuous casting, solidification process, convective heat transfer, anal. 78—84789
liquid metal turbulent heat fluxes, channel flow, nucl. reactor appl. 77—42035
liquid vertical layers, convective flows with spatially modulated temp. distrib. at boundaries *(Russian)* 79—32496
liquid-filled closed volumes, temp. stratification at const. heat flux density 79—81871
low-conductivity liquid, electroconvective stability 80—48814
magnetic convection, nonlinear, mean field approx., boundary layer method 80—69930
magnetic fluid, thermoconvective instability, with mag. field perturbations 78—94847
magnetic fluid (cable coolant), natural convection heat transfer 78—94846
magnetic fluid layer, thermocapillary instability with thermally insulated boundary 80—33595
magnetisable liquid, thermomagnetic convection between coaxial cylinders with distributed heat source 79—94622
magnetisable liquid layer, with solid boundaries, convective stability 79—94592
magnetizable liq., convective stability depend. on mag. field *(Russian)* 78—47051
magnetoelectrolysis in steady Hartmann flow cells, hydrodynamics, mass transport 77—36759
mass transfer by forced convection, at rough surfaces in annuli, rate meas. 77—27532
mass transfer of dissolved species, to planar electrode, combined effects 78—23949
measurement by differential light interferometer with achromatic $\lambda/2$ compensation 78—87419
melt, crystallising *(Russian)* 78—15385
melt, thermal convection as function of Grashof no., solidification kinetics 77—65661
melt crystallizing with conc.-depend. convection, impurity distrib. 80—10642
melt solidification, heat and mass transfer 79—14236
melted ice layer, onset of free convection criterion 77—58685
melting, of substrate into different miscible liq. layer, hydrodynamic instability, heat transfer 78—90695
melting at horizontal boundary, steady-state convection, interface corrugations 78—26118
melting process, with convective boundary condition, surface temp. rel. to time 79—76960
melting solid, role of natural convection 78—71275
melting with natural convection in melt region 78—30156

convection in liquids continued
- membranes, artificial, permeab. to pluridisperse soln. of ^{125}I-polyvinylpyrrolidone 77—12890
- metal, in annulus, natural convection 78—30294
- metal, laminar convective heat transfer along cylinder 77—914
- metals, w.r.t. Prandtl number and relative roughness *(Czech)* 77—7389
- metals with variable thermal cond. and capacity, forced convection 79—37310
- MHD, thermoelectric, appl. to fission and fusion reactors and metallurgy 79—50806
- MHD, unsteady free convection flow past vertical porous plate 78—30361
- MHD convection in rapidly rot. fluid layer, stability, rel. to geomagnetism 79—50808
- MHD convective flow through channel with conducting walls, Hall effects 78—5802
- MHD convective viscous flow past porous plate with suction, mass transfer effects 78—87398
- MHD Ekman layer on free convection past infinite porous flat plate 80—14830
- MHD flow, surface instability of nonisothermal layers 79—77272
- MHD forced convection in channel bounded by plate and permeable bed, Hall effects 80—69934
- MHD oscillatory flow past flat plate, Hall current effects 79—98816
- MHD Stokes problem for vertical plate, mass transfer and free convection current effects 79—90347
- MHD unsteady free convection flow, past hot vertical plate, calcs. 77—75986
- mixed laminar convection in vertical tube, thermophysical prop. temp. depend., effects 78—90895
- mixture, binary, oscillatory convective instability, thermodynamic anal. 78—94753
- molten salts, cellular convection near solidification point *(French)* 78—14004
- moving liquid, numerical method for convective diffusion problem 77—89120
- multi-layered geothermal reservoir, natural convection 80—8347
- multilayer flow, thermoconductive waves, interaction with radiation induced waves *(German)* 78—94803
- narrow vertical cavity, natural flow, visual obs. 78—34130
- natural, in closed cavity, approx. anal. methods 77—7390
- natural convection, in melted region around heated horizontal cylinder 79—46165
- natural convection boiling, heat-transfer coeff. 80—33421
- natural convection heating of liqs. in closed containers 77—15006
- natural convection in box of water-saturated porous media 77—31384
- natural convection in liqs. between sphere and cubical enclosure 77—23953
- natural convection in liquid layer in flat inclined solar energy panel *(French)* 79—18894
- natural convection in liquids with temperature dependent viscosity 78—94695
- natural convection patterns in inclined box, three-dimens. numerical anal. 77—19601
- natural convection patterns in inclined box, three-dimensional photography 77—19600
- natural convective transfer at low temp., thermal stratification effect 80—6039
- natural laminar convection flows, variable viscosity effect 80—33589
- natural motion, in confined porous medium, weakly nonlinear anal. 78—34136
- nematic film, phase grating produced by shear flow induced instability 78—9945
- nematic liquid cryst., anomalous convective temp. gradient crit. pt. *(Russian)* 77—7669
- nematic liquid crystal, electroconvective flow, vel. and orientation deform. angles *(Russian)* 79—37621
- nematic liquid crystal, Williams domain mode, non-linear analysis 77—62472
- nematics, homeotropic, heated from below, oscillatory convective instability, thermodynamic anal. 79—86690
- nematics, thermoconvective instabilities 79—77500
- Newtonian fluid, recirculating flow in rectangular cavity, free convective flow in enclosed container 80—74852
- nitrobenzene, liquid, electrohydrodynamic convection, laser light scatt. exam. 78—14094
- non-linear properties of thermal convection, review 79—18893
- non-Newtonian fluid, convection, stationary, vibr. instability 79—94683
- non-Newtonian fluid, effective diffusion of impurity in laminar flow of liquid 78—67228
- non-Newtonian fluid, free convection, heat and mass transfer 79—68765
- non-Newtonian fluid, hydrodynamic stability of free convection in vertical layer 78—59430
- non-Newtonian fluid, pipe flow, heat and mass transfer 79—46309
- non-Newtonian liquid, convective stability, energy method 80—38455
- non-stationary heat and mass transfer, coupled, with convective motion and relaxation, variational principle 80—106797
- nonisothermal two-phase flow in vertical channel, rel. to natural convection boiling 77—24013
- nonlinear at high Rayleigh number, viscous dissipation effect numerical integration 77—54994
- nonlinear thermosolutal convection 79—10557
- nonlinear two-dimens. Benard convection with Soret effect 77—19599
- nuclear reactor, convection effects on temp. distribs. during emergency cooling in SNR-300 77—26839
- nuclear reactor transient nonboiling heat transfer in cooling channel during flow coastdown 77—46267
- ocean, free convection development in upper quasi-homogeneous layer *(Russian)* 77—21784
- ocean, turbulence generation by convection *(Russian)* 78—16022
- ocean convection under ice sheet floating on warm salty water 77—70677
- open channel thermally stratified flow, eddy diffusivity buoyancy effects, obs. 78—90904
- oscillatory hydromagnetic free convection flow past an infinite vertical flat plate with suction 79—32687
- paraffin, solid-liq. interface motion during melting, convection effects, photographic obs. 79—18890
- paraffin plate heat storage element, fusion, periodic solidification, heat transfer kinetics *(French)* 80—40913
- parallel channel of forced convection boiling upflow system, instabilities 77—61494

convection in liquids continued
- parallel-plate channel, convectively-cooled, liq. solidification 77—68666
- Parowax, thermal energy storage, phase change material, time variation of storage and release 80—67008
- phase change region, cond. and natural convection, numerical method 79—41563
- photoabsorption convection in horizontal tube, unsteady-state convection, num. investig. 80—33594
- photoabsorptive convection, steady states in field of continuous laser radiation 79—14212
- pipe, containing anomalously viscous liq., convection intensification by spiral swirlers 79—94461
- pipe, horizontal, with different end temps., fully developed natural counterflow, temp. distrib. 78—75137
- pipe flow, turbulent, temp.-depend. viscosity effect on convective heat transfer 78—90884
- pipe with changing thermal power 80—23866
- plane-parallel channel, convection in turbulent liquid flow for Pai vel. profile 77—47013
- plate with steady state thermal boundary layer flow, appl. of governing principle of dissipative processes 79—50722
- plume, laminar, generated from heat source, temp. field 79—59984
- pollution dispersion-convection equation, soln. for bay with currents 77—91157
- polynary mixtures, natural convection boiling, heat transfer 78—90658
- pool boiling heat transfer from horizontal plates *(Japanese)* 78—67016
- pool heated volumetrically, reactor accident condition, phase change, free surface, thermal instability 78—89960
- pool-boiling and bubbling heat transfer, freely convecting liq. 79—32212
- porous bed with permeable boundary, natural convection 79—77238
- porous cylinder, water-saturated, heated, natural convection onset 78—59478
- porous media of low permeability, heat transfer in forced convection 78—83472
- porous medium, convective motions of saturating liquid near equilib. instability threshold 79—14398
- porous medium, heat transfer eqn. *(French)* 77—72298
- pseudoplastic fluid, flowing upward in vert. heated tube, variable physical props. 78—90945
- pseudoplastic non-Newtonian liquid, laminar natural convection heat transfer 79—64713
- pure liquid and binary soln. superheat, convective heat transfer from thin wire 80—92139
- radical species, tube electrode generation, laminar flow through EPR cavity, decomp., convection 77—24746
- Rayleigh-Benard convection, induced, pretransitional 79—55374
- Rayleigh-Benard convection, randomly forced, initial value problem 80—79314
- Rayleigh-Benard convection, time depend. vel., turbulence transition 77—3824
- Rayleigh-Benard convection, turbulence and intermittency, expt. 80—99998
- Rayleigh-Benard system, turbulence near onset of convection 80—48686
- Rayleigh-Benard-Marangoni instability, exptl. results 80—14700
- Rayleigh-Jeffreys convective stability problem with temp. and salinity gradients *(Russian)* 78—14012
- reacting particle in fluid, convective diffusion, nonlinear surface reaction kinetics 80—106854
- rivers, thermal convection downstream from thermal power plant warm water disposal constructions 79—83647
- rotating disc heat transfer with liq. jet impingement 79—4055
- rotating horizontal fluid layer, thermal instability 78—63438
- rotating liquid layer heated from below, form. and interaction of three-dimens. convective cells 79—14397
- saline water, side convection characteristics *(Russian)* 80—1580
- salt fingers, rot. effects 79—50767
- salt-brine interface, natural convection mass transport 78—30291
- saturated porous medium, completely confined, onset of thermal convection 78—83387
- second order liquid, convection flow past hot porous circular cylinder 79—14476
- second order liquid porous parallel walled channel flow with free and forced convection 78—42635
- second-order fluids, oscillatory free convection from infinite horizontal cylinder 77—72332
- sedimentation, settling convection, obs. and continuum fluid mechs. model 78—14070
- semi-infinite horizontal liquid layer with free boundaries, heat convection waves 77—11187
- silicone oil thin films, convective heat transfer, surface tension effect 78—94681
- simple fluid, energy stability method 79—27629
- smectic-A liq. crysts., sub-Rayleigh oscill. convection 80—87774
- smectic-A liquid crystals, oscillatory convective instabilities, caused by heating from below 80—103239
- solar absorbers, heat transfer by natural convection in an isothermal rectangular cavity open on one side *(French)* 80—61412
- solid spheres, reacting, in periodic array, convective mass transfer in liq. laminar flow 80—96176
- solidifying melt, concentration convection 79—14237
- solidifying melt thermal gravitational convection, impurity distrib. and transfer processes 80—19367
- solute layering, in low aspect enclosure, effect on lateral heat transfer 77—75776
- Soret-driven convective instability with rotation 78—46968
- sphere in current carrying liq., convection mass transfer, num. anal. 80—83851
- stability, convective, of weakly cond. liq. in electrostatic field *(Russian)* 77—27601
- stability of convective motion caused by internal heat sources *(Russian)* 79—14390
- stability of convective motion in fluid due to internal heat sources 79—77091
- statistical mechanics of stationary states, appl. to low-density systems 79—58624
- steady-state MHD convection in a vertical annular duct in a radial magnetic field 80—48809
- Stokes problem for infinite vert. plate, hydromagnetic free convection effects 80—10318
- stratified fluid, sugar soln., cellular convection, effect of inclination of heated wall 77—39323

convection in liquids continued
  stratified fluid layer, propagative thermal excitations *(French)* 80—33590
  stratified liquid, convective flow struct. after lateral heating *(Russian)* 77—11232
  stratified liquid, convective free flow struct. above heated cylinder 80—79322
  stratified liquid, free convective flow struct. over point heat source 80—79323
  subcooled forced convection film boiling in forward stagnation region 80—43702
  sugar solution, boiling, natural convection mechanisms on horizontal tube 77—24396
  supercritical, via layer of finite thermal conductivity *(Russian)* 78—38313
  surface tension driven convection, solidification effects 80—43703
  surface tension driven instability of liq. film flow down heated incline 79—27620
  surface-tension induced convection at reduced gravity 78—83374
  suspension, dielectric, convective heat transfer, rheodynamics, in horizontal coaxial cylindrical channel 78—59494
  temperature fluctuations in wake of linear heat source 79—77118
  thermal convection suppression by distributed automatic regulator *(Russian)* 78—30364
  thermal instability anal. for horizontal liq. layers with a density max. 78—67193
  thermocapillary convection, in floating zone melting, influence of zone geometry and Prandtl no. at zero gravity 79—66002
  thermocapillary convection, unevenly heated liq. stream near gas bubble 78—59460
  thermoconvective waves in horizontal bounded layer of incompressible fluid 77—89134
  thermocouple hot-wire anemometer for boundary layer meas. with free convection in liquids *(German)* 80—10329
  thermogravitation column, thermodiffusion and convection, flow distrib. and conc. profiles *(French)* 78—14493
  thermohaline convection in upper ocean, numerical simulation 80—48714
  thin film, viscous, between two nearly parallel walls, temp. distrib., convection effects 80—83801
  toroidal vessels, liquid filled, convective heat and temp. fields 80—1567
  transformer, oil-cooled, heat exchange anal., network method *(Russian)* 78—83399
  transient forced convection eqn. soln., circular pipe flow 78—30282
  transient hot wire method, role of convection 78—26121
  transient natural convection heat transfer 79—1050
  transient natural convection in a liquid during cooling 80—87770
  transient natural convection in single-phase heat-generating pool 80—9350
  transition boiling heat transfer with forced convection, composite test section, steady state method 79—19361
  tube, vert., uniformly heated, forced convection boiling, crit. heat flux 79—27498
  tube, with heated inner eccentric rod, steady convective laminar heat transfer 78—38311
  turbulence, free-stream, near semiinfinite flat plate, vortex array representations interaction 78—90842
  turbulent, laser beam propagation 79—98831
  turbulent channel liquid flows, nonsteady convective heat transfer 80—59023
  turbulent convection between parallel plates, result plotting method 80—24001
  turbulent convection in a cubic cavity heated from below 79—77092
  turbulent free convection in fresh and salt water, characts., visualisation 79—18888
  turbulent liquid flow in heated tube at supercritical press., heat transfer 78—71316
  turbulent natural convection boundary layer, space-time correl. meas. 78—71322
  turbulent natural convection in liq. metals in narrow cell *(French)* 78—94701
  turbulent tube flow, of water, with nonuniform heating 79—32513
  turbulent viscous incompressible flow in tube, nonsteady convective heat transfer 80—19393
  two-component liquid layer heated from below, convective instability, analogy with laser with saturable absorber 80—79319
  two-phase laminar channel flow, forced convection energy eqns. 77—55090
  Udimet 700, superalloy, convective processes during epitaxial regrowth 79—69919
  underground cable system, convectively cooled, temp. distribs., heat transfer correlations 78—71262
  underground cable system, convectively cooled, vel. distribs., press. drop correlations 78—71330
  uniformly heated fluid between vertical parallel plates, thermal convection 79—98727
  unsteady convection study, simultaneous velocity and interferometric meas. 79—98839
  unsteady convective heat transfer in heating liq. in pipe 77—89117
  unsteady free convection flow past a vertical porous plate with variable suction and transverse magnetic field 79—32691
  unsteady laminar forced convections in elliptic pipe 77—11184
  variational thermodynamics of viscous compressible heat conducting fluids 77—50868
  vertical channel flow, heat convection, fluid injection problem, Newton-Raphson method solns. 79—10556
  vertical cylinder, internal flow, with const. heat flux 79—46307
  vertical layers, struct. of laminar-turbulence transition and turbulent convection conditions 80—6040
  vertical natural laminar convection flows in cold water, buoyancy force reversals 80—59034
  vertical object in liq., total surface flux 79—37314
  vertical surface with suction, oscillatory flow, free convection effects 80—53865
  vertical tube with laminar combined convection, water, finite difference anal. 78—90894
  visco-elastic liquid, flow past hot porous circular cylinder, free and forced convection 78—83386
  viscoelastic liquid, flow through porous channel, free and forced convection effects 80—53861
  viscoelastic liquid, horizontal layer, thermal instability 77—68545

convection in liquids continued
  viscous convective flow, mixed finite element soln., discrete least squares approach 80—74851
  viscous fluid, incompressible, hydromagnetic free convective flow past vertical porous wall, mass transfer 80—64645
  viscous fluid, smooth transition to convection 78—83396
  viscous fluid in channel, laminar steady forced convection flow 79—32505
  viscous incompressible heat generating flow past porous plate with free stream oscillations, laminar free convection 79—37312
  viscous incompressible heat generating flow past porous plate with free stream oscillations, laminar free convection 79—37311
  viscous liquid, three-dimensional flow and convective diffusion toward particle, nonlinear kinetics 80—19397
  wall, plane, nonsteady heat transfer, conjugate problem soln. 79—37128
  wall with one-way heat flow, vertical inclined cavity stack 79—3899
  water, at 4°C, free convective flow, past infinite porous plate with const. suction 78—42606
  water, boiling, natural convection mechanisms on horizontal tube 77—24396
  water, boiling on finned surface, heat transfer crisis 78—9540
  water, convective heat transfer, free, with density inversion, in confined rectangular vessel *(German)* 79—18671
  water, cooling from surface under free and forced convection regimes *(Russian)* 78—36179
  water, forced laminar convection in horizontal pipe, density inversion effects, numerical anal. 78—90900
  water, horizontal layer, convection onset with max. density effects, nucl. plant waste heat storage 79—46164
  water, impinging on ice block, heat transfer in melting process 77—935
  water, MHD free convection flow past infinite porous plate 80—33703
  water, natural convection at density extremum 78—94696
  water, natural convection heat transfer from horizontal ice cylinder, anal. and obs. 77—27521
  water, non-Boussinesq convective struct. near 4°C 79—18886
  water, penetrative convection instabilities *(French)* 79—46304
  water, supercooled, effect on dendritic ice growth 77—7999
  water, thermally stratified, cooled, barrier effects on temperature structure and mixing *(German)* 79—41687
  water, thermally-stratified, cooled from above, free convection 79—46315
  water, thermoconvective instabilities, 0 to 4°C *(French)* 78—18300
  water, transient natural convection in horizontal pipe with const. cooling rate through 4°C 77—42828
  water, transition boiling under forced convective conditions, reactor accident condition 78—89961
  water, vertical boundary layer convection, salinity and press. depends. 79—37316
  water adjacent to vertical uniform flux surface, buoyancy driven flow, transition and transport 79—27631
  water at 4°C, unsteady free convection past infinite vertical plate 80—69822
  water between two horizontal concentric cylinders, free convective heat transfer analysis, density inversion effect 77—42836
  water boiling in annuli under forced convection, boiling noise 79—1062
  water cooling through free surface, critical value of boundary Rayleigh number *(Russian)* 78—61426
  water evaporative cooling, convection and mass transfer, fog formation in boundary layers 80—79293
  water evaporative cooling, heat and mass transfer coeffs., fog formation effects 80—79294
  water in cavity heated from below, convective instability *(Russian)* 79—14391
  water jet impinging on horizontal heated surface, single-phase convection and nucleate boiling regions *(Japanese)* 80—48761
  water near 4°C, plane-parallel convective flow instability 80—92137
  water saturated porous box with conducting walls, convection onset anal. 79—18949
  wedge, forced-convection film boiling, boundary layer flow 79—46366
  Ag-Cu (6.6% at.wt.), convective processes during epitaxial regrowth, expt. results 79—69919
  Al-Cu alloy, nonstationary mass transfer in front of moving phase boundaries in mormal freezing *(German)* 77—44238
  Al_2O_3, floating zone melting, forced convection, computer simulation 78—88422
  B_2O_3-$Na_2O(K_2O)(V_2O_5)$, thermal cond. of melt in region 900 to 1100°C, effect of convection 78—2309
  $CuSO_4$ soln., electrochemical analogue of Benard instability, isothermal and potentiostatic conditions 80—76530
  He distrib. system for Large Coil Test Facility 78—55001
  He, heat transfer by natural convection to liquid contained in high-speed rotating frame 79—58720
  He, heat transport in thermosiphon loops for superconducting turbogenerators 79—58718
  He I cryo-fluid, free convection at supercritical pressures 78—26745
  He, liq., Rayleigh-Benard expt., freq. locking and turbulence onset 79—90255
  He, supercrit., free convection heat transfer, 4.2-25K, 3-35 atm. 77—23961
  He, supercritical, high heat flux heat transfer, non-bulk Prandtl and Reynolds numbers 78—22346
  He, supercritical, laminar free convection heat transfer, analytical study 79—23311
  He, time depend. effects above convection, Rayleigh-Benard expt. using local probe 79—7718
  ^{3}He superfluid ^{4}He mixture, dil. soln. of ^{3}He convection 80—107600
  ^{3}He-^{4}He mixture, Benard instability near λ-temperature 80—34268
  ^{4}He, superfluid, thermo-osmotic convection, at incipient lambda transition, above crit. press. 78—95199
  Hg, inductively stirred, convective flow rate controlled by Lorentz's number rel. to solidified struct. 79—10444
  Hg layer with rot. and mag. field, cell sizes at thermal convection onset 77—54991
  Hg, natural convection in mag. field parallel to the gravity vector 79—81990
  InSb, convection in melts, and cryst. growth under large inertial accelerations 80—66421
  Li:NH_3, soln., free MHD convection near horizontal cylinder *(Russian)* 77—7467
  $MnCl_2$, aq. soln., thermomagnetic convection, in transverse flow round cylinder *(Russian)* 77—47100
  N_2, boiling liq., infuence of electric field on heat transfer 80—53770

convection in liquids continued
N_2, evaporating in horizontal tube, local heat transfer coeff. 77—23959
N_2, transient pool boiling, premature transition to stable film boiling 79—81709
NH_4Cl transparent soln., basaltic equiaxed solidification, visualisation of convection *(French)* 80—44297
NH_4Cl-H_2O, solidification microstructs., effect of reduced gravity 80—96632
Na, liquid, natural convection from vert. plate in fast breeder reactor 79—3202
Na, liquid, natural convection from plane surfaces, LMFBR design, review 80—37417
$NaClO_3$, cryst. growth from soln., convection phenomena 79—74074
$NaClO_3$, growth and dissolution kinetics, diffusion and convection regimes 78—63684
NaK, liquid metal natural convection under transverse magnetic field 80—69827
$NaNO_3$ melt, depend. of oscillatory Marangoni convection on zone length in cryst. growth melts 79—23555
Si, cooling rates of large diameter crysts. 78—35291
Si Czochralski growth, large crystal, convection and segregation 78—6843
Si, floating zone melting, forced convection, computer simulation 78—88422

convergence
see also convergence of numerical methods
adaptive beam forming processor formulation 80—91967
almost periodic functions with values in Banach spaces, convergence of Fourier series 77—82367
aquifer parameters, invariant imbedding and identification 79—57992
biorthogonal series convergence, biharmonic and Stokes flow edge problems 78—81847
Boltzmann eqn. on lattice, convergence 79—97314
boson expansions, convergence of various methods 79—93037
CI calculations, virtual orbitals for rapid convergence 79—85906
conditions of convergence of particle in cell method *(Russian)* 79—76567
convergence rates for elastic solutions method and variable elasticity parameters *(Russian)* 79—44740
degenerate-kernel methods, Fredholm integral eqns. approx. soln. 78—12543
diatomic molecules, one-electron, heteronuclear, partial wave treatment 79—10017
earthquake model, nonstationary, identification, nonlinear filtering approach 79—5458
eigenfunction expansions assoc. with vector-matrix differential eqn., convergence 78—69965
electrostatics, conditionally convergent series, for teachers 79—71201
ergodic processes, moving averages 77—37805
Feynman path integral, pointwise convergence 80—8778
Hartree-Fock wave functions, convergence in Roothaan's SCF eqns., 'level-shifting' method 78—41920
laser adaptive optical control with closed-loop estimation and predictive filtering 77—19298
Maxwell's initial boundary value problem, horizontal line (Rothe) method, convergence and error estimates 80—94957
Michaelis-Menten mechanism for quasi-steady state and quasi-equilibrium, approx. soln. 79—70511
Molodensky series, convergence improvement for geodetic boundary value problem soln. 79—62424
multiple Fourier series, convergence of rectangular partial sums 78—73831
neuron models Volterra-like polynomial representation 77—90754
nonlinear differential eqns., single and multistep methods 77—53733
nonlinear recursive estimation procedure, convergence and hybrid simulation 77—53850
nonstatistical parameter estimation adaptive algorithms 80—91995
nuclear reactor cylindrical models, diffusional approx., finite element anal., rate of convergence of solution *(Russian)* 80—18414
off shell scattering amplitude, S-matrix, pot. scatt., Mittag-Leffler expansions of Green's function, convergence 78—73874
one-dimensional oscillator, matrix elements of position coord., upper and lower bounds 79—35578
perturbation theory, Pade approximants and convergence, appl. intermolecular interactions 79—31635
perturbed Hamiltonian systems solution, quadratic convergence of accelerated elimination technique 77—60585
potential scattering, JWKB phase shifts, using Gauss-Mehler quadrature formulas 78—46411
quantum mechanical perturbation theory, convergence props., energy series 78—80
rotationally symmetric mag. field expansions into zonal harmonic functions 79—31772
scattering, algebraic theory, existence of wave operators *(French)* 78—24692
sequence of series of one-dimensional random variables with arbitrary depend. character, limit theorems *(Russian)* 77—49571
stochastic approx. procedures in continuous time 78—69969
thermonuclear device flute plasma oscillation stability algorithm 78—26336
two-body transition matrix and UPA model, convergence props. of generalised separable expansion 78—16939
Wigner-Kirkwood expansion of second virial coeff., convergence accel. 78—91052
$H+H^+$, interaction energy, perturbation expansion, symmetry forcing 79—22785
H_2^+, intramol. interaction energy, convergence of perturbation expansions 78—17745

convergence of numerical methods
ω-β-variable method, convergence props. 77—18792
accelerating fluid flow, finite-element soln. convergence 77—75873
Aitken's δ^2 transformation generalisation, summing perturbation series 78—24652
Aitken δ^2 transformation, geometric approx. 77—10595
approximate method for solving the integral equation of transport theory 77—87707
approximation method for solution of nonlinear integral equation with error estimation for problems in heat or mass transfer *(Russian)* 78—57879

convergence of numerical methods continued
aqueous solutions, Monte Carlo simulation, convergence of new algorithm 78—63649
asymptotic method using projection iteration, linear and nonlinear differential eqn. systems, errors, convergence *(Russian)* 77—57169
atmospheric wave propag. in distorted background flows, spectral series convergence 77—29375
atomic struct., numerical HF radial function during SCF iteration, convergence 78—58574
averaging methods, n-th order asymptotic convergence for autonomous systems 79—97188
Bayesian deconvolution, convergent props. 78—57861
Bayesian deconvolution, noise props. 78—57862
beam, with attached concentrated mass, nonlinear vibrs. 77—19557
Bertaut series convergence, for extended cryst. lattice electrostatic energy calc. 79—55693
boundary layer problems, singular perturbations, stability and convergence 78—90827
capillary surfaces approx. in gravitational field 77—55415
Chandresekhar's H-equations in multigroup neutron transport, iterative solns. 78—37389
CLEAN method, iterative beam removal, mathematical-statistical description 78—57464
collocation finite element method for groundwater flow simulation 78—93018
collocation variational method for solving Fredholm integral eqns., convergence condition 78—57764
collocation with piecewise continuous polynomials, stellar models appl. 77—87370
Compton effect, multiple scatt., operator formalism, nonstationary electrons 78—12846
condensation method for acceleration of convergence of solns. to partial differential eqns. 77—67253
conjugate gradient method, soln. of sparse linear eqns. 78—24647
conjugate gradient method for singular capacitance matrix equations., algorithm 78—36791
conjugate gradient solution to discrete ordinates equation 78—21622
connector choice in finite element anal. 78—45
constrained finite element solns., convergence proof 78—54168
constrained finite element solns., convergence proof 79—21537
continued fractions method for Mie scatt. calcs. 78—82914
cooperative stereo algorithm anal. 78—53413
coupled differential equation method calcs. of X-ray absorpt. spectra of molecules 77—88466
curved plate bending problem solved with nonconforming finite elements 79—37202
cylinder, infinite, solid, diametrically opposite conc. load deform. and stress 78—63287
density series, analysis of tail for Coulomb crystal energy 78—91300
diatomic molecule vibr. pots., representations accuracy 78—66531
difference equations solution *(German)* 80—36
differential equations, first order, convergence of averaging method and two-timescale method 78—85835
differential equations solution, parabolic, with M-matrices, iterative processes comparison *(German)* 80—1405
diffusion, linear eqn., improved series soln. method 80—8939
diffusion of immiscible fluids in porous media 79—90329
diffusion-type problems, mixed explicit-implicit iterative finite element scheme, soln. and examples 77—26155
direct gravity formula for 1967 Geodetic Reference System 78—92775
dynamic systems, numerical anal. of stable motions *(Russian)* 77—57181
echelette grating scatt., smoothing process for mode-matching soln. 78—1134
eigensystem derivatives, convergence of iterative method 78—28926
elastic-plastic initial value problem, iterative numerical integration 77—62170
electronic structure calcs., self-consistent, accelerating convergence of iterative process 80—87037
EM wave scattering integral eqn. 79—22882
epicyclic approximation for plane galactic orbits 80—36674
explicit iterative technique for FX2 reactor analysis computer code 78—17302
exponential operators, Zassenhaus and Baker-Campbell-Hausdorff formulae 78—20947
extended Fermi systems, hypernetted-chain calcs., convergence props. 78—24733
extended Graetz problem, approx. soln. by orthogonal collocation 77—89118
Fermi-hypernetted chain methods, appl. to ground-state Fermi systems 78—16727
fibrous materials, chain of bundles probability model for strength, numerical study of convergence 78—88496
field solution convergence in nonlinear environment by network method *(Czech)* 79—81350
finite element anal. of buckling of simply supported skew plates 78—59319
finite element analysis, patch test and general convergence criteria 77—31210
finite element approximation, Stokes problem 80—27138
finite element approximation singularities, two dimens. diffusion problems, nuclear reactor structs. 77—6496
finite element method, singular functions for convergence improvement 77—26152
finite element method for plastic flow theory problems *(Russian)* 77—58569
finite element method groundwater two-dimensional flow digital simulation 78—93018
finite element methods, 'moment schema', structural design computing *(German)* 80—14563
finite elements construction for natural boundary conditions satisfaction 79—2610
flow, confined, numerical simulation, anal. of higher order methods 80—19316
flow, plane parallel, finite amplitude stability, perturbative and iterative methods 78—38293
flow at high Reynolds numbers, convergence of real-time statistical laser Doppler velocimeter system 77—3895
flow-duct acoustics with eigenvalue depend. boundary conditions modal expansion convergence 77—50787

convergence of numerical methods continued
  fluid wave theories, Stokes, cnoidal, higher order solns. *(Japanese)* 78—42625
  Fourier-Bessel series summation *(Polish)* 78—12544
  fracture mechanics, appl. of method of pots. 78—51121
  function minimum norm approximation 78—54166
  Galerkin's method, non-uniform convergence 78—83304
  Galerkin-type spectral synthesis of neutron diffusion eqn., asymptotic error estimates 77—82989
  Gauss-Seidel convergence criterion for elastic structural stability 77—53781
  gradient-type methods convergence, singular parameter optimisation problems 77—82375
  gravitational potential of asymmetrical body, convergence of expansion in spherical harmonics 78—24479
  groundwater flow, unconfined, tunnel opening, 2-D finite element anal. 78—11922
  Hartree iterative solution of general SCF eqns., convergence criteria 77—61675
  Hartree-Fock-Roothaan equations, program for soln. by Roothaan's method 77—88395
  heat equation, semilinear, blowing up of finite difference soln. 77—54854
  heat exchanger true vibrations numerical soln. 78—75094
  heat transfer, nonlinear, iterative-variational method 78—94511
  heat transfer in laminar freely convecting boundary layer, series soln. predictive capability 78—71335
  Hermitian matrix, low lying eigenvectors, pseudo-convergence in iterative method 79—92970
  hybrid finite element methods 77—49581
  hydraulics variational inequality finite element approx. 77—13613
  hydrocode convergence 78—36834
  implicit finite element algorithms for geometrically nonlinear problems of struct. dynamics, accuracy anal. 78—86158
  inclusive iterative processes, convergence *(German)* 77—9876
  incompletely integrated shape functions, numerical stability, finite element stiffness matrices 78—1567
  integro-difference equations, degenerative, reduction method *(German)* 80—33
  interpolation by linear least squares, numerical stability of soln. *(German)* 77—9322
  inverse iteration method convergence, for nonlinear elliptic eigenvalue problems 79—40353
  ionospheric data processing, improvement of convergence of least squares method *(Russian)* 78—85700
  iterative methods, convergence rate, comparative study, appl. to hypersonic flow problem 79—40374
  iterative methods in finite element anal. of reinforced concrete 78—38186
  iterative procedures for penalty function solns. of algebraic systems 78—57770
  laminar flow with separation, successive approx. algorithm, convergence *(Russian)* 78—75117
  lattice sums from electronic struct. of crystalline solids 78—30577
  Legendre Pade approximants, convergence, to Coulomb and other scatt. amplitudes 78—28983
  light scatt. from three-dimensional obstacles with complex refractive index 77—75415
  linear difference equation, optimal estimates for soln. on circle 77—25920
  linear operator equations, convergence rates of variational solns. 77—33
  linear system solution by modified Stone finite element method *(French)* 79—41279
  liquid, Zwanzig perturbation expansion convergence, free energy 77—76274
  lumped mass approximation of heat eqn., uniform convergence 79—18669
  lunar motion, literal soln., formal convergence *(French)* 80—36482
  LWR core power distrib. calc., convergence of reiterating process *(French)* 80—5200
  M-matrices, differential eqns. soln. *(German)* 77—82377
  MacCormack's scheme, acceleration 78—36808
  MacCormack finite-difference scheme, over-relax. procedure 77—26161
  MC-SCF theory, orthonormality-constrained orbital optimisations 78—86766
  MCSCF method improvement 80—52857
  mesh analysis processes *(German)* 78—87257
  MHD equilibrium equations, convergence of iterative schemes 80—59115
  molecular collisions, differential scatt. cross sections from classical trajectories, Legendre moment method 78—3314
  molecular orbital CI calcs., convergence rate 78—70750
  molecular orbital SCF calcs., accel. convergence using reverse level shifting technique 78—70735
  moment-method solutions, convergence improvement using interpolants 79—18335
  Monte Carlo simulation of Brownian dynamics, new method, convergence props. 79—12719
  multicompartment diffusion and reaction modeling system applied to transmitter-mediated photoreception 79—70547
  multiconfigurational Hartree-Fock procedures, 2nd- and approx. 2nd-order 79—93907
  multipole expansion, choice of orders and density partitioning techniques 77—61677
  Navier-Stokes equations, theory and numerical analysis, book 78—77721
  neutron transport, 2-D, diffusion synthetic acceleration method 79—22357
  neutron transport, diffusion acceleration 80—13528
  neutron transport theory, Chandrasekhar H-eqns., comparison of iterative methods 80—47521
  Newton's method for solving nonlinear inequation systems, convergence 77—30001
  Newton Raphson algorithm, standard and damped least squares methods 77—9878
  NMR bandshape, complex exchange-broadened, iterative computer anal. 79—35805
  nonlinear chaotic iterations, local convergence *(French)* 77—67241
  nonlinear fluid dynamics, spectral decomposition in advection-diffusion analysis by finite element methods 79—49053
  nonlinear free surface flow problems, divergent low Froude number series expansion 78—51146
  nonlinear transformations for accelerating convergence of infinite integrals and series 77—67260

convergence of numerical methods continued
  nonlinear two-point boundary value problem with Newton method solution, mesh refinement process 78—36809
  nonlinear variation eqns., convergence of finite element solns. 78—86127
  nonselfadjoint operator eigenvalues approx. 77—54952
  nonseparable system semiclassical quantisation, invariant tori and energy levels calc. scheme 79—97225
  nozzle, convective heat transfer, turbulent boundary layer regime 78—9670
  nuclear reaction problem, iterative solutions, method of moments 80—18251
  ordinary fourth order differential eqn., numerical soln., convergence 77—87636
  orthogonal polynomials expansions, summation procedure 78—81805
  Pade approximants, punctual, partial wave expansion summations in scatt. by long range pots. 78—49707
  parabolic problem exact control finite element collocation method 77—26156
  partial-wave Schrodinger differential and integral eqns., comparison of numerical solns. 78—16671
  perturbation method and boundary conditions at noncanonical surfaces *(Russian)* 78—77696
  perturbation method in fission reactor calcs., convergence criterion and error estimate 77—14216
  perturbed energies, 2nd order, coupled HF iterative procedure, geometric approx. 79—9991
  plane restricted three body problem, asymptotic solns. *(Russian)* 77—22049
  planetary disturbing function expansion, convergence of Newton's iteration 77—64629
  plate, rectangular, with clamped/simply supported edge conditions, free-vibr. anal. 78—59340
  Pocklington integral eqn. basis function continuity requirements 77—74208
  Poisson's equation, finite difference form, numerical soln., unconditionally stable scheme 79—50
  potential flow, mixed hybrid finite element methods, book contrib. 79—32445
  pseudo nonlinear regression 77—64933
  radiowave propagation, numerical approximations of Sommerfeld integral for fast convergence 78—66727
  rarefied flow, low-speed flow over sphere, convergence of integral methods 78—22375
  renal counterflow systems differential equation, soln. by numerical method 78—24082
  residual correction applied to a sequence of block tridiagonal matrices 79—72800
  response matrix eqns., convergence of iterative solns. 77—67795
  Riccati equation, matrix differential, steady-state soln. calc., iterative algorithm *(Russian)* 77—49585
  Saint Venant partial differential eqn. four-point implicit numerical method 79—10582
  scattering, inelastic, R-matrix soln. of coupled eqns. 79—10163
  SCF theory, general many shell, level shifters 78—17548
  Schrodinger one-dimens. eqn. 77—64963
  second order hyperbolic differential equations, initial value problems *(German)* 78—20952
  Seidel's process for linear eqns. with non-negative elements *(Ukrainian)* 78—54165
  seismic stratum velocities determination, iterative method convergence *(Russian)* 79—74982
  self-consistent convergence, effect of electron distrib. nonuniformity 77—18778
  semiconductor, impurity ion pot., screening charge density expansion convergence 79—7799
  shells, cylindrical, mixed finite element approx. convergence 80—33450
  shifted Chebyshev polynomials, soln. of second kind operation eqns., convergence 78—62059
  singular finite elements, improvement of convergence *(French)* 77—49579
  skew plate free vibration, B-spline coordinate functions 79—68623
  spectroscopic measurement, convergence of iterative deconvolution technique, effect of errors 77—53849
  speed of convergence of a posteriori variance estimation *(German)* 79—100984
  spherical dome, three-dimens. elasticity soln. and edge effects 78—59306
  stability of numerical solution to problem of moving force on nonlinear elastic material 78—13944
  stable operational processes appl. to inverse geophys. problems 78—85718
  steady state Navier-Stokes equation, numerical method and appl. *(Japanese)* 77—68564
  steam generators, steady 2-dimens. two-phase flow and heat transfer calc. 79—1237
  stochastic collection eqn., sources of computational instability 77—2211
  Stoke's problem in velocity pressure formulation, mixed finite element approx. *(French)* 78—86164
  structural wt. optimisation, optimality criteria and mathematical programming 78—26029
  superconducting transition temp. theory, soln. of series expression for T_c and its radius of convergence 79—78251
  superposition method, appl. to free vibr. anal. of cantilever plates 77—39249
  thermoviscoelastic transient responses, stability and accuracy of finite element solns. 80—5951
  thermoviscoelasticity problems, numerical soln. processes, stability, convergence *(Russian)* 79—27536
  three-dimensional neutron transport, discrete ordinate solution 80—63222
  transition matrices for Markov chain sampling, model systems, convergence rate comparisons 77—57165
  transonic flow, relaxation solutions, convergence acceleration using cyclic iterative method 77—62272
  transonic flow solution method using acceleration technique based on Wynn's ε-algorithm 77—58724
  transport calculations in cylindrical geometry 79—58655
  transport equation, S_N methods of soln., exponential supplementary eqns., one-dimens. case 77—50189
  two dimensional bound state problems, finite element method comparison with spectral method 80—47856
  two-dimensional neutron diffusion eqn. for triangular region, finite Fourier transform soln. 78—78432
  unbounded two-dimensional linear eddy current algorithm 79—41300

convergence of numerical methods continued
underwater sound, convergence of Gaussian quadrature ranges, with observed sound-speed profiles 77—46851
vibration analysis, of singly curved rectangular sandwich plates with clamped boundaries, iterative calc. using Kantorovich method *(Japanese)* 80—5970
viscoplastic limit load problem, kinematic soln. method *(French)* 78—30195
viscous flow, 2nd order upwind scheme critique 78—94744
von Karman plate bending equations approx. 79—50598
vortex methods for Euler's equations 80—33614
water, liq., Monte Carlo simulation, convergence of new algorithm 78—63649
water, liq., Monte Carlo-Metropolis computer simulation, convergence characts. 80—10485
weather forecasting, balance eqn. soln. with min. correction of mass field 78—36246
Wiener-Hopf eqns. in non-LTE radiative transfer, rapidly convergent iterative method 78—12089
wind tunnel, convergence to interference-free conditions 78—38419
wings, low aspect ratio, computation of nonlinear characts. 79—41690
X-ray tomography, iterative reconstruction algorithms 77—12988
Cu, Fermi surface, electron mass enhancement, orthornormal function enhancement 80—96777
Nb, Fermi surface, electron mass enhancement, orthornormal function enhancement 80—96777

conversion electron spectra
conversion electron Mossbauer spectroscopy down to 4.2K, applications to thin film and surface studies 78—84504
depth selective Mossbauer effect spectroscopy empirical method of quantitative anal. using conversion electrons 78—20130
double focusing Fe core electron spectrometer BILL for (n,e^-) meas. 78—82566
high-spin states, means and methods of investig. 78—86722
isomer shifts, total conversion coefficients, nuclear electron and gamma transitions importance 79—85411
kinematic Doppler correction method for high resolution in-beam conversion electron spectroscopy after (HI,xn) reactions 79—54739
liquid scintillation spectrom. meas. of internal conversion electrons 79—89520
microfoil conversion electron detector for Mossbauer spectroscopy 78—70698
mini-orange spectrometers, conversion electron spectroscopy 79—93864
Mossbauer depth selective spectra 79—35909
Mossbauer depth selective spectroscopy, low energy electrons in matter 80—15930
Mossbauer depth selective spectroscopy influence of atomic number of inert component in surface layer 80—15931
Mossbauer radiation scatt. by condensed matter, review 79—78596
Mossbauer spectra, electrons below 10 eV 80—37145
Mossbauer spectra, X-ray prod. of secondary electrons 77—59498
Mossbauer spectrometry, back-scatter-type gas flow detector 80—37680
Mossbauer spectroscopy, cryogenic proportional He counter 80—69010
Mossbauer spectroscopy, dynamic theory 77—51997
Mossbauer spectroscopy, electron transport anal. 78—94159
Mossbauer spectroscopy at high temp., proportional counter 80—27886
nuclear isomers, 10^{-4} to 10^{-1} sec lifetime, decay spectra, meas. procedure 79—36167
polarisation of conversion electrons, parity violating nuclear forces 78—50125
standard spectrometric source conversion peak half-width determ. 77—79499
thin foils, depth selection, Monte Carlo calc. of energy distrib. 79—45598
(n,e) reactions study using internal target β-spectrometer with transport solenoid, background suppression 77—6612
Ag, odd-mass isotopes, $9/2^+ \rightarrow 7/2^+$ transitions, transition probabilities, half-lives 77—18475
Am, 240-3, spontaneous fission, conversion electron spectra obs. 77—82864
^{75}As populated in ^{75}Se decay, E0 transitions 80—22752
^{206}At→^{206}Po, EC-β^+ decay, Po excited levels 77—79340
^{194}Au, isomeric states anal. conversion electron and γ-ray spectra from ^{194}Pt(p,n) and ^{195}Pt(p,2n) 77—71582
^{143}Ba, nuclear spectroscopy of neutron rich A=143 nuclei 79—59039
^{80}Br, level struct. determ. from thermal (n,γ) meas. 78—41667
^{82}Br, level struct. determ. from thermal (n,γ) meas. 78—41667
^{109}Cd EC decay data revision 80—5095
^{112}Cd, $0_1{}^+ \rightarrow 0^+$ elec. monopole transition in low-lying ^{112}Cd levels prod. in ^{112}I decay 79—54406
^{114}Cd(n,e^+e^-), thermal 77—26624
^{140}Ce, hexadecapole motion obs. from α-scatt., EM transitions and conversion electron spectra 78—25097
^{139m}Ce, internal conversion of N=81 isotones 78—13027
^{123}Cs(^{123m}Cs), gamma and conversion electron radiation 80—106017
^{131}Cs populated in ^{131}Ba decay. E0 transitions 80—22752
^{156}Dy, prompt transitions multipolarities, γ and conversion electron spectra, energy level bands, spin, parity 78—8768
^{152}Eu, spectra meas. with Si(Li) detector 79—36460
Fe film, vacuum-evaporated contamination, conversion electron Mossbauer spectroscopic obs. 78—23985
^{57}Fe backscatt. electron Mossbauer spectroscopy 80—29661
^{224}Fr→^{224}Ra, γrays, internal conversion, eγ coincidence spectra meas. 80—78216
^{146}Gd decay, γ- and internal conversion electron spectra 79—75916
^{147}Gd, γ-transitions, internal conversion electron spectra meas. 79—6475
^{151}Gd, high spin states, gamma ray and conversion electron obs., level struct 77—46130
^{152}Gd populated in ^{152}Eu decay 80—22768
^{155}Gd, K X-ray intensity following thermal neutron capture 77—26691
^{155}Gd, vibr. state, level scheme, γ and conversion electron spectra from ^{154}Gd(n,γ) 80—57696
^{157}Gd(n,γ), γ and conversion electron spectra, ^{158}Gd collective bands 78—89819
^{180}Hf, polarisation of internal conversion electron calc. 78—50125
Hg, A=191,2,3,5,7,9, rot. aligned bands, high spin states, energy levels B(E2) values 78—70483
^{197}Hg energy levels from ^{195}Pt(α,2n), γ and conversion electron spectra, spins, parities 78—25149
^{199}Hg, K X-ray intensity following thermal neutron capture 77—26691

conversion electron spectra continued
^{157}Ho→^{157}Dy decay, internal conversion electron spectra and eγ coincidences *(Russian)* 80—68604
^{159}Ho, level scheme, γ-singles, conversion electron spectra via ^{159}Er decay 78—547
^{129}I, internal conversion electron and Mossbauer spectra, calibration of isomer shift 80—39921
^{111}In, rotational band detect., internal conversion electron spectra from ^{111}Cd(p,nγ)^{111}In 79—6362
^{114}In, internal conversion on outer electron shells, 191 keV E4 transition 80—42587
^{131}La→^{131} decay scheme, γ, X-ray and conversion electron spectra *(Russian)* 80—32241
^{172}Lu, decay scheme, γ-ray, conversion electron spectra 79—75913
^{172}Lu, internal conversion electron spectra 79—75906
^{172}Lu, radioactive decay, γ-ray spectra, internal conversion electron spectra 79—75912
^{176}Lu, K X-ray intensity following thermal neutron capture 77—26691
^{150}Nd(α,4n)^{150}Sm, 45 MeV, yrast bands in Sm anal. in interacting boson approx. 78—13124
^{141m}Nd, internal conversion of N=81 isotones 78—13027
^{60}Ni, hexadecapole motion obs. from α-scatt., EM transitions and conversion electron spectra 78—25097
^{200}Pb, obs. of levels in ^{198}Hg(α,2n) 78—66192
^{206}Pb, level scheme including conversion electrons ≲40 eV 78—21518
^{104}Pd, characts. of the levels excited in ^{104,104m}Ag decay 79—9515
Pm, A=143, 144, 145, ICC, γ-spectra, multipolarities for low-lying levels 77—50081
^{147}Pm decay, K-orbital shake off electrons and X-ray spectra 77—46141
^{204}Po, γ-rays, conversion electron spectra, γγ coincidences 80—83061
^{207}Po^m(2.79 s), ^{207}Po^g decay, spin from conversion electrons meas. 78—58252
^{141}Pr, ICC, γ-spectra, multipolarities for low-lying levels 77—50081
^{A}Pt, A=190-193, lifetimes of rotation-aligned states 78—93969
^{191}Pt energy levels, γ and conversion electron spectra, spins, parities 78—25149
Pu, A=239, 241, spontaneous fission, conversion electron spectra obs. 77—82864
^{239}Pu, spectroscopy in second minimum of pot. energy surface 79—30805
^{90}Rb, β,γ, conversion electron spectra obs. 77—71583
^{184}Re decay, energies, relative intensities, of conversion electrons and γ rays 77—61381
^{189}Re, beta-decay, ^{189}Os scheme 79—54388
^{208}Rn→^{208}At, γ-ray, conversion electron spectra 80—83072
^{221}Rn, decay scheme, α-, β-, γ-spectra meas. 79—6507
^{224}Rn→^{224}Fr±^{224}Ra, γ—rays, internal conversion, eγ coincidence spectra meas. 80—78216
^{100}Ru, negative parity bands obs. in ^{100}Mo(α,4n)^{100}Ru 77—6291
^{106}Ru β-decay, e^+ spectra, ^{106}Pd levels and E0 transitions 79—75894
^{121}Sb(n,γ), γ and conversion electron spectra, ^{122}Sb energy level scheme 78—54721
^{123}Sb populated in ^{123}Sn^m decay, γ-ray, X-ray and electron spectra 77—88073
^{152}Sm populated in ^{152}Eu decay 80—22768
^{119}Sn conversion electron Mossbauer spectroscopy in β-Sn, $CaSnO_3$ and SnO_2 79—33575
^{119}Sn, thin foil, 19.6 keV conversion e^- energy, ang. contrib., Monte Carlo calc. 79—11360
^{181}Ta, anomalous M1-conversion, 482-keV transition, penetration parameter meas. 77—61382
^{182}Ta decay, K-conversion coeff. of γ-rays above 800 keV 77—14069
^{182}Ta, decay scheme, conversion electron spectra, K-line transitions 78—13025
^{154}Tb, elec. monopole and quadrupole matrix elements for the $K^\pi=0^+$ bands in ^{154}Gd 77—57626
^{96}Tc low lying states, level scheme, parities, from conversion electron, γ spectra 78—46024
^{186}Tl decay, γ, conversion electron spectra and coincidences, ^{186}Hg bands, shape coexistence 78—25156
^{205}Tl(α,3n), 35-51 MeV, ^{206}Bi high-spin states anal. 78—82368
Tl(α,xn)^{205}Bi, population of high spin states, γ and conversion electron spectra 77—30616
^{157}Tm, ^{155}Tm decay, nucl. energy levels determ. of ^{157}Er and ^{155}Er *(French)* 77—57630
^{163}Tm decay, ^{163}Er excited state obs. 78—17146
^{165}Tm, levels from ^{165}Yb β-decay, γ and conversion electron spectra 78—74334
^{169}Tm, double K-shell vacancy creation by internal conversion in ^{169}Yb, EC decay 77—57627
UF_4, inner conversion electron spectra, electron orbit hybridisation *(Russian)* 80—87227
γ-UO_3, inner conversion electron spectra, electron orbit hybridisation *(Russian)* 80—87227
^{235}U(n_{th},f), investigation of conversion electrons in range 150 to 1500 keV *(Russian)* 77—10458
^{238}U, spontaneous fission, conversion electron spectra obs. 77—82864
^{235m}U differential spectra, isomer excitation energy *(Russian)* 80—13416
^{167}Yb, spin and parity determ. from ^{167}Lu→^{167}Yb data, ε/β^+ anomaly 79—6380
^{169}Yb, conversion electron spectrum below 300 keV 77—6303
^{169}Yb, populated in ^{169}Lu decay, meas. of γ-ray and conversion electron spectra 80—22766
^{169}Yb populated in ^{169}Lu decay, γ-ray and conversion electron spectra 80—22767

convertors
see also analogue-digital conversion; code convertors; digital-analogue conversion; direct energy conversion; frequency convertors; image convertors; impedance convertors; magnetohydrodynamic convertors; magnitude convertors; phase convertors; power convertors; solar absorber-convertors
adaptive amplifier convertor using sensitivity stabilisation for resistance thermometer and strain gauge *(Russian)* 77—41593
air flow consumption meas., respiratory process parameters determ. using electric model *(Bulgarian)* 80—76867
bolometric laser emission convertors, thin wire, thermal processes, EM energy absorption *(Russian)* 77—18094
capacitance to voltage, for automatic test set 78—24818
charge to time convertor, gated seven channel 78—13388
charge to voltage convertor, for ionisation chamber dosimeters 78—78505

convertors continued
- circular magnetoelectric convertors, angle-of-rotation conversion errors 77—17968
- D/A, use in photoelectronic spectrometer and coincidence instrum. 80—22473
- displacement A/D convertor with multichannel phase shifter 77—5823
- E_{112} mode, rectangular sensitivity analysis, nondestruct. control of epitaxial layers sim. structure appl. *(Russian)* 77—18052
- electrohydrodynamic and electropneumatic, flow regime alteration by corona discharge *(Russian)* 77—11269
- energy, efficiency increase, 1978 state and development trends 79—52917
- fluorimeters, weak fluoresc. detect., analogue method 77—40581
- frequency to magnetic field convertor for NMR magnetometer 79—71490
- frequency to voltage convertor using SAW linear FM chirp filter 80—19182
- frequency-voltage convertor for angular velocity meas. *(Polish)* 78—70101
- frequency-voltage convertor using Nb-oxide-Pb tunnel junctions, design 77—82555
- galvanomagneto-recombination, used in multichannel magnetometer 80—31810
- graphics calculator system using X-Y recorder and computer as digitiser 80—13046
- Hough-Powell digitizer for processing film from bubble chamber Mirabelle in K^+p expt. at 32 GeV/c 80—69040
- left ventricular assist system microprocessor controlled electromechanical convertor 78—15928
- liquid level-to-frequency converter 79—6080
- logarithmic, principle and appl. *(German)* 79—9233
- logarithmic frequency-voltage convertor design 77—13775
- magnetocumulative generator, megampere pulse shaping, explosively compressed plasma column *(Russian)* 78—1912
- measuring, linear, integrated parameters determination, experimental 77—74385
- mirror field ion-electron convertor, particle trajectories, IBM 360/91 computer calcs. 77—6626
- multijunction thermal, for AC voltage and current meas. 77—18033
- neuron firing rate meas. by freq.-to-voltage converter 79—70715
- NMR freq. to magnetic field convertor, digital circuit 77—61097
- O/E and E/O, connected to both ends of optical fibre giving low-loss, broad band, non-inductive line *(Japanese)* 80—87510
- parametric convertor type pulse amplifiers, AC Josephson effect appls. 78—19184
- percentage ohmmeter, wide-range, linear convertor-voltmeter construction 78—239
- radioisotope, parameter calc., thickness monitoring appl. *(Russian)* 78—25403
- RC, capacitor discharge through bolometer, RF power, energy measurement, digital output *(Russian)* 77—37940
- readout conversion, mechanical to electrical, of differential oil flowmeter 80—75013
- readout conversion, mechanical to electrical 80—75012
- sea wave energy conversion, using half-plane and omni-directional convertors 79—52875
- semiconductor current-freq. convertor circuit for digital integrator 78—21196
- sidereal time source, electronic convertor for mean to sidereal time 79—84677
- TDC, high precision calib. method 77—57831
- TE-TM light mode convertor using acousto-optic interaction in $LiNbO_3$, expt. 78—46794
- temperature-to-frequency, thermistor multivibrator applic. 77—26289
- temperature-to-time, using op amps 77—26290
- temperature-to-voltage linear convertor 78—32811
- temperature/frequency wide range convertor, expt. and cct. 77—17978
- thermal current convertor, for accurate AC meas. 77—18032
- thermometer with automatic balancing, for liquid streams temperature meas. 80—47055
- thyristor convertors, in regulated current source 77—37921
- time to amplitude, performance tests at high conversion rates 80—62648
- time to digital convertor, wide-range 79—18090
- time-to-amplitude convertor, rel. to decay time coincidence spectra anal. 77—38575
- time-to-amplitude convertors, spectral distortion *(Japanese)* 77—46469
- time-to-number convertor, wide-range high-resolution 78—9039
- total exposure error, digital instrum. for cameras with or without built in exposure meter 79—6208
- US field intensity meas. *(Russian)* 80—38209
- voltage-frequency convertor, bipolar, with transfer charact. linearisation 78—8414
- voltage-frequency convertor for astronomical photometry 78—45233
- voltage-frequency convertor using equal-weight conversion method 78—4650
- voltage/pH convertor, using operational amplifiers *(French)* 79—63267
- Al plate ion-electron convertor, for secondary ion intensity changes correction 78—12796
- $LiNbO_3$:Ti electro-optic TE-TM mode convertor structure 80—64215
- Pt-Rh resistance thermometer temp. convertor for nonlinearity error correction *(Russian)* 78—70124

convex programming
- design optimisation of reinforced plastic cylindrical shell under dynamic loading 79—59935

conveyors
- NDT, conveyor belts with steel reinforcing cables, computer-aided magnetic defectoscopy 77—73417
- pendulum oscillation optimal passive suppression *(Russian)* 79—10454
- polymer powder, pneumatic conveyance through metal pipes, charging tendency meas. 79—50186
- solid particle pnuematic conveyance, flow characts. 79—37380

cooling
- *see also Joule-Thomson effect; low-temperature production; magnetic cooling; refrigeration; supercooling*
- ablation of elastic solid, variational principle 78—90698
- absorption chillers, solar-fired, capacity modulation 80—66952
- absorption refrigeration machine driven by solar heat for air conditioning, math. modelling 80—76651
- AC conductor, cooled by cryogenic liq., heat transfer models 80—5926
- acoustooptical effects of cooling liquid, absorption of flashlamp radiation with phase transition in medium 80—5868

cooling continued
- aerodynamic heat transfer meas. using transient techniques 77—80258
- aerosol, particle fallout rate under nonisothermal conditions 78—7238
- aerospace solar panels with concentrating reflectors 79—96472
- agitated vessels with bare and finned vertical tube baffles, heat transfer, power expenditure 79—1052
- air, radiative cooling behind strong shock waves 78—91030
- air bearing and diamond machine design for optics 80—1365
- air warming and cooling rates, urban and rural sites 79—88454
- air-stream cooling device for precession photography of proteins 77—27781
- Alae lava lake, Hawaii, numerical analysis of cooling 77—64248
- alkali metal based liquid coolants, sp. ht. 79—86902
- alkylbenzenes, jet-cooled, vibr. relax., absorpt. spectra 80—74236
- alkylbenzenes, jet-cooled, vibr. relax., fluoresc. spectra 80—78694
- alloy, ternary, transition of univariant form. equiliv. into decomposition equilib. *(German)* 79—43196
- alloys, apparatus for rapid hardening from liquid state 80—76275
- annular gap with axial flow and rot. inner cylinder, heat transfer coeffs. 79—27489
- annular rib cooled by boiling liq. on surface, heat cond. anal. 79—55315
- atmosphere, IR cooling rates, effect of tropospheric aerosols 78—88886
- atmosphere, standard, IR cooling rate 80—26609
- atmospheric radiation climate of Thailand, calcs. from routine meteorological data 79—29814
- atomisation of water drops on hot metal wall *(French)* 80—79112
- atoms, laser cooling, Raman mechanism 80—23371
- bimetal, high-speed steel + machine steel, chem. comp. influence on magnitude of residual stresses in cooling *(Russian)* 79—74183
- Bitter solenoid efficiency factor, allowance for cooling holes 79—30502
- boiling burnout, for heaters cooled by liquid jets 79—59979
- boundary value problems, mixed and oblique derivative boundary conditions 80—69820
- brass, free cutting, machinability and mech. props., cooling rate effects *(Korean)* 77—63695
- brass cap cooling with liquid N_2, heat transfer 77—61071
- breeder reactor liquid Na pressure meas. *(German)* 77—88270
- bubble growth, noncondensing gas-vap. injected into liquid 78—55553
- building structures, harmonic temperature waves obs., thermoconductometer development and appl. 77—49720
- trans-butadiene, $^1B_{1u}$-state dynamics in cooled supersonic expansion, electronic absorpt. spectra obs. 80—78629
- cable oil, EHD pumping 78—87414
- capillary porous layer, statistical model of boiling 77—89196
- ceramics, porous, frost resistance under 1-d cooling, pore size distrib. effect *(Japanese)* 78—44069
- ceramics treatment methods, drying, cooling, heat treatment, reln. to material props. *(French)* 77—90296
- chalcogenide glasses, O-free, cooling rate influence on optical consts. 80—88952
- circulating cooling system, based on commercial 6.3 helium liquefier 78—57961
- closed-cycle cooling system, at UPM Cryogenic Facility, Saudia Arabia 79—71459
- cloud-free atmosphere long wave cooling rate determ. method *(German)* 77—64474
- cold liquid spray interaction with hot gas stream in channels 77—15108
- cold-bath, precision, laboratory appl. construction 79—26048
- combustion product plasma, discharge on cooled Cu electrodes, rel. to erosion damage in MHD channels 78—1925
- concave surface with single jet in crossflow, influence on heat transfer 80—1661
- condensed film, flow down vertical surface, effect cooling conditions on heat exchange *(Russian)* 78—46934
- condenser efficiency and performance enhancement, evaporative cooling *(German)* 79—72781
- condenser system, submerged, buble pumped augmented natural convection 78—94535
- conduction cooling device for low temp. phosphorimetry 80—90855
- conduction-controlled rewetting with precursory cooling, two-dimens. analysis 77—15019
- conical tube, heat transfer with internal cooling by swirling air jet 77—55063
- container wall, quasistatic stress distrib. due to internal press. and external temp. changing 77—84113
- continuous flow cooling unit, for the cryostat 80—31761
- continuous flow unit, for Mossbauer experiments, 4.2 to 300K 80—31954
- convective heat transfer, calc., quasisteady approach 78—34131
- cool diode sputter coater for heat-sensitive SEM specimens 78—24204
- Copiapo group IA Fe meteorite, cooling history 80—36578
- cosmic gas clouds, cooling rel. to fragmentation and galaxies form. 77—33628
- cosmic microwave background, cooling by intergalactic hot gas in distant rich clusters of galaxies 78—12369
- cryogenic conduit, calc. of stationary heat transfer zone under cooldown 80—10129
- cryogenic fluids cooling and freezing by vapour space evacuation 77—57331
- cryogenic systems, circulating cooling time for laminar and turbulent flow coolant 77—5849
- cryogenics, a critical review 78—89485
- cryolite, molten, struct. charact. by IR spectroscopy and splat cooling *(French)* 79—69835
- cryorefrigerator, double-stage for cooling to 10K on a 4-circle diffractometer 80—98919
- CTR blanket design *(Japanese)* 78—46164
- curtain cooling, behind permeable surface section, effect of injected gas flow distrib. 78—42657
- cylinder in still air, DC corona cooling obs. 80—70071
- cylindrical ingot, continuous casting, elastic-plastic temp. stresses and deformation *(Russian)* 79—61576
- cylindrical mould, heat cond. with phase change 79—37108
- DC thermocouple, with variable cross-section, thermoelec. cooling 78—24787
- deflecting septum magnet for cyclic accelerator 78—78525
- degenerate stars with H atmospheres, cooling law from space freq. 80—17576
- dendritic ice form. in pipe, cooling rate effect 78—90690
- diesel-driven chiller system simulation, with multi-tank thermal storage system, for large commercial buildings 79—48187

cooling continued

- 1,2-difluoroethane, internal rotation temp. frozen in supersonic jet, matrix IR spectroscopy 80—9594
- dilution refrigeration, history from 1951 79—41
- dilution refrigerator, anomalous cooling power, heat transport of ^3He-^4He solutions 80—37045
- direct contact cooling of crystallising $MgCl_2$ brine using kerosene drops 79—1053
- discrete-hole cooling, near-field character of jet discharged normal to main stream 77—15088
- discrete-hole cooling, three-dimens. num. prediction for laminar flow case 77—15089
- duct, annular, turbulent flow and heat transfer over backward facing step, finite difference soln. 79—1175
- Earth, interior cooling contrib. to surface heat flow rel. to Earth thermal evolution 80—89988
- Earth core, cooling rel. to geomag. field generation and surface heat flux 77—73638
- Earth lithosphere cooling, continental mantle heat flow var. with age 79—70764
- EBBA, liq. cryst., rapid cooling and mag. field effects on NMR relax. and thermal behaviour 79—82321
- efficiency in flow around wall, initial turbulence effects 80—79315
- electric machine using evaporative thermosiphon, design nomogram 77—71194
- electrical circuit, slowly modulated dissipative steady state, dQ=TdS far from equilib. 78—81934
- electron cooling experiments, mag. and vacuum system for NAP-M proton storage ring 77—65362
- electron cooling of proton beam in storage ring 77—14281
- electron microscope, 1.2 MV, high-resolution double-tilt cooling stage 80—68322
- electronic components cooling tube, calc. method *(Russian)* 78—59271
- electronic cooling, developments *(Russian)* 78—86712
- electrophotographic copier photoconductor drum cooling methods 78—62245
- electrostatically assisted, steel plate at 500°C 80—69628
- epoxy impregnated superconducting composites, mech. props., strain effect at 4K 80—25822
- epoxy resins, correlation between valence energies and low temp. flexibility 80—25815
- epoxy-rubber glass transition rel. to filler, cooling rate 79—4403
- ethyl acetate, gas, radiatively heated by CO_2 laser, cooling mechanism investig. 80—75021
- Ettingshausen device, transient cooling effects, theory 80—80304
- evacuated tubular solar collector integration with LiBr absorption cooling systems 80—3493
- evaporation cooling, radiation effect on heat transfer and Lewis no. *(German)* 79—41562
- evaporation cooling system based on porous heat emitting element, hydrodynamic and thermal characts. *(Russian)* 77—67430
- evaporation cooling system based on porous heat emitting element, stability anal. *(Russian)* 77—71322
- evaporative, on vapour cooled transmitter tubes, physical fundamentals *(German)* 77—11114
- evaporative cooling of porous wall, thermal state of vapour zone *(Russian)* 79—64763
- expansion cloud chamber with thermoelectric cooling 78—90034
- explosive r process cooling process 78—69791
- extraction electrode of ion source, cooling in long-pulse operation 80—52360
- fibre optic image tube, cooling effect 78—96401
- film, by injection from porous section 77—51041
- film, use of cholesteric liquid crystals for thermal flow visualisation 79—186
- film coating of flat wall, effect of coolant supply injection angle 77—23951
- film cooling, comparison with combined and external cooling of flat plate 77—23950
- film cooling, from single hole and hole row, free stream turbulence effect 79—46310
- film cooling, influence of surface longit. curvature 79—81878
- film cooling, leading edge effectiveness 79—1185
- film cooling, with upstream injection and intermediate panel temp. 79—1184
- film cooling at separated zone 79—1187
- film cooling effectiveness of tube wall, axially and radially flowing coolant 79—1186
- film cooling efficiency, axisymmetric air flow rot. cylinder, main flow swirl effect 78—75132
- film cooling in subsonic boundary layers, tangential slot injection 77—3839
- film cooling of rotating surface, efficiency 79—98718
- film cooling with density difference between mainstream and secondary fluid, heat-mass transfer analogy 78—30293
- fins, cooling efficiency rel. to that of smooth wall *(Russian)* 78—38182
- fission product decay heat removal with fusion-fission hybrid mobile blanket 80—99282
- fission reactor HCDA, natural convection heat transfer in fuel debris bed cooled at top and bottom 79—93785
- flame, atm. press., supersonic sampling, boundary layer cooling 77—60143
- flow rates through porous media, heat and mass transfer *(Russian)* 78—59479
- fluidised bed, fluidisation uniformity, disturbance criterion with uniform coding medium flow distrib. 80—43772
- fluidised bed, plasma jet cooling mechanism 78—79371
- fluidised bed two-level coolers, heat transfer 78—9705
- freely flowing liquid film, cooling, heat transfer, turbulent transport model calcs. 80—64560
- Freon-12 in heated tube, flow boiling dryout, transient heat transfer investigation, reactor LOCA 80—32359
- frost growth rate prediction eqn. for cooled surfaces 78—87248
- fuel cell stacks, H_3PO_4 79—48121
- fusion reactor, long pulse high current ion source electrode cooling 80—91360
- fusion reactor, press. induced flow cooling, highly stable superconducting mag. systems 80—106192
- fusion reactor, TFTR, field coils cooling water system 80—106160
- fusion reactor blankets, MHD coolant flows, 3-D model 80—23119
- fusion reactor magnet coil, 125 kG, 1 m, design, fabrication 78—55008

cooling continued

- fusion reactors, large Coil Program, Westinghouse coil cooldown and warmup 80 106193
- fusion reactors, Large Coil Test Facility, liq. He cooling system 80—102321
- galettes for cooled solenoids 77—22580
- galvanothermomagnetic refrigerating element, cooling mechanism *(Russian)* 77—26308
- gas, with variable physical props., pipe flow, turbulent momentum and heat transfer calc. 78—90869
- gas atmosphere quantitative analysis adsorption chamber 80—85234
- gas cooling to broad band reson. light press. 80—48835
- gas stream, thermally nonequilibrated flow through supersonic nozzle, cooling, population inversion *(Russian)* 77—7412
- gas transport by pipelines, temp. and pressure distrib. determ. 79—23326
- gas-film cooling efficiency in supersonic axisymmetric nozzles 79—98715
- gas-solid particle suspension, turbulent flow in curvilinear channel, local heat exchange 78—63484
- gases, radiatively heated by CO_2 laser, cooling mechanism investig. 80—75021
- generators, H_2 production, on-site, electrolysis of H_2O 80—72097
- generators, H_2 technology, solid polymer electrolyte H_2O electrolysis 80—67012
- glass, isobaric thermal behaviour during heating and cooling, rate of recovery, one-parameter model 80—75165
- glass, solidification kinetic eqn., derivation from heat transfer and viscosity eqns. 80—25679
- glass, viscous deformation during heating and cooling 80—89314
- glass fibre, cooling during drawing 79—52253
- glasses, thermal behaviour during heating or cooling, retardation kinetics 77—4049
- half-space, plane Stefan problem soln., degenerate hypergeometric transformations method 79—86332
- heat demonstration, enhancement using coolant sprays 80—8761
- heat pump, chemical, hydride conversion and storage system 80—72077
- heat transfer, total coeff. determ. tests for industrial cooling system of continuous hot rolling mills *(German)* 77—89005
- heat transfer and evaporation from cooled surfaces, nonlinear eqns. numerical soln. *(German)* 80—58893
- heated cylinder in still air, cooling by corona wind expt. 80—84023
- heated pounds, turbulent boundary layer of stratified airflow, surface waves 80—92133
- heavy ion+electron radiative recombination as cooling process, dipole approx. *(Russian)* 79—3565
- heavy particle beam cooling in an electron flux, mag. field effects 78—82557
- hexahedrite meteorites, cooling rates 78—57511
- high temperature nuclear reactors, He gas behaviour anal. *(German)* 77—67855
- high thermal input sputtering heat transfer process 79—28914
- hollow cathode lamp, cooling system 78—45718
- hot surfaces, cooling by jets of dispersed liquid 80—48558
- hot wall with impinging liq. droplet, transient temp. profile 78—75050
- houses, low-cost, in Brazil, evaporative and night sky cooling system design and testing 79—62132
- hydraulic resistance of channel during rot. about axis perp. to channel axis 77—58698
- hygroscopic materials handling, method for drying and cooling chamber 77—61054
- hypersonic gas flow, radiant heat and evaporative cooling 78—91028
- hypersonic transitional/turbulent boundary layer, wall cooling effect 78—26149
- hypersonic turbulent boundary layer, surface cooling, multiple slot injection 78—9653
- III-V compounds, Stefan problem, exact soln. describing growth rate with linear cooling 80—59411
- industrial solar total energy systems in United States 79—96426
- ingot forming from melt, liq. containment by EM field 80—35120
- ingots, cooling regime in conditions of minimal thermal stress, modelling *(Russian)* 80—65194
- interface segregation through cooling 79—43294
- interstellar clouds, cooling by C atoms and ions rel. to struct. *(Russian)* 80—12801
- interstellar H_2 cooling, dissociation and IR emission in shocked clouds 78—41009
- interstellar H II/OH maser regions, radiative cooling rel. to ion stream heating 80—56912
- interstellar hot gases, cooling by H_2 molecules 79—12505
- interstellar ionisation fronts, models with mag. fields and cooling 77—33594
- ion, electromagnetically confined, laser cooled, double resonance and optical pumping 80—87155
- ionosphere, cooling by 0 I, 63 μm emission, meas. 79—16732
- ionosphere, elect. heating and cooling rates discrepancy, Atmosphere Explorer-C meas. 77—29564
- IR cooling calcs., simple strategies for inclusion of Voigt effects 79—94768
- IR detectors, thermoelectrically cooled, features and appls. 79—2828
- ISABELLE superconducting dipole magnets, forced flow cooling 77—26907
- jet, cross stream injection boundary layer, flow and temp. field 79—1225
- jet cooling of metal plates, heat transfer coeff. 80—10107
- jet cooling on heated plate, surrounding fluid effect 78—79350
- jets, film cooling effectiveness 78—14052
- Jupiter, surface condition and cooling rate 77—29714
- Jupiter cooling time, effect of dense cores on evolutionary models 80—98603
- Lake Shlavantas, deep autumnal cooling and freezing *(Russian)* 78—36213
- lakes, winter season energy balance aspects *(Polish)* 78—24315
- laminar film cooling experiments in hypersonic flow 79—94648
- lamps, pulsed, destruction in liq. coolants 79—94312
- land basin with snow, radiative cooling 78—88872
- Landes group IA Fe meteorite, cooling history 80—36578
- laser, low-temp. ruby, with optical delay line inside resonator, cooling system 79—36922
- laser, solid state, plane active element initial cooling period *(Russian)* 79—36904
- laser cooled ion storage frequency standard possibilities 79—54102
- laser/component, using mechanical refrigerators, heat pump and thermoelectric coolers 78—22136

cooling continued
lava lake cooling model, numerical analysis method 77−64247
line-focus parabolic-trough photovoltaic arrays, active and passive cooling 80−93988
liquid, superheated, gas content effect on boil-up and cooling 79−1061
liquid, transient natural convection during cooling 80−87770
liquid flow around cylinder, thermophys. charact. rel. to friction and heat transfer *(Russian)* 78−38328
liquid-glass transition, glass transition depend. on heating and cooling rates 80−79920
liquids for cooling and index matching of Nd:glass laser systems 80−33015
LOCA, rewetting of hot surface, development of cooling wave 80−27767
low heat resistance cylinders, nonlinear radiative cooling, matched asymptotic expansion anal. 79−41559
low temp. device with DRON or URS-50 spectrometers 78−24910
low temp. melt spinning device 80−100825
low temp. testing machines of IMASh-5S-65 type, new cooling techniques, exam. of machine design 79−52520
lunar pyroxenes, cation distrib. and exsolution as chronological indicator of thermal history 78−45246
magnetic fluid (cable coolant), natural convection heat transfer 78−94846
magnetron sputtering equipment and application status 79−83124
mainstream acceleration effect on heat transfer and wall temp. downstream of gas injection 79−1251
mammal, brain-cooling system 80−3597
Manicouagan impact melt sheet, Quebec, thermal history 78−81167
meltspinning, theoretical anal. of ribbon thickness formation 80−104143
Mesozoic pillow lavas from French Alps, cooling rates rel. to clinopyroxene comp. trends 77−5154
metal cryostat, evacuation of ^{3}He vapour by an absorpt. pump 80−73369
metal growth in space, theoretical models, comparison with ground expts. 78−84786
metal-semiconductor thermoelectric coolers, effects of contact resist. and dopant conc. 80−81481
metallic alloy glasses, continuous cooling versus isothermal transformation diagrams, critical cooling rate 80−15012
metallic sputtered powder, stuct. and phase composition, cooling rate effect *(Russian)* 79−56941
metals and alloys, thermal fatigue testing, installation for −180 to 1100°C 80−3266
meteorites, cooling rate rel. to schreibersite growth for Emery mesosiderite 79−35211
methane-d$_4$, selectively excited, cooling, vibr.-vibr., vibr.-translational relax. 80−33723
methyl nitrite, internal rotation temp. frozen in supersonic jet, matrix IR spectroscopy 80−9594
methyl polymethacrylate, heat emission coeff. and cooling const., Angstrom periodic heat wave method 77−72706
MHD generator cooling by gas injection through channel *(Russian)* 78−38557
microclimatic modification by small water droplet evaporation 77−17248
microcooler, threestage, with cascade thermocouples 79−2765
micropolar incompressible fluids, kinetic and thermal energy decay 78−5648
microwave hyperthermia simulation *(French)* 80−3770
mineral cooling rates, implications of antiphase domains exptl. coarsening in pigeonite 80−81886
mirror surface, high power optical damage threshold elevation by hypervapotron cooling 79−23002
mixture, binary, time-depend. solidification, series soln. 78−75058
molecular gas, laser-stimulated cooling 80−5594
molecular gas, rot. temp. decrease due to stimulated transitions *(Russian)* 79−86152
molecular gas, thermalisation under reson. excitation by laser radiation *(Russian)* 78−26231
Moon, eclipse cooling curves, 1978 March 24, 3.4 mm obs. 80−31220
Mossbauer experiments, efficient continuous flow He cooling unit 77−33992
N$_2$O refrigerator, thermodynamics and thermoelectric condenser design 80−108809
negative ion source, nucleated boiling water cooled cathode, design and testing 80−102370
Neptune thermal evolution, convective cooling model and comparison with Uranus 78−85903
neutral beam, continuously operating, convectively cooled ion accelerator, mech. design and fabrication 80−102374
neutral beam injector, continuous operation, water cooled U-tube extraction grid 80−99392
neutron four-circle diffractometer, cooling down to 3.9K 77−27789
neutron stars, cooling 80−77443
neutron stars, possible temp. determ. 78−40984
neutron stars cooling, calcs. 79−101170
neutron stars thermal properties and detectability, cooling and heating processes 80−31323
nozzle, convergent-divergent, compressible turbulent boundary-layer heat transfer *(German)* 78−22399
nozzles, supersonic axisymmetric, film cooling efficiency 80−48710
nuclear fuel storage options compared, dry, shallow pool and deep pool 79−9843
nuclear fuel storage pools, local distrib. of temp., design *(German)* 79−49816
nuclear power station cooling water impact on water surface temps. and ice conditions *(Finnish)* 79−20868
nuclear power station spray cooling, heat and mass atmospheric transfer 78−94078
nuclear power stations, accumulation ponds cooling possibility analysis *(Slovenian)* 80−91208
nuclear reactors, operational principles *(Slovenian)* 77−67858
nuclear steam condenser, contamination control using atomic absorption spectrophotometer method 77−373
oceanic lithospheric plates, cooling rel. to subsidence of aseismic ridges 77−37162
oil-cooling baffled shell-and-tube heat exchanger expt. 78−83395
optical component blank pressure shaping, semiautomatic apparatus 79−72731
optical fibres, convective cooling during high speed coating 80−23815
optical fibres, cooling rates during drawing 80−66538

cooling continued
orbiting astronomical telescopes, IR detector cryogenic cooling requirements 78−96400
orbiting IR detector cooling by multimission solid cryogen cooler 80−86423
oscillating liquid-filled cylinders, heat transfer 80−10117
parallel-plate channel, convectively-cooled, liq. solidification 77−68666
particle accelerators, radiation exposure 80−5350
perforated plate composite cooling in turbulent gas flow 79−98716
PETRA storage ring, RF power supply and cooling systems 79−68054
phase change material physical and chemical props. for space heating and cooling 79−57479
phosphorimetry, low-temp., conduction cooling system for sample introduction 80−87158
photomultiplier, cooling system 78−45718
photomultiplier cooling by semiconductor microrefrigerators 78−57942
photoreceivers, cooling system 79−93218
phthalocyanine, free base, fluoresc. excitation spectrum, cooling in supersonic free jet 80−95670
pipe, of variable thermal and elec. conds., elec.-heated, flow-cooled, temp. distrib. 78−90626
pipe flow, laminar with nonlinear wall heat fluxes, axial cond. 79−27636
planets, internal cooling rel. to crustal tectonics, appl. to Moon and Mercury 78−12116
plasma, heavy-impurity control by light-impurity radiation, wall layer cooling 77−65879
plasma sources, cooling pattern of acceleration grids meas. by IR scanning 80−86303
plate, downward-facing, flat, heat transfer augmentation by nonuniform elec. field corona 78−94873
plate, infinite, asymmetric cooling, direct and inverse heat cond. problems 79−37113
plate, permeable, turbulent boundary layer with injection, heat transfer 79−1247
plate, vertical, unsteady free convection of water at 4°C 80−69822
plate quenching in water, heat flux calcs. for unsteady heat cond. 77−23853
PMMA, viscoelastic props. in plastic zone, cooling rate effect 80−40418
point-focus Fresnel lens photovoltaic arrays, active and passive cooling 80−93988
Poiseuille flow between porous flat plates, transpiration cooling, variable viscosity 77−47082
polarised target in high energy physics, horizontal dilution refrigerator with high cooling power 80−73372
polycarbonate, viscoelastic props. in plastic zone, cooling rate effect 80−40418
polycrystals, deform. during cooling, revealed by deposited graphite layer *(Polish)* 80−25755
polyethylene, correlation between valence energies and low temp. flexibility 80−25815
polyethylene terephthalate, low temp. sp. ht., effect of cooling rate 80−100336
polymer melt spinning, mechanics of nonisothermal process 77−51010
polystyrene, stress birefringence under nonisothermal conditions 78−15468
polystyrene-SiO$_2$, glass transition rel. to filler, cooling rate 79−4403
porous construction elements, evaporative cooling for subcritical, critical, supercritical liq. coolant parameters 79−55372
porous structures for cooling laser reflectors, theoretical study 80−91809
power plant cooling system design, optimal system synthesis, tower, pond 77−14260
power stations water effluents, effects on rivers and water basins, power engineering and water conservation viewpoints *(Czech)* 79−57505
protogalactic gas cooling mechanisms *(Russian)* 79−17107
pulsed solid laser radiation reproducibility *(German)* 77−58331
PVC, enthalpy determ. of order 79−7556
pyroelectric substance, adiabatic depolarization under cryogenic conditions 80−55045
quenching temperature, 0.03-1.3 MPa, base material thermal props. depend. 78−94587
radiation detector, effect of cooling element shape on heat removal efficiency 78−12691
radiation press cooling of ions in Penning EM trap 78−66527
radiative cooling by use of inverse greenhouse effect 79−25329
rarefied hypersonic flow over blunt wedge, cooling 77−35169
reactor pressure vessel, cooling by nitrine coolant *(Russian)* 79−59158
real liquids, quenched to glassy state, struct., one dimens. Ising model appl. 80−54134
resin slab, stress response, fluctuating external moisture (temp.) effects 78−55620
resonant absorbers, kinetic energy reduction by near-reson. EM irrad. 80−23371
rivers, well-mixed, simple non-linear cooling models 79−20902
rocks, igneous intrusions, convective cooling of infinite sill 79−20787
rod, expanding, conductive heat transfer computation, fast numerical technique 78−75029
Saturn cooling time, effect of dense cores on evolutionary models 80−98603
Saturn rings, IR brightness and eclipse cooling obs. 80−56763
selective covers for natural cooling devices 79−43750
shell cooled by evaporating liq. drops, temp. fields 78−9546
shock waves, metagalactic, cooling and thermal instability 80−46678
silicate melts, cooling rate rel. to chondrules textures experimental reproduction 80−94763
single localised ions, prep., cooling and fluoresc. 80−52929
snow surfaces cooling, impact of atmospheric CO$_2$ 79−92569
solar, CAD of windows as passive solar collectors, using interactive program 79−62146
solar, correlation between diffuse and hemispherical and between daily and hourly insolation 79−87975
solar, evacuated tubular solar collectors and LiBr absorption system integration 79−62135
solar, for moderately insolated regions, European research 79−57457
solar, of buildings in Turkmenian SSR, using open water evaporation, from LiCl solution 79−57463
solar, of mobile home, performance in Kuwait environment obs. 79−62130
solar, office complex design, with up to 70% energy savings 80−40831
solar, passive, of poultry sheds 79−70437
solar, periodic heat transfer analysis 79−62148
solar, residential, evacuated-tube collectors, design 79−88002

cooling continued
solar, US national demonstration program 79—62128
solar absorption and vapour compression, residential cooling systems 80—72017
solar absorption cooling systems, small scale, feasibility study 79—74502
solar air conditioning with solid absorbents, earth and underground water cooling 80—72018
solar assisted thermoelec. air conditioner humidifer (SATEACH) 80—108802
solar cell modules, high-efficiency with improved glass, adhesives and heat dissipation 80—76636
solar collector wall, bi-coolant, heating cycle, thermosiphoning, building heating and cooling 80—72083
solar collectors appl., standards establishment 80—7915
solar cooling, thermodynamic anal. of sorption machines, coeff. of performance calcs. *(French)* 80—55814
solar cooling performance predictions via stochastic weather algorithms 80—35642
solar energy: four sites demonstrate potential 79—61946
solar energy cooling, operating systems and current developments, review 80—85265
solar energy storage system, ammoniated salt heat pump using $MgCl_2$, $CaCl_2$, NH_4Cl 80—81484
solar energy systems, Conf., San Francisco, CA, USA, (Dec. 1978) 79—83635
solar evaporation and refrigeration units, assurance of specified energy parameter values, statistical analysis 80—93848
solar flare plasma, evaporative cooling 78—40890
solar heat collection and storage system evolution 79—62085
solar heat pump house, Dunham-Bush development 80—40830
solar heating and cooling of buildings, economic problems 79—57451
solar photosphere, adiabatic cooling and mag. fields hydraulic conc. in downdraughts 78—45300
solar powered Rankine cycle system, 18-ton, analysis and design 79—52897
solar quiescent prominences, heating and cooling, calc. 80—12738
solar system, for industrial plant, located in Southern Europe 79—62131
solar system optimisation, using continuous flow control 79—62127
solar thermoelectric generators, efficiency evaluation and improvement 79—62017
solar town in Iran, conceptual development 79—57408
solar wind protons cooling, evidence from Mariner 2 data 78—40789
solid laser active element, circular, cooling process, variation in ambient temp. *(Russian)* 78—74915
solid laser planar active element convective cooling *(Russian)* 78—82978
solid laser with superfluid He cooling 80—48282
solid state energy conversion, appl. of solid state cooling to spaceborne IR focal planes 80—107772
sonic nozzle expansions, rot. relax. theory 80—43827
space vehicle radioisotope power system, using Rankine conversion cycle, emergency cooling by multifoil insulation melting 79—48168
spacecraft components, liquid-trap heat pipe thermal diode 80—27292
spacecraft nuclear dynamic power system, thermally-integrated 79—48166
spacecraft radioisotope thermoelectric generator, in Shuttle 79—48142
spectroscopic cooled and intensified array detectors 78—65983
spent nuclear fuel cooling time determ. utilising gamma-ray meas. 80—63268
spheres, concentric, cooling by forced convection, at low Reynolds no. 79—1183
spray cooling, characts. and minicomputer control *(French)* 79—3889
stable low-temperature source to test for cold urticaria 78—61276
standard long-range operating stations in shelters with integrated thermal-syphon system 80—53616
stars, accretion disc stability, viscosity and cooling mechanism effects 78—49476
steam condenser, supersonic nozzle discharge, heat transfer and gasdynamics 78—55671
steel, 0.2 to 0.8% C, ferrite-pearlite transformation, tensile strength, cooling rate effect 80—7549
steel, C, mech. props. rel. to heat treatment, ferrite-pearlite transform. *(French)* 79—20043
steel, case carburised, residual stress effect in mech. performance 79—24659
steel, complex alloy, Cr (12-18 wt.%), transformation behaviour *(German)* 80—40349
steel, Cr-Ni, tensile strength and cooling curve, regression anal. 79—57070
steel, Cr-Ni-C (3, 1, 0.6 wt.%), grain boundary sulphide precip. and hot ductility *(Japanese)* 80—71654
steel, high speed, microstruct. effect of splat cooling 79—61624
steel, low C, low alloy, ferritic-pearlitic, high temp. mech. treatment, cooling effect 80—104193
steel, low-C, fully pearlitic, struct. and mech. characts. rel. to cooling conditions *(French)* 80—40425
steel, magnetite film formation at metal scale interface, during cooling 78—88575
steel, Mn-Mo-Nb-C, transform. charact. and struct. during continuous cooling 79—29057
steel, Mn-Si-Cr-Mo, dual phase, as-rolled, continuous cooling transformation diagram to optimize composition 80—100829
steel, Ni-Cu-Mo-C, powdered, influence of cooling rate after sintering on preps. 79—95969
steel, parts, stress calcs. during cooling, program system THEPLA *(German)* 80—35237
steel, stainless, 15Kh25T, embrittlement at 400 to 550 degrees C, grain size and cooling rate effects 78—44203
steel, stainless, Cr-Ni type, low temp. plasticity, effects of deform. rate and cooling conditions 77—70099
steel, stainless, fibre reinforced Al alloy, tensile props., cryogenic cooling effect 79—61623
steel, W-Mo-Co, high-speed tool, struct. and props., cooling rate effect at primary crystn. temp. 80—76241
steel forgings, expt.-calc. model of quenching, temp. meas. across cross section 80—16345
steel ingot, state of viscoelasticoplastic stress deformation, in process of solidification *(Russian)* 80—45295
Stefanian cell diffusion coefficients, effect of heat of vaporisation *(Japanese)* 79—86882
Stirling cryocooler, milliwatt refrigeration at temps. 3 to 4K 79—67307
stochastic cooling of particle beams, review 80—37675

cooling continued
stochastic cooling techniques for heavy particle beams 79—72175
stochastic cooling tests on proton beams, initial cooling expt. 78—90006
stratocumulus water clouds, radiation transfer and cooling rates 77—45146
Sun, photospheric cooling with increased sunspot activity 78—40896
sunspots, cooling by Alfven waves refl., theory 79—5799
superconducting magnet, fusion reactor appl., cooling system design 77—23289
superconducting magnet circulation cooling system based on He liquefaction apparatus 78—57992
superconducting magnet cooling, optimal cryogenic gas flow 79—93149
superconducting magnets, cooling system using liquid He 78—54998
superconducting magnets, force-cooled conductors design 78—54999
superconducting magnets, hollow conductors, cooled by supercritical He 78—54997
superconducting magnets, precooling using Cryomech GB02 cryocooler and gas-filled thermal switches 80—52245
superconductor, hard, critical state stability and oscillations 80—107959
superheated steam, turbulent flow, local heat transfer during cooling *(Russian)* 79—59985
supernova shock-accelerated cosmic rays, early radiation spectrum, cooling and escape 79—48626
supersonic diffuser with surface cooling, flow and heat transfer meas. in pseudo-shock region 77—42868
swirling film cooling in initial tube section 79—1256
TEM liquid He cooled environmental cell 80—68323
temperature control system for biological preparations 79—57830
temperature cycling apparatus using liquid He storage Dewar 78—65938
terrestrial planets, subsolidus convective cooling histories 79—66939
tetracene, intramol. dynamics and energetics in isolated ultracold state 79—98144
thermal stresses and temps. determ. in cooling bodies by finite elements 77—14881
thermodynamic cycle with air cooling, expt. determ. of efficiency *(Russian)* 79—59917
thermoelectric, rectangular monolithic infinite cascade thermojunctions 78—57944
thermoelectric convertor, generalised surface, quadratic form heat balance equations 79—83609
thermoelectric coolers, heat load estimation curves 78—45613
thermoelectric coolers, numerical anal. of transient behaviour 78—21140
thermoelectric coolers for micromodules 79—6120
thermoelectric cooling unit in mag. field 79—9218
thermoelectric devices, maximum refrigerating capacity determ. 80—86318
thermoelectric element, arbitrary shape, cooling efficency 78—67010
thermoelectric heat pumps, two-stage, design criteria anal. for cool-down speed maximisation 80—108812
thermoelement cooling control by variation of geometric shape 78—62195
thermoplastic sheet, extruded, thickness adjustment and cooling between calender rolls 79—68597
thermosphere, cooling by 0 I, 63 μm emission meas. 79—16732
thin film coating on polymer substrate, cooling means requiring no power 78—197
thin film evaporator with cooled rotatable RF cathode 79—78876
three-actuator deformable water-cooled mirror 80—33134
tissue, microwave heating, effect of surface cooling and blood flow 78—57038
transformer, oil-cooled heat exchange anal., network method *(Russian)* 78—83399
transition metal hydrides and deuterides, conc.-temp. depend. of mag. susceptibility 80—29523
transition metals and alloys, high-melting-point, fast cooling from melt, cooling rate influence on struct. *(German)* 79—43287
transpiration-cooled system, thermal response in radiative and convective environment 78—32323
transport fluids, spray evaporator for spacecraft thermal control systems 80—29160
trapped ion, laser cooling, theory 80—58414
tube wall, gas film-cooled, turbulent heat exchange, coolant turbulence intensity influence *(German)* 79—18895
turbine blade cooling, calc. of required level 79—64487
turbogenerators, high capacity, heating reduction measures for enhanced reliability and interval between maintenance *(Russian)* 80—96175
turbogenerators by H_2, heating-up detect. by gas stream chromatography and mass spectrography *(French)* 79—48024
turbomolecular pumps with corrosion resistant oil 77—87776
turbulent air flow in round tube, high-temp., friction resistance, cooling *(Russian)* 78—75135
turbulent channel liquid flows, nonsteady convective heat transfer 80—59023
turbulent water film, with different initial flow conditions and high temp. gradients, heat transfer 78—90862
two-phase nodules, heat treatment, stressed state, connection with nodule size, cooling rate and phase ratio *(Russian)* 80—16334
two-phase porous cooling system, hydrodynamic and thermal characteristics 77—10012
two-phase porous cooling system development 78—59477
two-phase transpiration cooling system 78—22418
type II superconductor, pinning strength, rel. to cooling of sample 80—11141
ultrahigh vacuum rotary manipulator with direct cooling 77—26317
underground cable system, convectively cooled, temp. distribs., heat transfer correlations 78—71262
underground cable system, convectively cooled, vel. distribs., press. drop correlations 78—71330
underwater plasma weld cooling 79—1932
Uranus thermal evolution, convective cooling model and comparison with Neptune 78—85903
USA demonstration solar heating and cooling collector thermal performances 79—62059
USA solar heating and cooling R&D programme 79—57373
vacuum chamber-bell jar with built-in cooling body 80—90860
vaporising coolant enthalpy for cryodevice initial cooling *(Russian)* 78—70130
vapour bubble collapse, effect of initial radius and subcooling 77—80196
vertical surface, cooling by liquid spray, heat transfer 80—74711
viscous incompressible flow problems, two-dimens., Navier-Stokes eqns soln. and contaminant effects 77—58638

cooling continued
  vortex cooling tube, in two-stage refrigeration and power producing arrangement 78—21142
  vortex tube efficiency, hot end inner rifling influence 79—94462
  wall, perforated, relative effects of external and internal convection *(French)* 79—1248
  walls, permeable, cooling characts., heat exchange, rad. emitter design 80—64535
  waste heat dissipation from cooling ponds at power generating stations 79—48191
  water, cooling from surface under free and forced convection regimes *(Russian)* 78—36179
  water, layer, semiinfinite, cooled (heated) from below, convection onset, density anomaly influence *(German)* 78—22350
  water, thermally-stratified, cooled from above, free convection 79—46315
  water, transient natural convection in horizontal pipe with const. cooling rate through 4°C 77—42828
  water cooling system, fluid relay responding to flow rate 77—37879
  water cooling through free surface, critical value of boundary Rayleigh number *(Russian)* 78—61426
  water droplets in hot gas flow, transient cooling 79—1063
  water evaporative cooling, convection and mass transfer, fog formation in boundary layers 80—79293
  water evaporative cooling, heat and mass transfer coeffs., fog formation effects 80—79294
  water films, subcooled, flowing down vertical tube, heat transfer 80—79318
  water jet, round, impinging, heat transfer in interference zone of film flow along wall 77—58750
  water surfaces cooling, impact of atmospheric CO_2 79—92569
  wear resistant material, US welding effect on struct. *(Slovak)* 79—74185
  X-ray diffraction, gas stream method of cooling 78—219
  X-ray emitting gas in clusters of galaxies, bremsstrahlung cooling evolution 79—40266
  Ag composite, SiC whisker-reinforced, prep. aboard Skylab. 78—84741
  Ag-Ga (27 at.%), cooling rate depend. of thermal arrest, transform. temp. 79—29053
  Al, heat transfer during cooling with water *(German)* 80—23873
  Al-Cr (3 to 11 at.%), cooling rate effect on solidification struct. and mech. props. *(Japanese)* 78—39755
  Al-In (40, 70 wt.%), liq. phase immiscible system, solidification in microgravity 78—84770
  Au-Cd (47.5 at.%), effect of cooling rates on stress-strain behaviour 78—76721
  Ba^+ ion cloud containment in RF trap, <50 ions, optical sideband cooling 78—75407
  Be, containerless melts in terrestrial and space environment, thermodynamic props. calc. from solidification and cooling curves 79—70052
  Bi-Sb, conditions for dendritic crystallisation, accompanying rapid cooling *(Russian)* 79—34020
  C fibre layers on arc anodes props. and cooling behaviour 79—52245
  C-O white dwarfs, effect of C-O eutectic form. on cooling time 80—77405
  $C^+ + H_2$, C^+ fine-struct. excitation, interstellar cloud cooling 78—25675
  CO_2, inversion transitions in aerodynamic cooling region *(Russian)* 77—34869
  CO_2, laminar free convection at supercrit. press. under cooling conditions, heat transfer analysis 79—86428
  CO_2, turbulent cooling tube flow, at supercrit. press. 78—14005
  CO_2-N_2, kinetic cooling effect by CO_2 laser radiation, temp. dependence 80—10347
  CO_2-N_2 gas mixture, kinetic cooling by CO_2 laser radiation *(Russian)* 77—89229
  CaO-SiO_2, melt, effect of cooling rate upon glass transition, X-ray analysis 79—27920
  $CaWO_4$, crystal growth from soln. in Na_2WO_4 melts, by continuous cooling, growth kinetics exam. 78—48303
  Co-Sn system, phase Co_3Sn obtained by splat cooling *(German)* 80—104147
  countercurrent single- and two-phase flow effects on hot surface quenching rate 78—59451
  Cr-Fe microstructural changes, heating and cooling cycles 79—78956
  $Cr(CO)_5$, multiphoton ionisation, mol. cooling in pulsed supersonic beam 80—28070
  Cu alloys, optimal secondary cooling condition estimation in continuous casting *(German)* 77—73295
  Cu, heat transfer during cooling with water *(German)* 80—23873
  Cu-Al-Fe-Mn, phase transform. during continuous cooling *(German, English)* 79—70044
  Cu-Al-Fe-Mn (10,3,2 wt.%), phase comp. struct., continuous cooling from β-phase effect 79—24499
  Cu-Al-Ni (13.8, 7.9 wt.%), cooling rates effect on internal friction *(Japanese)* 80—39217
  Fe, cast, dispersed with interdendritic graphite, eutectoid transformation of austenite during cooling 78—84800
  Fe, cast, graphite nodule form., ion microprobe mass anal. appl. 79—43295
  Fe, cast, spheroidal graphite, cooling velocity and C effect on matrix struct. *(Korean)* 78—19789
  Fe meteorites, group IC, comp. and mineralogy rel. to cooling rates 78—32414
  Fe-Al(16 wt.%), ordered, antiphase region obs. cooling rate effects *(French)* 77—59834
  Fe-Cu, modulated microstruct., continuous cooling effect, hardness and electron microscope obs. 79—87665
  Fe-Ni-Al-Co-Cu-Ti, 38 to 40 wt.% Co, 8 to 8.5 wt.% Ti, alloy YuNDKT tempering and thermomagnetic treatments 78—3154
  Fe-Ti-C, rapidly quenched by splat-cooling 80—84923
  $Fe(CO)_5$, multiphoton ionisation, mol. cooling in pulsed supersonic beam 80—28070
  Fe_3O_4, Fe_2O_3, magnetite and haematite nodules with fayalite and Ca ferrite additives, stressed state parameters *(Russian)* 80—45352
  GaAs, cryst. growth from large Ga:As solns., critical cooling rate 80—64938
  GaAs n-n^+ epitaxial structure for CW microwave electroacoustic amplifier 78—59235
  Ge-GaAs, crystallisation at superhigh cooling rates 80—54349
  Ge-Sn solid solution, cooling rate effect on partition coeff. of Sn between liq. phase and crysts. 77—12510
  H in thermosphere, cooling by 63 μm radiation field 79—80066

cooling continued
  HD interstellar cooling function in primary gas condensation and star birth *(Russian)* 77—33623
  ^2H-^2H molten-salt-cooled fusion reactor blankets, nuclear heating and radiation leakage 78—78490
  He cooling systems, large, review of hydrodynamics and heat transfer 79—204
  He distrib. system for Large Coil Test Facility 78—55001
  He for cryogenerators, system selection and efficiency *(French)* 77—26305
  He for superconducting generator *(French)* 77—26304
  He, forced flow cooling system for superconducting magnet, numerical anal. of heat-induced transients 80—82773
  He, liquid, heat transfer in narrow cooling channel below 4.2K 77—30170
  He, liquid, Helitex test facility for large-scale experiments 79—63232
  ^4He, superfluid saturated liq., recovery heat flux from silent and noisy film boiling states 79—72784
  In-Tl alloy, FCC→FCT martensitic transformation, on cooling, enthalpy meas. and X-ray exam. 78—39773
  (In+InP) melt, critical undercooling determ. and P content change after annealing *(Slovak)* 80—55430
  KCl melt, effect of cooling rate upon glass transition, X-ray analysis 79—27920
  KCl with Al_2O_3 disperse spheres, dislocation mechanism for stress relaxation in cooling crystal *(Russian)* 80—54347
  Li, liq. cooled pulsed fusion reactor blanket heat transfer, numerical calc. 78—94141
  Mg atoms, cooling to broad band reson. light press. 80—48835
  Mg^+, Penning trap, laser cooling, optical spectrum from laser freq. sweeping 80—52916
  MgO-SiO_2, melt, effect of cooling rate upon glass transition, X-ray analysis 79—27920
  Mo-low alloys, C enrichment mechanism of intercrystallite zones *(Russian)* 80—20963
  $Mo(CO)_6$, multiphoton ionisation, mol. cooling in pulsed supersonic beam 80—28070
  N cooled discharge plasma electron energy distrib. function 78—63633
  N_2, hypersonic nozzle flow, supercooling and spontaneous condensation 78—1549
  N_2 supply, liquid, to vacuum installations 80—31762
  NH_3 continuous absorption cooling flat plate collector design and optimisation 79—62081
  NO_2, rot. cooled, vibronic band lifetimes, time resolved fluoresc. excitation spectra obs. 79—94025
  N_2O_4 dissociating coolant, chemical reaction kinetics in transient regimes *(Russian)* 78—58344
  N_2O_4 dissociating coolant, O_2 generation time constant, enthalpy change *(Russian)* 78—58345
  $2NO_2 \rightleftarrows N_2O_4$, condensation, heat transfer and aerodynamics *(Russian)* 80—19932
  Na, liquid, heat transfer in crossflow around circular cylinder *(Japanese)* 77—57706
  NaCl melt, effect of cooling rate upon glass transition, X-ray analysis 79—27920
  Na_2O-$2SiO_2$, melt, effect of cooling rate upon glass transition, X-ray analysis 79—27920
  Nd:YAG laser, influence of birefraction and cooling on output characteristics *(Italian)* 79—50299
  Nd:YAG laser, pumped by Kr arc lamp, conductive cooling, for space operation 77—88775
  Ni, heat transfer during cooling with water *(German)* 80—23873
  β'-NiAl, dislocation climb, hot stage TEM 77—24318
  O_2, attachment cooling, press. depend. 80—91663
  O_2-N_2 mixture, attachment cooling, press. depend. 80—91663
  Pb-Bi, temp. regime of crystn. on rapid cooling *(Russian)* 80—66495
  Pb-Sb battery grids, ageing behaviour obs. 79—100517
  $2PbO.SiO_2$ melt, coding rate influence on constitution of silicate anions, crystn. kinetics 80—103248
  SF_6, supersonic jet, condensation and gasdynamic cooling 80—6089
  SF_6, supersonic jet expanding into vac., interaction with CO_2 laser beam 80—5584
  a-Se, hole form. energy, heating time and cooling rate depend. 79—41958
  Si solar cells with concentrating collectors and integrated heat use system 80—45701
  Si/Li spectrometer, using Peltier elements *(Czech)* 78—49947
  Si(Li) detector, cooling system with liq. N_2 *(Rumanian)* 79—85867
  SiO film on Al, radiative cooling surface 80—50439
  Sn molten drops, gas evolution on quenching 78—39818
  Sn-Bi(Pb)(Ga), temp. regime of crystn. on rapid cooling *(Russian)* 80—66495
  Sn-Sb-Ag, splat cooled foils, TEM study 80—40344
  SrW_2O_4, kinetics of crystal growth from solns. in $Na_2W_2O_4$ melts, by continuous cooling 80—11550
  $Te_{80}Ge_{15}Pb_5$, DSC sensitivity to controlled ageing in glass transition region 80—71673
  Ti-Al (27.3 wt.%), arc melted, microstruct. 79—61577
  Ti-Al-Zr alloy, TA6Zr5D, structural evolution during continuous cooling at different rates *(French)* 80—45300
  U-Al, transform. and struct. changes, cooling, cooling rate effect *(Korean)* 77—63660
  W, containerless melts in terrestrial and space environment, thermodynamic props. calc. from solidification and cooling curves 79—70052
  Xe arc lamp, air-water cooling system, DKsSh-1000 high pressure lamp (USSR) 80—74452
  Zn-Ga, temp. regime of crystn. on rapid cooling *(Russian)* 80—66495
  ZrO_2-Al_2O_3, cooling effects on mech. props. *(Russian)* 79—78999

cooling towers
  see also water supply
  Arizona Nuclear Power Project waste water reclamation for cooling 79—9861
  buoyant jet entrainment from single and multiple sources in draft cooling tower 79—32617
  with column supports, free vibration analysis 78—83292
  convection caused by rejected waste energy 79—12169
  design, global optimisation methods appl. 79—59840
  designs resulting from environmental pressures to waste heat rejection 78—7758
  drift eliminators, design study for collection efficiency 78—7760

cooling towers continued
- dry cooling, feasibility study, for industrial applications 80—87705
- environmental effects and their reduction *(Czech)* 80—51021
- EPRI research program for improved technology and environmental impact 78—7759
- geothermal plant optimum design conditions, Geysers Unit 16, Northern California (USA) 79—52877
- glazed solar cooler soln. regenerator, thermotechnical characts. 79—83620
- induced draft cooling towers, noise prediction and control 80—16878
- Lagrangian convection, application to simulation of cooling tower buoyant plume *(French)* 79—88450
- meteorological effects, review *(German)* 77—73800
- meteorological effects *(German)* 77—73799
- model and full-scale cooling tower resonance tests 78—83291
- moist plume convection *(French)* 79—84400
- natural draft, salt emission and deposition 80—40941
- plume models, importance of meas. *(German)* 77—66985
- plume vortices, time-lapse photography 79—20950
- plumes, interaction with atm., numerical model simulation *(French)* 80—94126
- plumes, Lagrangian conveection model, representation of isolated thermals *(French)* 79—88449
- plumes, lidar meas. *(German)* 77—25781
- plumes, max. rise formula appl. 77—45142
- plumes, stationary model *(German)* 80—4082
- plumes and drift, mathematical models 80—45836
- plumes simulation, model calibration at Meppen power station *(German)* 80—94130
- power plant cooling system design, optimal system synthesis, tower, pond 77—14260
- supporting columns and reinforcing rings, displacement analyses 78—38187
- Texas nuclear power plant cooling water requirements 79—9859
- water noise, meas. and reduction techniques 79—52997
- wet cooling system for power plants, atm. impact of plumes and fogging 78—7761
- wet-bulb temp. and moist air heat content meas. 80—52211
- wet/dry surface for cooling towers 79—32199

Cooper Hewitt lamps *see mercury vapour lamps*

Cooper pairing *see Cooper pairs*

Cooper pairs
- *see also BCS theory; Josephson effect*
- AC Josephson-Fiske effect, coherence 78—88082
- coupling, Cooper, increase due to strong longitudinal sound 80—49990
- critical pair-breaking current density, temp. depend. *(Russian)* 80—70887
- dirty proximity-effect sandwich system, theoretical investigation of transition temp. 79—73638
- ferromagnetic superconductor, paramagnetic fluctuations, influence on superconductivity 80—70900
- formation, and nature of supercond. currents 80—65736
- hadronic matter, Pomeron and critical temp., Yang-Mills gauge boson pairs 80—22566
- Josephson effect in weak link, phenomenological model 77—8241
- Josephson junction, coherently driven, bistability model 80—15661
- Josephson junction, pair transfer, quantum-mechanical description, commutator and anticommutator of collective operators 80—60146
- Josephson tunnelling as probe of Ginzburg Landau theory 77—89905
- Kondo superconductor, self-consistent theory of pairbreaking 78—26989
- magnetic flux quantum, in supercond. ring, theory, teaching approach 79—84902
- magnetic properties of superconductors, effect of insulating pairing of electrons 80—15651
- metal, p-wave pairing, and superconductivity 77—39998
- metal-insulator transition, electron pairing, effect on optical props. of supercond. 80—60139
- Mott insulator superconductor transition, Bari model, tricrit. behaviour and phase diagrams 78—14876
- multi-valley semimetals with Coulomb interaction between electrons *(Russian)* 78—64165
- narrow-band crystal, electron pairing mechanism in strong elec. fields 79—95542
- non-adiabatic systems, supercond. originating from quasi-orbital conduction electrons 79—33382
- nuclear quadrupole vibration theory, potential oscillations and collective motion *(Russian)* 79—13222
- one-dimensional superconductivity, response functions, from renormalisation group theory 80—54829
- photon induced electron pairing 78—26901
- plastic deformation of superconductors, Cooper pair scatt. model 80—39709
- pseudopotential, Bragg planes, effect on superconducting pairing and crit. temp. 80—15648
- rel. to quasiparticle and phonon lifetimes, theory 77—20488
- self-consistent selection of a superconducting representation for the BCS model 78—88067
- semimetal, mixed superconducting-excitonic insulator phase, diamagnetism, virtual intraband transitions 80—2520
- semimetal, simultaneous Cooper and insulating pairing, physical states 80—93036
- superconducting ground state of quasi-orbital electrons 78—39252
- superconducting order parameter, rel. to macrowave function, near T_c 79—47191
- superconductirg thin films Cooper pains, photon scatt. on plasmons, Landau-Ginzburg theory 80—65738
- superconductivity and phonons, review 80—84543
- superconductor, triplet pairing, strong Kohn anomaly *(Russian)* 78—19179
- tunnel triode, anharmonic wave coherent radiation *(Chinese)* 79—65604
- two-band systems, BCS pairing and Peierls distortion compatibility 78—88068
- Al granular films, inhomogeneous supercond. transitions, microwave meas. 80—103789
- Al, superconducting, yield stress increase by destruction of Cooper pairs by dislocations 79—43313
- Al-formvar superconductive junction, Ginzburg's generalised jellium model 80—15663
- Al-Mg, superconducting, yield stress increase by destruction of Cooper pairs by dislocations 79—43313

Cooper pairs continued
- Cd-Mn, dil., lattice state effects on pair breaking 77—8219
- ^{3}He, B-phase, existence of states with J=1 and 2 *(Russian)* 77—35779
- ^{3}He, superfluid A-phase, Cooper pairs vs. Bose condensed mols., ground-state current 80—49451
- ^{3}He, superfluid A-phase, mass current, intrinsic orbital angular momentum 80—84338
- La-Eu, dil., DHCP, impurity effects on T_c, electron pair breaking 77—36013
- La-Gd, dil., DHCP, impurity effects on T_c, electron pair breaking 77—36013
- $La_{1-c}Ce_cAl_2$, Kondo superconductor, self-consistent theory of pairbreaking 78—26989
- Pb-Cd-Pb junctions, pair pot., mag. field depend., crit. currents meas. 80—84555
- Sn superconducting films, Ge-covered, effect on excess elec. cond. 80—65741
- Sn thin film, HF pair breaking current *(Russian)* 77—32130
- YRh_4B_4, supercond., anomalous cond.-electron polaris. 80—25047

coordination complexes
- *inorganic complexes are indexed under the appropriate metal compound headings*
- chemistry, electronic excitation, luminesc. methods 79—54880
- EPR of doped mag. centres 78—64259
- fuel cell electrocatalytic O_2 reduction mechanism with metal chelate coating 78—23951
- metal complexes, NQR spectrosc. appls. 80—54986
- nuclear power station decontamination, chelating agent appl. 78—50280
- oxine, impregnation of activated charcoal, adsorption of ^{60}Co from waste water 78—58365
- radiolytically formed chelating agents, corrosion prevention appls. 78—64745
- tetraoxomanganese compounds, electronic spectra of tetrahedral $[MnO_4]^{m-}$ chromophore 77—58032
- trace elements, in acid solns., solvent extraction, chelation and thermodynamic activity *(French)* 78—27816
- transition metal, electronic energy transfer process 78—56907
- transition metal complexes, O containing, coordinate bonding, charge transfer electronic bands, complex struct. determ. 80—52977

copolymerisation *see polymerisation*

copper
- *see also nuclei with ......*
- (100) surface electron momentum distrib., reconstruction from point-geometry positron-annihilation data 79—56883
- (111) surface, PES and band struct. calcs. 80—89118
- abrasion, low speed, strain rate effects 79—20208
- ABS-2 plastic, etching rate rel. to electroless Cu adhesion *(Russian)* 78—35542
- absorbed O_2, ion-bombardment, ejected particle ang. distrib. 78—95643
- absorptivity under laser radiation action, time and temp. depend. 79—95724
- abundance in ordinary chondritic meteorites 80—8595
- acoustic emission rel. to stacking fault energy 78—14365
- acoustic emission signals in plastic deform., amplitude distrib. *(Japanese)* 78—6978
- acoustic emission under action of single elec. pulse discharge *(Russian)* 77—59071
- acoustic losses due to strong ultrasonic and static stress fields 80—79886
- acoustic non-linearity parameter in cubic cryst. 77—51444
- acoustic velocity, shock-compressed uniform solid, lateral discharge ang. semiempirical formula *(Russian)* 78—55910
- activation detector for thermal neutron meas., use of Cu 80—52814
- activation vol. and dislocation density determ. from relaxation obs. 78—3264
- activity distribs., UO_2 natural reactor fuel in ZED-2 hot loop facilities 78—58347
- adhesion to Au, surface treatments and surface impurities 77—15701
- adhesion to glass 77—44386
- adhesion to polyethylene, substrate topography effect 79—74340
- adhesion to polyethylene reactions of CuO with Cu or polymer 79—39118
- adhesive layers on ferrite substrates, prep. *(Polish)* 78—35537
- adiabatic demagnetisation for nucl. refrigeration of ^{3}He 79—67315
- admixture in Sn bath effect on Nb_3Sn critical current and stability temp. 80—7059
- adsorbed atoms on Pt electrode, optical props., electronic struct. 77—69855
- adsorbed CO, on (100) surfaces, LEED study of c(2×2) struct. 79—86983
- adsorbed CO on (100), vibr. excitation cross-sections 80—75441
- adsorbed CO on Cu(100) and Cu(111), struct., LEED pattern reinterpretation 79—28209
- adsorbed formate and acetate species on (100), EELS study 80—76120
- adsorbed I_2 on (111) and (110) surfaces, surface EXAFS study 80—40186
- adsorbed layers of N, O and S, electronic props., UPS, XPS and Auger spectra 77—66088
- adsorbed NO_2, ultrahigh vacuum ESR studies 80—97729
- adsorbed O c(2×2) on (001) face surface geometry determ. by deep-core-level XPS 80—40224
- adsorbed on Ag (001), electronic states calc. 78—6318
- adsorbed on polystyrene, unusual core level spectra, XPS obs. 79—24415
- adsorbed on W (100), electron field emission revealing unmasked surface reson. 79—15595
- adsorbed Xe on stepped and disordered surfaces, two-dimens. phase transformations 80—103580
- adsorption, dissociative, of H_2, on stepped and unstepped surfaces, theory 77—89636
- adsorption, effect on W(100) surface reson. 77—59201
- adsorption, ion-induced, of O_2 on (110) surface 80—54510
- adsorption, of Cs, on (111) surface, photoelectron spectra, angle averaging 79—83100
- adsorption, of H, potential energy curves, pairwise additive model calcs. 78—73087
- adsorption and chemisorption of CO, high resolution UPS 78—39666
- adsorption and desorption of water vapour, relative humidity effects 80—49505
- adsorption and surface reaction of formic acid 80—40741
- adsorption energies on W calc. 79—51464

copper continued
adsorption of Ag, pairwise interaction approach to adsorpt. of oriented overgrowths 77—62759
adsorption of amino acids, surface struct., LEED 78—38968
adsorption of CO, angle-resolved UPS and adsorbate induced struct. 78—71983
adsorption of CO on (110), LEED, surface pot., IR spectra 77—66092
adsorption of CO on polycryst., SIMS 78—14585
adsorption of Cs, struct. and electronic props. 78—23147
adsorption of Cs, XPS exam. of Cu surface state and Cs valence electrons 79—19647
adsorption of Cs and O, (111) surface band energy shift, angle-resolved UPS study 80—40228
adsorption of Cs on (111) surface, oxidation effect on UPS 79—78826
adsorption of Hg, effect on mech. strength, creep, fatigue, embrittlement *(Russian)* 79—29267
adsorption of I_2, surface EXAFS exam. 79—82446
adsorption of NO, NH_3 and N_2H_4, photoelectron spectra 78—6830
adsorption of O_2, N_2O by Cu (110) surface, ellipsometry, AES, LEED study 80—6635
adsorption of O_2, N_2O on (100) surface, reaction with CO 80—103583
adsorption of O_2 and its reaction with CO on (110) surface 80—15373
adsorption of O_2 on (210) surface, LEED and AES meas. 78—71998
adsorption of O, on (001) surface, deep core level XPS anisotropy 78—72690
adsorption of O and S on (100) surface, ang. resolved AES and LEED 78—18908
adsorption of Pb, Auger electron spectroscopy 77—85851
adsorption of Pd on stepped and low index surfaces, LEED, AES and desorption anal. 79—46942
adsorption of pyridine on (110) surface, angle-resolved photoemission, selection rules 80—40231
adsorption of Xe monolayers on (100) surface, thermodynamics and kinetics, LEED and AES obs. 79—99423
adsorption on W, pairwise interaction approach to adsorpt. of oriented overgrowths 77—62759
adsorption on W (100), effect on surface reson. 79—65983
adsorption on W field emitter, field emission energy distribs. 77—59677
adsorption on W single crysts. 78—14612
Aegean Sea, Cu, As and Hg conc. determ. 79—2292
in aerosol particles produced by ocean, meas. 79—58050
AES, valence band spectra, solid-state and atomic features 78—72646
AES excited by X-rays, satellite lines 79—33893
aggregated film, optical props., 0.35-1 μm 77—66548
L-alanine:Cu(II), EPR and ligand-ENDOR measurements 80—44907
alkali halide: Cu^-, charge transfer absorpt. band 79—73977
alkali halide:Cu^+, absorpt., emission and lifetime data, temp. depend. 77—4671
alkali halide:Cu^+, high press. studies of luminesc. phenomena 79—43017
alkali halide:Cu^+, luminesc. spectra and lifetime, high-press. effects 78—35194
alkali silicate glass, CuO doped, ESR spectra of Cu^+, quadrupole effects 78—64265
alkaline earth oxide:Cu phosphors, electroluminesc. 77—32440
amalgam, anodic oxidation in LiOH at room temp. 79—61865
amorphous, bombard. by Ar^+ ions, collision cascades, computer simulation 79—46731
amorphous, sputtering, computer simulation in binary collision approx. 79—56900
amplitude and freq. response to 1-dimens., transient stress waves, for annealed single crysts. 78—14399
amplitude depend. modulus effect 78—64573
analysis in electroplating solution, electrochemical, in presence of cyanide ions 77—1965
angle resolved photoemission spectra 78—43986
angle-resolved photoemission, band struct. 78—95680
angle-resolved photoemission, prediction of spectral peak intensities 78—72695
angle-resolved UPS, free electron final state model calcs. 78—31302
anisothermal annealing, effect on props. of MOOB bands 78—23719
anisotropic electron-phonon interaction theory 79—78022
annealed, cyclic plasticity under cyclic nonproportional strain histories, cyclic hardening, memory erasure, strain hardening 78—88510
annealed and cold rolled, with bamboo structure, exam. of grain boundaries as vacancy sources in diffusional creep 78—88508
annealed O free, high cond., proportional biaxial cyclic hardening 78—84844
annealed OFHC Cu, plastic behaviour 80—59559
annealed OFHC Cu, thick walled cylinder, finite strain pressure-tension loading 77—32632
annealed polycryst., torsional vibrations decrement, deformed vol. effect 80—76326
annealing of lightly deformed samples, effect of press. *(Russian)* 78—39795
annealing twins, density, effect of recrystallisation temp. and electron microscope resolution *(French)* 78—31423
annealing twins density, photoemission microscopy 80—35208
anode, passivating behaviour and illum. effects in alkaline soln. 80—104449
anode spot form., in vac. arc, threshold current time depend. 78—87515
anodic dissolution, of (100) plane, in acidic $CuSO_4$ soln., caffeine additive effects 78—27672
anodic oxidation, photoelectrochemical effects *(French)* 80—93701
anodisation, in NaOH soln., Cu_2O form., chronopotentiometry, SEM and TEM obs. 77—48573
arc, fluctuating, diagnostics using spectral-image photographs *(Japanese)* 79—41896
arc cathode craters, oxide film thickness effects, meas. using SEM *(German)* 78—38558
atom, γ-ray absorption cross-sections, 10-160 MeV 78—90136
atom, absolute effective electron impact excitation cross sections, spectral obs. 80—53147
atom, beam foil spectra, 20 to 350 nm wavelength, 16 to 110 MeV beam energy 78—78655
atom, CC $K\beta_{1,3}$ emission spectrum, double vacancy transitions 79—59393
atom, Compton profile asymmetry obs., Al, Ti, Fe, Cu, using $K\alpha$ fluoresc. 77—57937
atom, crossing effect in 3249Å emission line, mag. field strength depend. 78—25491
atom, Doppler-free laser spectroscopy in hollow cathode discharge 80—9537

copper continued
atom, effective ionisation cross section determ. for H, Li, Na, Cu, Ag, Au and Fr, classical theory *(Russian)* 77—30998
atom, electron bombard., 300 to 600 keV, K_α/K_β X-ray intensity ratios, K-shell ionis. cross sections 78—37747
atom, electron impact, excitation function (maxima, cross-sections) 78—50650
atom, electron impact cross section, elastic and ^2P and ^2D states, inversion ratios 78—9256
atom, electron impact ionisation cross-section, calc. *(Russian)* 79—89789
atom, emission spectra lines in hollow cathode discharge, radial inhomogeneities 77—4974
atom, highly ionised, spectral classifications below 55 Å 79—13658
atom, intensities of reson. lines *(French)* 77—57912
atom, isoelectronic series, semi-empirical oscillator strengths, lifetime, transition probability 80—32672
atom, isolated in mol. matrix, absorption spectra 79—22724
atom, $K\beta_{1,3}$ X-ray emission spectra, low energy plasmon satellites 80—19560
atom, $K\beta/K\alpha$ ratio anomalies, K-capture rel. to bremsstrahlung excitation 77—18825
atom, K-shell X-ray prod. by H^+ and He^+ bombardment, cross sections, energy depend. 78—5337
atom, L_{23}-$M_{4\ 5}M_{4\ 5}$ principal and satellite Auger spectra 78—42030
atom, L and M Auger spectra, CI effects, anomalies 78—33488
atom, L-shell soft X-ray emission spectra, oscillator strengths 80—32651
atom, large angle K-shell ionisation probabilities, projectile charge and mass depend. 78—74750
atom, $O^{2+,3+,4+,5+}$ induced K-shell X-ray production cross section, 7 to 24 MeV 77—61850
atom, orbital energies and X-ray K-absorpt. spectra 80—69060
atom, oscillator strengths, relativistic HF, core-polarisation model pot. 78—86818
atom, oscillator strengths of reson. transitions 79—22666
atom, photoelectric cross section, derived from total absorpt. cross sections 77—10646
atom, photoelectric cross sections for 323 keV gamma rays 77—88432
atom, photon-bound-electron scatt. meas. 77—14394
atom, reson. X-ray Raman scattering, IR divergence of Compton effect 78—21873
atom, resonance line, degree of coordination of clusters in metallic vapours *(French)* 77—58218
atom, resonance lines, relative oscill. strengths, absorpt. spectra 78—42005
atom, semiempirical, relativistic oscillator strengths including core polarisation for p-, s-, d-series 78—74609
atom, stabilized, contact HFS const., matrix shifts 77—42254
atom, Sternheimer shielding functions calcs. 79—76352
atom, total to K-shell photoelectric cross section ratios, 145 to 662 keV γ-rays 77—54545
atom, two-electron one-photon transition rate 77—71772
atom+$H^+(D^+)$, K shell ionisation, nuclear Coulomb effect 80—91650
atom+O ion collisions, A=16, 18, K-X-ray production 77—23554
atom and ions, isoelectronic sequence, coherent photon scatt. cross section calc. 78—5177
atom displacement threshold energy, around ⟨110⟩ directions, direct evidence 78—14379
atom in bulk, local density of states 79—37947
atom K-shell ionis., X-ray prod. cross section for incident H^+, ^4He and ^{14}N ions 78—70923
atom X-ray spectra, mass absorpt. coeffs. in ultrasoft region, spectral depend. 77—10622
atomic and metallic 3p excitation 79—22633
atomic cluster, EXAFS study of bond length and binding energy 79—81317
atomic clusters, struct. and electronic props., Mulliken-Walsh diagrams, extended Huckel procedure 78—46479
atomic electron collision cross sections 77—42410
atomic fluorescence, intensity profile in acetylene-air flame 77—52680
atomic ground and metastable populations, buffer gas effect 78—82955
atomic oscillator strengths, formula for cancellation disappearances 78—90124
atomisation, for graphite furnace AAS, using graphite platform 78—32877
atomistic images of field ion microscopy at high temps. 78—55792
atoms, electron scatt., ang. distrib. for 98.6 keV electrons 79—18295
Auger effect, $K\rightarrow M^2$ radiative, low energy satellites meas. 80—45174
Auger emission from (100) surface, ang. depend., overlayer effects 78—39637
Auger emission spectra, angular resolved 77—81182
Auger energy calc. using XPS, effect of 3d-4s admixed screening on relax energies 77—1782
Auger line shapes, $L_3M_{4,5}M_{4,5}$ and $M_{2,3}M_{4,5}M_{4,5}$ independent electron calc. 77—63500
Auger LMM spectra, transition probabilities, term splittings and effective Coulomb interaction 77—44126
Auger M_1VV line shape, bandlike and atomiclike features 79—43075
Auger spectra, comparison with multiplet struct. calc. 78—31287
Auger spectra, $L_{2,3}VV$ and MVV 78—68583
Auger spectra, LMM, rel. to L_{23} photoelectron spectra 77—77348
Auger spectra, MVV, atomic model and valence band features 78—72644
Auger-photoelectron coincidence measurements 79—19968
backscattering of fission products 80—16138
backscattering of H_1^+, H_2^+, H_3^+, 4-30 keV, O_2 effect 78—15268
band electron momentum distributions calc. 78—18950
band structure, MAPW method, asymptotic behaviour of Fourier coeffs. 77—24510
band structure, optical cond., Compton profile, self consistent calcs. 80—65435
band structure, parametrisation via Hubbard's scheme 77—31938
band structure and high-resolution normal emission UPS 80—6712
band structure calcs., optimised LCAO version, appl. to Wannier states 79—33220
Bauschinger AE peak detection of back stress component in flow stress *(Japanese)* 78—6977
beam, creep rupture under variable load, rupture life lower bound 77—3785
beta-ray backscattering variation with target thickness, self-absorpt. coeff., Z depend. 79—78801

copper continued
  bicrystal, {110ϵ⟨112⟩, deform. *(German)* 77−48513
  bicrystal, intergranular fracture 78−39883
  bicrystalline thin films, characterisation of [001] tilt boundaries 80−75473
  bicrystals, effect of grain boundary on tensile deformation *(Japanese)* 78−88495
  bidirectional twisting; effect on elongation and ductility changes 77−44315
  bimetal Nb-steel Kh18N10T with Cu interlayer, cyclic heating effect 77−16687
  binding energies, stable phase and elastic constants calc., appl. of reson. model pot. 77−69263
  biological specimen Cu content determ. using flameless atomic absorption spectroscopy, effects of sample prep. and matrix 80−98200
  blacked, sunlight absorber, struct. and thermal efficiency 77−125
  blistering by He atoms, (10-20 keV), exam. of skin structure, thickness, He distribution and swelling 79−60412
  blistering by plasma focus discharge deuterons, statical anal., plasma diagnostics 77−35351
  blisters due to He irrad., proton backscatt. study 80−75273
  Bloch states, photoelectron spectra, angle resolved 78−92175
  borate glass:Cu^{2+}, EPR spectra 77−8394
  Bordoni effect in single crysts., 10.2 and 30.6 MHz 80−66566
  boriding W and Mo, Cu effect 80−21165
  Borrmann transmission topography, for quantitative depth meas. of dislocations 79−86795
  Bragg diffraction, anharmonic contributions, Mossbauer study 78−76358
  brazed butt joint, static torsional deform. 77−16657
  bremsstrahlung, β generated, spectral shape depend. on target thickness 78−56545
  bremsstrahlung spectra, 10 to 30 keV, thick target expts. 77−8687
  bright galvanic coatings, crystallite size determ. 79−66221
  Brillouin zone integration special directions, electronic density of states calcs. application 80−49569
  cadmium maleate dihydrate:Cu^{2+}, EPR at 77 and 303K 79−33530
  calcium tartrate tetrahydrate:Cu^{2+}, spin-orbit coupling, optical absorpt. spectra 80−45120
  California harbours, vessel-related contamination by Cu and other metals 79−88010
  carrier scattering rate, temp. dependence, magnetoacoustic experiments 80−44671
  cascade energy density effect on isochronal recovery 78−47431
  catalyst, Al_2O_3 supported, effect on reduction of SO_2 by Cu 79−24819
  cathode, electrically stressed, broad area, surface elec. phenomena, electrolum. K-spot radiation identification with electron emission 80−20711
  cathode, electrolytic deposition of Cu-Cd alloys on (100) and (110) surfaces *(Polish)* 80−44435
  cathode, motion of cathode spot of vacuum arc 80−54069
  cathode, moving arc, microcrater current and spectral fluctuations, simultaneous meas. 80−38828
  cathode, ns voltage pulse breakdown of emitting sites, field emission microscopy obs. *(German)* 77−63547
  cathode, oxide-coated, arc erosion rates, SEM expts. 77−55185
  cathode, regeneration of microscopic tips and cathode polishing by explosive emission 77−16472
  cathode, vacuum arc, current parameters, theory 80−54068
  cathode erosion components, vac. arc, fusion temp. and charge transfer depend. 77−4010
  cathode spot, MHD generator channel conditions, temp. calc. 78−26359
  cathode spots on vac. arc discharge electrodes, model 78−91179
  cathode vacuum arc, cathode spot and cell areas, meas. 80−96405
  cathodes, broad area type, electrolum. regions, current-voltage characts. 80−84019
  cathodes, erosion, vacuum to atmospheric press. arcs 78−79482
  cathodes, heat sources of the arc cathode spot ion impact and neutralisation heating 80−38733
  cathodes arced in vacuum, erosion structs. 80−1872
  cathodoluminescence, film and polycryst. samples, low energy electron irrad., visible and UV emission 78−2921
  CdS:Cu, V, photoluminescence spectra 79−83027
  cell structures, in deformed single crysts., TEM 80−70209
  cellular method calc. for nonspherical potential 78−56063
  cementation, characterisation of nucleation and growth from aq. soln., TEM and SEM study 79−28972
  cementation, electrochem. nucleation and growth on Fe and Al, TEM 80−104451
  cementation, on Fe, deposit struct., reaction rates, SEM 80−104421
  cementation on Fe, expt. study *(Japanese)* 79−70002
  cementation on W substrate field ion microscopy of cementation vs. substrate dissolution, pH effect 80−16206
  CESR, influence of freq. and surface effects 79−51856
  CESR due to edge dislocations 78−19328
  CESR linewidth and g-value, freq. and temp. influence, 4.2-50K 79−87318
  CESR linewidth and g-shift in presence of spin-orbit perturbation, spin-phonon scatt. 77−63285
  CESR meas., 4.2K, selective transmission method 78−39401
  chalcogenide glasses:Cu(Mn), elec. cond. increase on impurity addition 77−11920
  channelling of ions for atom location, continuum approx. calc. of scatt. yield 77−7778
  channelling of Xe ions, Xe(M) radn. yield 79−73234
  chemical plating of glass ceramic with Ni and Cu 77−44379
  chemisorbed CO on (100) face, vibr. excitations and struct., EELS and LEED study 80−39437
  chemisorption, competitive, on metallic films, IR spectra, oil matrix technique 77−9118
  chemisorption, of acetic acid, on (100) surface, acetate species struct. obs. 79−98232
  chemisorption, of CO, SIMS, AES, desorpt. meas. 78−87875
  chemisorption, of O_2, enhancement during Ne^+ bombard. 80−65070
  chemisorption and decomp. of formic acid on (100) surface, EELS study 80−16729
  chemisorption and oxidation of ethanol on (110) surface 78−61044
  chemisorption of CO, angle resolved UV photoemission spectroscopy exam. 78−10284
  chemisorption of CO, coverage depend. photoelectron spectra, adsorption sites 78−95647
  chemisorption of CO, N_2, NO, semiempirical calcs. 78−14611

copper continued
  chemisorption of CO, on (001) face, electronic struct. of $(M)_5CO$ clusters 78−95948
  chemisorption of CO, on (100) face, XPS of core levels 79−15589
  chemisorption of CO, on (100) surface, XPS shake-up satellites, Xα-SW cluster model calcs. 79−95899
  chemisorption of CO on (111) face, IR spectra, LEED, and surface pot. meas. 80−39438
  chemisorption of CO on differently prepared (111) surfaces 78−6223
  chemisorption of H, density of states and chemisorption energy calc. 80−34315
  chemisorption of N_2-containing gases at high-press., XPS 77−20990
  chemisorption of O, Ar^+ bombardment, angle resolved SIMS, surface struct. 79−77913
  chemisorption of O, S, Se, NO and O_2, cluster theory 80−29264
  chemisorption of P and P compounds, Auger spectra 78−43248
  chemisorption of S on (001) surface, thermodynamics, AES study 79−82452
  chemisorption on low-index and stepped surfaces, LEED, AES and UPS obs. 80−84391
  chlorophyll a: Cu^{2+}, in pyridine fluoresc. quenching mechanism 79−56837
  circular plate perforation and deformation by square section punch 79−34100
  clad steel, bond strength through intermediate Zn layer *(Korean)* 79−66213
  clad superconducting Nb and NbTi wires, proximity effect 79−60996
  cluster, and bulk, struct. and electronic props. 78−95592
  cluster, optical spectroscopy, atom to bulk 78−95591
  clusters, electronic struct. and mag. props., MO calc. 77−20219
  clusters, interaction with CO, Cu_nCO form., chemisorpt. bond 78−31631
  clusters, size, geometric effects, catalysis implications 78−73131
  clusters, valence band and core binding energies, UPS meas. 79−38721
  clusters, visible and near-UV spectra 78−19503
  co-adsorption with O_2 on W{100} surface 78−38950
  coadsorption of H_2O and Br, on (100) face, Helmholtz layer model system 80−92777
  coadsorption with Ba on W faces, work function changes 80−65378
  coalescence of SiO_2 particles 78−92271
  coated C fibre, coating struct., SEM study 80−97605
  coated heat sink materials for fusion appl., thermal shock testing 80−18651
  coated InSb, surface contamination, ion microprobe mass analyser obs. 77−52729
  coated steel tube, segmental specimens, tensile testing 79−70255
  coated with Au and Ag, corrosion by thermal degradation products of chloroprene and silicone rubber 79−47801
  coated with polyethylene, in vac., adhesion 79−61793
  coating, bias sputter parameters effect, hollow cathode 77−40369
  coating, vacuum deposited, separation from leucosapphire substrate during annealing *(Russian)* 77−7997
  coating on Ni and Zr, thickness monitoring by back scattering of single energy electrons, density meas. 79−97362
  coating onto $BaFe_{12}O_{19}$ and $SrFe_{12}O_{19}$ 80−25593
  coating with biphenyl, freeze and viscous coating technique 78−48350
  cohesion, electron statistical model 77−27846
  cohesive and elastic props. model *(Hungarian)* 80−34120
  cohesive properties, augmented-spherical-wave calcs. 79−94952
  coincidence site lattice and DSC dislocation network model of high angle grain boundary structure 80−54260
  cold rolled, positron annihilation examination of recrystallisation *(German)* 77−70252
  cold rolled sheet, anisotropy of elastic and strength props. 80−81077
  cold rolling, mechanical props., ageing, annealing, recrystallisation, plastic strain *(Russian)* 80−35202
  cold work, P effect on annealing 79−47707
  cold worked, determ. of dislocation pinning and unpinning stages, using internal friction meas. 78−92278
  cold worked, dislocation production 77−32597
  cold worked, grain size effects on short-term strength *(Russian)* 78−56693
  cold-drawn, contact resist. against metals, for high compressive stress and high current density 77−59324
  cold-rolled, microstruct. 79−83216
  cold-rolled, thickness depend. of G_c for shear lip propag. from single crack propag. 78−11305
  collection mirrors for synchrotron radiation, Cu material 78−62275
  coloured surface layer form. by diffusion into glass 77−36677
  commercial pure, creep-rupture props., vacuum, *(Japanese)* 78−72843
  compact, exam. of anisotropic shrinkage, as function of pressure 79−8257
  compact, on H_2 permeated backing, precipitation *(Russian)* 78−27520
  compacted powder, thermal agglomeration, green strength 77−36417
  compressed powder, elec. cond. −30 to +30°C *(German)* 79−28335
  compressed powder, thermal cond. meas. *(German)* 80−70669
  compressed powder, thermoelectric effects 80−20155
  compressed spherical powder, electrical conductivity *(German)* 78−6343
  concentration in a.c. arc, during interruption, time depend. *(Russian)* 78−22597
  concentration in atmospheric sedimentable powder, in Vizcaya, Spain *(Spanish)* 78−57265
  concentration in snow of Mt. Blanc rel. to air pollution 78−81258
  condensates of different thicknesses, polycrystalline, mech. props. 79−65350
  condensation on Mo(100) and W(100), early stage comparison 80−80072
  conduction band, high momentum components determ. from annihilation radn. ang. correlation 79−19508
  conduction electron mirror refl. from cryst. surface *(Russian)* 77−35985
  conduction electron spin props., g-factor, de Haas-van Alphen oscill. amplitudes 77−35858
  conduction-electron spin flip by phonons, expt. data anal. 79−61219
  constantan junctions with solder, shock-induced elec. response 80−75626
  contact, texture rel. to manufacturing procedure 77−16611
  contact area, effect of loading time *(Japanese)* 78−6230
  contact formation and cohesion, influence of multiple contacting *(Russian)* 80−40548
  contact junction formation by ion evaporation 77−90285
  contact tarnishing and Cu-Au interdiffusion obs. 78−7098

copper continued
contaminant, effect on Hall mobility of VPE n-GaAs, photolum. expts. 80—54810
continuous casting, heat transfer and surface temp. meas. apparatus *(Russian)* 77—66631
continuously cast, O free, effect of nonmetallic inclusion on microstruct. and props. 77—81280
continuum representation of computer simulated dislocations 78—30623
coolant, for two stage nuclear demagnetisation refrigerator *(Japanese)* 80—47063
core-electron excitation edges 80—66345
corrosion, by applied alternating currents 79—70205
corrosion, effect of addition of bromides and iodides, in seawater 78—80670
corrosion, indoor, rate meas. 80—76404
corrosion, monitoring using polarisation resistance meas., techniques and correlations 77—16711
corrosion, noble metal additions effect, Auger spectra 78—35579
corrosion, photo-assisted, in anaerobic acidic medium 79—43466
corrosion, use in reaction kinetic investigation 79—70213
corrosion and wetting in presence of thiol reagents 80—11822
corrosion by org. insulant thermal destruction products *(Ukrainian)* 77—52525
corrosion in Ar-O_2-SO_2 *(Japanese)* 78—11410
corrosion in atmosphere, environmental test 79—66205
corrosion in HNO_3, inhibiting effect of monosaccharides 79—70209
corrosion in seawater, hydrostatic pressure effects 79—52420
corrosion inhibiting surface films of 2-mercaptobenzothiazole and 2-mercaptobenzimidazole, XPS and X-ray induced Auger spectra obs. 80—40600
corrosion inhibition, by benztriazole, chem. aspects 80—16545
corrosion inhibition, by mercaptobenzothiazole, spectro-electrochem. studies 80—30138
corrosion inhibition, chem. nature and struct. of protective films 77—60001
corrosion inhibition through decreasing rate of mass transfer by drag reducing agents 78—19920
corrosion inhibitive films formed by corrosion determination of thickness by X-ray photoelectron spectra 79—15845
corrosion inhibitor study by XPS, adsorbed benzotriazole 78—35554
corrosion of wire in $AgNO_3$, effective corrosion time, resistance variation 78—11404
corrosion protection by benzotriazole from SO_2 attack 78—11385
corrosion protection by benzotriazole pretreatment 80—16555
corrosion protection in chlorosubstituted acetic acids, use of 2-methyl benzothiazole corrosion inhibitor 79—57149
corrosion protection of powder during manufacture and storage 77—25200
corrosion resistance in chlorinated lime slurry and calcium hypochlorite soln. 79—83390
corrosion resistance in seawater *(Rumanian)* 79—74284
corrosion resistant coating Ti-Fe on Cu obtained by contact eutectic fusion 80—50772
corrosionprotection by ion implantation of Al and Cr 80—71789
crack nucleation and stage I propag. in high strain fatigue, microscopic and interferometric obs. 78—52936
crack nucleation and stage I propag. in high strain fatigue, mechanism 78—52937
crack propag. and fracutre kinetics in creep, optical microscopy and SEM obs. *(Russian)* 79—52342
cracks in earlier stages of fatigue, fractography *(Japanese)* 77—8924
cracks in fatigue early stages, direct obs. of substruct. by electron microscope *(Japanese)* 78—7028
creep, 200 to 600°C, within framework of structural phenomenological model 78—27585
creep, low-temp., during dynamic relaxation, effect of dislocation struct. *(Russian)* 77—25103
creep cavitation topology in high purity Cu, high temperature region *(Czech)* 80—65138
creep curves, comparison with theory 78—79232
creep damage and cavity growth, assessment using density meas. 80—104217
creep data, anal. at very low stresses 80—7636
creep data, comparison with dislocation creep theory 80—71708
creep rate, effect of pre-torsional deform at room temp. or 350°C 77—84836
creep rate, effect of surface anodic dissolution in acetate buffer soln. 78—3249
creep resistance, yield point and hardening under alternating torsional strains *(Russian)* 77—32587
creep stimulated by interrupted loading 79—74213
creep-fatigue failures, damage concept appl. 80—40535
creep-fatigue interaction of polycryst. specimens at elevated temp., hydrostatic press. effect on crack behaviour 77—59890
creep-rupture interaction, crack behaviour 79—52334
critical temp. determ. by exploding wires method, liquid metal enthalpy 78—6149
cross-slip at low stresses 77—11564
cross-slipping, stress orientation depend. 79—95022
cryogenic constructing material, far IR spectral refl. 77—24855
crystal, cohesion and vacancy form., electron statistical model 80—54169
crystal Cr-plated, const. strain rate tests, yield stress 79—83276
crystal defects, study with muon probes 78—47314
crystal faces, (100) and (111), response function with d orbital effects on electronic screening 77—62977
crystal growth, method for large oriented single crystal plates 77—90267
crystal growth, oriented, by vacuum intake method *(Russian)* 77—4732
crystal growth from melt 78—48308
crystal growth new technique for prep. from bulk using four pts., RHEED anal. 79—8240
crystal lattice behaviour under intense unidimensional compression *(Russian)* 78—6123
crystal potential in electron diffr. and band theory 78—83677
crystal structure stability, collinear three-ion interaction theory 80—49173
crystalline particles at sphere-plane contact, nondiffusional deform. under capillary forces 78—15329
crystallographic fatigue fracture of single crystal 77—44352
crystals, thick, imperfect, dynamical X-ray diffr., topographic effects 77—68898

copper continued
cubic crystals, anisotropic, dislocation loops, electron microscope image contrast 80—39101
current leads, gas-cooled, for superconducting dipole magnets, experimental study 79—67995
current-carrying conductor, MHD instability suppression, skin effect in strong electric field 77—951
curvature factor, interpretation of de Haas-van Alphen oscillation amplitudes 79—47000
cutting of bicrystal to compare mechanism for large crystals and polycrystals *(Japanese)* 78—60871
cyclable solid-state cell based on intercalated electrodes 79—100511
cyclic creep reversal 80—25766
cyclic hardening role in crack nucleation at high strain amplitude 78—64633
cyclic loading, change in mech. props. rel. to heat treatment 80—104282
cyclic strain hardening under deform. at various temps. 79—43273
cyclic straining anal., discrete polycrystal model 77—47507
cyclic torsional deform. at high deform. amplitudes *(German)* 79—87701
cyclic torsional deformation, final texture 80—7595
cyclic work hardening during frequency change fatigue tests *(German)* 79—34068
cyclic work hardening frequency effects *(German)* 79—29090
cyclically deformed, nucleation of persistent slip bands 78—72830
cyclically deformed polycrystals, elastic limit contrib. of thermally active processes *(Spanish)* 79—91732
cyclotron mass and Fermi velocity meas. by de Haas-van Alphen effect 77—76734
cyclotron masses using tetrahedron method 79—90946
cylindrical metal liners, explosion-accelerated, form stability anal. 78—83425
cylindrical shells, thickness determ. by inductive meas. 79—12760
Czochralski growth, meas. of contact angle between melt and cryst. 77—28708
damage production by high energy d-Be neutrons, elec. reist. meas. 77—62564
de Haas-van Alphen effect, accurate meas. of Dingle temp. changes 77—51638
Debye Waller determ. from modified Cheveau model 78—59918
Debye-Waller factor temp. parameter 78—30725
Debye-Waller factors, modified ang. force model 77—66013
decoration technique, lattice imperfection characterisation, of Si wafer *(Japanese)* 79—65069
defect annealing around stage III, $\gamma\gamma$ ang. correlation expt. 79—14846
defect annealing study by positron annihilation, and elec. resistivity meas. 78—51584
defect clusters, electron microscope exam. 78—47380
defect removal, obs. by positron annihilation 78—84677
defect-phonon perturbations after neutron irrad., neutron scatt. study 80—44278
defects, thermal relaxation, positron experiments *(German)* 80—50455
defects at thermal equilib. and melting, positron annihilation meas. 77—76391
deformation and fracture under dynamic loading 78—35442
deformation band, role in fatigue crack nucleation and propag. 79—24585
deformation hardening by shock front, quasiisentropic compression, front width effects 79—100209
deformation in ultramicrotomy 77—8874
deformation instability and tensile elongation 77—32655
deformation mechanism under high hydrostatic pressure *(Ukrainian)* 80—25758
deformation of ⟨100⟩ single crystal *(Japanese)* 77—59864
deformation of single cryst., effect of surface layer 79—8315
deformation potentials for isotropic strains 79—42506
deformation process, stage-by-stage nature investigation using acoustic emission *(Russian)* 80—40434
deformation under mutual indentation in contact with Pb-Bi eutectic melt *(Russian)* 77—59853
deformed, intensity and lattice strain distrib., exam. *(German)* 78—52885
deformed, positron lifetimes, trapping model 77—15451
deformed, temp. depend. of positron trapping 77—48270
deformed, texture development 79—87653
deformed and annealed, positron lifetime investig. of recovery and recrystn. 77—70064
deformed by hydrostatic extrusion, drawing or drawing under press., dislocation struct. obs. *(Russian)* 77—21213
deformed by rolling and torsion, stored energy *(German)* 79—29160
deformed single crysts., extinction, γ-ray diffr. and neutron struct. refinement 77—84588
dendrite growth from supercooled melt 77—51628
dendrites, electrodeposited, growth kinetics, cathode surface effects 79—70007
densification of particulate materials, general law 78—19692
densification of two layered powder medium 80—35138
deposits, keweenawan-type, exploration using LANDSAT-1 imagery 79—2398
deposits, morphology, polymer codeposition effects 79—74102
deposits on Cu (110) electrode, morphology and crystal growth 79—47644
depth resolution for MeV $^4He^+$ backscattering in C, Al, Cu 79—14840
desorption, of Ar, H_2, CO and methane production and meas. of atomically clean surface environment 80—52250
determ. in water and organic materials, flameless atomic absorpt. spectrometry with wire loop atomiser 80—45586
determination, by Zeeman effect at. absorpt. spectroscopy 77—32866
determination, in beef extract, by NAA 78—27856
determination, in cement, by direct atomisation AAS *(Japanese)* 79—70413
determination, in $Cu(NO_3)_2$, soln., by flameless at. absorpt. 77—40596
determination, in Italian chondritic meteorites, by destructive neutron activation anal. 78—12172
determination, in powder rock samples, by at. absorpt. *(Russian)* 78—85278
determination, in salt, spectrochem. method *(Russian)* 79—29440
determination, separation from Sb in Cu alloys, inverse voltamperometry method 78—61099
determination by computerised thermal neutron activation anal., interference correction 77—44544

copper continued
determination by cyclic and anodic stripping voltammetry, appl. to natural waters anal. 79−74446
determination by proton-induced X-ray emission anal. in blood and liver tissue 79−53291
determination in Al alloys by at. emission spectroscopy with spark source, photodiode array detector *(German)* 79−87926
determination in NaCl, serum or urine, AAS, background correction 78−27834
deuteron bombarded, annealing elec. resist. changes freq. factors, activation energy distrib. 79−77648
diatomic molecule, bonding, ab initio pseudopot. calcs. 79−6857
dibarium cobalt formate tetrahydrate:Cu, EPR of Cu-Co interactions 78−60334
dielectric const. by multiangle reflection meas., optical props. 79−95723
differential ranges of fission products by a coulometric method 80−65097
diffraction of He from (117) stepped surface, 70 to 773K 80−35031
diffusion, in Al, isotope effect 78−84006
diffusion, in CdS thin films, 20 to 200°C *(French)* 80−15424
diffusion and oxidation of Cu^+ in glass 80−79980
diffusion and solubility in Fe, 690-1050°C 77−59146
diffusion bonding with Ni, Ag and Al 77−62687
diffusion coefficient of H, steady-state flow method 80−10795
diffusion coefficient of Sn via surface segregation 77−7905
diffusion coefficients calc. for H and D *(Russian)* 78−91483
diffusion in Ag, SIMS investigations 80−59717
diffusion in Al films 78−2303
diffusion in Au, 75-150°C, AES, device appls. 77−1262
diffusion in Au, rate rel. to Ni 77−80652
diffusion in Au electrodeposited coating, under high temperature, influence on contacts performance *(Czech)* 78−91486
diffusion in Au grain boundaries, determ. using AES data 77−11742
diffusion in CdSe, effect of laser radiation on diffusion 79−10983
diffusion in $Ga_xIn_{1-x}P$, epitaxial film, effect of intrinsic impurities 78−87825
diffusion in GaAs epitaxial layers, grain boundaries, deep level transient spectroscopy study 80−49234
diffusion in $LiNbO_3$, and its effect on acoustic velocity 77−84847
diffusion in Nb, radiotracer and electron microprobe meas. 77−76615
diffusion in P_2O_5-glass, fluoresc. meas. 78−59980
diffusion in systems involving group VA elements, review 77−39697
diffusion layer cathodic deposition and anodic dissolution rates 80−93503
diffusion mobility of gas bubbles in Cu 80−39357
diffusion of ^{110}Ag, activation energy, form. enthalpy of vacancies 78−51736
diffusion of ^{33}P in single- and polycrystals, 548 to 1046°C 77−1265
diffusion of Ag, 759-1081°C 79−10982
diffusion of Au(Pb)(Bi), diffusion coefficient temp. depend. *(Russian)* 77−84987
diffusion of Fe, resistometric technique 78−38880
diffusion of Fe, study at high temp. using molten salt electrochemistry 77−84997
diffusion of Ge, isotope effect 78−2285
diffusion of H_2, isotope depend. 80−59727
diffusion of H and trapping 80−70447
diffusion of impurities, electrostatic model 78−2300
diffusion of interstitial O_2, sink/barrier phenomena 79−60553
diffusion of muons and protons 79−56689
diffusion of Ni, resistometric meas. 80−29222
diffusion of O_2, temp. depend. 650-1020°C *(Russian)* 77−84996
diffusion of S 78−47599
diffusion of stable Ge isotopes, isotope effect 79−60552
diffusion of V, Cr, Mn 77−62674
diffusion of Zn 79−77825
diffusion of Zr, microstruct. and microanal. study of coating formed *(Rumanian)* 78−19917
diffusion welding, tensile fracture strength *(Japanese)* 80−7663
diffusion/oxidation through Au, rate-controlling step 80−34240
diffusivity and solubility in LEC GaP 78−51743
diglycine barium chloride monohydrate:Cu^{2+}, optical absorpt. and EPR, lattice sites, hybridisation 77−43872
dimethylammonium manganese trichloride:Cu, impurities in quasi-one-dimens. Heisenberg systems, anisotropy effect 80−80502
discharge, high-current, hollow-cathode, excited states population meas. *(Russian)* 77−35421
discharge, hollow cathode in pulse mode, spectral lines and intensities 78−34376
discontinuous film, ageing effect on elec. cond. 79−24084
discontinuous film, light absorpt. spectra, dielec. function calcs. 79−51507
dislocation annihilation during tensile and cyclic deform. and limits of dislocation densities 80−34007
dislocation breakaway, in single crysts. etch pit study 78−6064
dislocation cell form. during plastic deform., TEM obs. 80−60935
dislocation core energy, core tension, Peierls model 79−27984
dislocation damping during electron irrad. 77−35632
dislocation damping during electron irrad. 77−76462
dislocation damping during electron irradiation, new model for peaking effect 78−87683
dislocation damping strain amplitude depend. on 1 MeV electron irrad. and quenching 79−95023
dislocation density, at large plastic strains 79−74224
dislocation density, calcs. as function of plastic strain in cold worked polycrystn. sample 79−38924
dislocation density, limiting value, theory 77−27882
dislocation density in fatigue, approx. determ. by resonant bending fatigue apparatus 77−86279
dislocation etch pit obs. on {111} surfaces 79−10861
dislocation etch pits on {111} surfaces *(Japanese)* 77−62536
dislocation formation during sintering *(German)* 78−31361
dislocation increase by electron wind *(Russian)* 79−95024
dislocation mean free path at 77K under elastic deform. 78−44162
dislocation mechanism of luminescence during fracture 79−24376
dislocation motion in highly perfect crystals *(Japanese)* 79−60373
dislocation motion obs. in briefly perfect crystal *(Japanese)* 79−60372
dislocation path length after pulse loading 78−30630
dislocation pinning rate, neutron and electron irrad., meas. by internal friction method 80−96570
dislocation point defect sink strengths, mutual recomb. effects 79−73207

copper continued
dislocation sources, grain boundaries in the premacroyield strain region 79−34096
dislocation structure, around tips of propagating fatigue cracks 79−29211
dislocation structure, evolution at heating 80−103337
dislocation substructure formation under hydrostatic extrusion 78−56696
dislocation velocity, thermal activation exam. of applied stress and temp. depend., expt. methods *(French)* 80−59474
dislocation-defect dragging in electron irradiated samples, 4.2 to 350K 78−43027
dislocation-dislocation interaction inducing cross slip in thin Cu plates, X-ray topographic anal. 80−49233
dislocation-free, melt growth conditions 78−3025
dislocations, zigzag stress-induced, X-ray topography obs. 79−99205
dislocations gliding on (001) planes, bright field and weak-beam images 80−107266
dispersion hardened, mobile dislocation density and length of slip lines 77−51387
dissolved Cu concs. in E.Atlantic Ocean, 23°N to 47°N 77−5239
distribution in waters of Yarra River estuary 79−16552
drawability, mech. props., effect of O impurities 79−83272
drawing deform. band form., axial orientation force meas., X-ray pole figure determ., on single crystal *(Japanese)* 78−76710
drilling with CO_2 laser pulses, influence of laser-supported detonation waves 79−28866
ductile fatigue crack growth mechanism in single crystals, in situ SEM obs. 79−61695
ductility minimum, strain rate depend. at intermediate temps. 79−79056
dynamic material behaviour under nearly uniaxial strain conditions, modified Kolsky apparatus 78−85070
dynamic strength and logarithmic modulus of plasticity 77−16655
dynamic uniaxial tension and compression curves 80−100884
elastic constants, third-order 79−51184
elastic constants, up to 2500 bar, −196-25°C, US pulse echo obs. 79−87680
elastic grain boundary responses, thermodynamic props., computer calc. 77−39593
elastic moduli rel. to Gruneisen elastic parameters 79−95070
elastic moduli second press. derivatives 79−96058
elastic modulus and internal friction during plastic deform., dislocation props. determ. 80−35244
elastic strain wave generation, by electron beam pulse *(Russian)* 77−76463
elastoresistivity of Frenkel pairs, defect migration *(French)* 80−2073
electric field gradient due to interstitial positive muon 78−31142
electrical cond., effects of impurities 78−43355
electrical conductivity, effect of cyclic strains and work hardening at 4.2K 78−91655
electrical conductivity exam. in solid and liquid phase *(Russian)* 77−62895
electrical conductivity measurement at MM wave freqs. 80−42235
electrical grade, fatigue damage eval. from freq. change of natural vibrs. 79−52498
electrical resistance of edge dislocations *(German)* 80−96859
electrical resistivity, at low temp., temp. depend. 78−23071
electrical resistivity, electron-electron scatt. and Fermi surface calc. 78−64023
electrical resistivity, linear strain effect at elevated temps. 79−91022
electrical resistivity, press. variation 78−84193
electrical resistivity, pseudoharmonic effect of phonons 80−34414
electrical resistivity, temp. depend. data 80−51967
electrical resistivity changes at high temp. due to vacancies 78−26565
electrical resistivity of dislocations, calc. *(Russian)* 78−60117
electrical resistivity under torsional deform., impurities and tensile loads 78−30898
electrically exploded foils, heating and burst phenomena 77−39488
electrochemical deoxidation, of induction stirred melts 78−39718
electrochemical displacement reactions, electron microscope obs. of nucleation and growth, comparison of Cu/Fe and Cu/Al cementation systems 79−47939
electrochemical dissolution and deposition kinetics, in aq. SO_4^{2-} soln. 78−27773
electrochemical nucleation, and growth on Fe and Al, TEM 80−104451
electrochemical overgrowths, role of substrate dislocations and grain boundaries in nucleation and growth 79−51454
electrocrystallisation, multiple twin form. 77−39750
electrocrystallisation from $CuSO_4$ solns., current density under stationary surface diffusion *(Russian)* 79−8237
electrocrystallisation from $CuSO_4$ solns., current density/overvoltage curves *(Russian)* 79−8236
electrocrystallisation from $CuSO_4$ solns., expt. and slow surface diffusion theory *(Russian)* 79−11505
electrocrystallisation from $CuSO_4$ solns., exptl. methods *(Russian)* 79−8235
electrocrystallisation in chloride aq. soln. 77−73241
electrocrystallisation of Cd on Cu single cryst., asymm. AC influence 78−10292
electrocrystallisation on graphite electrodes, nucleation 80−93504
electrode, adsorption of pyridine, angle-resolved Raman spectroscopy 80−52991
electrode, broad area, high-β emission sites, energy spectra 78−35253
electrode, deposition on InSb, ohmic contact formation, SEM obs. 77−51817
electrode, electrical breakdown of water in μs region 80−103917
electrode, electrodeposition of Cd, conditions for granular growth 80−55310
electrode, erosion due to high-current pulses, effect of media 79−10735
electrode, ionic mass transfer coeffs. determ. in open channels 80−59110
electrode, photopotentials, rel. to corrosion 79−24648
electrode degradation in coaxial plasmatron 79−14629
electrode material, influence on electric breakdown in dielectric liquids *(Russian)* 80−50265
electrode potential, transient response to elastic straining rel. to reaction kinetics 79−70212
electrodeposit, US agitation effect on hardness, porosity and grain size, work-hardening 77−60075
electrodeposit on (111) Cu substrate in presence of halo-compd. of acetic acid 80−15413
electrodeposit on Al and Fe, defects and their effect on props. 80−39474
electrodeposited, struct., physical and mech. props. *(Russian)* 79−56939

copper continued
electrodeposited, work function, heating temp. influence 79–33331
electrodeposited coating, annealing effect on struct. and microhardness *(Russian)* 78–76668
electrodeposited coating on Fe membrane, effect on H permeation, proposed catalytic mechanism 78–53252
electrodeposited single crystal film, fatigue cracking investigation *(Japanese)* 78–84975
electrodeposition, chemical factors 80–16207
electrodeposition, influence of specific adsorpt. of S, Cl 79–20001
electrodeposition, layer growth form. rate on (100) face, anions effect 80–35540
electrodeposition, on a Cu single cryst. (110) face in presence of sulphaguanidine 80–76203
electrodeposition, on Cu single cryst. (111) plane in presence of sulphaguanidine 80–76204
electrodeposition, using fluidised bed electrodes, at high current density 79–100063
electrodeposition and formation of crystallised layers on Ni(111) surface, twinning 77–24495
electrodeposition at vertical electrode, H_2 evolution effect on current distrib. 80–35543
electrodeposition by pulsating overpotential electrolysis, digital simulation 77–81410
electrodeposition from cyanide solns., interaction with 2-butynediol-1,4, obs. *(Russian)* 79–47936
electrodeposition from nitrate solns., cathode polarisation obs. *(Russian)* 79–47937
electrodeposition in acid $CuSO_4$, ridge growth on (110) face 77–11807
electrodeposition in cylindrical pores by pulse plating 80–81330
electrodeposition in flow-through electrodes 77–16514
electrodeposition on Cu single crystal (100) face, in presence of Br ions 78–84723
electrodeposition on Cu single crystal (100) face and Cu polycrystal surface in presence of sulphaguanidine 80–16210
electrodeposition on plane vertical cathode, distrib. of local current densities 79–70338
electrodeposition potential and electrolyte composition effects on surface morphology *(Russian)* 78–48337
electrodeposits, bright, low conc. of ions effect on internal stress 80–25909
electrodeposits obtained under influence of asymmetric AC, microscopic characts. 79–70003
electrodes, breakdown voltage, prebreakdown current in vacuum, crossed elec. mag. fields depend. 80–79604
electrodes, coaxial, field emission at low H_2 press., I-V characts. 77–28702
electrodes for static voltage breakdown of vac. in mag. field, pretreatment effects 77–19781
electrodissolution kinetics in acidic chloride solns. 80–16695
electroforming, study of process variables in the electromagnetic bulging of tubes 78–80582
electroless bath, electrochem. control system 80–71601
electroless deposition, electrochemistry 79–61520
electroless deposition, pH effect, computer study 78–39709
electroless film, room temp. oxidation 77–48572
electroluminescence from Cu cathode, semicond. impurities on surface 77–90200
electrolytic, powder mean normal contact stress in rolling 77–12571
electrolytic coating, brighness and adsorption of surface-active additives 80–100963
electrolytic Cu foil, determ. of oxides on surface 77–90682
electrolytic deposition, adsorption of substances used as brighteners 79–66220
electrolytic deposition, collagen and chloride additions effects obs., on morphology and crystal orientation 78–51852
electrolytic deposition from $CuSO_4$ solns. 78–61022
electrolytic epitaxial nucleation and growth, on (111) Ag 80–104081
electrolytic form. by electrodeposition, structural defects 77–39749
electrolytically deposited on Al, annealing, ring-like pattern *(Japanese)* 78–44139
electromigration, thermomigration, and solubility, in Pb 78–71882
electromigration and diffusion in Al films on Si substrates 79–77820
electromigration in Al, apparent effective charge, 325-500°C 77–39695
electromigration in $BaO-P_2O_5$ glasses at 400°C, luminesc. meas. 77–76610
electromigration in Pb 78–84003
electromigration of ^{113}Sn 80–6557
electron backscatter fractions, exptl. determ. 80–18617
electron backscattering, X-ray prod., energy distrib. calc. 79–38698
electron backscattering by bulk target, theoretical model *(French)* 80–60722
electron beam irradiated, influence of created pulsed press. on struct. and props. *(Russian)* 78–34539
electron beam reflection, high current *(Russian)* 78–84690
electron bombardment effects, gas evolution obs. *(Russian)* 79–1460
electron diffraction study, ECP contrast, Bloch wave model 80–96419
electron dose distribs. from plane infinite oblique sources, Monte Carlo calcs. 77–65339
electron drag on mobile dislocations at low temps., strain rate, temp., and field depend. 80–19808
electron emission depend. on surface mechanical treatment *(Russian)* 80–100945
electron emission induced by low energy light ions 79–61482
electron energy loss spectra, microanal. appl. 77–44099
electron energy loss spectrum, (311), 30-300 eV, CO or Xe adsorption effects 77–63507
electron energy loss spectrum, complex dielec. function calc. 77–11862
electron inelastic mean free paths and energy losses, electron gas statisitcal model 79–46733
electron irrad., positron lifetime exam. of annealing recovery 78–47354
electron irrad., very low atomic displacement threshold energy obs. 78–95078
electron irradiated, additional recovery around 200K 78–38755
electron irradiated, dia- and paraelastic effects 77–76482
electron irradiated, elastic point defect-dislocation interactions, defect dragging model extension 80–65050
electron irradiated, evidence for vacancy migration in stage III 78–38693
electron irradiated, exam. of vacancy migration energies, and annealing kinetics 78–47571

copper continued
electron irradiated, migration and thermal conversion of defects, 100 to 330K 80–59519
electron irradiated, secondary defect formation, effect of refl. condition *(Japanese)* 77–43248
electron irradiated, selfinterstitial atomic defect interaction radii, recovery expts. and error sources 80–65049
electron irradiated, small-angle X-ray scatt. investig. of stage III recovery 77–7763
electron irradiated, stage III recovery kinetics 78–63792
electron irradiated, temp. depend. of threshold energy for atom displacement 80–34055
electron irradiated, thermal variation of dislocation pinning by point defects 79–51150
electron irradiated, void nucleation, Monte Carlo simulation method *(French)* 77–59046
electron irradiated, void swelling and dislocation loops 79–99206
electron irradiated at 100K, comparison of irrad. hardening with dislocation vel. 80–54284
electron irradiated at 100K, dislocation vel. meas., etch pit technique 80–49271
electron irradiated at 4.7K, recovery of Frenkel defects, defect-agglomerate effects *(German)* 77–84797
electron irradiation, bremsstrahlung yield and absorbed energy distrib. 79–99245
electron irradiation at 130K, positron lifetime investig. of stage III recovery mechanism 77–47484
electron irradiation damage, dislocation pinning investig. of crowdion model 77–69000
electron mean free paths and stopping powers calc. using statistical model 77–19996
electron microscope obs. of shear bands *(German)* 77–48454
electron radiated, formation of Frenkel pairs 79–23598
electron range, low-energies continuous-slowing-down approx. and range straggling calcs. 80–39183
electron scattering cross sections, 300 to 1200 keV 78–9922
electron states, parametrised, separable potential for band structure calculations 78–79912
electron states of (111) surface 77–62979
electron transmission and absorpt. in bulk solids, 5 to 30 keV 77–89491
electron transmission and absorption, 70 keV initial energy 78–71777
electron transmission and absorption at 0.6 to 4 keV, obs. 77–84818
electron-dislocation interaction, influence of mag. fields on flow stress meas. 77–31672
electron-irradiated, monovacancy migration during stage III annealing, NQR study 80–107576
electron-irradiated, point defect agglomerates, HVEM invest. during in-situ annealing 80–84213
electron-irradiated crystals, electron diffr. channelling effect on atom displacement 80–39158
electron-irradiation, internal friction behaviour, shear modulus and damping meas. 80–55444
electron-phonon interaction, scatt. and transport props. 79–91037
electron-phonon interaction anisotropy, microcontact spectroscopy *(Russian)* 78–43372
electronic barrier resonances of (001) surface, LEED study 80–39651
electronic contribution to thermal cond. at low temps. 79–95384
electronic density of states, cluster approx., compared with photoemission spectra 79–60675
electronic energy loss of protons (deuterons), 80-800 keV 79–23666
electronic props., pseudopotential calc. 78–51960
electronic relax. time in Sondheimer size effect, temp. depend. 79–87086
electronic stopping function for He^+ and Li^+, 50-300 keV 79–69169
electronic structure, bulk and (001) film, extended tight-binding calcs. 80–70592
electronic structure, bulk d-band densities of states calc., optimisation of local orbitals 77–47711
electronic structure, empirical parametrisation scheme 78–91585
electronic structure, linear APW method 79–51467
electronic structure and d-holes of films and surfaces 78–39180
electronic transport properties, OPW calcs. 77–43553
electronic work function, temp. derivative from 2.9 to 6.2K 79–56284
electroplastic drawing, deformation zone current delivery schemes 79–91761
electroplated coating, levelling kinetics, interferometric investigation *(Bulgarian)* 78–79864
electroplated surface roughness and brightness rel. to periodic reverse current 79–96201
electroplating, raising temp. by gelatin addition to plating soln. *(Japanese)* 79–38754
electroplating, using cyanide copper baths, Rochelle salt influence and analysis *(German)* 77–25328
electroplating acid-Cu electrolytes, effect of periodic reverse current process on deposit props. 79–33951
electroplating method for sensitizing stress meas. *(Japanese)* 80–68197
electroplating of Ni alloy, protection against hydrogen embrittlement, aerospace engine appl. 80–76416
electroplating onto C fibre reinforced epoxy resin, coating props. *(Japanese)* 77–36412
electropolishing behaviour rel. to polarisation charact. 79–83386
electropolishing in alcoholic soln. of H_2SO_4 77–16718
electropolishing of horizontal surfaces, role of natural convection mass transfer 79–57143
electrorefining process, quantitative evaluation of Ag transfer 80–30246
electroreflectance, influence of surface microtopography 79–15437
electroreflectance of single cryst. electrodes, obs. in aqueous solns. 80–25342
electroreflectance spectra of monocrysts., anisotropic surface effects 79–8123
electrospark alloying to Ag, residual stresses obs. *(Russian)* 77–56145
electrospark machining, spreading and form. of surface layer, in solid-alloy-liquid-metal systems, kinetics *(Russian)* 78–27668
electrowinning from solvent extraction acid strip soln. using Pb-Sb anodes 77–48653
EM cascades caused by electrons and photons, 10-100 GeV, longit. development 79–21120
emissivity, 140-300K 77–35729
emissivity, 335-1100K, polishing effect 77–39682
emissivity, total hemispherical, temp decay method meas. 78–26708
energy band calc. by model-pseudopotential method 79–7779

copper continued
energy band dispersions, absolute determ. using ang.-resolved photoelectron spectrosc., symmetry method 79—15590
energy band dispersions and lifetimes using angle-resolved photoemission 79—77998
energy losses and straggling for H^+ and He^+ beams *(Russian)* 80—84226
energy reflection coefficient for 5 to 10 keV He ions 78—95639
epitaxial, on (111) Au, periodic arrays of misfit dislocations, electron diffr. 78—51857
epitaxial electrocrystallisation, substrate imperfections effect 78—18921
epitaxial growth on Au, alloying effects 77—62785
epitaxial growth on W, FIM and FEM obs. of nucleation and growth 78—26800
epitaxially grown film, on Au (111), twin form., LEED detection 80—88442
epitaxy in aqu. oxidation of (001) single crystal 80—11844
epitaxy on W (001) 78—60041
equation of state, isentropic expansion method 78—91414
equation of state for all press. between 300-200000K, numerical calcs. *(French)* 77—72672
equation of state from statistical electronic free energy 79—99495
equilibrium relations between Cu, white metal and SiO_2 saturated slag, under controlled SO_2 press. 77—52294
equivalent sphere diameter calc., Saltykov method 78—31362
erosive wear mechanisms, combined TEM and SEM obs. 80—108601
in estuarine environments, inorganic speciation 78—69371
estuarine river water, particulate heavy metal content, Cochin backwater, India 80—7964
etch pit formation on single cryst. planes by dil. H_2SO_4 78—14348
evaporated coating on Al single crysts., surface strengthening effects 77—8972
evaporated film , surface struct. 79—69381
evaporated layer, secondary electron energy distrib. and work function *(French)* 79—99993
evaporated layer on Ge, RHEED Kikuchi bands, anomalous contrast 78—87597
evaporated metal nuclei on C, SiO_2 films, atm. contamination, AES meas. 77—4264
evaporation, by absorption of Nd laser pulse, numerical anal. *(Russian)* 77—40312
EXAFS, with conventional X-ray source 77—69933
EXAFS amplitudes, many-body effects 80—97379
EXAFS analysis of interatomic distances, coord. numbers, and mean relative displacements 80—89087
EXAFS beats, determ. of differences in bond lengths 78—23552
EXAFS Debye-Waller factors 80—45168
EXAFS in photoelectron yield spectra and optimisation of the photon glancing angle 78—80435
expansion, isentropic, vaporisation and condensation kinetics anal. 77—66623
exploding foils, rapid mag. energy transfer, conductivity law *(French)* 78—91135
exploding wire unduloids, preferred grain orientations, lattice distortions, zonal texture 77—36568
exploding wire with inductive energy bank, quasistatic model, resistivity meas. 78—47199
explosion clad bonding, TEM obs. 77—62763
explosion of double wire, optical flashes, photographic appl. 80—1865
explosive cladding, TEM obs. and thermomech. model 79—96041
explosive compaction of metal powders 78—64501
explosive loading, depend. of struct. on deform. *(Russian)* 78—3177
extended screw dislocation, ⟨110⟩ misfit defect elastic interactions 80—100232
extended single crystal wire, orientation of cross section ellipse 77—86115
extended X-ray fine struct., lattice consts. 80—89085
extraction, from aq. soln., hydroxyoxime and hydroxyquinoline derivative reagents 79—74115
extraction by Kelex 100, meas. and correl. of solvent extraction equilibria 77—29034
extraction equilirbium, with versatic acid 911 79—43620
extruded at 77K, defect struct. and elastic limit *(Russian)* 80—30016
facing Cr steel, thermodynamic anal. 78—60878
failure under hydrostatic press., kinetics 78—52944
fast electron multiple scattering, and inner secondary electron generation 77—1160
fast electron transmission, contrib. of high-angle deflections 79—28024
fatigue, effect of active liquid media on struct. and stress condition *(Russian)* 77—28929
fatigue, high frequency, modulus meas. *(German)* 77—59938
fatigue, implications of hysteresis behaviour, plastic strain cycling 80—3191
fatigue, low-temp., effect of ambient environment *(Russian)* 77—59896
fatigue and fretting iniatiated fatigue in single crystal, crystallographic orientation effect 77—70182
fatigue behaviour effect of Zn, Au diffused coatings 78—72850
fatigue crack growth and threshold measured at very high frequencies 80—71742
fatigue crack initiation, model using probabilistic technique 78—68800
fatigue crack propag., environmental effects *(French)* 77—66711
fatigue crack propag., influence of specimen thickness *(German)* 80—66669
fatigue crack propag., role of dislocation substruct. 80—60963
fatigue crack propagation, effect of stacking fault energy as deduced from dislocation patterns, TEM study 79—61719
fatigue cracks, propagation, model, low cycle, cyclic stress-strain response determinations 79—68653
fatigue hardening and failure at intermediate life 77—48548
fatigue hardening and high cycle fatigue under reversed bending 79—20180
fatigue of single crystals and low const. plastic strain amplitude 79—20174
fatigued, early stage crack tip dislocation morphology, electron microscope obs. 78—27628
fatigued, relationship between stress and point defect cluster density 80—10592
fatigued, structural changes, damping and modulus 77—28906
fatigued high-purity polycrystals, temp. depend. of flow stress 77—44316
fatigued polycrystals, impure, temp. depend. of flow stress 77—44317

copper continued
fatigued polycrystals, point defect cluster rel. with yield stress temp. depend. 78—6989
fatigued specimens, 'etch pit slip', SEM obs 79—100258
FCC, appl. of model for lattice dynamics 78—91387
FCC, dislocations, elastic instability 79—82235
FCC, electrodeposition of HCP Co layer 79—11527
FCC, Gruneisen parameters, effect of temp. variation 78—22812
FCC, high-angle (001) CSL twist boundaries, struct. 79—46677
FCC, polycrystalline, deformation-strain curve description using substruct. parameters *(Russian)* 79—87690
FCC, props. of vacancies and divacancies 80—10545
FCC, single and multiple interstitials 77—68964
FCC, stacking fault, antiphase boundary energies, investig. methods, review *(French)* 79—42080
FCC, thermal expansion coeffs., Morse pot. calcs. 79—77775
FCC, twist boundaries, struct. invest. using computer simulation technique 80—84185
FCC(111) substrate, orientation relationship with Fe vac. deposits 80—59836
FCC crystal, stress-strain curve, stage I to stage II transition *(Japanese)* 78—19834
FCC single crystal, crystal rotation accompanying scratch deform. *(Japanese)* 79—15733
Fermi surface, electron mass enhancement, orthornormal function enhancement 80—96777
Fermi surface, electron-phonon enhancement factor 77—1357
Fermi surface, positron annihilation study 79—4869
Fermi surface, self-energy nonlocality effect 77—62805
Fermi surface and thermoelec. power, de Haås-van Alphen calc. 79—4503
Fermi surface orbit integrals, tetrahedron method, cyclotron mass orientation depend. 80—44476
Fermi surface orbit integrals, tetrahedron method, Dingle temps. for 3d transition metal impurities 80—44477
Fermi surface studies by the positron annihilation technique 79—82515
Fermi surface topology by two dimens. angular correlation of annihilation radiation 79—65359
fibre texture of filaments produced by glass coated melt spinning 77—85966
field ion appearance spectroscopy, ion generating processes at field emitter surface 79—52086
filament produced by glass-coated melt spinning, tensile strength 77—48508
film, 1/f noise, role of substrate 79—28388
film, 1/f noise and its temp. depend. 79—60939
film, 1/f noise and its temp. depend. 79—60940
film, (100), chemisorbed N_2, electronic struct. 77—59315
film, (110), energy bands, tight binding calc. 77—15761
film, (111), energy bands, tight-binding calc. 77—15760
film, absolute work function meas. by field-emission retarding-pot. device 77—59322
film, adhesion, on thermally oxidised Si, EM tensile adhesion test method 80—50804
film, adhesion changes on 10 MeV electron irrad. *(Russian)* 77—43460
film, adhesion to ABS polymers deposited in internal magnet magnetron sputttering system 79—83121
film, adsorption of CO, effect on resist., negative p-values 77—85083
film, ageing effect of thermoelectric power 78—2584
film, aggregated, absorpt. peaks, collective oscills. of electrons 78—80428
film, angular depend. UPS, surface electronic struct. 79—83095
film, annealing effect on grain size 78—72015
film, APW band struct. calc., muffin-tin potential 78—87899
film, band struct., appl. of extended rigorous cellular method 78—52055
film, complex impedance, IR transmission and refl. meas. 79—78216
film, continuous, 1/f noise, temp. and substrate depend. 79—24086
film, damping and vel. of longit. elastic waves at 9.4 GHz 80—10596
film, deposited on polystyrene substrate formation of Cu-O-polymer complex 78—92372
film, deposition with sputter gun 77—44162
film, diffuse optical scattering from variable roughness surfaces 80—100704
film, EELS, anomalous L_3/L_2 white-line ratios 80—93444
film, elec. resist. temp. coefficient 77—89883
film, electrodeposited, recrystallisation kinetics, X-ray scatt. *(Russian)* 78—60045
film, electron beam transmission, reflection, and absorp., $35 \leq E \leq 70$ keV 77—39754
film, electron energy loss spectra meas., optical functions calc. 78—19618
film, electron transmission, calc. 80—60724
film, electron transport props., struct. defects role 77—40117
film, electronic struct., self-consistent calc. 77—76959
film, energy losses of 20-40 keV electrons 78—92153
film, epitaxial on Mo, S impurity segregation at interface 78—84076
film, evaporated, adhesion meas. 80—50822
film, evaporated, interaction with BCl_3, HCl, adsorpt. 78—75945
film, evaporated, oxidation resistivity change meas. *(Japanese)* 79—11723
film, EXAFS determination using high-pass photocathode X-ray ionization chamber 79—68164
film, EXAFS meas. by total refl. 80—55228
film, excess (1/f) voltage noise 79—42598
film, five atomic layers, electronic band struct. using linearised APW method 79—69393
film, Frenkel pair prod. by light energetic ions, elec. cond. changes 77—59050
film, Gorsky effect, internal friction maxima, atom diffusional mobility *(Russian)* 80—70446
film, grown by ion plating method on Si wafers and glass plates *(Japanese)* 77—21039
film, growth by ionised-cluster beam deposition, adhesion to substrate 77—32527
film, growth on amorphous C, electronic props., UPS and XPS obs. 79—82476
film, in situ struct. determ. by internal stress meas. 80—54569
film, inert gas ion refl., semiempirical analysis, compared with expt., 10-30 keV 78—6823
film, inertialess glow induced by picosecond laser pulses *(Russian)* 80—100714
film, interaction with adsorbed dye mols., absorpt. and luminesc. 80—103981

copper continued
film, internal stress determ. by stress relaxation method *(Russian)* 77—62787
film, ion bombardment induced preferential orientation 79—19293
film, ion plated, defect growth structs., SEM obs. 80—24768
film, ion-plated, stainless steel, porosity depend. on process parameters 78—84720
film, Maxwell stresses at charged surface from elastoresistance 80—49957
film, microporosity induced by nucleation and growth processes, TEM expts. 78—10303
film, modulated surface-plasmon reson. in situ meas., O_2 adsorpt. 77—77311
film, Monte Carlo simulation of energy distrib. of low energy protons 77—15466
film, on (001) Ag, FCC and BCC metal-on-metal epitaxy, geometric factors, electron microscopy 78—22980
film, on amorphous C and Si substrates, dispersion force contrib. to adhesion *(French)* 80—59842
film, on Au substrate, oxidation and interfacial behaviour, ion scatt. spectroscopy study 80—66691
film, on Ni, recrystallisation and interdiffusion, electron microscope obs., 450-600°C 80—39363
film, on Ni single cryst., diffusion coeff. using method of nets 78—22903
film, on W substrate, cementation, vac. deposition, and electroplating, growth characts. 79—95291
film, optical consts. deduced from surface EM wave propag. 80—60697
film, optical props. in intermediate region between pure Drude and interband absorption 77—81170
film, oxidised in ^{18}O, ion scatt. anal. 77—40463
film, partially oxidised, EXAFS studies on superficial regions 80—75474
film, partially oxidised, oxide removal and O_2 desorption on vac. annealing 77—12738
film, photoelectron emission, intershell interaction influence on 3d and 5d branching ratio 80—104038
film, polycryst., nodule mechanism of diffusion-induced disintegration *(Russian)* 78—51829
film, pure and CO covered, optical consts., ellipsometry meas. 79—78645
film, pure and CO covered, work functions 79—91570
film, RF impedance temp. and freq. depend. 77—4453
film, simulation of transmission of 1 keV electrons 77—12475
film, single cryst., new technique for prep. employing two stages of evaporation 79—33932
film, single layer and multilayer systems, thickness determ. by X-ray fluoresc. 80—68180
film, strain coeff. of resist., film thickness and grain size depend. 77—55620
film, struct., oxidation, and exoelectron emission rel. to bulk samples *(Russian)* 79—37927
film, surface electronic struct. determ. by ab initio calc. 77—43679
film, surface-plasmon modulated reson. for adsorption studies 79—83045
film, temp. depend. of 1/f noise meas. 77—85277
film, thermal phonon radiation into α-quartz substrates 79—42363
film, thermoelec. power meas. 77—79092
film, ultra thin, EXAFS 79—15559
film, ultrathin, quench-condensed, two-dimensional elec. cond. 78—39233
film, vacuum deposited, O^+ bombardment sputtering rates 78—88390
film, vacuum deposited, surface struct., HEED meas. 78—6234
film, vacuum deposited, thickness meas. using X-ray fluoresc. technique 79—90911
film, vacuum deposited breakdown stress, thickness depend. *(Russian)* 77—59238
film, vacuum deposition on Pb (111), substrate diffusion effects, RHEED, LEED, AES 80—65410
film, vacuum-deposited, and filings, interrelation between dynamic and static distortions, X-ray diffr. meas. *(Russian)* 77—43305
film, valence bands, XPS excited by Zr $M\zeta$ radiation 80—40236
film, vapour deposited on polymer, ageing, adhesion, elec. cond., electrochem. pot. *(Russian)* 79—33362
film, work function and density of states of (100) surface, self-consistent calc. 77—35978
film, work function changes upon water contamination 80—44705
film continuity, observations by Auger spectroscopy 78—64433
film deposition, reactive sputtering in RF discharge, glow discharge mass spectrometry 77—44155
film deposition, thermal effects, influence on internal stress meas. 80—96767
film deposition from metal plasmas 78—6859
film growth, diffusion-induced redistribution of atoms between islands 77—89672
film growth on amorphous C, energy characts., in situ electron microscope determ. 79—11027
film growth on graphite and amorphous C, electronic struct. by photoemission and Auger obs. 79—77947
film machining by laser-induced explosion 78—15258
film on Fe foil, EM excitation of sound, Mossbauer study *(Russian)* 79—99795
film on Mo substrates, film stability on reinforced fibre substrates *(Russian)* 80—39462
film on Ni, AES comparison of ion plated and vacuum evaporated films 79—28250
film on Ni substrate, EXAFS in photoelectron yield spectra 80—16123
film sandwich structures Auger anal. 78—72030
film self-generation on Cu doped glass ceramics, for low-expansion IR laser mirrors 79—14127
films, adsorption of O, study of gravimetric uptake and work function 79—33179
films, on Ru (0001), growth, struct. and electronic props. 79—77958
films, resistance changes due to bombardment by N, C, or Ar ions 80—103670
films, sputtering yields due to Ar^+ milling, He^+ Rutherford backscattering and AES obs. 79—65969
films, vac. condensed at oblique vapour incidence, oriented cryst. growth, electron diffr. study 80—97432
final energy bands, high energy, angle resolved photoemission 80—2327
fine interaction of surface electrons, IR spectra 80—16041
fine particles, prep. by gas evaporation technique, crystal habit 77—52239
fine struct. in elastic-electron-yield spectra at transition-metal core energies 79—69938

copper continued
finely divided-polycaprolactam metallic polymer, impregnation depth determ. in porous sintered Fe-graphite 79—70272
flameless atomic absorption spectrophotometric determination of Ni and Co traces 77—90674
floating zone method growth, X-ray diffr. study of preferred growth 80—7490
flow detector tube filter use 78—56857
flow stress during cutting 77—59881
flow stress of single crysts., strain rate sensitivity analysis 77—16645
flow stress temp. depend., effect of interstitial atom clustering and embrittlement *(Russian)* 78—34538
flux adhesion, and spreading coefficient 80—15379
foil, 8 ns laser pulse-target interactions, ion-expansion struct. 79—14575
foil, conduction electron spin disorientation at surface 80—75855
foil, destruction by laser pulse in presence of plasma cloud *(Russian)* 77—80338
foil, elec. explosion, dielec. breakdown 78—67388
foil, electron irradiated at low temps., annealing, form. of clusters of atomic defects 77—15416
foil, electron scatt., appl. of Monte Carlo type calc. *(French)* 77—7636
foil, electron scattering, most probable transmitted scatt. angle calc. *(French)* 77—68901
foil, electron-irradiated, interstitial trapping on impurities 79—99242
foil, energy straggling of 6.74 MeV protons 78—79641
foil, high purity, identification of imperfections by thermal resistivity meas. 80—59951
foil, interstitial impurity interaction investigation by stage II isochronal recovery expts. 78—47423
foil, laser irradiated, low-angle X-ray scatt., angular block misalignment and hardness *(Russian)* 80—103413
foil, naturally passivated, ESCA, sputter etching 77—70218
foil, polycrystalline struct. influence on transmitted 300 keV ion energy loss 79—95057
foil, recrystallisation during annealing in high voltage electron microscope, grain growth *(Russian)* 79—100159
foil, role of grain-boundary porosity in superplasticity *(Russian)* 78—56690
foil, sputtering with ^{252}Cf fission products, desorbed secondary ions 78—68596
foil, total emissivity meas. by calorimetric technique 80—17941
foil relative activity, proton accelerating mechanisms in vacuum diodes, induced radioactivity 79—97470
foils, cyclotron beam intensity monitors 77—38578
foils, faulted defect formation by moving boundaries 80—107281
foils, near $\Sigma 9$ grain boundary properties, boundary dissociation 80—100251
fracture character and time-to-rupture, near MP *(Russian)* 77—21245
fracture criterion, expt. verification 78—64648
fracture due to shock waves leaving surface, shear stresses 78—51128
fracture speed during phase explosion due to electron beam irrad. *(Russian)* 80—76336
fracture under influence of high power US waves *(Russian)* 79—5034
fragmentation and dynamic recrystallisation after heavy and very heavy deform. *(Russian)* 78—39793
free electrolytic films, tensile creep for various film thicknesses calcs. *(Russian)* 80—11697
freezing point, precise determ. 78—30740
Frenkel defects, diffuse X-ray scatt. obs. *(German)* 79—23600
Frenkel pair production threshold energy, temp. depend., exam. 78—51530
Frenkel pair recombination radius, temp. depend. 77—89427
frequency spectra, and correlated spectral density between bulk atoms 79—19330
friction, He environment 4.2-80K 78—48543
friction and prow form. in scratch process by diamond cone 78—11349
friction mechanism, HV TEM expts. 80—35341
friction pair with bronze, C steel or Armco Fe, seizure centres on contacting surface *(Russian)* 77—70185
friction props. of surface films in air and high vacuum 78—60850
friction stress in high temp. creep 80—11723
friction stress meas. during high temp. creep of polycrystalline samples 79—1898
friction surface structural investigation, O_2 surface diffusion *(Russian)* 80—96726
friction under electrolyte immersion condition 78—64738
frictional behaviour, effect of mechanical properties 80—55548
fusion reactor material, low energy ion erosion expts., Kaufman source appl. 80—68942
fusion reactor shield, neutron induced activity and γ-ray source investigation 78—54872
galvanic couple with Al alloys, velocity effect on corrosion 78—35566
galvanomagnetic size effect meas. 77—11896
gamma-ray attenuation coeff. meas., 1115, 1173, 1332 keV 77—55303
gamma-ray impact, absolute pair production cross-section meas. 78 —43958
gamma-ray scatt., incoherent 80—40179
gamma-ray scattering, incoherent, total at. cross section 79—13679
gas desorption coeffs., electron- and ion-induced, bakeout temp. effect 79—65329
gas phase, He I photoelectron spectra, photoionisation cross section meas. 79—98051
geochemistry, chemical speciation in mixed freshwater, seawater and bine solns. 78—20409
geochemistry in sediments of Gulf of St. Lawrence and estuary 78—92855
glass:Cu^{2+}, near IR electronic spectra, effect of alkali contents 78—27267
glass/Cu-polymer compound powders, prep. and corona charging props. *(Japanese)* 78—19679
glow discharge sputtering redeposition, in noncond. compound chem. anal. 77—77860
grain boundaries, energy-misorientation relationship 79—60377
grain boundaries, intrinsic struct., electron diffr. anal. 80—84186
grain boundaries, near $\Sigma 9$, structure and dislocation interactions 80—79808
grain boundaries, nucl. gamma reson. *(Russian)* 79—8080
grain boundaries, struct. and energy, effect of temp. up to melting point 79—37718
grain boundaries effect on thermal cond. 79—51546

copper continued
grain boundary, near $\Sigma 9$, props., identification by image matching of Burgers vectors 80—79810
grain boundary anal. by TEM, CSL condition determ. 80—15117
grain boundary behaviour, validity of coincidence site lattice model of grain boundary struct. 79—51120
grain boundary character, revealed by etching and slip line continuity 79—33001
grain boundary intrinsic structure, boundary mobility 80—103368
grain boundary migration, TEM obs. on mechanism 80—79812
grain boundary morphology effect on void form. 78—48533
grain boundary sliding and intergranular fracture, in bicrystals 78—75717
grain growth during isothermal annealing *(Russian)* 79—52259
grain growth in strained $\{110\}<112>$ low stacking fault FCC crystals after artificial nucleation 79—91722
grain growth rate, 520-970°C *(Russian)* 80—29972
grain refinement by dynamic recrystallisation during hot working *(Japanese)* 77—52345
grain size effect on acoustic emission generated during plastic deformation 78—80609
grain-boundary sliding component in high temp. fatigue 80—50706
graphite-Cu, brushes, friction and wear under severe sliding conditions against steel 79—38991
Gruneisen number and nonlinearity const., elastic moduli data, US attenuation 80—65165
Gruneisen parameter, behaviour at high press. 78—83899
Gruneisen parameter determ. using thermoelastic effect 79—28068
Gruneisen parameters, 10-100K, phonon wave vector depend. 78—38801
Gruneisen parameters, dynamical study using modified Bhatia model 79—37797
guanadinium zinc sulphate:Cu^{2+}, EPR of Cu^{2+} at tetrahedrally coordinated Zn^{2+} sites 78—39388
H_2O_3/H_2SO_4 etching system 79—96227
Hall coefficient, relaxation times, Fermi surface 80—84460
Hall resist., anisotropic temp. depend. rel. to Fermi surface 77—62897
hard drawn wire, stress corrosion cracking *(Japanese)* 77—25193
hardness, temp. depend. 77—40440
hardness-flow stress rel. during strain-controlled bending fatigue 79—74245
He, bubbles in Cu, volume change calc. from isotropic elasticity theory 78—47445
heat capacity, 2 to 6.5K, using resistive SQUID 79—63213
heat content between 300.05 and T (T from 400 to 1000K) drop calorimetry *(French)* 80—10682
heat pipe meas. of corrosion and vapour press. 80—23878
heat pipes for radioisotope thermoelectric generator, Cu/H_2O, axially-grooved 79—48144
heat transfer during cooling with water *(German)* 80—23873
heat transfer during film boiling of small Cu drop in water 77—1219
heavily drawn ETP wire, secondary recrystallization 77—36537
heavily rolled, electron microscope obs. of cube oriented region, rolling texture 79—29093
HEED, virtual inelastic scattering estimated 78—26390
helicon attenuation below 1K, metal with diamag. domains *(Russian)* 77—85254
hepatic Cu measurement in vivo by nucl. reson. scatt. 77—9245
heterogeneous, new polishing technique *(German, English)* 79—20322
HF ultrasound, viscous and relax. components of dislocation attenuation 80—15196
high conductivity, high sp. ht., for cryogenic appl., prep. 78—76670
high purity, low cycle fatigue, cumulative damage, absorbed plastic energy anal. 79—38932
high strain rate behaviour, incremental elastic-viscoplastic constitutive eqns. integration 80—85138
high-conductivity, treatment technique for low temp. applics. 78—27650
high-purity, grain size and strain rate influence on mech. behaviour, precursors existence 80—85016
hollow cathode discharge population mechanism for highly-excited states *(Russian)* 78—63610
hollow cathode discharges, IR laser transitions, discharge conditions, excitation mechanisms 79—68383
hollow cathode laser, ion laser transitions 80—69366
hollow-cathode emission spectra, 200 to 430 nm 79—72264
hollow-charge jet, density meas., appl. of light radiography *(French)* 78—44344
horizontal cylinder, electropolishing in phosphoric acid 79—47835
horizontal plate, pool-boiling heat transfer, nucleation centre size, surface roughness 78—90652
horse shoe corrosion in flowing sea water, mechanism, cathodic protection possibility 79—66199
hot cathodoluminescence study, electron-hole recombination 80—93410
hot ductility and torsional deformation *(Japanese)* 79—57069
hot forged powder compact 77—24981
hot worked, recovery and recrystallization 79—91661
Hubbard model, photoemission spectrum, effect of electron correlation 79—78828
Hugoniots, third and fourth order, isotherms, Lagrangian and Eulerian strain measures 77—69068
human serum Cu, EPR spectrum obs. 80—91582
hydrocarbon catalysis 78—11550
hydroextrusion, effect of longitudinal US oscills. *(Russian)* 79—34071
hydrogen embrittlement, effect of disperse Al_2O_3 particles and matrix struct. *(Russian)* 78—3207
II-IV-V_2-Cu, pseudo-straight-zone semiconductor, Schottky barriers, IR photosensitivity and photocond. *(Russian)* 77—8195
impact of H and D ion beams, energy spectra negative component 79—65967
impact welding, viscous energy, dissipation 77—70058
impact welding to steel, fundamental parameters 80—97679
impact welding to steel, wavy interface characts. and formation 80—97680
implantation in Fe, effect on corrosion by H_2SO_4 soln. 80—71793
implantation in mild steel, annealing and rolling behaviour of conc. profile 78—75684
implantation of He ions, TEM exam. of He gas bubble lattice 79—46726
implantation of O^+ ions along channelling directions, stopping power 77—69021
implanted ^{222}Rn TIPAC measurements 78—43732
implanted ion detection by X-ray emission anal. in TEM 78—51575

copper continued
implanted with Cu^+, effect on cryst. orientation, Kr penetration meas. 80—88174
impurities removal using high-current-rectifier 77—9089
impurity and electron-phonon rates for orbit on Fermi surface 79—69541
impurity diffusion, mass depend. of energy factor of isotope effect 78—30795
impurity diffusion of ^{113}Sn and ^{124}Sb 79—77828
impurity diffusion of V^{th} period elements and self-diffusion 80—65301
impurity distribution between crude Cu, white metal and SiO_2 saturated slag 78—44055
impurity in Cr-Mo-V low-alloy steel, effect on high-temp. ductility and crack growth 80—66652
impurity in Li aluminosilicate glasses, ESR spectra 80—66027
impurity in Mn-Mo steel, effect on mech. props. 80—66596
impurity in rare earth oxides, determ. by at. absorpt. 79—87905
inclusion, in Si, behaviour during annealing in elec. field *(Russian)* 79—23779
inelastic cyclic deform. and fatigue 77—63795
inelastic electron scatt. data anal., appl. to Cu 77—73199
inhomogeneous clustering of radiation damage after neutron irradiation between 200 and 400°C 80—15161
initial sintering, method for obtaining surface diffusion coeffs., appl. to shrinkage data 78—95713
p-InSb:Cu, Ag, deep impurity centres, acceptor conc. effect on conduction type 80—44602
interaction of annealing twins in fcc metals and alloys 78—68712
interatomic force consts. from lattice vibrs. 77—20020
interatomic pot., vacancy form., migration energy from phonon dispersion curves 78—42950
interatomic potential from intermediate and low energy data 78—55829
interatomic potentials from experimental phonon spectra 78—75621
interatomic potentials from phonon spectra 80—19744
interdiffusion with sintered Al powder, struct. effect at high press. 78—60606
interdiffusion with SiO_x and Al_2O_3 films 77—85000
interface with ^4He, static and transient anomalous Kapitza conductance 79—19444
interface with ^4He, time depend. of anomalous Kapitza conductance 79—56066
interface with polymer, electronic struct., XPS study 80—45204
interface with polyvinyl alcohol, XPS study 79—83093
interface with superfluid ^4He, exponentially damped surface solutions generated by heat flow 79—55980
intergranular creep fracture surfaces, with slip band spacing, dimple spacing 80—76345
intergranular damage parameters in creep *(Czech)* 80—89342
internal friction, impurity effect *(Russian)* 79—87677
internal stress meas. by decremental unloading technique 78—64576
internal stresses in plastically deformed crystals *(Russian)* 78—79615
interstitial trapping configuration study by ion channelling 78—47455
intraband optical conductivity, electron-electron scatt. 78—35166
intracrystalline slip bands in high temp. creep, polycrystal, comparison with brass single crystal *(Czech)* 79—77604
intrinsic stacking fault energy, effect on cyclic hardening 79—11638
ion, in alkali silicate glass, oxidation reduction equilibria and optical absorption *(Japanese)* 77—12824
ion bombard. by 5 keV Ar^+, sub-surface damage 80—103399
ion bombarded, cone form. and associated surface features 77—59054
ion bombarded, energy distributions of fast ionized recoils 79—24402
ion bombarded, He gas-bubble superlattice form. 80—2086
ion bombarded surface, stability of pyramidal structures 79—51170
ion bombardment, development of pyramidal structures on surfaces 80—84177
ion bombardment, energy distrib. of positive secondary ions and sputtered atoms 77—32485
ion bombardment, low energy He^+, origin of autoionisation electron emission 77—20973
ion bombardment by Ar^+, blocking effect for fast ionized recoils 79—8221
ion bombardment induced preferential orientation of vacuum deposited layer 80—100290
ion bombardment-induced photon emission as function of target temp. 80—100698
ion etching, dispersion coeff. determ. *(German)* 80—40597
ion impact phenomena, computer simulation 78—88396
ion implantation, oxidation mechanisms study 77—8980
ion implanted in Al, doping after laser pulse irradiation 80—88194
ion irradiated, Auger electron spectra struct., possible surface diagnostic methods 79—69946
ion irradiated, Frank loops, electron microscope image contrast 80—6326
ion irradiated, impurity defect configuration, by DPAC-technique with ^{111}In 79—28021
ion laser, hollow cathode He-Cu discharge, at. emission obs. of plasma props. 80—19021
ion plating, on ceramic substrate, and coating struct. 78—11132
ion polishing for diamond-turned mirror dielectric coating adhesion 80—1370
ion radiation damage 78—22773
ion scattering from (100) face, expt. verification of two-atom model 77—12481
ion scattering from Cu (100), spatial distribs. under blocking conditions 77—59659
ion scattering on Cu crystal, 10-35 keV, diatomic models *(Russian)* 77—77337
ion selectivity, chalcogenide ceramic membrane as Cu-selective electrode *(Chinese)* 80—81357
ion-bombarded, particle ejection, SIMS obs. 79—78810
ion-electron emission yield, ang. depend., atomic order effects 77—85877
ion-irradiation studies of damage function 79—37746
ions, beam-foil spectra from 20 to 238 MeV energy, 5 to 60 nm, lifetime meas. problems 80—9722
ions, XVI to XIX, relativistic Dirac-Fock-Slater orbital binding energies, one-electron transition energies 79—25778
irradiated, containing self-interstitials and vacancies, electronic transport props. 78—60105
irradiated, exam. of dislocation bias for interstitials to edge dislocations 78—79612
irradiated, small edge dislocation loops, electron microscope image contrast, Burger's vector determ. 77—76410

copper continued
irradiated with 20 keV He$^+$, surface damage and gas trapping profile meas. *(French)* 80–84219
irradiated with electrons and neutrons, positron annihilation meas. *(German)* 77–62563
irradiated with protons, α-particles and C ions, increase of elec. resist. meas. 77–84808
irradiation effects at low temp., components for supercond. mag. for high energy phys. appl. 77–69012
irradiation induced defects, electron microscope images 78–83854
irradiation with 4 to 6 kV Ar$^+$ ions, Ar-vacancy cluster form. and stability 77–43259
irradiation with O$_2$ ions, defect production and annealing 80–88214
isochronal recovery of high energy d-Be neutron damage 78–51592
isoelectrionic series, collision strengths and Gaunt factors 79–98227
isoelectronic sequence, 4s-4p reson. transition in highly charged ions 77–75087
isoelectronic sequence, fine structure separations for ^{2}D terms 79–89804
isoelectronic series, core polarisation influence on oscillator strengths 79–45672
isoelectronic series, dipole polarisability, numerical Coulomb approx. 80–43199
isoelectronic series, hard-core pseudopotentials and struct. maps 80–44168
isoelectronic series, Hartree-Fock line strengths 78–9122
isoelectronic series, ionisation energy, multiplet strengths, diagrammatic MBPT theory calcs. 80–9500
isomer shift values of implanted ^{133}Xe/^{133}Cs, Mossbauer spectra 80–7240
jets produced by shaped explosive charges, particle size distribution in breakup 80–23957
K$\beta_{1,3}$ intensity distribution, line strength calcs., single vacancy scheme 80–32650
K shell photoelectric cross section, at 74.409 keV 79–72288
K shell prod. cross section of Ti, Cr, Fe, Ni, Cu, Zn for 75 to 150 keV p and e excitation 79–47552
K-shell ionisation cross sections, slow electron impact 80–83498
K-shell X-ray prod. by ^{14}N$^+$ bombardment 80–91482
K-shell X-ray production, projectile Z, energy and incident charge state depend. 79–78794
K-shell X-ray yield, following Cl^{n+} bombardment, residual vacancy effects 77–10623
Kapitza resistance, anomalous power depend. 77–28072
Kapitza resistance at solid He boundary, heavy thermal load, 0.45-1.5K *(Russian)* 77–11767
Kapitza resistance of interfaces with liq. ^{3}He and ^{4}He, 0.3-1.4K 77–24475
kfor=for 78–80822
kinetic friction re-examination using modified pin and disc machine 80–55547
Krasko-Gurskii model potential, test of validity 80–39485
Krupkowski's formula for strain hardening curve, physical interpretation, appl. to polycrystalline samples 79–100158
Lake Monona, Wisconsin, Cu environmental chemistry 79–44214
Langmuir films on Cu surface, surface EM wave absorpt. study 80–97359
large angle grain boundaries formed during cold work, TEM obs. of orientation relationships in single crystal 79–90678
laser, 1.54 Å, travelling wave source pumping, numerical anal. 77–83864
laser, 40 kV discharge, pulsed 400 μJ/cm^3 output *(Russian)* 77–10895
laser, atomic, finely dispersed metal particle active medium 80–91777
laser, coaxial, operation at above atm. buffer gas press. 79–59690
laser, coherent props., dynamic holography in VO$_2$ films 79–13929
laser, comparison of copper acetate, acetylacetonate and CuCl lasants 79–31875
laser, comparison of CuCl, CuBr and CuI lasants 77–34875
laser, CuBr lasant, continuously pulsed, long duration, high efficiency operation 78–79029
laser, discharge heated longit., scaling 78–50790
laser, discharge-heated vapour 79–7149
laser, electron energy distribs. in Cu-Ne(He) mixtures 79–13956
laser, energy conversion efficiency, reson. levels excitation 80–99715
laser, exploding wire *(Russian)* 77–38863
laser, for pumping jet dye laser 77–7128
laser, halide mixtures, continuously pulsed, kinetic processes 77–88702
laser, He buffer gas effect on output parameters 78–9368
laser, long lived sealed off halide discharge 77–88770
laser, mode-locked, high pulse rate operation 77–61967
laser, nanosecond pulsed, Milan-1, technical specification 78–17979
laser, operation at buffer gas atm. press. 80–38033
laser, optimisation of excitation conditions 80–9900
laser, pulsed, stimulated emission mechanism 79–64213
laser, pulsed emission at elevated powers 78–25895
laser, sealed vapour, service life and efficiency 79–27292
laser, self heating, optimum discharge parameters 77–75563
laser, steady multiply pulsed discharge heated vap., halide lasant 77–38911
laser, time depend. of electron density, resist. and interferometric meas. 78–25864
laser, transversely excited pulsed, gas discharge parameters influence 79–10291
laser, used for single crystal impurity luminesc. attenuation in Raman spectra 79–15467
laser, using Cu(NO$_3$)$_2$ as working substance 79–79244
laser, using Cu acetylacetonate as Cu atom donor 78–82956
laser, using Cu vap., fabrication, green and yellow emission *(French)* 80–43360
laser, using CuCl, double pulse, output characts. at small pumping characts. at small pumping pulse delays 78–13690
laser, using CuCl in hollow cathode config. 77–14742
laser, vapour, population inversion kinetics, modified hook method meas. 80–53275
laser action on 5106, 5782 Å lines in copper acetylacetonate, Cu(NO$_3$)$_2$ vapours 77–88712
laser damage threshold at 10.6 μm, up to 10^{10} W/cm^2 77–50707
laser discharge with He, metastable decay rates 79–86164
laser impact, multiple crater refl., effect on refl. props. 78–52596
laser irradiation of metal targets absorpt. coeff., air breakdown effect 79–52052
laser light absorpt. by plasma with very steep density gradient 80–96348

copper continued
laser line structure at 510.6, 578.2 nm 80–53274
laser lines, broadening, induced emission cross-sections 79–26928
laser microprobe emission spectroscopy, matrix effects 77–16870
laser oscillation at 2703 Å in Ne-Cu II hollow cathode discharge 78–13689
laser produced plasma corona development, X-ray streak camera obs. 77–15245
laser pulse irrad. of Cu targets, absorpt. studies 80–79455
laser radiation absorption in craters on metal targets 80–97386
laser radiation pulsed action, on foils and powder compacts, dimens. effect *(Russian)* 77–16437
laser using CuCl, double pulsed, scaling to 10 mJ 78–46624
laser using halide vap. transverse discharge 77–88716
laser-produced plasma, X-ray bremsstrahlung and fast ion meas. 78–5936
laser-produced plasma X-ray spectral lines identification *(Chinese)* 80–54036
lateral spread distribution widths MeV He ions in C, Al, Cu from energy spectra 79–14860
lattice and force consts., pairwise atomic repulsions in cluster model 79–32939
lattice and grain boundary diffusion of P, exam. of diffusion rates by tracer sectioning technique 78–79817
lattice atom displacements near end of implanted μ^+ tracks 78–55890
lattice diffusion and grain boundary diffusion in γ-Fe *(Japanese)* 78–18836
lattice dimensions, difference between vacuum condensates and massive specimens *(Russian)* 77–31912
lattice dynamics, energy wave number charact., by reson. model 80–10612
lattice dynamics, ion-ion and ion-electron interactions 80–49321
lattice dynamics, model incorporating second neighbour shell-shell interactions 77–59082
lattice dynamics, modified Bhatia model, phonon dispersion, Debye-Waller factor temp. depend. 77–31729
lattice dynamics, modified CGW model calcs., phonon dispersion, sp. ht. and equiv. Debye temp. 78–10135
lattice relaxation around μ^+ 79–56658
lattice specific heat, from two-parameter lattice dynamical model with dispersion 80–10678
lattice vibrations and ideal elec. resistivity 79–46770
Laue X-ray back reflection pattern solving, algorithm and statistical error analysis 79–99030
layer on W tip, field ion microscopy study 78–23587
layered cell structures and slip lines in deformed cryst., TEM obs. 79–99209
LEED anal. of surface struct. 78–71914
LEED from (311) surface, measured intensities, function of energy 77–89623
Lifshitz constant for calc. of van der Waals force between two solids *(French)* 80–107658
light ion (H, D, He, Li) irrad., defect prod. and electronic stopping power 80–34088
light pipe, submm. wave transmission, and refl. of surfaces, 50-10 cm^{-1} 78–18050
liq., thermal cond. and elec. resistivity 80–103661
liquid, 3d bandwidths, photoelectron spectrum 77–4286
liquid, absorption of gaseous O$_2$ 78–51686
liquid, coordination numbers, calc. in microinhomogeneous struct. model *(Russian)* 80–38902
liquid, deoxidation kinetics using CO 78–44403
liquid, deoxidation mechanism by reducing gas mixture *(Japanese)* 77–52638
liquid, deoxidation rates by CO$_2$-CO gas mixture *(Japanese)* 80–89394
liquid, diffusion coeffs. of ^{124}Sb, ^{113}Sn, ^{110m}Ag and ^{195}Au 79–95196
liquid, diffusion of Tl, Ir, Pb and Bi *(Japanese)* 78–59962
liquid, dissolved O below 0.02 wt.% effect on surface tension 80–107618
liquid, effective interionic interaction, pseudopot. method *(Russian)* 77–84622
liquid, effective interionic pots. determ. from expt. data 77–47338
liquid, electrical resistivity and thermoelectric power using t matrix approach 77–31988
liquid, electrical transport 79–38040
liquid, electronic spectrum 77–51646
liquid, electronic structure, structured medium approx. 80–84421
liquid, impurity diffusion, shear cell assembly meas *(French)* 80–75375
liquid, impurity diffusion of Ru, In, Sn, Sb *(Japanese)* 78–10204
liquid, multiple scatt. calcs. of resist. 78–76039
liquid, neutron scattering experiments up to 1900K using sapphire container 79–63215
liquid, normal spectral emissivity meas., 1376 to 1687K 80–10687
liquid, oxidation kinetics, by CO$_2$ 77–28986
liquid, pure, surface tension meas. *(German)* 77–35799
liquid, solubility of S, Se and Te 77–21096
liquid, struct. factor, neutron diffr. meas. and Monte Carlo calc. 80–38903
liquid, surface tension temp. depend. 77–4248
liquid, thermodynamic study of O$_2$ 80–88342
liquid, viscosity 77–4138
liquid, viscosity calc. using microinhomogeneous struct. model *(Russian)* 80–15284
liquid, wetting of W surface, depend. on preliminary surface treatment *(Russian)* 80–35388
liquid, X-ray diffraction analysis 79–4232
liquid 78–38912
liquid droplets, surface tension meas., 1000 to 1330°C 77–62711
liquid metals, structure factor modelling using quasi-crystallised model *(Russian)* 80–54118
liquid surface tension meas. with levitated metal droplets, influence of oscill. amplitude 78–51798
loosely packed powder, sintering SEM and dilatometry obs. 80–20843
loss rate in lakewater 80–7967
low energy ion sputtering, theory 79–28880
low temperature internal friction and microplastic strain 77–84839
low-cycle fatigue effect of plastic strain and stress factor 77–63766
luminosity spectrum bombardment of Cu target by Ar$^+$-ion beam 79–4884
magnetic focusing of electrons 79–65540
magnetic susceptibility, Animalu transition metal model pot. invest. 80–75711

copper continued
magnetic susceptibility, model pot. theory 80—75710
magnetic susceptibility, thermal density of states, non-local exchange-correlation effects 78—14924
magnetoresistance, temp. depend., impurity effects 80—70682
magnetoresistance of polycryst., effective medium approx. 79—87083
marine pollution determ. in Gulf of Fos, NW Mediterranean 79—12141
matrix, small oxide precipitates, two-phase system, sputtering and secondary ion emission 78—39650
matrix for filamentary Nb_3Sn superconductor, thermal strain effects of superconducting critical temp. 80—93032
matrix for Ti-Nb supercond. composite effect of temp. decrease on ductility 79—57119
matrix isolated atoms, matrix influence, theory 78—46288
matrix isolated atoms, matrix influence, theory 78—46290
matrix-isolated, matrix-induced changes in opt. spectra 77—57913
matte, thermodynamics of converting, distrib. of Au, Ag, Pb, Zn, Ni, Se, Te, Bi, Sb, As, Noranda process 79—47648
mechanical twinning characts., 4.2 to 300K *(Russian)* 79—37714
mechanical twinning in (110)$[\bar{1}12]$ single crystal under plane strain compression *(German)* 77—36616
melting curve to 60 kbar press., reinvestigation 80—39260
melts, supercooled, influence of impurities in crystallisation 79—29042
membrane, kinetics of permeation of H_2 79—99371
membrane, lifetime prediction and design 80—71752
membranes, life testing 79—70256
metabolic model and dosimetric data 78—65130
metal cathodes, oxidised and clean, basic erosion processes in electric arcs 80—103211
metal cluster, adsorption of CO, mol. orbital calc. 78—18895
metallic adhesion, use of fracture mechanics and contact resistance meas. 77—70271
metallised coating on polyethylene terephthalate film, fracture under laser irrad. *(Russian)* 80—76333
metallization of glass fibre reinforced epoxy laminate *(German)* 80—93670
metastable atoms, high current hollow cathode tube production 80—10445
microalloyed with B, elec. cond. and strength props. *(Polish)* 80—89285
microcrack propagation and plastic strain 80—81187
microcrystal, melting and solidification, temp. gradient, mol. dynamics model calc. *(German)* 77—76527
microdeformation distrib., effect of form of stressed condition 77—63759
microplastic deform. and amplitude depend. of internal friction *(Russian)* 80—45349
microstructure inhomogeneities, cold neutron small angle elastic scatt. 77—84736
microvoid form., gaseous impurity atom effects, positron annihilation study 80—49275
minerals suspended in ocean waters 79—74904
mirror, acted on by laser radiation, reflectivity meas. 79—10342
mirror, diamond turned, surface and optical studies 78—79098
mirror, laser damage, temp. depend. of absorptance, vaporisation and vap. heating 79—81471
mirror, polished, optical props. ageing 77—79912
mirror, single-point diamond-turned, evaluation for 8-beam CO_2 laser, Helios 79—23044
mirror, surface defect layer form. on mech. polishing 80—33122
mirror, vapour-deposited, on SiC substrate, pulsed laser damage characts. 80—48314
mirror film, ultraclean DC sputtered, optical props. 77—50748
mirror for laser, microstruct. effect on Ag overlayer deposition, 10.6 μm reflectivity 77—42543
mirror preparation as student expt., electroless plating of Cu on treated glass 80—36817
molecule, emission band spectra and vibr. const. 79—36656
molecule, VB calcs., wave functions, interatomic distance and dissoc. energy values 77—57883
molten, determ. of Ag activity by two component method *(Japanese)* 78—11547
molten, O_2 absorption, surface tension driven flow effect 78—6199
molten surface layer thickness, emissivity and AES meas. 80—39261
monolayer, (001), level ordering of states 78—91748
monolayer, electronic struct. 78—72233
monolayer (001), electronic struct., self-consistent LCAO calc. 79—4606
monolayer (100), self consistent electronic struct. 80—6926
monolayer deposition on Au electrode in underpotential region, RHEED investig. 80—54539
monolayer formation on Pt (100), (110), and (111), optical and electrochem. studies 79—99419
monopyrazine zinc sulphate trihydrate:Cu^{2+}, ESR meas. 78—84478
monovacancy formation enthalpy 79—65217
mosaic single cryst., neutron integrated reflectivities 79—86656
Mossbauer fraction, press. depend. 77—59493
Mossbauer fraction for ^{57}Fe, press. depend. 77—16226
multipole wave functions, singular points in band struct. and Wannier function tails, Cu cond. band appl. 79—37956
multipole wave functions for photoelectrons, constant-energy-surface harmonics, s-d band appl. 79—37955
muon$^+$ spin resonance, diffusion, temp. depend. 78—39490
muon diffusion, theory for FCC metals, compared with expt. 78—22883
muon diffusion at low temp., effect of nuclear elec. field gradients 77—52005
muon diffusion data anal., theory of incoherent direct and indirect multiphonon transitions 80—70448
muon localisation and lattice dilation, μSR 79—56694
muon localisation method *(Russian)* 77—32313
muon spin rotation, EFG, site of localisation 78—2785
muon trapping, Knight shift, rel. to H interstitials 80—50247
muonic Coulomb capture, ionic charge effect 78—66694
muons, positive, as light isotopes of H, book 79—82907
met-myoglobin:Cu^{2+}, single cryst., EPR, conform. changes 77—73505
nearest-neighbour atom displacements derived from EXAFS spectra, temp. depend. 79—87524
neutron and electron irrad., interstitial formation, dislocation pinning, internal friction meas. 80—100284
neutron damage, defect clusters 80—34067
neutron damage and gas prod. spatial variation in Li(d,n) radiation damage facility 77—42207
neutron damage calcs., deuteron break-up source, sputtering appl. 77—35593

copper continued
neutron effects, inertial confinement reactor first wall response to thermonuclear radiation 79—76133
neutron irrad. cryst., edge and screw dislocation groups, mean vel 79—7607
neutron irradiated, effect on internal friction 78—15445
neutron irradiated, replacement sequences, calcs. using ADDES and COMENT codes 79—46714
neutron irradiated, stage II recovery 77—31695
neutron irradiation, mobile interstitials production 80—34080
neutron irradiation at 200 to 400°C, decoration of dislocations, damage clusters 77—24332
neutron irradiation damage inhomogeneous clustering, TEM obs. 79—73223
neutron irradiation induced dislocation loops and point defects, temp. depend., 316 to 483K 77—51410
neutron production of free interstitials 80—34071
neutron spectra for fusion + hybrid reactor materials 80—23142
neutron yield calcs., electron beam incidence 78—95622
Nimonic alloy reinforced laminate composites, low-temp creep singularities, structural defect changes *(Russian)* 80—11696
nitroxide free radical mag. interaction with lanthanides or Cu^{2+} in liqs., ESR 78—68380
NMR at high polarisation and low field, nuclear spin exchange interaction 80—34790
NMR study on nuclear ordering below 1 μk 80—93187
noncrystalline, electronic density of states, multiple scatt. calcs. 78—91578
nonlinear acoustics, third-order elastic const. meas. 80—33292
nonlinear diffusion equations, identification of thermal cond. and sp. ht. *(French)* 77—47614
nonstationary temperature fields due to moving heat sources, heat capacity, thermal cond. *(Russian)* 80—107448
normal metal in composite superconductor, neutron irradiation effects 79—38049
Norton-Bailey parameters, from creep rupture data 80—30098
nuclear antiferromagnetism, low temp. NMR study 80—66049
nuclear antiferromagnetism, NMR obs. 79—78538
nuclear demagnetisation expts. 77—45851
nuclear susceptibility thermometer rel. to ^{199}Sn Mossbauer effect thermometer, 6 mk to 1K 79—35737
nuclei, antiferromag. ordering, mean field theory 79—78333
O free, annealing in photoemission electron microscope, twin density recrystallised grain size relation *(German)* 78—52850
OFHC, creep and relaxation curves for torsion-tension members at elevated temps. 78—83260
OFHC, strain rate variation effects on flow stress 79—43324
open orbit microwave transmission peaks 78—10491
optical constants, 5461 and 6328 Å, nearly ideal surface 77—36192
optical constants direct determination, d absorpt., reflectivity 77—69791
optical elements, US cleaning, deleterious effects 77—42631
ordered monolayer on Zn (0001), electronic struct., photoelectron spectra 78—39660
ore, leaching, effects of ultrasonics and their appls. 78—92214
ore processing materials, nondispersive X-ray fluoresc. anal. 78—92575
oriented bicrystal, sintering prod. technique 80—108371
oscilloscopic polarography determ. in environmental pollution anal. *(Chinese)* 79—53002
oxidation, electron scattering study 79—83377
oxidation, misfit dislocations between Cu_2O and substrate, TEM obs. 78—14629
oxidation, monolayer form., SIMS 79—89038
oxidation, of (100) single crystal surface 80—11846
oxidation, secondary ion energy spectra 80—71788
oxidation, two stage metastable and stable surface Cu_2O nucleation, 800-1000°C 77—70214
oxidation in CO_2, 800-1000°C 78—76784
oxidation in controlled clean air and standard laboratory air, 50-150°C 79—70202
oxidation in controlled clean air and standard laboratory air at 50 to 150°C 79—79154
oxidation kinetics, influence of intermediate annealing treatment 80—89412
oxidation of (111) single cryst. surface, laminar Cu_2O growth 78—72025
oxidation of surface (111), growth modes of (111)Cu_2O, UHV-RHEED and TEM obs. 79—19481
oxidation processes, EXAFS investigation 80—71808
oxidation zones, nucleation and growth during diffusional creep *(Russian)* 79—52431
oxide double layer form. on pure Cu 77—77637
N.Pacific, trace metal vertical profiles 80—67381
pair potentials calc., appl. to point defect props. 80—19798
pair potentials calcs., elastic props. calc. 80—49176
paramagnetic, conduction electron spin transmission 77—69693
partial densities of states, electron-phonon interaction 78—51869
particles, light scatt. spectra, size and shape effects 77—44015
particles in fluidised bed, electrical conductivity of electrodes, expt. meas. 77—48652
passivation by protective glassy layers at 500°C 78—76785
passivation using protective glassy layers at 500°C 80—3246
peaking effect existence in kHz internal friction meas. 80—24531
peptide-Cu II interaction, EPR and optical absorpt. 78—27881
phonon density of states determ. from thermodynamic functions *(Russian)* 77—7800
phonon dispersion, model pseudopotential method 79—23685
phonon dispersion relation in resonant model potential 80—6473
phonon dispersion relations and Debye-Waller factor calcs. 78—51630
phonon frequency determ. in noninteracting band scheme 78—47483
phonon limited electrical resistivity, temp. depend. 80—24876
phonon spectra, pseudopotential calc. 77—89508
phonon spectra, self-consistency condition for force const. models 80—44264
phonon-limited elec. and thermal resistivity 79—42517
phosphate glasses:Cu^{2+}, EPR, optical spectra 78—72399
photocorrosion in $CuCl_2$ and $FeCl_3$ aq. solns. 79—57145
photoelectric cross section in region 187 to 662 keV 79—69952
photoelectric cross sections of low energy photons 78—46309
photoelectric cross-section at K-edge measurements 78—2983
photoelectric interaction around the K edge 78—5183
photoelectron spectra, photon angle depend. of Cu (100) cryst. 77—59674

copper continued
photoelectron spectra 77—73218
photoelectrons, energy-angle depend. for UV light *(German)* 79—11495
photoemission, angle resolved, thermally induced breakdown of direct-transition model 77—77346
photoemission, angle-resolved, energy band symmetries 79—43104
photoemission, angle-resolved, from clean surface 78—15294
photoemission, bulk versus surface effects 78—52626
photoemission, temp. and photon-energy induced breakdown of direct transition model 78—95681
photoemission angular dependence, direct transition interpretation 77—21004
photoemission from indirect optical excitations 79—43103
photoemission from valence bands 77—20996
photoemission spectra, interpretation in terms of surface density of states 79—52081
photoemission spectra and band struct., extensions of combined interpolation scheme 79—78844
photoemission with polarised light, cryst. symm. effects 78—23581
photon activation analysis of coins and art objects 78—349
photon emission from inert gas-surface impact 78—11059
photoneutron yields released by incident electrons, improved calc. 80—27630
pickling in HCl waste free system 80—71795
pin, heavily deformed surface layer after dry sliding against steel ring, TEM obs. 77—60033
pin against steel ring, dry sliding wear, role of dynamic recrystallisation 80—108599
pin-on-disc friction and wear under boundary lubrication, dissolved O$_2$ effect 80—76365
pionic atom, 2p level shifts and widths 78—46469
pipe carrying potable water, corrosion 78—92409
planar channelling of α-particles, stopping power of solids 78—51602
plane coalescence, at grain boundaries 80—70221
plane shock wave loading, microdistortion X-ray anal. *(Russian)* 77—52399
plane strain deformed, electron microscope obs. of morphology 78—31424
plasma, accelerated, velocity meas. using fast-scanning Fabry-Perot spectrometer 79—41869
plasma, dense, nondegenerate, electron transport, thermal cond. *(Russian)* 79—98865
plasma, in fault current limiter mode vac. arc, temp. distrib. diagnostics 78—9851
plasma, laser-produced, high energy X-ray bremsstrahlung evidence of reson. absorpt. 78—42776
plasma, produced by CO$_2$ laser beam irrad. of solid, expansion of spontaneous mag. field 77—72495
plasma arc srapying, chem. reaction with plasma gases 80—66427
plasma EM macroparticle acceleration, high press. gas temp. density 80—79583
plastic deform., strain rate history and temp. effects depend. 79—11684
plastic deform. and prominent cross slip of ⟨100⟩ oriented single crystal 78—19852
plastic deform. build-up during low cycle fatigue *(Russian)* 77—25207
plastic deform. micropattern under various loading conditions 77—44321
plastic deformation, energy storage efficiency 77—4807
plastic deformation, formation of double twist boundaries *(Russian)* 77—81295
plastic deformation, steady state, transients due to strain rate changes 77—81302
plastic deformation, thermoactivated creep and stress relax. 79—87692
plastic deformation at low temps., structural defects, elec. resist. meas. *(Russian)* 78—39844
plastic deformation singularities, under periodic loading conditions 79—91766
plastic deformation thermal activation parameters from creep kinetics and stress relaxation 80—71717
plastic props., room temp. to recrystallisation temp., stress-strain relations, computer programs 77—1865
plastic rate calc. *(French)* 77—73303
plastic strain, during non-proportional loading 80—89291
plastic strain meas. due to sliding wear 78—64731
plastic working of wires, high-density current appl. 79—57002
plastically deformed, containing dislocation distribs., X-ray diffr. line broadening 77—43218
plastically deformed, lattice strain distrib. *(German)* 80—85012
plastically deformed, recovery, isochronal annealing, positron lifetime meas. 77—59807
plastically deformed at room temp., glide on {001} planes, TEM obs. 79—19257
plastically deformed crystals, SEM exam. of light and dark etch pits, dislocation arrangements 78—87679
plasticity, athermal and thermal *(Russian)* 79—11685
plasticity, temp. and rate dependence for different rigidities of stressed state *(Russian)* 79—29139
plate, electric current distortion effects 77—72853
plate, Sn-Pb solder, spreadability, effect of fluoride and iodide addition to ZnCl$_2$ flux *(Japanese)* 80—29251
plate, spreadability of Cd *(Japanese)* 80—29252
plated C fabric, plasma sputtering influence on strength and elec. cond. *(Russian)* 80—21008
plated substrates for Antares CO$_2$ laser mirrors 80—14349
plates, high speed collisions, dynamic pressures, shock wave parameters 77—68491
plates, Kapitza resist. to solid ^{4}He 78—34673
plating C steel nails, barrel plating efficiency 80—100964
platings on C steel filaments, porosity determ. 79—70239
point and planar defects, computer simulation 80—59455
point cathodes, explosive electron emission 77—55873
point emitter, surface microrelief under explosive electron emission 78—2973
point geometry angular correlation curves, enhancement in positron annihilation 79—95873
polarised, NMR spectra from below 1 kHz to 100 kHz, use of transverse SQUID 80—37064
polishing for optical appl. 78—5587
polishing in H$_3$PO$_4$, polarisation curves 78—56851
pollution conc. determ. in estuarine waters, Raritan and Lower New York Bays 79—12139
pollution levels in Belfast Lough 80—3539

copper continued
polyamide-Cu system, antifrictional props., struct. 80—40552
polycryst., creep and fracture behaviour, effects of prestrain and O 80—97544
polycryst. surface, Ar$^+$ sputtered, ion to neutral yield ratio, SIMS anal. 78—72659
polycrystal, grain boundary orientation determ. by struct. protonography *(Russian)* 78—38726
polycrystalline, Ar ion double scatt. 78—88399
polycrystalline, effect of grain size, specimen thickness, on mech. props. 78—84945
polycrystalline, elastic consts., inelastic coherent neutron scatt. meas. 80—34122
polycrystalline, grain size and high-temp. yield strength 80—7641
polycrystalline, low energy H$^+$ scatt., computer study 77—36338
polycrystalline, magnetoresist. due to crystal defects 78—56128
polycrystalline, probabilistic micromech. theory 77—863
polycrystalline, recovery and recrystn. kinetics 80—81081
polycrystalline, secondary ion energy spectra, ionisation mechanisms 79—38700
polycrystalline aggregate, various grain sizes, specimen thickness effect on mech props. 79—61645
polycrystalline material, plasticity analysis using stat. model *(Russian)* 78—26619
polycrystalline target, ion-atom cross-sections for sputtering of inert-gas ion incident at low energy 79—52059
polycrystalline target, X-ray intensity, microfocus source, non-linear rise studies 80—77927
polycrystalline target back sputtering of 100 to 500 eV Ne ions, computer simulation 78—60537
polycrystals, Ar$^+$ double-scattered energy distrib., compared to monocryst. *(Russian)* 77—55859
polycrystals, Bi segregation embrittlement 79—83318
polyethylene, cross-linked, thermal oxidation stability, influence of Cu 80—30128
polyethylene/Cu(Zn) adhesion, role of surface topography 80—35500
polygonisation, impurity effects rel. to stacking fault energy 77—63685
polymer laminate, fracture surface exam. by XPS *(German)* 78—84992
polyvinyl acetate:Cu, and undoped, thermally stimulated currents exam. 78—35083
pores, produced in high temp. fatigue, small-angle neutron scatt. study 79—14795
porous, shock compression calcs. using approx. eqn. of state 77—35657
porous, sintered, deform. diagram based on theory of plasticity *(Russian)* 78—88494
position annihilation radiation, two-dimensional ang. correlation, momentum density meas. 78—10331
positive muon dipolarisation rate 79—56692
positive muon spin rotation frequency, Knight shift meas. 79—38421
positive-muon spin depolarisation rate field depend. 79—33585
positron annihilation, high current densities, ang. distrib. of annihilation quanta *(German)* 77—12462
positron annihilation, source effects 78—31272
positron annihilation, umklapp process, rot.-specimen method 78—2410
positron annihilation ang. correl., trapping by mono- and multi-vacancies 77—32466
positron annihilation characteristics, effect of temp. 78—64427
positron annihilation measurements, monovacancy and divacancy parameters 77—35550
positron annihilation quanta ang. correl., point defect effects 77—76729
positron annihilation radiation, ang. correlation, APW calc. 80—7435
positron annihilation studies using high-density proportional chambers 80—25478
positron annihilation with high-momentum core electrons, vacancies study 80—25481
positron implantation, profiles in mono- and polycryst. samples, channelling 77—48273
positron lifetime, Doppler broadening of annihilation spectrum, temp. effect 78—2941
positron lifetime as a function of grain size 77—15427
positron lifetime changes, during cyclic fatigue 79—43060
positron source using Na^{22} ion-implantation for annihilation lifetime expts. 79—45489
positron trapping, defect specific temp. depend. 78—47336
positron trapping by vacancies using ^{19}Ne source 78—47341
positron trapping rate by dislocations in plastically deformed sample, 6 to 77K 77—11592
positron trapping rate in plastically deformed cryst., temp. depend. 78—31276
positron-lifetime study of 4.5-25 MeV proton irrad. effects 79—33021
positron-vacancy interactions, equilib. temp. depend. of positron annihilation 78—76547
positronium form. in two-photon positron annihilation 79—61462
powder, compression and stress relaxation *(Japanese)* 79—96060
powder, electric discharge sintering, struct. changes 77—77446
powder, electrodeposition, mathematical model for current efficiency and electric power consumption 80—20831
powder, electrodeposition prep. conditions, statistical anal. 80—20828
powder, electroless tinning 80—25607
powder, exam. of consolidation process based on electronic structure of solid 80—20842
powder, flowability, apparent density and comp., effect of Na, Mg, and Al additions 79—28986
powder, hot pressing on steel substrate, densification kinetics 80—40290
powder, positron annihilation *(Russian)* 77—63485
powder, sp. ht. cond. and sp. elec. cond. meas., Wiedemann Franz Lorenz law *(German)* 80—92872
powder, sprayed, effect of start props. on struct. and porosity of sintered products *(Czech)* 77—85960
powder compact, elec. resistivity 78—64028
powder compacts, improving cond. by pretreatment of green compact 80—20824
powder compacts, yield curve comparison, different loading paths *(Japanese)* 80—93621
powder formation by constant and pulsating overpotential electrolysis 77—81234
powder props. and sintered samples with Al$_2$O$_3$ 77—55909
powder under press., elec. cond. *(German)* 79—69485
powder-epoxy mixtures, cryo-tip refrigerator appl., heat transport 78—37013

copper continued
- powder-water-oil system, cohesion of powder particles with water, rheological prop. *(Japanese)* 80—14647
- powders, packed, complex mag. permeability calcs. 80—29583
- powders, prep. of spherical starting particles, for suspension electrolysis 78—60689
- preferred crystallographic orientation of melt grown single crystals *(Czech)* 79—43134
- preferred crystallographic orientation of unidirectionally solidified polycrystals *(Czech)* 79—43233
- pressing pressure effect on consolidation 79—74116
- prestrained, tough pitch and sintered, ductile fracture, voids *(Japanese)* 77—52472
- prevacancy temperature depend. of positron annihilation, Doppler broadening lineshape parameters 80—60709
- prismatic dislocation loops, (g.b)s product sign determ. *(Russian)* 78—38705
- prismatic dislocation loops revealed by X-ray topography and etching 77—11563
- production and extractive metallurgy, developments, review 80—20821
- projected range distrib. of 5-25 keV ^{4}He^{+} 80—65094
- protective coating on Al powder *(Russian)* 78—60881
- protective coatings, thermal shock performance 78—7081
- proton diffusion, config. and activation energies 79—37878
- proton impact X-ray emission, ang. distrib. and polarisation fraction 78—56546
- proton irradiated, muon spin rotation study at low temps. 78—92011
- proton irradiated, radiation-annealing effects in energetic displacement cascades, film resist. meas. 78—26603
- proton irradiation, 10 to 16 MeV, isochronal annealing meas. 80—2083
- proton irradiation, 10-16 MeV, neutron damage simulation 80—34089
- proton irradition, 10 to 16 MeV, resistivity changes 80—2082
- proton movement, activation energy 77—62678
- proton stopping power meas. at 100 keV, using ion induced X-ray emission 78—48725
- proton-induced L-shell ionisation cross-sections 80—100707
- proton-irradiated, H_2 gas-bubble struct., study at 300K 80—92569
- protoporphyrin: Cu^{2+}, in pyridine fluoresc. quenching mechanism 79—56837
- pseudopotential nonlocal model 78—14659
- pulsed gas laser with unstable resonator, beam shaping 78—17987
- pure, dynamic stress strain relations in combined tension and torsion, testing device 80—21197
- pure, vacuum environment and grain size effects on creep rupture props. at elevated temps. *(Japanese)* 80—81162
- PVC:Cu film, struct. and optical props., soln. growth technique 78—51837
- PVC:Cu films, electron transport and dielec. props. 79—82700
- PVC, Cu evaporated film, electron-induced metallochromic reaction for metal image formation 80—86476
- PVC, filler effect on adhesion to Cu 80—45476
- PVC film, Cu doping effect on chain vibrs. 79—95868
- PVC-Cu composite, annealing effects on elec. resist. 78—68060
- PVC-Cu composites, elec. resistivity rel. to compacting pressure 80—34495
- PVC-Cu composites with chemically deposited ultrafine copper particles 80—93534
- α-quartz:Cu^{2+}, γ-irradiated, stabilisation of impurity atoms 79—8047
- quartz:Cu, glassy and cryst., luminesc. centres 77—4679
- quartz:Cu, paramagnetic centre formation after α-irradiation *(French)* 77—69690
- radiation damage, vacancy migration induced by subthreshold focused collisions 77—19982
- radiation damage and diffusion 80—24645
- radiation damage due to protons, μSR 79—56702
- radiation damage effect of 800 MeV protons on thin target 77—69016
- radiation damage with radioactive probes, TDPAC meas. 77—24336
- radiation damaged, elec. field gradient, temp. depend. 78—39481
- radiation damaged, temp. depend. of elec. field gradient, DPAC expt. 78—43727
- radiation induced low-energy collision cascades, effects of thermal vibr. and zero-point motion 78—87705
- range of ^{27}Al^{+} ions, meas. by (p,γ) reson. broadening 79—46729
- range of Ni^{+} ions, increase due to ion bombardment induced crystalline reorientation 78—26611
- reaction with liq. Zn 77—9127
- recovered dislocation arrays, HVEM determ. of true segment length and interforest spacings 78—30631
- recovery for Cu_2O_y ore by segregation roasting *(Japanese)* 79—52136
- recovery from secondary sources, recent development 80—100800
- recovery of electrical resist. in weakly deformed single crystal 77—81304
- recovery substages, I_D and I_E, after thermal neutron damage 77—35590
- recovery-creep, high temp., cross-slip and climb of dislocations 77—19965
- recrystallisation and recovery during temperature strain *(Czech)* 77—70071
- recrystallisation and recovery during temperature strain *(Czech)* 77—73287
- recrystallisation annealing *(Russian)* 78—15430
- recrystallisation centre growth kinetics, impurity effects *(Russian)* 80—89253
- recrystallisation diagram for fine grained metal in region of small deformation *(Czech)* 77—59811
- recrystallisation kinetics *(Russian)* 78—11238
- recrystallisation kinetics after small deform. and grain growth *(Czechoslovakian)* 77—32592
- recrystallisation of cold rolled samples *(French)* 79—43269
- recrystallisation of room-temp. deformed torsion samples, microcalorimetry 77—28827
- recrystallisation retardation, two-phase Cu crysals, particle size, spacing effects 80—89242
- recrystallisation texture, of deformed single crysts., HVEM study 80—104179
- recrystallisation texture, rel. to rolling temp. 80—11664
- recrystallisation textures, and deformation formed by dry sliding against steel 79—91698
- recrystallised, inhomogeneous deform. due to texture changes *(German)* 79—29158
- recrystallised state, of single crysts., ⟨110⟩ oriented, tensile deformed, HVEM of recrystn. 80—89256

copper continued
- recrystallization annealing, grain growth, effect of type of deform. 80—100847
- recycling, effect on comp. 80—66455
- reference standards for radiation pyrometry, silver and copper freezing points 78—57888
- refinery electrolyte, glue determ., electrochem. method 79—48021
- refinery electrolyte containing thiourea, electrochemical method of meas. active glue conc. 77—4966
- reflection coefficients, changes at high temps. 78—19440
- reflective coatings, refr. index, UV polariser mirror coating appl. *(Russian)* 77—34928
- reflectivity at high temps., pulsed laser heating 77—63388
- reorientation following ion bombard. 80—70269
- residual resistivity for electrons scatt. by spin-depend. potentials, for Cu with 3d impurity 77—39829
- residual temperature, meas. during quasi-isentropic compression *(Russian)* 77—89495
- resin:Cu^{2+}, interaction with ligands, EPR meas. 78—10756
- resistance thermometer, heat shock influence on elec. cond. and thermophysical props. *(Russian)* 80—52210
- resistance welding, apparatus using C rod electrodes 77—79077
- resistivity and thermoelec. ratio, electron-electron scatt. contrib. 80—70670
- resistivity and thermoelectric ratio at low temp., 0.04 to 7K 79—73497
- resistivity changes with deform., subsequent recovery 77—52397
- resistometric study of anodic oxide films in neutral soln. 77—16739
- resonant and nonresonant conduction-electron-spin transmission 80—75857
- resonant cavities, RF loss reduction at 35 GHz by cryogenic cooling 78—93761
- resonant model potential, energy depend. 78—18952
- resonant model potential and phonon frequencies 78—30713
- rod, dynamic bending and residual deformation *(Russian)* 80—75293
- rod, tensile loaded, internal friction and Young's modulus measuring equipment, inelastic phenomena exam. *(Hungarian)* 79—52546
- rolled, dislocation struct. and recovery during annealing *(Russian)* 79—29084
- rolled at room temp. and 200°C, variation in props., hardness and X-ray meas. *(Russian)* 77—73285
- rolled sheet, texture transform. during primary recrystallisation as function of annealing time 79—91683
- rolled single crystal with defined solute content, stored energy and recrystallization temp. 79—96037
- rolling textures and texture inhomogeneities, exam. of development in single- and poly-crystals 79—11637
- saturation resistivity charges, ion and fission fragment irrad. induced 78—79643
- scattering and radiation damage for 14 MeV neutrons and 10 to 20 MeV protons 77—15458
- scattering of low energy He ions and atoms, elastic and inelastic effects 77—8708
- screening charge density round $\Delta Z=-1$ impurities, vacancies, NQR study 80—103897
- screw-fastened joints, low temp. thermal cond. and elec. resistance 79—95469
- second-order elastic consts., method of homogeneous deform. 79—55808
- secondary charge emission coeffs., low energy H^{0} flux meas. 80—25509
- secondary electron emission, Boltzmann eqn. appl. *(French)* 80—55238
- secondary electron emission, spurious peaks from grid of retarding field analyser 77—20968
- secondary electron low energy distrib. meas. using double-pass cylindrical mirror analyser 80—68293
- secondary electron spectra, low energy peaks interpretation 78—39638
- secondary electron yields from ion impacts, stopping power calcs. 78—11053
- secondary ion emission, chain effect for fast recoils Ar^{+} ion beam impact 78—56554
- secondary ion emission, energy spectra, 0-55 eV, contamination levels 79—15573
- secondary negative ion emission, effect of adsorbed O_2 *(Russian)* 79—28881
- secondary slip, in neutron irradiated crystals 80—88161
- secondary slip, in neutron irradiated monocrystals, secondary slip between overlapping dislocation arrays 80—88162
- selective recovery from Ca-Ni sulphides by segregation technology 79—61534
- selective surfaces on Al-Cu alloy, chemical brightening and etching 79—62037
- self diffusion at low temp., low energy ion beam sputtering 78—18821
- self interstitial struct. determ., and vacancy clustering, X-ray exam. 78—47351
- self-diffusion of ^{64}Cu, 737-1079°C, monovacancy and divacancy contribs. 79—19394
- self-interstitial interaction with solutes, resistivity meas. 78—47331
- self-ion-irradiated, axial channelling along ⟨110⟩, by Rutherford backscatt. of He ions 79—4342
- self-sputtered, secondary ion mass spectra 79—74044
- SEM, contrast of electron channelling patterns, estimation from low index refl. 78—9921
- SEM, electron channelling patterns 78—83697
- shear mode of ductile fracture 78—31525
- shear modulus and internal friction under press., EM reson. technique 77—31709
- sheet metal, texture heterogeneity, numerical simulation *(French)* 78—92274
- sheets, earing, R-values and 3-D orientation distrib. functions, comparisons 79—91702
- shell, deposited in vacuum, elastic characts. meas. by short time static extension *(Russian)* 78—39961
- shell, explosive expansion, deform. and rupture modes and mechanisms 80—85064
- shock adiabatics at ultrahigh press. *(Russian)* 77—27941
- shock compressed, release isentropes, eqn. of state at high energy density *(Russian)* 80—54340
- shock compressed, thermal energy relaxation 77—69043
- shock loaded, work hardening and press. depend. of dislocation arrangement and density 78—48429
- shock transition rise-time meas., limiting viscosity coeffs. 79—77680
- shock wave compression, reduced Hugoniot curve and eqn. of state *(Chinese)* 80—44259

copper continued
- shock wave data, 'solid Hugoniot' rel. to 'fluid Hugoniot' 80—65155
- shock-compressed, compression and rarefaction waves obs., 150-250 kbar 77—77535
- silicate glasses:Cu^+, effect of UV irrad., absorption bands 78—31222
- SIMS depth profiling, surface roughening by low energy ion irrad. 80—60727
- single cryst., latent hardening in tension 80—60878
- single crystal sintering model evaluation, Kossel interference and digital graphic simulation appl. *(German)* 80—2980
- single crystals, absorbed H, strain anal., X-ray divergent beam method 78—15463
- single crystals, effect of stacking fault energy on extrusion and intrusion development 78—72826
- single crystals, in high temp. creep, meas. of internal stress 78—80608
- single crystals, influence of friction and geometry of deformation, on texture inhomogeneities during rolling 78—72792
- single crystals, positron trapping by edge dislocations, producing by bending 78—80606
- single crystals Au ion implanted, pulsed electron beam irrad. 80—65019
- single particle lifetime 80—103612
- single-crystal thin foil, determination of struct. potentials from Kossel Mollenstedt diagrams 80—6324
- sinter, in contact with ^{3}He, thermal conductance, rel. to elec. resist., heat flow model calc. 80—10728
- sintered, appl. of stereological charact. of interface interaction 77—63589
- sintered, deform., temp. and loading rate effects 77—77548
- sintered, residual voids, quantitative anal. of morphological changes by metallography 79—47854
- sintered, use for exchange of heat with flow of superfluid ^{4}He 77—82526
- sintered preform, porous, ductile fracture criterion, rel. to forging process 77—56105
- sintered strip, external friction of rolling 77—1845
- sintering, cold working, recrystn. annealing, mech. props. and microstruct., porosity recrystallisation and grain growth, survey 78—76660
- sintering, contact resist. determ. of neck growth rate and mass tranport mechanism 77—55899
- sintering, isothermal, surface area reduction 77—8779
- sintering powder compacts, depend. of neck form. on particle size and sintering temp. 79—28988
- size effect in metallic sandwiches 79—73604
- skin lesion Mn, Cu and Zn conc. meas. by neutron activation 80—17063
- sliding behaviour, against polymers laminates and coated surfaces at cryogenic temps. 80—66671
- sliding charact., friction and wear *(Japanese)* 78—56778
- slip line length for single crysts. oriented along [100] and [111] 78—76664
- slip ring elemental surface composition as function of temp. 80—66901
- small particles, CO interaction, IR spectra obs. 77—20195
- small vacancy clusters, structures and energies, computer simulation 80—39073
- smelting, exam. of vacuum lift refining 78—60621
- sodium oxalate:Cu^{2+}, anhydrous spin Hamiltonian and bonding parameters and orbital-reduction factors 80—60408
- soft crystal, US irrad. induced dislocation distrib. 77—32584
- soil-water system interfacial reactions and heavy metal adsorption 78—3832
- solar selective absorbers, graphite on Cu, interf. films deposited on diffr. gratings 79—14103
- solderability, annealing effect *(Japanese)* 80—89244
- solid, $K\alpha$ hypersatellite spectrum, double K ionis. 77—18829
- solid cylinder, annealed, dynamic forming by compression *(Japanese)* 77—70267
- solid phase welding, behaviour of solid phase bonded interface, of poly and single crystalline Cu *(Japanese)* 78—48611
- solid state sintering, compact length change 80—11593
- solubility, low temp., in Be, Be-Al, and Be-Si, ion implantation and backscattering 77—62646
- solubility and diffusivity of F, electrochem. meas. 79—46808
- solubility in CdSe in presence of Ga 78—22856
- solubility of O_2 in solid Cu 77—69089
- SOMS, effect of impurities 80—50925
- sound propagation, anomalous, by cond. electrons 80—11048
- spallation, temp. effect on breaking strength 78—31536
- spark-source mass spectrometry, relative sensitivity coeffs. 79—92045
- spatial electron beam-matter interaction, model calcs. for Cu *(German)* 80—84815
- specific heat, 0-100 kbar, press. depend. 77—51512
- specific heat, 2 to 30K, meas. equipment *(German)* 77—87763
- specific volume meas., for ruby R_1 fluoresc. press. gauge calibration, 0.06-1 Mbar 78—70150
- spectral distrib. of X-ray braking radiation, due to electrons, calc. using Monte Carlo method 78—56538
- spheres, electrically augmented pneumatic transport at low particle and duct Reynolds numbers 78—87409
- spheres, rotation and translation during sintering onto a substrate, grain boundary energy SEM study 79—38759
- spheres, single cryst., dissolution, formation of etch pits, surface structure study using SEM 79—23735
- spin density wave fluctuations in nuclear spins, susceptibility, internal energy 80—50115
- spin properties of conduction electrons 79—46999
- spreading of high-press. polyethylene melt, index 79—37902
- sputter deposit, thick, microstruct., tensile props. 77—40461
- sputter deposit PIXE expt. 80—61196
- sputter deposited at high rate, microstruct. and props. 78—22988
- sputter deposition, isotope enrichment 77—27198
- sputtered, ionisation probability, energy dependence 80—35041
- sputtered atom angular distrib., mass effects in Mg plasma 79—87538
- sputtered Cu_1^+ ion energies by low energy inert gas ion bombard. 80—71555
- sputtered surfaces, stability of cones and pyramids 79—78812
- sputtered with 15 or 30 keV H^+, He^+ and Ar^+ ions, energy and angular distrib. 78—95625
- sputtered-deposited, damage-resistant high reflectivity material for high energy laser appl. 79—47181
- sputtering, binding energies 80—108312
- sputtering, Cu bombarded by Ne^+, Ar^+, Kr^+, average kinetic energy of sputtered atoms *(German)* 78—19619
- sputtering, surface topography, appl. of thermodynamics of capillarity 80—20749

copper continued
- sputtering by Ar^+, appl. of torsion vacuum microbalance to sputtering yield meas. *(Japanese)* 78—19622
- sputtering by Ar^+ ions, thickness distrib. and struct. characts. of Wehner's spot 77—59655
- sputtering by Ar, Brinkman cross section, approx. for sputtering yield 78—76571
- sputtering by Hg ions, isotope enrichment 77—59656
- sputtering coefficient, temp. depend. 78—19625
- sputtering efficiency ang. distrib. meas. using thermal particle detector 77—28671
- sputtering in inert atm., with uncooled cathode, oxidation of metallic coatings, X-ray diffr. obs. 78—3041
- sputtering intensities, ang. depend., for single crysts. 77—8709
- sputtering of atoms and positive ions along [011] and [101] directions, ang. depend. 77—24917
- sputtering processes, due to Ar^+ bombardment, computer modelling 79—19957
- sputtering rate on Ar ion bombard. 80—55245
- stabiliser for fusion reactor supercond. mag., neutron irrad. effects on magnetoresistance 80—34062
- steady wear mechanism, against Pyrex glass, expt. study to confirm theoretical anal. 80—45404
- steel, low C-Cu composite plates, vol. fraction and residual stress, effect on fatigue strength *(Japanese)* 79—8349
- steel, martensitic, age hardening with Cu, Nb additions, exam. of hardness 80—7681
- steel, reinforced, fatigue strength, surface layer effects 77—12697
- steel, stainless, laminated with Cu interlayers, mech. props. 77—48506
- steel fibre reinforced Cu, exam. of creep behaviour *(German)* 78—52931
- steel fibre reinforced Cu, fatigue 79—29221
- steel-Cu M3 bimetal, eutectic alloy, crack development, failure energy capacity *(Russian)* 80—40480
- steel/Cu bemetallic pipe, determ. of yield, tensile strength 80—25771
- STEM, extinction distances and anomalous absorpt. coeffs. 78—42872
- stepped substrate-adsorbed layer (S) interaction, selective effect on epitaxy 78—14616
- stepped surface exam., LEED vs. RHEED 77—72762
- stimulated emission, Cu in radial transverse discharge 77—50658
- stimulated emission from Cu atoms, discharge excitation in $CuBr_2$, $CuCl_2$ 77—23663
- stimulated emission from explosively formed vapour, apparatus for obs. 78—50764
- stopping of 3-7 MeV α-particles and 4-6 MeV protons *(Russian)* 79—51181
- stopping power for 0.3-1.5 MeV protons 79—55801
- stopping power for 28 MeV α-particles, re-evaluation 78—79651
- stopping power for MeV H^+, D^+, $^4He^{2+}$, $^7Li^{3+}$ ions, deviations from Bethe formula 78—26612
- stopping power meas. for 4-5 MeV/N ^{16}O, ^{40}Ar, ^{65}Cu, and ^{84}Kr 78—70720
- stopping powers, projectile range for Z=8-20, 0.0125-12.0 MeV/nucleon 78—83856
- stopping powers for 28.8 MeV α-particles 77—80556
- stopping powers for 8.78 MeV α-particles 77—80557
- stopping ratios of 50-300 keV H^+, He^+, $^7Li^+$, and $^8Be^+$ 80—42903
- stored energy meas. by new deform. calorimetry method, in single crystal 78—39834
- strain amplitude cycling, in fatigued single crysts. 80—3146
- strain hardening curve computation 77—90363
- strain hardening parameters, 4.2 to 300K *(Russian)* 79—20063
- strain hardening relation, method of error rectangles 77—55980
- strain localisation, during hot deform. 80—104195
- strain tempering by rapid heating and cooling of cold drawn wires *(Japanese)* 78—84863
- strained, interpolation functions for Fermi surface 80—65425
- stray X-rays from Cu components in transmission electron microscope, reduction 80—73550
- strength differential effect, temp. and strain rate sensitivity in saturation cycling 79—66094
- strengthening by dislocation substructures 77—36538
- stress component determination during loading cycle *(Czech)* 79—91725
- stress induced ordering of self-interstitial clusters 78—47358
- stress reduction at straining single crystal due to anodic dissolution *(Japanese)* 78—15579
- stress relaxation, dislocation motion through random array of point obstacles 77—7732
- stress relaxation in cyclic deformation 80—3119
- stress removal during annealing after hydrostatic extrusion 79—83215
- stress-strain behaviour over large strain range 79—15745
- strip, formed by high deform., mech. props. charact. *(Russian)* 78—27534
- strontium acetate hemihydrate:Cu^{2+}, EPR of cryst. 78—19312
- strontium acetate hemihydrate:$Mn^{2+}(Cu^{2+})$, EPR, spin Hamiltonian anal. and unit cell symmetry 80—29603
- structure changes in single cryst. under influence of static and dynamic stresses *(Russian)* 78—92300
- structure factor, absolute measured value of f(220), importance of extrapolation to zero extinction 79—19123
- substrate, (001), Ni electrodeposition, three-dimens. epitaxial crystallites, TEM image contrast 80—88457
- substrate, electrodeposition of Au film 80—81329
- substrate, ion induced intermixing of Au or Ag surface film 80—15420
- substrate, Sn autocatalytic deposition 80—100965
- substrate, surface topography influence on growth struct. of sputtered Cr 80—20058
- substrate, underpotential deposition of Pb, phase formation 80—54538
- substrate for polystyrene film, electrode effect on carrier injection, TSC, I-V characts. 80—34463
- substrate for SiO_2 film, surface EM wave absorpt. optical consts. *(Russian)* 80—108216
- substrate for solar selective surfaces, graphite coating props. 78—74952
- sulphidation, rapid data acquisition in slow electrode processes by simultaneous potentiostats 79—96236
- superconducting magnet stabiliser, 400 GeV proton irrad., resist. meas. 77—37948
- supercooled melt, dendrite growth morphology *(Japanese)* 78—11216
- superradiance at 511, 578 nm during two discharge current pulse vaporis. *(Russian)* 78—29942
- surface, 10-30 keV H ion bombardment, energy refl. meas. 78—27359

copper continued
surface, 10-35 keV Ar$^+$ bombarded, energy distribs. of ejected fast ionised recoils 79—47579
surface, ^{4}He$^+$ scattered ion yields, ang. depend. 78—15272
surface, ^{4}He backscatt., Rutherford scatt. cross section correction test 80—66369
surface, (001), adsorbed c(2×2)CO layer, struct. 80—88428
surface, (001), angle-resolved photoemission spectra calc. 77—40323
surface, (001), electronic struct. of steps 78—34884
surface, (001), inelastic scatt. of He atoms, 20K 79—8222
surface, (001), intensity profiles, barrier reson. features, LEED 78—64089
surface, (001), O$_2$ adsorption effect on surface barrier, LEED study 80—84378
surface, (001), scatt. of He and Ne atoms at 20K 78—80451
surface, (001), surface relax. and thermal expansion calcs. 79—23820
surface, (001), with adsorbed O, Ar$^+$ bombarded, particle ejection, ang. depend. 80—50489
surface, (001) and (110), electronic wave functions by spherical wave method 79—42604
surface, (001) and (111), angular resolved photoelectron spectroscopy 78—95652
surface, (100), 30 keV Ar ion impact, scatt. ion-electron emission correlation 77—52209
surface, (100), 5-10 keV Ne$^+$ bombarded, time of flight meas. of ion fractions 79—47578
surface, (100), adsorpt. of CO, UV and X-ray photoelectron spectra, LEED 78—56037
surface, (100), adsorption and incorporation of O$_2$ 78—56042
surface, (100), adsorption of O$_2$, angularly resolved UPS meas. 78—71956
surface, (100), angle-resolved PES study 80—55273
surface, (100), Ar ion sputtering, collision cascades and disturbed zone, computational model 79—74037
surface, (100), coadsorption of Pb and Bi, LEED and AES meas. 79—15017
surface, (100), d-like surface state band, angle-resolved photoemission obs. 79—78840
surface, (100), diatomic mol. scatt., energy transfer and dissociative adsorption 79—46961
surface, (100), elastic scatt. of He 79—95892
surface, (100), electronic struct., self-consistent local-orbital calc. 80—80348
surface, (100), interaction with O$_2$, AES, EELS, LEED and work function studies 80—24731
surface, (100), N chemisorption, bonding, MO theory 77—76659
surface, (100), O chemisorption, angle-resolved UPS study 80—84384
surface, (100), ordered Cl overlayer, adatom bonding effects, photoemission study 80—104044
surface, (100), oxidation studied by angle-dispersive photoemission spectra 78—15585
surface, (100), self-diffusion near ambient temp. by surface pot. meas. *(French)* 79—51397
surface, (100) and (110), classical trajectory calc. of dissociation of H$_2$ and D$_2$ 77—60114
surface, (100) and (111), high resolution normal and near-normal UPS 80—80933
surface, (100) coherent elastic scatt. of He, Ne, thermal attenuation 80—89105
surface, (110), adsorbed pyridine, photoemission selection rules 80—100751
surface, (110), adsorption of CO, electron energy loss vibr. spectra and LEED obs. 79—77902
surface, (110), Ar bombardment, fast recoil atom blocking effect 79—69172
surface, (110), contraction determ. by LEED intensity anal. 79—73385
surface, (110), ion-electron emission, crit. energy variations 80—55246
surface, (110), methanol adsorption, XPS, UPS and thermal desorpt. study 80—84388
surface, (110), N implanted, temp. depend. evolution, Auger line shape 78—2376
surface, (110), photoemission obs. of new surface state band 79—91121
surface, (110) 79—74056
surface, (111), (100), (110), energy band parameters, EHT calc. 78—34883
surface, (111), bulk s orbital bands, sensitivity to oxidation, photoelectron spectra 79—47597
surface, (111), Cs adsorption system, electronic surface band energy 80—2443
surface, (111), final state band gap effects in UPS 80—89120
surface, (111), high resolution photoemission spectra 79—52082
surface, (111), photoelectron angle resolved spectra, perpendicular momentum conservation oxidation induced breakdown 79—24412
surface, (111), polarisation depend. of angle resolved photoemission spectra 78—56557
surface, (111), positronium form. due to slow positron trapping 80—107748
surface, (111), structural determ. using reliability factor proposed for LEED 78—43224
surface, (111), UPS at const. wavevector component 80—16151
surface, (111) and (100), Sn segregation 78—14554
surface, (311), struct. determ. by multiple scatt. calcs. of LEED intensities 78—56028
surface, (410), edge atom depression, ion scatt. spectroscopy study 80—54492
surface, accel. heat transfer to boiling n-octane, due to porous Ni layer 77—85056
surface, active nucleation site spatial distrib., bubble flow density 78—71267
surface, adsorbed H$_2$, adsorbate induced photoemission, book contrib. 78—95668
surface, adsorbed monolayer of Kr, many-body interactions 78—84068.
surface, adsorbed N$_2$, H, O and ethylene monolayers, UV-visible polarised modulation spectra obs. 78—72619
surface, adsorbed NO, species identification, struct., dissoc. chemisorption, desorption, UV photoelectron spectroscopy 78—52635
surface, adsorption of Sr^{2+}, ^{90}Sr tracer expt., immersion time, conc. and temp. depends. 78—87863
surface, Ar$^+$ ion bombardment, O$_2$ enhancement of sputtered ion yields 79—38705

copper continued
surface, Ar$^+$ ion irradiated, electron micrscopy study of defects *(German)* 80—2087
surface, Ar$^+$ ion irradiated, small defect clusters, electron microscopy contrast *(German)* 79—99253
surface, Ar$^+$ low energy refl., surface thermal vibrs. effect 77—16448
surface, Ar ion bombardment, fast ionized recoils, thermal lattice vibr. effects 80—100737
surface, boiling props. of H$_2$O rel. to organics 78—90654
surface, bombarded with electron, proton and rare-gas ion, direct and recoil-induced electron emission 80—11526
surface, C and H ion bombardment, secondary electron emission coeff. experimental technique 79—78804
surface, charged-particle emission caused by laser beam scanning 80—11518
surface, chemisorbed CO vibr. spectrum 79—69347
surface, chemisorbed N, self-consistent electronic struct. calc. 78—2544
surface, clean and O-covered, ion-bombarded, molecular cluster ejection, model 79—87543
surface, conditions for total refl. of low-energy atoms 79—19958
surface, contact angs. meas., aq. ethanol (glycerine) solns., 20-70°C 78—56025
surface, Cs$^+$ impact, 5.5 keV, negative secondary ion emission obs., comparison with phosphor bronzes *(French)* 77—66562
surface, d-band narrowing, obs. using angle-resolved XPS 80—11062
surface, deuteron irradiated, dynamics of radiation blistering and near-surface deuterium retention 77—84807
surface, dissociation of H$_2$, effect of surface roughness, classical trajectory calcs. 78—76925
surface, effect of mag. field on spreading kinetics of Ga, In, and In-Bi(Ni) alloys 80—10742
surface, electron emission, ang. distrib., final state effects 77—66580
surface, electron stimulated desorption, glow discharge treatment 79—65964
surface, excited state formed by B$^+$ impact, light emission coeffs. 78—64417
surface, fast D$_2$ desorpt. mechanism, time-of-flight spectra 80—84379
surface, fine interaction of conduction electrons 80—34500
surface, grazing incidence reflection of nuclear polarised ^{7}Li and ^{14}N ions 79—64077
surface, H$_2$ dissociation, classical trajectory calcs. 77—1947
surface, H$^+$(H$_2^+$)(H$_3^+$) impact, backscattered H Balmer-β line intensity 77—23470
surface, H$^+$(H$_2^+$) ion impact, energy refl. coeffs. 78—54969
surface, hard corrugated, elastic He atom scatt. 79—69944
surface, He, Ne, and Ar ion irrad., 0.05 to 3 MeV, orientation of fast ions excited in surface collisions 79—4876
surface, He ion irrad., 1 to 25 keV, range profiles, reemission, blistering 78—38758
surface, heated, water droplet evaporation, heat transfer characts. 78—59269
surface, HMO study of H and H$_2$ adsorption 77—15682
surface, horiz., min. film boiling temp. of saturated ethanol-water mixture 78—90692
surface, inert gas ion irrad., fast ionised recoils, blocking effect 80—71550
surface, interacting mechanisms with organic sulphides rel. to friction and lubrication behaviour 80—45546
surface, intermediate UPS/XPS synchrotron radiation study 78—52633
surface, ion bombarded, cone struct. initiation 79—51171
surface, ion impact, mol. effects in electron emission 78—80446
surface, ion impact, surface atomic struct., effect on recoil atom energy distrib. 80—35050
surface, ion irrad., tertiary effects in pyramid form. 80—2090
surface, ion irrad., topographical features relative stability 80—2092
surface, low energy Ar$^+$ ion scatt., binary collision approx., SIMS meas. 79—47582
surface, low energy ion scattering, meas. of energy spectra of neutral particles, apparatus and expts. 80—55242
surface, low energy noble gas ion refl., surface thermal vibrs. effect 77—69955
surface, low energy noble gas ion refl., surface thermal vibrs. effect 77—73203
surface, luminesc. accompanied by ion implantation 80—60683
surface, Lyman-α emission from proton bombard. 79—91503
surface, mirror electron microscopy for total electron refl. coeff. determ. 78—5994
surface, negative affinity, narrow beam emission of slow positrons 80—89091
surface, negatively biased, positron impact, positronium form 80—35024
surface, obs. of positron Bragg refl. 80—103221
surface, photoelectron spectra electron refraction and light polarisation effects 78—72700
surface, photoemission 78—52619
surface, plasma cleaning and etching, removal of C 80—97645
surface, polished, with H$_2$O cryofilm, bidirectional visible and near IR reflectance 78—88274
surface, polycryst., 16 keV Ar$^+$ scatt., diatomic model 78—11044
surface, polycrystalline, Ar ion bombard., regular pyramid production 78—59843
surface, positronium emission 80—80897
surface, relative intensities of L$_{2,3}$M$_{4,5}$M$_{4,5}$ principal and satellite Auger spectra 79—52054
surface, small angle scatt. of low energy K$^+$ ions 80—20752
surface, spherical and plane, ion-electron emission 79—65966
surface, sputtering with 30 keV Ar$^+$ ions *(German)* 79—24407
surface, stay time meas. for physisorbing Xe 78—56044
surface, thermal activation meas. of positron binding energies 79—95371
surface, total hemispherical emissivity 79—28115
surface, transient heat transfer, to liq. He 79—72785
surface, with chemisorbed CO, cluster calc. using SCF-Xα-scatt. wave method 77—62742
surface, X-ray prod. by 5 MeV/amu deuterons (oxygen ions), projectile Z depend. 80—42982
surface (001), adsorbed O, core-level XPS, azimuthal anisotropy 79—19969
surface (001), barrier struct, LEED study 80—65354
surface (001), chemisorption of N atoms, electronic struct. of Cu$_5$N cluster, Xα scattered-wave calcs. 79—60902
surface (001), $\bar{M}$-point surface state, high-resolution angle resolved photoemission study 80—108322

copper continued
surface (001), O chemisorption, Cu3d-O2p interaction study by angular-resolved photoemission using synchrotron radiation 80—84836
surface (100), adsorption of O_2, CO and water, EELS study 80—2260
surface (100), adsorption of O_2, LEED study 80—100408
surface (100), Ar^+ ion scatt., 10-35 keV 77—36348
surface (100), clean and with adsorbed O, ion bombard., ejected atom energy distrib., classical trajectory calc. 79—100011
surface (100), focusing of Ar^+ ions, incident ion energy effects, E_i=15-35 keV 78—2965
surface (100), influence of coadsorbed O_2 on work function of Cs 79—15014
surface (100), interaction of CO and CO_2, molecular orbital calc. 77—31898
surface (100), linearized secondary-electron cascades, line-shape synthesis 79—74035
surface (100), O and O_2 ejection on ion bombard. 79—42373
surface (100), oxidation electron spectroscopic study 78—64782
surface (100), reaction with ethanol and methanol, EELS study 80—16728
surface (100), self-consistent electronic struct. calcs. 79—1614
surface (100), surface state-surface resonance density 79—28392
surface (100), UPS, two-electron reson. at 3p threshold, rel. to Ni 80—25522
surface (100), with adsorbed CO, Xα-scatt. wave cluster approach 80—49851
surface (100) crystallography, LEED I-V profile anal. 80—75415
surface (110), electroreflectance, surface state contrib. 80—80755
surface (110), $M_{23}VV$, $L_{23}VV$ spectra, cascade background corrections 79—43079
surface (110), O adsorption, low-energy ion bombardment investigation 80—34302
surface (110), oxidation of formaldehyde, temp. programmed desorption meas. 79—87878
surface (111), adsorpt.-desorpt. props. and surface struct. chem. of Cl 77—89648
surface (111), dilution of electron gas in Cs monolayer by O adsorption, plasmon energy losses 79—47036
surface (111), epitaxial growth of Pb and Tl, LEED, RHEED, AES study 78—84090
surface (111), frequency depend. photoelectric surface state cross section periodic oscills., PES study 80—50522
surface (111), interaction kinetics of N_2O using AES, LED and ellipsometry 79—65317
surface (111), interaction kinetics of O_2 using AES, LED and ellipsometry 79—65317
surface (111), interfacial photoemission into electrolyte, 3.4-5.0 eV, vectorial volume effect 77—36375
surface (111), LEED crystallography and reliability indices 80—54081
surface (111), low-energy positron diffr. 80—70511
surface (111), room-temp. oxidation, press. effects 79—79283
surface (111) atomic steps obs. using TEM 77—20173
surface ($\bar{1}$10), adsorption of O_2, low energy Ne^+ ion scatt. meas. 79—51431
surface analyses, quantitative, by collision spectroscopy of backscatt. medium energy ions 77—8704
surface angle resolved photoemission 79—83097
surface barrier influence on C diffusion in stainless steel type 1Kh18N9T *(Russian)* 80—54434
surface channelling of Ar ions, energy depend, 10-35 keV 77—27928
surface cleaning, by electron cyclotron resonance plasma of hydrogen 79—47822
surface cleaning by H^+ bombard., AES study 78—53022
surface coated with C, effect of pulsed thermal heating 80—23146
surface coated with plasma-sprayed TiC, TiB_2 Be and VBe_{12} coatings, fusion reactor appl. 80—18619
surface contaminant anal. by ion-electron spectroscopy 80—54490
surface contamination by H_2, shortening of ultracold neutron storage time 78—17461
surface crater form., by laser pulse, frontal method, approx. soln. 77—77327
surface damage and thermal effects from transient thermonuclear radiation in inertial confinement fusion reactors 79—648
surface dissolution effect on fatigue damage and crack nucleation 78—39936
surface electron states, (111) terrace of stepped (211) face, photoemission meas. 78—84697
surface electronic struct. and UV photoemission 77—62975
surface electronic structure, tight-binding calcs., self consistency effects 77—39909
surface energy band calc., significance for photoemission 78—95330
surface ionisation, elemental anal. of sputtering products *(French)* 80—50905
surface irregularity statistics for laser component materials 79—14057
surface layer hardening by multiple impact 80—108469
surface layer of Ge, heterodiffusion due to H atom surface recombination stimulation *(Russian)* 80—59726
surface melt of spherical crysts., microscopic obs. 78—34599
surface melting on spherically shaped crysts., IR emission obs. 77—20050
surface morphology influence on sputtered yield angular distribution 80—65338
surface phenomena, electron microscopy 80—103556
surface plasma waves 79—47151
surface polariton absorption and emission spectra, edge effects 78—10375
surface pretreatment effect on joint bond strength by cyanoacrylate adhesive Kanokonlit-E *(German)* 79—57202
surface reaction with NO_x, relative humidity depend. 79—5176
surface reflection and penetration of 25 eV to 10 keV He, T and H atoms 77—59657
surface roughness, liq. superheat and heterogeneous nucleation 79—37146
surface scattering elastic, $Na^+(K^+)(Rb^+)$, ang. and energy relationships, 1-3 keV *(Russian)* 79—78802
surface scattering of He from (117) ordered stepped surface 78—15277
surface scattering of low energy He ions from (100) face, neutralisation of ionisation 78—23572
surface semichannelling effects on spatial distrib. of reflected ions, computer simulation 80—35030
surface shot blasting, prep. for plasma deposition 80—16586

copper continued
surface sliding damage, no lubrication, materials depend. *(Japanese)* 78—56780
surface spin-flip probability from TESR 78—91953
surface state band on (111) face, photoemission cross section 77—90252
surface states, (100) and (111), polarisation depend. photoemission 80—100495
surface states, d-band, angle-resolved photoemission spectra obs., Cu (100) and (111) 80—20768
surface states, intrinsic, UV photoemission meas. 77—20983
surface states and surface pot. of (111) face 77—4418
surface structure, (100)/N, LEED, data averaging, objective approach 77—15668
surface structure, (110) ion focusing effect *(Russian)* 78—26757
surface subjected to friction, wear, exoelectron emission, rel. to O_2, H_2O, gaseous adsorpt. 79—1816
surface tension at intermediate and high temps., influence of additional elements 78—15476
surface tension cct. cavities under Cu^+ ion irradiation, O_2 and He effects *(French)* 77—35611
surface topographical features formed by ion bombard., crystallographic depend. 80—70266
surface treatment by the low-energy ions of plasma accelerators 80—97608
surface-grazing scattering, 1 MeV Ar^+ beam, excited-state orientation depend. on scatt. angle 77—61847
surface-water interface, natural boiling site cavities, SEM obs. 77—31763
surfaces, O_2 adsorbed, exam. of structure by LEED, O_2 pressure-temp. diagram *(Japanese)* 78—79884
surfaces, Van der Waals forces computation 79—15204
surfaces, with Langmuir films, surface EM wave absorpt. using CO_2 laser excitation 80—97365
surfaces (001), (110), and (111), ang. resolved Auger emission, model 78—39635
surfaces (100) and (111), angle-resolved photoemission and band struct. 79—95904
surfaces (111), (100), temp. depend. of bulk and surface energy bands using angle-resolved photoemission 79—69572
surfaces and twin faults, electronic states calc. by surface Green's functions 80—39647
suspension, determination of dielectric constant 77—40579
suspension electrolysis 79—61542
swaged, inhomogeneous work hardening *(German)* 80—76267
Swift effect, dynamic and static response to simple compression, tension and torsion 77—28858
Swift effect, in twisted tubes 77—28859
Swift effect, rel. to stress/strain behaviour in simple compression, tension and torsion 77—28860
target X-ray diffr. tubes, K_α charact. radiation rel. intensities calc. 78—4754
tarnishing in humid atmosphere 79—70210
telephone cable conductor, coaxial, resistivity measurements *(French)* 79—69487
tellurite glass, Cu^{2+} and Ni^{2+} doped, band-pass filters for 550 to 616 nm, transmission characts. 78—71166
TEM exam. of ion damage in FCC metals 78—87727
tensile curve and specific value of anisotropy coefficient *(French)* 77—28867
tensile deformed ⟨110⟩ orientated single cryst., recrystn., high voltage electron microscopy study 80—84958
tensile fracture mech. 77—63782
tensile strength, three separate first-principles calcs. 80—50683
tensile tests, −196 to +20°C 79—61692
tension deformed single crystal, dynamic recrystallisation 79—47716
tension-torsion impact testing, instantaneous plastic property 79—52474
tetra-ammine cadmium acetate:Cu, EPR dynamical effects 79—61204
tetramethylammonium manganous chloride:Cu, impure Heisenberg chain paramagnet, EPR sidebands, intensity, linewidths 78—76300
texture after rolling of single crystal at room temp. 77—25067
TGS:Cu, growth from soln., dislocation density 79—52096
TGSe:Cu^{2+}, EPR ang. depend., coord. of Cu^{2+}, Cu-ligand bond obs. and ferroelec. transition anomaly 80—7156
theoretical strength 80—104229
thermal boundary resistance of interfaces with solid ^4He, H_2, D_2 and Ne, 1-3K 77—20178
thermal conductivity, effect of material on working parameters of cryosurgery instruments 78—36037
thermal conductivity, low temp., influence of plastic deform. 78—30899
thermal conductivity maximum, temp. range 4.2 to 70K, plastic deform. influence 78—76049
thermal conductivity under high pressure 78—30901
thermal diffusivity meas. by flash with negative pulse, plasma jet heating 79—37888
thermal disorder, EXAFS determ. 80—45167
thermal displacement of surface atoms, elastic backscatt. of He atomic beam *(French)* 77—4709
thermal emissivities and diffusivities, expt. transient technique and theory for foils 78—43353
thermal expansion, 300-700K, standard material 78—43152
thermal expansion coeff. meas. using [illegible] in gauges and thermocouple 78—53059
thermal expansion meas., 5 to 320K, [illegible]ng dilatometer of parallel-plate capacitor type 77—51523
thermal expansion reference data: 1-1000K 80—96669
thermal expansivity at low temps. measurement using Si cell 80—37027
thermal neutron cross sections, in single crysts. 80—19672
thermal neutron irradiated, isochronal resist. recovery, 30-400K 79—19287
thermal oxidation, influence of ion implantation 78—64768
thermal quenching, by liq. N_2, for boiling curve of N_2 79—14232
thermal resistivity temp. depend., free electron approx., phonon spectrum 77—66152
thermal stress role in dislocation form. during growth from melt 80—6374
thermally stimulated exo-electron emission 80—11547
thermoelectric power at low temps. of pure samples 77—76798
thermomodulation spectra of high-energy interband transitions 80—108226
thermopower temp. depend. 79—65436
thick probes, subthermal neutron transmission curves for grain size and texture eval. *(German)* 80—71667

copper continued
thickness meas. of Au and Ni layers on Cu substrates simultaneously 80—13041
thin conductor, dynamic moduli of elasticity meas. by travelling normal wave method 78—53110
thin film, elec. resist., effect of annealing In electrodes 80—80416
thin film, electromigration, adhesion layer effects 80—96685
thin film, oxidation, RMEED/SEM studies 80—100968
thin film, transport prop. investig. 80—13011
thin film, vac. deposited, Auger spectroscopy 80—2952
thin films, ion plated on polyethersulphone, structural and resistivity study 79—42411
thin interlayer between high-strength alloy rods, tensile strength *(Russian)* 78—19821
thin layers, thickness meas. by proton-induced X-ray emission 80—4690
thin targets, electron transmission below 3 keV *(French)* 80—60725
TMMC:Cu, dynamic props. using local-moment pair correl. functions 80—15728
TMMC:Cu, EPR lines, dynamic effect of low-symmetric spin distrib. 80—39854
TMMC:Cu, EPR linewidth freq. depend., spin dynamics 80—15794
TMMC:Cu, mag. and non-mag. impurity effects on suscept. and Neel temp. 77—66312
TMMC:Cu, random one-dimens. Heisenberg antiferromag., spin fluctuations 79—61140
torsion deformation texture *(French)* 79—70082
total backscatt. coeffs., MeV electrons obliquely incident on target 77—63508
tracer diffusion, atom size effect 78—84005
transgranular cracking in 1M NaNo$_2$ solution 79—100287
tribological investigation using two-cylinder tribometer *(German)* 77—25164
triglycine calcium bromide:Cu^{2+}, ESR studies 80—97136
triglycine sulphate: Cu^{2+}, cryst., struct., hyperfine coupling consts., ^{1}H ENDOR, isotope effects 77—71822
trimethylammonium cobalt trichloride:CU, bound impurity effect, heat capacity meas. 79—61146
tropospheric fallout fluxes in Antarctica and Greenland 79—58007
tube, ambient axial electric field, temp. depend. surface shielding effect 77—58221
tube and plate solar collector geometry optimisation 79—62040
tubes, anisotropic, plastic deformation in hydraulic bulging 79—61688
twist boundary structure, plane translations 79—69113
two photon photoelectric emission, photocurrent vectorial depend. 79—95906
two-photon photoemission near single-photon photoelec. effect threshold 80—89121
type M1, primary recrystallisation kinetics depend. on state of impurities *(Russian)* 79—66069
type MOb, primary recrystallisation kinetics depend. on state of impurities *(Russian)* 79—66069
ultracold neutron scattering, one-phonon process 77—61480
ultrasonic velocity meas., mag. field depend. 78—19104
ultrasonic velocity response to stepwise change of stress *(Japanese)* 79—38905
underpotential deposition, on Pt substrate, XPS 77—59672
unidirectionally solidified morphology of solid liquid interface and solute redistribution *(Japanese)* 77—21133
upper electrode effect on MIM cathode emission 77—85344
UPS, 14-45 eV, density of states function 77—90244
UPS, rel. to band struct. 79—52080
US attenuation, nonlinearity parameter temp. depend. 79—42152
US attenuation by open-orbit electrons, role of deformation potential 79—73428
US fatigue crack propagation obs. 77—40451
US hardening kinetics rel. to dislocations 80—50644
US spot welding of metallic alloy glass 79—21730
US torsional vibrations in metals, measurement of absorpt. 80—58856
US velocity, depend. of applied stress and third order elastic const. *(Japanese)* 79—29124
US velocity, temp. depend., stress effects 80—75307
vacancies, formation entropy, diffusion const. by determinant and Green's function methods 79—77595
vacancies-gas impurity interactions in vacuum condensates *(Russian)* 79—15036
vacancy, lattice vibrs., reson. and localised modes 80—39236
vacancy, mechanical multipole moments determ. 78—55868
vacancy and divacancy diffusion 79—82377
vacancy annealing exam. by positron annihilation 79—14801
vacancy clustering, in e-irradiated Cu by small-angle X-ray scatt. 79—14845
vacancy clusters with He, computer simulation 77—39583
vacancy diffusion along single edge dislocations, computer modelling *(Russian)* 77—47612
vacancy form. enthalpy, positron annihilation meas. 80—97371
vacancy formation and migration, entropy factors 78—75866
vacancy migration energy in FCC lattice by computer simulation 77—11722
vacancy migration near twin boundaries and stacking faults 80—39075
vacancy model, electron statistical, formation energies determ. 77—76390
vacuum coating on steel substrate, influence of precipitation conditions on porosity *(Russian)* 80—54578
vacuum condensate, struct. and mech. props. depend. on depositionconditons 80—15417
vacuum condensate on PET film 77—77385
vacuum deposited epitaxial layer on Fe (001) substrate, orientation relationship 80—65415
vacuum deposited on Al substrate, recrystallisation 78—60044
vacuum gaskets, basic problems 80—47064
vacuum-condensed film, structural changes under glow discharge *(Russian)* 79—15852
valence band Auger spectra 78—76563
valence band splitting, X-ray K-emission spectroscopy 80—40189
valence bands, angle-resolved photoemission meas. using synchrotron radiation 77—24930
vaporisation and condensation coating on Mo and steel, substrate limiting temp. *(Russian)* 80—100787
vaporisation of cone, solution by wave front method 78—5640
vaporization, thermodynamic props. determ. by mass spectroscopy 78—22841

copper continued
vapour, conc. determ. in hollow-cathode discharge from autoionised line intensity *(Russian)* 77—84547
vapour, laser action at 5106 Å and 5782 Å, using copper acetate lasant 78—25854
vapour annular discharge laser, laser powers, device efficiency 80—19043
vapour deposition on polystyrene surface complex, XPS obs. 78—72026
vapour electron energy distrib. function computation 78—71091
vapour impulsive production after discharge current pulses through halide vapour *(Russian)* 79—90492
vapour laser, characts. comparison with 80—102711
vapour laser, discharge-heated high-power high-pressure 79—81453
vapour laser, electron temp. meas. using a microwave radiometer 77—7072
vapour laser, excited in pulsed radially transverse discharge, efficiency 80—14331
vapour laser, gas temp. meas. using Doppler broadening of Ne buffer gas lines 80—19020
vapour laser, induced emission, spectral comp., time evolution 80—74344
vapour laser, non heated, kinetic processes 80—37999
vapour laser, preionisation effect 80—87377
vapour laser, pulse repetition freq. up to 100 kHz 77—669
vapour laser, rate processes, computer simulation 80—69371
vapour laser, unstable resonator oscillator and oscillator-amplifier characts. 80—23720
vapour laser, using CuCl metal source, Cu ground state and metastable level population densities 77—83860
vapour laser assembly 80—9896
vapour laser discharge, power deposited, pump pulse repetition freq. influence 80—74350
vapour laser emission, pulse characteristics rel. to plasma parameters 78—71090
vapour laser excited by single elec. pulse, lasing characts. 80—87386
vapour laser excited by transverse discharge 80—53280
vapour laser output conversion by dye solution to 5782 Å 80—48241
vapour press. above different crystallographic planes *(Russian)* 78—18762
vapour production, in sputtered Cu$_2$O and CuO pulse discharge, laser appl. *(Russian)* 77—84556
vapour production method, hollow cathode arc, Ar buffer gas 78—86981
vapour pulsed laser, spectral comp. of superradiance, stimulated and spontaneous radiation 80—102713
vibratory cavitation tests, gas content and temp. effects 79—61744
vicinal surfaces, LEED study, S, O and Pb adsorption effects 80—103575
viscoplastic constitutive equation, for metal with strain rate history and temp. effects 79—61686
void growth and localisation of shear in plane strain tension 78—64613
voids, neutron radiation induced, in US and in 80US-10UC-10UC$_2$ 79—50951
VPE on W (110), alignment of (111)FCC-(110)BCC epitaxial metal pairs 79—19488
W, wire reinforced Cu 77—70114
wall-stabilised arc conductivities with Cu vapour contamination 78—75458
water:Cu(II) adsorbed on silica surface, EPR spectrum, freezing props. of water 77—4555
water, natural, trace metals, energy dispersive X-ray fluoresc., at absorpt. anals., comparison 77—60175
wear, atmos. press. effect, rel. to fatigue 77—70189
wear, effect of Mn$_5$Si$_3$ content *(Japanese)* 78—35525
wear, recrystallisation as controlling process, FCC metals 77—56117
wear and deform. of surface against conical mild steel rider 78—88542
wear under reversed friction, temp. effect 80—108588
wear volume/sliding time relationship 79—61743
well annealed crystal, etch pit technique refinement, dislocation config. study *(Japanese)* 79—4307
whisker, H$_2$ reduction of CuI, growth mechanism 78—30853
whisker blades, RF size effect, expt. technique and line shapes 79—65511
whisker growth in Zn reduction, morphological change to dendrites 79—28261
whiskers, Ar$^+$ ion implanted, X-ray study on lattice defects *(Japanese)* 79—99230
whiskers, current induced 1/f noise 77—32058
whiskers, hardening during uniaxial extension, preliminary torsion deform. *(Russian)* 78—15420
wick, sintered, effective thermal cond. meas. 78—94582
wire, axial texture after electroplastic drawing, X-ray struct. investigation *(Russian)* 80—104177
wire, drawn through diamond die, deformation zone EMF *(Russian)* 77—81327
wire, ductile fracture in drawing process, defect exam. *(French)* 77—21242
wire, electroplastic drawing X-ray diffr. anal. and mech. props. exam. *(Russian)* 79—29138
wire, exploding, resistance increase phase, elec. characts., applications 77 -55192
wire, exploding underwater in closed chamber, vap. bubbles, air effect *(Japanese)* 78—22596
wire, mech. props. and struct. after high-speed recrystallisation *(Russian)* 79—47704
wire, negative longitudinal magnetoresist. size effect 80—80252
wire, polycryst., internal friction, ultrasonic vibrations effect *(Russian)* 78—76685
wire, recrystallisation *(German)* 77—86055
wire, residual elec. resist., size effect and grain boundary contribs., heat treatment effects *(Russian)* 78—56126
wire, residual resistivity reduction by internal oxidation 79—87747
wire, stranded and solid, rel. stability of thermal EMF in cryogenic environment 78—60111
wire, tough pitch, rel. between oxygen contents and cupping *(Japanese)* 79—79087
wire, tough-pitch, cupping fracture, Cu$_2$O particle size effect 80—66668
wire, transient current pulsed heating, explosive inhomogeneous boiling 78—38562
wire rod, rolling temp. effects 77—70084
wires, effect of heat treatment during drawing 78—56659
wires, electrolytic, Young's modulus, working temp. effects 80—50667
work function, influence of cryst. orientation with and without adsorbed S *(French)* 78—76134

copper continued
work function temp. depend. at low temp. 77—47928
work hardened, meas. of stored energy *(French)* 77—44273
work hardening curves, critical points 79—43263
X-radiation generation via electrons, nonlinear rise and line-narrowing, book contrib. 79—28865
X-ray absorption, discontinuities and limits, chem. combination effects 80—93435
X-ray absorption edge, chem. shift, electron binding energy in compounds 78—62822
X-ray and microhardness meas. at high strain rates *(German)* 78—3184
X-ray attenuation, 5-40 MV, rel. sensitivities of materials for half-value-layer meas. 77—45927
X-ray characteristic absorption, study using diffractometer DRON-2,0 80—20733
X-ray Debye-Waller factors, CGW vs. DAF models 79—37794
X-ray emission spectra, $L_{\rm I}$ and L_η 78—39631
X-ray emission spectra in $PbO-B_2O_3$ glass 77—44089
X-ray fluorescence analysis for Cu content determ. of cuprous ores *(Rumanian)* 77—29508
X-ray K-absorpt. edge shifts, plasmon energies correlation 80—20734
X-ray K-absorpt. edges, plasma oscills. effects 77—59640
X-ray K-absorption discontinuity, extended fine struct. 78—76556
X-ray K-emission satellites, quasi-stationary states and origin 80—80903
X-ray $L_{\alpha 1,2}$ radiation, test of ESCA apparatus used as soft X-ray spectrometer *(French)* 77—13832
X-ray photoelectron spectra ang. depend. *(German)* 78—72679
X-ray photoemission, electron yield, 30-90 keV 77—8726
X-ray resonant Raman scatt. and fluoresc. near K-absorpt. edge 79—52042
X-ray studies of fusion energy neutron damage 78—51593
XPS, angle resolved core level, from (100) crystals 79—33895
XPS, angle-resolved, interpretation 78—72696
XPS, angle-resolved, valence band density of states distrib. 77—44123
XPS, D-orbital directed emission 77—40328
XPS, electron level binding, energy determ., and spectrometer calibration method 77—16458
XPS, single cryst. and polycryst. comparison 77—12493
XPS angular depend. *(Russian)* 79—38722
XPS core line asymmetries in muffin tin approximation 79—69953
XPS escape depths and relative photoionisation cross section for 3p subshell 77—73212
XPS valence-band spectra, angular-depend., meas. 77—21006
yield and flow behaviour, effect of cold drawing under combined stress 80—60912
yield condition for isotropic hardening 79—61653
yield stress decrease in compression, rel. to previous elongation *(Polish)* 80—50665
yield stress of electron irrad. cryst., isochronal annealing effects 79—79037
yield stress variation 78—56652
Young's modulus depend. on temp. and mech. action *(Russian)* 80—92584
Z dependence of thick target β-ray backscattering 80—76118
zero to first sound transition, inelastic neutron scatt. data 77—31738
zero-temperature equation of state, statistical model with density gradient correction 80—15215
zinc bisdiethyldithiocarbamate:Cu^{2+}, exchange interaction of Cu^{2+}-Cu^{2+} pairs, spin-lattice relax. 78—48034
ZnS:Mn,Cu, thin-film phosphors, LV DC electroluminescence 79—11472
μ^+ localisation in Cu, Al and Al-Mn, temp. depend. 80—44993
μ^+ meson spin relax. in cryst. lattices *(Russian)* 79—28664
Ag, Frenkel defect production associated with He and light ion implantation, exam. 78—47443
Ag halide photochromic glass:Cu^{2+}, characterisation of Cu ions 78—5530
Ag halide:Cu^{2+} photochromic glasses, darkening mechanisms, from flash photolysis and EPR studies 77—16156
Ag halides:Cu, in photochromic glass, formation and theoretical models, review 80—43418
Ag vacuum condensates, on Cu substrate, struct. and substruct *(Russian)* 79—73412
Ag-Cu, composite, fibre and layer structs., anomalous props. caused by internal phase boundaries 78—72754
Ag-Cu composite wires, size effect and interface contribution to diamagnetism 77—69490
Ag-Cu couple, grain boundary diffusion of Ag through Cu film, Rutherford backscattering obs. 80—34252
Ag-Cu flex leads, microstruct. study of corrosion 80—76406
Ag-Cu-Ag, layered struct., proton induced X-rays, impurity atom depth determ. 77—11582
AgBr:$Cu^+(Cu^{2+})$, luminesc., ion interactions 77—66534
$AgBr_{1-x}Cl_x$:Cu^{2+}, EPR of $(AgBr_6)^{4-}$, Jahn-Teller effect 79—91294
AgCl:$Cu^+(Cu^{2+})$, luminesc., ion interactions 77—66534
AgCuAg sandwich target, proton induced K-shell X-ray yield ratios 77—48724
β-AgI:Cu, pure and doped, photoconductivity, band struct., trap nature 79—95449
Al alloy A3B2, stress depend. of US velocity *(Japanese)* 78—26629
Al:Cu, CESR, effect of ion implantation 77—20701
Al/Cu laminates, vapour deposited, strength enhancement 79—24576
Al/Cu thin film couples, TEM study of intermetallic nucleation at interface 80—65305
Al-Cu, thin-layered laminates, yield strength rel. to dislocation generation and motion 79—20137
Al-Cu thin film couple, interdiffusion, AES obs. 80—6569
Al-Ox-Ag-Cu-Pb and Al-Ox-Cu-Ag-Pb trilayer junctions, tunnelling characts. 79—87208
$Al_2Be_3Si_6O_{18}$:Cu^{2+}, synthetic beryl, ESR, optical spectra and X-ray diffr. meas. 77—16166
$Al_xGa_{1-x}As$:Cu, LPE film, impurity levels, elec. and optical props. meas. 78—26862
$Al_xGa_{1-x}As$:Cu, variable-gap semicond., impurity props., carrier recomb. 80—96907
β-Al_2O_3-Ag_2O:Cu^{2+}, EPR of Cu^{2+} ions in conduction plane 77—69678
Al_2O_3-Cu composite, dispersion-strengthened, hardness, tensile strength and struct. 77—70063
Al_2O_3-Cu composite, vapour deposition, microstruct., texture and surface topography 77—70001
β-Al_2O_3-Na_2O:Cu^{2+}, EPR of Cu^{2+} ions in conduction plane 77—69678
β-Al_2O_3-Tl_2O:Cu^{2+}, EPR of Cu^{2+} ions in conduction plane 77—69678

copper continued
β-$Al_2O_3.Na_2O$:Cu, EPR, localisation of Cu^{2+} and linewidth effect 78—39395
Ar bubbles injected into Sn, Pb and Cu melts, under laminar flow, characts. 78—38394
Ar-Cu, Cu diffusion coeff. determ. volatile salt dissoc. in pulsed discharge 80—33721
$Ar+Cu^{x+}(11\leq x\leq 22)$, 1 MeV/amu, X-ray production cross-sections 78—37714
As_2S_3, vitreous, Ag, Cu, Sn and Ge impurities effect on electrophys. props. 77—76826
As_2Se_3, glassy, Cu, Ag and O impurities influence on electronic energy spectrum and mol. vibr. spectrum 77—90181
As_2Se_3:X (X=Cu, Ag, Tl, I, Ge), effect of doping, NMR meas. 80—11282
As_2Se_3+Cu, amorphous, diffusion, electrodiffusion profile determ., migrating impurities charge determ. 78—6185
As_3Se_3:Cu, glassy, broadening of electrodiffusion profiles at high elec. fields 79—55939
Au/Cu, double layer film, oxidation *(Japanese)* 80—61010
BaS:Cu, thermoluminesc. and decay 78—80426
BaS:Cu phosphor, photo- and electro-luminescence 79—43030
BaS-CaS:Cu phosphors, X-ray diffr. and fluoresc. spectra 80—40148
$BaTiO_3$:Cu, Γ_{15} phonon freezing, electronic instability, LCAO calc. 80—25318
$BaTiO_3$:Cu, photoferroelec. props., Jahn-Teller effect, laser irrad. effect on pyroelec. props. 78—60400
Bi_2Te_3-Sb_2Te_3:Cu, electrical cond. and thermopower, disorder effects *(German)* 77—1422
C content determ., isotope-spectral method *(Russian)* 80—55766
C fibre reinforced, thermal cond., temp. depend., 80 to 350K 77—24452
C fibre reinforced, thermal expansion and thermal fatigue *(Russian)* 79—38936
C fibre reinforced Cu, electrodeposited, tensile strength *(Japanese)* 79—43333
C fibre reinforced Cu, mech. props. *(Japanese)* 77—63723
C fibre reinforced Cu, specific elec. resistivity, 77 to 550K *(Russian)* 77—72895
C fibre reinforced Cu composite, fatigue strength under constant strain *(Russian)* 78—95796
CaO:Cu, thermoluminesc. following UV excitation, 290-500K 77—40292
$Ca(OD)_2$:Cu^{2+}, ESR, secondary spectra 78—88174
$Ca_3(PO_4)_2$:Cu^{2+}, ESR, high press. struct. transition 80—97134
CaS:Cu, colour centres, optical and thermal depths determ. 80—66275
CaS:Cu, colour centres and photoluminesc., flash stimulation bands *(Russian)* 77—20923
CaS:Nd, Cu, phosphor, electroluminesc., spectral characts. 79—19936
Cd complex, dichlorobis (pyrazole) cadmium:Cu(II), ESR, compressed tetragonal symmetry 78—6568
Cd-Cu-Se, phase diag. 77—52303
$CdBr_2$:Cu^+, polarised absorption spectra 77—59594
$CdCl_2$:Cu, optical props. 78—43918
$CdCl_2$:Cu^+, polarised absorption spectra 77—59594
$CdCl_2$:Cu^{2+}, meas. of covalency in tetragonal complexes 77—47781
$CdCr_2S_4$:Cu, magnetic microregions caused by s-d exchange 77—77050
$CdCr_2S_4$:Cu magnetic semiconductor growth, structural defects, physical properties 80—60759
$CdCr_2Se_4$:Cu, elec. props., temp. depend. *(Russian)* 78—72181
$CdCr_2Se_4$:Cu, ferromag. reson. and ESR line widths 80—60413
$CdCr_2Se_4$:Cu, mag. props., near Curie temp. *(Russian)* 77—63234
CdF_2:Cu, paramagnetic centre coordination, g-tensor orientation by anisotropy of ^{19}F ENDOR 80—54993
$Cd_{1-x}Fe_xCr_2S_4$:Cu, effect of doping on elec. props. and Curie temp. 78—84214
$Cd(NH_3)_4Cl_2$:Cu, EPR dynamical effects 79—61204
CdP_2:Cu, photoluminescence and photocond. characts., interimpurity recomb. of carriers 77—8637
Cd_3P_2:Cu, zero field Seebeck coeff. meas. 77—15883
CdS with Cu traces, γ-radiation dosimeter, prod. and characts. 78—8999
CdS:Cd, Cu, single crysts., IR restoration after optical degradation of photosensitivity 79—60867
CdS:Cd,Cu crystal, formation and bleaching of optically-induced absorption bands 78—31221
CdS:Cd(In), Cu- or defect-compensated, optical ageing rel. to storage cond. 78—84247
CdS:Cl, $Cu^+(Cu^{2+})$, photoconductive sensitivity 77—43648
CdS:Cu, Auger excitation mech. of 1.6-2.0 micron luminesc. band 79—8184
CdS:Cu, C-V curves of MIS diode used to examine trapping levels 80—65697
CdS:Cu, Cd, data storage, optical and photoelec. reading 78—1193
CdS:Cu, charge and transport mechanism of impurities, electrodiffusion doping 80—59725
CdS:Cu, Cl films, photocond. growth and decay time 80—60041
CdS:Cu, diffusion doping, photolum. 79—91493
CdS:Cu, electrodiffusion of shallow donors, photocurrent, TSC, and exciton luminesc. meas. 80—79992
CdS:Cu, fast electron irradiated, isochronous annealing of IR photocond. quenching spectra 77—1450
CdS:Cu, Fermi level position, luminesc., and photosensitivity, electron irrad. effects *(Russian)* 78—14652
CdS:Cu, heavily doped, defect struct. 78—22756
CdS:Cu, IR photolum. at 10K 79—28824
CdS:Cu, In, Ga, spray deposited film, struct., X-ray obs. 78—71713
CdS:Cu, photocond. under high excitation intensity 78—52033
CdS:Cu, photocurrent, elec. field effect on recombination processes *(Russian)* 80—100484
CdS:Cu, photosensitivity degradation mechanism 80—107851
CdS:Cu, recording holographic medium, exposure characts. *(Russian)* 77—635
n-CdS:Cu, Si, photocond., carrier lifetime, X-ray effects 77—59300
CdS:Cu, spectral sensitisation by cyanine dyes 78—64064
CdS:Cu, thin layer, electron pulse induced cond. relax. 80—2501
CdS:Cu, two-photon absorpt., impurity effects 77—16353
CdS:Cu, US absorpt. in heavily doped piezoelec. semicond. 79—11189
CdS:Cu,Cl, film, photocond., applied voltage freq. effect on props. 80—39635
CdS:Cu,Cl film, photocond., use in laser-addressed electrolum. display screen 77 51777
CdS:Cu,Pb reflectivity of Ni-salt coated powder, pre-irrad. effect on defect form. 79—27973

copper continued
- CdS:Cu binder layer, photoactive, AC impedance meas. 80—25299
- CdS:Cu film, dynamic quenching of photocapacitance, deep levels obs. 77—85175
- CdS:Cu films IR quenching of photocapacitance, deep level detection 79—56258
- CdS:Cu sintered layers, relaxation photocurrent kinetics *(Russian)* 80—107852
- CdS:Cu thin films, surface and bulk photoconc. 80—88653
- $CdS:CuCl_2$, sintered film, dopant conc. effects on carrier mobility 78—2484
- $CdS_{1-x}Se_x$-Cu, electrophotographic props. 77—45910
- CdSe:Cd, Cu, photo-induced changes in absorpt. spectra 78—80382
- CdSe:Cu, diffused in Se atm., photocond. props. 79—99580
- CdSe:Cu, doping profile rel. to photoelec. props. in alloyed surface layers *(Russian)* 77—85268
- CdSe:Cu, impurity photocurrent, kinetics and oscills. 80—65624
- CdSe:Cu,Cl film, induced impurity photocond., 0.6 to 1.2 eV 79—24012
- CdSe:Cu surface layer of CdSe, microstruct., photoelec. props. 78—43221
- $CdSnP_2$:Cu, deep centres, emission transitions, polarisation *(Russian)* 78—84650
- n-$CdSnP_2$:Cu, Hall mobility of electrons meas., 120-300K 77—4373
- CdTe:Cu, diffusion of Cu at 250 to 500°C, interstitial process 77—11737
- CdTe:Cu, doping effects on evaporation kinetics and electronic props. during high-temp. annealing in vacuum 78—22743
- CdTe:Cu films, impurity behaviour, Hall mobility and hole density meas. 80—80420
- $CdTl_2Se_4$:Cu, doping effect on surface tension of melt and cryst. microhardness 80—49464
- Cl^{n+} + Cu, effect on projectile charact. X-rays and REC of target thickness 79—45662
- Cl^{n+} + Cu film on C foil, X-ray production, radiative electron capture 77—19063
- Co-Cu interface, Co fine particles in Cu, interface magnetisation 80—88858
- Cr/Cu/Cr layer composite, influence of phase boundary on flow stress 78—60717
- Cr-Cu bilayer system, optical mechanical and corrosion properties 77—32707
- CsBr:Cu, polarisation study of tetragonal Cu^{2+} aggregate centres 78—39590
- $CsBr:Cu^-$, excitation and absorpt. spectra 80—108255
- $CsBr:Cu^+$, X-ray irrad., thermoluminesc. 80—16107
- $CsBr:Cu^+$ off-centre, optical absorpt. meas. 79—33740
- $CsBr(Cl):Cu^+$, γ-irradiated, thermolum. emission 80—104001
- $CsCl:Cu^+$, X-ray irrad., thermoluminesc. 80—16107
- $CsI:Cu^{2+}$, cryst., influence of impurities on yield stress 79—15748
- $CsMnCl_3.2H_2O$:Cu, parallel susceptibility, impurity effect on spin-flop field *(French)* 78—43569
- $CsMnCl_3.2H_2O$:Cu, mag. impurity effect on Neel temp. and spin-flop field 79—61099
- $Cs_2ZnCl_4:Cu^{2+}$, single cryst. and powdered single cryst., EPR, linear elec. field effect 80—11250
- $Cs_2ZnCl_4:Cu^{2+}$ electron spin echo envelope, Fourier transform ^{133}Cs modulation 80—58291
- Cu (111), hydroxylation and dehydroxylation, XPS obs. 80—7850
- Cu (111)/Cs, adsorption-induced changes of photoemission spectra and surface electronic struct. 80—55260
- Cu (111)/Na interface, UPS study of surface electronic struct. 80—80350
- Cu complex, with acetylene, Ar matrix-isolated EPR obs., bonding 78—50564
- Cu, conduction electron g-factor, Fermi surface 78—23011
- Cu corrosion, by COS, kinetic and morphological study *(French)* 79—43488
- Cu Cu^{2+} doped Cd complexes, ESR study 80—108059
- Cu, dendrites electrodeposited, growth kinetics, cathode surface effects 79—70007
- Cu, electrolytic, particle profiles, morphological characterisation derived from Walsh coeffs. 80—50816
- Cu, electrolytic epitaxial nucleation and growth, on (111) Ag 80—104081
- Cu, electrolytic powder, sintering, gas effects, finite size bodies 77—77447
- Cu, electronic and mag. structure calcs. of mag. impurities 80—80213
- Cu, fatigued single crysts., temp. depend. of saturation stress and dislocation substruct. 80—44211
- Cu film, effect of thermal strain on orientation 80—49294
- Cu film, stability and rupture using perturbation analysis 78—79911
- Cu I, high-dispersion absorpt. spectrum obs. 1570 to 2500 Å 80—78564
- Cu I, radiative lifetime meas. 79—3409
- Cu I isoelectric sequence, fine struct. separations for reson. transitions 78—17588
- Cu I lines, superradiance obs. in pulse vaporisation of pulverised Cu_2O, CuO 79—45934
- Cu I relaxation processes in Cu halide pulsed discharge lasers 78—25865
- Cu II, 1 W continuous output from 780.8 nm transition 78—82953
- Cu II, determ. by ion selective electrode, ligand interference preventive buffer appls. 78—20099
- Cu II, laser construction and performance, novel hollow cathode discharge structs. 80—38000
- Cu II, VUV wavelength comparison using imaging system 79—35686
- Cu II laser, CW, hollow anode-cathode discharge 78—17963
- Cu II laser, UV, operating period extension by Ar admixture 80—74342
- Cu II laser with cylindrical hollow cathodes, UV performance 80—102709
- Cu II spectral lines, vacuum UV wavelength standards 77—82619
- Cu III, calc. of configurations, CI effects 77—42228
- Cu IV, wavelength region 700-1200 Å, extended analysis 80—99473
- Cu ingots, solidification, quality and optimal modes of solidification, prediction from temp. fields 79—83187
- Cu, ion irrad., tertiary effects in pyramid form. 80—2090
- Cu, Johnson noise, rel. to absolute temp. 77—47872
- Cu liquid/liquid CuS, miscibility gap *(German)* 80—49370
- Cu plates, gap magnitude effect on their thermal interaction at cryogenic temps. 79—86323
- Cu polycrystal, fatigued, interior dislocation struct. 80—88147
- Cu, positive muon spin rotation meas. 78—10819
- ε-Cu precipitates, effect of H discharging phenomena in steels *(Japanese)* 80—7583

copper continued
- Cu, pure and Ge doped, vacancy formation energy 79—51464
- Cu sequence, ^2S-^2P transitions, oscill. strengths calc. 77—50406
- Cu single crystals, [100]- and [111], dislocation density meas. using TEM 80—79803
- Cu single crystals, dispersion strengthened, low temp. recovery of work-hardening and creep 79—83211
- Cu, single crysts., cyclically and unidirectionally deform. X-ray diffr. study 80—89319
- Cu, single crysts., deformed and annealed, neutron small angle scattering 79—82127
- Cu spheres, on Cu single cryst. surface, grain boundary energy anisotropy using gravitational torques 79—60385
- Cu, stress strain anal. of single crystal induced by absorbed H_2 *(Japanese)* 78—11276
- Cu, surface d-band narrowing, angle resolved XPS 78—19635
- Cu, ultra-microhardness testing for vacuum deposited film and bulk specimen 78—79910
- Cu V, spectra, config. levels 77—18820
- Cu vapour 78—46584
- Cu whiskers, Bragg case diffr. curves by X-ray triple cryst. diffr. method 79—51461
- Cu, with Al_2O_3 inclusions, breakdown and emission props., effect of inclusions 79—87389
- Cu XXI, 2p-4d and 2p-4s transition arrays, wavelengths and oscillator strengths 80—47933
- Cu XXI, spectra and energy levels of F isoelectronic series 79—93948
- Cu XXII, X-ray spectra in laser plasma, $2p^6\ {}^1S_0 \rightarrow 2s2p^5\ {}^1P_1$ 79—1340
- Cu XXVIII ion effects impeding obs. of parity nonconservation *(Russian)* 77—75078
- Cu^+, approximate relativistic Hartree-Fock eqns., soln. using Slater-type functions 80—58168
- Cu^+ formation during contact of Cu with Cu^{2+} aq. soln., rot. disk-ring electrode mechanism 79—61872
- Cu^+, generation by laser ionis. source for ICR spectroscopy, chem. appls. 80—45597
- Cu^+, Hartree-Fock calcs., exchange pot. simplification 77—75054
- Cu^+ hollow-cathode laser, IR output depend. on He-Ar press. ratio 80—48223
- Cu^+, in LiCl-KCl fused eutectic, diffusion and surface effects, chronopotentiometry *(French)* 78—11524
- Cu^+, reson. transition, effect of correl. in $3d^n$ core, HF calcs. 80—47911
- Cu^+ transitions in He-Cu halide gas discharges, CW laser oscill. 79—7116
- Cu^{18+}, $3^2P_{1/2}$ level decay, time-resolved obs., intensity modulations 77—61704
- Cu^{18+}, Na-like, low-lying levels, radiative lifetimes, f-values obs. 78—25482
- Cu^{2+} adsorption on SiO_2, zeolite surface bonding, EPR, optical spectroscopy investig. *(German)* 79—95266
- Cu^{2+}, complex formation with carboxylic acids in aqueous soln., thermodynamic parameters *(Italian)* 77—48669
- Cu^{2+} containing Ag halide photochromic glasses, optical props. 80—93364
- Cu^{2+}, dopant, ground state wavefunctions and Δg 78—64012
- Cu^{2+} effect on DNA helix-ball transition 79—70514
- Cu^{2+}, fluoresc. quenching of 1-methylpyrene in micellar system, general kinetic model 80—32753
- Cu^{2+}, g-anisotropy and ground state wave functions in crysts. *(German)* 78—23065
- Cu^{2+}, impurity ion in frozen aq. solns., effect on Fe^{3+} spin-spin relax., Mossbauer obs. 79—33573
- Cu^{2+}, in Zn (II) complex, ground state ion wavefunction calcs. 78—895
- Cu^{2+} ion, ground state wavefunctions and ESR parameters 80—88868
- Cu^{2+} ions, ground state wave functions, cryst. field effect, ESR data anal. 78—23060
- Cu^{2+} ions, influence on I^R spectra of H_2O 78—72501
- Cu^{2+}, removal using Itaya-zeolite *(Japanese)* 78—95951
- Cu:$^{69}Ge(^{67}Zn)$, nucl. alignment temp. depend. rel. to radiation damage during PAC obs. 77—27919
- Cu:^{85}Kr 80—15145
- Cu:Au:C, surface, obs. at very low accel. voltage (200 V-1 kV) by SEM 80—10764
- Cu:B, two site occupation by implanted ^{12}B 78—6077
- Cu:Be, alloy formation kinetics at solid cathodes, metal electrodeposition from molten salt electrolytes 80—26028
- Cu:Co precipitates, mag. anisotropy, precipitate shape, coercive force 80—80500
- Cu:Cr(Mn)(Fe), NMR satellite data rel. to impurity struct. 78—35052
- $Cu:Du^{3+}$, EPR, g-factor, hyperfine struct. 77—48046
- Cu:H, interaction of H and vacancies, positron annihilation, Doppler broadening 78—80434
- Cu:He, doubly peaked He depth profile and blistering 78—10078
- Cu:In, He, lattice defect struct., PAC meas. 80—70190
- $Cu:\mu^+$, lattice distortions, microscopic calc. 78—87665
- Cu:Ni, Dingle temps. calcs., tetrahedron method 80—6699
- Cu:O channelling, analytical model and computer simulation calcs. 79—1450
- Cu:O single crystal, $^{18}O^+$ ion implantation in channelling directions, expt. conditions and range profile obs. 80—65022
- Cu:O single crystal, $^{18}O^+$ ions implantation in channelling directions, stopping power meas. from max. range 80—65078
- Cu/Ag (111), metastable 2D condensations, epitaxy, growth modes, exp. techniques, book contrib. 80—49558
- Cu/Al bimetal film, structure, macroscopic defects *(Russian)* 79—1555
- Cu/Al film system, interdiffusion and phase growth kinetics 77—69122
- Cu/Al thin film couples, interfacial reactions, low temp. contact resist. meas. 80—44709
- Cu/Au, bilayers, interdiffusion phenomena, lattice dislocations, TEM obs. 80—59736
- Cu/Au, initial epitaxial growth at room temp. 80—59829
- Cu/Au + 0.03 at.% Fe, thermocouple characteristics, in mag. field at low temps. *(Russian)* 78—54365
- Cu/Cr-Ni-steel fibres, primary creep *(German)* 80—11734
- Cu/Cu_2O, relative chemical potential of oxygen *(German)* 78—31642
- Cu/CuCl double pulse laser, continuous glow discharge appl. 80—1190
- Cu/CuCl double pulse laser, pumping pulse and output pulse characts. 80—87380
- Cu/CuCl double pulse laser, dissoc. pulse, afterglow, and laser pulse model 80—91775

copper continued
Cu/CuCl double pulsed laser, extrema by electron density and output pulse energy 79−10283
$Cu/CuGaSe_2$ Schottky-barrier cells, photovoltaic effect 79−96440
Cu/graphite-SbF_5 wire composites, synthesis and elec. props. 80−70781
Cu/Nb layered ultrathin coherent struct. 80−80122
Cu/Ni coherent modulated structures, electronic struct. and magnetism 80−103620
Cu/Ni double layer evaporated film, misfit dislocation effect on strength *(Japanese)* 79−42425
Cu/Ni film counter, surface counting method for diffusion study 79−42321
Cu/Ni interface, diffr. studies of conc. variations 79−42322
Cu/Ni multilayer films, electron beam induced diffusion during AES depth profiling 80−19993
Cu/SbF_5 intercalated graphite/Cu composite wires, elec. cond. 80−44687
Cu/Sn (Pb)(W) interface, thermal conductance at low temps. 80−49436
Cu/Sn-Ni/Au tricouples, electrodeposited, interdiffusion obs. 80−84331
Cu/Zn galvanic couple, potential distrib. meas. technique, appl. to corrosion study, apparatus *(Japanese)* 78−53049
Cu-Ag interface, interdiffusion, X-ray and electron microprobe data 77−4225
Cu-Al composites, laminar, polycryst., electron diffr. proportional anal. 77−44444
Cu-Al thin film multistructure, Xe^+ ion beam cratering 80−66708
Cu-Al_2O_3, composite coatings, prep. by precip., props. 78−23841
Cu-Al_2O_3 cermet film, solar absorbing, production by dual cathode DC magnetron sputtering 80−16186
Cu-Al_2O_3 cermet films, temp. depend. of AC and DC cond. 79−87166
Cu-Al_2O_3 composite coating, codeposition kinetics from $CuSO_4$ plating bath 78−15555
Cu-Al_2O_3 composite coating, electrodeposited, exam. of particle-cathode adhesion during formation 79−33954
Cu-Al_2O_3 dispersed composite, electron beam deposition, struct. characterisation 77−44197
Cu-Al_2O_3 dispersed system, electron beam evaporated thick film, struct./prop. relations 77−44198
Cu-Al_2O_3 dispersion hardened wires, drawn, substruct. and strength 78−35405
Cu-Al_2O_3 electrodeposits, dispersion hardened, props. 79−28258
Cu-Al_2O_3 thin film ceramets, TEM study of composition and struct. 79−99437
Cu-Al_2O_3(Al_2O_3-MgO) cermet selective surfaces for evacuated solar collectors 79−43785
Cu-Au thin film system, interdiffusion coeff. from cond. and Auger anal., 25 to 250°C 77−59154
Cu-Au thin films after accelerated ageing, failure by Kirkendall porosity 80−6675
Cu-Au-Cu, thin films, sandwich struct., bombarded by 3-15 keV Ar^+ at angle of incidence of 30°, sputtering yield coeff. 79−65968
Cu-Be-O surface, $O(^5S)$ impact, secondary electron yield 78−58797
Cu-Cd electrodeposit on Cu, corrosion and its inhibition 79−74287
Cu-CdS, Schottky barrier, Cu diffusion and photovolt. mechanism 80−6980
Cu-$CdSiP_2$ surface-barrier diode, photoelec. props. 77−4442
Cu-Constantan junction, elec. response to shock compression 79−95470
Cu-Cu_2O diode junction, Schottky barrier, electronic struct. and minority carrier diffusion length *(French)* 80−65682
Cu-Cu_xO film, numerical anal. of normal reflect. data 79−99457
Cu-dimethyl terephthalate contacts, effect of elec. field on contact electrification 79−19660
Cu-epoxy-Cu sandwich, thermal boundary resist., 0.05-10K 78−14564
Cu-Fe, composite, fibre and layer structs., anomalous props. caused by internal phase boundaries 78−72754
Cu-Fe, interface, ferromagnetic and cond. spin reson. mode coupling 79−78521
Cu-$Fe_{78}Mo_2B_{20}$ wire composite, mech. props. 80−40441
Cu-ferrous alloy, hard inclusion composite exam. of wear resistance props. 79−34153
Cu-Gd_2O_3, high sp. ht. metal for supercond. composite 77−40404
Cu-Ge, amorphous, junction, current-voltage charact. 80−44725
Cu-Ge Schottky barrier photodetectors, near IR interband transitions and optical parameters 80−73449
Cu-GeO_2/BaO-Cu thin film, amorphous, effect of electroforming on conductance and capacitance 80−34537
Cu-graphite starter brushes, effect of high velocities, current densities on wear, friction 78−88544
Cu-H system, de Haas-van Alphen Dingle temps. for scatt. of cond. electrons determ. 77−76731
Cu-H_3PO_4 system, instability and oscillations *(French)* 78−64850
Cu-He, discharges, new ion laser transitions in near IR region, CW excitation 79−59673
Cu-In solid/liquid interface, laws governing diffusive interaction *(Russian)* 78−95156
Cu-KELEX 100 (alkyl β-hydroxy quinoline), distribution coeffs., model 78−53244
Cu-LIX 65N (β-hydroxy benzophenone oxime) distribution coeffs., model 78−53244
Cu-like ions, 4s-4p reson. lines and transitions obs. by means of laser prod. plasma, appl. to Tokamaks 80−99468
Cu-like ions, E1 transitions, wavelengths, oscillator strengths and transition probabilities, data tables 80−37780
Cu-liquid ^4He interface, macroscopic calc. of Kapitza resistance 77−11754
Cu-metal thin film couples, room temperature interactions 80−96699
Cu-Mg catalyst, cyclohexanol dehydrogenation, kinetic model depend. of reaction rate 77−90583
Cu-mild steel explosively welded interface, SEM examination *(German, English)* 80−96746
Cu-N mixture, partially ionised, transport and thermodynamic props. 77−80276
Cu-N_2, effect of Cu vapour on wall stabilised arc extinguishing times 78−87548
Cu-n-Si diodes, fabrication by electroless deposition method, characts. 80−100520
Cu-Nb multifilamentary composite, in situ formed, high temp. tensile strength 79−61602
Cu-Nb_3Sn, in situ formed multifilamentary composite, supercond. and mech. props. 78−39279

copper continued
Cu-Nb_3Sn multifilamentary tapes, in situ formed, crit. current density anisotropy 80−84576
Cu-Nb_3Sn superconducting composite, electron beam co-evaporated, TEM study 79−28247
Cu-Nb_3Sn superconducting composite, crit. props., AC hysteretic losses 80−50014
Cu-NbTi, composite conductor, acoustic emission 80−97032
Cu-Ne, hollow cathode laser discharge, spectroscopic temp. meas. 79−7490
Cu-Ne CW mW-level laser source at 250 nm 80−43352
Cu-Ne laser, spectral lines emission of gas-discharge pulse plasma 79−31883
Cu-Ne mixture, 3-20 kHz pulse discharge obs. 78−71092
Cu-Ni, bimetallic film, exam. of diffusion by electrical resistivity meas. *(Russian)* 79−14970
Cu-Ni, interface, ferromagnetic and cond. spin reson. mode coupling 79−78521
Cu-Ni bicrystal, misfit dislocation config., moire patterns, interdiffusion effects 78−84110
Cu-Ni bicrystals, epitaxial growth, chemical interdiffusion, X-ray diffr. line profile anal. 79−1527
Cu-Ni bilayer system, optical mechanical and corrosion props. 77−32707
Cu-Ni bimetallic film, Moire patterns, interdiffusion effects 77−51621
Cu-Ni bimetallic films, dislocation wall form. during interdiffusion, TEM obs. 78−51856
Cu-Ni bimetallic thin film, effect of microstructre on interdiffusion 79−77840
Cu-Ni evaporated thin film couple interdiffusion obs. 78−43187
Cu-Ni film system, time depend. diffusion coeffs., grain boundary and dislocation effects 77−80656
Cu-Ni interface, diffusion coeff., using method of nets 78−22903
Cu-Ni system, X-ray diffr. line broadening from small subgrains containing gradients of spacing 78−67612
Cu-Ni thin film couples, interfacial reactions, contact resistance meas. 78−63882
Cu-Ni thin thin film couples, polycryst., interdiffusion singularities, Frenkel and Kirkendall effects *(Russian)* 77−24447
Cu-Ni-CuCl-KCl/NaCl system, isothermal chem. metal transport *(German)* 77−63569
Cu-O single crystals, solid solution hardening, Cu crystal dislocations interaction with O atoms 79−52225
Cu-Pb proximity sandwiches, tunnelling expt., barrier transmission effects 80−50002
Cu-Pb thin film couple, interdiffusion and recrystallisation, grain size effects 77−76625
Cu-PbI_2, thin sprayed layer, glass substrate, hologram recording *(Russian)* 77−71956
Cu-PbI_2 photosystems, null-refl., cermet and Fabry-Perot types 78−46738
Cu-Permalloy, interafce, ferromagnetic and cond. spin reson. mode coupling 79−78521
Cu-Permalloy two-layer films, mag. anisotropy, grain boundary diffusion *(Russian)* 80−71122
Cu-phthalocyanine, photoemission multielectron effects from quasi atomic Cu 80−93458
Cu-Plexiglas double layer barrier, deform. of electron spectra *(Russian)* 78−84292
Cu-plexiglass (steel) channel with parallel flat walls, ice growth in laminar flow 79−3908
Cu-rare earth oxide-Y composite coatings, oxide and Y effect on coating precipitation 80−55554
Cu-sapphire interface, effect on shear strength of adsorbed species 80−49485
Cu-SiO/B_2O_3-Cu thin film, amorphous, conductance and capacitance, effect of electroforming 80−34537
Cu-SiO_2, low-temp. recovery creep, Orowan loop accumulation 80−81126
Cu-SiO_2 (0.0052 vol. fraction), work hardened, low temp. softening, particle size effects 77−52342
Cu-SiO_2 codeposited film, optical, elec., mechanical and corrosion props. 77−32708
Cu-SiO_2 single crystals, dispersion hardened, exam. of yield stress between 77 to 1200K 78−76720
Cu-steel and Cu-brass system, realisation of selective transport mode with friction, effects of normal stresses 79−87735
Cu-V_3Ga composites, supercond. props. 79−95557
Cu-W composite powder, prod. by H_2 reduction of $CuWO_4$ 79−20006
Cu-Xe film, metal-nonmetal transition, optical and resist. meas. 77−89818
Cu-Zn bilayer system, optical mechanical and corrosion properties 77−32707
Cu-Zn heterocontacts, microcontact spectra *(Russian)* 80−34502
Cu-Zn multilayer condensate, diffusion process, brass formation 78−43186
Cu^{2+}-1,5-dimethyl-2,4-hexadiene, fluoresc. quenching method for determ. binding const. 80−89530
$Cu+{}_5^{10}B^{n+}$, 4-38 MeV, K-shell ionis., X-ray obs. 79−59549
$Cu+{}^{28}Si^{n+}$, K-shell ionisation, projectile charge state depend., theory 78−17786
$Cu+C^{n+}$, radiative electron capture, target electron momentum distrib. 78−1075
$Cu+Cl_2(Br_2)(I_2)$, beam-gas chemiluminesc. reactions 80−85151
$Cu+Cl^{q+}$, K X-ray production and radiative electron capture, fluoresc. yield determ. 80−99553
$Cu+Cl^{q+}$, X-ray cross sections, projectile fluoresc. yields 78−74751
Cu+Cu collisions, Kα X-ray energy shifts, target thickness depend. 80−83311
$Cu+F_2$, chemiluminesc. reactions, mol. beam study 80−97702
$Cu+H^+$, 4 MeV beam-foil X-ray production cross-section 79−7003
$Cu+H^+$, atomic K-shell ionis., X-ray emission 79−18280
$Cu+H^+$, Cu K-shell ionis., probability ang. depend. 77−14553
$Cu+H^+$, K-shell ionis., Coulomb deflection effects, 0.5-2 MeV 78−17779
$Cu+H^+$, K-shell ionisation cross-sections calcs. 80−43165
$Cu+H^+$, K-shell ionisation cross-section determ. 80−48077
$Cu+H^+$, K-shell ionisation 0.5 to 40 MeV, meas. and PWBA-BEA calcs. 80−78699
$Cu+H^+$, X-ray emission, optical transition radn. 78−58618
$Cu+H^+$(He ions), K-shell ionisation cross-section, 85 to 790 keV 80−106390

copper continued
- Cu+N_2, preferential energy transfer from N_2 to specific Cu energy levels 80—43152
- Cu+N^+, X-ray production cross section, $K\beta/K\alpha$ ratio, 0.5-2.5 MeV/amu 77—54526
- Cu+Ni foil target, 50-65.5 MeV, K-vacancy production, impact parameter depend. 79—54958
- Cu+oxidant, chemiluminescence spectra and photon yields, population inversion 79—79255
- Cu+$Si^{n+}(Al^{n+})(Cl^{n+})(Ar^{n+})$, K-shell vacancy sharing ratio 78—42198
- Cu+X^{n+}, X=F, Al, Si, S, K X-ray production, target thickness depend. 77—75280
- Cu^{q+}+Kr, K-vacancy production, impact parameter depend. 79—72390
- Cu_2 contracted Gaussian-type orbital basis sets, test with and without outer orbital splitting 80—47872
- Cu_2, fluoresc., A-X system, rot. consts. *(French)* 78—33544
- Cu_2, Harris-Pohl selected valence electron split-shell MO calcs. 80—91439
- Cu_2, in supersonic free jet expansion, laser induced excitation spectrum obs. 80—14151
- Cu_4 clusters, electronic structures, SCF-Xα-SW method 80—88468
- Cu_n, cluster formation, by ion bombardment of single cryst. surface 78—92157
- Cu_n^+ ion cluster yield intensity from Cu target bombard. by H^+, Ne^+, Xe^+, Kr^+ 80—100728
- $CuCl_xBr_{1-x}$, binary melt, Cu solubility, temp. and conc. depend. 80—10677
- Cu(I) olfactory binding site 78—96060
- Cu(II), biamperometric iodometric determ. using Pt-graphite electrode system 77—70359
- CuII lasers with cylindrical hollow cathodes, performance 80—5751
- Cu(II), selective separation from rare earth elements on chelate ion exchangers 78—58861
- Cu(II)-nucleic acid base interaction, MO calcs. 79—10013
- Cu(X), resonance transitions, classification 80—42985
- ^{62}Cu generator for medical and biological uses 80—30890
- ^{63}Cu, ^{65}Cu, Fourier transform NMR studies 78—94262
- $^{63}Cu_2$, $B^1\Sigma_u^+$-$X^1\Sigma_g^+$ transition, Franck-Condon factors, r-centroids and pot. curves 80—43114
- $^{63}Cu_2$ $A^1\Pi_u$-$X^1\Sigma_g^+$ transition, Franck-Condon factors and r-centroids 80—95690
- ^{64}Cu β^- decay, K-shell autoionis. 80—956
- ^{65}Cu, excited states lifetimes, Doppler shift attenuation meas. 78—42009
- ^{67}Cu use in lung tumour diagnosis *(French)* 77—70519
- ^{67}Cu, whole-body counting of retention in man 79—62378
- Cu(100), photoemission via Bloch states and evanescent band gap states, polarised synchrotron irradiation 79—61492
- D^+ irradiated, radiation blistering onset at low temp. 80—2081
- Fe alloy granule reinforced Cu M2 wear resistance in rubbing with lubrication 80—16490
- Fe alloy granule reinforced Cu, friction in vacuum 80—25880
- Fe alloy granules in Cu binder, exam. of wear characteristics without lubrication 79—96154
- Fe, ferromagnetic transmission resonance, nonlinear phenomena 77—81016
- Fe/Cu composite, prop. of fatigue crack crossing interface under residual thermal stress effect 80—45371
- Fe-Cu, bimetallic molecule, matrix isolated, Mossbauer spectrum 78—68425
- Fe-Cu, bimetallic molecule, matrix isolated, Mossbauer spectrum 78—88233
- FeNi-Cu, composite fibre and layer structs., anomalous props. caused by internal phase boundaries 78—72754
- FeO-Fe_2O_3-SiO_2 -Al_2O_3-$CuO_{0.5}$/Cu slag-metal system, distrib. equilib. of Sn, Se, Te 78—44111
- $Fe(OH)_3$, coprecipitation with Cu, Ag, Au; Ge, Sn, Pb; Mn and Ca 79—70415
- Fe_2P:Cu, Mossbauer spectra, mag. transition 80—50240
- Ga, small Cu additives effect on cryst. growth from melt 77—32515
- p-GaAs:Cu, carrier drag by photons, rel. to IR detection 79—11185
- n-GaAs:Cu, contaminated single cryst., deep level photoluminesc. model 78—68554
- GaAs:Cu, diffused layers, photocond. spectra, hole conc. and mobility *(Russian)* 78—14758
- n-GaAs:Cu, electron-phonon interaction in optical transitions between deep impurity level and allowed bands 79—42591
- p-GaAs:Cu, impurity photocond. and absorpt. coeff., Hall meas. 80—6770
- GaAs:Cu, in MSM struct., phototrigger effect 78—56238
- GaAs:Cu, LPE, photoelec. meas. of electron density for different Cu introduction methods 78—43437
- GaAs:Cu, multiple scatt. Xalpha cluster model, impurity electronic states, dangling bond effect elimination 79—99504
- GaAs:Cu, photoionisation spectrum of deep impurities in presence of weak electron-phonon interactions 79—51529
- GaAs:Cu, S-type diodes, thermal quenching of injection currents and current-voltage characts. 78—26942
- GaAs:Cu, sensitivity of impurity photocond., ordered surface irregularities 79—24018
- GaAs:Cu, substitutional impurity elec. struct. 80—88513
- GaAs:Cu, supersaturated solid solns., decomp., surface impurity content 78—51681
- GaAs:Cu, Te, photoelec. props. 80—92936
- GaAs:Cu contamination equlib. assessment 79—51134
- GaAs:Cu electrode photographic device, CO_2 pulsed laser output high-speed meas. 79—14008
- GaAs:Cu melt grown, 1.36 eV band luminescence studies, edge emission 79—87510
- GaAs-Cu:Tl, cathode luminescence spectra, Hall effect, cryst. defects 80—76087
- GaAs;Cu, epitaxial and bulk conductivities compared *(Russian)* 78—10585
- GaP:Cu, deep levels, photoluminesc. and optical cross sections 79—38653
- GaP:Cu, elec. and optical props., rel. to doping and heat treatment 80—16056
- GaP:Cu, impurity absorpt. bands at 1.05, 0.75 eV 77—44032
- GaP:Cu, LPE, photoconductive props. obs. 78—47836
- GaP:Cu, Raman scatt. from acceptor state 80—11408
- GaP:Cu, thermally and optical excited cond., deep level centres 78—72190

copper continued
- GaP:Cu p^+-n junction, deep level parameters, TSC meas., rel. to photocurrent techniques 78—72249
- GaP:Cu-Ni, Schottky barrier, TSC meas., trap levels 78—91709
- GaSe:Cu(Cd, Sb), photovoltaic spectra 80—20240
- Ge:Cu, anelastic relax., internal friction temp. depend. meas. 79—65143
- n- Ge:Cu, characts. of radiation defects 78—55893
- Ge:Cu, deep-level impurities, insulating props. 78—39124
- Ge:Cu, degree of Cu contamination in heat treated Ge 80—2359
- Ge:Cu, displacement of Ge-Cu inclusions in const. elec. field, 700-850°C *(Russian)* 77—15634
- Ge:Cu, electron irrad. effects on carrier density, defect form. 80—19843
- Ge:Cu, electron irradiation effects on elec. props. 78—6103
- Ge:Cu, hot photoexcited holes at low temp. 78—30954
- Ge:Cu, IR detector, impurity photoconductivity *(German)* 78—82036
- Ge:Cu, polycrystalline film, electron transport props. 79—99642
- Ge:Cu, press. effect on energy spectrum of carriers, elec. cond. and Hall coeff. expts. 79—23930
- Ge:Cu, quenched, energy levels of thermal acceptors, annealing effect 78—34798
- Ge:Cu, quenched, interaction between shallow-level defects and Cu atoms, Hall effect meas. 78—64002
- Ge:Cu, solubility and behaviour of Cu, internal friction investigations 80—92678
- Ge:Cu, surface waves at static domain boundaries *(Russian)* 80—80288
- Ge:Cu photodetector, I-V characts. 78—19141
- Ge:Cu photoresistor, liquid H_2 cooled, detectability 78—80019
- Ge:Cu short wavelength quenching of photoconductivity 78—26907
- p-Ge:Cu^-, deep levels, optical-phonon-assisted capture of carriers 79—51597
- Ge:O, Cu, amorphous thin film, impurity effects on struct. 80—107054
- Ge:Sb,Cu, exactly compensated, impurity absorpt. and photocond. spectra 78—56189
- n-Ge:Sb,Cu, exactly compensated, static photocurrent-voltage characts. 79—38131
- n-Ge:Sb,Cu, exactly compensated, unipolar injection influence on photoconductivity 79—42592
- Ge:Sb,Cu, high resist. compensated, impurity of photocond., pulsed unipolar injection carriers 80—92935
- Ge:Sb,Cu, photoelec. props., fast electron irrad. effects 80—60036
- Ge-Cu, contacts, surface electron state spectrum, surface treatment effects *(Russian)* 80—34497
- Ge-Cu-Ge, layered struct., proton induced X-rays, impurity atom depth determ. 77—11582
- $GeS_{1.5}$:Cu, interpretation of dielectric behaviour 79—33595
- $Ge_{40}S_{60}$ glass, Cu doped, EPR study 79—65713
- $Ge_{40}S_{60}$:Cu, bond struct. and character in Ge-S system, EPR obs. 80—66014
- $Ge_{42}S_{58}$:Cu, glass, impurity effect on e.p.r., dangling bonds 77—4553
- Ge_xSi_{1-x}:Cu, solid soln., single cryst., photocond. spectra 79—24015
- H_2O vapour bubble formation, along grain boundaries, effect on intergranular creep fracture 80—71722
- He conc. profile meas. rel. to blistering 78—95089
- He defect complexes and depth distribution, production theory 77—31686
- He-Cu hollow cathode discharge, Cu II CW laser oscill. at 8096 Å 79—31878
- He-Cu hollow cathode laser, three phase excitation 80—48279
- $(HfO_2)_{0.9}(Y_2O_3)_{0.1}$:$Cu^{2+}$, ESR at room temp., spin Hamiltonian parameter determ. 77—16167
- $HgCl_2$, reaction on metallic Cu, reaction velocities, effect of neutral salt addition 78—64887
- HgTe:Cu, effect of prep. conditions on impurity distrib., hole conc. 77—8743
- In powders, uncoated and Cu-coated, fluctuation diamag. susceptibility above T_c 79—78309
- In-GaAs:Cu-In S-type diode, role of deep trapping levels in form. of current-volt. characts. 77—76948
- InAs:Cu, contamination equilib. assessment 79—51134
- InI:Cu, impurity behaviour during directional crystallisation, partition coeffs. 77—16491
- InP-Cu contact system, low temp. alloyed contact formation 80—100519
- p-InSb:Cu, ionisation energy of multiply charged impurities, compensation effects 78—18996
- p-InSb:Cu film, heavily doped, ionized impurity scatt., Hall effect and DC cond. meas. 79—99643
- InSb-Cu non-rectifying contacts by immersion plating 78—30984
- ingot, cast, exam. of nonmetallic inclusions, size freq. distrib. 78—39989
- KBr(Cl):Sr^{2+},Cu^+, thermolum. response, extension of two-step reaction model 80—89075
- $K_2C_2O_4.H_2O$:Cu^{2+}, ESR and isomorphism of Cu^{2+} 77—32252
- KCl, cryst., two-layer colloidal K and Cu colour centre light absorption 77—12408
- KCl:Cu, additively-coloured crysts., for hologram recording plates *(Russian)* 78—29914
- KCl:Cu, EPR, optical absorpt. and luminesc. investig. of anisotropic Cu_F^0 centres 77—20893
- KCl:Cu,Tl, plastic deform., charge exchange of hole centres *(Russian)* 77—11876
- KCl:Cu^-, absorpt. and emission spectra, $3d^{10}4s^2 \rightarrow 3d^94s^24p$ bands 79—24343
- KCl:Cu^- excitation and absorpt. spectra 80—108255
- KCl:Cu^+, exciton bands, optical absorpt. and MCD spectra 80—80821
- KCl:Cu^+, Kerr electro-optical effect 80—34890
- KCl:Cu^+ US attenuation meas., 80-300K 77—43285
- $KHSO_4$:Cu, DC electrical cond. 79—37874
- KI:Cu^-, absorpt. and emission spectra, $3d^{10}4s^2 \rightarrow 3d^94s^24p$ bands 79—24343
- KI:Cu^+, exciton bands, optical absorpt. and MCD spectra 80—80821
- KI-KCl:Cu^+ mixed cryst., off-centre Cu^+ 79—65112
- K_2O-B_2O_3:Cu II, glass, O basicity, ESR study 78—80199
- K_2O-CaO-B_2O_3:CuII, immiscibility, ESR detect. 78—80200
- K_2O-MgO-B_2O_3:Cu^{2+}, micro-inhomogeneities, EPR and Raman study 80—84080
- K_2SO_4-$ZnSO_4$ glass:Cu^{2+}, visible spectra 79—51990
- K_2SO_4-$ZnSO_4$:Cu II, glass, O basicity, ESR study 78—80199
- $KZnF_3$, Cu^{2+} and Mn^{2+} exchange interactions, luminesc. line temp. depend. 79—69480
- $KZnF_3$:Mn^{2+}, Cu^{2+}, exchange coupled, luminesc. props. 79—33781
- Kr+Cu^{q+}, ($16 \leq q \leq 23$), 1.4 MeV/amu, X-ray emission, charge state dependence 78—37713

copper continued

- LaMg(NO$_3$)$_2$:Cu^{2+}, spin-lattice recovery rate 78—10760
- Li ions stopping power and straggling 80—42908
- Li/Cu interface, CESR meas. 78—80218
- LiAlSiO$_4$:Cu, β-eucryptite solid electrolyte, Cu^{2+} EPR obs. of ion exchange props. 80—108056
- Li$_2$B$_4$O$_7$:Cu, Ag, as thermoluminescence dosimeter *(Japanese)* 78—31906
- LiCl:Cu, electron transfer absorption bands 79—95810
- LiCl:Cu$^+$, 3d→4p transitions, near UV absorpt. spectrum assignment 78—27272
- LiCl:Cu$^+$, luminescent centre, cluster MO calculation of energy levels 78—64411
- LiCl:Cu$^+$, MO calc. of luminesc. Cu$^+$ centres 79—38609
- LiCl(Br):Cu^{2+}, optical absorpt., charge transfer spectra 80—2797
- LiNbO$_3$:Cu, pure and doped, nonlinear excitation, multiphoton photorefractive process 79—36950
- LiNbO$_3$:Cu^{2+}, EPR and optical spectra 80—20453
- LiNbO$_3$:Cu(Fe), light induced charge transport, photovoltaic effects, impurity states 80—80317
- LiTaO$_3$:Cu, waveguide with periodic electrodes, mode conversion 78—33840
- LiTaO$_3$:Cu(Fe), light induced charge transport, photovoltaic effects, impurity states 80—80317
- Mg complex, Mg(H$_2$O)$_6$H$_2$(EDTA), Cu^2 doped EPR and ground state wavefunction of Cu^{2+} 79—56605
- MgF$_2$-Al film substrate tunable external-reflector retarder, computer based anal. 80—53407
- MgO:Cu, dopant conc., refr. index profile rel. to integrated optics 78—5583
- MgO:Cu, X-ray stimulated luminesc. 79—28802
- MgO:Cu^{2+}, next-nearest-neighbour ion effects on impurity 2p levels 77—20987
- Mg$_2$TiO$_4$: Cu ESR of Cu^{2+} 80—97131
- γ-Mn electrodeposition influence of Cu, Ag, and Be impurities *(Russian)* 79—47938
- Mn^{2+}-Cu^{2+} coupled pair, ESR spectrum, strong isotropic exchange model 80—29606
- Mo, arc, steady, vac., plasma ion mass and energy diagnostics 78—51385
- Mo fibre reinforced Cu, rule of mixtures of deform. parameters in stage III 80—97532
- Mo fibre reinforced Cu with weak interfaces, stability of tensile deform. 80—97533
- Mo reinforced, fatigue strength. surface layer effects 77—12697
- Mo-Cu cathode, spot motion and nature in UHV 80—79597
- Mo-Cu nonmiscible system, sputter yields 79—87546
- N$_2$-Cu arc plasma, transport coeffs. 80—96344
- ND$_4$Br, phase states and transition, from ESR of Cu^{2+} 79—99762
- ND$_4$Br:Cu^{2+}, pseudo-Jahn-Teller effect manifestation in ESR spectrum 80—71168
- ND$_4$Cl:Cu^{2+}, high-press. EPR, order-disorder transitions 78—19310
- NH$_4$Br:Cu$^+$, luminesc., orientation phase transition 80—100687
- NH$_4$Br:Cu^{2+}, ESR and absorpt. spectra, 300-1500 nm 78—60492
- NH$_4$Cl(Br):Cu^{2+}, compressed D$_{4h}$ cluster, g_{zz}-g_0 value 77—80756
- NH$_4$ClO$_4$:Cu^{2+}, dislocation etch pits exam., rel. to thermal decomp. 77—11555
- (NH$_4$)$_2$SO$_4$:Cu^{2+}, ESR parameters, effect of pH of mother soln., trapping sites 80—15791
- (NH$_4$)$_2$SO$_4$:Cu^{2+}, ferroelec., ESR, Cu^{2+} in trigonal bipyramidal coord. 78—23330
- (NH$_4$)$_2$SO$_4$:Cu^{2+}, ferroelec. transition, ESR study 79—91286
- NaBr:Cu$^+$, absorpt. spectra, pressure effects up to 6 kbar, comparison with NaCl:Cu$^+$ 79—4826
- NaBr:Cu$^+$, luminesc. and lifetimes, press. depend. 79—33809
- NaBr:Cu$^+$, off to on centre defect transitions under hydrostatic press. 78—15199
- NaBr:Cu$^+$, press. tuning of motional behaviour in shallow off-centre pots. 79—78718
- NaCl:^{63}Cu$^+$, resonant bandmode, stress spectroscopy with far IR laser 78—2847
- NaCl:Cu, UV absorpt., emission, excitation spectra, Cu$^-$ centres 77—81127
- NaCl:Cu, X-irrad., thermoluminesc., F-centres 79—33849
- NaCl:Cu$^+$, electrolytically coloured, electron trapping, optical absorpt. 80—100672
- NaCl:Cu$^+$, far IR props. of lattice resonant modes, hydrostatic press. effects 77—28574
- NaCl:Cu$^+$, luminesc. and lifetimes, press. depend. 79—33809
- NaCl:Cu$^+$, X-irrad., anisotropic Cu centre anal. 79—78714
- NaCl:Cu$^+$, X-irrad., thermoluminesc. centre, EPR anal. 79—43045
- NaCl:Cu$^+$, X-irrad. at room temp., ESR of Cu^{2+} centres 78—52343
- NaCl:Cu$^+$, X-ray irrad., role of Cu$^+$ in thermoluminesc. 78—56526
- NaCl:Cu^{++}, EPR spectra anal. spin-Hamiltonian parameters determ. *(Spanish)* 77—69673
- NaCl-Cu$^-$, absorpt. and emission spectra, 3d^{10}4s^2→3d^{9}4s^{2}4p bands 79—24343
- Na$_2$HAsO$_4$.7H$_2$O:Cu^{2+}, ESR, Cu lattice location 78—52342
- NaI:Cu$^+$, luminesc. of iolated V$_K$-centres 78—84641
- Na$_2$O-Al$_2$O$_3$-B$_2$O$_3$ glasses, kinetic study of Cu$^+$-Cu^{2+} equilib. 79—8448
- Na$_2$O-B$_2$O$_3$:Cu^{2+}, glasses, ESR and optical absorpt. 80—34760
- Na$_2$O-B$_2$O$_3$:Cu^{2+}, Mn^{2+} glasses, Cu^{2+}-Mn^{2+} interaction studied by ESR 80—93166
- Na$_2$O-MgO-B$_2$O$_3$:Cu^{2+}, micro-inhomogeneities, EPR and Raman study 80—84080
- Na$_2$O-P$_2$O$_5$:Cu II, glass, O basicity, ESR study 78—80199
- Nb reinforced, fatigue strength, surface layer effects 77—12697
- Nb/Cu, layered ultrathin coherent structs., supercond. props. 80—84525
- Nb-Cu bilayers used in refractory lift-off process, appl. to high Tc supercond. circuits 79—47626
- Nb-Cu-Nb junctions, Josephson effect meas., critical current, temp. depend. 80—93041
- Nb-stainless steel bimetallic strip Cu interlayer struct. during thermal fatigue *(Russian)* 78—15498
- Nb-Ti/Cu composite disc, crit. state model for crit. current determ. 79—99665
- Nb-Ti/Cu sheet composite, flux trapping and shielding capabilities in transverse fields 80—15667
- Nb$_3$Sn-Cu multifilamentary composite wire, Nb$_3$Sn filament morphology and grain size 80—100855
- Nb$_3$Sn-Cu superconducting composite with submicrometer filaments, fabrication and props. 79—38282

copper continued

- Nb$_3$Sn-Cu superconducting composites, produced by cold extrusion of fine powders 79—38767
- NbTi filament reinforced Cu, superconducting composite, elastic const., temp. depend. 78—68717
- NbTi-Cu, composite superconductor, acoustic emission 80—84546
- NbTi-Cu, supercond. composite, use in temp. and heat transfer coeff. meas. 80—77780
- Ne-Cu, UV ion laser, dominant transition at 260 nm 79—942
- Ne-Cu hollow-cathode laser discharge sputtering obs. 78—66800
- Ne-Cu laser, discharge processes, cathode sputtering 78—5463
- Ne-Cu pulsed discharge, electron energy distrib., ionis. rate 78—51387
- Ne-Cu UV laser, spectral range, threshold, power output 78—66809
- Ni complex, Cu^{2+} doped, spin lattice relax. 77—59453
- Ni complex:Cu^{2+}, Ni(II)bis(diethyl-dithiocarbamate):Cu^{2+}, electron spin-lattice relax. 77—1589
- Ni-Cu conductor system for Si solar cells 80—93991
- Ni-Cu diffusion couple surface, epitaxial, AES, CO chemisorption and LEED 77—31891
- Ni-Ti/Cu composite, plastic deform. influence on internal friction *(Russian)* 80—100871
- Pb ceramic glaze, Cu^{2+} doped, Pb^{2+} release 80—49101
- Pb diffusion and Pb melting curve, high press. effect 80—49337
- Pb glazes, Cu^{2+} doped, alkaline substitution, crystal field modifications, EPR study 79—95634
- Pb/Cu proximity effect sandwiches, US surface wave attenuation 79—60994
- Pb-Cu contacts, proximity effect *(Russian)* 80—34558
- Pb-Cu-Pb superconducting microbridges, response times and low-voltage behaviour 79—65602
- Pb-Cu(Ag) double layers, intermetallic boundary effects, tunnelling 80—88692
- PbI$_2$-Cu, light sensitive, internal photoelectric emission 80—107910
- PbO-B$_2$O$_3$:Cu^{2+}, glasses, ESR and optical absorpt. 80—34760
- PbO-B$_2$O$_3$(SiO$_2$) glasses, absorpt. spectra of Cu^{2+} ions and interpret. 78—27276
- PbO-SiO$_2$-Cu^{2+} glass, EPR 78—39392
- n-PbTe:Cu epitaxial films, elec. transport props. 80—75659
- p-PbTe-Cu, barrier props. 79—7898
- Pt-Cu$_2$O-Cu double injection diodes, I-V characts. and photomemory effects 77—47900
- Pt-Cu$_2$O-Cu single carrier space charge limited diodes, I-V characts. 77—47901
- RbCl:Cu, X-irrad., ESR of noncentral Cu^0 atoms, 20-180K 77—24739
- p-Si:Cu, Cn precipitation effects, for solar cells appl. 79—69249
- Si:Cu, diffusion-induced defects, X-ray triple cryst. diffractometry 80—2213
- Si:Cu, dopant profile changes induced by laser irrad. using SIM and backscatt. meas. 79—69148
- Si:Cu, electronic states of impurities 77—43531
- Si:Cu, implant redistrib. and enhanced solubility following laser irrad. 79—69129
- Si:Cu, impurity segregation and microstructural changes by pulsed laser irrad. 79—82254
- p-Si:Cu, influence of Cu on diffusion of Au 77—62679
- Si:Cu, interaction between vacancy emitting absorbing precipitates and dislocations, TEM obs. 78—71755
- Si:Cu, ion implanted, doping profile, pulsed laser annealing effects 80—88197
- Si:Cu, parameters of Cu levels determ. by photocapacitance meas. 77—62869
- Si:Cu, photocond. spectra and IR quenching 77—55568
- Si:Cu, precipitate morphology, IR microscopy study *(Chinese)* 80—103539
- Si:Cu, recoil implantation from thin surface films, backscatt. obs. 78—63783
- Si:Cu, segregation effects after laser pulse melting 79—1843
- Si:Cu extinction of X-ray topographic images of Cu precipitates 80—45310
- Si:Ga, Cu, Au, gettering of Cu and Au during Ga diffusion 78—91350
- Si:Ga, sealed tube diffusion, Au and Cu gettering behaviour 77—76445
- p-Si:P, Cu, influence of Cu on diffusion of P meas. 77—1267
- Si:P, Cu, radiation-doped, influence of growth defects in elec. props. 79—69144
- n-Si-Cu Schottky contacts, electrochem. deposition, barrier height and ideality factor 80—75641
- Si-SiO$_2$-Mg-Cu powder compact, nitridation to form Si$_2$ON$_2$ whiskers *(Japanese)* 80—93674
- SiO$_2$:Cu, XPS line broadening and extra-atomic relax. energies 80—71561
- Sn coated, fine struct. in diffusion zone and mech. props. 77—11739
- Sn coating on Cu wire, growth of diffusion layer due to ageing effect *(Polish)* 80—34227
- Sn/CU electroplated bimetallic films, interfacial reaction 80—96765
- SnO$_2$:Sb,Cu CVD thin film, resist. temp. coeff. 79—38198
- SnO$_2$-Cu$_x$S-ZnS:Mn,Cu-Al$_2$O$_3$-Al, light-emitting struct., cond. and electrolum., heat treatment 80—97345
- SrCl$_2$:Cu$^+$, exciton bands, optical absorpt. and MCD spectra 80—80821
- SrO:Cu^{2+}, ESR spectrum averaging due to motion near paramagnetic centres 77—24737
- SrO:Cu^{2+}, phonon-induced tunnel hopping, ESR obs. 79—69714
- SrS:Cu, phosphor, photolum. meas. 78—80393
- SrS:Cu, phosphor electroluminescence characts. 79—33838
- TGSe:Cu^{2+}, EPR studies 80—7153
- Te:Cu films, elec. transport props. 80—60120
- TiC-steel cermet with Cu additions, precip. hardening and ht. treatment temp. 77—40414
- TiO$_2$ particle, Cu-coated prep., ceramic composites 80—89159
- TiO$_2$:Cu, anodic, effect of Cu on optical props., rel. to possible appl. in solar energy conversion 80—16115
- α-V$_2$O$_5$:Cu, far IR absorption spectra meas. 77—73158
- W fibre reinforced Cu composite, work hardening 77—52341
- W fibre reinforced Cu composite, temp.-load depend. of time-to-rupture *(Russian)* 78—11299
- W fibre reinforced Cu composites, correl. between thermal cycling-induced microstructural changes at interphase boundaries and tensile behaviour *(Japanese)* 80—71674
- W wire reinforced Cu, exam. of thermal cycling induced deformation 79—5050
- W wire reinforced Cu, microfield, flow stress 78—27575

copper continued
W/Cu, Stoneley waves at (001) interface between cubic symm. cryst. 80−100388
W/Cu powders, liq. phase sintering, particle rearrangement 80−45253
W-Cu composite materials, vel. dispersion and scatt. of transverse US waves 78−91383
Xe+Cu^{q+}, ($16 \leq q \leq 23$), 1.4 MeV/amu, X-ray emission, charge state dependence 78−37713
(Zn, Cd, Hg)S:Cu,In, electroluminesc. temp. depend. 77−1732
(Zn,Cd,Hg)S:Cu,In, electroluminesc., brightness waves 77−59616
(Zn,Cd)S:Cu,Al, luminesc. efficiency deterioration due to surface oxidation by $(NH_4)_2Cr_2O_7$ thermal decomp. 80−29810
(Zn, Hg)S:Cu, Cl, effect of superposition of two sinusoidal fields and freq. on electroluminesc. 78−39606
Zn (II) complex, β-diketonate, 5-coord. adducts, Cu^{2+}, ground state ion wavefunction calcs. 78−895
Zn complex, Cu^{2+} doped, spin lattice relax. 77−59453
Zn/Cu film system, UPS during atomic diffusion 79−43097
Zn-Cu-Zn system, galvanic corrosion, anal. for coplanar electrodes with one electrode infinitely large 79−8398
Zn_3As_2:Cu, single crysts., gas phase growth, elec. props. 79−15598
$Zn(BrO_3)_2.6H_2O$:Cu^{2+}, Jahn-Teller system, EPR and spin-lattice relax. 78−10760
ZnCdS:Cu, binders effect on electrophotographic characts. 79−80712
ZnCdS:Cu, high field photoconduction in binder layer 79−47121
$Zn_{0.1}Cd_{0.9}S$:Cu, doping effect on two-photon absorpt. spectra, deep levels 77−69870
$Zn_xCd_{1-x}S$:Cl, Cu$^+$(Ag$^+$), high pressure luminesc. 78−19533
$Zn_xCd_{1-x}S$:Cu, photoluminesc., Birman effect *(Russian)* 79−28837
$Zn_xCd_{1-x}S$:Cu, photoluminescence 80−29783
$Zn_xCd_{1-x}S$:Cu, thermoemission of positive ions in simple gas atmos. *(Russian)* 77−28676
$Zn_xCd_{1-x}S$:Cu crystallophosphors, spectra of IR electrophotographic sensitivity *(Russian)* 80−50423
ZnO:Cu, excited state, zero phonon lines in emission and Zeeman spectra 79−38026
ZnO:Cu, H(D), OH and OD centres, IR-active absorpt. line spectra 79−15496
ZnO:Cu, O, Fe(Co)(Ni) photocond., electron escape probabilities and trap depths 77−32041
ZnO:Cu,H, motional effects in EPR spectra 78−80207
ZnO:Cu^{2+}, electronic struct., optical absorpt. and ESR 79−87312
ZnO:Cu^{2+}, phosphors, emission spectra, impurity effects 77−32420
ZnO-B_2O_3:Cu^{2+}, glasses, ESR and optical absorpt. 80−34760
(ZnO-ZnS)Cu:I, double band electroluminophors, form., props. 78−19568
ZnS, Fe^{3+}-Cu$^+$ complexes and A-centres, g-factor anisotropy *(Russian)* 77−20271
ZnS:(Cu, Cl), electroluminesc., voltage effect on ageing rate 79−95848
ZnS:Cl$^-$, Cu$^+$, phosphor, high press. effect on thermoluminesc. 78−64419
ZnS:Cu, Al phosphors, mechanism of IR stimulated and quenching 77−69881
ZnS:Cu, Br based electroluminesc. cells, light, const. field effects on electroluminesc. 78−84658
ZnS:Cu, Cl, I, anisotropy of blue Cu luminesc. centres 77−81137
ZnS:Cu, Cl, Mn film, AC electrolum. 80−60680
ZnS:Cu, Cl luminophor, photoluminesc. and struct. props. 77−32414
ZnS:Cu, Co, deep traps and stationary luminescence *(Russian)* 78−48227
ZnS:Cu, current pulses stimulated by elec. field at low temp. 78−39121
ZnS:Cu, deep transition metal impurity states, SCF CNDO cluster calcs. 80−100442
ZnS:Cu, effect of elec. field on photoluminescence, model of luminogen centre 78−76522
ZnS:Cu, electroluminesc. spectra fine struct. 79−95847
ZnS:Cu, film effect of Cu valency on cond. 79−11246
ZnS:Cu, Gudden-Pohl effect, flash kinetics 79−24367
ZnS:Cu, H, double band phosphor, electrolum., −100 to +100°C 78−10987
ZnS:Cu, Mn DC electroluminescent powder panels, bulk and junction effects 80−89068
ZnS:Cu, O(Fe,Co,Ni) photoconductors, killer impurities effect on electron escape probabilities and trap depths 77−4392
ZnS:Cu, Pb, phosphors, ruby laser stimulated time delayed emission spectra 77−69874
ZnS:Cu, phosphor, photocapacitive effect and Gudden-Pohl effect 79−65520
ZnS:Cu, polycryst. phosphor, excitation storage, recombination barrier participation 78−27316
ZnS:Cu, spectral distrib., rise and decay behaviour *(German)* 80−60625
ZnS:Cu, Tb phosphors, luminesc. props. 80−100690
ZnS:Cu, trap parameters, thermostimulated luminesc. and cond. meas. *(Russian)* 77−72868
ZnS:Cu,Al, LV cathodoluminesc. 79−33844
ZnS:Cu,Al phosphor, shallow hole traps 78−31237
ZnS:Cu,Al phosphors, luminesc. excitation spectra and exciton struct. 80−55164
ZnS:Cu,Cl, electrolum. brightness wave, effect of square pulses 77−52184
ZnS:Cu,Cl, electrolum. voltmeter design, accurate high-voltage meas. 78−24813
ZnS:Cu,Cl, exciton refl. spectra, hexagonal struct. 77−44021
ZnS:Cu,Cl phosphor, effect of charged imperfections on electrolum. 77−32443
ZnS:Cu,Cl(Br)(I), green luminesc., interimpurity phototransitions investig. *(Russian)* 77−66541
ZnS:Cu,Er,Cl film, ageing and forming, DC electroluminesc., impact excitation 79−47522
ZnS:Cu,O, photocurrent spectral distrib., Fe, Co and Ni impurity effects 77−8135
ZnS:Cu,Pb, thermoemission of positive ions in simple gas atmos. *(Russian)* 77−28676
ZnS:Cu,Pb film, sublimated, pulse electrolum. meas. *(Russian)* 77−85806
ZnS:Cu,Pt phosphors, photoluminesc., thermoluminesc. 78−43915
ZnS:Cu 79−24350
ZnS:Cu AC electroluminescent patterns and polytypic transformations 78−6784
ZnS:Cu crystal, powder, epitaxial film, luminescence anomalous thermal 80−76077

copper continued
ZnS:Cu crystallophosphors, spectra of IR electrophotographic sensitivity *(Russian)* 80−50423
ZnS:Cu phosphor, electric field quenching of photoluminesc. and flashlike rise in luminesc. 78−2911
ZnS:Cu powder exam. of dielectric constant anomaly, in terms of polarisation catastrophe phenomena 79−51897
ZnS:Cu$^+$:Cu$^-$(Al^{3+})(Ga^{3+})(In^{3+}), interimpurity luminesc. at high press. 78−19532
ZnS:Cu^{2+}, Jahn-Teller effect, stacking faults and formation of polytypes, absorption and emission spectra 77−4660
ZnS:Cu^{2+}, motional averaging in excited state 77−66137
ZnS:Cu(Cl), electroluminesc. and photoluminesc. spectra, fine struct. *(Russian)* 78−84661
ZnS:Mn, Cu, Cl films, AC electrolum. 80−60679
ZnS:Mn, Cu powder devices, DC electroluminesc. 79−38674
ZnS-CdS:Cu, cathodoluminesc. investig., appl. to cathode ray tube screening 80−108282
ZnS-CdS:Cu, cryst. struct., electron traps and glow curves 79−61437
ZnS-CdS:Cu, phospors, nature of fluorescent centres and traps 79−91484
ZnS-Cu, comet shaped electroluminesc. lines 78−52578
ZnS-Cu, polycryst., influence of alternating elec. field and UV light on struct. defects, electrolum. expts. 79−43041
(ZnS-ZnSe):Cu, H systems, electrolum. 77−4690
$ZnS_{1-x}Se_x$:Cu,Br ceramic, current oscills. and electrolum. under high elec. fields 79−38677
ZnS_xSe_{1-x}:Mn(Cu), luminesc. obs. 78−60519
ZnS(Se)(Te):Cu^{2+}, absence of EPR spectra due to strong spin-lattice coupling of Kramers doublets 77−85181
ZnSe:Cu, Al, single cryst., low-voltage red cathodolum. 78−80423
ZnSe:Cu, Cl, high press. luminesc. 78−19532
ZnSe:Cu, deep centres, photolum., photocapacitance and photocurrent expts. 78−39053
ZnSe:Cu, discovery of bound exciton, electroabsorption 80−45038
ZnSe:Cu, elec. props. after heat treatment in Zn or Se vapour 79−99505
ZnSe:Cu, I, ceramic, electroluminesc., electric field induced switching effect under illum. 77−1460
ZnSe:Cu, I ceramic, injection electroluminesc. of p-n microjunctions 80−40163
ZnSe:Cu, luminescence and diffusion behaviour of Cu impurities 78−35188
ZnSe:Cu, melt growth, dopant partition coeffs. 79−14837
ZnSe:Cu,Al, LV cathodoluminesc. 79−33844
ZnSeCu, double comet shaped electroluminesc. 78−52577
$ZnSeO_4.6H_2O$:Cu^{2+}, crystal struct. orientational degeneracy removal scheme, space groups, ESR spectra 78−47267
$ZnSiF_6$:Cu^{2+}, spin-spin interactions of impurity pairs *(Russian)* 78−72397
ZnTe:Cu, doping behaviour, SEM in cathodoluminesc. and photoluminesc. exam. 79−65927
ZnTe:Cu, elec. and optical identification of persistent acceptor 79−60764
ZnTe:Cu, elec. field and impurity conc. effect on ionisation energy 80−88514
ZnTe:Cu, precipitates, electron microscopic investigation 80−45312
ZnTe:Cu, red centre, electric and optical props. 80−20239
ZnTe:Cu, voltage depend. on precip. contrast 79−1433
ZnTe:Cu films, high cond., elec. and optical props. 80−88651
^{62}Zn/^{62}Cu generator, source of ^{62}Cu for radiopharmaceuticals 80−67248
ZrO_2:Cu, point defects, electrochem. characterisation 80−35599

copper alloys
see also brass; copper compounds
admiralty brass, stress corrosion cracking, aqueous $CuSO_4$ 77−59961
Admiralty Metal, transgranular stress corrosion crack propag. 80−89402
Al-Cu(4wt.%), θ' precipitation, effect on Young's modulus, electron microscope obs. *(French)* 79−47689
Alnico 5 alloy, S and Ti additions effect rel. to non-metallic inclusions, coercive force and grindability 80−89375
Alnico alloy, C addition effects on struct. and mag. props. 78−23835
analysis by ion microprobe, quantitative, using matrix ion species ratios 78−61070
ancient, epithermal neutron activation anal. method 78−8490
Babbitt-steel bimetal, exam. of structure of transition layer 79−100293
bearing and frictional material, current state of prod. and development trends review 78−19902
binary, liquid, activity meas. 77−20085
brass, corrosion protection in chlorosubstituted acetic acids, use of 2-methyl benzothiazole corrosion inhibitor 79−57149
brass (70/30), interaction of annealing twins in fcc metals and alloys 78−68712
Br.AZhNMts 7-2.5-1.5-9 bronze, Mg-Al, type, fatigue and stress corrosion cracking, welding effects 80−3233
bronze, Al, electrode strip, short-time sintering 77−1824
bronze, Al, wear on 13% Cr steel in presence of aviation fuel 80−11781
bronze, Al and Ti, sintered frictional material, wear resistance, effect of matrix struct. 77−28911
bronze, anisotropic bend ductility in single phase alloys 78−60726
bronze, Be, elastic elements made from spring alloy bands 79−87678
bronze, BrB2, thin-rolled sheets, thermostress treatment 79−52273
bronze, deformability, quantitative determ. in drawing 79−52229
bronze, diffusion of Ga in V_3Ga layer, grain boundaries *(Russian)* 80−65297
bronze, effect on compression of Nb_3Sn multifilamentary conductors 79−61012
bronze, friction pair with Cu, Armco Fe or C steel, seizure centres on contacting surface *(Russian)* 77−70185
bronze, low-cycle fatigue, NH_3 effect 80−104348
bronze, P type, experimental analysis of junction growth with a junction model 79−47783
bronze, powders, electric-pressure sintering onto cylindrical parts in fluidised bed 80−100960
bronze, shell, deposited in vacuum, elastic characts. meas. by short time static extension *(Russian)* 78−39961
bronze, sintered, mech. props. 77−28839
bronze, sintered, Zr addition effects on struct., hardness, wear resistance *(Russian)* 77−70019
bronze, spherical powder, negative magnetic resistance changes 77−1410

copper alloys continued
- bronze, spheroidal, equivalent sphere diameter calc., Saltykov method 78—31362
- bronze, surface pretreatment effect on joint bond strength by cyanoacrylate adhesive Kanokonlit-E *(German)* 79—57202
- bronze 905, partially solid, die thermal behaviour in machine casting 78—6917
- bronze bearings, TEM exam. of wear debris 77—77595
- bronze casting, graphite dispersed, graphite particle size effect on wear *(Japanese)* 79—15804
- bronze layered-steel composite, water lubricated bearing mat., manuf. and props. 78—11341
- bronze matrix, Be alloying addition effects on supercond. props. of Nb_3Sn monofilament wires 79—87222
- bronze P, friction with steel, boundary lubrication conditions, element conc. anal. of films 78—85001
- bronze P, friction with steel, lubricant friction boundary behaviour *(German)* 77—86190
- bronze P, heavily cold rolled, yield strength enhancement mech. 77—36539
- bronze porous, PTFE impregnated, coeff. of friction, temp. effect 78—64737
- bronze powder, granulated, porosity of starting mat., zinc stearate additive, effects on sintering kinetics 77—63599
- bronze powders preparation by electrodeposition 78—20026
- bronze scrapers, wear by rubber 79—66173
- bronze-Be BrB2, struct. and phase transform. during mechano-thermal treatment *(Russian)* 80—11667
- bronze-on-steel contact, lubricated, effect of zinc di-n-butyl dithiophosphate on wear 79—20219
- bronze-steel, phase composition and struct. of diffusional interlayer in fusion zone, X-ray analysis 78—56821
- cavitation during superplastic flow, affecting factors 78—60728
- charge perturbations around impurities, NMR anal. 77—85582
- compositional modulation spectra, line shape 78—76491
- Constantan, fatigue, grain size effect 77—21260
- Constantan single wire, thermal expansion +20 to −60°C, strain gauge use 77—67427
- continuous precipitation, nucleation, spinodal decomposition 80—3061
- copel-chromel thermocouples, neutron irradiation effects *(Russian)* 77—82515
- corrosion, monitoring using polarisation resistance meas., techniques and correlations 77—16711
- corrosion in putrid seawater 79—91838
- corrosion inhibitor study by XPS, adsorbed benzotriazole 78—35554
- corrosion resistance in chlorinated lime slurry and calcium hypochlorite soln. 79—83390
- Corson alloys, AE during tensile deform. *(Japanese)* 79—61654
- creep fracture prediction, intergranular damage meas. 77—21268
- Cu-Al, FCC, study of dipoles using weak-beam electron microscopy 78—22724
- Cu-Co, dil., rotational hysteresis of Co fine particles 78—23301
- Cu-Mn alloys, thermodynamics, suitability as electrodes 79—66339
- Cu-Zn-Mn, de-alloying props. 80—104332
- Cunial MNA13-3, Mn addition effect on props. 80—21035
- cyclic hardening and saturation behaviour of single crystals 78—64555
- D16 extruded rod, substruct, anisotropy and decomp. at subboundaries *(Russian)* 77—25095
- deformed, texture development 79—87653
- dental amalgam, exam. of fracture toughness and critical strain energy release rate 78—48933
- dental amalgams, Cu-rich, SEM and energy dispersive X-ray analysis 78—24184
- determination of Cu, Sb, inverse voltamperometry method 78—61099
- diffusion in systems involving group VA elements, review 77—39697
- dilute, containing rare earth impurities, magneto-transport props. 78—68015
- dilute, dislocation inertial effects in plastic deform., internal friction meas. 77—36609
- dilute, Frenkel pair recombination radius, temp. depend. 77—89427
- dilute, optical props. and electronic struct. 78—35164
- dilute, size effect, valency factor and point defect interactions 79—51143
- dilute, size effect of impurity atoms rel. to trapping radii for migrating self-interstitials 78—75690
- dilute, transport props. 78—76046
- dilute binary solid solutions, enthalpies of mixing and excess free enthalpies *(French)* 80—107427
- dilute compositional changes in oxide thin films, Auger electron microanalysis *(Japanese)* 77—21319
- dilute metastable alloy formation by ion implantation 80—15130
- dilute nonmagnetic alloys, electric field gradient tensor 77—72843
- dispersion type, with low temp. gradient of resist. 80—49686
- ductile fracture during tensile testing 80—45381
- duralumin, shock-compressed, compression and rarefaction waves obs., 150-250 kbar 77—77535
- elastic moduli, temp. depend., −196 to 1000°C 80—6451
- electric connectors, Al/Cu bimetal, galvanic corrosion elimination 80—35387
- electroless-replacement film, room temp. oxidation 77—48572
- electronic charge density around 3d-transition metal impurities 78—34799
- electrospark machining, bronze, spreading and form. of surface layer, in solid-alloy-liquid-metal systems, kinetics *(Russian)* 78—27668
- fatigue cavitation, high temp. 77—36658
- FCC, climb of extended dislocations due to irradiation HVEM 80—103343
- FCC ternary, solid soln. hardening model, compared with expt. results 77—44262
- fretting corrosion, exam. of secondary structures 79—100292
- graphite dispersed casting, damping capacity *(Japanese)* 79—96059
- hardness, elec. cond., photo emission, and mag. props. *(Norwegian)* 79—32909
- hardness testing, depth of impression meas., automated 79—15892
- high strength Al-Zn-Mg-Cu alloys, mechanical props. *(Japanese)* 79—91654
- horse shoe corrosion in flowing sea water, mechanism, cathodic protection possibility 79—66199
- inelastic cyclic deform. and fatigue 77—63795
- inelastic electron scattering by dislocations *(Russian)* 78—79988
- interdiffusion, evaporated couple with Al alloys *(Russian)* 77—43389
- intergranular damage parameters in creep *(Czech)* 80—89342

copper alloys continued
- internally deformed struct. as source of homogeneous linear struct. 78—26497
- internally oxidised, FIM 77—20074
- ion-selective membrane electrodes development, Ag ion conduction ceramic systems *(Japanese)* 80—61203
- jog formation and glide on dissociated dislocations, direct obs. 77—68977
- liquid, thermal cond. and elec. resistivity 80—103661
- liquid, viscosity 77—4138
- (LMM) Auger electron emission by keV Ar^+ bombardment 79—95880
- localised phonons due to substitutional impurities 79—77711
- low-cycle fatigue and cyclic creep, −196-20°C 80—100913
- magnetic susceptibility, correl. with lattice parameter for α-phase alloys 78—68154
- Magnico alloy, with Si, Nb, Ti and La, low-temp. thermomag. treatment 77—63812
- Magnico alloy, with Si, Nb, Ti effect of Ub on mag. props. and grindability 77—63811
- manganin foil like gauge calibration in planar shock wave expts. 80—95091
- manganin pressure gauges, effects of shock compression and relief *(Russian)* 78—70149
- manganin resistance gauge for high pressure meas. 77—10036
- manganin thin film microtransducers for elastohydrodynamic lubrication studies 80—37048
- melts, supercooled, influence of impurities in crystallisation 79—29042
- metal-glass mats. alloyed with Cu, powder prep. and props. 78—72912
- metallisation systems, electrolytic and galvanic corrosion due to SO_2 contamination 79—74304
- metastable alloy form. by ion implantation 79—82252
- metastable alloy formation by ion implantation 79—14828
- microconductors, cast, struct. and physical props. exam 78—44232
- microcrystalline, rapidly quenched particulates, appl. 80—84887
- mischmetal-Co-Cu-Fe-Mg, mag. props. 80—35353
- mischmetal-Co-Cu-Mg, mag. props. 80—35353
- $Mn_{1-x}Cu_xSb$ films, $0 \leq X \leq 0.3$, magneto-optical props. 79—51981
- mobility of boundaries, transition metal addition effects *(Russian)* 77—21160
- molten, gas content meas., reduced pressure test *(Chinese)* 80—81390
- Monel, in thermoluminesc. dosimeter, low dose meas. *(Japanese)* 78—86696
- Monel, Ni-Cu-Fe-Mn, resistance spot weld quality evaluation, using stress wave emission technique 78—53066
- Monel 400, corrosion susceptibilities in synthetic geothermal brines 77—86223
- Monel 400, stress corrosion cracking in NaOH soln. 79—66196
- Monel K-500, environmental fatigue crack growth in H_2 79—5084
- Monel K-500, fatigue crack growth rates in vacuum and O_2 environment 79—5083
- Monel metal, cast, electrochemical behaviour in NaCl soln. 79—87763
- multicomponent, film, secondary ion emission meas. of composition var. laws *(Russian)* 77—80704
- multicomponent alloy films, struct. form. laws and elec. prop. changes obs. during vacuum condensation 78—6850
- mutual alloying behaviour of the elements straddling the line Li-Mg-Cu-Au in the long periodic table 78—84769
- Nilomag alloy 771 coloured, X-ray photoelectron spectroscopy of surface film 78—64899
- optimal secondary cooling condition estimation in continuous casting *(German)* 77—73295
- ordered equiatomic, lattice specific heat meas., Debye temp. 80—54396
- orientation dependence, of mechanically induced transformations 79—87660
- phosphor bronze, beam, cylindrical, flexurally vibrating, Timoshenko's shear coeff. 78—83866
- phosphor bronzes, surface Cs^+ impact, 5.5 keV, negative secondary ion emission obs., rel. to Cu *(French)* 77—66562
- positron trapping in liq., and solid state 78—48255
- precipitation hardened, anomalous elastic props. 77—86071
- pseudoelastic single crystal fatigue 79—52364
- purification of solid metals by electrotransport *(German)* 78—51745
- rare earth alloys, RCu_4Al_8, mag. struct. and interactions 80—25092
- rare earth alloys, RCu_x, mag. props., 4.2 to 200K 79—87233
- rare earth intermetallic, RCu_4Ag, mag. props. and cryst. struct. 77—20562
- rare earth intermetallic, RCu_4Ag and RCu_4Al, struct. study 78—30587
- rare earth intermetallic $RCo_{5x}Cu_{5-5x}$, narrow Bloch walls, magnetisation, 4.2K 77—8333
- rare earth ternary alloys, RT_6Al_6, T=Cr, Mn, Fe, Cu, cryst. struct. 80—107110
- rare earth-copper intermetallic cpds., RCu_2, metamag., mag. props. 79—87242
- rare earth-copper intermetallic cpds., RCu_2, metamag., mag. props. 79—87243
- rare earth-Cu, amorphous, mag. and transport props. 80—34605
- rare earth-Cu intermetallic compds., single crysts., mag. props. 80—54892
- recrystallisation retardation, Al_2O_3 dispersion effect on kinetics 80—89242
- sintering, reduction processes, resist. meas. *(German)* 80—25597
- solid solution condensed films, influence of alloying components on phase composition and lattice spacing *(Russian)* 80—20047
- solid solutions, single phase FCC metal, stacking fault energy and delamination wear 78—3239
- solid solutions with 3d alloying impurities, exam. of thermoelectricity *(Russian)* 79—28339
- sputter deposited at high rate, microstruct. and props. 78—22988
- sputtered, microstructure and tensile props. 78—11368
- sputtering, alloy surface topography obs., Stewart-Thompson theory 78—43977
- stacking faults, weak-beam contrast in TEM 80—75132
- steel, alloy, Cr-Cu-Mn-C, HT80, effect of grain size on sensitivity to reheat cracking *(German)* 78—72856
- steel, alloy, Mn-Cr-Cu, exam. of ductility when deformed, alloying addition effects 78—44175
- steel, Cr and Cr-Ni, tempering resist., mech. props., Cu addition effect 79—79012
- steel, Cr-Cu-Mn, fatigue crack propag. rate eval. by J integral method *(Japanese)* 79—8346
- steel, Cr-Ni-Cu (14, 5, 2 wt.%), phase transform. and props., preliminary heat treatment effect 79—79011

copper alloys continued
- steel, Cu-Mn-Zn, Zn addition effects in powder forgings produced by liquid solid alloying 78—11157
- steel, Cu-Ni-Mo (2, 2, 0.25 wt.%), sintering, kinetic characts. 80—60805
- steel, low alloy, cold resistance, effect of nitrides, carbonitrides, carbides, Cu precipitates 77—16594
- steel, low C, cold rolled sheet, Cu effect on recrystallization texture *(Chinese)* 79—74173
- steel, precipitation hardening, strength and struct. *(German)* 79—47701
- steel, precipitation hardening, struct. and fracture *(German)* 79—61696
- steel, stainless, recrystallisation texture, effect of Cu, Ti additions on development *(Japanese)* 78—80558
- steel, stainless complex alloy, hot ductility, B effect 80—30038
- steel, WC reinforced surface layer, serviceability improvement by Ni, Cu-Ni, V alloying additions 77—21290
- steel composites for intense pulsed mag. field generation 80—42245
- steel-bronze bimetal mech. props., diffusional interlayer effects 79—29169
- STEM imaging of alloy containing Cr and SiO_2 particles 80—108685
- strain hardened, struct. factor effect on stress relaxation *(Russian)* 80—25748
- stress corrosion cracking control measures 77—90509
- stress relaxation, effect of surrounding medium *(Russian)* 79—100199
- stress relaxation estimation for electric connectors, expts. 77—21206
- superplastic, activation energy of plastic flow 78—64584
- superplastic, microscopic examination of internal void formation 80—16383
- thermal conductivity measurement, cryostat for meas. of plastically deformed specimens at liq. He temps. 78—81985
- thermoelectric power determ. 77—24549
- thermopower and resistivities, validity of Nordheim-Gorter relation 78—91671
- thermopower and resistivity, Nordheim-Gorter relation 79—65438
- Ticonal, effect of rare earth metals on mag. props., struct., and phase transformations 79—99732
- ticonal, grindability improvement, thermomagnetic and heat treatments 77—16625
- Ticonal with Sm, magnetic props., phase transform. after thermomagnetic treatment 78—3155
- time and spatially resolved at. absorpt. anal. 80—40760
- transition metal dilute alloys, residual resist., Dingle temp. 77—1409
- transition metal silicides, V(Nb)(Ta)(Cr)(Mo)(W)-Si-Cu, struct. and supercond., Cu influence 80—50592
- unidirectionally solidified morphology of solid liquid interface and solute redistribution *(Japanese)* 77—21133
- vacuum condensate, struct. and props. rel. to deposition conditions 78—11369
- vacuum condensed film, alloying addition influence on electrophysical props., elec. cond. *(Russian)* 80—34529
- Ag-Au-Cu, sputtering and AES 80—50503
- Ag-Au-Cu, surface composition change on sputtering with 2 keV Ar ions 80—66365
- Ag-Cu, α-phase alloy, thermopower at low temps. 78—84196
- Ag-Cu, dil., elec. quadrupole interactions on ^{111}Cd probe nuclei, time differential PAC meas. 78—15066
- Ag-Cu, dil. alloys, EFG at impurity, ^{111}Cd TDPAC 77—16213
- Ag-Cu, directionally solidified, obs. of cutting deform. zone *(Japanese)* 78—15422
- Ag-Cu, highly deformed eutectic composite wire, anomalous props., fibre diameter and foreign atom effects *(German)* 77—36566
- Ag-Cu, laser induced atomisation in graphite furnace, for at. absorption spectroscopy 77—44566
- Ag-Cu, liquid, surface tension 78—43217
- Ag-Cu, metastable alloy film, optical props. 77—12460
- Ag-Cu, metastable solubility lines on Ag side 78—39737
- Ag-Cu, optical spectra, 0.5-6 eV, d-band struct. 77—48168
- Ag-Cu, residual elec. resist., pseudopot. calc. 80—6813
- Ag-Cu, surface comp. after sputtering, AES obs. 77—55858
- Ag-Cu, surface segregation, electronic theory, density of states, cluster-Bethe-lattice approx. 80—49369
- Ag-Cu, temp. depend. of elec. field gradient, TDPAC meas. 77—32304
- Ag-Cu (10 wt.%), contact material, contamination layer thickness, resist., ESCA study *(German)* 80—55561
- Ag-Cu (39.9 at.%), eutectic composites, solidification and deform. *(Czech)* 77—59773
- Ag-Cu (5 at.%) solid solution, pre-fatigued, strain hardening at high temp. 78—15426
- Ag-Cu (50 at.%), splat-cooled, struct. of γ' extended solid solution 78—3147
- Ag-Cu (6.2 at.%), tricrystalline specimen, discontinuous precipitation, specific grain boundary energy *(German)* 77—86039
- Ag-Cu (6.2 at.%), tricrystalline specimens, fine lamellar discontinuous precipitation *(German)* 78—52822
- Ag-Cu (6.2 at.%), tricrystalline specimen, discontinuous precipitation, thermodynamics *(German)* 79—34043
- Ag-Cu (6.2 at.%), with discontinuous precipitates, quantitative struct. anal. using SEM 79—43527
- Ag-Cu (6.6% at.wt.), laser melt quenching and alloying 79—69919
- Ag-Cu (8 wt.%), plastic deform. effect on discontinuous precipitation 80—3053
- Ag-Cu alloy filaments, prod. by glass coated melt spinning, microstruct. and tensile strength 79—91667
- Ag-Cu eutectic, mechanism of lamellar spacing adjustment 78—31395
- Ag-Cu eutectic and off-eutectic alloys, thermal stability 77—25077
- Ag-Cu eutectic composite wire, HF conductivity and skin effect 79—33305
- Ag-Cu metastable solid soln., form. by ion-beam mixing 80—75244
- Ag-Cu solid soln., spectral determ. of comp. using UHF plasmotron as source 79—52812
- Ag-Cu surface alloyed films, laser melt quenched, microstruct. 80—76423
- Ag-Cu-Ni, phase diagram determ. 77—63634
- Ag-Cu-Pb coin chem. anal. by low energy γ-rays and neutron transmission meas. 80—35591
- Ag-Cu-Sn(Zn)(Au), effect of additions on eutectic and peritectic temp., of binary alloys 78—84801
- Ag-Cu-Zn-Cd solid metal lubricant in self lubricating composite steels 78—11340
- Ag-Cu-Zn-(Cd)(Mn), solder, UTS, room temp. to 4.2K 79—57064
- Ag-Pd-Cu, contact-spring props., fatigue and spring limit *(Japanese)* 79—29117

copper alloys continued
- Ag-Pd-Cu alloys, contact-spring props. and age hardening 78—88473
- Ag-Pd-Cu-Au dental alloy, age-hardening characts. 79—87646
- Ag-Sn-Cu-Hg, constitution of quaternary amalgam at 37°C *(German)* 77—81250
- $Ag_3Au_{1-x}Cu_x$, phase relations, X-ray diffr. and differential thermal anal. 80—108395
- AgCu and AuCu, mols., VB calcs. 77—57883
- Al bronze, anisotropic bend ductility in single phase alloys 78—60726
- Al bronze, creep forging 77—59848
- Al bronze, duplex alloy, corrosion fatigue behaviour 79—70218
- Al bronze, elastic limit after repeated transverse deformation *(Russian)* 77—66668
- Al bronze, G, Si additions, corrosion resistance 77—16714
- Al bronze, O free, annealing in photoemission electron microscope, twin density recrystallised grain size relation *(German)* 78—52850
- Al bronze, plasticity of two-phase, coarse microstruct. material *(German)* 77—59882
- Al bronze, superplastic low cycle fatigue 78—27632
- Al-Ag-Cu alloy precipitation and heat of evolution, microcalometric obs. *(Japanese)* 78—15406
- Al-Al_2 eutectic, abrasive fragmentation *(Czech)* 78—64715
- Al-Al_2Cu, aligned eutectic, precipitation, TEM and microhardness meas. 78—27529
- Al-Al_2Cu, eutectic composite, abrasive fragmentation *(Czech)* 80—30110
- Al-bronze, input energy, hysteresis, and fracture in low cycle buckling fatigue, superelastic range 78—31527
- Al-bronze, single crystal rod, energy dissipation, deformed by cyclic buckling in superelastic range 78—31479
- Al-Cu, age hardened, coherency stresses, composition and dislocation interactions for θ'' precipitates 77—36525
- Al-Cu, age-hardenable, US cavitation erosion mechanisms, effects of comp. and heat treatment 78—53002
- Al-Cu, Al_2O_3 fibre reinforced, exam. of interface interactions during fabrication 78—76616
- Al-Cu, alloying effect on phonon spectrum and lattice heat cond. 77—62695
- Al-Cu, anal. of electron diffr. micrographs using Patterson function *(French)* 79—20044
- Al-Cu, Bauschinger effect 79—61646
- Al-Cu, bicrystals, neutron irrad. effects on grain boundaries, intergranular fracture and precip. 77—48520
- Al-Cu, binary, solidification, predicted volume change 77—28802
- Al-Cu, cast, chilled zone composition and thickness obs. *(Japanese)* 80—7541
- Al-Cu, cast and directionally solidified, porosity 79—74145
- Al-Cu, cathodes for He-Ne lasers, cold, vapour deposited 80—5748
- Al-Cu, cold working causing preprecipitation, thermoelec. power *(French)* 79—8306
- Al-Cu, comparison of liquid impact erosion and cavitation erosion 80—104302
- Al-Cu, condensed films, metastable states 79—15046
- Al-Cu, corrosion of chill zone, solidification microstruct. effect 77—36687
- Al-Cu, couple phase diagrams and thermochemical data 79—66037
- Al-Cu, crack advance during fatigue, effect of cyclic hardening and COD 77—16675
- Al-Cu, decomposition of Guinier-Preston zones *(German)* 80—30014
- Al-Cu, dendritic solidification, fluid flow effect 78—11215
- Al-Cu, diffuse light scattering method for in situ obs. of pitting corrosion 80—25930
- Al-Cu, dil., anisotropic scattering of conduction electrons on dilute Cu impurities 79—47082
- Al-Cu, dil., core and valence band spectra, XPS study 80—84837
- Al-Cu, dil., deviation from Matthiessen's rule at high temps. 78—64025
- Al-Cu, dil., electronic states, XPS meas. 77—44117
- Al-Cu, dil., pulsed ruby laser irrad., noncryst. phase form 80—35012
- Al-Cu, dil., virtual bound states 77—43528
- Al-Cu, dil. alloy, quench condensed thin films, supercond. and struct. from electron diffr. patterns 78—47901
- Al-Cu, dil. binary alloy, planar interface stability during solidification *(Slovak)* 80—108424
- Al-Cu, disordered, electron energy struct. and X-ray emission bands, average t-matrix approx. *(Russian)* 80—24779
- Al-Cu, effect of alloy purity and ageing on fracture mechanism, and resultant toughness 79—5049
- Al-Cu, elastic interaction energy calcs. for Guinier-Preston zones 79—11617
- Al-Cu, electric discharge sintering of powder mixtures 78—60605
- Al-Cu, electrical resist. of Guinier-Preston zones during age hardening 77—72848
- Al-Cu, electronic structure exam. by soft X-ray and X-ray photoelectron spectroscopy 77—85136
- Al-Cu, epitaxial film, vac. deposited on NaCl(001), orientation obs. *(French)* 79—95294
- Al-Cu, evaporation, successive dilution method for reproducible control 77—69994
- Al-Cu, film, prep. by planar magnetron sputtering *(Japanese)* 80—16184
- Al-Cu, flow stress, origin of high strain rate sensitivity 78—44186
- Al-Cu, growth kinetics of plate precipitates 77—66649
- Al-Cu, growth kinetics of plate shaped precipitates 78—6932
- Al-Cu, growth kinetics of plate shaped precipitates 78—6933
- Al-Cu, growth kinetics of plate-like precipitates, vol. diffusion controlled growth 78—6935
- Al-Cu, growth kinetivs of plate-shaped precipitates 78—6934
- Al-Cu, high strength, type 2024-T3, crack growth, fatigue induced surface deform., holographic detect. 80—85120
- Al-Cu, high temp. internal friction peaks 77—48470
- Al-Cu, implanted metal system, Cu redistrib. after laser irrad. 79—69163
- Al-Cu, ingots, solidified, formation of equiaxed eutectic grains *(Japanese)* 78—39756
- Al-Cu, intergranular morphology of θ' precipitates, angle between grain boundary/precipitate plane 78—48413
- Al-Cu, isothermal coarsening of liquid inclusions 77—21166
- Al-Cu, lattice thermal cond. at low temps. 77—62889
- Al-Cu, liq., dissoln. and diffusion of alloying components, 700-1000°C *(Russian)* 80—15275
- Al-Cu, liq. alloys, surface tension meas. *(French)* 78—18875

copper alloys continued
Al-Cu, liq. alloys, with zero superheat, fluidity 80—70289
Al-Cu, liq. diffusion coeff. meas. using temp. gradient zone melting 78—26710
Al-Cu, liquid, surface tension model using surrounded atom concept 77—15665
Al-Cu, liquid alloys, exam. of Si diffusion *(Russian)* 79—28118
Al-Cu, liquid impact erosion 80—108598
Al-Cu, low freq. internal friction during plastic deform. *(Chinese)* 80—103420
Al-Cu, melt near solid-liquid interface, diffusion during crystallisation *(German)* 79—29046
Al-Cu, molten, showering cryst. form. in mould cooled from top *(Japanese)* 80—66498
Al-Cu, O transport during fatigue crack growth 78—52981
Al-Cu, partially solidified, viscosity and struct. *(Japanese)* 79—14950
Al-Cu, pitting potential 78—35550
Al-Cu, precipitate plate growth kinetics 79—15679
Al-Cu, precipitation hardened, hysteretic plastic work as failure criterion in Coffin-Manson type relation 77—32657
Al-Cu, rapid quenching, struct. and decomp. 80—76244
Al-Cu, recrystallization texture 79—91679
Al-Cu, single and two phase, superplastic behaviour 80—11709
Al-Cu, solidification, solid-liq. interface, solute conc. effects 80—59632
Al-Cu, solidification, stability of spherical particle growing from stirred melt 77—47365
Al-Cu, solute atom displacement in mixed dumbbell interstitials for FCC lattice 78—79631
Al-Cu, splat quenched, amorphous regions 77—4047
Al-Cu, splat quenched, amorphous regions, comment 77—4048
Al-Cu, splat quenching, electron transparent area prod. 77—4754
Al-Cu, splat-quenched, microstruct. thickness and comp. depend., TEM 77—8863
Al-Cu, stir cast microstructure, turbulent flow and solidification 79—20036
Al-Cu, superconducting amorphous films of high stability 80—70889
Al-Cu, surface enrichment of Cu due to Xe sputtering, AES and He ion backscatt. meas. 77—4250
Al-Cu, type 1100, synchrotron radiation microradiography 80—85121
Al-Cu, type 2036-T4, plane-strain work hardening, meas. and anal. 80—81073
Al-Cu, type 2219-T851, fracture mechanics and surface chemistry of fatigue crack growth 80—81168
Al-Cu, US wave propag. velocity, exam. 78—72982
Al-Cu, vertically solidified, effect of fluid flow on solidification struct., and macrosegregation *(Japanese)* 78—48391
Al-Cu, work hardening under tension at 1.6-900K 79—38842
Al-Cu (0.1 wt.%) alloy, unidirectional solidification, stability of planar solid liquid interface 77—86020
Al-Cu (0.5, 2 and 4.5 wt.%), solidification, apparent solid region *(Japanese)* 77—63653
Al-Cu (0.5 to 40 wt.%), morphology of quenched solid-liquid interface *(Czech)* 77—86021
Al-Cu (0.5 to 4.6 wt.%), cathode foil for electrolytic capacitors, relationship between comp., struct., and etchability 79—74314
Al-Cu (0.5 wt.%), evaporated layers, electromigration, linewidth depend. 80—65277
Al-Cu (1 to 10 wt.%), vapour deposited films, ion scattering spectrometry characterisation 80—15386
Al-Cu (1 wt.%), electron irradiated, dislocation damage, HVEM study 80—103389
Al-Cu (1 wt.%) alloy, plasmon dislocation interactions, electron microscope investig. 77—15421
Al-Cu (10 wt.%), inverse segregation 78—52819
Al-Cu (1.5 at.%), vacancy charact. study by electrical resistance derivative method, rel. to temp. 78—47361
Al-Cu (1.7 at.%), EXAFS study of precipitation 79—100151
Al-Cu (1.9 at.%), solute fluctuations, EXAFS study 80—79949
Al-Cu (2-5 wt.%), precipitation total surface influence on resistivity *(French)* 80—71650
Al-Cu (2%), metallisation for SAW devices 80—23856
Al-Cu (2.12 at.%), irradiated by 8J CO_2 laser pulses, metastable precipitate and amorphous phase *(French)* 78—80552
Al-Cu (2.6 wt.%), sheets, effect of strain path changes on formability 79—43347
Al-Cu (3 wt.%), stress aged, GP zone struct. by X-ray diffuse scatt. meas. *(Japanese)* 80—71653
Al-Cu (3 wt.%) single cryst., stress aging, oriented precipitation *(Japanese)* 80—71652
Al-Cu (33 wt.%) eutectic, superplasticity, in-situ obs. by TEM 77—28876
Al-Cu (33 wt.%) eutectic, solidification under reduced gravity, behaviour of suspended Al_2O_3 particles *(German)* 80—60853
Al-Cu (3.5 wt.%), precip. on stationary and non-stationary grain boundaries 78—84820
Al-Cu (3.71 wt.%), stress oriented precipitation of Guinier-Preston zones and θ' 78—52809
Al-Cu (3.93 wt.%), planar defects within theta precipitates 77—16583
Al-Cu (3.97 wt.%), containing Guinier-Preston zones, high resolution lattice images 80—107114
Al-Cu (4 wt.%), AE during deform., effect of ageing at 170°C 78—64597
Al-Cu (4 wt.%), age hardening, conditions leading to localised plastic deform. and fracture in slip bands during fatigue 78—64670
Al-Cu (4 wt.%), aged to contain Guinier Preston zones, crystallographic fatigue crack growth 78—60832
Al-Cu (4 wt.%), effect of semicoherent precipitation on void swelling, when neutron irradiated 79—42115
Al-Cu (4 wt.%), elastic accommodation of semicoherent θ' 78—64543
Al-Cu (4 wt.%), enhanced precipitation under electron irradiation in HVEM 78—52818
Al-Cu (4 wt.%), fatigue crack propag. role of adsorption in H_2S, Hg and moist air *(French)* 78—15580
Al-Cu (4 wt.%), high temp. cyclic deform., θ' particle dissolution obs. 80—108515
Al-Cu (4 wt.%), interparticle spacing influence on cyclic deformation and fatigue crack propag. 79—61717
Al-Cu (4 wt.%), naturally aged, early stages of G.P. zone form. 77—90355
Al-Cu (4 wt.%), neutron irrad., weak-beam dark-field obs. of dislocations near θ' precipitates 80—107333

copper alloys continued
Al-Cu (4 wt.%), non IPS geometric surface relief effects associated with diffusional phase transform. 77—32575
Al-Cu (4 wt.%), precipitation sequence of metastable phases, NMR meas. 78—23713
Al-Cu (4 wt.%), precipitation hardened and fatigued alloys, solute loss at fracture surface, EPMA exam. 78—39893
Al-Cu (4 wt.%), relationship between enthalpy, yield strength, and size of Guinier-Preston zone *(French)* 78—19767
Al-Cu (4 wt.%), reversion charact. *(Japanese)* 77—21150
Al-Cu (4 wt.%), reversion process of Guinier-Preston zones, ^{63}Cu NMR obs. 80—60871
Al-Cu (4 wt.%), single crystal, anisotropy in plane strain compression 77—36599
Al-Cu (4 wt.%), single cryst., small angle X-ray scatt. map after spinodal decomp. 79—15645
Al-Cu (4 wt.%), size distrib. and form. mechanism of GP zones *(Japanese)* 77—25054
Al-Cu (4 wt.%), stress corrosion cracking, effect of cold reduction *(Japanese)* 77—48580
Al-Cu (4 wt.%), supersaturated and aged conditions, high strain deform. 80—60907
Al-Cu (4 wt.%), TEM obs. of intergranular corrosion 79—91835
Al-Cu (4 wt.%), tensile ductility, effect of ageing and impact velocity *(Japanese)* 78—15465
Al-Cu (4 wt.%), θ' phase coalescence 79—56985
Al-Cu (4 wt.%), θ'-phase precipitation, characterisation of stages 79—56984
Al-Cu (4 wt.%), with θ' precipitates, relation between elastic limit and hardness *(French)* 79—5018
Al-Cu (4 wt.%) alloy, coherency loss of θ'-phase due to deform. 77—15424
Al-Cu (4 wt.%) alloy, precipitation hardened, single crystal, directional plastic behaviour, exam. 78—39788
Al-Cu (4 wt.%) alloy, reversion characts. *(Japanese)* 79—56989
Al-Cu (4 wt.%) alloy, θ' precipitate growth kinetics, electron microscope obs. *(French)* 77—44253
Al-Cu (4 wt.%) fractography *(German)* 78—19982
Al-Cu (4 wt.%) partially coherent precipitation hardened alloy, high temp. cyclic deform. 80—25710
Al-Cu (4% wt.), single crystals, positron trapping at precipitates 78—76554
Al-Cu (4.2 wt.%), precipitation strengthened, solute depletion at fatigue facets, AES study 79—38973
Al-Cu (4.3 wt.%), containing Guinier-Preston zones, high resolution lattice images 80—107115
Al-Cu (4.3 wt.%) alloy, lattice electron micrograph interpretation 79—86659
Al-Cu (4.5 wt.%), cast alloy, ductile intergranular fracture 77—28908
Al-Cu (4.5 wt.%), growth structs. with dendrite growth directions differing from heat flow direction during solidification 79—43235
Al-Cu (4.5 wt.%), volume contraction accompanying solidification 78—52791
Al-Cu (4.5 wt.%) alloy, controlled electropotential corrosion in NaCl soln., microstruct. exam 78—39948
Al-Cu (4.5 wt.%) cast alloy, press. effect during solidification on struct. and mech. props. *(Korean)* 77—77469
Al-Cu (4.5% at.wt.), laser surface melting and subsequent solidification, computer heat flow models 79—69916
Al-Cu (4.6 wt.%), cold work and ageing influence on ductility and fracture behaviour *(Japanese)* 80—89295
Al-Cu (4.8 wt.%), homogenization, temp. gradient driver process 77—52362
Al-Cu (4.8 wt.%), secondary arms in dendritic growth, solidification effects *(Japanese)* 78—15387
Al-Cu (4wt.%), elastic limit, precipitation effects *(French)* 79—47738
Al-Cu (5 wt.%), ageing, extinction effects *(Russian)* 77—81283
Al-Cu (5 wt.%), ageing during relax. of elastic stresses, X-ray diffr. expts. *(Russian)* 77—59821
Al-Cu (5 wt.%), fatigue strength, coarse precipitation effect *(German)* 79—91660
Al-Cu (5.7wt.%), unidirectionally solidified, dendritic morphology and dendrite arm spacing 79—29043
Al-Cu (6.3 wt.%), fatigue crack propag., plastic work role 79—79070
Al-Cu (96.5, 3.5 wt.%), characts. of disappearance of excess vacancies on dislocations 80—33991
Al-Cu (up to 0.5 at.%), neutron damage rate, interpretation of results 78—63794
Al-Cu alloy, deposition from RF induction source, onto laminated polyimide substrates and characterisation 80—16535
Al-Cu alloy, microsegregation *(Japanese)* 77—16589
Al-Cu alloy, nonstationary mass transfer in front of moving phase boundaries in mormal freezing *(German)* 77—44238
Al-Cu alloy, Portevin-Le Chatelier effect, influence of specimen dimensions and machine stiffness 77—70128
Al-Cu alloy, press-forming under coexisting state of liquid and solid, mech. props. 77—81240
Al-Cu alloy, vacuum deposited thin film, abnormal grain growth before melting transition and subsequent struct. change 79—60663
Al-Cu alloy 1201, thermomech. treatment effect on strength characts. and fracture toughness *(Russian)* 80—40391
Al-Cu alloy 2011, extraction and phase anal. 79—15673
Al-Cu alloy D16, riveted, low-cycle fatigue strength 80—30097
Al-Cu alloy dendritic solidification kinetics 80—81041
Al-Cu alloy in NaOH, aminophenols as corrosion inhibitors 80—30136
Al-Cu alloy precipitation and heat of evolution, microcalometric obs. *(Japanese)* 78—15406
Al-Cu alloy prod., Cu interdiffusion with sintered Al powder, struct. effect at high press. 78—60606
Al-Cu alloy RR58, high strain fatigue life, prior treatment effect 78—60835
Al-Cu alloys, anisotropy function determ. 77—43565
Al-Cu alloys, coarsening mechanisms of secondary dendrite arm, and organic analogue 80—81049
Al-Cu alloys, Cu precipitate detect. by positron annihilation, GP zone development 80—3051
Al-Cu alloys, dil., EXAFS spectra 80—2898
Al-Cu alloys, Guinier-Preston zones study by stress ageing 79—100152
Al-Cu alloys, hypo- and hyper-eutectic, dendrite coarsening during solidification 77—63651
Al-Cu alloys, positive muons diffusion and trapping 79—11372

copper alloys continued
Al-Cu alloys, quenched rapidly, microstruct. 78—56668
Al-Cu dil. alloys, elec. resist. temp. depend. 77—8068
Al-Cu dilute alloys, vein closing mechanism in fluidity tests 80—84924
Al-Cu edges in Permalloy conductor crossing effect on bubble propagation margins 80—29588
Al-Cu eutectic, mechanism of lamellar spacing adjustment 78—31395
Al-Cu eutectic alloy, cooling rate in rapid solidification, estimation from cell spacing 80—50623
Al-Cu eutectic melts, struct. determ. *(Russian)* 77—80408
Al-Cu film, anodic oxidation, corrosion props. 78—35581
Al-Cu film, galvanostatic formation anodic oxide, Rutherford backscattering and depth profiling 78—92395
Al-Cu film, magnetron sputtered deposition, characts. 79—91587
Al-Cu film bilayers, growth kinetics of θ phase, He$^+$ backscatt. and X-ray exam. 78—84105
Al-Cu films, DC sputtered, Cu distrib. 80—80113
Al-Cu films, deposition rate, mol. beam incidence angle influence on struct., film props. *(Russian)* 79—60646
Al-Cu full coherent precipitation hardened alloy, high temp. cyclic deform. 80—25711
Al-Cu hypoeutectic, solidification cycle, thermal anal. 80—29945
Al-Cu layer, photolithographically patterned, separation from substrate using plasma etching *(Slovak)* 80—45405
Al-Cu liquid alloys, rapid quenching prep. of metastable solids, apparatus *(German)* 79—28990
Al-Cu samples (0.5, 2.0 and 4.0 wt.%) polycryst., precipitation, positron annihilation and TEM 80—50639
Al-Cu single cryst., hardening due to oriented GP zones 80—55414
Al-Cu solid soln., supersaturated, plastic deform. effects *(French)* 79—91748
Al-Cu thin films, microstruct. rel. to electromigration 80—44355
Al-Cu type 2024 alloy, erosion in cavitating venturi 80—108602
Al-Cu-Fe, liquid, mag. moment and transition from mag. to nonmag. state 79—24132
Al-Cu-Fe alloys, solid and liquid, exam. of constitution and mag. props. *(German)* 78—52206
Al-Cu-Mg, acoustic emission power, strain rate depend. 77—4808
Al-Cu-Mg, acoustic emission during tensile testing 80—7632
Al-Cu-Mg, aged, stress corrosion cracking in NaCl soln. 80—7709
Al-Cu-Mg, alloy 2124-T351, crack tip closure assessment by electronfractography 80—16427
Al-Cu-Mg, alloy Al2048, early stages of fatigue crack propag. 77—63780
Al-Cu-Mg, alloys A-U4, A-U4G1, A-U2GN, effect of environment on fatigue crack growth 78—64677
Al-Cu-Mg, cold plastic deformation, stress/strain relations 79—56991
Al-Cu-Mg, dil. alloys, ageing response *(Korean)* 77—28832
Al-Cu-Mg, rolled plate fatigue charact. *(Russian)* 80—16437
Al-Cu-Mg, string ghost form. during solidification *(Japanese)* 79—100130
Al-Cu-Mg, tpye RR55, high strength, creep behaviour, effect rel. to anodic coatings, SEM study 80—97542
Al-Cu-Mg, tube drawing, tensile forces, plastic deformation *(French)* 79—70130
Al-Cu-Mg, type 2036, deformation at ageing temp., effect on struct. and props. 80—7605
Al-Cu-Mg, type D16 alloy, stress intensity coeff. determ. 79—87711
Al-Cu-Mg, type D16T, thin-wall cylinder cold rolling method 80—66535
Al-Cu-Mg (1.3, 1.3 at.%) alloy, natural ageing, meas. of quenching vacancy dislocation loops 79—15704
Al-Cu-Mg (2.0, 1.1 wt.%), Ostwald ripening of S′ precipitates *(Korean)* 79—38831
Al-Cu-Mg (2.6, 0.4 wt.%), Fe, Si, Mn and Ti addition effects on age-precipitation *(Japanese)* 80—20937
Al-Cu-Mg (4, 1.5 wt.%), mica dispersed, wear characts. and bearing performance 80—108591
Al-Cu-Mg (4,1 wt.%), behaviour during ductile fracture, SEM *(Rumanian)* 80—21062
Al-Cu-Mg alloy, extruded, press forming in liquid/solid coexisting state, mech. props., Mg effects 78—11151
Al-Cu-Mg alloy, influence of plastic deformation on fatigue limits, for prestrained components 78—68799
Al-Cu-Mg alloy, struct. of Guinier-Preston zones *(Russian)* 79—1870
Al-Cu-Mg alloy D16T, fatigue cracking under cyclic bending *(Russian)* 78—31506
Al-Cu-Mg alloy RR58, comparison of methods of correlating creep crack growth 78—60826
Al-Cu-Mg based, RR58, remaining creep life estimation from creep crack density meas. 78—44194
Al-Cu-Mg/mica particulate composite mech. props. 80—100919
Al-Cu-Mg-Ag casting alloy, precipitation hardening in artificially aged condition 79—1874
Al-Cu-Mg-Fe-Ni, Hiduminium RR58, crack propag. rates in air and salt soln. 80—21063
Al-Cu-Mg-Li alloy extrusions, microstruct., embrittlement and fracture props. 80—60965
Al-Cu-Mg-Mn, shot peened, positron annihilation meas. 77—63833
Al-Cu-Mg-Mn (4.5, 1.5, 0.6 wt.%), alloy 2024-T3, exam. of residual strength of plate containing crack, fracture anal. 78—90792
Al-Cu-Mg-Mn (4.5, 1.5, 0.6, wt.%), alloy 2024-T81, plates, adhesively bonded, exam. of fatigue crack growth 78—92349
Al-Cu-Mg-Mn (4.5, 1.5, 0.6 wt.%), thin sheet, exam. of fracture toughness, and fatigue crack growth 78—92353
Al-Cu-Mg-Mn-Fe-Si, alloy D16, effect of mechanisothermal treatment on mech. props. 78—56674
Al-Cu-Mg-Mn-Si-Fe, endurance with cyclic bending, effect of loading conditions 80—50724
Al-Cu-Mg-Mn-Si-Fe, subcritical crack growth under static plane stress 80—55528
Al-Cu-Mg-Mn-Si-Fe, torsional vibrations decrement, deformed vol. effect 80—76326
Al-Cu-Mg-Mn(-Zn-Cr), low temp. deformed, ageing and mech. props. 79—1881
Al-Cu-Mg-Ni-Fe alloy RR 58, creep resistance at elevated temps., thermomechanical treatment effects 77—59836
Al-Cu-Mg-Si-Fe-Mn-Ti, Si, Fe, Mn and Ti effect on precipitation in solid soln. *(Korean)* 79—66064
Al-Cu-Mg-Si-Mn (2.5, 0.7, 0.7, 0.5 wt.%), alloy AK6, US inspection of heat treatment quality 78—76681

copper alloys continued
Al-Cu-Mg-Si-Mn alloy AK8, fatigue strength, effect of residual stresses and cold working 77—56101
Al-Cu-Mg-Zn, Mg and Zn addition effects on dendrite struct. and mech. props. *(Korean)* 77—28796
Al-Cu-Mg-(Ag), effect of addition on fatigue microstructure relationships 80—40483
Al-Cu-Mg(:Fe,Si) alloys, double-ageing, resist., hardness meas. 77—28822
Al-Cu-Mg(-Si), inclusions, oriented distrib. metallography and effects on anisotropy *(Russian)* 78—80589
Al-Cu-Mn, long term strength and creep 80—60925
Al-Cu-Mn, type 2219, synchrotron radiation microradiography 80—85121
Al-Cu-Mn (1-5.2, 0-0.6 wt.%), N alloying and comp. effect on mech. props. *(Bulgarian)* 80—71719
Al-Cu-Mn (6.3, 0.3 wt.%), Al 2219-T851, fatigue crack initiation and early propag. 77—32684
Al-Cu-Mn (6.3, 0.3 wt.%), alloy Al 2219-T851, crack closure load meas. during fatigue 77—63870
Al-Cu-Mn (6.3,0.3 wt.%), alloy Al 2219-T851, crack closure load development for surface microcracks 77—86226
Al-Cu-Mn-Mg alloy D16, sheet, corrosion fatigue strength, with anodised and painted surfaces *(Russian)* 78—35575
Al-Cu-Mn-Mg-Fe-Si, corrosive environment effect on fatigue crack growth rate 80—55584
Al-Cu-Mn-Mg-Fe-Si (4.48, 0.66, 1.55, 0.43, o.23 wt.%), alloy D16, relationship between intercrystallite corrosion depth, and elec. cond. 79—20220
Al-Cu-Mn-Mg-Fe-Si-Zn alloy D16, surface layers chem. composition rel. to fatigue resist., corrosion-fatigue resist. 79—29275
Al-Cu-Mn-Zr, type 2219, particle, coarsening of disk shaped Θ' particles 80—45315
Al-Cu-Mn-Zr-Fe-Si (6,0.3,0.18,0.3,0.1 wt.%) experimental evidence of Mn enrichment in Al_2Cu precipitates by EDS in TEM 78—15415
Al-Cu-Ni, alloy RR 350, θ'-hardened, deform. induced microstructural instability, high temps. 80—16321
Al-Cu-Ni, directionally solidified, exam. of struct. of two phase alloys 78—80537
Al-Cu-Ni, vacancy ordering, electron microscope and electron diffr. obs. 79—27954
Al-Cu-Si, Al rich, unidirectionally solidified, microstruct. 79—34021
Al-Cu-Si, effect of sample conditions on sputtering and intensities, emission spectrochem. anal. using glow discharge *(Japanese)* 80—21349
Al-Cu-Si-Mg, deform. simulation using torsional test, elastoplastic constitutive eqn. 80—93594
Al-Cu-Si-Mg (4, 0.8, 0.8 wt.%), GPB zone formation during room temp. ageing 77—44263
Al-Cu-Si-Mn, type 2017S-T4, crack initiation at root of circumferential notch of round bar specimens *(Japanese)* 80—60947
Al-Cu-Sn, ageing process, effect of Sn atoms, ^{119}Sn Mossbauer spectra obs. 80—7598
Al-Cu-Sn (3.4, 0.28 wt.%), Mossbauer anal. of Sn behaviour during ageing 78—31431
Al-Cu-Zn alloy, ageing, X-ray and electron diffr. meas. *(Russian)* 78—39806
Al-Cu-Zn system, solid-phase reactions, phase diagram 80—50603
Al-Cu-Zr, particle stabilized structures, hot deform. 79—47733
Al-Cu-Zr, superplastic alloy Supral, solidification and recrystallisation 80—7550
Al-Cu-Zr (6, 0.3 wt.%), superplastic, texture studies 79—83210
Al-Cu-Zr (6, 0.3 wt.%), superplastic, mech. anisotropy and deformation mechanisms 79—83254
Al-Cu-Zr (6, 0.4 wt.%), superplastic flow activation energy 80—11701
Al-Cu-Zr (6, 0.4 wt.%), superplastic deformation characts. 80—16387
Al-Cu-(Mg), precipitation strengthened, Bauschinger effect 77—36585
Al-$CuAl_2$, directionally solidified eutectic alloy, effect of heat treatment 77—55977
Al-$CuAl_2$, eutectic system, interlamellar spacing meas. 77—36492
Al-$CuAl_2$, interface undercooling-growth vel. relationship, horizontal and vertical solidification 79—8294
Al-$CuAl_2$ aligned, fracture, effect of growth speed, orientation, environment 77—28907
Al-$CuAl_2$ eutectic, deformed, thermal stability 77—52348
Al-$CuAl_2$ eutectic, heat treatment and interlamellar spacing effect on tensile deformation 80—29979
Al-$CuAl_2$ eutectic, superplastic behaviour during compressive deform. 77—52429
Al-$CuAl_2$ eutectic, thermal instability in temp. gradient 78—52851
Al-$CuAl_2$ eutectics, microstruct. after solidification, heat pipe influence 80—76243
Al-$CuAl_2$ lamellar composite, creep, microstruct. obs. 79—8331
Al-$CuAl_2$ lamellar composite, stress and temp. depend. of creep 79—52330
Al-$CuAl_2$ lamellar eutectic, computer simulation of two dimensional Zn diffusion 78—30799
Al-Cu(-Mg), dimensional changes in heat treatment. 80—89271
Al-Cu(-Mg), normal and gravity segregation in ingots, expt. study *(Japanese)* 79—24526
Al-Cu(Zn, Ag, Mg_2Si), intermediate precipitates, stability, X-ray, elec. resist. and hardness study 80—3063
Al-Cu(0-10 wt.%) sintered alloys using composite powder 80—76210
Al-Cu(0.1 at.%), μ^+ depolarisation 79—56697
Al-Cu(4 wt.%), alloy AU4, θ' precipitation, apparent hardening maxima *(French)* 77—16598
Al-Cu(5.5 wt.%), macrosegregation during solidification *(Japanese)* 79 100150
Al-Cv (0.3 wt.%), moving solid-liq. interface, diffusion in liq. 80—107456
Al-Mg, dynamic uniaxial tension and compression curves 80—100884
Al-Mg-Cu, Al_2O_3 fibre reinforced, exam. of interface interactions during fabrication 78—76616
Al-Mg-Cu-Si-Cr (1,2.7,0.6,0.2wt.%), laser shock hardening of weld zones 78—39800
Al-Mg-Si-Cu, cold plastic deformation, stress/strain relations 79—56991
Al-Mg-Si-Cu, tube drawing, tensile forces, plastic deformation *(French)* 79—70130
Al-Mg-Zn-Cu, exam. of precipitation struct. by neutron scattering 78—92270
Al-Mg-Zn-Cu, type 7050, calorimetric study of fatigue induced microstructural changes 80—85034

copper alloys continued
Al-Mg(Cu)(Si), (5.0(4.5)(11.8) wt.%), ingots, vibr. effect during solidification on porosity formation 80—108426
Al-Mn-Cu, permanent magnetic materials, grain struct. effect *(Rumanian)* 79—73773
Al-Si-Cn-Mg, alloy AL32, ageing of castings produced by pressure die castings 78—56650
Al-Si-Cu, fracture resistance at low temps. 80—104284
Al-Si-Cu, granules, energy conditions of rolling 77—12578
Al-Si-Cu, LM30, crack propag. rates in air and salt soln. 80—21063
Al-Si-Cu casting alloy, optimum selection of chem. contents for optimum strength *(Czech)* 79—15625
Al-Si-Cu-Be alloys, phase equilib. *(Russian)* 77—59748
Al-Si-Cu-Mg-Ni, piston, depend. between min. creep rate and time of beginning of secondary creep *(Czech)* 80—35267
Al-Si-Cu-Mg-Ni cast alloy, fractography *(German, English)* 79—87809
Al-Si-Cu-Ni alloy casting, thermal props. 78—95814
Al-Si-Cu-Zr, ageing kinetics *(Russian)* 80—76274
Al-Zn-Cu (22, 0-3 at.%) alloys, coherent spinodal curve 79—87605
Al-Zn-Cu-Mg (V95T1), subcritical crack growth under static plane stress 80—55528
Al-Zn-Mg-Co, crazing tendency *(Russian)* 80—30068
Al-Zn-Mg-Cu, age hardened, effect of strain rate, temp. and environment on ductility 80—45368
Al-Zn-Mg-Cu, alloy 7075, hydrostatic pressure effects on ductile fracture 78—60779
Al-Zn-Mg-Cu, alloy 7075, fatigue, loading sequence, normal and reversed sequence effect 78—68791
Al-Zn-Mg-Cu, alloy 7075, effect of purity level, dispersoid type, heat treatment, on fracture toughness 78—80636
Al-Zn-Mg-Cu, alloy 7075-T6, corrosion in halide solutions, exam. of anion dependency 78—60867
Al-Zn-Mg-Cu, alloy 7075-T6, fatigue crack closure with negative stress ratio, following single tensile overloads 78—64687
Al-Zn-Mg-Cu, flaw growth in stress corrosion environment 79—66198
Al-Zn-Mg-Cu, fracture toughness 78—7044
Al-Zn-Mg-Cu, inclusions, oriented distrib. metallography and effects on anisotropy *(Russian)* 78—80589
Al-Zn-Mg-Cu, optimum treatment combination for thermochemical processing 77—44278
Al-Zn-Mg-Cu, type 7075, microstruct. role in hydrogen assisted fracture 80—30091
Al-Zn-Mg-Cu 7075, extraction and phase anal. 79—15673
Al-Zn-Mg-Cu (6, 2.5, 1.5 wt.%), deform. simulation using torsional test, elastoplastic constitutive eqn. 80—93594
Al-Zn-Mg-Cu (6,2, xwt.%) type alloy, fatigue crack propag., Cu content and recryst. effect 80—60960
Al-Zn-Mg-Cu (6.76, 2.37, 1.80 wt.%), cyclic SCC in salt water *(Japanese)* 80—45435
Al-Zn-Mg-Cu age-hardened alloys, fatigue crack propagation rel. to grain size in vac. and NaCl soln. 80—16538
Al-Zn-Mg-Cu alloy, laminated, adhesively bonded alloy 7075-T6, exam. of fracture resistance 78—76754
Al-Zn-Mg-Cu alloy, stress corrosion cracking mechanisms, rel. to micrographic obs. *(French)* 77—73376
Al-Zn-Mg-Cu alloy, type 7050 and AZ 74.61, engineering props. 79—70219
Al-Zn-Mg-Cu alloy, X-ray microanalysis in scanning transmission electron microscope, limitations 78—20122
Al-Zn-Mg-Cu alloy 7075, SCC from T6 to overaged T7X 77—90487
Al-Zn-Mg-Cu alloy 7075, overaged, precracked stress corrosion specimen, incubation effects 79—91832
Al-Zn-Mg-Cu alloy 7075-T651, adiabatic shear localisation and erosion 79—96157
Al-Zn-Mg-Cu alloys, effect of alloying elements as stress corrosion failure using regression analysis 78—80669
Al-Zn-Mg-Cu foil, STEM-microanal., specimen thickness effect on X-ray count rates 77—70374
Al-Zn-Mg-Cu type 7XXX, Cu effect and recrystallisation, low cycle corrosion fatigue 79—91852
Al-Zn-Mg-Cu type 7075, heat treatment optimisation 80—60888
Al-Zn-Mg-Cu-Co (6.5, 2.5, 1.5, 0.4 wt.%), fatigue crack propag. 80—55521
Al-Zn-Mg-Cu-Co-Fe-Si, powder alloy, fatigue crack tip plasticity, from load interactions 80—21066
Al-Zn-Mg-Cu-Cr, (5.6, 2.5, 1.6, 0.3 wt.%), laminates, 8 and 22 layers, adhesively bonded exam. of fatigue crack propag. 78—92345
Al-Zn-Mg-Cu-Cr, (5.6, 2.5, 1.6, 0.3 wt.%), alloy 7075, plates, adhesively bonded, exam. of fatigue crack growths 78—92348
Al-Zn-Mg-Cu-Cr, shot peened, positron annihilation meas. 77—63833
Al-Zn-Mg-Cu-Cr-Zr, high strength Cr and Zr addition effects 77—59820
(Al-Cu)/Si system, Si regrowth minimisation through overlying Al or Al alloy film 80—70569
AlCu, electron microscope spot prep. of deform. bands 79—15922
AlCu-NiCo (5 at.%), Θ′ hardened, creep mechanism 80—85013
Al_2Cu crystal, Young's modulus, Poisson ratio, elastic consts. determ. by extensometry and US meas., anisotropy discussion *(French)* 79—50683
Al_2Cu, de Haas-van Alphen effect and LMTO band struct. 79—69396
Al_2Cu, single cryst. elastic consts., 4.2-300K 78—72803
Al_4Cu_9, rhombohedral γ-brass, direct imaging of struct. and structural defects 80—15115
AlCuMgPb, microstruct. and flow stress during deform. at 573K 77—81307
$Al_{20}Cu_{25}Zr_{55}$ metallic glass, inelastic deform., free energy spectra 80—71699
AlZnMgCuO.5, crack propag. under monotone and cyclic load 78—7006
AlZnMgCuO.5, static crack growth, stress state effect, elec. pot. meas. 78—7007
Au-Ag-Cu, chem. surface anal., low energy ISS compared with SIMS 78—64908
Au-Ag-Cu, optical props. study using automatic nulling spectroellipsometer 80—55058
Au-Co, molten, US vel. meas., compressibility and partial struct. factors determ. 77—69045
Au-Cr, dil. spin glass elec. resist., press. and conc. depend. 80—24864
Au-Cu, cold worked, impurity conc. rel. to internal friction Bordoni peak, solid soln. hardening mech. 80—16363
Au-Cu, dielectric const. by multiangle reflection meas., optical props. 79—95723

copper alloys continued
Au-Cu, dil., electron irradiated, interstitials and their clusters, diffuse X-ray scatt. study 80—33997
Au-Cu, dil., quenched, vacancy cluster form. 77—62546
Au-Cu, dilute, low temp. thermoelec. power, electron diffusion and phonon drag. 77—20301
Au-Cu, Ising FCC and antiferromag., mag. phase diagram, ordering, Monte Carlo calc. 80—103833
Au-Cu, optical spectra, 0.5-6 eV, d-band struct. 77—48168
Au-Cu, oxidation kinetics of Cu out of Au soln. at 50-150°C 80—21171
Au-Cu, preferential sputtering 79—83080
Au-Cu, refr. index and absorpt. coeff., 1-5 eV *(Russian)* 78—60484
Au-Cu, residual elec. resist., pseudopot. calc. 80—6813
Au-Cu, short-range order and energy of ordering, diffuse X-ray diffr. meas. *(Russian)* 77—43174
Au-Cu, surface comp. after sputtering, AES obs. 77—55858
Au-Cu, surface comp. as function of temp., AES expts. 78—95212
Au-Cu, surface conc. profile and surface energy 80—84350
Au-Cu, surface segregation, electronic theory, density of states, cluster-Bethe-lattice approx. 80—49369
Au-Cu (4 wt.%), fatigue crack propag., environmental effects *(French)* 77—66711
Au-Cu (50% at.), pretransitional fluctuations *(French)* 80—2160
Au-Cu alloy, internal oxidation, calorimetric meas. 79—43258
Au-Cu film, elec. resist. and temp. coeff. of resist. 77—39968
Au-Cu solid soln., spectral determ. of comp. using UHF plasmotron as source 79—52812
Au-Cu-Ag, phase transform. effect on mech. props. *(Russian)* 78—3122
Au-Cu-Ag dental alloy, age-hardened, struct. and morphology 78—92272
Au-Cu-Ag-Pd (35.4, 17.8, 9.7 at.%), dental alloy, age-hardenable, TEM obs. 77—21156
Au-Cu-Cr, thin layer, deposited on glass or Si substrate, X-ray microanalysis *(French)* 80—50902
Au-Cu-Fe spin glass alloys, impurity mag. resist. meas. 80—59972
Au-Cu-Ga, solid soln., phase systems, valence electron density effects *(French)* 78—19724
Au-Cu-Ni, computer characterisation, exam. of phase equilibria and miscibility gap 79—11561
Au-Cu-Ni(Ag), phase precipitation on domain boundaries *(Russian)* 78—39777
Au-Cu-O surface, quantitative Auger analysis using relative sensitivity factors 78—7295
β-Au-Cu-Zn, martensitic transformation temps. ageing and quenching effect 79—47687
Au-Cu-Zn-Ni (13, 3.4, 8.5 wt.%), white gold, metallographic structure after cold rolling, effect of heat treatment, recrystallisation *(French)* 79—52238
Au-Ni-Cu phase diagrams, thermodynamic calc. *(Korean)* 78—68672
Au-Ni-Cu-Zn, white gold, metallographic struct., heat treatment and plastic working effect 80—40403
Au-Pt-Pd-Ag-Cu, commercial dental alloy, age-hardening characts. 80—89235
Au-Zn(Cu), electrolytic thinning for use in transmission electron microscopy 78—57918
AuCu II, periodic antiphase struct. *(French)* 79—14937
AuCu II, rational and irrational long period struct. 79—95175
AuCu II plates, growth mechanisms 77—48423
AuCu II plates, growth mechanism 79—56976
AuCu, optical constants direct determination, d absorpt., reflectivity 77—69791
AuCu-Al thin film bilayer system, phase formation, backscattering spectra 80—96728
$AuCu_3$, ordered, band struct. and optical props. at 30K 79—60696
$AuCu_3$, quantum theory of order-disorder transition energy 77—62640
$Au_{1-x}Cu_x$-Fe, dil., resistance maximum 79—61056
Au_3Cu, ht. of order-disorder transform., differential microcalorimetry *(French)* 78—57950
$Au_3Cu_{1-x}Ag_x$, phase relations, X-ray diffr. and differential thermal anal. 80—108395
$Au_2(MnCu)_2$, Heusler alloy, magnetic order and coupling 79—38303
BaCu, X-ray cryst. struct. determ. 80—92478
Be bronze, BrB2 grade, heat treatment quality evaluation, using eddy current device 77—90562
Be bronze, electrolytic polishing using cylindrical stationary electrode 78—64783
Be bronze, electropolishing using cylindrical electrode moving forwards 78—64784
Be bronze, struct. and props. after ageing under load 78—84932
Be bronze BrB2, quenched deformed, substruct. and props., effect of prerecrystallisation annealing *(Russian)* 78—60677
Be depth profiling by d and α detection in $^9Be(p,d)$ and $^9Be(p,\alpha)$ 79—5203
Be-Cu, calibration line introduction for comp. determ. by AES 79—56892
Be-Cu, ductile erosion, prediction, mechanistic model 77—12709
Be-Cu, optical elements, US cleaning, deleterious effects 77—42631
Be-Cu, props., precipitation hardening effects and appl. *(Italian)* 79—83207
Be-Cu, seawater corrosion protection, of repeater housings 78—15583
Be-Cu, thermal expansion, vibr. characteristics at low temp., effect of substitution impurities *(Russian)* 80—103439
Be-Cu alloy stress relaxation in bending, 63° to 343°C 80—50693
Be-Cu dynode, depth profiling anal. of surface layer 80—2253
Be-Cu high-strength alloy characteristics for electrical components 78—48547
Be-Cu K-band high-pressure cell for EPR-ENDOR studies 79—67336
Be-Cu mill-hardened strip stress relaxation obs. 78—48485
Be-Cu strip surface quality and preparation 80—50779
Be-Cu surface, secondary electron yield, for electron multiplier ion detector 78—74094
Be-Cu surface preparation for Au electrodeposition 78—7100
Be-Cu wire for high-speed matrix printers, wear resistivity obs. *(Japanese)* 80—55540
BeCu pressure clamp cell, for low temp. specific heat and magnetisation meas. 80—17956
Bi-Cu, liquid, interstitial index, definition and variation with temp. *(French)* 80—2011
Bi-Cu, molten, struct., cold neutron scatt. in region of small momentum transfer 77—39527
Bi-Cu, molten, struct., thermal neutron diffr. meas. 77—39526

copper alloys continued
Bi-Cu melts, struct., neutron scatt., conc. of segregated regions calc. 77—39528
Bu-Cu coating on steel 45, effect of abrasive particle size on wear 78—44225
CU-Zr-(Cr), powder metallurgical alloys, thermomech. treatment effect on props. 80—50660
CaCu$_5$, γ-phase in Ca-Cu system, calorimetric determ. of enthalpy of form. *(French)* 80—84915
Cd-CuCd$_3$, off-eutectic alloys, controlled grain growth *(Japanese)* 77—55958
Ce-Co-Cu-Fe-Ti, sintered magnet, prep. and mag. props. 77—73043
Ce-Cu, liq., charge transfer effect 78—94967
Ce-Cu, liquid, normal spectral emissivity 80—103506
Ce-Mn-Cu systems, phase equilibria at 600 and 400°C *(Ukrainian)* 80—11625
Ce-Sm-Co-Fe-Cu, permanent magnet props. 79—8013
CeCo$_{3.5}$Cu$_{1.5}$, and alloys of similar comp., cryst. structs., X-ray diffr. exam. 79—99120
CeCo$_{5-x}$Cu$_x$, $0\leq x\leq$ internal oxidation kinetics, oxide struct., X-ray study 80—104329
Ce(Cu,Ni)$_2$, pseudobinary phases, struct. and mag. props. rel. to Ce valence 78—6032
CeCu$_4$ Knight shifts and mag. susceptibility 79—95656
CeCu$_5$, Knight shift and mag. susceptibilities 79—95656
CeCu$_2$Si$_2$, collective phenomena 80—65933
CeCu$_2$Si$_2$, local mag. moments, neutron scatt. study 79—61058
CeCu$_2$Si$_2$, resistivity, thermal conductivity and thermopower between 1.5 and 300K 78—87963
CeCu$_2$Si$_2$, strong Pauli paramagnetism, superconductivity obs. 80—29499
CeCu$_2$Si$_2$, transport anomalies 80—20148
CeCu$_2$Si$_2$, tunnelling anomalies due to intermediate valence phenomenon 77—62873
CeCu$_2$Si$_2$, valence fluctuations, ^{29}Si NMR and mag. susceptibility 79—61246
Ce(Mn$_{1-x}$Cu$_x$)$_2$Si$_2$, mag. props. 80—25134
(Co, Cu, Fe)$_5$Ce, sintered permanent magnets, magnetic charact. 78—60608
(Co,Cu,Fe)$_5$Ce, sintered, mag. props. 78—68302
Co-Cr, fibrous eutectic, thermal stability 77—36547
Co-Cu, cryst. struct. and stacking fault influence on mag. props. *(Russian)* 80—25164
Co-Cu, electrodeposited alloy, struct. and physicochem. props. 78—35327
Co-Cu, multilayer α'-phase form. during martensitic transform. *(Russian)* 77—59785
Co-Cu, neutron radiation stimulated diffusion, electrical resistivity exam. *(Russian)* 79—14959
Co-Cu (8 wt.%), X-ray anal. of 126-layer rhombohedral martensite α'-phase 77—44251
Co-Cu-Fe-Ce, mag. characteristics of sintered permanent magnets 78—60312
Co-Cu-Fe-Ce alloys, sintered permanent magnets, mag. characts. 77—43855
Co-Cu-Fe-Sm magnet, microstruct. exam. after ageing, TEM meas. 77—48555
Co-Ni, selective catalytic surface behaviour, tight-binding approx. calcs. 78—76924
Co-Sm-Cu, phase diagram 79—91632
(Co$_{0.83}$Cu$_{0.17}$)$_6$Ce, cryst. struct. and mag. props., decomp. during ageing *(Russian)* 79—37661
Co$_4$CuCe, cryst. struct., mag. characts., ageing and decomposition *(Russian)* 79—4272
Co$_4$CuCe$_{0.9}$, correl. of cryst. struct. and coercive force *(Russian)* 77—80962
β-CoGa, Cu addition effects on defect struct. *(German)* 77—11546
Co$_2$Ga$_{2-x}$Cu$_x$, mag. and struct. phases from magnetisation, neutron, X-ray diffr. techniques 78—52253
Cr bronze Sn, recrystn. props., hot rolling, annealing, polygonisation *(Russian)* 80—55419
Cr-Ni-Mo-Cu-Nb steel, martensitic precipitation hardenable, corrosion-resistant, heat treatment, structure and props. 79—74169
Cu -Sn (0.05 at.%), grain boundary relax., misalignment angle effect *(Russian)* 78—3159
Cu alloy-Nb composite wires, resist.-temp. meas., percolation theory 79—28490
Cu based dilute alloys, enthalpy of formation and excess entropy 80—55347
Cu bearing substitutional solutions, thermodynamics, Kapoor model applicability 79—77761
Cu binary alloy, polarisation studies, electrode design 80—93761
Cu solid soln., wear 78—3233
Cu/Au planar interface, formation of ordered phases CuAu and Cu$_3$Au 79—82392
Cu-(Sn-)Ti melts, wetting of SiC 78—68664
Cu-Ag, alloys, activation vol. stress depend., single crysts. 77—48499
Cu-Ag, Auger spectroscopy, effect of composition on matrix parameters *(German)* 79—11489
Cu-Ag, deformed, recrystallization nucleation at second phase particles, electron microscope obs. 79—34059
Cu-Ag, dil., dose depend. of impurity detrapping stages after electron irradiation 78—51582
Cu-Ag, dil. molten alloy, Ag activity determ. by two-component evap. *(Japanese)* 77—48395
Cu-Ag, electron density change during Cu decay 79—99519
Cu-Ag, ion implantation as an ultrafast quenching technique for alloy production 77—55902
Cu-Ag, liquid alloy, solubility and activity of O$_2$ 79—29028
Cu-Ag, metastable alloy layer formed by Ag$^+$ ion implantation 78—71709
Cu-Ag, order-disorder transforms., s-band model 79—60502
Cu-Ag, solid soln., nonhomogeneity of deform. 78—84889
Cu-Ag, surface segregation of S, Auger spectral study diffusion 80—76549
Cu-Ag (Pb)(Bi), evaporation of Ag, Pb, Bi in vacuum induction melting 77—28742
Cu-Ag (0.1 wt.%), cold-worked, internal friction peaks in kHz range 80—89276
Cu-Ag (3 at.%), plastically deformed, lattice strain distrib. *(German)* 80—85012
Cu-Ag (8 wt.%), deformed, free energy changes in process of discontinuous precipitation 80—3054

copper alloys continued
Cu-Ag (8 wt.%), plastic deform. effect on discontinuous precipitation 80—3053
Cu-Ag film, amorphous resistivity, Hall coeff., thermopower and annealing kinetics 77—43744
Cu-Ag film, vac. deposited, thickness meas. using X-ray fluoresc. technique 79—90911
Cu-Ag film preparation with const. comp., by diffusion-limited evaporation from liquid 77—21038
Cu-Ag metastable alloy form. by ion implantation, combined TEM and ion channelling obs. 78—34530
Cu-Ag solder composite, plastic deform. below worn surfaces 77—36670
Cu-Ag-Au, coherent phase diagram, theoretical calc. 80—70373
Cu-Ag-Ge, Hume-Rothery glass form. 80—96449
Cu-Ag-O alloys, dil., O-metal interactions, activity coeff. meas. at 1423K 80—93792
Cu-Ag-P alloy wetting of Mo, Nb and Ta 79—82417
Cu-Ag-P amorphous alloys, strain gauge factor and elec. props. *(Japanese)* 79—79130
Cu-Ag-P(6-14, 11-14 wt.%) amorphous, crystn. and elec. props., X-ray diffr., elec. resist. and DTA meas. *(Japanese)* 80—84088
Cu-Ag-X, X=metals, P, S, Se, phase diagrams and thermodynamic props., iso-activity coeff. curves 77—81249
Cu-Ag-Zn, exam. of phase diagrams and thermodynamics props. 79—8275
Cu-Ag(Bi)-O, evaporation of Ag, Bi in vacuum induction melting 77—28742
Cu-Ag(Mn)(Ni)(Si)(Zn), alloying effect on embrittlement of stainless steel during soldering 79—47773
Cu-Ag(Pb)(Bi)(Ag-O)(Bi-O)(Si-S), stirred at different speeds under press., evaporation of Ag, Pb, Bi, S 77—47555
Cu-Ag(Se)(Sn)(Ag-Se-Sn), Ag, Se, and Sn effects, singly and together, on recrystallisation 79—100164
Cu-Ag(Sn), effective atomic number from β-ray produced bremsstrahlung meas. 78—22046
α_2-Cu-Al, antiphase period and tetragonality 78—15374
Cu-Al, α_2 phase, config. of periodic antiphase boundaries 79—95029
Cu-Al, α_2 phase form. process 77—48464
α-Cu-Al, binary substitutional, short-range ordering kinetics, vacancy behaviour 78—55867
Cu-Al, change in force constant due to volume effects 78—75778
Cu-Al, chemical emission by Ar$^+$ ion bombardment *(French)* 77—86410
Cu-Al, cold worked solid soln., anneal hardening, grain boundary effects 78—48420
Cu-Al, dil., thermal expansion *(French)* 79—95185
Cu-Al, directionally solidified eutectic composite alloy, form. and strength 77—90294
Cu-Al, dislocation core cut-off parameter, estimation from stacking fault nodes 80—103370
Cu-Al, dislocation core energy, core tension, Peierls model 79—27984
Cu-Al, dislocations, dissociated, climb mechanism, nucleated loops, Burgers vectors 80—65002
Cu-Al, disordered alloys, interatomic distances, coord. numbers, and mean relative displacements, EXAFS anal. 80—89087
Cu-Al, dispersion hardening by internal oxidation 78—56649
Cu-Al, effect of original grain size on struct. and props., after deformation and annealing 78—44178
Cu-Al, eutectic composition, exam. of high temp. mechanical behaviour *(French)* 78—72818
Cu-Al, explosive loading, depend. of struct. on deform. *(Russian)* 78—3177
α-Cu-Al, FCC, fractographic obs. of SCC 78—64786
Cu-Al, fatigue cracks, propagation, model, low cycle, cyclic stress-strain response determinations 79—68653
Cu-Al, faulted dipoles, geometry and form. 78—59809
Cu-Al, fission under weightlessness conditions *(Russian)* 78—31357
Cu-Al, gamma-2 phase intermetallic cpd., mech. props., effect of inversion domains 79—61599
Cu-Al, HV electron microscopy, crit. voltages depend. on comp., temp. and short-range order 80—100146
Cu-Al, heat capacity of phases, 233 to 800K, heat of transform. and entropy 77—47589
Cu-Al, heavily deformed martensites, annealing 79—38873
Cu-Al, impurity concentration effects 78—75777
Cu-Al, internally oxidised, elec. resist. meas. 77—35753
Cu-Al, internally oxidised, structural, elec. and mech. characts. 78—60761
Cu-Al, intrinsic temp. depend. of stacking-fault energy 78—51564
Cu-Al, irrad. in HVEM, climb of dissociated dislocations and point defect absorpt. 80—107257
α-Cu-Al, kinetic behaviour of vacancies and atoms 79—28129
Cu-Al, lattice thermal cond. meas., 0.06-2K 77—15822
Cu-Al, linear dislocation multipoles, weak-beam TEM 80—75233
Cu-Al, liq., elec. cond., temp. and conc. depend., model interpret. and alloy struct. *(Russian)* 80—88528
Cu-Al, low temp. deform., heating of dislocation sources 78—18660
Cu-Al, magnetic susceptibility, comp. and temp. depend., melting effects 78—52202
α-Cu-Al, mechanical twinning characts., 4.2 to 300K *(Russian)* 79—37714
Cu-Al, morphological stability study, phase transformations, two phase structure 78—11231
Cu-Al, negative muon capture ratios 80—55007
Cu-Al, optical composition modulation spectra, dielec. const. var., Fermi surface and electronic level shifts 80—6707
Cu-Al, ordered, superlattice fringe images, computer simulation 80—103296
Cu-Al, planar faults, faint electron microscopic image contrast obs. 80—107283
Cu-Al, plasticity, athermal and thermal *(Russian)* 79—11685
Cu-Al, positive muon trapping at vacancies 79—56704
Cu-Al, short range order and static distortion contribution to residual elec. resistivity *(Russian)* 80—70672
α-Cu-Al, short range order effect, atomic potential appl. 77—27850
α-Cu-Al, short range ordered, struct. and new superlattice phase 78—52756
Cu-Al, single crystal, dislocation velocity meas. 78—3171
Cu-Al, single crystal, dislocation velocity meas. 78—3172
α-Cu-Al, single crystal, low cycle fatigue 79—43405

copper alloys continued
- α-Cu-Al, single crysts., deformed and annealed, neutron small angle scattering 79—82127
- Cu-Al, single crysts., hysteresis behaviour implications rel. to fatigue, plastic strain cycling 80—3191
- Cu-Al, sintering, reduction processes, resist. meas. *(German)* 80—25597
- α-Cu-Al, solid soln., residual elec. resist. *(Russian)* 79—51547
- Cu-Al, strength and substruct., strain point influence *(Russian)* 79—52233
- α-Cu-Al, stress-strain behaviour, effect of grain size and composition 77—56038
- Cu-Al, sulphurisation solid state phenomena 78—64781
- Cu-Al, surface ionisation, elemental anal. of sputtering products *(French)* 80—50905
- Cu-Al, surface segregation during adsorption and low pressure oxidation *(French)* 78—75932
- Cu-Al, thermal conductivity, data anal. and synthesis 78—95284
- Cu-Al, two-phase Cu-rich alloy, influence of microstruct. on stress-strain behaviour 80—7631
- Cu-Al, vacuum condensate, struct. and mech. props. depend. on deposition conditons 80—15417
- Cu-Al (In), eutectic systems, specific phase boundary enthalpy, calorimetric study *(German)* 79—29016
- Cu-Al (0.05 wt.%), dil. alloy, anisotropic oxidation, electron microprobe Auger spectroscopy 77—12748
- α-Cu-Al (0.5 to 10 at.%), latent hardening and dislocation density 78—19853
- Cu-Al (0.5-17.6 at.%), mol. ions in spark source mass spectra 78—44427
- Cu-Al (10, 16 at.%), dislocation interactions, influence of jogs on extension of dislocation nodes 80—84176
- Cu-Al (10 at.%), dislocation glide source, TEM obs. 77—19958
- Cu-Al (10 at.%), single crystal, orientation depend. of work hardening near [111] axis 77—12646
- Cu-Al (10 at.%), single crystal, variation of flow stress after changes in strain rate 77—28879
- Cu-Al (10 at.%) alloy, work hardening at high temp. 77—32589
- Cu-Al (10 wt.%), annealed, tensile fatigue strength at high temp. in vacuum *(Japanese)* 78—35493
- Cu-Al (10 wt.%), deformed and tempered transform. during heat treatment of β' martensite *(Rumanian)* 79—34031
- Cu-Al (10 wt.%), water-quenched, tensile fatigue strength at high temp. in vacuo *(Japanese)* 78—72837
- Cu-Al (10.4%), creep, absence of instantaneous plastic strain upon stress changes 78—75718
- Cu-Al (10.5 at.%), dislocation generation and displacement in single crystal in bending 79—60368
- Cu-Al (11 at.%) single cryst., dislocation reactions during deform. twinning 80—79795
- Cu-Al (11.47 wt.%), high temp. phase transforms., effect of pre-exposure to neutrons 79—20045
- Cu-Al (11.6 wt.%), mech. props., tempering temps. effects 78—76669
- Cu-Al (12 wt.%), acoustic emission related to props. 79—34032
- Cu-Al (13 at.%), polycryst., effect of grain size, specimen thickness, on mech. props. 78—84945
- Cu-Al (13 at.%), polycrystalline aggregate, various grain sizes, specimen thickness effect on mech props. 79—61645
- Cu-Al (13wt.%), polycrystn. rod specimens; effect of specimen size on flow stress 79—79051
- Cu-Al (14.3 wt.%), ^{110}Ag diffusion in β/γ_2 interphase boundary 80—79989
- Cu-Al (14.8 at.%), vacancy formation energy determ. 78—63756
- Cu-Al (15 at.%), CC Cu-Al(Si), single crysts., latent hardening study by meas. of flow stress on secondary systems *(Japanese)* 79—24538
- Cu-Al (15 at.%), FCC, dislocations, elastic instability 79—82235
- α-Cu-Al (15 at.%), low temp. neutron irrad. induced point defects behaviour 77—43251
- Cu-Al (15 at.%), rolled single crysts., metallographic study of deformation struct., orientational change, shear bonds *(Japanese)* 79—24582
- Cu-Al (15 at.%), single crystal, steady state deform. with ⟨001⟩ axis at high temp. *(Japanese)* 78—6980
- Cu-Al (15 at.%), vacancy migration, and short range ordering, comparison of exp. results with theory 78—47356
- Cu-Al (15 wt.%), residual resistivity, influence of short range order and size effect *(Ukrainian)* 79—99528
- Cu-Al (15 wt.%) single crystal, steady state deform. at high temps. *(Japanese)* 78—19833
- Cu-Al (15.8 at.%), extension of jogs on dissociated dislocations, electron microscopy obs. 79—95017
- Cu-Al (2, 6.8 and 15 at.% Al), electron irrad. at 300 and 575 kV, exam. of damage rate 78—47425
- Cu-Al (21 at.%) transition state, tempered and quenched alloy *(French)* 80—55392
- Cu-Al (25 at.%), BCC β phase, high temp. creep, existence of master curve 80—55473
- Cu-Al (2.2 or 4.9 at.%), stacking fault energies, weak beam method of electron microscopy 77—19971
- Cu-Al (2.5 at.%), single crystal, steady state deform. at high temps. *(Japanese)* 77—52415
- Cu-Al (3 wt.%), annealing twins density, photoemission microscopy 80—35208
- Cu-Al (4.5 at.%), dislocation recovery anomalies *(Russian)* 77—21163
- Cu-Al (5 wt.%), subjected to tension-compression fatigue, deform. and fracture strength *(Japanese)* 80—93644
- Cu-Al (5.5, 7.3, 6.3 and 2.5 wt.%), Hg embrittlement under cyclic loading 77—86225
- Cu-Al (5.8 at.%) dislocation multipoles, weak-beam electron microscope obs. 79—73171
- α- Cu-Al (6 to 17 at.%), short-range order investigated by diffuse X-ray scatt. *(Russian)* 80—104187
- Cu-Al (6.4 wt.%), rolled low stacking fault energy alloy, struct. and texture 78—52844
- Cu-Al (7.5 at.%), single crystal, etched under load, slip bands 77—89446
- Cu-Al (7.9 wt.%), burst acoustic emission during Bauschinger effect 77—48475
- Cu-Al (8 at.%), coplanar slip, related with specimen size and axis *(Japanese)* 78—34518
- Cu-Al (8 wt.%) single crystal, surface dissolution effect on fatigue damage and crack nucleation 78—39936
- Cu-Al (9 wt.%), deformed, fatigue crack propag. 78—27621
- Cu-Al (9 wt.%), sudden mean stress variations during fatigue crack propag. 80—7668

copper alloys continued
- Cu-Al (9 wt.%) deformed, dispersed, ordered, microcalorimetry of plastic zones during fatigue crack propag. 79—47769
- α-Cu-Al (9.13, 13.56, 14.76, wt.%) short-range ordered, characterisation of locally ordered regions 80—79747
- Cu-Al (9.3 wt.%), in torsion, deformation temp. depend., superplasticity due to grain size, dislocation density *(Russian)* 79—74200
- Cu-Al ($<$3 at.%), new type of discontinuous slip at low temps. 77—12676
- Cu-Al alloy, dil., lattice expansion and localised vibr. mode 79—37789
- α- Cu-Al alloy, short range order structure 78—91303
- Cu-Al alloy, vacancy formation energy, determ., using new method, elect. cond. meas. 78—47345
- Cu-Al alloy, vibrs., average local information transfer approx. 79—46774
- Cu-Al alloy film, vacuum deposited, comp. struct., resistivity 78—6852
- Cu-Al alloy UA10, heat treatment *(French)* 80—35225
- Cu-Al alloys, laser microprobe emission spectroscopy, matrix effects 77—16870
- Cu-Al alloys, spark-source mass spectrosc. chem. anal., using mol. ions 79—92031
- Cu-Al alloys, strain hardening parameters, conc. and temp. depend., 4.2 to 300K *(Russian)* 79—20063
- Cu-Al bulk and thin-film forms, reflecting surface absorpt. coeffs. at 10.6 μm 80—95984
- Cu-Al composite, simulation of tensile behaviour and fracture void initiation *(Japanese)* 78—52948
- Cu-Al dil. alloy crystal, dislocation etch pits on {111} surfaces *(Japanese)* 77—62536
- Cu-Al dil. alloys, dislocation etch pit obs. on {111} surfaces 79—10861
- Cu-Al electrode, photopotentials, rel. to corrosion 79—24648
- Cu-Al eutectic alloy, unidirection transform. controlled by heat flow *(Japanese)* 78—15386
- Cu-Al film, electron energy loss spectra meas., optical functions calc. 78—19618
- Cu-Al films, elec. cond. of vacuum condensates depend. on composition, annealing *(Russian)* 80—65709
- β'Cu-Al martensite, stacking order, disorder anal. by continuous Fourier transformation of diffracted intensities 80—39115
- Cu-Al martensite, temper hardening, study by TEM, DTA, microhardness and yield strength meas. 79—43260
- Cu-Al powder compacts, elec. resist., temp. depend. 80—49690
- Cu-Al powder mixture, elec. discharge reaction sintering 78—64507
- α-Cu-Al single crystal, strain burst during low cycle fatigue 80—25866
- Cu-Al solid soln., internally oxidised, mech. props. *(Japanese)* 77—52411
- Cu-Al spherical crysts. grown from drop of melt, topography 80—84353
- Cu-Al system, high temp. lattice parameters by X-ray diffr. 80—28950
- Cu-Al_2O_3, dispersion strengthened, plasticity qualities, fractographical analysis *(Czech)* 80—50680
- Cu-Al_2O_3, dispersion-strengthened, vapour-deposited, tensile creep 78—11115
- Cu-Al_2O_3, internally oxidised, orientational relationships of precip. oxide phase 77—4783
- Cu-Al_2O_3, sinterec, deform., temp. and loading rate effects 77—77548
- Cu-Al_2O_3 (1 vol.%), effect of second phase particles on diffusional creep 78—31472
- Cu-Al_2O_3 coatings, electrodeposited, dispersion hardened, exam. of props. 79—34181
- Cu-Al_2O_3 disperse phase alloy oxidation kinetics 77—48584
- Cu-Al_2O_3 extruded bars, strength anisotropy 77—16597
- Cu-$Al_2O_3(SiO_2)$ dispersion hardening single crystal, cyclic deform. *(French)* 79—1893
- Cu-$Al_2O_3(SiO_2)(TiO_2)$ alloys, internally oxidised, plastically deformed, influence of particle form on primary loop nature *(French)* 80—103344
- Cu-Al-Co, precipitate-free zones near grain boundaries, growth kinetics, TEM obs. 80—40368
- Cu-Al-Co liquid alloys, constant Co-content of 5 wt.%, mag. props. *(German)* 80—88720
- Cu-Al-Fe, dil. liq. alloy, localised mag. state interactions *(German)* 77—1539
- Cu-Al-Fe, mech. props. rel. to heat treatment 80—50682
- Cu-Al-Fe, strength increase from intermediate annealing determ. of annealing temp. by recrystallisation 78—44136
- Cu-Al-Fe (11, 2 and 1 wt.%), Fe effects on microstruct. and mech. props. *(Korean)* 77—28807
- Cu-Al-Fe-Mn, phase transform. during continuous cooling *(German, English)* 79—70044
- Cu-Al-Fe-Mn (10,3,2 wt.%), phase comp. struct., continuous cooling from β-phase effect 79—24499
- Cu-Al-Mn, Heusler alloy, magnetic prop. investig. of struct. transitions *(German)* 77—8289
- Cu-Al-Mn, partial decomp. of β_1 phase, effect on mag. props. and martensitic transform. *(Russian)* 80—45306
- Cu-Al-Mn liq. alloys, susceptibility behaviour 80—93077
- Cu-Al-Mn spin glass, field depend. suscept. 79—73739
- Cu-Al-Mn(Ni)(Fe)(Co), hypereutectic, martensitic transform., effect of β_1-phase decomposition *(Russian)* 78—23705
- Cu-Al-Ni, 2H to 6R lattice restructurization during deform., anomalous elasticity 78—19753
- Cu-Al-Ni, elastic const. behaviour near Ms 77—12623
- Cu-Al-Ni, formation of martensitic phases during deform. by extension 79—20048
- Cu-Al-Ni, habit plane for SIM $\gamma' \rightleftarrows \beta_1'$ transform. 78—56640
- Cu-Al-Ni, heredity of martensitic transformations 79—47688
- Cu-Al-Ni, long period martensite phases, X-ray diffr obs. 80—7571
- Cu-Al-Ni, mixed powder compacts, Ni content influence in sintering behaviour *(Japanese)* 80—35130
- Cu-Al-Ni, phase diagram associated with stress induced martensitic transform. 79—8272
- Cu-Al-Ni, positron annihilation study of vacancies before and after martensitic transform. 79—99971
- Cu-Al-Ni, quenched, complex martensite form. 79—56977
- Cu-Al-Ni, rubber like behaviour 77—86114
- Cu-Al-Ni, single variant twinned martensites, pseudoelasticity 77—28849
- Cu-Al-Ni, sintered, internal friction after heat treatment *(Japanese)* 80—11686
- Cu-Al-Ni, stress induced martensite 77—36500
- Cu-Al-Ni, struct. anal. of stress induced β_1'' martensite by neutron diffr. 79—60308
- Cu-Al-Ni (13.8, 7.9 wt.%), cooling rates effect on internal friction *(Japanese)* 80—39217

copper alloys continued
- Cu-Al-Ni (14, 2.5 wt.%), thermodynamics of thermoelastic martensitic transform. 79—61585
- β-Cu-Al-Ni (14, 3 wt.%), single cryst., thermal effect due to stress induced martensite formation 80—81059
- Cu-Al-Ni (14, 4.5 wt.%), premartensitic alterations 77—12655
- Cu-Al-Ni (14, 8 wt.%), γ'-martensitic, sintered high damping 80—50577
- Cu-Al-Ni (14.0 4.2 wt.%), two stage superelasticity, successive martensite to martensite transform. 77—8826
- Cu-Al-Ni (14.1, 3 wt.%), autooscillations and nonlinear anelasticity 80—70307
- β_1-Cu-Al-Ni (14.2, 4.3 wt.%), quenched, metastable 2H type phase characts., TEM and electron diffr. study 79—74149
- Cu-Al-Ni (14.3, 4 wt.%), ω-phase form. during quenching and ageing *(Russian)* 80—25686
- Cu-Al-Ni (14.5, 3 wt.%), polycrystalline, pseudoelastic, cyclic stress strain response 77—86144
- Cu-Al-Ni (14.5, 3 wt.%), fatigued, polycrystn., pseudoelastic, dislocation and martensite substructs. 79—82223
- Cu-Al-Ni alloy, thermoelastic transformation hysteresis loop width strain rate depend. *(Russian)* 79—100138
- Cu-Al-Ni alloy single crystals, anomalous elasticity orientation depend., martensitic phase struct. during strain 79—87634
- Cu-Al-Ni alloys, deformed, fine struct. of martensite *(Russian)* 78—6923
- Cu-Al-Ni alloys, successive stress-induced martensitic transformations and associated transformation pseudoelasticity 79—43245
- Cu-Al-Ni Marmen alloys, rapid solidification and ageing 80—76245
- β-Cu-Al-Ni$_3$(DO$_3$), nonradial diffuse streaks and complex diffuse scatt. patterns of electrons 79—7527
- Cu-Al-Ni-Fe, (10, 5, 5 wt.%), cast microstruct. 78—80535
- Cu-Al-Ni-Fe system, corrosion behaviour in sea water 80—45421
- Cu-Al-Ni-Fe-Mn, cast Ni-Al bronze, fracture metallography 78—27597
- Cu-Al-Ni(Mn), duplex shape memory effect after nonuniform plastic deform. *(Russian)* 80—25759
- Cu-Al-Si, Si effect on mech. props. and microstructure *(Korean)* 79—38903
- Cu-Al-Si-C (95, 2.8, 1.8, 0.4 wt.%) fracture characts. of superplastic single phase, exam. 78—48500
- Cu-Al-Si-Co (2.8, 1.8, 0.4 wt.%), superplastic phase, exam. of mech. props. 78—52891
- Cu-Al-Sn system, coexistence of different and brass like phases 80—89206
- Cu-Al-Ti, formation of modulated structure rel. to barrier nucleation of new phase *(Russian)* 77—32580
- Cu-Al-Ti-Zr, internally oxidized, morphology of precipitates and dispersion hardening *(Russian)* 79—52217
- Cu-Al-Zn, period of periodic antiphases, quant. metallography *(French)* 79—100111
- Cu-Al-Zn, structural phenomena preceding martensitic transform. 77—12624
- Cu-Al(Au), critical voltage effect *(Japanese)* 78—91206
- Cu-Al(Au)(Ga)(Ni)(Pd)(Rh)(Zn) (4 at.%), anneal hardening mechanism 80—60879
- α-Cu-Al(Fe) dil. alloys, Al ion charge screening, elec. resist. obs. 77—4500
- Cu-Al(Ge)(Sn) alloy films, electron transport props. 77—76955
- Cu-Al(Ge)(Sn) film, thermoelec. power, 80-350K 78—68096
- Cu-Al(In), lamellar eutectoids, calorimetric determ. of interfacial enthalpy 78—60668
- α-Cu-Al(Ni)(Si), solid soln., ductility, comp. effect *(Japanese)* 79—43334
- Cu-Al(Si), preferred crystallographic orientation of melt grown single crystals *(Czech)* 79—43134
- Cu-Al(Si)(Fe)(Ni)(Pb), preferred crystallographic orientation of unidirectionally solidified polycrystals *(Czech)* 79—43233
- Cu-Al(Sn), effect of Al and Sn on friction and wear 78—11348
- Cu-Al(Sn), wear, recrystallisation as controlling process, FCC metals 77—56117
- Cu-Al(10 at.%) foils, trapezoidal splitting of partial dislocations 77—51376
- Cu-Al(23.5 at.% and 25.3 at.%), martensitic transform., positron annihilation meas. 77—16578
- Cu-Al(8 at.%), single crystal, twinning deform. 77—21236
- Cu-Au, (0.02-5 at.%), cold worked, internal friction peaks 79—11652
- Cu-Au, calc. of coherent phase diagram, using cluster variation method 79—11564
- Cu-Au, cold worked solid solution, flow stress and activation volume 80—16393
- Cu-Au, corrosion in HNO$_3$ 80—85091
- Cu-Au, dil., dose depend. of impurity detrapping stages after electron irradiation 78—51582
- Cu-Au, dil., enhanced lattice sp.ht. 78—51699
- Cu-Au, dil., magnetoresist., temp. depend. 80—70682
- Cu-Au, dil., Matthiessen's rule deviations above room temp. 79—91023
- Cu-Au, dil., O$_2$ solubility, thermodynamic and residual resist. study 78—59952
- Cu-Au, dil., thermal neutron irradiated, isochronal resist. recovery, 30-400K 79—19287
- Cu-Au, dose depend. of recovery after thermal neutron irrad. 77—69011
- Cu-Au, elastic modulus and internal friction during plastic deform., dislocation props. determ. 80—35244
- Cu-Au, elec. resist., pseudopot. calc. *(Russian)* 78—2460
- Cu-Au, H and D permeation, in situ growth of oxide barriers 78—75883
- Cu-Au, HV electron microscopy, crit. voltages depend. on comp., temp and short-range order 80—100146
- Cu-Au, long-range ordered, periodic antiphase domain boundary struct., X-ray diffr. obs. 79—95028
- Cu-Au, order-disorder transform, influence of strain energy 78—84796
- Cu-Au, plastic deformation, energy storage efficiency 77—4807
- Cu-Au, surface anal. by LEED and AES 77—69153
- Cu-Au, thermal conductivity, data anal. and synthesis 78—95284
- Cu-Au, vacancies and divacancies, quenching effects and elec. resist. meas. 80—39072
- Cu-Au (50 at.%), ordered, influence of elastic stresses on mech. props. *(Russian)* 78—92298
- Cu-Au alloys, electron density at Cu nucleus 79—54408
- Cu-Au alloys, vacancy and divacancy migration activation energies, elec. cond. meas. 80—88140
- Cu-Au film, aged, strength failure due to Kirkendall porosity 79—77969
- Cu-Au film, optical props. of ordered and disordered alloys 77—20945

copper alloys continued
- Cu-Au film, short wavelength composition modulation, interdiffusion exam. 77—72723
- Cu-Au off-stoichiometric alloys, long period superlattice 79—55699
- Cu-Au solid soln., Cu rich, meas. of interdiffusion, intrinsic and tracer diffusion coeff. 78—47608
- Cu-Au solid soln., Cu rich, elastic const. 79—87681
- Cu-Au system, grain boundary adsorption thermodynamics *(Russian)* 80—44317
- Cu-Au system, theory of interphase and antiphase boundaries 79—83174
- Cu-Au system, two-phase mixtures, long-period superlattices 80—84140
- Cu-Au-Cu thin film, diffusion induced grain boundary migration 79—77833
- Cu-Au-Fe, ferromag. ordering in FCC γ-Fe precipitates, Mossbauer study 80—71267
- Cu-Au-O alloys, dil., O-metal interactions, activity coeff. meas. at 1423K 80—93792
- Cu-Au(Be)(Sb), dil., electron high dosage source for residual resistance specimens and irradiation expts. *(German)* 78—21274
- Cu-Au(Pd), surface structures, LEED obs. 80—10761
- Cu-B, microvoid form., gaseous impurity atom effects, positron annihilation study 80—49275
- Cu-BN composite electromachining tools, dynamic hot pressing 80—84889
- Cu-Be, age hardening characts. *(Japanese)* 78—35398
- Cu-Be, condensation *(Russian)* 78—44014
- Cu-Be, dilute, electron irradiated, Be segregation 79—77637
- Cu-Be, dynamic segregation, ESCA obs. 77—8718
- Cu-Be, dynamic strain age hardening 77—52375
- Cu-Be, dynode surface, SEM and Auger microanalysis 80—100384
- Cu-Be, electrical resist. of Guinier-Preston zones during age-hardening 77—72848
- Cu-Be, explosive loading, depend. of struct. on deform. *(Russian)* 78—3177
- Cu-Be, impurity concentration effects 78—75777
- Cu-Be, quasiperiod struct. form. mechanism in eutectoid dissoc. 77—44257
- Cu-Be, relationship between discontinuous precipitation and continuous precipitation 79—100144
- Cu-Be, SCC in NH$_3$ 80—104326
- Cu-Be, solute atom displacement in mixed dumbbell interstitials for FCC lattice 78—79631
- Cu-Be, Young's modulus and yield point obs., dependence on heat treatment *(Czech)* 80—55448
- Cu-Be (0.0182 at.%), radiation induced Be segregation 78—23710
- Cu-Be (0.25 at.%), channelling meas. of trapping efficiencies of solute atoms for self-interstitials 79—86829
- Cu-Be (0.25 at.%), cryst., Cu self-interstitial atom, trapping, nucl. reactions and ion channelling obs. 78—14384
- Cu-Be (0.99 wt.%), direct obs. of small Guinier-Preston zones 78—72776
- Cu-Be (1.8 wt.%), discontinuous precip. form. and growth, TEM, obs. 80—104169
- Cu-Be (2 at.%), plastic deform. and dislocation substruct. 80—76307
- Cu-Be (2 wt.%), alloying addition effects on grain boundary reaction *(Japanese)* 80—49236
- Cu-Be (2 wt.%), plastic deformation influence on ageing, granular microhardness *(Russian)* 80—55474
- Cu-Be (2 wt.%), precipitation sequence, TEM obs. 80—108450
- Cu-Be (2.1 wt.%), discontinuous precipitation *(Japanese)* 78—19766
- Cu-Be (6.2, 9.3, 13.4 at.%), cell growth of discontinuous precipitation *(Japanese)* 79—24525
- Cu-Be alloy, CA 172, flat spring, mechanical props. in bending, stress relax. test, 23 to 232°C 78—72806
- Cu-Be alloy, notched specimen, static and dynamic behaviour 78—27634
- Cu-Be alloy, X-ray diffr. pattern singularities *(Russian)* 78—67682
- Cu-Be alloys, ageing kinetics, ultrasonic effects *(Russian)* 79—78997
- Cu-Be alloys, CuBe precipitation 80—29966
- Cu-Be search coil for measurement of magnetisation and susceptibility in pulsed magnetic field 79—63281
- Cu-Be solid solutions, local oscill. conc. depend., impurity bands *(Russian)* 80—75318
- Cu-Be-Co, cuboid (Co, Cu, Ni, Fe)Be inclusions, metallography, ageing effects 80—11645
- Cu-Be-Co, discontinuous reaction, analytical TEM 80—100842
- Cu-Be-Co (1.8, 0.2 wt.%), TEM obs. of precipitates, ageing charact. *(Korean)* 77—66648
- Cu-Be-Co (2,0.3 wt.%) alloy, heat treatment, influence of tempering on hardness, tensile props. transform diagram *(French)* 78—31384
- Cu-Be-Co(0.1,0.2 wt.%), discontinuous precipitation *(Japanese)* 80—55402
- Cu-Be-Ni (1.9, 0.32 wt.%) solution treated alloy, age induced vol. changes in structural transformations *(Russian)* 79—100179
- Cu-Be-Ni-Ti-Mg (2, 0.3, 0.2, 0.02 to 0.4 wt.%), multiple step ageing *(Russian)* 78—19786
- Cu-Be-Ni-Ti-Mg bronze, alloying element influence on minimum thermo EMF, cold working *(Russian)* 80—34426
- Cu-Be-Ni-Zr, anodic behaviour of intermetallic phase 78—72895
- Cu-BeCo (1.85, 0.29 wt.%), type CA172 (TH04), strengthened by spinodal decomp., stress relax. in bending 80—7616
- Cu-Be(Al)(Mg)(Ti), study of internal oxidation using central diffusion of X-rays *(French)* 79—37839
- Cu-Be(2 wt.%), tarnish surface films, formed in ammoniacal Cu(II) solns. 80—97624
- Cu-Be(25 wt.%), discontinuous precipitation *(Japanese)* 80—55402
- Cu-Be(30 at.%), eutectoid decomp., elastic interaction between precip. phase particles *(Russian)* 77—8833
- Cu-Bi, embrittled grain boundary obs. using STEM, Cu-SiO$_2$ comparison 78—38730
- Cu-Bi, grain boundary struct. intergranular fracture, segregation role 80—66648
- Cu-Bi, grain boundary thickness obs. using electron diffr. techniques 80—79811
- Cu-Bi (0.0115 wt.%), embrittled, grain boundary faceting, TEM study 79—27998
- Cu-Bi (0.02 wt.%), intergranular fracture, Kossel X-ray diffr. in SEM obs. 80—108579
- Cu-Bi alloys, grain boundaries, electron microscopy 77—12694
- Cu-Bi alloys, grain boundary segregation 79—61596
- Cu-Bi foil, electron diffr. effects and images from inclined grain boundaries 79—82241
- Cu-Bi-Fe, Fe effects on embrittlement 77—28900

copper alloys continued
Cu-Bi-S, evaporation of Bi in vacuum induction melting 77—28742
Cu-C bushings, powder metallurgically prepared, exam. of friction and wear charact. 79—15813
Cu-Cd, exam. of diamagnetic susceptibilities *(Russian)* 79—28504
Cu-Cd, magnetic susceptibility, comp. and temp. depend., melting effects 78—52202
Cu-Cd, structure, electrolytic deposition on monocrystalline Cu cathodes *(Polish)* 80—44435
Cu-Cd (0.03 at.%), single cryst., deformed, dislocation arrangement 79—10856
Cu-Cd (1 wt.%), creep stimulated by interrupted loading 79—74213
Cu-Cd (1.0 wt.%), yield stress and flow stress 80—97524
Cu-Cd alloy, CA 162, flat spring, mechanical props. in bending, stress relax. test, 23 to 232°C 78—72806
Cu-Cd alloy electro deposits on Cu substrate, struct. *(Polish)* 79—51437
Cu-Cd alloys obtained by electrolysis, struct. 78—91552
Cu-Cd electrodeposit on Cu, corrosion and its inhibition 79—74287
Cu-Cd-Cr, precipitation hardened, low temp. elastic props. 77—73299
Cu-Cd(In)(Sb), electron work function, contact pot. difference meas. 78—80041
Cu-Cd(2.7 wt.%), cellular precipitation kinetics and dissolution *(German)* 80—11651
Cu-Ce, effect of alloying additions on elec. cond. and mech. strength 78—44233
Cu-Ce effect of alloying additions on electrical cond., and mech. strength 78—44233
Cu-Co, age hardenable single crystal., fatigue and fatigue cracks *(German)* 77—16689
Cu-Co, dil., binding and caging of impurities and trapped interstitials 78—39462
Cu-Co, dil., valence and core level spectra, XPS study 80—84838
Cu-Co, Kondo system, NMR, spin-lattice relax., impurity spin dynamics 77—69724
Cu-Co, solid soln., mag. susceptibility near solubility boundary *(Russian)* 79—15281
Cu-Co, superparamagnetic, mag. aftereffects, dynamic neutron depolarisation study 80—50147
Cu-Co, thermoelectric power, precipitation effects *(German)* 77—85200
Cu-Co, time of flight atom probe, quantitative microanal., metallurgical appl. 80—86498
Cu-Co (1.5 and 4 wt.%), coherent Co-rich separations obs. by positron annihilation *(Russian)* 80—89082
Cu-Co (2 at.%), age hardened, stage I fatigue crack propag. 78—3203
Cu-Co (2 wt.%), single crysts., fatigued age-hardenable, dislocation structure *(German)* 80—54247
Cu-Co (2.48 wt.%), two-phase, surface meas. study of grain boundary sliding during creep 77—81299
Cu-Co alloy, ageing and reversion phenomena 79—91718
Cu-Co single cryst., precip. hardening *(German)* 80—84946
Cu-Co superparamagnetic particles, macrospin glass form. *(Russian)* 80—25165
Cu-Co-Fe, dil. alloy, low temp. resistivity maxima *(Russian)* 79—87091
Cu-Co-O system, distrib. of Co between Cu and Cu_2O *(Russian)* 77—16540
Cu-Co-S system, phase equilibria determ. by silica tube techniques 79—60482
Cu-Co-Si (0.36, 0.11 wt.%), surface layer struct. on annealing, SIMS and AES exam. 80—88415
Cu-Co(Cr)(Ni)(Ti), (1-1.3 at.%), elec. cond. exam. in solid and liquid phase *(Russian)* 77—62895
Cu-Co(Fe)(Ni), dil. mag. alloy, NMR of ^{63}Cu around impurities 77—16187
Cu-Cr, age hardened, fine precipitates struct., TEM study 80—3066
Cu-Cr, dil., elec. cond. meas., 1.5 to 30K 77—62914
Cu-Cr, dil., in supercond. proximity, localised bands 78—10613
Cu-Cr, dil., mag. susceptibility 77—63092
Cu-Cr, dil., negative magnetoresist. in pulsed fields up to 35T 77—62899
Cu-Cr, dil., spin glass, elec. resist., press. and conc. effects 78—52278
Cu-Cr, dil., spin-density magnetisation near Cr atoms, NMR study 80—80626
Cu-Cr, dil., thermal and elec. cond., deviations from Wiedemann-Franz law 77—66151
Cu-Cr, dil. alloy, Knight shift temp. depend., electronic struct. 78—84488
Cu-Cr, dil. alloy, Kondo resist. at 35 GHz 79—60814
Cu-Cr, dil. alloys, Frenkel defects, effects on anomalous resistivity and thermopower 77—8084
Cu-Cr, eutectic, effect of comp. and solidification conditions on microstruct. *(Russian)* 79—29037
Cu-Cr, formation of internal oxidation band 79—47820
Cu-Cr, isothermal decomp. diagrams 79—38791
Cu-Cr, Kondo alloy, Josephson tunnelling effect 80—60145
Cu-Cr, Kondo alloy, NMR of Cu satellites, 1 to 4K 79—73837
Cu-Cr, precipitation hardened, wear 78—3234
Cu-Cr, vapour deposited, electron irrad., resistance behaviour *(German)* 78—47779
Cu-Cr (0.55 wt.%), crystallography of precipitates, strain field study 80—25699
Cu-Cr (0.6 wt.%), electron microscope obs. of shear bands *(German)* 77—48454
Cu-Cr (0.75 wt.%), deformation characts., fully reversed cyclic strain with fatigue cracks and dislocation struct. 80—81148
Cu-Cr (1 wt.%), exam. of low cycle fatigue props. at elevated temp. 78—64674
Cu-Cr (1.45 wt.%), unidirectionally solidified eutectic, cooperative growth 77—90341
Cu-Cr alloy, laser irrad., structural changes *(Russian)* 80—100247
Cu-Cr eutectic, thermal stability in temp. gradient 79—61611
Cu-Cr system, optimal mutual orientations between FCC and BCC phases *(French)* 78—15371
Cu-Cr-SiO_2 system, age and dispersion strengthened, dislocation struct. around SiO_2 particles 80—108468
Cu-Cr-Zr-Mg (0.5, 0.1, 0.03 wt.%), exam. of low cycle fatigue props. at elevated temp. 78—64674
Cu-Cr-Zr-Ti-B alloy system, solidification cracks formed during welding, reduction by microalloying with B 79—96148
Cu-Cr(-SiO_2), single crysts., yield and pre-yield behaviour rel. to aging time 80—81103
Cu-Cr(Mn)(Fe), dil., NMR satellite data, rel. to electronic struct. 78—68398

copper alloys continued
Cu-Cr(Mn)(Fe), dil., NMR data, ionic model and Kondo temp. 78—68399
Cu-Cr(Nb), formation of two phase microstructure, during volumetric, and directional crystallisation *(Russian)* 79—29040
Cu-Cr(Ni), coating on Ti alloy VT9, plastic deform. and diffusion annealing effect on props. *(Russian)* 78—35425
Cu-Cu Zr eutectic composite, struct. and props., heat treatment and crystn. rate influence *(Russian)* 79—38813
Cu-Cu_2O crystallisation from melt, influence of crystn. conditions on struct. *(Russian)* 79—38814
Cu-Cu_6Y eutectic alloy, cast and directionally solidified, struct. and props. *(Russian)* 80—104138
Cu-Fe, classical Kondo system, impurity spin dynamics, NMR relax. of impurity neighbour nuclei 77—36056
Cu-Fe, cluster form., Fe solubility determ., 450 to 1000°C, Mossbauer spectra obs. *(German)* 79—29021
Cu-Fe, composite, simulation of tensile behaviour and fracture void initiation *(Japanese)* 78—52948
Cu-Fe, dil., diffusion and ageing processes, Mossbauer study 80—7245
Cu-Fe, dil., in supercond. proximity, localised bands 78—10613
Cu-Fe, dil., internally oxidised mag. and electrical prop. 77—12100
Cu-Fe, dil., ion implanted, phase comp., Mossbauer study 80—7244
Cu-Fe, dil., local mag. moments, neutron scatt. study 79—61058
Cu-Fe, dil., local susceptibility, Mossbauer meas. 78—19400
Cu-Fe, dil., powder, transferred orbital hyperfine field on near neighbours, NMR meas. 78—27098
Cu-Fe, dil., thermopower, interconfig. fluctuations 79—65412
Cu-Fe, dil., transmission ESR meas. 2 to 40K 78—68364
Cu-Fe, dil., valence and core level spectra, XPS study 80—84838
Cu-Fe, dil. alloy, anomalous thermoelec. power, sensitivity to defects, annealing effect 77—51728
Cu-Fe, dil. alloy, quench-condensed thin film, annealing effect on resistivity 78—43488
Cu-Fe, dil. alloy, spin relaxation rates, neutron scatt. study 79—47235
Cu-Fe, dil. alloy solubility and diffusion of Fe 78—43170
Cu-Fe, dilute, low temp. heat capacity in mag. field, superparamagnetism 80—39804
Cu-Fe, explosive plasma sputtered coatings, struct. and props. *(Russian)* 80—100783
Cu-Fe, force constant change with pressure, relative Mossbauer fraction 80—34163
Cu-Fe, growth kinetics and interfacial energy of coherent γ-Fe particles *(Japanese)* 78—19765
Cu-Fe, highly dil., mag. impurity scatt., and deviations from Matthiessen's rule 78—43371
Cu-Fe, implanted, Mossbauer effect meas. 78—31134
Cu-Fe, implanted, Mossbauer study, rel. to annealing temp. 78—31135
Cu-Fe, Kondo system, Cu-Fe, static and dynamic susceptibilities, hyperfine studies 77—63090
Cu-Fe, Kondo system, magnetisation, Mossbauer expts. 77—77028
Cu-Fe, local moment system, low temp. susceptibility, Mossbauer effect meas. 77—43810
Cu-Fe, metastable solid solutions, production by explosive plasma compressor *(Russian)* 77—90289
Cu-Fe, mixed cryst., Debye-Waller factors, Mossbauer spectra obs. *(German)* 78—52412
Cu-Fe, Mossbauer studies of ageing and precip. 79—38415
Cu-Fe, precipitation kinetics study by thermoelectric power measurement *(French)* 79—20050
Cu-Fe, precipitation processes during aging, TEM, resistivity, hardness study *(Japanese)* 80—35221
Cu-Fe, single crystal with coherent γ-Fe particles, precipitation hardening 78—31416
Cu-Fe, supersaturated, spontaneous magnetisation region development, Mossbauer obs. *(German)* 78—64306
Cu-Fe, thermal treatment effect on thermoelec. power *(French)* 77—32000
Cu-Fe, vapour deposited, electron irrad., resistance behaviour *(German)* 78—47779
Cu-Fe (0.04 to 0.9 at.%), film, resistivity temp. depend., 1.5 to 17K, impurity interactions 77—63007
Cu-Fe (0.2 at.%), clustering, precipitation, and oxidation, 298 to 919K, Mossbauer study 80—7242
Cu-Fe (0.2 at.%), quenched, Fe dimers and defects 80—40007
Cu-Fe (0.2 at.%), surface oxidation, Mossbauer obs. 80—55564
Cu-Fe (1 wt.%), stress induced martensitic transformation of spherical Fe particles, exam. 78—52803
Cu-Fe (1.2 at.%), Fe moment and lattice distortion, neutron scatt. meas. 79—24133
Cu-Fe (1.5 wt.%), precipitation-effect on void formation during electron irradiation 80—84211
Cu-Fe (1.5 wt.%), void form. during irrad. in HVEM, reactor irrad. simulation and ageing effects 80—107327
Cu-Fe (2.46 wt.%), reversion phenomena and cold-working effect *(Japanese)* 80—35204
Cu-Fe (<4 wt.%), solubility determ. by thermoelectric power meas. *(French)* 77—62644
Cu-Fe alloy film, mag. susceptibility max. 79—24173
Cu-Fe binary system, high-temp. phase relations in Fe-rich region 77—81249
Cu-Fe clusters, electronic states and mag. props., MO calc., appl. to Kondo problem 77—20219
Cu-Fe dilute alloy, host NMR spin lattice relaxation 79—51873
Cu-Fe group, dil., NMR satellite data calc., struct. of mag. impurities 80—103894
Cu-Fe phase diagram, 650 to 1050°C *(German)* 78—60658
Cu-Fe system, ageing and reversion phenomena study 80—89274
Cu-Fe-Mn-Ni-Pb-Zn copper based alloys optimisation of atomic absorption analysis 77—56274
Cu-Fe-O system, distrib. of Fe between Cu and Cu_2O *(Russian)* 77—16540
Cu-Fe-P alloy, CA 196, flat spring, mechanical props. in bending, stress relax. test, 23 to 232°C 78—72806
Cu-Fe(Co)(Ni), liquid, surface tension *(Japanese)* 79—19431
Cu-Fe(Mn), dil., interaction between local mag. moments 77—1540
Cu-Fe(2.5 wt.%), isothermally reacted austenite stability in very small particles 77—48432
Cu-Ga, binary alloy constituent EDS anal., secondary fluorescence, SEM study *(Chinese)* 80—85231
Cu-Ga, dil., Matthiessen's rule deviations above room temp. 79—91023

copper alloys continued

- Cu-Ga, disordered, phonon dispersion curves, inelastic neutron scatt. study 79—51223
- Cu-Ga, effect of ion bombardment on surface composition using differential reflectometry and AES 77—59189
- Cu-Ga, high dislocation density alloys and oxide precipitated struct., NMR, spin echo 80—39892
- Cu-Ga, ion bomard. effect on surface comp., reflectometry AES 77—81190
- Cu-Ga, lattice dynamical meas. and anal. *(Russian)* 77—62599
- Cu-Ga, liq., elec. cond., temp. and conc. depend., model interpret. and alloy struct. *(Russian)* 80—88528
- Cu-Ga, liq., mag. susceptibility, diamag. 78—72326
- Cu-Ga, magnetic susceptibility, comp. and temp. depend., melting effects 78—52202
- Cu-Ga, plastic flow enhancement during massive transformations 78—48468
- Cu-Ga (17 wt.%), elec. resist. and TEM studies 80—108604
- α-Cu-Ga (3.4-15 at.%) cold-worked, lattice imperfections, X-ray obs. 77—55291
- Cu-Ga alloys, massive phase ζ tempering, kinetics, order-disorder transform. *(French)* 78—44118
- Cu-Ga bulk and thin-film forms, reflecting surface absorpt. coeffs. at 10.6 μm 80—95984
- Cu-Ga periodic antiphases obs. *(French)* 77—4772
- Cu-Ga porous solid formed by shock compression 80—29905
- Cu-Ge, dil., Matthiessen's rule deviations above room temp. 79—91023
- Cu-Ge, dil., point defect props., density functional approach 80—29013
- Cu-Ge, disordered, phonon dispersion curves, inelastic neutron scatt. study 79—51223
- α-Cu-Ge, Fermi surface, high resolution positron annihilation study 78—6261
- Cu-Ge, lattice dynamical meas. and anal. *(Russian)* 77—62599
- Cu-Ge, liq., hard-sphere struct. factors 77—51301
- Cu-Ge, liq., mag. susceptibility, diamag. 78—72326
- Cu-Ge, liq. alloy, thermodynamic activity meas. by Knudsen-cell mass spectrometry *(French)* 80—10684
- Cu-Ge, liq. and solid, positron trapping 78—48255
- Cu-Ge, primary coplanar slip, role in deform. of FCC crystals *(Japanese)* 77—52412
- Cu-Ge, single cryst., dislocation motion obstacles, effective strength 80—15107
- α- Cu-Ge, superconducting transition temp. depend. on electron per atom ratio, lattice deform. 77—8222
- Cu-Ge, system, atomic struct. and electronic props. *(Russian)* 77—20289
- Cu-Ge, thermal expansion, X-ray determ. 78—26697
- Cu-Ge, thin films, elec. cond., Ge influence 79—82690
- Cu-Ge (0.44 to 7.3 wt.%), concentrated single crystal, yield region investigation, CRSS, slip 77—48478
- Cu-Ge (0.7 or 1.5 at.%), stacking fault energies, weak beam method of electron microscopy 77—19971
- Cu-Ge (1 at.%), FCC crystal, stress-strain curve, stage I to stage II transition *(Japanese)* 78—19834
- Cu-Ge (10-12 wt.%), intermediate ξ′-phase form. during deform. *(Russian)* 78—19747
- Cu-Ge (2 wt.%), positron annihilation, photon ang. distrib. meas. effect of deformation, annealing temp. *(Russian)* 78—35220
- Cu-Ge (5 at.%), single crystal, Bridgman growth, neutron diffraction topographic obs. of layer substructure 79—27938
- Cu-Ge (8 wt.%), anelastic effect due to deform. twins *(Japanese)* 79—20095
- Cu-Ge (8.7 at.%), pulse duration effects in shock hardening 77—12644
- Cu-Ge (8.7 wt.%) pulse duration effects on shock hardening 78—80561
- Cu-Ge (8.7 wt.%) shock hardening behaviour at very short pulse durations 78—80560
- Cu-Ge alloys, equilib. defects *(German)* 79—86789
- Cu-Ge codeposited film, elec. resist. and thermoelec. power, rel. to struct. 79—87168
- Cu-Ge single cryst. containing heavily faulted regions, X-ray diffr. profiles 80—24462
- Cu-Ge solid soln., isotope effect for Ge diffusion 78—2285
- Cu-Ge-La, Cu+Misch metal, eutectic alloy, internally oxidised, mech props. *(Japanese)* 77—52411
- Cu-Ge-Te system, DTA, crystallographic and metallographic analysis *(French)* 77—25019
- Cu-Ge(Zn), conc. single crystal, yield region investigation, flow stress and obstacle charact. 78—3173
- Cu-H, rolled sheet, plastic anisotropy theory based on yield function of fourth order 78—31458
- Cu-H system, de Haas-van Alphen Dingle temps. for scatt. of cond. electrons determ. 77—76731
- Cu-Hg, dil., pool electrodes, passivation in alkaline soln. 79—70214
- Cu-Hg amalgam electrode, standard pot. 78—76874
- Cu-In, dil., point defect trapping after ion implantation, DPAC meas. 78—43728
- β-Cu-In, directionally transformed eutectoid, morphology exam. by metallography *(German)* 78—92257
- Cu-In, effect of alloying additions on elec. cond. and mech. strength 78—44233
- Cu-In, liq., elec. cond., temp. and conc. depend., model interpret. and alloy struct. *(Russian)* 80—88528
- Cu-In, liq., solubility and activity of O 77—43331
- Cu-In, magnetic susceptibility, comp. and temp. depend., melting effects 78—52202
- Cu-In, thermally cycled, effect on mech. props. and microstruct. 79—4987
- Cu-In, undirectionally transformed, mechanical props. 78—48492
- β-Cu-In, unidirectionally transformed eutectoid, lamellar microstructure, influence of grain boundaries on thermal stability 78—72795
- Cu-In alloy, thermodynamics, calorimetric exam. *(French)* 77—21105
- Cu-In dilute, In^{114} impurity diffusion 79—65256
- β-Cu-In eutectic, unidirectionally decomposed discontinuous coarsening reaction 78—27472
- Cu-In eutectoid, coarsening at 829K 79—1885
- Cu-In eutectoid, directional eutectoid decomposition growth, crystallography 80—29874
- Cu-In liquid alloy, thermodynamic props., potentiometric exam. *(French)* 77—59126
- Cu-In liquid alloys, heat of form meas. *(Korean)* 77—9116

copper alloys continued

- Cu-In(Sb), growth kinetics, of discontinuous precipitation, third element effects 77—36511
- Cu-Ir, dil., impurity diffusion, temp. depend. *(Russian)* 78—67851
- Cu-M alloys (M=Zn,Al,Sn,Mn,Pb), diffusive redistrib. during friction *(Russian)* 78—52999
- Cu-M-O ternary liquid alloys, thermochem. calcs. 80—85209
- Cu-Mg, high temp. oxidation 79—43485
- Cu-MgO, dispersion hardened, prep. by milling Cu and Mg oxidising atmos. *(German)* 78—64509
- Cu-MgO, dispersion hardened alloys, prep. and props. 80—40291
- Cu-Mg(Sn), precipitating phase nuclei, diffuse X-ray scattering intensity determ. *(Russian)* 77—86031
- Cu-Mn, classical RKKY model, thermodynamic props. 78—39333
- Cu-Mn, de-alloying props. 80—104332
- Cu-Mn, dil., anomalous thermal expansion below 50K 78—51710
- Cu-Mn, dil., in supercond. proximity, localised bands 78—10613
- Cu-Mn, dil., Kondo deviations of Mn electron spin relax. and g-factor, NMR meas. 79—51747
- Cu-Mn, dil., local mag. moments, neutron scatt. study 79—61058
- Cu-Mn, dil., local moment fluctuations, NMR meas. 77—63091
- Cu-Mn, dil., mag. heat capacity, conc. and temp. depend. 79—61164
- Cu-Mn, dil., spin density magnetisation near magnetic atoms 79—33545
- Cu-Mn, dil., spin glass, thermopower, rel. to spin glass freezing temp. 78—79983
- Cu-Mn, dil., spin-glass dynamics, NMR meas. 78—31120
- Cu-Mn, dil. alloy, spin glass, host NMR, spin freezing 77—40138
- Cu-Mn, dil. alloy, spin glass, host NMR, spin freezing 77—40139
- Cu-Mn, dil. alloys, conc. depend. of resist. maximum 77—62893
- Cu-Mn, dilute, magnetoresist. and Hall effect, field-depend. electron scatt. 77—43581
- Cu-Mn, effect of ageing on mag. props. 77—28366
- Cu-Mn, exchange-coupled localised moments, Korringa relaxation rate 80—75851
- Cu-Mn, γ-phase interdiffusion obs., chem. comp. depend. *(Japanese)* 78—2307
- Cu-Mn, impurity spin dynamics in magnetic glasses at low frequencies *(French)* 78—88126
- Cu-Mn, interdiffusion *(Japanese)* 77—51554
- Cu-Mn, interdiffusion 78—18848
- Cu-Mn, itinerant to local moment magnetism transition with comp. 77—72984
- Cu-Mn, mag. irreversibility and metastability 78—19279
- Cu-Mn, mag. viscosity below freezing temp. 80—65910
- Cu-Mn, magnetisation curves 79—24172
- Cu-Mn, mictomag., massive short-range antiferromagnetism 77—12139
- Cu-Mn, Mn K X-ray emission and XPS lines, width and asymm. 78—19605
- Cu-Mn, molecular field distribution function in disordered Ising model *(Russian)* 80—54859
- Cu-Mn, positrons as probe of phase transforms. 78—31401
- Cu-Mn, spin glass, ^{63}Cu NMR linewidth and relax. meas. 77—69583
- Cu-Mn, spin glass, anomalous Hall effect 78—30908
- Cu-Mn, spin glass, meas. of order parameter 80—34642
- Cu-Mn, spin glass, transition temp., freq. depend. 80—97113
- Cu-Mn, spin glass, US meas. of crit. exponent α' 79—78384
- Cu-Mn, spin glass alloy, elec. resist. 77—8067
- Cu-Mn, spin glass alloy, magnetic excitations, neutron scatt. 78—10695
- Cu-Mn, spin glass materials, mag. field dependence of susceptibility peak 80—103840
- Cu-Mn, spin glasses, alternating susceptibility 80—65912
- Cu-Mn, zero field ESR in spin glass state 80—66017
- Cu-Mn (10 at.%), meas. of mag. viscosity below freezing temp. 79—24171
- Cu-Mn (15 at.%), mictomagnetic, short-range ordering, neutron scatt. polarisation anal. 80—50110
- Cu-Mn (16.7 at.%), spin glasses, alternating magnetisation 79—91241
- Cu-Mn (3, 5, 10 at.%), surface segregation of Mn and oxide film form., AES study *(French)* 79—66065
- Cu-Mn (3 to 20 at.%), high temp. steady state tensile deform. *(Japanese)* 78—52917
- Cu-Mn (38 to 58 wt.%), age hardened, exam. of precipitation and strengthing 78—72782
- Cu-Mn (3.%), specific heat below 3K 79—61165
- Cu-Mn (4.7 at.%), spin glass, spin correlations, neutron scatt. cross section meas. 79—51790
- Cu-Mn (7 at.%), magnetic susceptibility, clustering, band model of heterogeneous magnetics 77—43823
- Cu-Mn (8 at.%), spin glass, neutron scatt. and susceptibility investig. of spin dynamics 77—40076
- Cu-Mn (8 to 75 at.%), spin correl., neutron polarisation anal. study 80—65905
- Cu-Mn alloy, classical RKKY model, zero temp. dynamic struct. factor 78—68271
- Cu-Mn alloy, manganin, hysteresis-corrected calibration under shock loading 80—74818
- Cu-Mn alloy, spin glass, neutron scatt. 78—68265
- Cu-Mn alloy, spin-glass, US exam. 78—68351
- Cu-Mn alloys, Cu-rich, heat treated, segregation obs. *(Russian)* 78—27517
- Cu-Mn alloys, vacuum deposited, electrophys. props. 77—63006
- Cu-Mn dil., evidence for Mn clustering from high field magnetisation curves 79—78426
- Cu-Mn dil. spin glass alloy, impurity-impurity interaction press. depend., resistivity meas. 77—20308
- Cu-Mn Kondo system, ^{54}Mn nucl. orientation 78—68421
- Cu-Mn mictomagnet, effect of ageing on mag. moment 77—43841
- Cu-Mn spin glass, hysteresis loops, temp. and field depend. 80—15742
- Cu-Mn spin glass, magnetisation reversal and macroscopic mag. domain obs. 79—61168
- Cu-Mn spin glass, magnetisation curves, time depend. 80—15743
- Cu-Mn spin glass, saturated thermoremanent magnetisation, time and temp. evolution 79—61167
- Cu-Mn spin glass, specific heat below 3K, spin glass freezing temp. 79—95600
- Cu-Mn spin glass, spin freezing and exchange narrowing of mag. reson. 80—60411
- Cu-Mn spin glass alloy, neutron scatt. meas. of Edwards-Anderson order parameters 79—11323
- Cu-Mn spin glass alloy, spin correl. function, combined neutron spin echo and polarisation anal. 80—50107

copper alloys continued
Cu-Mn spin glass neutron diffr. expts. *(French)* 78—43593
Cu-Mn spin glasses, spin dynamics, neutron scatt. meas. 79—8002
Cu-Mn-Al, constricted hysteresis loop rel. to microstruct. 78—19273
Cu-Mn-Al, Heusler alloy, single cryst. and polycryst., martensitic transform. *(Russian)* 78—48398
Cu-Mn-Al, Heusler alloys, ferromag. inclusions, mag. props. and struct. study *(Russian)* 80—80570
Cu-Mn-Al, mag. props. and atomic ordering 79—24139
Cu-Mn-Al alloys, displaced hysteresis loop and microstructure obs. 80—84613
Cu-Mn-Au(Pt) spin glasses, anisotropic exchange interactions, effect of nonmag. impurities 80—80534
Cu-Mn-Ni, thin film, vacuum deposited, struct., elec. cond. *(Russian)* 78—19668
Cu-Mn-Ni alloy, Manganin, elec. resist. under static pressures up to 110 kbar, pressure gauge appl. 79—1594
Cu-Mn-P alloys, phase diagram *(Russian)* 80—20891
Cu-Mn-S, Mn surface segregation and Mn/S cosegregation 80—40367
Cu-Mn-Ti film, physical and electrical props. *(Russian)* 77—66208
Cu-Mn(Fe)(Co), Kondo system, host NMR exam. 78—80246
Cu-Mn(Fe)(Ni)(Zn)(Ge), dilute solid soln., exam. of recrystallisation and stored energy 78—52836
Cu-Mn(Ti)(Sn)(Si), dil., oxide film form. in ammoniacal Cu(II) solns., AES obs. 80—45415
Cu-Mn(1%) spin glass, remanent mag., zero-field NMR obs. 79—33492
Cu-N, quenched, complex martensite form. 79—56977
Cu-Nb, exam. of monotectic reaction, using chill casting technique 78—68679
Cu-Nb, supercond. wire, directional solidification of melts, supercond. ionisation temp. *(Russian)* 78—76596
Cu-Nb (0,4 at.%), splat quenched, aged, superconductivity *(Japanese)* 77—63018
Cu-Nb (17 wt.%) multifilamentary wires, fabrication and supercond. characts. 79—56476
Cu-Nb (7 wt.%), solidification microstruct., SEM 77—12611
Cu-Nb alloy, chill casting, consumable arc melting, ingot prep. techniques 80—84879
Cu-Nb alloys, origin of superconductivity 77—47918
Cu-Nb alloys for superconducting wire, casting of dendritic structure 80—2976
Cu-Nb composite superconductor produced by rapid quenching 78—48351
Cu-Nb filamentary composites, powder metallurgy prod., supercond. props. 79—56477
Cu-Nb multifilamentary composites, in situ formed, anomalous strength increase 79—43323
Cu-Nb multifilamentary composite, dislocation resistivity 80—70671
Cu-Nb_2Sr, multifilamentary supercond. composites, in situ formed, critical currents 79—65625
Cu-Nb_3Sn, high-current A-15 microcomposite material 80—44781
Cu-Nb_3Sn composite wires, powder metallurgically produced, supercond. props. 78—31026
Cu-Nb-Sn, multifilamentary supercond. composite wires, fabrication on laboratory scale and mech. props. 80—29897
Cu-Nb-Sn composites, cold-powder-metallurgy processed, supercond. critical currents 79—78279
Cu-Nb-Sn dil. alloys containing Nb_3Sn precipitates, superconductivity 78—43507
Cu-Nb-Sn system, phase equilibria and supercond. props. *(Russian)* 80—50589
Cu-Nb-Sn(Ge), phase relations and diffusion layer form. 77—36458
Cu-Nb(Nb_3-Sn) composite wires, powder metallurgy prod., supercond. props. and annealing 79—33428
Cu-Ni, (10 at.%), magnetisation in high mag. field, Arrott-Noakes plot 80—54919
Cu-Ni, AES analysis of protective oxide film 79—39035
Cu-Ni, adsorption of H_2+CO on (110) surface, TDS and UPS obs. 80—80052
Cu-Ni, alloys, electronic states, KKR-CPA calc. 78—84125
Cu-Ni, annealing effect on oxidation kinetics, reduction in vacancy level 80—50760
Cu-Ni, cast, strength and hot ductility, alloying and residual elements effect 80—66595
Cu-Ni, chemical emission by Ar^+ ion bombardment *(French)* 77—86410
Cu-Ni, chemisorpt. of CO, SIMS, AES, desorpt. meas. 78—87875
Cu-Ni, clean surface, surface segregation and growth process of altered layer *(Japanese)* 80—24720
Cu-Ni, cold worked solid solution, flow stress and activation volume 80—16393
Cu-Ni, comp. modulated alloy films, transport props., 10 to 300K 79—95515
Cu-Ni, corrosion, performance for condenser tube 79—39046
Cu-Ni, critical concentration for ferromagnetism 78—14969
Cu-Ni, crystal growth from melt Monte-Carlo method modelling, surface roughness *(Russian)* 79—77536
Cu-Ni, crystallisation temp., overcooling temp. *(Russian)* 80—97472
Cu-Ni, Cu rich, chemical and intrinsic diffusion coeff. determ. 79—28130
Cu-Ni, cyclically deformed, electrical resistance changes 79—57096
Cu-Ni, density of states of d-electrons, tight binding approx. calcs. 80—59863
Cu-Ni, diffusion of Ni, resistometric meas. 80—29222
Cu-Ni, diffusional homogenisation in compacted powder blends, X-ray diffr. line profile analysis 78—80491
Cu-Ni, dil., dislocation damping, 95-297K, at high strain amplitudes 78—39824
Cu-Ni, dil., electronic struct., virtual bound state due to s-d hybridisation 78—75990
Cu-Ni, dil., far IR absorptivity meas. using multireflection cell 77—18075
Cu-Ni, dil., screening charge density round $\Delta Z = -1$ impurities, vacancies, NQR study 80—103897
Cu-Ni, dil., valence and core level spectra, XPS study 80—84838
Cu-Ni, dil. alloy, optical reflectivity meas. virtual bound state model analysis 78—2873
Cu-Ni, disordered ferromag., spin density asphericity, neutron diffr. study 79—47251
Cu-Ni, disordered muffin tin type, coherent pot. approx. appl. 79—15062
Cu-Ni, effect of alloying and residual elements 78—85033

copper alloys continued
Cu-Ni, electrolytic plating 80—35425
Cu-Ni, erosive wear by impinging SiC particles, surface hardness and material props. effect 77—66705
Cu-Ni, evaporation limited segregation 80—70513
Cu-Ni, film, compositionally modulated, enhanced magnetisation density 78—84460
Cu-Ni, film, preferential sputtering due to altered layer struct., AES meas. 78—76573
Cu-Ni, foils, supermodulus effect, one-dimens. modulated structs. 79—95068
Cu-Ni, galvanic corrosion in sulphide modified seawater 80—100953
Cu-Ni, in 0.1 M NaCl, electric pot. and pH meas., crevice corrosion 78—31564
Cu-Ni, initial oxidation study by microprobe-AES method *(Japanese)* 79—15867
Cu-Ni, liq., surface conc. profile and surface energy 80—84350
Cu-Ni, long and short range electronic effects in bonding of CO and H_2 77—7974
Cu-Ni, mag. ordering temp. depend. on atomic short-range order from susceptibility meas. 79—61159
Cu-Ni, melt, accel. by shock wave treatment, crystallisation *(German)* 77—86022
Cu-Ni, microvoid form., gaseous impurity atom effects, positron annihilation study 80—49275
Cu-Ni, neutron irradiation, enhanced diffusion, elec. resist. meas. 80—6440
Cu-Ni, neutron radiation stimulated diffusion, electrical resistivity exam. *(Russian)* 79—14959
Cu-Ni, nucleation and growth of oxidation zones during diffusional creep *(Russian)* 79—52431
Cu-Ni, optical absorption and photoemission spectra 80—45216
Cu-Ni, oscills. in composition depth profile, UPS meas. 78—71919
Cu-Ni, parametric eval. of susceptibility to sulphide induced corrosion in sea water 80—16560
Cu-Ni, powder, sintered, effect of cold and hot dynamic pressing, upon structure and props. 79—33970
Cu-Ni, powder mixture electric discharge sintering, struct. changes 77—77446
Cu-Ni, powder mixtures, form. using electric discharge sintering 77—12563
Cu-Ni, preferential sputtering Auger electron spectra obs. 79—33880
Cu-Ni, quantitative AES anal. of M_1 VV transition, computer simulation 79—91542
Cu-Ni, random ferromag. alloy, local mag. moment calc. 80—70974
Cu-Ni, rubbing contact with cast Fe, surface temperature effect on dry sliding wear 80—60983
Cu-Ni, sintered, props. and degree of nonhomogeneity 80—20848
Cu-Ni, sintering, Kirkendall effect 80—93518
Cu-Ni, soft X-ray emission and local densities of states 79—83059
Cu-Ni, sputter-induced subsurface segregation, Auger electrons obs. 80—10757
Cu-Ni, sputtered and sputter-deposited surfaces, in-situ AES meas. 77—48296
Cu-Ni, sputtering yield, surface binding energies 80—50503
Cu-Ni, strength and substruct., strain point influence *(Russian)* 79—52233
Cu-Ni, sulphidation between 653 to 770K, exam. of scale morphologies, using X-ray diffr., and electron microprobe anal. 78—88559
Cu-Ni, surface comp. and catalysis, AES and thermal desorption meas. 79—46898
Cu-Ni, surface comp. calc. by regular soln. theory, surface relax. effects 79—42355
Cu-Ni, surface composition cluster size distrib., Monte Carlo method calc. 78—63915
Cu-Ni, surface layer, effect of Ar^+ bombardment, AES and SIMS 80—25504
Cu-Ni, surface segregation and in-depth profile, AES 77—31856
Cu-Ni, surface segregation, comparison of low-energy ion-scatt. results with theory 78—38923
Cu-Ni, thermal conductivity, data anal. and synthesis 78—95284
Cu-Ni, UPS, surface and bulk density of states, comp. depend. 77—44125
Cu-Ni (10 at.%), creep, substruct. and internal stresses *(Russian)* 80—97527
Cu-Ni (10 at.%), hardening, recovery, and struct. changes during high temp. creep *(Russian)* 80—89288
Cu-Ni (10 at.%), struct. changes during deform. *(Russian)* 78—19818
Cu-Ni (10 at.%) alloy, creep, dislocation density variation *(Russian)* 79—96101
Cu-Ni (10 wt.%), deformed bars, cold rolled, exam. of microstruct. by thin foil TEM 78—88502
Cu-Ni (100), UPS spectra, direct transition and matrix element effects 80—55268
Cu-Ni (110), adsorption of CO and H_2, UPS, thermal desorption, AES,and LEED study 80—80087
Cu-Ni (20 and 50 wt.%), sulphidation, exam. of scale growth kinetics 78—88560
Cu-Ni (20 wt.%) contour plate, for relay appl. creep characts. obs., use of Larson-Miller method *(Japanese)* 80—55454
Cu-Ni (20-80 at.%), clustering, diffuse neutron scatt. study, conc., temp. depend., miscibility gap location 78—47529
Cu-Ni (30-90 wt.%), elect. resist. rel. to cold working and heat treatment 80—71765
Cu-Ni (40 at.%), grain boundary migration, intergrain liq. layer effects *(Russian)* 77—15633
Cu-Ni (50 wt.%), preferential sputtering, thickness and in-depth comp. profile of altered layer, AES 78—39649
Cu-Ni (50 wt.%) alloys, estimation of sublimation energy of Cu atoms, evaporation rate and surface composition, AES meas. *(Japanese)* 80—49352
Cu-Ni (70 at.%), mech. behaviour in microplastic strain region *(Russian)* 78—39838
Cu-Ni alloy, dislocation density during deform., comparison of electron microscopy and X-ray diffr. *(Russian)* 79—5002
Cu-Ni alloy, sputtered altered layers, in-depth profile, model 78—19613
Cu-Ni alloy prep. by sulphide-oxide reactions 77—48366
Cu-Ni alloy surfaces, chemisorption of CO, LEED, AES, thermal desorption, and work function meas. 79—90879
Cu-Ni alloys, activity of most oxidizable element *(French)* 79—61868

copper alloys continued
Cu-Ni alloys, alloying additions effect on thermal conductivity, 20-400°C *(Russian)* 77—59159
Cu-Ni alloys, artefacts in thin foil images 80—3056
Cu-Ni alloys, chemical interdiffusion under uniaxial stress 80—65307
Cu-Ni alloys, density of states determ. by continued fraction method 78—47690
Cu-Ni alloys, dislocation climb sources activated by 1 MeV electron irradiation 77—89443
Cu-Ni alloys, electron irradiated, dissociated struct. of dislocation loops with Burgers vector a⟨100⟩ 77—89444
Cu-Ni alloys, magnetic diffuse neutron scatt. 78—14931
Cu-Ni alloys, sulphide induced corrosion 79—91836
Cu-Ni alloys, XPS apparatus appls. *(Dutch)* 79—1982
Cu-Ni alloys 706 and 715, corrosion in flowing seawater, O_2 effect 79—43460
Cu-Ni alloys 706 and 715, corrosion in flowing sea water, dissolved sulfide effect 80—35379
Cu-Ni bimetallic cluster, segregation and short range order props. at boundaries 79—29071
Cu-Ni clusters, electronic states and mag. props., MO calc. 77—20219
Cu-Ni composite formation by electric discharge sintering 77—63594
Cu-Ni crystals, growth, H_2 reduction of CuI-$NiBr_2$ mixture, habit study by X-ray difr., optical and SEM 79—60665
Cu-Ni diffusion couple, diffusion bonding process, fracture surface exam. *(German)* 77—35762
Cu-Ni dil. paramagnetic alloys, sp. elec. resist., effect of Ni clusters *(German)* 78—95293
Cu-Ni electrode, photopotentials, rel. to corrosion 79—24648
Cu-Ni film, (001), in situ oxidation, TEM obs. 78—23874
Cu-Ni film, coevaporated, AES anal. and ion sputtering effects 79—15044
Cu-Ni film, ferromag. mag. susceptibility meas., 30-130°C 79—95615
Cu-Ni film, struct. and mag. order effects on electron transport props. 78—6460
Cu-Ni films, compositionally modulated, magnetic anisotropy, magnetisation curves 80—88840
Cu-Ni films, thickness depend. of Curie temp., resist. meas. 78—6545
Cu-Ni oxidised with NO, surface comp., AES obs. 77—20176
Cu-Ni single phase alloy, sputter yields 79—87546
Cu-Ni sulphidised alloys, Ru and Os behaviour during carbonylation *(Russian)* 80—40584
Cu-Ni system, composition depend. of third-order elastic consts. 77—62579
Cu-Ni textured alloys, grain boundary effusion of Ni to surface 79—90680
Cu-Ni thin films, ferromag., Hall effect meas. 80—80428
Cu-Ni tubing, viscoplastic bending 78—35464
Cu-Ni:polyethylene, surface, obs. at very low accel. voltage (200 V-1 kV) by SEM 80—10764
Cu-Ni/Au-Ni multilayer films, ohmic behaviour, use as strain gauge 80—65713
Cu-Ni/Au-Ni multilayers obtained by co-evaporation in UHV, ohmic stability and TCR 79—78226
Cu-Ni-Al, ageing charact., optical TEM, X-ray, hardness obs. 79—29079
Cu-Ni-Al, grain boundary reaction under isothermal ageing at 623 to 973K *(Japanese)* 79—70090
Cu-Ni-Al, review 80—7564
Cu-Ni-Al (5, 2.5 at.%), precip. hardening *(Japanese)* 80—71663
Cu-Ni-Be (30, 0.5 wt.%), grain boundary reaction after ageing and quenching, obs. *(Japanese)* 79—70089
Cu-Ni-Be-(Al) (30,0.5,(0.2-2) wt.%), Al addition effect on grain boundary reaction *(Japanese)* 80—54254
Cu-Ni-Co, alloy pre-form prep. through reduction of sintered oxides 80—40284
Cu-Ni-Co, mag. props. of system of disperse ferromag. particles, 73 to 673K *(Russian)* 80—65968
Cu-Ni-Cr, lattice imaging and optical microanalysis of spinodal decomp. 78—52754
Cu-Ni-Cr, microstruct. behaviour and mechanical hardening 78—47281
Cu-Ni-Cr (28, 2.8 wt.%), spinodal alloy, microstruct. and tensile props. 78—39858
Cu-Ni-Cr system, coarsening in the $(\gamma_1+\gamma_2)$ region, metallographic study 78—84762
Cu-Ni-Fe, age hardenable, dislocation interactions with internal coherency stresses 77—36528
Cu-Ni-Fe, age hardened, yield strength correlation with internal coherency strains 77—44254
Cu-Ni-Fe, alloy pre-form prep. through reduction of sintered oxides 80—40284
Cu-Ni-Fe, corrosion resistant, SCC, crevice corrosion in seawater 79—96177
Cu-Ni-Fe, magnetic properties, heat treatment and compressive stress effects 80—60367
Cu-Ni-Fe, permanent magnet, temp. effect 80—34701
Cu-Ni-Fe, quenched and aged, deformed, low-temp. elec. resist. meas. *(Russian)* 77—52514
Cu-Ni-Fe, spinodal alloy, heat treatments for improved mech. props. 79—5024
Cu-Ni-Fe, spinodally decomposable, densification using four different powder methods 80—40283
Cu-Ni-Fe, synergistic effect of Ni and Fe on sea water corrosion 78—35561
Cu-Ni-Fe (14, 7 wt.%), solid soln., decomposed, magnetostatic interaction between ferromag. particles *(Russian)* 77—80967
Cu-Ni-Fe (26,8 wt.%), microduplex struct. form., hardness meas., optical and electron microscopy *(Japanese)* 78—76659
Cu-Ni-Fe alloys superparamag. early stages of decomp. *(Russian)* 78—6890
Cu-Ni-Fe solid solution, after precip., susceptibility of interacting superparamag. grains 79—99733
Cu-Ni-Fe tube, stressed, corrosion failure caused by cooling water, denickelation *(German)* 79—29286
Cu-Ni-Mn (20,20wt.%), structural transform., X-ray and hardness study *(French)* 78—39760
Cu-Ni-Nb (30, 0.9 at.%), precipitate free zones, X-ray microanal. 80—108768
Cu-Ni-Nb (30,1 wt.%), precipitation 77—86035
Cu-Ni-Nb-Al, correlation of γ' and γ'' precipitates phase stability 80—25704
Cu-Ni-Nb-Al, formation of γ' and γ'' precipitates 78—76655

copper alloys continued
Cu-Ni-O, liquid alloy, thermodynamic study by EME method *(Japanese)* 78—15367
Cu-Ni-O system, distrib. of Ni between Cu and Cu_2O *(Russian)* 77—16540
Cu-Ni-P, precipitation hardening 77—12633
Cu-Ni-S, molten, thermodynamic props. 80—104122
Cu-Ni-Sn, liq. alloy, calc. and anal. of mixing enthalpies *(German)* 80—44325
Cu-Ni-Sn, liq. alloy, mixing enthalpies determ. using a SETARAM high temp. calorimeter *(German)* 80—44324
Cu-Ni-Sn, thermal decomposition after prior cold work 78—15427
Cu-Ni-Sn (10, 6 wt.%), spinodal decomposition, X-ray and electron diffr. study 80—81063
Cu-Ni-Sn (10, 6 wt.%), temp. depend of yield stress and work hardening 80—21026
Cu-Ni-Sn (15, 8 wt.%), prior deform. effect on spinodal age hardening 80—108465
Cu-Ni-Sn (15, 9 wt.%), age hardening accompanying phase transition 78—64551
Cu-Ni-Sn (4,4 wt.%) resistance spot weld quality evaluation, using stress wave emission technique 78—53066
Cu-Ni-Sn (4-15, 4-8 wt.%), strip strengthened by spinodal decomp., stress relax. in bending 80—7616
Cu-Ni-Sn (9, 2 wt.%), surface comp., Auger electron spectroscopy study, manufacture and storage influence 80—65348
Cu-Ni-Sn (9, 6 wt.%), decomposition, initial stages, TEM study 80—2992
Cu-Ni-Sn alloy, flat spring, mechanical props. in bending, stress relax. test, 23 to 232°C 78—72806
Cu-Ni-Sn spinodal substitute for Be-Cu alloy 80—35217
Cu-Ni-Ti, ordering within precipitates, TEM obs. 80—108461
Cu-Ni-Ti system, phase equilibria in Cu rich region and Cu-T quasibinary constitution *(Japanese)* 80—89203
Cu-Ni-Ti system, reactions with melt in Cu-rich region *(Japanese)* 80—89202
Cu-Ni-W melt, solubility of W, primary solidification 78—19726
Cu-Ni-Zn, Cu rich, penetration tendency model for diffusion 77—39701
Cu-Ni-Zn, diffusion couples, zero-flux planes and flux reversals 80—15313
Cu-Ni-Zn, microduplex, superplastic deform., cavitation and fracture 78—64640
Cu-Ni-Zn, multiphase couples, diffusion paths and struct. at 775°C 77—62666
Cu-Ni-Zn, Portevin-Le Chatelier effect during tensile deform. *(German)* 79—8330
Cu-Ni-Zn (18, 27 wt.%), surface comp., Auger electron spectroscopy study, manufacture and storage influence 80—65348
Cu-Ni-Zn alloy, at 775 degrees C, diffusional and thermodynamic interactions 78—38883
Cu-Ni-Zn alloy, FCC, cold-worked, microstruct., X-ray obs. 78—3143
Cu-Ni-Zn alloy, surface comp., outdoor exposure influence 80—59770
Cu-Ni-Zn system, tie lines in a two phase region 80—24404
Cu-Ni-Zn-Mn fine grained precipitation-hardenable alloy, high strength and ductility 80—100805
α-Cu-Ni-Zn-Pb, fire cracking and ordering *(German)* 78—60760
α-Cu-Ni-Zn-Pb, fire cracking, effect of pores and impurities 79—29207
Cu-$NiAl_2O_4$, internally oxidised, orientational relationships of precip. oxide phase 77—4783
Cu-Ni; preferential sputtering, Auger meas. 78—27358
Cu-Ni(Fe,Co,Cr,Ti) powder based composite, high temp. strength of W reinforcing fibres 79—70021
Cu-Ni(Fe)(Mn)(V), dil., local mag. moments and Kondo effect, theoretical model 79—69651
Cu-Ni(Pd), composition modulated foils, layer struct. and mech. props. 79—95300
Cu-Ni(Su), supercooled melt, dendrite growth morphology *(Japanese)* 78—11216
Cu-Ni(Zn)(Ga)(Ge), dil. impurity electron struct., self-consistent Korringa-Kohn-Rostoker Green's function calc. 79—78040
Cu-Ni(10 (30) wt.%), seawater corrosion rate meas., electrochem. method validity 80—45426
Cu-O, effect of Se, S, Pb impurities on annealability and resistivity 77—28834
Cu-O (0.05 to 0.1 wt.%) liquid alloy, deoxidation kinetics by rotating graphite cylinders 80—61084
Cu-O-Zn dilute liquid alloy, Zn-O interaction parameter 80—55694
Cu-P (8.4 wt.%) metallic laminate, laws governing development and retardation of fast cracks 78—15527
Cu-P wire, phosphor bronze, magnetoresist. upper limit 77—43567
Cu-Pb, gas-atomised, particle profiles, morphological characterisation derived from Walsh coeffs. 80—50816
Cu-Pb, liquid, surface tension, size effect *(French)* 80—15341
Cu-Pb (Fe), liq., thermodynamic props. *(Polish)* 80—89199
Cu-Pb liquid alloys, exam. of O diffusivity at 1430K using electrochemical cell 78—51713
Cu-Pb-O, liquid, dil. alloy, O_2 activity, 1100 to 1200°C 80—25662
Cu-Pb-O system, ternary miscibility gap activity determ., thermodynamic method 77—28783
Cu-Pb-S system, at 1473K, thermodynamic anal. 78—39746
Cu-Pd, (100) and (110) surfaces, LEED patterns 77—85031
Cu-Pd, dil, perturbed angular correlation exam. of Pd impurity, ^{111}Cd probe 79—78588
Cu-Pd, dil., screening charge density round $\Delta Z=-1$ impurities, vacancies, NQR study 80—103897
Cu-Pd, disordered, antiphase domain boundaries, high resolution electron microscopy obs. 79—95030
Cu-Pd, disordered, shaft range order diffuse scatt., electron diffr., reinterpretation 77—84596
Cu-Pd, Fermi surface comp. depend. by positron annihilation ang. correl. 77—76727
Cu-Pd, mag. susceptibility and electronic struct. of ordering *(Russian)* 80—11161
Cu-Pd, surface comp. changes under ion bombardment, AES study 80—55250
Cu-Pd, surface struct. from LEED and AES meas. 79—77882
Cu-Pd, thermal conductivity, data anal. and synthesis 78—95284
Cu-Pd alloy, pressure effect on β-phase transition by elec. resist. meas. 79—15660
Cu-Pd alloy, singularities of physical props. and ordering *(Russian)* 78—76643

copper alloys continued
Cu-Pd dil. alloys, electronic states, virtual bound states model test *(French)* 77—62809
Cu-Pd foil, composition-modulated, elastic modulus enhancement 77—52382
Cu-Pt, dil., screening charge density round $\Delta Z=-1$ impurities, vacancies, NQR study 80—103897
Cu-Pt, disordered, shaft range order diffuse scatt., electron diffr., reinterpretation 77—84596
Cu-Pt, order-disorder transform, influence of strain energy 78—84796
Cu-Pt, quenched, microdomain model anal. of diffuse X-ray scatt. 79—52276
Cu-Pt, surface segregation, comparison of low-energy ion-scatt. results with theory 78—38923
Cu-Pt, temp.-press. phase diagram *(Russian)* 78—3100
Cu-Pt alloy, quenched, SRO, microdiffr. obs. 77—76360
Cu-Pt existence regions of FCC superstructs. *(Russian)* 78—52760
Cu-Pt system, phonon dispersion relations, force constant disorder effect 80—84263
Cu-Pt type alloys, theory of ordering *(Russian)* 77—1100
Cu-Pt-O alloys, dil., O-metal interactions, activity coeff. meas. at 1423K 80—93792
Cu-Rh (0.5 at.%), nucl. quad. relax. 79—82898
Cu-S, liquid, oxidation kinetics, by CO_2 77—28986
Cu-SO_2 system, melt, blow hole form. during solidification 79—43238
Cu-Sb, cold-worked, lattice defects, convolution relations for X-ray line breadth calcs. 78—51394
Cu-Sb, dil., grain growth rate, 520-970°C *(Russian)* 80—29972
Cu-Sb, liq., partial interference functions, short range chem. order effects 79—7541
Cu-Sb, peculiarities in temp. behaviour of internal adsorption *(Russian)* 79—55890
Cu-Sb, thermodynamic investigation 78—39750
Cu-Sb (1 wt.%), stress removal during annealing after hydrostatic extrusion 79—83215
Cu-Sb (10-50 wt.%), thermal dilatometric anal. 79—56954
Cu-Sb (24-45 wt.%), phase transform. exam. by thermal expansion 77—63629
Cu-Sb alloy, splat-quenched, energy dispersive X-ray diffr. 78—23728
Cu-Sb melt, eutectic struct. by neutron diffr., isotopic substitution 78—47233
Cu-Sb solid soln., finely lamellar discontinuous precipitation, ternary addition effects 77—36510
Cu-Sb solid solution, dil., FCC, intergranular solid shortness mechanism *(Russian)* 79—5032
Cu-Sb system, atomic struct. and electronic props. *(Russian)* 77—20289
Cu-Sc, dil., impurity effects on annealing and resist., vacancy-Sc interaction 79—51142
Cu-Si, change in force constant due to volume effects 78—75778
Cu-Si, deformation and fracture under dynamic loading 78—35442
Cu-Si, high dislocation density alloys and oxide precipitated struct., NMR, spin echo 80—39892
Cu-Si, impurity concentration effects 78—75777
Cu-Si, mech. of formation of martensitic struct. *(Russian)* 78—23702
Cu-Si, melt, enthalpy of formation at 1370K 80—26042
Cu-Si, phase transform, exam. *(Russian)* 77—8822
Cu-Si, reaction diffusion, effect of compressive stress 77—28050
Cu-Si, stacking fault energy meas. by tensile deform. of polycrystalline samples 78—95060
α- Cu-Si, superconducting transition temp. depend. on electrons per atom ratio, lattice deform. 77—8222
Cu-Si (0.7 to 3.3 at.%), stacking fault energies, weak beam method of electron microscopy 77—19971
Cu-Si (6.5 at.%), CC Cu-Al(Si), single crysts., latent hardening study by meas. of flow stress on secondary systems *(Japanese)* 79—24538
Cu-Si (6.5 at.%), plastic deformation, HVEM study *(French)* 80—66605
Cu-Si (6.5 at.%) alloy, easy glide deform., obs. and mechanism 77—8887
Cu-Si (7 at.%), dislocation interactions, influence of jogs on extension of dislocation nodes 80—84176
Cu-Si (8 wt.%), intrinsic struct. in grain boundaries and boundary mobility 80—103368
Cu-Si (up to 4.75 wt.%), exam. of high temp. oxidation in low O_2 and pure CO_2 atmospheres, by thermogravimetry 78—88574
Cu-Si alloy, FCC→HCP transition mechanism 77—77479
Cu-Si correl. of periodicities in diffr. patterns and images from grain boundary 78—14362
Cu-Si-Ni, undercooled, grain refinement 79—34079
Cu-Si-Zn wire, silicon bronze, magnetoresist. upper limit 77—43567
Cu-SiO_2, deformed, lattice rotations at second phase particles 80—25709
Cu-SiO_2, dispersion hardened, surface plasticity effect 78—52832
Cu-SiO_2 alloy, fracture at elevated temp. 78—39896
Cu-Si(Ge), dissoc. dislocations pinning by Suzuki effect *(French)* 79—100223
Cu-Si(Sb), dil., chemical etching and X-ray topography obs. of cellular struct. *(French)* 79—96249
Cu-Sn, amorphous, electron-phonon interaction effect on thermopower 80—29393
α-Cu-Sn, cyclic work hardening frequency effects *(German)* 79—29090
A-Cu-Sn, cyclic work hardening during frequency change fatigue tests *(German)* 79—34068
Cu-Sn, deformed, martensitic transformation *(Russian)* 79—15668
Cu-Sn, exam. of surface segregation equilibrium and kinetics, by Auger spectroscopy *(Russian)* 79—56981
Cu-Sn, ε and η phases, surface struct. changes due to sputtering 77—73206
Cu-Sn, graphite dispersed, wear, effect of graphite content *(Japanese)* 77—56114
Cu-Sn, graphite fibre reinforced, high speed tribological props. against steel 79—15809
Cu-Sn, mean square strain, use of approx. methods for Fourier series coeffs. for X-ray diffr. lines *(French)* 77—31549
Cu-Sn, self-diffusion of Sn, correl. with other props. *(Russian)* 79—23764
Cu-Sn, Sn surface segregation in monolayer regime, model of kinetics and equilib., AES data explained 79—7739
Cu-Sn, thermodynamics of Cu and Sn solns. using copper β-alumina solid electrolyte, 800-1100K 80—107502
Cu-Sn, vacuum condensed, reflecting surface absorpt. coeffs. at 10.6 μm 80—95984

copper alloys continued
Cu-Sn (1 wt.%), stress removal during annealing after hydrostatic extrusion 79—83215
Cu-Sn (15 at.%), temp. depend. of elastic consts. above martensitic transition temp., US exam. 78—76695
Cu-Sn (16.5 wt.%) alloy, stress induced martensite from γ phase 79—70066
Cu-Sn (2 wt.%), effect of undercooling on crystal multiplication 78—84866
Cu-Sn (25 wt.%), liq., struct. from thermodynamic and diffr. studies 80—6350
Cu-Sn (25 wt.%), struct. after ultrahigh-speed quenching *(Russian)* 78—80563
Cu-Sn (25 wt.%), struct. changes with ageing *(Russian)* 77—40421
Cu-Sn (4.9 wt.%), role of mech. twinning on stress/strain behaviour 80—85004
Cu-Sn alloy, surface comp., outdoor exposure influence 80—59770
Cu-Sn alloy chemical deposition process *(Russian)* 79—47642
Cu-Sn alloy components, photometric determ. *(Russian)* 79—11842
Cu-Sn binary system, wettability and interaction between solids and liqs. *(Japanese)* 80—92760
Cu-Sn industrial bronzes, Sn diffusion in deform. zone influence on wear resistance, friction *(Russian)* 80—108582
Cu-Sn liquid, optical reflectivity spectra of virtual bound states 80—89021
Cu-Sn liquid alloy, surface energy meas. by const. temp. method on solid alumina 78—6208
Cu-Sn liquid alloys, thermodynamic meas. 78—52765
Cu-Sn solid soln. steady state deform. *(Japanese)* 78—19832
Cu-Sn system, long period superlattice obs. and impurity effects 80—103297
Cu-Sn system, thermodynamic study of gaseous molecules of $CuSn_2$ and Cu_2Sn 79—70360
Cu-Sn system intermetallic formation rate, H_2 adsorption effect 79—90819
Cu-Sn warm pressed compact prep. 80—35136
Cu-Sn-Al, deform at high temps. *(Polish)* 80—89284
Cu-Sn-Mg, precipitation, effect of thermomechanical treatment *(Japanese)* 79—4970
Cu-Sn-Nb multifilamentary alloy, high field crit. current density 78—27004
Cu-Sn-Ni, mech. props. after thermomech. treatment 79—79009
Cu-Sn-P (5, 1-5 wt.%), effect of P on friction and wear characts. 80—16494
Cu-Sn-Pb-Fe-graphite, bronze-based, sintered alloy, silica additions effect 77—63807
Cu-Sn-Te system, phase diagram exam. *(French)* 77—21107
Cu-Sn-Ti, wetting of alumina and vitreous C 78—71904
Cu-Sn(-Al), quenched and aged, struct. of phases *(Russian)* 80—49184
Cu-Sn(Zn)(Al), wear, effect of Mn_5Si_3 content *(Japanese)* 78—35525
Cu-Sn(5 wt.%), electrical resistivity, annealing, cold rolling 77—8070
Cu-Ta, metastable alloy layer formed by Ta^+ ion implantation 78—71709
Cu-Ta metastable alloy form. by ion implantation, combined TEM and ion channelling obs. 78—34530
Cu-Te, liq., struct. and elec. props. 80—49083
Cu-ThO_2(ZrO_2) alloys, dispersion hardened, electrical cond. and mech. props. 78—44133
Cu-Ti, ageing effect on internal friction and elastic props. *(Russian)* 77—28842
Cu-Ti, and Cu-Ti-Si(Fe), struct. and coalesc. of oxide particles during internal oxidation *(Russian)* 79—90781
Cu-Ti, deform. effect on precipitation and recrystallisation, electron microscope study 77—70115
Cu-Ti, dil. alloy, cellular precipitates, nucleation, TEM study 80—3069
β-Cu-Ti, dil. alloy, growth phenomena associated with precipitation, TEM study 80—3070
Cu-Ti, internally oxidised, morphology, struct., particle precipitation singularities *(Russian)* 79—70067
Cu-Ti, lattice parameter change during ageing *(Japanese)* 78—35411
Cu-Ti, liquid phase sintering, metallographic electron beam microanalytical investigation 78—95888
Cu-Ti, small-angle electron scattering in TEM, intensity meas. Grigson method 79—14658
Cu-Ti, solubility of Ti, exam. using NMR of ^{63}Cu *(French)* 80—7179
Cu-Ti, strengthened by modulated structs., anomalous age hardening effects 80—97497
Cu-Ti, Zr effects on cellular precipitation 77—16587
Cu-Ti (Zr), strength improvement by thermomechanical treatment *(Japanese)* 78—48426
Cu-Ti (0.9 at.%), age hardening effect on critical resolved shear stress 79—61603
Cu-Ti (1.07 wt.%), containing coherent precipitation, observations of flow and fracture 78—80643
Cu-Ti (3.5 wt.%), aged by US strain, struct. and props. *(Russian)* 80—21003
Cu-Ti (3.5 wt.%), internal friction in dissociating alloy following deform. by US *(Russian)* 78—35419
Cu-Ti (3.5%), coherent precipitates, US irrad. effect on struct. and hardness *(Russian)* 77—48446
Cu-Ti (4 wt.%), aged, stress corrosion cracking in Cu-NH_3 solutions, effect of pH, Cu and NHz conc. 78—88562
Cu-Ti (4 wt.%), ageing, X-ray study 77—56012
Cu-Ti (4 wt.%), combined recrystallization and precipitation 79—29072
Cu-Ti (4 wt.%), isothermal transformation, electron and optical microscopy obs. of microstructure 80—16307
Cu-Ti (4 wt.%), lamellar multiphase, struct. and spatial comp. variation, analytical STEM 78—24011
Cu-Ti (5 wt.%), effect of cold work on ageing behaviour, TEM study *(Japanese)* 79—78991
Cu-Ti (5.7 at.%), dil., β-phase struct. 79—55700
Cu-Ti alloys, activation vol. stress depend., single crysts. 77—48499
Cu-Ti alloys, CuTi, $CuTi_2$, solubility of H_2, decomp. reacts. 79—65197
Cu-Ti alloys (0.5 to 4.0 wt%) ageing charact. determ. 79—20089
Cu-Ti matrix of diamond composite, microstresses, X-ray diffr. exam. 78—56679
Cu-Ti system, diffusion obs. *(German)* 78—63881
Cu-Ti-Al(Ga)(Au)(In)(Ag)(Ni), wetting of Al_2O_3, alloying effects 80—107617
Cu-Ti-Cr(Fe), internally oxidised, morphology, struct., particle precipitation singularities *(Russian)* 79—70067

copper alloys continued
- Cu-Ti-Fe (0.7, 0.9 wt.%) film, dispersion-strengthened, form. by high rate magnetron/plasmatron sputtering, and props. 80—25715
- Cu-TiC precipitation hardened composite, struct. effect on friction 78—11337
- Cu-Ti(0.7 at.%), plastic deform. and precip. hardened, annealing time 78—48446
- Cu-transition metal, alloys, satellite NMR study, lineshifts and splitting 80—34786
- Cu-transition metal, dil., mag. impurities, electronic struct., KKR-Green's function calc. 80—65783
- Cu-transition metal, residual resistivity, effect of 4d and 5d transition metal impurities 79—60791
- Cu-transition metal alloy, internal adsorpt. and mag. susceptibility, grain size effects *(Russian)* 78—19759
- Cu-transition metal dil. alloy, virtual bound states 79—37975
- Cu-V, dilute, Knight shift of ^{51}V reson., and host satellite resonances 77—85594
- Cu-V alloy, phase equilib. diagram exam. *(French)* 77—21100
- Cu-V_3Ga, high-current A-15 microcomposite material 80—44781
- Cu-V_3Ga, supercond. in situ composites, stress effects on crit. props. 80—65757
- Cu-V-Ga dil. alloys with V_3Ga particles, supercond. props. and microstruct. 78—39278
- Cu-V-Si, partial diag., V_3Si formation by bronze process 77—86032
- Cu-V-Si, supercond. props. 80—107945
- Cu-V-Si, two-step supercond. transition 80—34539
- Cu-W, powder, prod. by controlled reduction in H_2O/H_2 mixture of $CuWO_4$ 79—24458
- Cu-W sintered materials, porous, mech. and X-ray elastic const. *(German)* 77—81288
- Cu-W(Fe)(Ag), biphase material X-ray stress determ. *(Russian)* 79—5097
- Cu-Y, effect of alloying additions on elec. cond. and mech. strength 78—44233
- Cu-Zn, amorphous, viscoelastic behaviour *(Japanese)* 77—86110
- Cu-Zn, α-phase, photoelectron meas. 78—35247
- Cu-Zn, charge transfer, core-electron binding-energy shift 80—2676
- Cu-Zn, cohesive props., augmented-spherical-wave calcs. 79—94952
- Cu-Zn, cold worked solid solution, flow stress and activation volume 80—16393
- Cu-Zn, cyclic stress/strain curves in monocrystalline and polycrystalline samples, cold work and Zn addition effects 78—95786
- Cu-Zn, de-alloying props. 80—104332
- Cu-Zn, dil., Matthiessen's rule deviations above room temp. 79—91023
- Cu-Zn, interface sliding of FCC and BCC boundaries 80—104240
- Cu-Zn, magnetic susceptibility, comp. and temp. depend., melting effects 78—52202
- Cu-Zn, optical composition modulation spectra, dielec. const. var., Fermi surface and electronic level shifts 80—6707
- Cu-Zn, order-disorder transform, influence of strain energy 78—84796
- Cu-Zn, phase boundary motion kinetic during interdiffusion *(Russian)* 79—60559
- Cu-Zn, solid soln., rheological study of crystallographic order on creep *(French)* 80—97548
- β_1Cu-Zn, structural Umklapp processes at low and high temp. lattice kinetics of phase transformation isotherms *(German)* 78—30707
- Cu-Zn, thermal conductivity, data anal. and synthesis 78—95284
- Cu-Zn, thermally stimulated exo-electron emission 80—11547
- α-Cu-Zn, whiskers, X-ray topography, substruct. 77—11831
- Cu-Zn (0.25 wt.%), ductility minimum, strain rate depend. at intermediate temps. 79—79056
- Cu-Zn (2 at.%), stacking fault energies, weak beam method of electron microscopy 77—19971
- Cu-Zn (30 wt.%), rolled, electron microscope exam. of recrystallisation 78—76663
- Cu-Zn (30 wt.%), single crysts., quantitative anal. of stress relax., obstacle strength and athermal stress variation 80—89277
- Cu-Zn (36 wt.%), hardness-flow stress rel. during strain-controlled bending fatigue 79—74245
- Cu-Zn (38.9 wt.%), β-brass, spinodal decomposition, electron microscope and diffr. study 79—78930
- Cu-Zn (47.3 wt.%), spinodal decomposition, electron microscope and diffr. study 79—78930
- Cu-Zn (50 at.%), BCC β phase, high temp. creep, existence of master curve 80—55473
- α-Cu-Zn (5.3 to 21.8 wt.%), single crystals, effect of stacking fault energy on extrusion and intrusion development 78—72826
- Cu-Zn alloy, molecular dynamic exam. of perfect and imperfect cryst. 77—39647
- Cu-Zn alloy, surface layer composition determ. by XPS 79—43682
- Cu-Zn alloys, surface comp., outdoor exposure influence 80—59770
- β-Cu-Zn elec. resist. change with degree of order *(Japanese)* 78—34817
- β_1-Cu-Zn mixed crystal, metastable structural Umklapp process, isothermal phase transform. *(German)* 78—22798
- Cu-Zn-Al, β_1' martensite crystal crossing rel. to reversible shape memory effect *(Japanese)* 80—108499
- β-Cu-Zn-Al, diffr. effects., obs. and interpretation of extra maxima 80—44173
- β-Cu-Zn-Al, electron microscope exam. of premartensitic state 78—72801
- Cu-Zn-Al, internal friction, temp. and amplitude depend. 78—11262
- Cu-Zn-Al, internally faulted martensite, TEM obs. 78—3124
- Cu-Zn-Al, martensitic phase transformation effect on low cycle fatigue behaviour 80—7666
- Cu-Zn-Al, martensitic transform., short range order effect 79—61586
- Cu-Zn-Al, memory alloy wire and ribbon reversible martensitic transformation, ageing effect, review 80—7564
- β-Cu-Zn-Al, ordering, TEM obs. 78—39768
- β-Cu-Zn-Al, ordering 78—68687
- Cu-Zn-Al, polycrystn., β-phase, fatigue life, intergranular cracking 79—38974
- Cu-Zn-Al, pseudoelastic alloy, exam. of fatigue props. 78—76744
- Cu-Zn-Al, reversible shape memory effect associated with $\beta_1 \rightleftarrows \beta_1' \rightleftarrows \alpha_1'$, transform. *(Japanese)* 79—43242
- Cu-Zn-Al, reversible shape memory effect obtained by heating under constraint *(Japanese)* 79—43335
- Cu-Zn-Al, reversible shape memory effect *(Japanese)* 80—108500
- Cu-Zn-Al, single cryst., stress induced martensitic transformation 80—45308
- Cu-Zn-Al, TTT diagrams *(German)* 79—43208

copper alloys continued
- β-Cu-Zn-Al, US elastic const. meas. near martensitic transform. temp. 78—39827
- Cu-Zn-Al, Zener relaxation *(Russian)* 77—21198
- α-Cu-Zn-Al (18, 7 at.%), deform. and mech. props. 79—29159
- Cu-Zn-Al (19.3, 13.0 wt.%), effect of hydrostatic or uniaxial stress on elastic consts., near martensitic transformation point 78—76697
- Cu-Zn-Al (19.5, 6.35 wt.%), martensitic, static stresses influences on damping behaviour 80—10594
- Cu-Zn-Al (26, 4 wt.%), martensitic transform. temp. variation after low temp. ageing 79—15666
- β-Cu-Zn-Al (27.5, 4.0 wt.%), strain induced martensite, exam. of structure, microstructure 80—7648
- Cu-Zn-Al (35.45, 1.72 wt.%), memory effect and martensitic transform. *(Russian)* 79—43320
- Cu-Zn-Al alloy, lattice dynamical study of premartensitic state, phonon meas. 79—77696
- Cu-Zn-Al alloys, dendritic struct. obs. 77—8810
- Cu-Zn-Al cubic alloy, phonon sp. ht. near martensitic transform. 79—60521
- Cu-Zn-Al Marmem alloy, β_1 phase superstruct. obs., rel. to transform. mode 78—39776
- Cu-Zn-Al martensite, β-phase, single cryst., elastic waves behaviour as function of temp. 79—55807
- Cu-Zn-Al martensite, lattice dynamics, neutron scatt. meas. 80—88286
- Cu-Zn-Al martensite, the rubber effect 79—47684
- Cu-Zn-Al martensites, model for rubber like behaviour 79—47685
- β-Cu-Zn-Al pseudoelasticity 79—29126
- Cu-Zn-Al wire, made from pendant drop melt extraction technique from bulk material, X-ray diffr. and thermal anal. 79—43227
- Cu-Zn-Be, precipitation hardening 77—16599
- Cu-Zn-Ga configs. of martensite variants, shape deform. matrices 77—12620
- Cu-Zn-Ga martensite, thermally produced large single crystals 77—12615
- Cu-Zn-Ga(Al), martensites, internally faulted, shape memory mechanism 80—30010
- Cu-Zn-Mn, steady-state diffusion of Zn and Mn 80—70445
- Cu-Zn-Si, deform. close to martensitic transform. temp. 77—63714
- β-Cu-Zn-Si, premartensitic instability 77—12625
- Cu-Zn-Sn (24-34, 1.0 wt.%), cold-worked microstruct., X-ray diffr. obs. 80—3088
- Cu-Zn-Sn-Pb (5, 5, 5 wt.%) analysis in glow discharge lamp and in ion microprobe, sputtering processes 77—52730
- β-Cu-Zn(-Ni)(-Mn), order-disorder transformation temperature effect on quench hardening 78—95745
- Cu-Zn(Ga)(Ge)(As), dil., magnetic susceptibility, impurities effect, free electron gas model 79—91206
- Cu-Zn(Ga)(Ge)(As), dil., magnetic susceptibility, impurities effect, Fermi surface effects 79—91207
- Cu-Zn(Ga)(Ge)(As), Mossbauer effect of Fe impurities 78—31131
- Cu-Zn(Ge)(Ni)(Ga), α-phase alloys, lattice sp. ht. calcs. 80—65246
- Cu-Zn(30 at.%), electron irrad., positron annihilation, defect recovery 79—74018
- β- Cu-Zn(47.4 wt.%), heat content between 300.05 and T (T from 400 to 1000K) drop calorimetry *(French)* 80—10682
- Cu-Zr, amorphous, struct., X-ray scatt., rel. to Ni-P alloys 77—51324
- Cu-Zr, amorphous, viscoelastic behaviour *(Japanese)* 77—86110
- Cu-Zr, intermediary phases of equilib. diagram 78—84771
- Cu-Zr, metallic glasses, valence band struct. investigation 80—11533
- Cu-Zr, vapour quenching prod. (thermal evaporation and r.f. sputtering), amorphous film for electron microscopy 78—6851
- Cu-Zr (50 or 54 at.%), splat-quenched, glass transition and crystn. temps. determ. 78—22659
- Cu-Zr alloys, isothermal transformation diagram 80—20902
- Cu-Zr amorphous alloy, splat cooled, local order and amorphous struct. 80—88061
- Cu-Zr amorphous alloys, mech. props. *(Japanese)* 77—86179
- Cu-ZrO_2, internally oxidised, orientational relationships of precip. oxide phase 77—4783
- α-$Cu_{0.7}$ $Zn_{0.3}$, point-geometry ang. correl. curves, enhancement in positron annihilation 79—95873
- Cu_x Zn_{1-x}, sputtering, binding energies 80—108312
- (Cu-Au)-Co, single crysts., solid soln. and particle strengthening, superposition 80—97495
- $Cu_3Ag_{1-x}Au_x$, phase relations, X-ray diffr. and differential thermal anal. 80—108395
- α-CuAl, kinetic study of short-range ordering 78—23726
- $CuAl_2$ and Al crystals, mutual orientations in terms of lattice disorientations 80—28936
- $CuAl_2$, chemical effects on Al and Cu AES 77—59651
- $CuAl_2$, constitutional defect struct., from X-ray and density meas. proposed substitutional-vacancy model 79—37696
- $CuAl_2$, Kossel interferences of proton-induced Alk_α radiation 77—43112
- $CuAl_2$, single cryst., embrittlement and subboundary hardening via interstitial segregation *(Russian)* 77—12679
- $CuAl_2$, topological evolution during soln. heat treatment 77—32607
- $CuAl_2$-Al, directionally solidified eutectic, structural changes during strength tests *(Russian)* 80—7543
- $Cu_{0.7}Al_{0.3}$, chemical effect on valence electronic states, AES and SXAPS meas. 79—47558
- Cu_3Al-Al_2O_3 dispersion hardenend, short range order, quenching effect on yield stresS 78—35399
- γ-Cu_9Al_4, struct. refining from diffr. meas. 78—55834
- CuAu, calc. of elastic interaction between locally transformed regions with screw and edge dislocations 78—83844
- CuAu, electrical resistivity meas. to detect phase changes 77—48425
- CuAu, exam. of streaming due to intrinsic fluctuations 79—11602
- CuAu I, ordered equiatomic, lattice specific heat meas., Debye temp. 80—54396
- CuAu, mag. susceptibility and electronic struct. of ordering *(Russian)* 80—11161
- CuAu, order-disorder transform., band theory for internal energy 79—19539
- CuAu, ordered, vacuum deposited epitaxial films, orientation control by external stress 80—100426
- CuAu, thermal-neutron damaged, I_D and I_E recovery substages 77—35590
- CuAu type structures, interstitial atom redistrib. in octahedral and tetrahedral interstices *(Russian)* 77—55280

copper alloys continued

- CuAu-type superstructure, interaction of reacting dislocations *(Russian)* 78—83814
- $Cu_{1-x}Au$, neutron scatt., selection rules for phonon mass operator 79—28065
- Cu_3Au, 5-100 keV Cu^+ ion bombardment, displacement cascades, TEM investig. 77—11601
- Cu_3Au alloy, dynamics of ordering clusters in thermal non-equilib. state 79—51257
- Cu_3Au, alloys, superlattice-fringe imaging theory, images formed from two beams 80—79649
- Cu_3Au and $CuAu_3$, band theory of order-disorder transforms. 79—60501
- Cu_3Au, antiphase domain growth, quantitative comparison between theory and expt. 79—77606
- Cu_3Au, antiphase domain growth 80—55346
- Cu_3Au, atomic rearrangements during fast and thermal neutron irradiation 79—42114
- Cu_3Au, compound formation rel. to heat of mixing 80—55689
- Cu_3Au, Debye-Waller factor measurement in anal. of diffuse scattering data 79—23494
- Cu_3Au, deformation twinning 77—63717
- Cu_3Au, dislocation slip band mobility, critical stress 80—2032
- Cu_3Au, disordered [001]-orientated single crysts., plastic deform., TEM and slip line studies 80—97541
- Cu_3Au, displacement cascades prod. by Cu^+ bombardment 79—99251
- Cu_3Au, dynamics on transitional ordering process from disordered to ordered state 79—4267
- Cu_3Au, effects of temp. an order-depend. elec. resist. 77—31992
- Cu_3Au, elec. resistivity, temp. depend. 79—47078
- Cu_3Au, electrical resistivity and LRO, energy gap formation in Fermi surface 80—88533
- Cu_3Au, eqn. of state, applicability of semiempirical function of binding energy *(Russian)* 77—15533
- Cu_3Au, fast neutron irrad., displacement cascades 78—83852
- Cu_3Au, flow stress 77—21231
- Cu_3Au, heavy-ion or neutron bombardment, disordered zone form., TEM diffr. contrast 77—11600
- Cu_3Au, heterophase fluctuations near order-disorder transform., X-ray and neutron diffr. 77—73272
- Cu_3Au, interaction between superdislocations of opposite signs gliding in parallel planes *(Russian)* 77—80506
- Cu_3Au, long-range order parameter from electron micrograph thickness fringes 77—65938
- Cu_3Au, mag. susceptibility and electronic struct. of ordering *(Russian)* 80—11161
- Cu_3Au, meas. of ordering instability 79—38818
- Cu_3Au, mechanical damping in terms of Granato-Lucke theory, comparison with leaded and unleaded brass 78—95772
- Cu_3Au, metastable states domain existence, phase transition ordering energy, press. effect *(Russian)* 80—45303
- Cu_3Au, neutron irrad., displacement cascades, direct obs. method 80 107335
- Cu_3Au, ordered and disordered, cavitation induced erosion 77—16743
- Cu_3Au, ordering process, cluster size evolution 78—39766
- Cu_3Au, partial sputtering yields 77—8696
- Cu_3Au, radiation disorder model of phase stability 80—16297
- Cu_3Au, superdislocation motion resistance due to atoms in incorrect positions *(Russian)* 79—99189
- Cu_3Au, surface effects on order-disorder phase transition 77—76556
- Cu_3Au, TEM diffr. contrast of dislocation loop 77—24253
- Cu_3Au thin films, fine-grained and disordered, low temp. ordering 80—97433
- Cu_3Au type antiferromagnet Ising lattice, finite entropy at T=0, phase transition 77—89958
- Cu_3Au, under irradiation, microstructural-based estimate of disordering 80—2067
- Cu_3Au, X-ray and inelastic neutron scatt. investig. of spinodal ordering 77—77473
- Cu_3Au-Co, single crystal, overaging mechanism 79—20081
- Cu_3Au-Co, underaged, ordered and disordered single crystal, hardening mechanisms 78—3134
- Cu_3Au-Co single cryst., precip. hardening *(German)* 80—84946
- Cu_3Au-Cu_3Pd(Pt), quasibinary system, order-disorder transform., superlattice form. 80—2159
- Cu_3Au-Ni, antiphase domains morphology 80—108460
- $Cu_{81.5}Au_{18.5}$, meas. of ordering instability 79—38818
- CuAuI superlattice, (101) lattice twinning mode assoc. with ordering transition 77—15431
- Cu_2AuPd, struct., TEM and electron diffr. meas. 78—38666
- CuAu(Pt), quenched, short-range order X-ray diffuse scatt., microdomain model anal. 79—96043
- $Cu_3Au(-xCo)$, x=0.64 and 1.5 at.% Co, LRO 78—18584
- CuBe, electron emission following ion bombardment of electron multiplier dynode 78—23576
- CuBe, SIMS quantitative anal. of Be distrib. in vicinity of oxidation boundary *(French)* 80—11984
- CuBe, secondary electron emission coeffs. for multiply charged ion bombard. 78—11051
- CuCr alloys, supersaturated solid soln. dissociation *(Russian)* 79—52201
- CuCr, dil., anisotropic hyperfine coupling, NMR study 80—65784
- CuCr, dil., specific heat, impurity contrib. Kondo temp. 80—65903
- CuCr-Pb, proximity effect, tunnelling conductance 78—52160
- CuFe, dil., anisotropic hyperfine coupling, NMR study 80—65784
- CuFe film, metastable polycrystalline optical props. 79—83044
- CuFe solid solns., quenched from vap. phase, mag. props. 80—60307
- CuGa alloys with Mn impurities, liq., elec. resistivity 79—51545
- $Cu_{0.83}Ga_{0.17}$, α-phase, photoelectron meas., impurity level 78—35247
- $Cu_{1-x}Ga_x$ liquid alloys, elec. resistivity 79—47073
- Cu_3Ga, interpretation of diffuse contours in electron diffr. *(French)* 79—19377
- Cu_3Ga, transition state between long range order and short range order, model, computer simulation *(French)* 80—49371
- CuGe (1 wt.%), stress removal during annealing after hydrostatic extrusion 79—83215
- $Cu_{0.87}Ge_{0.13}$, α-phase, photoelectron meas., impurity level 78—35247
- CuH dilute alloy, Hall coefficient, relaxation times, Fermi surface 80—84460
- Cu_xLa_{1-x}, splat-cooled, phase diagram and supercond. props. 80—70881
- Cu_2Mg, electronic struct. volume depend. 79—65366
- CuMn, acceleration of coarsening by temp. changes, study by resistivity meas. 79—47718

copper alloys continued

- r-CuMn, annealing ordered phase study by neutron diffr. 80—89265
- CuMn, dil., anisotropic hyperfine coupling, NMR study 80—65784
- CuMn, hysteresis, spin orbit scattering effect on anisotropy in spin glass state 80—71095
- CuMn, magnetisation processes below freezing temp. 80—15748
- CuMn spin glass, AC susceptibility 80—60305
- CuMn, spin glass, mag. correls., neutron scatt. study 80—50105
- CuMn, spin glass, mag. hysteresis meas. 80—34691
- CuMn spin glass, μ^+ zero-field spin relax. probe for spin dynamics 80—97177
- CuMn, spin glass, random moments time correl., zero field muon spin relax. meas. 80—60335
- CuMn, spin glass, remanence, new approach from zero field NMR 80—34785
- CuMn spin glass, specific heat and entropy 80—60354
- CuMn, spin glass low DC field mag. susceptibility using SQUID 79—69684
- CuMn-like alloys, model calcs. on magnetisation processes in moderate fields below freezing temp. 79—24188
- $Cu_{0.86}Mn_{0.14}$, hysteresis loop development 80—65922
- $Cu_{0.95}Mn_{0.05}$, spin glass, inelastic neutron scatt., time-of-flight and three-axis techniques 80—50108
- $Cu_{0.95}Mn_{0.05}$, spin glass, low temp. mag. excitation spectrum, inelastic neutron scatt. obs. 80—50109
- $Cu_{0.98}Mn_{0.02}$, spin glass, Heisenberg mode, RPA approx. 80—65904
- γ-$Cu_{15}Mn_{85}$, antiferromag., neutron diffr. 80—2550
- Cu_3Mn, atomic short-range order, TOF neutron diffraction 79—10831
- Cu_3Mn, interaction between local mag. moments 77—1540
- $Cu_{75}Mn_{25}$, concentrated spin glass, elec. resist., depend. on hydrostatic press. 79—69685
- $Cu_{75}Mn_{25}$, spin glass, EPR line breadth, exchange-narrowed 79—15345
- Cu_2MnAl, alloy, energy band calc. by nonrelativistic SAPW method 79—4507
- Cu_2MnAl, dislocation structure, antiphase boundary energies, deformation behaviour prediction *(Russian)* 79—65085
- Cu_2MnAl, dynamical mag. susceptibility, spin waves, calc. from band struct. 80—54871
- Cu_2MnAl, ferromag. Heusler alloy, polarised neutron study of mag. moment density 78—84391
- Cu_2MnAl Heusler alloy, inelastic magnon scatt. of neutrons 77—4509
- Cu_2MnAl, Heusler alloy, single crystal, plastic deform. 77—44308
- Cu_2MnAl, Heusler alloy, spin waves, neutron inelastic scatt. meas. 77—80921
- Cu_2MnAl, Heusler alloy, magnetisation mag. anisotropy, magnetostriction and elastic consts. 78—23318
- Cu_2MnAl Heusler alloy, elec. resistivity 79—91020
- Cu_2MnAl, Heusler alloy, decomposition at 360°C 80—7536
- Cu_2MnAl, plastically deformed, domain struct., X-ray diffr. and electron microscope obs. *(Russian)* 79—20110
- Cu_2MnAl superparamagnetic particles in Cu_3Al lattice, magnetic moment ferromagnetic ordering *(Russian)* 79—78444
- Cu_2MnAl-Pd_2 MnAl mixed Heusler alloys, mag. props. 80—60269
- $Cu_2Mn_{0.863}Al_{1.057}$, Heusler alloy, mag. moment distrib., polarised neutron study 79—47247
- $Cu_2Mn_{0.98}Al_{1.02}$, Heusler alloy, hyperfine fields at sp elements, spin echo NMR meas. 78—84496
- $Cu_{2+x}Mn_{1-x}Al$, omega phase, roles of electron microscopy and electron diffraction *(French)* 78—27524
- $Cu_{3-x}Mn_xAl$, and $Cu_2Mn_{2-y}Al_y$, Heusler alloys, order-disorder transitions 80—59619
- $Cu_2Mn(Al_{1-x}Sn_x)$, Heusler alloys, thermal effects, saturation magnetisation 77—85499
- $Cu_2MnAl_{1-x}Sn_x$, Mossbauer effect study 80—60473
- $Cu_{2.0}Mn_{0.94}In_{1.0}$, In-Heusler single crystal, elec. resist. 78—60107
- $Cu_2MnIn_{1-x}Sn_x$ alloy, compositional SRO, hyperfine interactions 80—71065
- $Cu_2MnSn(In)$, Heusler alloy, hyperfine field at ^{111}Cd, TDPAC meas. 78—43705
- $Cu_{40}Nb_{30}X_{30}$ (X=Ti, Zr, Hf), superconductors with metastable ordered structs. 80—108484
- CuNi alloys, electronic theory of surface segregation 79—23819
- CuNi molecule, electronic states determ. by ab initio HF and CI methods 80—69087
- $Cu_{0.435}Ni_{0.565}$, clustering, temp. depend., diffuse neutron scatt. study 79—42013
- $Cu_{0.85}Ni_{0.15}$, liq., 3d bandwidths, photoelectron spectrum 77—4286
- $Cu_{1-x}Ni$, disordered muffin-tin, electron momentum density in average-t-matrix approx. 79—69390
- $Cu_{1-x}Ni_x$, mag. transition, NMR meas. by spin-echo technique 77—32267
- Cu_2Ni_{1-c}, solutions of KKR-CPA equations for paramagnetic alloys 78—95256
- Cu_cNi_{1-c}, Fermi surface of concentrated paramag. alloys 78—95257
- Cu_cNi_{1-c}, soft X-ray emission spectra 78—95620
- Cu_xNi_{1-x}, bulk electronic structure, comparison of CPA and ATA techniques 80—44467
- Cu_xNi_{1-x}, disordered alloy, muffin-tin model, electronic struct. and density of states calc. 80—29302
- Cu_xNi_{1-x}, low-temp. elec. resist. meas. *(Russian)* 77—52514
- Cu_xNi_{1-x}, magnetism of surface 78—95511
- Cu_xNi_{1-x}, paramag., electronic struct., atomic sphere approx. to KKR-CPA 79—19502
- Cu_xNi_{1-x} random alloy, angle-resolved photoemission 78—95683
- CuNiCr, IN838, heat treatment effect on fatigue and corrosion fatigue behaviour 80—20982
- Cu_2NiSn, Heusler alloy, elec. resist., 4.2 to 300K 80—75547
- α-CuNiZn alloys, Zener-relaxation effect 80—3121
- β-(CuNi)Zn, anomalous strengthening 77—48503
- Cu_2NiZn, atomistic approach to ordering 79—94944
- Cu_2NiZn, characterisation of superlattice dislocations by TEM 79—55748
- Cu_2NiZn, comparison between different theories predicting stacking fault energy from extended nodes 80—75240
- Cu_2NiZn, separation of partials of superlattice dislocations, anisotropic elasticity theory, ordering 79—65082
- Cu_2NiZn, stacking fault energy determ. from extended nodes 80 107280
- Cu_2NiZn, superlattice dislocations 78—83816
- Cu_3P, single crystal, prep. and props. 80—40250

copper alloys continued
CuPb, coexistence of ordered and disordered phases, elec. resist. meas. 77—85992
CuPd, chemical shift effects and origin of Pd 3d core level satellite 80—104039
Cu_3Pd, electron irrad. in electron microscope, radn. ordering 79—86818
Cu_3Pd, periodic antiphase boundaries, electron microscopy study *(French)* 80—59481
$Cu_{83}Pd_{17}$, Cu^+ (Au^+) ion-bombarded, displacement cascades and disordered zones, TEM studies 80—15167
$Cu_{1-x}Pd_xMnSb$, mag. phase transition 80—60268
$Cu_{0.5}Pd_{0.5}Ti_2$, solubility of H_2, decomp. reacts. 79—65197
CuPt alloy, equiatomic, ordering processes, anisothermal annealing exam. *(Japanese)* 78—39765
CuPt equiatomic alloy, effects of quenching temp. on ordering, study by elec. resistivity meas. *(Japanese)* 79—43285
CuPt, quenched, state of local order 79—47722
CuPt, specific heat, Debye temp. below 30K 78—55956
CuPt type alloys, static stress influence on ordering, theory *(Russian)* 77—59775
Cu_3Pt, antiphase domains morphology 80—108460
$(Cu_3Pt)_{1-c}Mn_c$, mag. suscept. and effect of atomic order and disorder 77—24669
Cu_2Sb, linear muffin-tin calc. for Fermi surface 77—62802
Cu_3Sb, formed by saturation of Cu grains with Sb, electron diffraction exam. of diffusion layer *(Russian)* 79—33119
$Cu_{82.5}Sb_{17.5}$, X-ray K-absorption discontinuity, extended fine struct. 78—76556
$Cu_{0.9}Si_{0.1}$, chemical effect on valence electronic states, AES and SXAPS meas. 79—47558
η-Cu_3Si precipitates in Si, cryst. struct. 78—91304
CuSn, amorphous, elec. resistivity temp. depend. comparison to Einstein oscillator model 78—6342
Cu(Sn)/Nb(Al), composite superconductor fabrication and characts. 77—81242
Cu_3Sn, modulated struct. phenomena, survey 79—95033
Cu_3Sn, one-dimens. long period superstructs. with Zn and Ni additions 78—83777
ε-(Cu_3Sn)-Cu diffusion couples, growth of intermediate phase layers *(Japanese)* 80—49431
CuSnMg, crystal struct. anal. 78—91306
Cu_4SnMg, crystal struct. anal. 78—91306
$Cu_{50}Ti_{50}$, amorphous and cryst. alloy, corrosion rates and anodic polarisation curves 79—24650
$Cu_{66}Ti_{34}$, metallic glass, neutron diffr. meas. of struct. factor 80—24367
$Cu_{40}Z4_{60}$, $Cu_{56}Zr_{44}$, and $Cu_{60}Zr_{40}$ metallic glass, inelastic deform., free energy spectra 80—71699
β-CuZn, acoustic emission rel. to stress induced martensitic transformation 80—81061
CuZn, omega phase, roles of electron microscopy and electron diffraction *(French)* 78—27524
CuZn, planar faults, faint electron microscopic image contrast obs. 80—107283
Cu_3Zn clusters, electronic structures, SCF-Xα-SW method 80—88468
Cu_xZn_{1-x}, disordered alloy, muffin-tin model, electronic struct. and density of states calc. 80—29302
Cu_xZn_{1-x}, positron annihilation and Mossbauer effect exam. 79—65775
CuZnAl, martensitic, ordering effect on yield stress 79—100133
CuZnAl single crystal, thermodynamic anal. of martensitic transform. under stress 79—87635
CuZr, photoemission study 80—104046
$CuZr_2+H_2$, 550 to 850°C, absorption isotherms, thermodynamics 79—87841
$Cu_{0.57}Zr_{0.43}$, amorphous, partial struct. factor, TOF pulsed neutron 79—14684
$Cu_{0.57}Zr_{0.43}$ amorphous alloy, neutron diffr. obs. of struct. 80—88060
$Cu_{40}Zr_{60}$, amorphous alloys, supercond. transition temp., press. depend. 80—84524
$Cu_{46}Zr_{54}$, devitrification effect on mech. props. 80—30082
$Cu_{46}Zr_{54}$, metallic glass, dynamical struct. factor and freq. distrib. meas. 80—54136
$Cu_{50}Zr_{50}$, amorphous and cryst. alloy, corrosion rates and anodic polarisation curves 79—24650
$Cu_{50}Zr_{50}$, metallic glass, internal friction peaks 80—25753
$Cu_{56}Zr_{44}$ metallic glass, devitrification and its effect on mech. props. 80—33893
$Cu_{57}Zr_{43}$, amorphous alloy, computer simulation of atomic structure 80—70125
$Cu_{60}Zr_{40}$, amorphous, ductility and stress relief, low-temp. annealing effects 80—76296
$Cu_{60}Zr_{40}$, amorphous, elec. resist. calc. and temp. coeff., using t-matrix 78—72130
$Cu_{60}Zr_{40}$, amorphous powder, production using gas-water atomisation unit 80—7518
$Cu_{60}Zr_{40}$ glassy metal, photoemission and mag. susceptibility 79—28896
$Cu_{60}Zr_{40}$, metallic glass, composition, mech. props., simulation 80—49117
$Cu_{60}Zr_{40}$, stability, crystallisation, ductility meas. 78—47246
$Cu_{66}Zr_{34}$, amorphous metallic glass, differences caused by preparation technique *(French)* 80—103247
Dy-Cu, amorphous, mag. phase diagram, magnetisation and sp. ht. meas. 80—80532
Dy-Cu amorphous mag. alloy, linear sp. ht. due to single-ion excitation 78—91874
DyCu, direct Coulomb contrib. of cond. electrons to crystalline elec. field 77—76784
DyCu, direct coulombic contrib. of cond. electrons to cryst. elec. field 79—91005
DyCu, exchange coulombic contrib. of cond. electrons to cryst. elec. field 79—95376
DyCu film, amorphous, asperomagnetic domains, Barkhausen jumps in hysteresis loop 80—75822
Dy_xCu_{1-x}, amorphous film, magnetisation meas., local anisotropy effects 78—68309
$DyCu_2Si_2$, Mossbauer spectra 80—20558
ErCu, cubic antiferromag., mag. excitations inelastic neutron scatt. meas. 78—72341
ErCu, magnetic excitations 80—25115
$Er_xLa_{1-x}Cu$, and $Er_xY_{1-x}Cu$, antiferromag., mag. and resist. behaviour 80—34412
$ErNi_{0.6}Cu_{0.4}$, sp. ht. and modulated mag. struct. 77—32167

copper alloys continued
$EuCu_2$, and $EuCu_5$, hyperfine interactions, high press. Mossbauer expts. 78—43714
$EuCu_5$, cond. electron spin polarisation 77—63136
$EuCu_5$, indirect exchange, spin echo NMR meas. 80—15822
$EuCu_2Si_2$, fluctuating valence system, quadrupole interaction temp. depend. 80—54972
$EuCu_2Si_2$, interconfiguration fluctuation, NMR expts. 80—66069
$EuCu_2Si_2$, valence fluctuation and temp. depend. of Cu nuclear quadrupole interaction 80—15818
$EuCu_2Si_2$, XPS studies, valence band, 4-f region 78—6831
$Eu(Ni_{1-x}Cu_x)_5$, mixed valency, isomer shift temp. depend. 78—84511
$EuNi_xCu_{5-x}$, mixed valency of Eu, Mossbauer expts. 78—52407
Fe, cast-Mg, 78—44149
Fe, grey cast, corrosion resist., Cu alloying additions effect *(Russian)* 78—56807
Fe/Fe-Cu composites, microplastic deformation development 78—39877
Fe-Ag-Cu melts, phase interface props., Cu influence *(Russian)* 79—51261
Fe-Al-Ni-Co-Cu alloys, Ti alloying and deoxidising addition *(Russian)* 78—80181
Fe-C-Cu (0.21, 0.2 wt.%), neutron-irradiated, resolution of C atoms, internal friction meas. 78—31442
Fe-C-Cu (0.21, 0.2 wt.%), neutron irradiated, torsional props. effect of Cu additions and annealing temp. 78—56699
Fe-C(graphite)-Ni-Cu, dynamically hot pressed mech. props., effect of Ni-Cu additives 78—60620
Fe-Co-Al-Cu-Ti (40, 14, 7.5, 4.5 wt.%), metastable equilibrium, high coercive state *(Russian)* 80—66476
Fe-Co-Ni-Al-Cu, polycryst. hard mag., C diffusion 79—77827
Fe-Cr-Ni-Cu-Sn, Cu and Sn effect on Cr and Ni segregation *(German)* 78—72777
α-Fe-Cu, coordination fields of crystal struct., rigid-sphere model 78—47266
Fe-Cu, dil., size effects on mag. hyperfine fields at non-mag. impurities 78—43586
Fe-Cu, dilute, coercive field, initial permeability and relax. loss, non-mag. impurity effect 77—69628
Fe-Cu, dissolution rate into molten Al, convection mass transfer *(Japanese)* 78—71858
Fe-Cu, generation of self-consistent Gibbs energy functions 79—11565
Fe-Cu, lath martensite habit planes, TEM study 80—84942
γ-Fe-Cu, lattice and grain boundary diffusion of Cu 79—23765
Fe-Cu, layers formed by reaction with molten Al, X-ray, EPMA and hardness meas. *(Japanese)* 78—72926
Fe-Cu, liq., thermodynamic characts. calc. *(Russian)* 80—15264
Fe-Cu, liquid phase sintering 80—16232
Fe-Cu, mag. moment distrib., elastic neutron scatt. obs. 79—78340
Fe-Cu, modulated microstruct., continuous cooling effect, hardness and electron microscope obs. 79—87665
Fe-Cu, precipitation hardening of α-Fe containing weak and strong particles 80—20946
Fe-Cu, protective coating on Al powder *(Russian)* 78—60881
Fe-Cu, sintered compacts, cooling effect on strength 77—73293
Fe-Cu, thermodynamic analysis of phase relationships 77—73260
Fe-Cu, vapour-deposited struct. and thermal stability 78—43265
Fe-Cu (0.34 wt.%), neutron irradiated, field-ion microscope detection of ultra-fine defects 79—42116
Fe-Cu (1.2 wt.%) effect of precipitation on recrystallisation, texture 78—88476
Fe-Cu (1.77%) alloy, influence of neutron irrad. on electric resist. *(Russian)* 79—38041
Fe-Cu (2 wt.%), furnace cooled, ageing and steam oxidation 78—23744
Fe-Cu (30 wt.%) alloy, dendrite remelting during isothermal holding, microspin obs. *(Japanese)* 78—71836
Fe-Cu (4.54 wt.%) alloy, scaling behaviour, 700-1000°C, 1 atm. O_2 80—93679
Fe-Cu (75 ppm), internal oxidation, local struct. determ. by EXAFS 80—25916
Fe-Cu alloy, effect of ε-Cu phase on strain ageing *(Japanese)* 80—7582
Fe-Cu alloys, transform. substruct., lath microstructure after quenching 80—16298
Fe-Cu clusters, mag. interaction, Mossbauer study 79—82895
Fe-Cu liquid alloy, heats of mixing, mixing entropies *(Russian)* 80—65224
Fe-Cu metastable dil. alloy film, hyperfine interactions 78—52398
Fe-Cu pseudoalloy, contact corrosion in tropical marine environment 78—11422
Fe-Cu-C, fatigue behaviour for tempering at 500°C, precip. hardening 77—40442
Fe-Cu-C, mixed powder compact, sintering mechanism 78—15343
Fe-Cu-C, phase equilibria, 950 to 1500°C 80—60836
Fe-Cu-C, sintered parts, struct. stabilisation with C potential control of protective atmosphere 78—60614
Fe-Cu-C sintered porous materials, machinability 80—66457
Fe-Cu-C sintered with added S, thermophys. props. 79—61541
Fe-Cu-C-O(-Ni) powder, atomized, reduction and decarburizing annealing parameters 80—25603
Fe-Cu-D, ion implanted, D trapping, 90-500K 80—15131
Fe-Cu-Mn(Ni), analysis and synthesis of phase diagrams 79—11563
Fe-Cu-Ni, austenite to ferrite+precipitate reaction, TEM/STEM study 80—3075
Fe-Cu-Ni, Ni effect on austenite decomposition 80—3048
Fe-Cu-Ni (2, 5 wt.%), interphase precipitation obs. in assoc. with Widmanstatten ferrite lateral growth 80—40365
Fe-Cu-Ni (2,2 wt.%), isothermally transformed, precipitate orientations 80—50640
Fe-Cu-Ni-Cr_3C_2-C based sintered friction material, wear, surface geometry and struct. effects 80—25875
Fe-Cu-Ti, improvement of irradiation-enhanced Cu embrittlement by Ti addition 79—43393
Fe-Cu-Zn, high-temperature phase diagrams *(German)* 80—108390
Fe-Cu(-C), alloyed with graphitising elements, geometrical thermodynamics *(Russian)* 79—52261
Fe-Cu(2, 4 and 6 wt.%), sintered, precipitation hardening 77—66653
Fe-glass-Cu sintered material, Cu effects on strength 77—77443
Fe-Mn-Cu-C, Cu effect on ε'-martensite, X-ray obs. of heating effects *(Russian)* 79—87667
Fe-Ni-Al-Co-Cu alloy, sintered single-crystal mag. prod., props. 77—66709

copper alloys continued
Fe-Ni-Al-Co-Cu-Sn alloy YuNDK35T5, Sn addition effects on physicomechanical and magnetic props. and workability *(Russian)* 77—70101
Fe-Ni-Al-Co-Cu-Ti, 38 to 40 wt.% Co, 8 to 8.5 wt.% Ti, alloy YuNDKT tempering and thermomagnetic treatments 78—3154
Fe-Ni-Al-Co-Cu-Ti alloy YuNDKT, nature of X-phase heat treatment effect on microstruct. 77—90380
Fe-Ni-Al-Co-Cu-Ti magnetic alloy electrolytic treatment with programmed pulse current *(Russian)* 79—100282
Fe-Ni-Al-Co-Cu-Ti YuNDK type, S effect on mech. props. 80—60927
Fe-Ni-Al-(Cu) (12, 0.5, 0.5 to 3 wt.%), Cu addition strengthening at 77K, mech. props. 80—60875
Fe-Ni-Co-Cu-Ti YuNDKT alloys, impaired mag. props. with C and S additions 80—60368
Fe-Ni-Cu alloy components, dynamics of arrival to arc discharge during roasting *(Russian)* 77—16895
Fe-Ni-Ti-(Cu) (12, 0.25, 2 wt.%), Cu addition strengthening at 77K, mech. props. 80—60875
Fe-Ni-V-(Cu) (12, 2, 2 wt.%), Cu addition strengthening at 77K, mech. props. 80—60875
Fe-Ni-(Cu) (12, 0.5 to 3 wt.%), Cu addition strengthening at 77K, mech. props. 80—60875
Fe-P-Cu-SiO_2-$FeAl_3$-asbestos composite, thermal and elec. conds., temp. and composition depends. 77—66609
Fe_3Al-Cu, ternary ordered solid soln., formation by substitution 77—43177
Ga-Cu, fast quenching of A15-phases *(German)* 77—36014
Ga-Cu, liq., mag. susceptibility *(Russian)* 78—6513
Ga-Cu liquid alloy, solubility and activity of O_2 77—59122
Ga-Cu-Sn solders, exam. of structural transformations due to hardening, heat treatment *(Russian)* 80—7578
Gd-Co-Cu, sputter deposited amorphous alloy, substrate bias, magnetic anisotropy, annealing 78—48006
Gd-Co-Cu film, amorphous, influence of biased magnetron deposition parameters on props. 77—43856
Gd-Cu, amorphous, mag. and elec. props. 80—80499
Gd-Cu, amorphous, mag. props. and ferromag. reson. 80—75862
Gd-Cu, amorphous alloy, mag. coupling 78—88108
Gd-Cu, amorphous alloy films, mag. phase diagram, spin glass and ferromag. regions 78—68234
Gd-Cu, splat-cooled, internal friction exam. 77—20012
Gd-Cu alloy film, amorphous, struct. and mag. props. 78—52318
Gd-Cu amorphous alloy film, mag. props. 77—16121
Gd-Cu sputtered amorphous films, ferromag. props. 77—66393
$Gd(Al_{1-x}Cu_x)_2$, C15 struct., elec. resist., comp. depend. 78—14705
$Gd(Al_{1-x}Cu_x)_2$, thermoelec. power, exchange interactions 80—24881
$Gd_{1-x}Co_x$, CPA calcs., mean mag. moments 77—72997
$Gd_{0.12}Co_{0.59}Cu_{0.29}$, sputtered film prep. for bubble device 77—16493
GdCu, electrical resistivity and length changes with temp., hysteretic behaviour 80—97600
Gd_xCu_{1-x}, amorphous film, magnetisation meas., fully aligned moment 78—68309
$Gd_2Cu_6Al_{11}$, NMR and mag. susceptibility 79—15367
$Gd(Cu_{1-x}Gd_x)$, pseudobinary alloy, mag. susceptibility and elec. resist. at low temp. 80—34602
GdCuGe, $Gd_6Cu_8Ge_8$ and $GdCu_2Ge_2$, magnetic props. 77—32180
$GdCu_2Si_2$/Mo, point contact spectroscopy of magnons 79—38312
GdCuSn, mag. props. 77—85439
$GdCu_{1-x}Zn_x$, mag. struct. determ. 79—87238
$Gd(Ni,Cu)_2$, spin disorder resist. evaluation, influence of antiferromagnetic order 77—73035
$(Gd_{1-x}R_x)(Co_{1-y}Cu_y)_5$, origin of hyperfine fields acting on Gd, Mossbauer study 80—44967
Ge-Cu, alloying effects on elec. transport props. of amorphous and crystalline Ge films 79—51689
Ge-Cu, liquid, solubility of O_2 at 1373K, in equilibrium with GeO_2 78—44109
Ge-Cu (0, 23, 40 at.%), amorphous film struct. *(German)* 78—95391
Ge-Cu film, amorphous, EPR meas. 78—80212
Ge-Cu film, codeposited, amorphous and polycryst., struct. and elec. props. 80—24766
Ge-Cu film, polycryst., struct. props. determ. 79—4494
Ge-Sn-M, M=Cu, As, Sb, formation of Ge-based solid solns. during crystallisation 77—80625
$Ge_{0.6}Cu_{0.2}Au_{0.2}$ film, superconducting transition temp., resistivity meas. 77—43774
Hf-Cu, amorphous, thermal stability, crystn., DSC and elec. resist. study 80—107060
Hf-Cu, oxidation of intermetallic phases 79—100298
Hf-Cu-Ge, alloys, phase diagrams and cryst. struct. *(Russian)* 80—25658
Ho-Cu, crystal field parameters from neutron spectra, rel. to mag. props. in ordered state 77—43546
Ho-Cu intermetallics, resist. and magnetoresist., mag. ordering obs. 80—70677
$HoCo_{5-x}Cu_x$, lattice parameters and mag. props. 79—82817
$HoCo_{5.5-x}Cu_x$, cryst. struct. and mag. props. 80—75800
$HoCu_2$, mag. struct. and elec. resist., neutron diffr. obs. 80—60206
Ho_xCu_{1-x}, amorphous film, magnetisation meas., local anisotropy effects 78—68309
$HoNi_{0.5}Cu_{0.5}$, sp. ht. and modulated mag. struct. 77—32167
$HoNi_{0.7}Cu_{0.3}$, mag. behaviour 79—99688
La-Cu alloys, cryst. struct. exam. 77—58978
LaB_6-Cu, form. by wetting of LaB_6 with Cu 80—100813
$La_{70}Cu_{30}$, disordered ribbons, production of quenched samples using arc furnace 80—71612
$LaCu_2Si_2$, ^{29}Si NMR and mag. susceptibility 79—61246
$LaCu_2Si_2$, resistivity, thermal conductivity and thermopower between 1.5 and 300K 78—87963
$La(Ni_{1-x}Cu_x)_5$, H_2 sorption props. 78—91533
$LaNi_4Cu$, H_2 absorption, cell volumes and desorption pressures correlation 78—22860
Ma-Cu (10 at.%), antiferromag. defect scatt., neutron polarisation anal. 78—2652
Mg/Mg_2Cu eutectic, hydriding and dehydriding kinetics obs. by press. sweep method 80—35765
Mg-Ag-Cu, phase comp. in Mg-rich region *(Russian)* 80—40331
Mg-Cu, binary system, nonstoichiometry, of Laves phases, $MgCu_2$ *(French)* 78—52770
Mg-Cu, electronic struct., X-ray emission obs. 77—16428
Mg-Cu (15.1 wt.%), damping capacity 77—48474

copper alloys continued
Mg-Cu-Pb system, phase equilibria in Mg-rich corner *(French)* 78—76630
$MgCu_2$, Fermi surface investig. by de Haas-van Alphen effect 77—35857
$MgCu_2$-$MgAl_2$, Friauf-Laves phase, long-period stacking variants, electron conc. depend. 77—80444
$MgCu_2$-$MgNi_2$, electronic sp. ht. 1.5 to 4.2K, Fe impurity effects *(German)* 77—59125
$MgCu_2$-$MgZn_2$ system, heats of form. of Laves phases *(German)* 79—66337
Mg_2Cu, industrial hydride reservoir, characts., technological aspects 80—45792
Mg_2Cu polycrystals, surface study by AES, XPES and X-ray induced AES 80—65346
Mg_2Cu sorption capacity, grain size distrib., and compactness for H_2 storage appl. 79—74547
$Mg(Cu_{0.535}Al_{0.465})_2$, 2D lattice images of Friauf-Laves phase and defect type 80—24324
$Mg(Cu_{1-x}Al_x)$ with x=0.465, Friauf-Laves phase, electron microscope obs. 77—19908
$MgCu_{2-x}Ni_2$, X-ray and neutron diffr. investigation of Laves phases of $MgCu_2$-type *(German)* 80—15050
$Mg(Cu_{1-x}Zn_x)_2$, crystal struct. and lattice spacing under high press. comp. depend. 77—72581
$MgCu_{2-x}Zn_x$, X-ray and neutron diffr. investigation of Laves phases of $MgCu_2$-type *(German)* 80—15050
Mn-Cu, acoustic shock pulse characts., stress amplitude and temp. depend. 79—19323
Mn-Cu, alloying addition and heat treatment effects on damping capacity 78—3165
Mn-Cu, alloying behaviour and high damping capacity 80—35160
γ-Mn-Cu, antiferromag. defect neutron scatt. study 79—47252
γ-Mn-Cu, antiferromagnetism, martensitic transformation 79—1673
γ-Mn-Cu, changes in cell dimensions at martensitic transform. 78—19750
Mn-Cu, fatigue, stability of energy dissipative charact. 77—21209
Mn-Cu, high-damping, acoustic shock pulse attenuation and vel., stress amplitude and temp. depend. 77—15503
Mn-Cu, liquid alloys, thermochemistry 79—56962
Mn-Cu, mag. and cryst. struct., neutron and X-ray diffr. meas. *(Russian)* 78—22694
Mn-Cu, melt, solubility and activity of S *(Russian)* 77—25012
γ-Mn-Cu, metastable, structural aspects of decomposition 79—1871
Mn-Cu, mictomagnetic props., neutron diffr. obs. 80—65906
Mn-Cu, plastic deform. mechanism and shape-memory effect, mag. struct. obs. *(Russian)* 78—60705
Mn-Cu, shape-memory effect at martensitic transform., cryst. and mag. struct. 77—36610
γ-Mn-Cu (10 at.%), spin wave studies using neutron diffraction 80—70991
Mn-Cu (25, 62 wt.%), elast. consts., temp. depend., 170-300K *(Russian)* 80—81095
Mn-Cu (25 wt.%) alloy, critical shear stresses of twinning and glide 79—87693
Mn-Cu (25 wt.%) rod, transverse vibrations, energy dissipation, static longitudinal load effect 80—81099
Mn-Cu (75, 25 wt.%), rod, coupled flexural and torsional vibrs., energy dissipation 80—89281
Mn-Cu (9.3 wt.%), cryst. struct. at FCC to FCT transform. *(Russian)* 80—11643
Mn-Cu alloy, local premartensitic instability in FCC phase 80—40355
Mn-Cu alloy, volume effect, paramagnetic-antiferromagnetic and structural transition, lattice consts. 80—39007
Mn-Cu alloys, mechanical damping at 40 kHz 78—23755
Mn-Cu alloys, spinodal decomp. at 380°C, neutron diffr. anal. *(Russian)* 79—20023
Mn-Cu alloys, stressed, diffuse neutron scatt. exam. 78—47950
Mn-Cu structural alloys, physicomechanical props. 77—12652
Mn-Cu-Al alloy under torsion, anomalous elasticity and transformation plasticity obs. *(Russian)* 78—75834
Mn-Cu-Bi ternary cpd. thin films for magneto-optic memory applic. *(Japanese)* 77—63238
Mn-Cu-Ni-Bi, magneto-optic film for storage appl. 77—12165
Mn-Cu-Zn system, optimum heat-treatment routine for max. damping 79—87670
γ-MnCu, antiferromag., stressed, mag. defects meas. by neutron polarisation anal. 80—50076
γ-MnCu crystals, antiferromag. Czochralski growth 80—97420
γ-MnCu, Mn-rich, inclined spin axis, neutron diffr. study 80—75723
MnCu, neutron scatt. near crit. comp., effects of stress and ageing 79—19722
$Mn_{17.5}Cu_{82.5}$, mictomag. process, susceptibility and resist. meas. 78—3157
MnCuBi film, coated with SiO layer Kerr readout characts. 77—85509
MnCuBi film, for mag. storage appl., prep. by RF sputtering, and props. 77—8369
MnCuBi film, optical and magneto-optical props. 77—4695
$MnCu_{1-x}Dy_xBi_{0.86}$ film, mag. and magneto-optic props., appl. as storage medium 77—8550
$Mn_{1-x}Cu_xSb$, ferromag., NMR exam. 77—12207
$Mn_{1-x}Cu_xSb$ film, ferromag. reson. 78—31114
Mo-Cu, electrical erosion resistance during electrospark machining 78—35531
Mo-Cu-Al, phase equilibrium *(Russian)* 78—15361
Monel, Norton-Bailey parameters, from creep rupture data 80—30098
Nb/Cu-Sn-Mg, superconductor, effect of Mg addition to Cu-Sn matrix 80—25028
Nb-Al-Ge-Cu, rapidly quenched, comp. and phase equilib. 80—76235
Nb-Al-Ge-Cu, supercond. influence of Cu on crit. current of diffused layers *(Russian)* 79—69643
Nb-Al(Ga, Si, Ge, Sn)-Cu, rapidly quenched, comp. and phase equilib. 80—76235
Nb-Cu, neutron radiation stimulated diffusion, electrical resistivity exam. *(Russian)* 79—14959
Nb-Cu (0.02 wt.%), Cu electron Nb_5Si, $NbSi_2$ and NbB_2 form. *(Russian)* 78—15400
Nb-Cu-Sn, cast supercond. alloy, crit. current, degradation resistance 78—76203
Nb-Ga-Cu, fast quenching of A15-phases *(German)* 77—36014
Nb-Ga-Cu, phase diagram, metallographic and X-ray study, annealed and as-cast supercond. crit. temp. *(Russian)* 78—56617

copper alloys continued
Nb-Ge-Cu, phase equilib. and supercond. props. *(Russian)* 80−40332
Nb-Sn-Cu, Cu effect on Nb solubility and peritectic transform. temp. in Sn bath *(Czech)* 77−59754
Nb_3/Sn-Cu composites, in situ processed, supercond. props. 80−75698
Nb_3Sn-Cu multifilamentary wires, in situ prep., supercond. and mech. props. 79−38768
Nb_3Su-Cu supercond. composites, fabrication, magnet appl. 80−11602
NbTi-Al-(Cu-Ni) multifilamentary composite supercond. wire, stability, AC losses 77−76998
$Nd(Co_{1-x}Cu_x)_5$, coercive force temp. depend. 79−82823
Ni alloy, precipitation strengthened compositions with oxide particles, condensed, struct. criteria and thin layer possibilities *(Russian)* 80−89236
Ni-Al bronze, fracture resistance of tubes 78−19867
Ni-Al bronze, fracture toughness 77−81312
Ni-Be bronze, Fe and Si alloying addition effect on phase composition *(Russian)* 78−15360
Ni-Cr, O transport, during fatigue crack growth, exam. 78−52981
Ni-Cr-Al-Cu, Evanohm, Kapitza conductance meas. using superconducting current comparator 77−41645
Ni-Cu, chemisorption of CO, inhibition by Cu *(French)* 77−1295
Ni-Cu, crystal growth, oriented, by vacuum intake method *(Russian)* 77−4732
Ni-Cu, dil., ferromagnetic, hyperfine field and relax. time obs. of impurity heavy nuclei 80−75533
Ni-Cu, directional order anisotropy energy induced by neutron irradiation, temp. depend. 77−66294
Ni-Cu, electron-irrad., neutron-scatt. studies 80−75268
Ni-Cu, ferromag., influence of local ordering on spin wave stiffness const. 77−89937
Ni-Cu, ferromag., mag. moment, local environment effects, HF CPA cluster calc. 80−65817
Ni-Cu, ferromag., polarised neutron scatt., evidence for mag. environment effect 77−40039
Ni-Cu, ferromag., press. effect on Curie temp. 79−51781
Ni-Cu, ferromagnetic, Hall effect, anomalous, rel. to scatt. processes 80−44572
Ni-Cu, ferromagnetic and spin glass transition, DC magnetisation meas. 79−78369
Ni-Cu, high temp. compatibility with pyrolytic C 79−65261
Ni-Cu, high-field susceptibility, spin-wave spectrum, CPA calc. 80−65818
Ni-Cu, hydrogenated, Curie point, cluster magnetism 78−14960
Ni-Cu, implantation damaged, crit. behaviour, perturbed ang. distrib. meas. anal. 80−60476
Ni-Cu, itinerant electron ferromagnet, magnetovolume effects 80−60397
Ni-Cu, liq., activity meas. of O_2 by EMF method *(Japanese)* 80−54408
Ni-Cu, local environment effects, magnetisation decrease 79−65664
Ni-Cu, local mag. field on μ^+ 79−56665
Ni-Cu, low field magnetisation meas., mag. props. comp. depend. 78−91879
Ni-Cu, mag. anisotropy, temp. and conc. depend. 77−63172
Ni-Cu, mag. moment distrib. 77−32178
Ni-Cu, magnetoresistivity anisotropy, spin mixing 80−88538
Ni-Cu, matrix effect in SIMS anal. using O_2^+ primary beam 80−76576
Ni-Cu, nearly ferromag., heat capacity meas. in mag. field 0.3 to 4K, superparamag. clusters 77−69579
Ni-Cu, nearly ferromag., spin-glass-like distrib. of interaction fields 79−91243
Ni-Cu, Ni rich alloys, magnetic phase transition, elec. resistivity meas. 300-700K 79−82781
Ni-Cu, Ni-rich, temp. depend. resist. 80−10943
Ni-Cu, protective coating on Al powder *(Russian)* 78−60881
Ni-Cu, short-range atomic clustering, residual resist. meas. 80−29386
Ni-Cu, sp. ht. in mag. field, 1.2-15K 78−68262
Ni-Cu, spin fluctuations effect on temp. depend. of elec. resistivity 78−47776
Ni-Cu, spin polarised tunnelling expts. 78−39372
Ni-Cu, sputtered using Hg^+ and Ar^+ beams, comp. variation as function of ejection angle, AES exam. 77−44105
Ni-Cu, sputtering rate, radiation-induced segregation and preferential sputtering effects, kinetic model 80−40199
Ni-Cu, surface composition, AES 78−14558
Ni-Cu, surface segregation using atom-probe FIM 79−77883
Ni-Cu, surface segregation, computerised atom-probe FIM study 80−75412
Ni-Cu, tunnelling electron spin polarisation 77−73058
Ni-Cu, W fibre reinforced, liquid phase sintering under press. 78−19695
Ni-Cu (30 at.%), H(D) penetration, reversed kinetic isotope effects 77−43387
Ni-Cu (30 wt.%), cast cold- and warm-worked, recrystallization 79−29092
Ni-Cu (30 wt.%), cast single phase, solidified from undercooled melt, mech. props. 77−48540
Ni-Cu alloy, asymmetry of XPS of shell electrons *(Russian)* 78−76579
Ni-Cu alloy, magnetoresistance anisotropy, planar Hall effect 79−23947
Ni-Cu alloy, optical absorpt. meas. 78−19518
Ni-Cu alloy, surface comp. and catalysis 80−54489
Ni-Cu alloys, spontaneous resist. anisotropy 77−89752
Ni-Cu film, deposited by cylindrical magnetron sputtering, internal stresses 80−24773
Ni-Cu semiconducting cast ingots, effect of EM stirring on struct. *(Russian)* 78−6915
Ni-Cu-Al(Si), spinodal decomposition, morphology of microstructure, elastic strain energy anisotropy effect 78−15354
Ni-Cu-H systems, Curie temp. during phase transitions under high press. H_2 80−71029
Ni-Cu-Mn, dil. alloys, NMR freq. temp. depend., spin echo meas. 78−64296
Ni-Cu-Mn, mag. and galvanomag. meas. 77−89928
Ni-Cu-Si, Si effect on structural changes during ageing, TEM and X-ray obs. 78−15438
Ni-Cu-Si (38,5 at.%), changes in modulated struct. during ageing early stages *(Japanese)* 79−100183
Ni-Cu-X (X=Sn, Nb, Ti), spinodal decomp. alloys, linear expansion coeff. influence on morphological anisotropy *(Japanese)* 80−70431
β-Ni-Cu-Zn, electron microscopy of premartensitic state 79−66059
Ni-Cu(5%), absolute composition depth profile, surface segregation, field-ion microscope obs. 79−33166
Ni-Fe-Cu, Mu-metal, mag. aftereffects, dynamic neutron depolarisation study 80−50147

copper alloys continued
Ni-Fe-Cu, thermodynamic activities of components in pseudobinary section Ni_3Fe-Cu at 1520K 77−59752
Ni-Fe-Mo-Cu (79, 16, 4.3, 0.7 wt.%) K-state formation, physical props. exam. 78−47761
Ni-Mn-Cu, interdiffusion at 1173K *(Japanese)* 79−99375
Ni-Nb-Cu-C, NbC dispersed supercond. tapes, fabrication and characts. 78−19773
α'_2-Ni-Zn-Cu martensite, thermoelastic, microscope obs., TEM 77−55966
$Ni_x\,Cu_{1-x}$ paramag., coherent pot. approx. for nonoverlapping muffin tin potentials 78−2451
NiCu, dil., disordered, virtual bound states, reson. model pot. theory 79−23934
$Ni_{1-x}Cu_x$ (x=0.03, 0.16, 0.24), photoemission study, surface, bulk electronic struct. 78−48281
$Ni_{1-x}Cu_x+CO$, $Ni(CO)_4$ form. activation energy, mag. phase depend. 80−3409
$Ni_{23}Cu_{77}$ random substitutional alloy, (001) surface, angle resolved photoemission 77−85895
$(Ni_xCu_{1-x})_2MnSn$, mag. props. and lattice parameter, composition depend. 77−80916
$Ni_{0.7}Cu_{0.3-x}Si_x$, magnetic props., 4.2 to 800K 77−8290
$(Ni_{1-x}Cu_x)Ti$, martensitic, shape memory effect kinetics and thermodynamics 80−3021
$Ni_3(Fe,Cu)$, kinetic phenomena rel. to ordering and electron struct. *(Russian)* 78−76043
$Ni_3(Mn,Cu)$, ordering kinetics, neutron diffr. and elec. resist. meas. *(Russian)* 77−47379
NiTiCu, shape memory alloys, electron microscope and X-ray diffr. study of struct. 79−82179
$NpCu_2Ge_2$, Neel point and hyperfine interactions, Mossbauer and magnetisation meas. 77−1555
$NpCu_2Si_2$, mag. struct., neutron diffr. determ. 80−93084
$NpCu_2Si_2$, Mossbauer and magnetisation expts. 78−31138
Pb-Cu, charged particle irrad., damage and recovery processes 77−69002
Pb-Cu, hypoeutectic, grain refinement, and structural stability by S, Se and Te additions *(German)* 80−55387
Pb-$Cu_{91}Ni_9$-Pb superconducting junction, crit. currents 79−69633
Pb-$Cu_{99.8}Mn_{0.2}$-Pb superconducting junction, crit. currents 79−69633
Pb-Sb-Te-Cu-Sn, influence of specimen and grain size on mech. props. *(Russian)* 77−81297
PbCu film, amorphous supercond., phonon heat transport, thermal cond. meas. 78−19181
$Pb_{0.9}Cu_{0.1}$, film, polycryst. or amorphous, thermal cond., 0.5-11K 78−39260
Pd-Ag-Cu (35,25 at.%), determ. of ageing transformations by resist. meas., metallography, TEM and X-ray diffr. 79−4967
Pd-Cu, alloys-H solid solutions, superconducting transition temp. behaviour *(Russian)* 80−70879
Pd-Cu, H solubility enthalpy and entropy, effect on elec. cond. 77−35699
Pd-Cu, influence of adsorbed H on positron lifetime spectra 80−25480
Pd-Cu, positron annihilation, absorbed H_2 effect *(Russian)* 79−91528
Pd-Cu, T diffusion, effect on freq. factor and activation energy 78−63880
Pd-Cu alloy, asymmetry of XPS of shell electrons *(Russian)* 78−76579
Pd-Cu alloys, epitaxial growth and surface characterisation 78−14638
Pd-Cu compound, KKR electronic struct. 80−59864
Pd-Cu film on $BaTiO_3$ dielectric ceramic substrate, interaction between film and substrate during sintering 79−33958
Pd-Cu-Ga, cold work and annealing-induced hardening, X-ray diffr. anal. and metallographic exam. *(Russian)* 79−38844
Pd-Cu-H(D) dilute alloy soln., thermodynamic props. at high-temp. 79−99334
Pd-Cu-Si, glass form., crit. cooling rate 80−75169
Pd-Cu-Si, laser melting and splat quenching to form foils for TEM obs. 80−29986
Pd-Cu-Si, metallic glass, miscibility limits, computer study 79−65198
Pd-Cu-Si glass, cold drawn, serrated plastic flow, optical and SEM study 79−79052
Pd-Cu-Si metallic glass, energy loss spectra and Auger spectra 78−23563
Pd-Si-Cu, amorphous, Hall effect meas. and electronic struct. 80−75551
Pd-Si-Cu amorphous ribbons, low temp. sp. ht., density of states trends 80−79957
Pd-Si-Cu metallic glass tips, appl. as electron field emission source 79−8229
Pd_2AlCu-PdAl system, interactions and solid-state transforms *(Russian)* 80−16272
$Pd_{1-x}Cu_xH_c$, superconducting transition temp. conc. var. 77−8221
$Pd_{0.775}Cu_{0.06}Si_{0.165}$ alloys, glassy and crystallised, low-temp. specific heat 79−60516
$Pd_{0.775}Cu_{0.06}Si_{0.165}$ glass, optical props. in energy range 0.67 to 5.6 eV 80−34872
$Pd_{0.775}Cu_{0.06}Si_{0.165}$, undercooled metallic melt, viscous behaviour 77−66037
$Pd_{68.5}Cu_{15}Si_{16.5}$ glass, elec. resist., struct. and mag. props. 79−65423
$Pd_{77.5}Cu_6Si_{16.5}$, cold drawn wires, surface markings, fracture stresses 79−56997
$Pd_{77.5}Cu_6Si_{16.5}$, glassy, liq. and cryst. mag. and elec. props. 77−66249
$Pd_{77.5}Cu_6Si_{16.5}$, heat of crystn. and viscous behaviour 80−75166
$Pd_{77.5}Cu_6Si_{16.5}$ metallic glass, diffusion of Au 78−55983
$Pd_{77.5}Cu_6Si_{16.5}$, metallic glass, composition, mech. props., simulation 80−49117
$Pd_{77.5}Cu_6Si_{16.5}$ metallic glass wire, cold drawing 80−50650
$Pd_{77.5}Cu_6Si_{16.5}$, ternary miscibility gap, simulation, dispersed phase composite form. 80−54379
$Pd_{77.5}Cu_{6.0}Si_{16.5}$ metallic glass, glass transition temp., cooling rate depend. 80−75181
$Pd_{77.6}Cu_6Si_{16.5}$, metallic glass, viscosity meas. from rates of thermal transformations 78−26713
$Pd_{781}Cu_{55}Si_{164}$ glass, erosion craters produced by spark machining, scanning microscopy obs. 78−44268
$Pd_{781}Cu_{55}Si_{164}$, liquid quenched metallic glass, wear resistance 79−66079
PdSiCu, amorphous, US attenuation and vel. studies 80−19881
PdSiCu, amorphous, US attenuation and vel. studies at low temps. 80−88278
$Pd_{0.775}Si_{0.165}Cu_{0.06}$, glassy alloy, resist. minimum associated with mag. impurities 79−56187

copper alloys continued

- $Pd_{0.775}Si_{0.165}Cu_{0.06}$, metallic glass, intensity-depend. US attenuation at low temps. 78-79671
- $Pd_{0.775}Si_{0.165}Cu_{0.06}$, metallic glass, 0.01-10K, relax of tunnelling systems by conduction electrons, US expts. 79-14889
- $Pd_{0.78}Si_{0.16}Cu_{0.06}$, phonon propagation below 1K 78-71824
- $Pd_{1-x-y}Si_xCu_y$, glassy, low temp. specific heat 78-83969
- $Pd_{18}Si_{14}Cu_6$, glass, changes in density of states with alloys comp. UPS obs. 80-50531
- $Pd_{77}Si_{17}Cu_6$, amorphous, struct. changes due to cold rolling and low temp. annealing 79-66072
- $Pd_{77.5}Si_{16.5}Cu_6$ amorphous, indentation recovery, defect struct. produced by deformation 79-43275
- $Pd_{80}Si_{17}Cu_3$, glass, changes in density of states with alloys comp., UPS obs. 80-50531
- Pr-Cu-Al system, X-ray and microscopic anal. *(Ukrainian)* 78-84774
- $Pr(Co_{0.7}Cu_{0.3})_5$, anomalous magnetisation curves 80-15757
- $Pr(Co_{1-x}Cu_x)_5$, coercive force temp. depend. 79-82823
- $Pr(Co_{1-x}Cu_x)_5$, magnetocrystalline anisotropy exam. 78-39315
- $Pr(Co_{1-x}Cu_x)_5$, saturation magnetisation anisotropy 78-47960
- $PrCu_2$, cryst. field transitions near cooperative Jahn-Teller transition 78-84178
- $PrCu_2$, Jahn-Teller transition, susceptibility, elec. resist., thermal expansion and acoustic meas. 77-20276
- $PrCu_2$, mag. excitations and cooperative Jahn-Teller transition 79-65196
- $PrCu_4$, Knight shift, mag. susceptibility, 80-800K 79-95570
- $PrCu_5$, cryst. field effects on transport props. 78-72133
- $PrCu_5$, Knight shift, mag. susceptibility, 140-400K 79-95570
- $PrCu_5$, nuclear induced ferromagnetism 79-61069
- $PrCu_6$, coolant for two stage nuclear demagnetisation refrigerator *(Japanese)* 80-47063
- $PrCu_6$, nucl. mag. ordering, heat capacity and magnetisation obs. 79-87272
- $PrCu_2Ge_2$, magnetic props. 77-32180
- Pt-Cu, ESCA study 80-2923
- Pt-Cu, surface composition, XPS *(Portuguese)* 80-24722
- Pt-Cu, surface segregation, ion scatt. spectroscopy meas. 79-82423
- Pt-Cu (49.37 at.%), coexistent phases in homogeneous ordering 79-29052
- Pt-Cu alloy, asymmetry of XPS of shell electrons *(Russian)* 78-76579
- Pt-Cu alloys, ESCA determ. of electronic struct. 80-34352
- Re-Cu-Al phase diagram, X-ray structural and microscopic anal. *(Russian)* 80-20895
- Rh-Cu, melts, surface props. *(Russian)* 78-26750
- Rh-Cu catalyst, Al_2O_3 supported, chemisorbed CO, IR spectra *(French)* 80-60559
- Ru-Cu catalyst, electron spectroscopy exam. 78-44405
- Ru-Cu clusters, EXAFS study 80-84804
- S-Cu-Fe, phase diagram calc. 78-10172
- Sc-Cu, electronic struct., susceptibility, sp. ht. and Knight shift meas. 77-43485
- Sc-Cu, phase diagram determination, using X-ray diffr., metallography and DTA techniques *(Russian)* 79-34004
- Sc-Cu-Ga, phase equilibria, diagrams of state, X-ray, microstructural study *(Russian)* 80-55356
- ScCu, electronic struct., NMR relax. times meas. 79-51871
- Si-Cu alloys, direct synthesis by implantation of Cu^+ *(Japanese)* 79-28006
- Sm-Co-Cu, with Sm_2Co_{17} struct., aged, TEM high coercivity material, TEM obs. of microstruct. 77-77073
- Sm-Co-Cu permanent magnets, phase diagram 77-21106
- Sm-Co-Cu-Fe, single phase 2-17 sample, hard mag. props. 77-8349
- Sm-Co-Cu-Fe-Ti magnets, comp. and sintering effects on coercivity 79-15326
- Sm-Co-Cu-Fe-Zr, reversible changes in coercive force and struct. state during heat treatment 400-800°C *(Russian)* 80-29574
- Sm-Co-Cu-Fe-Zr magnet, production and mag. props. 77-40085
- Sm-Cu phase diagram *(Russian)* 78-27477
- Sm-Cu system, phase struct. investigation by X-ray diffr. *(Russian)* 80-49185
- $Sm_{1-u}Ce_u(Co_{1-x-y-w}Fe_xCu_yCr_w)_z$, permanent mag., improved mech. props. 79-87593
- $Sm_2(Co, Cu, Fe, M)_{17}$, M=Nb, V, Ta, Zr, effect of M on mag. props. 77-89978
- Sm(Co, Cu) alloys, coercivity mech. 80-44862
- $Sm(Co,Cu)_5$, eutectoid transform. 77-8799
- $Sm(Co,Cu)_z$, precip.-hardened, mag. and metallographic props. 77-8339
- $SmCo_5$, Cu-modified, magnetisation reversal mechanism 77-8350
- $Sm(Co_{0.65}Cu_{0.35})_{5.6}$, cryst. struct. and coercive force, heat treatment effects *(Russian)* 80-44170
- $Sm(Co_{0.84}Cu_{0.16})_{6.9}$, microstruct. and domain struct., mag. reversal *(Russian)* 80-20429
- $Sm(Co_{0.87}Cu_{0.13})_{7.8}$, coercivity and microstruct. 79-56569
- $Sm(Co_{1-x}Cu_x)_{7.8}$ alloys, coercive fields, domain wall energies, mag. and metallographic exam. 78-91897
- $SmCo_{3.5}Cu_{1.5}$, anisotropy and coercivity, Kerr effect, magnetisation and aftereffect expts. 77-8300
- $SmCo_{3.5}Cu_{1.5}$, mag. aftereffects, coercive mechanism, magnetisation reversal 77-69634
- $SmCo_{3.5}Cu_{1.5}$, single cryst., domain wall motion and domain form. 78-39359
- $SmCo_{3.5}Cu_{1.5}$, single crysts., mag. props. study and role of anisotropy *(French)* 79-38356
- $SmCo_{3.5}Cu_{1.5}$, time dependent magnetisation 78-80176
- $SmCo_4Cu$, domain boundaries shift, mag. reversal processes 79-87286
- $SmCo_4Cu$, nonuniform comp., domain struct. and mag. reversals process *(Russian)* 79-1681
- $SmCo_{4.3}Cu_{0.7}$, highly anisotropic ferromag., mag. state after large Barkhausen jump *(Russian)* 79-4699
- $SmCo_{5-x}Cu_x$, giant intrinsic mag. hardness obs. 77-59432
- $SmCo_{5-x}Cu_x$, giant intrinsic mag. hardness 79-91255
- $SmCo_{5-x}Cu_x$ magnet alloy, metallurgical study *(Korean)* 77-8853
- $Sm(Co_{0.81}Cu_{0.15}Fe_{0.04})_{6.9}$ and $Sm(Co_{0.84}Cu_{0.16})_{6.9}$ powders, mag. props. *(Russian)* 80-20434
- $Sm(Co_{0.86-x}Cu_{0.14}Fe_x)_7$, permanent magnet, sintering and heat treatment effects 80-39817
- $Sm(Co_{0.85}Fe_{0.05}Cu_{0.10})_7$, coercive force meas. 77-4530
- $Sm(CoFeCuMn)_7$, coercive force and anisotropy temp. depend. 78-68297
- $SmCu_5$, X-ray K absorpt., chem. shift 79-91531
- $Sm_2Cu_{1.6}Zr_{0.16}Fe_{3.3}Co_{12}$, enhancement of mag. props. 79-82825

copper alloys continued

- $Sm_{1-w}MM_w(Co_{1-x-y}Cu_xFe)_z$, (MM-mischmetal), mag. meas. and metallographic exam. 77-56119
- $SmNi_4Cu$, intrinsic mag. hardness 77-85506
- $SmNi_{5-x}Cu_x$, giant intrinsic mag. hardness due to randomised cryst. field interactions 78-68208
- $Sm_{0.91}Zr_{0.09}(Co_{0.68}Cu_{0.10}Fe_{0.22})_{6.7}$, alloy permanent magnet, coercive force *(Russian)* 80-65966
- Sn bronze, air atomised, densification and pressure requirements during extrusion 77-59713
- Sn bronze, extruded atomized powders, struct. and props. 79-38763
- Sn-Cu, amorphous film, optical props. 79-69895
- Sn-Cu, strong coupling superconductor, LF EM response function 78-10605
- Sn-Cu film, amorphous and polycrystalline, thermopower meas. *(German)* 77-80857
- Sn-Cu film, metastable supercond. alloys produced by low temp. ion implantation 80-88670
- Sn-Cu film, spreading kinetics on Nb substrate in vacuum, 700 to 800°C *(Russian)* 77-80680
- Sn-Pb-Cu, microduplex eutectic, cavitation during superplastic flow 78-48457
- $Sn_{11}Cu_{41}$, γ-brass struct., F-cells, X-ray diffr. 77-19903
- $Sn_{90}Cu_{10}$, quench-condensed films, superconducting transition temp., elastic stress and strain effects 80-70883
- Sn_3Cu_9Ni, γ-brass struct., F-cells, X-ray diffr. 77-19903
- SrCu, X-ray cryst. struct. determ. 80-92478
- Tb-Cu-Ag, mag. props. *(Russian)* 77-51905
- Tb-Cu-Zn(Al), mag. props. *(Russian)* 77-51905
- $TbCu_2$, collinear mag. struct., neutron diffr. meas. 79-87242
- Tb_xCu_{1-x}, amorphous film, magnetisation meas., local anisotropy effects 78-68309
- $TbNi_{2-x}Cu_x$, elec. resist. and mag. props. 78-72348
- Th-Cu, amorphous, thermal stability, crystn., DSC and elec. resist. study 80-107060
- Ti-Al-V-Fe-Cu, melt-extracted polycryst., mech. props. 80-76360
- Ti-bronze, friction with diamond, characts. 78-48541
- Ti-Cu, eutectoid decomposition 79-24491
- Ti-Cu, evaporated adhesion after electroplating 79-82475
- Ti-Cu, oxidation high temp., comparative study with Ti *(French)* 79-20285
- Ti-Cu, oxidation of intermetallic phases 79-100298
- Ti-Cu, struct. damage and internal fatigue cracks *(French)* 77-73341
- Ti-Cu (2.5 wt.%), corrosion resist. in marine environments *(French)* 80-50767
- Ti-Cu alloys, in acidic media, electrochemical behaviour *(French)* 78-23863
- Ti-Cu alloys, mag. susceptibility meas., paramagnetic susceptibility meas. Curie temp. and mag. moments calc. *(Russian)* 78-34956
- Ti-Cu dissolution mechanisms, photoelectron spectra study *(French)* 80-45198
- Ti-Cu interdiffusion 77-89596
- Ti-Cu metallisation systems, in 85°C 78% RH SO_2 contaminated environment, performance 79-74304
- Ti-Cu solid solution, determ. of Cu solubility, stability by thermoelec. power meas. 79-77753
- Ti-Cu system, appl. of metal-hydrogen equilibration determ. thermodynamic props. 79-77772
- Ti-Cu thin films, oxidation kinetics in air at 100 to 300°C, meas. 80-40590
- Ti-Cu-Al(Zr)(Sn)(Nb)(Mo), heat treatable alloys, effect of alloying on strength, tensile props. 78-56671
- Ti-Cu-H, catalytic props. 80-30274
- Ti-Cu-Ni-Au metallisation systems, in 85°C 78% RH SO_2 contaminated environment, performance 79-74304
- Ti-Cu-Si system, transforms. in Ti-Ti_5Si_3-TiCu region, 800-1600°C *(Russian)* 77-21099
- Ti-Ni-Cu (44.5, 10 wt%), opposing stress effect on shape memory and martensitic reversion 78-44185
- Ti-Ni-Cu system, phase relations at 800 and 870°C 78-27481
- Ti-Pd-Cu-Ni-Au metallisation systems, in 85°C 78% RH SO_2 contaminated environment, performance 79-74304
- Ti_3Al, Cu, Fe, Mo (1 at.%) additions, oxidation resistance, 700 to 800 degrees C 77-12744
- $TiBe_{1.8}Cu_{0.2}$, ferromag., magnetisation density 80-103817
- $TiBe_{2-x}Cu_x$, C-15 lower phase, itinerant ferromagnetism 80-15723
- $TiBe_{2-x}Cu_x$, high press. study of Curie temp. and mag. susceptibility 80-84600
- TiCu intermetallic compounds, decomposition reaction by H_2 absorption *(Japanese)* 78-23668
- TiNi-TiCu, exam. of shape memory effect, specific work 79-100216
- $TmCu_5$, crystal field level scheme, neutron inelastic scatt. and specific heat meas. 79-51536
- U/(Zr-Cu-Mo alloy) welded joints, mech. characts. determ. 20 to 750°C 79-29113
- UCu_5, core and valence band spectra, XPS obs. 80-50530
- UCu_5, mag. props. and NMR 77-20734
- $UNi_{0.5}Cu_{4.5}$, core and valence band spectra, XPS obs. 80-50530
- $UNi_{5-5x}Cu_{5x}$, NMR and press. effects 80-25230
- $UNi_{5-x}Cu_x$, thermoelectric power, 5-300K 79-65444
- V/Cu-Ga, composite superconductor, V_3Ga phase form., TEM obs. *(Russian)* 80-84933
- V-Al/Cu-Ge composite superconductors, transition temp. and upper crit. field, heat treatment effects 79-38268
- V-Al/Cu-Ge composite tape, transition temp., upper crit. field 78-68126
- V-Al(Ga,Si,Ge,Sn)-Cu, rapidly quenched, comp. and phase equilib. 80-76235
- V-Ga-Cu, phase diagram *(Russian)* 77-25014
- W/Cu powder with varying W particle size, burning behaviour and crack form. tests *(German)* 78-7005
- W-Cu, electrical erosion resistance during electrospark machining 78-35531
- W-Cu, porous material, skeletal type, produced by liquid phase sintering, exam. of mech. strength, determ. resistance 80-16245
- W-Cu (92.8, 7.2 wt.%), liq.-phase sintered, embrittlement and interfacial impurity segregation 80-66647
- W-Cu amorphous metal films, struct. and elec. characterisation 79-87017
- W-Cu composite materials, vel. dispersion and scatt. of transverse US waves 78-91383
- W-Cu contact materials with Ni and Co dopants, sintering 77-55908

copper alloys continued
  W-Cu fibre reinforced composites, interface shear strength, critical aspect ratio 77—4826
  W-Cu permeable materials, development 77—28755
  W-Cu powder, liquid phase sintering, stabilisation of porous structure and control of volume changes 79—95974
  W-Cu pseudoalloy, porous, chromising 80—100959
  W-Cu sintered alloy, produced from coreduced powders, densification 78—11154
  W-Cu-Co(Ni) electrical contact material, comparison of Co and Ni effects *(Korean)* 78—10539
  W-Cu-Ni powder, liquid phase sintering, stabilisation of porous structure and control of volume changes 79—95974
  W-Cu-Ni(6), contact materials, activated sintering, Ni and Co effects 79—95967
  W-Cu-(Ti)(Zr), exam. of mech. props. as function of temp., composition, and oxidation props. 80—16472
  W-Ni-Cu, liquid phase sintered, interfacial embrittlement 79—57101
  W-Ni-Cu(4, 2 wt%), radionuclide calorimeter for liquid He range 4.2 to 8K 79—18093
  WC-Co-Cu, interdiffusion up to 1120°C 78—11492
  WCuB prep. by infiltration of W skeleton by CuB, hardness meas. *(German)* 78—64508
  $Y_{1-x}Co_x$, CPA calcs., mean mag. moments 77—72997
  $Y(Co_{1-x}Cu_x)_5$, neutron diffr., thermal expsn. *(French)* 80—19749
  $Y(Co_{1-x}Cu_x)_5$, neutron diffraction study *(Chinese)* 80—39000
  $Y_2(Co_{1-x}Cu_x)_{17}$, single crystal, mag. props. 77—47993
  YbCu, mag. susceptibility, thermally excited interconfiguration crossover 77—16042
  YbCuAl, intermediate valency cpds., paramag. susceptibility, 1.4 to 1060K 77—63079
  YbCuAl, intermediate-valent, nucl. reson. and relax. 79—78550
  YbCuAl, mixed valence behaviour, mag. props. 78—68150
  YbCuAl, mixed valence cpd., dynamic susceptibility, neutron inelastic scatt. 80—65807
  YbCuAl, mixed-valence behaviour, mag. susceptibility and sp. ht. 77—80939
  YbCuAl, mixed-valent cpd., thermal expansion and magneto-volume effects 80—66005
  YbCuAl, phase diagrams, lattice props., electron hole symmetry 79—91002
  YbCuAl, susceptibility, sp. ht. and magnetisation 79—28512
  $YbCu_2Si_2$, interconfiguration fluctuation, NMR expts. 80—66069
  $YbCu_2Si_2$, local mag. moments, neutron scatt. study 79—61058
  $YbCu_2Si_2$, mag. 4f Zeeman-level power spectrum using diffuse mag. neutron scatt. 79—60775
  $YbCu_2Si_2$, tunnelling anomalies due to intermediate valence phenomenon 77—62873
  $YbCu_2Si_2$, valence fluctuation and temp. depend. of Cu nuclear quadrupole interaction 80—15818
  $Yb_{0.99}Gd_{0.01}CuAl$, intermediate Yb valence states, mag. props. 79—51743
  $YbNi_2$-$YbCu_2$ system, valency state, Yb behaviour *(French)* 80—45277
  $Yb_{1-x}Y_xCuAl$, disordered extended Anderson model, CPA-alloy analogue treatment 80—65506
  $Yb_{1-x}Y_xCuAl$, intermediate Yb valence states, mag. props. 79—51743
  Zn, determ. by at. absorpt. spectroscopy *(Russian)* 78—23998
  Zn-Ag-Cu alloy powder, brazing solder, production using electrodeposition and heating in reducing atm. 79—100079
  Zn-Al-Cu, mech. and technological props. *(Polish)* 80—89286
  Zn-Al-Cu (18, 4 wt.%), plastic deform. at room temp., superplastic props., tensile strength *(Czech)* 80—45360
  Zn-Al-Cu (18, 5 wt.%) alloy, superplasticity *(Russian)* 77—59856
  Zn-Al-Cu casting alloys, mech. props. and dendritic morphology, Al content effect *(Korean)* 80—93612
  Zn-Al-Cu-Mg (4.1, 3.1, 0.05 at.%), thermal cond. and sp. ht. meas. below 4.2K 77—20081
  Zn-Al-Cu-Mg-Pb-Sn, Cu, Mg, Pb, Sn effects on corrosion in wet steam 77—48585
  Zn-Al-Cu-Mg-Pb-Sn (12, 1, 0.02, 0.01, 0.015, wt.%), combined effects of Pb and Sn additions on corrosion, in wet steam 78—39952
  Zn-Cu, dil. alloy, creep ductility 79—38899
  Zn-Cu system, sputtering during atomic diffusion, UPS meas. 78—92159
  Zr-Cr-Cu, phase diagram in Zr corner *(Russian)* 78—19721
  Zr-Cu, amorphous alloy, sheet production by plasma spray quenching 77—44193
  Zr-Cu, dil. martensites, struct. and strength 79—29077
  Zr-Cu, glassy alloy, struct. anal. using X-ray diffr. 79—51004
  Zr-Cu, metallic glasses, glass transition temp., crystallisation temp., exothermal relaxation effect 79—52747
  Zr-Cu, optical elements, US cleaning, deleterious effects 77—42631
  Zr-Cu, oxidation of intermetallic phases 79—100298
  Zr-Cu, role of oxide plasticity in oxidation behaviour 77—36680
  Zr-Cu (1.6 wt.%), mechanical equation of state, stress relax. meas. 78—52880
  Zr-Cu (1.6 wt.%), near eutectoid, active eutectoid decomposition ageing and quenching effects 80—2993
  Zr-Cu amorphous alloys, glass transition and ductility, O additions effect 80—75168
  Zr-Cu metallic glasses, glass form. and thermal stability 80—75177
  Zr-Cu-H, catalytic props. 80—30274
  Zr-Cu-Ti (2.5, 0.15 wt.%), indentation irregularity at elastic limit after heat treatment *(French)* 79—79004
  Zr-Fe-Cu-W, Mossbauer spectra parameters of Zr_2Fe particles *(Russian)* 80—29654
  Zr-Ni-Cu-H, catalytic activity, exam. by conversion of toluene, and bicyclic aromatic hydrocarbons 80—30276
  Zr-Ni-Cu-H, catalytic props. 80—30274
  $Zr_3Co_{1-x}Cu_x$, phase stability and supercond. T_c 78—80519
  ZrCu, constitutional and struct. studies, by mag. susceptibility, metallography and X-ray diffr. 80—70166
  $Zr_{0.35}Cu_{0.65}$ metallic glass, Young's modulus meas. by impulse induced resonance technique 80—40411
  $Zr_{65}Cu_{35}$, metallic glass, low temp. resist., supercond. T_c 79—38235
  $Zr_{40}Cu_{50}Fe_{10}$, magnetically dil. glass, 3d moments, mag. susceptibility and magnetisation meas. 79—95574
  $Zr_{40}Cu_{60-x}Fe_x$, electronic and mag. props. 77—8271
  $Zr_{40}Cu_{60-x}Gd_x$, magnetically dil. glass, 4f moments, mag. susceptibility and magnetisation meas. 79—95575
  $Zr_{0.475}Cu_{0.475}M_{0.05}$, glass transition temp., comp. depend. 80—79702
  $Zr_{40}Cu_{60-x}M_x$ (M=Fe,Mn,Gd,Tb), amorphous, mag. ordering and local random anisotropy 78—68273

copper alloys continued
  $Zr_{40}Cu_{60-x}M_x$, (M=Gd, Tb, Fe or Mn), amorphous alloy, mag. interactions 78—95432
  $Zr_{40}Cu_{50}Mn_{10}$, magnetically dil. glass, 3d moments, mag. susceptibility and magnetisation meas. 79—95574
  $Zr_{40}Cu_{60-x}Tb_x$, magnetically dil. glass, 4f moments, mag. susceptibility and magnetisation meas. 79—95575
  $ZuCuZn_2$, martensitic transition, shear elastic const. meas. 77—28810

copper compounds
  see also copper alloys
  acetate, lasant for Cu vapour laser 79—31875
  acetate, use as lasant for Cu vapour laser 78—25854
  acetate monohydrate, pure quadrupole reson., covalency 77—16205
  acetates, antiferromag. exchange coupling, superexchange mech. 78—39310
  β-Al_2O_3-Cu_2O, phys. and chem. props., use in determ. of thermodynamics of Cu-Sn alloys 80—107502
  alaninium copper tetrahalides, exchange, mag. anisotropy, and spin diffusion contribs. to EPR linewidth 80—80597
  alkyl ammonium copper chloride, two-dimensional ferromag., low temp. lattice cond., phonon spectrum 77—4227
  alkylammonium copper halides, mag. sp. ht., two-dimens. S1/2 Heisenberg ferromag. behaviour 77—32206
  di-alkylammonium copper tetrachloride, weakly discontinuous phase transition, linear birefringence obs. 80—11362
  benzoate, antiferromag., spin dynamics at low temp. 77—32278
  benzoate, EPR sidebands 79—78508
  benzoate, one-dimens. antiferromag., heat capacity, field-induced crossover of spin-dimensionality 80—97099
  benzoate low-dimensional Heisenberg antiferromag., high field magnetisation 80—80558
  benzoate trihydrate, half-field EPR, 1.5-300K 78—60333
  bis(triethylbenzylammonium)tetrachlorocuprate(II), mag. anisotropy, susceptibility, EPR of Cu^{2+} 78—52344
  bis(trimethylbenzylammonium)tetrachlorocuprate(II), mag. anisotropy, susceptibility, EPR of Cu^{2+} 78—52344
  boride coatings on steel effect of Cu impurities in reaction mixture on brittleness, acoustic emission meas. 80—16581
  calcium copper acetate hexahydrate, and deuterated cpd., tunnelling reson. effects in nonreson. spin-lattice relax. 79—86726
  calcium copper acetate hexahydrate, $CaCu(CH_3COO)_4.6H_2O$ and $CaCu(CD_3COO)_4.6H_2O$, antiferromag. transition obs. 78—2680
  calcium copper acetate hexahydrate, mag. susceptibility behaviour at low temp. 77—24679
  calcium copper acetate hexahydrate, mag. susceptibility field depend. 79—87241
  calcium copper acetate hexahydrate, PMR at low temp., atomic position determ. 77—20728
  carboxylates, magnetic and spectroscopic props. 79—91204
  chalcogen compounds NMR chemical shifts 80—29636
  chalcogenide spinels, thermal stability, thermochemical, thermodynamic and crystallochemical props. 77—51519
  chalcogenides, single-phase, preparation 78—35293
  chalcopyrite, aq. oxidation in hydrochloric acid 79—61764
  chalcopyrite, electrooxidation in ACl, stoichiometry and reaction mechanism, Cu extraction appl. *(French)* 80—16231
  chalcopyrite films, (112), lattice mismatch with (0001) CdS substrates 79—87012
  chalcopyrite ternary semiconductor, lattice thermal cond. and ionicity, dielectric model 79—77846
  chalcopyrites, acidic fermic sulphate leaching, reaction mechanism 79—83511
  chalcopyrites, refr. index dispersion 80—55057
  chloride layered compound with graphitised PAN fibre, struct. and elec. cond. 79—91600
  complex, mixed-valence, X-ray K-absorption spectra 79—33863
  complex, strong antisymmetric exchange 78—34976
  complexes, EXAFS obs. 80—998
  complexes, N ligands, X-ray K-absorpt. edge, expt. 80—89084
  contact fusion in complex metallic systems 78—26664
  copper (I)-butyrate, dimorphism, X-ray diffr. and fluoresc. *(German)* 79—51090
  copper acetate mono-α-picoline, binuclear, cryst. and mol. struct. 79—99174
  copper benzoate, mag. heat capacity and Neel temp. in mag. field 79—61147
  copper complex $CuBr_2$ (pyrimidine)$_2$, mag. susceptibility and magnetisation curve, 1.2-4.2K 80—11177
  copper dichloride dipyridine, ground state wave function and superexchange interaction 79—42752
  copper dipyridine dichloride, antiferromag. reson. below 1K 79—28619
  copper formate tetrahydrate, ferrielectricity 80—2706
  copper formate tetrahydrate, stress effect on antiferroelec. phase transition, dielec. meas. 79—38498
  copper formate urea hydrate, two dimens. antiferromagnet, EPR, temp. depend. 80—54937
  copper phthalocyanine, chlorinated, radiation damage mechanism 80—88000
  copper phthalocyanine, on graphite, epitaxial growth of new polymorph 77—80712
  copper phthalocyanine dye on Si, optical modulation of low energy transmission electrons 79—69939
  copper porphin, Zeeman expt. on phosphoresc. triplet and quartet states 79—33786
  Cu_2S-CdS solar cell, interface recombination and junction field studies, exptl. technique 80—45683
  p-$CuInTe_2$, single cryst., IR study of lattice and free carrier effects 80—45074
  cupric amines, hydrolysis 77—29004
  cupric formate tetrahydrate, uniaxial stress effect on dielec. props. 78—48125
  cuprous halide photochromic glasses, spectral props., shell model *(Russian)* 79—27354
  cuprous halide-metal halide systems, AC cond. rel. to phase diagram 77—72712
  cuprous halides, cation or anion doped, ionic cond. 79—46837
  cyclo-hexyl-ammonium-copper-trichloride, specific heat, ferromagnetic chain system 80—103491
  determination, in seawater, chromatographic-at. spectrosc. method 78—68972

copper compounds continued
- di(alkyl ammonium)copper tetrachloride, two-dimens. magnon and phonon thermal cond. in high mag. fields 77—69123
- di(propylammonium) copper tetrachloride, mag. suscept. meas. 77—63131
- dialkylammonium copper chloride, nearly 2-D ferromag., low temp. NMR 77—28455
- dialkylammonium copper chloride, two-dimens. ferromag., energy transport by paramag. magnons 77—80909
- dialkylammonium copper chlorides, mag. and struct. transitions, IR absorption 77—52097
- dialkylammonium copper chlorides nearly two dimens. Heisenberg ferromagnet, NMR study of magnetisation 77—85586
- dialkylammonium copper tetrachloride, ferromagnetic layer compound, magnetostatic mode excitation 80—29538
- dialkylammonium copper tetracholorides, quasi 2-dimens., lattice- and spin-dimens. crossovers 77—59416
- diammonium layer compound, ND_3-$(CH_2)_2$-ND_3CuCl_4, antiferromag., magneto-optical meas. birefringence 78—68483
- dibutylammonium copper chloride, parallel pumping of two-dimens. spin waves, spin wave bandwidth 77—66425
- diethylammonium copper chloride, non-Lorentzian EPR lineshape and magnetostatic modes 77—43862
- diethylammonium copper tetrabromide, mag. struct., NMR meas. 80—71192
- diethylammonium copper tetrachloride, ^{63}Cu NMR, hyperfine interactions 80—54956
- diethylammonium copper tetrachloride, ferromag., static and dynamic mag. props. 80—50074
- diethyldithiocarbamate single crystal, EPR exchange coupled pairs, low temp. hyperfine anomaly 77—90021
- diisopropylammonium copper chloride, mag. interactions, susceptibility, 2-230K 80—60237
- dimethyl ammonium copper chloride, nearly two-dimensional ferromag., nucl. transverse relax. rates meas. 77—81024
- dimethyl ammonium copper chloride, spin dynamics near crit. pt. 80—7112
- dimethylammonium copper chloride, magneto-optical props., 0.03-13.5 eV 77—52132
- dimethylammonium copper chloride bromide, mag. props., pulsed NMR expts. 80—11292
- dimethylammonium copper manganese chloride, two-dimens. mixed magnet, EPR 80—66030
- dimethylammonium copper tetra(chlorobromide), mag. susceptibility, 1 to 30K, mag. phase transition 79—4675
- dimethylammonium copper tetrachloride, crit. slowing down and anomalous relax. near Curie temp. 80—71053
- dimethylammonium copper tetrachloride, ferromag., static and dynamic mag. props. 80—50074
- dimethylammonium copper tetrachloride-tetrabromide mixed cryst., mag. transition 80—65874
- dipropylammonium copper chloride, nearly 2D ferromag., spin wave theory 77—85436
- dipropylammonium coppertetrabromide, Faraday effect obs. of mag. struct., and domains 77—63399
- dipyridine dichloride, dynamic shift of the ESR field 80—2630
- dipyridinium copper bromide, $Py_2Cu_5Br_7$, Cu^+ ion conductor, cryst. struct. 78—51527
- ESCA shake-up satellites, spin density intensity ratio relation 78—50590
- ethylenediammonium copper chloride, struct. and mag. props., vibr. spectra 79—10842
- EXAFS investigation of Cu-O, Cu-N, Cu-Br bond lengths 78—52593
- ferrite, hot pressed, powders, influence of CoO and CuO alloying on physicomechanical characts. *(Russian)* 77—66600
- ferrite, spinel type catalytic oxidation of CO, role of mag. exchange interactions 78—56916
- ferrite bubble film struct., EM and RHEED, Mn and Mn-Cu ferrites 77—11801
- ferrite films, Mn-, Ni- and Al-substituted, LPE growth 80—96752
- ferrites, crystallisation of monocrystals from high temp. soln. 78—60561
- formate.$4D_2O$, field-induced antiferromag. order above T_N 78—84389
- formate anhydrate, cryst. struct. and mag. props. 80—79768
- formate bisurea dihydrate, magnetisation curves 78—23298
- formate tetradeuterate, deuterated, paraelec. and antiferroelec. phases, neutron diffr. obs. of struct. 79—87404
- formate tetradeuterate, paramag., induced staggered magnetisation, NMR 77—12212
- formate tetrahydrate, antiferromag. phase, neutron diffr. study 80—93085
- formate tetrahydrate, dielec. anisotropy and dimer theory 79—38427
- formate tetrahydrate, dielec. props. under hydrostatic press. 77—20789
- formate tetrahydrate, ice rule ferroelectric, polarisation correlations 80—97190
- formate tetrahydrate, press. effect on dielec. props. *(Japanese)* 79—65787
- formate tetrahydrate, short-range order, diffuse neutron scatt. 78—15124
- formate tetrahydrate, two-dimens. spin 1/2 Heisenberg antiferromag., phase transition characts. 77—66352
- glass:CuO, band-pass characts. improvement by doping 77—54797
- glycylglycines, isotope substituted, IR and Raman vibr. spectra 78—42051
- halide based photochromic glasses, spectral props. 80—29708
- halide laser, continuously pulsed, degradation due to axial cataphoresis effects 77—31093
- halide laser, long lived sealed off discharge 77—88770
- halide laser, pumping efficiency 79—68385
- halide laser, rapid differential decay of Cu metastable populations 80—53270
- halide laser driving ccts., parametric study 80—83610
- halide laser mixtures, continuously pulsed, kinetic processes 77—88702
- halide laser systems, high average power pulser design 78—5497
- halide lasers, transverse excitation, large active volume 78—59021
- halide vapour, transverse discharge, stimulated emission in Cu 77—88716
- halide vapour laser, kinetic model 79—94222
- halides, anal. of cryst. binding and Anderson-Gruneisen parameters 80—15040
- halides, appl. to Cu discharge laser 77—38911
- halides, comparison as lasants for Cu vap. laser 77—34875
- halides, correlation between electronic dielec. constant and ionic separation 79—4758
- halides, cryst. ionic radii and electronic polarisabilities 77—1091

copper compounds continued
- halides, exciton-phonon interactions, optical absorpt. spectra, theory 80—49614
- halides, phonon anomalies, dynamical model 79—73272
- halides, phonon anomalies for Cu^+ at off-centre sites, dynamical model and Raman meas. 80—10618
- halides, photoelastic consts. 79—65837
- halides, refl. spectra, 4.5-7.5 eV 79—61402
- halides, tetrahedrally coordinated, band struct. and optical props. 77—51655
- halides, two photon spectra, quantitative investigation 80—50373
- halides, van der Waals energy, cohesive energy calc. 77—51343
- hexadecachlorophthalocyanato-copper discrimination of individual atoms in mol. images 80—100226
- hexadecachlorophthalocyanine, radiation damage 77—19987
- I_5-III-VI_4, synthesis and props. 77—52231
- iminodiacetate dihydrate, X-ray cryst. struct. and molecular struct. determ. 79—19237
- layered, anisotropic and dipolar interaction terms effect on mag. phase transition 77—63210
- manganese copper formate dihydrate, conc. depend. of EPR linewidth 79—38376
- matte converting, thermodynamics of process, Noranda process, exam. using computer model 78—80492
- molybdates, oxidation, reduction and thermal decomp. mechanisms 80—50847
- molybdates, valence band X-ray induced Auger spectra and XPS 78—80813
- nitrocomplexes, planar dynamic Jahn-Teller effects 77—15804
- oxalate, crystal growth in silicate gel, X-ray diffr. and i.r. spectrum 77—4724
- oxalate, decomposition kinetics, in polymeric medium, thermogravimetry and DTA 78—52749
- oxalate, two dimens. antiferromag., proton reson. exam. 77—28453
- oxalate cathodes for seawater cells 79—92067
- oxalate complex with aliphatic amines, X-band ESR line width 77—20687
- oxalate hemihydrate, photographic props. eval. for use as high-speed photographic materials 77—44497
- oxide reduction by electron cyclotron reson. plasma of H, model study on discharge cleaning 80—76548
- oxides, valence band X-ray induced Auger spectra and XPS 78—80813
- oxides, X-ray absorption, discontinuities and limits, chem. combination effects 80—93435
- phenyl alkyl ammonium copper chloride, quasi-two-dimens. Heisenberg ferromag., mag. props. 77—66273
- phthalocyanide, cryst. struct. sensitivity of band struct. 79—42444
- phthalocyanide, thermal stability obs., by DTA *(German)* 80—11945
- phthalocyanin film, thermal behaviour *(Japanese)* 80—24753
- phthalocyanine, β-phase, large single crystal growth from vapour *(German)* 77—32513
- phthalocyanine, chlorinated, stacking disorder 78—34622
- phthalocyanine, cryst., electron damage, electron microscope study 78—22762
- phthalocyanine, cryst. growth from vapour, hollow cryst. form, mechanism *(German)* 77—55252
- phthalocyanine, imperfect cryst., elec. transport phenomena, charge carrier conc. and trap. distrib. 77—1421
- phthalocyanine, polycryst. film, charge transfer state and optical spectra *(Russian)* 78—84607
- phthalocyanine, polycrystalline, forbidden ESR transition 79—95638
- phthalocyanine, simulated mol. images, point models and kinematical struct. amplitudes 80—103223
- β-phthalocyanine, single cryst., equilib. shape, growth shape, vapour phase growth *(German)* 77—43163
- phthalocyanine, size distribs., transient elec. birefr. 80—85223
- phthalocyanine, struct. and susceptibility to radiation dmdamage 79—32986
- phthalocyanine, valence band studies, UPS meas. 77—52221
- α′ phthalocyanine and chlorinated derivative mol. crysts., radiation damage in electron microscope 80—107328
- phthalocyanine dye deposition on Si (111), low energy electron optically modulated transmission increase 79—78133
- phthalocyanine film, photocelectrochem. behaviour on SnO_2 electrodes 80—15626
- phthalocyanine film, surface photovoltage, central ligand effect 79—78231
- phthalocyanine-iodine, amorphous cpd. prep. by I_2 diffusion in polycrysts., triplet EPR signals obs. *(Russian)* 80—66016
- platino-oxalate, one-dimens. conductors, prep., struct. and elec. cond. 80—24900
- polyphosphinate, bulk compressibility meas. to 30 kbar 80—76306
- polyvinyl alcohol film containing Cu^{2+} complexes, photoconductivity 80—107849
- porphinatocopper(II), phosphoresc., appl. to porphyrin 78—11574
- porphins, vibr. spectra, planar vibrs., normal coord. anal. 77—65474
- porphyrins mag. susceptibility and EPR, sample grinding effects 80—60420
- 1-3-propanediammonium-$CuCl_4$, ferromag., antisymmetric and anisotropic exchange, EPR linewidth 78—10761
- di-i-propyldiselenophosphate, soln. anisotropic g and hyperfine tensors, ESR linewidth meas. 79—85978
- pyridinium cuprous bromide, solid electrolyte, crystal growth from melt 78—64462
- pyrite-solvent boundaries, two-layer capacitance meas. *(Russian)* 78—10551
- rare-earth-Cu double oxides, catalytic props., mag. props., elec. conductivity 79—66350
- salicylaldoxime, vitrified solution, additional absorpt., in axially symmetric ESR spectra 77—16151
- sphalerite materials, complex, spray pyrolysis 79—43574
- TCNQ salt, Cu-TCNQ thin film between Cu and Al electrodes, elec. switching and memory phenomena 79—65562
- tellurites, acousto-optical criterion estimation 79—82945
- ternary compounds, chemical shifts of K X-ray absorption discontinuities 78—19599
- tetraamine sulphate two-dimensional Heisenberg antiferromag., high field magnetisation 80—80558
- tetramethylammonium copper chloride, S=1/2 Heisenberg 1-dimens. ferromag., mag. props. 79—82766

copper compounds continued
tetrammine sulphate monohydrate, evidence for exchange-coupled quadratic nets 77—24705
TGS:($CuSO_4$), internal friction 80—44257
thiospinels, quaternary, mag. and elec. props. *(French)* 80—65771
TMMC, Cu-substituted, spin dynamics, neutron scatt. cross section 80—60312
trimethylammonium copper heptachloride, one-dimens. ferromag., mag. susceptibility, 2 to 300K 79—61077
tripolyphosphate complexes, electrolyte development for direct deposition of Cu 80—45246
TTF.CuBDt, spin 1/2 Heisenberg chain, spin-Peierls transition 79—61135
TTFCuBDT, spin-Peierls transition in spin 1/2 Heisenberg chains, RPA calcs. 80—25150
TTG-BDT(Cu), giant struct. distortion, high speed photography obs. 78—43121
turquoise, crystalline, Nogales Mexico, SEM and TEM study 79—29760
vanadates, elec. and mag. props., stoichiometry 78—51991
$\{Cu(NH_3)_4\}^{2+}$ complex, superhyperfine interaction 79—91284
Ag-Cu_2O-Ag bistable switching devices, freq. distrib. of threshold voltage 77—32091
AgBr(Cl)-CuBr(Cl), photochromic film for hologram recording 79—64184
$Ag_{0.85}Cu_{0.15}Br$, far IR spectra, cond., cation local motion 79—1754
AgCuSe, mixed conduction 79—78140
AgCuSe, X-ray photoelectron and Auger spectra 78—56561
Al_2O_3/CuO, thin film interaction, $CuAl_2O_4$ form. *(Russian)* 78—52697
As-Se-Cu system glass films, elec. and photoelec. props. variation with photostruct. transforms. 77—76980
As-Te-Cu system glasses, DC and AC cond., thermo-EMF, freq. depend., 100 to 370K 77—76827
As-Te-Cu system glasses, elec. cond. and thermo-EMF 79—42540
As-Te-Cu system glasses, absorpt. coeff. and optical band gap 79—65829
$(As_{0.4}S_{0.6})_{100-x}Cu_x$, glassy, struct. and elec. cond. study 80—59399
As_2Se_3, effect of Cu and I, investigated by Mn^{2+} EPR spectra 77—73075
As_2Se_3-Cu (10-20%) film, glassy, darkening kinetics, and hologram diffr. efficiency 77—62027
$AsTeCu_x$ ($0 \leq x \leq 0.4$) glass, effect of Cu on elec. cond. and thermoelectricity, 100 to 370K 78—87978
B_4C-Cu cermet fabrication for neutron shielding appls. 80—102354
$BaCuO_2$, prep. and props. *(French)* 77—43201
$BaCuO_{2+x}$ ($0 \leq x \leq 0.12$), study of mag. and elec. props. rel. to the non-stoichiometry *(French)* 78—95051
$Ba_2Cu(OH)_6$, EPR, g-values 79—19770
BaO-B_2O_3-$V_2O_5(Fe_2O_3)(Cu_2O)$, glass, resist. and activation energy, reduced valency 77—51749
BaO-V_2O_5-CuO glass, EPR, Cu impurity effect on elec. props. 79—51849
BaO-V_2O_5-CuO semiconducting glasses, impurity effects, elec. resist. and EPR study 80—103692
$BaTiO_3$-CuO mixture, exam. of liquid phase sintering, densification 79—33979
$Ba_2Zn_{2-2(x+y)}Cu_{2x}Cd_{2y}Fe_{12}O_{22}$, mag. props. and Mossbauer spectrum 80—75765
$Ba_2Zn_{2-2x}Cu_{2x}Fe_{12}O_{22}$, hexagonal ferrites, prep. and mag. characterisation 79—1727
Bi_2S_3-$CuPbBi_5S_9$, solid solution, semiconductor and dielectric props. 79—69511
Bi_2S_3-$CuPbBiS_3$ series, ordered chem. twinning 79—55717
β'-$Cu_xV_2O_5$, mag. and spectroscopic study, semiconductor to metal transition 80—2628
C fibre reinforced CuO-H_3PO_4 microconcrete, effect of C fibre on props. 79—43192
CU_2O high press. phase transforms, optical and X-ray studies 80—44313
$CaCu_3Ge_4O_{12}$, bond length determ. 78—14318
$Ca_2Cu(UO_2)(CO_3)_4.6H_2O$, voglite, cryst. and powder diffr. data 80—24421
$Ca_{1+x}Ga_{1-x}N_y$, prep. *(French)* 77—44206
CaO-Cu concentrate pellet, fluidised bed roasting 77—4934
CaO-CuO-P_2O_5-V_2O_5 glass EPR, Cu impurity effect on elec. props. 79—51849
Cd-Cu-Se, phase diag. 77—52303
$Cd_{1-x}Cu_xCr_2S_4$, elec. resist., temp. depend., behaviour at Curie point 77—62929
$Cd_{1-x}Cu_xCr_2Se_4$ solid solution, spinel struct., X-ray investigation 79—78940
n-$CdIn_2S_4$/p-$CuInSe_2$ heterostructure, form. and photovolt. meas. 80—10831
$CdS{:}Cu_2S$ sputtered solar cells, energy anal. of cell fabrication techniques 80—50966
$CdS{:}CuCl_2$, sintered film, dopant conc. effects on carrier mobility 78—2484
$CdS{:}CuCl_2$, sintered layer, distrib. of energy levels of local centres 80—15568
CdS/Cu_2S heterojunction solar cells, optimal material props. theory and experimental verification 80—45686
CdS/Cu_2S solar cells, polycryst. thin film photovoltaic materials, photon loss anal., expt. determ. 80—93888
CdS/Cu_2S thin film heterojunctions, photocapacitance meas. of solar cell parameters 80—93897
CdS/Cu_2S thin film solar cells, design and fabrication, 9.15% conversion efficiency 80—81438
CdS-Cu_2S, thin film heterojunction, dark I-V characts. and heat treatment 79—56294
CdS-Cu_2S heterojunctions, photovoltaic mechanism, model 77—43715
CdS-Cu_2S heterojunction, slow relax. of photocurrent 78—26943
CdS-Cu_2S heterojunction, energy-band struct., capacitance-voltage characts., illumination effects 80—96982
CdS-Cu_2S junctions, carrier trap density, deep level defects 80—107801
CdS-Cu_2S photovoltaic cell, effects of O_2 on efficiency 78—14807
CdS-Cu_2S single cryst. heterojunction, trap depths in depletion region 78—52064
CdS-Cu_2S solar cell, minority carrier generation and transport in emitter 77—43649
CdS-Cu_2S solar cells, design and fabrication, 8.5% conversion efficiency 80—72047
CdS-Cu_2S solar cells, microstructural study of heterojunction materials 80—93978

copper compounds continued
CdS-Cu_xS solar cells, electron diffusion length determ. using spectral response meas. 80—81475
CdS-CuI film heterojunction photocells, prep., photoelec. props. 78—80044
CdS-$CuInSe_2$ solar cells, grain boundary and interface recomb. effects 79—39311
$(CdZn)S$-Cu_2S solar cell, film form. and characts. 78—68080
$Cd_{1-x}Zn_xS/Cu_2S$ thin film heterojunction solar cells, operational charact. 80—45687
$Cd_xZn_{1-x}S$-Cu_2S solar cell, interface chemistry modification of current-voltage charact. 79—100523
$Cd_zZn_{1-z}S$-Cu_2S, heterojunction interface double layer, dislocation field, charge compensation 79—7855
$Co_{1-x}Cu_xCr_2S_4$, paramag. susceptibility 80—20373
$Co_{0.08}(Ni,Cu)_{0.92}Fe_2O_4$ sphere, rotational hysteresis, mag. field strength and orientation depend. *(Russian)* 77—16110
$Co_x(Ni_{0.5}Cu_{0.5})_{1-x}Fe_2O_4$ ferrite, relation between elec. cond. and mag. anisotropy 80—75548
CoU_2S_5, mag. struct., exchange energy, magnetisation and neutron diffr. expts. 78—68170
$CsCuCl_3$ submillimetre spectra phasons, low freq. modes, phase fluctuations *(Russian)* 80—50333
$Cs_2Cu(SO_4)_2.6H_2O$, long exchange paths between mag. ion pairs, singlet-triplet separation determ. 77—69283
$(Cu,Ag)_2Se$, p-type, thermoelectric, vaporisation suppression, using inert and reactive coatings 79—48149
$(Cu,Ag)_2Se/(Bi, Sb)_2Te_3$, P type selenide segmented element fabrication, thermoelectric props. 80—107835
(Cu,Ag)X, (X=Cl, Br, I), molten, thermoelec. power determ. 78—26711
$(Cu,Zn)Cs_2(SO_4)_26(H,D)_2O$, thermal contact between nucl. Zeeman and electron dipole-dipole interaction system 77—90065
$(Cu,Zn)Cs_2(SO_4)_2.6(H,D)_2O$, proton spin-lattice relax. exam., rel. to EPR 77—90064
$(Cu,Zn)Cs_2(SO_4)_2.6(H,D)_2O$ Tutton salt, proton spin-lattice relax. time, proton conc. depend. and spin diffusion role 80—71221
$(Cu,Zn)_3Pb(A_3O_4)_2(OH)_2$, bayldonite, struct. chem., complex layer struct. 79—46609
Cu bi-univalent cpds., soln., activity and osmotic coeffs., H_2O activity, Gibbs energy, molality depend. 80—51964
Cu complex, 1-(2-thiazolylazo)-2-naphtholato Cu (II), cryst. struct. 77—11536
Cu complex, $(CH_3NH_3)_2Cu(Cl_{1-x}Br_x)_4$, ferromag., Br NMR mas. 80—29642
Cu complex, $(Cu[H_2O]_6)^{2+}$ in $MgSO_4.7H_2O$, EPR and optical spectra anal. 79—38377
Cu complex, (4,4′-bipy H_2)$CuCl_6$, with infinite linear chains of dimeric units, struct. and mag. susceptibility 80—96498
Cu complex, $[C_6H_5(CH_2)_nNH_3]_2CuCl_4$, n=1,2,3, two-dimens. ferromagnet, NMR and mag. susceptibility 77—16058
Cu complex, [Cu(1,4,7,10-tetrabenzyl-1,4,7-10-tetraazacyclododecane)Cl]NO_3, cryst., struct. 80—64966
Cu complex, $[(CH_3)_2NH_2]_3CuCl_5$, single cryst. Raman spectra 78—39535
Cu complex, acetylacetonate, appl. as Cu atom donor in 5106 Å Cu laser 78—82956
Cu complex, acetylacetonate, lasant for Cu vapour laser 79—31875
Cu complex, α-CuNSal, one-dimensional $S={}^1/_2$ Heisenberg system, nucl. relax. at high temp. 77—85610
Cu complex, bis-L-tyrosinato copper(II) complex, electronic spectra and dichroism 79—41183
Cu complex, bis-2-acetyl pyridine $CuCl_2$, space group and lattice parameters, X-ray diffr. meas. 77—31643
Cu complex, bis-(2,2′-bipyridyl) thiourea copper II perchlorate, single cryst., ESR 79—38373
Cu complex, bis-(alkylammonium) (11) tetrachloride, perovskite, lattice perfection 78—87633
Cu complex, bis-(alkylammonium) Cu(11)tetrachloride, perovskite, face struct. and growth rate 78—87634
Cu complex, bis-(salicyladoximato) Cu(II), ENDOR multiplet HFS, energy level non-crossing 79—72341
Cu complex, bis-acetylacetonatocopper II, in stretched PVA film, ESR 79—51847
Cu complex, bis-ethylene diamine copper(II) sulphate, dielectric relaxation studies 78—84519
Cu complex, bis-salycylal-1,2-ethylenediiminatocopper II, in stretched PVA film, ESR 79—51847
Cu complex, bis(N,N-diethyl-N′-benzoylthioureato)Cu(II), ESR 77—8393
Cu complex, bis(N-benzylsalicylaldiminato) Cu (II) lattice consts. and space group 79—37680
Cu complex, bis(1,1-diisobutyl-3-benzoyl-selenoureato)Cu(II), single cryst. ESR, ^{77}Se hyperfine struct., bonding 77—77086
Cu complex, bis(1,5-cyclooctadiene)copper(I) perchlorate, IR and Raman spectra 79—19877
Cu complex, bis(triphenylphosphine) phenanthroline copper (I), luminesc. spectra, decay times 80—60648
Cu complex, β-diketonate complexes, CNDO calcs. 79—59358
Cu complex, catena-μ-formato-formatobis(pyridine)Cu(II) monohydrate, X-ray cryst. struct. determ. 79—46610
Cu complex, catena-μ-isothiocyanato-(N′-pyridylmethylene-N″-salicyloylhydrazinato-NN′O) copper (II), EPR and visible spectra 80—5566
Cu complex, chloride monodimethylsulfoxide, spin ${}^1/_2$ ferromag. Heisenberg linear chain, cryst. struct. and mag. susceptibility 80—15706
Cu complex, chloride tetramethylsulfoxide, spin ${}^1/_2$ ferromag. Heisenberg linear chain, cryst. struct. and mag. susceptibility 80—15706
Cu complex, chlorocuprates (II), octahedral and tetrahedral, Jahn-Teller effect, parametrisation method 79—78052
Cu complex, copper (II) [2,5-diphenyloxazole]$_2$ $(ClO_4)_2.4H_2O$, ESR studies 80—88867
Cu complex, Cu (II), co-ordination cpd. with condensation product of salicylaldehyde and salicylaldehyde S-propylthiosemicarbazone X-ray struct. anal. 79—1425
Cu complex, Cu (II) ammonia, phenanthroline complexes, ion exchanged, EPR anal. precision 77—56261
Cu complex, Cu (II)-substituted ethylenediamines and monocarboxylates, cryst. and mol. struct., X-ray diffr. obs. 79—82182
Cu complex, $Cu_3Cl_6(H_2O)_2.2$ tetramethylsulphone, mag. interactions, susceptibility, 2-230K 80—60237

copper compounds continued
Cu complex, Cu-glycine in water, EPR spectral parameters, temp. depend. 80−2623
Cu complex, $CuCl_2.2NC_5H_5$, spin 1/2 system, one-dimensional nucl. relax. 78−39427
Cu complex, $Cu(H_2O)_6^{2+}$, ligand hyperfine interactions, orbital angular momentum contrib. 80−96833
Cu complex, Cu(II) acetylacetonates, X-ray K-absorpt. edges, edge widths and shifts 78−50556
Cu complex, Cu(II) bis(dithiocarbamate), ^1H ENDOR 80−87154
Cu complex, Cu(II) dimers. temp. depend. PMR relax., singlet-triplet separation determ. 80−43073
Cu complex, Cu(II) impurity in α-glycine crysts., ligand ENDOR spectra 79−65765
Cu complex, Cu(II)-L-asparagin complexes, ESR spectra, mag. and bonding parameters 78−23326
Cu complex, $Cu(NH_3)_2(NCX)_2$, X=O, S, electronic struct., stereochem. 80−58156
Cu complex, $Cu(NO_2)_6^{4-}$, bond. props. and Jahn-Teller distortion, INDO-LCAO-MO calcs. 80−75532
Cu complex, $Cu(ONC_5H_5)_6X_2$, $X=ClO_4$, BF_4, cooperative Jahn-Teller ordering and mag. struct., EPR meas. 79−60505
Cu complex, $Cu(en)_3Cl_2.0.75$ en, X-ray and ESR data, Jahn-Teller distortions 78−80206
Cu complex, di-μ-chlorobis[(1,5-cyclooctadiene)copper(I)], IR and Raman spectra 79−19877
Cu complex, di-μ-thiocyanato bis[di-(2-aminoethyl)amine] dicopper II diperchlorate, ESR 79−38374
Cu complex, diaquobis(2,3-dihydroxy-2-methyl propanato) copper(II), cryst., EPR, room-temp. 79−82861
Cu complex, dichloro-bis-pyridine copper II, one-dimens. antiferromagnet, dynamic props., review 80−15737
Cu complex, dichloro(N-nitrosopiperidine) Cu II, ^{14}N NQR obs. 80−54988
Cu complex, dichloro(dimethylnitrosamine)copper(II), magnetic phase transition, ^{14}N NQR obs. 80−11289
Cu complex, dichloro(dimethylnitrosamine) Cu II, mag. props., ^{14}N NQR obs. 80−54988
Cu complex, glycylglycinatocopper trihydrate, mol. g values, EPR meas. *(French)* 77−43874
Cu complex, glycylglycine, isotope substituted, IR and Raman vibr. spectra 78−42051
Cu complex, halocuprates, ferromagnetic insulator, two-dimens. Heisenberg layers, mag. susceptibility 80−50068
Cu complex, hexa(pyridine-N-oxide)$(BF_4)_2$, Heisenberg antiferromag., mag. props. and sp. ht. 78−23287
Cu complex, hexadecachlorophthalocyanatocopper (II), atomic resolution by computer image processing from electron micrographs 80−100149
Cu complex, hexakis pyridine-N-oxide cuprate ion, pure and Zn doped, EPR, Jahn-Teller effect 78−10754
Cu complex, $K(Cu(CN)_2)$, NQR spectrum of $^{63,65}Cu$ 77−12235
Cu complex, L-alanyl-L-serine, PMR, EPR and absorpt. spectra 78−46367
Cu complex, N,N′-ethylenebis (salicylaldiminato) copper (II)-thiourea, in solns., bond strength and hyperfine linewidth, EPR 80−74186
Cu complex, N,N′-o-phenylenebis (salicylaldiminato) copper (II)-thiourea, in solns., bond strength and hyperfine linewidth, EPR 80−74186
Cu complex, N,N′-tetramethylene bis-(2-pyridinaldimine) thiourea copper II perchlorate, single cryst., ESR 79−38373
Cu complex, polyacrylic acid-polyethyleneimine-Cu(II), struct. *(Russian)* 79−55018
Cu complex, polyvinylimidazole.Cu(II) complex, ESR studies on dimer form. between copper ions 80−100613
Cu complex, redox enzyme, electron transfer peculiarities 80−16896
Cu complex, Schiff-base, ESR and optical absorpt. in soln. and powder 79−65892
Cu complex, semiconducting polymer synthesis from Cu^{2+} chelate of PVA and iodine, optimum prep. conditions 79−91612
Cu complex, substituted Cu(II) acetates, exchange interactions, EPR, struct. 79−42829
Cu complex, TTF-bisdithiolene complex, spin Peierls transition 77−4523
Cu complex, tetrameric Cu(II) complex, higher-order spin coupling 79−99690
Cu complex, triazene-1-oxide complexes, EPR spectra in frozen nematic liq. cryst. glass 80−88871
Cu complex, triazole complexes, finite Heisenberg chain effects, temp. depend. 79−47230
Cu complex, with 1,2,4-triazole, mag. susceptibility, 2-300K struct. 77−77045
Cu complex, with S-methylthiosemicarbazone of salicylic aldehyde, structure 77−7702
Cu complex, with Schiff base of o-aminobenzaldehyde and S-methyldithiocarbazate, cryst. struct. 78−95040
Cu complex, with Schiff base of diacetylmonoxine and methylhydrazine dithiocarbazate, X-ray cryst. struct. determ. 79−14784
Cu complex (acetylacetonate), in vitreous liq. cryst. matrix, ang. depend. of EPR spectrum 78−9175
Cu complex phthalocyanine, optical density spectra, charge transfer states 79−95800
Cu complex with adenine, powder, physical properties obs. *(Japanese)* 77−43878
Cu complex with carboxylate, channel model in exchange theory 78−14950
Cu complex with L-phenylalanine amino acid, ESR spectra and magnetic susceptibility measurement 80−34761
Cu complexes, Cu(I)-P tetrahedral, ^{63}Cu FT-NMR 80−53021
Cu complexes, dimeric carboxylate complexes, X-ray K-absorption edge position and EXAFS 77−85841
Cu complexes, electronic transitions polaris. determ. by dichroism in nematic solvents 77−42344
Cu, complexes, FT NMR, ^{63}Cu and ^{65}Cu chemical shifts and coupling constants 78−94260
Cu complexes, involving metal-metal exchange interaction, shifts in X-ray K-absorption edge 77−16422
Cu complexes, of polyamines, ESR in soln., coordination around Cu(II) ions 78−5254
Cu complexes, paramag., XPS, temp. depend. 79−15582
Cu complexes, spin coupled ion pair, singlet-triplet splitting 77−85552
Cu complexes, spin-labelled, EPR, electron-electron coupling 79−51858
Cu complexes, with L-glutamic acid and DL-aspartic acid, EPR, bonding and hyperfine linewidth 78−25572

copper compounds continued
Cu complexes, with tridentate Schiff bases, exchange interactions, EPR, mag. susceptibility 78−23324
Cu complexes of 2-amino-5-methyl-1,3,4-thiadiazole and 2,5-dimethyl-1,3,4-thiadiazole, conductometric and IR meas. 80−87121
Cu complexes of amino acids and α-hydroxy acids, bonding effect on spin-orbit coupling 77−1399
Cu complexes with amino acids, static mag. susceptibility and effective mag. moment 77−12082
Cu complexes with dipeptides, EPR spectra of high pH aq. solns. 77−32248
Cu complexes with glycine, in aqueous soln., EPR meas. 77−36115
Cu compounds, chemical shifts of X-ray electron and Auger lines 78−86912
Cu I, press.-induced phase transitions, Raman scatt. obs. 77−43995
Cu II acetylacetonate, XPS 80−74196
Cu II complex, bis(pyrrolidonecarbodithioato) copper II, ESR, solvent effects 78−1008
Cu II complex, extended X-ray absorpt. fine struct. study 80−104011
Cu II complex with poly(vinyl alcohol), polyacrylamide and poly(vinyl pyrrolidone) films, ESR study 79−61199
Cu II complexes, 5-coord., ESR, optical absorpt., solvent effects 78−5253
Cu II complexes, 5-coord., ESR and optical absorpt. spectra 79−64020
Cu liquid/liquid CuS, miscibility gap *(German)* 80−49370
Cu oxalate complex with aliphatic amines, X-band ESR line width 77−20687
Cu phthalocyanine, grain boundary struct., crystallographic planes 80−103366
β-Cu phthalocyanine electrophotographic props. rel. to particle size *(Japanese)* 80−13171
Cu SCN-based photographic system, characts. of development process *(Russian)* 79−58834
Cu^{2+} complex, in water-ethanol soln., struct., EPR 78−50565
Cu^{2+} complexes, ground state wave functions, g-factor anisotropy, lattice structs. 77−24536
Cu^{2+} ions influence on $PbSO_4$ flotation, with sodium hexadecyl sulphate, metallurgical waste treatment appl. *(Japanese)* 80−55701
Cu^{2+} systems, magnetic, nuclear spin Hamiltonians *(Japanese)* 80−60430
Cu/Cu_2O, relative chemical potential of oxygen *(German)* 78−31642
Cu/CuCl double pulse laser, pumping pulse and output pulse characts. 80−87380
Cu/CuCl double pulse laser, dissoc. pulse, afterglow, and laser pulse model 80−91775
Cu/CuCl double pulsed laser, extrema by electron density and output pulse energy 79−10283
Cu-Ag-Se, computation of component activities from ternary miscibility gap data 79−11591
$Cu-Al_2O_3$ powder, electrolytic deposition 78−84743
Cu-As-Se glass, localised states exam. *(Russian)* 78−34806
Cu-As-Se glasses, recording and erasure by laser beam *(Russian)* 78−71170
Cu-ascorbic acid, physical development process (non-Ag) *(Russian)* 79−67413
Cu-B system, interactions, product chem., phase, struct. anal., book contrib. 78−47305
Cu-CaO concentrate pellet, oxidation kinetics 77−4894
Cu-Cd-Cl stretched photochromic glass, polorisation effects 79−95729
Cu-Cd-Se system, Cu-CdSe cross section and props. of cpds. formed 78−27491
Cu-Cl boracite, ferroelec., X-ray study on phase transition 79−33622
Cu-Cl boracite, pyroelec. coeff. meas. 80−75951
Cu-Co heterobinuclear complex, cryst., mag. susceptibility of $Cu-Co(fsa)_2$ en, $3H_2O$ 80−2556
Cu-complex, 2-diethylaminoethanolato(trichloroacetato)Cu(II) tetramer, cryst. struct. 80−28962
Cu-Cs diluted deuterated Tutton salts, electron non-Zeeman system, nuclear relaxation study 80−44951
$Cu-Cu_xO$ film, numerical anal. of normal reflect. data 79−99457
Cu-CuI-graphite secondary cell, transient ionic current obs. 80−108790
Cu-CuI-graphite secondary cell, steady state hole current obs. 80−108791
Cu-Fe-O ferrite system, thermodynamic stability, dissociation and phase relations *(Japanese)* 80−55378
Cu-Fe-O system, ternary phases, activities in spinel solid soln., phase equilibria and thermodynamic props. 78−6910
Cu-Fe-S-O, sulfide ore, use of phase equilibria in pyrometallurgy 79−11588
Cu-Fe-S-O matte, appl. of Gibbs-Duhem eqn. 77−4923
Cu-Ge-O, phase diagram and thermodynamics, electrochem. study 80−50617
Cu-H, evolution of gas during heating, mass spectroscopic exam. 80−30221
Cu-In-Se system cubic ordered phase existence and characts. 78−34495
Cu-Mg-FeO system spinel solid solns., synthesis, struct., and mag. props. 79−52142
Cu-Mn ferrites, heat treatment effect on props. 77−28838
Cu-O system, liq., thermodynamic study *(Japanese)* 78−64529
Cu-P-Se system, glasses, semicond., density, microhardness, softening point rel. to conc. 77−7674
Cu-phthalocyanine, chlorinated effects of dynamical scattering on mol. images, in high resolution electron microscopy 78−14255
Cu-Pt complex, $[Cu\ (C_2N_2H_8)_2][Pt(C_2O_4)_2]$, cryst. struct. determ. 77−4072
Cu-S, thin film, phase formation conditions *(Russian)* 79−56078
Cu-Sb-I system, glass form., struct. and IR spectra 80−64915
Cu-Sb-S-I, chalcogenide glass film, prep. by laser evaporation, and characterisation 77−12533
Cu-Sb-S-I amorphous film formation and stimulated crystallisation, electrophysial props. *(Russian)* 78−30838
Cu-Se mixture, activity of Se *(German)* 78−27492
Cu-Si-Te, phase equilib., DTA and metallographic anal. *(French)* 79 52182
$Cu-SiO_2$, in-situ deform. in HVEM 80−103338
$Cu-SiO_2$ systems, cavity nucleation, by plastic deform. 79−29127
Cu-Te system, cryst. chem., Mossbauer investig. 77−16220
Cu-Tl-S, phases, semiconductor and metallic behaviour *(French)* 79−96011
Cu-U-O system, equilib. relationships *(German)* 80−35163

copper compounds continued
Cu^{2+}-imidazole complex, electron spin echo, nuclear modulation effect 79—18211
P-Cu_{2-x}-n-CdS, heterojunction, energy band diagram 79—24070
$CuAg_3I_4$, co-ionic cond. obs. 80—34231
$Cu_xAg_{1-x}I$ crystals, layer structs., X-ray diffr. studies 80—96457
$Cu_{1-y}Ag_yInS_{2-x}Se_{2x}$, for solar photovoltaic cells 80—10982
$Cu_{1-y}Ag_yInS_{2(1-x)}Se_{2x}$, lattice consts. and band gap variations 79—78000
$Cu_{1-y}Ag_yInS_{2(1-x)}Se_{2x}$ pentenary alloy system, appl. to photovoltaic solar-energy conversion 80—35680
$CuAl_2Cl_8$, Raman resonance spectra of vapour 78—94251
$CuAl_{1-x}Fe_xS_2$ system, delocalisation of d-electrons, mag., elec. and optical obs. 78—34804
$CuAl_2O_4$, pure and NiO promoted catalysts, surface oxidation state and comp., XPS study 80—76134
$CuAlS_2$, reflectvvity and XPS meas. 78—35165
$CuAlS_2$, X-ray spectroscopic study 78—39626
$CuAl_5S_8$, cryst. growth, struct., and fluoresc. 77—48328
$CuAlS_{2x}Se_{2(1-x)}$, excitonic structure, phase-shift-difference spectra 78—2872
$CuAlS_2(Se_2)(Te_2)$, tetragonal distortion 79—32942
$Cu_3AlTl_2Te_4(Se_4)$, struct. and phys. props. *(French)* 79—86758
$(Cu_xAn_{1-x})_2AsO_4(OH)$, olivenite-adamite solid soln., ordering 78—42962
$Cu_2(AsO_4)Cl$, cryst. struct., X-ray diffr. meas. 77—47380
$Cu_2(AsO_4)Cl$, temp. depend. of mag. susceptibility 80—70962
$Cu_2AsO_4(OH)$, olivenite, symmetry and cryst. struct. determ. 77—80457
Cu_3AsS_4, thermal cond. in solid and liq. phases, 300 to 1100K, thermoelec. Q-factor 80—19997
$Cu_3As_2S_3I$, space group, determ. by convergent-beam electron diffr. 80—49154
$Cu_{15}(AsSe)_{85}$ photographic layers, temp. depend. of reverse optical recording *(Russian)* 79—67415
$Cu_x(As_{0.4}Se_{0.6})_{1.x}$, amorphous, ^{77}Se NMR, comp. depend. 78—76329
$Cu_{10}As_{31}Se_{38}O_{21}$, chalcogenide glass, exam. of electron mechanism of photo induced changes 78—87998
Cu_3AsTe_4, elec. and thermal conds., thermo-EMF, solid and liq. states, temp. depends. 78—43384
CuB_{24}, elec. props. at high temps. and in strong elec. fields, thermistor appls. 80—92903
$Cu_2{}^{I}B^{II}C^{IV}X_4$, ($B^{II}$=Zn, Mn, Fe, Co; C^{IV}=Si, Ge, Sn; X=S, Se), X-ray elec. and mag. meas. 79—65660
$Cu_3B_7O_{13}Cl$, cubic, approx. nonlinear optical susceptibility 80—78904
$Cu_3B_7O_{13}Cl$, dielec. const. and elec. resist. 77—69783
$Cu_3B_7O_{13}Cl$, ferroelec. 43m-mm2 phase transition, molar heat capacity meas. 80—93249
$Cu_3B_7O_{13}Cl$, Raman study of ferroelec. phase transition 79—38529
$Cu_3B_7O_{13}Cl(Br)$, piezoelectric, elastic and electromechanical coefficients *(French)* 78—39504
$Cu_3B_7O_{13}X$, X=Cl, Br, ferromag. ferroelectrics *(Japanese)* 79—65804
$CuBeF_4.5H_2O$, linear-chain antiferromag., mag. phase transition investig. 77—55684
$CuBeF_4.5H_2O$, mag. ordering in external mag. field, NMR obs. 77—66350
$CuBeF_4.5H_2O$, NMR, interactions between paramag. ion system and antiferromag. linear chains 77—63295
$CuBi_2O_4$, struct. determ. by Fourier and least squares method *(French)* 77—27852
Cu_3BiS_3, wittichenite, NQR of $^{63,65}Cu$ and ^{209}Bi 80—20490
$Cu_3Bi_5S_9$, modulated struct. 79—99147
CuBr, 1S exciton triplet state, magneto-optical props. 80—25345
CuBr, biexciton dispersion, two-photon absorpt. 80—76045
CuBr, biexciton luminesc. 77—44056
CuBr, biexciton two-photon absorption 79—47480
CuBr, biexciton two-photon absorpt. 80—11432
CuBr, charged excitons, band struct., electron-hole exchange interaction 77—69233
CuBr, cond. mechanisms and struct. at high temps. 77—84711
CuBr, continuously pulsed laser, cable-capacitor Blumlein discharge circuit, expt. characts. 78—82981
CuBr, Debye-Waller factors and Debye temp., powder neutron diffr., 295K 78—91407
CuBr, density of states of cond. band calc. 77—62819
CuBr, direct gap semiconductors, charged excitons 77—62840
CuBr, dispersion of multicomponent exciton polaritons, hyper-Raman emission spectra 80—20096
CuBr, EXAFS amplitudes, many-body effects 80—97379
CuBr, effective Hamiltonian for few-particle systems 77—15776
CuBr, electric field gradient-elastic tensor components, acoustic NMR obs. 80—25229
CuBr, electron-exciton inelastic collision cross sections 79—90967
CuBr, electronic dielec. const., vol. depend., Clausius-Mossotti model 80—100630
CuBr, emission spectra after two-photon excitation, Raman scatt. 79—47518
CuBr, energy bands, relativistic KKR method, UV absorpt. spectra 80—39501
CuBr, evaporated film, magneto-optical effects on exciton bands 78—72624
CuBr, exciton, energies, oscillator strengths, and phonon side bands 80—44512
CuBr, exciton absorpt. band shape, dielectric const. real part derivatives *(Russian)* 80—25413
CuBr, exciton bands, oscillator forces, temp. depend. *(Russian)* 79—28284
CuBr, excitonic mols., two photon generation 77—43511
β-CuBr, far IR spectra, cond., cation local motion 79—1754
CuBr, LF light scatt. spectra in superionic cond. phases, ion motion obs. 80—108217
CuBr laser, bubble gas effects on ground and metastable populations 78—82955
CuBr laser, burst-mode, laser power variation and time depend. of populations 79—50284
CuBr laser, rapid differential decay of Cu metastable populations 80—53270
CuBr laser, tunable dye laser radiation, gas temp. atomic density meas. technique 79—82037
CuBr, lattice dynamics of binary superionic conductors 80—107393
CuBr, multiphonon far IR absorpt., 2-80K 78—60462
CuBr, multiplet struct. of P-excitons due to valence band degeneracy 78—39035

copper compounds continued
CuBr, NMR chemical shifts, temp. depend. 78—68401
CuBr, neutron scatt. investig. of anharmonic effects on Debye-Waller factor 77—11658
CuBr, new bands in emission spectrum 77—68052
CuBr, optical props. 4 to 30 eV, band struct. 77—90166
CuBr, P exciton fine struct. 80—20091
CuBr, phonon dispersion 9-parameter shell model, compared with expt., and Debye temp. evaluation 78—59891
β-CuBr, phonon spectra, dispersion curves parameter calc. from zinc blende zone boundary conditions 78—51632
CuBr, photoelastic tensor, acousto-optical meas. 77—12359
CuBr, photoelasticity theory 78—10868
CuBr, piezo-optical effects on excitons, importance of k-linear terms 79—95802
CuBr, polariton Raman spectra, oscillator strengths, temp. depend. 80—66197
CuBr, press. depend. of Raman scatt. meas., Gruneisen parameters determ. 77—24845
CuBr, Raman spectra, Cu ions vibr. and diffractive motions 80—11412
CuBr, reflectance and thermoreflectance spectra, electronic struct. 80—71444
CuBr, rot. spectrum hyperfine struct., coupling consts., microwave spectroscopy study 80—18844
CuBr, single oriented crystals., electroreflectance, exciton transitions 77—66517
CuBr, specific heat and lattice dynamics 79—37798
CuBr, superionic behaviour at high temp., EXAFS study 80—107496
CuBr, superionic cond., cryst. struct,, neutron diffr. study 79—42041
CuBr, surface exciton polariton, ATR meas. 77—77236
CuBr, theory of photoelectric consts. 79—61335
CuBr, two-phonon optical absorpt. spectra 78—52485
CuBr, UPS, temp. depend., dynamic hybridisation 77—20998
CuBr vapour laser, characts. comparison with Cu, CuCl lasers 80—102711
CuBr, XPS, satellite of Br 4s line 78—56556
CuBr:Cl(I), lattice-dynamical study of impurity modes 80—29129
CuBr-Ag system, spectral distrib. of photosensitivity *(Russian)* 78—56535
CuBr-AgI system, ionic cond. and phase diagram 80—2198
CuBr-He-Ne pulsed discharge laser, Cu I relax. processes 78—25865
CuBr-$PbBr_2$ system, phase diagram, DTA and X-ray diffr. analysis 77—47552
$CuBr_2$, ^{63}Cu and ^{81}Br NQR line width obs. 80—50219
$CuBr_2$, aq. soln., structural transition, neutron diffr. study 80—64872
$CuBr_2$, aq. solns., EXAFS meas. 80—60714
$CuBr_2$, finite Heisenberg chain effects, temp. depend. 79—47230
$CuBr_2$, highly conc. aqueous soln., local ordering, extended X-ray absorb. fine struct. spectra 78—79520
$CuBr_2$, NQR freqs. temp. depend., paramag.-antiferromag. transition 79—42867
$CuBr_2$, quasi-1-dimens., NQR obs. 80—54987
$(CuBr)_3$, gas, He(I) photoelectron spectra 80—43103
$(CuBr)_3$, photoelectron spectrum and valence shell struct. 78—62843
$CuBr_4{}^{2-}$, ground state Zeeman splittings, reson. Raman spectra and mag.-optical activity 80—5579
CuBr(Cl), biexcitons, many exciton effects 78—51901
$CuBr_xI_{1-x}$, disorder-induced TA Raman lines 79—73929
$CuBrSe_3$, cryst. struct. 79—86750
$7CuBr.C_6H_{12}N_4CH_3Br$, solid electrolyte galvanic cell appl. 77—77775
$Cu(C_5H_5NO_6)(BF_4)_2$, sp. ht. and susceptibility, comparison with quadratic spin 1/2 Heisenberg antiferromag. calcs. 77—66353
$Cu(CN)_3{}^{2-}$, UV absorpt. spectra, electronic struct., MO calcs. *(French)* 77—34655
CuCO, linear, ab initio RHF-MO calcs., rel. to adsorption 79—26883
$Cu(CO)_4{}^{+}$, laser Raman spectra, CO stretching region 79—59469
Cu_nCO, interaction of Cu small particles with CO, IR matrix isolation spectra obs. 77—20195
$CuCd_2GaTe_4$, semiconductor, physicochem. and transport props. 77—59762
Cu_5CdSb, electrophys. props. 78—27491
CuCl (100), obs. of p- and d-like surface states, angle resolved UPS study 80—104045
CuCl, absorpt. coeff., 0.4-25 μm, band struct. determ. 77—73155
CuCl, amorphous/cryst. interface, supercond. mechanism 80—44783
CuCl, anharmonic thermal vibr. X-ray diffr. exam. 78—30728
CuCl, anomalous diamagnetism, high temp. Meissner effect *(Russian)* 78—34955
CuCl, anomalous Raman spectrum in transverse optic phonon region 77—24846
CuCl, anomalous TO-doublet origin for light scatt. study 78—43872
CuCl, anomalously slow group velocity of upper branch polariton 80—10893
CuCl, band struct., OPW calc. and X-ray spectra meas. 80—75506
CuCl, band struct. calc. using layer method 79—60704
CuCl, behaviour under press., possibility of superconductivity 79—38239
CuCl, biexciton first excited state, LO phonon assisted two-photon absorption 77—40260
CuCl, biexciton luminesc. 77—44056
CuCl, biexciton luminesc., subnanosecond time resolved spectroscopy 77—73167
CuCl, biexciton luminescence and two photon Raman emission, polarisation props. 78—80406
CuCl, biexciton resonant two-photon absorption 78—23491
CuCl, biexciton two-photon absorpt. 80—11432
CuCl, biexcitons, two-photon absorption and luminesc. 77—43513
CuCl, biexcitons existence, review 77—69239
CuCl, bonding, ab initio pseudopot. calcs. 79—6857
CuCl, Bose-Einstein condensation of biexcitons 79—56138
CuCl, charged excitons, band struct., electron-hole exchange interaction 77—69233
CuCl, continuously pulsed laser, cable-capacitor Blumlein discharge circuit, expt. characts. 78—82981
CuCl crystal activated photochromic glasses, absorpt. spectra 79—27353
CuCl crystal resonant Raman scatt. and luminescence competition *(Japanese)* 80—80770
CuCl, decay time mas. of biexcitonic photoluminesc. 78—10935
CuCl, defect and impurity bands, lattice consts. 80—54638
CuCl, density of states of cond. band calc. 77—62819
CuCl, dielectric function for semiconductors with high exciton conc. 80—84443

copper compounds continued
CuCl, difference Fourier maps, effects of phase errors 79—99033
CuCl, direct creation of high biexciton density at K=0, two-photon absorpt. and emission spectra 79—33727
CuCl, direct-gap semiconductors, charged excitons 77—62840
CuCl, disordered, diamag. transition 80—34636
CuCl, donor-acceptor recomb. spectra 80—45131
CuCl, double pulse laser, output characts. 78—13690
CuCl, double pulsed laser, scaling to 10 mJ 78—46624
CuCl double-pulse laser, weak axial mag. field effects on energy output 78—42327
CuCl, double-pulsed laser, energy output, initial current rise effect on pumping 78—13687
CuCl, effect of dispersed Al_2O_3 particles on ionic cond. 80—24649
CuCl, effective electron-hole interaction for intermediate and strong electron-phonon coupling 77—80735
CuCl, effective Hamiltonian for few-particle systems 77—15776
CuCl, electric field gradient-elastic tensor components, acoustic NMR obs. 80—25229
CuCl, electron-exciton inelastic collision cross sections 79—90967
CuCl, electron-hole pairs behaviour in energetic ion tracks 80—65457
CuCl, electronic dielec. const., vol. depend., Clausius-Mossotti model 80—100630
CuCl, electronic struct., ab initio HF SCF MO calcs. of $CuCl_4^{3-}$ cluster 78—95262
CuCl, electronic struct., self consistent all electron approach 80—2333
CuCl, electronic struct. by LCAO and LMTO methods, direct gap semiconductor 80—59868
CuCl, electrooptic props. below absorpt. edge 77—28548
CuCl, emission spectra after two-photon excitation, Raman scatt. 79—47518
CuCl, energy bands, relativistic KKR method, UV absorpt. spectra 80—39501
CuCl, energy bands and effective mass 80—10859
CuCl, evaporated film, magneto-optical effects on exciton bands 78—72624
CuCl exciton, energies, oscillator strengths, and phonon side bands 80—44512
CuCl, exciton bands, oscillator forces, temp. depend. *(Russian)* 79—28284
CuCl, exciton energy determ., electron beam excited luminesc. 79—38680
CuCl, exciton luminesc., reabsorpt. and polariton effects 80—50430
CuCl, exciton mol. creation by pure and phonon-assisted two-photon transitions 78—63987
CuCl, exciton spatial dispersion determ., two-photon Raman scatt. via excitonic mol. state 80—60595
CuCl, exciton spectra, extended effective mass theory 79—69424
CuCl, excitonic mol., two-photon excitation via polariton state 80—54612
CuCl, excitonic mol. luminesc. spectra, picosecond time anal. 78—52548
CuCl, excitonic molecules, secondary emission under two-photon reson. excitation 80—11468
CuCl, excitonic mols., ps time resolved luminesc. spectra 77—16383
CuCl, excitonic mols., two photon generation 77—43511
CuCl, excitonic polariton-polariton resonance scattering 79—24306
CuCl, excitonic polariton, picosecond time of flight meas. 80—29337
CuCl, excitons bound to neutral donor impurities, magneto absorption spectra 79—56816
CuCl, existence of charged excitons 78—76496
CuCl film, exciton absorption bands *(Russian)* 79—51985
CuCl film tunnel conductivity *(Russian)* 79—51726
CuCl, fission of relaxed excitonic mols. into upper and lower branch polaritons induced by M_L emission 80—11380
CuCl, four-wave mixing spectroscopy in crysts., nonlinear spectroscopy developments 80—91861
CuCl, frequency dependent optical phonons contrib. to small radius excitons binding energy 77—69236
CuCl, giant two-photon absorption into excitonic mol., anomalous dispersion of excitonic polariton 78—27211
CuCl, ground state of electron subsystem, quasimolecular model 79—69055
CuCl, H^+ irrad., luminesc., high density excitons in particle tracks 79—47020
CuCl, high press. phases and anomalous props. 79—7689
CuCl, high-temp. supercond., BCS strong-coupling limit for transition temp. 80—2511
CuCl, hollow cathode laser using metal tube 77—14742
CuCl, hyperfine struct., microwave rot. spectrum obs. 78—21917
CuCl, induced absorption due to exciton-biexciton transitions 78—15187
CuCl, interface superconductivity? 80—39696
CuCl, interface supercond., piezoelec. hypothesis 80—60128
CuCl, ionic mobility meas. method 77—15625
CuCl, ismorphic transitions at high press., 4.2 to 800K *(Russian)* 77—31774
CuCl, LF light scatt. spectra in superionic cond. phases, ion motion obs. 80—108217
CuCl, lasant for Cu vapour laser 79—31875
CuCl laser, dissoc. pulse cct. inductance effect 78—29936
CuCl laser, double-pulse, addition of HCl 77—50654
CuCl laser, double-pulsed, parametric study 77—50681
CuCl laser, potential, high-energy large vol. device 78—50807
CuCl, laser gas-discharge tubes, output characts. 79—64251
CuCl, lattice dynamics at 4.2K 79—19344
CuCl, lattice dynamics of binary superionic conductors 80—107393
CuCl, light mixing induced by giant two-photon absorpt. of excitonic mols. 78—42383
CuCl, liq., partial struct. factors, hard sphere model calc. 77—15299
CuCl, luminesc. and Raman processes under reson. two-photon excitation 79—33796
CuCl, luminesc. and reson. Raman scatt. of excitonic mols. 79—33814
CuCl, luminesc. from Bose-condensed state of biexcitons 79—23905
CuCl, luminesc. of excitonic mols. 80—2817
CuCl, luminesc. spectra, excitonic mol. reson. two phonon excitation 78—19514
CuCl, mech. vibrs. in piezoelec. solid, excitation by light pulses 80—75305
CuCl, metal source in Cu vapour laser, Cu ground state and metastable level population densities 77—83860
CuCl, metal vapour lasers excited by pulse trains 79—13955
CuCl, mol. emission spectrum, 5900-6800 angstrom, rot. anal. of A-X system 80—58273

copper compounds continued
CuCl, molten, ionic liquid description from NMR meas. 77—24257
CuCl, molten, struct. and transport props. 79—19134
CuCl, multiphonon far IR absorpt., 2-80K 78—60462
CuCl, NMR chemical shifts, temp. depend. 78—68401
CuCl, neutron scatt. of TO phonon at 5K 79—60446
CuCl, nonlinear light absorpt., picosec. pulse, exciton-biexciton transitions 79—47483
CuCl, nonrelativistic calcs., rel. to Ag halide photoelectron spectra 80—95679
CuCl, optical absorpt. meas., evidence against intrinsic electron-hole supercond. 80—108172
CuCl, optical absorption under press. 80—34949
CuCl, optical consts. in exciton absorption region, spectral depend. *(Russian)* 77—81125
CuCl, optical microscopic, X-ray diffr. and elec. resist. studies at high press. 80—11051
CuCl, optical props. 4 to 30 eV, band struct. 77—90166
CuCl, phonon dispersion 9-parameter shell model, compared with expt., and Debye temp. evaluation 78—59891
CuCl, phonon interaction of excitonic molecule 80—50316
CuCl, phonon spectrum and its temp. depend., phonon dispersion curves determ. by inelastic neutron scatt., at 4.2K 78—6132
CuCl, phonon-assisted two-photon absorpt. of excitonic mol., bare-exciton approach 79—78702
CuCl, photoelastic tensor, acousto-optical meas. 77—12359
CuCl, photoelasticity theory 78—10868
CuCl, photosensitive film formation on Cu 77—9105
CuCl, picosecond spectroscopy of secondary radiation from resonantly excited excitonic molecules 79—15461
CuCl, polariton effects in resonant Raman scatt. 78—10881
CuCl, polariton Raman spectra, oscillator strengths, temp. depend. 80—66197
CuCl, polariton vel. direct obs. 79—28297
CuCl, polycryst., thermal expansion and sp. ht., low temp. meas. 77—55367
CuCl, possibility of excitonic dielectric-supercond. phase transition 77—43797
CuCl, possibility of high temp. superconductivity 79—38238
CuCl, possibility of high temp. superconductivity 79—51711
CuCl powder compacts, DC voltage depend. resist. under press. 80—80334
CuCl, press. depend. of Raman scatt. meas., Gruneisen parameters determ. 77—24845
CuCl, pressure depend. of structural, chemical, elec. and mag. props. 80—96596
CuCl, propagation process of polaritons *(Japanese)* 80—24809
CuCl, ps. luminesc. spectra, resonantly excited excitonic mols. 78—19555
CuCl, psec time resolved spectroscopy, excitonic mols. 79—47500
CuCl pulsed laser, time depend. of Cu-atom conc. in ground and metastable states 78—66806
CuCl, pure and Cu_2S doped, ionic cond., 60-370°C 77—47617
CuCl, Raman and luminesc. processes under reson. two-photon excitation of excitonic mol. 79—8143
CuCl, Raman spectra, Cu ions vibr. and diffractive motions 80—11412
CuCl, refl. spectra, 4.5-30 eV, vel. to band struct. 80—103969
CuCl, relaxation of excitonic molecules generated by two-photon excitation, forward Raman scatt. 78—2838
CuCl, renormalisation of polaritons by biexciton virtual formation 79—99490
CuCl, reson. coherent nonlinear scatt., biexciton autoionising states 79—51978
CuCl, reson. Raman scatt. and luminesc. of biexcitons 79—38618
CuCl, reson. Raman scatt. and luminesc. due to excitonic mols. 79—91425
CuCl, reson. Raman scatt. and luminesc. under two-photon excitation 79—95765
CuCl, reson. two-photon Raman scatt., excitonic polariton dispersion 78—72509
CuCl, reson. two-photon excitation of excitonic mol. using circ. polarised light 78—84566
CuCl, resonant emission, lifetime of excitons 77—69887
CuCl, resonantly excited excitonic molecules, time resolved spectroscopy 78—92109
CuCl, self-consistent energy-band study 79—69408
CuCl, self-consistent zonal struct. calcs., electron spectrum gap *(Russian)* 80—34359
CuCl, struct. types in phase diagram, DTA and dilatometry meas. up to 35 kbar 78—18770
CuCl, superionic behaviour at high temp., EXAFS study 80—107496
CuCl, surface exciton polariton, ATR meas. 77—77236
CuCl, theory of photoelectric consts. 79—61335
CuCl third-order elastic and piezoelec. constants 79—46739
CuCl, third-order nonlinear optical spectroscopy 77—23713
CuCl, three-branch polariton dispersion curve, two-oscillator model 80—92832
CuCl, time resolved exciton-biexciton transitions, UV excitation, luminescence spectra 79—69883
CuCl, time-resolved study of induced absorption due to exciton-biexciton transitions 79—38658
CuCl, two photon reson. Raman scatt. by excitons 77—52086
CuCl, two-phonon optical absorption 77—63406
CuCl, two-phonon optical absorpt. spectra 78—52485
CuCl, two-photon absorpt. and luminesc., biexcitons 80—11434
CuCl, two-photon excitation of first vibr. state of biexciton, giant oscillator strength calc. 79—7789
CuCl, two-photon reson. Raman scatt. with recoiling excitonic polariton 77—36223
CuCl, two-photon reson. Raman scatt. by excitons via intermediate excitonic mol., polarisation and polariton effects 78—10880
CuCl, two-photon reson. Raman scatt., recoil of upper-branch excitonic polariton 78—27212
CuCl, two-photon reson. Raman scatt. and luminesc. of excitonic mols. 79—28819
CuCl, two-photon reson. scatt. in excitonic mol., population instability 79—28826
CuCl, two-photon resonant Raman scatt. via biexcitons 78—43302
CuCl, UPS meas., electronic struct. 80—50529
CuCl, UV spectra, Γ_1 biexciton level, appl. of nonlinear spectroscopic technique 79—8156

copper compounds continued
$CuCl$, Urbach rule at excitonic absorpt. edge, theoretical model tests 80—50299
$CuCl$ vapour laser, characts. comparison with Cu, CuBr lasers 80—102711
$CuCl$ vapour laser, output power limiting processes 80—91776
$CuCl$ vapour laser, use for image amplification in projection microscope system 79—98407
$CuCl$, XPS and Auger spectroscopy, elec. struct. 80—29852
$CuCl$, Z_3-exciton, temp. dependent TPA linewidth 78—67946
$CuCl$, zincblende struct., high press. Raman scatt., 77K 78—60463
$CuCl:Ag$ system, light sensitivity spectrum, exciton struct. *(Russian)* 79—51985
$CuCl:Br(I)$, lattice-dynamical study of impurity modes 80—29129
$CuCl$-Ag system, photosensitivity spectrum in region of CuCl exciton absorpt. *(Russian)* 79—78707
$CuCl$-Cl^- complex formation, UV absorpt. spectra 77—60064
$CuCl$-$TlCl$ system, phase diagram and high ionic cond. obs. 78—79802
$CuCl_2$, anhydrous, mag. phase transition 80—80506
$CuCl_2$, anhydrous, single crysts., prep. 77—85932
$CuCl_2$, anhydrous, single cryst., mag. behaviour in low temp. ordered phase 79—7974
$CuCl_2$, anhydrous paramagnetic phase, mag. susceptibility depend. on temp. 79—7965
$CuCl_2$, aq. soln., Raman spectrum, local order 78—84563
$CuCl_2$, aq. soln., structural transition, neutron diffr. study 80—64872
$CuCl_2$, aq. solns., EXAFS meas. 80—60714
$CuCl_2$, aq. solns., IR spectral reflectance meas., Kramers-Kronig anal. 77—4633
$CuCl_2$, aqueous soln., nonlinear conversion of acoustic pulses with thermooptic excitation 80—14510
$CuCl_2$, finite Heisenberg chain effects, temp. depend. 79—47230
$CuCl_2$, positron annihilation ang. correl., bonding depend. 77—20951
$CuCl_2$, quasi-1-dimens., NQR obs. 80—54987
$CuCl_2$, saturated soln., jet flow Raman spectroscopy for highly absorbing liq. systems 80—52323
$CuCl_2$-$2H_2O$, mag. g-tensors for ion complexes, spin-orbit coupling 78—10752
$CuCl_2$-brass, chemically deposited photosensitive cells, photovoltaic characts. 79—39303
$CuCl_2$-water solution, Nd-glass laser radiation induced vaporisation, press. history 80—2153
$(CuCl)_3$, gas, He(I) photoelectron spectra 80—43103
$(CuCl)_3$ photoelectron spectrum and valence shell struct. 78—62843
$CuCl_4^-$, ESCA satellite intensity, ab initio SCF calcs. 80—74103
$CuCl_4^{2-}$ anion, [g] tensor calcs. 77—28343
$CuCl_4^{2-}$, charge distrib. and ligand field splitting calc. 77—62879
$CuCl_4^{2-}$, core ionisation in 3d, 4f and 5f series, rearrangement effects 80—53065
$CuCl_4^{2-}$, electronic energy levels calc. by conventional and X alpha Hartree-Fock methods 78—66470
$CuCl_n$, electronic struct., INDO theory 80—42948
$Cu_2Cl_8^{4-}$, in Co (III), Cu (II) complex, single cryst. EPR 77—16157
Cu_3Cl_3, cyclic, nonrelativistic calcs., rel. to Ag halide photoelectron spectra 80—95679
$CuCl_xBr_{1-x}$, binary melt, Cu solubility, temp. and conc. depend. 80—10677
$CuCl_xBr_{1-x}$, disorder-induced TA Raman lines 79—73929
$CuCl(Br)(I)$, luminesc. due to exciton-electron scatt., calc. 77—16379
$CuCl(Br)(I)$, static polaris. and effect charge parameters, Born-Mayer pot. 77—31628
$CuCl(Br)(I)$, van der Waal dipole-dipole and dipole-quadrupole energies, Born and Slater-Kirkwood models 79—27947
$CuCl_2(Br_2)(I_2)$, prep. using chem. transport via gas complexes *(German)* 79—15599
$CuCl_2(Cl_4^{2-})(Cl_6^{4-})$, electronic struct. studies by SCF, MSXα and INDO method 80—74119
$Cu(ClO_3)_2$, mol. torsional oscills., cooperative study by NQR 80—25244
$CuClO_4$, neutron activated, radiation annealing 80—93569
$Cu(ClO_4)_2$ in ethylene glycol solns., US absorpt., relaxation rel. to temp. 77—31727
$2CuCl.CsCl$, and $3CsCl.2CuCl$, phase transform. heats, DTA obs. *(Russian)* 80—55698
$CuCl_2.CuCl_2.2D_2O$, neutron scatt. aspherical effects, mag. form factor 78—27017
$CuCl_2.H_2O$ additive in ethanol, effect on dissolution, selective etching of CsI crysts. 77—72618
$CuCl_2.TMSO$, ferromag. spin $^1/_2$ linear chain, mag. susceptibility 78—68180
$CuCl_2.2D_2O$, cryst. struct., mag. and reson. props. 80—60424
$CuCl_2.2D_2O$, staggered magnetisation, neutron diffr. obs. 78—39296
$CuCl_2.2H_2O$, antiferromag. reson., HF, press. depend. *(Russian)* 77—36137
$CuCl_2.2H_2O$, antiferromag. reson. in tilted mag. fields *(Russian)* 77—51961
$CuCl_2.2H_2O$, antiferromag., range of existence of intermediate state, NMR expt. 77—59410
$CuCl_2.2H_2O$, antiferromagnetic relax., autocorrel. function time evolution 77—59464
$CuCl_2.2H_2O$, antiferromag. reson. temp. depend., spin-flop phase *(Russian)* 78—23348
$CuCl_2.2H_2O$, antiferromag. to paramag. transition, high field magnetisation meas. 78—64204
$CuCl_2.2H_2O$, EPR linewidth and relax., effect of antisymmetric exchange 77—59448
$CuCl_2.2H_2O$, effect of press. on mag. phase transition, NMR meas. 78—19253
$CuCl_2.2H_2O$, energy gaps mag. field depend., antiferromag. reson. 79—87320
$CuCl_2.2H_2O$, flop of sublattice moments and Neel temp., press. effects, NMR obs. 77—40058
$CuCl_2.2H_2O$, group theoretical anal. of second order phase transitions 79—91239
$CuCl_2.2H_2O$, H_2O intramol. force fields calcs. 79—51229
$CuCl_2.2H_2O$, influence of high hydrostatic press. on intermediate state associated with spin flopping 78—35020
$CuCl_2.2H_2O$, magnetoelastic props. under press., antiferromagnetic resonance, lattice parameters 80—29598
$CuCl_2.2H_2O$, NMR, high press. effect on existence domain width of intermediate state 79—87255

copper compounds continued
$CuCl_2.2H_2O$, nearly one dimensional mag. system, EPR line shape 79—99759
$CuCl_2.2H_2O$, submillimetre ESR meas. using pulsed high mag. field 80—44905
$CuCl_2.2H_2O$, X-band ESR magneto-microwave effects 77—28434
$CuCl.2N(C_5D_5)$, one-dimens. antiferromag., mag. excitation line-shape, field depend., neutron study 79—38314
$CuCl_2.2NC_5H_5$, antiferromag. spin dynamics at low temp. 77—32278
$CuCl_4.2NH_3$, g-tensor components, LCAO calcs. 77—18794
$CuCl.2RbCl$, and $3CuCl.2RbCl$, phase transform. heats, DTA obs. *(Russian)* 80—55698
$Cu_{0.5}Co_{0.5}Cr_{2-x}Rh_xS_4$, K absorpt. discontinuity chem. shift, bonding parameters 77—77318
$CuCoNi$ ferrite magnetoacoustic oscills. rel. to microstruct. 77—85536
$CuCo_2S_4$, $Cu_{0.5}Co_{2.5}S_4$, spinels, ht. of formation 78—53237
$CuCr_{2-x}Fe_xO_4$, charge transfer, Mossbauer spectroscopy 80—15836
$CuCr_2O_4$ and $CuCrO_4$, IR spectrometry and EPR study *(French)* 79—47452
$CuCr_2O_4$, heat capacity, entropy, polymorphic transition, 298-1000K 78—10196
$CuCr_2O_4$, spinel, K X-ray absorption spectrum 78—19600
$CuCr_2O_4$, thermal decomp. mechanism *(French)* 80—50834
$CuCr_2O_4$-$CuFe_2O_4$ (2 mol.%), Mossbauer expts., existence of Fe^{2+} 78—43721
$CuCr_2O_4$-$MgCr_2O_4$, X-ray investig. 77—44224
$CuCr_2O_7.2H_2O$, chemical prep. and crystal data *(French)* 80—24417
$CuCr_2O_7.2H_2O$, X-ray cryst. struct. determ. *(French)* 80—54185
$CuCrS_2$, domain struct. and superstructure, TEM obs. 80—79779
$CuCrS_2$ single cryst., spectral study and phys. props. *(French)* 80—29002
$CuCr_2S_4$, electronic struct., mixed valence 80—70612
$CuCr_2S_4$, ferromag., spin wave contrib. to nucl. spin-lattice relax. time meas. 77—36147
$CuCr_2S_4$, mechanism for phase transition from ferromag.-ferrimag. state *(Russian)* 77—36075
$CuCr_2S_4$, neutron diffr. study of mag. struct. *(Russian)* 79—95580
$CuCr_2S_4$, spinel, K X-ray absorption spectrum 78—19600
$CuCr_2S_{4-\gamma}$, spinel, anomalies in paramag. susceptibility, Curie pt. *(Russian)* 77—80910
$(CuCr_2S_4)_x$-$(Cu_{0.5}In_{0.5}Cr_2S_4)_{1-x}$ solid solution, piezoelectric effect, X-ray struct. anal. *(Russian)* 80—15978
$CuCr_2S_{4-x}Se_x$ spinels, NMR spin echo study 80—71238
$CuCr_2S_4(Se_4)(Te_4)$, specific heats 79—11315
$CuCrSe_2$, influence of excess Cu on physical props. 80—103836
$CuCr_2Se_4$, crit. behaviour near Curie point 78—31068
$CuCr_2Se_4$, Crit. relax. processes, mag. reson. expts. 80—60425
$CuCr_2Se_4$, cryst., preparation, elec. cond., thermo EMF 77—8125
$CuCr_2Se_4$, crystal growth from melt, exam. of props. 80—55283
$CuCr_2Se_4$, electronic state, polarized neutron diffr. obs. 79—56501
$CuCr_2Se_4$, electronic struct., mixed valence 80—70612
$CuCr_2Se_4$, mag. moment distrib. by neutron diffr., Goodenough model 80—70945
$CuCr_2Se_4$, mag. reson. and valence state of Cu and Cr ions 80—60413
$CuCr_2Se_4$, magnetic properties obs. 78—76227
$CuCr_2Se_4$, mechanism for phase transition from ferromag.-ferrimag. state *(Russian)* 77—36075
$CuCr_2Se_4$, prep., thermal cond., temp. depend., 100 to 500K 77—24451
$CuCr_2Se_4$ single crystal, magnetic props. *(Japanese)* 78—6520
$CuCr_2Se_4$, spinel, K X-ray absorption spectrum 78—19600
$Cu_{1-x}Cr_2Se_4$, influence of excess Cu on physical props. 80—103836
$CuCr_2Se_{4-x}Br_x$, elec. resistance, Hall const., magnetoresistance singularities *(Russian)* 79—91078
$CuCr_2Se_{4-x}Br_x$, magnetisation, Curie const., exchange stiffness const. 79—91225
$Cu_{0.67}Cr_{1.78}Se_{2.67}Br_{1.34}$, polycrystalline mag. semicond., mag. and elec. props. 79—7846
$Cu_yCr_2Se_{4-x}Br_x$, ferromag. magneto-resistance exam. *(Russian)* 78—84238
$Cu_yCr_2Se_{4-x}Br_x$, ferromagnetic semicond., Hall effect 80—60012
$Cu_yCr_2Se_{4-z}Br_x$, degenerate ferromag. semicond., resist. minimum 79—73517
$Cu_yCr_2Se_{4-z}Br_x$, paramagnetic-ferromagnetic phase transition temp. depend. on element conc. 79—69672
$CuCr_2Se_{4-x}Cl_x$, magnetisation, Curie const., exchange stiffness const. 79—91225
$CuCr_2Se_4(S_4)(Te_4)$, binary and ternary solid solns., mag. and elec. props. 80—2407
$CuCr_2Te_4$, spinel, K X-ray absorption spectrum 78—19600
$CuCr_2X_4$ ($X=O,S,Se,Te$), K absorpt. discontinuity chem. shift., bonding parameters 77—77318
$CuCr_2X_4$ ($X=S,Se,Te$), excess entropy terms 79—86905
$Cu_{12}^{2+}Cu_4^{+}O_{16}$, paramelaconite, cryst. struct. determ. 78—26506
$CuErTe_2$, synthesis 78—26529
CuF, fast Li^+ ion stopping, chem. bonding effects 77—27929
CuF from $Cu+F_2$ chemiluminesc. reactions, mol. beam study 80—97702
CuF, from gas phase reaction, photon yields, chemi- and photo-luminesc., excitation spectra 79—5157
$Cu^{2+}F^-$ and $Cu^{2+}F^-Cu^{2+}$, transferred hyperfine interactions 80—70659
CuF_2, ^{63}Cu NQR meas. 80—50219
CuF_2, heat capacity, entropy, 10-300K, mag. ordering effects 79—87264
CuF_2, high temp. polymorphism and thermal props. 80—75199
CuF_2, stress-induced birefringence meas., 1-12 μm 77—24818
CuF_2, thermochemical props. 78—31674
Cu_xF_x, ($x=2$-5), heats of formation at 900K 78—31674
$CuF_2(F_6^{4-})$, electronic struct. studies by SCF, MSXα and INDO method 80—74119
$CuF_2.2H_2O$ powder, EPR and Cotton-Mouton Voigt effect in Q-band *(French)* 79—8045
$CuF_2.2H_2O$, synthesis, appl. for carrier-distillation emission spectroscopy 80—89164
$CuF_2.2H_2O$, X-band ESR powder spectrum and related magneto-microwave effects 79—24214
$CuFeCrMn$ spinel oxides, struct. determ., mag. states of Mn^{3+} ions *(Russian)* 78—19227
Cu_2FeGeS_4, crystallographic and magnetic structure *(French)* 80—28998
$CuFeO_2$, EFG tensor, nucl. quadrupole coupling const., O^{2-} polarisability 77—72844
$CuFeO_2$, oxidation, thermogravimetric obs. 77—86203

copper compounds continued
$CuFeO_2$-Fe_2O_3, decomposition kinetics and mechanism of spinel solid soln., composition and precipitation effects *(Japanese)* 77—77489
$CuFe_2O_4$, Jahn-Teller type crystal distortions 80—103904
$CuFe_2O_4$, LPE grown, domain struct. rel. to tetragonal distortion 78—92205
$CuFe_2O_4$, superexchange interactions, three-sublattice anal. 79—61095
$CuFe_2O_4$ thermally induced surface chemistry and struct., XPS 78—22939
$CuFe_2O_4$-$CuGa_2O_4$, physicochem. props. *(French)* 77—44233
$CuFe_5O_3$, cation substitution effect on eutectoid decomposition 78—68890
$CuFe_5O_8$, sintered, eutectoid decomposition study by elec. resist. meas. *(Japanese)* 78—19711
$Cu_{0.5}Fe_{2.5}O_4$, ferrite, determination of specific heat at 298-800K 80—2579
$Cu_{0.5}Fe_{2.5}O_4$-$ZnFe_2O_4$, cation distrib., mag. moment, Mossbauer spectra, chem. anal. 80—75210
$Cu_{1-x}Fe_{2+x}O_4$, cation distrib. and valence state 78—63732
$Cu_{1-x}Fe_{2+x}O_4$, elec. resist., Seebeck coeffs., 20 to 900°C, cation distrib. 79—4575
$CuFeS_2$, antiferromag., NQR local mag. field effects 80—71234
$CuFeS_2$, chalcopyrite, electrode surface reduction kinetics 78—56897
$CuFeS_2$, chalcopyrite, ionic diffusion obs., use of cathodolum. and AES 80—71497
$CuFeS_2$, electronic struct., Mossbauer expt. 78—27150
$CuFeS_2$, exam. of dissolution kinetics, for dissolution in $FeCl_3$-HCl and $Fe_2(SO_4)_3$-H_2SO_4 solns. 79—11790
$CuFeS_2$, explosive-shock deform. 78—95108
$CuFeS_2$, natural chalcopyrite, defect struct., TEM 77—62535
$CuFeS_2$ single crystal, optical reflectivity spectrum 80—40129
$CuFeS_2$, superficial degradation in air and water, XPS obs. *(French)* 80—89110
$CuFeS_2$, X-ray spectroscopic study 78—39626
$CuFe_2S_3$, cubanite, spontaneous magnetisation, polarised neutron obs. *(French)* 78—23245
Cu_2FeS_3, pseudocubic mineral, twinning obs. in point electron-diffr. photographs 77—43225
Cu_5FeS_4, bornite, AES investig. of surface struct., O_2 adsorpt. effects 77—15669
Cu_5FeS_4, bornite, cathodolum. and AES, ionic diffusion obs. 80—71497
Cu_5FeS_4, bornite, superstructuring, vacancy clustering, high-resolution electron microscopy 78—42981
Cu_5FeS_4, mag. ordering and vacancy clustering, mag. susceptibility and Mossbauer spectra meas. 77—85625
Cu_5FeS_4, S and S^{2-} states, identification from Auger line shapes 79—92034
$Cu_2FeSn_3S_8$, synthetic rhodostannite, X-ray cryst. struct. determ. *(French)* 79—99137
$Cu_3FeTl_2Se_4(Cu_3FeTl_2Te_4)$, crystallographic studies 77—31640
$Cu_3FeTl_2Te_4(Se_4)$, struct. and phys. props. *(French)* 79—86758
$Cu_{0.5}Ga_{0.5}Cr_2S_4$, mag. struct. determ. 77—8272
$CuGaCr_4S_8(Se_8)$, 1:1 ordering on tetrahedral sites, IR spectra obs. *(German)* 78—6669
$CuGa_xIn_{1-x}S_2$ solid soln., IR refl. spectra, comp. depend. 78—52498
$Cu(Ga_xIn_{1-x})(S_ySe_{1-y})_2$, spray pyrolysis 79—70004
$CuGa_{0.5}In_{0.5}Se_2/Zn_{0.29}Cd_{0.71}S$ heterojunction solar cell, preparation and props. 80—101110
$CuGa_xIn_{1-x}Se_2$, CVD, elec. and optical props., use as heterojunction solar cell absorber 79—52095
$CuGa_xIn_{1-x}Se_2$, X-ray diffr. cryst. data 80—84147
$CuGaO_2$, Gibbs free energy of formation, 680-1000°C 77—36489
$CuGa_2O_4$, Gibbs free energy of formation, 680-1000°C 77—36489
$CuGaS_2$, coloration, pure and Fe doped, EPR and optical absorpt. obs. 78—88336
$CuGaS_2$, crystal growth and luminesc. *(Japanese)* 78—23515
$CuGaS_2$, crystal growth by I_2 vapour transport, using temperature variation method 78—68610
$CuGaS_2$, crystal growth by solid phase crystallisation 80—25556
$CuGaS_2$, direct gap semicond., exciton energy at 300K from reabsorption of luminesc. 79—78728
$CuGaS_2$, ESR assessment of S diffusion behaviour on annealing 78—35036
$CuGaS_2$, exciton absorption energies, appl. of modulated phase-shift-difference method 78—39565
$CuGaS_2$, exciton energy determ., electron beam excited luminesc. 79—38680
$CuGaS_2$, IR lattice reflectivity spectra obs. 78—19477
$CuGaS_2$, ionic cond., galvanic cell meas. 77—47616
$CuGaS_2$, lattice vibr. modes, Fourier transform spectroscopy 79—33701
$CuGaS_2$, photoelectronic props., 77 to 300K 78—34865
$CuGaS_2$, press. depend. of energy gap, absorption edge obs. 77—12401
$CuGaS_2$, reabsorpt. of excitonic luminesc. in direct band gap semiconds. 77—63469
$CuGaS_2$, reflectvvity and XPS meas. 78—35165
$CuGaS_2$, reson. Raman scatt. by extraordinary phonons obs. 77—85704
$CuGaS_2$, single cryst., photocond. spectra 78—84252
$CuGaS_2$, single crysts. and thin films, absorpt. edge temp. depend., gap energy changes 79—42991
$CuGaS_2$, tetragonal distortion, crystal field splitting, temp. depend. 79—47060
$CuGaS_2$ thermo-optic coefficient, dispersion 80—71396
$CuGaS_2$, X-ray spectroscopic study 78—39626
$CuGaS_2$-CuGaSe, solid solutions, IR lattice reflectivity spectra obs. 78—19477
$CuGaS_2$-$CuGaSe_2$ system, forbidden-band width 78—35280
$CuGaS_2$-ZnS heterodiodes, LPE, emission spectra 79—33335
$CuGaS_2$-ZnS p-n heterojunction, for LED appl., prep. and characterisation 79—1831
$CuGaS_{2-2x}Se_{2x}$, mixed crysts., luminesc. spectra, lattice consts. and band gap energy 77—63454
$CuGaS_{2x}Se_{2(1-x)}$, excitonic structure, phase-shift-difference spectra 78—2872
$CuGa(S_xSe_{1-x})_2$, refl. spectra, comp. depend. 78—39570
$CuGa_5S_8(Se_8)$, ionic cond., galvanic cell meas. 77—47616
$CuGaS_2(Se_2)(Te_2)$, tetragonal distortion 79—32942
CuGaSe, Schottky diodes with tunnel device characts. 78—39215
$CuGaSe_2$, cryst. struct., X-ray powder data 77—39565
$CuGaSe_2$ crystals, electron probe microanal., correction procedure 80—2171

copper compounds continued
$CuGaSe_2$ crystals, I_2 vapour transport grown, luminesc. spectra 78—88349
p-$CuGaSe_2$, electrolum. obs. 77—32444
$CuGaSe_2$, epitaxial layers, lattice parameters meas. using RHEED 79—90913
$CuGaSe_2$, evidence of donor-acceptor type transition 80—93375
$CuGaSe_2$ film, optical props. near and above fundamental absorption edge 78—35215
$CuGaSe_2$, film, spray pyrolysis prod. 79—95953
$CuGaSe_2$, IR lattice reflectivity spectra obs. 78—19477
$CuGaSe_2$, obs. of energy transitions from lower valence band states 78—95576
$CuGaSe_2$, photoluminesc. spectra at 76K 79—38655
$CuGaSe_2$, single cryst. growth from melt, doping 77—12522
$CuGaSe_2$ single crysts., Hall effect and resist., acceptor states 80—10975
$CuGaSe_2$ single crystals, elect. and optical props. for solar cell appl. 80—10981
$CuGaSe_2$ single crystals, electrical and photovoltaic props. 80—92940
$CuGaSe_2$, temp. depend. of fundamental absorpt. edge 78—92090
$CuGaSe_2$ thin films, on GaAs substrates, structural and elec. props., photoluminesc. meas. 79—65564
$CuGaSe_2$/Cu Schottky-barrier cells, photovoltaic effect 79—96440
$CuGaTe_2$, elec. and optical props. 80—6829
$CuGaTe_2$ epitaxial layers, elec. props. as function of growth temp. 79—65565
$CuGaTe_2$, exam. of kinematic viscosity of melts, and short range ordering 79—1383
$CuGaTe_2$ film, flash evaporated, growth and optical props. 79—95296
$CuGaTe_2$ films deposited on GaAs substrates by flash evaporation, struct. and elec. cond. 80—24755
$CuGaTe_2$, IR lattice vibr. spectra 79—28765
$CuGaTe_2$, refr. indices meas. 80—93259
$(CuGaTe_2)_{1-x}$-$(2CdTe)_x$, phase diagram and microstruct. DTA and X-ray diffr. 77—59762
$Cu_3GaTl_2Te_4(Se_4)$, struct. and phys. props. *(French)* 79—86758
$CuGdTe_2$, synthesis and elec. props. 78—26529
$CuGeTe_2$, electroreflectance data, direct gap obs., cryst. field splitting and hybridisation degree 78—39557
Cu_2GeTe_3, tetrahedral phase stability 77—48415
CuH, CuLi, AgCu and AuCu, VB calcs., wave functions, interatomic distance and dissoc. energy values 77—57883
CuH, electronic struct., heat of formation, single particle lifetimes, Dingle temp. meas. 78—51923
CuH, gaseous, dissociation 79—91925
CuH, relativistic (non-relativistic) HF one-centre expansion calcs. 80—52908
CuH, UV absorpt. spectra 80—87143
CuH, vibr.-rot. interaction influence on band intensity parameters 79—49999
Cu_2HgI_4, fast ionic cond. and order-disorder transition 79—99363
Cu_2HgI_4, ordered and disordered phases Raman spectra temp. depend., ion hopping 78—23438
Cu_2HgI_4, polycryst., Raman spectra, press. depend. 77—73137
Cu_2HgI_4, superionic cond., cation disordering 77—84692
Cu_2HgI_4, thermochromic material, IR hologram recording 79—86135
Cu_2HgI_4, valence electron spectrum, SRO and LRO effects 78—52639
Cu_2HgI_4, XPES, lattice instability 79—33904
CuHgSBr, cryst. struct. *(French)* 79—90620
CuHgSCl, cryst. struct. *(French)* 79—90620
$Cu_{3.75}Hg_{1.75}S_2S_8$, velikite, cryst. struct. determ. 78—2097
CuI and CuI:CdI_2, ionic cond., vacancy and interstitial mobilities, phase transitions 77—20116
CuI, α and melt phases, light scatt. from correl. ion fluctuations 79—95771
Cu(I) complex, oxidation, fast reactions meas. by pulsed-flow instrument 80—66890
Cu(I) complexes, cuprous halide triphenylphosphines, NQR, Zeeman effect 80—54980
CuI, cond. mechanisms and struct. at high temps. 77—84711
γ-CuI crystalline film, excitonic spectra *(French)* 79—78771
CuI dissoc. energy A-X system vibr. bands 77—50434
CuI, EXAFS investigation of struct. and ion motion 80—108302
CuI, elec. props. 78—56193
CuI, electric field gradient-elastic tensor components, acoustic NMR obs. 80—25229
CuI, electron-exciton inelastic collision cross sections 79—90967
CuI, energy bands, relativistic KKR method, UV absorpt. spectra 80—39501
CuI, film, prep. on NaCl by reactive sputtering, struct. and composition investigation 79—90900
CuI films, reactively sputtered, epitaxial growth on rocksalt substrates 79—4918
CuI, γ and β phases, phonon contribs. to Gibbs free energy and entropy 77—80633
CuI, H_2 reduction, Cu whisker growth mechanism 78—30853
CuI, hyperfine struct., quadrupole coupling const., rot. spectrum 77—88447
CuI, ionic mobility meas. method 77—15625
CuI, ionic motions nature, mol. dynamics calcs., sp. ht. anomaly due to order-disorder transform. 80—107533
CuI, LF light scatt. spectra in superionic cond. phases, ion motion obs. 80—108217
CuI, lattice dynamics of binary superionic conductors 80—107393
CuI, marshite, ^{129}I concs. determ. by radiogenic ^{129}Xe meas. 77—63983
CuI, NMR chemical shifts, temp. depend. 78—68401
CuI, optical props. 4 to 30 eV, band struct. 77—90166
CuI, parameter calc. from zinc blende zone boundary conditions 77—1194
CuI, phonon dispersion 9-parameter shell model, compared with expt., and Debye temp. evaluation 78—59891
β-CuI, phonon spectra, model 77—89511
β-CuI, phonon spectra calc. 78—10138
CuI photocathodes, efficiency evaluation for soft X-ray diagnostics 80—57442
CuI, photoelastic tensor, acousto-optical meas. 77—12359
CuI, photoelasticity theory 78—10868
CuI, photolum., effect of heat treatment temp. 77—52151
CuI, polariton Raman spectra, oscillator strengths, temp. depend. 80—66197

copper compounds continued
- CuI, press. depend. of Raman scatt. meas., Gruneisen parameters determ. 77–24845
- CuI, pure and CdI_2 doped, ionic cond. obs. 77–15626
- CuI, Raman spectra, Cu ions vibr. and diffractive motions 80–11412
- CuI, reflectance and thermoreflectance spectra, electronic struct. 80–71444
- CuI single cryst., linear electro-optical props., temp. depend. 80–71376
- CuI, single crysts., growth and optical props. 80–93470
- CuI solid electrolyte α-phase stabilisation 80–29209
- CuI, specific heat and lattice dynamics 79–37798
- CuI, superionic, NMR relax. evidence for sublattice melting 77–15623
- CuI, superionic cond., cryst. struct., neutron diffr. study 79–42041
- CuI, superionic cond., EXAFS study 80–50462
- CuI, superionic cond., Raman spectra in all 3 phases 78–19486
- CuI, superionic conductor, Raman study 78–80353
- CuI, superionic conductor, lattice dynamics 79–95111
- CuI, superionic conductor, lattice dynamic meas. and calcs. 79–99880
- CuI, theory of photoelectric consts. 79–61335
- CuI, thermoreflectance spectrum, 4-7 eV region 79–19904
- CuI, visible spectra, A-X system, rot. anal. 79–72326
- CuI:Br(Cl), lattice-dynamical study of impurity modes 80–29129
- CuI-He-Ne pulsed discharge laser, Cu I relax. processes 78–25865
- CuI-PbI_2 system, phase diagram, DTA and X-ray diffr. analysis 77–47552
- $(CuI)_3$, photoelectron spectrum and valence shell struct. 78–62843
- Cu(II) complex, 2,2′,2″-triaminotriethylamine, EPR and optical absorpt. obs. 80–108055
- Cu(II) complex, hexamethyltriaminotriethylamine, EPR and optical absorpt. obs. 80–108055
- Cu(II) complex, $K_{0.4}[(Cu_{0.9}HCO_3)_2(OH)_2]1.66H_2O$, crystal struct. *(French)* 77–1111
- Cu(II) complexes, electronic transitions, dispersion induced circular dichroism spectra 77–27101
- Cu(II) complexes, reversible excited-state electron transfer reactions for solar energy conversion 80–89655
- Cu(II) ethylenediamine $(acetylacetone)_2$, electric dichroism spectroscopy 78–1013
- Cu(II) iminodiacetates in aqueous solution, gamma-ray radiolysis 80–35560
- Cu(II)-DL-proline complex, ESR, magnetic susceptibility and optical absorption 80–93167
- γ-$Cu(IO_3)_2$, cryst. struct. and mag. behaviour 78–79571
- $CuInCr_4S_8$, 1:1 ordering on tetrahedral sites, IR spectra obs. *(German)* 78–6669
- $Cu_{0.5}In_{0.5}Cr_2S_4$, piezoelectric effect, X-ray struct. anal. *(Russian)* 80–15978
- $Cu_{1/2}In_{1/2}Cr_2S_4$, transition from long-range to short-range mag. ordering 77–36087
- $Cu_{1-x}In_xCr_2S_4$, light induced magnetisation 78–76275
- $CuIn_{0.7}Ga_{0.3}Se_2$ epitaxial layers, on GaAs substrates, struct. and elec. props. 80–107670
- $CuIn_{1-x}Ga_xSe_2$ mixed cryst., optical transmission spectrum and gap energy temp. depend. 79–65896
- $CuIn_{1-y}Ga_ySe_{2(1-x)}Te_{2x}$ pentenary alloy compounds for photovoltaic solar energy conversion 80–93971
- $CuInS_2$, cathodolum. spectra, heat treatment and electron irrad. effects 78–10996
- $CuInS_2$, crystal growth by I_2 vapour transport, using temperature variation method 78–68610
- $CuInS_2$, crystals and thin films, growth, struct., and elec. props. 79–38729
- $CuInS_2$, epitaxial thin film on GaAs, exam. of growth, electrical props. 80–24754
- $CuInS_2$ film, photoconductivity effects 77–43662
- $CuInS_2$, film, spray pyrolysis prod. 79–95953
- $CuInS_2$ film homojunction solar cell, fabrication, performance 77–80832
- $CuInS_2$ films, RF sputtered, growth and props. 80–80124
- $CuInS_2$, films and heterojunctions, grain boundary and interdiffusion studies, AES and SIMS 79–77842
- $CuInS_2$ films prepared by spray pyrolysis, elec., optical and struct. props. 79–73609
- $CuInS_2$ films prod. by RF sputtered Cu-In films exposure to H_2S 79–95926
- $CuInS_2$, fund. reflectivity, 2 to 6 eV, band struct. implications 78–39574
- $CuInS_2$, homogeneity region and intrinsic dopant mechanism 78–34630
- n-$CuInS_2$, mag. props., obs. 80–70939
- $CuInS_2$, minority carriers lifetime, photoelectromag. effect meas. 79–47125
- $CuInS_2$, optical and elec. phenomena 78–39605
- $CuInS_2$, p-n junction photovoltaic props. and detectors 79–99574
- $CuInS_2$, region of existence, determ. by quenching and X-ray anal., phase transition 79–66054
- $CuInS_2$ single phase thin film prep. by flash evaporation 80–100796
- $CuInS_2$, X-ray spectroscopic study 78–39626
- $CuInS_2$:Cd(Zn), elec. props. 77–62927
- $CuInS_2$-CdS photovoltaic heterojunctions, growth and characts. 77–39931
- $CuInS_2$-SnS_2, spinel phase $Cu_xIn_xSn_{1-x}S_2$ obs., stoichiometry *(French)* 80–44326
- $CuIn_{11}S_{17}$, defect spinel, cryst. growth, search for new superionic cond. cpds. 78–31307
- $CuIn_5S_8$, single crystn. phase, CVD prep., X-ray cryst. struct. determ. 79–65990
- $CuIn_5S_8$, sulphospinel electron diffr. and electron microscopy study, order-disorder transform obs. 80–88080
- $CuIn_5S_8$ thiospinel, space group assignment by X-ray diffractometry 79–99141
- $CuInS_2(Se_2)$ film, vacuum deposited, absorpt. coeff. 78–72621
- $CuInS_2(Se_2)$-$GeS_2(Se_2)$, degree of solid solubility and phases characts. 78–35377
- $CuIn(S_xSe_{1-x})_2$, spray pyrolysis 79–70004
- $CuInS_2(Se_2)(Te_2)$, film, electron and X-ray diffr. 77–11819
- $CuInS_2(Se_2)(Te_2)$, tetragonal distortion 79–32942
- $CuInS_2(Se_2)(Te_2)$, thin films and photovoltaic devices, AES evaluation 78–67928
- $CuInS_2(Se_2)(Te_2)$, thin film, bulk polycryst. and single cryst. samples, AES 78–72648
- CuInSe, reflectvvity and XPS meas. 78–35165
- $CuInSe_2$, acceptor levels, elec. props. study 80–39578

copper compounds continued
- $CuInSe_2$ amorphous thin film, flash evaporation, struct., stoichiometry 80–89150
- $CuInSe_2$ crystals, electron probe microanal., correction procedure 80–2171
- $CuInSe_2$, dielectric const. from capacitance meas. 79–61292
- n-$CuInSe_2$, effective electron mass, IR free-carrier Faraday rot. meas. 77–55783
- $CuInSe_2$, energy gap, temp. depend., 15-300K, optical absorpt. obs. 77–36266
- $CuInSe_2$ epitaxial growth on GaAs 78–84104
- $CuInSe_2$, far IR refl. spectra, ionic bonds 79–55695
- $CuInSe_2$ film, evaporation source temp. effect, on comp. 80–39478
- $CuInSe_2$ film, MBE growth, AES and optical absorpt. obs. 79–78903
- $CuInSe_2$ film, photoconductivity effects 77–43662
- p-$CuInSe_2$ film, prep. from vac. evaporation of $CuInSe_2$, optical and elec. props. 79–82697
- $CuInSe_2$, film, spray pyrolysis prod. 79–95953
- $CuInSe_2$, films and heterojunctions, grain boundary and interdiffusion studies, AES and SIMS 79–77842
- $CuInSe_2$, growth on CdS (0001) surface using MBE 79–56936
- $CuInSe_2$, heteroepitaxy on {111} oriented Ge by flash evaporation, struct. 80–108333
- $CuInSe_2$, IR lattice vibr. spectra 79–28765
- $CuInSe_2$, influence of impurities and free carriers on optical props. 80–108225
- $CuInSe_2$, large single crystals growth by iodine transport and Bridgman methods 78–35300
- $CuInSe_2$, melt-grown, EPR characts. 78–35030
- p-$CuInSe_2$, minority carrier lifetime and surface recomb. velocity, photoelectromag. meas. 78–19085
- $CuInSe_2$, n- and p-type, elec. resist. and Hall effect, 80 to 500K 79–87096
- $CuInSe_2$ on GaAs, epitaxy grown RHEED exam. of epitaxial overgrowth *(German)* 79–11042
- $CuInSe_2$, photovoltaic props. and p-n junction form. 77–69371
- $CuInSe_2$ polycrystalline thin film anomalous photovoltaic effect *(German)* 78–68102
- $CuInSe_2$, refr. indices meas. 80–93259
- $CuInSe_2$, Schottky diodes with tunnel device characts. 78–39215
- $CuInSe_2$ semicond. films, optical props., 1-3 eV 78–27346
- n-$CuInSe_2$, single cryst., elec. props. 78–43397
- $CuInSe_2$, spray pyrolysis 79–70004
- p-$CuInSe_2$, thermal props. 80–96705
- $CuInSe_2$ thin film fabrication by RF-sputtering for solar cell appls. 80–100786
- $CuInSe_2$ thin films, prep. by spray pyrolysis, struct., elect. and optical props. for solar cell appls. 80–100781
- $CuInSe_2$ thin films for solar cells, radiofrequency sputtering technique, elec. props. 80–93487
- $CuInSe_2$, Zn implantation profiles by AES 77–31692
- $CuInSe_2$/CdS solar cell, grain boundary effects on performance 79–83603
- $CuInSe_2$-CdS heterojunction, photovoltaic effect, rel. to optimum conditions for solar cell fabrication 77–51810
- $CuInSe_2$-CdS photovoltaic heterojunctions, growth and charact. 77–39931
- $CuInSe_2$-CdS solar cell, polycrystalline thin film, high photocurrent, characts. 80–61339
- $CuInSe_2$-$CuInS_2$, melts, viscosity, elec. cond., density composition prop. graphs 79–14948
- $CuInSe_2$-$CuInS_2$, solid soln., photo-EMF spectra 80–20248
- $CuIn_2Se_{3.5}$, cubic ordered compound, optical gap 78–48175
- $Cu_{0.5}In_{2.5}Se_4$, transition state and domain struct. by electron microscopy and diffr. studies 80–15095
- $CuInSe_{2-x}S_x$, phase equilibria 77–90328
- $CuInSe_2(S_2)(Te_2)$, Debye temp., standard entropies and enthalpies, sp. ht. meas. 78–30769
- $CuInSnS_4$, spinel, cryst. growth, search for new superionic cond. cpds. 78–31307
- $CuInTe_2$, direct energy band gap determ., electroreflectance meas. 78–2418
- $CuInTe_2$, electroreflectance data, direct gap obs., cryst. field splitting and hybridisation degree 78–39557
- $CuInTe_2$ epitaxial layers, on GaAs, growth and props. 80–108359
- $CuInTe_2$, exam. of kinematic viscosity of melts, and short range ordering 79–1383
- $CuInTe_2$, far IR refl. spectra, ionic bonds 79–55695
- $CuInTe_2$ film, photoconductivity effects 77–43662
- $CuInTe_2$, grown from near stoichiometric comp., elec. and optical props. 78–68504
- $CuInTe_2$, infrared optical properties 79–82974
- $CuInTe_2$, optical transitions from valence band states 79–87416
- $CuInTe_2$, pressure-induced phase transformations 78–30748
- $CuInTe_2$, refr. indices meas. 80–93259
- $CuInTe_2$ single crystals, directional freezing growth and doping, resist. changes on annealing 80–60768
- $CuInTe_2$, vac. deposited film, growth, struct. and elec. characts. 77 69995
- $CuInTe_2$-CdS photovoltaic heterojunctions, growth and charact. 77 39931
- $(CuInTe_2)_{1-x}$-$(2ZnTe)_x$, phase diagram and cryst. growth of $CuZn_2InTe$ from $ZnCl_2$ flux 80–16287
- $Cu_xIn_xZr_{1-x}S_2$ system, struct. and cond. meas. *(French)* 80–88354
- $CuK_2Cl_4.2H_2O$, 3-dimens. Heisenberg ferromag., crit. behaviour 77–20594
- $CuK_2Cl_4.2H_2O$, Heisenberg ferromag., press. effect on Curie temp. and susceptibility 77–28386
- $CuK_2Cl_4.2H_2O$, Heisenberg ferromagnet, spontaneous magnetisation under press. *(Russian)* 77–36058
- $CuK_2Cl_4.2H_2O$, Heisenberg ferromag., mag. props. at high press. 77–69512
- $CuK_2Cl_4.2H_2O$, Heisenberg ferromag., mag. field effect on susceptibility near crit. point 80–39758
- $CuK_2Cl_4.2H_2O$, proton spin-lattice relax. and exchange interactions, temp. depend. 79–95663
- $CuK_2H_2(PCrO_7)_2$, cryst. struct. determ. 80–28989
- $CuK_2(SO_4)_2.6H_2O$-liquid ^3He interface, thermal boundary resist. from 8.5 to 110 mK 79–56001
- Cu_xMS_2, $(0<x\leq 0.50)$ (M=Zr, Hf), intercalation compounds, ordered phases obs. 80–33962

copper compounds continued
$CuM_2X_4.2D_2O$, MX=alkali or ammonium halide, quadrupolar interaction, 4-300K, reorientation 79—73848
$Cu_xMg_{1-x}Al_2O_4$, spinel solid solns., solid-state and surface props. 77—66415
$CuMn_2O_4$, comment on cryst. struct. determs. by neutron diffr. 79—23585
$CuMn_2O_4$, formation in phase transition during ht. treatment of $Cu(OH)_2$-$\alpha Mn(OH)_2$ 78—23659
$CuMn_2O_4$, ionic config., re-exam. of expt. evidence 77—19897
$CuMn_2O_4$, neutron diffr. exam., crystallographic props. 78—14329
$Cu_2Mn_3O_8$, cryst. struct. *(French)* 77—58987
$Cu_4Mn_2S_4$, spinel, prep. and elec. props., 100 to 650K 79—43127
$Cu_4Mn_2Se_4$, spinel, prep. and elec. props., 100 to 650K 79—43127
Cu_2MnSnS_4, mag. struct. rel. to Cu_2FeGeS_4 *(French)* 80—28998
$Cu_2Mn_2Te_4$, spinel, prep. and elec. props., 100-650K 79—43127
$CuMoO_4$, cathodic props. in Li primary batteries 80—3502
$Cu(Mo_2Re_2)S_8$, synthesis and electrical props. of mixed tetrahedral cluster phases 80—2971
$Cu_{0.9}Mo_3S_4$, triclinic low-temp. struct. 80—28959
$Cu_{1.8}Mo_6S_8$, supercond. energy gap and phonon-induced structs. in tunnelling density of states 79—51728
$Cu_{1.8}Mo_6S_8$, supercond. Chevrel phase, electron tunnelling spectroscopy expts. *(German)* 80—107966
$Cu_{1.8}Mo_6S_8$, superconducting state, triclinic struct., X-ray powder diffr. anal. 80—6388
$Cu_{2-x}Mo_3S_4$, X-ray cryst. struct. exam., effect of Cu conc. variation 78—2071
$Cu_2Mo_6S_8$, normal state and superconducting property measurements 78—91660
$Cu_2Mo_6S_8$, phonon density of states, mode softening correl. with supercond. transition temp. 79—51714
$Cu_{2.0}Mo_6S_8$, Chevrel phase supercond., compressibility and vol. depend. of Tc 78—31008
$Cu_{2.5}Mo_6S_8$, evaporated two-phase, crit. current and scaling laws 78—91831
$Cu_xMo_3S_4$, chevrel phase, charge transfer and valence electron conc. 78—6029
$Cu_xMo_3S_4$, superconductivity, lattice transforms., electronic instabilities 77—39990
$Cu_xMo_3S_4$, superconductivity and cryst. struct. 79—78250
$Cu_xMo_6S_8$, $1.5 \leq x \leq 3.55$, low temp. phase diagram, 1.2-320K 77—85371
$Cu_xMo_6S_8$, Chevrel phase, lattice instabilities, X-ray diffr. meas. 78—34491
$Cu_xMo_6S_8$, Chevrel phase supercond. prep. and supercond. props. 79—28434
$Cu_xMo_6S_8$ Chevrel phase, synthesis, stability and characts. 80—71608
$Cu_xMo_6S_8$, Chevrel-phase sputtered film, supercond. critical currents 77—80892
$Cu_xMo_6S_8$, constitution diagram, 11-2000K 80—108407
$Cu_xMo_6S_8$, evap. film prep., supercond. props., lattice parameters 78—23195
$Cu_xMo_6S_8$, evaporated and sputtered Chevrel phase films, indirect meas. of Fermi surface parameters 79—60686
$Cu_xMo_6S_8$, evaporated films, superconducting upper crit. fields, crit. currents 79—42714
$Cu_xMo_6S_8$, Hall effect and magnetoresistivity 78—95400
$Cu_xMo_6S_8$, inhomogeneous superconductor, scaling laws for pinning forces 79—47214
$Cu_xMo_6S_8$, normal-state electronic props., Fermi surface and supercond. parameter derivations 79—60850
$Cu_xMo_6S_8$, prep. by topotactic electrode reactions, struct., supercond. 79—99158
$Cu_xMo_6S_8$, sintered and sputtered, supercond. upper crit. field 78—23215
$Cu_xMo_6S_8$, sputtered, supercond. crit. currents and scaling laws 78—47923
$Cu_xMo_6S_8$, supercond., two-phase, upper crit. field meas. 80—29509
$Cu_xMo_6S_8$, superconducting reactively evaporated film, crit. currents 79—28492
$Cu_xMo_6S_8$ system, low temp. modifications *(French)* 80—50606
$Cu_xMo_6S_8$, thin films, low temp. normal state, resist., temp. depend. 78—91783
$Cu_xMo_6S_{8-y}$ electrodes, thermodynamic and transport props. 80—66963
$Cu_xMo_6S_{8-y}$, mixed conductor, partial Cu ion cond. and chem. diffusion 80—84323
$Cu_xMo_6S_{8-y}$, mixed conductor, equilib. partial thermodynamic props. 80—85270
$Cu_xMo_6S_6I_2$, Chevrel phase, synthesis and supercond. *(German)* 80—25038
$Cu_xMo_6S_6I_2$, $x=0$ to 1.2, superconducting Chevrel-phase system, synthesis and transition temps. 79—69618
$Cu_2Mo_6S_6O_2$, O-containing Chevrel phases, synthesis and props. 80—108368
$Cu_xMo_6S_8(Se_8)$, prep., metallurgical and supercond. props. 77—32102
$Cu_xMo_3S_4(Se_4)(Te_4)$, chevrel phase, anomalous elec. resist. 79—56221
$Cu_{0.7}Mo_3Se_4$, Chevrel-phase, low temp. struct. instability rel. to supercond. 77—47919
$Cu_{1.4}Mo_6Se_8$, Chevrel phase supercond., compressibility and vol. depend. of Tc 78—31008
$Cu(NH_4)_2Br_4.2H_2O$, 3-dimens. Heisenberg ferromag., crit. behaviour 77—20594
$Cu(NH_4)_2Br_4.2H_2O$, Heisenberg ferromag. press. effect on Curie temp. and susceptibility 77—28386
$Cu(NH_4)_2Br_4.2H_2O$, Heisenberg ferromag., corrections to scaling in sp. ht. 77—66328
$Cu(NH_4)_2Br_4.2H_2O$, Heisenberg ferromag., mag. props. at high press. 77—69512
$Cu(NH_4)_2Br_4.2H_2O$, uniaxial ferromag. insulator, influence of press. on magnetisation 77—69661
$Cu(NH_4)_2Br_4.2H_2O$, Heisenberg ferromagnet, phase transition in mag. field 79—7992
$Cu(NH_4)_2Br_4.2H_2O$ Heisenberg ferromagnet, mag. props. in mag. field 80—34637
$Cu(NH_3)_n(ClO_4)_2$, ($n=4$ or 5), EPR parameters and dilatometry 80—39850
$Cu(NH_3)_4(NO_3)_2$, single cryst., low temp. susceptibility and sp. ht., 10 behaviour 77—89929
$Cu(NH_3)_4PtCl_4$, $Cu(NH_3)_4^{2+}$ cation mol. orbital parameters 78—64011
$Cu(NH_3)_4SO_4.H_2O$, interface with liq. ^3He, Kapitza resist. anomaly near Neel temp. 77—69139
$Cu(NH_3)_4SO_4.H_2O$, EPR around Neel temp. 78—39390

copper compounds continued
$Cu(NH_3)_4SO_4.H_2O$, submillimetre ESR meas. using pulsed high mag. field 80—44905
$Cu(NH_4SO_4)_2.6H_2O$, X-band ESR magneto-microwave effects 77—28434
$Cu(NH_3)TeO_3.H_2O$, crystal struct. determ. 77—80450
$Cu(NH_3)_4.(H_2O)^{2+}$ solns., effect on working of Ti-Ni alloy *(Russian)* 78—53017
$Cu(NO_3)_2$, aq. electrolyte, apparent molar heat capacity and volume, of 298.15K 79—65208
$Cu(NO_3)_2$, aq. soln., Raman spectrum, local order 78—84563
$Cu(NO_3)_2$, decomp., prod. of free Cu atoms 79—79244
$Cu(NO_3)_2$, electronic struct., relative energies, iterative EHT calculations 77—38615
$Cu(NO_3)_2$, frozen aq. soln., phase transitions, struct., ESR 77—16154
$Cu(NO_3)_2$, in ethylene glycol solns., US absorpt., relaxation rel. to temp. 77—31727
$Cu(NO_3)_2 2.5H_2O$, spin-pair system, spin ordering, XY-model in external field 77—73033
$Cu(NO_3)_2.2^1/_2H_2O$, ^1H spin-lattice relax. time, 4.2K, 5-60 kOe 79—15371
$Cu(NO_3)_2.2^1/_2H_2O$, high field phase transition, susceptibility and NMR meas. 77—69559
$Cu(NO_3)_2.2^1/_2H_2O$, long-range ordered state, mag. props. 78—39417
$Cu(NO_3)_2.2^1/_2H_2O$, singlet ground-state system, mag. props., short-range ordered state 78—23289
$Cu(NO_3)_2.2^1/_2H_2O$, singlet ground state system, mag. props. 80—44850
$Cu(NO_3)_2.2.5\ D_2O$, magnetic ordering, neutron diffr. meas., 0.08-0.25K 80—39749
$Cu(NO_3)_2.2.5H_2O$, adiabatic magnetisation cooling by pulsed mag. field 77—20600
$Cu(NO_3)_2.2.5H_2O$, linear Heisenberg antiferromag., mag. and thermodynamic props. 79—61136
$Cu(NO_3)_2.2.5H_2O$, linear Heisenberg antiferromag., proton spin-lattice relax. times 79—61257
$Cu(NO_3)_2.2.5H_2O$, single cryst., $S={}^1/_2$ alternating linear antiferromag. spin dynamics 79—51793
$Cu(NO_3)_2$(pyrazine), single cryst. PMR 78—2761
$CuNa_2Si_4O_{10}$, synthetic, cryst. struct. determ. 77—47383
$CuNb_2O_6$, bonding characterisation 78—38680
$Cu_{0.5}NbS_2$, phase transformations of order-disorder and displacive type, domain-type microstruct. 77—4195
Cu_xNbS_2, $0.8<x<1$, order-disorder transitions and incommensurate superstruct. 77—15587
Cu_xNbS_2, electron diffuse scatt., microstruct., of transition state 77—31771
$Cu_xNi_yO_z$, protective oxide film on Cu-Ni alloy, AES 79—39035
$(Cu_xNi_{1-x})S_2$, XPS of valence band meas. 77—85885
$Cu_4NiSi_2S_7$, X-ray cryst. struct. determ., mag. props. 80—107172
CuO, $^4\Sigma_{1/2}$-$^2\Pi_{1/2}$ transition, rot. anal. 78—82748
CuO, 4182 Å band spectrum, rot. anal. 79—89685
CuO, ab initio HF-MC-SCF with GTO basis set, dissoc. energy and bond length 80—47890
CuO addition to molten salt heat transfer fluid, solar absorbing properties enhancement 78—87112
CuO, additive for activated sintering of SnO_2 77—36415
CuO aggregates, solid, aerosols, dynamic shape factors meas. 80—61165
CuO, black Zn-dust pigmented solar selective coatings for solar photothermal conversion 80—66997
CuO, $C^2\Pi_i$-$X^2\Pi_i$ and $D^2\Delta_i$-$X^2\Pi_i$ band systems, rot. anal. 78—82747
CuO, catalytic effect on thermal transitions of $Na_2S_2O_8$ and $K_2S_2O_8$ 79—15983
CuO, colorant, bandpass filter glass, 550-616 nm, transmission characts. 78—66919
CuO, Cu_2O, formation of internal oxidation band of Cu-Cr 79—47820
CuO, desorpt. of ions by low power laser beam 80—80092
CuO, EXAFS beats, determ. of differences in bond lengths 78—23552
CuO, effect on PTFE-Al adhesion joints 78—53183
CuO, electronic spectra in rare gas matrix 78—996
CuO film, electron energy loss spectra meas., optical functions calc. 78—19618
CuO film, positron annihilation meas. 77—40300
CuO, fluoresc., matrix isolation spectra 78—46381
CuO formed anodically in phosphorus medium, photoelectrochemical effects *(French)* 80—93701
CuO, isoelectric point meas. 80—88609
CuO, L_l and L_η X-ray emission spectra 78—39631
CuO, mol. orbital energies and X-ray K-absorpt. spectra 80—69060
CuO, monolayer on Cu, SIMS anal. of oxidation 79—89038
CuO, on Al or Cu, solar selective coating, figure of merit 80—72082
CuO, on Cu, identification by electron spectroscopic methods 80—60747
CuO, plasmochemical synthesis, oxidised from metals, exam. of props. 80—2984
CuO powder, surface area determ. by adsorpt. of stearic acid and pyridine 80—107636
CuO, reaction with solid K_2O and liq. K 79—66277
CuO, reactions with Cu or polyethylene in adhesion 79—39118
CuO, red $^2\Delta$-$x^2\Pi_i$ transition, $^2\Delta_{5/2}$ state consts. 78—9163
CuO, rot. anal. of red $A'\ ^2\Sigma^+ - X\ ^2\Pi_i$ system 78—13508
CuO selective surfaces on Al-Cu alloy, chemical brightening and etching 79—62037
CuO, sol, mixtures with TiO_2 and α-FeOOH sols, differential surface coagulation 79—79303
CuO solar selective black coatings for large area appls., prep. and props. 80—21411
CuO, solid, XPS satellite struct. 79—56908
CuO, sputtered pulse discharge, Cu vap. production, laser appl. *(Russian)* 77—84556
CuO surface, contaminated, cleaning treatments, ion scatt. anal. 78—53307
CuO surface, solar radiation absorpt., comparison with Planckian black body *(German)* 77—35026
CuO-Ag film solar absorbers, mechanism of high-temp. instability 78—22971
CuO-CaO-P_2O_5 glass devices, memory switching 78—56192
CuO-CaO-P_2O_5 system glasses, DC cond., hopping transport, 300 to 620K 78—23096
CuO-CdO-Fe_2O_3, sintered ferrite, preparation, mag. susceptibility, DC resistivity 80—34598
CuO-Cr_2O_3 based oxide, catalyst, adsorption of fluorobenzene, binding energy of F 1s electrons *(French)* 79—69346

copper compounds continued
- CuO-Cu_2O-TiO_2, phase equilibria, thermodynamics of Cu_3TiO_4 phase 80−55374
- CuO-Fe_2O_3, isoelectric point meas. 80−88609
- CuO-MgO system, Cu ions valence states, electronic refl. spectra 78−35168
- CuO-Nb_2O_5, phase anal., density determ. 78−10015
- CuO-V_2O_5-P_2O_5 glass, elec. cond. and switching *(Japanese)* 80−34492
- CuO-ZnO-Fe_2O_3, sintered ferrite, preparation, mag. susceptibility, DC resistivity 80−34598
- CuO+WO_3 solid state reaction kinetics, $CuWO_{4-x}$ formation study 80−66796
- CuO_2, width of reson. Raman scatt. enhancement profiles, phenon-lifetime contrib. 79−19883
- CuO_2/Cu junction solar cell, photovoltaic conversion characts. *(French)* 79−24900
- $Cu_{12}O$, solid, XPS satellite struct. 79−56908
- Cu_2O, ^{18}O conc. profile, secondary emission of negative or positive ions *(French)* 79−60395
- Cu_2O, ^{65}Cu NQR spectrum using digital freq. modulation 78−21189
- Cu_2O, 1s yellow exciton, lineshape studies by reson. Raman scatt. 78−76465
- Cu_2O, adsorption and desorption of water vapour, relative humidity effects 80−49505
- Cu_2O and CuO, smoke particles prep. by burning metal in Ar-O_2 gas, electron microscope obs. 77−52238
- Cu_2O and CuO powders, contact resistance, temp. and pressure dependence, obs. *(German)* 79−4555
- Cu_2O, anodic form. on Cu electrodes immersed in NaOH, chronopotentiometry, SEM and TEM obs. 77−48573
- Cu_2O, Auger quantitative anal. 78−73104
- Cu_2O, CVD from Cu-O-H-Cl-N system, thermodynamic anal. 78−39676
- Cu_2O, cond. filament props. and bistable switching effect *(German)* 78−2532
- Cu_2O containing Pb glass, crystallisation 78−47241
- Cu_2O, creep substruct. under compression, X-ray diffr. study 78−95785
- Cu_2O, creep tests, exam. of a creep machine mech. ability *(French)* 79−20325
- Cu_2O, Cu inclusions and annealing, optical and IR absorpt. obs. 80−60630
- Cu_2O, defect levels, TSC 77−66138
- Cu_2O, deposition by chem. transport using HU, HI *(German)* 78−31344
- Cu_2O, effective Hamiltonian for few-particle systems 77−15776
- Cu_2O, electric field screening by surface electron states 78−52058
- Cu_2O, electro-optic effects due to the Stark splitting of energy bands 79−82950
- Cu_2O, electroless deposition 78−27419
- Cu_2O, electron-exciton inelastic collision cross sections 79−90967
- Cu_2O, electron-exciton scatt. cross sections, central field and exchange approxs.. 77−62919
- Cu_2O, energy band interactions under uniaxial compression 80−25412
- Cu_2O, epitaxial, on Cu (111), misfit dislocations, TEM obs. 78−14629
- Cu_2O, epitaxial, on Cu(111), misfit dislocation annealing, TEM obs. 79−82228
- Cu_2O, even-parity excitons assignment, from two-photon spectrum 80−6731
- Cu_2O, evidence of competitive phenomenon between 0.72 μm and 0.93 μm luminesc. 78−27310
- Cu_2O, exciton luminesc. spectra, mag. field influence 80−80860
- Cu_2O, exciton speetra, extended effective mass theory 79−69423
- Cu_2O, exciton spectrum, effect of isotopic substitution 78−67955
- Cu_2O, exciton-phonon dynamics, reson. Raman scatt. 80−11406
- Cu_2O, exciton-phonon interactions, optical absorpt. spectra. theory 80−49614
- Cu_2O, excitons, exciton-phonon interactions, review, book contrib. 80−49624
- Cu_2O, excitons and structural defects at low temp. 78−84255
- Cu_2O film, electron energy loss spectra meas., optical functions calc. 78−19618
- Cu_2O film, positron annihilation meas. 77−40300
- Cu_2O film, reactively sputtered, photovoltaic props. rel. to solar cell applic. 79−7914
- Cu_2O film, reactively-sputtered, phase comp., resist. and optical consts. 79−95534
- Cu_2O films arc cathode emission study 78−23583
- Cu_2O, fine struct. of exciton spectrum 78−18972
- Cu_2O foils, electron microscope exam., Cu precipitates and CuO form. 79−1462
- Cu_2O, forbidden energy gap oxide semicond. crystals, review of spectroscopic props. 78−2876
- Cu_2O, form. by Cu oxidation in CO_2, 800-1000°C 78−76784
- Cu_2O formed anodically in phosphoric medium, photoelectrochemical effects *(French)* 80−93701
- Cu_2O, front wall solar cells, chemical origin of space-charge layer 79−70449
- Cu_2O, growth by melting, photocond. spectra 78−52029
- Cu_2O, heat of adsorpt. of pyridine and ethyl pyridine, flow microcalorimetry 78−85193
- Cu_2O, heterogeneous deform. during high temp. compression creep 78−48456
- Cu_2O, high-temperature investig. of recovery creep, 700 to 1000°C *(French)* 77−72650
- Cu_2O, hole mobility, scatt. mechanisms, elec. field effect 77−80786
- Cu_2O, L_I and L_{η} X-ray emission spectra 78−39631
- Cu_2O, laminar growth on (111) Cu single cryst. surface, microstruct. 78−72025
- Cu_2O, layer-planes form. at anodic overpotential after dissolution of Cu hydroxy complexes on Cu amalgam 79−61865
- Cu_2O MIS solar cell with SiO_2 interfacial layers, semi-transparent layers of Au, Cu, Ag and Al 80−93946
- Cu_2O, meas. of standard molar free energy of form. by EMF method of high temps. *(Japanese)* 78−11546
- Cu_2O, mol. orbital energies and X-ray K-absorpt. spectra 80−69060
- Cu_2O, NQR freq. of ^{63}Cu, temp. depend., mol. dynamics 77−12227
- Cu_2O, NQR frequency, appl. in pulsed NQR thermometer 77−13749
- Cu_2O, NQR press. depend. 77−12225
- Cu_2O, NQR spectrum of $^{63,65}Cu$ 77−12235
- Cu_2O, odd photomag. effect. meas. 77−89805
- Cu_2O, on Cu, identification by electron spectroscopic methods 80−60747

copper compounds continued
- Cu_2O on Cu, two stage metastable and stable surface nucleation, 800-1000°C 77−70214
- Cu_2O, optical absorpt. due to paraexciton in strong mag. field 77−28596
- Cu_2O, ortho and para exciton lifetime meas. 80−6730
- Cu_2O, photoconductivity in 1S excitonic line 80−34366
- Cu_2O, photoconductivity of crystals grown under hydrothermal conditions 78−14765
- Cu_2O, photomemory effect, EPR expts. 78−52353
- Cu_2O, photosensitive etching in nonoxidising etchants 80−78813
- Cu_2O, polar semicond., effective exciton-exciton interaction 79−42465
- Cu_2O polycrystalline and single cryst. mech. behaviour 78−95777
- Cu_2O polycrysts., dislocation obs. by elecron microscope *(Spanish)* 80−75230
- Cu_2O, positive and negative photomemory, IR luminesc. spectra, illum. effect 79−69557
- Cu_2O, pure and Fe doped, impurity scattering effect on carrier cyclotron resonance 79−56614
- Cu_2O, radiation damage 77−84809
- Cu_2O, reaction with solid K_2O and liq. K 79−66277
- Cu_2O, refl.-absorpt. IR spectroscopy 78−84555
- Cu_2O, relationship between interband transitions and spectrum of diagmagnetic excitons in moderate mag. fields 79−91412
- Cu_2O, residual conductivity, role of vacancies, photoluminesc. and photocond. 77−15901
- Cu_2O, reson. Raman scatt., yellow and green excitonic series 78−72511
- Cu_2O, reson. Raman scatt. from stress-split forbidden excitons 80−93332
- Cu_2O, sample thickness depend. of exciton polariton absorption coeff. 80−34941
- Cu_2O, Schottky barriers, low barrier heights, Auger spectra obs. 79−15224
- Cu_2O, self-consistent energy bands 80−59869
- Cu_2O, self-diffusion of Cu 77−84983
- Cu_2O, self-induced transmission and radiation echo for intraseries and interseries exciton transitions 78−5528
- Cu_2O, self-induced transparency, two-photon interaction of laser radiation with Frenkel excitons 78−25931
- Cu_2O single cryst. diodes, IR electroluminesc. 79−83034
- Cu_2O, single crystal, thermoelectric behaviour *(French)* 78−71786
- Cu_2O single crystals, photomemory effect, kinetics of excitation and deexcitation processes 77−85262
- Cu_2O, slip systems, Kroop hardness anisotropy meas. 77−31714
- Cu_2O solar cells, electrical and optical props., photocurrent anal. 80−101116
- Cu_2O, space group selection rules, symm. points and lines 77−35499
- Cu_2O, sputtered pulse discharge, Cu vap. production, laser appl. *(Russian)* 77−84556
- Cu_2O, standard free energy of formation, by EMF method with solid oxide electrolyte at low temps. *(Japanese)* 80−88338
- Cu_2O, switching channel electron probe microanalysis, switching cycle number (life) 77−32056
- Cu_2O, theory of large-radius excitons 78−47710
- Cu_2O, theory of lattice dynamics 78−59896
- Cu_2O, thermal activation of plastic deform. *(French)* 80−16394
- Cu_2O, thermal breakdown mechanism of switching process, expt. obs. *(German)* 77−28225
- Cu_2O, thermal expansion at low temp. 78−59959
- Cu_2O, thermal switching, resist.-temp. charact. 78−64071
- Cu_2O thin film solar cells, fabrication and anal. 80−55865
- Cu_2O, uniaxial stress effects on excitons 80−60589
- Cu_2O, with impurities, exciton absorpt. line shape calc. *(Russian)* 78−10934
- Cu_2O, yellow exciton series, silver impurity influence on spectrum 78−64388
- Cu_2O, yellow exciton series, 1s paraexciton levels, phonon assisted transitions, optical absorpt. edge 78−79934
- Cu_2O, yellow exciton states investig. by forbidden resonant Raman scatt. 77−48165
- $Cu_2O:Ag^+$, exciton-neutral and exciton-charged impurity scatt. cross sections 80−70618
- $Cu_2O:Ag^+$, yellow series line width, exciton-impurity scatt. 78−64386
- Cu_2O:Cd, dipolar and quadrupolar bound excitons, absorption spectrum *(Russian)* 78−92099
- $Cu_2O:Cd^{2+}$ implanted, reson. Raman scatt., annealing effect 77−24838
- Cu_2O:He(Na)(Cd), ion-implanted, resonance Raman studies of annealing 79−55765
- Cu_2O:Mn, photomemory mobility components, charged centre conc. 80−103725
- Cu_2O-Al_2O_3-SiO_2 glass, thermal expsn. coeff. 79−51284
- Cu_2O-Al_2O_3-SiO_2 glasses, strengthening by alkali-Cu ions exchange 80−55467
- Cu_2O-Au(Mg)(Mn)(Yb) Schottky barrier solar cells, surface anal. using AES 79−43759
- Cu_2O-Cu diode junction, Schottky barrier, electronic structure and minority carrier diffusion length *(French)* 80−65682
- Cu_2O-CuO-MoO_3, subsolidus phase diagram, mag. props. 80−50615
- Cu_2O-CuO-(β)Ga_2O_3 system, thermodynamics and phase equilibria, 680-1000°C 77−36489
- Cu_2O-electrolyte contact, electrolytic decomposition and photodecomposition 78−95357
- Cu_2O-Nb_2O_5, phase anal., density determ. 78−10015
- Cu_2O-PbO(NiO)-SiO_2, equilibrated with liquid Cu, Pb and Ni distrib. 77−28790
- $Cu_{2-x}O$, nonlinear elastic props., nonstoichiometry effects *(French)* 80−34133
- Cu_xO film, growth by anodisation, switching characts. 77−55898
- Cu_xO film, sputter deposited on Cu, induced stresses 80−24774
- Cu_xO, film, thermoelec. power, activation energy variation with electrode spacing in DC sputtering 78−76099
- Cu_xO formation on Cu oxidation, EXAFS obs. 80−71808
- Cu_xO_y ore, recovery of Cu by segregation roasting *(Japanese)* 79−52136
- $Cu(OH)_2$-α-$Mn(OH)_2$, phase transition during ht. treatment 78−23659
- $Cu_2(OH)_2CO_3$, malachite, vibr. assignments, force consts., coincidence method appl. 78−62953
- Cu(OH)Cl, temp depend. of elec. cond., solid state thermal decomp. 78−19042
- $Cu_5O_2(PO_4)_2$, crystal prep. and struct. *(French)* 78−10004
- $(Cu_2O)_{1-x}U_{1.4}M_{4.6}O_{18}$, M=Mo, W, $0 \leq x \leq 0.4$, crystallographic identification, paramag. props. *(French)* 79−46633

copper compounds continued
$(CuO)_nV_2O_5$, (n=1, 2, 3), elec. and mag. props. 79—78094
$Cu_2O(111)$ growth modes, on (111)Cu surfaces, UHV-RHEED and TEM study 79—19481
CuP_2, Cu_3P, electronic struct. of valence bands, X-ray spectra and XPS 78—92176
CuP_2 d-electron participation in chem. bonds 77—28682
$Cu_{0.75}P_{0.25}$, chemical effect on valence electronic states, AES and SXAPS meas. 79—47558
$Cu_3P_2H_3(NO_3)(OH)_2.H_2O$, likasite, comp. and struct. *(French)* 77—47405
$Cu_3(PO_4)_2$, cryst. struct. determ. 77—80476
$Cu_3(PO_4)_2$, polystyrene based membranes, parameters, biionic pot. 79—57294
$Cu_4(PO_4)_2O$, cryst. struct. *(French)* 78—55854
$Cu_4(PO_4)_2O$, cryst. struct. 78—55855
Cu_3PS_4, solid, reson. Raman spectra at low temp. 79—8129
Cu_6PS_5Br, cryst. struct. of new superionic conductor 78—26514
Cu_6PS_5Br, cryst. struct. at 293 and 473K, thermal parameters, neutron diffr. obs. 80—59450
$CuPSe_2$, refinement of cryst. struct. *(French)* 77—43182
CuPbBiS, ferroelec. semicond., elec. cond., photocond. permittivity, phase transitions 77—47822
$CuPb_3Br_7$, ionic cond. meas. 77—47552
$CuPbSbS_3$, piezoelectric semiconductor, electron-phonon interaction, temp. depend. 77—51464
Cu_3RSe_3, R=rare earth, synthesis and form. mechanism 77—36736
$CuRb_2Br_1.2H_2O$, three-dimens. ferromag., crit. susceptibility exponents in Curie temp. region using relax. techniques 77—66304
$CuRb_2Br_4.2H_2O$, 3-dimens. Heisenberg, ferromag., crit. behaviour 77—20594
$Cu(Rh_{1-x}Cr_x)S_4$, spinel system, susceptibility and metallic resistivity, anomalies due to s-d interaction 80—70958
$Cu_xRh_{3-x}S_4$, thermal stability and thermochem. props. 79—86904
$CuRhS_4(Se_4)$, press. depend. of supercond. transition temp. meas. 77—12050
CuS aerosol prepared by burning pyrotechnic mixture, crystallisation activity 78—96279
CuS, black Zn-dust pigmented solar selective coatings for solar photothermal conversion 80—66997
CuS, covellite, dissolution in aq. NH_3 via hydrolysis of cupric amines 77—29004
CuS, covellite substrates, growth of epitaxial cryst. growth, influence of saturation and elec. field 79—42408
CuS, electronic struct. from X-ray emission spectra 77—28661
CuS, molecule, emission spectra, rotational analysis of O-O band of green system *(French)* 77—3372
CuS, S recovery by ammoniacal leaching 79—52618
CuS solar selective black coatings for large area appls., prep. and props. 80—21411
CuS/Cds solar cells, developments, appls., and economics of solar photovoltaic conversion *(German)* 80—26132
CuS-PbS, black Zn-dust pigmented solar selective coatings for solar photothermal conversion 80—66997
CuS+PbS solar selective black coatings for large area appls., prep. and props. 80—21411
CuS_2, mag. props. rel. to Hubbard model 79—78373
$Cu_{0.67}S_{0.33}$, chemical effect on valence electronic states, AES and SXAPS meas. 79—47558
$Cu_{1.8}S$ film, vacuum evaporated, props. rel. to elec. cond. 77—36001
$Cu_{1.8}S$-Cu_2S thin films, phase transforms kinematic electron diffr. study 80—29295
$Cu_{1.94}S$, djurleite, cryst. struct., X-ray study 79—42033
Cu_2S and $CuS.CuS_2$, NQR spectrum of $^{63,65}Cu$ 77—12235
Cu_2S, bulk contact ice nucleation threshold under illum. 77—55343
Cu_2S, $Cu_{1.8}S$, $\alpha \to \beta$ transition, thermographic investigation of heats, entropies and activation energies 80—88314
Cu_2S, Cu_2Se and Cu_2Te, TE properties, research obs. 77—28163
Cu_2S, d-electron participation in chem. bonds 77—28682
Cu_2S, defect models of different allotropic varieties, thermal reactions of Hall coeff. *(French)* 77—47448
Cu_2S, diffusion length meas. using scanned laser beam tech. 80—93886
Cu_2S, electrodeposition, using nonaqueous solvents 80—76200
Cu_2S, electromechanical props. *(Russian)* 79—11117
Cu_2S epitaxial films, reactive sputtering prep. and electronic props. 79—78885
Cu_2S, epitaxial layers grown from liq. soln. RHEED obs. 78—91558
Cu_2S, epitaxial overgrowths on Cu films, characts., TEM and RHEED obs. 78—84101
Cu_2S, epitaxial overgrowths on Cu(111), struct. and morphology 79—82494
Cu_2S film, deposited by cylindrical magnetron reactive sputtering for solar cell appl. 79—11258
Cu_2S film, for CdS/Cu_2S photovoltaic devices, formation and props. 79—11257
Cu_2S film, on rough $Zn_xCd_{1-x}S$ substrate, film substrate lattice mismatch calcs. 78—43263
Cu_2S film, reactively sputtered, Hall effect meas., 90-300K 80—15541
Cu_2S, film preparation for solar cells, elec., optical, struct. props. 78—76602
Cu_2S films, prpe. methods, appl. to Cu_2S-CdS solar cells 80—80980
Cu_2S, HP-FCC polymorphic transition stages 80—33924
Cu_2S layer spray preparation and CuCl-thiourea complex formation 78—64471
Cu_2S, low chalcocite, cryst. struct., X-ray study 79—42033
Cu_2S, low temp. modification, elec. props. 77—8092
Cu_2S, mats. props. rel. to CdS/Cu_2S solar cells 77—77426
Cu_2S, microstructure, work hardening in polymorphic transform. and subsequent annealing effect 79—52199
Cu_2S, molten, oxidation, exam. of product phase composition by X-ray anal. *(Russian)* 79—34166
Cu_2S, on Cu, solar selective coating, figure of merit 80—72082
Cu_2S, optical and calorimetric meas. of thin films for Cu_2S-CdS solar cells 80—55863
Cu_2S, polycryst. thin films, struct., optical and elect. props. for solar energy appl. 80—10837
Cu_2S, polymorphic transition from hexagonal to FCC packing and struct. of 12H and 14H polytypes 79—55692
Cu_2S, S and S^{2-} states, identification from Auger line shapes 79—92034
Cu_2S, solid, oxidation mechanism, kinetic factors 78—85133
Cu_2S sputtered coating on CdS layer for solar cell fabrication 78—39692

copper compounds continued
Cu_2S stoichiometric thin films for solar cells 79—61991
Cu_2S, thermal cond. changes on melting 77—7848
Cu_2S, thermoelectric props. 80—54726
Cu_2S thin film fabrication processes and conduction mechanism for solar cells, review 79—74522
Cu_2S, threshold photoelectric emission *(French)* 78—60549
Cu_2S, XPES, lattice instability 79—33904
Cu_2S:Cd(Zn), effects of doping on elec. and optical props. 78—38743
Cu_2S/CdS heterojunction solar cells, diffusion length determ. using minority carrier SEM 80—61359
Cu_2S/CdS solar cell, design and fabrication 80—30481
Cu_2S/CdS solar cells, performance, obs. 80—30480
$Cu_2S/Zn_xCd_{1-x}S$ heterojunction solar cells, junction anal. 79—92080
Cu_2S-CdS, photovoltaic junction, prep. by chemical deposition 79—66019
Cu_2S-CdS, solar cell, photocurrent, spectral depend. 79—7853
Cu_2S-CdS back illuminated high efficiency thin film solar cells 79—74515
Cu_2S-CdS film junction formation by dry-barrier process 78—64109
Cu_2S-CdS heterojunction, influence of surface recomb. on photoelec. props. 77—43711
Cu_2S-CdS heterojunction characteristics and CdS polarity *(Japanese)* 78—23154
Cu_2S-CdS heterojunction model 78—39205
Cu_2S-CdS heterojunction, elec. and photoelec. characts., effect of etching of CdS 78—80048
Cu_2S-CdS heterojunctions, electron trap characterisation by capacitance transient meas. 79—78163
Cu_2S-CdS heterojunction diodes, barrier model estimated from photovoltage and cathodoluminesc. spectra 79—78165
Cu_2S-CdS heterojunction, photoelectric props. 80—29467
Cu_2S-CdS heterojunction solar cell, interface recomb. vel. determ. by capacitance/collection efficiency variation 80—50959
Cu_2S-CdS heterojunction solar cells, carrier transport, nonmonotonic band profiles 80—61361
Cu_2S-CdS heterojunction interface, depth distribution profiles, Auger spectra 80—88622
Cu_2S-CdS heterojunctions, role of deep levels in controlling photovoltaic props. 80—92941
Cu_2S-CdS heterophotocells based on CdS films of stoichiometric composition, elec. and photoelec. props. 80—93873
Cu_2S-CdS integrated thin film solar cell generators, fabrication techniques 80—55857
Cu_2S-CdS p-i-n structure diode, photoelec. characts. 78—2557
Cu_2S-CdS photocell characteristics, for various solar radiation incidence angles 79—83593
Cu_2S-CdS solar cell, fabrication using solid state reaction 77—16498
Cu_2S-CdS solar cell applications, CdS film spray fabrication, physical props. *(French)* 80—60113
Cu_2S-CdS solar cell fabrication by magnetron reactive sputtering deposition 80—61363
Cu_2S-CdS solar cells, EBIC and capacitance measurements, stability problems 80—45684
Cu_2S-CdS solar cells, interface recombination phenomena and tunnel effect 80—66978
Cu_2S-CdS solar cells, optical absorption coefficient changes in Cu_2S 80—93980
Cu_2S-CdS solar cells, optimised grid patterns 80—108798
Cu_2S-CdS solar cells, prep. and stoichiometric control of Cu_2S film 78—2560
Cu_2S-CdS solar cells in backwall configuration, model of photovoltaic effect 80—55861
Cu_2S-CdS solar cells with interdigitated grid, current-voltage analysis 80—93981
Cu_2S-CdS solar photopiles, tunnel conduction mechanism *(French)* 79—29480
Cu_2S-CdS sprayed solar cells, chemical spray deposition 80—93979
Cu_2S-CdS thin film heterojunctions, base doping effect on elec. and photoelec. props. 78—80043
Cu_2S-CdS thin film planar junction devices, quantitative photon loss anal. 80—61362
Cu_2S-CdS thin film solar cells, Cu_2S layer separation, struct. 79—95282
Cu_2S-CdS thin film solar cell fabrication by electrophoresis 80—55862
Cu_2S-CdS thin-film solar cells, low-cost manufacturing process outline, economic anal. 80—93930
Cu_2S-CdS thin-film solar cells, high open-cct. voltage and low refl. losses 80—94088
Cu_2S-Fe S mattes equilibration with Fe-O-SiO_2 slags under controlled partial pressures of SiO_2 79—83152
Cu_2S-Ga_2S_3 alloys, cryst. growth, struct. and fluoresc. 77—48328
Cu_2S-GeS_2 and Cu_2S-SnS_2 systems dissoc. of ternary congruently melting cpds. 79—87832
Cu_2S-Ge(Sn)S, phase diagrams 78—44100
Cu_2S-Ni_3S_2, melt viscosity 77—51536
Cu_2S-Tl_2S system, phase diagram 80—20906
Cu_2S-Zn_xCd_{1-x}, heterojunction, composition meas. near interface using aqueous ion-exchange 80—29465
Cu_2S-$Zn_xCd_{1-x}S$ and Cu_2S-CdS thin film solar cells by solid state reaction, comparison 80—101109
Cu_2S-$Zn_xCd_{1-x}S$ heterojunction, improved model of electro-optic behaviour 80—94023
$Cu_{2-\delta}S$, Cu chem. diffusion, and nonstoichiometry, 400°C, electrochem. determ. 79—28132
$Cu_2S+Ln_2S_3$, powdered mixtures, reaction rate, production of ionic semiconductors 80—93741
$Cu_{2-\delta}S$, thin films, determ. of stoichiometry from optical props. 79—60656
$Cu_{2-\delta}(S+Se)$ solid soln., deviation from stoichiometry, effective hole mass 77—31775
$Cu_{2-x}S$, and related disordered crystals, diffr. pattern, cluster theory 80—75123
$Cu_{2-x}S$, carrier mobility rel. to x 78—43389
$Cu_{2-x}S$, digenite, epitaxial layer, electron diffr. 77—85117
$Cu_{2-x}S$, digenite, X-ray determ. of structural transitions 80—92474
$Cu_{2-x}S$, digenite related phases, electron microscope study 79—10840
$Cu_{2-x}S$ film, evaporated, ordering process, electron diffr. study 80—39477
$Cu_{2-x}S$ films, vacuum deposited, electrical conduction and phase transitions 78—84332
$Cu_{2-x}S$ in chem. formed $Cu_{2-x}S$-CdS heterojunction, photosensitivity characts. 78—72199

copper compounds continued
- $Cu_{2-x}S$ on CdS, low temp. growth, AES obs. 79—28924
- $Cu_{2-x}S$, single cryst., as p-component of heterojunction, props. 77—39926
- $Cu_{2-x}S$ single cryst., struct. and elec. props. 77—24302
- $Cu_{2-x}S$/CdS heterostructures, heat treated, capacitance voltage meas. anal. 80—20292
- $Cu_{2-x}S$-CdS, solns. cell, photo-emf, depend. on degree of doping of CdS 79—52934
- $Cu_{2-x}S$-CdS ceramic solar cells, solar batteries operating characts. 80—93874
- $Cu_{2-x}S$-CdS heterojunction, current flow characts. and energy band struct. 77—43709
- $Cu_{2-x}S$-CdS heterojunction V-I characteristic and max. photovoltage, long-term changes *(Russian)* 78—43468
- $Cu_{2-x}S$-CdS heterojunctions, nature of longwave photo EMF 78—84284
- $Cu_{2-x}S$-CdS p-n heterojunction solar cells, props., Burstein-Moss effects 80—21404
- $Cu_{2-x}S$-CdS p-n heterojunction, optical energy convertor, struct. and recomb. props. 80—72065
- $Cu_{2-x}S$-CdS p-n heterojunction, copper sulphide growth features during formation *(Russian)* 80—107898
- $Cu_{2\delta}S$, ionic and electronic cond., thermopower and Hall effect in galvanic cell 77—20117
- Cu_7S_4, alternative transform. behaviour, direct obs. by TEM 77—1227
- Cu_9S_5, digenite, superstructuring, vacancy clustering, high-resolution electron microscopy 78—42981
- Cu_xS, $1 \leq x \leq 2$, quantum temp. size effect and magnetism *(Russian)* 80—103764
- Cu_xS chalcocite thin films, solar cell fabrication appl., characts. 78—39240
- Cu_xS, diffusion length determ., resolution limit of EBIC technique 79—21865
- Cu_xS evaporated layer growth in vacuum, compositional and optical characterisation, solar cell appls. 80—97437
- Cu_xS evaporated thin films, composition, prep. and characts. 80—25569
- Cu_xS film, deposited on Si and CdS, props. rel. to solar cell applic. 79—15240
- Cu_xS film, reactively sputtered, photovoltaic props. 79—11256
- Cu_xS film, thermally induced changes, effect on CdS-Cu_xS solar cell response 77—8181
- Cu_xS film for Cu-Cd-S solar cell, cathodolum. spectrum rel. to prod. method 79—56866
- Cu_xS films, magnetron reactive sputtering deposition and elec. props. 79—78884
- Cu_xS layer, on CdS, electron diffr. obs. of phases 78—51847
- Cu_xS, layers produced by reactive RF sputtering, struct., elec. and optical props. 79—90908
- Cu_xS, photon and electron excitation phenomena 79—7865
- Cu_xS/CdS, sequential evaporation, for solar cell applic. 80—93902
- Cu_xS-CdS heterojunctions produced by RF sputtering, for thin film solar cells 79—100053
- Cu_xS-CdS heterojunction solar cells, time evolution of spectral characts. 80—30478
- Cu_xS-CdS heterojunction solar cells spectral distrib. and photocapacitance 80—55864
- Cu_xS-CdS solar cell, minority carrier diffusion length, SEM determ. 77—72911
- Cu_xS-CdS solar cell, prep. and characts. *(Croatian)* 80—93876
- Cu_xS-CdS solar cells, Cu_xS transform. behaviour rel. to topotaxial growth, cell efficiency 77—11814
- Cu_xS-CdS solar cells, cu_xS growth kinetics and composition analysis by absorbance transient and galvanic electrochemical measurements 80—92797
- Cu_xS-CdS solar cells, screen printed, prep. and photovoltaic props. 80—40863
- Cu_xS-CdS solar cells, SCL current 80—76634
- Cu_xS-CdS thin film solar cell using chem. sprayed CdS film 78—43465
- Cu_xS-CdS thin film solar cells, using all film vacuum deposited process 80—93977
- $CuS_4C_4(CF_3)_4$.TTF, 1-dimens. mag. props. 77—66271
- CuSCN, $Cu(SCN)_2$, muonic Coulomb capture, ionic charge effect 78—66694
- $Cu(SCN)_{1/3}$, synthesis and high elec. cond., activated and metallic cond. obs. 80—96957
- $Cu_9S_5(Cu_{2-x}S)$, high temp. digenite, cryst. struct. refining by X-ray diffr. method 79—23587
- $CuSO_4$, aq. soln., electrolytic resistance variation in mag. field 80—11897
- $CuSO_4$, aq. soln., Soret coeff. and heat of transport 78—18809
- $CuSO_4$, aq. soln., viscosity meas., viscous flow activation energy, entropy *(Japanese)* 77—43363
- $CuSO_4$, aq. solns., densities, viscosities, elec. cond. meas., 20 to 70°C 80—59688
- $CuSO_4$, effect of press. on ion pair dissoc., cond. of aq. solns. 78—53218
- $CuSO_4$, single cryst., IR optical consts., comparison with soln. 77—66470
- $CuSO_4$ soln., electrochemical analogue of Benard instability, isothermal and potentiostatic conditions 80—76530
- $CuSO_4$, solution, activity coeff. determ. 78—76874
- $CuSO_4$, solution, dielectric relaxation studies 78—84519
- $CuSO_4$ solution, thermooptical excitation of sound by ns. laser pulses 80—79884
- $CuSO_4/H_2SO_4$ electrolytes, densities, elec. cond., viscosities 80—107455
- $CuSO_4$-$5H_2O$, decomposition anisotropy, reaction ellipsoid for transform. to trihydrate *(French)* 77—29003
- $CuSO_4$-H_2SO_4, electrodeposition of Cu on plane vertical cathode, distrib. of local current densities 79—70338
- $CuSO_4.3CO(NH_2)_2$, cryst. struct. determ. 78—34506
- $CuSO_4.3CO(NH_2)_2$, X-ray determ. of electron density distrib. 78—67699
- $CuSO_4.5H_2O$ and $CuSO_4.5D_2O$, Raman and IR spectra, mode assignments 77—66493
- $CuSO_4.5H_2O$, anisotropy of decomposition, thermal gradient obs. by IR thermography *(French)* 78—40048
- $CuSO_4.5H_2O$ dehydration kinetics depend. on water vapour press. 79 -15986
- $CuSO_4.5H_2O$, dehydration into trihydrate obs. using monocryst. platelets, product domains shape 80—71905
- $CuSO_4.5H_2O$, EXAFS, rel. between Debye-Waller factor and thermal parameters meas. by neutron diffr. 80—84803
- $CuSO_4.5H_2O$, IR spectra, internal modes and pot. environment, isotope effects 77—8563

copper compounds continued
- $CuSO_4.5H_2O$, linear-chain antiferromag., mag. phase transition investig. 77—55684
- $CuSO_4.5H_2O$, low freq. spin dynamics, proton relax. study 80—71218
- $CuSO_4.5H_2O$, mag. ordering in external field, NMR obs. 77—66350
- $CuSO_4.5H_2O$ monocryst. platelets, dehydration into trihydrate, displacement rate modulation of reaction front 80—108711
- $CuSO_4.5H_2O$, $S={}^1/_2$ antiferromag. Heisenberg chain, spin dynamics 80—11285
- $CuSO_4.5H_2O$, secondary nucleation and growth in a fluidized bed 80—50542
- $CuS_2(Se_2)$, electronic struct., UPS and XPS study 80—80935
- $Cu_2S(Se)$, ionic-electronic mixed conductor, solid state controlled growth using cryst. rotation 78—31338
- $Cu_2S(Se)$-CdS(Se) p-n heterophotoelements of optronic converters, props. on X-irrad. of scintillator 80—34505
- $CuSbS_2$ crystals, growth and characterisation 80—60770
- Cu_3SbS_3, NQR spectrum of ${}^{63,65}Cu$ 77—12235
- Cu_3SbS_3, skinnerite, polymorphism, X-ray diffr. and NQR meas. 80—49165
- Cu_3SbS_4, thermal cond. in solid and liq. phases, 300 to 1100K, thermoelec. Q-factor 80—19997
- Cu_3SbSe_4, cathodoluminesc., 90-298K 77—40290
- Cu_3SbTe_4, elec. and thermal conds., thermo-EMF, solid and liq. states, temp. depends. 78—43384
- $Cu_{2-\delta}(Se,S)$, ionic and electronic cond., thermopower and Hall effect in galvanic cell 77—20117
- CuSe film, phase transforms. and decomp., electron diffr. obs. 79—42418
- CuSe, lattice expansion, elec. cond. and sp. ht. at 326K transition 77—51491
- CuSe, presence as 2nd phase in p-type films from vac. evaporated $CuInSe_2$ 79—82697
- CuSe, X-ray photoelectron and Auger spectra 78—56561
- $CuSe_2$, CuSe, Cu_3Se_2 and Cu_2Se, thermodynamic props., 298 to 420K *(Russian)* 77—69098
- $CuSe_2$, mag. props. rel. to Hubbard model 79—78373
- $Cu_{1.8}Se$, I-V characts., switching effects, nonstoichiometry effects *(Russian)* 78—84266
- Cu_2Se, kinetics of polymorphic $\alpha \rightleftarrows \beta$ transformation *(Russian)* 80—70152
- Cu_2Se, oxidation by atmos. O_2 and SeO_2 vapour 77—52520
- Cu_2Se, thermal cond. changes on melting 77—7848
- Cu_2Se, VPE on mica, defect struct., temp. depend. 77—35837
- Cu_2Se, X-ray photoelectron and Auger spectra 78—56561
- Cu_2Se-$AgInSe_2$ heterojunction, photodetection props. 78—39195
- Cu_2Se-Cu_2Te, intermolecular interaction, thermodynamic anal. of dissociation pressure 80—53088
- Cu_2Se-GeSe quasibinary system, phase diagram and struct. 77—8802
- Cu_2Se-$GeSe_2$ and Cu_2Se-$SnSe_2$ systems, dissoc. of ternary congruently melting cpds. 79—87832
- $Cu_{2-\delta}Se$, ionic and electronic cond., thermopower and Hall effect in galvanic cell 77—20117
- $Cu_{2-x}Se$, carrier mobility rel. to x 78—43389
- $Cu_{2-x}Se$, cryst. struct. and density 79—90608
- $Cu_{2-x}Se$, elec. props. and band struct. 79—73513
- $Cu_{2-x}Se$, electric, thermal and magnetic props. investigation in low temp. phase *(Croatian)* 79—11299
- $Cu_{2-x}Se$, electrical activity of Cu vacancies 80—39606
- $Cu_{2-x}Se$, nonstoichiometric, diamag. and paramag. props., susceptibility meas. 80—70936
- $Cu_{2-x}Se$, single cryst., as p-component of heterojunction, props. 77—39926
- $Cu_{2-X}Se$, X=0-0.23, cond. transition to superionic state, crit. conc. 79—55924
- $CuSeO_4$, $S={}^1/_2$ Heisenberg antiferromag. linear chain, proton spin-lattice relax. 78—39433
- $CuSe_2O_5$, strongly antiferromag. coupled Cu linear chain, orbital props. 80—100580
- Cu_2SeO_4, ferrimag., spontaneous magnetisation meas. 77—63128
- $CuSeO4.5H_2O$, $S=1/2$ antiferromag. chain, proton relax. near saturation field 79—15370
- $CuSeO_4.5H_2O$, antiferromag. chain system, proton spin-lattice relax. near saturation field 79—61256
- $CuSeO_4.5H_2O$, $CuSO_4.5H_2O$ and $CuBeF_4.5H_2O$, linear-chain antiferromag., mag. phase transition investig. 77—55684
- $CuSeO_4.5H_2O$, linear-chain antiferromag., mag. phase transition investig. 77—55684
- $CuSeO_4.5H_2O$, mag. ordering in external mag. field, NMR obs. 77—66350
- $CuSeO_4.5H_2O$, Raman and IR spectra, mode assignments 77—66493
- $CuSiF_6.6H_2O$, paramag., nucl. and electron spin lattice relax. 78—84494
- $CuSiO_3.2H_2O$, chrysocolla, electronic absorpt. speotra 78—92087
- p-Cu_2Sn-n-ZnS heterojunction, I-V characts., photocond. and electrolum. 78—72251
- Cu_2SnS_3-CdSe, diamond-type semiconductor, Mossbauer spectrum of ${}^{119}Sn$ 80—44991
- $(Cu_2SnS_3)_x$-$(3CdS)_{1-x}$, diamond-type semiconductor, Mossbauer spectrum of ${}^{119}Sn$ 80—44991
- $(Cu_2SnS_3)_x$-$(3ZnS)_{1-x}$, diamond-type semiconductor, Mossbauer spectrum of ${}^{119}Sn$ 80—44991
- Cu_4SnS_4, cryst. struct. obs. *(French)* 77—19931
- $Cu_2SnS_3(Se_3)(Te_3)$, Mossbauer effect, lattice dynamics obs. 77—43923
- $(Cu_2SnS_3)_x(3CdS)_{1-x}$, second co-ordination sphere atoms effect on ${}^{119}Sm$ Mossbauer spectra *(Russian)* 77—63348
- $(Cu_2SnS_3)_x(3ZnS)_{1-x}$, second co-ordination sphere atoms effect on ${}^{119}Sn$ Mossbauer spectra *(Russian)* 77—63348
- Cu_2SnSe_3, single cryst. growth and morphology 77—85908
- Cu_2SnSe_3-CdS, diamond-type semiconductor, Mossbauer spectrum of ${}^{119}Sn$ 80—44991
- $(Cu_2SnSe_3)_x$-$(Cu_2SnS_3)_{1-x}$, diamond-type semiconductor, Mossbauer spectrum of ${}^{119}Sn$ 80—44991
- $Cu_2SnSe_3(Te_3)$, tetrahedral phase stability 77—48415
- $Cu^+(TCNQ)^-$ and $Cu^+(TCNQ)_2{}^-$, low temp. EPR of impurity reson. 77—85548
- Cu_2TE, annealing and deform. of defects induced by phase work hardening during thermal cycling 79—52230
- $CuTa_2O_6$, cryst. struct. *(French)* 78—51497
- $Cu_{0.5}TaO_3$, X-ray structural study 77—39575
- Cu_xTaS_2, electron diffuse scatt., microstruct., of transition state 77—31771
- $CuTbTe_2$, synthesis 78—26529

copper compounds continued
CuTe, Cu_2Te and $Cu_{2-x}Te$ alloys, struct., electron diffraction investigation 79—51066
$Cu_{1.7}Te$, and Cu_2Te, I-V characts., switching effects, nonstoichiometry effects *(Russian)* 78—84266
Cu_2Te, HP-FCC polymorphic transition stages 80—33924
Cu_2Te, microstructure, work hardening in polymorphic transform. and subsequent annealing effect 79—52199
Cu_2Te, thermal cond. changes on melting 77—7848
Cu_2Te-Ag_2S, kinetic props. of solid solutions 79—7827
Cu_2Te-Ge(Sn)Te_2, phase equilib., microstructural, DTA investigs. 77—16560
$Cu_{2-x}Te$, carrier mobility rel. to x 78—43389
$Cu_{2-x}Te$, cryst. struct. and density 79—90608
$Cu_{2-x}Te$, electrical activity of Cu vacancies 80—39606
$Cu_{2-x}Te$, single cryst., p-component of heterojunction, props. 77—39926
$Cu_{2-x}Te$, $x=0$ to 0.3, elec. cond., Hall const., carrier mobility, conc., thermoelec., density, lattice parameter 77—11915
$Cu_{2-x}Te$, $x<0.22$, phase diagram, electronic and ionic cond. meas. 80—6917
$Cu_{2-x}Te$-CdSe heterojunction, elec. and opt. props. *(Korean)* 77—51811
$Cu_{3-x}Te_2$, non-stoichiometric phases, electron microscopic and electron diffraction studies 80—64977
$Cu_{3\pm x}Te_2$, modulated struct. phenomena, survey 79—95033
CuTeBr, ionic cond., phase transition obs. by millimetre wave spectroscopy 78—22855
CuTeBr, superionic conductor, microwave absorption spectrum 80—11515
$CuTe_2Cl$, cryst. struct., X-ray diffr. meas. 77—4075
CuTeCl(Br)(I), struct., partial Cu^+ ionic cond. 77—84981
CuTeI, X-ray cryst. struct. determ. *(German)* 79—32957
$CuTeO_4$, cryst. struct. determ. 78—55845
Cu_3TeO_6, cryst. struct. 78—42972
CuTeX (X=Cl, Br, I), solid ionic cond., props. 79—14963
$Cu_2Th_4(MoO_4)_9$, crystallographic data determ. *(French)* 78—10013
Cu_3TiO_4, phase equilibria and thermodynamics 80—55374
CuTlS, melting heat and melting entropy *(Russian)* 80—70374
$Cu_2TlSe_2(Cu_2TlTe_2)$, crystallographic studies 77—31640
Cu_2TlX_2 (X=Se, Te), struct. and physical props. *(French)* 79—86758
$CuTmTe_2$, synthesis 78—26529
$Cu_2U_6S_{13}$, cryst. struct. and magnetic props. *(French)* 80—96496
$Cu_2U_6Se_{13}$, cryst. struct. and magnetic props. *(French)* 80—96496
$Cu_xV_{12}O_{30}$, oxygen bronze synthesis and thermal props. of single crysts. 77—84717
α-$Cu_xV_2O_5$, EPR and mag. susceptibility meas. 80—2627
$Cu_xV_2O_5$, metallic, Raman scatt. 78—80358
$Cu_xV_2O_5$, nonmetallic bronze, low field sp. ht. and mag. suscept. 78—72357
CuV_2S_4, preparation, cryst. struct. and physical props. *(French)* 79—55714
$Cu_{0.65}VS_2$, cryst. struct. and phys. props. *(French)* 79—60334
$Cu_{0.75}VS_2$, cryst. struct. and phys. props. *(French)* 78—14328
Cu_3VS_4, conducting ions as mobile donors 80—11055
p-Cu_3VS_4, mixed conduction due to cationic interstitials 80—70772
Cu_3VS_4, mixed conductor, fast ion transport at room temp. 78—72214
Cu_3VS_4, out of equil. mixed cond., electronic cond. decrease in ionic soln. 80—107874
Cu_3VS_4, out of equil. mixed cond., off-centre positions and order-disorder transition, ultrafast nucl. relax. obs. 80—108103
Cu_3VS_4, out of equil. mixed cond., chem. origin of mobile ions, spin-lattice relax. and NQR obs. 80—108104
Cu_3VS_4, Raman active modes 80—11414
Cu_3VS_4, Raman linewidth of A_1 mode under high press., reson. effects 80—108210
$CuWO_4$, cathodic props. in Li primary batteries 80—3502
$CuWO_4$, controlled reduction in H_2O/H_2 mixture 79—24458
$CuWO_4$, elec. cond., thermoelectric power and dielectric constant temp. depend. 80—96886
$CuWO_{4-x}$ prod. from $CuO+WO_3$ solid state reaction 80—66796
Cu_2ZnGeX_4, (X=S,Se), optical and electrical props. 77—35941
$Cu_xZn_{1-x}SiF_6.6H_2O$, heat capacities and thermodynamic props., 14 to 300K, cooperative Jahn-Teller transition 80—21314
Cu_2ZnSiX_4, (X=S,Se), optical and electrical props. 77—35941
$Cu_xZn_{1-x}ZrF_6.6H_2O$, distortions of nearest Jahn-Teller $[Cu(H_2O)_6]^{2+}$ centres 78—68000
^{64}Cu-bleomycin complex, lethal effects on Ehrlich ascites tumour cells 79—57709
$Cu_2[Fe(CN)_6]$, and $Cu_3[Fe(CN)_6]$, mag. susceptibility, reflectivity spectra and cryst. field 79—56808
$Cu[Ni_{0.5}Mn_{1.5}]O_4$, magnetisation and magnetostriction, fields up to 11 kOe, 4-160K *(Russian)* 78—19304
$Cu_6[Si_6O_{18}].6H_2O$, dioptase, cryst. struct. refining by X-ray and neutron diffr. methods 79—23586
cu_2S-CdS sprayed layer solar photopiles, CdS sprayed layer props. *(French)* 79—24901
$EuCu_2Si_2$, mixed valence system, X-ray absorption spectroscopic study 80—80906
Fe/Cu_2O displacement reaction kinetics at temps. between 800 and 1050°C 80—21278
$Fe_{0.5}Cu_{0.5}Cr_2S_4$, ESR spectra, elec. and mag. props., Curie temp. 80—97137
$Fe_{1-x}Cu_xCr_2S_4$, Hall effect and magnetoresist. 79—78119
$Fe_{1-x}Cu_xCr_2S_4$, mag. semicond., mag. props. and elec. cond. *(Japanese)* 79—47111
$Fe_xCu_{1-x}Cr_2Se_4$, crystallographic and image props. 80—39049
$(Fe_{1-x}Cu_x)_2O_3$, yH_2O crystal growth, characterisation by Mossbauer spectroscopy, mag. meas. and electron microscopy *(French)* 80—80655
$Fe_xCu_{1-x}Rh_2S_4$, mag. tetrahedral intrasublattice interaction, X-ray, magnetisation and Mossbauer expts. 78—52241
$(Fe_{0.55}{}^{2+}Mg_{0.32}{}^{2+}Mn_{0.03}{}^{2+}Cu_{0.10}{}^{2+})$ $[Fe_{1.74}{}^{3+}Al_{0.26}{}^{3+}]O_4{}^{2-}$, influence of Fe^{2+} ion substitution on electron hopping, Mossbauer study 80—71247
FeO-Fe_2O_3-SiO_2-Al_2O_3-$CuO_{0.5}$ slag, and Cu, distribution equilibria of Sn, Se, Te 77—51502
FeS-Cu_2S, melt viscosity 77—51536
FeS-Ni_3S_2-Cu_2 S melt, enthalpy *(Russian)* 78—95730
FeS-Li_2S-Cu_2S system, Mossbauer spectra and lattice parameters 79—78584
$FeSO_4$-$CuSO_4$ dosimeter, intense γ-radiation field effects *(Spanish)* 77—48876
Ga_2Te_3-Cu system solid solns., elec. cond. 78—51988

copper compounds continued
Ge:Li, Cu p-n junctions, current stimulated LiCu complex formation, photocurrents 80—107897
Ge-S-Cu, phase separation in melt centrifugal quenching 80—25701
$GuGaS_2$, temp. depend. Sellmeier coeffs. and coherence lengths for chalcopyrite crystals 79—76752
In_2Se_3-Cu_2S system, electrophys. props., influence of 1-4% Cu_2S 80—20219
KCl-CuCl eutectic fused salt, potential as intermediate temp. solar heat transfer and storage medium 80—101135
KCl-CuCl solid solution supersaturated, precipitation, impurity aggregation 80—29174
KCl-$CuCl_2$ solution, optical absorption of complex ions *(Russian)* 77—28592
$K_3Cu(CN)_4$, isotopic mixed crystal with ^{12}C and ^{13}C, Raman scattering 78—76476
$K_2CuCl_4.2H_2O$, paramag. single cryst., PMR temp. depend., hyperfine const. and exchange interaction *(Korean)* 80—29630
$KCuF_3$, ^{63}Cu NQR meas. 80—50219
K_2CuF_4, layered spin system, planar rotator symmetry, phase transition 80—65951
K_2CuF_4, magnon condensation 79—91220
K_2CuF_4, spin-wave relaxation, parallel pumping expt. 79—4729
K_2CuF_4, two-dimensional planar ferromagnet, giant fluctuation of spins *(Japanese)* 80—54894
$K_2Cu_{1-x}Zn_xF_4$, two-dimens., ferromag., spin wave excitations 78—80140
$K_2Cu_xZn_{1-x}F_4$, Curie temp., Cu conc. depend. 80—60255
$K_2PbCu(NO_2)_6$, incommensurate Jahn-Teller phase transition 78—79730
$K_2PbCu(NO_2)_6$, Jahn-Teller phase transitions, order-disorder model 78—79762
$K_2PbCu(NO_2)_6$, phase transitions induced by Jahn-Teller effect, uniaxial stress effects 80—6512
$K_2PbCu(NO_2)_6$, US vel. near cooperative Jahn-Teller phase transitions 79—23680
(Li,Na,Cu,Zn) ferrites, nonceramic synthesis, electrochem. investig. 78—35339
$Li_2Cu_5(Si_2O_7)_2$, cryst. struct. and proposal of new values for effective ionic radii of Cu^{2+} 79—4276
$Li_{0.5}Fe_{2.5}O_4$-$CuFe_2O_4$-$MnFe_2O_4$, structural characteristics and mag. props. of solid solutions 77—35696
$Li_{0.5}Fe_{2.5}O_4$-$CuFe_2O_4$-$ZnFe_2O_4$, order-disorder transition, quadratic transformation *(French)* 78—76447
$(Li_{0.5}Fe_{2.5}O_4)_{0.8}(CuFe_2O_4)_{0.2}$, struct., magnetic props., rectangular hysteresis loop 77—20645
$Li_{0.5}Ga_{2.5}O_4$-$CuCr_2O_4$ system, phase diagrams, IR spectra, Cu^{2+} electronic spectra *(French)* 78—51461
Mg-Cu-Mn-Ni-Fe-O, UHF ferrites, synthesis, physicochem. state, mag. and dielec. parameters 79—11536
$Mg_{0.7}Cu_{0.3}Fe_2O_{4+\delta}$, disaccommodation and accommodation 77—20641
$Mg(NH_4)(SO_2)_4.6H_2O:Cu(H_2O)_6{}^{2+}$, ^1H ENDOR 79—73854
MgO-$Al_2O_3(Cr_2O_3)(Fe_xO_y)$-CuO, phase relations and microstruct. 79—74140
$MgTaCuO_4$, cryst. struct., synthesis 78—83790
$Mn_{1-x}Cu_xCr_2S_4$, phase relationships and mag. phase diagram 79—78374
MnS-$CuInS_2$, phase relations, 400 to 1300°C, X-ray and microscopic exam. 79—1853
$(ND_4)_2Cu(OD_2)_2Cl_4$, Raman spectra, order-disorder transition *(French)* 79—91436
$NH_4Cu_4Cl_3(I_{2-x}Cl_x)$, highly conducting solid electrolyte 80—65280
$(NH_4)_2CuCl_4.2\ H_2O$, lattice dynamics, anal. of Raman scatt. measurements 80—34149
$(NH_4)_2CuCl_4.2H_2O$, HDO and NH_3D^+ species, IR spectrum, low-temp., phase transitions 77—77182
$(NH_4)_2CuCl_4.2H_2O$, Raman sepctra, dynamics, struct., phase transition 79—47434
$(NH_4)_2CuCl_4.2H_2O$, order-disorder transition, Raman spectra obs. 79—61357
$(NH_4)_2(Cu(H_2O)_6)(CuSO_4)_4$, cryst. struct. determ. by X-ray diffr. 78—55839
$((NH_4)_{1-x}K_x)_2\ CuCl_4.2H_2O$, Raman scatt. spectra 79—15459
NaCl-KCl-CuCl system diagram investig. *(Russian)* 79—96015
Na_2O-B_2O_3-CuO, γ-irrad., CuO effects on EPR 80—84645
Na_2O-P_2O_5-CuO, γ-irrad., CuO effects on EPR 80—84645
Na_2O-SiO_2:CuO glass, gamma-irradiated, EPR and optical spectra 80—103885
Na_2O-SiO_2-CuO, γ-irrad., CuO effects on EPR 80—84645
$Na_4[M^{II}(NH_3)_4][M^I(S_2O_3)_2]_2.L$, ($M^{II}$=Cu, Ni), ($M^I$=Cu, Ag), (L=$H_2O$, NH_3), IR spectra, vibr. anal. *(French)* 78—52477
$(NdCu_3)(Ti_3Fe)O_{12}$, synthesis, cryst. struct. and Mossbauer exam. 78—84505
NiO-CuO, equilibrium relations 80—55375
P_2O_5-WO_3:CuO glass, EPR, Cu impurity effect on elec. props. 79—51849
$PbMo_6S_8$, Hall effect and magnetoresistivity 78—95400
PbO-B_2O_3-SiO_2-Al_2O_3-ZnO-CuO-Bi_2O_3 solder glass, crystallisation prevention by Cu addition 80—11654
PbO-B_2O_3-SiO_2-Li_2O-ZrO_2-CuO, coloured, glass enamel, chemical durability and microstruct., CuO addition effect 79—29256
PbS-$CuS_{1.8}$-ZnS, phase equilib. *(Russian)* 77—28786
Pt-Cu_2O-Cu double injection diodes, I-V characts. and photomemory effects 77—47900
Pt-Cu_2O-Cu single carrier space charge limited diodes, I-V characts. 77—47901
$Pt(NH_3)_4CuCl_4$, ferromag., antisymmetric and anisotropic exchange, EPR linewidth 78—10761
RbCl-CuCl, solid electrolyte, AC cond. and phase relations meas. 77—72713
$RbCu_4Cl_3I_2$, development of Cu^+ ion cond. 80—107532
α-$RbCu_4Cl_3I_2$, solid electrolyte, cryst. struct. and anal. 79—82382
$Rb_2CuCl_4.2H_2O$, NMR spectra, second-order effects of mag. hyperfine interaction, pseudoquadrupole interaction 79—78540
$RbCuF_3$, ^{63}Cu NQR meas. 80—50219
$Rb_4Cu_{16}I_7Cl_{13}$ in CuCl-CuI-RbCl system, high Cu ion cond. solid electrolyte, elec. props. and powder X-ray diffr. anal. 80—15295
$Rb_2Cu(SO_4)_2.6H_2O$, single cryst., fine struct., mag. dipole coupling, EPR obs. 78—68360
$Rb_2CuX_4.2H_2O$, (X=Cl, Br), fine struct. due to indirect coupling of nuclear spins 79—78541
$Rb_2PbCu(NO_2)_6$, incommensurate Jahn-Teller phase transitions 79—65185

copper compounds continued
- $SbCu_2Si_2$, mixed valence system, X-ray absorption spectroscopic study 80—80906
- SiO_2-Al_2O_3-Cu_2O glass alkaline durability, corrosion rate, heat capacity and elastic moduli 80—93673
- SnO_2-copper phthalocyanine-Ag systems, elec. and electroluminescent behaviour 80—80864
- SnO_2-Cu_xS-ZnS:Mn,Cu-Al_2O_3-Al, light-emitting struct., cond. and electrolum., heat treatment 80—97345
- $Sr_2Cu(OH)_6$, EPR, g-values 79—19770
- $(ThCu_3)(Mn_2Fe_2)O_{12}$, synthesis, cryst. struct. and Mossbauer exam. 78—84505
- $ThCu_3Mn_4O_{12}$, mag. struct. of new perovskite-type ferrimag. 78—52222
- $TiCuD_{0.90}$, neutron powder diffr. study for cryst. struct. refinement 78—95018
- Tl_2CuI_3, melting point, cryst. struct., DTA, X-ray diffr. *(French)* 77—84710
- $Tl_2PbCu(NO_2)_6$, incommensurate Jahn-Teller phase transitions 79—65185
- V_2O_5-CuO-BaO glass, unpaired electron localisation, ESR study 80—66026
- V_2O_5-P_2O_5-CuO system glasses, phase separation, crystn. and EPR spectra 77—76321
- $Y_{1.62}Sm_{0.21}$ $Lu_{0.27}Cu_{0.9}Ge_{0.9}Fe_{4.1}O_{12}$, implanted bubble garnet, anisotropy profile, FMR study 80—7103
- Zn-Cu-Se system, condensed phase equilibria, 800-1000°C, vapour pressures of Zn, Se_2 77—16553
- Zn-Cu-Se system, region of existence of ZnSe phase 77—16554
- $Zn_xCd_{1-x}S$-Cu_2S heterojunction solar cells, props., comp. meas. of interfacial region 80—81472
- $Zn_xCn_{0.1}Fe_{2.9}O_4$, Cu, Zn substituted magnetite, domain wall resonance, mag. props. 80—15756
- $Zn_xCu_{0.1}Fe_{2.9-x}$ O_4, ferromag. reson., g-factors, Jahn-Teller ion effects 80—66043
- $Zn_xCu_{0.1}Fe_{2.9-x}O_4$, ferromag. relax. 80—60422
- $Zn_xCu_{1-x}Fe_2O_4$, mag. props., Mossbauer spectra 79—87344
- $Zn_{1-x}Cu_xGeF_6.6H_2O$, depression of dynamic Jahn-Teller effect 77—16164
- $Zn(NO_3)_2$-$Cu(NO_3)_2$ glass forming melts, density and viscosity 79—77794
- ZnO-Cu_2O heterojunction solar cells, prop. by RF sputtering 80—93945
- ZnS:Cu, Er, Na, phosphor, mechanism of sensitisation effect of Cu and Na ions 77—16369
- ZnS-Cu_2S solid soln., phase transform. during crystn., 850 or 1150°C 77—48362
- ZnS-$CuGaS_2$ heterodiodes, LPE, emission spectra 79—33335
- ZnS-$CuInS_2$, phase relations, 400 to 1300°C, X-ray and microscopic exam. 79—1853
- ZnS-MnS-$CuInS_2$, sobsolidus equilib., phase diagrams 80—3016

copper-oxide rectifiers
- No entries

copper zinc alloys *see brass*

copying *see reproduction (copying)*

copyright *see industrial property*

Corbino effect
- *see also Hall effect*
- n-InSb Corbino disc, acoustic noise effect on I-V characts. *(Russian)* 80—100492
- metal, closed-orbit, uncompensated, elec. and thermal magnetoresist., quadratic field depend. 79—95388
- Ba-ferrite, corresponding to remanent magnetization 79—38109
- GaAs, carrier mobility profiles meas. at room temp. by Corbino effect 78—60128
- Gd-transition metal, amorphous film, galvanomag. effects, Hall detector 77—89882
- n-InSb Corbino disc power meter for 3 cm wavelengths 79—71428
- n-Si inversion layers, electronic g-factor, spin-split Landau levels 80—80346

Coriolis force
- *see also rotation*
- (3×3) order systems, force const. calcs. using isotopic freqs., parametric method 78—21907
- A-type stars, mag. field generation by Coriolis EMF 78—8027
- acetonitrile, soln., IR perpendicular bands, profiles, rot. models 78—58695
- alkali metal+inert gas, role of different interactions in intramultiplet relax. at nonresonant interactions 77—6902
- allene(-d_4), IR absorption intensities 80—1026
- antisymmetric light scattering of molecules with non-degenerate electronic state 79—18192
- Atlantic Ocean, Coriolis parameter variability rel. to cyclic currents vortex 77—53466
- atmosphere, E.African jet dynamics, July mean conditions simulation 80—77045
- atmosphere, geostrophic adjustment on the spherical Earth 77—45064
- atmosphere, rot. rel. to gravity waves and equatorial ionosphere 78—36232
- atmosphere general circulation model with variable Coriolis parameter, energetics *(Russian)* 80—21791
- atmospheric geopotential in presence of mountains 80—26602
- atmospheric movements, spatial problem on influence of orography with Coriolis force included *(Russian)* 80—94565
- Baltic Sea two-dimensional seiches, effects of Earth rot. 80—8323
- benzene, and -d_6, $^1B_{2u}$ excited state, force field, normal coords. 78—5193
- benzene, doubly degenerate high-resolution rot.-vibr. Raman bands 79—6941
- benzene-d_3, gas phase Raman spectrum, E′ and E″ species, Coriolis consts. *(French)* 78—5235
- boron trihalides, quadratic potential functions, Coriolis consts. calcs. 79—72239
- chloromethane, and isotopes, $\nu_2+\nu_3$ band, Coriolis reson. with $\nu_3+\nu_5$ band *(French)* 78—5229
- chloromethane, IR spectrum, evidence for $2\nu_3$ overtone 79—68226
- coupling constants, spectroscopic determ., extremal props., book contrib. 78—78678
- cyclopropane, IR band intensities, anal. using Coriolis interaction and CNDO/2 calcs. 79—41172
- deformed nuclei, effect on Coriolis interaction, Nilsson model and Woods-Saxon pot. calcs. 80—63071

Coriolis force continued
- 1,1′-dicyanoethene(-d_2), microwave spectrum, Coriolis interaction, rot. assignments 78—82721
- dimethylallene, excited states, microwave spectrum and strong Coriolis coupling 78—9141
- Earth, elastic tides and natural oscills. with Coriolis force included 77—37122
- education, Coriolis machine, inertial motion viewed from rot. reference frame, coordinate transformation 78—69934
- effects in fixed frame, physical meaing 77—75788
- ethane, doubly degenerate torsional states, pure rot. transitions, theory 79—72299
- ethane, liq., IR torsion band, 98-173K mechanism, Coriolis coupling 77—38662
- ethyl iodide, microwave spectra and internal rot. anal. 80—69130
- ethylene, IR absorpt. spectra of ν_1, ν_{10} and ν_4 interacting band 80—83369
- ethylene-d_0,-d_4, IR band intensity and Coriolis interactions 79—54851
- ethylene-d_1, ν_9 B-type band analysis, ground state rot. parameters 77—42316
- ethylene-d_1, IR absorpt., ν_{12} and $\nu_2+\nu_9$ bands, rot. consts., Fermi and Coriolis coupling consts. 77—27070
- ethylene-d_4, Raman spectrum, fundamental bands 79—59473
- fluid dynamics on rotating plane, averaged equations 78—42617
- fluid motion within ellipsoidal cavity, influence of Coriolis force field *(Russian)* 78—81296
- fluoromethane, microwave spectrum, and 2nd order Coriolis reson., mol. consts. 77—18915
- fluoromethane, very high resolution IR spectrum anal. 77—34630
- fluoromethyl methyl mercury-d_0, -d_3, vibr. spectra, normal coord. anal. 79—50017
- formaldehyde, CO laser Stark and IR absorpt. spectra, dipole moment and rot. consts. 77—75150
- formaldehyde, IR spectra, Coriolis-coupled ν_4, ν_6 and ν_3 fundamental bands 78—5227
- formaldehyde, IR spectrum, rot. anal., P-and Q-branch assignments 77—18923
- formaldehyde, mag. rot. spectrum, A^1A_2 state, singlet-triplet perturbations 79—98126
- formaldehyde, vibr. excited states, RF spectrum *(French)* 77—30863
- formaldehyde(-d_1, d_2), and isotopic forms, microwave spectrum, ν_4-ν_6 vibr. states Coriolis reson. 78—82719
- formaldehyde-d_1, ν_5 and ν_6 vibr. excited states, microwave spectrum obs. 79—72304
- formaldehyde-d_2, laser Stark spectra, Coriolis coupled ν_4 and ν_6 fundamentals 77—27065
- formic acid, vibr. states, rot. and Coriolis parameters IR Fourier transform spectra 80—32709
- formic acid and isotopic species, microwave spectra, Coriolis reson. between vibr. excited states 79—13700
- Friedmann universes, distance functions for Coriolis interaction 80—51925
- Group IIIA metal tetrahalide ions, vibr. anal. 80—63608
- Group IV tetrabromides, intramol. force fields and mean vibr. amplitudes 80—106316
- group IV tetrahalides, isotope shifts, Coriolis coupling and force consts., isotope substitution and matrix isolation 77—42322
- Group V trideuterides, Coriolis coupling consts., progressive rigidity method calcs. 78—929
- Group V trihalides, Coriolis coupling consts., progressive rigidity method calcs. 78—929
- hexahalo ions, octahedral, mol. consts. calcs. 80—106317
- hexaoxy ions, octahedral, mol. consts. calcs. 80—106317
- hot-wire sensor, effect of centrifugal and Coriolis forces on rotating probe 78—94862
- infinitesimal operators of translation and rot., dynamic eqns. lineage 80—17788
- influence on LF waves in rotating plasmas 78—75309
- ion+atom collision, electron spin coupling in rot. frame, X-ray emission 79—36724
- ion cyclotron motion, Coriolis coupling of ion internal degrees of freedom 80—87246
- ionized medium, technique for rot. freq. meas. 80—41730
- Jupiter, Coriolis parameter variability rel. to Great Red Spot vortex theory 77—53466
- ketene, IR spectra, rot.-vibr. anal. of Coriolis coupled bands 78—86859
- ketene-d_0, -d_2, Coriolis coupling, centrifugal distortion and force consts., mean vibr. amplitudes calcs. 79—36607
- liquid films, thin, effect of Coriolis force on film dynamics 78—94747
- liquid-gas flow without mass transfer, centrifugal scaling 77—35209
- mass flow meter using Coriolis principle, electro-optical force sensing techniques 80—103094
- mass flowmeter, meas. Coriolis effect on mols., electro-optical sensing 80—96327
- ^{13}C-methane, ν_1 fund., quasi-CW inverse Raman spectra 80—48004
- methane, ν_2 and ν_4 bands Coriolis interaction, using a general Hamiltonian formalism *(French)* 78—5192
- methane, mol. rot.-vibr. consts., calc. using ν_1 band data 79—76529
- methane, phase II, IR and Raman spectra of ν_3 and ν_4 modes 78—2834
- methane, simultaneous analysis of ν_2 and ν_4 bands 77—10662
- methane-d_1, ν_3 band anal., 7.6 micron 80—47980
- methane-d_1, ν_6 band at 8.6 μm, vibr.-rot. band 78—21923
- methane-d_2, IR spectrum, ν_2 and ν_8 bands, rot. struct. and consts. 77—27066
- methane-d_4, ν_2 and ν_4 IR bands meas. and anal. 80—18851
- methane-d_4, ν_2 Raman band anal. 79—31536
- methanol (d_3), OH stretch fund., torsion-rot. levels, IR spectra obs. 80—32711
- methyl chloride, microwave spectrum of excited vibr. states, Coriolis coupling, rot. consts. 77—14420
- methyl fluoride, second-order Coriolis resonance between ν_2 and ν_5 states, microwave spectra 78—74646
- methylene fluoride, excited vibr. state, microwave spectrum 78—58672
- mol. consts. and mean vibr. amplitudes calcs. 80—106318
- molecular, symmetry coordinates construction, arbitrariness limitation 78—55252
- molecular IR integrated intensities, rel. to mol. consts., isotopic sum rule 77 27118
- molecular rotation vibration, Coriolis coupling of degenerate vibr. states 79 63977

Coriolis force continued
molecular rotational and vibrational relaxation autocorrelation functions 80—32856
molecular structure, isotopic relations for rot. and Coriolis consts. 79—3377
molecule, intensities dipolaris. ratios, polarisability, matrix rotation, isotopic rules 78—5288
molecule, vibr. problem in Cartesian displacement coords., Coriolis and transition moment calcs. 77—83573
molecule vibrational-rotational line intensities, accidental resonances effect 77—18987
molecules, isolated, intersystem crossing, rot. motion effect 80—95669
nonlinear symmetric XY_2 type molecules, isotopic invariants, Coriolis coupling constants, centrifugal distortion constants 80—923
normal co-ordinates through coriolis coupling constants 80—28005
nuclear mag. dipole moment model, Coriolis coupling, odd-A deformed nuclei 77—30488
nuclear rotational motion, particle-rotation coupling 79—17838
ocean, deformed eddy shape, with varying Coriolis force 79—66708
ocean internal waves, wind-generated, role of Coriolis force *(French)* 79—62518
ocean residual circulation, topographic generation by oscillatory tidal currents 79—57954
ocean surface intrusions, Coriolis force rel. to fronts and internal waves 79—2262
ocean turbine energy system status 80—45628
octahedral systems, intramolecular force fields and vibr. amplitudes, Wilson's FG matrix method 77—31021
odd nuclei states, Coriolis mixing, phonon admixture and non-adiabatic effects in even-even core 78—74310
phosphine, IR spectrum, ν_1 and ν_3 band analysis 80—83366
pipes carrying fluid flow, oscillation stability *(German)* 78—87298
plasma, rotating, axially symmetric, continuous MHD spectrum 79—60180
Poiseuille flow, plane, horiz., rot., stability, effect of Coriolis force 78—67203
polyatomic molecule, sextic centrifugal distortion consts., Watson Hamiltonian, perturbation method 77—10785
quantitative demonstration, apparatus design 77—49532
ring, oscillatory behaviour, influence of Coriolis forces on power transmission belts *(German)* 78—87255
roll-cell instability, rot. laminar and turbulent channel flows 77—946
rotary ether drag, Coriolis contribution 80—4556
rotating fluid, differential Coriolis force rel. to spread of mixing 79—57949
rotating radial pipe with liq. film, Coriolis effect, film width and vaporisation 79—18955
rotational alignment in nuclei and planets 80—90636
salt fingers, rot. effects 79—50767
sea straits geostrophic adjustment, theory and laboratory expts. for two-layer system 79—48503
spherical top mols., $T(\nu_3)$ rovibrational bands, level cluster patterns, centrifugal and Coriolis effects 79—18175
stationary cellular convection, rotation effects *(German)* 79—81904
Sun convective zone, Coriolis forces rel. to differential rot. mechanism 79—25556
Sun external layer, Coriolis EMF rel. to mag. field semi-dynamo 77—49349
symmetric-top molecules in liquids, Coriolis coupling 77—10657
tetrafluoromethane, ^{19}F chem. shielding, depend. on internal coords. 78—5249
tetrafluoromethane, $\nu_2+\nu_4$ band, high resolution diode laser spectra 80—69138
tetrafluoromethane, ν_4 fundamental of three isotopic species 78—70835
tetrafluoromethane, mol. consts. and mean vibr. amplitudes calcs. 80—106318
tetrahalide of group IV A, molecular consts. 78—66528
tetrahedral and octahedral complexes, mol. vibrs. and reaction pathways, min. energy coords. and compliance consts. 77—57966
tetrahedral XY_4 ions, normal coord. treatment and mol. consts. 79—93968
tetramethyls, of IVA metals, pseudo-exact force consts., force fields 77—31022
transition metal ammine complex, mol. force consts. and vibr. amplitude 79—31727
triatomic mol. in solvent, rot. induced vibr. energy relax., Coriolis effect 80—47921
s-triazine(-d_3), gas phase IR band contours obs., computer simulation 77—6774
tsunami type plane wave, Coriolis force effect *(Russian)* 78—77193
turbulence, linear spectral study *(French)* 79—84408
wide estuaries geostrophic adjustment, theory and laboratory expts. for two-layer system 79—48503
XY_2 bent symmetrical molecules, Coriolis coupling consts., centrifugal distortion consts. 80—58236
XY_2 molecules, nonlinear, inertia defects and dipole moments by kinetic consts. method 80—928
XY_2 nonlinear system, mol. dynamics calcs. 78—41975
XY_3, pyramidal halides, mean amplitude, Coriolis coupling const. and centrifugal distortion const. 78—29735
XY_3 pyramidal-type mols., mol. consts., kinetic consts. and L-approx. methods 80—18839
XY_3 type molecules, centrifugal distortion constants and inertia defects *(Russian)* 79—800
XY_4 oxygenated ions, tetrahedral, mol. consts. 79—36555
XY_6-type molecules, Coriolis coupling consts., at. mass effect, XCl_6 appls. 78—66684
XYZ type system, bent, force field determ. Redington's method applicability 79—81168
^{27}Al, inelastic electron scatt., charge distrib., Coriolis band mixing calc., C2 form factors 79—529
BF_3, ^{19}F chem. shielding, depend. on internal coords. 78—5249
B_2F_4, mol. force consts. and vibr. amplitude, force field study 79—31729
$BF(OH)_2$, identification, rot. and centrifugal consts., mol. struct., microwave spectra obs. 80—32705
B_2H_6, quadratic valence force field, rel. to ethene 79—3382
$BHBr_2$, and isotopic forms, mol. pot. consts., amplitudes, Coriolis coupling, centrifugal distortion 78—50662
$BHCl_2$, and isotopic forms, mol. pot. consts., amplitudes, Coriolis coupling, centrifugal distortion 78—50662

Coriolis force continued
BHF_2, and isotopic forms, mol. pot. consts., amplitudes, Coriolis coupling, centrifugal distortion 78—50662
BrF_5, excited vibr. states, microwave spectrum, rot. const. determ. 78—94237
BrF_5, microwave spectrum, Coriolis interaction, A_1-A_2 splitting of kl levels 77—38657
CF_2S, mol. consts., kinetic consts. method calcs. 80—58235
CF^2Se, mol. consts., kinetics consts. method calcs. 80—58235
CO_2, IR band intensity 80—83425
CO_2+N_2, semiclassical energy transfer method, Coriolis coupling 78—90266
COF_2, force field analysis using parametric represent. method 80—27990
CeF_3, force consts., Coriolis coupling consts., vibr. amplitudes 78—17650
CeF_3, mol. force, compliance and Coriolis consts. 79—31726
$CrCl_4$, mol. consts. and mean vibr. amplitudes calcs. 80—106318
CuBr, rot. spectrum hyperfine struct., coupling consts., microwave spectroscopy study 80—18844
DO_2, ν_2 fundamental band, 9.8 micron, laser mag. reson. spectroscopy 79—85961
EuF_3, mol. force, compliance and Coriolis consts. 79—31726
Ga trihalides, vibr. anal., pot. const. determ., mol., compliance and Coriolis coupling const. calc. 80—95579
GdF_3, mol. force, compliance and Coriolis consts. 79—31726
GeF_4, $\nu_3(F_2)$ IR band contour, isotopically pure cpds., mol. consts. 77—61746
GeH_4, tetrahedral mol., force field calcs. 78—29734
GeH_3X, mol. consts. calcs. 79—36606
H_2 Se, potential function and vibrational spectra 77—68030
HBS, and isotopic forms, force consts., coriolis consts., vibr. amplitudes, shrinkage effects 80—43021
HNCO, microwave and RF spectra, b-type rot. transitions 78—21914
HNCS, a-type rot. spectrum in excited bending vibr. states 79—3437
HNO, fundamental vibr. bands, laser Stark spectra 77—38692
H_2O, IR line and band strengths, 5000-5750 cm^{-1} 78—5292
$HfBr_4(HfI_4)$, struct., force field and Coriolis const. calcs. 78—86843
HoF_3, mol. force, compliance and Coriolis consts. 79—31726
In trihalides, vibr. anal., pot. const. determ., mol., compliance and Coriolis coupling const. calc. 80—95579
KrHCl, van der Waals complexes, struct., RF and microwave spectra, isotope effects 80—37806
LaF_3, force consts., Coriolis coupling consts., vibr. amplitudes 78—17650
LaF_3, mol. force, compliance and Coriolis consts. 79—31726
LuF_3, mol. force, compliance and Coriolis consts. 79—31726
MgX_2 (X=F, Cl, Br, I), 2Z 80—43021
NF_3, Raman spectra, Coriolis coupling and transition dipole 78—39533
NH_3, Coriolis and l-type interactions, ν_2, $2\nu_2$ and ν_4 states, IR spectra 80—47993
NH_4^+, mol. consts. and mean vibr. amplitudes calcs. 80—106318
N_2O_4, mol. force consts. and vibr. amplitude, force field study 79—31730
NdF_3, mol. force, compliance and Coriolis consts. 79—31726
O_3, combination bands $(\nu_1+\nu_2)$ and $(\nu_2+\nu_3)$, anal. 78—9150
O_3, IR and microwave spectra, ν_3 vibr.-rot. band 77—38663
O_3, line position and intensities of $2\nu_3$, $\nu_1+\nu_3$ bands 80—87181
ONCN, far IR spectra, pure rot. and vibr.-rot. bands 78—82731
$P^{35}Cl_3$, microwave, rotational spectra, excited vibrational states 79—98080
PF_3, anharmonic force field from mm wave spectra of vibr. excited states 79—13701
POF_3, IR rot.-vibr. spectrum, mol. consts., laser Stark spectroscopy obs. 78—33508
RuO_4, $\nu_3(F_2)$ IR band contour, isotopically pure cpds., mol. consts. 77—61746
SO_2, IR spectra, Coriolis intensity perturbations 80—95617
SPF_3 band contours of E fundamentals, IR spectra 79—98089
SPF_3, isotopic forms, microwave spectra, centrifugal distortion consts., vibr. and rot. states, IR matrix spectra 77—10665
$Sc+NO_2$, chemiluminesc., nonequilib. product distrib. 80—101014
SiD_3F, microwave spectrum, rot.-vibr. interaction consts., Coriolis reson., El moment 77—6766
SiF_4, ^{19}F chem. shielding, depend. on internal coords. 78—5249
SiF_4, $\nu_3(F_2)$ IR band contour, isotopically pure cpds., mol. consts. 77—61746
Si_2F_6, normal coord. analysis, vibr. freqs. and amplitudes, shrinkage and distortion consts., force consts. 80—27989
SiH_4, tetrahedral mol., force field calcs. 78—29734
$^{28}SiH_4$, analysis of ν_4 band interacting with ν_2 band *(French)* 78—9152
SiH_3F, microwave spectrum, rot.-vibr. interaction consts., Coriolis reson., El moment 77—6766
SnH_4, tetrahedral mol., force field calcs. 78—29734
$TiBr_4$, (TiI_4), struct., force field and Coriolis const. calcs. 78—86843
TiF_4, equilib. config., force field, Coriolis consts., vibr. freqs. and amplitudes 80—32835
Tl halide dimers, kinetic consts. method for vibr. analysis 79—26968
Tl_2Cl_2, mol. consts., IR and Raman freqs. assignments 78—17648
Tl_2F_2, mol. consts., IR and Raman freqs. assignments 78—17648
WO_3, vibr. anal., mol. consts., kinetic consts. method 80—23393
XBr_4, Coriolis coupling const., at. mass effect 79—31728
XI_4, Coriolis coupling const., at. mass effect 79—31728
XeO_3F_2, mol. consts., general valence force field calcs. 78—21906
YF_3, force consts., Coriolis coupling consts., vibr. amplitudes 78—17650
YbF_3, mol. force, compliance and Coriolis consts. 79—31726
$ZrBr_4(ZrI_4)$, struct., force field and Coriolis const. calcs. 78—86843

cornea *see eye*

corona
see also electric breakdown; flashover; solar corona
AC, at 50 Hz, DC electric field influence obs. *(German)* 80—70052
AC, point-plate arrangement, behaviour near threshold voltage obs. *(German)* 80—70051
AC corona meas. using field-filter probes 80—47082
aerosol particle neutralisation to Boltzmann's equilib. by corona discharge 78—61064
air, low-velocity heat transfer to flat plate 79—77112
air, negative corona current O_3 density depend., 46-87 kPa 80—1852
air, negative point-plane corona, electrical characts. 78—71567
air, negative pulseless corona to spark breakdown transition condition 80—54062
air, positive corona discharge time lag obs. 79—27849
air, pulsed corona discharge channel fast heating process 78—67560
air, Trichel corona, negative ion form. 77—35425

corona continued
- air, unionized, enhanced light emission from positive corona 79—37568
- air corona discharge, thermal energy positive ion extraction through Al and Au films 80—38801
- air corona discharge ion density and mobility obs. 78—67594
- air gap, drift vel. meas. of ionized particles 80—24298
- air gap corona pulse delay obs. and HV insulation design 79—19117
- air gap discharge zone probabilistic features 78—67582
- air HF corona discharge ignition characteristics 78—67589
- air positive point corona current continuous component 78—67586
- air positive point-to-plane corona, continuous and pulse components 79—19119
- air-intake flowmeter using corona discharge principle, automobile engine appl. 80—33716
- alpha-particle streamer counter performance characts. 78—25402
- alternating corona, with superimposed DC field, at threshold voltage 80—1860
- analogy with dynamic plasticity 79—41888
- asymmetrical gaps as high-voltage rectifiers 77—57352
- atmosphere frozen precipitation, corona charging 77—5295
- atmospheric air, onset of corona 80—36354
- atmospheric positive streamer corona, primary wave emission, secondary electron emission 80—44008
- back corona, formation 79—50908
- back corona, sparkover voltage 79—50909
- breakdown field strength of gas mixtures and unitary attaching gases 79—55445
- charged insulating film high-field conduction and breakdown 80—15975
- charged polyethylene thermally stimulated current and surface potential decay obs. 80—15945
- charged PVF_2 α_c relaxation obs. 80—15956
- charging devices for electrophotography, characterisation and modelling 79—19110
- charging props. of PMMA-metal oxide composite powder *(Japanese)* 78—95708
- cloud chamber, coronal discharge effect on cloud droplet growth 77—34514
- computing process for electrons and ions distribution determ., based on physical model 79—4204
- convective heat transfer coeffs. for corona wind cooling of flat surface 78—87234
- corona to glow discharge transition mechanism, morphologic discussion 79—99014
- corona to spark transition, cathode zone activity, Schlieren obs. 78—87585
- counter resolution rel. to current, gas pressure and anode wire diameter *(Russian)* 78—90018
- current density in ionised gas in macroscopic field, direct meas. by Stark broadening of H lines *(French)* 78—9839
- current flow in corona discharges with arbitrary outer-conductor geometries 77—62418
- cylinder in still air, DC corona cooling obs. 80—70071
- cylindrical electrode under corona discharge, elec. field intensity meas. 79—23473
- DC, transient regime determ. *(Russian)* 77—35412
- DC corona discharge in rarefied air, coherent ion plasma oscillations 77—76230
- DC corona discharges in coaxial cylinder electrode 80—33837
- DC corona Trichel pulse development at atm. pressure, obs. 78—67588
- DC corotron, two dimens., for electrophotography, numerical modelling 79—19109
- DC transmission conductors, corona discharge and elec. charge on water drops, obs. 79—82114
- dielectric liquids, corona light emission 77—8508
- diffuse electrical gas discharge, in turbulent flows 79—94834
- discharge, anomalous cathode drop, elec. field form. *(German)* 77—43088
- discharge, decomposition of CO, qualitative chemical anal. of reaction products 78—60992
- discharge, gaseous ion stabilisation by H_2O drop capacitors *(Russian)* 77—62420
- discharge, spherical probe I-V characts., electrostatic precipitator testing appl. 78—79467
- discharge by negative ion decomposition, investigation *(Russian)* 77—55179
- discharge characts., influence of ion mobility, anal. 79—50902
- discharge in air gap, drift rel. meas. of charged particles 80—52267
- discharge in atmosphere, review 78—26363
- discharge over insulating surfaces, interaction study *(French)* 77—4016
- discharge pulses, field strength and electron density calcs. 80—38814
- discharges and applications, conference, London, England, Dec 1979 80—33848
- discharges from ice points on metal electrodes 78—67587
- discharges in atmospheric air under AC voltage, observation *(Japanese)* 79—84417
- effects of neutral gas density reduction on negative pulseless glow-spark transition 80—33850
- EHD augmented baking, corona wind impingement effects 78—87235
- EHD study of corona wind between wire and plate electrodes 78—71561
- electric discharge, appls. review 80—33849
- electrification of objects under DC transmission lines, charge simulation calcs. 78—78853
- electro-gas dynamic technologies, corona discharge industrial applications, qualitative analysis *(Rumanian)* 80—70061
- electrographical imaging of objects, in electric discharge *(Czech)* 80—37104
- electron density meas. by microwave resonant cavity method 77—68881
- electrostatic deposition of thin particulate layer, resistivity meas. under ionic bombardment 80—68218
- electrostatic precipitation, charge measurement, positive and negative corona 80—96403
- electrostatic precipitator, initiation condition and mode of back discharge 78—16814
- electrostatic precipitator, wire-duct type, back corona effects, math. model 80—49028
- electrostatic precipitator system, under neg. direct and pulsed voltage, characts. 79—19107
- electrostatic precipitators, corona discharge theory analytic developments *(Rumanian)* 80—70062
- electrostatic spraying, corona discharge effect *(Japanese)* 79—5186
- electrostatically assisted heat transfer 80—69628

corona continued
- energy spectrum of corona impulses generated from insulated wires under high AC voltages 78—71621
- excimer laser preionisation techniques, spark and corona preionisers 80—33016
- flow regime alteration, of liquid (gas), use in automatic systems *(Russian)* 77—11269
- force exerted on electrode in O_2 and N_2 corona discharge 77—19803
- glass electrets obs., bonded, under corona discharge and electron irradiation conditions *(Russian)* 79—4759
- heat transfer augmentation around downward facing flat plate by nonuniform elec. field 78—94873
- heated cylinder in radial elec. field, corona characts. power freq. variation effects 78—87538
- heated cylinder in still air, cooling by corona wind expt. 80—84023
- heated discharge electrode, breakdown streamers, expt. 77—76228
- high-pressure corona discharge current oscillations and role of excited atoms 78—67590
- homopolar, of conductor-two plane electrodes, volt-ampere characts. calc. *(Russian)* 78—26353
- homopolar corona, plane parallel field, outer region electrical characts. calc. *(Russian)* 78—67447
- hot gases electrostatic precipitators, air temp. influences on negative corona integral characts. *(Russian)* 79—41892
- impulse corona development in rod/plane gaps—negative polarity 78—87541
- impulsive discharges around conductors, phys. aspects consideration *(French)* 80—92406
- inert gases, high press. corona discharge ionisation instability 77—11430
- insulation corona discharge, ageing process, expt. 77—43095
- inverse, in electron-ion technology, influence of chlorine and use of conditioning reagents *(Russian)* 79—1355
- inverse, in sputtered polymer powder layers, characteristics meas. by electrostatic method *(Russian)* 77—10042
- Kirlian photography, image modulation 77—5952
- laboratory air, positive point to plane corona, critical parameters 80—49035
- laser compression of inertially confined plasmas, future energy developments 80—23120
- laser diagnostics, probing radiation Raman scatt. *(Russian)* 80—19618
- laser induced microsphere, electron density profile, interaction and transport profile 80—107008
- laser produced plasma corona development, X-ray streak camera obs. 77—15245
- leader channel temp. rise, initial stage, elec. field strength determ. *(Russian)* 77—35411
- Lichtenburg figures of corona discharge at LF 77—4006
- long spark form. mechanism 80—59326
- low press. discharge, attractive forces on electrodes 80—49041
- low-pressure wire-cylinder corona discharge with wire at positive potential, and mag. field effect 79—94831
- mass spectroscopic atmospherical pressure ionisation by corona discharge, ionisation characts. 77—60156
- multifluid behaviour between elec.-stressed spherical cathode and spherical anode 80—10443
- multiwire proportional chamber, corona discharge region effects *(Chinese)* 79—93887
- needle-to-plane electrode corona inception voltage and streamer length 78—67583
- negative, discharge effects over surfaces, investigation by spectrophotometry and granulometry methods *(French)* 77—4014
- negative, from sharp needles, threshold voltage calc. 80—49036
- negative air corona, low energy humid air ions, etching effect on Al foil 80—40593
- negative corona current, time depend. in air and oxygen 79—64930
- negative corona discharge in air, current distrib. 78—87539
- negative corona Trichel pulse mechanism, unified theory 80—49039
- negative DC corona study in atmospheric air using Schlieren and interferometric techniques 80—49023
- negative discharge, surface potential decaying process, for polypyrimidines with azomethine in main chain *(Japanese)* 79—24095
- negative impulse corona and sparkover, background ionisation effects 78—87540
- negative impulse corona structure in rod/plane gap 79—86636
- negative point to plane gap, in air, pulseless corona 78—47195
- negative unipolar, in air at high temp. and pressure, investigation 77—80392
- ns surface discharge study in low press. 80—19640
- onset and breakdown in non-uniform air gaps, physical models 77—15268
- onset voltage calculation, effect of avalanche space charge fields 79—86632
- onset voltage in bipolar fields 78—67580
- onset voltage in nonuniform air gap, calc. methods 77—15253
- optical component protection in dusty environments, electrostatic techniques 80—58657
- optoelectronics, appl. in measuring gas discharge phenomena 80—107007
- PET-CdS photoreceptors, air space effects on electrophotographic props. *(Japanese)* 79—44962
- plant growth and development, effect of 60Hz elec. field 77—81534
- plasma, of corona and HF discharge, technological process appls. 80—1855
- PMMA, treeing effects on electric breakdown *(Korean)* 77—81053
- PMMA coated frit powder prep., corona-charging props. *(Japanese)* 80—25891
- point discharge current magnitude 78—44935
- point source current distrib. in external field 79—10727
- point to plane electrodes, corona current experimental equations *(Japanese)* 79—50918
- point-to-plane air gap, corona onset, breakdown voltage 78—47194
- point-to-plane gap corona and breakdown in supersonic airstream 78—67573
- point-to-plane negative corona discharge in axial airstream 78—67585
- polyethylene, surface activation by corona treatment *(Japanese)* 77—77604
- polyethylene films, adhesive props. improvement by corona discharge appl. *(French)* 78—92438
- polyethylene films, corona charged, charge trapping 80—88571
- polyethylene films, high density, corona-charged, surface pot. decay 79—24254

corona continued
polyethylene terephthalate film, surface modification by corona discharge, adsorption and wettability 77—86212
polymer powder deposition, reverse corona influence obs. *(Russian)* 77—12526
polyolefin film, corona discharge treatment 77—56129
polyvinylidene fluoride, corona-charged, surface effects 80—66102
polyvinylidene fluoride, poling by corona charging, pyroelec. effect 78—19423
polyvinylidene fluoride films, corona-charged, struct. changes, piezo- and pyroelec. props. 79—11389
polyvinylidene fluoride films, corona-poled, piezoelectricity *(Japanese)* 80—55040
polyvinylidine fluoride, corona charging at 12.5 kV, obs. 78—92027
positive, initiated by negative ion decay, expt. 77—55182
positive, unipolar, gas purification appl., expt. 77—39492
positive corona, conditions for flare discharge on direct voltage appl. *(Russian)* 80—14948
positive corona discharge, current oscills. 77—11431
positive corona discharge, mag. field effects 77—43089
positive corona electrode, negative ion counterflow, elec. field strength meas. 80—38817
positive corona from two interacting thin points in air 80—49040
positive corona onset in atmospheric air—A multiple avalanche process 80—38786
positive discharge in atmospheric air, cathodic sputtering investigation by spectrophotometry method *(French)* 77—4015
positive glow corona along a cylindrical rod between two parallel plates 80—38768
positive pulses on conductors of different dia., statistical anal. *(Russian)* 77—7610
probes for electric field measurement in corona discharges 80—33822
pulse character in strongly heterogeneous field formed by electrodes point-plate arrangement *(Czech)* 80—70048
pulsed corona discharge, pulse isolation 77—41641
pulsed corona meas. in coaxial electrode structures 79—19114
pulsed electrical discharge, displacement currents compensation *(Russian)* 78—9870
pulseless corona, space-charge limited current flow, computer solutions of Poisson and current continuity equations 79—86627
rarefaction shocks in laser plasma corona 79—19037
respiration rate meter, corona discharge identification and ionisation current control *(French)* 79—92411
rod to plane gap in atmospheric air, breakdown and corona characteristics under AC voltage *(Japanese)* 79—84416
rod-to-plane air gap breakdown under negative impulse voltage 78—67563
rod-to-plate system, initial corona voltage calculated according to Townsend's Theory *(Czech)* 80—87961
rod/plane gap, first corona inception as function of electrode radius and voltage rate *(German)* 77—7607
secondary electron emission due to negative corona discharges 78—67592
similitude between ionic wind, discharge pattern and corona current 79—32833
sound effects of positive corona discharge 80—28858
sphere-plane gap avalanche current pulse meas. in nonuniform fields 78—67556
temperature anomalies, wire to cylinder discharge 79—1358
temporal space-charge field change meas. at high voltage electrodes in negative corona 80—38770
theta-pinch, striated corona, theory 79—41897
thin film, Kirlian-type images and transport in high-voltage corona discharges 79—55590
on three-electrode systems, floating potential determ., test *(German)* 77 7611
threshold voltage, noncoaxial cylinders in air 80—28857
thundercloud elec. field meas. by balloon-borne coronasonde 78—61577
thunderstorms, coronae effects on elec. fields beneath thunderstorms 79—79978
thunderstorms, microwave radiometric detect. of corona from chaff 78—16106
transition corona effect arc, cathode zone effect 78—1934
transition region, downflow of spicular material 77—33448
transition region and inner corona, energy balance 80—90379
transmission lines, high voltage, depend. of coronal discharge power loss on instantaneous rainfall rate 80—98471
Trichel corona, negative ion mass spectra 78—87537
Trichel corona negative ion transit times 79—19115
Van de Graaf accelerator, corona stabilisation system 79—18061
Van de Graaff accelerator, corona stabiliser, effect of insulating gas comp. 79—13559
Van de Graaff generator, corona stabilisation systems 78—29668
visible ionisation layer radius for positive and negative coronas 79—10728
water drops on HV overhead power lines, expt. 80—33851
wire-to-cylinder corona, current distrib. on cylinder surface 80—6302
xerographic discharge in binder layers 80—47140
CO_2, negative point-plane corona, electrical characts. 78—71567
CO_2, Trichel corona, negative ions 78—30503
H_2O vapour under point corona discharge, microprocessor control for vapour generator and EHD phenomena 80—106852
He II Balmer α line components 77—33436
He-O_2 corona discharge CV characteristics 78—91168
KrF, efficient 1/4 J laser with corona preionisation 79—59713
N glow discharges surface coronas and photopreionisation stability, demonstration 80—105475
N-O mixtures, positive glow corona in quasi-uniform fields 80—100104
N_2 positive corona into spark, prebreakdown phase, spectroscopic anal. 80—38790
N_2 UV laser, travelling-wave corona excitation 77—7121
N_2-Ar corona dishcharge, convection and mixing, atm. press., mass spectra obs. 80—1853
NO_x generation from heated corona wires 80—47081
O_2 $^1\Sigma_g^+$ state lifetime obs., using spectroscopic analysis *(French)* 77—24230
O_2, negative point-plane corona, electrical characts. 78—71567
O_2, Trichel corona, negative ions 78—30503
SF_6 and SF_6-N_2 mixture, elec. breakdown and corona stabilisation obs. 78—87582
SF_6 and SF_6-air mixture gas under impulse voltage, discharge phenomena *(Japanese)* 80—96409
SF_6, compressed in positive rod-to-plane gaps, static breakdown anal. 80—38796
SF_6, compressed in space-charge stabilised nonuniform fields, corona threshold computation 79—19118
SF_6 corona-stabilised breakdown, computations and obs. 80—64804
SF_6 gas, electrode surface roughness effects obs., on initial corona voltage *(Croatian)* 80—54074
SF_6, negative point-plane corona, electrical characts. 78—71567
SF_6 positive-point corona phenomena, breakdown voltage/press. characts. 80—38859
SF_6 rod-to-plate corona discharge characteristic obs. 78—67584
SF_6/N_2 mixtures, positive-point corona phenomena breakdown voltage/press. characts. 80—38859
SF_6-air mixture impulse discharge characteristics of 30 cm gaps 78—67572
SF_6-N_2 mixture in rod-plane gaps, static field breakdown 79—68965
ZnO resin layer leakage current in corona charging *(Japanese)* 78—24877
ZnO-resin electrophotographic photosensitive layers, dark decay mechanism of corona charge *(Japanese)* 79—24002

coronagraphs
see also solar corona
Apollo Telescope Mount and solar instruments of Skylab, overview 77—60593
diffraction limit problems and design approaches 80—82200
external occulting disc coronograph, scattered light reduction 78—36455
external shading disc, diffracted light intensity, calcs. 77—87267
High Altitude Observatory Coronagraph/Polarimeter on the Solar Maximum Mission 80—51662
Lyman alpha coronagraph 79—25486
Norikura Observatory equipment for polarimetry *(Japanese)* 80—82223
objective component surface scatt. angular distrib. obs. 80—74463
Skylab, solar occultation technique for atmospheric aerosol layer obs. 77—9540
Skylab experiment on contaminant particulate environment 77—78633
Skylab particulate expt. T025, photographic coronagraph for atm. aerosol meas. 77—60568
Solwind, NRL coronograph, initial obs. 80—82325
white light coronagraph and X-ray XUV solar telescope, CCD camera systems and support electronics 80—62023
white light coronagraph/XUV telescope expt., quadratic A/D converter 80—62024
white-light coronagraph, on Skylab, instrumental stray radiance meas. 77—60607
white-light coronagraph, on Skylab, radiance calibration 77—60606

corpuscular streams *see cosmic rays; solar wind*

correlation methods
see also correlators
Abell and Shane-Wirtanen catalogues, cross-correl. anal. 78—4118
acoustic absorption coeff. in situ meas. by correlation technique 77—27444
acoustic array gain, rel. to correl. coeffs. and patch size 77—31158
acoustic correlation measurement method for rotating sources of noise 80—64279
acoustic emission amplitude estimation model 79—68476
acoustic emission sources, localisation 78—87220
acoustic FM signals, correl. methods for underwater sound meas. 77—62086
acoustic noise and vibration anal. appls. 79—81617
acoustic noise measurement of rotating sources *(Croatian)* 78—46869
acoustic noise path diagnostics in dispersive structural systems, crosscorrelation anal. 77—23807
acoustic wave reflection from ocean bottom and surface, correlation measurement of coeff. 80—58848
acoustics, correlation coeff. meas. for signals with stationary additive noise 78—94489
acoustics, lagged signal power spectrum in cross correl. 78—9502
air pollutants remote sensing by correl. spectroscopy, instrumental response characts. 79—5623
air pollution data in urban area, spatial correlation analysis 79—12236
air pollution monitoring by satellite, correl. spectroscopy techniques 77—64456
air pollution remote sensing, use of computer-assisted correl. spectrometer 78—4002
aircraft noise identification system by correlation technique 79—23131
altimetric data file acquisition automatic digital correlation method 78—61633
amorphous polymer multiple dielectric relaxation, time-correlation function representation 80—15951
analysis code for automated reduction of gamma ray data 78—23978
arc meas. appl., natural fluctuations of voltage and emitted light correlation *(French)* 80—19654
artifact-free region-of-interest reconstruction from coded-aperture recordings 79—89863
associative parallel-search memory, correlation search using coded key words 79—10265
astronomical distance determination, method for extragalactic objects with active nuclei *(Russian)* 80—51880
astronomical H_2O radio sources, autocorrel. anal. of spectra 78—65713
astronomical images optimal classification into stars or galaxies, Bayesian approach 80—21920
astronomy, cross correl. detection of rapid stellar var. using two telescopes 77—82127
atmospheric temperature rel. to geographic latit., correl. charts construction by graphical method 79—29905
auto and cross-correlation analysis techniques on-board spacecraft *(French)* 79—70925
auto-correlations with irregular signals, time series anal. 77—18767
autocorrelation, surface texture assessment 80—47013
autocorrelation analysis, two-dimensional, appl. to block tectonics in E. Mongolia 80—56469
autocorrelation of meas. signal, dynamic characteristics of stroboscopic transducers determining 77—5824
automatic speaker recognition, cepstral/spectral and linear prediction techniques compared 80—91993
avian heart rate meas. using autocorrel. techniques 78—31989
Backward stochastic partial differential eqns. and diffusion processes with noisy observations *(French)* 79—54052

correlation methods continued
- binary image correlator in absence of geometric distortion, statistical analysis 79—22907
- binaural signal analysis by cross correl. 78—27958
- biological rhythm research, second-order correlation functions and bispectra 78—3441
- biological specimen recognition with partially matched spatial filter 80—46113
- biopolymer Brownian diffusion, fluoresc. correl. spectroscopy 79—62193
- blood velocity, catheter meas., cross correl. technique 78—80943
- body control mechanism, human, investigation using analysis of body's period signals 79—66576
- brain, 40 Hz activity in sigmoid gyrus, nucleus accumbens and amygdala, cross correl. anal. 80—76730
- cardiac arrhythmia monitoring, joint interval histogram and correlation coeff. scatter diagram techniques 77—25572
- cardiovascular flow disturbance, US detection 77—60231
- cardiovascular flow disturbance detection by pulsed US Doppler velocimeter autocorrelograms 77—25526
- cepheids, double mode, in northern hemisphere, search using existing obs. 80—8634
- chloroplast conformational vars., auto-correl. anal. 80—30680
- chromatography, correlation type, noise sources eval. and practical considerations 80—40771
- clusters of galaxies, mean density and correl. function, theory and obs. 78—24559
- coherent Doppler anemometer for turbulent vel. meas., potential accuracy anal. *(Russian)* 78—71406
- coherent optical correlation techniques, review 80—43277
- coherent optical defectoscopy, signal processing, materials testing appl. *(German)* 78—7110
- coherent radiation beams, parameters from correlation method *(Russian)* 78—50705
- coherent-optics image recognition by hybrid series-parallel processing *(Russian)* 77—58265
- collisionless molecular multiphoton processes, rate eqns. 79—98173
- colloid size distrib., photon correl. spectroscopy, methods of cumulants, histogram and Laplace transform 79—58801
- complex plates, anal. non-stationary random vibrations 80—102991
- complex surface shape inspection, coherent optical method evaluation 79—81578
- computer-evaluated ECG parameter correlation with constitutional variables in infants and children 79—39406
- computerised classical tomography, optimum coding sequences appl. 79—8530
- conditional sampling, detection and data signal phase relation, turbulent boundary layer appl. 78—24772
- Continental Shelf sediment sonar signal processing 78—61622
- correlation TOF technique, real modulation 79—49898
- cosmic ray diffusion theory, vel. correl. function 77—73913
- coupled-core nuclear reactor, distributed parameters identification, pseudorandom perturbation and correlation anal. 80—86966
- creep rupture data analysis, development of correlation and extrapolation methods 80—58975
- cross correlation techniques for remote river velocity and level meas. 78—57328
- cross-correlation flow meas. error estimation and reduction 79—3194
- cross-section data adjustment iteration procedure 79—9696
- data extraction from film using optical and/or digital and/or electronic devices 78—63024
- decimal/residue/decimal optical converters 79—22905
- deep galaxy samples correlation anal., techniques and appl. to two-colour sample 78—41056
- density meter characteristics, stochastic models *(Russian)* 77—9987
- depolarising diffusers, autocorrelation by holography *(French)* 79—31801
- diffusing surface optical autocorrelation 80—99646
- digital filtration in correlation time-of-flight spectrometry 79—49894
- dislocations and microplasma sites, STEBIC/STEM/EELS correlation 80—96528
- distributed type associative memory model with quantised Hadamard transform 80—108867
- Earth crust, dielectric const. determ. from rocks elec. parameters correl. at high temps. *(Russian)* 79—8628
- ECG, ambulatory arrhythmia quantification by correl. technique 78—81020
- ECG body surface potential map estimation, limited lead selection 78—57111
- ECG monitoring by contour comparison, QRS triggering with real-time correlator *(German)* 78—92715
- echography, in vivo A-scan dynamic autocorrel. anal. 80—51192
- echolocation, bat, accuracy of meas. of target angular coords. using equisignal zone 78—77071
- EEG automatic segmentation based on autocorrelation function 79—96673
- EEG eye movement artefact removal 77—44826
- EM wave attenuation and rainfall rates dual-polarisation radar meas. technique, precision 79—25371
- errors, signal parameter meas. 80—57241
- European air temperature band-pass filtered series, correls. and phases 80—26579
- evoked potential averaging, cross correlation and iatency-corrected averaging comparison 79—53268
- exercise vectorcardiogram, spatial velocity and magnitude ECG correlation 79—43846
- exercise vectorcardiogram changes rel. to left ventricular function at rest 79—43859
- fast image recognition by generalised harmonic analysis *(Russian)* 80—63930
- fermions, constrained variation in Jastrow method at high density, neutron system, liquid ^{3}He appls. 77—5753
- filter functions, Savitzky-Golay, freq. response plots 77—53741
- fission reactor theory, resonance reaction rates, group averaged, correl. technique 79—59129
- flat plate solar collector efficiency and heat loss characteristic meas. 79—62064
- flow statistics derived from laser anemometry, retrieval via photon correl. 77—3896
- fluctuations of intensity at two wavelengths in turbulent medium 80—87318

correlation methods continued
- fluorescence correlation spectroscopy, profile of focused collimated laser beam near focal minimum 80—43386
- fluorescence spectroscopy applied to biopolymer dynamics and struct. 77—60329
- Fourier interference spectrometric detection of atmospheric pollutants 80—35813
- Frank ECG correlates of left ventricular ejection fraction 79—39405
- fundamental voice freq., correl. anal. of physiological factors 78—40201
- galaxies, distant, space distribution, evolution effects 79—40260
- galaxies, distrib. in 36 square degree field near North Galactic Pole 79—40261
- galaxies deep samples, correl. anals. 79—67104
- galaxies optical redshifts determ., Fourier transform filtering and cross correl. techniques 80—56936
- galaxy clustering, correlation analysis of space and surface distribs. 78—16546
- galaxy clustering rel. to correlation functions hierarchy 79—30138
- galaxy correlation function evolution, N-body Monte Carlo model 80—62292
- galaxy n-point correlation functions, applicability to clustering models discrimination 80—8699
- galaxy redshifts survey, data reduction techniques 80—22074
- Galaxy turbulent structure from radio sources Faraday rot., correl. functions 78—20885
- gastro-intestinal electrical rhythms, freq. estimation using auto-correlation and auto-regressive modelling 77—44875
- geodesy, influence on window functions on prediction *(German)* 77—86749
- geodesy, strict determ. of adjusted straight line from correlated obs. *(German)* 77—86751
- geoelectric sounding, correl. analysis of induced polarisation curves *(Russian)* 77—9565
- geomagnetic field reversals, correl. function anal. 80—21622
- geomagnetic pulsations, cross-correlation and cross-spectral analyses *(French)* 79—70928
- geophysical fields correl. anal., input conditions *(German)* 79—35014
- geophysics, combined anal. of geophysical and geological data for ancient metamorphic forms. study *(Russian)* 79—8630
- geophysics, complex exponentiated data digital correl. *(German)* 79—44279
- gravitational waves, possible detection using correlation techniques 78—89393
- hepatic tissue in vitro acoustic attenuation slope spatial correlation obs. 79—57702
- high-pressure asymmetric mixture vapour-liquid equilibrium calc. 79—4408
- holograms of diffuse objects, autocorrel. of transmittance 78—1185
- holographic information, photoelec. recording, correl. methods 77—79784
- homogeneous random fields, modelling realisations 80—8911
- hourly diffused solar radiation, horizontal surface, computer simulation appl. 77—81981
- hydrometeorologic elements in coastal zone, long-term var. from correl. anal. *(Russian)* 78—77258
- identification of acoustic pathways through barriers 80—102880
- image alignment errors due to aliasing 80—106480
- image correlation based on extracted edges 80—99658
- image correlation in white light by wavelength multiplexing 79—55072
- image correlation with geometric distortion acquisition performance 78—71039
- image correlation with geometric distortion effect on local accuracy 78—71040
- image degradation identification 78—58941
- image matching using struct. information, edge vector correlation 78—63036
- image registration and differencing by coherent optical pattern recognition 80—99648
- image registration using material information 80—99664
- implicit sampling for noncoherent optical data processing 80—99652
- improvement of cross-correlation peaks by image filtering 79—76610
- incoherent optical correlation operations 80—99650
- incoherent scatter radar correlation function meas. 77—73888
- interferometer signal processing by acoustooptic correlation devices, radio astronomy applications 80—8543
- intestinal motility study by computerised anal. of sounds and EMG wall pots. *(German)* 78—31944
- ionosphere sounding, filtering effect on drift parameters determined by full correl. anal. 78—65450
- IR correlation process analyser, non-dispersive instrument 77—82628
- isostasy investigation, correl. coeffs. between elevations and Bouguer anomalies 77—86850
- jet engine noise source location, polar correl. technique 77—62105
- jet flows, correlation techniques to detect azimuthally coherent structures 80—53765
- jet turbulence, laser velocimeter correlation meas. 80—106785
- Jupiter decamatric radio emission and solar activity, short-term correl. anal 79—21222
- Landeu model, critical multiple correlations 79—75440
- LANDSAT-1 digital image registration and cloud effect rectification 77—78490
- laser anemometry, high Reynolds number flow, review, data anal. for photon correl. method, simulation 79—60082
- laser crossed beam correl. technique, meas. turbulence parameters, in rocket exhaust 79—86541
- laser Doppler anemometry in internal combustion engine cylinder 79—77296
- laser scattered light intensity, recurrence rate correl. 78—66760
- laser surface speed measurement by correlation, industrial paper machine test *(French)* 80—95082
- left ventricular hypertrophy with bundle branch block, ECG/VCG and echocardiogram correlation 79—44035
- leg loading components correlation in snow skiing 79—96608
- Lennard-Jones and Stockmayer pot. parameters, crit. evaluation, correl. methods 78—1966
- linear predictive coded speech digitisers, background noise spectral subtraction 80—96140
- liquid mixture, surface tension theory 80—88404
- liquid two-dimensional itinerant oscillator model testing by molecular dynamics 79—32868
- LMFBR Na vapour bubble collapse detection by acoustic emission 79—13451

correlation methods continued

M-sequence modulated acoustic signal propagation meas. *(Japanese)* 78—18132

magnetic anomaly field vertical intensity, autocovariance function analytic derivation for sources statistical distrib. *(German)* 79—34746

mammographic US image correlation with histopathologic sections 80—101240

maximum entropy method, accuracy improvement via autocorrel. method 80—56712

maximum-entropy correlation and spectral analysis of short-length biomedical signals 79—66577

maximum-likelihood method, measuring baseline coordinate vectors of multielement radio interferometer 80—26753

measurement data equal accuracy verification 78—8378

meteorology, optimum difference schemes, synthesis on sphere 78—93011

missing values in time series, effect on autocorrelation analysis 79—17197

model, with distributed parameters, inverse problem 79—75322

Mohorovicic relict discontinuities, multidimensional correl. anal. rel. to tectonic cycle recurrence *(Russian)* 77—44947

molecular dynamics, high speed computation of correl. functions 77—7648

molecular rotational and vibrational relaxation autocorrelation functions 80—32856

moonlit object real-time optical matched filtering 77—19192

motif detect. in quantum noise limited electron micrographs 77—67546

multiband image spatial domain filtering by Karhunen-Loeve transform 78—78952

multiple-frequency heterodyne correlation radiometer, min. detectable power 77—74508

multisensor image pattern recognition, statistical and deterministic aspects 80—99647

multisignal time difference estimator for transient sound source location 80—96127

multispeaker phoneme classification by canonical correlation analysis 80—91988

multispectral digital images, intensity variations and false colour display correlation 77—78514

myocardial ^{201}Tl scintigram anal. by coded aperture imaging 79—79647

myocardial injury, correlation of US and enzymatic indices 77—21581

natural terrain scenes, segmentation-based boundary-modelling processor 80—99661

nerve axon automatic counting 78—31994

noise sources in open turbulent pre-mixed flames, correl. methods expts. 77—51127

nonlinear operator realisation, coherent optics method *(Russian)* 79—94157

nonperiodic objects, reconstruction from electron micrographs using correlation methods 80—86527

northern hemisphere annual temperature approximation, simple method 78—81345

nuclear power system and fuel channels stochastic identification and parameter estimation 79—3201

nuclear reactor transit time estimation coolant bubbles appl. 78—94067

oblique incidence sound absorpt. characts. of materials using cross-correlation methods *(Japanese)* 78—83172

ocean bottom relief description using spatial correl. function 77—21760

ocean transparency field, statistical relationships with hydrological and biological characts. *(Russian)* 79—88361

ocean wave synthetic aperture radar imagery rel. to surface structure 80—46197

OCR by spatial filtering with light beam deflection 78—1370

OCR systems based on nonredundant correlation meas. 79—94162

optical, precision of detail recognition *(German)* 78—9340

optical, speckle appls. 77—19189

optical analogue computer performance advantages 78—78949

optical cross correlation by complex exponentiation of input data 77—71942

optical cross-correlation of complex exponentiated input data 78—42290

optical data cross-correlation matrix processing 79—13910

optical determination of real or complex correlation functions between the signals *(Spanish)* 79—76611

optical information storage, seminar, Washington, USA (Apr. 1979) 80—41942

optical Mellin transform using computer generated hologram 77—10850

optical pattern recognition, discriminant hypersurface prod. by average filters 80—99649

optical pattern recognition by thermoplastic complex filter 80—99656

optical polarisation meas. amplitude correlation method 80—53206

optical residue arithmetic, correlation approach 79—31809

optical signal and image processing, US Air Force research programme 80—78791

optical space-variant pattern recognition, using polar camera 78—66767

orthogonalization of random variables, weather forecasting appl. 77—74203

outputs of acoustic arrays, crossarray beamforming with a parametric receiving array and a line array 80—79078

PARCOR anal. lattice, inverse filter reflection coeff. calc. *(German)* 80—96114

passive time-delay estimation with moving source or receivers, correlator compensation requirements 80—58843

pattern recognition using wavelength-multiplexed matched spatial filters 79—76603

periodic sampling in periodic fluid flow measurement by laser anemometry 80—64657

perturbation computation with correlated sampling, nuclear reactor neutron transport 79—588

Photoelectric recording of optical fields by correlation processing 78—71048

photographic development, correlation analysis of developing ability and structural data of pyrocatechol derivatives 79—20448

photon correl. laser anemometry, information extraction method 79—60081

photon correl. laser anemometry, on-line data reduction system 79—60080

photon correl. spectroscopy, macromolecular soln. dynamics, review 79—59603

photon correl. velocimetry, turbomachinery and industrial burner velocity and turbulence profiles 79—60083

photon correlation in nanosecond range using programmable digital counter, photomultiplier evaluation 78—54464

correlation methods continued

photon correlator, near ideal, with SAW device 80—68252

plasma, streaming in crossed fields, conductivity tensor calc. using correl. function of microscopic current 77—19675

Plurimat 20 data acquisition system, phys. appls., automatic simultaneous data recording *(French)* 77—41579

polarity correlations in nuclear reactor anal. using noise techniques 77—14219

polymer molecular weight correlation with physical and rheological props. 77—51011

polymer viscoelasticity and strength characterisation, advanced light scatt. techniques 80—11857

positive column, striation dynamics, velocity/amplitude correlation 78—67517

power curve regression equations for Ohio River, statistical computer program 78—61472

precipitation over Central Europe, large-scale field components extraction for forecasting purposes 78—92940

propeller cavitation tunnel hydroacoustic transfer function, meas. and anal. *(Croatian)* 80—92002

pseudonoise signals reflected from ocean bottom, correlation with transmitted signal 80—58846

pulmonary artery press. estimation using pulse wave velocity 80—12203

pulsar scintillations, freq. cross-correl. and finite bandwidth effects 80—4392

pulse sequences, mixed spectrum, appl. to linear atom chains 79—84944

PWR components vibrations meas. *(German)* 80—79247

PWR neutron noise interpretation by vibration analysis 78—94073

PWR pressure vessel vibration excitation, noise correlation and modelling 79—13442

QSOs and Lick galaxy counts, correl. from extragalactic objects catalogues statistical anal. 79—25700

quantum chemistry, matching model calcs. with experiment through linear regression 80—58243

quasar redshifts distributions, periodicity from correl. and power-spectrum anal. 80—62313

quasicoherent light source image synthesis by phase measurable interferometry 77—58284

radar ambiguity function display and one-dimensional correlation/convolution by coherent optical processors 78—78950

radar signals reflected from sea waviness 80—46190

radiographs, industrial, discontinuous registration using profile analysis and piecewise correlation techniques 80—102645

radiowave reflection from ionosphere, large-scale screen speed determ. 77—9602

rain parameters, meas. by optical scintillation, correl. method simulation 78—36290

rainfall, monthly, in NW.Georgia, spatial correls. rel. to climatology and weather modification expts. 80—51479

random data filtering, effects of detrending and smoothing 78—40685

random process correlation coefficient sign determ. 79—71232

rank correlation, appl. to variant selection for automatic solar stratospheric station construction *(Russian)* 79—96913

real 1D signal convolution and correlation by freq. plane filtering 80—32919

real-time moving object tracking by optical correlation, using liq. cryst. image transducer 79—32035

reflected-beam laser anemometry using photon correlator 80—106861

remote measuring techniques, three-channel correlation *(German)* 79—50512

repetitive signal, signal processing via surface acoustic wave recirculation loops 78—22228

residential building heat loss estimation by aerial IR imaging 79—74586

ring pseudorandom aperture for transverse section radioisotope tomography 77—64129

ripple noise pitch detection by human, adaptive model 78—73166

rocket exhaust anemometry, Doppler difference and two focus methods, correlator and photon counting 79—60084

rotated image correlation by gradient vector sum histograms 79—75647

rotating noise sources, correl. meas. method, math. model construction *(Croatian)* 77—39150

SAW information storage and correlation in semiconductor diode arrays 78—9505

scale and rotation invariant optical pattern recognition and classification 80—99655

scanning optical sensor signal peak extraction and multiframe correlation methods 79—81380

scintigram change obs. by crosscorrelation 78—80961

seismic events correlation in time section, algorithm *(Russian)* 79—39962

seismic events visual correlation quantitative estimates based on min. average risk criteria *(Russian)* 79—44133

seismic shear waves, Q estimation from S-SS amplitude correls. 77—64218

seismology, noise-resistance of optically generated correlograms *(Russian)* 78—40699

seismology, rapid convolution and correl. *(Russian)* 79—39959

seismometers, automated high-precision amplitude and phase calibration 77—9519

semiconductor junction noisy transient meas. 78—62205

semielliptic notch with crack, micro- and macro-stress concentration correlation *(German)* 78—83330

ship model wake meas. in wind tunnel, laser anemometer autocorrelation *(German)* 79—60085

sideways-looking radar using synthetic aerial, remote sensing appl. 78—69537

siesmic surface waves correlation method, appl. to tectonic dislocations prospecting in complex media *(Russian)* 79—8605

signal processing, time-integrating, acousto-optic 80—102641

signal processing activities of United States Army 80—48172

sleep EEG activity and hormonal change correlation 77—9314

solar cycles 14 to 19, large sunspot groups occurrence frequency 77—17467

solar energy system simulation, diffuse and total solar radiation relationship 79—57398

solar insolation at Fort Hood, Texas, prediction correl. 78—24333

solar radiation, correlations between diffuse and hemispherical and between daily and hourly insolation 79—87975

solar radiation data, statistical correl. between daily and monthly averages 80—8409

correlation methods continued
solar wind velocity recurrence period, depend. on heliographic latit. 80—62106
sound pressure in rectangular reverberent room, correl. coeffs. 78—18115
SPAC, speech processing using the autocorrelation function, noise reduction in speech communication *(Japanese)* 80—33371
space research, signals auto-correl. and cross-correl. preprocessing on spacecraft 77—64609
spaced fading records, correlation analysis, occurrence of negative V_c^2 79—88540
spatial coherence meas. by correlated diffusers 80—74296
spatial convolution and correlation of optical fields via degenerate four-wave mixing 78—71044
spatial pattern recognition by spectral feature classification and coherent optical correlation 80—99644
speckle pattern time-space cross-correlation for in-plane vel. meas. 80—105623
speckle wavelength decorrelation for surface roughness meas. 79—30418
speech, aspects of grammatical coding in correls. of duration for nonadjacent segments 77—56387
speech synthesis from partial autocorrelation vowel-consonant-vowel concatenation units 79—46135
spread-spectrum signal optical processing 79—72518
statistical treatment of experimental data, book 78—77834
stellar radial velocities determ. via cross-correl. techniques and TV detector, appl. to (NGC 6327) 78—16305
stellar speckle interferometry for stars cold satellites searches, autocorrel. functions *(Russian)* 80—12672
stellar spectrograms, relative Zeeman and Doppler shifts determ. via statistical approach 78—36467
stereophotogrammetry, automatic, using structural pattern recognition techniques 78—61632
Stockmayer and Lennard-Jones pot. parameters, crit. evaluation, correl. methods 78—1966
stratigraphic correlation by principal components, effects of missing data 79—25350
structural-vibr. related noise, anal. via statistical correl. theory 77—84077
subcellular motions in Nitella flexilis, photon correl. spectroscopy 79—66465
Sun glitter on sea, correl. function appl. to sea surface slope distrib. function determ. *(Russian)* 80—94611
surface displacement meas., coherent optical correlation technique 79—75499
synoptic climatology development for NE.Gulf of Alaska, automated correl. technique appl. 80—98405
tape recording, low freq. FM, of nerve action potentials 79—57832
thoracic X-ray image comparison automation *(Japanese)* 79—29615
time, for measuring fluorescence decays with CW He-Cd laser 79—50072
time and temp. correl. functions, calc. method with quasi-particle appls. *(Russian)* 78—12641
time integrating acousto-optic signal processors 80—48176
time-resolved fluorimetry, cross-correlation method 79—79331
tissue pulse-echo US absorption estimation model 79—48304
tissue US signal analysis methods 79—57737
TOF spectra, parameter estimation and gain of correlation method 79—49895
transionospheric propagation from a satellite, observations on the beyond-the-horizon statistics 77—25825
transionospheric radio signal time delay spatial correlation 78—45117
transparency optical thickness irregularity processing by laser heterodyne correlation 79—14119
two-frequency dispersion interferometers for space plasma nonuniformity 79—70964
two-phase fluid velocity meas. by radiation intensity correlation 77—75996
two-tone image analysis using one-dimensional autocorrelation function *(Russian)* 80—63931
ULF wave-particle interactions, dynamic cross correlation studies *(French)* 79—70926
underwater acoustic source location and motion estimation, joint reduction of bias and variance 80—96087
underwater acoustic time delay estimation, cross-correl. and smoothed coherence transform methods compared 80—96086
underwater acoustic transducers, reciprocity calibration by FM signal correl. methods 77—68298
underwater camera data correl. and interpretation, systems approach 79—5688
underwater sound, acoustically relevant statistics for stochastic internal-wave models 77—46854
underwater sound arrival angle estimation by multiple cross-correlation meas. 78—66978
underwater sunlight fluctuations in sea spatial and temporal correlation 80—94533
US crack detection, emission pulses amplitude and crack size correlation 77—90568
US filtering and correlation by SAW devices 78—60969
US flowmeter, correlation and spectral props. of flow modulated US signals 77—42948
US lateral and range resolution improvement by optical computer 79—53203
US materials testing, under industrial conditions 77—75759
US tissue characterisation by backscattered field space-time processing 79—48305
US vel. meas. using quartz transducer transmitter-receiver 78—30139
US-optical correlator for spatial freq. meas. 80—95995
vectorcardiogram and ECG correlation with angiocardiographic left ventricular mass 79—44027
vectorcardiogram and ECG correlation with coronary arteriorgram and left ventriculogram 79—44041
vectorcardiographic P loop correlation with left atrial volume echocardiogram 79—44025
vehicle noise meas., expt. 77—68349
Vela supernova remnant, rot. measure correl. function and assoc. power spectrum rel. to turbulence 80—51836
velocity distribution measuring system, 2D, using multiple line detectors and correlation analysis 80—14851
velocity measurement by light scattering techniques, digital correlation appl. 78—57916

correlation methods continued
Venera 9 televised pictures of Venus cloud layer, geometrical correl. methods 80—67604
virometer, real time virus detect. and identification in biological fluids 78—7555
visual evoked response of humans, nonlinear anal. 78—92622
VLF signals propagation, multi-mode, statistical anal. *(Russian)* 79—5702
voice tremor EMG correlation, psychological stress evaluators 77—9214
Volterra kernel estimation of bilinear systems, cross correlation algorithm 79—80919
water waves, wind-generated, spatial correls. rel. to freq. independent phase vels. 80—98333
wave propagation in one-dimensional medium with space-time inhomogeneities, spectral-correlation characts. evolution *(Russian)* 79—2634
wind characteristics for energy conversion systems, variance anal. 78—49100
wind remote measurements, individual particle scatt. and single-burst digital correl. 79—100980
workpiece quality control by optical correlation 77—50644
OH, submicron airglow bands correl. studies during Spacelab simulation 79—25381

correlation theory
see also correlators; information theory
20 GHz multi relay links, simultaneous probability of rain attenuation 78—3898
atmosphere optics, phase correlation scale effects rel. to atmospheric imaging characts. 80—94604
auditory system pitch detection mechanism model 77—90811
bat echolocation system, optimum phase modulation for insensitivity to acceleration 79—53163
bidimensional surface waves, periodic correlational random field model *(Russian)* 78—20430
bilinear system Volterra-kernel estimation 79—26512
biomedical signals, development of common struct. for filters, correlators and Fourier analysers *(German)* 78—88748
complex meas. system error correlation matrix *(Russian)* 77—9979
contrast of time-averaged speckle patterns produced by small vibrations of diffuse objects 79—94169
density perturbations in expanding universe, linear theory 78—4417
diffusing object surface state study by double speckle photography 79—85120
discrete process, one-dimens., invariant distribs. and stationary correlation functions 78—21059
distributed parameters' correlation effect on meas. system output *(Russian)* 77—9980
expanding universe, density perturbations three-point correl. function and higher order functions prediction 78—65730
focused radiation scintillations, freq. correl. by speckle interferometry 79—94153
Fresnel plane interference fringe generation by correlated speckle patterns 80—106462
function determination problem 79—71396
galaxy pair-correlation function, clustering evolution effects, cosmological N-body simulations 78—96550
galaxy two-point correlation function, integral constraint on evolution 77—5578
geomagnetic field quiet time var. rel. to interplanetary mag. field, autocorrel. effects 78—61697
geophysical interpretation problems, soln., correl. theory of homogeneous random fields appl. 79—100986
interferometer model for binaural perception and resolving power of bats *(French)* 78—80883
IR staring mosaic sensor performance, effect of spacecraft-induced line-of-sight jitter 80—86416
jet propulsion aircraft noise, two-point correlation model 78—42493
laser cavity resonators, spatial field configuration with nonresonant feedback 79—18453
measurement accuracy influence factor grouping and correlation 78—41262
non-gaussian field, clipped time autocorrelation function of intensity fluctuations 80—106472
non-purely ferromagnetic systems, correlation inequalities 79—47219
phase expansion coefficients spatial correlation, propag. through atm. turbulence 79—80021
photon correl. and analogue signal processing, clip-level crossing rates 77—88650
quantiles, use in construction of correls. 77—91291
radiowave phase fluctuations in anisotropic turbulent atmosphere when emitted by moving source 80—17352
reverberant sound field spatial cross-correlation 79—68496
ring laser mode competition and anticorrelation calc. and expt. 80—102740
skin impedance parameter dispersion and correlation 79—29518
SPAC speech processing system using autocorrelation function, operation and characts. 79—68510
space-time optics, speckle phenomena and white light correlations 80—106460
spatial-correlation theory, evaluation of integral 77—88981
speech quality and intelligibility measures and their correlations 80—91978
speech quality parametric objective measures correlated with subjective results 80—91980
speech quality subjective and objective measures and their correlations 80—91979
stationary random processes, correlation between level-crossing time interval lengths 80—22292
statistical properties of light, change by multiphoton absorbers with intermediate reson. 79—86208
statistical treatment of experimental data, book 78—77834
stereo-pair images, correlation error prediction 80—102636
surface roughness estimation using linear FM signal *(Russian)* 78—77353
tube turbulent convection, effective power dependence of heat transfer coeff. 79—4006
underwater sound propagation in presence of randomly perturbed parabolic profile 78—94477

correlators
  see also correlation methods; correlation theory; information theory
  5120-channel digital cross-correlator for Westerbork radiotelescope 77—64650
  acousto-optic correlators, real-time and memory devices 78—46533
  acousto-optic correlators, spatial or time integrating, review 78—9341
  acousto-optic memory correlator, long duration, using acousto-photorefractive effect 78—79124
  acousto-optic memory correlator using acousto-photorefractive effect 78—71248
  acousto-optic real time two crystal correlator 78—42497
  acousto-optic real-time radar and sonar signal processing 79—72515
  acousto-optic signal correlators, review 77—58473
  acousto-optical, with two-dimensional reference transparency, testing 80—106485
  acousto-optical devices for real- and near-real-time signal processing 80—10024
  acoustoelectric memory correlators, fabrication, experimentation and anal. 79—32179
  active optical devices, seminar, San Diego, CA, USA (August 1979) 80—101664
  adaptive, appl. of DIAM acoustic signal storage device *(French)* 77—7272
  add-subtract digital correlator, design and performance 77—61053
  aerial reconnaissance film interrogation by optical matched filtering 77—78484
  ambiguity processing by joint Fourier transform holography 80—58468
  astronomical telescope speckle interferometry, online digital autocorrelator 78—81548
  automated correlation spectrometer with two Ge(Li) detectors 78—82562
  biomedical signals, development of common struct. for filters, correlators and Fourier analysers *(German)* 78—88748
  Chinese character recognition with real time optical correlator 78—29904
  clip-correlator, fluorescence intensity correlation, photon counting *(Russian)* 80—42271
  clip-correlator, for fluorescence correlation experiments *(Russian)* 80—42270
  coded aperture imaging, analogical deconvolution appl. to nucl. medicine *(French)* 78—35943
  coherent optical correlation techniques, review 80—43277
  coherent optical correlators, filter plane resolution requirements 77—34828
  coherent optical processor for vehicle tracking and identification using laser diode light sources 80—37957
  coherent optical processor with interference contrast microscope input 80—43281
  coherent optical signal processor for passive ambiguity function generation 79—72520
  composite bioelectric potential analysis, online hybrid system 77—9313
  cross correlator, wide bandwidth, construction and appls. 78—4658
  cross-correlator for broad-band impedance meas. using high-speed CMOS switches 77—26324
  detector integration acouto-optic signal processing 79—72519
  diffused p-n diode memory correlator 77—23831
  digital correlator, for signal preprocessing on spacecraft 77—64609
  digital correlator signal preprocessing 80—83556
  digital correlator with blinker facility for photon correlation spectroscopy 80—37092
  digital receiver, 5000 channel, radiotelescope appl. *(Dutch)* 77—67040
  diode array SAW correlator model and expt. 78—9508
  equalizing and coherence measure correlators 79—13911
  geodesic lens design for integrated optics signal processing 80—33247
  HF random process statistical characteristics meas. 77—18045
  high-speed correlometer, based on US delay line 77—75757
  hologram filter for three dimens. object recognition *(French)* 79—18359
  holographic, expts. to improve accuracy 77—65583
  holographic correlator, noise sources, accuracy improvement 77—23636
  holographic interference correlators, theory 78—78969
  hybrid optical corelator system for automated stereo compilation 78—63035
  image Fourier transform correlator using US light modulator *(Russian)* 77—58264
  imaging system using intensity triple correlator 78—74846
  incoherent diffraction correlator with a holographic filter 80—37955
  incoherent optical correlator using projected fringes patterns, for object shape and contour control 79—97357
  integrated optics coherent correlator for real-time signal processing 80—79007
  joint transform correlator performance rel. to wavefront modulator characteristics 80—102651
  kit of instruments for statistical research 78—87215
  large time-bandwidth acousto-optic signal processors 79—46118
  laser diode lensless MSF holographic optical element correlator, optical pattern recognition 80—102663
  liquid crystal image transducer, performance effects of liquid crystal thickness 80—102838
  Malvern, based on photon correlation and laser scattering spectroscopy, development and appl. 80—5741
  matched filter, multicapacity, for correlator appl., using birefr. object film 80—74478
  matched filtering using band-limited illumination 80—69531
  memory-correlator cells employing acoustically induced charge hologram in piezoelectric semiconductors 78—86290
  multichannel digital correlator for optical mixing spectroscopy 79—93234
  one-bit correlation method for aneurysm detect. 80—17175
  optical, incoherent, analogue techniques 77—10863
  optical, joint-Fourier-transform correlator, dual-axis, hologram recording 79—59649
  optical, laser damage to photographic emulsions 79—27303
  optical, nonlinear t-E curve effects for matched spatial filter material 80—95812
  optical, spatially coherent white light 79—3642
  optical, using real time chromatic filtering and extended white light source *(French)* 79—3641
  optical coherent correlator operation in image segment identification, aerial photograph anal. 80—102654
  optical convolvers and correlators, generalised model 78—55303
  optical correlation instrument field-of-view, intensity distrib. selection 79—72688
  optical correlator, wavefront propagation error effects 79—50232

correlators continued
  optical correlator length shortening using Fourier transform lens array 79—59646
  optical correlator with shift invariant linear matched filter 80—37962
  optical diffraction correlators invariant to optical element shifts 80—106471
  optical frequency plane correlator, degradation sources 77—71924
  optical image and signal processing, United States Air Force programmes 78—74854
  optical image correlation, real-time high-resolvance, by Bragg diffr. in saturable absorbers 80—48159
  optical image plane correlator for ambiguity surface computation 79—76598
  optical image-forming system for T-type correlation antennas 79—27180
  optical information storage, seminar, Washington, USA (Apr. 1979) 80—41942
  optical joint Fourier transform processing with thermoplastic device 79—72512
  optical matched filter correlator memory techniques and capacity 80—43280
  optical matched filter correlator memory techniques and storage capacity 80—102643
  optical matched filter image correlator, for aerial reconnaissance film screening 78—94371
  optical Mellin transform, freq. plane and joint transform correlators 77—10849
  optical multiple-invariant space-variant processors 78—42279
  optical pattern recognition, coordinate transform. preprocessing 77—61921
  optical pattern recognition, deformation invariant, space variant, book contrib. 79—76619
  optical wideband ambiguity function generator with Doppler compensation 78—78936
  OTF measurement using autocorrelation method 80—58469
  photodichroic spatial light modulator for joint Fourier transform correlation 80—106617
  photon correlator for meas. transient waveforms of very weak fluorescence 80—87250
  plasma line correlator and filter bank, appl. to plasma line meas. at Chatanika 80—98507
  positional coding optical correlator, tabular coordinate search method *(Russian)* 79—98292
  pressure modulator radiometer for atm. gas emission meas. 78—81457
  pseudorandom binary noise US correlation system for nondestructive evaluation 79—52612
  radio antenna arrays, incoherent optical 1-bit cross-correlators, radioastron. appls. 80—98555
  radio astronomy, interference-excising correlator 79—75110
  real time optical correlation of 3-D scenes 77—27262
  SAW acousto-optic time integrating correlator 80—64295
  SAW correlators for US flaw detection 77—19470
  SAW delay line acousto-optic signal processing devices 79—94328
  SAW device analogue signal processing appl. 77—27437
  SAW memory correlators, charge storage 79—64455
  SAW monolithic storage correlator, appl. to adaptive filter 78—87208
  SAW storage correlator, input correlation 77—84085
  SAW storage correlator equivalent circuit models 78—9506
  SAw/CCD accumulating correlator for analogue signal processing 79—72757
  semiconductor injection lasers in correlative data processing systems 80—74307
  side-entry surface acousto-optic interaction signal processor 80—48174
  signal time delay estimation, quantitative study of optimum and sub-optimum filters in generalized correlator 79—59866
  sonar Doppler phased array coherent imaging and processing by metaxial optics 79—72521
  space variant optical correlators, accuracy and space bandwidth 78—17864
  space-blur bandwidth product in correlator performance evaluation 80—43270
  spatial filter correlator, coherent optical matched, for microfilm data base word recognition 80—43279
  storage convolution, correlation using SAW, piezoelectric devices, signal processing appl. *(French)* 79—32146
  surface wave memory correlator using nonlinear interactions *(French)* 80—33294
  surface-wave acousto-optic signal processors 80—102640
  time-integrating acousto-optical correlator design and performance 80—106618
  tracking correlation receiver with feedback for radio astronomical interferometry 78—57445
  unclipped digital correlator for quasielastic light scattering 80—57387
  US return signals, correlation with bipolar digital representation of broadcast waveform 80—99897
  velocity measurement, correlator design 79—40544
  video correlating system for blood flow vel. meas. in microvessels 78—53543
  wide bandwidth analogue correlator, appl. to mode-locked ion laser meas. 79—88983
  wideband chirp and Barker code correlations with storage convolver 77—23832
  LiNbO$_3$ acoustophotorefractive memory correlator enhancement 79—55080
  Si diode storage correlator optical imaging and memory characteristics 77—23772
  TeO$_2$ time-integrating acousto-optical correlator for chirp spectrum analyses 80—106474
  ZnO monolithic SAW device, separation of storage effects 79—18611
  ZnO Sezawa mode pn-diode array memory correlator 79—78178
  ZnO-Si p-n diode monolithic storage correlator 78—18119

correspondence principle
  classical action in nonrelativistic quantum mechs. 77—71235
  Einstein, quantum mechanics, conceptual problems 80—46783
  electron self-energy problem, correspondence principle 79—93321
  Feynman path integral and quantum mech. as $\hbar \to 0$ 77—2557
  general relativity theory, logical status 77—68
  general system quantisation, rigid sphere appl., wave eqn. using correspondence principle 78—57801
  gravitation theory, energy aspect of correspondence principle *(Russian)* 77—2576

correspondence principle continued
hadrons, uncharmed, rotational states 80—22596
indeterminacy, classical tests without corresponding quantum tests 80—62527
intrinsic geometry of quantum mech. phase space Hamiltonian systems, correspondence principle 79—83
Liouville mechanics for systems with singular Lagrangian, quantisation 78—62096
multiphoton inverse bremsstrahlung, plasma laser absorpt. coeff., correspondence principle method 79—32749
orbital correspondence anal. in max. symm., appl. to spin-forbidden processes 78—78631
potential step scattering, theory 80—46761
quantisation as a nontrivial deformation of classical mechs. *(Czech)* 78—86171
quantum mechanics, development and Heisenberg's role *(Polish)* 78—89291
semiclassical amplitudes, generalised theory, overlap states 78—4499
stochastic action integral interpretation of quantum mechanical transformation function 80—77644
temporal logic 80—27176
weak gravitational field, connection between Dirac and Dixon eqns. 78—124
Wheeler's superspace, correspondence eqns., variational principles 78—24696

corrosion
see also corrosion protection; corrosion testing; electrochemistry; stress corrosion cracking; surface chemistry
AC induced, alternating voltage effect on electrode under charge transfer control 80—21156
accident of plant *(Japanese)* 79—29248
Al alloy, welded, behaviour in sea water desalting conditions *(Japanese)* 77—25192
alite paste, mature, microstructure study by SEM, TG and X-ray diffr., corrosion 78—92381
alkali metals, liq., compatibility with ceramics 77—44387
alkali silicate glasses in aqueous solutions, leaching kinetics rel. to surface pot. 80—11803
alloy, high temperature, mechanical, thermal and corrosion props. 78—95763
alloy, HTR material, oxidation and carburization in He 80—108645
alloy, super- and heat resisting, thermodynamic study of corrosion 79—57161
ALLOY 713LC, corrosion kinetics and products under low oxygen partial pressures *(German)* 79—87764
alloy colour and colour stability as alloy design criteria 80—101005
alloy steel, austenitic, Ni free, TEM exam. of corrosion process 78—85029
alloy steel, corrosion resistance in liquid metals *(Czech)* 77—50245
alloys, corrosion resistance in geoethermal brine environments 78—85032
alloys, ion implantation in tribology and corrosion science, overview 79—14830
alloys, potential-pH diagrams for interpretation in high salinity geothermal brines 79—96191
alternating current electrode processes, review 80—61107
alumina, wear, effect of liquid environment, use of pendulum scratching sclerometer *(Russian)* 77—16693
amalgam, dental, corrosion, immersion conditions 79—12037
amalgam, dental, corrosion behaviour, market survey 79—12038
amorphous metals, book contrib. 79—66225
anorthite, ceramic, chem. resist. and struct. 79—61756
atmosphere, corrosion test site selection *(French)* 80—16893
atmospheric corrosion by local microelement participation 78—7067
austenitic alloys, corrosion performance in automobile exhaust environments 78—7091
austenitic alloys in hot water, low cycle fatigue, appl. to nuclear reactors 77—4871
austenitic stainless steel tubes in liquid Na, 873K and 973K 77—57722
austenitic steel, Cr-Ni alloyed, Ti stabilised, nuclear reactor pipeline appl. *(Hungarian)* 77—18658
automatic corrosion rate monitoring, in near-neutral soln., using a microcomputer 80—50749
basalt fibres, alkali resist. in cement soln. 80—89377
boiler tube, investigation using gamma-ray transmission meas. technique 77—9011
bonding material of basic refractories, effect of SO_3, Na_2SO_4 and V_2O_5 79—83343
boronised coating on steel, sliding and abrasive wear, corrosion resist. 78—11428
brass, admiralty, dezincification conditions in fresh or seawater, thermogalvanic method 80—16548
brass, Auger spectral anal. of oxide corrosion films, quantitative methods 78—35557
brass, corrosion and dezincification in water 77—16740
brass, corrosion inhibitors, triazole, benzotriazole, naphthotriazole 77—25182
brass, corrosion pretreatment effect on corrosion inhibition 79—100280
brass, galvanic, anal., coplanar electrodes with radial symm. 79—52416
brass, hot stamping type, resistant to dezincification 79—70208
brass, sphere, dissolution in H_2SO_4 in elec. field *(Russian)* 77—4867
brass photocorrosion in $CuCl_2$ and $FeCl_3$ aq. solns. 79—57145
brass plate corrosion by HNO_3 vap., holographic interferometry 79—3658
brass-Sn couple in souring substances, corrosion 79—87760
brittle material, wear, acoustic emission obs., effect of ion aggregates in Rebinder-Westwood environment 78—48536
butadiene coatings, on steel, delamination by corrosion 78—64765
BWR, calc. of shutdown dose rate around recirculation pipes, radioactive corrosion products in primary cooling water 80—68734
BWR, high temp., high press. water circuit, NiOH injection effect on ass transfer 80—13533
BWR, primary coolant piping, Co deposition into corrosion films, model 80—13532
BWR radioactive products, behaviour 78—21661
BWR stainless steel piping, corrosion film charact. 79—54498
BWR with forward-pumped heater drains, water quality performance 79—67918
CANDU-PHW reactors, primary and secondary water chemistry, review 79—22382

corrosion continued
carbide, effect of mech. props. on erosion resist. under spark machining conditions 78—11421
carbon steel water tubes in alkali loaded solvents, corrosion speed investigation *(Hungarian)* 78—48559
Carpenter 20 Cb-3 alloy, pitting resist. in low salinity geothermal brines 80—93681
cathodic reaction during localised corrosion, theoretical model of location 79—70337
cavitational corrosion of materials in molten metals on const. mag. field appl. *(Russian)* 80—60987
celsian, ceramic, chem. resist. and struct. 79—61756
cement, regulated set, sulphate resistance and long term strength 78—35438
chemical states at surfaces exposed to high-temp. vapours 78—11559
chemically stabilised, sensitisation and corrosion resist., heat treatment depend., precipitation steel, stainless, Cr-Ni 79—38827
CIRENE reactor power channel, fuel string dynamics and pressure tube fretting corrosion 79—30950
coal conversion plant material, corrosion and wear 78—53012
coal gasification plant using nuclear process heat, material corrosion 78—13348
colloidal corrosion products model, prep. and charact. 80—16561
colorimeters, used for corrosion meas. production control, quality monitoring *(German)* 77—48603
commercial refractories, soln. in soda-lime glass, 1200-1350°C 78—95821
concrete, autoclaved, polymer impregnated and water cured, chemical resistance *(Japanese)* 78—31554
condenser tube corrosion resistance performance review 79—39046
conference, Electrochem. Society fall meeting, Las Vegas, USA (Oct. 1976) 77—16831
conference, electrochem. society fall meeting, Las Vegas, USA (Oct. 1976) 77—77787
contact current distrib. calcs. 77—21394
convective diffusion in pits 80—40601
corrosion products in main technological systems of atomic power plants with an RBMK-1000 reactor during operation 80—5236
corrosion resistance and mech. parameters of sheaths and tubes for nuclear power appl. 79—97813
corundum, corrosion resist. in fused Li rel. to phase and microstruct. changes 77—44378
crown glass, corrosion by organic acid solns., exam. of corrosion depth by interferometry *(Japanese)* 79—20237
Cu-Zn-Mn, de-alloying props. 80—104332
damage in nonmagnetic parts electromagnetic determ. of degree, apparatus *(Russian)* 77—70207
defect processes, theory, rate eqns., chemical rules 80—33990
defect theory and processes, review 80—2009
deformation effects in nuclear reactors and mech. structures 80—3211
dental amalgam, corrosion rates in Ringer solns. and artificial saliva 79—87758
dentin, human, effects of irradiation on wear resistance, microhardness and acid solubility 79—96634
design principles in corrosion research, expt. appl. 80—16515
destructive materials testing anal. by nondestructive electromagnetic methods *(German)* 77—86267
Duralumin, endurance limit and corrosion resistance *(Russian)* 77—16720
dynamic, in power units in hot industrial gas stream 78—35567
economic evaluation of loss *(Japanese)* 79—39005
education and role of professional societies *(Japanese)* 77—26105
elastomer compound O-rings for service in hot water, evaluation 79—29257
electrical contact material, sintered, corrosion under tropical marine climate 78—11366
electrochemical, linear polarisation equation 78—48661
electrochemical corrosion, kinetics anal. 79—96335
electrochemistry, steady-state conversion rate rel. to surface reaction process, catastrophe theory 80—108717
electrode, impedance and polaris. resistance 79—83466
electrode erosion, under pulse discharge for various materials *(Russian)* 77—51255
electrolytic coatings, corrosion of stainless steel and Ni in 40% wt. KOH 80—30175
electronic device dendritic growth mechanisms 78—56058
engineering, eval. and performance *(Japanese)* 79—20231
engineering, introduction *(Japanese)* 78—31555
epoxy meas. of H_2O diffusion by radionuclides, corrosion effects *(Czech)* 77—48566
eucryptite, ceramic, chem. resist. and struct. 79—61756
evaluation and performance in corrosion engineering. I *(Japanese)* 79—8378
examination, appl. of small cyclotrons *(Hungarian)* 78—70656
failure, metallographic anal. 79—61836
fatigue, review 77—8991
fatigue 77—4151
FBR fuel pin cladding attack model 80—45446
fibre reinforced composites, conf. Moscow, USSR (Nov. 1978) 80—8733
field-ion microscope specimens caused by polymer gaskets 80—57425
fission reactor materials, UO_2 high temp. reaction with Zr-Nb 78—66344
fission reactor structural materials, corrosion resistance in liquid metals *(Czech)* 77—50245
fluoride mixture, molten, resist. of materials to corrosion by 80—60797
freeze-drying corrosive materials 77—41580
fretting corrosion water-cooled nucl. reactor 77—79431
fusion reactor first wall materials, mechanical, corrosion and irrad. behaviour requirements 77—67875
n-GaAs, stabilisation against photodecomposition, surface damage influence 80—76390
galvanic, anal., coplanar electrodes with radial symm. 79—52416
galvanic current meas. instrumentation, function of velocity of metal electrolyte 77—10040
galvanising baths, premature leakage, corrosion effects 78—35539
gas bubble detection recording and measuring system with nanolitre resolution for use in liquid environment 78—31739
geothermal energy utilisation, fouling problem overcoming 79—43740
germanate optical glass, resistance to humidity and spotting agents 77—58404
glass, ancient samples, trace element anal. by neutron activation, rel. to corrosion and devitrification 78—12801

corrosion continued
glass, chemical durability, thermodyn. approach 78—7063
glass, corrosion, effect of EDTA, ethyl alcohol and sugar in leach soln., chem. durability 79—74269
glass, effect of surface area to solution volume ratio 79—96167
glass, excavation type, layers and profiles of SiOH, CaOH, and KOH polyatomic ion groups special corrosion effect 80—81387
glass, float, low-Fe, weathered, surface, characterisation 80—93666
glass, influence of complexing agents and nature of buffer soln. on chem. durability, theory 79—74268
glass, medieval, simulated, durability anal. using IR reflection spectroscopy 80—40777
glass, silicate, resist. to NaOH 80—21143
glass, stained, deterioration by atmospheric corrosion and microorganisms 80—93664
glass, wear, acoustic emission obs., effect of ion aggregates in Rebinder-Westwood environment 78—48536
glass fibre, chemical durability in alkali, powder method of testing *(Polish)* 78—7065
glass fibre, preparation, appl. in Portland cement reinforcement, alkali resistance 80—81019
glass fibre reinforced plastics, ageing by boiling in water, effect on physicomech. props. 80—60892
glass fibre reinforced plastics, creeping tests on flat specimens in liq. media, clamping device 78—7126
glass fibre reinforced polyester, creep life, effect of liquid environment and increased temp. *(Russian)* 77—16723
glass reactions with aq. solns., influence of surface pot. on kinetics 80—108612
glass surfaces, corrosion, passivation and anal. 78—60854
grain boundary grooving under action of surface diffusion and evaporation or corrosion 80—39397
grain boundary grooving under influence of evaporation or corrosion 79—28179
graphite, corrosion by CO_2, CO production radiolytically induced gas pressure effects 80—106115
graphite, from reactor, quantitative microanalysis by laser emission spectroscopy 80—81384
graphite, high density, erosion in molten Si rel. to cryst. growth technology 78—3244
graphite, nuclear, CO formation at initial stages of H corrosion 78—11355
graphite, oxidation, corrosion resistance, bend strength, assessment for rotary glass fibre making apparatus 78—64753
graphite, synergistic effect of electrons on atomic H activity 80—106112
graphite corrosion in PBHTGR process heat reactor following massive air ingress *(German)* 80—83181
graphite fuel elements, irrad., catalysed corrosion, laser emission spectroscopy anal. 79—87924
graphite moderator structure design and manufacturing specification 80—23110
graphite oxidation and coolant chemistry of CEGB gas-cooled reactors 80—42774
H_2SO_4 vapour corrosion, in general atomic S-I thermochem. water-splitting cycle 80—45449
haematite particles, crud deposition on heat transfer surface, surface chemistry 80—35376
Hastelloy, corrosion behaviour in simulated HTGR He environment 79—54495
Hastelloy G, and C-276, pitting resist. in low salinity geothermal brines 80—93681
Hastelloy-Z, carbonisation and carburisation in high press. He environment *(Japanese)* 79—26516
Hayes alloy no.716, Fe-Cr-Ni-Co-W-Mo-Si-C-B (26, 22, 12, 3.5, 3, 1.2, 1.1, 0.4 wt.%), hardfacing alloy 80—100802
Haynes alloy 20 Mod, pitting resist. in low salinity geothermal brines 80—93681
heat exchanger testing, liquid-fluidised bed, for geothermal power plant appl. 79—48090
high temp., in oil firing boilers and turbines *(Japanese)* 77—28932
high temperature corrosion, review *(Japanese)* 78—72911
high temperature hot corrosion, SO_2 and NaCl effects 78—48563
high-temperature alloys, hot corrosion, book contrib. 78—11444
hip replacements, total, causes of failure 77—81662
holographic interferometry 79—3658
HTGR primary circuit components, metallurgical eval. of structural materials 79—67867
implantation in Al and Al-Zn-Mg-Cu, effect on corrosion behaviour 80—71794
implanted prosthesis failure analysis techniques and results 80—89906
Incoloy, evaluation for use in nuclear process heat appl. 78—13234
Incoloy 600 and 800, surface film in hot conc. NaOH, XPS study 80—11824
Incoloy 600 vacuum heat treatment for improved corrosion resistance of PWR steam generator tubing 80—5246
Incoloy 800, corrosion and carburization in liquid Na up to 973K 79—47841
Incoloy 800, high temp. gaseous corrosion in sulphidising environments 79—47838
Incoloy 800, mechanical props., heat treatment and appl., conf., Petten, Netherlands (March 1978) 79—43296
Incoloy 800, mechanisms of corrosion in He 79—47843
Incoloy 800, pretreatment potential effect on pit generation *(Japanese)* 79—43474
Incoloy 800, review on high temp. gaseous corrosion in carburising and oxidising environments 79—47837
Incoloy 800, thin wall tubing, creep-rupture testing in steam under constant and cyclic load 79—47774
Incoloy 800 for HTR appls., correlation of carburization behavior, mechanical property degradation, and exposure conditions 80—5244
Incoloy 800H, H_2SO_4 vapour corrosion,, in general atomic S-I thermochem. water-splitting cycle 80—45449
Incoloy 825, corrosion resistance as structural material for denitrification vessel 77—36685
Inconel, 617, 800, corrosion behaviour in simulated HTGR He environment 79—54495
Inconel, chloride corrosion in hot acidic media 78—35552
Inconel, corrosion in acidic chloride soln. at 25°C 77—70202
Inconel 600, effects of ageing and misorientation on intergranular corrosion *(Japanese)* 79—79158

corrosion continued
Inconel 600, H_2SO_4 vapour corrosion, in general atomic S-I thermochem. water-splitting cycle 80—45449
Inconel 600, nuclear reactor boiler corrosion, XPS 80—66709
Inconel 600, nuclear reactor boiler corrosion, XPS 80—71816
Inconel 600, PWR primary corrosion products 80—13578
Inconel 600, S penetration leading to sulphide form. *(French)* 79—74306
INCONEL 617, corrosion kinetics and products under low oxygen partial pressures *(German)* 79—87764
Inconel 625, pitting resist. in low salinity geothermal brines 80—93681
Inconel alloy 600, precipitation effect on corrosion 77—25180
instrument operation in adverse environments, conference, London (1976) 78—189
ion beam appl. 77—8963
ion implantation studies, review 77—43236
ion implantation surface alloy creation, corrosion resistance 78—88569
ion techniques, conf., Manchester, England, (Apr. 1975) 77—8962
ion-implanted alloys, surface props. effects and appls. 80—79824
jute, cement reinforcing fibre, alkali resist. 80—89377
KER 110 hard porcelain in conditions of practical use *(German)* 79—100270
latent heat storage materials, high temp. corrosion resistance and thermodynamic stability 80—30582
LMFBR, H burden from steam side corrosion in Na heated steam generators 78—58355
LMFBR evaporator tubes, corrosion and heat transfer 79—1088
LMFBR mixed oxide fuel pins, proposed mechanism for internal cladding corrosion 79—8384
LMFBR type mixed oxide fuel pins, composition of corrosion product oxide phases in pin gaps 78—70599
load-bearing structures, behaviour prediction of materials degradation 79—34133
lubricated load-bearing surfaces, zeta potential effects 79—87761
LWR materials, pressure boundary problems, corrosion, cracking and radiation embrittlement props. 78—46142
LWR primary circuit structural materials, phase comp. of corrosion products by Mossbauer spectroscopy 80—5237
Magnex AL 80, aqu. corrosion, silicate effects 77—70230
Magnox AL 80, ion beam analysis of corrosion films 77—8978
MAGNOX fuel canning material, corroded, F conc. profiles determ. using $^{19}F(p,\alpha\gamma)^{16}O$ reaction 79—92035
Magnox reactors, remote corrosion monitoring, laser based instrument 78—41822
marine corrosion, and its prevention 80—104333
marine struct. protection *(Japanese)* 77—28931
mass transfer model in high temp. high press. water circuits 79—67813
materials interactions, stability, phase transformations, thermodynamics and corrosion 78—88444
materials science and technology problems, present situation in Japan *(Japanese)* 77—28918
mechanical treatment in aq. salt soln., material transport rel. to wear 80—16506
mechanism and protection *(Italian)* 79—83342
metal, anal. using ion beam and nucl. techniques 79—52448
metal, candidate current collector for Li-FeS_x battery, anodic corrosion rate in LiCL-KCl eutectic 79—100512
metal, corrosion in electrolytes, pit growth 80—21186
metal, corrosion pit initiation and growth, salt film form. 80—16563
metal, crater deepening, expt. testing of models *(Russian)* 77—20962
metal, electrochemical reaction on surface in aq. soln. 79—83387
metal, refractory, water vapour attack, immersion heater appl. in vacuum radiation furnace *(German)* 80—21184
metal, tarnish layer nucleation and growth 77—11827
metal, wear characts., mechanisms 77—32697
metal corrosion meas. specifications and quality assurance 77—12764
metal parts, sintered, corrosion and protection 78—44278
metal pipelines for natural fresh water supply, fundamental criteria *(Russian)* 79—1921
metal substrate, thin film form., appl. of AES and ESCA *(French)* 80—50903
metal surface, newly generated, occurrence of salt films during repassivation 79—15860
metal-glass mats. alloyed with Cu, powder prep. and props. 78—72912
metal-metal metal-polymer sliding, wear mechanisms, review 79—70174
metal-to-metal bonds, stress analysis in hostile environments 79—20338
metal/metal ion system, instantaneous corrosion rate deform. by Faradaic rectification 78—80667
metal/metal ion systems, instantaneous corrosion rate determ. by Faradaic rectification 78—80666
metal/solution reactions, possible Mossbauer studies 80—39988
metallic glass, corrosion behaviour, metalloid elements influence, review 80—89421
metallic glasses, mats. props. review 77—4043
metallic glasses, review *(German)* 79—41962
metallic glasses manufacture, struct. and stability *(Norwegian)* 79—14687
metallic surfaces in contact with flowing electrolyte, mag. field effects on electrochemical reactions 77—73369
metallisation, IR microscopy failure anal. 80—98976
metallurgical viewpoint *(Japanese)* 78—39947
metals, alloys and oxides, AES investigation of corrosion and growth nature of surface layers 77—77330
metals, colloid chem. appls. 80—89541
metals, indoor corrosion rates meas. 80—76404
metals, precipitate films, ion selectivity effects on passivation and corrosion 80—35377
metals, pure, corrosion due to V_2O_5 melts *(Japanese)* 80—93691
metals, rapidly quenched, conf., Brighton, England (July 1978) 80—67934
metals, scaling, theory, electrochem. transport model 78—64761
metals, strength and corrosion tests, NDT, electromagnetic methods, use in anal. of destructive materials testing *(German)* 77—73396
metals, strength and corrosion tests, quantitative noncontact meas. of physical and geometric props. *(German)* 78—23909
metals and alloys, corrosion conditions simulation in crack-like defects using electrochemical cell *(Russian)* 79—52445
metals and alloys, finishing, use of ion implantation techniques, effect on wear and corrosion props. 79—34204
metals and alloys, gas corrosion, in composite atmospheres *(Polish)* 79—79142

corrosion continued
metals and alloys, sulphidation mechanism, review *(Polish)* 80–45413
metals in aqueous soln., effects of ion implantation 77–25290
metals in ionising solvents, review 77–8973
metals used in coal gasification, demands made on materials used in process *(German)* 80–45438
MHD generator insulation wall deterioration *(Japanese)* 77–24200
mirrors *(Polish)* 80–11811
molten salts, corrosion and containment props., bibliography 80–41971
Monel 400, corrosion susceptibilities in synthetic geothermal brines 77–86223
Monel metal, cast, electrochemical behaviour in NaCl soln. 79–87763
monitoring using polarisation resistance meas., sources of error 77–16712
monitoring using polarisation resistance meas., techniques and correlations 77–16711
Mossbauer spectroscopy applics. 77–12749
Mossbauer study of corrosion processes and products 80–40572
mullite fibre reinforced mullite, in vitro degradation, bending strength, Young's modulus, density meas. 78–85011
Nb-O, effect of O_2 on penetration of Li at 400°C 79–11719
nickeliferous materials, properties and appls. *(German)* 79–79182
NIMONIC 80A, corrosion kinetics and products under low oxygen partial pressures *(German)* 79–87764
noble metal, interfacial corrosion in metal to ceramic reaction welding 78–53035
noble metal alloy, dil., solute segregation and subsequent film growth in corrosive environment, model 79–24649
noble metal contact, substrate material diffusion and corrosion film formation, model 80–2312
North Sea oil production platforms, use of steel and concrete in construction 79–78985
nuclear fuel element cladding, corrosion product deposition, heat transfer model *(Bulgarian)* 80–71818
nuclear fuel rods steel-coated, effect of impurities on clad-corrosion *(German)* 79–49693
nuclear fuel sheath in boiling water, corrosion product deposition and release 79–91839
nuclear power station corrosion research, review of problems *(Czech)* 78–62598
nuclear power stations, corrosion damage, influence of water chemistry 79–54517
nuclear power stations, overview of water chemistry 79–54553
nuclear power stations with RBMK reactors, structural materials corrosion monitoring 79–9756
nuclear reactor, particulate corrosion product transients in primary coolant 80–47540
nuclear reactor components, lubrication, friction system in liquid Na and Ar 79–59176
nuclear reactors, corrosion product transport, high temp. water loops 79–91840
nuclear reactors, steam generator tube survey, causes of failures, repair procedure 78–54826
nuclear steam generator tubes testing and evaluation, using CIS/DASIO system *(Czech)* 80–63301
nuclear water-cooled reactor systems, water chemistry 79–93694
nucleation and growth at surfaces, kinetic studies, review 78–72046
numerical modelling of fatigue, crack, creep and corrosion test results, review 78–30243
ohmic potential drop, rel. to crit. pitting and protection pots. 78–72900
optical examination and monitoring of surfaces, review 79–67375
optical glass, chem., durability, pragmatic view 80–78921
optoacoustic spectroscopy using cell with ultimate corrosion resistance 80–42269
parylene polymers, synthesis, elec., phys., corrosion props. *(German)* 78–64521
periclase refractories, props. after testing at over 2000°C 80–104317
Permalloy, corrosion resist. and mag. props., effect of Cr addition 77–86219
Permalloy film, corrosion induced defects, scanning Auger microscopy 77–40464
Permalloy film, corrosion kinetics, mass and resist. change techniques, comparison 78–27675
Permalloy film corrosion characterisation by crystal oscillator microbalance and resistance meas. 78–7101
Permalloy films, oxidation effects on atmospheric corrosion, AES, XPS and ion sputtering anal. 80–11829
Permalloy-Rh, film, influence of Rh on corrosion resist. and mag. props. 80–3235
phase change material physical and chemical props. for space heating and cooling 79–57479
phosphate glass-Al alloy seals, elec. and mech. props., glass transition 80–81018
photographic development rate, effect of developer ion charge 79–24753
physical methods in corrosion technology 77–16753
pipe, internal, radiographic method of exam., NDT 77–32737
pit growth, convective diffusion in pits, ionic components conc. calc. 80–45409
pitting, kinetic theory 77–90469
pitting, stochastic theory 78–7077
plastic clad metal, corrosion charact. by electrical resist. and capacitance meas. *(German)* 80–30171
plastic encapsulated and hermetic modules, permeation properties 80–100937
plastic-encapsulated IC, metallisation corrosion test 78–11486
plastics, reinforced, resin selection rel. to corrosion props. 80–40322
plastics and reinforced plastics, tabulated data as design guide 77–21087
polarisation resistance meas., technique and instrumentation 78–15609
polarisation resistance meas. for accurate rate determ. 78–31562
polarisation resistance measurements, determ. of corrosion mechanis. 78–80656
polarisation resistances method of determ. effectiveness of inhibitor 77–28930
polarography, in glass-corroding media, using polyethylene capillary tubes 78–61090
polyester resin, water diff. meas. by radionuclides, corrosion effects *(Czech)* 77–48566
polyesters, corrosion-resistant, based on TMPD glycol, prep., phys. and corrosion props. 80–21136
polyethylene, high-density, longevity prediction, effect of surface active media 77–12729

corrosion continued
polyethylene, oxidised, low-temp. dielectric spectrum 79–61304
polymer-polymer and metal-polymer sliding wear mechanisms, review 79–70174
polymers, atmospheric resistance, distrib. function determ. and anal. *(German)* 80–81225
porcelain, charge carrier prod. by degradation in SF_6 80–7707
porcelain enamel, resistance to aqueous attack, expt. results 78–56788
porcelain enamel, resistance to aqueous attack, prediction eqn. 78–60853
Portland cement, corrosion by H_2S 80–21129
portland cement paste, microstructure study by SEM, TG and X-ray diffr., corrosion 78–92381
potential/time, and potentiostatic polarisation curves as a method of predicting corrosion 80–45419
power line equipment, field work investigating corrosive effects *(Norwegian)* 80–97631
pressure vessel for corrosion testing at high temps. 77–12754
prevention in process industries *(Japanese)* 77–28919
problem areas, unsolved, review 77–4864
PTFE, anisotropic electrochemical attack 79–39004
PVC, biological media effect on. physiomech. props. 79–96168
PVC, unplasticized, evaluation method for chemical resistance *(Japanese)* 80–25893
PWR, computer code for the study of migration and deposition of corrosion products 80–13700
PWR, in-reactor loop expts. on corrosion product transport and water chemistry 78–58335
PWR, materials corrosion, steam generator operations, influence of water chemistry 79–54555
PWR, radionuclide surface activities meas. 80–13941
PWR boiler tubes, corrosion risk reduction methods 79–39045
PWR CANDU, corrosion product transport, deposition on fuel bundles, press. tubes 77–61492
PWR coolant system corrosion product composition and significance 79–9689
PWR crud descriptive model 79–9691
PWR reactor, steam generator accidents, rel. to impurity enrichment in boiling on surface coated with porous struct. 78–2365
PWR secondary water chemistry, EPRI program 77–54356
PWR steam generator corrosion problems and design implications 79–93812
PWR steam generator tubing, corrosion problems 79–24683
PWR steam generators, corrosion resistance of tubes 77–79432
radioactive corrosion product accumulation in nuclear steam generators 80–13579
random exposure conditions, total accumulated corrosion 80–40579
rate calc. from low polarization data, IR-drop effect 79–47791
rate evaluated from nonlinear polarisation data 77–77600
rate meas. by differential pulse method 78–19962
rate measurement, with dual electrodes 80–85180
rates, error anal. in using 2 and 3 electrode polarisation resist. meas. 80–100930
RBMK reactors, startup and shutdown, H_2O_2 and Fe compounds behaviour investigation 79–9822
reactor steam generator tube perform. anal., corrosion failure 79–59178
refractories, corrosion rate in glass melt 79–70196
refractory metals, oxidation, high-temp., mechanism, review *(Polish)* 79–34184
refractory metals and oxides, reactions of liq. alkali metals, relevance to reactor technology 80–85173
refractory solid/liquid reaction zones, electron probe micro analysis applic. *(French)* 77–32848
replication, NDT anal. and inspection technique 78–11467
resistant alloys, metastable microcrystalline, appl. 80–84887
review, (1978) *(Japanese)* 79–34174
review in corrosion science and control–1979 *(Japanese)* 80–45408
Roschenbleck equation 77–21297
rotating metal disc electrode, mass transfer under turbulent conditions, suspended particle effects 78–27772
scanning electron microscopy, appl. to surface anal. 80–99004
semiconductor photoanodes, corrosion stability 80–21130
silicate glass, hydration in steam atmosphere 80–85211
silicate glass, IR reflection spectra relation to corrosion state of surface *(Japanese)* 78–88554
silicate glass corroded by moisture, IR refl. spectra change *(Japanese)* 78–53013
silicate glass. IR reflection spectra change due to moisture corona *(Japanese)* 78–19914
silicate glasses, corrosion by aq. solns. 78–64752
silicate glasses, exam. of chemical stability, in alkali solns. 78–88557
silicate glasses, relation between IR reflection spectra and corrosion state *(Japanese)* 78–23850
silicate thermoplastic pigments for glassware, chem. resist. 79–61755
silicides, oxidation and hot corrosion resistance kinetics 80–25896
simultaneous potential current time meas. during polarisation studies 77–90515
sintered mats., complex diffusion alloying 78–68650
solar water heating system, corrosion 80–30131
speed meas. via polarised resistance methods *(Dutch)* 78–3245
spodumene, ceramic, chem. resist. and struct. 79–61756
stainless steel, in $MgCl_2$ solutions, Cl distrib. in oxide films, SIMS *(French)* 80–108765
stainless steel bins for storage of high level radioactive wastes 77–6535
stainless steel cladding, effect of stoichiometry on attack in UO_2-PuO_2 fuel 79–26523
steam generating equipment, liquid/vapour flow visualisation and localised fast meas., instrumentation 79–46404
steam generators of water cooled nuclear power plants, corrosion phenomena, Review 80–558
steam-generating channels with cosine law heat liberation, mass exchange conditions 79–81710
steel, 12 MKh, strength, ductility rel. to H_2 corrosion at 1000 kg/cm^2 press., 450°C *(Russian)* 79–15723
steel, 12Kh18N9T-TiB_2, eutectic alloy, high temp. props. 78–84931
steel, AGR boilers, gas side corrosion, breakaway oxidisation treatment 78–48558
steel, alloy, 55Kh20G9AN4, corrosion resistance, alloying effects 77–70225
steel, alloy, Cr-Mo, pitting and crevice corrosion, exam. *(Japanese)* 78–64769

corrosion continued
steel, alloy, Fe-Cr-Ni-Mo-Al, (13, 8, 2, 1, wt.%), H_2 effects on fracture, exam. 78−60809
steel, alloy, fretting corrosion, exam. of secondary structures 79−100292
steel, AISI 1010, corrosion susceptibilities in synthetic geothermal brines 77−86223
steel, aluminized, atmospheric corrosion kinetics 79−47808
steel, austenite, effect of neutron irradiation on intercrystallite corrosion 78−688
steel, austenitic, Cr-Ni-Ti, X5CrNiTi18.10, corrosion in HNO_3 *(German)* 78−44253
steel, austenitic, CrNi, high Mo, corrosion, effect of struct. *(German)* 77−90481
steel, austenitic, high alloyed, low C, polarization resistance meas. in boiling HNO_3 80−16557
steel, austenitic, in liquid Na, corrosion resistance and degradation of mechanical props., influence of N 80−16567
steel, austenitic, intercrystalline corrosion, N_2, C and Cr effects 79−83374
steel, austenitic, intercrystn. corrosion and mech. props., inflence of Cr, N and Nb *(German)* 80−50747
steel, austenitic, intergranular defectiveness determ. using inductive instruments 78−53075
steel, austenitic, Ni-Cr, corrosion tests with stray currents after manufacturing operation and welding *(German)* 77−86274
steel, austenitic, stainless, intercrystalline corrosion in low and high oxidizing environment *(Russian)* 79−43477
steel, austenitic, stainless, pitting and crevice corrosion, effect of Mo, Si and N *(Japanese)* 78−92399
steel, austenitic, tensile props. after corrosion by UO_{2+x} and fission products *(German)* 77−70216
steel, austenitic, X5CrNiN19.7 and X5CrNi18.10 corrosion in HNO_3 *(German)* 78−44253
steel, austenitic and duplex 308 stainless, mech. of intergranular corrosion and pitting corrosion 79−91846
steel, austenitic and ferritic, corrosion effects of Li 80−35398
steel, austenitic and martensitic, cavitation failure in liq. 77−44405
steel, austenitic and martensitic, corrosion under boiled conditions, Mossbauer spectroscopy study 79−47800
steel, austenitic stainless, 12Kh18N10T, intercrystalline corrosion, hot rolling effect 79−79010
steel, austenitic stainless, 317L, potentiostatic tests, use of free-corrosion potential time transients to distinguish between pitting and crevice corrosion 79−39058
steel, austenitic stainless, anodic polarization, Cr content effect 80−35382
steel, austenitic stainless, B effect on corrosion resistance 78−35569
steel, austenitic stainless, chloride corrosion in hot acidic media 78−35552
steel, austenitic stainless, corrosion by Li and Li:LiH at 873K 80−35397
steel, austenitic stainless, corrosion in acidic chloride soln. at 25°C 77−70202
steel, austenitic stainless, corrosion in hot conc. aqu. NaOH soln. 80−7710
steel, austenitic stainless, corrosion in hot conc. caustic soda, NaCl addition effects *(Japanese)* 77−8990
steel, austenitic stainless, corrosion pits, specimen position effect on shape 78−11387
steel, austenitic stainless, corrosion resistance *(Russian)* 78−15572
steel, austenitic stainless, corrosion resistance in passive state, cold work effects *(Czech)* 77−59987
steel, austenitic stainless, corrosion resistance of cold deformed Cr-Ni austenitic stainless steel in N_2O_4 media at 433K *(Russian)* 80−76422
steel, austenitic stainless, corrosion resistance testing, urea plant applications *(Czech)* 80−61012
steel, austenitic stainless, corrosion testing for chemical plants, corrosion rate forecast automatic instrumentation *(German)* 78−44289
steel, austenitic stainless, Cr-Ni-(Mo), intercrystalline corrosion sensitivity, electrochemical determ. *(Czech)* 77−59989
steel, austenitic stainless, effect of autogenous welding on chloride pitting corrosion 79−91842
steel, austenitic stainless, fretting corrosion of orthopaedic implant materials by bone cement 80−104813
steel, austenitic stainless, fretting wear in air and CO_2 at elevated temps. 80−21119
steel, austenitic stainless, influence of Cr, Mo, N, content on resist. to pitting corrosion 78−80668
steel, austenitic stainless, influence of steel comp. on corrosion in high temp. Na 78−80675
steel, austenitic stainless, intercrystalline corrosion, stressed state effect 80−55582
steel, austenitic stainless, intergranular corrosion evaluation 77−16741
steel, austenitic stainless, Ni free, corrosion obs. 79−24652
steel, austenitic stainless, nonsensitized, fatigue strength, intergranular corrosion effect *(Japanese)* 80−85027
steel, austenitic stainless, props., nuclear reactor appl. 77−3101
steel, austenitic stainless, sensitivity of intergranular corrosion, effect of Mo content, heat treatment and degree of stabilization *(Czech)* 79−70095
steel, austenitic stainless, sensitized forgings, corrosion resistance restoration, computer calc. *(German)* 79−66074
steel, austenitic stainless, TRIP, fretting corrosion of surgical implant material, electrochemical investigation 79−66197
steel, austenitic stainless, type 00Kh18N20S3M3D3B, anticorrosion props., heat treatment effects 80−30168
steel, austenitic stainless, types 304L and 316L, work-hardened, electrochem. and corrosion behaviour in acid solns. 80−50757
steel, austenitic stainless, welded joints, cold working effects on mech. and corrosion props. *(Hungarian)* 78−52838
steel, austenitic stainless in liq. Na, mechanical props., review 79−20150
steel, austenitic stainless type 316, corrosion mechanism in hot flowing Na, computer simulation 80−3251
steel, austenitic types AISI 316, 347 and Esshete 1250, corrosion in molten SO_4 deposits 80−97625
steel, bearing, M50, localised corrosion resistance, improvement by ion implantation 80−16602
steel, boronised, corrosion resistivity *(Japanese)* 77−52544
steel, C, brazed joints, corrosion mechanical strength 79−43491
steel, C, corrosion and self protection in hot saline soln. 79−1925
steel, C, corrosion by aq. H_2S solns. 80−100946
steel, C, corrosion by freshwater *(Russian)* 79−1921

corrosion continued
steel, C, corrosion by wet elemental S, exam. as function of pH and particle size 78−92388
steel, C, corrosion during cyclical exposure, to wet elemental S, and He atmosphere 78−92391
steel, C, corrosion in concentrated H_2SO_4 78−64767
steel, C, corrosion in H_2S soln., Fe dissolution 79−79145
steel, C, corrosion inhibition by 2-ethylamino-ethanol in aerated 3% NaCl soln., pH effect 80−21160
steel, C, corrosion products, chem. state anal. by conversion electron Mossbauer spectroscopy 80−40595
steel, C, corrosivity in conc. chloride soln. 79−96193
steel, C, Cr-Mo ferritic and austenitic stainless, corrosion behaviour in reducing environment of coal fired MHD generator 80−104322
steel, C, electric resistance welded pipe, grooving corrosion in seawater 78−35556
steel, C, erosion-corrosion in aqu. H_2S soln. up to 120°C, 1.6 MPa press. 80−21155
steel, C, fatigue crack growth in air and seawater, under constant amplitude and random loading 78−64679
steel, C, hot concentrated saline solns., aerated and nonaerated environments 80−25926
steel, C, naval, corrosion in harbour anaerobic sediments, rolling direction and tensile stress effects 80−30135
steel, C, naval, corrosion in natural seawater, rolling direction and tensile stress effects 80−30134
steel, C, pitting corrosion and scaling in geothermal brine 79−91843
steel, C, potentiodynamic behaviour, in conc. NaOH, cyclic voltammetric obs. 79−16006
steel, C, rotating disc electrode in 3 wt.% NaCl solution, corrosion rate meas. *(French)* 79−43470
steel, C, rust prevention control by changing sulphide type 79−47813
steel, C, type 1020, H_2 attack, effect of H_2S 79−96192
steel, C, type St37 80−40594
steel, C and austenitic stainless, cold working effect on corrosion behaviour 79−74299
steel, C-Mn, corrosion in acidic soln., metallurgical factor effects 79−70206
steel, case-hardened cast, contact endurance rel. to austenizing *(Russian)* 78−56805
steel, cold worked, AISI type 304 L and 316 L, pitting resistance in NaCl solns. 80−35393
steel, cold-rolled, corrosion resistance in 1M $LiAsF_6$/THF, suitability for organic electrolyte Li secondary batteries 79−100387
steel, corroded, Mossbauer effect anal. of corrosion products 78−19943
steel, corroding surface in nuclear reactor, mixed cation spinel form. 78−35565
steel, corrosion, Na loop system, analysis of radioactive corrosion product transfer 78−78464
steel, corrosion and polarization and electrocapillary behaviour in H_2SO_4, radioactive n-dibutyl sulphide effect 79−70215
steel, corrosion by hydrazine, electrochemical mechanism for room temp. inhibition 78−44249
steel, corrosion in Pb bath up to 1400K, corrosion prevention *(German)* 77−90482
steel, corrosion resistance, effect of diffusion Fe plating *(Russian)* 77−70208
steel, corrosion resistance rel. to electroerosion treatment conditions *(Russian)* 79−15848
steel, corrosion resistant, review of heat treatment, mech. and corrosion resist. characts. *(Korean)* 79−24653
steel, Cr, ferritic, corrosion morphology, electrochem. pot. and Mo additions effect *(French)* 80−45439
steel, Cr, pitting corrosion, temp. depend. *(Czech)* 79−39039
steel, Cr (17 wt.%), influence of Mo on intergranular corrosion *(French)* 80−21182
steel, Cr (9 wt.%), SiO_2 vapour deposited coatings, exam. of corrosion protective props. 78−88563
steel, Cr or Ni ion implanted, corrosion behaviour 80−11840
steel, Cr-Mn(Ni), Mn and Ni additions, effect on corrosion resistance and hardness 80−104342
steel, Cr-Mo (2.25, 1 wt.%), corrosion in molten NaOH, rel. to reactor boiler wastage 77−90497
steel, Cr-Mo-(Nb)-(Ni)(Ti), low-alloy selection for nuclear steam generator tubes 78−54834
steel, Cr-Ni-Mo, resist. to corrosion and corrosion-fatigue in seawater 80−104346
steel, deformed and welded mild, potential distrib. meas. technique, appl. to corrosion study, apparatus *(Japanese)* 78−53049
steel, dissolution in HNO_3, thermometric method of rate estimation, a limitation 77−56138
steel, electric, EO-100 and E-11, surface cleansing with ML-51 combined with monoethanolamine, corrosive action study 79−39052
steel, erosion by high-press., high-temp., short gas pulse 78−7092
steel, ferritic, base material for powder flame spraying process, intercrystn. corrosion *(Czech)* 80−30158
steel, ferritic, Cr-Al corrosion in S vapour and H_2S-H_2 mixtures 78−23875
steel, ferritic, Cr-Mo, containing less than 12 wt.% Cr, sensitisation during welding, to intergranular corrosion 78−88566
steel, ferritic, Cr-Mo-Nb, intergranular corrosion resistance 80−104319
steel, ferritic, Mo addition effect on corrosion resistance, X-ray photoelectron study 79−74285
steel, ferritic, screening studies for evaluation for nucl. process heat system 78−13236
steel, ferritic, tests for intergranular corrosion 77−73384
steel, ferritic (17 wt.% Cr), influence of Mo on intergranular corrosion 80−30139
steel, ferritic and austenitic, corrosion in NaOH contaminated Na *(French)* 77−52541
steel, ferritic stainless, Cr-Mo, Mo effect on pitting pot., AES anal. 78−95852
steel, ferritic stainless, Cr-Mo (12,1wt.%) microstructure influence on localised corrosion behaviour 80−61018
steel, ferritic/austenitic high Cr, development, mech. props. and corrosion resist. 80−45422
steel, galvanised, pipe carrying potable water 78−92409
steel, galvanised, with paint coating, adhesion failure, XPS study 80−40671
steel, heat-exchanger alloys for use in nuclear steam coal gasification plant 78−15589

corrosion continued
steel, heat-resistant, martensitic, Kh12NMFB weldability 80—20987
steel, high and low C, wires, electroheated, thermal cycling and corrosion behaviour 80—61006
steel, high strength 0.77%C, plastic deform., surface dissolution effect 77—8883
steel, high temperature strength, corrosion-erosion effect of gas metal mixtures stream *(Russian)* 78—35576
steel, high-strength, fatigue, interaction effects between trace impurities and environment 80—66651
steel, high-strength low alloy, H_2 attack, 350-510°C 80—97636
steel, hydrogen absorption, anilines surfactants effectiveness, HCl conc. effect 80—108638
steel, hydrogenation and cracking in H_2 S, cathodic polarization and surface layer effects *(Russian)* 77—52528
steel, low alloy, atmospheric corrosion in marine environments 80—30142
steel, low alloy, corrosion in artificial seawater, alloying element effect *(Chinese)* 80—21150
steel, low alloy, corrosion in artificial seawater, alloying element effect *(Chinese)* 80—21151
steel, low alloy, influence of accelerated weathering on corrosion 80—55565
steel, low alloy 79—43487
steel, low alloy and C, corrosion, alternating current effect 80—30141
steel, low C, alloy, nonmagnetic 40KhNM, corrosion resistance, melting procedure effects 77—70226
steel, low C, corrosion, heat treatment and plastic deform. effects 77—63825
steel, low-alloy hydrogenation and embrittlement under neutron irrad. in contact with water *(Russian)* 77—52529
steel, low-C, pitting resist. in low salinity geothermal brines 80—93681
steel, martensitic, low C, nitriding, exam. of case props. 78—85045
steel, martensitic cutlery, pitting corrosion 80—100962
steel, mech. strength, effect of H_2 sorption and Al and N_2 surface treatment *(Russian)* 78—31570
steel, metallurgical stability and corrosion in He atmos., HTR appl. 79—36329
steel, mild, AC effects 79—15864
steel, mild, AISI 1009 and 1018, corrosion incipient processes in hypersaline geothermal brine at 90°C 80—50753
steel, mild, corrosion, by applied alternating currents 79—70205
steel, mild, corrosion and passivation in benzoate solutions 79—79180
steel, mild, corrosion by Fe^{3+}, inhibition by potassium oxalate 79—39019
steel, mild, corrosion in complex aq. environment, linear polarisation investig. 78—76782
steel, mild, corrosion kinetics in presence of cyanoguanidine formaldehyde resin 78—19926
steel, mild, corrosion rate meas. in H_2SO_4 using microprocessor controlled potentiostat 80—71798
steel, mild, critical soil moisture content in underground corrosion 79—96186
steel, mild, decomp. of CCl_4 and corrosive action 80—45420
steel, mild, in Na_2SO_4 soln., anodic polarisation study of corrosion by AC 80—40582
steel, mild, nonmetallic inclusion effect on pitting 80—35381
steel, mild, oxidation of contaminated crevices exposed to CO_2 79—20243
steel, mild, pitting corrosion in O_2 bearing water, nonpassivating metal/environment system 80—30147
steel, mild, plastic deform. and pitting corrosion in neutral media 79—52415
steel, mild, radioactive waste form containers 80—18493
steel, mild, surface oxide effect on acid corrosion inhibition 78—11384
steel, mild, Zn gluconate inhibitor against corrosion in sea water 77—56136
steel, Mn, effect of Mn on corrosion *(Czechoslovakian)* 77—28933
steel, N-Cr-Mn, influence of nitride phase on corrosion behaviour *(Bulgarian)* 79—61798
steel, nature of iron sulphides in H_2S-O_2 environment 79—96195
steel, Ni-Cr, corrosion on N_2O_4 flow 520-890K and 8-9 MPa *(Russian)* 80—3256
steel, notched specimens in sea water, endurance limit enhancement, specimen size, freq. effects 80—93678
steel, passivation by sulphochromic soln. *(French)* 78—23869
steel, polymer coated, electrolyte permeation and elect. permittivity rel. to metal substrate corrosion 79—96175
steel, pressure vessel type, H_2 effect on corrosion, fatigue strength and embrittlent *(French)* 79—47770
steel, quenched and tempered, localised corrosion sensitivity *(German)* 78—19949
steel, rare earth additions, effect on physicomechanical props. 77—12639
steel, sheet, type 08Kp, blackness degree rel. to heat treatment in controlled atms. 79—57165
steel, sintered, diffusion treatment with B, Si, Cr and C, corrosion and wear improvement 77—77642
steel, sphere, dissolution in H_2SO_4 in elec. field *(Russian)* 77—4867
steel, spring alloy, microstruct. and props. at low temps. 77—44286
steel, stainless, 08Kh18N10T, long-term strength in He atm. containing impurities 79—24662
steel, stainless, 18-8, impedance diagram in passive and transpassive state in Na_2SO_4 soln. *(Japanese)* 77—21318
steel, stainless, 18Cr-2Mo-Ti, atmospheric corrosion 80—85078
steel, stainless, 304, H_2SO_4 vapour corrosion, in general atomic S-I thermochem. water-splitting cycle 80—45449
steel, stainless, 304, weld decay, precip. of $M_{23}C_6$ during thermal cycles *(Japanese)* 79—52468
steel, stainless, 316L, corrosion, comparison of powder metallurgy and conventionally produced specimens 79—15863
steel, stainless, 316L, fretting corrosion of surgical implant material, electrochemical investigation 79—66197
steel, stainless, 95Kh18, vacuum quenching 78—85047
steel, stainless, amorphous films, corrosion resist. and ion plating use 80—89423
steel, stainless, attack by liquid and vaporised CsOH 78—68840
steel, stainless, austenitic, H_2 induced transformation obs. *(Japanese)* 80—11640
steel, stainless, basic corrosion studies 77—34402
steel, stainless, boiling water reactor, corrosion and oxidation potentials monitoring 79—20252
steel, stainless, C and alloy, corrosion behaviour in simulated HTGR He environment 79—54495

corrosion continued
steel, stainless, candidate current collector for Li-FeS_x battery, anodic corrosion rate in LiCl-KCl eutectic 79—100513
steel, stainless, carbonisation and carburisation in high press. He environment *(Japanese)* 79—26516
steel, stainless, cavitation erosion in chemically aggressive liquids, acetic acid effects *(German)* 79—39050
steel, stainless, cavitation-erosion in fresh water, electron microscope and electrochem. study 80—55580
steel, stainless, clad oxide fuel pin, thermodynamic model for attack 79—97807
steel, stainless, corrosion, localised, in acidic Cl^- solns., exam. of galvanic reactions 79—20250
steel, stainless, corrosion, performance for condenser tube 79—39046
steel, stainless, corrosion and grain boundary penetration on exposure to coal gasification environment 80—61003
steel, stainless, corrosion behaviour of composite materials in N_2O_4 oxidising atmospheres *(Russian)* 80—76421
steel, stainless, corrosion due to molten LiF-LiCl-LiBr, fusion reactor appl. 78—53217
steel, stainless, corrosion in nonisothermal Li flow 79—79177
steel, stainless, corrosion in seawater circulation plant, comparison with Ti *(German)* 80—25897
steel, stainless, corrosion resistance in chlorinated lime slurry and calcium hypochlorite soln. 79—83390
steel, stainless, corrosion resistance in sea water 78—85028
steel, stainless, Cr, Mo effects on passivation AES and electrochemical anal. 79—74292
steel, stainless, Cr-Ni, localized corrosion 78—35555
steel, stainless, Cr-Ni (18,10 wt.%) Ti stabilised, cavitation failure, relationship of corrosive and erosive factors *(Russian)* 77—16722
steel, stainless, Cr-Ni (18, 10 wt.%), long-term strength in H at high pressure 80—55485
steel, stainless, Cr-Ni-Mo (16, 14, 3 wt.%), corrosion resist., vacuum heat treatment effect 79—87754
steel, stainless, crevice corrosion, mathematical model 78—95834
steel, stainless, crevice corrosion in chloride solns. 79—52414
steel, stainless, crevice corrosion in marine conditions 77—56135
steel, stainless, crevice corrosion in NaCl soln. 79—52422
steel, stainless, crevice corrosion resistance S mechanism effect *(French)* 77—77635
steel, stainless, CrNi, localized corrosion *(Slovak)* 78—19948
steel, stainless, Cs enhanced corrosion, Te influence 78—23866
steel, stainless, diffusion of Cs study using ion beams 77—20125
steel, stainless, duplex, STEM obs. of localized corrosion 80—104324
steel, stainless, durability in H_2 up to 500°C 80—30170
steel, stainless, E-brite 26-1, pitting resist. in low salinity geothermal brines 80—93681
steel, stainless, ferrite to austenite decomposition 80—3073
steel, stainless, ferritic, corrosion in formic acid at 70°C, effect of Mo additions 78—35551
steel, stainless, ferritic, corrosion resistance improvement by Mo and Ti additions 77—90505
steel, stainless, heat treated, oxide comp. and corrosion susceptibility of grades 410 and 430, AES study 80—66692
steel, stainless, interaction with (U-Pu)O_2 fuel, electron microprobe anal. 79—26524
steel, stainless, intercrystalline corrosion, effect of alloying elements, thermodynamic anal. 77—90504
steel, stainless, intercrystallite corrosion, testing using potentiostatic etching method 78—7113
steel, stainless, intercrystn. corrosion, depletion theory *(Czech)* 80—35408
steel, stainless, investigation techniques *(Dutch)* 78—15582
steel, stainless, knife line attack phenomenon, carbide precipitation during post heat treatment 79—20288
steel, stainless, Li compatibility, H_2 influence 78—68844
steel, stainless, liq. Li corrosion rate expressions, 600-1000°C 80—93682
steel, stainless, LMFBR fuel pin cladding long-term in-reactor corrosion by liquid Na 80—16593
steel, stainless, long-term corrosion stability rel. to use in joint endoprostheses 78—36059
steel, stainless, LWR and FBR material *(Japanese)* 77—83033
steel, stainless, Na exposed, corrosion in chloride containing aq. soln. 79—57151
steel, stainless, neutron irradiation and N_2O_4 corrosion effects *(Russian)* 80—52741
steel, stainless, Ni-Cr-Mo-W (29, 13, 3, 2 wt.%), long-term strength in H at high pressure 80—55485
steel, stainless, oxidation in N_2O_4, 200-700°C, anal. using Fick's second law *(Russian)* 77—73377
steel, stainless, pitting, rotation effects 79—100281
steel, stainless, pitting corrosion, stochastic theory 78—7077
steel, stainless, pitting corrosion in chloride media, electrochem. aspects 80—61007
steel, stainless, pitting potential in 0.1 M NaCl soln. at 280°C 79—61799
steel, stainless, PWR primary corrosion products 80—13578
steel, stainless, radiation-thermal treatment, N_2O_4 coolant action, intergranular corrosion *(Russian)* 78—58357
steel, stainless, resulphurated, Cr-Mo (18,2 wt.%), Mo effect on corrosion resistance *(French)* 77—63830
steel, stainless, sensitization, C content and ferrite morphology effect 80—89400
steel, stainless, sintered Kh18N10T, friction and corrosion props. for frictional units of nuclear plants 78—60845
steel, stainless, spectrochem. anal. using luminesc. discharge *(Spanish)* 79—92029
steel, stainless, sputtering and chem. attack by H ions of 100 eV energy 78—95635
steel, stainless, stabilised with Cr-Ni-Nb, reaction with Te vapour 77—8986
steel, stainless, surgical implants, corrosion 79—70706
steel, stainless, TRIP and 316L, orthopaedic implant material, metallurgical cond. effect on pitting resistance 79—70704
steel, stainless, type 12Kh18N10T, US inspection for intergranular corrosion 78—60912
steel, stainless, type 304, effect of cold work as sensitization 79—66071
steel, stainless, Type 304, pitting corrosion in Na_2SO_4 soln. *(French)* 80—40581

corrosion continued
steel, stainless, type 316, corrosion behaviour in high temp. impure He gas 80—76402
steel, stainless, type 316, corrosion in flowing Li 80—35399
steel, stainless, type 316, corrosion obs. in impure phosphoric acid 79 79179
steel, stainless, type 316, corrosion rates in molten Li salts 80—35400
steel, stainless, type 316, surface comp. rel. to crevice corrosion initiation 80—93680
steel, stainless, type 316L, pitting resist. in low salinity geothermal brines 80—93681
steel, stainless, type 430, Ni^+-implanted, struct., comp. and electrochem. anal. of surface alloy 80—16603
steel, stainless, type AISI 304, corrosive reactions obs. by polarimetric Mossbauer spectroscopy 80—40594
steel, stainless, type Kh17N13M2T, strengthening by plastic deformation and cold working *(Russian)* 78—52839
steel, stainless, types 304 and 316, corrosion susceptibilities in synthetic geothermal brines 77—86223
steel, stainless 304, metallurgical factors on the corrosion and mass transfer in liq. Na *(Japanese)* 80—71804
steel, stainless 304L, pitting potential of single and duplex phase, test method and surface cond. effect 80—16550
steel, stainless 310, sulphidation kinetics temp. effect and Cr role 78—64773
steel, stainless and C, radioactive contamination under applied potential in high temp. water 79—24646
steel, stainless and plain C, brazed joints used in thermal power plants, corrosion resistance 79—43492
steel, stainless austenitic, Cr-Ni (18,11 wt.%), corrosion resistance in urea *(Czech)* 77—70220
steel, stainless austenitic type 304, corrosion by molten Cs_2O_3-CsO_2 79—57141
steel, stainless ferritic *(Japanese)* 79—34194
steel, stainless knife line attack phenomena, addition of rare earth metals 79—20289
steel, stainless passive film, inhibitive action of bound water against Cl corrosion 80—35372
steel, stainless tubing 316, attack by $Te/O_2/Cs$ corrodents 80—50770
steel, stainless type 304, evaluating tendency for sensitization using Jominy bar test 80—16337
steel, stainless-glass composite, sintered, corrosion resistance 77—77608
steel, structural, naturally and artificially weathered, SEM characteris. 78—23882
steel, structural H_2, embrittlement and H_2S cracking resist., effect of alloying elements and struct. 79—38953
steel, structural martensitic, corrosion resist. under stress effect of strain ageing with hydroextrusion *(Russian)* 79—38853
steel, structural types St. 3PS, 10CrNiCuP, corrosion rates 80—108681
steel, type 12X18H10T, defect development in contact area with coolant *(Russian)* 80—57859
steel, volatile products from reaction with H_2O-CO_2, high temp. 80—81233
steel, wear resistance of low temp. nitriding treatment 80—89357
steel 03Kh12N10MT, mech. props. at low temps. 77—16615
steel and alloys, corrosion stability to double iodate-iodide salt melt in H prod. *(Russian)* 80—55593
steel austenitic stainless, pitting corrosion susceptibility, non-metallic inclusion effect 80—11816
steel corrosion in NH_3 and NH_3-N_2-H_2 mixture at high press. and temp., testing unit 77—56174
steel electrode, erosion resist., influence of C and carbide-forming elements *(Russian)* 78—11389
steel electrodes, pitting corrosion currents rel. to conc. of inhibitive and corrosive anions under corrosion conditions 80—85181
steel fibre reinforced Al_2O_3-Al, production and mech. props. 80—11619
steel fibre reinforced Al alloy, corrosion resistance, electrochemical characts. 80—11806
steel fibre reinforced concrete, accelerated corrosion test at high temps. *(Japanese)* 78—31553
steel high strength X 3 CrNiMoNbN 2317, Bauschinger effect and creep at room temp., effect of heat treatment *(German)* 77—36543
steel matrix-bronze surface, water lubricated bearing material, manufacture, friction, corrosion and erosion 78—11341
steel pipe corrosion, mass transfer coeffs. under isothermal flow conditions 80—97628
steel reinforced concrete, steel corrosion *(Japanese)* 79—39038
steel stainless, type 316, corrosion by molten alkali metal hydroxides and liquid Li 77—44414
steel wires, pre-strained electroheated, corrosion behaviour, direct resist. heating technique study *(German)* 80—40580
steel-polymer wear mechanism during fretting corrosion 78—35522
subscale form., limiting cases 79—20239
surface, mech. and corrosion props. improvement using US energy *(Rumanian)* 79—15821
surface analytic techniques, review 80—31929
surface coatings, materials conservation and optimum tribological performance 80—34130
surface crack growth due to corrosion under low cyclic loading *(Russian)* 79—100285
surface preparation of corrosion test samples, specimen holder 77—28937
surface science, rel. to energy development and technology 78—88553
surgical implant materials, corrosion props. 79—39605
Tafel slope determ. and corrosion rate from cathodic polarisation curves, graphical method 79—66177
tapered corrosion sections, light element profiling using nucl. reaction analysis and scanned microbeam 79—92036
testing, trends in standards and expt. procedures *(Japanese)* 77—28953
testing for chemical plants, use of electrochemical methods, corrosion rate forecast automatic instrumentation *(German)* 78—44289
theory, rel. to protective coatings 78—19918
thermal insulating materials in steel-sheathed pipe system *(German)* 78—31580
thermodynamics and electrochemistry, energy considerations 78—88643
thick capillary-porous structure, mass exchange during boiling 80—19503
THTR fuel element, irradiation testing in DRAGON reactor *(German)* 78—25295
transistors package, potential source of corrosion 79—70230
transition metal diborides, C32-type, phys., chem. props., appls., review, book contrib. 78—47308

corrosion continued
transition metal oxides, corrosion, defect. struct. and cation transport 79—100277
Tribaloy 700, hard surfacing in Na, friction, wear and corrosion 79—24628
turbomolecular pumps with corrosion resistant oil 77—87776
ultramicrotomy in corrosion and protection TEM 77—81358
Vitallium alloy, fretting corrosion of surgical implant material, electrochemical investigation 79—66197
water-cooled reactor materials, corrosion control in CIRENE plant *(Spanish)* 77—34392
Westinghouse steam generator experience with all volatile treatment 79—9853
Westinghouse steam generators, operations update 78—21683
Westinghouse steam generators, operations update 78—21751
wire for high-speed matrix printers *(Japanese)* 80—55540
wire samples, programmed control machine for corrosion testing 77—56172
X-ray diffraction apparatus, for in-situ high temp. water corrosion 80—90936
zircalloy, in-reactor, effects of water radiolysis 77—12817
Zircalloy in thermal gradient, calc. of supercharging effect of H_2 and hydride distrib. 78—21639
Zircaloy, accelerated corrosion in BWR and high temp. high press. steam, correlation 77—3104
Zircaloy, breakaway mechanism, corrosion kinetics in steam 80—61030
Zircaloy, claddings for irradiated UO_2 fuel, stability during long-term storage 79—26588
zircaloy, nuclear microprobe methods for investigating oxidative corrosion 80—71787
Zircaloy, PWR primary corrosion products 80—13578
Zircaloy corrosion in water reactors, comparison of uniform and nodular forms 79—47817
Zircaloy fuel cladding, irradiation-induced in-reactor corrosion in CANDU reactors 80—104352
Zircaloy heated surface, FeO deposition in boiling water 78—58353
Zircaloy-2, Cd metal embrittlement in 300-340°C 77—16747
Zircaloy-2, electrochemical pitting in alkaline chloride soln., H_2 evolution and anodic disintegration 80—16553
Zircaloy-2, hot-pressed, influence of diffused C on structure and oxidation 80—61016
Zircaloy-2, radiation and isotope effects on corrosion in H_2O/D_2O mixture 77—21314
Zircaloy-4, accelerated corrosion in high temp., high press. steam, effect of heat treatment 78—44263
Zircaloy-4, cyclic nature of corrosion in 633K water, optical and electron microscope study 79—66207
zircaloy-4, Nb additions, corrosion behaviour 77—40469
Zircaloy-4, PWR tubes, ZrO_2 scales formed in steam, microstruct. 77—6524
Zircaloy-4 BWR channels, corrosion resistance 80—104351
zirconosilicate glass fibre, strength, stiffness and Young's modulus, effect of cement environment 77—44335
$33K_2O.7Al_2O_3.60P_2O_5$, high expansion glass, chemical durability improvement by ion exchange 79—66180
Ag, contact material, contamination layer thickness, resist., ESCA study *(German)* 80—55561
Ag, corrosion in atmosphere, environmental test 79—66205
Ag, corrosion in marine atm., potentiometric technique, appls. 79—24693
Ag galvanic coatings, by org. insulant thermal destruction products *(Ukrainian)* 77—52525
Ag, heat pipe meas. of corrosion and vapour press. 80—23878
Ag on Cu, corrosion by thermal degradation products of chloroprene and silicone rubber 79—47801
$Ag/Na_2SO_4(WO_4)$, and $Ag/Ag_2SO_4(WO_4)$ solid cell systems interface form., intergrain contact growth 77—16827
Ag-AgCl reference electrode for high temp. eqn. environments, construction and performance 77—12803
Ag-As-Se system glasses, soln. rate 79—43456
Ag-Au, corrosion in HNO_3 80—85091
Ag-Cu (10 wt.%), contact material, contamination layer thickness, resist., ESCA study *(German)* 80—55561
Ag-Cu flex leads, microstruct. study of corrosion 80—76406
Ag-Pb (30 wt.%), contact material, contamination layer thickness, resist., ESCA study *(German)* 80—55561
Ag-Pd-Ni, corrosion in marine atm., potentiometric technique, appls. 79—24693
Ag-Sn alloys and amalgams, electrochem. considerations, corrosion in physiological soln. 80—93760
Ag-Sn-Au, dental amalgams, effect of small additions of Au, struct. and corrosion study 79—20718
Al alloy, 51S, modified by misch metal, for space appl. 80—55466
Al alloy, corrosion in uninhibited alcohol/water coolants 78—44248
Al alloy, fretting corrosion, exam. of secondary structures 79—100292
Al alloy, galvanic corrosion monitored by acoustic emission 77—90499
Al alloy, galvanic couple with Cu, steels, Zn and Ti-Al-V, velocity effect on corrosion 78—35566
Al alloy, pitting resistance short duration test and new characterization test 77—90513
Al alloy, powder, erosion resist. to hot propellant gases 77—56165
Al alloy 6061, pitting, rotation effects 79—100281
Al alloy electrode, corroding, acoustic emission 80—60997
Al alloy O1920, corrosion testing in industrial atmos. *(Russian)* 77—70205
Al alloy type 7075, pit initiation mechanism 77—12733
Al alloys, basic corrosion studies for nucl. reactor applic. 77—34402
Al alloys, corrosion inhibition by organic dyes, protective compound form. 78—44255
Al alloys, pit propagation, influence of anions in halide solution 78—72917
Al alloys, pitting corrosion rel. to load-carrying capacity of sheets *(Russian)* 78—56806
Al, alloys, thermomechanical working effect on mech. props. *(Russian)* 77—21181
Al alloys, type 1050, 5086, 2024 and 7075, galvanic corrosion in tap and artificial sea water 80—21162
Al and alloys, critical pitting potential meas., review 79—43501
Al and alloys, monitoring using polarisation resistance meas. techniques and correlations 77—16711
Al and alloys corrosion characteristics in ethylene glycol-water mixtures 78—7095

corrosion continued
Al, annealing in moist atm., causes and kinetics of H_2 blister form. *(German)* 80–25923
Al anode, implanted in heart-blocked dog, AC impedance and corrosion investig. 77–60297
Al, anode current oscillations during potentiostatic pitting 77–90496
Al, anodic film formed in H_2SO_4, thin film TEM obs. by direct vertical sectioning 78–7106
Al, anodized, inorganic glass coating, solution deposited, environmental protection 79–34205
Al, barrier film growth in soln. of film promoting and aggressive ions 77–8975
Al bronze, G, Si additions, corrosion resistance 77–16714
Al, cathodic polarization 80–21153
Al, chemical polishing, electrochem. props. of soln. 79–29282
Al, conversion coating formed in chromate/fluoride soln., TEM obs. 79–74289
Al, corrosion, general and pitting, Mo and Ar ion implantation effects 80–71794
Al, corrosion and anodic polarization in NaOH soln., effect of aldehydes 78–19923
Al, corrosion by carbon tetrachloride, IETS obs. 80–81230
Al, corrosion during 10 years at coastal site at Alicante 79–20244
Al, corrosion in uninhibited ethylene glycol-water solutions 79–70222
Al, corrosion resistant pure metal, passivity and pitting in chloride solutions 78–44258
Al, electron irrad. induced aqueous corrosion 77–81343
Al film, evaporated, in distilled water, ellipsometric obs. 77–48590
Al, galvanic corrosion, anal. for coplanar electrodes with one electrode infinitely large 79–8398
Al, localised corrosion, blister form. in oxide film as pitting precursor 78–27678
Al, oxide coated, inhibitive and aggressive ion effects, secondary ion mass spectrometry 77–8974
Al pitting corrosion in Cl solns., electrochemical exam. 79–20248
Al, pitting mechanism, obs. using Engell-Stolica potentiostatic method 80–25905
Al, polishing, electrolytic and chemical, SEM exam. of gassing defects 79–34206
Al, protection potential 79–52427
Al, sputtering and chem. attack by H ions of 100 eV energy 78–95635
Al, strained, localised corrosion on slip steps 79–20265
Al-(Mn), effects of Mn on electrode or free corrosion potentials 80–100942
Al-Al_4Cin eutectic alloy, extruded and unidirectionally solidified, corrosion a neutral NaCl soln. 80–21154
Al-Ca-Zn (5,5 wt.%) superplastic sheet alloy, mechanical properties, superplastic forming behaviour 80–60920
Al-Cr alloys, corrosion inhibition by o-substituted phenols in NaOH soln. 78–44250
Al-Cu, diffuse light scattering method for in situ obs. of pitting corrosion 80–25930
Al-Cu (Mg)(Zn), corrosion of chill zone, solidification microstruct. effect 77–36687
Al-Cu (4 wt.%), TEM obs. of intergranular corrosion 79–91835
Al-Cu (4.5 wt.%) alloy, controlled electropotential corrosion in NaCl soln., microstruct. exam 78–39948
Al-Cu film, anodic oxidation, corrosion props. 78–35581
Al-Cu-Mn-Mg-Fe-Si (4.48, 0.66, 1.55, 0.43, o.23 wt.%), alloy D16, relationship between intercrystallite corrosion depth, and elec. cond. 79–20220
Al-Mg, ageing process, effects of Ag additions and pressure *(Russian)* 80–45321
Al-Mg (7 wt.%), bare surface reaction rates in aq. solns. 80–101022
Al-Mg(Zn)(Cu), pitting potential 78–35550
Al-Mn (1 wt.%) corrosion in uninhibited ethylene glycol-water solutions 79–70222
Al-Si-Mg, corrosion inhibition in 0.1 N NaOH soln. 78–19924
Al-Sn, (<0.28 wt.%) corrosion behaviour in 16% HCl 78–85054
Al-Zn alloy cladding materials, corrosion behaviour under vacuum heating *(Japanese)* 79–91845
Al-Zn-Mg (6,3 wt.%) high-strength alloy, dislocations distrib., corrosive environment influence *(Russian)* 79–52442
Al-Zn-Mg alloy V95, two-stage ageing kinetics, mech. props. effects 79–83238
Al-Zn-Mg alloys, role of dispersed transition metal intermetallic compounds 79–96088
Al-Zn-Mg-Cu, alloy 7075-T6, corrosion in halide solutions, exam. of anion dependency 78–60867
AlMgSi, adhesive jointing, acoustic anal. *(German)* 78–7168
AlO_2, corrosion resistance of phosphate bonded castable, and dense fired types in steam CO at 199°C 79–20222
Al_2O_3 ceramic, surface elec. resist. in Cs vapour 77–51802
β''-Al_2O_3, Li_2O-stabilised, deterioration under electrolytic conditions 80–40592
Al_2O_3-$MoSi_2$ for use as heating element, anti-oxidation and anti-erosion props. *(Japanese)* 79–95989
Al_2O_3-SiO_2 glass, annealed and tempered, fracture strength studies under dynamic conditions 79–96132
Al_2O_3-SiO_2-Fe_2O_3-CaO-MgO-TiO_2, refractory, corrosion and mech. behaviour correlations 80–40563
Al_2O_3-SiO_2-X_2O (X=alkali metal) glass, acid resist. 80–21140
Al_2O_3-SiO_2-ZrO_2 refractories, corrosion behaviour in glassmelting furnaces *(Polish)* 80–71783
Au, corrosion in H_2SO_4 solutions, effect of pH 79–70344
Au galvanic coatings, by org. insulant thermal destruction products *(Ukrainian)* 77–52525
Au, heat pipe meas. of corrosion and vapour press. 80–23878
Au on Cu, corrosion by thermal degradation products of chloroprene and silicone rubber 79–47801
Au, sputtering and chem. attack by H ions of 100 eV energy 78–95635
Au-In, electrodeposited from acid cyanide electrolyte, exam. of wear and corrosion resistance 78–80482
B fibre reinforced Al alloy, corrosion resistance, electrochemistry 80–11806
B fibre reinforced Al composites, corrosion, electrochem. behaviour 79–20225
B fibre reinforced Mg, exam. of fatigue props. and corrosion 80–11751
B_4C, chem. erosion by H-plasma, first wall of fusion reactor 77–36676
BN fibres, prep., struct., thermal, mech. and elec. props., appls., book contrib. 78–48360

corrosion continued
BaO-Al_2O_3-SiO_2 ceramic, chem. resist. and struct. 79–61756
BaO-K_2O-Na_2O-ZnO-SiO_2, corrosion and microhardness, effect of detergents 80–16518
Ba_2SiO_4 cement, hardened, H_2SO_4 resistance *(Japanese)* 77–77602
$BaTi_4O_9$ effect of chemical treatment on loss quality, at microwave wavelengths 79–34159
$Ba_2Ti_9O_{20}$, effect of chemical treatment on loss quality, at microwave wavelengths 79–34159
Be powders, gas evolution during heating from 20-700°C 79–61796
Be-Cu, seawater corrosion protection, of repeater housings 78–15583
C fibre reinforced Al alloy, corrosion resistance, electrochemistry 80–11806
C, glassy, electrolytic durability 80–66809
C, pyrolytic, oxidation resist. in liq. corrosive medium 77–90471
C, vitreous, erosion in molten Si rel. to cryst. growth technology 78–3244
CC Fe-Ni-Cr (35, 15 wt.%): Nb(Ti)(Mo), corrosion in HTGR He environment 80–61021
$CaAl_2O_4$ cement bond phases, corrosion in steam-CO at 199°C 79–29234
CaO, by K_2O melt, SEM obs. 77–44383
CaO-Al_2O_3-SiO_2 ceramic, chem. resist. and struct. 79–61756
$Ca_5(PO_4)_3OH$ bioceramic, material props. 80–93523
Cd dissolution in sulphate solutions, effects of O_2 on mechanism 77–77631
$CdAl_2O_4$, LWR burnable poison, irradiation and corrosion beahviour *(German)* 79–67846
Co, atmospheric corrosion, H_2O adsorption and chem. kinetics 80–11826
Co base amorphous alloys, alloying elements influence on corrosion behaviour, XPS obs. 80–89422
Co, corrosion by molten alkali metal hydroxides and liquid Li 77–44414
Co, corrosion in Ar-SO_2 atmospheres, scale struct. obs. *(Japanese)* 80–55568
Co, model for cond. mechanism in CoO, rel. to basic atomic processes of metal corrosion 77–25198
Co, reaction, in Ar-SO_2 atmosphere, 500 to 900°C 78–39953
Co-B(-Cr) thin film glasses, mag. props. and corrosion resist. 80–80576
Co-based amorphous alloys, effect of alloying additions on corrosion resistance *(Japanese)* 79–96215
Co-based superalloys, low temp. hot corrosion, Na_2SO_4-induced, mechanism, burner rig tests 80–40610
Co-Cr, high temp. sulphide corrosion 78–64775
Co-Cr (up to 25 wt.%), sulphidation and oxidation in Ar-SO_2, effects of increase in Cr content 80–11839
Co-Cr orthopedic implants, surface oxide layer investigations using ESCA technique 79–25157
Co-Cr-Al-Y, turbine blade coating, hot corrosion by Na_2SO_4 and vaporous NaCl 78–19941
Co-Cr-Ni alloy FSX 414, electrochemical corrosion meas. in molten sulphate 79–96178
Co-Cr-Ni-Ta-Al-Y (25, 10, 5, 3, 0.5 wt%), exam. of hot corrosion 79–20251
Co-Cr-Si alloy hot corrosion and oxidation expts. for ionic conducting scale 78–11446
Co-Cr-WC, corrosion and corrosive wear in sea water 78–92408
Co-Fe-B and Co-Fe-Cr-P-B sputtered amorphous films, mag. props. and corrosion resist. 79–28567
Co-Mo-Cr-Si, plasma and detonation coatings, Laves- and carbide-strengthened, comparative props. 78–15562
Co-Ni-Cr-Al-Ta, S-57 alloy hot corrosion, cyclic oxidation, depth of attack determinations 80–11837
Co-Ni-Cr-Mo, hip joint anchorage stem, superior fatigue strength, high corrosion resist. 79–29671
Co-Ni-Cr-W-Fe, HA-188 alloy, hot corrosion, cyclic oxidation, depth of attack determinations 80–11837
Co-WC, corrosion and corrosive wear in sea water 78–92408
$(CoFeB)_{100-x}Cr_x$ thin films, magnetic props. and corrosion resist. 80–34709
Co_3O_4 anode, wear-resistant, use in applied electrochem. 80–40701
Co_3O_4 film anode, electrochem. and corrosion processes in $HClO_4$ 79–61875
^{58}Co dissolution during PWR refuelling shutdown, control with H_2O_2 78–21698
$(Cr,Al)_2O_3$-$ZrSiO_4$ refractories, glass resist. and corrosion mechanism 79–61757
Cr, corrosion by O_2 containing H_2O and gaseous NaCl, volatile products 78–27674
Cr, corrosion in SO_2, 700-1000°C 80–97642
Cr, corrosion resistant pure metal, passivity and pitting in chloride solutions 78–44258
Cr, electrochemical behaviour, in molten V_2O_5 *(Japanese)* 80–89498
Cr film, on mild steel, hardness and protective props., rel. to grain size 78–11436
Cr, high temp. corrosion in Cl_2 and Cl_2-O_2 mixtures 77–77629
Cr, high temp. in Cl_2 and Cl_2-O_2 mixture 78–15601
Cr, pure, corrosion due to V_2O_5 melts *(Japanese)* 80–93691
Cr steel and alloys, long-time exposure to N_2O_4, effect on mech. props. *(Russian)* 78–48573
Cr-Ni steel and alloys, long-time exposure to N_2O_4, effect on mech. props. *(Russian)* 78–48573
Cr-Y_2O_3 dispersion hardened, oxidation and nitridation resistance, embrittlement 78–44267
Cr_2O_3 corrosion, high-temp., in Cl_2 and Cl_2-O_2 mixtures 78–15601
Cr_2O_3, high temp. corrosion in Cl_2 and Cl_2-O_2 mixtures 77–77629
Cr_2O_3-Al_2O_3-$ZrSiO_4$ system, electrosmelted refractories, phase comp., corrosion and glass resist. Cr^{3+} conc. depend. 79–33982
Cu, adsorption and desorption of water vapour, relative humidity effects 80–49505
Cu alloy, fretting corrosion, exam. of secondary structures 79–100292
Cu and alloys, monitoring using polarisation resistance meas., techniques and correlations 77–16711
Cu and Cu alloys, corrosion inhibitor study by XPS, adsorbed benzotriazole 78–35554
Cu and Cu alloys, corrosion resistance in chlorinated lime slurry and calcium hypochlorite soln. 79–83390
Cu and Cu alloys, horse shoe corrosion in flowing sea water, mechanism, cathodic protection possibility 79–66199
Cu base alloys, in putrid seawater 79–91838

corrosion continued
- Cu, by org. insulant thermal destruction products *(Ukrainian)* 77—52525
- Cu, chem. aspects of corrosion inhibition by benztriazole 80—16545
- Cu contact tarnishing and Cu-Au interdiffusion obs. 78—7098
- Cu, corrosion, by applied alternating currents 79—70205
- Cu corrosion, by COS, kinetic and morphological study *(French)* 79—43488
- Cu, corrosion, use in reaction kinetic investigation 79—70213
- Cu, corrosion and wetting in presence of thiol reagents 80—11822
- Cu, corrosion in atmosphere, environmental test 79—66205
- Cu, corrosion in HNO_3, inhibiting effect of monosaccharides 79—70209
- Cu corrosion inhibition, by mercaptobenzothiazole, spectro-electrochem. studies 80—30138
- Cu, corrosion inhibition through decreasing rate of mass transfer by drag reducing agents 78—19920
- Cu, corrosion inhibitive films formed by corrosion determination of thickness by X-ray photoelectron spectra 79—15845
- Cu, effect of addition of bromides and iodides on corrosion in seawater 78—80670
- Cu electrode, photopotentials, rel. to corrosion 79—24648
- Cu foil, determ. of oxides on surface 77—90682
- Cu, heat pipe meas. of corrosion and vapour press. 80—23878
- Cu, in Ar-O_2-SO_2 *(Japanese)* 78—11410
- Cu, in seawater, hydrostatic pressure effects 79—52420
- Cu, noble metal additions effect, Auger spectra 78—35579
- Cu, photo-assisted corrosion in anaerobic acidic medium 79—43466
- Cu photocorrosion in $CuCl_2$ and $FeCl_3$ aq. solns. 79—57145
- Cu, pipe carrying potable water 78—92409
- Cu powder, corrosion protection during manufacture and storage 77—25200
- Cu, resistance in seawater *(Rumanian)* 79—74284
- Cu rich dental amalgams, SEM and energy dispersive X-ray analysis 78—24184
- Cu wire, corrosion in $AgNO_3$, effective corrosion time, resistance variation 78—11404
- Cu with Au electroplate, water vap. adsorption 77—69168
- Cu/Zn galvanic couple, potential distrib. meas. technique, appl. to corrosion study, apparatus *(Japanese)* 78—53049
- Cu-Al-Ni-Fe system, corrosion behaviour in sea water 80—45421
- Cu-Au, corrosion in HNO_3 80—85091
- Cu-Cd electrodeposit on Cu, corrosion and its inhibition 79—74287
- Cu-Cu_6Y eutectic alloy, cast and directionally solidified, struct. and props. *(Russian)* 80—104138
- Cu-Mn, de-alloying props. 80—104332
- Cu-Ni, corrosion, performance for condenser tube 79—39046
- Cu-Ni, galvanic corrosion in sulphide modified seawater 80—100953
- Cu-Ni, parametric eval. of susceptibility to sulphide induced corrosion in sea water 80—16560
- Cu-Ni, sulphidation between 653 to 770K, exam. of scale morphologies, using X-ray diffr., and electron microprobe anal. 78—88559
- Cu-Ni (20 and 50 wt.%), sulphidation, exam. of scale growth kinetics 78—88560
- Cu-Ni alloy, in 0.1 M NaCl, electric pot. and pH meas. 78—31564
- Cu-Ni alloys, sulphide induced corrosion 79—91836
- Cu-Ni alloys 706 and 715, corrosion in flowing seawater, O_2 effect 79—43460
- Cu-Ni alloys 706 and 715, corrosion in flowing sea water, dissolved sulfide effect 80—35379
- Cu-Ni cast alloy, effect of alloying and residual elements 78—85033
- Cu-Ni-Fe, synergistic effect of Ni and Fe on sea water corrosion 78—35561
- Cu-Ni-Zn-Mn fine grained precipitation-hardenable alloy, high strength and ductility 80—100805
- Cu-Ni(Al) alloy electrode, photopotentials, rel. to corrosion 79—24648
- Cu-Ni(10 (30) wt.%), seawater corrosion rate meas., electrochem. method validity 80—45426
- Cu-Zn, de-alloying props. 80—104332
- Cu_3Au, ordered and disordered, cavitation induced erosion 77—16743
- CuNiCr, IN838, heat treatment effect on fatigue and corrosion fatigue behaviour 80—20982
- Cu_2O, adsorption and desorption of water vapour, relative humidity effects 80—49505
- $Cu_{50}Ti_{50}$, amorphous and cryst. alloy, corrosion rates and anodic polarisation curves 79—24650
- $Cu_{50}Zr_{50}$, amorphous and cryst. alloy, corrosion rates and anodic polarisation curves 79—24650
- D isotope effect, corrosion stability in high temp. aqu. soln. 78—9091
- Fe (001) surface, initial reaction with water vap. 77—69173
- Fe, acidic corrosion, effect of aromatic and arylaliphatic sulphides 78—35560
- Fe alloy containers for liquid Li, corrosion resistance properties 79—47815
- Fe and alloys, monitoring using polarisation resistance meas., techniques and correlations 77—16711
- Fe, anodic behaviour, in acidic solns. of liq. NH_3 78—27671
- Fe, anodic dissolution in acidic chloride solns., exam. 78—92389
- Fe, Armco, coated and uncoated, laser interferometric obs. of corrosion 79—47810
- Fe Armco, corrosion and mechanical behaviour in liquid Li 78—53036
- Fe, Armco, inter- and intragranular sulphidation 80—55570
- Fe, Armco, pitting corrosion in Na_2SO_4 78—35559
- Fe, Armco, plastic deform., surface dissolution effect 77—8883
- Fe base amorphous alloys, Ni addition effect on corrosion resistance 77—4869
- Fe based amorphous alloys, delayed fracture in atmosphere, effect of alloying additions *(Japanese)* 79—96212
- Fe, cast, anodic protection under boiling H_2SO_4 in industrial conditions 79—20245
- Fe, cast, corrosion in uninhibited alcohol/water coolants, and graphitization 78—44248
- Fe, cast, grey, corrosion in water at 50°C dissolved O_2 conc. effect 80—11820
- Fe, colloid chem. appls. 80—89541
- Fe commercial piping, corrosion under flow conditions, SO_4 ion effect 80—97629
- Fe, corrosion, inhibition by Pb azelate, uptake and distrib. of azelate and Pb ions 77—56137
- Fe, corrosion, oxidation, ion-, electron-beam techniques appl. 79—43700
- Fe, corrosion and conservation of unearthed objects *(Japanese)* 79—79161

corrosion continued
- Fe, corrosion and electrochem. behaviour in NaOH soln. containing ClO_3^- *(Japanese)* 78—72928
- Fe, corrosion and oxidation, new technique for simultaneous acquisition of Mossbauer spectra and microbalance data 78—44252
- Fe, corrosion and passivation in presence of halide ions in aq. solns. 80—50758
- Fe, corrosion and passivation in LiCl soln., peripheral velocity effect 80—61000
- Fe, corrosion behaviour in H_2SO_4 soln., ion implantation effect 80—71793
- Fe, corrosion by molten alkali metal hydroxides and liquid Li 77—44414
- Fe corrosion in acids, inhibition by thiurea and its derivatives 79—20262
- Fe corrosion in aq. H_2S, FeS polymorph form. 80—81231
- Fe, corrosion in H_2SO_4, substituted purine effect 80—30148
- Fe, corrosion in H_2SO_4 soln., inhibiting effect of Mn, Cd, and Zn ions, H_2 evolution 79—47803
- Fe, corrosion in hot conc. caustic soda soln. *(Japanese)* 79—43473
- Fe, corrosion in O_2 free water, catalytic effect of certain metals 79—47804
- Fe, corrosion in phosphoric acid, kinetics and mechanisms 79—96188
- Fe, corrosion inhibition in pH range 9.3 to 12.6, tartrate ion effect on oxide film thickening 78—44251
- Fe, corrosion of tubes in air saturated soln. under turbulent flow conditions *(Japanese)* 79—61783
- Fe, corrosion product analysis by Mossbauer spectroscopy 77—28927
- Fe corrosion products, Raman spectroscopic detect. 79—16063
- Fe, crevice corrosion in chloride solns. by chromate 79—91847
- Fe, dissolution and passivation, effect of phosphate and chromate corrosion inhibitors 80—21152
- Fe, dissolution and passivation kinetics in solns. containing O 80—76547
- Fe, dissolution under cathodic polarization 80—25899
- Fe, effect of Pb ion implantation 79—39015
- Fe, electrochemical behaviour, in molten V_2O_5 *(Japanese)* 80—89498
- Fe grain boundary grooving by N contaminated liquid Li, corrosion mech. 77—6522
- Fe, grey cast, corrosion resist., Cu alloying additions effect *(Russian)* 78—56807
- Fe in distilled H_2O, initial corrosion behavior, velocity and dissolved O_2, influence 80—35375
- Fe, intergranular corrosion in NO_3 solns., electrochem. and AES study 80—50751
- Fe, passivity in aq. soln., correlation with mol. struct. 80—16541
- Fe, pure, corrosion behaviour, effect of Ta ion implantation 78—31559
- Fe, pure, corrosion due to V_2O_5 melts *(Japanese)* 80—93691
- Fe, pure, in Na loop systems 77—48576
- Fe, pure, surface oxide effect on acid corrosion inhibition 78—11384
- Fe, pure circular disc electrodes in (Na, H)ClO_4 solns., complex formation meas. 80—55569
- Fe, rotating disc electrode, corrosion in acidic chloride soln. O_2 and benzotriazole effects 78—35564
- Fe, surface films formed in inhibitive solns., optical props., protective quality 79—20260
- Fe, temp. and Zn aggregates influence *(Dutch)* 78—48571
- Fe, water sorption visualisation using THO and autoradiography 78—26761
- Fe-(Mo)-CaF_2, sintered, friction and corrosion props. for frictional units of nuclear plants 78—60845
- Fe-(Ni), cast, influence of Ni content on corrosion props. *(German)* 80—35370
- Fe-Al-Cr (10, 5 to 10, wt.%), corrosion by coal char, SEM and X-ray diffr. exam. 78—88573
- Fe-B-Cr(Si) thin film glasses, mag. props. and corrosion resist. 80—80576
- Fe-c, Fe-Si-B, and Fe-Cr-P-C sputtered amorphous films, mag. props. and corrosion resist. 79—28567
- Fe-C amorphous alloys, corrosion resistance improvement by Cr and/or Mo addition 79—66211
- Fe-Cr, amorphous alloy, effect of metalloidal impurities on corrosion resistance and electrochem. behaviour 78—72925
- Fe-Cr, corrosion in hot conc. caustic soda soln. *(Japanese)* 79—70225
- Fe-Cr, ellipsometric study of films formed in orthophosphoric acid 79—74290
- Fe-Cr (12 wt.%), corrosion in o-phosphoric acid 80—97622
- Fe-Cr (28 wt.%), intergranular corrosion and anodic polarization at grain boundary groove *(Japanese)* 79—15869
- Fe-Cr alloys, corrosion, oxidation, combined ion-, electron-beam techniques appl. 79—43700
- Fe-Cr alloys, $NaClO_3$ and NaCl effects on corrosion behaviour in hot NaOH soln. *(Japanese)* 80—35407
- Fe-Cr surface alloy formed by ion implantation, anodic polarisation 78—48561
- Fe-Cr-Al, kinetics and mechanism of high temp. S corrosion 80—25911
- Fe-Cr-Al (17, 4 or 6 wt.%), high temp. corrosion in S vapour 80—40591
- Fe-Cr-Al (7, 5 wt.%), expt. stainless alloys, phys. and mech. props. 80—97637
- Fe-Cr-Al-Y, high temp. corrosion depend. on Y, oxidation, stress growth *(Russian)* 80—40588
- Fe-Cr-Al(Ni) alloys, corrosion by coal char at 871° and 982°C 80—3237
- Fe-Cr-B, amorphous, Elinvar and Invar charact. *(Japanese)* 80—11832
- Fe-Cr-B amorphous alloys, corrosion resistance, Invar and Elinvar characts. *(Japanese)* 79—96213
- Fe-Cr-Mn (11.5, 3 wt.%), microduplex ferritic-martensitic steel, exam. 78—39862
- Fe-Cr-Mo and Fe-Cr-Mo-Si alloys, amorphous films, corrosion resist. and ion plating use 80—89423
- Fe-Cr-Ni, corrosion behaviour in hot conc. NaOH soln. *(Japanese)* 80—85082
- Fe-Cr-Ni, thermodynamic prediction in coal gasifier environment 79—43206
- Fe-Cr-Ni alloy 800, sensitization times for intergranular corrosion 77—16746
- Fe-Cr-Ni alloys, oxidation-sulphidation in gas mixture, parabolic kinetics, thermochem. diagram 78—72932
- Fe-Cr-Ni-Al alloys, 25 keV ion implanted, metallic corrosion behaviour 79—52447
- Fe-Cr-P-C alloy, amorphous, corrosion resist. in 1N HCl 78—80678
- Fe-Cr(Ni) surface alloys, corrosion resistant, formation by ion implantation 79—28009

corrosion continued
- Fe-Cu (4.54 wt.%) alloy, scaling behaviour, 700-1000°C, 1 atm. O_2 80–93679
- Fe-Mn, high-temp. sulphidation, scale struct., corrosion kinetics 80–50777
- Fe-Mo (0 to 6 wt.%), alloys, in chloride solns., role of Mo as localised corrosion inhibitor 79–20255
- Fe-Mo alloys, pitting 80–16549
- Fe-Mo-C amorphous alloys, Mo effect corrosion resistance in HCl *(Japanese)* 79–96214
- Fe-Mo-P-C alloy, amorphous, corrosion resist. in 1N HCl 78–80678
- Fe-Ni surface alloy formed by ion implantation, anodic polarisation 78–48562
- Fe-Ni-C (23, 0.39 wt.%), austenitic or martensitic structs., corrosion faces anal. *(French)* 80–21181
- Fe-Ni-Cr, compatibility with Li_2O pellets, mass spectrometric study of Li_5FeO_4 evaporation 79–8385
- Fe-Ni-Cr, high Ni content, intergranular corrosion, effect of Cr *(French)* 80–7708
- Fe-Ni-Cr (35, 15 wt.%), high temp. alloys, for HTR primary components, alloying additions for carburisation protection 80–5243
- Fe-Ni-Cr (44, 17 wt.%), nuclear microprobe methods for investigating oxidative corrosion 80–71787
- Fe-Ni-Cr base alloy, oxidation and hot corrosion *(Chinese)* 80–21149
- Fe-Ni-Cr-Mn-Al-Ti Incoloy 800, exam. of scale morphology, alloying element distrib. after oxidation 78–80677
- Fe-Ni-Cr-P-B amorphous alloy, localized corrosion 80–16559
- Fe-Ni-Cr-S, phase relations rel. to sulphidation of austenitic stainless steel 79–38800
- Fe-Ni-Cr-base superalloys, characterization for PNP components 80–5242
- Fe-P-C amorphous alloys, corrosion resistance by alloying with metallic elements 79–66212
- Fe-Si binary alloys, anodic behaviour using cyclic voltammetry 79–52417
- Fe-W-P-C alloy, amorphous, corrosion resist. in 1N HCl 78–80678
- Fe-Zn, stable and metastable alloys, order-disorder, mag. interactions and corrosion behaviour 78–68422
- Fe-Zn alloys, electrochem. corrosion of ζ, δ_1 phases *(French)* 79–20274
- FeB_x coatings on steel, formed by B diffusion, pack cementation process, microstruct. and mech. props. 78–15592
- FeNi superlattice form., by corrosion of Santa Catharina meteorite 79–8885
- $Fe_{32}Ni_{36}Cr_{14}P_{12}B_6$, Metglas amorphous films, corrosion resist. and ion plating use 80–89423
- Fe_2O_3 deposition on Zircaloy heated surfaces in pressurised boiling water 79–93714
- Fe_2O_3, haematite, effect of boiling on the mass transfer of corrosion products in high temperature, high pressure water circuits 80–71766
- α-Fe_2O_3, surface struct., adsorptive interactions rel. to rusting process, IR spectra 79–34363
- α-FeOOH, surface struct., adsorptive interactions rel. to rusting process, IR spectra 79–34363
- $Fe_{1-x}Pd_x$ film, vac. deposited, oxidation and corrosion, AES, XPS and STEM obs. 79–100286
- $Fe_{1-x}Pd_x$ films, vacuum deposited, mag. and corrosion props. 79–56574
- Ga, heat pipe meas. of corrosion and vapour press. 80–23878
- Ga_2O_3-SiO_2-X_2O (X=alkali metal) glass, acid resist. 80–21140
- p-GaP, cathode of photoelectrochemical cell 78–10552
- Ge, heat pipe meas. of corrosion and vapour press. 80–23878
- GeTe, oxidation kinetics 77–44380
- glass, PbO cryst., chem., electrochem. corrosion *(French)* 79–20232
- H_2SO_4 decomposition, corrosion tests on possible containment materials 80–45448
- Hf, corrosion in buffer soln., revealed by impedance and potential meas. 79–96182
- Hf electrode, surface oxide film, impedance and pot. behaviour 80–61001
- Hf-Fe(Co)(Ni)(Cu), alloys, oxidation of intermetallic phases 79–100298
- $HfPt_3$, corrosion resist. and elec. cond., bulk and film samples 78–72285
- Hg-Ag-Sn, dental amalgams, corrosion penetration in crevices 80–3238
- In, heat pipe meas. of corrosion and vapour press. 80–23878
- InP surface, interaction with Cl, electron spectroscopic obs. 78–56036
- IrO_x film, anodic, electrochromism, pH effects on corrosion stability, coloration and bleaching mech. 80–2726
- K_2O-Na_2O-BaO-SiO_2 glass, corrosion kinetics in aqn. KOH, transition metal oxide addition effects 77–56125
- K_2O-PbO-ZnO-B_2O_3-SiO_2, corrosion and microhardness, effect of detergents 80–16518
- K_2O-SiO_2 glass, IR reflection spectra change due to moisture corrosion *(Japanese)* 78–19914
- K_2O-SiO_2 glass, improvement in water resist. by ion exchange 78–85012
- K_2O-ZnO-P_2O_5, exam. of chemical durability, glass transformation temp. 79–20221
- Li, anodic behaviour in aq. LiOH solns. 78–39941
- Li, corrosion in alkaline soln. 77–73367
- LiO_2-SiO_2 glass, improvement in water resist. by ion exchange 78–85012
- Li_2O-Al_2O_3-SiO_2 ceramic, chem. resist. and struct. 79–61756
- Li_2O-Al_2O_3-SiO_2 glass, aq. corrosion 79–61753
- Li_2O-GeO_2-Ga_2O_3, glass, electrode props., dissolution kinetics 80–89387
- Li_2O-SiO_2, corrosion behaviour in aq. solns. of Al compounds 80–66679
- Li_2O-ZnO-P_2O_5, exam. of chemical durability, glass transformation temp. 79–20221
- Mg, electron irrad. induced aqueous corrosion 77–81343
- Mg, in aqu. NaCl soln. at room temp. *(French)* 77–59990
- Mg-Be, reactor fuel element cladding, corrosion resistance in $K_2Cr_2O_7$ aq. soln. 79–76074
- Mg-noble metal alloy, sintered, supercorroding for heat and H_2 gas generation, seawater reaction 78–15607
- $MgAl_2O_4$, corrosion resist. in fused Li rel. to phase and microstruct. changes 77–44378
- MgIn, atmospheric corrosion, SEM, electron diffraction and electron probe obs. 79–24681
- MgO, corrosion resist. in fused Li rel. to phase and microstruct. changes 77–44378
- MgO, molten K_2SO_4 treated, phys. and chem. props. *(Japanese)* 79–57133
- MgO refractory ceramic, erosion resistance in reaction products flow *(Russian)* 77–25173
- MgO single crystal, corrosion by BOF slag 79–24635

corrosion continued
- MgO, sintered, refractories, props. after testing at over 2000°C 80–104317
- MgO-C in melts, corrosion resist., rel to oxidation, porosity, content 80–40578
- Mn, corrosion, at high temp. in pure SO_4 80–50774
- Mn, model for cond. mechanism in MnO, rel. to basic atomic processes of metal corrosion 77–25198
- Mo alloy, metallurgical stability and corrosion in He atmos., HTR appl. 79–36329
- Mo, candidate current collector for Li-FeS_x battery, anodic corrosion rate in LiCl-KCl eutectic 79–100513
- Mo, corrosion behaviour in high temp. impure He gas 80–76402
- Mo, corrosion by O_2 containing H_2O and gaseous NaCl, volatile products 78–27674
- Mo, corrosion susceptibilities in synthetic geothermal brines 77–86223
- Mo, electrochemical behaviour in alcoholic KOH soln. 79–87762
- Mo, film, vacuum deposited, elec. cond., internal stresses, surface corrosion, MOS gate appl. *(Japanese)* 78–80073
- Mo-Ru-V alloys, phase equilib. and corrosion resist. *(Russian)* 79–52165
- Mo-Ti-Zr, TZM, corrosion behaviour in high temp. impure He gas 80–76402
- Mo_2C, corrosion and electrochem. props. in aq. H_2SO_4, HCl, HNO_3 and KOH solns. 80–11813
- $MoSi_2$, oxidation in CO_2, 1200-1700°C 77–40454
- $N_2O_4 \rightleftarrows 2NO_2 \rightleftarrows 2NO+O_2$, precipitation of corrosion products in a fractionating column *(Russian)* 80–25707
- Na heated steam generators, tube degradation induced by dryout instability 77–46213
- Na-cooled fast reactors, material corrosion problems 79–36328
- NaCl:Ca crystals, surface recrystn., moisture effect 80–84950
- Na_2O-$2SiO_2$ high expansion glass, chemical durability improvement by ion exchnage 78–48361
- Na_2O-(BaO)-SiO_2 glass, chemical durability of surface, heat treatment effect 79–52405
- Na_2O-(CaO)-SiO_2, corroded, quantitative anal. by IR frequency shifts 78–19909
- Na_2O-(CaO)-SiO_2, diffusion controlled attack by aq. solns. 80–81218
- Na_2O-Al_2O_3-SnO_2-SiO_2 glass, chemical stability in NaOH and Na_2CO_3 solns. 80–16532
- Na_2O-Al_2O_3-ZrO_2-SiO_2 glass, chemical stability in NaOH and Na_2CO_3 solns. 80–16532
- Na_2O-B_2O_3-SiO_2 glass, phase separated, HCl leaching rate and microstruct. 79–29242
- Na_2O-CaO-FeO-Fe_2O_3-MnO-SiO_2 glass, alkaline durability 78–23842
- Na_2O-CaO-MgO-Al_2O_3-SiO_2, corrosion and microhardness, effect of detergents 80–16518
- Na_2O-CaO-SiO_2 glass, SIMS anal. of aq. corrosion profile 79–66182
- Na_2O-CaO-SiO_2 glass, annealed and tempered, fracture strength studies under dynamic conditions 79–96132
- Na_2O-CaO-SiO_2 glass, corrosion in alkaline soln. *(Japanese)* 79–96174
- Na_2O-CaO-SiO_2 glass, microprobe anal. of corroded surface 80–7704
- Na_2O-FeO-Fe_2O_3-SiO_2, chemical durability at different pH values 78–72902
- Na_2O-K_2O-CaO-SiO_2 glasses, chemical durability, mixed alkali effect 79–8377
- Na_2O-MgO-Al_2O_3-SiO_2, chemical durability at different pH values 78–72902
- Na_2O-SiO_2 glass, IR reflection spectra change due to moisture corrosion *(Japanese)* 78–19914
- Na_2O-SiO_2 glass, improvement in water resist. by ion exchange 78–85012
- Na_2O-SnO_2-ZrO_2-SiO_2 glass, chemical stability in NaOH and Na_2CO_3 solns. 80–16532
- Na_2O-ZnO-P_2O_5, exam. of chemical durability, glass transformation temp. 79–20221
- Na_2O-ZrO_2-SiO_2 glass, treated with 2 N solns. of $NaCO_3$ and NaOH, surface layer comp. 80–35366
- Na_2O-ZrO_2-SiO_2 system, glass corrosion in NaOH and Na_2CO_3 solns. at 90-150°C 79–66187
- Nb, corrosion by molten alkali metal hydroxides and liquid Li 77–44414
- Nb, corrosion kinetics in sulphidizing atm. 80–35396
- Nb, corrosion resistant pure metal, passivity and pitting in chloride solutions 78–44258
- Nb, corrosion susceptibilities in synthetic geothermal brines 77–86223
- Nb, film, evaporated, adsorpt. of SO_2, corrosion 78–79897
- Nb-Ni, cathodic polarization in conc. KOH soln. 80–16591
- Nb-Zr (1 wt.%), corrosion behaviour in high temp. impure He gas 80–76402
- Nb-Zr-O, corrosion resistance in molten Li *(Russian)* 78–31567
- Ni 78–7099
- Ni alloys, anodic charact. meas. by AC impedance method *(Japanese)* 79–70224
- Ni alloys, corrosion behaviour in reducing environment of coal fired MHD generator 80–104322
- Ni alloys, crevice corrosion in marine conditions 77–56135
- Ni alloys, metallurgical stability and corrosion in impure He atmospheres, HTR appl. 79–36329
- Ni alloys, Nimonic PE 16, corrosion behaviour in high temp. impure He gas 80–76402
- Ni and alloys, monitoring using polarisation resistance meas., techniques and correlations 77–16711
- Ni, atmospheric corrosion, moisture adsorption and indoor corrosion rates 80–71799
- Ni base alloys, hot corrosion in coal conversion system atmos. 79–96200
- Ni base alloys, oxidation reaction investigation by X-ray diffr. and fluorescence *(German)* 79–57345
- Ni based superalloys 713C and Mar-M200, Si effect on oxidation, hot corrosion and mech. behaviour 78–39950
- Ni, bright, rest potential meas. and interpretation in NaCl and dil. H_2SO_4 *(French)* 78–85056
- Ni, candidate current collector for Li-FeS_x battery, anodic corrosion rate in LiCl-KCl eutectic 79–100513
- Ni, cavitation-erosive wear in surface-active media, dislocation struct. and fracture study by FMR *(Russian)* 79–52384
- Ni, corrosion and passivation in phosphate soln., pH depend., ellipsometric study 80–104448
- Ni, corrosion by molten alkali metal hydroxides and liquid Li 77–44414
- Ni, corrosion HCl, thiourea and derivatives effect 79–96179
- Ni, corrosion in atmosphere, environmental test 79–66205

corrosion continued
- Ni, corrosion in LiCl-KCl eutectic melt containing nitrate ions *(Japanese)* 78—92398
- Ni, corrosion in molten Na_2SO_4 at 1173K, E-pO^2 diagram 78—44247
- Ni, corrosion in SO_2, high temp. 79—20281
- Ni, corrosion mechanism, localized, in alcoholic H_2SO_4 77—86218
- Ni, corrosion rates in SO_2-O_2-SO_3 atmospheres under simultaneous sulfidation-oxidation 79—79162
- Ni, corrosion resistance in 1M $LiAsF_6$/THF, suitability for organic electrolyte Li secondary batteries 79—100387
- Ni, dissolution in methanolic soln. *(Rumanian)* 79—74283
- Ni, electrochemical behaviour, in molten V_2O_5 *(Japanese)* 80—89498
- Ni, film thickening in aqn. soln., rel. to anion type and conc. 79—96180
- Ni, high temp., SO_4 induced, studied at 900°C in O_2+4.2% SO_2 80—97639
- Ni in 0.1 N $HClO_4$, Cl^- effect 79—39020
- Ni, intergranular corrosion in dil. H_2SO_4 solns., S segregation effects 80—30152
- Ni, model for cond. mechanism in NiO, rel. to basic atomic processes of metal corrosion 77—25198
- Ni, preoxidised, reaction with SO_2 at high temp. 79—39047
- Ni, pure, corrosion due to V_2O_5 melts *(Japanese)* 80—93691
- Ni, pure, corrosion susceptibilities in synthetic geothermal brines 77—86223
- Ni, S penetration of NiO scales 78—64776
- Ni, simultaneous sulfidation-oxidation at 603°C in Ar-SO_2 atmospheres 79—8389
- Ni-(W,Cr)C, corrosion and corrosive wear in sea water 78—92408
- Ni-Ag, corrosion in marine atm., potentiometric technique, appls. 79—24693
- Ni-Al-Cr-Ti-W-Mo, US vibration applied during solidification, improved strength, corrosion resistance *(Russian)* 78—15382
- Ni-B thin film glasses, mag. props. and corrosion resist. 80—80576
- Ni-base alloy, screening studies for evaluation for nucl. process heat system 78—13236
- Ni-base alloy creep, corrosion and fatigue testing for appl. in nucl. process heat system 78—13237
- Ni-based superalloys, corrosion by O_2 containing H_2O and gaseous NaCl, volatile products 78—27674
- Ni-based superalloys, low temp. hot corrosion, Na_2SO_4-induced, mechanism, burner rig tests 80—40610
- Ni-based superalloys, mechanical integrities of surface scales, contaminant corrosion 78—95845
- Ni-Ce-Fe-Ti (77, 20, 4, 2.5 wt.%), long-term strength in H at high pressure 80—55485
- Ni-Cr, corrosion resistance of dental casting alloys 78—31561
- Ni-Cr, degradation after exposure to 1% H_2S/H_2 gas mixture at 1000°C 80—89408
- Ni-Cr (23 and 33 wt.%), kinetic and morphological study of sulphidation in S_2, H_2S and H_2S/H_2 79—52424
- Ni-Cr-Al, hot corrosion resist. of Na_2SO_4 cooled specimens 78—44264
- Ni-Cr-Al, oxidation, NaCl vapour effects on microstruct. 78—44274
- Ni-Cr-Al-ThO_2, hot corrosion, cyclic oxidation depth of attack determinations 80—11837
- Ni-Cr-Co alloy IN738, electrochemical corrosion meas. in molten sulphate 79—96178
- Ni-Cr-Co-Mo, long-term corrosion stability rel. to use in joint endoprostheses 78—36059
- Ni-Cr-Co-Mo-Al, IN-67 alloy, hot corrosion, cyclic oxidation, depth of attack determinations 80—11837
- Ni-Cr-Fe (15.7, 7.63 wt.%), Inconel 600, anal. of pit generation by 3.5% NaCl, by stochastic theory *(Japanese)* 78—85038
- Ni-Cr-Fe Alloy 600, acid intergranular corrosion rel. to caustic stress corrosion cracking stress relieving effect 77—66712
- Ni-Cr-M alloys, M=minor alloying addition Y, La, Ce, Sm, Th, U, Zr, V, corrosion rates 77—16750
- Ni-Cr-Mo (74, 20, 4 wt.%), long-term strength in H at high pressure 80—55485
- Ni-Cr-Mo steel, corrosion and cavitation-erosion resist. *(Russian)* 78—11395
- Ni-Cr-Nb-Al eutectic alloys, sulphidation/oxidation at high temps., corrosion mechanism 78—72934
- Ni-Cr-P, amorphous, corrosion behaviour, immersion tests and electrochem. meas. *(Japanese)* 80—85085
- Ni-Cr-W-C(Si) hardness, corrosion resistance, wear resistance tests in 10% HCl *(German)* 78—92368
- Ni-Cr-W-Co-(Al)(Ti)(Mo), high-temp. sulphide corrosion 80—76408
- Ni-Cr-Zr, degradation after exposure to 1% H_2S/H_2 gas mixture at 1000°C 80—89408
- Ni-Cr-base superalloys, characterization for PNP components 80—5242
- Ni-Fe-Pd thin films, mag., surface and corrosion props. 80—34707
- Ni-Fe-Rh films, mag. and corrosion props. 80—34702
- Ni-Mo-Cr-Si, plasma and detonation coatings, Laves- and carbide-strengthened, comparative props. 78—15562
- Ni-Si, intergranular segregation of Si, electron energy loss spectrometers, X-ray anal. *(French)* 79—8388
- Ni-Ti-P, amorphous, corrosion behaviour, immersion tests and electrochem. meas. *(Japanese)* 80—85085
- γ'-Ni_3Al and β-NiAl, pure and alloyed environmental resistance 77—59962
- NiCoPd, anodic dissolution, SFE effect *(German)* 80—25924
- $Ni_xFe_yCr_{1-x-y}$ films, struct., mag. props., and corrosion resist. 80—34706
- $Ni_{35}Fe_{30}Cr_{15}P_{14}B_6$, amorphous, anodic polarisation and localised corrosion 77—21310
- $Ni_{36}Fe_{32}Cr_{14}P_{12}B_6$, amorphous, electrochem. corrosion in chloride solns. 80—50763
- $Ni_xFe_{3-x}O_4$, solubility in high-temp. aqueous soln., appl. to PWR 78—4987
- Ni_4Mo alloy, high temp. oxidation, oxide layer growth, struct., mech. behaviour 78—44269
- Pb, aq. corrosion film, IR and Raman spectroscopy 80—55567
- Pb, corrosion, by applied alternating currents 79—70205
- Pb, electrode, potential effect on surface struct. in H_2SO_4 in anodic region 80—16592
- Pb, patination, IR spectroscopic study 77—56140
- Pb sheathed cables in plastic multiway ducts 80—7721
- Pb, sphere, dissolution in H_2SO_4 in elec. field *(Russian)* 77—4867
- Pb/$PbCl_2$ electrode, in chloride media, low temp. props. 78—68899
- Pb-acid battery, effect of H_3PO_4 on positve electrode, constant pot. corrosion studies 79—92071

corrosion continued
- Pb-acid battery, grid corrosion, effect of addition agents 80—3505
- Pb-acid battery positive, cyclic corrosion 79—92072
- Pb-Ca-Sn, chill cast and wrought, cyclic voltammetry and electrochemical meas. of anodic activity, PbO_2 form. 78—31582
- Pb-Ca-Sn alloys for battery grids, proposed phase diagram, grain struct. development, corrosion phenomena 77—16546
- Pb-Sb, chill cast and wrought, cyclic voltammetry and electrochemical meas. of anodic activity, PbO_2 form. 78—31582
- Pb-Sb alloy, Sb distrib. profile as function of depth in corrosion films 80—21177
- Pb-Sb-Sr alloys, corrosion props. by simplex-lattice planning method 77—56148
- PbO-attack, thermodynamic activity in liquid PbO-$PbCl_3$ 78—7227
- PbO-B_2O_3-SiO_2, glass enamel, heat treated, exam. of microstructure and chemical durability 79—29254
- PbO-B_2O_3-SiO_2-Li_2O-ZrO_2-CdO(CoO)(CuO), glass enamel, chemical durability, microstruct., CuO, CdO and CoO addition effects 79—29256
- PbO-B_2O_3-SiO_2-Li_2O-MgO(CaO)(ZnO)(Al_2O_3)(TiO_2)(ZrO_2), glass enamel, heat treated, chemical durability, MgO, CaO, ZnO, Al_2O_3, TiO_2, ZrO_2 addition effects 79—29255
- PbO-K_2O-SiO_2-(Al_2O_3) glass, corrosion in acid, leaching kinetics 78—92378
- PbO-SiO_2, corroded in acid, IR reflectance spectra 77—20846
- PbO-SiO_2 glass, corrosion in acid, conc. profile meas. 78—92379
- PbO-SiO_2 glass, modifier release in acid soln. 79—43450
- PbO-SiO_2-(Al_2O_3) glass, corrosion in acid, leaching kinetics 78—92378
- PbO_2, corrosion in HBF_4, redox mediator effects 77—90480
- PbO_2 electrode, cyclic voltammetry for accelerated life tests 78—31582
- Pb(Sb)/H_2SO_4, $PbSO_4$(sat.), rates, instantaneous, Faradaic rectification, experimental verification part II 78—80667
- Pt, boiling water reactor, corrosion and oxidation potentials monitoring 79—20252
- Pt electrode, electrochemical studies in $NaHCO_3$ solutions at elevated temps. 78—85026
- Pt-Rh-W alloy corrosion by radioisotopic power system insulating and thermoelec. materials 78—7094
- Ru, as elec. contact material, environmental interactions and prep. 80—29463
- RuO_2, as elec. contact material, environmental interactions and prep. 80—29463
- RuO_2-TiO_2 anode, wear-resistant, use in applied electrochem. 80—40701
- RuO_x, catalyst at anode of solid polymer electrolyte cell, corrosion 79—20376
- Si, electron irradiation induced corrosion 77—59960
- Si, ion-implanted surface, profiling method 78—95075
- SiAlON system, β', 15 R phases, oxidation resist. *(French)* 78—72899
- SiC, chem. erosion by H-plasma, first wall of fusion reactor 77—36676
- SiC coating corrosion by fission product Pd in HTGR coated particle fuels 80—102237
- SiC, corrosion in gases and alkaline melts 77—8967
- SiC corrosion in HTGR fuel particles 77—67817
- SiC corrosion in HTGR fuel particles 77—74932
- SiC, corrosion resist. in residual fuel oil fired environment 79—39010
- SiC, oxidation and corrosion behaviour, formation of protective SiO_2 coatings *(German)* 80—25885
- SiC, oxidation and hot corrosion resistance kinetics 80—25896
- SiC, resist. to oxidation and corrosion at high temps. *(German)* 80—35357
- β-SiC, submicron powder, prep. by siliconization of C black, props. *(Japanese)* 79—66192
- SiC-Si, wear resist., props. under abrasion and corrosion 80—100927
- Si_3N_4, corrosion resist. in residual fuel oil fired environment 79—39010
- Si_3N_4, oxidation and hot corrosion resistance kinetics 80—25896
- Si_3N_4, reaction bonded, exam. of Na_2SO_4 induced heat corrosion 79—20224
- Si_3N_4, reaction-bonded, added oxides effect on strength after oxidation 79—39012
- Si_3N_4, reaction-bonded, Na ion assisted oxidation, 800 to 1300°C 79—39011
- Si_3N_4, synthesis and props. of shapes 79—47650
- Si_3N_4-Y_2O_3, hot-pressed, oxidation kinetics 80—16520
- SiO_2 fibre reinforced Al, thermal degradation kinetics 77—44194
- SiO_2, fused, slide glass surface, Ca^{2+} ion deposition as inhibitor to alkaline attack 80—50737
- SiO_2, vaporisation in steam atmosphere 80—44306
- SiO_2, vitreous, resist. to NaOH 80—21143
- SiO_2-Al_2O_3-B_2O_3, glass fibre, water and acid resistance 80—11799
- SiO_2-Al_2O_3-CaO-MgO-B_2O_3, E-glass, acid resist. studies 80—60991
- SiO_2-Al_2O_3-Cu_2O glass alkaline durability, corrosion rate, heat capacity and elastic moduli 80—93673
- SiO_2-Al_2O_3-Y_2O_3-La_2O_3-TiO_2 glasses with high elastic moduli, alkaline durability 80—85071
- SiO_2-B_2O_3-Na_2O-K_2O system glass, phase separated, loss of oxides during acid leaching, atomic absorpt. anal. 79—11716
- SiO_2-CaO-Na_2O-M_mO_n systems, M=Zr, Sn, Ti, Al, La, Ta, P, Mn, Fe, Pb, Cr, water, alkali, acid resist., chem. durability 79—34162
- SiO_2-ZrO_2-Al_2O_3-CaO-Na_2O-K_2O-Li_2O, chemical resistant glass for glass fibres 80—21128
- Sn, heat pipe meas. of corrosion and vapour press. 80—23878
- Sn, pitting corrosion in aqn. soln. 79—52426
- Sn, pitting corrosion in aq. solns., influence of Cl^-, ClO_4^-, SO_4^{2-}, and NO_3^- *(French)* 80—89389
- Sn powder, incorporated into lacquers, applied to tinplate containers 78—80671
- Sn-Ni electrodeposit, contact resist. corrosion effect 78—47847
- Sn-Ni electrodeposits, worn, and Au coated, corrosion resist. 77—77633
- SnO_2, electrodes, effect of DC on corrosion in lead glass melt 80—85075
- SrO-Al_2O_3-B_2O_3-SiO_2, glass, corrosion by Cs vapour or liq. 77—16706
- $SrZrO_3$ ceramic, high-temp. corrosion resist. *(Polish)* 79—52409
- Sr_2ZrO_3, resist. to corrosion by Al_2O_3, CaO, MgO, SiO_2, K_2CO_3 and coal ash 80—16516
- T, metal and alloys, mechanical props., electrochemistry, oxidation and corrosion resist., conference, Nantes, France (Nov. 1978) 80—41932
- Ta, corrosion by molten alkali metal hydroxides and liquid Li 77—44414
- Ta, corrosion resistance in 1M $LiAsF_6$/THF, suitability for organic electrolyte Li secondary batteries 79—100387
- Ta, corrosion resistant pure metal, passivity and pitting in chloride solutions 78—44258
- Ta, film, evaporated, adsorpt. of SO_2, corrosion 78—79897

corrosion continued
- Ta-Pt, electrospark alloying for obtaining stable effective electrodes for electrochemical processing *(Russian)* 79—39157
- TaN film, growth by CVD, microhardness and corrosion resist. 77—36404
- Te film, stability in moist air, rel. to information storage capability, atmospheric corrosion model 80—71774
- Te film in Sn/Te/electrolyte system 77—63923
- Th-U alloy fuel behaviour in organic-cooled reactor 78—86605
- Ti alloy, VT3-1, vacuum-chromized, fretting-corrosion in couple with unprotected BT3-1 and steel 40KhNMA *(Russian)* 78—56804
- Ti and Ti alloys, mechanical, thermal and elec. props., data sheet 79—43317
- Ti and Ti alloys, resistance in HNO_3 *(French)* 77—59992
- Ti anode, Pt-Ir coated, corrosion and passivation behaviour in Cu electrowinning appl. 80—55573
- Ti, behaviour close to corrosion potential in aerated sulphuric solution *(French)* 78—23862
- Ti, conference, Rennes, France (Nov. 1976) 78—23857
- Ti corrosion by a hot perfluoropolyether 80—93684
- Ti, corrosion by molten alkali metal hydroxides and liquid Li 77—44414
- Ti, corrosion by O_2 containing H_2O and gaseous NaCl, volatile products 78—27674
- Ti, corrosion in H_2SO_4, estimated from weight loss meas. at 270°C and 56 bar *(French)* 80—85080
- Ti, corrosion in seawater circulation plant, comparison with stainless steel *(German)* 80—25897
- Ti, corrosion inhibition in acid medium, electrochem., Auger investigs. *(French)* 78—44430
- Ti, corrosion resist. in marine environments *(French)* 80—50767
- Ti, corrosion resistance in 1M $LiAsF_6$/THF, suitability for organic electrolyte Li secondary batteries 79—100387
- Ti, corrosion resistant pure metal, passivity and pitting in chloride solutions 78—44258
- Ti, corrosion susceptibilities in synthetic geothermal brines 77—86223
- Ti, crevice corrosion in NaCl soln., 100 to 250°C *(Japanese)* 78—72927
- Ti electrodes, RuO_2 coated, corrosion during O evolution rel. to electrode prep. *(French)* 80—76420
- Ti, film, evaporated, adsorpt. of SO_2, corrosion 78—79897
- Ti in acidic chloride solns., anodic dissolution and passivation 80—35541
- Ti in conc. H_2SO_4, effect of oxidation product coating on corrosion rate 79—74282
- Ti, oxide layer form. in acid soln., electrochem. and optical props. 78—48560
- Ti, physical props., implant surgery appl. 77—73615
- Ti, pit nucleation in bromide media, ion beam anal. 80—93683
- Ti, repassivation and pitting corrosion 80—30143
- Ti, sulphurisation kinetics, 450-550°C, thermogravimetric determ. 77—25197
- Ti:Pd, ion implanted, corrosion behaviour and Rutherford backscatt. anal. 80—71792
- Ti-Al, Al effects on susceptibility to salt corrosion *(Russian)* 77—25185
- Ti-Al, phase diagram in Ti rich region *(Russian)* 77—25013
- Ti-Al-Cr-Fe-Si alloy AT6, and weldments, mech. and corrosion props. 77—90409
- Ti-Al-Sn(V), corrosion resist. in marine environments *(French)* 80—50767
- Ti-Al-V, long-term corrosion stability rel. to use in joint endoprostheses 78—36059
- Ti-Al-V (6, 4 wt.%), fretting corrosion of orthopaedic implant materials by bone cement 80—104813
- Ti-Al-V (6, 4 wt.%), repassivation and pitting corrosion 80—30143
- Ti-Cu, corrosion resist. in marine environments *(French)* 80—50767
- Ti-Cu alloys, in acidic media, electrochemical behaviour *(French)* 78—23863
- Ti-Cu metallisation systems, in 85°C 78% RH SO_2 contaminated environment, performance 79—74304
- Ti-Fe, corrosion, effect of microstruct. caused by casting, annealing, beating *(Russian)* 79—57140
- Ti-Fe-C, type 50A, pitting resist. in low salinity geothermal brines 80—93681
- Ti-Fe(Co)(Ni)(Cu), alloys, oxidation of intermetallic phases 79—100298
- Ti-Ni-Mo, Ticode 12, pitting resist. in low salinity geothermal brines 80—93681
- Ti-Pd, crevice corrosion in NaCl soln., 100 to 250°C *(Japanese)* 78—72927
- Ti-Pd, dil., ion implanted, corrosion rate and electrochemical props. 79—43467
- Ti-Pd-Cu-Ni-Au metallisation systems, in 85°C 78% RH SO_2 contaminated environment, performance 79—74304
- Ti-Pt, electrospark alloying for obtaining stable effective electrodes for electrochemical processing *(Russian)* 79—39157
- Ti_3Al-Sn-Zr, alloy, Sn and Zr alloying influence on creep and scaling resist. *(Russian)* 79—52302
- TiN, from high-temp. reaction of NH_3 and $TiCl_4$, physicochem. props. 80—55334
- TiN-AlN, composite, erosion resist. in electron stream 78—11365
- TiO_2 amorphous film, alkali resistance, refractive index, IR spectra *(Japanese)* 78—23546
- TiO_2, anodically formed layers, film instability obs. 78—72916
- n-TiO_2 photoanodes, corrosion suppression mechanism 80—2462
- TiO_2, photoelectrochemical systems, solar energy utilisation *(German)* 80—45713
- TiO_2-RuO_2 anode, wear-resistant, use in applied electrochem. 80—40701
- TiO_2-ZrO_2-SiO_2 amorphous film, alkali resistance, refractive index, IR spectra *(Japanese)* 78—23546
- UO_2-PuO_2 fuel pin, hyperstoichiometric, post irradiation examination 80—63258
- V-Mo, effect of ion plated Mo on corrosion in liquid Na, mech. props. 78—53020
- V-Mo (25 wt.%), corrosion behaviour in high temp. impure He gas 80—76402
- V-Mo alloys, corrosion in high purity liquid Na containing ≈ 1 ppm O, at 700°C for 500 h 79—8383
- V-Nb-Mo(Cr), corrosion in liquid Na, O_2 effects 77—8987
- V-Si(Ti)(Sn-Ti), corrosion resistance and some physicomechanical props. 77—70229
- V-Ti (20wt.%), corrosion in liquid Na, O_2 effects 77—8987
- Vitallium, orthopaedic implant material, metallurgical cond. effect on pitting resistance 79—70704
- W, gas-surface interaction in atom-probe FIM 77—40336

corrosion continued
- W, reaction with SO_2, 1600-2100K, kinetics 79—20266
- WC-Co alloy, hard metal, resistance of cavitation erosion *(Japanese)* 80—16575
- WSi_2, oxidation in CO_2, 1200-1700°C 77—40454
- Y_2O_3, corrosion resist. in fused Li rel. to phase and microstruct. changes 77—44378
- Y_2O_3 sintered body, luminous pipe of high press. Na discharge lamp, corrosion resistivity *(Japanese)* 78—19915
- Zircaloy, dispersion and spheroidisation treatment of δ ZrH, effect on corrosion resistance 79—76072
- Zn alloys, anodic corrosion in seawater 77—77628
- Zn and Zn coated surfaces, cathodic pretreatment 78—19929
- Zn, chromated, electroplate on steel, corrosion, effect of chromate content 79—20286
- Zn, corrosion, by applied alternating currents 79—70205
- Zn, corrosion in de-aerated 0.1 M NaCl, pH range 1.6 to 13.3 78—19921
- Zn, corrosion in HCl under forced convection 80—35426
- Zn, corrosion inhibition, role of thiocyanate ion in perchloric acid with n-decylamine 79—96223
- Zn, corrosion inhibition by n-decylamine, synergistic effect of halide ions 80—11819
- Zn, corrosion rate, electrochem. meas. using differential pulse polarograph 77—59980
- Zn, rate meas. by differential pulse method 78—19962
- Zn, wear resistant coating, effect of surface-active substances in electrodeposition on props. *(Russian)* 78—11359
- Zn-Al (22 at.%), heat treatment and straining effect on fracture and corrosion 79—87672
- Zn-Al-Cu-Mg-Pb-Sn, Cu, Mg, Pb, Sn effects on corrosion in wet steam 77—48585
- Zn-Al-Cu-Mg-Pb-Sn (12, 1, 0.02, 0.01, 0.015, wt.%), combined effects of Pb and Sn additions on corrosion, in wet steam 78—39952
- Zn-Ti, environmental factors affecting pitting corrosion potential in NaOH solns. 80—45423
- Zn(Hg)/KOH, ZnO(sat.), rates, instantaneous, Faradaic rectification, experimental verification part II 78—80667
- Zr alloy, thermal neutron capture cross-section var. with time, calc., and corrosion props. var. 77—61505
- Zr alloys, effect of steel presence on corrosion stability 77—56162
- Zr and alloy, cathodic behaviour in conc. hot H_2SO_4 79—52423
- Zr and alloys, basic corrosion studies for nucl. reactor applic. 77—34402
- Zr and Zircaloy, polarisation in high temp. water 77—52540
- Zr, corrosion by molten alkali metal hydroxides and liquid Li 77—44414
- Zr, corrosion resistant pure metal, passivity and pitting in chloride solutions 78—44258
- Zr, electrochemical pitting in alkaline chloride soln., H_2 evolution and anodic disintegration 80—16553
- Zr-Al(8.6 wt.%), mech. props., corrosion and fast neutron irrad. influence 78—84948
- Zr-Fe(Co)(Ni)(Cu), alloys, oxidation of intermetallic phases 79—100298
- Zr-Nb (1 wt.%), corrosion in water at 285°C 77—56161
- Zr-Nb-Sn (3,1 wt.%), corrosion resist. depend. on mech. and heat treatments 80—653
- ZrB_2, prod., oxidation rate, corrosion resistance 77—52274
- ZrB_2-TiB_2 solid solns., prod., oxidation rate corrosion resist. 77—52274
- Zr(C,N), coating on Zr substrate, oxidation by water vap., kinetics, 0.2-20 torr, 500-600°C *(French)* 78—44266
- $Zr(HPO_4)_2$, cryst., heat treated, acid strength distrib. 78—92377
- ZrN, coating on Zr substrate, oxidation by water vap., kinetics, 0.2-20 torr, 550-700°C *(French)* 78—44266
- ZrN-AlN, composite, erosion resist. in electron stream 78—11365
- ZrO_2 amorphous film, alkali resistance, refractive index, IR spectra *(Japanese)* 78—23546
- ZrO_2-SiO_2(-Na_2O) glass fibres, prep. from metal alkoxides, resistance to NaOH soln. 80—97454
- $ZrPt_3$, corrosion resist. and elec. cond., bulk and film samples 78—72285
- ZrSi/$ZrSi_2$ coating on Ar, exam. of oxidation behaviour by O_2, H_2O *(French)* 79—20284

corrosion control *see corrosion protection*

corrosion fatigue *see stress corrosion cracking*

corrosion fatique testing *see corrosion testing*

corrosion prevention *see corrosion protection*

corrosion protection
- *see also anodisation; corrosion; corrosion protective coatings; packaging; pH control*
- AGR, moderator corrosion problems, soln. 77—18688
- Al, electrodes, use of soluble corrosion inhibitors to suppress electrode dissolution 78—88565
- boiler feedwater redox potential meas. by Pt thin-layer electrodes 80—89578
- boric acid solutions, extractive purification from radioactive corrosion and fission products 80—18458
- brass, corrosion in acetic acid soln., inhibitive action of thioureas 79—87759
- brass, in chlorosubstituted acetic acids, use of 2-methyl benzothiazole corrosion inhibitor 79—57149
- brass corrosion in HCl, HNO_3 and NaOH, p-thiocresol inhibitor effectiveness 79—57147
- cathodic protection, conc. changes 79—70181
- cathodic protection, of pipelines, using photoelectric solar plant 79—39286
- cathodic protection for small plant, economic method *(German)* 80—100943
- cathodic protection in seawater, sacrificial anode performance 79—57246
- cathodic protection meas. methods *(Dutch)* 78—3297
- chlor-alkali and related industries *(Japanese)* 79—34173
- coatings, prevention role and corrosion types 78—11354
- condenser tube corrosion resistance performance review 79—39046
- control in chemical plant engng. *(Japanese)* 79—34172
- controlled environment exposure of atomically clean surfaces 78—19954
- corrosion resistance for long-term implants *(German)* 79—8565
- disaster prevention *(Japanese)* 79—39006
- drum boilers, working at 11.0 to 15.5 MPa, pH control by addition of caustic soda *(Russian)* 80—89420
- electric connectors, Al/Cu bimetal, galvanic corrosion elimination 80—35387
- electrical resistance alloys, oxidation mechanism *(Polish)* 79—79143

corrosion protection continued
- electrochemical electrodes linearly polarised, electrolyte stationary electric field calc. *(Russian)* 80−21289
- electrode, disc type, current distrib., analogue model investig. 79−34321
- electrodes, stainless steel, cathodic protection, biomedical appl. 77−90923
- fracture preservation and cleaning, for fractography 80−71866
- fusion reactor, Li cooling system, corrosion inhibition by Al additions 80−108646
- galvanic corrosion cell types and aversion methods 77−81329
- galvanic corrosion control, new methods 80−40598
- hard plated pit props., vacuum impregnation by immersion, secondary anticorrosion treatment *(German)* 79−79144
- Incoloy 800, stress corrosion cracking in NaOH solns., electrochem. aspects, peening treatment 80−97618
- Inconel, type 600, Li corrosion inhibitions by Al additions 80−108646
- Inconel 600, stress corrosion cracking in NaOH solns., electrochem. aspects, peening treatment 80−97618
- LWR local corrosion causes and preventive methods *(French)* 78−8963
- magnetic thin films, Fe-Sr-Cr, produced by sputtering process 80−80573
- Magnox reactors, moderator graphite, coolant comp. effect on radiolytic graphite/CO_2 reaction 77−6489
- Magnox reactors, moderator graphite, He injection into Wylfa reactor I coolant gas 77−6490
- marine corrosion, and its prevention 80−104333
- metal pipelines for natural fresh water supply, fundamental criteria *(Russian)* 79−1921
- metal surfaces, laser heat treatment, wear resist., corrosion protection, hardening, review 78−72939
- metals, stress corrosion cracking avoidance, critical potential data appl. 79−74308
- metals and concrete reinforcements, cathodic protection using lightning conductors connected with diodes 79−52418
- motor-car corrosion protection improvement, primer paint appl. by electrocoating effect *(Dutch)* 80−71915
- multilayer Ni deposits, simultaneous thickness and electrochemical potential determination for individual layers 80−71813
- nervous system electrostimulation, stainless steel electrode corrosion control 78−7464
- nuclear industries, corrosion problems and prevention *(Japanese)* 80−42711
- in nuclear reactor, radiolytically formed chelating agents appl. 78−64745
- offshore seismic exploration streamer cable connector design and programming 77−25803
- painting *(Japanese)* 78−95829
- Permalloy corrosion resistance enhancement 79−79150
- physical principles, meas. and protection *(Italian)* 79−83342
- pipeline systems, cathodic protection, polarisation effect calc. using spline function method *(Russian)* 78−31566
- plastics, managing problems of corrosion *(Japanese)* 78−92382
- pollution control equipment appl. 78−77317
- polyethylene terephthalate sheeting, storage in aqueous media rel. to props. *(German)* 79−29250
- PWR boiler tubes, denting type corrosion, control by use of neutralisers 80−106109
- radionuclide corrosion and fission products, ion exchange separation 80−18460
- radionuclide corrosion and fission products, liquid-liquid extractions with metal diethyldithiocarbamates 80−18459
- review, (1978) *(Japanese)* 79−34174
- review in corrosion science and control−1979 *(Japanese)* 80−45408
- rust prevention in lubricants, test method 78−15635
- scale protection criteria in natural waters 79−70182
- sheet metal, deep-drawn, for implant device encapsulation, mech. and metallographic props. *(German)* 79−8564
- stainless steel, laser surface melting 80−93698
- steel, austenitic, corrosion-resistant, strengthening by alloying with N_2 78 95757
- steel, austenitic type 304, sensitised, intergranular stress corrosion cracking inhibition study 80−100939
- steel, borided, nitrided, corrosion behaviour in aqueous media 78−95837
- steel, corrosion protection, NAA obs. 78−53038
- steel, galvanised, prepassivation, chem. nature of film and corrosion resist. *(French)* 79−43480
- steel, high-strength, type 4340, new inhibitors for crack arrestment in corrosion fatigue 80−100941
- steel, low C, corrosion in HCl inhibited by 2-hydroxy-3-(2-undecyl, pentadecyl or heptadecyl amidoethylamine) propane-1-triethyl ammonium hydroxides, acid-corrosion inhibitors 80−50761
- steel, low C, corrosion inhibition by Na_2MoO_4 77−86221
- steel, low-alloy, feasibility of electrochem. corrosion protection 79−70220
- steel, martensitic, corrosion resistance and mechanical performance in medical instruments 79−39537
- steel, mild, acid dissolution inhibition by aniline and thiourea, iodide effect 79−79181
- steel, mild, cathodic protection against corrosion fatigue cracks 79−74281
- steel, mild, corrosion inhibitor, zinc potassium chromate 78−95839
- steel, mild, protection by Zn-rich paint in flowing aerated 0.5 M NaCl solution, Zn particle size effect 78−95840
- steel, mild, protection by Zn-rich paint in flowing aerated 0.5 M NaCl solution, exposed area ratio effect 78−95841
- steel, mild, protection by Zn-rich paint in flowing aerated 0.5 M NaCl solution, zinc content effect 78−95842
- steel, mild, protection by Zn-rich paint in flowing aerated 0.5 M NaCl solution, zinc oxide addition effect 78−95843
- steel, protective props. of N-containing inhibitors *(Russian)* 78−56809
- steel, rusted, exam. of tannin treatment action mode 78−88564
- steel, stainless, 18-8 Ti and 18-8 Nb, against stress corrosion cracking in polythionic acid solution 78−56824
- steel, stainless, crack resistance in chloride soln., electrochem. protection, polarization effect 80−55589
- steel, stainless, highly protective film development by surface treatment 80−66699
- steel, stainless, sensitised surface normalisation by laser melting 78−60869
- steel, stainless, surface cathodic alloying, for increased passivation and corrosion resist. 80−100940
- steel, stainless type 316, Li corrosion inhibition by Al additions 80−108646

corrosion protection continued
- steel, unalloyed, electric metallisation, corrosion resistance tests *(Russian)* 78−19935
- steel 20, protective props. of diammonium salt-based inhibitors *(Russian)* 78−56808
- steel in concrete, cathodic protection 79−70216
- steel surface, ellipsometric obs. of corrosion inhibitor action, propargyl alcohol film growth *(Rumanian)* 80−60996
- strain gauge, vulcanized-rubber protection and waterproofing in seawater environment 78−16787
- synergism 80−30173
- tensoresistors, protection methods from phenol formaldehyde resin medium 79−54121
- ultramicrotomy in corrosion and protection TEM 77−81358
- underwater repeater housing, of Be-Cu alloy 78−15583
- water pipe, by natural scale layers, microstruct. and chem. comp. 79−74293
- Zion Generating Station steam generator operating experience 79−9851
- Al corrosion in chloroacetic acids, 2-mercaptobenzothiazole inhibitor effectivenes 79−57148
- Al dissolution in HCl soln., inhibition by hydrazine derivatives 80−50759
- Al tube, polyethylene oxide drag reducing polymer effect on corrosion rate 80−45445
- Al-brass tubes, passivation treatment for atmospheric corrosion protection during storage and transport 80−85079
- Al-Cu alloy in NaOH, aminophenols as corrosion inhibitors 80−30136
- Al-Mn (1.3 wt.%) alloy, corrosion inhibition in trichloroacetic acid using chloroanilines 79−83389
- Al_2O_3, anodic, passified, inhibition of reaction with water 80−89390
- Au electrodeposition, heavy metal ion induced depolarisation effects 77−16511
- $CaSO_4$, scale mineral form., kinetics and mechanism, inhibitor effect 80−30115
- Cr, surface cathodic alloying, for increased passivation and corrosion resist. 80−100940
- Cr/Au metallisation system, corrosion inhibition using intermediary Pd layer 79−79155
- Cu, (100) plane, anodic dissolution in acidic $CuSO_4$ soln., caffeine additive effects 78−27672
- Cu, corrosion protection by benzotriazole pretreatment 80−16555
- Cu, corrosionprotection by ion implantation of Al and Cr 80−71789
- Cu, in chlorosubstituted acetic acids, use of 2-methyl benzothiazole corrosion inhibitor 79−57149
- Cu, passivation by protective glassy layers at 500°C 78−76785
- Cu, passivation using protective glassy layers at 500°C 80−3246
- Cu-Ni-Fe, corrosion resistant, SCC, crevice corrosion in seawater 79−96177
- Fe 80−30173
- Fe, atomically clean, N_2 treatment, corrosion inhibition 78−19954
- Fe base amorphous alloys, alloying element role in improving corrosion resist., ESCA study 80−50754
- Fe, carboxylic acid surface film struct. 79−74294
- α-Fe, chem. interaction with aluminophosphate and alumino-chromophosphate adhesives, Mossbauer obs. 80−40596
- Fe, corrosion, inhibition and monitoring techniques 80−30132
- Fe, corrosion, substituted methylamines as inhibitors 79−83384
- Fe corrosion in HCl, inhibition by thiourea and derivatives 78−7097
- Fe, corrosion pitting in acid, alkaline solution, gelatin effect 78−95838
- Fe, dissolution and passivation, effect of phosphate and chromate corrosion inhibitors 80−21152
- Fe, effect of anion and organic corrosion inhibitors on H_2 penetration rate 80−100938
- Fe, film growth under organic coatings, qualitative ellipsometric-electrochem. approach 80−104344
- Fe, grey cast, in ethanediol/water, inhibition of corrosion by benzoate/benzotriazole mixture. synergistic effect 80−45425
- Fe, influence of acid Na_3PO_4 soln. in tap water as a corrosion inhibitor 80−45424
- Fe, inhibition in Na_2SO_4 soln. containing aliphatic acids, electrochemical and ellipsometric study 79−74309
- Fe, mechanism of action of weak acids and their salts on passivation by O_2 80−50886
- Fe polarised wire, elongation in presence of acetylene type acid corrosion inhibitors 80−55590
- Fe powder, acid dissolution inhibition by aniline and thiourea, iodide effect 79−79181
- Fe surface, purposeful modification by gas adsorption, charact. by photoemission 78−71955
- Fe-B-Mo-Cr, amorphous, Mo and Cr addition effect on corrosion behaviour 80−16568
- Fe-Cr alloys, feasibility of electrochem. corrosion protection 79−70220
- Fe-Cr-Pd, Pd alloying effects on passivation 80−35373
- Fe-Mo (0 to 6 wt.%), alloys, in chloride solns., role of Mo as localised corrosion inhibitor 79−20255
- GaP photoelectrode, role of Au overlayers 78−14812
- $Gd_2(MoO_4)_3$, passivation of c surface against attack by HF by inert ion beam irradiation 78−35545
- Mn-Bi alloys, improvement study *(Japanese)* 78−43617
- NaO-CaO-SiO_2 glasses, fluorinating agents effect on comp. and surface struct. 80−35364
- Ni-Cr, austenitic alloy, oxidation mechanism, adhesion of Cr_2O_3 scale *(Polish)* 79−79143
- Ni-Cr-Al, hot corrosion resist. of Na_2SO_4 cooled specimens 78−44264
- Si solar cells for cathode protection of submerged marine structures 80−40859
- $SmCo_5$, powder, exam. of protective preps. of organic media against oxidation 79−96220
- Ti, surface cathodic alloying, for increased passivation and corrosion resist. 80−100940
- Ti/Ag metallisation system, corrosion inhibition using intermediary Pd layer 79−79155
- Ti-Al-Mo-V, crack resistance in chloride soln., electrochem. protection, polarization effect 80−55589
- TiO_2 (rutile) photoanode, corrosion suppression by high-energy redox reactions 78−23163
- TiO_2 anodes, corrosion suppression by high energy redox reactions 77−77599
- Zn, and corrosion inhibition by surface active substances 80−40589
- Zn corrosion in HCl and H_2SO_4, alkaloid inhibitor effectiveness 79−57146

corrosion protective coatings
acrylic thermosetting powders, parameters 79—20003
alumina on stainless steels and Inconel, gasless ion plated films 77—40476
aluminide on superalloys, high temp. 79—57138
alumino-chromo-phosphate adhesive, chem. interaction with α-Fe substrate, Mossbauer obs. 80—40596
aluminophosphate adhesive, chem. interaction with α-Fe substrate, Mossbauer obs. 80—40596
anodic oxide in Al, quality testing *(German)* 77—28943
anodised Al rods, humidity and coating thickness effects on fatigue in reversed torsion 77—25205
anticorrosive and antifouling coatings, laboratory and environmental testing 78—64746
benzoic acid inhibitor film on Fe, passivation and inhibitor props., X-ray photoemission spectroscopy exam. 78—88561
boilers, steam generating, operation reliability 78—11424
boride coatings, technology, props., book contrib. 78—48574
boride on stainless steel, mech., elec. props., boronising sintering method investig. 78—60594
carbide coating, oxidation protection 77—32704
carborundum, oxidation protection via phosphate impregnation 77—44374
clear, protection of sputtered metal layers 80—35392
composite material deposition by electrolysis *(French)* 77—73375
controlled nucleation thermochemical deposition, improvements over chemical vapour deposition 78—92387
corrosion types and role of coatings 78—11354
diaphragm for corrosive atm. pressure or vacuum meas. isolation chamber 77—30174
dip-applied coating for water-immersed wedge-gate valve of cast Fe with stainless steel trim 80—93677
electrocoating from molten salts 79—83394
electrolytic coatings, corrosion of stainless steel and Ni in 40% wt. KOH 80—30175
electron beam deposited alloy coating for gas turbine superalloy, defects 77—40473
electron beam deposition, principles and technology 79—24439
electroplated coatings thickness test standards 79—8405
electroplating, surface finishing for protection and component build up 78—35586
enamel, melted vitreous, for protective coating appls., gas generation in highly viscous phase *(Russian)* 77—73360
engineering component ion implantation 79—83360
erosion damage prevention 77—21306
fluoroplastic, fretting corrosion resistance, effect of fillers *(Russian)* 77—59972
fretting corrosion control using coatings and surface treatments 80—35368
gas turbine blading by plasma spraying, description 77—12728
inorganic glass coatings, solution deposited, for anodized Al 79—34205
Ioncote coating process, using field emission systems for corrosion and abrasion protection *(German)* 80—76205
metal barrier-layer protective deposits, inorganic finish selection and appl. 80—71812
metal flame spray coating acceptance factors and tests in steelworks environment 79—83397
metal protective coating on metals and alloys, anticorrosion mechanism *(Rumanian)* 78—23853
metallic, book 77—44413
metallic, optimum, selection method 78—19956
metallic, testing standardisation 78—11454
metallurgical coatings, vapour deposition processes in vac. 80—35430
Nicralloy-coated 80—40611
organic, performance evaluation of adhesion and permeability 78—64764
overlay coatings for turbine parts, physical vapour deposition techniques, economic evaluation 80—35429
oxidation resistant coatings, electron beam deposition techniques 80—35100
oxide coating protection effectiveness estimation 77—86198
oxide films, corrosion resist. determ. method 79—24689
oxide layer stress accumulation and perturbation of parabolic kinetics 79—5076
oxides on Al alloys, mech. props. and influence on substrate fatigue 77—44408
paint, zinc-rich, for protection of mild steel, dust particle size effect 78—95840
paint, zinc-rich, for protection of mild steel, Zn content effect 78—95842
paint, zinc-rich, for protection of mild steel, ZnO addition effect 78—95843
paint, zinc-rich for protection of mild steel, exposed area ratio effect 78—95841
paint coatings on steel, corrosion fatigue resistance *(Russian)* 77—59979
passivation films on ferritic stainless steel, anal. by glow discharge emission spectrometry *(French)* 79—87923
phosphate binder based, for steel 79—79151
Phosphate conversion coatings on steel 78—3251
phosphosilicate glass, on Si or Al, corrosion in high temp. water and moisture 77—48564
plasma sprayed coating consolidation by laser remelting 80—93697
plasma spraying technique appl. *(Japanese)* 80—55558
plastic clad metal, corrosion charact. by electrical resist. and capacitance meas. *(German)* 80—30171
plastic powder coating, technique and appl. 79—38786
plastics on metals 79—96211
polyester thermosetting powders, parameters 79—20003
polymer, electrochem. techniques for performance monitoring 80—3234
polymer film coating of Al particles *(Russian)* 77—86232
polymer film coatings on metal electrodes, through electroinitiated polymerisation 77--77632
polymer powder coatings, water permeability eval. by radioactive tracers *(Czech)* 78—11362
polymer transparent film, protective ability for optical surfaces 77—31135
polymer-coated steels, electrolyte permeation and elect. permittivity rel. to metal substrate corrosion 79—96175
polystyrene, fatigue props., effect of environment and surface coatings 79—43455
polyurethane thermosetting powders, parameters 79—20003
pressure vessels, operation reliability 78—11424

corrosion protective coatings continued
protective coatings, role in mechanical failure prevention, conf., Caithersburg, USA (Oct. 1975) 77—21327
protective coatings for metals, chemically vapour deposited 78—44261
recent development *(Japanese)* 77—28920
semiconductor, implantation of Si, Al, Hf, Ta into InP and GaAs, form. of protective oxide 78—79622
silicide coating, oxidation protection 77—32704
stainless steel passivating film, comp., AES obs. 77—48571
steam turbines, operation reliability 78—11424
steel, 30KhGSA, fatigue strength under fretting corrosion, effect of plasma-sprayed coatings *(Russian)* 78—11394
steel, alloy, structure and properties after nitriding in molten salts, steel 08kp with Al diffusion coating 80—35418
steel, aluminized, atmospheric corrosion kinetics 79—47808
steel, butadiene coatings, delamination by corrosion 78—64765
steel, C, corrosion and self protection in hot saline soln. 79—1925
steel, corrosion and organic coatings, possible Mossbauer studies 80—39988
steel, corrosion fatigue, cathodic coatings effects *(Russian)* 77—52532
steel, corrosion protective organic coating failure by contamination 77—90486
steel, corrosion resistant coatings 77—56141
steel, data sheet 79—70211
on steel, economic considerations *(German)* 79—39054
steel, galvanized, Fe-Zn phases, Mossbauer study 80—50233
steel, high alloy ledeburitic, wear and corrosion resistant coating by chemical vapour deposition 78—92403
steel, low C, anticorrosion films, quality rating using colour indication method 80—21209
steel, medium C, 45, fatigue strength increase by plasma steel coatings, fretting corrosive cond. 79—15875
steel, mild, Ta coating at atm. press. using CVD method 80—55591
steel, mild, UV cured coating, protective and elec. props. 79—43489
steel, Ni-Cr on perlitic steel, viscous-failure characts. from dynamic failure energy 79—43391
steel, organic, adhesion and permeability 78—64764
steel, sintered, oxidation in superheated steam, corrosion protection 79—39049
steel, stainless, austenitic, surface films grown in Cl solns., ellipsometric investig. 79—20261
steel, stainless, corrosion protection by heat treatment method 78—68836
steel, stainless, type 316, surface comp. rel. to crevice corrosion initiation 80—93680
steel, stainless 18-8, ellipsometric meas. of optical const. and thickness of passive film 77—21326
steel, stainless type 304, anodically polarised, Cl ion effect on passive film 80—97621
steel, surface treatment process in nontoxic salt bath 79—83398
steel, surface treatment protective coatings for scuffing and adhesive wear resistance 77—86217
steel, with anodic coating, corrosion fatigue *(Russian)* 77—70206
steel antioxidation protective glass enamel cladding exam. of development 78—85031
steel structure, off-shore splash zone corrosion 77—59996
surface alloys prod. by ion implantation 78—88569
thermosetting powders, parameters 79—20003
XPS, review of use in corrosion science 78—15586
Zircaloy, breakaway mechanism, corrosion kinetics in steam 80—61030
AL, thermal sprayed coating on steel substrate, cavitation and corrosion resist. in sea water 80—35427
Ag galvanic coatings, corrosion by org. insulant thermal destruction products *(Ukrainian)* 77—52525
Al alloys, corrosion inhibition by organic dyes, protective compound form. 78—44255
Al alloys, stress corrosion cracking protection, by $\gamma_1 Al_2O_3$ anodic film 78—95836
Al coating on directional Ni_3Al-Ni_3Nb eutectic alloy, microstruct. exam. 78 - 15593
Al, corrosion-protective chromate coatings, characterisation 79—47798
Al hermetic jacketing on SiO_2 fibres, reductions in static fatigue 79—43448
Al, high rate electron beam deposition of strip steel 79—24440
Al, ion plated coating on steel *(Japanese)* 78—80477
Al, ion plating on Ti, graded interface form. 78—11442
Al on Ni base alloys, transport agent comparison 78—11429
Al, on unalloyed steel, electric metallisation, corrosion resistance tests *(Russian)* 78—19935
Al treated steel for sulphide corrosion resistance 77—63826
Al-based coatings, for high temp. alloys, process development and props. 80—40614
Al-coated IN-100, microstruct. degradation, influence of corrosioin protective coating 80—40611
Al-Zn coated steel sheet, chromate passivation protection against wet-storage stain 78—95854
Al-Zn-Hg alloy, cathodic protection characts., surface free energy, lattice struct. 79—29281
AlC_xN_y, refractory deposit, prep. by thermal decomp. of Al dialkylamides and characterisation 80—11572
Al_2O_3, on Si, dissolution and corrosion in high temp. water and moisture 77—48564
Au ion plating process 79—66186
Au overlayer, on GaP photoelectrode 78—14812
B-A on steel 43, creep and long term strength in NH_3 79—91854
BP coatings, on Mo by CVD and their composition and microhardness 79—28942
Cd, protective coating, on 30KhGSA steel, in Black Sea 78—19956
Co coated Ti, produced by electrospark alloying, corrosion behaviour in Cl saturated NaCl solns. *(Russian)* 79—39026
Co-Al, low temp. hot corrosion, Na_2SO_4-induced, mechanism, burner rig tests 80—40610
Co-Cr-Al based coating, electron beam evaporation of low vapour press. elements 80—40613
Co-Cr-Al-Y, low temp. hot corrosion, Na_2SO_4-induced, mechanism, burner rig tests 80—40610
Co-Cr-Al-Y, Pt-modified, oxidation and hot corrosion resist. 78—11437
Co-Cr-Al-Y, turbine blade coating, hot corrosion by Na_2SO_4 and vaporous NaCl 78—19941
Co-Cr-Al-Y protective coating for combustion turbines, hot corrosion evaluation 80—40608

corrosion protective coatings continued
- Co-Cr(-Al-Y) coatings, hot corrosion resist., ductile-brittle transition 79—24674
- Co-Mo-Cr-Si, plasma and detonation coatings, Laves- and carbide-strengthened, comparative props. 78—15562
- Co-Ni-Cr-B, X-306 centrifugally cast cylinder lining alloy, compatibility with hardfacing alloys 77—32726
- CoB and Co_2B, electrochem. behaviour in H_2SO_4 79—39030
- CoNiB, corrosion-resistant amorphous mag. thin films 80—54923
- Cr, CVD protective coating on steel, struct. and carbide form. 77—40387
- Cr, electroplate, effect on props. of substrate 77—21330
- Cr electroplated steel, laser treatment 80—21191
- Cr, on mild steel, hardness and protective props., rel. to grain size 78 11436
- Cr plated steel, factors influencing durability 80—108643
- Cr-C, deposited by hollow cathode discharge, characterisation 78—11371
- Cr-N, deposited by hollow cathode discharge, characterisation 78—11371
- Cr-Si, corrosion and failure mechanisms of coatings for gas turbine applications 79—29284
- Cr_3C_2, $Cr_{23}C_6$, plasma sprayed coatings for gas-cooled reactor appl. 79—24676
- Cr_xC_y-(Ni-Cr) sprayed coatings, for gas cooled reactor heat exchangers, factors affecting performance 80—40609
- Cr(Ni) films on steel, type AISI 316, thermal passivation in controlled vacuum 80—76276
- Cu, corrosion inhibition, chem. nature and struct. of protective films 77—60001
- Cu, corrosion inhibitive films formed by corrosion determination of thickness by X-ray photoelectron spectra 79—15845
- Cu, corrosion protection by benzotriazole from SO_2 attack 78—11385
- Cu, surface film of 2-mercaptobenzothiazole and 2-mercaptobenzimidazole, XPS and X-ray induced Auger spectra obs. 80—40600
- $Cu_xNi_yO_z$, protective oxide film on Cu-Ni alloy, AES 79—39035
- Fe alloy, corrosion inhibition, chem. nature and struct. of protective films 77—60001
- Fe, Armco, coated and uncoated, laser interferometric obs. of corrosion 79—47810
- Fe, Armco, siliciding with Si-SiO_2 mixture, exam. of corrosion resistance 80—16584
- Fe coated Ti, produced by electrospark alloying, corrosion behaviour in Cl saturated NaCl solns. *(Russian)* 79—39026
- Fe, data sheet 79—70211
- Fe powders, Co- or Cu-plated, prep. by rad. and chem. plating, mag. props. 80—44867
- Fe, surface films formed in inhibitive solns., optical props., protective quality 79—20260
- Fe, surface treatment process in nontoxic salt bath 79—83398
- Fe-Cr, passivity in H_2SO_4, XPS study 78—44256
- Fe-Cr based coatings, hot corrosion resist. 79—24674
- Fe-Cr-Pd, electrospark coating on alloys, corrosion resist. increase *(Russian)* 78—27669
- Fe-Ni-Cr on steel 78—48572
- Fe-Ni-Cr-B, X-101 centrifugally cast cylinder lining alloy, compatibility with hardfacing alloys 77—32726
- Fe-X-MoS_2 (X=WC, HfC, Al_2O_3, ZrO_2, HfB_2, ZrB_2), self lubricating coatings, exam. of props. 79—96217
- Fe-Zn, on low C rimming steel, effect of addition of Al to Zn on phase composition and morphology *(Polish)* 78—53014
- FeB, Fe_2B on steel, formed by B diffusion, pack cementation process, microstruct. and mech. props. 78—15592
- FeCoB, corrosion-resistant amorphous mag. thin films 80—54923
- FeO inhibitor film on Fe, passivation and inhibitor props., X-ray photoemission spectroscopy exam. 78—88561
- FeTiB, corrosion-resistant amorphous mag. thin films 80—54923
- Ge, aluminising coating 78—11430
- HfC, CVD, on filaments of W-ThO_2 and SiC, coating effect on high temp. mech. props. 78—15347
- Ir, electron beam deposition and ion plating 77—44166
- KCl, water repellant coatings, optical absorption 77—46769
- $LiAlO_2$, on 316 stainless steel, molten carbonate fuel cell gas seal protection 79—39293
- LiO_2-Na_2O-CaO-SiO_2 glass-ceramic coating, high temp. effects on steel substrate 79—61776
- MgF_2 layered Al, coating effects on diffraction grating efficiency 77—39064
- Mo alloy TZM bonding to Fe by vacuum rolling, corrosion protection appl. 79—29283
- Mo, oxidation resistant coating of Nichrome, electrophoretic deposition *(Japanese)* 79—20270
- Mo, siliconised thermal stress and thermal expansion 77—21324
- Mo-Si coating on Nb and Nb alloys, protection against high temp. oxidation *(Russian)* 79—39029
- Na_2SO_4 on Ni-Cr-Al, cyclically oxidised, hot corrosion resist. 78—44264
- Nb alloy, oxidation protection from $MoSi_2$ coating, diffusion-slip casting appl. method 80—21187
- Ni, B-containing multicomponent diffusion layer formation *(Russian)* 77—44400
- Ni base superalloy IN 100, corrosion resistant intermetallic coating, microstruct. effect on mech. props. 78—85058
- Ni based Rene 80 superalloy, initial stages of pack aluminisation 80—76188
- Ni based superalloys, aluminide and MCrAlY (M=Ni, Co, Fe) coating characterization by phase diagrams 79—8276
- Ni coated Ti, produced by electrospark alloying, corrosion behaviour in Cl saturated NaCl solns. *(Russian)* 79—39026
- Ni coating, heat treated, as plated, electrochemical study of corrosive wear 80—16536
- Ni coating, self lubricating containing oxides, carbides and borides on steel 80—21189
- Ni superalloy, electroless codeposition of Si and Ti 77—16513
- Ni/ZrO_2-Y_2O_3, sputtered multilayered ceramic/metal coatings, props. 80—40620
- Ni-(Co)-Cr, aluminide coating, microstruct. and chem. 80—76189
- Ni-Al, low temp. hot corrosion, Na_2SO_4-induced, mechanism, burner rig tests 80—40610
- Ni-Co-Cr-Al-Y, electron beam evap., low press. gas scatt. 77—40474
- Ni-Co-Cr-Al-Y, electron beam deposited, for Ni-base superalloy, fatigue crack initiation and propag. 78—11438
- Ni-Co-Cr-Al-Y, plasma-arc-sprayed, metallurgical characts. and oxidation behaviour 80—40618

corrosion protective coatings continued
- Ni-Co-Cr-Al-Y protective coating for combustion turbines, hot corrosion evaluation 80—40608
- Ni-Cr based coatings, hot corrosion resist. 79—24674
- Ni-Cr coatings on steel, standardisation 79—57139
- Ni-Cr/ZrO_2-Y_2O_3 sputtered multilayered ceramic/metal coatings, props. 80—40620
- Ni-Cr-Al aluminised coating, diffusion paths for formation and degradation of oxidation resistant coatings 78—11431
- Ni-Cr-Al coatings, corrosion and thermal shock resist. in diesel engines 79—24675
- Ni-Cr-Al-Y for Ni base TaC eutectics 77—40475
- Ni-Cr-Fe, Nimonic-75, electroless siliconization 78—27679
- Ni-Cr-Fe-Si-B wear-resist. and corrosion-resist. coatings by furnace melting 80—35428
- Ni-Cr-Si, corrosion and failure mechanisms of coatings for gas turbine applications 79—29284
- Ni-Cr-W-C(-Si), struct. and props. of corrosion and wear resistant alloys 79—24627
- Ni-Fe-Cr soft magnetic film plating bath 79—43465
- Ni-In alloy, on Kovar, vacuum seal for borosilicate glass appl. *(Italian)* 80—40621
- Ni-Mo-Cr-Si, plasma and detonation coatings, Laves- and carbide-strengthened, comparative props. 78—15562
- Ni-Nb-Cr-Al, directionally solidified eutectic superalloy, high temp. oxidation resistant coatings 78—39937
- Ni-P (8 wt.%), protective coating for wear and corrosion resistance of steel 77—21329
- Ni-SiC coating, heat treated, as plated, electrochemical study of corrosive wear 80—16536
- Ni-SiC(WC), dispersion hardened coating, chemically deposited using electroless baths, exam. of protection props. 79—34208
- Ni-W-C, X-800 centrifugally cast cylinder lining alloy, compatibility with hardfacing alloys 77—32726
- (NiCo)-Cr-Al-Y/ZrO_2-Y_2O_3 plasma sprayed ceramic coating for turbine engine components 80—40616
- Ni_2P, CVD on Mo plate, microhardness and resist. to chem. attack 79—66009
- Pb coated Ti, produced by electrospark alloying, corrosion behaviour in Cl saturated NaCl solns. *(Russian)* 79—39026
- PbO-ZnO-B_2O_3:TiO_2 glass, circuit corrosion protection on alumina substrates 79—29236
- Pd, electron beam deposition and ion plating 77—44166
- Pd, electrospark coating on alloys, corrosion resist. increase *(Russian)* 78—27669
- Pd, H-permeable, on V, Nb and Ta foils, Auger and secondary ion mass spectroscopy 79—52467
- Pt, electron beam deposition and ion plating 77—44166
- Si-B based CVD coating for gas turbine blading, props. 80—40615
- Si-based coatings, for high temp. alloys, process development and props. 80—40614
- SiC, oxidation protective coating on C fibres *(Polish)* 79—52408
- SiC protective coatings, on graphite for HTR, corrosion *(German)* 78—3248
- SiC, pyrolytic, on C fibres, rate of oxidation 78—60857
- Si_3N_4 films, prep. by thermal nitridation of Si in NH_3, comp. and oxidation resist. 80—3215
- Si_3N_4 on Mo, RF reactive ion plating 78—3250
- Si_3N_4, on Si, dissolution and corrosion in high temp. water and moisture 77 48564
- Si_3N_4, pyrolytic, prep. by CVD, bulk and coatings, exam. of electrical, optical and physical props. 79—95935
- SiO_2 9% Cr steel, vapour deposited, exam. of corrosion protection props. 78—88563
- SiO_2 coating on $MoSi_2$, effect on oxidation, AES study *(German)* 79—74298
- SiO_2, on Si, dissolution and corrosion in high temp. water and moisture 77—48564
- SiO_2 protective coating formation on SiC *(German)* 80—25885
- SiO_2 thin films, comparison of RI and IR spectra 80—11497
- SiO_2-based glassy layers, passivating Cu at 500°C 80—3246
- SiO_2-ZrO_2-Li_2O-Na_2O based crystallisable glasses composition and properties 80—50731
- Sn, autocatalytic deposition on steel, Ni, Cu, polypropylene and ABS 80—100965
- Sn-Ni metastable equiatomic alloy, sputter deposition 78—3043
- Sn-plate passivation films, TEM struct. obs. 80—45416
- Ta coating of mild steel by CVD 78—15594
- TaC, CVD, on filaments of W-ThO_2 and SiC, coating effect on high temp. mech. props. 78—15347
- Te coating of PbTe surfaces, struct. and junction characts. 80—50743
- Ti alloy, commercial, creep, effect of environment and coating 78—31480
- Ti alloy, mechanical props. at high temp., effect of Pt ion plating 79—29156
- Ti alloy, VT3-1, vacuum-chromized, fretting-corrosion in couple with unprotected BT3-1 and steel 40KhNMA *(Russian)* 78—56804
- Ti alloy substrate, Ni-Cr plasma spray coated, interface interaction 77—21323
- Ti bonding to Fe by vacuum rolling, corrosion protection appl. 79—29283
- Ti, coatings, electrolytically deposited, texture, anti-corrosional props. *(Russian)* 80—66532
- Ti on steel, ion plated, process parameters rel. to props. 77—70217
- Ti, wear and corrosion resistance, effect of surface alloying with Nb and Si *(Russian)* 77—25191
- Ti with metallic coatings produced by electrospark alloying, corrosion behaviour in Cl saturated NaCl solns. *(Russian)* 79—39026
- Ti-coated C steel, effect of heat treatment on struct. and props. 77—56159
- Ti-Fe corrosion resistant coating on Cu, obtained by contact eutectic fusion 80—50772
- Ti-Zr-Nb-Si, Nb and Si surface alloying effects on wear and corrosion resistance *(Russian)* 77—25191
- Ti+Al on steel 45, failure during high temp. creep in NH_3 79—11731
- TiB_2-$TiSi_2$ composites, high-temp. oxidation, scale comp. 78—15561
- TiC-Ni composite coating, activated reactive evaporation prep., structure 77—44393
- TiN film as protective coating for vacuum deposition chamber, Auger electron spectroscopy study 80—25922
- TiN, reactive ion plating with auxiliary discharge deposition conditions influence on film props. 80—20801

corrosion protective coatings continued

TlI, on KCl, epitaxial growth habit rel. to optical scatt. 77—50738
V-Mo, effect of ion plated Mo on corrosion in liquid Na, mech. props. 78—53020
W, CVD, on filaments of W-ThO_2 and SiC, coating effect on high temp. mech. props. 78—15347
W coated Ti, produced by electrospark alloying, corrosion behaviour in Cl saturated NaCl solns. *(Russian)* 79—39026
W, contact interaction between oxide film and graphite, interference effect *(Russian)* 79—11721
W, for Al_2O_3-Y_2O_3 ceramics 80—35367
W-Al_2O_3 cermet films, oxide evaporation deposited on Mo, Ti, Al_2O_3 substrates, struct., props. 80—25581
WC-Co, phase comp. and oxidation resist. of coatings deposited by thermal diffusion using TiB_2 80—21173
Y_2O_3, coating for graphite crucible used in melting U 77—32712
Zn bright coating, rack parts or bulk goods, in GTL-barrel units *(German)* 80—84862
Zn, chromated, electroplate on steel, corrosion, effect of chromate content 79—20286
Zn coated steel sheet, chromate passivation protection against wet-storage stain 78—95854
Zn, on steel *(Dutch)* 78—48571
Zn, thermal sprayed coating on steel substrate, cavitation and corrosion resist. in sea water 80—35427
Zn thin metal primer systems for steelwork 79—79148
Zn-Al (15 wt.%), thermal sprayed coating on steel substrate, cavitation and corrosion resist. in sea water 80—35427
Zr-based plasma-sprayed thermal barrier coating evaluation 80—40619
ZrC_xN_{1-x}, on Zr, oxidation kinetics, 450-600°C, 50-400 Torr O_2 press. *(French)* 77—25171
ZrN, on Zr, oxidation kinetics, 550-700°C, 50-500 Torr O_2 press. *(French)* 77—25170
ZrO_2, stabilized by Y_2O_3, corrosion and thermal shock resist. in diesel engines 79—24675
ZrO_2-SiO_2, protective antirefl. coatings, electron beam evaporation on glass 77—31143
$ZrO_2Y_2O_3$/Ni-Cr-Al-Y, NASA two-layer thermal barrier coating, for gas turbine engines, test results 80—40617
ZrSi/$ZrSi_2$ coating on Ar, exam. of oxidation behaviour by O_2, H_2O *(French)* 79—20284

corrosion testing

Ag, corrosion in atmosphere, environmental test 79—66205
alloys, corrosion resistance in geothermal brine environments 78—85032
bending fatigue testing machine, multispecimen 79—39060
brass, corrosion and dezincification in water 77—16740
brass, dezincification testing in laboratory 79—34226
cathodic protection meas. methods *(Dutch)* 78—3297
cell construction for metal SCC obs. in boiling $MgCl_2$ 78—39962
chemical plants, corrosion rate forecast automatic instrumentation *(German)* 78—44289
conference on electrochem. test methods for stress corrosion cracking, Firminy, France (Sep. 78) 80—94910
diffuse light scattering method for in situ obs. 80—25930
eddy current monitoring 78—88584
electrical contact materials, corrosion test *(German)* 80—55561
electrical contacts, gentle accelerated corrosion test 79—61814
electrochemical methods, appl. and limitations in corrosion studies *(Japanese)* 80—45465
fatigue crack arrest, corrosive environment, at low stress intensities 78—92415
fatigue failure, flat specimens and struct. elements in liq. corrosive media, test method 80—40646
field testing, NBS program 80—76427
galvanic couples in seawater, flow effects, circling-foil apparatus 79—96238
glass bottles, qualitative method for monitoring chemical corrosion 78—85068
glass water resistance, rapid meas. method 79—61812
heat exchange tube thickness meas. by eddy current for corrosion testing, computer study 78—68852
holographic interferometry of corrosion 80—71853
Inconel 600 alloys, stress corrosion cracking, prediction in 10% NaOH soln. at 315°C 80—97616
Inconel 718, environment effect on high temp. fatigue crack growth 80—30090
machine for testing materials under biaxial cyclic stress in corrosive medium 79—52537
machine with asymmetric loading 80—100983
mechanicochemical testing of metals, electrochemical cell for mechanico-chem. behaviour determ. 78—60905
metal, stress corrosion cracking testing apparatus in rapidly flowing liquid environment *(Russian)* 77—70249
metal corrosion meas. specifications and quality assurance 77—12764
metal corrosion rate in soln., appl. of coulostatic method for rapid evaluation 79—20310
metal corrosion rate in soln., new rapid electrochem. eval. method 79—1931
metallic coatings, corrosion testing standardisation 78—11454
metals, apparatus for exam. of localized behaviour 79—91863
metals, corrosion in marine atm., potentiometric technique, appls. 79—24693
metals, rods with temp. gradient, apparatus for examining corrosion along surface 79—52513
metals and alloys, under stress, unit for producing biaxial tensile stresses 79—57174
metals under stress, test apparatus 79—70248
monitoring by magnetic susceptibility variation meas. 79—29292
monitoring review 78—68849
monitoring survey 79—24684
monitoring techniques 79—83404
nuclear reactor structural materials, WR-1 irradiation facility 78—89945
nuclear steam generators, inservice inspection, book contrib. 79—100322
optical glass, chem., durability, pragmatic view 80—78921
oxidative stability determ. technique 80—45412
oxide films, corrosion resist. determ. method 79—24689
pacemaker battery microcalorimetric testing 80—30933
pit propagation rate curves, new method assessing corrosion resistance 77—90514

corrosion testing continued

plant condition monitoring in nuclear power generating industry, review 80—47612
plastic-encapsulated IC, metallisation corrosion test 78—11486
polarisation resistance method, using 2 and 3 electrodes, error anal. in corrosion rates 80—100930
polymer bound glass article, rapid kinematic corrosion test, method and apparatus 79—39063
polymer test apparatus for chem. resist. and penetrability in corrosive medium under hydrostatic pressure 79—39065
potentiostat, P-04, for electrochem. meas. 80—61185
potentiostat appl. 79—96237
potentiostatic tests, use of free-corrosion potential time transients to distinguish between pitting and crevice corrosion 79—39058
pressure vessel for corrosion testing at high temps. 77—12754
radioactive tracers, distant-reading method of corrosion monitoring in chem. equipment 80—50795
rig for S-N data determ. of welded joints in corrosive environment 79—66227
scale-resistant metallic materials, cyclic oxidation method for spalling and scale resist. determ. 77—77695
seawater deaeration procedure for conducting electrochemical expt. 79—29366
sheet glass, chemical resistance to water testing by surface cond. meas. *(Polish)* 79—70271
sheet materials, failure kinetics, method for investigating under long-term static loading in corrosive medium 80—85110
simulated boiling water reactor conditions 78—80696
simulated industrial atmospheres, equipment for establishment and maintenance of SO_2 conc. 79—52512
simultaneous potential current time meas. during polarisation studies 77—90515
specimen holder for surface prep. 77—28937
steel, austenitic, Ni-Cr, corrosion tests with stray currents after manufacturing operation and welding *(German)* 77—86274
steel, austenitic stainless, of type 55 23 33, slow strain rate testing under electrochem. control in high temp. water 80—97650
steel, austenitic stainless, tube carburised layer metallographic determ. 78—85077
steel, ferritic, tests for intergranular corrosion 77—73384
steel, high-speed, portable salt bath for rapid anal., high frequency current heating 77—70256
steel, hydrogenation during acid corrosion under stress, laboratory apparatus for study *(Russian)* 77—77656
steel, low alloy, constructional, fatigue cracking in corrosive media 78—85081
steel, low alloy, sulphide corrosion cracking resistance, test procedure and eval. 77—63842
steel, low C, anticorrosion films, quality rating using colour indication method 80—21209
steel, martensitic stainless, in SO_4 solns., activation pH and susceptibility to H_2 assisted stress corrosion cracking 80—97619
steel, mild, aerosol container, electrochemical cell for corrosion study 80—30180
steel, mild, cyclic strain enhanced dissolution in NH_4NO_3, corrosion fatigue props. 80—85083
steel, Si-Mn-Ni-Cr-Mo, acoustic emission during stress corrosion cracking appl. to materials testing 78—53042
steel, Si-Ni and Cr gas turbine blade material, corrosion fatigue testing 79—70247
steel, spalling and scale resist. determ. by cyclic oxidation method 77—77695
steel, stainless, crevice corrosion rate prediction, short duration test method 80—30179
steel, stainless, intercrystallite corrosion, testing using potentiostatic etching method 78—7113
steel, stainless, repassivation ability in 3% NaCl at 80°C, stress effect, testing device *(French)* 77—77693
steel, stainless, stress corrosion testing, slow strain rate, elevated temp. and high press. study 80—97615
steel, stainless, US methods for intergranular corrosion inspection 78—95898
steel, stainless intercrystalline corrosion, electrochemical testing method 80—55611
steel, stainless type 10CrNiCuP, and St. 3PS, suitability for power station chimney flue structural material 80—108681
steel, testing in moist H_2S 78—23901
steel corrosion in NH_3 and NH_3-N_2-H_2 mixture at high press. and temp., testing unit 77—56174
steel stainless, intergranular corrosion, effect on acoustic props. for US inspection 79—11745
steels, austenitic stainless, stress corrosion cracking, correl. between electrochem. and mech. parameters 80—97613
stress corrosion crack growth over extended period, US pulse high difference method of recording 79—70235
stress corrosion cracking, multisection plan for H_2 absorpt. of metals for tests under cathodic polarisation conditions 79—52504
stress corrosion cracking test machine, design and construction, appl. to Fe-Cr-Ni alloys 80—97649
stress corrosion test specimen-fixture interaction for slow crack-growth 77—56166
stress corrosion testing device, lab. and autoclave testing 79—52502
thin layer activation, appl. to wear and corrosion meas., surface treatment and sputtering 79—87810
trends in standards and expt. procedures *(Japanese)* 77—28953
Al alloy, pitting resistance short duration test and new characterization test 77—90513
Al alloy V95T1 sheets, failure kinetics, method for investigating under long-term static loading in corrosive medium 80—85110
Al alloys, stress corrosion cracking testing, constant strain rate test method evaluation 79—20296
Al alloys, types Indal 3S and 6061-T6, corrosion behaviour evaluation, for heat exchanger appls. 80—85092
CO_2 conc. regulation in climatic cabinets for corrosion testing *(German)* 78—53069
Cu, corrosion in atmosphere, environmental test 79—66205
Cu, sulphidation, rapid data acquisition in slow electrode processes by simultaneous potentiostats 79—96236
Cu-Ni-Zn alloy, surface comp., outdoor exposure influence 80—59770
Cu-Sn alloy, surface comp., outdoor exposure influence 80—59770
Cu-Zn alloys, surface comp., outdoor exposure influence 80—59770

corrosion testing continued
Fe, corrosion, inhibition and monitoring techniques 80−30132
Fe-Cr-Al, scale and spalling resist. determ., appl. of cyclic oxidation method 77−77695
Fe-Ni-Cr-Mo, exam. of tapered tensile specimen, for stress corrosion threshold stress testing 78−53055
He corrosion test facility at Springfields nucl. power development lab. 79−29327
Mo electrode, corrosion rate in molten glass *(Chinese)* 80−66687
Na corrosion of LMFBR structural materials *(Spanish)* 80−55595
Ni, corrosion in atmosphere, environmental test 79−66205
Pb battery anode reverse polarisation corrosion test method *(Bulgarian)* 80−50950
Ti alloys, structural materials for liquid metal radiation loops 78−72958
Zn/$ZnSO_4$/Zn system, laser interferometric study of corrosion of coated and uncoated metals, technique standardisation 79−35815

corundum
see also ruby; sapphire
γ-irrad., colour centres, growth method effect 77−1710
abrasive, evaluation of brittleness, contact endurance by cyclic microhardness 79−15890
acoustic enhancement of NMR lines 80−29632
additive for CaO based refractory from industrial lime 80−89184
attachment energy as habit controlling factor 80−59422
baddeleyite-corundum refractories, fused, elec. resist., 1300-2300°C 79−28345
baddeleyite-corundum refractories, thermophysical props. 79−82398
band structure, calc. using semiempirical Mulliken-Rudenberg method 80−80177
bladed crystals, morphology and struct. 77−84680
ceramic, composition and phase struct., effect of Na_2O and CaO 77−81244
ceramic, effects of Na_2O, CaO additions on sintering struct., props. 79−15630
ceramic, prod. from etching wastes of Al foils 80−108376
ceramic, roughness depend. on initial grain size of alumina *(Polish)* 78−30816
colour centres, AES, electron energy loss, and optical spectroscopy obs. 78−35176
corrosion resist. in fused Li rel. to phase and microstruct. changes 77−44378
cracks, jump determ. from specific failure and elastic energy 79−87712
creep under low partial pressure of O_2, 1200-1600°C 80−35255
crystal growth by Verneuil method, effect of thermal conditions on quality 77−44152
crystal growth mechanism in cryolite flux 78−30563
crystallization during bauxite reduction at 800-180°C 77−86296
CVD film on III-V semicond. substrate, ion beam etching, defect detection 80−89155
defect crystal structure 80−103316
defects in unirradiated cryst., optical absorpt. spectra 79−61409
dielectric constant, effect of degree of purity and perfection 77−48117
doped, induced absorption spectra, low temp. irrad. effects *(Russian)* 78−72570
electrocorundum, subjected to thermal shock, study of substruct. and surface morpholoy 79−43292
electrocorundum hydrothermal etching method 80−50790
electronic struct. determ. by X-ray spectroscopy 79−8210
energy levels of donor and acceptor and electron and hole mobilities 80−59911
enthalpy, 800-2300K, empirical eqn., α-phase 78−14478
enthalpy of α-corundum, 800-2300K 77−47592
fibre FP, manufacture, strength and modulus 80−81013
fibre FP reinforced Al and Mg composites, fabrication and props. 80−81004
filamentary crystal reinforced mullite-corundum ceramics, filaments strength, eval. 80−104230
Fourier transform Ir spectroscopy of vibr. states at high temp. 80−97256
fusion cast refractory, effects of glassy phase on thermal cycling resist. 78−84956
glass-ceramic second-order microstresses 78−27468
grinding, effect of grinding wheel material, particle size, temp. *(German)* 79−43173
grinding material, review *(Polish)* 80−29917
growth and adhesion on Pt-Al alloys 77−8994
growth of single crysts. from Na_3AlF_6-xLi_3AlF_6 system fluxes 78−11094
hexadecapole transitions, acoustically induced, of ^{27}Al nuclei *(Russian)* 80−50205
hydrostatic compression, X-ray diffr. meas. 79−99269
impurity striation, light scatt., optical and electron microscopy meas. 78−22757
ion bombarded, vol. expansion, annealing compaction, surface props. 78−67748
IR intensities, valence-band dynamic and electrooptic models 80−34906
Jahn-Teller effect of $3d^n$ ions in trigonal symm. 77−35894
large optical crystal production with zero orientation 79−50457
luminescence, vacuum UV range spectra *(Russian)* 77−24903
mantle related, thermodynamic props. at high press. and temp. 80−81874
mechanical strength rel. to tension intensity factor *(Polish)* 80−11725
mullite-corundum, electroceramic, low temp. meas. of linear thermal expansion coeff. 79−60526
mullite-corundum ceramics, electron microscopy of damaged surface 80−88413
mullite-corundum ceramics, thread-like crystals reinforced, props. 80−108525
neutron damage, fusion/fission ratio 80−34066
optical, polished, surface layer obs. by IR reflection spectra *(Russian)* 78 19458
optical crystal block structure 79−72637
optical quality crystal growth 77−34916
packing errors in structure, X-ray diffr. obs., charact. features 79−46655
particle aerosol, nonlinear propag. of laser radiation 79−23033
periodic regular texture 79−99328
polishing of single cryst. corundum, dispersion medium formulation 80−102870
porous refractories, production 80−35149
powder medium effect on microstruct., comp., strength and dielec props. during high temp treatment 79−33984
powdered mixture, compaction, optimum porosity and particle sizes 77−85971
premetallizing with Mo-Mn-SiO_2 79−47792
recombination luminescence excitation by synchrotron radiation 79−95841
reduction products above 1700°C 77−16522
reflection spectrum, dispersional anal. 77−36239
refractory ceramic deformation curve analysis *(Russian)* 79−90716
refractory lining, wear resistance in combustion gas flow *(Russian)* 79−8370
refractory lining specimen, thermal softening assessment *(Russian)* 79−83237
shaped crystal, grown from melt, struct. perfection 78−3021
single crystal transmission and reflectance IR phonon spectra, polariton dispersion 80−66170
sintering, activated, kinetic parameters analysis 77−63580
spherical ground samples, extinction effects, inhomogeneous mosaicity 78−75494
spinel formation during reducing heating 77−36427
Stepanov method for shaped crystal growth, development prospects 78−3013
stress relaxation in single crysts. 78−47263
surface microstructural changes due to reduction by C *(Russian)* 80−100378
thermal expansion of monocrysts., temp. depend., 28-800°C 79−82361
thread-like crystals reinforced mullite-corundum ceramics, props. 80−108525
three beam diffraction, divergent beam photographs 79−23483
transparent ceramic prod., synthesis of initial alumina 77−52270
Verneuil growth, directional depend. of crystallisation *(German)* 77−35496
whiskers nucleation, effect of machining support surface *(Russian)* 79−65352
Ag:Al_2O_3:Al tunnel-junction struct., surface polariton mean free path, roughness 80−93008
α-Al_2O_3, charge distribution determ., SCF calc., Slater-type orbitals, Madelung type const. 80−107100
Al_2O_3:Co^{3+}, corundum, Jahn-Teller effect in trigonal symmetry 79−82563
α-Al_2O_3:Co^{3+}, local deform. due to uniaxial stress 80−34140
Al_2O_3:Cr_2O_3(Ti_2O_3), dopant influence on struct. and mech. props. 80−24471
Al_2O_3:Cr^{3+}, corundum and ruby, ^{27}Al quadrupole, transitions, acoustic and elec. saturation 77−90071
α-Al_2O_3:Cr^{3+}, local deform. due to uniaxial stress 80−34140
Al_2O_3:Cr^{3+}, standard reference material for EPR 79−12757
α-Al_2O_3:Cr^{3+}, stress-induced linear dichroism in $^3A_2(^3T_1) \rightarrow {}^3T_2$ transition, Jahn-Teller effect 80−34884
α-Al_2O_3:Cr^{4+}(V^{3+}), ground state spin Hamiltonian parameters and electric field effect 77−15801
α-Al_2O_3:Fe, ferrimagnetic resonance exam. precipitate nature and size determ. 78−48405
Al_2O_3:Mo^{3+}, zero field splitting study by ESR 80−7159
Al_2O_3:Ni^{2+}, corundum, phaser production of transverse phonons by impurity centres *(Russian)* 78−91390
Al_2O_3:Si(Ti)(V)(Fe)(Co)(Ni), gamma-irrad., low temp., induced absorpt. spectra 79−56820
Al_2O_3:Ti^{3+}, corundum, point defect diffusion and interaction with impurity, Ti^{3+} to Ti^{4+} reaction 79−10985
Al_2O_3:Ti(Si), annealing, electron irrad., absorpt. spectra 77−20890
α-Al_2O_3:V^{3+}, local deform. due to uniaxial stress 80−34140
α-Al_2O_3:V^{3+}, stress-induced linear dichroism in $^3A_2(^3T_1) \rightarrow {}^3T_2$ transition, Jahn-Teller effect 80−34884
α-Al_2O_3:V^{3+}(Cr^{3+})(Co^{3+}), optical absorption spectra, DC and AC field effects 78−10925
α-Al_2O_3:V^{4+}, emission spectrum, Jahn-Teller effect in $^2T_{2g}$ and ^2E_g states 79−83007
α-Al_2O_3/graphite mixtures, high corrosion resistance refractory materials, fracture anal. *(French)* 79−70137
Al_2O_3-ZrO_2 cast refractories, nucleation processes reconstruction by SEM, TEM and STEM 78−35380
Al_2O_3-$ZrSiO_4$, granular corundum-zircon refractory, development 80−66462
Li_2O-Al_2O_3, rapidly quenched glasses, Li ion cond., elec. cond. 80−100346
$MgAl_2O_4$-Al_2O_3 powder prep., for plasma arc spraying, coating props. 77−66612
Ni-Al_2O_3, high temp. plasticity, oxide inclusion effect 80−50681
Si-Al-Al_2O_3 system, solid phase Si regrowth on sapphire 80−100413
SiAlON, prepared from siliceous sand and Al powder, hot pressing, steatite contamination effects *(Japanese)* 80−93528
SiO_2-α-Al_2O_3, metastable phase equilib. diagram without mullite 79−4398
ZrO_2-Al_2O_3, cooling effects on mech. props. *(Russian)* 79−78999
ZrO_2.SiO_2-αAl_2O_3 mixed powders, solid state reactions 80−40337

cosmic dust
see also meteoroids
Abell 30, 78, planetary nebulae, warm and cool dust populations rel. to unusual struct. 80−51855
absorption of trapped line photons 79−25460
active radio galaxies, dust lane origin, explosion model 79−62910
AFGL 333, far IR obs., evidence for star form. at ionization front 79−53932
V1301 Aquilae (Nova Aquilae 1975), dust grain IR emission model 80−105254
atmospheric cosmogenic radioisotope flux variation due to cosmic dust and meteoritic matter 78−61634
ε Aurigae, extinction by circumstellar matter rel. to wavelength-depend. fluctuations 80−62190
B361, rotating dust globule, CO obs. 77−33582
Barnard Loop Nebula, far UV imagery rel. to dust grains albedo 77−29911
Becklin's star, in Orion, IR spectrum rel. to carbonate grains abundance 77−29903
bipolar nebula, new, in Centaurus, dust thermal IR emission 79−84837
bipolar nebulae, IR polarimetry rel. to dust scatt. and grain sizes 78−36658
bipolar reflection nebulae, photoelec. polarization maps 78−28742

cosmic dust continued
- black hole, thin spherical dust shell, dynamics, Russner-Nordstrom geometry 78—77481
- black magnetic spherules in marine sediments, origin 78—24494
- black spherules collected at Mt. Norikura, Japan, accretion rate 78—96445
- book, general aspects 78—57498
- 3C 120, radio galaxy, dust rel. to vars. in optical spectrum *(Russian)* 80—90540
- 3C 273, quasar containing dust, IR spectra obs. 80—56970
- VY Canis Majoris, apparent orbit, rotating holey dust cloud hypothesis 79—40191
- Y Canum Venaticorum, C star, circumstellar SiC IR emission obs. 80—46544
- TX Canum Venaticorum, cataclysmic variable shell and dust emission, visible spectra obs. 80—105249
- carbyne as possible constituent 80—90514
- Carina I and II H II regions, dust far IR emission 79—25657
- Carina spiral feature, distrib. of stars and interstellar dust along inner side 80—51871
- η Carinae, dust condensation 79—17066
- η Carinae, high angular resolution obs. (35-175 μ) 79—8925
- η Carinae, high-resolution IR radiation maps of homunculus, spectral and spatial distrib. 80—12767
- η Carinae, IR ang. diameter 78—93271
- η Carinae, silicate grains size distrib. in Homunculus Nebula 80—4382
- η Carinae, spherical circumstellar dust shell model, radiative transfer 78—36577
- η Carinae and Carina Nebula, polarimetric study rel. to dust grains props. 79—67043
- *o* Ceti circumstellar dust, 11 micron radiation vars. 79—5828
- charged dust grains accretion, role of induced charges 79—8966
- charged grains, thermal coagulation in dense interstellar clouds 79—53872
- charged interstellar grains, motion in interplanetary space 80—4300
- charged spherical dust shell, gravitational collapse, maximal time slicing condition 80—67554
- charged spherical grains, electrostatic attraction 77—3509
- chemistry, organic compounds and relation to origin of life 78—73660
- chromite grains in Fe formation from Early Precambrian Isua supracrustal belt, W. Greenland, probable cosmic origin 80—72508
- circumsolar dust cloud, inner F-corona, model and composition 80—82162
- circumstellar clouds, scattered stellar radiation circular polarisation theory 78—96428
- circumstellar dust envelopes, calc. of eclipse light curves and fringe visibilities 79—35234
- circumstellar dust shells, contrib. to young stars reddening and polarisation 78—93199
- circumstellar dust shells, models rel. to compact IR sources spectra 77—29948
- circumstellar dust shells, Monte Carlo simulation of polarised light transfer 78—81608
- circumstellar dust shells, polarisation by Mie scatt., Monte Carlo anal. 80—98650
- circumstellar dust shells, radiative transfer 77—13318
- circumstellar dust shells and mass loss, from luminous O-B3 stars in open clusters *(German)* 78—53925
- circumstellar grains, evaporation and growth 79—35240
- circumstellar matter round OB3 type stars in young clusters, 2200 Å hump interpretation 80—82351
- circumstellar shells, silicate dust content from thermal CO and SiO millimetre line emission 78—49423
- clouds rel. to diffuse galactic light and Milky Way brightness fluctuations 78—61921
- in clusters of galaxies, IR and radio radiation, upper limits *(Russian)* 79—21449
- cocoon stars, grain temps. and IR spectra 77—64824
- cold clouds and interstellar grains *(Italian)* 77—87516
- collisional growth to planetesimals, relative vel. 80—82247
- colloidal plasmas in space: some aspects of condensation and growth of solids 79—41795
- comet dust particles, impact mass spectrometer for chemical analysis on fly-by mission 78—93112
- Comet Ikeya-Seki (1965 VIII), polarization reversal, grain segregation due to radiation press. 79—8881
- comet low vel. particle meas. during fly-by mission using capacity type detector 78—93113
- comet nuclei, dust layer models 80—77350
- Comet West (1975n), scatt. phase function of cometary dust, 0.5 to 18 μ 77—29731
- Comet West (1976 VI), coma mols. and dust distrib., visible emission profiles 80—101562
- Comet West (1976 VI), dust rel. to polarisation of head 80—8587
- Comet West (1976 VI), IR obs., dust model 78—81592
- Comet West (1976 VI), polarisation obs. rel. to elongated particles scatt. indicatrix 79—62794
- Comet West (1976 VI), striated tail study 79—35194
- cometary coma, dust grains props. rel. to IR continuum interpretation 78—7923
- cometary dust in atmosphere, rel. to ice ages and ecological catastrophes 78—53714
- cometary grains, simulation *(Russian)* 78—36532
- cometary nuclei origin in presolar nebula, dust gravit. instability 79—2523
- comets, dust mantle model rel. to monochromatic brightness vars. 78—81589
- comets, dust release and mantle development 79—44412
- comets, origins, research and interplanetary relationships 78—57507
- comets, recent, periodic, gas/dust ratios and dust grains colours 79—70997
- compact H II regions, large beam IR obs. 78—16488
- compact H II regions two-component dust models for near IR emission 77—33600
- condensation from gas phase, nucleation, growth and transform. of amorphous and crystalline solids 80—24745
- condensation in interstellar clouds, theoretical aspects 80—26939
- condensation onset, role of association reactions 80—26931
- condensation processes investigation, expt. techniques 80—26940
- R Coronae Austrinae interstellar molecular cloud, for IR study and dust temp. profiles 80—62237

cosmic dust continued
- cosmological anisotropic dust filled model, closure result 77—37676
- CRL 2104, CRL 2179, late WC stars, 2 to 4 μm spectrophotometry and circumstellar dust 78—96491
- CRL 3068, dust-enshrouded star 77—91664
- crystalline physiology, model for non-chemical form of life 77—90978
- CH Cygni, dust grains form. in circumstellar shell from linear polarisation vars. 78—69808
- V1016 Cygni, IR spectrum and circumstellar dust shell 78—93266
- V1668 Cygni (Nova 1978), dust form. phase time from linear polarisation obs. 80—26875
- V 1668 Cygni (Nova 1978) ejecta shell, dust form. rel. to spectral development 80—51789
- V1668 Cygni (Nova 1978) envelope, dust form. rel. to multifilter photometry and polarimetry 80—90454
- dark nebulae in M31, catalogue 80—72787
- dense clouds, grain size control 77—33607
- density, and composition rel. to expansion of Universe 77—41403
- destruction mechanism by X-ray bombardment 77—26046
- differential photoelectric charging of nonconducting surfaces in space 79—25439
- diffusion and sedimentation of dust in molecular clouds 79—17062
- disequilibrium condensation environments in space, frontier in thermodynamics 80—26942
- distribution from obs. of OB stars near Carina arm, UBVβ photometry 80—85941
- distribution from UBVβ photometry of OB stars in Puppis 80—85937
- distribution of dust in giant extragalactic H II regions 79—35320
- 30 Doradus complex, in LMC, UV reddening law 78—96516
- dust grains in early solar system, formation of planets with Fe cores 78—85869
- dynamic evolution of dusty H II region 79—88719
- dynamical evolution of spherical gas-dust nebulae including diffusion effects 79—80342
- dynamics in collapsing protostellar cloud, planet formation 79—58401
- Einstein's eqns. for dust, gravit. collapse and radiation 78—99
- Einstein eqns., nonexistence of solns. 78—49736
- emission-line stars, far IR obs., cool dust cloud evidence 79—92771
- expanding spherical nebulae with dust, H I Lyman α formation 79—8975
- extraterrestrial matter in fresh snow, preliminary results 79—84302
- far IR emission, rel. to translational anisotropy of cosmic microwave background 77—33706
- fine particles clustering, experiment 80—26937
- formation, in circumstellar shell around protostar 77—13327
- formation and composition, evidence from interstellar Fe, Mn and Mg depletion obs. 79—2563
- formation in space medium thermodynamics and kinetics, workshop, Houston, Texas (1978 September 6 to 8) 80—22131
- formation time scale in novae 77—67093
- free radical recombination onto grain surfaces, isotope effects by hyperfine interaction 77—33609
- galactic central region and anomalous IR source 79—44588
- galactic centre, distrib. of stars and dust, black hole hypothesis 78—86010
- galactic centre, dust thermal emission in compact IR sources 78—24551
- galactic centre, gas, dust, high energy particles and star form. 80—36713
- galactic centre, IR polarization due to silicate dust grains 77—9794
- galactic centre, radiation model, dust grains heating by O-stars and K-giants 78—36697
- Galactic Centre direction, 2.2 micron polarisation obs. rel. to grain alignment 77—64850
- galactic centre direction, near IR polarisation due to aligned interstellar grains 78—96534
- galactic distribution, rel. to integrated starlight synthetic spectrum between 3000 and 10000 Å 80—46536
- galactic dust and IR astronomy, review *(French)* 78—12352
- galactic dust emission rel. to microwave background anisotropy 80—77524
- galactic dust globules, microwave spectral lines obs. 78—57609
- galactic gas-to-dust ratio determ. from globular cluster obs. 79—88747
- galactic interstellar extinction law, vars. 78—85990
- galactic photometric disc model, direct starlight intensities and interstellar dust clumping effects 80—22077
- N.Galactic Pole region, dust cloud complex detect. from polarisation meas. 79—62814
- in galaxies, effect on optical surface brightness 80—90518
- galaxies, extinction in IR-emitting nuclei 79—44599
- galaxies, nearby, interstellar reddening law and dust content *(German)* 80—67850
- galaxies active nuclei, emission line spectra rel. to ionised gas and dust 79—88730
- Galaxy high latitude nebulosity, as source of enigmatic dark lines crossing (M81) 80—56947
- gas-to-dust ratio and galactic reddening determ. 79—5875
- giant stars with IR excesses, gas-dust shells rel. to optical emission linear polarisation 78—96481
- globular clusters, UBVR photometric obs., dust patches 78—81662
- Gould's belt, anomalous extinction, grain growth 79—44603
- grain accretion in protoplanetary nebula, liquid drop effects 78—85862
- grain formation in cool stellar envelopes 80—56814
- grain formation in nova envelope 77—82254
- grain growth, by radiation pressure induced coagulation 80—94851
- grain growth in interstellar clouds, theory and obs. 80—67834
- grain mantles interstellar mol. form., laboratory analogue expts. results and implications 80—26944
- grain motions in the solar nebula 79—84686
- grain sedimentation in solar nebula 77—87284
- grain surface ion reactions, S interstellar molecule formation 80—101632
- grain temps. and IR emission from interstellar dust clouds 77—74119
- grain vels. in turbulent gas in protostellar cloud 79—58402
- grains, review 78—16516
- grains, size distrib. from 0.11-1.0 μm obs. 78—8084
- grains distrib. in intercloud medium, from K-type giant stars colour excesses 79—40251
- grains electric charge, effects of interstellar radioactivity 77—87499
- grains in H II regions *(Italian)* 79—48897
- grains in hot gas 79—92820
- grains in IR sources, possible origin for unidentified IR features 80—82452

cosmic dust continued
grains sudden nucleation and growth, in supernova and nova ejecta 80—26941
grains surrounding variable source of heating radiation, IR flow development 80—105324
grains with resonant impurities, model for optical behaviour 77—53660
graphite, hydrocarbon formation on interstellar grain surfaces 80—82458
graphite grain surface reactions in interstellar and protostellar environments 78—4316
graphite grains, in Venus atmosphere, as source of UV absorpt. 78—20665
graphite grains, rel. to H_2 form. in interstellar medium 77—71136
graphite grains temperature, effect of IR optical consts. 78—12324
gravitational collapse, Oppenheimer-Snyder solution, Newtonian analogue 77—73945
HD 193793, Wolf-Rayet star, circumstellar dust form. episode 80—31301
HD 193793, Wolf-Rayet star, IR obs., cooling of circumstellar dust shell 79—48823
HD 193793, Wolf-Rayet star, photometric evidence for C-rich dust cloud 80—26861
HD 44179 (Red Rectangle), IR spectrum obs. rel. to dust comp. 77—78859
HD 45677 or 50138, hot Bep stars with circumstellar dust IR excesses, UV obs. 78—93250
HD 80077, superluminous supergiant, evidence for circumstellar dust shell 77—17555
heating of spherical dust cloud with embedded stars, model 80—26952
HR 5999, circumstellar dust around variable shell star 79—8926
HR 5999, variable shell star, photometry rel. to circumstellar dust shell 78—28701
IC 1396 interstellar molecular cloud, for IR study and dust temp. profiles 80—62237
IC 342, Scd galaxy dust thermal IR emission obs. rel. to star form. in central regions 80—62256
IC 3568, planetary nebula, struct. and internal extinction 80—31338
ice, 45μm signature possible identification in Orion 79—17068
ice, identification as carrier of 3 μm absorpt. in IR sources questioned 78—49499
ice grains, amorphous, H_2 form. and importance for planetary atmospheres 80—26933
ice grains in interplanetary and interstellar media, low energy cosmic ray erosion 78—45177
ice particles in solar system, lifetime 77—29721
insulating dust grains, photoelectric yield 80—90507
intercluster dust tests and CGCG selection effects 79—9012
intergalactic, obs. near NGC 300 77—45553
intergalactic dust, effect on meas. of cosmological deceleration parameter q_0 77—5564
intergalactic dust, possible existence 77—53678
intergalactic dust extinction effects on quasar distribution 80—17651
intergalactic dust grains in Coma cluster, rel. to surface brightness photometry 77—87550
intergalactic dust in galaxy clusters, evidence from Zel'dovich effect 78—54041
intergalactic dust in M81 group, appl. to explosionless model of (M82) 77—33632
intergalactic dust rel. to pregalactic fluctuations visibility, upper limit on q_0 80—8717
intergalactic pyrolitic graphite whiskers, absorpt. effects rel. to cosmic microwave background 80—94866
intergalactic relativistic dust grains, as source of cosmic gamma-ray bursts 79—88764
intergalactic relativistic grains, transition radiation 79—75272
intergalactic suprathermal grains, prod. by scatt. on mag. field 79—48911
International Solar Polar Mission, predictions for zodiacal light and local interstellar dust obs. 79—92717
interplanetary, large fluffy particles as explanation of optical props. 78—57499
interplanetary, orbit distribution, Pioneer 8 and 9 obs. 78—89031
interplanetary, origin and comp., review 79—75154
interplanetary, origin and evolution 80—101555
interplanetary, scatt. meas. of irregular particles versus Mie theory 78—58918
interplanetary charged grains, Lorentz scatt. 79—70996
interplanetary dust, effect of spin and solar radiation on motion *(Japanese)* 78—20732
interplanetary dust, light scatt. function rel. to zodiacal light photometric axis 78—20727
interplanetary dust, light scatt. intensity, theory 80—109324
interplanetary dust, symmetry plane in inner solar system 80—56767
interplanetary dust, two independent populations suggested 79—21227
interplanetary dust, zodiacal light circular polarisation theory 78—96428
interplanetary dust, zodiacal light indications 78—57500
interplanetary dust and electrons spatial distrib. round Sun, contrib. to corona 80—46514
interplanetary dust between 1 and 5 AU, conflicting Pioneer 10 and 11 data 79—44410
interplanetary dust complex, azimuthal asymmetry mechanism from restricted three-body problem 80—85843
interplanetary dust components in inner Solar System 80—85914
interplanetary dust concentration toward Venus orbital plane, zodiacal light obs. 79—21228
interplanetary dust grains, H-implanted, role in upper atmosphere H chemistry 78—65445
interplanetary dust in stratosphere, visible absorpt. spectra 80—101554
interplanetary dust particles, effects of solar radiation on orbits 77—5493
interplanetary dust particles, Mg isotopic composition 80—72879
interplanetary dust spatial distrib., new results from zodiacal light obs. *(German)* 79—80268
interplanetary dust spatial distrib. near 1 AU, Helios 1 and 2 obs. 78—36511
interplanetary grains in outer planetary magnetospheres, physical and dynamical processes 80—41745
interplanetary meteoric material distrib. near terrestrial planets, methematical modelling 79—96976
interplanetary micrometeoroids, rel. to meteoric night-glow 77—91488
interplanetary particle dynamics 78—57501
interplanetary particles, sampling techniques 78—57459

cosmic dust continued
interplanetary particles rot. bursting caused by solar radiation press. 77—9644
interplanetary small particles in solar system, radiation forces 80—17461
interplanetary submicron dust, cometary origin 79—30008
interplanetary submicron grain orbits, gravit. attraction, radiation press. and electrodynamics 79—8879
interplantary, causing dark patches in zodiacal light 78—93153
interstellar, Apollo 17 far UV search for starlight scatt. 78—65726
interstellar, composition, origins *(French)* 79—30116
interstellar, turbulence effect on coagulation 79—35356
interstellar, UV scatt. props. and size distrib. 80—26932
interstellar 10 and 20 μm absorpt. bands, comparison with Nogoya meteorite IR spectrum. 79—48741
interstellar 10 micrometer absorpt. band, comparison with phyllosilicates laboratory spectra 79—80344
interstellar bacterial grains, prod. of 3μ spectral feature in galactic IR sources 80—62227
interstellar clouds, dust grains effects on H to H_2 transition region 79—25672
interstellar clouds, grain absorption rel. to UV radiation field *(Russian)* 80—73026
interstellar clouds above galactic plane, light scatt. detect. possibility 79—30124
interstellar clouds heating due to molecules desorption from grains 77—9786
interstellar cold grains as seeds of life 77—91606
interstellar dark dust cloud model, lifetime of molecules 78—85999
interstellar dense clouds, dust condensation, cooling, IR emission 79—62897
interstellar dense molecular clouds, chem. evolution 78—28749
interstellar diatomic oxide grains, IR absorption features 78—49509
interstellar dust, chemical composition 78—57624
interstellar dust, cloudlike distrib. rel. to integrated starlight synthetic spectrum between 3000 and 10000 Å 80—62200
interstellar dust, effect on cosmic background radiation spectrum *(Russian)* 80—8719
interstellar dust, far IR emission from galactic plane at longit. ($l^{II}=27.5°$) 80—62231
interstellar dust, IR extinction meas. rel. to diffuse interstellar bands strengths 78—93198
interstellar dust, new model of mixed oxide grains 80—26934
interstellar dust, pre-solar, in Allende meteorite, evidence from pre-4550 Myr inclusions 79—35212
interstellar dust, pre-stellar 79—84844
interstellar dust, submillimetre thermal emission obs. from L1641 and Orion Nebula 80—36685
interstellar dust accretion by Sun, influence on neutrino prod. 79—12441
interstellar dust around λ Orionis, scattered UV radiation obs. 80—56918
interstellar dust clouds, among brightest IR sources of AFCRL Survey 77—87283
interstellar dust clouds, nonthermal OH main lines and OH abundance 80—36683
interstellar dust diffuse IR emission, rel. to extended low-density H II region and star form. 79—17047
interstellar dust distrib. within 3 kpc in galactic plane 80—109512
interstellar dust distribution perpendicular to galactic plane, fine struct. study *(Russian)* 80—73036
interstellar dust far IR emission, large-beam sky survey at millimetre and submillimetre wavelengths 79—97045
interstellar dust grains, photoelectric effect rel. to gas heating by galactic UV radiation 80—67839
interstellar dust grains, temp. fluctuations 80—26938
interstellar dust temperature and far IR emission, implications of 2 μm intensity in solar neighbourhood 80—36744
interstellar dust temperature statistical distrib. resulting from star random distrib. 80—98700
interstellar dusty H II blisters, appearance at radio and IR wavelengths 80—85979
interstellar extinction at UV wavelengths, role of biochemical chromophores 80—26945
interstellar extinction curve, comparison with visible and UV extinction of silicate, C and SiC smokes 80—82180
interstellar extinction curve, rel. to plasma reson. in Fe granular deposits 79—21387
interstellar Fe grains, temp. 77—71135
interstellar gas-dust clouds assoc. with open star clusters, effect on cluster dynamics 80—101622
interstellar grain clumps, assoc. with prebiotic molecules 77—26042
interstellar grain clumps in meteoritic inclusions, spectroscopic evidence 77—25987
interstellar grain composition constraints from 10 μm data 80—82471
interstellar grain destruction by chemical reactions, collisions and photodesorption 78—54021
interstellar grain destruction by sputtering 78—54020
interstellar grain mantle growth in UV-shielded dense clouds 78—54022
interstellar grain mantle molecules, middle IR fluoresc. and absorpt. spectra 79—88716
interstellar grain models, rel. to extinction curves and R values in Southern Milky Way 77—13443
interstellar grain motions, role in star form. 78—69788
interstellar grain size, polarimetric obs. of four deviating stars 80—12792
interstellar grain size distrib. 79—21388
interstellar grain size versus colour excess ratios 79—17040
interstellar grain streaming in solar system 80—26810
interstellar grain synthesis and Be and B abundances in meteorites 79—16894
interstellar grains, accretion by chemically peculiar A-type stars 79—67017
interstellar grains, carbyne as major constituent 78—69859
interstellar grains, characts. near stars with peculiar interstellar polarisations 77—53659
interstellar grains, chemical role 80—82470
interstellar grains, collisions in turbulent gas 80—77470
interstellar grains, destruction by sputtering 78—45382
interstellar grains, destruction mechanisms 79—92825
interstellar grains, disorientation in suprathermal rotation 79—92824
interstellar grains, effects on gravit. instability of rotating plasma 80—109347
interstellar grains, H_2 form. on surfaces 79—21367

cosmic dust continued
interstellar grains, ice mantle and silicate core, emission props. *(Italian)* 79−48898
interstellar grains, interaction of light with small-particle system 77−74111
interstellar grains, IR spectra compared to IR extinction of irradiated and amorphous olivine 79−53873
interstellar grains, K and Ar isotopic anomalies 78−28761
interstellar grains, luminesc. emission 79−8967
interstellar grains, magnetic alignment 78−41017
interstellar grains, max. temps. 77−49449
interstellar grains, organic compositon, IR obs. 80−77460
interstellar grains, polarisation reversal by small particles over strong resons. 79−2564
interstellar grains, shape and size rel. to near IR linear polarisation wavelength depend. 80−51833
interstellar grains, spin-related magnetism 79−5883
interstellar grains, suprathermal rotation 79−92823
interstellar grains, surface reactions rel. to mol. form. in dark clouds 79−44593
interstellar grains, temperature fluctuations and size distrib. 79−71087
interstellar grains, temperatures in diffuse clouds rel. to interstellar Ar depletion 80−51848
interstellar grains, UV phase function 79−97047
interstellar grains and molecules, UV obs. from Spacelab 80−41871
interstellar grains causing IR polarisation of mol. coulds 80−82469
interstellar grains comprised of organic cpds., 3.4 microns absorpt. obs. 80−109514
interstellar grains formation, time-depend. nucleation theory 80−26946
interstellar grains in interplanetary space, optical detection during out-of-ecliptic mission 78−85906
interstellar grains in SNRs, effect on X-ray spectra 80−94849
interstellar grains surface reactions contrib. to molecular form. 77−9784
interstellar grains with water ice mantles, max. linear polarisation wavelength 79−5882
interstellar graphite grains, chemical sputtering 79−62880
interstellar graphite grains rel. to 2175 Å feature, implications of C depletion meas. 80−17638
interstellar low mass dust clouds in solar vicinity, photometric survey results 80−36512
interstellar Mg silicates, mid IR extinction from laboratory silicates IR optical consts. 80−31337
interstellar oxide grains, mol. prod. 79−25690
interstellar oxide grains, S and Cl depletion 80−17635
interstellar particles, scattering of starlight, origin and composition 79−88729
interstellar perturbed grains, optical and thermal props. 77−45523
interstellar plasma clouds, dust sedimentation rel. to star form. 78−73744
interstellar polysaccharides and related hydrocarbons, identification from IR spectra 78−28763
interstellar porous grains, free-space equilib. temps. calc., rel. to optical props. 80−62223
interstellar radiating dust clouds, review 77−78863
interstellar reddening in high-latit. field around ω Bootis 79−101185
interstellar reddening material, distrib. in solar neighbourhood from stellar colour excesses 78−49502
interstellar refractory grains, abundances rel. to metal depletions and hot medium filling factor 80−17634
interstellar transition metal grains, of H, rel. to H_2 catalytic form. 78−54005
interstellar UV extinction obs. in galactic plane from TD1 satellite 78−93382
intracluster dust, contrib. to Orion young stars reddening and polarisation 78−93199
IR emission by dust grains near variable primary sources 79−44358
IR emission from dust in stellar aggregates *(Italian)* 79−48869
IR emission of dusty H II regions 79−71091
IR observations at Jena University Observatory *(German)* 77−26047
IR properties of grains in space, review 80−26943
IR sources, 10 μm silicate absorpt. band equivalent widths and dust temps. 78−57614
IR sources, effect of multiple grain components on radiation transfer and 10 micron silicate feature 78−36659
IR sources, middle IR polarisation by dust 79−67078
IR sources, unidentified spectral features review 80−26936
IR sources assoc. with double-lobed refl. nebulae, far IR obs. rel. to dust emissivity 78−54009
IR sources showing 10 μm silicate absorpt. feature, dust temps. 79−101217
IRC+10216, circumstellar dust shell model rel. to IR energy distrib. 80−56972
IRC +10216, C star, circumstellar dust cloud size from far IR obs. 80−82539
irregular absorbing particles, new scatt. model rel. to zodiacal light 80−67543
isotopically anomalous material, injection into early solar nebula 79−101094
Jupiter ring, dust EM scatt. lifetimes 80−82273
K3-50, compact H II region, 2 to 4 micron spectrophotometry dust thermal emission 77−13422
Kleinmann-Low nebula, 29 to 125 microns spectrum rel. to dust thermal emission 77−33680
L134 dark cloud, CO emission and visual extinction 77−13425
L134 dark cloud, detect. of DNC at 152.6 GHz 78−4334
L134 dust cloud, formaldehyde excitation temp. 77−5552
L 183 (L 134 N) dust cloud, NH_3 and cyanoacetylene mapping at 23 GHz 80−105307
laboratory analogues 79−58397
large interstellar grains towards ρ Ophiuchi, origin 80−41870
late-type stars, O-rich, 16 to 39 micron spectroscopy rel. to circumstellar silicate dust 80−22002
CW Leonis (IRC+10216), IR C star, circumstellar dust orientation by paramag. relaxation rel. to intrinsic polarisation 80−67730
limit on density by microwave background obs. 77−17653
LMC, dark clouds distrib. rel. to spiral struct. 77−29924
LMC, interstellar extinction meas., UV sky-survey telescope obs. 79−35384
lunar dust sample 61501, light rare gases abundances in primary particles *(French)* 80−51674

cosmic dust continued
lunar rock surfaces, accretionary grain populations development under meteoroid and solar wind bombardment 80−94731
lunar rock surfaces, accretionary grain populations development obs. from Apollo samples 80−94732
Lynds 134 interstellar dust cloud, visual extinction rel. to CO isotopic fractionation 80−26924
M17, far IR obs. rel. to H II region interaction with mol. cloud 80−22053
M17, Platt particles and spatial temp. fluctuations 78−61907
in M31, gas-to-dust ratio determ. 78−8120
M43, small diffuse nebulae in Orion complex, optical linear polarization map 80−46644
M82, intergalactic cloud encounter model 79−75279
M82 nucleus, Brackett-line obs. rel. to visual extinction 79−25704
M8, Dragon dust cloud obs., isophotometry 78−36673
M8, silicate dust absorpt. in IR sources 77−64817
M8 (Lagoon Nebula), far IR obs. rel. to dust temp. 80−4413
Markarian 231, IR emission from silicate dust grains 77−5570
Markarian 3, 231, Seyfert galaxies, evidence for asymmetric dust envelopes from optical polarisation 80−90533
Mars, 1877-1971 dust storms and polar cap recession rate correl. *(Italian)* 77−91461
Mars, 1971 dust clouds physical characts. 79−84704
Mars, 1973, dust storm, maps from hourly photographs 77−5477
Mars, aeolian environment, differential redistrib. rates 79−44399
Mars, aeolian features, bright and dark crater streaks 78−32381
Mars, atm. optical props. during 1971 dust storm 77−13274
Mars, dust clouds and frictional generation of glow discharges 77−78708
Mars, dust clouds and prebiotic molecules 77−64688
Mars, dust clouds physical props., surface layer particles mean radius 78−45258
Mars, dust redistrib. and erosion during one Mars year from Viking landers imaging obs. 79−80265
Mars, dust storms, opacity from Viking IR thermal mapping 80−82253
Mars, dust storms 77−49324
Mars, dust storms interplay with perennial ice cover rel. to polar landscapes evolution 79−84721
Mars, dust storms monitoring using atm. transparency meas. *(Russian)* 78−36481
Mars, global dust storm effect on S polar cap seasonal recession 79−84715
Mars, global dust storms effects on pressure vars. meas. by Viking landers 1 and 2 80−72812
Mars, saltation threshold, interparticle force, surface roughness and low atm. density effects 77−5478
Mars, scattering by nonspherical particles and optical props. of dust 79−25535
Mars, wind speed requirements for particle motion 77−5479
Mars atmosphere, dust content rel. to longit. var. of 2.8 cm brightness temp. 80−105191
Mars atmosphere, dust effects on thermal IR props. at 7, 9, 11 and 20 μm 79−84709
Mars atmosphere, dust rel. to thermal IR props., 15 μm band meas. 79−84710
Mars atmosphere, dust storms coupling with thermal tides 79−84719
Mars atmosphere, general circulation model, including dust and topography 80−90354
Mars atmosphere, local dust clouds effects on thermal IR props. 79−84711
Mars atmosphere, solar heating rates during global dust storm 78−85878
Mars atmosphere, suspended dust particles props. and effects 79−84717
Mars atmosphere dust, Viking orbiter imaging obs. 79−84707
Mars atmosphere thermal IR properties, dust and ice clouds detect. from Viking IRTM spectral meas. 79−84712
Mars dust storm of 1971, cloud form., multicolour TV photometry obs. 80−101546
Mars major dust storms, surface meas. of atmospheric phenomena 79−84708
Mars north polar region, dust deposits evolution 80−31225
maser sources, role of dust in pumping 78−36716
mass transport on lunar surface 80−8558
Merope nebula, uvby photometry and dust grains phase function in UV 78−32553
metal abundances, three-level models of chemical evolution 79−48873
meteoritic material, meas. from spacecraft near Earth and in interplanetary space 77−53486
microparticle studies by space-borne instrumentation 78−57460
microwave background spectrum distortion by dust 80−27022
millimetre temps. of planets, galactic and extragalactic sources 78−28556
Mira variable stars, grain opacity rel. to supersonic mass flow 79−35270
models for dusty and diffuse H II regions, IR emission 78−41010
in molecular clouds NGC 2264, ρ Ophiuchi, B335 and S140, dust/gas ratio and mass 80−94842
molecule formation by surface reactions on interstellar grains 78−28753
molecule synthesis by ion implantation, photon emission studies of N^+ and N_2^+ bombardment of Si 77−70297
Monoceros R2 association, interstellar extinction and grains characts. 77−13409
nebulae, dusty, non on-the-spot (OTS) models 78−85995
nebulae, emission lines due to interstellar dust in visible spectra 79−53874
NGC 1068, Seyfert galaxy, radiative transfer in dust rel. to spectral flux distrib. 77−29914
NGC 1068, Seyfert galaxy, silicate emission feature from IR photometry 78−54035
NGC 2023, reflection nebula, far IR study rel. to dust temp. and mass density distrib. 80−51831
NGC 2024, H II region, near IR obs. rel. to hot dust thermal radiation 79−58393
NGC 2024 (Orion B), dust rel. to recomb. line obs. 77−29895
NGC 2264, dust props. rel. to interstellar circular polarisation in (Walker No.67) 78−12223
NGC 2264, young open cluster, differential reddening due to intracluster dust clouds 78−53996
NGC 3227, 3516, Seyfert galaxies, evidence for asymmetric dust envelopes from optical polarisation 80−90533
NGC 4151, Seyfert galaxy, optical polarimetry, circumnuclear dust envelope 78−61916

cosmic dust continued
- in NGC 4314, barred spiral galaxy, distrib. from UBV surface photometry of central region 80—77482
- NGC 5102, lenticular galaxy, dust and young stars obs. 79—44609
- NGC 5128 (Centaurus A), high-resolution spectroscopy and tubelike model of dust band 80—56945
- NGC 604, 5471, giant extragalactic H II regions, internal dust extinction from UV spectra 80—77467
- NGC 604, H II region in M 33, dust densities in nebula core and halo 80—85984
- NGC 6250, young southern cluster, extinction law and high R-values in dust clouds 78—16490
- NGC 6888, ring nebula assoc. with Wolf-Rayet star, dust comp. 77—29905
- NGC 7000 (North America Nebula), dust scatt. of stellar continua rel. to rocket UV imagery 80—82440
- NGC 7023, refl. nebula, far UV brightness rel. to HD 200775 reddening and dust albedo and scatt. 80—51832
- in NGC 7023, refl. nebula, optical and UV extinction of HD 200775 by dust 80—109515
- NGC 7027, 16-38 μ spectral obs. and dust model of planetary nebula 78—93354
- NGC 7027, planetary nebula, effect of dust on [O II] emission 80—8667
- NGC 7027, planetary nebula, far IR emission 77—22288
- NGC 7027, planetary nebula, interstellar, local and internal dust extinction from UV spectrum 80—82459
- NGC 7538 (IRS 1+2), compact H II region, 2 to 4 μm spectrophotometry, dust thermal emission 77—13422
- North America and Pelican Nebular Complex, struct., visual extinction map 80—22063
- nova envelopes, dust form. and ionisation theory 80—98678
- Nova Sagittarii 1977, IR obs., high temp. dust shell form 77—60766
- Nova Serpentis 1978, evolution of dust shell 80—90430
- Nova Serpentis 1978, IR photometry rel. to dust shell condensation 80—4365
- novae, dusty circumstellar envelopes *(French)* 77—56940
- nucleation in finite systems, theory and computer simulation 80—26038
- ρ Ophiuchi dark cloud, high ang. resolution obs. of far IR source 79—40235
- optical props. of heterogeneous grains 77—79750
- organic grains in interstellar medium, existence questioned 79—21397
- organic molecules in interstellar dust, possible spectral signature at 2200Å 77—57074
- Orion Nebula, evidence for scatt. by dust from long-slit spectroscopy in rocket UV 80—105297
- Orion Nebula, intracluster dust, circumstellar shells and wavelength depend. of polarisation 77—78839
- Orion Nebula, polarisation at 11.1 and 19.6 μm meas., aligned absorbing grains 80—36690
- Orion Nebula, starlight scatt. by dust rel. to UV imagery 78—4326
- Orion Nebula, stellar radiation scatt. by dust, contrib. to nebula UV continuous spectrum 80—90499
- Orion Nebula peripheral regions, O/H ratio rel. to dust grains form. 80—36686
- λ Orionis H II region, absorption shell and core 78—77590
- oxide grains, role in formaldehyde prod. in diffuse interstellar clouds 79—40246
- oxide grains surface reactions rel. to interstellar medium elemental depletions 78—36654
- Periodic Comet Encke dust, large grains in short supply 78—85908
- α Persei star cluster, dust props. from polarisation wavelength depend. meas. 79—48865
- PHL 938, quasar, continuum spectrum reddening due to dust 78—96561
- plane-symmetric cosmological model, Einstein eqn. solns. for dust 78—49733
- planetary nebulae, 8 to 13 micron spectrophotometry rel. to silicate and SiC grains 80—22057
- planetary nebulae, dust absorpt. effect on C IV 1550 Å lines fluxes 79—17051
- in planetary nebulae, dust continuous IR emission 80—109525
- planetary nebulae, dust model for IR emission 80—56900
- planetary nebulae, dust temp. and mass, IR photometry obs. 80—94850
- planetary nebulae, dust to gas ratio and internal extinction 77—45519
- planetary nebulae, Fe condensation and nebula form. models 79—40238
- planetary nebulae, grain temps. rel. to 10 micron props. 79—48879
- planetary nebulae, obs. of Abell 30 and 78 rel. to dust thermal radiation 77—91602
- planetary nebulae, theoretical data review 80—109536
- planetary nebulae dust, observational review 80—109535
- planetary surface, dust covered, polarimetric model 79—25528
- in plasma environments, physical and dynamic props. 80—26930
- Pleiades reflection nebulosity, dust clumps shearing rel. to filamentary struct. 78—8082
- polysaccharide grain model for galactic IR sources, IR fluxes calcs. 78—54008
- possible cold source of life 79—21203
- pre-main-sequence A and F stars in NGC 2264, circumstellar dust rel. to IR excesses 78—32461
- prebiotic polymers, possibilities in IR spectra of galactic sources 78—4336
- pregalactic dust, distortion of cosmological microwave black body radiation spectrum 80—67915
- pregalactic dust and distortions of the cosmic-background spectrum 80—67916
- presolar grains, as source of extinct radioactivities 77—45367
- presolar grains, as source of extinct radioactivities in meteorites 77—49342
- presolar grains in meteorites, prod. by supernovae 78—24520
- presolar grains in Murchison meteorite, evidence from inert gases 79—21243
- presolar interstellar grains in Allende meteorite, evidence from ^{40}Ar-^{39}Ar ages 80—98621
- primary cosmic rays origin, intergalactic suprathermal grains, accel. mechanisms 79—25412
- primitive grain clumps and organic compounds in carbonaceous chondrites 77—2374
- protoplanetary nebula, grain accretion time and mass limit 77—73976
- protosilicate particles, IR laboratory spectra rel. to interstellar silicate absorption bands 80—56907
- protosolar nebula, dust grain motion time evolution 80—82234
- QSOs, dust opacity and photoionization in far UV 80—46696

cosmic dust continued
- QSOs, high redshift, dust in emission-line regions 79—21458
- quasar absorption line systems, lack of dust 77—49493
- quasar emission lines, dust absorption and scattering models 80—27009
- R50 dusty star in SMC, IR photometry 77—45461
- radiative transfer in spherical dust shells, generalised two-stream Eddington approx. 79—35120
- radio galaxies with dust lanes 79—44604
- Rayleigh scatt., unusual extinction profiles 77—45527
- Red Rectangle, refl. nebula assoc. with HD 44179, spectrum interpretation 77—49462
- reddening and quasars intrinsic spectra 79—67113
- reflection nebula, inhomogeneous, scatt. function for grains of silicates and ice 79—21405
- reflection nebula, optical colours, polarisation, composite and mixture of nebula grains 78—16502
- reflection nebulae, scattering props. of interstellar grains 79—53867
- reflection nebulae, simplified models rel. to dust comp. and particle size 78—96526
- reflection nebulae, spherical core-mantle dust grains rel. to colour and polarization 79—62896
- reflection of light from thick slabs of dust in reflection nebulae 79—62881
- refractory grain destruction in low-velocity shocks 79—17041
- refractory silicate grains, nonequilib. phases condensation from SiO vapour 79—60497
- relativistic and non-relativistic dust grains, rel. to high energy particles in EAS 80—61975
- relativistic dust grains, and EAS initiation 80—46360
- relativistic dust grains survival mechanism *(Russian)* 78—49493
- relativistic dust universes, comoving metrics, Newtonian interpretation 78—65732
- S140 interstellar molecular cloud, for IR study and dust temp. profiles 80—62237
- HM Sagittae, emission-line star, polarimetry rel. to circumstellar dust shell *(Russian)* 80—36649
- HM Sagittae, IR spectrum and circumstellar dust shell 78—93266
- RY Sagittarii, pulsating R Coronae Borealis star, circumstellar dust shell rel. to IR vars. 77—45462
- Sagittarius B2, dust for UV absorpt. rel. to He abundance problem 78—49496
- scattering from a cylindrical dust cloud in an isotropic radiation field 79—30107
- RY Scuti, silicate grains IR emission from early-type supergiant binary system 80—41827
- sedimentation of grains in interstellar clouds 78—93349
- FH Serpentis (Nova Serpentis 1970), dust grain IR emission model 80—105254
- Seyfert galaxies, dust thermal emission contrib. to IR energy distribs. 78—57645
- Seyfert galaxies, dust thermal IR emission obs. 79—17083
- Seyfert galaxies, interstellar dust heating rel. to thermal IR emission vars. 80—67865
- Seyfert galaxies, type 1, dust as source of IR luminosity 78—12357
- Seyfert galaxies nuclei, dust effects on continuous optical spectra 78—57644
- shell around α Orionis, scattered polarized light 79—12473
- silicate dust, radiation effects rel. to diffuse interstellar bands origin 77—13432
- silicate grain condensation, laboratory expt. 78—54015
- silicates, emission and extinction in 4-14 μ range 79—44581
- silicates, optical props. in far UV 78—53875
- SMC, dust content from five colour photometry of Cepheids 77—29923
- solar corona, colours during eclipse and dust composition 80—51730
- solar nebula, primitive dust material evaporation metamorphism 79—58279
- solar nebula, role of grains as isotopic anomalies carriers 80—26757
- solar neighbourhood, galaxy counts/H I column densities relation rel. to local interstellar cloud 80—26953
- solar system, interstellar dust penetration, Lorentz force versus gravit. focusing 77—13315
- solid particles growth in contracting interstellar clouds, influence of turbulence 80—62251
- Southern Coalsack, CO emission assoc. with globule complex 77—29902
- space vehicle erosion by dust and particles during interstellar flight 77—49266
- spherical dust shell around central star, two-shell moment method for radiative transfer 80—62001
- spiral and elliptical, optical surface brightness, dust effects 80—90518
- in spiral galaxies, galaxy classification from dust lane strength 80—82484
- in spiral galaxies, late type, optical anal. method, visible obs. 80—101638
- spiral galaxies, light absorpt. by interstellar dust 79—35393
- spiral structure and dust lane gravitational collapse in galaxies 79—92849
- star dust, interstellar and circumstellar 77—41404
- starlight scattering, diffuse galactic light interpretation 78—8118
- static spherically symmetric distrib. of charge, complete field, charged dust appl. 78—21026
- stratosphere, upper, evidence for extraterrestrial dust layers 78—73445
- submicron particles of solar origin 77—9727
- supergiant radial vel. meas., expanding dust cloud effects on maser source 79—5816
- supergiant stars, circumstellar dust shell, stellar interferometry 79—80309
- suprathermal grain production by radiation pressure 79—58391
- SU Tauri, R Coronae Borealis star, circumstellar dust shell discovery from optical and IR photometry 80—101601
- RV Tauri and yellow semiregular variables, circumstellar dust prod. rel. to metallicity 80—26865
- temperature probability function and IR emissivity of dust heated by randomly distributed stars 78—28756
- thermal emission spectrum from small interstellar grains with temp. fluctuation 78—69864
- transparency to microwave background at $z=40$ rel. to big bang model 78—28869
- UV absorpt. cross section, He abundances *(Italian)* 78—32551
- UV absorption and scattering, obs. of galactic latit. depend. of 1530 Å radiation field 77—33704
- UV grain albedos rel. to C I in interstellar medium 79—92818
- UV opacity effects on stellar spectra 80—90505

cosmic dust continued
- UV scattering albedos, determ. from galactic UV background meas. 77−13504
- Venus, surface dust detected by Venera 9 and 10 radiant flux obs. 80−72803
- Venus dust ring, evidence from Venera 9, 10 obs. 79−75131
- volatile dust effects in H II regions *(Italian)* 79−21394
- NQ Vulpeculae (Nova 1976), CO emission during η Carinae stage rel. to grain form. 79−25609
- NQ Vulpeculae (Nova 1976), IR photometry, dust form. in exploded shell 79−48832
- W3, IR maps from 4.9 μm to 20 μm 78−49495
- W3/W4/W5 region, heavy optical obscuration obs. 80−62301
- W51, W49, airborne for IR spectroscopic obs. rel. to dust cloud model 80−36684
- W51 (IRS 2), compact H II region, 2 to 4 micron spectrophotometry, dust thermal emission 77−13422
- W51A, H II region, dust thermal emission obs. at 3.9 mm 79−35333
- W58, IR obs. of H II regions and dust clouds near K3-50 77−49457
- Wolf Rayet stars, late type with circumstellar dust shell, 8-13 micron spectral obs. 80−101599
- X-ray burst propag. through interstellar dust, small-angle scatt. effects 78−57433
- X-rays scattering rel. to cosmic X-ray bursts tails, refutation 79−12546
- yellow semiregular and RV Tauri variables, circumstellar dust prod. rel. to metallicity 80−26865
- young galaxies, dust. distrib. rel. to galaxy form. 77−33645
- young stars, circumstellar dust rel. to interstellar gas and EHF continuum emission 80−51766
- young stellar objects, circumstellar dust shells rel. to polarisation 79−8911
- zodiacal dust, solar flare protons interaction, γ-ray and X-ray lines prod. 79−53771
- zodiacal dust cloud, charged dust particles motion in interplanetary space 80−4299
- zodiacal dust cloud, thermal emission at 11 and 20 microns 80−90367
- zodiacal light, three-dimensional eqn. for brightness integral inversion 79−75155
- zodiacal light, wavelength dependent model, Mie scatt. and thermal emission 78−81587
- zodiacal light dust, orbits from Doppler shift meas. 78−85904
- zodiacal light Fraunhofer lines Doppler shift, interplanetary dust dynamics 78−45278
- zodiacal light obs., serach for dust free zone around Sun 78−45277
- II Zw 40, dwarf galaxy, radio obs. rel. to gas/dust ratio 79−8992
- ^{26}Al, rel. to activity in N.Pacific deep sea sediment 77−5181
- Fe, condensation rel. to astrophysical dust grains form. 80−26927
- H II regions, compact, IR silicate absorpt. obs. 77−22287
- H II regions, dust content, review 78−16508
- in H II regions, effects on struct. 77−33588
- H II regions, galactic, dust far IR emission compared with high-radiofrequency obs. 78−49497
- H II regions, galactic, forbidden S III 18-71 micron emission obs. rel. to dust extinction 79−97046
- H II regions, Lyman continuum photons selective absorpt. by dust 78−28759
- H$_2$O ice, amorphous, as source of 3.1 μm absorpt. in mol. clouds 80−26956
- Mg silicates, interstellar, effects of M proton irradiation on IR spectra 77−45534
- MgO, CaO, zero phonon lines rel. to origin of diffuse interstellar absorpt. bands 77−57073
- ^{59}Ni formation cross section in Fe$+\alpha$ at 7-24 MeV, poss. prod. in cosmic dust 78−78399
- OH 26.5+0.6, late-type variable star, 2 to 40 micron spectrophotometry rel. to dust shell 78−24568
- OH maser sources, dust effects on radiative transport and inversion 80−17681
- OH/IR stars, dust far IR emission rel. to OH main lines masers inversion 78−28664
- SiO mass loss and grain formation in expanding envelopes around evolved stars 79−48782
- SiO particles and 9.6 μ interstellar extinction feature 78−45378

cosmic radiation *see cosmic rays*

cosmic radiations, radiofrequency *see radiofrequency cosmic radiation*

cosmic radio waves *see radiofrequency cosmic radiation*

cosmic ray absorption
- EAS sea level absorption length, integral size spectra simulation 80−51634
- heavy ions, charge and LET distrib. meas., radiation damage in biological objects 80−94664
- interstellar arks, cosmic-ray shielding 77−49264
- ultraheavy cosmic ray charge determ. in emulsion, Mott cross section effects 79−18084

cosmic ray alpha-particles and helium nuclei
- α in solar wind, heating and acceleration 79−12376
- antihelium, relative abundance in primary cosmic radiation 78−73594
- charge state of anomalous He component, expt. test 78−7847
- energetic particles intensity meas., 1973 Sept., by interplanetary probes 77−29604
- energy spectra between 1-9 AU 78−4046
- Fort Churchill obs. of He and heavy nuclei fluxes 77−70959
- galactic cosmic rays differential spectra, model description, solar modulation theory 79−80130
- interplanetary α-particles intensity increases at shock wave front 79−53695
- interplanetary corotating nucleon fluxes separation from solar flare fluxes by radial gradients and nuclear comp. 79−25413
- interplanetary intensity gradient, 1973 April-August, Pioneer 10 and 11 meas. 77−13192
- low energy He flux, modulation in 1974-1975 near solar minimum 77−33304
- magnetosphere, α-particles accel. 79−62675
- primary cosmic rays, isotopic comp. meas. and anal. from 123 and 279 MeV per nucleon 78−49251
- recurrent particle streams at 1 AU 79−96867
- sea-level flux determination for heavy cosmic-ray particles 79−29956
- solar, alpha-particles and protons streaming velocities relative magnitude at 1 AU 77−9643
- solar alpha particles during August 1972, review of obs. 77−25895

cosmic ray alpha-particles and helium nuclei continued
- solar cosmic rays, obs. of events with high relative ^{3}He abundances during 1976 November to December 80−61972
- solar energetic storm particle events, ^{4}He/H ratio vars., theory 77−9636
- solar flare energetic particle events from same active region, p/α enhancement 79−40151
- solar flares, energetic particle composition temporal development 78−89148
- solar heavy-ion-rich particle events, ^{3}He/^{4}He ratios energy depend. and temporal evolution, ^{3}He/^{4}He in heavy-ion-rich solar energetic particle events, energy depend. and temporal evolution 80−90299
- solar protons and α particles, rigidity-independent coronal propag. and escape 78−77444
- solar wind α-particles after interplanetary shock wave passage 77−33301
- solar wind alpha component dynamics, Prognoz obs. 77−53388
- solar wind He ions superheating and superacceleration 80−12631
- sunward flowing moderate intensity proton and alpha particle fluxes, characts. 78−89016
- ^{3}He in lunar rocks, method for solar flare cosmic ray proton flux determ. 80−98576
- ^{3}He/^{4}He isotopic composition of solar cosmic rays 80−72725
- ^{4}He anomalous component, solar latit. and radial depend. 79−35080

cosmic ray apparatus
- *see also particle detectors*
- 1 km^{3} seawater detector for ultrahigh-energy neutrinos, sources detectability 78−49264
- acoustic detection of hadronic showers induced by cosmic neutrinos 79−76265
- acoustic detectors, technique for $>$10 TeV air shower expts. 79−62691
- air shower arrays, response to air showers 79−739
- air shower remote sensing using light emission and optical detection 78−4050
- air showers for 10^{4} to 10^{6} particles, lateral distrib. of EM component, detection 80−17459
- Akenon Air Shower project, e and μ obs., core energy flow, device description 79−72184
- Aryabhata satellite payload for detection of energetic solar neutrons and gamma rays 79−84636
- atmospheric electrons, MeV range registration instrument 79−5645
- automatic pressure recorder for cosmic ray recording system 77−53337
- background radiation, meas. methods 78−82588
- balloon borne neutron flux meas. system 77−91437
- calorimeter to study cosmic ray muon interactions 80−37686
- cavitation detection, of heavy nuclei and multiparticle effects in ultrarelativistic particles interaction 79−84617
- cellulose nitrate plastic detector, charge resolution improvement for cosmic ray particles 79−84671
- cerenkov counter for spacecraft application 78−86734
- charge meas., minimum pulse selection method, energy levels 80−37712
- charge sensitive high resolution amplifier 77−88352
- Cherenkov hodoscope spectrum of TF-1 Pb glass, determ. of photon coords. 77−30707
- Cherenkov light meas. method for individual showers direct obs. 77−17309
- Cherenkov photographic detector appl. to search for Dirac monopole 78−70700
- Cherenkov pulse duration during EAS 78−73595
- conference on cosmic rays and particle physics, Newark, USA, Oct. 1976 79−58987
- conference on long distance neutrino detection, Washington, DC, USA (April 1978) 79−80217
- cosmic ray variation spectrograph, data reliability ensurance 79−84610
- Deep Underwater Muon and Neutrino Detector (DUMAND), appl. to galactic nuclei probing 80−4432
- deep underwater muon and neutrino detector (DUMAND) 80−8546
- detector geometry effect on directional flux distrib. meas. 77−17362
- detector size determ. for high energy interactions above 10 TeV, summary 79−62706
- detector system for spectra of nuclei above 100 GeV/nucleon 79−58249
- digital onboard processor, for directional charged particle flux meas. in space 77−64610
- drift chamber detector for high resolution gamma-ray astronomy 77−9660
- DUMAND array, study of ultrahigh energy neutrino interactions 79−80108
- DUMAND detector, neutrinos in the depth of the sea *(French)* 79−75104
- DUMAND detector, objectives in weak interaction studies 79−63463
- DUMAND project, optical acoustic detection, programme status 79−80109
- Durham air shower array, Monte Carlo anal. of response 78−36460
- EAS, 10^{14} to 10^{16} GeV, characteristics of peripheral master system of Tien-Shan exptl. arrangement *(Russian)* 78−32310
- EAS, response of scintillators, Ne flash tubes and water Cerenkov detectors 78−49259
- EAS, simultaneous detection of γ-ray bundles and air showers 79−62700
- EAS array, at Durham, data anal. 77−91392
- EAS array at Durham 77−91391
- EAS detectors, pulse profiles studies 79−25421
- EAS research, primary cosmic ray energy $>10^{17}$ eV, equipment system parameters, capabilities 77−64569
- Elbrus spectrographic system, appl. to cosmic ray vars. 79−84605
- electron spectrometers, pulse shape anal. in fosfich detector 77−65387
- electrons and nuclei expt. on International Sun-Earth, Explorer C spacecraft 78−85792
- emulsion chamber, high energy primary electron spectrum obs. *(Japanese)* 79−80153
- emulsion chamber for cosmic gamma-ray detection 79−29959
- emulsion chamber for high energy gamma-ray spectra 79−29958
- emulsion stack connected with ionis. calorimeter for high energy cosmic ray obs. 78−25386
- energetic particle flux meas. in magnetosphere and interplanetary space, International Sun-Earth Explorer A and B spacecraft 78−85799
- EOSCOR: A light weight, microprocessor controlled solar neutron detector 79−101063
- fast 32-channel hodoscopic gating module, with memory and data output into CAMAC data way 78−7885
- FEU-49 photomultiplier, gain stability study 77−41663
- flexible geometry hodoscope using proportional chamber cathode read-out 79−3297

cosmic ray apparatus continued
galactic neutrino sources, expt. neutrino astronomy, test of stellar evolution theories 77—70964
gamma ray spark chamber telescope for range 10-100 MeV 78—36459
gamma-ray burst astronomy, critical comparison of detectors 77—64648
gamma-ray Compton telescope, high ang. resolution, 0.3-10.0 MeV directivity *(Portuguese)* 78—85847
gamma-ray detectors, counters and telescopes *(Polish)* 78—96394
gamma-ray spectrometer with various shaped scintillators, for gamma-ray spatial pattern anal. 79—16831
gamma-ray telescope, large area, coordinate-sensitive time-of-flight scintillation system 79—84676
gamma-ray telescope in 10-30 MeV range 78—73638
gas Cherenkov counter with ionisation spectrometer, appl. to cosmic ray studies 80—94662
gas proportional scintillation counter for use in large area detector systems without photomultipliers 79—59302
Geiger-Muller counter hodoscope, protection from spark chamber noise 77—18742
global network of cosmic-ray stations, appl. as spectrographic instrument set 79—12404
HEAO-B, focal plane crystal X-ray spectrom. 78—40825
HEAO-B, imaging proportional X-ray counter 78—40823
HEAO-B, solid state X-ray spectrom. 78—40824
HEAO-B monitor proportional counter instrument 78—40822
HEAO-B X-ray spectrometer, high voltage power module and charge amplifier design 78—40826
HEAO-B X-ray telescope, gas control system 78—40827
HEAO-B X-ray telescope, high resolution imaging instrument 78—40821
HEAO-B X-ray telescope 78—40820
heterodyne gravitational wave detector, sensitivity 77—41298
high energy neutrinos of extraterrestrial origin, possible detection with DUMAND 79—80179
high resolution gas scintillation proportional counter for studying low energy cosmic X-ray sources 80—58052
hodoscope, high resolution, using spherical mirror 77—393
hodoscope Cherenkov spectrometer, particle identification 77—88343
hodoscope read-out, fast sparse-data-scan system using CAMAC compatible elements 79—45609
hodoscopes, scintillation, with hodoscope photomultipliers 80—47817
Homestake long-range neutrino detector research program 79—80107
horizontal air shower detection apparatus 78—36457
inclined muon monitors, muon spectra, generating functions, rel. to diurnal variation at Kiruna 78—85783
inclined muon telescopes, appl. of spectrographic method for cosmic ray vars. study 78—45167
instrumental variations during continuous detection of nucleons and ionising components 77—14323
intensity variations, ground level recording methods, progress 77—53336
International Sun-Earth Explorer spacecraft, expts. and instruments 78—85785
interplanetary and solar electrons meas. instrumentation on International Sun-Earth Explorer spacecraft 78—85786
ion sensor, low-energy, for space meas. with reduced photosensitivity 78—53764
ionisation calorimeter, fluctuations in cascade showers generated by muons 79—84618
isotope analyser for C to Ni at 1 GeV/nucleon 77—60555
isotope spectrometer on International Sun-Earth Explorer C spacecraft 78—85797
large area multiwire ionisation hodoscope 77—30714
Lexan and nuclear emulsion data, reassessment of 1975 magnetic monopole candidate results 79—3333
Lexan detectors from Apollo 17 mission, Fe peak isotopic resolution 77—56801
Lexan foil, and nuclear emulsion sandwich stacks, obs. of cosmic rays with $Z \geq 34$ 78—20597
Lexan track detector, appl. to ultra heavy comsic ray nuclei 78—20596
Lexan track detectors, cosmic ray element abundances from Ni-Kr 78—20598
liquid scintillation counters, large area, calibration 77—397
low energy proton expt. on International Sun-Earth Explorer C spacecraft 78—85791
magnetic spectrometers, cosmic ray muons multiple scatt. 80—4215
manned submersibles for cosmic ray detect. in deep sea 78—81510
Mariner-Jupiter-Saturn low energy charged particle expt. 77—70971
mass composition from μ multiplicity meas. using Homestake neutrino detector 79—66903
medium energy expt. on International Sun-Earth Explorer C spacecraft 78—85798
MISO low energy γ-ray telescope 79—25472
MOS rectangular vol., distrib. function for ion track lengths 79—85872
multidetector telescope expt. on International Sun-Earth Explorer C spacecraft for isotopic abundance determ. 78—85789
multilayer metal targets, comp. and energy spectrum 77—53391
multilayer wide-gap spark chamber for a gamma telescope 79—76267
multiplane hodoscope, D/A system for charged particle track analysis 77—14325
multiple telescope systems, particle anisotropies meas. technique 77—82103
multiplicative core selector for EAS axis determ. 80—41682
muon hodoscope, appl. to orebodies location in mineworkings 79—84491
muon telescope for slow muon spectra and zenith angle depend. meas. 78—49324
muon telescopes, coupling functions at sea level and underground 79—16784
MUTRON, cosmic ray mag. spectrometer, MWPC trigger system 78—55081
MWPC, for cosmic drift X-ray imaging 79—41063
National Cosmic Ray Facility, for high energy physics and primary comp. studies, 10^{14} to 10^{18} eV 79—62704
neutrino detection, high-energy, using acoustic pulse from hadron shower *(Russian)* 77—38580
neutrinos, high energy, emission from point sources and detect. techniques 79—2484
neutron detector, efficiency determ. by Monte Carlo method 78—21809
neutron detector, large underground telescope, Russia *(Russian)* 78—73589
neutron monitor diurnal anisotropy, effects of fluctuations and noise 77—45264
neutron supermonitor, neutrons energy and time distribs. 79—84611

cosmic ray apparatus continued
neutron supermonitor 4-NM-64 with control of long term stability of meas. 78—21808
nuclear and ionic charge distrib. particle expts. on International Sun-Earth Explorer spacecraft 78—85790
nuclear emulsion, appl. to ultra heavy cosmic ray nuclei 78—20596
nuclear emulsion, nonrelativistic nuclei interactions rel. to fast doubly-charged particles form. 79—80175
nuclear emulsion, photometric meas. of thin CNO particle tracks 79—76281
nuclear emulsion, test of Katz's track formation theory of cosmic ray tracks Be to Mg 79—54754
nuclear emulsion type BA-2, pulsed electric field effect on cosmic ray detection 79—26829
nuclear emulsions, hydrodynamic effects in cosmic ray nucleus-nucleus interactions 79—80176
oblique muon telescopes, method of difference coupling coeffs. 78—28461
particle pitch angle measurement using telescopes with multiple view directions 78—24425
particle telescope of Sydney Univ., results 78—25388
pellicle stack, γ-ray family from cosmic-ray hadron reactions, accelerated scanning method 78—78546
photodensitometry of tracks of highly ionizing particles in the cosmic rays 79—22551
photographic appls. for expts. on ocean floor 80—36509
photomultipliers with large photocathodes, intrinsic amplitude resolution 77—41664
plastic detectors, meas. of high-linear-energy transfer particles on Apollo, Skylab and ASTP space missions 77—41272
plastic total absorption track detector of high energy particles 78—55107
plastic track detector CR-39, detection of relativistic cosmic ray Fe group nuclei 79—80154
progress in cosmic ray astronomy *(Chinese)* 79—75058
proportional counter for cosmic X-radiation recording, 2 to 25 keV, optimal characts. 77—23375
radiochemical detector, cosmic ray muon induced neutrons meas., depth depend. 77—61670
radiochemical solar neutrino detectors using (ν,e^-) reaction, (p,n) background from cosmic ray muons 77—61650
Sayan spectrograph data, on intensity vars. of interplanetary, magnetospheric and atmospheric origins 79—84606
scintillation and Cherenkov counter system, for EAS research above 2×10^{14} eV 77—61649
scintillation counter characteristics, optimum design for elongated detector 77—61652
scintillation counter hodoscopes, LED test system 78—58556
scintillation counters, large area, light collection 78—74538
scintillation detector array, 200 m^2 for examining central section of EAS 77—61648
scintillation hodoscope for meas. of ionisation losses of relativistic particles 80—42892
scintillation proportional counter, built in K getter 78—29707
scintillation proportional large area gas counter for X-ray astronomy 78—49321
scintillation proportional large area gas counter for X-ray astronomy 78—49322
scintillation supertelescope, computation of meteorological coeffs. 77—13202
scintillation time-of-flight telescope for cosmic γ-ray preselection 78—82572
Signe II MP, satellite expt. for study of solar and cosmic X-ray and γ-ray bursts 80—41696
SILYA-4 light nucleus isotope spectrometer for cosmic ray obs. above atmosphere 79—80111
small emulsion chambers, design, scanning and energy meas. 79—59299
small emulsion chambers, materials, construction, anal. techniques, cosmic ray expt. 79—59300
SNM-57 proportional neutron counter, intrinsic background meas. 77—65399
snow gauge, cosmic-ray, snowpile meas. *(Japanese)* 77—5347
soft X-ray spectrometer, for diffuse cosmic sources 77—5440
solar wind ion comp. expt. on International Sun-Earth Explorer C spacecraft 78—85793
space instrumentation for charged particles meas., review *(Russian)* 77—17368
spacecraft expt. determ. of cosmic-ray particle fluxes 78—85778
spark calorimeter, for locally generated penetrating-particle beams obs. 79—84603
spark chamber and time of flight detector for 15-150 MeV neutrons from extended source 77—83447
spark chambers and scintillation counters combination array, for multicored EAS obs. 77—60557
spark counter, localised-discharge, as new particle detector 79—81119
spectrometer, for study of 6 to 50 MeV, cosmic ray electrons 78—45235
Sun-blind photomultipliers for near UV 77—41665
superconducting mag. spectrom. for cosmic ray flux meas. 78—25383
superheavy primary cosmic ray nuclei, obs. with solid-state track detectors and X-ray films *(Japanese)* 78—61688
thin ionisation calorimeters for cosmic ray spectra meas., Monte Carlo calcs. 77—30713
time of flight system as directional counter in gamma ray telescopes 77—390
time of flight telescope, compensated, for spaceborne cosmic ray measurements 77—67939
TLD system for meas. of cosmic dose on board a spacecraft 80—109047
TOF technique for particle identification at 2-400 keV/N 80—5435
transceiver, inexpensive, use in cosmic ray time coincidence expts. with long baselines 80—52837
transition radiation detector system for high energy hadron interactions research 77—61651
transition-radiation detector and shower detector combination for galactic electron meas. 77—57844
Tskhra-Tskaro system, for research on cosmic rays of 0.4 to 10 TeV energy 79—84626
two-dimensional buffer store based on a multichannel amplitude analyzer for neutrino detect. 79—26838
undersea detection system, located in deep ocean 80—98522
upper atmosphere, background effects in scintillation telescopes 78—85823
Utah Fly's Eye, optical detection sytem, data acquisition system and status report 79—63864

- **cosmic ray apparatus** continued
  - Voyager cosmic ray detector system, energetic particle studies in outer heliosphere 78—24434
  - Voyager low energy charged particle experiment 78—20618
  - X-ray emulsion chambers, electron-photon cascade energy determ. errors 79—84613
  - Yakutsk improved system, for examination of EAS Cherenkov pulse shapes 79—80169
  - γ-rays in range 3.5 to 100 MeV, system for meas. ang. and energy distribs. 77—50324
  - Al chamber, air-filled, 900 l, for sea level ionisation meas. 79—35081
  - Ar liquid calorimeter with very thin sampling 77—34518
  - CdTe detector, Cl doped, for reentry vehicle appl., development electronics 77—45288
  - CsI crystals, in scintillation counters, nonstatistical counting rates due to phosphoresc. 78—95597
  - Fe calorimeter, hadronic cascade curves between 20 and 8000 GeV 80—36464
  - Fe-liquid scintillator multilayer calorimeter transition effects, muon burst rates 78—90019
  - H_2 streamer chamber up to atmospheric pressure 77—38553
  - H_2O, acoustic rad. from ionising particles 78—71793
  - NaI(Tl) large area multi-crystal detectors for X-ray and gamma-ray astronomy 77—22070
  - Si solid state detector telescopes, neutral particle background effects 78—28472
  - Si(Li) thin window detectors for NASA ISEE-C cosmic ray telescope 78—40819
  - Si(Li)-emulsion shower counter for cosmic ray electron obs. 80—58033
  - W scintillator ionisation spectrometer, meas. of cascades initiated by 5 to 300 GeV hadrons 77—34526

- **cosmic ray composition**
  - *see also cosmic ray alpha-particles and helium nuclei; cosmic ray deuterons; cosmic ray electrons; cosmic ray mesons; cosmic ray muons; cosmic ray neutrinos; cosmic ray nuclei; cosmic ray photons*
  - age determ. from comp. of cosmic rays on Earth 77—53341
  - anomalous component, source material from comets 79—71003
  - anomalous component of low-energy particles, obs. and calc. spectra 78—28465
  - antimatter content in cosmic rays 77—53375
  - antiprotons and antihelium, relative abundance in primary cosmic radiation 78—73594
  - atmospheric shower development 80—17458
  - baryon pair production with large decay Q-value. Brasil-Japan emulsion chamber collaboration 79—58992
  - Biobloc II expt. results for high-LET particles 80—94663
  - charge meas., minimum pulse selection method, energy levels 80—37712
  - charged cosmic ray particles, fiftieth anniversary of discovery, review 79—2448
  - charged hadrons, negative/positive ratio, 3220 m above sea level *(Chinese)* 79—12369
  - closed galaxy, cosmic ray propag. model, nuclear abundances 77—70951
  - composition, influence on atmospheric hadron families characts. 79—80160
  - conference, Yakutsk, USSR (Jun. 1977) 79—80110
  - conference on cosmic rays and particle physics, Newark, USA, Oct. 1976 79—58987
  - Dirac monopole, search with Cherenkov photographic detector 78—70700
  - EAS, characts. of gamma ray and hadron families, Monte Carlo calcs. 77—53377
  - EAS, energies of electron-photon and hadron components near axis, 3330 m above sea level 77—64563
  - EAS, low-energy hadron meas. 79—80165
  - EAS, very large, sea-level characts., particle number spectra 79—80168
  - EAS hadrons, lateral distrib. at mountain level 80—21881
  - EAS radioemission, freq. spectrum, lateral distrib., primary cosmic rays comp. 77—87219
  - EAS with N of 10^4 to 10^5, energy and charge compositions of nuclear-active component 77—64553
  - electron-proton abundance ratio, rel. to origin 77—49252
  - electron/proton ratio, gradients rel. to galactic gamma-ray spectra 78—40784
  - element abundances from Ni-Kr, meas. with Lexan track detectors 78—20598
  - element ions, interval $6 \leq Z \leq 28$, energies composition, Skylab study 80—8501
  - elements in $26 \leq Z \leq 30$ interval, relative abundances 79—40044
  - galactic cosmic nuclei abundance, time averaged for $Z \geq 50$, tracks in meteorite minerals 80—101513
  - galactic cosmic ray composition determ. from tracks in lunar and meteoritic feldspars 78—20603
  - galactic cosmic rays, charge and energy spectra rel. to short pathlengths deficiency 79—84596
  - galactic cosmic rays, Fe nuclei isotopic comp. 80—72729
  - galactic cosmic rays, Ne, Mg and Si isotopes high resolution meas. 80—51631
  - galactic proton/electron ratio 78—69633
  - geomagnetic and solar disturbance effects on cosmic rays and neutrons 77—13195
  - geomagnetically forbidden cosmic ray nuclei, kinetic energies and charges 77—37489
  - hadron and γ-ray spectra with $\Sigma E_\gamma > 500$ TeV 77—64575
  - hadron families, high-energy, Monte Carlo studies 79—80158
  - hadron flux composition at mountain altitudes *(Russian)* 80—61973
  - hadron interactions, transverse momenta at 10^{14} to 10^{15} eV in Pamir expt. 79—80170
  - hadron interactions with Pb and Fe at 3260 m above sea level 77—64552
  - hadron spectrum, ground level, 30 to 1000 GeV 79—75064
  - hadron unaccompanied flux at depth 730 g cm^{-2}, energy spectra in range 10^2-10^4 GeV 78—73593
  - hadronic component and momentum spectrum at 2 km altitude in 70-350 GeV/c range *(Russian)* 80—67486
  - hadronic interactions, 10^{12} to 10^{15}eV, and cosmic ray components in atmosphere 79—62708
  - hadrons, spectra above 2 TeV 79—80147
  - hadrons of high energy, neutral to charged ratio at mountain altitude 79—62698
  - hadrons of tens of TeV energies, energy characts. of gamma-ray quanta produced 79—80148
  - heavy antinucleus interpretation of event of Price et al. 77—45272

- **cosmic ray composition** continued
  - heavy leptons in cosmic radiation underground, search using scintillation+Cherenkov detectors 78—65470
  - heavy long lived cosmic ray particles 80—90300
  - heavy nuclei, cavitation detect 79—84617
  - horizontal cosmic ray penetrating particles identification, fractional charge search *(Chinese)* 80—101514
  - interplanetary corotating nucleon fluxes separation from solar flare fluxes by radial gradients and nuclear comp. 79—25413
  - isotope abundance meas. for C to Ni 77—60555
  - isotope abundances, Cr to Ni 79—70937
  - isotopic composition, rel. to cosmic ray origin and containment time 78—53781
  - isotopic composition, review 78—20599
  - isotopic composition of B, C, N, Ne, Mg and Si, mean mass determ. 78—93060
  - light elements, possible existence of cosmological cosmic rays 78—7841
  - light isotopes abundances in galactic cosmic rays, rel. to interstellar gas density 80—17456
  - long lived heavy particles with fractional charge, evidence in cosmic ray events 79—2447
  - long term composition changes from lunar fossil tracks 77—60552
  - low energy cosmic rays, Skylab meas. of heavy ions 80—56689
  - low energy nuclei, ionization states and origin 77—53339
  - low-energy interplanetary background, proton/He nuclei meas. by Venera 9 and (Venera 10) 78—4049
  - lunar charged particle environment, irradiation and accretion of lunar rocks and grains 77—60562
  - medium energy cosmic rays, comp. from Si to Ni meas. with nuclear emulsion 77—5404
  - medium energy expt. on International Sun-Earth Explorer C spacecraft 78—85798
  - medium energy nuclei, Ne to Fe, charge comp. 79—84608
  - National Cosmic Ray Facility, for high energy physics and primary comp. studies, 10^{14} to 10^{18} eV 79—62704
  - near-Earth cosmic rays, short-term fluctuations in electron and γ quanta components 80—67483
  - neutron/proton ratio at different atmospheric depths, from primary nucleon spectrum 80—8499
  - nuclear component of galactic cosmic rays, light nuclei/medium nuclei ratio from diffusion model 79—53678
  - nuclei, charge comp. and energy spectra, energies >5 GeV per nucleon 78—16259
  - nuclei, low energy, props., Skylab expt. 78—69632
  - nuclei, ultrahigh-energy, metagalactic, spectrum calc. 77—53342
  - nuclei from 3000 MeV to 50 GeV per nucleon, charge comp. and energy spectra 78—93059
  - nuclei with $4 \leq Z \leq 26$ and $0.3 \leq E \leq 2$ GeV amu^{-1}, energy spectra and abundance ratios 77—56800
  - nuclei with $Z \geq 50$ in olivine from meteorites 80—105139
  - nucleon rays with $Z \geq 34$, high resolution study with track detectors 78—20597
  - origin, energy spectrum, composition, general review 79—80117
  - particle masses, determ. from Cherenkov radiation from large air showers 79—25420
  - particle telescope meas. at Sydney Univ., results 78—25388
  - penetrating radiation composition, Cosmos 721 obs. 77—53279
  - pion spectrum, at top of atmosphere 78—53780
  - plastic detectors, calib., heavy cosmic ray charge distrib. 78—17500
  - primaries, mass composition meas. with Homestake neutrino detector 79—66903
  - primary, air shower cores, energetic hadron, $>10^{13}$ eV, arrival time distrib. 79—44321
  - primary composition near 10^7 GeV, from underground muon meas. 80—41681
  - primary cosmic ray N and O, isotopic comp. with consequences for source models 79—84609
  - primary cosmic rays, $>10^{13}$ eV, comp. study, from hadron time distribs. near air shower cores 79—62697
  - primary cosmic rays, anal. of number of nucl. cascade avalanches in ionisation calorimeter 78—12064
  - primary cosmic rays, energy 10^{14}-10^{16} eV, comp. and interactions, Tien-Shan data 79—80149
  - primary heavy nuclei diffusion in atmosphere, spectra and comp. 80—41680
  - primary nuclei composition effect on cosmic ray muons response function 80—41683
  - propagation of 1-100 GeV cosmic rays in Galaxy 78—20590
  - proton nucleon component, rel. to galactic cosmic ray origin models with halo 80—61971
  - quarks, monopoles, tachyons etc., review of expts. 78—12872
  - quiet time comp. and energy spectra for cosmic rays between 0.6-24 MeV per nucleon 77—29609
  - range distribution function of cosmic rays in matter 79—80113
  - relative abundances of nuclei with $Z \geq 7$ from plastic detectors 78—16260
  - satellite and balloon research projects, problems 79—8785
  - secondary neutral pion-nucleon flux ratio at atm. top from $pp \rightarrow \pi^0 + X$ data 80—8500
  - solar activity, cosmic-ray variations, and neutrino fluxes, review 79—84599
  - solar cosmic rays, energy spectrum of Fe-group nuclei 77—53353
  - solar cosmic rays, interpretations of isotopic comp. of H and He 77—45266
  - solar cosmic rays, obs. of events with high relative ^{3}He abundances during 1976 November to December 80—61972
  - solar energetic particle event of 1974 July 4, Fe/O charge comp. spatial and temporal vars. 77—22199
  - solar energetic particles in corotating events, comp. 79—25414
  - solar flare accelerated particles, charge spectrum and comp. form. 80—46529
  - solar flare energetic particle abundances in range $2 \leq Z \leq 28$, Voyager obs. 80—90382
  - solar flares, energetic particle composition temporal development 78—89148
  - solar flares, particle emission comp. *(Italian)* 78—96461
  - solar particle event, November 18, 1968, abundance ratios rel. to interplanetary propag. 77—29607
  - solar particles, isotope composition form., effect of ion-sonic turbulence 80—101574
  - solar particles, Z-rich event characts., (1972 to 1976) 79—5717

cosmic ray composition continued
solar proton/He ratios, rel. to nucleons, interplanetary accel. in corotating interaction regions 77—9635
source composition, energy depend. at high energies 77—67013
source composition probe of acceleration mechanisms 80—31178
spectral shape of cosmic rays over Galaxy 78—20589
sunward flowing proton and alpha particle fluxes, comp. and spectra 78—89016
tachyon monopole, search 79—16770
tachyon search, ray energy $\geq 10^{14}$ eV, 290 μs preceding period 77—78588
ultra heavy cosmic ray nuclei meas. with Lexan and emulsion detectors 78—20596
ultraheavy ($Z>52$) nuclei in galactic cosmic rays, long-term average abundances from pallasites 77—9641
ultraheavy cosmic rays just beyond Fe, comp. and origin rel. to solar system material 77—70952
ultraheavy cosmic-rays rel. to r-process models 78—49250
$Z \gtrsim 60$ cosmic rays, charge and energy spectra from Skylab expt. 78—40782
γ-ray spectrum from pp collisions, fireball model 77—18364
μ to e ratio fluctuations with shower size 78—7848
$\pi^{\pm}$ charge ratio in atmosphere 78—28463
Be isotopes meas., 200-1500 MeV/nucleon 79—12366
^{7}Be, cosmic ray accel. probe 78—81512
^{7}Be/^{9}Be data rel. to cosmic ray acceleration mechanisms 80—31183
^{10}Be abundance, implications for origin 79—44314
^{10}Be abundance and age of galactic cosmic rays 78—12060
^{10}Be abundance rel. to age, balloon meas. technique 77—29602
^{10}Be nuclei, rel. to galactic cosmic ray origin models with halo 80—61971
^{14}C measurement in known age specimens, cosmic ray intensity determ. 80—101516
Ca, cosmic ray source abundance 78—28467
^{40}Ca source abundance meas. 80—8502
Fe, Co, Ni abundance, time delay between nucleosynthesis and accel. to relativistic energies 78—28455
Fe group nuclei, detection in CR-39 plastic track detector 79—80154
Fe peak isotopic resolution, Lexan detectors from Apollo 17 mission 77—56801
Fe primaries, 10^{14} eV, proposed direct meas. 77—37490
Fe+p, high energy spallation, studies, cosmic ray implications, isotope abundances 77—2998
He isotope composition of solar cosmic rays from Venera 9 obs. 80—72725
He isotopic composition from 123 to 279 MeV per nucleon, meas. and anal. 78—49251
^{3}He/^{4}He in heavy-ion-rich solar energetic particle events, energy depend. and temporal evolution 80—90299
Li abundance, balloon borne telescope obs. 78—40785
Li to Fe nuclei for 2-150 GeV/nucleon, abundances and spectra 79—21116
Me to Fe nuclei, primary, 200 to 650 MeV/ nucleon, relative abundances 80—77246
Ne isotopes, ratio in galactic cosmic rays 79—101036
Ne, Mg, Si, mean mass meas. 78—7845

cosmic ray deuterons
production mechanisms 79—29955
sea-level flux, meas. by Sydney University particle telescope 78—25388
sea-level flux determination for heavy cosmic-ray particles 79—29956

cosmic ray effects and interactions
see also high-energy cosmic ray interactions
air showers impact on water surface, acoustic pulses generation and detect. 79—66901
artificial satellites electrostatic shielding from cosmic radiation, Cosmos 605 meas. 77—29622
astronaut dosages, Apollo 7 to 14 and Soyuz 3 to 9 missions, TL meas. *(Hungarian)* 79—29639
atmosphere, ion-pair production rate above 18 km altitude, parametrisation 78—65469
atmospheric nucleon and charged pion unidirectional diffusion eqns. 78—57417
Barwell meteorite, preatmospheric size, particle track study 78—53893
Biostack experiment, high precision localisation methods for cosmic high energy loss particles 78—20235
Biostack experiment, radiobiology of cosmic high energy loss particles using visual track detectors 78—20234
Biostack experiments, radiobiology of cosmic galactic radiation heavy nuclei 78—20236
Biostack III Zea mays expt., high LET particle dosimetry 78—20287
carbonaceous chondrites, cosmic ray irradiation rel. to parent bodies form. 80—36580
Centaurus A, nuclear gamma-ray lines, origin in relativistic plasma 80—41890
charge coupled devices, cosmic ray background model 80—51669
charged cosmic ray scatt. in stochastic mag. field, above 1 GeV 78—61689
chondrite Kirin H, inert gas content interpretation *(German)* 80—46505
chondrite Yamato-74191, inert gas composition and neutron capture effects 80—46504
clusters of galaxies, intracluster gas heating by relativistic electrons rel. to X-ray and radio emission 78—57655
cosmic dust, radiation effects rel. to diffuse interstellar bands origin 77—13432
D-region, ionisation effects from cosmic X-ray sources 79—35048
Dhajala meteorite, India, cosmic radiation effects, fossil track studies 80—72733
Dhajala meteorite, unequilibrated H3 chondrite, K-Ar and cosmic ray exposure ages 78—32425
Djermaia (H) chondritic breccia, preirradiation history 80—36579
dosimetric significance at altitude of supersonic transport and in free space 78—20295
dosimetry in nucl. emulsions for Apollo and Apollo-Soyuz Biostack expts. 78—20288
Earth atmosphere, effects of energetic particle precip. on middle atmosphere chemical comp. 80—109213
EAS, muon spectrum at sea-level, Maeda's model, using pion-kaon ratio 78—85781
EAS, violation of scale invariance in hadron interactions, 10^{15} to 10^{17} eV 78—7849

cosmic ray effects and interactions continued
EAS and radiowaves produced from secondary electrons in geoelectric field, 10 kHz-10 MHz 79—21118
EAS radio emission, field strength at 44, 60 and 80 MHz 80—8505
EAS radio pulses, correlation at 60 and 80 MHz 80—8504
electrons, relativistic, form. of regions of nonlinear electron spectrum rel. to synchrotron spectrum generation 80—109555
electrons in clusters of galaxies, spatial distrib. of Compton-produced X-ray flux 77—33686
EM cascade, particle-induced, in water, thermoacoustic effect, neutrino detection appl. 79—29960
event of Price et al., heavy antinucleus interpretation 77—45272
eye, astronaut light flash obs. on Skylab 4, role of nucl. stars 77—5089
Fabry-Perot etalon, optically contacted, stability to cosmic radiation 80—98544
FJM 6 molecular cloud, IR and radio mol. line studies rel. to cosmic ray heating 80—26929
fossil tracks in pallasites, abundances of ultraheavy ($Z>52$) nuclei 77—9641
fragmentation parameters meas. in nuclear emulsions, validity 78—90017
galactic cosmic ray composition determ. from tracks in lunar and meteoritic feldspars 78—20603
galactic cosmic rays, effect on solar wind vel. 80—101506
galactic cosmic-ray diffusion in low-latitude solar wind 77—53344
galactic diffusion, interaction effects on cosmic ray age distrib. 77—5401
galaxies active nuclei, cosmic ray driving of gas 77—29915
gamma-ray spectrometers; calc. of radioactivity induced during spaceflight 80—102382
gamma-rays, origin of galactic diffuse component 80—17450
gamma-rays generation, implications for galactic struct. studies 77—26083
gamma-rays origin in cosmic ray interactions with matter *(Polish)* 78—96571
hadron interactions, violation of scaling model *(Russian)* 78—78231
heavy cosmic rays ($Z=30$-40), Linear Energy Transfer (LET) spectra and biological implications 80—3828
heavy stable particles, cosmic ray produced, search in heavy water 79—40048
high energy interactions, scaling, limited fragmentation, cosmic ray models 77—10211
high-LET particle exposure of Skylab astronauts 77—29212
ice grains in interplanetary and interstellar media, low energy cosmic ray erosion 78—45177
immunology, Ni plated slides, effect of metallic shield on cosmic radiation effects 80—56317
intercloud cosmic ray ionisation rate 78—85989
interfering background influence on orbiting IR sensor systems 77—22011
interstellar Alfven waves generation, cosmic rays from dense mol. clouds 77—13190
interstellar clouds, cosmic ray ionisation rate upper limit from electron abundance determ. 80—41866
interstellar clouds, cosmic ray ionization 79—17063
interstellar gas interaction with cosmic rays, X-rays prod. 77—68110
interstellar grains, destruction by sputtering 78—45382
interstellar grains destruction by cosmic rays, hydrodynamic mechanism 78—24546
interstellar H$_2$, ionisation, dissociation and heating efficiencies of cosmic rays 78—28454
interstellar material interaction, contrib. to galactic gamma-ray flux 79—25763
interstellar medium, cosmic ray generated anisotropic MHD turbulence 77—45532
interstellar medium, cosmic ray ionisation coupling to acoustic instability 79—97044
interstellar medium, electrons contrib. to diffuse X-ray flux in 2 to 7 keV range 80—98745
interstellar medium, gamma-ray flux from Cygnus X region rel. to CG 78+1 nature 79—92895
ionisation events in stratosphere, effects on NO$_2$, O$_3$ and climate, rel. to life extinction 78—96273
ionisation of interstellar matter, rel. to spatial inhomogeneities in diffusion model 77—5402
ionization of Jupiter atmosphere 80—17538
Jupiter atmosphere, low order effect of cosmic ray albedo neutron decay (CRAND) input 78—45271
Kirin meteorite, cosmogenic radionuclides study *(Chinese)* 79—21237
light elements origin, prod. by cosmological cosmic rays 78—12436
Luna 24 soil samples, cosmic ray irradiation rel. to depositional history 79—88608
Luna-24 regolith column, particle track based irradiation and accretion history 78—45244
lunar rocks, cosmic ray exposure ages and burial depths from cosmogenic Xe ratios 77—57661
lunar rocks and grains, obs. rel. to irradiation and accretion of solids in space 77—60562
lunar samples, charged particle track anal., thermoluminesc. and microcratering studies 77—60665
lunar soil samples from Luna-24, radioactivity and cosmic ray dose rate, thermolum. obs. 80—67596
lunar surface materials, nature and composition of species formed 77—41334
Marjalahti pallasite, cosmic ray induced ^{53}Mn production 80—72891
Mars, cosmic-ray interactions with rocks and atmosphere, gamma-ray spectra 77—53448
meson decay, effect on stratospheric cosmic rays height-intensity distrib. 79—12364
meteorite, Unter-Massing iron, cosmic-ray exposure age and preatmospheric size *(German)* 80—46507
meteorite thermoluminescence as measure of irrad. history, validity of method 80—36584
meteorites, ^{39}Ar prod. as evidence for Maunder minimum in solar activity 78—57529
meteorites, mass ablation, cosmic-ray track study 78—53894
meteorites, role of cosmic rays in thermoluminesc. prod. 80—31262
meteorites, secondary cosmic ray interactions rel. to isotopically anomalous Ag in Santa Clara and Pinon Fe meteorites 80—85902
meteorites, stony, thermoluminesc. gradients due to cosmic ray bombardment 77—74020
meteorites capturing ^{22}Na, ^{10}Be, ^{26}Al from solar flare cosmic rays 80—36461

cosmic ray effects and interactions continued
- meteoritic chondrules, origin through relativstic electrons heating 80—4310
- meteoritic hypersthene, fresh and fossil tracks, rel. to Fe abundance in cosmic ray flux 77—41276
- MeV protons, effects on IR spectra of interstellar Mg silicates 77—45534
- minerals, thermal annealing of ion tracks 78—20604
- multilayer metal targets, comp. and energy spectrum 77—53391
- muons atmospheric production, high energy 77—64583
- neutral particle background, effects in cosmic ray telescopes composed of Si solid state detectors 78—28472
- neutron integral generation factors rel. to atmospheric depth 77—53380
- nonrelativistic nuclei interactions, fast doubly-charged particles form. 79—80175
- nuclear active particle prod. without pions, possible evidence 77—91395
- nuclear and space radiation effects, conf., Albuquerque, USA (Jul. 78) 79—19276
- nuclide production in Fe meteorites, rare gas concs. 78—65473
- one-dimensional diffusion eqn. integration, one-fireball model 78—57416
- particle identification from tracketch rates in minerals 79—16788
- positron initiated showers in Pb, 0.5-3.5 GeV, test of cosmic ray shower calcs. 78—37332
- positrons, galactic, primary source, interactions and fates 80—109319
- proton interaction with lunar and planetary material, gamma-ray production, simulation 78—16318
- radiation belt around Earth, electron energies above 100 MeV, produced by primary cosmic rays 78—36409
- radiobiological studies in space and at ground-based accelerators 80—41266
- San Juan Capistrano meteorite, cosmic ray record 78—57512
- scintillation, 1/f fluctuations *(Japanese)* 78—43448
- seawater and atm. surface layer gamma radiation field rel. to cosmic ray neutrons *(Russian)* 79—39746
- secondary electrons in dense interstellar clouds, origin and effects 77—33593
- solar CNO particles, rel. to carbonaceous chondrite fission Kr and Xe origin 79—35199
- solar flare tracks in Luna 24 core samples, thermolum. obs. 80—82246
- solar system ^{16}O and ^{26}Al isotopic anomalies, local proton irradiation model 78—93128
- solar wind, deposition of momentum and energy by MHD waves 77—37493
- solar wind particles trapping and accel. at Earth 80—98532
- space colonies, radiation effects and protection 77—86651
- spaceflight, radioactivity induced in scintillator materials 78—85822
- spores of Bacillus subtilis inactivation rel. to heavy ion impact parameters 80—26288
- St. Mesmin brecciated chondrite, irradiation history from noble gases abundances 78—28593
- St. Severin chondrite, ^{53}Mn production due to nucl. spallation, depth-depend. 80—82316
- St. Severin meteorite, flux of low energy particles in solar system 77—82096
- ultra heavy cosmic ray nuclei meas. with Lexan and emulsion detectors 78—20596
- ultraheavy cosmic ray charge determ. in emulsion, Mott cross section effects 79—18084
- visual phenomena in space 78—20297
- NN interactions, cosmic ray clusters, size and mass determ. 77—71548
- NN semi-inclusive reactions, secondary pion production, 1000 GeV, scaling phenomena 79—22157
- p-nucleus cross sections characts. appl. to calc. of muon sea level momentum spectrum and charge ratio 77—41275
- ^{26}Al production in atmosphere, rel. to ^{26}Al activity in deep sea sediment 77—5181
- B production in interstellar medium, evidence from B detect. in front of κ Orionis 80—51841
- ^{14}C form. in atm., diffusion distrib. 80—101510
- ^{14}C, production rel. to cosmic rays and solar activity cyclic vars. 79—16776
- Ca isotope enrichment in magnetic spherules in marine sediments 79—44423
- CsI crystals, in scintillation counters, nonstatistical counting rates due to phosphoresc. 78—95597
- Fe meteorites, cosmic ray produced nuclides, ^{41}K/^{40}K-^{4}He/^{21}Ne exposure ages and age distribs. 79—30015
- Fe meteorites, radial distrib. of spallogenic K, Ca, Cr, Ti, V and Mn isotopes 80—67488
- ^{56}Fe, hadron generated cascades, energy flux absorption length, 1-20 TeV *(Russian)* 78—28468
- H_2O, acoustic rad. from ionising particles 78—71793
- He, Ne, Ar isotopes and ^{236}U prod. by solar cosmic ray protons in lunar materials 77—17311
- Li, Be, B, cosmic-ray nucleosynthesis and extragalactic matter local infall rate 79—17084
- ^{53}Mn, in stony meteorites, determ. by activation anal. for cosmic ray effects investig. 78—12018
- ^{53}Mn produced in meteorites, neutron activation anal. 79—30018
- ^{15}N, enrichment in Mars atm. due to cosmic ray interactions in early solar system 78—73669
- ^{22}Na production rates at mountain altitudes 78—12065
- O_3 levels in stratosphere, solar activity, cosmic rays effects 77—53362
- SF_6, breakdown at high pressure, possible cosmic ray effects 78—87577

cosmic ray electrons
- atmosphere MeV gamma rays prod., theoretical zenith angle distrib. at high balloon altitudes 77—45208
- atmospheric showers, γ-ray initiated, computer simulations, Cherenkov radiation, geomag. field effects 77—49254
- atmospheric showers, electron and muon components, correl. with nucleon MFP in air *(Russian)* 77—73916
- black holes, primordial, electron-positron radiation, spectrum rel. to galactic radio spectrum 80—62179
- cascade shower, electron energy density, lateral struct. function 79—66900
- cascade shower electrons, approx. determ. of lateral struct. function 77—33307
- Cassiopeia A, relativistic electrons streaming at speeds above Alfven vel. 79—40068

cosmic ray electrons continued
- charge coupled devices interaction model, event rate and electron number distrib. 80—51669
- clusters of galaxies, Compton-produced X-ray emission, spatial distrib. 77—33686
- clusters of galaxies, intracluster gas heating by relativistic electrons rel. to X-ray and radio emission 78—57655
- clusters of galaxies, intracluster relativistic electrons hard X-ray spectra and gas heating 79—25735
- Coma cluster of galaxies, origin and transport of electrons in halo radio source 77—26073
- Coma galaxy cluster, relativistic electrons streaming at speeds above Alfven vel. 79—40068
- confinement in dynamical galactic halo 78—4044
- coronal and interplanetary propagation of solar particles following E45° solar flare on 29/7/73 78—49248
- cosmic betatron model *(Rumanian)* 78—49315
- cosmic rays propagation and distribution in Galaxy 78—69621
- Crab Nebula, nonlinear plasma effects rel. to wisp struct. 79—25682
- doubly scattered electron fluxes in atmosphere 77—53358
- EAS, Akeno Air Shower project, e and μ obs., core energy flow, device description 79—72184
- EAS, characts. for primary energy <200 TeV, electron and muon fluxes 79—80162
- EAS, correlations between muon and electron component characteristics 79—44324
- EAS, electron and muon number distrib., anal. of primary cosmic ray spectrum, 10^{13} to 10^{16} eV 77—67014
- EAS, electron and muon spatial distribs., mountain heights 77—64562
- EAS, electron component sensitivity to fragmentation range in inclusive spectra 79—84614
- EAS, electron flux, spatial distrib. 77—49256
- EAS, electron lateral distrib. at mountain altitude 78—28470
- EAS, electron spatial distrib. at 1700 m above sea level 79—80163
- EAS, electron-photon and muon components, simulation 77—49255
- EAS, energies of electron-photon and hadron components near axis, 3330 m above sea level 77—64563
- EAS, energy ratio of electron-photon and hadron components in core 77—82093
- EAS, hadron interactions, comp. of primary particles of energy 10^{14}-10^{16} eV, Tien-Shan data 79—80149
- EAS, lateral age parameter and radial electron distribs. 80—85828
- EAS, muon to electron ratio fluctuations 78—7848
- EAS, response of scintillators, Ne flash tubes and water Cerenkov detectors 78—49259
- EAS and radiowaves produced from secondary electrons in geoelectric field, 10 kHz-10 MHz 79—21118
- EAS near core, struct. of electron-photon component *(Russian)* 78—57414
- electron and γ interaction ranges, Monte Carlo calc. *(Russian)* 79—12370
- electron showers, Cherenkov radiation from electron ang. distrib. function *(Russian)* 79—80861
- electron-nucleus and EM cascade build up in layered medium, Landau-Pomeranchuk effect 77—64558
- electron-photon cascade energy determ., effects of optical density and energy spectrum meas. errors 79—84613
- electron-photon cascade in air, simulation of energy and lateral characteristics 79—44323
- electron-photon cascades, Monte Carlo simulation of cascade development 79—44322
- electron-photon cascades, spectra above 2 TeV 79—80147
- electron-photon cascades in homogeneous absorbers 77—61669
- electron-photon shower, range fluctuations in unbounded medium 79—80152
- electron-photon showers, successive approximation method 77—64559
- EM cascade showers, electron/photon energy flow 77—22027
- EM cascade theory equations, approx. solution *(Russian)* 77—49257
- EM cascades in air, 10-100 GeV, longit. development 79—21120
- energetic secondary electrons, in dense interstellar clouds 77—33593
- energy spectra, 0.3-3.0 MeV 80—51632
- energy spectra between 9-300 GeV 79—29954
- energy spectrum, theory of lifetime distrib. of particles 78—96368
- energy spectrum and propag. 80—67485
- energy spectrum of galactic cosmic rays, fundamental props. *(Chinese)* 80—105138
- excess radiation flux at heights of 200-300 km meas. 77—53278
- extragalactic radio sources, relativistic electrons in situ accel. by shock waves 78—49241
- fast electrons long-term vars. in Earth's outer radiation belt 78—49226
- galactic, evidence for large-scale gradients 77—33299
- galactic disc, non-thermal electron bremsstrahlung rel. to gamma-rays prod. 78—24414
- galactic disc, primary electron component estimate from gamma-ray emission obs. 80—82540
- galactic discrete sources 79—35078
- galactic electron spectrum below 1000 MeV 79—5718
- galactic electrons, contrib. to diffuse X-ray flux in 2 to 7 keV range 80—98745
- galactic electrons, distrib. rel. to spiral struct. and continuum radiation 77—13465
- galactic electrons, flux and gradients rel. to galactic gamma-ray spectra 78—40784
- galactic electrons, propag. rel. to galactic radio background distrib. 77—5602
- galactic electrons, radio emission rel. to cosmic ray confinement 77—73910
- galactic electrons, source spectrum rel. to diffusion model of propag. 79—53677
- galactic electrons, spectrum determ. from radio emission rel. to Galaxy gamma-rays prod. 80—62257
- galactic electrons and positrons, fluxes in closed galaxy model 77—13189
- galactic halo, diffusion models for low-freq. radio emission 78—12433
- galactic halo, inverse Compton scatt., diffuse γ-ray background prod. 77—53711
- galactic halo, relativistic electrons spectrum from radio obs. 78—96544
- galactic positrons, annihilation and gamma radiation spectrum 79—44309
- galactic primary cosmic-ray electrons, 30-1000 GeV, emulsion chamber obs. 80—85827
- galactic proton/electron ratio 78—69633
- galactic radio emission rel. to cosmic ray electron spectra 77—29610

cosmic ray electrons continued
galactic radio halo, electron spectra 77−9631
high energy EM showers in atmosphere, Monte Carlo simulation 77−56802
high energy interactions and cosmic ray components in the atmosphere 79−62707
high energy primary electron spectrum, emulsion chamber obs. *(Japanese)* 79−80153
interplanetary, detect. expt. on International Sun-Earth, Explorer C spacecraft 78−85792
interplanetary and solar, meas. instrumentation on International Sun-Earth Explorer spacecraft 78−85786
interplanetary intensity gradient, 1973 April-August, Pioneer 10 and 11 meas. 77−13192
interplanetary modulation and transport of Jovian electrons 78−45175
interplanetary space and magnetosphere, electrons with energy 0.3 to 3 MeV, Prognoz 4 obs. 79−62693
interplantary propagation, Mars spacecraft meas. 78−53779
interstellar electron spectrum in local interstellar medium, determ. from bremsstrahlung gamma radiation 79−25417
interstellar local electron spectrum determ. from galactic radio background 78−93056
Jovian electrons, propag. close to Sun ($\lesssim$0.5 AU) 79−101034
Jupiter, electron propag. out of solar equatorial plane, Pioneer 11 obs. 79−40123
Jupiter, surface temp. excess, attributed to cosmic radiation from galactic nucleus *(French)* 77−60714
Jupiter origin for energetic electrons, study of 1972-7 intensity variations 80−72726
large air showers, arrival-time distribs. of μ's and e's, obs. at 5200 m above sea level 79−62699
low-energy, interplanetary background meas. on Venera 9 and (Venera 10) 78−4049
low-energy electrons, quiet-time increases, Jovian origin 77−2367
in M51, diffusion model rel. to radio spectral index distrib. 78−8119
M87 jet, relativistic electrons anisotropic flux rel. to synchrotron emission *(Russian)* 80−8694
magnetosphere, particles distrib. above 400 km altitude beneath radiation belts 78−49227
magnetosphere and interplanetary space, fast electron intensity 77−33282
modulation of Jupiter electrons, Pioneer 10 and 11 obs. 78−61690
muon-electron ratio and particle mass for primary cosmic rays of $10^{15}10^{16}$ eV energy 79−80150
muons, high-energy, EM component density spectrum 77−82092
National Cosmic Ray Facility, for high energy physics and primary comp. studies, 10^{14} to 10^{18} eV 79−62704
near-Earth cosmic rays, short-term fluctuations in electron and γ quanta components 80−67483
Pamir and Fuji electron-nuclear cascades, high energy γ-families 79−25423
polar, magnetotail lobe and interplanetary low energy electrons, satellite obs. 78−73587
positron energy spectrum, effect of interstellar medium anal. 77−49253
positrons, galactic, primary source, prod. rate, and escape probability 80−109319
positrons in primary cosmic radiation and collisions in interstellar medium 80−77241
primary electron intensity and energy spectrum 77−45270
primary electrons, detect. by synchrotron radiation in geomag. and interstellar mag. fields 78−57412
primary spectrum data at EAS energies 80−46359
primary-electron spectrum above 3 GeV meas. 77−53374
propagation, diffusion model 79−53679
propagation in atmos., energy spectra evolution allowing for secondary electron production 80−41676
propagation in Galaxy, leaky-box model 78−57409
propagation of 1-100 GeV cosmic rays in Galaxy 78−20590
quasiperiodic pulsations in stratosphere 79−80133
quasitrapped electrons, 100 MeV, in geomag. field 200-250 km above equator *(Russian)* 78−49223
radio sources, compact, extragalactic, synchrotron and relativistic Maxwellian source models rel. to spectra 80−62299
radio sources, extragalactic, relativistic electron clouds rel. to variable radio emission temporal characts. *(Russian)* 80−62307
in radio sources, form. of universal and diffusion regions of relativistic electrons non-linear spectra 80−109555
relativistic electron spectra, inference from meas. of inverse Compton radiation 80−90339
relativistic electrons, inverse Compton interactions rel. to astrophysical gamma-ray prod. 80−17448
Saturn, surface temp. excess, attributed to cosmic radiation from galactic nucleus *(French)* 77−60714
scaling and charge ratio at 1-10 TeV 77−64576
secondary electron fluxes at equator, Kosmos-428 data 78−45168
short-period fluctuations, in upper atm., correl. with solar diameter vars. 79−21115
showers, lateral structure function, electronic component 77−91394
solar, nonrelativistic, coherent propag. 77−91506
solar, review of obs. during August (1972) 77−25895
solar electrons, Prognoz-6 fluxes and spectra meas. during large scale interplanetary disturbances 80−90315
solar electrons from E45° flare, 1973, July 29, coronal and interplanetary propag. 77−82090
solar electrons from September and November 1977, flares, spectra and time profiles 78−77446
solar flare, 1973 April 29, cosmic ray anisotropy, Cosmos 555 obs. 77−45268
solar flare electrons, peculiarity of ejection into interplanetary space *(Russian)* 78−77445
solar flare energetic particles, interplanetary propag. model 78−65468
solar flare particle accel. and generation 80−,101575
solar impulsive electron events not assoc. with flares, ISEE 3 obs. 80−67683
solar modulation, 1969-1977 period 80−26706
solar nebula, relativistic electrons rel. to meteoritic chondrules origin 80−4310
solar nonrelativistic electron diffusion mechanism in interplanetary medium 77−53349
solar nonrelativistic electron stream, propag. in solar atmosphere rel. to type III radio bursts 78−28623

cosmic ray electrons continued
solar wind, very low electron and proton temps., statistical anal., origin 78−65477
solar wind electrons, vel. distrib. at 1 AU, steady state theory 79−101041
spatial distrib. perpendicular to galactic plane 77−53338
spectra in 100 MeV-100 GeV range, Interkosmos 17 spectrometer 80−8503
spectra in Earth's radiation belts during mag. storms 77−53314
spectral shape of cosmic rays over Galaxy 78−20589
splash and re-entrant albedo electrons, energy spectra 78−69630
transition-radiation detector and shower detector combination for galactic electron meas. 77−57844
transitional emission detector, electron identification in cosmic ray background, X-ray detection study 80−4213
Tycho supernova remnant, relativistic electrons distrib. from radio struct. obs. 80−56919
ultrahigh energy electrons traversing cosmic blackbody photon gas, effective penetration distance 79−5742
Voyager cosmic ray detector system, energetic particle studies in outer heliosphere 78−24434
Voyager Cosmic Ray Experiment, telescopes, electron energy meas., pulse height analysers 79−48643
X-ray transient radiation detection, comparison with theoretical predictions *(Russian)* 79−66896
e/μ ratio in 10^6 GeV cosmic ray shower, interaction model, Feynman scaling 77−45271

cosmic ray energy spectra
11 year variations during 19th and 20th solar cycles 79−84602
air shower muons lateral distrib. and spatial separation of distrib. 80−109320
anomalous component of low-energy particles, obs. and calc. spectra 78−28465
antiproton spectrum, at top of atm., scaling law 79−12365
atmospheric neutrinos, 10-10^7 GeV, energy spectra and ang. distribs. *(Russian)* 80−85830
atmospheric neutron and gamma ray fluxes and energy spectra 79−75063
atmospheric secondary nucleon spectra, 10^2-10^4 GeV, 2-component model *(Russian)* 78−41612
charged particle acceleration to relativistic energies in interplanetary shock waves 79−80123
clusters of galaxies, intracluster relativistic electrons spectra and hard X-ray emission 79−25735
Compton scattering at nonzero particle fluxes, radiation and relativistic electrons spectra 79−8825
conference on cosmic rays and particle physics, Newark, USA, Oct. 1976 79−58987
cosmic ray electrons, X-ray transient radiation detection, comparison with theoretical predictions *(Russian)* 79−66896
deep underground muons at Mt. Blanc station, integral energy spectrum 80−31184
density spectrum of cosmic-ray air showers at very high densities 79−16783
detector system for spectra of nuclei above 100 GeV/nucleon 79−58249
diffuse gamma-ray flux, 2-25 MeV energy range 78−32309
diurnal anisotropy energy spectrum in 1971-75 period 79−80136
diurnal anisotropy of intensity, solar flare location effect 79−44318
EAS, 10^{14} to 10^{16} GeV, characteristics of peripheral master system of Tien-Shan exptl. arrangement *(Russian)* 78−32310
EAS, characts. for primary energy <200 TeV, electron and muon fluxes 79−80162
EAS, energy spectrum for 10^{17}-10^{20} eV 79−80151
EAS, high energy muon density 80−36466
EAS, muon density meas., $E>10^{15}$ eV using scintillators and spark chambers *(Italian)* 79−21119
EAS, muon spatial and energy distribs., magnetic spectrometer study 77−67017
EAS, response of scintillators, Ne flash tubes and water Cerenkov detectors 78−49259
EAS, size fluctuation effect on size spectrum 79−58207
EAS growth, significance of fragmentation and pionisation ranges in inclusive spectra 79−84614
EAS sea level absorption length, integral size spectra simulation 80−51634
EAS with $E_0>2\times10^{16}$ eV, position of maximum energy *(Russian)* 79−96870
EeV cosmic rays, energy spectrum and arrival direction 80−67480
electron component of galactic cosmic rays, spectrum spatial distrib. from propag. diffusion model 79−53679
electron spectra in cosmic extragalactic radio sources, rel. to radio spectra 80−62299
electron spectrum determ. from galactic radio background 78−93056
electron-photon cascade energy determ., effects of optical density and energy spectrum meas. errors 79−84613
electron-photon cascade in air, simulation of energy and lateral characteristics 79−44323
electron-photon cascades, spectra above 2 TeV 79−80147
electron-photon shower, range fluctuations in unbounded medium 79−80152
electron-positron radiation from primordial black holes, spectrum rel. to galactic radio spectrum 80−62179
electrons, confinement in dynamical galactic halo 78−4044
electrons, discrete galactic sources 79−35078
electrons, energy spectrum and propag. 80−67485
electrons, energy spectrum of galactic cosmic rays and fundamental props. *(Chinese)* 80−105138
electrons, high energy, primary, spectrum obs. by emulsion chamber *(Japanese)* 79−80153
electrons, in M51, injection spectral index rel. to galaxy radio index distrib. 78−8119
electrons, relativistic, in radio sources, form. of universal and diffusion regions of non-linear spectra 80−109555
electrons, spectra between 9-300 GeV 79−29954
electrons and nuclei expt. on International Sun-Earth, Explorer C spacecraft 78−85792
electrons in 100 MeV-100 GeV range, Interkosmos 17 spectrometer study 80−8503
electrons of energy 0.3-3.0 MeV 80−51632
electrons solar modulation, 1969-1977 period 80−26706

cosmic ray energy spectra continued
electrons traversing atmosphere, energy spectra evolution allowing for secondary electron production 80−41676
electrons with energy 0.3 to 3 MeV, Prognoz 4 obs. in interplanetary space and magnetosphere 79−62693
element ions, interval $6\leq Z\leq 28$, energies composition, Skylab study 80−8501
energetic storm particle events connection with interplanetary shock wave parameters 79−70935
environmental radiation fields prod. by cosmic rays 80−51630
extragalactic cosmic rays, 10^{20} eV, energy spectrum and arrival direction 80−82157
fast timing ang. distrib. meas., data anal. 78−49256
for interaction in graphite 79−29959
Forbush decreases and solar anisotropy, 11-year vars. 79−44317
galactic cosmic ray electrons, source spectrum rel. to diffusion model of propag. 79−53677
galactic cosmic rays, accel. mechanism and transport, model 79−35077
galactic cosmic rays, charge and energy spectra rel. to short pathlengths deficiency 79−84596
galactic cosmic rays, energy spectra from modulation models including particle drift effects 80−31180
galactic cosmic rays, inside magnetosphere, local energy spectra calc. *(Russian)* 78−16258
galactic cosmic rays, modulation coeff. energy depend. in 11-year cycle 78−28460
galactic cosmic rays, obs. between 1-9 AU 78−4046
galactic cosmic rays, propag. and spectra in finite solar cavity 78−69623
galactic cosmic rays, spectrum determ. from stratospheric cosmic rays eleven-year cycle 80−4212
galactic cosmic rays differential spectra, model description, solar modulation theory 79−80130
galactic cosmic rays modulation by solar total mag. field 79−80131
galactic electron spectrum below 1000 MeV 79−5718
galactic electrons, spectrum determ. from radio emission rel. to Galaxy gamma-rays prod. 80−62257
galactic gamma-ray spectra, rel. to cosmic ray electrons flux and cosmic ray gradients 78−40784
galactic halo, relativistic electrons spectrum from radio obs. 78−96544
galactic positron annihilation radiation, spectrum 79−44309
galactic primary cosmic-ray electrons, 30-1000 GeV, emulsion chamber obs. 80−85827
galactic protons, spectrum vars. meas. by Venera 9 and Venera 10 probes 77−91388
gamma quanta produced by cosmic-ray hadrons of tens of TeV energies, energy characts. 79−80148
gamma ray high energy families, f′ spectrum 78−28466
gamma ray spectroscopy, review 80−67582
gamma-quanta, spectra above 2 TeV 79−80147
gamma-quantum families of 10 to 100 TeV energy, height depend. 79−80159
gamma-quantum families with $\Sigma E_{\gamma}>30$ TeV, energy characts. in Pamir expt. 79−80156
gamma-ray astronomy, use of artificial satellites 79−53727
gamma-ray background, spectrum rel. to primordial heavy leptons annihilation contrib. 78−93479
gamma-ray bursts, hard X-ray spectra 78−7846
gamma-ray bursts, multiple Compton scatts. effect on X-ray emission spectrum 78−96389
gamma-ray emission, high-energy, from galactic disc, spectral characts. COS-B obs. 78−36695
gamma-ray spectra, high energy, near top of atmos. detection+meas. by emulsion chamber 79−29958
geomagnetic shielding of artificial satellite, cutoff probability for nuclei 80−12626
hadron energy spectra produced by primary cosmic ray particles, $E>10^{14}$ eV 80−21880
hadron spectrum, ground level, 30 to 1000 GeV 79−75064
hadron unaccompanied flux at depth 730 g cm^{-2}, energy spectra in range 10^{2}-10^{4} GeV 78−73593
hadronic component and momentum spectrum at 2 km altitude in 70-350 GeV/c range *(Russian)* 80−67486
hadronic interactions, 10^{12} to 10^{15}eV, and cosmic ray components in atmosphere 79−62708
hadrons, spectra above 2 TeV 79−80147
heavy ions, charge and LET distrib. meas., radiation damage in biological objects 80−94664
heavy ions, low energy, Skylab obs. of energy spectra 80−56689
heavy nuclei, charge and energy spectra 79−25418
heavy nuclei, LET spectra vs. absorber depth 78−20296
heavy nuclei (Z=30-40), charge spectra and biological implications 80−3828
high energy cosmic rays, EAS and energy deposition 79−66898
high-energy, cosmic rays, solar anisotropy spectrum 80−51628
highest energy cosmic rays, spectrum rel. to diffusion from Virgo cluster 80−4208
horizontal muon intensity and momentum spectrum at 3220m above sea level *(Chinese)* 80−101515
inclined muon monitors, muon spectra, generating functions, rel. to diurnal variation at Kiruna 78−85783
interplanetary cosmic ray protons, 1-4.5 MeV, spectral anal. and correl. study 80−77243
interstellar electron spectrum in local interstellar medium, determ. from bremsstrahlung gamma radiation 79−25417
leakage error in cosmic ray spectra 78−89023
meteorological, geomag. and interplanetary vars., separation via spectrographic instrument set 79−12404
multiple scattering cosmic ray energy balance in randomly nonuniform mag. field *(Russian)* 78−49252
muon, absolute intensities in vertical and zenith angles 55°-85° 80−17460
muon charge ratio, sea level, phenomenological model, review 80−67487
muon energy at sea-level, Cocconi-Koester-Perkins model 79−48634
muon flux density fluctuations in EAS 80−21884
muon momentum spectrum and charge ratio in vertical direction 80−41685
muon spectra at sea-level, solar modulation at geomag. equator 79−16775
muon spectrum at sea-level, Maeda's model, using pion-kaon ratio 78−85781
muon spectrum up to 1 TeV at 75° zenith angle 79−53689

cosmic ray energy spectra continued
muons, at different altitudes, Bose-type model calcs. 79−44326
muons, integral and differential absolute intensity meas. below 1 GeV 80−41684
muons, parent nucleons, energy distrib., at sea level and underground, phenomenological model 80−61974
muons, spectra above 2 TeV 79−80147
Musala anisotropy, 10^{11}-10^{14} eV range 78−49255
Musala station, obs. of anisotropy 78−49253
NAP flux at 735 g cm^{-2} altitude, energy spectrum 77−73914
neutrinos, high-energy prod. spectra and diffuse fluxes 79−44327
neutrinos and cosmic rays from pulsars 80−31319
neutron spectrum, sea level, calc. from primary nucleon spectrum 80−8499
neutron spectrum variations meas., Elbrus spectrographic system appl. 79−84605
neutrons, energy and time distribs. in neutron supermonitor 79−84611
nuclei, charge comp. and energy spectra, energies >5 GeV per nucleon 78−16259
nuclei, energy spectra determ. by gas Cherenkov counter with ionisation spectrometer 80−94662
nuclei, low energy, props., Skylab expt. 78−69632
nuclei, mass composition at EAS energies 80−46359
nuclei from 3000 MeV to 50 GeV per nucleon, charge comp. and energy spectra 78−93059
nuclei recurrent fluxes, 1-8 MeV/nucleon energies, Prognoz-4 meas. 79−21112
origin, energy spectrum, composition, general review 79−80117
pion spectrum, at top of atmosphere 78−53780
power type spectrum for particle accel. at spherical shock wave *(Russian)* 80−72730
primary cosmic ray fluctuations, Musala Peak obs. 78−49254
primary cosmic ray nucleon and sea level muon energy interrelation, scaling model 80−51633
primary cosmic ray nucleon spectrum from sea level μ-spectrum using scaling model 79−29957
primary cosmic rays, 10^{13} to 10^{16} eV, for EAS data 77−67014
primary cosmic rays, $>10^{13}$ eV, comp. study, from hadron time distribs. near air shower cores 79−62697
primary cosmic-radiation spectrum from 10^{12} eV to 10^{15} eV from atmospheric Cerenkov-radiation measurements 79−66895
primary energy spectrum of Grigorov et al., interpretation 80−36462
primary heavy nuclei diffusion in atmosphere, spectra and comp. 80−41680
primary nucleon spectra from atmospheric γ-ray and muon data 79−44320
primary nucleon spectrum from sea level muon spectrum *(Russian)* 79−62709
protons, high-energy meas. in Proton satellites 78−28462
protons, low-energy, interplanetary background meas. on Venera 9 and (Venera 10) 78−4049
relativistic and non-relativistic dust grains, rel. to high energy particles in EAS 80−61975
relativistic electron spectra, inference from meas. of inverse Compton radiation 80−90339
relativistic particles acceleration in shock fronts 78−24415
review of energy spectrum and anisotropy of the cosmic radiation *(Hungarian)* 79−44319
sea level muon spectrum and charge ratio, derivation from CERN (p.pπ) results 80−8506
sea level muon spectrum and primary nucleon spectrum, Cocconi-Koester-Perkins model 79−84612
sea-level muon spectra, calc. from ISR kaon-pion ratio 79−8784
secondary electron fluxes at equator, integral energy spectra 78−45168
secondary gamma-rays, energy spectra rel. to atmos. depth 79−58205
solar ^{3}He rich cosmic ray events, ^{3}He and ^{4}He nuclei energy spectra 80−61972
solar active region protons at 1 AU, energy spectra from Prognoz-3 80−101512
solar and galactic subcosmic rays; interstellar space spectrum of role in cosmos 78−61693
solar charged particles generated in 1972, August 7 flare accel. and injection spectrum 79−12360
solar cosmic rays, spectra rel. to particles shock accel. in solar wind corotating interaction regions 80−82159
solar energetic particle events following September and November, 1977, flares, proton and electron spectra 78−77446
solar energetic particles, Pronoz-6 fluxes and spectra meas. during large scale interplanetary disturbance 80−90315
solar flare particles absolute spectra for flares of 1966-76 period 79−84598
solar flare particles meas. and integral proton spectra anal. 79−62695
solar flare proton energy spectra slope from radio burst data 79−53683
solar flare protons, flux intensity function determ. via radio bursts 78−45165
solar flare protons, spectrum determ. from latitudinal effect, using minimal Stormer pulse 78−45308
solar flare protons, spectrum from stochastic accel. model 80−21953
solar gamma-rays during 1972 Aug. 4 flare *(Russian)* 78−12185
solar heavy nuclei enhancement at high energies, 1974 July 4 event 78−28641
solar particles, origin, nature and effects, interplanetary propag., review *(Russian)* 79−66893
solar particles, spectrum formation near Earth, propagation and acceleration *(Russian)* 80−4211
solar particles, Z-rich event characts., (1972 to 1976) 79−5717
solar particles from E45° solar flare on 29/7/73, coronal and interplanetary propagation 78−49248
solar proton flare, 1971 September 2, simultaneous satellite obs. 77−67083
solar proton spectra determ., comparison of methods 78−28459
solar protons, energy spectrum shape at 1 AU *(Russian)* 78−16255
spacecraft expt. determ. of cosmic-ray particle fluxes 78−85778
splash and re-entrant albedo electrons, energy spectra 78−69630
sunward flowing proton and alpha particle fluxes, comp. and spectra 78−89016
theory of lifetime distrib. of particles 78−96368
two-component spectrum, evidence from cosmic ray nucleosynthesis 79−17084
ultra high energy cosmic rays, discussion *(French)* 80−21879

cosmic ray energy spectra continued
- underground obs. of fluctuations, nonlinearities effect on power spectrum 80—41679
- underground observations, difference coupling coeffs. and difference meteorological coeffs. 78—28464
- variation spectrograph data, reliability ensurance 79—84610
- $Z \gtrsim 60$ cosmic rays, charge and energy spectra from Skylab expt. 78—40782
- K-π ratio from diffusion model and sea level μ spectrum shape 79—35083
- μ, charge ratio, momentum spectra, zenith-angle depend. anal. 78—45171
- μ, directional cosmic-ray range spectra 78—45172
- Ge detectors in space, computer spectral anal. of cosmic ray proton induced radioactivity 79—12413
- He nuclei, energy spectra and isotopic comp. meas. from 123 to 279 MeV 78—49251
- Li to Fe nuclei for 2-150 GeV/nucleon, abundances and spectra 79—21116

cosmic ray geophysical effects *see geophysical aspects of cosmic rays*

cosmic ray jets *see cosmic ray showers and bursts*

cosmic ray mesons
- atmospheric nucleon and charged pion unidirectional diffusion eqns. 78—57417
- axion, astrophysical limitations on mass *(Russian)* 78—61835
- C-ray emulsion-chamber study 77—64557
- charged hadrons, negative/positive ratio, 3220 m above sea level *(Chinese)* 79—12369
- charged particle flux meas. at sea level between 250 and 10000 GeV 77—73915
- decay effect on height-intensity distrib. of stratospheric cosmic rays 79—12364
- diffusion equations for nucleon and charged pions in atmosphere 79—70936
- EAS, energy ratio of electron-photon and hadron components in core 77—82093
- EAS, violation of scale invariance in hadron interactions, 10^{15} to 10^{17} eV 78—7849
- high-energy hadron spectrum depend. on hadron inelastic cross-section increase *(Russian)* 77—46093
- lunar variations of intensity 79—80146
- meson-neutrino spectrum from GSFC 78—85782
- multiple meson production by 10^{13}-10^{16} eV cosmic rays, longitudinal behaviour of γ air family 77—33309
- negative pions, multiple charged-particle generation in inclusive reactions with nuclei 79—76022
- nuclear interactions around 20 TeV, characts., comparison with Monte Carlo simulation 79—58991
- pion spectrum, at top of atmosphere 78—53780
- pions, cosmic ray composition at 2 km altitude in 70-350 GeV/c range *(Russian)* 80—67486
- secondary neutral pion-nucleon flux ratio at atm. top from $pp \rightarrow \pi^0 + X$ data 80—8500
- K prod. in nN interactions, effect on μ charge ratio 77—18363
- K-π ratio from diffusion model and sea level μ spectrum shape 79—35083
- NN interactions, cosmic ray clusters, size and mass determ. 77—71548
- π production spectrum derivation from primary cosmic ray spectrum and scaling consts. 77—25897
- π^-, RBE and OER values from Vicia Faba root growth inhibition obs. 80—26271

cosmic ray muons
- absolute intensities of medium-energy muons in the vertical and at zenith angles 55°-85° 80—17460
- air shower, fluctuations of low-energy muons, composition models 77—37491
- air showers, muonic component lateral structure function 77—70963
- altitude depend. meas. by scintillation telescopes 77—30469
- angular distribution of low-energy cosmic ray muons underground 78—40786
- atmospheric production of high energy muons 77—64583
- atmospheric showers, electron and muon components, correl. with nucleon MFP in air *(Russian)* 77—73916
- C-ray emulsion-chamber study 77—64557
- cascade showers generated by muons in ionisation calorimeter, fluctuations anal. 79—84618
- cascade showers prod. by muons in Fe at 0.3-3 TeV 77—64570
- charge coupled devices interaction model, event rate and electron number distrib. 80—51669
- charge ratio, momentum spectra, zenith-angle depend. anal. 78—45171
- charge ratio, sea level, phenomenological model review 80—67487
- charge ratio at sea level, depend. on K prod. in nN interactions 77—18363
- coupling functions for muon telescopes at sea level and underground 79—16784
- deep underground muons at Mt. Blanc station, integral energy spectrum 80—31184
- deep underwater muon and neutrino detector (DUMAND) 80—8546
- detection in deep sea using manned submersibles 78—81510
- directional cosmic-ray range spectra 78—45172
- diurnal harmonics, underground muon data, corotational model 77—70958
- dose rate and flux density estimations by TLD method 79—58208
- EAS, π photoprod. as source of low-energy muons 80—4214
- EAS, Akeno Air Shower project, e and μ obs., core energy flow, device description 79—72184
- EAS, ave. lateral muon density distrib., arrival direction studies 78—73596
- EAS, characts. for primary energy <200 TeV, electron and muon fluxes 79—80162
- EAS, correlations between muon and electron component characteristics 79—44324
- EAS, electron and muon number distrib., anal. of primary cosmic ray spectrum, 10^{13} to 10^{16} eV 77—67014
- EAS, electron and muon spatial distribs., mountain heights 77—64562
- EAS, electron-photon and muon components, simulation 77—49255
- EAS, energetic muons and multiple penetrating particles 77—53378
- EAS, hadron interactions, comp. of primary particles of energy 10^{14}-10^{16} eV, Tien-Shan data 79—80149
- EAS, high energy muon density 80—36466

cosmic ray muons continued
- EAS, method of searching for anomalous muon generation 78—89026
- EAS, muon component sensitivity to fragmentation range in inclusive spectra 79—84614
- EAS, muon density meas., $E > 10^{15}$ eV using scintillators and spark chambers *(Italian)* 79—21119
- EAS, muon momenta meas. 78—20600
- EAS, muon spatial and energy distribs., magnetic spectrometer study 77—67017
- EAS, muon spatial distrib., expt. and calc. 79—80167
- EAS, muon spatial distrib. and age parameter correl. 79—80166
- EAS, muon spatial distrib. correl. with shower age 77—64582
- EAS, muon spectrum at sea-level, Maeda's model, using pion-kaon ratio 78—85781
- EAS, muon to electron ratio fluctuations 78—7848
- EAS, single and muon pairs, 20-1000 GeV, showers of 10^4 to 10^7 particles 78—28473
- EAS, violation of scale invariance in hadron interactions, 10^{15} to 10^{17} eV 78—7849
- EAS arrival direction distributions 78—28471
- EAS at 690 g/cm^2, fluctuations of muon component 78—36411
- EAS at mountain altitudes, comparison with numerical calcs. 77—87218
- EAS high energy muons, array and data analysis 78—89027
- electron-muon ratio and particle mass for primary cosmic rays of $10^{15}10^{16}$ eV energy 79—80150
- EM interactions of muons and muon pairs, 5-1200 GeV *(Russian)* 78—73598
- energy spectrum at sea level, 1-10 TeV, with emulsion chamber 79—25424
- flux deep underground, intensity vs. depth, neutrino induced component 79—16786
- flux density fluctuations in EAS 80—21884
- ground level high-energy muons, spectra and generation processes 77—25898
- high energy, exptl. work, review 77—82095
- high energy cosmic rays, EAS and energy deposition 79—66898
- high energy interactions, muons penetrating large depths in rock and water 77—29612
- high energy interactions and cosmic ray components in the atmosphere 79—62707
- high-energy, EM component density spectrum 77—82092
- hodoscope, appl. to orebodies location in mineworkings 79—84491
- horizontal muon intensity and momentum spectrum at 3220m above sea level *(Chinese)* 80—101515
- inclined muon monitors, muon spectra, generating functions, rel. to diurnal variation at Kiruna 78—85783
- inclined muon telescopes, for spectrographic investigation of cosmic ray vars. using difference coupling coeffs. 78—45167
- inelastic interaction with Fe nuclei 79—84616
- inelastic scatt. with NaCl nuclei, above 300 GeV *(Russian)* 79—22106
- integral μ momentum spectrum, absolute intensity meas. 0.4 to 3.0 GeV/c 79—5720
- integral and differential absolute intensity meas. below 1 GeV 80—41684
- integral intensity meas. at low latit. station 79—53690
- intensity of secondaries in atmos., solar activity affecting height distrib. 80—41675
- large air showers, arrival-time distribs. of μ's and e's, obs. at 5200 m above sea level 79—62699
- large cosmic ray showers, muon component computer simulation using hadronic collisions models 78—57415
- lateral density distrib. of muons in air showers at different heights 79—40045
- lateral distribution at different altitudes in atmosphere 80—26708
- momentum spectra in vertical for 100-3000 GeV/c range 77—73918
- momentum spectrum and charge ratio in vertical direction 80—41685
- multiple scatt. by Pb nuclei at sea level, anomalous scatt. distrib. 78—7851
- multiple scatt. by Pb nuclei at sea level, Rainwater-Cooper theory, 230 MeV/c muons 78—7850
- multiple scattering in mag. spectrometers theory 80—4215
- multiplicity meas., mass composition of cosmic ray primaries using Homestake neutrino detector 79—66903
- National Cosmic Ray Facility, for high energy physics and primary comp. studies, 10^{14} to 10^{18} eV 79—62704
- oblique muon telescopes, generalisation of difference coupling coeffs. method 78—28461
- pair generation, nucleon cascade role 80—91120
- parent nucleons, energy distrib., at sea level and underground, phenomenological model 80—61974
- primary cosmic ray nucleon and sea level muon energy interrelation, scaling model 80—51633
- primary cosmic ray nucleon spectrum from sea level μ-spectrum using scaling model 79—29957
- primary nucleon spectrum from sea level muon spectrum *(Russian)* 79—62709
- radiative energy losses in ground 79—84619
- radiochemical measurement of cosmic ray muon induced neutrons, depth depend. 77—61670
- response functions, primary nuclei comp. effect 80—41683
- scaling and charge ratio 79—12371
- scaling and charge ratio at 1-10 TeV 77—64576
- scintillation detector system, cosmic ray muon lifetime, undergraduate teaching 78—81752
- scintillation supertelescope obs., meteorological coeffs. computation 77—13202
- sea level charge ratio, energy depend. 80—94665
- sea level momentum spectrum and charge ratio, 1 to 5000 GeV/c, based on hadron+nucleus characts. 77—41275
- sea level muon spectrum, Bugaev model 77—82094
- sea level muon spectrum, Cocconi-Koester-Perkins model calcs., using nucleon spectrum 77—49258
- sea level muon spectrum, determ. from $pp \rightarrow \Pi^- + X$ scaling variable 77—13995
- sea level muon spectrum and charge ratio, derivation from CERN (p.pπ) results 80—8506
- sea level muon spectrum and primary nucleon spectrum, Cocconi-Koester-Perkins model 79—84612
- sea-level energy spectra from primary nucleon spectra, Cocconi-Koester-Perkins model 79—48634
- sea-level expt., analytical and Monte Carlo interpretations 77—67016
- sea-level expt., hadronic and muonic fluxes obs. 77—67015

cosmic ray muons continued
sea-level muon charge ratio, energy up to 1 TeV 78—89029
sea-level muon spectra, calc. from ISR kaon-pion ratio 79—8784
sea-level muon spectra, model using kaon-pion ratio 78—93064
sea-level muon spectrum, primary cosmic ray chem. comp. calcs. 77—64555
sea-level spectrum, Dao scaling model for $pp \to \pi^- X$ 78—61694
sea-level spectrum 80—98527
sea-level spectrum and charge ratio, reln. to. accelerator data 77—9640
shower, muon energy spectra at large zenith angles, 0.28 to 35 TeV *(Russian)* 77—9639
showers underground, multiplicity distribs., local interactions in absorbers 77—5406
sidereal daily variation, rel. to cosmic rays ang. distrib. at heliosphere boundary 79—80116
sidereal variations, muon obs. at 150 m underground 79—53687
solar harmonics, variation of upper limit rigidity, 1958-63 78—49265
solar modulated low-energy sea-level spectra, at geomag. equator 79—16775
solar neutrino radiochemical detectors, cosmic ray muon induced proton background effects 77—61650
spatial characts. in large showers 77—22031
spectra, at different altitudes, Bose-type model calcs. 79—44326
spectra above 2 TeV 79—80147
spectral index between 10 and 150 GeV by end-of-range meas. 77—70960
spectrum and charge ratio, 100 GeV/c to 10 TeV/c, using mass spectrograph 80—4216
spectrum up to 1 TeV at 75° zenith angle 79—53689
stellar daily variation, semiannual modulation 78—69626
temperature variations, spectrographic obs. of secondary cosmic rays 78—69628
time correlation of muon pairs and multiple hadron production 79—80178
time distribution, random and nonrandom components of arrival times 80—72732
underground muons, response functions for different depths 80—82160
underground observations, difference coupling coeffs. and difference meteorological coeffs. 78—28464
variation in particle fluxes, correlation with atmospheric variables 77—22030
vertical integrated momentum spectra, 3220 m above sea level *(Chinese)* 79—12372
e/μ ratio in 10^6 GeV cosmic ray shower, interaction model, Feynman scaling 77—45271
K-π ratio from diffusion model and sea level μ spectrum shape 79—35083
$\mu+\mu$ ratio, calc. from pp inclusive reactions at ISR energies 78—58212
μe collisions, 10 MeV to 10 GeV electron energy transfer, target Z/A depend. of cross section 77—30355
μN inelastic scatt., four-momentum depend. determ. 77—61337
Fe+cosmic ray photon, prod. of 300-1000 GeV muons, cross section, shadowing 77—64580
Fe+μ, 2 to 800 GeV, EM interactions of cosmic ray muons, e^+e^- prod. and knock-on e^- prod. 79—66902
Fe(μ,μ'), small Q^2 and >200 GeV, implications for photonuclear process 77 -23001
LiF thermoluminescent dosimeters, response to ground-level cosmic-ray background 79—59265
NaCl+cosmic ray muons, photonuclear cross section, nuclear muon losses 77—64581
^{92,94}Nb production in Earth crust by cosmic-ray muons 77—49045

cosmic ray neutrinos
acoustic detection of high energy particle showers in water 79—85862
atmospheric neutrinos, 10-10^7 GeV, energy spectra and ang. distribs. *(Russian)* 80—85830
background neutrinos and Friedmann model *(Polish)* 78—89276
Bianchi type IX universes, neutrino viscosity 78—77633
Brookhaven experiment sensitivity to solar neutrinos, collapsing stars and cosmic neutrinos, ^{37}Cl neutrino absorpt. cross-sections 78—4929
Brookhaven solar neutrino experiment, results and solar model calcs., new solar ν-detectors 79—80286
conference on long distance neutrino detection, Washington, DC, USA (April 1978) 79—80217
deep underwater muon and neutrino detector (DUMAND) 80—8546
detection, using acoustic pulse from hadron shower *(Russian)* 77—38580
detection and expts. with very high energy cosmic neutrinos 78—36413
detection in deep sea using manned submersibles 78—81510
detection in ocean by nonlinear sound generation by hadron showers 80—36465
DUMAND array, study of ultrahigh energy neutrino interactions 79—80108
DUMAND detector, neutrinos in the depth of the sea *(French)* 79—75104
DUMAND project, optical acoustic detection, programme status 79—80109
EM cascade, particle-induced, in water, thermoacoustic effect, neutrino detection appl. 79—29960
energy spectra from pulsars 80—31319
fermion nonminimal gravitational coupling and the solar-neutrino problem 79—75761
galactic neutrino sources, expt. neutrino astronomy, test of stellar evolution theories 77—70964
galactic neutrinos and decay to UV photons 80—109566
hadronic showers, cosmic neutrino induced, acoustic detection 79—76265
heavy neutrino lifetime upper bound in big-bang cosmological model 77—74170
heavy neutrino mass, cosmological upper limit from big bang model 80—8728
heavy-neutrino mass lower bound in big-bang cosmological model 77 -78904
high energy, exptl. work, review 77—82095
high energy neutrino astronomy, possible point sources 79—2484
high energy neutrinos, emission by binary pulsars 79—2550
high energy neutrinos, prod. by galactic nuclei and detectability 80—4432
high energy neutrinos of extraterrestrial origin, possible detection with DUMAND 79—80179
high-energy background D production model limitations 79—44328

cosmic ray neutrinos continued
high-energy neutrinos, diffuse fluxes prediction 79—44327
Homestake long-range neutrino detector research program 79—80107
identification and research at Laue Langevin Institute, Grenoble *(French)* 80—21883
lepton degeneracy and cosmological constraints on the number of neutrinos 80—8538
lepton mixing and neutrino oscillations, cosmic neutrinos, heavy leptons, μ decay 78—82193
lepton mixing and neutrino oscills. review, 'solar neutrino puzzle' 78—66182
light element production by neutrinos emitted by collapsing stellar cores 79—21173
meson-neutrino spectrum from GSFC nucleon spectrum 78—85782
neutrino oscillation hypothesis and time depend. of Brookhaven solar-ν counting rate 79—80288
neutron star crust, contribution to neutrino luminosity 79—97018
neutron stars, neutrino emissivities 79—97016
oscillations, evidence from Brookhaven solar neutrino expt. 79—16787
pulsars with expanding dense envelopes, high energy neutrino sources 78—8034
radiative lifetimes, limits from supernovae 79—16785
solar, detect. possibility using $^{81}Br(\nu,e)^{81}Kr$ reaction 77—22160
solar, proposed Earth flux determ. by mass spectrometric assay of ^{205}Pb in Tl minerals 77—5447
solar ^{37}Cl neutrino expt., theory 79—84763
solar ^{8}B neutrinos, cross-section constraints in $^{37}Cl(\nu_e,e^-)^{37}Ar$ 77—26675
solar ν flux for inhomogeneous models 78—4166
solar activity, cosmic-ray variations, and neutrino fluxes, review 79—84599
solar flux and ^{6}Be reson., $^4He(^3He,n)^6Be$ 38.61 MeV cross-section 78—619
solar flux calcs., neutrino oscills. constraint 80—109410
solar neutrino, and role of exchange currents in pp reactions *(Russian)* 77—74710
solar neutrino capture rate, disagreement between theory and expt. 78—4171
solar neutrino detection, new expts. proposal 80—31181
solar neutrino experiments 79—8902
solar neutrino flux correls. with solar activity 80—46522
solar neutrino flux rel. to catalytic role of third particle in H burning 79—80287
solar neutrino problem, chemistry of Brookhaven expt. 77—78735
solar neutrino problem, fermion nonminimal gravit. coupling 78—29294
solar neutrino problem, prod. of ϕ meson from neutrinoless fusion process 79—8898
solar neutrino problem, results versus predictions *(Polish)* 77—71081
solar neutrino problem and $^3He(^3He,de^+\nu)^4He$ 15, 25 MeV cross-section 77—50142
solar neutrino problem rel. to Fe limited solubility in central Fe-H plasma 78—89149
solar neutrino problem rel. to solar interior struct. *(Italian)* 78—81598
solar neutrino puzzle, explanations for missing neutrinos 80—51723
solar neutrino puzzle, lepton mixing explanation 78—16373
solar neutrino radiochemical detectors, cosmic ray muon induced proton background effects 77—61650
supernovae, neutron stars, $\nu(\bar{\nu})$ emission 78—8038
two-dimensional buffer store based on a multichannel amplitude analyzer for neutrino detect. 79—26838
ultrahigh energy neutrino emission from cosmic ray sources 78—65723
ultrahigh energy neutrino flux from galactic neutron stars, calc. 79—53851
ultrahigh-energy neutrinos, prod., fluxes and detect. 78—49264
undersea detection system, located in deep ocean 80—98522
(ν,e) reaction on ^{55}Mn, ^{71}Ga, ^{87}Rb, cross section calcs., to solar neutrino expts. *(Russian)* 77—50119
$\bar{\nu}_e e^- \to W$, intermediate boson prod. by prompt high energy atm. neutrinos 79—3014
$\bar{\nu}_e e^- \to W \to$hadrons, 30 to 100 GeV W-boson underwater detection from cosmic ν *(Russian)* 77—38159
^{37}Ar production rate in tests for solar neutrinos, cosmic ray neutrinos contrib. 79—16837
$^{37}Cl(v,e^-)^{37}Ar$, shell model cross section calc., appl. to cosmic ray and background elimination *(Russian)* 80—5131
$^{71}Ga(v,e^-)^{71}Ge$, shell model cross section calc., appl. to cosmic ray and background elimination *(Russian)* 80—5131

cosmic ray neutrons
aircraft altitudes, Ames collaborative study on mid-latitude flights 78—53538
altitude variation, Feynman scaling hypothesis calcs. 80—77245
atmospheric neutron and gamma ray fluxes and energy spectra 79—75063
atmospheric spectra, 50 MeV$\leq$E$\leq$100 GeV, Monte Carlo simulation *(German)* 77—13197
balloon borne neutron flux meas. system 77—91437
Climax neutron monitor flux, modulation in 1974-1975 near solar minimum 77—33304
cutoff rigidity vars. during mag. storm, magnetospheric ring current radii determ. 79—62685
detector, large underground telescope, Russia *(Russian)* 78—73589
diffusion equations for nucleon and charged pions in atmosphere 79—70936
diurnal anisotropy, anal. of 80—94660
diurnal anisotropy, effects of non-field-aligned diffusion 78—32304
diurnal anisotropy effects of fluctuations and noise 77—45264
Earth's albedo flux meas. with Aryabhata satellite 77—22023
emulsion-chamber study 77—64557
energy and time distributions, in neutron supermonitor 79—84611
fast neutrons in atmosphere, energy spectrum and flux meas. 78—12063
flux variations meas., Elbrus spectrographic system appl. 79—84605
galactic cosmic rays density and current inside interplanetary mag. sector 79—80120
geomagnetic cutoff rigidity decrease, 1973, April 1 over Europe *(German)* 77—13194
integral generation factors rel. to atmospheric depth 77—53380
intensity delay rel. to latitude solar activity index 77—53364
intensity variations, hysteresis, fluctuations and barometric and ionospheric effects 79—84604
intensity variations in interplanetary space, 1972-7 period 80—72726

cosmic ray neutrons continued
- Jupiter atmosphere, low order effect of cosmic ray albedo neutron decay (CRAND) input 78—45271
- latitude course meas. with mobile system 77—53372
- long period intensity variations freq. spectra 77—25892
- neutron-proton ratio determ. 77—70961
- neutrons and mesons, lunar variations of intensity 79—80146
- nucleon cascade in atmosphere 79—12363
- polar coupling coeffs. for multiple neutrons up to 15 GeV 77—70954
- primary cosmic ray nucleon and sea level muon energy interrelation, scaling model 80—51633
- primary cosmic ray nucleon spectrum from sea level μ-spectrum using scaling model 79—29957
- radiochemical measurement of cosmic ray muon induced neutrons, depth depend. 77—61670
- sea level neutron spectrum, atm. neutron-proton ratio, from primary nucleon spectrum 80—8499
- sea level spectra meas. with anthracene scintillator 77—5405
- seawater and atm. surface layer gamma radiation field rel. to cosmic ray neutrons *(Russian)* 79—39746
- short-period variations, meas. by Kiev station neutron supermonitor *(Russian)* 79—96865
- solar, produced by (p,n) reactions with flare accel. protons 77—25997
- solar disturbance effects on cosmic rays and neutrons 77—13195
- solar neutrons, prod. in solar flares and expected fluxes 78—32306
- solar proton albedo neutron flux north-south asymm. meas. 79—75061
- total vector anisotropy obs. by neutron monitors 79—53685
- transport in upper atmosphere, Monte Carlo calcs. 80—8468
- underground observations, difference coupling coeffs. and difference meteorological coeffs. 78—28464
- variation in particle fluxes, correlation with atmospheric variables 77—22030
- variations during September 1977, Mirny and Moscow obs. 80—105137
- nN inelastic scatt. cross-section meas. 77—61413
- NN interactions, cosmic ray clusters, size and mass determ. 77—71548
- Mg(n,α)Ne reaction, cross sections at 14.1 and 14.7 MeV and implications for meteorites 79—96874

cosmic ray nuclei
- *see also cosmic ray alpha-particles and helium nuclei; cosmic ray neutrons; cosmic ray protons*
- abundance, statistical post-acceleration effects 79—96869
- antimatter, in laboratories and Universe, expts. and obs. data *(Polish)* 79—88588
- atmospheric secondary nucleon spectra, 10^2-10^4 GeV, 2-component model *(Russian)* 78—41612
- Biostack experiments, radiobiology of cosmic galactic radiation heavy nuclei 78—20236
- Centauro event, high density nuclear matter, and quark model interpretation 79—63565
- charge composition and energy spectra, energies >5 GeV per nucleon 78—16259
- charge spectrum of high energy nuclei *(Korean)* 79—48633
- charged particle flux meas. at sea level between 250 and 10000 GeV 77—73915
- confinement in dynamical galactic halo 78—4043
- cosmic rays propagation and distribution in Galaxy 78—69621
- detection of heavy cosmic rays aboard Cosmos-936 using plastic nuclear track detectors 80—94663
- detector system for spectra of nuclei above 100 GeV/nucleon 79—58249
- dosimetry in nucl. emulsions for Apollo and Apollo-Soyuz Biostack expts. 78—20288
- Earth atmosphere penetration by energetic heavy nuclei 80—85826
- EAS, energy ratio of electron-photon and hadron components in core 77—82093
- element ions, interval $6\leq Z\leq 28$, energies composition, Skylab study 80—8501
- emulsion plastic sandwich stack event, cosmic ray nucleus interpretation 78—69635
- energy loss params., appl. on mass determ. of cosmic ray nuclei in nuclear emulsion 78—94175
- energy spectra, determ. by gas Cherenkov counter with ionisation spectrometer 80—94662
- Fort Churchill obs. of He and heavy nuclei fluxes 77—70959
- fragmentation parameters meas. in nuclear emulsions, validity 78—90017
- galactic abundance, time averaged for $Z\geq 50$, tracks in meteorite minerals 80—101513
- galactic cosmic rays, energy dependent diffusion in dynamic halo model 80—82156
- geomagnetic shielding of artificial satellite, cutoff probability for nuclei 80—12626
- heavy ions, charge and LET distrib. meas., radiation damage in biological objects 80—94664
- heavy nuclei, charge and energy spectra 79—25418
- high energy cosmic nuclei+emulsion nuclei collisions, cross sections, multiplicity distribs. 78—41744
- interplanetary, detect. expt. on International Sun-Earth, Explorer C spacecraft 78—85792
- interplanetary recurrent fluxes, 1-8 MeV/nucleon energies, Prognoz-4 meas. 79—21112
- interstellar grains destruction by cosmic rays, hydrodynamic mechanism 78—24546
- isotopic composition of B, C, N, Ne, Mg and Si, mean mass determ. 78—93060
- isotopic composition of Fe-group elements, galactic cosmic rays 78—89024
- K-captured isotopes content calc. in galactic cosmic rays 79—80114
- LET spectra vs. absorber depth, heavy nuclei 78—20296
- low energy, ionisation states and origin 78—69634
- low energy, props., Skylab expt. 78—69632
- magnetic monopole candidate, reassessment of 1975 Lexan and emulsion meas. 79—3333
- mass composition at EAS energies 80—46359
- medium energy nuclei, Ne to Fe, charge comp. 79—84608
- multidetector telescope expt. on International Sun-Earth Explorer C spacecraft 78—85789
- particle production in cosmic ray collisions, multiplicities and rapidity distrib., collective tube model 80—8507
- primary cosmic ray N and O, isotopic comp. with consequences for source models 79—84609

cosmic ray nuclei continued
- primary cosmic rays, $>10^{13}$ eV, comp. study, from hadron time distribs. near air shower cores 79—62697
- primary cosmic rays, isotope abundances, Cr to Ni 79—70937
- primary nuclei, high-energy gamma-quantum and hadron families prod., Monte Carlo studies 79—80158
- primary nuclei composition effect on cosmic ray muons response function 80—41683
- propagation, diffusion model 79—53678
- propagation in Galaxy, leaky-box model 78—57409
- proton generation in solar flares 80—101575
- range distribution function of cosmic rays in matter 79—80113
- slow heavy penetrating particles, meas. by Sydney University particle telescope 78—25388
- solar active region protons at 1 AU, energy spectra from Prognoz-3 80—101512
- solar CNO particles, rel. to carbonaceous chondrite fission Kr and Xe origin 79—35199
- solar flare energetic particle abundances in range $2\leq Z\leq 28$, Voyager obs. 80—90382
- superheavy element search in Earth samples, meteorites and cosmic rays *(Russian)* 79—84277
- superheavy primary cosmic ray nuclei, obs. with solid-state track detectors and X-ray films *(Japanese)* 78—61688
- tracks in olivine from Marjalahti meteorite, abundance of VVH nuclei 78—36414
- Voyager cosmic ray detector system, energetic particle studies in outer heliosphere 78—24434
- Voyager Cosmic Ray Experiment, telescopes, electron energy meas., pulse height analysers 79—48643
- VVH nuclei in meteorite olivines, fossil track studies 80—105139
- Z=30-40, charge spectra and Earth orbit biological hazard 80—3828
- NN collision events, modified Duller-Walker approach, 100-10000 GeV 78—49261
- B, primary cosmic ray nuclei, isotopic composition using nuclear emulsions 79—80155
- ^{10}Be deposition rates at Earth surface, seasonal vars. 80—26707
- ^{10}Be nuclei, rel. to galactic cosmic ray origin models with halo 80—61971
- C, primary cosmic ray nuclei, isotopic composition using nuclear emulsions 79—80155
- ^{40}Ca source abundance meas. 80—8502
- (Fe,X), 1.9 GeV/N, in emulsion, mean free paths, and fragmentation parameters 80—102197
- Fe and other Z=20-25 nuclei, isotopic composition 77—82091
- Fe group nuclei, detection in CR-39 plastic track detector 79—80154
- Fe, hydrodynamic effects in cosmic ray nucleus-nucleus interactions 79—80176
- ^{3}H, sea level flux determination 79—29956
- He nuclei isotopic comp. in primary cosmic rays 79—80145
- Li abundance, balloon borne telescope obs. 78—40785
- ^{53}Mn meas. in lunar soil and chondrites, evidence for solar modulation absence during glacial period 79—80129
- Ne, Mg, Si, mean mass meas. 78—7845
- Ne to Fe nuclei, 200 to 650 MeV/nucleon, relative abundances 80—77246

cosmic ray-nucleus reactions
- *for inelastic cosmic ray-nucleus scattering, see "cosmic ray-nucleus scattering"*
- atmospheric nucleon and charged pion unidirectional diffusion eqns. 78—57417
- book, spallation reactions and their applications 77—42005
- electron-nucleus cascade build up, Landau-Pomeranchuk effect 77—64558
- emulsion nuclei, spallations produced by 0.1 to 1 GeV/nucleon nuclei, low energy particles *(Russian)* 78—33234
- emulsion nuclei$+\pi^0(\eta)$, 20 TeV, balloon-borne chamber, Monte Carlo simulation 80—9309
- energy estimates of incident particles in high-energy cosmic-ray collisions 80—22647
- fragmentation parameters of ^{12}C, ^{14}N, ^{16}O accelerated 2.1 GeV/nucleon ions in emulsion 77—3027
- galactic centre, cosmic ray flux, predicted from high energy γ ray observations 80—72731
- gamma ray spectroscopy, review 80—67582
- gamma ray-charged particle correlations, 20 TeV 78—45170
- gamma-ray spectra, high energy, near top of atmos. detection+meas. by emulsion chamber 79—29958
- gamma-rays production, cosmological cosmic rays hypothesis 78—16251
- graphite in emulsion chamber, high-energy cosmic gamma-ray prod. spectra 79—29959
- hadron+nucleus cross-section, energy depend., multiplicity, scaling violation model *(Russian)* 79—22350
- hadron+nucleus energy spectra of secondary leading particles 77—61468
- hadron multiple prod., cosmic-ray-nucleus reactions, muon time-correl. meas. *(Russian)* 77—14133
- hadron-nucleus collision, super high energy, pseudorapidity distrib. characts. 80—5170
- hadrons with $E>2$ TeV, integral flux, attenuation in air, NN cross section *(Russian)* 77—78589
- heavy ion reactions, 0.1 to 1.0 GeV/nucleon, characts. of peripheral and central collisions 77—61448
- heavy ion-nucleus, complete target fragmentation, shock waves 77—61447
- heavy nuclei reactions, meson generation 77—61446
- high energy interactions in emulsion stack combined with ionisation calorimeter 78—49263
- high energy interactions of nuclei, review 79—22326
- high-energy cosmic-ray components in atmosphere, scaling features 78—93062
- Judek effect and nuclear hidden colour excitations in heavy cosmic ray-nucleus reactions 80—27567
- multiple meson production, total $E_\gamma>2\times 10^{13}$eV 79—58989
- multiple production of particles, energy $>10^{12}$ eV *(Russian)* 77—71549
- multiplicity distrib. of particles *(Russian)* 79—5719
- muon charge ratio, sea level, phenomenological model, review 80—67487
- nuclear emulsion, $\sim$20 GeV/nucleon, mean meson multiplicity and angl. distribs. 79—58988
- one-dimensional diffusion eqn. integration, one-fireball model 78—57416

cosmic ray-nucleus reactions continued
- Pamir and Fuji electron-nuclear cascades, high energy γ-families 79—25423
- particle production in cosmic ray collisions, multiplicities and rapidity distrib., collective tube model 80—8507
- pionless nuclear active particle prod., possible evidence 77—91395
- polyethylene+hadrons, 400 GeV, secondary particle ang. distrib. and multiplicity meas. 77—64571
- proton-nucleus, 50-200 GeV/c, ang. distrib. of charged shower particles *(Korean)* 80—27641
- protons, local irradiation model for solar system ^{16}O and ^{26}Al isotopic anomalies 78—93128
- secondary particle ang. distrib. and multiplicity meas. 77—64571
- shower ang. distribs., anisotropy coeffs., multiple prod. mechanism 10^{10} to 10^{13} eV/nucleon *(Russian)* 77—79385
- spallation reactions, rel. to Be abundance in Hyades 77—53584
- ultra-high energy nuclear interaction event with large transverse momentum at 445 TeV *(Chinese)* 80—105140
- very high energy cosmic ray-nuclear interactions, new particle search, X particles 80—8508
- (p,xn) reactions, cross-sections and astrophysical appls. 78—28504
- p-nucleus around 20 TeV, momentum and energy spectra 77—22029
- pp$\rightarrow\pi$+anything, pion spectrum at top of atmosphere 78—53780
- Al+hadrons, 400 GeV, secondary particle ang. distrib. and multiplicity meas. 77—64571
- ^{37}Ar production rate due to cosmic ray neutrinos, contrib. to solar neutrinos tests 79—16837
- ^{81}Br(ν,e)^{81}Kr, solar neutrinos detect. possibility 77—22160
- ^{41}Ca production in Earth surface layers, possible use for radioactive dating 79—21063
- ^{36}Cl prod. in proton induced high-energy spallation, cosmic ray effects 77—61421
- Cu+hadrons, 400 GeV, secondary particle ang. distrib. and multiplicity meas. 77—64571
- Fe group relativistic nuclei interaction with max. number of nucleons, on Ag, Br *(Russian)* 77—30634
- Fe+μ, 2 to 800 GeV, EM interactions of cosmic ray muons, e$^+$e$^-$ prod. and knock-on e$^-$ prod. 79—66902
- Fe+p, high energy spallation, studies, cosmic ray implications, isotope abundances 77—2998
- Fe+p inclusive react., structure function of conserved hadrons, 100-1600 GeV *(Russian)* 78—41611
- ^{6}Li(d,α), 100-180 keV, low energy cross sections, astrophysical region extrapolation 80—22843
- ^{6}Li(d,p), 100-180 keV, low energy cross sections, astrophysical region extrapolation 80—22843
- Mg(n,α)Ne reaction, cross sections at 14.1 and 14.7 MeV and implications for meteorites 79—96874
- ^{15}N, enrichment in Mars atm. due to cosmic ray interactions in early solar system 78—73669
- ^{92,94}Nb production in Earth crust by cosmic-ray muons 77—49045
- ^{17}O(p,α) cross section for astrophysical energies 80—18267

cosmic ray-nucleus scattering
- effective inelastic cross-section for high-energy protons 77—61412
- gamma-rays production, cosmological cosmic rays hypothesis 78—16251
- muons, multiple scattering in mag. spectrometers 80—4215
- nucleon-nucleus inelastic scatt. cross-section meas. 77—61413
- μ-NaCl scatt., above 300 GeV *(Russian)* 79—22106

cosmic ray origin
- *see also cosmology; element origin*
- 1-100 MeV gamma-ray background, spectrum rel. to cosmological cosmic rays and light elements prod. 78—12436
- acceleration, by galactic mass infall 77—78583
- acceleration, implications of particle streaming at speeds above Alfvan vel. 79—40068
- acceleration by shock waves in astrophysical plasma, implications for origin 80—82192
- acceleration of cosmic rays in shock fronts 78—32302
- acceleration to relativistic energies, time delay after nucleosynthesis 78—28455
- age determ. from comp. of cosmic rays on Earth 77—53341
- air showers, arrival direction distrib. of high-energy particles, Northern Hemisphere 78—20601
- Alfven wave accelerated particles, distrib. function self-similar soln. 80—56702
- anisotropy, 10^{11} to 10^{20} eV 79—66892
- anisotropy, implications for cosmic ray origin and local anisotropy 79—44313
- anisotropy at extremely high energies, from EAS data, rel. to origin 79—80115
- background radiation nonequilib. distrib., radiation flux spectrum source 80—46710
- black hole particle emission process, high energy limit 77—5544
- Coma cluster of galaxies, origin and transport of electrons in halo radio source 77—26073
- cosmological cosmic rays existence, light-elements and γ-rays prod. 78—7841
- cosmological cosmic rays existence, obs. constraints set by γ-ray background, Li and D abundances 78—7842
- diffuse X-ray background, implications of Hubble const. for discrete source models 79—101226
- electrons, discrete galactic sources 79—35078
- electrons, galactic, evidence for continuous ejection model from energy spectrum *(Chinese)* 80—105138
- energy spectrum, composition, origin, general review 79—80117
- extragalactic cosmic rays, 10^{20} eV, energy spectrum and arrival direction 80—82157
- extremely high energy cosmic rays, role of neutrons in propagation 77—29603
- Fermi acceleration, effects of particle pitch angle scatt. 78—53775
- galactic cosmic ray Fe nuclei source, neutron excess from isotopic comp. 80—72729
- galactic cosmic rays, age derived from ^{10}Be abundance 78—12060
- galactic cosmic rays, distrib. rel. to pulsar source model 80—4207
- galactic cosmic rays, flare stars as source, hypothesis 80—46559
- galactic cosmic rays, Ne isotopes abundances rel. to source region 79—101036
- galactic cosmic rays, particle accel. by shock waves 78—49241
- galactic cosmic rays, short pathlengths deficiency rel. to no-near-sources model 79—84596

cosmic ray origin continued
- galactic cosmic rays, source model rel. to electron-proton abundance ratio 77—49252
- galactic cosmic rays, source-dominated diffusion model rel. to halo size constraints 78—12353
- galactic dynamo action and ultra-high-energy cosmic ray propag. 77—74146
- galactic electrons, source spectrum rel. to diffusion model of propag. 79—53677
- galactic gamma radiation, possible origin, data from COS-B and SAS-2 satellites *(French)* 78—85776
- galactic gamma rays, discrete source component 79—35436
- galactic gamma-rays, diffuse component origin in elementary interactions 80—17450
- galactic gamma-rays and origin 77—78584
- galactic gamma-rays implications for galactic struct. studies 77—26083
- galactic radiation belts, trapped electrons as radiowave source 80—26982
- galactic sources, coronal-type ionisation model and flare star contributions 78—49240
- galactic vector and tensor anisotropy rel. to Musala expt. 77—17302
- gamma ray astronomy obs. implication 80—46352
- gamma rays, cosmic sources identified with H II regions 77—91669
- gamma rays, medium energy, from galactic centre region, emission mechanisms 79—9030
- gamma rays, origin 77—87213
- gamma-ray burst origin, episodic gas accretion on neutron star 77—5600
- gamma-ray burst sources, galactic distrib. models 80—22117
- gamma-ray burst sources, new limits on distrib. 78—93465
- gamma-ray bursts, multiple Compton scatts. effect on X-ray emission spectrum 78—96389
- gamma-ray bursts, prod. by intergalactic relativistic dust grains 79—88764
- gamma-ray bursts, sources models 77—9823
- gamma-ray burts, distance limit for non-relativistic source models 78—32612
- gamma-ray origin in protogalaxy formation, model 80—62325
- gamma-ray sources, SNRs and OB assocs. 79—92887
- gamma-ray transient event of 1979 March 5, location 80—73074
- gamma-rays, non-thermal electron bremsstrahlung prod. in galactic disc. 78—24414
- gamma-rays originating from external galaxies, electron-microwave interaction 80—22121
- gamma-rays production, cosmological cosmic rays hypothesis 78—16251
- Gould belt OB type stars 80—77512
- high energy cosmic rays, identification with intergalactic suprathermal dust grains 79—48911
- highest energy cosmic rays, diffusion from Virgo cluster 80—4208
- historical aspects and proof of cosmic ray and radio halos in Galaxy 79—44314
- injection into dense supernova shells by pulsars 78—65638
- intensity of cosmic radiation on Earth and in Galaxy, diffusion restriction by mag. fields 77—13191
- interplanetary cosmic ray protons, 1-4.5 MeV, spectral anal. and correl. study 80—77243
- interstellar matter acceleration, evidence from cosmic rays isotopic comp. 78—53781
- interstellar medium interaction with stellar wind, cosmic ray accel. 80—77512
- Jupiter origin for energetic electrons, study of 1972-7 intensity variations 80—72726
- K-captured isotopes content calc. in galactic cosmic rays 79—80114
- low energy nuclei, ionization states and origin 77—53339
- low-energy cosmic rays, origin determ. 77—53376
- low-energy electrons, quiet-time increases, Jovian origin 77—2367
- low-energy interplanetary background, evidence for galactic origin from Venera 9 and 10 meas. 78—4049
- 3K microwave background, in Universe expansion model 80—98746
- multiply charged nuclei, spectra rel. to origin and propag. 77—5403
- neutrino sources, fluxes rel. to deep underwater muon and neutrino detector (DUMAND) size 80—8546
- neutrinos, emission by binary pulsars 79—2550
- neutrinos, high-energy prod. spectra and diffuse fluxes 79—44327
- neutrinos, ultrahigh energy, prod., fluxes and detect. techniques 78—49264
- neutron star, episodic accretion of gas and cosmic Γ-ray bursts 78—69824
- nonrelativistic cosmic rays, source distrib. rel. to path-length distrib. 79—88558
- nuclei, abundance, statistical post-acceleration effects 79—96869
- nuclei, low energy, ionisation states and origin 78—69634
- nuclei and electrons propag. and distrib. in Galaxy, rel. to origin 78—69621
- nuclei with $4\leq Z\leq 26$ and $0.3\leq E\leq 2$ GeV amu^{-1} 77—56800
- plasma turbulent reactor, power law distribs., cosmic ray source model *(Russian)* 78—26244
- positron production by pulsars, galactic 511 keV gamma-ray line from positron annihilation 80—46590
- positrons, galactic, primary source, prod. rate, and escape probability 80—109319
- primary cosmic ray N and O, isotopic comp. with consequences for source models 79—84609
- primary cosmic rays, intergalactic suprathermal grains, accel. mechanisms 79—25412
- protons, origin rel. to electron fluxes in closed galaxy model 77—13189
- protons in upstream region of Earth's bow shock 79—48622
- quiet time comp. and energy spectra for cosmic rays between 0.6-24 MeV per nucleon 77—29609
- recent experimental work 77—56799
- review, cosmic gamma radiation, sources and detection 78—12059
- review of past and present research *(Russian)* 78—73590
- soft gamma-ray pulses, prod. in high-temp. astrophysical plasmas 77—78736
- soft X-rays diffuse background, astrophysics and origin of 0.1-2.0 keV 78—16581
- solar energetic storm particles, accel. rel. to interplanetary shock wave parameters 79—35079
- solar flare accelerated particles, charge spectrum and comp. form. 80—46529
- solar protons and electrons, accel. by shock waves during large flares 80—21974
- source composition, energy depend. at high energies 77—67013

cosmic ray origin continued
source isotopic abundances, secondary tracer approach for galactic cosmic rays 79—96864
source material synthesis, evidence from Ne, Mg and Si isotopes meas. 80—51631
source spectrum and abundances, evidence from nuclei charge comp. and energy spectra 78—93059
sources of ultra-high energy cosmic rays 78—61941
steady state Universe using stochastic electrodynamics, cosmic background radiation and red shift 78—77631
supernova remnants, cosmic rays escape and adiabatic energy losses 79—16771
supernova remnants, cosmic rays trapping by hydromag. waves in high β plasmas 80—17482
supernova shock-accelerated cosmic rays, early radiation spectrum, cooling and escape 79—48626
supernovae, low-energy cosmic rays diffusion model, spatial inhomogeneities 77—5402
supernovae and cosmic ray sources *(Italian)* 79—53846
two source model, evidence from cosmic ray nucleosynthesis 79—17084
ultra high energy cosmic rays, discussion *(French)* 80—21879
ultraheavy cosmic rays just beyond Fe, comp. and origin rel. to solar system material 77—70952
ultrahigh energy cosmic ray origin and propagation 78—49242
ultrahigh-energy cosmic rays, possible source in galactic centre 80—46351
Voyager cosmic ray detector system, energetic particle studies in outer heliosphere 78—24434
X-ray bursts, mechanism assoc. with max. mass of neutron stars 77—33545
$Z \gtrsim 60$ cosmic rays, charge and energy spectra rel. to source comp. 78—40782
^{7}Be, cosmic ray accel. probe 78—81512
^{10}Be abundance rel. to age, balloon meas. technique 77—29602
Ne to Fe nuclei, primary, 200 to 650 MeV/nucleon, relative abundances 80—77246

cosmic ray photons
see also cosmic ray X-rays; solar cosmic ray photons
1-100 MeV gamma-ray background, spectrum rel. to cosmological cosmic rays and light elements prod. 78—12436
γ-ray and hadron spectra with $\Sigma E_{\gamma} > 500$ TeV 77—64575
γ-ray spectra at 30-500 TeV 77—64574
γ-ray spectra recorded in X-ray emulsion chambers, decascading 77—64578
γ-rays, scaling and charge ratio at 1-10 TeV 77—64576
γ-rays from hadron interactions above 2.5 TeV 77—64573
γ-rays recorded by nucl. emulsion and X-ray film 77—64572
γ-rays ultra-high energy, emulsion chamber anal. *(Chinese)* 78—89028
air shower cores, high-energy γ-rays and their bursts 77—91393
atmospheric Cherenkov radiation in large cosmic ray showers, computer simulation using hadronic collisions models 78—57415
atmospheric neutron and gamma ray fluxes and energy spectra 79—75063
atmospheric radiation, north-south anisotropy at balloon altitudes 77—29608
background radiation density, accreting black holes contrib. 80—4461
Cherenkov light in EAS, time struct. 77—33306
Cherenkov photons, effect on IR interferometric search for non-solar planets 80—98523
condensation in hot Universe, longitudinal relict. rad. *(Russian)* 78—65734
conference, non-solar gamma-rays (Bangalore, India, May-June 1979) 80—77548
damping in discrete space-time rel. to galaxy redshifts *(Chinese)* 77—67145
diffuse cosmic gamma-ray spectrum, Apollo data in 0.3-10 MeV region 77—33705
diffuse gamma radiation, galactic and isotropic components 78—65725
diffuse gamma-ray flux, 2-25 MeV energy range 78—32309
diffuse X-ray and gamma-ray background, primeval galaxies contrib. 80—8692
EAS, π photoprod. as source of low-energy muons 80—4214
EAS, characts. of gamma ray and hadron families, Monte Carlo calcs. 77—53377
EAS, electron-photon and muon components, simulation 77—49255
EAS, EM component 78—49258
EAS, energies of electron-photon and hadron components near axis, 3330 m above sea level 77—64563
EAS, energy ratio of electron-photon and hadron components in core 77—82093
EAS, high transverse momentum of γ-ray bundles, $>10^{12}$ eV 79—62701
EAS, response of scintillators, Ne flash tubes and water Cerenkov detectors 78—49259
EAS, simultaneous detection of γ-ray bundles and air showers 79—62700
EAS arrival direction distributions 78—28471
EAS near core, struct. of electron-photon component *(Russian)* 78—57414
EAS proton-initiated EM component at 690 g.cm^{-2}, Monte Carlo simulation 77—91390
electron and γ interaction ranges, Monte Carlo calc. *(Russian)* 79—12370
electron-photon cascade energy determ., effects of optical density and energy spectrum meas. errors 79—84613
electron-photon cascade in air, simulation of energy and lateral characteristics 79—44323
electron-photon cascades, Monte Carlo simulation of cascade development 79—44322
electron-photon cascades in homogeneous absorbers 77—61669
electron-photon shower, range fluctuations in unbounded medium 79—80152
electron-photon showers, successive approximation method 77—64559
EM cascade showers, electron/photon energy flow 77—22027
EM cascade theory equations, approx. solution *(Russian)* 77—49257
EM cascades in air, 10-100 GeV, longit. development 79—21120
emission power spectra described by solns. of Kompanyets' kinetic eqn. *(Russian)* 78—152
energy and flux meas. of high energy γ-rays, emulsion chamber detection *(Japanese)* 78—20595
EUV background, point source contribs. 80—62324

cosmic ray photons continued
galactic 0.511 MeV annihilation radiation, theory of positrons primary source, prod. rate, and escape probability 80—109319
galactic γ-ray lines, balloon investigation using Ge(Li) spectrometer 80—8677
galactic γ-rays from low energy cosmic ray interactions with interstellar medium 80—8678
galactic disc gamma-ray emission, implications of γ-ray sources number-intensity relation 80—46702
galactic gamma radiation, possible origin, data from COS-B and SAS-2 satellites *(French)* 78—85776
galactic gamma radiation in 0.03-4.1 MeV range, Kosmos 461 meas. 77—67144
galactic gamma rays, discrete source component 79—35436
galactic gamma-ray emission, data rel. to new constraints on galactic halo size 78—12353
galactic gamma-ray emission, rel. to Galaxy cosmic rays and mag. field distrib. 80—4207
galactic gamma-ray flux, 60 keV to 5 MeV range, from ensemble of point sources 79—53933
galactic gamma-ray spectra, rel. to cosmic ray electrons flux and cosmic ray gradients 78—40784
galactic gamma-rays implications for galactic struct. studies 77—26083
galactic plane gamma-radiation 79—71105
galactic positron annihilation radiation, spectrum 79—44309
Galaxy gamma-ray emission, fluxes determ. from cosmic ray electron spectrum 80—62257
gamma burst detector on Pioneer Venus Orbiter 80—67505
gamma quanta produced by cosmic-ray hadrons of tens of TeV energies, energy characts. 79—80148
gamma ray astronomy *(Korean)* 79—12368
gamma ray burst, 1979 March 5, evidence for periodicity 80—31389
gamma ray high energy families, f′ spectrum 78—28466
gamma ray observations interpretation *(Polish)* 79—58451
gamma rays, 6.13 MeV, detect. within and at top of atm., extraterrestrial source hypothesis 80—46354
gamma rays, above 100 MeV, prod. by electron bremsstrahlung 77—13189
gamma rays, cosmic sources identified with H II regions 77—91669
gamma rays, flux from Cygnus X region rel. to nature of CG 78+1 79—92895
gamma rays, galactic distrib. from diffusion model for nuclear component propag. 79—53678
gamma rays, medium energy, from galactic centre region, obs. 79—9030
gamma rays, origin 77—87213
gamma rays, prod. by relativistic electrons inverse Compton interactions 80—17448
gamma rays from annihilation of positrons produced by pulsars, 511 keV line 80—46590
gamma rays from galactic disc, obs. between $-45° < l^{II} < 45°$ in 80 keV to 8 MeV energy range 80—82540
gamma-quanta, spectra above 2 TeV 79—80147
gamma-quantum, high energy, prod. by nucleon diffr. fragmentation by 10 TeV NN collisions 79—80174
gamma-quantum families, obs. rel. to hadron interactions transverse momenta to 10^{14} to 10^{15} eV 79—80170
gamma-quantum families, released cluster mass determ. 79—80171
gamma-quantum families of 10 to 100 TeV energy, height depend. 79—80159
gamma-quantum families with $\Sigma E_{\gamma} > 30$ TeV, energy characts. in Pamir expt. 79—80156
gamma-ray 511 keV positron annihilation line in upper atmosphere 80—41582
gamma-ray air family, lateral structure function 77—41274
gamma-ray angle and energy distrib., sea level to 39 km altitude 2.25 meV 80—26705
gamma-ray astronomy, present status 79—25763
gamma-ray astronomy, review *(Polish)* 78—96394
gamma-ray astronomy, use of artificial satellites 79—53727
gamma-ray astronomy and cosmic ray origin 79—29951
gamma-ray background, prod. by annihilation of primordial stable neutral heavy leptons 78—93479
gamma-ray background and protogalaxy formation model 80—62325
gamma-ray burst astronomy, critical comparison of detectors 77—64648
gamma-ray burst origin, episodic gas accretion on neutron star 77—5600
gamma-ray burst source, position from Helios 2-Vela-Ariel 5 obs. 79—48956
gamma-ray burst sources, galactic distrib. models 80—22117
gamma-ray burst sources, new limits on distrib. 78—93465
gamma-ray bursts, distance limit for non-relativistic source models 78—32612
gamma-ray bursts, galactic origin 78—32303
gamma-ray bursts, hard X-ray spectra 78—7846
gamma-ray bursts, intensity distrib., galactic origin *(Russian)* 79—16772
gamma-ray bursts, multiple Compton scatts. effect on X-ray emission spectrum 78—96389
gamma-ray bursts, preliminary results from Solrad 11 detectors 77—57108
gamma-ray bursts, prod. by intergalactic relativistic dust grains 79—88764
gamma-ray bursts, search with coincident balloon flights 77—49506
gamma-ray bursts, sources models 77—9823
gamma-ray bursts, stellar superflare model *(Chinese)* 77—22021
gamma-ray bursts, ultra high energy, from celestial sources, unsuccessful search 80—67911
gamma-ray diffuse background, new look at universe 79—80373
gamma-ray diffuse background, rel. to D prod. by high-energy particles 77—33709
gamma-ray diffuse background from galactic halo 77—53711
gamma-ray diffuse component from galactic centre and anticentre 79—62901
gamma-ray emission, high-energy, from galactic disc, spectral characts. COS-B obs. 78—36695
gamma-ray families from hadron reactions, accel. scanning in X-ray pellicle stack 78—78546
gamma-ray fast intense transient (1979 March 5), detect. 80—73073
gamma-ray isotropic metagalactic background in 0.03-4.1 MeV range, Kosmos 461 meas. 77—67144
gamma-ray prod. spectra for high energy reactions in graphite 79—29959

cosmic ray photons continued
- gamma-ray spectra, high energy, near top of atmos. detection+meas. by emulsion chamber 79—29958
- gamma-ray transient event of 1979 March 5, location 80—73074
- gamma-rays, 0.511 MeV energy, meas. with balloon-borne Ge(Li) spectrometer 77—53373
- gamma-rays, diffuse background obs. *(German)* 77—60853
- gamma-rays, galactic, diffuse component origin in elementary interactions 80—17450
- gamma-rays, galactic disc bremsstrahlung emissivity and local interstellar electron spectrum 79—25417
- gamma-rays, galactic line emission from ^{26}Al beta-decay 77—33692
- gamma-rays, hard intensity radiation pulsations in the atmosphere *(Russian)* 80—17454
- gamma-rays, non-thermal electron bremsstrahlung prod. in galactic disc. 78—24414
- gamma-rays, possible existence of cosmological cosmic rays 78—7841
- gamma-rays, quasi-periodic intensity variations in stratosphere *(Russian)* 80—90177
- gamma-rays, short-period fluctuations, in upper atm., correl. with solar diameter vars. 79—21115
- gamma-rays, sky survey with fine energy resolution using Ge spectrometer 77—53701
- gamma-rays, spatial pattern anal. via spectrometer with various shaped scintillators 79—16831
- gamma-rays from galactic disk and inverse Compton effect of electrons on starlight 80—26702
- gamma-rays from supernovae, Antarctic ice core record 80—31314
- gamma-rays origin in cosmic ray interactions with matter *(Polish)* 78—96571
- gamma-rays originating from external galaxies, electron-microwave interaction 80—22121
- gamma-rays production, cosmological cosmic rays hypothesis 78—16251
- hard gamma-rays from galactic centre and diffuse background, Kosmos 561 obs. 79—84597
- high energy γ-ray family events, large emulsion chamber expt. on Mt. Fuji 79—63562
- high energy EM showers in atmosphere, Monte Carlo simulation 77—56802
- high energy interactions and cosmic ray components in the atmosphere 79—62707
- high-energy gamma-quantum families, Monte Carlo studies 79—80158
- high-energy spectra obs. with Fe emulsion chamber 77—60556
- ionising background radiation, influence on H at periphery of galaxies 78—65729
- Jupiter, surface temp. excess, attributed to cosmic radiation from galactic nucleus *(French)* 77—60714
- 3K microwave background, in Universe expansion model 80—98746
- Monte Carlo simulation of high-energy EM air showers 77—64577
- multiple meson production by 10^{13}-10^{16} eV cosmic rays, longitudinal behaviour of γ air family 77—33309
- near-Earth cosmic rays, short-term fluctuations in electron and γ quanta components 80—67483
- neutron star, episodic accretion of gas and cosmic Γ-ray bursts 78—69824
- nuclear interactions around 20 TeV, characts., comparison with Monte Carlo simulation 79—58991
- review, cosmic gamma radiation, sources and detection 78—12059
- Saturn, surface temp. excess, attributed to cosmic radiation from galactic nucleus *(French)* 77—60714
- scintillation time-of-flight telescope for cosmic γ-ray preselection 78—82572
- secondary gamma-rays, energy spectra rel. to atmos. depth 79—58205
- soft gamma-ray pulses, prod. in high-temp. astrophysical plasmas 77—78736
- solar and cosmic X-rays and gamma-rays, obs. by Signe II MP satellite expt. 80—41696
- time of flight telescope, compensated, for spaceborne cosmic ray measurements 77—67939
- ultrahigh energy photons traversing cosmic blackbody photon gas, effective penetration distance 79—5742
- γ, primaries meas., 10 to 100 GeV, using air showers Cherenkov light distrib., detector system 78—73597
- γ ray natural background, exposure rate variations in open air *(Czech)* 77—67900
- γ-ray families, multiparticle prod. above 10^{14} eV, Monte Carlo anal. 78—49257
- γ-ray families and high-energy interactions 77—87221
- γ-ray fluxes meas. at 4370 and 4880 m above sea level 77—64551
- γ-ray initiated atmospheric showers, computer simulations, Cherenkov radiation, geomag. field effects 77—49254
- γ-ray lateral distrib. from fireball prod. behaviour, multiple meson prod. 77—53381
- γ-rays in range 3.5 to 100 MeV, system for meas. ang. and energy distribs. 77—50324
- Fe+cosmic ray photon, prod. of 300-1000 GeV muons, cross section, shadowing 77—64580

cosmic ray propagation
- accel. in expanding coronal mag. bottle 80—77244
- acceleration by shock waves in astrophysical plasma 80—82192
- acceleration in shock waves, energy loss effect *(Russian)* 80—17449
- anisotropic diffusion equations 77—91384
- anisotropic inhomogeneous diffusion around Sun 79—21113
- anisotropic propag., transport eqn., Green's function 78—77441
- anisotropy, 10^{11} to 10^{20} eV 79—66892
- anisotropy at extremely high energies, from EAS data, rel. to origin 79—80115
- atmospheric nucleon and charged pion unidirectional diffusion eqns. 78—57417
- Cassiopeia A, relativistic electrons streaming at speeds above Alfven vel. 79—40068
- charged particle acceleration on front of shock wave, regular mechanism 78—36410
- charged particle acceleration to relativistic energies in interplanetary shock waves 79—80123
- charged particle diffusion in turbulent mag. field 77—70989
- charged particles acceleration, role of mag. mirrors in shock waves 79—80122
- charged particles acceleration on shock front, temporal characts. 79—80121

cosmic ray propagation continued
- charged particles drifts in mag. field with arbitrary spatial var. 80—46382
- charged particles propag. through random EM fields in space, kinetic eqn. 77—91382
- closed galaxy, cosmic ray propag. model, nuclear abundances 77—70951
- Coma galaxy cluster, relativistic electrons streaming at speeds above Alfven vel. 79—40068
- conference, Yakutsk, USSR (Jun. 1977) 79—80110
- coronal and interplanetary propagation of solar particles following E45° solar flare on 29/7/73 78—49248
- deuterons and antiprotons production mechanisms 79—29955
- diffusion, in solar wind deformed by interstellar medium 79—53680
- diffusion, mean and local coeffs., connection 79—21110
- diffusion and turbulent galactic mag. field 79—48627
- diffusion average properties in solar wind streams 79—75067
- diffusion coefficients heliographic latit. distrib. in 11-year solar cycle 77—91386
- diffusion in interplanetary space with allowance for second spherical harmonic 79—80118
- diffusion in large-scale turbulent magnetic field 79—58203
- diffusion in random magnetic field, weak particle-field interaction theory validity 79—21109
- diffusion model, source spectrum of galactic cosmic-ray electrons 79—53677
- diffusion model for galactic cosmic ray propag. 80—56684
- diffusion model of cosmic ray propag., appl. to electron component 79—53679
- diffusion model of cosmic ray propag., appl. to nuclear component 79—53678
- diffusion theory, vel. correl. function 77—73913
- discrete galactic sources, statistical theory of propag. 79—44312
- dynamical halo model and cosmic ray path length var. with energy 79—53675
- electron-photon shower, range fluctuations in unbounded medium 79—80152
- electrons, energy spectrum and propag. 80—67485
- electrons, in M51, diffusion model rel. to radio spectral index distrib. 78—8119
- electrons, relativistic, in radio sources, form. of universal and diffusion regions of non-linear spectra 80—109555
- electrons from Jupiter, interplanetary modulation and transport 78—45175
- electrons in galactic halo, diffusion models for low-freq. radio emission 78—12433
- energetic storm particle events connection with interplanetary shock wave parameters 79—70935
- energy changes in solar system 79—48628
- energy variation in interplanetary space of solar and galactic cosmic rays 80—101505
- equivalent diffusion coefficients of solar cosmic rays 80—85825
- Fermi-accelerated cosmic rays mediation of shock front 80—85829
- galactic anisotropy of 1-100 TeV particles 80—17451
- galactic cosmic modulation, isotropic and anisotropic diffusion, asymm. conditions 78—40777
- galactic cosmic ray acceleration by supernova shock waves 80—82154
- galactic cosmic ray energy loss and modulation in solar system 78—49245
- galactic cosmic ray modulation, numerical models of particle drift effect on cosmic ray transport 80—31180
- galactic cosmic rays, accel. mechanism and transport, model 79—35077
- galactic cosmic rays, age and propag. derived from ^{10}Be abundance 78—12060
- galactic cosmic rays, effect on solar wind vel. 80—101506
- galactic cosmic rays, energy dependent diffusion in dynamic halo model 80—82156
- galactic cosmic rays, equilib. configs. stability, hydromagnetic energy principle 80—82448
- galactic cosmic rays, interplanetary modulation allowing for generalised anisotropic diffusion tensor 80—101504
- galactic cosmic rays, interplanetary propag., and solar mag. cycle depend. semiannual var. 79—16777
- galactic cosmic rays, interplanetary propag. rel. to ang. distrib. at heliosphere boundary 79—80116
- galactic cosmic rays, propag. in finite solar cavity 78—69623
- galactic cosmic rays, propag. in spherically symmetric solar wind 79—53681
- galactic cosmic rays, propag. rel. to light isotopes abundances and interstellar gas density 80—17456
- galactic cosmic rays, short pathlengths deficiency rel. to no-near-sources model 79—84596
- galactic cosmic rays, ultrahigh energy, propag. rel. to origin in galactic centre 80—46351
- galactic cosmic rays acceleration by EM radiation 78—7840
- galactic cosmic rays density and current inside interplanetary mag. sector 79—80120
- galactic cosmic rays interplanetary propagation, energy depend. of modulation coeff. 78—28460
- galactic dynamical halo, retrodictive probability approach 78—65467
- galactic electrons, propag. rel. to energy spectrum and fundamental props. *(Chinese)* 80—105138
- galactic halo, dynamical model, age, matter traversal distrib. and anisotropy for nuclei 78—4043
- galactic halo, dynamical model, electrons energy spectrum and spatial distrib. 78—4044
- galactic halo, size constraints from galactic gamma-ray data 78—12353
- galactic primary cosmic-ray electrons, 30-1000 GeV, emulsion chamber obs. 80—85827
- galactic propagation and distribution 78—69621
- galactic protons, interplanetary propag. rel. to meas. by Venera 9 and Venera 10 probes 77—91388
- gamma-rays originating from external galaxies, electron-microwave interaction 80—22121
- ground level enhancements, comparison of 1977 Nov. 22 and 1969 Feb. 25 events 79—40042
- hadronic interactions, 10^{12} to 10^{15}eV, and cosmic ray components in atmosphere 79—62708
- highest energy cosmic rays, diffusion from Virgo cluster 80—4208
- interplaetary propagation, drift as essential energy loss process 80—8498
- interplanetary, accel. to relativistic energies 79—21111

cosmic ray propagation continued
- interplanetary, charged particles transport in fluctuating mag. fields, Fokker-Planck eqn. soln. 79—27752
- interplanetary, Mars spacecraft meas. 78—53779
- interplanetary accel., one-dimens. model with moving MHD shock wave 79—80119
- interplanetary anisotropic diffusion, solar daily vars. vector computation 80—4209
- interplanetary corotating nucleon fluxes separation from solar flare fluxes by radial gradients and nuclear comp. 79—25413
- interplanetary diffusion, solar latitude depend. 80—12622
- interplanetary diffusion coefficients, calcs. from diurnal intensity var. 79—29952
- interplanetary diffusion of solar cosmic rays, Monte Carlo method 80—12623
- interplanetary magnetic field sector structure and anisotropy of 50-1000 GV cosmic rays 80—62072
- interplanetary modulation characts., determ. from stratospheric cosmic rays eleven-year cycle 80—4212
- interplanetary modulation processes, evidence from stratosphere obs. 80—101508
- interplanetary plasma, cosmic propag. rel. to Forbush decreases struct. 77—91385
- interplanetary propagation, anal. of large amplitude wave-trains of cosmic-ray intensity 80—94660
- interplanetary propagation, cosmic ray flow lines and energy changes 80—82158
- interplanetary propagation, cosmic ray intensity diurnal vars. anal. 79—29953
- interplanetary propagation, energetic particles interaction with shock wave front in turbulent medium 80—4210
- interplanetary propagation, energy density depend. on cosmic rays radial gradient orientation *(Russian)* 79—53682
- interplanetary propagation, non-field-aligned diffusion effects on neutron monitor diurnal anisotropy 78—32304
- interplanetary propagation, origin of transient cosmic ray intensity vars. 78—89021
- interplanetary propagation, quiet time anisotropies obs. from Pioneer 10 and 11 78—77442
- interplanetary propagation, role of outer solar system fields and plasmas 79—58213
- interplanetary propagation, scatt. in simulated mag. field fluctuations 80—51626
- interplanetary propagation, semidiurnal var. prod. by mag. field imperfect corotation 80—8497
- interplanetary propagation, transient diurnal var. spectrum anal. rel. to scintillation model 79—25416
- interplanetary propagation, two-particle distrib. function and cosmic-ray intensity fluctuations 78—28457
- interplanetary region, transport eqn. 79—44315
- interplanetary scintillations at 250 GV, statistical props. 80—8496
- interplanetary shock acceleration of energetic protons 80—56686
- interplanetary space, effects of microinstability onset in solar wind 77—87222
- interplanetary steady-state transport eqn., Green's theorem and Green's functions 77—87214
- interplanetary transport, particle drift effects and analytical soln. to modulation problem 78—28456
- interplanetary variations, determ. via spectrographic instrument set 79—12404
- interstellar and interplanetary mag. discontinuities, causing cosmic rays isotropy 78—4045
- interstellar cosmic ray acceleration models, inconsistencies 80—82155
- interstellar diffusion in galactic models with halo, appl. to proton nucleon component 80—61971
- interstellar H_2, ionisation, dissociation and heating efficiencies of cosmic rays 78—28454
- interstellar medium interaction with stellar wind, cosmic ray accel. 80—77512
- interstellar molecular clouds, cosmic ray penetration 79—8979
- interstellar propag. of low-energy cosmic rays, charge equilib. and radiation 79—53676
- interstellar propagation, column density from He isotopic comp. from 123 to 279 MeV 78—49251
- interstellar propagation, compound diffusion in inhomogeneous mag. field 77—67127
- interstellar propagation, evidence from 3000 MeV to 50 GeV nuclei charge comp. and energy spectra 78—93059
- interstellar propagation of primary Ne to Fe nuclei, 200 to 650 MeV/nucleon, relative abundance 80—77246
- Jovian electrons, propag. close to Sun ($\leq$0.5 AU) 79—101034
- Jupiter, electron propag. out of solar equatorial plane, Pioneer 11 obs. 79—40123
- kinetic equation, limits of applicability of quasilinear approximation 77—91383
- leaky-box model for galactic propag. 78—57409
- linear and nonlinear modulation theory, model calcs. 79—80140
- local interstellar medium and cosmic ray anisotropy 79—44313
- magnetosphere, asymm. periodic oscills. in Stormer problem 77—78586
- magnetospheres, effect on cosmic ray propag. 80—101517
- mean free path of low-rigidity cosmic rays, weak turbulence diffusion theory 80—98524
- medium energy expt. on International Sun-Earth Explorer C spacecraft 78—85798
- Monte Carlo propagation model 78—20591
- north-south anisotropy of intensity pulses 80—56687
- ρ Ophiuchi cloud, cosmic ray accel. by stellar winds 80—77512
- particle accel. at spherical shock wave front, power spectrum *(Russian)* 80—72730
- particle acceleration by moving magnetic mirrors, efficiency 79—44310
- particle acceleration in collisionless shocks, regulated injection and high efficiency 79—44311
- path tracing in time independ. mag. field, helix predictor corrector method 79—62692
- path-length distribution, concept extension to nonrelativistic energies 79—88558
- polar orbiting satellite obs. of flux altitude depend. 80—46353
- positrons, galactic, prod. rate and probability of escape from Galaxy 80—109319
- primary cosmic radiation, antiprotons relative abundance rel. to galactic propag. model 78—73594
- proton generation in solar flares 80—101575
- pulsar magnetospheres, cosmic ray acceleration mechanisms *(Russian)* 78—16448
- range distribution function of cosmic rays in matter 79—80113
- recurrent proton streams, 1.3 to 2.3 MeV protons radial diffusion coeff. 79—16774
- relativistic particles acceleration in shock fronts 78—24415
- Saturn magnetic field, cosmic ray cutoff rigidities 80—72873
- screening effect on interstellar cloud stability 79—67077
- solar charged particles generated in 1972, August 7 flare, interplanetary propag. 79—12360
- solar cosmic ray events, solar and interplanetary diffusion 78—28458
- solar cosmic ray propagation correlations detected on Mars-7 and Prognoz-3 78—49247
- solar cosmic ray propagation in interplanetary medium, solns. to Fokker-Planck eqn. 80—77242
- solar cosmic rays, fast azimuthal transport by coronal mag. bottle 78—32305
- solar cosmic rays, injection processes and interplanetary propag. influence on intensity and anisotropy 78—12195
- solar cosmic rays interplanetary propag. *(Chinese)* 79—101035
- solar cosmic rays propag., diffusion in mag. fields, convection in solar wind, dimens. method soln. *(Chinese)* 78—81511
- solar energetic particle events following September and November, 1977, flares, diffusion model 78—77446
- solar energetic storm particles, accel. rel. to interplanetary shock wave parameters 79—35079
- solar equator vicinity, daily cosmic ray flows during solar cycle 78—69622
- solar flare electrons, peculiarity of ejection into interplanetary space *(Russian)* 78—77445
- solar flare energetic particles, interplanetary propag. model 78—65468
- solar flare particle accel., injection energy concept 80—101509
- solar flare particle events, exponential decay 78—4047
- solar flare particles meas. and integral proton spectra anal. 79—62695
- solar flare particles propag. in interplanetary medium, model 79—80128
- solar flare protons, escape into interplanetary space rel. to 9 GHz microwave bursts characts. 80—4323
- solar flare protons, flux limit due to accel. mechanism saturation effects 80—98645
- solar magnetic dipole orientation effects 79—44316
- solar nonrelativistic electrons coherent propag. 77—91506
- solar particle event, 1973 April 29, mean free paths near Earth 78—89017
- solar particle events with high relative ^{3}He abundances, interplanetary propag. conditions 80—61972
- solar particles, origin, nature and effects, interplanetary propag., review *(Russian)* 79—66893
- solar particles, propag. from 1 to 5 AU 78—20594
- solar particles, spectrum formation near Earth, propagation and acceleration *(Russian)* 80—4211
- solar particles from E45° flare, 1973, July 29, coronal and interplanetary propag. 77—82090
- solar particles motion in coronal magnetic field 79—75196
- solar proton and electron events, interplanetary scatt. mean free path 78—57421
- solar wind high speed streams and galactic cosmic ray modulation 80—41673
- solar wind particles trapping and accel. at Earth 80—98532
- spallation production during propag., secondary nuclide as tracer 79—96864
- statistical particle acceleration models for Cassiopeia A supernova remnant 78—57606
- steady-state transport eqn., monoenergetic source solns. 77—82088
- streaming along galactic magnetic fields, effect on pulsar scintillations 80—51845
- streaming perpendicular to mean mag. field, gyrophase distrib. function 78—53778
- Sun's inner heliosphere, longit. modulation of galactic cosmic rays 80—90298
- sunward flowing proton and alpha particle fluxes, interplanetary propag. model 78—89016
- supernova remnants, cosmic rays accel. in shock fronts 78—32302
- supernova remnants, cosmic rays escape and adiabatic energy losses 79—16771
- supernova remnants, cosmic rays trapping by hydromag. waves in high β plasmas 80—17482
- supernova shell, cosmic ray accel. *(Russian)* 77—87454
- supernova shock-accelerated cosmic rays, early radiation spectrum, cooling and escape 79—48626
- transport coeffs. in supernova remnants 79—101033
- transport eqn., steady-state, nonenergetic-source soln. 78—96366
- turbulent diffusion, partially averaged field approach 78—53776
- two-zone model, radioactive cosmic ray isotope appl. 79—66891
- ultrahigh energy cosmic ray origin and propagation 78—49242
- velocity diffusion, turbulent mag. field, Monte Carlo calc. 78—53777
- $\bar{p}$ flux, upper limit for secondary production 78—12062
- ^{7}Be, cosmic ray accel. probe 78—81512

cosmic ray protons
- 11 year cosmic-ray cycle, galactic and sdlar protons anal. 77—53360
- acceleration by zero-point background radiation, stochastic electrodynamic theory 79—21117
- acceleration into interplanetary medium during 1972, August 4 flare *(Russian)* 77—33303
- altitude variation, Feynman scaling hypothesis calcs. 80—77245
- anti-proton detection *(French)* 80—56688
- antiproton component at 3220 m altitude *(Chinese)* 79—25419
- antiproton spectrum, at top of atm., scaling law 79—12365
- antiprotons, production mechanisms 79—29955
- antiprotons, relative abundance in primary cosmic radiation 78—73594
- antiprotons balloon-borne superconducting-mag. spectrometer obs. 80—17457
- antiprotons in primary cosmic radiation and collisions in interstellar medium 80—77241
- atmospheric interactions, direct lepton prod. *(Russian)* 80—12627
- atmospheric neutron-proton ratio, from primary nucleon spectrum 80—8499
- atmospheric spectra, $50\ \mathrm{MeV} \leq E \leq 100\ \mathrm{GeV}$, Monte Carlo simulation *(German)* 77—13197

cosmic ray protons continued
auroral proton source in magnetosheath 77—33240
charged particle fluxes meas. on geostationary orbit 79—80082
coronal and interplanetary propagation of solar particles following E45° solar flare on 29/7/73 78—49248
coronal propag. at medium and high energies 77—53355
diffusion equations for nucleon and charged pions in atmosphere 79—70936
diffusive Sunward flow of 1.6 MeV protons at 1 AU 77—33302
directional flux meas. in space, digital onboard processor appl. 77—64610
EAS, violation of scale invariance in hadron interactions, 10^{15} to 10^{17} eV 78—7849
EAS radioemission, freq. spectrum, lateral distrib., primary cosmic rays comp. 77—87219
emulsion-chamber study 77—64557
energetic particles intensity meas., 1973 Sept., by interplanetary probes 77—29604
energetic protons near Earth's bow shock, pitch angle distribs. 80—26683
excess radiation flux at heights of 200-300 km meas. 77—53278
extremely high energy cosmic rays, role of neutrons in propagation 77—29603
flux increases, rel. to solar flares and storm sudden commencements 77—9637
Forbush effect in intensity of solar protons 79—80126
galactic, inside magnetosphere, local energy spectra calc. *(Russian)* 78—16258
galactic cosmic ray intensity out to 18 AU, Pioneer 10 and 11 obs. 80—90297
galactic cosmic rays differential spectra, model description, solar modulation theory 79—80130
galactic cosmic rays origin, galactic models with halo 80—61971
galactic proton/electron ratio 78—69633
galactic protons, as extraterrestrial source of atmospheric water vapour 78—69416
galactic protons, origin rel. to electron fluxes in closed galaxy model 77—13189
galactic protons, spectrum vars. meas. by Venera 9 and Venera 10 probes 77—91388
generation in solar flares 80—101575
high-energy meas. on Proton satellites 78—28462
interaction with lunar and planetary material, gamma-ray production, simulation 78—16318
interplanetary, 1-4.5 MeV, spectral anal. and correl. study 80—77243
interplanetary, assoc. with active regions at 1-5 AU 78—45176
interplanetary, low-energy, interaction with shock waves, 1975 January, Helios 1 obs. 78—20609
interplanetary, use in galactic modulation parameter determ. 80—82156
interplanetary acceleration by transit time damping 77—2311
interplanetary acceleration mechanisms 77—2312
interplanetary corotating nucleon fluxes separation from solar flare fluxes by radial gradients and nuclear comp. 79—25413
interplanetary corotating regions, nucleon accel. and modulation of Jupiter electrons 78—61690
interplanetary flux enhancements and solar wind speed, Mars 7 meas. 79—84620
interplanetary flux rises, 1973 Aug.-Sept., correl. with solar wind vars. 79—21123
interplanetary intensity gradient, 1973 April-August, Pioneer 10 and 11 meas. 77—13192
interplanetary intensity increases at shock wave front 79—53695
interplanetary shock acceleration of energetic protons 80—56686
interplantary propagation, Mars spacecraft meas. 78—53779
low energy proton expt. on International Sun-Earth Explorer C spacecraft 78—85791
low energy protons, modulation in 1974-1975 near solar minimum 77—33304
low-energy, interplanetary background meas. on Venera 9 and (Venera 10) 78—4049
mean free path between Compton interactions with microwave background photons 77—87211
MeV streams after interplanetary magnetic sector boundary, effect on troposphere 79—53491
multiplicity functions in rigidity interval 1 to 15 GV 79—66894
neutron-proton ratio determ. 77—70961
nucleon cascade in atmosphere 79—12363
origin of 30-100 keV protons in upstream region of Earth's bow shock 79—48622
pitch angle distrib. in high-latitude magnetotail during 1970 April 16 solar proton event 79—53670
primary cosmic ray nucleon and sea level muon energy interrelation, scaling model 80—51633
primary cosmic ray nucleon spectrum from sea level μ-spectrum using scaling model 79—29957
primary cosmic rays, $>10^{13}$ eV, comp. study, from hadron time distribs. near air shower cores 79—62697
primary nuclear air showers, phenomenological model 77—22028
primary proton spectrum, 10^{12}-10^{14} eV 77—91389
quasiperiodic pulsations in stratosphere 79—80133
recurrent particle streams at 1 AU 79—96867
recurrent proton streams, 1.3 to 2.3 MeV protons radial diffusion coeff. 79—16774
secondary $\bar{p}$, confinement models 78—12061
secondary protons, fluxes above 500 MeV at 200-300 km altitudes 77—64497
slow protons, sea-level flux meas. by Sydney University particle telescope 78—25388
solar, alpha-particles and protons streaming velocities relative magnitude at 1 AU 77—9643
solar, characts. determ. near Earth from radio burst obs., longit. attenuation function 78—45309
solar, energy spectrum shape at 1 AU *(Russian)* 78—16255
solar, He, Ne and Ar isotopes and ^{236}U prod. in lunar materials, rate calc. 77—17311
solar, high-energy, from 1973 April 29 flare, arrival delay at Earth 79—62694
solar, high-energy, upper cutoff 77—17306
solar, intensity north-south asymm. rel. to plasma sheet and daytime polar cusp dynamics 77—17297
solar, interplanetary scatt. mean free path, energy depend. 77—9633
solar, low-energy events, assoc. with mag. sector boundaries 77—45265

cosmic ray protons continued
solar, polar cap aurora induction, secondary electrons prod. 79—53605
solar active region protons at 1 AU, energy spectra from Prognoz-3 80—101512
solar charged particles generated in 1972, August 7 flare, accel. 79—12360
solar cosmic ray protons, spatial distrib. in Earth's mag. field 77—53357
solar energetic proton events at large heliocentric distances, shock-assoc. 78—77451
solar energetic storm particle events, ^{4}He/H ratio vars., theory 77—9636
solar energetic storm particle events, correl. with interplanetary shock wave parameters 79—35079
solar flare, 1973 April 29, cosmic ray anisotropy, Cosmos 555 obs. 77—45268
solar flare, spectrum determ. from latitudinal effect, using minimal Stormer pulse 78—45308
solar flare effect on proton propag. in interplanetary medium 77—53502
solar flare energetic particle events from same active region, p/α enhancement 79—40151
solar flare energetic particles, interplanetary propag. model 78—65468
solar flare flux determ. from ^{3}He meas. in lunar rocks 80—98576
solar flare particle events, exponential decay 78—4047
solar flare particles absolute spectra for flares of 1966-76 period 79—84598
solar flare proton energy spectra slope from radio burst data 79—53683
solar flare protons, flux limit due to accel. mechanism saturation effects 80—98645
solar flare protons, identification from accompanying EM emission 79—12443
solar flare protons, in August 1972, role in polar cap absorpt. and auroral events 77—29567
solar flare protons, Mars 7 probe meas. 78—69624
solar flare protons, near-Earth parameters determ. from radio bursts 78—45165
solar flare protons, radiation hazard in shielded spacecraft 80—8194
solar flare protons, stochastic accel. 80—21953
solar flare protons during August 1972, review of obs. 77—25895
solar flare protons near-Earth radiation hazard, dosage estimation technique 80—67482
solar flare related cosmic rays, $\geq$130 MeV, May 1979 obs. 80—51627
solar flares, energetic particle composition temporal development 78—89148
solar flares, excessive particle emission mechanism 78—45310
solar high latitude flares *(Russian)* 77—64729
solar high-energy protons in August 1972, review of obs. 77—25894
solar particles, magnetotail lobe and plasma sheet entry in 1971 April 22 event 79—101026
solar proton albedo neutron flux north-south asymm. meas. 79—75061
solar proton event, 1970, April 16, features in interplanetary space and magnetosheath 77—87215
solar proton event of 1978 May 7, neutron monitor obs. 80—67686
solar proton event of 1978 May 7 arrival times of scatter free particles 79—75066
solar proton flares, temporal ref. functions from microwave radio bursts 78—73591
solar proton flares 1942-76 and their prediction 78—20811
solar proton flares during August 1972, summary of solar/interplanetary events 77—25991
solar proton fluxes at 1 AU during solar min., Prognoz 3 obs. 78—69769
solar proton irradiation model for solar system ^{16}O and ^{26}Al isotopic anomalies 78—93128
solar proton region development in 1973, September 7 flare 77—37588
solar proton spectra determ., comparison of methods 78—28459
solar protons, 1970, April 16, pitch angle distribs. transform. from solar wind into magnetosheath 77—87216
solar protons, as extraterrestrial source of atmospheric water vapour 78—69416
solar protons, auroral zone precip. assoc. with storm sudden commencements 77—82081
solar protons, flux anisotropy and inhomogeneity meas. 77—53351
solar protons, polar region fluxes rel. to sector struct. of interplanetary magnetic field 77—49251
solar protons, Prognoz-6 fluxes and spectra meas. during large scale interplanetary disturbance 80—90315
solar protons, relationships to ionospheric polar cap riometer absorpt. 78—28413
solar protons, struct. of fluxes in high-latit. magnetosphere in April (1972) 77—64532
solar protons and α particles, rigidity-independent coronal propag. and escape 78—77444
solar protons from E45° flare, 1973, July 29, coronal and interplanetary propag. 77—82090
solar protons from September and November, 1977, flares, spectra and time profiles 78—77446
solar protons in Earth's magnetosphere, vars. and spectra (August 1970) 78—16256
solar protons in magnetosphere, flare-time asymmetry and anisotropy 77—33280
solar protons in magnetosphere (1971 September 1-16) 79—2446
solar protons prod. by flare of 7 Aug. 1972 anal. 77—53356
solar protons reflected by Earth's bow shock, upstream wave boundary determ. method *(Italian)* 78—24409
solar relativistic protons from flare of 1 September 1971, anisotropy 77—22022
solar wind, very low electron and proton temps., statistical anal., origin 78—65477
solar wind protons after interplanetary shock wave passage 77—33301
solar wind protons vel., effect of galactic cosmic rays 80—101506
spectrum and spatial distrib. in Earth's radiation belts 77—53313
star, interplanetary accel. in corotating interaction regions 77—9635
sun, flare proton generation 80—109413
sunward flowing moderate intensity proton and alpha particle fluxes, characts. 78—89016
supernova shell, cosmic ray accel. *(Russian)* 77—87454
theoretical proton spectra at atm. depths 40 g cm $^{-2}\leq h \leq 350$ g cm *(German)* 79—12367
transitional emission detector, electron identification in cosmic ray background, X-ray detection study 80—4213
(p,xn) reactions, cross-sections and astrophysical appls. 78—28504
$\bar{p}$ flux, upper limit for secondary production 78—12062
pN inelastic scatt. cross-section meas. 77—61413

- **cosmic ray protons** continued
  - pp interactions, cosmic γ-ray spectrum, fireball model 77−18364
  - $pp \rightarrow \bar{p}X$, upper atmosphere, $p/\bar{p}$ flux ratio calc. 78−40783
  - pp total cross section at cosmic ray energies up to 100 TeV 79−96868
  - Ge detectors in space, computer spectral anal. of cosmic ray proton induced radioactivity 79−12413

- **cosmic ray showers and bursts**
  - *see also cosmic ray electrons; cosmic ray X-rays*
  - γ-ray families and high energy reaction asymptotic props. 79−16779
  - air shower, fluctuations of low-energy muons, composition models 77−37491
  - air shower arrays, response to air showers 79−739
  - air shower cores, energetic hadron, $>10^{13}$ eV, arrival time distrib. 79−44321
  - air shower cores, high-energy γ-rays and their bursts 77−91393
  - air showers, >10 TeV, acoustic detection 79−62691
  - air showers, acoustic detect. 79−66901
  - air showers, muonic component lateral structure function 77−70963
  - air showers for 10^4 to 10^6 particles, lateral distrib. of EM component, detection 80−17459
  - angular distribution of shower particles, changes with increasing multiplicity, models 78−36412
  - arrival direction distrib. of high-energy particles, Northern Hemisphere 78−20601
  - atmosphere prompt neutrinos, W-bosons prod. 79−3014
  - atmospheric Cherenkov pulse duration, depend. on cosmic ray shower parameters 78−89025
  - atmospheric nuclear cascade characts., calc. for Pamir expt. 79−80157
  - atmospheric shower hadronic component, lateral struct. function 77−56804
  - cascade shower, electron energy density, lateral struct. function 79−66900
  - cascade shower electrons, approx. determ. of lateral struct. function 77−33307
  - cascade showers from cosmic ray muons interaction with Fe nuclei, anal. 79−84616
  - cascade showers generated by muons in ionisation calorimeter, fluctuations anal. 79−84618
  - cascade showers prod. by muons in Fe at 0.3-3 TeV 77−64570
  - cascade theory, one dimensional, fluctuations of the particle number *(Russian)* 79−96871
  - Cherenkov light in EAS, time struct. 77−33306
  - clean atmospheric jet, 878 TeV, cascade degradation absence 79−35084
  - clusters of particle prod. at high energies 77−64579
  - coherent hadron radiation at TeV energies *(Russian)* 79−92641
  - coherent hadron radiation interpretation of cosmic ray anomalous events *(Russian)* 79−92642
  - composition from atmospheric shower development 80−17458
  - conference on cosmic rays and particle physics, Newark, USA, Oct. 1976 79−58987
  - Cygnus X-3, 1974 EAS obs. of high-energy gamma-ray source *(Russian)* 77−64881
  - decay law of cascade processes *(Chinese)* 79−58206
  - density spectrum of cosmic-ray air showers at very high densities 79−16783
  - development repudiation of putative primary mass composition change 80−61976
  - direct cosmic ray muon pair generation, nuclear cascade role 80−91120
  - Durham air shower array, Monte Carlo anal. of response 78−36460
  - EAS, 10^{14} to 10^{16} GeV, characteristics of peripheral master system of Tien-Shan exptl. arrangement *(Russian)* 78−32310
  - EAS, 10^{15}-10^{18} eV, experimental data, implications for particle accelerators, review 79−8786
  - EAS, π photoprod. as source of low-energy muons 80−4214
  - EAS, Akeno Air Shower project, e and μ obs., core energy flow, device description 79−72184
  - EAS, array density spectrum 80−90301
  - EAS, associated prod. of radiopulses and optical Cherenkov radiation 77−60559
  - EAS, atmospheric elec. field, rapid vars. connected with high energy primary particles 79−66739
  - EAS, atomic nuclei fragmentation, analytical method *(Russian)* 78−65472
  - EAS, ave. lateral muon density distrib., arrival direction studies 78−73596
  - EAS, axis determ. using new multiplicative core selector 80−41682
  - EAS, characts. for primary energy <200 TeV, electron and muon fluxes 79−80162
  - EAS, characts. of gamma ray and hadron families, Monte Carlo calcs. 77−53377
  - EAS, Chenenkov flashes obs. for detec. of ultrahigh energy cosmic γ-rays 79−80368
  - EAS, Cherenkov pulse shapes obs. using improved Yakutsk apparatus 79−80169
  - EAS, computer simulations of Cherenkov radiation 79−66899
  - EAS, conflict with scaling, 10^{15} to 10^{17} eV 77−61336
  - EAS, correl. between optical Cherenkov pulses and radiopulses anal. 77−60560
  - EAS, correlations between muon and electron component characteristics 79−44324
  - EAS, detection of muons 78−28473
  - EAS, detectors pulse profiles studies 79−25421
  - EAS, development, atm. Cherenkov study 79−84615
  - EAS, duration of atmospheric Cherenkov pulses 78−73595
  - EAS, electron and muon number distrib., anal. of primary cosmic ray spectrum, 10^{13} to 10^{16} eV 77−67014
  - EAS, electron and muon spatial distribs., mountain heights 77−64562
  - EAS, electron flux, spatial distrib. 77−49256
  - EAS, electron lateral distrib. at mountain altitude 78−28470
  - EAS, electron spatial distrib. at 1700 m above sea level 79−80163
  - EAS, electron-photon and muon components, simulation 77−49255
  - EAS, EM component 78−49258
  - EAS, energetic muons and multiple penetrating particles 77−53378
  - EAS, energies of electron-photon and hadron components near axis, 3330 m above sea level 77−64563
  - EAS, energy ratio of electron-photon and hadron components in core 77−82093
  - EAS, energy spectrum for 10^{17}-10^{20} eV 79−80151
  - EAS, hadron interactions, comp. of primary particles of energy 10^{14}-10^{16} eV, Tien-Shan data 79−80149

- **cosmic ray showers and bursts** continued
  - EAS, high energy, Cherenkov light meas. 78−45169
  - EAS, high energy muon density 80−36466
  - EAS, high p_T cross section from multiple core rates 79−62703
  - EAS, high transverse momentum of γ-ray bundles, $>10^{12}$ eV 79−62701
  - EAS, lateral age parameter and radial electron distribs. 80−85828
  - EAS, low-energy hadron meas. 79−80165
  - EAS, multi-cored obs. by combination array of spark chambers and scintillation counters 77−60557
  - EAS, multicored, at Mt. Norikura, preliminary results 79−62702
  - EAS, muon and EM components 78−28471
  - EAS, muon density meas., $E>10^{15}$ eV using scintillators and spark chambers *(Italian)* 79−21119
  - EAS, muon flux density fluctuations 80−21884
  - EAS, muon momenta meas. 78−20600
  - EAS, muon spatial and energy distribs., magnetic spectrometer study 77−67017
  - EAS, muon spatial distrib., expt. and calc. 79−80167
  - EAS, muon spatial distrib. and age parameter correl. 79−80166
  - EAS, muon spatial distrib. correl. with shower age 77−64582
  - EAS, muon to electron ratio fluctuations 78−7848
  - EAS, Musala Peak obs., fluctuations of 10^{14} eV rays 78−49254
  - EAS, nuclei mass composition spectrum 80−46359
  - EAS, optical detection system—Utah Fly's Eye, data acquisition system and status report 79−63864
  - EAS, particle flux densities calc. 77−64561
  - EAS, radio pulse detec. and anal. 77−53379
  - EAS, response of scintillators, Ne flash tubes and water Cerenkov detectors 78−49259
  - EAS, results of highest energy nuclei 78−57413
  - EAS, scintillation detector array, 200 m^2 for examining central section 77−61648
  - EAS, search for tachyons 79−16780
  - EAS, simultaneous detection of γ-ray bundles and air showers 79−62700
  - EAS, size fluctuation effect on size spectrum 79−58207
  - EAS, small atm. elec. field variations 77−60558
  - EAS, spatial distrib. near axis, multicore struct. 79−80164
  - EAS, ultrahigh energy interactions scaling deviations and modified models 79−80172
  - EAS, upper troposphere, balloon obs., nuclear reactions, 10^{15} eV energy particles 79−80161
  - EAS, validity of Feynman scaling 78−28469
  - EAS, very large, sea-level characts., particle number spectra 79−80168
  - EAS age parameters, elementary act parameters, primary cosmic ray spectrum 77−64567
  - EAS array, at Durham, data anal. 77−91392
  - EAS array at Durham 77−91391
  - EAS at 690 g/cm^2, fluctuations of muon component 78−36411
  - EAS Cherenkov radiation impulse shape *(Russian)* 78−49260
  - EAS Cherenkov radiation meas. by photomultiplier, cosmic ray induced noise 77−18735
  - EAS containing 10^5 to 10^6 particles, expt. study 77−64560
  - EAS data on primary particle spectrum at 10^8-10^{10} GeV 77−64568
  - EAS data relation to high-energy particle prod. models, simulation 77−70962
  - EAS growth, significance of fragmentation and pionisation ranges in inclusive spectra 79−84614
  - EAS hadrons, lateral distrib. at mountain level 80−21881
  - EAS heavy mass particle search in S.India 77−29611
  - EAS initiated by relativistic dust grains, hypothesis refuted 80−46360
  - EAS lateral distribution function fluctuations at distances <50 m from axis *(Russian)* 79−53688
  - EAS longitudinal development for primary particle energies above 10^{17} eV 77−64564
  - EAS muon data, primary energy spectrum 77−2315
  - EAS near core, struct. of electron-photon component *(Russian)* 78−57414
  - EAS proton-initiated EM component at 690 g.cm^{-2}, Monte Carlo simulation 77−91390
  - EAS radio emission, electric field strength *(Russian)* 78−93061
  - EAS radio emission, field strength at 44, 60 and 80 MHz 80−8505
  - EAS radio emission spectra, Cherenkov and synchrotron radiation mechanisms 77−64566
  - EAS radio pulses, correlation at 60 and 80 MHz 80−8504
  - EAS radioemission, freq. spectrum, lateral distrib., primary cosmic rays comp. 77−87219
  - EAS research, primary cosmic ray energy $>10^{17}$ eV, equipment system parameters, capabilities 77−64569
  - EAS research above 2×10^{14} eV, scintillation and Cherenkov counter system 77−61649
  - EAS sea level absorption length, integral size spectra simulation 80−51634
  - EAS with N of 10^4 to 10^5, energy and charge compositions of nuclear-active component 77−64553
  - electron and γ interaction ranges, Monte Carlo calc. *(Russian)* 79−12370
  - electron and muon components in wide atm. avalanches, correl. with nucleon MFP in air *(Russian)* 77−73916
  - electron-photon cascade energy determ., effects of optical density and energy spectrum meas. errors 79−84613
  - electron-photon cascade in air, simulation of energy and lateral characteristics 79−44323
  - electron-photon cascades, Monte Carlo simulation of cascade development 79−44322
  - electron-photon cascades, spectra above 2 TeV 79−80147
  - electron-photon shower, range fluctuations in unbounded medium 79−80152
  - electron-photon showers, successive approximation method 77−64559
  - electrons in large air showers observed at 5200 m above sea level 79−16781
  - EM cascade, particle-induced, in water, thermoacoustic effect, neutrino detection appl. 79−29960
  - EM cascade build up in layered medium, Landau-Pomeranchuk effect 77−64558
  - EM cascade eqns., numerical integration, results for air, Cu, Pb and Fe 78−20602
  - EM cascade showers, electron/photon energy flow 77−22027
  - EM cascade theory, calc. of collision integral and fundamental eqn. soln. *(Russian)* 78−16261
  - EM cascade theory equations, approx. solution *(Russian)* 77−49257

cosmic ray showers and bursts continued
- EM cascades in air, caused by 10-100 GeV electrons and photons 79−21120
- energetic delayed hadrons in air showers, possible new massive particle 79−75065
- energy, position of maximum for EAS with $E_0>2\times10^{16}$ eV, shape of Cerenkov impulses *(Russian)* 79−96870
- energy and flux meas. of high energy γ-rays, emulsion chamber detection *(Japanese)* 78−20595
- fast doubly-charged particles, form. in nonrelativistic nuclei interactions 79−80175
- fast timing ang. distrib. meas., data anal. 78−49256
- gamma quanta produced by cosmic-ray hadrons of tens of TeV energies, energy characts. 79−80148
- gamma rays in 10^{11}-10^{14} eV range using atmospheric Cherenkov technique 79−25422
- gamma-quanta, spectra above 2 TeV 79−80147
- gamma-quantum, high energy, prod. by nucleon diffr. fragmentation by 10 TeV NN collisions 79−80174
- gamma-quantum families, obs. rel. to hadron interactions transverse momenta to 10^{14} to 10^{15} eV 79−80170
- gamma-quantum families, released cluster mass determ. 79−80171
- gamma-quantum families of 10 to 100 TeV energy, height depend. 79−80159
- gamma-quantum families with $\Sigma E_\gamma>30$ TeV, energy characts. in Pamir expt. 79−80156
- gamma-ray air family, lateral structure function 77−41274
- gamma-ray bundles, high transverse momentum estimated from RE distribs. 79−40046
- gamma-ray burst origin, episodic gas accretion on neutron star 77−5600
- gamma-ray prod. spectra for high energy reactions in graphite 79−29959
- gamma-ray spectra, high energy, near top of atmos. detection+meas. by emulsion chamber 79−29958
- hadron energy spectra produced by primary cosmic ray particles, $E>10^{14}$ eV 80−21880
- hadron families, characts. calc. 79−80160
- hadron interaction model, superhigh energy, characteristics of hadron and gamma-ray families *(Russian)* 79−96873
- hadron-induced cascade showers in Pb and Fe, Monte-Carlo anal. 77−60561
- hadronic showers, cosmic neutrino induced, acoustic detection 79−76265
- hadrons, spectra above 2 TeV 79−80147
- hadrons >300 GeV in EAS, Durham array obs. 77−73917
- high energy EM showers in atmosphere, Monte Carlo simulation 77−56802
- high-energy cosmic-ray components in atmosphere, scaling features 78−93062
- high-energy gamma-quantum and hadron families, Monte Carlo studies 79−80158
- highest-energy cosmic rays, detected by EAS obs. 79−2450
- horizontal air shower detection apparatus 78−36457
- inclined muon monitors, muon spectra, generating functions, rel. to diurnal variation at Kiruna 78−85783
- individual showers direct obs. by method using Cherenkov light meas. 77−17309
- large air showers, arrival-time distribs. of μ's and e's, obs. at 5200 m above sea level 79−62699
- large air showers, Cherenkov radiation image reconstruction 79−25420
- large cosmic ray showers, computer simulation using models of hadronic collisions 78−57415
- lateral density distrib. of muons in air showers at different heights 79−40045
- lateral electron structure in EAS, simulation study 78−81513
- lateral structure function, electronic component 77−91394
- model for 10^6 GeV cosmic rays in atm., Feynman scaling, e/μ ratio 77−45271
- Monte Carlo simulation of high-energy EM air showers 77−64577
- multicore observations in our showers, appl. of C+200 GeV neutrons multiplicity distribs. 77−50127
- multiple charged particle showers, generation by negative pion-nucleus inclusive reactions 79−76022
- multiple meson production by 10^{13}-10^{16} eV cosmic rays, longitudinal behaviour of γ air family 77−33309
- muon charge ratio, energy up to 1 TeV 78−89029
- muon energy spectra at large zenity angles, 0.28 to 35 TeV *(Russian)* 77−9639
- muon generation, anomalous, method of searching in EAS 78−89026
- muon lateral distribution at different altitudes in atmosphere 80−26708
- muon showers underground, multiplicity distribs., local interactions in absorbers 77−5406
- muon spectrum at sea-level, Maeda's model, using pion-kaon ratio 78−85781
- muon-electron ratio and particle mass for primary cosmic rays of $10^{15}10^{16}$ eV energy 79−80150
- muons, high-energy, EM component density spectrum 77−82092
- muons, lateral distrib. and spatial separation of distrib. 80−109320
- muons, spectra above 2 TeV 79−80147
- muons in EAS, array and data analysis 78−89027
- muons in EAS at mountain altitudes, comparison with numerical calcs. 77−87218
- muons in large air showers observed at 5200 m above sea level 79−16782
- muons in large showers, spatial characts. 77−22031
- National Cosmic Ray Facility, for high energy physics and primary comp. studies, 10^{14} to 10^{18} eV 79−62704
- neutrino detection, high-energy, using acoustic pulse from hadron shower *(Russian)* 77−38580
- neutron star, episodic accretion of gas and cosmic Γ-ray bursts 78−69824
- nuclear primary air showers, phenomenological model 77−22028
- particle anisotropy at ultrarelativistic energies, EAS distribs. 77−64565
- particle lateral distribution at large distances from EAS axis with numbers 10^7-10^8 *(Russian)* 77−87220
- path fluctuations in EM cascade in infinite medium *(Russian)* 78−65471
- pellicle stack, γ-ray family from cosmic-ray hadron reactions, accelerated scanning method 78−78546
- penetrating-particle beams, locally generated, at air equivalent depth 200 m 79−84603

cosmic ray showers and bursts continued
- pionisation region gauge invariance violation for hadrons, K and γ in EAS *(Russian)* 79−40676
- pions, high energy, prod. by nucleon diffr. fragmentation by 10 TeV NN collisions 79−80174
- positron initiated showers in Pb, 0.5-3.5 GeV, test of cosmic ray shower calcs. 78−37332
- primary cosmic rays, $>10^{13}$ eV, comp. study, from hadron time distribs. near air shower cores 79−62697
- primary cosmic-radiation spectrum from 10^{12} eV to 10^{15} eV from atmospheric Cerenkov-radiation measurements 79−66895
- proportional counter for air shower observation, counter prod. characts. and lifetime determ. 80−98526
- proton-nucleus, 50-200 GeV/c, ang. distrib. of charged shower particles *(Korean)* 80−27641
- radiowaves produced from secondary electrons in geoelectric field, 10 kHz-10 MHz 79−21118
- relativistic and non-relativistic dust grains, rel. to high energy particles in EAS 80−61975
- remote sensing using light emission and optical detection 78−4050
- review, cosmic gamma radiation, sources and detection 78−12059
- scale invariance violation in hadron interactions, 10^{15} to 10^{17} eV 78−7849
- sea level muon spectrum, Bugaev model 77−82094
- sea-level expt., analytical and Monte Carlo interpretations 77−67016
- sea-level expt., hadronic and muonic fluxes obs. 77−67015
- secondary particles from cosmic ray nucleus-nucleus interactions, hydrodynamic effects search 79−80176
- shower front curvature, determ. by fast timing data of cosmic ray air shower arrays 79−2449
- simulation of nucl. cascades in atmosphere 77−64556
- slow particles from hadron-nucleus interactions, characts. rel. to interaction models 79−80177
- solar and cosmic X-rays and gamma-rays, obs. by Signe II MP satellite expt. 80−41696
- tachyon search, ray energy $\geq10^{14}$ eV, 290 μs preceding period 77−78588
- theoretical proton spectra at atm. depths 40 g cm$^{-2}\leq h\leq350$ g cm ^{2} *(German)* 79−12367
- time correlation of muon pairs and multiple hadron production 79−80178
- time of flight telescope, compensated, for spaceborne cosmic ray measurements 77−67939
- ultra high energy cosmic rays, discussion *(French)* 80−21879
- wide atmospheric shower development, cascade curves restoration *(Russian)* 80−36463
- eγ cascade widths, review of expt. evidence and calcs. 78−85779
- γ, primaries meas., 10 to 100 GeV, using air showers Cherenkov light distrib., detector system 78−73597
- γ-ray families, multiparticle prod. above 10^{14} eV, Monte Carlo anal. 78−49257
- γ-ray initiated atmospheric showers, computer simulations, Cherenkov radiation, geomag. field effects 77−49254
- μ burst rates, Fe-liquid scintillator multilayer calorimeter transition effects 78−90019
- ^{56}Fe, hadron generated cascades, energy flux absorption length, 1-20 TeV *(Russian)* 78−28468
- He nuclei prod. at high energy, correlation with shower particles generation *(Russian)* 77−41273

cosmic ray solar modulation
- 11 year cosmic-ray cycle, galactic and sdlar protons anal. 77−53360
- 11 year galactic cosmic-ray cycle, anomalous effects 77−53359
- 11 year modulation cycle rel. to sunspots and solar general mag. field 79−21114
- 11-year modulation cycle obs., review 77−13196
- 27-day cycle, amplitude, quasistationary treatment 77−53369
- 27-day cycle and anisotropy rel. to solar activity epoch 77−53370
- 27-day modulation with solar wind radial attenuation 78−73592
- activity cycle 20 effects 79−53684
- amplitude modulation in 27-day variations 80−26703
- annual and semiannual variations, phase reversals. rel. to Sun polar mag. fields reversals 78−40780
- conference, Yakutsk, USSR (Jun. 1977) 79−80110
- corona holes correlated to cosmic ray intensity, during solar cycle 80−94661
- coronal holes modulation effects 80−77370
- cyclic variations in cosmic rays and solar activity, detect. from radiocarbon meas. 79−16776
- daily variations, 50-200 GeV 80−17455
- diffusion, in solar wind deformed by interstellar medium 79−53680
- diffusion coefficients heliographic latit. distrib. in 11-year solar cycle 77−91386
- effect on cosmogenic isotope production in Earth atmosphere, secular vars. 79−53686
- electrons, modulation, 1969-1977 period 80−26706
- flare particles production and modulation, analytical solns. 78−16368
- Forbush decrease propag. to 16 AU 79−96866
- galactic cosmic ray energy loss and modulation in solar system 78−49245
- galactic cosmic ray intensity out to 18 AU, Pioneer 10 and 11 obs. 80−90297
- galactic cosmic ray modulation, numerical models of particle drift effect on cosmic ray transport 80−31180
- galactic cosmic rays, analytic solns. 78−7844
- galactic cosmic rays, annual vars. from anisotropic diffusion in interplanetary space 77−60550
- galactic cosmic rays, drift motion rel. to energy loss and eleven-year modulation 80−8498
- galactic cosmic rays, effect of directional medium-scale interplanetary vars. 77−29605
- galactic cosmic rays, energy loss and modulation in solar system 78−32308
- galactic cosmic rays, isotropic and anisotropic diffusion, asymm. conditions 78−40777
- galactic cosmic rays, latit. depend. modulation 77−2314
- galactic cosmic rays, nucleonic flux and solar indices correl. 77−22026
- galactic cosmic rays, particle drift effects 77−37488
- galactic cosmic rays, propag. in finite solar cavity 78−69623
- galactic cosmic rays, propag. in spherically symmetric solar wind 79−53681

cosmic ray solar modulation continued
galactic cosmic rays, spatial vars., meteorite radioactivity record *(Bulgarian)* 80—72728
galactic cosmic rays 11-year cycle, modulation coeff. energy depend. 78—28460
galactic cosmic rays anomalous intensity during 20th solar cycle rel. to solar total mag. field 79—80132
galactic cosmic rays differential spectra, model description, solar modulation theory 79—80130
galactic cosmic rays equatorial modulation and north-south asymm. 78—16253
galactic cosmic rays modulation absence during glacial period 79—80129
galactic cosmic rays modulation by solar total mag. field 79—80131
galactic cosmic rays modulation depth in interplanetary space, pitch-angle depend. 79—80139
galactic cosmic rays north-south gradient rel. to solar polar coronal holes 78—89019
galactic cosmic rays var. with solar cycle and coronal mag. field 78—7974
galactic cosmic-ray flux, origin of solar mag. cycle depend. semiannual var. 79—16777
galactic protons, spectrum vars. meas. by Venera 9 and Venera 10 probes 77—91388
ground level enhancements, comparison of 1977 Nov. 22 and 1969 Feb. 25 events 79—40042
Helios 1 measurements, 1974 Dec.-1975 Sept., quiet time spectra, radial gradients 78—20592
high energy particles anisotropy characts. near solar minimum 79—84607
high-energy, cosmic rays, solar anisotropy spectrum 80—51628
intensity modulation in interplanetary space taking into account royal zones in solar activity distrib. 79—80138
intensity var. rel. to solar activity 78—69625
intensity variations in interplanetary space, 1972-7 period 80—72726
intensity variations of interplanetary, magnetospheric and atmospheric origins, Sayan spectrograph data 79—84606
intenstiy variations in midlatit. stratosphere, total solar mag. field effect 79—62696
interplanetary corotating regions, nucleon accel. and modulation of Jupiter electrons 78—61690
interplanetary diffusion in presence of Alfven waves, Fokker-Planck theory 77—29606
interplanetary magnetic field polarity changes, cosmic ray modulation and D-region effects 77—33272
interplanetary modulation and solar activity 79—80135
linear and nonlinear modulation theory, model calcs. 79—80140
long term modulation, rel. to solar modulating region 80—51629
longitudinal intensity modulation of galactic cosmic rays, models 80—90298
Maunder minimum in solar activity, meteoritic evidence for reduced cosmic ray modulation 78—57529
multiply charged nuclei, charge depend. of solar modulation 77—5403
muon intensity in atmos., solar activity affecting height depend. of intensity 80—41675
muon solar harmonics, variation of upper limit rigidity, 1958-63 78—49265
muon spectra at sea-level, solar modulation at geomag. equator 79—16775
neutron component, short period vars. *(Russian)* 79—96865
neutron intensity, effects of solar disturbance and geomagnetism on cosmic rays 77—13195
neutron intensity, vars. rel. to interplanetary modulation zones 79—84604
nonstationary modulation theory, self-similar solns., rel. to vars. obs. on Aragats Mountain 79—80143
north-south asymmetry of solar activity and cosmic rays 79—80137
nuclei, low energy, ionisation states and origin 78—69634
particle drift effects on cosmic ray transport, analytical soln. to modulation problem 78—28456
past solar activity by means of cosmogenic isotope conc. in lunar samples 78—61828
polarity reversal of solar magnetic field, 22 year modulation 80—46357
positron energy spectrum, effect of interstellar medium anal. 77—49253
protons of ≥ 130 MeV, April and May 1979 obs. 80—51627
recurrent proton streams, 1.3 to 2.3 MeV protons radial diffusion coeff. 79—16774
relativistic galactic cosmic rays, anisotropies assoc. with solar rotation 80—67481
rotation of Sun, causing variation of diurnal anisotropy 80—41677
semi-diurnal anisotropy on flare days 80—46356
short-term fluctuations, evidence for solar origin 80—67483
short-term variations of galactic cosmic ray intensity, 1964-67 period 77—64550
solar daily variation anisotropy 80—46355
solar equator vicinity, daily cosmic ray flows during solar cycle 78—69622
solar flare of 1976 April 30, modulation region 80—67484
solar surface oscillations, cosmic ray flux modulation 79—8777
solar wind, high speed stream effects on solar cycle 20 cosmic ray modulation 80—72914
solar wind, origin, space charged particle repulsion by light *(Chinese)* 78—16388
solar wind plasma/cosmic rays energy exchange, depend. on cosmic rays radial gradient orientation *(Russian)* 79—53682
stationary solar particles modulation in interplanetary space 77—25896
stellar daily variation, semiannual modulation 78—69626
storm, symmetrical equator-pole anisotropy rel. to solar plasma regime 78—89020
stratosphere cosmic rays, eleven-year cycle 80—4212
sunspot cycle, cosmic rays and LF radio-waves signal vars. 77—78560
sunward flowing proton and alpha particle fluxes, solar wind vel. depend. 78—89016
transient cosmic ray intensity vars., solar flare origin 78—89021
transient cosmic ray intensity vars., solar source 78—89022
transient diurnal variation, spectrum anal. and correl. with interplanetary mag. field fluctuations 79—25416
transient variation origin, rel. to flares with type IV radioemission 79—40043
transport theory, effects of particle drift 77—45263
tridiurnal intensity variations, theory 77—33305
μ, long-period variation in galactic cosmic-ray distrib. 77—53382

cosmic ray solar modulation continued
H and He fluxes, modulation in 1974-1975 near solar minimum 77—33304
^{4}He anomalous component, solar latit. and radial depend. 79—35080

cosmic ray variations
see also geomagnetism
11 year cosmic-ray cycle, galactic and sdlar protons anal. 77—53360
11 year galactic cosmic-ray cycle, anomalous effects 77—53359
11 year modulation cycle rel. to sunspots and solar general mag. field 79—21114
11 year variations during 19th and 20th solar cycles 79—84602
27-day cycle, amplitude, quasistationary treatment 77—53369
27-day cycle and anisotropy rel. to solar activity epoch 77—53370
1972, August cosmic ray storm, north-south anisotropies and related phenomena 78—89018
1977, September, cosmic ray storm obs. in wide rigidity range 79—48632
active solar processes, manifestation in interplanetary space from data of cosmic ray variations 78—57411
altitude differences and geomag. field secular changes effects 78—93058
anisotropy of 50-1000 GV radiation and IMF sector structure 79—48639
annnual and semiannual vars. 80—26704
annual and semiannual variations, phase reversals. rel. to Sun polar mag. fields reversals 78—40780
charged-particle scatt. in interplanetary mag. field, cosmic-ray fluctuations 77—53352
conference, Yakutsk, USSR (Jun. 1977) 79—80110
cosmogenic isotope production in Earth atmosphere, secular vars. 79—53686
cyclic variations in cosmic rays and solar activity, detect. from radiocarbon meas. 79—16776
daily intensity variation, depend. on mag. storms, sunspot no., and solar flux 79—35082
differential, ionospheric and ^{14}C coupling coeffs. for investigation of variations 79—80142
diurnal anisotropy, anal. of 80—94660
diurnal anisotropy energy spectrum in 1971-75 period 79—80136
diurnal anisotropy of cosmic rays, 1937 to 1973 period 77—22025
diurnal anisotropy of intensity, solar flare location effect 79—44318
diurnal harmonics, underground muon data, corotational model 77—70958
diurnal variation, fundamental and second harmonic 77—53363
diurnal variation, power spectrum anal. 79—25416
diurnal variation of cosmic ray intensity, interplanetary diffusion coeffs. calcs. 79—29952
diurnal variation of cosmic ray intensity, two approaches to study 79—29953
electrons and γ-rays, short-period fluctuations, in upper atm., correl. with solar diameter vars. 79—21115
electrons and protons quasiperiodic pulsations in stratosphere 79—80133
eleven-year cycle, in stratosphere cosmic rays 80—4212
energetic particles intensity meas., 1973 Sept., by interplanetary probes 77—29604
energetic storm particle events connection with interplanetary shock wave parameters 79—70935
energy variation in interplanetary space of solar and galactic cosmic rays 80—101505
fast electrons long-term vars. in Earth's outer radiation belt 78—49226
fast timing ang. distrib. meas., data anal. 78—49256
fluctuations at 250 GV, spectral analysis 79—75062
flux in atmosphere, primary and splash albedo components, polar orbiting satellite meas. 79—25415
Forbush decrease, 1978 February 14-15, bidirectional anisotropy 80—41678
Forbush decrease in model of solar wind shock wave *(Chinese)* 80—90302
Forbush decrease of February 1978, Australian neutron monitor recordings 79—48630
Forbush decrease propag. to 16 AU 79—96866
forbush decreases: origin and development in the interplanetary space 79—75059
Forbush decreases, initiation and propag. from solar flares *(Korean)* 77—53335
Forbush decreases, origin of transient north-south anisotropy of cosmic rays 77—9634
Forbush decreases, struct. 77—91385
Forbush decreases and corresponding solar flares during solar cycle 20, 1965-72 period 78—49249
Forbush decreases and geomagnetic storms rel. to interplanetary parameters 77—70956
Forbush decreases and interplanetary mag. field disturbances 77—60551
Forbush decreases and interplanetary mag. field structure 77—53365
Forbush decreases and solar anisotropy, 11-year vars. 79—44317
Forbush decreases during August 1972, review of obs. 77—25894
Forbush decreases in 1973-1974, unusual characts. 80—12624
Forbush decreases in August 1972, summary of solar/interplanetary events 77—25991
Forbush effect, 1969-1970 world data 77—53367
Forbush effect, galactic cosmic ray currents obs., interplanetary mag. field inhomogeneity 79—80124
Forbush effect in intensity of solar protons 79—80126
Forbush effect in solar wind particles 80—98532
Forbush fine structure and interplanetary shock-wave fronts 77—53366
galactic cosmic ray intensity out to 18 AU, Pioneer 10 and 11 obs. 80—90297
galactic cosmic rays, annual vars. from anisotropic diffusion in interplanetary space 77—60550
galactic cosmic rays, solar latitude variations from chondrite cosmogenic isotope radioactivity 80—101507
galactic cosmic rays 11-year cycle, modulation coeff. energy depend. 78—28460
galactic cosmic rays affected by Sun's inner heliosphere, models 80—90298
galactic cosmic rays anisotropic diffusion in interplanetary space, 11-year var. 77—25891
galactic cosmic rays anomalous intensity during 20th solar cycle rel. to solar total mag. field 79—80132
galactic cosmic rays equatorial modulation and north-south asymm. 78—16253
galactic cosmic rays var. with solar cycle and coronal mag. field 78—7974

cosmic ray variations continued

- galactic cosmic-ray flux, origin of solar mag. cycle depend. semiannual var. 79—16777
- galactic protons, spectrum vars. meas. by Venera 9 and Venera 10 probes 77—91388
- geomagnetic field effects, development of cosmic ray studies 77—17308
- geomagnetic field interaction, influence of partially magnetospheric current systems on cosmic ray flux *(German)* 80—51609
- ground level enhancements, comparison of 1977 Nov. 22 and 1969 Feb. 25 events 79—40042
- ground level recording methods, progress 77—53336
- high energy particles anisotropy characts. near solar minimum 79—84607
- inclined muon monitors, muon spectra, generating functions, rel. to diurnal variation at Kiruna 78—85783
- inner solar system, past cosmic ray intensity from ^{26}Al in Fe meteorites 79—44422
- intensity, long term, ^{14}C obs. in known age specimens 80—101516
- intensity at Earth of supernovae cosmic rays, cosmogenic isotope obs. 80—101503
- intensity data, for atmosphere mean-mass temp. vars. determ. 77—91387
- intensity fluctuations, semi-diurnal anisotropy 80—12625
- intensity fluctuations, sudden increases and sharp decreases 77—70955
- intensity of cosmic radiation on Earth and in Galaxy, diffusion restriction by mag. fields 77—13191
- intensity pulses, north-south anisotropy of Earth based obs. 80—56687
- intensity solar diurnal variation, interplanetary mag. field north-south component correl. 78—93057
- intensity variations in interplanetary space, 1972-7 period 80—72726
- intenstiy variations in midlatit. stratosphere, total solar mag. field effect 79—62696
- interplanetary, rel. to Dhajala chondrite cosmogenic radioisotopes 79—35207
- interplanetary disturbances rel. to mag. and comsic ray storms 77—33313
- interplanetary intensity fluctuations 77—78585
- interplanetary magnetic field related variations, rel. to lower ionosphere and lower atmosphere 80—8510
- interplanetary magnetic field sector structure effect on cosmic ray diurnal var. 79—84622
- interplanetary propagation, two-particle distrib. function and cosmic-ray intensity fluctuations 78—28457
- interplanetary proton flux rises, 1973 Aug.-Sept., correl. with solar wind vars. 79—21123
- interplanetary scintillations at 250 GV, statistical props. 80—8496
- latitude distribution var. with time of cosmic rays in atm. 79—84601
- limits from ^{10}Be var. in marine sediments 79—29748
- long period intensity variations freq. spectra 77—25892
- long term composition changes from lunar fossil tracks 77—60552
- low-energy electrons, quiet-time increases, Jovian origin 77—2367
- meteorological, geomag. and interplanetary vars., separation via spectrographic instrument set 79—12404
- meteorological conditions determ. from cosmic ray obs., spectrographic method 78—69627
- muons, sidereal daily var. rel. to cosmic rays ang. distrib. at heliosphere boundary 79—80116
- Musala anisotropy, 10^{11}-10^{14} eV range 78—49255
- Musala station, obs. of anisotropy 78—49253
- neutron component, short period vars. *(Russian)* 79—96865
- neutron component vars. during September 1977, Mirny and Moscow obs. 80—105137
- neutron flux variations meas., Elbrus spectrographic system appl. 79—84605
- neutron intensity variations, hysteresis, fluctuations and barometric and ionospheric effects 79—84604
- neutron monitor diurnal anisotropy, effects of fluctuations and noise 77—45264
- neutron monitor diurnal anisotropy, effects of non-field-aligned diffusion 78—32304
- neutron monitor total vector anisotropy 79—53685
- neutrons and mesons, lunar variations of intensity 79—80146
- nonstationary modulation theory, self-similar solns., rel. to vars. obs. on Aragats Mountain 79—80143
- north-south anisotropy at balloon altitudes 77—29608
- north-south asymmetry, interplanetary mag. field sector polarity determ. 79—30009
- north-south asymmetry of solar activity and cosmic rays 79—80137
- nucleonic component of cosmic rays, diurnal variation coeff. 79—75060
- particle anisotropy at ultrarelativistic energies, EAS distribs. 77—64565
- particle flux variation, correlation with atmospheric variables 77—22030
- past cosmic ray intensity using time variations of tree ring stable isotope conc. 78—61692
- primary cosmic ray fluctuations, Musala Peak obs. 78—49254
- protons and α-particles intensity increases at front of interplanetary shock wave 79—53695
- protons flares, fast particles flight time from cosmic ray increases 77—17469
- recurrent Forbush decreases and solar active regions rel. to M-regions 78—96367
- Sayan spectrograph data, on intensity vars. of interplanetary, magnetospheric and atmospheric origins 79—84606
- semidiurnal anisotropy, latitude dependence 79—48631
- semidiurnal variation, possible source in imperfect corotation 80—8497
- short period, 2-60 cycles/hr., possible meteorological variations 77—53371
- short-period variations, interplanetary shock wave struct. determ. 79—80125
- short-term cosmic ray fluctuations, time anal. 80—67483
- short-term variations of galactic cosmic ray intensity, 1964-67 period 77—64550
- sidereal variation of 10^{11} eV particles and interplanetary mag. fields 80—17452
- sidereal variations, muon obs. at 150 m underground 79—53687
- solar activity, cosmic-ray variations, and neutrino fluxes, review 79—84599
- solar activity effect on cosmic rays 77—53340
- solar activity rel. to intensity vars. 78—69625
- solar activity variations and origin of ^{10}Be, ^{26}Al 77—53361
- solar anisotropy of high-energy cosmic rays, var. with solar activity cycle 80—51628
- solar cosmic rays, preflare enhancements rel. to solar X-ray emission 78—45166

cosmic ray variations continued

- solar cosmic rays during August 1972, square wave var. 77—25895
- solar cycle variation, effect of directional medium-scale interplanetary vars. 77—29605
- solar daily variations, computation from anisotropic diffusion theory 80—4209
- solar energetic storm particle events, ^{4}He/H ratio vars., theory 77—9636
- solar flare particle intensity variations, depend on interplanetary mag. field and solar wind 80—77372
- solar flares effects 79—84764
- solar modulation, climate record from tree ring ^{14}C link with solar variability 80—101424
- solar particles intensity vars. assoc. with interplanetary mag. field disturbances 78—40779
- solar proton flux affected by photosphere and interplanetary field 80—41672
- south-north asymmetry in high latit. magnetosphere, 1969-77 period 79—84600
- spectrographic investigation method and mean-mass temp. 78—73588
- spectrographic investigation via inclined muon telescopes, using difference coupling coeffs. 78—45167
- spectrographic method for extraterrestrial and magnetospheric cosmic-ray variations studies, penumbra 77—87217
- spectrographic variations data, reliability ensurance 79—84610
- stellar daily variation, semiannual modulation 78—69626
- stratosphere obs., evidence for interplanetary modulation processes 80—101508
- sunspot cycle, cosmic rays and LF radio-waves signal vars. 77—78560
- temperature variations, spectrographic obs. of secondary cosmic rays 78—69628
- transient cosmic ray intensity variations, origin 77—70957
- transient cosmic ray intensity vars., solar flare origin 78—89021
- transient cosmic ray intensity vars., solar source 78—89022
- transient variation origin, rel. to flares with type IV radioemission 79—40043
- tridiurnal intensity variations, theory 77—33305
- two year variations in Earth atm., sonde obs. 80—101511
- ultrahigh energy cosmic ray origin and propagation 78—49242
- underground obs. of fluctuations, nonlinearities effect on power spectrum 80—41679
- underground observations, difference coupling coeffs. and difference meteorological coeffs. 78—28464
- underground observations, spectrographic method, medium to high energy range 78—32307
- unusual cosmic ray storm (1978, February), symmetrical equator-pole anisotropy 78—89020
- μ, long-period variation in galactic cosmic-ray distrib. 77—53382
- ^{14}C concentration in Earth's atmosphere, corrections with astrophysical and geophysical phenomena 78—61477
- ^{14}C in atmosphere content variation, past geomagnetic and cosmic ray intensity variations 78—61691
- He isotope composition of solar cosmic rays from Venera 9 obs. 80—72725
- O_3 levels in stratosphere, solar activity, cosmic rays effects 77—53362

cosmic ray X-rays

- background of hard X-rays, produced by pregalactic black holes? 80—56978
- background radiation, possible origin 80—94898
- background sources, detectability in deep X-ray surveys 78—96567
- bursts, origin rel. to max. mass of neutron stars 77—33545
- bursts tails, interpretation 79—12546
- diffuse 80—82551
- diffuse 2 to 10 keV background, contrib. from, Seyfert galaxies emission 78—93392
- diffuse background, active galactic nuclei contrib. 78—36733
- diffuse background, contrib. of intermediate-luminosity X-ray galaxies 79—2578
- diffuse cosmic and atmospheric MeV γ-rays, balloon obs. 78—4048
- diffuse soft X-ray sky, astrophysics rel. to 0.1-2.0 keV cosmic X-rays 78—16581
- diffuse soft X-rays, galactic, brightness distrib. 79—53942
- diffuse soft X-rays from H I deficient region in Hercules, O VII emission line obs. 79—25759
- diffuse X-radiation background above 20 keV, balloon obs. 78—54096
- diffuse X-ray background, constraints on non-thermal source syntheses 80—27021
- diffuse X-ray background, contrib. of distant quasars 79—92892
- diffuse X-ray background, contrib. of intercluster medium emission 80—4426
- diffuse X-ray background, implications of Hubble const. for discrete source models 79—101226
- diffuse X-ray background, implications of luminosity functions of Seyfert 1 galaxy nuclei and BL Lacertae objects 80—8682
- diffuse X-ray background, normal galaxies contrib. 79—17141
- diffuse X-ray background, rel. to intergalactic matter 80—109543
- diffuse X-ray background, search for correl. with light of galaxies 80—56977
- diffuse X-ray background, source 78—8168
- diffuse X-ray background, spectrum from 3 to 50 keV 80—41916
- diffuse X-ray background and extragalactic X-ray sources 79—58447
- diffuse X-ray background intensity, implications of uniformity of quasars radial distrib. in chronometric cosmology 80—105409
- diffuse X-ray flux in 2 to 7 keV range, galactic component obs. 80—98745
- diffuse X-rays component, separation method using growth curves 79—25512
- galactic soft X-ray background rel. to coronal gas O VI absorpt. 78—36653
- proportional counter for cosmic X-radiation recording, 2 to 25 keV, optimal characts. 77—23375
- soft X-ray background, three-band obs. rel. to thermal emission models 77—45604
- soft X-rays, spectrometer for diffuse background 77—5440
- solar and cosmic X-rays and gamma-rays, obs. by Signe II MP satellite expt. 80—41696
- supernova γ- and X-rays, recorded by Antarctic ice NO_3 content 80—31314
- ultrasoft X-ray background, obs. in S galactic hemisphere 77—45615
- X-ray bursts, OGO-5 satellite obs. 77—13492

cosmic rays
- *see also cosmic ray absorption; cosmic ray apparatus; cosmic ray composition; cosmic ray effects and interactions; cosmic ray energy spectra; cosmic ray origin; cosmic ray propagation; cosmic ray showers and bursts; cosmic ray solar modulation; cosmic ray variations; galactic cosmic rays; geophysical aspects of cosmic rays; high-energy cosmic ray interactions; primary cosmic rays; radiofrequency cosmic radiation; solar cosmic ray particles; solar radiation*
- astronomical observations, research programme at Blackett Lab., Imperial College, review 79—66890
- coherent propagation in random mag. field, perturb. calc. 77—17303
- conference on nuclear cosmic physics, Leningrad, USSR (Oct. 1978) 80—98755
- conference proceedings, 15th IUPAP International Conf. Plovdiv, Bulgaria (Aug. 1977) 78—49239
- confinement, effect of interstellar MHD turbulence 77—49246
- cosmological, existence, nuclear gamma-ray prod. 78—16251
- cosmological cosmic rays, prod. of light elements 78—12436
- detection, acoustic radiation by charged atomic particles in liquids, theoretical anal. 79—89526
- distribution in vicinity of front of nonstationary shock wave 77—17304
- energy loss in solar wind magnetic field 77—53347
- energy spectra and anisotropy *(Hungarian)* 79—44319
- galactic centre γ-rays from trapped cosmic rays 77—87212
- HZE particle radiation studies, Kosmos 782 biosatellite 79—16778
- intensity spectrum correl. with interplanetary mag. field inhomogeneity spectrum 77—53348
- ionosphere, cosmic ray layer, electron density distrib., radiowave absorpt. 77—22024
- lunar charged particle albedo, Luna 22 data 80—56729
- magnetoelectric dipole structure hypothesis, biological and cosmic appls. 80—91124
- nature and astrophysical sources, review 78—77486
- new particles, balloon meas. *(Japanese)* 79—80112
- particle anisotropies, meas. via multiple telescopes 77—82103
- progress in cosmic ray astronomy *(Chinese)* 79—75058
- propagation, modulation and acceleration in magnetised plasma 77—53346
- propagation in interplanetary mag. field, diffusion approx. of kinetic eqn. 77 - 13193
- protosolar system, cosmic ray fluxes determ. from meteorites B isotopic anomalies 80—4462
- Salyut-6 orbital station, cosmic radiation dose field meas. 80—89876
- scattering on magnetic inhomogeneity, spectrum, transport range 77—53345
- space sciences, conf., Trivandrum, India (Jan. 1977) 78—69586
- spacecraft interiors high linear energy transfer particle meas. 77—41272
- spatial cosmic ray gradient from ^{37,39}Ar content of meteorites 77—17312
- threshold rigidity correl. with secular variations in geomagnetic field 77—53368
- transport, steady-state eqn., similarity solns. 78—16254

cosmic X-rays *see cosmic ray X-rays*

cosmogony *see cosmology*

cosmology
- *see also black holes; element origin; general relativity; red shift*
- $\lambda\phi^4$ theory, conformal symmetry breaking, cosmological particle creation 80—90998
- Abell clusters, 3-D nearest neighbours test 80—90545
- abundance of stable particles prod. in early Universe 79—44653
- accelerating Universe models 78—57707
- acoustic nonlinear adiabatic waves in self-gravitating gas, astrophys. appl. 78—28512
- acoustic wave spontaneous birth in early Universe *(Russian)* 80—90593
- adiabatic cosmological perturbations, propag. through matter-radiation decoupling era rel. to galaxies form. 80—62337
- adiabatic density perturbations, evolution in radiation era 79—25769
- adiabatic regularisation, quantum field in Robert-Walker metric 78—73916
- aether drift experiments, nonuniformity of background radiation 78—93482
- age of universe, from ^{186}Os, ^{187}Os neutron capture cross section ratio 77—6384
- age of Universe, impossibility of an infinite past 78—62029
- Ambartsumian's proto-matter hadronic nature from ang. momentum-mass relation 80—77528
- amorphous state analogy 79—54370
- ancient Chinese cosmology 77—33816
- angular diameter-redshift relation for matter and radiation filled universes 78—20917
- anisotropic and homogeneous cosmological models in renormalised theory of gravitation 79—2703
- anisotropic Bianchi II cosmological models with matter and electromagnetic fields 79—48976
- anisotropic cosmological solutions in theory with quadratic invariants *(Russian)* 77—91673
- anisotropic dust filled model, closure result 77—37676
- anisotropic incoherent fluid cosmological model in general relativity 79—40303
- anisotropic uniform model universes with cosmical const., flat space 78—73788
- anisotropic universe, particle generation and vacuum polarisation 77—74626
- anisotropic universe, relict radiation polarisation and anisotropy 80—67917
- anisotropic universe, scalar particle creation 78—77487
- anisotropy damping through quantum effects in early universe 78—57708
- anisotropy dissipation by scalar particle prod. in early universe 80—86025
- anomalous Hubble expansion, local supercluster of galaxies 78—4419
- anomalous Hubble expansion and inhomogeneous cosmological models 77 13513
- anomalous nuclei, primordial synthesis 80—46719
- anthropic principle, rel. to physical world struct. 79—48973
- antimatter, in laboratories and Universe, expts. and obs. data *(Polish)* 79—88588
- antimatter, origin, whereabouts 80—62340
- antimatter cosmologies, observational tests, review 77—26095
- antimatter in Universe, hiding place in primordial black holes 80—22126
- antimatter near Galaxy from information on neutral pion production processes *(Polish)* 77—70999

cosmology continued
- aspherical gravitational collapse, matter associated perturbations, linear Einstein field and conservation eqns. 79—5843
- aspherical structure growth, Local Supercluster kinematics 79—92899
- astronomical bodies, mag. field, cosmological interpretation 80—46714
- asymmetric creation of matter and antimatter in the expanding Universe 79—75302
- asymptotic freedom condition and temp. of relict radiation of Universe *(Russian)* 77—91676
- axions and Higgs particles, astrophysical mass bounds 79—5745
- axisymmetric gravitational collapse with escaping neutrinos, Einstein's field eqns. 80—26888
- background 2.7K radiation coherence rel. to black body and cosmological models 79—97108
- background 3K radiation, cosmological implications 79—97117
- background gravitational radiation spectra in early state of the Universe *(Russian)* 80—36745
- background isotropic radiation excess at 1 MeV, possible origin from Seyfert galaxies 80—77522
- background microwave radiation, cosmological explanation *(Polish)* 80—41920
- background radiation, meas. at 2 mm *(French)* 77—13503
- background radiation, ray aberration large-scale anisotropy 78—24576
- background radiation *(Italian)* 79—48966
- background radiation density, accreting black holes contrib. 80—4461
- background radiation fluctuations at 1394 MHz 79—53941
- background radiation nonequilib. distrib., radiation flux spectrum source 80—46710
- background radiation small-scale angular fluctuations 77—82332
- background radiation spectrum, cosmological significance of obs. *(Italian)* 79—48972
- background radiation spectrum, early energy release distortion in Rayleigh-Jeans region 80—73077
- background radiosources, Westerbork survey, angular size distrib. and source count 78—96553
- baryon annihilation 80—90590
- baryon asymmetry in Universe, thermodynamic equilib. departure *(Russian)* 79—48975
- baryon asymmetry magnitude in CP violation model 80—36754
- baryon asymmetry of the Universe, unitarity and possible origins, comments 79—88589
- baryon asymmetry of Universe *(Russian)* 79—62945
- baryon asymmetry origin, unification mass 80—31398
- baryon asymmetry with cosmological asymmetries, theory 80—4464
- baryon excess, finite temp. gauge theory effects, entropy 80—51933
- baryon number domain structure, from symmetry breaking in grand unified field theories 79—84876
- baryon number generation in grand unified theories 79—26279
- baryon number generation mechanism in expanding universe 80—51931
- baryon number of the Universe 79—30163
- baryon number of universe and $\bar{p}$ decay 77—91422
- baryon production, expanding Universe, baryon to entropy ratio, number nonconservation 79—44652
- baryon production, kinematical constraints for heavy boson decay 80—51932
- baryon production mechanisms, and formulas 80—36753
- baryon symmetric big bang cosmology 78—61945
- baryon synthesis from unconfined primordial quarks 80—57566
- baryon-symmetric, cosmic microwave background distortions 78—65727
- baryon/photon ratio bounds due to human existence, grand unification 80—62345
- baryons, origin in Universe 79—62938
- Belavin Yang-Mills pseudoparticle soln., metric representation, isotropic Universe relation 80—27404
- Bertotti-Robinson EM universe 78—36741
- Bianchi cosmologies, classification in conformal flat space times 80—56985
- Bianchi cosmologies, singularities, Einstein eqn. solns., review 80—12837
- Bianchi IV cosmological model, exact solns. 77—67151
- Bianchi IX model, spectral asymmetry and QFT in curved spacetime 80—56982
- Bianchi IX type bouncing mixmaster universe, size 80—56989
- Bianchi model Lie groups, automorphisms 79—30313
- Bianchi model universes, hypersurfaces of transitivity, Riemann curvature 80—67922
- Bianchi models, inhomogeneous generalisation 80—46718
- Bianchi type I anisotropic universe, quantum gravitational effects *(Russian)* 78—24588
- Bianchi type I cosmological soln. in new gravitational theory 79—88775
- Bianchi type I model, viscous dissipation 77—13507
- Bianchi type I space-time gravitational field, particles eqn. of state 80—77664
- Bianchi type I universe, quantized scalar field 78—4549
- Bianchi type I universes, scalar field propagators 77—41427
- Bianchi type II exact cosmological model with matter and EM field 80—105560
- Bianchi type II model, effect of viscosity *(Russian)* 77—45624
- Bianchi type IX universes, neutrino viscosity 78—77633
- Bianchi type V model, matter dynamics, horizon and singularity problems 80—36749
- Bianchi type VI model with EM field, comment 77—33711
- Bianchi type VII homogeneous cosmological models 77—17734
- Bianchi type VIII spatially homogeneous cosmologies 77—17729
- Bianchi type-I cosmologies and spinor fields 80—62347
- Bianchi type-I universe, entropy per particle in early stage 77—17732
- Bianchi type-I universes, entropy prod. and viscous dissipation 78—8179
- Bianchi type-V universes, neutrino viscosity 79—9042
- Bianchi universes, magnetic fields and fluids with conductivity 80—83864
- Bianchi V LRS dust space-times, intermediate singularities, whimpers, instability 80—36750
- Bianchi V type universe, red shift and anisotropic microwave background 80—98744
- Bianchi VI$_0$, VII$_0$ cosmological models with spin and torsion 80—46720
- Bianchi VIII/IX cosmological models, anisotropic, with matter and EM fields 78—73784
- Bianchi-type I universe, causally connected DeWitt's two vacuum states 78—12608
- Bianchi-V cosmological space-time, Einstein-Weyl equations, neutrino currents 80—86023
- Bianchi-V universe with Proca field, torsion singularities 77—67149

cosmology continued
- big bang, evidence from quasars and microwave background radiation 77—37611
- big bang, evidence from radiosource obs. 77—2503
- big bang, helium synthesis, neutrino flavors, and cosmological implications 80—73084
- big bang, photon condensation and longit. background radiation in Universe 79—40307
- Big Bang evolutionary eras *(German)* 80—17707
- big bang model, element prod. 78—8177
- Big Bang model, galaxy cluster missing mass from massive leptons, additional ν species 78—81719
- big bang model, hot, observational cosmology 78—12444
- big bang model and cosmic black body radiation 77—9830
- big bang model and microwave background at $z=40$, transparency of dust grains 78—28869
- big bang nucleosynthesis, cosmology and neutrino physics constraints 79—30154
- big bang nucleosynthesis, lifetime and mass constraints of heavy lepton neutrinos 79—40308
- Big Bang primordial fluctuations and Universe smoothness in grand unified theories 80—56987
- big bang theory and phys. singularities in general relativity theory *(Russian)* 78—81893
- big-bang model and ^{4}He abundance, review, book contrib. 78—89277
- big-bang nucleosynthesis with nonzero lepton numbers 78—16583
- bimetric gravitation theory, cosmological basis, closed universe 78—65844
- bimetric gravitation theory, cosmological model 77—33710
- bimetric theory of gravitation, cosmological models 77—41424
- binary galaxies, late type, mass-to-light ratios from luminosity-weighted averages 78—8113
- binary stars and cosmology 77—41393
- black hole, Kerr-Newmann, spontaneous discharge 78—12288
- black hole, point source spherical model, Schwarschild coord. frame, nature of interior universe 77—67107
- black hole and galaxy form. in cold early universe 78—16585
- black hole in external mag. field, relativistic particle radiation 80—22035
- black hole particle emission process, high energy limit 77—5544
- black hole quantum evaporation, baryon asymmetry of the Universe *(Russian)* 80—109577
- black hole thermodynamics, cosmological event horizons and particle creation 77—67152
- black holes, cosmological density 78—77573
- black holes, gravitation, charges, cosmology and coherence, elementary particles and Dirac large numbers 79—2477
- black holes, primordial, possibility of cold cosmological singularity *(Russian)* 77—22266
- black holes in closed universes 78—16454
- Bose-Einstein condensation in an Einstein universe 78—77797
- Brans-Dicke and relativistic cosmologies, differences and possible tests *(Polish)* 80—27024
- Brans-Dicke closed space cosmology, exact soln. for radiation-filled era 78—93488
- Brans-Dicke cosmology, nonhomogeneous space-time 80—86024
- Brans-Dicke cosmology, the cosmological term 78—24582
- Brans-Dicke theory, cosmological solns. for homogeneous isotropic universe 78—96579
- bright phase in galactic evolution, intergalactic gas ionization 77—26065
- 3C 273, UV spectrum, 1200-1700 Å, cosmological implications 78—45425
- calibration theory and gravitational const. variation in early universe *(Russian)* 80—17706
- canonical quantisation of gravity, QFT in curved spacetime, Bianchi I cosmology 80—27202
- Cauchy problem for general relativistic perfect magnetofluid 78—70024
- causal universe, cosmological matter creation 79—53945
- causality problems in special relativity, tachyons in an expanding universe 79—67155
- causally continuous closed universes, props. 78—29011
- causally symmetric spacetimes 77—74281
- chaotic cosmology, theory and appls. 77—57112
- chaotic Universe, Friedmannian expansion, degree of chaos and He abundance 80—67920
- chaotic Universe, Friedmannian expansion 80—67919
- charge in cosmological models, effect on curvature parameter 78—69921
- charged homogeneous cosmologies, theory 79—25767
- charged universe, cosmology 79—25766
- chronometric cosmology, appl. to radio sources apparent superrelativistic vels. 79—25768
- chronometric cosmology, uniformity of quasars radial distrib. rel. to X-ray background 80—105409
- chronometric predictions, tests using galaxy and quasar samples 80—86022
- chronometric redshift theory, erroneous presentation correction 78—85839
- chronometric redshift theory and QSO superluminal vels. 79—9023
- classical field component of galaxies, test 77—33658
- classical spontaneous breakdown of symmetry and induction of inertia 79—40417
- classification scheme for non-rotating inhomogeneous cosmologies 80—8726
- clock paradox as cosmological problem 78—36907
- closed Friedmann cosmos, entropy prod. density for chem. reactions *(German)* 77—26101
- closed Friedmann model, metric perturbations, closed form solns. 80—22129
- closed Universe, elliptical de Sitter metric 80—109570
- closed universe, S^3 topology, rel. to Dante's Divine Comedy 80—41980
- closure hypothesis in cosmic turbulence theory 79—35438
- clusters of galaxies, ang. size-redshift relation for nearby clusters 78—4372
- clusters of galaxies, mean density and correl. function, theory and obs. 78—24559
- clusters of galaxies, self-similar gravitational clustering theory 80—4447
- clusters of galaxies, space distrib. compared with radio sources *(Chinese)* 79—17111
- clusters of galaxies, tidal forces in inhomogeneous cosmological models 80—62338
- clusters of galaxies, X-ray sources evolution 79—17133

cosmology continued
- cold dense universes, photoionisation by quasars, QSO spectral indices and cut off energy determ. 80—77526
- collapsing gas cloud, stopping of fragmentation 77—60856
- collective relaxation in galaxy correlations 78—24579
- coloured cosmological black holes, soln. of Einstein-Yang-Mills system 79—12492
- composite Hubble diagram, rel. to Friedmann cosmology 77—22333
- composite particle formation in explosive nucleosynthesis 78—69678
- conference, singularities in general relativity, Waterloo, Canada (Aug. 1977) 80—31405
- conference on Universe at large redshifts, Copenhagen (June 1979) 80—57000
- conformal and gauge spontaneous symm. breaking, cosmology quantum effects 80—37185
- constraints, galactic evolution from light-element abundances, models 80—31401
- continuous creation cosmologies and large number hypothesis 77—78902
- contracting and expanding universe without singularity, thermal particle prod. 78—73785
- correctionless observational cosmology 79—53946
- correlation function for density perturbations in expanding universe, linear theory 78—4417
- correlation function for density perturbations in expanding universe, non-linear theory 78—8173
- cosmic blackbody radiation, anisotropy detect. 78—4415
- cosmic censorship and test particles, black hole destruction 80—105552
- cosmic dust density and composition rel. to expansion of Universe 77—41403
- cosmic gas clouds of fragmentation, form. of galaxies and first generation of stars 77—33628
- cosmic glack body radiation meas. using low temp. optical techniques, 2-40 cm^{-1} 79—71161
- cosmic inhomogeneities physical origin, conjecture 80—56986
- cosmic microwave background, Sunyaev-Zel'dovich effect in millimetric region 79—25765
- cosmic microwave background, translational anisotropy and galactic dust clouds far IR emission 77—33706
- cosmic microwave background spectrum, G-varying cosmology 80—86020
- cosmic rays existence, light-elements and γ-rays prod. 78—7841
- cosmic rays existence, obs. constraints set by γ-ray background, Li and D abundances 78—7842
- cosmic turbulence evolution through period of recombination 77—64895
- cosmic virial theorem 77—17726
- cosmic X-ray background, search for correl. with light of galaxies 80—56977
- cosmogony, Earth and Moon origin, book 80—17266
- cosmogony, exact soln. of general relativity eqns. for oscillatory collapse *(Russian)* 77—87256
- cosmogony, model comparisons 80—17508
- cosmogony of solar system 80—41736
- cosmological bounce 77—49514
- cosmological changes in atomic and nuclear constants 77—49286
- cosmological const. and Einstein eqns. Kerr-Schild soln. 77—30059
- cosmological const. modification from correspondence limits of general relativity 78—24581
- cosmological constant, broken gauge theories and 3K black-body radiation 78—28870
- cosmological constant and supergravity 77—74171
- cosmological models, rel. to bimetric gravit. 77—17352
- cosmological principle, new look 78—86042
- cosmological red shift, Doppler and gravitational components using Birkhoff's theorem 78—86041
- cosmology and geophysics, book 79—12552
- 3CR radiosources, source counts and V/V_{max} tests for complete sample 78—77613
- curvature collineations in Godel and steady state universes 78—32620
- curved space-time, post geometric optics, dispersive effects of EM polaris. 78—96
- cylindrical general relativistic systems, numerical codes 80—67549
- cylindrically symmetric space-time, coupled EM and scalar fields 79—85035
- cylindrically symmetric universe in general relativity, Petrov type I degenerate 80—17705
- dark night sky paradox, expansion and hierarchical struct. of the universe 78—86055
- dark sky paradox and origin of universe 79—25770
- data reduction and cosmological constant 80—41923
- de Sitter universe and mechanics 78—21034
- decay of fluctuations in the early universe and high energy particle interaction 80—109573
- deceleration parameter, comparison of various cosmological tests, static Euclidean model 80—73081
- deceleration parameter, direct meas. via 3C 286 radio absorpt. line 78—20902
- deceleration parameter, influence on double radio sources separation depend. on redshift 80—22096
- deceleration parameter, test from galaxy clusters ang. size-red shift relation 78—12437
- deceleration parameter (q_0), determ. using galaxy clusters charact. size 78—36703
- deceleration parameter and Sunyaev-Zeldovich effect 79—62936
- deceleration parameter determ. method 77—29966
- deceleration parameter determ. using local data 80—62351
- deceleration parameter determ. using X-ray and microwave obs. of galaxy clusters 79—21476
- deceleration parameter meas., effect of intergalactic dust 77—5564
- deep galaxy samples correlation anal., techniques and appl. to two-colour sample 78—41056
- density fluctuations and vel. fields evolution through H recomb. 77—17727
- density irregularities on large scale, X-ray background evidence 80—105405
- density parameter, determ. from redshifts of complete sample of galaxies 77—29965
- density parameter, lower limit from NGC 1023 galaxy group dynamics 80—82521
- density perturbations development after recomb. 78—49569
- density perturbations in expanding universe, three-point correl. function and higher order functions prediction 78—65730
- diffuse cosmic far UV background, rocket obs. 80—46708

cosmology continued
diffuse gamma radiation, SAS-2 obs. 78—8169
diffuse gamma-ray emission from active galaxies 80—12806
diffuse gamma-ray isotropic background 80—51923
diffuse X-ray background, active galactic nuclei contrib. 78—36733
dimensionality and the generation of matter 79—101231
dimensionless gravitational coupling constant magnitude and cosmogony 77—33714
Dirac, Hubble-Sandage diagram for first ranked galaxies 77—57110
Dirac, matter creation, solar model tests 79—71163
Dirac, significance of microwave background 77—13508
Dirac's large number hypothesis, fundamental const. variability 77—67153
Dirac's large number theory, consequences for cosmology *(French)* 77—60859
Dirac's Large Numbers hypothesis testing using precision ranging to Mars 77—45616
Dirac's large-number hypothesis, angular momentum for Regge trajectory with n=2 80—18091
Dirac's multiplicative cosmology, stellar clusters theoretical isochrones with decreasing gravit. const. 78—16586
Dirac cosmology, comparison of theory with obs. 77—22334
Dirac cosmology, onset of galactic nucleosynthesis, and age of Universe 77—13514
Dirac cosmology, rel. to microwave background and QSOs 78—8176
Dirac Large Numbers Hypothesis, incompatibility with primordial nucleosynthesis 79—92900
discrete redshifts, anal. and absolute solar motion determ. 78—49530
discrete space-time, photon damping and galaxy redshifts *(Chinese)* 77—67145
distance determination, new method, appl. to weighing of Universe 79—9003
distance scale, Cepheid variables and cosmic distance measurement 79—84920
distance scale, spiral galaxies distances from tertiary indicators 79—30120
Doppler shift distributions in Universe, extragalactic peculiar motions 78—4416
double radio sources, cosmological implications of ang. size-redshift test 77—57100
dynamical eqns., variation of parameters 80—109568
dynamical space and gravitation within a purely geometrical framework including Machian ideas 78—93587
early big bang, asymptotic freedom, rel. to cosmic microwave background isotropy 80—46712
early nucleosynthesis and He and D abundances 80—62356
early Universe, baryon asymmetry development in big bang 80—62346
early Universe, baryon number generation due to CP- and B-violating interactions 80—109571
early Universe, EM and gravit. Green's functions 78—73786
early Universe, gauge theories, grav. constant time depend. and antigravity 80—90591
early universe, gauge theory symmetry breaking at high-temp. and density 77—22664
early Universe, horizon problem and the broken-symmetric theory of gravity 80—62344
early Universe, inhomogeneity and origin of entropy 80—62350
early universe, tepid model 78—20919
early universe density-temp. fluctuations, present observability 80—82554
early universe structure, spectral appearance of non-uniform gas at high z 79—92898
Earth as part of the Universe 79—5438
earthquake phenomena as cosmological manifestations 79—57856
education, Friedmann cosmology luminosity distance eqn. 78—6
education, Mach's principle, Einstein's equation and classical physics anal. 77—49524
education, nonscience majors, innovative course based on mass-radius diagram of states of matter 78—62002
education, Olbers' paradox, comment 78—86070
effective Lagrangian and pair prod. 80—22123
eigenvalue problem formulation, from Einstein eqn. 78—16704
Einstein's and Godel's universes, a unified treatment 78—41101
Einstein's contribution 79—71165
Einstein's contribution 1905 to 1915 80—77530
Einstein's contribution to relativity and cosmology *(Norwegian)* 80—4598
Einstein's cosmological constant, lunar ranging data anal. by Seelinger's theory 79—6040
Einstein's cosmological works *(Czech)* 80—27097
Einstein's equations, special exact solutions 77—41516
Einstein's field eqns., perfect fluid distrib. with eqn. of state., spherical symmetric space-time 78—32615
Einstein's field equations, inhomogeneous soln., for $p=\mu$ eqn. of state 79—12666
Einstein's theory of gravitation, for homogeneous cosmological models 79—12547
Einstein's theory of relativity, acceptance in Canada 80—68012
Einstein's universe, radiating charged particle 79—17302
Einstein eqn. spherically symm. solution in presence of conformally invariant scalar field 80—17846
Einstein eqns. with stiff eqn. of state, exact soln. 79—2677
Einstein equations, general cosmological solution, singularity problems 80—82686
Einstein equations, generalised de Sitter solution 77—26100
Einstein equations, plane-symmetric solns., dynamical consequences 80—31639
Einstein field eqns., exact soln. for metric with rotation in presence of matter *(Russian)* 77—74275
Einstein static universe, generalised, equilib. configs. for perfect fluids 77—45748
Einstein Universe, with source-free EM field 79—85036
Einstein-Cartan, Friedmann-like cosmological models without singularities 78—77632
Einstein-Cartan cosmology and singularity prevention *(Polish)* 77—71162
Einstein-Cartan theory, bounce of spheres 78—93572
Einstein-Cartan theory, rel. especially to elementary particle weak interactions 78—37171
Einstein-Cartan theory of gravitation, homogeneous isotropic cosmological model *(Russian)* 77—49510
Einstein-de Sitter model and metric, book contrib. 80—22248

cosmology continued
Einstein-de Sitter model for Universe at any epoch 79—17147
Einstein-de Sitter universe, classical predictive electrodynamics 80—86175
Einstein-Godel universe 79—2583
Einstein-Godel Universe with EM field 79—80376
Einstein-Lichnerowicz eqns., spatially homogeneous solns. 78—16708
Einstein-Maxwell eqns., some exceptional electrovac type D metrics with cosmological constant 79—75419
Einstein-Maxwell equations, inhomogeneous stationary cosmological solns. 80—62556
Einstein-Maxwell null field metric, exact cosmological solns. 79—67122
Einstein-Maxwell theory, cosmological model with gravitational, electromagnetic, and scalar waves 80—86188
Einstein-Straus unified field theory, cosmological appl. 79—67123
Einsteins eqns. of general relativity, cosmological soln. 78—12617
elastic spacetime rel. to black holes and gravitational waves 78—73625
electric charge polarisation of cosmic systems, appl. to stars and universe 79—48771
electrically polarized Universe model 78—36738
electromagnetic vacuum, isotropy, testing 77—87254
electrons, rest mass, continuous increase hypothesis *(Chinese)* 77—71209
element formation, inhomogeneity in D prod. 79—21471
element origin rel. to cosmology, review 80—62359
elemental abundances and origin *(French)* 77—26097
elemental evolution and isotopic composition, teaching 78—41128
elementary particle constants and cosmic object size, empirical relation 77—82338
elementary particle physics, Bose-Einstein condensation 80—27430
elementary particle physics, cosmological approach, review, book contrib. 80—68440
elementary particle physics, influence on understanding of Universe 80—51935
elements origin and evolution 78—32619
elliptical protogalaxies, dynamical evolution 78—32571
EM and gravitation fields in flat space time, relationship, hierarchy hypothesis 77—5732
EM Gowdy universe with 3-torus topology, primordial homogeneous EM field influence 79—88774
EM space isotropy, possible expt. check 77—13228
empty space Einstein eqn. solns., Mach's principle in spatially homogeneous spacetimes 79—17295
entropy perturbations rel. to microwave background fluctuations *(Russian)* 78—36735
entropy prod. in very early universe 78—32624
entropy production and viscous phenomena in early universe 77—82337
equivalence principle according to Mach 79—44823
ether as a neutrino sea 77—53728
ether as neutrino sea, materialistic basis for physical explanation 77—53729
event horizons, thermodynamic quantities and props. 79—97113
evolution of extragalactic radiosources 77—17728
evolution of large-scale structure from relict radiation temp. fluctuations 80—105360
evolutive mechanics, relativistic analytic mechanics 77—17800
evolving hierarchical cosmologies, cosmic background radiation fluctuations 80—101655
excitable ether composed of neutrinos, anomalous structural interactions explained 77—53730
expanding Mach-Einstein universes 80—51926
expanding shearfree spatially homogeneous universes, nonsynchronous time coord. 78—36740
expanding universe, BBGKY eqns. integration for development of strongly nonlinear clustering 78—8175
expanding universe, Bolyai-Lobachevsky vel. space, astron. obs. corollaries 77—71156
expanding universe, density correl. of gravitating point masses 77—33715
expanding Universe, density perturbations, correlation function evolution 79—44646
expanding universe, galaxy correls. time evolution, gravit. instability, model 79—17145
expanding universe, high freq. EM field propag., with Dirac coupling 79—58913
expanding universe, pseudo-Euclidean metaspace hypothesis 77—37677
expanding universe, scalar field propagator, particle creation 77—17733
expanding universe, shear growth 77—41425
expanding universe effect on quantum mechanics of electromag. bounded spin 1/2 particles 78—54271
expanding universe model with continuous mass creation 79—44647
expanding Universe primodial inhomogeneities, cluster halos density and vel. distribs. as cosmological probe 80—22122
expanding universe with bulk and shear viscosity in conformally flat coords. 78—96575
expanding universes, positive frequency and Hamiltonians 80—4624
extragalactic astronomy meeting (Paris, 11-13 December 1978) 79—97121
extragalactic background light, upper limit 79—17142
extragalactic distance scale, review of distance indicators 78—93396
extragalactic distance scale, tertiary distance indicators 79—25708
extragalactic distance scale 77—91640
extragalactic distance scale applied to galaxies in Local Group 78—89247
extragalactic distance scale using H II region fluxes and parent galaxy diameters 79—44576
extragalactic distance scale using H II region isophotal diameters 79—44575
extragalactic objects clustering in Universe *(Polish)* 78—96580
extragalactic radiosource counts rel. to big bang model 78—69920
extragalactic radiosources, cosmological evolution rel. to young galaxies and quasars 78—28799
faint extragalactic radio sources, counts estimate at 5 GHz 78—32588
faint galaxy counts, rel. to Friedmann cosmological model *(Russian)* 77—87584
fermion asymmetry of the Universe and the W condensate, Weinberg Salam model *(Russian)* 80—73087
fermion number nonconservation in cosmological models, Big Bang theory 79—80381
fermion pair creation near Friedmann singularity, energy density and press. *(Russian)* 77—57114
field equations for spatially homogeneous space-times 80—52083
field galaxies, luminosity function and space distrib. 79—88731

cosmology continued

- field galaxies space distrib., redshifts and photometry of complete sample 79−21418
- fine-scale anisotropy of microwave background, long-wavelength gravitational wave effects 78−81535
- finite universe, estimation of correl. using two stage sampling design 77−67146
- finite universe, idealistic concept *(Chinese)* 77−13509
- fluid drops as cosmological models, stellar evolution, solar system origin, planetary geology 80−73086
- formation of clusters of galaxies and secondary peak 80−77497
- formation of galaxies and clusters: violent gas dynamics 78−86018
- free quarks, production in early universe 80−393
- Friedman imperfect fluid cosmology, local EM field propagation 79−84872
- Friedman models, particle creation from vac. 77−5603
- Friedman models, the cosmological constant 77−64896
- Friedman models, viscosity effects *(Russian)* 77−29969
- Friedman universe, parallax depend. on redshift 78−12438
- Friedman universe asymptotic states, energy conditions using phase variable method 80−41922
- Friedmann, equations with cosmological constant, exact solns. 78−8180
- Friedmann cosmological model, explicit canonical quantisation. 79−21644
- Friedmann cosmological model quantisation, geometrical-dynamical anal. *(Russian)* 77−64636
- Friedmann cosmological models, relativity of space finiteness-infiniteness 78−96582
- Friedmann cosmological models, relativity of spatial and temporal finiteness and infinity 79−62941
- Friedmann cosmology in modern context *(French)* 79−2581
- Friedmann model, classical and quantum gravit. collapse problems *(Russian)* 77−87257
- Friedmann model, expanding Universe, nonlinear acoustic effects *(French)* 80−67921
- Friedmann model, hot hadronic matter in early universe, relativistic eqn. of state 78−45438
- Friedmann model, large distance meas. by triangulation 78−86047
- Friedmann model, quantum effects *(Russian)* 77−79025
- Friedmann model, spontaneous breaking of symmetry and evolution of Universe *(Russian)* 77−5607
- Friedmann model, spontaneous symmetry breakdown 80−51929
- Friedmann model anisotropic homogeneous generalisation, dynamics *(Russian)* 77−49515
- Friedmann model universes with decoupled radiation field, density perturbations growth 80−109567
- Friedmann model with eqn. of state of non-ideal hadron gas, evolution *(Russian)* 79−44649
- Friedmann models, fermion pair creation by gravit. field and singularity *(Russian)* 78−93493
- Friedmann models, scale parameter 80−77527
- Friedmann models, views of the evolving Universe, for teaching 78−24598
- Friedmann models and correlation analysis of space and surface distribs. of galaxy clustering 78−16546
- Friedmann universe, black holes in quasi-isotropic Tolman soln. *(Russian)* 77−91561
- Friedmann universe, closed black-body spectrum evolution, for teaching 78−24599
- Friedmann universe, photon gas 78−4543
- Friedmann universe, statistical model, geometrical props. determined by neutrino gas 77−53717
- Friedmann universe long wavelength perturbs. rel. to microwave background anisotropy 79−21478
- Friedmann universes, binding energy of primeval fluctuations 77−64894
- Friedmann universes, cosmological principle appl. to variational methods *(French)* 80−77529
- Friedmann universes, distance functions for Coriolis interaction 80−51925
- Friedmann-Lemaitre zero pressure universe, growth of density perturbations 77−49512
- Friedmannian universe, cosmological fluctuations produced near a singularity 80−101656
- friedmon gas model 80−41926
- fundamental dimensionless numbers and possibility of life, historical data in cosmic cycle 79−80245
- fundamental dimensionless numbers and possibility of life, Machian variational cosmology 79−80246
- fundamental distance scale, max. likelihood technique tests 80−51745
- fundamental distance scale, variable star distances 80−51746
- fundamental physical constants and their development in time *(Hungarian)* 79−25922
- fundamentals of relativity, general, special and cosmological, book 78−29007
- G-varying cosmology, galaxy and QSO magnitude/red shift relations 80−56980
- G-varying cosmology, radio source counts and models 80−56981
- G-varying cosmology, thermodynamic relations and 3K background radiation 80−56979
- Galactic disc evolution 77−29928
- galactic evolution, determ. via apparent surface brightness 77−9801
- galactic evolution, via surface brightness parameters 77−13462
- galaxies, angular redshift anisotropy, additional evidence and interpretation 77−2472
- galaxies, counts up to 25th apparent magnitude *(Russian)* 80−51879
- galaxies, deep samples, cosmological implications 80−62285
- galaxies, distant, space distribution, evolution effects 79−40260
- galaxies, distrib. in 36 square degree field near North Galactic Pole 79−40261
- galaxies, early-type accretion from gas-rich dwarfs cosmological implications 80−31349
- galaxies, luminosity evolution from 2.2 μm of giant ellipticals 80−105358
- galaxies, origin and early evolution 80−17669
- galaxies, redshift-magnitude bands and evolution from Perseus and A1367 clusters obs. 78−54033
- galaxies, two-component, chemical evolution, analytical approach 79 25711
- galaxies active nuclei, local space density 78−57676
- galaxies and clusters form., large-scale distrib. and motion in adiabatic theory 78−54056

cosmology continued

- galaxies and clusters of galaxies formation, anisotropic gravit. collapse 78−4344
- galaxies binary systems, luminosity/separation correl. as dynamical friction effect 80−36700
- galaxies covariance function, explanation for 9 Mpc break 78−65688
- galaxies dimensions and masses, relationship to fundamental constants *(French)* 80−22081
- galaxies distribution, hierarchical clustering pattern stability 78−86026
- galaxies evolution, evidence from redshift distrib. in extragalactic objects 80−90527
- galaxies evolution, state of fundamental knowledge inferred from study of globular clusters 80−90488
- galaxies fields stochastic simulation 80−62295
- galaxies formation, dissipation and merging rel. to rotation 80−4444
- galaxies formation, pregalactic evolution model 79−92863
- galaxies formation and evolution, review 79−17100
- galaxies formation by gravit. instability, role of ang. momentum 80−98722
- galaxies global orientation, position angle distrib. of Uppsala Catalogue galaxies *(Russian)* 78−41049
- galaxies mean mass density estimation 77−49486
- galaxies primordial protoclusters, search for H I emission at Z=3.33 and (4.92) 78−41066
- galaxies space distribution determination, statistical anal. of galaxy catalogues 80−46417
- galaxy, fragmentation and interaction, rel. to evolution *(Russian)* 77−82312
- Galaxy age, determ. from ^{187}Re-^{187}Os systematics in meteorites 80−41778
- galaxy clumps, formation and evolution in expanding Universe 78−93432
- galaxy cluster evolution evidence from ang. size-redshift relation 80−41903
- galaxy cluster interaction with supercluster, model of Emden sphere embedded in background 80−62296
- galaxy cluster X-ray sources, luminosity function evolution rel. to source counts 80−62314
- galaxy clustering, N-body computer simulations in expanding Universe 79−97114
- galaxy clustering, search for evolutionary effects from galaxy fields stochastic simulation 80−90530
- galaxy clustering, statistical test, covariance 80−56955
- galaxy clustering depend. on cosmological density parameter 79−48971
- galaxy clustering evolution, cosmological N-body simulations 78−96550
- galaxy clustering hierarchy 78−49546
- galaxy clustering in Friedmann model, N-body simulation 80−17670
- galaxy clustering models, discrimination of statistical measures 79−35404
- galaxy clustering N-body simulations, fraction in groups as function of density enhancement 80−67879
- galaxy clustering N-point simulations, covariance function 80−31373
- galaxy clustering spectrum, low mass portion anal. 78−81695
- galaxy clusters, as relativistic spherically-symmetric inhomogeneities 77−71147
- galaxy clusters, brightness spectrum and cosmic luminosity 78−81696
- galaxy clusters, covariance function, Limber's relativistic formula, relativistic inversion 78−69891
- galaxy correlation function evolution, N-body Monte Carlo model 80−62292
- galaxy correlations, gravit. instability evidence in dense universe 77−33712
- galaxy cosmogony based on spatial distrib. of matter 77−37652
- galaxy counts and colour-redshift relations rel. to cosmology and galactic evolution 77−33627
- galaxy counts and colours for faint objects 80−105351
- galaxy counts in 21<B<25 apparent mag. range 80−105352
- galaxy covariance function, extension to small scales 79−101197
- galaxy covariance function, technique for shape determ. at small scales 80−82506
- galaxy development in expanding Universe *(Danish)* 78−86019
- galaxy distribution, statistical anal. of galaxy catalogues 80−26987
- galaxy distribution correl., appl. to Universe structure and evolution theory, review 79−62912
- galaxy distribution evolution 80−62287
- galaxy evolution and automated faint galaxy counts 80−105350
- galaxy formation, dissipative processes 78−4343
- galaxy formation, Hubble sequence rel. to mag. fields 77−71142
- galaxy formation, origin of rotation *(Russian)* 77−82334
- galaxy formation and entropy prod. from nonlinear adiabatic fluctuations 78−8172
- galaxy formation and gravit. clustering, efficiency 79−48903
- galaxy formation and vacuum quantum fluctuation of the gravitational field 79−30156
- galaxy formation in Eddington-Lemaitre universe 79−62909
- galaxy groups, mass-to-light ratios and crossing times rel. to universe density 77−45572
- galaxy luminosity evolution, evidence from faint galaxies number magnitude counts 80−26976
- galaxy merging, cosmological N-body simulations 80−56922
- galaxy n-point correlation functions, applicability to clustering models discrimination 80−8699
- galaxy origin and evolution, developments 80−36718
- galaxy spatial distrib., spatial pair-correl. function 78−4350
- galaxy two-point correlation function, integral constraint on evolution 77 5578
- galaxy vel.-distance relations and Local Supercluster Hubble ratio 80−17698
- gamma-ray diffuse background, new look at universe 79−80373
- gas clouds, inhomogeneous, one-dimensional collapse, role of small perturbations *(Russian)* 80−36497
- gas density in galaxy superclusters rel. to closed Universe 78−41064
- GB2 sky survey at 1400 MHz, differential radiosource counts 78−54063
- general relativistic hierarchical cosmology, exact model 78−69917
- general relativity, anisotropic MHD model 79−35437
- general relativity, big bang model, nucleosynthesis, scale covariant theory, review 78−73789
- general relativity, caustics and singularities, gravitational converging effects 80−77654
- general relativity, cosmological tests 77−49662
- general relativity, gauge field theory 78−36898

cosmology continued
general relativity, initial value formulation, anti-Machian nature 78—8276
general relativity, vacuum field equations, fifth dimension, ratio of EM to gravitational force 80—77679
general relativity appls. and Friedmann models of Universe 79—97110
general relativity conference, Trieste, Italy, 1975, July 78—8285
generalised cosmological principle, in Newtonian and relativistic theories *(Polish)* 80—27025
generalized Godel Universe with heavy photons 80—46713
geodesic deviation and absolute motion 78—41099
geometrical approach to general-relativistic cosmology 77—5606
geometrized theories of gravitation 79—21636
geometrodynamical theory of subatomic particles as singularities and pseudogroup classification 77—57111
geometrodynamics, inclusion of observer in wave function 78—54234
globally hyperbolic spacetimes, conformal deform., Ricci curvature and energy condition 79—9159
globular clusters ages, effects of He settling in low mass stars 80—73013
Godel's metric 78—62125
Godel's space-time, rotating universe with successive causal and noncausal regions, solns. to Einstein eqns. 79—67200
Godel metric, world function 80—31624
Godel universe, dynamics 78—32622
Godel universe, scalar perturbations 78—57709
Gowdy universes, particle creation 80—56990
grand unification mass scale, cosmological origin 79—88773
grand unified theories, baryon asymmetry of the Universe, SO(10) model 80—4619
grand unified theories, compatibility with big bang cosmology, superheavy monopoles 80—86647
grand unified theories, mag. monopoles and cosmological implications 80—86643
gravitating sphere in Lyra's geom., thermodynamic equilib. 78—65840
gravitation, background depend. approach, quasistatic limit 77—9937
gravitation, background depend. approach, relativistic gravitational eqns. 77—9938
gravitation, gauge covariant theory, cosmological constant 79—88865
gravitation, modified theory with regular solns. *(German)* 79—88844
gravitation, relativistic theory, static solutions and Poincare press. 80—31648
gravitation and dynamical space, geometrical framework, Mach's principle 80—95001
gravitation and inertia in general relativity 78—8317
gravitation bimetric theory, flat metric election 80—62004
gravitation wave propagation in expanding universe 78—73787
gravitational collapse, classical and quantum, problems *(Russian)* 78—53815
gravitational collapse of hadron system, rel. to contraction of closed oscillating Universe *(Russian)* 80—4466
gravitational const. var. cosmological light element abundance constraint, comment on errors 80—72767
gravitational const. variations rel. to Earth struct. 77—73626
gravitational constant, cosmological var. rel. to solar luminosity 80—82182
gravitational constant changes and planetary expansion limits 78—28155
gravitational constant decrease, two-body problem and cosmological implications 77—13219
gravitational constant possible var., cosmological limit 78—93492
gravitational constant rel. to cosmological parameters 79—48974
gravitational constant time variation, influence on cosmic He abundance 79—92667
gravitational constant variation, anal. using scale covariant theory 79—92666
gravitational constant variation, determ. from visual binary stars obs. *(Russian)* 79—44537
gravitational constant variation, Dirac's Large Numbers Hypothesis 79—16819
gravitational constant variations, effect on stellar evolutionary tracks 80—82186
gravitational constant variations, effects on Earth moment of inertia 78—49302
gravitational curvature, Einstein's theory, an introduction, book 80—22161
gravitational field eqns., gauge covariant, exact one body soln. 78—36899
gravitational field stochastic fluctuations 79—44837
gravitational force and cosmic matter-antimatter asymmetry 80—90586
gravitational gauge field theory, renormalisable 79—44839
gravitational indistinguishability of neutrino field and stokesian fluids 79—30159
gravitational inertial field and critical systems, free motion 78—93484
gravitational inertial field eqns., Lagrangian density, Hubble law 78—93483
gravitational instability in early Universe, cluster-sized perturbations 78—93487
gravitational interaction variations, theories and effects 77—60858
gravitational particle creation, role of asymptotic in-out calculations 79—88772
gravitational perturbations growth, collisionless particles effect *(Russian)* 79—101233
gravitational radiation, high freq., cosmological field, energy 78—57837
gravitational radiation, long-wave, primordial, interaction with galaxies 80—17661
gravitational radiation 77—9825
gravitational source strength of matter, cosmological problem 77—82119
gravitational theories generated by groups of transformation and Dirac's large number hypothesis 79—12677
gravitational theory, cosmological soln, with matter 80—86021
gravitational wave noise, from spontaneous prod. of gravitons, energy density distrib. *(Russian)* 79—12551
gravitational waves, dispersion in cold matter 80—12967
gravitational waves, origin and consequences for Universe 80—109569
gravitational waves stochastic background, energy density upper limit from pulsar timing meas. 80—36743
gravitational-inertial field of Universe, crit. systems struct. 80—8720
gravitational-inertial field of Universe, generalised metric tensor theory 78—89275
gravitationally nondegenerate Bianchi type I cosmological model, in general relativity 78—93490
gravito-C-field, in cylindrically symmetric space-time, rigorous solns. 78—69926

cosmology continued
graviton pair production in early Universe, effective pot. approach 78—24587
graviton production by cosmological background, role of conformal (non) invariance 79—49131
graviton viscosity in early Universe 77—74169
Great Debate of galactic astronomy, actual proceedings 77—29979
groups and clusters of galaxies, cosmological implications of virial mass discrepancy 78—28803
H_0 and q_0 determ. from Baade's distance method 80—73082
H_0 global value from galaxy distance meas. 77—9827
hadron matter phase transformation at high temps., cosmological consequences *(Russian)* 77—91674
hadron plasma theory *(Russian)* 78—37148
Hagedorn's big-bang model, strongly degenerate heavy neutrino decay, free quark-baryon ratio 78—16589
Hagedorn's bootstrap model of early Universe, dense matter eqn. of state, external mag. field 78—86044
Hagedorn early universe dissipation, Boltzmann kinetic eqn. soln. 80—8723
Hagedorn temperature and Dirac's large numbers hypothesis 80—105410
Hamiltonian formalism for self gravitating relativistic perfect fluid, Lagrangian variational principle 78—16289
Hawking effect, thermal nature of the density matrix for black hole particle prod. *(Russian)* 78—89644
Hawking mini black-holes origin and cold early Universe 78—93298
heavy element origin, dispersion into interstellar space by stellar winds 77—41404
heavy lepton massive neutrinos in big bang model, mass and number 78—45444
heavy leptons, number of types, cosmological limits from ^{4}He primordial abundance 77—33716
heavy Majorana particles, cosmological and astrophysical implications 80—90331
heavy neutrino lifetime upper bound in big-bang cosmological model 77—74170
heavy neutrino mass, cosmological upper limit from big bang model 80—8728
heavy stable neutral lepton, astrophysical consequences of existence 78—93091
heavy-neutrino mass lower bound in big-bang cosmological model 77—78904
hierarchical and relativised models of Universe *(Russian)* 78—86043
high-energy gravity and the very early universe 80—98847
historical review of theories of origin of Universe *(French)* 79—84931
history, fire and evolutionary cosmology in Wright and Kant 79—5764
homogeneous collapsing star, orthogonal vector and tensor harmonics, matter and field asymmetries 79—5841
homogeneous cosmological models, entropy prod., viscous damping of anisotropy, Bianchi type-I spaces 78—49572
homogeneous cosmological models, Hamiltonian systems 77—13703
homogeneous cosmologies, dipole and quadrupole anisotropies 80—109572
homogeneous isotropic closed universe, spontaneous breaking of gauge symm. *(Russian)* 77—45979
homogeneous isotropic Universe models, radiation theory 77—37501
homogeneous models and kinetic equation of gases in general relativity 80—21914
homogeneous type IX model with EM field, Hamiltonian formalism 77—53716
homogeneous universes, qualitative behaviour 80—94904
homoheneous isotropic universe, influence of extra dimensions 80—51928
hot Universe, entropy perturbations and cosmogenic processes 80—105411
hot universe with primordial black holes, neutrino radiation kinetics *(Russian)* 78—93485
Hoyle's hypothesis, cosmological models 78—86045
Hoyle-Narlikar conformal gravitation, cosmological tests 80—56698
Hubble's constant, doubling rel. to superluminal radio sources model 78—81722
Hubble's law, equivalence with universal law of gravitation *(Italian)* 78—24577
Hubble's law, galaxies recession and quasar redshifts *(Swedish)* 77—71144
Hubble's law, laboratory exercise in astronomy 78—65740
Hubble's law and universal gravitational constant *(Italian)* 78—24578
Hubble const. distance depend. caused by ScI galaxy luminosity distrib. *(German)* 77—45620
Hubble const. estimate from Galaxy rotation curves 77—33640
Hubble constant, determ. from H II region dias. 80—41887
Hubble constant, determ. from new method of galaxies distance meas. 77—29920
Hubble constant, determ. outside Local Supercluster from new galaxy distance scale 80—105325
Hubble constant, from late-type galaxies H I obs. 78—86015
Hubble constant, implications for discrete source models of diffuse X-ray background 79—101226
Hubble constant, local value from Sb galaxies luminosity classification 80—62339
Hubble constant, new determ. 79—92902
Hubble constant, value from Virgo cluster distance and redshift 78—89265
Hubble constant and extragalactic distance indicators *(German)* 78—45442
Hubble constant and Virgo I cluster distance 79—62917
Hubble constant determ., large turbulent Universe model 78—96578
Hubble constant determ., large turbulent Universe model 79—58453
Hubble constant determ. from super-luminal radiosources 78—12439
Hubble constant determ. from Type I supernovae envelope model 77 -53617
Hubble constant determ. from Type I supernovae enveloped model 77—87459
Hubble constant determ. using galaxy diameter luminosity relation *(French)* 79—30128
Hubble constant determination, Type I supernovae appl. 79—40304
Hubble constant rel. to H I profile width distances for disc galaxies 78 41050
Hubble constant value limits from obs. of galaxy clusters 79—67099
Hubble diagram, deceleration parameter rederivation 77—13457
Hubble diagram as cosmological test, dynamics friction effects 77—9826

cosmology continued
Hubble diagram curvature, from redshifts and photometry of distant galaxy clusters 78—49515
Hubble diagram for E and S0 galaxies in the local region 79—35359
Hubble diagram for QSOs 78—77616
Hubble diagram statistics, form of luminosity function and density vars. with appl. to quasars 79—97093
Hubble diagram statistics, q_0 determ. and luminosity evolution rel. to quasars 79—71102
Hubble diagrams for brightest quasars 78—28845
Hubble expansion in Euclidean framework 80—31395
Hubble flow, Virgocentric perturbation rel. to elliptical galaxies mass to light ratios 80—98707
Hubble law, laboratory exercise for students 79—35500
Hubble law isotropy test on quasars 79—97111
Hubble moduli, generalised, use in study of homogeneity and isotropy of Universe expansion *(French)* 79—53944
Hubble Modulus, numerical simulation test of cluster effect 79—2569
Hubble modulus for Markarian galaxies 78—49538
Hubble modulus increase behind clusters of galaxies 77—78872
Hubble parameter, anisotropy rel. to large-scale cosmological inhomogeneity 77—91675
Hubble parameter determination, homogeneity of galaxies sample 77—13506
Hubble ratio, determ. from accurate H I profiles of nearby galaxies 80—41895
Hubble ratio, local value, and extragalactic distance scale *(French)* 77—60826
Hubble sequence, ang. momenta and time scales of galaxies early evolution 79—8997
ideal Fermi gas, thermodynamics and eqn. of state 77—30117
ideal liquid, generalised Lagrangian energy density, nonsingular cosmological space-time model *(Russian)* 79—9040
inertial frame dragging effect, and contrib. of matter to gravit. constant, Brans-Dicke theory 79—67206
inertial mass isotropy 79—58455
information from new types of radio obs. 78—28872
inhomogeneous cosmological model solns. of Einstein eqns. for perfect fluid 78—24585
inhomogeneous cosmological models containing spacelike and timelike singularities alternately 78—69925
inhomogeneous cosmologies, anal. of conformally flat slices 80—17704
inhomogeneous cosmologies, conformally flat slices and invariant classification 80—17703
inhomogeneous cosmologies, exact solns. to Einstein field eqns. for perfect fluid 77—74285
inhomogeneous cosmologies, intrinsic symmetries 80—17702
inhomogeneous cosmologies as algebraically, special spacetimes, rot. dust soln. generalisation 77—49646
inhomogeneous models of early universe 77—17736
inhomogeneous perfect fluid cosmologies 77—74284
inhomogeneous self-similar model, observable relations 79—44645
inhomogeneous Universe, gravitational wave effects, on orbital motions 80—61998
interacting EM waves in general relativity exact solns. of Einstein-Maxwell eqns. 77—60985
interacting quantum fields chromatic principle 77—34086
intercluster intergalactic medium, theory for expanding cosmologies 80—4426
intergalactic C model abundance, X-ray absorpt. effects 80—62270
intergalactic clouds rel. to origin of universe *(French)* 80—67874
intergalactic graphite whiskers, RF adsorpt. props. rel. to microwave background radiation 80—31357
intergalactic hot gas formation by ejection from galaxy in early explosive era 78—45408
interstellar dust, pre-stellar 79—84844
interstellar He abundance, rel to stellar models and cosmological models 78—16518
invariance group instability, spacetime, group contractions and models of Universe 79—9041
ionising background radiation, meas. from effects on H at periphery of galaxies 78—65729
IR diffuse background, upper bound on metagalactic flux 77—29964
IR Hubble diagram for giant elliptical galaxies 80—105359
IR night sky background, 2.4 μm meas. 78—81715
irreversibility, time and anisotropies, cosmological origin 77—13510
isotropic closed universe, quantised scalar field formulae 79—12550
isotropic cosmological models, vacuum stress energy tensor and particle creation *(German)* 80—94901
isotropic cosmological models without singularity, Einstein eqn. solns., Universe description 80—56988
isotropic homogeneous universe, modified field equations rel. to cosmological model without big-bang *(German)* 80—51927
isotropic models of Universe, regularisation of fermion stress-energy tensor 78—81725
isotropic universe, gravit. perturb. propag., using general relativistic kinetic theory 78—20920
isotropic Universe, kinetics of small perturbations *(Russian)* 78—54102
isotropic Universe, kinetics of small perturbations *(Russian)* 78—54103
isotropic universe, kinetics of small perturbations *(Russian)* 78—65731
isotropic universe, particle creation and vacuum polarisation, cosmological models 80—90582
isotropic Universe, quantum gravitational effects, spontaneous particle production *(Russian)* 80—94711
isotropic universes construction of symmetric vectors 79—71166
isotropically expanding universes, effect of graviton creation 78—16588
isotropy, vacuum polarisation contrib. to energy content of Universe 80—73083
isotropy of relict radiation, coherence of Universe *(Russian)* 79—85024
JBD theory, exact cosmological soln. with particle creation 78—96576
Kantowski-Sachs models, global struct. 78—24584
Kasner metric, direct variational theory for general relativity eqn. soln. *(Russian)* 78—12610
Kasner spacetime, conformal energy-momentum tensor trace anomaly calc. 79—21603
Kerr metric in cosmological background, event horizon radius 77—74082
Killing vectors in plane HH spaces 78—54104
Klein paradox and vacuum polarization 78—8329
Klein-Alfven cosmology, theory of matter-antimatter boundary layers 77—49284

cosmology continued
Lagrangian or Hamiltonian formulations, shift vector field restrictions, symmetry group 80—67923
Lambert, J.H., self-taught scientist, life and work on cosmology 77—82354
large cosmical masses, expansion and rot. momenta *(Russian)* 77—17351
large number theory with constant G 80—46715
large numbers, cosmic coincidences rel. to gravit. const. 79—48969
large numbers hypothesis, review *(Polish)* 77—64897
large numbers hypothesis and the Einstein theory of gravitation 79—21477
Large Numbers Hypothesis implications for Earth rotation 79—12063
Large Numbers Theory with constant G 80—31400
large-scale structure in universe, formation and development 79—12526
large-scale universal inhomogeneities, X-ray background evidence 79—75299
Lemaitre's cosmology, review *(Polish)* 77—17737
Lemaitre cosmology in modern context *(French)* 79—2581
Lemaitre Universes, Jeans instability 78—12445
lepton degeneracy and cosmological constraints on the number of neutrinos 80—8538
lepton era, transport coeffs., Weinberg-Salam model 78—32623
light element abundances, galactic evolution and universal baryon density 79—40302
light element synthesis in big bang Universe 79—9044
light elements origin, prod. by cosmological cosmic rays 78—12436
linear density perturbation, general relativistic and Brans-Dicke cosmologies 77—22336
linearly expanding universes in Jordan-Brans-Dicke theory 80—46711
local mean mass density and galaxy clustering 78—45436
local missing, mass problem, undetected M3-M8 dwarfs 77—67123
Local Supercluster, redshift anisotropy, luminosity selection effects 77—74147
locally rotationally symm., spatially homogeneous cosmological model, decomposable differential operators 78—57825
locally rotationally symmetric cosmological model containing a nonrotationally symmetric electromagnetic field 79—30161
Lorentzian gravity, appl. to hadron struct. and galaxy clusters 79—97288
low density Bianchi type VII_h models, isotropisation 79—80379
low-density Universe, cosmological const. and isotropy 79—101227
low-density universes, linear clustering, of galaxies 80—85993
Mach's inertial interaction to produce gravitational force 77—2589
Mach's principle, gravity and inertia, Leibniz invariant theory 77—41426
Mach's principle, modification of general relativity theory *(German)* 79—88843
Mach's principle, the cosmological constant, and the scale-covariant theory of gravity 79—25774
Mach's principle and general principle of relativity, elementary physical approach and observational basis 80—52080
Mach's principle equivalence principle, violation, for teachers 78—61998
mach principle and the quantal response of the Universe 79—12549
Machian argument in Friedmann models of Universe 77—74168
Machian effects in compact rapidly spinning shells 79—2684
Machian framework, purely geometrical, for describing gravity and inertia 79—44651
magnetohydrodynamic Bianchi type-I models 77—67150
magnetoviscous fluid cosmological models in general relativity 79—63095
magnitude-redshift relation for matter and radiation filled universes 78—20917
many worlds cosmology, entropy per baryon 77—53714
Marinov coupled mirrors expt., a critique, preferred cosmological reference frame 80—27120
mass and number limits of neutral weakly interacting particles 77—71000
mass changing cosmology, solar evolution and neutrino flux 78—45441
mass integral formulation of general relativity, cosmological solns. 78—12618
mass limits of neutral leptons *(Russian)* 77—82800
mass/light ratio of Universe from mean overdensity toward Virgo supercluster 80—94877
massive galactic haloes, form. and evolution, rel. to missing mass problem 78—28777
massive gas clouds, cooling, dynamics and fragmentation rel. to masses and radii of galaxies and clusters 77—60857
massive particle production in anisotropic space-times 80—90583
massive unstable neutrinos, cosmological implications 78—45437
massless scalar field in a de Sitter universe and its thermal flux 79—127
massless scalar particle creation, classical and quantum gravit. collapse *(Russian)* 79—9039
massless scalar particle prod. by cosmological torsion field 80—51936
mathematical theories and philosophical insights in cosmology 80—90650
matter,-antimatter antiproton studies 78—54654
matter and antimatter cosmological separation 78—69918
matter and radiation fluctuations after decoupling epoch 80—62354
matter creation, dynamic meas. technique 78—28868
matter distrib. now and at matter-radiation decoupling epoch 80—62355
matter distribution in nuclei far from β stability valley, charact. features 77—64635
matter formation, photon condensation, treatment using Bose-Einstein statistics 78—12435
matter in universe, origin 78—20918
matter-antimatter accounting, thermodynamics, and black-hole radiation 79—49136
matter-antimatter asymmetry of Universe, review of speculations and data *(French)* 79—35439
matter-antimatter boundary layers with mag. neutral sheet, model 78—53807
matter-antimatter hydrodynamics, annihilation rate calc. 78—73780
matter-antimatter symmetric universe, random geometry 78—86046
matter-filled universe, relativity of space and time finiteness-infiniteness 78—96581
maximal surfaces in closed and open spacetimes 78—8294
maximum information universe 79—30157
Maxwell equations, in Minkowski space-time and Poincare group 79—30301
Mayan astronomy, Venus studies 79—88782
meaningless questions, philosophy 77—13515
meta universe, tachyon energy and momentum, contribution to gravitational field 77—45760
metagalactic shock waves, thermal processes 80—46678

cosmology continued
  - metagalaxy, model *(Chinese)* 79—67121
  - metagalaxy rotation and cosmic numbers *(Russian)* 77—82333
  - meteorites, isotope abundance anomalies, astrophysical implications 80—46511
  - meteorites, isotope abundance anomalies, cosmological implications 80—46510
  - metric tensor components interpretation, astrophys. implications 78—93097
  - metrical connection in space-time, Newton's and Hubble's laws 78—57435
  - MHD cosmological models, plane symmetry 80—82556
  - MHD kinks in nonresistive plasma, astrophys. appl. 79—27763
  - microwave background, interaction with crosmic ray protons, Hubble radius 77—87211
  - microwave background, residual fluctuations, gravitational effects 80—62332
  - microwave background, review 80—62336
  - microwave background angular distrib., large scale fluctuations 80—62328
  - microwave background angular distrib., small scale fluctuations 80—62329
  - microwave background dipole anisotropy, dynamical inferences 80—62330
  - microwave background fluctuations, recombination epoch effects 80—62333
  - microwave background longward of 3 mm, spectral distortions 80—62326
  - microwave background radiation, anisotropy meas. 80—41918
  - microwave background radiation, search for linear polarisation 79—21470
  - microwave background radiation fluctuations, in adiabatic and entropic theories of galaxy form. 79—62942
  - microwave background radiation isotropy and spectral distrib. as test of Dirac cosmologies 78—49570
  - microwave background radiation large-scale anisotropy meas. 80—8718
  - microwave background radiation polarisation, anisotropic cosmological expansion 78—73778
  - microwave background radiation polarisation, IR survey 78—73779
  - microwave background radiation rel. to big bang cosmologies 77—49508
  - microwave background radiation spectrum, statistical anal. of data 78—86039
  - microwave background radiation spectrum deform. by lasting recomb. 77—9824
  - microwave background small-scale fluctuations, consequences of neutrino rest mass *(Russian)* 80—109576
  - microwave background spectrum, distortion by pregalactic dust 80—67916
  - microwave black body radiation spectrum, implications for Population III stars 80—67915
  - millimetre region cosmic background radiation, large scale anisotropy meas. 80—82553
  - mini black holes, formation in condensed stellar mass object core 77—49425
  - minicompact objects according to the bimetric theory of gravitation 79—49140
  - missing dark mass rel. to primordial star generation 78—61946
  - missing mass in massive, slow-moving neutrinos, decay 80—109566
  - mm emission from extragalactic objects, luminosities, spectra, microwave background contrib. 77—17677
  - model, with gravit. and scalar waves 79—53949
  - model hierarchical Universe based on trema sets, correlations and texture *(French)* 79—48970
  - model with inhomogeneous space and nonuniform time 79—58452
  - models, obs. and theoretical approaches and expectations 78—77636
  - models with gravitational waves, exact solns. 79—88771
  - molecule formation in pregalactic stage of Universe *(Russian)* 77—87583
  - multiply-connected space-time, black holes and tachyons 79—30315
  - muon neutrino mass limit in absence of muon-lepton-number conservation 78—21368
  - net baryon number and CP nonconservation with unified fields 80—62349
  - neutrino, Maxwell, and scalar fields in the cylindrical magnetic or plasm universe 80—120
  - neutrino background radiation, cosmological significance 78—77486
  - neutrino cosmology, open universe with neutrino and graviton dominance 77—17731
  - neutrino number and isotropy of Universe in grand unified theories 80—85852
  - neutrino number constraints in big-bang theory 79—62940
  - neutrino stability and cosmological He production 78—73783
  - neutrino systems, relativistic kinetic theory of transport processes 80—73283
  - neutrino viscosity and isotropization of anisotropic-curvature cosmological models 80—8729
  - neutrino viscosity and isotropization of Bianchi type-VIII and type-IX cosmological models 79—75300
  - neutrinos and Friedmann model *(Polish)* 78—89276
  - Newtonian, generalised Clebsch representation for velocity field of fluid, variational formulation 80—51930
  - Newtonian, global particular solution to initial value problem of stellar dynamics 79—35314
  - Newtonian, homogeneous, review 78—16584
  - Newtonian cosmology, derivation of law of gravitation from Hubble's law *(Italian)* 80—8722
  - Newtonian cosmology, extension to whole of space *(Italian)* 79—21475
  - Newtonian cosmology, universe energy conjecture *(Italian)* 79—21474
  - Newtonian cosmology and universal gravitation constant *(Italian)* 79—21473
  - Newtonian cosmology for unbounded Universe, review *(Italian)* 80—12836
  - Newtonian cosmology if G varies 77—17730
  - Newtonian cosmology with time-varying gravitational constant 78—65733
  - Newtonian gravitation theory and mechanics and Hubbles law, homogeneous fluid theory of Universe *(Italian)* 80—12835
  - Newtonian mechanics and expansion of the universe *(Italian)* 79—21472
  - Newtonian model with diminishing gravitational constant 78—54100
  - Newtonian model with varying gravitational constant, alternative approach 78—54101
  - Newtonian non rotating cosmological model *(Spanish)* 79—48978

cosmology continued
  - Newtonian unified models, time-mirror interaction *(French)* 77—78901
  - Newtonian universes with shear, singular states 79—2582
  - non singular cosmologies in conformally invariant gravitation theory 77 22337
  - non-linear high-frequency waves in relativistic cosmology 79—48968
  - non-zero cosmological constant, evolution free test 80—4465
  - nonempty space, relativity of finiteness and infinity 79—9045
  - nonlinear primordial fluctuations, theory 79—25773
  - nonlinear viscous cosmology, Bianchi type-I model anal. 80—41921
  - nonsingular, as quantum vacuum effect 79—53947
  - nonsingular gravitational collapse, Yang-Mills cosmos 79—21621
  - nonsingular isotropic cosmological model, physical reality *(Russian)* 78—77635
  - nonstatic universe, generalised Doppler formula 77—78900
  - nonsymmetric field theories, Mach's principle 77—9920
  - nonsymmetric unified field theory implied cosmology metric 79—53943
  - nonsymmetric unified field theory of Einstein, cosmological implications, Universe expansion 78—73911
  - nonuniqueness of solutions to Einstein's equations, symmetries in T_{ij} 80—12953
  - nuclear astrophysics, introduction to form. and evolution of matter in Universe, book 80—105447
  - nucleosynthesis, conventional and unconventional 80—46722
  - objects in nonradial motion, redshifts, special and general relativistic anal. 79—80212
  - observational cosmology since 1958, progress and problems 78—28873
  - observational test of cosmological particle production theories 80—109574
  - observational tests of the cosmic turbulence theory 80—98747
  - 'Olbers' paradox', history and resolution 77—33758
  - one-electron atom in curved space-time 80—78509
  - open cosmological model of Friedmann type, physics and biology in an open universe 79—97119
  - open Universe geometrical struct., deceleration parameter and spatial curvature 80—62343
  - open Universe supported by HEAO-2 quasar data 79—62946
  - optical isotropy of space, equivalence principle *(Russian)* 79—62944
  - origin of galaxies in expanding Universe, plasma cond. and instabilities, MHD soln. 80—62283
  - origin of matter in the Universe 77—26096
  - origin of the elements, review 79—97118
  - oscillating universe cosmologies, review 77—87579
  - pair creation as above barrier reflection, WKB approx. 79—80377
  - pair creation in presence of EM fields 80—41924
  - pair production in intense mag. fields, cosmological appls. 77—13505
  - parallactic distances in locally inhomogeneous Universe 79—97120
  - parallaxes of objects at cosmological distances, meas. via radiointerferometric techniques 78—53796
  - particle creation and geometry 78—12442
  - particle creation by time-depend. gravitational field, quantum equivalence principle 80—41925
  - particle creation classical analogue, WKB approx. 79—30160
  - particle creation in curved space-time, covariant treatment 78—12443
  - particle detection and creation for scalar quantum field in curved space-time 77—67597
  - particle emission in the de Sitter universe for massless fields with spin 79—40434
  - particle pair creation, canonical quantisation for Chitre-Hartle model 80—62342
  - particle production in expanding universes 80—27023
  - particle production models using Lewis invariant 80—36755
  - particle production rate in gravitational fields *(Russian)* 77—91423
  - particles and fields conference, Argonne, IL, USA (Oct. 1977) 78—78130
  - path integral quantisation and cosmological particle prod. 78—12440
  - perfect fluid cosmology with geodesic world lines 79—25775
  - perfect fluid cosmology with geodesic world lines 80—67924
  - perfect fluids expanding with both vorticity and shear, cosmological appl. 79—48669
  - perihelion precession as Machian effect 77—26098
  - perturbations growth in isotropic cosmological model, kinetic theory, ultrarelativistic limit 79—62943
  - perturbations larger than horizon size in big-bang cosmology, tenacious myths 80—105408
  - perturbed spherically symmetric collapsing star, initial value problem in quasi-Newtonian background 79—5842
  - philosophical relevance *(German)* 80—90652
  - photon condensation in hot Universe, longitudinal relict rad. *(Russian)* 78—65734
  - photon decay in curved space-time, Hubble red shift and solar limb effect explanation 79—35606
  - photon gas, Friedmann model, self-similar motions, cosmological solns. *(Russian)* 78—16590
  - photon parametric creation in model cosmological problems, nonlinear optics equivalence 80—73085
  - photon splitting into 3, cosomological limits, spectral broadening, frequency-dependent and multiple red-shifts 80—77284
  - photon-tachyon interactions and the isotropic photon flux 80—446
  - physical laws large-scale uniformity, evidence from QSO absorpt. redshifts 80—73079
  - physics of microwave background, conference Jodlowy Dwor, Poland, 1978 September 80—62389
  - Planck's const. time variation on cosmological scales 77—57113
  - Planck's constant, time invariance 78—93556
  - Planck's constant cosmological var. upper limit from microwave background radiation spectrum 78—12434
  - Planck's radiation laws, scalar photons and Hubble effect *(German)* 77—45305
  - plane symmetric universe model with disordered radiation 77—22335
  - plane-symmetric cosmological model, Einstein eqn. solns. for dust 78—49733
  - plane-symmetric cosmologies 79—71162
  - planetary formation, current theories and problems 79—84685
  - Poincare and cosmic evolution 80—57073
  - Poincare cycle, general relativity, cosmology and thermodynamics 79—80378
  - Poincare gauge theory with Weyl-type Lagrangian and gravitation 78—4545
  - polarisation effects in cosmological models with anisotropic curvature 80—94903

cosmology continued
polarization transport in anisotropic universes 78−8174
polytropic universe, exact solns. of field eqns. 77−64891
positive energy conjecture and cosmic censor hypothesis 77−29640
pregalactic black holes, constraint an abundance 80−12777
pregalactic gas cloud, thermal instability, fragmentation 78−4421
pregalactic H-He stars formation and nucleosynthesis 77−71157
pregalactic microwave background, origin 78−86040
primaeval cosmic microwave background radiation, polarisation in anisotropic universe 80−82552
primaeval entropy fluctuations and gravit. clustering 78−28867
primaeval galaxies, model emission spectra 80−46655
primaeval giant elliptical galaxies, observable props. 78−89260
primaeval hot gas clouds fragmentation and diffuse X-ray background radiation 78−28861
primeval galaxies, appearance in X- and γ-ray regions, contrib. to background rad. 80−8692
primeval galaxies, investigation of red shift 80−31372
primeval galaxies at very large redshifts, spectral energy distribs. from massive halos 77−78866
primordial, small mass black holes and fundamental length *(Russian)* 77−22264
primordial abundances rel. to light element-relic radiation interaction *(Russian)* 78−4423
primordial background radiation, temp. fluctuations due to gravit. waves 78−65728
primordial baryons, generation by black holes 80−98750
primordial black hole development 78−93299
primordial black hole evaporation rel. to D origin *(Russian)* 77−74172
primordial black hole explosions, gamma-ray bursts rate upper limit 77−29873
primordial black holes, evaporating, observational consequences of positron prod. 80−46599
primordial black holes, evaporating, rel. to galactic positrons primary source and fates 80−109319
primordial black holes, evaporation, effects on background EM radiation spectrum 79−88695
primordial black holes, evolution 77−17614
primordial black holes, form. in anisotropic universe 78−32507
primordial black holes, form. in stiff universe *(Russian)* 80−51802
primordial black holes, influence on galactic radio spectrum 80−62179
primordial black holes, radiation accretion in early Universe 80−67918
primordial black holes, self-similar growth, stiff eqn. of state 78−36629
primordial black holes, self-similar growth for general sound speed case 79−5856
primordial black holes, small mass, obs. consequences of evaporation *(Russian)* 77−78818
primordial black holes, statistical clustering 77−49423
primordial black holes, upper bound on number density calc. 78−65649
primordial black holes and big bang nucleosynthesis *(Russian)* 79−17151
primordial black holes evaporation, cosmological implications 79−21325
primordial black holes form. and accretion of matter 80−36660
primordial black holes formation, hydrodynamics 79−21324
primordial black holes formation 80−12776
primordial cosmic turbulence, spectrum evolution 80−90589
primordial gravitational waves, galaxy tidal deform. 79−92865
primordial inhomogeneities in expanding Universe, galaxy density and vel. distribs. in rich clusters 79−44644
primordial low mass black holes evaporation and H recomb. kinetics *(Russian)* 78−61943
primordial matter cooling by H_2, rel. to star form. 79−35440
primordial microwave radiation, recomb. lines calc. 78−54097
primordial mini black holes explosion rate, upper limit from gamma-ray bursts search 80−67911
primordial neutrino gas, viscosity and thermal conductivity 79−84874
primordial neutrino gas 79−53950
primordial neutrino-antineutrino gas, diffusion effects 79−84875
primordial neutrino-antineutrino gas, separation process 79−67126
primordial nucleosynthesis, limits on props. of massive neutral leptons 78−57438
primordial star formation in cold early universe 77−87578
projective relativity based on De Sitter universe 77−41423
prospects for 1980s period 79−97112
protogalactic hot gas cooling by H_2^+ vibr. excitation *(Russian)* 79−17149
protogalactic medium, vortex generation 80−62360
protogalaxy formation age and γ-ray background 80−62325
q_0, deceleration parameter, upper limit from pregalactic fluctuations visibility 80−8717
q_0 determ. from supernovae obs. 77−49509
QCD and superdense matter, quark and gluon plasma, hadronic structure, neutron stars, hadron collisions, review 80−73683
QCD black body radiation, big bang universe hadron era 80−62341
QSO radio emission, Faraday rotation and cosmological magnetic fields 80−22087
QSO redshifts and field galaxies 78−89271
QSO resonance lines as luminosity calibrators 80−105388
QSO/galaxy associations, redshifts and distances 80−31369
QSOs and Lick galaxy counts, correl. from extragalactic objects catalogues statistical anal. 79−25700
QSOs number density excess and initially inhomogeneous cosmologies 79−2576
qualitative isotropic cosmology involving a cosmological constant with allowance for dissipation *(Russian)* 79−5927
quantisation of scalar field in cosmological spaces *(Russian)* 77−45621
quantisation of space and time *(Danish)* 80−8724
quantised gravitational wave perturbations in Robertson-Walker universes 78−12636
quantum effects, black and white holes 78−12441
quantum effects and evolution of cosmological models 77−17735
quantum effects and regular cosmological models *(Russian)* 80−27206
quantum effects in early universe, effective action for scalar fields 80−22128
quantum effects in early universe, trace anomaly influence 80−22127
quantum fluctuations in gravitational collapse and cosmology 78−49571
quantum fluctuations near the classical space-time singularity 80−8893
quantum gravity, semiclassical theory, appl. book contrib. 80−22268
quantum gravity, tadpole diagrams, Ward identities, induced cosmological term 78−125

cosmology continued
quantum gravity and path integrals, supersymmetric theory, virtual Planck-mass black holes 79−2706
quantum many-particle systems in curved spacetime 80−98751
quantum particle creation of Hawking effect in nonstationary black holes 78−4278
quantum processes at large redshifts 80−62357
quantum theory, a general framework 79−9043
quantum Universe, non-singular model 79−30158
quantum vacuum cosmology 77−5728
quark binding, explained by strong gravity with cosmological const. 78−4820
quark confinement, relevant cosmological f-g fields 80−86659
quark era in primaeval Universe 80−36746
quark-nucleon phase transitions, rel. to density fluctuations in early Universe 79−75301
quarks, unbound, attempts to reconcile recent evidence for existence in stable matter 78−58160
quasar absorption lines origin, cosmological hypothesis predictions and observational evidence 78−57684
quasar evolution 78−57688
quasar evolution with resolved components, deceleration parameter determ. 80−31386
quasar Hubble diagrams, nonparametric statistics 79−40289
quasar number counts and X-ray background 79−75294
quasar red shifts, anal. for randomness 78−12400
quasar red shifts, cosmological implications of ln (1+z) parameter periodicity 80−17687
quasar redshift data, cosmological interpretation using V/V_{max} test 78−28844
quasar redshifts, gravit. and cosmological components 77−13229
quasar redshifts cosmological nature, new test 77−17713
quasar-galaxy associations, results from optically variable quasars and bright galaxies 79−58438
quasars, absolute magnitudes and Hubble plot 77−91662
quasars, angular diameter−redshift test for large redshift objects 78−28841
quasars, complete samples, volumes analysis 80−51899
quasars, evidence for nature of redshifts from brightness cyclic depend. on parameter ln (1+z) 80−105382
quasars, faint, number limits 79−92884
quasars, flat spectrum, evidence for cosmological evolution 78−54074
quasars, Hubble diagrams 78−57691
quasars, Hubble diagrams and optical luminosity functions 78−61930
quasars, local space density 78−57676
quasars, luminosity function, const. density model with luminosity evolution 77−5586
quasars, nonuniform radial distrib. regardless of redshift 78−32593
quasars, number-magnitude relation rel. to luminosity function and cosmological evolution 80−77507
quasars, periodicity in ln(1+z) distrib. 77−22327
quasars, red-shift hypothesis implies Earth-centred universe 78−16563
quasars, redshift-magnitude relation, statistical study and chronometric cosmology 78−93455
quasars, redshifts and Hubble diagrams 78−96559
quasars, redshifts clumping and geocentric universe 77−87565
quasars, space density evolution 79−9027
quasars and cosmology, theoretical anal. *(French)* 80−8705
quasars and young galaxies, relations and cosmological implications 78−32582
quasars from B2 catalogue, 1415 MHz structs. and redshift-angular size plot 79−35422
quasars greatest redshifts rel. to parent galaxies masses 77−49480
quasars of Michigan-Tololo survey, spectrophotometry and redshift distrib. 80−22105
quasars relative luminosities determ. from emission line strengths, rel. to Universe model 78−61931
quasi-stellar objects, luminosity indicators in emission-line spectra 77−57103
quasi-stellar objects, variable, photometry and completeness of faint blue objects in Sandage-Luyten field 78−54069
quasi-stellar radio sources from 4C and Parkes catalogues, cosmological implications 78−65714
quasi-stellar radio sources with large redshifts, angular dia.-redshift test 78−24565
quiescent isotropic homogeneous initial universe model 78−41103
radiation accretion by primordial black holes in the early Universe 79−44519
radiation damping and expansion of universe, Robertson-Walker metric 77−33717
radiation damping in universe with topologically closed space sections 78−57828
radiation era, magnetic field amplification 78−96577
radiation-dominated era, perturbations, Purcell clustering effect 79−58454
radiation-matter flat universe, small perturbations and black hole form. effects 80−94900
radio galaxies, red shift dependence of proper densities and colours 80−62286
radio sources, cosmological evolution rel. to source counts freq. depend. and spectral index distribs. 78−96554
radio sources, extragalactic, ang. distrib., no evidence for anisotropy from deep survey at 4.85 GHz 80−77502
radio sources, extragalactic, ang. size-redshift diagram interpretation 80−22101
radio sources, extragalactic, space distrib. compared with clusters of galaxies *(Chinese)* 79−17111
radio sources, faint, evidence for cosmological evolution from statistical study at 81.5 MHz 80−90554
radio sources cosmological evolution, free-form anal. method 78−41070
radio sources redshift-apparent, cosmological implications 77−87559
radio-quiet quasars, Hubble diagram, luminosity function and density evolution 80−51903
radioastronomy, pioneering work by Jansky, and Penzias and Wilson 79−44655
radioastronomy and cosmology, IAU Symposium 74 (Cambridge, England, 16-20 Aug. 1976) 78−28871
radiogalaxies, redshift-magnitude relation and cosmological test 78−28798
radiogalaxies anomalous redshifts, prod. by foreground galaxy clusters 77−9798

cosmology continued
radional field theory, corpuscular theory, origin of natural forces 78—77785
radiosource angular sizes and cosmological tests 78—28821
radiosource clustering, statistical analysis of surveys 78—28818
radiosource counts and isotropy of faint sources in B2 survey 80—105374
radiosource counts and spectral index distribs. 80—98732
radiosource population, isotropy at 1400 MHz, new GB sky survey 77—45584
radiosource populations and redshift interpretation in evolutionary use 78—28832
radiosources, aggregate flux and space volume emissivity at 1404 MHz 77—13480
radiosources, angular diameter-redshift relation for scintillating sources 78—28824
radiosources, angular size-flux density relation rel. to evolution 78—28822
radiosources, cosmological information interpretation 78—28831
radiosources, flux density-angular size distrib. for extragalactic sources 78—28823
radiosources, number-flux density counts of unidentified objects, noncosmological effect 78—12395
radiosources, rot. measures origin, cosmological implications 77—5584
radiosources, space distrib. from short wavelength surveys 80—62305
radiosources, statistical test on complete sample of identified sources 78—89269
radiosources cosmological evolution, free-form analysis, self-consistent luminosity function 80—46716
radiosources hot spots as cosmological probes 77—13483
radiosources isotropy in B2 catalogue 78—73766
radiosources with components, flux densities and source parameters, cosmological aspects 78—28833
Rayner model, elastic sphere in general relativity theory *(Russian)* 79—92671
recession vels. greater than light 77—87585
recombination epoch, density fluctuation evolution 79—67124
recombination epoch and microwave background, spectrum distortions 80—62334
recurrent Finsler space, infinitesimal affine motion 79—71305
red shift controversy rel. to Seyferts and quasars 77—2476
red shift of light traversing clusters of galaxies, photon prop. 77—29642
red shifts, critical anal. of explanation by new field 77—9828
redshift-distance relation, evidence for linearly expanding Universe 80—31354
redshift-distance square law 79—67095
redshift-magnitude bands and galaxies evolution, data anal. 78—57629
redshifts and superluminal expansion vels. of galaxies and quasars 77—26050
reference coordinate system concept, development history *(German)* 77—13642
regular isotropic cosmological model, graviton generation *(Russian)* 77—22338
Reissner-Nordstrom-de Sitter metric, the third law, and cosmic censorship 79—35609
relativistic, radiative transfer for polarized light, eqn. soln. method 78—73781
relativistic cosmologies with synge gas and blackbody radiation 80—36751
relativistic dense matter, statistical mechanics using phenomenological quantum field model 78—89814
relativistic dust universes, comoving metrics, Newtonian interpretation 78—65732
relativistic ejection, kinematics *(French)* 77—73943
relativistic EM fluid flow geometry 79—4091
relativistic EM fluid flow with geometrical symmetry 79—4092
relativistic gas expansion 77—64892
relativistic gravitational potential, relation to mass-energy 80—22239
relativistic hierarchical cosmology, mathematical formalism and Einstein eqns. 80—82555
relativistic interpretation of cosmological const. *(French)* 77—87580
relativistic interpretation of redshift related to light crossing clusters of galaxies 77—17685
relativistic mechanics, generalised, spacetime quantisation and Mach's principle 78—73867
relativistic non-ideal hadron gas universe, gravit. collapse *(Russian)* 79—44650
relativistic scalar entropy 79—62939
relativistic shock waves, damping 77—75994
relativistic simple waves, shock damping and entropy prod. 77—17725
relativistic star, curved space-time, vac. stability, polarisation, phase transition 77—49290
relic θ particle concentration in the Universe *(Russian)* 80—86026
relic 't Hooft Polyakov mag. monopoles in the Universe 79—9317
relic monopoles from big bang, cosmological problem for standard unified theories 80—77532
relic radiation, as possible product of quantum era in universe expansion *(Russian)* 78—81717
relict black-body radiation temp. fluctuations prod. by cosmological turbulence *(Russian, English)* 78—77630
relict radiation spectrum distortion by 21 cm absorpt. line *(Russian)* 78—4422
repulsive gravitational forces, possible clustering mechanism 77—37674
reversed causality illustration, Kac ring, expt. searches 77—49704
review 77—53715
review of relationship between cosmology and elementary particle physics 79—101061
rich clusters of galaxies, form. times and gravit. const. var. 78—69892
Riemann-Cartan space-time with cosmological principle, torsion tensor 80—31633
Riemannian manifolds, symmetric vectors and algebraic classification 80—68094
rigidly rotating relativistic dust cylinder, Riemann tensor, ultrarelativistic case 80—86158
rival cosmologies to big bang, review 78—57705
Robertson-Walker and Petrov G_4 VIII cosmologies, general relativistic kinetic theory 78—24586
Robertson-Walker cosmologies, Kostant-Souriau quantisation 80—12838
Robertson-Walker expanding universe, energy spectrum of H-atom 78—73869
Robertson-Walker metric, elementary particles in homogeneous isotropic universe 77—5734

cosmology continued
Robertson-Walker metric and symmetries belonging to contracted Ricci collineations 78—24580
Robertson-Walker spacetime, energy-momentum tensor and particle state definition 79—25934
Robertson-Walker spacetime, trace anomaly of energy-momentum tensor of quantised scalar fields 79—63360
Robertson-Walker type solutions in unitary theory *(French)* 79—17287
Robertson-Walker universe, density constraint on local inhomogeneities 78—8281
Robertson-Walker universe, finite temp. effects 78—45440
Robertson-Walker Universe, quantum statistics 79—88769
Robertson-Walker universe, stress tensor and conformal anomalies for massless fields 77—78903
Robertson-Walker universes, particle creation, self-interacting quantised fields 80—17699
rotating black hole, Kerr metric, spontaneous creation of massive spin 1/2 particles 78—89217
rotating metrics, scalar perturbations 80—62348
rotating pressure-free space-time, thin self-similar disc config. 78—96387
rotating sphere, internal gravit. field in weak-field approx., appl. to astrophysical objects *(Russian)* 79—25939
rotating universe, stability 79—17146
rotating universe with violation of causality 79—44828
rotation measures, intergalactic magnetic field and cosmology 78—28800
Rubin-Ford effects of Milky Way galactic absorpt. on Sc-type galaxies sample 78—49533
Sakharov's thoery of gravitation 79—25950
SC galaxies, space distrib., large-scale struct. 79—71106
scalar field, anisotropic, with cosmical time 79—88847
scalar fields, self-interacting, with geometrical interpretations 80—31397
scalar matter production, global effects in quantum cosmology 79—92903
scalar particles creation in isotropic universe, Feynman propagator behaviour 78—45445
scalar-particle prod. near anisotropic universe singularity due to gravit. field 77—91421
scalar-tensor cosmology of Jordan-Brans-Dicke, influence of massless EM fields 77—45617
scalar-tensor theory of gravity with const. G, cosmological solns. 78—21041
scale covariant cosmology, coupling of matter and radiation 79—62937
scale covariant cosmology, primordial He prod. 80—105412
scale covariant cosmology, props. of early generation stars 78—36739
scale covariant gravitation theory, rel. to stellar vel. dispersion age depend. 78—65661
scale covariant gravitation theory appls. 77—79019
scale covariant gravity theories, astrophysical tests 80—73216
scale covariant models and early Earth temp. 78—57704
scale invariance, metrical connection and the motions of astronomical bodies 79—44648
scale-covariant, 3K background and Large Numbers Hypothesis 78—93480
scale-covariant gravitation theory, appl. to stellar dynamics 80—26913
second viscosity effects *(Russian)* 78—41102
Segal chronogeometric redshift, classical anal. 77—45618
self-consistent variational theory, Machian model 80—67558
self-similar hierarchical cosmology and atomic scale phenomena 79—101230
self-similar space-times, perturbation scheme 78—54099
self-similar space-times, solutions to general relativity eqns. 78—54098
semiclassical theory of scalar field in globally hyperbolic universe 78—54250
Seyfert-like galaxies, medium-redshift, redshift-magnitude-ang. dia. data statistical anal. 78—86016
shear-free and acceleration-free fluids in Einstein's theory of gravitation *(German)* 77—22467
shock formation and shock structure in the cosmological radiative era 80—4463
single galaxies abundance and cosmological significance 77—53688
single soliton cosmological waves, Friedmann cosmological model background *(Russian)* 80—17708
singular points and projective limits in relativity 80—52077
singularities, specific examples 80—36748
singularities in general relativity theory 79—35591
singularities in spatially homogeneous cosmologies 80—36747
singularity avoidance and quantum conformal anomalies 77—67148
singularity generic, studies by Belinskii, Khalatnikov and Lifschitz 80—31399
singularity theorems and universe rejuvenation 78—32616
solar He abundance inferred from global oscills. obs. in spectra, cosmology implications 80—51724
solar neutrino problem, implications for cosmological hypotheses 79—16918
solar system formation, re-evaporation of condensed matter, evidence from meteorite mineral content 78—85864
solar system formation, role of supernova, isotopes found in primitive meteorites 79—44380
solar system motion rel. to diffuse X-ray background, evidence from Compton-Getting anisotropy 80—98745
space curvature, universal evolution and density 77—91677
space time permeated by compressible, thermally conducting self-gravitating field, props. 79—71315
space-time homogeneous models with torsion 79—58607
space-time infinity of Universe, various problems *(Polish)* 78—61948
space-time metric, quantised field influence, external grav. field *(Russian)* 80—86027
space-time metrical fluctuations induced by cosmic turbulence 80—82557
space-time properties, local and global, Einstein's eqns., Universe matter density 78—61942
space-time spinorial structs., and EM hyperheavens 77—74283
spacelike dust, 4-parameter Lie isometry groups 77—57246
spacetime singularities 78—8291
spatial conformal flatness in homogeneous and inhomogeneous cosmologies 78—69924
spatial distribution of different types of galaxies 79—84862
spatially homogeneous and inhomogeneous cosmologies with equation of state $p=\mu$ 79—49122
spatially homogeneous anisotropically expanding universe, Heckmann-Schucking models 79—88768
spatially homogeneous cosmologies with EM field 80—51924

cosmology continued
spatially homogeneous cosmology, dynamical degrees of freedom 79–30155
spatially homogeneous neutrino cosmologies 80–90585
spatially homogeneous universes which admit source-free magnetic fields 80–12973
spatially homothetic cosmological models 79–25771
spatially inhomogeneous models of the universe, early stages of evolution *(Russian)* 80–4467
spectral lines of prestellar origin, prediction in cosmic relic radiation *(Russian)* 78–77628
spectral shifts, variational study, relativistic aspects *(French)* 80–21909
spherical models at late times, general features 80–17697
spherical multicomponent fluid, hydrostatic equilib., thermodynamic interpretation, 3-component neutron star 79–49135
spherically symmetric distrib. of matter with press., Einstein eqns. soln. 78–32617
spherically symmetric self-similar universe, theory 80–8727
spherically symmetric vacuum manifold, effect of nonvanishing cosmological const. 77–74288
spinor field cosmological models, Einstein-Cartan theory of gravitation 78–32618
spiral galaxy orientation anisotropy in Abastumani Catalogue of Bright Galaxies 77–17678
spiral structures, geophysical and astrophysical 80–77287
spontaneous breaking of gauge symmetry in a nonstationary isotropic metric 79–21643
spontaneous symmetry breaking, Eddington's no. cosmic variablity, inertia, and gravitation 79–80375
stability of expanding Universe 79–17148
stable hadrons containing massive stable quarks, cosmological constraints 79–54308
stable heavy neutrinos, dynamical interactions and astrophys. effects 79–5743
stable method heavy leptons, astrophysical mass constraint, condensation in stars and galaxies *(Russian)* 80–72768
standard candle location, giant elliptical galaxy selection 80–105353
standard hot big bang model of Universe, dynamics 78–69922
star formation before galaxies, missing mass soln. 78–57654
star formation from hot matter with primordial chemical comp., role of H_2^+ mol. ion *(Russian)* 78–40924
static and near-static semiclosed configs. and cosmological term *(Russian)* 78–93486
static axially symmetric electrovac universes, Einstein-Maxwell field eqns. exact solns. 79–85034
static inhomogeneous cosmological model 77–67147
static Universe model with two centres, red shift explanation 78–57706
static Weyl solutions, for Brans-Dicke Maxwell fields 79–85033
statically homogeneous cosmological models, Einstein-Cartan theory *(Russian)* 77–49511
statistical mechanics, relativistic formulation, appl. of bootstrap theory to thermodynamics and cosmology 79–40452
statistical mechanics of complex systems, linkages from fundamental particles to cosmology 79–25964
statistical mechanics of gravitating systems 79–35311
statistical virial theorem appl. 79–5926
steady state cosmology within stochastic electrodynamics framework 80–56983
steady state universe, hawking process and cosmic microwave background 79–80380
steady state Universe using stochastic electrodynamics, cosmic background radiation and red shift 78–77631
strong and gravitational interaction unified theory, hierarchy of universes, large numbers explanation 79–17654
strong gravitational field and general relativity 80–67548
strong gravity and Dirac numbers 78–21372
strong gravity equations, spin and torsion effects, rel. to spin of Universe 79–97116
structure development in expanding universe, new model 78–93489
structure of early Universe 80–90594
structure of the universe, book 78–32628
structure of Universe in most recent epoch 77–37675
SU(5) grand unification, cosmological baryon asymmetry 80–86640
SU(5) theories with both proton stability and cosmological baryon-number generation 80–86642
super-dense matter, phase transitions in gauge theories and cosmology, review 79–44654
superclusters, existence and role in cosmic hierarchy 77–71151
superconducting early Universe, cosmological baryon prod., CP invariance grand unification 80–90592
superconductivity and elementary particles theory, review 80–4911
superdense cosmogony and magnetic field origin *(Russian)* 79–8985
superdense nonequilibrium cosmic objects, coherent boson graviton avalanche catastrophes 78–85844
superfluid as a source of all interactions 79–21620
superfluid vacuum state, time-varying constant and nonsingular models 77–13512
supergravity, local supersymmetry in (2+1) dimens., differential forms. 78–49980
superheavy magnetic monopoles, cosmological prod. in grand unified models 80–8884
superluminal radio sources, cosmological proper motion-redshift relation 80–22095
superluminal velocities in extragalactic radiosources, review 77–78882
superluminally expanding radiosources and radio-quiet QSOs 79–30142
supernovae as standard candle 79–101167
supernovae at great distance, luminosity and temporal var. as cosmological probes 80–94821
superweak particle cosmological constraints, ν with neutral current interactions, ^{4}He primordial abundance 79–84667
symmetric big-bang cosmologies, implications of antiproton instability 78–41104
symmetric universe models testing *(Polish)* 79–101229
symmetric vectors and Ricci directions 80–8725
symmetries and metrics of homogeneous cosmologies 80–90584
symmetry breaking, and nature of weak interactions 80–27428
symmetry breaking and phase transition in early hot universe 77–22661
symmetry restoration in the early Universe 78–73782
Szekeres inhomogeneous cosmological models, intrinsic symmetries in general relativity 80–12955

cosmology continued
Szekeres inhomogeneous models, isotropic blackbody radiation inc. 80–46717
tachyon dust universe 78–24583
tachyons interaction with gravity, rel. to cosmology and black holes 79–25839
tachyons nature and role in cosmological evolution *(Russian)* 79–17150
telescopic principles in the theory of gravitation *(German)* 79–40416
test particle mass in gravitational field, rel. to Mach's principle 79–12670
theoretical isochrones for stellar evolution with variable G, Brans-Dicke theory 79–67125
theories and predictions, general review 79–88770
thermal history of Universe, and relic rad. theory 78–20921
thermal particle prod. spectra in Taub-Nut spacetime 77–13382
thermal particle production in a radiation dominated Robertson-Walker universe 78–81721
thermal radiation, parity violating currents 79–17633
thermodynamics of Universe 78–4418
tidal interactions in expanding Universe, prolate systems form. 79–71164
tidal theory for origin of solar nebula 79–84687
tilted Bianchi type-III cosmologies 79–53948
time asymmetry, in Riemann gravit. theory *(German)* 79–35610
time asymmetry, rel. to black hole thermodynamics 77–2451
time symmetric gravitational waves evolution, initial data, apparent horizon 78–12626
time varying Newtonian gravity, Q 78–77634
time-asymptotic particle interpretation in the Friedman-de Sitter space 78–81720
Tolman-Omer and Godel universes, closed conformal transforms. *(French)* 77–71159
Tomimatsu Sata space-times, Einstein eqns. soln., effective pot. for equatorial motion 78–32621
trace anomalies in a two-dimensional de Sitter metric and black-body radiation 78–65841
traditional assumptions, critical comments 77–13511
transfer coefficients, behaviour at relativistic temps., dissipative effects *(Russian)* 79–6062
trouser type universe metric 77–45623
turbulence, Kurskov-Ozernoi transformation appl. 77–5604
turbulence decay rel. to galaxy form. 78–49568
turbulence in cosmology, non-linear interactions rel. to universe expansion, quantum turbulence 78–77629
turbulence origin rel. to galaxy form. 77–49513
twin enantiomorphic universes, with opposite proper times *(French)* 77–74167
Type I supernovae as cosmological clocks 77–2446
Type VI$_0$ cosmologies, tilting and viscous models 78–57703
type VI$_0$ modes with EM field, plasma conductivity 78–8171
unborn galaxy clusters, microwave and X-ray emission 78–8131
unidentified high latitude radiosources 78–57672
unified fields in pentadimensional theory 79–44832
unified gauge theories and the baryon number of the universe 78–85842
unified theory of strong and gravitational interactions 79–17662
uniform electrovacuum space time, observer dependent effects, Bertotti-Robinson line element 79–122
uniform gravitational collapse, lepton pair creation, macroscopic gauge theory of gravity 78–81724
unitary fields, model of Newtonian theory *(French)* 77–53407
universal anisotropy and gravit. waves, effect on microwave background fluctuations 78–28866
universal anisotropy limits and He production 78–36737
universal atomic standard, Einstein field eqn. considerations 80–107
universal baryon density, constraint from ^{7}Li abundance 78–4420
universal CP noninvariant superweak interaction and baryon asymmetry of the universe 78–66072
universal evolution, steady-state and big-bang theories *(Italian)* 80–98748
Universal evolution and fate 77–64890
universal expansion and big-bang theory rel. to stellar cluster formation *(Dutch)* 80–62212
universal fragmentation model, appl. to spiral galaxies form. 80–90529
universal large scale shearing, Ariel V X-ray background data 80–62352
universal origin and exploding black holes 78–8178
universal structural evolution 80–17700
Universal structure, galaxy formation and young objects 77–29968
universe, book 77–26102
Universe, closed or open, Fornax system density profile, strong gravitational interactions 80–90587
Universe, consistent age 78–81723
universe, history from origin to earliest geological times, rel. to origin of life 78–69923
Universe, hydrodynamics, book contrib. 77–49516
Universe, initial isotropy and homegeneity questioned 80–22125
Universe, spatial homogeneity, philosophical problems 80–56984
Universe, structure and future, Olber's Paradox 80–8773
Universe, very massive unstable particles, prop. bounds 80–82558
Universe age effects on stellar evolution with variable gravitational constant 79–30052
Universe and general field clumpy structure 78–45443
Universe and microcosm, gravitational-inertial field theory 80–8721
Universe baryon asymmetry, left-right symmetric grand unified models 80–82559
Universe baryon number asymmetry mechanism, unified calibration theory calcs. *(Russian)* 80–36756
Universe before nucleosynthesis, first three minutes 80–62358
Universe creation as quantum phenomenon, fireball model 79–9038
universe density, H I obs. rel. to density of unseen galaxies 77–29925
universe density, results from groups of galaxies 78–12385
Universe density perturbations, consequences for evolution nonlinear stage of neutrino rest mass *(Russian)* 80–105414
Universe density perturbations spectrum, consequences of neutrino rest mass *(Russian)* 80–109576
Universe early stages, expansion, entropy, and struct. 80–46721
Universe expansion 78–93491
Universe expansion and time variation of atomic mass 80–90588
Universe expansion far from singularity, density fluctuations *(Russian)* 77–33713
Universe expansion kinematics, motion in space and time 80–17701
Universe expansion model, explanation of 3K background 80–98746

cosmology continued
  universe expansion or reference system contraction 79—101228
  Universe fluctuations, spontaneous prod. 80—94902
  Universe global structure and nonhomogeneous large scale mag. field *(Russian)* 77—82335
  universe homogeneity, relation to dimensionality of space 77—64893
  Universe homogeneity and isotropy 78—16587
  universe inhomogeneities, power law relating mass fraction to density enhancement 78—57656
  Universe initial regularity, effects of matter-antimatter symmetry breaking 80—22124
  Universe isotropy, test using radiosource rot. measures and red shifts 77—2502
  Universe large-scale inhomogeneity, spherically symmetric models 77—64889
  Universe large-scale struct. form., two-dimensional simulation of gravit. system dynamics 80—98749
  Universe long-term future, review 80—41927
  Universe mass density and age, implications of neutrino rest mass *(Russian)* 80—109575
  universe matter-antimatter model, light element abundances 78—45439
  Universe mean density, implications of intergalactic matter obs. 80—109543
  universe mean luminosity density, from luminosity function of field galaxies 78—16526
  universe mean mass density, estimate from Kirshner, Oemler, Schechter, galaxy redshift sample 79—75298
  universe model, Brans-Dicke theory, props. 78—45446
  universe model, computer simulation of galaxy distrib . in Lick catalogue 78—81718
  Universe model, homogeneous, isotropic, close to cosmological singularity, long-wave disturbances 80—73078
  universe models, development of modern cosmology *(Chinese)* 77—9829
  universe models containing matter and gravitational radiation 77—87679
  universe models with Rastall's theory of gravity 78—41100
  universe models with variable past gravit. constant and macroscopic masses, solar and stellar tests 77—45619
  Universe neutrino species and lepton numbers 80—8730
  Universe origin and evolution 79—40306
  Universe preferred frame optical test, Earthbound ring laser interferometry 80—77531
  Universe primeval perturbs., search for microwave background fluctuations *(Russian)* 78—36734
  Universe structure, open and closed curved spaces 78—77652
  universe ultimate fate, effect of finite proton lifetime 80—82560
  Universe ultimate fate 77—71163
  universe ultimate fate 79—75303
  Universe uniqueness, cosmological theories and large number hypothesis 77—82336
  universe with variable G and c, initial conditions 79—48977
  vacuum cosmologies, repulsive and attractive timelike singularities 79—92901
  vacuum instability *(Chinese)* 79—97115
  vacuum instability and inhomogeneous distrib. of celestial objects *(Chinese)* 77—87581
  vacuum quantum effects, isotropic cosmological models *(Russian)* 80—51937
  vacuum state, influence of gravitation and cosmological effects on symmetry breaking *(Chinese)* 78—65858
  vacuum structure in calibration theories, CP violation *(Russian)* 80—27478
  vacuum structure in gauge theories, strong CP violation and cosmology 80—86578
  vacuum superfluidity near anisotropic singularity, phase transitions *(Russian)* 80—94905
  variable rest mass field theory and the cosmological singularity models 80—77525
  variable rest masses, black hole solutions and neutron star models 79—30162
  variable rest masses, relativistic theories, tests and consequences 80—31396
  velocity-distance relation, history 80—12880
  very early Universe, baryon asymmetry 79—40309
  very early Universe, nonequilib., grand unified particle interactions, baryon number violating bosons 80—36752
  very early Universe, phase transitions and mag. monopole prod., grand unification 80—51934
  viscoelastic matter cosmological evolution, causal thermodynamics *(Russian)* 79—101232
  viscous fluid cosmological model in general relativity 78—61944
  Vlasov-Einstein eqns. in spherical symmetry, self-similar analysis 80—67535
  vortex cosmologies, light element synthesis 77—45622
  wave propagation and evolution in self-gravit. medium *(Chinese)* 79—80211
  weak currents role in 'pair creation' universe, quasar model 77—5605
  weak interaction and isotropy of Universe 78—61947
  weak interactions, conf., Bloomington, USA, (May, 1977) 78—414
  weak interactions in astrophysics and cosmology 77—25934
  Weinberg-Salam model, vacuum instability, cosmology and particle mass constraints 80—78007
  Weyl's geometry rel. to dynamical mass excess in clusters of galaxies 78—69919
  Wheeler's 'rule of unanimity' in quantum cosmology 80—98846
  Wheeler-Feynman electrodynamics, advanced wave emergence in steady state universe 80—17816
  whimper space-time solns. to Einstein eqn. 80—31614
  white holes, local big bang inhomogeneities and observability 78—45353
  white holes, optical appearance 79—21323
  white holes, tachyon emission 77—33718
  white holes spectral features in Nordstrom and Kerr-Newman metrics 77—29967
  world model, relativistic free particle case 77—71158
  X-ray and γ-ray background radiations origin 77—33703
  X-ray background, constraints rel. to X-ray background synthesis 80—27021
  X-ray background, contrib. of discrete evolving sources 80—82551
  X-ray background, contribution from young galaxies 80—82550
  X-ray background, produced by pregalactic black holes? 80—56978
  X-ray background, source 78—8168
  X-ray background irregularities 80—62331

cosmology continued
  X-ray background sources 80—94898
  X-ray clusters of galaxies, evolution over cosmological time scales 78—28770
  X-ray diffuse background, spectrum from 3 to 50 keV 80—41916
  X-ray source counts 79—40305
  Yang's gravitation theory, homogeneous cosmological models 79—17304
  Yang-Mills gravity dynamics homogeneous and isotropic world models 78—45543
  Zeldovich spectrum of cosmological fluctuations from spontaneous symmetry breaking 80—62353
  zero mass surfaces, rel. to cosmological singularities 79—25772
  Zwicky galaxies, luminosity function slope 80—36709
  $\gamma\gamma \to \nu\bar{\nu}$, nonzero neutrino mass, early Universe process 78—21483
  ν sea, cosmological, EM wave propagation, torsionic background 80—77283
  $\bar{p}$ decay and baryon number of universe 77—49964
  D abundance in Galaxy rel. to cosmology 78—69883
  D and density of matter in open, expanding Universe 79—12548
  D origin, prod. by high energy particles 77—33709
  H II region vel. dispersions rel. to linear diameters 77—33595
  H recombination, kinetics in presence of low mass primordial black holes *(Russian)* 79—17152
  He origin, evidence from subdwarfs He abundance 80—22003
  He primordial abundance, obs. of chemical abundances in new halo planetary nebula 77—45510
  ^{4}He production, nonzero neutrino rest mass effects 80—105413
  Re/Os cosmochronology, nuclear correction factor 80—17485
  Re-Os, rel. abundance, rel. to nuclear chronometer reliability 78—85919
cosmotrons
  No entries
Costa Ribeiro effect *see dielectric phenomena; phase transformations*
Cotton-Mouton effect *see birefringence; magneto-optical effects*
Cottrell atmospheres
  composite dislocations, asymm. equilib. positions and line tensions 79—51108
  diffusion length and lifetime meas. and assessment by SEM 80—96902
  edge dislocation motion, glide and climb resist. due to dragging a Cottrell atm. 79—99194
  metals, research at Birmingham, (1945-55) 80—62444
  solid solution alloys, creep behaviour at intermediate stresses and creep power law breakdown 79—57058
  steel, C, rel. to effect of temp., deform. rate and stress state on ductility *(Russian)* 78—35428
  steel, C, strain ageing and fatigue limit 80—40378
  steel, mild, work hardening and strain ageing during fatigue *(Japanese)* 77—8931
  Ag, deformed at room temp., glide on {001} planes, TEM obs. 79—19257
  Cu, deformed at room temp., glide on {001} planes, TEM obs. 79—19257
  Cu-Ni alloy, dil., rel. to dislocation damping, 95-297K, at high strain amplitudes 78—39824
  Fe, damping during and after deformation 79—43344
  Fe-Al(Ti), O containing, mag. aftereffect and disaccommodation meas., time depend., activation energy, and ageing props. 80—88836
  n-Ge:Bi,O, plastically deformed, dislocation scatt. anisotropy, effect of state of O in Cottrell atm. 78—19028
  H_2 transport by dislocations 77—21263
  LiF:Ni, dislocation behaviour in diffusion zone, Cottrell clouds *(Russian)* 80—70212
  Ni 200, static strain ageing, 373 to 473K 77—36558
  Ni, deformed at room temp., glide on {001} planes, TEM obs. 79—19257
  Ti-Al-V-Sn (6,6,2 wt.%), depend. of K_{ISCC} on loading rate and crack orientation 80—45427
Cottrell locking *see Cottrell atmospheres*
Couette flow
  see also jets
  13 GK model, numerical results for Couette, Poiseuille and thermal creep flow between parallel plates 79—77057
  accelerating shear flow, internal gravity waves 79—32628
  anemometry, hot-wire, in very low velocity flow, calibration of probes 80—75008
  anisotropic liquid, axially symmetric flow 80—103050
  autooscillations, azimuthal wave type, rot. Couette flow stability loss 77—75882
  bead-spring-type model in nonuniform vel. gradient, dil. soln. kinetic theory results 80—64628
  BGK scattering model, Boltzmann eqn. solved by local Green's function method 79—97327
  bifurcation in steady flows of viscous fluid, expt. 78—30267
  bifurcation in steady flows of viscous fluid, theory 78—30266
  blood cell suspensions, stability to small disturbances in circular Couette flow 80—56099
  blood droplet deformation in Couette flow suspension, expt. *(German)* 79—16227
  blood suspension aggregation in Couette flow *(French)* 80—97991
  buoyancy effect on plane Couette flow past permeable bed 80—92215
  centrifugally stratified helical Couette flow, stability 77—89183
  chaotic circular Couette flow, reemergent order 79—27651
  chemically reactive flow, heat and mass transfer, approximate theory 79—68821
  circular Couette flow, centrifugal instabilities in cylindrical annulus 79—18956
  classical fluid near critical point, nonequilib. steady state fluctuations with laminar shear flow 79—81844
  coagulated colloidal suspensions, couette flow, viscosity effect 79—90317
  cone/plate system in fluid, friction heating and convection 78—87238
  convective cells, stochastic oscill. spatial-time spectra *(Russian)* 80—103029
  Couette flow, turbulence transition, Landau picture, stochastic attractor representation *(Russian)* 79—98692
  Couette flow stability, transformation of perturbation eqns. 77—7474
  Couette-Taylor flow, laser Doppler velocimetry obs. of transition to turbulence 80—92163
  cylindrical Couette flow, perturbation by Coulomb force induced secondary flow, electroviscous effect *(French)* 80—24100
  cylindrical Couette flow and electrically induced secondary flow, superposition 80—28575

Couette flow continued
Czochralski growth, fluid flow changes, depth depend. 77−69981
discrete kinetic theory, maths. and numerical aspects, Couette flow appls. 80−19413
discrete velocity gas, kinetic theory boundary conditions 78−30254
dusty gas between two infinite coaxial cylinders 78−55685
early nonperiodic transitions in Couette flow 80−59056
electrically conducting fluid, with time-depend. suction, between parallel walls 79−37279
electrorheological suspensions, struct. form. in electric fields *(Russian)* 77−86391
finite amplitude stability, perturbative and iterative methods 78−38293
finite linear viscoelasticity, Couette flow *(French)* 77−65767
gas, nonlinear shear viscosity in steady Couette flow 80−28588
gas creep along solid surface, half-space moments method calcs. 78−67222
gas kinetic boundary value problem, non-equilibrium thermodynamics 80−19544
half-range expansions soln., for arbitrary Knudsen nos. 77−51088
Hall effects in unsteady Couette flow 77−15127
hard-sphere fluid, shear viscosity, nonequilib. molecular dynamics calcs. 79−68996
hydrodynamic instabilities, transition to turbulence, Couette flow, vertex streets, Rayleigh-Benard instability 78−83362
hydrodynamic instabilities and turbulence, flow states, examples and meas. methods 80−92116
hydrodynamic stability of cylindrical flow 79−46288
hydrodynamic stability rel. to finite amplitude perturb. *(Russian)* 79−37291
hydrodynamic thermal breakdown in viscous fluid, Couette flow between cylinders 78−83391
incompressible viscous fluid, entrance region heat transfer in plane Couette flow, num. procedure 77−15020
instability, finite amplitude 78−13993
instability of longitudinal convection rolls 78−26122
laminar Couette flow between parallel plates, heat transfer 77−31299
laminar Couette flow in rot. fluid between coaxial cylinders, Taylor instability 77−51066
laminar equalising flow in Couette-type channel flow *(German)* 78−51239
laminar to turbulent transition spectrum evolution 80−103034
linearised plane Couette flow, rarefied gas with infinite range molecular interactions, asymptotic anal. 79−23340
liquid flow in-rotating spherical layers, stability and nonuniqueness 79−77135
liquid in rot. system, Hall effects on MHD Couette flow and heat transfer 79−41681
low Reynolds number motion of particles with 2 or 3 perpendicular planes of symmetry 80−24034
macromolecular dilute aqueous solns., flow in various geometries 79−41757
magnetic fluid, motion in external mag. field, Couette and Poiseuille flow 79−14491
MHD, effects of couple stresses for electrically conducting fluid, skin effect 78−91020
MHD, Hall and ion-slip effects, heat transfer 79−94726
MHD, unsteady, between two plates when one subjected to random pulses 80−69938
MHD Couette flow, Hall effect in rot. system 80−74991
MHD Couette flow, with variable wall temp., heat transfer 79−27640
MHD Couette flow and heat transfer in rotating system 77−35246
MHD Couette flow stability in presence of mag. field 79−23373
MHD Couette flow with Hall currents, stability, numerical soln. 77−72360
MHD Couette flow with porous boundary 80−53876
MHD flow instability, cond. liq., finite disturbances effect *(Russian)* 77−65808
MHD laminar flow, suspended particle motion stabiity *(Russian)* 78−5808
MHD supercritical Taylor-Couette flow 80−33702
modulated, stability 77−3810
modulated circular flow, energy stability 77−31313
nematic liquid crystal, cylindrical Couette flow, stability 79−32526
nematic liquid crystal, hydrodynamic instability phenomena and mechanisms, book contrib. *(French)* 77−84229
nematic liquid crystals, book contrib. 78−59531
nematic liquid crystals, Couette flow, orientation instability for finite anchoring energies 80−74923
non-Newtonian flow with moving boundaries 79−23343
non-Newtonian fluid, Couette flow, vel. profile determ. 77−15074
non-Newtonian fluids, heat transfer in plane Couette flow with additional pressure gradient including entrance effects 79−50760
non-Newtonian incompressible fluids, with uniform suction at stationary plate 79−32637
non-Newtonian liquid, isothermal Couette flow in slowly converging channel with complex shear 77−15069
nonlinear stability of motion of viscous liquid between concentric rotating cylinders 79−14409
nonlinearity viscoplastic liquid, convective dissipative heat exchange 80−87772
nonlinearly viscoplastic fluid, Couette flow 79−18918
ordinary differential eqns., invariant imbedding, Riccati transformations and eigenvalue poblems 77−37
p-azoxyanisole, nematic phase Couette flow mag. field and boundary condition effects 77−3887
periodic secondary motions in plane channel, num. soln. method 77−55092
permeable wall layer, heat transfer and temp. distrib. 78−51165
pipe flow, finite amplitude stability theory 78−63498
plane, bifurcation from infinity, nonlinear differential eqn. 79−98806
plane, critical Reynolds number 79−81931
plane, experimental facility for realization 80−53900
plane, finite amplitude, instability shear layer parallel flow, cellular motion 80−1601
plane, stability, Orr-Sommerfeld eqn. exact soln. 79−98685
plane, transition to turbulence and finite amplitude disturbances 80−33558
plane non-Newtonian Couette flow, heat transfer 79−86471
plane parallel flow, free convection in Couette and Poiseuille flows, numerical simulation 80−99995
plane turbulent Couette-Poiseuille flow, asymptotic anal. 80−33674

Couette flow continued
plane two-layer flows, effect of fluid microstructure on stability 79−77212
polyatomic gas, plane Couette flow in Knudsen regime, wall induced polarisation 80−19443
polymer solution, dil., rotating Couette flow, elongational viscosity and stability 79−27669
polymer solution, stability in Couette flow *(German)* 77−47047
polymer solutions, concentrated, rheological relationships 77−75867
porous annular region, steady flow 78−75201
power law fluid Couette flow, entrance region heat transfer 79−32587
power spectra for chaotic transitions in Rossler dynamical system 80−53898
pressurised turbulent flow in circular annular slot, calc. 79−90229
quasiperiodic flow between rot. cylinders, second charact. mode visualisation 80−28519
radiative magnetogasdynamic Couette flow with variable parameters 80−14840
rarefied gas, heat transfer in plane Couette flow, ellipsoidal model 77−72330
rarefied gas dynamics projection and variational methods 80−6189
rarefied gas mixture flow along surface, isothermal slip 78−67220
resonance mechanism, small 3-D disturbances 80−79269
rigid sphere suspensions, micropolar fluid model, viscous Couette flow 77−84302
rotating cylinders, Taylor vortex form. and spectral props. of boundary value problems 79−90262
rotating system between parallel plates, heat transfer 77−75878
rotatory, amplitude steady secondary flow past marginal state, Landau's conjecture 79−77128
secondary flows and stability study of rotating spherical layers at arbitrary Rossby numbers 79−18899
shpere between plane parallel boundaries, creeping parallel motion, strong interaction theory 80−103075
slip flow analogy 80−1508
spherical, in thick layer, with revolving inner sphere, stability, review 79−81969
spherical Couette flows, loss of stability between two rotating spheres 80−1527
stability, Green's functions 77−31279
statistical linear algebraic model 78−47002
stratified viscous plane Couette flow, stability, const. buoyancy freq. 77−47059
stratified viscous plane Couette flow, stability, variable buoyancy freq. 77−47060
stress near rigid boundaries 77−80200
striated boundary effect on viscous drag 78−59367
symmetric Couette and Taylor flow between rotating coaxial cylinders, Navier-Stokes eqn. solns. *(German)* 78−94750
Taylor cells hydrodynamics instability and vortex currents in Couette flow 80−64571
Taylor vortex flow, finite difference transient implicit method, stability 79 14404
Taylor vortices, finite difference numerical computation 77−62259
Taylor vortices in Couette flow, temporal development 79−64672
Taylor vortices near instability point, amplitude, mode-coupling theory 77−68598
Taylor-Couette flows at very high Taylor number, marginal instability 80−1599
Taylor-vortex flow between rot. cylinders, amplification rates and torques 77−42848
thixotropic fluid, shear flow, oscillatory Couette flow, apparent viscoelasticity 79−90288
transition regime, Couette flow between cylinders *(Chinese)* 80−59042
turbulence creation, review *(Hungarian)* 79−23312
turbulence in rotational Couette flow, power spectra of nonlinearly coupled waves 78−30261
turbulent, eddy viscosity decay, phenomenological theory 79−98700
turbulent Couette flow with adverse press. grad., zero net flow 77−72281
turbulent plane Couette flow, probability distrib. functions 77−54983
turbulent pressure-head, of capsule pipeline transportation system 77−35125
two layer flow stability *(Russian)* 79−14380
two parallel infinite plates, Couette flow of dusty gas 80−1681
two-dimensional shear flow, viscosity effects, microscopic model 77−89085
two-phase flow, asymptotic solns. 79−77223
unsteady Couette flow through porous wall in presence of mag. field 80−53856
viscometer, shear rate determ. 77−68723
viscometer measurement error correction, non-Newtonian liquids appl. *(German)* 78−94868
viscoplastic fluid Couette flow, heat transfer 80−10270
viscous flow equations num. soln. using integral represents. 77−54966
viscous heating at low Reynolds number, stability anal. 77−72280
vortex flows, between rotating cylinders, axisymmetric Navier-Stokes equations 80−59044
wall conductance effects on convective horizontal channel flow 79−23374
He-I, liquid, Taylor vortex instability in Couette flow 79−98683
^{4}He, superfluid, axial heat transport through annular duct with rotating inner cylinder 79−60575
^{4}He, superfluid, rotating Couette flow, hydrodynamic instabilities, attenuation of second sound resonances 79−55964

counter accessories
see also counting circuits
multiwire proportional chamber with short resolution time, high accuracy bidimensional readout 77−57810

counters
see also Cherenkov counters; counting tubes; fission counters; Geiger counters; proportional counters; scintillation counters; semiconductor counters; spark counters
active well coincidence counters, expt. comparison with random drivers for U assay 80−78503
aerosol, Knollenberg light scattering counters, response characts. 79−66369
aerosol, photoelectric, calibration by sedimentation method 80−99031
aerosol particle size distribution errors of ratio-type single-particle counters 77−21898

counters continued
- aerosol particle sizing by optical scattering counters 77—21896
- alpha-particle corona streamer type, performance characts. 78—25402
- alpha-particle corona-streamer counter, performance characts. 79—9962
- automatic light scattering cloud condensation nucleus counter 78—3980
- bivariate point process connected with electronic counters 77—67406
- cell counter, electronic, model 927-TC for cell culture laboratories 79—39616
- charged particle counters in the pre-modern period, historical perspective 79—72190
- co-axial type, summertime obs. in Hyogo Prefecture, Japan 80—31109
- coincidence type ion electron converter device, neutron decay weak interaction obs. 80—58100
- condensation nuclei, counter with inherent size resolution capability 78—81470
- coronary blood flow meas., precordial counting collimator 77—77967
- counters and timers, accurate meas. techniques 78—45605
- counting statistics with variable dead time, generalised expressions for distribs. *(French)* 78—21828
- dead time correction by the pulser method for single channel nuclear counting systems 79—13611
- dead time correction for a counting rate measured with a system of buffer memories 78—86756
- digital, principles 79—67256
- digital US vel. meter using freq. counter 80—38202
- Electrokinetic measurements with submicron particles and pores by the resistive pulse technique 77—86384
- electron counting frequency meters with integrated electronics components *(Russian)* 79—72205
- electron multiplier, channel, effect of count rate 77—6623
- Euratom variable dead-time neutron counter, use for Pu passive assay 80—69042
- frequency, selection principles 79—12775
- gamma counting and self-shielding efficiency, activated thick foil 80—69043
- gas chromatography-mass-spectrometry, ion counting operational characts. *(Japanese)* 77—60157
- gas discharge flow counter for high-temp. gas radiochromatography 79—24859
- halide, photon-induced discharges propag. 77—26942
- heart beat counter, versatile digital SAMI 80—85510
- high-vacuum gas-discharge electron counter 79—18086
- historical perspective of early detectors and counters 79—72189
- ion counting with CEM on double focusing mass spectrometer 77—79194
- lightning counter, multichannel, with digital display 80—51570
- lightning flash counters, for ground flash density meas. 80—51552
- lossy integrator, response for time variable counting rate *(Rumanian)* 78—90045
- medical external counting procedures, history 80—42033
- megachannel pulse height analyser for gamma-ray coincidence analysis 80—99430
- mirror field ion-electron convertor, particle trajectories, IBM 360/91 computer calcs. 77—6626
- multifunction nuclear, monochannel spectrometer Numecint 88 *(Rumanian)* 77—79515
- multistage time averaging filters for timing measurements with large counters 80—99425
- neutron coincidence methods with thermal neutron, appl. limitations *(Bulgarian)* 79—85874
- neutron coincidence system without delay cycle *(Bulgarian)* 79—85873
- neutron ionization chambers, development and characts. 79—68157
- neutron thermal flux, absolute determ., $4\pi\alpha$-γ coincidence meas. 79—85576
- nuclear materials accountability, U and P NDA of crated waste by gamma-ray and neutron coincidence counting 80—83166
- nuclear radiation measurement, pulse processing technique, pulse shaping *(Japanese)* 79—81138
- nuclear radiation pulse counter control cct. *(Spanish)* 80—95508
- optical particle counter, portable, using He-Ne laser, for particles with 0.06 to 10 μm diameter 79—75674
- optical single-particle-size spectrometer calibration and testing, monofilament fibres as substitute particles 80—58819
- paralysable event detectors, improved counting technique 78—57928
- paralyzable event counters, method for partial recovery of lost events 79—18094
- portable neutron coincidence counter for assaying large Pu samples 80—69041
- pulse counter, four-function pocket calculator adaption, for teachers 78—12497
- pulse height analysis programs for high event rates, organisation 77—407
- radiation counting-rate meter output arrival at threshold value, simulation *(Japanese)* 79—93897
- resistance strip magnetic electron multiplier counting system, protons and H atoms detect. efficiency 77—10552
- reversible with digital indication, for oscillograph logging *(Russian)* 77—41209
- Rossi counter for neutron equivalent-dose measurement 80—18678
- statistical behaviour described by goodness-of-fit tests 77—54476
- submicron particulates size determ. by sideway light scattering method 80—98883
- Swiss watch and clock industry, microprogrammed counter logic *(French)* 80—8963
- synchronous reversing decade counter, memorisation, display 77—71728
- thermal neutron coincidence counting, correction for variable moderation and multiplication 80—69045
- time-interval digital extensometer appl. *(Russian)* 77—53888
- total energy coincidence meas. of complementary particles, charged particle anal. of light elements 79—5201
- whole body counters, international intercomparison 80—78504
- X-ray detectors, counting losses, electron storage ring synchrotron radiation 78—86752
- X-ray photometer proportional counter design and characts. *(Polish)* 78—41388
- yield correction by event-time interval transformation 78—9043
- Pb/liq. Ar shower counter systems of SPEAR Mark II detector 78—37495
- Si $\Delta E.E$ counter telescope, particle identification limits *(Japanese)* 79—81133

counters (circuits) *see counting circuits*

counting circuits
- *see also coincidence circuits; pulse height analysers; scaling circuits*
- acoustic detector for beta and gamma radiation *(German)* 79—63876
- AGC pulse processing circuits for photomultiplier tube 79—97955
- amplifier, fast DC coupled linear pulse, gain and phase response design 80—58088
- automatic nuclear emulsion scanner with moving microscope 79—13595
- balloon born cosmic ray electron detectors, curious random counting statistics, electric circuit 78—17540
- baseline restorer, deterioration of S/N *(French)* 77—3237
- beam analyser for electrons and protons 78—37482
- Bellcord—a multilevel fast preprocessor for 1024 ECL channels 79—45577
- CAMAC standard 160-MHz decade counter with digital readout 78—9041
- charge sensitive preamplifiers, signal and noise response 78—33404
- charge transfer transversal filters, applications in nuclear detectors 77—54466
- charged particle detector system for high rate expts., drift-proportional chambers, operating parameters 78—33379
- composite amplifier-discriminator cct., RMS noise meas. 77—54473
- constant fraction 100 MHz discriminator using hybrid microcircuit technology 78—33402
- constant fraction differential discriminator for use in fast timing coincidence systems 79—45580
- constant slope timing for nuclear semiconductor detectors 79—76305
- constant-display frequency meter 79—21718
- count-doubling time monitor, new reactor safety circuit for low-power-level operation 79—41004
- counter-timer-frequency meter for teaching, evaluation 78—28901
- DC coupled discriminator with continuously variable width, fast switching characts. 77—6643
- dead time correction system using standard modules 78—17532
- diagnostic radiation counter, meas. of ^{131,132}I conc. in thyroid gland 77—81557
- digital drift chamber digitizer system 79—45602
- digital freq. counters and counter-timers, new range using MSI 80—27318
- digital interval synthesiser, computer-controlled 78—8386
- digital leaky integrator 79—22560
- digital micrometer/counter accuracy assessment *(Polish)* 78—45654
- digital processor for position sensitive proportional counters 77—26941
- digital scattering angle pre-processors 80—23268
- digital universal counter TTL, amateur constr. *(German)* 78—12727
- digitisers, nonlinear clock 79—18091
- digitisers of time and pulse height, monolithic flash A/D convertor 80—63475
- dissector one-electron current pulse timing, delayed self-coincidence method 79—26846
- dissector pickup tube operating as a counter 80—95153
- Doppler signal centre freq. estimation using quadrature zero-crossing counter, US blood flowmeters 78—31879
- dosimeter system, transit type, for ^{60}Co rot. therapy, electronic modification 77—2053
- drift chamber counter, missed counts and registration efficiency calc. 78—78594
- drift chamber electronics for time and pulse height meas. 79—3326
- drift chamber system for BNL mag. spectrometer expt., design constraints, readout electronics 78—33382
- drift chambers, losses and recording efficiency of electronic cct. 77—88347
- dual NIM standard 52 fold multiplicity unit 79—49914
- electro-optical stabilisation of subnanosecond lifetime spectrom. 77—34508
- electronic measurement apparatus development at ATOMKI *(Hungarian)* 80—18768
- event counter, with selectable time gate, for neurophysiological applic. 77—40944
- fast event recorder utilizing a CCD analog shift register 79—45578
- fast trigger cct. for electron identification in scintillation shower detector 79—81124
- FASTBUS, medium energy physics appls. 80—42912
- FASTBUS, molecular data bus system for high energy physics 80—42911
- femtoamp current preamp for microprocessor controlled isotope calibrator 79—45586
- Fluke model 1953 A, 125 MHz counter *(German)* 77—82541
- frequency counter, LSI design, for microwave band 80—213
- frequency counter sophistication 77—71307
- frequency counters, phase-locked transfer oscillator automatic computing system 77—5862
- frequency counters, review 78—21164
- friction machine, type SMTs-2, exam. of electronic loading cycle counter 79—52527
- gain stabilized NaI(Tl) γ-ray detector, electronics, disc-based minicomputer, power shape in LWR core 78—33284
- gamma ray spectroscopy, time dependent deadtime and pile up corrections 77—23385
- gas scintillation proportional counter, burst length discrimination system 78—21824
- Geiger-Mueller survey meter, portable, compensated count rate cct. 80—99426
- Gray counter, fast synchronous 80—37708
- high rate 4π β-γ coincidence counting system 79—45588
- high speed decade counter, binary-decimal convertor, integrated circuitry 77—75028
- high speed trigger system for total deposited energy measurement in a liquid argon calorimeter 79—45576
- hybrid impedance matching circuit for surface barrier detectors *(French)* 78—90035
- hybrid pulse pile-up rejection system, appl. to Rutherford backscatt. 77—54468
- IEEE conf., scintillation and semiconductor counters and nucl. power systems 77—54389
- instrument selection tables, recent developments 80—13055
- ionisation loss sampling detectors, readout techniques, particle identification 78—46232
- Lass spectrom., performance of PWC cluster logic trigger 79—76262
- LF measurement using counters and monostables 77—113

counting circuits continued
  - lightning ground-flash multiple-stroke discriminator cct. 78—81446
  - liquid H chamber Lyudmila, electronic apparatus for expanded diagnostic system 80—23265
  - logarithmic converter stabilized by a baseline restorer employing gain switching 79—45582
  - lossy integrator, response for time variable counting rate *(Rumanian)* 78—90045
  - magnetostriction spark cameras data readout cct. 78—78576
  - modular 125 ps resolution time interval digitizer for 10 MHz stop burst rates and 33 ms range 79—45591
  - Mossbauer const. velocity spectrometer, control circuits 79—93866
  - multichannel analyser, programmable power supply for nonlinear scaling 77—42218
  - multichannel counter for molecular beam time-of-flight experiments 80—37119
  - multistage parallel-serial time averaging filters to reduce time jitter in scintillation counter time meas. 80—102405
  - multistage time averaging filters for timing measurements with large counters 80—99425
  - multitrack pulse height electronics 79—3325
  - multiwire proportional chamber, shift register read out system 78—86736
  - multiwire proportional chamber, small design, construct., performance, electronics 78—17507
  - multiwire proportional chamber with analogue data plotting 78—78566
  - multiwire proportional counter, linear read out electronics, hybrid preamplifier realisation 80—58091
  - MWPC, cylindrical, event triggers, correlation of wire addresses 80—58092
  - MWPC, drift time meas. electronics 79—3327
  - MWPC, fast analogue logic 79—13605
  - MWPC, multi-delay line cathode readout 79—45573
  - MWPC compact chambers and electronics for crystal ball detector 79—45534
  - neutron-gamma pulse shape discrimination, digital technique 77—403
  - neutron-gamma separation cct. in liquid B scintillation counter 78—862
  - NQR spectrometer, super-regenerative, continuous freq. monitoring 79—63190
  - nuclear event simulation, green LED, trigger circuit, wavelength matched to photomultiplier 77—3238
  - nuclear reactor instrumentation, microprocessor controlled, digital period meter, hardware and software 80—63473
  - nucleonic dual charge sensitive preamplifier 78—55110
  - nucleonic probe ccts with noise rejection, low-level activity meas. 80—52833
  - opto-coupled system for photomultiplier blanking 79—81137
  - parallel plate avalanche counter, timing props. determ. 77—88339
  - particle counter, programmable command data acquisition equipment *(French)* 77—54464
  - particle simulation unit for counter circuitry testing 78—81002
  - Petri dish autoradiographed cell counter 79—70723
  - phoswich detector, reduction of low energy background 77—23369
  - photomultiplier assemblies and associated electronics for high energy physics large counter expts. 77—83469
  - photon count cct. using high-speed comparator in discriminator 78—77979
  - pile-up rejection system for high threshold experiments 80—95509
  - PIXE, trace element anal. with triggered beam pulsing 77—46453
  - plastic scintillation detector system for low level environmental radiation meas. 77—38567
  - portable neutron spectrometer/kerma-rate meter, design, performance 78—33361
  - preamplifier, charge sensitive, loop phase shift and delays 80—58089
  - preamplifier, wideband low-noise system, spectroscopy with Si surface barrier detectors 77—54467
  - precision gated current integrator and live time meter system 79—9973
  - printing scalar, single channel, for photon counting 77—5919
  - programmable line using microstrip transmission line and temp. compensated ECL gates 79—26845
  - programmable NIM-standard logic unit 77—6657
  - proportional counter, position-sensitive, direct position and time digitizer 80—58090
  - proportional counters, position-sensitive, delay-line termination, timing-signals extraction 77—402
  - proportional drift tube for large calorimeter ν detector 79—13592
  - pulse counter, high-speed DC coupled, sensitivity and performance 79—89524
  - pulse counting, high precision, limitations, optimal conditions 77—54463
  - pulse counting circuit, in time-interval series meter 78—176
  - pulse counting measurement systems, optimum parameters determ. 79—89523
  - pulse discriminator, high-speed nonoverloading 77—401
  - pulse discriminator, timing distrib., effect of randomizing time 78—58555
  - pulse shape discriminator for n,γ separation, appl. to TOF spectroscopy 79—6786
  - pulse stacking method of counting in position sensitive detection 77—10556
  - pulse-shape discrimination cct. for liquid scintillation alpha particle spectroscopy 78—21823
  - pulse-train counter and recorder, automatic, with preset program 79—3319
  - pulsed, statistically distributed flow converted into pseudorandom flow 77—18753
  - pulser events, separate storage method 78—46235
  - PWC electronics system for high rate situations 79—26844
  - quadrupole CAMAC universal timer 78—9040
  - radiation counting rate meter output at threshold, fluctuation and arrival shift by computer simulation 80—106240
  - random events, student lab. apparatus demonstrating time distrib. 78—41124
  - reversing, seven decade, LED display, quadrupole mass spectrometer appl. 77—18129
  - scintillation camera electronics capable of high processing rates, clinical significance 77—40740
  - scintillation counter 77—3219
  - scintillation counter hodoscopes, LED test system 78—58556
  - scintillation counters, time-of-flight, electronics system for Mark II Detector 80—58093
  - scintillation detectors, statistical resolution meas. 79—93874

counting circuits continued
  - scintillation probe containing long plastic scintillator, AGC circuit 77—57833
  - secondary beam profile monitor based on MWPC 79—6783
  - semiconductor detector to cold resistance preamplifier, signal coupling through cable or delay-line transformer 78—33401
  - sferics counter, uses two ICs 77—29360
  - signal processing system for high counting rate spectrom. 77—44788
  - single channel analyser, temp. stability, resolution 78—33399
  - single channel counting rate monitor 77—30729
  - solar gamma ray emissions study, Solar maximum mission, detector assembly and electronic assembly 80—63476
  - stationary counting process, first and second order props., estimation technique 80—52834
  - student laboratory apparatus three-digit or four-digit counter-timers 77—17743
  - subnanosecond lifetime measurements, system using microchannel plate photomultiplier 78—37520
  - synchronous reversing decade counter, memorisation, display 77—71728
  - TAC-MCA systems, distortion of spectra by measuring process 79—63877
  - TDC, high precision calib. method 77—57831
  - teaching apparatus, counter-timer cct. 78—28900
  - temperature controlled hybrid substrate for use as a building block in precision instrumentation design 79—45583
  - test instrument survey *(German)* 78—8394
  - Thornton's electronics modules for physics courses, evaluation 77—57133
  - time counter design 78—8385
  - time interval digitiser *(French)* 79—76309
  - time measurement, live, dead or clock, in gamma-ray spectrometry 77—34524
  - time stretcher with high resolution 77—6642
  - time to amplitude converters, precision 1 GHz time calibration 80—27903
  - time to digital convertor, wide-range 79—18090
  - time to digital convertor in real time, low cost 78—55111
  - time-to-number convertor, wide-range high-resolution 78—9039
  - track correlator as fast trigger in π-μ Coulomb bound states detection 79—45574
  - transuranic element meas. in vivo at CRNL 77—77993
  - triple const. fraction discriminator evaluation 78—70708
  - universal, HP 5328A, digital voltmeter appl. 78—29125
  - universal counted and dual-trace delayed-sweep oscilloscope used for precise timing measurements 78—24763
  - US pulse velocity meas. by time selector and frequency counter *(German)* 78—13876
  - very fast time pick-off for low intensity pulsed particle beams 80—63478
  - very low frequency counters, use digital time interval conversion with microprocessor control 77—74430
  - wide-band measuring system for studying charge-coupled device characteristics 79—45585
  - wire spark chambers, capacitive read-out system 80—102407
  - X-ray intensity meas., twin channel method with one special counter, circuit *(German)* 77—6644
  - X-ray spectrometer, proportional counter as input for meas. chain electronics 78—40826
  - zero crossing discrimination technique for constant fraction timing 79—76308
  - CdTe detector, Cl doped, for reentry vehicle appl., development electronics 77—45288
  - CdTe photovoltaic mode γ- and X-radiation dosimeters 79—13594
  - HgI_2, detectors, novel pulse processing system 78—41902
  - H(n,γ), parity violation study, high-rate counting circuitry for γ-rays 78—62527
  - NaI(Tl), pile up reduction in low intensity rad. counting, fractional charge collection technique 77—88345
  - Pr wire thermal cond. automatic meas. device 78—54362
  - Pu low-background assay equipment, liquid scintillation detector, sample changer, electronics 77—54474
  - Si p-n junction, radiation detector DC cct., transient processes 77—70556
  - Si p-n junction radiation detector behaviour in temp.-compensated cct. 78—33389
  - Si(Li) X-ray spectrom., dead-time meas. system 77—79503

counting tubes
  - *see also dekatrons*
  - internal-gas radioactivity-counting with pure H_2S as counting gas 78—854

country planning *see town and country planning*

county planning *see town and country planning*

coupled circuits
  - Cole-Cole dielectric relaxation distrib. function, circuit model 80—7291
  - four-terminal meas. circuit stray-impedance errors 78—77940
  - interacting SAW transducer equivalent circuits 77—27456
  - magnetic field stabilisation using directly coupled IC op. amps, for EPR spectrometer *(Czech)* 79—26095
  - nonlinear coupled dynamic physiological systems, network thermodynamic simulation 79—96504
  - planar waveguide structure for integrated optics, props. *(Czech)* 80—96018
  - power amplifier coupling to resonators 79—68052
  - selective limiter-amplifier, high phase-amplitude stability 78—4632
  - US transducer arrays, acoustic imaging, electric coupling effects 80—43587

coupled networks *see coupled circuits*

coupled superconductor devices *see superconducting junction devices*

couplers (electric connectors) *see electric connectors*

couplers (waveguide) *see waveguide couplers*

coupling (process) *see joining processes*

coupling circuits *see coupled circuits*

CP invariance
  - 't Hooft-Polyakov mag. monopole electric charge in CP nonconserving theories, $e\theta/2\pi$ charge dyon 79—97534
  - Abelian lattice gauge theories, θ-vacua construction in compact gauge theories 79—58874
  - asymmetric creation of matter and antimatter in the expanding Universe 79—75302
  - axion, Gargamelle beam dump expt. 78—50003
  - axion effect on two-dimens. CP problem 80—42358

CP invariance continued
baryon asymmetry of the Universe, quantum black hole evaporation *(Russian)* 80—109577
baryon electric dipole moments in CP noninvariant Kobayashi-Maskawa theory *(Russian)* 80—105897
baryon hadronic decay, $3/2^+$ decuplet isobars in SU(3) symmetry, dynamical assumption 79—26333
baryon mesonic decays, two quarks transition amplitude, baryons taken as symmetric three quark states 78—17013
baryon number generation mechanism in expanding universe 80—51931
baryon number of the Universe 79—30163
broken symmetries at high temperature 80—42357
Cabibbo angle, CP violation quark masses 78—33016
Cabibbo angle and CP violation in a gauge model with discrete symmetry 79—45028
Cabibbo angle and discrete symm. 78—29288
Cabibbo angle in six quark $SU(2)_L \times SU(2)_R \times U(1)$ gauge model 79—17683
Cabibbo current and CP violation in a six quark gauge model 78—70329
chiral asymmetry in vectorlike weak SU(3), CP violation, one loop correction 79—287
cosmic matter-antimatter asymmetry and gravitational force 80—90586
cosmological baryon asymmetry magnitude in CP violation model 80—36754
CP^{n-1} model, embeddings of classical solns. of O(2p+1) nonlinear σ-models, instantons 80—86562
CP noninvariance test in nonleptonic decay of mesons containing one 6-quark 79—71654
CP violation via Higgs boson exchange, Weinberg-Salam model anal. 79—63384
critical magnetic field for CP violation 80—369
dynamical symmetry breakdown at the two-dressed-loop level and beyond 79—294
early Universe, baryon number generation due to CP- and B-violating interactions 80—109571
eight quark model, CP violation, heavy quark degeneracy, explanation of $K_L \rightarrow 2\pi$ 77—26490
electroweak interactions, dynamically broken gauge theories, CP nonconservation without elementary scalar fields 80—86613
EM interactions, gauge formulation, $SU_\gamma(2)$ internal symmetry and P- and CP-violation *(Russian)* 80—42368
flavour-changing neutral currents, CP-violation 80—22553
gauge chiral U(1) symmetry and CP invariance in presence of instantons 78—78075
gauge model with spontaneous P-violation, anal. of spontaneous CP violation 77—38113
in gauge theories applied to weak interactions, review 77—26479
gauge theories of weak, EM, and strong interactions, book contrib. 79—30694
gauge theory, radiative symm.-breaking effects, Higgs boson masses 78—41435
grand unified theories, baryon asymmetry of the Universe, SO(10) model 80—4619
gravitationally induced CP effects, quantum gravidynamics, QCD quark sector 80—86616
heavy charged quark system decays, CP noninvariance, six-quark model/QCD anal. 79—80826
hierarchy of quark masses, Cabibbo angles and CP violation 79—22030
Higgs exchange in guage models with right-handed charged currents P and CP invariance 78—12824
Higgs-boson exchange P and CP violation, Weinberg model 78—8575
high energy lepton pair prod. with pol. hadrons, P and C violations 80—99068
historical introduction, weak interactions, book 78—78133
horizontal gauge symmetry as a natural CP-violation source at the two-generation level 79—93310
$K^0 \rightarrow \bar{K}^0$ transition in the standard $SU(3) \otimes SU(2) \otimes U(1)$ scheme *(Russian)* 80—82951
Kobayashi Maskawa model, QCD effects and CP violation 80—42427
left-right symm. gauge theories, CP violation, absolutely stable hadrons 78—74155
left-right symmetric model from general horizontal symmetry, Cabibbo angle, CP violation 80—101972
lepton mixing matrix, sequential Weinberg-Salem theory, CP conservation 80—47238
leptons, EM characts. and CP disturbance in SU(3)×U(1) model *(Russian)* 78—29327
maximal CP violation in SU(2)×U(1) theory with very heavy quarks 77—38123
microweak violation, SU(2)×U(1) gauge model 77—71456
milliweak gauge models of CP violation 80—73633
mixing matrix and CP violation for n quark generations 80—101986
muon electric dipole moment meas. restriction of models of CP violation 78—37209
net baryon number and CP nonconservation with unified fields 80—62349
neutral currents, flavour- and muon-number changing in SU(2)×U(1) model with CP isolation 77—26484
neutrino reactions at high energy, weak interaction props. and hadron struct. investigation, book contrib. 79—30727
nonconservation, weak-current angles of six quark model, constraints, from K^0-$\bar{K}^0$ system 79—71685
noninvariant vacuum domains, cosmological role of weak currents 77—5605
nonleptonic hyperon decays, CP violation, deviations from $\Delta I = {}^1/_2$ rule 78—70367
nucleus, mag. field, Cabibbo angle, and CP violation 77—41918
Okun-Zakharov-Pontecorvo model of CP nonconservation 77—67621
Poincare group, irreducible representations of groups containing subgroup of finite index 80—68384
Pontecorvo neutrino oscillations for Dirac and Majorana masses, CP nonconservation 80—105829
potentially CP violating phase in QCD, alleged axion mass, PCAC quark masses 78—66080
pseudoparticle solutions in gauges with unique pots., physical interpretation 77—79222
QCD, CP-nonconserving effects 79—63430
QCD, neutron electric dipole moment, chiral estimate, current algebra, CP violating reactions 80—27471
QCD, six-quark model, $\Delta S = 1$ weak nonleptonic decays 80—22582
QCD confinement of colour, modification of axion scheme 80—73663

CP invariance continued
QCD theories of interactions, CP conservation, in presence of pseudoparticles 78—16923
quark electric dipole moment from CP noninvariant gauge theory, left handed currents *(Russian)* 78—74218
quark field quantum fluctuation computation in arbitrary Yang-Mills instanton background 80—13268
quark models and unified field theories, review 79—80805
quarks and leptons, fermion physics in terms of SU(2)×SU(1) gauge theory 78—74197
quaternion model, gauge theory for leptons and quarks *(Russian)* 78—62315
quaternion model, quark mass matrix, CP violation and Cabbibo angle *(Russian)* 79—40751
Reggeization of elementary fermions in arbitrary renormalizable gauge theories 80—68367
relativistic two fermion equations, Lorentz, parity and charge conjugation invariance 80—90976
self-coupled vector fields, calcs. using Dirac quantisation procedure 78—89610
six quark model, CP nonconservation upper bounds in neutral theory meson systems 80—42397
six quark model without right handed currents 77—6081
six-quark model, spontaneous CP violation *(Russian)* 79—93379
SO_{10}, soft CP violation and complex Majorana mass relations 80—78010
soft CP violation, renormalisable gauge model for strong, weak and EM interactions 78—74196
soft CP-invariance violation at high temperature 79—75697
spontaneous CP nonconservation in theories with more than four quarks 80—47212
spontaneous CP violation in vector-like model of weak interactions 77—54071
spontaneous symmetry breaking in nonstationary isotropic metric 79—89079
spontaneously broken chiral $U(1)_4$, weak-interaction singlet and strong CP invariance 79—80781
statistical theory of CP violation in K^0 decay 77—41784
strong CP problems, soln. in Weinberg-Salam model, colour group extension 79—75699
strong interactions, CP invariance and pseudoparticles 77—61213
strong P and T noninvariances in a superweak theory 78—82123
$SU(2)_L \times SU(2)_R \times U(1)$, CP invariance, global chiral U(1) symmetry, axion-quark coupling 79—22009
$SU(2)_L \times U(1)$, strong CP-violating phase, one-loop corrections, Higgs particles 80—62910
$SU(2)_L \times U(1)$ gauge model, mixing angles and CP violation 80—73648
$SU(2)_L \otimes SU(2)_R \otimes U(1)$ calculability, fermion mass matrix and CP invariance violation 80—13252
$SU(2)_L \otimes U(1)$ theory, CP violation and Cabibbo angle 80—52447
$SU(2) \times U(1) \times S_3$ model, CP violations and Kobayashi-Maskawa matrix elements 79—85243
$SU(2) \times U(1) \times SU_F(2)$ gauge model, CP violation and off-diagonal neutral currents 79—13008
$SU(2) \times U(1) \times SU_F(2)$ gauge symmetry, CP violation, neutron elec. dipole moment, muon number changing process 79—89091
SU(2)×U(1) gauge model, right-handed charm current, CP violation 78—45795
SU(2)×U(1) gauge models, CP violation origin, Yukawa interaction 79—40712
SU(2)×U(1) gauge theory, μ-e mass ratio and CP violation as quantum effect 79—30691
SU(2)×U(1) gauge theory, natural suppression of CP violation 78—41421
SU(2)×U(1) scheme, CP violation parametrization, quark n-doublet weak interaction *(Russian)* 80—13231
SU(2)×U(1) six quark model, uniquely determined discrete symmetry 79—93360
$SU(2) \otimes U(1) \otimes U(1)'$ gauge theories and extensions, one-loop generated CP violation 79—89078
$SU(2) \otimes U(1)$ gauge model, strange baryon weak radiative decays and CP violation 79—6260
$SU(2) \otimes U(1)$ gauge models of weak and electromagnetic interactions and the μe universality *(Russian)* 80—13257
SU(3)×U(1) gauge models, exam. of weak currents and associated features 78—16975
SU(3)×U(1) gauge models, generalised mixing and CP violation in hadron decays 78—41473
SU(4)×U(1) gauge theory, Cabibbo mixing, new approach, CP nonconservation calc. 79—71657
SU(4)×U(1) unified gauge theory, CP nonconservation 79—71656
SU(5), unification of weak, EM and strong interactions, review 80—105814
SU(5) gauge model, masses, mixing angles, CP violation and b-quark decay 80—78006
SU(5) grand unification, cosmological baryon asymmetry 80—86640
SU(5) grand unification, strong CP violation, quark-lepton mass ratio 80—32057
SU(6) exotic gauge model, lepton-quark symm., CP-violation and $\mu \rightarrow e\gamma$ decay 78—12875
SU(N)×SU(N) symmetry breaking with extremum constraints 80—68385
SU(n) decomposition theorem, appl. to CP violation through quark mass diagonalisation 80—47216
superconducting early Universe, cosmological baryon prod., CP invariance grand unification 80—90592
superheavy boson decay, neutrino number and isotropy of Universe in grand unified theories 80—85852
supersymmetry, OSp(1,4), superfield formulation in anti-de Sitter space 80—57508
superweak CP violation mediated by neutral Higgs bosons 80—363
superweak gauge theory of CP-invariance violation 79—75710
superweak gauge theory without charm 77—10195
superweak model of CP violation, gauge theory realisation 77—10194
symmetry violation natural suppression, muon and electron lepton number nonconservation 78—8574
unified gauge theories and Higgs bosons 77—45948
unified SU(6) gauge theory, hierarchy of gauge symm. and CP nonconservation 78—41464
universal CP noninvariant superweak interaction and baryon asymmetry of the universe 78—66072

CP invariance continued
Universe baryon number asymmetry mechanism, unified calibration theory calcs. *(Russian)* 80—36756
vacuum neutrino oscillations between ν_e, ν_μ, ν_τ, CP violation 79—291
vacuum structure in calibration theories, CP violation, cosmology *(Russian)* 80—27478
vacuum structure in gauge theories, strong CP violation and cosmology 80—86578
very early Universe, baryon asymmetry 79—40309
violation in weak interaction, renormalization of QCD vacuum parameter θ 79—40683
weak interaction, vector-like theories, CP violation, spontaneous breaking 78—62333
weak interactions, CP violation and instantons 80—354
weak interactions, lepton-hadron symmetry, CP violation and $\Delta I = {}^1/_2$ rule 80—82934
weak mass mixing and CP violation with heavy quarks, V-A model anal., possible meas. in e^+e^- expts. 79—30695
Weinberg's model of CP violation in gauge theories, valence quark hypothesis 79—12940
Weinberg-Salam model, Higgs doublets and $\Delta I = 1/2$ rule 77—65132
Yang heavy axion, contradiction of muon anomalous mag. moment data *(Russian)* 79—49484
B meson, cascade decays, CP nonconservation 80—105811
b-quark meson, decay, weak mass mixing, CP violation 80—32086
$B^0\bar{B}^0$ mixing in six quark model, decay, mass mixing and CP nonconservation 80—42406
$D \to K^*\mu\nu$, in e^+e^- annihilation, T-odd asymmetry in CP violation model *(Russian)* 80—105885
$D^0\bar{D}^0$, mixed spinless charmed mesons from e^+e^- annihilation, decay, CP violation tests 77—46067
e^+e^- annihilation, CP violating effects, D^0, G^0 and H^0 meson decays 79—80769
$e^+e^- \to \gamma\gamma$, Einstein-Podolsky-Rosen nonseparability, Feynman nonlocality 77—34110
$\gamma N \to N\pi$, dispersion relations assuming no CP violation *(Russian)* 79—93435
$K \to 3\pi$, CP violation, current algebra anal., six quark Weinberg-Salam model 80—47281
$K \to \pi\pi$, Kobayashi Maskawa model, QCD effects 80—42427
$K^- \to \pi\mu\nu$, μ polarisation and T-odd correlations, Weinberg model of CP violation *(Russian)* 80—62969
K^0 CP violating decays, review 77—57532
$K^0 \to \pi^0\pi^0$, phase and magnitude of CP nonconservation parameter η_{00} 80—4988
$K^0 \to \pi^+\pi^-$, CP nonconservation parameter η_{+-} phase and magnitude 80—4989
$K^0 \to \pi\pi$, six-quark model, $\Delta I = 1/2$ rule and CP violation 79—54323
K^0-$\bar{K}^0$ type systems, CP invariance under particle phase choices 80—52433
$K_1{}^0$-$K_2{}^0$ system, violation, CPT conservation, book contrib. 78—78173
$K_L \to \pi^+\pi^-$, branching fraction meas., CP violation parameter determ. 78—8663
$K_L \to \pi^+\pi^-(\pi^0\pi^0)$, CP violation parameters in six quark model *(Russian)* 80—62974
$K_L{}^0{}_{\mu 3}$ decays, CP invariance violation limits 79—89146
$K_L - K_S$ mass difference, Kobayashi-Maskawa six quark model, mixing angles, mass matrix and CP violation 80—13284
$KL_L{}^0 \to \pi^+\pi^-\gamma$, branching ratio meas. 77—18280
$l\bar{l} \to \text{meson} \to \gamma\gamma$, CP nonconservation 79—58899
μ decay correlations and lifetime meas. 80—77996
$\mu \to e\gamma$ or 3e, heavy leptons, CP violation 77—82727
n electric dipole moment, CP violation in gauge theories 80—91041
ν, massless, left-right symmetric gauge models, $SU_{2,L} \times SU_{2,R} \times U_1$ 80—27461
ν oscillation, CP or T violation effects 78—21349
$\tau \to K^*\pi\nu$, in e^+e^- annihilation, T-odd asymmetry in CP violation model *(Russian)* 80—105885
Cs cell, laser beam excitation, multipass, optical pumping and weak neutral current parity violation 80—58207
$K \to \pi e^+e^-$, six-quark model, CP violation 80—78055

CPA calculations
actinides and alloys, metallurgical props. rel. to electronic struct., energies calc. method 77—20221
adsorption, coherent potential approximation 79—33193
alloy, binary, ordering, residual resist. in CPA *(Russian)* 77—24545
alloy, disordered, DC conductivity temp. depend. meas. in off-diagonal CPA 77—28153
alloy, disordered, energy band struct. and elec. cond., effect of short-range order 80—10860
alloy, disordered muffin tin type, coherent pot. approx. appl. 79—15062
alloy, pseudobinary, ferromag., magnon energy derivation 80—107996
alloy, substitutional, analytic approximation for Herglotz property 79—37946
alloy, with off-diagonal randomness, phonon-modulated electronic transport 77—15813
alloy thin film, thickness depend. of CPA electronic densities of states 80—65644
alloys, binary, 50-50, singularities at metal-insulator transition, CPA calc. 80—84428
alloys, CPA for props. 80—75493
alloys, disordered, charge density function calculation method 79—42433
alloys, disordered, muffin-tin model, electronic struct. and density of states, theory 80—29301
alloys, disordered, orbital mag. susceptibility of conduction electrons CPA calc. 78—76217
alloys, highly resistive, temp. depend. on elec. resist. 78—91657
alloys, positron annihilation CPA calc. for spatial and momentum distrib. 77—80720
alloys, random, equilib. and transport props., single-site approxs. 80—92801
alloys, random binary, single-particle Hamiltonian and self-consistency 79—37953
alloys, self-consistent cluster theories for diagonal and off-diagonal disorder 79—37950
alloys, substitutionally disordered, optical cond., intraband transitions 80—103933
alloys, with off-diagonal disorder, density of states and cond., CPA calc. 80—24780

CPA calculations continued
amorphous semiconductor, tetrahedrally bonded, effects of quantitative disorder on electronic struct. 79—47003
amorphous tetrahedrally-bonded solid, electronic struct., theoretical approach 80—29315
Anderson transition in systems with purely off-diagonal disorder 79—19518
anthracene, isotopically mixed cryst., exciton dynamics 80—29329
antiferromagnet, dil. paired, bond dilution problem, CPA theory 79—78389
antiferromagnet, Heisenberg model, randomly dil., excitations 78—23258
antiferromagnetic alloy, stoichiometric depend. of elec. resist. 77—69312
antiferromagnetic alloys, spin disorder resistivity, coherent potential approx. 78—14722
antiferromagnetism onset in Hubbard model 78—19206
binary alloy, completely disordered, position of electronic energy bonds, CPA calc. *(French)* 78—22999
binary alloy, density of states, CPA with nonretracing paths 77—31924
binary alloy, model substitutionally disordered, electron momentum density 78—56061
binary alloy, one-dimens., embedded-cluster calcs. of phonon spectra 79—77703
binary alloy, partially ordered, elec. resist., CPA calc. 78—43356
binary alloy, short range order effect on density of states *(Russian)* 78—67929
binary alloys, acoustic modes in random and correlated alloys, order-disorder transform. 80—65189
binary alloys, charge transfer and transport props. in tight-binding model 79—82577
binary alloys, density of states in CPA 77—51633
binary alloys, disordered, electron-electron correl, T-matrix approx. 79—78026
binary alloys, random, dielec. matrix and related props. 78—51916
binary disordered alloy with long range order, elec. cond., single band model 77—28154
binary disordered system, effective-medium and augmented space method, pseudofermion approach 79—60668
bond-type disorder system, electrical cond. and electron localization calcs. 78—2475
cluster, at., homomorphic CPA analyticity 78—82872
cluster, at., homomorphic CPA for off-diagonal randomness 78—82873
Compton profiles, struct. depend. 78—35223
and CSEM methods, comparison 77—4280
Cu_cNi_{1-c}, soft X-ray emission spectra 78—95620
diagonal vertex approx. for Gaussian random systems 78—23003
dilute ferromagnet, spin wave excitations, multicomponent CPA theory 78—68135
dilute systems, donor fluorescence at high trap concentration 80—71479
disorder at surfaces and interfaces, effect on electronic props. 78—26932
disordered alloy, electron correl. in Hubbard model, and spin susceptibility 77—76762
disordered alloy, electronic transport, effect of thermal and off-diagonal disorder 78—30902
disordered alloy, quantum transport theory, CPA 77—20282
disordered alloys, electronic density of states in muffin tin model 80—88467
disordered alloys, electronic struct., CPA calcs., short-range order 78—63964
disordered alloys, influence of strong hybridization on elec. cond. 79—11097
disordered alloys, optical absorpt. at high temp., CPA calc. *(Russian)* 77—44028
disordered alloys, temp. depend. of elec. resist., elastic electron-phonon scatt. 79—56185
disordered alloys, transport phenomena theory, coherent pot. approx. 78—87958
disordered crystal, biphonon spectra, light absorpt. coeff. and density of states, CPA calc. 80—84271
disordered crystals, biphonon spectra, CPA calc. 80—70341
disordered extended Anderson model, CPA-alloy analogue treatment 80—65506
disordered metal, resistivity, anomalous temp. coeff. at high temp. 78—2458
disordered quasi-one-dimensional systems with electron correlation, electronic properties 78—87966
disordered surfaces, lattice dynamics 79—60616
disordered system with n orbitals per site, n=infinity limit 79—60768
disordered systems, bond-type, elec. cond., effects of fluctuations of transfer energies 77—80757
distorted one dimensional system with bond disorder, electron density of states 80—24778
electronic transport in substitutionally disordered system, derivation of cluster approx. 78—84184
electronic transport in substitutionally disordered systems, MCPA and Monte Carlo calc. 78—84185
electrons in disordered metals and at metallic surfaces, conf., Ghent, Belgium (Sept. 1978) 80—41946
EM wave multiple scatt. by random distribs. of discrete scatterers with coherent pot. and quantum mech. formulism 80—95768
extended Hubbard model, antiferromagnetic solution, degenerate d-band 78—19208
ferroelectric, mixed order-disorder displacive transition, model 77—59540
ferroelectric mixed crystals, dielectric constant, dynamics, transition temp. theory 78—10855
ferromagnetic alloys, conc., spin fluctuations, SCR theory and CPA calcs. 78—64290
ferromagnetic binary alloys, narrow-band with random hopping, spin wave stiffness const. 79—56524
ferromagnetic disordered binary alloy, CPA theory of magnetoabsorption, electron scatt. mechanisms *(Russian)* 77—8549
ferromagnetic instability in two-band Hubbard model 79—1653
ferromagnetic metals, spin fluctuation theory, Curie temp., mag. susceptibility 80—65937
ferromagnetic partially ordered alloy, spin wave stiffness const. 79—24150
ferromagnetic random binary alloys, elastic neutron scatt. cross section 78—91845
ferromagnetic semiconductor, theory review 80—20369
ferromagnetic ternary alloy, spin-disorder resist. in CPA weak scatt. limit 78—39100

CPA calculations continued
ferromagnetic ternary alloys, elec. resist., cond. electron scatt. and heterogeneities of spin system *(Russian)* 79−56189
ferromagnetic transition metal alloys, CPA appls. 77−72983
ferromagnetism, Hubbard model, mag. susceptibility, modified Stoner criterion 79−51736
ferromagnets, random, large exchange interaction, Green function theory 78−6537
Friedel sum rule, high conc. extension, appl. to coherent pot. approx. 80−44462
fundamental Korringa-Kohn-Rostoker eqn. version of coherent potential approx. 80−59847
Heisenberg amorphous ferromagnet, magnetisation and Curie temp., CPA calc. 80−75703
Heisenberg antiferromagnet, anisotropic, excitations at finite temp. 79−95562
Heisenberg antiferromagnet, dil., CPA calc. 78−68263
Heisenberg antiferromagnet, dil. with random first- and second-neighbour exchange bonds, CPA theory 78−52187
Heisenberg antiferromagnet, excitations at finite temp. using CPA 79−56554
Heisenberg antiferromagnet, spin waves at finite temp., CPA calc. 79−73728
Heisenberg ferromagnet, dil., CPA theory, spin-wave stiffness and Curie temp. 78−31080
Heisenberg ferromagnet, disordered, pair effects in bond model 79−78290
Heisenberg ferromagnet, disordered, two spin species, spin-wave spectra calc. 77−59375
Heisenberg ferromagnet, disordered two-dimens., CPA theory of bond model 80−60163
Heisenberg ferromagnet, spin wave excitations at finite temp., CPA calc. 77−32142
Heisenberg model, amorphisation *(Russian)* 78−80118
homomorphic cluster coherent pot. approx., appl. to random systems 79−90930
homomorphic cluster CPA, rigorous proof for analyticity 79−19504
homomorphic cluster CPA analyticity 79−90929
Hubbard model, doubly degenerate, CPA alloy analogy 77−32151
Hubbard model, doubly degenerate, long range order 80−50029
Hubbard model, local moments 78−95414
III-V semiconductor alloys, energy gap variation, CPA calcs. 78−43294
impurity crystal, transport of energy of electron excitations 77−40283
insulator-to-metal transition for half-filled Hubbard band in paramagnetic state 80−92817
Ising, quenched dil. random-bond model, CPA difference eqn. and crit. curves 80−2584
Ising model, random, in transverse field, CPA approach 77−36040
Ising model, random, susceptibility and magnetisation 77−80899
Ising transverse bond-diluted model, appl. of CPA 79−56551
itinerant magnetic-systems, general alloy analogues 77−85410
itinerant magnetism, quasispin model 77−66239
IV-VI mixed compounds, structural phase transition 80−15242
KKR-CPA equations, numerical solution 80−44474
liquid and amorphous metals, electronic states, optical theorem, multiple scatt. theory 80−49578
liquid-like random Kronig-Penney model, electronic density of states, CPA calc. 79−1567
Lloyd formula and muffin-tin CPA local density of states 80−70577
magnetic alloy, highly concentrated Kondo effect 79−24134
magnetic semiconductors, electron propag., s-d model, red shift theory 77−51736
magnetic semiconductors, excitation spectrum, temp. and band occupation depend. 80−49588
magnetic ternary alloys, statistical theory of electrical resistivity 78−87969
metal surface electronic density of states, random distribution of impurity atoms 78−6424
metallic alloys, ordered and disordered, positron localisation 78−79962
metallic disordered alloy, strongly correlated, extended CPA anal. 77−20217
mixed crystal, semi-infinite, local electronic states, CPA extension 79−65401
mixed valence cpds., mag susceptibility and sp. ht., periodic Anderson model, CPA alloy analogue method 80−15474
mixed valence state, electronic structure 79−11092
muffin-tin potentials, nonoverlapping CC Ni_x Cu_{1-x} paramag., coherent pot. approx. for nonoverlapping muffin tin potentials 78−2451
n-type semiconductors, plasmon-local phonon mode interaction, RPA, CPA theory 78−87932
narrow gap semiconductor, resonant scatt., Green's function method and CPA 80−6827
noble metal alloys, disordered, bulk electronic structure 80−44467
phonons in disordered shell models 80−70347
Potts model, dil. random bond 80−29556
quantum transport theory, CPA calcs. 77−85186
quantum transport theory in CPA, limit of small carrier number 77−69285
quantum transport theory in CPA, using diagrammatic expansion and resummation approach 77−69284
quasi-low dimensional spin system, 3-D mag. ordering, randomness effects 78−10710
quasi-one-dimensional conductors, alloys, Peiels distortion 80−59965
random alloys, CPA calcs. cluster extensions, appraisal of applicability 79−15063
random anharmonic system, self-consistent approx. 77−62798
random binary alloy, charge and spin struct. factors, CPA theory 77−28374
random chain of oscillators, CCPA calcs. of spectral density 79−37792
random Ising bond interactions, paramag. phase, thermodynamic props. 77−20523
random lattice, atom site diagonal perturbation, functional integral approach 80−57218
random lattice, with purely off-diagonal disorder, electron localisation 80−49672
rare earth alloys, CPA calc. of mag. moments and transition temps. 78−84423
rare earth alloys, magnetic properties, impurity effects, CPA calc. 80−44784
rare earth compound, intermediate valence induced by alloying, CPA calculations 78−67986

CPA calculations continued
rare earth-transition metal alloy, disordered, saturation mag. moment using CPA 77−20515
rare earth-transition metal alloys, CPA calcs., moments and transition temps. 78−52252
s-d alloys, density of states calc. using coherent potential approx. *(Japanese)* 77−76721
semiconductor, impurity band props. 79−23888
semiconductor alloys, ternary, energy band calc., compositional disorder effect determ. 79−42442
semiconductor solid solutions, influence of lattice disorder on elec. props. 77−8100
semiinfinite crystal with surface substitutional disorder, electronic struct. 77−72903
site-disordered spin systems, generalised CPA 77−20513
solid solution, vol., electron correl. effect 77−28133
structurally disordered materials, CPA theory of excitations, lattice model 79−87030
substitutional alloys of intermediate valence systems, static mag. susceptibility con. and temp. depend. 80−84586
substitutionally disordered systems, analytic extension of CPA to clusters 79−19503
surface excitons in mixed molecular crystals, theory 79−47135
TCNQ complex salts, temp. depend. of elec. cond. 77−8078
ternary alloy, disordered DC elec. cond. calc. 77−15812
ternary alloy semiconductor, band struct., CPA calc. based on linear combination of bond orbitals 79−87035
ternary alloys, density of states, CPA calc., off-diagonal disorder 78−22998
ternary alloys, disordered, elec. cond. and density of states, CPA calc. *(Russian)* 79−47072
ternary alloys, vibr. freq. distrib. spectra, small cluster statistical theory 79−24317
thin film, 11-layered, CPA calc. of local density of electronic states 80−65643
transition metal alloy, electronic structure, mag. props. 78−95254
transition metal alloy disordered host, actinide impurity localised magnetism 77−51883
transition metal alloys, binary, state density curves, relation between short-range order and Fermi level position, CPA calculations 80−107687
transition metal alloys, cohesive properties and press.-vol. relation 80−92476
transition metal alloys, disordered, bulk electronic structure 80−44467
transition metal alloys, disordered, local densities of states 77−59244
transition metal alloys, ferromag. local ordering effect on spin wave stiffness const. 77−66282
transition metal alloys, spin glass behaviour, simple itinerant model 78−84436
transition metal alloys, static magnetic suscept. calc. *(Russian)* 77−77036
transition metal alloys, temp. depend. of asphericity of mag. moment distrib. 77−20538
transition metal carbonitrides, carboxides and oxynitrides, electronic struct., theoretical approach 80−54584
transition metal-actinide dilute alloy, disordered occurrence of localised magnetism, CPA calc. 77−63096
transition metals, energy of cohesion calc., Hubbard Hamiltonian with exchange interaction 77−69261
transition metals and alloys, metallurgical props. rel. to electronic struct., energies calc. method 77−20221
two-dimensional white noise problem and inversion layer localisation 78−84271
X-Y model, on linear chain in random fields, thermal props., appl. to praseodymium ethyl sulphate 79−65679
zincblende structured ternary alloy semiconductor valence bands, LCBO coherent potential approximation *(Japanese)* 78−47699
Au-Cu alloy, rel. to refr. index and absorpt. coeff., 1-5 eV *(Russian)* 78−60484
Au_xAg_{1-x}, density of states and resist., CPA calc. 80−24780
Ce-Sn, liq., elec. resistivity negative temp. coeff., CPA calcs. 79−42515
Co-Ni, Hall effect, anomalous, residual coeff. calcs. using coherent pot. method *(Russian)* 80−80249
Cu-Ni, alloys, electronic states, KKR-CPA calc. 78−84125
Cu-Ni, disordered muffin tin type, coherent pot. approx. appl. 79−15062
Cu-Ni, random ferromag. alloy, local mag. moment calc. 80−70974
Cu-Ni, soft X-ray emission and local densities of states 79−83059
Cu-Ni, UPS, surface and bulk density of states, comp. depend. 77−44125
Cu-Ni alloys, density of states determ. by continued fraction method 78−47690
Cu-Pt system, phonon dispersion relations, force constant disorder effect 80−84263
Cu_cNi_{1-c}, Fermi surface of concentrated paramag. alloys 78−95257
Cu_xNi_{1-x}, bulk electronic structure, comparison of CPA and ATA techniques 80−44467
Cu_xNi_{1-x}, disordered alloy, muffin-tin model, electronic struct. and density of states calc. 80−29302
Cu_xNi_{1-x}, paramag., electronic struct., atomic sphere approx. to KKR-CPA 79−19502
Cu_xZn_{1-x}, disordered alloy, muffin-tin model, electronic struct. and density of states calc. 80−29302
EuO magnetic semiconductor, quasiparticle lifetimes, CPA study 80−65443
Fe, liq., CPA theory of excitations, lattice model 79−87030
Fe-Co, Hall effect, anomalous, residual coeff. calcs. using coherent pot. method *(Russian)* 80−80249
Fe-Cr, random ferromag. alloys, local mag. moment calc. 80−70974
Fe-Ni, fcc alloys, spin wave energy calc. 79−87247
Fe-Ni, Hall effect, anomalous, residual coeff. calcs. using coherent pot. method *(Russian)* 80−80249
Fe-Ni alloy, FCC, high-field susceptibility and spin wave spectrum 79−56493
Fe-Ni alloys, electronic struct. by XPS obs., Elk's CPA results comparison 79−33226
Fe-Ni alloys, FCC, mag. props. calc. 79−65659
Fe-Ti, mag. moment distrib. and environmental effects around Ti impurity 80−7092
Fe-V alloys, BCC, ferromag. polarised neutron diffr., appl. of multiband CPA theory 77−77033
$Fe_3Al(Si)$, electronic structure, magnetic moments 80−107695

CPA calculations continued
FeTi alloy, elec. and mag. props. near order-disorder transition 79-82576
$Fe_xZn_{1-x}F_2$, Neel temp., CPA calc. 78-68233
$Fe_xZn_{1-x}F_2$, Neel temp. mag. cone depend., CPA calcs. 78-88122
GaAs, valence band structure, CPA, bond orbital calcs. 78-87909
$GaAs_xP_{1-x}$, band struct., CPA calc. based on linear combination of bond orbitals 79-87035
GaP, valence band structure, CPA, bond orbital calcs. 78-87909
GaP_xAs_{1-x}:N, luminesc. of N bound state excitons, local-environment effects 80-100691
GaSb, valence band structure, CPA, bond orbital calcs. 78-87909
Gd-Co, CPA calcs., moments and transition temps. 78-52252
Gd-Fe, CPA calcs., moments and transition temps. 78-52252
Gd-Ni, CPA calcs., moments and transition temps. 78-52252
$Gd_{1-x}M_x$, M=Co, Ni, Fe, temp. depend. of magnetisation 77-77043
$Gd_{1-x}M_x$, M=Ni, Fe, Co, mean mag. moment calcs. 77-72997
o-H_2:p-H_2, solid, librons, CPA theory 77-47536
HCN, valence shell correl. energies, pair correls., unlinked cluster effects, CPA calc. 79-13648
HNC, valence shell correl. energies, pair correls., unlinked cluster effects, CPA calc. 79-13648
$Hg_{1-x}Cd_xTe$, acceptor impurity band form. 80-20119
InAs, valence band structure, CPA, bond orbital calcs. 78-87909
$In_xGa_{1-x}As_yP_{1-y}$, valence band struct., CPA calc. 79-73435
InP, valence band structure, CPA, bond orbital calcs. 78-87909
InSb, valence band structure, CPA, bond orbital calcs. 78-87909
$K(H_{1-x}D_x)_2PO_4$, ferroelec., dielec. susceptibility, pseudo-spin model 77-52024
$K_2Pt(CN)_4Br_{0.3}.xH_2O$, transport props. x depend., CPA calc. of screened random pot. 77-39828
$Mn_{1-c}Zn_cF_2$, antiferromag. reson., far IR spectrum, CPA calc. 77-20716
$Mn_{1-x}Zn_xF_2$, randomly diluted uniaxial antiferromagnet, CPA theory 79-78388
$Mn_xZn_{1-x}F_2$, CPA estimate for Neel temp. 78-76245
Mo_cNb_{1-c}, is the rigid-band model valid? 78-95258
N_2, vertical valence ionis. pot. calc., by perturbation, CI and CPA techniques 80-69263
Nb-Mo, electronic struct., thermoreflectance meas. 0.5-5.0 eV 80-45050
Ne, vertical valence ionis. pot. calc. by perturbation, CI and CPA techniques 80-69263
Ni, spin-wave exchange stiffness const. 77-4510
Ni-Co, high-field susceptibility, spin-wave spectrum, CPA calc. 80-65818
Ni-Cr, residual resist., CPA calc. to muffin tin pot. 77-62892
Ni-Cr(V)(Co)(Mn)(Mo)(Ru)(Fe), spin wave stiffness consts., RPA CPA band model 79-61088
Ni-Cu, ferromag., mag. moment, local environment effects, HF CPA cluster calc. 80-65817
Ni-Cu, high-field susceptibility, spin-wave spectrum, CPA calc. 80-65818
Ni-Fe, high-field susceptibility, spin-wave spectrum, CPA calc. 80-65818
Ni-Fe, residual resist., CPA calc. to muffin tin pot. 77-62892
Ni-Mn alloys, ferromagnetism-to-spin glass phase transition and strong mag. field effect 80-75773
Ni-Pd alloys, mag. props., average and local density of states, CPA calc. 77-59242
Ni-Ti, mag. moment distrib. and environmental effects around Ti impurity 80-7092
Ni-V(Mo)(Ru)(Cr), weak ferromag., stiffness const., low-temp. meas., rel. to RPA-CPA theories 78-31063
Ni_x Cu_{1-x} paramag., coherent pot. approx. for nonoverlapping muffin tin potentials 78-2451
$Ni_{0.89}Cr_{0.11}$, phonons with disorder caused by force consts., neutron diffr. obs. and CPA calc. 80-96602
NiFe alloys, spin-wave exchange stiffness const. calcs., weak ferromagnetism 77-4510
Pb-In, CPA interpretation of positron annihilation *(Russian)* 80-11507
Pd-Ni-P, amorphous, elec. resistivity negative temp. coeff., CAP calcs. 79-42515
Pd-Pt, resonant modes, rel. to CPA predictions 78-75757
Pd-Pt alloys, mag. props., average and local density of states, CPA calc. 77-59242
Pd_cAg_{1-c}, possibility of superconductivity 80-10862
PdH_x, CPA calculations of density of states 79-23882
Pr-Nd (5 at.%), paramag. excitation spectrum, CPA calc. 80-50043
Pr-Nd (5%), impurity modes and mag. ordering 78-84422
Rb-K, lattice vibrs. in CPA, comparison to neutron scatt. meas. 79-42165
$Rb_{1-c}K_c$, phonon spectra, single site CPA 78-10142
$(SN)_x$, with H impurities, CPA calculations 80-44468
$(SNH)_x$, density of states, CPA calcs., effect of H impurities 79-42431
$Sm_{1-x}B_xS$, valence transition induced by alloying 80-96829
$Sm_{1-x}La_xS$, valence transitions, theoretical model 79-69474
$Sm_{1-x}Y_xS$, valence transitions, theoretical model 79-69474
TiC_{1-x}, substoichiometric, electronic density of states 80-2319
TiN_{1-x}, substoichiometric, electronic density of states, CPA method calcs. 80-88464
$U_xTh_{1-x}As$ (Sb), electronic struct., relativistic KKR-averaged $\dot{T}$-matrix approx. method 80-107702
Y-Co, CPA calcs., moments and transition temps. 78-52252
$Y_{1-x}Co_x$, mean mag. moment calcs. 77-72997
$Y_{1-x}Co_x$, temp. depend. of magnetisation 77-77043
$Yb_{1-x}Y_xCuAl$, disordered extended Anderson model, CPA-alloy analogue treatment 80-65506

CPT invariance
baryon number generation, examples unitary and CPT invariance 79-35960
black hole evaporation, predictability, CPT invariant superscatt. operator and S-matrix 80-46600
book, axiomatic QFT, PCT, spin and statistics 78-78102
causality, macroscopic, Einstein correlation, CPT symmetry, decreasing probabilities, advanced waves, antiparticles 80-68073
conformal invariant supersymmetric theory, CPT transformation 77-13884
covariant representation of microscopic charge and current densities in terms of polarisation and magnetisation fields 79-71
CPT invariance and the arrow of time *(Chinese)* 79-63380

CPT invariance continued
K_L^0-K_S^0 transmission regeneration in H, comparison of expt. data and theoretical prediction *(Russian)* 77-49955
Lagrangian formalisms with CPT violation, causal Lagrangian, gauge theories 78-62303
local quantized superfield, invariance of 'Wightman's superfunction' 77 ·57435
modular operator, local observables, in von Neumann algebras, duality in QFT, CPT invariance 78-81793
nonlocal Wightman fields, PCT and spin statistics 79-35915
Poincare group, irreducible representations of groups containing subgroup of finite index 80-68384
quantum electrodynamics, CPT invariance, permutation symmetry and crossing symmetry 79-55176
quantum gravity and time reversibility 80-82704
quantum mechanical interpretation 80-105805
relativistic QFT, spontaneous symmetry violations 80-52411
$Yukawa_2$ QFT, Lorentz invariance of CPT invariant states 80-52381
$e^+e^- \to W^+W^-$, polarisation amplitudes 80-42484
$e^+e^- \to ZZ$, polarisation amplitudes 80-42484
$K_2^0 \to k\pi$, k=2 or 3, Racah time reversal, a C,P,T scheme 80-78056
μ decay correlations and lifetime meas. 80-77996
$\mu \to e\gamma$, decay ang. distribs. and polarisation effects 77-41835
$\nu(\bar{\nu})N$ elastic scatt., symmetry relations CPT invariance of current matrix elements 78-54627
p-$\bar{p}$ symmetry, mass difference, Dirac and CPT theory test 78-82125

crack detection
see also cracks
1300 MW cross compound turbine unit IP rotor coupling, fatigue crack due to combined corrosion and low alternating stresses, report 80-16611
acoustic, emission pulses amplitude and crack size correlation theory and expt. 77-90568
acoustic emission, digital memory storage and source isolation 78-27712
acoustic emission appl. to materials testing plastic strain and growing cracks identification 80-81252
acoustic emission crack growth measurement, instrum., expt. 77-73421
acoustic emission detection for small components production testing, review 80-16632
acoustic emission method and development of equipment for monitoring crack formation during welding 80-89451
acoustic emission system for monitoring components and struct. in severe fatigue noise environment 77-63869
acoustic emission transients meas. rel. to crack propag., appl. to low alloy steel 79-8407
acoustic flaw detection, contactless electrogasdynamics 78-53120
acoustic flaw detector with sound indicator 78-53140
acoustic imaging techniques for NDT 77-81381
acoustic signalling unit for US echo type flaw detector 78-53117
acoustic spectral flaw detector 79-39089
acoustic spectral flaw detector 79-34248
acoustic wave scattering by flaws, reciprocity theory appl. 78-72941
active thermal meas. optimisation 77-77702
AE monitoring of multipass submerged arc welding 77-73394
aircraft wing fatigue crack using acoustic emission source technique 77-16769
amplifier for US flaw detector, special frequency response 79-70276
artillery projectile inspection by noncontact EM transducers 79-47872
automated rail flaw detection, US wheel probe variation problems 79-47862
automatic mechanical scanning, TV signal form. on basis of digital memory 80-71864
automatic radiometric flaw detection with X-rays on series production parts *(German)* 80-21240
automatic US equipment for monitoring drill and casing tubes 78-53085
betatron flaw detection, signal processing algorithm 77-81375
bleeding system, used for flaw detection in aircraft industry 79-66226
bone acoustic emission diagnosis, soft tissue effects 79-48362
boundaries, effect on cylindrical defect field 78-53093
bovine femur crack detection by acoustic emission 79-48312
brass wire, US inspection, immersion method 80-66757
brittle porous materials, US fractography appl., expts. on glass 77-44336
building product, nonmetallic, first crack determ. device, during load test *(Czech)* 80-45471
BUS-2 scan control unit for automatic interference reduction 79-5126
BWR, surface inspection methods, in-service inspection of reactor pressure vessel 80-27759
ceramic, automatic US defect detection for tile grading and packing processes 78-23885
ceramic surface flaw detection by SAW scatt. 79-47866
ceramics, crack and inclusion detection, NDT microwave evaluation 78-95866
ceramics, surface cracks, acoustic surface wave meas. 80-61055
cold strip surface, flaw inspection with optoelectronic equipment 78-60967
cold strip surfaces with opto-electronic equipment *(German)* 79-66253
compact fracture mechanics specimens, crack and load monitoring using strain gauges 79-83411
compact test pieces, optimization of electric potential technique for crack growth monitoring using finite element anal. 79-87799
composite material, testing with fluctuating components using monoenergetic electrons, sensitivity 79-79209
computerised tomography, principles and methods for medical and industrial appl. 79-74755
computerized US signal processing for crack detect. under installed fasteners 77-19490
concrete, surface crack width meas. by light-dependent resistor 79-96250
conducting material, eddy current losses 78-19965
conference, England, (Dec. 1974) 77-32754
contact tip of transducer, method of joining 78-53086
crack opening displacement testing 77-36722
crack polarisation when magnetised in a longitudinal alternating field, detection method 78-53094
crack scattering in polycrystalline media 78-75089
CRISP-E penetrant system 79-15917
critical opening determination method using double-displacement sensor 77-63848

crack detection continued
- cylindrical and conical components, thermal flaw detector 79—5127
- cylindrical defect detection, boundary effect calc. during magnetic study 78—53150
- defect characterisation from magnetic leakage fields 77—12750
- defect classification, automatic, by US spectral method 79—66240
- defect coordinate determ. by calibration of AE method 80—35473
- defect coordinate determ. in struct. with arbitrary surface, AE method 79—66239
- defect depth determ. by radiographic inspection 79—66241
- defect reconstruction, from US methods, mathematical model *(German)* 78—44295
- defect size measurement by radiography 79—91858
- defect thickness determ., radiographic visual comparative method 79—11737
- defectoscope, portable, using Schmitt-trigger based annunciator, without hysteresis 77—90567
- defectoscopy of permanent magnets, using electromagnetic method 78—39998
- depth measurement by US techniques 80—71859
- dielectric material, electro-optical inspection of internal defects 78—56869
- dielectric waveguide, flow detection using UHF EM field pattern display 80—104378
- diffraction model for US frequency analysis and flaw characterisation 77—21337
- dimensions of flaws in direction of irradiation determ. from radiographs with aid of defectometer 80—71863
- double layer article, detection of defective layer by electron flaw detection 79—47859
- drill pipe with welded end couplings, US inspection 79—5124
- dye penetrant and magnetic particle methods 77—9022
- echo signal amplitude of US flaw detector, automatic measuring instrument 79—79212
- echo type flaw detector, frontal resolution investigation 78—53109
- eddy current flaw detector, feedback phase effects on response to displacements 77—73418
- eddy current imaging flaw detection system 80—89426
- eddy current modulation type defectoscope, signal and sensitivity calc. 78—44327
- eddy current nondestructive evaluation, finite element analysis appl. 80—35439
- eddy current probe, high saturation with internal reference, design and specifications 80—40658
- eddy current technique 79—43500
- eddy current tester, for nonferrous tubes and rods 78—85099
- eddy current through type transducer, operating condition simulation when inspecting ferromagnetic rods 78—53077
- eddy currents in cylindrical conductor with surface crack, calc. 80—23601
- eddy-current flaw detect., suppression of interf. parameters 80—89442
- eddy-current flaw detection of long ferromag. products, magnetizing device parameters 80—89447
- eddy-current rotating probe for tubular condenser examination *(German)* 77—1897
- eddy-current transducers, double-ended, signal calc. for nonferromag. cylindrical products 80—89443
- elastic body, framework model appl. 79—41607
- elastic rod, stress-wave detection of an edge crack 78—30236
- elastic wave radiation, rel. to AE signal charact. 78—60952
- elastic wave scatt. from localised defects in solids, long-wavelengths 79—87794
- elastic wave scatt. theory for anal. and design of flaw characterisation expts., long-wavelength limit 79—83408
- electrical potential probe method *(German)* 77—1898
- electrically cond. materials, pulsed elec. meas. method *(French)* 79—29324
- electrically welded tubes, magnetic method with ferroprobe 78—53080
- electromagnetic flaw detector, differential eddy current transducer asymmetry effect on sensitivity 79—39092
- electromagnetic method *(Russian)* 78—35605
- electromagnetic NDT, digital method of edge effect suppression 78—56866
- electromagnetic transducer for crack exam. 78—76816
- electron radiography, feasibility for microcrack detection 78—72967
- electronic spectromatic flaw detectors, functional schemes 78—44322
- electrostatic defectoscopy, of cylindrical specimens using cylindrical capacitors 78—40000
- elongated defects representation on magnetic tape 79—39094
- EM scattering for rectangular slot estimation 80—18965
- emulsion containing water from crack detection processes using penetrating agents, purification *(German)* 79—5517
- failed steam accumulator anal., role of NDT 78—95877
- fatigue crack depth meas. in threaded part of drill pipe by US inspection 79—1930
- fatigue crack dimensions, recording method and sensor 77—63856
- fatigue crack growth in aircraft wing test, AE detection 78—60925
- fatigue crack propag. meas. and crack closure at low stress intensity level by unloading elastic compliance method *(Japanese)* 77—9016
- fatigue cracks, electrical detection method 77—73382
- fatigue cracks, microwave detection of third-order nonlinearities 80—55594
- fatigue cracks, US visualization, advantages over pulse-echo methods 80—66738
- fatigue detection and rating by acoustic emission, review 80—104380
- ferrite, US testing 78—53084
- ferrites, microwave flaw detection 78—53122
- ferromagnetic material, flaw detected hy high freq. magnetization, harmonic content in mag. field 80—71857
- ferromagnetic probe inspection unit for automatic inspection of welded tubing 78—56860
- ferromagnetic thin parts crack detection, mag. powder inspection using electromagnet 77—73424
- ferroprobe, basic concepts 78—60959
- ferroprobe flaw detector with RF pulse excitation 78—53081
- ferroprobe monitoring of rolled steel products with local transverse alternating magnetisation 77—73420
- ferrous metal rolled repetitive sections, ultrasonic quality inspection 79—87770
- fibre composite structure, thermal field techniques for NDT 80—66737
- fibreglass laminates, thermal NDT using liq. crysts. 80—93709

crack detection continued
- fibrous cracking, COD and initiation, replication technique 77—56069
- field meas. by Hall probes, accurate estimate 78—53155
- field of a strongly elongated elliptical cylinder in a nonlinear medium 79—91895
- fission reactor component reliability, non-destructive testing and flaw evaluation *(French)* 79—24711
- fission reactor pressure vessel and circuit development, conf. report 80—47541
- fission reactor pressure vessel walls, ultrasonic inspection reliability 79—24713
- fission reactor US testing to ensure safety, trends *(German)* 77—26847
- flaw detection, combined techniques classification choice of optimal NDT system 79—11752
- flaw detection, US reference reflection parameter determ. from amplitude and time of travel meas. *(German)* 79—91877
- flaw detection during leak tests, mech. treatment effects 78—60956
- flaw detection methods, planning statistical acceptance monitoring 79—91901
- flaw detection probability estimation from inspection data 79—24712
- flaw detection systems based on semicond. detectors and scintillation crysts. for hard bremsstrahlung 79—11748
- flaw detection using optical filters 78—53163
- flaw detector, eddy current, feedback phase effects on response to displacements 77—73418
- flaw detector, UD-22UM, materials with large US attenuation appl. 79—52585
- flaw detector for revealing fatigue cracks 79—66244
- flaw detector magnetizing units with semiconductor rectifiers, magnetic field meas. 78—53076
- flaw detectors modernisation, depth probe readjustment avoidance 77—90564
- flaw image produced with high energy scattered radiation, scattered radiation effects 79—34239
- flaw size determ. accuracy by US focusing probes and holography 79—29296
- flaw sizing of real defects, review 78—53041
- flaw-detection apparatus, noise immunity, sounding signal freq. modulation 80—89441
- flaws, size and shape meas. by US spectrum method 80—7745
- flaws, size and shape meas. method of ultrasonic spectrum pt.II 80—7746
- flaws in solids, low-frequency props. from scattering meas. 80—76475
- flow detectors, radiation type, electron bremsstrahlung irrad. field dia. calc. 78—56857
- fluorescent magnetic powder appl. *(German)* 79—91879
- fluorescent penetrant inspection, heat assisted 80—45466
- fracture mechanics evaluation, role of NDT 78—68862
- gamma flaw detector, multichannel 77—90565
- gamma radiation scattering appl. 78—44331
- gamma-ray and betatron integrated flaw detector, exam. of design 79—5103
- gamma-ray and betatron integrated flaw detector, exam. of design 79—15938
- gamma-ray back scattering flaw detector and thickness gauge 78—44333
- gamma-ray flaw detection, use of Kalman filter 79—5121
- gamma-ray flaw detector with analogue data processing, design and error calc. 77—73406
- gamma-ray flaw detector with analogue data processing, param. optimisation 77—81374
- glass fibre reinforced plastic, filament wound tube, US defect detection 80—7734
- glass reinforced plastic, acoustic emission investigation of deformation and fracture 77—16756
- glued members, low frequency acoustic flaw detector inspection 78—60954
- gradiometer, ferromagnetic probe, fault detection optimisation 78—53096
- graphite composite aircraft structures, flaw detection by US methods 78—44288
- grating acoustic scanner for material defects 79—47878
- growth and coordinate determ. by acoustic emission 79—5119
- growth gauge for assessing flaw growth potential in structural components 78—68859
- growth measurement using thin conductor film 79—74324
- holographic fringe multiplication appl. 79—41357
- holographic interferometry, using He in test chamber 80—93723
- holographic interferometry and speckle 78—60933
- hot-rolled rods, surface defect detection without scale removal by NDT 78—95890
- hydraulic component fatigue crack acoustic emission inspection 77—40513
- impedance flaw detector, acoustic, feasibility of standardless check 78—53158
- impedance flaw detector, resonant transducer 79—52572
- impedance flaw detectors, unified procedure for transducer calc. 79—90109
- Incoloy 800, eddy current testing *(German)* 79—96257
- industrial NDT computed transverse axial tomography system 80—89430
- inspection penetrants, evaluation 80—61056
- instrument for crack detection by AE 79—52582
- insulating material monitoring by electroluminescent screens, defect imaging 78—53083
- insulation, foam, spray-on, using dye solution or X-ray opaque solution 80—76440
- internal flaw, transverse dimension determ. by thermal control 80—104400
- ion microprobe mass analyzer appl. *(Japanese)* 77—25233
- IR defectoscopy, optimum algorithm in case of noncontent temp. meas. 78—60947
- IR non-destructive testing of bonded materials, theory and practice 80—93708
- laser speckle interferometry for nondestructive evaluation 78—60976
- leakage flux probe, inspection of tubing and round billets 77—12753
- length determ. by electric potential meas., automatic instrument *(German)* 79—96258
- length meas., inductive and videoelectronic methods *(German)* 77—63866
- liquid penetrant testing, continuum fluid mechanics aspects 80—43818
- liquid-filled crack, Rayleigh wave reflection and transmission calc. 77—32762

crack detection continued
- local magnetic field image recording on magnetic tape without bias 78—53129
- magnetic flaw detector, thyristor magnetising current switch, exam. 78—44311
- magnetic flaw detector, using magnetic powder method 77—90571
- magnetic flow detector, general purpose, portable 79—5107
- magnetic flux leakage, model 79—43499
- magnetic particle, penetrant and eddy current techniques, reliability 77—66718
- magnetic particle crack detection, remanent magnetism 77—63841
- magnetic particle inspection, combined magnetization of parts by rectified single half-period fields 79—52575
- magnetic particle inspection oxides, evaluation 80—40657
- magnetic powder, circulation method/magnetic field effect *(German)* 78—60928
- magnetic powder flaw detection, contact recording of patterns 78—53102
- magnetic powder inspection of thin parts using electromagnet 77—73424
- magnetic stray fields, optical detection 78—31602
- magnetisation method evaluation, for components with difficult shape 77—90556
- magnetizing flaw detection system for underground pipeline inspection 78—53103
- magnetographic flaw detector for monitoring cylindrical articles 80—35478
- magnetographic method, depending on coordinates in weld seam 80—108668
- metal, holographic interferometry, double impulse method 77—9033
- metal, microcrack, generated in oxides during high temp. oxidation, detection by slight sulphidisation 77—8999
- metal, stress wave emissions wideband recording facilities 77—37873
- metal crack depth meas. by potential probe method, principle *(German)* 77—86234
- metal ellipsoidal flaw characterisation 79—47865
- metal fatigue crack detection using nondestructive evaluation (NDE) methods 80—71826
- metal surface, exoelectron emission as observation technique 77—81202
- metal surface, microwave ferromag. resonance probe for eddy current detection 79—34254
- metallic and non-metallic surface defects, optical method 77—28973
- metals, contactless transducer, for thickness meas. and flaw detection 78—44312
- metals, crack propag. signals wideband recording facility 77—37873
- metals, microwaves non-conventional appl. survey *(Italian)* 80—13093
- metals, ultrasonic inspection, echo-mirror method with transform. of elastic waves 80—108663
- microtrons, appl. in nondestructive inspection of industrial products 80—81267
- microwave, adaptive filtering 79—52576
- moire method, speckle shearing, qualitative appl. for structural flow detect. *(German)* 78—82015
- multichannel flaw detector, optimal parameters 79—34247
- multifrequency US flaw detectors, parameters 79—5118
- multiparametric SHF flaw detection 79—70281
- natural frequency meas. method 80—30191
- near-surface defects, US detection and analysis *(German)* 80—93728
- neutron radiography examination of TRIGA reactor fuel rods 77—50229
- new measurement and observation techniques 80—45463
- noise immunity of flaw detection system 80—104385
- noise suppression circuit for automatic flaw indicator 79—5111
- non-destructive measurement of crack depth by DC conduction or potential methods *(German)* 79—52550
- non-metallic materials, flaw detection by tomodensitometry *(French)* 79—20295
- nuclear power station, US metalwork flaw detection system *(Russian)* 78—25302
- one-sided thermal monitoring, effect of flaw parameters on sensitivity and speed 79—5122
- optical heterodyne interferometer, appl. to surface inspection 77—90529
- optical instrument, for measuring depth and dimensions of surface microdefects 78—76812
- optical spatial filtering, of visualised results of flaw detection monitoring, rational regions of appl. 80—7751
- optical strong fibres, fatigue strength and flaw size distribution 77—11056
- optimal relation between geometric charact. of flaw and radiator optical focus 79—34246
- oxide thermal-sprayed coating on steel, acoustic emission 80—21247
- phase sensitive eddy current detectors, effect of compensation conditions, on transducer-product clearance inductions 78—85103
- photoelastic dynamic studies of fracture 80—38358
- physical optics farfield inverse scatt., mathematical inversion technique for nondestructive eval. 80—69580
- piezoelectric ceramics, using phase method of microwave flaw detection 78—72968
- piezoelectric transducer, composite, of low freq. acoustic flaw detector, natural freq. calc. 80—89450
- pipe, thick walled, increasing efficiency of automated ultrasonic inspection of segregate defects 79—11755
- pipe end, by magnetic particle device *(German)* 77—90535
- pipes, large-diameter, US testing of welds 78—3267
- plate, flaw reconstruction by automatic US testing *(German)* 80—61059
- polyethylene pipes, lifetime determ., crack growth in thermoplastics under various conditions 78—39981
- portable depth gauge 79—34251
- precision tubes, US inspection system *(German)* 77—90539
- pressure vessel, defect detection, strain evaluation laser holographic and speckle photography methods 77—81365
- pressure vessel crack detection by magnetic crack detection and dye-penetrant inspection 80—100994
- pressure vessels, AE during fatigue crack expansion 80—108675
- pressure vessels, probability of flaw nondetection 78—78479
- pressure vessels weld quality assessment, NDT methods and equipment 78—56871
- propagation rate meas. by fracture sensors 80—50796
- pulsed reflectometry, shape filtering method 80—35476
- PWR acoustic monitoring instrumentation 78—17309
- quantitative, model study using IR scanning 79—83400
- radiation crack detection, use of luminescent convertors 78—53125
- radiation flaw detection, automatic control systems 78—48596
- radiation flaw detection, correction of shadow images 80—89456

crack detection continued
- radiation flaw detector, optimal relative sensitivity 77—90554
- radiographic image quality, effect of inadequate screen-film contact *(German)* 80—61057
- radiographic inspection algorithm speedup by array processor 80—108659
- radiographic technique with object and film rotating rel. to X-ray beam 77—66716
- radiography, effect of stress on crack detection 80—40653
- radiography inspection, improved 77—86262
- radioisotope X-radiation sources in defectoscopy 77—56176
- radiological methods 79—79191
- radiometric defectoscope with feedback, charact. of operation 78—44321
- radiometric flaw detector, relay-type with time delay signal smoothing, prob. anal. 77—81377
- radiometric flaw detectors, results of practical appl. 78—40004
- radiometric flaw-detector, performance evaluation and parameter choice for smoothing filter 79—15945
- radioscopic inspection data of pore defects, statistical anal. 78—48606
- rate meter-type flaw detector, measuring circuits 78—60963
- refractories, elastic props., test unit for up to 1500°C 79—57167
- refractory, fissure fixing for struct. anal. with television microscope 77—63846
- reinforced plastics, low frequency acoustic flaw detector inspection 78—60954
- remote sensing of flaws in solids using laser system 78—60975
- resistance introduced by a defect in modulation inspection method 79—91892
- resonant radio flaw detector, 2 mm band for low temp. investigations 78—53115
- rolled sheet, artificial surface cracks, reflection of normal shear waves 80—89448
- rotating machine flaw detection, acoustic signature analysis and time-domain techniques 79—50525
- rotor forgings, US holographic inspection 77—66730
- rubber, thermal defectoscopy study 80—89445
- SAW scattering from surface cracks, angular and frequency dependence obs. 79—57197
- scan control unit, BUS-1 78—53143
- scanning laser beam system with defined flaw analysis, microcomputer-controlled *(German)* 80—3278
- scanning radiography beam-absorption system, param. selection for extended sources 77—81376
- seams, welded and soldered, Fourier hologram appl. for flaw detection in ICs 79—52580
- semiautomatic ultrasonic flaw detector for studs 79—66247
- sensitivity, of various nondestructive inspection methods 78—72974
- servo-hydraulic test system, for fatigue crack propagation studies under biaxial loading 80—76431
- shadow flaw detector, acoustic section anal. 77—77706
- shadow immersion flaw detector, pulsed US, operating characts. for multiple shadow mode 78—44304
- shear wave echo, from subsurface planar flaws, calc. model 77—25228
- sheet samples, crack length automatic recording 78—60907
- small surface cracks, size estimation using SAW 78—76793
- soap built-up multilayers, defect visualisation by optical microscopy 77—59186
- Space Shuttle external insulation, acoustic emission inspection 78—16276
- spherical material parts, defect coordinates, location via acoustic emission method 78—35626
- Splav-VM, automated US device for inspecting hollow extruded profiles 80—7747
- sputter target cracking, acoustic emission testing 80—81248
- stainless steel, pipe, small-diameter ribbed-bore, Lamb-wave ultrasonic inspection for defect detection 79—15944
- stainless steel type 316, ductile crack initiation, detection and toughness characterisation 77—16662
- steam generator tubes, EM acoustic transducer 80—76464
- steel, acoustic emission associated with phase conversions 79—70275
- steel, austenitic, crack determ. using mag. permeability probe *(German)* 79—52549
- steel, austenitic, eddy current testing of welds, cladding and cast materials *(German)* 78—44293
- steel, austenitic, optimum freq. for US testing *(German)* 80—30195
- steel, austenitic, weld, with natural flaws, US test techniques *(German)* 78—27713
- steel, austenitic stainless weld, US inspection, focusing probe significance *(German)* 77—73397
- steel, austenitic weld joints and surface claddings, eddy current testing *(German)* 77—1895
- steel, austentic stainless, butt welds, US exam. 80—93710
- steel, ball bearing rods, inspection installation 80—81268
- steel, billet, high speed automatic surface inspection, MIDAS 79—83420
- steel, C and Mn, rails, surface crack exam. by eddy current technique 77—9007
- steel, Co-Cr-Mo, type HY 180 correl. between advanced NDT evaluation methods and fracture mech. parameters 80—97675
- steel, coarse grained Kh18N9T, US amplitude inspection, efficiency estimation 78—48592
- steel, Cr-Mo-V, high temp. steam pipe weld, defect distrib. and growth 80—25979
- steel, Cr-Ni-Mn, AISI 4340, correl. between advanced NDT evaluation methods and fracture mech. parameters 80—97675
- steel, crack detectability by radiography 79—91857
- steel, crack detection using image quality indicators, comparison 77—25232
- steel, crack initiation detection by AC potential method *(Chinese)* 80—21196
- steel, eddy current surface crack detection *(French)* 79—61831
- steel, fatigue crack depth meas. by US technique 77—9006
- steel, ferritic weldment, US testing of defects, charact. and size 78—7104
- steel, ferromagnetic round bar, eddy current crack detection *(German)* 79—91880
- steel, flaw detection in macrostruct. of large specimens 79—87777
- steel, high strength low-alloy, AE appl. to nondestructive testing 79—83419
- steel, low alloy, welded joints, cracking during heat treatment 80—7724
- steel, nuclear reactor pressure vessel materials, AE assessment 79—83422
- steel, potential-drop meas. system 79—34225
- steel, single probe US technique, NDT 77—66732

crack detection continued
steel, stainless, US methods for intergranular corrosion inspection 78—95898
steel, stainless 1Kh18N9T, flaw detection by X-ray television system 79—5120
steel, stainless austenitic welds, time domain approach to crack location and sizing 80—50781
steel, statistical methods in US anal. of real defects 78—72976
steel, strip inspection for cracks, magnetic instrument 79—52584
steel, surface defect detection by magnetographic method 78—44332
steel, tape, US inspection for segregate type defects 79—15943
steel, thick rolled sheet with unfinished surface, US defect assessment expt. 77—77720
steel, thin sheet flaw detector, magnetisation system 77—12751
steel, types A533B and KAS, fracture toughness meas. using elect. potential method *(Japanese)* 80—93722
steel, US inspection to 1000°C, hot-metal defectoscopy 80—66750
steel, US internal flaw detection system 77—66717
steel, US testing, sensitivity adjustment for focusing probes, testing of planar and curves surfaces *(German)* 78—7152
steel, weld, flaw-size meas. by US frequency anal. 77—44429
steel, welded joint, standardization of radiographic flaw detection 79—91900
steel band used as pulling member, device for inspecting mechanical state 78—76810
steel bars, type 3102 bright steel, automatic combined inspection line 77—77714
steel forgings, variable attenuation coeff. effect on flaw detect. 77—77707
steel pipe, flaw detection by US pulse-echo method 80—66756
steel plates, US testing, dynamic evaluation of flaw size 79—15949
steel pressure vessel, notched, acoustic emission meas. during pressurisation 78—21638
steel wire, US inspection, immersion method 80—66757
structural failure detection by vibration detector 78—15641
structural fatigue crack acoustic emission monitoring 77—32755
structural material defect characterisation by US signal processing 79—52614
surface crack parameter determ. by diffr. method 79—66237
surface cracks, SAW excitation, length and depth resonances 79—8403
surface layer structure determ. using Barkhousen noise probe *(German)* 79—24710
surface wave scatt. from elliptical cracks for failure prediction 80—55608
Temp-1 system for the ultrasonic inspection of bulky aluminium alloy plates 80—66755
thermal defectoscopy, two-dimensional numerical soln. with convective heat loss 77—81378
thermal detection of delamination and inclusion flaws, ID anal. 80—71820
thermovision flaw detector 'Stator-1', meas. channel 80—76449
transducer, low frequency US flaw detector appl. 79—98580
transducers, applied, resistance due to cracks, eddy current calc. and hodograph 78—53095
tube flaw detection by annular US transducers 78—60971
tubing, testing and failure localisation by electrodynamic method 77—63847
turbine blades, crack detect., holographic interferometric method 78—35625
turbine blades, fatigue crack detect., strobed hologram method 78—35624
turbine rotor shaft, US testing, sensitivity multiplication factor 80—85125
two coordinate defect marker, design, and operation for rolled stock flowline inspection 78—44309
two-axis tensile test machine, for static and dynamic tests *(French)* 78—15627
ultrasonic flaw detector, automatic, for butt welds *(Japanese)* 80—25976
ultrasonic testing of austenitic collars in a computer controlled immersion test-plant *(German)* 79—96256
US, crack dimensions, studies survey 79—11744
US, development of reference fatigue cracks, book contrib. 79—100327
US, differential probe head for impedance type defectoscopes 77—73408
US, differential probe head for impedance type defectoscopes, transducer design 77—73409
US, flaw detection equipment, acoustic section bandwidth increasing techniques 77—73410
US, informative shape index for nature of flaws 77—73407
US, metal fatigue detect. in shafts of power plant machinery 77—77716
US, pressure vessel of PWR reactor, in-service inspection *(Czech)* 78—29658
US, structural products and structures, restricting portion of signal analysis 78—44318
US, using equivalent defect sizes, sliderule construction 77—90576
US attenuation, precrack damage and crack propag. study 80—40656
US automatic defect recording and heat treatment monitoring system 77—90542
US automatic inspection of tubing 78—56865
US basic instrument crack and flaw detection, basic instrument 79—5108
US bulk wave electromagnetoacoustic excitation 79—57195
US defectoscopy of parts hard-faced by electric-arc welding, expt. 77—73411
US diffraction sizing 79—29291
US echo pulse flaw detectors, use of auxiliary sensitivity regulation 78—60951
US fault detection, MatEval computerised test system *(French)* 79—52564
US flaw detect., tolerance on operating freq., sensitivity standardisation 78—53089
US flaw detection, diffraction of normal modes by a compliant disk 80—87603
US flaw detection, focusing probes 80—,104383
US flaw detection for welded seams, with automatic registration of flaw parameters 77—90570
US flaw detection sensitivity enhancement by focusing system, theory 78—53112
US flaw detection sensitivity enhancement by focusing system 78—53113
US flaw detector, microprocessor controlled, for flaw classification in welded plates 80—100992
US flaw detector, portable, supply voltage stabilisation 77—90573

crack detection continued
US flaw detector UDM-3, measurement errors 79—8409
US flow detection, mirror shadow method sensitivity expression and analysis 78—53088
US flow detectors, tuning methods for time depend. sensitivity control unit 80—108667
US holography for defect size meas. at inservice inspections of nuclear components 79—45372
US imaging cell for direct visualisation of defects in solids 79—20324
US inclined probe, construction improvements 80—33411
US inspection, automatic, thin walled large diameter pipes, flaw size classification 78—60949
US inspection of cast explosive billets for air voids 78—3287
US inspection of large diameter pipe and stock 78—48593
US inspection of rails for flakes, mechanised US unit 78—44330
US materials testing for crack-like flaw identification and crack parameter determ. *(German)* 80—50794
US methods, progress in theory and principles 80—81262
US multichannel shadow flaw detectors, accuracy and reliability of inspection 78—44306
US probe, rocking-beam, radiation pattern 77—90572
US probe of plastics and rubber materials 79—52558
US resonance method, appl. in inspection of symmetrical products 80—89449
US shadow flaw detectors, metrological peculiarities when inspecting thick rolled steel sheet 80—81263
US shadow immersion exam. of defects, dimension determ., error anal. 78—44305
US shadow immersion flaw detection in rough surfaced objects, registration threshold selection 77—73413
US sizing, diffraction technique 79—83429
US sonoprobe for Si crystal microcracks detection 80—76462
US spectral anal. of flaws, theoretical study 78—95897
US spectral method for determ. of nature of defects 79—5115
US spectroscopic NDT 78—76805
US test procedure for early detect. and remaining life prediction 80—71848
US testing, instrument limitation, flaw detection instruments, programmed automatic corrections 78—7103
US testing of T-joint welds, acoustic system characts., optimisation 77—73412
vitreous enamel, bubble struct. and flaw forecasting 78—53118
weld defects and plant structures 79—79192
weld flaw study using ultrasonic holography *(Dutch)* 78—68855
weld interrogation distance amplitude curve, attenuation effects 77—40505
weld joint, furnace welded pipe inspection unit for above 1000°C 78—53134
weld joint in stainless steel tubing of OK18T1 steel, ferromag. probe inspection unit 77—77721
welded corner pipes flow detection, method 77—77711
welded joint, radiographic inspection, standardization of sensitivity and flaw size 80—89455
welded joint, US reflection from irregularities 80—104389
welded joints, radiographic inspection, real flaws detectability evaluation 80—81266
welded joints, strain concentration zone detection by holographic interferometry 77—40512
welded plates, flaw classification using microprocessor controlled flaw detector 80—100992
welded tee joint, using US method, echo-signal amplitude characteristics calc. 77—90549
width investigation by inclined scanner with regulated directivity diagram 80—89452
wood, standing trees, US pulse echo method for flaw detection 80—66731
X-ray, electroluminescent storage screens, expt. results 77—77722
X-ray flaw detection, electroluminescent storage screens, expt. results 77—77722
X-ray television system applic. to flaw detection in welded joints 77—81380
Al alloy cylindrical parts, crack detection by two channel eddy current inspection unit 78—72998
Al alloy sheets, type 7075-T6 used in aircraft, early detection of fatigue cracks 80—66730
Al, plate, defect location by natural frequency meas. method 80—30191
Al, subsurface flaw detection by photoacoustic microscopy 80—66725
Al, surface wave scatt. from elliptical cracks for failure prediction 80—55608
Al, US and X-ray testing of castings, moulds and die-casting machines 78—53097
Al-Cu, high strength, type 2024-T3, crack growth, fatigue induced surface deform., holographic detect. 80—85120
Al-Cu, type 1100, synchrotron radiation microradiography 80—85121
Al-Cu-Mn, type 2219, synchrotron radiation microradiography 80—85121
Al_2O_3, crack detection caused by thermal shock, AE technique *(Japanese)* 80—21248
B fibre, US inspection, immersion method 80—66757
C fibre reinforced plastic, crossply defect location by natural frequency meas. method 80—30191
Fe, cast, parts inspection of unmachined surfaces using fluorescent penetrant method 79—11754
Fe, cast, US flaw detection by boxcar integration 80—89437
Fe-Co-Ti-Al alloy type YuNDK magnets, metallographic method of distinguishing cracks 80—85096
Ge, microflaw vol. conc. determ., etching method 79—24688
MgO and MgO-dolomite, crack detection caused by thermal shock, AE technique *(Japanese)* 80—21248
Mo film, constrained, 20 MHz thermoelastic wave generation 79—47880
Mo wire, US inspection, immersion method 80—66757
Mo/Nb welded joints in sheet metal, detect. and exam. of cracks, initiation, development 77—73385
Na_2O-Li_2O-Al_2O_3, local electrode current density and flow decoration 80—100935
Nb ingot, US flaw detection sensitivity enhancement by focusing system 78—53113
Si crystal microcrack detection by ultrasonoprobe 80—66733
Si textured solar cell, hairline crack detect. using focused laser scanner 79—48123

crack detection continued
  Si_3N_4, hot pressed, surface wave scatt. from elliptical cracks for failure prediction 80—55608
  SiO_2 film, local defects detection by electrolytic decoration *(Bulgarian)* 78—60896
  W wire, US inspection, immersion method 80—66757

crack-edge stress field analysis
  see also penny-shaped cracks
  Γ-shaped crack elastic energy evolution rate in laminate determ. by pliability vibr. meas. 78—83348
  a mixed boundary value problem in elasticity 79—23274
  adhesive fracture specimen, DCB, crack tip stress field anal. 78—55602
  adhesively bonded metallic panels, 2-ply, finite element and integral eqns. anal. of fatigue crack growth 78—92347
  adhesively bonded sheets, fracture anal. 77—50996
  anisotropic composites, bounds and self consistent estimates for overall props. 78—5654
  anisotropic elastic slab containing crack, deformation 79—68570
  anisotropic medium under polynomial form applied stress, elliptical crack elastic field 79—46263
  anisotropic slab, thermoelastic crack problem 80—23960
  annular crack at spherical voids, stress intensity factor estimates 80—106757
  annulus, infinite, with two pairs of cracks at inner boundary, plain strain problem 77—14963
  asymptotic techniques for stress conc. regions in plane problems 78—28953
  bar, circular, in tension, strain energy release rate for edge crack 79—18815
  bar, rectangular, torsion crack problem, harmonic function continuation technique soln. 80—99969
  beam, cracked, transverse loading by stamp, stress and fracture anal. 80—10187
  beam, curved, Dugdale plastic zone sizes for edge cracks 79—72853
  beam, double cantilever, dynamic crack propagation modelling, 1D anal. validation 79—72857
  beam, stress distrib. around slender notch, two-dimens. photoelastic investig. 78—34069
  beam (plate) pure bending, dynamic fracture, axial force effect 78—63385
  biaxial load effect on crack border elastic strain and strain energy rate 78—18231
  biaxial load effects 78—55594
  biaxial stress field, stress ratio effect on fatigue crack growth 77—58617
  bimaterial bodies, stress intensity factor eval. using numerical crack flank displacement data 79—50660
  bimaterial composite, influence on elasto-dynamic stress intensity factors of crack straddling interface 77—68532
  birefringent plates, cracks, stress intensity factors, refl. caustics method 80—93718
  body force method, to calculate stress intensity factors, for crack, in arbitrarily shaped plate 78—90775
  body loading with cracks, energy conditions for brittle failure *(Russian)* 80—96234
  bonded anisotropic bodies, arbitrarily oriented crack near interface *(Japanese)* 78—9611
  bonded dissimilar materials, crack along bond, stress intensity factors 78—55607
  bonded elastic half-plane, intersecting crack anal. 77—14953
  bonded half plane containing inclined cracks subject to antiplane shear loading 79—81813
  bonded half planes containing inclined cracks subject to antiplane shear loading stress intensity factors 79—50661
  border stress and displacement eqns., validity for qualitative predictions 77—54926
  branched cracks, plane strain stress intensity factors 78—1608
  branched cracks in 2-D, numerical soln. 79—46269
  brittle cracks, stability, propagation, fracture mech. *(Czech)* 78—79257
  brittle elastic body, stability and post-critical growth of system of cooling or shrinkage cracks 80—1486
  brittle fracture from loss of stability near crack 78—55597
  brittle materials, crack propagation under compression, finite element anal. *(Japanese)* 78—42567
  brittle materials, intergranular creep crack growth, diffusion controlled theory 78—84950
  brittle materials, water drop impacted, damage thresholds 80—81149
  brittle rupture, strength time depend. *(Russian)* 78—46912
  brittle solid, residual stress about pointed indentation impression 77—12686
  BWR piping cracks, relation between crack and stress 79—40995
  C-shaped fracture-toughness test specimens, stress, strain and deflection meas. 78—19963
  cap, cracked, transverse shear and material orthotropy effects 80—10144
  Cauchy type singular integral eqns. with complex singularities, numerical soln., stress intensity factors 78—55611
  caustics equations for crack and dynamic plane elasticity problems 80—43669
  centre cracked plate under quadratic thermal gradient, stress intensity factors analysis 80—43665
  ceramic, stress intensity factor estimates for a peripherally cracked spherical void and a hemispherical surface pit 79—29196
  ceramics, process zone surrounding crack tip, theory 78—67154
  ceramics, transformation toughening, martensitic transforms. in crack-tip stress fields 80—104154
  circular craze analysis, simple membrane model 77—3779
  circular cylinder with circumferential edge crack under uniform heat flow, thermal stresses 80—48641
  circular disc, stress intensity factors and crack energy 78—79260
  circular flaws, forced torsional oscillations at low frequencies 80—53703
  circular in infinite isotropic elastic plate, elastic field evaluation 77—55319
  circumferential edge-crack in cylindrical cavity, stress anal. 77—80116
  classification of stress-intensity factors from isochromatic-fringe patterns 79—55339
  closed cylindrical shells, crack propagation criteria 80—38341
  closed form stress intensity factors for common crack configurations 77—58606
  closure of crack related to crack propag., prediction method for crack growth 78—67099
  collinear edge cracks in rotating disc 77—65717

crack-edge stress field analysis continued
  combined mode bend specimens, calc. of stress intensity factors, 3 alternate methods 79—77025
  compact tension specimens, stress intensity and crack openings 80—1474
  component containing cracks, critical review of creep 78—63321
  composite full-planes, stress singularities 78—34077
  composite material crack tip fatigue behaviour and stress state study *(Japanese)* 80—28470
  composite material/metal sheet bonded, finite element anal. of patched cracks 80—10192
  composite materials, bimaterial plate, cracked, finite element anal. of stress distribution 78—75104
  composite plane, periodic problem *(Russian)* 77—50987
  composite structural elements, stress intensity factors determ. 80—99973
  composite systems, cracked, finite element microscopic stress anal. 78—34083
  composites, stress singularities for crack meeting interface 77—3776
  compression wave diffraction by penny-shaped crack in presence of mag. field 79—47318
  computer analysis of crack propagation 77—35094
  concrete, reinforced, failed slabs, nonlinear analysis by finite element method *(Japanese)* 77—42785
  concrete, stress distribs. under splitting loads *(Japanese)* 78—35495
  conforming crack tip element with quadratic variation in singular fields 78—38251
  coplanar cracks in infinite transversely isotropic medium, stress distrib. 78—51122
  coplanar Griffith cracks in infinite elastic medium, dynamic stress conc. 79—46270
  corrosion-fatigue crack propagation modelling 78—90779
  couple stresses effect on crack tip 78—18240
  crack, dislocation model of plastic zone 77—84837
  crack extension angle, influence of specimen's geometry 80—99965
  crack extension criterion of maximum shear or principal stress 78—79278
  crack extension forces in elasto-plastic stress fields 78—18250
  crack growth, anal., crack tip deform. modelling 79—41626
  crack loaded in anti-plane shear under creep 79—27598
  crack propagated perpendicular to dissimilar material interface, calc. of stress intensity coefficient *(Russian)* 79—55340
  crack tip finite element anals. 79—41624
  crack tip plastic zone, thermal props. calcs. 80—7659
  crack tip plasticity in dynamic fracture mech. 79—41627
  crack tip singularity analysis by global-local model of large finite elements 80—28466
  crack tip singularity models, assessments for use with isoparametric elements 79—50652
  crack tip strain and stress, experimental investigation 79—68669
  crack tips, near boundaries or other geometrical discontinuities, stress intensity factors 80—1484
  crack-tip, from field values of displacements using complementary energy 78—67114
  crack-tip problems and quarter-point triangular elements 78—83333
  crack-tip slip band blocked by grain boundaries, simple model 79—50665
  cracked infinite elastic wedge loaded by rigid punch, stress intensity factors 79—77019
  cracked plates, symmetric bending by reflected caustics method 80—19283
  cracked stiffened panels, biaxially loaded, elastic and elastic-plastic analysis, using finite element method 79—68656
  cracking problem in timber, optimisation and finite element methods 77—39261
  creep deform., stress field and modified J-integral near crack tip. *(Japanese)* 80—103411
  creep fracture, failure mechanism involving grain boundary sliding and brittle crack extension 80—97557
  critical state of matrix near sharp-pointed rigid inclusion *(Russian)* 77—58600
  critical stress characts. in multicracked brittle plates in complex stress state *(Russian)* 77—58601
  cruciform crack, unsymmetric, soln. in infinite plane isotropic elastic medium 79—14342
  curved crack, propag. finite element anal. 80—1485
  curvilinear, in elastic body with cyclic symmetry *(Russian)* 78—34075
  curvilinear cracks, star-shaped array in infinite isotropic elastic medium 78—55609
  curvilinear cracks in bonded dissimilar materials, expt. soln. based on caustics 77—58622
  cylinder, hollow, with external crack, axially symmetric torsion problem soln. 80—14614
  cylinder, internally pressurised, stress intensity factors of inner and outer cracks 77—58610
  cylinder, stress-intensity factor for penny-shaped crack 78—30237
  cylinder, tensile, of infinite length, with circumferential edge crack, stress intensity factors 77—68533
  cylinder, transversely isotropic with circumferential edge crack, singular stresses 80—19284
  cylinder, weakened by penny-shaped cracks, thermoelastic stresses 80—10191
  cylinder elongation, containing periodically located disk-shaped cracks 79—90186
  cylinder with oblate spheroidal cavity or internal penny shaped crack under tension, stresses 80—69736
  cylindrical shell, transverse shear effect on axial crack 78—67090
  cylindrical shell under axial tension, crack tip stress anal. using caustics 77—3775
  cylindrical shells, anal. of through cracks by quarter point elements 79—72856
  damage model, crack growth and instability 79—41614
  disc, circular, edge cracked, plane stress under symmetric pin loading 79—50595
  disc, circular, linearly elastic, radial edge crack, const. internal press., stress anal. 77—54932
  disc, circular rotating, diametral edge cracks, stress-intensity factors 80—14572
  disc, with crack, stress and strain calcs. *(German)* 80—106760
  discontinuous deformation gradients near crack tip in finite anti-plane shear 80—58973
  discs, rotating hollow circular, stress intensity factors for multiple edge cracks 80—38334
  disk specimen 80—28468

crack-edge stress field analysis continued

- dislocation theory, elastic energy momentum tensor and crack propagation 80—69741
- double cantilever beam adhesive joint, cohesive fract., stress anal. 77—65721
- double torsion fracture toughness test, 3-dimens. finite element anal. 80—30203
- double torsion specimens, crack velocity correction factor for crack-front shape 79—98668
- dual theory of elasticity for media with regularly distributed cracks 77—68534
- ductile materials, crack extension rates 80—96230
- ductile notched fracture toughness specimens, instability prediction, approx. flow stress model 78—34082
- Dugdale crack, dynamic effects in propagation, Hankel and Laplace transform methods 80—87741
- Dugdale crack model, von Mises combined stress surface 77—54936
- Dugdale model, calcs. using weight functions 78—55590
- Dugdale model solution, of cracked bodies, finite element analysis 78—67116
- Dugdale model validity limits for thin cracked plates under biaxial loading 80—43667
- dynamic crack growth under stress wave loading 79—81815
- dynamic crack-tip fields according to deformation theory 80—64481
- dynamic finite element analysis of cracked bodies subjected to impact loading 80—69742
- dynamic propagation in anti-plane shear, anal. by finite differences 80—84240
- dynamic propagation of a finite crack, stress intensity factors 79—90183
- dynamic stress-intensity-factor determination from isopachics 80—28416
- dynamic stresses induced by moving cracks, numerical soln. 77—11146
- edge crack, oblique, in semi-infinite plate, stress anal. 80—64463
- edge cracked sheets with mixed boundary conditions, stress intensity factors, displacements, stresses 80—64477
- edge notch, semicircular, in semi-infinite plate, stress anal. 78—38258
- edge notch stress anal., book contrib. 78—94621
- edge notched brittle plates, virgin waves and boundary reflections at fracture 80—79233
- edge-cracked plates subjected to transient thermal singularities, stress intensity factors 77—58612
- elastic body, system of curved cracks under different boundary conditions on their lips 80—53713
- elastic body with crack-like inhomogeneities, influence on effective mech. characts. *(Russian)* 78—26088
- elastic crack, with arbitrary surface loads, stress singularities 77—65680
- elastic crack behaviour model from thermodynamic considerations *(French)* 79—10534
- elastic crack tip enclave model, fracture stress 80—71730
- elastic cracked members, anal. by optimisation techniques 80—1470
- elastic cylinder with internal circular crack *(Russian)* 79—59944
- elastic dielectric, crack tip stresses, EM field distrib. 79—68641
- elastic dielectric, crack tip stresses generated by EM field 79—68642
- elastic dielectric, crack tip stresses in EM field, Williams method 79—68640
- elastic infinite plate with parabolic crack 78—30239
- elastic interaction between solute atoms and stress field at tip of cracks and notches 78—34067
- elastic layer containing cylindrical cavity, stress distrib. near external crack 77—72171
- elastic medium, infinite homogeneous isotropic, with external crack, thermal stress anal. 77—42778
- elastic plane, stress-strain state at brittle crack vertex, geometric nonlinearity effects *(Russian)* 80—79221
- elastic plate, crack closure in bending, sixth order anal. 80—96231
- elastic pressured shells, stress intensity factors for very short cracks 77—50997
- elastic solid, cracked or notched, general numerical method for three dimensional singularities 78—67137
- elastic solid with doubly periodic array of cracks, fracture mechs. 78—34085
- elastic stress intensity factor calcs. using elastostatics M-integral conservation law, plane cracks 78—46913
- elastic strip bonded to rigid support 79—23277
- elastic strip with isolated crack, equilibrium 80—14620
- elastic strip with two coplanar Griffith cracks, thermal stress distrib. 77—42779
- elastic thin semi-circular plate containing edge crack 78—13972
- elastic-plastic anal. of asymmetric cracked specimen under longit. shear 77—14954
- elastic-plastic crack tip characterisation, relation to R-curves 78—56767
- elastic-plastic material with plastic orthotropy, crack tip singular behaviour 79—81816
- elastic-plastic materials, finite deformation anal. of crack-tip opening 78—51126
- elastic-plastic plane-strain crack growth, comparison of theory and experiment 80—108560
- elastic-plastic solids, crack tip deformation and fracture 79—27591
- elastic-plastic stress fiield, plane stress and plane strain, blunting of tip *(Chinese)* 80—64469
- elasticity, mixed boundary value problems, numerical scheme 78—26038
- elasticity, singular eqn. soln. 79—68639
- elasticity, soln. by superposition of finite elements and singular fields 78—38249
- elasto-diffusive solids, singularity movement, appl. to fracture propag. 78—30235
- elasto-plastic flow in computer simulated, A533 steel 78—56720
- elasto-plastic material, crack tip stress and strain fields and fracture behaviour 78—22304
- elastodynamic anal. by finite element method using singular element 78—55603
- elastodynamic effects on crack branching 78—67113
- elastodynamic fracture analysis of plane crack extension 78—5693
- elastodynamic stress intensity factors, ray theory approach 79—7339
- elastodynamics, stress and crack-displacement intensity factors 78—67112
- elastoplastic body, depend. of crack opening and plastic zone size on type of stress state 79—14348
- elastoplastic crack problems front soln. appl. 77—27493
- elements with curved boundaries and variable nodes 79—98663
- elliptic crack and punch problems, Lame polynomial solns. 78—75069
- elliptic plate, with curvilinear cracks, elastic equilibrium *(Ukrainian)* 77—68521

crack-edge stress field analysis continued

- elliptic slit in plate, thermal stress concentration 77—39262
- embedded semicircular surface crack, stress intensity factors, superposition methods 80—79217
- energy release rates calc., inverse flexibility method 79—41617
- energy-balance approach to fatigue crack growth 78—90773
- epoxy composites, dynamic crack propag. 80—40497
- epoxy resin, sheet, stress intensity distrib. through plate thickness along crack front 79—43390
- exact linear elastic solutions for Mode I, II and III crack problems 78—34072
- explicit finite difference method, anal. of dynamic crack and fracture 77—75860
- extension due to nonuniform internal press. 78—51124
- exterior interface cracks, shear and tensile tractions, stress anal. 80—58971
- external crack, stress distrib. using dislocation layers 79—98664
- externally cracked cylinder, elastoplastic response anal. by method of lines, computer program 80—28435
- face cracked plate, subjected to rotationally constrained end displacements, mode I anal. 79—23280
- fast fracture and crack arrest, finite difference anal., appl. to steel, epoxy resin 78—1607
- fast reactor, dynamic elastic response of subassembly ducts to impact loading, finite element anal. 80—18536
- fatigue crack, macroscopic residual stress at tip, X-ray obs. and finite element anal. *(Slovak)* 78—19885
- fatigue crack growth, closure, prediction and fracture mechanics 79—50653
- fatigue crack growth, threshold 78—63392
- fatigue crack growth in notched components 78—83329
- fatigue crack path prediction by finite element method *(Japanese)* 78—42568
- fatigue crack propagation, crack closure, effective stress range factors 80—100924
- fatigue crack propagation, theoretical expl. of delaying effects of overloads 78—67093
- fatigue crack propagation theory, threshold derivation 78—83337
- fatigue cracks, Dugdale crack closure analysis, under const. amplitude loading 79—50650
- fatigue cracks in side notches, stress intensity factor formula 78—79264
- fatigue cracks threshold stress intensity for crack growth, prediction using dislocation model 78—83870
- ferromagnetic elastic solid, two coplanar Griffith cracks, singular stresses 80—65985
- fibre reinforced composites, angle ply, delamination mechanics and failure mode 80—79236
- fibre reinforced composites, exam. of thermal stress fracture 78—75103
- fibre reinforced composites, transverse plane, elastic, failure behaviour *(Japanese)* 78—48510
- fibre reinforced composites, unidirectional, anal. of cracks emanating from circular hole 80—100301
- fibre reinforced elastic materials, crack tip anal. 79—27594
- finite deformation crack in infinite body under antiplane simple shear 78—18242
- finite element anal. using isoparametric elements 79—3973
- finite element anal. using special tip elements 77—58605
- finite element analysis of elastodynamic fields near running cracks 78—34066
- finite element mesh optimisation for fracture problems soln. 78—34070
- finite plane region, problem soln., using indirect boundary integral method 79—77014
- finite plate, propag. mode III crack, dynamic stress intensity factor, reflected stress waves 80—103001
- finite plate, stress intensity factor for deep surface crack 80—28467
- finite-geometry solids, rectangular surface cracks, stress anal. and stress-intensity factors 78—38256
- fission reactor fatigue loading, growth of underclad flaws 79—22429
- fission reactor pipework integrity assessment 79—22431
- flat cylindrical shell, with infinite series of cracks, stress state 80—53716
- flat elliptical crack, in infinite solid, mixed boundary value problems 78—9602
- flexible plate, stress distrib. through crack 77—89074
- fracture, arbitrary criterion, weakest link theory reformulated 78—90786
- fracture, dynamic analysis with Lagrangrian finite difference method 77—35095
- fracture, energy scaling, size effects and ductile-brittle transitions 79—43394
- fracture, nonlinear, and stable crack extension process, finite element anal. 80—53702
- fracture, plane strain cumulative, criterion 79—60432
- fracture criterion of Sih, formal extension, elastic stress field near crack *(German)* 79—1139
- fracture mech., conf., Washington, USA (Sept. 78) 79—43422
- fracture toughness, J-integral rel. to crack tip opening displacement *(Japanese)* 78—42569
- fretting fatigue, stress intensity factors 79—90184
- frozen stress fields, study of crack-tip nonlinearities 79—37239
- generalised stress intensity factor theory *(Chinese)* 79—94554
- generalised stress intensity factors, numerical determ. method, crack problem appl. 79—72851
- glass, fracture and fatigue, crack tip radii influence 80—89335
- glass, stress intensity factors by double torsion method, crack growth *(French)* 77—73345
- glass fibre reinforced plastic, brittle coating technique 80—35299
- glass plate, flexure crack propag., expt. and anal. 78—80620
- glass plate, physically or chemically tempered, contact fracture resist., model 78—19895
- gradient stress fields, stress intensity factor determ., nuclear safety appl. 78—34089
- grain boundary crack, stress depend. of growth rate during creep 77—80575
- granular solids, cracks, stress concentrations and shapes, Fourier transform methods 80—83761
- graphite, pyrolytic, ion bombard., flaking, stress fields around penny-shaped cracks 78—52946
- graphite reinforced epoxy laminate plates with cracks, strain and failure anal. 79—29170
- Green's function analysis, crack emanation from circular hole in infinite sheet 80—92084
- Green's function for thru-crack emanating from fastener holes 78—67118

crack-edge stress field analysis continued
- Griffith crack, asymmetrically loaded in infinite anisotropic medium 79—50649
- Griffith crack, at interface of two bonded dissimilar elastic wedges, stress field, inverse Mellin transforms 80—53718
- Griffith crack, cross shaped, surface stress distrib. 78—30240
- Griffith crack, initial motion 77—14959
- Griffith crack, interface of layer bonded to half plane, approx. method 78—79258
- Griffith crack, stress distrib. at interface of elastic layer bonded to half plane 80—23955
- Griffith crack at interface of bonded wedges, Mellin transform technique 79—40369
- Griffith crack at rigid-elastic media interface, transform soln. method 77—897
- griffith crack in an infinite nonhomgeneous elastic medium under shear 78—87300
- Griffith crack in infinite elastic solid, stress distrib. 77—80107
- Griffith crack in nonhomogeneous medium under shear, asymmetric problem 79—18813
- Griffith crack in transversely isotropic material stress anal. 79—64583
- Griffith crack opened by rigid inclusion, stress distrib. 80—79228
- Griffith crack opened by thin symmetric wedge, stress intensity factor 77—75807
- Griffith crack opened by thin symmetric wedge 78—46911
- Griffith crack problems in non local elasticity, solutions for one and two dimensional problems 78—51125
- Griffith crack system stress field, at 2-bonded dissimilar elastic halfplane interface 79—64584
- Griffith crack-antiplane shear wave interaction at interface of two bonded elastic half-spaces, geophys., seismological appl. 80—92087
- Griffith cracks, coplanar in infinite elastic layer under torsion 78—1610
- Griffith cracks, in infinitely long elastic strip, stress intensity factors for variable pressure 79—77022
- Griffith cracks in infinite elastic strip, stress distrib. 79—40370
- Griffith energy criterion of fracture for edge cracks 80—5992
- growth determination, in mixed mode loading system 78—67105
- half space, elastic, edge cracks, dynamic growth 80—58972
- half-plane with internal line crack, elastic problem, stress intensity factors and crack form. energy 77—42782
- half-space with crack nonperpendicular to edge, exact soln. and stress intensity factors *(Russian)* 80—53711
- harmonic solid, crack parallel compression, crack plane strain buckling 80—64475
- Hertzian cracking, anti-plane elastic solid model, surface energy meas. *(Spanish)* 77—31260
- high strength ductile materials, condition for crack growth 80—10190
- high temp. cracks, discrete dislocation anal. 78—48514
- high-temperature reactor structural displacement and strain analysis by picture processing *(Japanese)* 80—78352
- highly deformed zone and cyclic strain history near fatigue crack tip *(Japanese)* 79—34145
- hole and vicinity crack stress intensity factor calc., program *(Japanese)* 78—9603
- hollow elastic solid, cracked, torsion anal. 78—51134
- Homalite-100 plates, modified compact-tension specimens, dynamic anal. 80—97561
- inclined crack under biaxial load problem 78—34071
- inclined-strip-yield crack tip plasticity model, appl. to fatigue crack growth 80—38333
- infinite anisotropic elastic medium, simple smooth crack 77—46967
- infinite body, stress and displacement from arbitrary load on circular crack 79—32381
- infinite cracked isotropic sheet, under symmetric loads, Green's functions for stresses, stress intensity factors and displacements 80—99967
- infinite elastic medium, diffraction of torsional waves by flat annular crack 80—64447
- infinite elastic medium with cylindrical inclusion, axisymmetric external crack stress intensity 79—72859
- infinite elastic medium with cylindrical inclusion, external crack in torsion, stress distrib. 80—79216
- infinite elastic solid, with flat annular crack, axisymm. stress distrib. under torsion 77—23913
- infinite hollow cylinder with external crack, boundary value problem 78—90712
- infinite power law viscoelastic body, crack propag. by rigid wedge, stress intensity 80—64476
- infinite sheet, radial cracks from circular hole, stress intensity factor under tension, shear 78—34081
- infinite solid, elliptical crack under shear 78—75096
- infinite transversely isotropic medium with pressurised annular crack, stress distrib. 77—46973
- infinite transversely isotropic solid, containing penny-shaped crack, stress intensity factor 80—69738
- infinite transversely isotropic solid containing penny shaped crack, stress intensity factor *(French)* 80—43663
- influence function method, fracture mechs. and residual fatigue life anal. of power station cracked components 77—80109
- inhomogeneous layered medium, time-depend. behaviour of stress intensity factor after sudden crack appearance *(German)* 77—35085
- integral eqn. formulation for plane crack in free surface *(French)* 79—55338
- intensity factor determ., using numerical method *(Italian)* 80—14625
- intensity factors at arched crack tip, caustics method 80—19298
- intensive finite element grading for stress concs. 78—55587
- interactions on radial lines in infinite elastic plane 77—35083
- interface crack, incompletely open, nonoscill. singularities 78—59346
- interface crack, singularity anal. 80—10201
- interface crack, stress singularity 80—53707
- interface crack in a shear field 79—18828
- interface crack in bonded elastic half-planes 77—14952
- interface crack tip, adhesion loss model 80—38335
- interface cracks, periodic array, interaction anal. 80—10186
- interface edge cracks, energy release rate calc. based on M-integral 80—87742
- interface flaw extension with friction, basic mathematical anal. 79—18810
- interface penny-shaped crack, Fredholm integral eqn. soln. 78—90784
- isochromatic crack tip fringe patterns, dynamic 3-parameter method for stress intensity factors 80—38365

crack-edge stress field analysis continued
- isochromatic-fringe patterns, classification of stress-intensity factors 80—33527
- isotropic elastic half spaces with circular crack, stress at interfaces *(Russian)* 79—27582
- isotropic strip with transverse crack, Green's function for stress intensity coeff. *(Russian)* 77—35093
- J-integral, interrelation with crack opening displacement 79—50648
- J-integral appl. for stress intensity factors 79—81811
- J-integral values, determ. from notch testing of silicone rubber crack tip replica 79—52475
- kinked crack tip, elastic stress intensity factors 80—53709
- laminate, ±45°, multilayer hybrid-stress finite element analysis of through-thickness edge crack 77—54928
- laminated composite media, crack tip propagation, model by two-dimens. mixture theory 79—10528
- laminates, fracture, effect of adhesive layers 78—90791
- layered materials, stress free and problem, plane elastostatic problem, crack across interfaces 78—34076
- limiting stresses for brittle body with elliptical hole with edge cracks, diag. construction *(Russian)* 78—55600
- line crack subject to shear 78—79268
- linear elastostatics, combined boundary integral eqn./finite element anal. of cracks 77—72178
- LMFBR hexagonal ducts, cracking, effect on safety and fuel pin failure 78—17318
- loaded notch apex crack, tip intensity factor 77—62207
- local destruction near pointed inclusions, material struct. effect *(Russian)* 77—35630
- longitudinal shear crack, stress-deform. state near end *(Russian)* 78—22305
- magnetoelastic problem for soft ferromag. elastic solid with finite crack, linear theory 77—66410
- maximum energy release rate problem, explicit asymptotic soln. 79—77021
- metal elements, adhesively bonded, cracked or with discontinuities, analysis procedures 78—90793
- metal panels, adhesively bonded, cracked, fracture anal., crack tip stress intensity factors 78—90792
- method of potentials, appl. to fracture mechanics 78—51121
- misfitting elastic inclusion in infinite plane containing crack 77—65718
- mixed boundary-value problems soln. by direct variational method 78—83331
- mixed mode crack tip finite element 77—14962
- mixed mode stress intensity factor determ. from isochromatic fringe patterns, general method 79—77030
- mixed-mode stress intensity factors, photoelastic determ. method 79—18841
- mode I stress intensity factors, method of caustics 80—38364
- mode II fracture test specimen, boundary-collocation anal. and photoelastic expt. 77—50982
- mode III cracks, steady propag. followed by nonuniform growth, stress intensity factor 77—65716
- modified Dugdale model appl. to parabolic stress distrib. 79—41615
- moving crack tip energy flux density vector *(Russian)* 79—10532
- moving interfacial cracks, dynamic stresses, finite difference approx., iterative process 77—46966
- multiple crack interaction, effects on stress-intensity factor 77—62204
- near-tip elastodynamic fields, stress intensity factors 77—68535
- neo-Hookean elastic layer, Griffith cracks, plane strain problem 79—50666
- non-hardening material, under plane strain, stress distrib. around crack tip 80—10189
- nonlinear fracture mechanics, matched asymptotic expansions method, longit. shear of elastic-perfectly-plastic specimen 77—35087
- nonlinear fracture mechanics, matched asymptotic expansions method, longit, shear of elastic work hardening plastic specimens 77—35088
- notch fatigue cracks, propag. and initiation, elastic-plastic fracture mechanics 80—38329
- notch problems, book 78—94617
- notched member fatigue life predictions combining crack initiation and propagation 80—38328
- notched or cracked specimens, fracture criterion based on micro and macro crack mechanisms 80—1476
- nozzle corners, cracked, determination of flaw shapes, stress intensity distributions, using frozen photoelastic stress method 79—43547
- nuclear reactor Pilgrim I nozzle-to-press. vessel weld discontinuities, fracture mechs. anal. 77—80110
- numerical model analysis of stable crack growth 78—55596
- numerical solutions of three dimensional dynamic crack problems and simulation of dynamic fracture phenomena by a 'non-standard' finite difference method 79—41613
- opening mode crack problems, Westergaard method, critical re-examination 80—38337
- optically isotropic mats., stress intensity factor determ. by dynamic method of caustics 80—33546
- optically transparent materials, evaluation of elastic ratio by interferometry 78—90804
- orthogonal polynomial solns. to crack problems in linear elasticity 77—75857
- orthotropic laminate composite, broken layer 78—38254
- orthotropic laminate composite containing layer with crack, stress intensity factors 78—5694
- orthotropic sandwich plate containing part-through crack under mixed mode deform., stress intensity factors 78—34068
- orthotropic strip, internal and edge cracks 77—80114
- orthotropic strip with Griffith crack, stress and displacement fields 78—26087
- Paris differential eqn. for fatigue cracks, numerical calc. of eqn. parameters 78—63384
- part-circular cracks at various openings under complex loading conditions 80—30105
- penny shaped crack in inhomogeneous medium, high freq. torsional oscills. 78—26086
- penny-shaped crack, elastodynamic response in cylinder of finite radius 79—37240
- penny-shaped crack, interaction of longitudinal wave at interface of two bonded dissimilar elastic solids 80—33532
- penny-shaped crack, sudden twisting in a finite elastic cylinder, stress calcs. 78—67110
- penny-shaped crack in infinite viscoelastic medium 77—31254

crack-edge stress field analysis continued
- penny-shaped crack problem, deformed incompressible elastic solid 80—92085
- penny-shaped cracks, in elastic sphere embedding in infinite elastic space, thermal stresses 80—64460
- penny-shaped cracks, transverse tension, stresses, micropolar elasticity 80—64459
- perfectly plastic medium, elastic-plastic field at tip of steadily growing crack *(Chinese)* 80—58968
- perforated plate, stretched, cracks emerging from circular openings 78—51129
- periodic elastic inclusion-rectilinear crack system in isotropic medium 79—41619
- periodic semi-infinite cracks, Gauss-Hermite numerical integration 77—39260
- photoelastic determination, of mode I stress intensity factors 78—90781
- photoelastic isochromatic fringe loops use for stress intensity factor determ. 78—34097
- plane crack, in infinite solid, stress intensity factor under normal pressure 79—72855
- plane crack of arbitrary configuration in elastic medium, stress concentration coeff. *(Russian)* 79—81805
- plane crack of arbitrary shape, integral eqns. method of soln. 77—68530
- plane elastic crack, dynamics under variable loading *(Russian)* 80—79222
- plane elasticity, curvilinear crack edges concentrated forces and edge dislocations, numerical soln. 80—58970
- plane elasticity, periodic contact and crack problems, closed form solns. 77—42783
- plane isotropic elastic medium, photoelastic determ. of complex stress intensity factors 80—43664
- plane isotropic elasticity, crack stress intensity factors using singular integral eqns. 79—72858
- plane stress crack geometries, comparison of finite element and expt. studies 77—89069
- plastic asymmetric edge crack under longitudinal shear 77—80117
- plastic blunting at tip, relationship with J-integral *(Japanese)* 80—103414
- plastic crack in bending, tension, anal. 79—41623
- plastic deformation at the tip of an edge crack 80—69734
- plastic zones at crack tips during uniaxial deformation *(Russian)* 79—50655
- plasticity spread from stack of cracks, under tensile loading 77—46969
- plate, anisotropic, stress intensity factor for crack 80—48643
- plate, asymmetric crack branching under plane stress and loading 78—59344
- plate, circ., thin, elastic, containing Griffith crack, in infinite elastic medium, stress distrib. 79—32374
- plate, cracked, finite element technqiue for stress intensity factor computing 79—72854
- plate, elastic, containing through crack, skew symmetric loading, transverse shear effects 80—64478
- plate, elastic, under uniform twisting, periodic collinear cracks *(Japanese)* 78—67097
- plate, interference fit fastener-filled hole, stress intensity factors for through cracks 77—58609
- plate, laminated composite, notch tip stresses, experimental and numerical 79—77006
- plate, out of plane bending, steady state crack propagation, rotatory inertial effects 79—7340
- plate, semi-infinite with crack on end of stiffened edge, uniform tension 79—68659
- plate, state of stress and strain near crack vertex in nonlinear bending 80—5991
- plate, wide, analysis on crack in high strain zone *(Chinese)* 78—83326
- plate boundary and extension problems, stress intensity factors, finite element anal. 79—55341
- plate containing cracks, varying temp. cond. at edges, thermal conductivity and thermoelasticity *(Russian)* 77—23915
- plate structure, crack simulation computer program *(Japanese)* 80—79218
- plate structures, two-dimensional, computer program based on superposition method *(Japanese)* 78—51123
- plate with crack, effect of couple stresses in bending *(Ukrainian)* 77—31258
- plate with initial crack subject to extension, brittle fracture energy conditions *(Russian)* 80—103002
- plate with line crack subject to antiplane shear 80—14618
- plate with periodic system of internal parallel cracks with asymmetrical loading *(Russian)* 77—50988
- plate with transverse compression zone, crack arrest phenomena 79—4369
- plates, cracked, buckling under tension, finite element anal. 80—53666
- plates, thin, with a crack, strain edge dissipation rate evaluation 80—14623
- plates and tubes, thick-walled growth characts. of part-through cracks 77—58613
- plates under uniaxial load, optimum hole shapes, cracks and fracture appl. 80—64479
- plates with flows or cracks; twisting and bending theory 79—64545
- PMMA, craze zones at crack tips, validity of Dugdale model, comment 80—108535
- PMMA, craze zones at crack tips, validity of Dugdale model 80—108534
- PMMA, craze zones at crack tips at different temps., meas. correl. with Dugdale model 78—23826
- PMMA, indentation fracture mechanics 78—35490
- PMMA, methanol crazes, mech. props., craze-strain profile 78—72844
- PMMA bar, notched and perforated, fracture produced by longitudinal impact 79—43388
- PMMA biaxially stressed plate, fracture trajectories 77—70152
- PMMA plate with angled elliptic notch in tension, exptl. investig. 78—38257
- point loaded circular disc with two diametrical cracks 79—27589
- polycarbonate, bisphenol A, birefringent plates, cracks, stress intensity factors, refl. caustics method 80—93718
- polycarbonate, theoretical prediction of temp. rise at tip of running crack 80—2114
- polycarbonate of bisphenol bar, notched and perforated, fracture produced by longitudinal impact 79—43388

crack-edge stress field analysis continued
- polycarbonate plates, modified compact-tension specimens, dynamic anal. 80—97561
- polymer, principal stress distrib. meas. at running crack tip *(Japanese)* 77—42784
- polymer craze mechanics, elastic model 77—48519
- polynomial solutions for an ellipse on an anisotropic elastic half-space 79—10480
- polystyrene, n-heptane and methanol crazes, micromechanics 77—12680
- pop-in behaviour induced by crack interaction 77—54923
- porous elastic media, boundary-layer analysis of propagating mode II cracks 78—5696
- post-yield fracture mechanics to penny-shaped and semicircular cracks 77—54925
- power-law hardening material, pre-cracked plate, unstable fracture criterion 80—84238
- pressure vessel, crack initiation during thermal shock, warm pre-stress 78—41816
- pressure vessel nozzles, cracks, stress intensity factors, photoelastic anal. 77—80125
- pressurised cylindrical shell with clamped crack, stress intensity factors 77—80119
- pressurized pipeline, double cantilever beam, dynamic crack growth, finite element method 78—34080
- propagating interface crack, transition zone asymptotic fields 79—64587
- propagating rectangular fracture in semi-infinite elastic medium 78—57168
- propagation in system of parallel internal plano-circular cracks *(Russian)* 77—23916
- propagation through finite element mesh, nodal grafting method 77—75854
- quadrature rule for conforming quadratic crack tip elements 79—27587
- quadrupole trigonometrical integral eqn. soln., appl. to crack problems 79—72852
- quarter elliptical cracks in irregular bodies, exam. using finite element alternating method 78—90796
- quasi static crack growth, in sheet materials 78—67106
- quasibrittle body with internal determ. of crack growth kinetics and life expectancy 78—63383
- radial cracks emanating from outer and inner surface of circular ring, elastic anal. 79—68645
- radiation blistering, fracture model, stress fields around lenticular bubble 79—86823
- randomly heterogeneous body, shear crack propag. 77—54931
- reactor LOCA, crack extension limiting, warm prestress for small ΔT 80—27784
- reactor pressure vessel, stress intensities for nozzle cracks 78—70583
- reactor pressure vessels, 3D finite element anal. of surface cracks 79—10535
- reactor vessel nozzle cracks, stress intensity factors 79—15796
- rectangular orthotropic region, plane shear, stress free edge effects 79—18830
- rectilinear anisotropic material hybrid crack element 77—27492
- rectilinear anisotropic solids, mixed-mode crack anal. using conservation laws of elasticity 80—84239
- rectilinear crack, isolated, growing at const. rate under antiplane deform. conditions, dynamics 79—7338
- rigid indentation and plane crack extension 79—18835
- rim of semi infinite plate, crack originating from triangular notch under transverse bending 79—77009
- ring segments, radially cracked, displacement coeffs. from boundary collocation anal. 78—71298
- rings, cracked, Dugdale plastic zone sizes for edge cracks 79—72853
- rock, symmetrically extending plane crack, self-similar pressure profiles 78—69340
- rotating circular elastic disc, diametral edge cracks, stress anal. 79—32386
- round compact specimen, mode I stress intensity factor testing, boundary collocation method 78—27702
- rubber, peeling initiation and propag. 78—76824
- running crack tip, effect of strain rate depend. Young's modulus on stress and strain fields 78—75097
- running penny-shaped crack, elastodynamic stress field and bifurcation 77—14969
- semi-elliptical crack in finite plate, stress intensity factors *(Japanese)* 77—23914
- semi-elliptical fault fatigue propagation, three-dimensional anal. *(French)* 79—23283
- semi-elliptical surface crack in semi-infinite solid, stress intensity factors 80—84241
- semi-elliptical surface cracks in finite thickness plates, stress intensity factors 79—77013
- semi-infinite crack, kinking under dynamic loading conditions, elastodynamic stress intensity factors 79—68660
- semi-infinite crack, response to point forces 77—65719
- semi-infinite crack tips, practical evaluation of stress intensity factors 80—99962
- semi-infinite medium, transient thermal loadings, stress intensity factors 80—10193
- semi-infinite plate, crack from triangular notch 79—41570
- semielliptic notch with crack, micro- and macro-stress concentration correlation *(German)* 78—83330
- semielliptical surface cracks, stress intensity factors in bending *(Japanese)* 78—26089
- semiinfinite solid, stress distrib. near external crack 80—23954
- separation energy rate for crack advance 78—56765
- SH-wave diffraction by edge crack in elastic medium 79—64573
- shadow methods, reflected, transmitted, obs. of sharp V-notched plates, under pure bending 78—90777
- shallow shells, arbitrarily oriented cracks, stress intensity factor 79—7341
- sharp crack tip, reverse shear on inclined planes 79—77023
- shear crack, stress distrib., finite elastic anal. 78—51119
- shear loaded interface crack, friction effects, contact zones, stress fields 80—79225
- shear of infinite elastic space with plane crack *(Russian)* 77—75853
- shear wave scattering by cracks in elastic medium, stress intensity factors 80—74787
- sheets, semi-infinite, Dugdale plastic zone sizes for edge cracks 79—72853
- singular stress field at crack front edge in elastic body, crack propagation 79—50656

crack-edge stress field analysis continued
singularity analysis at elastic crack tip *(Chinese)* 79—94555
singularity at corner of wedge shaped punch or crack 78—83252
singularity at crack tip, order changing at discontinuity 78—59345
skew crack propagation, induced dynamic stresses, numerical soln. 79—1137
slab containing annular crack, thermal stresses, integral transform techniques 80—96229
slab with pressurised annular crack, antisymmetrical problem analysis 77—58599
slitlike crack arrays, plastic and strain hardened materials, fracture characts. 78—90798
soft ferromagnetic elastic solid, magnetoelastic interaction with penny shaped crack in const. mag. field 79—18829
solid rocket fuel propellant, modified propagation law 80—53712
solids weakened (strengthened) by inhomogeneity, tensile and compressive strength 78—42571
spherical crack in elastic space *(Ukrainian)* 77—68522
stable crack-growth, fracture criteria, numerical approach 78—67104
stacked stress concentrations in elastic solid, spread of plasticity 77—31259
state of stress, role in crack tip failure 80—106758
state of stress in vicinity of crack, approx. three dimensionsal 78—67135
steady crack growth with linear strain hardening, crack-tip fields 78—5695
steel, 0.40/0.50 C, crack growth, Weibull analysis 78—92319
steel, AISI 1018, dynamic crit. stress intensity vs. crack vel. 80—2115
steel, alloy A533B1, neutron irrad., flow growth characts. by acoustic monitoring 80—100918
steel, austenitic, reliability of stress intensity factor values 80—55530
steel, austenitic stainless, analysis of fracture surface in stress corrosion cracking *(Japanese)* 80—16573
steel, austenitic stainless, reliability of stress intensity factor values 80—55530
steel, austenitic stainless type SUS 316, low cycle fatigue tests, freq. effect on notch sensitivity at elevated temps. *(Japanese)* 80—104260
steel, C, crack initiation and propagation life under repeated impact tensile loads *(Japanese)* 80—104264
steel, C 0.75%, crack, with straight front perp. to wire under tension, strain energy release rate *(French)* 79—1136
steel, crack propagation stress wave obs. of brittle fracture *(German)* 77—56110
steel, effect of H_2 on phys. and mech. props. 80—101657
steel, eutectoid, fatigue crack tip props. in rotary bending and cyclic torsion 77—32668
steel, ferritic, cleavage fracture toughness, temp. and strain rate depend. 80—85028
steel, fracture toughness determination, from crack propagation measurements *(German)* 79—43421
steel, low C, low cycle fatigue, cumulative damage, absorbed plastic energy anal. 79—38932
steel, SAE 4340, depend. of fracture roughness on crack velocity 79—47772
steel, stainless, failure analysis at elevated temperatures 80—55499
steel, structural, slow stable crack growth, exam. of crack profile 78—84965
steel for nuclear reactor press. vessels, criteria for brittle fracture, neutron effects *(German)* 77—34389
steel plates, explosively clad, fatigue crack propagation behaviour *(Japanese)* 80—104262
steel-Al-steel plate, fatigue damage analysis and life predictor 77—25120
stiffened panels, stringers bonded to cracked orthotropic sheet, stress intensity factors 79—50647
stiffened panels with rectangular cut outs, stresses and deform. *(Japanese)* 79—3977
strain energy density and surface layer energy for blunt cracks or notches, book contrib. 78—94618
strain intensity criterion for crack branching in brittle mats. 78—55592
strain velocity effects on critical crack opening displacement 79—18818
strain-energy density factor, crack tip plastic zones 79—50654
stress and deformation field, for cracks with two and three corners 78—34087
stress corrosion cracking failure, predictive approaches 80—97611
stress distribution near a crack crossing an interface 79—81807
stress gradients, crack propagation and arrest 77—68527
stress inteisity factors, time depend., singular finite element 80—1471
stress intensity factor, simplified three parameter method 79—1138
stress intensity factor calc., infinite similar element method 78—79277
stress intensity factor crack opening displacement relationship for compact tension specimen 78—90778
stress intensity factor determ., accurate finite element method 77—54878
stress intensity factor for a crack at the edge of a loaded hole 80—10185
stress intensity factor for a flat elliptical crack in an elastic solid under uniform tension 79—27525
stress intensity factor for stress singular problems, energy convergence and eval. by mixed finite element method 79—23276
stress intensity factor from stress conc. factor, calc. 78—55588
stress intensity factors, anal. determ. by variational method for eccentric cracks 78—67115
stress intensity factors, modified Lobatto-Chebyshev method 80—99972
stress intensity factors, single-edge cracked bar loaded by in-plane transverse forces *(Chinese)* 78—83327
stress intensity factors, UNCLE finite element system calcs., appls. in fracture mechanics 78—67098
stress intensity factors by enriched finite elements 78—90774
stress intensity factors determ. from isochromatic fringe loops, three-parameter method 79—18843
stress intensity factors estimation, tensometric methods 79—32424
stress intensity factors for circumferential crack from notch in round tensile bar 79—41618
stress intensity factors for crack at edge of pressurised hole 80—33528
stress intensity factors for internal multiple cracks in thick-walled cylinders stressed by internal pressure using load relief factors 79—46261
stress intensity factors for self similar cracks derived from path independ. integrals 79—23213
stress intensity factors for semi-infinite crack under 3-D loading 77—80115
stress-hardening material, ductile fracture, J-integral estimates 77—89064
stretched finite elastic strip, central crack dynamic response 79—18826

crack-edge stress field analysis continued
strip, elastic, Griffith crack interactions, mixed boundary value problem 80—58969
strip under residual stress, crack-contact and free-end problem 77—65720
strip under three-point load, integral transform method 77—72244
strip with crack, coefficient of stress intensity at end of crack, reinforcing half-planes *(Russian)* 77—14951
strip with semi-elliptic notches or cracks, stress anal. by rational mapping function 79—14257
subcritical crack growth depend. on effective stress intensities 78—56726
surface crack in a clamped circular plate subjected to uniform lateral pressure, bending stress anal. 80—74811
surface cracks, formation during uniaxial extension, development rules *(Russian)* 80—1477
symmetrical pair in circular disc, stress and crack energy 78—46914
symmetrically branched crack, infinite elastic medium, stress intensity factors at tips 77—14970
tensile fracture stress pulse emission in glass rods 77—15486
tensile strips, Dugdale plastic zone sizes for edge cracks 79—72853
thermal stress singularities at crack tips, effect of insulated circular hole 77—68525
thermal stresses in elastic plane with circular boundary and thermally isolated cracks *(Russian)* 78—55599
thermoelastic cracks in plane, boundary integral eqn. method *(German)* 80—106761
thermoelastic problem for a half-plane with an internal line crack 79—32259
thermoelastic semiinfinite solid with heated boundary, thermally insulated line crack 78—55610
thermoelasticity, anisotropic, crack problems, temp., displacement, stress field 77—80105
thick walled cylinder, internal or edge crack, stress intensity factors 79—18827
thick walled tube in tension, stress intensity factor of annular cracks 77—62214
thin elastic plate, bending problem soln. in fracture mech. using specialized finite element technique 79—77011
three dimensional anal. using integral equation system 77—46968
three dimensional cracks, stress intensity factors 78—55601
three dimensional structures, finite element technique for stress intensity factor computing 79—72854
three-dimensional crack anal. by finite element method 78—83332
threshold for cracking after overloadings, rel. to efficient stress intensity factor *(French)* 77—72247
tip opening displacement by finite element anal. *(Czech)* 78—59343
trajectory, unstable crack extension 80—64462
transitions elements for use with quarter point crack-tip elements 78—63376
transversely isotropic composite with penny shaped crack, stress intensity, crack energy 79—98660
transversely isotropic cylinder, thermal stresses for penny-shaped crack 77—89070
transversely isotropic solid, penny shaped crack, stress anal. 80—92083
two bonded elastic solids interface, penny shaped crack, torsional wave interaction 80—64484
unbounded body, weakened by circular cracks, elastic equilib. 80—53717
US caustics in non destructive evaluation, diffraction at crack like defects 80—43680
vertex stress of quarter-infinite crack in half-space 77—46970
vertical crack inside semi-infinite plane, stress-intensity factors 77—3772
viscoelastic, crack growth relations, for orthotropic, prestrained media 78—90772
viscoelastic cracked linear bodies, stress and strain under tension and compression 77—7342
viscoelastic medium, linear, semi-infinite crack propagation, tip stresses and displacements 80—53700
void growth, coalescence, ahead of moving crack tip, finite element anal. 78—1609
weakening of an elastic solid by a periodic array of penny-shaped cracks 79—68658
wearing half-space, determ. of stress intensification factors 80—99964
wedge, symmetric cracking by transverse displacements, stress intensity factors 80—79226
wedge loading of a semi-infinite strip with an edge crack 78—79270
wedge opening load specimen, side grooved, stress intensity factor soln. and calibration 78—51130
wedge shaped crack, apex singularities under all modes 80—64480
wedge shaped crack or inclusion, stress singularity at corner 79—46268
wedge symmetric cracking by concentrated loads 77—19568
wedge-shaped crack plastic zone, superdislocation model 79—94557
wedged crack, propag, data with static compliance calibration 80—2115
weight function calcs. from stress intensity factor 78—55591
weight function concept, crack closure method, method, stress intensity factors calcs. in plane or axisymm. problems 78—67102
weight functions from virtual crack extension 80—10188
Westergaard equations for expt. evaluation of stress intensity factors, limitations 77—7345
work-hardened material, elastic-plastic stress distrib. near flat surfaced notch with cycloidal tip 77—35084
yielding on inclined planes at crack tip 80—33525
yielding on inclined planes at tip of crack loaded in uniform tension 77—42780
yielding on inclined slip planes at crack tip 77—42781
Al alloy, 7175 T 651, crack tip opening under cyclic loading, effect of environmental and R-ratio 80—45377
Al alloy, type 7175 T 651 *(French)* 80—65145
Al alloys, fatigue crack propagation rates, stress intensity factors *(French)* 77—25154
Al alloys selection using fracture mechanics 78—56725
Al, fatigue crack propagation rates, stress intensity factors *(French)* 77—25154
Al-Zn-Mg-Cu-Cr, (5.6, 2.5, 1.6, 0.3 wt.%), alloy 7075, plates, adhesively bonded, exam. of fatigue crack growths 78—92348
Al_2O_3-SiO_2 glasses, thermally toughened, residual compressive stresses evaluation 78—31523
B fibre reinforced epoxy laminate, energy release approach for stable crack growth in free edge delamination problem 78—19878
B reinforced Al laminates, applic. of linear elastic fracture mechanics 77—28893

crack-edge stress field analysis continued
- Cu high purity, low cycle fatigue, cumulative damage, absorbed plastic energy anal. 79—38932
- LiF, dislocation mobility near fast-moving crack tip 78—47389
- Ni, H diffusion, trapping and mobility near vacancies, dislocations and cracks 80—49426
- Ti-Al-V (6,4 wt.%), dynamic crit. stress intensity vs. crack vel. 80—2115
- Ti-V (40 at.%), microcracks intersecting fatigue crack, exam of origin 78—80638
- WC-Co alloys fracture, spatially constrained crack tip opening displacement 77—77580
- Zr-Nb (2.5 wt.%) pressure type rel. between stess intensity factor, crack opening displacement and J-integral 80—100920
- ZrO_2 microsphere stabilised ceramic, fracture characts., thermal stability *(Russian)* 80—76335

crack inspection *see crack detection*

crack-tip stress field analysis *see crack-edge stress field analysis*

cracking *see fracture*

cracks
- *see also crack detection; crack-edge stress field analysis; crazing; fatigue cracks; penny-shaped cracks; stress corrosion cracking; thermal stress cracking*
- β-eucrypite, glass-ceramics, internal stresses 79—15770
- β-spodumene, glass-ceramics, internal stresses 79—15770
- Γ-shaped crack elastic energy evolution rate in laminate determ. by pliability vibr. meas. 78—83348
- acoustic emission from a brief crack propagation event 79—64397
- adsorbed molecule vibr. excitation due to plastic deform. accompanying fracture 77—15488
- aircraft parts, microfractographic fracture analysis exam., SEM exam. *(Japanese)* 78—52950
- β-Al_2O_3-Na_2O, geometrical aspects of breakdown, TEM study 79—79096
- Al alloy 2024-T81, adhesive bonded multi-ply laminate, effective remote stresses and stress intensity factors 77—73328
- alabaster, US waves in crack preparation region rel. to seismic waves 77—9405
- alkali halide crystals, defect state change during electrolysis 78—95057
- alkali halides, cryst., optical emission following pulsed 10.6 μ irrad. 79—28847
- alkaline silicate glass, surface layers, plasticity and microcrack formation, electron microscopy *(German)* 80—40469
- alloy B95T1 with surface cracks, fracture toughness determ. *(Russian)* 77—25141
- alumina, polycryst., compressive strength, microplasticity 77—36620
- alumina, polycryst., crack resist. and sub-crit. crack extension 78—19874
- alumina, polycrystalline, subcritical crack extension and crack resist. 77—8911
- amber, natural, optical strength and laser induced rupturing 78—7039
- ammonium tartrate, triboluminescence and cryst. fracture dynamics 80—50437
- amorphous thin films, crack networks of voids 78—2399
- anisotropic elastic slab, stress field and crack energy 77—50908
- anisotropic material, stress intensity factor near crack type defects 78—38255
- anisotropic slab, thermoelastic crack problem 80—23960
- anisotropic solids, cracks, interaction energies 77—80576
- annular, crack resistance, characteristics correlation of material α_p and γ 80—21075
- annular pressurised crack in transversely isotropic slab 77—72236
- antiplane strain, crack at boundary between two materials with branch into one of them 80—79231
- anvil, truncated, compressive strength, high press. apparatus appl. 78—84906
- Araldite B, crack arrest toughness determination 78—72867
- Araldite B specimens, dynamic fracture toughness, influence on dynamic crack propag. 80—99966
- arrest, concepts, appl., review 79—41621
- arrest, sudden, steadily moving 77—44363
- articulated medium, elec. and thermal cond. anisotropy, crack density tensor 77—55505
- asbestos cement, resistance to crack growth 79—29185
- automotive materials, microfractography appl. to ductile failure, brittle fracture, crack studies 77—56199
- axisymmetrical homogeneous elastic solid with internal circular cracks, energy release rates 78—67139
- bar, rectangular, torsion crack problem, harmonic function continuation technique soln. 80—99969
- Barre granite, crack growth and development during creep 79—84237
- beam, cracked, dynamic weight function from finite element soln. 80—79234
- beam, cracked, transverse loading by stamp, stress and fracture anal. 80—10187
- beam, double cantilever, dynamic crack propagation modelling, 1D anal. validation 79—72857
- beams, effects on bending frequency *(Japanese)* 77—27487
- beams in pure bending, distributed damage theory, cracks, fracture 80—64474
- bending induced edge cracks, growth rate in acoustically excited panels 78—5697
- biaxially fibre reinforced composites, two dimens. mixture theory, dynamic crack appl. 78—87301
- bimaterial full-plane with crack at any angle to interface 77—14965
- birefringent plates, cracks, stress intensity factors, refl. caustics method 80—93718
- body loading with cracks, energy conditions for brittle failure *(Russian)* 80—96234
- body with period system of cracks laminar plastic zone development during longitudinal shear *(Russian)* 77—68442
- body with thermally insulated cracks, periodic thermoelastic situation 77—68417
- bonded dissimilar half planes having Griffith crack at interface, elastic wave interaction 78—67091
- bonded ductile half planes, plastic yielding through interface from cracks under antiplane deformation 77—14960
- bonded orthotropic strips with cracks, elastostatic problem 79—81809
- bone, compact, fracture mechs., effects of density and specimen thickness 78—3534
- bone tissue, human, subjected to longit. extension, acoustic emission 77—25495

cracks continued
- borosilicate glass, microparticle impact, high speed photography obs. 78—44223
- borosilicate glass surface, damage due to impact of small glass and steel spheres 78—52994
- bounded elastic body containing a crack, mode 1 deform., integral eqn. soln. 79—3976
- branched, growth determ. by numerical methods 79—68649
- branched crack, under biaxial stress 78—67125
- brass, crack opening displacement, rel. to flow stress 78—68810
- brass, fracture initiation and propagation during strip drawing 78—64663
- α-brass, plane stress ductile fracture, prestrain effects 80—108532
- brass 70/30, fatigue crack propagation, effect of stacking fault energy as deduced from dislocation patterns, TEM study 79—61719
- brittle elastic body, stability and post-critical growth of system of cooling or shrinkage cracks 80—1486
- brittle fracture, precedence of stability loss near crack *(Ukrainian)* 79—77007
- brittle fracture, statistical theory, dislocation mechanism, crack propagation *(Chinese)* 80—106755
- brittle fracture, structure design, method of calculation 78—72869
- brittle material, compressive strength, statistical and micromech. theory 78—64618
- brittle material, dynamic solid particle damage, elastic and elastic-plastic response regimes 77—8910
- brittle material, fast crack propagation, computer simulation 80—38331
- brittle material, phase transform., plane stress anal. 77—86024
- brittle material under compressive load, crack extension from flaws 78—95812
- brittle materials, crack interaction effects on critical stress for fracture propag. 79—25234
- brittle materials, crack jump determ. from specific failure and elastic energy 79—87712
- brittle materials, grain size dependence of microcrack initiation 80—40505
- brittle materials, influence of structural parameters on fracture toughness 79—96133
- brittle materials under complex loading systems, design parameters 79—38917
- brittle porous materials, critical stress and crack size evaluation *(Russian)* 78—35494
- brittle rupture in solid body, distribution function at threshold *(Russian)* 77—84192
- brittle solid, crack system propagation, stability conditions 78—51131
- brittle solids, unstable growth of tension cracks 80—106756
- built-up edge form., direct SEM obs. 80—104303
- bulk constitutive relations for cracked materials 80—8790
- bulk crack propag., use of partial props. in coarse two-phase materials 80—108531
- butadiene, stressed, microcrack generation under const. elongation, struct. depend. 77—90459
- butadiene-nitrile, stressed, crack generation under const. elongation, struct. depend. 77—90459
- BWR, Dodewaard, fuel pin failures 77—67834
- BWR fuel rod relocation, gap conductance anal. 80—83192
- calcite, crack propagation obs. 77—73725
- cap, cracked, transverse shear and material orthotropy effects 80—10144
- capacitance, mech. loads effects 80—84242
- case hardened components, exam. of fracture surface by TEM. *(Japanese)* 78—52949
- castings, economic testing by mag. powder method *(German)* 80—3277
- caustics equations for dynamic plane elasticity problems 80—43669
- cement, hardened paste, internal stresses and microcrack form. caused by drying 78—92325
- cement, Portland, static and fatigue cracking morphology, SEM obs. 77—52493
- cement and mortar, flexural strength, loading rate effect on crack growth 77—77556
- cement paste, direct tensile tests and tied crack model 78—11306
- cement paste, direct tensile tests and tied crack model 78—11307
- cemented carbide, simple evaluation method 77—32748
- ceramic, strength recovery by diffusive crack healing 77—77555
- ceramic, stress intensity factor estimates for a peripherally cracked spherical void and a hemispherical surface pit 79—29196
- ceramic composite, toughening by oriented nucleation of microcracks 77—8921
- ceramic material fracture mechanics, n review 80—45373
- ceramic multilayer capacitors, fracture mechanics approach to structural reliability assessment 80—89328
- ceramics, coarse-grained, dimensional anal. of grain size depend. of fracture strength 80—70299
- ceramics, crack extension micromechanisms, review 80—108567
- ceramics, crack propagation, microstructural aspects 79—15771
- ceramics, fracture mech., probability, micromech. models of crack growth 80—108571
- ceramics, microcracks, and thin intergranular films obs. by TEM 80—68295
- ceramics, polycrystalline, fracture mirror form. 77—48541
- ceramics, polycrystn., strength-grain size relations 79—79081
- chemically assisted fracture, atomic models of crack growth 80—64466
- chemically assisted fracture, general reaction rate theory and thermodynamics 80—64465
- chevron notched short bar specimens, compliance and stress intensity coefficients 80—96232
- circular crack under general asymmetric loads, related integral eqns. 80—64483
- circular elastoplastic torsional shaft, crack tip plastic zone propag. 80—48649
- circumferentially notched tensile specimen, finite element anal. 78—67150
- citric acid monohydrate, triboluminescence and cryst. fracture dynamics 80—50437
- cladding, cracks under stainless steel cladding of pressure vessel, detection, causes, danger 80—52760
- cleavage crack extension, discreteness of atomic struct. effect, one dimensional model 77—81314
- cleavage crack tip lattice trapping, relation between macroscopic and microscopic thermodynamic surface energies 80—59572
- closed crack tip terminating at interface, asymptotic anal., friction effects 79—64595

cracks continued
  closed cylindrical shell with insulated cross crack *(Ukrainian)* 78—90638
  closed cylindrical shells, crack propagation criteria 80—38341
  closed cylindrical shells with longitudinal cracks, limit equilib. criteria *(Ukrainian)* 79—50646
  coal, permeability to methane, influence of temp., geostatic and stratal press. *(Russian)* 79—66695
  cohesive strength of constructional components with crack-type defects, stress intensity coeff. *(Russian)* 78—30234
  cokes, metallurgical, struct. and strength 80—93610
  combined mode cracks, energy fracture criteria, complex variable method 79—27596
  combined mode cracks, fracture criteria 78—79285
  compliance, review and extension of information for common crack growth specimens 79—3974
  composite, brittle particulate, fracture, theoretical aspects, crack-front interaction with pores 79—70156
  composite, crack extension micromechanism 80—108566
  composite, crack propag. *(Russian)* 77—25147
  composite, laminate, crack normal to interface, impact response 80—14628
  composite, layered, Love wave diffr. by stress-free crack in plane interface 80—33501
  composite, metal-based fibre-type, designing for structural integrity 79—83155
  composite elastic media, crack retardation at boundary *(Russian)* 79—23275
  composite fracture with bonding strength defects between components, computer simulation 80—11771
  composite laminate in combined stress state, fracture models 80—10211
  composite material, longitudinally cracked, exam. of plane deformation 78—67096
  composite material strength criteria 80—10208
  composite materials, fracture, elastic mismatch and interfacial bonding influence 80—40506
  composite materials, fracture kinetics 80—11770
  composite materials, fracture mechanics 80—10202
  composite mode cracks, K_I-K_{II}, brittle fracture study *(Chinese)* 80—55494
  composites, micro- and macro cracks 80—11767
  composites with stress gradients, failure anal. 80—10199
  compressed crack development at circular inclusion boundary with elastic medium *(Russian)* 79—46265
  compression failure anal., glassy materials investigation 78—55608
  concentric circular arc cracks in anti-plane strain, screw dislocation pile-up model 77—54927
  concrete, crack propagation, uniaxial compressive stress *(Japanese)* 78—11330
  concrete, interaction of matrix crack and aggregate particle 79—79076
  concrete, microcrack phenomena, geometric probability calcs. 79—57091
  concrete, reinforced cross-section, reponse to short-term and sustained loads 79—52358
  concrete, US wave propag. and microcracking *(French)* 80—39225
  conic-section simulation finite element anal. 77—3773
  continuous beams with concrete slabs under load, method for crack prevention in slab *(Japanese)* 80—83760
  continuous growth or quantized growth steps 79—32377
  continuous plastic cracks in ordered alloys, discrete dislocation analysis 78—80625
  continuum mechanics, non-local, at atomic scale 78—12563
  corners and cracks, finite element approx., hybrid finite elements 79—64585
  corundum, mech. strength rel. to tension intensity factor *(Polish)* 80—11725
  couple stresses effect on crack tip 78—18240
  covalent crystals, nanosec. electron beam effects, size depend., Ioffe effect 80—88211
  Cr film, vacuum deposited, macrostruct. due to intrinsic stress, cracks following scratches in substrates 78—6238
  crack, dislocation model of plastic zone 77—84837
  crack branching, elastodynamic effects 78—67113
  crack growth, 3-D geometric effects, implications for composite material structures 80—10204
  crack propagation, fracture viscosity and plastic flow calc. *(German)* 77—54934
  crack tip disintegration by strong EM field 78—83339
  crack tip integral for non-elastic materials 77—68528
  crack tip mixed mode isochromatic fringe patterns 80—28464
  crack tip opening displacement, rel. to J-integral, discussion *(Chinese)* 78—83328
  crack tip plasticity, inclined strip yield superdislocation model 77—68526
  cracked elastic body statics, three-dimensional problem *(Russian)* 78—73858
  cracked elastic surface layer bonded to half-space, fracture anal. 79—27586
  cracked thick walled cylinder, elastic plastic fracture anal. under displacement controlled loading 78—67119
  crater form. at tip, under powerful local electromagnetic field *(Russian)* 77—70149
  creep crack growth, appl. of fracture mechanics 78—18237
  creep crack growth, diffusion and deformation controlled 80—79867
  creep crack growth initiation theory 77—58604
  creep crack propag. anal. on basis of plastic singular stress field 79—68647
  creep crack propag. by cavitation near crack tips 80—107364
  creep fracture model, plastic growth of cavities at tip of grain boundary wedge cracks 77—52446
  critical opening, determ. in fracture toughness testing *(Russian)* 79—52479
  critical opening calc., improved method 77—3780
  critical opening displacement *(Czech)* 77—70164
  critical size for accidental loading *(Russian)* 80—53704
  cropping and blanking, plastic flow, fracture, crack propagation 80—74761
  cross-plied factors controlling transverse cracking 77—77566
  crystal cleavage due to dislocation tilt wall splitting 78—91377
  cubic single crystals, hardness meas. by spherical indentation 80—16622
  curved crack propagation 80—1485
  curved macro-element for cracks and corners 80—33448

cracks continued
  curvilinear crack along the interface of two plane isotropic elastic media 79—37246
  curvilinear crack theory *(Russian)* 79—46266
  CVD coating, crack and pore imaging by electrographic printing 80—34333
  cylinder, finite, of anisotropic material, thermal stresses due to thermal crack 77—39233
  cylinder, hollow with external annular crack, bending, stress intensity coeff. *(Russian)* 79—27537
  cylinder, thick walled, stability loss and crack formation in failure *(Russian)* 79—77016
  cylindrical ingot, continuous casting, elastic-plastic temp. stresses and deformation *(Russian)* 79—61576
  cylindrical shell, circumferentially cracked, transverse shear effect 80—28472
  cylindrical shell mixed boundary value problem, integral eqn. 77—35
  cylindrical shells, anal. of through cracks by quarter point elements 79—72856
  cylindrical specimen with external crack reaching surface of annular stress concentrator, tension and bending 79—14349
  damage model, crack growth and instability 79—41614
  damage model of creep-fatigue interaction 79—77008
  damage rupture, phenomenological approach to plasticity, creep and fatigue *(French)* 79—37245
  DBCS model under biaxial modes of loading, crack separation energy rate 79—81814
  DCB specimen, fast fracture simulation using Kanninen's model 78—19866
  Debonding of circular second phase particles 78—5688
  defect dimension determination by acoustic emission 80—104381
  defected stripe, current crowding and flux divergence 78—71885
  deformable body with central vertical crack, destruction in homogeneous force field *(Russian)* 79—27554
  deformable solids, fracture and hardening kinetics 80—35210
  deformation and fracture of materials in creep range, effects of nonlinear stress-strain rate relations 80—58938
  delamination failure mode of composite bars in compression 80—11772
  delamination wear, mechanics of crack propag. 78—3231
  dental amalgam, exam. of fracture toughness and critical strain energy release rate 78—48933
  deposited film thickness and grain size determ. on non-conductive SEM specimens 78—77170
  depth measurement, ultrasonic techniques, review 78—95903
  development kinetics, with varied rigidity under low cycle loading 77—90464
  development resistance anal., stereoscopic fractography anal. 79—90189
  diamond, brittle failure due to liq. Si, SiC layer form. in cracks 77—15720
  diamond, mechanical strength depend. on thermal working parameters, microcracks *(Russian)* 80—55501
  diamond, optically active centre effect on strength props. 80—40462
  diamond subsurface damage exam. using cathodoluminescent mode of SEM 77—80398
  differential geometry of fracture 79—27581
  diffraction by a crack of a cylindrical longitudinal pulse 80—92082
  diffraction of simple harmonic waves by Griffith cracks in infinite nonhomogeneous elastic medium 77—54913
  diffusion of H_2 towards crack in stressed solid, eigensoln. 77—24446
  diffusional growth of intergranular cavities in uniform stress field and ahead of crack-like stress concentrator 80—107366
  diffusive growth in plastically deforming solid 79—20182
  directivity pattern of radiation 78—87305
  disc, circular, linearly elastic, radial edge crack, const. internal press., stress anal. 77—54932
  discrete dislocation anal. 79—64590
  discrete dislocation analysis 80—84236
  dislocation distrib., fracture relation, plastic flow at crack tip, slip line theory 80—64482
  dislocation layers and crack problems in elasticity theory 80—33533
  dislocation model for interaction between tensile crack and hole 78—67092
  dislocation struct. effect on motion 77—86182
  dislocation theory for stress intensity factors around a crack tip 80—69741
  dispersed fracture of unidirectional composites 80—11768
  dissolved species, advection-diffusion eqn. in pulsating crack 80—96312
  double cantilever beam, dynamic stress intensity factors computation and crack arrest stress intensity factors 78—34088
  double cantilever beam, fracture behaviour, quasistatic energy anal. 79—18817
  double cantilever beam crack propagation specimen, simple model 77—68531
  doubly-periodic array of cracks in an infinite isotropic medium 78—87303
  dual elastic continuum model of media with quasicracks, tensional medium with mobility effects 77—72153
  ductile crack extension, hybrid displacement finite element model 80—28471
  ductile fracture surfaces, statistical characts. of microcracks *(Russian)* 78—23807
  Dugdale, in material with continuous damage form. 78—18234
  Dugdale model solution, of cracked bodies, finite element analysis 78—67116
  Dugdale model validity limits for thin cracked plates under biaxial loading 80—43667
  dynamic crack behavior at initiation 80—7676
  dynamic crack propagation and arrest 78—68758
  dynamic finite element analysis of cracked bodies subjected to impact loading 80—69742
  dynamic fracture toughness, influence on dynamic crack propag. 80—99966
  dynamic shear crack propag. mechanics, earthquake source model 79—84147
  dynamic thermoelasticity of body with crack, two- and three-dimensional *(Russian)* 77—68400
  dynamically loaded in strain rate sensitive materials 78—60820
  earthquakes stress relaxation models, finite difference calc. of crack propag. 77—73682
  elastic bimaterial problems and cracks, integral equations 79—44741
  elastic body, crack dynamics *(Russian)* 80—1480

cracks continued
- elastic body, dynamic crack system interactions, elastic antiplane deformation conditions 78—9609
- elastic body with crack-like inhomogeneities, influence on effective mech. characts. *(Russian)* 78—26088
- elastic body with plane cracks of normal fracture, 3D problems *(Russian)* 80—79219
- elastic cracked members, anal. by optimisation techniques 80—1470
- elastic dielectric, EM wave effect on displacement field of crack 78—30231
- elastic equilibrium of a wedge with a crack 80—69733
- elastic fracture mechanics, power type singularities analysis, using finite elements 77—80106
- elastic fracture mechanics problem, two-dimensional, Green's function method 79—23272
- elastic fracture of solids containing arrays of cracks 80—1473
- elastic isotropic dielectric medium with crack, EM wave diffr. 78—26084
- elastic layer containing cylindrical cavity, stress distrib. near external crack 77—72171
- elastic material, finite element anal. of crack problems 78—67146
- elastic medium, crack propag. in dynamic thermoelasticity *(French)* 80—38327
- elastic medium, opening of two coplanar Griffith cracks 79—32379
- elastic plane, stress-strain state at brittle crack vertex, geometric nonlinearity effects *(Russian)* 80—79221
- elastic plane wave scatt. by crack of finite width 77—80092
- elastic plate, crack closure in bending, sixth order anal. 80—96231
- elastic plate with unsymmetrical cruciform crack, stress distrib. 77—31256
- elastic solid with annular crack, bending effect 79—72806
- elastic strip, arbitrarily oriented, crack distrib. *(Russian)* 78—63378
- elastic strip debound dynamics, simple transient motion 78—67040
- elastic strip with isolated crack, equilibrium 80—14620
- elastic surface wave guidance by stress free crack 79—46250
- elastic wave scattering, crack characts. using quasistatic approx. 79—37241
- elastic-perfectly plastic material, theory of stable crack growth 78—79272
- elastic-plastic anal. of asymmetric cracked specimen under longit. shear 77—14954
- elastic-plastic crack problem, comparison of finite element soln. 78—79263
- elastic-plastic fracture mechanics, crack separation energy rates 78—46915
- elastic-plastic fracture mechanics for structure design 77—14961
- elastic-plastic media, invariant integral in crack theory 77—14966
- elasticity, crack energy in initially stressed neo-Hookean anisotropic infinite medium 80—48642
- elasticity parameters, calc. for cracked material 79—55346
- elasticity plane problem formulation using dislocation layers, contact and crack problems 79—64507
- elasticity theory for body with curvilinear cracks, integral eqn. construction, two dimensional problem *(Russian)* 77—27490
- elasto-plastic stress and strain in cracked bars under torsion and shear 79—68654
- elastodynamic anal. by finite element method using singular element 78—55603
- elastodynamic diffraction, two-dimens., by cracks, matched asymptotic expansions 80—1468
- elastodynamics, longit. wave diffr. by semi-infinite crack, geometrical theory 77—46829
- elastoplastic bodies with cracks in complex states of stress, limiting equilib. 80—53715
- elastoplastic body, tensor dislocation density near crack vertex 78—26090
- elastoplastic fracture mechanics, finite element analysis *(German)* 77—54935
- elastoplastic solutions, theory of cracks, special characts. *(Russian)* 79—32375
- elastostatic problems, three-dimens., mode I loading, soln. method 80—92086
- electrical conductivity of cracked solid 79—91117
- electrical determination method of crack fronts in metallic parts *(French)* 79—77037
- elliptical crack section, line singularity fields 77—51433
- elstic-plastic crack and hole interaction in elastic medium under uniform shear load 78—51117
- EM field effect on crack propagation in elastic dielectric 79—68576
- energy release rates calc., inverse flexibility method 79—41617
- epoxide resin, amine-cured, crack propag. 78—27596
- epoxide resin, low temp. crack propag. 80—85020
- epoxy composites, dynamic crack propag. 80—40497
- epoxy materials, crack blunting mechanisms 80—66624
- epoxy polymers, high temp./press. materials test for undersea environment 78—3213
- epoxy resin, crack propagation, photoelasticity investig. 79—8341
- epoxy resin, thermoelastic stress creation and motion picture recording of interaction with dynamic crack 78—56697
- epoxy resin adhesives, crack propag. and mech. props. 78—68783
- epoxy resins, crack propag. stability, effects of water, temp., specimen geometry, hardener 78—11324
- equilibrium and kinetic aspects of brittle fracture 78—79271
- equivalent inclusion method for a three-dimensional lens-shaped crack in anisotropic media 78—67123
- ethylene-propylene rubber, highly deformable, fracture surface roughness 78—44197
- expansion process, associated differential geometry 79—67159
- explicit finite difference method, anal. of dynamic crack and fracture 77—75860
- extension, initial stage in time depend. and/or ductile fracture 78—67107
- extension angle, influence of specimen's geometry 80—99965
- extension calc. *(Chinese)* 80—19279
- extension criterion *(Chinese)* 78—13971
- extension due to nonuniform internal press. 78—51124
- extension due to rigid inclusions 79—81812
- extension forces in elasto-plastic stress fields 78—18250
- exterior interface cracks, shear and tensile tractions, stress anal. 80—58971
- external, crack extension condition derivation, non uniform pressure, using dislocation approach 79—68657
- failure analysis, ductile crack growth 79—90724
- failure criterion considering stress state at crack apex 79—57113

cracks continued
- failure kinetics and stability 77—883
- failure through crack growth, discussion of different stages 77—68536
- femoral bone, bovine, slow fracture propagation obs. 79—79592
- ferroconcrete, cracked, strain meas. *(German)* 79—34275
- ferromagnet, single domain, isolated pores and brittle cracks *(Russian)* 78—39381
- ferromagnetic solids, magnetomechanical effects, magnetostriction, hysteresis, stress, yielding, fatigue damage, crack growth *(Polish)* 80—71150
- fibre fracture, in composites, influence of cracks 79—79039
- fibre reinforced composite, energy release rate for cracks 77—66690
- fibre reinforced composite, fibre geometry and filler vol. influence on fracture stresses 80—45397
- fibre reinforced composite, initial yield surface, in plane stressed state 77—86106
- fibre reinforced composite, with additional matrix toughening component, crack growth 77—56076
- fibre reinforced composites, brittle zone on fibre surface, deform. and fracture 77—56104
- fibre reinforced composites, crack growth 80—10212
- fibre reinforced composites, cracking and fracture, review 78—60772
- fibre reinforced composites, micro- and macrocracks 80—65148
- fibre reinforced composites, unidirectional, anal. of cracks emanating from circular hole 80—100301
- fibre reinforced composites, weakened by periodic system of cracks, longitudinal shear 80—35323
- fibre reinforced plastics, creep damage *(Japanese)* 77—32702
- fibre reinforced polymer, pressurised wound tube, failure from longitudinal defects 77—16660
- fibrous composite, short steel wire reinforced (polymer impregnated) concretes, cracking and toughening 78—80626
- fibrous composite, thermal crack propagation anal. 80—10205
- fibrous cracking, COD and initiation, replication technique 77—56069
- fibrous laminated composite, tensile failure, quantitative fault tree anal. 77—59891
- fibrous media, crack interactions 80—10203
- filament-wound pipe, microscopy of failure mechanisms 79—24604
- fine relaxation crack form. along compressive max. shear crack 79—23281
- finite antiplane shear field near crack tip in elastic solid 78—18245
- finite centre crack specimen, biaxial and nonlinear effects on energy release rate, J-integral 78—18232
- finite element anal. of problems with non-removable singularities 77—72250
- finite element model of crack movement with fracture propagation *(Russian)* 79—77017
- finite plate with circular hole, summary of SIF design graphs for cracks 79—23278
- fission reactor cladding, power ramp investigations, clad hoop strain and pellet clad interaction 80—16440
- fission reactor fuel rod hairline cracks, effect on thermoelastic stress in surrounding can, iterative method of determ. 77—54285
- fission reactor pressure vessel and circuit development, conf. report 80—47541
- fission reactor pressure vessel safety and reliability evaluation, two-criteria approach 79—18016
- flat elliptical crack, behaviour in an anisotropic elastic body 79—7336
- flaw size measurement, nondestructive evaluation 80—71855
- flawed elastoplastic structure, method of lines applied to crack problem 79—46259
- flaws, 2D, irregularly shaped, fracture mechanics transfer function 80—99970
- fluoroplastics, mech. props., accumulation of submicrocracks, thermal treatment effects 77—4850
- fracture, appl. of continuum theory of dislocations fracture mechanics 78—67767
- fracture, chemically-assisted, atomic modelling at crack tips 80—106754
- fracture, post-yield, numerical investigation 78—18249
- fracture, statistics in brittle materials with surface shear-sensitive cracks 79—41616
- fracture energy rel. to inelastic behaviour 79—60429
- fracture initiation, crack opening displacement and crack tip plastic strain energy 79—18819
- fracture mech., linear elastic, appl. to crack stability in brittle struct., elastic-plastic conditions 78—90800
- fracture mech. during creep, interference microscopy exam. of 12Kh18N9, 08Kh18N10T 78—56756
- fracture mechanics, fundamental aspects and new developments, safety evaluation aspects *(Italian)* 78—34086
- fracture mechanics, influence function method computer program 77—75859
- fracture mechanics, plasticity, finite element anal., review 79—41612
- fracture mechanism 78—63380
- fracture of compact tensile test pieces with starting notches *(German)* 77—58619
- fracture parameter estimation by long wavelength scatt. 79—24709
- fracture resistance, dependence on crack length 78—67120
- fracture toughness parameters J and $G^{\perp}$, effect of load biaxiality 78—67128
- fracture toughness testing by US, crack extension monitoring 77—16758
- fracture under combined loads by maximum-energy-release-rate criterion 79—32384
- frictional contact in crack analysis 80—1475
- frictional slip progressing into contact zone of crack 80—16417
- fully yielded components, stable and unstable cleavage fracture, moving cracks 79—64586
- fusion reactor ceramics, Weibull probabilistic design approach 79—93822
- fusion reactor materials, material requirements exam., review 78—50257
- gas flow through cracks, surface roughness influence 80—69929
- GFRP cross-ply laminate, constrained cracking 78—19870
- glaciers, spacing of water-free crevasses 80—21784
- glass, co-acting (synergistic) flaws and strength 77—20168
- glass, electron bombarded, brittle failure 77—28909
- glass, fracture, by impulse loading, splitting method tests strength properties 79—57118
- glass, fracture mechanics studies, specimen *(French)* 77—73401
- glass, hardness testing, mechanical property determ. *(German)* 80—40669
- glass, impact damage, localised 77—44306
- glass, minimum life prediction, uncertainty 77—16665
- glass, strength degradation from impact with spheres 78—27663

cracks continued
glass, tempered, stress meas. in surface, indentation technique 77—44341
glass, Vickers indentation, slow surface crack growth 77—12688
glass and ceramics, strength and failure predictions 77—21256
glass fibre pipe, subject to external press., layering 77—52485
glass fibre reinforced composite, thick-walled shell, crack prevention during heat treatment 77—52376
glass fibre reinforced epoxy and unsaturated polyester resins, crack form. *(German)* 78—19887
glass fibre reinforced epoxy-aniline, laminate, work required to rupture along interfaces 79—43413
glass fibre reinforced plastic, acoustic emission 80—104294
glass fibre reinforced plastic, fracture dynamics 80—100906
glass fibre reinforced plastic laminate, crack resistance under prolonged loading 77—21276
glass fibre reinforced plastics, under compressive load *(Japanese)* 78—92301
glass fibre reinforced polycarbonate, creep crack growth *(Japanese)* 78—39887
glass fibre reinforced polyester, 90° cross-ply laminates, multiple transverse fracture 77—8913
glass fibre reinforced polyester, behaviour under bending load *(Japanese)* 79—38904
glass fibre reinforced polyester filament wound pipe, failure 78—44192
glass fibres, flaw generation by indentation fracture technique 80—81156
glass plate, flexure crack propag., expt. and anal. 78—80620
glass plate impacted by glass spheres, localised impact damage 77—56089
glass plates, effect of localized damage on energy losses, during impact by glass spheres 78—52973
glass-ceramic, randomly oriented, physical props. 78—48501
glass-ceramic, randomly oriented, physical props. 78—48502
glass-glass-ceramic composites, crack growth, elec.-mech. analogue 80—85022
glassfibre reinforced composites, accumulation of fatigue damage using diffuse light transmission *(Russian)* 78—19896
glassy materials, compression cracking theory and failure 80—7677
grain boundary crack, diffusional growth 78—47471
grain boundary estimation of creep rupture time *(Chinese)* 78—83325
granite, stressed, crack-crack and crack-pore interactions 79—84238
granite plate, crack propagation by projectile impact load 78—60741
granites microcracking and heating, new evidence from cathodoluminescence 80—51391
graphite, bending strength, surface roughness effect at high temp. *(Japanese)* 79—70131
graphite, crack propag. kinetics 79—66161
graphite, failure in lab. tests, fracture mech. approach, finite element stress anal. 77—4149
graphite, fusion reactor applications, mechanical constitutive laws for irradiation behaviour 80—32448
graphite, pyrolytic, numerical discussion of flaking mechanism from ion bombard. 78—52947
graphite, silicized, fracture analysis, deform. 78—15530
graphite epoxy laminate, mixed mode fracture, fracture strength 77—70156
graphite fibre reinforced epoxy matrix laminates, microscopical anal. 78—3288
graphite reinforced epoxy laminates, cracked, deformation and failure in biaxial stress fields 79—47763
graphite/epoxy laminates, T300/5208, effect of curing stresses on first ply failure 79—43329
graphitic materials deformation, crack and fracture behaviour, SEM exam 80—11706
Green's function analysis, crack emanation from circular hole in infinite sheet 80—92084
Green's function for thru-crack emanating from fastener holes 78—67118
Griffith crack, asymmetrically loaded in infinite anisotropic medium 79—50649
Griffith crack, at interface of two bonded dissimilar elastic wedges, stress field, inverse Mellin transforms 80—53718
Griffith crack, initial motion 77—14959
Griffith crack in transversely isotropic material stress anal. 79—64583
Griffith crack opened by rigid inclusion, stress distrib. 80—79228
Griffith crack quasi-static growth, irreversible thermodynamics 79—18812
Griffith crack-antiplane shear wave interaction at interface of two bonded elastic half-spaces, geophys., seismological appl. 80—92087
Griffith cracks, partial immobile equilib. in two media plates 80—33529
Griffith cracks, stresses due to rigid inclusions 79—32373
Griffith criterion for brittle fracture in nonlinear thermoelasticity 79—77020
Griffiths cracks in a piezoelectric medium, critical load calcs. *(Russian)* 79—46264
growth, elastoplastic finite element anal. 79—46260
growth, three-dimensional problem 78—79266
growth characts., anal. modelling 79—41622
growth control under biaxial low-cycle loading *(Russian)* 80—23952
growth determination, in mixed mode loading system 78—67105
growth in conditions of creep *(Russian)* 78—63379
growth monitoring using finite element analysis, calibration of electric potential technique 79—32380
growth prediction in nonhomogeneous viscoelastic media 78—75098
growth thermodynamics for elastic, almost elastic and viscous bodies *(Russian)* 80—1481
haematite, degree of reduction, potential relaxation due to cracks *(Russian)* 80—66770
half space, elastic, edge cracks, dynamic growth 80—58972
half-space with crack, local loss of stability *(Russian)* 79—18821
harmonic solid, crack parallel compression, crack plane strain buckling 80—64475
Hastelloy, C-276, H-induced crack growth 80—71747
Haynes Stellite 6B, particle erosion damage, TEM obs. 78—88546
heat generation at the tip of a moving crack 79—27590
heat resistant KhN80TBYuA and KHN62VMkYu, microscopic intergranular crack form. prediction in high temp. deform. 77—81325
heat shrinkage tubing, crack resistance *(Japanese)* 79—61709
heat transfer and flow through hydraulically induced fracturesin hot dry rock 79—34424
heterogeneous media, struct. fracture and formation 79—86385
hexagonal 2-dimens. cryst., stable microcut, computer modelling 78—18704

cracks continued
hexagonal crystals, elastic energy of slit cracks 79—60431
high strength, crack propagation behaviour, stress, temp. and fracture toughness effects *(German)* 78—31494
high temp. cracks, discrete dislocation anal. 78—48514
high temp. relief cavitation, SEM, STEM, TEM, SIMS and EDX anal. 79—5039
hole and vicinity crack stress intensity factor calc., program *(Japanese)* 78—9603
Holmalite-100, dynamic photoelastic and dynamic finite-element analyses of dynamic-tear-test specimens 79—55348
Homalite, specimen geometry effect on crack propag. and arrest 79—34148
Homalite-100 plates, modified compact-tension specimens, dynamic anal. 80—97561
Homalite-epoxy duplex specimens, crack arrest study via dynamic photoelasticity 78—31515
homogeneous solids, crack size distrib. 79—81808
hot-pressed with crystn. grain boundary phases 78—95716
HSLA steel 78—52943
hydraulic losses due to cracks in electrodialysis machine *(Russian)* 77—32964
hydrogen embrittlement, adsorpt. model. and equilibrium crack growth meas. 80—108574
hydrostatically compressed crystals, crack nucleation mechanism 79—10893
ice, Antarctic deep core, X-ray diffr. topographic studies 78—63803
ice, dislocation processes and tensile crack formation in glaciers 78—20438
ice shelves, floating, tidal flexure cracks, fracture mechanics 78—69368
ice-metal interface, mech. behaviour and crack prod. of single cryst. 78—43230
Iceland spar, crystal, interaction of crack and elastic twin 77—12698
impact of microparticles, on brittle solids, high speed photography obs. 78—44223
impact penetration damage, probability based fracture mechs., appl. to Al panels 78—1606
Impact response of a finite crack in a finite strip under anti-plane shear 78—5691
impact viscosity resolution, using Otani method 79—50657
impacted pretensioned plate, dynamic finite element and photoelastic analyses 78—67111
impermeable rock hydrofailure, plane circular crack propagation *(Russian)* 79—70788
inclined crack in orthotropic strip, elastostatic problem 79—64594
Incoloy 800, creep crack growth, age hardening effect 79—43436
Inconel 600 safe-end cracking failure at Duane Arnold reactor 80—104295
Inconel 718, low cycle fatigue at 298 and 823K 77—86151
Inconel 718, surface flawed tensile bars, utility in cyclic life studies 77—21342
inelastic loading, crack propagation criterion *(German)* 79—50668
inequality conditions, consequences in crack and friction contact problems 79—37242
infinite elastic dielectric with Griffith crack, EM wave propag., Voigt-Toupin model 80—1469
infinite elastic medium, diffraction of torsional waves by flat annular crack 80—64447
infinite elastic solid, with flat annular crack, axisymm. stress distrib. under torsion 77—23913
infinite isotropic elastic medium, crack and misfitting inclusion interaction 79—37244
infinite plane with crack in nonuniform steady field, stress intensity coeffs. 80—38343
infinite plate, with cut along arc of circle, limiting equilibrium state 77—84195
infinite power law viscoelastic body, crack propag. by rigid wedge, stress intensity 80—64476
infinitesimal deviation, in arbitrary direction *(French)* 80—19281
inhomogeneous elastic material, antiplane crack problems 79—14343
initiation in notches, pure strain rate role, finite element computer program 77—70166
inorganic glass, effect of liq. medium on process of mechanical destruction 80—89283
instability, directional criteria 78—90789
insulated line in semiinfinite medium under uniform heat flow, thermal stress near tip 77—72242
integral J_1, calculation by finite element analysis 78—67129
intensity factor for mode I loaded cracks, exam. using shadow spot method *(German)* 79—41642
interacting cracks, in a cruciform pattern, spontaneous growth 80—99961
interaction between cracks positioned at an angle 78—83871
interactions on radial lines in infinite elastic plane 77—35083
interface crack, singularity anal. 80—10201
interface crack in combined tension-compression and shear field 80—48647
interface cracks, periodic array, interaction anal. 80—10186
interface edge cracks, energy release rate calc. based on M-integral 80—87742
interfacial crack between dissimilar media, biaxial load effects 80—99968
internal plane crack in elastic half-space, integral eqns. 80—38336
internally loaded elastic plate, containing infinite row of closely spaced parallel cracks, approx. anal. 79—68644
ionic crystal, dislocation mechanism of electrification during cleavage 77—24353
ionic crystals, fracture in mag. field 78—59855
ionic crystals, nanosec. electron beam effects, size depend., Ioffe effect 80—88211
isoprene, stressed, microcrack generation under const. elongation, struct. depend. 77—90459
isotropic and anisotropic crystals, stress fields around defects of dislocation-aggregate type 77—39591
isotropic body with many cracks or intrusions, transport processes 77—11116
isotropic elastic half-plane, curvilinear crack system 79—81806
J_{Ic} determ. from single specimen *(Chinese)* 78—30230
J-integral, interrelation with crack opening displacement 79—50648
J-integral determ. under elastic-plastic strain 79—64515
J-integral estimation 77—1876
jade, fracture parameters and crack propag. resist., rel. to fibrous microstruct. 77—8908

cracks continued
- Joule heat concentrators, metal foil expts. max. heat release, cracks in conductors 80—92022
- kinetic model of crack propagation *(Russian)* 78—63381
- Lamb wave diffraction by finite crack in elastic layer 80—64244
- laminate, reinforced in two directions, cracking 79—96139
- laminates, combined fracture and delamination, simple idealised example 77—68529
- laminates, failure mechanics, damage development 79—43427
- laminates, multiple fracture 80—10206
- laser crack development and light absorption 78—2193
- in layered composite, effect on impact response 77—50991
- layered cylinder, axisymmetric delaminations 78—79269
- layered material with through cracks, transverse conductivity 77—84122
- length determ., analysis of crack-opening-displacement meas. 78—5702
- limestone plate, crack propagation by projectile impact load 78—60741
- line crack subject to shear 78—79268
- linear elastic media, horizontally polarised shear wave diffraction by a finite crack extending uniformly 79—68652
- linear elastic solid, expanding crack under conc. load, dynamic problem 79—68646
- linear elastic solids, time-depend. crack propag. 78—75099
- linear elastostatics, combined boundary integral eqn./finite element anal. of cracks 77—72178
- linear viscoelastic material, crack propagation due to increasing applied stress 78—18246
- linear viscoelastic solid, crack propag. 79—23225
- LMFBR, effect of cracks in fast neutron embrittled hexagonal subassembly ducts 78—74446
- LMFBR concrete containment struct., exptl. anal. of dynamic loading 78—41867
- LMFBR fuel pin transient behaviour, effect of shutdown cracks in TREAT tested pins 79—31001
- LMFBR materials, exam. of material requirement 78—50256
- load nonalignment effects on crack propagation 77—3797
- loaded in anti-plane shear under creep 79—27598
- longitudinal-shear crack refraction, Wiener-Hopf method calcs. 80—87743
- lug, test and analysis 78—67153
- LWR materials, pressure boundary problems, corrosion, cracking and radiation embrittlement props. 78—46142
- magnetic tapes, calcs. of field reflections due to extensive flaws 80—104387
- maximum-energy-release-rate criterion applied to a tension-compression specimen with crack 79—23212
- measurement, recording instrument 80—100984
- medium with large no. of cracks, direct elec. current calcs. 80—96233
- metal, brittle, ductility improvement by plating *(German)* 77—8954
- metal, brittle fracture, low temp. statistical strength criterion 77—73318
- metal, dissolved species in cracks, linear differential eqn. problem 79—51316
- metal, ductile fracture, crack initiation at dislocation cell boundaries 77—66692
- metal, hard, brittle, correlation between wear, crack resistance and stress intensity factor *(German)* 77—36666
- metal, hydrogen crack development 79—20189
- metal, microstructure and strength *(German)* 77—70138
- metal, notched sheet, thickness effect on deform. and fracture under tension 79—70113
- metal, surface strain meas. by intensity of reflected light flux 77—17972
- metal, thin sheet, crack growth, effect of strain rate 77—1869
- metal, very thin foils, crack propag., electron microscope obs. 77—63792
- metal structures, thin walled, crack growth problems 80—55527
- metal surface deformation obs. by interference microscopy *(German)* 77—56210
- metal weld, submerged arc, metallographic study of chevron cracking 78—56761
- metallic laminate, laws governing development and retardation of fast cracks 78—15527
- metallic laminated composite, crack growth retardation *(Russian)* 77—70144
- metallic materials, crack propag. mech. and fracture toughness, microstruct. effects 78—19859
- metallisation stripe, cracked, temp. gradient and current crowding, electromigration 77—51828
- metals and alloys, corrosion conditions simulation in crack-like defects using electrochemical cell *(Russian)* 79—52445
- metals and alloys, relaxation, rel. to defect struct. *(Russian)* 78—19801
- microcrack enlargement in heterogeneous materials, conc. criterion 80—11769
- microcrack formation, disclination mech. 79—23674
- microcracks, statistical linking theory consistent with classical reliability theory 78—84952
- micropolar elasticity, uniqueness for anti-plane crack problems 79—30235
- mild steel, effects of CO_2-O_2 mixture compositions on hot cracking resistance 77—21239
- minerals, cracks rel. to effective seismic vels. var. with press. 79—44179
- mixed boundary-value problems, orthogonal polynomial solns. 78—54193
- mixed-boundary value problems, numerical scheme 77—68432
- mode I crack, non-steady growth 78—18241
- mode III cracks, steady propag. followed by nonuniform growth, stress intensity factor 77—65716
- model, deduced from thermodynamics *(French)* 78—63386
- modified crack closure integral, finite element calc. of stress intensity factors 78—18235
- modified Westergaard equations 78—67122
- modulus of elasticity for bodies weakened with oriented cracks *(Russian)* 77—14898
- monolithic component glasses and rigid sintered fibre-optic elements, microcrack form. during grinding 78—87175
- movement, isothermal conditions, heat liberation, finite element method *(Russian)* 79—27583
- multibarrier kinetics, subcritical crack velocity stress depend., review 80—23958
- multilayer built-up plate with crack, rigidity determ. 79—90190
- multiple crack interaction, effects on stress-intensity factor 77—62204
- neo-Hookean elastic layer, Griffith cracks, plane strain problem 79—50666
- nitrided layer, fracture toughness determ. from hardness impressions *(German, English)* 80—97575

cracks continued
- noise intensity during cracking 77—846
- non-linear theories for onset of stable and unstable crack growth 77—72248
- non-randomly cracked body, elastic moduli 79—23209
- nonhomogeneous medium under shear, elasticity theory 78—86166
- nonlinear elasticity of medium with stable random frictionless cracks 79—64581
- nonlinear materials, Mode I fracture behaviour, finite element anal. 80—84237
- nonlocal thin elastic plates, impact by cylindrical projectile, shearing stress anal. 79—10467
- nonpropagation crack notch *(Japanese)* 77—59912
- notch apex crack, tip intensity factor 77—62207
- notched and bend specimens with equivalent geometries, cyclic deform. *(German)* 77—86271
- nuclear fuel, quantitative metallographic anal., computer program, QMA 79—15951
- nuclear fuel compacts for HTR, irrad.-induced creep 78—44168
- nuclear fuel element model for cladding performance during power changes, strain defects 78—58359
- nuclear fuel rods, thermal and mechanical anal. with URANUS code 78—41803
- nuclear fuel-cladding interaction between cracked surfaces, mechanical and temp. contact 78—66341
- nuclear reactor, cracked fuel elements, temp. distrib. calc. 78—78446
- nuclear reactor materials, crack propag., fracture, and ductile-brittle transition *(Spanish)* 79—36316
- nuclear reactor materials, crack-front tunnelling, investigated by single specimen compliance technique 80—70300
- nuclear reactor piping system, crack initiation and propagation, fracture mechanics 80—83193
- nuclear reactor pressure vessels, radiation embrittlement, allowable crack size, unstable fracture 77—10465
- nuclear reactor vessel cracks and elastic fracture mechanics 77—67843
- numerical modelling of fatigue, crack, creep and corrosion test results, review 78—30243
- optical components, polishing defects obs. by etching 77—75724
- optically isotropic mats., stress intensity factor determ. by dynamic method of caustics 80—33546
- orthotropic layer weakened by double periodic plane cracks, compound problem of theory of elasticity 79—90139
- orthotropic parallelepiped, weakened by double periodic plane cracks, theory of elasticity 79—86340
- orthotropic strip, stress intensity factors and crack opening displacements 80—53710
- othortropic medium in presence of symmetrical body forces, stress intensity factor 79—7337
- overlapping interacting cracks 78—55593
- perforated plate with cracks, stress intensity factor 79—14263
- periodic curvilinear cracks in isotropic medium, integral eqn. soln. 78—51118
- perspex, explosively end-loaded bars with transverse holes or section changes 77—63769
- photoelastic, isochromatic fringes, comparison of stress intensity factor determ. methods 77—84197
- photoelastic prediction of crack propag. angle 80—87748
- phthalic anhydride+8-hydroxyquinoline, solid-state reaction kinetics 77—36746
- piecewise homogeneous elastic medium, crack with finite branch, slip lines 80—38342
- piecewise-uniform plane, curvilinear cracks, integral eqns. of heat conductivity and thermoelasticity *(Russian)* 78—38250
- piezoelectric materials, fracture mechanics, deform. anal., crack development 77—24349
- pillow lava, spreading cracks props. 79—79780
- pin loaded single edge notched tension specimens, K-COD relationship 78—67133
- pipe, axial crack, elastic-plastic dynamic finite element anal. 77—3795
- pipe, straight, fracture under large deflection, pipe pressures, finite difference code 77—58616
- pipeline, pressurized, steady-state crack propagation 77—58614
- pipeline girth weld, determ. of acceptable defect level 79—34143
- pipes, straight, fracture under large deflection conditions, structural deformation 77—58615
- piping for PWR, Aquitaine 1 loop for studies of crack growth rate and propagation 77—3796
- plain strain arrest charact. 77—44367
- planar, growth under hydraulic fracture 80—28469
- planar body, with circ. boundary and thermally insulated cracks, temp. distrib. 78—67002
- plane, arbitrary shape, soln. of three dimensional problem 78—79265
- plane brittle crack, crit. size *(Russian)* 77—44329
- plane compressional wave attenuation by random distrib. of thin circular cracks 79—27561
- plane crack, in infinite solid, stress intensity factor under normal pressure 79—72855
- plane crack problems in micropolar theory of elasticity 78—54191
- plane cracks, occupying two-connected domain, elasticity theory problems *(Ukrainian)* 80—74804
- plane elastic crack, dynamics under variable loading *(Russian)* 80—79222
- plane elasticity, cracks, Cauchy type integrals and integral eqns. with logarithmic singularities 79—30252
- plane elasticity, curvilinear crack edges concentrated forces and edge dislocations, numerical soln. 80—58970
- plane elasticity theory, use of automorphic functions *(Russian)* 79—35563
- plane finite elastostatics, discontinuous deformation gradients, ellipticity failure and cracks 79—32264
- plane notch and crack problems, appl. of displacement and hybrid stress methods 78—63375
- plane problems and antiplane shear probs., approx. path independ. integrals 77—7337
- plane strain conditions, crack propag., fracture energy criteria, displacement discontinuity method 80—48648
- plane strain shear cracks, rupture vel., rel. to earthquakes 77—17043
- plane stress crack problems, fully plastic soln. and large scale yielding estimates 77—19573
- plane stress to plane strain thickness dependent transition, anal. model 78—67126

cracks continued
- plane-strain buckling of cracks in incompressible elastic solids 80—79186
- plaster of Paris, explosively end-loaded bars with transverse holes or section changes 77—63769
- plastic deformation at the tip of an edge crack 80—69734
- plastic flow conc., blunting of crack tips *(Russian)* 78—7013
- plastic flow round crack under friction and combined stress 78—79280
- plastic material in planar stressed state, crack growth influence of thermal stabilities 79—69190
- plastic materials, crack resistance *(Russian)* 78—63377
- plastic relaxation, time dependent at crack tip 77—63765
- plastic shear crack, discrete dislocation anal. 79—50659
- plastic tensile crack behaviour, discrete dislocation analysis 78—22788
- plastic yielding, modelling at a crack tip by inclined slip planes 80—33472
- plastic zone ahead of crack, development under creep conditions, computer simulation 78—34091
- plastic zones at crack tips during uniaxial deformation *(Russian)* 79—50655
- plastics, crack growth stability anal. using catastrophe theory 80—74810
- plate, bounded by curvilinear contour, weakened by cracks, elastic equilibrium *(Russian)* 77—68524
- plate, elastic, containing through crack, skew symmetric loading, transverse shear effects 80—64478
- plate, three dimensional theories 78—67136
- plate, wide, analysis on crack in high strain zone *(Chinese)* 78—83326
- plate, with internal crack, in tension, instability of plane solution *(Russian)* 79—50616
- plate structure, crack simulation computer program *(Japanese)* 80—79218
- plate temp. dependent props. under linear temp. distrib., thermoelastic problem for crack 80—48579
- plate weakened by equal-armed cross-shaped crack, plastic strain and fracture 80—69740
- plate with crack close to one edge, elastoplastic equilib. 80—14624
- plate with crack or ribbon like inclusion subjected to uniform heat flow, thermoelasticity 80—48578
- plate with transverse compression zone, arrest phenomena 79—4369
- plates, effect of curvature of front of through slit 80—23953
- plates, open and loaded holes, exam. of part elliptical cracks 80—10195
- Plexiglas, fast cracks propag. and interaction 80—100905
- Plexiglas, rod, breakdown charact. by longitudinal stress waves 78—38773
- plexiglas plates, static and dynamic stress intensity factor meas. by method of optical transmitted caustics 77—66740
- PMMA, crack growth rate effect, fracture surface structure 80—16466
- PMMA, crack velocity depend. on critical stress in fracture, static and dynamic loading 77—63768
- PMMA, cracking kinetics, effect of small vibrs. 79—57108
- PMMA, expt. checking of ultimate equilibrium for crack in plane stress field 77—90462
- PMMA, fracture toughness for moving crack 77—44365
- PMMA, glassy, craze and crack growth *(Japanese)* 77—8970
- PMMA, instantaneous crack resist. during stable crack propag. 80—85058
- PMMA, mech. degradation in presence of metals, effect of low mol. wt. environment generated during mech. working *(Russian)* 78—31422
- PMMA, methanol crazes, grown from cracks, exam. of growth criteria 78—48551
- PMMA, overlapping skew-parallel crack dynamic propag. and arrest meas., method of caustics 78—84962
- PMMA, rain erosion behaviour, exam. 78—53001
- PMMA, stress fields round indentations 77—28861
- PMMA, submicroscopic cracking in dynamic extension, light scatt. meas. 79—70171
- PMMA, uniaxial tension, fractographic anal. of crack growth kinetics 80—40519
- PMMA plates with flawed fastner holes, static fracture testing 80—97651
- PMMA with stress-raising flaw, deform. 80—25799
- polished glass surface, reflected light phase rotation 80—66147
- polycarbonate, bisphenol A, birefringent plates, cracks, stress intensity factors, refl. caustics method 80—93718
- polycarbonate, theoretical prediction of temp. rise at tip of running crack 80—2114
- polycarbonate plates, modified compact-tension specimens, dynamic anal. 80—97561
- polycarbonate structure foams, fracture toughness 78—15500
- polycarbonate-steel surfaces, changes in morphology induced by fretting 78—15538
- polycrystalline material, diffusional growth of cracks *(Russian)* 78—91376
- polyester resin, reinforced with glass chopped strand mat and woven roving fabric, fracture toughness and crack-growth meas. 79—83299
- polyethylene, high-density, submicroscopic cracks form. and residual strength, hydrostatic press. influence 79—20185
- polyethylene, high-density, tensile necking, specimen size and loading conditions effects 79—61672
- polyethylene, low density, highly deformable, fracture surface roughness 78—44197
- polyethylene, of low density, determ. of avoiding of tensile cracks *(German)* 80—19874
- polyethylene glass sphere filled, crack form. and necking *(German)* 78—35452
- polymer, birefringent, stress intensity factor determ. 80—14633
- polymer, crack extension micromechanisms, review 80—108561
- polymer, crack tip failure mechanism modelling 80—108565
- polymer, crosslinked, amorphous probabilistic theory of time to fracture 77—90448
- polymer, fracture kinetics, book 79—29222
- polymer, loaded, mech. of macrocrack generation and propag., photometric and X-ray meas. 77—4886
- polymer, transparent, high-temp. zone form. in laser induced mech. breakdown 77—56086
- polymer, ultimate lifetime at high loads 79—20184
- polymer concrete, fracture toughness meas. 79—70168
- polymer crystals, deform. and fracture, submicrocrack nucleation and supermod. struct. 78—52918
- polymer multilayer composite, wire-reinforced, dynamically loaded, crack propagation and arrest 80—97567

cracks continued
- polymer plate, crack growth kinetics in uniaxially extended specimen *(Russian)* 80—1483
- polymer reinforcement, fracture mechanics 80—10207
- polymer with macrodefects, fracture mechanism *(Russian)* 78—35500
- polymeric composites, sliding wear mechanisms at metal surfaces, microscope obs. 79—87742
- polymeric foam, cell cracking 79—11701
- polymeric glasses, kinetic theory of brittle fracture 78—48526
- polymers, glassy, craze surface displacements, model 80—93651
- polymers, orientation of plane of large cracks prod. by laser pulses 80—11753
- polymers, vitreous, quasibrittle fracture 80—21094
- polypropylene, fracture exam. using microscopic obs. *(German, English)* 79—20186
- polysiloxane dizwitterionomers, mech. props., microstruct. 80—49131
- polystyrene, intersections of coarse shear bands 79—100212
- polyurethane, high temp./press. materials test for undersea environment 78—3213
- polyurethane, rate dependent criterion of crack growth 79—32376
- polyurethane rigid foam, fracture props. over range of densities 79—79106
- porcelain, correlation between wear, crack resistance and stress intensity factor *(German)* 77—36666
- porcelain, crack propag. data applicability to failure prediction 80—81154
- porcelain, strength eval. after grinding 77—52518
- post yield solutions for fracture mechanics analyses of cracks emanating from elliptic holes 79—68643
- power-law hardening material, pre-cracked plate, unstable fracture criterion 80—84238
- prefracture zone, similarity conditions in vicinity of contour of microcrack *(Russian)* 78—30233
- pressure vessel, reinforced concrete, stress anal. of cracked shell 78—44213
- pressure vessel, strength analysis, by thermal shock 78—68819
- pressure vessel nozzles, stress intensity factors, photoelastic meas. 77—44360
- pressure vessel reliability, sensitivity to material and other factors 79—18018
- pressurised cylindrical shell with clamped crack, stress intensity factors 77—80119
- pressurized containers, crack propagation and arrest 77—58611
- prismatic beams with circular cracks under tensile loading 80—53714
- propag. of cracks, effect of humidity 77—86133
- propag. rate variation with resistance to crack movement 77—59926
- propag. simulation, using moving grid based finite difference scheme 78—83334
- propagaion, quasistatic energy anal. 77—46972
- propagation, branching model 77—23918
- propagation, computer simulation 80—59573
- propagation, material struct. effect under body compression *(Russian)* 77—15485
- propagation, Stefan problem approach 77—14964
- propagation, subjected to mode I and II loading, rupture criteria *(French)* 80—14616
- propagation anal. technique using catastrophe theory 79—55342
- propagation and arrest, in plates, pipes and pressure vessels 78—56770
- propagation in creep, finite element analysis *(Japanese)* 77—8926
- propagation in creep, rate obs. on stainless steels *(Japanese)* 77—8927
- propagation in elastic bodies, review of expt. and theoretical results 77—14958
- propagation in nonproportionally scaled elastic structures 79—18807
- propagation initiation, meas. by elec. resist. meth. *(Chinese)* 77—9005
- propagation model, rel. to appl. of stress wave emission to propag. in metals 77—63837
- propagation theory, analytic source mechanisms for crack extension 79—98662
- propagation toughness testing 77—44449
- propagation under compression, finite element analysis 78—67148
- propergol, rheological props. during polymerisation *(French)* 78—23762
- propylene, isotactic, crack propag. rel. to morphology *(German)* 78—76749
- pulsed stress effects 78—56724
- PVC, highly deformable, fracture surface roughness 78—44197
- PVC, rigid, internal struct. of diamond shaped cavities 80—66628
- PVC, rigid, tensile fracture morphology, rel. to mol. props. 77—59883
- PVC, slightly plasticised, fracture toughness tests, impact tests 79—5037
- PVC sheet, notched, yielding 78—56708
- PWR piping, circumferential cracks, opening and extension, MARC finite element program 80—78364
- Pyrex, stress intensity factors of surface cracks and fracture stress, acoustic meas. 79—47845
- pyrocarbon coatings, deposition in fluidized bed, TEM, changes by irradiation 80—34084
- quarter elliptical cracks in irregular bodies, exam. using finite element alternating method 78—90796
- quarter infinite crack in half space, solns. 80—43672
- quartz, phase transform. in brittle materials, plane stress anal. 77—86024
- quartz film, microcrack growth, electron microscope obs. 77—69037
- quartz substrate, SAW attenuation due to platelet defects 79—95253
- quasi static crack growth, in sheet materials 78—67106
- quasi-Newtonian force 78—63765
- quasi-state hyperelastic crack propagation, energy release rate 79—68661
- quasi-static crack propagation in single cells of fibre reinforced materials under tension *(German)* 80—106759
- quasistatic crack growth, nonlocal model, thermodynamics of irreversible processes basis 78—83324
- quasistatic problems in non-homogeneous elastic layer 77—72235
- random walk theory applied to crack propagation 80—43666
- rapid mode II shear crack with finite cohesive traction, stability, earthquake model 79—84148
- rate dependent criterion of growth 79—32376
- Rayleigh scatt. of elastic waves 79—55343
- Rayleigh waves interaction, with microcracks on brittle solids 80—39214
- reactor fuel cladding failure under reactivity initiated accident conditions *(Japanese)* 79—30955
- reactor press. vessel nozzle under internal press. safety against bursting *(German)* 78—17326
- reactor technology, conference, Berlin, Germany (Aug. 1979) 80—77539
- reactor vessel, determ. of stress intensity factor 80—37455

cracks continued
rectilinear anisotropic solids, mixed-mode crack anal. using conservation laws of elasticity 80—84239
refraction of propagating crack by stress wave, brittle amorphous mat. 78—92337
refractories, thermal cond., microcracks contrib. 80—19999
refractories, thermal cond. rel. to gas phase mass transfer in pores and microcracks 79—73352
reinforced concrete, cracking strength and max. rack width *(Chinese)* 80—5988
reinforced concrete, elasto-plastic anal. of plane frame *(Chinese)* 80—5950
reinforced concrete structs., initial stress approach to nonlinear dynamic anal. 77—83036
reinforced concrete structures, under missile loading, finite difference code 80—13956
reinforced masonry shear wall, elastoplasticity and crack-growth anal. *(Chinese)* 79—94506
reinforced plastics, failure of thin walled flexural structures 80—10209
reinforced plastics, subject to short-term tensioning, failure 79—61725
residual stress effect in quasi-static cracking of materials 77—84193
residual stress effects in failure from flaws 79—66228
resin beams with glass fibres, crack propag. expt. 78—15521
ring, axially cracked, numerical anal. of residual stress effect on crack closure 79—77012
Rochelle salt, mechanoluminescence and crack mobility, charge prod. during fracture 78—88370
rock, crack propag. in diametrically-compressed discs 79—48463
rock, cracked, slip surface development 78—15480
rock, dry, quantitative model of dilatancy and appl. to Westerly granite 79—16445
rock, failure process under compression, fracture mechanics *(Japanese)* 79—57915
rock, symmetrically extending plane crack, self-similar pressure profiles 78—69340
rock compressibility, nonelliptical crack effects 79—2227
rock plate, loaded by projectile impact, crack propag. 79—83296
rock rupture by elastic shock wave superposition in multiple detonations *(Russian)* 77—35082
rocks, crack growth and thermoelastic behaviour 80—26502
rocks, crystalline, from 5.3 km depth in Michigan Basin, microcracks obs. 79—39705
rocks, effect of cracks on thermal expansion 78—28218
rocks, hot, dry, hydraulically fractured linearly expanding cracks, eqns. *(Japanese)* 79—34809
rocks, hot, dry, water circulation through large crack rel. to geothermal heat extraction 79—57355
rocks, internal cracks, nondestructive obs. in stressed state 77—73726
rocks, microcracks and joints effect on compressibility, anal. using new model 80—8300
rocks, microfracture *(Japanese)* 78—7020
rocks, oriented cracks, differential strain analysis 78—53647
rocks, rings, discs, under diametral compression, tensile strength calcs. *(French)* 77—70638
rocks of Stone Canyon, California, macrocracks rel. to P-waves in situ vel. study 79—57865
rod, theory of resistance to failure of technical materials, macrocrack instability criteria 79—10536
rolled sheet, artificial surface cracks, reflection of normal shear waves 80—89448
rotating discs, with radial cracks, appl. of linear-elastic fracture mechanics 77—54929
rubber abrasion pattern analysis and obs. 79—38988
rubber springs, bonded, crack growth energy calc. and meas. 79—83316
ruby, structural defects due to laser irrad. *(Russian)* 80—100303
running crack, cohesive fracture zone, thermodynamic laws 80—43676
running crack, three-dimens. problem, elasticity dynamic eqns. 79—18811
running crack problem, thermodynamic calc. *(French)* 79—64582
running crack tip, effect of strain rate depend. Young's modulus on stress and strain fields 78—75097
sapphire, fracture anisotropy of $\langle 1\bar{2}10\rangle$ zone 79—61726
sapphire 0°, creep deform., fracture anal. 77—56035
SAW scattering by surface breaking cracks 79—56058
second fundamental crack problem and the rigid line inclusion problem in plane elasticity 80—27129
SEM/acoustic emission in situ techniques *(German)* 79—96240
semi-elliptical surface crack in semi-infinite solid, stress intensity factors 80—84241
semi-infinite crack, extension against antisymmetric quasiuniform body force 79—98661
semi-infinite crack, kinking under dynamic loading conditions, elastodynamic stress intensity factors 79—68660
semi-infinite crack tips, practical evaluation of stress intensity factors 80—99962
semicircular surface crack, elastic fracture mechanics, boundary integral eqn. anal. 80—14622
semielliptic crack, elastic fracture mechanics, boundary integral eqn. anal. 80—14622
semielliptical, in cast components, relation between axes 78—11326
SH sudden crack, displacement far-field spectrum, earthquake appl. 77—25641
SH wave diffraction in half-space with crack 79—53981
sharp contact cracking, residual stress effects 79—100245
shear crack propagation under cohesive-type tractions 79—3972
shear cracks nucleation and initial propag. 79—81804
shear loaded interface crack, friction effects, contact zones, stress fields 80—79225
shear microcrack propag. in triaxially-compressed brittle rocks 80—90080
sheel, cylindrical, closed, laminated, longitudinal crack, elastic eqn., energy approach *(Russian)* 80—87740
sheet, misfitting inclusion and circular arc cracks 78—67117
sheet drawing, slip line field for mid-plane cracking or splitting 80—50648
sheet metals, ductile, shearing process 78—84841
silica optical fibres, surface flaws obs., fracture strength 77—14793
silica paricle filled epoxy resin, mech. props., fracture by slow crack growth 77—40443
silicate glasses, fused, cone cracks around Vickers indentations 79—29189
singular crack borders, constitutive preps. 78—67108

cracks continued
size distrib. function under dynamic loading conditions *(Russian)* 79—46262
slender Z-crack, elasticity problems 78—87304
slow crack growth rate and creep strain, relationship under tensile loading 77—3778
small particles, crack propag. rel. to impossibility of comminution by compression 78—52709
soda lime glass, microparticle impact, high speed photography obs. 78—44223
soda-lime glass surface, damage due to impact of small glass and steel spheres 78—52994
solar cells, faulty, scanning light spot anal. 80—89625
solid popellant, delayed fracture and crack propagation *(French)* 80—108521
spalling of cold mill work rolls, prevention measures 77—55981
specimen configuration effect on crack initiation in delayed fracture, apparent stress intensity factor anal. *(Japanese)* 79—77676
specimen configuration effects, tensile and precracked data 80—16413
split birefringent coating on birefringent material, determ. of dynamic stress intensity factors 79—50684
stabilisation of trajectories 77—62213
stability of parallel cracks in solids reinforced by bars 80—43671
stable crack extension and nonlinear fracture criteria, finite element anal. *(Chinese)* 80—10184
stable crack-growth, fracture criteria, numerical approach 78—67104
stable growth in antiplane shear, finite element investigation 79—3975
stable growth props. 79—68648
stainless steel, effects of flux during submerged arc welding 77—21238
stainless steel rod adaptor, failure anal. in Fast Burst Reactor 77—54307
stainless steel type 316, ductile crack initiation, detection and toughness characterisation 77—16662
star crack development, elastic antiplane deformation conditions, self similar problem 78—5698
static bend testing by unit with energy accumulator 77—86251
stationary heat conduction in an anisotropic slab containing a crack 79—94470
steady state crack propagation, media with variable elastic moduli 78—90783
steady state creep analysis of a cracked body using the superposition method 79—94507
steady-state heat conduction of solids with inclusions and cracks, analogy with longitudinal shear *(Russian)* 77—68371
steel, 0.45% C, annealed, roller, macroscopic and microscopic changes in surface layer due to rolling contact 77—77518
steel, 12Kh1M1F, pipe with axial surface crack, resistance of failure in plastic deform. 79—100235
steel, A533B, crack branching 78—64705
steel, acoustic-emission analysis of fracture-toughness tests 80—55596
steel, alloy, crack arrest toughness determination 78—72867
steel, alloy, nonmartensitic decomposition of austenite, fracture strength of high tempered products *(Russian)* 78—11304
steel, austenitic, 30KhGSA, heat treatment, preliminary, cold deform., elec. heating rel. to mech. props. 79—24554
steel, austenitic, martensitic transform. at crack tip 77—70051
steel, austenitic, Mn-Ni-Cr, Mn effects on cracking *(German)* 77—59889
steel, austenitic, precipitation hardened, ductility of grain boundaries and crack propag. *(German)* 78—52834
steel, austenitic decomposition kinetics, crack sensitivity, H_2 effect *(Russian)* 80—20885
steel, austenitic stainless, crack growth-tertiary creep relation 77—28863
steel, austenitic stainless, Cu-Mo substituted 18/8 type, austenitic stability 79—91716
steel, austenitic stainless, propagation 78—60797
steel, C, crack opening displacement, rel. to flow stress 78—68810
steel, C, crack propag. and sealing, effect of thermal working *(Russian)* 79—34078
steel, C, crack resistance, preliminary loading condition effects in crack appl. 78—56739
steel, C, ductile fracture under cold forming conditions, press. effect 78—52938
steel, C, hollow pipe body with internal crack pattern, ingot segregation, hot shortness 77—32693
steel, C, rod, breakdown charact. by longitudinal stress waves 78—38773
steel, C, torsional prework effect on fatigue strength, crack propagation *(Japanese)* 80—55514
steel, C and low alloy, structural, ductile and brittle fracture resist. in stable crack growth stage 79—52369
steel, carbide cracking as source of acoustic emission 78—19872
steel, carbon type, hydrogen press. effect on morphology of hydrogen attack 80—85052
steel, cast, fractographic features of coarse grained intercrystalline fractures *(Czechoslovakian)* 77—36627
steel, cast, high speed, solidification, (Fe,Mo)$_6$C form., struct. 79—24514
steel, cast C and C-Mn steels, fracture toughness 77—4836
steel, cold crack formation following laser welding *(Russian)* 79—38938
steel, continuously cast, segregation at halfway cracks 80—60869
steel, continuously cast billets, influence of hot working on internal cracks 79—83242
steel, continuously cast slabs, formation of longitudinal midface cracks 79—83315
steel, Cr, hypereutectic, structural, critical rates of impact, kinetics of failure 80—35325
steel, Cr-Mo, crack decoration in oxides by electrodeposited metals *(German, English)* 79—70266
steel, Cr-Mo, martensite to ferrite transform. by fatigue deform. *(French)* 79—66056
steel, Cr-Mo, oxidised, mechanism of crack decoration of oxides by electrodeposition 80—97560
steel, Cr-Mo (2.25, 1 wt.%), weld metal, high temp. crack growth, effect of tempering, prestrain and grain refinement 78—27622
steel, Cr-Mo-V, medium strength, correlation between crack initiation, propag. and microstruct. 78—60787
steel, Cr-Mo-V, normalised and tempered, size and geometry effect on creep cracking behaviour 78—64630
steel, Cr-Mo-V, stress relief cracking mechanism 78—64669
steel, Cr-Mo-V (0.5, 0.5, 0.25 wt.%), bainitic and martensitic, tempered, creep crack growth 77—86136
steel, Cr-Mo-V (0.5, 0.5, 0.25 wt.%), comparison of methods of correlating creep crack growth 78—60826

cracks continued
  steel, Cr-Mo-V (0.5, 0.5, 0.25 wt.%), creep crack growth, temp. effect 78—64667
  steel, Cr-Mo-V (0.5, 0.5, 0.25 wt.%), creep crack growth at 565°C 77—73323
  steel, Cr-Mo-V (0.5, 0.5, 0.25 wt.%), creep crack growth in notched bend test, microstruct. effect 77—21261
  steel, Cr-Mo-V (1, 1.25, 0.25 wt.%), creep crack growth *(Japanese)* 79—43399
  steel, Cr-Mo-V press. vessel, crack growth under creep 78—60827
  steel, Cr-Ni, case hardened rollers, surface fatigue failure under pure rolling and sliding rolling contacts 79—52472
  steel, Cr-Ni-Al, intergranular crack investigation by etching *(Chinese)* 79—43457
  steel, Cr-Ni-Cu (14, 5, 2 wt.%), phase transform. and props., preliminary heat treatment effect 79—79011
  steel, Cr-Ni-Mo, 'light spots', fractographic anal. 79—29204
  steel, crack form. during continuous casting 78—7038
  steel, crack opening displacement in deeply notched specimens 78—27617
  steel, crack resistance, J-integral approach 77—66699
  steel, crack tip opening displacement and J-integral fracture criteria 77—3777
  steel, crack tip studies, stretched zone and COD 78—68812
  steel, CrNiMoV, weld metal, hot cracking resistance during electroslag welding, effects of Cr 79—87732
  steel, dispersion hardening type 0Kh12NDL, cast, resistance to cold crack formation during welding 79—87731
  steel, ductile struct., crack propag. 78—68805
  steel, ferrite-pearlite, ductile fracture, pearlite colony morphology and hydrostatic press. effect *(Japanese)* 78—15510
  steel, ferritic, underclad cracking mechanism, effects of residual strain and heat affected zone ductility 77—25158
  steel, fibrous crack extension, micromechanisms 80—108563
  steel, fracture ductility, determ. in bending tests and US emission 78—23899
  steel, fracture toughness testing, obs. of crack initiation and stable growth processes *(Japanese)* 78—52954
  steel, H_2 cracking mechanism *(Russian)* 77—25130
  steel, H_2 embrittlement and selective adsorption 77—36645
  steel, H embrittlement mechanism, microcrack formation, dislocation model *(Russian)* 80—65143
  steel, hardened, exoelectron emission from torsion fatigue damage 77—86142
  steel, heat resist., crack growth resist. on long-term loading 79—29178
  steel, heat resistant 15Kh1M1FL, cast, crack development at various stages of fracture, prolonged load 77—63802
  steel, heat resistant Kh15N24VChT, microscopic intergranular crack form. prediction in high temp. deform. 77—81325
  steel, high alloy, strain induced martensite and austenite influence on crack formation *(Russian)* 80—21007
  steel, high strength, alloy, initiation of cracks at delayed fracture, AE study 78—72868
  steel, high strength, hypereutectoid, low alloy, microcrack frequency and fracture toughness rel. to martensitic struct. *(Czech)* 77—70163
  steel, high strength, low alloy, plate, impaired ductility in sheared edges 78—60727
  steel, high strength, weld cold cracking, anal. of fracture morphology, using SEM *(Japanese)* 78—52960
  steel, high strength, weld zone resistance to welding induced cold cracking, preliminary heat treatment effects 79—91720
  steel, high strength low alloy, acoustic emission meas. from crack opening displacements 80—7732
  steel, high strength sheets, finite element anal. of crack propag. expts. 80—40498
  steel, high-speed, cast, mech. props. at high temps. 79—20135
  steel, HSLA, HAZ microcrack study in multilayer welding *(Chinese)* 79—100172
  steel, HY 100 and 130, fibrous cracking, COD and initiation, replication technique 77—56069
  steel, inclusion, grain boundaries and H_2 attack, fracture analysis 77—32695
  steel, lamellar pearlite, containing proeutectoid cementite, brittle-fracture study *(Japanese)* 80—93648
  steel, laminar composite, crack extension, rising tensile load effect 77—36642
  steel, lightly alloyed, S effect on failure following controlled rolling *(Russian)* 79—57086
  steel, low alloy, crack branching in delayed fracture 79—79067
  steel, low alloy, crack form. during stress relief in heated zones *(German)* 79—74242
  steel, low alloy, crack tip stress and strain fields and fracture behaviour 78—22304
  steel, low alloy, fracture strength investigation under various types of loading 78—7042
  steel, low alloy, high strength, correlation between fracture toughness, tensile props., fracture morphology 78—60789
  steel, low alloy, naval, stretch zone width meas., COD for ductile crack initiation 78—68813
  steel, low alloy, quenched and tempered, formation of stony fracture during forging 79—79059
  steel, low alloy creep resisting, causes of weldment cracking 78—56760
  steel, low alloy press. vessel, fracture toughness determ. from invalid compact tension specimens 77—4848
  steel, low alloy-high strength, deforms. during cold crack developments in welded joints 80—81142
  steel, low C, brittle fracture susceptibility, low temp. deform. effects 77—56103
  steel, low C, fractographic study of stage 1 cracking, endurance limit *(Japanese)* 77—8936
  steel, low C, nucleation and increase of discontinuities in environment of non-metallic inclusions *(Polish)* 79—79022
  steel, low C, slip band expt. studies during fatigue process 80—45374
  steel, low C, structural, AE rel. to crack tip plasticity *(Japanese)* 79—66150
  steel, low C, Ti inclusion nucleation, effect on crack formation *(Czech)* 79—91782
  steel, low C, transition behaviour, bending speed effect *(Japanese)* 78—11222
  steel, low C, type 08Yu, influence of nonmetallic inclusions on microfailures, during strain *(Russian)* 79—34128

cracks continued
  steel, low C, type 17G2SF, crack critical opening evaluation using plasticity diagram 80—45382
  steel, low C, under rotating bending and torsion, overstressing effects *(Japanese)* 77—8935
  steel, low S, overheating 77—21185
  steel, low-alloy, fracture resist. assessment from stable crack length *(Russian)* 79—15765
  steel, low-C, S10C and 520C, tensile fracture at low temps. *(Japanese)* 80—81163
  steel, maraging, high strength, gaseous H_2 embrittlement 77—86147
  steel, maraging, Ni, H_2 assisted crack growth 77—73346
  steel, maraging, pressure vessel, with defects, failure anal. 77—44361
  steel, martensitic, grinding crack formation, impingement cracks and strain influence *(Japanese)* 78—56747
  steel, martensitic, impact bending failure resistance, initial crack length and tempering effects 78—31530
  steel, martensitic, tEM examination of microcracking in plate martensite *(German, English)* 79—91887
  steel, martensitic grain size effects in H_2 assisted cracking, austenitising 77—28901
  steel, medium C, internal cracks in continuous casting billet and rolling products *(Chinese)* 79—43375
  steel, metastable austenitic, resistance to failure 77—4852
  steel, mild, and stainless, ferritic and austenitic, susceptibility of underclad cracking, rel. to chem. comp. 77—21280
  steel, mild, resistance to slow stable crack growth, use of J integral 78—68809
  steel, mild, X-ray meas. of conc. stress at crack tip *(Japanese)* 77—77570
  steel, Mn-Cr-V, crack propag. resist. at hardness indentation, and fracture toughness *(German)* 79—29220
  steel, MnMoNi(Cr), pressure vessel, stress relief cracking 79—43404
  steel, Ni (23 wt.%), crack propag. in the presence of H_2 *(French)* 78—15517
  steel, Ni-Cr, case hardened rollers, macroscopic and microscopic changes in surface layer due to rolling contact 77—77518
  steel, Ni-Cr-Mo, exam. of delayed fracture using fracture mechanics *(Japanese)* 78—52961
  steel, Ni-Cr-Mo-V, temper embrittled, crack initiation strength *(Japanese)* 77—52474
  steel, Ni-Mo-Cr, critical value of J-integral determ. *(German)* 80—25827
  steel, perlitic, ferritoperlitic and bainitic, stress state influence on fracture *(French)* 79—79093
  steel, pressure vessel, A533B, ductile, plane strain crack growth 78—80621
  steel, quenched, adsorption of P on austenite grain boundaries rel. to tendency to delayed fracture of type 18Kh2N4VA *(Russian)* 80—45378
  steel, quenched 40Kh2N5SM and 18KhNVA, nature of delayed fracture 77—90456
  steel, rail, fracture rough exam. of wear in rollers, subject to creep 79—15808
  steel, rolled 15 MND 6, nuclear reactor cell material, determination of non-cracking threshold *(French)* 79—52367
  steel, SAE 4340, depend. of fracture roughness on crack velocity 79—47772
  steel, Si, braking cracks by pulse by current 77—16683
  steel, sintered, maraging, N14K7M5T, mech. props., effect of Ti additions 77—25081
  steel, spheroidised AISI 1095, U-notched bend specimens, hydrogen effect on fracture 79—52363
  steel, St.3, fatigue fracture near slot shaped stress concentrators 77—1870
  steel, stainless, 20% cold worked, type 316, creep failure time 78—19894
  steel, stainless, 316, intergranular crack growth by diffusion 79—24608
  steel, stainless, 316, nuclear fuel cladding, crack nucleation 78—72864
  steel, stainless, creep crack growth rate, correlation of tension and bending type specimens *(Japanese)* 79—38944
  steel, stainless, diffusive crack growth under plastic deform. 79—20182
  steel, stainless, duplex, hot ductility and fracture mechanism 78—60731
  steel, stainless, He ion irrad., fracture behaviour, in-situ HV electron microscopy 80—29089
  steel, stainless, single crystals, shear cracks, electron microscope study 80—40522
  steel, stainless, type 304, creep crack extension rates 80—3160
  steel, stainless, type 316, cyclic creep behaviour, as func. of max. applied stress 78—48460
  steel, stainless 304, crack initiation obs. in low-cycle fatigue specimens 77—52490
  steel, stainless 304, crack propagation under intermittent overloading at elevated temperatures *(Japanese)* 79—38947
  steel, stainless 304, fracture mech. appl. to crack propag. under creep *(Japanese)* 78—27606
  steel, stainless AISI 304, single phase FCC, stacking fault energy and delamination wear 78—3239
  steel, stainless brittle zone Al 3 component composites deform. and fracture 77—56104
  steel, stainless SUS 316, creep fracture at elevated temps. vacuum environment effect *(Japanese)* 77—8942
  steel, stainless wire reinforced Al-Zn-Mg system, resistance to crack propagation 79—43409
  steel, static bend testing of cracked samples until failure, −60 to 20°C 78—23893
  steel, structural, arrested brittle cracks in Robertson test with temp. gradient 77—56052
  steel, structural, impurity effect on crack initiation, dynamical loading *(Czech)* 80—60955
  steel, structural, rel. between static and dynamic fracture toughness 78—68815
  steel, structural, St37-2, crack tip displacement and flow curves *(German)* 79—47747
  steel, structural 15Kh2NMFA, use of linear and nonlinear fracture mech. for crack propagation resist. determ. 79—5056
  steel, structures, failure assessment method and fracture mechanics 78—48488
  steel, Ti (0.1 to 0.55 wt.%), strengthening by carbide precipitation 77—25062
  steel, tool, maraging, based on N12M10, exam. of hardening, crack resistance and wear *(Russian)* 79—34047

cracks continued
- steel, two-phase austenitic-ferritic, plastic deformation under hot working conditions 77—48466
- steel, type 27KhGSNL., castings, exam. of cracks due to treatment 78—44205
- steel, type 316, wedge crack nucleation 77—73339
- steel, type 4140, elastic-plastic plane-strain crack growth, comparison of theory and experiment 80—108560
- steel, type A508, Cl 2, microcrack formation during stress-relief annealing of a weldment 78—80629
- steel, type Kh13N9D2MT martensitic aged, struct. and mech. props. *(Russian)* 80—93600
- steel, types A533B and KAS, fracture toughness meas. using elect. potential method *(Japanese)* 80—93722
- steel, types S25C and S45C surface damage produced by pulsating impact contact load *(Japanese)* 80—104263
- steel, very low C, delamination study by impact testing 78—3218
- steel, welded-joints, H_2 induced cracking, S content effect 80—97562
- steel, Zn coated, cold rolling influence on struct. and deform. of diffusional layer *(Russian)* 80—55465
- steel 18 Gps, ductile fracture, rel. between plastic deform. in fracture zone and fracture characts. *(Russian)* 77—52457
- steel 35GS and 20GS, thermally strengthened rolled, H_2 embrittlement and cracking resistance *(Russian)* 78—35479
- steel AISI 304 tubes, fatigue crack growth under mixed loading conditions 77—3114
- steel compact specimens, finite element analyses of dynamic stress intensity factors, and crack arrest stress intensity factors 79—61732
- steel fibre reinforced concrete, tensile strength and ultimate strain *(Polish)* 80—21027
- steel for nuclear pressure vessels, transient finite element crack propag. model 77—3106
- steel layer types St3+0Kh13, acoustic emission parameters, brittle fracture, crack propagation *(Russian)* 80—93633
- steel layers, types St3+Kh18N9T, acoustic emission parameters, brittle fracture, crack propagation *(Russian)* 80—93633
- steel low alloy, 30KhGSA, sheet, regression anal. of critical stages of fracture process 79—15786
- steel low C, fatigue strength of notched specimen, low-temp. quenching and quench ageing effects 79—100173
- steel parts, martensite form., hardening cracks, acoustic emission investig. possibility 79—29177
- steel structural components, flaw assessment based on cleavage fracture hypothesis 78—60804
- steel wire reinforced polymer, crack growth matrix toughening effect of glass fibres 77—56076
- steel-Cu M3 bimetal, eutectic alloy, crack development, failure energy capacity *(Russian)* 80—40480
- steels, cleavage fracture model at low temperatures *(German)* 80—35293
- steels, high strength, optical crack profile meas. and correlation with mech. props. *(German)* 80—21108
- steels, hydrogen cracking under long-term strength tests 77—86243
- steels, low alloy, grain boundary anal.,, H_2 embrittlement, scanning AES 79—43256
- steels, low-C, aged after quenching, rel. between micro-cracks and coaxing effect *(Japanese)* 80—81159
- stochastic models, appl. to composites and polymers 80—10198
- straight, in grooved and ungrooved shafts, stress intensity factor calc. 77—56061
- strain energy density and surface layer energy for blunt cracks or notches, book contrib. 78—94618
- stress analysis of crack, elastoplastic range 78—67144
- stress and crack-displacement intensity factors, in elastodynamics 78—67112
- stress concentration near apex, elasticity theory and photoelastic expts. 80—23959
- stress fields generated by defects in continuum 79—69104
- stress gradients, crack propagation and arrest 77—68527
- stress intensity factor, near doubly riveted stiffeners 78—67152
- stress intensity factor, three dimens. speckle interferometry, along crack front 77—84196
- stress intensity factor determ., using numerical method *(Italian)* 80—14625
- stress intensity factor determ. along crack path., numerical method 80—74808
- stress intensity factor for crack and nearby slip band, two-phase material 77—56097
- stress intensity factor formula for side notches 78—79264
- stress intensity factor measurement, dynamic fracture toughness determination from isopachics of a running crack [holographic interferometry] 79—34257
- stress intensity factors, anal. determ. by variational method for eccentric cracks 78—67115
- stress intensity factors, single-edge cracked bar loaded by in-plane transverse forces *(Chinese)* 78—83327
- stress intensity factors at the tips of kinked and forked cracks 78—67124
- stress intensity factors calc. by finite element methods, 3-D 77—27491
- stress intensity factors for circumferential crack from notch in round tensile bar 79—41618
- Stress singularity for a crack with an arbitrarily curved front 78—5690
- stress-intensity factor determ. by strain-gauge method 80—76445
- stressed rocks, crack induced anisotropy, effective elastic moduli and attenuation 80—56461
- strip, elastic, Griffith crack interactions, mixed boundary value problem 80—58969
- structural changes in single crystal under single electric impulse discharge *(Russian)* 79—65086
- structural steel cracking, plastic deform. and fracture toughness obs. *(German)* 77—59936
- styrene-butadiene rubber, highly deformable, fracture surface roughness 78—44197
- subcritical growth of cracks in thin viscoelastic plates 80—28465
- sugar, triboluminescence and cryst. fracture dynamics 80—50437
- sulphide group minerals, effects of cracks on electrical conductivity 78—64045
- surface, oxide wedging 79—5046
- surface crack growth due to corrosion under low cyclic loading *(Russian)* 79—100285
- surface crack in a clamped circular plate subjected to uniform lateral pressure, bending stress anal. 80—74811

cracks continued
- surface energy density wedging method 77—75858
- symmetrical branches at end of crack, effects on growth 80—103003
- symmetrical Lamb wave scatt. at pair of thin slots 79—47868
- symposium, USA-USSR, 1978, on composite materials fracture 80—11766
- tartaric acid, triboluminescence and cryst. fracture dynamics 80—50437
- teeth, human, laser interactions 77—52840
- tensile cracks and shear faults, elastic wave radiation 79—16411
- tensile impact tests with rupture diagram recording on pendulum machines, testing procedure 79—29313
- tensile stability, effect of crack and cavitation generation 77—16659
- tetramethyl-p-silphenylenesiloxane-dimethylsiloxane block copolymer films, deformation 79—15739
- TGS, deuterated, undoped and alanine-doped, growth by rotating disc method and elec. props. 79—47611
- theory, doubly periodic problem 78—1611
- theory, soln. of two dimensional problems 77—72241
- thermal anal., finite element techniques 77—3793
- thermally activated crack propagation 78—18247
- thermoelastic cracks in plane, boundary integral eqn. method *(German)* 80—106761
- thermoelastic periodic problems for infinite solid with disc shaped cracks, integral eqn. solns. *(Ukrainian)* 78—55559
- thin bodies with cracks, deform. stability problem statement *(Russian)* 77—35081
- thin plate, elastic-plastic equilibrium, cracks running to orifice contour *(Russian)* 80—23956
- thin plates with cracks, local buckling *(Ukrainian)* 77—68461
- thin sheet impact strength study *(Czech)* 80—59571
- three dimensional, stress intensity factors 78—55601
- tip elements, singularity reconsiderations 80—1479
- tip opening displacement by finite element anal. *(Czech)* 78—59343
- tip opening displacement/J-integral relation *(Chinese)* 77—72237
- tip strain distribution measurement by recrystn. *(German, English)* 77—56203
- tip strain meas. by electron micrograph stereoscopy 80—69752
- tip stress and strain *(Chinese)* 79—73249
- transient piezoelectric wave scatt. 79—52615
- transversely isotropic medium with cylindrical cavity and external crack, stress distrib. 78—79259
- triangular quarter point element as elastic and perfectly-plastic crack tip elements 77—14956
- triboluminescence kinetics in crysts. 77—77306
- tube with hexagonal bore, crack formation during rolling *(Russian)* 78—80622
- twisted circular cylinder with radiating internal cracks stress intensity factor *(Chinese)* 80—5984
- two dimensional, reinforced concrete, finite element analysis of structures taking account of nonlinear physical behaviour and discrete crack development 79—57121
- two-component media, macrocrack problem *(Ukrainian)* 79—98666
- two-dimensional, in plate structures, stress analysis, computer program based on superposition method *(Japanese)* 78—51123
- underground nuclear explosion, gas flow in permeable Earth formation with crack 78—61372
- US attenuation, precrack damage and crack propag. study 80—40656
- US scattering of elastic waves, quasistatic approx. 78—67080
- Van der Waals interactions between brittle cracks and gaseous environments 77—90440
- virtual crack extension method, nonlinear material behaviour 78—18230
- virtual extension method for combined tensile and shear loading 78—67149
- viscoelastic, crack growth relations, for orthotropic, prestrained media 78—90772
- viscoelastic bodies, crack growth kinetics under cyclic loads *(Russian)* 80—87739
- viscoelastic body containing cracks, durability calcs. 80—79227
- viscoelastic mass, detachment of glass sphere, crack tip *(French)* 78—42536
- viscoelastic medium, crack growth *(Russian)* 78—18252
- viscoelastic medium, linear, semi-infinite crack propagation, tip stresses and displacements 80—53700
- viscoelastic plate of arbitrary shape, crack growth kinetics *(Ukrainian)* 77—68523
- viscoelastic solid, crack growth law using energy and COD fracture criteria 79—32378
- viscoelastic solid, kinetics of propagation *(French)* 77—89065
- viscoelastic solids, linear, crack growth law derivation, fracture process zone concept 80—92088
- viscoelastic strip, dynamic crack propagation due to antiplane loading 80—64464
- wear, delamination theory, review 78—3229
- wearing half-space, determ. of stress intensification factors 80—99964
- wedge loading of a semi-infinite strip with an edge crack 78—79270
- wedge shaped crack, apex singularities under all modes 80—64480
- wedge-shaped crack plastic zone, superdislocation model 79—94557
- wedged crack, propag, data with static compliance calibration 80—2115
- Weibull distribution, adding static and dynamic fatigue effects 80—70298
- Westerly granite, stress effects on cracks 77—25676
- Westerly granite, vel. anisotropy, dilatancy effect 79—2226
- wood, cracked beam, mode II stress intensity factor 77—73325
- wood, Douglas fir, crack front width effect on fracture toughness 77—56060
- yield stress, crack opening displacement and stress intensity factor relationship, appl. of modified Dugdale model 79—41615
- yield zone form., fracture resistance, influence of specimen configuration 78—68817
- Zircaloy-2, hydride precipitation and growth at crack tips, electron optical obs. 80—108449
- Zircaloy-2, role of oxide plasticity in oxidation behaviour 77—36680
- zirconate-titanate ceramics, K_{IC} eval. by double torsion technique 77—90444
- Al 6061 alloy, B fibre reinforced, fracture 80—11773
- Al alloy, 2219-T851, crack closure 78—7012
- Al alloy, crack arrest toughness, used to estimate plane strain for toughness 77—63863
- Al alloy, crack propag. toughness testing 77—44449
- Al alloy, crack tip studies, stretched zone and COD 78—68812
- Al alloy, K_{1c} determ. method, results scatter *(French)* 77—70167

cracks continued
- Al alloy, RR58, remaining creep life estimation from creep crack density meas. 78—44194
- Al alloy 2017-T3, part-through crack propagation, by alternating bending stress *(Japanese)* 78—27607
- Al alloy 6061-T6, fracture initiation and propagation during strip drawing 78—64663
- Al alloy AK4-1 with surface cracks, fracture toughness determ. *(Russian)* 77—25141
- Al alloy Al 7075-T651, microcrack closure load development for stage I and II cracking 77—86150
- Al alloy type 7010-T7651, high toughness, cyclic and monotonic crack propag. 80—108528
- Al alloys, fracture toughness under plane stress 78—92316
- Al alloys 7075-T6 and 2024-T3, crack propag./wear rate relationship 78—3232
- Al, anodised surface, neutral particle emission during tensile deform. 79—78856
- Al, crack growth resistance, J-integral approach, crack line wedge loaded specimen 78—35513
- Al, crack resistance, J-integral approach 77—66699
- Al, deformed surface layer, block misorientation 79—99405
- Al epoxy bonded joint, determ. and appl. of COD 80—30078
- Al, fracture due to shock waves leaving surface, shear stresses 78—51128
- Al, liquid metal embrittlement by Ga 78—64653
- Al, oxide covered, tensile deform. in high vac., particle and photon emission 78—39672
- Al sheet alloy D16AT, regression anal. of critical stages of fracture process 79—15786
- Al sheet D16AT, plastic strain distrib. at crack tip by coordinate-grid method 80—16400
- Al, single phase FCC, stacking fault energy and delamination wear 78—3239
- Al, step coverage optimisation by computer simulation and SEM 78—51838
- Al-Ag (7.27 wt.%), peculiarities exhibited during fatigue loading *(Chinese)* 80—71723
- Al-Al_2O_3 composite, brittle zone on fibre surface deform. and fracture 77—56104
- Al-Cu, type 1100, synchrotron radiation microradiography 80—85121
- Al-Cu-Mg alloy RR58, comparison of methods of correlating creep crack growth 78—60826
- Al-Cu-Mg-Mn (4.5, 1.5, 0.6 wt.%), thin sheet, exam. of fracture toughness, and fatigue crack growth 78—92353
- Al-Cu-Mn, type 2219, synchrotron radiation microradiography 80—85121
- Al-$CuAl_2$ eutectic, deformed, thermal stability 77—52348
- Al-Zn-Mg, ductile intercrystalline fracture obs. 77—77554
- $AlNbO_4$, polycrystalline, thermal diffusivity, effect of microcracking 78—26743
- Al_2O_3, bending strength, surface roughness effect at high temp. *(Japanese)* 79—70131
- Al_2O_3, fracture stress rel. to flaw and fracture mirror sizes 79—11689
- Al_2O_3, fracture toughness meas. using Knoop indentation method *(German)* 80—25830
- Al_2O_3, fracture toughness determ. using four-point-bend specimens 80—108536
- Al_2O_3, hot pressed, fracture stress-reflecting spot relations 80—71731
- Al_2O_3, sintered, correlation between wear, crack resistance and stress intensity factor *(German)* 77—36666
- Al_2O_3, spalling and cracking by compression 77—81313
- Al_2O_3 strength-size relation 77—21255
- Al_2O_3 substrates, tape-casted, fracture strength analysis 80--60948
- Al_2O_3, thermally shocked, strengthening kinetics 77—8920
- Al_2O_3, twinning and microcrack nucleation during indentation 77—63793
- Al_2O_3, unflawed polycryst., tensile failure, SEM and acoustic emission expts. 78—27598
- β-Al_2O_3-MgO ceramic, formation and structure of atomic scale cracks 80—45395
- Al_2O_3-SiO_2 (3 wt.%), J-integral meas. at high temps. *(German)* 80—93624
- Al_2O_3-ZrO_2 composite, fracture toughness increase by microcracking in energy dissipative zone near crack tip 79—20156
- Al_2O_3-ZrO_2 dispersed system, thermal diffusivity/conductivity, effect on microcracking resulting from phase transform. 78—10231
- Al_2TiO_5, grain size pseudobrookite oxide, microcracking relations 79—29194
- AlZnMgCuO.5, crack propag. under monotone and cyclic load 78—7006
- AlZnMgCuO.5, static crack growth, stress state effect, elec. pot. meas. 78—7007
- B fibre reinforced epoxy laminate, energy release approach for stable crack growth in free edge delamination problem 78—19878
- B fibres, radial cracks 78—15505
- B_2O_3-SiO_2 glass, crack front shape corrections for crack velocities in double torsion specimens 79—91778
- B_2O_3-SiO_2 glass, crack growth, phase separation effects 80—89336
- $BaTiO_3$, effect of phase transformation on fracture behaviour 78—48507
- C fibre reinforced epoxy and unsaturated polyester resins, crack form. *(German)* 78—19887
- C fibre reinforced plastic, shear props., effects of flaws and voids 77—44334
- C, glassy, size effect on bending strength 79--52309
- C-C composite, structure model, Rosen model with fractional matrix 80—11719
- $CaCO_3$, Iceland spar, crack interactions with twin interlayers 77—7790
- CaF_2, hot forged, laser window material, fabrication, props. 77—46773
- CaF_2, strength-controlling fracture energy depend. on flaw-size to grain-size ratio 80—81152
- Co-Mo alloy electrodeposits, codeposited impurities rel. to H_2 permeation, props. 79—19493
- Cr film, evaporated, on die-cast Zn, microstruct. and intrinsic stresses, substrate temp. effects 78—10304
- Cr-Mo-V, steamline bends, restorative heat treatment effects 78—68716
- Cu and Cu-Sn(Zn)(Al) alloys, wear, effect of Mn_5Si_3 content *(Japanese)* 78—35525
- Cu, continuously cast, O free, effect of nonmetallic inclusion on microstruct. and props. 77—81280
- Cu, crack propag. and fracutre kinetics in creep, optical microscopy and SEM obs. *(Russian)* 79—52342
- Cu, fracture due to shock waves leaving surface, shear stresses 78—51128

cracks continued
- Cu solid soln., wear 78—3233
- Cu solid solutions, single phase FCC metal, stacking fault energy and delamination wear 78—3239
- Cu, tough pitch wire, microcrack and cupping formation *(Japanese)* 79—79087
- Cu-Al (5.5, 7.3, 6.3 and 2.5 wt.%), Hg embrittlement under cyclic loading 77—86225
- Cu-Al-Ni-Fe-Mn, cast Ni-Al bronze, fracture metallography 78—27597
- Cu-Be (2 at.%), plastic deform. and dislocation substruct. 80—76307
- Cu-Cr, precipitation hardened, wear 78—3234
- Cu-Cr-Zr-Ti-B alloy system, solidification cracks formed during welding, reduction by microalloying with B 79—96148
- α-Cu-Ni-Zn-Pb, fire cracking and ordering *(German)* 78—60760
- Cu-P (8.4 wt.%) metallic laminate, laws governing development and retardation of fast cracks 78—15527
- Eu_2O_3-Ta_2O_5, microcracking, elastic props., internal friction 78—92326
- FE, electrolytic, dissolved H precip., effect on flow stress *(Japanese)* 78—39848
- Fe alloy MA-956E, oxide dispersion strengthened sheet, tensile and creep props. at 1365K 78—48470
- Fe and Fe alloys, polymorphism effect on failure accompanying electrospark action *(Russian)* 79—74236
- Fe, Armco, microstructure in quasibrittle and plastic fracture 77—1863
- Fe, Armco, sleeve, deformed by cold drawing, exam. of surface and texture *(Russian)* 79—34057
- Fe, Armco, transform. of observed crack traces on section to true crack density for fracture calcs. 79—10533
- Fe, BCC, atomistic studies of H_2 enhanced crack propag. 78—31538
- Fe, cast, fracture mech. and fractography *(Japanese)* 78—7031
- Fe, cast, grey, martensitic, lamellar, internal notch effect on abrasive wear *(German)* 79—29231
- Fe, cast, rare-earth-Mg nodular, fracture toughness and fatigue *(Chinese)* 78—95791
- Fe, cast rod, breakdown charact. by longitudinal stress waves 78—38773
- Fe, H_2 adsorption at dislocations and cracks 79—20146
- Fe, metallised pellet, factors influencing crushing strength after H_2 reduction 79—11531
- Fe, microcracks formed by H_2 precipitation, SEM and TEM obs. *(Japanese)* 79—70071
- Fe, polycrystalline, fracture surface singularities under single loading conditions *(Russian)* 80—50696
- Fe, pure, hydrogen-charged, initial cracking obs. 80—108580
- Fe, volume changes and defect healing due to plastic deform. *(Russian)* 80—81139
- Fe-Al-Si (6.22, 9.63 wt.%), bending test under high press., high temp. 80—85057
- Fe-Cr-Ni-Si, sintered, carbide coated, crack propag. energy in impact bending 79—66162
- Fe-Ni base alloy, precracked specimen, K_{Ihcc} threshold value under const. load at high temp. *(Chinese)* 78—31499
- Fe-Ni single crystal, lattice strain induced by anisotropic distrib. of M_2 *(Japanese)* 80—35262
- Fe-Ni-Al (18.2 wt.%) aged, fracture toughness and mode, grain size depend. 77—12700
- Fe-Ni-C, martensitic delayed fracture *(Slovak)* 79—43401
- Fe-Ni-C, mech. and structural props. under cathodic H_2 at elevated temps. *(French)* 77—59920
- Fe-Ni-Cr, austenitic, creep strength and ductility, effect of γ' precipitation 77—36597
- Fe-Si, crack propag. kinetics, effect of current pulses 78—31531
- Fe-Si, dislocation struct. of plastic relax. zone at tip of brittle crack 77 77582
- Fe-Si(3.25 wt.%), crack nucleation depend. on twins during intense slip *(Russian)* 79—100239
- Fe_2TiO_5, grain size pseudobrookite oxide, microcracking relations 79—29194
- GaN, formed from initial oxidation and nitridation of GaAs, surface and contact props. 77—20436
- GaP crystal, structure defect formation due to annealing and stress, dendrites, slip, dislocations 80—29026
- p-Ge film, fragmented struct., elec. cond., Hall coeff. and magnetoresist. meas. 77—15979
- H embrittlement cracking at notches, model, based on stress induced diffusion of H atoms 78—39897
- H embrittlement cracking at notches 78—84985
- H_2, distrib. kinetics in vicinity of crack *(Russian)* 77—25132
- HfO_2, monoclinic, microcracking, elasticity, internal friction, thermal expansion meas. 79—29195
- InBi single crystal, deform. mode under dynamic indentation 80—88163
- InP, damage induced during handling for TEM obs. 80—2024
- InP-$Ga_xIn_{1\ x}$As-InP, DH fabrication, crack form. due to lattice mismatch 77—15704
- KCl, annealed in KBr vapour, crack and pore formation, diffusionally induced stress relaxation *(Russian)* 80—40388
- KCl, brittle fracture on electron bombardment, probability distrib. functions 79—86820
- KCl, spontaneous cleavage, step line propag., macroscopic defects 78—87662
- KH_2PO_4, cryst. growth, splitting due to colloidal inclusions 77—7681
- Li-Sn, phase relationships between Li_7Sn_2 and LiSn, microcracking obs. in quenched alloys 79—78933
- $LiAlSiO_4$ glass-ceramic, fracture phenomena as function of initial flaw size and temp. 78—95797
- LiF bicrystal, high-angle tilt boundary and edge dislocation intersection effects 80—79836
- LiF, dislocation mechanism of electrification during cleavage 77—24353
- LiF, dislocation mobility near fast-moving crack tip 78—47389
- LiF, plasic deform., cleavage-crack propag., X-ray topography 77—39625
- LiF single cryst. with vac. deposited Bi film, surface failure induced by laser impulse *(Russian)* 77—35585
- LiF, stressed state and dynamics of dislocations near tip of fast growing crack 77—62541
- $LiNbO_3$ waveguide, diffusion of Ti, exam. by electron probe anal. and X-ray diffr. 78—47588
- $LiNb_{1\ y}Ta_yO_3$, Czochralski growth and basic props. 77—63556
- Li_2SO_4, triboluminescence and cryst. fracture dynamics 80—50437
- $MgAl_2O_4$, strength-controlling fracture energy depend. on flaw-size to grain-size ratio 80—81152
- MgO, anisotropy of grinding damage, chem. polishing and etching 79—47793

cracks continued
MgO, crack propagation during in-situ deform., plastic zone formation 80—16468
MgO, crack tip dislocations and dislocation-free zones 80—96533
MgO, lattice misorientation and displaced vol. for microhardness indentation 78—64617
MgO single cryst., impact wear damage 80—76375
MgO, single crystal, wear damage, surface cracks 78—68825
MgO single crystals, crack formation process, micro-deformation and fracture *(Japanese)* 80—24530
MgO, thermally shocked, strengthening kinetics 77—8920
$MgTi_2O_5$, grain size pseudobrookite oxide, microcracking relations 79—29194
$MgTi_2O_5$, thermal diffusivity, grain size and microcracking effects 78—10233
Mo, dislocation structure, temp. depend., at crack tip, of fractured single cryst. 79—29210
Mo, fracture and crack propag. tested in tension along [001] axis *(Russian)* 80—50697
Mo, microcrack formation, structural singularities, TEM obs. *(Russian)* 79—1905
Mo, neutron irradiation effects on microcracks *(Ukrainian)* 79—77639
Mo sheet, 45° brittleness due to partial recrystallisation, 45° crack formation and propagation *(Russian)* 79—100238
Mo sheet, shock-induced intergranular cracks 79—57087
Mo, siliconised thermal stress and thermal expansion 77—21324
Mo/Nb welded joints in sheet metal, detect. and exam. of cracks, initiation, development 77—73385
Mo-C (0.07 wt.%), two-phase alloy, fracture and deform. characts., struct. depend. *(Russian)* 77—32635
Mo-Hf-C, superior powder metallurgy die alloys for isothermal forging mech. props. 79—74201
Mo-Re alloy wire, high-strength, fracture mechanism *(Russian)* 77—25126
Mo-Ti-Zr alloys TZM and TZC, superior powder metallurgy die alloys for isothermal forging mech. props. 79—74201
Mo-Ti(B)-Zr(Al)-C, stress cycling at room temp. *(Russian)* 77—25148
NaCl, damage process preceding semi-brittle fracture in depend. on deform. microcrack development 77—44272
NaCl, deformed surface layer, block misorientation 79—99405
NaCl, plastic deform., cleavage crack propag., X-ray topography 77 39625
NaCl, single cryst., crack healing at low temp. 77—36622
NaCl, single crystal, surface markings, left by unsteady cleavage crack propag. 79—46746
NaCl, tricrystal, crack propag. 77—70177
Na_2O-Al_2O_3-SiO_2, porous glass, crack shape, US fractography obs. 77—44336
Na_2O-Ca_2O-SiO_2 glass, crack nucleation about pointed indentations 79—91779
Na_2O-CaO glass, crack nucleation during indentation, micromechanics 80—30069
Na_2O-CaO glass, shear deform. under pyramidal indentations 80—84989
Na_2O-CaO glass, strength and failure predictions 77—21256
Na_2O-CaO-SiO_2, double torsion specimens, compliance and fracture load as crack length function 78—48508
Na_2O-CaO-SiO_2, expt. errors in estimating time to failure 77—16666
Na_2O-CaO-SiO_2, fracture mirror form. 77—48541
Na_2O-CaO-SiO_2, glass, surface indentation effect on mech. strength, and thermal stress resistance 78—48463
Na_2O-CaO-SiO_2 glass, K_{IC} eval. by double torsion technique 77—90444
Na_2O-CaO-SiO_2 glass, crack nucleation around plastic indents 78—92327
Na_2O-CaO-SiO_2 glass, sharp contact cracking, residual stress effects 79—100245
Na_2O-CaO-SiO_2 glass, fractographic anal. of delayed failure 80—45387
Na_2O-CaO-SiO_2 glass, high-vel. liq. impact, oblique impact anomaly 80—89329
Na_2O-CaO-SiO_2 glass foils, HVEM in-situ straining expts. 80—104216
Na_2O-SiO_2, crack front shape corrections for crack velocities in double torsion specimens 79—91778
Na_2O-SiO_2 glass, microcracking about NiS inclusions, fracture mech. description 80—89333
Na_2O-SiO_2 glass, OH^- content effect on mech. and other props. 80—89337
Na_2O-SiO_2 glass, scoring, deform. and fracture mech. approach 80—89332
Na_3O-CaO-SiO_2, fracture initiation, influence of temperature and composition 79—100246
Nb, H_2 embrittlement, microscopic obs. at low temps. 77—32666
Nb_3Sn composite wires, supercond., degradation mech. under tensile strain at 4.2K 79—38284
Nb_3Sn filamentary superconducting composites, mechanical property variations between composites 79—57054
Nb_3Sn superconductors, mech. behaviour, diffusion *(German)* 78—39880
Ni alloy 718, creep crack growth 77—63776
Ni base alloy 718, crack growth behaviour at 425°C 79—61731
Ni, oxide covered, tensile deform. in high vac., particle and photon emission 78—39672
Ni plated Fe single crystal, deformed at 77K, surface obs. 78—19916
Ni single crystal foil, H_2 induced deform. during thinning, electron-optical obs. 79—57059
Ni, single phase FCC stacking fault energy and delamination wear 78—3239
Ni, volume changes and defect healing due to plastic deform. *(Russian)* 80—81139
Ni wire reinforced epoxy resin, crack propagation 79—29188
Ni-Al bronze, fracture resistance of tubes 78—19867
Ni-base superalloys, powder metallurgical, creep-rupture at intermediate temps. 80—97568
Ni-base wrought superalloy, creep and stress rupture behaviour in air and vacuum 80—60918
Ni-Cr-Al-TaC, eutectic composite, microstructure, fatigue props. 80—85038
Ni-Cr-Co superalloy, σ-phase effect on mech. props. *(Chinese)* 79—74229
Ni-Cr-Co superalloy IN-792, crack growth resistance, metallurgical effects 77—36655
Ni-Cr-Co-Mo-Al-Ti alloys, Waspaloy, Astroloy, exam. of microstruct. effect on crack growth 78—52977

cracks continued
Ni-Cr-W-Mo-Ti-Al alloy KhN67MVTYu, heat treatment effect on mech. props. 77—70082
Ni-Mo alloy electrodeposits, codeposited impurities rel. to H_2 permeation, props. 79—19493
Ni-Mo-Cr steel, elastic-plastic material characterisation 78—72854
Ni-Nb-Al-(Cr), eutectic, mech. props., high press. H_2 effects 77—63779
Ni-W (45.5 wt.%), eutectic, mech. props., high press. H_2 effects 77—63779
Ni_3Al-Ni_3Nb, eutectic alloy, crack development, failure energy capacity *(Russian)* 80—40480
Pb(Zr,Ti)O_3, fracture and deform. 80—79870
Pb(Zr,Ti)O_3, K_{IC} eval. by double torsion technique 77—90444
Se glass, flexural strength in transition range 77—56032
Se-Ni-Mylar multilayered struct., interfacial bonding effect on adhesion, ESCA obs. 79—95274
Si, crack-tip dislocation pattern, X-ray topography *(French)* 80—107253
Si, dangling bonds, EPR, localised states and unpaired electrons on microcrack surfaces 78—52351
Si, mechanically damaged surfaces, EPR meas., role of microcracks 79—42836
Si, near (111), fracture by painted indenter, SEM study 80—71734
Si, near (111) slices, scratches made by diamond stylus 77—12726
Si, surface, stacking fault generation due to mech. damage, preoxidation annealing influence 80—54261
Si wafers, scribing and subsequent fracture 80—11743
Si-Al-O-N, high-temp. fracture and diffusional deform. mechanisms 80—40509
SiC, fracture toughness and high-temp. slow crack growth 80—81153
SiC, polycrystn., crack length and indentation dimension versus indentation load 79—70157
Si_3N_4, evidence for cavitation crack growth, SEM study 79—79086
Si_3N_4, fracture toughness meas. using Knoop indentation method *(German)* 80—25830
Si_3N_4, hot pressed, crack healing *(German)* 79—24599
Si_3N_4, hot pressed, fracture phenomenology, fracture surface energy, crack propagation 79—57090
Si_3N_4, hot-pressed, fracture mech. parameters, indentation-precracking and double-torsion methods 80—104364
Si_3N_4, hot-pressed, fracture toughness determ. using specimens with chevron and straight through notches 80—108538
Si_3N_4, hot-pressed, strength anisotropy origins 80—89330
Si_3N_4-Al_2O_3, hot-pressed with crystn. grain boundary phases 78—95716
SiO_2 films sputtered in H-Ar mixed gas, enhanced step coverage 80—75470
SiO_2, fused, crack nucleation about pointed indentations 79—91779
SiO_2, fused, fibres, lifetime predictions, applicability of crack velocity date 77—52467
SiO_2, fused, single particle impact damage 80—40508
SiO_2 glasses surface textures and defects, exam. using liq. crysts. 80—6364
SiO_2 reinforced decorative laminates, abrasion resistance, abrasive paper deterioration 77—16696
SiO_2-Na_2O glass, fracture initiating flaws, depth meas., crack propag., SEM exam. 78—48494
SiO_2-PSG-Si_3N_4 composite layer, on Si, crack occurrence, PSG film thickness and comp. effects 77—72806
Ta foil, crack growth resistance, straining stage in SEM 77—25124
Ti alloy, crack resistance, J-integral approach 77—66699
α-Ti, crack growth under tensile loading, in-situ obs. *(Chinese)* 79—96121
Ti, oxidation behaviour under pure O_2 atmos., temp. range 600-800°C 80—89415
Ti, volume changes and defect healing due to plastic deform. *(Russian)* 80—81139
Ti-Al-Mo-Cr (4.5, 5, 1.5 wt.%), weld metal, α/β interace sliding 80—108512
Ti-Al-Mo-Sn-Si (4,4,2,0.5 wt.%), fracture toughness and crack propagation 78—39892
α-βTi-Al-Sn-Zr-Mo (6, 2, 4, 6 wt.%), deformation associated with surface cracks and α particles 79—79107
Ti-Al-U (6,4 wt.%), low and high cycle fatigue rupture at same load 78—3217
Ti-Al-V, plane strain toughness and resistance to crack propagation *(French)* 78—23813
Ti-Al-V (6, 4 wt.%) slow crack growth in air and fracture toughness, H content effect *(French)* 80—45385
Ti-Al-V (6,4 wt.%), sustained loading charact. and H_2 effects 78—48515
Ti-Al-Zr-Mo-Si (6,5,0.5,0.25 wt.%) fracture toughness and crack propag. 78—39892
Ti-Al-(V) (6,4 wt.%), hot salt stress corrosion susceptibility, microstruct. effects 77—36688
TiC hard coating on Co, effect of martensitic transform. in substrate causing cracks 79—29060
(U,Pu)O_2, ceramographic exam. of Dounreay PFR fuels, data bank storage 79—49811
UO_2, isothermal crack healing and strength recovery, thermal shock effects 77—36625
UO_2, strength recovery and crack healing 77—8918
UO_2, surface energy, determ. by Hertzian indentation 80—93641
UO_2-U_4O_9, thermal cond., effect of microstruct. and microcracking 79—97810
(V,Ti)C+(Ni,Mo) cermet systems, performance through hardness vs crack resist. plots 79—79099
V_3Ga superconducting tape, stress effect on critical current *(Japanese)* 80—50020
W, (100) oriented cryst., plastic relax. effect on semi-brittle fracture 77—69036
W alloy, nonlinear compliance curves, caused by crack closure and fracture tests 77—56064
W bicrysts., crack propag. across grain boundaries, crack speed meas. technique appl. 80—108575
W, cyclically deformed, electrical resistivity 77—52491
W, fan shaped twins of type II, struct. 79—90676
W surface layer struct. during milling, plastic deform., failure *(Russian)* 80—40586
W wires, KSiAl doped cavity formation *(German)* 78—31524
W/Cu powder with varying W particle size, burning behaviour and crack form. tests *(German)* 78—7005
W-Ni-Fe(Co)(Cr), structural characterisation *(French)* 77—56074
WC-Co, creep rupture strength meas. 78—31475

cracks continued
- WC-Co (10 wt.%), vacuum sintered, short-time bending creep rupture strength *(Japanese)* 78—15508
- WC-Co carbide, crack paths, SEM study *(Japanese)* 80—50710
- WC-Co cemented carbide, indentation fracture, operative fracture mode survey 77—70183
- WC-Co particle-matrix composite, fracture and cleavage strength 77—73342
- WC-TiC-TaC-Co cemented carbides, transverse-rupture strength at 600 to 1000°C obs. *(Japanese)* 79—43374
- YAG brittleness anisotropy, microcrack formation due to surface treatment 80—40526
- YIG, film, LPE, annealing-induced relief of compressive misfit strain 78—2386
- Y_2O_3, strength-controlling fracture energy depend. on flaw-size to grain-size ratio 80—81152
- Zn, dislocation mechanism of Rose channel formation under impact loading conditions *(Russian)* 79—79073
- Zn, liquid metal embrittlement 78—64653
- ZnSe, growth centres, crystallographic parameters and etching patterns study *(French)* 79—41998
- Zr alloys with Fe, Cu, Cr, Nb, role of oxide plasticity in oxidation behaviour 77—36680
- Zr and Zr alloys, cracking, H_2 induced delay, strain energy effect on H_2 solubility 78—92364
- Zr, hydride precipitation and growth at crack tips, electron optical obs. 80—108449
- Zr-base alloy as reactor core material, microstruct., deform. and fracture 78—4988
- Zr-Nb, (2.5 wt.%), cold-worked pressure tubing for CANDU reactors, slit burst testing 79—26532
- Zr-Nb (2.5 wt.%), cold worked, in reactor oxidation of crevices and cracks 78—23865
- Zr-Nb (2.5 wt.%), fractographic aspects of H_2 induced delayed cracking 79—47767
- Zr-Nb (2.5 wt.%), H_2 induced subcritical crack growth meas., application of potential drop method 78—27645
- Zr-Nb (2.5 wt.%), heat treatment effects on slow crack growth, cold working effects 77—28836
- Zr-Nb (2.5 wt.%), hydride precipitation and growth at crack tips, electron optical obs. 80—108449
- Zr-Nb (2.5 wt.%), meas. of crack growth at elevated temp. by holographic interferometry 79—38933
- Zr-Nb (2.5 wt.%) pressure type rel. between stess intensity factor, crack opening displacement and J-integral 80—100920
- Zr-Nb alloy, pressure tubes of PWR reactor, cracks identification and avoidance 78—82472
- ZrC, fracture by laser beams, macrocrack propag. 79—15789
- ZrO_2, MgO partially stabilized, microstruct. development during ageing 79—91710
- ZrO_2, partially stabilised, toughening mechanism 77—56084
- ZrO_2-Zr cermet composite, hot pressed, fracture toughness 78—27604
- $ZrSiO_4$, plasma dissociated, improved thermal shock resistant refractories 79—52350

cranes
- bridge, vibration damping calc. 80—101711

cranking model, nuclear *see nuclear cranking model*

crazing
- *see also stress corrosion cracking*
- ABS polymer, fracture behaviour, rubber content effects 77—32676
- ABS polymer, transparent, fracture of notched tensile specimens 77—63772
- ABS resin, craze growth and fracture 80—50705
- acrylonitrile-butadiene-styrene copolymers, micromechanism of deform. and rupture *(German)* 80—35276
- bisphenol-A-diglycidyl ether epoxies, amine-cured, microscopic failure 77—90441
- bisphenol-A-diglycidyl ether epoxies, struct., fracture and mech. response, cure and crystallisation conditions effects 79—15779
- bromostyrene-crosslinked polyester, craze resistance 80—35421
- chinaware, semivitreous, eval. of crazing resistance by stress meas., after autoclaving *(Japanese)* 79—20235
- chinaware, vitreous, elimination of crazing by repeating glost firing *(Japanese)* 79—20236
- circular craze analysis, simple membrane model 77—3779
- compressive stress effect, local stress role 78—19875
- copolyimide glass based on benzophenone tetracarboxylic acid dianhydride 77—63720
- craze density measurement by quantitative TEM 79—24701
- dicyano bisphenol polycarbonate, crazing, polar group incorporation 78—85017
- environment effect on stability of cracking 79—100273
- lacquer coating, brittle, plasticizer *(Japanese)* 77—52479
- micromechanisms of crack extension, conf., Cambridge, England (March 1980) 80—105421
- Nylons, inorganic salt influence on fracture 80—30119
- Nylons, morphology and crack propag. in inorganic salts 80—30118
- PCTFE, work to produce environmental crazing at low temps. 78—15553
- PMMA, correlations of craze profile with Dugdale's plastic zone profile 79—100272
- PMMA, craze shape, fracture toughness, —30 to 45°C 77—48542
- PMMA, craze shape and fracture, temp. depend. 77—52486
- PMMA, craze zones at crack tips, validity of Dugdale model, comment 80—108535
- PMMA, craze zones at crack tips, validity of Dugdale model 80—108534
- PMMA, craze zones at crack tips at different temps., meas. correl. with Dugdale model 78—23826
- PMMA, crazing, deform. kinetics 80—84990
- PMMA, creep meas. in N_2 atmos., craze parameters 79—15734
- PMMA, effect of surface finish on strength, and craze reistance 78—76724
- PMMA, fatigue life enhancement, prior crazing 80—89331
- PMMA, fracture surface parabola markings, temp. 78—52969
- PMMA, glassy, craze growth, expt. and model 78—15520
- PMMA, glassy, in methanol, growth kinetics of solvent crazes, hydrodynamics 79—15836
- PMMA, glassy rods, craze initiation, kerosene wetting effects 77—25172
- PMMA, influence of craze configuration on fracture 78—76758

crazing continued
- PMMA, large deforms. at tip of running crack, opt. interference obs 80—85062
- PMMA, methanol crazes, grown from cracks, exam. of growth criteria 78—48551
- PMMA, methanol crazes, mech. props., craze-strain profile 78—72844
- PMMA, plastic deform. by crazing *(Japanese)* 80—93619
- PMMA, stress relaxation during crazing, eqn. 79—61762
- PMMA, struct.-prop. relationship between mol. wt. and fracture surface energy 78—80633
- PMMA, ultrasonically modulated tensile stress produced fracture surface 79—91815
- PMMA, work to produce environmental crazing at low temps. 78—15553
- PMMA sheet in methanol, pre-soak, dissolved gas content rel. to craze nucleation, creep 79—66185
- PMMA with stress-raising flaw, deform. 80—25799
- polyarylate, solvent crazing *(Japanese)* 79—29246
- polybutadiene, cross linked, deform. below T_g, radical form. and crazing 79—52307
- polycarbonate, craze morphology, 77 to 375K, gaseous environment effect 77—63819
- polycarbonate, craze roles in fatigue 79—29183
- polycarbonate, craze thickening mechanism during craze growth 79—91823
- polycarbonate, crazes, statistical aspects optical microscopic obs. *(Japanese)* 79—29247
- polycarbonate, creep deform. caused by crazing 80—21133
- polycarbonate, criterion for craze nucleation 78—19881
- polycarbonate, cyclic deformation and craze growth 78—76759
- polycarbonate, deform. and failure modes, surface craze characts. 79—91753
- polycarbonate, effect of mol. weight on craze shape and fracture toughness 80—25858
- polycarbonate, environmental stress crazing 78—68832
- polycarbonate, exposed to ethanol, craze nucleation and growth 79—24639
- polycarbonate, fatigue crack propag., mol. wt. depend. 80—50700
- polycarbonate, glassy, fatigue crack initiation in high strain fatigue tests 80—97564
- polycarbonate, impact behaviour, effects of thermal pre-treatment and mol. wt. 78—95798
- polycarbonate, neck propag., rel. to dry craze growth mechanism 80—59563
- polycarbonate, plane strain fracture energy instability and mixed mode crack propag. 78—68775
- polycarbonate, plastic deform. by crazing 79—52310
- polycarbonate, solvent crazing *(Japanese)* 79—29246
- polycarbonate, stress crazing, liq. environment effects 78—84970
- polycarbonate, stress relaxation during crazing, eqn. 79—61762
- polycarbonate, yielding and crazing behaviour in torsion under superimposed hydrostatic press. 78—52898
- polycarbonate craze shape temp. depend. 78—48529
- polychlorotrifluoroethylene, creep meas. in N_2 atmos., craze parameters 79—15734
- polychlorotrifluoroethylene, tensile deform. in He, N_2, Ar, O_2 and CO_2 gaseous environments 77—56040
- polyethylene, high-density, environmental stress crack growth 80—25895
- polyethylene, low density, SEM exam. of environmental stress cracking 78—53011
- polyethylene, low-density, fatigue fracture surfaces produced by monatonic and cyclic loading 80—40510
- polyethylene, stress cracking in aqueous detergent 77—12727
- polyethylene terephthalate, crazing and shear deformation on stretching in air and liquids *(Russian)* 78—88558
- polymer, crack extension micromechanisms, review 80—108561
- polymer, crack tip failure mechanism modelling 80—108565
- polymer, crazing limit in creep and stress relax. 79—34177
- polymer, fatigue crack growth, model 78—15506
- polymer, fracture and crazing under plain strain *(Japanese)* 80—25850
- polymer, fracture kinetics, book 79—29222
- polymer, fracture mechanism and surface crazing 77—90446
- polymer, gas environment effects 77—4845
- polymer, glassy, generality of discontinuous fatigue crack growth 77—32677
- polymer, specimen size effect on mech. behaviour associated with crazing 77—73337
- polymer, toughened glassy, crazing within glassy occlusions in rubber particles, micromech. analysis 79—91824
- polymer craze mechanics, elastic model 77—48519
- polymer materials, characterisation 80—103270
- polymers, glassy, craze surface displacements, model 80—93651
- polymers, glassy, glass bead filled, crazing characts., slope-discontinuity method 79—11712
- polymers, glassy, initiation and growth of crazes 78—60767
- polymers, HVEM in-situ deform. 80—104215
- polymers, low mol. wt., mol. theory of fracture toughness 79—66140
- polymers, stress analysis of circular craze, extension of linear membrane model 78—75081
- polymers, vitreous, quasibrittle fracture 80—21094
- polymers glassy, stress analysis aspects of crazing 80—21148
- polypropylene, crystalline spherulitic, shear bands formed under compression at low temp. 80—40507
- polypropylene, fracture toughness eval. with surface crack specimens 79—15777
- polypropylene, microstruct. changes during large strain cyclic deform. 80—66627
- polystyrene, amorphous, failure in methanol and ambient air 80—3165
- polystyrene, coarse shear bands and fracture, SEM study, craze fracture surfaces 79—29191
- polystyrene, craze and fracture surface morphology 77—12682
- polystyrene, craze density meas. by quantitative TEM 79—24701
- polystyrene, craze initiation, in tension-torsion expts. 78—15519
- polystyrene, crazed, orientation and struct., electron diffr. meas. 80—30122
- polystyrene, crazed, orientation and struct., optical meas. 80—30121
- polystyrene, effect of pressure and environment on fracture and yield 78—76757
- polystyrene, fracture toughness eval. with surface crack specimens 79—15777
- polystyrene, glassy, craze growth, expt. and model 78—15520

crazing continued
  polystyrene, glassy, crazing and brittle fracture on flat die indentation 80—60970
  polystyrene, glassy, fracture surface, formation and struct. of striations 77—28892
  polystyrene, glassy, in methanol, growth kinetics of solvent crazes, hydrodynamics 79—15836
  polystyrene, high impact, under press., mech. behaviour 79—52305
  polystyrene, high-impact type, deformation and microvoid form. 78—80602
  polystyrene, mol. conform., craze fracture 79—15835
  polystyrene, n-heptane and methanol crazes, micromechanics 77—12680
  polystyrene, n-heptane and methanol crazes, structure 77—12681
  polystyrene, oblique laser diffr. and reflection from surface crazes 77—47508
  polystyrene, polymerisation route and internal lubricant effects 77—12683
  polystyrene, rubber-modified, crazing and fracture, Dugdale model 77 8907
  polystyrene, rubber-modified, fracture mechanics anal. of effect of rubber content, craze formation 79—29190
  polystyrene, stress cracking, pressure-induced, mechanism 80—35361
  polystyrene, stress relaxation during crazing, eqn. 79—61762
  polystyrene, unmodified and rubber modified, craze initiation in n-alcohols, kinetics 80—25894
  polystyrene film, craze growth and fracture 79—83319
  polystyrene fracture surfaces prod. by monotonic and cyclic loading 79—47768
  polystyrene-poly(styrene-b-butadiene-b-styrene) polyblends, electron micrographs for struct. 78—51442
  polystyrene-polyethylene(ethylene-propylene) blends, copolymer modified, mech. props., morphology 79—57088
  polystyrene-polyethylene block copolymer, deformation ratios, Poisson ratio and adhesion, dilatometric obs. 80—60937
  polystyrene-tetrachloroxylene(tetrachlorobenzene) glassy solns., additive morphology rel. to mech. props. 79—65007
  polysulphone, craze appearance effect on mech. props. 80—21135
  polysulphone, solvent crazing *(Japanese)* 79—29246
  polythene, finite element anal. of crazing and cavitation by dil. aq. detergent 78—53006
  porcelain, relation of crazing to stress in porcelain glaze, method of stress determ. *(Japanese)* 78—31537
  porcelain wave, crazing resistance, glaze fitness *(Japanese)* 79—74278
  PVC, crazes, statistical aspects optical microscopic obs. *(Japanese)* 79—29247
  PVC, crazing, deform. kinetics 80—84990
  PVC, creep deform. caused by crazing 80—21133
  PVC, ductile fracture, SEM investig. 77—44343
  PVC, effects of mol. wt. and plasticiser on fatigue cracking 79—5044
  PVC, glassy, fatigue crack initiation in high strain fatigue tests 80—97564
  PVC, glassy rods, craze initiation, kerosene wetting effects 77—25172
  PVC, rigid, craze and yield zones in fracture 80—50701
  PVC, rigid, tensile fracture morphology, rel. to mol. props. 77—59883
  PVC, slightly plasticised, fracture toughness tests, impact tests 79—5037
  quartz, crazing resistance, particle size effect *(Japanese)* 79—39014
  steel, Cr-Mo, oxidised, mechanism of crack decoration of oxides by electrodeposition 80—97560
  styrene-acrylonitrile copolymer, crazing and brittle fracture on flat die indentation 80—60970
  styrene-acrylonitrile copolymer swelling, glass transition and crazing, polar group incorporation 78—85017
  tetraglycidyl 4,4′ diaminodiphenyl methane, diaminodiphenyl sulphone cured, failure and tensile mech. props., moisture effect 80—50735
  tetraglycidyl 4,4′ diaminodiphenyl methane epoxy, diaminodiphenyl sulphone cured, struct., deform. mode, failure 79—29141
  thermoplastics, homogeneous, fracture under plane strain and plane stress conditions 78—52941
  thermoplastics, structural changes during deformation, rel. to impact resistance 80—25800
  vitreous china, crazing tendency, rel. to thermal expansion and quartz and cristobalite content *(Japanese)* 78—44243
  Al-Zn-Mg-Co, crazing tendency *(Russian)* 80—30068
  B_2O_3-SiO_2-Na_2O phase-separated glass, creep fracture morphology 80—81151
  Fe, cast, craze crack form. 78—44221
  Fe, cast, crazing with directionally arrayed flake graphite 77—59935

creation hypothesis, continuous *see cosmology*

creation of electron pairs *see electron pair production*

creep
  see also creep fracture; creep testing; diffusion creep; elastic aftereffect; irradiation induced creep; recovery-creep; stress relaxation
  13 GK model, numerical results for Couette, Poiseuille and thermal creep flow between parallel plates 79—77057
  acrylonitrile-styrene copolymer melts, rheological behaviour *(German)* 77—51012
  activation energy determ. by temp. pulse method 77—86257
  activation parameters under monotonic heating conditions *(Russian)* 78—23764
  ageing bodies, with growing slit, creep theory 78—63329
  ageing media, thermodynamic pots. in creep theory *(Russian)* 78—63318
  aggregate, polycrystalline, grain boundary sliding contrib. to total strain 77—25114
  alkali halide, dislocation struct. formation under creep conditions *(Russian)* 77—7733
  alkali silicate glasses, secondary relax. transitions 80—88261
  alloy, creep elongation, modification of Monkman-Grant relation *(Czech)* 77—63726
  alloy, cryogenic, creep, review 80—104222
  alloy, heterogeneous with coarse microstruct., steady state power law creep 79—61644
  alloy, high temperature, mechanical, thermal and corrosion props. 78—95763
  alloy, single and two-phase, power law representations, deviations at high strain rates 77—48504
  alloy, solid solution, large grained, creep ductility 78—48479
  alloy, solid substitutional soln., diffusive creep *(Russian)* 79—55816
  alloy, structural, time-depend. fatigue, nuclear reactor materials 79—1909

creep continued
  alloy, substitutional solid soln., irradiated creep rate enhancement theory 77—63739
  alloys, industrial, stacking fault energy rel. to mech. props. *(French)* 79—43339
  alloys, intergranular precipitate effect on diffusion growth of creep voids 79—34041
  amorphous-crystalline substances, high temp. plastic deform. interpret. 77—35627
  ampule for inside fission reactor exam. of materials, examining creep, long term strength in plane stress state 78—85098
  anelastic, contrib. of climb rate of dislocation links and config. 77—52431
  anelastic, fluctuation-dissipation theorem derivation for linear anelasticity 78—43066
  anisotropic, phenomenological descriptions 77—24347
  anisotropic reinforced resin laminate, cyclically reversing load, strain behaviour determ., approx. method *(German)* 79—5096
  arterial wall empirical linear response models 77—90831
  articular cartilage in compression, biphasic creep and stress relax., theory and expts. 80—94275
  austenitic stainless steel, type 316, anelasticity and creep transients 78—84880
  austenitic stainless steel tubes in liquid Na, 873K and 973K 77—57722
  baddeleyite-corundum refractories, creep and annealing 78—84907
  Bakor 33, refractory, stress relaxation capacity determ. 80—60910
  Barre granite, crack growth and development during creep 79—84237
  beam, nonlinear viscoelastic, torsion creep 79—18745
  beam, rectangular cantilever, loaded by external force and own weight, optimum design *(Polish)* 79—64497
  bending crack test, for fatigue crack propag. laws determ. *(French)* 77—51007
  biaxial creep behaviour, ribbed GCFR cladding at 650C 78—86597
  bone, compact, long-term torsional creep obs. 80—104619
  bone tissue, human, on stretching 80—3702
  bony tissue, compact, from human tibia, creep under tension 77—25487
  boundary value problems solution, rational approach 77—58560
  brass, adsorpt. of Hg, effect on mech. strength, creep, fatigue, embrittlement *(Russian)* 79—29267
  brass, creep of β and β' phases, influence of order *(French)* 79—38921
  brass, cyclic creep under increasing stress condition, constitutive eqn. 80—93593
  brass, cyclic strain induced creep, relation between modes of stress and strain superposition 78—60733
  brass bicrystals, two-phase (α/β), interphase boundary sliding at high temperature 80—88164
  brass single crystal, intracrystalline slip bands in high temp. creep *(Czech)* 79—77604
  buckling of complete spherical shell, perturbation method 77—19552
  carboxyl terminated butadiene nitride-diglycidyl ether of bisphenol A epoxy resin, struct. and mech. props. 78—52901
  cartilage deformation and interstitial fluid flow, nonlinear interaction 77—32931
  cavitation failure, incorporating cavity nucleation with strain 80—16451
  cavities under stress at high temps., rel. to metal creep 77—32625
  cavity growth, creep mechanisms, independent and sequential 80—55480
  cavity growth anal. during superplasticity 80—60923
  cavity growth diagram, for high temp. creep 80—65140
  celluloid, nonlinear viscoelastic deform. under superimposed hydrostatic pressure 79—34116
  cellulose acetate films, light scatt., tensile creep, desalination 80—16050
  cellulose film, meas. of shear modulus and damping in a torsion pendulum 79—4989
  cellulose nitrate, creep behaviour under superimposed tensile and hydrostatic loading 77—56029
  cement, hardened paste, transitional thermal creep 80—25785
  cement grog bodies, high Al_2O_3 content, creep characts. obs. 80—66578
  cement paste, heat-cured, recoverable and irrecoverable deform. 77—63732
  ceramic, polycrystn. creep stress exponents rel. to slip and ductility 77—90400
  ceramic, porosity depend. 80—97530
  ceramic and glass ceramic, AE meas. under maintained load *(German)* 79—43315
  ceramics, microstructure dependence of mechanical behaviour 78—88533
  ceramics, oxide, TEM study of deform., review 79—87686
  ceramics, synthetic raw materials, sintered and fused, use in refractories industry, slagging, creep, thermal thick resistance *(German)* 79—4937
  ceramics, tensile and compressive creep behaviour, bend tests 78—48455
  chamotte concrete, alumina-based cement, thermomech. props. 78—35455
  circular cylinder, creep transition in torsion 79—59929
  circular plate, anisotropic and homogeneous, with circular hole at centre, creep behaviour 80—48597
  circular specimen subject to pure bend, ultimate tensile and compressive strength *(Russian)* 80—74768
  component cantaining cracks, critical review 78—63321
  composite, steady creep bending stresses 78—71280
  composite materials, self-consistent estimates for viscoelastic creep 78 13921
  composite spherical shells under uniform internal pressure, transition theory of creep 78—90724
  concrete, creep, elasticity and strength in tension and compression 78—11287
  concrete, creep, long term prediction and shrinkage from short term tests 79—20122
  concrete, creep, time dependent behaviour under high tensile stress *(Japanese)* 78—31465
  concrete, creep activation energy under short-term static and cyclic stresses 77—63730
  concrete, creep during drying and wetting 79—52319
  concrete, creep theory *(Chinese)* 79—74196
  concrete, creep under combined shear and compression stresses *(Japanese)* 77—40511
  concrete, high strength, made with a special cement admixture, mech. props. *(Japanese)* 80—89297
  concrete, reinforced cross-section, reponse to short-term and sustained loads 79—52358
  concrete, unified concepts of constitutive modelling and numerical soln. 77 25093

creep continued
- concrete, unsaturated, dynamic props. of impulsive-type loading 79—70106
- concrete creep under nonuniform temp. distrib., linear viscoelastic analysis 77—62172
- concrete reactor pressure vessels, finite element creep anal. 78—41813
- concrete reactor vessels, behaviour of perforated slabs under temp. and external load 79—30917
- concrete structs., steady-state stresses under sustained and cyclic temp. 77—83024
- consistent creep and rupture properties for creep-fatigue evaluation of nuclear components 80—35329
- const. determ. from stress-relaxation meas. in bending and torsion 78—9572
- constitutive eqn. *(Japanese)* 79—64532
- constitutive equations of continuum creep damage mechanics 78—67054
- constructional element load carrying capacity anal *(Russian)* 79—98631
- constructional materials, creep, viscosity, resist. to inelastic deform. 80—89309
- corrosion resist. depend. on mech. and heat treatments 80—653
- corundum, polycrystalline, creep under low partial pressure of O_2, 1200-1600°C 80—35255
- Cotac 74, directionally solidified composite, creep behaviour prediction *(French)* 78—68754
- covalent crystal, creep and dislocation structure under tension *(Russian)* 78—19839
- Cr-Mo (2.25, 1 wt.%), annealed, tertiary creep behaviour 79—43326
- crack growth at high-temp., fracture mech. appl., review 79—41628
- crack growth in conditions of creep *(Russian)* 78—63379
- crack retardation at elev. temp., hold time effect of single overload 79—79068
- cracktip under incipient creep deform., stress field and modified J-integral *(Japanese)* 80—103411
- creep buckling, effects of small deflexion approximations on predicted behaviour 79—7309
- creep data, 3- and 4-element response curve fitting 77—90395
- creep scatter as an inherent material property 79—68590
- creeping structs. bounding solns. for load varyings above shakedown limit 77—89039
- creeping structs. under load variations above shakedown limit, appl. of bounds 77—89040
- cryogenic, back stress model 79—99265
- crystalline rocks, transient creep and semibrittle behaviour 79—16460
- crystals, quantum effects in plasticity 80—59561
- Cu, highly conductive, cyclic creep reversal 80—25766
- curve approximation, rapid method using electron beam indicator 80—10166
- curves, theoretical exam. of curve shape, comparison with Cu creep curves 78—79232
- cyclic creep, enhnaced, high temp. theory for polycrystalline materials 78—7018
- cyclic creep under increasing stress condition, constitutive eqn. 80—93593
- cyclic plasticity, creep recovery unified approach to interaction prediction 79—8329
- cylinder, thick walled, thermal stress calc. taking nonlinear creep into account 79—46184
- cylinder, thick-walled, creep transition under internal pressure 80—53659
- cylinder under uniform pressure, transition functions 80—10158
- cylindrical punch, three-dimensional stress field, photoelastic studies 80—93272
- cylindrical shell, buckling, combined action of axial compression and internal pressure 80—28447
- cylindrical shell with elliptic cross section, subject to torsion, creep buckling 78—34040
- cylindrical thick shells, elastic-plastic creep anal. 80—5960
- cylindrical wound shell with viscoelastic core in axial compression, optimisation 77—4821
- cylindrically loaded creeping structures for short cycle times 77—11135
- damage analysis under nonproportional cycling 80—97556
- damage induced structural instability 80—28445
- damage model of creep-fatigue interaction 79—77008
- damage parameter in continual fracture mechanics review *(Polish)* 79—32382
- damage rupture, phenomenological approach to plasticity, creep and fatigue *(French)* 79—37245
- deformation, and diffusion controlled creep crack growth 80—79867
- deformation, effect of damage 78—79664
- deformation and fracture of materials in creep range, effects of nonlinear stress-strain rate relations 80—58938
- deformation mechanism diagram, 3D presentation 80—3141
- deformation mechanism map, for high temp. creep 78—35439
- deformation mechanism maps 80—3143
- deformation rate of vibrating structs. 77—11136
- dental amalgam, simultaneous description of transient- and steady-state creep 79—83266
- diagrams for polycryst. ceramics with ambipolar diffusion inc. grain size 77—73304
- diamond grain configuration in high temp. creep and fatigue 77—21221
- diffusion controlled dislocation creep 79—46745
- diffusion controlled dislocation creep 79—46744
- diffusion welded joints, creep deformation effect on characts. 80—25806
- discs, circularly symmetric, rupture, ductile-brittle creep 80—69735
- Dislocation creep in particle-strength systems 78—3182
- dislocation creep under cylcic stressing, physical model and theoretical eqns. 78—39833
- dislocation structure and stress/strain velocities, thermodynamics theory *(Russian)* 79—43319
- dislocation-creep, ratio of cell diameter to dislocation spacing 77—24348
- dislocations model, compatibility with transient and steady state creep *(Italian)* 80—33487
- dispersion hardened alloy, friction stress for high-temp. creep 78—11289
- Dorn relationship for creep prediction, introduction of force factor *(Russian)* 78—18185
- Drucker postulate verification at high temp. 80—30025
- Duralumin, adsorpt. of Hg, effect on mech. strength, creep, fatigue, embrittlement *(Russian)* 79—29267
- Duralumin, lifetime after preliminary plastic deform., kinetic theory of strength 79—43395
- Duralumin D16T, creep, energy variant of theory expt. verification 78—6993

creep continued
- dynamics in stress relax. regime, analyt. expressions 77—11627
- Earth mantle, creep laws 78—69305
- Earth mantle, structural superplastic creep and linear viscosity 77—5155
- EBR-II, fabrication of in-reactor creep capsules using previously irradiated cladding tubes 79—54478
- EBR-II irradiation subassembly and creep specimen container design 79—54479
- elastic creep fatigue rules fo ASME B&PV code case 1592 78—44211
- elastic-plastic fatigue crack growth under load cycling 77—59913
- elastic-plastic-creep-large strain analysis at elevated temperature by the finite element method 79—37185
- elastic-viscoplastic materials, uniaxial cyclic loading, stresses, relaxation, creep 80—64402
- elasticity and damage, interrelation *(French)* 79—90182
- elasto-viscoplastic flow, finite element anal. by initial stress rate method 78—26047
- electric connector materials, estimation for Cu alloys and plastics, expts. 77—21206
- energy variant of theory 78—6992
- energy variant of theory 78—6993
- engineering materials, elev. temp. fatigue interactions 77—86173
- engineering materials relation between deform., rupture, power-law creep 79—5020
- enhanced thermal creep deformation, secondary stress cycling conditions, elastic region, LMFBR fuel rod 77—4832
- epichlorohydrin/bisphenol A epoxy polymer concrete, viscoelastic props. 80—45340
- epoxide polymer, cellular, in vitreous state, creep 79—96092
- epoxy, crosslinked, time-temp. superposition applied in creep with superimposed hydrostatic press. 77—70127
- epoxy C plastics, under tensile stress, effect of whiskerization of polymer matrix on creep resist. 79—87699
- epoxy composites, with different degrees of hardening, bulk-creep prediction 80—104223
- epoxy resin, Cl-containing, relation between static and dynamic deform. characts 80—3137
- epoxy resin, filled and unfilled, subjected to extensional creep, dynamic props. 80—71697
- epoxy resin, meas. of glass transition temp., linear viscoelasticity 80—29157
- epoxy resin, time-temp. superposition of creep data, linear viscoelastic props. 80—30045
- epoxy resin composites, cooldown residual thermal stresses, viscoelastic response 80—60941
- epoxy resin parabolic shells, exam. of viscoelastic creep 79—43307
- epoxy resin systems, synthesis review, phys. and mech. props. at low temps. 80—25650
- epoxy-graphite laminate creep behaviour humidity effects 77—66682
- exoelectron emission during creep 77—44312
- expansion bellows, flexibility of axially loaded toroidal bellows in creep 79 32299
- Eyring creep model, effective stress 79—90722
- failure, high temp., life fraction rule and probabilistic approach 80—93608
- fatigue high temp., hold time effects, cavitation nucleation, creep interaction 78—60734
- FBR mixed-oxide fuel crusts, thermal fracturing and the effect of creep 79—49698
- FCC metals and alloys, deform. behaviour 77—8892
- ferrite, polycrystalline, ionic diffusion and dislocation movement during creep deform. *(Japanese)* 77—28039
- fibre glass laminate in tension, creep 80—71718
- fibre reinforced composites, conf. Moscow, USSR (Nov. 1978) 80—8733
- fibre reinforced composites, materials properties, unsolved problems, review 77—4843
- fibre reinforced composites, thermal cycling, elastoplastic strain calc. under action of external stresses *(Russian)* 79—38896
- fibre reinforced metals, creep behaviour exam. *(German)* 78—52931
- filled polymer mechanical properties, particle shape effect, review 80—100864
- finite element anal., variable stiffness method 78—22278
- finite element solution of creep problems involving rapid cyclic loading 77—3750
- fission reactor, FAXMOD anal. of creep and sheath ballooning 80—42759
- fission reactor fuel rod deformation code FEMAXI-II and its application 80—37446
- fraction model, numerical plasticity and creep anal. 77—3743
- fracture mechanics parameters, applicability to creep, fatigue crack propag., at evalated temp., exam. using various materials *(Japanese)* 78—52962
- friction stress for high-temp. creep 78—11289
- friction stress meas. validity for high-temp. creep 79—74219
- friction stress measurement, in high temp. creep 79—74223
- fusion reactor blanket, thermal stresses and cyclic creep-fatigue 78—62655
- gabbro, long-term creep, large and small specimen results obtained over 20 and 3 years respectively *(Japanese)* 78—56705
- galena, polycryst. synthetic, stress relax. 500 to 800°C 78—87737
- gel, appl. to study of viscoelastic props. at small constant shear stresses 79—54123
- geodynamic processes 78—3744
- geological faults, fracture, creep and strain 78—69345
- glacier ice secondary and tertiary creep meas. by borehole closure rates 77—64339
- glaciers and ice sheets, strain heating and creep instability 77—86954
- glass, flat, dependence of creep, viscosity on cooling intensity, during quenching 80—20964
- glass fibre composite, creep calc. in nonstationary temp. distrib., temp.-time analogy 77—70132
- glass fibre filled polycarbonate, compressive creep *(Japanese)* 77—8888
- glass fibre reinforced plastics mechanical properties measurement, use of electrical resistance strain gauges, effects on props. 79—43541
- glass fibre reinforced polyamide, GFPA 66, rel. strain meas. during creep in liq. environments 80—30046
- glass fibre reinforced polyester, creep life, effect of liquid environment and increased temp. *(Russian)* 77—16723
- glass reinforced epoxide, winding in transverse direction, creep and thermal expansion 79—96093

creep continued
- glassy polymer, relationship between activation energy of creep and cohesive energy 79—69188
- glassy state and highly viscous liq., rheology 80—70130
- grain and phase boundaries between crystals, conf., Konigstein, Germany (Oct. 1977) 78—72762
- grain boundary, role of dislocations 78—43065
- grain boundary and interphase boundary sliding in power law creep 79—61643
- grain boundary cavities, star-shaped unstable growth 79—46679
- grain boundary offsets during creep 77—7735
- grain boundary sliding and intercrystalline fracture in high temp. creep *(Czechoslovakian)* 77—32642
- grain boundary sliding and its accommodation during creep and superplasticity 77—40436
- grain-boundary sliding controlled, grain rolling, superplasticity 77—90399
- granite, long-term creep, large and small specimen results obtained over 20 and 3 years respectively *(Japanese)* 78—56705
- granodiorite, fracture under uniaxial compression, mech. and AE meas. *(Japanese)* 78—56748
- graphite fibre reinforced Al, temp. and press. effect on interface chemistry, mech. prop. meas. 78—64595
- graphites, reactor, strength and deformation under conditions of cyclic variation in load and temp. 79—43355
- hardening during creep, effect of interstitial and vacancy dislocation loop *(Russian)* 77—81271
- Hastelloy X, carburisation and dimens. stability in HTGR, He environment, effect on creep rate 80—45366
- Hastelloy X, creep, effect of He environment and grain size *(Japanese)* 77—48488
- Hastelloy X, creep and creep rupture props. in air and helium at 900°C *(Japanese)* 77—52405
- Hastelloy X, creep props. and appl. to structural design *(Japanese)* 77—59862
- Hastelloy X, grain size effect. creep and creep-rupture *(Japanese)* 80—16382
- Hastelloy X, heat resistant superalloys, for nuclear plants in He, creep props. *(Japanese)* 79—83263
- Hastelloy X, high temp. low cycle fatigue strength *(Japanese)* 77—59910
- heat evolution during cyclic deformation of a hereditary medium *(Russian)* 79—46227
- heteroolastic beam, progressive creep under loading *(French)* 79—7290
- hexagonal polycrystals, creep and plasticity, rel. to single crystal slip 78—13920
- high temp., steady state, anelasticity and measured internal stress 78—35456
- high temp. relief cavitation, SEM, STEM, TEM, SIMS and EDX anal. 79—5039
- high temperature, remarks with respect to zero creep method 77—12671
- high temperature plant design methods, reference stresses and bounding theorems 80—58937
- high-temp. nucl. reactor components, elastic-plastic-creep response, computer program 77—3112
- high-temperature creep model incorporating recovery and thermally activated glide 79—64534
- high-temperature materials for space power systems, mech. props. 79—57045
- hollow sphere with stamps on external surface, creep stresses 77—84152
- HTGR, structural materials, effect of coolant impurities on mech. props. *(German)* 78—25297
- hybrid, identification 79—10506
- hyperbolic sine creep, flow potential function 79—32304
- ice, columnar grained, rheology 79—57044
- ice, polycrystalline cores, creep laws for various stress states *(French)* 77—53077
- ice sheets, a creep instability analysis, Antarctic and Greenland 79—84304
- Incoloy, 800 and 807, heat resistant superalloys, for nuclear plants in He, creep props. *(Japanese)* 79—83263
- Incoloy 800, austenitic, creep fatigue interaction at 600°C 78—64672
- Incoloy 800, carburisation, oxidation and creep, review 79—47837
- Incoloy 800, cast, microstruct. evolution during creep, TEM obs. 79—43366
- Incoloy 800, creep rupture, creep strength and tensile data, 500 to 800°C 79—43371
- Incoloy 800, creep rupture props. at 525°C 79—43437
- Incoloy 800, exam. of mech. and microstructural props. 79—5022
- Incoloy 800, mech. props. above 600°C 79—43370
- Incoloy 800, mechanical props., heat treatment and appl., conf., Petten, Netherlands (March 1978) 79—43296
- Incoloy 800, microstruct. effect on mech. props. 79—43367
- Incoloy 800, review of mech. props. up to 600°C 79—43368
- Incoloy 800, use up to 550°C, creep ductility 79—43369
- Incoloy-800, creep-fatigue interaction 77—70113
- Inconel, 617 and 625, heat resistant superalloys, for nuclear plants in He, creep props. *(Japanese)* 79—83263
- Inconel 606, discontinuous creep process 79—66124
- Inconel 617, morphological changes of carbides, effect on creep props. 80—108509
- Inconel 82, discontinuous creep process 79—66124
- Inconel X750, positron annihilation study of ageing and creep 80—29824
- Inconel X750 springs, in-reactor stress relaxation 78—11256
- incubation period following stress reduction during creep 79—7603
- independent and sequential processes, charact. 78—52921
- inelastic deformation of structures, repeated actions of load temp., structural model 77—3747
- inelastic solids, anelastic relaxation anal., extended to creep at high temp., appl. to internal friction *(French)* 78—63806
- inorganic solid, stress depend. of activation volumes in creep and stress relaxation 79—19312
- interdependent processes, analysis 78—80594
- intergranular fracture during power-law creep 79—96105
- internal stress, stochastic model for dip test in steady-state creep 80—58915
- internal stress measurement, in creep, anelasticity influence 80—70306
- irradiation-induced swelling, and creep, effects of pt. defect trapping and solute segregation 79—79040
- isoperimetric gradient bounds for Poisson and torsional creep problems 79—98639

creep continued
- isotropic stable media, stress tensors and creep-strain rates correl. 80—87722
- izod polystyrene, influence of dimensions in mech. props. *(German)* 80—21039
- kernal determ. from short time test results 79—86350
- kinetics, analytical description 77—11139
- Lagneborg particle by-passing model, creep rate stress exponents and friction stress 80—55481
- lamellar composites, development of microplastic strain *(Russian)* 79—34102
- laminate, time and temp. effects, mech. response, computer simulation 78—35466
- Larson-Miller parameter, rel. to stress rupture and creep 77—72192
- life prediction from transient creep data 77—48512
- life prediction modelling for creep damage 80—59574
- LMFBR claddings with axial fins, stress anal. including creep effects 77—88224
- LMFBR materials, exam. of material requirement 78—50256
- loaded column, creep and ageing optimisation problems stress-strain state *(Russian)* 79—46226
- long-term strength prediction by stepwise loading based on theory of damage accumulation 80—48644
- lubricated elastomers in contact with regularly spaced sliders, frictional dynamics 79—20213
- machine, for creep tests, conditions of plane state of stress 80—21232
- material creep deform. determ. *(Bulgarian)* 79—61681
- mechanical stability in creep conditions *(Russian)* 79—18758
- metal, creep, point defects 78—48462
- metal, creep movement of dislocations, effect of stress distrib. at grain boundaries *(Russian)* 78—27564
- metal, creep-electron emission relation 78—6994
- metal, dislocation kinetics of superplasticity and creep 77—76404
- metal, electron state effect on mech. props. and electroplasticity 78—14725
- metal, FCC, creep rate, stress depend. *(Russian)* 79—1896
- metal, FCC, transitional creep *(Russian)* 77—25101
- metal, FCC and BCC, high temp. creep, influence of dislocation splitting width *(Russian)* 79—5004
- metal, flow stress, subgrain size and subgrain stability of elev. temps. 77—86094
- metal, hardening due to increased subgrain boundary stability 78—52934
- metal, heat resistant charact. extrapolation by temp.-time methods, creep data 78—15477
- metal, high temp. steady state creep, activation energy determ. *(Russian)* 77—50920
- metal, nonlinear integral eqn., existence and approx. solns. 78—13931
- metal, power law representations, deviations at high strain rates 77—48504
- metal, pure, friction stress for high temp. creep 78—11289
- metal, recovered dislocation substructure, prod. and utility, review 77—84749
- metal, secondary creep rate, comparison of sinh and effective stress creep 79—52321
- metal, strength characteristic, high temp., prediction from creep processes 77—86119
- metal, stress conc. caused by grain boundary sliding under power law creep 78—60732
- metal, surface energy meas. by zero creep method at extremely low O_2 partial press. *(Czech)* 78—63926
- metal creep, deform. struct. modeling, compatibility conditions *(Russian)* 78—13924
- metal deformation, elevated temps., effect of creep deterioration 77—3787
- metal failure, due to hydrostatic pressure, exam. of kinetics 78—52944
- metal matrix fibre reinforced composite, high tem. appl., creep, dislocation processes 77—48369
- metal structures, creep, stress and stability anal. rules and methods 79—32302
- metal structures, inelastic anal. 78—70586
- metal wire, influence of grain boundaries on high temp. creep *(German)* 78—72812
- metallic materials, numerical soln. algorithm of extrapolation and interpolation problems of limiting stress characts. 79—83281
- metallic media, varying loads, elevated temp. inelastic anal. using state variable theories 78—83264
- metals, BCC, effect of screw dislocations, on mech. props. *(Russian)* 78—60704
- metals, continuum props. of constitutive relationships 77—35053
- metals, crack resistance, high temp., during creep due to stress relaxation *(Russian)* 79—52348
- metals, creep anal. using boundary integral eqn. method 79—46231
- metals, creep limit and long-term strength, parametric eval. method 80—100996
- metals, creep prediction using analytical tabular method *(Ukrainian)* 78—68725
- metals, dislocation cell diameter rel. to free energy during creep 79—91756
- metals, engineering, multi-axial creep characts. 80—64398
- metals, exam. of multiaxial creep charact. 79—43364
- metals, polycrystn., creep damage and cavity growth, assessment using density meas. 80—104217
- metals, recrystallisation during hot deform. 78—68714
- metals, strain hardening, creep, stress relaxation correlation with high temp. processes *(Russian)* 79—34053
- metals, time depend. inelastic deform., boundary integral eqn. calcs. 78—51090
- metals and alloys, creep and stress relaxation curves, phenomenological description 79—100231
- metals and alloys, high-temp. creep conditions 77—77550
- metals under combined stresses, review of creep behaviour 80—59567
- metals under creep loading, cumulative damage, engineering approach 80—58935
- metals used in coal gasification, demands made on materials used in process *(German)* 80—45438
- methacrylic polymers, multiple dielectric relaxations, investigation by thermally stimulated creep method 80—93238
- microcreep, low temp., quantum effects *(Russian)* 78—71784
- micromechanical modelling of interacting creep processes in polycrystals 78—30205

creep continued
  microscopic models, stress drop test interpretation during creep 77−75814
  microstructural phenomena, physical chemistry 79−11550
  minimum creep rate rel. to time to fracture 77−7346
  minimum principle for the problem of torsional creep 79−75337
  modelling of creep incorporating initial strain and ageing 80−58939
  mortar containing Ca lignosulphonate, creep, effect of degree of hydration 77−63731
  Mt. Burnet Dunite, high-temp. creep meas. 78−7624
  mullite, high temp. mech. props. in compression 77−56033
  mullite, refractory ceramic creep, struct. effects 77−66679
  multiaxial creep-fatigue damage, determ. of strain range 79−7650
  multibar structure strength from heteroplasticity concept *(French)* 79−18742
  multilayer shells, stress-strain state and stability at high temps. 77−54903
  multilayer winding around hollow cylinder, creep and ageing optimisation problems stress-strain state *(Russian)* 79−46226
  mylonites, grainsize reduction and grain boundary sliding rel. to flow strength 80−21721
  Nabarro-Herring creep, internal stress 78−43067
  naphthalene, cryst. plasticizing by surface active organic media, creep rate meas. 79−55813
  naphthalene single crysts., steady creep obs. 80−75296
  naphthalene single crysts., surface active substances effect on plastic flow 80−44248
  natural rubber vulcanisates, creep under tension, O_3 effects 78−92302
  Nimonic, IN100, γ' precipitates, casting conditions effect on morphology 80−7548
  Nimonic 105, creep and stress rupture props., trace elements influence 80−66602
  Nimonic 105, friction stress meas. during creep 79−61665
  Nimonic 105, overaged, creep and fatigue crack growth 77−86138
  Nimonic 105, temp. and stress depend. of microstruct., small angle neutron scatt. study 79−15726
  Nimonic 80A, creep rapture under non-proportional loading 80−108518
  Nimonic 90, creep rate stress exponents and friction stress, comparison with Lagneborg particle by-passing model 80−55481
  Nimonic 90, dispersion hardened, friction stress rel. to initial and secondary creep 80−11711
  Nimonic alloy reinforced Al, Cu and brass, laminated composites, low-temp creep singularities, structural defect changes *(Russian)* 80−11696
  Nimonic cylinder, stress redistribution obs. 77−4831
  non-linear uniaxial integral constitutive equation incorporating rate effects, creep and relaxation 80−28436
  non-linear viscoelastic behaviour, numerical anal. 78−59318
  non-Newtonian fluid, creeping motion past sphere 80−24057
  noncrystalline solids, thermally stimulated creep method for mol. motions investig. 78−22787
  nonisothermal creep, reference stress and temp. 80−64401
  nonisothermal theories, of plastic flow and theory of work hardening in creep 79−57077
  nonlinear creep problems in symm. press. vessels, uniqueness of integral eqns. positive solns. 77−65694
  nonlinear creep theory of an ageing body, principle of correspondence *(Russian)* 80−33469
  nonlinear material and structural behaviors, soln. procedure, theoretical basis for program composite−III 78−30204
  nonlinear monotonic functions with selectable intervals 79−46230
  nonlinear theory of hereditary media, functional relationship between stress, strain and temp. 78−26054
  nonlinear viscoelastic materials, creep and relax., book 77−11141
  nonlinear viscoelastic materials, stress formulation relations *(German)* 79−76987
  nonsteady inelastic deform., stress anal. by photoviscoplasticity 79−94563
  nonuniform hereditory-ageing media, creep theory 77−35059
  nonuniformly ageing materials, equations of state in nonlinear creep theory 77−75824
  notched bar design for creep-rupture testing under tri-axial stresses 77−62165
  notched bars, creep stress redistrib., finite element anal. 77−62164
  nuclear fuel cladding, slightly oval cylindrical shells, creep anal. 78−78468
  nuclear fuel element behaviour in transients 77−88202
  nuclear fuel element model for cladding performance during power changes, strain defects 78−58359
  nuclear fuel pin inelastic modelling and stress analysis using FULMOD code 77−46233
  nuclear piping, impact loading *(Japanese)* 79−43373
  nuclear reactor materials, radiation damage, fast breeder and fusion reactors *(Japanese)* 79−81011
  nuclear reactor structural materials assessment, AISI 316 and 9Cr-1Mo steels, for UK LMFBR 78−86581
  numerical modelling of fatigue, crack, creep and corrosion test results, review 78−30243
  numerical solution methods 80−14582
  nylon-6,6, creep meas. at const. temp., humidity 78−95883
  nylon-6,6, creep prediction for different physical conditions, by superposition of creep curves 79−68603
  olivine, creep mechanisms 78−69332
  olivine, high temp. creep, edge dislocation control 79−79815
  olivine, plastic flow of oriented single crystals, dislocation struct. interpretation 78−36156
  organic glass, creep under shear with superposition of hydrostatic press. 78−31482
  paper, meas. of shear modulus and damping in a torsion pendulum 79−4989
  paper strip reinforced paraffin, model composite, optimum reinforced plates, tension/compression tests 77−86124
  paraffin oil, aq. emulsion, polyelectrolyte stabilised, mech. props. 79−39223
  parametric data handling method development, creep and creep-rupture data 80−58934
  PCTFE, work to produce environmental crazing at low temps. 78−15553
  peridotite, high-temp. anelasticity and elasticity 80−17256
  phenomenological theory, dislocation kinetics 77−63755
  phenylone, deformability in physiological salt soln. 80−12305
  pipe, curved, in creep, flexibility 78−34039

creep continued
  pipe, curved, thin-walled, steady creep problem, stress distrib. *(Russian)* 80−23905
  pipe bends, short radius, creep bending 77−6517
  pitch and coke-pitch disperse system, viscoelastic props. 80−1500
  plastic elasticity, hardness, creep, and relaxation meas. with Vickers indenter by electroacoustic method *(German)* 78−48584
  plastic flow, order-disorder transform. effect on creep, traction and relaxation *(French)* 80−35180
  plastic yielding, stationary state, recovery creep model 77−7314
  plastically deforming solid, creep cavitation by vacancy diffusion 78−48471
  plasticity, large deflections and creep problems, soln. strategy 77−42750
  plasticity and creep, theory, microhomogeneity in plastic strain 79−14281
  plastics, nonlinear viscoelastic anisotropic, creep 80−35249
  plastics under combined stresses, review of creep behaviour 80−59567
  plate, rectangular, finite bending in creep conditions *(Russian)* 80−79169
  plate, round, viscoelastic, deformation and creep *(Russian)* 79−32291
  plate, simply supported rectangular under axial compression, creep buckling and deformation 79−68605
  plate with central hole, effect of J_3 on creep and relaxation 77−54905
  plexiglas tube exposed to const. axial loads, deform. and creep, loading regime effect 77−90416
  PMMA, activation parameters of creep 79−38925
  PMMA, biaxially oriented, shrinking kinetics in transform. range 78−27588
  PMMA, crazing, deform. kinetics 80−84990
  PMMA, creep compliance calc. from short-term creep expts. 80−89303
  PMMA, creep meas. in N_2 atmos., craze parameters 79−15734
  PMMA, in distilled water, influence of liquid environmental media on mech. behaviour 78−52902
  PMMA, influence of craze configuration on fracture 78−76758
  PMMA, work to produce environmental crazing at low temps. 78−15553
  PMMA organic glass, stress relax. calc. from creep curves 80−71709
  PMMA sheet in methanol, pre-soak, dissolved gas content rel. to craze nucleation, creep 79−66185
  polyamide, PA 66, rel. strain meas. during creep in liq. environments 80−30046
  polyamide, viscoelastic behaviour determ. from reln. between creep and relaxation *(German)* 77−62174
  polyamide coating on steel roller, experimental exam. of contact parameters 78−68842
  polyamide resin, computer approx. of families of curves of physically nonlinear creep 77−66684
  polyanide, thermorheological and mech. props. 79−96067
  polyarylate, F-2 influence of water on mech. props. *(Russian)* 78−88513
  polycarbonate,, creep deform. caused by crazing 80−21133
  polycarbonate, creep deform. caused by crazing 80−21133
  polycarbonate, delayed yiedling under const. load 79−38906
  polycarbonate, viscoelastic behaviour determ. from relationship between creep and relaxation *(German)* 77−62174
  polycarbonate film, struct. and mech. props. 79−19160
  polychlorotrifluoroethylene, creep meas. in N_2 atmos., craze parameters 79−15734
  polycomponent metallic solid soln., creep and diffusion of vacancies *(Czech)* 79−43340
  polycrystal creep props., derivation from single crystal data 77−65696
  polycrystalline materials, high temp. creep, role of grain boundary sliding 80−34128
  polycrystalline metals, effect of grain boundary sliding on steady creep 80−96590
  polycrystalline wires, small dia., formulation of zero creep method 78−52922
  polyester laminates, glass fibre-reinforced, due to natural weathering 79−66107
  polyester resin, creep, temp. and humidity effects under shear and tensile strains 77−86105
  polyester resin, creep, uniaxial elongation under variable temperature humidity 77−52434
  polyester resin, PN-3, creep, effect of temp. and moisture 77−4820
  polyethylene, creep during shear deform. with applied hydrostatic press. 80−76324
  polyethylene, creep in plane stressed state under programmed loads 79−11680
  polyethylene, environmental stress cracking, liq. efficiency criteria 80−21134
  polyethylene, high density, creep, computer program calc. *(German)* 78−60715
  polyethylene, high density, creep curves, exponential functions for description *(German)* 78−90732
  polyethylene, high density, crystalline, creep under plane stress state with const. loading 79−1903
  polyethylene, high density, fracture buildup due to prolonged loading, exam. 78−68779
  polyethylene, high density, influence of dimensions in mech. props. *(German)* 80−21039
  polyethylene, high mol. wt., deformability in physiological salt soln. 80−12305
  polyethylene, high-density, damage accumulation kinetics under creep during prolonged loading 80−40447
  polyethylene, high-density unorientated, damage buildup kinetics under creep conditions, during prolonged loading 80−60932
  polyethylene, low density, meas. of shear modulus and damping in a torsion pendulum 79−4989
  polyethylene, low density, nonlinear variable temp. creep 79−38908
  polyethylene, low density, nonlinear viscoelastic model, creep and recoil rates 77−42794
  polyethylene, low density, shear and tensile creep at finite strains 78−52903
  polyethylene, low density melts, temp. depend. of the elongational behaviour 80−6012
  polyethylene, mech. retardation time spectrum, thermostimulated creep 79−5014
  polyethylene, nonoriented partially cryst., kinetic damage accumulation cure 80−71753
  polyethylene, ultrahigh modulus linear, annealing effects on mech. stiffness and struct. 79−91717

creep continued
- polyethylene pipes, lifetime determ., crack growth in thermoplastics under various conditions 78—39981
- polyethylene terephthalate, amorphous, thermally stimulated creep and TSC expts., retardation modes 79—69768
- polyethylene terephthalate, thermally stimulated creep method for mol. motions investig. 78—22787
- polyethylene terephthalate, TSC and thermally stimulated creep, dielec. and mech. retardation modes 79—78613
- polyisobutylene, undiluted, mol. wt. influence on creep behaviour 80—45370
- polymer, crazing limit in creep and stress relax. 79—34177
- polymer, creep, effect of temp. and humidity, field test results 78—23793
- polymer, creep curves, correl. between isothermal and thermomech. 78—64587
- polymer, creep in tension under hydrostatic press. 77—70124
- polymer, creep prediction during random changes in load, ambient temp. and humidity, computer calc. 77—70121
- polymer, creep prediction during random load changes and random stationary temp.-humidity conditions 77—86104
- polymer, linear viscoleastic creep under arbitrary temp. variations 79—95075
- polymer, thermally stimulated creep 78—11245
- polymer concrete, longitudinal deformation modulus investigation in creep conditions *(Bulgarian)* 80—71685
- polymer films and sheets 78—80590
- polymer materials, hysteresis flow model applicability for degree of inelasticity 80—28422
- polymer networks, creep during scission reactions 79—15738
- polymer rod, fluid-permeable, longit. stability during creep 79—57066
- polymer solution, conc., appl. to study of viscoelastic props. at small constant shear stresses 79—54123
- polymeric fibre-reinforced plastic, creep prediction from components props. 80—40448
- polymeric material, temperature shear function and temp.-time analogy in linear thermoviscoelasticity region 79—18747
- polymeric solid, molecules motion, thermally stimulated creep 77—90402
- polymeric solids, mech. retardation time spectrum, thermostimulated creep 79—5014
- polymeric systems, rheology, review 78—87317
- polymers, amorphous, glass-rubber transition, time-temp. superposition, shear creep compliance meas. 80—88309
- polymers, and their solns., dynamic storage and loss compliances determ. from creep data 80—5948
- polymers, construction of single relaxation time spectrum 78—44160
- polymers, creep under plane stress, nonlinear viscoelasticity models appl. 80—89308
- polymers, cross-linked, with different degrees of hardening, bulk-creep prediction 80—104223
- polymers, energy considerations *(German)* 77—80081
- polymers, long-term strength prediction, review 80—104226
- polymers, partially crystalline, nonlinear mech. relax. *(Russian)* 80—40467
- polymers, temp. depend. under dynamic conditions, linear theory of thermoviscoelasticity 79—61642
- polymers, Volterra eqns. approx. soln. 79—50614
- polyolefin, amorphous, thermostimulated creep, 77-350K 79—69185
- polyolefin, amorphous, thermostimulated creep and glass transition 79—69186
- polyolefins, amorphous, compensation temp., thermostimulated creep 79—14919
- polyolefins 79—100221
- polypropylene, creep and failure under low frequency cyclic loading 77—1858
- polypropylene, creep curves *(German)* 78—64599
- polypropylene, glass fibre reinforced, injection moulded discs, struct. and mech. props. 78—19706
- polypropylene, linear viscoelastic region, creep prediction using temp. pulse technique 78—68732
- polypropylene, oriented, stress relax. process characts., 20-100°C 79—20097
- polypropylene, oriented, thermooxidative degradation kinetics, durability, influence of mech. initiated processes *(Russian)* 79—24591
- polypropylene, shear and tensile creep at finite strains 78—52903
- polystyrene, Millar interpenetrating network, viscoelasticity and phase domain form. 78—83749
- polystyrene-tricresyl phosphate solns., viscoelastic props., conc. depend. 80—76299
- polyurethane, dithiodiglycol-plasticised, time-crosslinked density reduction, photochem. scission obs. 78—52920
- polyurethane, filled, relation between static and dynamic deform. characts. 80—3137
- polyurethane solid foams, creep laws *(German)* 80—65139
- polyvinyl butyral, activation parameters of creep 79—38925
- POM, creep compliance calc. from short-term creep expts. 80—89303
- porous crystals, nonsteady state high temp. creep and after-effect *(Russian)* 78—39835
- Portland cement paste, hardened, creep under cyclic temp. 79—8320
- post buckling characteristics, influence on creep buckling 79—7308
- power law representations, deviations at high strain rates 77—48504
- power plant pipelines under creep conditions, allowable thermal stresses *(Russian)* 78—13930
- precipitate hardened material, intergranular cavity growth inhibition 80—50677
- pressure sintering, inhomogeneous flow and effective press. 80—93512
- pressure vessels, creep bounds and brittle damage estimates 80—23908
- pressure vessels, secondary creep problem, lower bound approx. soln. sequence 79—14284
- PTFE, relaxational props. effect of temp. and hydrostatic press. *(Russian)* 77—44325
- PTFE, stress-time analogy under shear and hydrostatic pressure in creep regime 80—104227
- PTFE and filled PTFE, nonlinear creep, compression bulk modulus 80—66593
- PVC, amorphous, orientation study by creep thermomechanical method, computer anal. 78—75561
- PVC, antiplasticisation rel. to ageing and nonlinear viscoelasticity 78—52929
- PVC, antiplasticised, linear-nonlinear viscoelasticity transition 79—5015
- PVC, crazing, deform. kinetics 80—84990

creep continued
- PVC, creep meas., use of computer in rational determination of material values *(German)* 78—31474
- PVC, crosslinked, mech. and thermal props. with plasticisers *(Japanese)* 79—15741
- PVC, high temp. creep 78—48453
- PVC, mech. behaviour in nonlinear viscoelasticity range 79—4996
- PVC, plasticised, history-independent recovery, creep, stress relaxation 78—80607
- PVC, plasticised, thermomechanical and dielec. relax. props. rel. to degree of processing 79—70124
- PVC, rigid, physical ageing effect on elec. props. 78—10836
- PVC, rigid, tertiary creep *(German)* 77—52433
- PVC, tensile tests at low strain rate, secondary instability form. *(German)* 77—66727
- PVC, unplasticized, evaluation method for chemical resistance *(Japanese)* 80—25893
- PVC, viscoelasticity, plasticiser influence 79—52292
- PVC with mineral fillers, mech. props. 80—21042
- pyrocarbon coating of Biso fuel, neutron effects on stress and strain 77—79437
- pyrocarbon coating of Biso fuel, neutron effects on stresses and strains 77—79436
- pyrolysis furnace tube, materials evaluation with creep damage model 77—52445
- quartz, creep and mechanism by which water accommodates dislocation glide 77—90414
- quartz, naturally deformed, dynamic recrystn. during creep, dislocation substruct., Mg alloy comparison 80—109142
- quartz, synthetic hydrolytically-weakened α-β phase transform. effects on creep props. 77—43274
- quartz ceramic, SiO_2-Cr_2O_3-TiO_2, creep and porosity, for ceramics with different structures 80—21011
- rapid cycling problems, finite element soln. 78—63317
- rare earths, elastic and mechanical properties, review 79—70132
- rate equations for elevated temperature creep 80—65141
- reactor fuel pin claddings, fission gas driven creep calcs. 79—26531
- reference stress method, consistent interpretation for basic creep data 77—50929
- reference stress method for creep design, approx. 80—48592
- refractories, high-temp. installation for thermomech. testing 79—83425
- refractories, hot compressive strength 77—12677
- refractory, flexural creep 79—29155
- refractory, rheological behaviour at high temp. *(French)* 77—56016
- refractory alloys, creep mechanism and struct. changes *(Russian)* 79—52299
- refractory ceramic creep meas. in tension and compression 78—31486
- reinforced UP resin laminate under dynamic stress, anisotropic, mech. behaviour determ. *(German)* 79—83268
- relaxation and creep curves for torsion-tension members, at elevated temps. 78—83260
- remaining creep life for components under stress at elevated temperatures 80—59566
- rheological analysis of stress change experiments during high temperature creep 79—37193
- rheological property meas. apparatus *(French)* 80—14644
- rheonomic shell, cylindrical, local stability in creep conditions *(Russian)* 80—92069
- rheonomic viscoelastic materials, under prolonged loading, failure hypothesis 80—3180
- rock creep, stable sliding, and premonitory slip 79—16410
- rocks, acoustic emission and creep at high confining press. and differential stress 77—73716
- rocks, olivine-rich, activation vol. for creep, rel. to Earth upper mantle 79—44184
- rod-shaped elements, under simultaneous static loads and elevated temps., linear limited stress relax. 80—14590
- rotating discs, variable thickness, transition theory of creep, stress determ. 78—90725
- rotating orthotropic disks 80—33476
- rubber, creep processes associated with uniaxial compression 78—68734
- rubber hydrochloride, meas. of shear modulus and damping in a torsion pendulum 79—4989
- Saint-Venant pure bending problems, transient creep bounds 80—19249
- San Andreas fault, California, bimodal distrib. of creep event amplitudes 77—78145
- San Andreas fault, California, short-period nonseismic tilts rel. to episodic slip 77—29276
- sapphire 0°, creep deform., fracture anal. 77—56035
- screw subboundaries as dislocation sources, creep 80—100234
- secondary, nonconst. loading, test procedure effects 79—51195
- secondary creep, quasistatic and dynamic, uniqueness of solns. 77—80078
- SEM of bulk specimens using imaging of subgrains 80—66609
- shallow spherical shell, parametric anal. of creep buckling by finite element method 77—46938
- shell, circular cylindrical with varying wall thickness, creep buckling, variational methods 80—14595
- shell, cylindrical, creep buckling, perturbation method 77—11134
- shell, finite circular cylindrical, rate formulation for elastic-plastic creep anal. 77—58568
- shell, spherical, externally pressurised, axisymmetric and bifurcation creep buckling 80—43637
- shell and plate, reinforced, viscoelastic and elastic, with transverse shear strain, stability 77—84171
- shell buckling under creep conditions, sequential loading method, deformations anisotropy 80—33495
- shells, circular cylindrical, creep buckling and post buckling under axial compression 77—46949
- shells, circular cylindrical, in axial compression, axisymmetric creep buckling, isotropic elasticity 80—69704
- shells, compressed viscoelastic orthotropic, stability 79—7305
- shells of resolution under asymmetrical loading, creep deformation anal. 77—3751
- sialon, high temp. creep 77—77530
- sign-reversing loading *(Russian)* 79—23224
- SiN, hot-pressed, creep 80—16380
- smooth circular pipe bends, under combined in-plane bending/internal press. creep anal. 77—46936
- smooth circular pipe bends, under combined in-plane bending/internal press. creep anal. 77—50927
- soil, viscous nonlinear, stresses and strains 78—73363

creep continued
soil creep induced by freeze-thaw cycles, rate meas., lab. expt. 77—81868
solid solution alloys, creep behaviour at intermediate stresses and creep power law breakdown 79—57058
spherical thick walled vessels under internal press. 78—30190
stainless steel in reactor cladding, const.-load creep curves 77—7322
stainless steel type 316 weld metal with controlled residual elements, creep behaviour 77—8902
stationary creep in structures with random material props. 78—67053
stationary predictions from model tests using reference stresses 78—18192
stationary state creep anal., struct. with non-uniform temp. distrib. 77—14915
statistical methods for creep, fatigue and fracture data analysis 80—58936
steady creep, defining equns. construction *(Russian)* 79—80436
steady state, climb controlled, at high and intermediate temps., theoretical description 79—95074
steady state creep analysis of a cracked body using the superposition method 79—94507
steady-state creep determ. eqns., microscopic stability restrictions *(Russian)* 79—10493
steel, 12Kh1MF, structural changes during creep tests 77—63746
steel, 15Kh1M1F, thermal cycling and cyclic stress effects on strength and creep resist. *(Russian)* 79—52341
steel, 17249, creep and creep fracture *(Czech)* 77—86089
steel, 1Kh12V2MF, pore formation in creep, precip. hardening 77—63747
steel, 50 and 1Kh18N9T, strength, effect of H_2 78—3197
steel, alloy type 15G2AFDps describing cyclic-creep processes with parametric eqn. 79—57074
steel, alloy X8CrNiNb1613, creep limit and long-term strength, parametric eval. method 80—100996
steel, austenitic, Cr-Ni, precipitation strengthened, anomalous stress-depend. of creep rate 80—11712
steel, austenitic, creep, low-temp., during dynamic relaxation, effect of dislocation struct. *(Russian)* 77—25103
steel, austenitic, grain boundary sliding, exam. by tensile creep tests 78—76715
steel, austenitic, high tensile X 3 CrNiMoNbN 23 17, creep at room temp., effect of Bauschinger effect *(German)* 77—1852
steel, austenitic, intermittent loading effect on creep *(Japanese)* 79—29147
steel, austenitic, measured internal stress and anelasticity in creep *(Czech)* 79—38909
steel, austenitic, metastable, alloy 000Kh18N10 creep at low temps. 77—1861
steel, austenitic, Ni-Cr, precipitation strengthened, anelasticity, plastic creep limit, 823K 79—1899
steel, austenitic, nitrided, creep, effect of N_2 and Ti and prior deform. 78—23789
steel, austenitic, under creep and cyclic loading at 823K *(German)* 77—90435
steel, austenitic 316, grain boundary, sliding, grain size depend. 77—25108
steel, austenitic 316, grain boundary sliding, creep strain and stress depend. 77—25109
steel, austenitic and martensitic, structural sensitivity of Bauschinger effect *(Russian)* 79—52303
steel, austenitic heat resistant, zig-zag grain boundaries, strength 77—73308
steel, austenitic stainless, 304 and 316, creep-fatigue interaction 77—70113
steel, austenitic stainless, ageing at high temp., effect on creep props. SEM 80—97516
steel, austenitic stainless, Cr-Ni (16, 16 wt.%), in-pile rupture strength, cold work and soln. annealing effects 77—63687
steel, austenitic stainless, Cr-Ni (25, 25 wt.%) grain size, temp. and stress influence on creep 80—30021
steel, austenitic stainless, Cr-Ni-Ti, creep deform. effects on intergranular TiC dispersion stability 78—84912
steel, austenitic stainless, creep, performing effect under tensile and compressive load, rel. to Bauschinger effect 79—96103
steel, austenitic stainless, creep, rel. to radiation swelling and stacking fault energy *(Russian)* 78—27562
steel, austenitic stainless, creep curve jumps 80—30037
steel, austenitic stainless, creep deform. effect on struct. of twin boundaries 79—8332
steel, austenitic stainless, deformation induced cavitation, exam. 79—43363
steel, austenitic stainless, fatigue crack propag., stable and unstable, role of precipitation 80—40534
steel, austenitic stainless, grain boundary migration during high temp. creep, TEM exam. 78—88509
steel, austenitic stainless, grain boundary segregation studies, intergranular fracturing technique for stress corrosion cracking investigation 79—39057
steel, austenitic stainless, He implanted 1.4970, high temp. fracture 77—86186
steel, austenitic stainless, high temp. alternating torsion behaviour, saturation state phenomenology 79—70111
steel, austenitic stainless, microstructure and transient creep 79—61675
steel, austenitic stainless, stabilized, creep improvement, effect of B precipitation and hyperquenching *(French)* 78—23784
steel, austenitic stainless, type 304, cyclic creep during unbalanced tension-compression loading at elevated temp. 80—97545
steel, austenitic stainless, type 316, effect of hold times on fatigue life, explanation in terms of grain boundary sliding damage 78—72851
steel, austenitic stainless, type 800, tensile creep props. rel. to intergranular microstruct. at 800°C, TEM study 79—38885
steel, austenitic stainless, types 304 and 316, environment effect on crack growth, under creep and fatigue conditions 80—85035
steel, austenitic stainless, V alloyed, creep inhibition at grain boundaries, dislocation struct., TEM study 79—43346
steel, austenitic stainless, V alloyed, creep mechanism 77—36591
steel, austenitic stainless, V alloyed, creep mechanism 77—48514
steel, austenitic stainless AISI 304, dislocation substruct., carbide precipitation and deform. mech. map 77—70116
steel, austenitic stainless in liq. Na, mechanical props., review 79—20150
steel, austenitic stainless Ni-Cr, heat resist. and comp. of non-metallic inclusions, effect of La, Nd, Pr and Ce 80—76315

creep continued
steel, austenitic stainless type 304, time-depend. fatigue, mechanistic model 80—100925
steel, austenitic stainless type 316, σ phase precipitation during long term high temp. creep, fracture 79—74157
steel, C, accelerated deform. by to H_2 absorption *(Japanese)* 79—70121
steel, C, accumulation of longitudinal strain under cyclic torsion 78—64615
steel, C expt. investigation above 900°C 80—81134
steel, cast 20KhML, deform. resistance and low cycle fatigue in pure shear creep effect 78—3192
steel, CC Cr-Mo-V, heat resisting, creep, probabilistic physical granulation *(Czech)* 79—70125
steel, Cr and Mn, cyclic creep in complex stress system, 20-400°C 79—91764
steel, Cr-C (3.74, 0.86 wt.%), stress assisted bainitic transform. *(Czechoslovakian)* 77—32573
steel, Cr-Mn, annealing effect on mech. props. for cryogenic appl. *(Russian)* 78—19788
steel, Cr-Mo, annealed, creep and rupture, heat treatment effects 79—24548
steel, Cr-Mo, annealed, interaction solid soln. hardening, precipitation effects on creep 79—4974
steel, Cr-Mo, constitutive eqn. model for high temp. behaviour of fast reactor structural alloys 78—66343
steel, Cr-Mo, creep resistant, creep, effect of carbide precipitation *(German)* 77—52398
steel, Cr-Mo, secondary relaxation, correspondence of steady state creep *(Japanese)* 79—83250
steel, Cr-Mo (1.25, 0.5 wt.%), creep, fracture, Ti and Ti+B effects 77—36603
steel, Cr-Mo (1.25, 0.5 wt.%), creep and rupture, temp. and stress effects 77—86096
steel, Cr-Mo (2.25, 1 wt.%), creep and high temp. low-cycle fatigue tests 80—85061
steel, Cr-Mo (2.25, 1 wt.%), creep-fatigue testing from thermal transient effects in CRBRP reactor 78—21660
steel, Cr-Mo (2.25, 1 wt.%), damage accumulation and microstruct. changes during creep 80—3129
steel, Cr-Mo (2.25, 1 wt.%), interrelationship between creep deform. and creep rupture 79—61664
steel, Cr-Mo (2.25, 1 wt.%), small changes effect in impurity elements, creep life 80—25790
steel, Cr-Mo (2.25, 1 wt.%) pipe, high temp. fatigue and creep strength 80—85060
steel, Cr-Mo (9, 1 wt.%) microstructural instability during creep, heat treatment effects 78—48472
steel, Cr-Mo type, tube, long-time stressed condition *(German)* 77—59888
steel, Cr-Mo-(V), microstruct. effect on high-temp. props. *(Czech)* 80—89300
steel, Cr-Mo-(V) austenitic, creep resist., high-temp. props. residuals effect 80—66600
steel, Cr-Mo-V, creep, effect of microstruct., heat treatment, transform. temp. 78—11248
steel, Cr-Mo-V, creep deform. under const. and cyclic temp. 79—38914
steel, Cr-Mo-V, creep fatigue interaction 78—60841
steel, Cr-Mo-V, creep fatigue interactions obs., strain controlled and load controlled tests 78—44214
steel, Cr-Mo-V, creep/fatigue interaction 78—64632
steel, Cr-Mo-V, excessive temp. effect on creep behaviour, structure and hardness *(German)* 80—30054
steel, Cr-Mo-V, heat treated, mech. props. *(German)* 80—25724
steel, Cr-Mo-V, low alloy, creep fatigue interaction 78—64673
steel, Cr-Mo-V, low alloy, V effect on creep *(Czech)* 77—86088
steel, Cr-Mo-V, rupture ductility rel. to cavitation, density and SEM obs. 79—34142
steel, Cr-Mo-V, steamline bends, restorative heat treatment effects 78—68716
steel, Cr-Mo-V, strength and ductility in creep, purity influence 80—66598
steel, Cr-Mo-V (1, 0.5, 0.25 wt.%), long-time stress relaxation props. 77—12666
steel, Cr-Mo-V low-alloy, mech. props. and stress relief cracking, effects of impurities and deoxidation practice 80—66599
steel, Cr-Ni-Nb, containing controlled particle dispersions, creep strength 77—52425
steel, Cr-Ni-Ti-B, grain size effect on mech. and struct. props. *(French)* 80—45361
steel, Cr-V (1.5, 0.5 wt.%), ferritic, effect of temp. and microstruct. on creep damage 79—5023
steel, creep and fatigue fracture prevention 78—60837
steel, creep resistant, AISI 304, residual lifetime assessment by low cycle fatigue testing *(German)* 78—15485
steel, CrMoV, creep and creep strength under alternate tension/compression *(Czech)* 77—63728
steel, CrMoV, creep resistant, cast, creep rupture and creep *(German)* 77—70098
steel, CrMoV, creep-resistant, quantitative struct. parameter *(Czech)* 80—35266
steel, CrMoV, low alloy, creep resistant, temp. and stress depend. of time to rupture *(Czech)* 77—70160
steel, CrMoV, low alloy, quantitative stereological anal. of carbide phase, struct. stability during creep *(German, English)* 79—96262
steel, CrMoV, quantitative stereological anal. and creep-resistance *(Czech)* 80—30030
steel, CrMoV (1 wt.%), high temp. creep and fracture 77—36598
steel, cryogenic, creep, review 80—104222
steel, cyclic creep and mean stress influence on fatigue life *(Czech)* 79—43403
steel, Dorn relationship for creep prediction, introduction of force factor *(Russian)* 78—18185
steel, elbow-pipe assembly, high-temp. elastic-plastic creep test 77—77551
steel, ferritic, Cr-Mo-V (0.5, 0.5, 0.25 wt.%), creep and fracture, microstructural instability effects 77—63734
steel, ferritic, creep resist., high-temp. props. residuals effect 80—66600
steel, ferritic, screening studies for evaluation for nucl. process heat system 78—13236
steel, heat resistance, thermal stability, stress-rupture strength, and creep 80—81194

creep continued
steel, heat resistant, explosive loading effects on struct. and mech. props. *(Russian)* 78—39787
steel, heat resistant, tensile strain and endurance, normal and radiation conditions, linear load variation 80—81189
steel, heat resistant charact. extrapolation by temp.-time methods, creep data 78—15477
steel, heat-resist., C replica method of investigating creep damage in TEM 80—21012
steel, high strength 0.77%C, surface dissolution effect 77—8883
steel, low alloy, creep behaviour at engineering stresses 79—74218
steel, low alloy Cr-Mo, heat fatigue, effect of technical factors 79—79058
steel, low alloy type 12Kh1MF, effect of thermal cycling on life under creep conds. 79—57075
steel, low and high-alloy, expt. investigation above 900°C 80—81134
steel, low C, creep, prestrain effects *(Korean)* 77—21227
steel, low C, high temp. plastic flow under thermal cycling in superplasticity interval 77—70130
steel, low C, strain ageing, effect of prestrain *(Korean)* 77—8865
steel, low C and mild, fatigue deformation, phenomenological exam. 78—64691
steel, low-alloy, impurities, segregation and creep embrittlement 80—66653
steel, medium C, 45, Ti+Al coated, failure during high temp. creep in NH$_3$ 79—11731
steel, medium C and austenic stainless, cyclic strain induced creep, relation between modes of stress and strain superposition 78—60733
steel, mild, cyclic creep reversal 80—25766
steel, Ni-Cr-Mo, cyclic creep under increasing stress condition, constitutive eqn. 80—93593
steel, pearlitic, Cr-Mo, Cr-Mo-V and Mo-V, heat resist., Mo content rel. to mech. props. 79—20134
steel, pearlitic, creep-induced micropore healing kinetics of 12MKh and 15Kh1M1F, TEM obs. *(Russian)* 80—71690
steel, pearlitic, heat-resist., secondary phase precipitation, deform., and fracture during creep *(Russian)* 80—50669
steel, plain C, cyclic induced creep at room temp. 80—25765
steel, plastic deform., density changes *(German)* 80—60908
steel, rail, fracture rough exam. of wear in rollers, subject to creep 79—15808
steel, spring, 60C2A, tempered under stess, influence of tempering conditions on mech. props. *(Russian)* 79—47724
steel, stainless, 20% cold worked type 316, creep deform. 77—66688
steel, stainless, 304, creep/fatigue interaction at elevated temps. 77—86174
steel, stainless, 304, thermal fatigue and strength estimation, creep fatigue interaction 79—11708
steel, stainless, 304 and 316, evaluation of tensile and creep data 77—77552
steel, stainless, 316, creep and rupture, 525 to 900°C, creep rate 79—11678
steel, stainless, 316, creep and rupture, 525 to 900°C, rupture and ductility 79—8327
steel, stainless, 316, creep and rupture, 525 to 900°C 79—8328
steel, stainless, 316, creep fatigue interaction failure 78—80652
steel, stainless, 316, intergranular crack growth by diffusion 79—24608
steel, stainless, aged 304, twin boundary cavitation during creep 77—86099
steel, stainless, AISI 304, dislocation struct., carbides, deform. mech. map 77—16650
steel, stainless, AISI 316, high-temp. mech. props. 80—66601
steel, stainless, austenitic Ni-Cr type, creep deformed, dislocation multipole obs. 80—107258
steel, stainless, Cr-Ni-Nb stabilised, Te vapour effect on creep and tensile props. 79—24583
steel, stainless, creep ductility, intergranular particle size and spacing effect 80—40461
steel, stainless, creep ductility, sigmal phase influence 80—55478
steel, stainless, creep limit, cyclic load component effect at high temps. 80—104231
steel, stainless, FBR fuel rod cladding damage correl. for rod perform. predictions 80—18424
steel, stainless, Fecralloy, creep-rupture props., 650-800°C 80—97535
steel, stainless, HK40 and HP, centrifugal cast tube, creep damage estimation from creep void obs. *(Japanese)* 79—87687
steel, stainless, massive particle form. during creep, precipitation 77—63679
steel, stainless, phase instability effect on cladding deform. profile of LMFBR fuel elements 77—74921
steel, stainless, steady state creep, microstructural parameters 78—39870
steel, stainless, SUS 304, creep-fatigue interaction, creep effect *(Japanese)* 79—83264
steel, stainless, SUS 316, creep-fatigue interaction at 600°C 79—34123
steel, stainless, Ti stabilised, creep props. rel. to B conc. *(French)* 79—20132
steel, stainless, type 304, creep crack extension rates 80—3160
steel, stainless, type 304, creep surface determ. from multiple integral representation 79—47761
steel, stainless, type 304, viscoplastic model, uniaxial, based on total strain and overstress 80—64387
steel, stainless, type 316, 20% cold worked, exam. of creep 78—72817
steel, stainless, type 316, cyclic creep behaviour, as func. of max. applied stress 78—48460
steel, stainless 78—64583
steel, stainless 20/25/Nb, biaxial creep meas., reactor fuel cladding tubes performance obs. 78—82442
steel, stainless 304, cyclic plasticity, exponential stress-strain law 77—25157
steel, stainless 304, elevated temp. low cycle fatigue, heat treatment effect 78—27626
steel, stainless 304, high-temp. 77—63743
steel, stainless 316, creep under high stress 78—52892
steel, stainless 316, recovery by annealing of creep produced dislocations 80—11702
steel, stainless cold-worked austenitic, fatigue and creep crack growth at elevated temp. 78—48524
steel, stainless type 316, set of master curves for creep ductility 79—66112
steel, stainless type 316, thermally aged, accelerated creep-fatigue crack propag. 80—89326

creep continued
steel, stainless type KH18N10T creep and long term strength tests *(Russian)* 80—3123
steel, steam pipes, 12Cr1MoV, selection of allowable stresses based on minimum possible strength data 80—104237
steel, stress relaxation, short-term, creep and strain hardening *(Russian)* 80—30005
steel, structural bending moments and tensile creep, relaxation bending test device 79—70245
steel, SUS 304 and S15C, creep deform. under reversed cyclic stresses *(Japanese)* 80—81114
steel, type 12Kh1Mf and 15Kh1M1F, damage accumulation during prolonged high-temp. creep 79—57026
steel, type 1Kh18N9T, stress state form influence on creep and plasticity characts. rel. to cyclic stress intensity change 79—87694
steel, under high H$_2$ press. *(Russian)* 78—35423
steel 15Kh1M1F, microstruct. changes rel. to creep and fracture *(Russian)* 79—24572
steel 45, B-Al coated, creep and long term strength in NH$_3$ 79—91854
steel austenitic stainless, fatigue, low cycle, temp. and strain rate effects *(Japanese)* 79—29198
steel austenitic stainless 316, grain boundary sliding, temp. depend. 77—25110
steel bar with inhomogeneous props. of lagging creep, deform. 79—15731
steel creep resistant, rare earth metal effect on inclusion charact. *(Czech)* 77—86134
steel EI736, creep, viscosity, resist. to inelastic deform. 80—89309
steel fibre reinforced Al$_2$O$_3$-Al, production and mech. props. 80—11619
steel fibre reinforced Cu, exam. of creep behaviour *(German)* 78—52931
steel high strength, Cd plated, effect of composition and thermal treatment, on hydrogen embrittlement susceptibility *(Russian)* 79—15769
steel high strength X 3 CrNiMoNbN 2317, Bauschinger effect and creep at room temp., effect of heat treatment *(German)* 77—36543
steel reinforced concrete, computer expt. on slender beam columns 79—70127
steel tubes, 12 Kh1MF, cross-section shape change, during creep of bent tubes loaded with internal pressure 78—31485
steels, austenitic stainless, stress corrosion cracking, correl. between electrochem. and mech. parameters 80—97613
steels, martensitic-ferritic, austenitic, microdefect accumulation during creep, effects of heat treatment, hardening 79—24550
steels, ultrahigh C, superplastic, mech. behaviour at elevated temps 80—21028
stiff constitutive models, numerical integration, inelastic deform. 80—96208
strain gauge, based on polyimide adhesive, effect of cyclic heat exchanges, 20 to 300°C 77—16775
strength effect for given strain *(Russian)* 79—55815
stress and deform. conc. in plastic region during creep, approx. calc. 77—56045
stress clock function in viscoelasticity 80—99941
stress relaxation curve prediction from creep data *(German)* 77—70097
strictly momentless shell with zero gauss curvature 79—90152
structural anal., underlying concepts of finite element analysis 78—66337
structural deformation under non-proportional cyclic loading, approx. method of calc. 77—46930
structural element design calc. under creep conditions 80—48598
structural elements, creep limit eval. by method of charact. parameters 80—79174
structures subjected to arbitrary cyclic loading, creep life estimation 78—90722
structures with load variations above shakedown limit, boundary solns. 80—10156
strut creep buckling, damage effects 80—102976
subgrain size importance in creep rate 77—90415
superalloy, microstructure resulting from alloying and heat treatment, effect on creep, fatigue, fracture strength 78—11246
superconductors, plastic deformation, Cooper pair scatt. model 80—39709
superplastic alloys, cavity growth 80—93627
superplasticity, mechanism rel. to hyperfine grain struct. 78—84930
surface energy measurement for solid, new technique 78—44187
surface science in metallurgy, review 79—42388
T-jump expt., effect of finite rates of temp. change 77—72191
Teflon, creep in shear, hydrostatic pressure effect 79—57065
Teflon, creep under flat cyclic stress 78—23800
Teflon, creep under joint action of tension, hydrostatic pressure 78—68750
Teflon, viscoelastic behaviour prediction of low temp., creep curves exam. 79—20141
tendon, rat tail, creep failure obs. 79—62289
tensile creep and early failure, model 80—15185
tension creep, finite element anal. of void growth 79—18739
tension determination in elastic element on motionless sheave, hybrid calculator appl. *(Bulgarian)* 80—23894
textolite glass, stress relax. calc. from creep curves 80—71709
theory problems for ageing bodies with growing slits and cavities 80—69678
thermal creep slip problem, rel. profiles, collision freq. effects 77—3738
thermal stress simulation in continuous casting, finite element method 78—30170
thermoplastics, short-fibre-reinforced, 100-s creep modulus prediction, at small strains 78—15473
thin wafer method, analytical examination for rate independ. and rate depend. materials *(Japanese)* 79—59931
thin wall structures, subject to transient heating and loading 80—33486
thin walled tubes, exam. of steady creep under combined loading 78—83269
thin wallled tube, limiting deform. in creep deform. 79—41593
threaded plastic parts, load distrib., taking into account vibr. creep 79—83282
threshold stress, importance in anal. of creep data 80—64389
α-Ti, effect of Pt ion plating on creep behaviour 79—66123
time to fracture under static and cyclic loads 77—70176
Tokamaks, lifetime of reactor components 80—32445
torsional creep problem, appl. of maximum principle 78—71284
transient, phenomenological theory 79—60428
transient creep analysis, finite-element and analytical soln. superposition 77—75820
transient problems, bounds and approx. solns. 80—43623
transition behaviour, exam. of diffusion term significance in criteria 78—75719

creep continued
transition from Nabarro-Herring to Harper-Dorn mechanism at low stress levels 78—13926
transition in transversely isotropic shells under uniform pressure 79—14277
transversely-isotropic metallic materials, constitutive eqn. for modelling secondary creep 78—6974
tubes, thick-walled, thermoelastoplastic creep stress anal. 80—58922
tubes, thin wall, long-time strength, steady creep conditions *(Russian)* 78—46900
tubes, thin wall, model for collapse due to creep *(Spanish)* 78—87276
two-bar struct., creep problems with variable temp. 77—50935
two-dimensional creeping flow of simple viscoelastic fluid through finite gap *(German)* 77—46979
two-phase structures, high-temp. deform. 78—68738
Udimet 520, γ' distribution in slip plane, dislocation loop form. during creep *(Japanese)* 79—42075
Udimet 700, creep, rupture, grain size effects 77—21229
Udimet 700, Ni-Co-Cr-Al-Ti (18.8, 15.2, 4.5, 3.39 wt.%) exam. of high temp. creep 79—61684
Udimet 700, Ni-Co-Cr-Al-Ti (18.8, 15.2, 4.5, 3.39 wt.%) exam. of high temp. creep, viscoplastic flow 79—61685
uniaxial stretching curve data anal. using creep with anisotropic hardening theory *(Russian)* 79—76981
urethane elastomer, temp. strain relaxation investigation by opticomechanical method and IR spectroscopy 77—4805
variable temperature creep problems, behaviour of structs., theoretical expt., investigations 77—3748
variational principles, generalised, Lagrange multiplier method applied to flow theory *(Chinese)* 80—79171
vibrational, circular cylindrical shell stability study *(Bulgarian)* 79—64536
visceral smooth muscles in vertebrates, viscoelastic and plastic props. 78—73169
visco-plastic approach to plasticity and creep problems, involving geom. nonlinearities 78—26050
viscoelastic and inelastic fluid flow past sphere, creeping and boundary layer flows, drag coeff. 77—51090
viscoelastic bodies, deformation taking into account influence of accumulated defects 80—19252
viscoelastic deformation, apparent activation energy, creep T-jump expt. 79—37264
viscoelastic linear on non-linear bodies, creep and relax. phenomena generalisation 77—876
viscoelastic material, linear, creep function, information theory approach to its monotonicity, concavity and symm. 77—84156
viscoelastic materials, linear, numerical cond. between creep and relaxation *(German)* 77—62174
viscoelastic materials with fading memory, thermodynamics of relaxation and creep processes 78—71282
viscoelastic properties dynamic evaluation for use in cardiac prosthetics 78—40405
viscoelastic solid, crack growth law using energy and COD fracture criteria 79—32378
viscoelastic stationary bodies with non-stationary loading, creep generalisation 77—877
viscoelastic-plastic tube, successive deformation under cyclic, temp. variation 80—92074
viscoelasticity, linearised theory, variational principles *(Russian)* 78—87279
viscoelasticity linear theory solns. by model γ-irradiation, polarisation-optical method 80—33485
viscoelastoplastic deformation of isotropic body, tensor laws of behaviour *(French)* 77—62160
viscous metal sheets, creep bulging, theoretical anal. 80—1439
woven epoxyphenol glass plastic, creep prediction during random changes in load, ambient temp. and humidity, computer calc. 77—70121
β-Zircalloy, creep charact. 79—8317
Zircalloy-4 fuel sheathing, inverted primary creep 78—86615
Zircaloy 4, creep anal. and appl. in prediction of residual stress relaxation 79—43325
Zircaloy 4, stress relaxation in bending 78—68719
Zircaloy creep collapse, hot cell examination 78—86596
Zircaloy PWR fuel cladding deformation tests under mainly convective cooling conditions 80—57862
β-Zircaloy-2, tensile creep and creep rupture props. under vacuum 78—52915
Zircaloy-2 cladding, beta-phase creep and creep rupture props., 1000 to 1500°C 78—78470
Zircaloy-2 tube, external pressure creep behaviour 79—57083
Zircaloy-4, creep damage at LWR temp. 79—52312
Zircaloy-4, failure strain prediction under non-stationary loading conditions 80—93640
Zircaloy-4, fuel cladding, steady-state creep from 940 to 1873K 79—74206
Zircaloy-4 cladding, creep transients, plastic hoop strain meas. 79—57068
Zircaloy-4 cladding, steady-state creep, 940 to 1873K 79—15759
Zircaloy-4 fuel cladding axial deform. in PWR LOCA 80—13585
ZrC$_{0.98}$, porosity influence on high temp. creep. *(Russian)* 80—25764
Ag, large grain boundary cavity coalescence during tension creep 78—52894
Ag-Cd (50 at.%), BCC β phase, high temp. creep, existence of master curve 80—55473
Ag-Cu (5 at.%) solid solution, pre-fatigued, strain hardening at high temp. 78—15426
Ag-Mg (18.5 wt.%), rheological study of crystallographic order on creep *(French)* 80—97548
Ag-MgO (0.1 wt.%), intergranular cavity growth at elev. temps. 79—66068
Ag-Zn (50 at.%), BCC β phase, high temp. creep, existence of master curve 80—55473
Ag-Zn equiatomic, creep of β phase *(French)* 78—48477
AgCl, single crystal, recovery controlled transient creep, substructural obs., phenomenological anal. 77—77526
Al, 2618, creep under step stress changes, viscous viscoelastic model 80—81138
Al, activation energy at low temp., thermoactivation anal. *(Russian)* 77—31717
Al alloy, 2618-T61, creep bahaviour prediction, physically consistent method 80—66610

creep continued
Al alloy, creep crack growth 80—60976
Al alloy, particle strengthened, yield drop and creep minimum *(German)* 78—39881
Al alloy, precipitation hardening, creep deform. effect 77—16601
Al alloy, type AK4-1T bar, verification of existence of thermal force surface of creep process 79—87695
Al alloy, type AK4-1T1, effect of high temp. ageing, on endurance of thin walled joints 78—80570
Al alloy 2618, creep and recovery under combined stress, viscous-viscoelastic model representation 79—34117
Al alloy AK4-1, crack growth rate prediction under creep conditions 80—85107
Al alloy AL22, influence of ultrasonics application on creep during multistage ageing *(Russian)* 79—91708
Al alloy AMg6, multilayer shells, stress-strain state and stability at high temps. 77—54903
Al alloy D16T, stress concentration under creep, two dimensional problem solution 77—56044
Al alloy with different props. in tension and compression, creep 80—81129
Al alloys D16T and Amg6, creep curve scatter 77—63762
Al and Al-Mg (5.5 wt.%), instantaneous plastic strain associated with stress increments during steady state creep 78—48478
Al bronze, creep forging 77—59848
Al cell structures produced by cycling and monotonic creep 80—55452
Al, creep, low-temp., during dynamic relaxation, effect of dislocation *(Russian)* 77—25103
Al, creep, rel. to radiation swelling and stacking fault energy *(Russian)* 78—27562
Al, creep and dislocation distribution, influence of electron irradiation *(Russian)* 78—95775
Al, creep and rupture, 77 to 273K *(Russian)* 79—43386
Al, creep at intermediate temps., in situ study of cell boundary evolution, HVEM 78—48480
Al creep behaviour, 3D presentation of deformation mechanism diagrams 80—3141
Al, creep data anal. at very low stresses 78—27570
Al, creep strength and rupture under combined stresses 79—20133
Al, deformation, internal friction, dynamic modulus and creep meas. 79—91727
Al, deformed surface layer, block misorientation 79—99405
Al, high purity, deformed at 573K, stress reductions effect on creep behaviour 79—74216
Al, high temp. fracture, SEM obs. 77—59918
Al, high-purity, high temp. creep, approx. determ. of parameters *(German)* 80—50688
Al, microrupture singularities in low stress range at elevated temp. *(Russian)* 79—29172
Al, non-elastic deformation, phenomenological model with solute strengthening effect incorporation 78—39832
Al, oxidation, influence on deformation map 80—40599
Al, plastic deformation thermal activation parameters from creep kinetics and stress relaxation 80—71717
Al, polycryst. in annealed and creep conds., dislocation interactions with grain boundaries 79—42067
Al, polycrystalline, movement of 3-fold nodes of boundaries in high temp. creep 80—89317
Al, polycrystn., HVEM in-situ investigation of creep mechanism 80—104214
Al, pure, creep, grain size effect on rate at 408K 77—52428
Al, singularities of effect of pressure on stages of creep *(Russian)* 79—29134
Al, stationary creep in HVEM, cell struct. evolution 80—104242
Al, stiffness and damping in creep 78—23780
Al, superpure, anomalous primary creep behaviour, precipitate form. 80—7646
Al, superpure, rate-controlling processes 80—85009
Al, thermoactivated creep and stress relax. 79—87692
Al, threshold stress, importance in anal. of creep data 80—64389
Al, transient creep, effect of pre-torsional deform., dislocation glide and density 77—4147
Al-Ag (up to 4 wt.%), 570-630°C, influence of Ag addition *(Russian)* 79—5003
Al-Al$_2$O$_3$, dispersion hardened, creep *(Czech)* 80—108463
Al-Al$_3$Ni, eutectic, creep model 77—36588
Al-Au (0.2 wt.%), precipitation mechanism and creep behaviour 80—3058
Al-Ca-Zn (5,5 wt.%) superplastic sheet alloy, mechanical properties, superplastic forming behaviour 80—60920
Al-Cu-Mg, tpye RR55, high strength, creep behaviour, effect rel. to anodic coatings, SEM study 80—97542
Al-Cu-Mg-Mn-Fe-Si, alloy D16, effect of mechanisothermal treatment on mech. props. 78—56674
Al-Cu-Mg-Ni-Fe alloy RR 58, creep resistance at elevated temps., thermomechanical treatment effects 77—59836
Al-Cu-Mn, long term strength and creep 80—60925
Al-Cu-Mn-Zr, type 2219, particle, coarsening of disk shaped Θ' particles 80—45315
Al-Cu-Ni, alloy RR 350, θ'-hardened, deform. induced microstructural instability, high temps. 80—16321
Al-CuAl$_2$ lamellar composite, creep, microstruct. obs. 79—8331
Al-CuAl$_2$ lamellar composite, stress and temp. depend. of creep 79—52330
Al-Ge (4 wt.%), superplasticity exam. *(Russian)* 78—39836
Al-Mg, creep behaviour in broad stress interval at 623K 80—30044
Al-Mg (2 wt%), high temp. creep, effect of cold working on mechanism 79—43351
Al-Mg (2 wt.%), exam. of Harper-Dorn creep 79—5026
Al-Mg (2 wt.%), steady creep characts., precip. effect 80—35189
Al-Mg (2 wt.%) subgrain formation at low stresses 78—84928
Al-Mg (2.2 at.%), creep at 573K 79—20145
Al-Mg (2.2 at.%), high temp. creep mech. determ. by stress-relaxation 77—12670
Al-Mg (4.6 wt.%) alloy, mech. effects during static or cyclic creep 78—39865
Al-Mg (5.5 at.%), applied stress change effect in creep *(Czech)* 79—70126
Al-Mg (5.5 at.%), internal stress during creep at high temp. 79—91749
Al-Mg (5.5 at.%), stress change expt. on creep 79—24584

creep continued
- Al-Mg (5.5 at.%), theory of internal stress for class I high temp. creep 78—19807
- Al-Mg (5.5 wt.%), effect of stress changes during creep on dislocation struct., TEM study 79—74214
- Al-Mg (5.5%), creep, absence of instantaneous plastic strain upon stress changes 78—75718
- Al-Mg alloy, creep rate, effect of dislocation pinning by impurity atoms *(Russian)* 78—38719
- Al-Mg-Si alloy, descriptive method for alloy creep tests by nonstationary loadings 78—23759
- Al-Mg(Zn-Mg), long term strength and creep 80—60925
- Al-Si, dilute, anomalous primary creep behaviour, precipitate form. 80—7646
- Al-Si alloy, eutectic, quasiisotropic 80—79165
- Al-Si crystals, work hardened, softening and creep rates on annealing 80—11663
- Al-Si eutectic, high temp. creep, two regimes of flow, modified Dorn eqn. anal. 79—74215
- Al-Si-Cu-Mg-Ni, piston, depend. between min. creep rate and time of beginning of secondary creep *(Czech)* 80—35267
- Al-Si-N-O system, comps. corresponding to β'-sialon phase reaction hot-pressing 80—84891
- Al-W(Mo)(Nb), struct. and props. of alloys obtained from granules 80—50717
- Al-Zn (11 wt.%), stress depend. of strain rate at elev. temps. 78—23757
- Al-Zn (20 (30) (35) (40) (60) at.%), effect of UTS on cyclic creep strength *(Korean)* 80—25778
- Al-Zn (22 wt.%), superplastic strain rate sensitivity, rel. to ductility 78—31478
- Al-Zn solid soln., controlling creep mechanisms, role of diffusion 78—31469
- Al-Zn solid soln., controlling creep mechanisms role of diffusion 78—31470
- Al-Zn-Mg superplastic alloy, cavity growth under creep conditions 80—60940
- AlCu, electron microscope spot prep. of deform. bands 79—15922
- AlCu-NiCo (5 at.%), Θ' hardened, creep mechanism 80—85013
- AlGe (4 wt.%), struct. peculiarities of superplastic behaviour due to porosity 79—34111
- AlN, creep during hot pressing 78—23650
- Al_2O_3, acceptor-dominated polycrystn., cond. and creep 79—78109
- α-Al_2O_3, atomic disorder, dominant type 78—63757
- Al_2O_3, creep and long term strength 78—23802
- Al_2O_3, polycrystalline, creep and grain boundary sliding 77—36576
- Al_2O_3, pure and Fe or Cr doped, polycryst., creep, diffusion mechanisms 78—11272
- Al_2O_3, vacuum condensate, struct. and mech. props., second phase effect *(Russian)* 80—71705
- Al_2O_3-AlN, creep 77—21235
- Al_2O_3-SiO_2 refractory, creep, viscosity, resist. to inelastic deform. 80—89309
- $(Al_2O_3)_nMgO$, n=1.1, high temp. creep, dislocation behaviour 78—80593
- Ar, solid, diffusion processes in plastic deform. *(Russian)* 80—92591
- Au-Ni solid soln., creep 78—15475
- B fibre reinforcement of thermoplastics, creep resist. and elastic moduli 80—55458
- B-Al, fibre reinforced composite, transverse creep, comparison with laminated Al 77—36587
- Be, creep mechanism 77—36586
- Be-Si-Al-O-N ceramic, phase assemblages, relationships with props. 80—60848
- C fibre reinforced epoxide resin, torsion creep 78—44172
- C fibre reinforced epoxy resin, transverse creep compliance, time and temp. depend. *(Japanese)* 80—45358
- C fibre reinforced plastic, ±45° orientation, creep, fatigue, repeated loading and crack growth 78—68729
- C, pyrolytic, high-temp. deform. under mech. loads 77—16644
- CaO-MgO, doloma, composition effect on creep, impurity effects 79—43318
- Cd, creep, low-temp., thermal heating and quantum mechanisms 80—79868
- Cd, creep mechanism at low temps. *(Russian)* 79—11659
- CdTe, creep activation energy and velocity *(Russian)* 78—56716
- Ce-Si-Al-O-N ceramic, phase assemblages, relationships with props. 80—60848
- (Co,Cr)-$(Co,Cr)_7C_3$, eutectic creep model 77—36588
- $(Co,Cr)(Co,Cr)_7C_3$ eutectic composite, creep anisotropy 78—19840
- Co alloy, X-40, creep-fatigue interaction at high-temp. 78—84958
- Co base alloy, creep-fatigue interaction in aligned eutectic and solid soln. 80—108554
- β-Co, creep at low stresses 79—79028
- β-Co, grain size independent viscous creep 80—40460
- Co, powder, hot pressing on steel substrate, densification kinetics 80—40290
- Co, steady creep rate, stress depend., exam. at phase transformation at 390°C 78—52923
- Co, steady state creep rate, stress depend. rel. to FCC to HCP phase change 78—64598
- Co-Cr-C eutectic, creep and fatigue crack propag. 78—39859
- $(Co_{1-x}Ni_x)O$, single crysts., morphology change during compressive creep testing 79—29144
- CoO, polycrystalline, high temp. deform. 78—3174
- CoO, pure and Li doped, dislocation spacing effect on high-temp. creep 78—35444
- CoO single crystal, compressive creep morphology 77—56034
- CoO single crystal, compressive creep 78—11275
- CoO, single crystal and polycryst., subgrain boundary form. and creep mechanism 77—39594
- Cr-Fe, with Si and Ta additions, metallurgical and mechanical characterisation *(Italian)* 77—66674
- Cr-Mo-V rotor steel, austenite to bainite transformation under cooling conditions, effect on creep 80—3033
- Cr_3C_2 fibre reinforced Ni-based composite, oxidation and creep, Y additions effect 80—66685
- Cr_2O_3, O diffusion coeff. from creep meas. 78—18823
- Cu, aftereffect deformation, creep duration effect on structure, rupture time 79—91766
- Cu alloy, superplastic, activation energy of plastic flow 78—64584
- Cu alloys, low-cycle fatigue and cyclic creep, −196-20°C 80—100913

creep continued
- Cu, commercial, pure, creep-rupture times and creep rate, in vacuum *(Japanese)* 78—72843
- Cu, creep, 200 to 600°C, within framework of structural phenomenological model 78—27585
- Cu, creep, low-temp., during dynamic relaxation, effect of dislocation struct. *(Russian)* 77—25103
- Cu, creep curves, comparison with theory 78—79232
- Cu, creep damage and cavity growth, assessment using density meas. 80—104217
- Cu, creep data, anal. at very low stresses 80—7636
- Cu, creep rate, effect of surface anodic dissolution in acetate buffer soln. 78—3249
- Cu, creep-fatigue failures, damage concept appl. 80—40535
- Cu, creep-rupture interaction, crack behaviour 79—52334
- Cu foil, role of grain-boundary porosity in superplasticity *(Russian)* 78—56690
- Cu free electrolytic films, tensile creep for various film thicknesses calcs. *(Russian)* 80—11697
- Cu, friction stress in high temp. creep 80—11723
- Cu, grain-boundary sliding component in high temp. fatigue 80—50706
- Cu, high purity, creep cavitation topology, high temperature region *(Czech)* 80—65138
- Cu, OFHC effect of cold drawing under combined stress 80—60912
- Cu, plastic deformation, steady state, transients due to strain rate changes 77—81302
- Cu, plastic deformation thermal activation parameters from creep kinetics and stress relaxation 80—71717
- Cu, polycryst., creep and fracture behaviour, effects of prestrain and O 80—97544
- Cu, polycrystalline, friction stress meas. during high temp. creep 79—1898
- Cu, polycrystalline, intracrystalline slip bands in high temp. creep, comparison with brass single crystal *(Czech)* 79—77604
- Cu, powder, hot pressing on steel substrate, densification kinetics 80—40290
- Cu single crystals, in high temp. creep, meas. of internal stress 78—80608
- Cu, surface tension at intermediate and high temps., influence of additional elements 78—15476
- Cu, thermoactivated creep and stress relax. 79—87692
- Cu wire, creep rate, effect of pre-torsional deform. at room temp. or 350°C 77—84836
- Cu, wire, polycryst., internal friction, ultrasonic vibrations effect *(Russian)* 78—76685
- Cu/Cr-Ni-steel fibres, primary creep *(German)* 80—11734
- Cu-Al, eutectic composition, exam. of high temp. mechanical behaviour *(French)* 78—72818
- Cu-Al (10.4%), creep, absence of instantaneous plastic strain upon stress changes 78—75718
- Cu-Al (25 at.%), BCC β phase, high temp. creep, existence of master curve 80—55473
- Cu-Al_2O_3, dispersion-strengthened, vapour-deposited, tensile creep 78—11115
- Cu-Al-Si-Co (2.8, 1.8, 0.4 wt.%), superplastic phase, exam. of mech. props. 78—52891
- Cu-Co (2.48 wt.%), two-phase, surface meas. study of grain boundary sliding during creep 77—81299
- Cu-Ni (10 at.%), creep, substruct. and internal stresses *(Russian)* 80—97527
- Cu-Ni (10 at.%) alloy, creep, dislocation density variation *(Russian)* 79—96101
- Cu-Ni (20 wt.%) alloy, contour plate for relay appl. use of Larson-Miller method *(Japanese)* 80—55454
- Cu-Zn, amorphous, viscoelastic behaviour *(Japanese)* 77—86110
- Cu-Zn, interface sliding of FCC and BCC boundaries 80—104240
- Cu-Zn, rheological study of crystallographic order on creep *(French)* 80—97548
- Cu-Zn (50 at.%), BCC β phase, high temp. creep, existence of master curve 80—55473
- Cu-Zr, amorphous, viscoelastic behaviour *(Japanese)* 77—86110
- Cu_2O, creep substruct. under compression, X-ray diffr. study 78—95785
- Cu_2O, creep tests, exam. of a creep machine mech. ability *(French)* 79—20325
- Cu_2O, heterogeneous deform. during high temp. compression creep 78—48456
- $(Fe,Ni,Co)_3V$, long-range ordered alloy for fusion reactor appl. 80—32481
- α-Fe, 0.14 wt.% P addition effect on creep 77—90420
- α-Fe, $(\bar{1}\bar{1}2)$ $[\bar{1}\bar{1}\bar{1}]$ anti-twinning slip system, low temp. strengthening, dislocation struct. 77—21164
- Fe alloy MA-956E, oxide dispersion strengthened sheet, tensile and creep props. at 1365K 78—48470
- Fe and Fe-Cr, flow stress, effect of cathodic, H_2 charging *(Japanese)* 79—52313
- Fe, Armco, corrosion and mechanical behaviour in liquid Li 78—53036
- Fe, Armco, dislocation struct. effect on creep *(Russian)* 78—39841
- Fe, Armco, screw dislocation effect on mech. props. *(Russian)* 78—60704
- Fe, Armco, surface dissolution effect 77—8883
- Fe, Armco and carbonyl, kinetic singularities of plastic deform. during $\gamma\rightarrow\alpha$ transform. *(Russian)* 78—92262
- α-Fe, cavitation and sliding distrib. changes during creep at 500°C 78—6991
- α-Fe, cold rolled, hydrostatic press. effect on microstructural changes during creep 78—39871
- Fe, creep, effect of H_2 on struct. 77—16652
- α-Fe, creep and fracture between 77 and 673K 79—7649
- Fe, creep at 77, 295K, formation of five struct. 80—60926
- α-Fe, creep life, meas. by microstruct. changes 78—35443
- Fe, deformation, influence of crystallographic lattice type *(Russian)* 79—34106
- α-Fe, deformation induced intergranular creep cavitation 78—31473
- Fe, deformation twin form. during high temp. creep *(Russian)* 79—24573
- α-Fe, high temp. deform. and substruct. *(Japanese)* 77—21226
- α-Fe, hydrostatic pressure effect on creep rate and failure time 78—92306
- α-Fe, influence of C and ZrH_2 on static and cyclic creep behaviour 78—39856

creep continued
- Fe, polycryst., influence of α-γ transform. on creep *(Russian)* 80–89289
- Fe, powder, hot pressing on steel substrate, densification kinetics 80–40290
- Fe, pure, cathodic charging effect on creep and tensile deformation 80–76320
- Fe-bearing olivine and pure forsterite, creep props. comparison 77–78168
- α-Fe-C (0.03 wt.%), structural singularities of transition from thermally activated to force-induced fracture *(Russian)* 78–56731
- Fe-Co-V (33, 33 at.%), BCC β phase, high temp. creep, existence of master curve 80–55473
- α-Fe-Mo (1.5 and 1.8 at.%), deform., testing mode effect at stages prior to steady states 77–66721
- Fe-Mo (1.8 at.%), high temp. creep mech., use of stress exponent 79–5025
- Fe-Mo (1.8%), creep, absence of instantaneous plastic strain upon stress changes 78–75718
- Fe-Mo (4.1 wt.%), substructs. developed during steady state creep at 1100-1200K, TEM obs. *(Japanese)* 79–38900
- Fe-Mo-Cr alloys, creep tests *(German)* 79–61648
- Fe-Mo(4.1 wt.%), steady state creep at high temps. 80–89316
- Fe-Ni-Cr, austenitic, creep strength and ductility, effect of γ' precipitation 77–36597
- Fe-Ni-Cr (25, 15 wt.%), high temp. creep, dispersed γ'-$Ni_3(Al, Ti)$ effects *(Czech)* 78–64590
- Fe-Ni-Cr (25, 15 wt.%), mobile dislocation density in steady state creep, strain transient dip test, TEM exam. 80–7650
- Fe-Ni-Cr alloy 800, creep ductility decline 77–48502
- Fe-Ni-Cr alloy 800, minor alloying element effect on creep, ageing microstruct. 78–27572
- Fe-Ni-Cr austenitic alloy, homogeneous and dispersion strengthened, internal stresses and high temp. creep 78–19841
- Fe-Ni-Cr-Si alloy 800, Si effect on creep and age hardening 77–48444
- Fe-P-C, viscoelastic behaviour of amorphous alloys *(Japanese)* 77–86110
- Fe_3-Al, solid soln., rheological study of crystallographic order on creep *(French)* 80–97548
- $Fe_{40}Ni_{40}P_{14}B_6$, amorphous, steady-state creep rate, cryst. effect 80–81102
- $Fe_xNi_yP_{14}B_6(S_2)$, coiled ribbons, stress relaxation 79–29120
- Ga, creep near MP, influence of cryst. orientation *(Russian)* 77–8878
- GaAs cryst., creep and dislocation vel. at different doping and temps. 78–95783
- Ge, creep and self-diffusion activation energies 78–38772
- Ge, heavily doped, microcreep breakdown 80–97549
- Ge, hot microdeformation and simultaneous X-ray topography apparatus *(French)* 80–38871
- Ge, plastically deformed under high temp. creep conditions, elec. props. 80–92915
- Ge, stationary creep depend. on deform. stabilisation of material struct. *(Russian)* 80–100300
- H_2, solid, 2-4.2K, o-H_2 content effects *(Russian)* 77–7787
- n-H_2, solid, controlling mechanisms *(Russian)* 77–89493
- HfC, pressing regime influence on high-temp. creep *(Russian)* 80–100852
- HgTe, creep activation energy and velocity *(Russian)* 78–56716
- In, twin boundary movement by creep 80–24460
- KCl, Czochralski-grown, creep and struct. changes, 77-300K *(German)* 77–28862
- KCl single crystal, dislocation velocity stress exponent estimation by stress relaxation and creep tests *(Japanese)* 78–55875
- LiF, deform. mech. map. 77–81298
- LiF, single cryst., impression creep 78–6986
- LiF single crystals, stepwise creep, 300K, in dislocation depletion conditions, thermal cycling effects *(Russian)* 77–15484
- LiF, strong reorientation resulting from creep, X-ray obs. 79–100228
- Li_2O-Al_2O_3-$4SiO_2$, glass-ceramic, tensile creep and high temp. fracture 78–52914
- Mg alloy, dil., dynamic recrystn. during creep, dislocation substruct., quartz comparison 80–109142
- Mg-Al (0.8 wt.%), grain-boundary sliding component in high temp. fatigue 80–50706
- Mg-Al-Zn, anelastic creep and recovery 77–63709
- Mg-Si-Al-O-N ceramic, phase assemblages, relationships with props. 80–60848
- $MgAl_2O_4$, dislocations, sessile dissoc. 79–46663
- MgO, effect of B_2O_3, CaO and SiO_2 minor additives on high temp. creep 78–48450
- MgO, MgO-CaO (58 wt.%), comparison of high temp. creep and fracture 77–16658
- MgO, polycryst., creep diagrams inc. ambipolar diffusion and grain size for polycryst. ceramics with ambipolar diffusion, incl. grain size 77–73304
- MgO, polycrystalline, stress depend. of creep 79–70120
- MgO polycrystals, ultrafine grained, compressive creep 77–32639
- MgO, single cryst., tensile creep, stress induced dislocation structs. 80–96539
- MgO, single crysts., work hardening and creep 79–43262
- MgO, tensile creep of single crystals, substruct. effect 79–66113
- MgO, ultrafine grained Fe doped, high temp. creep 79–15727
- $MgO{:}CaO(SiO_2)(B_2O_3)(Cr_2O_3)$, effective of impurities on high temp. creep 80–40455
- MgO-C dispersion, creep, effect of C on grain size and growth 79–100213
- MgO-$CaMgSiO_4$, exam. of high temp. creep behaviour 78–80601
- MgO-$MgAl_2O_4(FeCr_2O_4)$, thermoplastic and thermophys. props. for steel vacuuming installations 80–35281
- $MgO(Al_2O_3)_{1.8}$, spinel, X-ray refl. topography, dislocation substructures during creep form. *(French)* 78–68737
- MgO.1.1 Al_2O_3 spinel, high temp. deform., cryst. orientation effect 80–107263
- MgO.3.5Al_2O_3, precipitation during creep experiments 79–47694
- Mg_2SiO_4, forsterite, glissile splitting of dislocations, cross-slip-controlled creep and mantle rheology 78–61406
- Mg_2SiO_4, pure forsterite, transient and steady-state creep at low stress 79–79827
- Mo alloy TsM-6, creep rate in vacuum, grain size effect 80–108514
- Mo, block boundary dislocation struct. singularities under high temp. steady state creep conditions *(Russian)* 79–90670

creep continued
- Mo, creep deformed single crysts., subboundary struct. obs., dislocation sets 80–103348
- Mo, irradiated with fission fragments, creep, 20-30K *(French)* 77–48493
- Mo, monocrystalline, exam. of microplasticity at ambient temps. *(French)* 78–52888
- Mo, single crystal, ductility and high temp. strength in routine tests 77–90427
- Mo single crystal, effect of prior ultrasonic working on hardness, crystal orientation and creep resistance *(Russian)* 79–34056
- Mo single crystal, thermocyclic strength of high temps. of single crystal 77–16685
- Mo single crystal 78–15478
- Mo, single crystals, creep deformed, Burgers vectors, block boundary dislocation struct. *(Russian)* 79–77603
- Mo, single crystals, high temp. creep and strength depend. on thermomechanical treatment *(Russian)* 79–79034
- Mo, US working effect on single cryst. during deform., strengthening effect, plasticity resource *(Russian)* 79–34107
- Mo wire, struct. and high-temp. creep, dopant elements influence 80–66603
- Mo-Hf-C, superior powder metallurgy die alloys for isothermal forging mech. props. 79–74201
- Mo-Ti-La-C, influence of high pressure on mech. preps. after nitriding *(Russian)* 79–57137
- Mo-Ti-Zr alloys TZM and TZC, superior powder metallurgy die alloys for isothermal forging mech. props. 79–74201
- Mo-V-C, hot-worked, substructural hardening and high-temp. strength *(Russian)* 80–25731
- Mo-W-Mo (4.74, 2.17 wt.%), creep resistance in ultrahigh vacuum 79–5027
- Mo_2 single crysts., surface orientation effect as high temp. creep and fracture type 80–16403
- Mo_3C_2, pressing regime influence on high-temp. creep *(Russian)* 80–100852
- NH_4Cl, transitional plasticity, light scatt. study 79–77674
- NaCl, deform. mech. map. 77–81298
- NaCl, deformed surface layer, block misorientation 79–99405
- NaCl, halite, dynamic recrystn. during compression creep, geophys. appl. 80–25772
- NaCl, rock salt, progressively mined soln. cavities, struct. behaviour 78–61409
- NaCl single crystal, plasticity, effect of alternating electric field 78–15481
- NaCl, single crystal, recovery controlled transient creep, substructural obs., phenomenological anal. 77–77526
- Nb base alloy, high temp. creep estimation and long term strength charact. 78–3195
- Nb, creep rate in vacuum, grain size effect 80–108514
- Nb:He, mech. props. and microstruct. 80–85003
- Nb-Mo-Ti-Zr, influence of C content on creep charact. and creep-rupture strength *(Russian)* 77–48483
- Nb-O, cyclic creep, effect of O_2 conc. and temp. 78–48466
- Nb-W-Mo-Zr (5, 2.1, 0.92 wt.%), creep resist., high temp. ageing in vacuum 80–71716
- Nb-W-Zr-Ta (90, 4.5, 3.5, 2 wt.%) creep and creep limit in super vac. at 1100°C, heat treatment effect 80–81133
- Nb-Zr (1 wt.%), high temp. creep, under O_2 stream pressure *(Russian)* 77–52404
- Nb-Zr-C, strengthening phase struct. and morphology after prolonged high temp. stress in vacuum *(Russian)* 77–25065
- Nb-Zr-C alloy, creep in vacuum, prolonged high-temp. ageing effects *(Russian)* 78–56692
- Nb-Zr-C alloy, effect of ageing on high temp. strength *(Ukrainian)* 79–52249
- Nb-Zr-C alloy, long term loading at high temps. effect on struct. and morphology of carbide phase 79–15754
- Nb-Zr-C alloy, strengthening phase, struct. and morphology after stress ageing *(Russian)* 78–31454
- NbC, pressing regime influence on high-temp. creep *(Russian)* 80–100852
- NbC, vacuum condensate, struct. and mech. props., second phase effect *(Russian)* 80–71705
- $NbC_{0.98}$, single crysts., creep, 1800-2700°C *(Russian)* 79–5005
- NbC_x, creep-comp. curves for homogeneous region 78–52911
- Nb_3Sn, hot isostatically pressed, plastic deform. 80–108510
- Ni alloy 718, creep crack growth 77–63776
- Ni alloy EI617, creep, effect of preliminary heat treatment on struct. and props. 77–21195
- Ni alloy IN-738, Y_2O_3 (1.5 wt.%) addition, mechanical alloying 77–40427
- Ni alloy KhN56VMKYu, creep, viscosity, resist. to inelastic deform. 80–89309
- Ni alloys, cyclic creep of heat resistant alloys *(Russian)* 78–19845
- Ni alloys, heat resistant, creep resistant deform. 79–100234
- Ni base alloy IN 738 LC, overaged, creep and fatigue crack growth 77–86138
- Ni base superalloy, directionally solidified, struct. and props. *(Chinese)* 80–20918
- Ni base superalloy, internal stresses due to dislocation walls around second phase particles 79–99210
- Ni base superalloy, single crystal, apparent and effective creep parameters, incubation period 77–63715
- Ni base superalloy IN 100, corrosion resistant intermetallic coating, microstruct. effect on mech. props. 78–85058
- Ni base superalloy IN-738, γ' precipitate coarsening during ageing and creep 79–52271
- Ni coating, electron beam evaporated, ductility and struct. 78–11439
- Ni, creep, effect of AC mag. field, 1.5-4.2K *(Russian)* 79–11657
- Ni, creep, rel. to radiation swelling and stacking fault energy *(Russian)* 78–27562
- Ni, creep, single crystals, 1.5-50K, orientation effects *(Russian)* 79–15757
- Ni, creep, struct. and activation characts., effective stress, electron microscopy and resistometric obs. *(Russian)* 80–40427
- Ni, creep, substruct. and internal stresses *(Russian)* 80–97527
- Ni, creep at 77, 295K, formation of five struct. 80–60926
- Ni, creep parameters, high temp. 80–50685
- Ni, creep rates, stress depend., and activation energies, constant stress tests, comparison with dislocation creep theory 80–71708

creep continued

Ni, cyclic creep in single crystals 79—66129

Ni, Dorn relationship for creep prediction, introduction of force factor *(Russian)* 78—18185

Ni, mag. field effect on creep, 4.2K *(Russian)* 77—90000

Ni, mag. field effects, 30-250 Oe 77—16141

Ni, magnetic aftereffect reactivation of single crystal by plastic deform. 79—65697

Ni, magnetically ordered state, softening with varying mag. field *(Russian)* 78—35017

Ni, oxidation, high temp., effect of C on cavity form., SEM study 80—97638

Ni, oxide dispersion strengthened, creep and tensile props. 77—86042

Ni, powder, hot pressing on steel substrate, densification kinetics 80—40290

Ni, simultaneous obs. of Barkhausen and magnetoplastic effect 79—28583

Ni, structural changes, creep mechanism, multiple dislocation cross slip *(Russian)* 80—59476

Ni superalloy, dispersion strengthened, creep stress component rationalisation *(Korean)* 79—66115

Ni, transient creep stress depend. at $T<T_{0.2MP}$, dislocation struct. *(Russian)* 77—48482

Ni, variation in dislocation density during creep, determ. by X-ray diffr. analysis *(Russian)* 80—76302

Ni-Al, rheological study of crystallographic order on creep *(French)* 80—97548

Ni-Al, solid soln. and solid soln. hardened, stead state creep 78—27578

Ni-Al (1.18 wt.%), substruct. hardening effect, depend. on mechanism controlling creep rate, 700°C 79—20144

Ni-Al (6.2 wt.%), high temp. creep *(Czech)* 77—63727

Ni-Al_2O_3 alloy, electron beam evaporated, struct. and mech. props. 78—11114

Ni-Al-Cr alloy Ehi 826 77—86120

Ni-Al-Cr superalloy IN-100, crack retardation at elev. temp., hold time effect of single overload 79—79068

Ni-base alloy, heat resistant charact. extrapolation by temp.-time methods, creep data 78—15477

Ni-base alloy, screening studies for evaluation for nucl. process heat system 78—13236

Ni-base alloy creep, corrosion and fatigue testing for appl. in nucl. process heat system 78—13237

Ni-base superalloy, effects of grain boundary carbides on creep and back stress 80—3130

Ni-base wrought superalloy, creep and stress rupture behaviour in air and vacuum 80—60918

Ni-based alloys, binary, ternary, complex, TiC additions, effects 78—92305

Ni-based heat resisting alloys, strain resistance under complex loading program conditions 79—57073

Ni-Co (5(66) wt.%), internal stresses during creep 80—3142

Ni-Co-Cr-Al-Ti-Mo superalloy IN738, casking porosity removal using hydrostatic press. sintering 80—55322

Ni-Cr, creep-fatigue failures, damage concept appl. 80—40535

Ni-Cr, low short-term creep resist. at 700°C 80—76313

Ni-Cr, solid soln., exam. of back stress role in creep behaviour of particle strengthened alloys 78—52889

Ni-Cr (2 wt.%), role of hydrostatic pressure on sintering of creep cavities 79—28980

Ni-Cr alloy, ÉI 437B, vibrocreep at normal and high temps. 77—4824

Ni-Cr alloy, KhN70VMTYu, gas turbine blades, thermocyclic strength characts., exam. 78—60743

Ni-Cr alloy Ehi 617, equation of condition for creep, expt. checking 77—86120

Ni-Cr alloy KhN70VMTYu, heat resistant, explosive loading effect on struct. and mech. props. *(Russian)* 78—39787

Ni-Cr complex alloy with good creep resistance, friction stress/flow stress relation 79—8337

Ni-Cr superalloy, interactions between creep and low cycle fatigue *(Chinese)* 80—66572

Ni-Cr-Al-TaC, eutectic composite, microstructure, fatigue props. 80—85038

Ni-Cr-Al-Ti (Ti-Co), exam. of back stress role in creep behaviour of particle strengthened alloys 78—52889

Ni-Cr-Al-Ti alloy type ZhS6U, effects of heat treatment in high vel. gas streams on props. 79—57025

Ni-Cr-Co alloys, relax. resist. exam. by bending and tension 79—24564

Ni-Cr-Co superalloy, σ-phase effect on mech. props. *(Chinese)* 79—74229

Ni-Cr-Co-Mo-Al-Ti (10, 15, 3, 5.5, 4.5 wt.%), superalloy, exam. of creep and fracture behaviour 78—48464

Ni-Cr-Co-Mo-Al-Ti alloys, Waspaloy, Astroloy, exam. of microstruct. effect on crack growth 78—52977

Ni-Cr-Co-Ti-Mo-W-Al (14, 9.8, 5, 4, 3.9, 3 wt.%), low cycle fatigue, prior heat treatment effect 80—60962

Ni-Cr-Ta-Ti-Si, EP557 precipitation hardening alloy, mech. props., heat treatment effect 80—60877

Ni-Cr-W (20, 10 to 40 wt.%), phase composition, struct. and props. 80—21034

Ni-Cr-W (20, 3 wt.%), high temp. creep, atmospheric effect on anomalous behaviour 78—80617

Ni-Cr-(Al), oxide dispersion strengthened, creep and tensile props. 77—86042

Ni-Cr(-Mo), creep parameters, high temp. 80—50685

Ni-Fe metallic glass, METGLAS 2826, creep props. 79—15746

Ni-Fe-Cr-Nb-Ta-Mo alloy, fatigue crack growth, stress ratio and hold-time effects 80—40531

Ni-Ni_3Al-Cr_3C_2 eutectic composite, creep 77—40431

Ni-P, struct. obs. by X-ray diffr., low temp. annealing and deform. effects 79—56995

Ni-ThO_2, dispersion hardened, fracture mechanism map 78—60823

Ni_3Al based alloys, mean square atomic displacements, rel. to steady creep rate 79—28053

γ'-Ni_3Al-Fe (10 at.%) alloy, steady-state creep 78—15460

$Ni_{2/3}Fe_{7/3}O_4$, precipitation of α-Fe_2O_3, optical microscopy, SEM and TEM studies *(French)* 80—11650

NiO, polycrystalline, high temp. deform. 78—3174

NiO single crysts., creep along $\langle 100\rangle$, stresses 50 MPa-120 MPa, 950-1200°C *(French)* 79—20121

NiO, stress relief and plastic flow in temp. range 1323-1473K 80—89302

creep continued

NiTa C-13, advanced fibre reinforced eutectic superalloy, creep and rupture 77—63744

Nr-Cr-ThO_2 (20, 2 vol.%), Orowan stress/creep threshold stress comparison 77—8901

Pb creep, low-temp., thermal heating and quantum mechanisms, supercond. transition effects 80—79868

Pb, Pb-Bi, supercond., anomalous thermal cond., transition induced creep *(Russian)* 77—36020

Pb, pure, friction stress for high temp. creep 78—11289

Pb, strain hardening and recovery, during primary creep 78—39799

Pb:Ni, paramag. impurity effect on work hardening at superconducting transition *(Russian)* 77—47915

Pb-Al_2O_3 composites, creep rate and creep behaviour *(Japanese)* 78—84830

Pb-Bi(Ni), creep, low-temp., thermal heating and quantum mechanisms, supercond. transition effects 80—79868

Pb-Sb-Te-Cu-Sn, influence of specimen and grain size on mech. props. *(Russian)* 77—81297

Pb-Sn(Bi)(Ni), strength loss in supercond. transition, nonmag. and paramag. impurities influence *(Russian)* 80—70875

Pb-Tl, sliding and its accommodation during creep and superplasticity 77—40436

PbTe based thermoelec. materials, creep mechanisms 77—16643

Pd-Si, amorphous, viscoelastic behaviour *(Japanese)* 77—86110

Pd-Si, struct. obs. by X-ray diffr., low temp. annealing and deform. effects 79—56995

$Pd_{82}Si_{18}$ glassy, long term creep tests, isoconfigurational viscosity rel. to annealing treatment 79—66122

Pt alloys, influence of Rh, Au, Mo, W, Zr, Hf alloying elements on creep activation energy at high temp. *(Chinese)* 80—66573

Se, amorphous, struct. relax. effects, obs. by mech. props. *(French)* 79—51201

Se amorphous films, structural relax., viscosity, creep, heat capacitors, and IR spectra meas. 79—42424

Si, creep and self-diffusion activation energies 78—38772

Si, heavily doped, microcreep breakdown 80—97549

Si, stationary creep depend. on deform. stabilisation of material struct. *(Russian)* 80—100300

Si-Al-O-N, compression creep, comparison with SiC and Si_3N_4 79—15728

Si-Al-O-N, high-temp. fracture and diffusional deform. mechanisms 80—40509

Si-Al-O-N sintered ceramic, microstruct., phase composition and transformation mech., mech. props. 80—40309

SiC, chem. stability, mech. and thermal props. rel. to appls. 80—21103

SiC, compression creep, comparison with Si_3N_4 and sialon 79—15728

SiC, high temp. creep. 77—77530

SiC, high-temp. creep interpretation by deform. mapping techniques 77—21230

SiC, pyrolitic coating for nuclear fuel particles 77—79465

SiC single crystal, hot hardness and creep behaviour 79—100247

Si_3N_4, CVD, struct., optical and mech. props. 77—1816

Si_3N_4, effect of oxide impurities on physicomechanical props. 80—16396

Si_3N_4, high temp. creep. 77—77530

Si_3N_4, oxidised ceramic, O_2 depth profiling using ^{4}He backscatt. 77—89463

Si_3N_4, pyrolytically-deposited, engng. significance 79—38746

Si_3N_4, reaction bonded, creep, internal oxidation effects 78—56701

Si_3N_4, reaction bonded, effect of Si powder grain size on microstructure, and mech. props. *(German)* 79—4998

Si_3N_4, reaction bonded and hot pressed, compression creep, comparison with sialon and SiC 79—15728

Si_3N_4, reaction-bonded, internal oxidation processes role in high-temp. mech. props. 79—38915

Si_3N_4, reaction-bonded and hot pressed, deform. and fracture during creep 79—38916

Si_3N_4-Mg_2SiO_4-Si_2N_2O, compressive creep, composition effect 80—50674

Si_3N_4-MgO, compressive creep, oxidation induced compositional change 80—50676

Si_3N_4-MgO (2-5 wt.%) hot pressed, tensile creep testing 80—40423

β-Sn, impress creep of single crystal 79—91743

Ta, bamboo struct., wire, high-temp. rheology 77—1851

Ta-W-Hf (8,2 wt.%), T-111, O_2 absorption, effect on lattice parameter and specimen dilation 78—83958

TaC, pressing regime influence on high-temp. creep *(Russian)* 80—100852

(Ti, Cr)B_2-based alloys, densification of powder mixtures by hot-pressing, elec. and mech. props. 80—20812

Ti alloy, commercial, effect of environment and coating 78—31480

Ti alloy, crack initiation on planar shear bands, H_2 assisted 80—71749

Ti alloy, creep and long-term strength under cyclic loading 78—3191

Ti alloy, creep strain increments rel. to stresses, nonstationary loading 80—25776

Ti alloy, cyclic creep 77—81323

Ti alloy, heat resistance, thermal stability, stress-rupture strength, and creep 80—81194

Ti alloy, mechanical props. at high temp., effect of Pt ion plating 79—29156

Ti alloy, microstruct. and mech. props., room and elevated temps. 77—36554

Ti alloy, microstructure resulting from heat treatment, alloying, effect on creep, fatigue, fracture strength 78—11246

Ti alloy, OT-4, 800-1050°C *(Russian)* 77—59859

Ti alloy, VT3-1 mech. props. and low-temp. creep 77—44314

Ti alloy creep strength rel. to diamond electrochem. cutting conditions *(Russian)* 79—96081

Ti alloys, 685 and 6242, creep resist. and thermal stability in air and in vac., role of Si 80—30020

Ti alloys, data handbook of low temp. mech. and phys. props. 80—22153

Ti alloys, strength characts., elastoplasticity, creep 78—6976

Ti based alloy, type VT65 and VT5-1, describing cyclic-creep processes with parametric eqn. 79—57074

Ti, commercial, creep behaviour, 25 to 400°C, role of impurities and/or alloying elements *(French)* 80—45354

Ti, Cr coating effect on mech. props. *(Russian)* 77—44290

α-Ti, grain size independent viscous creep 80—40460

Ti, high purity, data handbook of low temp. mech. and phys. props. 80—22153

Ti, surface and grain boundary free energy, zero-creep determ. 79—4313

Ti, tensile properties and creep behaviour at high temp. 78—23773

creep continued
Ti-(Al)-Zr-Si (5, 0.5 wt.%), creep 77—36595
Ti-Al-Cr-Mo-V(Fe), low cycle fatigue in repeated tension 80—76348
Ti-Al-Mo-Zr, type VT-9, creep eqns. rel. to extension and compression props. 80—100875
Ti-Al-Nb-Ta-Mo (6, 2, 1, 0.8 wt.%), elevated temp. flow strength, creep resist., diffusion welding characts. 80—30033
Ti-Al-Sn-Zr-Mo alloy, Ti-6242, α+β, creep property improvement by Pt ion plating 80—16408
Ti-Al-Sn-Zr-Mo-Si-O-H, Si, O, H effects on fatigue, fracture and creep charact. 79—11697
α-Ti-Al-Sn(5, 2.5 wt.%), effect of Pt ion plating on creep behaviour 79—66123
Ti-Al-V, (6,4 wt.%), history dependent steady state creep rate 78—39866
Ti-Al-V, alloy 685, fatigue life, creep and dynamic strain ageing effect, 25 to 400°C *(French)* 80—45384
Ti-Al-V (6, 4 wt.%), α-β anneal, recrystn. anneal, β-anneal, room temp. creep 79—61662
Ti-Al-V (6,4 wt%), cyclic temp. creep, transition effect 80—97539
Ti-Al-V (6,4 wt.%), surface and grain boundary free energy, zero-creep determ. 79—4313
Ti-Al-Zr-Mo-Si (6, 5, 0.5, 0.25 wt.%), β-processed, fatigue props., hold time effect 80—60961
Ti-Al-(V) (6,4 wt.%), hot salt stress corrosion susceptibility, microstruct. effects 77—36688
Ti_3Al-Sn-Zr, alloy, Sn and Zr alloying influence on creep and scaling resist. *(Russian)* 79—52302
TiB_2, TiC, vacuum condensate, struct. and mech. props., second phase effect *(Russian)* 80—71705
TiC, activation energy for creep, from micro-Vickers hardness expts. 77—28890
$(U,Pu)O_2$, thermal creep in 40 to 100 N/mm^2 stress range 77—28881
UC, polycrystalline, creep mechanism interpretation 78—8898
UC-NbC, UC-ZrC and UC-ZrC-NbC, solid soln. strengthening rules, physicomech. prop. changes 77—28826
$UC_{1.5}$, creep behaviour and phase change under compression stress 78—35432
UO_2, config. and climb rate of dislocation links, contrib. to anelastic creep 77—52431
UO_2 pellet, interaction between cladding in water reactor fuel pins 78—25286
UO_2, superplastic creep 79—15730
UO_2, thermal creep in 40 to 100 N/mm^2 stress range 77—28881
US-UC-UC_2 system, potential nuclear fuels, phase solid soln. studies, prep. and props. exam. 79—40996
V, polycryst., creep behaviour, 790-880°C 79—24578
V, substrct. changes during creep dislocation density *(Russian)* 78—23782
V_3Si single cryst., creep deform. 80—71695
V_3Si, supercond. structure and properties *(German)* 80—93631
Va, creep rate in vacuum, grain size effect 80—108514
W alloy wire reinforced stainless steel, fibre/matrix interaction, fabrication and heat treatment effect 79—91607
W alloys, deformed, vacuum technology appl., mech. props. *(German)* 79—57046
W, block boundary dislocation struct. singularities under high temp. steady state creep conditions *(Russian)* 79—90670
W, creep in monocrystal at 0.57 T_m *(Russian)* 77—1856
W fibre reinforced Ni composites, high temp. tensile and creep props. 77—52444
W fibre reinforced Ni composite, prep. by hot isotactic pressing, mech. props. *(Slovak)* 78—19694
W single cryst., high temp. creep and dislocation struct. 80—71715
W single crystal, creep, excess edge and screw dislocation density calc. *(Russian)* 78—34519
W, single crystals, creep deformed, Burgers vectors, block boundary dislocation struct. *(Russian)* 79—77603
W, single crystals, high temp. creep and strength depend. on thermomechanical treatment *(Russian)* 79—79034
W, US working effect on single cryst. during deform., strengthening effect, plasticity resource *(Russian)* 79—34107
W, wire, doped, high temp. creep behaviour 78—88499
W wire, struct. and high-temp. creep, dopant elements influence 80—66603
Y-Si-Al-O-N ceramic, phase assemblages, relationships with props. 80—60848
$YH_{1.92}$, tensile strength and creep 80—55459
Y_2O_3, plastically deformed monocryst., HV electron microscopy obs. of dislocation config. *(French)* 79—55747
Y_2O_3-AlN, creep 77—21235
Zn alloys, rolled and press. die-cast, creep and deformation behaviour *(German)* 80—66611
Zn, creep, compression anisotropy effects 79—83275
Zn, creep, low-temp., thermal heating and quantum mechanisms 80—79868
Zn, microrupture singularities in low stress range at elevated temp. *(Russian)* 79—29172
Zn single crystal, discontinuous creep *(Russian)* 77—81292
Zn, singularities of effect of pressure on stages of creep *(Russian)* 79—29134
Zn-Al (22 wt.%), eutectoid, low stress and superplastic creep behaviour 80—81120
Zn-Al (22 wt.%), superplastic eutectoid, concurrent grain growth and deformation mechanism 79—74222
Zn-Al eutectoid alloy sheets, creep bulging 80—1439
Zn-Al superplastic eutectoid alloy, low strain rate behaviour 80—40458
Zn-Al(Cu), dil. alloy, creep ductility 79—38899
Zr alloy, creep, steady state creep rate, stress depend. at low stress *(Czechoslovakian)* 77—32640
Zr, creep, optical and electron metallographic anal., 473 to 873K 78—39986
α-Zr, creep stress characts., 300-900K 77—66675
Zr, crept single crystal, nature of γ-hydride 77—21147
α-Zr, effect of stress changes on creep *(Czech)* 79—96085
α-Zr, grain-boundary sliding component in high temp. fatigue 80—50706
α-Zr, some stress change expts. on creep 80—3125
Zr-Cr-Fe, irradiation damage, metallurgical struct. effect 77—51412
Zr-H, tensile strength and creep 80—55459
Zr-Nb (1 wt.%) exam. of creep behaviour, 373 to 773K 78—80599
Zr-Sn-Mo (4.5,1 wt.%) and (4.5,2 wt.%), creep behaviour at room temp. *(Czech)* 79—24590

creep continued
Zr-Sn-Mo (6, 1 wt.%), creep and creep rupture 78—23778
Zr-Sn-Mo-(Nb), creep and creep fract. at 623 to 823K *(Czechoslovakian)* 77—32643
Zr-Sn-Mo(Nb), creep and creep fracture, 623 to 823K *(Czech)* 77—59916
Zr-Sn-No-(Nb), steady state creep 77—36580
α-Zr-Sn(Mo), creep characts., influence of Sn and Mo *(Czech)* 80—81119
ZrC-TaC solid solns., high-temp. creep 79—11661
ZrC_x, creep-comp. curves for homogeneous region 78—52911
ZrO_2, ZrB_2, vacuum condensate, struct. and mech. props., second phase effect *(Russian)* 80—71705

creep fracture
ageing at high temp., effect on creep props. SEM 80—97516
Al alloys D16T and AK4-IT, effective thermal force surface in process of damage and time until failure 80—35324
alloy, creep elongation, modification of Monkman-Grant relation *(Czech)* 77—63726
alloys, creep cavitation control, intergranular precipitates role 80—66664
alloys, high temperature, creep failure criteria 80—65150
alloys, intergranular precipitate effect on diffusion growth of creep voids 79—34041
alloys for fission reactor components, mech. props. at high temp., failure prediction 80—5241
brass, cyclic creep and fracture under stress-controlled cyclic conditions 79—74232
α-βbrass, exam. of creep fracture by tensile tests 78—88531
α-brass, metallographic and fractographic study of void formation during creep 80—16449
brittle materials, intergranular creep crack growth, diffusion controlled theory 78—84950
cavitation failure, incorporating cavity nucleation with strain 80—16451
cavity, growth mechanisms, stress depend., rel. to creep fracture 79—99266
cavity growth controlled by surface diffusion, numerical study 79—90668
complex-stress criterion governing creep fracture 77—3783
composite, fracture time under tensile loading 78—88521
concrete, creep, time dependent behaviour under high tensile stress *(Japanese)* 78—31465
concrete *(Japanese)* 78—31519
concrete prestressed members, creep fracture during manufacture 78—76767
consistent creep and rupture properties for creep-fatigue evaluation of nuclear components 80—35329
constitutive equations 78—3202
continuous damage parameter for non-ageing materials 80—16418
correlation and extrapolation methods, creep rupture data analysis 80—58975
Cotac 74, directionally solidified composite, creep behaviour prediction *(French)* 78—68754
Cr-Mo (2.25, 1 wt.%), annealed, tertiary creep behaviour 79—43326
crack growth, appl. of fracture mechanics 78—18237
crack growth, model, diffusion of vacancies along grain boundaries 78—75716
crack growth initiation theory 77—58604
crack growth rate estimation by reference stress methods 79—50663
crack loaded in anti-plane shear under creep 79—27598
crack propag. anal. on basis of plastic singular stress field 79—68647
crack propag. by cavitation near crack tips 80—107364
crack propag. rates, prediction using C* parameter 77—90449
crack propagation in creep, rate obs. on stainless steels *(Japanese)* 77—8927
crack propagation in creep finite element analysis *(Japanese)* 77—8926
cracked bodies, failure prediction in creep range 79—27592
creep strength of deformed material, conditions of physico-chemical action *(Russian)* 77—16703
damage bounds in creeping struct. approaching rupture 79—50612
damage criteria, cavity config., use of density meas. 78—60818
damage parameter, energy based, for fatigue and creep-fatigue appl. 78—59347
damage-induced tensile instability 77—4854
deformation and fracture of materials in creep range, effects of nonlinear stress-strain rate relations 80—58938
determination, miniature test-pieces, multipurpose apparatus *(Russian)* 77—52558
dislocation source activation by load impulses 78—14350
Dugdale model for crack opening and growth 78—5699
EBR-II, mixed-oxide fuel pins, results from expt. F11A after cladding break 79—67861
engineering alloys, prediction of creep fracture, exam. 78—56776
engineering materials relation between deform., rupture, power-law creep 79—5020
failure by cavitation under non-steady conditions, exam. 78—56774
failure mechanism involving grain boundary sliding and brittle crack extension 80—97557
fatigue-life model, under stationary and non-stationary loading, based on wedge crack development 78—38248
α-Fe, long-time strength *(Russian)* 77—44330
fibre reinforced plastics, crack growth *(Japanese)* 77—32702
fracture mech. during creep, interference microscopy exam. of 12Kh18N9, 08Kh18N10T 78—56756
fusion reactor first wall/blanket system, thermal-hydraulics and fatigue life modelling 78—58453
fusion reactor metals, He embrittlement, grain boundary cavity model 80—34075
geofracture creep, meas. using interference of light with equal optical paths *(Chinese)* 80—82113
glass fibre reinforced polycarbonate, creep crack growth *(Japanese)* 78—39887
grain boundary crack, stress depend. of growth rate during creep 77—80575
grain boundary estimation of creep rupture time *(Chinese)* 78—83325
grain boundary sliding and intercrystalline fracture in high temp. creep *(Czechoslovakian)* 77—32642
granodiorite, fracture under uniaxial compression, mech. and AE meas. *(Japanese)* 78—56748
Hastelloy X, creep and creep rupture props. in air and helium at 900°C *(Japanese)* 77—52405

creep fracture continued
heat-resisting alloy, EP199, creep-rupture strength in NH_3 and decomp. products *(Russian)* 77—52534
high temperature fracture under cyclic loading, book contrib. 79—66171
high temperature plant design methods, reference stresses and bounding theorems 80—58937
HTR annular compacts, creep strain limit expt. 77—42069
ice sheet, creep rupture obs. at depth 79—2306
Incaloy IN 738, dispersion hardened superalloy 78—11156
Incoloy, evaluation for use in nuclear process heat appl. 78—13234
Incoloy 800, chem. behaviour and mech. performance in HTR He at high temps. 79—47842
Incoloy 800, creep and fatigue props. in high temp. gas cooled reactor He environment 79—47776
Incoloy 800, creep crack growth, age hardening effect 79—43436
Incoloy 800, creep rupture, creep strength and tensile data, 500 to 800°C 79—43371
Incoloy 800, creep rupture ductility, 500 to 600°C, hardness and metallurgic exam. 79—43435
Incoloy 800, creep rupture props. at 525°C 79—43437
Incoloy 800, design codes and lifetime prediction aspects for nuclear and non nuclear appls. 79—47778
Incoloy 800, effect of liquid Na on creep and rupture props. 79—47775
Incoloy 800, mechanical props., heat treatment and appl., conf., Petten, Netherlands (March 1978) 79—43296
Incoloy 800, thin wall tubing, creep-rupture testing in steam under constant and cyclic load 79—47774
Inconel, type 706, precipitation and creep rupture behaviour, optical and TEM study 79—74158
Inconel 625, creep rupture behaviour in Ag environment 80—25853
Inconel 625, creep rupture strength and corrosion in HTC in He *(German)* 77—77557
Inconel 718, creep fracture characts. 79—52339
Inconel 718, surface flawed tensile bars, utility in cyclic life studies 77—21342
Inconel X750, positron annihilation study of ageing and creep 80—29824
intergranular fracture during power-law creep 79—96105
intergranular fracture during power-law creep under multiaxial stresses 80—107365
Larson-Miller parameter, exam. 78—76742
Larson-Miller parameter, exam. 78—76743
life prediction modelling for creep damage 80—59574
like improvement mechanism, reheat treatment 78—64666
LMFBR, LOCA, fuel pin failure mechanisms 80—13587
Local stress and strain during crack growth by steady state creep 77—90442
macroscopic growth, relation between engineering and metallurgical factors 78—11321
macroscopic growth 78—79282
materials under load, durability and accumulation of damage *(Russian)* 77—59892
metal, strength characteristic, high temp., prediction from creep processes 77—86119
metal disintegration effect on struct. performance 77—3787
metal structs., creep rupture life upper bounds, variable load and temp. 77—62206
metals, engineering, multi-axial creep characts. 80—64398
metals, fracture during creep 78—68778
metals, time to rupture and accumulation of damage under load *(Russian)* 79—5029
metals under creep loading, cumulative damage, engineering approach 80—58935
microcracks, statistical linking theory consistent with classical reliability theory 78—84952
micromechanisms of crack extension, conf., Cambridge, England (March 1980) 80—105421
minimum creep rate rel. to time to fracture 77—7346
Ni-base alloy 713LC, creep rupture strength and corrosion in HTR in He *(German)* 77—77557
Nimonic 105, temp. and stress depend. of microstruct., small angle neutron scatt. study 79—15726
Nimonic 115, superalloy, critical strain model for creep fracture 77—32648
Nimonic 80A, creep in tension and torsion 77—25113
Nimonic 80A, creep rapture under non-proportional loading 80—108518
Nimonic 80A, creep rupture strength and corrosion in HTR in He *(German)* 77—77557
Nimonic 80A, intergranular creep fracture under const. cavity density 78—60825
Nimonic PE16, creep rupture props. in CO_2, air and vacuum environments at 700°C 79—74248
Norton-Bailey parameters, from creep rupture data 80—30098
notch creep rupture strength under longit. shear and torsion 78—5689
notched bars, creep rupture, stress and damage history calcs. 78—39901
parametric data handling method development, creep and creep-rupture data 80—58934
plastic growth of cavities at tip of grain boundary wedge cracks 77—52446
plastic zone ahead of crack, development under creep conditions, computer simulation 78—34091
plate weakened by equal-armed cross-shaped crack, plastic strain and fracture 80—69740
PMMA, durability over extensive time temp. range 77—90460
PMMA, plastic deform. by crazing *(Japanese)* 80—93619
cis-1,4polybutadiene, lightly crosslinked, isothermal and nonisothermal creep 77—25106
polycarbonate film, struct. and mech. props. 79—19160
polycrystalline body, rupture curves, isochronous, in plane stress 80—69739
polycrystalline material, diffusional growth of cracks *(Russian)* 78—91376
polyethylene, dynamic mechanical behaviour during creep to failure in uniaxial extension 78—15455
polyethylene, environmental stress cracking correl. with liq. sorption for low-swelling liqs. 80—81165
polyethylene, environmental stress cracking due to liq. viscosity, kinetic effect 77—4863
polymer fibre, lifetime under load, in presence of UV radiation stress depend. 78—48534
polymer fibre, lifetime under load, in presence of UV radiation, stress depend. 78—48535

creep fracture continued
polymer with macrodefects, fracture mechanism *(Russian)* 78—35500
polystyrene fibre, ageing effects on elongation to fracture *(German)* 78—76750
polyvinylethylal, durability over extensive time temp. range 77—90460
PVC, high temp. creep 78—48453
PVC, rolled, anisotropic, creep fracture *(Japanese)* 79—34132
reactor piping components, fracture mech. methods, safety anal. 79—11698
reactor piping components, safety anal., fracture mechanics methods 79—11699
refractory fibre, effect on high-temp. strength of refractory coatings *(Russian)* 77—52536
remaining creep life for components under stress at elevated temperatures 80—59566
review 77—8944
rocks, critical dilatant vol. at tertiary creep onset 78—28220
roving glass cloth fibre reinforced plastic, fracture mech., time depend. *(Japanese)* 80—55508
rupture life lower bound, structs. subjected to variable load, steady state creep 77—3785
rupture of specimens with random material props. 79—10491
rupture of structures subjected to variable loading and temp. 77—3786
rupture strength of nonstationary loading, stress conc. influence 78—31514
size effect on time to rupture *(Czech)* 79—77024
slow crack growth rate and creep strain, relationship under tensile loading 77—3778
stainless steel, 18Cr-11Ni, for nuclear reactors, mech. props., neutron effects 77—34383
steel, 12 MKh, creep-respective strength and fracture mode in H_2 *(Russian)* 77—52461
steel, 12Cr1MoV, thermal fatigue and creep effect in fracture 80—104297
steel, 12Kh1MF, fracture in creep at temp. near 0.5 MP *(Russian)* 77—32675
steel, 17249, creep and creep fracture *(Czech)* 77—86089
steel, austenitic, 316, creep failure at 625°C, grain size effect 78—27631
steel, austenitic, Cr-Ni (18,12 wt.%), containing coarse grain boundary precipitates, thermomechanical treatment 78—27545
steel, austenitic, Cr-Ni (18, 11 wt.%), creep rupture *(German)* 78—11297
steel, austenitic, creep, low-temp., during dynamic relaxation, effect of dislocation struct. *(Russian)* 77—25103
steel, austenitic, creep exposure, partial recovery of mech. props. by subsequent annealing *(German)* 77—59886
steel, austenitic, creep exposure, propag. rate of intercryst. cracks *(German)* 77—59887
steel, austenitic, creep fatigue cycling, electric crack growth 79—29209
steel, austenitic, fracture state in creep *(Czech)* 80—30081
steel, austenitic Cr-Ni, intergranular damage parameters in creep *(Czech)* 80—89342
steel, austenitic Cr-Ni (18,12 wt.%), containing coarse irregular carbide precipitates along grain boundaries, ductility 78—60718
steel, austenitic ferritic welded transition joint, type 316. thermal fatigue life *(Japanese)* 79—83307
steel, austenitic heat resisting, creep rupture props., effect of grain- and grain boundary-strengths 80—97573
steel, austenitic stainless, crack growth-tertiary creep relation 77—28863
steel, austenitic stainless, creep crack propag. at elevated temps. 78—19862
steel, austenitic stainless, fast neutron irrad., effect on mech. props. 78—92309
steel, austenitic stainless, stabilized, creep improvement, effect of B precipitation and hyperquenching *(French)* 78—23784
steel, austenitic stainless, type 347 and 316, accelerated creep anal. under constant sustaining load 79—83311
steel, austenitic stainless, weldments, creep fracture, correlation with time-temperature parameters 79—29219
steel, austenitic stainless tensile ductility in air and H_2 77—66687
steel, austenitic stainless type 304, time-depend. fatigue, mechanistic model 80—100925
steel, austenitic type 347, nucleation and growth of creep cavities 80—40513
steel, austensitic stainless, creep crack growth, environmental sensitivity 80—85030
steel, C, and stainless 304 and 316, creep crack propagation, J-integral application 80—35331
steel, C, S15C, crack propag. under combined creep and fatigue, J-integral approach *(Japanese)* 79—83303
steel, C-Mn, pressure vessel usage, elevated temp. mech. beahviour 78—35462
steel, CC Cr-Mo-V (1,1,.25 wt.%), Mo_2C-V_4C_3 precipitation, creep rupture test *(Japanese)* 79—70070
steel, Cr-Mn, X-ray diffr. exam. of fine struct. during deform. *(Russian)* 78—38661
steel, Cr-Mo, annealed, creep and rupture, heat treatment effects 79—24548
steel, Cr-Mo, annealed, microstructural effects on creep-rupture behaviour 79—57120
steel, Cr-Mo, effect of Mo on high-temp. props. 80—85005
steel, Cr-Mo, high-temp. props. and constitutive equations 79—34146
steel, Cr-Mo (10-14, 2-6 wt.%), heat-resist., creep-rupture strengths 80—104271
steel, Cr-Mo (1.25, 0.5 wt.%), creep and rupture, temp. and stress effects 77—86096
steel, Cr-Mo (1, 0.5 wt.%), heat treated creep failure, role of stress state 79—5047
steel, Cr-Mo (20, 1 wt.%), creep rupture tests, at 500°C loading times up to 300000 hours *(German)* 80—25828
steel, Cr-Mo (2.25, 1.0 wt.%), thermally aged and Na decarburised, stress-rupture props. 80—21102
steel, Cr-Mo (2.25, 1 wt.%), creep and high temp. low-cycle fatigue tests 80—85061
steel, Cr-Mo (2.25, 1 wt.%), creep-fatigue testing from thermal transient effects in CRBRP reactor 78—21660
steel, Cr-Mo (2.25, 1 wt.%), interrelationship between creep deform. and creep rupture 79—61664
steel, Cr-Mo (2.25, 1 wt.%), relationship between minimum creep rate and time to fracture 78—56759

creep fracture continued
- steel, Cr-Mo type, tube, long-time stressed condition *(German)* 77—59888
- steel, Cr-Mo weld metal, trace element embrittlement suppression by creep strength effects 80—66656
- steel, Cr-Mo-V, creep crack growth temp. depend., 525 to 600°C 78—64634
- steel, Cr-Mo-V, creep fracture, microstruct. effects 78—64668
- steel, Cr-Mo-V, normalised and tempered, size and geometry effect on creep cracking behaviour 78—64630
- steel, Cr-Mo-V, notch geometry influence on creep rupture props. *(German)* 80—30055
- steel, Cr-Mo-V, stress rupture, notch influence, temp. depend. *(German)* 80—60945
- steel, Cr-Mo-V (0.5, 0.5, 0.25 wt.%), bainitic and martensitic, tempered, creep crack growth 77—86136
- steel, Cr-Mo-V (0.5, 0.5, 0.25 wt.%), comparison of methods of correlating creep crack growth 78—60826
- steel, Cr-Mo-V (0.5, 0.5, 0.25 wt.%), creep crack growth, temp. effect 78—64667
- steel, Cr-Mo-V (0.5, 0.5, 0.25 wt.%), creep crack growth at 565°C 77—73323
- steel, Cr-Mo-V (0.5, 0.5, 0.25 wt.%), creep crack growth in notched bend test, microstruct. effect 77—21261
- steel, Cr-Mo-V (1, 1.25, 0.25 wt.%), creep crack growth *(Japanese)* 79—43399
- steel, Cr-Mo-V creep crack growth, relation between engineering and metallurgical factors 78—11321
- steel, Cr-Mo-V press. vessel, crack growth under creep 78—60827
- steel, Cr-Mo-V-Nb-B, creep rupture strength *(Japanese)* 79—83301
- steel, Cr-Mo-W-V, long term creep rupture props., turbine blade *(Japanese)* 77—59909
- steel, Cr-Ni-Ti (18, 8, 0.7 wt.%), creep rupture tests, at 500°C loading times up to 300000 hours *(German)* 80—25828
- steel, Cr-V (1.5, 0.5 wt.%), ferritic, effect of temp. and microstruct. on creep damage 79—5023
- steel, creep fracture, temp. effect on data scattering 79—74258
- steel, creep rate mismatch interaction in stress relief cracking 80—97578
- steel, creep resistant, fine grained, structural, welded-joints, cause of cracking during stress relieving *(German)* 77—70141
- steel, creep rupture testing between 400 and 700°C const. stress, accel. temp. method 78—31495
- steel, creep-resistant, creep rupture under variable stress and temp. *(German)* 79—24597
- steel, CrMo(W)V, creep rupture tests, at 500°C loading times up to 300000 hours *(German)* 80—25828
- steel, CrMoV, creep resistant, cast, creep rupture and creep *(German)* 77—70098
- steel, CrMoV, low alloy, creep resistant, temp. and stress depend. of time to rupture *(Czech)* 77—70160
- steel, CrMoV (1 wt.%), creep crack propag. rates, prediction using C* parameter 77—90449
- steel, CrMoV (1 wt.%), high temp. creep and fracture 77—36598
- steel, ferritic, Cr-Mo-V (0.5, 0.5, 0.25 wt.%), creep and fracture, microstructural instability effects 77—63734
- steel, ferritic, low alloy, effect of microstruct. on creep fracture 78—80640
- steel, finite life characteristics, notch effects *(German)* 77—90434
- steel, heat resistant cast and wrought for petrochemical industry, creep rupture *(German)* 77—36618
- steel, high Mn, heat resistant, alloying additions, effect on mech. props. *(Korean)* 77—12631
- steel, high Mn austenitic, creep rupture, p addition and two-step soln. heat treatment effects *(Korean)* 80—93646
- steel, high-strength reinforcing, 20GS2, local microstresses on creep strength in hydrogenating media *(Russian)* 77—52462
- steel, long-term strength prediction, nature of temperature-time parameter 77—21275
- steel, low alloy, creep behaviour at engineering stresses 79—74218
- steel, low alloy, creep crack growth, microstruct., fatigue effects 80—7672
- steel, low alloy, relationship between stationary creep rate and time to rupture *(Czech)* 79—70165
- steel, low alloy creep resisting, causes of weldment cracking 78—56760
- steel, low C, creep rupture strength, precracked round bars under torsion *(Japanese)* 77—59908
- steel, mild, low endurance fatigue 78—19865
- steel, Mo-V, creep rupture strength, heat treatment effects *(German)* 78—72834
- steel, Mo-V, creep rupture strength, rel. to microstruct. *(German)* 78—35467
- steel, plan C, creep rupture tests, at 500°C loading times up to 300000 hours *(German)* 80—25828
- steel, stainless, 20% cold worked, type 316, creep failure time 78—19894
- steel, stainless, 304, creep fracture propag., elongation, tensile strength, yield stress meas. applicability of fracture mechanics parameters 78—35508
- steel, stainless, 304, thermal fatigue strength *(Japanese)* 79—83306
- steel, stainless, 304 and 316, creep-fatigue life, strainrange partitioning applic. 77—77586
- steel, stainless, 316, 304, LMFBR primary piping materials, mech. props., review 77—25151
- steel, stainless, 316, creep and rupture, 525 to 900°C, creep rate 79—11678
- steel, stainless, 316, creep and rupture, 525 to 900°C, rupture and ductility 79—8327
- steel, stainless, 316, creep and rupture, 525 to 900°C 79—8328
- steel, stainless, 321, internal pressure creep rupture strength of boiler tubes, anisotropy effect 78—23825
- steel, stainless, annealed type 304, LMFBR, creep rupture mode of failure, reliability anal. 77—3113
- steel, stainless, cold-worked, 316, chem. comp. effects on rupture life, tensile props. 77—25152
- steel, stainless, Cr-Ni-Nb-Ti, effect of I_2 vapour on creep fracture props. 78—72814
- steel, stainless, creep crack growth rate, correlation of tension and bending type specimens *(Japanese)* 79—38944
- steel, stainless, cumulative damage in creep 79—70140
- steel, stainless, Fecralloy, creep-rupture props., 650-800°C 80—97535
- steel, stainless, GCFR ribbed cladding, post-irradiation creep rupture tests 80—18430
- steel, stainless, HK40 and HP, centrifugal cast tube, creep damage estimation from creep void obs. *(Japanese)* 79—87687
- steel, stainless, oxide dispersed, prod. by spray dispersion method, mech. props. exam. of mech. props. *(Japanese)* 78—48419
- steel, stainless, plastic zones around creep and fatigue cracks at 650°C 78—48523
- steel, stainless, stress-rupture data correlation 77—44346
- steel, stainless, SUS 316, creep-fatigue interaction at 600°C 79—34123
- steel, stainless, type 304, uniaxial damage accumulation law for time depend. loading with creep-fatigue interaction 79—83324
- steel, stainless, type 316, fatigue crack propagation, J-integral application 80—35332
- steel, stainless, type 316, microstruct. changes in creep ductility, SEM, TEM, optical microscopy and X-ray diffr. study 79—38927
- steel, stainless, type DIN 1.4970 exam. of creep fracture in vacuum at 923 to 1073K 78—72817
- steel, stainless, weld overlaid, creep-rupture props. 78—13230
- steel, stainless 304, crack propagation under fatigue-creep conditions and fractography *(Japanese)* 80—104267
- steel, stainless 304, crack propagation under intermittent overloading at elevated temperatures *(Japanese)* 79—38947
- steel, stainless 304, creep and fatigue crack propag. at elevated temps., fract. mech. and fractography 77—21279
- steel, stainless 304, fracture mech. appl. to crack propag. under creep *(Japanese)* 78—27606
- steel, stainless 316, creep fracture maps 80—30083
- steel, stainless 316, fusion reactor first wall, thermal stress and creep fatigue limitations 79—76132
- steel, stainless casts, creep ductility, Auger spectroscopy study 80—60917
- steel, stainless creep behavior of ribbed cladding in prototypic GCFR coolant environment 80—16480
- steel, stainless SUS 316, creep fracture at elevated temps. vacuum environment effect *(Japanese)* 77—8942
- steel, type DIN 1.4970, tensile creep rupture at cyclic load variation at 700°C 79—66143
- steel plate, austenitic stainless, with crack, expts. and finite element analysis *(Japanese)* 80—50694
- steel stainless type 304, Norton-Bailey parameters, from creep rupture data 80—30098
- steel/steel bimetal, creep-rupture strength in corrosive environment *(Russian)* 77—52533
- strength of precracked round bars under torsion, expt. and anal. investigation *(Japanese)* 77—59908
- strength of structural materials with complex stress state 77—14967
- stress rupture regression lines in reactor materials, statistical determination 80—30106
- stress-rupture data correlation 77—44346
- strip yield models for crack incubation and growth 78—55605
- structural components subjected to proportional cyclic loading, rupture life estimates 77—35089
- styrene-butadiene rubber, fracture time variability, endochronic prediction 78—76734
- superimposed non-stationary stress and temp. loading, creep rupture 80—66630
- temperature ramp loading, and monotonous stress, creep rupture, calcs. 79—74240
- temperature ramp loading 80—3170
- tensile creep and early failure, model 80—15185
- Udimet 700, creep, rupture, grain size effects 77—21229
- Udimet 700, creep crack growth 78—48517
- Udimet 700, Ni-Co-Cr-Ti, hold time effects on high temp. fatigue crack growth 79—5036
- uniaxial damage accumulation law for time depend. loading with creep-fatigue interaction 79—83324
- VHTR system, material requirements for intermediate heat exchanger, rel. to creep-rupture tests 78—13235
- Zircaloy cladding ballooning, analytical model for transient gas flow in LWR 80—18499
- β-Zircaloy-2, tensile creep and creep rupture props. under vacuum 78—52915
- Zircaloy-2 cladding, beta-phase, creep and creep rupture props., 1000 to 1500°C 78—78470
- Zircaloy-4, creep rupture at monotonous stress and temp. ramp loading 79—74241
- Zircaloy-4, creep rupture at superimposed non-stationary stress and temp. loading 80—66630
- Zircaloy-4 cladding rubes, burst strain and stress corrosion cracking, I influence 80—3248
- Ag, gas bubble embrittlement mechanism 78—60824
- Ag, implanted grain boundary cavities effect on cavity growth kinetics and creep fracture 78—52935
- Ag, microcrack propagation and plastic strain 80—81187
- Al alloy, accumulation of damages in stress concentration zones in alternating creep and fatigue 79—100261
- Al alloy, fatigue life estimation from creep rupture data *(Japanese)* 79—79089
- Al alloy, RR58, prior stress history effects on creep rate and fracture 77—4829
- Al alloy, RR58, remaining creep life estimation from creep crack density meas. 78—44194
- Al alloy 2024, creep crack growth rate, temp. and cyclic load effect *(Japanese)* 79—83302
- Al alloy 7075, stress-rupture data correlation 77—44346
- Al alloy AL22, influence of ultrasonics application on creep during multistage ageing *(Russian)* 79—91708
- Al alloy A356-T61, creep rupture props. 78—27612
- Al alloys, types 1100 and 5454, long-time rupture tests 80—76434
- Al, creep, low-temp., during dynamic relaxation, effect of dislocation *(Russian)* 77—25103
- Al, creep and rupture, 77 to 273K *(Russian)* 79—43386
- Al, creep and rupture, in torsion, mech. *(Russian)* 79—5030
- Al, creep strength and rupture under combined stresses 79—20133
- Al, cumulative damage in creep 79—70140
- Al, high temp. fracture, SEM obs. 77—59918
- Al, microcrack propagation and plastic strain 80—81187
- Al, microrupture singularities in low stress range at elevated temp. *(Russian)* 79—29172
- Al, time-to-rupture and character of fracture, near MP *(Russian)* 77—21245

creep fracture continued
- Al-Cu-Mg alloy RR58, comparison of methods of correlating creep crack growth 78−60826
- B_2O_3-SiO_2-Na_2O phase-separated glass, creep fracture morphology 80−81151
- C fibre, Al-coated, stress rupture 78−80628
- C steel, prior stress history effects on creep rate and fracture 77−4829
- Co alloys, binary, and MAR-M322 type, influence of phase transform. on diffusion and mech. props. *(Russian)* 79−5000
- Co(Cr,Ni)-TaC fibrous eutectic, deformed, thermal stability of microstruct. *(Russian)* 79−1895
- Cr-Mo-Ni-Ti alloy A-286, stress-rupture data correlation 77−44346
- Cr-Mo-V steel, creep rupture tests on notched cylindrical specimens at 600°C 77−32670
- Cu alloy, creep fracture prediction, intergranular damage meas. 77−21268
- Cu and alloys, intergranular damage parameters in creep *(Czech)* 80−89342
- Cu bicrystals, grain boundary sliding and intergranular fracture studies 78−75717
- Cu, commercial, pure, creep-rupture times and creep rate, in vacuum *(Japanese)* 78−72843
- Cu, commercial, pure, vacuum environment end grain size effects on creep rupture props. at elevated temps. *(Japanese)* 80−81162
- Cu, crack propag. and fracutre kinetics in creep, optical microscopy and SEM obs. *(Russian)* 79−52342
- Cu, creep, low-temp., during dynamic relaxation, effect of dislocation struct. *(Russian)* 77−25103
- Cu, creep-fatigue interaction of polycryst. specimens at elevated temp., hydrostatic press. effect on crack behaviour 77−59890
- Cu, dimple spacing on intergranular creep fracture surfaces with slip band spacing 80−76345
- Cu, formation of H_2O vapour bubbles, effect as intergranular creep fracture 80−71722
- Cu, microcrack propagation and plastic strain 80−81187
- Cu, polycryst., creep and fracture behaviour, effects of prestrain and O 80−97544
- Cu, pure, Norton-Bailey parameters, from creep rupture data 80−30098
- Cu, time-to-rupture and character of fracture, near MP *(Russian)* 77−21245
- Cu-Cr (1 wt.%), exam. of low cycle fatigue props. at elevated temp. 78−64674
- Cu-Cr-Zr-Mg (0.5, 0.1, 0.03 wt.%), exam. of low cycle fatigue props. at elevated temp. 78−64674
- Cu-SiO_2 alloy, fracture at elevated temp. 78−39896
- α-Fe, creep and fracture between 77 and 673K 79−7649
- α-Fe, hydrostatic pressure effect on creep rate and failure time 78−92306
- α-Fe-C (0.03 wt.%), structural singularities of transition from thermally activated to force-induced fracture *(Russian)* 78−56731
- Fe-Cr-Al-Ti-Y_2O_3 (20, 4.5, 0.5, 0.5) type MA956, strain rate effect on fracture behaviour at 1366K 80−16458
- Fe-Cr-Al-Y (Y-Al_2O_3)(Y_2O_3), preparation and exam. of mech. props. 78−52720
- Fe-Ni-Cr, austenitic, creep strength and ductility, effect of γ' precipitation 77−36597
- Fe-Ni-Cr (40, 15.8 wt.%), precipitation and creep rupture behaviour, optical and TEM study 79−74158
- Fe-Ni-Cr-base superalloys, characterization for PNP components 80−5242
- KCl, microcrack propagation and plastic strain 80−81187
- LiF, microcrack propagation and plastic strain 80−81187
- MgO, MgO-CaO (58 wt.%), comparison of high temp. creep and fracture 77−16658
- Mo, single crystal, ductility and high temp. strength in routine tests 77−90427
- Monel, Norton-Bailey parameters, from creep rupture data 80−30098
- NaCl, microcrack propagation and plastic strain 80−81187
- Nb-Mo-Ti-Zr, influence of C content on creep charact. and creep-rupture strength *(Russian)* 77−48483
- Nb-Ti superconducting multifilamentary wires, mechanisms for crit. current degradation 77−28324
- Nb_3Sn superconducting multifilamentary wires, mechanisms for crit.current degradation 77−28324
- Ni alloy 718, creep crack growth 77−63776
- Ni alloy Mar M200, directionally solidified Hf additions, effect of vol.% γ' on creep rupture 78−27526
- Ni, deformed in uniaxial tension, fracture map 78−56764
- Ni, microcrack propagation and plastic strain 80−81187
- Ni/Ni_3Al+Ni_3Nb, directionally solidified eutectic alloy, crack growth rate under creep fatigue conditions 79−52361
- Ni-Al, intercrystalline creep rupture *(Czech)* 77−86135
- Ni-base superalloys, powder metallurgical, creep-rupture at intermediate temps. 80−97568
- Ni-based alloys, binary, ternary, complex, TiC additions, effects 78−92305
- Ni-Cr, heat resistant cast and wrought for petrochemical industry, creep rupture *(German)* 77−36618
- Ni-Cr (20 wt.%), Norton-Bailey parameters, from creep rupture data 80−30098
- Ni-Cr alloys, creep crack growth, environmental sensitivity 80−85030
- Ni-Cr-Co, Nimocast alloy 738, γ'' precipitate morphology and creep rupture, thermal stress crack effect 78−11318
- Ni-Cr-Co superalloy IN-792, crack growth resistance, metallurgical effects 77−36655
- Ni-Cr-Co-Al alloy IN-738, uniaxial damage accumulation law for time depend. loading with creep-fatigue interaction 79−83324
- Ni-Cr-Fe, high temp. corrosion and creep in carburizing and oxidising atmos. 79−11727
- Ni-Cr-base superalloys, characterization for PNP components 80−5242
- Ni-ThO_2 dispersion strengthened, high temp. strength, grain size and shape effects 77−48447
- Pt alloys, influence of Rh, Au, Mo, W, Zr, Hf alloying elements on creep activation energy at high temp. *(Chinese)* 80−66573
- Si-Al-O-N ceramic, grain boundary desegregation and intergranular cohesion 80−100872
- Si-SiC composite, high temp. time depend. strength 77−56083
- Si_3N_4, reaction-bonded and hot pressed, deform. and fracture during creep 79−38916
- strengthened by lattice transformations, mech. props. study *(Japanese)* 79−43332

creep fracture continued
- Ti alloys, 685 and 6242, creep resist. and thermal stability in air and in vac., role of Si 80−30020
- Ti alloys, heat-resistant, mech. props., alloying addition effects *(Russian)* 77−59861
- Ti, fracture mechanism maps 80−3188
- Ti-Al, Al effects on susceptibility to salt corrosion *(Russian)* 77−25185
- Ti-Al-Cr-Mo-Zr hard alloy VK15, shot blasting in strength improvement 77−81272
- Ti-Al-V-Sn (5.5, 5.5, 2 wt%), crack growth, slow, H-induced 80−104272
- V alloy, fusion reactor first wall, thermal stress and creep fatigue limitations 79−76132
- WC-Co, creep rupture strength meas. 78−31475
- WC-Co (10 wt.%), vacuum sintered, short-time bending creep rupture strength *(Japanese)* 78−15508
- WC-Co alloy, short-time creep rupture strength, C content effect 400° to 900°C *(Japanese)* 78−48487
- WC-Co alloy time-depend. strength params. 78−31516
- Zn, microcrack propagation and plastic strain 80−81187
- Zn, microrupture singularities in low stress range at elevated temp. *(Russian)* 79−29172
- Zr-Sn-Mo (6, 1 wt.%), creep and creep rupture 78−23778
- Zr-Sn-Mo-(Nb), creep and creep fract. at 623 to 823K *(Czechoslovakian)* 77−32643
- Zr-Sn-Mo-(Nb), fracture in creep 77−36581
- Zr-Sn-Mo(Nb), creep and creep fracture, 623 to 823K *(Czech)* 77−59916
- α-Zr-Sn(Mo), creep characts., influence of Sn and Mo *(Czech)* 80−81119

creep-recovery *see recovery-creep*

creep testing
- ampoule, testing materials subject to reactor irradiation and dissociating coolant 78−3301
- anisotropy due to steady creep, effects on subsequent creep, investig. method 78−7135
- apparatus for creep and long-term strength tests, with cyclic temp. var. 80−61046
- automatic deformation recording instrument 78−7122
- automatic temperature regulation system 77−63853
- boiler tubes in service inspection, creep testing techniques assessment *(Japanese)* 77−81356
- canisters for radioactive waste vitrification 78−86648
- ceramic compression tests, machine for high temp. testing *(French)* 79−20325
- ceramic samples with initially nonlinear axis creep, expt. errors *(Russian)* 77−25224
- compression creep, precision testing apparatus *(Spanish)* 77−48608
- concrete, creep under combined shear and compression stresses *(Japanese)* 77−40511
- concrete, low cost rig 78−11466
- constant tensile stress with elastic compressibility, creep test *(Bulgarian)* 80−108680
- creep capsules, multiaxially stressed, remote pressurization and laser closure welding 79−54514
- descriptive method for alloy creep tests by nonstationary loadings 78−23759
- device for examining under radiation, −196 to 250°C 78−60920
- device for producing constant stress 80−71835
- electronic constant-stress device 80−25965
- extensometric method, for inside nuclear reactor channels 80−100998
- fatigue and creep testing installation for wide range of strain rates 80−76447
- fission reactor irradiated cladding, in-cell facility for mechanical testing 80−21244
- furnace tube HK40 alloy in petroleum industry *(Japanese)* 77−28950
- glass fibre reinforced plastics, creeping tests on flat specimens in liq. media, clamping device 78−7126
- high temp. furnace control methods 80−30187
- HS-188 alloy crack growth anal. 77−40509
- hydraulic loading system for testing under irradiation 78−31609
- impression creep, digital simulation by finite element method 78−7142
- in-pile creep measuring rig 77−42083
- indentation test 78−3281
- installation for in-reactor study of creep and stress-to-rupture, plane stress mode 78−39996
- irradiation creep facility, materials testing for fast and fusion reactors 79−57192
- light ion irradiation creep apparatus 79−70264
- LMFBR structure materials in liquid Na, capsule type creep tester *(Japanese)* 80−108653
- low-cycle testing unit for use in vacuum and at high temp. 79−52503
- machine using torsion, in radiation zone of nuclear reactor 78−11480
- measurements, using capacitance type strain gauge 80−21256
- metal, torsional creep under accelerator irradiation, meas. instrument 78−3262
- metals, mechanical props., testing and modelling 80−25811
- metals and alloys relaxation resistance testing using constantly loaded sample 78−39965
- microcreep, meas. device for high-temp. thin samples *(French)* 77−73388
- microspecimens in strong mag. fields, device for tensile and creep tests 79−15903
- miniature test-pieces, multipurpose apparatus *(Russian)* 77−52558
- mono and polycrystalline pure metal 77−66736
- multicycle creep curves, device for recording at elevated temps. 79−43512
- neutron irradiated materials, high-energy, in situ testing apparatus 79−79200
- nuclear steam generator tubes testing and evaluation, using CIS/DASIO system *(Czech)* 80−63301
- plastic deformation, creep test method *(Hungarian)* 80−97660
- plastic specimens under compression, multiposition device for creep exam. 80−25946
- plastics testing, automation 80−76443
- polymer, creep tests for determining degree of cross-linking *(German)* 78−76822
- polymer, long-term durability prediction methods 79−20320
- polymer, plane materials stress relax. and creep under biaxial loading, test procedure 78−3279

creep testing continued
- polymer, relaxation properties investigation method and instrument 78—39967
- polymer coating, creep determ. by impression of rigid sphere 78—85084
- polymers, elastic and creep moduli meas. by contact methods 80—11852
- polymers, hygroscopic, creep testing machines in environmental chamber, nylon-6,6 appl. 78—95883
- pressurised tubes, laser interferometer system, in-reactor creep, reference fuel cladding appl. *(German)* 77—74925
- programmed automatic unit, complex stressed condition 77—56208
- proton simulation of fusion reactor first wall environment apparatus 79—24707
- rate determination using Michelson interferometer 78—68856
- reactor fuel cladding, in-reactor creep testing 77—23211
- refractories high-temp. tests, at different loadings, laboratory equipment *(Russian)* 78—19970
- refractory ceramic, equipment combination 78—11477
- refractory materials, high temp. installation in vacuum and rarefied gas flows 79—91864
- relaxation bending test device 79—70245
- rock, triaxial creep loading apparatus for time dependent behaviour investigation 77—9538
- rocks, long-term creep tests, rel. to Earth crust rheology 79—79828
- rotating viscoelastic disks 80—38360
- rubber, stretching strength, long-term, testing apparatus 79—15907
- rupture strength testing under cycic loading, AIMA-5 machine modification 79—52506
- SAE 1045, creep and relaxation curves for torsion-tension members at elevated temps. 78—83260
- space shuttle insulation coating, combined load testing at 1100°C 79—34261
- spring-loaded device, compact, to obtain constant stress in simple tension 79—43503
- steel, austenitic, approx. method for high-temp. cracking resistance estimation 78—23914
- steel, Kh20N80, during creep resist. testing *(Russian)* 77—44294
- steel, stainless, type 304, viscoplastic behaviour, strain rate sensitivity, creep, relaxation, tensile tests 80—66727
- steel, stainless in service inspection, techniques assessment *(Japanese)* 77—81356
- strain gauge, load cells, characterisation of creep response 79—35718
- strain measurement, design and construction of apparatus 78—15634
- strain range partitioning method for anal. of material creep fatigue behaviour 80—104361
- tensile testing, prolonged high temp. testing method with subseqeunt microscopic exam. 77—52581
- tension creep test, continuous meas. of low freq. shear modulus *(French)* 78—23913
- thermoelectric heating and cooling device, automatic 80—21218
- thyristor temp. regulation circuits, for creep testing devices 80—25956
- Zircaloy 2 irradiation creep strain meas. technique 77—42084
- Zircaloy fuel cladding, irrad. capsule design for continuously monitoring creepdown 79—34513
- Al alloy, creep rupture testing, metallographic studies of fracture test specimen 77—63862
- Al alloys, creep deformation investig. using method of precision lattices 77—86250
- Al bicrystal, tensile and creep deform. obs. by holographic interferometry *(Japanese)* 77—56197
- Al-Si-Zn alloy, creep rates, pre-torsional deformation effect 79—96096
- C materials, radiation creep 77—12769
- C paste, viscoelastic props., depend. on coke grain size 80—1501
- Cu-Ni (20 wt.%) alloy, contour plate for relay appl. use of Larson-Miller method *(Japanese)* 80—55454
- Na ML-3 circuit for testing mech. props. of structural materials of LMF-BRs *(Spanish)* 80—55595
- Ni, light ion irradiation creep apparatus 79—70264
- Si wafers, using stress provided by deposited Si_3N_4 film 77—66000
- $(\alpha+\beta)$-Ti-Al-Mo-Fe alloy VT-22, behaviour during creep testing, solid soln. dissoc. *(Russian)* 80—40346
- Zn polycryst., compressive strength, temp. and strain rate effects 80—16616

crestatrons *see travelling-wave-tubes*

crimping
- collagen with planar crimp, tensile deformation 80—84235
- filaments, slender, with planar crimp, tensile deformation 80—84235
- textiles with planar crimp, tensile deformation 80—84235

critical constants, thermal *see critical points*

critical current density (superconductivity)
- A15 films, electron beam codeposition, synthesis and props. 78—72296
- A15-type compounds, review of superconducting props. and structure 80—70909
- composite superconductivity, multifilamentary, current distrib., external field effects 77—28338
- composite superconductor, flux jump nucleation theory, critical state stability 77—28290
- composite superconductor, multifilamentary, self-field losses 77—28315
- composite superconductor, propagation velocity expressions 80—60155
- composite superconductors for fusion magnets, current distrib. and losses 77—28331
- composite wire critical current density rel. to tensile stress at 4.2K, obs. 79—33439
- compound superconductors, radiation effects on critical currents 78—52175
- DC SQUID, ultra-low-noise tunnel junction, design, fabrication and noise props. 80—29506
- dipole magnet models of combined type 79—31301
- film, inversion temp. in pinning of vortices by periodic struct. 78—56274
- film, pin-free, vortex chain size effect and negative resist. 77—80888
- foil, pin distribution effect on DC voltage-current characts. 79—99666
- granular films, percolation threshold and crit. current, theory 80—88706
- hard superconductor, flux jump nucleation theory, critical state stability 77—28290
- hard superconductor flux jumps under time depend. external conditions 80—7038
- hard superconductor influence of thermally activated flux creep on AC response 79—33416
- high current density magnet, thermal stability 80—37057
- intermetallic phases, technical superconductor applications *(German)* 78—27005

critical current density continued
- Josephson array, relation between critical current and order parameter 79—87197
- Josephson tunnel junctions, current density distrib. Fiske mode field depend. 79—78264
- junction, superconductor-normal metal-supercond., impurities in normal metal layer, pair penetration depth determ. 80—29508
- long thin superconductor, resistive domain of small cross section in microwave EM field 79—28446
- lossless and dissipative current carrying states of quasi-one dimens. superconductor 77—32109
- magnet stability, critical current margin design criterion 80—31807
- molybdenum chalcogenides, multicomponent, physical props. 80—84577
- multifilament supercond. composites, transverse resistivity 77—72956
- multilayered supercond. films, critical currents as functions of mag. field and temp. *(French)* 77—72955
- pair-breaking current density, temp. depend. *(Russian)* 80—70887
- percolating two-dimens. square lattice, normal-state cond. and crit. current density, crit. exponents 80—84541
- proximity effect weak links, steady-state and RF props. 80—84563
- rare earth lead molybdenum sulphides, $R_xPb_{1\pm x}Mo_{6+y}S_8$, R=La, Nd, Pr, Gd, sputtered, supercond. props. 80—50019
- resistive domains in long supercond. of small cross section, close to crit. temp. 78—26995
- scaling relations in mag., mechanical and superconducting pinning theory 77—76403
- SQUID, granular supercond. characterisation 79—28489
- superconducting contacts, critical currents, density, penetration depth 80—25059
- superconducting magnets, pulsed, hysteretic and mechanical loss calcs. 79—80649
- superconductors, type II, review of mechanical behaviour and stress effects 77—86083
- technical superconductor radiation damage obs. 79—33422
- technical superconductors, preparation velocity of normal-conducting zone 79—24096
- two-band superconductors, external mag. field depend. *(Russian)* 80—88707
- type I, metastable current states meas. *(Russian)* 78—43529
- type II, irreversible, flux flow in transverse mag. field 79—7949
- type II supercond., rot. in mag. field, flux density distrib. 78—43536
- type II superconductor, current density distrib. in cylindrical sample 79—38270
- type II superconductor, cylindrical, rotating in mag. field, dissipation determ. 77—28309
- type II superconductor, neutron irradiation effects *(Rumanian)* 78—52144
- type II superconductors, order parameter change near H_{c2}, influence of transport current 80—75690
- type II superconductors, oscillations, resistive state, current density 80—44782
- type II wires, general crit. state model in two dimens. and zero applied field, uniqueness theorem 80—93062
- type superconductor with field-dependent surface barrier, AC losses 79—87216
- volume pinning force, crit. current density, depend. on mag. field and temp. 78—6491
- volume pinning force for combined attractive-repulsive flux-line defect interaction pots. 77—59363
- vortex array, pinning of flux lines by randomly-spaced pinning centres 78—52172
- weak links, symmetric, crit. current densities and current phase relations 79—87207
- Ag-Sn, supercond. proximity-effect bridge, thermal effects 79—78265
- Al granular film, vortex chain size effect and negative resist. 77—80888
- $Al-Al_2O_3$ granular film, normal state resist. depend. 77—40013
- CdS-In, photosensitive granular superconductor 79—78246
- Cu alloy-Nb composite wires, resist.-temp. meas., percolation theory 79—28490
- Cu-Nb (0,4 at.%), splat quenched, aged, superconductivity *(Japanese)* 77—63018
- Cu-Nb (17 wt.%) multifilamentary wires, fabrication and supercond. characts. 79—56476
- Cu-Nb alloys, origin of superconductivity 77—47918
- Cu-Nb filamentary composites, powder metallurgy prod., supercond. props. 79—56477
- $Cu-Nb_2Sr$, multifilamentary supercond. composites, in situ formed, critical currents 79—65625
- $Cu-Nb_3Sn$, in situ formed multifilamentary composite, supercond. and mech. props. 78—39279
- $Cu-Nb_3Sn$ composite wires, powder metallurgically produced, supercond. props. 78—31026
- $Cu-Nb_3Sn$ multifilamentary tapes, in situ formed, crit. current density anisotropy 80—84576
- Cu-Nb-Sn, multifilamentary supercond. composite wires, fabrication on laboratory scale and mech. props. 80—29897
- Cu-Sn-Nb multifilamentary alloy, high field crit. current density 78—27004
- $Cu-V_3Ga$, supercond. in situ composites, stress effects on crit. props. 80—65757
- $Cu_xMo_6S_8$, sputtered, supercond. crit. currents and scaling laws 78—47923
- Cu(Sn)/Nb(Al), composite superconductor fabrication and characts. 77—81242
- Ge-Sn barriers, Josephson tunnelling 79—28468
- In_2Bi-In(Bi) laminar eutectic alloy, SNS struct., Josephson behaviour *(French)* 78—26996
- $LaMo_6S_8$ thin films, crit. currents and pinning forces 80—34575
- $LiTi_2O_4$, prep., characterisation and supercond. props. 77—40010
- Mo sulphides, ternary $M_xMo_6S_8$, crit. currents in strong mag. fields *(Russian)* 77—43796
- $(Mo_{0.6}Ru_{0.4})_{80}Si_{10}B_{10}$, amorphous supercond. matrix, flux pinning by MoRu precips. 80—65756
- $Mo_{70}Si_{20}B_{10}$, amorphous alloys obtained by liq. quenching, superconductivity 80—75670
- Nb, critical current density, deviation from critical state model 80—84578
- Nb film, deposited in quasi-closed vol., supercond. props. 79—91180
- Nb, single crysts., fluxoid pinning by small nitride precips. 80—70913
- Nb, superconducting, hysteresis in time depend. fields up to 3 kOe 77—24637

critical current density continued
  Nb, superconducting bridges by electron beam lithography and ion implantation Josephson effect 80—20355
  Nb, superconductor, neutron irradiation, low temp., effect on critical current 78—52180
  Nb, surface effect on crit. current density 79—61014
  Nb, surface effect on critical current density 79—65627
  Nb:He, implant saturation and annealing, effect on struct. and supercond. props. *(Russian)* 78—43538
  Nb-Al-(Ge) film, depend. of supercond. props. on sputter deposition conditions and heat treatment 77—36399
  Nb-Ge, A15 struct. superconductor, high field transport props. TEM study 80—34574
  Nb-Ge film, CVD and sputter deposited, critical current density and stability 77—28327
  Nb-Ge-Si, A15 struct. superconductor, high field transport props. TEM study 80—34574
  Nb-NbO$_x$-Pb, miniature tunnel junction, current density, determ. by $I_c(\Phi)$-curve 79—7939
  Nb-Si(—V)(Zr)(Mo)(Ta)(W)(C)(B)(Ge), ductile amorphous, superconductivity 80—60131
  Nb-Sn filamentary composite, as function of reaction conditions 77—28330
  Nb-Ti, Helmholtz coils, optimisation, critical current rel. to mag. induction 79—67353
  Nb-Ti, multifilament superconductor, metallurgical design 79—33434
  Nb-Ti, optimised pinning struct., crit. data 1.8-4.2K 77—89913
  Nb-Ti, radiation effects on critical currents 78—52175
  Nb-Ti, superconductivity after heavy ion irradiation at low temps. and high fluence 77—69437
  Nb-Ti, wire drawn and hydrostatically extruded supercond., crit. current density 79—38275
  Nb-Ti 10 kA conductor development for Tokamak toroidal coil 79—31217
  Nb-Ti alloys, crit. current density, scaling law 78—31027
  Nb-Ti filamentary superconductor critical current density rel. to thermal treatment 79—33440
  Nb-Ti multifilamentary supercond., commercial, crit. current density 79—38274
  Nb-Ti superconducting alloy, critical current density, heat treatment effects *(Japanese)* 78—14909
  Nb-Ti/Cu sheet composite, flux trapping and shielding capabilities in transverse fields 80—15667
  Nb-Ti-Ta alloys, metallurgical anal. and crit. current densities 79—38286
  Nb-Ti-Zr, superconducting, ageing effect on critical current density *(Japanese)* 79—61747
  Nb-Ti-Zr, superconducting, critical current density and microstruct. correlation *(Japanese)* 79—61748
  Nb-Ti-Zr ternary system, high-field supercond. 80—97045
  Nb-Zr, deformed strip, pinning force, widely varied j_c, temp. and mag. field variations *(Russian)* 79—7948
  Nb-Zr sputtered films on Ta, struct. and supercond. props. *(Japanese)* 78—52138
  Nb_3(Al,Ge) and Nb_3(Al,Si), liq. quenched, supercond. props. 80—84580
  Nb_3Al, liq.-quenched, crit. current density and T_c 77—72957
  Nb_3Al multifilamentary composite, metallurgy, fabrication and supercond. props. 77—28764
  Nb_3Al multifilamentary cable fabrication and props. 79—33438
  NbC, ultrafine powders and sintered compacts, prep. and supercond. props. 77—40015
  NbCN superconducting films, high field critical current densities and resistive transition 79—61018
  NbCn, superconducting film, high field critical current densities and resistive transition 79—73648
  Nb_3(Ge, X), X=Si, Ga, CVD tapes, supercond. props. at high mag. fields 79—38279
  Nb_3Ge, CVD, AC losses, temp. depend., 4-20K 77—28311
  Nb_3Ge, CVD, hysteretic losses, precipitates and deposition temp. effects 77—28319
  Nb_3Ge, CVD, impurity doping effect on supercond. crit. props. 78—52174
  Nb_3Ge CVD supercond. tape critical current anisotropy obs. 79—33372
  Nb_3Ge CVD tapes, supercond. props. at high mag. fields 79—38279
  Nb_3Ge, CVD-prepared, high field props. and scaling 79—56455
  Nb_3Ge, crit. current density temp. depend. 77—47951
  Nb_3Ge film, CVD, critical current density rel. to second phase (tetr. Nb_5Ge_3) 77—32131
  Nb_3Ge film, critical current density and flux pinning 77—20510
  Nb_3Ge film, prep. by coevaporation, supercond. props. 78—91830
  Nb_3Ge film, prepared by cosputtering, supercond. props. 79—4634
  Nb_3Ge film, sputtered and evaporated, transition temp., critical field and current anisotropy 77—28328
  Nb_3Ge films, correl. between crit. current density and microstruct. 79—38277
  Nb_3Ge films, magnetron sputtered preps. and microstruct. 79—38276
  Nb_3Ge, hysteretic losses in parallel AC and DC mag. fields 79—87217
  Nb_3Ge, projected critical current, comparison with $PbMo_6S_8$ 79—69642
  Nb_3Ge sputtered film, struct. and superconducting props. 77—28337
  Nb_3Ge, supercond., projected upper limits to crit. current density 77—36037
  Nb_3Ge, supercond. film, prep. by chem. transport reaction, critical props. 79—47635
  Nb_3Ge superconducting long tapes, CVD prepared, high current densities at 20 T 79—33436
  Nb_3Ge tape, prepared continuously by CVD, props. 78—60257
  Nb_3Ge tape conductors, strain depend. of crit. current density 79—38278
  $Nb_2Ge_{1-x}Ga_x(Sn_x)$ CVD films, supercond. props., 4.2 to 19K 79—42713
  NbN, ultrafine powders and sintered compacts, prep. and supercond. props. 77—40015
  NbSn multifilamentary superconducting composites, micromechanics 79—38878
  Nb_3Sn, alloying agent influence on struct. and supercond. props. *(Russian)* 80—39698
  Nb_3Sn bronze process, flux pinning scaling law depend. on strain 80—75696
  Nb_3Sn, bronze processed, effect of third element additions 77—28333
  Nb_3Sn composite processes with Cu-Sn-Zn matrix, superconducting props. 78—84370
  Nb_3Sn, crit. current enhancement by low temp. fast neutron irradiation 77—40014

critical current density continued
  Nb_3Sn, critical current density 78—52176
  Nb_3Sn, fast neutron irradiation, effect on critical current density 78—19197
  Nb_3Sn filamentary composite conductor design 79—30515
  Nb_3Sn film, growth by high-rate magnetron sputtering, transition temp. and crit. currents 77—28718
  Nb_3Sn, flux density gradient determ. by Faraday effect 80—107969
  Nb_3Sn, flux trapping and shielding capabilities in transverse fields 80—15667
  Nb_3Sn, grain size in A15 reaction layers 78—14911
  Nb_3Sn, high-current A-15 microcomposite material 80—44781
  Nb_3Sn, irradiated, critical current density 79—38293
  Nb_3Sn, low dose fast neutron irrad. effect 78—14910
  Nb_3Sn microfilamentary superconducting composite, critical currents, fracture props. 80—107970
  Nb_3Sn monofilament wires, supercond. props., effect of Be alloying additions to bronze matrix 79—87222
  Nb_3Sn monofilamentary composite conductors, tensile stress influence on critical current 80—97046
  Nb_3Sn monofilamentary wires, supercond. crit. current density, bending effects 80—50018
  Nb_3Sn, monofilaments, radiation-enhanced diffusion growth, crit. current density 80—65758
  Nb_3Sn multifilament conductor critical current rel. to mech. strain 79—31215
  Nb_3Sn multifilament superconductors produced by ECN technique, prep. and props. 79—33975
  Nb_3Sn, multifilament superconductor, metallurgical design 79—33434
  Nb_3Sn, multifilament superconductor, pulsed mag. field losses and critical current densities 80—54853
  Nb_3Sn, multifilamentary, optimization of high field crit. current density 79—38288
  Nb_3Sn multifilamentary conductor, for fusion research magnets, manufacture and props. 77—28760
  Nb_3Sn multifilamentary composite superconductor, effect of heat treatment on supercond. props. 79—33376
  Nb_3Sn multifilamentary composite wires, supercond. crit. current density, temp. and mag. field depend. 79—33425
  Nb_3Sn, multifilamentary high-field superconductor, status of development 79—61004
  Nb_3Sn, multifilamentary supercond., prod. by ECN powder metallurgy method and props. 77—28762
  Nb_3Sn multifilamentary superconductor AC hysteresis losses 79—33437
  Nb_3Sn multifilamentary superconducting wires, crit. current density in high mag. field 79—38281
  Nb_3Sn multifilamentary superconducting wires, improved high-field props. 79—47215
  Nb_3Sn, multifilamentary superconductor preparation by 'in situ' and cold powder methods, review 80—93522
  Nb_3Sn, neutron irrad., crit. current change rel. to temp. and metallurgy 78—80109
  Nb_3Sn, supercond., fast particle irradiation effects, using anti-site defect model, electronic state influences 79—56346
  Nb_3Sn, supercond., production of high current carrying strip *(Russian)* 79—33435
  Nb_3Sn, supercond., projected upper limits to crit. current density 77—36037
  Nb_3Sn superconducting wires, in situ multifilamentary, mech. props. 79—47746
  Nb_3Sn superconducting wire, fabrication from Cu-Nb-Sn alloy using controlled high temp. gradient 80—25056
  Nb_3Sn superconductor, low temp. deuteron irradiation 78—52182
  Nb_3Sn superconductors, Kirkendall voids, effects on mech. and supercond. props. 79—33429
  Nb_3Sn-Cu, high-current A-15 microcomposite material 80—44781
  Nb_3Sn-Cu composite superconductors, in-situ, AC losses 79—38283
  Nb_3Sn-Cu multifilamentary wires, in situ prep., supercond. and mech. props. 79—38768
  Nb_3Sn-Cu superconducting composites, produced by cold extrusion of fine powders 79—38767
  $Nb_3(Sn_{1-x}Ga_x)$, bronze processed wires, critical current densities in fields up to 23.5 T 78—47922
  Nb_3(SnIn) wires, prep. by ductile fabrication process and props. 79—38265
  NbTi, monocore and filament conductors, crit. current densities and anisotropy factors, heat treatment effects 79—38285
  NbTi multifilamentary composite wires, supercond. crit. current density, temp. and mag. field depend. 79—33425
  NbTi multifilamentary superconductor, production samples, performance 77—40012
  NbTi, processing parameter optimisation for high mag. field appls. 79—38290
  NbTi, solid soln. supercond., crit. current anisotropy 79—38273
  NbTi supercond. threads in Cu matrix, struct. composition and props. *(French)* 79—73649
  NbTi, superconducting multifilamentary conductors, crit. current density, bending effects *(German)* 80—39727
  NbTi wire, supercond., magnetisation rel. to field orient. 78—52151
  NbZr, thermally activated flux creep, effect on AC response 79—33416
  Ni-Nb(-Cu)-C, NbC dispersed supercond. tapes, fabrication and characts. 78—19773
  Pb foil, crit. current density, pinning force density, shadow electron microscopy obs. 80—88696
  Pb-Cd, oriented lamellar superconductor-normal composite, supercond. 79—1650
  Pb-$Cu_{91}Ni_9$-Pb superconducting junction, crit. currents 79—69633
  Pb-$Cu_{99.8}Mn_{0.2}$-Pb superconducting junction, crit. currents 79—69633
  Pb-In, series-connected Josephson tunnel junctions, fabrication procedure diagnostics 78—47909
  Pb-In, vortex pinning on grain boundaries *(Russian)* 77—89910
  Pb-In alloys, supercond., AC losses of EM energy, critical current densities 79—33423
  Pb-In-Ag, transport current distribution in longitudinal mag. field 80—25057
  Pb-In-Au, series-connected Josephson tunnel junctions, fabrication procedure diagnostics 78—47909
  Pb-Sn Josephson junctions, small area high current density normal resistance, RC times 80—34555
  Pb-Sn lamellar eutectic alloy, supercond. normal-supercond. junction arrays 77—24641

critical current density continued
  Pb-Tl (20 wt.%) rod, supercond., critical current densities in surface pinning region 79–47216
  $PbMo_{5.1}S_6$, supercond. wire prep. by powder technique 78–52705
  $PbMo_6S_8$, crit. current density, effect of prep. technique and press. 78–14908
  $PbMo_6S_8$, projected critical current, comparison with Nb_3Ge 79–69642
  $PbMo_6S_8$, sputtered film, critical current density meas. 78–84369
  $PbMo_6S_8$, temp. depend. of crit. currents 80–20363
  $PbMo_6S_8$ wire, powder processed, crit. current density and field 80–80466
  Sn, cylindrical and plane films, crit. current transverse distrib. 77–43795
  Sn, single crystal cylinder, threshold current of paramagnetic effect *(Russian)* 79–87194
  $SnMo_6S_8$, crit. current density, effect of prep. technique and press. 78–14908
  $U_xPb_{1\pm x}Mo_{6+y}S_8$, sputtered supercond. props. 80–50019
  V (-Ti), supercond., rotating discs, hysteresis losses and mag. phenomena 80–75695
  V, superconductor, neutron irradiation, low temp., effect on critical current 78–52180
  V-Hf-Nb(Zr), multifilamentary, superconducting props. improvement 79–38267
  V_3Ga, composite-processed, with improved current carrying capacities in high mag. fields 79–38272
  V_3Ga, grain size in A-15 reaction layers 78–14911
  V_3Ga, high-current A-15 microcomposite material 80–44781
  V_3Ga, multifilament superconductor, pulsed mag. field losses and critical current densities 80–54853
  V_3Ga, multifilamentary supercond., prod. by ECN powder metallurgy method, and props. 77–28762
  V_3Ga multifilamentary supercond. wire, fabrication and props., crit. review 79–38271
  V_3Ga, multifilamentary wire, crit. current props. with third element additions 79–61013
  V_3Ga multifilamentary wires 79–69645
  V_3Ga, supercond., projected upper limits to crit. current density 77–36037
  V_3Ga-Cu, high-current A-15 microcomposite material 80–44781
  V_2Hf base Laves phase compound tapes, supercond. props., prep. 77–40011
  V_3Si, grain size in A-15 reaction layers 78–14911
  V_3Si, neutron irrad., grain boundary pinning, field-depend. change of crit. current density 80–65759
  V_3Si, plastic deform. effect on supercond. props. 80–29500
  $W_{70}Si_{20}B_{10}$, amorphous alloys obtained by liq. quenching, superconductivity 80–75670
  $Y_xPb_{1\pm x}Mo_{6+y}S_8$, sputtered supercond. props. 80–50019
  Zr-Nb (20%), low-j_c supercond. vortex pinning *(Russian)* 77–80885

critical currents
  see also critical current density (superconductivity); flux creep; flux flow; flux pinning
  A-15 diffusion layers, influence of additions of growth and supercond. props. *(German)* 80–11130
  angular dependence in supercond. with long narrow defects 77–69463
  Clarke solder-blob junctions, hysteresis studies 79–28478
  composite superconductor, power increase at current close to crit. current, expt. meas. 77–28314
  coupled Josephson weak links, phase locking 78–72309
  definitions of terms for supercond. phenomenology, meas. practices 78–52117
  digital Josephson technology—present and future 79–28472
  dilutely pinned superconductors, nonlinear I-V characts. 79–56479
  dislocation structures, supercond. states 79–69627
  dislocation systems, superconducting states, impurity effects *(Russian)* 80–11131
  ferromagnetic thin film, long reentrant, self-heating-induced phenomena 80–50013
  filament, current-carrying, mode softening near crit. current 77–72959
  film, long, second crit. current in perpendicular mag. field 77–63045
  film, ordering parameter and current density, depend. on paramag. impurity conc. and electron pair rel. *(Russian)* 78–6489
  film bridge, supercond. stimulated by UHF radiation, crit. currents 77–16008
  film bridges, supercond. stimulation by microwaves, threshold *(Russian)* 79–33409
  film structure with degenerate semiconductor bridge, Josephson effect 80–20359
  flux-flow noise voltages, oscillations in V-I curves 80–15671
  fluxon pinning in supercond. with regularly spaced defects 78–39276
  Ginzburg-Landau theory, time depend., dissipative current carrying states in supercond. filaments 78–47906
  granular microbridges, fluctuations and crit. current determ. 80–84562
  granular superconductor, quantum interference, coherence and percolation *(French)* 79–56434
  granular superconductors, coherence transition, structural disorder effects 80–88657
  granular superconductors, percolation theory, crit. props. 80–84575
  high performance wire development 77–20487
  hysteresis in nonequilibrium superconducting proximity-effect bridges 79–15258
  inhomogeneous superconductors, nonlocal pinning, inversion temp., and crit. current 79–56475
  Josephson array, crit. current and order parameter 79–33410
  Josephson contacts with semicond. layer, critical current *(Russian)* 79–99661
  Josephson current in superconductors with nonmagnetic impurities 78–39269
  Josephson effect in weak link, phenomenological model 77–8241
  Josephson elements, elec. controlled *(Russian)* 79–91189
  Josephson FET, hybrid, feasibility 80–80451
  Josephson junction, barrier inhomogeneities, effect on junction behaviour *(German)* 78–91818
  Josephson junction, diffr. and interference phenomena 77–69457
  Josephson junctions, inelastic tunnelling, pair-quasiparticle interference current 80–84566
  Josephson junctions, natural fluctuations in tunnel current *(Russian)* 77–47937
  Josephson two-dimensional junction, stationary current flow, approximate linear analysis 77–8240

critical currents continued
  large-scale applications of supercond. materials, review 79–69640
  local state form. along dislocation, crit. field and current for destruction *(Russian)* 78–14905
  long superconducting bridges with variable thickness, Josephson effects 78–14897
  long superconductor film second crit. current, microwave power depend. 77–43794
  magnetic field dependence of critical current, peak effect in second order supercond. *(Russian)* 78–47924
  MB DC-SQUID, crit. current mag. modulation, logic device appl. 78–84371
  measurement method, for continuous meas. on supercond. tapes and composites 77–24656
  microbridge Josephson junction, fabrication using electron beam lithography, crit. current meas. 79–28457
  microbridges, response times and low-voltage behaviour 79–65602
  microjunction, supercond.-normal metal-supercond., microwave enhanced crit. current 79–82720
  microscopic theory of Josephson effect in supercond. constrictions 79–60989
  microwave-induced effects 79–87202
  multifilament composite superconductor, production and characterisation 77–28766
  multifilamentary superconducting wires, in situ, anal. of continuity proximity effect conductivity 79–60997
  multifilamentary superconductor, current transfer, expt. results for NbTi and Nb_3Sn 78–72316
  multifilamentary superconductor, current transfer, theory 78–72315
  multifilamentary superconductor, flexibility and elec. characts. 77–24990
  nonequilibrium superconductivity, theory in coherent longitudinal phonon field 79–47205
  normal metal-constriction-superconductor microbridge, I-V characts. and excess current 79–73641
  peak effect, static and dynamic crit. currents obs. *(Russian)* 77–85399
  periodic pinning structures, supercond. vortices 79–38269
  point contacts, three-dimens. assembly, crit. currents and penetration depth 80–84560
  proximity effect bridge, thermal effects 77–63030
  proximity effect weak links, control of characts. 79–65615
  quenching of technical superconductors by ht. and mag. field pulses 78–43537
  radiation stimulated superconductor, Eliashberg theory 77–89895
  randomly pinned type II superconductors, I-V characts. 79–56478
  rare earth lead molybdenum sulphides, $R_xPb_{1\pm x}Mo_{6+y}S_8$, R = La, Nd, Pr, Gd, sputtered, supercond. props. 80–50019
  split planar thin-film superconductor, anomalous crit. currents 79–51731
  SQUID, with V-VO_x-Pb Josephson tunnel junctions, quantum interference, critical currents 78–91821
  standard definition for practical superconds. 77–28322
  standards for practical superconductors, development 79–33442
  superconducting bridge, DC Josephson effect, microscopic theory *(Russian)* 78–56258
  superconducting contact, effect of UHF field *(Russian)* 78–72313
  superconducting filament formation near edge dislocation *(Russian)* 79–4635
  superconducting film, critical electric fields and currents in two dimensional systems *(Russian)* 80–107972
  superconducting film, inhomogeneous, pair-breaking current, Ginzburg-Landau theory 80–97029
  superconducting film, resistive state, linear depend. on applied microwave power of second crit. current 77–32121
  superconducting magnets, tape-wound cylindrical, trapped fields, diamag. effects 77–26355
  superconducting short bridges, critical current depend. on high. freq. field 80–44774
  superconducting short microbridges, dynamic props. 79–47202
  superconducting-normal metal-superconducting junction, crit. currents, mag. field depend. 80–50008
  superconductor, long thin-film, paradox in crossover of mech. causing hysteresis 80–107971
  superconductor, standard measurement techniques for determ. of props. 79–69622
  superconductor critical temp. depend. on radiation defects, electron density of states calcs. 80–44758
  superconductor-constriction-superconductor, microbridge, I-V characts. and excess current 79–73641
  superconductor-degenerate semiconductor-superconductor structures, critical Josephson current calc. 78–52162
  superconductor-normal metal boundary, effect on crit. current of depairing *(Russian)* 80–34557
  superconductor-normal metal interface, boundary conditions and critical currents *(Russian)* 80–15665
  superconductors, critical parameters during field emission of electrons 80–88682
  superconductors, tilted vortices, mixed state features in surface layers *(Russian)* 80–29512
  superconductors, type I, surface impedance, anomalous skin effect, surface supercond. regime *(Russian)* 80–80459
  tokamak induction heating coils, 50 kA prototype superconducting cable, critical current 80–106196
  transport current effects on superconducting thin-walled cylinder in mag. field *(Russian)* 80–100573
  tunnel junction, paramag. impurities effect on Josephson current *(Russian)* 80–70903
  type I superconductor, critical current, in circ. mag. field 78–68124
  type II annular superconductor, field replication and flux shielding 77–28286
  type II superconductor, pinning, deformation of flux line lattice 79–47213
  type II superconductors, critical currents, in non-transverse mag. fields theory 77–55646
  type II superconductors, flux pinning investigation using one-dimens. analogue model 78–88086
  type-II superconductor with flux pinning, max. possible loss-free current 80–84579
  vortex chain interaction with periodic pinning pot., crit. currents 79–56469
  weak links, interaction in stationary states 78–31020
  weak links, SNS and SS_1S types, current-phase relation 79–60991
  Ag-Sn proximity effect bridge, crit. current anomaly 78–76194

critical currents continued
- Ag-Sn proximity effect bridges, nonequilibrium state, hysteresis of crit. current 79—56411
- Ag-Sn proximity-effect bridges, crit. current hysteresis under phonon injection 79—87206
- Ag-Sn proximity-effect bridges, T* anomaly under phonon injection 80—34566
- Al film, metastable current states, mean free path variation *(Russian)* 80—2538
- Al film perforated with triangular lattice of 1 μm holes, critical currents due to flux pinning 77—28332
- Al film strips, radiation stimulated supercond. 77—28298
- Al granular bridges, with different thicknesses and widths, crit. current, temp. depend. 80—88688
- Al, point contact Josephson junction, microwave-enhanced critical currents 77—8242
- Al strips, freq. depend. of microwave-enhanced supercond., and local injection of electrons 78—6492
- Al strips, microwave-enhanced supercond. meas. 80—2509
- Al strips, on Si substrates, microwave-enhanced crit. currents, phonon effects 79—56451
- Al supercond. film, perforated, crit. currents associated with interaction of commensurate flux-line sublattices 78—34937
- Al superconducting film, cylindrical, granular, crit. currents and electron mean free paths 80—7057
- Al, superconducting film, microwave enhanced critical current, charact. time const. meas. 79—24102
- Al superconducting strips, with local injection of electrons, microwave-enhanced crit. currents 77—63044
- Al-Ge thin film alloy, critical currents near metal-insulator transition 79—65626
- Bi, amorphous, microbridge prep. and transition from superconducting to normal state 78—34933
- Cu-Nb-Sn composites, cold-powder-metallurgy processed, supercond. critical currents 79—78279
- Cu-Nb-Sn dil. alloys containing Nb_3Sn precipitates, superconductivity 78—43507
- Cu-Nb(Nb_3-Sn) composite wires, powder metallurgy prod., supercond. props. and annealing 79—33428
- Cu-V-Ga dil. alloys with V_3Ga particles, supercond. props. and microstruct. 78—39278
- $Cu_{2.5}Mo_6S_8$, evaporated two-phase, crit. current and scaling laws 78—91831
- $Cu_xMo_6S_8$, Chevrel-phase sputtered film, supercond. critical currents 77—80892
- $Cu_xMo_6S_8$, evaporated films, superconducting upper crit. fields, crit. currents 79—42714
- $Cu_xMo_6S_8$, superconducting reactively evaporated film, crit. currents 79—28492
- ^3He, superflow, gap functions, critical currents, susceptibilities 80—103531
- ^3He, superfluid B-phase, anisotropic gap distortion due to superflow and depairing crit. current 80—88383
- Hf-V foil, rapidly quenched and heat treated, supercond. props. 80—54852
- In film, crit. current hysteresis prod. by electron overheating 79—56449
- In, film, embedded with He particles, superconductor ion implantation study of inhomogeneities 78—52181
- In film, metastable current states, mean free path variation *(Russian)* 80—2538
- In superconducting microbridge, voltage locking and other interactions 80—39720
- In-Sn film, supercond. transition temp. and crit. currents *(Russian)* 77—55632
- Nb and alloys, dynamic destruction of supercond. 77—69461
- Nb and Nb alloys, superconductor, flux pinning under heavy ion irradiation 78—52167
- Nb, bicrystal, resistive crit. current, depend. on transverse mag. field 79—24114
- Nb film, critical currents due to microwave field 80—25058
- Nb, film, critical mag. fields and currents, temp. depend. *(Russian)* 80—103798
- Nb film, Gd ion implantation effects 77—39986
- Nb film, struct. and electrophys. props. at 4.2K 80—80436
- Nb, film, switching, storage and erasure effects 77—8253
- Nb, film microbridge, fabrication and I-V characts. 79—87198
- Nb, flux pinning by voids during neutron irrad. 77—40008
- Nb, granulated film, critical current temp. depend. *(Russian)* 80—103803
- Nb microbridges, vertical type, fabrication and DC characts. 80—103788
- Nb, neutron irradiation, low temp., 15 MeV, effect on superconducting props. 78—52179
- Nb, superconducting, deformed, oscillation in current-voltage characts. near H_{c2} 79—28491
- Nb, superconducting film, vac. deposited, deposition parameter effects on crit. temp. 80—2514
- Nb superconducting films, crit. depairing currents, temp. and mag. field depend. 80—7058
- Nb superconducting point contact, high freq. props. in far IR 80—54840
- Nb:O, type II supercond., radiation-induced flux pinning 78—80106
- Nb/Cu-Sn-Mg, superconductor, effect of Mg addition to Cu-Sn matrix 80—25028
- Nb/In composite superconductor, transport props. 80—88658
- Nb-Cu-Nb junctions, Josephson effect meas., critical current, temp. depend. 80—93041
- Nb-Cu-Sn, cast supercond. alloy, crit. current, degradation resistance 78—76203
- Nb-Cu-Sn, diffusion couple, chemical driving force and couple size, effect on reaction rate and crit. current 79—56462
- Nb-H single crysts., critical current and flux pinning *(Russian)* 77—47946
- Nb-Nb_3(Al,Ge) multifilamentary supercond., fabrication and props. 77—20480
- Nb-Nb_xO_y-Pb(In) Josephson junctions, preparation and props. *(Russian)* 79—91188
- Nb-NbO_x-Pb Josephson junctions with high current densities, critical current 80—100552
- Nb-NbO_x-Pb tunnel junctions with high normal resists., 79—56399
- Nb-NbO_x-PbIn window type junctions, critical Josephson current depend. on magnetic field 79—65607
- Nb-NbO_xPb tunnel junctions, current density distrib. 80—39717

critical currents continued
- Nb-Nb(Nb_3Sn) supercond. point contacts, crit. currents, effect of laser radiation *(Russian)* 79—28484
- Nb-Ta (13 wt.%) alloy, flux line bending by transport currents, neutron diffr. 77—8247
- Nb-Ta (54 at.%) cylinder, superconducting mag. and resistive behaviour 77—8252
- Nb-Ti, optimised pinning struct., crit. data 1.8-4.2K 77—89913
- Nb-Ti, pinning curves, high field J_c and scaling behaviour 80—93064
- Nb-Ti alloy, supercond. and mag. props., anisotropy *(Russian)* 77—59361
- Nb-Ti alloy strip, crit. current anisotropy 78—10624
- Nb-Ti composites, multifilamentary, high current, crit. current degradation 77—24659
- Nb-Ti in Cu matrix composite superconductor, cyclic stress effects on transport props. 77—28336
- Nb-Ti superconducting composites, crit. current changes and fatigue damage after 4.2K strain cycling 77—28323
- Nb-Ti superconducting multifilamentary wires, mechanisms for crit. current degradation 77—28324
- Nb-Ti/Cu composite disc, crit. state model for crit. current determ. 79—99665
- Nb-Ti-Ta, pinning curves, high field J_c and scaling behaviour 80—93064
- Nb-Ti-Zr, wire, anomalous crit. AC 77—16014
- Nb-Ti-Zr wire, longit. critical currents in AC mag. field, flux flow instability [-] type II superconductors 77—72958
- Nb-Zr, crit. current, flow-flow resist. depend., allowance for superheating *(Russian)* 80—93061
- Nb-Zr, type II supercond., radiation-induced flux pinning 78—80106
- Nb_3/Sn-Cu composites, in situ processed, supercond. props. 80—75698
- Nb_3(Al,Ge) supercond., diffused layer critical current depend. on Cu before and after annealing *(Russian)* 79—69643
- Nb_3(Al, Ge) tape, effect of thermal treatment on supercond. props. 79—61016
- Nb_3Al, A-15 struct., converted from cold worked BCC struct., crit. currents 80—75697
- Nb_3Al tape, effect of thermal treatment on supercond. props. 79—61016
- Nb_3Ga, critical data, under hydrostatic pressure to 15 kbar 79—47217
- Nb_3Ge, bridge contact, Josephson effect 80—70906
- Nb_3Ge continuous supercond. tape, prep. by CVD 77—80893
- Nb_3Ge sputtered and evaporated, struct.-depend. anisotropy of supercond. crit. currents 79—38292
- Nb_3Ge, supercond. film, CVD, crit. temp., crit. current density 78—76204
- $Nb_3Ge_{1-x}M_x$ (M=Ga,Sn), pseudo-binary, scaling laws for supercond. crit. currents 79—24118
- NbN, critical data, under hydrostatic pressure to 15 kbar 79—47217
- NbN diffusion wires, crit. currents and supercond. crit. field under high press. 79—38287
- NbN granular films, crit. current behaviour 80—15672
- NbN granular films, supercond., crit. props. 80—88661
- NbN granular microbridges, Josephson effects 80—84556
- NbN, granulated film, critical current temp. depend. *(Russian)* 80—103803
- $NbSe_2$ microbridges, current-voltage curves, hysteresis of crit. current *(Russian)* 77—69452
- Nb_3Sn, AC losses, low field behaviour, morphology depend. 77—24655
- Nb_3Sn composite supercond., current transfer, theory 78—72315
- Nb_3Sn composite supercond., current transfer, expt. results 78—72316
- Nb_3Sn, composite superconducting wire, critical current-bend strain relationships 80—93063
- Nb_3Sn composite wires, supercond., degradation mech. under tensile strain at 4.2K 79—38284
- Nb_3Sn composites, crit. currents and microstruct. 79—38280
- Nb_3Sn conductor, bronze-process fine-filament, development and props. 79—33426
- Nb_3Sn, crit. current ang. depend., prep. conditions effect 77—47949
- Nb_3Sn, critical current enhancement by low temp. fast neutron induced flux pinning centres 78—52177
- Nb_3Sn, critical currents, ang. depend., prep. conditions effects 77—43793
- Nb_3Sn, critical data, under hydrostatic pressure to 15 kbar 79—47217
- Nb_3Sn, Cu admixture in Sn bath effect on critical current and stability temp. 80—7059
- Nb_3Sn, current carrying capacity increase by Hf addition 80—7056
- Nb_3Sn filament, crit. current stress induced degradation 77—24658
- Nb_3Sn, filamentary, fatigue tests on small coils 78—64652
- Nb_3Sn, filamentary, mech. props. and crit. current 77—24657
- Nb_3Sn, filamentary conductors, type-II, low temp. 30 GeV proton effects on critical props. 78—52178
- Nb_3Sn filamentary wires, fabricated by infiltration method, supercond. props. 77—28761
- Nb_3Sn film contacts, quantum interference at H_2 temp. *(Russian)* 77—12041
- Nb_3Sn in bronze, supercond. props. thermally induced matrix stresses 77—32134
- Nb_3Sn in Cu matrix composite superconductor, cyclic stress effects on transport props. 77—28336
- Nb_3Sn, low temp. neutron irrad. expts., $E_n=14$ MeV 79—33424
- Nb_3Sn, multifilament conductors, strain-crit. current meas. 78—64174
- Nb_3Sn multifilament conductors, strain effect on crit. props. 78—80108
- Nb_3Sn multifilament conductors, fabrication and props. 79—33427
- Nb_3Sn, multifilamentary composite wires, critical current strain depend. 77—20511
- Nb_3Sn multifilamentary conductor, tensile stress effects 77—28329
- Nb_3Sn multifilamentary conductors, crit. current under tensile stress 77—89912
- Nb_3Sn multifilamentary conductors, enhancement of supercond. crit. current by tensile stress 78—6490
- Nb_3Sn multifilamentary conductors for large-scale magnets, crit. currents, stability, and stress effects 79—38291
- Nb_3Sn multifilamentary composite superconductor, effect of heat treatment on supercond. props. 79—33376
- Nb_3Sn multifilamentary composite superconductor, reaction treatment, crit. current, transition temp. and bend props. 79—33430
- Nb_3Sn multifilamentary composites, supercond. destruction by current, long N-S interfaces 79—56480
- Nb_3Sn, multifilamentary conductors, effect of bronze on compression 79—61012
- Nb_3Sn, multifilamentary conductors, stress-induced enhancement of critical currents 79—69644

critical currents continued
- Nb_3Sn multifilamentary composites, crit. currents, flux pinning, and crit. field 79—78280
- Nb_3Sn multifilamentary dipole magnets, supercond. props., 4.2 to 15K 79—31275
- Nb_3Sn multifilamentary hollow superconductor and magnet, fabrication and crit. currents 79—38289
- Nb_3Sn, multifilamentary supercond., flexibility and elec. characts. 77—24990
- Nb_3Sn, multifilamentary supercond., crit. current, bend tests 77—28335
- Nb_3Sn, multifilamentary supercond., stress effects 77—32133
- Nb_3Sn multifilamentary superconductors crit. current up to 18 T 77—47950
- Nb_3Sn multifilamentary superconductor, stress induced normal$\rightleftarrows$supercond. transition 79—33377
- Nb_3Sn multilayered supercond. power line conductors, elec. props. and growth morphology 77—28325
- Nb_3Sn, neutron irrad. effect on upper crit. field and crit. current 77—72954
- Nb_3Sn, neutron irradiation at 8K, supercond. crit. current and crit. temp. meas. 77—28334
- Nb_3Sn, radiation damage effect on superconducting props. 78—52127
- Nb_3Sn strip, made by diffusion method, crit. curent anisotropy, Zr alloying addition effects *(Russian)* 78—47921
- Nb_3Sn, supercond., production of high current carrying strip *(Russian)* 79—33435
- Nb_3Sn, supercond. composite, residual stress state, crit. currents 80—80468
- Nb_3Sn, supercond. diffusion layer, Zr content and Nb cold working effects 77—16015
- Nb_3Sn superconducting bridge junction, crit. current temp. depend. *(Russian)* 78—34938
- Nb_3Sn superconducting layers, struct. and prep. *(Slovak)* 78—56273
- Nb_3Sn superconducting multifilamentary wires, mechanisms for crit.current degradation 77—28324
- Nb_3Sn superconducting multifilamentary wire, stress effects 79—33431
- Nb_3Sn superconducting multifilamentary composites, strain depend. of crit. current and crit. field 79—33432
- Nb_3Sn superconducting multifilamentary conductors, localisation of defects by inductive procedure 79—33433
- Nb_3Sn, superconducting props., effect of radiation induced atomic disorder 78—52133
- Nb_3Sn superconductors, bronze-processed, effect of Ta additions 78—95404
- Nb_3Sn tapes, appl. of continuous meas. method 77—24656
- Nb_3Sn thin film bridges, AC Josephson effect 79—42702
- Nb_3Sn, thin film weak-links SQUIDs, localised region radiation damage, fabrication and properties 78—47912
- Nb_3Sn, vap. deposited supercond. film, effect of N_2 and tape heating 78—34939
- Nb_3Sn-Cu superconducting composite with submicrometer filaments, fabrication and props. 79—38282
- Nb_3Sn-Nb_3Sn supercond. point contacts, crit. currents, effect of laser radiation *(Russian)* 79—28484
- Nb_3Sn-Zr (0.8%), supercond. tape, crit. current, two stage annealing effect *(Russian)* 77—63046
- Nb_3Sn_4 film, critical currents due to microwave field 80—25058
- $Nb_3(SnGa)$, wire, neutron effect on T_c, I_c and flux pinning 79—38216
- $Nb_3(SnIn)$ tapes, diffusion processed, high field props. 79—38266
- Nb_3Su-Cu supercond. composites, fabrication, magnet appl. 80—11602
- NbTi composite supercond., current transfer, theory 78—72315
- NbTi composite supercond., current transfer, expt. results 78—72316
- NbTi, filamentary conductors, type-II, low temp. 30 GeV proton effects on critical props. 78—52178
- NbTi in Al composite superconductor, AC losses and crit. current 77—28310
- NbTi, multifilamentary composite wires, critical current strain depend. 77—20511
- NbTi multifilamentary wires, 30 GeV proton irradiated, effect on crit. currents 77—89911
- NbTi multilfilamentary composite, appl. of continuous meas. method 77—24656
- NbTi superconducting tapes, mag. field profiles 77—28326
- NbTi/In composite superconductor, transport props. 80—88658
- NbV-VO_x-Pb Josephson tunnel junction, VO_x effect on props. 79—87203
- Pb film, monocryst., heteroepitaxial growth, struct. defects, and elec. props. *(Russian)* 80—84403
- Pb thin strips, supercond., optical wave illum., critical current behaviour 80—50012
- Pb-Cd-Pb, supercond.—normal-metal—supercond. junction, crit. currents 80—107965
- Pb-Cd-Pb junctions, pair pot., mag. field depend., crit. currents meas. 80—84555
- Pb-Ge thin film alloy, critical currents near metal-insulator transition 79—65626
- Pb-In alloys, flux pinning at grain boundaries 80—34572
- Pb-In cylinder, vortex-surface interaction, vortex field *(Russian)* 78—27003
- Pb-In multilayered superconducting film 79—61017
- Pb-In/Sn-In proximity sandwiches, crit. currents 79—60992
- Pb-Na alloy, with Pb_3Na precips., flux pinning, crit. currents obs. *(German)* 78—14907
- Pb-Sb, dynamic destruction of supercond. 80—2529
- $Pb_{80}In_{20}$ foil, deformed, annealed, correlation between pinning strength and flux flow noise charges 77—43792
- $PbMo_6S_8$, supercond. wires prod. and characteris. 77—69462
- PbNa, type-II superconductor, regularly ordered precipitates, peak effect, crit. current meas. *(German)* 78—19196
- $Pb_{0.871}Sn_{0.129}$, supercond., hysteresis in flux flow characts., normal metal precipitates 78—80107
- Sn film, crit. current hysteresis prod. by electron overheating 79—56449
- Sn film, limitation in microwave stimulation of supercond., crit. current meas. *(Russian)* 80—88695
- Sn film, long, order parameter relax. during flow of crit. current 77—59364
- Sn film, metastable current states, mean free path variation *(Russian)* 80—2538
- Sn, long film, crit. currents in microwave EM fields 80—70898
- Sn microstrip, optically illuminated, resistive transition and supercond. props. 80—54821

critical currents continued
- Sn, supercond. film, electron mean free path depend. of crit. currents and pair-breaking limit 77—20504
- Sn superconducting film, phonon-injection-induced destruction of supercond. 80—6956
- Sn, superconductivity destruction by current in hollow cylindrical sample *(Russian)* 79—78278
- Sn thin film, HF pair-breaking current *(Russian)* 77—32130
- Sn-In multilayered superconducting film 79—61017
- Ta wire, emission current effect on superconductor critical parameters 79—91185
- Ta wires, supercond. destruction by current, long N-S interfaces 79—56480
- Ti-Nb superconducting alloys and cmpds. with A15 struct., H_2 effect on supercond. props 79—28438
- Ti-Nb-Si, amorphous alloy, supercond. props. and crystn. behaviour, TEM and DTA study *(Japanese)* 80—84536
- Ti-Nb-Zr-Ta, superconducting props. comp. depend., stress effects and precipitation behaviour, X-ray scatt. 80—93059
- TiN, low-energy ion-stimulated deposited, supercond. props. 80—88664
- $U_xPb_{1\pm x}Mo_{6+y}S_8$, sputtered supercond. props. 80—50019
- V/Al-Al_xO_y-Pb tunnel junction, superconducting transition, critical currents, Josephson effect *(Russian)* 80—29507
- V-H single crysts., critical current and flux pinning *(Russian)* 77—47946
- V-V_xO_y-Pb tunnel junctions, Josephson characteristics *(Russian)* 77—47938
- V-VO_x-Pb Josephson tunnel junction, crit. currents exam. 78—23209
- V_3Ga, filamentary conductors, type-II, low temp. 30 GeV proton effects on critical props. 78—52178
- V_3Ga multifilament wire, crit. current props. above 4.2K 77—32135
- V_3Ga multifilamentary wires, effect of low temp. neutron irrad. 77—32132
- V_3Ga, multifilamentary wire, stress effect on critical currents 77—80891
- V_3Ga, neutron irrad. effect on upper crit. field and crit. current 77—72954
- V_3Ga superconducting tape, stress effect on critical current *(Japanese)* 80—50020
- V_3Ga-Cu composites, supercond. props. 79—95557
- V_3Si, supercond. structure and properties *(German)* 80—93631
- V_3Si superconducting bridge junctions, vortex model appl. *(Russian)* 79—60986
- $Y_xPb_{1\pm x}Mo_{6+y}S_8$, sputtered supercond. props. 80—50019
- Zr-V foil, rapidly quenched and heat treated, supercond. props. 80—54852

critical field, superconducting *see superconducting critical field*

critical fluctuations
- *see also fluctuations in superconductors*
- ϕ^4 system, metastable state, decay rate calc. 80—22301
- actinide systems, spin fluctuations effect, model approach 77—28404
- aniline-cyclohexane, crit. mixture with shear flow, light scatt. obs. 80—6521
- anthracene-TCNB, 1:1 charge transfer complex, phase transition at 206K, NMR meas. 79—7690
- azoxy-4,4′-(di-undecyl α-methylcinnamate), smectic A to smectic C phase transition, optical tilt angle meas. 78—95141
- binary alloy, elec. resist. due to crit. fluctuations near order-disorder temp., theory 77—40071
- binary critical mixture near crit. temp., temp.-jump expts. 77—21407
- binary mixture, entropy fluctuations, light beating spectroscopy 77—10119
- binary mixture, high-frequency sound absorpt. near crit. separation point 78—83881
- binary mixture, pretransitional effects near convective instability 77—41536
- binary mixtures and simple fluids near crit. point, Rayleigh and Brillouin scatt. 77—36256
- boiling, nucleate, superheating, heterogeneous nucleation theory calc. 79—46170
- Bose glass, marginal fluctuations 80—2586
- boson systems, critical dynamics and fluctuation-dissipation theorem 79—40467
- Brownian motion in fluid near critical point, fluctuation-dissiptation theorem 80—4647
- CBOOA, liq. cryst., mag. aligned, smectic A-nematic transition, US absorpt meas. 78—95137
- CBOOA, liq. cryst., nematic to smectic A transition, high resolution X-ray scatt. exam. 78—94984
- CBOOA, liq. cryst., smectic A to nematic phase transition, crit. neutron scatt. 78—95135
- CBOOA, US attenuation near nematic-smectic A transition 78—87773
- chemical fluctuations near nonequilibrium phase transitions to nonuniform states 80—45542
- chemical model, Schlogl's, critical fluctuations near non-equilib. critical point 80—85150
- chemical system, nonlinear, open, information, critical fluctuations and phase-transition-like phenomena 79—24720
- chloroform, liq., crit. fluctuations, proton spin relax. obs. 78—19358
- cholesteryl 2-(2-ethoxy-ethoxy) ethyl carbonate, dynamics of isotropic-cholesteric transition, normal and blue phases 79—95134
- classical fluids, laminar flow critical phenomena in mean field approx. 80—59001
- cluster dynamics near critical points, linear and nonlinear relax. 77—13725
- COC, dynamics of isotropic-cholesteric transition, normal and blue phases 79—95134
- condensation point, thermodynamic function singularities, vapour fluctuations 77—41558
- correlation functions, lasing systems exhibiting first order like phase transition threshold behaviour 77—71969
- cyclohexane-methanol, crit. opalescence, elec. field effect 79—28775
- dielectric fluid, Debye absorption at crit. liq.-vapour transition 80—100322
- dielectrics, partial polarisation fluctuations, macroscopic phenomenological eqn. and thermodynamic fluctuation theory study 79—78615
- diffusion process, description of crit. fluctuations by means of most probable path 79—49166
- dimethylammonium copper tetrachloride, crit. slowing down and anomalous relax. near Curie temp. 80—71053
- DNA, soln., phase transitions, light absorption oscills. obs. 80—26197

critical fluctuations continued
dye laser, tunable, dye dissolved in liq. cryst., second order phase transform. 80—43328
dynamical renormalisation group method, mode coupling theory 80—27254
dynamics, far from equilibrium 80—27258
elastic phase transitions, order parameter and mode softening 80—75325
electron-phonon quasi-one-dimensional system, fluctuations anal. 77—89703
electronic and spin Peierls transition, gap eqns. 80—24801
ferrites, critical dynamics, influence of static impurities *(Russian)* 78—10713
ferroelectric, displacive type, Ginzburg-Lavanyuk parameter 79—8106
ferroelectric, uniaxial, static and dynamic crit. phenomena, Larkin-Khmelnitzkii theory 78—64327
ferroelectric antiferromagnetics, spin wave fluctuations in strong mag. fields *(Russian)* 79—82773
ferroelectric crystal, fluctuons, calc. by method of parametric potential *(Russian)* 79—69784
ferroelectrics, sp. ht. calc., soft mode contrib., near T_c 78—64338
ferromagnet, magnetic moment fluctuations and sp. ht. near crit. point 77—28388
ferromagnetic semiconductors, conduction electron heating, critical scatt. effects 79—91040
ferromagnetic-paramagnetic transition, exciton migration in crit. region 79—73440
field theoretic method 80—27255
first-order phase transition, nonlinear relaxation, Ginzburg-Landau theory including fluctuations 79—35658
fluid, crit. state conditions *(Russian)* 78—47496
fluid, ion mobility, effect of long-wavelength fluctuations 80—49393
fluid, Rayleigh linewidth, simulation using emulsion 77—16324
fluid, shear flow effects 77—20045
fluid, Stokes-Einstein diffusion coeff. determ. 80—90783
gels, crit. conc. fluctuation dynamics, near phase separation 78—56921
Ginzburg-Landau model, time-depend., critical dynamics near dimens. 2 77—61021
Ginzburg-Landau systems *(Russian)* 79—75484
hard superconductor flux jumps under time depend. external conditions 80—7038
Heisenberg ferromagnet, structurally and chemically disordered, critical behaviour 77—43838
Heisenberg spin system, one-dimensional, dynamical behaviour 80—29567
helicoidal ferroelectric smectic A-smectic C phase transition, low freq. polarisation fluctuation spectrum 79—95714
4'-n-heptyl-4-cyanobiphenyl, nematic, mag. field depend. of birefringence and order parameter 77—76534
incommensurate Peierls-Frohlich system, fluctuation cond., Green's function calc. 80—24886
incommensurate phase transition, Bethe-Peierls and mol. field approx. 80—20599
Ising model, critical behaviour in transverse field 77—66330
Ising model, spin fluctuation waves in critical point region *(Russian)* 77—33970
Ising pair correlation function Gaussian basis distrib. of density fluctuations *(Russian)* 77—33969
Ising system, finite, statistically layered, crit. phenomena 78—95446
isobutyric acid-water, crit. mixture, conc. fluctuation mean relax. time, US absorpt. and vel. meas 80—29163
Lennard-Jones fluid, phase separation by spinodal decomposition, mol. dynamics computer simulation 79—10766
Lifshits points for bidimensional representations *(Russian)* 79—93086
light generation at impurity atoms in ferroelectrics and LC, fluctuation effects *(Russian)* 80—91767
limit cycle fluctutions near bifurcation point, Fokker Planck, Langevin eqn. calcs. 80—77709
liquid, binary, crit. conc. fluctuations, nonexponential decay, 3-methylpentane-nitroethane expt. 80—44309
liquid, vibr. dephasing and gas-liq. crit. density fluctuations 79—51954
liquid crystal, refractive index near smectic-A/smectic-C transition, orientational order 80—24572
liquid-liquid mixtures, critical region fluctuations, centrifuging effects 78—63850
2,6-lutidine-water critical mixture, spinodal decomposition, Rayleigh scatt. 80—70416
macrovariables in nonequilibrium states, normal fluctuation critical dimensionality 77—57280
magnetic material, fluctuational breakdown of metastable states at phase transitions *(Russian)* 78—52245
magnetic metals, crit. transverse US attenuation, spin fluctuations 78—48022
magnetic systems, effect on resistivity 78—87955
magnetic transition at T=0, impurity effects 78—76259
magnetically ordered materials, anomalous spin-flip scatt. rate near ordering temp. 79—82802
master equation, instability point, relax., fluctuation 77—13681
MBBA, dynamic critical behaviour in NLC above nematic-isotropic transition 80—49096
MBBA, proton spin-lattice relax. in crit. regime 80—80631
micellar solutions, crit. behaviour 80—105601
mixture, binary, fluctuations near liq.-liq. crit. point, neutron small-ang. scatt. appl. 79—82347
Mossbauer radiation crit. scatt. in condensed matter 79—56635
multicritical points, fluctuation dynamics *(Russian)* 77—27977
nematic bend-splay elasticity near the nematic-smectic-A transition 80—24360
nematic liquid cryst., 3D convective instability in AC field 77—62475
nematic liquid crystal, acoustic attenuation anomaly above clearing point 78—75816
nematic liquid crystal, order parameter fluctuations and anomalous sound propag. just above clearing point, critical dynamics 80—15224
nematic liquid crystal, quasi-elastic light scatt. near instability point, dielec. regime 78—75535
nematic liquid crystal-isotropic liquid phase transition, fluctuations effect *(Russian)* 79—86879
nematic liquid crystals, orientation fluctuations in high mag. field, quenching, birefringence effects 80—64892
nematic mesophase, mode-coupling theory near clearing point 77—89377
nematic-isotropic phase transition character, molecular bending fluctuations critical growth *(Russian)* 80—79919

critical fluctuations continued
nematic-smectic A(C) phase transitions, contribs. to viscosities from order parameter fluctuations 79—60489
nematic-smectic-A transition, high-resolution X-ray and light scatt. study 79—73297
nematic-smectic-C phase transition fluctuations, ring model 77—24392
neutron scattering, transitional, ambiguity in exptl. results 77—47546
nitrobenzene-n-heptane, crit. mixture, conc. fluctuation mean relax. time, US absorpt. and vel. meas 80—29163
nitrobenzene-n-hexane, shear viscosity, critical conc. fluctuation rate, verification of renormalisation prediction 78—47514
nitroethane-isoctane, crit. mixture, conc. fluctuation mean relax. time, US absorpt. and vel. meas 80—29163
NLC inelastic light scattering by order parameter biaxial and longitudinal fluctuations *(Russian)* 80—75160
non equilibrium systems, stochastic model, master eqns. *(Chinese)* 80—68126
nonequilibrium phase transitions in chemical systems 78—54325
nonlinear dynamics of first order phase transitions 79—11322
p-nonyloxy benzoate p-butyloxyphenol, smectic A to smectic C transition, crit. ang. fluctuations, Rayleigh scatt. obs. 79—95131
p-nonyloxybenzoate p-butyloxyphenol, smectic A to smectic C transition, crit. fluctuations, Rayleigh scatt. obs. 78—95140
one-dimensional electron system, generalised susceptibilities in mag. field, fluctuations *(Russian)* 77—80750
one-dimensional system, phase fluctuations, disorder, nonlinearity 80—54331
order-parameter fluctuations with two time scales, critical growth and saturation effects 77—9975
PAA, nonlinear soft mode at Rayleigh-Benard instability, neutron cond. spectrosc. obs. 80—79266
PAA-di, nematic liquid crystal, NMR data, appl. of Landau-de Gennes theory 80—64893
pentane-o-nitrotoluene critical solution, nonlinear dielectric effect 78—55952
4-n-pentylbenzenethio-4′-n-alkoxybenzoates, birefr., crit. behaviour near smectic A-C transition 80—80745
phase transformation, second kind, critical fluctuation pattern, effect of large-scale inhomogeneities *(Russian)* 78—18741
phase transition, fluctuation-induced ordering in system of two interacting fields 79—80556
phase transitions, caused by inhomogeneity of transition parameter *(Russian)* 79—23698
phase transitions to non-uniform states 79—86870
plasma, nonlinear wave interactions and critical fluctuations 80—38626
polyacrylamide gel, network density fluctuations, crit. behaviour 77—44518
polyacrylamide gel and single chain in soln., laser light scatt. obs. near phase transitions 80—93808
polymer dynamics in binary critical mixture 77—58943
polystyrene networks swollen in cyclohexane, swelling equil. and light scatt. at theta conditions 80—107036
probabilistic aspects of crit. fluctuations 77—22516
quasi-one-dimensional metallic system, phase transitions problem, Gorkov-Dzyaloshinskii model 78—6296
random ferromagnets, Ginzburg criterion, critical fluctuations 80—71032
random $n \geq 4$ vector models, renormalisation group technique in $4-\varepsilon$ dimensions 77—16088
random uniaxial systems with dipolar interactions, phase transitions 77—72677
real-space renormalisation group approach, Migdal approx., review 80—27257
real-space renormalisation group approach 80—31699
roughness fluctuation in layer between two phases 80—85147
scaling hypothesis with finite correl. length at phase transition point 79—73743
scaling techniques, near second-order phase transitions 79—35626
short-term local phase and polymorphic transforms. and changes of inner states in solids 79—14913
simple fluids, order-parameter fluctuations near crit. point, Ornstein-Zernike theory 78—34416
solid, near phase transition, light scatt., review 80—29752
solitons near critical point, neutron scattering observation 80—34650
solutions with critical point of unmixing, acoustic relax. *(Russian)* 79—95085
spin glass, fluctuation effects 79—78381
spin glass, theory 78—52279
spin systems with quenched random impurities, dynamics, replicas and frustration approaches 80—34673
spinodal decomposition in critical fluid mixtures, fluctuation spectrum 78—22825
stochastic n-vector model below T_c, hydrodynamic excit. spectra 77—74326
structural transitions, method of self consistent phonon field 79—33065
superfluid, two-dimensional, dissipation near crit. point 78—47619
superradiance, scaling theory and exact soln., fluctuations and relax. near instability point 78—37864
TBBA, liq. cryst., smectic A-nematic transition, cybotactic cluster form., X-ray obs. 78—95138
TBBA, smectic C to smectic A transition, crit. exponent, neutron diffr. obs. 78—95143
p-terphenyl, crit. slowing down at struct. phase transition, high resolution neutron spectroscopy 79—82329
tetragonal ferroelectric, crit. fluctuations, phase transition splitting *(Russian)* 78—48131
TGS:Cr^{3+}, EPR obs. of fluctuations near phase transition 78—43820
TGSe, sp. ht. anomaly, AC calorimetric obs. 78—23414
thermodynamics, nonequilib., with crit. fluctuations, master eqn. derivation of Keizer's theory 79—67240
thin films, superconducting fluctuation influence on magnetoresistance *(Russian)* 80—54815
TTF-TCNQ, impurity effects on CDW fluctuations 80—44576
turbulence analogy with crit. fluctuations, intermittency exponents, book contrib. 77—84214
turbulence spectrum, fluctuation corrections by renormalisation group methods 77—42806
uniaxial dipolar magnet, critical dynamics and statics 77—59422
uniform treatment of fluctuations at critical points 80—181
unstable equilibrium state decay near crit. point 79—80557
zero-point fluctuations in direct-action electrodynamics 80—57528
CoF_2, antiferromag. crit. props., neutron scatt. obs. 80—88749

critical fluctuations continued
  $Co_{1-x}Zn_xF_2$, antiferromag. crit. props., neutron scatt. obs. 80–88749
  Cr, critical coeff. of resistivity near Neel temp. 77–59417
  Cr_2O_3, rel. to EPR linewidth, near Neel temp. 78–23327
  $CsPbBr_3$, cubic-to-tetragonal phase transition, critical anomalies, phenomenological eqns. 80–39275
  $CsPbCl_3$, cubic-to-tetragonal phase transition, critical anomalies, phenomenological eqns. 80–39275
  Cu_3Au, heterophase fluctuations near order-disorder transform., X-ray and neutron diffr. 77–73272
  Cu_3Au, X-ray and inelastic neutron scatt. investig. of spinodal ordering 77–77473
  EuO, crit. behaviour of opt. absorpt. edge 77–59418
  EuS, thermo- and magnetorefl. spectra, dynamical spin fluctuation effect on exciton state 77–52126
  Fe, crit. fluctuations, Mossbauer obs. 78–43724
  Fe whiskers, AC susceptibility, critical slowing down of mag. fluctuations 77–69594
  Fe-Ni (33-38 at.%), low-angle neutron diffr., anomalous crit. scatt. *(Russian)* 80–60193
  Fe-Ni Invar alloys of crit. conc., mag. props., flow theory methods *(Russian)* 80–65894
  $FeCl_2$, metamagnetic, sound propag. near tricritical point 78–48024
  $Fe_{65}Ni_{35}$, mag. cluster structs., 25-422°C 77–69493
  ferromagnets, critical dynamics, influence of static impurities *(Russian)* 78–10713
  He, liq., critical and tricritical dynamics, renormalisation group calc. 80–29239
  He, superfluid phase transition, fluctuational character *(Russian)* 77–47633
  He^3 liquid, Anderson-Morel phase stabilisation *(Russian)* 79–73368
  ^3He fluid-superfluid transition phase diagram, thermodynamic stability, fluctuations *(Russian)* 80–80023
  ^3He, liquid, fluctuation contrib. to sound vel. and damping above superfluid transition temp. 80–15324
  ^3He, spin flow density fluctuations, superfluidity *(Russian)* 80–65328
  ^3He-^4He mixture, critical and tricritical dynamics, renormalisation group calc. 80–29239
  ^3He-A, superfluid, first order current induced textural transition 79–95237
  ^4He, critical fluctuations near lambda point, energy-density correl. function 79–12753
  ^4He, liq., critical thermal cond. near λ-point, light scatt. spectrum 80–24697
  ^4He, liq., dynamic scaling near T_λ 80–34264
  ^4He, liq., dynamical behaviour to λ-line, light scattering review 79–7717
  ^4He, liquid, order parameter fluctuation critical attenuation near critical temp., first sound 80–2229
  K solution, in KBr, conc. fluctuations, neutron small-angle scatt. study in electrolyte-metal transition range 79–14668
  $KCr(SO_4)_2.12H_2O$, phase transition associated fluctuations, Cr^{3+} EPR obs. 77–32247
  KD_2PO_4, polarisation fluctuations, wavevector depend. 80–71295
  K_2FeO_4, crit. slowing down of spin fluctuations, Mossbauer spectra and relax. theory 80–65882
  KH_2PO_4, light scatt. in elec. field, ferroelec.-paraelec. transition 80–2707
  KH_2PO_4:SeO_4^{3-}, slowing down of fluctuations near T_c, EPR obs. 78–60403
  $KMnF_3$, cubic-to-tetragonal phase transition, critical anomalies, phenomenological eqns. 80–39275
  $KMn_{1-x}Ni_xF_3$, antiferromag. crit. props., neutron scatt. obs. 80–88749
  $KMn_xZn_{1-x}F_4$, three dimens. Heisenberg antiferromag., fluctuations near percolation threshold 79–78390
  Li-ND_3, near liq.-liq. crit. point, conc. fluctuations, neutron diffr. long wavelength thermodynamic limit 79–10948
  $Mn_{1.88}Cr_{0.12}Sb$, antiferromag.-ferrimag. transition, neutron crit. scatt. and crossover effect 80–71023
  MnSi, crit. transverse US attenuation, spin fluctuations 78–48022
  $Mn_xZn_{1-x}F_2$, three dimens. Heisenberg-Ising antiferromag., fluctuations near percolation threshold 79–78390
  NH_4Br, β-γ phase transition, critical anomalies, phenomenological eqns. 80–39275
  $NH_4Br(Cl)$, anomalous sound attenuation above lambda point 78–51617
  $NaNO_2$, ferroelectric, NMR of ^{23}Na small particles 79–28629
  Ni-Mn (17-27 at.%), low-angle neutron diffr., anomalous crit. scatt. *(Russian)* 80–60193
  PLZT ceramics, diffuse phase transitions and thermodynamics 80–29694
  $PbMg_{1/3}Nb_{2/3}O_3$, ferroelec., crit. electron-phonon phenomena and diffuse phase transition in elec. field 79–38497
  PbO-B_2O_3-Al_2O_3 system melts and glasses, viscosity, phase separation, and supercritical fluctuations effects 79–65235
  $RbAg_4I_5$, depolarisation of light by crit. fluctuations 79–61333
  Rb_2CoF_4, critical fluctuations near Neel temp., US attenuation study 80–108013
  $Rb_2Co_xMg_{1-x}F_4$, two-dimens. Ising antiferromag., fluctuations near percolation threshold 79–78390
  $Rb_2Mn_xMg_{1-x}F_4$, two dimens. Heisenberg-Ising antiferromag., fluctuations near percolation threshold 79–78390
  SF_6, long-range correlation length near liquid-vapour transition, Rayleigh scatt. 77–8593
  SiO_2, glassy-amorphous, light scatt. exam. 78–14281
  SiO_2 glassy-amorphous system, struct. *(German)* 78–38626
  $Sr_xBa_{1-x}Nb_2O_6$, neutron and light scatt. in phase transition region 78–64336
  $SrTiO_3$, central peak in spectrum of ferroelec. mode fluctuations and dielec. losses, 4.2K 78–19432
  $SrTiO_3$, EPR of Fe^{3+}-V_O centre, above T_c 80–39870
  $SrTiO_3$:Cr^{5+}, nonlinear Jahn-Teller coupling, local dynamics, near struct. transition 80–2625
  V_3Si, d-spacing fluctuations above Martensitic phase transition 80–7570
  Xe, positronium formation in Xe gas near crit. pt. 79–86091

critical mixtures
  3--phenylpropanol-n-hexane, Kerr effect near crit. pt. 79–61336
  acetic acid, in cyclohexane soln., Raman scatt. near crit. stratification, temp. depend. *(Russian)* 79–11420
  acetic anhydride-cyclohexane, crit. resistivity, H_2O impurity effect 79–51565
  acetonitrile+CS_2 liquid mixture, elec. cond. crit. phenomena 77–4212

critical mixtures continued
  acoustic relaxation in solutions with crit. pt. of unmixing *(Russian)* 79–95085
  alcohol-aliphatic hydrocarbon mixture, critical soln. temp. 79–37844
  alkali metal vapour-He(Ar)(N_2), alkali condensation in flow, heat and mass transfer 78–75192
  aniline+cyclohexane critical mixture, gravity-induced concentration gradients 77–28004
  aniline-cyclohexane, crit. mixture with shear flow, light scatt. obs. 80–6521
  aniline-cyclohexane, hypersound velocity, absorption temp. depend *(Russian)* 80–75303
  aniline-cyclohexane, viscosity conc. and temp. depend. in crit. mixing region 77–35686
  aqueous mixtures, lower crit. soln. pt. theory 79–4415
  benzonitrile, hexane and CCL_4 solns., nonlinear dielec. effect 79–78602
  benzonitrile-isooctane mixture, dielec. const. near consolute point, temp. and freq. depend. meas. 80–71292
  binary, entropy fluctuations, light beating spectroscopy 77–10119
  binary, fluctuations near liq.-liq. crit. point, neutron small-ang. scatt. appl. 79–82347
  binary, gravity induced gradients, optical meas. 77–4203
  binary, latent heat of vaporisation, prediction 78–83930
  binary, off-critical, quenched, struct. functions and mobilities renormalisation 79–82343
  binary, shear viscosity, pseudospinodal curves and scaling 78–22844
  binary critical mixture, critical turbidity, kinetics, press. jump investig. 77–47548
  binary critical mixture near crit. temp., temp.-jump expts. 77–21407
  binary gas mixture thermal fluctuations in renormalised kinetic theory 77–22492
  binary hydrocarbon mixtures, critical points calc. using Soave eqn. of state 77–1209
  binary liquid, critical conc. determ. from dielectric const. meas. 77–20788
  binary liquid mixtures, vibr. and rot. relax., crit. point effects 79–50969
  binary liquid mixtures near crit. pt., nonlinear dielectric effect 78–23384
  binary mixture, high-frequency sound absorpt. near crit. separation point 78–83881
  binary mixture, Kerr effect near crit. pt. 79–61336
  binary mixture, nucleate boiling heat transfer, conc. depend. 78–87249
  binary mixture, time-depend. solidification, series soln. 78–75058
  binary mixture in external field, crit. opalescence 78–84595
  binary mixture near crit. point, singly and multiply scattered light distrib. 78–56494
  binary mixtures, dielec. props., droplet model 79–69762
  binary mixtures, multiple light scatt. 77–48183
  binary mixtures, near critical, metastable, phase separation and nucleation and drop growth, rate eqns. 80–65232
  binary mixtures, recent developments in phase transitions and critical phenomena 77–87713
  binary mixtures, sound propag., mode coupling theory, validity breakdown 80–65159
  binary system cluster dynamics, critical diffusion and phase separation kinetics 77–61042
  n-butanol-water-Ca $(SCN)_2$ system with hypercrit. point, US absorpt. 80–49306
  carbon tetrachloride-perfluoroethylcyclohexane, crit. mixture, brilliant total refl. from liq.-liq. interface 79–90786
  o-chloroaniline-iso-octane, crit. system, comp. depend. of absorpt., US obs. *(German)* 80–19879
  o-chloroaniline-iso-octane critical system, US absorpt. meas. 77–51440
  o-chloroaniline-n-heptane, crit. system, comp. depend. of absorpt., US obs. *(German)* 80–19879
  condensation, simplified mass transfer anal. 80–10675
  critical fluids, light scatt. in presence of uniform shear flow 79–78693
  cyclohexane+acetic anhydride, elec. resist. near crit. soln. temp. 78–71874
  cyclohexane-aniline critical mixture, shear and critical fluctuations, instantaneous mapping of velocity gradients 80–79420
  decahydronaphthalene-H_2O, liq.-liq. phase equilib., crit. phenomena 78–18764
  n-decane-nitrobenzene critical system, US absorpt. meas. 78–6126
  diffusion near crit. point in solns. with large conc. gradients in capillary *(Russian)* 77–84958
  n-dodecane-β,β′-dichlorediethyl ether crit. mixture, Rayleigh line wing 77–20864
  ethane-propane, binary mixture near crit. point, conc. fluctuation decay rate, spectrosc. obs. 77–81108
  ethanol-CS_2 mixture, Rayleigh and depolarised Raman scatt. lines near crit. temp. 77–20863
  ethanol-water mixture, saturated, min. film boiling temp. on horiz. stainless steel and Cu surfaces 78–90692
  ethanol-water-chloroform mixture, light scatt. near plait point 78–72532
  ethylene glycol-H_2O-lauryl alcohol-nitromethane-nitroethane, liq., multicrit. pts., 37-42°C 79–86868
  fluid, binary mixture, in centrifugal field, crit. dynamics 80–44310
  fluid binary mixtures at high press., phase equilibria, critical phenomena calcs. 77–35664
  fluid mixture in homogeneous states near line of tricritical or polycritical pts., generalised Pippard's relns. 80–6485
  fluid mixture near tricritical point, light scatt., mean field behaviour 80–34930
  fluid near crit. point, rapid evaluation of multiple scatt. 78–84594
  gaseous, conc. fluctuations meas. using catalytic wire 77–26291
  n-heptane+acetic anhydride, elec. resist. near crit. soln. temp. 78–71874
  n-heptane-nitrobenzene, critical fluid, ratio of sound dispersion to attenuation 79–55826
  n-heptane-nitrobenzene, US study of crit. mixing 78–75732
  n-hexadecane-acetone, noncritical interface near crit. end point, surface tension meas. 79–69322
  ionic fluids binary mixtures, critical conc. fluctuations 78–34596
  isobutyric acid+water, thermal expansion near upper crit. soln. temp. 77–29031
  isobutyric acid and water, shear viscosity of critical mixture, amplitude ratios 80–2188
  isobutyric acid-d_{10}-D_2O, coexistence curve, liq. densities 78–18780
  isobutyric acid-H_2O, crit. mixture, partial molar vol., temp. depend. 78–18800
  isobutyric acid-water, conc. fluctuation mean relax. time, US absorpt. and vel. meas 80–29163

critical mixtures continued
isobutyric acid-water, US and hyprosonic study 80—88268
isobutyric acid-water critical mixtures, shear viscosity, pseudospinodal curves and scaling 78—22844
isobutyric acid-water mixture, heat of transport, crit. exponent 80—15277
isobutyric-acid-H_2O, crit. fluid, refr. index, α and Δ components 79—82940
liquid, binary, crit. conc. fluctuations, nonexponential decay, 3-methylpentane-nitroethane expt. 80—44309
liquid, near tricrit. pt., light scatt. and sum rules, appl. to ethanol-benzene-water-$(NH_4)_2SO_4$ 80—34933
liquid, near tricrit. pt., thermodynamic model and sum rules, appl. to benzene-ethanol-water-$(NH_4)_2SO_4$ 80—34196
liquid mixtures, critical equilib., gravity effects 77—74340
liquid mixtures, intermol. forces effect on phase diagram and excess props., perturbation theory 80—39287
liquid-liquid mixtures, critical region fluctuations, centrifuging effects 78—63850
liquid-liquid solubility, critical phenomena in binary mixtures 80—54376
2,6-lutidine-H_2O, phase separation, hydrodynamic effects 78—83960
2-6-lutidine-water, anomalous supercooling near critical point 80—70384
2,6-lutidine-water, fluid film, crit. phenomena, scaling, law of corresponding states 79—90787
2,6-lutidine-water, fluid film, crit. temp. shift, crossover temp., coexistence curve amplitude, fluid-boundary interaction 79—90788
2,6-lutidine-water critical mixture, spinodal decomposition, Rayleigh scatt. 80—70416
2,6-lutidine-water thick films, interferometric obs. of crit. behaviour 80—93266
lysozyme-salt water soln., critical mixing point, turbidity and viscosity meas. 77—86437
methane-trifluoromethane, liq.-liq. phase equilib., crit. phenomena 78—18764
methanol-cyclohexane, crit. exponents *(Russian)* 79—77766
methanol-cyclohexane, crit. mixture, single and multiple light scatt., autocorrel. spectroscopy 77—85734
methanol-cyclohexane, mixture, thermal expansion near crit. soln. point 78—71871
methanol-n-heptane, elec. resistance, crit. phenomena, freq. depends. 79—60884
3-methylpentane-nitroethane, binary liq. mixture, crit. correlation function, universality 77—7840
3-methylpentane-nitroethane, correl. function near crit. mixing point 79—55893
3-methylpentane-nitroethane crit. mixture, dynamical scaling for sound propag. 80—49305
multicomponent fluid mixtures, critical phases 77—26258
multicomponent fluid mixtures, renormalised one-chain approx. 77—11452
multicomponent mixtures, phase envelopes and crit. points calc. 80—54337
multicomponent mixtures, tricritical behaviour, possible exptl. tests 77—47543
multiply scatt. light, LF spectrum 77—52125
nitrobenzene, solns., elec. permittivity near crit. point 78—76372
nitrobenzene and n-heptane, US and hypersonic acoustical props. 80—65170
nitrobenzene-hexane critical solutions, crit. exponent determ. by nonlinear dielec. method 79—87373
nitrobenzene-hexane solution, double-scatt. light intensity near critical point of mixing *(Russian)* 80—55117
nitrobenzene-i-octane, with critical point, US dispersion 77—1179
nitrobenzene-n-heptane, conc. fluctuation mean relax. time, US absorpt. and vel. meas 80—29163
nitrobenzene-n-hexane, crit. mixtures, reorientation spectra, linewidths and intensities 79—28777
nitrobenzene-n-hexane, liq. mixture, static and dynamic viscosities near crit. point 77—69108
nitrobenzene-n-hexane, multiply scatt. light, LF spectrum 77—52125
nitrobenzene-n-hexane, shear viscosity, critical conc. fluctuation rate, verification of renormalisation prediction 78—47514
nitrobenzene-n-hexane crit. mixture, depolarised Rayleigh linewidth meas. 77—81112
nitrobenzene-n-hexane crit. mixture, Rayleigh line and depolarised scatt. 77—20864
nitrobenzene-n-hexane critical mixture, shear viscosity meas. 77—72689
nitrobenzene-n-hexane critical mixture, ultrasound absorpt. 77—1178
nitrobenzol-n-hexane, hypersound velocity, absorption temp. depend *(Russian)* 80—75303
nitroethane, cyclohexane and benzene solns., nonlinear dielec. effect 79—78602
nitroethane-3-methylpentane, binary liq., depolarised light scatt. at crit. point 78—39558
nitroethane-3-methylpentane mixture, crit. temp. press. variation 80—15235
nitroethane-cyclohexane, pretransitional effects above phase transition temp., nonlinear dielectric meas. 79—15390
nitroethane-iso-octane(hexane), crit. exponents *(Russian)* 79—77766
nitroethane-isoctane, conc. fluctuation mean relax. time, US absorpt. and vel. meas 80—29163
nitroethane-isooctane, crit. fluid, refr. index, α and Δ components 79—82940
nitroethane-isooctane mixture, crit. temp. press. variation 80—15235
nitroethane/iso-octane, crit. mixture, refractive index 79—87413
nitromethane+CS_2 liquid mixture, elec. resist. crit. phenomena 77—4212
nitromethane-CS_2, elec. resistance, crit. phenomena, freq. depends. 79—60884
nitromethane-isooctane, liq. mixture, coexistence curve, refr. index meas. 80—10655
nitrotoluene-pentane, pretransitional effects above phase transition temp., nonlinear dielectric meas. 79—15390
o-nitrotoluene-saturated hydrocarbon soln., critical exponent, permittivity meas. 78—22858
one-fluid approx. transport coeffs., critical region behaviour 79—14951
pentane-o-nitrotoluene critical solution, nonlinear dielectric effect 78—55952
4-n-pentyl-4′-cyanobiphenyl, isotropic, optical and electrical Kerr effect 79—32886
perfluoromethylcyclohexane-tetrachloromethane, specific heat temp. depend., critical composition mixture near critical temp. 78—26689

critical mixtures continued
phase separation kinetics, percolation effects 80—65233
3-phenylpropanol-hexane, nonlinear dielectric effect, critical exponent 80—93227
polar substance containing, corresponding states principle use in crit. states calc. 80—39196
poly(vinyl methyl ether)-polystyrene mixture, electric field depend. of cloud point temp., laser scatt. meas. 80—6519
poly-γ-benzyl-glutamate, conc. soln., rheology, liq. cryst. transition 79—94574
polyethylene oxide, aq. salt soln., meas.-based thermodynamic quantities 78—75525
polymer solution, intermolecular interpenetration and entanglement, crit. concs. 79—27900
polystyrene, diethyl malonate soln., near-crit., osmotic compressibility, correlation length, scaled functions 80—11422
polystyrene-diethyl malonate, strongly opalescent critical isochore, scattered light intensity 80—71436
propionitrile-hydrocarbon systems, critical solns., Kerr electrooptical Kerr effect meas. 80—100645
PVC-THF-H_2O, precipitation fractionation, influence of stereoregularity 79—7046
Rayleigh line narrowing near critical mixing pt. 79—56803
solutions with closed loop coexistence curves, directionality depend. of lattice models 78—95158
spinodal decomposition in critical fluid mixtures, fluctuation spectrum 78—22825
steam-inert gas, uncondensable gas content effect on steam condensation heat transfer in vert. tube 78—75041
1,2,3,4-tetrahydronaphthalene-H_2O, liq.-liq. phase equilib., crit. phenomena 78—18764
transport properties, theory 78—14497
tricritical points of model fluid mixture 77—31752
triethylamine-H_2O, crit. fluid, refr. index, α and Δ components 79—82940
triethylamine-H_2O, crit. phenomena, US vel. and absorpt. 78—91382
triethylamine-water, critical mixture, specific heat anomaly 79—42268
triethylamine-water, near crit. soln. pt., sp. ht. at const. press. and crit. conc., −1-22°C 78—38847
triethylamine-water critical mixtures, US absorpt. 79—28045
trimethylamine-water critical fluid, ratio of sound dispersion to attenuation 79—55826
water, subcooled, choked expansion and the isentropic homogeneous equilib. model for 2-phase flow 78—91034
water-isobutyric acid, crit. mixture 80—24601
water-isobutyric acid (2,6-lutidine) mixtures, critically quenched, phase separation and coalescence 80—24581
wetting, three phase junction 77—59177
Widom-Rowlinson hard-sphere mixture model, transport props. 80—14981
CS_2-ethanol mixture, Rayleigh and depolarised Raman scatt. lines near crit. temp. 77—20863
CS_2+acetic anhydride, elec. resist. near crit. soln. temp. 78—71874
Cs-NH_3, Cs-ND_3, solns., US absorption, metal-nonmetal transition 79—69194
^3He-^4He, tricritical normal phase liq., ion mobility 78—79850
^3He-^4He films, tricritical behaviour in vicinity of walls 79—51387
Li-ND_3, near liq.-liq. crit. point, conc. fluctuations, neutron diffr. long wavelength thermodynamic limit 79—10948
$(NH_4)_2SO_4$-H_2O-ethanol-benzene, tricritical mixture, light scatt. 79—15473
Ne-H_2 liq. mixtures, phase equilib. effects, thermodynamic perturb. theory *(Russian)* 80—92663
SF_6-Ar, condensing flow, gasdynamic and IR meas. 80—6501
SO_2-tetrachloromethane, solns., near critical point, ultrasound absorpt. obs. 80—65160
^{235}U, ^{235}U systems, criticality anal. using KENO and SU-HAMMER codes 78—89949

critical opalescence
binary mixture in external field, crit. opalescence 78—84595
cyclohexane-methanol, crit. opalescence, AC elec. field effect 78—35159
cyclohexane-methanol, elec. field effect 79—28775
density fluctuations and critical opalescence in a gravitational field 80—66137
dipalmitoyl lecithin vesicles in dil. suspension, light scatt. obs., of phase transitions 77—16915
liquid-vapour transformation, light scattering study, crit. opalescence 80—44307
methane-2,2-dimethylbutane-2,3-dimethylbutane, tricritical point obs., opalescence 77—76562
methane-n-pentane-2,3-dimethylbutane, tricritical point obs., opalescence 77—76562
multiple scattering contribution, dynamical similarity hypothesis 79—8151
nonisotropic medium near critical point, space-time correlation functions of hydrodynamic fluctuations 77—30123
nonuniform fluid state, Van der Waals theory, thermodynamics, struct. and phase stability 79—77475
poly-α-methylstyrene, in cyclohexane, crit. opalescence *(Russian)* 77—62463
polystyrene, diethyl malonate soln., near-crit., osmotic compressibility, correlation length, scaled functions 80—11422
polystyrene-diethyl malonate, strongly opalescent critical isochore, scattered light intensity 80—71436
polystyrene-polyisobutylene, solns., incompatibility, light scatt., crit. opalescence 77—24408
propionitrile-hydrocarbon systems, critical solns., Kerr electrooptical Kerr effect meas. 80—100645
quartz crystal, opalescence near α-β transition, static model rel. to domain wall form. 80—11420
self action of incoherent light beam in a randomly inhomogeneous medium *(Russian)* 78—18025
structure factor, nonuniform fluid, thermodynamical treatment 77—40198
$BaTiO_3$, periodic domain struct. and opalescence at tetragonal to orthorhombic transition 80—66131

critical path analysis
see also project engineering; systems analysis
binary alloys, electronic density of states, generalized cluster-Bethe-lattice approach 79—42432

critical path analysis continued
- fission reactors, BWR, Enrico Fermi-2, system turnover, test and startup program 80—63338
- nuclear power plant, Virgil C., startup, conduct of operations, organisation and personnel 80—63340

critical path scheduling *see critical path analysis*

critical phenomena
- *see also critical fluctuations; critical mixtures; magnetic transitions; phase equilibrium; phase transformations; renormalisation*
- $1/n$ expansion to order $1/n^2$, crit. exponent β for $d=3$ 79—35636
- $1/n$ expansion to order $1/n^2$, crit. exponents γ, ν for $d=3$ 79—35637
- $1/n$ expansion up to order $1/n^2$, critical amplitude ratio R_x 79—58646
- ε expansion for critical amplitude ratio 78—65896
- ε-expansion technique, appl. to integral evaluation in critical dynamics 80—57187
- $\lambda\phi^4$ theory, high temp. expansion, crit. exponent γ calc. 77—2743
- σ model, two dimens., nonlinear, three loop calc., minimal subtraction method 78—62289
- ϕ_1^4 field theory, eigenvalues, Schwinger functions, critical behaviour 77—45931
- ϕ_2^4 multiphase field theory, asymptotic 77—10167
- ϕ^4 field theory, crit. point existence 77—10170
- ϕ^4 fields, critical exponents and elementary particles 77—26243
- ϕ^4 theory, spontaneous symmetry breakdown in finite systems 79—45011
- ϕ^4 theory, three dimens. second order phase transitions, infrared singularities 80—37161
- ϕ^4-model in two and three dimensions, real-space renormalisation for arbitrary single-site pot. 80—22307
- ϕ^6 operators in scalar systems near four dimensions, tricritical scaling and renormalisation 79—58863
- ψ^6 theory, Gell-Mann and Low renormalisation group 77—71439
- Abelian lattice gauge theories, phase transitions 78—12812
- acetone, heat emission in crit. region, press. and heating surface temp. effects *(Russian)* 80—69634
- alloys with competing interactions, phase diagrams and crit. props. 79—40514
- amorphous ferromagnet, thermal cycling and annealing, critical behaviour 79—42790
- amplitude ratio in $1/n$ and ε expansions, consistency 77—67397
- Anderson-Mott transition, crit. dimensionality 80—10876
- anisotropic bond percolation in d-dimens. hypercubic lattice 79—75464
- anisotropic critical line from anisotropic scaling 80—12997
- anisotropic cubic system with long-range interactions, critical behaviour 78—36941
- antiferromagnetic Fermi liquid, critical phenomena, neutron scatt., Neel point *(Russian)* 80—71077
- arbitrary N critical phenomena in three dimens., critical exponents 79—80746
- Ashkin-Teller-Potts model, in two dimensions, renormalisation group study 77—53837
- Ashkin-Teller-Potts model, renormalisation group anal. 79—154
- asymptotic number of lattice animals in bond and site percolation 78—54310
- Baxter and Ashkin-Teller models, critical line correlation functions 80—4681
- Bell-Lavis 2-D bonded lattice model, critical behaviour 79—17356
- Benard instability, critical fluctuation, slowing, optical and acoustic study 79—77075
- Bethe lattice, high density percolation 79—58643
- binary ionic highly dissymmetric mixtures, phase separation 79—46425
- binary liquid mixtures, first order transitions, pseudo-critical slowing down 79—55627
- binary mixtures an and liquid-gas transitions, model for coupling between molecule polarisation and order parameter 78—22823
- biological multiparticle systems; stat.-thermodynamic treatment, phase transitions *(German)* 79—16119
- bistable system, catastrophe prediction using externally applied force 78—77823
- block-cluster approach to percolation 80—161
- bond and site percolation, renormalisation group results 79—149
- bond percolation processes in d dimensions 78—70066
- Bose condensate, bounds in dimensions $\nu\geq 3$ 78—54294
- Bose fluid, interacting, renormalisation group approach 78—45562
- Bose system condensed, crit. behaviour, renormalisation group approach 78—41231
- Bose system passing through crit. point, time evolution 77—37815
- Bose systems, critical exponents, η and z to second order in $\varepsilon=2-d$ at $T=0$ 80—77696
- boson system, λ-transition, renormalisation-group theory 80—143
- boson system, multicomponent, transport coeffs., crit. behaviour, kinetic theory 77—2611
- boson system, scaling equation of state, renormalisation group transformation 78—12643
- Brownian motion of interacting and noninteracting particles in periodic potential driven by external field, analogy 79—2726
- Brownian particle, freq.-depend. friction coeff. in fluid near crit. pt. 78—73929
- Buckingham-Gunton inequality for critical exponents, scaling limits 79—54083
- butene isomers, gaseous, density and temp. effects on electron mobilities 80—33725
- cis-butene-2, high density vapour thermal electron attachment density depend. 79—90369
- capillarity, van der Waals' thermodynamic theory under hypothesis of continuous variation of density 79—56043
- catastrophe theory, violation of certain conservation laws at crit. values of parameters 78—4575
- catastrophes, phase transitions 80—8948
- cell membrane nuclear hydrodynamic shear, non-equil. Ising model, master eqn. 78—61146
- chemical instabilities, rel. to equilibrium phase transitions 78—65897
- chemical reaction, exothermic, criticality, Frank-Kamenetzki parameter, upper and lower bounds 79—66335
- chemically oscillatory systems, critical fluctuation universality, soluble master eqn. 79—75454
- classical fluid, crit. dynamics, double scatt. correction 79—42979
- classical fluid near critical point, nonequilib. steady state fluctuations with laminar shear flow 79—81844
- classical n-vector model, critical temp. shifts 78—36939
- classical n-vector model, eqn. of state in $1/n$ expansion 77—65005

critical phenomena continued
- classical n-vector model, spin-dimensionality dependence of critical parameters 79—40479
- classical n-vector models, d-2 and 4-d expansions 79—30387
- classical system crit. dynamics, Fokker-Planck description 78—21057
- cluster shapes at percolation threshold, cluster dimensionality, reln. to critical point exponents 78—4561
- cluster shapes at percolation threshold, effective cluster dimensionality, connection with percolation critical exponents 79—63166
- coexistence curve of liquid system with global eqn. of state 79—1487
- coexisting phases, interfacial profile near tricrit. points 80—19906
- compressible dilute Ising systems, critical behaviour 80—108017
- conductance network, random, simple, triangular, site percolation, crit. conc., comparison with exact value and Yuge's value 79—12746
- conference, critical phenomena, Sitges, Spain (June 1976) 77—22510
- conference, statistical physics, Budapest, Hungary (Aug. 1975) 77—49664
- conference on dynamical critical phenomena, Geneva (Apr. 1979) 80—27040
- conformal-invariant field theory, anomalous dimensions, coupling consts. 80—4870
- continuous renormalisation transformation, variational calcs., rel. to Potts model 78—93618
- correction-to-scaling amplitudes on coexistence curve 80—57234
- correlation functions in X-Y models and step free energies in roughening models 78—67675
- Coulombic fluid, correlation function critical behaviour Ornstein-Zernike theory 79—1957
- coupled order system in $1/n$ expansion, fixed points critical exponent ϕ^4 theory 78—4578
- critical exponents by quantum field theory methods *(Russian)* 80—4869
- critical exponents to order ε^3 for ϕ^3 models of critical phenomena in $6-\varepsilon$ dimensions 80—86547
- critical fluids, droplet model 77—53846
- critical indices, conformally invariant bootstrap method 79—12955
- critical principal connections and gauge-invariance 79—6287
- critical scattering theory, book 79—25913
- crossover exponents, crit. behaviour of quadrupole ordering parameter 77—66339
- crossover scaling functions for two-point correlations near tricritical points 79—40510
- cubic crossover, approx. renormalisation group calc. 77—49701
- cyclohexane-aniline mixture, shear induced transition to mean-field crit. behaviour 80—7364
- cylindrical shell deform., effect of loading history on bifurcation *(Ukrainian)* 78—55578
- d-dimens., quantal spin systems, reln. with $(d+1)$ dimens. Ising systems 77—16031
- decimation transformation for 2-D and 3-D systems 78—12649
- decimation transformations in lattice systems of continuous spins 79—25997
- decorated lattice gas model of critical phenomena in fluids and fluid mixtures, review 78—36944
- Dicke model for multi-level systems, thermodynamic critical behaviour 77—61038
- dielectric liquid, isomorphism in crit. phenomena 79—33649
- diffraction catastrophe patterns, two dimens., caustics anal. 77—17827
- diffusion in the one-dimensional Ising model 80—77719
- dilute ferromagnet, Ising model, crit. props. in percolation limit 79—1677
- disordered, two-dimens. Ising models, real space renormalisation group 79—42788
- disordered spin system 79—40516
- disordered systems, renormalisation-group approach 77—5784
- divergent series summation by order depend. mappings 79—88819
- dual resonance amplitudes, satisfactory invariant measure 78—66093
- dynamic crit. phenomena and renormalisation group, appl. to lattice dynamic model 77—22515
- dynamic critical exponents, inequalities 80—79662
- dynamic critical phenomena, real-space renormalisation group methods, appl. two-dimens. kinetic Ising model 78—77810
- dynamic critical phenomena 77—82477
- dynamic critical phenomena closed-form differential renormalisation group generator 78—86413
- dynamic models, scale transformations 77—22513
- dynamic scaling near lambda point of liq. He and at bicritical points 80—15321
- dynamical scaling. mode coupling, and dynamic renormalization group, book contrib. 79—60480
- dynamical systems, critical transition to stochasticity 80—73265
- dynamical systems, global first integrals, connections with critical phenomena 78—32667
- dynamics in Fokker-Planck formalism 77—22514
- Dyson's hierarchical model, critical isotherm 77—59370
- Dyson's hierarchical model, critical props. 79—40481
- Dyson's hierarchical model, one-dimens., crit. props. 77—79038
- effective critical exponents in spherical limit 79—12749
- effective medium approach to real space renormalization 79—80539
- elastic phase transitions, crit. dynamics 80—2146
- elastic transitions of second order, dynamical renormalisation group method 79—40512
- elastically coupled systems at marginal dimensionalities, crit. dynamics and stability 80—101769
- electronic transport coeff., soln. between Mori-Green-Kubo formulae and Boltzmann approx. 78—79971
- energy density fluctuation, at fixed wavevector, max. below T_c 79—69225
- excitonic phase transition in mag. field, quantum renormalization group 79—87045
- experiments in orbiting laboratory 79—67278
- explosion, thermal, crit. parameters analysis 80—11891
- exponent renormalisation, first order transition 78—70085
- ferroelectrics, uniaxial, critical behaviour studied via renormalisation group theory 78—8367
- ferromagnet, impurity spin critical dynamics 80—2593
- ferromagnet, Ising-Heisenberg-XY crossover, bicritical point, partial differential approximants for susceptibility series 77—85466
- Feynman-Wilson gas, statistical model for multiparticle physics 79—22071
- field theory in $2+\varepsilon$ dimensions, critical dimen. in string model 77—57503
- field-theory approach to crit. dynamics far from equilib. 77—57295

critical phenomena continued
- field-theory renormalization and critical dynamics above T_c: helium, antiferromagnets, and liquid-gas systems 78—87767
- finite size scaling theory, static, dynamic, based on renormalisation group approach, critical phenomena exam. 78—16745
- first order transition and critical behaviour, mean-field theory, master eqn. and nonlinear Fokker-Planck eqn. 78—8375
- first-order transition induced by cubic anisotropy 79—4688
- Fisher renormalised Ising exponents in compressible spherical model 77—30113
- Fisher-Domb cluster model, pseudospinodals in first order transitions 80—57213
- fixed-point interactions with wave vector depend. struct. 77—65000
- fluid, critical maxima and minima of thermodynamic functions 77—27974
- fluid, dynamic droplet model, freq. and temp. scaling 78—26625
- fluids, crit. pt., scaling and extended scaling eqns. of state implementation, program 79—46780
- fluids, critical-point universality 78—22826
- fluids in steep field gradients and near critical points, hydrostatic density distrib. 77—76523
- frequency splitting, gauge invariant, of continuum Yang-Mills field 77—87905
- gases, chem. pot. near crit. density, Thom's catastrophe theory 78—91063
- Gaussian random field, ferromagnets in $4+\varepsilon$ space dimens. 78—73954
- Gaussian-Heisenberg crossover behaviour, cutoff corrections 77—79042
- geometrical aspects of statistical physics, scaling and fractals 79—58625
- Ginzburg-Landau field, eqn. of motion and nonlinear response near critical point 77—15991
- Ginzburg-Landau model, crossover and scaling at low temp. 77—61023
- Glauber-Ising model, 2-dimens., crit. dynamics, real-space renormalisation group theory 78—70070
- Glauber-Ising model, real space-time depend. renormalisation group 78—49774
- graph-like state of matter, electrical cond. of random networks, gelation and elasticity 78—65875
- gravity effects in fluids near the gas-liquid critical point 79—58667
- hadronic matter, statistical bootstrap model and critical behaviour 80—42430
- Heisenberg model, crit. behaviour, Bose expansion 79—42785
- hierarchical model, ε-expansion anal. 77—71284
- hierarchical model, renormalisation group approach 80—34580
- high energy physics, conf., Schladming, Austria (Feb.-Mar., 1977) 78—8494
- honeycomb bond lattice, renormalisation group approach 79—85089
- hydrodynamic contrib. to two-time correlation functions, using nonequilibrium distrib. function 77—49703
- hyperscaling and the critical exponent ν 79—80747
- impurity effect, critical exponent 80—36961
- induced moment systems, effect of spin fluctuations 80—2585
- interface, noncritical, near a crit. end pt., struct. and tension 77—84885
- interline region heat transfer, London-Van der Waals dispersion force effect 78—71276
- invariance of critical exponents for renormalisation groups generated by flow vector 77—67402
- ionic fluids binary mixtures, critical conc. fluctuations 78—34596
- ionic mixtures phase separation, critical parameters 80—77279
- irregular networks, self-avoiding walks, critical parameters 77—20607
- Ising, quenched dil. random-bond model, CPA difference eqn. and crit. curves 80—2584
- Ising chain in transverse magnetic field, SLAC renormalisation group approach 79—67476
- Ising ferromagnet, crit. correlation-function approxs. 78—56324
- Ising ferromagnet, equivalence of different order parameters 77—36082
- Ising ferromgnet, rectangular, n-point functions 78—76250
- Ising lattice, collective excitations in 1-D systems with extended interactions 77—65006
- Ising lattice, two-dimens. finite square, sp. ht. anomaly 80—27230
- Ising lattices critical behaviour, stochastic model simulation method 77—45804
- Ising mean cluster size near T_c, exponent interpretation 77—37820
- Ising model, adiabatic susceptibility and specific heat at const. magnetisation 80—7114
- Ising model, compressible, crit. behaviour, applic. of renormalisation group methods 77—82464
- Ising model, correlation length, renormalisation group calc. *(Russian)* 78—77811
- Ising model, cubic, site impure, crit. behaviour 77—66357
- Ising model, duality relations and replica method 80—77722
- Ising model, high-temperature low field expansions extension 79—93045
- Ising model, kinetic, Migdal type renormalisation group calcs. 79—93069
- Ising model, kinetic, nonlinear crit. relax. 77—32140
- Ising model, one-dimens., real-space renormalization group 79—15317
- Ising model, Percus-Yevick type approx. 78—148
- Ising model, phase transition near percolation threshold 77—33956
- Ising model, quantum-classical crossover crit. behaviour in transverse field 77—5766
- Ising model, renormalisation group calcs. on critical phenomena 80—42171
- Ising model, spin-one system, correlation functions with bilinear and biquadratic interactions 78—91876
- Ising model, three dimens., critical indices, high temp. series anal. 80—22295
- Ising model, two dimensional, second neighbour interaction, Pade approximant, critical behaviour 79—4682
- Ising model, two point correlation, renormalisation group methods 78—8353
- Ising model, two- and three-dimens., cumulant expansion for renormalisation transform. 77—49691
- Ising model, two-dimensional kinetic, dynamic correlation functions, real space renormalisation group approach 80—62589
- Ising model critical region two-point correl. function, quantum field theory 77—69471
- Ising model in 3-D, critical exponent γ 79—12727
- Ising model in 4-D, critical isotherm 79—44871
- Ising model kinetic, finite size effects in critical dynamics 80—46990
- Ising model on square and triangular lattice, variational renormalisation group method 78—16740
- Ising model simulation, random mixture critical props. 77—69573

critical phenomena continued
- Ising model with nearest and next-nearest neighbour interactions, nonuniversality 79—44870
- Ising model with second neighbour and four body interactions, thermostatistical props. 80—31682
- Ising models, three-dimens., renormalisation group transform. 78—62163
- Ising n-spin correlation function for 2-dimens. model in quantum field theory 77—37821
- Ising n-spin correlation functions for 2-dimens. model in quantum field theory 77—37821
- Ising site model, random mixtures, Monte Carlo simulation 78—73935
- Ising site model, random mixtures, Monte Carlo simulation 78—73936
- Ising spin 1/2 model, confluent singularities and hyperscaling 79—73655
- Ising spin $^1/_2$ model, renormalisation group approach 80—2582
- Ising system, exactly soluble with new boundary conditions 77—85472
- Ising system, periodically layered, cooperative effects in crit. phenomena in sp. ht. 78—23284
- Ising system, two-dimens., transverse field crit. props., renormalisation and scaling 78—21080
- Ising system, two-state, crit. behaviour, Bragg-Williams approx. calcs. 78—86223
- Ising system, with lattice anisotropy, two dimens., crit. props. 78—73932
- Ising system on triangular lattice, critical dynamics, time dependent real-space renormalisation group 78—60289
- Ising systems, coupled, variational renormalization group approach 77—2616
- Ising triplet model, numerical evidence for two critical points 77—37819
- Ising two-dimensional spin systems, decimation transforms. 77—77017
- Ising-system, two-state, crit. behaviour, Monte Carlo calcs. 78—86222
- isobutene, droplet nucleation from crit. gas-phase+positive ions 79—39222
- isotropic N-component spin systems with long and short range interaction, critical behaviour 80—54907
- isotropic spin systems, with long and short-range interactions, crit. exponent η 77—65013
- Kagome lattice, renormalisation group approach 79—85089
- kinetic Ising model, quenched relaxing impurities, critical dynamics 79—40484
- kinetic Ising model of ferromagnetism, simulation of equilib. critical props. 78—89410
- Landau-Ginsburg model, droplets free energy, Jost function 79—40469
- Landau-Ginzburg-Wilson model, 2 and $2+\varepsilon$ dimensions 78—36940
- laser theory, statistical mechanics of open systems *(Japanese)* 79—76658
- laser theory, statistical mechanics of open systems *(Japanese)* 79—76659
- lattice animals, critical dimension 80—57208
- lattice dynamic model, renormalisation group 77—2624
- lattice gas model, critical cond., rel. to cond. in superionic conductors 78—93614
- lattice gas model, double spin 1/2, for mag. annealed binary alloy and nematic mixture 77—66342
- lattice gas of big interacting mols., phase transitions *(Russian)* 79—157
- lattice Higgs models, (non)Abelian, diamag. and crit. props. 79—67465
- lattice renormalisation group and thermodynamic limit 78—8359
- lattice Schwinger model, massive QED for fermions in 1+1 dimens. 78—78121
- lattice spin systems, matching conditions for crit. props., group struct. of block transforms 80—22305
- lattice-lattice scaling, reln. to scaled eqn. of state, appl. to Ising model 78—70067
- lattices of effective nonintegral space dimensionality, critical behaviour 77—49688
- layered periodic system, crit. temp., 1/n expansion 79—40519
- Lennard-Jones gas, Ising model, critical parameters from cluster integrals 77—11297
- Lifshitz point, crit. exponents calc., k-space instability on λ line 77—65014
- Lifshitz point, critical wavevector 78—36954
- Lifshitz point, low-temp. renormalisation group 78—65898
- linear Ising chain, differential real space renormalisation 79—85092
- liquid mixtures, critical equilib., gravity effects 77—74340
- liquids, acoustic absorption near critical points 79—95082
- liquids, summer school, Aleria, Corsica, France (Sept. 1977) 80—6339
- local critical properties, near isolated impurity 78—6142
- local equilibrium theory for steady states with heat flow near critical points 80—105599
- localisation of particle moving in given pot., renormalisation group theory 77—66135
- logarithmic corrections to a simple power law at $d=4$ in 1/n expansion 78—65895
- long-range site percolation, crossover from mean-field to crit. behaviour 80—82728
- low temperature critical phenomena, review 80—73297
- low-temp. approach to renormalisation-group eqn. for lattice of discrete spins 77—61030
- 2, 6-lutidine-water mixture, phase separation near crit. point, spatial and temporal fluctuations 79—82346
- magnetic disordered systems, Monte Carlo anal., review, book contrib. 79—82809
- magnetic systems and mixtures, phase diagrams, Monte Carlo studies, book contrib., review 79—82313
- magnetism, spin-S Heisenberg model mapped onto interacting Bose field 79—47291
- magnetism and magnetic materials, conference, Cleveland, USA (Nov. 1978) 79—73651
- magnets, randomly distributed point defects, critical exponents, renormalisation theory 80—60346
- Malthus-Verhulst process, crit. point calcs. 80—42176
- master eqn., dynamical renormalisation group transform., Ginzburg-Landau model, kinetic Ising model 80—42170
- Meissner effect in gauge fields 78—29250
- metastable states close to instability, phase transition parameter eqn. of motion 80—57230
- mixed, spin-$^1/_2$ Ising ferromagnet, crit. props. 80—34655
- models and mathematics of quantum dynamics, conf., Bielefeld, Germany (Sept. 1975) 77—10158
- modern theory, including renormalisation group, graduate level text 77—102
- modified F model, rel. to nearest-neighbour Ising model, crit. polarisation 79—93058

critical phenomena continued
- molecular thermodynamics appl. to phase separation and critical phenomena *(German)* 78–14447
- Monte Carlo methods in statistical physics, book 79–80528
- Monte Carlo studies, surface physics appl., book contrib. 79–82426
- Mossbauer radiation scatt. by condensed matter, review 79–78596
- Mott transition, spin glass description 79–65386
- multicomponent fluid mixtures, critical phases 77–26258
- multicomponent systems, critical props. prediction from eqn. of state 77–57289
- multicritical phase transitions, review 79–30385
- multiplicative renormalisation group, relation to critical phenomena in phase changes *(Hungarian)* 77–54042
- n-component compressible model with cubic anisotropy, critical behaviour RG calc. 78–145
- n-component spin system, anisotropic Brillouin zone, Wilson-Feynman graph technique, universality 77–5764
- n-vector lattice spin model near two-dimens., crit. temp. 77–8324
- n-vector model, n=0 limit, zero field susceptibility and pair correlation function 79–97332
- n-vector model, stochastic, dynamic critical props. 77–24362
- n-vector model in 3-dimens., critical exponents from field theory 77–67398
- neutron star matter at high temp. and density, bulk props. 78–89812
- non-equilib. instability, k=0 hard mode transition, appl. of dynamic renormalisation group 79–21686
- non-ideal systm, generalisation of scaling hypothesis 79–19356
- non-uniform system, crit. behaviour 78–12660
- nonequilibrium critical phenomena, probability density functions, fluctuations 78–54327
- nonequilibrium open systems, phase transitions, expt. studies, review 79–75483
- nonisotropic medium near critical point, space-time correlation functions of hydrodynamic fluctuations 77–30123
- nonisotropic systems near liquid-vapour critical point, similarity hypothesis, gravitational effects 80–17913
- nonlinear relaxation and fluctuation 79–30373
- nonuniform external force field effects 80–73296
- nuclear critical opalescence, percursor to pion condensation 78–62498
- nuclear dense matter phase transitions, cusp catastrophe theory 77–22920
- nucleation near a critical temperature 79–80553
- $O(1/n^2)$, critical indices for 3-dimens. system with short range forces 78–49775
- O(n)-symmetric systems dynamic crit. exponents, renormalized field theory 79–12754
- one-particle-irreducible renormalisation group generator for crit. phenomena 77–82475
- order parameter, n-component, of O(n)-symmetric system, crit. dynamics renormalised field theory 77–22509
- Pade approximation method as renormalisation group method 80–17909
- percolation, universal critical amplitude ratios 80–101765
- percolation cluster sizes and perimeters, scaling form 79–2728
- percolation clusters, as teaching aid for Monte Carlo simulation and crit. exponents 78–12477
- percolation clusters, teaching film 79–58509
- percolation clusters and lattice animals, similarity laws for density profile, Monte Carlo data anal. 79–44881
- percolation in 3-D, renormalisation group approach 80–22299
- percolation problem, high order behaviour in 0^3 field theories 78–65883
- percolation problem, microscopic similarity theory *(Russian)* 77–2634
- percolation problem, universality, anomalous dimensions of ϕ^4 operators 77–79045
- percolation processes in three and more dimens. 77–65007
- percolation theory, bond problèm, critical probabilities, bond clusters 78–86224
- percolation theory, review 80–98868
- percolation theory at the critical dimension 79–152
- percolation threshold of heterogeneous system 79–42889
- perfluoromethylcyclohexane-tetrachloromethane, specific heat temp. depend., critical composition mixture near critical temp. 78–26689
- perturbation theory, large-order behaviour, critical exponents, Callan-Symanzik eqns. 79–30397
- phase behavour of multicomponent fluids, method of pseudocomponents 77–59094
- phase transformations in intermediate spherical model 79–30403
- phase transition in 2-D sine-Gordon system 79–12736
- phase transition theory, renormalization group method 77–80601
- phase transitions, external constraints, critical indices 77–33967
- phase transitions, influence of interaction energy terms quadratic in deformation 77–37836
- phase transitions, percolation clusters and lattice animals 79–6057
- phase transitions and critical phenomena, recent developments 77–87713
- phase transitions at tetracritical point, Landau theory *(Russian)* 79–17379
- phase transitions in strongly random systems, review 79–58647
- physics of transitions, introduction 78–26660
- planar-rotator model with short range interaction 79–80540
- plane rotor model, static and dynamic crit. behaviour, Monte Carlo simulation 79–38334
- polycritical point vicinity, scaling 77–45815
- polymer solutions, free energy of mixing, modelling, critical exponents 80–44106
- polymer solutions, tricritical effects, small angle neutron scatt. studies 79–41939
- polymer statistics of long chains in solns. or melts 79–31758
- Pomeron and critical temp. 79–12982
- pomeron and critical temperature 79–3003
- position space renormalisation of spin systems with long-range forces, critical exponents 78–24755
- position space renormalizations and the breakdown of hyperscaling 79–40482
- position-space renormalization approach 79–30404
- Potts model, appl. of Legendre transformation 78–80156
- Potts model, crit. behaviour, renormalisation group calcs. *(Russian)* 79–6059
- Potts model, critical dynamics 80–101766
- Potts model, dilute random bond, critical curve 80–80518
- Potts model, quenched bond disorder, single-bond effective interaction approx. 80–27229

critical phenomena continued
- Potts model, three-state, high field series expansions and critical props. 79–85090
- Potts model, triangular, at transition temp., related models 78–8358
- Potts model, triangular, with two- and three-site interactions 80–36951
- Potts model, zero state, in $2+\varepsilon$ dimensions, crit. exponents 78–77809
- Potts model and percolation 78–54312
- Potts model on square lattice, specific heat critical exponents 77–20606
- Potts s-state model, exact critical surface on triangular and honeycomb lattices 79–148
- probability theory, for critical point behaviour 79–44889
- pseudo-critical dynamics in first-order transitions 79–71391
- pseudocritical phenomena near the spinodal point 78–65894
- pure component liquid-vapour transition, two component decorated lattice gas model 79–35650
- q-state Potts model multicritical point, singularities and scaling functions 80–57215
- quadratic lattice, correlated percolation 80–68149
- quantum spin model, appl. of projective renormalisation group 80–84607
- quantum spin systems, exact boson representation and crit. behaviour 79–78423
- quantum X-Y model, crossover scaling near zero temp. 79–28535
- quenched critical fluid, time evolution of fluctuation spectrum 78–65893
- quenched random spin systems, dynamical replica methods, nonequilib. critical phenomena 78–43602
- random fields, lowering of dimensionality in phase transitions 77–17923
- random resistor network, scaling and critical behaviour near percolation threshold 77–41545
- random resistor networks, critical behaviour near percolation threshold 78–87956
- random spin system, 1/n expansion 78–62173
- random spin systems with long-range interactions, critical behaviour 78–36942
- random system, absence of long range order, classical X-Y model 77–30103
- real fluids, static and dynamic crit. phenomena, theory, summer school lecture series 80–6344
- real-space renormalisation group approach, Migdal approx. 79–63088
- real-space renormalisation group study of crit. dynamics 78–49785
- recurrence technique for confluent singularity analysis of power series 80–73277
- Reggeon field theory, critical exponents calc. by convergent numerical method 77–45991
- Reggeon field theory, critical Pomeron intercept with block-spin methods 79–71615
- Reggeon field theory on a lattice, critical behaviour, Monte Carlo calc. 80–18126
- Reggeon quantum spin model, critical exponents 78–62338
- relaxational dynamics, renormalisation group anal., scaling fields and variables 80–105602
- relaxational dynamics in systems with many-component order-parameter, scaling fields and variables 80–101772
- renormalisation group, invariance props. of crit. exponents 77–22512
- renormalisation group, scale breaking model 78–49972
- renormalisation group applications 77–57296
- renormalisation group approach to critical phenomena, ferromagnetic example 78–8497
- renormalisation group eqns. in large-n limit, nonlinear solns. 77–61039
- renormalisation group equations in critical dynamics, scaling far from equilib. 77–28395
- renormalisation group theory, critical props. of generalised 2D Ising model 80–4665
- renormalisation group theory, general principles of phenomenological theory 80–4663
- renormalisation group theory, numerical method for calc. of free energy and correl. length of generalised Ising model 80–4664
- renormalisation group theory rel. to hamiltonian symm. *(Russian)* 77–11666
- renormalisation group transformations *(Chinese)* 78–95128
- renormalisation theory, variational principles 78–73951
- renormalization transformations for quantum spin systems 79–40511
- resistivity of mag. solids 79–42213
- retarded Josephson eqn., critical limit cycles 79–1644
- Riemann-Hugoniot catastrophe and P, ρ, T surfaces of real gases 79–6066
- Riemannian curvature and classification of Riemann and Ricci tensors in space-time 80–36914
- rocks, partially melted, rheology 78–32080
- roughening transition, crit. slowing down of solid on solid cryst. surface model 77–5773
- roughening transition in one dimension, dynamics at low temps. 80–159
- scale invariance and critical phenomena 77–22511
- scaling and multiplicative renormalising in solid state physics, review *(Hungarian)* 79–11289
- scaling critical exponents with neglect of cutoff, dimensional anal. 79–93087
- scaling properties of models of nonequilibrium phenomena, 't Hooft renorm. group method 79–26015
- scaling relations, dynamic, linear and nonlinear, in renormalisation group theory 77–8321
- scaling relations in mag., mechanical and superconducting pinning theory 77–76403
- second order transformations in ideal and disordered systems *(German)* 79–40508
- second-order expansion of indices in the generalised Villain model 80–90801
- segregation of two molten polymers of different lengths, critical props. 78–55801
- self-avoiding lattice walks, renormalisation by non-linear transforms. 79–75468
- self-avoiding walks on the hyper face-centred cubic lattice in four dimensions 79–17355
- self-consistent screening approximation, long range interactions and the critical exponent η 80–101761
- semi-infinite system n-vector model in large-n limit 77–41557
- semi-infinite systems, critical behaviour 78–4563
- series analysis methods, integral approx. methods, appl. to Ising model susceptibility 79–71392
- simulation, using Wien bridge oscillator, threshold instabilities 77–1211
- sine Gordon theory, equivalence to z-dimens. ferromag. classical X-Y model low temp. behaviour 77–13873

critical phenomena continued
- smectic A to nematic phase transition, critical dynamics 79—1493
- smectic A-nematic transition, defect model, crit., director fluctuation 79—14916
- solitons in condensed matter physics, theory 80—50122
- solution, binary, and pure material, isomorphism of crit. vapour form phenomena *(Russian)* 77—13723
- space environment applications for critical phenomena and condensation, second order phase transformations 79—46783
- spherical and mean spherical models, correlation phenomena 77—74327
- spherical limit of coupled time depend. n-vector models, relaxation phenomena 80—86238
- spherical model, nonlinear critical dynamics 77—22506
- spherical model on hypercubic lattice modified 1/d expansion for critical temp. 77—2621
- spherical model with layered impurities, critical behaviour 80—93124
- spherical models, critical behaviour 77—61025
- spherical random field model, low dimensionality for transition 80—68150
- spin, discrete cubic model, displacive phase transitions 77—32198
- spin lattice models, continuous-integral method 78—93615
- spin system, isotropic, critical behaviour with long-range interaction 77—89966
- spin system, isotropic, N-component, with long- and short-range interactions, crit. behaviour 78—76256
- spin system, Wilson's renormalisation group recursion eqns. 78—4581
- spin systems, crit. behaviour at $n=-2$ 78—43600
- spin systems with long-range interactions 79—40515
- spin-1/2 models, on square lattice, sublattice renormalisation transformations 78—65878
- spinodal line in constrained systems 79—40520
- square site percolating system, renormalisation group approach 78—41241
- stability of critical behaviour, critical-exponent renormalization and first-order transitions 79—44895
- statistical equality connecting zero Fourier harmonics with average quantities 80—133
- steam critical behaviour of thermodynamic potential 80—42175
- stochastic eight-vertex model, universality in critical dynamics, Ising model appl. 78—41246
- stochastic n-vector model below T_c, critical dynamics 78—36959
- stochastic n-vector model dynamic crit. props. 77—45805
- structural phase transformations, static critical behaviour 80—92640
- structural phase transition, intrinsic and extrinsic central peak properties, review 80—34168
- structural phase transitions, crit. dynamics and quasi-elastic scatt. 80—92641
- structural stability in physics (conference, Tubingen, Germany, May and Dec. 1978) 80—8739
- structure of the BBGKY hierarchy near phase transition 80—88013
- superconductors, critical slowing down, dynamic-exponents, Ginzburg-Landau theory 80—103783
- superfluidity and the two dimensional XY model 79—28498
- surface critical exponents in terms of bulk exponents 77—49702
- surface percolation processes, scaling theory and real space renormalisation group 80—86223
- Takagi model, critical and tricritical behaviour using double-time Green's functions 77—45816
- thermal radiation, critical phenomena for periodically rough water surface *(Russian)* 78—81188
- thermodynamic properties, crit. behaviour, correction-to-scaling amplitudes, crit. exponents 80—57233
- three dimensional system with short-range interaction, critical exponents calc. 80—42348
- three-dimensional flow problem, calc. of crit. indices *(Russian)* 77—82474
- three-dimensional model, cubic anisotropy effect 78—10170
- threshold-phase transition analogy 78—70081
- time-local gaussian processes, path integrals and nonequilib. nonlinear diffusion 77—13726
- topological excitations in Abelian Higgs model 78—70275
- transformation methods in anal. of crit. prop. 78—49771
- transport coefficients near critical point, dynamical spherical model 77—49695
- transverse Ising model, dipolar interaction, crit. relax. function 79—40487
- triangular lattice bond problem, series expansion study of percolation probability 79—2727
- triangular spin lattice, renormalisation theory anal. of triplet interactions 77—5771
- tricritical behaviour, nonuniversality 78—93640
- tricritical coexistence in three dimensions, multicomponent limit 80—19907
- tricritical phase transition, critical exponents, classical N-component spin systems 78—4579
- trifluoromethane, dielectric const. near critical point 79—15394
- triplet Ising model on triangulated dice lattice, phase transitions 77—17918
- turbulence, crossover dimensions 79—50713
- two dimensional percolation, crit. amplitudes, universality test 77—13727
- two dimensional XY model, critical behaviour review 80—52149
- two thermodynamic phase interface and critical behaviour, surface fluctuation dynamical symmetry 79—97333
- two-dimensional anisotropic N-vector models 79—85095
- two-dimensional quantum systems at zero temp., liquid to gas phase transitions 78—77798
- two-dimensional systems, crit. percolation behaviour, renormalisation-group approach 79—4396
- two-spin correlation function, dipolar crossover 80—80516
- universal relations among crit. amplitude, calc. up to order ε^2 for systems with continuous symm. 77—17936
- universal relations among crit. amplitudes 77—66341
- universality hypothesis in classical statistical mechanics 79—12712
- Universe, spontaneous prod. of cosmological fluctuations 80—94902
- Van der Waals fluid near critical pt., transport props. 79—46537
- van der Waals theory, renormalisation 77—17935
- water, Ising lattice model with directional bonding, renormalisation group study 80—28894
- Wilson and Wegner-Houghton generators, equivalence at arbitrary anisotropic fixed points 77—22507

critical phenomena continued
- XY model, $S={}^1/_2$, in transverse field in two and three dimensions, zero temp. renormalisation group method 80—108025
- Z(N) topological excitations in Yang-Mills theories: duality and confinement 79—12938
- zero field susceptibility in $d=4$, $n=0$ limit, confluent logarithmic singularities 78—54308
- zero-component field theories, high order behaviour without $n\to0$ limit 79—75438
- zero-temperature phase transition in rigorously solvable model, crit. exponent and scaling law 79—11321
- ϕ^3 field theory in $6+\varepsilon$ dimensions, anomalous dimens. calc. 78—134
- ϕ^4 3-D field theory, IR behaviour and connection with critical phenomena 79—71601
- ϕ^6 theory, Gell-Mann and Low renormalisation group appls. 78—29224
- Gd, thermal conductivity critical behaviour near Curie point 80—75540
- $g\phi^4$ model, large-order behaviour of the 1/N expansion in zero and one dimensions 79—58862
- He, density correlation function and dynamic transient exponents at and above T_λ 79—51325
- ^{3}He-^{4}He liquid mixtures, holographic obs. of diffusion waves 79—60595
- ^{3}He-^{4}He mixtures, tri-critical phenomena, Callan Symanzik study of $\lambda\phi_3{}^4+g\phi_3{}^6$ theory 77—35788
- ^{4}He, superfluid, film thinning during crit. and subcrit. flow 80—20002
- ^{4}He, superfluid, thermo-osmotic convection, at incipient lambda transition, above crit. press. 78—95199
- ^{4}He, transients in critical dynamics 79—40513
- MnF_2, mag. susceptibility, crit. behaviour near Neel point 79—91217
- ND_4Cl, ultrasonic exam. near order-disorder transition, elastic consts. 79—46799
- NH_4Cl, molar heat capacity near order-disorder transform. under high press. 78—51697
- Ni-H system, phase diagram and thermodynamic properties calcs. 80—66480
- Pd-H system, phase diagram and thermodynamic properties calcs. 80—66480
- SF_6, critical isochore, dielectric const. critical anomaly upper bound 80—84679
- $SrTiO_3$, critical elastic compliance, acoustic resonance meas. 80—65118
- Xe, light scattering, in crit. region, scaling interpretation 79—46420

critical points
- *see also boiling point; melting point*
- ϕ^4 field theory with Gaussian propagation in three dimens. 80—4686
- acetonitrile, Rayleigh linewidth, in crit. region 79—24329
- acrylamide gel, spinodal line and critical point, light scatt. meas. 79—79315
- adsorbed monolayer of orientable molecules, lattice fluid model, real-space renormalisation group method 80—17882
- air flows in triple point shock configurations, anal. thermodynamics *(Russian)* 79—32569
- alkali halides, molten, crit. consts. calc., dense gas formulation 80—44100
- alloy, FCC closed packed, ordering-type transitions 80—2140
- alloy between ferromag. and antiferromag. species, competing order parameters, Bethe-Peierls approx. 77—48003
- alloys, binary, BCC, order-disorder transform., three-body interaction effects 80—39257
- alloys, binary, elec. resist. near crit. point 80—96847
- analytical method for determ. from expt. data on $\rho_s(T)$ boundary curve 77—15539
- aniline+cyclohexane critical mixture, gravity-induced concentration gradients 77—28004
- aniline-cyclohexane, viscosity conc. and temp. depend. in crit. mixing region 77—35686
- anisotropic spin system, field theoretic approach to bi-critical point 79—40518
- antiferroelectrics, multicritical points in structural phase transitions, renormalisation 80—75982
- antiferromagnets, disordered spin flop, bicritical behaviour, critical experiments 80—65899
- aspirator saturator, performance, dew point data of air *(Japanese)* 79—40580
- asymmetrical Ising model, phase transitions 80—17891
- BCC Ising model with competing interactions, fluction-induced first-order transition 80—20424
- benzene, gas, liq. and crit., cation mobility 80—48842
- benzene, soln., light deflection, near crit. point, due to gravitational effect 78—2818
- benzene, tables of thermodynamic props. 77—24419
- bicritical point crossover, asymptotic behaviour of a field theory with quadratic symmetry breaking 79—1488
- binary critical mixture, critical turbidity, kinetics, press. jump investig. 77—47548
- binary fluid, molecular dynamics 80—88014
- binary fluids, universal const. $R_\xi{}^+$ meas. 80—19952
- binary lattice gas, crit. phenomena, cluster expansions and transcriptions 80—4670
- binary lattice gas, crit. phenomena, series anal. 80—4671
- binary liquid mixture, critical conc. determ. from dielectric const. meas. 77—20788
- binary liquid mixtures near crit. pt., nonlinear dielectric effect 78—23384
- binary mixtures and simple fluids near crit. point, Rayleigh and Brillouin scatt. 77—36256
- binary ordering alloy, theory of surface effects 79—19434
- binodal decomposition near crit. point, scaling hypothesis 80—79912
- block-cluster approach to percolation 80—161
- boson systems, dynamical plane rotator model, dynamical correl. functions in mol. field approx. 80—88758
- β-brass order-disorder transition, crit. temps. and exponents rel. to composition 77—8818
- Brownian diffusion, in fluid near its critical point *(Russian)* 77—22496
- Brownian motion of interacting and noninteracting particles in periodic potential driven by external field, analogy 79—2726
- catastrophe polynomials, thermodynamic phase diagrams 80—8946
- catastrophe theory, phase diagram classification 80—22313
- charged hard sphere dense classical fluid, equation of state and crit. point 80—64849
- chiral field, BPHZL renormalisation and 1/N expansion and critical behaviour 80—52383

critical points continued
o-chloroaniline-iso-octane, crit. system, comp. depend. of absorpt., US obs. *(German)* 80−19879
o-chloroaniline-n-heptane, crit. system, comp. depend. of absorpt., US obs. *(German)* 80−19879
chlorotrifluoromethane, self-diffusion coeff. near crit. temp., density depend. obs. 78−95530
classical and quantum lattice systems critical lengths and critical temp. estimates 79−56556
classical fluids, thermodynamic behaviour near crit. point, book contrib. 79−60479
classical fluids in crit. region, generalised perturbation theory 79−77474
coexisting phases, interfacial profile near tricrit. points 80−19906
Coulomb gas 2-D, interaction potential, screening length, critical temp. 80−62571
Coulomb gas in d-dimensions, roughening transition 77−89718
crystal lattice stability and deform. phase transitions under press. 80−59624
cubic margules solution model, miscibility gap and crit. point behaviour 78−59925
cubic Margules solution model, miscibility gap and critical point 79−65199
cyclohexane, vap. press. from 451K to crit. temp. and press. 78−47512
cyclohexane-acetic anhydride mixture, impurity effects on crit. behaviour of elec. resist. 79−65527
trans-decahydronaphthalene-polystyrene system, press. and mol. wt. depend. of polymer solubility 79−23734
degenerate semiconductors, heterogeneous state, first-order phase transition, Ginzberg-Landau method analogue 80−70372
dicalcium lead propionate, ferroelec., annealed, crit. exponents, dielec. const. temp. depend. 80−55050
β,β'-dichloroethyl ether-iso-octane, critical indices, allowance for light double scatt. *(Russian)* 80−60624
Dicke model phase transition, thermodynamic Green's function method 80−5715
dielectric fluid near critical point, effect of elec. field *(Russian)* 77−62647
dielectric liquids, critical point and eqn. of state investig. by optothermodynamic method *(Russian)* 79−33068
diffusion process with critical point, eigenvalues discretisation technique 80−172
dimethylsulphoxide, density up to 257°C, vap. press. up to 189°C, crit. density 79−90768
dimethyltetraphenylmethylphenylsiloxanes, density, viscosity, surface tension and crit. temps. 79−86830
diphenyl ether, preparation, purification and use in triple-point cell 79−21750
disordered anisotropic antiferromagnet. random field effects 80−2580
n-dodecane-β,β'-dichlorediethyl ether crit. mixture, Rayleigh line wing 77−20864
double spin $^1/_2$ lattice gas model, phase diagrams 77−20521
dynamic scaling near bicrit. points 78−6535
dynamics, far from equilibrium 80−27258
elements and refractories with high crit. temp., review 78−59931
equation of state, perturbed-hard-sphere, applicable to sub- and supercritical temps. 79−19350
equation of state calcs. with Wilson-Kogut renormalisation group 79−97249
equation of state near critical point, thermodynamical scaling hypothesis 77−74341
ethane, gas, liq., and crit., electron mobility, density and temp. effects 80−92246
ethane, solid, thermodynamic props. between double solid-to-solid transition and triple point temp. 78−75828
ethane, use of high press. recycle-flow calorimeter 80−42228
ethane+CO_2 system, isothermal vapour-liq. equilibrium data, 10 to 25°C and high press., critical points 78−79754
ethanol-CS_2 mixture, Rayleigh and depolarised Raman scatt. lines near crit. temp. 77−20863
ethylene, high density behaviour, extrapolated $P\rho T$ surfaces and critical density 80−87834
ethylene deuterates, deuteration and isomeric effects on triple point temp. 77−43337
ethylene glycol-H_2O-lauryl alcohol-nitromethane-nitroethane, liq., multicrit. pts., 37-42°C 79−86868
ethylene-polyethylene mixtures, phase behaviour under high-press., polymer mean mol. wt. influence 79−24745
exponent inequalities for the percolation problem 79−63165
extinction coefficient 79−65889
FCC Blume-Capel model, Monte Carlo study 80−103453
Fermi liquid, normal, mag. ordering at absolute zero 79−38344
ferroelectric ferromagnet, soft modes and ferromag. reson. 80−11275
ferromagnet, total spin distrib. in spherical model with long-range pot. 79−30383
ferromagnetic classical vector model, extension of high temp. free energy series 80−7062
ferromagnetic metals, resist. anisotropy, crit. behaviour and temp. depend. 80−96858
ferromagnets and simple fluids, thermodynamic stability, crit. points 78−16766
first-order transition induced by cubic anisotropy, tricritical point, location 79−4688
flexible polymers, in soln., obs. of pair correlation function, temp. and conc. effects small neutron scatt. anal. 79−10780
fluctuations in Ginzburg-Landau systems *(Russian)* 79−75484
fluid, classical, elementary molecular theory 77−19859
fluid, simple, light scatt., gravity effects on crit. exponents determ. 80−20650
fluid density bibliography, temp. range exceeding 40K 80−51980
fluid mixture near tricritical point, light scatt., mean field behaviour 80−34930
fluid near crit. point, rapid evaluation of multiple scatt. 78−84594
fluid near critical point, spin-lattice relaxation time 80−80630
fluid of hard charged spheres at low density 77−9974
fluid properties, near critical point, student apparatus 77−60881
fluids, dynamical scaling and crit. point universality 80−88297
fluids with triple point, lattice and continuous one-dimens. models 77−31571
Fokker-Planck eqn. expansion, weak diffusion, critical point 80−57228
fractal lattices, crit. phenomena 80−105587
Freon-113, correlative and optical props. near critical pt. 79−65822

critical points continued
gas-gas equilibrium, thermodynamics at high press. 78−18734
Goldstone mode singularities, eqn. of state of isotropic magnet 79−42803
hadronic matter, critical point exponents 79−58944
hard-sphere system, with square well attraction, Percus-Yevick theory 77−43123
heat fluctuations near crit. point 80−47005
heat flux at flow boiling of N_2 in horizontal tube up to critical press. *(German)* 80−99921
Heisenberg, spin $^1/_2$ dil. magnet, crit. props. 80−15733
Heisenberg ferromagnet, critical points and two-magnon spectrum 79−87274
p-n-heptyloxybenzylidene-aminofluorenone/COOB mixtures, dynamic twist viscosity near polycrit. points 79−95133
n-hexadecane-β,β'-dichlordiethyl ether exfoliating mixture, light scatt. and hypersound vel. 77−28586
HMTTF-TCNQ chain, three dimensional ordering critical temp. 78−95152
Husimi-Temperley model under a random field 79−97313
hydrodynamics of fluid near critical points 78−59361
inert gas adsorbed on graphite, phase transitions using Landau model 79−69243
inert gas fluid, localised excess-electron states, quasilocalisation 80−44529
infinite type, exact sol. in one dimens. 79−9199
infinite type critical points 78−8374
Ising, spin $^1/_2$ dil. magnet, crit. props. 80−15733
Ising ferromagnet, 2-D, with quenched bond disorder, critical temp. 78−56328
Ising ferromagnet crit. props. of site and bond diluted model 79−42766
Ising like model, tricritical two-dimensional behaviour, finite size effects, model depend. 79−35641
Ising model, 3-D, partition function integration, collective variables method *(Russian)* 77−37824
Ising model, basis distrib. 78−16748
Ising model, boundary free energy, natural iteration and cluster variation methods, critical points 77−17913
Ising model, free energy, variational calc. for 3 dimens. system 80−42167
Ising model, Percus-Yevick type approx. 78−148
Ising model, spin 1/2, susceptibility and fourth field derivative for $T>T_c$ and $d=4$ 79−61024
Ising model, spin-one, bilinear and biquadratic interactions, phase diagram 80−75772
Ising model, three-spin triangular, nature of critical point 77−2617
Ising model, tricritical phenomena, nearest neighbour and next nearest neighbour interactions 77−69566
Ising model, tricritical two dimensional behaviour, ε expansion universal quantities 79−35642
Ising model correlation quadratic identities, discrete-time Toda eqn. 80−105582
Ising model for monolayers of coadsorbed atoms, phase transitions 80−19909
Ising model strips, scaling theory, wall effects in crit. systems 80−80539
Ising O(2), O(3) and O(4) spin systems, Hamiltonian string-coupling expansions 80−20426
Ising systems of different spin values, random system 80−11144
isobutyric acid+water, thermal expansion near upper crit. soln. temp. 77−29031
isobutyric acid-water mixture, electrical conductivity near crit. pt. 77−15612
isostructural phase transition by Landau phenomenological anal. 79−90757
Kosterlitz-Thouless critical point, multicritical behaviour 79−85104
Landau crit. point, mean-field theory, scaling theory and crit. exponents to second order in ε^2 79−4395
Landau critical point, low temp. renormalisation group and 1/N expansion 79−35656
Landau model with several order parameters 78−41244
Landau point crit. exponents to order ε^2 78−41259
Landeu model, critical multiple correlations 79−75440
Legendre transform notation for critical point criteria 78−12657
Lennard-Jones 12-6 system, triple pt. props., mol. dynamics simulation 78−2231
Lennard-Jones (100) crystal-liquid interface, structure 78−91284
Lennard-Jones pot. fluid, locating of crit. point 79−37826
Lennard-Jones system, 2- and 3-dimens., crit. point parameters, quantum corrections 79−4227
Lennard-Jones system, molecular dynamics simulation of interfacial and co-existence props. at triple point 78−83916
Lennard-Jones two-dimens. fluid, Percus Yevick eqn., radial distrib. function, critical point 77−76272
Lifshits critical points 79−7796
Lifshits points for bidimensional representations *(Russian)* 79−93086
Lifshitz point, critical exponents, ε-expansion 78−65899
Lifshitz point, physical realisation 79−41957
Lifshitz points of higher character 77−67395
Lifshitz pts., magnets with competing interactions 79−42214
light multiple scatt. in inhomogeneous medium near critical point, spectral comp. *(Russian)* 77−42483
light scattering near phase transition points 79−15415
light scattering near phase transition pts. in pure and defect containing crysts., review 80−93361
liquid, critical pt. exponents, significant struct. theory appl. 77−7837
liquid, low mol. weight, glass transition temp. and crit. props. 80−39265
liquid crystal, binary mixtures, phase transition, entropy, relation to smectic plane tilt angle 80−65203
liquid metals, surface tension and critical props. 79−28176
liquid solidification press. meas., dielectric loss method 77−45868
liquid-gas critical point, quantum mechanical effects, theory 80−103452
liquid-gas critical point in 3.3 dimensions 79−7684
liquid-gas equilibrium, crit. density, temp., and press. calc. using cell theory *(Spanish)* 79−90767
liquid-gas transitions in the spin-1 asymmetrical Ising model 79−42212
liquid-vapour crit. pt. region, NMR freq. shift anomalous behaviour 80−44938
liquid-vapour transition, non-Ising-like effects, eqn. of state, renormalisation group calc. 80−84286
liquidons and gasons, continuity of state historical controversies 80−12882

critical points continued
liquids, simple, corresponding states correls. and triple point solid vol. 80—92649
2-6-lutidine-water, anomalous supercooling near critical point 80—70384
macromolecular system, critical branching, a statistical theory 80—3413
magnetic disordered system, critical phenomena 78—52269
MBBA, pretransitional effects above phase transition temp., nonlinear dielectric meas. 79—15390
metal, critical temp. determ. by exploding wires method, liquid metal enthalpy 78—6149
metal, thermopower near magnetic and order-disorder critical points 79—65454
metals and alloys, critical temperatures determination, elec. resist. method, IMASh-5S-69 installation 80—71827
metamagnet, two-dimens., tricritical spinodal decomp., Monte Carlo study 80—93117
metamagnetic tricritical point, anisotropic Ising model high-field expansions 77—63198
metastable state relaxation, critical point region nucleation in thermodynamic systems *(Russian)* 80—13026
metastable states near tricritical point *(Russian)* 78—63841
methane, dense gaseous and liq., thermal cond.-viscosity correlation, up to 500 atm., 95-500 K 77—80657
methane, effects of impurities and annealing on triple point 78—83919
methane, high-purity, triple point temp. and press. meas. 77—31753
methane, nuclear spin conversion at triple point 79—77723
methane adsorbed on graphite basal plane, first order melting transition, triple point 80—2269
methane triple point sealed cells using stainless steel envelope 80—95099
methane-2,2-dimethylbutane-2,3-dimethylbutane, tricritical point obs., opalescence 77—76562
methane-n-pentane-2,3-dimethylbutane, tricritical point obs., opalescence 77—76562
methanol, Rayleigh linewidth, in crit. region 79—24329
3-methylpentane-nitroethane, binary fluid, Rayleigh linewidth meas. near crit. point 78—48190
methylphenylsiloxanes, density, viscosity, surface tension and crit. temps. 79—86830
2-methylpyridine+D_2O, p-T-X miscibility dome critical point, US vel. meas. 77—27979
3-methylpyridine-D_2O soln., consolute points, crit. soln. temps., light scatt. obs. 77—77230
micellar solutions, crit. behaviour 80—105601
mixtures, analogy with pure fluids 78—67819
multicomponent, multiphase systems near critical point, phase volume behaviour 80—15212
multicomponent mixtures, phase envelopes and crit. points calc. 80—54337
multicomponent mixtures, tricritical behaviour, possible exptl. tests 77—47543
multicritical (order O) magnetisation eqn. of state, renormalisation group calc. 78—31085
multicritical point and problem of coexistence of two ordered phases 79—77717
multicritical points, fluctuation dynamics *(Russian)* 77—27977
n-component spin system, energy-energy correl. function calc. 80—31697
near-critical fluids in turbulent flow through tubes, heat transfer num. prediction method 77—42832
nematic liquid cryst., tricritical behaviour near transition to isotropic fluid *(Russian)* 80—15001
nematic/smectic A/smectic C triple point, Landau theory 79—95142
neutron diffraction studies of phase transitions and crit. phenomena, book contrib. 79—60229
nitrobenzene:n-hexane, depolarised Rayleigh scatt., crit. anomalies 78—68524
nitrobenzene-hexane solution, double-scatt. light intensity near critical point of mixing *(Russian)* 80—55117
nitrobenzene-n-hexane, liq. mixture, static and dynamic viscosities near crit. point 77—69108
nitrobenzene-n-hexane crit. mixture, Rayleigh line and depolarised scatt. 77—20864
nitrobenzene/n-hexane (n-heptane), critical exponent β, phase coexistence curve anal., viscosity coeff. meas. 80—100327
nitroethane-isooctane mixture, depolarised Rayleigh scatt. near crit. point 80—45089
nonclassical equations of state for critical and tricritical points 80—4683
nonequilibrium phase transition, dynamical features *(Chinese)* 78—83030
nonisotropic systems near liquid-vapour critical point, similarity hypothesis, gravitational effects 80—17913
nonpolar fluid, excessive electrons near crit. points 80—92836
nucleation theory and first order phase transition dynamics near critical points 80—84284
O(N) Heisenberg spin systems, $N=2,3,4$, and Ising model, strong coupling expansions and phase diagrams 79—71378
one-component Ginzburg-Landau field, nonlinear crit. slowing down 80—27252
one-dimensional system, Bose-Einstein condensation at const. press. 80—22276
optical double scattering method for condensed systems parameters determ. 80—28161
ordering alloys, nonlinear critical relaxation of the Ginzburg Landau field coupled to a conserved density 80—90803
organic compounds, crit. temps. correl. with boiling pts. 78—91421
organic compounds, vapour liquid critical pressures and volumes 79—99306
oriented bond percolation, threshold probability and correlation length exponent calc. 80—68146
pair correlations, asymptotic decay, Percus-Yevick eqn. solns. 77—47311
partition function of the three-dimensional Ising model 79—71381
pentane-benzene solution, vapour-liquid equilibrium study, vaporisation critical state *(Russian)* 80—79931
4-n- pentyl-phenylthiol-4′-alkoxybenzoate, homologous series, specific heat meas., nematic-smectic-A tricritical point 80—15227
phase diagram and critical points *(Japanese)* 80—24568
phase diagram with first-order transition close to second-order transition 80—59625
phenol-water mixture, pure and KCl-doped, electrical conductivity near crit. pt. 77—15612
3-phenylpropanol-hexane, nonlinear dielectric effect, critical exponent 80—93227

critical points continued
planar rotator model, one-hypercube renormalisation group transform. 78—72353
plane Ising lattice, local magnetisation depend. on linear defects *(Russian)* 80—2595
polariton Fermi-resonance, EM wave dispersion 80—2344
polymer, flexible chain collapse 78—87628
polymer, high mol. wt., glass transition temp. and crit. props. 80—39265
polymer chains, θ-domain, tricrit. props. in poor solvent 80—103450
polymer demixtion, crit. points 78—26419
polymer glass tricritical points, symm., in binary polymeric glass mixture 79—82320
polymer mixtures, molten, interface props. near consolute point 78—87792
polymer solns., phase diagrams, pulse-induced critical scatt. 79—1490
polymer solution, semidilute, chain size 78—87607
polymethylene in binary n-alkane solvents, lower critical soln. temp. 79—37841
polymethylene in n-alkanes, lower critical soln. temp. 79—37840
polystyrene-cyclohexane, polymer solns., coexistence curve 79—28101
position space renormalisation group transformation peculiarities in thermodynamic limit 79—97245
Potts lattice gas, crit. and tricrit. exponents using Kadanoff transform. 80—101768
Potts model, four state, series studies 79—85088
Potts model, Monte Carlo simulation in three dimens. 80—163
Potts model, presence of instability 80—17892
Potts model, three-state, effects of symmetry-breaking perturbations 80—105579
Potts model, two dimensional three state, critical exponents 80—105583
Potts model in 2-D, exact results 79—58644
Potts models, planar, critical points for various lattices 79—93061
propylene, high density behaviour, extrapolated $P\rho T$ surfaces and critical density 80—87834
PTFE, γ-ray effects on 19 and 30°C phase transitions, Fourier transform IR spectroscopy 80—103387
pure fluids, critical point change of variables 79—93065
quasielastic light scattering near phase transitions 80—93362
quenched bond disorder, effective medium approx. in Ising model 80—42163
random fields, multicritical points and dimensionality shift 79—40468
random Ising ferromagnet, upper bounds 80—34663
random magnet, Ginzburg-Landau model 78—10704
rarefied shock wave existence near thermodynamic critical point of a substance *(Russian)* 80—88263
Rayleigh linewidth meas. on crit. fluid, double scatt. effect 77—20865
Rayleigh scattering linewidth near pt., simple fluid, gravity effect 77—85735
Rayleigh scattering near crit. pt., nonzero beam diameter and gravity effect 77—85737
Rayleigh scattering near crit. pt., nonzero beam diameter effect 77—85736
reference materials for critical temp. and press. meas. 77—71289
reference standards for radiation pyrometry, silver and copper freezing points 78—57888
relaxation model near the Lifshitz point 79—17376
relaxation phenomena, Monte Carlo studies, review, book contrib. 79—80531
relaxation phenomena, stochastic and deterministic theory 80—182
relaxational dynamics in systems with many-component order parameter, renormalisation group anal. 80—42181
relaxational dynamics in systems with many-component order-parameter, scaling fields and variables 80—101772
renormalisation group eqns. and thermodynamic anomalies near tricritical point *(Russian)* 80—13027
rigid-rod fluid, thermodynamic props., crit. points and transitions 78—73919
secondary ref. stand., MP of Y_2O_3 77—45821
sedimentation and density gradients, near liq.-liq. crit. soln. point, high gravit. field 78—47526
semiconductor, crit. points for electron-hole system 80—44511
significant liquid structure theory, liquid-vapour transition, reduced eqn. of state for real fluids 79—32869
single component system near critical point, equilibrium achievement delay 80—90799
smectic liquid crystal, Lifshitz point in H-T phase diagram 77—84904
smectic liquid crystals, chiral polarised electric field induced tricritical point 78—10176
solid electrolyte, transition temperature to high cond. state as function of press. 80—44365
solidification press., spindle and castor oils, silicone liqs., and viscosity, 20-180°C, $0\text{-}10^4$ Pa 77—43266
solids and liquids, dielec. characts., temp. depend., laboratory installation for meas. 80—37051
solvent-polymer system, liquid multi-phase separation 78—14468
spherical model, isotropic Lifshitz point in $2<d<4$ dimens. 78—29062
spin dimensionality dependence of T_c in the 1/n expansion 78—32772
spin systems, dynamical plane rotator model, dynamical correl. functions in mol. field approx. 80—88758
spin-spin correlation function near the critical point 79—11319
spinodal decomposition, early stage, of fluids near crit. point 77—55340
square lattice, critical dynamics and potential moving approx., renormalisation group approach 80—57209
square-well fluid, nonclassical crit. behaviour 80—44291
squaric acid, structural phase transition, US vel. meas. as function of temp. below and above T_c 79—14927
star-triangle transformation, phase boundary for planar site-bond percolation problems 80—95042
steel, martensitic transform. critical temp. determ. 77—90349
structural phase transition, intrinsic and extrinsic central peak properties, review 80—34168
superfluid, two-dimensional, dissipation near crit. point 78—47619
superheated binary solns., flashing kinetics, nucleation and critical bubble 80—92035
surface polariton scattering by order, parameter fluctuations near crit. pts. 80—92835
surface tension, solid-liq. interphase, thermal meas. procedure *(French)* 77—66072
surface tension of liquid at triple point, and bulk modulus, theoretical relationship 78—47638

critical points continued
surface tension temp. dependence from triple point to critical point *(German)* 80—100376
surfaces, multicritical phenomena 77—32208
symmetry breaking fields, destruction of first order transitions 79—40517
system with two parameters, Mott and ferromagnetic transitions, phase diagram of the extended Caron Pratt model 79—15083
Teit's equation modification in critical region *(Russian)* 77—27976
temp. shifts for finite slabs in ε-expansion 78—41242
temperature, critical dynamics below T_c 80—27256
ternary alloy with three-body potentials, transition temp. calc. using correl. function approach 79—69451
ternary fluid mixture exhibiting tricritical points, model 78—26659
ternary liquid mixtures, shear viscosity at plait points 77—35685
tetrafluoromethane adsorbed on graphite, adsorption isotherms, crit. temps. *(French)* 80—34312
tetramethylsilane, liq., electron mobility up to crit. point 77—76809
TGFB, high press. influence on anomalous specific heat, tricritical point 80—25322
three dimens. pure substance with two critical points, model 79—69239
three-component model, global phase diagram 77—37835
three-dimensional Ising model, crit. behaviour 80—4672
toluene, gas, liq. and crit., cation mobility 80—48842
toluene, tables of thermodynamic props. 77—24419
transition metal dichalcogenides, trigonal-prismatically coordinated layers, phenomenological theory of CDW state 80—80200
transition point of random Ising model with bond dilution 79—93060
transition state determination by the X-method 77—90580
triangular lattice, self-avoiding walks 79—40478
triangular lattice gas model, multicritical behaviour 77—74328
tricritical coexistence in three dimensions, multicomponent limit 80—19907
tricritical crossover exponent 77—4239
tricritical phenomena, ternary, quaternary fluid mixtures, classical models 78—91416
tricritical point determ. by NQR 79—77746
tricritical points and thermodynamic quantity singularities, renormalisation group method *(Russian)* 77—69071
tricritical points and universality in three dimensions 80—42179
tricritical points of model fluid mixture 77—31752
tricriticality and the failure of scaling in the many-component limit 79—6071
triple point, 180° rule violation criteria, thermodynamic stability 77—7841
triple point temperature meas., theoretical aspects, thermometric reference materials 77—67436
triple points, 180° Rule, Butterfly model 80—8945
triple points cells, Ar, O_2, comparison 78—73996
triple points of Kr, Ar, N_2, Ne, reference temperature appl. 78—73997
two dimensional system, melting and condensation theory 80—57231
two-dimens. planar model, universality class of crit. lines determ. 78—4566
two-dimensional Ising model, real space renormalisation transform. 78—2687
two-dimensional Ising spin glass, crit. temp. 80—11206
two-dimensional lattice embeddings of connected graphs of cyclomatic index two 78—41243
two-dimensional square Ising model in transverse magnetic field, renormalisation-group method 80—20428
uniaxial Heisenberg antiferromagnet, phase diagrams 80—15730
unijunction transistor transition critical exponents, negative resistance phenomena 80—44713
universality class of asymmetric fluid critical points 80—57098
US velocity in crit. region water 80—59582
vapour pressure critical exponent optimal determ. 79—51271
vapour-liquid equilibrium, supercritical components, standard state fugacities 80—15230
volume at critical temp., estimation procedure 79—91981
water, supercooled liq., high freq. sound vel. and absorpt., thermodynamic singularity, 228K 77—76489
water, triple point as temp. fixed point 80—59626
water and steam, thermal cond. equation, 0 to 800°C, triple pt. press. to 1000 bars, crit. region 80—39364
water triple point cell prep. for calibrating thermometers 78—204
wetting, three phase junction, at critical point 77—59177
X-Y model, one dimens., transverse correl. function at zero temp. 79—40493
Yang-Lee edge singularity and ϕ^3 field theory 78—65882
Yang-Mills gravity dynamics homogeneous and isotropic world models 78—45543
Ag_3AsS_3; NQR study of phase transitions, high press., tricrit. pt. determ. 79—77746
Al-Zn alloy, small-angle neutron scatt. in crit. point regions, 324-435°C *(German)* 77—85993
Ar, liq., critical exponent, η, X-ray scatt. 80—92660
Ar, liq., surface thickness, near triple point, using surface tension data 79—99400
Ar, liquid, depolarized Rayleigh scatt. at triple point, mol. dynamics simulation 80—60617
Ar, liquid surface thickness near crit. point 80—34180
Ar, phase transition, anharmonic cryst.-gas transition 80—6510
Ar, simple classical liq. at triple pt., long-time anomalies suppression 80—24339
Ar, triple point, depolarized Rayleigh scattering from fluids of spherical molecules 78—88319
Ar, triple point, rel. to IPTS reference pt. 77—104
Ar, triple point, surface tension effect on transition zone 77—35798
Ar triple point determ. by thermal anal. *(Japanese)* 79—95123
Ar triple point sealed cells using stainless steel envelope 80—95099
B_2O_3-BaO, liquid immiscibility region, equilibration and quenching expts. 80—45288
$Ba_2TiGe_2O_8$-$Ba_2TiSi_2O_8$, pseudobinary system, pyroelectricity and related props. 78—95553
$BaTiO_3$:Co, tricritical point, X-ray diffr. meas. 80—71341
C, graphite-liquid-vapour triple point pressure and liq. C density 77—62618
C, solid-liquid-vapour triple point pressure 79—14914
CH_4, triple point, International Practical Temp. Scale, comparisons 79—40566
β-CO, single cryst., adiabatic elastic consts., at triple pt., Brillouin scatt. obs. 79—47466

critical points continued
CO_2, high density behaviour, extrapolated $P\rho T$ surfaces and critical density 80—87834
CO_2, near critical point Rayleigh and Raman scatt., Fermi diad 80—80765
CO_2, specific heat, meas., near crit. point 77—51490
CO_2, thermal diffusivity and cond. in crit. region meas. by holographic interferometry *(German)* 78—59942
CO_2 triple point, overheating and undercooling phenomena 80—2142
COS, vapour pressure and critical properties 79—95149
CS_2-ethanol mixture, Rayleigh and depolarised Raman scatt. lines near crit. temp. 77—20863
Ce, critical isomorphic $\gamma \rightleftarrows \alpha$ transition, phase equilibrium curve *(Russian)* 80—55397
Cs, liquid-vapour coexistence curve and critical exponent β 77—76538
$CsMnBr_3.2D_20$, spin-flop system, extended scaling near bicrit. pt. 79—51752
$CsMnCl_3.2H_2O$, mag. phase diagram near bicritical point 80—71021
n-D_2, triple point determ. 79—95124
DyAG, cubic antiferromagnet, multiaxis phase transitions 79—78377
$DyAl_2$, magnetisation, three-state Potts model 79—42804
ErB_4, mag. phase diagram, neutron diffr. study 80—50091
Fe complex, $Fe(Cl)[S_2CN(C_2H_5)_2]_2$, 3-D Ising ferromag., cryst. susceptibility, 1.5-20K 80—20390
Fe, structural stabilisation, influence of C interstitials on transition temp. between α and γ phases 79—11611
Fe-H system, influence of H press. on Fe crit. points and H solubility 78—52758
$FeCl_2$, magnetic phase diagram, optical studies 78—88121
$(Fe_{1-x}Mn_x)_{75}P_{16}B_6Al_3$, amorphous, spin-glass-ferromag. multicritical point, AC susceptibility meas. 80—50117
Fe_3O_4, crit. exponents meas. by polarized neutron scatt. 80—44828
Ga triple point temp. determ. 80—42223
Ge, electron-hole droplet condensation, crit. point 80—49612
GeH_4, Lorenz-Lorentz coeff., refr. index, crit. consts. and density depend. 78—92041
H_2, thermometric fixed points determ. 77—82511
H_2 triple, boiling and 17K equilib. points realization, cryostat and method 80—27314
n-H_2, vap. press. eqn. between triple and critical pts. 77—55351
H_2-Ar, liq.-vapor equilib. 83 to 141K, to 52 MPa 79—42226
HBr, triple-point temp. and pressure, vapour pressure of liquid to 205K 79—7683
H_2O, vapour pressure meas. at triple point 77—43338
He II, superfluid behaviour near λ point 77—59166
^3He, equation of state and crit. exponents near liq.-vapour crit. point 80—24707
^3He-^4He mixture, equation of state and crit. exponents near liq.-vapour crit. point 80—24707
^3He-^4He mixture, ion trapping at tricritical point, depend on temp. and elec. field 79—7729
^3He-^4He mixture, transport props. near superfluid transition and tricritical point 80—29242
^3He-^4He mixture, tricritical dynamics and λ-line behaviour, model 77—39719
^3He-^4He mixture near tricritical point, thermal diffusion ratio and thermal conc. gradients 77—76640
^3He-^4He mixtures, interfacial tension near tricritical point 77—69141
^3He-^4He mixtures, sound propag. near superfluid transition and tricritical point 79—65284
^3He-^4He tricritical mixture, universality under press. 80—103533
^4He, HCP-FCC transition, near triple point, thermal anal. 79—60596
^4He superfluidity, macroscopic quantum waves, bound quasi-particles 80—39378
^4He, universality under press. near superfluid transition, critical exponents and scaling corrections 77—47638
Hg, expanded fluid, thermoelec. power near crit. point 79—23951
Hg, liq., vapour press. and crit. points determ. from elec. cond. meas. 77—59273
Hg, liq.-vap. interface, density profile near triple point, X-ray refl. 78—75821
Hg, liquid-vapour coexistence curve and critical exponent β 77—76538
Hg-Cd, liq. amalgam, vapour press. and crit. points determ. from elec. cond. meas. 77—59273
$Hg_{3-\delta}AsF_6$, theory of phase transitions 80—6486
K, liq., density, at near critical temp. 80—103407
K solution, in KBr, conc. fluctuations, neutron small-angle scatt. study in electrolyte-metal transition range 79—14668
KAg_4I_5, superionic phase transition, dynamical and crit. pt. props. 80—107535
KBr, molten, solutions of K, conc. fluctuations, small angle neutron scatt. study 80—92448
KBr:Tl, impurity-induced first-order Raman scatt., critical-point and critical-line anal. 79—19884
KCl:Tl, impurity-induced first-order Raman scatt., critical-point and critical-line anal. 79—19884
KDP monocrystal, expansion and contraction coeffs., tricritical point, Landau theory explanation *(Russian)* 80—44340
KH_2PO_4-type crystals, H bond in ferroelectricity, role of high pressure research, tricritical point 79—15414
Li soaps, n.C_{13}-n.C_{20}, phase transition temps. and enthalpies, DSC obs. 80—45544
MnF_2, spin-flop bicritical point, susceptibility and RF absorpt. meas. 79—87277
Mo, liq., exptl. determ. of crit. data 78—75531
MoF_6, critical parameters determ. using thermodynamic and mol. similarities 77—43310
N_2, high density behaviour, extrapolated $P\rho T$ surfaces and critical density 80—87834
N_2, liq., Raman Q branch temp. depend., interferometric obs. 77—43987
N_2, viscosity near liquid-vapour transition 79—77799
NH_3-ethylene (propylene) mixtures, crit. curves at high-press. 79—23715
$NH_4Ag_4I_5$, superionic phase transition, dynamical and crit. pt. props. 80—107535
NH_4Cl, order parameter, electro-optic measurement 78—88280
NH_4Cl, order parameter variation near multicritical pt., SHG 79—81484
NH_4Cl, order-disorder phase transition, type of multicritical point, nonlinear quadratic susceptibility 78—83947
$NH_4Cl_{1-x}Br_x$ mixed cryst., phase diagram and characts. of phase transitions 77—62637

critical points continued
$(NH_4)_3H(SO_4)_2$, press.-temp. phase diagram, dielec. and DTA meas. 77−81067
$(NH_4)_2SO_4$-H_2O-ethanol-benzene, tricritical mixture, light scatt. 79−15473
NH_4X, (X=Cl, Br, I), tricritical points 79−7695
NO, first monolayer on MgBr cleavage face, triple point 78−6227
Na thermodynamic props. for reactor safety analysis 79−13478
Na-NH_3, solns., US absorpt. and vel. near crit. point 79−28047
Nb-V system, H_2 absorpt. 80−59808
Nd-H, weak depend. of T_c on press. 79−52174
Ne, vapour press. and triple point, influence of impurities 78−79756
Ne-Kr, time-dependent props. near crit. mixing point, 2000 bar, mol. dynamics calcs. 80−24580
O_2, liq., Raman Q branch temp. depend., interferometric obs. 77−43987
O_2, triple point, determination at low temp. *(Japanese)* 80−31749
O_2 triple point, realisation rel. to IPTS 77−105
O_2 triple point, rel. to IPTS reference pt. 77−104
$Pb_{1-x}Ge_xTe$, degenerate semiconducting ferroelectric, structural phase transition temp., mag. field effects 80−45017
$Pb_3(P_xV_{1-x}O_4)_2$, ferroelastic phase transition, DTA, dilatometric and Brillouin scatt. study 80−70398
$PbZr_xTi_{1-x}O_3$, ferroelec. phase transition under high press. 79−99833
$PbZr_xTi_{1-x}O_3$ solid solutions, tricritical behaviour 78−80296
$RbAg_4I_5$, superionic phase transition, dynamical and crit. pt. props. 80−107535
$RbCaF_3$, cubic to tetragonal phase transition, ^{87}NMR meas. 80−7187
S-benzene systems, liq.-liq. phase separation 80−96658
SF_6, coexisting densities, revised and extended scaling 78−34613
SF_6, critical parameters determ. using thermodynamic and mol. similarities 77−43310
SbSI, ferroelec. transition critical phenomena *(Russian)* 80−7314
Si, electron-hole droplet condensation, crit. point 80−49612
Ti-Ni, effect of alloying on crit. points and martensitic transform. hysteresis 80−20935
$TlMnCl_3$, transition temp., variation with press. 79−7694
UF_6, critical parameters determ. using thermodynamic and mol. similarities 77−43310
UO_2, vapour press. meas. up to 5000K, appl. of laser pulse heating 80−52230
$V_{0.986}Fe_{0.014}O_2$, metal-insulator phase transition, effect of hydrostatic press. 80−6725
WF_6, critical parameters determ. using thermodynamic and mol. similarities 77−43310
Xe, fluid, near crit. point, correl. range and Rayleigh linewidth 80−93352
Xe, high density behaviour, extrapolated $P\rho T$ surfaces and critical density 80−87834
Xe, sound propag. near critical pt. 79−82285
Xe, triple light scatt. along crit. isochore 77−58838

critical temperature, superconducting *see superconducting transition temperature*

CRO *see cathode-ray oscilloscopes*

crocidolite *see asbestos*

crops *see farming*

cross-sections (nuclear) *see nuclear reactions and scattering*

crosstalk
45 Mb/s fibre-optic transmission system performance 77−27376
bidirectional optical fibre, crosstalk, review 78−66901
bidirectional optical fibre, Rayleigh scattering freq. depend. meas. 79−64317
colour image recording on monochrome film by carrier frequency photography *(Japanese)* 77−41711
data buses, angle optical fibre, signal distribution systems and crosstalk isolation 79−3802
electro-optic waveguide deflector performance characteristics 80−33213
electrooptic polarisation switch for multimode fibres 77−27335
holographic interferometry, two-reference-beam, nonlinear cross talk 77−14675
light pipes, crosstalk power between modes 77−785
nosetip recession meas. using implanted radioactive sources, error analysis 78−16272
optical fibre 78−50923
optical fibre link, end-to-end cross coupling loss meas. 78−90502
optical fibre switch, four-way, mechanically operated 80−53464
optical fibre transmission system filtering prism *(Japanese)* 78−9441
optical heterodyne interferometer, elimination of two-channel crosstalk 77−10100
optical multiplexer design for wavelength-division multiplexing transmission via single fibre 80−33222
optical video discs, adjacent track crosstalk 79−50338
optical waveguide 4×4 switching network 77−3683
optical waveguide switches and modulators, crosstalk due to two polarisations 77−7175
optical waveguides, multichannel, cross-talk noise anal. 80−91922
phase hologram multiple storage, crosstalk noise 77−38827
polarisation-independent optical switch using weighted directional coupler 80−58798
single-mode fibre tapered velocity coupler performance 79−55246
stepped switched optical directional couplers with unequal section lengths 80−33235
$LiNbO_3$:Ti waveguide directional coupler switches, optically-induced crosstalk 80−48417
$LiTaO_3$ monolithic pyroelectric array, IR detectors 80−77857
$LiTaO_3$/CCD hybrid focal plane, IR imaging and detection, crosstalk 80−77856

crowdions
elastic interaction with extended at. defects in isotropic media 77−76454
metal, FCC, investigation of stage-I_E interstitial nature by TEM 78−47329
metal, HCP, long-range interstitial migration rel. to c/a ratio 79−28125
property analysis using Frenkel-Kontorova model 79−42056
Ag, TEM exam. of ion damage in FCC metals 78−87727
Au, prop. anal. using Frenkel-Kontorova model 79−42056
Au, TEM exam. of ion damage in FCC metals 78−87727
Au-Ag, radiation damage and diffusion 80−24645
Cu, electron irradiation damage, dislocation pinning investig. of crowdion model 77−69000
Cu, TEM exam. of ion damage in FCC metals 78−87727
KBr, defect accumulation under electron irrad. at 4K 80−107233

crowdions continued
KCl:H, dichroic H- and U-centres by polarised bleaching of interstitial H, Cl_2^- crowdion form. 80−29766
Ni, computer simulation of point defects and planar defects 78−43013
Ni, pure and doped, mech., mag. relax. meas. dumb-bell self-interstitital reorientation *(German)* 78−52879
Ni, self interstitial migration and crowdion conversion, dislocation pinning expts. 77−84762
Ni, TEM exam. of ion damage in FCC metals 78−87727
Ni-Be alloys, struct. and phase stability in neutron bombardment field *(Russian)* 77−76467
Ni_3Fe, disaccommodation meas. after low temp. electron and neutron irrad. 80−88832
Pt, crowdion conversion to dumbbell, two-interstitial model, thermal neutron irrad. 80−33992
Pt, interstitial thermal conversion study by elec. cond. meas. 80−15096
Pt, ion irrad. damage, temp. depend., electron microscopy obs. of defect kinetics 80−107339
Pt, radiation damage, self-interstitials migration modes and thermal conversion 79−65126
Pt, TEM exam. of ion damage in FCC metals 78−87727
W, split crowdion interstitial, (111), computer simulation of TEM imaging 78−71723

CRT *see cathode-ray tubes*

crushing
granular material crushing strength determ. apparatus 79−70260
high-alloy die steel, heat resistance and crushing strength, low-temp. thermomech. treatment effects 77−52372
kaolin grog particles, shape and density 80−97450
metal tubes, crushed between rigid plates, large deformation compression 80−66579
particles, small, impossibility of comminution by compression 78−52709
powder, dry ball milling, breakage parameters variation with ball and powder loading 80−80999
triboluminescence measurement, crushing and high stress appl. device 78−27338
$CaHPO_4$, powder and granules with starch mucilage binder, surface topography variation under compression 80−80998
Ge powder/Au electrode contact pot. difference, grain size depend. 80−44723
$SrO.nFe_2O_3$ isotropic ferrite magnets, manuf. process and mag. props. *(Japanese)* 80−29915
U ore, ^{222}Rn release 78−89970
Y_2O_3, effect of roasting temp. of $Y_2(C_2O_4)_3$ on crushing, compressibility, sintering props. 77−8790

crushing strength *see compressive strength*

cryoelectric stores
see also cryotrons; superconducting devices
Josephson effect applications 77−20503
superconducting, conference, Stanford, Calif., USA (Aug. 1976) 77−28272
superconducting film, memory device storage of Abrikosov vortices 79−28487
Nb, supercond. film, switching, storage and erasure effects 77−8253

cryogenic pumps *see cryopumping*

cryogenics
see also cryoelectric stores; cryopumping; cryoscopy; cryostats; cryotrons; Joule-Thomson effect; low-temperature production; low-temperature techniques; magnetic cooling; refrigeration
AC conductor, cooled by cryogenic liq., heat transfer models 80−5926
acoustic microscopy, scanning 80−79080
alkanes, light, solubility in liq. N_2, IR spectroscopy obs. 80−59654
alloy, cryogenic, creep, review 80−104222
alloys, FCC base hard materials, low temp. toughness *(Japanese)* 80−100916
Australian National Measurement Laboratory and cryogenics 79−35753
automatic system for low temp. X-ray studies of phase transitions 77−15281
automobile, liquid H storage and refuelling 80−30604
BEBC, bell jars for research into strong interactions at SPS energies *(Dutch)* 77−46463
biological material, prep. for X-ray microanal. of diffusible elements, methods of drying ultrathin cryosections 78−77166
biological material cryofixation, fast freezing device 78−28138
biological material prep. for X-ray microanal. of diffusible elements, rapid freezing and ultrathin section prep. 78−77165
biological materials, low-temp. SEM, X-ray microanal. 79−39627
biological specimen freeze-drying process obs. by SEM 78−28142
biological specimens, cryosectioning for X-ray microanal. 79−39626
biomedical appl., development trends *(German)* 77−25590
blood cells, red, human, frozen section prep. for electron probe anal., fracturing or cutting 79−39625
boiling, critical heat fluxes, effect of cylindrical heater dimensions 79−35756
boiling heat transfer and vapour bubble dynamics in cryogenic liquid 77−31765
boiling in cryogenic liquids, investigations on heat transfer 79−60494
boiling of cryogenic liquids, crit. heat flux, heating surface props. effects 78−90662
brass cap cooling with liquid N_2, heat transfer 77−61071
calorimetric determ. of dielectric loss factors at 1 kHz and 4.2K 80−98921
calorimetry, review 79−40573
CERN ISR, cold bore expt. 79−76212
closed cycle refrigerator, low power, SQUID's appl. 78−77921
condensed gas films, thermal radiation absorpt. 78−32824
conference, Grenoble, France (May 1976) 77−17988
conference on cryogenic engineering, London, England, (July 1978) 79−54137
construction material magnetisation meas. *(Slovak)* 78−93693
contact heat transfer between heat-liberating element and surface of subliming solid cryoagent 78−81987
cooling and freezing cryogenic fluids by vapour space evacuation 77−57331
cryobiology, freezing and cryofixation 78−28136
cryobiology, struct. and functional aspects of freezing techniques 78−28137
cryoelectronics, appl. of multicontact thin-film superconducting switch 78−4661

cryogenics continued
- cryoelectrotechnics, thermodynamic and quantum interpretation *(Rumanian)* 77—61070
- cryogenic refrigerators for fusion research 79—679
- cryogenically cooled mixer for 80 to 120 GHz, improvements 79—40073
- cryomicrotomy of thick sections, cutting work 78—28139
- cryonuclear physics for radioactive decay and neutron+nucleus reaction studies *(Dutch)* 78—29416
- cryopreservation of cells and biological samples using electronically programmed freezer 79—62420
- cryopump and extremely high vacuum *(Japanese)* 79—71468
- cryosprayer improvements for surgery 77—78033
- cryosurgery, freezing patterns of normal and diseased tissues 78—44685
- cryosurgery instruments, effects of heat transfer material on working parameters 78—36037
- cryosurgical apparatus coolant supply system 77—81637
- cryosurgical applicator for dermatology 77—78034
- cryosurgical heat tube instrument design 77—78031
- cryosurgical instrument for proctological and gynaecological operations for malignant tumours 79—70699
- cryosurgical instruments for otorhinolaryngology 77—78032
- cryosurgical probe, Stefan-like problem in biological tissue analysis 77—17005
- cryoultramicrotomy, prep. of thin sections for electron probe anal. of calcifying cartilage 78—31988
- curve-fitting method based apparatus for thermal props. meas. at cryogenic temps., performance characts. 77—67441
- delivery systems for supercooled liquids in production and laboratory 79—80625
- density reference system for cryogenic fluids 78—54344
- dielectrics, thermal conductivity, temps. <1.5K, methods and apparatus *(French)* 77—1268
- digital Josephson technology—present and future 79—28472
- dilution refrigerators, molar flow rates determ. method 77—10032
- dispersion analysis of cryosols and suspended microadmixtures in cryogenic liquids using Doppler spectroscopic method 79—75535
- displacement transducer optimisation 80—86323
- distillation process for noble gas removal from gas streams at Japanese power stations 77—61538
- double-stage cryorefrigerator, for cooling to 10K on a 4-circle diffractometer 80—98919
- EBR-II cover-gas cleanup system 79—97874
- elastic body cryogenic gravitational wave antennae, sensitivity 79—12705
- electric discharge, at insulator surface in liq. He 77—84558
- electric lines, physical parameters anal. 80—82768
- electrical insulating polymeric materials immersed in liquid N_2, short-term insulating characts. 79—85145
- electrical leads carrying current, cooled by vapour 79—75534
- electrohydraulic fatigue apparatus for testing at cryogenic temperature 80—35463
- electronograph cryogenic trap construction 80—31766
- energy doubler quenches, pressure development 79—76200
- energy Doubler refrigeration system for particle accelerators 79—72013
- energy technology relationship 78—88053
- epoxies, commercial powder-filled, measurement of thermal diffusivity, 1.5 to 15K 79—58729
- epoxy polymer, with low thermal expansion coeff. 78—3094
- epoxy resin, low temp. irradiation effects on mechanical props., use in superconducting magnets 78—60737
- EPR method of appl. strong electric fields at low temp. 79—21792
- EPR spectra of γ-O_2 *(Russian)* 78—6565
- ESCAR magnet cooling system 79—30485
- ESCAR superconducting fully cryogenic accelerator 77—83236
- ethane, flow continuity in arterial capillary systems in cryogenic heat pipes 80—64536
- Ettingshausen refrigerator, longit., isothermal, nonstationary regimes, theory 78—18157
- European Space Agency cryogenic programme 79—63239
- European transonic wind-tunnel project for testing at cryogenic temps. 79—58713
- experimental precision, gravitation and general relativity 78—8333
- far IR spectral reflectance of cryogenic constructing materials 77—24855
- fast loading dilution refrigerator 79—58702
- Fermilab Central He liquefier, characts. of main components 79—67991
- Fermilab Tevatron He liquefier power supply 79—68044
- film boiling, heat-exchange intensification, nitrogen in pipes 79—81876
- film boiling mode, disperse, of cryogenic liqs., heat transfer and modified Reynolds model 80—5924
- film- and transition-boiling heat transfer to cryogenic fluids 80—92026
- flange joint design and characteristics 78—86277
- flexible cryogenic system for testing superconducting quadrupole magnets for CERN intersecting storage rings 79—58706
- flowmeter for dynamic flow rate meas. 79—60075
- flowmetering, three-year experience at NBS 77—27637
- fluid boiling in capillary tubes, heat transfer 79—59915
- fluidic/pneumatic level meas. 77—26310
- food and medical industrial appls., equipment for freezing and temp. control 79—58714
- force cooled superconductor cryostability expt. 78—50378
- force-cooled superconductor design for large fusion magnets 79—31216
- forced oscillations of liquid in straight tube *(Russian)* 79—97393
- freeze-etching results interpretation 78—28141
- freeze-fracturing preparation technique, methods and results, review 78—24776
- fusion, toroidal field superconducting coil cryogenic stability and field anal., design parameter 80—106200
- fusion reactor, high current density superconducting coils, cryostability 80—106201
- fusion reactor, MFTF, cryogenic system 80—106163
- fusion reactor, MFTF, mag. cryostability 80—106198
- fusion reactor, press. induced flow cooling, highly stable superconducting mag. systems 80—106192
- fusion reactor, TMX, config., liq. N_2 supply and operation of vacuum system 80—95448
- fusion reactor toroidal field coil thermal design and anal. 78—50368
- fusion reactors, Large Coil Program, pool boiling mag. quench press. calc. 80—106199
- fusion reactors, large Coil Program, Westinghouse coil cooldown and warmup 80—106193
- fusion reactors, Large Coil Test Facility, liq. He cooling system 80—102321

cryogenics continued
- fusion reactors, TMX, installation and operation of cryoliners in vacuum system 80—95449
- gas flow meas. using cryogenic method 78—34245
- gas liquefaction cryogenic microhead 79—95150
- generators, He cooling system selection and efficiency *(French)* 77—26305
- generators, magnet field transient change calc. *(French)* 77—26303
- glass-ceramic capacitance thermometers, low temp., accuracy and stability 77—61074
- heat exchanger, low cost, ultra-compact 79—35758
- heat influx through electrical cable, calc. 78—81988
- heat pipe, cryogenic, gas-controlled performance anal. 78—75034
- heat pipe, internal heat transfer visualisation 78—94533
- heat pipe, with metal-fibre wick, thermophys. characts. investig. 80—4725
- heat pipe/radiator dynamic testing 78—94532
- helium refrigeration system and cryogenic system for superconducting Switchyard magnets at Fermilab 79—67990
- HEUB superconducting dipoles, operating experience 77—83234
- high-pressure apparatus, appl. of sintered diamond tipped, opposed piston apparatus 80—86322
- high-pressure cell for gas-mixture expts. 80—86334
- insulation breakdown characteristics, liq. N_2 partial discharge, polymer films 78—1920
- intermolecular free-length determination in liquids at cryogenic temp. 79—82131
- ion implantation in samples colder than 0.5K, low temp. nuclear orientation studies 80—34033
- IPTS, β-γ transition in O_2 as reference temp. 77—103
- IPTS, boiling and triple points of O_2 and Ar 77—104
- IPTS, O_2 boiling point and triple point realisation 77—105
- IR detector balanced common module coolers 80—95142
- IR detector-preamplifier for cryogenic spectrometer, optimization 80—95164
- IR detectors, non-evacuated cryogenic package 79—97395
- ISABELLE, superconducting magnet quench protection system 77—83233
- Jacobson's const. and intermolecular free-length eval. w.r.t. pressure and temp. 80—15176
- Japanese National Research Institute for Metals, cryogenic appls. 80—4693
- Josephson junction position measurement method 77—69458
- laminar-vacuum insulation, nonstationary heat and mass transfer 78—59279
- laminar-vacuum insulation, nonstationary heat and mass transfer 78—59280
- laser beam waveguide propag. in frozen gaseous layers at 4.2K 80—64168
- laser fusion cryogenic target characterisation by wavefront shearing interferometer 80—74008
- laser fusion fuel configurations, cryogenic, survival in fluorescence energy 77—50288
- laser fusion target, solid-fuel-layer technology 79—49834
- laser fusion target materials, cryogenic processing 80—32443
- laser fusion targets, cryogenic technology 80—68939
- laser fusion targets, fabrication 78—58485
- laser fusion targets, fabrication and characterisation 78—58484
- laser fusion targets, irrad. systems 78—58486
- LBL 88 inch cyclotrons, cryogenic pumping system 79—54681
- leak detect. device for cryogenic fluid tank 78—37016
- Linde cycle, max. thermodynamic efficiency determ. *(Russian)* 77—17984
- liquefier-cryogenic vessel, energy and economical aspects of vapour-cooled shield theory 79—58739
- liquid density meas., radio-isotopic method using γ-ray attenuation *(Russian)* 77—37847
- liquid He cryopump for 1 MV accelerator, cryogenic supply and boil-off removal 79—72011
- liquid methane density meas. at cryogenic temp., commercial densimeters eval. 78—54343
- liquid N monitor for Li drifted Ge detectors 78—29122
- liquid surface, floating insulation beads effect on evaporation rate 77—30164
- liquid to vapour transformations, mechanics of two phase flows 77—89532
- liquids, cryogenic, nucleate boiling, influence of thermal props. of heating surface material 77—46888
- liquids, electrical breakdown, time lag 80—29684
- liquids, simple, generalised charts for computation of two-phase choked flow 77—47061
- liquids, vibr. kinetics, nonlinear optics appls. 80—13082
- low and ultralow temp. cryogenic coolers for space missions 80—77790
- low permeability meas. at cryogenic temperatures 79—30514
- magnet technology, conference, Bratislava (1977) 79—30499
- magnetic field, weak, meas. of absolute intensity, use of RF biased SQUID 80—82794
- magnetic flux-free environment creation 80—101797
- magnetic suspension densitometer for cryogenic meas. 79—12805
- measurements at liquid He temperatures *(German)* 79—5760
- Meissner coils in high-vacuum applications, anomalous behaviour 78—32826
- metal-insulator pairs, frictional heating at cryogenic temps., rel. to supercond. magnet technology 80—66671
- Michelson interferometer, cryogenic, rocket-borne, for EXCEDE II expt. 80—95133
- microbeam anal., conf., Ann Arbor, MI, USA (June 1978) 79—39258
- microminiature cryogenic refrigerators, design, construction 79—26059
- miniature cryogenic liquefier, heat exchange characts. 77—67440
- molecular adsorption refrigeration systems, design theory and performance 79—58722
- MSU superconducting cyclotron cryogenic system, operating experience 79—54672
- multilayer insulation, heat and mass transfer during evacuation 77—30167
- multilayer insulation, heat flux, residual gas press. distrib. 77—30163
- multilayer insulation, heat transfer model 79—94465
- natural gas, liquefied, low-temp. US/USSR materials, mechanical and weld props. 79—61735
- natural gas, liquefied, low-temp. US/USSR materials, mechanical and weld props. 79—61736

cryogenics continued
- neodymium ethyl sulphate, magnetothermodynamics, absolute temp. scale, mag. moment and magnetization , below 0.5K 78—34984
- neoplasm treatment, oral cavity and pharynx 77—78030
- neutron polarisation filter, cryogenic, construction 77—23341
- NMR meas. at ultra-low tapes, S/N ratio, appl. to thermometry 80—73400
- nonisothermal pumping lines, conductance calcs. *(Spanish)* 80—82776
- nuclear cryogenically pumped gas target for γ-ray ang. distrib. meas. 78—55076
- nuclear demagnetisation expts. on Cu, heat leaks 77—45851
- nuclear fusion appl. *(French)* 79—93677
- nuclear magnetic order determ. using low-temperature techniques *(French)* 80—5062
- nuclear magnetism, review *(Japanese)* 80—86806
- nucleate boiling crisis in supercond. magnet cooling channels 79—32196
- nucleate pool boiling in liquid Ar, N_2, and their mixtures 79—60495
- optical system, cryogenic and contamination effects 80—38113
- optics test chamber for cryogenic meas. at high vacuum, upgrading design 79—23098
- orbiting IR detector cooling by multimission solid cryogen cooler 80—86423
- organ cryopreservation apparatus 77—37060
- piston pumps, double-acting, for cryogenic He and N_2 79—58716
- PMMA, solid, stress-strain behaviour, strain rate and temp. effects, cryogenic temps. *(Japanese)* 78—11315
- polymer, solid, impact compression crushing at low temps. *(Japanese)* 78—7032
- polymeric cryoprotectants in preservation of biological ultrastruct., aq. soln. low temp. states 78—65157
- polymeric cryoprotectants in preservation of biological ultrastructure, physiological effects 78—65158
- polymeric cryoprotectants in preservation of biological ultrastructure, morphological aspects 78—65159
- porous solids, gradientless heat transfer, cryogenic liq. crystn. 79—59903
- porous solids, gradientless heat transfer, metallic thermal cond. theory 79—59902
- power packs, using liquid N_2, for operating pneumatic tools 79—58715
- power plants, current lead thermodynamic optimisation using indefinite Lagrange multipliers 77—87768
- pressure-vacuum valve 78—37020
- progress report 79—208
- PVC, solid, stress-strain behaviour, strain rate and temp. effects, cryogenic temps. *(Japanese)* 78—11315
- radiant heat transfer at cryogenic temperatures 79—76950
- radioactive waste, gaseous, cryogenic rectification system for ^{85}Kr and ^{133}Xe removal 78—50268
- radiometer, using a cryogenically cooled two-channel paramp for 47 GHz 77—37982
- radionuclide calorimeter for liquid He range 4.2 to 8K 79—18093
- refrigeration cycle using phase separation phenomena 79—58721
- refrigerators, two-stage operating mode optimisation *(Russian)* 80—22368
- research activities and facilities, low temp., in Italy 79—93146
- review, and applications *(French)* 77—53920
- review, of low temp. physics and technology 78—89485
- review of concepts and trends 78—37022
- review of investigations near absolute zero early investigation to present day discoveries 78—69958
- rocket-borne cryogenically cooled field-widened interferometer for the 2 to 8 μm spectral region 80—95163
- sample rotation, biaxial, in supercond. solenoid *(Czech)* 80—37010
- satellite-borne passive radiative cooler, flight measurements 79—54140
- SEM, X-ray microanalysis, cryogenic stage for sample preparation 80—42306
- semiconductor thermometry at low and very low temperatures 80—4713
- Senftleben-Beenakker thermal conductivity effect apparatus 78—81989
- separation of Kr and Xe from dissolver off-gas in fuel reprocessing plant 77—61590
- solar cooling, Rankine-cycle systems, selection of working fluids 80—104515
- solar receiver convective losses determ., using cryogenic heat transfer tunnel 79—83636
- solid insulating materials, dielectric properties at cryogenic temps. 80—90867
- solitons in low temperature physics 79—63057
- solutions, spectrosc. and photochem. 80—16713
- space chamber, tracer slug leak detection 79—80627
- space research, appl. and requirements *(French)* 79—70942
- space research appls., 1 mK to 10K temp. range, survey 78—93712
- spaceborne refrigerator, ultra-reliable 79—54139
- spacecraft, cryogenic instrumentation 80—86319
- spacecraft instrumentation 79—54138
- specific heat and thermal conductivity measurements, down to 25 mK, heat pulse technique 77—45850
- specific heat measurement, dynamic differential calorimetry 77—74405
- spectrophotometer UR-10 attachment for investigation of small objects at low temps. 79—21822
- Speer carbon resistors as pressure gauges 80—95108
- spherical shell target implosion by laser 77—74977
- spherical target preparation and placement in laser forces by cryogenic device 77—80335
- spray-freezing unit for prep. of specimens for freeze-etching 77—41581
- SQUID appl. to nuclear gyros and magnetometers, high stability and sensitivity 80—98949
- standard resistors, search for appropriate Al alloy 77—17997
- steel, cryogenic, creep, review 80—104222
- steel, Fe-Mn, improvement of cryogenic mech. props. through thermal/mech. treatments 79—79098
- steel, stainless, Cr-Ni, for cryogenic engineering, mech. props. 78—11240
- structural materials 77—17989
- stycast 1266 epoxy, thermal contraction, 4-300K 80—4724
- superconducting 50 MVA generator, thermal design of cryogenic rotor 79—58710
- superconducting dipole magnet system design, for MHD facility 79—52948
- superconducting generators aspects *(French)* 77—26304
- superconducting lens, electron microscope appl. 80—86530
- superconducting magnet energy doubler central liquefier 77—82530
- superconducting magnets, cooling system using liquid He 78—54998
- superconducting magnets, force-cooled conductors design 78—54999

cryogenics continued
- superconducting magnets, hollow conductors, cooled by supercritical He 78—54997
- superconducting magnets cryostabilisation using superfluid He 78—54996
- superconducting quadrupoles used in CERN hyperon-beam, cryogenic design and performance 79—54220
- superconducting telecommunication cables, cryogenic envelope, determination of struct. and thermal insulation performance 79—58731
- superconducting temperature sensor, NbTi monofilamentary wire in current sharing state 80—57288
- superconducting turbogenerators, heat transfer in rotating excitation winding using He in rotating thermosiphon loops 79—58718
- superconductive electronics, conf., Charlottesville, USA (Mar. 1978) 79—28447
- superconductivity, computerised measurement instrumentation 80—98920
- superconductivity at Intermagnetics General Corp. 79—58699
- supercritical liquid air storage plant for elec. energy 78—74006
- target, cryogenic, produced for laser-driven fusion, frozen H_2 78—86688
- temperature calibration device, appl. of miniature sealed cells, and precision cyrostat 77—22559
- temperature controller, use of ICs 80—90856
- temperature cycling apparatus using liquid He storage Dewar 78—65938
- temperature measurement in high mag. fields, instrumentation and methods, review 78—37003
- temperature regulator for use with resistive and capacitive sensors 77—82534
- temperature sensing element calibration 77—26311
- Tevatron Central Helium Liquefier, Fermilab, process control system 79—72012
- TFTR, neutral beam line cryopanels, cryogenic supply systems 78—55027
- thermal insulation, porous gas-filled, configurational effects on heat transfer 79—58734
- thermal insulation, porous multilayer, with diffraction shields 79—58732
- thermometer using Si diode, 4.2-300K range 77—137
- thermonuclear reaction programs, controlled, cryogenic technology and superconductivity 79—54600
- thermosiphon, liquid N_2, effects of heater geometry on flow stability 79—58728
- thermostat, fast reacting, for meas. below 1K, design and testing 77—33994
- thin film ultrahigh-vaccum evaporation/sputtering apparatus 80—20790
- tissue destruction, choice of instrument working temps. 78—36036
- Tokamak power reactor supercond. poloidal magnet system design, experimental 79—31207
- toroidal vessel partially filled with liquid, heat transfer meas. rel. to leakage 80—5913
- trace impurities in gasses, IR spectrometric detect., cryogenic method 79—16053
- transition boiling of cryogenic liquids 79—65182
- treatment device for (sub)atrophic rhinitis and pharyngitis 77—78028
- triple point cells, Ar, O_2, comparison 78—73996
- triple points of Kr, Ar, N_2, Ne, reference temperature appl. 78—73997
- tumour treatment, head and neck, cryogenic instruments 77—78029
- turbogenerator, stability study *(Russian)* 77—53919
- two-stage solid cryogen cooler development, orbital operation, IR radiometer for spacecraft appl. 78—89040
- ultralow temperature physics, future prospects 79—65268
- vacuum chamber at 4.2K, 10^{-14} Torr 77—67449
- vacuum technology, medium, high and ultrahigh, conf., Oxford, England (Apr. 1978) 79—63242
- vacuum-powder insulation, radiative heat transfer determ. by IR spectroscopy 77—13759
- valve design and materials 79—71462
- vapour formation and heat transfer in supercond. magnet cooling channels 79—32197
- vapour pressure meas. gauge of ^{3}He for use up to 0.3K 80—68207
- variable-temperature trap, for separation of gas mixtures 79—16026
- very low temp. physics and meas. *(Japanese)* 78—45636
- Vespel SP-22 resin, thermal contraction, 4-300K 80—4724
- Weber-type gravitational wave antenna, obs. of mechanical Nyquist noise 77—30078
- world energy economy role *(Rumanian)* 80—7933
- zero gravity refrigeration and liquid control by capillary confinement of helium-3 78—43198
- Al, anodized, as cryogenic material, IR reflectance 79—61387
- Ar, porous solid, contact heat transfer of sublimation 77—31767
- Au, thermal radiative props. at cryogenic temps., comparison with model predictions 77—15604
- Cu, high-cond., high spt. ht., for cryogenic appl., prep. 78—76670
- D-T laser fusion target, fabrication using cold-gas jets 79—49833
- Fe-Ni-Al-(Cu) (12, 0.5, 0.5 to 3 wt.%), Cu addition strengthening at 77K, mech. props. 80—60875
- Fe-Ni-Ti-(Cu) (12, 0.25, 2 wt.%), Cu addition strengthening at 77K, mech. props. 80—60875
- Fe-Ni-V-(Cu) (12, 2, 2 wt.%), Cu addition strengthening at 77K, mech. props. 80—60875
- Fe-Ni-(Cu) (12, 0.5 to 3 wt.%), Cu addition strengthening at 77K, mech. props. 80—60875
- H cryogenic storage, liquefaction processes, storage and distrib. equipt. 80—45784
- H fuel, survey of liquid hydrogen container technology for highway vehicle fuel system applications 80—30607
- H_2 liquefier with He refrigeration cycle 79—58740
- H_2, pool boiling, heat transfer coeffs. determ. 78—30165
- H_2 target, liquid, microprocessor-based cryogenic refrigerator controller 79—45491
- ^{2}H cryogenic gas garget design for neutron therapy 77—75020
- He, boiling in tubes, heat transfer, cryogenic stabilisation 78—30162
- He cryogenic discharge, current oscills. 78—67463
- He cryorefrigerator, exergy method of anal. 80—4723
- He cycles, minimal losses due to thermodynamic irreversibility 80—86320
- He dewar, superfluid, for IRAS telescope 79—54143
- He, flowing, pressure and temp. oscillations near critical states 79—58744
- He I cryo-fluid, free convection at supercritical pressures 78—26745
- He II system for refrigerating Spacelab scanning IR telescope 79—54141
- He jet, cryogenic, and recoil TOF apparatus 78—17458
- He leak detection in large cryogenic vessels 78—93694
- He, liq., flow boiling in vertical channels, visualisation 77—42938

cryogenics continued
- He, liq., narrow channel flow and heat transfer characts., void fraction in steady and transient states 78—55000
- He, nucleate pool boiling, heat transfer 77—31823
- He refrigerator system for Fermilab switchyard, microprocessor based control facility 79—68006
- He refrigerator systems, trace impurity analyzer 79—70388
- He rotating rig, for research applied to superconductive alternators with rotating field windings 79—58719
- He, supercritical, heat transfer in turbulent tube flow 78—30287
- He, thermally induced oscills. in cryogenic apparatus 78—67875
- ^{4}He superfluid, precision second sound meas. 77—15648
- Kr, distillation from gaseous effluents 80—5309
- N_2, boiling in tubes, heat transfer, cryogenic stabilisation 78—30162
- N_2, heat transfer during boiling in field of centrifugal forces 79—60493
- N_2, liq., solubility of solidified hydrocarbons and halogen-hydrocarbons, calc. by Preston-Prausnitz method 78—26686
- N_2 pool boiling in high centrifugal accel. fields, peak nucleate boiling heat flux 79—59907
- N_2, porous solid, contact heat transfer in sublimation 77—31767
- N_2 vapour columns, improved natural convection heat transfer 79—59986
- N_2-He mixture, film condensation, appls. to condensers for cryogenic installations 78—59941
- NbTi composites, cryogenic stability due to boundary resistance between filament and matrix 79—58748
- NbTi solenoid, operating at 9 T in He gas 77—74461
- O_2, liquid, pool boiling in inhomogeneous mag. field 77—31766
- Pd-Pt-Au alloys for low-temp. precision resistors 79—69490
- Xe, distillation from gaseous effluents 80—5309

cryopumping
- adsorbent, new high-efficiency cryovacuum polymer type, N_2 adsorption obs. 79—63249
- aerodynamic molecular beam apparatus using cryopumping 77—71335
- annular cryopump in high vacuum evaporation apparatus for thin Cr film deposition 77—90277
- bakeable ion-cryopumped ultrahigh vac. system 80—77802
- balloon borne mass spectrometer, liquid He cryopump and opening device 78—77370
- circulating cooling system, exptl., with rotary pump, for supercond. mags. 77—82528
- cold traps, liq. N_2, automatic level controller, transfer system 78—24805
- condensation cryopump, CERN modified version 80—52253
- condensation cryopump, heat treatment and zone melting installation 80—20959
- cryopump, appl. in science and technology 79—63252
- cryopump, small cryorefrigerators and its appl. *(Japanese)* 78—37021
- cryopump system, for use in HV centre terminal of tandem Van de Graaff 79—63253
- cryosorption pumping of He by charcoal, cryopump design for fusion reactor 80—105654
- CTR cryosorption vac. pumping of D, H and He at 4.2K 77—50298
- cyclotrons, selection criteria 79—54670
- deposition system using liq. He cooled cryopumping panel 78—56581
- doublet III neutral beam source cryopanel system 79—76233
- electrostatic particle accelerator, cryogenic pump for long continous running *(French)* 78—32829
- Excalibur CVR 1106 cryosorption pump, He pumping at 4.2K by mol. sieve SA 79—44914
- freeze-drying technique for prep. biological tissue for electron microscopy 78—65164
- fusion JET machine, cyropumps and cryogenic ancillary equipment 77—30670
- fusion reactor, cryopump neutral beam compatibility test 78—17423
- fusion reactor, cryosorption pumping, D_2-He (5 at.%), on mol. sieve, 5A, 4.2K 78—74499
- fusion reactor, neutral beam injecto cryogenic pumping panel chevron baffles, black coating materials, selection 80—95456
- fusion reactor, radiation-induced degassing 79—85780
- fusion reactor, STARFIRE project, T handling and vacuum requirements 80—106187
- fusion reactor and injector devices, large cryopumps 78—50399
- fusion reactor high power neutral injector cryopumps, design and performance 78—74494
- fusion reactor vacuum pumping using compound cryopumps, performance 80—95452
- fusion research, and fusion reactors, vacuum energy 77—57746
- GSV-250, heated cryogenic pumps 77—74415
- Helios Laser Facility, cryopump high-vac. system for 25000-l. target chamber, design and operational characts. 80—77801
- high vacuum generation, using cryomethods, discussion of types and performance of cryopumps *(German)* 79—88967
- hydrocarbon contamination, of vacuum dependent scientific instruments 79—63259
- industrial vacuum system, cryopump design and performance 77—87777
- ion pump-cryopump system, performance 78—70142
- large area cryopump, pumping speed 80—52255
- liquid He boil-off reduction 77—30157
- liquid He cryopump, for fusion machines, degassing 78—54382
- liquid He cryopumps for PLT neutral beam injectors 78—58439
- magnet spectrometer, QQDDQ Big Karl, cryopump system 79—63257
- magnetron sputtering systems, 20K cryopumping cryopumping sputtering 79—80634
- metallurgical installation, for heat treatment and zone melting 80—20959
- microbalance, vac. type, cryopump 80—77803
- molecular capture coefficient calc. of cryopump cell 77—58538
- neutral beam injection system cryopump, liq. He-cooled, for fusion reactor H_2 pumping 78—74495
- neutral beam injection vac. components, for fusion reactor 78—74493
- neutral beam line injectors, cryopumping system, for Tokamak Fusion Test Reactors 78—55028
- neutral beam line pipe, He cryotrapping capability 80—18638
- neutral beam proximity operation of cryopump, meas. relating to safety, pumping speed and radiation outgassing 79—88968
- neutral beam source, cryopumping and mag. shielding, fabrication and operating cost 80—106229
- neutral injector modular cryopumping system 80—105656
- neutron irrad. effects on pumping characts. appl. to fusion reactors 79—44915
- porosity of solid gas layers *(Japanese)* 80—20031
- quartz crystal production, cryopump appls. 80—90861

cryopumping continued
- refrigerator cooled 20K cryopump with adsorption panels 77—30172
- rough exhaust cryogenic pump 78—228
- sputtering application, cryogenic versus turbomolecular pumping 79—80629
- Stirling cryogenerator 79—67331
- superconducting magnet cooling, optimal cryogenic gas flow 79—93149
- thermal design criteria for optimised cryopump 80—22377
- thermal spike effects on cryosorption pumps with condensed CO_2 layers 79—80635
- thermonuclear fusion appl. *(Russian)* 79—36417
- Tokamak fusion reactors, pumping problems 77—30672
- Tokamak type fusion machine, boundary conditions for cryopumping 77—30671
- Tokamaks, experimental system for studying cryopumping under operating conditions 79—58753
- ultra high vacuum system for MBE of Si 77—67448
- ultrafine particle production *(Japanese)* 80—52252
- ultrahigh vacuum pumps 78—89488
- vacuum production, past, present and future 80—31775
- BN, low-Z material, outgassing expts. 79—209
- BeO, low-Z material, outgassing expts. 79—209
- D, cryosorption pumping, 6 to 20K, fusion reactor appl. 78—70626
- D_2 and H_2 for nucl. fusion, large capacity cryocondensation pump 78—21151
- H^+, energetic beam direct cryosorption pumping 80—105655
- H_2, cluster beam source 79—63258
- H_2, pumping speed of Excalibur CVV2008 liq. He cryosorption pump 79—80633
- H_2, v.p. meas. 2 to 4.5K, influence of thermal radiation 77—5848
- H_2-He mixture, pumping speed of Excalibur CVV2008 liq. He cryosorption pump 79—80633
- He adsorption, cryopump, heat treatment and zone melting installation 80—20959
- He closed-loop cryopumps, design, appl. 79—26062
- He condensation pump for supersonic gas jet, vacuum UV source 79—93155
- He cryosorption pumping at 4.2K by type 5A molecular sieve 78—17422
- He, pumping speed of Excalibur CVV2008 liq. He cryosorption pump 79—80633
- He, supercritical, reciprocating pump for forced flow 78—41317
- ^{4}He adsorption cryostat, 0.5K production 77—10029
- Si_3N_4, low-Z material, outgassing expts. 79—209
- T_2, cryocondensation pumping, smooth surface at 4.2K, fusion reactor application 78—74492

cryoscopes *see cryoscopy*

cryoscopy
- alkali metal salts, heat of melting and activities using cryoscopic data 77—40573
- alloy systems assessment of accuracy of cryoscopic calcs. from fusibility diagrams 77—25010
- cell water permeability during freezing and thawing, cryomicroscope multiple nonlinear regression analysis 79—92197
- fluoride-oxide-SiO_2 system, containing Mg^{2+}, Ca^{2+}, Ba^{2+}, Pb^{2+} 77—28798
- fluoride-oxide-SiO_2 system, containing Na^+, K^+, Li^+, cryoscopy 77—28797
- hydrocarbons, C_1 to C_3, cryoscopic system for purity assessment in range 0 to −190°C 78—3418
- living cell volumetric changes in freezing and thawing, thermodynamic model and expt. 79—92192
- molecular weight measurement using recording thermistor cryoscope based on standard components 77—50572
- solutes, differential concentration by cryoscopic effect 77—36856
- BaF_2-xBaO.ySiO_2, activities rel. to liquidus comp. 77—28798
- CaF_2-xMgO.ySiO_2, activities rel. to liquidus comp. 77—28798
- KF_2-3K_2O.2SiO_2 freezing point depression meas., effect of silica compound additions 77—28797
- LiF-Li_2O.SiO_2, activities rel. to liquidus comp. 77—28797
- MgF_2-xMgO.ySiO_2, activities rel. to liquidus comp. 77—28798
- NaF-3Na_2O.2SiO_2, freezing point depression meas., effect of silica compound additions 77—28797
- Na_2O-SiO_2 melts, cryoscopic struct. study 80—14994
- PbF_2-xPbO.ySiO_2, activities rel. to liquidus comp. 77—28798
- PbO mixtures with various oxides, solvents for garnet growth, cryoscopic study 80—24393
- $UO_2(NO_3)_2$ solutions, cryoscopy and activity coeffs. 78—11544

cryosorption *see sorption*

cryostats
- AC loss measurement apparatus for multifilament superconductor 77—22576
- adiabatic demagnetisation of nucl. spins, refrigeration 78—49844
- adjustable He level cryostat 79—88961
- adjustable temperature system for radiation investigs. in 5-300K range 79—88960
- adsorbed gases, sp. ht. meas. 79—58695
- adsorption cryostats, high cooling power, temp. below 0.7K 77—17995
- air-bath cryostat for enzymology at subzero temps. 78—48949
- apparatus for low-temp./high pressure Mossbauer absorber study, modified 79—17591
- bell-jar for low temp. optical spectrometry *(French)* 77—175
- biological freezing, multipurpose cryostat 78—40437
- biological material freezing, multi-purpose cryostat 78—15940
- calibrating apparatus for resistance thermometers, thermodiodes and thermocouples, 4.2-300K range 78—45624
- calorimetric cryostat, low-temp., with ^{3}He/^{4}He refrigeration, metal-H_2 systems sp. ht. meas. 80—49378
- cold-finger support for Ge shielded γ-ray detector 79—93868
- collective accelerator, superconducting solenoids resonators and cryogenic system 78—46187
- compact transportable He cryostat for optical investigations *(German)* 77—41623
- compact vacuum vessel-cryostat for absorption spectra meas. 77—41689
- conference on cryogenic engineering, London, England, (July 1978) 79—54137
- contact potential difference changes meas. between metal and supercond. at transition temp. 77—22573
- continuous flow, design and application 79—21759
- continuous flow cryostat, for measurement in pulsed magnetic fields 78—37017

cryostats continued
  continuous flow cryostat for low temp. expts. in reactor pile *(Japanese)* 79—54471
  continuous flow He for metal and insulating material thermal conductivity meas. *(Croatian)* 77—26302
  continuous flow helium cryostat for optical studies at fixed high pressure 78—81984
  continuous flow system using supercrit. He, for meas. on superconductors 77—30155
  with continuous He flux, for optical investigations, construction 78—74008
  continuously variable cryostat giving accurate settings at any temperature between 77 and 300K 79—67311
  cooling circuit, 1.8K for Karlsruhe superconducting proton-linac 79—58707
  counterflow gas-liquid helium heat exchanger with copper grid 80—17947
  cryoturbogenerator transition process simulation, cryostat damping casings electrical characteristics determination *(Russian)* 80—8996
  design, and thermal cond. meas. on nylon and graphite, near 100 mK 77—82535
  device for obtaining temperatures of 4.2-300K with considerable heat flow into specimen 78—77922
  dewar, liq. He, for space expts., long-term cooling feasibility 77—33323
  Dewar system for trapped radical study down to 1.5K 79—17427
  dilution refrigerator for low temperature nuclear orientation experiments on line to an isotope separator 79—752
  dipstick cryostat, with temp. controller for high thermal stability 80—37044
  for electron irradiation of crystals 77—41619
  electron microscope, 400 kV superconducting, new cryostat *(French)* 77—192
  emergency cold valve, operating in He II 80—22367
  EPR method of appl. strong electric fields at low temp. 79—21792
  EPR spectroscopy in strong elec. fields at 77 and 4.2K 78—86310
  EPR study 80—86321
  evaporation cryostat for vac. meas. on ultrathin metal film 77—87769
  evaporation-type, for thermal conductivity meas., 4-100K and 0.004-400 W/cm K 77—37878
  far IR absorbent solid dispersive reflection meas., using Fourier spectrometer and cryostat 79—30580
  Fermilab energy doubler magnets, support design and cryostat system 79—31257
  fibreglass insert to liquid He Dewar 78—57967
  fibreglass nonmagnetic He cryostat construction 79—67309
  flow cryostat, for use between 3.5-300K 77—82533
  flow rate meas. in liq. N_2, anemometrical technique 77—31409
  flowing gas He cryostat for Raman spectroscopy 79—67312
  flowthrough opt. cryostat for operation with superconducting solenoid, for magnetoopt. investigations 80—105651
  fusion target prep. of solid H_2, D_2 using cryostat, laser fusion research 78—17417
  gas high pressure cell for optical studies at low temp. and hydrostatic pressure 78—82016
  glass He cryostat for optical and magneto-optical investigations 78—74007
  glass He cryostat for Raman scattering meas. 78—290
  glass He cryostat for spectroscopic investigation and electron irradiation of crystals 77—37899
  glass helium cryostat for optical and magneto-optical studies 78—81981
  glass liquid He cryostat for Mossbauer spectroscopy 79—58853
  He cooled, closed cycle, for accelerator based radiation damage studies 77—41622
  heat capacity cryostat for small specimens in 1.5 to 10K range 80—68204
  IR absorption spectrometer cryostat 79—67396
  IR cell, variable-temp., for studies of adsorption on alkali halides, 80 to 300K 79—80604
  ISABELLE storage rings magnet cryostats, mech. design 77—83218
  lambda-tight In rings, simple demountable device for fixing 77—30160
  large cooling power, for polarised target of electron synchrotron 77—34496
  large scale He II, for supercond. RF particle separator 77—30742
  Linde cycle, max. thermodynamic efficiency determ. *(Russian)* 77—17984
  liquid He automatic replenishment system 79—67308
  liquid He boil-off reduction 77—30157
  liquid He cryostat for collection of 3-dimensional X-ray intensity data down to 20K 80—22369
  liquid He cryostat for optical meas. 79—88962
  liquid He transfer controller, semiautomatic 79—17428
  liquid nitrogen level monitor, for parametric amp. using diode sensor 78—29121
  low cost simple cryogenic controller, temps. 78 to 300K 77—22555
  for low temperature thermometer calibration *(German)* 77—37897
  magneto-optical, optical meas. at 0.4K, cooling by evacuation of ^{3}He vapour by an absorpt. pump optical meas. at 0.4K, cooling 80—73369
  magneto-optics cryostat with balanced thermal dilatations, 1.7 to 300K 79—63203
  magnetofluid seals appl. to rot. cryostats 80—4721
  magnetooptical, with superconducting solenoid at 83 kOe 79—71461
  mass production for large particle accelerators 79—68045
  matrix isolation apparatus for magneto-optical obs. 78—82057
  mechanical testing devices for high and cryogenic temps. 78—7137
  metal, optical window 77—33996
  microfluorometric measurements of DNA dye complex using cryostat 80—17949
  mini-cryostat for planar solid state detectors 79—22550
  miniature continuously filled He^4 cryostat 78—41316
  Mossbauer effect measurement apparatus for use at high press. and low temps. 77—67548
  Mossbauer effect study at 65 and 77K 79—67364
  Mossbauer spectroscopy, cryostat and proportional counter design 79—54238
  multipurpose, for low temp. electron irrad. of semicond. 79—35755
  neurosurgical cryoprobe, self-contained, with replaceable flask, features 78—7526
  NMR probe assembly, He-cooled, for proton-enhanced ^{13}C reson. 80—17978
  non-metallic, used with 1.5 MJ pulsed superconducting coil, performance tests 79—49259

cryostats continued
  nonvacuum X-ray cryostat with liquid N level control 77—41624
  normal boiling point determination for Ne 78—79757
  optical high-pressure chamber 80—31767
  for optical studies 77—41619
  Porous heat exchangers for continuous flow helium cryostats 78—16803
  portable ^{3}He cryostat for space appls. 77—22077
  portable ^{3}He detector cryostat for far IR 78—41352
  prototype supercond. quadrupole magnet for CERN intersecting storage rings 79—31265
  pulse radiolysis, var. temp. cell housing 78—27794
  reentrant Dewar, modified, for magneto-optical flux detection in superconductors 78—89486
  refrigerator cooled, design and performance 79—58754
  RF-biased SQUID, with half-wavelength transmission line 80—22342
  rotating, He flow, temp. distrib., thermodynamics 78—34666
  rotating, high-speed, containing liquid He, heat transfer by natural convection 79—58720
  rotating, vapour column flow anal. 80—4722
  ruby valve, lambda-tight, for liq. He II transfer 77—30159
  semiconductor galvanomagnetic effects meas. *(Hungarian)* 77—17986
  silica windows in liquid He cryostat, unwanted birefringence 78—66926
  small 77 to 400K for semicond. galvanomagnet effects meas. 77—30149
  small constant flow cryostat design 77—30156
  small flow-through cryostat for polarization microscope 78—86327
  small-sample mag. semiconductor thermoelectric power meas. installation 80—31795
  solid cryogen cryostat for cooling IR detector onboard spacecraft 79—54122
  space research instrumentation, use of solid cryogens *(French)* 77—134
  specific heat determination, powders, meas. apparatus for 4.3-300K 80—227
  spectrophotometer universal cryostat attachment 80—31765
  spectroscopy studies, of inorganic and organic molecules, sublimation temp. 300 to 3000K *(Russian)* 79—10094
  SQUID adjustment *(Polish)* 80—31768
  SQUID magnetometer with temp. control, spontaneous magnetisation and mag. susceptibility meas. 80—68221
  SQUID magnetometers, geophysical dewar systems design 80—101462
  student apparatus for laboratory course in supercond. 79—58494
  student demonstration He cryostat for superfluidity and superconductivity obs. *(Polish)* 80—86059
  superconducting electron microscope lenses, construction of cryostat for testing 77—22627
  superconducting lens system for 500 kV electron microscope 80—68321
  superconducting magnet, low evaporation cryostat *(Japanese)* 79—44910
  superconducting magnet system, development for physical experiments 80—9008
  superconducting magnets, precooling using Cryomech GB02 cryocooler and gas-filled thermal switches 80—52245
  superconducting solenoid SUPER-SOLO, switch and cryostat 79—54222
  superconducting solenoids for polarized beam synchrotron, magnet and cryostat design 79—31252
  superconductive electronics, cryocoolers 79—26058
  surface tension meas. 79—17426
  TEM liquid He cooled environmental cell 80—68323
  temperature field inhomogeneity in cooled screen, effect on efficiency 78—62204
  temperature regulator for 77 to 340K range, Ge transistors use as heating elements 77—67442
  temperature regulator for liquid ^{4}He bath near 4.2K 78—41319
  temperature regulator for low-power cryostats 77—37880
  temperature variable cryostat, design and construction, for MCD spectroscopy 77—22554
  tensile testing cryostat for 200 kN tensions 79—96235
  thermal conductivity meas. of semiconductors, 90 to 450K 79—76957
  thermal conductivity measurement, of plastically deformed specimens at liq. He temps. 78—81985
  thermal load by radiation from the neck *(German)* 78—86276
  thermal transport in solids 80—52243
  thermostat for heat dissipating electronic devices 79—88941
  thin film, internal friction meas. apparatus for 4.2-300K 79—5093
  thin film fabrication and simultaneous computer-controlled measurement equipment, automatic 79—69984
  throat, with coaxial extension elements, heat exchange efficiency 80—77769
  transfer cryostat from liquid N_2 to He, for annealing meas. 77—45855
  twin-chamber flexible vacuum connection 80—73368
  two-channel cryostat for UR-20 spectrophotometer 78—24800
  US strengthening of cryst. mats., instrument for US attack at low temp. 77—49732
  vacuum deposition of thin films, cryostat *(Japanese)* 78—27403
  vacuum monochromator low-temp. attachment construction and optics 80—31764
  vacuum tight heat bridge, for use at temperatures below 0.1K 78—37018
  vacuumless, optical investigations of semiconductors 80—73370
  vapour pumping system, for obtaining temps. of 4.2 to 300K 78—81980
  volatile substances, cryostat for low-temp. investig. of IR spectra 79—54136
  X-irradiation of solids at low temps. 80—86321
  X-ray diffraction study, crystal structure of polyethylene at 4.5K 78—14288
  X-ray diffractometry of solid He, cryostat design 77—53921
  X-ray topography, cryogenic, using synchrotron radiation 77—39507
  Al-NbTi solenoid magnet for high energy particle detector, conductor and cryostat design 79—31319
  Ar triple point realisation cryostat for Pt resistance long stem thermometers 77—26307
  $Ce_2Mg_3(NO_3)_{12}.24H_2O$ demagnetization cryostats, appls. of nucl. cooling in nucl. orientation studies 79—63230
  H_2, cluster beam source, cryopumping 79—63258
  ^{3}H3, continuous flow cryostat, for polarised targets 80—52240
  He, cryostat, rotating, centrifugal field rel. to residual press. in vac. cavity 80—42232
  He cryostat for low temp. calorimetry 79—40577
  He cryostat modification for asymm. Michelson interferometer 78—74053
  He cryostat system for gas sorption meas. at 12-150K 78—32823
  He dewars, liquid, use of detachable leads for energising superconducting magnet 79—63240

cryostats continued
He evaporation cryostats for expts. in solid-state physics, 5K to 320K 79—58708
He, exptl. horizontal rotating, design 77—33993
He, for adjustable coding of open refrigeration tube 79—35759
He, for high press., low-temp. X-ray diffr. 77—11442
He, for prolonged low-cycle fatigue testing 79—52491
He immersion and gas-flow optical cryostat system 78—77923
He, liq., dewar, temp. profile 77—41621
He, liquid, as zero mechanical work thermal pump for superconducting AC machines 79—58717
He, liquid, for use in dispersive Fourier transform spectroscopy 79—54135
He, liquid, safety aspects 79—58730
He, liquid, wide-aperature dewar, heat analysis and reduction of evaporation rate 79—58743
He, liquid cryostat, design and construction for e$^+$e$^-$, annihilation $\gamma\gamma$ ang. correl. meas. 79—93148
He liquid rotating cryostat, design and tests 77—26309
He, superfluid, for Spacelab and ESA cryogenic programme 79—63239
He superfluid systems for space environment, porous-plug liquid-vapour separators 79—54142
He temperature, for use with dispersive Fourier Michelson interferometer 79—2841
He, temperature controller appl., using digital voltmeter *(Czech)* 78—29120
He underground rippled dewar system for 10000 MWh superconductive energy storage magnets 79—58705
He, with refrigerator, for superconducting magnet 79—58733
^{3}He cooled, for polarised targets 77—13760
^{3}He cryostat, continuously operating for Mossbauer investigation of biological samples 79—96725
^{3}He cryostat for calorimetric meas. of solids *(German)* 78—16805
^{3}He cryostat with automatically refilled condensation stage 77—17996
^{3}He, liquid, cryostats for different refrigerating capacities 79—58749
^{3}He liquid target for scatt. expts. 78—70663
^{4}He cryostat design, superconductive tunnelling study *(Spanish)* 80—73347
^{4}He, isotopically pure, apparatus for preparation 78—57959
N cryostat for −195 to +150°C range with sample heating 77—74406
N$_2$, liq., cryostat for obtaining temps. −195 to 150°C and forced heating of specimen 77—74403
N$_2$, liq., temp. distrib., appl. to microwave thermal noise source 79—58700
NH$_3$, solid, gamma-irrad., cryostats development 77—45856
Nb-Ti (50%), supercond., cryostat design for magnetisation study *(Spanish)* 80—75673

cryotrons
development in Japan *(Japanese)* 78—45637
Nb-NbO$_x$-Pb junction, static charact. of tunnelling cryotrons 79—28480
Nb$_2$Sn, thermally controlled, used in transformer-rectifier flux pump for superconducting magnet 80—4727

crystal atomic structure
see also crystal atomic structure of alloys; crystal atomic structure of elements; crystal atomic structure of inorganic compounds; crystal atomic structure of organic compounds; electron diffraction crystallography; lattice constants; neutron diffraction crystallography; space groups; superlattices; X-ray crystallography
atomic structure determination, experimental methods, review 79—68970
binary crystals, stability and average structure factors 78—91297
Bragg reflections, ratio of integral intensities, determ. struct. perfection of single crystals 80—87987
Bravais classes and superspace groups for the classification of structures with a one-dimensional modulation 79—94938
Bravais lattices, new group theoretical deriv. 79—77540
Bravais-lattice operator in one band of solid 80—10519
centrosymmetric crystals, triplet phase invariants, formula from fourth order determinantal joint probability distrib. 80—15030
Clebsch-Gordan reduction for cryst. irreducible representations problems 78—2052
coincidence site lattices, and pattern shift lattices *(French)* 79—69035
computer aided graphical representation, of projections onto coordinate planes 79—60217
condensed models based on square-type layers, derivation 77—55254
conference, International Crystallography Congress, Warsaw, Poland (Aug. 78) 79—23481
convergent beam electron diffraction, determ. of crystal point groups and space groups *(Japanese)* 79—77461
coordination number, proposed rigorous definition 79—99085
coordination numbers in solids, Pearson diagrams 80—107103
cubic crystal structures, Archimedean truncated octahedron and packing of geometrical units 80—15028
cumulative distributions, symmetry- and composition-dependent of normalized structure amplitude for use in intensity statistics 79—32847
density distribution of bonding electrons, simple refinement, method 78—18573
density distribution of bonding electrons, simple refinement, applic. to diborane 78—18574
development over 50 years, microscopic particles, microscopic struct. of matter *(Chinese)* 77—68929
diffraction methods, philosophic concepts and implementation 79—94932
discrepancy indices, in presence of random positional errors, crystals with similar atoms 79—73058
dislocation core, symmetry of dynamical electron microdiffraction patterns 80—100140
electron density maps, extrapolative filtering, resolution maximisation 78—75506
electron energy spectrum in crystals, use of atomic scatt. form factors 80—6688
electron microscopy of atoms in cryst. 77—43122
energy spectrum and transition probabilities, point group coupling, coeffs., props. and application 80—43033
ferroic point groups, four categories 79—82169
fluorite structured crystals, high temp. disorder and elastic consts. 78—30689
four-dimensional space, crystallographic groups, book 79—27942
framework structures, from 4- and 8-membered rings 79—73113
generating function techniques 80—44162
geometric properties of cryst. lattices in spaces of arbitrary dimension 79—90588

crystal atomic structure continued
group theory, space and point group factorization, appl. to crystallography and spectroscopy 79—60295
group theory applications to physical and chemical systems in relation to struct. and substructs. 80—42921
hard-disc system, structures of close-packed thin layer 79—27941
Heesch group struct., rel. to mag. prop. tensors 77—8274
Hirshfeld type deformation functions, and elec. field gradients calcs. by Fourier series 79—73479
historical review *(Danish)* 79—9071
homogeneous linear structures, systemisation according to charact. numbers of position symbols 78—95009
infinitely adaptive crystal structures, elastic energy, long range repulsive interaction 78—38647
inorganic cages, rel. to cubane and adamantane 80—19729
interatomic vectors construction, of crystal without calculating Fourier series 79—94840
ionic crystal, arrangement of ions, eutactic 78—9982
Karl-Hauptman matrix, joint probability distrib. of struct. factors in space group P1 79—23480
Karle-Hauptman matrix, conditional phase probability distributions of struct. factors 79—19120
kinematical (Universal limit), and freedom from extinction 79—23486
KKR method, structure constants, electronic struct. 80—80152
least-squares structure refinement, weighting scheme, using Chebyshev polynomial 79—73067
magnetic materials, symm. restrictions on constitutions eqns., group theoretical procedure 77—55255
magnetic point groups, rel. to mag. props. of cryst. 77—31622
metric tensors, in Hilbert space, geometrical approach to solving cryst. structs. 79—32846
microparacrystals in physics, review *(German)* 79—27933
Miller Index concept, teaching aids 79—84910
mixed crystals, 1D and 2D, ion distrib. statistics 80—49167
modulated non-commensurate layer structures, nomenclature and classification 79—94931
modulated structures, conference, Kailua Kona, Hawaii, USA (March 1979) 79—94928
modulated structures, general treatment 79—94966
modulation operations and derived structs. 79—94930
molecular assembly, two dimens. packings of elliptical mol. 79—37640
molecular cryst. struct., principles *(German)* 79—42000
molecular crystals, spectroscopy, bibliography (1977) 80—7317
molecular fragments, oriented, use of struct. factors to find origin 77—51266
molecular theories appl. to crystalline state struct. 79—55680
NMR spectra moments, props. of orientation dependences, cryst. struct. investigations 79—60239
noncentrosymmetric structures, antisymmetric atomic features, Bijvoet ratio 79—32925
noncentrosymmetric structures, correlation between third cumulants in refinement 78—91288
nonstoichiometric compounds, intermediate phase 79—65013
occupation statistics for 2-dimens. lattices of single particles 77—33951
ordered structure conditions, pairwise interaction model *(Japanese)* 79—51018
orientationally disordered structures, orientation and position correlations of a mol. 80—14966
orientationally disordered structures, positive definiteness of orientational distrib. functions 80—14958
p-orbital bands and crystal struct. stability 77—7691
Patterson method, multiple solutions for low symm. systems *(Chinese)* 80—87986
periodic structure homometric set, search algorithm 80—75118
perturbation stable cell comparison technique 80—49133
phase determination, appl. of quartet and quintet invariants 79—51034
planar molecules, molecular packing 80—24383
point group symmetry, derivation and recognition schemes, computer assisted learning programmes 77—29973
point groups, Cauchy symm., elastic work functions 77—72644
point groups, Racah coeffs., isoscalar factors, character formulae 77—13568
point groups, symmetry, teaching aid 78—77650
polyhedral cavity field tensors 80—100182
polytypic crystal structs., appl. of self-consistent field method to statistical model 79—37639
powder least-squares program, POWLS 80—1892
quantum field theory of crystals and extended objects, review 79—42164
quasi-symmetry and double point groups C$_4$ and D$_3$ 80—92472
quasisymmetry (P-symmetry) groups in crystallography, semidirect products method 78—51457
Racah coefficients for point groups, chemical space groups and mag. group symmetry 80—57214
Rietveld neutron profile refinement, interactive computer system, POWDER 80—1900
rigid molecules, with large librations, dynamic density and struct. factors 79—7515
Shubnikov point groups, PUA representations 79—55690
simple cubic lattices, coordination radii and numbers, distant neighbour potential energy contributions 79—77535
single-crystal diffractometry, peak searching, crystal setting and determining automatic cell constants 80—6319
solids, evaluation of finite strain eqns. of state using lattice models 80—96620
soliton lattice melting, functional integral method 80—17883
space groups, of low symmetry, comments on struct. refinement 79—90582
space groups, triclinic, cryst. struct. refinement by least squares 78—75607
spin point groups, nontrivial, rel. to mag. point groups 77—31620
stereoviews and morphological data on microcrystals 78—18510
struct. parameters determ. from NMR spectra anl. of two-spin system 77—89353
structural fragment, automatic construction, taking account of attainable chem. bond lengths 80—92419
structure analysis, separation of unknown parameters 80—28869
structure factor moduli, estimates from negative intensity obs. 78—75486
structure imaging, direct, in electron microscopy 79—68990
structure models, positional errors, their influence in the residual R_2 79—7563

crystal atomic structure continued
structure semiinvariants, extension concept, role in probabilistic theory 78−75608
STRUKTURA, program system for cryst. struct. investigations 80−44071
substitutionally disordered binary systems, existency domain 80−88068
superposition of similar structures, optimisation transformations 79−27865
swinging twinning on unit cell level as cryst. struct. building operation 77−31623
symmetry adaptation, operator equivalence, mag. reson., operator equivalent formalism *(French)* 78−84374
teaching, close packed crystal struct. model, for handling and overhead projection 78−24625
teaching, coordinated polyhedra approach 77−78934
tensorial covariants for the 32 crystal point groups 79−19173
tetrahedral molecules, structural relationships between plastic and ordered phases 79−55681
transplutonium element symposium, Baden-Baden, Germany (September 1975) 77−28974
triclinic lattices, planewise summation method 80−107069
triplet phase invariants, formula for acentric case 80−84115
two-phase cryst. structures, orientational electron microdiffr. anal. with aid of OMEGA program 80−103218
two-phase semi-invariants, probabilistic theory of first rank via method of representations, practical appls. and aspects 79−50921
unit cell, determinantal eqns. for scale factor, temp. factors, quantitative chem. contents 78−75609
vacancy modelling, topological approach 80−10543
Vavilov-Cerenkov parametric effect, to use in cryst. struct. investigation 80−1895
Wyckoff site description of cryst. struct., depend. on labelling of axes 79−23557
X-ray Bragg scattering, in the Born-Oppenheimer approximation 79−32850
X-ray high order refinements of H atoms, theoretical approach 79−19121
Zhdanov notation, resolution of ambiguities, homometric structs. 77−31619

crystal atomic structure of alloys
A15 structures, atomic radii and lattice parameters 77−89408
A-15 compounds, radical plane construction appl. to effective atomic radii rerivation 79−99109
A-15 type, derivation of related structs. 78−30573
AB_2 Friauf-Laves phases, atomic sites and H absorpt. 80−24406
actinide, metallurgical props. rel. to electronic struct., energies calc. method 77−20221
alkali metal binary intermetallic cpds., OPW calc. of struct., bonding and stability 77−43169
alkaline earth-group IVB intermetallic compounds, occurrence, struct. 78−38663
aluminides of non-magnetic transition metals, atomic volumes deviation from additivity 79−82178
atomic ordering, appl. of Green's temp. functions *(Russian)* 79−51051
binary alloys, and intermetallic cpds., struct. and stability, ab initio pseudopot. calcs. 78−34460
brass, nonradial diffuse streaks and complex diffuse scatt. patterns of electrons 79−7527
γ-brass type structures, factors determining adopting of I or P shell 77−24290
brass-like alloy phases, binding and cryst. struct., valence arguments 80−88081
γ-Cu_5Zn_8, high pressure effect on brass struct. 80−107108
cubic metallic structures, cryst. field coeffs., geometric struct. factors 77−43547
dimensional analysis, bonding information from valency effects appearing as artefacts 80−96471
disordered alloys, interatomic distances, coord. numbers, and mean relative displacements, EXAFS anal. 80−89087
$Fe_2Al_xSi_{1-x}$, DO_3 structured, ferromag., lattice parameters 79−42010
ferrous alloys, phase transforms. and ordering, Mossbauer spectroscopy 77−12619
germanides, $(T,Nb)_{11}Ge_8$, T=V, Cr, Mn *(French)* 78−38675
group VIII and nearly related elements, cmpd. and superlattice form. 79−94955
inhomogeneous binary alloys, X-ray diffr. profile calc. 78−67609
intermetallic phases, struct. description *(German)* 80−88090
intermetallic phases with $L1_2$ and $D0_{19}$ struct., atom incompressibility, lattice parameter approach 78−91294
interstitial compounds, electronic structure and useful phys. props. 77−89683
interstitial solid solns., HCP, ordering type transitions within thermodynamics theory framework 80−49162
Invar, Fe-Ni alloy, atomic struct., elastic neutron scatt. obs., phase diagram 79−94964
Kh20N40 alloys, phase composition after quenching, tempering 78−60650
$L1_2$ and $L1_0$ superstructure atomic ordering phase diagrams, order-disorder transition 80−38989
lattice images using high resolution TEM 78−34399
Laves phases C14, C15 and C36, electrostatic energy calcs. 77−1095
local atomic arrangements, associated with ordering, review 80−50632
long period stacking variants, stability in pairwise interaction model 79−94956
martensite, habit plane 78−18572
martensite crystal, struct. X-ray diffr. study 78−79565
martensite steel, cryst. struct. variation during heating, role of Mn and Al *(Russian)* 79−46600
martensitic transform. mech., martensite crystal lattice and C atom behaviour 77−25051
mischmetal-$Ni_{5-x}Al_x$ ternary alloys, Al addition effects on structural and H_2 absorpt. props. 79−52761
modulated structures, X-ray diffr. 77−39502
Nimonic 80A, struct., fracture characts. 80−3071
nonstoichiometric compounds, physicochem. props. depend. on short-range order struct. 80−100227
nonstoichiometric solid solutions, ordering 78−87794
order-disorder transitions, alloys with DO_{22} and $L1_0$ superstruct. 80−38990
ordered alloys, cryst. struct. and phase transforms. *(Russian)* 79−29047

crystal atomic structure of alloys continued
ordering, statistical theory including interatomic interaction energy change and anisotropy 77−15542
ordering, theory, crystal lattice parameters rel. to composition and order *(Russian)* 79−77543
phase diagrams and struct. under press., index of substances 79−60484
pyrochlore struct. and its relatives 79−14773
rare earth alloys, R_3Pt_4, cryst. struct. and lattice const. determ. 77−55266
rare earth alloys, R_3Ru and R_5Ru_2, cryst. struct. 80−1965
rare earth alloys, RBe_{13}, XPS, resist. and susceptibility study 80−71565
rare earth alloys, RCd_2, bonding props. 77−58969
rare earth alloys, RCo_2, elec. resistivity, thermopower, X-ray struct. meas. 80−24874
rare earth alloys, RFe_4Al_8, cryst. struct. mag. props. and hyperfine interactions 78−87648
rare earth alloys, $RGe_{2-y}Ni_y$ phases with AlB_2-type struct. 77−24292
rare earth alloys, RM_2X_2 (M=Rh, Pd,Ag,Ir,Pt,Au; X=Si,Ge), cryst. struct. 80−1964
rare earth alloys, RPt_2Si_2, struct. determ. 77−89407
rare earth cobaltides, RCo_3 type, hydride phase synthesis, thermal stability and struct. 80−59438
rare earth hydrides, props., book contrib. 80−45291
rare earth intermetallic, $R(Fe_{1-x}Mn_x)_2$, phase struct., mag. and Mossbauer meas. 77−20563
rare earth intermetallic, RCu_4Ag, $AuBe_5$ struct., mag. props. 77−20562
rare earth intermetallic, RCu_4Ag and RCu_4Al, struct. study 78−30587
rare earth intermetallic cpds., cryst. chemistry, book contrib. 80−39010
rare earth intermetallic cpds., R_3Os, cryst. struct. 80−96475
rare earth intermetallics, RMg_2, cryst. and mag. props., ordering 78−68185
rare earth intermetallics, RMn_2Si_2 and RMn_2Ge_2 78−59782
rare earth iron silicides, $R_2Fe_4Si_9$ and $RFeSi_3$, cryst. struct. and mag. suscept., temp. depend. *(Russian)* 78−34957
rare earth phase structure, dimens. anal. 80−96470
rare earth ternary alloys with Fe or Co and Si or Ge, $ThCu_2Si_2$ type 78−51469
rare earth trialuminides, long period polytypes, electron diffr., high resolution imaging 78−83781
rare earth-Cd alloys, existence and cryst. struct. 79−77555
rare earth-Ga alloys, phase diagrams 79−78932
rare earth-Hg alloys, cryst. struct. determ. 79−77555
rare earth-iron intermetallic, O-stabilised, $R_{12}Fe_{32}O_2$, prep., struct. and mag. props. 77−8956
rare earth-nonmagnetic metal intermetallic cpds., struct. and props., review 79−95377
rare earth-Pt alloys, cryst. struct. determ. 78−26491
rare earth-transition metal alloy, R_xT cryst. struct. 77−55265
rare earth-transition metal intermetallics, struct. and props. review 78−10668
rare earth-transition metal-aluminium intermetallics, RT_6Al_6, T=Cr, Mn, Fe, Cu, cryst. struct. 80−107110
rare earth-Zn alloys, existence and cryst. struct. 79−77555
Santa Catharina, Fe-Ni (50 wt.%) superstructure obs. 79−30024
silicides, $(Cr, Nb\ or\ Ta)_{11}Si_8$, $(Mn,Mo)_{11}Si_8$ *(French)* 78−38675
space filling elongated rhombic dodecahedron in alloy structs. 79−32946
stability and structure, pseudopotential calcs. *(German)* 80−38913
steel, 50N29 type, self-consistent junctions and spatial relative organisation 80−19750
steel, Cr-Mn, X-ray diffr. exam. of fine struct. during deform. *(Russian)* 78−38661
steel, galvanized, Fe-Zn phases, Mossbauer study 80−50233
steel, Ni, martensite decomposition *(Russian)* 79−1841
steel, thermodynamic props. of C in austenite, relationship with cryst. lattice anomalies of martensite *(Russian)* 78−59781
superconducting materials, properties, review and table 77−4460
superconducting materials properties 79−56366
superstructure, stability and crystallographic characts. *(Russian)* 78−18583
thermodynamic properties and struct., microscopic theory *(Japanese)* 80−29191
Ticonal, effect of rare earth metals on mag. props., struct., and phase transformations 79−99732
Ticonal, two- and one-dimens. modulated struct. after thermomag. treatment and water quenching *(Russian)* 80−29983
transition metal, metallurgical props. rel. to electronic struct., energies calc. method 77−20221
transition metal alloy, ground state properties, self-consistent calc. 78−91587
transition metal alloy phases, and σ phases, electron factors 79−46602
transition metal alloys, BCC crystal struct. dependence on band struct. 78−83778
transition metal-B subgroup element alloy, ordered BCC phases at high temp. 79−32948
transition metal-group IIIB alloys, relationship between struct. and thermodynamic props. *(German)* 78−91307
X-ray diffraction powder patterns, standard, for 112 substances 79−60223
X-ray diffraction powder patterns, standard, for 87 substances 80−64839
Ag-Ge system, atomic struct. and electronic props. *(Russian)* 77−20289
Ag-Nd *(German)* 78−51472
Ag-Pr *(German)* 78−51472
$Ag_xAu_{1-x}Zn$, resistivity and X-ray diffr. 78−47283
AgCd-AgMg(AgZn), quasibinary alloys, phase relations 79−8273
Ag_3Mg, long-period alloy, ordered struct. 79−27949
Ag_3Mg, long-period ordered, struct., high resolution electron microscopy obs. 79−94960
Ag_3Mg, structure of ordered alloy, electron diffraction, kinematical vs. dynamical diffraction calc. 80−10530
γ-Ag_5Zn_8, high pressure effect on brass struct. 80−107108
Al-Ag alloy, second ageing stage, diffuse electron and X-ray scatt. *(Russian)* 78−68711
Al-Al_3Ni eutectic, cryst. struct., orientation, electron microscopy, computer calcs. *(German)* 77−72582
Al-Cu (1.9 at.%), solute fluctuations, EXAFS study 80−79949
Al-Cu (3.97 wt.%), containing Guinier-Preston zones, high resolution lattice images 80−107114
Al-Cu (4.3 wt.%), containing Guinier-Preston zones, high resolution lattice images 80−107115
Al-Cu (4.3 wt.%) alloy, lattice electron micrograph interpretation 79−86659

crystal atomic structure of alloys continued
- Al-Cu-Ni, vacancy ordering, electron microscope and electron diffr. obs. 79—27954
- Al-Fe (49 at.%) quenched alloy, neutron diffuse scatt., diffuse ω phase obs. 80—84141
- Al-Fe-X-Si (X=transition metal), struct. and comp. by electron microscopy 80—88093
- Al-Ge (6.8 at.%), quenching from mushy state for production of metastable phases 80—35223
- Al-Mg (13 wt.%), aged single crysts., small angle neutron scattering 80—1961
- Al-Mg-Li alloy, metastable S′-phase, struct. *(Russian)* 80—103291
- Al-Ni-Si sintered SAS-1 alloy, struct. *(Russian)* 79—52135
- Al-Pd, rapidly solidified, new ordered phase, electron microscope obs. 79—11645
- Al-Pd (6 at.%), metastable Al_2Pd phase formed by rapid quenching, electron diffr. obs. 79—51054
- Al-Pt (2 at.%), splat cooled, $AlPt_2$ phase, electron diffr. obs. 79—15657
- Al-W(Mo)(Nb), struct. and props. of alloys obtained from granules 80—50717
- $Al_{1.1}Be_{0.6}B_{22}$, metal distrib., X-ray diffr. study 80—75204
- Al_4Ca, phase transformation, struct. and orientation relationships 79—78963
- α-AlFeSi, anomalous dispersion methods 78—9998
- $Al_4(Ni, Co)_3$ ternary phase in Al-Ni-Co system, cryst. struct., vacancy controlled phase *(Chinese)* 80—70164
- AlSc, lattice parameter changes in Al 3d alloys 77—62504
- $Al_{10}V$, well defined local modes, inelastic neutron scatt. study 78—26648
- $Al_{10}V$-Ga, dil., well defined local modes inelastic neutron scatt. study 78—26648
- AmB_2 (B=Al, Co, Fe, Rh, Ru), crystal structure, mag. props. of Laves phases 77—27851
- $AmPt_5$, preparation and cryst. struct. *(French)* 78—42959
- Au-Ge (27 at.%), metastable phase struct. determ. by electron diffr. 78—83780
- Au-Mg (18 at.%) alloy, superstruct. determ., electron microscope obs. 78—75630
- Au-Mg alloys, long-period superstructures, electron diffr. obs. 79—94959
- Au-Mn, orthorhombic struct., electron diffra. and electron microscopy obs. 80—15052
- Au-Mn alloys, equiatomic region of phase diagrams crystallographic and mag. exam. 78—52755
- Au-Mn system, AABB struct., experimental evidence for occurrence 78—63698
- Au-Mn-Cr(Pd) alloy, ferro- to non-mag. transform. 77—12117
- Au-Pd-Zn system, quasibinary phases investig. 77—12596
- AuAl formation by thin film interactions, identification by X-ray diffraction 79—99442
- Au_3Cd_5 and Au_5Ce_8.h, cryst. struct. and binding type *(German)* 79—86742
- AuCd.r, cryst. struct. determ. 77—84699
- $AuCu_{0.5}Zn_{0.5}$, internally deformed struct. as source of homogeneous linear struct. 78—26497
- $Au_{11}Mn_4$ ordered phase formation, electron diffr. and microscopy study 80—107418
- $Au_{11}Mn_4$, ordering, electron diffr. and high resolution TEM obs. 78—71707
- Au_4Mn, atomic short range order and pair interaction, neutron diffr. exam. 78—22695
- Au_4Mn, heat treated, short-range order, diffuse X-ray diffr. study *(German)* 80—88092
- Au_5Mn_2, electron microscope exam. of ordering 78—63697
- $Au_{35}Ni_{65}$, vapour quenched amorphous alloy, atomic arrangements 80—100173
- Au(Pd)-Zn, martensitic transformation, Hall coeff., specific elec. resistivity and X-ray powder diffraction 78—72774
- $AuSn_4$-Sn, unidirectionally solidified, X-ray diffr. anal. of crystal struct. 78—91308
- Ba-Pb system, intermediate phases, equilib. phase diagram, cryst. struct. 77—44213
- Ba_2Cd and Ba_2Hg 77—11505
- BaCu, X-ray cryst. struct. determ. 80—92478
- $Ba_{10}Ga$, cryst. struct. *(French)* 80—79749
- $BaNiSn_3$, cryst. struct. rel. to $ThCr_2Si_2$ type *(German)* 78—51470
- $BaPdSn_3$, prep. and crystal structure *(German)* 80—84138
- $Ba_{0.67}Pt_3B_2$, cryst. struct. and supercond. props. 79—38231
- $BaPtSn_3$, cryst. struct. rel. to $ThCr_2Si_2$ type *(German)* 78—51470
- Ca_3Cd_2 77—11505
- $CaCu_5$-type structure, intermediate phase, relative stability and struct. characts. 77—58968
- $Ca_{0.67}Pt_3B_2$, cryst. struct. and supercond. props. 79—38231
- $Ca_{31}Sn_{20}$, X-ray diffr. 78—14310
- $CaZn_3$, struct. with mixed $BaLi_4$- and $CeCu_2$-like ordering 80—107106
- $Cd_{65}Hg_{35}$ and $Cd_{55}Hg_{45}$, X-ray study of cryst. struct. and thermal expansion 80—24405
- Ce-Co-Al (0-33.3 at.% Ce), isothermal section, X-ray study *(Ukrainian)* 80—39002
- Ce-Ga system, phase equilib. and cryst. struct. of phases 80—35159
- Ce-In, phase equilibrium and cryst. struct. 80—66483
- Ce-Mn-Co, cryst. struct. determ. 77—11508
- Ce-Mn-Cu systems, phase equilibria at 600 and 400°C *(Ukrainian)* 80—11625
- Ce-Mn-Fe, cryst. struct. determ. 77—11508
- Ce-Mn-Ni, cryst. struct. determ. 77—11508
- Ce-Tl, phase equilibrium and cryst. struct. 80—66483
- $CeBe_{13}$, intermediate valence state, XPS, resist. and susceptibility study 80—71565
- $CeCoAl_4$, X-ray anal. of crystal struct. *(Russian)* 77—55263
- $CeCo_{3.5}Cu_{1.5}$, and alloys of similar comp., cryst. structs., X-ray diffr. exam. 79—99120
- $Ce(Cu,Ni)_2$, pseudobinary phases, struct. and mag. props. rel. to Ce valence 78—6032
- $CeMn_2Si_2$, cryst. and mag. struct. determ. 78—52225
- $CeNi_{8.5}Si_{4.5}$, X-ray cryst. struct. determ. 80—88089
- $CeRh_{3-x}Pd_x$, electronic and cryst. struct. comparison, catalytic behaviour 78—84398
- $CeRh_{3-x}Pd_x$, lattice spacing and mag. suscept., effect of prep. and hydrogenation 77—58976
- $CeRh_{3-x}Pd_x$, powdered alloys, catalytic behaviour correlation with electronic struct., lattice struct. and surface comp. 79—82181
- $Ce_2Rh_2(Pt_2)$, structure determ., rhombohedral Er_3Ni_2 type 77—80443

crystal atomic structure of alloys continued
- $Ce_2Sc_3Si_4$, X-ray cryst. struct. determ. 80—92480
- Ce_5Sn_3, low temp. modification with tetrogonal struct. 80—1963
- Co-Al alloy, multilayer martensite phases, illustration of polytype structures 80—84932
- Co-Cu (8 wt.%), X-ray anal. of 126-layer rhombohedral martensite α'-phase 77—44251
- Co-Fe, double hexagonal alloys, crystalline and mag. props. *(Japanese)* 79—73132
- Co-Ga, β' phases, evidence of non-cubic lattice distortions around vacant sites 78—42956
- Co-Ga alloys, phase diagrams and cryst. struct., DTA, X-ray diffr. and microprobe anal. *(French)* 79—47660
- Co-Gd-B, rules of cmpd. form. in related systems 79—34010
- Co-mischmetall system, phase relations, microstruct., mag. props. 80—104118
- Co-Ti alloys, martensitic transformation depend. on ageing, cryst. struct. 79—91649
- Co-V (20.7 wt.%), cryst. struct., electron and X-ray diffr. study 80—44172
- γ-Co-Zn, γ-brass, struct. obs. 77—24290
- $(Co_{0.83}Cu_{0.17})_6Ce$, cryst. struct. and mag. props., decomp. during ageing *(Russian)* 79—37661
- Co_4CuCe, cryst. struct., mag. characts., ageing and decomposition *(Russian)* 79—4272
- $Co_4CuCe_{0.9}$, correl. of cryst. struct. and coercive force *(Russian)* 77—80962
- Co_2FeGa, alloy, site preference of Co and Fe, Mossbauer and neutron study 79—78577
- β-CoGa, Cu addition effects on defect struct. *(German)* 77—11546
- $Co_2Ga_{2-x}Cu_x$, mag. and struct. phases from magnetisation, neutron, X-ray diffr. techniques 78—52253
- $Co_2Ga_{2-x}Ni_x$, mag. and struct. phases from magnetisation, neutron, X-ray diffr. techniques 78—52253
- $CoIn_3$, ordered phase, cryst. struct. determ. 78—2066
- CoMnP, cryst. mag. struct., neutron diffr. study *(French)* 80—59439
- Co_2P, struct. comparison with Co_2Si, $PbCl_2$, and SbSI *(French)* 80—84155
- CoSb, at. struct. and mag. susceptibility 77—39561
- Co_2Si, struct. comparison with Co_2P, $PbCl_2$, and SbSI *(French)* 80—84155
- Cr-Fe-Ni alloys, cryst. struct. and defects, high resolution electron microscopy obs. 79—94961
- Cr-Si-Cu, struct. and supercond., Cu influence 80—50592
- Cr_5Al_8, 26R cryst. struct., unit cell parameters 77—19904
- γ-Cr_5Al_8, γ-brass, cryst. struct. redeterm. 77—47377
- $(Cr_{1-x}Fe_x)_{1+\delta}Sb$, interstitial occupancy, Cr:Fe distrib., X-ray and neutron diffr. study 79—42012
- Cr_2Os, σ phases, ordering, X-ray cryst. struct. determ. 80—107107
- Cr_2Ru, σ phases, ordering, X-ray cryst. struct. determ. 80—107107
- Cr_3Si type phases, A-15, crystallographic interpretation of atomic volumes 79—10833
- Cu-Ag(Ta) metastable alloy form. by ion implantation, combined TEM and ion channelling obs. 78—34530
- Cu-Al, disordered alloys, interatomic distances, coord. numbers, and mean relative displacements, EXAFS anal. 80—89087
- α-Cu-Al, short range ordered, struct. and new superlattice phase 78—52756
- α-Cu-Al (9.13, 13.56, 14.76, wt.%) short-range ordered, characterisation of locally ordered regions 80—79747
- Cu-Al alloy, ordered, superlattice fringe images, computer simulation 80—103296
- α- Cu-Al alloy, short range order structure 78—91303
- Cu-Al-Ni, struct. anal. of stress induced β_1'' martensite by neutron diffr. 79—60308
- Cu-Au off-stoichiometric alloys, long period superlattice 79—55699
- Cu-Be alloy, X-ray diffr. pattern singularities *(Russian)* 78—67682
- Cu-Be-Ni (1.9, 0.32 wt.%) solution treated alloy, age induced vol. changes in structural transformations *(Russian)* 79—100179
- Cu-Co-S system, phase equilibria determ. by silica tube techniques 79—60482
- Cu-Cr, age hardened, fine precipitates struct., TEM study 80—3066
- Cu-Ga porous solid formed by shock compression 80—29905
- Cu-Ge(Sb) systems, atomic struct. and electronic props. *(Russian)* 77—20289
- Cu-In eutectoid, directional eutectoid decomposition growth, crystallography 80—29874
- Cu-Ni-Sn (10, 6 wt.%), spinodal decomposition, X-ray and electron diffr. study 80—81063
- Cu-Pt type alloys, theory of ordering *(Russian)* 77—1100
- Cu-Sn(-Al), quenched and aged, struct. of phases *(Russian)* 80—49184
- Cu-Ti (5.7 at.%), dil., β-phase struct. 79—55700
- β-Cu-Zn-Al, diffr. effects., obs. and interpretation of extra maxima 80—44173
- Cu-Zn-Al Marmem alloy, β_1 phase superstruct. obs., rel. to transform. mode 78—39776
- Cu-Zn-Ga configs. of martensite variants, shape deform. matrices 77—12620
- γ-Cu_9Al_4, struct. refining from diffr. meas. 78—55834
- Cu_2AuPd, struct., TEM and electron diffr. meas. 78—38666
- Cu_2MnAl, Heusler alloy, decomposition at 360°C 80—7536
- $Cu_{0.435}Ni_{0.565}$, clustering, temp. depend., diffuse neutron scatt. study 79—42013
- η-Cu_3Si precipitates in Si, cryst. struct. 78—91304
- Cu_3Sn, one-dimens. long period superstructs. with Zn and Ni additions 78—83777
- CuSnMg, crystal struct. anal. 78—91306
- Cu_4SnMg, crystal struct. anal. 78—91306
- Dy-Fe-Al, pseudobinary alloy, struct. exam. 77—58979
- DyC_x, $0.28<x<0.53$, cryst. struct. and Curie temp. 79—86741
- $DyCo_2$-$DyAl_2$ system, mag. and structural studies 80—108006
- Dy_5Pt_4, isotypic with Pu_5Rh_4, X-ray cryst. struct. refinement anal. 79—4271
- Er-Co-Ni, cryst. struct. and H_2 capacity 77—89543
- Er-Fe-Al(Mn)(Co), cryst. struct. and H_2 capacity 77—89543
- $(ErCo_2)_x(ErAl_2)_{1-x}$, mag. and struct. investigations of intermetallic systems 78—95440
- $Er(Fe_{1-x}Mn_x)_2$, struct. determ. by X-ray diffr. *(Russian)* 77—76358
- $Er_6Ga_{1.5}Ni_{2.5}$, struct. determ. by X-ray powder method *(Ukrainian)* 80—39001

crystal atomic structure of alloys continued
Er_5Pt_4, isotypic with Pu_5Rh_4, X-ray cryst. struct. refinement anal. 79−4271
Eu-As system, cryst. struct. of phases formed 78−26493
Eu-Cd compounds, Mossbauer effect, mag. props. and lattice consts. 77−36164
Eu-Ga alloys, phase diagrams, struct. and comp. *(Russian)* 79−52163
$Eu_{11}As_{10}$, Eu_5As_{10}, $Eu_{3+x}As$, Eu_5As_3, Eu_4As_2O, cryst. struct. 78−18585
Eu_5As_3, cryst. struct. of high and low temp. phases 78−75626
$EuPt_x$ compounds, partial valence change, ^{151}Eu Mossbauer and magnetisation obs. 80−70167
Fe cast with spheroidal graphite, fine cryst. struct. on tempering *(Russian)* 80−96476
Fe-Al, electron density distrib. vs. at. order 79−60309
Fe-Al alloy, ordered, superlattice fringe images, computer simulation 80−103296
Fe-Al eutectic alloy, duplex crystals, unit cell parameters, appl. of Weissenberg technique 78−67684
Fe-C martensite, crystal struct. and morphology of ordered phase 79−42011
Fe-Co, ferromagnetic micropowder, cryst. struct., coercivity, remanence, saturation 80−65967
Fe-Co alloy, V addition effect on atomic order parameters, dislocation struct., mechanical props. 79−91762
Fe-Co based alloys, redistrib. of elements, combined appl. of emission and absorption Mossbauer spectroscopy *(Russian)* 78−6031
Fe-Co-Si solid solutions, BCC, atomic configs., Mossbauer study 80−39006
α-Fe-Cu, coordination fields of crystal struct., rigid-sphere model 78−47266
Fe-Mn, effect of N on cryst. lattice parameter of austenite *(Russian)* 78−67683
α-Fe-Mn, singularities of martensite struct. *(Russian)* 80−28948
Fe-Mn-As, crystal struct. and magnetic props. of intermetallic cmpds. with Cu_2Sb type struct. *(Japanese)* 78−59785
Fe-Mn-C, atomic interaction structure in carbides 78−42955
Fe-Mn-Sb, phase comp. 80−16267
Fe-Mo alloys, cryst. struct. and defects, high resolution electron microscopy obs. 79−94961
Fe-Ni, ordered phase, Llo superstruct., Mossbauer spectrum, Debye-Scherrer pattern from LL-chondrite 80−50241
Fe-Ni, taenite, superstruct. in Fe meteorites 78−61820
Fe-Ni (25 to 50%), FCC, meteorites and thermodynamic equilib., Mossbauer and X-ray diffr. study 80−88087
Fe-Ni alloys, electrodeposit on Cu, texture investig. 77−11818
Fe-Ni-C-Mn (3.56, 3.25, 0.6 wt.%), solid soln., quenched, changes during annealing to crystal structure, mech. props. *(Russian)* 79−34076
Fe-Ni-Co-Ti, martensite cryst. lattice tetragonality, $\gamma \rightleftharpoons \alpha$ transform. *(Russian)* 79−61587
Fe-Ni-Pt system, ordered phase fields of equilibrium diagram 78−48373
Fe-Ni-Ti martensitic alloy, γ' particle effect on crystallisation struct. *(Russian)* 78−44129
Fe-Ni-Ti-Al, martensite, nature of tetragonality 79−32936
Fe-Ni-V-(CO) alloy, lattice parameter variation during ageing *(Russian)* 78−39812
Fe-Rh alloy, nonmag. and mag., band theory 79−37973
Fe-Si, electron density distrib. vs. at. order 79−60309
Fe-Si-Al (5,10 wt.%) struct. anal. by electron microscopy and electron diffr. *(Chinese)* 79−11618
Fe-Si-Al sendust type alloys, Co preferred substitution sites, Mossbauer spectra 79−91328
Fe-Zn, crystallographic relations by X-ray diffr. 80−24408
Fe-Zn, δ-phase, X-ray analysis 77−59758
δ-Fe-Zn layer formed on hot dip galvanising, texture 77−9001
Fe_3Al, containing C in solid solution., mag-permeability disaccommodation *(Polish)* 79−95613
Fe_3Al-M, ternary ordered solid solns. with M=Ti, Mn, Ni, Cu, Ge substituent 77−43177
$Fe_{73}Al_xSi_{27-x}$, DO_3 structured, ferromag., lattice parameters 79−42010
FeCo, isothermal annealing effect on lattice const. *(Japanese)* 79−20076
Fe_2CoGa, alloy, site preference of Co and Fe, Mossbauer and neutron study 79−78577
Fe_2Hf, ferromagnetism in hexagonal and cubic compounds 77−36074
$(FeMn)_3$ Si alloys, L2,A struct. of single phase alloy 77−59393
$Fe_{3-x}Mn_xAl$, ordering of Fe atoms, X-ray diffr. meas. and mid gamma reson. anal. *(Russian)* 80−96469
$(Fe_{1-x}Mn_x)_3Si$, $(Fe_{1-x}Co_x)_3Si$, order distrib., hardening effect *(Russian)* 77−89410
Fe_2MnSi, antiferro- and ferromag. props. 77−12104
$Fe_{3-x}Mn_xSi$, struct., magnetisation, and spin echo expts., rel. to local environment model 77−20518
$Fe_{0.7}Ni_{0.3}$, Invar alloy, bulk moduli, pressure effect on lattice spacing 79−55805
FePC molten and amorphous alloys, struct. factors 80−79674
FePt lattice, symmetry, state of order, vibration, temp. effects *(German)* 77−4067
$FeSb_2$, phase structure, X-ray crystallography *(French)* 78−91305
$Fe_{1+x}Sb$, phase structure, X-ray crystallography *(French)* 78−91305
Fe_3Si, 3d transition metal substituted, limits of solubility, mag. props. and electron conc. 78−10670
Fe_xSi_{1-x}, struct. exam. by electron diffr. and resist. meas. 77−89409
FeTi-D(H), γ-phase, neutron and electron diffr. 80−84156
$FeTiD_x(O \leq x \leq 1.9)$, neutron diffr. struct. anal. 80−75447
$(Fe_{1-x}V_x)_3Ge$, magnetic and X-ray studies 80−1966
$Fe_{3-x}V_xSi$, struct., magnetisation, and spin echo expts., rel. to local environment model 77−20518
Fe_4Zn_9, γ-brass struct. with I cell 77−24290
β'-Ga-In, metastable binary phase, X-ray diffr. determ. of cryst. struct. 80−1967
Ga-Ni-R, (R=Dy, Ho, Er, Tm, Lu), struct. determ. by X-ray powder method *(Ukrainian)* 80−39001
Ga-transition metal alloys, phase diagrams and cryst. struct. *(French)* 79−47659
Gd-Co-B system, phase composition, struct., phase equilibria 78−35355
Gd-Fe-B ternary systems, phase equilibria and cryst. struct. *(Ukrainian)* 80−11626
Gd-Mn alloy, mag. props. and effect of H_2 absorpt. 78−19250
Gd-Ni-Al, (Gd<33.3 at.%), isothermal section, 800°C, X-ray and microscopic anal. *(Russian)* 79−27950

crystal atomic structure of alloys continued
$Gd(Al_{1-x}Mn_x)_2$, ordering on crystallographic sites, X-ray diffr. 78−38662
$GdCO_2$, lattice parameter determ. 79−14737
Gd_3Co_3Ga, crystal struct., X-ray determ. *(Russian)* 79−27951
$Gd(Co_xIr_{1-x})_2$, C15 Laves phase struct., g shift, linewidth EPR meas., Fermi level movement interpretation 79−61210
$Gd(Co_xIr_{1-x})_2$, struct. and mag. moments, comp. depend. 79−86743
$Gd_{1-x}Dy_xNi$, FeB-CrB type stacking variations, cryst. struct. 80−64952
$GdMn_2$-$GdAl_2$ system, mag. and structural studies 80−108006
$(GdMn_2)_x(GdAl_2)_{1-x}$, mag. and struct. investigations of intermetallic systems 78−95440
$Gd_2Ni_{17-x}Al_x$, X-ray obs. 79−65034
$GdRh_2H_x$, $GdRu_2H_x$, struct. and mag. props., Mossbauer and magnetisation meas. 80−71271
$Gd_{1-x}Y_xNi$, FeB-CrB type stacking variations, cryst. struct. 80−64952
Ge-Ag, exam. of structure using electron microscope *(Russian)* 79−14738
Ge-Si:Sb, prepared in Universal Furnace expt. in Soyuz-Apollo programme, melting and crystn. 80−19737
Ge_2FeGa, and Fe_2CoGa, site preference and local environment effects, Mossbauer and NMR expts. 78−43710
GraNi-rare earth intermetallics, struct. by X-ray powder method *(Ukrainian)* 80−10529
Hf-Co-Ga system, crystal atomic struct. and phase equilibria *(Ukrainian)* 78−84772
Hf-Ge-B system, phase equilibria 78−35356
Hf-Ni (65 to 80 at.%), phase diagram and cryst. struct. of intermediate phases 79−52170
$HfFe_2Si_2$ 77−31633
$HfNi_3$, α and β modifications, X-ray cryst. struct. determ. 79−7578
Hf_3Ni_7, X-ray cryst. struct. determ. 79−4270
Hf_8Ni_{21}, single-cryst., X-ray cryst. struct. determ. 79−4269
$Hf_3Ni_2Si_3$, struct., lattice consts., space group, X-ray Weissenberg camera data 78−47284
HfV_2, C-15 struct., phase transitions, elec. cond., crystal lattice parameters *(Russian)* 80−54826
$Hf_{1-x}Zr_xV_2$, lattice consts. at 4K and room temp., phase division at $x=0.4$ 78−51474
Hg-Tl, metastable system, prep. by quenching, phase struct. 78−52762
$Hg_{99}As$, struct. reinterpretation 78−38660
β-$Hg_{0.80}In_{0.20}$, cryst. struct. from powder patterns 79−51052
Ho-Ga-Ni (60, 30 wt.%) cryst. struct., isostructural compound structural study 80−33930
$HoCo_{5.5-x}Mn_x(Fe_x)(Ni_x)(Cu_x)$, cryst. struct. and mag. props. 80−75800
$HoCo_{5-x}Ni_x(Cu_x)$, lattice parameters and mag. props. 79−82817
Ho_5Pt_4, isotypic with Pu_5Rh_4, X-ray cryst. struct. refinement anal. 79−4271
In-Sb, cryst. struct. after appl. of high press., supercond. transition temp. 80−70169
In_4Ag_9, γ-brass struct. with P-cell 77−24290
In_4Au_9, γ-brass struct. with P cell 77−24290
In_2Bi, cryst. struct. and density *(German)* 80−24407
$InMn_3$, crystallographic anal., new form of γ-brass struct. with a P cell 79−99116
Ir alloys, R_5Ir_2 (R=Pr, Nd, Sm, Gd, Tb, Dy, Ho, Er, Tm, Lu, Y), cryst. struct. 80−96473
IrLi and Ir_3Li 77−11506
$IrMn_{1+x}Sb$ alloys, crystal struct., and mag. props. 78−34466
Ir_5Sn_7, cryst. struct. determ. *(German)* 79−27952
α-IrV, internally deformed struct. as source of homogeneous linear struct. 78−26497
K_3Ga_{13}, X-ray cryst. struct. determ. 80−92479
La-Bi alloy system, phase diagram, struct. of intermetallic compounds 77−44214
La-Cu alloys, cryst. struct. exam. 77−58978
La-Fe, FCC, Mossbauer spectra, Fe atom position 80−20549
$LaCoAl_4$, X-ray anal. of crystal structure *(Russian)* 77−55263
$La(Co_{1-x}Ni_x)_5$, distrib. of Co and Ni atoms, neutron diffr. obs. *(Russian)* 80−64954
$La_3Co_2Sn_7$, prep. and crystal structure *(German)* 80−84138
$LaNi_{5-x}Al_x$ ternary alloys, Al addition effects on structural and H_2 absorpt. props. 79−52761
$LaNi_{5-y}Al_y$ alloys and related hydrides, thermodynamic and struct. props. for H_2 storage appl. 80−16847
La_3Pt_2, structure determ., rhombohedral Er_3Ni_2 type 77−80443
La_3Sn, cubic phase, high press. and high temp. synthesis, and characterisation 78−19687
La_5Sn_3, low temp. modification with tetrogonal struct. 80−1963
β-Li-Al, lattice parameters, density, defect struct. 80−24440
Li-Pd (60 to 75 at.%), phase diagram and cryst. struct. of $LiPd_2$ phase *(German)* 79−51055
Li-Rh-H system, intermetallic cpds. and phase relationships, cryst. struct. 78−44084
$Li_2Ag_{2-x}In_x$, optical props., struct., energy bands, interband transitions 78−72539
7LiAl, cryst. growth, Stockbarger method, struct. and homogeneity 80−89137
LiAl, pseudopotential method and ordering problem 77−35500
$Li_2Cd_{2-x}In_x$, optical props., struct., energy bands, interband transitions 78−72539
$LiCd_{1-x}Tl_x$, intermetallic, X-ray and Knight shift meas. of ^{205}Tl and ^{113}Cd 79−42851
LiIr, struct. and props. exam. 78−92245
Li_yPdH_x, production and cryst. props. *(German)* 77−43176
Li_yPtH_x, production and cryst. props. *(German)* 77−43176
$LiRh_3$ 77−11506
LiTl, pseudopotential method and ordering problem 77−35500
Lu-Mn alloy, mag. props. and effect of H_2 absorpt. 78−19250
Lu_5Pt_4, isotypic with Pu_5Rh_4, X-ray cryst. struct. refinement anal. 79−4271
Mg base Laves phase alloys, long period struct. classical lattice gas model method 79−94957
Mg-Er (<25%) alloys, struct. and props. 79−96001
Mg-Ga, metastable cryst. and glassy phases, X-ray struct. anal. and electron microscopy *(German)* 79−46601
Mg-Ga (6 wt.%), precipitation, lattice const., ageing effects *(Chinese)* 79−43279
Mg-Nd-Zn dilute alloy, metallography and precip. kinetics 80−71655
$MgCu_2$-$MgAl_2$, Friauf-Laves phase, long-period stacking variants, electron conc. depend. 77−80444

crystal atomic structure of alloys continued
$Mg(Cu_{1-x}Al_x)$ with $x=0.465$, Friauf-Laves phase, electron microscope obs. 77—19908
$MgCu_{2-x}Ni_2$, X-ray and neutron diffr. investigation of Laves phases of $MgCu_2$-type *(German)* 80—15050
$Mg(Cu_{1-x}Zn_x)_2$, crystal struct. and lattice spacing under high press. comp. depend. 77—72581
$MgCu_{2-x}Zn_x$, X-ray and neutron diffr. investigation of Laves phases of $MgCu_2$-type *(German)* 80—15050
$MgNi_2$, four-layer, Friauf-Laves phases, stacking variants 80—96468
$MgNi_{2-x}Zn_x$, X-ray and neutron diffr. investigation of Laves phases of $MgCu_2$-type *(German)* 80—15050
$MgZn_2$, struct. exam. using Shaw's model potential calc. 77—19906
$MgZn_2$, two-layer, Friauf-Laves phases, stacking variants 80—96468
$MgZn_2$-$MgAg_2$, Friauf-Laves phase, long-period stacking variants, electron conc. depend. 77—80444
$MgZn_2$-$MgAg_2$ system, Friauf-Laves phases, stacking variants 80—96468
Mn-Cu, mag. and cryst. struct., neutron and X-ray diffr. meas. *(Russian)* 78—22694
Mn-Cu (9.3 wt.%), cryst. struct. at FCC to FCT transform. *(Russian)* 80—11643
Mn-GA system, cryst. struct. and degree of order *(Chinese)* 79—51048
Mn-Ga, DO_{22} type alloys, magnetic props., crystal struct. *(Japanese)* 78—59784
Mn-Ga, mag. and cryst. struct. in conc. region of gamma phase, temp. depend. *(Russian)* 79—65649
Mn-Ga system, X-ray struct. investigation, solubility *(Chinese)* 80—88084
Mn-H(D), ferromag., thermal, struct. mag. props. 78—88145
Mn-Ni, γ-phase antiferromag., lattice distortion and elastic props., ΔE effect interpret. 77—20671
Mn-Ni(Pd), atomic and mag. order, neutron diffr. exam. 79—73697
Mn-Si (62.5 to 63.8 wt.%), phase anal. and cryst. struct. *(Japanese)* 80—15049
$Mn_{1.11}Al_{0.89}$, unit cell parameters, temp. depend. 79—55697
Mn_4Al_{11}, X-ray cryst. struct. 80—38999
γ-MnAu, antiferromag., phase diagram, X-ray diffr. and Young's modulus meas. 80—71024
$Mn_{77}Fe_4Si_{19}$, cryst. struct. and superstruct. 77—35511
Mn_2Ge_7, high-temp. phase, X-ray powder cryst. struct. *(German)* 80—39005
β-$Mn_{66}Ni_{20}Si_{14}$, X-ray crystal struct. refinement 79—14735
MnSb, interstitial cations, mag. and crystallographic study 79—55698
MnSi-Si system, striations and cryst. struct. of matrix 80—103292
$Mn_{85.5}Si_{14.5}$, R-phase 78—42953
$Mn_5(Si_{1-x}Ge_x)_3$, magnetic and cryst. struct., ferromag. props. 77—59391
$Mn_{23}Y_6D_x$, D atom location, neutron diffr. study *(French)* 80—24426
Mo-Al-Ge, new compounds, structure and props. 80—39003
Mo-Al-Ge, X-ray phase and microstructural anal. 80—93536
Mo-Co-Si alloys, cryst. struct. and defects, high resolution electron microscopy obs. 79—94961
Mo-Si-Cu, struct. and supercond., Cu influence 80—50592
Mo-Sn-Se system, supercond. crit. temp. and cryst. struct. *(Russian)* 80—107947
Mo-ZrC, internal oxidation, struct. formation law, microstruct. examination 78—84836
Mo_3CoSi, TEM study 79—51047
$Mo_{1.7}Ge_{0.3}B$ 77—52285
NaTl, pseudopotential method and ordering problem 77—35500
Nb A15 compounds, preferential order-disorder 77—84702
Nb-Al-Ir A-phase, crystal struct. determ., $MgZn_2$-Laves C14 type 77—1099
Nb-B, atomic order, stability, supercond. *(French)* 80—50021
Nb-Ga-Ir, phase equilib. at 1000°C, cryst. data for intermediate phases 78—52763
Nb-Ge, transition metal atom stabilised superconductivity 79—7924
Nb-Ge-Sn(Pt)(Ir), A15 cpds. prod. by liq. quenching, phase stability and supercond. props. 79—95538
Nb-H, ordering of hydride phases 77—19902
Nb-H interstitial alloy, props. and synthesis 79—69265
Nb-H system, phase diagram and transforms., struct. obs. of various phases 80—104125
Nb-Ir-O, H-phase, cryst. struct. 78—38664
Nb-Ir-O, phase struct., supercond. H-phase 78—39246
Nb-Ni-Al alloys, cryst. struct. and defects, high resolution electron microscopy obs. 79—94961
Nb-Pt-O system, phase equilibria, diagram, unit cell parameters, supercond. 80—55352
Nb-Si-Cu, struct. and supercond., Cu influence 80—50592
Nb-Si-Sn(Pt)(Ir), A15 cpds. prod. by liq. quenching, phase stability and supercond. props. 79—95538
NbAl, α phases, lattice parameter and order 77—76359
$Nb_3Al(Ge)$, bonding, electronic charge distribs. and struct. transform. from self-consistent pseudopotentials 79—69054
NbAlIr A′ phase, struct. 78—18587
Nb_3As, structural and supercond. props. press. effects 80—39700
Nb_4CoP, new ternary phosphide with Nb_4CoSi type struct. *(Russian)* 77—55262
NbD_x, λ-phase struct., neutron and electron diffr. meas. 79—94962
$NbFe_{2-x}Si_x$, crystalline struct., electron microscopy determ. *(French)* 80—54174
$Nb_{78}Fe_{40}Si_{80}$, X-ray cryst. struct. determ. *(French)* 80—15048
Nb_4Ga_5, cryst. struct. and homogeneity range 78—42957
Nb_3Ge, and $Nb_{0.82}$, structural and supercond. props. press. effects 80—39700
$Nb_3Ge_{0.8}Nb_{0.2}$, A-15 type struct. and order parameter 79—77552
NbH(D), ordered, TEM obs. of anisotropic lattice distortions 79—7579
Nb_3Si, high press. phase, prod. by recrystn. of metastable sputter deposits, struct. and supercond. props. 78—60571
Nb_3Si, structural and supercond. props. press. effects 80—39700
Nb_5Si_3, supercond. props. and cryst. struct. 79—78245
Nb_3Sn, atomic displacements induced by radiation damage, X-ray study 80—2085
Nb_3Sn, X-ray study of fission fragment induced structural damage 78—51589
NbSnSb, synthesis and struct. *(French)* 79—90596
Nd-Fe-B ternary systems, phase equilibria and cryst. struct. *(Ukrainian)* 80—11626
Nd-Ga alloy, phase diagram, DTA, X-ray and metallographic obs. 79—24494

crystal atomic structure of alloys continued
Nd-Ni-Al, isothermal section, 600°C, X-ray struct. anal. *(Ukrainian)* 80—33929
$NdAg_2$, high temp. modification, thermal effects 78—38665
Nd_3Co_3Ga, crystal struct., X-ray determ. *(Russian)* 79—27951
$Nd_3Rh_2(Pt_2)$, structure determ., rhombohedral Er_3Ni_2 type 77—80443
Ni-Al (36 at.%) martensite, ordering obs. *(Russian)* 77—80446
Ni-Al solid solution, Ni-rich, superordered martensite formed during quenching 77—32577
Ni-base cost multicomponent alloy, γ′, carbide, boride phases, quantities, composition *(Russian)* 78—75627
Ni-Co, low temperature lattice parameter, Gruneisen parameter 77—76357
Ni-Cr-Ti-Al-Mo-Nb-Fe (13-16, 2.35-2.75, 1.3-1.7, 2.8-3.2, 1.8-2.2, 2.0 wt%), heat resistant props, mech props. struct., stepwise ageing effects *(Russian)* 78—76666
Ni-Fe (67.7 at.%), noncommensurate atomic struct., neutron diffr. exam. *(Russian)* 77—84701
Ni-Fe-Al type B2 lattice alloys, Fe atom distribution, Mossbauer study *(Russian)* 79—99796
Ni-Fe-Mo(Cr), determ. of preferential locations of Mo or Cr on Fe and Ni sublattices, by X-ray intensity study 79—37662
Ni-Ga alloys, phase diagrams and cryst. struct., DTA, X-ray diffr. and microprobe anal. *(French)* 79—47660
Ni-Pd-Ge, phase relationships and struct. 77—36451
Ni-Ti alloy, struct. and props., self-propagating high temp. synthesis *(Russian)* 78—26492
Ni_3Al, at. displacements, characteristic temp. and lattice spacing, temp. depend. *(Russian)* 79—90598
Ni_3Fe, short-range order, diffusive elastic neutron scattering 80—24400
NiGa, point defects, lattice parameter determ. 78—38695
NiMnGe, crystal and spiral mag. struct., Neel temp., X-ray and neutron diffr. 77—16052
Ni_2MnIn, Heusler alloy, order-disorder phase transitions, X-ray diffr. meas. 77—66640
$NiPt_NGe_{N'}$, cryst. struct. *(German)* 80—44171
NiSb, at. struct. and mag. susceptibility 77—39561
Ni_5Sb_2, cryst. struct. *(German)* 78—83775
$NiSi_x$, cryst. struct. of phase *(German)* 79—99119
$Ni_{11}Zr_9$, X-ray obs. 79—65035
Ni_3Zr, cryst. struct. and stability 79—90597
$NpFe_2$, lattice distortions in ferromag. phase, X-ray obs. 80—15774
$NpNi_2$, lattice distortions in ferromag. phase, X-ray obs. 80—15774
Os intermetallic cpds., R_3Os (R = La, Pr, Nd, Gd, Tb, Dy, Ho, Er, Y), cryst. struct. 80—96474
Pb-Sb, crystal struct., supercond. after subjection to high press. 78—88064
Pd-Ag-Au, temp. effect on lattice parameters and thermal expansion 78—51473
Pd-H alloys, low temp. lattice parameter meas., β and mixed (α+β) phases study 78—26496
Pd-Mn system, superstructure, electron diffr. and X-ray powder diffr. study 79—94958
Pd-Sb film, rhombohedral phase, cryst. struct. electron diffr. determ. 80—39008
Pd-Se, thin layers, phase identification and struct., electron diffr. 77—51615
Pd-Zn system, phase characterisation *(German)* 78—60654
Pd-Zn system, struct. stability of B2 and $L1_0$ phases 78—26495
PdAl.r, cryst. struct. determ. 77—84700
Pd_5As, cryst. struct. and cryst. binding *(German)* 78—42958
PdBi, rhombic, cryst. struct. determ. *(German)* 79—77556
Pd_5Bi_2, cryst. struct. *(German)* 79—51053
γ-Pd_8Cd_{43}, X-ray cryst. struct. determ. 80—54172
$PdD_{0.73}$, (1, 1/2, 0)-superlattice reflection splitting near 50K, neutron diffr. studies 80—70168
$Pd_{21}Ge_8$, cryst. struct. *(German)* 78—18586
Pd_5Ge, cryst. struct. and cryst. binding *(German)* 78—42958
$Pd_2Mn_xV_{1-x}Sn$, Heusler alloy, structural disorder, Mossbauer study 80—80650
$Pd_{60}Ni_{20}Si_{20}$, amorphous, struct., high resolution electron microscopy 80—1969
Pd_2PbBi, and Pd_4PbBi_3, cryst. struct. *(German)* 79—94963
PdPb.r, crystal structure *(German)* 80—96472
$Pd_{13}Pb_9$.r, cryst. struct., X-ray study 80—103293
$Pd_{20}Sb_7$, cryst. struct. determ. *(German)* 77—19905
Pd_7Se_4, cryst. struct. determ. *(German)* 78—75628
$Pd_{80}Si_{20}$, vapour quenched amorphous alloy, atomic arrangements 80—100173
$Pd_{20}Te_7$, cryst. struct. determ. *(German)* 77—19905
Pd_9Te_4, cryst. struct. and binding *(German)* 78—51471
Pr-Cu-Al system, X-ray and microscopic anal. *(Ukrainian)* 78—84774
Pr-Ga (0 to 50 at.%), phase diagram and cryst. structs. of intermetallic cryst. 80—3002
Pr-In system, phase diagram determ. and intermediate phases characterisation 79—91621
$PrAg_2$, high temp. modification, thermal effects 78—38665
$PrCoAl_4$, X-ray anal. of crystal struct. *(Russian)* 77—55263
Pr_3Co_3Ga, crystal struct., X-ray determ. *(Russian)* 79—27951
$PrRh_x$, Sny, crystallography X-ray powder diffr. study 80—100217
$Pr_3Rh_2(Pt_2)$, structure determ., rhombohedral Er_3Ni_2 type 77—80443
Pr_5Sn_3, low temp. modification with tetrogonal struct. 80—1963
Pt-Au(Al)(In)(Sn)(Zr), solid soln., magnetic props. and lattice parameters *(German)* 79—87236
Pt-In, cryst. struct. determ. *(German)* 78—26494
$PtBi_2.h_3$, cryst. struct. *(German)* 80—107113
$β_1$-PtCd, structural parameters 79—27953
γ-$Pt_8Cd_{40(41)}$, X-ray cryst. struct. determ. 80—54172
$Pt_{13}In_9$, exam. of crystal structure, and phase diagrams *(German)* 78—83779
$PtPb_{0.7}Bi_{1.3}$, crystal structure *(German)* 80—84139
$PtPb_3Bi$ *(German)* 78—59783
Pt_4PbBi_7, cryst. struct. *(German)* 80—107113
δ-Pu, struct. rel. to anomalous props. 77—19910
Pu-Pt(Rh)(Pt-Rh), exam. of phases and crystal structure 78—80518
ζ-Pu-Zr, X-ray powder diffr. cryst. struct. determ. 79—19187
Pu_5Ir_3 77—58975
Pu_5Ir_4, X-ray diffr. meas. 77—55267
$Pu_5Ir_4(Rh_4)$ 77—19909
η-$Pu_{19}Os$ 78—42954
ζ-$Pu_{19}Os$, X-ray cryst. struct. determ. 79—99117

crystal atomic structure of alloys continued
Pu$_2$Pt, cryst. struct. determ. 78—79564
Pu$_{31}$Pt$_{20}$, crystal struct. determ. 77—80445
Pu$_{31}$Rh$_{20}$, crystal struct. determ. 77—80445
Pu$_5$Rh$_4$ 77—58974
Pu$_5$Rh$_4$, X-ray diffr. meas. 77—55267
Re-Al-Si system, phase equilibria, ReAl$_{1.2}$Si$_{0.8}$, ReAl$_{1.25}$Si$_{0.75}$ prod., struct. 78—35357
Re$_5$Si$_3$, X-ray cryst. struct. determ., microhardness rel. to Re content 80—84142
Rh$_7$Mg$_{44}$ structure types, alternative description of cryst. struct. 79—7577
Rh$_2$MnX, (X=Al, Ga, In, Tl, Sn, Pb, Sb), Heusler and Heusler-related cpds., mag. and cryst. props. 77—20568
SbBe$_{13}$, X-ray obs. 77—24291
Sb$_2$Tl$_7$, single-cryst. struct., X-ray diffr. determ. 77—65963
Sc-Co-Si, phase equil. and atomic struct. *(Russian)* 77—77462
Sc-Fe-Si system, phase obs. at 800°C *(Russian)* 78—23661
Sc$_3$Co, new struct. type related to Fe$_3$C and Re$_3$B by periodic unit-cell twinning 79—4268
ScGa$_2$ atomic structure determ. using single crystal method *(Ukrainian)* 80—70165
ScH$_2$, electron diffr. investigation 80—107112
Sc$_2$M$_3$Si, M=Fe, Co, Ni, struct. determ. by X-ray powder method *(Russian)* 77—55261
Sc$_2$Pt, X-ray powder struct. anal., Debye-Waller factors 79—77553
Sc$_{(3)}$Re$_2$Si$_3$, X-ray cryst. struct. determ. 80—39009
Sm-Co base ternary alloy, mag. props. and cryst. struct. 77—8352
Sm-Co deposit, arc plasma sprayed, crystal and micro struct. exam. 79—28248
Sm-Cu system, phase struct. investigation by X-ray diffr. *(Russian)* 80—49185
Sm-Fe-B ternary systems, phase equilibria and cryst. struct. *(Ukrainian)* 80—11626
Sm(-Pr)-Co, sintered, cryst. phases *(Russian)* 80—39004
Sm$_{11}$Cd$_{45}$, cryst. struct. similarity with γ-brass and α-Mn clusters 78—75625
Sm$_x$Co$_y$, mag. and struct. investigations of intermetallic systems 78—95440
Sm$_x$Co$_y$, mag. props. 78—43568
Sm(Co$_{0.65}$Cu$_{0.35}$)$_{5.6}$, cryst. struct. and coercive force, heat treatment effects *(Russian)* 80—44170
Sm$_3$Co$_3$Ga, crystal struct., X-ray determ. *(Russian)* 79—27951
Sm$_3$Ir, X-ray cryst. struct. determ., isotypic compound types 79—69057
Sm$_{10}$Pd$_{21}$, X-ray cryst. struct. anal. 79—99118
Sm$_3$Rh$_2$, structure determ., rhombohedral Er$_3$Ni$_2$ type 77—80443
Sn-Bi, crystal struct. and superconductivity after appl. of high press. and quenching 80—10531
Sn-Ni electrodeposited equatonic alloy, cryst. struct., X-ray, electron diffr. anal. 80—79748
Sn$_{11}$Cu$_{41}$, γ-brass struct., F-cells, X-ray diffr. 77—19903
Sn$_3$Cu$_9$Ni, γ-brass struct., F-cells, X-ray diffr. 77—19903
SrCu, X-ray cryst. struct. determ. 80—92478
SrNiSn$_3$, cryst. struct. rel. to ThCr$_2$Si$_2$ type *(German)* 78—51470
SrPdSn$_3$, prep. and crystal structure *(German)* 80—84138
Sr$_{0.67}$Pt$_3$B$_2$, cryst. struct. and supercond. props. 79—38231
Ta-Ga phase relationships, X-ray anal. of struct. 77—36453
Ta-H system, phase diagram and transforms., struct. obs. of various phases 80—104125
Ta-Si-Cu, struct. and supercond., Cu influence 80—50592
TaAl, α phases, lattice parameter and order 77—76359
β-Ta$_2$H, ordered alloy, electron microscope study of lattice distortions 77—11507
Ta$_2$H, single cryst., X-ray diffr. study on H ordering 79—14736
TbCo$_2$, X-ray obs. of low temp. modifications of crystal struct. *(Russian)* 78—75632
Tb$_3$Co$_3$Ga, crystal struct., X-ray determ. *(Russian)* 79—27951
TbFe$_2$, X-ray obs. of low temp. modifications of crystal struct. *(Russian)* 78—75632
TbRh$_x$Sny, crystallography X-ray powder diffr. study 80—100217
Th ternary alloy, Al$_4$Ba-ThCu$_2$Si$_2$-type struct., geometrical characts. 77—58977
Th-Mn alloy, mag. props. and effect of H$_2$ absorpt. 78—19250
ThC$_{0.063}$, cryst. struct. and lattice dynamics 80—88088
ThCo$_{5-x}$Al$_x$, homogeneity regions, X-ray powder diffr. study 79—77554
ThFe$_{5-x}$Al$_x$, homogeneity regions, X-ray powder diffr. study 79—77554
ThMn$_{5-x}$Al$_x$, homogeneity regions, X-ray powder diffr. study 79—77554
Th$_2$Zn$_{17}$, constant axial ratio of the hexagonal cell 79—69056
Ti alloy, BT22 quenched from 850-1200°C, X-ray study of structure *(Ukrainian)* 80—24402
Ti alloys, Fermi sphere limiting electronic capacitance, Brillouin zones *(Russian)* 80—92808
α,$\alpha+\beta$ Ti alloys, structural instability during prolonged periods of heating *(Russian)* 78—56664
α-Ti alloys VT1 and VT5, struct. and phys. props., H$_2$ effect 80—108576
Ti-Fe-H(D) system, struct. phase diagram, thermodynamics and diffusion *(German)* 79—56963
Ti-Hf-O system, ω(0) phase form. 79—11553
Ti-Mo (16 at.%), effect of H impurities on lattice spacing, hardness, and plastic strain *(Russian)* 79—11664
Ti-Mo (20 at.%), incommensurate struct., stacking soliton 80—107109
Ti-Mo(Nb)(Ta), BCC struct., tetragonal phase form. by cold deform. *(Russian)* 78—88462
Ti-Nb-Mo(V)(Ta)(Al)(Zr), BCC struct., tetragonal phase form. by cold deform. *(Russian)* 78—88462
Ti-Ni-Cu system, phase relations at 800 and 870°C 78—27481
Ti-O, dil. HCP solid soln., O interstitial distrib. effect on lattice parameters 78—30588
Ti(Al$_x$B$_{1-x}$)$_2$ (B=Cr, Mn, Fe, Co), $0<x<0.4$, influence of Al on H sorption props. X-ray cryst. struct. determ. 79—28198
η-Ti$_3$Be$_3$(O,N)$_x$, formation and struct. 79—73151
TiC, X-ray diffraction study of struct. of ordered phase and phase transform. *(Ukrainian)* 79—37660
Ti$_8$C$_5$, X-ray order struct. determ. 80—103295
TiD$_x$, α- and β-phases, D-site occupancy, neutron diffr. study 79—42014
TiFeD, cryst. struct., Mossbauer and neutron diffr. obs. 80—34839
Ti$_3$Ga, lattice period and crystallographic struct., temp. depend. *(Russian)* 78—55835
TiSnSb, synthesis and struct. *(French)* 79—90596
TlBi$_2$, cryst. struct. and density *(German)* 80—24407
Tm-H solid solution, struct., 20-500°C 79—90643

crystal atomic structure of alloys continued
Tm$_5$Pt$_4$, isotypic with Pu$_5$Rh$_4$, X-ray cryst. struct. refinement anal. 79—4271
γ-U, struct. rel. to anomalous props. 77—19910
U ternary alloy, Al$_4$Ba-ThCu$_2$Si$_2$-type structure, geometrical charact. 77—58977
U-Fe(Ni)(Co)-B, isothermal section of phase diagram, X-ray obs. 79—52157
UCo$_{5.3}$, mag. props., cryst. and domain struct. *(Russian)* 77—4529
UCo$_{5.3}$, mag. props. and cryst. struct. *(Russian)* 77—51925
U(Co$_x$Ni$_{1-x}$)$_2$, cryst. struct. and mag. props. at 4.2K 80—54175
U$_{10}$Co$_{51}$Si$_{33}$, crystal struct., dimensions, space group and coord. *(Russian)* 80—88085
U$_2$Co$_3$Si$_5$ 78—47285
U$_6$Co$_{30}$Si$_{19}$, X-ray cryst. struct. determ. 80—107111
UGa$_2$, cryst. struct., mag. and magnetoelastic props. *(Russian)* 79—38364
UIr$_2$X$_2$ (X=Si,Ge), cryst. struct. 80—1964
U$_3$Ni$_3$Sb$_4$, and related compounds, X-ray diffr. cryst. struct. determ. 79—42009
U$_3$Ni$_4$Si$_4$, X-ray cryst. struct. determ. 80—33931
U$_4$(Re$_{0.17}$Si$_{0.83}$)$_{13}$, X-ray diffraction anal. of crystal struct. *(Ukrainian)* 78—83773
U$_4$Re$_7$Si$_6$, X-ray diffraction anal. of crystal struct. *(Ukrainian)* 78—83773
U$_3$Si, X-ray diffr. exam. 78—75629
δ-UZr$_2$, computed X-ray powder diffr. patterns and densities 77—43172
V binary alloys with group IIIB and IVB elements, coord. polyhedra 78—9997
V-Rh alloys, short range atomic order exam. *(Russian)* 78—63696
V-Si-Cu, struct. and supercond., Cu influence 80—50592
γ-V$_5$Al$_8$, γ-brass, cryst. struct. redeterm. 77—47377
V$_4$As$_3$, defect struct. 77—4112
V$_3$(Fe,Ge), struct. and supercond. transition temp. *(Russian)* 79—7920
V$_{3-x}$M$_x$Ga, M=Ti, Cr, Mn, Fe, Co, Ni, cryst. struct. and microhardness meas. 79—86740
V$_{16}$N$_{1.5}$ solid solution, quenched, ordered structure *(Russian)* 80—88086
V$_3$Si, electron charge distrib., martensitically transforming single cryst., X-ray diffr. meas. 78—75631
V$_3$Si, Mossbauer spectra of ^{57}Fe *(Russian)* 79—24235
β-W type (A-15 type) structure, double space group selection rules 77—39551
W-Si-Cu, struct. and supercond., Cu influence 80—50592
Y-Mn alloy, mag. props. and effect of H$_2$ absorpt. 78—19250
Y$_3$Au$_3$Sb$_4$, cryst. struct., X-ray diffr. meas. 77—47378
YCo$_3$, hydride phase synthesis, thermal stability and struct. 80—59438
Y(Co$_{1-x}$Cu$_x$)$_5$, neutron diffr., thermal expsn. *(French)* 80—19749
Y(Co$_{1-x}$Cu$_x$)$_5$, neutron diffraction study *(Chinese)* 80—39000
Y$_2$(Co$_{0.31}$Fe$_{0.69}$)$_{19.2}$, statistical site occupancy deviations effect on cell parameters 77—7717
Y$_3$Co$_3$Ga, crystal struct., X-ray determ. *(Russian)* 79—27951
Y(Co$_{1-x}$Ni$_x$)$_5$, distrib. of Co and Ni atoms, neutron diffr. obs. *(Russian)* 80—64954
Y(Fe$_{1-x}$A$_x$)$_2$, A=Al or Ni, Laves phase, mag. props. and Mossbauer effect 77—85632
Y$_6$(Fe$_{1-x}$Al$_x$)$_{23}$, cryst. struct. and mag. props. 79—82180
Y$_3$Ni$_2$, crystal struct., tetragonal type 78—14309
Y$_3$Os, cryst. struct. 80—96475
Y$_3$Pd$_2$, structure determ., rhombohedral Er$_3$Ni$_2$ type 77—80443
Y$_5$Pt$_4$, isotypic with Pu$_5$Rh$_4$, X-ray cryst. struct. refinement anal. 79—4271
Y$_3$Ru(Pd), cryst. struct. 80—96474
Yb-Ga system, phase diagram, cryst. structs. of phases 79—52169
Zr-Ge-B system, phase equilibria 78—35356
Zr-Ir, high temp. modification, X-ray diffr. obs. *(Ukrainian)* 79—32947
Zr-Ni (65 to 80 at.%), phase diagram and cryst. struct. of intermediate phases 79—52170
Zr-Os quenched alloys, metastable phases *(Ukrainian)* 78—84804
Zr-Rh, high temp. modification, X-ray diffr. obs. *(Ukrainian)* 79—32947
ZrC-NbC-MoC$_{1-x}$ alloys, physicomech. props., comp. depend. 79—66097
Zr$_2$CoGa$_3$, crystal struct. determ. by single crystal method *(Ukrainian)* 79—51049
ZrCoSi, crystal struct. *(Ukrainian)* 78—83774
ZrCr$_2$D$_x$, site occupation modes and cryst. struct., neutron diffr. study 80—59440
ZrCu, constitutional and struct. studies, by mag. susceptibility, metallography and X-ray diffr. 80—70166
Zr(Fe$_{1-x}$A$_x$)$_2$, A=Al or Ni, Laves phase, mag. props. and Mossbauer effect 77—85632
Zr(Fe$_{1-x}$Al$_x$)$_2$, Curie temp., magnetisation, and cryst. struct., conc. depend. 80—75730
ZrRh$_{3-x}$Pd$_x$, electronic and cryst. struct. comparison 78—84398
ZrRh$_{3-x}$Pd$_x$, powdered alloys, catalytic behaviour correlation with electronic struct., lattice struct. and surface comp. 79—82181
Zr(V,Al)$_2$, struct., supercond. props., elec. resist. and mag. susceptibility, 4.2 to 300K *(Russian)* 79—15246
ZrV$_2$, C-15 struct., phase transitions, elec. cond., crystal lattice parameters *(Russian)* 80—54826
ZrV$_2$D$_x$(H$_x$), site occupation modes and cryst. struct., neutron diffr. study 80—59440
ZrX$_2$ alloy, Laves phases with MgZn$_2$, MgCu$_2$ structs., X-ray emission Zr spectra *(Russian)* 80—71517

crystal atomic structure of elements
actinides, metallurgical props. rel. to electronic struct., energies calc. method 77—20221
actinides, struct. props. rel. to F electrons 78—83951
alkali metal metastable magnetic crystal, aligned electronic spins, mag. props. 77—77035
alkali metals, atomic properties, pseudopot. calcs. 77—89512
cubic metallic structures, cryst. field coeffs., geometric struct. factors 77—43547
diamond, Compton profiles, X-ray struct. factors, band struct., LCAO calc. 78—51889
diamond, dislocation growth degree of supersaturation determ. 80—88145
diamond, effective supersystem cryst. simulation method, geometrical parameters, bulk moduli, impurity levels calcs. *(French)* 80—15430
diamond, electron density, neutron diffraction powder data 78—38655
diamond, electron density, X-ray powder diffraction data 78—38656

crystal atomic structure of elements continued
diamond, X-ray struct. factor calc., unrestricted Hartree-Fock procedure or small cluster 77—11866
diamond (113), scattering factor, Bragg reflection Pendellosung interference study 80—1885
graphite, neutron induced changes, exam. of lattice consts., elastic modulus, elec. cond 79—95053
graphitised viscose fibre, fluorination, change in struct. 80—88039
inert gas cryst. struct., induction energies, FCC and HCP 77—15343
inert gas crystallites of 5, 6, 7, 8 atoms, metastable states, Monte Carlo method 78—22687
inert gas solid, long range forces, book contrib. 77—51347
inert gases, book contrib. 77—51348
metal, BCC, fine particles formed by gas-evap. technique, cryst. struct. and habit 79—27935
metal, Bloch-Simon struct. index, chem. bond geometry interpretation 77—35508
metal, cryst. equilib. and Cauchy deficiency 79—19328
metals, structure and thermodynamic properties at high temperatures, microscopic theory *(Japanese)* 80—29191
α-N_2, computer-simulation with atomic pair pot., plastic cryst., phonon dispersion 77—7679
β-N_2, cryst. struct. at 25 kbar and 296K 80—10528
phase diagrams and struct. under press., index of substances 79—60484
rare earth metals, d-band occupancy rel. to cryst. struct. 77—35510
rare earth metals, preparation methods and properties, review 79—69969
rare earths, struct. props. rel. to F electrons 78—83951
structural and electronic changes under 200 kbar press. and above 80—24588
superconductors, review and table of props. 77—4460
Tl, time of flight neutron diffraction meas. of c/a ratio and vol. change at transition 77—15335
transition metal, band theory 78—34757
transition metal, metallurgical props. rel. to electronic struct., energies calc. method 77—20221
transition metal clusters, cohesive energy and level statistics 78—95267
transition metals, group IV, diffusion mechanism *(Russian)* 79—73335
β-W, coeff. for X×X and R×R irreducible representations 79—14732
Ag, stability of FCC struct. collinear three-ion interaction 80—49173
Al, computed X-ray powder diffr. patterns and densities 77—43172
Al, low-order Fourier coeff. of pot., modified thickness fringe method 80—75130
Al, powder, X-ray at scatt. factors at 80K 78—2065
Al, proton irradiation, Al atomic displacement position study 80—103401
Al, valence charge density calc. 78—6030
Am, high press. form, cryst. struct., X-ray diffr. obs. up to 14 GPa 80—24399
Am, phase transformation at high press., X-ray diffr. obs. 80—107422
Ar crystals, first order Raman scattering, evidence for HCP phase 78—23454
Ar small crystallite,s self consistent phonon calc. of struct. and thermodynamic props. 77—62596
Ar, solid, vacancy conc., X-ray study at const. vol. 80—64991
As, band structure on Jones zone boundary, pseudopot. calc. 80—54603
As, pseudopot. expansion method 77—27848
As, struct., pseudopotential method calcs., using untruncated pot. 78—18582
Au, atomic struct. of large angle [001] twist boundary, determ. by computer modelling and X-ray diffr. study 80—70162
Au, inner electron wavefunction, meas. using Bragg scatt. of 412 keV gamma-radiation 79—14734
Au, multiray calc. of cryst. lattice projection in ⟨111⟩ direction, from electron microscope image 79—94855
Au, stability of FCC struct. collinear three-ion interaction 80—49173
B, α-, and β-rhombohedral, struct. changes on Zn incorporation 78—79596
B, β-rhombohedral structure, accurate refinement 77—58973
B, conference, Varna, Bulgaria (Oct. 1978) 80—12842
B, IR-active phonons, reflectivity and absorption spectra 79—82294
B, polymorphism, cryst. chem., struct., growth, book contrib. 78—47278
β-B, rhombohedral, containing Sc, X-ray diffr. indicating ScB_{28} 78—34464
β-B, rhombohedral, containing Zr, X-ray obs. of $ZrB_{\sim 51}$ 79—23574
B, tetragonal, cryst. struct. 80—15045
B, tetragonal, phase I, prep. and struct., book contrib. 78—47277
B, tetragonal, X-ray diffr. and C doping obs. *(French)* 79—14731
β-B, tetragonal form, cryst. struct. related to α-AlB_{12} 79—77551
$B_{50}C_x$, $x=1$ to 2, prep. and struct., book contrib. 78—47277
$B_{50}N_x$, $x=1$ to 2, prep. and struct., book contrib. 78—47277
Be, electron density and bonding, Fourier method study 78—26481
Be, single cryst., mean square atomic displacement and antisymmetric atom vibrations, neutron data 80—49180
C, crystalline, intermediate form, CI lattice energy *(Russian)* 78—22693
C, high temperature behaviour, over 2600K, polymorphic carbyne forms 79—7575
C materials, thermodynamic props. rel. to struct. 77—80597
C_8 crystalline diamond-like form, cryst. struct. *(Russian)* 79—99114
$(C)_n$, cryst. struct. determ. from X-ray photoelectron and X-ray spectra 78—88384
CF, X-ray diffr., high press. effect 78—83766
Cd, single cryst., root-mean-square atom displacement, X-ray meas. 78—75624
Ce, $\alpha \rightarrow \alpha'$ high press. transition, volumetric study 78—83940
α''-Ce, high pressure phase 79—23565
Ce, new allotropic phase above 121 kbar, X-ray diffr. obs. 77—35509
α'-Ce, X-ray diffr. data, reappraisal 77—55260
^{248}Cm, prep. and cryst. struct. 79—99115
Co, ferromagnetic micropowder, cryst. struct., coercivity, remanence, saturation 80—65967
Cr, crystal structure below Neel temp., X-ray diffr. study 78—83772
Cs, accurate struct. factor determ. by X-ray and neutron diffr. 79—51046
Cs, crystal struct., van der Waals and repulsive interaction 80—84137
Cs, structural energies, pseudopotential formalism 80—39519
Cu, cementation, on Fe, deposit struct., reaction rates, SEM 80—104421
Cu, cryst., ion-electron emission yield, ang. depend., atomic order effects 77—85877
Cu, interatomic distances, coord. numbers, and mean relative displacements, EXAFS anal. 80—89087
Cu, stability of FCC struct. collinear three-ion interaction 80—49173

crystal atomic structure of elements continued
Cu struct. factor f(220), importance of extrapolation to zero extinction 79—19123
Dy, crystal structure, P-T phase diagram 78—84776
Er, effect of hydrostatic pressure on lattice consts. and volume 79—51272
Fe, ferromagnetic micropowder, cryst. struct., coercivity, remanence, saturation 80—65967
Fe, high-purity single crystals, X-ray topography and double-crystal diffraction 80—92534
Ga, cryst. struct., high press., X-ray diffr. obs. 78—42952
Ga, polymorphism at high press. *(French)* 78—47279
Gd, crystal structure, P-T phase diagram 78—84776
Ge (111) surface, annealed, atomic structure 78—75916
Ge, crystal struct. factor, at. scatt. factor, electron diffr. determ. 77—15291
Ge, electron microscopy, multi-beam lattice images in (011) orientation 77—24252
Ge, electronic and struct. props., nonlocal pseudopot. calc. 80—34349
Ge, film, elec. props., prep. by DC sputtering *(Japanese)* 79—78237
H, metallic, struct. and stability 78—14305
H_2, metallic, phonons, supercond. transition, nonlinear self consistent screening approach 79—95537
H_2, solid, HCP to FCC transition at 80 to 100 atm. *(Russian)* 77—55259
$Hg_{99}As$, struct. reinterpretation 78—38660
I, metallic solid, high press. struct., phase transition, X-ray diffr. study 78—87647
K, accurate struct. factor determ. by X-ray and neutron diffr. 79—51046
K, crystal struct., van der Waals and repulsive interaction 80—84137
K, structural energies, pseudopotential formalism 80—39519
Kr, HCP, vap. phase grown thin films 78—18917
Kr, solid, vacancy conc., X-ray study at const. vol. 80—64991
Li, anharmonicity and low temp. phase struct., neutron diffr. study 80—107105
Li linear chain, ab initio calcs., cryst. orbital method 79—37659
β-Mn, struct., polyhedron model 78—79563
β-Mn, X-ray crystal struct. refinement 79—14735
Mo, cryst., ion-electron emission yield, ang. depend., atomic order effects 77—85877
Mo, electronic and struct. props., nonlocal pseudopot. calc. 80—34349
Mo powder, struct. facators, time of flight neutron diffr. 78—47212
N_2, X-ray structure factors, mapping of electrostatic props. 79—94841
$^{15}N_2$, solid struct., and thermodynamic props. *(Russian)* 80—88083
Na, accurate struct. factor determ. by X-ray and neutron diffr. 79—51046
Na, dynamical structure factor calc., High temp. 80—15047
Nd, crystal structure, P-T phase diagram 78—84776
Ni, low temperature lattice parameter, Gruneisen parameter 77—76357
γ-O_2, mol.-dynamic study of struct., dynamics 80—96467
O_2, solid, struct. elementary excitation spectrum and thermodynamic props. *(Russian)* 79—55696
P, black, pseudopotential crystal-struct. stability calcs. as function of press. 79—60503
P, black allotrope, orthorhombic bonding, up to 26.6 kbar, neutron diffr. obs. 79—99106
Pa, lattice parameter variation at low temp., thermal expsn. 80—15046
Pa, preparation by Van Arkel method, cryst. struct. 78—39715
Pd, catalyst, Z-contrast, in STEM 79—46530
Pd, low temp. lattice parameter meas. 78—26496
Pt, catalyst, Z-contrast, in STEM 79—46530
Pt clusters, at. struct. 79—19186
Pt metals, lattice parameters, densities and atomic vols., tabulation 79—65033
Rb, crystal struct., van der Waals and repulsive interaction 80—84137
Rb, structural energies, pseudopotential formalism 80—39519
α-S, attachment energy as habit controlling factor 80—59421
α-S, monoclinic allotrope, thermal behaviour 78—67813
α-S, under hydrostatic press., deformable mol. lattice statics 80—49175
β-S, X-ray powder diffr. pattern at −150, −75, 100°C 78—95015
Sb, band structure on Jones zone boundary, pseudopot. calc. 80—54603
Sb, cryst. struct. to 26 kbar via diamond anvil cell and X-ray diffractometer 77—31560
Sb, film, liquid and vapour quenched, metastable struct. 79—56974
Se, atom positions, effect of press. 78—34465
Se, Bijvoet intensity differences, prediction in noncentrosymmetric structs. 79—7574
Se, habit variation of crystals of the $C3_12$-$C3_22$ space group 80—107090
Se, lattice distortion and p-orbital bands 77—89405
α-Se, monoclinic allotrope, thermal behaviour 78—67813
Se, trigonal and amorphous, electronic struct. and nonempirical calc. of struct. props. 80—59866
Si, (110) oriented, electron optical conditions for struct. image form. 80—75131
Si, effective supersystem cryst. simulation method, geometrical parameters, bulk moduli, impurity levels calcs. *(French)* 80—15430
Si, electron distribution re-evaluation 78—38657
Si, electron microscope images 78—14256
Si, electronic and struct. props., nonlocal pseudopot. calc. 80—34349
Si, hexagonal form existence in Si_3N_4 77—1112
Si lattice constraints on structure of Si-SiO_2 interface states 77—20379
Si powder, X-ray K_α doublet diffr. peak position rel. to lattice const. precision 77—68891
Si, structural props., self-consistent calc. 80—28947
Si, testing aspherical atom refinements 79—7516
Sm, crystal structure, P-T phase diagram 78—84776
β-Sn, covalency of bonding, (202) almost forbidden reflection meas. 79—94953
Ta BCC lattice, strain ordering in interstitial solutions 80—107420
Ta film, optical const. var. with struct., ellipsometric meas. 77—63478
Te, atom positions, effect of press. 78—34465
Te, habit variation of crystals of the $C3_12$-$C3_22$ space group 80—107090
Te, high pressure metallic phase, cryst. struct. 80—49161
Te, Kikuchi patterns, of non-centrosymmetrical crystal 80—100202
Te lattice distortion and p-orbital bands 77—89405
Te, trigonal and amorphous, electronic struct. and nonempirical calc. of struct. props. 80—59866
Th, atomic struct. by field ion microscopy 80—59437
Th, lattice parameter variation at low temp., thermal expsn. 80—15046
U, field emission microscopy, emissive props. 78—88409

crystal atomic structure of elements continued
V polycrystalline plate, struct. facators, time of flight neutron diffr. 78—47212
V, single cryst., (110) scatt. factor, absolute meas. 78—71706
V, small particles, crystal structure, magnetic and superconducting props. 80—97121
W, atom, high resolution phase contrast electron microscopy imaging 80—103224
W, electronic and struct. props., nonlocal pseudopot. calc. 80—34349
W:Re, polygonisation in diffusion process, glide dislocation interactions 80—38998
Xe, HCP, vap. phase grown thin films 78—18917
Yb, structural and electronic changes under 200 kbar press. and above 80—24588
Zr, α- and β-phases, computed X-ray powder diffr. patterns and densities 77—43172

crystal atomic structure of inorganic compounds
actinide compounds, structure, mag. and related props., review 80—6389
actinide dioxides, low temp. lattice parameters, Neel pt. behaviour 77—27867
actinide double orthovanadates and orthoarsenates, struct. evolution due to cationic and anionic substitutions 77—19938
$AgBi(CrO_4)_2$, synthesis, thermolysis, crystallography *(French)* 80—33946
β''-Al_2O_3, Mg- and Li-stabilized, high electron microscopy images of defects 79—73135
β-Al_2O_3-Cu_2O, phys. and chem. props., use in determ. of thermodynamics of Cu-Sn alloys 80—107502
$Al_5(BO_3)O_6$ synthetic, interplanar distances, struct. 79—86775
alkali borates, vitreous and cryst., vibr. spectra and struct. comparison 78—23470
alkali bromide-VBr_2 systems, cryst. struct., DTA investig. *(German)* 78—72766
alkali chloride:Mn^{2+}, spin Hamiltonian parameters, binding energies for cation vacancy complexes 80—96461
alkali germanate crystals and glasses, struct. and stability, IR spectra meas. 80—64911
alkali halides, structures in compressible ions theory 80—33971
alkali hydrides, bulk props. prediction from molecular behaviour 78—51468
alkali ionic conductors with sheet structures, ion mobility and influences 80—107522
alkali metal actinide complex halides, thermochem. and struct. props. 80—7847
alkali metal borides, prep., cryst. struct., thermal stability, phys. and chem. props., book contrib. 78—47304
alkali metal indates and thioindates, prep., props. and struct. 80—35517
alkali metal intercalation compounds, ionicity, struct., size, intercalation amount, ion mobility anal. 80—39041
alkali metal intercalation cpds., prep. methods and cryst. struct. 79—99156
alkali metal rare earth double metaphosphates, vibr. spectra, rel. to struct. 80—34905
alkali metal ternary sulphides, $A_xMo_3S_4$, and hydration products, cryst. struct. 78—42989
alkali metal ternary sulphides, A_xMoS_2, and hydration products, cryst. struct. 78—42989
alkali metal titanates, $(A_2Ti_6O_{13})_n.A'Ti_4O_9$, (A=Na, K, Rb)(A'=Ba, Pb, Sr), intergrowth in tunnel structures 80—28995
alkali metal-transition metal oxide, AMO_2, stability rel. to coordination *(French)* 77—19933
alkali suboxides, structure and bonding, book contrib. 80—972
alkali tungsten bronzes, struct. and supercond. 79—82703
alkali-trihalogeno-plumbates, $M[PbX_3]$, cryst. growth struct. and spectra *(German)* 79—90632
alkaline AlC_4, cryst. struct. comparison with pseudo-alkaline AlC_4 79—73145
alkaline earth compounds, $MB_{12}H_{12}.xH_2O$, M=Ca,Sr,Ba, cryst. growth from soln. and morphology 77—44145
alkaline earth halides, thermodynamic and structural props., computer simulation 78—75849
alkaline earth metal phosphites, $M^{II}PO_3H.xH_2O$, cryst. struct. *(French)* 80—24413
alkaline earth precious metal hexahydroxides, prep. and characterisation 79—90610
alkaline earth transition metal ternary and quaternary oxides, ATO_3, $ATi_{1-x}T_xO_3$, and $AZr_{1\ x}T_xO_3$, prep., mag. props. and struct. 79—15277
alkaline earth uranates, struct., phys. and chem. props., preparation methods, review *(Japanese)* 79—14764
alkaline earth-ReO_6, ordered or perovskite type struct., magnetic and elec. props. 79—65053
alkaline-earth-Os ternary oxide system, solid state prep. and reactions, cryst. struct., mag. and elec. props. 79—24739
aluminate:Ce^{3+}, hexagonal, luminesc. rel. to host lattice structure 78—6776
anadalusite, thermal expansion and cell parameters 79—90801
antimonates, double and triple, with perovskite structure, cationic distrib. *(French)* 77—1109
antimonates, $M_4{}^{II}M^{III}Sb^VO_8$ spinels, struct. determ., IR and Mossbauer spectra 79—91431
armstrongite, X-ray cryst. atomic struct. and refinement 79—60345
arsenates, $M^{II}M^{IV}(AsO_4)_2$, (M^{II}=Ba,Sr; M^{IV}=Ge,Ti,Sn,Zr,Hf), vibr. spectra, cryst. struct., bonding 77—36225
asbestiform chain silicates, new minerals and struct. groups 78—28227
asbestos, chrysotile, crushed, temp.-induced changes in struct. 77—24305
astrophyllite, electron diffr. characts. of polytypic forms 77—39573
astrophyllite, polytypic forms 77—39572
Au_2P_3, polyphosphides with weak Au-Au interactions, cryst. struct. determ. by X-ray techniques 79—37674
barium mordenite, dehydrated, position of cations and molecules, electron probe anal. 78—51509
beryllonite, Zn(Fe) analog, refined cryst. struct. allowing anisotropy of atomic thermal vibs., comparison with hurbutite 79—55722
$Bi_7Ni_4NbO_{21}$, crystal point group determ. by high resolution electron microscope image 79—51036
binary compounds, structural stability, nonlocal density-functional atomic pseudopot. method 80—49174
birnessite group mineral, new, with 14 Å spacing, in deep-sea micronodules 79—74892

crystal atomic structure of inorganic compounds continued
boracite, single cryst. prep. and phys. props. 80—100763
borides, B_{12}, cryst. chem. classification, book contrib. 78—47302
borides, B-rich, cryst. chem., struct., review, book contrib. 78—47278
borides, conference, Varna, Bulgaria (Oct. 1978) 80—12842
borides, hexa- and tetra-, prep., struct., elec., mag. props., book contrib. 78—47303
borides, refractory compounds, classification 79—94985
borides, spatial correls. of valence and external core electrons 80—10523
borides, ternary, struct. classification, props., book contrib. 78—47309
borides containing B_{12} polyhedral units, tetraborides, structural determinants, book contrib. 78—47301
borides of Ib and IIb elements, interactions, product chem., phase, struct. anal., book contrib. 78—47305
borides with ReB_2 and Mo_2IrB_2 type structures 78—42995
boulangerite, cryst. struct., superlattice variations, order-disorder struct. 79—86770
bytownite, quenched from 1723K, X-ray single cryst. struct. anal. and refinement 79—19193
calcite, luminescence spectral anal. of polycyclic aromatic hydrocarbon impurities 80—71483
carboborite, cryst. struct. *(Chinese)* 78—18615
carboborite, X-ray crystallographic investigation *(Chinese)* 78—18614
carbonate mineral, (Si, Cl)-bearing, from limestone-granite contact zone, X-ray powder diffr. pattern *(French)* 78—69339
carlfriesite, cryst. struct., chemical formula revision, and synthesis 79—55709
cation octahedral site preference energies 77—80483
CD $SO_2(NHAg)_2$, disilver sulphamide *(German)* 78—10008
α-celsian-leucospherite-tuhualite-milarite series of cpds., struct. types 79—19223
cemented carbides, physical and chem. nature 80—76265
ceramic mineral, exam. by X-ray diff. at high temp. *(French)* 79—96234
ceramics, local atomic arrangements, associated with ordering, review 80—50632
chabazite, Cu^{2+}-exchanged, cation and water mol. positions 78—15709
chalcogenide spinels, thermal stability, thermochemical, thermodynamic and crystallochemical props. 77—51519
chalcopyrites, for electrolum. device appl., props. and technology, book contrib. 77—73175
chevkinite from Oslo region, Norway, cryst. struct. and chemical comp. 78—85533
Chevrel phase compounds, bonding and phys. props. rel. to struct., book contrib. 80—49209
chlorite, cryst. struct. and compressibility at high press. 78—63717
chloritoid, topotactical dehydration, X-ray diffr. and TEM study 79—51057
chrysotile, cryst. struct. rel. to milling, X-ray diffr. 77—55278
CO_2 ferrite, crystal structure, X-ray absorpt. spectra, chemical shifts 80—88118
fac- $(Co(NH_3)_3(NO_2)_3)$, X-ray cryst. struct. determ. 79—60311
conference, Crystal XII, Canberra, Australia (Jan.-Feb. 1980) 80—62388
coordination polyhedra classification 77—4088
corundum, attachment energy as habit controlling factor 80—59422
covalent semiconductor, atom form factors of different atomic models, fitting theoretical struct. factors by varied temp. factors 80—1882
$Cr_2P_6O_{18}$, X-ray cryst. struct. determ. *(French)* 77—80452
$Cu_{1.8}Mo_6S_8$, superconducting state, triclinic struct., X-ray powder diffr. anal. 80—6388
cubic ionic structures, cryst. field coeffs., geometric struct. factors 77—43547
cubic perovskite, E2, topologically related structures 78—18570
diamond structure crystals, forbidden Bragg refl., electron distrib. 77—51265
1,5-diazo-3,7-dithiabicyclo (3,3,1) nonane, molecular and cryst. struct. 78—51528
dickite occurrence in Jamaica, ordered and disordered varieties 78—83786
divalent Sr, Ba, Ca, Zn, Cd iodates, complex salts, phase transitions, cryst. struct. *(Chinese)* 80—70171
electrochemically intercalated, ion ordering, X-ray diffr. meas. 80—44177
enstatite-diopside-wollastonite system, evidence for high press. phases with perovskite struct. 79—79825
ethylenediammonium metal chlorides, $(NH_3CH_2CH_2NH_3)MCl_4$, M=Ni,Pd,Cu,Cd,Mn, struct. and mag. props., vibr. spectra 79—10842
Eu-Sb system, X-ray powder diffr. data for phases Eu_5Sb_3, $Eu_{11}Sb_{10}$, Eu_2Sb_3 79—51075
ferrite, hexagonal, local lattice distortions, use of Mossbauer effect 78—43745
ferrite bubble film struct., EM and RHEED, Mn and Mn-Cu ferrites 77—11801
ferrite spinels, normal and inverse, solid state chem. expts. for students 80—36815
ferrites, polycryst., X-ray diffr. struct. anal., chem. anal. *(German)* 77—72598
ferroactive thin films, physical prop. optimisation 80—80698
ferrocyanides, $A_2BFe(CN)_6$, A=alkali metal, B=alkaline earth metal, structural aspects 78—14326
fluorapatites, $M_4R_6(SiO_4)_6F_2$, (M=alkaline earth; R=Nd, Y, or Yb), synthesis and characterisation 77—24992
fluorite-related phases, Ln_3MO_7, (Ln=rare earth, Y or Sc), (M=Nb, Sb or Ta) 79—46619
fluorite-related phases, Ln_3MO_7, (Ln=rare earth, Y or Sc), (M=Nb, Sb or Ta) 79—46620
garnet, body-centred cubic cylinder packing 77—62497
garnet, pretransition phenomena and long-range ordering 79—99151
garnets, cation-anion distances, Poix formula 78—67701
garnets, crystal and static mag. props. 79—99166
garnets, oxide and fluoride, relation between lattice parameters and ionic radii 80—1986
germanides, $(T,Nb)_{11}Ge_8$, T=V, Cr, Mn *(French)* 78—38675
graphite fluorides, $(CF)_n$ and $(C_2F)_n$, prep., struct., discharge characts., electrode props. 80—89502
graphite intercalate $C_{24}Cs$ positional and orientational correlations, X-ray study 80—33970
graphite intercalated with $PdCl_2$, $RuCl_3$ and $OsCl_3$, synthesis and cryst. struct. 79—8253
graphite intercalation compound, RbC_8, first stage intercalation cpd., X-ray crystallographic obs. *(French)* 79—32966
graphite intercalation compound with halogens, ionisation 78—26489

crystal atomic structure of inorganic compounds continued
graphite intercalation compounds, props. and appls. 78—71711
graphite intercalation compounds, X-ray charact. 80—19780
graphite intercalation compounds, X-ray struct. factor meas. applications 80—54207
graphite intercalation compounds with K and tetrahydrofuran *(French)* 78—26692
graphite intercalation with Hg and alkali metal 80—44183
graphite salts, $C_8^+MF_6^-$, (M=Os,Ir,As), struct. and elec. props. 80—70183
graphite-$FeCl_3$ intercalation compound form., effect of added O, Cl, and water vapour *(German)* 79—52634
graphite-HNO_3 intercalation compound, HNO_3 mol. orientation, model 80—24432
graphite-HSO_3F insertion compounds *(French)* 79—52635
graphite-ICl residue compounds, struct., X-ray diffr. 78—47287
graphite-Na-N-H intercalation compounds *(French)* 79—52633
graphite-Rb, intercalation cpd., superlattice struct., electron diffr. study 80—75214
group IIIa dihydrides, structs. and stabilities 80—107146
gypsum, struct., vibr. spectroscopic obs. *(Russian)* 78—15175
halide compounds, cryst. chem. and structs. of type $A_2B^+B^{3+}X_6$ 79—46639
halide compounds ABX_3 with perovskite struct., cryst. chem., X-ray diffr. anal. 78—95042
hard-core pseudopotentials and struct. maps 80—44168
hilgardite and parahilgardite, piezoelectric zeolite type structures and composition 78—16003
hornblendes, refinement of struct. characts. by reference to PMR data 78—22704
humite, real structs., mixed layer characts. 78—79567
I-III-VI_2 semiconductors, nucl. quadrupole coupling consts. and struct. parameters 79—42509
ice, cryst. Ic and Ih phases, diffr. patterns and far IR spectra, isotope effects 78—6662
ice, crystal structure, CNDO/2 calcs., unit cell polarity effects 78—22683
ice, hexagonal, lattice struct., computer simulation 78—14324
ice, Ih, elastic diffuse neutron scattering due to D-D correlation functions 80—96493
ice, Ih-phase, oriented single cryst., proton distrib., light scatt. obs. 77—16318
ice, rel. to thermal cond. of 9 solid phases 78—30801
ice, struct. factors using X-ray Pendellosung method 80—1981
ice-I, metastable structure effect of surface condition on crystallisation in capillaries 79—56037
ilmenite, cryst. struct. at various compositions 79—86769
intercalation compounds, metal guests in chalcogenide hosts, struct., review 79—46627
intercalation compounds, physical and chemical props. 79—19209
intercalation compounds, synthesis, reaction mechanism, struct. and bonding 80—39047
iodomercuroates, complex, NQR spectra of ^{127}I and struct. 77—12230
ionic crystals, relative stabilities of NaCl, CsCl and cubic ZnS structures 80—19745
iron-transition metal oxinates, Mossbauer spectra 77—90082
IV-VI semiconductors, crystal structure and symmetry of electron spectra, doping effects *(Russian)* 79—7696
jamesonite, cryst. struct., superlattice variations, order-disorder struct. 79—86770
layer structures, intercalation with N_2H_4, charge density waves or artefacts 80—100221
layered materials and intercalates, International Conference, Nijmegen, Netherlands (Aug. 1979) 80—36771
layered transition metal dichalcogenide, diffuse intensity contours in electron diffr. patterns, struct. interpretation 80—38878
$^6LiH_3(SeO_3)_2$, absolute atomic arrangement rel. to spontaneous polarisation, neutron diffr. study 80—15067
lithium formate monohydrate, X-N difference density and structural parameters from different expts. 78—18627
long period stacking variants, stability in pairwise interaction model 79—94956
lunar pyroxenes, cation distrib. and exsolution as chronological indicator of thermal history 78—45246
manganese (II) oxalate hydrates, prep. and cryst. props. 77—76377
metal fluoride hydrates, O-H...F bond geometry 78—34458
metal ionic radius and oxide structure chart 79—73152
metal pentahalides, $(MX_5)_2$, space groups and cell dimensions *(German)* 78—38668
metal silicides, fabrication technique and characterisation, review *(Japanese)* 80—60779
metal-rich compounds, pnictides, chalcides and halides, struct. and bonding, review 79—46626
metal-rich compounds, struct. and props. 78—95045
metallic glasses, structure and formation, thermodynamic props., cluster relaxation approx. 80—54143
3-methoxynaphthalide, cryst. and mol. structure. 77—31654
4,4′-methylenebis(1,3,5-trimethyl-4-imidazolin-2-one), cryst. and mol. struct. 80—107201
$Mg_{1.34}Fe_{0.16}Al_{0.12}Ti_{0.38}OBO_3$, warwickite, cation distrib. from X-ray struct. and Mossbauer spectra anal. 79—1424
mica, Fe^{3+} localisation determ. by EPR *(French)* 77—43196
microcline, maximum room temp. phase transition, unit cell parameters, thermal expansion 80—54208
minerals, bulk modulus-volume relationship, for cation-anion polyhedra 80—41434
minerals, elastic props., chemical comp. and crystal struct. 77—86862
mixed oxides, cryst. struct., electron microscopy study 78—91310
molybdates (double), of mono- and tri-valent metals, polymorphism, X-ray diffr. obs. 78—87642
monazites, nuclear waste, synthesis, ideal actinide hosts for geologic disposal, unit cell parameter data 79—22406
mordenite, dehydrated Na-exchanged, cation and molecular distrib. 79—90617
Mossbauer spectra, struct., electronic and mag. props. 79—91320
MX_4 mole cules, distortion from T_d symm. appl. to PO_4, SO_4, $AlCl_4$ 78—63706
MX_4 molecules, distortion from T_d symm. kernel, co-kernel and averaged configs. 78—63705
$Na_2Zn[SiO_4]$, X-ray cryst. struct determ., thermal vibration anisotropy allowance 80—92510

crystal atomic structure of inorganic compounds continued
neutron, construction, appl. to cation distrib. determ. in nonstoichiometric MnZn ferrite *(Bulgarian)* 78—83656
nifontovite, cryst. struct., H bonds 79—19232
niobate based ceramics, synthesis, struct., elec. cond., mag. props. *(Czech)* 80—45259
niobates of divalent metals, bonding characterisation 78—38680
noble metal complexes, hexafluoro, review of struct. obs., pseudorot., press. effects 78—6045
nonstoichiometry and structural disorder in some families of inorganic cpds. 79—51091
nontransition metal simple binary suboctet compounds, structural stability 77—58966
octahedral molecule MX_6 with close-packed arrangement of X-atoms, possible cryst. struct. *(German)* 79—27940
one-dimens. ionic conductor, modulation and incommensurability 80—19980
one-dimensional conductors, modulated structs., formation and nature 79—94968
one-dimensional conductors, struct. aspects, book contrib. 78—10429
opals, crystal struct. and IR spectra 80—40117
optical fibres, material dispersion 79—27377
orthopyroxene from lunar anorthosite 15415, crystal structure and thermal history 78—53842
oxide:U^{6+}, struct. sensitivity of luminesc. 77—90187
oxide, non-stoichiometric, pretransition phenomena and long-range ordering 79—99151
oxide hydrides, oxide halides and hydroxide halides, cryst. struct. data tables book *(German, English)* 80—51971
oxide spinel, systematic trends in geometry, ionic radii and electronegativity 80—19778
oxides, ABO_4 type, high press. phase transforms. and struct. types, cryst. chem. aspects 80—79940
oxides, $RCu_3Mn_4O_{12}$, R=La to Lu, Y, synthesis and mag. props. 80—75717
oxides, struct. and props. 79—27964
oxides, superstruct. based on fluorite lattice, conc. wave method 78—51393
oxides with spinel struct., interionic distances calc. 80—39057
oxo-compounds of halogens and Xe, cryst. struct. data tables, book *(German, English)* 80—51971
oxofluorotitanates, preparation and characterisation 79—99872
paragonite, $2M_1$, cryst. struct. refinement by HV electron diffr. 78—67696
paragonite, 3T, cryst. struct., oblique texture electron diffr. 78—67697
$Pb_4Sb_4S_{11}$, synthetic, cryst. struct. by X-ray goniometry 80—6394
penninite, one-layer triclinic chlorite, neutron diffraction study 80—84144
perovskite compound combination, Mossbauer spectroscopy study *(Russian)* 80—80666
perovskite family, monoclinic of 1:1 ordered $A_2(B'B'')O_6$ compounds caused by antiparallel displacement of A ions 79—10839
perovskite-like oxides, $ACu_3B_4O_{12}$ subseries, synthesis, struct. and mag. props. 77—68960
perovskite-like oxides, high-pressure series, rel. between structure and physical properties 78—51493
perovskites, $(AA')(BB')O_6$, ion valency pairs determ. from lattice consts. 77—43195
perovskites, $A_2^{2+}B^{3+}U_{5/6}^{6+}\nu_{1/6}O_6$, struct., cation vacancies, X-ray diffr. study *(German)* 80—107147
perovskites with space group I4/mcm, determ. by cryst. struct. 78—75643
perrierite from Oslo region, Norway, cryst. struct. and chemical comp. 78—85533
phase diagrams and struct. under press., index of substances 79—60484
phlogopite, cryst. struct. and compressibility at high press. 78—63717
phosphates, $M^{II}M^{IV}(PO_4)_2$, (M^{II}=Ba,Sr; M^{IV}=Ge,Ti,Sn,Zr,Hf), vibr. spectra, cryst. struct., bonding 77—36225
phosphates, $MCrTi(PO_4)_3$, M=Mg, Mn, Co, Ni, Zn, Cd, Pb, Ca, Sr, Ba *(French)* 77—84708
piezoelectrics, absolute config., bibliography 77—48129
plagioclase, labradorite, Al/Si distrib. in An_{66}, superstructure in An_{54} 79—94970
polysilicic acid, IR spectra, struct., crystallisation effects *(Russian)* 78—72528
pseudoboehmite, exam. of structure, using radial electron distrib. method, and X-ray diffraction 80—1977
pyrochlore, pyrochlore struct. and its relatives 79—14773
pyrochlore related structures, phases of type AM_2X_6, acentricity and phase transitions, X-ray diffr., DSC and NMR study 79—27943
pyroclore formation, structural characts. 80—54164
pyrophosphatase, inorganic, of yeast, cryst. growth, derivatives formation, heavy atoms positions 80—108842
pyroxenes, high Ca, of the diopside-hedenbergite series, cryst. struct. refinement 79—14783
quartz, $\alpha \rightarrow \beta$ transition obs. from nonlinear optics and bond polarisability model 77—15336
quartz, α-β phase transition point, struct., light scatt. *(Russian)* 78—47521
quartz, crystal structure rearrangement due to neutron irrad. 80—64981
quartz, habit variation of crystals of the $C3_12$-$C3_22$ space group 80—107090
quartz, impurity content and lattice consts., electrolysis influence 77—35580
quartz, low, cell parameter variations between 94 and 298K 80—96497
quartz, neutron irradiated, X-ray cryst. struct. anal. 79—14853
α-quartz, Renninger effect, forbidden X-ray reflections 80—64980
quartz, synthetic, growth forms and interface mol. group waveness *(Chinese)* 79—51027
rare earth aluminium borates, thermal stability, X-ray struct. anal., refractive indices 79—4297
rare earth antimonates, $RSbO_4$ (R=Nd-Lu or Y), high temp. modifications, cryst. chem. identification X-ray anal. 79—65059
rare earth antimony oxides, $RSbO_4$, low temp. form, prep., cryst. chem. identification 78—47300
rare earth arsenides and bismuthides, chemical bonding and structural features, coherent alloying theory 80—107101
rare earth beryllogallates with melilite struct., synthesis 77—81236
rare earth chalcobismuthites, $RBiTe_3$, prep., elec. props., and crystallographic date 80—59981
rare earth compound, perovskites, preparation, struct. *(French)* 79—46629

crystal atomic structure of inorganic compounds continued
rare earth compounds, R_2MoO_5, cryst. struct., IR spectra, elec. and mag. props. 80—33954
rare earth compounds, R_2MoO_5, preparation, exam. of higher oxygen pressure limit, mag. susceptibility *(French)* 78—76618
rare earth compounds, $R(Rh_{0.85}Ru_{0.15})_4B_4$, mag. ordering and supercond. 78—14861
rare earth compounds, $RNaMTa_5O_{15}$ (R=rare earth, M=K, Rb, Tl, Cs), relative stability of struct. types, and piezoelec. props. *(French)* 80—49206
rare earth compounds, $RThNbTiO_8$, synthesis and cryst. struct. *(French)* 78—83799
rare earth cpds., RM_4Sb_{12} (R=La, Ce, Pr, Nd, Sm, Eu; M=Fe, Ru, Os), prep. and cryst. struct. 80—100211
rare earth double orthophosphates with alkali metals, spectroscopic obs., struct. and chem. nature 80—100674
rare earth ferrite-garnets, compensation temp., rare earth ion influence 79—51775
rare earth gallium borates, high temperature crystallisation, composition, struct., props. 80—40253
rare earth garnets-$R_xR'_{3-x}Fe_{5-t}M_tO_{12}$, R,R′-rare earths, on Y ions, Mp=Al^{3+}, $Ga^{3+}Sc^{3+}$, In^{3+}, effect of ion replacements on lattice constant 79—1408
rare earth germanates, R_2O_3-GeO_2 system cpds., physicochem. characts. 80—97469
rare earth halides, prep. and props., book contrib. 80—54211
rare earth hydrides, props., book contrib. 80—45291
rare earth intermetallic, RNi_4AlH_x, Hz absorpt. and cryst. struct. of hydride 78—34487
rare earth intermetallics, RPt, (R=Gd, Tb, Dy, Ho, Er, Tm), structs. and mag. props. 80—50069
rare earth iodates, crystallographic and nonlinear optic data 78—6044
rare earth iridium borides, RIr_4B_4, supercond., magnetism and metastability 80—29501
rare earth mixed halides, RFX, synthesis and lattice parameters 78—30594
rare earth molybdates, cryst. growth, cryst. chem., and phys. props., book contrib. 80—44194
rare earth molybdates, $R_{12}Mo_6O_{35}$, R=La to Tb, synthesis and characterisation 79—1419
rare earth molybdenum chalcogenides, Chevrel phase correlation between struct. and supercond. transition temp. 80—7023
rare earth molybdo-perrhenates, synthesis and props., cryst. struct., IR spectra *(French)* 79—32976
rare earth orthoferrites, coord. number rel. to ionic radius 78—26548
rare earth orthophosphates, RPO_4 (R=Tb, Dy, Ho, Er, Tu, Yb, Lu), IR and Raman spectra 80—34904
rare earth orthotitanates and orthovanadates, interrelationship between cryst. struct., IR spectra and physiochem. props. 77—24835
rare earth orthovanadites, RVO_3, magnetic and cryst. struct., Jahn-Teller effect 77—32169
rare earth orthovanadites, X-ray diffraction investig., unit cell parameters 77—27859
rare earth oxides, binary, struct. and props., book contrib. 80—45292
rare earth oxides, mixed, phase relations and struct., book contrib. 80—45293
rare earth oxides, perovskite-like, synthesis, struct., elec. props. 80—65554
rare earth oxides, R_2MoO_5, preparation and struct. of R_2MoO_5 79—46624
rare earth oxymolybdates, growth from soln., struct., props. 77—28705
rare earth oxyorthotitanates, crystallochem. classification 80—107142
rare earth oxyphosphates, IR and Raman spectra, vibr. assignments, cryst. struct. characts. 80—97258
rare earth oxyphosphates, x Ln_2O_3.y P_2O_5, synthesis, characterisation and thermal stability 80—16256
rare earth perovskites and garnets, prep. and props. book contrib. 80—44193
rare earth phosphides, $R_2M_{12}P_7$ (M=Fe, Co, Ni), crystal. struct., X-ray diffr. obs. 79—1411
rare earth pnictides, prep. and props., book contrib. 80—54212
rare earth potassium molybdates, $RKMo_2O_8$, flux growth in R_2O_3-K_2O-MoO_3 system, and cryst. struct. 78—35289
rare earth rhenium silicides, $R_2Re_3Si_5$, RRe_4Si, crystal structs. 79—38806
rare earth RNb_3O_9, synthesis and physicochem. props. 77—90304
rare earth scandates, $RScO_3$ synthesis and lattice constant reevaluation 78—30593
rare earth silver tungstates, α,β and β' phases 77—31627
rare earth substituted lead apatites, $Pb_{10-2x}R_xM_x(PO_4)_6Z_2$, M=Na or K and Z=F or Cl, cryst. struct. and IR spectra 80—107167
rare earth sulphides, R_2S_3-In_2S_3, intermediate combinations, description of crystal types *(French)* 78—75648
rare earth sulphides, selenides and tellurides, cryst. struct., book contrib. 80—54210
rare earth ternary borides, RRh_4B_4, supercond. and ferromag., cryst. struct., X-ray diffr. 77—89423
rare earth ternary silicides, RRu_2Si_2 and RPt_2Si_2, crystallographic study *(French)* 78—47286
rare earth titanates, pseudoperovskite struct., nonlinear spectral and luminesc. characts. 80—29771
rare earth titanates, $R_2Ti_2O_7$, synthesis and phys. props. 79—43128
rare earth titanium oxides, $RTiO_3$ type, bulk mag. and struct. props., ferrimag. order 80—107993
rare earth titanoniobates, $RTiNbO_6$, physicochem. investig. 77—47422
rare earth trifluorides, coord. number rel. to ionic radius 78—26548
rare earth trihydroxides, cryst. structs., trends 77—35529
rare earth zirconate, $R_2Zr_2O_7$, Raman spectra, anion disorder characterization 80—25358
rare earth-Sn-S system, R_2SnS_5 compounds *(French)* 77—1104
rare earth-transition metal pnictides of $ThCr_2Si_2$ type 78—51502
rare-earth mixed sulphides, of type $L_4Lu_{11}S_{22}$, cryst. struct. *(French)* 79—77575
rare-earth trihydroxides, single cryst. X-ray lattice constants determ. 80—19766
refractory compounds, electron struct. and phys. props. 80—54585
ruby, cryst. struct. and compression up to 46 kbar 79—37682
ruby, single cryst. struct. determ. for press. up to 90 kbar 78—83875
rustumite, crystal structure, X-ray anal. 80—79766
rustumite, crystal structure determ. by X-ray diffr. method 80—70182
rustumite, naturally occurring 77—84727

crystal atomic structure of inorganic compounds continued
ruthenates, $ACu_3Ru_4O_{12}$, A=Na,Ca,Sr,Cd,La,Pr,Nd, synthesis, cryst. struct., mag. and elec. props. *(French)* 80—107151
sea ice, radar anisotropy due to horizontal c axes preferred aximuthal orientation 79—34836
semiconductor morphotropic and isomorphic series, cryst. struct. stability 77—51353
serpentine minerals, milling rel. to cryst. struct., X-ray diffr. 77—55278
silicate HV high-resolution electron microscopy 80—70096
silicates, plane Si-O rings with max. number of tetrahedra 78—18622
silicates with branched anions, crystallochemistry distinct class 79—57917
silicides, $(Cr, Nb or Ta)_{11}Si_8$, $(Mn,Mo)_{11}Si_8$ *(French)* 78—38675
α-SiO_2 cryst. struct. determ. up to 68×10^8 Pa by X-ray diffractometry 79—37668
sodalites, aluminogermanate- and aluminate-, IR spectra rel. to T-O bond length and T-O-T ang. 79—91445
solid soln. form., regions of existence 79—11581
solid state chemistry problems, appl. of electron microscopy and diffr. 79—46527
spinel structs., thermodynamic anal. of energy of cation octahedral sites 79—10827
spinel structure compounds, cation distrib., neutron diffr., determ., minimum errors 78—1958
spinels containing Fe^{3+} and Sb^{5+}, $M_4{}^{2+}Fe^{3+}Sb^{5+}O_8$, Mossbauer spectra 80—15892
6 $(SrAl_2O_4)$.SrO, cryst. struct. determ. by means of vector subsystems 79—94983
steel, bainite and martensite, ^{57}Fe Mossbauer spectra 80—15051
stilpnomelane, complex layer silicate, struct. of long-period polytypes 77—64266
stishovite (SiO_2), single cryst. anal. of struct. 78—53648
struct. and props. exam. 78—92245
structural diagram of compounds ABO_4 78—79548
sulphate based binary solid electrolytes, props., appls. 77—84971
sulphide compounds of Si, Ge and Sn, struct. and chem. bonding *(French)* 78—30580
sulphide spinel, systematic trends in geometry, ionic radii and electronegativity 80—19778
sulphides, RR'_3S_6, where R,R′=rare earth, Sc or Y, struct. organisation *(French)* 77—11519
superconducting materials properties 79—56366
superionic conductors, EXAFS studies of struct. and cond. process, book contrib. 80—25485
superionic conductors, struct. and dynamical props., X-ray and neutron scatt. studies, book contrib. 80—24433
superstructure reflection determ. from pseudostruct. reflections *(Chinese)* 79—10748
synthesis, structs. *(French)* 78—51519
taenite lamellae in Fe meteorite, Mossbauer study 78—65575
tantalates, double and triple, with perovskite structure, cationic distrib. *(French)* 77—1109
TaS_2, amine intercalation, water effects, X-ray diffr. meas. 80—44178
TCNQ complex, $(C_{13}H_{21}N_2S_2)^+(C_{12}H_4N_4)_2$, cryst. and mol. struct. 77—62514
ternary metal borides, struct. chem. 79—14769
ternary semiconductor, struct. effects on energy band struct. 78—39021
ternary W oxides with Mo_5O_{14} struct. 77—4084
tetraferriphlogopite, cryst. struct. refinement using least squares approx. 78—79594
tetrahalides of group IV elements, NQR spectra rel. to cryst. struct. 77—12231
tetrahedral structures, related to wurtzite type (B4), non-bonded interactions and cryst. chemistry 79—14743
tetratitanates, $M_2Ti_4O_9$ (M=Li, Na, K, Rb, Cs, Tl, Ag), preparation, cryst. struct. determ. 78—75646
tienshanite, X-ray determ. 78—83800
titanates, isostruct. with $[CaCu_3](Mn_4)O_{12}$, synthesis and characterisation *(French)* 79—90615
titanomaghemite, synthetic, cation distrib. 78—55856
titanomagnetites, temp. depend. cation distrib., mag. prop. obs. 80—85647
todorokites, natural, new forms crysts. structs. 79—48469
tooth enamel, human cryst. struct. refinement, Rietveld method 80—51040
tourmaline, Mossbauer spectra, struct. 80—20566
tourmaline, pyroelectricity, struct. mechanisms 78—10850
transition, metal nitride, atomic struct. *(German)* 79—90622
transition metal, polynary oxocompounds, struct. data, book 78—51521
transition metal borides, cryst. struct., prep. methods, chem., elec., mag. props., appls., book contrib. 78—47307
transition metal carbides and nitrides, M_2X, struct. and phase transitions 79—70051
transition metal carbonitrides, physicochem. props., comp. depend. 80—55370
transition metal chalcogenide layer compounds, convergent beam electron microscopy obs. 80—108689
transition metal chalcogenides, $MS_3(Se_3)$, present status of research *(Japanese)* 80—20100
transition metal chalcogenides, struct. and mag. props., book contrib. 77—43808
transition metal complex, linear chain type, synthesis 78—6047
transition metal complexes with 1,2,4-triazole, mag. susceptibility, 2-300K, struct., antiferromag. props. 77—77045
transition metal compounds, $M_{2-x}Mo_xAs(P)$ and $M_{2-x}W_xAs(P)$ *(French)* 77—47429
transition metal diborides, C32-type, phys., chem. props., appls., review, book contrib. 78—47308
transition metal dichalcogenides, deform. modulated superstruct., model explaining results for VSe_2 78—51515
transition metal dichalcogenides, physical props., review *(Japanese)* 80—33969
transition metal dichalcogenides, zone axis electron diffr. patterns 78—34497
transition metal dichalcogenides prep. and growth, book contrib. 78—19650
transition metal dioxides, elec. struct. props., two-band model calcs. 78—67934
transition metal ferrocyanides, crystal structures and ion-exchange props. 77—15362

crystal atomic structure of inorganic compounds continued
- transition metal hydride complexes, struct. geometry bonding, neutron diffr. studies 79−46641
- transition metal hydrides, struct. change from metal struct., due to interaction of metal with H 80−49196
- transition metal layered oxides, struct. classification and props. 80−39046
- transition metal precious metal hexahydroxides, prep. and characterisation 79−90610
- transition metal silicides, $(M,M')_6Si_5$ type *(French)* 77−43193
- transition metal sulphate hydrates, systematic cryst. struct. differences *(German)* 77−84724
- transition metal tetrametaphosphates, cryst. struct., high press. effects *(French)* 77−15373
- transition metal-O systems, exam. of phase diagrams and crystal structure 79−8291
- transition metal-rare earth-B systems, phase diagrams and struct. considerations 80−16286
- traskite, Ba mineral of variable comp., X-ray diffr. struct. anal. 77−44981
- tridymite, low, synthetic, struct. refinement, Si-O bond lengths and Si-O-Si bridging angles 77−80456
- $TTT_{1.2}NiS_4C_4H_4$, quasi-one-dimensional cond., cryst., mag. and elec. props. 78−10424
- $TTT\text{-}(I_3)_{0.5}$, one-dimens. metal, mag. susceptibility, elec. resist., thermopower meas. 78−87967
- tungstates, $A(B_1W)O_3$, $A(B_1C_1W)O_3$, perovskite struct. 77−51352
- tungstates, hexagonal bronze type struct., cryst. struct. and props. 77−39574
- tungstates (double), of mono- and tri-valent metals, polymorphism, X-ray diffr. obs. 78−87642
- tungsten-bronze ferroelectrics, $A_5B_{10}O_{30}$- and $A_6B_{10}O_{30}$-type, phase relations 78−35100
- tveitite, X-ray powder and single cryst. electron diffr. study *(German)* 79−99160
- vermiculite, interlayer space struct. anal., by replacing exchange cations with NH_4^+ 77−7700
- wustites, X-ray diffr. and electron microscopy study *(French)* 80−64973
- X-ray cryst. struct. determ. 79−14751
- X-ray diffraction powder patterns, standard, for 112 substances 79−60223
- X-ray diffraction powder patterns, standard, for 87 substances 80−64839
- YAG powder, X-ray K_α doublet diffr. peak position rel. to lattice const. precision 77−68891
- zeolite, hydrated, partly exchanged with Ce ions, cation distrib. *(Spanish)* 77−4080
- zeolite, synthetic, ZSM-11, synthesis and struct. 78−87657
- zeolite framework types, classification using coordination sequences 79−55718
- zeolites, coordination sequences 79−86751
- zeolites, type A, struct. studied by powder neutron diffr. 79−86655
- zinckenite, chem. and structural study *(French)* 77−43181
- ^{248}CmN, prep. and cryst. struct. 79−99115
- $ABCl_3$ cpds., basic struct. types and polymorphisms 78−79583
- Ag complex, dioxane perchlorate, cryst. struct., phase transitions, X-ray study 80−59646
- Ag orthophosphates and sulphates, anhydrous, struct. relationships w.r.t. fast ion cond. 80−107188
- Ag-Se system, formation of FCC thin films *(French)* 77−4267
- $AgAsSe_2$, X-ray diffr. exam. 77−7704
- Ag_3AsSe, X-ray diffr. exam. 77−7704
- Ag_3AsSe_3, synthesis and X-ray cryst. struct. anal. 79−4284
- $AgBi(CrO_4)$, cryst. struct., neutron diffr. time-of-flight study *(French)* 80−15057
- $AgBi(Cr_2O_7)$, cryst. struct. determ. by X-ray and neutron diffr. *(French)* 80−92492
- Ag_2BrNo_3, cryst. struct. 78−18594
- Ag_2CO_3, X-ray cryst. struct. determ. *(French)* 79−69071
- Ag_2ClNO_3, X-ray cryst. struct. determ. and refinement 79−69073
- $AgCoPO_4$, crystalline struct. *(French)* 79−1422
- $Ag_2Cr_2O_7$, X-ray cryst. structural anal. *(French)* 79−4288
- $AgGa_xIn_{1-x}Se_2$, X-ray diffr. cryst. data 80−84147
- Ag_9GaSe_6, crystn. in $Ag_2Se\text{-}GaSe_3$ system, lattice parameters *(French)* 77−51472
- $\beta\text{-}Ag_9GaSe_6$, X-ray cryst. struct. determ. *(French)* 79−4277
- $\beta'\text{-}Ag_8GeSe_6$, X-ray cryst. struct. determ. *(French)* 80−39020
- Ag_2HPO_4, X-ray cryst. struct. determ., Patterson method *(French)* 79−14755
- $AgHg_2AsO_4$, cryst. struct. by X-ray diffr. *(French)* 78−34490
- $AgHg_2PO_4$, cryst. struct. by X-ray diffr. *(French)* 78−34490
- AgI aerosols, particle size influence on cryst. struct. 80−2000
- AgI based, superionic conductors, geometric struct. principles 77−89574
- AgI, EXAFS investigation of struct. and ion motion 80−108302
- α-AgI, ionic motions nature, mol. dynamics calcs. 80−107533
- AgI large single crysts., gel and soln. growth and props. 80−35071
- AgI, mixed-polytype cryst. containing new 12H polytype 77−19911
- α-AgI, neutron powder diffr. meas. interpretation 80−10533
- AgI, position and dynamics of Ag ions using EXAFS, jump-diffusion cond. model 77−59643
- AgI, single cryst. neutron diffr. meas., Ag distrib. determ. 78−10025
- α-AgI, state of order, config. model 80−6390
- α-AgI, structural and dynamical behaviour 80−107544
- AgI, structural model for superionic conduction 78−79797
- α-AgI, structure, X-ray diffr. 77−84728
- α-AgI, superionic compound struct., cation distrib., powder neutron diffr. 77−72595
- AgI, superionic cond., cryst. struct., neutron diffr. study 79−42041
- α-AgI, superionic phase, struct., X-ray scatt. anal. 80−28983
- AgI type solid electrolytes, expt. props. 78−63877
- α-AgI type superionic conductors, struct. and phase transition *(Japanese)* 79−65250
- Ag_2INO_3, X-ray cryst. struct. determ. and refinement 79−32956
- $AgIO_3$, chem. prep. and cryst. struct. 80−75207
- $Ag_{26}I_{18}W_4O_{16}$, cryst. struct. and ionic conductivity 77−80647
- $AgInCr_4S_8(Se_8)$, 1:1 ordering on tetrahedral sites, IR spectra obs. *(German)* 78−6669
- $AgInS_2(Se_2)\text{-}SnS_2(Se_2)$, degree of solid solubility and phases characts. 78−35377
- $Ag_xMo_6S_8$, Chevrel phase, lattice instabilities, X-ray diffr. meas. 78−34491
- $AgN(CN)_2$ 77−35513

crystal atomic structure of inorganic compounds continued
- $AgNO_3$, ESCA contrib. to X-ray struct. determ. *(French)* 77−62508
- $AgNO_3$, polymorphic structural relationships, X-ray diffr. and microscopy 77−19930
- $AgNO_3$, struct. at room temp. and press., perfect cryst. *(French)* 78−55846
- $Ag_xNa_{2-x}Te_2^{IV}Te_3^{VI}O_{14}$, (x=0,4), mixed tellurate, cryst. chem. and elec. cond. *(French)* 80−107150
- $AgNbO_3$, cryst. growth and phase transitions 80−40243
- $Ag_2Nb_2O_5F_2$, cryst. struct. determ. from single cryst. diffr. data *(French)* 78−95030
- $Ag_2O\text{-}Al_2O_3\text{-}MgO\text{-}Na_2O$, β″-alumina, structure, X-ray determ. 80−107148
- Ag_3PO_4 78−42973
- $AgPS_2$, single crystal, prep. and structure 77−35524
- $Ag_2P_2S_6$, X-ray cryst. struct. determ. by direct methods *(French)* 79−14752
- $Ag_4P_2S_7$, cryst. struct., X-ray diffr. meas. *(French)* 77−47412
- $Ag_4P_2S_7$, single crystal, prep. and structure 77−35524
- $Ag_4P_2Se_6$ *(French)* 78−63703
- $Ag_4P_2Se_6$, orthorhombic system, crystal parameters determ. *(French)* 78−34481
- $Ag_5Rb(PO_4)_2$, struct., density and elec. cond. 80−33952
- $\alpha\text{-}Ag_2S$, cryst. struct., X-ray scatt. determ. 79−46613
- $\beta\text{-}Ag_2S$, fast-ion conductor, Ag ion density, neutron diffr. study 80−34234
- Ag_2S, metal-nonmetal transition, crystallographic, optical, mag. and transport props. 78−6418
- $\alpha\text{-}Ag_2S$, struct., X-ray scatt. intensity anal. 78−38672
- $\alpha\text{-}Ag_2S$, structure, comment on coherent scattering intensity 78−95027
- $Ag_2S\text{-}In_2S_3\text{-}SnS_2$ system quaternary and ternary sulphide spinels, solid solubility and struct. 78−35376
- Ag_3SBr, superionic conductor, phase transition, struct. 80−107144
- βAg_3SI, anharmonic thermal vibr. of cations 80−65214
- Ag_3SI, superionic conductor, ordered phase struct. 78−83792
- Ag_3SI, superionic conductor, struct. and phase transition *(Japanese)* 79−65250
- Ag_3SI, superionic cond., phase transition and cryst. structs., sp. ht., neutron and X-ray diffr. obs. 80−10662
- Ag_2SO_4, cryst. struct., form. 77−19928
- $Ag_4SO_2N_2$, X-ray cryst. struct. determ. 80−88101
- $Ag_8S_3SO_4$, new cryst. data 79−37685
- $AgSbS_2$, synthetic crystals, DTA and cryst. struct., phase transitions *(German)* 78−42943
- Ag_2Se, metal-nonmetal transition, crystallographic, optical, mag. and transport props. 78−6418
- $Ag_6Si_2O_7$, direct and Fourier methods *(German)* 78−10007
- $Ag_{1-x}Sn_{1+x}Se_{2-y}$, supercond. and normal state props. 77−36008
- Ag_2TeO_3, chem. prep. and cryst. struct. *(French)* 80−79755
- $Ag_2Te_xSe_{1-x}$ system, solid solns. of substitution existence, X-ray phase obs. 79−43217
- $Ag_2Th(MoO_4)_3$, crystallographic data determ. *(French)* 78−10013
- AgTlTe(S)(Se), cryst. struct. 80−107156
- Ag_2WO_4, preparation and characterisation 79−99873
- $Ag_2W_2O_7$, preparation and characterisation 79−99873
- $Ag_2W_4O_{13}$, preparation and characterisation 79−99873
- $\beta\text{-}Ag_xW_yV_{2-y}O_5$ bronzes, β-phase existence range, elec. cond. and Ag diffusion 78−35373
- (Al,B)N, produced by nitriding AlB_{12} powder 77−12560
- Al oxides and hydroxides, electro-erosional prep. *(Russian)* 80−81297
- Al saponite, evidence for inclusion in chlorite-like mineral group, X-ray and chem. anal. 79−12108
- Al-B(-C) system, synthesis and struct. of boride phases 80−45282
- $Al(Al_{1+2x}Si_{1-2x})O_{5-x}$, mullite, X-ray diffr. structural model 80−49191
- $\alpha\text{-}AlB_{12}$ 77−43197
- $\alpha\text{-}AlB_{12}$, cryst. struct. and refinement 77−15376
- $\gamma\text{-}AlB_{12}$, struct. rel. to isohedral B framework 78−2086
- $\alpha\text{-}AlB_{12}$, valence electron distrib. deform. 79−65042
- AlB_2, structure types, coordination 77−19913
- $AlBO_3$, B-O bond length determ. 78−10010
- $AlBeB_{24}$, and $\beta\text{-}(Al,Be)B_{12}$, prep. and struct., book contrib. 78−47277
- $Al_{1.0}Be_{0.7}B_{22}$, cryst. struct. by X-ray diffr. 80−15069
- $Al_4Bi_2O_9$, single cryst., struct., X-ray obs. 77−43191
- $Al_{10}Br_3(OH)_{27}(H_2O)_{13\pm2}$, cryst. struct., X-ray powder diffr. obs. *(French)* 78−2084
- $Al_{10}Br_4(OH)_{26}(H_2O)_{13\pm2}$, cryst. struct., X-ray powder diffr. obs. *(French)* 78−2084
- $Al_4C_3\text{-}Be_2C\text{-}SiC$ system, phase analysis and TEM struct. obs. 80−108420
- $Al_{10}Cl_3(OH)_{27}(H_2O)_{13\pm2}$, cryst. struct., X-ray powder diffr. obs. *(French)* 78−2084
- $Al_{10}Cl_4(OH)_{26}(H_2O)_{13\pm2}$, cryst. struct., X-ray powder diffr. obs. *(French)* 78−2084
- $\alpha\text{-}Al_2(CrO_4)_2Cr_2O_7.4H_2O$, cryst. struct. determ. 78−6038
- $AlCuCl(SO_4)_2.14H_2O$, aubertite, X-ray cryst. struct. determ. *(French)* 80−33932
- $Al_{2x}Ga_{2(1-x)}O_3:Cr^{3+}$, luminesc., lifetime, 77 and 4K, struct., energy transfer 79−28798
- $\alpha\text{-}AlH_3$, prep., thermal decomposition, transform., struct. *(French)* 80−3326
- $AlH(SO_4)_2.4H_2O$, cryst. parameters and X-ray powder diffr. data *(French)* 79−14765
- $AlHfTaO_6$, powder X-ray diffr. data 79−99155
- $Al(IO_3)_3.8H_2O$, crystal structure, thermal vibr. parameters, X-ray study 80−64979
- $AlInS_3$, X-ray cryst. struct. determ. 80−28968
- $Al_2In_{12}S_{21}$, preparation, struct. and elec. props. 77−59685
- $(Al_xIn_{1-x})_2S_3$, x=0-0.33, cryst. struct., X-ray diffr. 79−55710
- $Al_2In_{12}Se_{21}$, cryst. growth from melt, elec. props. 79−56922
- $\beta\text{-}Al_{11-y}Mg_yO_{16}$, X-ray diffuse scatt. obs. of struct. 80−107186
- $Al_3Mg_2[Si_5AlO_{18}]$, cordierite cryst., effect of face symmetry on structural ordering of Al 78−22703
- AlN, cryst. struct. refinement 77−84731
- $AlNH_4HP_3O_{10}$, cryst. struct. determ. *(French)* 77−47408
- $Al_{10}N_8O_3$, sublimation growth, cryst. struct. determ. 80−19751
- $Al_9N_7O_3$, sublimation growth, cryst. struct. determ. 80−19751
- $Al(NO_3)_3.9H_2O$, cryst., deuteration rel. to NO_3^- ion vibr. spectrum *(Russian)* 77−40240
- $Al_2Nb_2O_7$, new phase of mixed oxide 78−59787
- $\beta\text{-}Al_2O_3$, alkali-free water containing, cryst. struct. determ. *(German)* 77−47416

crystal atomic structure of inorganic compounds continued
α-Al_2O_3, computed X-ray powder diffr. patterns and densities 77—43172
Al_2O_3, corundum ceramic, effects of Na_2O, CaO additions on sintering struct., props. 79—15630
α-Al_2O_3, cryst. struct. determ. at 2170K 80—39015
β-Al_2O_3, long-period structs., electron microscope obs. 80—92501
β-Al_2O_3 phases, synthesized, effect of starting Al_2O_3 composition and halogen ion additions, on structural state 78—76620
η-Al_2O_3, prep. and struct. *(Japanese)* 77—55930
β-Al_2O_3:Gd^{3+}, EPR, ion site occupancy 77—81003
β-Al_2O_3-$(Na,K)_2O$, equil. distrib. of ionic species 80—107511
β-Al_2O_3-Ag_2O, cryst. structs. of stoichiometric and non-stoichiometric phases by X-ray diffr. *(French)* 80—28987
β-Al_2O_3-Ag_2O, stoichiometric A phase, X-ray diffuse scatt. obs., sublattice phase transition 80—64944
β-$11Al_2O_3$-Ag_2O, sublattice phase transition, stoichiometric 79—42241
β-Al_2O_3-$Ag_2O(D_2O)(NH_4^+)$ 80—107512
β''-Al_2O_3-$Ag_2O(K_2O)(Li_2O)(Na_2O)(Rb_2O)$, single cryst. Raman scatt., cond. mechanism and cryst. struct. 80—66209
β-Al_2O_3-D_2O, anhydrous, prep. and struct. of $DAl_{11}O_{17}$ 80—107187
Al_2O_3-Dy_2O_3, phase diagram at high temps. *(Japanese)* 79—38810
β-Al_2O_3-H_3O^+ protonic cond., struct. investig. 79—19213
β''-Al_2O_3-$H_3O^+(Na_2O)$, struct. basis for superionic cond. 80—107498
β-Al_2O_3-$H^+(H_2O)_n$, IR and Raman spectra, OH stretching freqs., struct. and cond. 78—27210
β-Al_2O_3-K_2O-MgO, cryst. struct., nonstoichiometry, ion-ion correlations 80—88129
Al_2O_3-La_2O_3:Eu^{3+} system, optical and struct. exam. 77—4674
β-Al_2O_3-Li_2O-Na_2O, solid electrolytes, elec. props., stability 77—84978
β-Al_2O_3-NH_4^+, protonic cond., struct. investig. 79—19213
β-Al_2O_3-NH_4^+, single cryst. characts. and AC cond. obs. 80—107514
Al_2O_3-Na_2O, β and β'' phases, stability, cond., paramag. impurity effects obs. 77—84976
β-Al_2O_3-Na_2O, cond. plane struct. and energetics 80—92715
β-Al_2O_3-Na_2O-Li_2O, struct. determ. by powder neutron diffr. 79—46623
Al_2O_3-Nd_2O_3, optical absorpt. spectrum and struct. of β-phase *(French)* 77—69848
Al_2O_3-NiCr composite, plasma sputtering of electroheating coatings, elec props. *(Russian)* 80—108350
Al_2O_3-TiO_2-$MgO.2TiO_2$, exam. of solid solutions by X-ray phase analysis 79--95981
$Al(OH)_3$, unit cell, determinantal eqns. for scale factor, temp. factors, quantitative chem. contents 78—75609
$Al_2(OH)_4(SO_4).7H_2O$, aluminite, cryst. struct. determ. and refined 78—83782
AlO_xN_y spinel, crystal struct. model 78—91333
γ-AlOOD, boehmite, hydrogen bond, neutron profile refinement of struct. 78—71701
γ-AlOOH and γ-AlOOD, IR and Raman spectra obs., struct. and ${D_{2h}}^{17}$ space group anal. 80—89000
γ-AlOOH, boehmite, proton pair obs. from NMR absorpt. spectra 80—75866
γ-AlOOH, boehmite, structural variability 78—38681
AlOOH, diaspore, cryst. struct. refinement and electron density distrib. 80—79758
β-$Al_2O_3.Na_2O$ type compounds, struct. and stoichiometry by TEM 77—11521
AlPO cristobalite form, polymorphic transform. investig., X-ray diffr. and IR spectra 77—4199
$AlPO_4$, low quartz struct., charge density refinement, use of elec. field gradient calcs. 79—73480
$AlPO_4.2H_20$, cryst. struct., X-ray diffr. 77—19924
α-Al_4SiC_4, $Al_4Si_2C_5$, X-ray crystallographic data 80—49197
Al_2SiO_5 polymorphs (sillimanite-andalusite-kyanite), thermal expansion and high-temp. cryst. chemistry 80—39319
Al_2SiO_5, sillimanite and andalusite, elastic constants, cryst. struct. 79—60422
$AlSiP_2$, wurtzite-pyrite intergrowth struct. 79—60328
$AlTiTaO_6$, powder X-ray diffr. data 79—99155
$AlWO_4$, form., struct. 77—16518
$Al_2[(OH)_2(PO_4)_2(UO_2)_3].(OH)_4.10H_2O$, phuralumite, X-ray cryst. struct. determ. 79—90606
$Al[(PO_4)_2(UO_2)_2].OH.8H_2O$, threadgoldite, X-ray cryst. struct. determ. 80—28969
alkali earth uranates, struct., phys. and chem. props., preparation methods, review *(Japanese)* 79—14764
$(Am,Cm)O_2$ solid soln., struct. changes under self- and reactor irrad. 77—27927
α-$Am_2(MoO_4)_3$, cryst. struct., lattice parameters 79—14774
AmOBr, cryst. struct. from powder patterns 79—46617
AmSi, $AmSi_2$, prep. and cryst. struct. 78—18607
$AmTe_{1\ 73(2)}$, X-ray single cryst. struct. determ. and refinement 79—19201
α-$Am_2(WO_4)_3$, cryst. struct., lattice parameters 79—14774
apatites, replacement by La, Nd, Sm, Gd by Ti, Ge, Mn^{IV}, V^V *(French)* 79—69093
$AsCl_3$, low temp. struct. study *(French)* 79—32968
AsF_3, 193K obs. *(French)* 80—49194
AsF_5-graphite intercalation compound nature 80—103308
AsI_3, X-ray cryst. struct. refinement 80—64961
AsO_2, X-ray cryst. struct. determ. 80—39026
As_2O_3 crystalline and amorphous, EXAFS study of struct. 80—19776
As_2O_3, cubic modification, struct. refinement *(German)* 78—30590
$AsSbO_4$, X-ray cryst. struct. determ. 80—107127
As_2Se_3, monoclinic, chem. bonds rel. to electronic and vibr. states 80—64951
$As_2(Se_{1-x}S_x)_3$, crystal growth and at. struct. 79—60289
As_2Te_3, $As_4Te_5I_2$, $TlAsTe_2$, local struct. changes on crystal-glass transition, Mossbauer spectra 77—36157
(Au, Ag)Te_2, calaverite, Te atom splitting and modulated struct. 79—99145
$AuAg_3Te_2$, petzite, X-ray cryst. struct. refinement 79—46634
AuBr, I and P forms, growth by vap. transport, cryst. struct. 78—38676
AuClO, X-ray cryst. struct. determ. 80—1973
Au_2O_3, X-ray cryst. struct. determ. 79—69074
$Au_7P_{10}I$, polyphosphides with weak Au-Au interactions, cryst. struct. determ. by X-ray techniques 79—37674
AuTeI 78—51504
B hydrides and related cpds., cryst. struct., secondary and multi-centre bonding 78—63751

crystal atomic structure of inorganic compounds continued
B modifications, exam. of physical props. and electron structure 79—94954
B-O(S)(Se)(Te)(Po) compounds, prep. and struct., book contrib. 78—47306
B-Zn solid soln., struct. changes on Zn incorporation into α- and β-rhombohedral B 78—79596
$(B_{12})_4B_2Ti_{1.3-2.0}$, tetragonal, cryst. struct. 77—15360
BC_x, IR-active phonons, reflectivity and absorption spectra 79—82294
$B_{13}C_2$, chem. bonding nature, static deform. densities and pictorial representation 80—92489
$B_{13}C_2$, crystal struct. refinement, X-ray diffr. 79—55702
$B_{13}C_2$, dynamic deformation densities and valence densities 80—1971
$B_{13}C_2$, infinite network struct., X-ray diffr. meas. 80—15070
$B_{13}C_2$, structural anal., electron density and bonding 80—15071
B_4C, morphology and struct. of vap. grown crysts. 79—7562
$B_{50}C_x$, x=1 to 2, prep. and struct., book contrib. 78—47277
$(B_{12})_4C_2Ti_{1.86}$, X-ray cryst. struct. determ. *(German)* 80—54188
$(B_{12})_4C_2V_{1.29}$, X-ray cryst. struct. determ. *(German)* 80—54188
$B_{10}H_{14}$, cryst. struct. *(Czech)* 78—87649
$B_{10}H_{14}$, molecular charge distrib. 78—26513
B_2H_6, cryst., mol. charge distrib. anal., using struct. factors from mol. densities 80—15068
BN, O content depend. on heat treatment temp., neutron activation analysis 80—16356
BN, wurtzite-type, prepared by static compression, struct. 77—35539
BN:C, hardening by doping, p-T diagram, cryst. struct. *(Russian)* 77—77491
BN-AlB, cubic phase solid soln., crystallographic and metallographic study, thermal resist. *(Russian)* 78—30599
$B_{50}N_x$, x=1 to 2, prep. and struct., book contrib. 78—47277
B_2O_3, struct. determ., continuous random network approach 78—67693
$B_{0.65}Ru_{2.7}Cr_{1.3}O_8$, short axis tripling, X-ray and electron diffr. study 79—77576
$(Ba,Gd)TiO_3$, flux growth and chem. characts. 78—23595
Ba ferrite compounds, microsyntactic intergrowth and cryst. defects, TEM obs. 79—10858
Ba hectorite, Ba ion position, water effect *(French)* 77—72593
$Ba_{3x}A_{2-2x}Ti_{6-x}O_{13}$, (A=Na, K, Rb), $0<x<0.2$, struct. evolution, tunnel struct. 79—65049
$BaAgP_3O_9.4H_2O$, cryst. struct. determ. *(French)* 77—80464
$BaAl_2Ge_2O_8$, structural parameters 78—14312
$BaB_{12}H_{12}.10H_2O$, struct. dehydration, intermediate phases and thermooxidative degradation 80—33951
$Ba_x(Ba_{1\ x}Al_x)Fe_2S_6[S_{1-y}(S_2)_y]$, cryst. struct., Mossbauer and mag. behaviour 77—55273
$BaBe(PO_4)F$, babefphite, cryst. struct. determ. using $P\bar{1}$ automatic diffractometer 80—107179
$Ba_2Bi^{3+}Bi^{5+}O_6$, structure and elec., mag., thermal props. vs. temp. X-ray and neutron powder diffr. study 79—19189
$Ba_2Bi^VBi^{III}O_6$, struct. determ. by powder neutron diffr. 78—34468
$BaBi_6Ti_3Nb_2O_{21}$, cryst. struct. and dielec. const. 77—47428
$BaBi_8Ti_7O_{27}$, cryst. struct. and dielec. const. 77—47428
$Ba_2Bi(Y)RuO_6$, perovskites, prep., struct., emission control catalysts 77—68957
BaBrF, cryst. at. struct. by X-ray diffr. 78—75641
$BaBr_2.2H_2O$, X-ray cryst. struct. redeterm. and refinement *(German)* 80—39025
$BaCaLu_2F_{10}$, single cryst. X-ray struct. determ. and refinement 79—69084
$BaCaLu_2F_{10}$, site occupancy from excitation and emission spectra *(French)* 77—81145
$BaCa_2Mg[SiO_4]_2$, synthesis and struct. characterization 78—22698
$Ba(ClO_3)_2.H_2O$, cryst., O-H bond lengths, H-O-H angles, corrections 79—32945
$Ba_5Cl(PO_4)_3$, X-ray cryst. struct. determ. and refinement 80—1974
$BaCl_2.2H_2O$, cryst. struct. determ. by neutron diffr. 78—75639
$BaCoO_3$, cryst. struct. determ. 77—47394
$BaCrO_3$, 27 layer polytype, struct. determ. 80—107162
$BaCr_2O_7$, α and β form, powder data, cryst. struct. *(French)* 80—39032
α-$BaCr_2O_7$, X-ray cryst. struct. determ. *(French)* 80—15064
$Ba_{1-p}Cr_2S_{4-p}(Se_{4-p})$, modulation of intergrowth struct. 79—94967
$BaCuO_2$, prep. and props. *(French)* 77—43201
BaF_2-MnF_2-$M'F_3$ (M'=V,Cr), comparative study of barium fluorides rel. to 1st transition series elements *(French)* 79—69090
BaFBr, cryst. struct. determ. 77—80465
$BaF_{2-x}H_x$, synthesis and struct. determ. using neutron diffr. *(French)* 80—24425
BaFI, cryst. struct. determ. 77—80465
$(BaF)_2[Zn_{1-x}Cu_xF_4]$, statistics of ion distrib. 80—49167
$Ba_3Fe_2BO_9$, (B=Re, Te, W, Mo), siegnette magnets with hexagonal barium titanate structure 78—76397
$Ba_3Fe_{2-x}Ho_xUO_9$, $O\leq x\leq 1.2$, perovskites, struct. and mag. props. *(French)* 78—18612
$Ba_3Fe_{2-x}Lu_xUO_9$, crystallographic and mag. props. *(French)* 77—15380
$BaFe_{12\ x}M_xO_{19}$ (M=Al, Ga, Sc, In) ferrites, mag. props. and struct. 80—15690
$BaFe_{12}O_{19}$, ferrite, DC cond., dielec. props., lattice consts. 80—80272
$BaFe_{12}O_{19}$, hexagonal ferrite, local lattice distortions, use of Mossbauer effect 78—43745
δ-$BaFe_2O_4$ room-temp. formation and polymorphism *(German)* 80—44192
$Ba_2Fe_6O_{11}$, cryst. struct. *(French)* 79—86755
β-$BaFe_2S_4$, cryst. struct., X-ray diffr. obs. 80—84153
$Ba_{1+x}Fe_2S_4$, electron diffr. study, orientation anomaly 80—107152
$Ba_9(Fe_2S_4)_8$, subcell and supercell structs. 77—35512
β-$Ba_9Fe_4S_{15}$, and low temp. α polymorph., cryst. struct. 78—67690
Ba_2FeSbO_6, siegnette magnets with hexagonal barium titanate structure 78—76397
$Ba_3Fe_3Se_7$, stella quadrangula as struct. building unit 80—15055
$Ba_3Fe_{0.2}Si_{0.8}S_5$, stabilisation of tetravalent Fe 79—60326
$Ba_2Fe[Ge_2O_7]$, hydrothermal growth, struct. and opt. props. 77—65971
$BaGaF_5$, X-ray cryst. struct. anal., lattice energy *(German)* 79—69094
$BaGa_2Ge_2O_8$, ordered synthetic feldspar, cryst. struct. 78—34469
$Ba_2Ga_2GeO_7$, gehlenite struct., synthesis and physicochem. props. 79—43181
$BaGa_2Si_2O_8$, ordered synthetic feldspar, cryst. struct. 78—34469
$Ba_3Ge_9O_{20}(OH)_2$, cryst. struct. determ. 77—11524
$BaH_6As_4O_{14}$, cryst. struct. exam., new cyclic anion *(French)* 78—2080
$BaHCr_2PO_{10}.H_2O$ and $BaHCr_2PO_{10}.3H_2O$, cryst. struct. determ. *(French)* 77—47407

crystal atomic structure of inorganic compounds continued
$Ba(H_2PO_4)_2$ 77–31649
$Ba(H_2PO_4)_2$, orthorhombic 78–10005
$Ba(H_2PO_4)_2$, orthorhombic, cryst. struct. determ. 78–26515
$Ba(H_2PO_4)_2$, triclinic, cryst. struct. *(French)* 78–55848
$Ba(H_2PO_4)_2$, X -ray cryst. struct. determ. 79–7589
$BaH[AsCr_2O_{10}]$, X-ray cryst. struct. determ. 79–42019
$Ba(IO_3)_2$, cryst. struct. determ. by X-ray diffractometry 80–107139
$BaIn_2Se_4$, cryst. struct. *(German)* 80–79760
$BaKP_3O_9.H_2O$ *(French)* 78–51480
$Ba_xLa_{1-x}CoO_3$, x=0 to 0.5, structural, elec. and mag. props., Zener double exchange and Goodenough's model 79–65663
$Ba_{1+x}La_{1-x}MnO_4$, X-ray obs. *(French)* 78–6042
$Ba_6La_2Na_2(PO_4)_6F_2$, cryst. structure 79–60332
$Ba_3M_{4-4x}Ti_{4+5x}O_{21}$ $(O \leq x \leq 0.3)$, M=Nb,Ta, synthesis and struct. anal. *(French)* 80–44185
$Ba_2MgCr(PO_4)_3$, cryst. data 77–39564
$BaMgTi_7O_{16}$, hollandite struct. electron-optical imaging at 3 Å resolution 77–65939
$Ba(NO_2)_2.H_2O$, pyroelec., room temp. cryst. struct. 80–96491
$Ba_2NaNb_5O_{15}$, effect of substituting Gd, Cr on lattice parameters 78–47291
$Ba_2NaNb_5O_{15}$, X-ray powder diffraction data determ. *(Chinese)* 80–70170
$Ba_3Nb_6Si_4O_{26}$-$Ba_3Nb_4Ti_4O_{21}$, intergrowth, nonstoichiometry, struct. obs. *(French)* 77–19932
$Ba_3Nb_{8-x}X_xO_{21}$ (X=Nb, Ti, Cr, Fe, Ni, Mg, Zn), X-ray diffr., layer struct. *(French)* 77–15368
$BaNd_2(MoO_4)_4$, X-ray cryst. struct. determ. 80–88128
$Ba_4Nd_3Na_3(PO_4)_6F_2$, cryst. structure 79–60332
$Ba_2Ni_3F_{10}$, cryst. struct. and antiferromag. props. 80–107153
Ba_2NiReO_6, mag. and cryst. struct. 77–20554
$BaNpO_2(H_3C_2O_2)_3.2H_2O$, structure and bonding study 77–27868
BaO, at. charge densities, X-ray struct. factors 78–79566
BaO-GeO_2-Na_2O-H_2O system, hydrothermal crystn., phase formation laws, interplanar spacings of phases 79–46636
BaO-TeO_2, cryst. chem. study, X-ray diffr. powder data *(French)* 80–15080
Ba_3OSiO_4, struct. refinement 78–34479
$BaO.GeO_2.5H_2O$, X-ray cryst. struct. determ. *(German)* 79–69067
α-$Ba_2P_2O_7$, Raman, IR spectra, factor group anal. and band assignment 78–35126
$Ba_2P_2O_7$, X-ray diffr. determ. 78–44371
$Ba_{10}(PO_4)_6F_2$, cryst. structure 79–60332
$BaPb_{1-x}Bi_xO_3$, semiconductor-metal transition and supercond., IR absorpt. and struct. meas. 77–28278
$BaPb_{1-x}Bi_xO_3$, struct. determ., X-ray and neutron diffr. study 79–42039
$BaPtO_3$, synthesis and struct. 77–80486
$Ba_3Pt_2O_7$, struct. model 77–72597
Ba_2RF_7, (R=Dy, Ho, Er, Tm, Yb, Lu, Y), superstructure phases, prep., thermal characterisation and X-ray powder diffr. 80–96494
$BaRMnO_4$, (R=La,Nd), X-ray obs. *(French)* 78–6042
$Ba_5(ReO_5)_3Cl$, X-ray cryst. struct. determ., $(ReO_5)^{3-}$ content *(French)* 79–90601
$Ba_{10}(ReO_5)_6X$(X=Br, I), single cryst. X-ray struct. refinement *(French)* 79–77578
$BaSO_4$, barite, crystal struct. and sulphate force consts. 78–83784
$BaS_2O_3.H_2O$, X-ray powder data 79–14767
$Ba_2Sb^VBi^{III}O_6$, struct. determ. by powder neutron diffr. 78–34468
$Ba_3Sb_2NiO_9$, 6H, cation ordering, powder neutron diffr. obs. 78–55852
$Ba_4Sb_4S_{11}$, cryst. struct., selenoantimonate (III) anions *(German)* 80–103305
$Ba_{0.7}Sn_{2.6}Cr_{1.4}O_8$, short axis tripling, X-ray and electron diffr. study 79–77576
$Ba_{0.7}Sn_{2.6}Cr_{1.4}O_8$, X-ray cryst. struct. and composition determ., new hollandite phase 79–14750
$Ba_{0.5}Sr_{1.5}Al_4Si_{12}O_{32}.10H_2O$, brewsterite cryst. struct. refinement 77–80471
$Ba_{0.725}Sr_{1.775}Li_xNb_{5-x}Ti_xO_{15}$, solid soln., prep., struct., dielec. props. *(French)* 77–69782
$Ba_{1.35}Sr_{0.65}NaNb_5O_{15}$ crystals, struct., dielec. and pyroelectric characts. 79–51913
$Ba_{0.25}Sr_{0.75}Nb_2O_6$, quadratic susceptibility dispersion meas., oscillator model including structure 78–59078
$Ba_xSr_{1-x}Nb_2O_6$ crystals, struct., dielec. and pyroelectric characts. 79–51913
$Ba_xSr_{1-x}Nb_2O_6$, struct. and dielec. props., isomorphic substitution effect 78–27165
$Ba_{1-x}Sr_xNiO_{3-y}$, Sr substitution effect, powder X-ray diffr. 78–51498
$BaTa_2O_6$, structural study X-ray diffr., IR absorpt. and Raman spectra *(French)* 80–107173
$BaTe_2O_6$, X-ray cryst. struct., O_2 coordination no. of Te *(German)* 79–69075
$BaTiO_3$, mean square atomic displacement temp. depend., sublattice vibration anharmonicity 80–79890
$Ba_2Ti_{5.5}O_{13}$, X-ray cryst. struct. determ. *(French)* 79–73148
$Ba_2V_2O_7$, cryst. struct. determ. and bond strength anal. 79–23576
$BaVO(EDTA).6H_2O$, cryst. and mol. struct., X-ray diffr. obs. *(Russian)* 78–30601
$BaVS_3$, annealing influence on lattice constants, neutron diffr. profile anal. 80–1976
$BaVS_3$, polycrystalline, elastic behaviour, 40 to 350K 79–60498
$BaVSe_3$, one-dimensional, struct. and mag. props. 80–28993
$Ba_3WFe_2O_9$ and $Ba_3WFe_2O_{8.42}$, crystallographic and mag. props., comparative study 80–103303
$Ba_3WFe_2O_9$-$Ba_3WCo_2O_{9-x}$ system, struct. evolution *(French)* 80–88110
$Ba_3W_2O_9$, X-ray powder struct., face shared octahedra with W(VI) 80–64974
Ba_xWO_3, $(0.01<x<0.33)$ series form. 79–65046
Ba_5X_3, α, intermediate phases, cryst. struct. (X=IIb, IIIb, IVb, Vb element) 78–83793
$BaX_{1/3}Ru_{2/3}O_3$ (X=Ca, Cd, Mg, Sr), crystal struct., mag. susceptibility and exchange integrals *(French)* 77–16037
Ba_2YbF_7 single crystals, electron diffr. cryst. struct. anal. *(French)* 80–92507
$BaZnGeO_4$, revised cryst. data 80–100210
Ba_2ZnS_3, cryst. struct. determ., X-ray powder diffr. data 77–76365
Ba_2ZnS_3, prep. by solid state reaction and melt growth, X-ray anal. 77–73226
α-$BaZrF_6$ with $[Zr_2F_{12}]^{4-}$ complex *(French)* 78–51477

crystal atomic structure of inorganic compounds continued
$BaZrO_3$, cryst. growth and thermoluminesc. *(Russian)* 78–23604
$Ba[Pt(CN)_4Br_2]4.5H_2O$, single crystal neutron diffr. struct. exam. 78–2082
$Ba[Pt(CN)_4].4H_2O$, neutron diffr. 77–35521
Be-Si-N system polytypes, struct. obs. using TEM 80–107192
$BeAs_2$, high temp. cryst. type, space groups and lattice parameters *(French)* 77–68948
BeB_{12}, prep. and struct., book contrib. 78–47277
$Be_2(BO_3)F$, cryst. struct. 79–42026
$BeCl_2.4H_2O$, IR and Raman spectra *(French)* 80–20618
$(BeH_2)_x$, polymer, ab initio calcs., cryst. orbital method 79–37659
Be_3N_2-$BeSiN_2$ system, crystallography and phase relationships, TEM and electron diffr. study 80–92502
BeO_4 tetrahedra, variabilities in interatomic distances and angles 79–46594
BeP_2, tetrahedral struct. of order-disorder type, coordination rule for short-range order 77–15370
$Be(PO_3)_2(II)$, X-ray diffr. *(French)* 78–14317
$BeSO_4.4H_2O$, IR and Raman spectra *(French)* 80–20618
$Be_9Si_3N_{10}$, TEM, direct obs. of cryst. struct. 79–60339
$Be_4(Si_2O_7)(OH)_2$, bertrandite, cryst. struct. determ. 77–76380
$Be_4{}^tTe^0[O_7\square]^c$, singularities of atomic arrays as compared with $Al_2{}^0Mg^5[O_4]^c$ spinel struct. type 79–19242
Bi-layered compounds, stability in rel. to structural mismatch 80–39040
$Bi_4Cl_2S_5$, X-ray single cryst. struct. determ. 79–19199
$BiF_2Si_2O_8OH$, crystal struct., space groups by RHEED 78–47297
$BiFeO_3$, ferroelec., antiferromag., cryst. and mag. struct., neutron diffr. study 80–65786
$Bi_{12}GeO_{20}$, laevorotatory, cryst. struct! redeterm. 80–15065
$Bi_6(H_2O)(NO_3)O_4(OH_4)[(NO_3)_5]$, X-ray cryst. struct. determ. and refinement 79–32958
BiI_3, structure, exciton states and physicochem. characteristics *(Russian)* 80–100435
$Bi_3In_5S_{12}$, X-ray cryst. struct. determ. 80–107126
$Bi_{2-x}La_xWO_6$, synthesis and crystallography 80–66459
BiNbS(Se), struct., X-ray powder diffr. meas 80–44175
Bi_2O_3, powder diffr. patterns and struct. 79–27961
Bi_2O_3-SrO, solid state phase diagram, thermal and high temp. X-ray anal. *(French)* 79–65190
Bi_2O_3-SrO system, stoichiometric cpds., cryst. data *(French)* 79–99153
Bi_2O_3-WO_3, X-ray diffraction studies 78–38677
BiOCl, exam. of crystal structure and morphology, as function of growth conditions, using electron microscopy 79–52103
$Bi_{12}O_{15}Cl_6$, struct. derivation from $Bi_6X_{7+n}Cl_3$ by chem. twinning 77–35520
$Bi_6O_7FCl_3$, struct. derivation from $Bi_6X_{7+n}Cl_3$ by chem. twinning 77–35520
$BiOI$-$2Bi_2O_3$ prep., cryst. struct. *(French)* 78–53205
$Bi_6O_5(OH)_3(NO_3)_5.3H_2O$, cryst. struct. determ. and refinement, X-ray anal. 79–7586
$BiReO_4$, prep. and cryst. struct. 80–28991
Bi_2S_3-$CuPbBiS_3$ series, ordered chem. twinning 79–55717
$Bi_{1-x}Sb_x$, semiconductor film, X-ray diffraction in thin cryst. with linear variation of lattice period 78–26373
$BiSbO_4$, synthesis, struct. and m.p. 77–84714
ρ-BiSe, single crystal, synthesis and elec. props. 77–16490
p-Bi_2Se cryst. growth, elec. props. 77–8748
$Bi_{12}SiO_{20}$, laevorotatory, cryst. struct., absolute piezoelec. d_{14} coeff. 79–94974
$Bi_2Sn_2O_7$, prep., stability, and crystallographic exam. *(French)* 78–51510
BiTaS(Se), struct., X-ray powder diffr. meas 80–44175
BiTe, X-ray powder cryst. struct. determ. and refinement 79–19203
Bi_4Te_3, X-ray powder cryst. struct. determ. and refinement 79–19203
BiTeI, and Bi_2Te_3-BiI_3 phase diagram 77–28788
$BiTiNbO_6$, cryst. struct. determ. *(German)* 78–79570
$Bi_7Ti_4NbO_{21}$, mixed-layer cryst. struct. determ. by super-high-resolution electron microscopy 77–84703
$Bi_5TiNbWO_{15}$, cryst. struct. and dielec. const. 77–47428
$Bi_7Ti_4TaO_{21}$, cryst. struct. and dielec. const. 77–47428
$BiVO_4$, cryst. growth and struct. 80–35078
$BiVO_4$, struct. and ferroelastic phase transition 80–29004
$Bi_2W_2O_9$, layered struct., 1 MV high-resolution electron microscopy obs. 79–27955
$Bi_2W_2O_9$, struct., dielec. props., melting character and thermal stability 79–23572
^{249}BkN, prep. and cryst. struct. 79–99115
$BrF_3.SbF_5$, NQR anal. of complex ion struct. 77–12238
C fibres, fibril dimension estimation, using lubricostatic structural models 80–54171
$C_8{}^+AsF_6{}^-$, synthesis of first stage graphite salt, relationship to first stage graphite/AsF_5 intercalate 79–24738
$C_{12.6}AuCl_3$, intercalation compound, struct. *(French)* 78–42982
$C_8Br_xCl_{1-x}$ intercalate, crystallographic, elec., mag. props. 80–107184
$C_{12}Cl$ and $C_{16}Cl$ intercalation compounds, form. and struct. *(French)* 80–40674
$C_{24}Cs$ and $C_{36}Cs$, graphite intercalated, ordering of intercalant layers, X-ray diffuse scatt. 80–44182
CEr_2S_4, spinel, crystal struct. *(French)* 78–91326
$C_{12n}K$, graphite intercalated, two-dimens. structurally disordered phases, X-ray diffr. profiles 80–44181
$C_{11.3}NiCl_{2.13}$ intercalation compounds, cryst. struct. *(French)* 80–33947
CO complex, with 1,2,4-triazole, mag. susceptibility, 2-300K, struct. 77–77045
$(CO(NO)_2CL)_2$, order-disorder struct., X-ray data 80–39037
$CONa_6(SO_4)_4$, vanthoffite cryst. struct., lattice parameters and thermal behaviour 77–19929
$C_{12}{}^{2+}PtF_6{}^-$, struct. and elec. props. 80–70183
$C_{24}Rb$, intercalated graphite, order struct. determ. by neutron scatt. 80–107143
$(Ca,Sr)_5(PO_4)_3Cl$, partially substituted chlorapatite, cryst. struct. from X-ray data 80–96478
$Ca\ 0.4B_2O_3.2H_2O$, X-ray cryst. struct. determ. and refinement 79–94976
Ca dichlorophosphate complexes, cryst. struct. ^{35}Cl NQR obs. 80–108108
Ca metaborates, endogeneous, H bonds in cryst. structs. 80–33975
Ca-Nb-O perovskites, struct. characterisation *(French)* 78–10021
Ca-water interactions, in crystalline hydrates, geometry 80–39024

crystal atomic structure of inorganic compounds continued
$Ca_2Al_2GeO_7$, gehlenite struct., synthesis and physicochem. props. 79−43181
$Ca_3Al_2O_6$, cubic, X-ray powder diffr. data 79−94975
$CaAl_2Si_2O_3$, anorthite, quenched from 1530°C 78−63700
$CaAl_2Si_2O_8$, anorthite, quenched from 1530°C, struct. refinement 77−15355
$Ca_3Al_2Si_3O_{12}$, grossular, cryst. struct. and compressibility to 60 kbar 78−63718
$CaAl_2Si_3O_{10}.3H_2O$, scolecite, from Poona, India, X-ray cryst. struct. determ. 79−90605
CaB_2C_2, cryst. struct. *(French)* 79−32969
$CaB_{12}H_{12}.10H_2O$, struct. dehydration, intermediate phases and thermooxidative degradation 80−33951
$CaB_{12}H_{12}.8H_2O$, cryst. struct. 77−51351
CaB_4O_7, cryst. struct. determ. 78−10029
$Ca_2B_6O_{11}$, cryst. struct. determ. 77−11526
$Ca_2(B_5O_9)Cl.H_2O$, triclinic chilgardite, cryst. struct. determ. 78−63737
$Ca_2(B_4O_4(OH)_8)$, uralborite, accurate cryst. struct. 78−34492
$CaB_2O_4.6H_2O$, diffractometric data 77−15391
$CaBa(PO_3)_4$, struct. from IR spectra 77−47421
$CaBr_2$-H_2O, ^{79}Br NQR, cryst. struct. 78−27110
$CaBr_2.4CH_3OH$, cryst. struct. determ. *(French)* 78−59788
$CaBr_2.4C_2H_5OH$, cryst. struct. determ. *(French)* 78−59788
$CaBr_2.6H_2O$, cryst. struct. determ. 77−80474
$CaCO_3$ calcite, neutron irrad. effects 77−39617
$CaCO_3$, thermal decomp. in vacuo, ultrastruct. and crystallography 78−71864
$Ca_3(CaTa_2)O_9$, monoclinic symm., layer like cation ordering 77−1105
$(Ca_xCd_{1-x})CO_3$, cryst. struct. and cation isomorphous miscibility 80−33972
$CaCeAl_3O_7$, melilite struct., prep. and props. 80−93524
$CaClNO_3.2H_2O$ *(French)* 78−42975
$CaCl_2.2H_2O$, cryst. struct., X-ray diffr. meas. *(French)* 77−47417
$CaCl_2.4H_2O$, β form *(French)* 78−42974
α-$CaCl_2.4H_2O$, redeterm. of cryst. struct., H bonding and Ca coordination *(French)* 79−37676
$CaCl_2.6H_2O$, cryst. struct. determ. 77−80474
$CaCrO_4.H_2O$, cryst. struct. *(French)* 78−18593
$CaCu_3Ge_4O_{12}$, bond length determ. 78−14318
CaD_2, neutron diffr., NMR 77−15378
$CaEuGa_3O_7$, synthesis, mechanism and kinetics, cryst. props. 77−52268
$Ca_{1-x}Eu_xSi_2$, solid solns., α-$ThSi_2$ struct. type, comp. and press depend. 78−91322
CaF_2 crystal structure, stability compared with TiO_2 *(Russian)* 80−64945
CaF_2-$(Y,R)F_3$ (R=any lanthanide except Pm, Eu), phase diagrams 78−84783
CaF_2-YbF_3 system, phase relationships *(German)* 79−24501
CaFCl, cryst. struct. determ. 77−80465
$CaF_{2-x}H_x$, solid soln. prep. and struct. determ. *(French)* 78−51505
$CaF_2.SiO_2$, dehydration product of fluorapophyllite, X-ray powder and cryst. data 79−37686
$CaFeO_3$, preparation, cryst. struct., mag. and elec. props. 78−44066
$CaFe_3O_5$, cryst. struct., isotypism with $Ca_3Y_2Fe_{19}O_{30}$ *(French)* 77−43203
$CaFe_5O_7$, cryst. struct. determ., unit cell parameters *(French)* 77−84709
$CaFeSbAs_2O_7$, stenhuggarite 77−58983
$Ca_{0.5}Gd_{0.5}H_n$, H_2 dissociation press., phase behaviour and struct. 78−2260
$Ca_2Ge_2(GeO_4)(Ge_4O_{12})$, cryst. struct., X-ray anal. 80−19783
$CaGe_2O_5$ crystal struct., X-ray and Patterson function anal. 80−39054
$Ca_2Ge_7O_{16}$, cryst. struct. interpretation by symmetrisation method 80−107180
$Ca_4(Ge_3O_{10}).H_2O$, cryst. struct. determ. 79−90627
$CaHPO_4$, monetite, cryst. struct. refinement, H bonding, neutron diffr. meas. 77−47389
$CaHPO_4$, monetite, low-temp. ordering of H atoms, X-ray and neutron diffr. study at 145K 80−39022
$Ca_2HPO_4SO_4.4H_2O$, synthetic, cryst. struct. and relation to brushite and gypsum 78−83785
$Ca(IO_3)_2$, synthetic lautarite, cryst. struct. determ. 78−26517
$CaIr_xRe_{1-x}O_3$, perovskite struct., X-ray and IR obs. 79−90621
$CaIr_xTi_{1-x}O_3$, semiconductor, struct., mag. and elec. props. 79−91046
$CaK_2As_2O_7$, cryst. struct., bond lengths 77−31639
$Ca_2K_2NaTiO[Si_7O_{18}(OH)]$, tinaxite, X-ray cryst. struct. determ. *(German)* 80−39023
$CaLaBO_4$, crystallographic and Pb^{2+} luminesc. data 79−32971
$CaLaFeO_4$, two-dimens. mag. ordered, structural and mag. props. *(French)* 80−70173
$CaLaFeO_4$, two-dimens. mag. props. rel. to cryst. struct. 80−75776
$CaLaFeO_4$, X-crystallog. and Mossbauer spectrum *(French)* 77−66447
$CaLa_{1-x}Gd_xGaO_4$, $(0 \leq x \leq 1)$, Gd^{3+} luminescence and cationic distrib. *(French)* 79−78734
$Ca_{1-x}La_xMgAl_xSi_{2\ x}O_6$, crystalline and vitreous phase comp. and props. 77−44221
$Ca_2La_8(SiO_4)_6O_2$, cation ordering, X-ray diffr. meas. 79−23577
$CaLu_2S_4$, cryst. struct., space group *(French)* 77−80479
$Ca_3(MTa_2)O_9$, M=Ca, Cd, Mn, Fe, Zn, Co, Mg, Ni, monoclinic perovskite-type struct. 77−84725
$Ca_2MTa_5O_{15}$(M=K, Rb, Tl, Cs), relative stability of struct. types, and piezoelec. props. *(French)* 80−49206
$CaMgB_2O_5$, computer analysis of Patterson functions 77−15388
$Ca_3Mg(BO_3)_2(CO_3).0.36\ H_2O$, natural sacchite, cryst. struct. determ. 79−23590
$CaMg_2Cl_6.12H_2O$, cryst. data, X-ray powder method 80−1978
$Ca_6Mg_5Mn(B_2O_5)_6$, kurchatovite 77−65967
β-$Ca_{3-x}Mg_x(PO_4)_2$, struct. and impurity distrib., stabilising role of Mg 78−10020
$Ca_3Mn_2Ge_3O_{12}$, crystal struct. distortion due to cooperative Jahn-Teller effect *(Russian)* 77−1119
$CaMn_3O_6$, X-ray diffr. data, lattice parameter determ. 79−24508
$CaMn_4O_8$, X-ray diffr. data, lattice parameter determ. 79−24508
$CaMn_4(Si_5O_{15})$, rhodonite cryst. struct., compared with synthetic germanates 78−30600
$CaMn[B_2O_5]$, synthetic Mn-kurchatovite, cryst. struct. 79−14777
$Ca_2Mn_7[Si_{10}O_{28}](OH)_2.5H_2O$, inesite, cryst. struct., X-ray determ. 79−19227
$CaNH_4HP_2O_7$, monoclinic, crystal struct. exam. 78−2070
$CaNH_4NaP_2O_7.2H_2O$, analysis of X-ray data *(French)* 78−14316

crystal atomic structure of inorganic compounds continued
$Ca(NO_3)_2.2h_2O$, β- to α-phase orientational transform., struct. interpretation *(French)* 77−80448
α-$Ca(NO_3)_2.4H_2O$, X-ray diffr., H bonds *(French)* 77−58986
$(Ca_{0.90}Na_{0.06}Mg_{0.71}Fe_{0.25}{}^{2+}Fe_{0.05}{}^{3+}Al_{0.03})(Si_{1.88}Al_{0.11}Ti_{0.01})_2O_6$, struct., space group, bond lengths, X-ray diffr. meas. 78−47298
α-$CaNa_2P_2O_7.4H_2O$, X-ray cryst. struct. determ. 80−64964
$CaNbF_7$, polymorphism, X-ray powder diffr. data *(French)* 80−19779
$Ca_2Nb_2O_7$, crystal struct. and phase transitions, rel. to isomorphous crystals *(Japanese)* 80−49208
$Ca_2Nb_2O_7$, monoclinic modification, cryst. struct., X-ray diffr. method 80−64955
$Ca_2Nb_2O_7$-Sm_3NbO_7 system, phase equilib. 80−20907
$Ca_{0.5}Nd_{0.5}H_n$, H_2 dissociation press., phase behaviour and struct. 78−2260
$CaNd_{3/2}Nb_{3/2}O_7$, pyrochlore struct., synthesis elec. props. 79−42543
$Ca_xNi_{1-x}Fe_2O_4$, X-ray struct. anal., determ. of lattice constant and interplanar distances *(French)* 80−96487
CaO, at. charge densities, X-ray struct. factors 78−79566
5CaO-$3Al_2O_3$, cryst. struct. determ. 78−55840
CaO-Fe_2O_3-Al_2O_3 system, solid soln. of $Ca_2Fe_{2(1-x)}Al_{2x}O_5$ *(Russian)* 80−16284
CaO-MnO system, solid soln. form. and analysis 80−28996
β-(CaO_2)-SiO_2-H_2O, SEM and X-ray diffr. exam. of structure, crystallisation props. 78−73012
$2CaO(Al_2O_3)_x(Fe_2O_3)_{1-x}$, Fe^{3+} distrib. in struct. 79−94980
β-$CaO.SiO_2$, parawollastonite, rel. between structs. proposed 80−15056
$CaO.SnO_2.SiO_2$, tin sphene, lattice parameters 77−7697
α-$Ca_2P_2O_7$, Raman, IR spectra, factor group anal. and band assignment 78−35126
α-$Ca_3(PO_4)_2$ 77−47395
$Ca_3(PO_4)_2$, new cryst. phase prep. and struct. *(French)* 78−83789
$Ca_5(PO_4)_3Cl$, structural interaction of Cl 78−55837
$Ca_5(PO_4)_3F$, structural interaction of F 78−55837
$Ca_5(PO_4)_3(F_{1-x}(OH)_x)$ apatites, lattice struct. NMR obs. 79−42845
$Ca_5(PO_4)_3OH$, structural interaction of OH 78−55837
$CaPb(OH)_6$, cryst. struct. determ. *(French)* 77−47419
$Ca_{0.5}Pr_{0.5}H_n$, H_2 dissociation press., phase behaviour and struct. 78−2260
$Ca_{1+x}Re_2O_6(OH)_{2x}$ (x=0,3), high pressure synthesis and structure *(French)* 78−51511
CaS:Nd phosphors, X-ray powder diffr. anal. 80−100204
$CaSO_4$, body centered matrix basis 80−79765
$CaSO_4$:Bi, cryst. growth, luminesc. props. 77−58993
$CaS_2O_3.6H_2O$, cryst. data and mag. susceptibility 77−76368
$CaSb_{10}O_{10}S_6$, sarabauite, X-ray cryst. struct. determ. and refinement 79−14754
$Ca_3Sc_2Si_3(Ge_3)O_{12}$, garnets, refined cryst. struct. 78−87654
$Ca_x(Si,Al)_{12}(O,N)_{16}$, α′-Sialon ceramics, prep. and characterisation 78−84750
$Ca_{11}(Si, Al)_4O_{18}Cl$, alinite, cryst. struct. determ. 79−19215
$CaSi_2$, high-pressure phase transform., cryst. struct. 77−35693
$CaSiO_3$ (wollastonite), individual silicate chains obs. by high resolution electron microscopy 79−100829
Ca_2SiO_4, K_2NiF_4-type structure, high pressure synthesis, crystal chemical and geophysical implications 79−69089
β-Ca_2SiO_4, struct. redeterm., hydraulic activity 77−58981
Ca_2SiO_4-BaO, conditions and mechanism in cryst.-chemical stabilisation of unstable phases 80−39302
Ca_2SiO_4-FeO, conditions and mechanism in cryst.-chemical stabilisation of unstable phases 80−39302
Ca_2SiO_4-MgO, conditions and mechanism in cryst.-chemical stabilisation of unstable phases 80−39302
Ca_3SiO_5, polymorphism, X-ray diffr. data *(French)* 79−94973
$Ca_{11}Si_4O_{18}Cl$ alinite, cryst. struct. interpretation by rhombus method 80−39052
$Ca_2SiO_3Cl_2$ 78−67694
$Ca_{10}(SiO_4)_3(SO_4)_3(OH,Cl,F)_2$, hydroxyellestadite, X-ray cryst. struct. determ. 80−96485
$(Ca_{1-x}Sr_x)(Ca_{1/3}Nb_{2/3})O_3$ perovskites, cryst. struct. *(French)* 79−65044
$Ca_{1-x}Sr_xSi_2$, solid solns., α-$ThSi_2$ struct. type, comp. and press depend. 78−91322
Ca_2TaLaO_6, perovskite structure, cationic distrib. *(French)* 77−1109
$CaTaRO_6$, (R=La, Nd, Gd, Sm, Er, Lu), synthesis and physicochem. props. 79−52139
$CaTeO_4$, powder diffr. cryst. struct. determ. 79−42020
$Ca_6Th_4(SiO_4)_6O_2$, cryst. struct. by X-ray diffr., cation distrib. *(German)* 78−43001
$Ca_n(Ti,Nb)_nO_{3n+2}$, (n=4.5,5 or 6), cryst. struct. determ. *(French)* 79−65039
$CaTiO_3$-$Ca_2Fe_2O_5$, Mossbauer resonance exam. of structure, phase equilibrium 78−76640
$Ca_2TlTa_5O_{15}$, cryst. struct. *(French)* 79−86749
$CaWO_4$, body centered matrix basis 80−79765
$CaWO_4$, scheelite, stella quadrangula as struct. building unit 80−15055
Ca_5X_3, α, intermediate phases, cryst. struct. (X=IIb, IIIb, IVb, Vb element) 78−83793
$Ca_2XFe_xTi_{3-x}O_8$, X=Ca, Sr, Ba, Y, La, Gd, struct. and O vacancy ordering *(French)* 77−11520
$Ca_4YFe_5O_{13}$, cryst. struct., electron microscopy and X-ray diffr. study 80−88116
$Ca_3Y_2Ge_3O_{12}$:Eu^{3+}, garnets, prep., struct., luminesc., absorpt. spectra, Eu^{3+} localisation 77−69884
$Ca_{0.5}Y_{0.5}H_n$, H_2 dissociation press., phase behaviour and struct. 78−2260
$CaZn(SiO_4).H_2O$, clinohedrite, cryst. struct., H bonds 78−79593
$CaZrO_3$:Pb^{2+} (Bi^{3+}) and related $Pb^{2+}(Bi^{3+})$-actuated hosts, cryst. struct. effects on luminesc. 77−16376
Ca2$(NH_4)H_7(PO_4)_4.2H_2O$, X-ray cryst. struct., PO_4 ion with 3 symmetric H bonds 80−64956
$Ca_8[Al_{12}O_{24}](WO_4)_2$, cryst. and powder diffr. data redeterm. 80−24423
$Ca[B(OH)_4]_2$, frolorite, refinement of cryst. struct. 77−58996
$Ca[B_2O_2(OH)_4]$, cryst. struct. determ. 77−15393
$Ca_2[B_8O_{13}(OH)_2]$, refinement of cryst. struct., H-bonding 77−89421
$Ca_2[B_3O_4(OH)_4]Cl$, solongoite, cryst. struct. refinement 78−26549
$Ca[B_2O(OH)_6].2H_2O$, refined cryst. struct. 78−2092
$Ca_2[B_5O_9]C.H_2O$, hilgardite, PMR of water mol. 80−84655
$Ca[Fe(CN)_5(NO)].4H_2O$, X-ray cryst. struct. determ., heavy-atom method 80−92494
$Ca_5[GeO_4]_2(OH)_2$ monoclinic cell struct., crystallographic consts. 79−82191
$Ca_5[SiO_4]_2(OH)_2$, cryst. struct. refinement 80−107181

crystal atomic structure of inorganic compounds continued

- $Ca_2[(UO_2)_3(PO_4)_2(OH)_2](OH)_2.4H_2O$, phurcalite, cryst. struct. determ. 78–55849
- $Ca[ZnSiO_4].H_2O$, clinohedrite, cryst. struct., comparison with $(Mn,Mg)Mg(OH)_2[ZnSiO_4]$, herstmannite 79–19228
- Cd complex, $(Cd[SC(CH_3)_2CH_2NH_2]_2CdCl_2)_2.2H_2O$ cryst. and mol. struct. 78–74787
- Cd compound with XO_4 tetrahedral, complex, var. of cation coordination numbers 79–86768
- Cd-As system, phase diagram, $CdAs_4$ struct. 79–74138
- Cd-Sb system, phase diagram, struct. and stability of phases *(German)* 78–60661
- CdA_2X_4 (A=Ga,In; X=S,Se), Fourier IR and Raman spectra, cryst. struct. and symm. *(German)* 79–24313
- $CdAs_2$, cryst. struct. and vitrification capacity 80–88126
- Cd_2AsCl_2, X-ray cryst. struct. anal. *(French)* 80–64957
- Cd_3AsCl_3, X-ray cryst. struct. determ. and refinement *(French)* 80–107119
- Cd_2As_3I, X-ray cryst. struct. determ. *(French)* 79–99138
- $Cd_5(AsO_4)_3Br$, halogen atom distrib. determ. 78–2078
- $Cd_5(AsO_4)_3Br$, X-ray diffr. cryst. struct. exam. and refinement 78–10000
- $Cd_2B_2O_5$, basalt atom coordinates isotropic temp. corrections, X-ray study 80–59449
- $Cd_4(BO_3)_2(OH)_2$, synthetic cryst., structural anal. 79–86764
- $CdBa_3(MO_4)_2$, (M=Ge, Si), cryst. struct., form. 77–19928
- $CdBa(PO_3)_4$, $CdSr(PO_3)_4$, struct. from IR spectra 77–47421
- $CdBr_2$, polytype 12R, cryst. struct. determ. 80–33937
- $Cd(BrO_3)_2.2H_2O$, cryst. struct. 80–1992
- $CdBr_2.4H_2O$, cryst. struct. determ. *(French)* 78–26502
- $CdCa_2Cl_6.12H_2O$, X-ray cryst. struct. anal. *(French)* 79–4291
- $CdCl_2 . 2.5H_2O$, rel. between cryst. struct. and morphology, PBC theory of Hartman and Perdok *(French)* 80–70148
- $CdCl_2.4H_2O$, cryst. struct. determ. by X-ray diffractometry *(French)* 79–37673
- $CdCr_2S_{4-x}Se_x(O_x)$ X=0, 4, and solid solns., imperfect struct. model from cryst.-chem. investigs. 79–42053
- $CdCr_2Se_4$, optical reflectivity, dielectric const. by expt. data Kramers-Kronig anal., spinel struct. 79–99903
- $CdCr_2Se_4$, spinel film, struct. SEM study, props. 78–79905
- $CdCsP_3O_4$, cryst. struct. exam. *(French)* 78–2076
- $CdF(OH)$, X-ray cryst. struct. determ. 79–99134
- $CdFe_{1/2}Nb_{1/2}O_3$, high temp. X-ray exam. 77–11527
- $CdFeTi(PO_4)_3$, cryst. struct. and prep., rhombohedral lattice *(French)* 77–27856
- $CdGa_2S_4$, IR light transmission, IR refl. spectra and cryst. struct. 79–56777
- $CdGa_2S_{4(1-x)}Se_{4x}$, solid soln., crystallographic studies 78–15301
- $CdGa_2Se_4$, IR refl. spectra and cryst. struct. 79–56777
- $CdGa_2Se_4$, ordered vacancy compound, Raman scatt. 79–95749
- $CdGa_2Se_4$ ordered vacancy compound, Raman scatt. 79–99870
- $CdGa_2Te_4$, IR refl. spectra and cryst. struct. 79–56777
- $CdGe_2O_5$, X-ray crystal struct. determ., comparison with sphene 77–4089
- $CdH_{10}(AsO_4)_4$, X-ray cryst. struct. determ. and refinement *(French)* 80–33941
- $Cd(H_2PO_3)_2.H_2O$, cryst. struct. determ. 78–26507
- CdI_2 crystal, method for identification of rhombohedral lattice 77–31637
- CdI_2 polytypes, crystal structure analysis, refinements for structure determination 78–91312
- CdI_2 polytypes, crystal structures using new refinements for structure determination 78–91313
- $Cd(IO_3)_2$, cryst. struct. determ. 78–26523
- $CdIn_2O_4$, crystal growth from flux, elec. and struct. props. 77–81206
- $CdIn_2S_{4-x}Se_x$, struct. types anal., X-ray diffr. exam. 79–86756
- $CdIn_2Se_4$, defect zincblende semicond., valence band, cryst. struct. effects 78–48278
- $CdK_2(Cr_2O_7)_2.2H_2O$, X-ray cryst. struct. determ. using MULTAN *(French)* 79–69082
- $CdK_2P_2O_7$, cryst. struct., bond lengths 77–31639
- $CdK_4(P_3O_9)_2.2H_2O$, cryst. chemistry and cryst. struct. determ. *(French)* 78–26505
- $CdLi_2(PO_3)_4$, cryst. struct. determ. *(French)* 77–4069
- $Cd_2MTa_5O_{15}$ (M=K, Rb, Tl, Cs), relative stability of struct. types, and piezoelec. props. *(French)* 80–49206
- $Cd_xMg_{1-x}Se$ single crystals, melt grown, struct. and microhardness anisotropy 79–86836
- $Cd(NH_4)_2(Cr_2O_7)_2.2H_2O$, chemical prep. and crystal data *(French)* 80–24416
- $Cd(NH_4)_2(Cr_2O_7)_2.2H_2O$, X-ray cryst. struct. determ. *(French)* 80–39012
- $CdNH_4NaP_2O_7.3H_2O$, analysis of X-ray data *(French)* 78–14316
- $Cd_4Na(PO_4)_3$, X-ray cryst. struct. determ. 79–73143
- $Cd_4Na(VO_4)_3$, X-ray single cryst. struct. determ. and refinement, Patterson synthesis 79–19196
- $Cd_2Nb_{2-2x}Sn_{2x}O_{7-2x}F_x$, solid soln., X-ray diffr. and Mossbauer study *(French)* 78–87659
- $CdNd_4(SiO_4)_3O$, synthesis, cryst. struct. 78–87653
- CdO, ionicity, X-ray powder diffraction meas. 78–18616
- $CdO-TeO_2$, cryst. chem. study, X-ray diffr. powder data *(French)* 80–15080
- CdOHF (II), polycrystn., X-ray cryst. struct. determ. 79–60344
- β-$Cd_2(OH)_2SO_4$ *(French)* 77–15353
- γ-$Cd_2(OH)_2SO_4$ *(French)* 77–15354
- Cd_3P_2, high press. phase relns. and cryst. structs. 78–59792
- Cd_7P_{10}, rel. to other Cd-P system structs. 80–33960
- $Cd_4P_2I_3$, X-ray cryst cryst. struct. determ. and refinement *(French)* 80–107120
- β-$Cd(PO_3)_2$, high temp. form, X-ray cryst. struct. anal. *(French)* 79–32953
- $Cd_5(PO_4)_3Br$, $Cd_5(PO_4)_3Cl$, halogen atom distrib. determ. 78–2078
- $Cd_5(PO_4)_3Br$, X-ray diffr. cryst. struct. exam. and refinement 78–10000
- $Cd_{14-x}P_4S_{24-2x}I_{2x}$, icosahedral structs., synthesis and characts. 77–1107
- $CdRbI.H_2O$, cryst. struct., X-ray diffr. 77–19918
- CdS, appl. of generalised temp.-factor formulation 78–26383
- CdS, electron micrograph equal thickness fringes, phase angles and absolute struct. pot. 77–76383
- CdS, prepared by ceramic Technol., physical props. 79–60837
- $CdS(PO_4)_3OH$, single crysts., X-ray struct. anal. 78–95019

crystal atomic structure of inorganic compounds continued

- CdS(Se)(Te), determ. of wurtzite, zincblende and rocksalt phases 80–100219
- $Cd_3Sc_2Ge_3O_{12}$, garnet, refined cryst. struct. 78–87654
- CdSe, cryst. struct. and Bijvoet ratios, X-ray diffr. meas. 77–55268
- $CdSiP_2$, bond strengths and bond lengths, thermal expansion coeff. meas. 78–87651
- $CdSnO_3$ and Cd_2SnO_4, crystal growth by flux or high press. method, elec. and struct. props. 77–81206
- Cd_2SnO_4, film, spinel struct., X-ray diffr. study 78–75644
- CdTe, physical props., review 77–39833
- $CdTeMoO_6$, prep. and cryst. struct., X-ray diffr. obs. 79–1414
- $CdTh(MoO_4)_3$, struct., DTA and X-ray diffr. obs. *(French)* 78–95024
- $CdTh(MoO_4)_3$, X-ray cryst. struct. determ. *(French)* 80–64959
- $CdTh(WO_4)_3$, struct., DTA and X-ray diffr. obs. *(French)* 78–95024
- $CdTl_2Se_4$, single cryst., preparation, elec. cond. 77–24554
- $Cd_5(VO_4)_3I$, $Cd_5(VO_4)_3Br$, halogen atom distrib. determ. 78–2078
- $Cd_5(VO_4)_3I$, $Cd_5(VO_4)_3Br$, X-ray diffr. cryst. struct. exam. and refinement 78–10000
- $CdWO_4$, X-ray cryst. struct. determ. 80–108410
- Cd_3X_2, X=P,As,Sb, phys. props. 78–26527
- $Cd_5[PO_4]_3Cl$, X-ray diffr. study of cryst. struct. 78–10022
- $(Ce,Ta)Ta_6O_{19}$, disordered struct., convergent-beam electron diffr. symmetry 80–54178
- Ce, cryst. structs. at high press. 77–19890
- $Ce_{1.25}Bi_{3.78}S_8$, cryst. struct. determ. *(French)* 77–80467
- $Ce(CO_3)_5^{6-}$, in Na and guanidinium salts, struct./props. correlation *(French)* 78–95032
- $CeCl_3.7H_2O$, X-ray cryst. struct. determ. 79–46606
- $Ce_2Co_5B_2$, X-ray anal. *(Ukrainian)* 79–51050
- $CeCo_{5-x}Cu_x$, $0\leq x\leq$ internal oxidation kinetics, oxide struct., X-ray study 80–104329
- $CeCrOS_2$, single cryst. X-ray diffr. struct. determ. *(French)* 79–23581
- $CeCrOS_2$, X-ray cryst. struct. determ. *(French)* 80–92485
- $CeDyS_3$, cryst. struct. determ. *(French)* 78–6034
- $Ce(HPO_4)_2\times 1.33H_2O$, crystalline, thermoanal. meas. 79–91938
- $Ce_5Ir_{3(4)}$, cryst. struct. determ. 80–64960
- $CeKFe(CN)_6.4H_2O$, struct., X-ray diffr. obs. 79–51065
- $Ce_6Mo_{10}O_{39}$, 22 77–76373
- $Ce_6(MoO_4)_8(Mo_2O_7)$, X-ray examination crystal struct. 78–67687
- $CeNbO_4$, cryst. chemistry exam. 78–38678
- $CeNiC_2$, struct. determ. using X-ray diffraction *(Ukrainian)* 80–33949
- $Ce_6Ni_6P_{17}$, synthesis and cryst. struct. 78–75634
- CeO, high press. synthesis, struct. and lattice consts. *(French)* 80–29913
- $Ce(OH)_3$, X-ray cryst. struct. determ. 80–19758
- $Ce_4O_4S_3$ and $Ce_6O_6S_4$, synthesis and cryst. struct. *(French)* 79–32965
- $Ce_4O_4S_3$, X-ray cryst. struct. determ., using Patterson and Fourier synthesis *(French)* 79–14753
- $Ce_6O_6S_4$, X-ray cryst. struct. determ., Fourier and Patterson synthesis *(French)* 79–73139
- $CeOSO_4.H_2O$, struct. refinement 77–15359
- $3Ce_2O_3.2Si_3N_4$, ceramic, prep. by cold compaction and firing, struct. anal. 77–21070
- $Ce_2O_3.2Si_3N_4$, preferred unit cell for indexing powder diffr. pattern 80–49200
- $3Ce_2O_3.2WO_3$, X-ray charact. and thermal props. 77–43194
- CeP_3O_9, X-ray powder data 79–51079
- $CeRe_4Si_2$, cryst. struct. determ. 78–2098
- CeS_2, orthorhombic, prepared at 1773K and 5.5 GPa X-ray single cryst. struct. determ. 79–19198
- $Ce(SeO_4)_2.4H_2O$, cryst. struct., X-ray powder diffr. meas. 78–34483
- $CeSiO_2N$, cryst. struct. 78–10017
- $CeSiO_2N$, cryst. struct. 78–10018
- $CeSiO_2N$, cryst. struct. 78–10019
- $Ce_4Si_2O_7N_2$, crystal struct., resemblance with lanthanite and yttrium analogues 80–39035
- $Ce_4Si_2O_7N_2$, preferred unit cell for indexing powder diffr. pattern 80–49200
- $Ce_5(SiO_4)_3N$, X-ray powder diffr. data 80–39036
- $CeTaO_4$, $CeTa_7O_{19}$, cryst. chemistry exam. 78–38678
- $CeTa_7O_{19}$, crystal struct. 79–60323
- $CeTi_2O_6$, cryst. chemistry exam. 78–38678
- CfI_2 and CfI_3, cryst. struct. determ., X-ray diffr., optical spectra 78–75645
- $^{249}CfBr_x$, spectral and X-ray diffr. data, 25 to 700°C 77–28584
- ClF_5, condensed phases, structural study by vibr. spectroscopy and X-ray and neutron diffr. 79–1405
- $ClF_5.xSbF_5$ and $ClF_3.xSbF_5$, NQR anal. of complex ion struct. 77–12238
- ClO_2F, cryst. struct., X-ray and neutron diffr., Raman spectra *(French)* 78–83788
- $(Cl_3PNPCl_3)(PCl_6)$, X-ray cryst. struct. determ. 80–88095
- CmO_2, struct. changes under self- and reactor irrad. 77–27927
- $^{244}Cm(OH_3)$, cryst., self-irrad. effects and lattice parameters 77–69013
- Co complex, 1-(2-thiazolylazo)-2-naphtholato Co (III), cryst. struct. 77–11536
- Co complex, $(NH_3C_6H_5)[Co(SO_3)DH_2(NH_2C_6H_5)](NH_3C_6H_5)ClO_4.H_2O$, cryst. and mol. struct. 80–33980
- Co complex, $(4\text{-methylpyridine})_4Ni(NCS)_2$, porosity 77–76364
- Co complex, bis(N-β-napthyl-salicylaldiminato) Co (II), space group, lattice consts., X-ray diffr. obs. 78–51496
- Co complex, bis(N-p-tolyl-salicylaldiminato) Co (II), space group, lattice consts., X-ray diffr. obs. 78–51496
- Co complex, bisdimethylglyoxime (thiosemicarbazide)-cobalt (III) nitrate, mol. and cryst. struct. of dihydrate 78–83803
- Co complex, monofumaratotetraaquocobalt(II) monohydrate, cryst. struct. and cryst. binding 79–37681
- Co complexes, N-substituted salicylaldimine Co(II) and Co(III) complexes, struct. 77–58994
- Co ferrite, growth on fine acicular γ-Fe_2O_3 particles 80–29871
- Co intercalation compound, electron microscopy 80–84164
- Co Y zeolite, absorpt. spectra, Co^{2+} ions location upon dehydration 77–73152
- Co/Na zeolite, -A and -Y type, local coordination of Co(II) ions studied by X-ray absorpt. fine struct. spectroscopy 80–93434
- Co-complex, dichlorobis(pyridinium-2-thiolate)Co(II), cryst. and mol. struct. 80–28963
- $CoAl_{2-x}Fe_xO_4$, cation distrib., lattice parameter determ., X-ray diffr. exam. 79–69088
- $CoAl_2O_4$, cation distribution, Mossbauer and X-ray diffr. obs. 78–95532

crystal atomic structure of inorganic compounds continued
$CoAl_2O_4$, electron density distrib. 78-51481
$CoAs_3$, prep. and characterisation 77-77356
$Co_3(AsO_4)_2$ polymorph, closest packing 80-70174
$Co_2(AsO_4)Cl$, cryst. struct., X-ray diffr. meas. 77-47380
$Co_3B_7O_{13}I$, neutron diffr. investig. of mag. and cryst. struct., ferro- and paraelec. phases 77-32170
$CoCl_2.6H_2O$, albrittonite, new mineral from Llano County, Texas 78-65286
$CoCl_2.nh_2O$, cryst. struct. *(German)* 80-1987
$CoCr_2O_4$, Mossbauer spectra and cryst. struct. determ. 79-56637
$Co_{2.94}Fe_{0.06}S_4$ Mossbauer ^{57}Fe spectrum, mag. transition, lattice atomic occupancy 77-48095
$Co(H_2O)_6[SnF_3]_2$, crystal structure *(French)* 80-59441
$Co^{II}(H_2PO_4)_2.2H_2O$, cryst. and powder diffr. data *(French)* 80-24419
$CoK_4(P_3O_9)_2.7H_2O$, cryst. data *(French)* 78-79568
$Co_xMg_{1-x}Al_2O_4$, struct., catalytic activity, Co^{2+} ion distrib. 78-30595
$Co^{2+}Mo^{4+}O_3$, defect spinel struct., elec. and mag. props. 80-70176
CoMoP, X-ray cryst. struct. anal. *(French)* 79-4281
$CoMo_2Re_2S_8$, cubic structure, mixed tetrahedral cluster *(French)* 77-15372
$Co(NH_4)_2(BeF_4)_2.6H_2O$, cryst. struct. refinement by X-ray diffr., comparison with neutron diffr. *(French)* 77-47387
$Co(NH_3)_6Cl_3$, proton second moment meas., 96 to 404K 79-95652
$Co(NH_3)_6(Cr(CN)_6)$, electron distrib., X-ray diffr. 77-19915
$Co(NH_3)_6(Pb_4Cl_{11})$, cryst. struct., and relationship with the chlorolead struct. moieties in $NH_4(Pb_2Cl_5)$ and $PbCl_2$ 79-32954
$Co_{0.32}NbS_2$, intercalation compound, struct. and photoemission meas. 77-16453
$Co_{3-x}Ni_xO_4$, $0\leq x\leq 1.1$, struct., semicond.-semimetal transition, Seebeck coeff. 78-87972
CoO, under controlled atmosphere, exam. of composition and temp. dependence, of lattice parameter *(French)* 79-19214
CoO, X-ray determ. of electron density distribs., atomic scatt. factors 80-15078
Co_3O_4, Mossbauer spectra and cryst. struct. determ. 79-56637
CoP_3, prep. and characterisation 77-77356
$CoRh_2O_4$, Mossbauer spectra and cryst. struct. determ. 79-56637
CoS-MnS(ZnS)(CdS), phase study by X-ray obs., lattice const. 79-1854
$CoSb_3$, prep. and characterisation 77-77356
$CoSeO_4.4H_2O$, cryst. chemical and X-ray powder data 79-51073
γ-Co_2SiO_4, electron density distrib. 77-35514
$Co(UO_2AsO_4)_2.8H_2O$, prep. cryst. struct. characterisation 78-30589
$Co_{1-x}Zn_xFe_{2(1-y)}Cr_{2y}O_4$ spinels, solid solns., struct. 80-19764
$Co_xZn_{1-x}Fe_2O_4$, ferrite, DC cond., dielec. props., lattice consts. 80-80272
$CoZrD_3$, polycrystn., neutron and X-ray diffr. anal. of struct. 79-65061
$Co^{2+}[Fe(CN)_6]^{3-}$, struct. determ. 80-15901
$Co(urea)_2Cl_2.2H_2O$, two-dimens. mag. props., cryst. struct., specific heat 80-75777
Cr complexes with glycilglycine, structure, optical, e.p.r. and mag. investig. 77-1103
Cr-Co complex, $[Cr(OCN_2H_4)_6][Co(NH_3)_2(NO_2)_4]_3.3H_2O$, cryst. struct. 80-6392
CrB, crystallographic relationship with αMoB, UBC, ThBC 79-42025
$CrBr_4$, $CrCl_4$, Raman spectra, struct. and thermodynamic functions 78-60443
$Cr(CO)_5(CS)$, cryst. struct. determ., Fourier method *(French)* 79-4282
$CrEr_2S_4$ *(French)* 77-15356
$Cr_2Er_6S_{11}$, X-ray cryst. struct. determ. and refinement *(French)* 80-103298
$Cr_{1-x}Fe_xOOH$, solid soln., cell dimensions, X-ray powder anal. 79-24740
$Cr_4H_2(SO_4)_7.24H_2O$, X-ray cryst. struct. determ., H bond study 80-92491
$CrH(SO_4)_2.7H_2O$, X-ray struct. determ., hydrated proton complex and H bonding 77-80449
$Cr_xMo_{1-x}O_2$ ($x\leq 0.5$), solid soln., trivalent Cr, X-ray powder diffr. anal. 80-70177
$Cr(NH_3)_5ONOCl_2$, cryst. struct. determ. at 245K 78-75637
$(Cr(NH_3)_6)[MnCl_5(H_2O)]$, X-ray cryst. struct. anal. 79-4285
$Cr_{0.5}NbSe_2$, cryst. struct., metallic cond., mag. and phys. props. *(French)* 80-33956
Cr_2O_3, monocrysts. formed on heat treatment of Ni-Cr based alloy in air, struct. obs. 79-52455
β-CrOOH, neutron diffr. exam., cryst. and magnetic struct. *(French)* 78-2654
β-CrOOH(D), crystal struct., isotope effects on bond lengths 77-15371
α-CrOOH(D), isotope effects in bond lengths 77-80488
$Cr_{12}P_7$, X-ray cryst. struct. redeterm. 79-19192
$CrPS_4$ 77-47401
$CrPS_4$, cryst. struct., X-ray diffr. *(French)* 77-19926
$CrPS_4$, phys. props. and Li intercalates 79-19788
CrS, X-ray diffr. obs., high press., diamond anvil camera method 77-4082
CrS-FeS, sulphorspinel, struct. and elec. props. 80-49834
$CrS_{1-x}Se_x$, antiferromag. props., struct., variations near Neel temp. 78-64199
$CrS_2(Se_2)$, and alkali metal intercalates, phys. props. 80-44179
$Cr_{3\pm x}Se_4$, struct., elec. and mag. props. 80-107160
$CrThS(Se)_3$, synthesis, cryst. characts. *(French)* 78-51517
$Cr_{1-x}Ti_xN$, cryst. and mag. struct., at low temps. *(French)* 80-29005
$CrTiNdO_5$, distrib. of Cr^{3+} and Ti^{4+} ions, Mossbauer spectrum 77-69747
Cr_2TiO_5, in Cr_2O_3-TiO_2 system, struct. determ. 79-60329
$Cr_{1-x}V_xN$ solid solution, X-ray diffr. structure exam. at low temp., deformation study *(French)* 78-2069
$CrWO_4$, cryst. growth and struct. *(French)* 77-43202
$Cr_{12-x}W_xP_7$, solid solns., prep., cryst. struct. *(French)* 78-63723
Cs-mordenite , dehydrated, positions of cations and molecules 79-1418
Cs_2 $CdBr_4$, room temp. struct. 80-29000
$CsAg_3Se_2$, crystal struct., X-ray study *(German)* 78-83795
$CsAlCl_4$, crystal struct. refinement 79-73145
$CsAlCl_4$, solid state Raman spectra, 298-80K, vibr., struct. 79-28745
$CsAlF_4$, single cryst., prep. and struct. *(French)* 80-79762
$CsAlSiO_4$, prep. and X-ray characterisation 78-39728
$Cs_2As_2O_7$, solid-state synthesis, X-ray powder data *(French)* 80-15079
CsAu, semicond. and metallic, NMR line shape, Knight shift, X-ray diffr. study 78-68402

crystal atomic structure of inorganic compounds continued
$Cs_2Au^IAu^{III}Cl_6$, influence of high hydrostatic pressure on cryst. struct. in pressure range up to 52×10^8 Pa 79-51249
$Cs_2B_{12}H_{12}$ and $Cs_2B_{12}H_{12}.CsX$, X=halogen cryst. growth from soln. and morphology 77-44145
$Cs(B_xW_{3-x})O_9$ (B=Na, Ca, Co, Ni, Cd, Ga, Bi, Nb, Ta) cryst. struct., temp. dielec. anomalies 80-1998
$Cs_2BaFe(CN)_6.2H_2O$ 77-72668
$Cs_3Bi_2Br_9$, cryst. struct. determ. 77-80475
$Cs_3Bi_2I_9$, hexagonal $Cs_3Cr_2Cl_9$ struct. type 78-34478
$Cs_5Bi(MoO_4)_4$, synthesis, X-ray and thermal investigations 77-36390
CsC_8 intercalation compound, cryst. atomic struct. study *(French)* 79-42021
$Cs_2C_2O_4(SbF_3)_2$, growth from soln. and X-ray diffr. study *(French)* 77-80481
$CsCdBr_3$, $CsMgBr_3$ and $CsMgI_3$, diamag. linear chain lattices 80-70172
$CsCdCl_3$, phase transition under pressure 78-51664
$CsCd(NO_2)_3$, pure and metal ion doped, cryst. struct., reflectance spectra and thermal decomp. 79-51081
CsCl structure, evaluation of finite strain eqns. of state using lattice models 80-96620
Cs_3CoCl_5, neutron diffr. struct. at 4.2K 80-54176
Cs_3CoI_5, cryst. struct. and thermal props. *(German)* 79-23578
$CsCrCl_3$, co-operative Jahn-Teller distorted struct. determ. 78-63713
$CsCrI_3$, Mossbauer spectra, struct., electronic and mag. props. 79-91320
$CsCrI_3$, neutron diffr. expts. at 300, 77 and 1.2K 80-107163
$CsCrI_3$, X-ray cryst. struct. determ. *(French)* 79-73140
$CsCuCl_3$, phys. props. 77-62511
CsD_2PO_4, neutron scatt. study of ferroelectric phase transitions 77-59538
Cs_3EuF_6, $CsEu_2F_7$, cryst. struct. by X-ray diffr., equilib. in CsF-EuF_3 *(French)* 78-44107
$Cs_2FeCl_5.H_2O$, cryst. struct., superconducting susceptometer mag. meas. 79-73717
$CsFeCl_3.2D_2O$, cryst. and mag. struct., neutron scatt. and NMR expts. 79-7969
$CsFeCrF_6$, $CsFeVF_6$, crystal struct., Mossbauer hyperfine spectra 78-52381
$CsGa_{1-x}Fe_xS_2$, tetrahedrally coordinated Fe atoms in low spin state, mag. props. and neutron diffr. study *(German)* 80-88714
$CsHF_2$, struct. and phase transformation, NMR study 77-90047
CsH_2PO_4, cryst. struct., neutron-diffraction study 78-79592
CsH_2PO_4, ferroelec., X-ray struct. study at room temp. 80-88113
CsH_2PO_4, paraelectric phase, struct. exam. by neutron diffr. 79-37679
$CsH_3(SeO_3)_2$, paraelec. phase, struct. determ. by neutron diffr. 78-34472
$Cs_2Hf(MoO_4)_3$, X-ray cryst. struct. determ. 80-107182
Cs_3HgBr_5, X-ray cryst. struct. determ. and refinement 79-46637
$CsInCl_3$, mixed-valence cpd., structural phase transition *(German)* 80-70406
$Cs_2KFe(CN)_6$, single cryst. neutron diffr. struct. determ. 80-28972
$CsLa(SO_4)_2$, X-ray cryst. struct. determ. 80-33939
$Cs_2LiCr(CN)_6$, cryst. struct., room temp., powder neutron diffr. obs. 77-19914
$Cs_2LiCr(CN)_6$, room temp. struct., phase transitions 78-51491
$CsLiSO_4$, crystal structures of I and III phases, twins 80-70181
$CsLiWO_4$, X-ray cryst. struct. determ., stuffed H-cristobalite struct. 80-54181
$Cs_{12}M_{33}O_{90}(.12H_2O)$, cation exchanger with intersecting tunnel struct. *(French)* 78-20014
$CsMgCl_3$, Cs_3MgCl_5, Raman spectrosc. investigation of struct. 80-49202
$CsMn_{1-x}Co_xF_3$, ferrimag., mag. props. and cryst. struct. 77-77056
$CsMnF_4$, planar ferromag., cryst. and mag. struct., Jahn-Teller effect 80-75715
$Cs_2MnF_2.H_2O$, X-ray cryst. struct. anal. 79-4289
$CsMn_{1-x}Ni_xF_3$, ferrimag., mag. props. and cryst. struct. 77-77056
Cs_2MnNiF_6, cation distrib. and mag. struct. *(French)* 78-14935
$CsNO_2$-$CsNO_3$ solid solns., cryst. struct. and phase changes 79-51082
$CsNO_3$, high pressure phases III and IV, X-ray struct. determ. 80-28953
Cs_2NaAlF_6, cryst. struct. determ. 78-95036
$Cs_2NaAl_3F_{12}$ *(French)* 77-15348
$Cs_2NaBiCl_6$, optical, photoelastic, acoustooptic props. 80-55064
$Cs_2NaFe(CN)_6$, structural phase transformations 79-19178
$Cs_8Nb_{22}O_{59}$, melt growth and struct., dielec. and optical characterisation 78-35294
$Cs_2Nb_6TiO_{18}$, X-ray obs. *(French)* 78-6040
α-$CsNd(PO_3)_4$, single cryst. struct. and spectral-luminescent props. 80-96490
$CsNdP_4O_{12}$, X-ray cryst. struct. anal. 79-7590
Cs_2NpBr_6, prep., cryst. struct. and enthalpy of formation 78-10014
CsO_2, low temp. phase study, crystallographic domains and unit cell dimens. 78-63728
$Cs_3P_3O_9.H_2O$, X-ray determ. *(French)* 77-24298
$CsPbBr_3$, struct., Debye-Waller factor, neutron diffr. study 79-90609
$CsPbCl_3$, high-resolution elastic neutron diffr. study 80-28984
$CsPbCl_3$, nucl. smearing functions, multipole analysis 80-88097
$CsPbCl_3$, phase transition under pressure 78-51664
$Cs_2PbCu(NO_2)_6$, α-modification, Jahn-Teller induced α to β transition, neutron diffr. obs. 79-1498
$Cs_2PbCu(NO_2)_6$, low-temp. γ-modification, struct., powder neutron diffr. study, 160K 80-84151
$CsPr(PO_3)_4$, cryst. struct. 79-42022
$Cs_2Pt(CN)_4.H_2O$, cryst. struct., neutron diffr. meas. 77-47393
$Cs_3R_2X_9$ (=Sc,Y,Ho-Lu, X=Cl and R=Sc,Sm-Lu, X=Br), prep. and Guinier-Simon X-ray study 80-49204
$Cs_{1-x}Rb_xMF_3$ (M=Mg, Co, Ni, Zn), hexagonal fluoride perovskite structural evolution by cationic substitution *(French)* 80-24430
Cs_2S_2, synthesis and cryst. struct. *(German)* 79-46618
$Cs_2S_2O_6$, piezoelectric, crystal struct. studied by X-ray diffr. 80-100208
$Cs_3Sb_2I_9$, hexagonal $Cs_3Cr_2Cl_9$ struct. type 78-34478
CsScSi, Laue obs. *(Ukrainian)* 79-51064
$CsSn_2I_5$, surface props., Auger study, elec. cond. meas., photochem. study 80-66339
$Cs_{10}Ta_{29.2}O_{78}$, cationic exchanger with crossed tunnel struct., cryst. struct. *(French)* 78-83797
$Cs_2Ta_6TiO_{18}$, X-ray obs. *(French)* 78-6040
Cs_2Te_3, synthesis and cryst. struct. 80-88115
$CsTiMO_5$ (M=Ta, Tb), ion exchange props., synthesis and crystallographic props. *(French)* 80-28997

crystal atomic structure of inorganic compounds continued
- $CsTi_2NbO_7$, layer struct., X-ray and electron diffr. study 80-79753
- $Cs_{1-x}(Ti_{1-x}Nb_{1+x})O_5$, layer compound, cryst. struct., nonstoichiometry 80-64972
- $CsTl(SeO_4)_2$, $Cs_3Tl(SeO_4)_3$, and $Cs_5Tl(SeO_4)_4$, cryst. struct. *(French)* 80-84148
- $Cs_2U_2O_7$, α-, β- and γ-phase structures, X-ray and neutron diffr. obs. 77-7696
- $CsUOF_5$, struct. obs. using neutron diffr. and NMR 79-32962
- $Cs_4(UO_2)_4O_2Cl_8(H_2O)_4$, cryst. data 77-76367
- $CsUO_2(PO_3)_3$, synthesis and struct. 79-86767
- Cs_xVF_3 (x=0.25,0.19), cryst. struct. examination by electron diffr. using TEM 79-23583
- $CsVI_3$, Mossbauer spectra, struct., electronic and mag. props. 79-91320
- $CsVO_3$, X-ray determ. 78-6043
- CsV_2O_5 77-35518
- $Cs_{0.3}V_2O_5$, cryst. struct., semicond. behaviour 77-35516
- $Cs_{0.35}V_3O_7$, cryst. struct., semicond. and antiferromag. behaviour 77-35515
- $Cs_2V_5O_{13}$ 77-35517
- $Cs_2(VOF_4(H_2O))$, neutron and X-ray diffr. struct. determ. 79-90613
- $Cs_{0.06}WO_3$, cryst. struct. determ. 79-23569
- $Cs_6W_{11}O_{36}$, cryst. struct. determ. 78-26512
- Cs_xWO_3, x=0.20 and 0.32, hexagonal W bronzes, X-ray cryst. struct. refinement 79-77577
- $Cs_9(XeO_3Cl_2)_4Cl$, neutron and X-ray diffr. struct. determ., Xe-Cl bonding 78-30591
- $Cs_2[Cu(H_2O)_6](SO_4)_2$, Tutton's salts, stereochem., neutron struct. determ. 78-18609
- $Cs_2[FeCl_5(H_2O)]$, X-ray cryst. struct. determ. 80-107129
- $Cs_2[M(CN_4)].H_2O$, M=Pt,Pd,Ni, cryst. data 79-51070
- $Cs_2[Pt(CN)_4](FHF)_{0.39}$, cryst. struct., X-ray diffr. meas. 78-59789
- $Cs_2[Pt(CN)_4].H_2O$, polarised emission, correlation to cryst. struct. 79-19917
- $Cs[SbF_5OH]$, X-ray cryst. struct. determ. 79-55707
- $Cs[SnI_3]$, X-ray cryst. struct. anal. 80-54192
- $Cs_{12}[U(GeW_{11}O_{39})_2].13\text{-}14H_2O$, X-ray cryst. struct. determ. *(French)* 80-107136
- $Cs[VOF_3].1/2H_2O$, cryst. struct. 79-60333
- $(Cu,Zn)_3Pb(A_3O_4)_2(OH)_2$, bayldonite, struct. chem., complex layer struct. 79-46609
- Cu complex, 1-(2-thiazolylazo)-2-naphtholato Cu (II), cryst. struct. 77-11536
- Cu complex, (4,4′-bipy H_2)$CuCl_6$, with infinite linear chains of dimeric units, struct. and mag. susceptibility 80-96498
- Cu complex, [Cu(1,4,7,10-tetrabenzyl-1,4,7-10-tetraazacyclododecane)Cl]NO_3, cryst., struct. 80-64966
- Cu complex, bis-2-acetyl pyridine $CuCl_2$, space group and lattice parameters, X-ray diffr. meas. 77-31643
- Cu complex, bis(N-benzylsalicylaldiminato) Cu (II) lattice consts. and space group 79-37680
- Cu complex, catena-μ-formato-formatobis(pyridine)Cu(II) monohydrate, X-ray cryst. struct. determ. 79-46610
- Cu complex, chloride monodimethylsulfoxide, spin $^1/_2$ ferromag. Heisenberg linear chain, cryst. struct. and mag. susceptibility 80-15706
- Cu complex, chloride tetramethylsulfoxide, spin $^1/_2$ ferromag. Heisenberg linear chain, cryst. struct. and mag. susceptibility 80-15706
- Cu complex, Cu (II), co-ordination cpd. with condensation product of salicylaldehyde and salicylaldehyde S-propylthiosemicarbazone X-ray struct. anal. 79-1425
- Cu complex, Cu (II)-substituted ethylenediamines and monocarboxylates, cryst. and mol. struct., X-ray diffr. obs. 79-82182
- Cu complex, with 1,2,4-triazole, mag. susceptibility, 2-300K struct. 77-77045
- Cu complex, with S-methylthiosemicarbazone of salicylic aldehyde, structure 77-7702
- Cu complex, with Schiff base of o-aminobenzaldehyde and S-methyldithiocarbazate, cryst. struct. 78-95040
- Cu complex, with Schiff base of diacetylmonoxine and methylhydrazine dithiocarbazate, X-ray cryst. struct. determ. 79-14784
- Cu-complex, 2-diethylaminoethanolato(trichloroacetato)Cu(II) tetramer, cryst. struct. 80-28962
- Cu-In-Se system cubic ordered phase existence and characts. 78-34495
- Cu-Pt complex, $[Cu\ (C_2N_2H_8)_2][Pt(C_2O_4)_2]$, cryst. struct. determ. 77-4072
- Cu-Te system, cryst. chem., Mossbauer investig. 77-16220
- $CuAl_5S_8$, cryst. growth, struct., and fluoresc. 77-48328
- $(Cu_xAn_{1-x})_2AsO_4(OH)$, olivenite-adamite solid soln., ordering 78-42962
- $Cu_2(AsO_4)Cl$, cryst. struct., X-ray diffr. meas. 77-47380
- $Cu_2AsO_4(OH)$, olivenite, symmetry and cryst. struct. determ. 77-80457
- $CuBi_2O_4$, struct. determ. by Fourier and least squares method *(French)* 77-27852
- $Cu_3Bi_5S_9$, modulated struct. 79-99147
- CuBr, cond. mechanisms and struct. at high temps. 77-84711
- CuBr, superionic behaviour at high temp., EXAFS study 80-107496
- CuBr, superionic cond., cryst. struct., neutron diffr. study 79-42041
- $CuBrSe_3$, cryst. struct. 79-86750
- Cu_5CdSb, electrophys. props. 78-27491
- CuCl, difference Fourier maps, effects of phase errors 79-99033
- CuCl, superionic behaviour at high temp., EXAFS study 80-107496
- $CuCl_2.CuCl_2.2D_2O$, neutron scatt. aspherical effects, mag. form factor 78-27017
- $CuCl_2.2D_2O$, cryst. struct., mag. and reson. props. 80-60424
- $CuCr_2O_7.2H_2O$, chemical prep. and crystal data *(French)* 80-24417
- $CuCr_2O_7.2H_2O$, X-ray cryst. struct. determ. *(French)* 80-54185
- $CuCrS_2$, domain struct. and superstructure, TEM obs. 80-79779
- $CuCrS_2$ single cryst., spectral study and phys. props. *(French)* 80-29002
- $CuCr_2Se_4$, cryst., preparation, elec. cond., thermo EMF 77-8125
- $Cu_{12}^{2+}Cu_4^{+}O_{16}$, paramelaconite, cryst. struct. determ. 78-26506
- Cu_2FeGeS_4, crystallographic and magnetic structure *(French)* 80-28998
- $Cu_{0.5}Fe_{2.5}O_4\text{-}ZnFe_2O_4$, cation distrib., mag. moment, Mossbauer spectra, chem. anal. 80-75210
- $Cu_{1-x}Fe_{2+x}O_4$, cation distrib. and valence state 78-63732
- Cu_5FeS_4, bornite, superstructuring, vacancy clustering, high-resolution electron microscopy 78-42981
- $Cu_2FeSn_3S_8$, synthetic rhodostannite, X-ray cryst. struct. determ. *(French)* 79-99137
- $Cu_3FeTl_2Se_4(Cu_3FeTl_2Te_4)$, crystallographic studies 77-31640
- $Cu_{0.5}Ga_{0.5}Cr_2S_4$, mag. struct. determ. 77-8272

crystal atomic structure of inorganic compounds continued
- $CuGaCr_4S_8(Se_8)$, 1:1 ordering on tetrahedral sites, IR spectra obs. *(German)* 78-6669
- $CuGa_xIn_{1-x}Se_2$, X-ray diffr. cryst. data 80-84147
- $CuGaSe_2$, cryst. struct., X-ray powder data 77-39565
- CuHgSBr, cryst. struct. *(French)* 79-90620
- CuHgSCl, cryst. struct. *(French)* 79-90620
- $Cu_{3.75}Hg_{1.75}S_2S_8$, velikite, cryst. struct. determ. 78-2097
- CuI, cond. mechanisms and struct. at high temps. 77-84711
- CuI, EXAFS investigation of struct. and ion motion 80-108302
- CuI, ionic motions nature, mol. dynamics calcs., sp. ht. anomaly due to order-disorder transform. 80-107533
- CuI, superionic cond., cryst. struct., neutron diffr. study 79-42041
- Cu(II) complex, $K_{0.4}[(Cu_{0.9}HCO_3)_2(OH)_2]1.66H_2O$, crystal struct. *(French)* 77-1111
- γ-$Cu(IO_3)_2$, cryst. struct. and mag. behaviour 78-79571
- $CuInCr_4S_8(Se_8)$, 1:1 ordering on tetrahedral sites, IR spectra obs. *(German)* 78-6669
- $CuIn_5S_8$, single crystn. phase, CVD prep., X-ray cryst. struct. determ. 79-65990
- $CuInS_2(Se_2)\text{-}GeS_2(Se_2)$, degree of solid solubility and phases characts. 78-35377
- $Cu_xIn_xZr_{1-x}S_2$ system, struct. and cond. meas. *(French)* 80-88354
- $CuK_2H_2(PCrO_7)_2$, cryst. struct. determ. 80-28989
- $Cu_3MTl_2X_4$ (X=Se, Te, M=Fe, Ga, Al), struct. and phys. props. *(French)* 79-86758
- $CuMn_2O_4$, comment on cryst. struct. determs. by neutron diffr. 79-23585
- $CuMn_2O_4$, neutron diffr. exam., crystallographic props. 78-14329
- $Cu_2Mn_3O_8$ *(French)* 77-58987
- $Cu_{0.9}Mo_3S_4$, triclinic low-temp. struct. 80-28959
- $Cu_{2-x}Mo_3S_4$, X-ray cryst. struct. exam., effect of Cu conc. variation 78-2071
- $Cu_xMo_3S_4$, superconductivity and cryst. struct. 79-78250
- $Cu_xMo_6S_8$, Chevrel phase, lattice instabilities, X-ray diffr. meas. 78-34491
- $Cu_xMo_6S_8$, prep. by topotactic electrode reactions, struct., supercond. 79-99158
- $Cu(NH_3)TeO_3.H_2O$, crystal struct. determ. 77-80450
- $CuNa_2Si_4O_{10}$, synthetic, cryst. struct. determ. 77-47383
- $Cu_4NiSi_2S_7$, X-ray cryst. struct. determ., mag. props. 80-107172
- $CuO\text{-}Nb_2O_5$, phase anal., density determ. 78-10015
- $Cu_2O\text{-}Nb_2O_5$, phase anal., density determ. 78-10015
- $Cu_5O_2(PO_4)_2$, crystal prep. and struct. *(French)* 78-10004
- $(Cu_2O)_{1-x}U_{1.4}M_{4.6}O_{18}$, M=Mo, W, $0\leq x\leq 0.4$, crystallographic identification, paramag. props. *(French)* 79-46633
- $Cu_3P_2H_3(NO_3)(OH)_2.H_2O$, likasite, comp. and struct. *(French)* 77-47405
- $Cu_3(PO_4)_2$, cryst. struct. determ. 77-80476
- $Cu_4(PO_4)_2O$ *(French)* 78-55854
- $Cu_4(PO_4)_2O$, X-ray obs. 78-55855
- Cu_6PS_5Br, cryst. struct. of new superionic conductor 78-26514
- Cu_6PS_5Br, cryst. struct. at 293 and 473K, thermal parameters, neutron diffr. obs. 80-59450
- $CuPSe_2$, refinement of cryst. struct. *(French)* 77-43182
- $Cu_{1.94}S$, djurleite, cryst. struct., X-ray study 79-42033
- Cu_2S, low chalcocite, cryst. struct., X-ray study 79-42033
- $Cu_2S\text{-}Ga_2S_3$ alloys, cryst. growth, struct. and fluoresc. 77-48328
- $Cu_{2-x}S$, digenite, epitaxial layer, electron diffr. 77-85117
- $Cu_{2-x}S$, digenite related phases, electron microscope study 79-10840
- $Cu_{2-x}S$, single cryst., as p-component of heterojunction, props. 77-39926
- $Cu_{2-x}S$ single crysts. 77-24302
- Cu_9S_5, digenite, superstructuring, vacancy clustering, high-resolution electron microscopy 78-42981
- $Cu_9S_5(Cu_{2-x}S)$, high temp. digenite, cryst. struct. refining by X-ray diffr. method 79-23587
- $CuSO_4.3CO(NH_2)_2$, X-ray determ. of electron density distrib. 78-67699
- $Cu_2Se\text{-}GeSe$ quasibinary system, phase diagram and struct. 77-8802
- $Cu_{2-x}Se$, single cryst., as p-component of heterojunction, props. 77-39926
- $Cu_{2-x}Se(Te)$ crystals, struct. 79-90608
- Cu_4SnS_4, X-ray obs. *(French)* 77-19931
- $CuTa_2O_6$ *(French)* 78-51497
- $Cu_{0.5}TaO_3$, X-ray structural study 77-39575
- $Cu_{2-x}Te$, single cryst., p-component of heterojunction, props. 77-39926
- $Cu_{3-x}Te_2$, non-stoichiometric phases, electron microscopic and electron diffraction studies 80-64977
- $CuTe_2Cl$, cryst. struct., X-ray diffr. meas. 77-4075
- CuTeCl(Br)(I), struct., partial Cu^+ ionic cond. 77-84981
- CuTeI, X-ray cryst. struct. determ. *(German)* 79-32957
- $CuTeO_4$, cryst. struct. determ. 78-55845
- Cu_3TeO_6 78-42972
- $Cu_2Th_4(MoO_4)_9$, crystallographic data determ. *(French)* 78-10013
- $Cu_2TlSe_2(Cu_2TlTe_2)$, crystallographic studies 77-31640
- Cu_2TlX_2 (X=Se, Te), struct. and physical props. *(French)* 79-86758
- $Cu_2U_6S_{13}(Se_{13})$, cryst. struct. and magnetic props. *(French)* 80-96496
- CuV_2S_4, preparation, cryst. struct. and physical props. *(French)* 79-55714
- $Cu_{0.65}VS_2$, cryst. struct. and phys. props. *(French)* 79-60334
- $Cu_{0.75}VS_2$, cryst. struct. and phys. props. *(French)* 78-14328
- $Cu_6[Si_6O_{18}].6H_2O$, dioptase, cryst. struct. refining by X-ray and neutron diffr. methods 79-23586
- $DAl_{11}O_{17}$, anhydrous, cryst. struct. from powder neutron diffr. 80-1983
- γ-$DBa(PO_3)_2$, polyphosphate, crystal structure determination *(French)* 78-91314
- $D_3O.ClO_4$, solid, neutron powder diffr. study 80-107176
- D_xTaS_2, struct., form. by cathodic reduction, neutron diffr. obs. 79-73150
- $DyAsO_4$, cryst. struct. by X-ray diffr. co-operative Jahn-Teller transition 77-89411
- DyB_4, cryst. and mag. struct., neutron diffr. meas. 80-15692
- $DyFe_2B_2$, compounds with $CeAl_2Ga_2$ structure type *(Ukrainian)* 79-32970
- $Dy_2Fe_3Si_5$, cryst. struct. determ. 78-18620
- $Dy_3Ni_7B_2$, struct., space groups, X-ray study *(Ukrainian)* 80-39029
- Dy_5Ru_2, Mn_5C_2-type struct., X-ray cryst. struct. determ. 80-96483
- $DySbO_3$, single crysts., hydrothermal synthesis and crystallographic characteristics 79-95916
- Er complex, $ErL_6(ClO_4)_3$, L=tetramethyl, urea, struct. 77-62512

crystal atomic structure of inorganic compounds continued
ErAG, rare earth impurity, spectral probe of stoichiometry variations 77−85790
$ErAgSe_2$, cryst. struct. determ. *(French)* 77−47413
ErB_4, cryst. and mag. struct., neutron diffr. meas. 80−15692
$ErCl_3.6H_2O$, single cryst., H^+ coords., NMR 80−97152
$ErFe_3$, H_2 sorption, mag. and struct. props. of hydrides 80−34831
$ErFe_2B_2$, compounds with $CeAl_2Ga_2$ structure type *(Ukrainian)* 79−32970
$ErFe_2H_{3.65}$, $ErFe_2H_{4.12}$, Mossbauer spectra, electronic and structural studies 80−15860
$Er_3Fe_{5-x}In_xO_{12}$, lattice consts., T_c, mag. saturation, K-absorpt. and Mossbauer spectra, 80K *(Russian)* 77−20954
ErGG, rare earth impurity, spectral probe of stoichiometry variations 77−85790
$Er_4O_2(OH)_8.HNO_3$, gel-grown, cryst. struct. 77−35528
ErP_5O_{14}, X-ray cryst. struct. determ. 80−96486
$Er_2Sr_3(BO_3)_4$, cryst. struct. from X-ray diffr. meas. 77−89419
$ErVO_3$, produced by $Er_2O_3+VO_2$ high-press. reaction, cryst. struct. and mag. props. meas. 80−19773
$^{253}EsBr_x$, spectral and X-ray diffr. data, 25 to 700°C 77−28584
Eu selenides, X-ray phase anal. 77−11514
Eu-Bi system, X-ray powder diffr. data for phases Eu_5Bi_3, Eu_4Bi_3, $Eu_{11}Bi_{10}$ 79−51075
Eu-Te, chalcogenides, exam. of crystal-chemical characts. 79−1407
$Eu(Al_{0.5}Ta_{0.5})O_3$, mag. props. 77−4587
Eu_2As_2, single cryst. struct. refinement, X-ray diffr. 77−19817
Eu_3As_4, X-ray cryst. struct. determ. 79−99135
Eu_4As_3, new synthesis, trigonal anti-Th_3P_4-type compound, X-ray characterisation 79−37687
Eu_4As_3, X-ray cryst. struct. anal. 80−39013
Eu_5As_4, cryst. struct. determ., symmetrical version of Sm_5Ge_4-type struct. 78−63710
Eu_4As_2O, X-ray cryst. struct. determ., least squares refinement 78−9999
$Eu_3As_3.TaO$, X-ray cryst. struct. determ. 80−33940
$EuB_{6-x}C_x$, magnetic and elec. props. 78−91842
EuB_2O_4, X-ray single cryst. struct. determ., Patterson synthesis 79−19204
EuB_4O_7, X-ray cryst. struct. determ. 80−107135
$Eu_2B_5O_9Cl(Br)$, synthesis and characterisation 80−39039
$EuBr_{1.5}Cl_{0.5}$, preparation and characterisation 79−77571
EuC_6, intercalation cpd. with graphite, synthesis and struct. 80−44184
$EuCo_2Si_2$, cryst. struct. and valence state 77−76375
$Eu_{1-p}Cr_2S_{4-p}(Se_{4-p})$, modulation of intergrowth struct. 79−94967
$EuCu_2Ge_2$, cryst. struct. and valence state 77−76375
$EuCuSi_3$, cryst. struct. and valence state 77−76375
EuFX mixed halides, synthesis and lattice parameters 78−30594
$EuFe_2Si_2$, cryst. struct. and valence state 77−76375
$EuGa_3(BO_3)_4$, luminesc. spectra, local symmetry of rare earth ion determ. 80−16095
$EuGa(In)_2X_4$, X=S,Se,Te, prep. and props. 77−85214
$EuGa_2S_4$, cryst. struct. determ. by direct methods with MULTAN 76 *(French)* 79−37669
$Eu_2(GeO_4)O$, X-ray cryst. struct. determ. 79−99140
Eu_2GeS_4, X-ray cryst. struct., thiogermanate ion *(French)* 80−15066
$Eu_3Ge_3S_9$, X-ray cryst. struct. determ. *(French)* 79−7587
Eu_2IrH_5, prep., cryst. struct., mag. and elec. props. 80−88117
$Eu(Lu_{0.5}Ta_{0.5})O_3$, mag props. 77−4587
$Eu(Lu_{0.5}Ta_{0.5})O_3$, mag. props. 77−4587
$Eu(Mg_{0.5}W_{0.5})O_3$, mag. props. 77−4587
$EuMn_2P_2(As_2,Sb_2)$, pnictides with Ce_2O_2S-type struct. 79−65055
$Eu_2Nb_2O_7$-$Sr_2Nb_2O_7$, new system preparation 78−42994
$EuNi_2Ge_2$, cryst. struct. and valence state 77−76375
$EuNiSi_3$, cryst. struct. and valence state 77−76375
$EuNi_2Si_2$, cryst. struct. and valence state 77−76375
B-Eu_2O_3, cryst. struct. refinement from X-ray scattering data 79−37672
Eu_2O_3-Sc_2O_3-Ta_2O_5 system, orthotantalate section, X-ray diffr. and luminesc. obs., conc. depend. 80−54205
Eu_2O_3-Y_2O_3-Ta_2O_5, struct., phase form., luminesc. and X-ray diffr., obs. *(Russian)* 78−6765
$Eu(OH)_3$, cryst. struct. 80−24424
EuO(S)(Se)(Te), cryst. and electronic struct., mag., elec., and optical props., book contrib. 80−39760
Eu_3S_4, single cryst., X-ray cryst. struct. refinement *(French)* 79−23579
$EuSb_2$, cryst. struct. and antiferromag. props. 79−32973
Eu_2Sb_3, cryst. struct., elec. and mag. props. 80−33958
$EuSi_2$, high-pressure phase transform., cryst. struct. 77−35693
β-Eu_2SiO_4 *(French)* 78−47293
Eu_2SnS_4, cryst. struct. *(French)* 79−86757
$Eu_3Sn_2S_7$, cryst. struct. *(French)* 78−18597
$Eu_3Sn_2S_7$, cryst. struct. *(French)* 79−86757
$Eu_4Sn_2S_9$, cryst. struct. *(French)* 79−86757
$Eu_5Sn_3S_{12}$, cryst. struct. determ. *(French)* 77−47388
$Eu_5Sn_3S_{12}$, cryst. struct. *(French)* 79−86757
$Eu_{1-x}Sr_xSi_2$, solid solns., α-$ThSi_2$ struct. type, comp. and press depend. 78−91322
$Eu_2Ta_2O_7$-$Sr_2Ta_2O_7$, new system preparation 78−42994
Eu_2VO_4, prep. and props. 77−15379
$Eu_3V_2O_7$, prep. and props. 77−15379
$Eu_3VTa_2O_9$, prep., characterisation and mag. props. 78−26535
Eu_xWO_3-Sn_yWO_3, prep. and struct. of mixed W bronzes 77−4085
Eu_4Y_2X, (Y=pnictogen, X=chalcogen), anti-Th_3P_4 type struct. 79−65048
$F_{1-x}O$, wustite, X-ray struct. anal. *(French)* 80−70175
F_2SnBr_6, cryst. struct. determ. at room temp. 79−19202
$(Fe,Mn)_3C$, crystallochemical struct. *(Russian)* 77−55271
$(Fe,Mn)_5C_2$, crystallochemical struct. *(Russian)* 77−55271
$(Fe,Mn)_7C_3$, crystallochemical struct. *(Russian)* 77−55271
Fe complex, 1-(2-thiazolylazo)-2-naphtholato Fe (II), cryst. struct. 77−11536
Fe complex, cis-dichlorotetrakis (dimethylformamide) iron (III) tetrachloroferrate, cryst. struct. 79−32981
Fe complex, $FeOCl[(ethyltetramethylcyclopentadienyl)_2Fe]_{0.16}$ synthesis and struct. 80−44176
Fe complex, nitrile nonacarbonyl, cryst., mol. structs. 80−64967
Fe complex, nitrile nonacarbonyl cryst., mol. struct. 80−64968
Fe complex, tris(1-pyrrolidinecarbodithioato)iron(III), and related cpds. mag. props., struct. 77−89933
Fe complex, with 1,2,4-triazole, mag. susceptibility, 2-300K, struct. 77−77045
Fe intercalation compound, electron microscopy 80−84164

crystal atomic structure of inorganic compounds continued
Fe-lanthanid-O systems, thermodynamic props., composition and lattice constants 78−31390
Fe-WO_3 system, struct. phase exam. by optical microscopy and X-ray diffr. 78−31389
$Fe_{3-x}Al_xO_4$, cation distrib., mag. and other phys. props. 77−43818
$FeBO_3$-MBO_3 solid soln., (M=Mn, Cr, Al, Ga, In), synthesis, crystal chem. and mag. props. 78−31058
$Fe_4Ca_3S_3O_6$, struct. and phase analysis *(Russian)* 77−58995
$FeCl_2$-graphite, intercalation compound, formation by reduction of Fe(III) compounds with $Fe(CO)_5$ 78−63721
$FeCl_2.nH_2O$, cryst. struct. *(German)* 80−1987
$(Fe_{1-x}Co_x)_3P$, cryst. struct. and mag. props. 78−19222
$Fe_xCo_{1-x}Rh_2S_4$, spinel struct., X-ray, mag., elec. and Mossbauer spectra meas. 77−12278
$FeCr_{2-x}In_xSe_4$, struct. and mag. props., comp. depend. 77−66262
$FeCr_2O_4$, Mossbauer spectra and cryst. struct. determ. 79−56637
$Fe_2(CrO_4)_2$ $Cr_2O_7.4H_2O$, synthesis and struct. determ. Patterson and electronic density functions *(French)* 77−27853
α-$Fe_2(CrO_4)_3.3H_2O$ *(French)* 78−42960
$FeCr_2S_4$, vapour grown, struct. and stoichiometry, X-ray fluoresc. anal. 79−4263
$Fe_xCu_{1-x}Cr_2Se_4$, crystallographic and image props. 80−39049
$Fe_xCu_{1-x}Rh_2S_4$, mag. tetrahedral intrasublattice interaction, X-ray, magnetisation and Mossbauer expts. 78−52241
FeF_2, EXAFS at high press., bond compressibility, at. spacings 78−39628
$FeF_3.3H_2O$, α and β phase, ^{57}Fe Mossbauer study of local struct. 80−39973
$Fe_2F_5.7H_2O$ and oxidation products, ^{57}Fe Mossbauer study of local struct. 80−39973
α-$FeGa_2S_4$, 1T polytype, cryst. struct. refinement *(French)* 80−103304
$Fe_3Ge_2O_8$, crystal struct. determ. 80−49207
$FeH_2P_3O_{10}.H_2O$, cryst. struct. determ. *(French)* 77−47418
$Fe^{II}(H_2PO_4)_2.2H_2O$, cryst. and powder diffr. data *(French)* 80−24419
$FeH(SO_4)_2.4H_2O$, cryst. parameters and X-ray powder diffr. data *(French)* 79−14765
Fe(III) compounds, $A_2FeX_5.H_2O$, (A=alkali ion, X=Cl or Br), antiferromag. props. and struct. 78−31056
$FeIn_2S_4$, indite, thiospinel, cation ordering in tetrahedral sites, X-ray diffr. meas. 78−95028
$Fe_{10.92}K_{1.55}O_{17}$, ferrite, cryst. struct., nonstoichiometry, ion-ion correlations 80−88130
$FeLu_2S_4$, structural study, X-ray diffr., Mossbauer spectroscopy 80−107159
$(Fe_{1-x}M_x)_3P$, cryst. struct. and mag. props. 78−19222
$FeMnGaO_4$, X-ray study of cryst. struct. and ionic config. 78−55851
$(Fe_{1-x}Mn_x)_3P$, cryst. struct. and mag. props. 78−19222
$Fe_2(MoO_4)_3$, cryst. struct. and twinning behaviour 80−33967
$FeMo_2Re_2S_8$, cubic structure, mixed tetrahedral cluster *(French)* 77−15372
$FeMo_2S_4$, cryst. struct., mag. struct. and props., neutron diffr. meas. *(French)* 77−47971
$FeMo_3S_4$, triclinic, containing Fe pairs, X-ray cryst. struct. anal. 80−54193
$Fe_2NaBa_6Ge_8O_{24}.4(OH,H_2O)$, growth and struct. 77−65971
$FeNa_6(SO_4)_4$, vanthoffite cryst. struct. lattice parameters and thermal behaviour 77−19929
$(Fe_{0.45}Nb_{0.53})O_2$, rutile, cation distrib. and mag. ordering *(German)* 80−107116
$Fe_{0.33}NbS_2$, intercalation compound, struct. and photoemission meas. 77−16453
$Fe(Nb_{1-x}W_x)O_4$, mag. and elec. props. and Mossbauer effect 79−78590
$(Fe_{1-x}Ni_x)_3P$, cryst. struct. and mag. props. 78−19222
FeO-Fe_2O_3-SiO_2 system, molten, struct. using high temp. X-ray method *(Japanese)* 80−14992
$Fe_{1-x}O$, wustite, defect struct. 80−107216
$Fe_{1-x}O$, wustite, modulated struct., struct. refinement 79−94966
$Fe_{1-z}O$, wustite, struct. evolution, mean isotropic thermal agitation factor, depend. on equil. temp. and comp. *(French)* 77−68947
$Fe_{1-z}O$, wustite, struct. at high temp., neutron diffr. obs. *(French)* 79−86754
$Fe_{1-z}O$, wustite, struct. at high temp., neutron diffr. *(French)* 80−1982
Fe_2O_3, haematite, X-ray diffr. of high temp. anomalous behaviour of cryst. lattice 77−58991
α-Fe_2O_3, hematite, high temp. anomalous behaviour of cryst. lattice 77−69087
α-Fe_2O_3, mutual orientations of different lattices *(French)* 79−51038
Fe_2O_3-TiO_2 system, high temp. intergrowth struct., metal atom ordering in intergrowth boundaries 78−79573
Fe_3O_4, magnetite, electronic struct. at low temps., NMR anal. 78−67686
Fe_3O_4 magnetite, polycryst., X-ray struct., anal. *(German)* 77−72598
Fe_3O_4, magnetite, X-ray diffr. investig. of low temp. phase symm. 77−15364
FeOCl, cathodic reduction in organic electrolytes, intercalation complex production 79−1833
FeOCl intercalation cpds. with Li and amines, cryst. struct. 78−51512
α-FeO_2H, asymmetric line shapes of Mossbauer spectra *(Chinese)* 80−103902
β-FeOOH, dehydration 80−79767
FeOOH, high-pressure phase, neutron diffraction study 78−52212
β-FeOOH, lattice imaging and pore struct., high resolution electron microscopy obs. 80−103310
δ-FeOOH, structure and phase transform., Mossbauer, X-ray, DTA study *(Chinese)* 80−54368
α-$FeOOH.nH_2O$, hydrogoethites, weak ferromag. props. 77−53042
FeP_4, prep. and props., struct. anal. 79−14775
FeP_4, twinned cryst., synthesis and cryst. struct. 79−4278
Fe_3P-type structures, atomic coord. and bonding 79−60330
FeS, zinc blende type, crystallographic and Mossbauer obs. 78−87650
FeS-Ga_2S_3 system, intermediate phases crystallographic study *(French)* 79−51061
FeS_2 (pyrite), glide elements study by electron microscopy and electron diffr. 78−83817
FeS_2, EXAFS at high press., bond compressibility, at. spacings 78−39628
$Fe_{1-x}S$, NC-type, wave distrib. of vacancies 79−99178
$Fe_{1-x}S$, pyrrhotite, modulated struct., struct. refinement 79−94966
Fe_7S_8, 3C pyrrhotite, cryst. struct. refinement 79−42017
$FeSO_3$, anhydrous, X-ray cryst. struct. determ. *(French)* 80−92486